HERMAN F. MARK

ENCYCLOPEDIA OF POLYMER SCIENCE AND TECHNOLOGY

THIRD EDITION

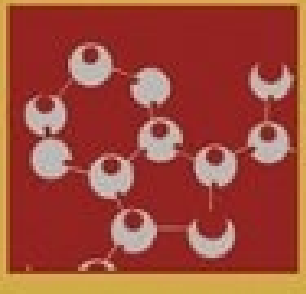

ACETYLENIC POLYMERS, SUBSTITUTED

Introduction

Polymerization of acetylene was first achieved by Natta and his co-workers using a Ti-based catalyst (1). Because of the lack of processability and stability, early studies on polyacetylenes were motivated by theoretical and spectroscopic interests only. Then the discovery of the metallic conductivity of doped polyacetylene (2–6) stimulated research into the chemistry of polyacetylene, and now polyacetylene is recognized as one of the most important conjugated polymers. The finding by Natta and co-workers was followed by the modification of their catalytic system. An explosive expansion in polyacetylene chemistry has been caused by the entry of the Shirakawa catalyst $Ti(O\text{-}n\text{-}C_4H_9)_4$–$(C_2H_5)_3Al$. Its very unique ability to give a thin film of polyacetylene (7,8) has attracted the interest of solid-state physicists, which has significantly contributed to the fundamental chemistry of conjugated macromolecules.

Unfortunately, the intractability and unstability of polyacetylene strictly inhibit its practical applications. Thus, an introduction of substituents onto polyacetylene backbone has been investigated to improve its processability. Early attempts led to the conclusion that only sterically unhindered monosubstituted acetylenes can be polymerized with the Ti-based Ziegler–Natta catalysts. Traditional ionic and radical initiators also lack the ability to provide high molecular weight polymers from substituted acetylenes. In 1974 the first successful polymerization of substituted acetylene was achieved when it was found that "Group 6" transition metals are quite active for the polymerization of phenylacetylene to a polymer with molecular weight over 10^4 (9). After this finding, there has been much effort to develop highly active catalysts, to tune the polymer properties, and

Encyclopedia of Polymer Science and Technology. Copyright John Wiley & Sons, Inc. All rights reserved.

also to precisely control the polymer structure. These energetic studies have produced a wide variety of polymers from acetylene derivatives including mono- and disubstituted acetylenes, α,ω-diynes, and 1,3-diacetylenes. The carbon–carbon alternating double bonds in main chains of these polymers provide an opportunity to obtain unique properties such as conductivity, nonlinear optical properties, magnetic properties, permeability, photo- and electroluminescent properties, and so on, which are not accessible from the corresponding vinyl polymers.

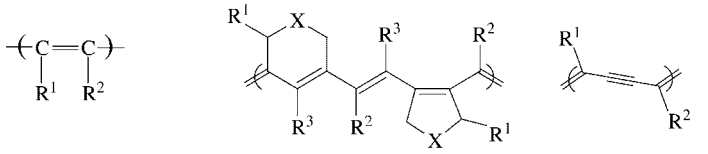

Many papers in the literature have followed the finding by Masuda and coworkers (9). This article covers the literature from the mid-1980s up to mid-2000. As a result of the rapid growth in the area, the chemistry of polymers from acetylene, 1,3-diacetylenes, and α,ω-diacetylenes are excluded (see POLYACETYLENE; DIACETYLENE and TRIACETYLENE POLYMERS). The first focus is on the polymerization reaction of substituted acetylenes with various transition metal catalysts. The synthesis of functionally designed polyacetylenes is also covered. Readers are encouraged to access other reviews and monographs on polyacetylene (10–14), on 1,3-diacetylenes (15–19), and on α,ω-diynes (20,21). Previous review articles are also helpful to survey the chemistry of substituted polyacetylenes (10,13,22–29).

Polymerization Catalysts

A variety of transition metal catalysts have been found to polymerize substituted acetylenes. Effective catalysts range from Group 3 to Group 10 metals. Activity of catalysts greatly depends on monomer structure; therefore, it is quite important to recognize the characteristics of each catalyst. Table 1 lists recent representative examples for the polymerization of substituted acetylenes with various transition metal catalysts, which will help readers to understand the general features of catalysts.

Group 3 Transition Metals. Examples for the polymerization of substituted acetylenes with "Group 3" transition metals are rather limited (134). Ziegler–Natta catalysts based on Group 3 transition metals polymerize acetylene and its derivatives (32,33,62). The combination of Sc or lanthanide transition metals with trialkylaluminum, eg, M(naphthenate)– and M(phosphonate)–*i*-$(C_4H_9)_3Al$, has been proven to provide high molecular weight polymers from terminal aliphatic and aromatic alkynes. High molecular weight polymers (M_n > 30,000) are available from aliphatic linear alkynes such as 1-hexyne and 1-pentyne, whereas 1-alkynes with branching at α or β-position, eg, 3-methyl-1-pentyne and 4-methyl-1-pentyne, result in polymers in low yields (32,33). In a similar way, phenylacetylene polymerizes in the presence of a ternary

Table 1. Substituted Acetylenes That Form High Molecular Weight Polymers with Transition Metal Catalysts

Monomer	Catalyst	M_n, 10^3	Reference
[A] Monosubstituted aliphatic acetylenes [HC≡CR]			
R = n-C_4H_9	$W(dmp)_4Cl_2$–C_2H_5MgBr(a)	170	30,31
	$Nd(naphthenate)_3$–i-$(C_4H_9)_3Al$	35	32,33
$CH(CH_3)C_2H_5$	$Fe(acac)_3$–$(C_2H_5)_3Al$[b]	27	34
	$MoCl_5$–$(C_6H_5)_4Sn$	13	34
$C(CH_3)_3$	$MoCl_5$	33	35
	$MoOCl_4$-n-Bu_4Sn-C_2H_5OH	149	36
	$MoCl_2(CO)_3(As\ C_6H_5)_2)_2$	335	37
	(nbd)$Rh^+[(\eta^6$-$C_6H_5)B^-(C_6H_5)_3]$[c]	28	38
(S)-$(CH_2)_2C(CH_3)C_2H_5$	$Fe(acac)_3$–i-$(C_4H_9)_3Al$[b]	[η]=1.22	39
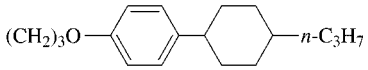	$Fe(acac)_3$–$(C_2H_5)_3Al$[b]	610	40
	$MoCl_5$–$(C_6H_5)_4Sn$	15	40
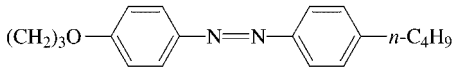	[(nbd)RhCl]$_2$–$(C_2H_5)_3N$[c]	96	41
	$Fe(acac)_3$–$(C_2H_5)_3Al$[b]	121	41
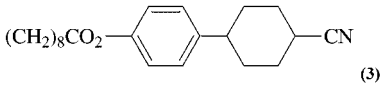 (3)	WCl_6–$(C_6H_5)_4Sn$	14	42
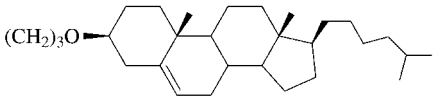			

Table 1. (Continued)

Monomer	Catalyst	M_n, 10^3	Reference
$Si(CH_3)_2$-*n*-C_6H_{13}	WCl_6–$(C_6H_5)_4Sn$	17	44
	$NbCl_5$	39	44
$CH(n\text{-}C_5H_{11})Si(CH_3)_3$	$Mo(CO)_6$–CCl_4–hν	105	45
n-C_6F_{13}	WCl_6–$(C_6H_5)_4Sn$	[η]=0.08	46
CO_2-*n*-C_4H_9	$[(nbd)RhCl]_2$	20	47
CO_2CH_3	$MoCl_5$–$(C_6H_5)_4Sn$	[η]=0.063	48
CO_2H	$MoCl_5$	[η]=0.047	48
	$(Cp*RuCl_2)_2$	4	49
CO_2-(−)-menthyl	$[(nbd)RhCl]_2$[c]	250	50
	$MoOCl_4$–*n*-$(C_4H_9)_4Sn$	18	50
$CH_2N(CH_3)_2$	$Ni(NCS)_2(P(C_6H_5)_3)_2$	16	51
	$Pd(P(C_6H_5)_3)_2[C{\equiv}CCH_2N(CH_3)_2]_2$	15	52
CH_2OH	$Pd(P(C_6H_5)_3)_2(C{\equiv}CCH_2OH)_2$	53	52
CH_2-*N*-indolyl	$[(nbd)RhCl]_2$–$(C_2H_5)_3N$[c]	71	53
$CH_2CH(CO_2C_2H_5)PO(OC_2H_5)_2$	WCl_6–$C_2H_5AlCl_2$	9	54
$CH_2{}^+P(C_6H_5)_3B(C_6H_5)_4{}^-$	$MoCl_5$-$(C_6H_5)_4Sn$	12	55
[B] Monosubstituted aromatic acetylenes			
Phenylacetylenes [$HC{\equiv}CC_6H_4R$]			
R = H	WCl_6–$(C_6H_5)_4Sn$	15	56
	$W(CO)_6$–CCl_4-hν	77	57
	$WCl_2(CO)_3(As(C_6H_5)_3)_2$	33	37
	$W(CO)_6$–$(C_6H_5)_2CCl_2$-hν	21	58,59
	$Fe(acac)_3$-$(C_2H_5)_3Al$[b]	4.2	60,61
	$Sm(naphthenate)_3$-*i*-$(C_4H_9)_3Al$	184	62
	$(cod)Rh(L)PF_6$–NaOH[d]	8.7	63
	$[(nbd)RhCl]_2$–$(C_2H_5)_3N$[c]	160	64
p-*n*-C_4H_9	$Fe(acac)_3$-$(C_2H_5)_3Al$[b]	39	65
	$[(nbd)RhCl]_2$–$(C_2H_5)_3N$[c]	240	65
	$MoCl_5$-*n*-$(C_4H_9)_4Sn$	9.2	65

p-Adm[e]	$[(nbd)RhCl]_2$–$(C_2H_5)_3N$[c]	>1000	65
p-OCH_3	$[(nbd)RhCl]_2$–$(C_2H_5)_3N$[c]	60 (*M*w)	66
p-Cl	$[(nbd)RhCl]_2$–$(C_2H_5)_3N$[c]	260 (*M*w)	66
p-NO_2	$[(cod)RhCl]_2$[d]	15.5	67
m-CH=NC_6H_5	$[(nbd)RhCl]_2$–$(C_2H_5)_3N$[c]	588	68
p-I	$WOCl_4$	19	69
p-CO_2CH_3	$(nbd)Rh^+[(\eta^6\text{-}C_6H_5)B^-(C_6H_5)_3]$[c]	218	38
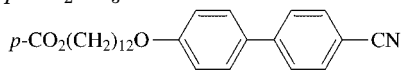	$[(nbd)RhCl]_2$–$(C_2H_5)_3N$[c]	158	70
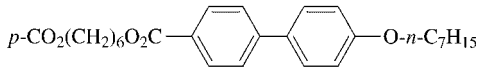	$[(nbd)RhCl]_2$–$(C_2H_5)_3N$[c]	122	71
p-CO_2-(-)-menthyl	$[(nbd)RhCl]_2$–$(C_2H_5)_3N$[c]	1260	72
p-(+)-OCONHC∗H(CH_3)C_6H_5	$[(nbd)RhCl]_2$–$(C_2H_5)_3N$[c]	320	73
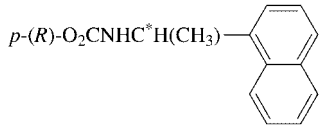	$[(nbd)RhCl]_2$–$(C_2H_5)_3N$[c]	51	74
p-(1*R*,2*S*)CH_2NHC∗H(CH_3)C∗H(OH)C_6H_5	$[(nbd)RhCl]_2$[c]	48	75
p-N-*n*-$(C_4H_9)_2$	$[(nbd)RhCl]_2$–$(C_2H_5)_3N$[c]	>1000	76
p-N-*i*-$(C_3H_7)_2$	$[(nbd)RhCl]_2$–$(C_2H_5)_3N$[c]	–	~

Table 1. (Continued)

Monomer	Catalyst	M_n, 10^3	Reference
o-CH_3	$W(CO)_6$–CCl_4–hν	170	78
	WCl_6–$(C_6H_5)_4Sn$	57	78
o-CF_3	$W(CO)_6$–CCl_4-hν	260	79
	WCl_6–$(C_6H_5)_4Sn$	190	80
	$MoCl_5$-$(C_6H_5)_4Sn$	280	80
2,5-$(CF_3)_2$	$W(CO)_6$–CCl_4-hν	[η]=0.352	81
o-$Si(CH_3)_3$	$W(CO)_6$–CCl_4-hν	1200	82
	$MoCl_5$-*n*-$(C_4H_9)_4Sn$-C_2H_5OH	43	83
	$Mo[OCH(CF_3)_2]_2$(=N-Adm)=$CHC(CH_3)_2C_6H_5$ (**7g**)[e]	14	84
o,*o*,*m*,*m*,*p*-F_5	WCl_6–$(C_6H_5)_4Sn$	[η]=0.61	85
o,*o*,*m*,*m*,-F_4-*p*-*n*-C_4H_9	WCl_6–$(C_6H_5)_4Sn$	110	85
m-N=NC_6H_5	[(nbd)RhCl]$_2$–$(C_2H_5)_3N$[c]	110	86
o-Fc (**14**)[f]	**7j**	16	87
p-CH=CHFc (**15**) [f]	**7j**	19	87
p-N=NFc (**16**)[f]	**7j**	11	87
p-C≡CC_6H_4-*p*-C≡CFc (**17**)[f]	**7j**	18	88
Other aromatic acetylenes [HC≡CAr]			
Ar = 1-Naphthyl	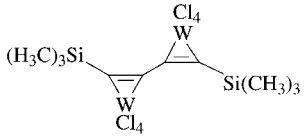	95	89
	(**3**)		
	WCl_6–$(C_6H_5)_3Bi$	46	90
	WCl_6/dioxane	36	91
2-Naphthyl	WCl_6–$(C_6H_5)_4Sn$	9	92
1-Anthryl	WCl_6–$(C_6H_5)_4Sn$	37	93
2-Anthryl	WCl_6–$(C_6H_5)_4Sn$	9	93
9-Anthryl	WCl_6	Insoluble	90

7	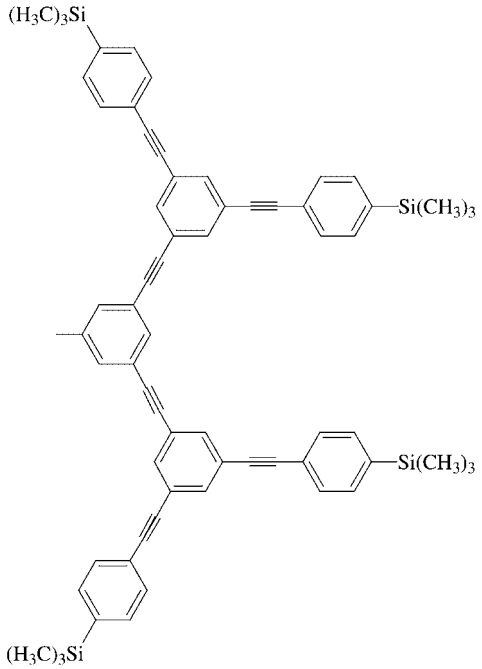	[(nbd)RhCl]$_2$–(C_2H_5)$_3$N[c]	340	97
	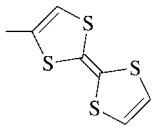	[(nbd)RhCl]$_2$–(C_2H_5)$_3$N[c]	11.7	98

Table 1. (Continued)

Monomer	Catalyst	M_n, 10^3	Reference
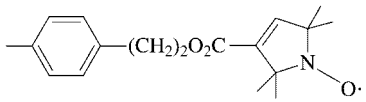	$[(cod)RhCl]_2$[d]	95.3	99
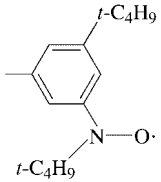	$[(nbd)RhCl]_2$–$(C_2H_5)_3N$[c]	11	100
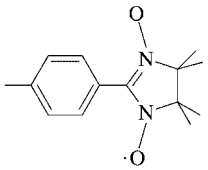	$(cod)Rh(NH_3)Cl$[d]	150	101
Ferrocenyl $[(\eta^6\text{-}C_5H_4)Fe(\eta^6\text{-}C_5H_5)]$ (**12**)	**7j**	16.4	102
Ruthenocenyl $[(\eta^6\text{-}C_5H_4)Ru(\eta^6\text{-}C_5H_5)]$ (**13**)	**7j**	16	102
[C] Disubstituted aliphatic acetylenes $[R^1C{\equiv}CR^2]$			
$R^1 = CH_3$ $R^2 = n\text{-}C_3H_7$	$MoCl_5$	1100 (M_w)	103
C_2H_5 C_2H_5	WCl_6–$(C_6H_5)_4Sn$	Insoluble	104
	$(OAr)_3Ta[C(CH_3)C(CH_3)CH\text{-}t\text{-}C_4H_9](py)$[g] (**3**)	17.9	105
Cl $n\text{-}C_6H_{13}$	$MoCl_5$–$n\text{-}(C_4H_9)_4Sn$	510	106
Br $n\text{-}C_4H_9$	WCl_6	7.1	107
CH_3 S-$n\text{-}C_4H_9$	$MoCl_5$-$(C_6H_5)_3SiH$	71	108
CH_3 Fc[f]	WCl_6–$(C_6H_5)_4Sn$	16	109

CH_3 $Si(CH_3)_3$ (**18**)	$TaCl_5$	130	110
	$NbCl_5$	210	110
	$TaCl_5$-$(C_6H_5)_3Bi$	1800	111
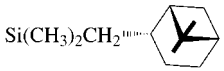			
CH_3	$TaCl_5$-$(C_6H_5)_3Bi$	80	112
CH_3 $Si(CH_3)_2C_6H_5$	$TaCl_5$-$(C_6H_5)_4Sn$	150	113
CH_3 $Ge(CH_3)_3$	$TaCl_5$	809	114
	$TaCl_5$	Insoluble	115
[D] Disubstituted aromatic acetylenes [RC≡CAr]			
R = CH_3 Ar=C_6H_5	$TaCl_5$	[η]=2.70	116
	$TaCl_5$-*n*-$(C_4H_9)_4Sn$	600	117
Cl C_6H_5	$MoCl_5$-*n*-$(C_4H_9)_4Sn$	690 (M_w)	118
Cl C_6H_4-*p*-Adm[e]	$MoCl_5$-*n*-$(C_4H_9)_4Sn$	110	119
C_6H_5 C_6H_5	WCl_6–$(C_6H_5)_4Sn$	Insoluble	120
C_6H_5 C_6H_4-*p*-$Si(CH_3)_3$	$TaCl_5$-*n*-$(C_4H_9)_4Sn$	750	121
			122
C_6H_5 C_6H_4-*p*-$Si(C_6H_5)_3$	$TaCl_5$-*n*-$(C_4H_9)_4Sn$	1900	123
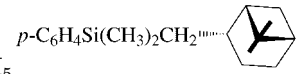			
C_6H_5	$TaCl_5$-*n*-$(C_4H_9)_4Sn$	>100	124

Table 1. (Continued)

Monomer	Catalyst	M_n, 10^3	Reference
C_6H_5 C_6H_4-*p*-$OC(CF_3)$=$C[CF(CF_3)_2]_2$	$TaCl_5$-*n*-$(C_4H_9)_4Sn$	$[\eta]$=0.87	125
C_6H_5 C_6H_4-*p*-C_6H_5	$TaCl_5$-*n*-$(C_4H_9)_4Sn$	Insoluble	126
C_6H_5 C_6H_4-*p*-*N*-Carbazolyl	$TaCl_5$-*n*-$(C_4H_9)_4Sn$	190	127
C_6H_5 C_6H_4-*p*-$Ge(CH_3)_3$	$TaCl_5$-9-BBN	1000	128
C_6H_5 C_6H_4-*p*-*t*-C_4H_9	$TaCl_5$-*n*-$(C_4H_9)_4Sn$	460	129
C_6H_5 C_6H_4-*p*-$CH_2C_6H_5$	$TaCl_5$-*n*-$(C_4H_9)_4Sn$	350	126
C_6H_5 C_6H_4-*p*-Adm[e]	$TaCl_5$-*n*-$(C_4H_9)_4Sn$	2200	119
[E] Cyclic acetylenes			
Cyclooctyne	$(CO)_5W$=$C(C_6H_5)OCH_3$ (**4**)	Insoluble	130
	(*t*-$C_4H_9O)_3Mo$≡C-*n*-C_3H_7[g]	Insoluble	131
	W_2(O-*t*-$C_4H_9)_6$[g]	Insoluble	132
	$PdCl_2(C_6H_5CN)_2$	Insoluble	133

[a] dmp = OC_6H_3-*o*,*o*-$(CH_3)_2$.
[b] acac. = acetyleacetonate.
[c] nbd = bicyclo[2.2.1]hepta-2,5-diene (2,5-norbornadiene).
[d] cod = 1,5-cyclooctadiene, 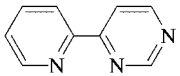
[e] Adm = 1-adamantyl.
[f] py = pyridine, Ar = *o*,*o*-*i*-$(C_3H_7)_2C_6H_3$.
[g] Ring-opening polymerization.

Ln(naphthenate)–*i*-$(C_4H_9)_3Al$–C_2H_5OH catalyst (62). Sc- and Nd-based catalysts are relatively effective among the other Group 3 transition metals including 15 lanthanide elements. One of the characteristic points of these catalytic systems is the selective formation of cis-cisoidal polymers. Thus, poly(phenylacetylene) formed with Ln(naphthenate)–*i*-$(C_4H_9)_3Al$–C_2H_5OH is crimson, crystalline, and insoluble. The resultant poly(phenylacetylene) gradually dissolves into *o*-dichlorobenzene at 135°C (62), which probably results from the thermally induced cis-to-trans isomerization of the main chain.

Group 5 Transition Metals. The most probable side reaction in the polymerization of acetylenes is cyclooligomerization that is well promoted by "Group 5" transition metals. For example, cyclotrimerization of 1-alkynes readily occurs in the presence of $NbCl_5$ (135–137). Thus, bulky substituents must be incorporated into the monomers for the successful formation of polymers by Group 5 transition metals. In other words, Ta and Nb catalysts suit the polymerization of disubstituted acetylenes.

The most convenient catalysts are $TaCl_5$ and $NbCl_5$. Both catalysts can polymerize disubstituted acetylenes such as 3-octyne (138) and 1-phenylpropyne (116). The use of cocatalysts such as *n*-$(C_4H_9)_4Sn$, $(C_2H_5)_3SiH$, $(C_6H_5)_3Sb$, $(C_6H_5)_3Bi$, and $(C_6H_5)_4Sn$ accelerates the polymerization and suppresses the polymer degradation, leading to the formation of ultra high molecular weight polymers. For example, polymers with molecular weight above 10^6 are obtained from 1-trimethylsilyl-1-propyne (113) and diphenylacetylenes (121) with $TaCl_5$–$(C_6H_5)_4Sn$. Without a cocatalyst, diphenylacetylenes give no polymers (120). It has been reported that well-characterized dinuclear Nb and Ta complexes (**1**) polymerize disubstituted acetylenes (139). Like $NbCl_5$ and $TaCl_5$, cyclooligomerization dominates over the polymerization in the case of monosubstituted acetylenes. The Nb version of (**1**) gives good yields of polymers compared with the Ta analogue. Ta carbene (**2**) induces living polymerization of 2-butyne (105).

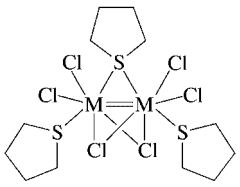

M = Ta, Nb

1

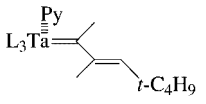

(L = OC_6H_3-*o*, *o*-*i*-$(C_3H_7)_2$)

2

Monosubstituted acetylenes generally prefer cyclotrimerization to polymerization in the presence of halides of "Group 5" metals as described earlier (135–137). The polymerization of monosubstituted acetylenes by $NbCl_5$ and $TaCl_5$ catalysts is possible only in the case of sterically crowded monomers, which is exemplified by the polymerization of 3-trialkylsilyl-1-alkynes with the formula of HC≡CCH($Si(CH_3)_2R$)R′ (R = CH_3, *n*-C_6H_{13}, C_6H_5; R′ = *n*-C_3H_7, *n*-C_5H_{11}, *n*-C_7H_{15}) (45). Even *tert*-butylacetylene affords a low yield of polymer in the presence of $TaCl_5$ or $NbCl_5$. Additionally, the molecular weights of these Ta- and Nb-based poly(*tert*-butylacetylene)s are lower than those of the W-based ones. However, there has been a demonstration of the unique ability of

2,6-dimethylphenoxyo (dmp) complexes of Nb, $Nb(dmp)_nCl_{5-n}$ (dmp = OC_6H_3-*o,o*-CH_3, $n = 1$ or 2) with cocatalysts such as C_2H_5MgBr or $(C_2H_5)_3Al$, to polymerize terminal acetylenes such as *tert*-butylacetylene and phenylacetylene (30,31). From *tert*-butylacetylene, extremely high molecular weight polymers are available. Even poly(phenylacetylene) prepared with $Nb(dmp)Cl_4$–*t*-C_4H_9MgCl possesses relatively high molecular weight ($M_n = 19{,}000$). Such an exceptional ability of $Nb(dmp)_nCl_{5-n}$–cocatalyst originates from the presence of bulky aryloxo groups that have the same effect as bulkiness on the monomer.

Group 6 Transition Metals. This class is most widely employed because of their high ability to polymerize a wide range of substituted acetylenes (10,23,25, 26). We shall classify "Group 6" transition metals into the following four categories: metal halide catalysts, metal carbonyl catalysts, metal carbene catalysts, and metal alkylidene catalysts.

Metal Halide Catalysts. $MoCl_5$ and WCl_6, the most convenient "Group 6" transition metal catalysts, give high yields of polymers from various monosubstituted acetylenes, especially from bulkily monosubstituted acetylenes. In the case of sterically not very crowded monomers such as 1-*n*-alkyne and phenylacetylene, the yields and molecular weights of polymers are unsatisfactory ($M_n < 1 \times 10^5$) because of the unavoidable formation of cyclotrimers (140). In contrast, sterically crowded monomers like *tert*-butylacetylene and ortho-substituted phenylacetylenes selectively polymerize with $MoCl_5$ and WCl_6 to give high molecular weight polymers. $MoCl_5$ or WCl_6 alone are unfortunately inactive for disubstituted acetylenes.

Appropriate organometallic cocatalysts such as *n*-$(C_4H_9)_4Sn$, $(C_2H_5)_3SiH$, $(C_6H_5)_3Sb$, $(C_6H_5)_3Bi$, and $(C_6H_5)_4Sn$ remarkably activate $MoCl_5$ and WCl_6 catalysts and allow the effective polymerization of even disubstituted acetylenes such as 2-octyne (103) and 1-chloro-1-octyne (106). Living polymerization is also possible by applying this catalyst system (141). For example, in the presence of an appropriate protic additive (*e*g, C_2H_5OH, *t*-C_4H_9OH), $MoOCl_4$–*n*-$(C_4H_9)_4Sn$ gives polymers with narrow molecular weight distributions ($M_w/M_n < 1.1$) from various mono- and disubstituted acetylenes (25,27,28).

A systematic study was made on the nature of W-based catalysts, $W(dmp)_nCl_{6-n}$–cocatalyst ($n = 1$–4), in the polymerization of terminal acetylenes (30,31). The catalytic activity of $W(dmp)_nCl_{6-n}$ is generally lower than that of WCl_6 because the electron-donating phenoxy ligands reduce the Lewis acidity of the metal. However, these catalysts are characterized by the ease of fine-tuning of the activity, which can be simply performed by varying the number of ligands. $W(dmp)_nCl_{6-n}$ catalyzes the polymerization of *tert*-butylacetylene to give an extremely high molecular weight polymer in the presence of cocatalysts such as C_2H_5MgBr and $(C_2H_5)_3Al$. Emphasis should be placed on the fact that the enhanced bulkiness around W in $W(dmp)_nCl_{6-n}$ enables the polymerization of *n*-alkylacetylenes, leading to high molecular weight polymers. This contrasts to the feature of the WCl_6–catalyzed polymerization that generally results in low molecular weight polymers from the less sterically hindered monomers such as 1-alkynes ($M_n \sim 10^4$). For example, $W(dmp)_4Cl_2$–C_2H_5MgBr transforms 1-octyne into an elastomer with M_n of 350,000, while WCl_6 provides yellow viscous oil.

It has been reported that a stable W-based butadiyne complex (**3**) polymerizes ortho-substituted phenylacetylenes (142) and monosubstituted arylacetylenes

having condensed aromatic rings to give polymers having extended main-chain conjugation (89).

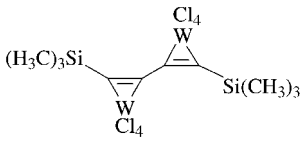

3

Metal Carbonyl Catalysts. Mo or W hexacarbonyl alone cause no polymerization of acetylenes. However, upon uv irradiation in halogenated solvents such as CCl_4, various substituted acetylenes readily polymerize with Mo and W hexacarbonyls (10,23,25,26). $Cr(CO)_6$ as well as other "Group 7" metal carbonyls such as $Mn_2(CO)_{10}$ and $Re_2(CO)_{10}$ yield no active species under similar conditions. CCl_4, used as a solvent, plays a very important role for the formation of active species, and therefore, cannot be replaced by toluene, that is often used for metal chloride-based catalysts. Although the activity of metal carbonyl catalysts is low compared with the metal halide catalysts, they provide extremely high molecular weight polymers. Another advantage of metal carbonyl catalysts is their stability, which facilitates the experimental procedure.

An alternative metal carbonyl catalyst, $(Mes)Mo(CO)_3$ (Mes = mesitylene), also catalyzes the polymerization of substituted acetylenes in CCl_4 (143). Photoirradiation is unnecessary for this system; the ligating mesitylene is readily released by heating, which allows the polymerization to proceed without photoirradiation. In a similar way, photoirradiation can be omitted by using $(CH_3CN)_3M(CO)_3$ as a catalyst (144).

The use of $(C_6H_5)_2CCl_2$ enables the omission of CCl_4 in the metal-carbonyl catalyzed polymerization of acetylenes. For example, the polymerization of phenylacetylene with $W(CO)_6$ in the presence of $(C_6H_5)_2CCl_2$ in toluene proceeds homogeneously and gives a polymer with M_n of 17,000 in 68% yield upon photoirradiation (58,59). Very high molecular weight polymers ($M_w > 10^5$) are attainable from sterically bulky aromatic and aliphatic acetylenes. An alternative metal carbonyl catalyst, $MCl_2(CO)_3[As(C_6H_5)_3]$ (M = Mo, W), that catalyzes the ring-opening polymerization of norbornenes has been shown to polymerize *tert*-butylacetylene and ortho-substituted phenylacetylenes without photoirradiation or the use of CCl_4 (37).

Metal Carbene Catalysts. The first use of isolated single-component carbene catalysts showed that the Fischer (**4**) and Casey carbenes (**5**) polymerize phenylacetylene, *tert*-butylacetylene, and cyclooctyne in low yields (130). For example, the bulk polymerization of *tert*-butylacetylene with (**4**) gives a high molecular weight (M_n = 260,000) polymer in 28% yield. Polymer-supported Fischer carbene (**4**) is also active for the polymerization of phenylacetylene under photoirradiation (145). As a catalyst, the Casey carbene (**5**) is less stable but more active than the Fischer carbene (130). The Rudler carbene (**6**) readily releases the intramolecularly ligated double bond upon the approach of an acetylenic monomer. Thus, it is more active than the Fischer and Casey carbenes (146–148). These carbene complexes are, however, unable to control the polymerization.

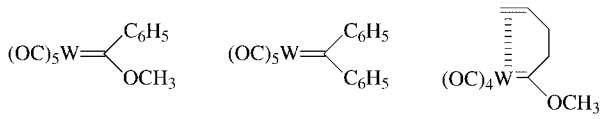

4 5 6

The polymerization chemistry of substituted acetylenes has been explosively evolved by the development of well-characterized Mo- and W-based metal carbenes with the structure of (**7**). Although the preparation of these catalysts is somewhat tedious, they elegantly function as living polymerization catalysts for substituted acetylenes such as ortho-substituted phenylacetylenes (84,149) and α,ω-diynes (150–152). Since the initiation efficiency is quantitative, polymers with a desired molecular weight are available. The structure of both terminal ends can be controlled by using appropriate terminating agents. The bifunctional Schrock carbene (**8**) bisinitiates the polymerization of diethyl dipropargylmalonate, $(HC{\equiv}CCH_2)_2C(CO_2C_2H_5)_2$, giving telechelic living polymers (151). Details for the living polymerization are described herein.

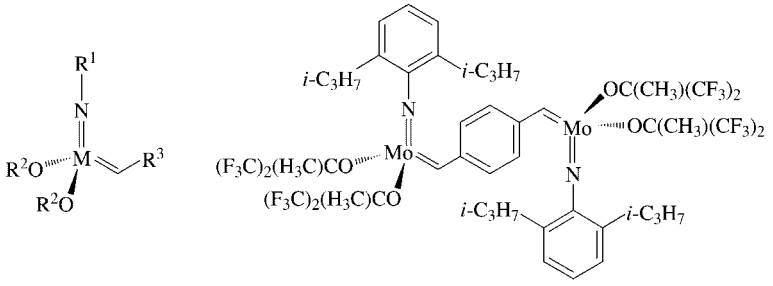

7 8

Metal Alkylidyne Catalysts. Metal alkylidyne complexes such as $(CO)_4BrW{\equiv}CC_6H_5$ (153) and $(t\text{-}C_4H_9O)_3Mo{\equiv}C\text{-}n\text{-}C_3H_7$ (131) serve as catalysts for the polymerization of substituted acetylenes. Speculated initiation mechanisms of $(CO)_4BrW{\equiv}CC_6H_5$-catalyzed polymerization involve its isomerization into a metal carbene species $(CO)_4W{=}CBrC_6H_5$. The complex, $(t\text{-}C_4H_9O)_3Mo{\equiv}C\text{-}n\text{-}C_3H_7$, which is formed by the reaction of $Mo_2(O\text{-}t\text{-}C_4H_9)_6$ with 4-octyne, catalyzes the polymerization of cyclic acetylene (131). The polymerization of cyclooctyne proceeds in a ring-opening fashion to give an insoluble linear polymer with M_n and M_w/M_n estimated to be 8600 and 7.0, respectively, after the hydrogenation of the polymer into polyethylene. Ring-opening polymerization of cyclooctyne is also achieved with a W catalyst, $W_2(O\text{-}t\text{-}C_4H_9)_6$ (132). The reaction of cyclooctyne with $W_2(O\text{-}t\text{-}C_4H_9)_6$ gives a bifunctional metal alkylidene complex *in situ* $(t\text{-}C_4H_9O)_3W{\equiv}C(CH_2)_6C{\equiv}W(O\text{-}t\text{-}C_4H_9)_3$; thus, bisinitiation takes place to give a polymer having active species at both terminal ends (132).

Group 8 Transition Metals. Iron-catalyzed polymerization of substituted acetylenes has a long history (22,25,60). Well-used iron catalysts have a general formula of $Fe(acac)_3{-}R_nAlCl_{3-n}$, and they are readily prepared *in situ*. $Fe(acac)_3{-}(C_2H_5)_3Al$ is employed most frequently. This is a heterogeneous catalyst and is able to polymerize sterically unhindered terminal acetylenes such as *n*-alkyl-, *sec*-alkyl-, and phenylacetylenes. On the contrary, monomers having bulky

substituents such as *tert*-alkylacetylenes and disubstituted acetylenes cannot be polymerized with the Fe catalysts. Although Fe catalysts cannot precisely control the polymerization, they show very high activity and often give very high molecular weight polymers. Poly(*n*-alkylacetylenes) obtained with Fe catalysts are orange-colored, soluble, rubbery, and have high molecular weights (154). Similar to the lanthanide catalysts as noted previously, Fe catalysts provide cis-cisoidal polymers, which was evidenced by the C—H out-of-plane deformation at 740 cm^{-1} in the ir spectrum. Thus, poly(phenylacetylene) formed with $Fe(acac)_3$–$(C_2H_5)_3Al$ is insoluble and crystalline (61). See later for the stereospecific polymerization with Fe catalysts.

Group 9 Transition Metals. A significant contribution to the recent tremendous strides in the chemistry of substituted polyacetylenes is undoubtedly based on the finding of excellent activity of Rh catalysts (25,26,29). The most characteristic feature of Rh catalysts is their very high activity for the polymerization of phenylacetylenes to give high molecular weight polymers with almost perfect stereoregularity (cis-transoidal). Furthermore, the excellent ability of Rh catalysts to tolerate various functional groups including amino, hydroxyl, azo, radical groups, and so on allows the production of highly functionalized polymers (Table 1).

The first example of the Rh-catalyzed polymerization employed $RhCl_3$–$LiBH_4$ for the polymerization of phenylacetylene (60). The use of protic solvent (ethanol) accelerates the polymerization, and a cis-transoidal polymer selectively forms. After this discovery, a variety of Rh catalysts have been developed (Table 2). Cationic Rh catalysts such as $(nbd)Rh^+[(\eta^6\text{-}C_6H_5)B^-(C_6H_5)_3]$ (38) and dinuclear Rh complexes, $[(nbd)RhCl]_2$ and $[(cod)RhCl]_2$ (29), are frequently employed. $[(nbd)RhCl]_2$ is usually more active and stable than $[(cod)RhCl]_2$ (64,157). The Rh-catalyzed polymerization proceeds in various solvents such as benzene, tetrahydrofuran, ethanol, and triethylamine (47,64). Among the solvents, ethanol and triethylamine are favorable for phenylacetylenes from the viewpoint of both polymerization rate and polymer molecular weight (64). The most widely applied catalyst is $[(nbd)RhCl]_2$–$(C_2H_5)_3N$ (29). Use of this catalyst allows the polymerization of phenylacetylenes to give excellent yields of stereoregular polymers with high molecular weights ($M_n > 10^5$). Living polymerization of phenylacetylenes is feasible using a well-characterized Rh catalyst such as $(nbd)C_6H_5C{\equiv}CRh(P(C_6H_5)_3)_2$ (**9**) (168–171). Multicomponent catalysts, $[(nbd)RhOCH_3]_2$–$P(C_6H_5)_3$ (172) and $[(nbd)RhCl]_2$–$LiC(C_6H_5){=}CPh_2$–$P(C_6H_5)_3$ (173), have been proven to be active for the living polymerization of phenylacetylenes. In the latter case, the initiation species is a vinylrhodium (**10**) that was isolated and well characterized by x-ray analysis (174). Details for the living polymerization are described in the next section.

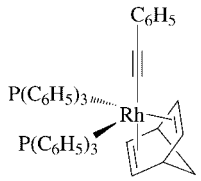

9

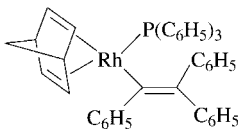

10

Table 2. Rh Catalysts for the Polymerization of Substituted Acetylenes

Catalyst	Reference	Catalyst	Reference
$RhCl_3$–$LiBH_4$	60	$[(cod)Rh(SC_6F_5)]_2$	164,165
$[(cod)RhCl]_2$	(29,63,155,156)	$(cod)Rh(SO_3C_6H_4$-*p*-$CH_3)(H_2O)$	166
$[(nbd)RhCl]_2$	(29,47,64,157–160)	$[(nbd)Rh(acac)]_2$	167
$(cod)Rh^+B(C_6H_5)_4^-$–$HSi(C_2H_5)_3$	161	$(nbd)Rh^+[(\eta^6$-$C_6H_5)B^-(C_6H_5)_3]$	38
$(nbd)Rh^+(dbn)_2PF_6^-$	162	$(nbd)C_6H_5C{\equiv}CRh(P(C_6H_5)_3)_2$ (**9**)	168–170–171
(nbd)Rh(dbn)Cl	162	$[(nbd)RhOCH_3]_2$–$P(C_6H_5)_3$	172
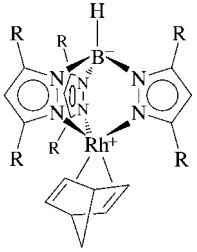	163	$[(nbd)RhCl]_2$–$(C_6H_5)_2C{=}C(C_6H_5)Li$–$P(C_6H_5)_3$	173
		$(nbd)(C_6H_5)_2C{=}C(C_6H_5)Rh(P(C_6H_5)_3)_2$ (**10**)	174
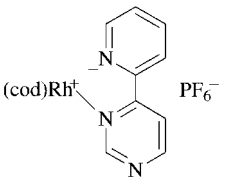	(63,155,156)	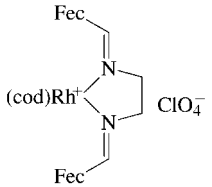	175

Polymerization of phenylacetylenes is feasible even in aqueous media by using water-soluble catalysts. For example, $(cod)Rh^{+}(mid)_2PF_6^{-}$ (mid = *N*-methylimidazole) provides cis-transoidal poly(phenylacetylene) (cis 98%) in high yield (98%) (166). Other catalysts, $(cod)Rh(SO_3C_6H_4\text{-}p\text{-}CH_3)(H_2O)$ and $(nbd)Rh(SO_3C_6H_4\text{-}p\text{-}CH_3)(H_2O)$, work as water-soluble catalysts to produce cis-transoidal polymer (166). The polymerizations can be done under air; thus, a poly(phenylacetylene) thin film (thickness ca 250 nm) is readily obtained by dropping a dilute chloroform solution of phenylacetylene onto the water surface of a dilute aqueous solution of $(cod)Rh(SO_3C_6H_4\text{-}p\text{-}CH_3)(H_2O)$ in an open beaker (166).

Polymerization of phenylacetylene in compressed (liquid or supercritical) CO_2 has been studied using a Rh catalyst, $[(nbd)Rh(acac)]_2$ (167). Higher polymerization rate is obtained in CO_2 than in conventional organic solvents such as THF and hexane. Polymerization in the presence of a phosphine ligand, $\{p\text{-}[F(CF_2)_6(CH_2)_2]\text{-}C_6H_4\}_3P$, predominantly produces cis-transoidal polymers, while, without the ligand, both cis-transoidal and cis-cisoidal polymers are formed.

Rh catalysts have been recently applied to the polymerization of propiolic esters (47). Amines cannot be used as cocatalysts in this case because of the high reactivity of propiolic esters toward nucleophiles. Rh-catalyzed polymerization of propiolic esters is accompanied by unavoidable side reactions such as linear- and cyclooligomerizations; thus, the yields of poly(propiolic esters) are rather unsatisfactory (15–60%). Relatively high yields of poly(propiolic esters) with high molecular weights are accessible when the polymerization is conducted in alcohols or acetonitrile at high monomer and catalyst concentrations (50). A characteristic feature is the almost perfect stereoregularity of the polymers, which is in contrast to the Mo-catalyzed polymerization of propiolic esters (48). Stereoregular cis poly(propiolic esters) exist in a well-ordered helical conformation. See later for details for the synthesis of helical polyacetylenes.

A disadvantage of the Rh-catalyzed polymerization is recognized in the poor availability of monomer. Monomers that can be effectively polymerized are limited to phenylacetylene and its para- and meta-substituted derivatives and propiolic esters. $[(nbd)RhCl]_2$–$(C_2H_5)_3N$-catalyzed polymerization of monosubstituted acetylenes having bulky substituents such as *tert*-butylacetylene and ortho-substituted phenylacetylenes is sluggish, and the latter gives insoluble polymers in low yield. However, a cationic rhodium complex, $(nbd)Rh^{+}[(\eta^6\text{–}C_6H_5)B^{-}(C_6H_5)_3]$, shows higher activity than $[(nbd)RhCl]_2$–$(C_2H_5)_3N$, and is able to effectively polymerize bulky monomers including *tert*-butylacetylene and 3-phenyl-1-butyne (38). Disubstituted acetylenes cannot be polymerized with Rh catalysts. Only one exceptional example has been found by using cyclooctyne as a monomer whose very large ring strain (∼38 kJ/mol) enables very rapid polymerization with $[(nbd)RhCl]_2$, giving an insoluble polymer in good yield (133).

Group 10 Transition Metals. Group 10 transition-metal catalysts including Ni and Pd are generally not adequate for the polymerization of acetylenes because these catalysts tend to lead to the cyclooligomerization rather than the polymerization. Exceptional examples have been found by using $Ni(NCS)_2P(C_6H_5)_3$ (51) and $[Pd(C{\equiv}CR)_2(P(C_6H_5)_3)_2]$ (R = $Si(CH_3)_3$, CH_2OH, $CH_2N(CH_3)_2$) (52,176). Polymers with a relatively high molecular weight are formed with these late transition metal catalysts. Another successful polymerization of substituted acetylenes with "Group 10" metals is achieved by utilizing enhanced free energy

difference between the monomer and polymer. Namely, highly strained cyclooctyne readily polymerizes with Pd and Ni catalysts including $PdCl_2$, $Pd_2(dba)_3$, $Pd(CH_3CN)_2(OTs)_2$, $Ni(cod)_2$, and so forth (133).

Ionic Catalysts. Preparation of polyacetylenes having satisfactory molecular weights is impossible by ionic processes. For example, anionic polymerization of phenylacetylene is claimed to be accompanied by the electron transfer from the active center to the conjugated chain, which causes the formation of low molecular weight oligomers (177). Attempts to ionically polymerize acetylene derivatives have been made using zwitterionic monomers such as *N*-methyl-2-ethynylpyridinium salts (178–180) and phosphonium acetylenes ($C_6H_5C{\equiv}C^+P(C_6H_5)_3Br^-$) (181). The degree of polymerization is generally below 25. However, the ability of these monomers to anionically polymerize offers block copolymers with common vinyl monomers such as styrene, which would provide a new route to functional materials. Relatively high molecular weight polymers ($\sim$10,000) can be obtained by the *tert*-C_4H_9OK-initiated proton transfer polymerization of acetyleneamides (182). Much higher reactivity of acetyleneamides than that of acrylamides allows one to conduct the polymerization under the mild conditions to give formally alternating copolymers of acetylene with isocyanates.

Precision Polymerization

In these two decades remarkable progress has been made in the development of excellent catalysts for living and stereospecific acetylene polymerizations (10,26–28). The π-conjugated polymers prepared by the sequential polymerization are strictly limited to polyacetylenes, except for only a few examples. Thus, synthesis of tailor-made conjugated macromolecules such as end-functionalized polymers, block copolymers, star-shaped polymers is possible only in the case of substituted acetylenes.

General. As stated in the preceding section, diverse transition metals from Group 3 to Group 10 elements initiate the polymerization of substituted acetylenes. Catalysts that achieve living polymerization, however, are quite limited, which contrasts to a wide variety of living polymerization catalysts for vinyl monomers. The catalysts are classified into the following groups: (1) metal halide catalysts, (2) metal carbenes, and (3) Rh complexes. As described later, attention should be paid on the fact that the structure of monomers undergoing living polymerization significantly depends on the type of catalyst. Thus, appropriate catalysts must be selected in order to synthesize well-defined polymers from the individual monomer.

Living Polymerization by Metal Halide Catalysts. Metal halide-based living polymerization catalysts possess a general formula of MO_nCl_m–cocatalyst–ROH (M = Mo or W, $n = 0$ or 1, $m = 5$ or 4) (10,25–28). The most striking feature of these catalysts is the ease in preparation. One can readily generate these catalysts *in situ* just by mixing these three components. The living polymerization of substituted acetylenes has been achieved, for the first time, by using a Mo-based multicomponent catalyst. The ability of a protic additive, ethanol, to control the polymerization of 1-chloro-1-octyne with $MoCl_5$–*n*-$(C_4H_9)_4Sn$ in toluene has been demonstrated (141). Poly(1-chloro-1-octyne) with narrow molecular weight

distribution ($M_w/M_n < 1.2$) is attainable in the presence of $MoCl_5$–*n*-$(C_4H_9)_4Sn$–C_2H_5OH. The living nature was confirmed by the linear dependence of molecular weight on monomer conversion and by the successful initiation of the polymerization of second-charged monomers with the living prepolymer. The use of $MoOCl_4$ instead of $MoCl_5$ provides propagation species with a longer lifetime (183). For example, in the case of $MoCl_5$–*n*-$(C_4H_9)_4Sn$–C_2H_5OH, bimodal poly(1-chloro-1-octyne) is formed if the monomer is further added after the complete consumption of the initially fed monomer. On the other hand, the deactivation of the active chain end is not observed under the $MoOCl_4$–*n*-$(C_4H_9)_4Sn$–C_2H_5OH system, which leads to the formation of unimodal polymers after a similar multistage polymerization (184). Other cocatalysts including $(C_6H_5)_4Sn$, $(C_2H_5)_3SiH$, and $(C_6H_5)_3Bi$ do not induce living polymerization, and only *n*-$(C_4H_9)_4Sn$ and $(CH_3)_4Sn$ give living poly(1-chloro-1-octyne). Internal acetylenes such as 2-nonyne also undergo living polymerization (185). The living nature of the polymerization of 2-nonyne is remarkably enhanced by conducting the polymerization in anisole instead of toluene. Although the polymerization rate is not dependent on the length of alkyl chain, the position of the acetylenic triple bond drastically affects the polymerization rate; that is, the polymerization rate decreases in the order of 2-alkyne > 3-alkyne > 4 alkyne (185). In a similar way, $MoCl_5$–*n*-$(C_4H_9)_4Sn$–C_2H_5OH induces living polymerization of ring-substituted phenylacetylenes (141). Bulky substituents (*eg*, CF_3, $Si(CH_3)_3$, *i*-C_3H_7), however, should be incorporated into the ortho position in order to exclude cyclotrimerization (140,186–189). Thus, living nature is slightly low in the case of *o*-methylphenylacetylene (190). It is interesting that phenylacetylene derivative, HC≡CC_6F_4-*p*-*n*-C_4H_9, having no bulky ortho substituent polymerizes with $MoOCl_4$–*n*-$(C_4H_9)_4Sn$–C_2H_5OH in a living fashion to yield a polymer with low polydispersity (191).

Replacement of toluene with anisole as polymerization solvent remarkably improves the living nature, leading to both an increase in initiation efficiency and a decrease in polydispersity. For instance, the initiation efficiency of *o*-trifluoromethylphenylacetylene increases from 9 to 42% in anisole (192). The ability of anisole to improve the living nature enables living polymerization of 1-chloro-2-phenylacetylene (192); living polymer from this monomer is inaccessible in toluene (193).

The effects of organometallic components have been systematically investigated. In toluene, only *n*-$(C_4H_9)_4Sn$ and $(CH_3)_4Sn$ cocatalyze living polymerization (184). However, the use of anisole expands the availability of cocatalyst; $(C_2H_5)_3Al$ (194), $(C_2H_5)_2Zn$ (195), and *n*-C_4H_9Li (196) can be used as cocatalysts. It is interesting that the addition of the third component, the protic additive, is not necessary in the case of *n*-C_4H_9Li. Variation of cocatalysts affects the initiation efficiency and block copolymerization behavior. Initiation efficiency decreases in the order of *n*-$(C_4H_9)_4Sn$ > $(C_2H_5)_3Al$ > $(C_2H_5)_2Zn$ > *n*-C_4H_9Li. Consequently, extremely high molecular weight polymers ($>10^5$) with very narrow molecular weight distribution (<1.03) are attainable by using $MoOCl_4$–*n*-C_4H_9Li (196). Block copolymerizations have been examined by using various monomers and cocatalysts (197). $MoOCl_4$–*n*-$(C_4H_9)_4Sn$–C_2H_5OH appears to be most effective for the selective formation of block copolymers from various monomers. For example, in the block copolymerization with $MoOCl_4$–$(C_2H_5)_3Al$–C_2H_5OH, reverse of the feed order often causes deactivation of the living chain end, giving a mixture of

homo- and copolymers. On the other hand, with $MoOCl_4$–*n*-$(C_4H_9)_4Sn$–C_2H_5OH, block copolymers with narrow molecular weight distributions selectively form from various substituted acetylenes even if the order of monomer addition is changed (197).

Tungsten-based multicomponent catalysts, $WOCl_4$–*n*-$(C_4H_9)_4Sn$–*t*-C_4H_9OH, $WOCl_4$–*n*-C_4H_9Li, and $WOCl_4$–C_2H_5MgBr, have been proven to achieve controlled polymerizations of *o*-trifluoromethylphenylacetylene, *o*-trimethylsilylphenylacetylene, HC≡CC_6F_4-*p*-*n*-C_4H_9, 3-decyne, and 5-dodecyne (198,199). On the other hand, analogous combinations of WCl_6 with cocatalysts are ineffective for living polymerization of these monomers.

$NbCl_5$ has been reported to polymerize 1-trimethylsilyl-1-propyne in nonpolar solvents such as cyclohexane, giving a polymer with low polydispersity (200). The molecular weight of this polymer increases in proportion to the monomer conversion. Either the replacement of $NbCl_5$ by $TaCl_5$ or the use of other solvents disrupts the living nature of the polymerization.

Living Polymerization by Single-Component Carbene Complexes. Much effort has been made to develop well-defined carbene complexes for the living polymerization of substituted acetylenes as well as cyclic olefins. The first example for the isolated metal-carbene catalyzed polymerization of acetylenes appeared in the literature for the acetylene oligomerization with a W-based carbene (**11**) (201). Soluble oligoacetylenes, $(C_2H_2)_n$ (n = 3–9), are obtained by the reaction of acetylene with (**11**) in the presence of quinuclidine. The living chain ends of these oligoacetylenes quantitatively react with pivaldehyde to give oligomers having *tert*-butyl groups at both ends. Trans geometrical main-chain structure dominates over the cis one. The living nature of this polymerization system allows selective formation of an ABA-type triblock copolymer of norbornene with acetylene.

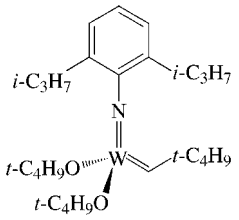

11

After the work with W-based catalysts, Mo carbene catalysts (**7a–d**) were synthesized (Table 3) and have been proven to elegantly induce living cyclopolymerization of 1,6-heptadiynes (150,151). Mo carbenes ligated by bulky imido and alkoxy groups are quite effective. Because there is no significant difference between the propagation and initiation rates, the resultant polymers show relatively broad molecular weight distributions (∼1.25). However, these catalysts are able to quantitatively initiate the polymerization, which allows an easy control of the molecular weights simply by adjusting the monomer–initiator ratio. It is important to use appropriate solvent (DME) for selective cyclopolymerization; the polymerizations can be run in other solvents but give insoluble networked polymers. Bisinitiation of 1,6-heptadiynes is feasible if bifunctional initiator (**8**) is used (151). The ability of these Mo carbenes to tolerate polar functional groups

Table 3. Mo-Based Carbene Catalysts ((7)) for the Living Polymerization of Substituted Acetylenes

(**7**)	R^1	R^2	R^3	R^4
7a	C_6H_3-2,6-*i*-$(C_3H_7)_2$	$OC(CH_3)(CF_3)_2$	$C(CH_3)_2C_6H_5$	H
7b	C_6H_3-2,6-*i*-$(C_3H_7)_2$	$OC(CF_3)_3$	$C(CH_3)_2C_6H_5$	H
7c	1-Adm	$OC(CH_3)(CF_3)_2$	$C(CH_3)_2C_6H_5$	H
7d	C_6H_3-2-*t*-C_4H_9	$OC(CH_3)(CF_3)_2$	$C(CH_3)_3$	H
7e	C_6H_3-2-*t*-C_4H_9	$O_2C(C_6H_5)_3$	$C(CH_3)_3$	H
7f	C_6H_3-2-*t*-C_4H_9	$O_2C(C_6H_5)_3$	$C(CH_3)_2C_6H_5$	H
7g	1-Adm	$OCH(CF_3)_2$	$C(CH_3)_2C_6H_5$	H
7h	1-Adm	$OCH(CF_3)_2$	C_6H_5	CH_3
7i	1-Adm	$OCH(CF_3)_2$	C_6H_5	C_6H_5
7j	C_6H_3-2,6-$(CH_3)_2$	$OC(CH_3)(CF_3)_2$	$C(CH_3)_2C_6H_5$	H

permits living polymerization of functionalized monomers containing ester, sulfonic ester, and siloxy groups (151). Even a hydroxy group-containing monomer quantitatively provides a polymer. End-capping of the polymers is readily accomplished using aromatic aldehydes including *p-N,N*-dimethylaminobenzaldehyde and *p*-cyanobenzaldehyde. Cyclopolymerization of 1,6-heptadiynes with carbenes (**7a–d**) offers polymers having both five- and six-membered cyclic structures. In contrast, carbenes (**7e**) and (**7f**), which have bulky carboxylate ligands produce polymers bearing only six-membered rings (152).

Ring-substituted phenylacetylenes have been applied to the Mo carbene-initiated polymerization, leading to a finding that well-defined polymers are readily obtained with (**7g–i**) ligated by less bulky alkoxy groups (84,149). Unless an appropriate base is added, isolation of (**7g–i**) cannot be accomplished because of their instability. Like metal halide-induced living polymerizations, bulky ring substituents at the ortho position are required for controlled polymerization. The most characteristic point of these polymerization systems is that all the steps including initiation and propagation can be readily monitored by an nmr technique. For example, the detailed studies on the initiation step for various ring-substituted phenylacetylenes have revealed that the alkylidene groups of (**7**) selectively undergo α-addition onto *o*-trimethylsilylphenylacetylene. On the other hand, the selectivity of α-addition decreases with the decrease in the bulkiness of ortho substituents. Thus, the polymer main chain has both head-to-tail and head-to-head structures in the case of phenylacetylenes with small ortho substituents.

Metal-containing monomers, ferrocenylacetylene (**12**) and ruthenocenylacetylene (**13**) have been subjected to living polymerization with (**7j**) that has bulky alkoxide ligands (102). Living polymers are inaccessible with (**7g–i**) that suit ortho-substituted phenylacetylenes. Because of the insolubility of these polymers, the polymerization degree must be restricted below ca 40 in order to produce the soluble polymers. Similar metallocene-containing monomers, HC≡CC_6H_4-*o*-Fc (**14**), HC≡CC_6H_4-*p*-CH=CHFc (**15**), HC≡CC_6H_4-*p*-N=NFc (**16**), and HC≡CC_6H_4-*p*-C≡CC_6H_4-*p*-C≡CFc (**17**), polymerize in a living manner in the presence of (**7**) (87,88). The use of (**7j**) leads to successful formation of high molecular weight polymers ($\sim 10^4$) from terminal aliphatic acetylenes (202). Because the chain propagation is faster than initiation, narrow molecular weight distribution is not attained.

However, cyclotrimerization of 1-*n*-alkylacetylene can be completely suppressed, leading to the quantitative yields of polymers.

In addition to these Mo- and W-based carbene complexes, a Ta-based carbene (**2**) that is active for the living polymerization of 2-butyne has been developed (105). Again, the initiation efficiency is quantitative, and the living end can be endcapped with aromatic aldehydes. As polymers from symmetric acetylenes are generally insoluble, soluble poly(2-butyne) is accessible if the degree of polymerization is suppressed below 200. The nmr analysis of living oligomers of 2-butyne clearly indicates that both cis and trans structures exist in the main chain. This Ta carbene (**2**) is unfortunately ineffective for the polymerization of internal acetylenes having bulky substituents such as diphenylacetylene. Chain transfer inhibits the formation of polymers from terminal acetylenes with (**2**), giving oligomers having broad molecular weight distributions.

Stereospecific Living Polymerization by Rh Catalysts. As shown in the previous section, very high order of regulation for double bond geometry (cis-transoidal) is possible by using Rh catalysts. Although the presence of long-lived propagating species has been claimed in the Rh-catalyzed polymerization of phenylacetylene (157), the conventional Rh catalyst, $[(nbd)RhCl]_2$, cannot achieve well-controlled polymerization. Rh-catalyzed living polymerization was first accomplished in 1994 (168). The excellent ability of an isolated catalyst (**9**) to offer quantitative yields of poly(phenylacetylenes) with narrow molecular weight distribution was demonstrated (168) (Table 2). The structure of (**9**) was completely characterized by a single-crystal x-ray analysis, and more details of the polymerization have been disclosed (171). Polymerization of phenylacetylene with (**9**) in the presence of 4-(*N*,*N*-dimethylamino)pyridine (DMAP) provides a well-defined polymer having a long-lived active site at the propagation terminal. DMAP is indispensable, and without DMAP, the polydispersity increases to 1.3. High stability of the propagation centers allows the isolation of poly(phenylacetylene) having active propagation sites that can sequentially polymerize second monomers to give precisely controlled block copolymers (171).

One striking feature of the stereoregular polyacetylenes is their simple NMR spectral patterns, which facilitates investigation of the polymerization mechanism as well as the polymer structure. A copolymer of phenylacetylene with partly ^{13}C-labeled phenylacetylene ($C_6H_5{}^{13}C{\equiv}{}^{13}CH$) shows two doublet carbon signals with $J_{13C-13C}$ of 72 Hz, indicating the presence of $^{13}C{=}{}^{13}C$ bond in the polymer backbone (171). This is a clear indication of the insertion mechanism instead of the metathesis pathway. Solid-state NMR studies of poly(phenylacetylene) also verified the insertion mechanism for the Rh-catalyzed polymerizations (169).

After the finding of catalyst (**9**), further development of a new living polymerization system, $[(nbd)Rh(OCH_3)]_2$–$P(C_6H_5)_3$–DMAP, enabled the enhancement of the initiation efficiency from 35% to 70% (172). The polymerization with $[(nbd)Rh(OCH_3)]_2$–$P(C_6H_5)_3$–DMAP is 3–4 times faster than that with (**9**). The isolation of $[(nbd)Rh(OCH_3)]_2$ is not necessary; a simple mixture of commercially available $[(nbd)RhCl]_2$, $P(C_6H_5)_3$, $NaOCH_3$, and DMAP induces the living polymerization of phenylacetylene without broadening the polydispersity.

A new vinylrhodium complex (**10**) for the living polymerization of phenylacetylenes has been prepared, isolated, and fully characterized by x-ray analysis (174). Catalyst (**10**) polymerizes phenylacetylene and its para-substituted

analogues to give living polymers. Living polymerization is also possible even in the presence of water. The isolation of (**10**) is not necessary, and the complex formed *in situ* by the reaction of $[(nbd)RhCl]_2$ with $LiC(C_6H_5)=C(C_6H_5)_2$ and $P(C_6H_5)_3$ induces living polymerization in quantitative initiation efficiency (173). A remarkable feature of this polymerization system is the ability to introduce functional groups at the initiation terminal. For example, living poly(phenylacetylene) bearing a terminal hydroxy group is readily obtained by the polymerization with a three-component catalyst, comprising $[(nbd)RhCl]_2$, $LiC(C_6H_5)=C(Ph)C_6H_4$-*p*-$OSiCH_3$-*t*-C_4H_9, and $P(C_6H_5)_3$, followed by the desilylation of the formed polymer. Polymerization of β-propiolactone with the terminal phenoxide anion of this polymer gives a new block copolymer of phenylacetylene with β-propiolactone (203).

Stereospecific Polymerization with Fe Catalyst. As mentioned earlier, iron and lanthanide catalysts are able to form cis-cisoidal stereoregular polymers from phenylacetylenes. However, a quantitative discussion on the cis-cisoidal steric structure has not been made because of the insolubility of cis-cisoidal poly(phenylacetylene). Attempts have been made to prepare soluble cis-cisoidal poly(phenylacetylenes) by incorporating alkyl pendant onto the aromatic ring (65). nmr analyses of Rh- and Fe-based polymers from *p*-adamantyl-, *p*-*tert*-butyl-, and *p*-*n*-butylphenylacetylenes led to a conclusion that all of the Rh- and Fe-based polymers adopt cis-transoidal geometrical structure. From the NMR analysis, the cis content of these polymers was calculated to be more than 95% for Rh-based polymers. The cis content of Fe-based polymers significantly depends on the bulkiness of the ring substituents and decreased from 93 to 65% with an increase in the bulkiness. These data support the idea that cis-cisoidal polymers are specifically formed with Fe catalysts unless the ring substituents are extremely bulky. However, the thermodynamic instability of the initially formed cis-cisoidal conformation readily isomerizes the cis-cisoidal polymers into cis-transoidal ones upon dissolution.

Stereospecific Living Polymerization by Mo Catalysts. Apart from the stereospecific polymerizations through the insertion mechanism in the case of Rh and Fe catalysts, the metathesis approaches to stereoregular polymers are rather difficult. For instance, the cis content of poly(*o*-methylphenylacetylene) prepared with $MoOCl_4$–*n*-$(C_4H_9)_4Sn$–C_2H_5OH is 81% (190). A unique example for elegantly controlled stereospecific metathesis polymerization is limited to the Mo-catalyzed polymerization of *tert*-butylacetylene (36,204). Cis polymers are selectively obtained from *tert*-butylacetylene in the presence of $MoCl_5$. WCl_6 catalysts, in contrast, lead to less stereoregulation. Stereospecific living polymerization of *tert*-butylacetylene is possible with $MoOCl_4$–*n*-$(C_4H_9)_4Sn$–C_2H_5OH, which gives a polymer with a narrow molecular weight distribution (36). The cis content reaches 97% at a low temperature (−30°C). Cis content decreases if the polymerization is conducted with $MoOCl_4$ or $MoOCl_4$–*n*-$(C_4H_9)_4Sn$. A detailed nmr study on the stereoregularity of poly(*tert*-butylacetylene) showed that the cis content depends on the rate of Lewis-acid catalyzed isomerization from the cis to the trans form (205). That is, all catalysts including $MoOCl_4$, $MoOCl_4$–*n*-$(C_4H_9)_4Sn$, and $MoOCl_4$–*n*-$(C_4H_9)_4Sn$–C_2H_5OH specifically give cis polymers just after the polymerization. However, a rapid acid-catalyzed cis-to-trans isomerization reduces the cis content as well as the molecular weight after the completion of the polymerization. Thus, the difference in acidity of catalysts determines the rate of

isomerization and eventually influences the cis content of the polymer. The isomerization can be retarded by conducting the polymerization at low temperature or in poor solvents such as dichloromethane or anisole.

Functional Polyacetylenes

Thanks to the tremendous progress in the transition metal-catalyzed polymerization of substituted acetylenes as described in the previous sections, it is now possible to access various acetylene-based polymers having desired first-order structures. This, in combination with highly advanced organic synthetic technology, provides novel functional materials based on polyacetylenes, and the following surveys examples of the design and synthesis of functional substituted polyacetylenes.

Permeable Polyacetylenes. Application of substituted polyacetylenes as gas-permeable materials has been most intensively studied (206–213). These studies are motivated by the extremely high gas permeability of poly(1-trimethylsilyl-1-propyne) (**18**) (214). which is the most permeable material among the polymers available. Its oxygen permeability (P_{O2} = 1–2 mmol/(m·s·GPa), 3000–6000 barrers) is about 10 times larger than that of poly(dimethylsiloxane). In addition to its high permeability, the ability of (**18**) to give a free-standing film has attracted many membrane scientists. Poly(diphenylacetylenes) also exhibit large values for gas permeability (213). They are thermally very stable ($T_0 > 500^\circ$C) and possess film-forming ability. The ease in modifying ring substituents provides an opportunity to tune the permeability as well as the solubility and second-order conformation. Table 4 lists examples of the substituted polyacetylenes having high gas permeability. The permeability of poly(diphenylacetylenes) significantly depends on the shape of ring substituents. Generally, those with bulky ring substituents such as *tert*-butyl, trimethylsilyl, and trimethylgermyl groups exhibit very large P_{O2} values, up to 0.37–0.40 mmol/ (m·s·GPa) (1100–1200 barrers), which is about a quarter of that of (**18**) and approximately twice as large as that of poly(dimethylsiloxane). Poly(phenylacetylenes) tend to show lower permeability than poly(diphenylacetylenes).

Liquid crystalline Polyacetylenes. Several kinds of polyacetylenes with liquid-crystalline moiety in the side groups have been prepared with the motivation of improving main-chain orientation and effective conjugation through the alignment of the pendant mesogens. The polymer skeleton of poly(1-alkynes) shows liquid crystallinity, whereas poly(phenylacetylene)- based polymers exhibit poorer mesomorphism because of their high rigidity of the polymer backbone (71). Poly(1-alkynes) with phenylcyclohexyl mesogenic cores separated from the main chain by an alkylene spacer (**19**) have been synthesized (40,224). These polymers prepared with Fe and Mo catalysts show smectic A phase upon heating. Mo-based polymers show higher transition temperatures compared to the Fe-based polymers. X-ray diffraction (xrd) measurements indicate that these polymers adopt layered structures in the liquid crystalline state where the mesogenic side chains locate at both sides of the main chain (225). The main chain of the polymers has been claimed to comprise the head-head–tail-tail linkage from the xrd data. Novel photo-responsive liquid crystalline polyacetylenes (**20**) that have azobenzenes as

Table 4. Oxygen Permeability Coefficients (PO_2) and PO_2/PN_2 of Highly Permeable Substituted Polyacetylenes

R^1	R^2	Po_2 mmol/(m·s·GPa)	barrer[a]	Po_2/PN_2,	Reference
CH_3	$Si(CH_3)_3$ (**18**)	2.0	6100	1.8	214
CH_3	$Si(C_2H_5)_3$	0.29	860	2.0	113
		0.21	640	2.2	215
CH_3	$Si(CH_3)_2C_2H_5$	0.32	970	2.0	215,216
		0.17	500	2.2	217
CH_3	$Si(CH_3)(C_2H_5)_2$	0.15	440	2.1	215
CH_3	$Si(CH_3)_2$-*i*-C_3H_7	0.15	460	2.7	215,216
CH_3	$Si(CH_3)_2$-*n*-C_3H_7	0.033	100	2.8	217
CH_3	$Ge(CH_3)_3$	0.60	1800	1.5	115
		0.93	2800	–	114
CH_3	*n*-C_3H_7	0.90	2700	2.0	218
CH_3	$(CH_2)_3Si(CH_3)_3$	0.043	130	2.4	215
CH_3	C_6H_4-*p*-$Si(CH_3)_3$	0.080	240	2.4	215,216
C_6H_5	C_6H_4-*m*-$Si(CH_3)_3$	0.40	1200	2.0	121,122
C_6H_5	C_6H_4-*p*-$Si(CH_3)_3$	0.37	1100	2.1	121,122
C_6H_5	C_6H_4-*p*-$Si(CH_3)_2$-*i*-C_3H_7	0.067	200	2.3	219
C_6H_5	C_6H_4-*m*-$Si(CH_3)_2$-*t*-C_4H_9	0.037	110	2.5	219
C_6H_5	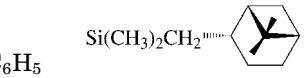	0.073	200	1.1	124
C_6H_5	C_6H_4-*m*-$Ge(CH_3)_3$	0.37	1100	2.0	128
C_6H_5	C_6H_4-*p*-*t*-C_4H_9	0.37	1100	2.2	129
C_6H_5	C_6H_4-*p*-*n*-C_4H_9	0.033	100	1.7	129
H	C_6H_4-*p*-$Si(CH_3)_3$	0.057	170	2.7	220
H	C_6H_3-*o*,*p*-$(Si(CH_3)_3)_2$	0.16	470	2.7	220
H	C_6H_3-*o*-$Ge(CH_3)_3$	0.037	110	2.0	221
H	C_6H_2-2,4,5-$(CF_3)_3$	0.26	780	2.1	222
H	C_6H_3-2,5-$(CF_3)_3$	0.15	450	2.3	222
H	*t*-C_4H_9	0.043	130	3.0	223

[a] 1 barrer = 1×10^{-10} cm^3(STP)·cm/(cm^2(·s·cm Hg).

mesogens have also been prepared (41,226). Thermally induced transitions from glassy to smectic and isotopic phases take place at 38 and 87°C, respectively. Polymer (**20**) undergoes reversible photochemical trans-to-cis and cis-to-trans isomerizations.

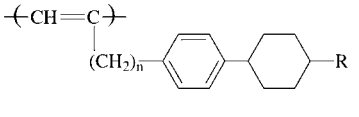

19 n = 1, 3, 4
R = H or *n*-C_3H_7

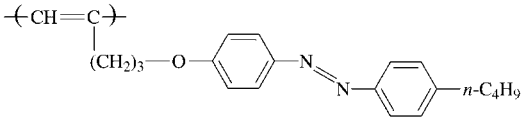

20

Similar liquid crystalline polyacetylenes (**21**) were synthesized. Polymers (**21**) possess 4′-cyano-4-biphenylyloxy mesogenic centers that are separated from

the main chain by long alkylene spacers (70). The cyano functionality does not deactivate the Mo- and W-based metathesis catalysts, and good yields of the polymers are obtained. All polymers (**21**) are mesomorphic, which was supported by the differential scanning calorimetry, polarizing optical microscopy, and x-ray diffraction analyses. The presence of a longer spacer favors better ordering of the mesogenic cores. These polymers adopt various morphologies, *e*g, monotropic nematicity, enantiotropic nematicity, and enantiotropic smecticity, depending on the length of the alkylene spacer.

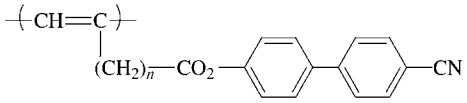

21 n = 2, 3, 8

A liquid crystalline-substituted polyacetylene bearing cholesteryl side groups (**22**) has been synthesized by using a well-defined Schrock-type catalyst (43). Upon cooling, the polymer exhibits a mesophase of the smectic A type before undergoing a glass transition. The ability of the Schrock catalyst to achieve the living polymerization of norbornenes provides a block copolymer (**23**) consisting of a mesogen-substituted polynorbornene and (**22**) (227). The acetylene-block exhibits a smectic A phase, while the polynorbornene domain is nematic. Thus, the block copolymer shows microphase separation retaining the mesophases of the homopolymers.

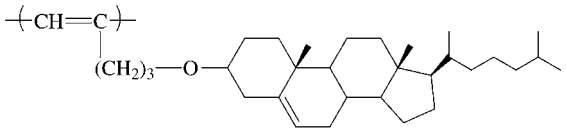

22

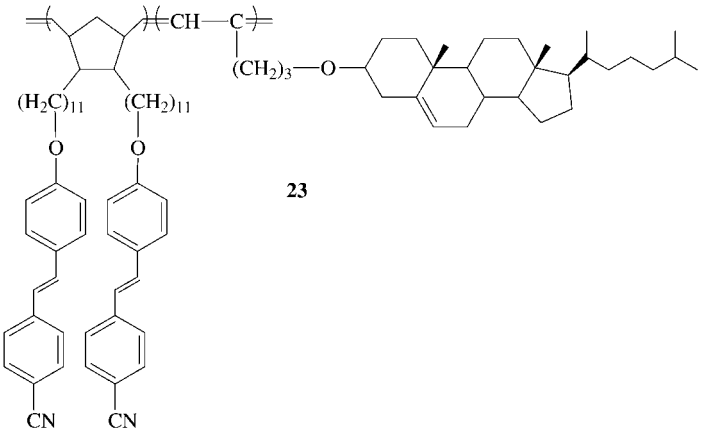

23

Polyacetylenes with Nonlinear Optical Properties. Substituted polyacetylenes are conjugated polymers; however, the repulsion between pendant

groups causes the twist of the main chain to reduce the degree of conjugation. Thus, many of substituted polyacetylenes show quite low unpaired-electron densities, which results in their poorer electrical conductivity (10,22–24,26). The main-chain conjugation can be improved by introducing ortho-substituents to monosubstituted arylacetylenes. For example, poly(phenylacetylenes) ortho-substituted by trimethylsilyl, trimethylgermyl, and trifluoromethyl groups are deeply colored and show large third-order nonlinear optical susceptibilities (228,229) (Table 5). Arylacetylenes bearing condensed aromatic rings such as naphthalene, anthracene, phenanthrene, and pyrene also belong to this category (52,90–95). Monomers designed so as to increase steric repulsion between the pendant groups and the main chain of the formed polymers give polymers having extremely expanded main-chain conjugation in the presence of W catalysts (94). Hence, 9-phenanthrylacetylene, 9-anthrylacetylene, and 1-pyrenylacetylene give deeply colored polymers in good yields with WCl_6–*n*-$(C_4H_9)_4Sn$. They show the absorption maxima around 600 nm, and the cut off wavelengths reach 800 nm. On the other hand, the less conjugated polymers are formed from 2-anthrylacetylene and 2-phenanthrylacetylene. Among the polymers from monosubstituted acetylenes, the polymer from 10-hexoxycarbonyl-9-anthrylacetylene (**24**) exhibits the largest third-order nonlinear optical susceptibility (230) (Table 5). Although the homopolymer of 9-anthrylacetylene obtained with W catalyst is insoluble (90), (**24**) is a soluble dark-purple polymer having an absorption maximum at 580 nm. The electric conductivity of I_2-doped (**24**) is 8.77×10^{-4} S/cm at 293 K. *N*-Carbazolylacetylene also polymerizes with W catalysts, giving a polymer with high degree of main-chain conjugation (95).

Luminescent Substituted Polyacetylenes. The luminescent property of conjugated polymers is one of the most important functions, and an energetic study of the photo- and electroluminescence of substituted polyacetylenes has been made (231–245). Polymers that show intense luminescence are those from diphenylacetylenes and 1-phenyl-1-alkynes, and so on. Only weak red emissions are observed from monosubstituted arylacetylene polymers (234,240). A systematic investigation on the luminescence of these kinds of polymers found that poly(diphenylacetylenes) exhibit photoluminescence around 530 nm and electroluminescence around 550 nm (232,242). In a similar way, poly(1-phenyl-1-alkynes) photochemically and electrochemically emit strong lights with spectral maxima located around 455 and 470 nm, respectively. Green and blue emissions are observed from the electroluminescent devices using poly(diphenylacetylenes) and poly(1-phenyl-1-alkynes) as the emission layers, respectively (235,236,240,242,243). The Stokes shift of photoluminescence of these polymers is quite large: 0.3 eV for poly(diphenylacetylenes) and 0.6 eV for poly(1-phenyl-1-alkynes). This series of studies varying the substituents on the polymers have revealed the following tendencies: (*1*) the introduction of bulky or long alkyl pendant groups enhances the efficiencies of the luminescence of poly(diphenylacetylenes) (235,242), and (*2*) the emission peaks blue-shift with the length of the alkyl pendant of poly(1-phenyl-1-alkynes) (234). Interestingly, both photo- and electroluminescences of the blend of blue emissive poly(1-phenyl-1-octyne) and green emissive poly(1-phenyl-2-*p*-*n*-butylphenylacetylene) vary between green and blue, which is dependent on the ratio of the two polymers (234,237). This result means that the emission

Table 5. Substituted Polyacetylenes That Show Large Third-Order Nonlinear Optical Susceptibilities

Polymer		λ_{max}, nm	$10^{12}\chi^{(3)}$, esu	Measurement[a]	Wavelength, nm	Reference
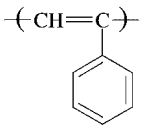	cis-rich	–	0.36	THG	1907	228
	trans-rich	352	0.54	THG	1907	229
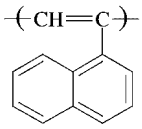		510	12	THG	1907	228
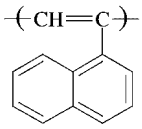		520	40	THG	1907	90
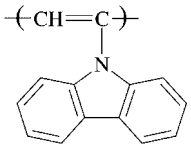		550	18	THG	1907	95
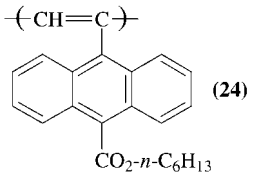 **(24)**		571	−190	EA	631	230
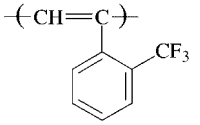		439	3.0	THG	1907	229
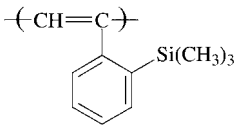		536	17	THG	1907	229
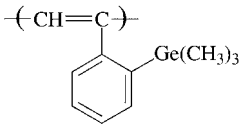		548	26	THG	1907	229
			28	EA	631	229

[a]THG: third-harmonic generation; EA: electroabsorption.

wavelength with desired color between blue and green can be obtained by controlling the mole ratio of these two polymers.

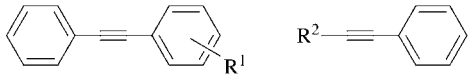

R^1 = Adm, $Si(CH_3)_3$, $Si(i\text{-}(C_3H_7)_3)$, $Si(C_6H_5)_3$, OC_6H_5, $t\text{-}C_4H_9$, $n\text{-}C_4H_9$, etc.
R^2 = CH_3, C_2H_5, $n\text{-}C_6H_{13}$, etc.

Polymers from monosubstituted terminal acetylenes strongly luminesce upon photoexcitation (246). Higher photoluminescent efficiency is observed for polymers (**25**) (**26**) (**27**), which emit strong deep-blue light (380 nm). This unexpected strong emission seems to originate from the ordering of the pendant mesogens that enhance the main-chain conjugation of the polymers. Similar to the case of other luminescent polyacetylenes, the increase in the length of the alkyl chain causes a slight blue-shift of the emission wavelength.

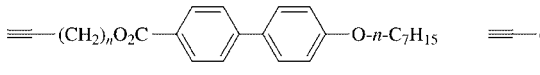

25 (n = 2–4, 9)

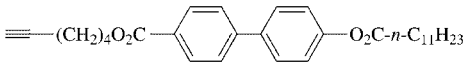

26

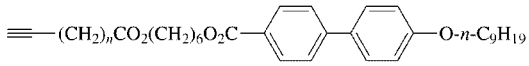

27 (n = 2, 8)

Chromic Substituted Polyacetylenes. In contrast to the extensive studies on the luminescent properties, less attention has been paid on the chromic properties of substituted polyacetylenes. The first demonstration of electrochromism was made using poly(*o*-trimethylsilylphenylacetylene) (247). Poly(*o*-trimethylsilylphenylacetylene) is cycled electrochemically between doped and undoped states. Upon electrochemical doping, poly(*o*-trimethylsilylphenylacetylene) film loses its red color to white. Similarly, poly[*p*-(*N,N*-diethylamino)phenylacetylene] can be electrochemically doped and exhibits a reversible color change between green ocher and deep blue (76).

Magnetic Substituted Polyacetylenes. Development of organic magnets is one of the most challenging and exciting targets for synthetic chemists. Theory predicts that free radicals in pendants of poly(phenylacetylene) are capable of ordering the ferromagnetic spin-interaction if the radicals conjugate with the phenyl rings. According to this theory many efforts have been made to prepare poly(phenylacetylenes) having stable radicals such as phenoxy, galvinoxyl, nitronyl nitroxide, and aminyl radicals. Figure 1 shows representative examples for poly(phenylacetylenes) having stable radicals such as phenoxy, galvinoxyl, nitronyl nitroxide, and aminyl radicals. Polymers (**28–31**) are prepared by the direct polymerization of the radical-containing monomers (99–101,248). Rh catalysts suit the polymerization of radical-containing monomers because the radical groups do not interfere with Rh catalysts. The other radical-containing polymers (**32–37**) are derived from the polymerization of the corresponding precursors followed by the oxidative polymer reaction (249–254). Under the appropriate

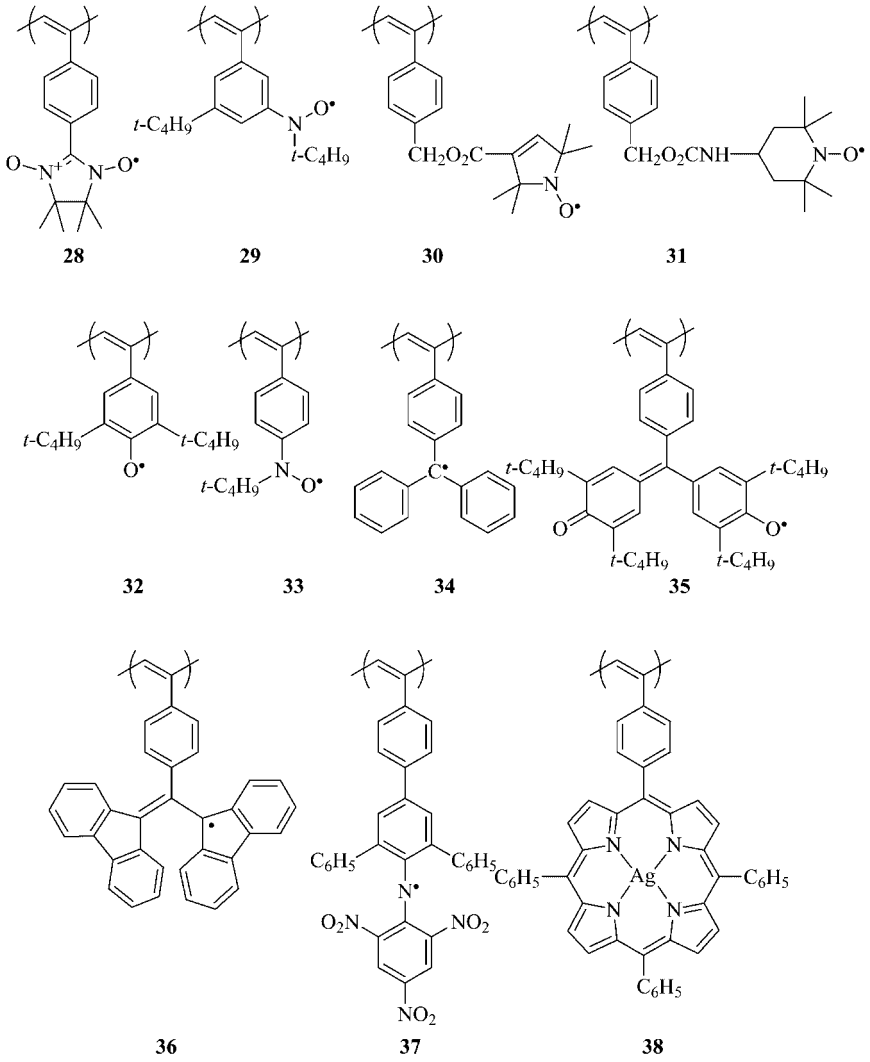

Fig. 1. Poly(phenylacetylenes) having stable radicals.

conditions, polymers with a very high spin concentration are available. Paramagnetic metalloporphyrins have been incorporated into poly(phenylacetylene) with the motivation of producing magnetically interacting polymers (**38**) (255). Unfortunately, no ferromagnetic interactions have been achieved because of the torsion in the polyene backbone. The twist of the main chain, caused by the steric repulsion between the pendants, inhibits the extended conjugative spin coupling through the alternating double bonds in the main chain.

Optically Active Substituted Polyacetylenes. The repulsion between the pendants in substituted polyacetylenes twists the main chain, which discourages the studies on the synthesis of acetylene-based polymer magnets. Recently, this main-chain torsion has been extensively applied to the synthesis of chiral

polymers having well-ordered helical conformations, which has expanded the potential utility of substituted acetylenes as the enantioselective permeable materials, polarization-sensitive electrooptical materials, asymmetric electrodes, and so on.

Helical Poly(1-alkynes). The first report of the synthesis of chiral substituted polyacetylenes involved the polymerization of terminal aliphatic acetylenes having a chiral pendant (**39**) with $Fe(acac)_3$ in the presence of trialkylaluminum (39). Relatively weak but clear Cotton effects appear in the electric absorption range of the main chain, suggesting the helical conformation of the polymers. The distance between the chiral carbon and the main chain remarkably influences the chiroptical properties of the polymers, and the intensity as well as the shape of the Cotton effects considerably changes with the variation of the number of methylene spacers between the chirogenic carbon and the main chain. A decrease in temperature results in the drastic enhancement of the Cotton effect, which indicates the short persistence length of the helical domain. Monomer (**40**) was polymerized with a cationic Rh catalyst, $(nbd)Rh^+[(\eta^{-6}\text{–}C_6H_5)B^-(C_6H_5)_3]$, to give a polymer displaying very intense Cotton effects (38). Thus, the increase in the bulkiness at the α-carbon is likely to advantageously induce helicity to the backbone.

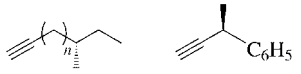

39 **40**

Helical Poly(phenylacetylenes). The most widely studied helical-substituted polyacetylenes are based on poly(phenylacetylene) with chiral ring substituents. Polymerization of chiral phenylacetylenes was first reported in 1995 (72). 4-(−)-Menthoxycarbonylphenylacetylene (**41**) was subjected to the polymerization with several transition metal catalysts such as $[(nbd)RhCl]_2$ and WCl_6. The resultant Rh-based polymer shows a large optical rotation and intense CD effects in the electric absorption region of the main chain. The polymer, thus, exists in a helical conformation with an excess of one-handed screw-sense. Poly(phenylacetylene) with small chiral pendants, poly(**42**), in contrast, displays poorer chiroptical properties. Interestingly, an increase in temperature steeply increases the optical rotation of poly(**41**) if the polymer is produced with a W catalyst. Such a drastic enhancement of chiroptical properties is not observed in the case of Rh-based poly(**41**).

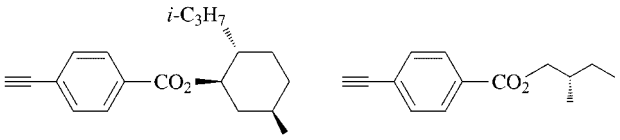

41 **42**

The ability of the helical poly(phenylacetylene) to recognize chiral molecules has been demonstrated (73). A stereoregular phenylacetylene-based polymer, poly(**43**), prepared with Rh catalyst has been shown to adopt a helical conformation. The corresponding polymer with ill-controlled stereoregularity, that is,

W-based poly(**43**), shows no distinct CD effects. High stereoregularity (cis) is, thus, required for the construction of well-ordered helical structures. The molecular recognition ability was demonstrated by the chromatographic enantioseparation of various racemates using poly(**43**) as a chiral stationary phase.

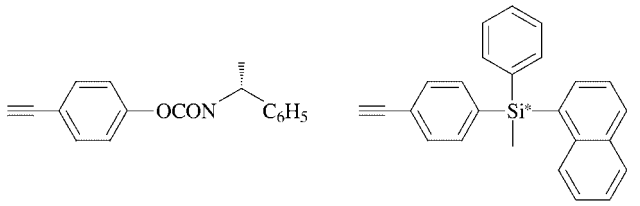

43 **44**

The nature of the helical conformation of poly(phenylacetylene) has been studied in detail (74). The stability of the helical conformation of poly(phenylacetylenes) was estimated by the chiroptical properties of the copolymers from chiral and achiral phenylacetylenes. When the monomer possesses sterically less bulky ring substituents, a clear cooperative nature on the copolymerization is not observed. A chiral amplification phenomenon is attainable only when the monomers have bulky ring substituents. This result coincides with the poor chiroptical property of poly(**42**) (73) and also with the very intense CD effects of poly(**44**) having bulky chiral silyl groups (256). Computational simulations verified that, unlike polyisocyanates which have a long persistence length of helical structure because of their stiff main chain, the main chain of poly(phenylacetylene) is quite flexible and that, unless bulky substituents are incorporated, poly(phenylacetylene) exists in essentially randomly coiled conformation or in a helical conformation with very short persistence length.

In an elegant application of the unique nature of poly(phenylacetylene), a new method has been established for the transformation of the randomly coiled conformation of poly(phenylacetylene) into a well-defined helix by using external chiral stimuli (Fig. 2) (77,257–260). For example, poly(4-carboxylphenylacetylene) adopts a stable helical conformation with an excess of one-handed screw-sense when the carboxyl groups complex with chiral molecules (258). Very intense CD effects as a result of the helical conformation of the main chain are observed in the presence of chiral amines or aminoalcohols. The absolute configuration of chiral molecules determines the sense of the helix. For instance, addition of (*R*)-amines results in a positive first Cotton effect around 440 nm, whereas negative first Cotton effects appear in the presence of (*S*)-amines. This behavior is almost universal for a wide range of amines and aminoalcohols. Therefore, poly(4-carboxylphenylacetylene) functions as a probe for chiral molecules. A similar phenomenon is attainable for poly(phenylacetylenes) having amino (77) or boronic acid groups (258). The former recognizes chiral carboxylic acids and α-hydroxy carboxylic acids, and the latter can be applied as a probe for a wide variety of chiral molecules that include not only diols, aminoalcohols, amines, α- and β-hydroxy carboxylic acids but also steroids and carbohydrates.

Aminoalcohols more strongly complex with carboxylic acid than amines. This characteristic allows substitution of the chiral amines, initially complexed with poly(4-carboxylphenylacetylene), by achiral aminoalcohols (260). The most

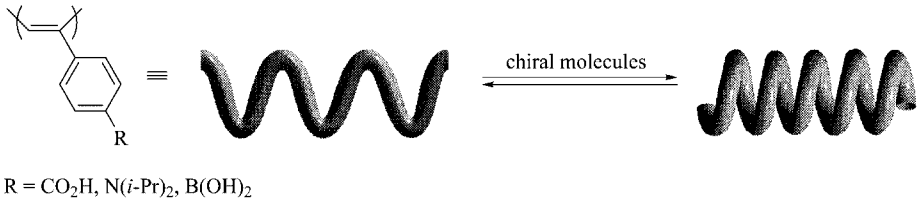

Fig. 2. Schematic illustration of the complexation of poly(phenylacetylenes) with chiral molecules.

characteristic point of this process is that the helix sense, determined by the priory complexed chiral amines, is maintained even after complete substitution by achiral aminoalcohols. In other words, the memory of macromolecular helicity is possible.

Helical Poly(propiolic esters). Comprehensive studies of the helical nature of poly(propiolic esters) (**45**) have shown that, apart from the flexibility of the main chain of polymers from poly(1-alkynes) and poly(phenylacetylenes), poly(propiolic esters) possess a stiff main chain (50,261,262). The Mark–Houwink–Sakurada plots of the stereoregular (cis-transoidal) poly(propiolic esters) clearly indicate the stiff main chain of poly(propiolic esters) (262). For example, the slope of the Mark–Houwink–Sakurada plot of poly(hexyl propiolate) is 1.2, which is comparable to that of poly(hexyl isocyanate). The stiffness of poly(propiolic esters) originates from the helical conformation with a large helical domain size. In contrast to other substituted polyacetylenes, a clearer cooperative effect of helical structure is observed in the chiral/achiral and the R/S copolymerizations (262). Therefore, only a small amount of chiral substituents in the pendant groups leads to well-ordered helical poly(propiolic esters) with an excess of one-handed screw sense. The most important factor to affect the secondary conformation of poly(propiolic esters) is the structure of pendants, and an introduction of methylene groups at the α-position of the ester group is indispensable for the construction of well-ordered helical polymers (261). For the polymers having α-methylene groups (**44**), $n = 1$–5), remote control of the screw sense is possible if the chiral information positions within the ε-carbon from the ester group. Temperature variable CD spectra also suggest that, if the chiral carbon locates within the δ-position, one screw sense dominates over the counterpart even at room temperature. When the chiral substituent on the ester group is a long alkyl chain such as (*S*)-3,7-dimethyloctyl group, helix sense inversion takes place, which is driven by the change of temperature or solvent composition (77).

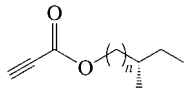

45 (n = 0–5)

A simple NMR technique can estimate not only the activation energy of helix–helix interconversion ($\Delta G‡$), but also the free energy difference between the right- and left-handed conformations (ΔG_r) (**262**). In the NMR spectra of poly(propiolic esters) without α-branching, α-methylene protons give two diastereotopic signals. This peak separation is contributed by the slow interconversion process between

the right- and left-handed helical conformations. Thus, the temperature variable NMR measurements readily give the activation energy $\Delta G^{\ddagger}$ for the helix–helix interconversion (71–79 kJ/mol, 17–19 kcal/mol), which is comparable to that of polyisocyanates. This means that poly(propiolic esters) undergo rapid helix inversion at ambient temperature. The ΔG_r of poly(hexyl propiolate) was also estimated by NMR to be 6.65 kJ/mol (1.59 kcal/mol) at 22°C.

Helical Polymers from Disubstituted Acetylenes. In contrast to the energetic studies on the helical polymers from monosubstituted acetylenes, those from disubstituted acetylenes are very limited. One of the reasons is the difficulty in controlling and elucidating the stereoregularity of the polymers from disubstituted acetylenes. However, in contrast to the instability of polymers from monosubstituted acetylenes (263–269), those from disubstituted acetylenes are quite stable. Another advantage of polymers from disubstituted acetylenes is their excellent permeability to small molecules. Thus, chiral polymers from disubstituted acetylenes are potentially applicable to the chiral resolution membranes.

The first example of chiral polymer from a disubstituted acetylene is a poly(1-trimethylsilyl-1-propyne)-based polymer, poly(**46**), which was synthesized in moderate yields using $TaCl_5$–Ph_3Bi (112). Poly(**46**) displays small optical rotations, and its molar ellipticities of the Cotton effects are up to a few hundreds. The main chain of poly(**46**) is, therefore, not a well-ordered helix. This is probably because of the less controlled geometrical structure (cis and trans) of the polymer backbone. However, the free-standing film of this polymer achieves an enantioselective permeation of various racemates including alcohols and amino acids. For example, the concentration-driven permeation of an aqueous solution of tryptophan by poly(**46**) gives 81% enantiomeric excess (ee) of the permeate at the initial stage. A characteristic of the membrane of poly(**46**) is its ability to enantioselectively recognize 2-butanol and 1,3-butanediol, because the direct resolution of these racemates by hplc is impossible.

Other chiral polymers from disubstituted acetylenes are based on the poly(phenylacetylene) derivatives that are also recognized as one of the most permeable polymers. Diphenylacetylene having a dimethyl-(−)-pinanylsilyl group (**47a**) was polymerized with Ta and Nb catalyst to give an extremely high molecular weight polymer in good yield (124). The produced polymer exhibits a very large optical rotation ($[\alpha]_D > 2000°$), and complicated but very intense CD effects appear in its absorption region. Although the first order structure (cis or trans, head-to-head or head-to-tail) of the polymer is unknown, these very rich chiroptical properties are indicative of the main-chain chirality based on helical structure. Similar polymers from disubstituted acetylenes (**47b**) and (**47c**) have been obtained; however, their chiroptical properties are poorer in comparison with those of poly(**47a**).

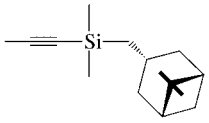

46

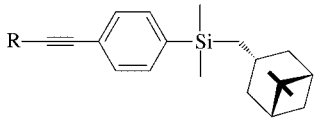

47a; R = C_6H_5
47b; R = CH_3
47c; R = Cl

Although poly(**47a**) exhibits large chiroptical properties, its ability to enantioselectively permeate racemates is unexpectedly low. In contrast, poly(**47b**) that possesses small $[\alpha]_D$ and $[\theta]$ values achieves the resolution of racemic mixtures of tryptophan. The initial % ee of permeate reached 52%. Thus, the size of the void in the membrane of helical poly(**47a**) appears to be very large, which may inhibit the racemate to interact with the chiral environment originating from the chiral pendant.

BIBLIOGRAPHY

"Acetylene and Acetylenic Polymers" in *EPST* 1st ed., Vol. 1, pp. 46–66, by E. M. Smolin, Diamond Alkali Co., and D. S. Hoffenberg, Gaylord Associates, Inc.; "Acetylenic Polymers" in *EPSE* 2nd ed., Vol. 1, pp. 87–130, by H. W. Gibson, Xerox Corp, and J. M. Pochan, Eastman Kodak Co.

1. G. Natta, G. Mazzanti, and P. Corradini, *Atti Accad. Naz. Lincei, Cl. Sci. Fis. Mat. Nat., Rend.* **25**, 3 (1958).
2. H. Shirakawa and co-workers, *J. Chem. Soc., Chem. Commun.* 578 (1977).
3. C. K. Chiang and co-workers, *Phys. Rev. Lett.* **39**, 1098 (1977).
4. C. K. Chiang and co-workers, *J. Am. Chem. Soc.* **100**, 1013 (1978).
5. H. Naarman, *Synth. Met.* **17**, 223 (1987).
6. J. Tsukamoto, A. Takahashi, and K. Kawasaki, *Jpn. J. Appl. Phys.* **29**, 125 (1990).
7. T. Ito, H. Shirakawa, and S. Ikeda, *J. Polym. Sci., Polym. Chem. Ed.* **12**, 11 (1974).
8. H. Shirakawa and S. Ikeda, *Polym. J.* **2**, 231 (1971).
9. T. Masuda, K. Hasegawa, and T. Higashimura, *Macromolecules* **7**, 728 (1974).
10. H. Shirakawa, T. Masuda, and K. Takeda, in S. Patai, ed., *The Chemistry of Triple-Bonded Functional Groups*, Suppl. C2, Vol. **2**, Wiley, Chichester, 1994, Chapt. "17".
11. A. M. Saxman, R. Liepens, and M. Aldissi, *Prog. Polym. Sci.* **11**, 57 (1985).
12. J. C. W. Chien, *Polyacetylene*, Academic Press, New York, 1984.
13. T. A. Skotheim, ed., *Handbook of Conducting Polymers*, Marcel Dekker, Inc., New York, 1986.
14. S. Curran, A. Star-Hauser, and S. Roth, in H. S. Nalwa, ed., *Handbook of Organic Conductive Molecules and Polymers*, Vol. **2**, John Wiley & Sons, Inc., Chichester, 1997, Chapt. "1".
15. J. Tsibouklis, *Adv. Mater.* **7**, 407 (1995).
16. T. Ogawa, *Prog. Polym. Sci.* **20**, 943 (1995).
17. J. Shinar, in H. S. Nalwa, ed., *Handbook of Organic Conductive Molecules and Polymers*, Vol. **3**, John Wiley & Sons Inc., Chichester, 1997, Chapt. "7".
18. F. Mohammad, in Ref. 17, Chapt. "16".
19. T. Kobayashi, in Ref. 17, Vol. **4**, Chapt. "7".
20. S.-K. Choi and co-workers, *Prog. Polym. Sci.* **22**, 693 (1997).
21. S.-K. Choi and co-workers, *Chem. Rev.* **100**, 1645 (2000).
22. G. Costa, in G. Allen, ed., *Comprehensive Polymer Science*, Vol. **4**, Pergamon Press, Oxford, 1989, Chapt. "9".
23. T. Masuda and T. Higashimura, *Adv. Polym. Sci.* **81**, 121 (1986).
24. C. I. Simonescu and V. Percec, *Prog. Polym. Sci.* **8**, 133 (1982).
25. T. Masuda, in S. Kobayashi, ed., *Catalysis in Precision Polymerization*, John Wiley & Sons, Inc., Chichester, 1997, Chapt. "2.4".
26. T. Masuda, in J. C. Salamone, ed., *Polymeric Material Encyclopedia*, Vol. **1**, CRC Press, Boca Raton Fla., 1996, p. 32.
27. T. Masuda and co-workers, *J. Mol. Catal.* **133**, 213 (1998).

28. T. Masuda and co-workers, *J. Macromol. Sci., A: Pure Appl. Chem.* **34**, 1977 (1997).
29. M. Tabata, T. Sone, and Y. Sadahiro, *Macromol. Chem. Phys.* **200**, 265 (1999).
30. Y. Nakayama, K. Mashima, and A. Nakamura, *J. Chem. Soc., Chem. Commun.* 1496 (1992).
31. Y. Nakayama, K. Mashima, and A. Nakamura, *Macromolecules* **26**, 6267 (1993).
32. Z. Shen and M. F. Farona, *J. Polym. Sci., Part A: Polym. Chem.* **22**, 1009 (1984).
33. Z. Shen and M. F. Farona, *Polym. Bull.* **10**, 298 (1983).
34. T. Masuda and co-workers, *Polym. J.* **14**, 371 (1982).
35. T. Masuda and co-workers, *Polym. J.* **12**, 907 (1980).
36. M. Nakano, T. Masuda, and T. Higashimura, *Macromolecules* **27**, 1344 (1994).
37. H. Nakako and co-workers, *Polym. J.* **30**, 577 (1998).
38. Y. Kishimoto and co-workers, *Macromolecules* **28**, 6662 (1995).
39. F. Ciardelli, S. Lanzillo, and O. Pieroni, *Macromolecules* **7**, 174 (1974).
40. S. Oh and co-workers, *J. Polym. Sci., Part A: Polym. Chem.* **31**, 2977 (1993).
41. H. Goto, K. Akagi, and H. Shirakawa, *Synth. Met.* **84**, 373 (1997).
42. B. Z. Tang and co-workers, *Macromolecules* **31**, 2419 (1998).
43. S. Koltzenburg, F. Stelzer, and O. Nuyken, *Macromol. Chem. Phys.* **200**, 821 (1999).
44. H. Tajima, T. Masuda, and T. Higashimura, *J. Polym. Sci., Part A: Polym. Chem.* **25**, 2033 (1987).
45. T. Masuda and co-workers, *Macromolecules* **20**, 1467 (1987).
46. K. Tsuchihara, T. Masuda, and T. Higashimura, *Polym. Bull.* **20**, 343 (1988).
47. M. Tabata and co-workers, *J. Macromol. Sci., A: Pure Appl. Chem.* **31**, 465 (1994).
48. T. Masuda, M. Kawai, and T. Higashimura, *Polymer* **23**, 744 (1982).
49. I. Yamaguchi, K. Osakada, and T. Yamamoto, *Inorg. Chim. Acta* **220**, 35 (1994).
50. H. Nakako and co-workers, *Macromolecules* **32**, 2861 (1999).
51. M. V. Russo and co-workers, *Polymer* **36**, 4867 (1995).
52. M. V. Russo and co-workers, *Polymer* **38**, 3677 (1997).
53. T. Sata, R. Nomura, and T. Masuda, *Polym. Bull.* **41**, 395 (1998).
54. Y.-S. Gal and co-workers, *Macromolecules* **28**, 2086 (1995).
55. Y.-S. Gal, *Eur. Polym. J.* **33**, 169 (1997).
56. T. Masuda and co-workers, *Macromoleucles* **9**, 661 (1976).
57. T. Masuda and co-workers, *Polym. Bull.* **2**, 823 (1980).
58. Y. Misumi and co-workers, *Polym. J.* **30**, 581 (1998).
59. Y. Tamura, Y. Misumi, and T. Masuda, *Chem. Commun.* 373 (1996).
60. R. J. Kern, *J. Polym. Sci., Part A1* **7**, 621 (1969).
61. B. Biyani and co-workers, *J. Macromol. Sci., Part A: Chem.* **9**, 327 (1975).
62. Z. Shen and M. F. Farona, *Polym. Bull.* **10**, 8 (1983).
63. A. Furlani, S. Licoccia, and M. V. Russo, *J. Polym. Sci., Part A: Polym. Chem.* **24**, 991 (1986).
64. W. Yang and co-workers, *Polym. J.* **23**, 1135 (1991).
65. Y. Fujita and co-workers, *J. Polym. Sci., Part A: Polym. Chem.* **36**, 3157 (1998).
66. M. Tabata, Y. Wu, and K. Yokotoa, *J. Polym. Sci., Part A: Polym. Chem.* **32**, 1113 (1994).
67. M. V. Russo, A. Furlani, and R. D'amato, *J. Polym. Sci., Part A: Polym. Chem.* **36**, 93 (1998).
68. A. M. A. Karim, R. Nomura, and T. Masuda, *Polym. Bull.* **43**, 305 (1999).
69. J. Vohlídal and co-workers, *Polymer* **38**, 3359 (1997).
70. B. Z. Tang and co-workers, *Macromolecules* **30**, 5620 (1998).
71. X. Kong, J. W. Y. Lam, and B. Z. Tang, *Macromolecules* **32**, 1722 (1999).
72. T. Aoki and co-workers, *Chem. Lett.* 2009 (1993).
73. E. Yashima, S. Huang, and Y. Okamoto, *J. Chem. Soc., Chem. Commun.* 1811 (1994).
74. E. Yashima and co-workers, *Macromolecules* **28**, 4184 (1995).
75. E. Yashima, Y. Maeda, and Y. Okamoto, *J. Am. Chem. Soc.* **120**, 8895 (1998).

76. T. Sugimoto and co-workers, *Polym. Bull.* **42**, 55 (1999).
77. E. Yashima and co-workers, *Chirality* **9**, 593 (1997).
78. Y. Abe, T. Masuda, and T. Higashimura, *J. Polym. Sci., Part A: Polym. Chem.* **27**, 4267 (1989).
79. H. Muramatsu, T. Ueda, and K. Ito, *Macromolecules* **18**, 1634 (1985).
80. T. Masuda and co-workers, *Macromolecules* **21**, 281 (1988).
81. K. Tsuchihara and co-workers, *Polym. Bull.* **23**, 505 (1990).
82. T. Masuda and co-workers, *Macromolecules* **23**, 1374 (1990).
83. T. Masuda and co-workers, *Polym. J.* **25**, 535 (1993).
84. R. R. Schrock and co-workers, *Organometallics* **13**, 3396 (1994).
85. T. Yoshimura and co-workers, *Macromolecules* **24**, 6053 (1991).
86. M. Teraguchi and T. Masuda, *Macromolecules* **33**, 240 (2000).
87. M. R. Buchmeiser and co-workers, *Macromolecules* **31**, 3175 (1998).
88. M. R. Buchmeiser, *Macromolecules* **30**, 2274 (1997).
89. M. Yamaguchi, M. Hirama, and H. Nishihara, *Chem. Lett.* 1667 (1992).
90. K. Nanjo and co-workers, *J. Polym. Sci., Part A: Polym. Chem.* **37**, 277 (1999).
91. M. Tabata, K. Yokota, and M. Namioka, *Macromol. Chem. Phys.* **196**, 2969 (1995).
92. T. Ohtori, T. Masuda, and T. Higashimura, *Polym. J.* **11**, 805 (1979).
93. K. Musikabhumma and T. Masuda, *J. Polym. Sci., Part A: Polym. Chem.* **36**, 3131 (1998).
94. S. M. A. Karim and co-workers, *Proc. Jpn. Acad. Ser. B* **75**, 97 (1999).
95. T. Sata and co-workers, *J. Polym. Sci., Part A: Polym. Chem.* **36**, 2489 (1998).
96. T. Kakuchi and co-workers, *J. Polym. Sci., Part A: Polym. Chem.* **33**, 1431 (1998).
97. T. Kaneko and co-workers, *Macromolecules* **30**, 3118 (1997).
98. T. Shimizu and T. Yamamoto, *Chem. Commun.* 515 (1999).
99. L. Dulog and S. Lutz, *Makromol. Chem., Rapid Commun.* **14**, 147 (1993).
100. Y. Miura, M. Matsumoto, and Y. Ushitani, *Macromolecules* **26**, 2628 (1993).
101. A. Fujii and co-workers, *Macromolecules* **24**, 1077 (1991).
102. M. Buchmeiser and R. R. Schrock, *Macromolecules* **28**, 6642 (1995).
103. T. Higashimura, Y.-X. Deng, and T. Masuda, *Macromolecules* **15**, 234 (1982).
104. T. Masuda, Y. Kuwane, and T. Higashimura, *Polym. J.* **13**, 301 (1981).
105. K. C. Wallace and co-workers, *Organometallics* **8**, 644 (1989).
106. T. Masuda and co-workers, *Macromolecules* **20**, 1734 (1987).
107. M. Kawasaki, T. Masuda, and T. Higashimura, *Polym. J.* **15**, 767 (1983).
108. T. Masuda and co-workers, *Macromolecules* **23**, 4902 (1990).
109. K. Tamura, T. Masuda, and T. Higashimura, *Polym. J.* **17**, 815 (1985).
110. T. Masuda, E. Isobe, and T. Higashimura, *Macromolecules* **18**, 841 (1985).
111. T. Masuda and co-workers, *Macromolecules* **19**, 2448 (1986).
112. T. Aoki and co-workers, *Macromolecules* **29**, 4192 (1996).
113. T. Masuda and co-workers, *J. Polym. Sci., Part A: Polym. Chem.* **25**, 1353 (1987).
114. K. Kaku and T. Masuda, *J. Polym. Sci., Part A: Polym. Chem.* **38**, 71 (2000).
115. U.S. Pat. 4759776 (Dec. 8, 1988), M. Langsam (to Air Products).
116. T. Masuda, T. Takahashi, and T. Higashimura, *Macromolecules* **18**, 311 (1985).
117. T. Masuda and co-workers, *Macromolecules* **18**, 2109 (1985).
118. T. Masuda, M. Yamagata, and T. Higashimura, *Macromolecules* **17**, 126 (1984).
119. M. Teraguchi and T. Masuda, *J. Polym. Sci., Part A: Polym. Chem.* **37**, 4546 (1999).
120. A. Niki, T. Masuda, and T. Higashimura, *J. Polym. Sci., Part A: Polym. Chem.* **25**, 1553 (1987).
121. K. Tsuchihara, T. Masuda, and T. Higashimura, *J. Am. Chem. Soc.* **113**, 8548 (1991).
122. K. Tsuchihara, T. Masuda, and T. Higashimura, *Macromolecules* **25**, 8516 (1992).
123. M. Teraguchi and T. Masuda, *J. Polym. Sci., Part A: Polym. Chem.* **36**, 2721 (1998).
124. T. Aoki and co-workers, *Macromolecules* **32**, 79 (1999).

125. T. Yoshimura and M. Asano, *Polym. J.* **26**, 159 (1994).
126. H. Kouzai, T. Masuda, and T. Higashimura, *Polymer* **35**, 4920 (1994).
127. H. Tachimori and T. Masuda, *J. Polym. Sci., Part A: Polym. Chem.* **33**, 2079 (1995).
128. H. Ito, T. Masuda, and T. Higashimura, *J. Polym. Sci., Part A: Polym. Chem.* **34**, 2925 (1996).
129. H. Kouzai, T. Masuda, and T. Higashimura, *J. Polym. Sci., Part A: Polym. Chem.* **32**, 2523 (1994).
130. T. J. Katz and S. J. Lee, *J. Am. Chem. Soc.* **102**, 422 (1980).
131. S. A. Krouse, R. R. Schrock, and R. E. Cohen, *Macromolecules* **20**, 904 (1987).
132. S. A. Krouse and R. R. Schrock, *Macromolecules* **22**, 2569 (1989).
133. K. Yamada, R. Nomura, and T. Masuda, *Macromolecules* **33**, 9179 (2000).
134. Z. Shen, *Macromol. Symp.* **84**, 5 (1994).
135. T. Masuda, T. Mouri, and T. Higashimura, *Bull. Chem. Soc. Jpn.* **53**, 1152 (1980).
136. G. Lachmann, J. A. K. Du Plessis, and C. J. Du Toit, *J. Mol. Catal.* **42**, 151 (1987).
137. G. Dändliker, *Helv. Chem. Acta* **52**, 1482 (1969).
138. T. Masuda, T. Takahashi, and T. Higashimura, *J. Chem. Soc., Chem. Commun.* 1297 (1982).
139. F. A. Cotton and co-workers, *Macromolecules* **14**, 233 (1981).
140. J. Kunzler and V. Percec, *Polym. Bull.* **29**, 335 (1992).
141. T. Masuda and co-workers, *J. Chem. Soc., Chem. Commun.* 1805 (1987).
142. M. Yamaguchi and co-workers, *Chem. Lett.* 1259 (1991).
143. K. Tamura, T. Masuda, and T. Higashimura, *Polym. Bull.* **30**, 537 (1993).
144. B. Z. Tang and N. Kotera, *Macromolecules* **22**, 4388 (1989).
145. R. Nomura, K. Watanabe, and T. Masuda, *Polym. Bull.* **43**, 177 (1999).
146. D.-J. Liaw and co-workers, *Makromol. Chem., Rapid Commun.* **6**, 309 (1985).
147. D.-J. Liaw and co-workers, *Polym. J.* **24**, 889 (1992).
148. D.-J. Liaw and C.-L. Lin, *J. Polym. Sci., Part A: Polym. Chem.* **31**, 3152 (1993).
149. R. R. Schrock and co-workers, *J. Am. Chem. Soc.* **118**, 3883 (1996).
150. H. H. Fox and R. R. Schrock, *Organometallics* **11**, 2763 (1992).
151. H. H. Fox and co-workers, *J. Am. Chem. Soc.* **116**, 2827 (1994).
152. F. J. Schattenmann, R. R. Schrock, and W. M. Davis, *J. Am. Chem. Soc.* **118**, 3295 (1996).
153. T. J. Katz and co-workers, *J. Am. Chem. Soc.* **106**, 2659 (1984).
154. K. Yokota and co-workers, *Polym. J.* **25**, 1079 (1993).
155. A. Furlani and co-workers, *Polym. Bull.* **16**, 311 (1986).
156. A. Furlani and co-workers, *J. Polym. Sci., Part A* **27**, 75 (1989).
157. M. Tabata, W. Yang, and K. Yokota, *Polym. J.* **22**, 1105 (1990).
158. M. Lindgren and co-workers, *Polymer* **32**, 1531 (1991).
159. M. Tabata, W. Yang, and K. Yokota, *J. Polym. Sci., Part A: Polym. Chem.* **32**, 1113 (1994).
160. M. Tabata and co-workers, *Macromolecules* **27**, 6234 (1994).
161. Y. Goldberg and H. Alper, *J. Chem. Soc., Chem. Commun.* 1209 (1994).
162. J. Schniedermeier and H.-J. Haupt, *J. Organomet. Chem.* **506**, 41 (1996).
163. H. Katayama and co-workers, *Organometallics* **16**, 4497 (1997).
164. R. Vilar and co-workers, *Eur. Polym. J.* **30**, 1237 (1994).
165. A. Escudero and co-workers, *Eur. Polym. J.* **31**, 1135 (1995).
166. B. Z. Tang and co-workers, *Macromolecules* **30**, 2209 (1997).
167. H. Hori, C. Six, and W. Leitner, *Macromolecules* **32**, 3178 (1999).
168. Y. Kishimoto and co-workers, *J. Am. Chem. Soc.* **116**, 12131 (1994).
169. K. Hirao and co-workers, *Macromolecules* **31**, 3405 (1998).
170. Y. Kishimoto, T. Noyori, P. Eckerle, T. Miyatake, and T. Ikariya, in J. C. Salamone, ed., *Polymeric Material Encyclopedia*, Vol. **7**, CRC Press, Boca Raton, Fla., 1996, p. 5051.

171. Y. Kishimoto and co-workers, *J. Am. Chem. Soc.* **121**, 12035 (1999).
172. Y. Kishimoto and co-workers, *Macromolecules* **29**, 5054 (1996).
173. Y. Misumi and T. Masuda, *Macromolecules* **31**, 7572 (1998).
174. M. Miyake, Y. Misumi, and T. Masuda, *Macromolecules* **33**, 6636 (2000).
175. S.-I. Lee, S.-C. Shim, and T.-J. Kim, *J. Polym. Sci., Part A: Polym. Chem.* **34**, 2377 (1996).
176. M. V. Russo and co-workers, *Polymer* **37**, 1715 (1995).
177. V. M. Kobryanskii, *J. Polym. Sci., Part A: Polym. Chem.* **30**, 1935 (1992).
178. S. Subramanyam, M. S. Chetan, and A. Blumstein, *Macromolecules* **26**, 3212 (1993).
179. L. Balogh and A. Blumstein, *Macromolecules* **28**, 3691 (1995).
180. L. Balogh and co-workers, *Macromolecules* **29**, 4180 (1996).
181. P. Zhou and A. Blumstein, *Polymer* **38**, 595 (1997).
182. R. Nomura, H. Nakako, and T. Masuda, *Polym. J.* **32**, 303 (2000).
183. T. Yoshimura, T. Masuda, and T. Higashimura, *Macromolecules* **21**, 1899 (1988).
184. T. Masuda, T. Yoshimura, and T. Higashimura, *Macromolecules* **22**, 3804 (1989).
185. H. Kubo, S. Hayano, and T. Masuda, *J. Polym. Sci., Part A: Polym. Chem.* **38**, 2697 (2000).
186. J. Kunzler and V. Percec, *J. Polym. Sci., Part A: Polym. Chem.* **28**, 1221 (1990).
187. T. Mizumoto, T. Masuda, and T. Higashimura, *Macromol. Chem. Phys.* **196**, 1769 (1995).
188. T. Masuda and co-workers, *Polym. J.* **25**, 535 (1993).
189. T. Masuda and co-workers, *Macromolecules* **25**, 1401 (1992).
190. H. Kaneshiro, T. Masuda, and T. Higashimura, *Polym. Bull.* **35**, 17 (1995).
191. T. Masuda and co-workers, *Polym. Bull.* **32**, 19 (1994).
192. S. Hayano and T. Masuda, *Polymer* **40**, 4071 (1999).
193. K. Akiyoshi, T. Masuda, and T. Higashimura, *Makromol. Chem.* **193**, 755 (1992).
194. H. Kaneshiro, S. Hayano, and T. Masuda, *Polym. J.* **31**, 348 (1999).
195. S. Hayano and T. Masuda, *Macromol. Chem. Phys.* **198**, 3041 (1997).
196. S. Hayano and T. Masuda, *Macromolecules* **31**, 3170 (1998).
197. E. Iwawaki, S. Hayano, and T. Masuda, *Polymer* **41**, 4429 (2000).
198. S. Hayano and T. Masuda, *Macromolecules* **32**, 7344 (1999).
199. S. Hayano and T. Masuda, *Macromol. Chem. Phys.* **201**, 233 (2000).
200. J. Fujimori, T. Masuda, and T. Higashimura, *Polym. Bull.* **20**, 1 (1995).
201. R. Schlund, R. R. Schrock, and W. E. Crowe, *J. Am. Chem. Soc.* **111**, 8004 (1989).
202. S. Koltzenburg and co-workers, *Macromolecules* **32**, 21 (1999).
203. K. Kanki, Y. Misumi, and T. Masuda, *Polym. Prepr.* **48**, 1702 (1999).
204. Y. Okano, T. Masuda, and T. Higashimura, *Polym. J.* **14**, 477 (1982).
205. T. Masuda and co-workers, *Macromolecules* **29**, 1167 (1996).
206. D. S. Breslow, *Prog. Polym. Sci.* **18**, 1141 (1993).
207. S. A. Stern, *J. Membr. Sci.* **94**, 1 (1994).
208. D. R. Paul and Y. P. Yampol'skii, *Polymeric Gas Separation Membranes*, CRC Press, Boca Raton, Fla., 1994.
209. R. E. Kesting and A. K. Fritzsche, *Polymeric Gas Separation Membranes*, John Wiley & Sons, Inc., New York, 1993.
210. H. Odani and T. Masuda, in N. Toshima, ed., *Polymers for Gas Separation*, VCH, New York, 1992, Chapt. "4".
211. Y. Osada and T. Nakagawa, eds., *Membrane Science and Technology*, Marcel Dekker, Inc., New York, 1992.
212. I. Cabasso, in J. I. Kroschwitz, ed., *Encyclopedia of Polymer Science and Engineering 1*, Vol. **9**, John Wiley & Sons, Inc., New York, 1987, p. 509.
213. B. D. Freeman and I. Pinau, eds., *Am. Chem. Soc., Symp. Ser.* **733** (1999).
214. T. Masuda and co-workers, *J. Am. Chem. Soc.* **105**, 7473 (1983).

215. L. M. Robeson and co-workers, *Polymer* **35**, 4970 (1994).
216. A. C. Savoca, A. D. Surnamer, and C. F. Tien, *Macromolecules* **26**, 6211 (1993).
217. K. Takada and co-workers, *J. Appl. Polym. Sci.* **30**, 1605 (1985).
218. A. Morisato and I. Pinnau, *J. Membr. Sci.* **121**, 243 (1996).
219. K. Tsuchihara, T. Masuda, and T. Higashimura, *J. Polym. Sci., Part A: Polym. Chem.* **31**, 547 (1993).
220. T. Aoki and co-workers, *J. Polym. Sci., Part A: Polym. Chem.* **32**, 849 (1994).
221. T. Mizumoto, T. Masuda, and T. Higashimura, *J. Polym. Sci., Part A: Polym. Chem.* **31**, 2555 (1993).
222. Y. Hayakawa and co-workers, *J. Polym. Sci., Part A: Polym. Chem.* **30**, 873 (1992).
223. T. Masuda and co-workers, *Polymer* **29**, 2041 (1988).
224. S.-Y. Oh and co-workers, *Macromolecules* **26**, 6203 (1993).
225. K. Iino and co-workers, *Synth. Met.* **84**, 967 (1997).
226. K. Akagi and co-workers, *J. Photopolym. Sci. Technol.* **10**, 233 (1997).
227. S. Koltzenburg and co-workers, *Macromol. Chem. Phys.* **200**, 814 (1999).
228. T. Wada and co-workers, *Mol. Cryst. Liq. Cryst.* **294**, 245 (1997).
229. T. Wada, T. Masuda, and H. Sasabe, *Mol. Cryst. Liq. Cryst.* **247**, 139 (1994).
230. R. Nomura and co-workers, *Macromolecules* **33**, 4313 (2000).
231. K. Tada and co-workers, *Jpn. J. Appl. Phys.* **34**, L1083 (1995).
232. K. Tada and co-workers, *Jpn. J. Appl. Phys.* **35**, L1138 (1996).
233. K. Yoshino and co-workers, *Synth. Met.* **91**, 283 (1997).
234. R. Hidayat and co-workers, *Jpn. J. Appl. Phys.* **38**, 931 (1999).
235. R. Hidayat and co-workers, *Jpn. J. Appl. Phys.* **36**, 3740 (1997).
236. M. Hirohata and co-workers, *Jpn. J. Appl. Phys.* **36**, L302 (1997).
237. R. Hidayat and co-workers, *Jpn. J. Appl. Phys.* **37**, L180 (1998).
238. Q. Zheng and co-workers, *Jpn. J. Appl. Phys.* **36**, L1508 (1997).
239. S. V. Frolov and co-workers, *Jpn. J. Appl. Phys.* **36**, L1268 (1997).
240. R. Sun, T. Masuda, and T. Kobayashi, *Synth. Met.* **91**, 301 (1997).
241. Q. Zheng and co-workers, *Jpn. J. Appl. Phys.* **36**, L1675 (1997).
242. R. Sun, T. Masuda, and T. Kobayashi, *Jpn. J. Appl. Phys.* **35**, L1673 (1996).
243. R. Sun, T. Masuda, and T. Kobayashi, *Jpn. J. Appl. Phys.* **35**, L1434 (1996).
244. Q. Zheng and co-workers, *Jpn. J. Appl. Phys.* **36**, L1508 (1997).
245. R. Sun and co-workers, *Jpn. J. Appl. Phys.* **38**, L1508 (1999).
246. Y. M. Huang and co-workers, *Macromolecules* **32**, 5976 (1999).
247. K. Yoshino and co-workers, *Jpn. Appl. Phys.* **33**, L254 (1994).
248. Y. Miura and co-workers, *Macromolecules* **26**, 6673 (1993).
249. H. Nishide and co-workers, *Macromolecules* **25**, 569 (1992).
250. H. Nishide and co-workers, *Macromolecules* **26**, 4567 (1993).
251. L. Dulog and P. Bognar, *Macromol. Rapid Commun.* **16**, 43 (1995).
252. N. Yoshioka and co-workers, *Macromolecules* **25**, 3838 (1992).
253. H. Nishide and co-workers, *J. Macromol. Sci., A: Pure Appl. Chem.* **29**, 775 (1992).
254. Y. Miura and co-workers, *J. Polym. Sci., Part A: Polym. Chem.* **30**, 959 (1992).
255. K. Aramata, A. Kajiwara, and M. Kamachi, *Macromolecules* **28**, 4774 (1995).
256. K. Kaku and T. Masuda, *Macromolecules* **33**, 6633 (2000).
257. E. Yashima, Y. Maeda, and Y. Okamoto, *Chem. Lett.* 955 (1996).
258. E. Yashima and co-workers, *J. Am. Chem. Soc.* **118**, 9800 (1996).
259. E. Yashima, T. Matsushima, and Y. Okamoto, *J. Am. Chem. Soc.* **119**, 6345 (1997).
260. E. Yashima, K. Maeda, and Y. Okamoto, *Nature* **399**, 449 (1999).
261. H. Nakako and co-workers, *Macromolecules* **33**, 39–78 (2000).
262. R. Nomura and co-workers, *J. Am. Chem. Soc.* **112**, 8830 (2000).
263. H. Nakako, R. Nomura, and T. Masuda, *Macromolecules* **34**, 1496 (2001).
264. T. Masuda and co-workers, *Macromolecules* **18**, 2369 (1985).

265. T. Higashimura and co-workers, *Polym. J.* **17**, 393 (1985).
266. B. Z. Tang and co-workers, *J. Polym. Sci., Part A: Polym. Chem.* **27**, 1197 (1989).
267. B. Z. Tang and co-workers, *J. Polym. Sci., Part B: Polym. Phys.* **28**, 281 (1990).
268. K. Tsuchihara, T. Masuda, and T. Higashimura, *J. Polym. Sci., Part A: Polym. Chem.* **29**, 471 (1991).
269. J. Vohlidal and co-workers, *Collect. Czech. Chem. Commun.* **58**, 2651 (1993).
270. J. Sedlácek and J. Vohlidal, *Makromol. Chem., Rapid Commun.* **14**, 51 (1993).

RYOJI NOMURA
TOSHIO MASUDA
Kyoto University

ACRYLAMIDE POLYMERS

Introduction

The terminology used to describe acrylamide-containing polymers in the technical literature varies in its precision. In order to avoid confusion, throughout this article the term "poly(acrylamide)" is reserved for the nonionic homopolymer of acrylamide, whereas the term "polyacrylamides" or "acrylamide polymers" refers to acrylamide-containing polymers, including the homopolymer and copolymers. Specific nomenclature is used for particular copolymers, for example, poly(acrylamide-*co*-sodium acrylate).

The diverse class of water-soluble and water-swellable polymers comprising polyacrylamides contains some of the most important synthetic polymeric materials used to improve the quality of life in our modern society. Acrylamide-containing polymers fall into three main categories: nonionic, anionic, and cationic. The projected annual sales growth rate of polyacrylamides between 1999 and 2002 is 4–7% (1). The multi-billion-dollar global market value of this class of materials makes it an economically important segment of the chemical industry.

Poly(acrylamide) is made by the free-radical polymerization of acrylamide, which is derived from acrylonitrile by either catalytic hydrolysis or bioconversion. The unique chemistry of acrylamide, its favorable reactivity ratios with many comonomers, and the ability of poly(acrylamide) to be derivatized allows for a substantial variety of polymers to be tailor-made over a wide range of molecular weights (approximately 10^3–50×10^6 Da), charge densities, and chemical functionalities.

A very large number of applications for acrylamide-containing polymers have been extensively reviewed (2–7). One major application area for polyacrylamides is in solid–liquid separations. The largest market segments therein are for use

Encyclopedia of Polymer Science and Technology. Copyright John Wiley & Sons, Inc. All rights reserved.

as flocculants and dewatering aids for municipal wastewater, thickening aids for industrial wastewater, secondary clarification and clarification of potable water, solids removal from biological broths, and animal feed recovery from waste. Because of major concern for the environment, the allowable suspended solids in most effluent streams are becoming more restricted by government regulations. New technologies for producing cationic polymers with a wide range of charge levels, novel structures, and very high molecular weights have addressed this need. These polymers have greatly improved the dewatering performances of centrifuges, screw presses, and belt presses used for such purposes. This has resulted in drier dewatered solids, which has translated into lower costs to either landfill or incinerate the solids.

The largest volume applications for polyacrylamides in paper mills are in on-machine wet-end processes. Paper retention aids and drainage aids are used to flocculate or bind fillers, fibers, and pigments. Glyoxalated cationic polyacrylamides are used as strengthening agents and promoters for paper sizing. Other papermaking applications include off-machine processes for recovering fiber from recycled paper waste and for deinking.

High molecular weight polyacrylamides have also traditionally been used in the minerals processing industry. Recent polymer technology developments, including ultra high molecular weight and novel anionic polyacrylamides, have yielded important materials. These products are used as flocculants in coal mining, the Bayer process for alumina recovery (red mud flocculants), precious metals recovery, and the solid–liquid separation of underflow streams in a variety of mining processes. Novel chemical modifications of low molecular weight polyacrylamides have resulted in materials that are used as modifiers in the selective separation of metal sulfides and magnetite and as depressants and flotation aids.

One large market segment for anionic polyacrylamides had traditionally been in enhanced oil recovery. However, low oil prices have resulted in a large decline in such applications. Since 1990, polymer flooding has virtually disappeared in the United States. However, during 1999 crude oil prices started to increase.

Other significant application areas for polyacrylamides include soil conditioning and erosion control, drag reduction, sugar processing, additives in cosmetics, and superabsorbents.

Physical Properties

Solid Polyacrylamides. Completely dry poly(acrylamide) is a brittle white solid. It is nontoxic, unlike the monomer. Dry polyacrylamides (including copolymers) are commercially available as nondusting powders and as spherical beads. These products can contain small amounts of additives that aid in both the stability and dissolution of the polymers in water. Commercially available acrylamide copolymer powders, which are typically dried under mild conditions, will usually contain about 5–15% water depending on their ionicity. The powders are hygroscopic, and generally become increasingly hygroscopic as the ionic character of the polymer increases. Cationic polymers are particularly hygroscopic.

Some physical properties of nonionic poly(acrylamide) are listed in Table 1. The tacticity and linearity of the polymer chain is claimed to be dependent on

Table 1. Physical Properties of Solid Poly(acrylamide)

Property	Value	Reference
Density	1.302 g/cm^3 (23°C)	8
Glass-transition temperature (T_g)	195°C	9
Critical surface tension (γ_c)	52.3 mN/m (= dyn/cm) (20°C)	10
Chain structure	Mainly heterotactic linear or branched, some head-to-head addition	11–14
Crystallinity	Amorphous (high molecular weight)	15
Solvents	Water, ethylene glycol, formamide	16
Nonsolvents	Ketones, hydrocarbons, ethers, alcohols	17
Fractionation solvents	Water–methanol	18
Gases evolved on combustion in air	H_2, CO, CO_2, NH_3, nitrogen oxides	19

the polymerization temperature. Syndiotacticity is favored at low temperatures (20). Linear polymer chains are reportedly obtained below 50°C, but branching begins to occur as the temperature is increased above this level (21). A wide range of values of the glass-transition temperature (T_g) of poly(acrylamide) have been published. This is because the measured value is highly sensitive to the presence of water and also to the presence of nonacrylamide species along the polymer backbone. For example, small amounts of acrylate groups can arise from hydrolysis of the amide group during or after polymerization. This can dramatically change the T_g.

Solution Properties. The amide group (—$CONH_2$) in poly(acrylamide) provides for its solubility in water and in a few other polar solvents such as glycerol, ethylene glycol, and formamide. We can acquire a sense of poly(acrylamide)'s affinity for water by examining a few characteristic parameters. Theta (Θ) conditions for a polymer delineate a particular combination of solvent and temperature at which the polymer acts in an ideal manner (22), ie, the chains behave as random coils. The Θ temperature of poly(acrylamide) in water has been determined to be −8°C (23). Thus, water at 25°C is a solvent of intermediate quality for poly(acrylamide). Aqueous methanol (40 vol%), however, is a Θ solvent for poly(acrylamide) at 25°C (24). The Flory χ parameter, which is a measure of the relative affinity between the polymer segments with each other vs with the solvent, is 0.5 under Θ conditions. The Flory χ parameter of poly(acrylamide) has been determined to be 0.48 in water at 30°C (25). These and other properties of poly(acrylamide) in solution are collected in Table 2.

Poly(acrylamide) is soluble in liquid water at all concentrations, temperatures, and pH values. However, at high pH (>10.5) the polymer will begin to hydrolyze on standing (29). Poly(acrylamide) is generally soluble in most salt solutions but can phase separate in some highly concentrated salt solutions, such as $(NH_4)_2SO_4$. Each amide group in poly(acrylamide) has roughly 2 strongly bound water molecules (30) associated with it, whereas the entire first hydration sheath contains a total of about 4–5 water molecules per monomer (31). This may be compared to poly(sodium acrylate), which has 4 strongly bound water molecules

Table 2. Physical Properties of Poly(acrylamide) in Solution

Property	Value	Conditions	Reference
Steric hindrance parameter (σ)	2.72	Water @ 30°C	26
Characteristic ratio (C_∞)	14.8	Water @ 30°C	26
Persistence length (y)	1.52 nm	Water @ 25°C	–[a]
Partial specific volume (ν)	0.693 cm^3/g	Water @ 20°C	27
Theta temperature (Θ)	−8°C	Water	23
Theta conditions	0.40 v/v methanol/water	25°C	24
Flory χ parameter	0.48 ± 0.01	Water @ 30°C	25
Refractive index increment (dn/dc)		Water @ 25°C	28
	0.187 cm^3/g	$\lambda = 546.1$ nm	
	0.185 cm^3/g	$\lambda = 632.8$ nm	

[a]Calculated from the values of K_0 (Mark–Houwink–Sakurada prefactor under Θ conditions) and Θ_0 (viscosity constant) found in Ref. (21), using the relationship: $y = (\frac{M_n}{2b})(\frac{K_n}{\Theta_0})^{2/3}$, where M_0 is the monomer molecular weight (71 g/mol), and b is the monomer length (0.25 nm).

per repeat unit (32) and a total of 11 water molecules of hydration per repeat unit (33). Certain salts, however, can alter the hydrogen bonding between the primary amide groups and water in individual chains. For example, addition of potassium iodide [7681-11-0] to a poly(acrylamide) solution can increase the solution viscosity slightly (34). The inferred coil expansion involves a change in the hydration sheath of the polymer.

The amide group is capable of strong hydrogen bonding, which has effects on both the monomer and polymer properties. The relative rates of acrylamide polymerization in various organic solvents (35–37) are influenced by solvent–monomer interactions, which depend on the polarity and hydrogen bonding ability of acrylamide. Hydrogen bonding has been evidenced (with nmr) to occur mainly with the carbonyl oxygen in the acrylamide (38,39).

The hydrogen bonding ability of the amide group is also well worth considering when rationalizing the solution properties of polymers containing acrylamide. Two examples are presented here. The slow evolution of hydrogen-bonded aggregates (see the following) have been implicated in explaining the time dependence of the viscosities of poly(acrylamide) solutions in aqueous media (12,40). Second, it is well known that copolymers of acrylamide and sodium acrylate exhibit maximum values of the mean square radius (R_g), second virial coefficient (A_2), and intrinsic viscosity [η] at 60–70 mol% acrylate content (41). This can be rationalized from a consideration of intermolecular hydrogen bonding and electrostatic interactions.

Copolymers of acrylamide with ionic comonomers are also generally quite soluble in water. However, the solution properties of ionized copolymers of acrylamide are substantially different from those of the homopolymer. The incorporation of ionic comonomers leads to all of the traditional polyion effects such as chain expansion and viscosification at low ionic strength (polyelectrolyte effect), ionization-dependent dissociation constants, counterion condensation, ion exchange with charged surfaces, and specific binding of certain multivalent ions. For example, anionic copolymers containing carboxylate groups will precipitate at certain multivalent salt concentrations (42–44). Poly(sodium acrylate) can phase

separate in the presence of divalent salts when there are about 0.8 equivalents of the divalent cations (45). The phase behavior of acrylamide–acrylic acid copolymers in mixtures of mono and divalent salts has been studied (46). Trivalent cations (eg, Al^{3+} and Cr^{3+}) are even more efficient at precipitating polyions containing carboxylate groups (47). Under the right conditions, these physical crosslinks can be used to form a reversible gel. This strategy has been employed in mobility control systems used in oil recovery (48).

The rate of dissolution of polyacrylamides can depend on the agitation conditions, dissolved salts, the material form of the polymer (eg, solid or emulsion), state of hydration, and the presence of other components. While salts only weakly affect the dissolution rate of poly(acrylamide), ionic copolymers tend to dissolve decidedly more slowly in salt solutions than in pure water. Increasing the mechanical energy input typically speeds up the dissolution process; however, mechanical degradation (chain scission) of very high molecular weight chains can occur. Flows with elongational components (eg turbulent and porous media flows) are usually most egregious in this regard. The coil-to-stretched transition initiated at a critical elongation rate in these flows can be responsible for such phenomena as drag reduction (49) and apparent viscosity enhancement in porous media flow (50,51). However, chain scission can also occur at a second critical elongation rate. These critical elongation rates are functions of the degree of polymerization, the solvent quality, and the polymer concentration (52–56). Care is often taken to avoid mechanical degradation of the polymer during mixing [especially in impeller-type mixers (57), gear pumps, and orifice flow], filtration, and flow through a packed column [eg, in high performance size-exclusion chromatography (HPSEC) analysis], all of which expose the polymer chains to some elongational flow kinematics.

Linear polyacrylamides in solution adopt nearly random coil configurations that are partially permeable (draining) to solvent. The coils are unassociated in dilute solution. The average shape of the isolated coils has been described as an ellipsoidal or bean-shaped structure (58). The individual chains are quite flexible, as is common with most vinyl polymers. This is indicated from several parameters shown in Table 2, such as the persistence length, steric hindrance parameter (σ), and characteristic ratio (C_∞). The persistence length of 1.52 nm for poly(acrylamide) in water is quite similar to the average intrinsic (bare) persistence length ($\sim$1.4 nm) of many vinyl polymers (59).

One measure of the size of a polymer in solution is its mean square radius (R_g), sometimes referred to as its radius of gyration. The mean square radius scales with the weight-average molecular weight (M_w) to a fractional power (a_r) for a homologous series of polymers all within the same topology class (eg, linear chains); $R_g = K_r M_w{}^a r$. The K_r and a_r values depend on the polymer, solvent, and temperature. Suggested values derived from the literature for poly(acrylamide) and a few copolymers are listed in Table 3.

Solution Rheology. Solutions of polyacrylamides tend to behave as pseudoplastic fluids in viscometric flows. Dilute solutions are Newtonian (viscosity is independent of shear rate) at low shear rates and transition to pseudoplastic, shear thinning behavior above a critical value of the shear rate. This critical shear rate decreases with the polymer molecular weight, polymer concentration, and the thermodynamic quality of the solvent. A second Newtonian plateau at high shear rates is not readily seen, probably because of mechanical degradation of the chains

Table 3. Suggested R_g–M_w Correlations for Polyacrylamides in Solution $R_g = K_r M_w{}^a r$ (R_g in nm)

Polymer	Solvent	Temp., °C	MW range (10^6 Da)	10^2 K_r, nm	a_r	Reference
Poly(acrylamide)	Water	25	0.83–13.4	0.725	0.64	23
Poly(acrylamide)	0.1 *M* NaCl + 0.2% NaN_3	20	0.16–8.2	0.749	0.64	60
Poly(Na acrylate$_{29}$–*co*-acrylamide$_{71}$)	0.1 *M* NaCl		0.96–6	2.50	0.60	44
Poly(Na acrylate$_{20}$–*co*-acrylamide$_{80}$)	1 *M* NaCl pH 9	Ambient	0.1–3.0	4.06	0.55	61
Poly(acrylamide$_{70}$–*co*-AETAC$_{30}$)	1 *M* NaCl + biocide		0.5–2.7	3.30	0.54	62

(12). Viscometric data for dilute and semidilute poly(acrylamide) solutions can often be fit to a Carreau model (63,64). It is wise to remember the cautions that were cited previously about mechanical degradation of the high molecular weight components of a polyacrylamide sample when analyzing rheological data.

The viscosities of fully dissolved, high molecular weight poly(acrylamide)s in aqueous solutions have often, but not always, been seen to change with time over the periods of days to weeks. Typically, the solution viscosity decreases with time. Extensive studies of this instability phenomenon have been made (12,40) and it was concluded that the evolution of intramolecular hydrogen bonds and the resulting change in macromolecular conformation were responsible for the time dependence, and not any molecular weight degradation. The instability can be avoided completely when the polymers are dissolved in formamide, aqueous ethylene glycol, or 2% 2-propanol in water. Competing viewpoints do exist about the interpretation of this solution aging (65,66).

The intrinsic viscosity $[\eta]$ of a polymer in solution is a measure of its molecular volume divided by its molecular weight. The $[\eta]$ value can be empirically correlated to the viscosity-average molecular weight (M_η) via the Mark–Houwink–Sakurada relationship (67): $[\eta] = K_\eta M_\eta a_\eta$. Poly(acrylamide) and ionic copolymers of acrylamide follow this empirical relationship, which is often used to estimate the polymer molecular weight. Table 4 lists suggested literature values of K_η and a_η for poly(acrylamide) and several copolymers in a variety of solvents.

At high concentrations of univalent ions ($\sim$1 M), the solution properties of ionic copolymers of acrylamide tend to resemble those of the homopolymer, but they are not exactly the same. Considering the intrinsic viscosity data, the exponents a_η for anionic and cationic polyacrylamides in high salt concentrations tend to cluster between 0.7 and 0.8, which is similar to that for poly(acrylamide) (12,23,60–62,71–75). However, the prefactors (K_η) vary over a larger range, and this cannot be rationalized simply by considering only the degree of polymerization. This means that there are real differences in the short-range interactions along the chains, which depend on the copolymer composition.

The polymer concentration (c) dependence of the zero-shear-rate viscosity (η_0) for aqueous poly(acrylamide) solutions of various viscosity-average molecular weights does not seem to follow the entanglement model, wherein polymer chain interpenetration would dominate the viscometric behavior, and a master curve should result when η_0 is plotted against cM_η. Instead, the data can be better described using a suspension model, wherein $c[\eta]$ correlates the η_0 data on a master plot. A concise presentation of the relationship between η_0, M_η, and c for poly(acrylamide) in water at 25°C has been made (12).

Solutions of poly(acrylamide) that are well in excess of the overlap concentration can display viscoelastic properties. Viscoelasticity of these polymeric fluids can be observed in a variety of ways, including the presence of a normal stress and/or flow irregularities (eg, vortices) in steady-shear flow, stress overshoot during shear flow startup, a measurable storage modulus (G') in oscillatory flow, an apparent shear thickening in flows with an elongational component (eg, porous media flow), a measurable elongational viscosity, or the ability to pull a solution "fiber" (tubeless siphon effect). A simple means for qualitatively assessing the molecular weight of a linear poly(acrylamide) in solution is to see how long a thread one can pull out of a semidilute solution of the polymer using a rod.

Table 4. Suggested Mark–Houwink–Sakurada Correlations for Polyacrylamides in Solution $[\eta] = K_\eta M_\eta a_\eta$ ($[\eta]$ in cm^3/g)

Polymer	Solvent	Temp., °C	MW range (10^6 Da)	$10^2\ K_\eta$, cm^3/g	a_η	Reference
Poly(acrylamide)	Water	25	0.038–9	1.00	0.76	68
Poly(acrylamide)	0.5 *M* NaCl	25	0.5–5.5	0.719	0.77	69
Poly(acrylamide)	1.0 *M* NaCl	25	1.1–14.6	2.57	0.67	70
Poly(Na acrylate$_{20}$–*co*-acrylamide$_{80}$)	0.5 *M* NaCl pH 9	25	0.12–3.0	1.40	0.75	61[a]
Poly(Na acrylate$_{20}$–*co*-acrylamide$_{80}$)	0.5 *M* NaCl pH 9	25	0.12–3.0	1.09	0.78	61[b]
Poly(Na acrylate$_{30}$–*co*-acrylamide$_{70}$)	0.5 *M* NaCl	25	0.77–5.5	1.12	0.79	69
Poly(Na acrylate$_{20}$–*co*-acrylamide$_{80}$)	1.0 *M* NaCl pH 9	25	0.12–3.0	1.41	0.74	61[a]
Poly(Na acrylate$_{20}$–*co*-acrylamide$_{80}$)	1.0 *M* NaCl pH 9	25	0.12–3.0	1.31	0.76	61[b]
Poly(acrylamide$_{70}$–*co*-AETAC$_{30}$)	1.0 *M* NaCl + biocide	25	0.5–2.7	1.05	0.73	62

[a]Uncorrected or polydispersity.
[b]Corrected for polydispersity.

Acrylamide Polymerization

Acrylamide [79-06-1] (2-propenamide, C_3H_5ON) readily undergoes free-radical polymerization to high molecular weight poly(acrylamide) [9003-05-8]. The synthetic methods have been reviewed extensively (12). Free-radical initiation can be accomplished using organic peroxides, azo compounds, inorganic peroxides including persulfates, redox pairs, photoinduction, radiation-induction, electroinitiation, or ultrasonication. Several reasons account for the ultrahigh molecular weights achievable. First, preparations of polyacrylamides are usually conducted in water, and the chain transfer constant to monomer and polymer appears to be zero in water (76). Second, the value of $k_p/k_t{}^{1/2}$, about 4.2, is unusually high (77) and is independent of the pH of the media. The rate of polymerization is proportional to the 1.2–1.5 power of the monomer concentration and to the square root of the initiator concentration (78–80). All this results in a high rate of propagation. Chain termination is primarily by disproportionation (81).

The large amount of heat (82.8 kJ/mol) that evolves during polymerization can result in a rapid temperature rise. One way in which this exotherm problem has been addressed in commercial high-solids and high-molecular-weight processes has been through the use of an adiabatic gel process in which the initiation temperature is 0°C. In another approach, controllable-rate redox polymerization of aqueous acrylamide-in-oil emulsions can be carried out at moderate temperatures of 40–60°C in order to accommodate the exotherm and to achieve very high molecular weights. At 70–100°C, a persulfate initiator can give a grafted or branched polymer (82). Additives greatly affect the rate and the kinetics of polymerization (83,84). These additives include metal ions, surfactants, chelating agents, and organic solvents. The high chain-transfer constant of compounds such as 2-propanol, bisulfite ion, or persulfate ion to active polymer has been reported (85). Chain-transfer agents have been used purposely to control molecular weight, minimize insoluble polymer, and control cross-linking and the degree of branching in commercial preparations.

Structural Modifications of Poly(acrylamide)

Poly(acrylamide) is a relatively stable organic polymer. However, poly(acrylamide) can be degraded (eg, molecular weight decreases) under certain conditions. The amide functionality is acidic in nature and is capable of undergoing most of the chemical reactions of primary amides. Consequently, acrylamide polymers can be functionalized by post-polymerization chemical reactions. Examples illustrated in the following constitute the most-used chemical modifications. To obtain anionic derivatives, poly(acrylamide) can be hydrolyzed with caustic. Sulfomethylated poly(acrylamide) can be prepared by reacting poly(acrylamide) with formaldehyde and sodium bisulfite under acidic conditions. Reacting poly(acrylamide) with hydroxylamine under alkaline conditions can yield hydroxamated poly(acrylamide). As an example of a cationic derivative, Mannich-base poly(acrylamide) can be obtained by reacting poly(acrylamide) with formaldehyde and dimethylamine to produce a cationic polymer with a charge that varies with pH. As an example of a nonionic derivative, poly(acrylamide) can be reacted with glyoxal to yield pendent

aldehyde functionality. These structurally modified polyacrylamides are successful commercial products.

Degradation. Dry poly(acrylamide) is relatively stable. The onset of dry poly(acrylamide) decomposition occurs at 180°C (86). Inter- or intra-amide condensation (87) to an imide can occur in acidic media at high temperatures (140–160°C). At temperatures above 160°C, thermal degradation, imidization, nitrile formation, and dehydration take place. Polymer stability is very important in actual applications in order to maintain consistent and excellent performance. In most applications, polymer solutions are prepared and used at moderate temperatures; however, there are exceptions such as in the harsh reservoir conditions (high temperature and high salinity) found in some enhanced oil recovery operations. Impurities such as residual persulfate from batch manufacturing can degrade the polymer (88,89). A residual Fe^{2+} EDTA complex in the product can also enhance degradation at both ambient and elevated temperatures (90–92). Hydroxy radicals, which can form in the presence of oxygen (93,94), can attack the polymer backbone. In the absence of oxygen, anionic polyacrylamide solutions were stable at 90°C for 20 months (95). Polyacrylamide in aqueous solution, in the presence of oxidizing agents such as $KMnO_4$, bromine, and $AgNO_3$, will degrade. The degraded polymer shows a reduced molecular weight, cross-linking, and chain stiffening (96). Recently, potassium peroxosulfate (97) was also reported to degrade hydrolyzed polyacrylamide. In the presence of ozone, very little degradation was found at low pH. However, random chain scission occurred at pH 10 (98). In the presence of sodium azide, a bactericide, a poly(acrylamide) in solution at room temperature showed no degradation for a long time (60). A combination of both pressure and elevated temperature can enhance polyacrylamide degradation. Polymer degradation can also occur under shear and elongational stresses (93,99). Backbone homolytic cleavage has been confirmed by a free-radical trap technique. Under certain shear conditions one macroradical per 12 monomer units can be formed.

Numerous types of oxygen scavengers are used to inhibit and prevent oxidative degradation. These stabilizers have been reviewed (96) extensively. Effective compounds are thio compounds, hydroquinone, bisulfite, phenolic compounds, hydroxylamine, hydrazine, and others.

The biodegradability of poly(acrylamide) has not been definitively delineated in the literature (96). Recently, however, microorganisms (100), enterobacter agglomerans and azomonas macrocytogenes, were isolated from soil and the molecular weight of poly(acrylamide) in the presence of these microorganisms was found to undergo a 40-fold reduction as a result of chain degradation. The rate of biodegradation was equivalent to 20% of the carbon being consumed each day.

Hydrolyzed Polyacrylamide. Hydrolysis of poly(acrylamide) proceeds smoothly over a wide range of pH. Fundamental studies have been reviewed extensively (13,101–103). At alkaline pH, three reaction kinetics constants have been described, k_0, k_1, and k_2. The subscripts characterize the number of neighboring carboxylate groups next to the amide group being hydrolyzed. The rate constant k_0 is for no carboxylate neighbors, k_1 is for one carboxylate neighbor, and k_2 is for two carboxylate neighbors. Indirect evidence has shown that $k_0 > k_1 > k_2$. Under alkaline conditions, the rate of hydrolysis of poly(acrylamide) decreases with increasing conversion. The electrostatic repulsion from the increasing number of

carboxylate groups in the backbone polymer opposes the approaching hydroxyl ion. Consequently, further hydrolysis will be severely retarded. Only about 80% of the amide groups (104) can be hydrolyzed by excess hydroxide ion even at elevated temperatures.

^{13}C nmr studies (105–107) have shown that hydrolysis at high pH results in a nearly random distribution of carboxylate groups. In one industrial process, a polyacrylamide with about 30 mol% hydrolysis is prepared by heating an aqueous poly(acrylamide) solution containing excess sodium carbonate [497-19-8] (108). Polymerization of acrylamide in a water-in-oil emulsion in the presence of sodium hydroxide has also yielded a copolymer with about 30 mol% hydrolysis (109). A method of preparing a hydrolyzed poly(acrylamide) (104) with a viscosity-average molecular weight greater than 30×10^6 Da was achieved in an inverse emulsion, in the presence of caustic, ethoxylated fatty amine, and oil.

Hydrolysis of poly(acrylamide) proceeds slowly under acidic conditions. The undissociated carboxylic acid groups are protonated, neutral species under those conditions. The intramolecular catalysis by means of undissociated—COOH groups at low pH has been proposed as the main mechanism (92). An imide structure has been proposed to be an intermediate in the low pH hydrolysis of poly(acrylamide), yielding short blocks of carboxyl groups distributed along the polymer chain. To date, there has been limited application of these block copolymer structures, and ones with high molecular weight have not been commercialized.

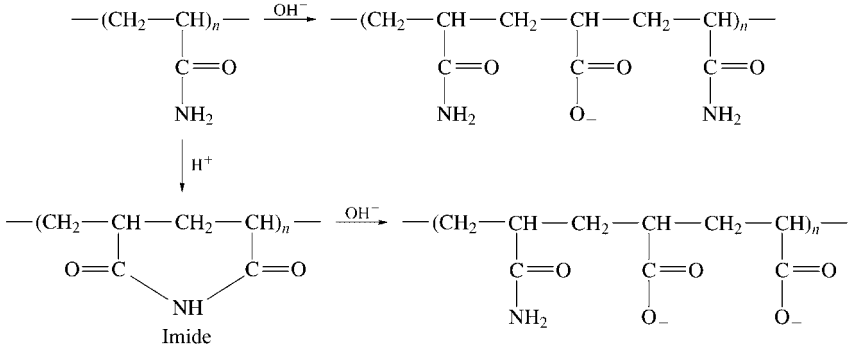

Under neutral conditions, the observed mechanism of hydrolysis cannot be explained by a simple superposition of the retardation kinetics at high pH and intramolecular catalysis at low pH (92).

Cationic Carbamoyl Polymers. Poly(acrylamide) reacts with formaldehyde [50-00-0], CH_2O, and dimethylamine [124-40-3], C_2H_7N, to produce aminomethylated polyacrylamide (a Mannich reaction). This reaction has been studied extensively (110–114). A wide range of substitution can be produced in solution or in water-in-oil emulsion. ^{13}C nmr studies (114) have verified that the Mannich substitution reaction follows second-order kinetics. The formation of the formaldehyde–dimethylamine adduct is very rapid. The high rate of Mannich substitution at high pH indicates a fast base-catalyzed condensation mechanism. The Mannich reaction is reversible and pH dependent. At low pH, the rate of substitution is very slow.

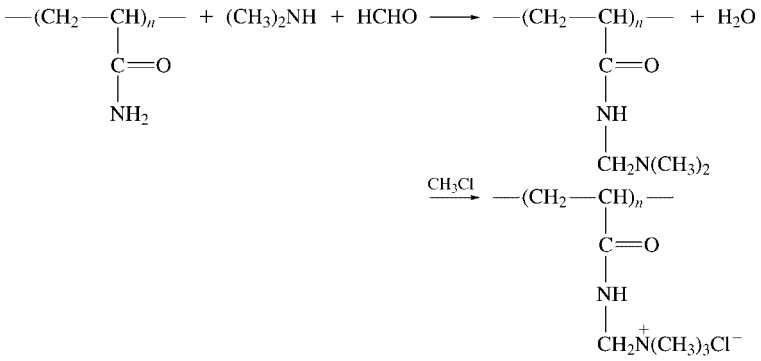

Mannich Reaction

Because of the simplicity of the process, the small capital investment for manufacturing equipment, and the low raw material costs, this group of cationic water-soluble polymers constitutes a substantial percentage of commercially important flocculants. Solution Mannich polyacrylamides are prepared and sold only at 4–6% solids, limited by the large solution viscosities and propensity for crosslinking on standing. The addition of formaldehyde scavengers such as guanidine compounds and dicyandiamide [461-58-5] (115) have improved the shelf stability. Aminomethylation of poly(acrylamide) is a reversible reaction. The reverse reaction can be retarded if the pendent amine groups are protonated by addition of an acid. Mannich base products protonated with organic acids or mineral acids have been patented (116). Low charge-density quaternized aminomethylated products are also sold at polymer solids less than 3% because of very high solution viscosities at higher polymer concentrations.

Several disadvantages of solution Mannich poly(acrylamide)s are the problem of handling high solution viscosities, the added expense of shipping low solids formulations, and the limitations to applications with low pH substrates because of the decrease in cationic charge with increasing pH. Quaternized aminomethylated products in water-in-oil emulsions with greater than 20% solids have been developed. The charges in both high and low charge products were nearly independent of pH (113,117–119). Microemulsion formulations have been developed and now they replace certain polymer macroemulsions. In one such case, poly(acrylamide) was functionalized in a microdroplet (∼100 nm in diameter) that contained only a few poly(acrylamide) molecules (120). Products based on this technology have been commercially successful as high performance cationic organic flocculants for municipal and industrial wastewater applications (121,122).

Sulfomethylation. The reaction of formaldehyde and sodium bisulfite [7631-90-5] with polyacrylamide under strongly alkaline conditions at low temperature to produce sulfomethylated polyacrylamides has been reported many times (123–125). A more recent publication (126) suggests, however, that the expected sulfomethyl substitution is not obtained under the previously described strongly alkaline conditions of pH 10–12. This nmr study indicates that hydrolysis of polyacrylamide occurs and the resulting ammonia reacts with the sodium bisulfite and formaldehyde to form sulfomethyl amines and hexamethylenetetramine

[100-97-0]. A recent patent describes a high pressure, high temperature process at slightly acid pH for the preparation of sulfomethylated polyacrylamide (127).

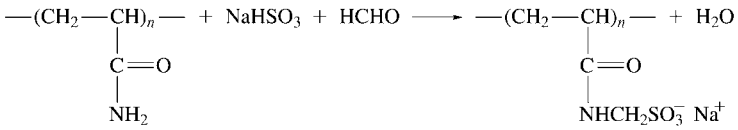

Reaction with Other Aldehydes. Poly(acrylamide) reacts with glyoxal [107-22-2], $C_2H_2O_2$, under mild alkaline conditions to yield a polymer with pendent aldehyde functionality.

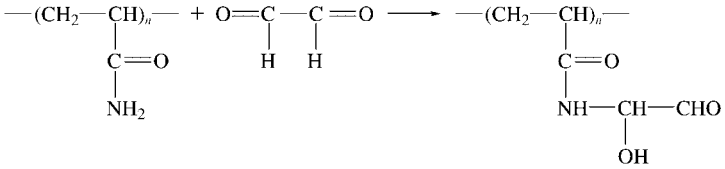

The rate of this reaction can be controlled by varying the pH and reaction temperature. Cross-linking is a competing reaction. The reaction rate increases rapidly with increasing pH and with increasing polymer concentration. In a typical commercial preparation, a 10% aqueous solution of a low molecular weight polyacrylamide reacts with glyoxal at pH 8–9 at room temperature. As the reaction proceeds, solution viscosity increases slowly and then more rapidly as the level of functionalization and cross-linking increases. When the desired extent of reaction is achieved, before the gel point, the reaction is acidified to a pH below 6 to slow the reaction down to a negligible rate. These glyoxalated polyacrylamides are used as paper additives for improving wet strength (128).

A similar reaction occurs when poly(acrylamide) is mixed with glyoxylic acid [298-12-4], $C_2H_2O_3$, at pH about 8. This reaction produces a polymer with the CONHCH(OH)COOH functionality, which has found application in phosphate ore processing (129).

Transamidation. Poly(acrylamide) reacts with hydroxylamine [7803-49-8], H_2NOH, to form hydroxamated polyacrylamides with loss of ammonia (130).

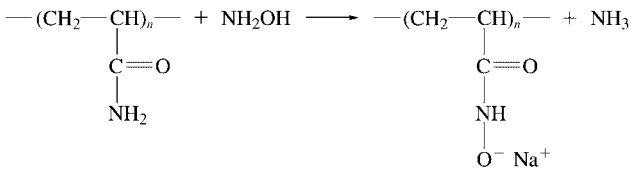

This hydroxamation reaction occurs under alkaline conditions (131–133). Carboxyl groups can be produced because of the hydrolysis of the amide (131, 132). Acrylamide polymers can also be reacted with primary amines such as 2-aminoethanesulfonic acid (taurine) [107-35-7] at high temperature and acid pH to yield N-substituted copolymers containing sulfoethyl groups (134).

Hofmann Reaction. Polyacrylamide reacts with alkaline sodium hypochlorite [7681-52-9], NaOCl, or calcium hypochlorite [7778-54-3], $Ca(OCl)_2$, to form a polymer with primary amine groups (135). Optimum conditions for the reaction include addition of a slight molar excess of sodium hypochlorite, followed by addition of concentrated sodium hydroxide at low temperature (136). A two-stage addition of sodium hydroxide minimizes a side reaction between the pendent amine groups and isocyanate groups formed by the Hofmann rearrangement (137). Cross-linking sometimes occurs if the polymer concentration is high. High temperatures can result in chain scission. If long reaction times are used, NaOCl will cause chain scission and molecular weight decline. If very short reaction times are used at temperatures above 50°C, then polymers with high primary amine content can be obtained (138).

Reaction with Chlorine. Poly(acrylamide) reacts with chlorine under acid conditions or with NaOCl under mild alkaline conditions at low temperature to form reasonably stable *N*-chloropolyacrylamides. The polymers are water soluble and can provide good dry strength, wet strength, and wet web strength in paper (139).

Chemistry of Acrylamide Copolymers

Cationic Copolymers. The largest segment of the acrylamide polymer market has been dominated by cationic copolymers. The copolymers of acrylamide (AMD) and cationic quaternary ammonium monomers are manufactured by various commercial processes, which will be discussed in a later section. The most widely used of these cationic comonomers are cationic quaternary amino derivatives of (meth)acrylic acid esters or (meth)acrylamides, and diallydimethylammonium chloride.

The quaternary ammonium monomer contents in these copolymers are typically between 5 and 80 mol% for most applications. The composition actually employed depends on cost–performance relationships. Costs are largely dominated by the cationic monomer. Thus, the cationic demand of the substrate for each application has to be optimized. Normally, low- to medium-charge copolymers are used for paper waste applications and medium- to high-charge copolymers are used for sludge dewatering. The molecular weights for flocculants are usually 5×10^6 Da or greater. The higher molecular weight polymers often have the advantage of lower dosages in water treating and better fines capture in paper manufacture. Commercially important cationic comonomers, along with their reactivity ratios with acrylamide, are listed in Table 5.

Copolymers [69418-26-4] of acrylamide and AETAC (see Table 5, footnote *b*) are the most important flocculants because of a uniform sequence distribution of comonomers (140,141). Reactivity ratios obtained under very different free-radical copolymerization conditions can agree very well. For example, in one case, a free-radical copolymerization was initiated using potassium persulfate (KPS) [7727-21-1] in aqueous solution at pH 6.1 (141), while in the other case the copolymerization was initiated using a TBHP/MBS redox pair in an inverse emulsion stabilized with sorbitan monooleate (SMO) at pH 3.5 (140). The surfactant in an inverse emulsion may alter the reactivity of both AMD and AETAC. For

Table 5. Acrylamide Monomer (M_1) Reactivity Ratios

Comonomer M_2	CAS registry number	Molecular formula	r_1	r_2	Initiators[a]	Temp., °C	Reference
Cationic comonomer M[b]							
AETAC	[44992-01-0]	$C_8H_{16}NO_2Cl$	0.61	0.47	TBHP/MBS	40	140
AETAC	[44992-01-0]	$C_8H_{16}NO_2Cl$	0.61	0.47	KPS	40	141
MAETAC	[5039-78-1]	$C_9H_{18}NO_2Cl$	0.24	2.47	TBHP/MBS	40	140
MAETAC	[5039-78-1]	$C_9H_{18}NO_2Cl$	0.25	1.71	KPS	40	141
MAETAC	[5039-78-1]	$C_9H_{18}NO_2Cl$	0.57	1.11	KPS/NAS	26	142
DMAPAA	[3845-76-9]	$C_6H_{16}N_2O$	0.47	1.1	KPS	40	141
MAPTAC	[51410-72-1]	$C_{10}H_{21}N_2OCl$	0.57	1.13	KPS	40	141
DADMAC	[7398-69-8]	$C_8H_{16}NCl$	6.4–7.54	0.05–0.58	APS, ACV	20–60	141,143,144
Anionic comonomer M[b]							
AA	[79-10-7]	$C_3H_4O_2$	0.25–0.95	0.3–0.95	KPS	30	144,145
AA	[79-10-7]	$C_3H_4O_2$	0.89	0.92	AIBN	45	146
MAA	[79-41-4]	$C_4H_6O_2$	2.8–0.39	0.2–0.51	KPS	30	144
NaAMPS	[5165-97-9]	$C_6H_{12}O_4NSNa$	0.98	0.49	APS	30	147

[a]TBHP: *tert*-Butylhydroperoxide, MBS: sodium metabisulfite, KPS: potassium persulfate, APS: ammonium persulfate, ACV: azocyanovaleric acid, NAS: sodium sulfite, AIBN: 2,2′-azobisisobutyronitrile.

[b]AETAC: Acryloyloxyethyltrimethylammonium chloride, $CH_2{=}CHCO_2(CH_2)_2N^+(CH_3)_3Cl^-$; MAETAC: methacryloyloxyethyltrimethylammonium chloride, $CH_2{=}CCH_3CO_2(CH_2)_2N^+(CH_3)_3Cl^-$; DMAPAA: dimethylaminopropylacrylamide, $CH_2{=}CHCONH(CH_2)_3N(CH_3)_2$; MAPTAC: methacrylamidopropylacrylamide, $CH_2{=}CCH_3CONH(CH_2)_3N^+(CH_3)_3Cl^-$; DADMAC: diallyldimethylammonium chloride, $(CH_2{=}CHCH_2)_2N^+(CH_3)_2Cl^-$; AA: acrylic acid, $CH_2{=}CHCO_2H$; MAA: methacrylic acid, $CH_2{=}CCH_3CO_2H$; NaAMPS: 2-acrylamido-2-methylpropanesulfonic acid, Na salt, $CH_2{=}CHCONH(CH_3)_2CH_2SO_3\text{-}Na^+$.

example, when SMO is utilized, in formulations made below the azeotropic monomer composition (ie, the copolymer composition is the same as the monomer feed composition, at about 58 mol% AETAC), AETAC is consumed slightly faster than AMD. On the other hand, if a block copolymeric surfactant, poly(ethylene oxide-*b*-12-hydroxysteric acid) (HB246), is utilized (148), then AMD is the faster reacting monomer. The results suggest that in the interfacial region near the discrete aqueous droplets, the AMD concentration is greater in the HB246 case than in the SMO case.

During AMD/MAETAC copolymerizations, MAETAC [5039-78-1] reacts with its own monomer significantly faster than with AMD. Consequently, copolymers [35429-19-7] can have severe compositional drift and often poor performance. How the sequence distribution can be improved if copolymerizations of AMD and MAETAC are conducted in water-in-oil microemulsion recipes has been studied (142). $K_2S_2O_8$-Na_2SO_3 redox initiator and the composite surfactants SMO and octylphenol ethoxylate were used. They found that reactivity ratios for AMD/MAETAC values were $r_{AMD} = 0.57$ and $r_{MAETAC} = 1.11$ (see Table 5).

Quaternary aminoester copolymers are very susceptible to base hydrolysis and are stable under very acidic conditions (140). In both manufacturing and in applications of these products, great care is needed to control the pH in order to prevent hydrolysis. These products should possess sufficient buffering acid to maintain very acidic conditions. The hydrolytic instability of ester copolymers is primarily attributed to a base-catalyzed ester cleavage reaction that forms cyclic imides between neighboring AMD and AETAC groups. The loss in cationic charge is not due to direct ester hydrolysis (149). The chemistry of the six-membered imide ring is shown below (140,150).

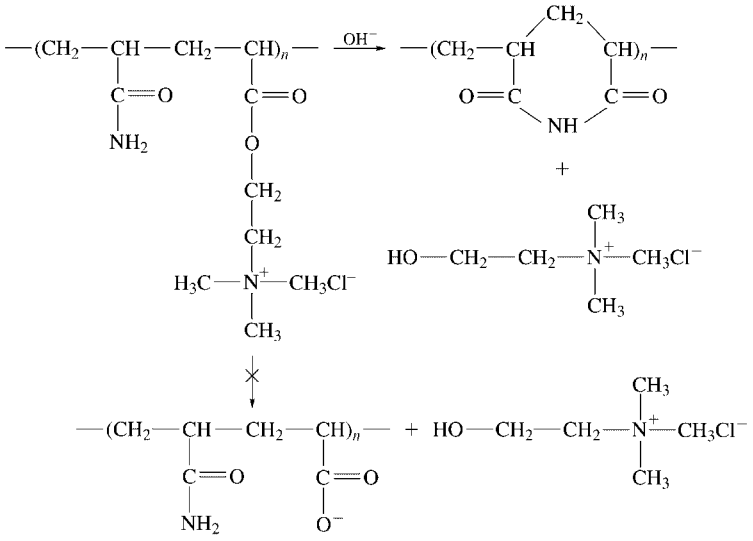

The effect of pH on hydrolytic stability of cationic ester–acrylamide copolymers has been long recognized (149). The decrease in viscosity and effectiveness, characteristic of this instability, do not take place in aqueous solutions at pH 2–5.

Cationicity loss in AETAC and MAETAC copolymers depends on both pH and composition. For example, in a 43 mol% AETAC copolymer, at least 95% of the ester groups have at least one AMD neighbor. The effect of pH on cationicity loss in this copolymer was minimal at a pH of 2–3 at 90°C for 9 h. Above pH 3, ester loss increased dramatically. Prolonged heating (24 h) resulted in a greater degree of ester loss. It was found that the rate of isolated ester hydrolysis was first order in hydroxide concentration at 60°C at constant buffer pH of 5.5. If there were neighboring acrylamide groups in the chain, then there was a second-order dependence of ester disappearance on hydroxide concentration. This indicated that the imidization reaction was also first order in hydroxide ion concentration. The percentage of esters cleaved increased as the number of AETAC groups with neighboring AMD groups increased. Polymers with esters and no AMD neighbors such as the homopolymers of AETAC or MAETAC were found to have a low degree of hydrolysis. The rate of hydrolysis of AETAC and MAETAC copolymers were the same only when both had the same number of AMD neighbors.

Cationic copolymers derived from amide monomers, such as MAPTAC [51410-72-1] and APTAC [45021-77-0], are reasonably random and are hydrolytically stable. However, they are more expensive. The molecular weights of high charge AMD/APTAC [75150-29-1] and AMD/MAPTAC [58627-30-8] copolymers typically do not reach the high molecular weights of AMD/AETAC copolymers because of impurities in the APTAC and MAPTAC. However, low charge AMD/MAPTAC copolymers, containing ∼3 mol% MAPTAC, are significant commercial products.

Diallydimethylammonium chloride (DADMAC) [7398-69-8] is the least expensive commercially available cationic monomer. This monomer has been successfully produced by reacting allyl chloride, dimethylamine, and sodium hydroxide in aqueous solution (151,152). Monomer solutions with solids of 60–70% can be achieved and used directly for polymerization without further isolation and purification. DADMAC is a nonconjugated diene monomer that was found to homopolymerize to high molecular weight linear cationic polymer without crosslinking (151,152). Poly(diallydimethylammonium chloride) (PDADMAC) [26062-79-3] was the first synthetic organic flocculant approved for potable water clarification by the U.S. Public Health Service (154). The polymerization of DADMAC is known as kinetically favorable to give 98% of inter–intra cycloaddition and 2% pendent double bonds (143). The initiator radical attacks the terminal carbon on one allyl group, and the radical formed attacks the internal carbon on the other allyl group in the same molecule to form a five-membered pyrrodinium ring with a cis-to-trans ratio of 6:1 (155).

The rate law for DADMAC polymerization in an aqueous system, when persulfate is used, is not simple: $R_p = (S_2O_8^{2-})^{0.8}(\text{DADMAC})^{2.9}$. A combination of complicated initiation reactions and dimeric DADMAC interactions can account for the unusually high exponent of the DADMAC concentration (156). High monomer concentrations (>1.5 mol/L) used in commercial processes result in greater rates of polymerization and higher molecular weights. PDADMAC with low residual unreacted monomer can be manufactured in water using either persulfate addition or ammonium persulfate with sodium metabisulfite (157). Polymerization of DADMAC has also been studied in water-in-oil emulsion in a continuous stirred tank reactor (158). In that case, the oil-soluble initiator,

2,2′-azobis(2,4-dimethylvaleronitrile) (ADVN), and the surfactants sodium di-2-ethylhexylsulfosuccinate (AOT) and SMO were used. The rate of polymerization was $R_p = k\,(\mathrm{ADVN})^{0.4}(\mathrm{AOT})^{0.5}(\mathrm{SMO})^{-0.4}(\mathrm{DADMAC})^3$. The negative order of SMO concentration was due to the fact that SMO is a radical scavenger. The influences of partitioning effects and ionic strength contributed to the third order in DADMAC concentration.

The molecular weight of PDADMAC is not as high as for acrylic polymers because of the large chain-transfer constant of allylic radicals. However, a molecular weight of 5×10^5 Da is sufficient for applications such as potable water clarification, color removal, and textile processing. These applications rely on the very high cationic charge of PDADMAC. This polymer is often used along with a high molecular weight anionic polyacrylamide in process-water clarification in paper deinking mills.

Anionic Copolymers. Anionic acrylamide copolymers such as poly(acrylamide-*co*-sodium acrylate) [25085-02-3], poly(acrylamide-*co*-ammonium acrylate) [26100-47-0], poly(acrylamide-*co*-sodium-2-acrylamido-2-methylpropanesulfonate) (AMD/NaAMPS) [38193-60-1], and poly(acrylamide-*co*-2-acrylamido-2-methyl-1-propanesulfonic acid) (AMD/AMPS) [40623-73-2] have considerable practical importance. They can be prepared in solution, inverse emulsion (144,145), and inverse microemulsion (146). Comonomer reactivity ratios of AMD with acrylic acid or acrylic acid salts are given in Table 5. Reactivity ratios vary with pH. At high pH the reactivity ratio for AMD is higher, but at low pH the reactivity ratio of acrylic acid is higher. At a pH of about 5, a random copolymer can be obtained. When AMD and sodium acrylate are copolymerized in a microemulsion at pH of about 10, copolymer composition is independent of conversion and the reactivity ratios are equal. The copolymer chain composition conforms to Bernoullian statistics (146). These copolymers are used extensively as industrial flocculants for water treating, mining and paper manufacture, drag reduction agents, and in secondary and tertiary oil recovery. Reasons for their extensive use include their low cost and very high molecular weights. Their limitations include poor solubility at low pH and precipitation of the salt form in the presence of calcium ions.

Comonomer reactivity ratios for AMD and NaAMPS are given in Table 5 (147). AMD/AMPS copolymers and AMD/NaAMPS copolymers maintain their anionic charge at low pH and have a high tolerance to many divalent cations. They are used as flocculants for phosphate slimes, uranium leach residues, and coal refuse. There are also many oilfield applications.

Commercial Processes

There are numerous laboratory methods to prepare polyacrylamides. However, there are only a few viable commercial processes used to manufacture materials that meet the necessary performance standards. There are many requirements for commercial materials: very low to very high molecular weights, low insolubles content, low residual monomer content, fast dissolution rate, ease of handling, minimal dusting (for dry solids), product uniformity, long-term storage stability (to ensure performance consistency), high solids (to reduce shipping costs), and

consistent performance characteristics. Several common commercial processes are summarized below.

Solution Polymerization. Commercial production of polyacrylamides by solution polymerization is conducted in aqueous solution, either adiabatically or isothermally. Process development is directed at molecular weight control, exotherm control, producing low levels of residual monomer, and control of the polymer solids to ensure that the final product is fluid and pumpable. A generic example of a solution polymerization follows.

An acrylamide monomer solution (2–30 wt% in water) is typically prepared, and deaerated by sparging it with an inert gas (eg, nitrogen) to reduce the oxygen content in solution. Stainless steel batch reactors or glass continuous stirred tank reactors are often used for solution polymerizations. A chelating agent is added to complex autopolymerization inhibitors such as copper or other metals, if they are present. The polymerization is then initiated using one of several free-radical initiator systems (azo, peroxy, persulfate, redox, or combinations) at concentrations ranging from 0.001 to 10 wt% on monomer. The rate of polymerization depends on reaction conditions, but it typically depends on the 1.2–1.6 order of monomer concentration and 0.5 order of initiator concentration. The heat evolved during polymerization (82.8 kJ/mol) can be removed by an external cooling system. For adiabatic processes, the temperature rise needs to be estimated and great care needs to be exercised to avoid exceeding the reflux temperature. Chain-transfer agents and inorganic salts can be added to improve processing and to reduce insolubles. Monomer-to-polymer conversions of 99.5% are achievable in 4–6 h of polymerization time. The products can have a molecular weight ranging from one thousand to four million. Polymer solids can be 2–30%. The process can be used in conjunction with thermal drying or precipitation methods in order to obtain products in either powder or granular form. Short residence times in drum drying have been used to avoid chain degradation and formation of insolubles. Precipitation in C_1—C_4 alcohols can be done to obtain nonsticky rubbery polymer gel that can be further extruded and then dried with hot air. The resulting granules can be milled and sieved to produce a uniform product. Care is taken to avoid very finely divided material that can cause dusting problems.

Some commercial low molecular weight polyacrylamides (LMPAM) are manufactured in solution and sold at 10–50% solids. For example, LMPAM containing DADMAC comonomer is made at 40% solids and can be reacted with glyoxal to produce a strengthening resin for paper. Furthermore, LMPAM hydrolyzed with sodium hydroxide to polyacrylate is manufactured at 30% solids and is used as an antiscalant. High molecular weight poly(acrylamide) is also prepared in solution at 2–6 wt% solids and is often further modified using, for example, the Mannich reaction.

Inverse Emulsion Process. A method of avoiding the high solution viscosities of high molecular weight water-soluble polymers comprises emulsifying the aqueous monomer solution in an oil containing surfactants, homogenizing the mixture to form a water-in-oil (inverse) emulsion, and then polymerizing the monomers in the emulsion. The resulting polymer latex can be inverted in water, releasing the polymer for use. A basic patent (159) illustrated this inverse emulsion process. Processes in which the inverse emulsion polymerization results in finely divided particles that are small enough to retard settling and can

be sold without further modification have been developed (160,161). Stability of the inverse emulsion to mechanical shear has recently been improved (162). Commercial production of inverse emulsion polymerization of AMD has been reviewed (163).

Polymerization on Moving Belts. Dry polyacrylamides are sometimes preferred, particularly when transportation distances are long. A variety of continuous processes has been developed for preparing dry polyacrylamides that consist of polymerizing aqueous acrylamide on a moving belt and drying the resulting polymer (164–166). In one such process (167), an aqueous solution of acrylamide and a photosensitizer is pumped onto a moving stainless steel belt, cooled on the underside by a water spray and covered on the upper side by a humid inert atmosphere. The belt passes under uv lamps that photoinitiate polymerization. The belt speed can be controlled so that the polymerization is complete when the polymer reaches the end of the belt. At the end of the belt the polymer gel that has formed can be sliced into small granules and dried in an oven. The dried polymer is then passed through a grinder to produce the desired particle size for handling and use.

Several recent patents describe improvements in the basic belt process. In one case, a higher solids polymerization is achieved by cooling the starting monomer solution until some monomer crystallizes, and then introducing the resulting monomer slurry onto a belt. The latent heat of fusion of the monomer crystals absorbs some of the heat of polymerization, which otherwise limits the solids content of the polymerization (168). In another patent, a concave belt that flattens near the end is described. This change is said to result in improved release of polymer from the belt (167).

Dry Bead Process. Dry polyacrylamides can also be prepared in the form of dry beads with bead sizes ranging from about 100–2000 μm (169,170). These beads are formed by azeotropically distilling water from inverse suspension polyacrylamides, collecting the beads by filtration, and further drying the beads in a fluid bed drier for short times. The resulting beads can be dissolved in water in a similar manner to other dry polyacrylamides. The size and shape of the beads prepared in the suspension polymerization process are a function of the types and amounts of surfactants and additives employed. Typically, 0.03–0.2 wt% (based on water plus polymer) of an oil-soluble polymeric surfactant is used to obtain the desired bead size. Greater amounts of surfactants lead to smaller beads (169). Certain water-soluble ionic organic compounds are said to be effective in improving the stability of the beads and providing a narrower bead size distribution when used in conjunction with the polymeric stabilizers (169). In the absence of the stabilizer, irregularly shaped, unstable particles can result. The choice of the stabilizer is considered to be dependent on the charge of the polyacrylamide being produced (169).

Microemulsion Polymerization. One inherent problem with water-in-oil emulsions of acrylamide-based polymers is the potential formation of unstable lattices both during production and in finished products. The coagulum that can form in the reactor can result in a time-consuming cleanout (171). Technology has continuously improved reactor configuration, types of agitation, proper cooling (171), and a proper balance of aqueous, oil, and emulsifier ratios (160,161). Microemulsion polymerization (qv) can provide improvements to address these

problems (172–182). Monomer microemulsions are thermodynamically stable systems comprising two liquids, insoluble in each other, and a surfactant. They form spontaneously without homogenization. The resulting polymer microlattices are typically nonsettling, transparent, and about 100 nm in diameter. These systems can have high emulsifier levels: more than 8 wt%, which is about 4–5 times more than emulsifier levels in conventional inverse emulsions. Consequently, the cost of producing microemulsions becomes less attractive. However, further refinements to technology lead to the development of cost-effective microemulsified Mannich acrylamide polymers (120–122,183). This technology was used to develop functionalized polyacrylamides (184). In one case, a poly(acrylamide) microlatex reacted with formaldehyde and dimethylamine (Mannich reaction), and then quaternized with methyl chloride to yield a very highly charged cationic carbamoyl polymer (120–122,185). These commercial products are widely used in many applications for solid–liquid separation. These products have been improved by treating them with buffer acid, a formaldehyde scavenger, and heat to produce a high performance cationic polymer (186).

Environmentally Friendly Polyacrylamides. In recent years, commercial processes that use biodegradable oils to replace petroleum hydrocarbons have received a great deal of attention. Also, there has been a great deal of interest in polymerization in supercritical fluids. These future directions for the manufacture of polyacrylamides are summarized in the following.

Dispersion Polymerization. Water-in-oil emulsions contain at least 30 wt% of a petroleum-based hydrocarbon that is a valuable natural resource. By using such formulations, oils are consumed unnecessarily and can enter the world's waterways as a source of secondary pollution. An aqueous polymer dispersion is one environmentally responsible formulation that contains no oil or surfactant, and near-zero amounts of volatile organic compounds. Dispersion polymerization can be used to prepare cationic, anionic, and nonionic polyacrylamides.

Inverse Emulsions with Biodegradable Oils. Some examples of inverse emulsion polymerization processes employing biodegradable oils include materials with aqueous phase monomer mixtures, such as AMD and AETAC or AMD and MAETAC, dispersed in a biodegradable oil, such as bis-(2-ethylhexyl)adipate (187), containing a polymeric emulsifier that is a copolymer of dimethylaminoethylmethacrylate and mixtures of methacrylates. A buffering acid, such as a dicarboxylic acid, is used to stabilize cationic copolymers. Aliphatic dialkylethers are also used as biodegradable oils (188), in conjunction with SMO as an emulsifier, to produce high-molecular-weight cationic copolymers.

Inverse Emulsion Polymerization Acrylamide in Near-Critical and Supercritical Fluid Conditions. Supercritical fluids exhibit both liquid-like properties (eg, solubilizing power), and gas-like properties (eg, low viscosities). Aqueous AMD has been dispersed and even microemulsified in near-supercritical ethane–propane mixtures using nonionic surfactants such as ethoxylated alcohols (eg, Brij 30 and Brij 52). Emulsion polymerization of AMD was then conducted at 60°C for 5 h and 379 bar, at the near-supercritical condition of certain ethane–propane mixtures (189). 2,2′-Azobis(isobutyronitrile) (AIBN) was used as the initiator. The resulting poly(acrylamide) had a low molecular weight in the range of $(2.7–5.8) \times 10^5$ Da. The ethane and propane can be easily recovered and recycled in a production plant.

Emulsion polymerization of AMD was also conducted at 60°C for 1 h and 345 bar in near-supercritical CO_2. AIBN was the initiator. An amide end-capped hexafluoropropylene oxide oligomer that has high solubility in the near-supercritical CO_2 was found to stabilize the dispersed particles (190–192). Only a few classes of polymers have good solubility in near-supercritical CO_2. The advantages of using carbon dioxide include very low viscosities during polymerization and ease of recovery.

Applications.

Dewatering. Polyelectrolyte-assisted dewatering constitutes one of the most important application areas of polyacrylamides (3). Solid–liquid separations in aqueous media can be enhanced by the flocculation of small suspended particles into larger aggregates, which increases separation rates. Floc formation requires a destabilization and adherence of the smaller particles. This is usually accomplished by means of surface charge neutralization, charge-patch formation, and/or polymer bridging (193). Acrylamide-containing polymers make ideal candidates for such flocculants because of the large molecular weights achievable with them. High molecular weight cationic copolymers are typically employed in wastewater treatment. Solid–liquid separations in mining industries often benefit from the use of anionic copolymers, or in some cases dual polymer systems (cationic and anionic in sequence). Various dewatering processes in the papermaking industry regularly make use of cationic, anionic, or dual addition systems (194). Nonionic poly(acrylamide) finds less use in solid–liquid separations, save for some mining applications.

Mineral Processing. Both synthetic and natural hydrophilic polymers are used in the mineral processing industry as flocculants and flotation modifiers. Most synthetic polymers in use are polyacrylamides. Nonionic polymers are effective as flocculants for the insoluble gangue minerals in the acid leaching of copper and uranium (195,196), for thickening of iron ore slimes (197), and for thickening of gold flotation tailings (198). In some uranium leach operations, a cationic polymer with a relatively low charge density is used along with the nonionic polymer to improve supernatant clarity.

Anionic polyacrylamides are extensively used in the mining industry. They are used as flocculants for insoluble residues formed in cyanide leaching of gold (199). Acrylamide–acrylic acid copolymers are used for thickening copper, lead, and zinc concentrates in flotation of sulfide ores. These copolymers, containing from 50 to 100% carboxylate groups, are used to flocculate fine iron oxide particles in the manufacture of alumina from bauxite at high pH (200). Hydroxamated polyacrylamides, prepared by reaction of nonionic polyacrylamide or anionic polyacrylamide with hydroxylamine salts, are also effective in this Bayer process (201). Other uses for hydroxamated polyacrylamides include reduction of titanaceous and siliceous scale in Bayer alumina processes (202) and flocculation of titanium or copper ore tailings in froth flotation processes (203). Copolymers [40623-73-2] of acrylamide and acrylamido-2-methylpropanesulfonic acid [15214-89-8] have been patented as phosphate slime dewatering aids (204).

Low molecular weight polyacrylamide derivatives with mineral specific functionalities have been developed as highly selective depressants for separation of valuable minerals from gangue minerals in froth flotation processes. These depressants have certain ecological advantages over natural depressants such

as starches and guar gums. The depressants provide efficient mineral recovery without flocculation. They are often used along with hydrophobic mineral collectors (eg, sodium alkyl xanthates) and froth modifiers. Partially hydrolyzed polyacrylamides with molecular weights of 7,000–85,000 can be used in sylvanite (KCl) recovery (205). Polymers having the functionality $-CONHCH_2OH$ are efficient modifiers in hematite–silica separations (206). Polymers containing the —CONHCH(OH)COOH functionality provide excellent selectivity in separation of apatite from siliceous gangue in phosphate benefication. Valuable sulfide minerals containing copper and nickel can be separated effectively from gangue sulfide minerals such as pyrite in froth flotation processes when acrylamide–allylthiourea copolymers or acrylamide–allylthiourea–hydroxyethylmethacrylate terpolymers are added to depress the pyrite (207). Acrylamide copolymers can be used as iron ore pellet binders (208). When the ore slurry in water has a pH above 8, anionic polymers are effective. If the ore is acid washed to remove manganese, then a cationic polymer is effective.

Paper Manufacture. Polyacrylamides are used as wet-end additives to promote drainage of water from the cellulose web, to retain white pigments and clay fillers in the sheet, to promote sheet uniformity, and to provide dry tensile strength improvements (209). An important advance in papermaking technology has been the use of microparticle retention aids. Organic microparticles, prepared from acrylamide and anionic comonomers by microemulsion polymerization, provide good sheet formation characteristics and controlled drainage (210,211). Cationic polyacrylamides that have been reacted with glyoxal are used to promote wet strength (212). These wet strength resins have been used in paper towels. Recently, these glyoxalated polymers have been modified so that they can be used in toilet tissue. These polymers provide an initial high wet tensile strength with rapid tensile strength decay in water so that sewers may not become clogged (213,214). Anionic polyacrylamides have been used with alum to increase dry strength (215). Primary amide functionality promotes strong interfiber bonds between cellulose fibers. Sometimes paper mills use dry strength additives so that recycled fiber, groundwood, thermomechanical pulp, and other low cost fiber can be used to produce liner board and other paper grades which must meet ICC requirements for burst strength and crush strength. Recently, there has been an increasing demand for writing papers and copy paper that have good print characteristics. Print quality can be improved by use of surface sizes combined with acrylamide polymers. The acrylamide polymer gives the paper sheet better surface strength (216). Details on paper manufacture can be found in Reference (217). All additives used for manufacture of food-grade papers are subject to FDA regulations and are listed in the *Code of Federal Regulations* [paragraphs 176.170, 176.180, 178.3400, and 178.3650] (1998).

Enhanced Oil Recovery. Polymer flooding is a potentially important use for anionic polyacrylamides having molecular weights greater than 5 million and carboxyl contents of about 30%. The ionic groups provide the proper viscosity and mobility ratio for efficient displacement. The anionic charge prevents excessive adsorption onto negatively charged pores in reservoir rock. Viscosity loss is observed in brines particularly when calcium ion is present. A primary advantage of anionic polyacrylamides is low cost (218). Profile modification is a process wherein flooding water is diverted from zones with high permeability to other zones of

lower permeability containing oil. Polymeric hydrogels are used for this. Metals such as chromium and aluminum can be injected with anionic polyacrylamides to cross-link the polymers in more permeable reservoir zones prior to the water flood (219,220). The development of new, more environmentally acceptable cross-linking systems has continued. A recent patent claims a composition consisting of hexamethylenetetramine [100-97-0] and 4-aminobenzoic acid [150-13-0] for this purpose (221).

Polyacrylamides are used in many other oilfield applications. These include cement additives for fluid loss control in well-cementing operations (222), viscosity control additives for drilling muds (223) and brines, and for fracturing fluids (224). Copolymers [40623-73-2] of acrylamide and acrylamidomethylpropanesulfonic acid do not degrade with the high concentrations of acids used in acid fracturing.

Hydrophobically Associating Polymers. Extensive research in the 1980s and 1990s focused on acrylamide copolymers containing small amounts of hydrophobic side chains. At zero or low shear rates, the apparent viscosity can be very large because of association of the hydrophobic groups between chains. In oil reservoir conditions, the polymers tolerate high salt concentrations while providing proper viscosifying properties (225). These associative thickeners are also used in coatings (226) and in oil spill cleanup (227). Reference (228) gives more information about associative polymers.

Hydrophobically associating acrylamide copolymers can be prepared by micellar polymerization. These copolymers have short blocks of hydrophobic groups randomly distributed in the backbone. A recent paper reviews the major advances in this area (229).

Superabsorbents. Water-swellable polymers are used extensively in consumer articles and for industrial applications. Most of these polymers are cross-linked acrylic copolymers of metal salts of acrylic acid and acrylamide or other monomers such as 2-acrylamido-2-methylpropanesulfonic acid. These hydrogel-forming systems can have high gel strength, as measured by the shear modulus (230). Sometimes, inorganic water-insoluble powder is blended with the polymer to increase gel strength (231). Patents describe processes for making cross-linked polyurethane foams that contain superabsorbent polymers (232,233). Recent patents describe grafted copolymers that are highly absorbent to aqueous electrolyte solutions (234).

Analytical Methods. Most of the traditional methods for polymer analysis (235) are applicable to polyacrylamides. We will only point out several special features regarding the use of some of these techniques for the analysis of polyacrylamides.

Oftentimes a preliminary step applied before many analytical methods is the isolation of the polymer. The isolation of polyacrylamides from the other components of the media in which they were prepared (eg, aqueous solution or inverse emulsion, with attendant surfactants and oil) is often readily accomplished by precipitation in short-chain alcohols or acetone. The individual solubilities of formulation components should be tested if there is any doubt. Experience shows that anionic copolymers are often best precipitated in the alcohols, and cationic copolymers in acetone (homopolyaminoesters are soluble in methanol). Since acrylamide is soluble in these organic solvents, it will also be separated from the polymer in this procedure.

Once the polymer is isolated, its chemical composition can be quantified using in or nmr spectroscopies (12,236). An nmr study can also give some information about chain architecture in the case of copolymers (237). Elemental analysis can be employed to confirm a composition. Ultraviolet spectroscopy is generally not used for compositional analysis per se; however, polymers containing acrylamide do absorb short-wavelength uv radiation, along with many other materials. A uv detector set around 215 nm is a common choice for measuring polymer concentration in the absence of interfering substances; many surfactants and some salts (eg, NO_3^-, SCN^-) are problematic in this regard. Differential refractometry is the logical alternative for concentration monitoring when uv-absorbing substances are present.

The extent of conversion during an acrylamide polymerization is most easily followed by determining the disappearance of the monomer. High performance liquid chromatography (hplc) is often found best for this purpose. An hplc method in which poly(acrylamide) inverse emulsions can be used directly has been developed (238). In the case of copolymers, hplc protocols that allow the simultaneous determination of all the unreacted monomers can be used to evaluate compositional drift as a function of conversion.

Global properties of the polymer chains (eg, molecular weight, coil dimensions, branching content) are most often evaluated using scattering, hydrodynamic, or viscometric techniques on dilute polymer solutions. The conventional methods appropriate for soluble polymeric materials typically apply equally well to polyacrylamides. In the case of high molecular weight polyacrylamides, the main difficulties in obtaining accurate information involve preparing a purified polymer solution that is in an equilibrium state, and passing it through the measurement device without substantially altering it in either process.

When using viscometric methods, experiment protocols can be designed to address any effects that instabilities may have on the viscosities of the polyacrylamide solutions, if not to alleviate the instabilities altogether. Mechanical degradation can also occur in high molecular weight polymers. This can happen during sample preparation (eg, mixing), purification (eg, filtration), or during the viscosity measurement itself (especially in elongational flows). In any case, one should estimate these handling effects for any set of protocols.

The presence of colloidal-size contamination ("dust") in polymer solutions can possibly affect either static or dynamic light scattering experiments (239,240). Neutron scattering is less afflicted by this kind of contamination (241). For high molecular weight polyacrylamides whose coil dimensions are roughly in the same size range as the colloidal contaminants, and which have a natural propensity to adsorb onto suspended materials (after all, many of these polymers are flocculants), any problem of sample purification should not be ignored. If one is simply looking for a clean sample, it is possible to exhaustively filter a solution in a recycle loop (242). Clarification of dilute polymer solutions by centrifugation is another method that can minimize mechanical degradation of the polymers. Centrifuging dilute solutions of high molecular weight linear polyacrylamides from 4 to 8 h in excess of $15{,}000 \times G$ is satisfactory in many instances. Good light scattering data can be acquired even in the case of a marginally clean polymer solution by attempting to "look through the dust." This is made easier by reducing the scattering volume, slowing (or stopping) the solution flow, and monitoring the scattering

volume (either manually or with the aid of a computer algorithm) for periods that are free of point scatterers.

The effects of sample clarification must be gauged when trying to preserve and analyze the polymer in its original form. This includes situations when samples are passed through packed columns, as in HPSEC analysis. A uv-absorbance study can be used to determine polymer loss if there are no interferences in the solution. A method that can monitor the molecular weight distribution (eg, HPSEC or dynamic light scattering), or one that is sensitive to the high molecular weight component (eg, elongational viscometry), can be used to assay for mechanical degradation.

The double extrapolation of light scattering data to zero polymer concentration and zero scattering angle yields an average property of the macromolecular ensemble: the weight-average molecular weight (M_w) from static light scattering and the z-average hydrodynamic radius ($<R_h>_z$) from dynamic light scattering. In some cases, the details of the distribution of these quantities are also of interest. Dynamic light scattering data can be analyzed directly to give a distribution of the hydrodynamic size distribution of a sample. How to derive molecular weight distributions from dynamic light scattering data has been demonstrated (243), but this involves knowing the correlation between the polymer diffusion coefficient and molecular weight, a relationship that is not always available.

Methods involving a physical separation of the components of the distribution, coupled with a method for measuring some feature of the macromolecules across this separated collection, find more use in determining molecular weight (or size) distributions. Size exclusion chromatography (sec) remains a popular way to separate macromolecular populations (244), including polyacrylamides (245). More recently, flow field flow fractionation (ffff) (246) has been shown to have some advantages over sec methods, especially for very high molecular weight polymers, including polyacrylamides. Since the fluid contact surface in ffff is a membrane, as opposed to a packed bed of finely divided particles in sec, there is less opportunity for altering the native distribution by means of polymer adsorption, retention, or mechanical degradation. High molecular weight cationic copolymers of acrylamide can be difficult to pass unaltered through commercial sec columns. Ultracentrifugation (63,247,248) has also been used to separate the components of polyacrylamide samples for subsequent analysis, but this is currently a less popular method than either sec or ffff.

The early approaches to characterizing the molecular weight distributions of samples separated using sec or ffff were based on retention time, requiring a correspondence to be made between the retention time and molecular weight. This was typically done by calibrating the separation device using fractionated (narrowly distributed) standards, which in some cases were only vaguely related chemically to the polymer of interest. More recently the use of in-line light scattering detectors for the purpose of directly determining M_w, R_g (static light scattering photometer), or R_h (dynamic light scattering photometer) for each "slice" of the separated distribution has been an alternative to these approaches (249). This has generally improved one's ability to characterize the details of the molecular weight or size distributions for many acrylamide-containing polymers, for which standards consisting of narrow fractions are not readily available.

Titration methods are mostly applicable to ionic copolymers of acrylamide. Typically, potentiometric titrations are used for high salt concentrations, and conductometric titrations are used for low salt concentrations. This kind of information can be important since ionogenic groups with weak acid or base properties will have both dissociation-dependent and salt-dependent pK_as when they are in a polymer chain. In addition to titrating ionic acrylamide copolymers with low molecular weight titrants, their titration with other oppositely charged polyelectrolytes has proven useful (250). For example, poly(potassium vinylsulfonate) can be used to titrate cationic copolymers of acrylamide. This titration gives information about the available charge on the host macromolecule. Usually the macroion titrant is of lower molecular weight than the polymer of interest. In any case, the conditions of the polyelectrolyte–polyelectrolyte complexation reaction must allow for complete 1:1 complex formation. Care must be taken such that the kinetics of the complex formation does not influence the results. The end point can be detected in any one of several ways, including turbidometrically, or using a dye indicator. The color change of the dye at the end point can be determined visually or spectrophotometrically with an "optrode."

Detecting Polyacrylamides. In order to detect low concentrations of polyacrylamides as part of an analysis scheme (251), to optimize the use of or to monitor the fate of these polymers in a variety of technological applications, an assay method for trace amounts of these polymers that remain in solution is usually needed. One approach, more appropriate for laboratory studies, has been to incorporate fluorescent groups in the polymer either by copolymerization or by postpolymerization derivatization. Acrylamide copolymers containing sodium fluorescein (252), various dyes [phenol red, or brilliant yellow (253)], *N*-2,4-dinitroanilineacrylamide (254), or a pyrene-labeled monomer (255) have been described. Early methods based on chemical derivatizations describe coupling fluorescein isothiocyanate to amine groups on Hofmann-reacted poly(acrylamide) (256,257). Various other approaches have been developed to add fluorescein (258), dansyl (259), 9-xanthydrol (260), and other fluorescent groups to acrylamide-containing chains (261).

A completely different approach to detecting low levels of high molecular weight polyacrylamides in solution without recourse to prelabeling the polymers has been used in a number of instances. Methods based on the flocculation capacity of these polymers are surprisingly sensitive. Both the turbidity and the settling rate of a suspension can change measurably after exposure to even low concentrations (several ppm) of a flocculant. Such changes were used in the settling rate of kaolin suspensions to assay for low levels of anionic polyacrylamides in runoff water from a soil amendment application involving those polymers (262). They were able to reliably detect residual polymer in the water at the ppm level.

Specifications, Shipping, and Storage. The amount of residual acrylamide is usually determined for commercial polyacrylamides. In one method, the monomer is extracted from the polymer and the acrylamide content is determined by hplc (263). A second method is based on analysis by cationic exchange chromatography (264). For dry products the particle size distribution can be quickly determined by use of a shaker and a series of test sieves. Batches with small particles can present a dust hazard. The percentage of insoluble material is determined in both dry and emulsion products.

Polyacrylamide powders are typically shipped in moisture-resistant bags or fiber packs. Emulsion and solution polymers are sold in drums, tote bins, tank trucks, and tank cars. The transportation of dry and solution products is not regulated in the United States by the Department of Transportation (DOT), but emulsions require a DOT NA 1693 label.

Under normal conditions, dry polymers are stable for 1 year or more. The emulsion and solution products have somewhat shorter shelf lives.

Safety and Health.

Commercial Polyacrylamides. Dry cationic polyacrylamides have been tested in subchronic and developmental toxicity studies in rats. No adverse effects were observed in either study. Chronic studies of polyacrylamides in rats and dogs indicated no chronic toxicity or carcinogenicity. Dry anionic and nonionic polyacrylamides (265) have acute oral (rat) and dermal (rabbit) LD_{50} values of greater than 2.5 and greater than 10 g/kg, respectively. Dry cationic polyacrylamides have acute oral (rat) and dermal (rabbit) LD_{50} values of greater than 5 and greater than 2 g/kg, respectively. Emulsion nonionic, anionic, and cationic polyacrylamides have both acute oral (rat) and dermal (rabbit) LD_{50} values of greater than 10 g/kg. Dry nonionic and cationic material caused no skin irritation and minimal eye irritation during primary irritation studies with rabbits. Dry anionic polyacrylamide did not produce any eye or skin irritation in laboratory animals. Emulsion nonionic polyacrylamide produced eye irritation in rabbits, while anionic and cationic material produced minimal eye irritation in rabbits. Emulsion nonionic, anionic, and cationic polyacrylamide produced severe, irreversible skin irritation when tested in rabbits that had the test material held in skin contact by a bandage for 24 h. This represents an exaggeration of spilling the product in a boot for several hours. When emulsion nonionic, cationic, and anionic polyacrylamides were tested under conditions representing spilling of product on clothing, only mild skin irritation was noted. Polyacrylamides are used safely for numerous indirect food packaging applications, potable water, and direct food applications.

Experimental Polyacrylamides. It is wise to treat any laboratory-prepared "experimental" polyacrylamide as if it contains substantial amounts of unreacted monomer unless it has been isolated and purified as described above.

Acrylamide is commercially available as a 50% solution in water with a copper salt as a polymerization inhibitor. Polymerization is very exothermic and autopolymerization can occur under certain conditions. In the interest of safety, acrylamide solutions should be stored under the following conditions:

(1) Maintain the storage temperature below 32°C (90°F) and above the solubility point.
(2) Keep the solution free of contaminants.
(3) Maintain the proper level of oxygen and Cu^{2+} inhibitors.
(4) Maintain the pH at 5.2–6.0.
(5) Store the solution in a container that is opaque to light.

It is recommended that these solutions be stored for no more than 3 months because of the depletion of the dissolved oxygen. All containers must be dated and no more than 93% full. Packaged acrylamide solutions should be consumed on a first-in, first-out basis.

Table 6. Suppliers of Polyacrylamides

Region	Companies
United States	Axchem
	Baker-Petrolite Co.
	BetzDearborn, Inc.
	Buckman Laboratories International, Inc.
	Calgon Corp.
	Callaway Chemical Co.
	Chemtall, Inc.
	CIBA Specialty Chemicals Corp. (Allied Colloids, Ltd.)
	Cytec Industries, Inc.
	Delta Chemical Corp.
	The Dow Chemical Co.
	Drew Chemical Corp. (Ashland Chemical, Inc.)
	Exxon Chemical Co.
	Hercules Inc.
	Nalco Chemical Co.
	Polydyne, Inc.
	S.N.F. Floerger SA
	Stockhausen, Inc.
Canada	Cytec Canada, Inc.
	Nalco Canada, Inc.
	Raisio Chemicals Canada, Inc.
	Rhodia Canada, Inc.
Mexico	BASF Mexicana, S.A. de C.V.
	Cytec, Atequiza Jalisco
	Nalco, Toluca
South America	Dispersol San Luis S.A. (Argentina)
	LaForestal Quimica S.A.I.C. (Argentina)
	Henkel Argentina S.A.
	Industrias Quimicas del Valle S.A. (Argentina)
	Proquima Productos Quimicos (Argentina)
	Adesol Produtos Quimicos Ltda. (Brazil)
	Quimicos Nacional Quiminasa S/A (Brazil)
	Cyquim de Columbia
	Quimicos Cyquim, C.A. (Venezuela)
Europe	BASF AG (Germany)
	Ciba Specialty Chemicals PLC (U.K.)
	Cytec Industries BV (Netherlands)
	Cytec Industries U.K. Ltd. (U.K.)
	Deutsche Nalco-Chemie GmbH (Germany)
	Kimira Oyj (Finland)
	Röhm GmbH (Germany)
	S.N.F. Floerger S.A. (France)
	Stockhausen GmbH (Germany)
Japan	Arakawa Chemical Industries, Ltd.
	Dai-Ichi Kogyo Seiyaku Company, Ltd.
	Diafloc Co., Ltd.
	Harima Chemicals, Inc.
	Hymo Corp.

Table 6. (Continued)

Region	Companies
	Kurita Water Industries, Ltd.
	Japan Polyacrylamide Ltd.
	Konan Chemical Industry Co., Ltd.
	Mitsubishi Chemical Industries Co., Ltd.
	Mitsui-Cytec, Ltd.
	Nippon Kayaku Co., Ltd.
	Sankyo Kasei Co., Ltd.
	Sanyo Chemical Industries, Ltd.
	Sumitomo Chemical Co., Ltd.
	Toa Gosei Chemical Industry Co., Ltd.
Republic of Korea	Cytec Korea, Inc.
	E-Yang Chemical Co., Ltd.
	Kolon Industries, Inc.
	Unico (Seoul)
Taiwan	Cytec Taiwan Corp.
	Taiwan Arakawa Chemical Ind., Ltd.
	Young Sun Chemical Works, Ltd.
China	China Petrochemical Corp.
India	Engineer's Poly-Chem
	Kaushal Aromatic Chemicals Pvt. Ltd.
	Somnath Products

Economic Aspects. Worldwide, there are many suppliers of polyacrylamides. Some of these are producers and some are repackagers. Suppliers are listed in Table 6. Selling prices for polyacrylamides vary considerably depending on the product form (solution, emulsion, dry), type (anionic, nonionic, cationic), and other factors. Prices on a polymer basis can range from as low as about $2/kg for simple dry nonionic polyacrylamides to $8/kg and more for highly charged cationic polymers. Prices in recent years have dropped because of price erosion and lower manufacturing costs of AETAC and DADMAC cationic monomers. In many applications, such as sludge dewatering in waste treatment, the need for increased performance has lead to increased functionalization (eg, higher cationicity) and increased cost.

In the United States, the major uses for polyacrylamides are in water treating, and paper manufacturing. For water treating, the best growth is expected to be for cationic copolymers because of use in dewatering equipment like belt presses that produce high solids sludge cakes that can be more easily incinerated or disposed of in scarcer landfills. For paper manufacturing, glyoxalated cationic copolymers for paper wet strength, high molecular weight retention aids, and drainage aids are considered to grow in use. Increased use of poly(acrylamide) flocculants in recycled paper mills, particularly in deinking mills where better process water clarification is necessary because of closed water circuits, is also expected. Polyacrylamides are beginning to be used along with surface sizes in paper to improve the control of ink adsorption and print quality. In the mineral process industry in the United States (and Australia), there has been a great

Table 7. Consumption of Polyacrylamides[a]

Year	Paper, %	Water treating, %	Mining, %	EOR, %	Other, %	Total 10^3 t
United States						
1989	21.9	59	7.9	6	5.4	68.5
1993	18.3	63	13.6	0	5.1	86.0
1997	25	60	10.8	0	4.2	120.0
Western Europe						
1997	38.4	53.5	5.8	0	2.3	86
Japan						
1985	62	38				42
1989	57.7	42.3				52
1993	51	49				53
1997	52.4	47.6				63

[a]From Ref. (1).

increase in the use of hydroxamated polyacrylamides in alumina manufacture. The market for polyacrylamides in enhanced oil recovery has decreased steadily in the United States. In 1985, the total market exceeded 10 million metric tons, but in 1999 the use has been almost none. Total consumption of polyacrylamides is expected to increase about 4% per year during the next few years after 1999 in the United States. In Europe, the use of water-treating chemicals on municipal sludge treatment will increase because of European Union legislation preventing sewage dumping. The treatment of wastewater is intensive, and many waste treatment plants and paper mills have closed circuits because of environmental concerns. The total consumption of poly(acrylamide)s is expected to increase about 3% per year in Europe. In Japan, the major consumption has been in paper manufacture (anionic and nonionic polyacrylamides) and water treatment (cationic and amphoteric copolymers). In municipal sludge treatment, highly cationic polyacrylamides are used for rapid flocculation in high speed centrifuges. The use of cationic copolymers is expected to grow at higher rates. Japan exports a considerable amount of polyacrylamides (and acrylamide monomer) to Asian and other markets. Another potential market will be enhanced oil recovery in China. Table 7 gives an estimated breakdown of polyacrylamide consumption (1).

BIBLIOGRAPHY

"Acrylamide Polymers" in *EPST* 1st ed., Vol. 1, pp. 177–197, by W. M. Thomas; American Cyanamid Co.; "Acrylamide Polymers" in *EPST* 2nd ed., Vol. 1, pp. 169–211, by W. M. Thomas, American Cyanamid Co. and D. W. Wang, (IBM Corp.).

1. *SRI Consulting*, Marketing Research Report on Water Soluble Polymers, *Chemical Economics Handbook*, Feb. 1999. Internet web site: http://ceh.sri.com/.
2. H. Dautzenberg and co-workers, *Polyelectrolytes: Formation, Characterization and Application*, Hanser Publishers, New York, 1994, p. 272.
3. R. S. Farinato, S.-Y. Huang, and P. Hawkins, in R. S. Farinato and P. L. Dubin, eds., *Colloid–Polymer Interactions: From Fundamentals to Practice*, John Wiley & Sons, Inc., New York, 1999, p. 3.

4. S.-Y. Huang and D. W. Lipp, in J. C. Salamone, ed., *Polymeric Materials Encyclopedia*, Vol. **5**, CRC Press, Inc., Boca Raton, Fla., 1996, p. 2427.
5. H. I. Heitner, *Kirk-Othmer: Encyclopedia of Chemical Technology*, 4th ed., Vol. **II**, John Wiley & Sons, Inc., New York, 1994, p. 61.
6. H. I. Heitner, T. Foster, and H. Panzer, in J. I. Kroschwitz, ed., *Encyclopedia of Polymer Science and Engineering*, 2nd ed., Vol. **9**, Wiley-Interscience, New York, 1987, p. 824.
7. D. A. Mortimer, *Polym. Int.* **25**, 29 (1991).
8. O. G. Lewis, *Physical Constants of Linear Homopolymers*, Springer-Verlag, New York, 1968, p. 23.
9. I. Janigová and co-workers, *Macromol. Chem. Phys.* **195**, 3609–3614 (1994).
10. J. Brandrup and E. H. Immergut, eds., *Polymer Handbook*, 3rd ed., John Wiley & Sons, Inc., New York, 1989, p. VI–416.
11. J. E. Lancaster and M. N. O'Connor, *J. Polym. Sci., Polym. Lett. Ed.* **20**, 547 (1982).
12. W.-M. Kulicke, R. Kniewske, and J. Klein, *Prog. Polym. Sci.* **8**, 373–468 (1982).
13. S. Sawant and H. Morawetz, *Macromolecules* **17**, 2427 (1984).
14. S. Sawant and H. Morawetz, *J. Polym. Sci., Polym. Lett. Ed.* **20**, 385–388 (1982).
15. S. J. Guerrero, P. B. Oldarino, and J. H. Zurimendi, *J. Appl. Polym. Sci.* **30**, 962 (1985).
16. W.-M. Kulicke, R. Kniewske, and J. Klein, *Prog. Polym. Sci.* **8**, 383 (1982).
17. Ref. 10, p. VII–383.
18. Ref. 10, p. VII–245.
19. *SUPERFLOC 127 Flocculant, Material Safety Data*, Cytec Industries, West Paterson, N.J. 1996.
20. F. A. Bovey, *High Resolution NMR of Macromolecules*, Academic Press, New York, 1972, p. 147.
21. W.-M. Kulicke, R. Kniewske, and J. Klein, *Prog. Polym. Sci.* **8**, 379 (1982).
22. P. J. Flory, *Principles of Polymer Chemistry*, Cornell University Press, Ithaca, N.Y., 1953.
23. G. Medjahdi, D. Sarazin, and J. Francois, *Eur. Polym. J.* **26**, 823–829 (1990).
24. A. L. Izyumnikov and co-workers, *Polym. Sci. USSR* **30**, 1062–1071 (1988).
25. H. H. Hooper and co-workers, *Macromolecules* **23**, 1096–1104 (1990).
26. Ref. 10, 1989 p. VII–34.
27. W.-M. Kulicke, R. Kniewske, and J. Klein, *Prog. Polym. Sci.* **8**, 386 (1982).
28. W.-M. Kulicke, R. Kniewske, and J. Klein, *Prog. Polym. Sci.* **8**, 392 (1982).
29. H. Volk and R. E. Friedrich, in R. L. Davidson, ed., *Handbook of Water-Soluble Gums and Resins*, McGraw-Hill, New York, 1980, Chapt. "16".
30. P. H. von Hippel and co-workers, *Biochemistry* **12**, 1256 (1973).
31. B. P. Makogon and T. A. Bondarenko, *Polym. Sci. USSR* **27**, 630–634 (1986).
32. A. J. Begala and U. P. Strauss, *J. Phys. Chem.* **76**, 254 (1972).
33. K. Hiraoka and T. Yokoyama, *Polym. Bull.* **2**, 183 (1980).
34. M. Leca, *Polym. Bull.* **16**, 537–543 (1986).
35. A. Chapiro and L. Perec-Spritzer, *Eur. Polym. J.* **11**, 59 (1975).
36. T. O. Osmanov and co-workers, *Dokl. Akad. Nauk SSSR* [Phys. Chem.] **240**, 910–913 (1978).
37. V. F. Gromov and co-workers, *Eur. Polym. J.* **16**, 529–535 (1980).
38. Ye. V. Bune and co-workers, *Vysokomol. Soyedin., Ser. A* **28**, 1279 (1986).
39. Yu. S. Bogachev and co-workers, *Polym. Sci.* **33**, 1357–1360 (1991).
40. W.-M. Kulicke, in B. Gampert, ed., *The Influence of Polymer Additives on Velocity and Temperature Fields—IUTAM Symposium*, Essen, Germany, 1984, Springer, Berlin, 1985, pp. 163–172.
41. W.-M. Kulicke and H. H. Horl, *Colloid. Polym. Sci.* **263**, 530 (1985).
42. P. Albonico and T. P. Lockhart, *J. Appl. Polym. Sci.* **55**, 69–73 (1995).
43. V. Ya. Kabo, L. A. Itskovich, and V. P. Budtov, *Polym. Sci. USSR* **31**, 2217–2225 (1989).

44. T. Schwartz and J. François, *Makromol. Chem.* **182**, 2775–2787 (1981).
45. A. Ikegami and N. Imai, *J. Polym. Sci.* **56**, 133 (1962).
46. J. François and co-workers, *Polymer* **38**, 6115–6127 (1997).
47. R. Rahbari and J. François, *Polymer* **33**, 1449 (1992).
48. R. K. Prud'homme and co-workers, *Soc. Petroleum Eng. J.* 804–808 (Oct. 1983).
49. W.-M. Kulicke, K. Kötter, and M. Gräger, *Adv. Poly. Sci.* **89**, 1 (1989).
50. F. Durst, R. Haas, and B. U. Kaczmar, *J. Appl. Polym. Sci.* **26**, 3125–3149 (1981).
51. G. Chauveteau, M. Moan, and A. Magueur, *J. Non-Newtonian Fluid Mech.* **16**, 315–327 (1984).
52. R. S. Farinato and W. S. Yen, *J. Appl. Polym. Sci.* **33**, 2353–2368 (1987).
53. W.-M. Kulicke and R. Haas, *Ind. Eng. Chem. Fundam.* **23**, 308–315 (1984).
54. S. A.-A. Ghoniem, *Rheol. Acta* **24**, 588–595 (1985).
55. K. A. Narh and co-workers, *Polym. Commun.* **31**, 2–5 (1990).
56. J. A. Odell and A. Keller, *J. Polym. Sci., Part B: Polym. Phys.* **24**, 1889–1916 (1986).
57. J. P. Scott and co-workers, *J. Appl. Polym. Sci.* **62**, 2097–2106 (1996).
58. W. M. Kulicke, M. Koetter, and H. Graeger, *Advances in Polymer Science*, Vol. **89**, Springer-Verlag, Berlin, 1989, p. 32.
59. Ref. 2, p. 224.
60. J. Francois and co-workers, *Polymer* **20**, 969 (1979).
61. K. J. McCarthy, C. W. Burkhardt, and D. P. Parazak, *J. Appl. Polym. Sci.* **33**, 1699–1714 (1987).
62. F. Mabire, R. Audebert, and C. Quivoron, *Polymer* **25**, 1317 (1984).
63. D. Vlassopoulos and W. R. Schowalter, *J. Rheol.* **38**, 1427–1446 (1994).
64. A. Ait-Kadi, P. J. Carreau, and G. Chauveteau, *J. Rheol.* **31**, 537–561 (1987).
65. H. C. Haas and R. L. MacDonald, *J. Appl. Polym. Sci.* **16**, 2709–2713 (1972).
66. M. Chmelir, A. Kunschner, and E. Barthell, *Angew. Makromol. Chem.* **89**, 145–165 (1980).
67. Ref. 10, p. VII–2.
68. W.-M. Kulicke, R. Kniewske, and J. Klein, *Prog. Polym. Sci.* **8**, 407 (1982).
69. J. Klein and K. D. Conrad, *Makromol.Chem.* **179**, 1635–1638 (1978).
70. T. Griebel, W.-M. Kulicke, and A. Hashemzadeh, *Colloid. Polym. Sci.* **269**, 113–120 (1991).
71. P. Munk and co-workers, *Macromolecules* **13**, 871–875 (1980).
72. J. Klein and K. D. Conrad, *Makromol. Chem.* **179**, 1635–1638 (1978).
73. W.-M. Kulicke and J. Klein, *Angew. Makromol. Chem.* **69**, 169–188 (1978).
74. W. Scholtan, *Makromol. Chem.* **14**, 169 (1954).
75. T. Griebel and W.-M. Kulicke, *Makromol. Chem.* **193**, 811–821 (1992).
76. S. M. Shawki and A. E. Hamielec, *J. Appl. Polym. Sci.* **23**, 3341 (1979).
77. D. J. Currie, F. S. Dainton, and W. S. Watt, *Polymer* **6**, 451 (1965).
78. J. P. Riggs and F. Rodriguez, *J. Polym. Sci., Part A1* **5**, 3151 (1967).
79. C. Y. Chen and J. F. Kuo, *J. Polym. Sci., Chem.* **26**, 1115 (1988).
80. S. K. Ghosh and B. J. Mandal, *Polymer* **34**, 4287 (1993).
81. T. J. Suen, A. M. Schiller, and W. N. Russel, *J. Appl. Polym. Sci.* **3**, 126 (1960).
82. E. H. Gleason, M. L. Miller, and G. F. Sheats, *J. Polym. Sci.* **38**, 133 (1959).
83. V. F. Kurenkov and V. A. Myagchenkov, *Eur. Polym. J.* **16**, 229 (1980).
84. J. Barton, V. Jurvanicova, and V. Vaskova, *Makromol. Chem.* **186**, 1935 (1985).
85. W. M. Thomas and D. W. Wang, *Encyclopedia of Polyme. Science and Engineering*, 2nd ed., Vol. **1**, John Wiley & Sons, Inc., New York, 1985, p. 182.
86. P. Molyneux, *Water Soluble Synthetic Polymers: Properties and Behavior*, Vol. **I**, CRC Press, Inc., Boca Raton, Fla., 1983, p. 91.
87. S. J. Guerrero, P. B. Oldarino, and J. H. Zurimendi, *J. Appl. Polym. Sci.* **30**, 955 (1985).

88. H. C. Hass and R. L. McDonald, *Polym. Lett.* **10**, 401 (1973).
89. H. C. Hass and R. L. McDonald, *J. Appl. Polym. Sci.* **16**, 2709 (1972).
90. T. V. Stupnikova and co-workers, *Visokomol. Soedin., Ser. A* **30**, 1380 (1988).
91. D. K. Ramsden and K. McKay, *Polym. Degrad. Stab.* **15**, 15 (1986).
92. D. K. Ramsden and K. McKay, *Polym. Degrad. Stab.* **14**, 217 (1986).
93. W. Nagashiro and co-workers, *Bull. Chem. Soc. Jpn.* **48**, 2597 (1975).
94. U. Grollman and W. Schnabel, *Polym. Degrad. Stab.* **4**, 203 (1982).
95. R. G. Ryles, *SPE* **389**, 1359 (1985).
96. L. I. Tolstikh and co-workers, *Intern. J. Polym. Mater.* **17**, 177 (1992).
97. V. F. Kurenkov and co-workers, *Izv. Vyssh. Uchebn. Zaved., Khim. Tekhnol.* **41**(2), 73 (1998).
98. J. Suzuki, S. Iizuka, and S. Suzuki, *J. Appl. Polym. Sci.* **22**, 2109 (1978).
99. F. L. Buchholz and L. R. Wilson, *J. Appl. Polym. Sci.* **32**, 5399 (1986).
100. K. Nakamiya and S. Kinoshita, *J. Ferment. Bioeng.* **80**(4), 418 (1995).
101. H. Kharadmand, J. Francois, and V. Plazanet, *Polymer* **29**, 860 (1988).
102. K. Ysuda, K. Okajima, and K. Kamide, *Polym. J.* **20**, 1101 (1988).
103. H. Morawetz, *Chemical Reactions on Polymers* , 1988, p. 317, Chapt. "23".
104. U.S. Pat. 5,286,806 (Feb. 15, 1994), R. E. Neff and R. G. Ryles (to American Cyanamid Co.).
105. F. Halverson, J. E. Lancaster, and M. N. O'Connor, *Macromolecules* **18**, 1139 (1984).
106. N. D. Truong and co-workers, *Polymer* **27**, 459 (1986).
107. N. D. Truong and co-workers, *Polymer* **27**, 467 (1986).
108. U.S. Pat. 3,022,279 (Feb. 20, 1962), A. C. Profitt (to The Dow Chemical Company).
109. V. F. Kurenkov, A. S. Verihznikova, and V. A. Myagehenkov, *Vysokomol. Soyedin., Ser. A* **28**, 488 (1986).
110. U.S. Pat. 3,171,805 (Mar. 2, 1965), T. J. Suen and A. M. Schiller (to American Cyanamid Co.).
111. U.S. Pat. 3,539,535 (Nov. 10, 1970), R. Wisner (to The Dow Chemical Company).
112. A. G. Agababyan, G. A. Gevorgyan, and O. L. Mndzhoyan, *Russian Chem. Rev.* **51**, 387 (1982).
113. U.S. Pat. 4,179,424 (Dec. 18, 1979), K. J. Phillips, E. G. Ballweber, and J. R. Hurlock (to Nalco Chemical Co.).
114. C. J. McDonald and R. H. Beaver, *Macromolecules* **12**, 203 (1979).
115. U.S. Pat. 3,988,277 (Feb. 20, 1976), C. R. Witschonke and R. Rabinowitz (to American Cyanamid Co.).
116. Eur. Pat. 0405712 A2 (Feb. 1, 1991), G. Nakra, J. P. Kane, and T. E. Sortwell (to Diatec Co.).
117. Ger. Offen. 2,333,927 (Jan. 23, 1975), K. Dahmen, W. H. Hübner, and E. Barthell (to Chemische Fabrik Stockhausen & Cie).
118. U.S. Pat. 4,230,608 (Dec. 18, 1980), L. A. Mura (to Nalco Chemical Co.).
119. Can. Pat. CA 1204535 (Mar. 6, 1986), K. G. Srinivasan (to Nalco Chemical Co.).
120. U.S. Pat. 4,956,399 (Sept. 11, 1990), J. J. Kozakiewicz and S.-Y. Huang, (to American Cyanamid Co.).
121. U.S. Pat. 5,037,881 (Aug. 6, 1991), J. J. Kozakiewicz and S.-Y. Huang, (to American Cyanamid Co.).
122. U.S. Pat. 5,132,023 (July 21, 1992), J. J. Kozakiewicz and S.-Y. Huang (to American Cyanamid Co.).
123. U.S. Pat. 3,332,927 (July 25, 1967), M. F. Hoover (to Calgon Corp.).
124. A. M. Schiller and T. J. Suen, *Ind. Eng. Chem.* **48**, 2132 (1956).
125. U.S. Pat. 3,979,348 (Sept. 7, 1976), E. G. Ballweber and K. G. Phillips (to Nalco Chemical Co.).
126. D. P. Bakalik and D. J. Kowalski, *Polym. Mater. Sci. Eng.* **57**, 845 (1987).

127. U.S. Pat. 5,120,797 (June 9, 1992), D. W. Fong and D. J. Kowalski (to Nalco Chemical Co.).
128. U.S. Pat. 3,556,932 (Jan. 19, 1971), A. T. Coscia and L. Williams (to American Cyanamid Co.).
129. D. R. Nagaraj and co-workers, *Int. J. of Miner. Process.* **20**, 291 (1987).
130. U.S. Pat. 4,587,306 (May 6, 1986), L. Vio and G. Meunier (to Societe Nationale Elf Aquitaine).
131. A. J. Domb, E. G. Cravalho, and R. Langer, *J. Polym. Sci., Polym. Chem. Ed.* **26**, 2623 (1988).
132. U.S. Pat. 5,128,420 (July 7, 1992) A. J. Domb and co-workers (to Massachusetts Institute of Technology).
133. U.S. Pat. 4,902,751 (Feb. 20, 1990), M. E. Lewellyn and D. P. Spitzer (to American Cyanamid Co.).
134. D. W. Fong and D. J. Kowalski, *Polym. Mater. Sci. Eng.* **75**, 145 (1996).
135. H. Tanaka and R. Senju, *Bull. Chem. Soc. Jpn.* **49**, 2821 (1976).
136. H. Tanaka, *J. Polym. Sci., Polym. Chem. Ed.* **17**, 1239 (1979).
137. A. El Achari and co-workers, *Makromol. Chem.* **194**, 1879 (1993).
138. U.S. Pats. 5,039,757 (Aug. 13, 1991), 5,239,014 (Mar. 8, 1994), and 5,292,821 (Mar. 8, 1994), T. Takaki and co-workers (to Mitsui Toatsu Chemicals, Inc.).
139. Eur. Pat. Appl. 289,823A (May 5, 1987), Y. L. Fu, S.-Y. Huang, and R. W. Dexter (to American Cyanamid Co.).
140. D. R. Draney and co-workers, *Polym. Prepr.* **31**, 500 (1990).
141. H. Tanaka, *J. Polym. Sci., Polym. Chem. Ed.* **24**, 29 (1986).
142. R. Ha and S. Hou, *Gaofenzi Xuebao* 570 (Oct. 1993); *Chem. Abstr.* **122**, 161506x (1995).
143. Ch. Wandrey, W. Jaeger, and G. Reinisch, *Acta Polym.* **32**, 197 (1981).
144. K. Plochocka, *J. Macromol. Sci., Rev. Macromol. Chem. C* **20**(1), 67 (1981).
145. U.S. Pat. 4,439,332 (Mar. 27, 1984), S. Frank, A. T. Coscia, and J. M. Schmitt (to American Cyanamid Co.).
146. F. Candau, Z. Zekhnini, and F. Heatley, *Macromolecules* **19**, 1895–1902 (1986).
147. C. L. McCormick and G. S. Chen, *J. Polym. Sci., Chem.* **20**, 817 (1982).
148. J. H. Barajas, Inverse-Emulsion and Inverse-Microemulsion Polymerization of Acrylic Water Soluble Monomers, Ph.D. Thesis, Vanderbilt University, 1996, Chapt. "4".
149. R. Aksberg and L. Wågberg, *Appl. Polym. Sci.* **38**, 297 (1989).
150. E. T. Hsieh, I. J. Westerman, and A. Moradi-Araghi, *Polym. Mater. Sci. Eng.* **56**, 700 (1986).
151. Y. Negi, S. Harada, and O. Ishizuka, *J. Polym. Sci., Part A-1: Chem.* **5**, 1951 (1967).
152. C. Wandrey, J. H. Barajas, and D. Hunkeler, *Adv. Polym. Sci.* **145**, 123–182 (1999).
153. U.S. Pat. 3,288,770 (Nov. 29, 1966), G. B. Butler (to Peninsular Chem. Research, Inc.).
154. Anon., *Chem. Eng. News* **46** (Jan. 15, 1968).
155. J. E. Lancaster, L. Baccei, and H. P. Panzer, *J. Polym. Sci., Polym. Lett. Ed.* **14**, 549 (1976).
156. M. Hahn and W. Jaeger, *Angew. Makromol. Chem.* **198**, 165 (1992).
157. U.S. Pat. 4,092,467 (May 30, 1978), R. P. Welcher, R. Rabinowitz, and A. S. Cibuslkas (to American Cyanamid Co.).
158. M. Chen and K. H. Reichert, *Polym. React. Eng.* **1**(1), 145 (1993).
159. U.S. Pat. 3,284,393 (Nov. 8, 1966), J. W. Vanderhoff and R. M. Wiley (to The Dow Chemical Company).
160. U.S. Pat. 3,826,771 (July 30, 1974), D. R. Anderson and A. J. Frisque (to Nalco Chemical Co.).
161. U.S. Pat. 5,376,713 (Dec. 27, 1994), M. N. O'Connor, L. J. Barker, and R. G. Ryles (to Cytec Technology Corp.).
162. U.S. Pat. 5,679,740 (Oct. 21, 1997), H. I. Heitner (to Cytec Technology Corp.).

163. D. Hunkeler and J. H. Barajas, in Ref. 4, p. 3330.
164. Fr. Pats. 2,428,053 and 2,428,054 (June 9, 1978), J. Boutin and J. Neel (to Rhône-Poulenc Industries).
165. U.S. Pat. 4,762,862 (Aug. 9, 1988), A. Yada and co-workers (to Dai-Ichi Kogyo Seiyaku Co.).
166. Ger. Pat. DE 3,621,429 (Jan. 8, 1987), J. M. Lucas and A. C. Pericone (to Milchem, Inc.); *Chem. Abstr.* **106**, 138949e (1987).
167. U.S. Pat. 4,857,610 (Aug. 15, 1989), M. Chmelir and J. Pauen (to Chemische Fabrik Stockhausen GmbH).
168. Eur. Pat. EP 296331B (Feb. 2, 1995), W. B. Davies (to Cytec Technology Corp.).
169. U.S. Pat. 4,506,062 (Mar. 19, 1985), P. Flesher and A. S. Allen (to Allied Colloids, Ltd.).
170. U.S. Pat. 4,962,150 (Oct. 9, 1990), A. S. Allen (to Allied Colloids, Ltd.).
171. D. Hunkeler and J. H. Barajas, in O. Olabisi, ed., *Handbook of Thermoplastics*, Vol. **10**, Marcel Dekker, Inc., New York, 1997, p. 237.
172. F. Candau, in M. A. El-Nokaly, ed., *Polymer Association Structures: Microemulsions and Liquid Crystals* , 1984, pp. 47–61.
173. U.S. Pat. 4,521,317 (June 4, 1985), F. Candau and co-workers (to Inst. Franacais du Petrole, Rueil-Malmaison).
174. F. Candau, Y. S. Leong, and R. M. Fitch, *J. Polym. Sci., Chem. Ed.* **23**, 193 (1985).
175. U.S. Pat. 4,681,912 (July 21, 1987), J.-P. Durand and co-workers (to Inst. Franacais du Petrole, Rueil-Malmaison).
176. WO 8810274 A1 (Dec. 29, 1988), F. Candau and P. Buchert (to Norsolor S.A.).
177. M. T. Carver and co-workers, *J. Phys. Chem.* **93**, 4867 (1989).
178. F. Candau and P. Buchert, *Colloids Surf.* **48**(1–3), 107 (1990).
179. F. Candau, D. Collin, and F. Kern, *Makromol. Chem., Makromol. Symp.* **35/36** (Copolym. Disperse Media), 105 (1990).
180. U.S. Pat. 5,093,009 (July 21, 1992), F. Candau, P. Buchert, and E. Esch (to Inst. Franacais du Petrole, Rueil-Malmaison).
181. D. Hunkeler and co-workers, *Adv. Polym. Sci.* **112**, 116 (1994).
182. J. Barton, *Prog. Polym. Sci.* **21**, 399 (1996).
183. U.S. Pat. 5,545,688 (Aug. 13, 1996), S.-Y. Huang (to American Cyanamid Co.).
184. U.S. Pats. 4,956,400 (Sept. 11, 1990) and 5,037,863 (Aug. 6, 1991), J. J. Kozakiewicz and co-workers, (to American Cyanamid Co.).
185. U.S. Pats. 5,883,181 (Dec. 10, 1996), and 5,723,548 (Mar. 3, 1998), J. J. Kozakiewicz and S.-Y. Huang (to Cytec Technology Corp.).
186. U.S. Pats. 5,627,260 (May 6, 1997), 5,670,615 (Jan. 26, 1997), and 5,863,982 (Jan. 26, 1999), S.-Y. Huang and co-workers (to Cytec Technology Corp.).
187. U.S. Pat. 4,824,894 (Apr. 25, 1989), R. Schnee, A. Scordialo, and J. Masanek (to Röhm GmbH, Chemische Fabrik).
188. WO 92/08744 (May 29, 1992), U.S. Pat. 5,358,988 (Oct. 25, 1994), L. Schieferstein and co-workers (to Henkel Co.).
189. U.S. Pat. 4,933,404 (Feb. 20, 1990), E. J. Beckman, E. J. Smith, and J. L. Fulton (to University of Pittsburgh).
190. E. J. Beckman, E. J. Smith, and J. L. Fulton, *J. Phys. Chem.* **94**, 345 (1990).
191. E. J. Beckman, E. J. Smith, and J. L. Fulton, *Macromolecules* **27**, 312 (1994); E. J. Beckman, E. J. Smith, and J. L. Fulton, **27**, 5238 (1994).
192. K. A. Shaffer and J. M. Desimone, *Trends in Polym. Sci.* **3**(5), 146 (1995).
193. J. Gregory, in C. A. Finch, ed., *Industrial Water Soluble Polymers*, The Royal Society of Chemistry, Cambridge, U.K., 1996, pp. 62–75.
194. G. Petzold, in R. S. Farinato and P. L. Dubin, eds., *Colloid–Polymer Interactions: From Fundamentals to Practice*, John Wiley & Sons, Inc., New York, 1999, pp. 83–100, Chapt. "3".

195. J. M. W. Mackenzie, *Eng. Min. J.* 80–87 (Oct. 1980).
196. J. P. MacDonald, P. L. Mattison, and J. M. W. MacKenzie, *J. S. Afr. Inst. Min. Metall.* **81**, 303 (1981).
197. *Superfloc 16 Plus Flocculant*, Cytec Industries, West Patterson, N.J., 1997.
198. R. W. Adams and co-workers, *Mining Chemicals Handbook* (rev. ed.), Cytec Mining Technical Services, Cytec Industries Inc., Stamford, Conn., 1986.
199. D. L. Dauplaise and M. F. Werneke, in *Proceedings of the Consolidation and Dewatering of Fine Particles Conference*, University of Alabama, Tuscaloosa, Ala., 1982, pp. 90–113.
200. Ref. 6, p. 830.
201. U.S. Pat. 4,767,540 (Aug. 30, 1988), D. P. Spitzer and W. S. Yen (to American Cyanamid Co.).
202. U.S. Pats. 5,733,459 and 5,733,460 (Mar. 31, 1998), A. S. Rothenberg and co-workers (to Cytec Technology Corp.).
203. U.S. Pat. 5,368,745 (Nov. 29, 1994), A. S. Rothenberg, R. G. Ryles, and P. So (to Cytec Technology Corp.).
204. U.S. Pat. 4,342,653 (Aug. 3, 1982), F. Halverson (to American Cyanamid Co.).
205. U.S. Pat. 4,533,465 (Aug. 6, 1985), R. M. Goodman and S. K. Lim (to American Cyanamid Co.).
206. D. R. Nagaraj and co-workers, *Int. J. of Miner. Process.* **20**, 291, 293 (1987).
207. U.S. Pat. 5,756,622 (May 26, 1998), S. S. Wang and D. R. Nagaraj (to Cytec Technology Corp.).
208. Eur. Pat. EP 288,150B (Feb. 23, 1994), A. Allen (to Allied Colloids, Ltd.).
209. U.S. Pat. 4,824,523 (June 1, 1987), L. Wågberg and T. Lindström (to Svenska Traforskningsinstitutet).
210. U.S. Pat. 5,167,766 (Dec. 1, 1992), D. S. Honig and E. Harris (to American Cyanamid Co.).
211. D. S. Honig and co-workers, *Tappi* **76**(9), 135–143 (1993).
212. C. E. Farley, in L. L. Chan, ed., *Wet Strength Resins and Their Application*, Tappi Press, Atlanta, Ga., 1994, p. 45.
213. U.S. Pat. 4,605,702 (Aug. 12, 1986), G. J. Guerro, R. J. Proverb, and R. F. Tarvin (to American Cyanamid Co.).
214. U.S. Pat. 5,723,022 (Mar. 3, 1998), D. L. Dauplaise and G. J. Guerro (to Cytec Technology Corp.).
215. W. F. Reynolds and R. B. Wasser, in J. P. Casey, ed., *Pulp and Paper Chemistry and Chemical Technology*, John Wiley & Sons, Inc., New York, 1981, pp. 1447–1470.
216. U.S. Pat. 5,824,190 (Oct. 20, 1998), G. Guerro, D. Dauplaise, and R. Bazaj (to Cytec Technology Corp.).
217. J. P. Casey, ed., *Pulp and Paper Chemistry and Chemical Technology* (**4** vols.), John Wiley & Sons, Inc., New York, 1987, pp. 1–2609.
218. J. K. Borchardt, in J. I. Kroschwitz, ed., *Encyclopedia of Polymer Science and Engineering*, 2nd ed., Vol. **10**, Wiley-Interscience, New York, 1987, p. 350.
219. U.S. Pat. 4,744,419 (May 17, 1988), R. Sydansk and P. Argabright (to Marathon Oil Co.).
220. U.S. Pat. 4,606,407 (Aug. 8, 1986), P. Shu (to Mobil Oil Corp.).
221. U.S. Pat. 5,905,100 (May 18, 1999), A. Moradi-Araghi (to Phillips Petroleum Co.).
222. U.S. Pat. 4,806,164 (Feb. 21, 1989), L. Brothers (to Halliburton Co.).
223. U.S. Pat. 4,423,199 (Dec. 27, 1983), C. J. Chang and T. E. Stevens (to Rohm and Haas Co.).
224. U.S. Pat. 4,417,989 (Nov. 29, 1983), W. D. Hunter (to Texaco Development Corp.).
225. J. Bock and co-workers, in G. A. Stahl and D. N. Schulz, eds., *Water-Soluble Polymers for Petroleum Recovery*, Plenum Press, New York, 1988, pp. 147–160.

226. U.S. Pat. 4,722,962 (Feb. 2, 1988), G. D. Shay (to DeSoto, Inc.).
227. U.S. Pat. 4,734,205 (Mar. 29, 1988), D. F. Jacques and J. Bock (to Exxon Research and Engineering Co.).
228. A. Karunasena, R. G. Brown, and J. E. Glass, in J. E. Glass, ed., *Polymers in Aqueous Media: Performance Through Association* (Adv. Chem. Ser. 223), American Chemical Society, Washington, D.C., 1989.
229. F. Candau and J. Selb, *Adv. Colloid Interface Sci.* **79**, 149–172 (1999).
230. U.S. Pat. 4,654,039 USRE 32649 (Apr. 19, 1988), K. Brandt, T. Inglin, and S. Goldman (to The Proctor and Gamble Co.).
231. U.S. Pat. 4,500,670 (Feb. 19, 1985), M. J. McKinley and D. P. Sheridan (to The Dow Chemical Company).
232. U.S. Pat. 4,725,628 (Feb. 16, 1988), C. Garvey, J. Pazos, and G. Ring (to Kimberly Clark Corp.).
233. U.S. Pat. 4,725,629 (Feb. 16, 1988), C. Garvey and J. Pazos (to Kimberly Clark Corp.).
234. U.S. Pats. 5,439,983 (Aug. 8, 1995) and 5,206,326 (Apr. 27, 1993), I. Ahmed and H. L. Hsieh (to Phillips Petroleum Co.).
235. E. Schröder, G. Müller, and K.-F. Arndt, *Polymer Characterization*, Hanser, Munich, 1989.
236. F. A. Bovey and G. V. D. Tiers, *J. Polym. Sci., Part A* **1**, 849 (163).
237. F. Halverson, J. E. Lancaster, and M. N. O'Connor, *Macromolecules* **18**, 1139–1144 (1985).
238. J. Hernandez-Barajas and D. J. Hunkeler, *J. Appl. Polym. Sci.* **61**, 1325 (1996).
239. P. Kratochvil, *Classical Light Scattering from Polymer Solutions*, Elsevier, New York, 1987.
240. B. Chu, *Laser Light Scattering: Basic Principles and Practice*, 2nd ed., Academic Press, New York, 1991.
241. J. S. Higgins and H. C. Benoit, *Polymers and Neutron Scattering*, Clarendon Press, Oxford, 1994.
242. W.-M. Kulicke and R. Kniewske, *Makromol. Chem., Rapid Commun.* **1**, 719–727 (1980).
243. A. DiNapoli, B. Chu, and C. Cha, *Macromolecules* **15**, 1174–1180 (1982).
244. M. G. Styring and A. E. Hamielec, in A. R. Cooper, ed., *Determination of Molecular Weight*, John Wiley & Sons, Inc., New York, 1989, Chapt. "10", p. 263.
245. L. A. Papazian, *J. Liquid Chromatogr.* **13**, 3389–3398 (1990).
246. J. C. Giddings, K. D. Caldwell, and L. F. Kesner, in Ref. 244, Chapt. 12, p. 337.
247. G. Holzwarth, L. Soni, and D. N. Schulz, *Macromolecules* **19**, 422–426 (1986).
248. G. Holzwarth, L. Soni, D. N. Schulz, and J. Bock, in Ref. 225, pp. 215–229.
249. P. J. Wyatt, *Anal. Chim. Acta* **272**, 1–40 (1993).
250. H. Terayama, *J. Polym. Sci.* **VIII**, 243 (1952).
251. M. A. Langhorst and co-workers, *Anal. Chem.* **58**, 2242–2247 (1980).
252. Y. Nishijima and co-workers, *J. Polym. Sci., Part A-2* **5**, 23–35 (1967).
253. U.S. Pat. 4,194,877 (Mar. 25, 1980), J. I. Peterson (to United States of America, Washington, D.C.).
254. P. Gramain and P. Myard, *Polym. Bull.* **3**, 627–631 (1980).
255. N. J. Turro and K. S. Arora, *Polymer* **27**, 783 (1986).
256. J. Rica and co-workers, *Macromolecules* **20**, 1407–1411 (1987).
257. H. Tanaka and R. Senju, *Bull. Chem. Soc. Jpn.* **49**, 2821 (1976).
258. J. K. Inman and H. M. Dintzis, *Biochem.* **8**, 4074–4082 (1969).
259. H. Tanaka and L. Odberg, *J. Polym. Sci., Part A: Polym. Chem.* **27**, 4329–4339 (1989).
260. U.S. Pat. 4,813,973 (Mar. 21, 1989), M. A. Winnik and R. M. Borg (to University Toronto Inventions Found.).

261. U.S. Pat. 5,389,548 (Feb. 14, 1995), J. E. Hoots, C. C. Pierce, and R. W. Kugel (to Nalco Chemical Co.).
262. R. D. Lentz, R. E. Sojka, and J. A. Foerster, *J. Environ. Qual.* **25**, 1015–1024 (1996).
263. *Methods Exam. Waters Assoc. Matl. 1988*, Department of the Environment, U.K.; *Chem. Abstr.* **108**, 197583v (1988).
264. G. Schmoetzer, *Chromatographia* **4**, 391–395 (1971); *Chem. Abstr.* **76**, 25744c (1972).
265. D. D. Mc-Collister and co-workers, *Toxicol. Appl. Pharmacol.* **7**(5), 639 (1965).

SUN-YI HUANG
DAVID W. LIPP
RAYMOND S. FARINATO
Cytec Industries

ACRYLIC (AND METHACRYLIC) ACID POLYMERS

Introduction

Almost all acrylic polymers produced commercially contain acrylic acid and/or methacrylic acid at some level, which gives them a special property. Content of the acidic monomers ranges from <5 wt% present in many widely used emulsion copolymers to100 wt% in water-soluble homopolymers. Between these extremes, by the inclusion of a wide variety of comonomers, the copolymers may be water-soluble, soluble only in their neutralized forms, the so-called alkali-soluble polymers, or swollen gels if cross-linkers are present. The less expensive acrylic acid produced by a simpler process is now more commercially available than methacrylic acid and dominates the polymer market especially in nonemulsion areas. This article focuses chiefly on water-soluble, alkali-soluble, and water-swellable gels, based on homopolymers and copolymers since these are very important commercially and they contain significant levels of the acidic monomers. Acrylic emulsion polymers have low acid content and are widely used in industry and household paint formulations: they are included here in a selected limited fashion because they have been widely studied and the open and patent literatures are so voluminous.

Monomers

The structures of propenoic acid, commonly called *acrylic acid*, and 2-methylpropenioc acid, commonly called *methacrylic acid*, are shown below:

Encyclopedia of Polymer Science and Technology. Copyright John Wiley & Sons, Inc. All rights reserved.

Table 1. Physical Properties of Acrylic and Methacrylic Acids

Property	Acrylic acid	Methacrylic acid
Formula weight	72.06	86.10
Melting point, °C	13.5	14.0
Boiling point, 101 kPa,[a] °C	141.0	159–163
Vapor pressure, 25°C, kPa[a]	0.57	0.13
Density, 25°C, g/mL	1.045	1.015
Heat of vaporization, J/g[b]	435	418
Heat of polymerization, kJ/g[b]	1.08	0.657
Heat of polymerization, kJ[b]/mol	76.99	56.32
Heat capacity, 25°C, J[b]/(g·°C)	2.1	2.1
Refractive index η_D	1.4185	1.4288
Viscosity, 25°C, mPa·s (=cP)	1.25	1.3
Flash point, tag closed cup, °C	50	67
Flash point, Cleveland open cup, °C	68	77
Surface tension, 25°C, mN/m (=dyn/cm)	–	26.5
Solubility in water	Miscible	Miscible
Autoignition temperature, °C	412	400
Dissociation constants (10^5)	5.5	2.2

[a]To convert kPa to mm Hg, multiply by 7.5.
[b]To convert J to cal, divide by 4.184.

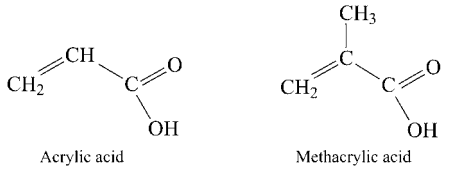

Acrylic acid and methacrylic acid are selective oxidation products of propylene and isobutylene, respectively. The minor difference in structure between the two acids, the α-methyl substituent of methacrylic acid, results in minimal physical property differences as indicated in Table 1. However, this structural difference distinctly affects polymerization and copolymerization kinetics and the characteristics of the resulting polymers.

Acrylic acid was first reported in 1843 as a product of the air oxidation of acrolein, which is obtained from the high temperature cracking of glycerol (1) (Fig. 1). However, large-scale production of acrylic acid was not introduced until the 1930s when industrial manufacturing processes were developed and safe-handling procedures adopted for this very reactive monomer (2). Since then, commercial growth has been phenomenal and, today, the production and use in

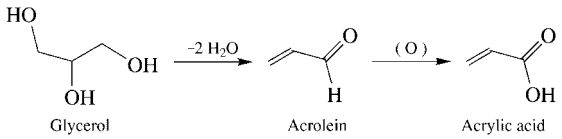

Fig. 1. Cracking of glycerol to acrylic acid.

polymerizations greatly predominates over methacrylic acid. This is due to its lower cost and relative ease of preparation by the oxidation of inexpensive propylene, and to a great extent to the global acceptance of superabsorbent acrylic acid-based polymers in diapers and feminine hygiene products.

Frankland and Duma first reported methacrylic acid in 1865 (3). However, like acrylic acid, its commercial development came many years later in 1933 (4). The development required pioneering chemistry on the monomer and its derivatives by Dr. Otto Rohm published in his doctoral thesis in 1901 and its evolution through the formation of the Rohm and Haas Co. in 1909 (5–8). Like the acrylic acid, methacrylic acid and its vinyl derivatives are used mainly in the preparation of polymers. There is little interest in small organic molecules based on the monomers.

Properties. The physical properties of the two acidic monomers are contrasted in Table 1. The major differences to note between the two acidic monomers with regard to polymerization reactions and polymer properties are the higher boiling point of the methacrylic acid and the higher heat of polymerization and higher acidity of acrylic acid.

Both monomers are bifunctional organic compounds, with each having carboxylic acid and conjugated unsaturated double bond functionalities. The carboxyl group undergoes all the reactions expected and readily forms salts and esters using conventional procedures. Caution must be exercised during these reactions because the conjugated unsaturation present in the molecules renders them susceptible to highly exothermic and potentially explosive Michael addition reactions and free-radical polymerizations under uncontrolled conditions. It is this high reactivity of the monomeric double bond that allows rapid carefully controlled polymerization to produce the expected result in polymerization reactions.

Manufacture of Acrylic Acid Monomer. Many synthetic routes to acrylic acid exist and are reported widely in the literature. However, the only currently commercially viable process is based on the direct high temperature gas-phase oxidation of propylene, as indicated schematically in Figure 2. This economical process, based on the availability and low cost of propylene, is expected to predominate commercially for many years. Other once practiced processes based on acrylonitrile, propiolactone, and ethylene cyanohydrin are no longer of importance (2).

The oxidation proceeds by the two-step catalytic process indicated above, without the isolation of the intermediate acrolein. Acrylic acid, obtained in high yield based on propylene, is isolated as an aqueous solution and purified by extraction and distillation. The principal impurities in the commercial monomer, termed glacial acrylic acid, that may affect subsequent polymerization reactions include acetaldehyde, acrolein, furfural, benzaldehyde, and acrylic acid dimer, 3-acryloxypropionic acid. Since these impurities are inhibitory in polymerization,

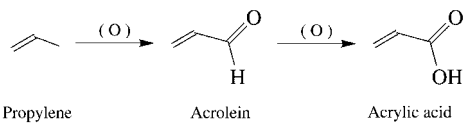

Fig. 2. Acrylic acid by propylene oxidation.

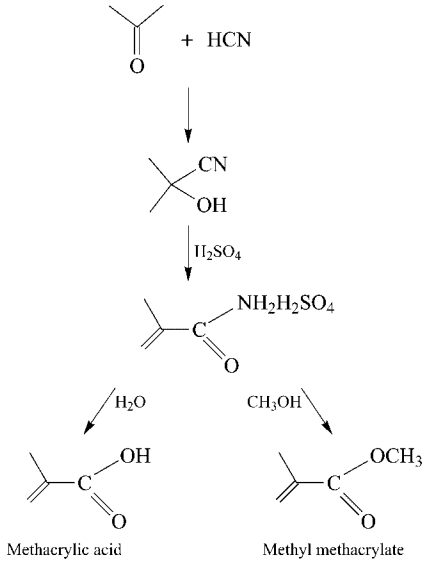

Fig. 3. Processes for methacrylic acid and methyl methacrylate.

they must be removed to facilitate the production of ultrahigh molecular weight polymers for use in superabsorbent manufacture, for example.

Manufacture of Methacrylic Acid Monomer. The commercial manufacture of methacrylates began in 1933 based on acetone cyanohydrin, which is still the basis for all current production (4). This well-established technology is based on the commercially inexpensive chemical starting compounds, acetone, hydrogen cyanide, and sulfuric acid. The process is represented by the schematic shown in Figure 3. Acetone reacts with hydrogen cyanide to form acetone cyanohydrin, which is readily converted into the methacrylamide sulfate salt in the presence of anhydrous sulfuric acid. This intermediate salt may be directly converted into either methacrylic acid or methyl methacrylate by reaction with water or anhydrous methanol, respectively. In commercial practice, the two steps are generally carried out simultaneously with an aqueous methanol solution to produce an ester rich mixture, since methyl methacrylate is the higher volume commercial product for the production of Plexiglas (Rohm and Haas Co.).

Handling and Storage of Acrylic and Methacrylic Acids. Acrylic acid is available commercially at 98%+ purity and contains a polymerization inhibitor such as hydroquinone (HQ), monomethylhydroquinone (MEHQ), or phenothiazine. Methacrylic acid, on the other hand, is available at 99%+ purity and is stabilized with either HQ or MEHQ. It is not usually necessary to purify the monomers to remove the inhibitors prior to polymerization, as the level of free-radical initiators used readily overwhelms them. However, where ultrahigh molecular weight polymers are required, for example in superabsorbent polymers, the impurities must be removed. The corrosiveness of the monomers toward many metals requires storage to be in stainless steel, glass, or aluminum or suitably lined vessels. Any metals leached from storage vessels could potentially promote dangerous runaway polymerizations in the presence of oxygen. Obviously, for

the same reasons, polymerization reactions must be carried out in similarly constructed equipment.

Since both acids have relatively high freezing points, 13–14°C, they must be prevented from freezing in cold conditions. If freezing occurs, thawing is a hazardous procedure since the distribution of inhibitor between solid and liquid is difficult to control, and runaway uncontrolled and potentially explosive polymerization of the liquid phase is always a threat. To avoid this potential hazard, monomer storage at temperatures in excess of their freezing points is recommended.

Health and Safety. Both acids are moderately toxic compounds when ingested or absorbed through the skin. Severe internal burns result from swallowing. Skin contact causes rapid tissue damage due to the highly corrosive nature of the monomers. The vapor of acrylic acid is more irritating to the eyes than that of methacrylic acid, but both may cause redness on prolonged exposure.

As with all industrial chemicals with similar characteristics, safe handling with suitable protection gear is highly recommended; gloves, facemask, and clothing are all important. These are all listed in the Material Safety Data Sheets (MSDS) that accompany the monomers and these sheets must be thoroughly read and understood before working with either monomer.

Polymerization of Acrylic and Methacrylic Acids

Dependence on pH. The rates of polymerization of both acidic monomers in dilute aqueous solutions are pH-dependent. The rate of polymerization is high at low pH for both monomers; it falls rapidly to a minimum at pH 6–7, and then increases to a maximum at pH 10 for acrylic acid and 12 for methacrylic acid (9–13). At high salt or monomer concentrations, the polymerization rate minimum at the pH range 6–7 becomes less pronounced.

The explanation of the observed rate minimum at pH 6–7 is generally considered to be due to the slower rate of propagation for the anion than for the free acid. However, as pH is increased, the rate of polymerization increases because of the decreased rate of termination of the radical anions promoted by coulombic repulsion (10). An alternative explanation of both the increase of polymerization with pH and the leveling of the rate by added salts at pH 6–7 is postulated to be due to the formation of terminal ion pair radicals with a propagation rate similar to that of the free-acid monomers (9).

Copolymerization. Acrylic and methacrylic acids readily copolymerize free radically with many vinyl monomers. This versatility results from a combination of their highly reactive double bonds and their miscibility with a wide variety of water- and solvent-soluble monomers. Reactivity ratios derived from copolymerizations with many monomers are tabulated in many books on polymerization, for example in Wiley's *Polymer Handbook* (14) (see also Wiley's Database of Polymer Properties). Q and e values are parameters that may be established for a monomer based on a large number of reactivity ratios with other monomers. These parameters are associated with interactions between the monomer and the growing chain via resonance (Q) and polar effects (e).

As mentioned, the rate of copolymerization of acrylic and methacrylic acids is dependent on pH effects and the resulting ionization as well as the comonomers.

Table 2. Comonomer Effects on Acidic Polymers

Comonomer	Polymer
None	Water-soluble
Water-soluble	Water-soluble
Water-insoluble, low level	Water-soluble
Water-insoluble, mid level	Alkali-soluble emulsion
Water-insoluble, high level	Emulsion polymer
Polyvinyl cross-linker	Gel

This conflict makes it difficult to describe the acidic monomers by single Q and e values derived from reactivity ratios. Neutralization changes both Q and e values. Particularly, e values reverse from a positive value to a negative value on neutralization (15). This is expected as e is a measure of electron-donating ability of the monomeric double bond and neutralization may be equated to a change from electron-withdrawing carboxylate group to an electron-donating carboxylate ion.

Alternative Synthesis of Acidic Polymers. There are two approaches to homo- and copolymers of acrylic and methacrylic acids. In addition to the conventional use of acrylic acid and methacrylic acid monomers, the main theme of this article, there exists the possibility of converting polymers of the derivatives of these two monomers to acidic polymers. There would obviously have to be very extenuating circumstances to take this route industrially because of cost penalties. However, there are situations where there is a reason to do this. Availability of monomers is a good example. Acrylonitrile was at one time more available than acrylic acid in some parts of the world and simple hydrolysis of the polymer gave poly(acrylic acid). Other potential routes exist from such homo- and copolymers of acrylamide, acrylic and methacrylic esters, and acid chlorides. Although not further discussed here, the reader is reminded that polymer synthesis with acrylic monomers is very versatile and forethought is always necessary before plunging ahead.

Polymerization Processes. A variety of processes are used commercially to homopolymerize and copolymerize acrylic acid and methacrylic acid. On the basis of economics and environmental considerations, water is generally the preferred industrial solvent or polymerization medium. However, the choice of process is usually dictated by the requirements of the polymer to be produced. As already indicated, pH influences the rate of polymerization. Comonomers and molecular weight of the polymer to be produced also have a profound effect on the type of polymerization process that can be used and on the type of product obtained. The contents of Table 2 indicate the change from water-soluble to alkali-soluble emulsions and ultimately emulsion polymers is dependent on the comonomers in copolymers of acrylic and methacrylic acids. This transition from water-soluble polymer to emulsion polymer as the acidic monomer is decreased depends on the hydrophobicity of the comonomer. Introduction of divinyl monomers causes transition to gel materials in all compositions. The gels may vary from highly swollen to tightly bound copolymers, depending on the cross-linker level.

The effect of molecular weight is very pronounced with the water-soluble polymers. The change of viscosity of aqueous solutions is shown schematically in Figure 4. A precipitous increase in viscosity occurs at lower concentrations with

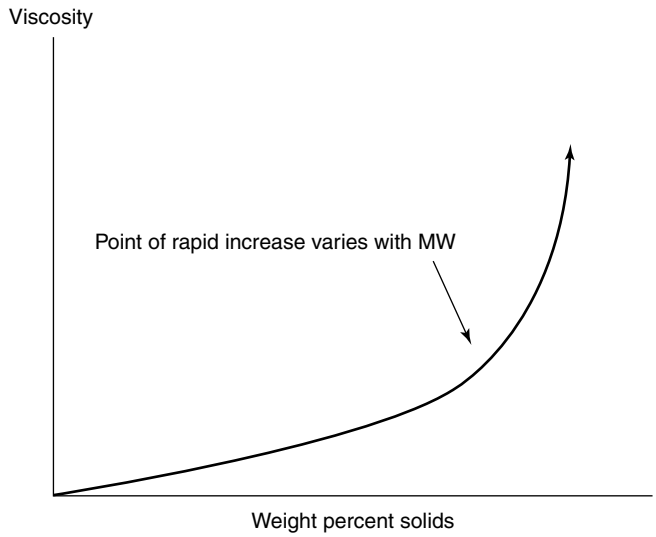

Fig. 4. Water-soluble polymers: viscosity/molecular weight in water.

higher molecular weights, essentially making it economically impossible to make polymer of greater than about 100,000 Da by aqueous solution polymerization. This can be controlled to some extent by polymerizing the monomers at lower concentration, but this becomes economically undesirable at some point, usually around 30 wt% solids. Hence, new technology is borne. Generally speaking, low molecular weight homopolymers, less than 100,000 Da, may be made in aqueous solution; higher molecular weights require technologies such as suspension and gel polymerization.

Copolymer synthesis suffers the same viscosity restrictions as the homopolymers when the comonomers are sufficiently water-soluble to produce water-soluble copolymers. When water-insoluble comonomers are used it is possible to resort to cosolvents with water or surfactants in micellar polymerizations to effect solubility to a limited degree, but this is only useful at low molecular weight and is undesirable environmentally. Higher molecular weight copolymers are usually made by emulsion, inverse emulsion, or suspension polymerization.

Polymer Characteristics

The polymer types considered here are primarily those that are soluble in water as prepared, soluble after neutralization of emulsion polymerized copolymers, the so-called alkali-soluble polymers, and cross-linked swellable gel polymers. Emulsion polymers are discussed in a limited fashion, as acrylic and methacrylic acids are used ubiquitously at low levels in almost all acrylic emulsion polymerizations to contribute some special characteristic. For example, the incorporation of acidic monomers contributes to such properties as adhesion, wettability, and emulsion polymer stability.

Emulsion Polymers.

Applications. Acrylic emulsion polymers containing insufficient acrylic or methacrylic acids to solubilize on neutralization are used in a myriad of applications including, coatings, floor polish, inks, dispersants, adhesives, and caulks. These are almost all thin film applications and the acid contributes hydrophilicity, stability, dispersancy, etc. The polymers are balanced by backbone hardness, hydrophobicity/hydrophilicity balance, functionality, all moderated by choice of comonomers and by molecular weight and morphology. Some examples from the literature of the use of emulsion copolymers containing low levels of acidic monomers include autodeposition coatings (16), paper saturants (17), wood coatings (18), corrosion-resistant coatings (19), printing ink binders with core-shell morphology (20), monodispersed particles for liquid toners (21), oil-repellent finishes based on fluoromonomers (22), dilatant dispersants for antistatic coatings (23), water-resistant coatings (24), water-dispersible polymers for building materials (25), surfactant-free emulsions for nonwovens (26), pressure-sensitive adhesives with good mechanical stability (27), water-resistant cosmetics (28), anticorrosion coatings for ferrous metals (29), hair styling shampoos (30), redispersible film-forming coatings (31), core-shell graft polymers for cement modifiers (32), coatings and inks (33), wood coatings (34), acrylic polyester hybrids (35), redispersible powders for cement (36), hair fixatives (37), redispersible core-shell polymers (38), core-shell coatings (39–42), coatings (43), pressure-sensitive adhesives (44), and emulsion paints (45).

Synthesis. The synthesis of emulsions is widely described in the literature, both patent and open. Ingredients are surfactants for setting particle size and stabilization of the emulsion, and initiators for polymerization. Leading reference books are by Blackley; although somewhat dated it is still an excellent book and another is Gilbert's recent publication (46). Other useful synthesis references include some specific interests, pressure-sensitive adhesives (47), styrene emulsion polymerization using alkali-soluble resins as emulsifiers (48), manufacture and use of curable emulsions (49), preparation of concentrated emulsions (50), multistage polymer preparation (51), core-shell vinyl acrylic emulsions (52), acrylic grafted to polyester emulsions (53), aqueous polymer dispersions (54), process for polyacrylate dispersions (55), sterically stabilized acrylic graft copolymers (56), polyacrylate dispersions without colloid protection (57) and with colloid protection (58), low VOC emulsions (59), design of latex polymers (60), random copolymers as emulsifiers (61), multihollow latex particles (62), modeling of acid distribution in lattices (63,64), modeling of microparticles and experimental verification (65), and effect of pH on properties of emulsion polymers (66). Since so many applications of acrylic emulsions are dependent interfacial science, film formation is very important and has received much interest (67–70).

Water-Soluble Polymers.

Synthesis. Water-soluble polymers are prepared by conventional free-radical polymerization methods with molecular weight control through the level of initiator and the use of chain transfer agents. Generally, molecular weights of the polymers range from a few thousand to several hundred thousand, which is useful in many applications from dispersants to rheology modifiers to thickeners to flocculants. The lower molecular weights from 1000 to about 30,000 have been most widely worked on. Typical initiators fall into two classes, the thermally activated

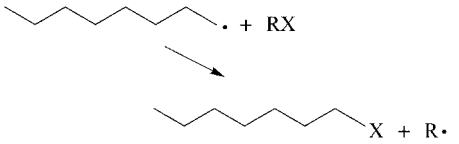

Fig. 5. Chain transfer in free-radical polymerization.

and the redox types. The thermally activated are persulfates, perphosphates, azos, hydroperoxides, etc, which are used in temperature ranges of 50–100°C. The redox initiators are generally designed for use at lower temperatures and function by using stoichiometric amount of reducing and oxidizing agents in the presence of a metal catalyst. The metal decomposes the peroxy compound to produce radicals for initiating polymerization and is converted to a higher oxidation state in the process; the reducing agent cycles the metal back to the lower oxidation state and the process is repeated.

Molecular weight control by using chain transfer agents (Fig. 5) results in the incorporation of the chain transfer agent at least on the polymer terminus.

RX is a general term for a chain transfer agent. The liberated R· radical then initiates another polymer chain and X, usually hydrogen from chain transfer agents, terminates the current chain. Phosphite chain transfer agents are exemplified in the aqueous preparation of low molecular weight acrylic homo- and copolymers (71,72). A similar utilization was patented by Coatex S. A. (73). Other chain transfer agents that have been used include alcohols such as isopropylalcohol (74), aminothiols (74), mercaptoethanol (75), mercaptoethanol (76), hypophosphorous acid (77), and copper salts that are extremely effective (78–82).

Other interesting polymerizations include the use of metal-activated hydrogen peroxide to deliver low molecular weight polymers (83,84), continuous polymerization of water-soluble monomers in extruders (85), dry polymerization of acrylic acid in super critical carbon dioxide (86,87) and on a powder bed (88), and the use of sodium nitrate mediated aqueous polymerization to allow high solids (89).

Transamidation allows the preparation of unique low molecular weight, water-soluble polymers from acrylic acid–acrylamide copolymers. The advantage is that functional amines such as sulfonic acid salts can be incorporated into preformed polymer to create new functional polymers without the need to synthesize new monomers (90–92).

Applications. Water-soluble homopolymers of acrylic and methacrylic acids and their copolymers are widely used in a myriad of applications. Poly(acrylic acid) and copolymers with maleic acid and other monomers are used in large quantities in solid detergents and dishwashing powders (80,93–107). Only minor modifications to composition and/or molecular weight to alter the balance of surface interactions allow use in many different applications. Changing hydrophile/hydrophobe ratio, charge density, introduction of other charged species, etc, all expand the application range. Scale formation in aqueous systems may be prevented by the presence of sulfonate groups (108–110) and allyloxy functionality (111,112). Cement additives used to reduce water requirements are based on acrylic acid copolymers with poly(ethylene oxide) acrylate monomers (113–116). Copolymers with acrylic alkyl esters are used in textile sizing agents (117).

Plant productivity in hydroponic media is reportedly enhanced by the presence of poly(acrylic acid) (118). Dispersing characteristics are imparted by copolymerizing a range of monomers and again they are used widely, for example, in inks (119), for inhibiting barium scale in seawater (120), ceramics (121,122), to disperse acrylic emulsion polymers (123), to disperse dyes (124). Copolymers are also used in oil drilling and recovery (125–129), in corrosion control (130–136), in paper for wet and dry strength (137), boiler water treatment (138–141), specialty cleansers (142–146), eliminating odor from animal excrement (147), reverse osmosis for scale inhibition (148), water clarification (149), soil conditioners (150), and seed coatings (151).

Environmental Issues of Water-Soluble Polymers. Because the water-soluble polymers based on acrylic and methacrylic acids are generally disposed off in the environment, there have been studies to determine their effect on the environment and to monitor their build. Acrylic acid polymers are not biodegradable except at the oligomer molecular weight, that is about 3 to 10 units (152). Elegant monitoring of low concentrations is available by two techniques, immunoassay (153) developed at Rohm and Haas, and fluorescence tagging (154). Tagging is useful both for environmental monitoring and for concentration control in applications.

Alkali-Soluble Polymers. Alkali-soluble polymers are generally emulsion polymers that have insufficient acid content to solubilize in water in the absence of neutralization. In addition to emulsion polymerization, polymerization in partial or complete organic solvents, as suspensions, and inverse emulsions are all reported. However, emulsion polymerization represents the most convenient route to these polymers, with suspension and inverse emulsions being very limited.

Alkali-soluble emulsion polymers were originally developed as thickeners based on copolymers of acrylic acid and methacrylic acid with simple acrylic and methacrylic esters, as exemplified by their preparation in patents to S.C. Johnson (155), BASF (156), and Goodyear (157). However, in the last two decades advanced hydrophobically modified alkali-soluble polymers have emerged as thickeners and rheology modifiers which function by association of their hydrophobic functionalities with themselves or other convenient centers in a formulation containing these polymers. Figure 6 represents this association schematically.

Both types of alkali soluble thickeners generally contain methacrylic acid rather than acrylic acid since this monomer is more readily incorporated into

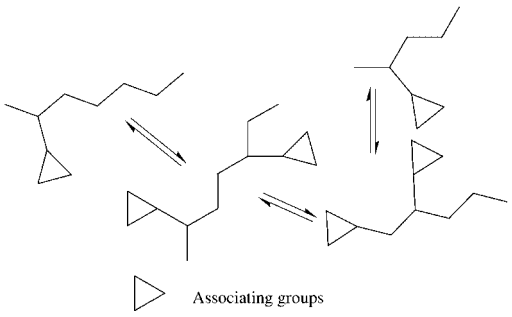

Fig. 6. Association of hydrophobic alkali-soluble polymers.

emulsion polymers, as it is more hydrophobic than acrylic acid and less likely to homopolymerize in the aqueous continuous phase. Patents to Dow (158), DeSoto (159), Union Carbide (160), and Rohm and Haas (161) represent the synthesis of hydrophobically modified alkali-soluble emulsion polymers. The hydrophobe may be attached to the acrylic polymer backbone by an ester or urethane linkage (162). The properties of hydrophobic associative thickeners and conventional thickeners in paint-making formulations have been compared (163). Several papers have appeared on the interactions of similar polymers in paint formulations (164–167) and on general hydrophobic interactions in water (168,169).

There are other less widely used syntheses of associative polymers including acid monomer grafting to poly(ethylene oxide) (170,171), inverse emulsion polymerization (172–174), suspension polymerization (175), micellar polymerization (176,177), and solid-phase extrusion polymerization (178).

Applications. In addition to latex paint applications already mentioned, applications include paper (179), oil spill clean-up (180), flocculants and mineral dewatering (181), emulsion polymerization stabilizers (182), and in mixed associative thickeners in paints (183).

Gel Polymers. Gel polymers based on the acidic monomers are high molecular weight (co)polymers that are cross-linked such that solubilization in water is prevented. The levels of swelling or gel formation are controlled by degree of cross-linking of the polymer. The major outlet for this chemistry is in the development of superabsorbent polymers now ubiquitous in diapers and feminine hygiene products. They have completely revolutionized a way of life for raising infants and caring for incontinent elderly. Hence, it is not surprising that most of the published information is patent literature that relates to manufacturing processes that have been or continue to be used for the preparation of superabsorbents. Some of these processes are referenced herein, but the patent literature is so voluminous that not all are included here.

Synthesis. Gel polymerization of acrylic acid with a polyvinyl cross-linking monomers in water is by far the most prevalent commercial process. Examples of cross-linkers used are triallylamine (184), *N*,*N*′-methylenebisacrylamide (185), tetraallyloxyethane (186,187), trimethylolpropane triacrylate (188), ethylene diamines (189), trimethylol triacrylate and diacrylate in combination (190), ethylene glycol diglycidyl ether (191), trimethylolpropane tris(3-aziridinylpropionate) (192), and poly(ethylene oxides) diacrylate (193). In an extension of cross-linking one process by Sanyo uses inefficient graft polymerization of acrylic acid onto starch as a source of the cross-linking required to introduce control over gel swelling (194).

Applications. Copolymers of acidic monomers and other water-soluble monomers obtained by gel polymerization for special effects, generally in medical applications, include hydroxyethyl methacrylate (195), hydroxypropyl methacrylate and acrylamide (196), and vinyl saccharides (197).

There has been a move from conventional granular gel materials to foamed (198) and flat plate (199) type superabsorbents based on poly(acrylic acid). In addition to superabsorbents for personal hygiene, the materials have wide ranging applications in many areas from biomedical to cosmetics. Some of these are petroleum recovery and sealing of sewer pipes when cross-linked with metals such as iron salts (200); flocculants in water purification (201); copolymers with

acrylamide in textile printing pastes (202); cosmetic gelling agents (203); surgical dressings (204); reversible gels (205); subterranean fault stabilization (206), and controlled release (207).

Block and Graft Polymers

Graft Synthesis. Free-radical-promoted grafting of acrylic and methacrylic acids and other water-soluble comonomers onto synthetic and natural substrates gives unique polymeric structures quite different from the random copolymers obtained in conventional copolymerization. These block and graft polymers bring a unique and different structure/property balance with applications in many areas.

Applications. Poly(ethylene oxides) are readily grafted with acrylic acid to give partially biodegradable detergent polymers (208–210). Grafts onto other substrates include poly(vinyl alcohol) (211), water-soluble maleic anhydride copolymers (212), polycaprolactone (213), and onto emulsion polymers of acrylates and methacrylates (214).

Natural substrates are often starch or cellulose derivatives. Grafts for detergent applications (215,216), thickening dispersions (217), leather tanning (218), water treatment (219), oil recovery (220), water-absorbents (221), and water-absorbents in fibers and sheets (222). More fundamental studies on grafting to polysaccharides have been published (223).

Block Synthesis. Water-soluble block copolymers are formed from the copolymerization of macromonomers of methacrylates with acrylic and methacrylic acid monomers and their solution properties compared with random copolymers of similar composition (224). Diblock and triblock copolymers may be prepared by a number of techniques and are also used on ink-jet inks (225) and scale inhibition in water boilers (226), respectively. Associative properties of block polymers to form micellar structures are well established (227,228). Triblock polyampholyte polymers are also known (229).

Inverse Emulsion Polymerization

Inverse emulsion polymerization is a term used for water in oil (monomer) dispersion polymerization as opposed to conventional emulsion polymerization where the monomer and polymer are largely insoluble and dispersed in water. The advantage is that high molecular weight polymers and copolymers of water-soluble monomers may be prepared without the attendant viscosity build mentioned earlier. The process chemistry is well established as indicated in the patent literature (230–233) but not widely used and likely to be less so as solvents are removed from processing. Spray drying is often used for polymer isolation (234).

BIBLIOGRAPHY

"Acrylic Acid Polymers" in *EPST* 1st ed., Vol. 1, pp. 197–226, by M. L. Miller, American Cyanamid Co.; "Acrylic and Methacrylic Acid Polymers" in *EPSE* 2nd ed., Vol. 1, pp. 211–234, by J. W. Nemec and W. Bauer Jr., Rohm and Haas Co.

1. J. Redtenbacher, *Annalen* **47**, 125 (1843).
2. J. W. Nemec and W. Bauer Jr., in M. Grayson, ed., *Kirk-Othmer Encyclopedia of Chemical Technology*, 3rd ed., Vol. **1**, Wiley-Interscience, New York, 1978, pp. 330–354.
3. E. Frankland and B. F. Duppa, *Ann.* **136**, 1 (1865).
4. J. W. Nemec and L. Kirch, in M. Grayson, ed., *Kirk-Othmer Encyclopedia of Chemical Technology*, 3rd ed., Vol. **15**, Wiley-Interscience, New York, 1981, pp. 346–376.
5. E. H. Riddle, *Monomeric Acrylic Esters*, Reinhold Publishing Corp., New York, 1954.
6. M. Salkind, E. H. Riddle, and R. W. Keefer, *Ind. Eng. Chem.* **51**, 1232 (1959).
7. L. S. Luskin, in E. C. Leonard, ed., *High Polymers, Vinyl and Diene Monomers*, Pt. 1, Vol. **24**, Wiley-Interscience, New York, 1970, pp. 105–203.
8. L. S. Luskin, in F. D. Snell and C. L. Hilton, eds., *Encyclopedia of Industrial Chemical Analysis*, Vol. **4**, John Wiley & Sons, Inc., New York, 1967, p. 181.
9. V. A. Kabanov and co-workers, *Eur. Polym. J.* **11**, 153 (1975).
10. G. Blauer, *Trans. Faraday Soc.* **56**, 606 (1960).
11. H. Ito, S. Shimizu, and S. Suzuki, *Kogyo Kagaku Zasshi* **58**, 194, 278 (1958).
12. S. Suzuki, H. Ito, and S. Shimizu, *Kogyo Kagaku Zasshi* **57**, 658 (1954).
13. Y. Kikuchi and K. Yamaoka, *J. Sci. Hiroshima Univ. Ser. A* **21**, 143 (1957).
14. J. Brandrup and E. H. Immergut, *Polymer Handbook*, 4th ed., John Wiley & Sons., Inc., New York, 1999.
15. L. J. Young, *J. Polym. Sci.* **54**, 411 (1961).
16. U.S. Pats. 5352726 (Oct. 4, 1994) and 5912297 (June 15, 1999), W. Hall (both to Henkel Corp.).
17. Eur. Pat. Appl. EP 942098 (Sept. 15, 1999) (to National Starch).
18. U.S. Pat. 5912293 (June 15, 1999) (to Allied Colloids).
19. World Pat. WO 9936192 (July 22, 1999) (to Henkel Corp.).
20. World Pat. WO 9923183 (May 14, 1999) (to Hewlett-Packard Co.).
21. U.S. Pat. 5902853 (May 11, 1999), A. Rudin (to Xerox Corp.).
22. Eur. Pat. Appl. EP 902073 (Mar. 17, 1999) (to Nippon Mektron).
23. Ger. Offen. DE 19757669 (Jan. 7, 1999) (to BASF AG).
24. World Pat. WO 9849205 (Nov. 5, 1998) (to Waker-Chemie GmbH).
25. Ger. Offen. DE 19653524 (June 25, 1998) (to BASF AG).
26. U.S. Pat. 5795932 (Aug. 18, 1998) (to Sequa Chemicals, Inc.).
27. Euro. Pat. Appl. EP 814140 (Feb. 29, 1997) (to Hercules, Inc.).
28. Ger. Offen. DE 19627204 (Jan. 8, 1998) (to BASF AG).
29. Pol. Pat. PL 165052 (Nov. 30, 1994) (to Instytut Mechaniki Precyzyjnej).
30. World Pat. WO 9709031 (Mar. 13, 1997) (to Procter & Gamble Co.).
31. World Pat. WO 9715616 (May 1, 1997) (to Rhone-Poulenc Chimie).
32. Eur. Pat. Appl. EP 727451 (Aug. 21, 1996) (to Rohm and Haas Co.).
33. Eur. Pat. Appl. EP 213895 (Mar. 11, 1987) (to Hercules Inc.).
34. Eur. Pat. Appl. EP 697423 (Feb. 21, 1996) (to Allied Colloids Ltd.).
35. Ger. Offen. DE 4419216 (Aug. 31, 1995) (to Bollig and Kemper KG).
36. Eur. Pat. Appl. EP 601518 (June 15, 1994) (to Air Products and Chemicals).
37. World Pat. WO 9402112 (Feb. 3, 1994) (to National Starch and Chemical Investments Holding Corp.).
38. Eur. Pat. Appl. EP 522791 (Jan. 13, 1993) (to Rohm and Haas Co.).
39. U.S. Pat. 4916171 (Apr. 10, 1990) (to Rohm and Haas Co.).
40. Eur. Pat. Appl. EP 348565 (Jan. 3, 1990) (to Rohm and Haas Co.).
41. U.S. Pat. 4876313 (Jan. 24, 1989) (to Rohm and Haas Co.).
42. Eur. Pat. Appl. EP 338486 (Jan. 25, 1989) (to S. C. Johnson and Sons, Inc.).
43. Brit. Pat. BR 8705620 (Aug. 16, 1988) (to BASF Corp.).
44. Eur. Pat. Appl. EP 258753 (Mar. 9, 1988) (to S. C. Johnson and Sons, Inc.).
45. U.S. Pat. 4477623 (Jan. 16, 1984) (to Synres International).

46. D. C. Blackley, *Emulsion Polymerization*, Applied Science Publishers, Barking, 1975; R. G. Gilbert, *Emulsion Polymerization: A Mechanistic Approach*, Academic Press, Inc., New York, 1995.
47. CN 1176986 (Mar. 25, 1998) (to Changsha Electric Powder College, PRC).
48. D. Y. Lee and J. H. Kim, *J. Polym. Sci., Part A: Polym. Chem.* **36**, 2865–2872 (1998).
49. Eur. Pat. Appl. EP 245021 (Nov. 11, 1987) (to The Dow Chemical Co.).
50. Ger. Offen. DE 3522419 (Jan. 2, 1987) (to Chemische Fabrik Stockhausen GmbH).
51. Eur. Pat. Appl. EP 555959 (Aug. 18, 1993) (to Rohm and Haas Co.).
52. World Pat. WO 9511265 (Apr. 27, 1995) (to Lucky Ltd.).
53. Ger. Offen DE 4345086 (July 21, 1994) (to Toyo Boseki KK).
54. Eur. Pat. Appl. EP 565825 (Feb. 1, 1993) (to Huels).
55. U.S. Pat. 4994537 (Feb. 19, 1991) (to Hercules, Inc.).
56. World Pat. WO 9008786 (Aug. 9, 1990) (to Akzo NV).
57. Eur. Pat. Appl. EP 252526 (Jan. 13, 1988) (to Hercules, Inc.).
58. World Pat. WO 9614357 (May 17, 1996) (to Hercules, Inc.).
59. Eur. Pat. Appl. EP 767180 (Apr. 9, 1997) (to Elf Atochem Italia SRL).
60. L. S. Park and co-workers, *Pollimo* **14**, 583–589 (1990).
61. D.-Y. Lee and J.-H. Kim, *Polym. Prepr. (Am. Chem. Soc., Div. Polym. Chem.)* **38**, 418–419 (1997).
62. D. Steinkopff, *Prog. Colloid Polym. Sci.*, Vol. 110 (Trends in Colloid and Interface Science XII), 1998, pp. 99–104.
63. D. Charmont, J. F. D'Allest, and F. Dobler, *DECHEMA Monograph 131 (5th International Workshop on Polymer Reaction Engineering)*, 1995, pp. 113–121.
64. D. Charmont, J. F. D'Allest, and F. Dobler, *Polymer* **37**, 5237–5245 (1996).
65. D. E. Mestach and W. H. Baan, *DECHEMA Monograph 131 (5th International Workshop on Polymer Engineering)*, 1995, pp. 35–44.
66. P. Hernandez and co-workers, *Annu. Tech. Conf. Soc. Plast. Eng.* **52**, 1672–1674 (1994).
67. D.-Y. Lee and co-workers, *Langmuir* **15**, 8252–8258 (1999).
68. I. C. Hodges, J. Hearn, and M. C. Wilkinson, *Polym. Mater. Sci. Eng.* **81**, 185–186 (1999).
69. Y.-J. Park and co-workers, *Colloid Polym. Sci.* **276**, 709–714 (1998).
70. H. Kast, *Makromol. Chem.* **10/11**, 447–461 (1985).
71. U.S. Pat. 5866664 (Feb. 2, 1999), B. Weinstein (to Rohm and Haas Co.).
72. Eur. Pat. Appl. EP 405818 (Jan. 2, 1991), G. Swift and K. Hughes (to Rohm and Haas Co.).
73. Fr. Pat. FR 2751335 (Jan. 23, 1998) (to Coatex A. S.).
74. Ger. Offen. DE 3346350 (June 13, 1985) (to Benckiser-Knapsack GmbH).
75. U.S. Pat. 6932671 (Aug. 3, 1999) (to Phillips Petroleum Co.).
76. Ger. Offen. DE 3620149 (Dec. 17, 1987) (to Roehm GmbH).
77. U.S. Pat. 5298585 (Mar. 29, 1994), B. Weinstein and co-workers (to Rohm and Haas Co.).
78. Eur. Pat. Appl. EP 429307 (May 29, 1991) (to Rohm and Haas Co.).
79. Eur. Pat. Appl. EP 441022 (Aug. 14, 1991) (to Rohm and Haas Co.).
80. Eur. Pat. Appl. EP 430574 (June 5, 1991) (to Rohm and Haas Co.).
81. Eur. Pat. Appl. EP 534695 (Mar. 31, 1993) (to Rohm and Haas Co.).
82. Pol. Pat. PL 164268 (July 29, 1994), S. Kudla (to Inst. Ciezkiej Syntezy Organicznej).
83. Uzbekistan 1641831 (Apr. 15, 1991) (to Institute of Chemistry, Acad. Sci.).
84. Eur. Pat. Appl. EP 398724 (Nov. 22, 1990) (to Rohm and Haas Co.).
85. Ger. Offen. DE 3621429 (Jan. 8, 1987) (to Milchem, Inc.).
86. CA 1274942 (Oct. 2, 1990) (to BASF).
87. H. Hu and co-workers, *Gaofenzi Xuebao* **6**, 740–743 (1998).
88. Ger. Offen. DE 3519013 (Nov. 27, 1986) (to BASF AG).

89. D. Fong, *J. Macromol. Sci., A: Pure Appl. Chem.* **35**, 401–409 (1998).
90. BE 905996 (June 19, 1987) (to Nalco Chemical Co.).
91. AT 395592 (Jan. 25, 1993) (to Nalco Chemical Co.).
92. U.S. Pat. 4604431 (Aug. 5, 1986) (to Nalco Chemical Co.).
93. U.S. Pat. 5360570 (Nov. 1, 1994) (to Rohm and Haas Co.).
94. U.S. Pat. 5100980 (Mar. 31, 1995) (to Rohm and Haas Co.).
95. U.S. Pat. 5223590 (June 29, 1993) (to Rohm and Haas Co.).
96. U.S. Pat. 5430114 (July 4, 1995) (to Rohm and Haas Co.).
97. Ger. Offen. DE 3812402 (Jan. 26, 1989) (to BASF AG).
98. World Pat. WO 9635728 (Nov. 14, 1996) (to Stockhausen).
99. World Pat. WO 9401477 (Jan. 20, 1944) (to Stockhausen).
100. Ger. Offen. DE 3818426 (Dec. 9, 1989) (to BASF AG).
101. U.S. Pat. 5482647 (Jan. 9, 1996) (to Church and Dwight Co.).
102. World Pat. WO 9742282 (Nov. 13, 1997) (to The Procter & Gamble Co.).
103. World Pat. WO 9813452 (Apr. 2, 1998) (to The Procter & Gamble Co.).
104. Eur. Pat. Appl. EP 877076 (Nov. 11, 1998) (to Rohm and Haas Co.).
105. Eur. Pat. Appl. EP 893491 (Jan. 27, 1990) (to Unilever PLC).
106. World Pat. WO 9958633 (Nov. 18, 1999) (to Unilever PLC).
107. GB 2322137 (Aug. 19, 1998) (to Unilever PLC).
108. U.S. Pat. 5516432 (May 14, 1996) (to Rohm and Haas Co.).
109. World Pat. WO 9710180 (Mar. 20, 1997) (to Ashland, Inc.).
110. U.S. Pat. 5866013 (Feb. 2, 1999) (to BetzDearborn, Inc.).
111. Eur. Pats. Appl. EP 774506 and EP 774507 (May 21, 1997) (both to Rohm and Haas Co.).
112. Ger. Offen. DE 4328817 (Mar. 2, 1995) (to BASF AG).
113. Eur. Pat. Appl. EP 924174 (June 23, 1999) (to Takemoto Yushi KK).
114. World Pat. WO 9947468 (Sept. 23, 1999) (to Lafarge SA).
115. Eur. Pat. Appl. EP 940374 (Sept. 8, 1999) (to Takemoto Yushi KK).
116. Ger. Offen. DE 19830760 (Jan. 13, 2000) (to SKW Trostberg AG).
117. Rom. Pat. 100582 (Oct. 28, 1991) (to Intreprinderea Chimica Risnov).
118. U.S. Pat. 5854177 (Dec. 29, 1998) (to Donlar Corp.).
119. Eur. Pats. Appl. EP 812888 (Dec. 17, 1997) and EP 908496 (Apr. 14, 1999) (both to Seiko Epson Corp.).
120. AU 613925 (Aug. 15, 1991) (to Ciba-Geigy AG).
121. U.S. Pats. 5726267 (Mar. 10, 1998) and 5880237 (Mar. 9, 1999) (both to Nalco Corp.).
122. Eur. Pat. Appl. EP 737656 (Oct. 16, 1996) (to Rohm and Haas Co.).
123. World Pat. WO 9718271 (May 22, 1997) (to Allied Colloids Ltd.).
124. Eur. Pat. Appl. EP 796876 (Sept. 24, 1997) (to National Starch and Chemical Investments Holding Corp.).
125. Eur. Appl. EP 649864 (Apr. 26, 1995) (to Wolff Walsrode AG).
126. CN 1152587 (June 25, 1997) (to Sichuan University).
127. Ger. Pat. DE 3418397 (Dec. 6, 1984) (to Sanyo Chemicals Industries Ltd.).
128. Eur. Pat. Appl. EP 483638 (May 6, 1992) (to Hoechst AG).
129. U.S. Pat. 4728445 (Mar. 1, 1988) (to Pony Industries, Inc.).
130. CA 1176049 (Oct. 16, 1984) (to Katayama Chemical Works).
131. U.S. Pat. 4756881 (July 12, 1988) (to Nalco Chemical Co.).
132. AU 595599 (Apr. 5, 1990) (to Betz International, Inc.).
133. Eur. Pat. Appl. EP 526786 (Feb. 10, 1993) (to Nalco Chemical Co.).
134. U.S. Pat. 5308498 (May 3, 1994) (to Nalco Chemical Co.).
135. Eur. Pat. Appl. EP 674022 (Sept. 27, 1995) (to Betz Europe, Inc.).
136. GB 2299331 (Oct. 2, 1996) (to Nalco Chemical Co.).
137. Eur. Appl. EP 713890 (May 29, 1996) (to Hercules, Inc.).

138. U.S. Pat. 4828713 (May 9, 1989) (to Betz Laboratories, Inc.).
139. U.S. Pat. 5271847 (Dec. 21, 1993) (to Betz Laboratories, Inc.).
140. U.S. Pat. 5078891 (Jan. 7, 1992) (to Betz Laboratories, Inc.).
141. Eur. Pat. Appl. EP 459661 (Dec. 4, 1991) (to Rohm and Haas Co.).
142. U.S. Pat. 5783200 (July 21, 1998) (to The Procter & Gamble Co.).
143. CA 1204361 (May 13, 1986) (to Bristol Myers Co.).
144. World Pat. WO 9426858 (Nov. 24, 1994) (to Unilever PLC).
145. U.S. Pat. 4869934 (Sept. 26, 1989) (to Sterling Drug, Inc.).
146. U.S. Pat. 4861511 (Aug. 29, 1989) (to Nalco Chemical Co.).
147. World Pat. WO 9830251 (July 16, 1998) (to Damar Holdings SA).
148. U.S. Pat. 5256303 (Jan. 26, 1993) (to Nalco Chemical Co.).
149. U.S. Pat. 5643462 (July 1, 1997) (to BetzDearborn, Inc.).
150. Eur. Pat. Appl. EP 415141 (Mar. 6, 1991) (to Chemie Linz GmbH).
151. Ger. Offen. DE 3713348 (Nov. 10, 1988) (to BASF AG).
152. R. J. Larson and co-workers, *J. Environ. Polym. Degrad.* **5**(1), 41–48 (1997).
153. Eur. Pat. Appl. EP 785431 (July 23, 1997) (to Rohm and Haas Co.).
154. World Pat. WO 9735192 (Sept. 25, 1997) (to Nalco Chemical Co.).
155. U.S. Pats. 4628071 (Dec. 9, 1986), 5073591 (Dec. 17, 1991), and 5093396 (Mar. 3, 1992) (all to S. C. Johnson and Sons, Inc.).
156. Ger. Offen. DE 19617633 (Nov. 6, 1997) (to BASF AG).
157. Eur. Pat. Appl. EP 317662 (May 31, 1989) (to Goodyear Tire and Rubber).
158. U.S. Pat. 4728696 (Mar. 1, 1988) (to The Dow Chemical Company).
159. U.S. Pat. 4514552 (Apr. 30, 1985) (to DeSoto, Inc.).
160. U.S. Pat. 5292828 (Mar. 8, 1994) and World Pat. WO 9965958 (Dec. 23, 1999) (both to Union Carbide Chemicals and Plastics Technology Corp.).
161. Eur. Pat. Appl. EP 896027 (Feb. 10, 1999) (to Rohm and Haas Co.).
162. G. D. Shay and A. F. Rich, *J. Coat. Technol.* **58**(732), 42–53, 1986.
163. B. J. Van Rooden and T. M. S. Annen, *Wochenbl. Papierfabr.* **124**, 854–861, (1996).
164. J. S. Berg, D. J. Lundberg, and E. J. Glass, *Prog. Org. Coat.* **17**(2), 155–173 (1989).
165. A. Karunasena, S. K. Jongewaard, and E. J. Glass, *Polym. Mater. Sci. Eng.* **57**, 632–636 (1987).
166. A. Karunesa and E. J. Glass, *Polym. Mater. Sci. Eng.* **56**, 624–628 (1987).
167. S. K. Jongewaard, R. H. Fernando, and E. J. Glass, *Polym. Mater. Sci. Eng.* **54**, 166–169 (1986).
168. C. W. Frank, D. J. Hemker, and H. T. Oyama, ACS Symposium Series, Vol. **467**: *Water-Soluble Polymers*, American Chemical Society, New York, 1991, pp. 303–319.
169. K. C. Tam and co-workers, *J. Polym. Sci., Part B: Polym. Phys.* **36**, 2275–2290 (1998).
170. D. Hourdet, F. L'Alloret, and R. Audebert, *Polymer* **38**, 2535–2547 (1997).
171. F. L'Alloret, D. Hourdet, and R. Audebert, *Colloid Polym. Sci.* **273**, 1163–1173 (1995).
172. U.S. Pat. 4656222 (Apr. 7, 1987) (to Celanese Corp.).
173. World Pat. WO 9736941 (Oct. 9, 1997) (to Cytec Technology Corp.).
174. World Pat. WO 9929745 (June 17, 1999) (to Cytec Technology Corp.).
175. Eur. Pat. Appl. EP 566930 (Jan. 27, 1993) (to BASF AG).
176. K. D. Branham and co-workders, *Macromolecules* **25**, 1201–1206 (1992); *Macromolecules* **27**, 5123–5128 (1994); *Macromolecules* **29**, 254–262 (1996).
177. World Pat. WO 9903895 (Jan. 28, 1999) (to Rhodia Chimie).
178. Eur. Pat. Appl. EP 143935 (June 12, 1985) (to Belland AG).
179. CA 2084851 (June 10, 1993) (to Hercules, Inc.).
180. U.S. Pat. 4734205 (Mar. 29, 1988) (to Exxon Research and Engineering Co.).
181. CA 1236939 (May 17, 1988) (to Nalco Chemical Co.).
182. D. Y. Lee, J. H. Kim, and T. I. Min, *Colloid Surf.* **153**(1–3), 89–97 (1999).
183. U.S. Pat. 4735981 (Apr. 5, 1988) (to DeSoto, Inc.).

184. Eur. Pat. Appl. EP 644207 (Mar. 22, 1995) (to Nalco Chemical Co.).
185. Eur. Pat. Appl. EP 522570 (Jan. 13, 1993) (to Mitsubishi Petrochemical Co., Ltd.).
186. Eur. Pat. Appl. EP 530438 (Mar. 10, 1993) (to Hoechst Celanese Corp.).
187. Ger. Offen. DE 4127814 (Mar. 12, 1992) and DE 4123889 (Mar. 12, 1992) (both to Sanyo Chemical Industries.).
188. Eur. Pat. Appl. EP 409136 (Jan. 23, 1991), World Pat. WO 9008789 (Aug. 9, 1990), and Eur. Pat. Appl. EP 312952 (Apr. 26, 1989) (all to The Dow Chemical Company).
189. U.S. Pat. 4921904 (May 1, 1990) (to Nalco Chemical Co.).
190. Eur. Pat. Appl. EP 632068 (Jan. 4, 1995) (to Nippon Shokubai Co., Ltd.).
191. U.S. Pat. 4698404 (Oct. 6, 1987) (to Nalco Chemical Co.).
192. U.S. Pat. 4645789 (Feb. 24, 1987) (to Personal Products Co.).
193. Eur. Pats. Appl. EP 827753 (Mar. 11, 1998) and EP 811636 (Dec. 10, 1997) (both to Nippon Shokubai Co., Ltd.).
194. Ger. Offen. DE 19628863 (Jan. 23, 1997), DE 19637190 (Mar. 20, 1997), and GB 2313124 (Nov. 19, 1997) (all to Sanyo Chemical Industries).
195. U.S. Pat. 5731387 (Mar. 24, 1998) (to Adhesives Research, Inc.).
196. U.S. Pat. 5726250 (Mar. 10, 1998) (to Adhesives Research, Inc.).
197. Eur. Pat. Appl. EP 283090 (Sept. 21, 1988) (to Shell International Research).
198. U.S. Pats. 5338766 (Aug. 16, 1994) and 5328935 (July 12, 1994) (both to The Procter & Gamble Co.).
199. Eur. Pat. Appl. EP 955086 (Nov. 10, 1999) (to Nippon Shokubai Co., Ltd.).
200. Eur. Pat. Appl. EP 476263 (Mar. 25, 1992) (to American Cyanamid Co.).
201. ZA 9104649 (Jan. 28, 1992) (to Chemical Services Ltd.).
202. Ger. Offen. DE 4435425 (Apr. 11, 1996) (to BASF AG).
203. World Pat. WO 9717055 (May 15, 1997) (to L'Oreal).
204. U.S. Pat. 4671267 (June 9, 1987) (to E. I. Stout).
205. Eur. Pat. Appl. EP 335653 (Oct. 4, 1989) (to Altalanos Iparfejlesztesi).
206. U.S. Pat. 6011075 (Jan. 4, 2000) (to Schlumberger Technology Corp.).
207. Eur. Pat. Appl. EP EP 970707 (Jan. 12, 2000) S. Morikane and D. Morikane (to Daiya Pharmaceutical Co., Ltd.).
208. Eur. Pat. Appl. EP 429307 (May 29, 1991) (to Rohm and Haas Co.).
209. Eur. Pat. Appl. 639592 (Feb. 22, 1995) (to Nippon Shokubai Co., Ltd.).
210. World Pat. WO 2000002938 (Jan. 20, 2000) (to Rhodia Chimie).
211. Ger. Offen. DE 4343993 (June 29, 1995) (to Stockhausen).
212. Eur. Pat. Appl. EP 725093 (Aug. 7, 1996) (to BASF Corp.).
213. Eur. Pat. Appl. EP 321913 (June 28, 1989) (to S. C. Johnson and Sons, Inc.).
214. World Pat. WO 9619512 (June 27, 1996) (to Zeneca).
215. Eur. Pat. Appl. EP 465287 (Jan. 8, 1992) (to Rhone-Poulenc Chimie).
216. Eur. Appl. EP 725131 (Aug. 7, 1996) (to BASF Corp.).
217. World Pat. WO 9321244 (Jan. 28, 1993) (to Raision Tehtaat Oy AB).
218. Ger. Offen. DE 4201452 (July 22, 1993) (to BASF AG).
219. Ger. Offen. DE 4038908 (June 11, 1992) (to BASF AG).
220. Eur. Pat. Appl. EP 356241 (Feb. 28, 1990) (to Allied Colloids Ltd.).
221. DE 3613309 (Jan. 22, 1987) (to Huels AG).
222. M. Yoshinobu, M. Morita, and I. Sakata, *Sen'i Gakkaishi* **47**(2), 102–108 (1991).
223. L. Zhang and A. F. Johnson, *China J. Polym. Sci.* **11**(2), 144–152 (1993).
224. Y. Tsukahara and co-workders, *J. Polym. Sci., Part A: Polym. Chem.* **27**, 1099–1114 (1989).
225. Eur. Pat. Appl. EP 851012 (July 1, 1998) (to E. I. du Pont de Nemours & Co., Inc.).
226. R. Xiong, G. Wei, and Y. Zhang, *Gongye Shuichuli* **18**(6), 11–13 (1998).
227. Ger. Offen. DE 19634328 (Apr. 1, 1997) (to Elf Atochem).
228. L. Zhang, R. Barlow, and A. Eisenberg, *Macromolecules* **28**, 6055–6066 (1995).

229. C. S. Patrickios and co-workders, *Langmuir* **15**, 1613–1620 (1999).
230. CN 1152053 (June 18, 1997), S. Yu and X. Li.
231. U.S. Pat. 4753981 (June 28, 1988) (to Phillips Petroleum Co.).
232. U.S. Pat. 4745154 (May 17, 1988) (to Alco Chemical Corp.).
233. Eur. Pat. Appl. EP 153506 (Sept. 4, 1985) and U.S. Pat. 4524175 (June 18, 1985) (both to The Dow Chemical Company).
234. U.S. Pats. 6011089 (Jan. 4, 2000), 5869542 (Feb. 9, 1999), and 5849862 (Dec. 15, 1998) (all to Cytec).

GRAHAM SWIFT
GS Polymer Consultants

ACRYLIC ELASTOMERS, ETHYLENE-ACRYLIC.

See ETHYLENE-ACRYLIC ELASTOMERS.

ACRYLIC ESTER POLYMERS

Introduction

The usage of acrylic esters as building blocks for polymers of industrial importance began in earnest with the experimentation of Otto Rohm (1). The first recorded preparation of the basic building block for acrylic ester polymers, acrylic acid, took place in 1843; this synthesis relied on the air oxidation of acrolein (2,3). The first acrylic acid derivatives to be made were methyl acrylate and ethyl acrylate. Although these two monomers were synthesized in 1873, their utility in the polymer area was not discovered until 1880 when Kahlbaum polymerized methyl acrylate and tested its thermal stability. To his surprise, the polymerized methyl acrylate did not depolymerize at temperatures up to 320°C (4). Despite this finding of incredibly high thermal stability, the industrial production of acrylic ester polymers did not take place for almost another 50 years.

The commercial discovery of acrylic ester polymers took place while Otto Rohm was conducting his doctoral research in 1901. Rohm obtained a U.S. patent in 1912 covering the vulcanization of acrylates with sulfur (5). Commercial production of acrylic ester polymers by the Rohm and Haas Co. of Darmstadt, Germany, commenced in 1927 (6).

Properties

The structure of the acrylic ester monomers is represented by the following:

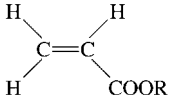

Encyclopedia of Polymer Science and Technology. Copyright John Wiley & Sons, Inc. All rights reserved.

The R ester group dominates the properties of the polymers formed. This R side-chain group conveys such a wide range of properties that acrylic ester polymers are used in applications varying from paints to adhesives and concrete modifiers and thickeners. The glass-transition range for a polymer describes the temperature range below which segmental pinning takes place and the polymer takes on a stiff, rigid, inflexible nature. This range can vary widely among the acrylic ester polymers from -54°C for butyl acrylate (R = C_4H_9) to 103°C for acrylic acid (R = H). Film properties are dramatically influenced by this changing of the polymer flexibility.

When copolymerized, the acrylic ester monomers typically randomly incorporate themselves into the polymer chains according to the percentage concentration of each monomer in the reactor initial charge. Alternatively, acrylic ester monomers can be copolymerized with styrene, methacrylic ester monomers, acrylonitrile, and vinyl acetate to produce commercially significant polymers.

Acrylic ester monomers are typically synthesized from the combination of acrylic acid and an alcohol. The properties of the polymers they form are dominated by the nature of the ester side chain as well as the molecular weight of the product. Acrylic ester polymers are similar to others in that they show an improvement in properties as a function of molecular weight until a certain threshold beyond which no further improvement is observed. This threshold is reached at a molecular weight value of 100,000–200,000 for acrylic polymers.

Glass-Transition Temperature. The Glass Transition temperature (T_g) (qv) describes the approximate temperature below which segmental rigidity (ie, loss of rotational and translational motion) sets in. Although a single value is often cited, in reality a polymer film undergoes the transition over a range of temperatures. The reason for this range of temperatures for the glass transition is that segmental mobility is a function of both the experimental method used [dynamic mechanical analysis (dma) vs differential scanning calorimetry (dsc)] as well as the experimental conditions. Factors such as hydroplasticization in varying degrees of humidity can skew T_g results. Most polymers experience an increase in the specific volume, coefficient of expansion, compressibility, specific heat, and refractive index. The T_g is typically measured as the midpoint of the range over which the discontinuity of these properties takes place. Care should be taken when analyzing T_g data, however, as some experimenters cite the onset of the discontinuity as the T_g value.

The rigidity upon cooling below T_g is manifested as an embrittlement of the polymer to the point where films are glass-like and incapable of handling significant mechanical stress without cracking. If, on the other hand, one raises the temperature to which a film is exposed above the glass-transition range, the polymer film becomes stretchable, soft, and elastic. For amorphous acrylic polymers, many physical properties show dramatic changes after passing through the glass-transition temperature range. Among these physical properties are diffusion, chemical reactivity, mechanical and dielectric relaxation, viscous flow, load-bearing capacity, hardness, tack, heat capacity, refractive index, thermal expansivity, creep, and crystallization.

The most common thermal analyses used to determine the glass-transition temperature are dma and dsc. More information on these techniques and how to interpret the results are contained in References 7–9. The T_g values for the most common homopolymers of acrylic esters are listed in Table 1.

Table 1. Physical Properties of Acrylic Polymers

Polymer	Monomer molecular formula	CAS registry number	T_g, °C[a]	Density, g/cm^3 [b]	Refractive index, n_D
Methyl acrylate	$C_4H_6O_2$	[9003-21-8]	6	1.22	1.479
Ethyl acrylate	$C_5H_8O_2$	[9003-32-1]	−24	1.12	1.464
Propyl acrylate	$C_6H_{10}O_2$	[24979-82-6]	−45		
Isopropyl acrylate	$C_6H_{10}O_2$	[26124-32-3]	−3	1.08	
n-Butyl acrylate	$C_7H_{12}O_2$	[9003-49-0]	−50	1.08	1.474
sec-Butyl acrylate	$C_7H_{12}O_2$	[30347-35-4]	−20		
Isobutyl acrylate	$C_7H_{12}O_2$	[26335-74-0]	−43		
tert-Butyl acrylate	$C_7H_{12}O_2$	[25232-27-3]	43		
Hexyl acrylate	$C_9H_{16}O_2$	[27103-47-5]	−57		
Heptyl acrylate	$C_{10}H_{18}O_2$	[29500-72-9]	−60		
2-Heptyl acrylate	$C_{10}H_{18}O_2$	[61634-83-1]	−38		
2-Ethylhexyl acrylate	$C_{11}H_{20}O_2$	[9003-77-4]	−65		
2-Ethylbutyl acrylate	$C_9H_{16}O_2$	[39979-32-3]	−50		
Dodecyl acrylate	$C_{15}H_{28}O_2$	[26246-92-4]	−30		
Hexadecyl acrylate	$C_{19}H_{36}O_2$	[25986-78-1]	35		
2-Ethoxyethyl acrylate	$C_7H_{12}O_3$	[26677-77-0]	−50		
Isobornyl acrylate	$C_{13}H_{20}O_2$	[30323-87-6]	94		
Cyclohexyl acrylate	$C_9H_{14}O_2$	[27458-65-7]	16		

[a]Refs. 7 and 10.
[b]Ref. 11.

The most common way of tailoring acrylic ester polymer properties is to copolymerize two or more monomers. In this fashion, the balance of hard (high T_g) and soft (low T_g) monomers used to make up the overall composition will determine the overall hardness and softness of the polymer film. An estimate of the T_g, and therefore the film hardness, can be calculated using the Fox equation (eq. (1)) (12):

$$1/T_g = \Sigma W(i)/T_g(i) \quad (1)$$

The factor W in this equation refers to the weight, or percent composition, of a given monomer with a given T_g value for the homopolymer.

As can be seen in Table 1, the most common acrylic ester polymers have low T_g values and, therefore, soften films in which they are copolymerized with other vinylic monomers. This effect results in an internal plasticization of the polymer. That is, the plasticization effect from acrylic esters, unlike plasticizer additives which are not covalently bound, will not be removed via volatilization or extraction.

Nondestructive techniques such as torsional modulus analysis can provide a great deal of information on the mechanical properties of viscoelastic materials (8,13–25). For this type of analysis, a higher modulus value is measured for those polymers which are stiffer, harder, or have a higher degree of cross-linking. The regions of elastic behavior are shown in Figure 1 with curve A representing a soft polymer and curve B a harder polymer. A copolymer with a composition between these two homopolymers would fall between the two depicted curves, with the

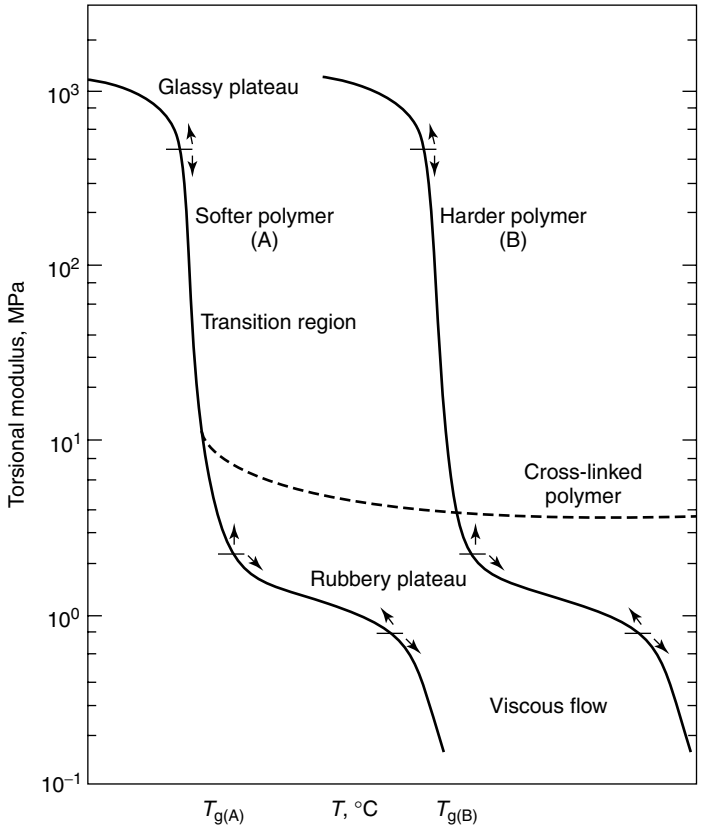

Fig. 1. Modulus–temperature curve of amorphous and cross-linked acrylic polymers. To convert MPa to kg/cm^2, multiply by 10.

relative distance from each curve determined by the similarity of the copolymer composition to one homopolymer or the other (26–28).

Acrylic ester polymers are susceptible to the covalent bonding of two or more polymer chains to form a cross-link (11,29–38). The above-described thermal analysis techniques are capable of distinguishing not only T_g but also varying degrees of cross-linking between polymers. A higher degree of cross-linking results in an elevation and extension of the rubbery plateau region. After a certain level of cross-linking is obtained, the segmental mobility of the polymer chains is impeded (23,25,28). This loss of mobility is measured as an increase in the T_g of the polymer. Further details on cross-linking within and between polymer chains can be found in References 11 and 29–38.

Molecular Weight. The properties of acrylic ester polymers (and most other types of polymers for that matter) improve as molecular weight increases. Beyond a certain level (100,000–200,000 for acrylic ester polymers) this improvement in polymer properties reaches a plateau. The glass-transition temperature can be described by the equation:

$$T_g = T_{gi} - k/M_n$$

Table 2. Mechanical Properties of Acrylic Polymers

Polyacrylate	Elongation, %	Tensile strength, kPa[a]
Methyl	750	6895
Ethyl	1800	228
Butyl	2000	21

[a]To convert kPa to psi, multiply by 0.145.

where T_{gi} is the glass-transition temperature for a polymer of infinite molecular weight and M_n is the number average molecular weight. Typical values of k fall in the range of 2×10^5 (39). Reference 40 summarizes the effect of molecular weight on polymer properties.

Mechanical and Thermal Properties. The mechanical and thermal properties of a polymer are strongly dependent on the nature of the ester side-chain groups of its composite monomers. With H as a side chain, poly(acrylic acid) is a brittle material at room temperature, which is capable of absorbing large quantities of water. The first member of the acrylic ester family, poly(methyl acrylate), is a tough, rubbery, tack-free material at room temperature. The next higher chain length material, poly(ethyl acrylate), is softer, more rubbery, and more extensible. Poly(butyl acrylate) has considerable tack at room temperature and is capable of serving as an adhesive material. Information on these homopolymers is summarized in Table 2 (41). Softness of these polymers increases with increasing chain length until one reaches poly(*n*-nonyl acrylate). Beginning with this chain length, the side chains start to crystallize, which leads to a stiffening of the polymer. This stiffening translates into an embrittlement of the polymer (42); poly(*n*-hexadecyl acrylate), for example, is a hard, waxy material at room temperature.

Acrylic ester polymers are quite resilient to extreme conditions. This resilience gives finished products the durability that has earned acrylic polymers their reputation for value over time. In contrast to polymers of methacrylic esters, acrylic esters are stable when heated to high temperatures. Poly(methyl acrylate) can withstand exposure to 292–399°C in vacuo without generating significant quantities of monomer (43,44). Acrylic ester polymers are also resistant to oxidation. Hydroperoxides can be formed from polymer radicals and oxygen under forcing conditions (45–47), but by and large this is a minor concern.

Solubility. Like most other properties, the side chain of acrylic ester polymers determines their solubility in organic solvents. Shorter side-chain polymers are relatively polar and will dissolve in polar solvents such as ether alcohols, ketones, and esters. With longer side-chain polymers, the solubility of a polymer shifts to the more hydrophobic solvents such as aromatic or aliphatic hydrocarbons. If a polymer is soluble in a given solvent, typically it is soluble in all proportions. Film formation occurs with the evaporation of the solvent, increase in solution viscosity, and the entanglement of the polymer chains. Phase separation and precipitation are not usually observed for solution polymers.

Solubility is determined by the free energy equation (the Flory–Huggins equation) governing the mutual miscibility of polymers (eq. (2)):

$$\Delta G_{Mix} = kT(N_1 \ln \nu_1 + N_2 \ln \nu_2 + \chi_1 N_1 \nu_2) \quad (2)$$

Table 3. Solubility Parameters of Acrylic Homopolymers Calculated by Small's Method[a]

Polymer	$(J/cm^3)^{1/2}$ [b]
Methyl acrylate	4.7
Ethyl acrylate	4.5
n-Butyl acrylate	4.3

[a] Refs. 23 and 53.
[b] To convert $(J/cm^3)^{1/2}$ to $(cal/cm^3)^{1/2}$, divide by 2.05.

where k is the Boltzmann's constant, T the temperature, N_1 the number of solvent molecules, N_2 the number of polymer molecules, ν_1 the volume fraction of the solvent, ν_2 the volume fraction of the polymer, and χ_1 the Flory–Huggins interaction parameter.

With this equation, polymer dissolution takes place when the free energy of mixing is negative. A polymer in solution always has a much higher entropy level than undissolved polymer since it is free to move to a far greater extent. This means the change in entropy term will always have a large positive value. Therefore, the factor which determines whether or not a polymer will dissolve in a particular solvent is the heat term. If the difference in the solubility parameters for two substances is small, dissolution will occur since the heat of mixing will be small and the entropy difference will be large (this translates into a negative overall energy of mixing). A polymer will dissolve in a particular solvent if the solubility parameters and the polarities for the polymer and the solvent are comparable (38,48–53). Some relevant solubility parameters are given in Table 3.

Polymer solution viscosity is a function of the polymer molecular weight, concentration in solvent, temperature, polymer composition, and solvent composition (9,54–56).

Chemical Resistance. Acrylic polymers and copolymers are highly resistant to hydrolysis. This property differentiates acrylic polymers from poly(vinyl acetate) and vinyl acetate copolymers. When exposed to highly extremely acidic or alkaline environments, acrylic ester polymers can hydrolyze to poly(acrylic acid) and the corresponding alcohol. Resistance to hydrolysis decreases in the order butyl acrylate > ethyl acrylate > methyl acrylate. Although it is the least hydrolytically stable, methyl acrylate is still far more resistant to hydrolysis than vinyl acetate (57,58).

Ultraviolet radiation is the other main stress encountered by polymers in the coatings arena. One hundred percent acrylic polymers are highly resistant to photodegradation because they are transparent to the vast majority of the solar spectrum (59). When uv-absorbing monomers, such as styrene, are incorporated into the polymer backbone, the uv-resistance of the resulting polymer decreases dramatically and a more rapid deterioration in polymer/coating properties is observed. On the other hand, a noncovalently bound uv absorber, such as hydroxybenzophenone [117-99-7], further improves the uv stability of 100% acrylic polymers (59).

Higher energy radiation such as from gamma ray or electron beam sources results in the scission of both main and side chains (60). The ratio of backbone to side-chain scission is determined by the nature of the side chain (61,62).

Acrylic Ester Monomers

A wide variety of properties are encountered in the acrylic monomers area. This range of properties is made accessible by the variability of the side chain for acrylic monomers. Some of the key physical properties of the most commercially important monomers are included in Table 4. A more complete listing of both monomers and their properties is found in the article Acrylic Acid and Derivatives.

The two most common methods for production of acrylic ester monomers are (*1*) the semicatalytic Reppe process which utilizes a highly toxic nickel carbonyl catalyst and (*2*) the propylene oxidation process which primarily employs molybdenum catalyst. Because of its decreased cost and increased level of safety, the propylene oxidation process accounts for most of the acrylic ester production currently. In this process, acrolein [107-02-8] is formed by the catalytic oxidation of propylene vapor at high temperature in the presence of steam. The acrolein intermediate is then oxidized to acrylic acid [79-10-7].

$$CH_2{=}CHCH_3 + O_2 \xrightarrow{\text{catalyst}} CH_2{=}CHCHO + H_2O$$

$$2\,CH_2{=}CHCHO + O_2 \xrightarrow{\text{catalyst}} 2\,CH_2{=}CHCOOH$$

Once the acrylic acid has been formed, the various acrylic ester monomers are synthesized by esterification of acrylic acid with the appropriate alocohol (63–66).

These monomers are then prevented from highly exothermic and hazardous autopolymerization processes during shipping and storage by the addition of a chemical inhibitor. The most common inhibitors currently used are hydroquinone [123-31-9], the methyl ether of hydroquinone (MEHQ) [150-76-5], and the newest member of the inhibitor family, 4-hydroxy TEMPO [2226-96-2]. 4-Hydroxy TEMPO, unlike the quinone inhibitors, does not require the presence of oxygen in order to be effective. Chemical inhibitors are only added at the $<$100 ppm level and are not typically removed prior to their commercial use. Finally, copper and its alloys can also function as inhibitors and should, therefore, be avoided when constructing a reactor for purposes of producing acrylic ester (co)polymers (67). With no inhibitor added, the monomers must be stored at temperatures below 10°C for no longer than a few weeks. Failure to exercise these precautions can result in violent, uncontrolled, and potentially deadly polymerizations.

Common acrylic ester monomers are combustible liquids. Commercial acrylic monomers are shipped with DOT (Department of Transportation) red labels in bulk quantities, tank cars, or tank trucks. Mild steel is the usual material of choice for the construction of bulk storage facilities for acrylic monomers; moisture is excluded to avoid rusting of the storage tanks and contamination of the monomers.

A variety of methods are available for determining the purity of monomers by the measurement of their saponification equivalent and bromine number, specific gravity, refractive index, and color (68–70). Minor components are determined by iodimetry or colorimetry for hydroquinone or MEHQ, Karl–Fisher method for water content, and turbidimetry for measuring trace levels of polymer. Gas–liquid chromatography is useful in both the general measurement of monomer purity as well as the identification of minor species within a monomer solution.

Although toxicities for acrylic ester monomers range from slight to moderate, they can be handled safely and without difficulty by trained, personnel, provided

Table 4. Physical Properties of Acrylic Monomers

Acrylate	CAS registry number	Molecular weight	Bp, °C[a]	d^{25}, g/cm^3	Flash point, °C[b]	Water solubility, g/100 g H_2O	Heat of evaporation, J/g[c]	Specific heat, J/g·K[c]
Methyl	[96-33-3]	86	79–81	0.950	10	5	385	2.01
Ethyl	[140-88-5]	100	99–100	0.917	10	1.5	347	1.97
n-Butyl	[141-32-2]	128	144–149	0.894	39	0.2	192	1.92
Isobutyl	[106-63-8]	128	61–63[d]	0.884	42	0.2	297	1.92
t-Butyl	[1663-39-4]	128	120	0.879	19	0.2		
2-Ethylhexyl	[103-11-7]	184	214–220	0.880	90[e]	0.01	255	1.92

[a] At 101.3 kPa unless otherwise noted.
[b] Tag open cup unless otherwise noted.
[c] To convert J to cal, divide by 4.184.
[d] At 6.7 kPa = 50 mm Hg.
[e] Cleveland open cup.

Table 5. Toxicities of Acrylic Monomers

Monomer	Acute oral LD_{50} (rats), mg/kg	Acute precutaneous LD_{50} (rabbits), mg/kg	Inhalation	
			LC_{50} (rats), mg/L	TLV, ppm
Methyl acrylate	300	1235	3.8	10
Ethyl acrylate	760	1800	7.4	25
Butyl acrylate	3730	3000	5.3	

that the proper safety instructions are followed (67,71). Table 5 contains animal toxicity data for common acrylic ester monomers under acute toxicity conditions.

Because of their higher vapor pressures, liquid methyl and ethyl acrylate are the two most potentially harmful acrylic ester monomers. Threshold limit values (TLV) for long-term low level exposures to these monomers in industrial situations have been established by OSHA (Table 5). Local regulations and classifications sometimes apply, however, to these monomers. Ethyl acrylate, for example, has been labeled a known carcinogen by the State of California (71).

Radical Polymerization

Free-radical initiators such as azo compounds, peroxides, or hydroperoxides are commonly used to initiate the polymerization of acrylic ester monomers. Photochemical (72–74) and radiation-initiated (75) polymerization are also possible. At constant temperature, the initial rate of polymerization is first order in monomer and one-half order in initiator. Rate data for the homopolymerization of several common acrylic ester monomers initiated by 2,2′-azobisisobutryonitrile (AIBN) [78-67-1] have been determined and are contained in Table 6. Also included in this table are heats of polymerization and volume shrinkage data (76).

The polymerization of both acrylic and methacrylic ester monomers is accompanied by the release of a large quantity of heat as well as a substantial decrease in sample volume. Commercial processes must account for both these phenomena. Excess heat must be removed from industrial reactors by the use of high surface area heat exchangers. As for the shrinkage issue, the percent shrinkage encountered upon polymerization of the monomer is, in general, inversely proportional to the length of the monomer side chain. Mole for mole, the shrinkage amount is relatively constant (77).

Table 6. Polymerization Data for Acrylic Ester Monomers in Solution[a]

Acrylate	Concentration, solvent	k_{sp}, L/mol·h[b]	Heat, kJ/mol[c]	Shrinkage, vol%
Methyl	3 *M*, Methyl propionate	250	78.7	24.8
Ethyl	3 *M*, Benzene	313	77.8	20.6
Butyl	1.5 *M*, Toluene	324	77.4	15.7

[a] Ref. 76.
[b] At 44.1°C.
[c] To convert kJ to kcal, divide by 4.184.

The free-radical polymerization of acrylic monomers takes place through the classical stepwise chain-growth mechanism, which is described as the head-to-tail addition of individual monomer units through attack of the monomer double bond and formation of a single bond between the newly incorporated monomer units.

This stepwise growth continues until either termination or chain transfer of the radical chain end takes place. Termination can occur by combination or disproportionation, depending on the conditions of the polymerization (78,79).

The addition step typically takes place as a head-to-tail process although head-to-head addition has been observed as well (80). Oxygen has a strong inhibitory effect on the rate of polymerization of acrylic ester polymers. Oxygen is, therefore, excluded from commercial reactors primarily through the use of positive nitrogen flow. The nature of the oxygen inhibition is known: an alternating copolymer can be formed between oxygen and acrylic ester monomers (81,82).

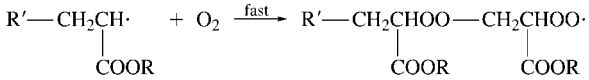

The oxygen chain end is relatively unreactive when compared to the acrylic chain end and reduces the overall rate of polymerization. Additionally, the peroxy radical undergoes a faster rate of termination than the standard acrylic-based radical:

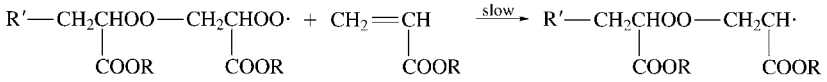

One will observe a drop in overall reaction rate, a change in polymer composition and properties, as well as a decrease in polymer molecular weight if oxygen is not excluded from a reactor when polymerizing acrylic ester monomers (83).

The wide variety of acrylic ester monomers dictates that a wide variety of homopolymers with radically different properties are accessible. An even wider variety of polymers can be formed through the copolymerization of two or more acrylic ester monomers (84,85).

Acrylic ester monomers are, in general, readily copolymerized with other acrylic and vinylic monomers. Table 7 presents data for the free-radical copolymerization of a variety of monomers 1:1 with acrylic ester monomers. These numbers are calculated through the use of reactivity ratios:

$$r_1 = k_{11}/k_{12}$$
$$r_2 = k_{22}/k_{21}$$

For a binary copolymer, the smaller reactivity ratio is divided by the larger r value and multiplied by 100. Values greater than 25 indicate that

Table 7. Relative Ease of Copolymer Formation for 1:1 Ratios of Acrylic and Other Monomers, $\frac{r(\text{smaller})}{r(\text{larger})} \times 100$

Monomer 2	CAS registry number	Monomer 1		
		Methyl acrylate	Ethyl acrylate	Butyl acrylate
Acrylonitrile	[107-13-1]	53	46	74
Butadiene	[106-99-0]	66	4.7	8.1
Methyl methacrylate	[80-62-6]	50.3	30.6	14.6
Styrene	[100-42-5]	21	16	26
Vinyl chloride	[75-01-4]	2.7	2.1	1.6
Vinylidene chloride	[75-35-4]	100	52	55
Vinyl acetate	[108-05-4]	1.1	0.7	0.6

Table 8. *Q* and *e* Values for Acrylic Monomers[a]

Monomer	Q	e
Methyl acrylate	0.44	+0.60
Ethyl acrylate	0.41	+0.46
Butyl acrylate	0.30	+0.74
Isobutyl acrylate	0.41	+0.34
2-Ethylhexyl acrylate	0.14	+0.90

[a]Ref. 88.

copolymerization proceeds smoothly; low values for the ease of copolymerization can be helped through the adjustment of comonomer composition as well as the monomer addition method (86).

A growing chain with monomer 1 as the chain-end radical has a rate constant for self-addition of k_{11}; the rate for addition of monomer 2 is k_{12}. The self-addition rate for a terminal monomer 2 radical is given as k_{22}; the rate for addition of monomer 1 is k_{21}. The reactivity ratios can also be calculated from the Price-Alfrey measures (87) of resonance stabilization (Q) and polarity (e) which are shown for common acrylic esters in Table 8. NMR can also be used to determine the composition distribution characteristics of acrylic copolymers (88,89).

In addition to the standard side-chain variation discussed above, special functionality can be added to acrylic ester monomers by use of the appropriate functional alcohol. Through the use of small levels of functional monomers, one can allow an acrylic ester polymer to react with metal ions, cross-linkers, or other types of resins. Table 9 contains information on some of the more common functional monomers.

Bulk Polymerization

Bulk polymerizations of acrylic ester monomers are characterized by the rapid formation of an insoluble network of polymers at low conversion with a concomitant rapid increase in reaction viscosity (90,91). These properties are thought to

Table 9. Functional Monomers for Copolymerization with Acrylic Monomers

Monomer	Structure	CAS registry number	Molecular formula
Carboxyl			
Methacrylic acid	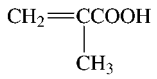	[79-41-4]	$C_4H_6O_2$
Acrylic acid	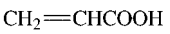	[79-10-7]	$C_3H_4O_2$
Itaconic acid	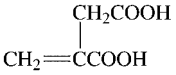	[97-65-4]	$C_5H_6O_4$
Amino			
t-Butylaminoethyl methacrylate	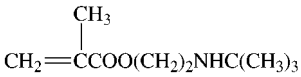	[24171-27-5]	$C_{10}H_{19}NO_2$
Dimethylaminoethyl methacrylate	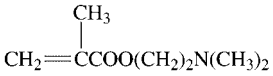	[2867-47-2]	$C_8H_{15}NO_2$
Hydroxyl			
2-Hydroxyethyl methacrylate	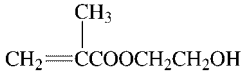	[868-77-9]	$C_6H_{10}O_3$
2-Hydroxyethyl acrylate		[818-61-1]	$C_5H_8O_3$
N-Hydroxymethyl			
N-Hydroxymethyl acrylamide		[924-42-5]	$C_4H_7NO_2$
N-Hydroxymethyl methacrylamide	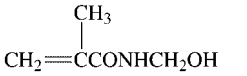	[923-02-4]	$C_5H_9NO_2$
Oxirane			
Glycidyl methacrylate	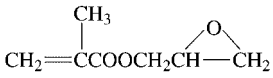	[106-91-2]	$C_7H_{10}O_3$
Multifunctional			
1,4-Butylene dimethacrylate	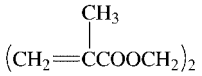	[2082-81-7]	$C_{12}H_{18}O_4$

come from the chain transfer of the active radical via hydrogen abstraction from the polymer backbone. When two of these backbone radical sites propagate toward one another and terminate, a cross-link is formed (91).

Solution Polymerization

Of far greater commercial value than that of simple bulk polymerizations, solution polymerizations employ a co-solvent to aid in minimizing reaction viscosity as well as controlling polymer molecular weight and architecture. Lower polyacrylates are, in general, soluble in aromatic hydrocarbons, esters, ketones, and chlorohydrocarbons. Solubilities in aliphatic hydrocarbons, ethers, and

Table 10. Chain-Transfer Constants to Common Solvents for Poly(ethyl acrylate)[a]

Solvent	$C_s \times 10^5$
Benzene	5.2
Toluene	26.0
Isopropyl alcohol	260
Isobutyl alcohol	46.5
Chloroform	14.9
Carbon tetrachloride	15.5

[a]Refs. 79, 92, and 93.

alcohols are somewhat lower. As one moves to longer alcohol side-chain lengths, acrylics become insoluble in oxygenated organic solvents and soluble in aliphatic and aromatic hydrocarbons and chlorohydrocarbons. Solvent choices for acrylic solution polymerizations are made on the basis of cost, toxicity, flammability, volatility, and chain-transfer activity. The chain-transfer constants (C_s) for a variety of solvents in the solution polymerization of poly(ethyl acrylate) are shown in Table 10.

Initiators serve the dual role of beginning the polymerization of an individual chain as well as controlling the molecular weight distribution of a polymer sample. Initiators are chosen based on their solubility, thermal stability (rate of decomposition), and the end use for the polymer. Additionally, initiators can be used to control polymer architecture by cross-linking control; this property also allows initiators to serve a role in the regulation of molecular weight distribution. Levels of usage vary from hundredths of a percent to several percent by weight on the polymer formed. The types of initiators most commonly employed in solution polymerizations are organic peroxides, hydroperoxides, and azo compounds.

Molecular weight control can also be achieved through the use of a chain-transfer agent. The most commonly used species in this class are chlorinated aliphatic compounds and thiols (94). The chain-transfer constants (C_s at 60°C) for some of these compounds in the formation of poly(methyl acrylate) are as follows (87): Carbon tetrabromide, 0.41; Ethanethiol, 1.57; and Butanethiol, 1.69.

Because of the volatile nature of the monomers used and high temperatures often employed, solution polymerizations are typically performed in reactors which can withstand pressures of at least 446 kPa (65 psi). Standard materials of construction include stainless steeel (which may be glass-lined) or nickel. Anchor-type agitators are used for solution polymerizations with viscosities up to 1.0 Pa·s (1000 cP), but when viscosity levels move above this range, a slow ribbon-type agitator is used to sweep material away from the reactor walls. Improper agitation can result in the severe fouling of a reactor. Most industrial reactors are jacketed for steam heating and/or water cooling of a batch and contain a rupture disk to relieve pressure buildup. Additionally, there are numerous inlets in a typical industrial reactor as well as a thermocouple for monitoring temperature. A valve is placed in the bottom of the reactor to release polymerized material to storage containers.

Cooling within a reactor is typically provided by a reflux condenser. Since polymerization is a highly exothermic process, temperature control is a safety concern as well as a product integrity issue. Temperature control is primarily

obtained through the gradual addition of monomers into the reactor by gravity from storage containers close to the reactor. In this manner, the rate of monomer addition and reaction can be matched to the cooling capacity of the reactor so that temperatures remain relatively constant throughout the polymerization. If these measures fail to control the temperature of a particular batch, a chemical inhibitor, such as a hydroquinone, can be added to retard the rate of polymerization.

Oxygen can serve as an inhibitor of polymerization. Reactors typically maintain a blanket of nitrogen over the entire reactor kettle. In polymerizations with temperatures below reflux, nitrogen is used to purge the reaction solution; a nitrogen blanket is then placed over the reactor prior to the addition of the initiator. Total cycle times for solution polymerizations run in the range of 24 h (95).

A typical solution polymerization recipe is shown below:

Composition	Parts
Reactor charge	
Ethyl acetate	61.4
Benzoyl peroxide	0.1
Monomer charge	
Ethyl acrylate	36.5
Acrylic acid	2.0

This copolymer has an overall composition of 94.8% ethyl acrylate/5.2% acrylic acid with the monomer charged at a level of 39 wt% in a solution of ethyl acetate. Initially, the solvent and initiator, benzoyl peroxide in this case, are added to the reactor and heated to reflux (80°C). Forty percent of the monomer mixture is added to the reactor in one charge. Then, four equal aliquots of monomer are added 24, 50, 79, and 110 min after the initial charge. Reflux is maintained within the reactor overnight to ensure complete reaction; the product is then cooled and packaged the next morning (96).

Storage and handling equipment are typically made from steel. In order to prevent corrosion and the transfer of rust to product, moisture is typically excluded from solution polymer handling and storage systems (97). Because of the temperature-sensitive nature of the viscosity of solution polymers, the temperature of the storage tanks and tranfer lines is regulated either through prudent location of these facilities or through the use of insulation, heating, and cooling equipment.

Emulsion Polymerization

Emulsion polymerization is the most industrially important method of polymerizing acrylic ester monomers (98,99). The principal ingredients within this type of polymerization are water, monomer, surfactant, and water-soluble initiator. Products generated by emulsion polymerization find usage as coatings or binders in paints, paper, adhesives, textile, floor care, and leather goods markets. Because of their film-forming properties at room temperature, most commercial acrylic ester polymers are copolymers of ethyl acrylate and butyl acrylate with methyl methacrylate.

Lower acrylates are capable of polymerizing in water in the presence of an emulsifier and a water-soluble initiator. The polymeric product is typically a milky-white dispersion of polymer in water at a polymer solids content of 30–60%. Particle sizes for these latices fall in the range of 0.1–1.0 μm. Because of the compartmentalized nature of the process (99), high molecular weights are obtained with most emulsion polymerizations without the resulting viscosity build encountered with solution polymerizations. Additionally, the use of water as a dispersion medium provides attractive safety, environmental, and heat removal benefits when compared to other methods of polymerizing acrylic ester monomers. The emulsion polymerization of the higher (relatively water insoluble) acrylates can even be accomplished now through the use of a patented method for catalytically transferring monomer from droplets to the growing polymer particles (100).

The types of surfactants used in an emulsion polymerization span the entire range of anionic, cationic, and nonionic species. The most commonly used soaps are alkyl sulfates such as sodium lauryl sulfate [151-21-3], alkylaryl sulfates such as sodium dodecyl benzene sulfonate [25155-30-0], and alkyl or aryl polyoxyethylene nonionic surfactants (87,101–104). Product stability and particle size control are the driving forces which determine the types of surfactants employed; mixtures of nonionic and anionic surfactants are commonly used to achieve these goals (105–108).

Water-soluble peroxides, such as sodium or ammonium persulfate, are commonly used in the industrial arena. The thermal dissociation of this initiator (109) results in the formation of sulfate radicals which initiate polymer chains in the aqueous phase. It is possible to use other oxidants, such as hydrogen peroxide [7722-84-1] or persulfates in the presence of reducing agents and/or polyvalent metal ions (87). In this manner, a redox initiator system is formed which allows the experimenter to initiate polymer chains over a much broader range of temperatures (25–90°C) than simple thermal initiation (75–90°C) (110). The primary disadvantage of this initiation method is that greater level of salt impurities are introduced to the reactor which could, perhaps, adversely influence final polymer properties such as stability.

Emulsion polymerization batches on the industrial scale are typically run in either stainless steel or glass-lined steel reactors which can safely handle internal pressures of 446 kPa (65 psi). Agitation within the reactors is controlled by use of a variable speed stirring shaft coupled at times with a baffling system within the reactor to improve mixing. Care must be taken to avoid excessive mixing forces being placed on the latex as coagulum will form under extreme conditions. Temperature control of batches is maintained through the use of either steam or cold water jacketing. Multiple feed lines are necessary to provide for the addition of multiple streams of reactants such as initiators, monomer emulsions, inihibitors if necessary, and cooling water. Monitoring equipment for batches typically consists of thermocouples, manometers, sightglasses, as well as an emergency stack with a rupture disk in case of pressure buildup within the reactor. A typical industrial emulsion polymerization plant is shown in Figure 2.

There are numerous examples of typical industrial emulsion polymerization recipes available in the open literature (111,112). A process for the synthesis of a polymer with a 50% methyl methacrylate, 49% butyl acrylate, and 1% methacrylic acid terpolymer at a solids content of 45% is described below:

Charge	Parts
Monomer emulsion charge	
Deionized water	13.65
Sodium lauryl sulfate	0.11
Methyl methacrylate	22.50
Butyl acrylate	22.05
Methacrylic acid	0.45
Initiator charge	
Ammonium persulfate	0.23
Reactor charge	
Deionized water	30.90
Sodium lauryl sulfate	0.11

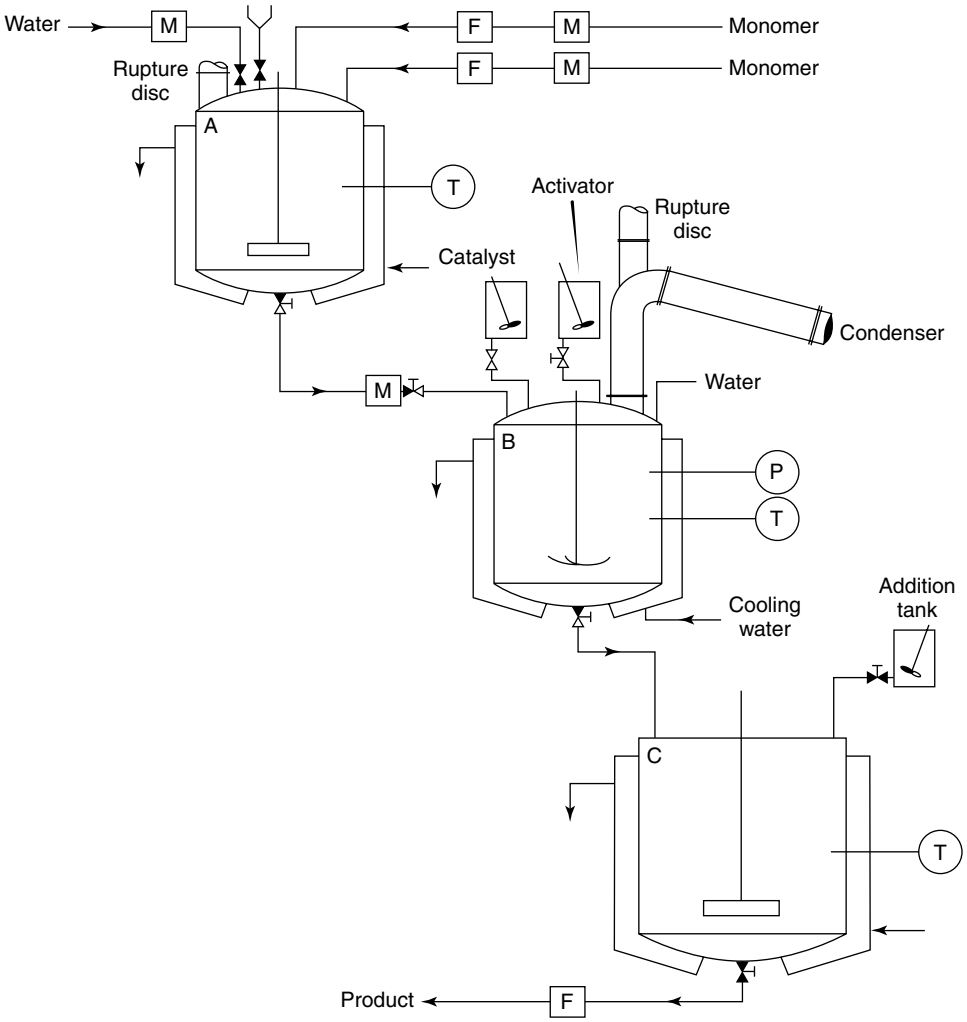

Fig. 2. Emulsion polymerization plant. A, Emulsion feed tank; B, polymerization reactor; C, drumming tank; F, filter; M, meter; P, pressure gauge; T, temperature indication.

The monomer emulsion is first formed in a separate agitation tank by combination of the water, soap, and monomer with a proper level of mixing. Care must be taken to avoid excessive levels of agitation in the monomer emulsion tank to avoid incorporating air into the emulsion. The reactor water is heated under a nitrogen blanket to a temperature of at least 75°C prior to the addition of the initiator. Following the addition of the initiator, the monomer emulsion is fed into the reactor over the course of approximately 2.5 h. Temperature control is maintained during this time through both control of the monomer feed rate as well as use of the reactor jacket heating/cooling system. After the monomer emulsion feed is completed, the temperature is held above 75°C for at least 30 min to reduce the level of residual standing monomer within the system. The product is then cooled, filtered, and packaged.

Once packaged, the storage of acrylic latices is a nontrivial matter; problems commonly encountered with these polymer colloids include skinning (surface film formation), sedimentation, grit formation within the latex, formation of coagulum on storage container walls, and sponging (aerogel formation). Exposure of the material to extremes in temperature is avoided through prudent location of these facilities or the use of insulation, heating, and cooling equipment. Acrylic emulsion polymers, like many other types of polymers, are subject to bacterial attack. Proper adjustment of pH, addition of bactericides, and good housekeeping practices (95) can alleviate the problems associated with bacterial growth. Some advances in the industrial application of emulsion polymerization have been described in the open literature (113).

Suspension Polymerization

Suspension polymers of acrylic esters are industrially used as molding powders and ion-exchange resins. In this type of polymerization, monomers are dispersed as 0.1- to 5-mm droplets in water and are stabilized by protective colloids or suspending agents. In contrast to emulsion polymerization, initiation is accomplished by means of a monomer-soluble agent and occurs within the suspended monomer droplet. Water serves the same dual purpose as in emulsion (heat removal and polymer dispersion). The particle size of the final material is controlled through the control of agitation levels as well as the nature and level of the suspending agent. Once formed, the 0.1- to 5-mm polymer beads can be isolated through centrifugation or filtration.

The most commonly used suspending agents are cellulose derivatives, polyacrylate salts, starch, poly(vinyl alcohol), gelatin, talc, and clay derivatives (95). The important function these agents must serve is to prevent the coalescence of monomer droplets during the course of the polymerization (114). Thickeners can also be added to improve suspension quality (95). Other additives such as lauryl alcohol, stearyl acid or cetyl alcohol lubricants and di- or trivinyl benzene, diallyl esters of dibasic acids, and glycol dimethacrylates cross-linkers are used to improve bead uniformity and bead performance properties.

Unlike emulsion polymerization, the initiators employed in suspension polymerization must not be water-soluble; organic peroxides and azo species are most commonly used. In similar fashion to bulk polymerization, the level of initiator

used directly influences the molecular weight of the product (95,115,116). Developments in the method of suspension polymerization have been reviewed in the open literature (117,118).

Graft Copolymerization

Polymer chains can be attached to a preexisting polymer backbone of a similar or completely different composition to form what is termed a graft copolymer. Acrylic branches can be added to either synthetic (119,120) or natural (121–124) backbones. Attachment of graft polymer branches to preformed backbones is accomplished by chemical (125–127), photochemical (128,129), radiation (130), and mechanical (131) means. The presence of distinct compositions in this branched geometry often conveys properties which cannot otherwise be attained (132,133).

Living Polymerization

One of the most exciting areas currently in the radical polymerization of acrylic ester monomers is the field of living polymerization. Living polymers are defined in Reference 134 as "polymers that retain their ability to propagate for a long time and grow to a desired maximum size while their degree of termination or chain transfer is still negligible." Because of these properties, exceptional control can be exercised over the topology (ie, linear, comb), composition (ie, block, graft), and functional form (ie, telechelic, macromonomer) of these polymers (135).

Atom-transfer radical polymerization (ATRP) and nitroxide-mediated (136–138) polymerization both show promise in terms of the ability to fine tune polymer architecture using living radical methods. ATRP has been successfully used in the polymerization of methyl acrylate (139,140) as well as functional acrylates containing alcohol (141), epoxide (142), and vinyl groups (143) on the side chain. The main drawbacks to the ATRP method of creating acrylic ester homo- and copolymers are the relatively long reaction times and the high levels of metal-containing initiator required (see LIVING POLYMERIZATION, RADICAL).

Radiation-Induced Polymerization

Coatings can be formed through the application of high energy radiation to either monomer or oligomer mixture. Ultraviolet curing is the most widely practiced method of radiation-based initiation (144–150); this method finds its main industrial applications in the areas of coatings, printing ink, and photoresists for computer chip manufacturing. The main disadvantage of the method is that uv radiation is incapable of penetrating highly pigmented systems.

To form a film via this method, a mixture of pigment, monomer, polymer, photoinitiator, and inhibitor are applied to a substrate and polymerized by controlled exposure to uv radiation. Polymers used as co-curing agents often have unsaturated methacrylate functionalities attached; higher order acrylates are often used as the solvent in photocure mixtures.

In order to avoid the problems associated with more highly pigmented systems, electron beam curing is employed (151). This high energy form of radiation is capable of penetrating through the entire coating regardless of the coating's pigment loading level.

Anionic Polymerization

The Anionic Polymerization of acrylic ester monomers is accomplished by use of organometallic initiators in organic solvents. The main advantage to the use of anionic polymerization as opposed to other methods is its ability to generate stereoregular or block copolymers. Some examples of this type of polymerization include the anionic formation of poyl(*t*-butyl acrylate) (152–155), poly(isopropyl acrylate) (156), and poly(isobutyl acrylate) (157,158). Solvent conditions primarily determine tacticity of the resulting polymer product with nonpolar solvents generating isotactic product and polar solvents resulting in the formation of syndiotactic polymers. The strikingly different physical properties and mechanistic discussions on the formation of these two different types of polymer have been described in the polymer literature (159–162).

The initiation step for anionic polymerizations takes place via a Michael reaction:

$$R_3C^-M^+ + CH_2{=}CHCOOR \longrightarrow R_3C{-}CH_2{-}\bar{C}H{-}COOR$$

A subsequent polymer growth occurs by head-to-tail addition of monomer to the growing polymer chain.

$$R_3C{-}CH_2{-}\bar{C}H{-}COOR + CH_2{=}CHCOOR \longrightarrow R_3C{-}CH_2{-}\underset{\displaystyle COOR}{CH}{-}CH_2{-}\underset{\displaystyle COOR}{\bar{C}H}$$

Because of cost constraints and toxicity issues involved with the organometallic initiators, anionic polymerization is of limited commercial significance. Both the living methods described above as well as DuPont's group-transfer polymerization method (163–167) are seen as alternative ways to achieve the same level of control over polymer architecture as that of anionic polymerization. All these methods offer the promise of narrow and controllable molecular weight distributions as well as the ability to form block copolymers through the sequential addition of monomers. Additionally, all the methods suffer from slow overall reaction rates and the difficulty of removing the specialty initiators after polymer formation has taken place.

Analytical Test Methods and Specifications

Emulsion Polymers. Current analytical methods allow for complete characterization of all crucial aspects of an acrylic latex (87). The main properties of interest are an acrylic latex's composition, percent solids content, viscosity, pH,

particle size distribution (168,169), glass-transition temperature, minimum film-forming temperature (170), and surfactant type. In addition to these basic properties, the stability of a latex with respect to mechanical shear, freeze-thaw cycles, and sedimentation on standing for long periods of time are of interest in commercial products.

Solution Polymers. A solution polymer's composition, solids content, viscosity, molecular weight distribution, glass-transition temperature, and solvent are of interest. Standard methods allow for all of these properties to be readily determined (171,172).

Environmental Health and Safety Factors

Acrylic polymers are categorized as nontoxic and have been approved for the handling and packaging by the FDA. The main concerns with acrylic polymers deal with the levels of residual monomers and the presence of nonacrylic additives (primarily surfactants) which contribute to the overall toxicity of a material. As a result, some acrylic latex dispersions can be mild skin or eye irritants.

During the manufacture of an acrylic polymer, precautions are taken to maintain temperature control (173). In addition to these measures, polymerizations are run under conditions wherein the reactor are closed to the outside environment to prevent the release of monomer vapor into the local environment. As for final product properties, acrylic latices are classified as nonflammable substances and solution polymers are classified as flammable mixtures.

Uses

Because of their wide property range, clarity, and resistance to degradation by environmental forces, acrylic polymers are used in an astounding variety of applications that span the range from very soft adhesive materials to rigid non-film-forming products (Table 11).

Coatings. Acrylic ester latex polymers are used widely as high quality paint binders because of their excellent durability, toughness, optical clarity, uv stability, and color retention. These properties allow acrylics to find use as binder vehicles in all types of paints (76): interior and exterior; flats, semigloss, and gloss; as well as primers to topcoats. Although all-acrylic compositions are most

Table 11. U.S. Production (10^3 t) of Acrylic Monomers[a]

Monomer	1969	1975	1980	1984
Methyl	14	20	22	28
Ethyl	91	109	136	138
n-Butyl	29	81	145	192
2-Ethylhexyl	15	15	31	39
Other	4	9	23	27
Acrylate esters, total	*153*	*234*	*357*	*424*

[a]Ref. 154.

favored in exterior applications because of their excellent durability (174), other types of copolymers such as vinyl-acrylics and styrene-acrylics benefit in terms of performance properties from the acrylic portion of the composition; methods of manufacturing acrylic-based paints have been described previously in the literature (175). Acrylic emulsion polymers even find use in the protection of structural steel (176) (see COATING METHODS, SURVEY).

The industrial finishing area sees both acrylic emulsions as well as solution polymers utilized in a wide variety of applications including factory finished wood (177,178), metal furniture and containers (179), and can and coil coatings (180). In order to harden acrylic polymers for this type of demanding application, the polymers are often cross-linked with melamines, epoxies, and isocyanates. The coatings are applied via spraying, roll dipping, or curtain coating. Radiation curing using uv radiation or electron beam radiation (181–186), powder coating (187–190), electrode deposition of latices (191–193), and the use of higher solids level emulsion (194) represent newer methods for applying acrylic coatings to form industrial finishes. Excellent reviews on the use of water-based emulsions (195,196) and solution acrylics (197–199) can be found in the open literature (see COATINGS).

Hydrophobically modified acrylics are finding extensive usage as thickening agents in the paints marketplace as well as the area of industrial finishes (200). Flow and leveling improvements are observed when changing a formulation over from hydroxyethylcellulose to acrylic-based thickeners. Unlike cellulosic thickeners, the modified acrylics act through an associative thickening mechanism; they stabilize the dispersed polymer phase rather than thickening the aqueous phase of a polymer latex. Two main types of modified acrylics are of commercial value: HASE (hydrophobically modified alkali-soluble emulsions) and HEUR (hydrophobically modified ethylene oxide urethane block copolymers). These acrylics compete with hydrophobically modified hydroxyethylcellulose in the marketplace (201–203).

Textiles. Because of their durability, soft feel, and resistance to discoloration, acrylic emulsion polymers find a variety of uses in the textiles area including binders for fiberfill and nonwoven fabrics, textile bonding or laminating, flocking, backcoating and pigment printing applications. *N*-Methylolacrylamide is often used as a self-cross-linker in acrylic textile binders to improve washing and dry cleaning durability as well as overall binder strength (204).

Polyester (205–208), glass (209), and rayon (210) nonwoven and fiberfill mats have been manufactured using acrylic binders to hold the mats together. In this process, the acrylic emulsions are applied to a loose web or mat and are then heated to form a film at the fiber crossover points which maintains the structural integrity of the mat. The final products generated using this technology include quilting, clothing, disposable diapers, towels, filters, and roofing (see NONWOVEN FABRICS).

Acrylic polymers find use in applications that take advantage of their exceptional resistance to environmental assaults such as uv radiation, ozone, heat, water, dry cleaning, and aging (211). Acrylics are often used as the backing material for automotive and furniture upholstery to improve the dimensional handling properties, prevent pattern distortion, prevent unraveling, and minimize seam slippage. Strike-through problems are averted through the use of foamed or

frothed acrylic coatings, which also yield a softer fabric and save on energy costs (212). Crushed acrylic latex foam are employed as backing materials for draperies. The foam protects the drapery from sun damage, mechanically stabilizes the fabric, improves drape, and gives a softer hand than conventional backing materials (213). Acrylics are also used as carpet-backings and to bond fabric-to-fabric, fabric-to-foam, and fabric-to-nonwoven materials (214).

The flocking process begins with the bonding of cut fibers to an adhesive-coated fabric to obtain a decorative and functional material (215). Acrylics can provide the softness and durability that are sought in flocked textiles; they also serve as binders for pigments in the printing of flocked fabrics (35,216,217).

The feel, soil release properties, and permanent-press behavior of a fabric can be finely tuned using acrylic as finishing polymers. Copolymers of acrylics with acrylic or methacrylic acid can be used as thickeners for textile coating formulation.

Adhesives. Acrylic emulsion polymers are used in a wide variety of adhesives. Pressure-sensitive Adhesives, which typically have T_g values less than 20°C, are the main type of acrylic adhesive. Acrylic polymers and copolymers find use as PSAs in tapes, decals, and labels. Along with their aforementioned superior chemical resistance properties, acrylics possess an excellent balance of tack, peel, and shear properties which is crucial in the adhesives market (218,219). Other types of adhesives that employ acrylics include construction formulations and film-to-film laminates.

Paper. Because of their excellent cost-performance balance, acrylic-vinyl acetate copolymer emulsion binders have been used as pigment binders for coated paper and boards. These binders provide higher brightness, opacity, coating solids, and improved adhesion versus styrene–butadiene copolymers (220,221). Acrylics also find usage as paper saturants with properties that compare favorably to natural rubber, butadiene–acrylonitrile, and butadiene–styrene (222). Finally, acrylic emulsion polymers are utilized in starch-latex-pigmented coatings (223) as well as size-press (224) and beater addition (225) applications.

Other Applications. The leather finishing area is a traditional stronghold of acrylic emulsion polymers (226). Acrylics are used throughout the entire process of pigskin leather production; the use of acrylics lends uniformity, break improvement, better durability, and surface resistance while preserving the natural appearance of the pigskin (227).

Acrylics have been used to impart impact strength and better substrate adhesion to cement (228). The ceramics industry uses both acrylic solution and emulsion polymers as temporary binders, deflocculants, and additives in ceramics bodies and glazes (229) (see CERAMICS).

Acrylics are used in the manufacture of aqueous and solvent-based caulks and sealants (230,231). Elastomeric acrylics are used in mastics to prevent uv radiation and chemical damage to the underlying polyurethane foam. Acrylics also impart hailstone resistance as well as flexibility over a broad temperature range (232). The manufacturing process for poly(vinyl chloride) uses acrylics as processing aids and plate-out scavengers in calendered and blown films. Acrylics allow for the manufacture of thick, smooth calendered vinyl sheets through modification of the melt viscosity of the vinyl sheet polymer (233). In the

agricultural area, thin layers of acrylic emulsions have been applied to citrus leaves and fruit to control "Greasy Spot," a disease which causes leaf-spotting and eventually leaf loss (234). Acrylics have found a great deal of use in the floor polish area; a guide to formulating these coatings has been published (235).

Acrylic polymers have been used as alternatives to nitrile rubbers in some hydraulic and gasket applications because of their excellent heat-resistance properties (236,237). Ethylene–acrylate copolymers have been used as transmission seals, vibration dampeners, dust boots, and steering and suspension seals (238).

BIBLIOGRAPHY

"Acrylic Ester Polymers" in *EPST* 1st ed., Vol. 1, pp. 246–328, by L. S. Luskin and R. J. Myers, Rohn and Haas Co.; "Acrylic and Methacrylic Ester Polymers" in *EPST* 2nd ed., Vol. 1, pp. 211–299, by B. B. Kine and R. W. Novak, Rohm and Haas Co.

1. J. Redtenbacher, *Ann.* **47**, 125 (1843).
2. Fr. Englehorn, *Berichte* **13**, 433 (1880); L. Balbiano and A. Testa, *Berichte* **13**, 1984 (1880).
3. W. Caspary and B. Tollens, *Ann.* **167**, 241 (1873).
4. G. W. A. Kahlbaum, *Berichte* **13**, 2348 (1880).
5. U.S. Pat. 1,121,134 (Dec. 15, 1914), O. Rohm.
6. E. H. Riddle, *Monomeric Acrylic Esters*, Reinhold Publishing Corp., New York, 1954.
7. J. Brandrup and E. H. Immergut, *Polymer Handbook*, 2nd ed., Wiley-Interscience, New York, 1975.
8. H. B. Burrell, *Off. Dig. Fed. Soc. Paint Technol.* 131 (Feb. 1962).
9. D. W. van Krevelen, *Properties of Polymers*, Elsevier, Amsterdam, 1972.
10. J. L. Gardon, in N. M. Bikales, ed., *Encyclopedia of Polymer Science and Technology*, Vol. **3**, Interscience Publishers, a division of John Wiley & Sons, Inc., New York, 1965, pp. 833–862.
11. T. G. Fox Jr., *Bull. Am. Phys. Soc.* **1**(3), 123 (1956).
12. J. A. Shetter, *J. Polym. Sci., Part B* **1**, 209 (1963).
13. L. E. Nielsen, *Mechanical Properties of Polymers*, Van Nostrand Reinhold Co., Inc., New York, 1962, p. 122.
14. I. Williamson, *Br. Plast.* **23**, 87 (1950).
15. R. F. Clark Jr. and R. M. Berg, *Ind. Eng. Chem.* **34**, 1218 (1942).
16. *ASTM Standards, ASTM D1043-61T*, Vol. 27, American Society for Testing and Materials, Philadelphia, Pa., 1964.
17. S. D. Gehman, D. E. Woodford, and C. S. Wikinson Jr., *Ind. Eng. Chem.* **39**, 1108 (1947).
18. *ASTM Standards, ASTM D1053-61*, Vol. 19, American Society for Testing and Materials, Philadelphia, Pa., 1974.
19. A. C. Nuessle and B. B. Kine, *Ind. Eng. Chem.* **45**, 1287 (1953).
20. A. C. Nuessle and B. B. Kine, *Am. Dyest. Rep.* **50**(26), 13 (1961).
21. V. J. Moser, *Am. Dyest. Rep.* **53**(38), 11 (1964).
22. M. K. Lindemann, *Appl. Polym. Symp.* **10**, 73 (1969).
23. W. H. Brendley Jr., *Paint Varn. Prod.* **63**(3), 23 (1973).
24. R. Zdanowski and G. L. Brown Jr., *Resin Review*, Vol. **9**, No. 1, Rohm and Haas Co., Philadelphia, Pa., 1959, p. 19.
25. R. Bakule and J. M. Blickensderfer, *Tappi* **56**(4), 70 (1973).

26. A. V. Tobolsky, *J. Polym. Sci., Polym. Symp.* **9**, 157 (1975).
27. L. J. Hughes and G. E. Britt, *J. Appl. Polym. Sci.* **5**(15), 337 (1961).
28. S. Krause and N. Roman, *J. Polym. Sci., Part A* **3**, 1631 (1965).
29. H. L. Gerhart, *Off. Dig. Fed. Soc. Paint Technol.* 680 (June 1961).
30. R. M. Christenson and D. P. Hart, *Off. Dig. Fed. Soc. Paint Technol.* 684 (June 1961).
31. H. A. Vogel and H. G. Brittle, *Off. Dig. Fed. Soc. Paint Technol.* 699 (June 1961).
32. J. D. Murdock and G. H. Segall, *Off. Dig. Fed. Soc. Paint Technol.* 709 (June 1961).
33. J. D. Petropoulous, C. Frazier, and L. E. Cadwell, *Off. Dig. Fed. Soc. Paint Technol.* 719 (June 1961).
34. D. G. Applegath, *Off. Dig. Fed. Soc. Paint Technol.* 737 (June 1961).
35. U.S. Pat. 2,886,474 (May 12, 1959), B. B. Kine and A. C. Nuessle (to Rohm and Haas Co.).
36. U.S. Pat. 2,923,653 (Feb. 2, 1960), N. A. Matlin and B. B. Kine (to Rohm and Haas Co.).
37. D. H. Klein, *J. Paint Technol.* **42**(545), 335 (1970).
38. S. H. Rider and E. E. Hardy, *Polymerization and Polycondensation Processes* (Adv. Chem. Ser. No. 34), American Chemical Society, Washington, D.C., 1962.
39. R. H. Wiley and G. M. Braver, *J. Polym. Sci.* **3**, 647 (1948).
40. J. R. Martin, J. F. Johnson, and A. R. Cooper, *J. Macrol. Sci. Rev. Macromol. Chem.* **8**, 57 (1972).
41. A. S. Craemer, *Kunststoffe* **30**, 337 (1940).
42. B. E. Rehberg and C. H. Fisher, *Ind. Eng. Chem.* **40**, 1429 (1948).
43. G. G. Cameron and D. R. Kane, *Makromol. Chem.* **109**, 194 (1967).
44. L. Gunawan and J. K. Haken, *J. Polym. Sci., Polym. Chem. Ed.* **23**, 2539 (1985).
45. A. R. Burgess, *Chem. Ind.* 78 (1952).
46. R. Stelle and H. Jacobs, *J. Appl. Polym. Sci.* **2**(4), 86 (1959).
47. B. G. Achhammer, *Mod. Plast.* **35**, 131 (1959).
48. K. L. Hoy, *J. Paint Technol.* **43**, 76 (1970).
49. A. F. M. Martin, *Handbook of Solubility Parameters and Other Cohesion Parameters*, CRC Press, Inc., Boca Raton, Fla., 1983.
50. J. H. Hildebrand and R. L. Scott, *The Solubility of Non-Electrolytes*, 3rd ed., Rheinhold Publishing Corp., New York, 1949.
51. P. A. Small, *J. Appl. Chem.* **3**, 71 (1953).
52. H. Burrell, *Off. Dig. Fed. Soc. Paint Technol.* 726 (Oct. 1955).
53. J. L. Gardon, *J. Paint Technol.* **38**, 43 (1966).
54. A. Rudin and H. K. Johnston, *J. Paint Technol.* **43**(559), 39 (1971).
55. T. P. Forbarth, *Chem. Eng.* **69**(5), 96 (1962).
56. M. Salkind, E. H. Riddle, and R. W. Keefer, *Ind. Eng. Chem.* **51**, 1328 (1959).
57. H. Warson, *The Applications of Synthetic Resin Emulsions*, Ernest Benn Ltd., London, 1972.
58. R. F. B. Davies and G. E. J. Reynolds, *J. Appl. Polym. Sci.* **12**, 47 (1968).
59. A. R. Burgess, *Chem. Ind.* 78 (1952).
60. M. Tabata, G. Nilsson, and A. Lund, *J. Polym. Sci., Polym. Chem. Ed.* **21**, 3257 (1983).
61. R. K. Graham, *J. Polym. Sci.* **38**, 209 (1959).
62. W. Burlant, J. Minsch, and C. Taylor, *J. Polym. Sci., Part A* **2**, 57 (1964).
63. S. Sakuyama and co-workers, *Chem. Technol.* 350 (June 1973).
64. F. T. Maler and W. Bayer, *Encycl. Chem. Process Des.* **1**, 401 (1976).
65. D. J. Hadley and E. M. Evans, *Propylene and Its Industrial Derivatives*, John Wiley & Sons, Inc., New York, 1973, pp. 416–497.
66. U.S. Pat. 3,875,212 (1975), T. Ohrui (to Sumitomo Chemical).
67. *Storage and Handling of Acrylic and Methacrylic Esters and Acids, CM-17*, Rohm and Haas Co., Philadelphia, Pa.

68. *Analytical Methods for the Acrylic Monomers, CM-18*, Rohm and Haas Co., Philadelphia, Pa.
69. *Acrylate Monomers, Bulletin F-40252*, Union Carbide Corp., New York.
70. *Celanese Acrylates, Product Manual N-70-1*, Celanese Chemical Co., New York.
71. *State of California Health and Welfare Agency Safe Drinking Water and Toxic Enforcement Act of 1986*.
72. M. H. Mackoy and H. W. Melville, *Trans. Faraday Soc.* **45**, 323 (1949).
73. G. M. Burnett and L. D. Loan, *International Symposium on Macromolecular Chemistry*, Prague, 1957, p. 113.
74. U.S. Pats. 2,367,660 and 2,367,661 (Jan. 23, 1945), C. L. Agre (to E. I. du Pont de Nemours & Co., Inc.).
75. A. Chapiro, *Radiative Chemistry of Polymeric Systems*, Wiley-Interscience, New York, 1972.
76. *Preparation, Properties and Uses of Acrylic Polymers*, CM-19, Rohm and Haas Co., Philadelphia, Pa.
77. T. G. Fox Jr. and R. Loshock, *J. Am. Chem. Soc.* **75**, 3544 (1953).
78. J. L. O'Brien, *J. Am. Chem. Soc.* **77**, 4757 (1955).
79. E. P. Bonsall, *Trans. Faraday Soc.* **49**, 686 (1953).
80. P. G. Griffiths and co-workers, *Tetrahedron Lett.* **23**, 1309 (1982).
81. G. V. Schulz and G. Henrici, *Makromol. Chem.* **18/19**, 473 (1956).
82. F. R. Mayo and A. A. Miller, *J. Am. Chem. Soc.* **80**, 2493 (1956).
83. M. M. Mogilevich, *Russ. Chem. Rev.* **48**, 199 (1979).
84. D. A. Tirrell, in J. I. Kroschwitz, ed., *Encyclopedia of Polymer Science and Engineering*, Wiley-Interscience, New York, 1986, pp. 192–233.
85. O. Yoshiahi and T. Imato, *Rev. Phys. Chem. Jpn.* **42**(1), 34 (1972).
86. F. W. Billmeyer Jr., *Textbook of Polymer Chemistry*, Interscience Publishers, New York, 1957.
87. *Emulsion Polymerization of Acrylic Monomers*, CM-104, Rohm and Haas Co., Philadelphia, Pa.
88. J. J. Uibel and F. J. Dinon, *J. Polym. Sci., Polym. Chem. Ed.* **21**, 1773 (1983).
89. F. A. Bovey, *High Resolution NMR of Macromolecules*, Academic Press, New York, 1972.
90. M. S. Matheson and co-workers, *J. Am. Chem. Soc.* **73**, 5395 (1951).
91. T. G. Fox and R. Gratch, *Ann. N.Y. Acad. Sci.* **57**, 367 (1953).
92. L. Maduga, *An. Quim.* **65**, 993 (1969).
93. P. G. Griffiths, E. Rizzardo, and D. H. Solomon, *J. Macromol. Sci., Chem.* **17**, 45 (1982).
94. J. G. Kloosterboer and H. L. Bressers, *Polym. Bull.* **2**, 205 (1982).
95. *The Manufacture of Acrylic Polymers, CM-107*, Rohm and Haas Co., Philadelphia, Pa.
96. *The Manufacture of Ethyl Acrylate–Acrylic Acid Copolymers, TMM–48*, Rohm and Haas Co., Philadelphia, Pa.
97. *Bulk Storage and Handling of Acryloid Coating Resins, C-186*, Rohm and Haas Co., Philadelphia, Pa.
98. P. A. Lovell and M. S. El-Aasser *Emulsion Polymerization and Emulsion Polymers*, John Wiley and Sons, Inc., New York, 1997.
99. R. G. Gilbert, *Emulsion Polymerization: A Mechanistic Approach*, Academic Press, New York, 1995.
100. U.S. Pat. 5,521,266 (May 28, 1996), W. Lau (to Rohm and Haas Co.).
101. B. B. Kine and G. H. Redlich, in D. T. Wasan, ed., *Surfactants in Chemical/Process Engineering*, Marcel Dekker, Inc., New York, 1988, p. 163.
102. A. E. Alexander, *J. Oil Colour Chem. Assoc.* **42**, 12 (1962).
103. C. E. McCoy Jr., *Off. Dig. Fed. Soc. Paint Technol.* **35**, 327 (1963).
104. A. F. Sirianni and R. D. Coleman, *Can. J. Chem.* **42**, 682 (1964).

105. G. L. Brown, *Off. Dig. Fed. Soc. Paint Technol.* **28**, 456 (1956).
106. Brit. Pat. 940,366 (Oct. 30, 1963), P. R. van Ess (to Shell Oil).
107. U.S. Pat. 3,080,333 (Mar. 5, 1963), R. J. Kray and C. A. DeFazio (to Celenese).
108. A. R. M. Azad, R. M. Fitch, and J. Ugelstad, *Colloidal Dispersions Micellar Behavior* (ACS Symp. Ser. No. 9), American Chemical Society, Washington, D.C., 1980.
109. H. Fikentscher, H. Gerrens, and H. Schuller, *Angew. Chem.* **72**, 856 (1960).
110. A. S. Sarac, *Prog. Polym. Sci.* **24**, 1149 (1999).
111. U.S. Pat. 3,458,466 (July 29, 1969), W. J. Lee (to The Dow Chemical Company).
112. U.S. Pat. 3,344,100 (Sept. 26, 1967), F. J. Donat and co-workers (to B. F. Goodrich Co.).
113. H. Warson, *Makromol. Chem. Suppl.* **10/11**, 265 (1985).
114. G. F. D'Alelio, *Fundamental Principles of Polymerization*, John Wiley & Sons, Inc., New York, 1952.
115. G. S. Whitby and co-workers, *J. Polym. Sci.* **16**, 549 (1955).
116. B. N. Rutovshii and co-workers, *J. Appl. Chem. USSR* **26**, 397 (1953).
117. H. Warson, *Polym. Paint Colour J.* **178**, 625 (1988).
118. H. Warson, *Polym. Paint Colour J.* **178**, 865 (1988).
119. L. J. Hughes and G. L. Brown, *J. Appl. Polym. Sci.* **7**, 59 (1963).
120. B. N. Kishore and co-workers, *J. Polym. Sci., Polym. Chem. Ed.* **24**, 2209 (1986).
121. G. Graczyk and V. Hornof, *J. Macromol. Sci., Chem.* **12**, 1633 (1988).
122. O. Y. Mansour and A. B. Moustafa, *J. Polym. Sci., Polym. Chem. Ed.* **13**, 2795 (1975).
123. T. Nagabhushanam and M. Santoppa, *J. Polym. Sci., Polym. Chem. Ed.* **14**, 507 (1976).
124. L. Zhi-Chong and co-workers, *J. Macromol. Sci., Chem.* **12**, 1487 (1988).
125. C. E. Brockway and K. B. Moser, *J. Polym. Sci., Part A-1* **1**, 1025 (1963).
126. G. Smets, A. Poot, and G. L. Dunean, *J. Polym. Sci.* **54**, 65 (1961).
127. C. H. Bamford and E. F. T. White, *Trans. Faraday Soc.* **52**, 719 (1956).
128. J. A. Hicks and H. W. Melville, *Nature (London)* **171**, 300 (1953).
129. I. Sahata and D. A. I. Goring, *J. Appl. Polym. Sci.*, **20**, 573 (1976).
130. R. K. Graham, M. J. Gluchman, and M. J. Kampf, *J. Polym. Sci.* **38**, 417 (1959).
131. D. J. Angier, E. D. Farlie, and W. F. Watson, *Trans. Inst. Rubber Ind.* **34**, 8 (1958).
132. W. J. Burlant and A. S. Hoffman, *Block and Graft Polymers*, Reinhold Publishing Corp., New York, 1960.
133. R. J. Ceresa, *Block and Graft Copolymers*, Butterworth, Inc., Washington, D.C., 1962.
134. M. Szwarc, *J. Polym. Sci., Part A: Polym. Chem.* **36**, ix, (1998).
135. T. E. Patten and K. Matyjaszewski, *Adv. Mater.* **10**, 901 (1998).
136. M. K. Georges and co-workers, *Macromolecules* **26**, 2987 (1993).
137. S. A. F. Bon and co-workers, *Macromolecules*, **30**, 324 (1997).
138. C. J. Hawker and co-workers, *Macromolecules* **31**, 213 (1998).
139. J. S. Wang and K. Matyjaszewski, *Macromolecules* **28**, 7901 (1995).
140. T. E. Patten and co-workers, *Science* **272**, 866 (1996).
141. S. Coca and co-workers, *J. Polym. Sci., Part A: Polym. Chem.* **36**, 1417 (1998).
142. K. Matyjaszewski, S. Coca, and C. B. Jasiaczek, *Macromol. Chem. Phys.* **198**, 4001 (1997).
143. S. Coca and K. Matyjaszewski, *Polym. Prepr. (Am. Chem. Soc., Div. Polym. Chem.)* **38**, 691 (1997).
144. D. McGinniss, *Ultraviolet Light Induced Reactions in Polymers* (ACS Symp. Ser. No. 25), American Chemical Society, Washington, D.C., 1976.
145. J. W. Vanderhoff, *J. Polym. Sci.* **38** (1959).
146. S. P. Pappas, ed., *U.V. Curing: Science and Technology*, Technology Marketing Corp., Stamford, Conn., 1978.
147. U.S. Pat. 3,418,295 (Dec. 24, 1968), A. C. Schwenthaler (to E. I. du Pont de Nemours & Co., Inc.).
148. V. D. McGinnis, SME Technical Paper (Ser.) FC 76-486, 1976.

149. J. V. Koleche, *Photochemistry of Cycloaliphatic Epoxides and Epoxy Acrylates*, Vol. **I**, ASTM International, 1989.
150. *The Curing of Coatings with Ultra-Violet Radiation, D8667 G.D.*, Tioxide of Canada, Sorel, P.Q., Canada.
151. T. A. Du Plessis and G. De Hollain, *J. Oil Colour Chem. Assoc.* **62**, 239 (1979).
152. M. L. Miller and C. E. Rauhut, *J. Polym. Sci.* **38**, 63 (1959).
153. B. Garret, *J. Am. Chem. Soc.* **81**, 1007 (1959).
154. A. Kawasahi and co-workers, *Makromol. Chem.* **49**, 76 (1961).
155. G. Smets and W. Van Hurnbeeck, *J. Polym. Sci., Part A-1* **1**, 1227 (1963).
156. W. E. Goode, R. P. Fellman, and F. H. Owens, in C. G. Overberger, ed., *Macromolecular Synthesis*, Vol. **1**, John Wiley & Sons, Inc., New York, 1963, p. 25.
157. J. Furukawa, T. Tsuruta, and T. Makimoto, *Makromol. Chem.* **42**, 162 (1960).
158. T. Makmoto, T. Tsuruta, and J. Furukawa, *Makromol. Chem.* **50**, 116 (1961).
159. Y. Heimei and co-workers, in N. A. J. Platzer, ed., *Appl. Polym. Symp.*, Vol. **26**, 1975, p. 39.
160. D. E. Glusker and co-workers, *J. Polym. Sci.* **49**, 315 (1961).
161. D. J. Cram and K. R. Kopecky, *J. Am. Chem. Soc.* **81**, 2748 (1959).
162. H. Yuki and co-workers, in O. Vogl and J. Furukawan, eds., *Ionic Polymerization*, Marcel Dekker, Inc., New York, 1976.
163. M. T. Reetz, *Angew. Chem., Int. Ed. Engl.* **27**, 994 (1988).
164. V. V. Korshak and co-workers, *Makromol. Chem. Suppl.* **6**, 55 (1984).
165. C. P. Bosmyak, I. W. Parsons, and J. N. Hay, *Polymer* **21**, 1488 (1980).
166. F. L. Keohan and co-workers, *J. Polym. Sci., Polym. Chem. Ed.* **22**, 679 (1984).
167. Y. D. Lee and H. B. Tsai, *Makromol. Chem.* **190**, 1413 (1989).
168. E. A. Collines and co-workers, *J. Coat. Technol.* **47**, 35 (1975).
169. E. B. Bradford and J. W. Vanderhoff, *J. Polym. Sci. Part C*, **1** 41 (1963).
170. T. F. Protxman and G. L. Brown, *J. Appl. Polym. Sci.* 81 (1960).
171. P. W. Allen, *Technique of Polymers Characterization*, Butterworths, London, 1959.
172. *Dilute Solution Properties of Acrylic and Methacrylic Polymers, SP-160*, Rohm and Haas Co., Philadelphia, Pa.
173. M. Harmon and J. King, U.S. NTIS AD Rept. AD-A0I7443, p. 142, 1974.
174. R. E. Harren, A. Mercurio, and J. D. Scott, *Aust. Oil Colour Chem. Assoc. Proc. News* 17 (Oct. 1977).
175. *Resin Review*, Vol. **18**, Rohm and Haas Co., Philadelphia, Pa., 1968.
176. R. N. Washburne, *Am. Paint Coatings J.* **67**, 40 (1983).
177. R. P. Hopkins, E. W. Lewandowski, and T. E. Purcell, *J. Paint Technol.* **44**, 85 (1972).
178. T. E. Purcell, *Am. Paint J.* (June 1972).
179. Technical Practices Committee, *Materials Performance*, Vol. **15**, National Assoc. of Corrosion Engineers, Houston, Tex., 1976, pp. 4, 13.
180. K. E. Buffington, *Maint. Eng.* (Mar. 1976).
181. I. K. Schahidi, J. C. Trebellas, and J. A. Vona, *Paint Varn. Prod.* **64**, 39 (1974).
182. C. B. Rybyn and co-workers, *J. Paint Technol.* **46**, 60 (1974).
183. *Multifunctional Acrylates in Radiation Curing*, Celanese Co., New York.
184. C. H. Carder, *Paint Varn. Prod.* **64**, 19 (1974).
185. *Materials for Photocurable Coatings and Inks*, Union Carbide Corp., New York.
186. R. A. Hickner and L. M. Ward, *Paint Varn. Prod.* **64**, 27 (1974).
187. F. Wingler and co-workers, *Farbe Lack* **78**, 1063 (1972).
188. R. Muller, *Farbe Lack* **78**, 1070 (1972).
189. J. K. Rankin, *J. Oil Colour Chem. Assoc.* **56**, 112 (1973).
190. F. A. Kyrlova, *Lakokras. Mater. Ikh Primen.* **3**, 20 (1969).
191. J. B. Zicherman, *Am. Paint J.* **56**(46), (23–28 1972).
192. U.S. Pat. 1,535,228 (Aug. 16, 1968), K. Shibayama (to Eiki Jidaito).

193. F. Beck and co-workers, *Farbe Lack* **73**, 298 (1967).
194. A. Mercurio and S. N. Lewis, *J. Paint Technol.* **47**, 37 (1975).
195. W. H. Brendley Jr. and E. C. Carl, *Paint Varn. Prod.* **63**, 23 (1973).
196. M. R. Yunaska and J. E. Gallagher, *Resin Review*, Vol. **19**, Rohm and Haas Co., Philadelphia, Pa., 1969, pp. 1–3.
197. G. Allyn, *Materials and Methods*, Reinhold Publishing Co., New York, 1956.
198. *Protecting the Surfaces of Copper and Copper-Base Alloys*, International Copper Research Association, New York.
199. R. R. Kuhn, N. Roman, and J. D. Whiteman, *Mod. Paint Coatings* **71**, 50 (1981).
200. J. C. Thiabault, P. R. Sperry, and E. J. Schaller, in J. E. Glass, ed., *Water-Soluble Polymers*, American Chemical Society, Washington, D.C., 1986, p. 375.
201. A. J. Reuvers, *Prog. Org. Coatings* **35**, 171 (1999).
202. T. L. Maver, *J. Coat. Technol.* **64**, 45 (1992).
203. T. Murakami, R. H. Fernando, and J. E. Glass, *Surf. Coat. Int.* **76**, 8 (1993).
204. N. Sutterlin, *Makromol. Chem. Suppl.* **10/11**, 403 (1985).
205. V. J. Moser, *Resin Review*, Vol. **14**, Rohm and Haas Co., Philadelphia, Pa., 1964, p. 25.
206. D. I. Lunde, *Nonwoven Fabrics Forum, Clemson University*, June 15–17, 1982.
207. U.S. Pat. 3,157,562 (Nov. 17, 1964), B. B. Kine, V. J. Moser, and H. A. Alps (to Rohm and Haas Co.).
208. U.S. Pat. 3,101,292 (Aug. 20, 1963), B. B. Kine and N. A. Matlin (to Rohm and Haas Co.).
209. J. R. Lawrence, *Resin Review*, Vol. **6**, Rohm and Haas Co., Philadelphia, Pa., 1956, p. 12.
210. U.S. Pat. 2,931,749 (Apr. 5, 1960), B. B. Kine and N. A. Matlin (to Rohm and Haas Co.).
211. G. C. Kantner, *Text. World* **132**, 89 (1982).
212. G. C. Kantner, *Am. Text.* **12**, 30 (Feb. 1983).
213. L. Thompson and H. Mayfield, *AATCC National Technical Conference*, 1974, p. 258.
214. F. X. Chancler and J. G. Brodnyan, *Resin Review*, Vol. **23**, Rohm and Haas Co., Philadelphia, Pa., 1973, p. 3.
215. V. J. Moser and D. G. Strong, *Am. Dyest. Rep.* **55**, 52 (1966).
216. U.S. Pat. 2,883,304 (Apr. 21, 1959), B. B. Kine and A. C. Nuessle (to Rohm and Haas Co.).
217. Brit. Pat. 1,011,041 (1962), K. Craemer (to Badische Anilin).
218. K. F. Foley and S. G. Chu, *Adhes. Age* 24 (Sept. 1986).
219. D. Satas, *Adhes. Age* 28 (Aug. 1988).
220. J. J. Latimer, *Pulp Pap. Can.* **82**, 83 (1981).
221. J. E. Young and J. J. Latimer, *South. Pulp Pap. J.* **45**, 5 (1982).
222. P. J. McLaughlin, *Tappi* **42**, 994 (1959).
223. L. Mlynar and R. W. McNamec Jr., *Tappi* **55**, 359 (1972).
224. F. L. Schucker, *Resin Review*, Vol. **7**, Rohm and Haas Co., Philadelphia, Pa., 1957, p. 20.
225. H. C. Adams, T. J. Drennen, and L. E. Kelley, *Tappi* **48**, 486 (1965).
226. J. A. Handscomb, *J. Soc. Leather Trades' Chem.* **43**, 237 (1959).
227. W. C. Prentiss, *J. Am. Leather Chem. Assoc.* **71**, 54 (1976).
228. J. A. Lavelle and P. E. Wright, *Resin Review*, Vol. **24**, Rohm and Haas Co., Philadelphia, Pa., 1974, p. 3.
229. J. R. Johnson, *Resin Review*, Vol. **11**, Rohm and Haas Co., Philadelphia, Pa., 1961, p. 3.
230. P. E. Wright and H. C. Young, *Resin Review*, Vol. **24**, Rohm and Haas Co., Philadelphia, Pa., 1974, p. 17.

231. P. H. Dougherty and H. T. Freund, *Resin Review*, Vol. **17**, Rohm and Haas Co., Philadelphia, Pa., 1967, p. 3.
232. L. S. Frankel, D. A. Perry, and J. J. Lavelle, *Resin Review*, Vol. **32**, Rohm and Haas Co., Philadelphia, Pa., 1982, p. 1.
233. J. T. Lutz Jr., in Ref. 197, p. 18.
234. M. Cohen, *Proc. Fl. State Hortic. Soc.* **72**, 56 (1959).
235. *Resin Review*, Vol. **16**, Rohm and Haas Co., Philadelphia, Pa., 1966, p. 12.
236. T. M. Vial, *Rubber Chem. Technol.* **44**, 344 (1971).
237. P. Fram, in N. M. Bikales, ed., *Encyclopedia of Polymer Science and Technology*, Vol. **1**, Interscience Publishers, New York, 1964, pp. 226–246.
238. D. L. Schultz, *Rubber World* **182**, 51 (May 1980).

ROBERT V. SLONE
Rohm and Haas Company

ACRYLONITRILE AND ACRYLONITRILE POLYMERS

Introduction

Acrylonitrile (also called acrylic acid nitrile, propylene nitrile, vinyl cyanide, propenoic acid nitrile) is a versatile and reactive monomer (1) which can be polymerized under a wide variety of conditions (2) and copolymerized with an extensive range of other vinyl monomers (3). Since its U.S. commercial debut in 1940, acrylonitrile has been one of the most important building blocks of the polymer industry. This has been demonstrated by the steady production growth of acrylonitrile to more than 4,000,000 t produced worldwide each year. Today, over 90% of the worldwide acrylonitrile production each year uses the Sohio-developed propylene ammoxidation process. Acrylonitrile is among the top 50 chemicals produced in the United States, as a result of the tremendous growth in its use as a starting material for a wide range of chemicals and polymer products. Acrylic fibers remain the largest user of acrylonitrile. Other significant uses are in styrene–acrylonitrile (SAN) and acrylonitrile–butadiene–styrene (ABS) resins and nitrile elastomers, and as an intermediate in the production of adiponitrile and acrylamide.

Acrylonitrile Monomer

Physical Properties. Acrylonitrile (C_3H_3N, mol wt = 53.064) is an unsaturated molecule having a carbon–carbon double bond conjugated with a nitrile group. It is a colorless liquid, with the faintly pungent odor of peach pits. Its properties are summarized in Table 1. Acrylonitrile is miscible with most organic solvents, including acetone, benzene, carbon tetrachloride, ether, ethanol,

Encyclopedia of Polymer Science and Technology. Copyright John Wiley & Sons, Inc. All rights reserved.

Table 1. Physical Properties of Acyrlonitrile Monomer[a]

Property	Value
Molecular weight	53.06
Boiling point, °C	
At 101.3 kPa[b]	77.3
At 66.65 kPa	64.7
At 33.33 kPa	45.5
At 13.33 kPa	23.6
At 6.665 kPa	8.7
Critical pressure, kPa	3.535×10^3
Critical temperature, °C	246.0
Cryoscopic constant, mol%/°C	2.7
Density, g/L	
At 20°C	806.0
At 25°C	800.4
At 41°C	783.9
Dielectric constant at 33.5 MHz	38
Dipole moment, C·m[c]	
Liquid	1.171×10^{-29}
Vapor	1.294×10^{-29}
Entropy, vapor at 25°C, 101.3 kPa, J/(mol·K)[d]	273.9
Entropy of polymerization, liquid, 25°C, J/(mol·K)	−109[e]
Explosive mixture with air at 25°C, vol%	
Lower limit	3.05
Upper limit	17.0 ± 0.5
Flash point (tag open cup), °C	−5
Freezing point, °C	-83.55 ± 0.05
Gibbs energy of formation, vapor at 25°C, kJ/mol	195.4
Heat capacity, specific, liquid, kJ/(kg·K)	2.094
Heat capacity, specific, vapor, kJ/(kg·K)	
At 50°C, 101.3 kPa	1.204
T (K) from 77–1000°C, at 101.3 kPa	$0.53 + 26.23 \times 10^{-4}T$ $-86.03 \times 10^{-8}T^2$
Heat of combustion, liquid at 25°C, kJ/mol	-1.7615×10^3
Heat of formation at 25°C, kJ/mol	
Vapor	189.83
Liquid	151.46
Heat of fusion, kJ/mol	6.635×10^3
Heat of polymerization, kJ/mol	-72.4 ± 2.1
Heat of polymerization at 74.5°C, kJ/mol	−76.5[f]
Heat of vaporization at 101.3 kPa, kJ/mol	32.65
Ignition temperature, °C	481.0
Molar refraction, D line	15.67
Parachor at 40.6°C	151.1
Polarizability at 25°C	266
Refractive index	
$n^{20}{}_{\mathrm{D}}$	1.3911–1.39142
$n^{25}{}_{\mathrm{D}}$	1.3888
t from 10–35°C	$n^{t}{}_{\mathrm{D}} = 1.4022 - 0.000539t$
$n^{20}{}_{\mathrm{C}}$	1.38836
$n^{20}{}_{\mathrm{F}}$	1.39890

Table 1. (Continued)

Property	Value
$n^{20}{}_G$	1.4078
Solubility parameter, $(J/mL)^{1/2}$	21.48
Surface tension at 24°C, mN/m (=dyn/cm)	27.3
Surface tension of aqueous solution, c from 0–6 wt%, d, mN/m (=dyn/cm)	$c = 0.223d - 0.0018d^2 + 0.00013d^3$
Vapor density, relative	1.83 (air = 1.0)
	$\log p = 6.6428 - 1.6447 \times 10^3/T$ (K)
Viscosity at 25°C, mPa·s (=cP)	0.34

[a] Refs. 4, 13, and 14.
[b] To convert kPa to mm Hg, multiply by 7.5.
[c] To convert C·m to debyes, multiply by 2.997×10^{29}.
[d] To convert J to cal, divide by 4.184.
[e] Ref. 15.
[f] Ref. 16.

ethyl acetate, ethylene cyanohydrin, liquid carbon dioxide, methanol, petroleum ether, toluene, xylene, and some kerosenes. Table 2 lists the azeotrope compositions of acrylonitrile with some of those solvents. Other important properties are reported in the literature: vapor pressure, solubility in water, and partial vapor pressure over its aqueous solutions (4,5); the partition of acrylonitrile between water and styrene (6); vapor–liquid equilibria and boiling temperatures for acrylonitrile–acetonitrile–water systems (7); high pressure–volume isotherms and temperature–volume isobar (8); electron diffraction and infrared spectral data (4); and Raman and uv spectra (9).

Chemical Properties. The presence of both a double bond and an electron-accepting nitrile group permits acrylonitrile to participate in a large number of addition reactions and polymerizations. The chemical reactions of acrylonitrile have been discussed in great length and detail (10,11). A brief summary follows.

Reactions of the Nitrile Group.

Hydration and Hydrolysis. In concentrated 85% sulfuric acid, partial hydrolysis of the nitrile group produces acrylamide sulfate, which upon neutralization yields acrylamide; this is the basis for acrylamide's commercial production. In dilute acid or alkali, complete hydrolysis occurs to yield acrylic acid.

Table 2. Azeotrope Compositions of Acrylonitrile[a]

Other component	Boiling point, °C	Acrylonitrile, wt%
Benzene	73.3	47
Carbon tetrachloride	66.2	21
Chlorotrimethylsilane	57	7
Methanol	61.4	39
2-Propanol	71.7	56
Tetrachlorosilane	51.2	11
Water	71	88

[a] Ref. 4.

Alcoholysis. Reactions with primary alcohols, catalyzed by sulfuric acid, convert acrylonitrile to acrylic esters. In the presence of alcohol and anhydrous halides, imido ethers are formed.

Reactions with Olefins and Alcohols. The Ritter reaction occurs with compounds such as olefins and secondary and tertiary alcohols which form carbonium ions in acid, and N-substituted acrylamides are formed.

Reactions with Aldehydes and Methylol Compounds. Catalyzed by sulfuric acid, formaldehyde and acrylonitrile react to form either 1,3,5-triacrylylhexahydro-*s*-triazine or *N*,*N*′-methylenebisacrylamide, depending on the conditions. Similarly, in the presence of sulfuric acid, *N*-methylolbenzamide reacts to yield mixed bisamides. *N*-Methylolphthalimide reacts to give *N*-phthalimidomethylacrylamide.

Reactions of the Double Bond.

Diels-Alder Reactions. Acrylonitrile acts as a dienophile with conjugated carbon–carbon double bonds to form cyclic compounds. On the other hand, acrylonitrile can act as a diene. For example, with tetrafluoroethylene 2,2,3,3-tetrafluorocyclobutanecarbonitrile forms; and with itself, dimers of *cis*- and *trans*-cyclobutanedicarbonitriles form at high temperatures and pressure. The activation energy for acrylonitrile cyclodimerization has been reported to be 90.4 kJ/mol (12).

Hydrogenation. With metal catalysts, an excellent yield of propionitrile is attained, which can be further hydrogenated to propylamine.

Halogenation. At low temperatures, halogenation proceeds slowly to produce 2,3-dihalopropionitriles. In the presence of pyridine, addition of chlorine forms 2,3-dichloropropionitrile quantitatively. At elevated temperatures, without uv light, 2,2,3-trihalopropionitrile is obtained; with uv light, both 2,2,3- and 2,3,3-isomers are formed. Simultaneous chlorination and alcholysis occur to give 2,3-dichloropropionic acid esters.

Hydroformylation. In a process also known as the oxo-synthesis, acrylonitrile reacts with a mixture of hydrogen and carbon monoxide, catalyzed by cobalt octacarbonyl, to give β-cyanopropionaldehyde. This reacts with hydrogen cyanide and ammonia, and then hydrolysis produces glutamic acid on a large commercial scale.

Hydrodimerization. The reductive dimerization of acrylonitrile can be done either chemically or electrochemically to form adiponitrile. Hydrodimerization with its derivatives also takes place.

Reactions with Azo Compounds. Meerwein reactions of diazonium halides with acrylonitrile take place at low temperatures, catalyzed by cupric chloride, to yield 2-halo-3-arylpropionitriles. Reactions with diazomethane compounds lead to pyrazolines and finally cyclopropanes. Reactions with 9-diazofluorene produce a cyanocyclopropane derivative, with the generation of nitrogen. Phenyl azide reacts with acrylonitrile to yield a heterocyclic nitrile at room temperature or an open-chain nitrile at elevated temperatures.

Reactions of Both Functional Groups. Hydrolysis of acrylonitrile catalyzed by hydrochloric acid yields 3-chloropropionic acid. Alcoholysis and chlorination occur simultaneously in the presence of sulfuric acid. Similarly, alcoholysis and hydrochlorination also occur. Addition of both ammonia and hydrogen produces both trimethylenediamine and propylamine. Treatment of acrylonitrile

with hydrogen peroxide at neutral to slightly alkaline pH, yields glycidamide. Similarly, treatment with water, containing ammonium sulfide or a weak base, forms bis(2-carboxamidoethyl)sulfide or poly(β-alanine).

Cyanoethylation Reactions (Michael-Type Additions). Most compounds with a labile hydrogen atom can add on the double bond of acrylonitrile to form cyanoethyl groups; that is, the primary products are 3-substituted propionitriles.

$$CH_2{=}CHCN + RH \longrightarrow RCH_2CH_2CN$$

A large number of useful reactions fall into this category. Examples of these reactions are carbon cyanoethylation in which aldehydes, ketones, esters, nitriles, nitro compounds, sulfones, aliphatic and aromatic hydrocarbons, or haloforms add to acrylonitrile; nitrogen cyanoethylation where amines, ammonia, anilines, or amides add; oxygen cyanoethylation where alcohols, phenols, water, hydroperoxides, oximes, or hydrogen peroxide react; sulfur cyanoethylation in which sulfides, bisulfides, or sulfhydryl compounds add; hydrogen halide cyanoethylaphonates, boranes, silanes, or tin hydrides. In addition, many natural and synthetic polymers possessing labile hydrogen atoms, such as cotton, jute, gums, lignin, proteins, modified cellulose, poly(vinyl alcohol) (PVC), and acetone–formaldehyde and methyl ethyl ketone–formaldehyde condensates, react with acrylonitrile to yield cyanoethyl derivatives.

Manufacture of Acrylonitrile. Acrylonitrile is produced in commercial quantities almost exclusively by the vapor-phase catalytic propylene ammoxidation process developed by Sohio (now BP Chemicals) (17).

$$C_3H_3 + NH_3 + 3/2\ O_2 \xrightarrow{\text{catalyst}} C_3H_3N + 3\ HO_2$$

A schematic diagram of the commercial process is shown in Figure 1. The commercial process uses a fluid-bed reactor in which propylene, ammonia, and air contact a solid catalyst at 400–510°C and 49–196 kPa (0.5–2.0 kg/cm^2) gage. It is a single-pass process with about 98% conversion of propylene, and uses about 1.1 kg of propylene per kg of acrylonitrile produced. Useful by-products from the process are HCN (about 0.1 kg per kg of acrylonitrile), which is used primarily in the manufacture of methyl methacrylate, and acetonitrile (about 0.03 kg per kg of acrylonitrile), a common industrial solvent. In the commercial operation the hot reactor effluent is quenched with water in a countercurrent absorber and any unreacted ammonia is neutralized with sulfuric acid. The resulting ammonium sulfate can be recovered and used as a fertilizer. The absorber off-gas containing primarily N_2, CO, CO_2, and unreacted hydrocarbon is either vented directly or first passed through an incinerator to combust the hydrocarbons and CO. The acrylonitrile-containing solution from the absorber is passed to a recovery column that produces a crude acrylonitrile stream overhead that also contains HCN. The column bottoms are passed to a second recovery column to remove water and produce a crude acetonitrile mixture. The crude acetonitrile is either incinerated or further treated to produce solvent quality acetonitrile. Acrylic fiber quality (99.2% minimum) acrylonitrile is obtained by fractionation of the crude acrylonitrile mixture to remove HCN, water, light ends, and high boiling impurities. Disposal of

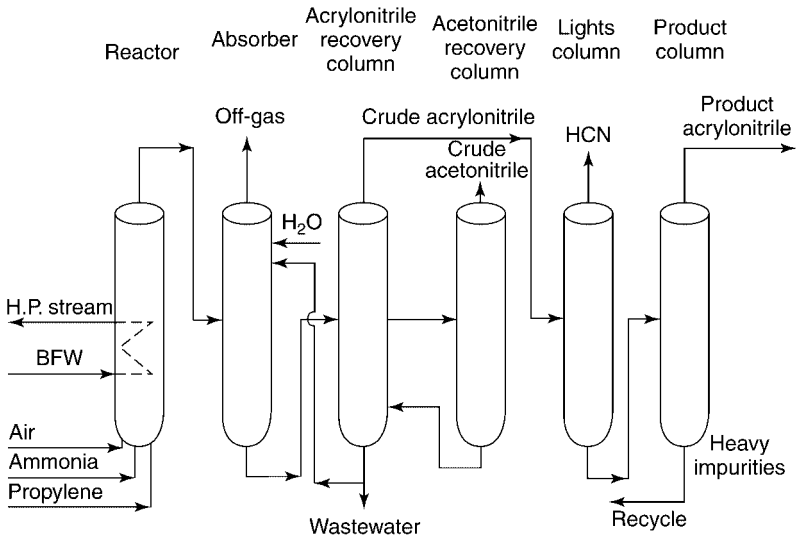

Fig. 1. Process flow diagram of the commercial propylene ammoxidation process for acrylonitrile. BFW is boiler feed water.

the process impurities has become an increasingly important aspect of the overall process, with significant attention being given to developing cost-effective and environmentally acceptable methods for treatment of the process waste streams. Current methods include deep-well disposal, wet air oxidation, ammonium sulfate separation, biological treatment, and incineration (18).

Although the manufacture of acrylonitrile from propylene and ammonia was first patented in 1949 (19), it was not until 1959 when Sohio developed a catalyst capable of producing acrylonitrile with high selectivity, that commercial manufacture from propylene became economically viable (20). Production improvements over the past 30 years have stemmed largely from development of several generations of increasingly more efficient catalysts. These catalysts are multicomponent-mixed metal oxides mostly based on bismuth–molybdenum oxide. Other types of catalysts that have been used commercially are based on iron–antimony oxide, uranium–antimony oxide, and tellurium–molybdenum oxide.

Fundamental understanding of these complex catalysts and the surface-reaction mechanism of propylene ammoxidation has advanced substantially since the first commercial plant began operation. Mechanisms for selective ammoxidation of propylene over bismuth molybdate and antimonate catalysts have been published (21). The rate-determining step is the abstraction of an α-hydrogen of propylene by oxygen in the catalyst to form a π-allyl complex on the surface (21–23). Lattice oxygens from the catalyst participate in further hydrogen abstraction, followed by oxygen insertion to produce acrolein in the absence of ammonia or nitrogen insertion to form acrylonitrile in the presence of ammonia (24–27). The oxygens removed from the catalyst in these steps are replenished by gas-phase oxygen, which is incorporated into the catalyst structure at a surface site separate from the site of propylene reaction. In the ammoxidation reaction, ammonia

is activated by an exchange with O^{2-} ions to form isoelectronic NH^{2-} moieties according to the following:

$$NH_3 + O^{2-} \longrightarrow NH^{2-} + H_2O$$

These are the species inserted into the allyl intermediate to produce acrylonitrile.

The active site on the surface of selective propylene ammoxidation catalyst contains three critical functionalities associated with the specific metal components of the catalyst (28–30): an α-H abstraction component such as Bi^{3+}, Sb^{3+}, or Te^{4+}; an olefin chemisorption and oxygen or nitrogen insertion component such as Mo^{6+} or Sb^{5+}; and a redox couple such as Fe^{2+}/Fe^{3+} or Ce^{3+}/Ce^{4+} to enhance transfer of lattice oxygen between the bulk and the surface of the catalyst. The surface and solid-state mechanisms of propylene ammoxidation catalysis have been determined using Raman spectroscopy (31,32), neutron diffraction (33–35), x-ray absorption spectroscopy (36,37), x-ray diffraction (38–40), pulse kinetic studies (26,27), and probe molecule investigations (41).

Other Acrylonitrile Processes. Processes rendered obsolete by the propylene ammoxidation process (42) include the ethylene cyanohydrin process (43–45) practiced commercially by American Cyanamid and Union Carbide in the United States and by I. G. Farben in Germany. The process involves the production of ethylene cyanohydrin by the base-catalyzed addition of HCN to ethylene oxide in the liquid phase at about 60°C, and subsequent dehydration.

A second commercial route to acrylonitrile used by DuPont, American Cyanamid, and Monsanto was the catalytic addition of HCN to acetylene (46). The reaction occurs by passing HCN and a 10:1 excess of acetylene into dilute HCl at 80°C in the presence of cuprous chloride as the catalyst. These processes use expensive C_2 hydrocarbons as feedstocks and thus have higher overall acrylonitrile production costs compared to the propylene-based process technology. The last commercial plants using these process technologies were shutdown by 1970.

Other routes to acrylonitrile, none of which achieved large-scale commercial application, are acetaldehyde and HCN (47), propionitrile dehydrogenation (48, 49), and propylene and nitric oxide (50,51).

Numerous patents have been issued disclosing catalysts and process schemes for the manufacture of acrylonitrile from propane. These include the direct heterogeneously catalyzed ammoxidation of propane to acrylonitrile, using mixed metal oxide catalysts (52–55).

A two-step process involving conventional nonoxidative dehydrogenation of propane to propylene in the presence of steam, followed by the catalytic ammoxidation to acrylonitrile of the propylene in the effluent stream without separation, is also disclosed (56).

Because of the large price differential between propane and propylene, which has ranged from $155/t to $355/t between 1987 and 1989, a propane-based process may have the economic potential to displace propylene ammoxidation technology eventually. Methane, ethane, and butane, which are also less expensive than propylene, and acetonitrile have been disclosed as starting materials for acrylonitrile synthesis in several catalytic process schemes (57,58).

Table 3. Worldwide Acrylonitrile Production,[a] 10^3 t

Region	1997	1998 (Estimated)
Western Europe	1073	1112
Eastern Europe	189	182
United States	1483	1324
Japan	729	730
Far East/Asia	779	841
African/Middle East	147	152
Latin America/Mexico	232	246
Total production	*4642*	*4587*

[a]Ref. 62.

Economic Aspects (Monomer). The propylene-based process developed by Sohio was able to displace almost all other commercial production technologies because of its substantial advantage in overall production costs, primarily due to lower raw material costs. Raw material costs, less by-product credits, account for about 60% of the total acrylonitrile production cost for a world-scale plant. The process has remained economically advantaged over other process technologies since the first commercial plant in 1960 because of the higher acrylonitrile yields, resulting from the introduction of improved commercial catalysts. Reported per-pass conversions of propylene to acrylonitrile have increased from about 65 to over 80% (17,59–61).

More than half of the worldwide acrylonitrile production is situated in Western Europe and the United States (Table 3). In the United States, production is dominated by BP Chemicals with the Sohio Process, with more than a third of the domestic capacity (Table 4). Nearly one-half of the U.S. production was exported in 1997 (Table 5), with most going to Far East Asia.

Far East Asian producers, especially in the People's Republic of China (PRC), have not been able to satisfy their increasing domestic demand in recent years. Consequently, the percentage of U.S. production exported grew from around 10% in the mid-1970s to approximately 42% in 1997.

In addition, the higher propylene costs relative to the United States generally makes it more economical to import acrylonitrile from the United States than to install new domestic production. Nevertheless, additions to Far East Asian acrylonitrile production capacity have been made in the 1990s, notably in South

Table 4. U.S. Acrylonitrile Producers[a]

Company	Approximate capacity,[b] 10^3 t/year
BP Chemcials	640
Solutia, Inc.	260
Sterling Chemicals	360
E. I. du Pont de Nemours & Co., Inc.	185
Cytec Indutries	220
Total production	*1665*

[a]Ref. 62.
[b]As of 1997.

Table 5. U.S. Acrylonitrile Exports,[a] 10^3 t

Destination	1997	1996
Far East/Asia	334	378
Japan	92	107
Western Europe	91	57
Canada	7	6
Latin America/Mexico	82	50
Middle East/Africa	91	57
Total export	*697*	*655*

[a]Ref. 62.

Table 6. World Acrylonitrile Demand, 10^3 t/year

Region	1998 (Estimated)	1997	1995	1990	1986
Western Europe	1109	1116	1045	1136	1187
Eastern Europe	141	150	171	311	262
Japan	726	723	674	664	640
North America	781	800	756	641	638
Far East/Asia	1297	1264	1025	646	462
Africa/Middle East	261	257	223	135	142
Latin America/Mexico	302	281	244	206	213
Total demand	*4617*	*4591*	*4138*	*3739*	*3543*

Korea. Table 6 provides a breakdown of worldwide demand between 1986 and 1998. Growth in demand has averaged about 3% per year.

Analytical and Test Methods. Numerous instrumental and chemical techniques are available for the determination of acrylonitrile. The method of choice is directed by the concentration and the medium involved. For direct assay of acrylonitrile, titrimetric procedures are frequently used. Dodecyl mercaptan reacts with acrylonitrile under base catalysis; excess mercaptan is then back-titrated with an acid bromate-iodide solution (63), or alternatively, for colored solutions, with silver nitrate (64). Hydrolysis of the nitrile with strong base generates ammonia, which can then be determined by Nessler's reagent (65).

For dilute solutions, both gas chromatography (66) and polarography (67) are rapid, sensitive, and precise. Small amounts of acrylonitrile can be separated from other components by azeotropic distillation with alcohols, followed by polarographic (67,68) or chromatographic (69,70) analysis.

For monitoring of acrylonitrile in ambient air, a measured quantity of an air sample is drawn through a charcoal tube, followed by quantitative extraction with a carbon disulfide–acetone (98:2) mixture for gas chromatographic analysis. Reliable results can be attained even when <1-ppm acrylonitrile is present (71). A comprehensive review and a description of the development of environmental test methods for air, water, soil, and sediment samples have been done (72).

Storage and Transport. Acrylonitrile must be stored in tightly closed containers in cool, dry, well-ventilated areas away from heat, sources of ignition, and incompatible chemicals. Storage vessels, such as steel drums, must be protected against physical damage, with outside detached storage preferred. Storage tanks

and equipment used for transferring acrylonitrile should be electrically grounded to reduce the possibility of static spark-initiated fire or explosion. Acrylonitrile is regulated in the workplace by OSHA (29 CFR 1910).

Acrylonitrile is transported by rail car, barge, and pipeline. Department of Transportation (DOT) regulations require labeling acrylonitrile as a flammable liquid and poison. Transport is regulated under DOT 49 CFR 172.101. Bill of lading description is Acrylonitrile, Inhibited, 3, 6.1, UN 1093, PGI, RQ.

Health and Safety Factors. Acrylonitrile is absorbed rapidly and distributed widely throughout the body following exposure by inhalation, skin contact, or ingestion. However, there is little potential for significant accumulation in any organ, with most of the compound being excreted primarily as metabolites in urine. Acrylonitrile is metabolized primarily by two pathways: conjugation with glutathione and oxidation. Oxidative metabolism leads to the formation of an epoxide, 2-cyanoethylene oxide, that is either conjugated with glutathione or directly hydrolyzed by epoxide hydrolase.

The acute toxicity of acrylonitrile is relatively high, with 4-h LC_{50}s in laboratory animals ranging from 300 to 900 mg/m^3 and LD_{50}s from 25 to 186 mg/kg (73,74). Signs of acute toxicity observed in animals include respiratory tract irritation and two phases of neurotoxicity, the first characterized by signs consistent with cholinergic overstimulation and the second being CNS (central nervous system) dysfunction, resembling cyanide poisoning. In cases of acute human intoxication, effects on the CNS, characteristic of cyanide poisoning, and effects on the liver, manifested as increased enzyme levels in the blood, have been observed.

Acrylonitrile is a severe irritant to the skin, eyes, respiratory tract, and mucous membranes. It is also a skin sensitizer. Acrylonitrile is a potent tumorigen in the rat. Tumors of the CNS, ear canal, and gastrointestinal tract have been observed in several studies following oral or inhalation exposure. The mechanism of acrylonitrile's tumorigenesis in the rat and the relevance of these findings to humans are not clear. Available data are insufficient to support a consensus view or a plausible mode of action. There is evidence for weak genotoxic potential, but no evidence of DNA-adduct formation in target tissues.

Indications are that oxidative stress and resulting oxidative DNA damage may play a role. There is extensive occupational epidemiology data on acrylonitrile workers. These investigations have not produced consistent, convincing evidence of an increase in cancer risk, although questions remain about the power of the database to detect small excesses of rare tumors. In 1998, The International Agency for Research on Cancer reevaluated the cancer data for acrylonitrile and made a rare decision to downgrade the cancer risk classification (from "probably carcinogenic to humans" to "possibly carcinogenic to humans") based primarily on the growing epidemiology database (75).

Experimental evaluations of acrylonitrile have not produced any clear evidence of adverse effects on reproductive function or development of offspring at doses below those producing paternal toxicity. The results of genotoxicity evaluations of acrylonitrile have been mixed. Positive findings *in vitro* have occurred mainly at exposures associated with cellular toxicity, and the most reliable *in vitro* tests have been negative.

Acrylonitrile will polymerize violently in the absence of oxygen if initiated by heat, light, pressure, peroxide, or strong acids and bases. It is unstable in

the presence of bromine, ammonia, amines, and copper or copper alloys. Neat acrylonitrile is generally stabilized against polymerization with trace levels of hydroquinone monomethyl ether and water.

Acrylonitrile is combustible and ignites readily, producing toxic combustion products such as hydrogen cyanide, nitrogen oxides, and carbon monoxide. It forms explosive mixtures with air and must be handled in well-ventilated areas and kept away from any source of ignition, since the vapor can spread to distant ignition sources and flash back.

Federal regulations, (40 CFR 261) classify acrylonitrile as a hazardous waste and it is listed as Hazardous Waste Number U009. Disposal must be in accordance with federal (40 CFR 262, 263, 264, 268, 270), state, and local regulations, and occur only at properly permitted facilities. Strict guidelines exist for clean-up and notification of leaks and spills. Federal notification regulations require that spills or leaks in excess of 100 lb (45.5 kg) be reported to the National Response Center. Substantial criminal and civil penalties can result from failure to report such discharges into the environment.

Acrylonitrile in Air. As a consequence of the 1977 interim results of both the Dow and DuPont studies, OSHA issued an emergency temporary standard on Jan. 17, 1978, specifying that the 8-h time-weighted average exposure to airborne acrylonitrile should not exceed 2 ppm; prior to 1977, 20 ppm was allowed. This standard covered all workplaces manufacturing or using acrylonitrile as a raw material, as well as fabrication facilities processing acrylonitrile-based polymers.

The permanent OSHA standard was implemented on Nov. 2, 1980, and it establishes a maximum permissible exposure limit for the vapor of acrylonitrile at 2 ppm as an 8-h time-weighted average, a ceiling limit at 10 ppm as a 15-min time-weighted average, and an action level at 1 ppm as an 8-h time-weighted average. Eye and skin contact with liquid acrylonitrile is prohibited. Other provisions include notification of regulated areas, methods of compliance, respiratory protection, emergency situations, protective clothing and equipment, housekeeping, waste disposal, hygiene facilities and practices, medical surveillance, employee information and training, signs and labels, record keeping, observation of monitoring, etc (76).

Environmental monitoring around 11 U.S. industrial sites which produce acrylonitrile, acrylamide, acrylic and modacrylic fibers, ABS, SAN, and nitrile elastomers was conducted in 1977. Acrylonitrile in the air was very low, ranging from 0.1 to 325 ng/L (4.3 ppm); and in soils or sediments, none (72). Studies of the atmosphere surrounding several types of commercial equipment processing a high acrylonitrile copolymer (Barex 210) indicate no evidence of acrylonitrile under normal operating conditions (1163). Some typical emission sources in the acrylonitrile-polymerization industry have been identified, control techniques suggested, and plan of action discussed (72). Approaches to remedy toxic chemical problems and provide a safe environment have also been suggested (77).

Acrylonitrile in Polymers. The very low amount of residual acrylonitrile in finished resins or products (ca 1 ppm in acrylic and modacrylic fibers, 20–50 ppm in ABS and SAN) does not pose the threat of acrylonitrile migration or release under normal intended use and handling conditions. Materials made from acrylonitrile are exempt from OSHA regulations, provided they are not capable of releasing acrylonitrile in airborne concentrations in excess of 1 ppm as a 9-h time-weighted

average, under the expected conditions of processing, use, and handling, and not heated above 77°C. Thus, certain finished polymers and their fabricated products, such as ABS, SAN, nitrile barrier resins, solid nitrile elastomers, and acrylic and modacrylic fibers, are exempt. Polymers and copolymers of acrylonitrile per se are riskless, but there is concern regarding acrylonitrile in food containers (qv) because of the possibility of migration from the finished products to the contained foodstuff. Therefore, the use of the polymers for food-contact applications requires compliance with governmental regulations.

Well-sealed containers of carbon or stainless, tin-coated metals, or brown glass bottles can be used and labeled DANGER, CONTAINS ACRYLONITRILE, CANCER HAZARD. They should be properly grounded and stored in a well-ventilated area free of excessive heat, flames, sparks, or other sources of ignition. Contamination with strong acids or bases, peroxides, or other initiators should be avoided. Acrylonitrile should be handled in a hood or a ventilated area where the concentration will not exceed OSHA-regulated standards. Testing should be done according to OSHA standards to ensure personnel protection and compliance. Protective equipment such as rubber gloves and apron (or liquid-proof uniform), goggles, and face shield should be used. When acrylonitrile is at or above the action level of 1 ppm, respiratory protection should be implemented. A half-face respirator with organic vapor cartridge can provide adequate protection up to 20 ppm; full-face respirator, up to 100 ppm; and supplied air respirator in positive pressure mode with full-face piece, helmet, suit, or hood, up to 4000 ppm.

Uses. Historically, synthetic fibers consume more than half of the acrylonitrile produced throughout the world, and ABS–SAN copolymers are the second largest users (see Table 7). Nitrile elastomers have the longest history of acrylonitrile usage. Worldwide consumption of acrylonitrile increased from 2.5×10^6 in 1976 to 4.6×10^6 t/year in 1998. The trend in consumption over this time period is shown in Table 7 for the principal uses of acrylonitrile: acrylic fiber, ABS resins, adiponitrile, nitrile rubbers, elastomers, and SAN resins. Since the 1960s acrylic fibers have remained the major outlet for acrylonitrile production in the United States and especially in Japan and the Far East. Acrylic fibers always contain a comonomer. Fibers containing 85 wt% or more acrylonitrile are usually referred to as *acrylics, whereas fibers containing 35–85 wt% acrylonitrile are* termed modacrylics (see FIBERS, ACRYLIC). Acrylic fibers are used primarily for the manufacture of apparel, including sweaters, fleece wear, and sportswear, as well as for home furnishings, including carpets, upholstery, and draperies. Acrylic

Table 7. Worldwide Acrylonitrile Uses and Consumption, 10^3 t

Use	1998 (Estimated)	1997	1995	1990	1986
Acrylic fibers	2615	2628	2313	2242	2350
ABS resins / SAN	1095	1079	996	781	598
Adiponitrile	494	477	446	330	281
NB (AN/BD) Copolymers	144	143	134	143	125
Miscellaneous	269	264	249	243	189
Total consumptions	*4617*	*4591*	*4138*	*3739*	*3543*

fibers consume about 57% of the acrylonitrile produced worldwide. Growth in demand for acrylic fibers in the 1990s was modest, between 2 and 3% per year, primarily from overseas markets. Domestic demand was flat.

ABS resins and adiponitrile are the fastest growing uses for acrylonitrile. ABS resins are second to acrylic fibers as an outlet for acrylonitrile. These resins normally contain about 25% acrylonitrile and are characterized by their chemical resistance, mechanical strength, and ease of manufacture. Consumption of ABS resins increased significantly in the 1980s and 1990s with its growing application as a specialty performance polymer in construction, automotive, machine, and appliance applications. Opportunities still exist for ABS resins to continue to replace more traditional materials for packaging, building, and automotive components. SAN resins typically contain between 25 and 30% acrylonitrile. Because of their high clarity, they are used primarily as a substitute for glass in drinking cups and tumblers, automobile instrument panels, and instrument lenses. The largest increase among the end uses for acrylonitrile has come from adiponitrile, which has grown to become the third largest outlet for acrylonitrile. It is used by Solutia as a precursor for hexamethylenediamine (HMDA, $C_6H_{16}N_2$) [124-09-4] and is made by a proprietary acrylonitrile electrohydrodimerization process (78). HMDA is used exclusively for the manufacture of nylon-6,6 (see POLYAMIDES). The growth of this acrylonitrile outlet in recent years stems largely from replacement of adipic acid ($C_6H_{10}O_4$) [124-04-9] with acrylonitrile in HMDA production, rather than from a significant increase in nylon-6,6 demand. The use of acrylonitrile for HMDA production should continue to grow at a faster rate than the other outlets for acrylonitrile, but it will not likely approach the size of the acrylic fiber market for acrylonitrile consumption.

Acrylamide is produced commercially by heterogeneous copper-catalyzed hydration of acrylonitrile (79–82). Acrylamide is used primarily in the form of a polymer, polyacrylamide, in the paper and pulp industry, and in wastewater treatment as a flocculant to separate solid material from wastewater streams (see ACRYLAMIDE POLYMERS). Other applications include mineral processing, coal processing, and enhanced oil recovery in which polyacrylamide solutions were found effective for displacing oil from rock.

Nitrile rubber finds broad application in industry because of its excellent resistance to oil and chemicals, its good flexibility at low temperatures, high abrasion and heat resistance (up to 120°C), and good mechanical properties. Nitrile rubber consists of butadiene–acrylonitrile copolymers, with an acrylonitrile content ranging from 15 to 45%. In addition to the traditional applications of nitrile rubber for hoses, gaskets, seals, and oil well equipment, new applications have emerged with the development of nitrile rubber blends with PVC. These blends combine the chemical resistance and low temperature flexibility characteristics of nitrile rubber, with the stability and ozone resistance of PVC. This has greatly expanded the use of nitrile rubber in outdoor applications for hoses, belts, and cable jackets, where ozone resistance is necessary.

Other acrylonitrile copolymers have found specialty applications with good gas-barrier and chemical-resistant properties. An example is BP Chemicals' Barex resins which are acrylonitrile–methyl acrylate copolymers grafted on a nitrile rubber. Barex resins are unique barrier resins with the combinations of excellent oxygen barrier, good chemical resistance, and antiscalping properties.

Another application for acrylonitrile is in the manufacture of Carbon fibers. They are produced by pyrolysis of oriented polyacrylonitrile fibers and are used to reinforce composites for high performance applications in the aircraft, defense, and aerospace industries. These applications include rocket engine nozzles, rocket nose cones, and structural components for aircraft and orbital vehicles where light weight and high strength are needed. Other small specialty applications of acrylonitrile are in the production of fatty amines, ion-exchange resins, and fatty amine amides used in cosmetics, adhesives, corrosion inhibitors, and water-treatment resins. Examples of these specialty amines include 2-acrylamido-2-methylpropanesulfonic acid ($C_7H_{13}NSO_4$) [15214-89-8], 3-methoxypropionitrile (C_4H_7NO) [110-67-8], and 3-methoxypropylamine ($C_4H_{11}NO$) [5332-73-0].

Polymerization of Acrylonitrile

Homopolymerization. Pure acrylonitrile does not polymerize readily without initiators or light, but polymerization proceeds rapidly and exothermically in the presence of free radicals or anionic initiators. Oxygen is a very strong inhibitor and forms peroxides. If oxygen is allowed to react to exhaustion, polymerization may then proceed at a very high rate through the thermal decomposition of peroxides, and explosion can occur. Conventional peroxide initiators, such as benzoyl peroxide and hydrogen peroxide, and azo compounds, such as 2,2′-azobis(isobutyronitrile) and 2,2′-azobis(2,4-dimethylvaleronitrile), can be used at moderate temperatures below 100°C. Redox catalysis systems can be used in aqueous media at low temperatures. Initiation can also be induced by light (83) and radiation (84). Polymerization can be carried out in bulk, emulsion, suspension, slurry, or solution.

Continuous Bulk Process. Polyacrylonitrile is not soluble in its monomer and precipitates from the medium. The polymerization exhibits autocatalytic behavior, and as polymerization proceeds, it becomes increasingly difficult to remove the heat of polymerization as viscosity increases. Consequently, in a batch process, the polymerization can run out of control. Therefore, continuous operation is used to overcome the difficulties (85–87). As an example, the following streams are continuously charged into a 2.5-L reactor at 40°C, equipped with an agitator and filled initially with acrylonitrile to one-half of its volume:

(1) cumene hydroperoxide 10 g/h
(2) SO_2 (gas) 120 g/h
(3) dimethylacetomide 3.2 g/h
(4) 2-mercaptoethanol 8 g/h

After the first 10 min, acrylonitrile is fed into the reactor at 4000 g/h. The effluent from the reactor has 54.6% conversion of acrylonitrile (85). The mechanisms and kinetic models for acrylonitrile bulk polymerization have been described (88–91), as has the study of high pressure polymerization (8).

Continuous Slurry Process. This process is similar to bulk polymerization, but the monomer is isolated into small suspended droplets in an aqueous medium.

This provides heat-removal capability and commercial feasibility. In one example (92), a 60-L stainless steel cylindrical reactor is equipped with a turbine agitator and a pump to circulate a portion of the polymerizing medium from the bottom through a heat exchanger, thus removing the heat of polymerization. Three separate streams of a 0.3% H_2SO_4 aqueous solution, a catalyst solution (15% Na_2SO_3 and 4.22% Na_2ClO_3 in water), and a monomer solution (97% acrylonitrile and 3% water) are continuously charged into the reactor at the rates of 22.4, 1.0, and 11.8 kg/h, respectively. At 35°C and 1.69 h of residence time, the conversion is 90% and the polymer has an average molecular weight of ca 75,000.

Emulsion Process. In the following example, redox catalysis is used to achieve rapid polymerization at low temperatures (20–60°C), yielding a polymer with better color than that obtained by the use of other initiator systems where higher temperatures are required.

(1) water 270 parts
(2) emulsifier (23% sodium salt of sulfonated cumar resin) 26 parts
(3) ammonium persulfate 0.6 parts
(4) ammonium bisulfite 0.5 parts
(5) sodium dihydrogen phosphate 0.8 parts
(6) dilute H_2SO_4 As required to adjust the solution of pH 4.6

One hundred parts of this solution and 50 parts of acrylonitrile are charged into a reactor. It is then purged with N_2, sealed, and polymerized at 40°C for 2 hs, achieving 85% conversion (93). After polymerization is completed, the polymer is recovered by coagulation with salt (see EMULSION POLYMERIZATION).

Solution Process. The solution process is rather straightforward and is generally used to prepare acrylic polymers suitable for direct wet- or dry-spinning fiber manufacture. Dimethylformamide is one of the best solvents for polyacrylonitrile and is used extensively. In this medium, an overall activation energy for the polymerization has been estimated to be 86.6 kJ/mol (94). Other important solvents are dimethylacetamide, dimethyl sulfoxide, ethylene or propylene carbonate, and concentrated aqueous solutions of NaSCN, HNO_3, H_2SO_4, and ZnC_{l2}.

Copolymerization. Acrylonitrile copolymerizes readily with electron-donor monomers, and >800 acrylonitrile copolymers have been registered with *Chemical Abstracts*. A comprehensive listing of reactivity ratios for acrylonitrile copolymerizations is available (95). Copolymerization is carried out by bulk emulsion, slurry, or suspension processes. The arrangement of monomer units in acrylonitrile copolymers is most commonly random. Special techniques can be used to achieve specific arrangements.

Alternating Copolymers. Copolymerization of a strong acceptor monomer with a strong donor monomer yields alternating equimolar copolymers; for example, this is the case for maleic anhydride or vinylidene cyanide with styrene. Acrylonitrile, a weak electron acceptor, complexes readily with charge-transfer agents, such as organoaluminum or metallic halides. These complexes are strong electron acceptors, which interact with strong donor monomers to form ground-state

comonomer complexes and undergo polymerization to form alternating copolymers. The probable reaction mechanism is as follows:

$$A + CTA \longrightarrow A{-}CTA$$

$$D + A{-}CTA \rightleftharpoons (D{\rightarrow}A{\cdots}CTA) \rightleftharpoons D^{+}\ {}^{-}A{-}CTA$$

$$D^{+}\ {}^{-}A{-}CTA \longrightarrow (DA)_x\,(D^{+}\ {}^{-}A{-}CTA) \longrightarrow {-}(DA)_n{-}$$

where A is acrylonitrile, CTA the charge-transfer agent, and D the strong electron-donor monomer.

The polymerization proceeds spontaneously at room temperature or elevated temperatures. The proposed matrix of the comonomer complexes is described in Reference 96. Examples of alternating acrylonitrile copolymerizations involve vinyl cyclohexanes with $AlEC_2H_5tCl_2$ (97), vinyl acetate with $ZnCl_2$ (98) or Ziegler–Natta catalyst (99), and styrene.

Block Copolymers. Several methods such as ultrasonics (100), radiation (101), and chemical techniques (102,103), including the use of polymer ions, polymer radicals, and organometallic initiators, are available to prepare Block Copolymers of acrylonitrile. Acrylonitrile can be used as either the first-or the second-phase monomer. Depending on the mechanism of termination, a diblock of the AB type and a triblock of the ABA type can be formed by disproportionation or transfer for the former, and recombination for the latter. Some of the comonomers are styrene, methyl acrylate, vinyl chloride, methyl methacrylate, vinyl acetate, acrylic acid, and *n*-butyl isocyanate. An overview and survey of alternating and block copolymers can be found in Reference 104.

Properties of Homopolymer

Polyacrylonitrile adopts the head-to-tail linkage of its monomer units, with nitrile groups on alternate carbon atoms at very close proximity:

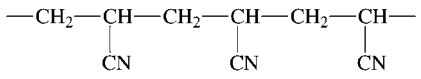

By conventional polymerization methods, polyacrylonitrile forms both isotactic and syndiotactic configurations in approximately equal proportion. However, primarily the isotactic polyacrylonitrile is formed in the polymerization.

The compact size and strong polarity of the nitrile groups make them very interactive with their surroundings. The lone pair orbital on nitrogen is suitable for hydrogen bonding, as well as for electron-donor–acceptor complex formation. In addition, the electrons in the π-orbitals of the nitrile triple bond are available for interactions, for example, with transition-metal ions.

The polar nitrile groups exert intramolecular repulsion, compelling the molecules into an irregular helical conformation (105,106), but they ensure intermolecular attraction between polymer molecules. The interactions of polyacrylonitrile molecules and their relationship to macroscopic properties have been reviewed (106).

Table 8. Estimate of Phases in Polyacrylonitrile[a, b]

Sample[c]	Crystalline	Quasi-crystalline	Amorphous
PAN B molded at 200°C	0.47	0.25	0.28
PAN B molded-annealed	0.45	0.34	0.21
PAN B cast	0.42	0.10	0.48
PAN A cast-annealed	0.44	0.23	0.33

[a] Ref. 109.
[b] Made by emulsion free-radical polymerization.
[c] PAN A: 120,000 M_v, cast from DMF, PAN B: 328,000 M_v, cast from DMSO.

The prevailing polar nature of polyacrylonitrile provides its unique and well-known characteristics, including hardness and rigidity, resistance to most chemicals and solvents, sunlight, heat, and microorganisms, slow burning and charring, reactivity toward nitrile reagents, compatibility with certain polar substances, ability to orient, and low permeability toward gases. Physical constants and an infrared spectrum of polyacrylonitrile are available (107).

Morphology. The heterogeneous system of polyacrylonitrile contains crystalline, quasicrystalline, and amorphous phases (108,109). The ratio of these three phases has been estimated (Table 8); there is little change in the crystalline phase regardless of specimen preparations. This indicates that the crystals, even though destroyed when dissolved in the solvents, form again to the same extent upon casting from the solvents. However, large differences are shown for the quasicrystalline and amorphous phases, depending on the methods of preparation.

Three regions of transition are defined by dynamic mechanical measurements (109): the main transition for the amorphous phase at 157°C, the dipole–dipole interaction for the quasicrystalline phase at 99°C [generally considered as the Glass Transition], and the secondary transition for the amorphous phase at 79°C (see DYNAMIC MECHANICAL PROPERTIES). The high temperature transition is usually ascribed to concerted motions of the pendent nitrile groups and is very sensitive to modifications. When the polymer is heat-treated (110) to form a conjugated ring system from the nitrile groups, this high temperature transition disappears as in the case of the dielectric transition (111) (see DIELECTRIC RELAXATION). Furthermore, when a small amount (5–10%) of methyl methacrylate is introduced as a comonomer, the transition behavior changes drastically; the high temperature transition disappears (112). Multiple-transition phenomena have also been shown by birefringence (113), dielectric (114–117), and x-ray diffraction (qv) (118) measurements (see MORPHOLOGY).

Crystallization. Using fractionated polyacrylonitrile, crystallization has been carried out at various temperatures (119), and several morphological growth features have been observed, namely, rectangular single crystals, twinned crystals, ovals, and spherulites. The lamellae are vertically arranged in a manner similar to polyethylene ovals. As in thin-film polystyrene, natural rubber, and gutta-percha, crack-like structure or space between lamellae is found to be associated with fibrils. The growth mechanism for polyacrylonitrile spherulites is similar to that for other polymers (see SEMICRYSTALLINE POLYMERS; CRYSTALLIZATION KINETICS).

Amorphous Polyacrylonitrile. This polymer has been synthesized successfully, using bis(pentamethyleneimino) magnesium as catalyst and *n*-heptane as solvent (120,121). By converting the polymer into poly(acrylic acid) by alkaline hydrolysis, and comparing its infrared spectrum to those of poly(acrylic acid) prepared with azobisisobutyronitrile as initiator, this amorphous polyacrylonitrile has been shown to have the normal head-to-tail structure of the usual, more crystalline polyacrylonitrile described previously. Its density is 1.2% higher, and its configuration is primarily isotactic, like the polymer synthesized through a radiation-induced urea canal complex. Its solubility is remarkably different; it is easily soluble in propylene carbonate at room temperature and in formamide at elevated temperatures. In addition, the viscoelastic properties of the amorphous material show only a single transition at high temperatures of ca 170°C with the absence of the transition at ca 100°C. This fact supports the assignment of the high temperature transition to the molecular motion related to the amorphous region and the low temperature transition to the quasicrystalline region (see AMORPHOUS POLYMERS).

Melting Point. Because polyacrylonitrile decomposes before reaching its melting temperature, the determination of its melting point requires rather unusual approaches. A melting point of 317°C has been obtained by dilatometry (qv) (105). Using a heating rate of 40°C/min, which is sufficiently fast to achieve melting prior to degradation, a value of 326°C has been measured by dta (122). By wide-angle x-ray and stereoscan measurements, at a heating rate of >1000°C/min, a melting point of 320 ± 5°C has been deduced (123).

Water is known to depress the melting point of acrylonitrile polymer and its vinyl acetate copolymers strongly; degradation during measurement becomes insignificant, and scanning calorimetry has been used effectively to probe the structure of the polymers (124,125). Addition of water continually depresses the polymer melting point until a critical water concentration is reached, whereupon the molten polymer separates from the water, and no further reduction in melting point is observed (Fig. 2). Both the minimum melting point and the critical water concentration decrease with increasing comonomer content. The melting-point reduction by water is consistent with the Flory theory (126) and can be expected from the nitrile–water interaction, which results in the disruption of the nitrile–nitrile bonding. On the other hand, the depressions of both the melting point and the heat of fusion by the presence of the comonomer (Fig. 3) are attributable to the crystal defect model (127) in which the noncrystallizable comonomer enters the lattice as defects rather than being relegated to an amorphous phase. Thus, the degree of the depressions is interpreted as a measure of the regularity and strength of the intermolecular dipole–dipole bonds that stabilize the lattice.

When the draw ratio of the fiber is extended from 1 to 6 times, the heat of fusion increases from 1.88 to 2.5 kJ/mol, and a secondary endotherm appears at 147°C; the primary endotherm is at 156°C (Fig. 4). These changes are reversible upon relaxation of the fiber. The appearance of the secondary endotherm is interpreted as a disruption in the crystalline phase at high threadline stress, whereas the increase in the heat of fusion reflects the formation of dipole–dipole bonds upon orientation of the polymer chains in the amorphous region of the fiber.

Polarization. Polyacrylonitrile can achieve very high, persistent electrical polarization as inferred from thermally stimulated discharge analysis (128). This

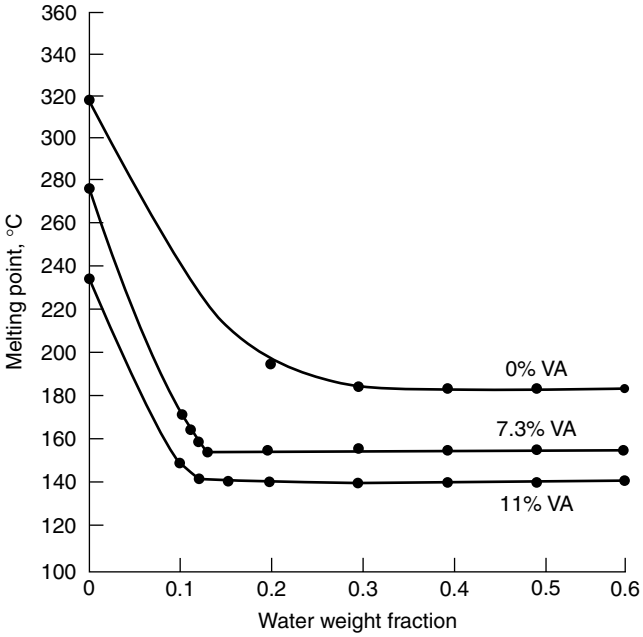

Fig. 2. Dependence of melting point of water content for acrylonitrile–vinyl acetate (VA) copolymer (125).

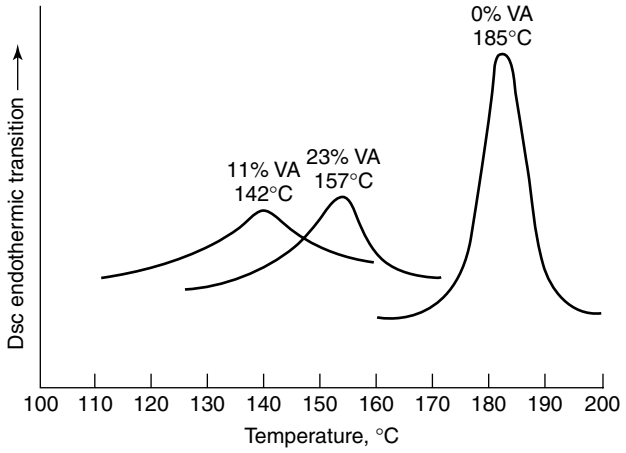

Fig. 3. Melting endotherms of acrylonitrile–vinyl acetate copolymers mixed with two parts of water (125).

can be explained by the strong dipole moment of the nitrile groups and the quasicrystalline nature of the polymer. Because of the strong dipole moment, an external electrical field can impose strong torque on the polymer chains and lead to a highly polarized state. Quasicrystallinity permits these chains to be rearranged

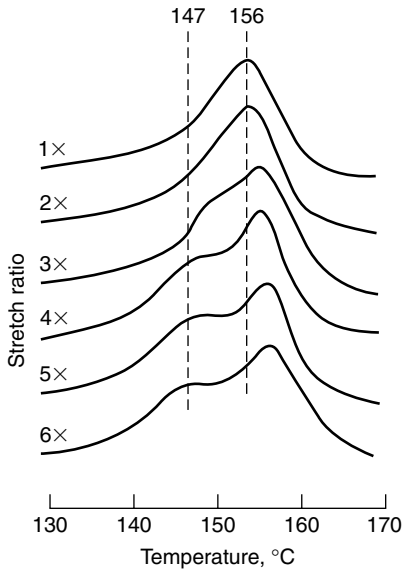

Fig. 4. Melting endotherms of acrylonitrile copolymer fiber (7% vinyl acetate) at different stretch ratios (124).

and packed together, providing a certain degree of molecular reorganization to store the energy. Both x-ray diffraction and high resolution internal-reflection infrared spectroscopy have been used to study the polarization characteristics of polyacrylonitrile films (129).

When the films are exposed to electric fields, x-ray diffraction indicates a densification of laterally ordered regions and an increase in the degree of local order or in the size of the ordered regions. Infrared spectroscopy suggests an intensification of dipolar bonding between adjacent nitriles, and the possibility of vibrational coupling among adjacent groups. It is envisioned that when polyacrylonitrile is subjected to thermoelectric treatment, the structural rearrangement of the polymer chains involves not only a biased orientation of dipoles, but also enhanced dipole–dipole associations forming dipolar clusters.

Solubility. Because of the properties of polyacrylonitrile, an active solvent capable of dissolving this polymer must satisfy some unique and critical chemical property of the polymer chains and, at the same time, separate the polymer molecules with a nonpolar segment. For example, dimethylformamide is an effective solvent, but formamide, methylformamide, and diethylformamide are not; dimethyl sulfone is, but diethyl sulfone is not. The following solvents are effective for polyacrylonitrile at either room temperature or elevated temperatures (107,130): dimethylformamide, dimethylthioformamide, dimethylacetamide, *N*-methyl-β-cyanoethyl formamide, α-cyanoacetamide, tetramethyl oxamide, malononitrile, fumaronitrile, succinonitrile, adiponitrile, α-chloro-β-hydroxypropionitrile, β-hydroxypropionitrile, hydroxyacetonitrile, *N*,*N*-di(cyanomethyl)aminoacetonitrile, ε-caprolactam, bis(β-cyanoethyl)ether, γ-butyrolactone, propiolactone, 1,3,5-tetracyanopentane, tetramethylene sulfoxide,

dimethyl sulfoxide, 2-hydroxythyl methyl sulfone, methyl ethyl sulfone, sulfolane, *m*-nitrophenol, *p*-nitrophenol, *o*-, *m*-, *p*-phenylene diamine, methylene dithiocyanate, trimethylene dithiocyanate, dimethyl cyanamide, ethylene carbonate, propylene carbonate, succinic anhydride, maleic anhydride, certain *N*-nitro- and nitrosoalkyl amines, some formylated primary and secondary amines, pyrrolidinone derivatives, concentrated sulfuric acid or nitric acid, and concentrated aqueous solutions of LiBr, NaCNS, or $ZnCl_2$. Copolymers of acrylonitrile are often soluble in dioxane, chlorobenzene, cyclohexanone, methyl ethyl ketone, acetone, dimethylformamide, butyrolactone, and tetrahydrofuran.

Barrier Properties. The remarkable barrier property of polyacrylonitrile to oxygen and carbon dioxide has been demonstrated (131), but high permeability toward helium is noticed. The high polarity of polyacrylonitrile leads to this high permeability and high sorption toward water vapor. This is perhaps the only limitation for the barrier application of the polymer. The activation energies for permeation and their preexponential factors for polyacrylonitrile are available (131). The value of the ratio of the permeabilities to helium and oxygen is exceptionally high; for example, the value for poly(vinylidene chloride), another high barrier polymer, is 58.5, whereas that for polyacrylonitrile is 1770. In addition, the activation energies for permeation are relatively low; for example, the activation energy for poly(vinylidene chloride) is 70.3 kJ/mol for nitrogen, while that for polyacrylonitrile is only 44.4. These two features suggest that the free volume of polyacrylonitrile for gas transport must be very small (see BARRIER POLYMERS; VINYLIDENE CHLORIDE POLYMERS).

The sorption of CO_2 has been studied at high pressures under various temperatures, and the characteristic dual-mode sorption isotherms (superposition of Henry's law and a Langmuir isotherm) of gas–glassy polymer systems have been observed (132). The Langmuir affinity constants and their enthalpy change are lower than expected. This is interpreted as resulting from the competition for available sites between CO_2 and the immobile residual in the film. The observed behavior suggests unique slow relaxations of polyacrylonitrile during the transient CO_2 permeation process, which are not observed in other glassy polymers. The sorption of water vapor has also been studied (133,134), and like CO_2, the water-vapor sorption follows the dual-mode model. At high vapor pressures, clustering of the penetrant molecules in nonrandom aggregation is suggested. Again, as in CO_2 sorption, non-Fickian time-lag behavior is observed, indicating relaxations of polyacrylonitrile during the transient sorption transport to accommodate the clustering process of the penetrant.

Chemical Reactions. Polyacrylonitrile is resistant to common solvents, oils, and chemicals, but its nitrile groups and α-hydrogens do react with certain reagents. Hydration with concentrated sulfuric acid forms a solution (135). Hydrogenation results in the formation of polymers with pendent aminonethylene groups (136,137). Hydrolysis with hot aqueous alkali yields a mixture which passes through a thick red stage and eventually becomes the yellow, water-soluble salt of poly(acrylic acid) (138) (see ACRYLIC (AND METHACRYLIC) ACID POLYMERS). Upon reaction with strong alkali in dilute dimethylformamide solution, rapid chain scission ensues (139). Reaction with hydroxylamine produces amidoximes and hydroxamic acids (140,141). Grafting with vinyl acetate proceeds in emulsion, with potassium persulfate as initiator (142). Irradiation induces free-radical sites

which initiate grafting or cross-linking (qv), depending upon the presence or the absence of a monomer (143).

Thermal Degradation. Upon heating, discoloration of polyacrylonitrile occurs; it first becomes yellow, then progressively red, and finally black. The mechanism of color formation is thought to be the reaction of the nitrile groups in forming a conjugated system. A comprehensive review of polyacrylonitrile color formation and thermal degradation reaction has been made (144). There are four main categories of Degradation reactions: chain scission, cross-linking, hydrogenation, and cyclization (145). Thermal degradation under reduced pressure, and in air at 200°C, has been studied using Fourier transform infrared spectroscopy (146). A mechanism involving imine–enamine tautomerism explains satisfactorily the observed spectral changes under reduced pressure (146). The reactions in air are more complex, and their interpretation is difficult.

The decomposition products of pure polyacrylonitrile yarn pyrolyzed at 400, 600, and 800°C in either air or nitrogen have been quantitatively analyzed using gas chromatography and gas chromatography–mass spectrometry (147). The main products are HCN, which is the predominant toxic product, and 16 other nitriles. At higher temperatures, the quantities of HCN, acetonitrile, acrylonitrile, and aromatic nitriles increase, whereas those of aliphatic dicyanides decrease. Ammonia is a decomposition product, but its toxicity is insignificant, compared to HCN, and has not been determined. The viscous condensates contain several homologous series of aliphatic nitriles. A similar study of polyacrylonitrile pyrolysis products in oxygen at 400, 700, and 900°C has shown the four chief products to be HCN, acetonitrile, acrylonitrile, and benzonitrile (148). The other 16 products are methane, acetylene, ethylene, ethane, propene, propane, 1,3-butadiene, ethyl nitrile, vinyl acetonitrile, crotonitrile, benzene, pyridine, dicyanobutene, adiponitrile, dicyanobenzene, and naphthalene. With increased temperature, the relative yields and complexity of products increase to a maximum of ca 700°C. Further increase in temperature produces thermally stable product, including low molecular weight nitriles and aromatic species.

Copolymers

Because of the combination of high melting point, high melt viscosity, and poor thermal stability, acrylonitrile homopolymer has little application. Even in synthetic fibers, small amounts of copolymers are incorporated to improve stability, dye receptivity, and certain other properties. By copolymerizing acrylonitrile with other monomers, the deficiencies of acrylonitrile homopolymer have been tempered and, at the same time, the unusual and desirable properties of acrylonitrile have been incorporated into various melt-processible resins. For general applications, acrylonitrile content ranges up to ca 50%; for barrier applications, to ca 75%. Acrylonitrile copolymer properties, such as rigidity, chemical resistance, melt viscosity, stability, and permeability, generally vary in proportion to the acrylonitrile content. However, the glass-transition temperature (T_g) shows unusual behavior; there is a maximum or a minimum T_g in certain cases, eg, for copolymers of styrene, vinylidene chloride, and methyl methacrylate.

The principal uses of acrylonitrile are in Acrylic fibers, copolymers with styrene (SAN), and in combination with butadiene and styrene (ABS). (see ACRYLONITRILE–BUTADIENE–STYRENE). SAN copolymers are discussed in detail in later sections of this article. Following are a few other copolymers and their properties.

Copolymers of Benzofuran. These alternating copolymers are optically active and are prepared in the presence of optically active aluminum compounds as complexing agents for acrylonitrile. Opposite signs of rotation are obtained using different complexing agents. The highest specific rotation of -8° has been attained with the stoichiometric ratio of menthoxyaluminum dichloride to acrylonitrile. The results indicate that the alternating dyad contributes to the optical activity, and the asymmetric configuration of the carbon atoms of the acrylonitrile unit influences the optical rotation. It is claimed that the optical activity is mainly induced by the copolymers themselves, not by the residual catalysts (149).

Copolymers of Carbon Dioxide. Copolymerization proceeds in the presence of triethylenediamine as initiator at 120–160°C under moderate pressure to yield an ester structure. The yield and molecular weight of the copolymers increase with initiator concentration, but the M_n of the synthesized copolymers is low, ie, 1500–2200. They are transparent viscous liquids or solids, depending on the molecular weight (150).

Copolymers of 2-Dimethylaminoethyl Methacrylate. The cationic nature of this copolymer has been shown to permit heparin attachment and cyclization of the nitrile groups with ethylene oxide gas for controlled structure alterations. The improved blood compatibility suggests Medical applications, including dialysis membranes, ultrafiltration membranes, and adsorbent coatings for hemoperfusion (151).

Copolymers of Methyl Acrylate. Barex® resins, commercial high barrier resins produced by BP Chemicals, are copolymers of acrylonitrile and methyl acrylate [96-33-3]. These resins are excellent examples of the use of acrylonitrile to provide gas and aroma/flavor barrier, chemical resistance, high tensile strength, stiffness, and utilization of a comonomer to provide thermal stability and processibility. In addition, modification with an elastomer provides toughness and impact strength. These materials have a unique combination of useful packaging qualities, including transparency, and are excellent barriers to permeation by gases, organic solvents, and most essential oils. Barex resins also prevent the migration and scalping of volatile flavors and odors from packaged foods and fruit juice products (152,153). They also provide protection from atmospheric oxygen. Barex resins meet FDA compliance for direct food contact applications. In April 2000, the FDA approved the use of Barex 210E resin for fruit/vegetable juices, ready-to-use teas, and other specified beverages for fill temperatures less than 150°F (66°C). This new ruling expands the application of Barex resins into the beverage market place.

Barex resin extruded sheet and/or calendered sheet (153) can be easily thermoformed into lightweight, rigid containers (152,154). Packages can be printed, laminated, or metallized. Recent developments in extrusion and injection blow molding (152,155), laminated film structures (152,156), and coextrusion (153,157) have led to packaging uses for a variety of products. Barex resins are especially well-suited for bottle production. These acrylonitrile copolymers also provide a

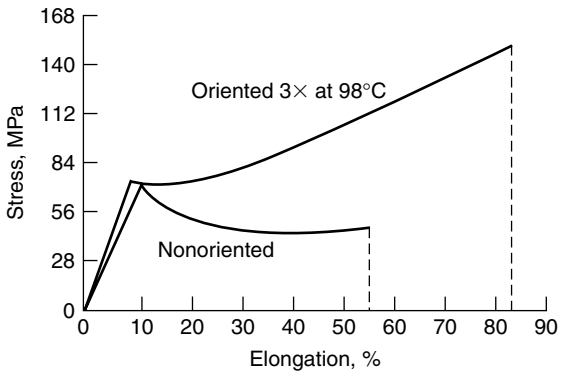

Fig. 5. Stess elongation of Barex 210 sheet (159). To convert MPa to psi, multiply by 145.

good example of the dependence of properties on the degree and temperature of orientation (158,159). Figure 5 illustrates the improvement in tensile strength, elongation, and the ability to absorb impact energy as a result of orientation (159) by Barex resins (for example, Barex 210). Tensile strength and impact strength increase with the extent of stretching, and decrease with the orientation temperature. Oxygen permeability decreases with orientation. These orientation properties have led to the commercialization of Barex resins to fruit juice containers in France (153). Some typical physical properties of Barex resins are shown in Table 9.

Table 9. Physicial/Mechanical Properties of Commercial Barex Resins[a]

Property	Barex 210[b]	Barex 218[b]	ASTM test method
Specific gravity at 23°C, g/cm^3	1.15	1.11	D792
Tensile strength (yield), MPa[c]	65.5	51.7	D638
Flexural modulas, GPa[d]	3.38	2.69	D790
Melt index (200c, 27.5 lb)	3	3	D1238
Notched Izod impact, J/m [e]	267	481	D790
Heat deflection temperature, °C	77	71	D648
Gas permeability			
Oxygen at 23°C and 100% rh [nmol/(m·s·GPa)[f]]	1.54	3.09	D3985
Carbon dioxide at 23°C and 100% rh [nmol/(m·s·GPa)[f]]	2.32	3.09	D3985
Water vapor at 38°C and 90% rh [nmol/(m·s·MPa)[g]]	12.7	19.1	F1249-90

[a] Product literature from BP Chemicals., m·s·MPa
[b] Extrusion grade.
[c] To convert MPa to psi, multiply by 145.
[d] To convert GPa to psi, multiply by 145,000.
[e] To convert J/m to ft·lb/in., divide by 53.39.
[f] To convert nmol/(m·s·GPa) to (cm^3·mm)/(m^2·24 h·bar), divide by 5.145.
[g] To convert nmol/(m·s·MPa) to (g·mm)/(m^2·24h · atm), divide by 6.35.

Copolymers of Methyl Methacrylate. The glass-transition temperatures of these copolymers exhibit a minimum of ca 87°C at ca 40 wt% acrylonitrile; the T_g's of the homopolymers are ca 105°C. This unusual behavior is explained by the interactions of the dyads and well predicted by the sequence-distribution equation (160).

Copolymers of Styrene. For thermoplastic applications, the largest volume comonomer for acrylonitrile is styrene. Styrene–acrylonitrile copolymers are designated SAN. SAN copolymers are discussed in detail in the later part of this article.

Copolymers of Poly(vinyl alcohol) with Formaldehyde and Hydroquinone. These electron-exchange resins are condensation products of partially cyanoethylated poly(vinyl alcohol) and have a weak acidic nature and lustrous black appearance. The polar groups of acrylonitrile improve the redox capacities over a standard weak-acid electron exchanger, hydroquinone–phenol–formaldehyde (161).

Copolymers of 4-Vinylpyridine. Acrylonitrile improves the tensile strength of these reverse-osmosis membranes. Cross-linking quaternization of the copolymers with diiodobutane improves the performance of the membranes, achieving salt rejection of 95% and hydraulic water permeability of up to 30×10^{-15} $cm^2/(s \cdot Pa)$. The quaternized membranes also are anion exchangeable; more than two-thirds of iodide exchanges with chloride (162).

Copolymers of Vinylidene Chloride. The glass-transition temperatures of these copolymers vary nonlinearly with composition, as is the case for copolymers of methyl methacrylate, but these show a maximum. It is a broad maximum around 105°C at 55–80 wt% acrylonitrile. (The T_g of vinylidene chloride homopolymer is ca −20°C, whereas PAN's is ca 100°C.) Again, sequence distribution explains such behavior (163). These copolymers have good barrier properties and are used for surface Coatings. Acrylonitrile grafting on starch imparts hydrophilic behavior to starch and results in exceptional water absorption capability (164–167). These copolymers can also immobilize enzymes by entrapment or covalent bonding (168).

Grafting on Fibers. By treatment with sodium hydroxide and a low degree of cyanoethylation, the moisture retention of cotton can be improved by as much as 14% (169). X-ray diffraction reveals a decrease in the crystallinity of the cotton, which provides the improved moisture retention (170). Modifications of fibers by grafting with acrylonitrile, followed by hydrolysis, produce water-receptive and soil-repellent fibers (171). Such treatments to nylon result in significant protein-coupling efficiency (172). Grafting onto polypropylene fibers enhances moisture absorption and dye absorption (173).

Other Copolymers. Acrylonitrile copolymerizes readily with many electron-donor monomers other than the copolymers mentioned above. More than 800 acrylonitrile copolymers have been registered with *Chemical Abstract* and a comprehensive listing of reativity ratios for acrylonitrile copolymerizations is readily available (174). Some of the other interesting acrylonitrile copolymers follows: acrylonitrile–methyl acrylate–indene terpolymers, by themselves, or in blends with acrylonitrile–methyl acrylate copolymers, exhibit even lower oxygen and water permeation rates than the indene-free copolymers (175,176). Terpolymers of acrylonitrile with indene and isobutylene also exhibit excellent barrier

Table 10. Monomers Commonly Copolymerized with Acrylonitrile

Monomer	Molecular formula	Structural formula	CAS registry number
Methyl methacrylate	$C_5H_8O_2$	$CH_2{=}C(CH_3)COOCH_3$	[80-62-6]
Methyl acrylate	$C_4H_6O_2$	$CH_2{=}CHCOOCH_3$	[96-33-3]
Indene	C_9H_8	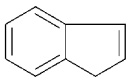	[95-13-6]
Isobutylene	C_4H_8	$CH_2{=}C(CH_3)_2$	[115-11-7]
Butyl acrylate	$C_7H_{12}O_2$	$CH_2{=}CHCOOC_4H_9$	[141-32-2]
Ethyl acrylate	$C_5H_8O_2$	$CH_2{=}CHCOOC_2H_5$	[140-88-5]
2-Ethylhexyl acrylate	$C_{11}H_{20}O_2$	$CH_2{=}CHCOOC_8H_{17}$	[103-11-7]
Hydroxyethyl acrylate	$C_5H_8O_3$	$CH_2{=}CHCOOC_2H_4OH$	[818-61-1]
Vinyl acetate	$C_4H_6O_2$	$CH_2{=}CHOOCCH_3$	[108-05-4]
Vinylidene chloride	$C_2H_2Cl_2$	$CH_2{=}C(Cl)_2$	[75-35-4]
Methyl vinyl ketone	C_4H_6O	$CH_2{=}CHCOCH_3$	[78-94-4]
α-Methylstyrene	C_9H_{10}	$CH_2{=}C(CH_3)C_6H_5$	[98-83-9]
Vinyl chloride	C_2H_3Cl	$CH_2{=}CHCl$	[75-01-4]
4-Vinylpyridine	C_7H_7N	$CH_2{=}CHC_5H_4N$	[100-43-6]
Acrylic acid	$C_3H_4O_2$	$CH_2{=}CHCOOH$	[79-10-7]

properties (177), and permeation of gas and water vapor through acrylonitrile–styrene–isobutylene terpolymers is also low (178,179).

Copolymers of acrylonitrile and methyl methacrylate (180) and terpolymers of acrylonitrile, styrene, and methyl methacrylate (181,182) are used as barrier polymers. Acrylonitrile copolymers and multipolymers containing butyl acrylate (183–186), ethyl acrylate (187), 2-ethylhexyl acrylate (183,186,188,189), hydroxyethyl acrylate (185), vinyl acetate (184,190), vinyl ethers (190,191), and vinylidene chloride (186,187,192–194) are also used in barrier films, laminates, and coatings. Environmentally degradable polymers useful in packaging are prepared from polymerization of acrylonitrile with styrene and methyl vinyl ketone (195).

Acrylonitrile multipolymers containing methyl methacrylate, α-methylstyrene, and indene are used as PVC modifiers to melt blend with PVC. These PVC modifiers not only enhance the heat distortion temperature, but also improve the processibility of the PVC compounds (196–200). The acrylonitrile multipolymers grafted on the elastomer phase provide the toughness and impact strength of the PVC compounds with high heat distortion temperature and good processibility (201,202). Table 10 gives the structures, formulas, and CAS registry numbers for several comonomers of acrylonitrile.

Although the arrangement of monomer units in acrylonitrile copolymers is usually random, alternating or block copolymers may be prepared using special techniques. For example, the copolymerization of acrylonitrile, like that of other vinyl monomers containing conjugated carbonyl or cyano groups, is changed in the presence of certain Lewis acids. Effective Lewis acids are metal compounds with nontransition metals as central atoms, including alkylaluminum halides, zinc halides, and triethylaluminum. The presence of the Lewis acid increases

the tendency of acrylonitrile to alternate with electron-donor molecules, such as styrene, α-methylstyrene, and olefins (203–207). This alternation is often attributed to a ternary molecular complex or charge-transfer mechanism, where complex formation with the Lewis acid increases the electron-accepting ability of acrylonitrile, which results in the formation of a molecular complex between the acrylonitrile–Lewis acid complex and the donor molecule. This ternary molecular complex polymerizes as a unit to yield an alternating polymer. Cross-propagation and complex radical mechanisms have also been proposed (208).

A number of methods such as ultrasonics (209), radiation (210), and chemical techniques (211–213), including the use of polymer radicals, polymer ions, and organometallic initiators, have been used to prepare acrylonitrile block copolymers. Block comonomers include styrene, methyl acrylate, methyl methacrylate, vinyl chloride, vinyl acetate, 4-vinylpyridine, acrylic acid, and n-butyl isocyanate.

Living radical polymerization (atom transfer radical polymerization) has been developed which allows for the controlled polymerization of acrylonitrile and comonomers to produce well defined linear homopolymer, statistical copolymers, block copolymers, and gradient copolymers (214–217). Well-defined diblock copolymers with a polystyrene and an acrylonitrile–styrene (or isoprene) copolymer sequence have been prepared (218,219). The stereospecific acrylonitrile polymers are made by solid-state urea clathrate polymerization (220) and organometallic compounds of alkali and alkaline-earth metals initiated polymerization (221).

Acrylonitrile has been grafted onto many polymeric systems. In particular, acrylonitrile grafting has been used to impart hydrophilic behavior to starch (124,222,223) and polymer fibers (224) as discussed above. Exceptional water absorption capability results from the grafting of acrylonitrile to starch, and the use of 2-acrylamido-2-methylpropanesulfonic acid [15214-89-8] along with acrylonitrile for grafting results in copolymers that can absorb over 5000 times their weight of deionized water (225). For example, one commercial product made by General Mills, Inc., Super Slurper, is a modified starch suitable for disposable diapers, surgical pads, and paper towel applications. Acrylonitrile polymers also provide some unique applications. Hollow fibers of acrylonitrile polymers as ultrafiltration membrane materials are used in the pharmaceutical and bioprocessing industries (226). Polyacrylonitrile-based electrolyte with $Li/LiMn_2O_4$ salts is used for solid-state batteries (227). Polyacrylonitrile is also used as a binding matrix for composite inorganic ion-exchanger (228).

SAN Copolymers

Because of the difficulty of melt processing the homopolymer, acrylonitrile is usually copolymerized to achieve a desirable thermal stability, melt flow, and physical properities. As a comonomer, acrylonitrile contributes hardness, rigidity, solvent and light resistance, gas impermeability, and the ability to orient. These properties have led to many copolymer application developments since 1950. The utility of acrylonitrile [107-13-1] in thermoplastics was first realized in its copolymer with styrene (C_8H_8) [100-42-5], in the late 1950s. Styrene is the largest volume of comonomer for acrylonitrile in thermoplastic applications. Styrene–acrylonitrile copolymers [9003-54-7] are inherently transparent plastics with high heat

resistance and excellent gloss and chemical resistance (229). They are also characterized by good hardness, rigidity, dimensional stability, and load-bearing strength (due to relatively high tensile and flexural strengths). Because of their inherent transparency, SAN copolymers are most frequently used in clear applications. These optically clear materials can be readily processed by extrusion and injection molding, but they lack real impact resistance.

The subsequent development of acrylonitrile–butadiene–styrene resins [9003-56-9], which contain an elastomeric component within a SAN matrix to provide toughness and impact strength, further boosted commercial application of the basic SAN copolymer as a portion of these rubber-toughened thermoplastics (see ACRYLONITRILE–BUTADIENE–STYRENE). When SAN is grafted onto a butadiene-based rubber, and optionally blended with additional SAN, the two-phase thermoplastic ABS is produced. ABS has the useful SAN properties of rigidity and resistance to chemicals and solvents, while the elastomeric component contributes real impact resistance. Because ABS is a two-phase system and each phase has a different refractive index, the final ABS is normally opaque. A clear ABS can be made by adjusting the refractive indexes through the inclusion of another monomer such as methyl methacrylate. ABS is a versatile material and modifications have brought out many specialty grades such as clear ABS and high temperature and flame-retardant grades. Saturated hydrocarbon elastomers or acrylic elastomers (230,231) can be used instead of those based on butadiene (C_4H_6) [106-99-0] as weatherable grade ABS.

SAN Physical Properties and Test Methods. SAN resins possess many physical properties desired for thermoplastic applications. They are characteristically hard, rigid, and dimensionally stable with load-bearing capabilities. They are also transparent, have high heat distortion temperatures, possess excellent gloss and chemical resistance, and adapt easily to conventional thermoplastic fabrication techniques (232).

SAN polymers are random linear amorphous copolymers. Physical properties are dependent on molecular weight and the percentage of acrylonitrile. An increase of either generally improves physical properties, but may cause a loss of processibility or an increase in yellowness. Various processing aids and modifiers can be used to achieve a specific set of properties. Modifiers may include mold release agents, uv stabilizers, antistatic aids, elastomers, flow and processing aids, and reinforcing agents such as fillers and fibers (232). Methods for testing and some typical physical properties are listed in Table 11.

The properties of SAN resins depend on their acrylonitrile content. Both melt viscosity and hardness of SAN resins increase with increasing acrylonitrile level. Unnotched impact and flexural strengths depict dramatic maxima at ca 87.5 mol% (78 wt%) acrylonitrile (233). With increasing acrylonitrile content, copolymers show continuous improvements in barrier properties and chemical and uv resistance, but thermal stability deteriorates (234). The glass-transition temperature (T_g) of SAN varies nonlinearly with acrylonitrile content, showing a maximum at 50 mol% acrylonitrile. The alternating SAN copolymer has the highest T_g (235,236). The fatigue resistance of SAN increases with acrylonitrile content to a maximum at 30 wt%, then decreases with higher acrylonitrile levels (237). The effect of acrylonitrile incorporation on SAN resin properties is shown in Table 12.

Table 11. Physical/Mechanical Properties of Commercial Injection-Molded SAN Resins[a]

Property	Lustran 31-2060	Tyril 100	ASTM test method
Specific gravity at 23°C	1.07	1.07	D792
Vicat softening point, °C	110	108	D1525
Tensile strength, MPa[b]	72.4	71.7	D638
Ultimate elongation @ breakage, %	3.0	2.5	D638
Flexural modulus, GPa[c]	3.45	3.87	D790
Impact strength notched Izod, J/m[d]	21.4 @ 0.125 in.	16.0 @ 0.125 in.	D256
Melt flow rate, g/10 min	8.0	8.0	D1238
Refractive index n_D	1.570	1.570	D542
Mold shrinkage, in./in.	0.003–0.004	0.004–0.005	D955
Transmittance at 0.125-in. thickness, %	89.0	89.0	D1003
Haze at 0.125-in. thickness, %	0.8	0.6	D1003

[a]Product literature from Bayer (Lustran 31-2060) and Dow (Tyril 100).
[b]To convert MPa to psi, multiply by 145.
[c]To convert GPa to psi, multiply by 145,000.
[d]To convert J/m to ft·lb/in., divide by 53.39.

Table 12. Compositional Effects on SAN Physical Properties[a]

Acrylonitrile, wt%	Tensile strength, MPa[b]	Elongation, %	Impact strength, notch[c], J/m[c]	Heat distortion temp., °C	Solution viscosity, MPa (=cP)
5.5	42.27	1.6	26.6	72	11.1
9.8	54.61	2.1	26.0	82	10.7
14.0	57.37	2.2	27.1	84	13.0
21.0	63.85	2.5	27.1	88	16.5
27.0	72.47	3.2	27.1	88	25.7

[a]Ref. 238.
[b]To convert MPa to psi, multiply by 145.
[c]To convert J/m to ft·lb/in., divide by 53.39.

SAN Chemical Properties and Analytical Methods. SAN resins show considerable resistance to solvents and are insoluble in carbon tetrachloride, ethyl alcohol, gasoline, and hydrocarbon solvents. They are swelled by solvents such as benzene, ether, and toluene. Polar solvents such as acetone, chloroform, dioxane, methyl ethyl ketone, and pyridine will dissolve SAN (239). The interactions of various solvents and SAN copolymers containing up to 52% acrylonitrile have been studied, along with their thermodynamic parameters such as the second virial coefficient, free-energy parameter, expansion factor, and intrinsic viscosity (240).

The properties of SAN are significantly altered by water absorption (241). The equilibrium water content increases with temperature while the time required decreases. A large decrease in T_g can result. Strong aqueous bases can degrade SAN by hydrolysis of the nitrile groups (242).

The molecular weight of SAN can be easily determined by either intrinsic viscosity or size-exclusion chromatography (sec). Relationships for both multipoint and single-point viscosity methods are available (243,244). The intrinsic viscosity and molecular weight relationships for azeotropic copolymers have been given (245,246):

(1) $[\eta] = 3.6 \times 10^{-4} M_w^{0.62}$ dL/g in MEK at 30°C

(2) $[\eta] = 2.15 \times 10^{-4} M_w^{0.68}$ dL/g in THF at 25°C

(3) $[\eta] = \frac{\eta_{sp}/c}{1+k_\eta \eta_{sp}}$, where $k^\eta = 0.21$ for MEK at 30°C and 0.25 for THF at 25°C

Chromatographic techniques are readily applied to SAN for molecular weight determination. Size-exclusion chromatography or gel permeation chromatography (247) columns and conditions have been described for SAN (248). Chromatographic detector differences have been shown to be of the order of only 2–3% (249). High pressure precipitation chromatography can achieve similar molecular weight separation (250). Liquid chromatography can be used with sec-fractioned samples to determine copolymer composition (251). Thin-layer chromatography will also separate SAN by compositional (monomer) variations (250).

Residual monomers in SAN have been a growing environmental concern and can be determined by a variety of methods. Monomer analysis can be achieved by polymer solution or directly from SAN emulsions (252), followed by "head space" gas chromatography (251,252). Liquid chromatography is also effective (253).

SAN Manufacture. The reactivities of acrylonitrile and styrene radicals toward their monomers are quite different, resulting in SAN copolymer compositions that vary from their monomer compositions (254). Further complicating the reaction is the fact that acrylonitrile is soluble in water and slightly different behavior is observed between water-based emulsion and suspension systems, and bulk or mass polymerizations (255). SAN copolymer compositions can be calculated from copolymerization equations (256) and published reactivity ratios (174). The difference in radical reactivity causes the copolymer composition to drift as polymerization proceeds, except at the azeotropic composition where copolymer composition matches monomer composition. Figure 6 shows these compositional variations (257). When SAN copolymer compositions vary significantly, incompatibility results, causing loss of optical clarity, mechanical strength, and moldability, as well as heat, solvent, and chemical resistance (258). The termination step has been found to be controlled by diffusion even at low conversions, and the termination rate constant varies with acrylonitrile content. The average half-life of the radicals increases with styrene concentration from 0.3 s at 20 mol% to 6.31 s with pure styrene (259). Further complicating SAN manufacture is the fact that both the heat (260,261) and rate (262) of copolymerization vary with monomer composition.

The early kinetic models for copolymerization, Mayo's terminal mechanism (263) and Alfrey's penultimate model (264), did not adequately predict the behavior of SAN systems. Copolymerizations in dimethylformamide and toluene indicated that both penultimate and antepenultimate effects had to be considered

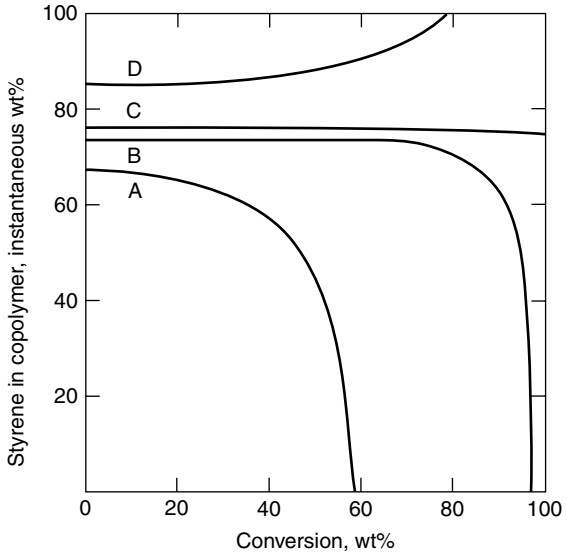

Fig. 6. Approximate compositions of SAN copolymers formed at different conversions starting with various monomer mixtures (256): S/AN = 65/36(A); 70/30(B); 76/24(C); 90/10(D).

(265,266). The resulting reactivity model is somewhat complicated, since there are eight reactivity ratios to consider.

The first quantitative model, which appeared in 1971, also accounted for possible charge-transfer complex formation (267). Deviation from the terminal model for bulk polymerization was shown to be due to antepenultimate effects (268). The work with numerical computation and ^{13}C- nmr spectroscopy data on SAN sequence distributions indicates that the penultimate model is the most appropriate for bulk SAN copolymerization (269,270). A kinetic model for azeotropic SAN copolymerization in toluene has been developed that successfully predicts conversion, rate, and average molecular weight for conversions up to 50% (271).

An emulsion model that assumes the locus of reaction to be inside the particles and considers the partition of acrylonitrile between the aqueous and oil phases has been developed (272). The model predicts copolymerization results very well when bulk reactivity ratios of 0.32 and 0.12 for styrene and acrylonitrile, respectively, are used. Commercially, SAN is manufactured by three processes: emulsion, suspension, and continuous mass (or bulk).

Emulsion Process. The emulsion polymerization process utilizes water as a continuous phase, with the reactants suspended as microscopic particles. This low viscosity system allows facile mixing and heat transfer for control purposes. An emulsifier is generally employed to stabilize the water insoluble monomers and other reactants, and to prevent reactor fouling. With SAN, the system is composed of water, monomers, chain-transfer agents for molecular weight control, emulsifiers, and initiators. Both batch and semibatch processes are employed. Copolymerization is normally carried out at 60–100°C to conversions of ~97%.

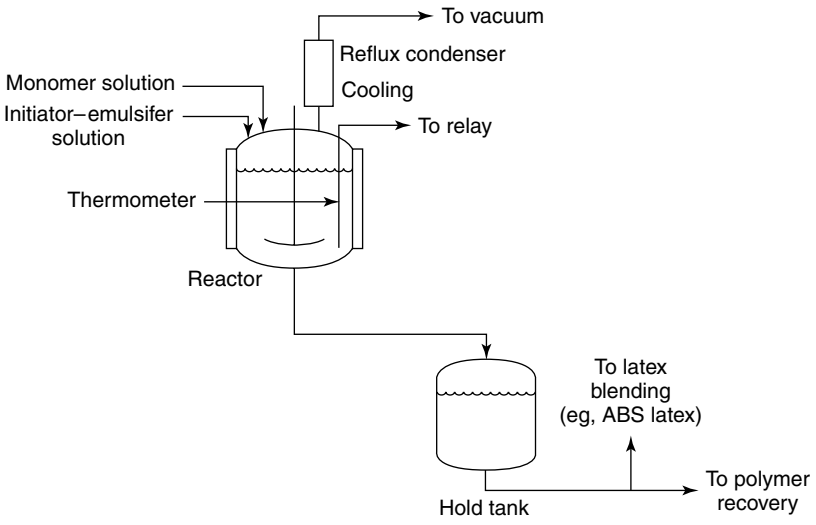

Fig. 7. SAN batch emulsion process (274).

Lower temperature polymerization can be achieved with redox-initiator systems (273).

Figure 7 shows a typical batch or semibatch emulsion process (274). A typical semibatch emulsion recipe is shown in Table 13 (275).

The initial charge is placed in the reactor, purged with an inert gas such as N_2, and brought to 80°C. The initiator is added, followed by addition of the remaining charge over 100 min. The reaction is completed by maintaining agitation at 80°C for 1 h after monomer addition is complete. The product is a free-flowing white latex with a total solids content of 35.6%. Compositional control for other than azeotropic compositions can be achieved with both batch and semibatch emulsion

Table 13. Semibatch-Mode Recipe for SAN Copolymers

Ingredient	Parts
Initial reactor charge	
Acrylonitrile	90
Styrene	111
Na alkanesulfonate (emulsifier)	63
$K_2S_2O_8$ (initiator)	0.44
4-(Benzyloxymethylene) cyclohexene (mol wt modifier)	1
Water	1400
Addition charge	
Acrylonitrile	350
Styrene	1000
Na alkanesulfonate (emulsifier)	15
$K_2S_2O_8$ (initiator)	4
4-(Benzyloxymethylene) cyclohexene (mol wt modifier)	10
Water	1600

processes. Continuous addition of the faster reacting monomer, styrene, can be practiced for batch systems, with the feed rate adjusted by computer through gas chromatographic monitoring during the course of the reaction (276). A calorimetric method to control the monomer feed rate has also been described (233). For semibatch processes, adding the monomers at a rate slower than that for copolymerization can achieve equilibrium. It has been found that constant composition in the emulsion can be achieved after ca 20% of the monomers have been charged (277).

Residual monomers in the latex are avoided either by effectively reacting the monomers to polymer or by physical or chemical removal. The use of *tert*-butyl peroxypivalate as a second initiator toward the end of the polymerization or the use of mixed initiator systems of $K_2S_2O_8$ and *tert*-butyl peroxybenzoate (278) effectively increases final conversion and decreases residual monomer levels. Spray devolatilization of hot latex under reduced pressure has been claimed to be effective (278). Residual acrylonitrile can also be reduced by postreaction with a number of agents such as monoamines (279) and dialkylamines (280), ammonium–alkali metal sulfites (281), unsaturated fatty acids or their glycerides (282,283) and their aldehydes, esters of olefinic alcohols, cyanuric acid (284), and myrcene (285).

The copolymer latex can be used "as is" for blending with other latexes, such as in the preparation of ABS, or the copolymer can be recovered by coagulation. The addition of electrolyte or freezing will break the latex and allow the polymer to be recovered, washed, and dried. Process refinements have been made to avoid the difficulties of fine particles during recovery (286,287).

The emulsion process can be modified for the continuous production of latex. One such process (288) uses two stirred-tank reactors in series, followed by insulated hold-tanks. During continuous operation, 60% of the monomers are continuously charged to the first reactor, with the remainder going into the second reactor. Surfactant is added only to the first reactor. The residence time is 2.5 h for the first reactor where the temperature is maintained at 65°C for 92% conversion. The second reactor is held at 68°C for a residence time of 2 h and conversion of 95%.

Suspension Process. Like the emulsion process, water is the continuous phase for suspension polymerization, but the resultant particle size is larger, well above the microscopic range. The suspension medium contains water, monomers, molecular weight control agents, initiators, and suspending aids. Stirred reactors are used in either batch or semibatch mode. Figure 8 illustrates a typical suspension manufacturing process while a typical batch recipe is shown in Table 14 (289). The components are charged into a pressure vessel and purged with N_2. Copolymerization is carried out at 128°C for 3 h and then at 150°C for 2 h. Steam stripping removes residual monomers (290), and the polymer beads are separated by centrifugation for washing and final dewatering.

Compositional control in suspension systems can be achieved with a corrected batch process. A suspension process has been described where styrene monomer is continuously added until 75–85% conversion, and then the excess acrylonitrile monomer is removed by stripping with an inert gas (291,292).

Elimination of unreacted monomers can be accomplished by two approaches: using dual initiators to enhance conversion of monomers to product (293,294)

Table 14. Batch-Mode Recipe for SAN Copolymers[a]

Ingredient	Parts
Acrylonitrile	30
Styrene	70
Dipentene (4-isopropenyl-1-methylcyclohexene)	1.2
Di-*tert*-butyl peroxide	0.03
Acrylic acid–2-ethylhexyl acrylate (90:10) Copolymer	0.03
Water	100

[a]Ref. 289.

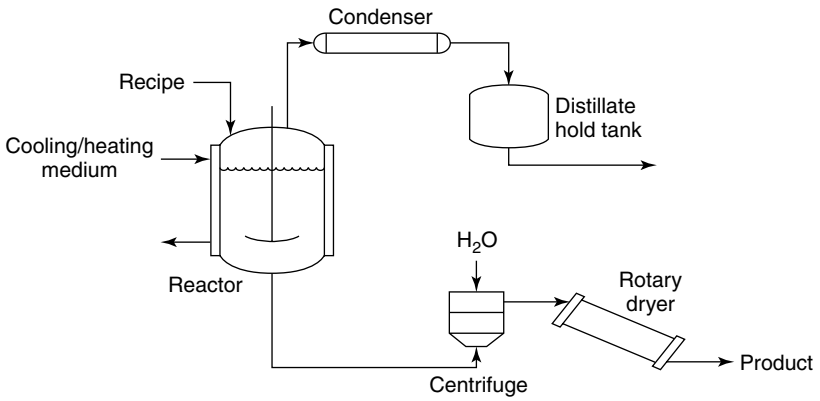

Fig. 8. SAN suspension process (289).

and steam stripping (290,295). Several process improvements have been claimed for dewatering beads (296), to reduce haze (297–300), improve color (301–305), remove monomer (306,307), and maintain homogeneous copolymer compositions (291,292,308).

Continuous Mass Process. The continuous mass process has several advantages, including high space-time yield, and good quality products uncontaminated with residual ingredients such as emulsifiers or suspending agents. SAN manufactured by this method generally has superior color and transparency, and is preferred for applications requiring good optical properties. It is a self-contained operation without waste treatment or environmental problems since the products are either polymer or recycled back to the process.

In practice, the continuous mass polymerization is rather complicated. Because of the high viscosity of the copolymerizing mixture, complex machinery is required to handle mixing, heat transfer, melt transport, and devolatilization. In addition, considerable time is required to establish steady-state conditions in both a stirred-tank reactor and a linear-flow reactor. Thus, system start-up and product grade changes produce some off-grade or intermediate grade products. Copolymerization is normally carried out between 100 and 200°C. Solvents are used to reduce viscosity or the conversion is kept to 40–70%, followed by devolatilization to remove solvents and monomers. Devolatilization is carried out from 120 to 260°C

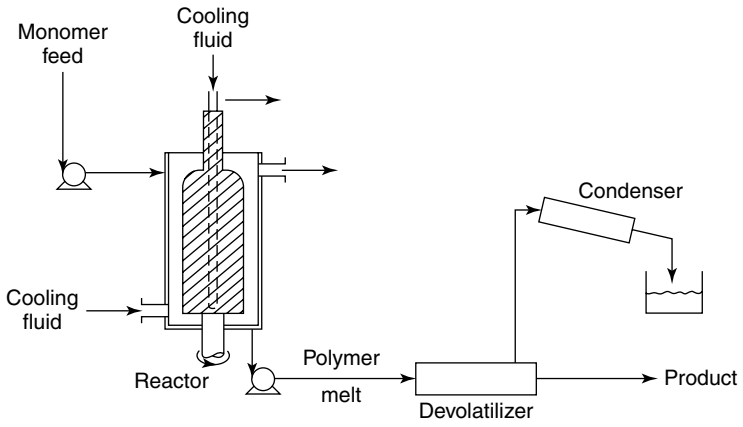

Fig. 9. SAN continuous mass process (309).

under vacuum at less than 20 kPa (2.9 psi). The devolatilized melt is then fed through a strand die, cooled, and pelletized.

A schematic of a continuous mass SAN polymerization process is shown in Figure 9 (309). The monomers are continuously fed into a screw reactor where copolymerization is carried out at 150°C to 73% conversion in 55 min. Heat of polymerization is removed through cooling of both the screw and the barrel walls. The polymeric melt is removed and fed to the devolatilizer to remove unreacted monomers under reduced pressure (4 kPa or 30 mm Hg) and high temperature (220°C). The final product is claimed to contain less than 0.7% volatiles. Two devolatilizers in series are found to yield a better quality product as well as better operational control (310,311).

Two basic reactor types are used in the continuous mass process: the stirred-tank reactor (312) and the linear-flow reactor. The stirred-tank reactor consists of a horizontal cylinder chamber equipped with various agitators (313,314) for mixing the viscous melt and an external cooling jacket for heat removal. With adequate mixing, the composition of the melt inside the reactor is homogeneous. Operation at a fixed conversion, with monomer make-up added at an amount and ratio equal to the amount and composition of copolymer withdrawn, produces a fixed composition copolymer. The two types of linear-flow reactors employed are the screw reactor (309) and the tower reactor (315). A screw reactor is composed of two concentric cylinders. The reaction mixture is conveyed toward the outlet by rotating the inner screw, which has helical threads, while heat is removed from both cylinders. A tower reactor with separate heating zones has a scraper agitator in the upper zone, while the lower portion generates plug flow. In the linear-flow reactors the conversion varies along the axial direction, as does the copolymer composition, except where operating at the azeotrope composition. A stream of monomer must be added along the reactor to maintain SAN compositional homogeneity at high conversions. A combined stirred-tank followed by a linear-flow reactor process has been disclosed (315). Through continuous recycle copolymerization, a copolymer of identical composition to monomer feed

can be achieved, regardless of the reactivity ratios of the monomers involved (316).

The devolatilization process has been developed in many configurations. Basically, the polymer melt is subjected to high temperatures and low pressures to remove unreacted monomer and solvent. A two-stage process using a tube and shell heat exchanger with enlarged bottom receiver to vaporize monomers has been described (311). A copolymer solution at 40–70% conversion is fed into the first-stage exchanger and heated to 120–190°C at a pressure of 20–133 kPa and then discharged into the enlarged bottom section to remove at least half of the unreacted acrylonitrile. The product from this section is then charged to a second stage and heated to 210–260°C at <20 kPa. The devolatilized product contains ~1% volatiles. Preheating the polymer solution and then flashing it into a multipassage heating zone at lower pressure than the preheater, produces essentially volatile-free product (310,317). SAN can be steam-stripped to quite low monomer levels in a vented extruder which has water injected at a pressure greater than the vapor pressure of water at that temperature (318).

A twin-screw extruder is used to reduce residual monomers from ca 50 to 0.6%, at 170°C and 3 kPa with a residence time of 2 min (313). In another design, a heated casing encloses the vented devolatilization chamber, which encloses a rotating shaft with specially designed blades (319,320). These continuously regenerate a large surface area to facilitate the efficient vaporization of monomers. The devolatilization equipment used for the production of polystyrene and ABS is generally suitable for SAN production.

Processing. SAN copolymers may be processed using the conventional fabrication methods of extrusion, blow molding, injection molding, thermoforming, and casting. SAN is hygroscopic and should be dried before use for best results. Small amounts of additives, such as antioxidants, lubricants, and colorants, may also be used. Typical temperature profiles for injection molding and extrusion of predried SAN resins are as follows (321):

(1) **Molding temperatures**

a. cylinder 193–288°C
b. mold 49–88°C
c. melt 218–260°C

(2) **Extrusion temperatures**

a. hopper zone water-cooled
b. rear zone 177–204°C
c. middle zone 210–232°C
d. torpedo zone and die 204–227°C

Health and Toxicology. SAN resins, in general, appear to pose few health problems, in that SAN resins are allowed by the FDA to be used by the food

and medical industries for certain applications under prescribed conditions (322). The main concern over SAN resin use is that of toxic residuals, eg, acrylonitrile, styrene, or other polymerization components such as emulsifiers, stabilizers, or solvents. Each component must be treated individually for toxic effects and safe exposure level.

Acrylonitrile is believed to behave as an enzyme inhibitor of cellular metabolism (323) and is classified as a possible human carcinogen of medium carcinogenic hazard (324), and can affect the cardiovascular system and kidney and liver functions (323). Direct potential consumer exposure to acrylonitrile through consumer product usage is low because of little migration of the monomer from such products. The concentrations of acrylonitrile in consumer products are estimated to be less than 15 ppm in SAN resins. OSHA's permissible exposure limit for acrylontrile is 2 ppm, an 8-h time-weighted average with no eye or skin contact; the acceptable ceiling limit is 10 ppm; and the action level, the concentration level that triggers the standard for monitoring, etc, is 1 ppm. Further information on the toxicology and human exposure to acrylonitrile is available (325–327).

Styrene, a main ingredient of SAN resins, is a possible human carcinogen (IARC Group 2B/EPA-ORD Group C). It is an irritant to the eyes and respiratory tract, and while prolonged exposure to the skin may cause irritation and CNS effects such as headache, weakness, and depression, harmful amounts are not likely to be absorbed through the skin. OSHA has set permissible exposure limits for styrene in an 8-h time-weighted average at 100 ppm, the acceptable ceiling limit (short-term, 15 min, exposure limit) at 200 ppm (328), and the acceptable maximum peak at 600 ppm (5-min max. peak in any 3 h). For more information on styrene environmental issues, see the CEH Styrene marketing research report (329,330).

In September 1996, the EPA issued a final rule requiring producers of certain thermoplastics to reduce emissions of hazardous air pollutants from their facilities. The final rule seeks to control air toxins released during the manufacture of seven types of polymers and resins, including SAN.

Economic Aspects (Polymers)

The first commercial applications of acrylonitrile polymers were developed by German scientists to provide oil- and gasoline-resistant rubbers during World War II. Although nitrile elastomers (Buna N) no longer account for a main portion of acrylonitrile use, they are still indispensable in many applications. Also, in response to the needs of the war, scientists at U.S. Rubber Company developed the forerunners of modern ABS, ie, tough, shatterproof blends of nitrile rubbers and SAN copolymers. Acrylic fiber manufacture was initiated around 1960, and world production of acrylonitrile has since increased to $>4.0 \times 10^6$ t. Historically, acrylic fibers have consumed >70% of the acrylonitrile in Europe, the Far East, and Latin America. In the United States, this outlet has been gradually decreasing from 50% to about a 30% share.

SAN Economic Aspects. SAN has shown steady growth since its introduction in the 1950s. The combined properties of SAN copolymers, such as optical

clarity, rigidity, chemical and heat resistance, high tensile strength, and flexible molding characteristics, along with reasonable price have secured their market position. Among the plastics with which SAN competes are acrylics, general-purpose polystyrene, and polycarbonate. SAN supply and demand are difficult to track because more than 75% of the resins produced are believed to be used captively for ABS compounding and in the production of acrylonitrile–styrene–acrylate (ASA) and acrylonitrile–EPDM–styrene (AES) weatherable copolymer (331). SAN is considered to be only an intermediate product and not a separate polymer in the production processes for these materials.

There are two major producers of SAN for the merchant market in the United States, Bayer Corp. and the Dow Chemical Co., which market these materials under the names of Lustran and Tyril, respectively. Bayer became a U.S. producer when it purchased Monsanto's styrenics business in December 1995 (332). Some typical physical properties of these SAN resins have been shown in Table 11. These two companies also captively consume the SAN for the production of ABS as well as SAN-containing weatherable polymers. The other two U.S. SAN producers, either mainly consume the resin captively for ABS and ASA polymers (GE Plastics) or toll produce for a single client (Zeon Chemicals). BASF is expected to become a more aggressive SAN supplier in the United States since its Altamira, Mexico, stryenics plant came on-line in early 1999. Overall, U.S. SAN consumption has been relatively stable for the last few years, ranging from 43×10^3 to 44.5×10^3 t (95–98 million pounds) between 1994 and 1996. Most markets for SAN are growing at only GDP rates. Consumption growth for SAN in 1996–2001 is expected

Table 15. U.S. Production/Consumption of SAN, 10^3 t (Dry-Weight Basis)

	Production	Consumption[a]
1985	39.5	34.1
1986	41.8	35.9
1987	57.3	38.6[b]
1988	67.3	41.4
1989	51.4	34.1
1990	61.4	37.3
1991	49.5	37.7
1992	51.4	38.2
1993	47.7	40
1994	62.7	44.5[c]
1995	59.1	43.6[c]
1996	55.5	43.6[c]
1997	43.6	–[c]

[a]Includes captive consumption for uses other than ABS compounding and ASA/AES polymers production.

[b]According to the SPI, 45 t of SAN resin was consumed domestically in 1987. Industry believes this figure to be incorrect. An estimate of 38.6 t is believed to be more accurate.

[c]Reported SPI data for 1996–1997 includes both U.S. and Canadian information and, therefore, are not included in this table. The stated CEH statistics represent consumption only.

to continue at an average annual rate approximation of GDP growth at 2%. Use for packaging will be flat and the automotive application may disappear altogether. Other markets, however, are expected to increase at annual rates between 2.3 and 5.9%. Production and consumption figures for SAN resin in recent years are shown in Table 15 (332).

Uses

Acrylonitrile copolymers offer useful properties, such as rigidity, gas barrier, chemical and solvent resistance, and toughness. These properties are dependent upon the acrylonitrile content in the copolymers. SAN copolymers offer low cost, rigidity, processibility, chemical and solvent resistance, transparency, and heat resistance, which provide advantages over other competing transparent/clear resins, such

Table 16. SAN Copolymer Uses[a]

Application	Articles
Appliances	Air conditioner parts, decorated escutcheons, washer and dryer instrument panels, washing machine filter bowls, refrigerator shelves, meat and vegetable drawers and covers, blender bowls, mixers, lenses, knobs, vacuum cleaner parts, humidifiers, and detergent dispensers
Automotive	Batteries, bezels, instrument lenses, signals, glass-filled dashboard components, and interior trim
Construction electronic	Safety glazing, water filter housings, and water faucet knobs battery cases, instrument lenses, cassette parts, computer reels, and phonograph covers
Furniture	Chair backs and furniture shells, drawer pulls, and caster rollers
Housewares	Brush blocks and handles, broom and brush bristles, cocktail glasses, disposable dining utensils, dishwasher-safe tumblers, mugs, salad bowls, carafes, serving trays, and assorted drinkware, hangers, ice buckets, jars, and soap containers
Industrial	Batteries, business machines, transmitter caps, instrument covers, and tape and data reels
Medical	Syringes, blood aspirators, intravenous connectors and valves, petri dishes, and artificial kidney devices
Packaging	Bottles, bottle overcaps, closures, containers, display boxes, films, jars, sprayers, cosmetic packaging, liners, and vials
Custom molding	Aerosol nozzles, camera parts, dentures, disposable lighter housings, fishing lures, pen and pencil barrels, sporting goods, toys, telephone parts, filter bowls, tape dispensers, terminal boxes, toothbrush handles, and typewriter keys

[a]Refs. 9 and 145.

as poly(methyl methacrylate), polystyrene, polycarbonate, and styrene–butadiene copolymers. SAN copolymers are widely used in goods such as housewares, packaging, appliances, interior automotive lenses, industrial battery cases and medical parts. U.S. consumption of SAN/ABS resins in major industrial markets is about 1095 t in 1998.

Acrylonitrile copolymers have been widely used in films and laminates for packaging (333–337) because of their excellent barrier properties. In addition to laminates (338–342), SAN copolymers are used in membranes (343–346), controlled-release formulations (347,348), polymeric foams (349,350), fire-resistant compositions (351,352), ion-exchange resins (353), reinforced paper (354), concrete and mortar compositions (355,356), safety glasses (357), solid ionic conductors (358), negative resist materials (359), electrophotographic toners (360), and optical recordings (361). SAN copolymers are also used as coatings (362), dispersing agents for colorants (363), carbon-fiber coatings for improved adhesion (364), and synthetic wood pulp (365). SAN copolymers have been blended with aromatic polyesters to improve hydrolytic stability (366), with methyl methacrylate polymers to form highly transparent resins (367), and with polycarbonate to form toughened compositions with good impact strength (368–371). Table 16 lists the most common uses of SAN copolymers in major industrial markets (232,319). Some important modifications of SAN copolymers are listed in Table 17.

Acrylonitrile has contributed the desirable properties of rigidity, high temperature resistance, clarity, solvent resistance, and gas impermeability to many polymeric systems. Its availability, reactivity, and low cost ensure a continuing market presence and provide potential for many new applications.

Table 17. Modified SAN Copolymers

Modifier	Remarks	Reference
Polybutadiene	ABS, impact resistant	[a]
EPDM rubber[b]	Impact and weather resistant	371,372
Polyacrylate	Impact and weather resistant	373,374
Poly(ethylene-*co*-vinyl acetate) (EVA)	Impact and weather resistant	375
EPDM+EVA	Impact and weather resistant	376
Silicones	Impact and weather resistant	377
Chlorinated polyethylene	Impact and weather resistant and flame retardant	378
Polyester, cross-linked	Impact resistant	379
Poly(α-methylstyrene)	Heat resistant	380
Poly(butylene terephthalate)	Wear and abrasion reisitant	381
Ethylene oxide–propylene oxide copolymers	Used as lubricants to improve processability	382
Sulfonation	Hydrogels of high water absorption	383
Glass fibers	High tensile strength and hardness	384

[a] See ACRYLONITRILE–BUTADIENE–STYRENE POLYMERS.
[b] Ethylene–propylene–diene monomer rubber.

BIBLIOGRAPHY

"Acrylonitrile Polymers" in *EPST* 1st ed., Vol. 1, pp. 375–425, by C. H. Bamford and G. C. Eastmond, University of Liverpool; "Acrylonitrile Polymers" in *EPSE* 2nd ed., Vol. 1, pp. 426–470, by F. M. Peng, Monsanto Co.

1. C. H. Bamford, W. G. Barb, A. D. Jenkins, and P. F. Onyon, *The Kinetics of Vinyl Polymerizations by Radical Mechanisms*, Butterworths, London, 1958.
2. W. M. Thomas, *Fortschr. Hochpolymer. Forsch*. **2**, 401 (1961).
3. *The Chemistry of Acrylonitrile*, 2nd ed., Petrochemical Division, American Cyanamid Co., New York, 1959, p. ix.
4. Ref. 3, pp. 2–10
5. C. E. Funk Jr., *Ind. Eng. Chem.* **43**, 1152 (1951).
6. W. V. Smith, *J. Am. Chem. Soc.* **70**, 2177 (1948).
7. D. S. Blackford and R. York, *J. Chem. Eng. Data* **10**, 313 (1965).
8. T. Sasuga and M. Takehisa, *J. Macromol. Sci. Chem., Part A* **12**, 1343 (1978).
9. T. Fukuyama and K. Kuchitsu, *J. Mol. Struct.* **5**(1/2), 131 (1970).
10. Ref. 3, pp. 11–29, 66–247.
11. K. Stueben, in E. C. Leonard, ed., *High Polymers*, Vol. **XXIV**, Part 1, Wiley-Interscience, New York, 1970, pp. 31–51.
12. V. N. Shuraeva and V. Ya Katsobashvill, *React. Kinet. Catal. Lett.* **7**, 267 (1977).
13. L. T. Groet, in M. Grayson and D. Eckroth, eds., *Encyclopedia of Chemical Technology*, 3rd ed., Vol. **1**, John Wiley & Sons, Inc., New York, 1978, pp. 415–416.
14. P. L. Morse, Acrylonitrile from Ethylene-Interim Report No. 17A1, Process Economics Program, SRI International, Menlo Park, Calif., Mar. 1970, pp. 97–98.
15. K. J. Ivin, in J. Brandrup and E. H. Immergut, eds., *Polymer Handbook*, 2nd ed., John Wiley and Sons, Inc., New York, 1975, p. II-433.
16. Ref. 15, p. II-424.
17. J. L. Callahan and co-workers, *Ind. Eng. Chem. Prod. Res. Dev.* **9**, 134 (1970).
18. *Chem. Eng. News* **67**(2), 23 (1989).
19. U.S. Pat. 2,481,826 (Sept. 13, 1949), J. N. Cosby (to Allied Chemical & Dye Corp.).
20. U.S. Pat. 2,904,580 (Sept. 15, 1959), J. D. Idol (to The Standard Oil Co.).
21. J. D. Burrington, C. T. Kartisek, and R. K. Grasselli, *J. Catal.* **87**, 363 (1984).
22. C. R. Adams and T. J. Jennings, *J. Catal.* **2**, 63 (1963).
23. C. R. Adams and T. J. Jennings, *J. Catal.* **3**, 549 (1964).
24. G. W. Keulks, *J. Catal.* **19**, 232 (1970).
25. G. W. Keulks and L. D. Krenzke, in *Proceedings of the 6th International Congress on Catalysis*, 1976, The Chemical Society, London, 1977, p. 806.
26. G. W. Keulks and L. D. Krenzke, *J. Catal.* **61**, 316 (1980).
27. J. F. Brazdil, D. D. Suresh, and R. K. Grasselli, *J. Catal.* **66**, 347 (1980).
28. R. K. Grasselli, J. F. Brazdil, and J. D. Burrington, in *Proceedings of the 8th International Congress on Catalysis*, 1984, Vol. V, Verlag Chemie, Weinheim, 1984, p. 369.
29. R. K. Grasselli, *Appl. Catal.* **15**, 127 (1985).
30. R. K. Grasselli, *React. Kinet. Catal. Lett.* **35**, 327 (1987).
31. J. F. Brazdil, L. C. Glaeser, and R. K. Grasselli, *J. Catal.* **81**, 142 (1983).
32. L. C. Glaeser and co-workers, *J. Chem. Soc. Faraday Trans. 1* **81**, 2903 (1985).
33. R. G. Teller, J. F. Brazdil, and R. K. Grasselli, *Acta Cryst. C* **40**, 2001 (1984).
34. R. G. Teller and co-workers, *J. Solid State Chem.* **52**, 313 (1984).
35. R. G. Teller and co-workers, *J. Chem. Soc. Faraday Trans. 1* **81**, 1693 (1985).
36. M. R. Antonio and co-workers, *J. Phys. Chem.* **92**, 2939 (1988).
37. M. R. Antonio and co-workers, *J. Phys. Chem.* **92**, 2338 (1988).
38. J. F. Brazdil and R. K. Grasselli, *J. Catal.* **79**, 104 (1983).
39. J. F. Brazdil, L. C. Glaeser, and R. K. Grasselli, *J. Phys. Chem.* **87**, 5485 (1983).

40. W. Sleight, in J. J. Burton, and R. L. Garten, eds., *Advanced Materials in Catalysis*, Academic Press, Inc., New York, 1977, pp. 181–208.
41. R. K. Grasselli and J. D. Burrington, *Adv. Catal.* **30**, 133 (1981).
42. K. Weissermel and H. J. Arpe, *Industrial Organic Chemistry* (A. Mullen, trans.), Verlag Chemie, New York, 1978, pp. 266–267.
43. U.S. Pat. 2,690,452 (Sept. 28, 1954), E. L. Carpenter (to American Cyanamid Co.).
44. U.S. Pat. 2,729,670 (Jan. 3, 1956), P. H. DeBruin (to Stamicarbon N.V.).
45. *Chem. Eng. News* **23**, 1841 (Oct. 25, 1945).
46. D. J. Hadley and E. G. Hancock, eds., *Propylene and Its Industrial Derivatives*, Halsted Press, a division of John Wiley & Sons, Inc., New York, 1973, p. 418.
47. K. Sennewald, in *5th World Petroleum Congress Proceedings*, 1959, Section IV, Paper 19.
48. U.S. Pat. 2,554,482 (May 29, 1951), N. Brown (to E. I. du Pont de Nemours & Co., Inc.).
49. U.S. Pat. 2,385,552 (Sept. 25, 1945), L. R. U. Spence and F. O. Haas (to Rohm and Haas Co.).
50. U.S. Pat. 2,736,739 (Feb. 28, 1956), D. C. England and G. V. Mock (to E. I. du Pont de Nemours & Co., Inc.).
51. U.S. Pat. 3,184,415 (May 18, 1965), E. B. Huntley, J. M. Kruse, and J. W. Way (to E. I. du Pont de Nemours & Co., Inc.).
52. U.S. Pats. 4,783,545 (Nov. 8, 1988), 4,837,233 (June 6, 1989), and 4,871,706 (Oct. 3, 1989), L. C. Glaeser, J. F. Brazdil, and M. A. Toft (all to The Standard Oil Co.).
53. Brit. Pats. 1,336,135 (Nov. 7, 1973), N. Harris and W. L. Wood; 1,336,136 (Nov. 7, 1973), N. Harris (both to Power-Gas Ltd.).
54. U.S. Pat. 3,833,638 (Sept. 3, 1974), W. R. Knox, K. M. Taylor, and G. M. Tullman (to Monsanto Co.).
55. U.S. Pats. 4,849,537 (July 18, 1989) and 4,849,538 (July 18, 1989), R. Ramachandran, D. L. MacLean, and D. P. Satchell Jr. (both to The BOC Group, Inc.).
56. U.S. Pat. 4,609,502 (Sept. 2, 1986), S. Khoobiar (to The Halcon SD Group, Inc.).
57. U.S. Pat. 3,751,443 (Aug. 7, 1973), K. E. Khchelan and co-workers.
58. J. Perkowski, *Przem. Chem.* **51**, 17 (1972).
59. U.S. Pat. 4,746,753 (May 24, 1988), J. F. Brazdil, D. D. Suresh, and R. K. Grasselli (to The Standard Oil Co.).
60. U.S. Pat. 4,503,001 (Mar. 5, 1985), R. K. Grasselli, A. F. Miller, and H. F. Hardman (to The Standard Oil Co.).
61. U.S. Pat. 4,228,098 (Oct. 14, 1980), K. Aoki and co-workers, (to Asahi Kasei Kogyo Kabushiki Kaisha).
62. World Acrylonitrile and Derivatives Supply/Demand Report, PCI-Fibres & Raw Materials, 1998.
63. D. W. Bessing and co-workers, *Anal. Chem.* **21**, 1073 (1949).
64. J. Janz and N. E. Duncan, *Anal. Chem.* **25**, 1410 (1953).
65. S. E. Aarato and E. Bittera, *Munkavedelem* **18**(10–12), 50 (1972).
66. L. K. Austin and G. P. Cunningham, *J. Coat. Technol.* **52**(665), 49 (1980).
67. G. W. Daves and W. F. Hamner, *Anal. Chem.* **29**, 1035 (1957).
68. L. I. Petrova and co-workers, *Gig. Sanit.* **37**(1), 63 (1972).
69. J. M. Stepanek and V. M. Cerna, *Analyst* **83**, 345 (1958).
70. J. M. Stepanek, V. M. Cerna, and V. J. Patkova, *Analyst* **84**, 65 (1959).
71. D. R. Marrs, R. L. Capbell, J. M. Boyko, A. L. Parish Jr., and N. W. Standish, in *SPE National Technical Conference*, Nov. 13–15, 1978, pp. 131–136.
72. J. E. Going and co-workers, Environmental Monitoring Near Industrial Sites: Acrylonitrile, Final Report No. EPS/560/6-7/003, Dec. 1978, PB 928, NTIS, U.S. Department of Commerce, Washington, D.C., 285 pp.

73. ASTM E299-97, *Annual Book of ASTM Standards*, American Society for Testing and Materials, Philadelphia, Pa., 1999.
74. *Material Safety Data Sheet Number 1386*, BP Chemicals Inc., Cleveland, Ohio, 1989.
75. Assessment of Human Exposures to Atmospheric Acrylonitrile, SRI International, Menlo Park, Calif., 1979.
76. *Code Federal Regulations, Title 29, Chapter XVII, Part 1910, Subpart 1045, Occupational Safety and Health Standards for General Industry.*
77. E. L. Miller, in *SPE National Technical Conference: Plastics in Packaging and Acrylonitrile—A Dual Meeting*, Chicago, Ill., Nov. 13–15, 1978, pp. 2261–2231.
78. U.S. Pat. 3,193,480 (July 6, 1965), M. M. Baizer and co-workers, (to Monsanto Chemical Co.).
79. U.S. Pats. 3,597,481 (Aug. 3, 1971), 3,631,104 (Dec. 28, 1971), and Re. 31,430 (Oct. 25, 1983), B. A. Tefertiller and C. E. Habermann (all to The Dow Chemical Company).
80. U.S. Pat. 4,048,226 (Sept. 13, 1977), W. A. Barber and J. A. Fetchin (to American Cyanamid Co.).
81. U.S. Pat. 4,086,275 (Apr. 25, 1978), K. Matsuda and W. A. Barber (to American Cyanamid Co.).
82. U.S. Pat. 4,178,310 (Dec. 11, 1979), J. A. Fetchin and K. H. Tsu (to American Cyanamid Co.).
83. J. Barton, I. Capek, and P. Hrdlovic, *J. Polym. Sci., Polym. Chem. Ed.* **13**, 2671 (1975).
84. N. S. Batty and J. T. Guthrie, *J. Polym. Sci., Polym. Chem. Ed.* **25**, 2539 (1980).
85. U.S. Pat. 3,879,360 (Apr. 22, 1975), L. patron and co-workers, (to Montedison Fibre S.p.A.).
86. U.S. Pat. 3,821,178 (June 28, 1974), P. Melacini and co-workers, (to Montedison Fibre S.p.A.).
87. U.S. Pat. 3,787,365 (Jan. 22, 1974), P. Melacini and co-workers, (to Montedison Fibre S.p.A.).
88. G. Burillo, A. Chapiro, and E. Mankowski, *J. Polym. Sci., Polym. Chem. Ed.* **18**, 327 (1980).
89. D. N. Bort, G. F. Zvereva, and S. I. Kuchanov, *Polym. Sci. U.S.S.R* **20**, 2050 (1978).
90. L. H. Garcia-Rubio, A. E. Hamielec, and J. F. MacGregor, *J. Appl. Polym. Sci.* **23**, 1413 (1979).
91. L. H. Garcia-Rubio and A. E. Hamielec, *J. Appl. Polym. Sci.* **23**, 1397 (1979).
92. U.S. Pat. 2,847,405 (Aug. 12, 1958), W. C. Mallison (to American Cyanamid Co.).
93. U.S. Pat. 2,462,354 (Feb. 22, 1949), M. M. Brubaker (to E. I. du Pont de Nemours & Co., Inc.).
94. K. Sugiyama, *J. Maromol. Sci., A: Chem. Ed.* **13**(1), 13 (1979).
95. L. J. Young, in Ref. 3, pp. II-128–II-139.
96. N. G. Gaylord, *J. Macromol. Sci., A: Chem. Ed.* **6**, 259 (1972).
97. G. B. Kharas and co-workers, *J. Polym. Sci., Polym. Chem. Ed.* **16**, 3233 (1978).
98. C. S. Hsia Chen, *J. Polym. Sci., Polym. Chem. Ed.* **14**, 2109 (1976).
99. Y. N. Sharma, V. G. Gandhi, and I. S. Bhardwaj, *J. Polym. Sci., Polym. Chem. Ed.* **18**, 59 (1980).
100. A. Henglein, *Makromol. Chem.* **14**, 128 (1954).
101. A. Chapiro, *J. Polym. Sci.* **23**, 377 (1957).
102. A. D. Jenkins, *Pure Appl. Chem.* **46**, 45 (1976).
103. H. Craubner, *J. Polym. Sci., Polym. Chem. Ed.* **18**, 2011 (1980).
104. Noshay and J. E. McGrath, *Block Copolymers: Overview and Critical Survey*, Academic Press, Inc., New York, 1977.
105. W. R. Krigbaum and N. Tokita, *J. Polym. Sci.* **43**, 467 (1960).
106. G. Henrici-Olive and S. Olive, *Adv. Polym. Sci.* **32**, 123 (1979).

107. R. Chiang, in J. Brandrup and E. H. Immergut, eds., *Polymer Handbook*, 1st ed., John Wiley & Sons, Inc., New York, 1966, pp. V1-69–70.
108. S. Minami, *Appl. Polym. Symp.* **25**, 145 (1974).
109. S. Kenyon and McC. J. Rayford, *J. Appl. Polym. Sci.* **23**, 717 (1979).
110. E. V. Thompson, *Am. Chem. Soc. Div., Polym. Chem. Prepr.* **19**, 952 (1979).
111. L. K. H. Van Beek, *J. Appl. Polym. Sci.* **9**, 553 (1965).
112. E. V. Thompson, *Am. Chem. Soc. Div., Polym. Chem. Prepr.* **20**, 952 (1979).
113. R. M. Kimmel and R. D. Andrews, *J. Appl. Phys.* **36**, 3063 (1965).
114. Y. Ishida, O. Amano, and Takayanagi, *Kolloid-Z.* **172**, 129 (1960).
115. Y. Ishida and co-workers, *Kolloid Z. Z. Polym.* **199**, 67 (1964).
116. K. Gupta and co-workers, *Eur. Polym. J.* **15**, 129 (1979).
117. K. Ogura, S. Kawamura, and H. Sobue, *Macromolecules* **4**, 79 (1971).
118. P. Bajaj, D. C. Gupta, and A. K. Gupta, *J. Appl. Polym. Sci.* **25**, 1673 (1980).
119. R. M. Gohil, K. C. Patel, and R. D. Patel, *Colloid Polym. Sci.* **254**(10), 859 (1976).
120. Y. Imai and co-workers, *J. Polym. Sci., Polym. Lett. Ed.* **8**, 281 (1970).
121. Y. Joh, *J. Polym. Sci., Polym. Chem. Ed.* **17**, 4051 (1979).
122. P. Dunn and B. C. Ennis, *J. Appl. Polym. Sci.* **14**, 1795 (1970).
123. V. G. Hinrichsen, *Angew. Makromol. Chem.* **20**(285), 121 (1971).
124. B. G. Frushour, *Polym. Bull. (Berlin)* **4**, 305 (1981).
125. B. G. Frushour, *Polym. Bull. (Berlin)* **7**, 1 (1982).
126. P. J. Flory, *J. Chem. Phys.* **17**, 233 (1949).
127. R. K. Eby, *J. Appl. Phys.* **34**, 2442 (1963).
128. S. H. Carr, in *SPE 35th Annual Technical Conference*, Montreal, Que. Canada, Apr. 25–28, 1977, pp. 373–375.
129. S. I. Stupp and S. H. Carr, *Colloid Polym. Sci.* **257**, 913 (1979).
130. C. E. Schildknecht, *Vinyl and Related Polymer*, John Wiley & Sons, Inc., New York, 1963, p. 271.
131. S. M. Allen and co-workers, *J. Membr. Sci.* **2**, 153 (1977).
132. G. S. Huvard and co-workers, *J. Membr. Sci.* **6**, 185 (1980).
133. G. Ranade, V. Stannett, and W. J. Koros, *J. Appl. Polym. Sci.* **25**, 2179 (1980).
134. V. Stannett and co-workers, *Polym. Eng. Sci.* **20**, 300 (1980).
135. U.S. Pat. 2,579,451 (Dec. 18, 1951), A. E. Polson (to E. I. du Pont de Nemours & Co., Inc.).
136. U.S. Pat. 2,682,525 (June 29, 1954), H. L. Jackson (to E. I. du Pont de Nemours & Co., Inc.).
137. U.S. Pat. 2,682,524 (June 29, 1954), D. D. Coffman (to E. I. du Pont de Nemours & Co., Inc.).
138. W. Kerr and H. Fernow, *J. Prakt. Chem.* **160**, 281 (1942).
139. J. R. McCartney, *Mod. Plast.* **30**, 118, 179 (July 1953).
140. F. L. M. Schouteden, *Makromol. Chem.* **24**(1), 15 (1957).
141. F. L. Schouteden, *Chim. Ind. (Paris)* **79**, 749 (1958).
142. R. A. Hayes, *J. Polym. Sci.* **11**, 531 (1953).
143. H. Sobue and Y. Tajima, *Kogyo Kogaku Zasshi* **63**, 660 (1960).
144. L. H. Peebles Jr., in N. Bikales, ed., *Encylopedia of Polymer Science and Technology*, 1st ed., Vol. **1**, Wiley-Interscience, New York, 1976, pp. 1–25.
145. A. H. DiEdwardo, *Am. Chem. Soc., Div. Org. Coat. Plast. Chem. Prepr.* **38**, 692 (1978).
146. M. M. Coleman and R. J. Petcaich, *J. Polym. Sci., Polym. Phys. Ed.* **16**, 821 (1978).
147. Y. Tsuchiya and K. Sumi, *J. Appl. Polym. Sci.* **21**, 975 (1977).
148. W. D. Woolley, S. A. Ames, and P. J. Fardell, *Fire Mater* **3**(2), 110 (1979).
149. E. Kobayashi, J. Furukawa, and S. Nagata, *J. Polym. Sci., Polym. Chem. Ed.* **17**, 2093 (1979).

150. W. Y. Chiang, *Proc. Natl. Sco. Council (Republic of China)* **2**(2), 170 (1978).
151. J. M. Courtney, G. B. Park, I. A. Fairweather, and R. M. Lindsay, *Biomater. Med. Dev. Artif. Organs* **4**, 263 (1976).
152. S. Woods, *Candian Packaging* **39**(9), 48 (1986).
153. *Barex Resins Technical Data Sheets*, BP Amoco Chemicals, Apr. 2000.
154. P. R. Lund and T. J. Bond, *Soc. Plast. Eng. Tech. Pap.* **24**, 61 (1975).
155. R. C. Adams and S. J. Waisala, in *TAPPI Pap. Synth. Conf. Prepr.*, Atlanta, Ga., 1975, p. 79.
156. Jpn. Pat. 85 097,823 (May 31, 1985) (to Mitsui Toatsu Chemicals, Inc.).
157. U.S. Pat. 4,452,835 (June 5, 1984), G. Vasudevan (to Union Carbide Corp.).
158. Ger. Pat. 2,656,993 (June 22, 1978), R. E. Isley (to The Standard Oil Co.).
159. J. A. Carlson Jr. and L. Borla, *Mod. Plast.* **57**(6), 117 (1980).
160. N. W. Johnston, *Appl. Polym. Symp.* **25**, 19 (1974).
161. H. K. Acharya, N. Krishnaswamy, and B. D. Dasare, *J. Appl. Polym. Sci.* **23**, 2945 (1979).
162. E. Oikawa and T. Ohsaki, *Desalination* **25**(2), 187 (1978).
163. D. B. Bailey and P. N. Heinrichs, *J. Polym. Sci., Chem. Ed.* **16**, 3185 (1978).
164. J. E. Turner, M. Shen, and C. C. Lin, *J. Appl. Polym. Sci.* **25**, 1287 (1980).
165. E. I. Stout and co-workers, *J. Appl. Polym. Sci.* **21**, 2565 (1977).
166. W. P. Lindsay, in *TAPPI Annual Meeting Preprints*, Atlanta, Ga., 1977, pp. 203–205.
167. U.S. Pat. 4,134,863 (Jan. 16, 1979), G. F. Fanta, E. I. Stout, and W. M. Doane (to U.S. Department of Agriculture).
168. U.S. Pat. 3,985,616 (Oct. 12, 1976), M. W. Weaver and co-workers, (to U.S. Department of Agriculture).
169. W. Tsuji, A. Hirai, and M. Hosono, *J. Appl. Polym. Sci.* **20**, 2837 (1976).
170. A. Hirai and co-workers, *J. Appl. Polym. Sco.* **20**, 3365 (1976).
171. J. W. Brickman, *TAPPI* **60**(6), 99 (1977).
172. F. I. Abdel-Hay, C. G. Beddows, and J. T. Guthrie, *Polym. Bull. (Berlin)* **2**, 607 (1980).
173. F. Sundardi, *J. Appl. Polym. Sci.* **22**, 3163 (1978).
174. L. J. Young, in Ref. 15, 2nd ed., pp. II-128–II-139; see also R. Z. Greenley, in Ref. 15 3rd ed., 1989, pp. II-165–II-171.
175. U.S. Pat. 3,926,871 (Dec. 16, 1975), L. W. Hensley and G. S. Li (to The Standard Oil Co.).
176. U.S. Pat. 4,195,135 (Mar. 25, 1980), G. S. Li and J. F. Jones (to The Standard Oil Co.).
177. U.S. Pat. 3,997,709 (Dec. 14, 1976), W. Y. Aziz, L. E. Ball, and G. S. Li (to The Standard Oil Co.).
178. Fr. Pat. 2,207,938 (June 21, 1974) (to Polysar Ltd.).
179. Can. Pat. 991,787 (June 22, 1976), M. H. Richmond and H. G. Wright (to Polysar Ltd.).
180. U.S. Pat. 4,301,112 (Nov. 17, 1981), M. M. Zwick (to American Cyanamid Co.).
181. U.S. Pat. 4,025,581 (May 24, 1977), J. A. Powell and A. Williams (to Rohm and Haas Co.).
182. Jpn. Pat. 79 058,794 (May 11, 1979), H. Furukawa and S. Matsumura (to Kanegafuchi Chemical Industry Co., Ltd.).
183. Fr. Pat. 2,389,644 (Dec. 1, 1978), P. Hubin-Eschger, (to ATO-Chimie S.A.).
184. Jpn. Pat. 75 124,970 (Oct. 1, 1975), A. Kobayashi and M. Ohya (to Kureha Chemical Industry Co., Ltd.).
185. Jpn. Pat. 87 013,425 (Jan. 22, 1987), M. Fujimoto, T. Yamashita, and T. Matsumoto (to Kanebo NSC K.K.).
186. U.S. Pat. 4,000,359 (Dec. 28, 1976), W. A. Watts and J. L. Wang (to Goodyear Tire and Rubber Co.).
187. U.S. Pat. 3,832,335 (Sept. 27, 1974), J. W. Bayer (to Owens-Illinois, Inc.).

188. Jpn. Pat. 74 021,105 (May 29, 1974), M. Takahashi, K. Yanagisawa, and T. Mori (to Sekisui Chemical Co., Ltd.).
189. U.S. Pat. 3,959,550 (May 25, 1976), M. S. Guillod and R. G. Bauer (to Goodyear Tire and Rubber Co.).
190. Fr. Pat. 2,041,137 (Mar. 5, 1971), Q. A. Trementozzi (to Monsanto Co.).
191. Ger. Pat. 2,134,814 (May 31, 1972), T. Yamawaki, M. Hayashi, and K. Endo (to Mitsubishi Chemical Industries Co., Ltd.).
192. U.S. Pat. 3,725,120 (Apr. 3, 1973), C. A. Suter (to Goodyear Tire and Rubber Co.).
193. Ger. Pat. 1,546,809 (Jan. 31, 1974), D. S. Dixler (to Air Products and Chemicals, Inc.).
194. Jpn. Pat. 87 256,871 (Nov. 9, 1987), H. Sakai and T. Kotani (to Asahi Chemical Industry Co., Ltd.).
195. Ger. Pat. 2,436,137 (Feb. 13, 1975), B. N. Hendy (to Imperial Chemical Industries Ltd.).
196. U.S. Pat. 4,596,856 (June 24, 1986), M. M. Wu, E. J. Dewitt, and G. S. Li (to The Standard Oil Co. (Ohio)).
197. U.S. Pat. 4,603,186 (Jul. 29,1986), M. M. Wu, E. J. Dewitt, and G. S. Li (to The Standard Oil Co. (Ohio)).
198. U.S. Pat. 4,638,042 (Jan 20, 1987), G. S. Li, M. M. Wu, and E. J. Dewitt (to The Standard Oil Co. (Ohio)).
199. U.S. Pat. 4,681,916 (Jul. 21, 1987), M. M. Wu, E. J. Dewitt, and G. S. Li (to The Standard Oil Co. (Ohio)).
200. U.S. Pat. 4,681,917 (Jul. 21, 1987), G. S. Li, M. M. Wu, and E. J. Dewitt (to The Standard Oil Co. (Ohio)).
201. U.S. Pat. 4,761,455 (Aug. 2, 1988), M. M. Wu, E. J. Dewitt, and G. S. Li (to The Standard Oil Co. (Ohio)).
202. U.S. Pat. 4,677,164 (Jun. 30, 1987), G. S. Li, M. M. Wu, and E. J. Dewitt (to The Standard Oil Co. (Ohio)).
203. S. Yabumoto, K. Ishii, and K. Arita, *J. Polym. Sci., Part A* **1**, 1577 (1969).
204. N. G. Gaylord, S. S. Dixit, and B. K. Patnaik, *J. Polym. Sci., Part B* **9**, 927 (1971).
205. N. G. Gaylord and co-workers, *J. Macromol. Sci. Chem.* **6**, 1495 (1972).
206. K. Arita, T. Ohtomo, and Y. Tsurumi, *J. Polym. Sci., Polym. Lett. Ed.* **19**, 211 (1981).
207. C. D. Eisenbach and co-workers, *Angew. Makromol. Chem.* **145/146**, 125 (1986).
208. H. Hirai, *J. Polym. Sci. Macromol. Rev.* **11**, 47 (1976).
209. A. Henglein, *Makromol. Chem.* **14**, 128 (1954).
210. A. Chapiro, *J. Polym. Sci.* **23**, 377 (1957).
211. A. D. Jenkins, *Pure Appl. Chem.* **46**, 45 (1976).
212. H. Craubner, *J. Polym. Sci., Polym. Chem. Ed.* **18**, 2011 (1980).
213. G. Krasnoselskaya and B. L. Erusalimskii, *Vysokomol. Soedin., Ser. B* **29**, 442 (1987).
214. J. Chiefari and co-workers, *Macromololecules* **31**, 5559 (1998).
215. K. Matyjaszewski, *J. Macromo. Sci., Part A* **10**, 1785 (1997).
216. M. Baumert and co-wokers, in *Polymeric Materials Science and Engineering*, vol. 79 (Fall Meeting 1998).
217. K. Tharanikkarasu and G. Radhakrishnan, *J. Polym. Chem. 34* **9**, 1723 (1996).
218. T. Fukuda and co-workers, *Macromolecules* **29**, 3050 (1996).
219. I. Q. Li and co-workers, *Macromolecules* **30**, 5195 (1997).
220. M. Minagawa and co-workers, *Polymer* **36**, 2343 (1995).
221. G. Optiz and co-workres, *Acta Polym.* **47**(2/3), 67 (1996).
222. J. E. Turner, M. Shen, and C. C. Lin, *J. Appl. Polym. Sci.* **25**, 1287 (1980).
223. E. I. Stout, D. Trimnell, W. M. Doane, and C. R. Russell, *J. Appl. Polym. Sci.* **21**, 2565 (1977).

224. F. Sundardi, *J. Appl. Polym. Sci.* **22**, 3163 (1978).
225. U.S. Pat. 4,134,863 (Jan. 16, 1979), G. F. Fanta, E. I. Stout, and W. M. Doane (to U.S. Department of Agriculture).
226. A. C. Orchard and L. J. Bates, *BHR Group Conf. Ser. Pub. 3*, 1993, pp. 59–66.
227. K. M. Abrham and M. Alamgir, in *Proc. of the 35th Int. Power Sources Symp.*, 1992, pp. 264–266.
228. F. Sebesta and coworkers, *Acta Polytec.* **38** (3), 119 (1998).
229. Ref. 1, p. 29.
230. J. L. Ziska, in R. Juran, ed., *Modern Plastics Encyclopedia*, Vol. **65**, No. 11, McGraw-Hill, Inc., New York, 1989, p. 105.
231. D. M. Bennett, in Ref. 272, in p. 96.
232. F. L. Reithel, in Ref. 232, p. 105.
233. B. N. Hendy, in N. A. J. Platzer, ed., *Copolymers, Polyblends, and Composites* (Adv. Chem. Ser. 142), American Chemical Society, Washington, D.C., 1975, p. 115.
234. W. J. Hall and H. K. Chi, in *SPE National Technical Conference: High Performance Plastics*, Cleveland, Ohio, Oct. 5–7, 1976, pp 1–5.
235. N. W. Johnston, *Polym. Prepr., Am. Chem. Soc.* **14**(1), 46 (1973).
236. N. W. Johnston, *J. Macromol. Sci., C: Rev. Macromol. Chem.* **14**, 215 (1976).
237. J. A. Sauer and C. C. Chen, *Polym. Eng. Sci.* **24**, 786 (1984).
238. W. Hanson and R. L. Zimmerman, *Ind. Eng. Chem.* **49**, 1803 (1957).
239. Brit. Pat. 590,247 (July 11, 1947) (to Bakelite Ltd.).
240. R. F. Blanks and B. N. Shah, *Polym. Prepr., Am. Chem. Soc.* **17**, 407 (1976).
241. S. A. Jabarin and E. A. Lofgren, *Polym. Eng. Sci.* **26**, 405 (1986).
242. M. Kopic, F. Flajsman, and Z. Janovic, *J. Macromol. Sci., A: Chem.* **24**(1), 17 (1987).
243. H. U. Khan and G. S. Bhargava, *J. Polym. Sci., Polym. Lett. Ed.* **22**(2), 95 (1984).
244. H. U. Khan, V. K. Gupta, and G. S. Bhargava, *Polym. Commun.* **24**(6), 191 (1983).
245. V. H. Gerrens, H. Ohlinger, and R. Fricker, *Makromol. Chem.* **87**, 209 (1965).
246. Y. Shimura, I. Mita, and H. Kambe, *J. Polym. Sci., Polym. Lett. Ed.* **2**, 403 (1964).
247. R. Cooper, in J. I. Kroschwitz, ed., *Encyclopedia of Polymer Science and Engineering*, 2nd ed., Vol. **10**, Wiley-Interscience, New York, 1987, pp. 1–19.
248. L. H. Garcia-Rubio, J. F. MacGregor, and A. E. Hamielec, *Polym. Prepr., Am. Chem. Soc.* **22**, 292 (1981).
249. K. Tsuchida, *Nempo—Fukui-ken Kogyo Shikenjo* **1980**, 74 (1981).
250. G. Gloeckner and R. Konigsveld, *Makromol. Chem., Rapid Commun.* **4**, 529 (1983).
251. G. Gloeckner, *Pure Appl. Chem.* **55**, 1553 (1983).
252. M. Alonso, F. Recasens, and L. Puiganer, *Chem. Eng. Sci.* **41**, 1039 (1986).
253. K. Hidaka, *Shokuhin Eiseigaku Zasshi* **22**, 536 (1981).
254. R. G. Fordyce and E. C. Chapin, *J. Am. Chem. Soc.* **69**, 581 (1947).
255. W. V. Smith, *J. Am. Chem. Soc.* **70**, 2177 (1948).
256. P. J. Flory, *Principles of Polymer Chemistry*, Cornell University Press, Ithaca, N.Y., 1957, Chapt. "V".
257. C. H. Basdekis, *ABS Plastics*, Reinhold Publishing Corp., New York, 1964, p. 47.
258. Brit. Pat. 1,328,625 (Aug. 30, 1973) (to Daicel Ltd.).
259. R. V. Kucher and co-worker, *Polym. Sci. U.S.S.R* **20**, 2793 (1978).
260. M. Suzuki, H. Miyama, and S. Fujimoto, *Bull. Chem. Soc. Jpn.* **35**, 60 (1962).
261. H. Miyama and S. Fujimoto, *J. Polym. Sci.* **54**, S32 (1961).
262. G. Mino, *J. Polym. Sci.* **22**, 369 (1956).
263. F. R. Mayo and F. M. Lewis, *J. Am. Chem. Soc.* **66**, 1594 (1944).
264. E. T. Mertz, T. Alfrey, and G. Goldfinger, *J. Polym. Sci.* **1**, 75 (1946).
265. A. Guyot and J. Guillot, *J. Macromol. Sci., A: Chem.* **1**, 793 (1967).

266. A. Guyot and J. Guillot, *J. Macromol. Sci., A: Chem.* **2**, 889 (1968).
267. J. A. Seiner and M. Litt, *Macromolecules* **4**, 308 (1971).
268. B. Sandner and E. Loth, *Faserforsch Textiltech.* **27**, 571 (1976).
269. D. J. T. Hill, J. H. O'Donnell, and P. W. O'Sullivan, *Macromolecules* **15**, 960 (1982).
270. G. S. Prementine and D. A. Tirrell, *Macromolecules* **20**, 3034 (1987).
271. C. C. Lin, W. Y. Chiu, and C. T. Wang, *J. Appl. Polym. Sci.* **23**, 1203 (1978).
272. T. Kikuta, S. Omi, and H. Kubota, *J. Chem. Eng. Jpn.* **9**, 64 (1976).
273. Brit. Pat. 1,093,349 (Nov. 29, 1967), T. M. Fisler (to Ministerul Industriei Chimice).
274. U.S. Pat. 3,772,257 (Nov. 13, 1973), G. K. Bochum and co-workers, (to Knapsack A.G.).
275. U.S. Pat. 4,439,589 (Mar. 27, 1984), H. Alberts, R. Schubart, and A. Pischtschan (to Bayer A.G.).
276. A. Guyot, J. Guillot, C. Pichot, and L. R. Gurerrero, in D. R. Bassett and A. E. Hamielec, eds., *Emulsion Polymers and Emulsion Polymerization* (ACS Symp. Ser. 165), American Chemical Society, Washington, D.C., 1981, p. 415.
277. J. Snuparek Jr. and F. Krska, *J. Appl. Polym. Sci.* **21**, 2253 (1977).
278. Ger. Pat. 141,314 (Apr. 23, 1980), H. P. Thiele and co-workers (to VEB Chemische Werke Buna).
279. Pol. Pat. PL 129,792 (Nov. 15, 1985), P. Penczek, E. Wardzinska, and G. Cynkowska (to Instytut Chemii Przemyslowej).
280. U.S. Pat. 4,251,412 (Feb. 17, 1981), G. P. Ferrini (to B. F. Goodrich Co.).
281. U.S. Pat. 4,255,307 (Mar. 10, 1981), J. R. Miller (to B. F. Goodrich Co.).
282. U.S. Pat. 4,228,119 (Oct. 14, 1980), I. L. Gomez and E. F. Tokas (to Monsanto Co.).
283. U.S. Pat. 4,215,024 (July 29, 1980), I. L. Gomez and E. F. Tokas (to Monsanto Co.).
284. U.S. Pat. 4,215,085 (July 29, 1980), I. L. Gomez (to Monsanto Co.).
285. U.S. Pat. 4,252,764 (Feb. 24, 1981), E. F. Tokas (to Monsanto Co.).
286. U.S. Pat. 3,248,455 (Apr. 26, 1966), J. E. Harsch and co-workers (to U.S. Rubber Co.).
287. Brit. Pat 1,034,228 (June 29, 1966) (to U.S. Rubber Co.).
288. U.S. Pat. 3,249,569 (May 3, 1966), J. Fantl (to Monsanto Co.).
289. U.S. Pat. 3,547,857 (Dec. 15, 1970), A. G. Murray (to Uniroyal, Inc.).
290. Brit. Pat. 971,214 (Sept. 30, 1964) (to Monsanto Co.).
291. U.S. Pat. 4,193,903 (Mar. 18, 1980), B. E. Giddings, E. Wardlow Jr., and B. L. Mehosky (to The Standard Oil Co.).
292. U.S. Pat. 3,738,972 (June 12, 1973), K. Moriyama and T. Osaka (to Daicel Ltd.).
293. Brit. Pat. 1,328,625 (Aug. 30, 1973), K. Moriyama and S. Takahashi (to Daicel Ltd.).
294. Jpn. Pat. 78 082,892 (July 21, 1978), S. Kato and M. Momoka (to Denki Kagaku Kogyo K.K.).
295. Jpn. Pat. 79 020,232 (July 20, 1979), S. Kato and M. Momoka (to Denki Kagaku Kogyo K.K.).
296. Jpn. Pat. 79 119,588 (Sept. 17, 1979), K. Kido and co-workers, (to Kureha Chemical Industry Co., Ltd.).
297. Jpn. Pat. 82 167,303 (Oct. 15, 1982) (to Toshiba Machine Co.).
298. U.S. Pat. 3,198,775 (Aug. 3, 1965), R. E. Delacretaz, S. P. Nemphos, and R. L. Walter (to Monsanto Co.).
299. U.S. Pat. 3,258,453 (June 28, 1966), H. K. Chi (to Monsanto Co.).
300. U.S. Pat. 3,287,331 (Nov. 22, 1966), Y. C. Lee and L. P. Paradis (to Monsanto Co.).
301. U.S. Pat. 3,681,310 (Aug. 1, 1972), K. Moriyama and T. Moriwaki (to Daicel Ltd.).
302. U.S. Pat. 3,243,407 (Mar. 29, 1966), Y. C. Lee (to Monsanto Co.).
303. U.S. Pat. 3,331,810 (July 18, 1967), Y. C. Lee (to Monsanto Co.).
304. U.S. Pat. 3,331,812 (July 18, 1967), Y. C. Lee and S. P. Nemphos (to Monsanto Co.).
305. U.S. Pat. 3,356,644 (Dec. 5, 1967), Y. C. Lee (to Monsanto Co.).
306. U.S. Pat. 3,491,071 (Jan. 20, 1970), R. Lanzo (to Montecatini Edison SpA).
307. Jpn. Pat. 83 103,506 (June 20, 1983) (to Mitsubishi Rayon, Ltd.).

308. Jpn. Pat. 88 039,908 (Feb. 20, 1988) (to Mitsui Toatsu Chemicals, Inc.).
309. Belg. Pat. 904,985 (Oct. 16, 1986), S. Ikuma (to Mitsubishi Monsanto Chemical Co.).
310. U.S. Pat. 3,141,868 (July 21, 1964), E. P. Fivel (to Resines et Verms Artificiels).
311. U.S. Pat. 3,201,365 (Aug. 17, 1965), R. K. Charlesworth and co-workers (to The Dow Chemical Company).
312. U.S. Pat. 2,941,985 (June 21, 1960), J. L. Amos and C. T. Miller (to The Dow Chemical Company).
313. U.S. Pat. 3,031,273 (Apr. 24, 1962), G. A. Latinen (to Monsanto Co.).
314. U.S. Pat. 2,745,824 (May 15, 1956), J. A. Melchore (to American Cyanamid Co.).
315. Jpn. Pat. 73 021,783 (Mar. 19, 1973), H. Sato and co-workers, (to Toray K.K., Ltd.).
316. R. L. Zimmerman, J. S. Best, P. N. Hall, and A. W. Hanson, in R. F. Gould, ed., *Polymerization and Polycondensation Processes* (Adv. Chem. Ser. 34), American Chemical Society, Washington, D.C., 1962, p. 225.
317. Jpn. Pat. 87 179,508 (Aug. 6, 1987), N. Ito and co-workers (to Mitsui Toatsu Chemicals, Inc.).
318. Jpn. Pat. 83 037,005 (Mar. 4, 1983) (to Mitsui Toatsu Chemicals, Inc.).
319. U.S. Pat. 3,067,812 (Dec. 11, 1962), G. A. Latinen and R. H. M. Simon (to Monsanto Co.).
320. U.S. Pat. 3,211,209 (Oct. 12, 1965), G. A. Latinen and R. H. M. Simon (to Monsanto Co.).
321. F. M. Peng, in J. I. Kroschwitz, ed., *Encyclopedia of Polymer Science and Engineering*, 2nd ed., Vol. **1**, Wiley-Interscience, New York, 1985, p. 463.
322. United States Food and Drug Administration, *Fed. Regist.* **52**, 33802–33803 (Sept. 8, 1987).
323. United States Food and Drug Administration, *Fed. Regist*. **43**, 2586 (Jan. 17, 1978).
324. National Institute for Occupational Safety and Health, "A Recommended Standard for Occupational Exposure to Acrylonitrile," DHEW Publ. No. 78116, U.S. Government Printing Office, Washington, D.C., 1978.
325. N. I. Sax and R. J. Lewis Sr., *Dangerous Properties of Industrial Materials*, 7th ed., Van Nostrand Reinhold Co., Inc., New York, 1989.
326. R. E. Lenga, *The Sigma-Aldrich Library of Chemical Safety Data*, Sigma-Aldrich Corp., Milwaukee, Wis., 1985.
327. M. Sittig, ed., *Priority Toxic Pollutants*, Noyes Data Corporation, Park Ridge, N.J., 1980.
328. *"Threshold Limit Values for Chemical Substances in the Work Environment Adopted by ACGIH for 1985–86,"* American Conference of Government Industrial Hygienists, Cincinnati, Ohio, 1985.
329. "Criteria for Recommended Standard Occupational Exposure to Styrene", U.S. Department of Health and Human Services (NIOSH), Washington, D.C., Rept. 83–119, pp. 18, 227, 1983; available from NTIS, Springfield, Va.
330. J. Santodonato and co-workers, *Monograph on Human Exposure to Chemicals in the Work Place; Styrene*, PB86-155132, Syracuse, N.Y., July 1985.
331. *Chem. Eng. News* **67**(25), 45 (June 19, 1989).
332. SRI Report, SRI International, Menlo Park, Calif., July 1998.
333. Jpn. Pat. 76 000,581 (Jan. 6, 1976), M. Nishizawa and co-workers (to Toray Industries, Inc.).
334. Jpn. Pat. 82 185,144 (Nov. 15, 1982) (to Gunze Ltd.).
335. Jpn. Pat. 81 117,652 (Sept. 16, 1981) (to Asahi Chemical Industry Co., Ltd.).
336. U.S. Pat. 4,389,437 (June 21, 1983), G. P. Hungerford (to Mobil Oil Corp.).
337. Jpn. Pat. 88 041,139 (Feb. 22, 1988) (to Mitsui Toatsu Chemicals, Inc.).
338. Jpn. Pat. 83 119,858 (July 16, 1983) (to Toyobo Co., Ltd.).

339. Jpn. Pat. 83 183,465 (Oct. 26, 1983) (to Dainippon Printing Co., Ltd.).
340. Jpn. Pat. 84 012,850 (Jan. 23, 1984) (to Asahi Chemical Industry Co., Ltd.).
341. Jpn. Pat. 85 009,739 (Jan. 18, 1985) (to Toyo Seikan Kaisha, Ltd.).
342. Eur. Pat. Appl. EP 138,194 (Apr. 24, 1985), J. H. Im and W. E. Shrum (to The Dow Chemical Company).
343. U.S. Pat. 4,364,759 (Dec. 21, 1982), A. A. Brooks, J. M. S. Henis, and M. K. Tripodi (to Monsanto Co.).
344. Jpn. Pat. 84 202,237 (Nov. 16, 1984) (to Toyota Central Research and Development Laboratories, Inc.).
345. Jpn. Pat. 85 202,701 (Oct. 14, 1985), T. Kawai and T. Nogi (to Toray Industries, Inc.).
346. H. Kawato and co-workers, *Kenkyu Hokoku–Asahi Garasu Kogyo Gijutsu Shoreikai* **49**, 77 (1986).
347. Eur. Pat. Appl. EP 141,584 (May 15, 1985), R. W. Baker (to Bend Research, Inc.).
348. Y. S. Ku and S. O. Kim, *Yakhak Hoechi* **31**(3), 182 (1987).
349. U.S. Pat. 4,330,635 (May 18, 1982), E. F. Tokas (to Monsanto Co.).
350. Ger. Pat. 3,523,612 (Jan. 23, 1986), N. Sakata and I. Hamada (to Asahi Chemical Industry Co., Ltd.).
351. Jpn. Pat. 84 024,752 (Feb. 8, 1984) (to Kanebo Synthetic Fibers, Ltd.).
352. Ger. Pat. 3,512,638 (Feb. 27, 1986), H. J. Kress and co-workers (to Bayer A.G.).
353. Jpn. Pat. 88 089,403 (Apr. 20, 1988) (to Sumitomo Chemical Co., Ltd.).
354. Jpn. Pat. 82 059,075 (Dec. 13, 1982) (to Nichimen Co., Ltd.).
355. S. Milkov and T. Abadzhieva, *Fiz. Khim. Mekh.* **11**, 81 (1983).
356. M. Gadalla and M. E. El-Derini, *Polym. Eng. Sci.* **24**, 1240 (1984).
357. Ger. Pat. 2,652,427 (May 26, 1977), G. E. Cartier and J. A. Snelgrove (to Monsanto Co.).
358. Jpn. Pat. 82 137,359 (Aug. 24, 1982) (to Nippon Electric Co., Ltd.).
359. Jpn. Pat. 83 001,143 (Jan. 6, 1983) (to Fujitsu Ltd.).
360. Jpn. Pat. 88 040,169 (Feb. 20, 1988), Y. Takahashi and co-workers, (to Sharp Corp.).
361. Jpn. Pat. 86 092,453 (May 10, 1986), Y. Ichihara and Y. Uratani (to Mitsubishi Petrochemical Co., Ltd.).
362. Braz. Pat. 87 818 (Dec. 22, 1987), T. P. Christini (to E. I. du Pont de Nemours & Co., Inc.).
363. Jpn. Pat. 84 018,750 (Jan. 31, 1984) (to Sanyo Chemical Industries, Ltd.).
364. Jpn. Pat. 84 080,447 (May 9, 1984) (to Mitsubishi Rayon Co., Ltd.).
365. P. Albihn and J. Kubat, *Plast. Rubber Process. Appl.* **3**, 249 (1983).
366. U.S. Pat. 4,327,012 (Apr. 27, 1982), G. Salee (to Hooker Chemicals and Plastics Corp.).
367. Jpn. Pat. 83 217,536 (Dec. 17, 1983) (to Asahi Chemical Industry Co., Ltd.).
368. Eur. Pat. Appl. EP 96,301 (Dec. 21, 1983), H. Peters and co-workers (to Bayer A.G.).
369. Y. Fujita and co-workers, *Kobunshi Ronbunshu* **43**(3), 119 (1986).
370. H. Takahashi and co-workers, *J. Appl. Polym. Sci.* **36**, 1821 (1988).
371. Ger. Pat. 2,830,232 (Mar. 29, 1979), W. J. Peascoe (to Uniroyal, Inc.).
372. Jpn. Pat. 79 083,088 (July 2, 1979), S. Ueda and co-workers, (to Asahi-Dow Ltd.).
373. Ger. Pat. 2,826,925 (Jan. 17, 1980), J. Swoboda, G. Lindenschmidt, and C. Bernhard (to BASF A.G.).
374. U.S. Pat. 3,944,631 (Mar. 16, 1976), A. J. Yu and R. E. Gallagher (to Stauffer Chemical Co.).
375. H. Bartl and co-workers, in *ACS National Meeting, Division of Industrial Engineering Chemistry*, Atlanta, Ga., Mar. 29–Apr. 3, 1981. Paper 15.
376. Jpn. Pat. 79 083,049 (July 2, 1979), S. Ueda and co-workers, (to Asahi-Dow Ltd.).
377. U.S. Pat. 4,071,577 (Jan. 31, 1978), J. R. Falender, C. M. Mettler, and J. C. Saam (to Dow Corning Corp.).
378. *Mod. Plast.* **60**(1), 92 (1983).

379. U.S. Pat. 4,224,207 (Sept. 23, 1980), J. C. Falk (to Borg-Warner Corp.).
380. U.S. Pat. 4,169,195 (Sept. 25, 1979), M. K. Rinehart (to Borg-Warner Corp.).
381. Jpn. Pat. 81 016,541 (Feb. 17, 1981) (to Asahi-Dow Ltd.).
382. Ger. Pat. 2,916,668 (Nov. 13, 1980), J. Hambrecht, G. Lindenschmidt, and W. Regel (to BASF A.G.).
383. Jpn. Pat. 80 157,604 (Dec. 8, 1980) (to Daicel Chemical Industries, Ltd.).
384. T. C. Wallace, in *SPE Regional Technical Conference*, Las Vegas, Nev., Sept. 16–18, 1975.

MICHAEL M. WU
BP Chemicals

ACRYLONITRILE–BUTADIENE–STYRENE POLYMERS

Introduction

Acrylonitrile–butadiene–styrene (ABS) polymers [9003-56-9] comprise a versatile family of readily processable resins used for producing products exhibiting excellent toughness, good dimensional stability, and good chemical resistance. Special product features can also be obtained such as transparency, unique coloration effects, higher heat performance, and flame retardancy. ABS is comprised of particulate rubber, usually polybutadiene or a butadiene copolymer, dispersed in a thermoplastic matrix of styrene and acrylonitrile copolymer (SAN) [9003-54-7]. The presence of SAN chemically attached or "grafted" to the elastomeric particles compatabilizes the rubber with the SAN component. Altering structural and compositional parameters allows considerable versatility in the tailoring of properties to meet specific product requirements.

Physical Properties

Typical mechanical properties of some commercially available ABS materials are listed in Table 1. It is indicated that a wide range of mechanical and impact properties are achievable for ABS materials.

These property variations are obtained through comonomers, additives, or by making structural changes such as the following: rubber content, extent of rubber cross-linking, rubber particle size and distribution, grafted SAN level and composition, and the composition and molecular weight of the matrix. Depending on the polymerization technique, SAN can be controlled to varying levels as the continuous phase, as grafted polymer attached to the rubber particles, and as

Encyclopedia of Polymer Science and Technology. Copyright John Wiley & Sons, Inc. All rights reserved.

Table 1. Material Properties of ABS Grades

Properties	ASTM method	Medium impact	High impact	Heat resistant	Flame retardant	High modulus[a]
Notched Izod impact at rt, J/m[b]	D256	160–270	270–530	75–300	140–320	50–150
Tensile yield strength, MPa[c]	D638	35–50	30–45	35–60	35–45	65–95
Elongation at break, %	D638	20–40	25–80	10–60	10–30	2–5
Flexural yield strength, MPa[c]	D790	55–75	50–75	55–90	55–75	95–160
Flexural modulus, GPa[d]	D790	2–3	1.5–2.5	2–3	2–2.5	4–9
Heat deflection[e], °C at 1825 kPa[f]	D648	75–90	75–85	90–110	70–80	95–105
Vicat softening pt, °C	D1525	100–110	95–105	110–125	85–100	100–110
Rockwell hardness	D785	100–115	80–110	105–115	95–105	110–115

[a] Filled with ~10–30% glass.
[b] To convert J/m to ft·lbs/in., divide by 53.4.
[c] To convert MPa to psi, multiply by 145.
[d] To convert GPa to psi, multiply by 145,000.
[e] Unannealed at 6.35-mm thickness.
[f] To convert kPa to psi, multiply by 0.145.

occlusions contained within the rubber particles. Thus, both the rubber content and the "rubber phase" (defined as rubber that may contain occluded SAN) volume fraction at a given rubber weight fraction can be independently controlled. Because of the capability to vary such structural and compositional parameters for property enhancements, ABS is a versatile engineering thermoplastic that can be customized to provide a wide range of mechanical and flow properties.

Structural and Compositional Effects. Being a multiphase polymer blend, the effects of the compositional and structural features in ABS are complex and interdependent. However, to a first approximation, the rubber phase contributes toughness, the styrene component contributes rigidity and processability, and the acrylonitrile (AN) phase contributes chemical resistance.

Effect of Dispersed Rubber Phase. The impact toughness of ABS is one of many properties affected by the rubber phase volume fraction, particle size and size distribution, and structure. SAN alone is quite brittle—it is the presence of the uniformly distributed rubber phase (ranging in size from 50 to 2000 nm) that imparts the ductility observed in ABS resins. It is widely reported that rubber particles induce plastic deformation in the SAN phase on a microscopic scale in the form of crazing and shear yielding accompanied (in most cases) by rubber voiding (1–4). A maximum in impact energy seems to occur when the micro deformation process is dominated by shear yielding at the deformation rates involved. The impact strength of ABS increases with rubber phase content usually leveling off at ~30% rubber by weight. Most commercial ABS resins have a rubber content in the range of 10–35 wt%. The volume fraction of the rubber phase at a given rubber level can be much higher for products manufactured by the mass (or sometimes termed a "bulk ABS") vs emulsion process because of the much higher level of occluded SAN produced in the mass process (see Figs. 1 and 2).

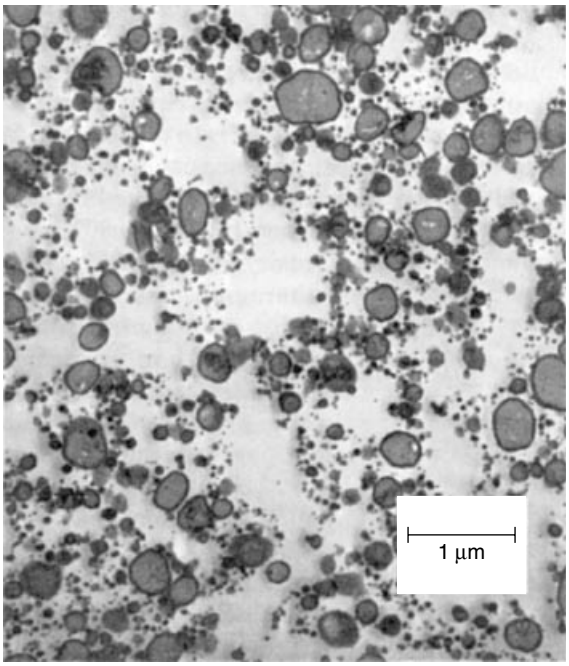

Fig. 1. Transmission electron micrograph of ABS produced by an emulsion process. Staining of the rubber bonds with osmium tetroxide provides contrast with the surrounding SAN matrix phase. To convert J/m^2 to ft·lbf/in.^{2}, divide by 2100.

The rubber phase size and size distribution is also affected by the manufacturing process. Typically, the size of the rubber phase averages ∼200–400 nm for resin produced by an emulsion process and ∼1000–2000 nm for resin produced by mass polymerization. The size distribution of the rubber particles can be very broad, narrow monomodal, or bimodal. The dependence of the impact toughness of ABS on rubber phase particle size and size distribution can be of a complex nature because of the interactions with the graft interface. A maximum impact is reported (1) to occur for emulsion ABS at a mean rubber particle size of about 300 nm for a matrix SAN containing 25% AN.

It has been reported (5) that the elastic modulus of ABS resins prepared by either mass or emulsion polymerization can be represented by a single relationship with the dispersed phase volume fraction. This is in agreement with the theory that the modulus of a blend with dispersed spherical particles depends only on the volume fraction and the modulus ratio of particles to matrix phase. Since the modulus of rubber is almost 1000 times smaller than the modulus of the matrix SAN, the rubber particle volume fraction alone is the most important parameter controlling modulus values of ABS resins. Even for rubber particles containing a high occlusion level, as in ABS produced by mass polymerization, the modulus of the composite particle still remains unchanged from pure rubber, suggesting a unique relationship between modulus and dispersed phase volume fraction. Also, the modulus of a material is a small strain elastic property and is independent of particle size in ABS. The effects of rubber content on modulus and on tensile

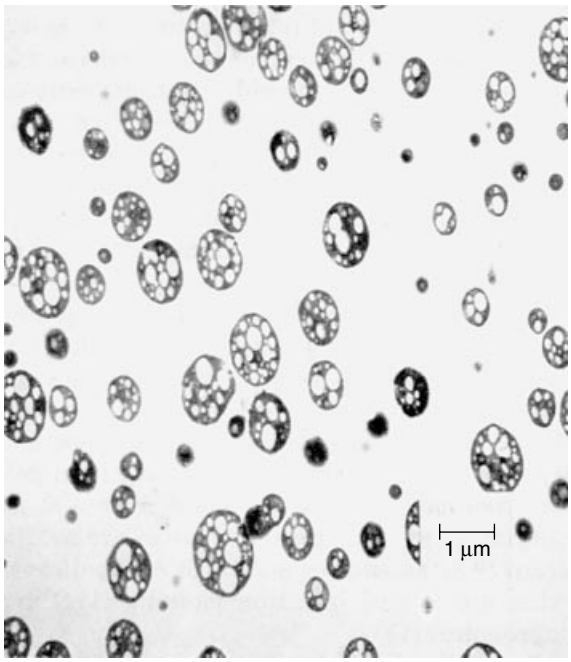

Fig. 2. Transmission electron micrograph of ABS produced by a mass process. The rubber domains are typically larger in size and contain a higher concentration of occluded SAN than those produced by emulsion technology. To convert J/m to ft·lbf/in., divide by 53.4.

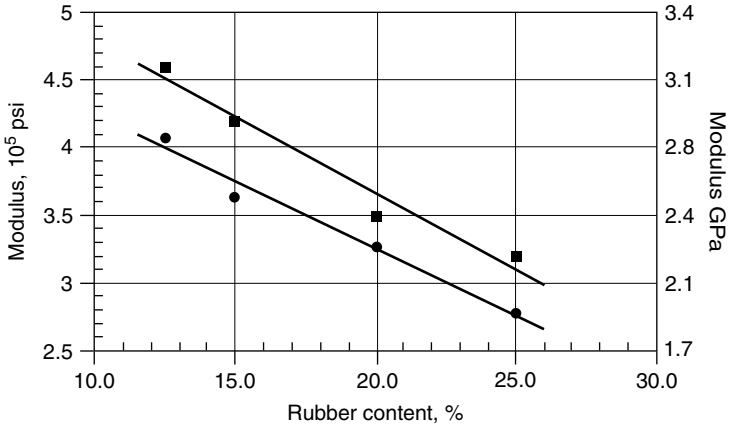

Fig. 3. Effect of rubber content on tensile and flexural modulus of emulsion ABS. The rubber particle volume fraction alone is the most important parameter controlling the modulus values of ABS. ● Tensile mod and ■ flex mod.

and flexural yield stress are shown in Figures 3 and 4 for an emulsion produced ABS. As illustrated, the tensile and flexural yield stress values are also strongly affected by the rubber volume fraction, although—unlike modulus—the stress values are not independent of rubber particle size. It is known that tensile yield stress decreases at a given rubber volume fraction with an increase in particle

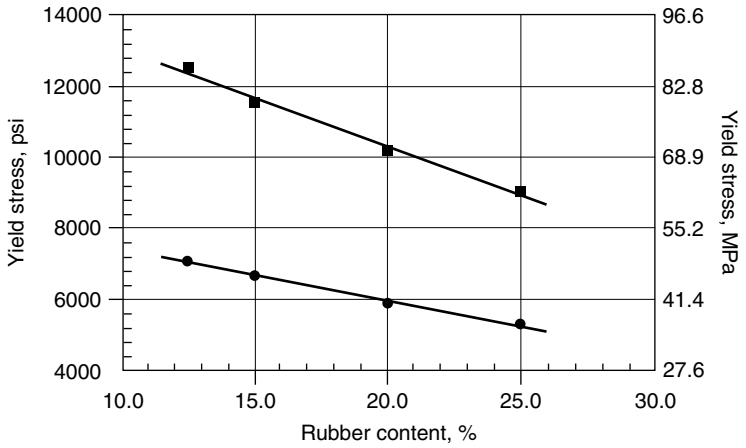

Fig. 4. Effect of rubber content on tensile and flexural yield stress of emulsion ABS at a fixed rubber particle size. ● Tensile stress and ■ flex stress.

diameter; this behavior is explained on the basis of having an increased volume of matrix SAN under higher stress near rubber particles (6).

Effect of Matrix SAN Composition and Molecular Weight. At a given rubber content and grafted rubber particle size and distribution, the mechanical properties of ABS are also strongly affected by the molecular weight and composition of the SAN present as the continuous, matrix phase. Increasing the molecular weight of the matrix SAN increases impact toughness, an effect which tends to level off at molecular weights higher than a number-average molecular weight (M_n) of ~60,000. If the SAN M_n is less than 25,000, no significant amount of crazing deformation is indicated, and therefore, no significant toughening takes place with rubber addition. Yield stress and modulus values of ABS appear to be independent of the molecular weight of the SAN, consistent with the observation that the craze initiation stress value for SAN is independent of molecular weight above an M_n of ~25,000 (7). A similar relationship between craze initiation stress and molecular weight has been reported for polystyrene (8).

The AN content of SAN has a significant influence on the environmental stress-cracking resistance of ABS, and it is generally observed that increasing AN content increases the stress-cracking resistance of ABS. Most general-purpose ABS materials contain SAN with AN content of 20–30%, whereas improved chemical resistance ABS grades employ SAN with AN content of about 35%. It is also indicated that AN in SAN improves the crazing resistance of SAN, which can explain the increased ductility of ABS as compared to rubber-modified polystyrene (high impact polystyrene). Creep and fatigue performance also improve as the AN content of the SAN is increased. In addition to the AN content of SAN matrix, the AN content of the grafted SAN plays an important role in ABS materials prepared by the melt blending of grafted rubber with SAN pellets. If the difference between AN levels of matrix SAN and grafted SAN is over 5%, some immiscibility and partial phase separation can take place (9), which can cause rubber aggregation during compounding and processing steps. Surface gloss of final article may

be lowered although mechanical properties and impact toughness can be maintained with an AN mismatch of as high as 10% between the grafted SAN and matrix SAN. Surface appearance can also be affected if two different matrix SAN components having a differing AN content are mixed because of the surface of the molded part becoming enriched with the SAN of lower AN content (10).

Effect of Grafted SAN. The extent of grafting is a critical parameter as well. If the level of grafted SAN is lowered, a nonuniform dispersion of rubber may occur, affecting toughness and aesthetic properties (eg, gloss). Furthermore, the rubber aggregates will also have an increased tendency to undergo deformation during processing, resulting in the loss of toughness, mechanical, and aesthetic properties. In commercial ABS materials, SAN molecular weight and composition, graft amount, and rubber particle size and structure are properly balanced to achieve an optimal balance of mechanical properties, toughness, melt viscosity, and aesthetics.

Rheology. The ABS manufacturer controls rheological properties through structure variations which can have a complex effect dependent on shear rate. Effects of structural variations on viscosity functions are more evident at lower shear rates (<10/s) vs higher shear rates. At high shear rates, the melt viscosity is controlled primarily by the composition and molecular weight of the ungrafted SAN and by the percentage of the grafted rubber phase. The modulus curves correspond in their shape to that of the ungrafted SAN component, and the rubber particle type and concentration have little effect on the temperature dependence of the viscosity function (11). The extrudate swell, however, becomes smaller with increasing rubber concentration (12).

By contrast, the graft phase structure has a marked effect on viscosity at small deformation rates. The long time relaxation spectra are affected by rubber particle–particle interactions (13,14), which are strongly dependent on particle size, grafting, morphology, and rubber content. Depending on particle surface area, a minimum amount of graft is needed to prevent the formation of three-dimensional networks of associated rubber particles (14). At low shear rates, the associated rubber particles behave similar to a cross-linked rubber; the network structure, however, is dissolved by shearing forces. Extensive studies on the viscoelastic properties of ABS in the molten state have been reported (11–18). Effects of lubricants and other nonpolymeric components have also been described (19). Techniques for characterizing melt-flow differences include melt-flow rate, melt index, spiral flow, and capillary rheometry.

High shear rate viscosity (eg, 1000/s) is considered more relevant to injection-molding applications, and, in general, molding grades have lower melt viscosities than extrusion grades. Designers are striving to further reduce costs through thinwall design. ABS exhibits both low melt viscosity and good impact strength, key characteristics making ABS suitable for thinwall applications (20).

Gloss. Surface gloss values can be achieved ranging from a very low matte finish at <10% (60° Gardner) to high gloss in excess of 95%. Gloss is dependent on the specific grade and the mold or polishing roll surface. Low gloss is achieved either through the use of large rubbery domains, aggregates of smaller rubber particles, or through the addition of dulling agents.

Thermal Properties. Higher heat ABS grades are achieved through copolymerization with monomers (eg, alpha methyl styrene or *N*-phenyl

maleimide) in the matrix phase or through the use of ABS as a base polymer in high performance alloys. Most common are ABS–polycarbonate alloys which extend the property balance achievable with ABS to offer even higher impact strength and heat resistance (21).

Color. ABS is sold as an unpigmented powder, unpigmented pellets, precolored pellets matched to exacting requirements, and "salt-and-pepper" blends of ABS and color concentrate. Color concentrates can also be used for on-line coloring during molding.

Transparency. Standard ABS grades are opaque because of the refractive index mismatch between the dispersed rubber phase and the continuous SAN matrix. However, ABS-type systems are available as transparent grades for clear applications, with transparency achieved by the matching of the refractive index of the rubber and matrix phases through the incorporation of comonomers. Typically, refractive index of the rubber phase is increased through the use of styrene–butadiene rubber and the matrix phase reduced and matched to the rubber phase through terpolymerization with methylmethacrylate.

Chemical Properties

The behavior of ABS may be inferred from consideration of the functional groups present within the polymer.

Chemical Resistance. The term *chemical resistance* is generally used in an applications context and refers to resistance to the action of solvents in causing swelling or stress cracking as well as to chemical reactivity. Environmental stress cracking can be assessed by applying a chemical to a prestressed sample and determining its stress-crack resistance over a specified period of time. As previously discussed, the presence of AN enhances environmental stress-cracking resistance. In ABS, the polar character of the nitrile group reduces interaction of the polymer with hydrocarbon solvents, mineral and vegetable oils, waxes, and related household and commercial materials. Good chemical resistance provided by the presence of AN as a comonomer combined with relatively low water absorptivity ($<1\%$) results in high resistance to staining agents (eg, coffee, grape juice, beef blood) typically encountered in household applications (22).

Similar to most polymers, ABS undergoes stress cracking when brought into contact with certain chemical agents under stress (22,23). Injection-molding conditions can significantly affect chemical resistance, and this sensitivity varies with the ABS grade. Certain combinations of melt temperature, fill rate, and packing pressure can significantly reduce stress-cracking resistance, and this effect is interactive in complex ways with the imposed stress level that the part is subjected to in service. Both polymer orientation and stress appear to be considerations; thus, critical strains can be higher in the flow direction (24). Consequently, all media to be in contact with the ABS part during service should be evaluated under anticipated end-use conditions.

Processing Stability. Processing can influence resultant properties by chemical and physical means (25,26). Degradation of the rubber and matrix phases has been reported under very severe conditions (27). Morphological changes may become evident as agglomeration of dispersed rubber particles during injection

molding at higher temperatures (26). Physical effects such as orientation and molded-in stress can have marked effects on mechanical properties. Thus, the proper selection and control of process variables are important to maintain optimum performance in molded parts. Antioxidants added at the compounding step have been shown to help retention of physical properties upon processing (25).

Appearance changes evident under certain processing conditions include color development (25), changes in gloss (27), and splaying. Discoloration may be minimized by reducing stock temperatures during molding or extrusion. *Splaying* is the formation of surface imperfections elongated in the direction of flow and is typically caused by moisture, occluded air, or gaseous degradation products; proper drying conditions are essential to prevent moisture-induced splay.

Techniques for evaluating processing stability and mechanochemical effects include using a Brabender torque rheometer (28,29), injection molding (26,28), capillary rheometry (26,28), and measuring melt index as a function of residence time (25).

Thermal Oxidative Stability. ABS undergoes autoxidation and the kinetic features of the oxygen consumption reaction are consistent with an autocatalytic free-radical chain mechanism. Comparisons of the rate of oxidation of ABS with that of polybutadiene and SAN indicate that the polybutadiene component is significantly more sensitive to oxidation than the thermoplastic component (30–32). Oxidation of polybutadiene under these conditions results in embrittlement of the rubber because of cross-linking and the introduction of polar oxidized groups; such embrittlement of the elastomer in ABS results in the loss of impact strength. Studies have also indicated that oxidation causes detachment of the grafted SAN from the elastomer, which contributes to impact deterioration (33).

Examination of oven-aged samples has demonstrated that substantial degradation is limited to the outer surface (33), ie, the oxidation process is diffusion limited. Consistent with this conclusion is the observation that oxidation rates are dependent on sample thickness (31). Impact property measurements by high speed puncture tests have shown that the critical thickness of the degraded layer at which surface fracture changes from ductile to brittle is about 0.2 mm. Removal of the degraded layer restores ductility (33). A demonstration of the effects of an embrittled surface on impact was achieved using ABS coated with SAN (34). Rates of oxidation can be significantly affected by additives such as colorants (31).

Test methods for assessing thermal oxidative stability include oxygen absorption (30,31,35), thermal analysis (36,37), oven aging (33,38,39), and chemiluminescence (40,41). Such techniques primarily reflect the reactivity of the rubber component in ABS with oxygen.

Antioxidants have been shown to improve oxidative stability substantially (42,43). Hindered phenols, thiodipropionates, and phosphites can be effective in improving processing or end-use stability (44). In multiphase systems like ABS, stabilizers can partition between the component phases. Thus, the additive concentration in each phase can differ significantly from the added or average concentration potentially influencing additive effectiveness. The use of rubber-bound stabilizers to permit concentration of the additive in the rubber phase has been reported (45–47). Scanning electron microscopy (sem) using xeds (energy dispersive x-ray analysis) has been used to determine the partitioning behavior of stabilizers in ABS. The partitioning of various conventional stabilizers between the rubber

and thermoplastic phases has been shown to correlate with solubility parameter values (48).

Photo-oxidative Degradation. Unsaturation present as a structural feature in the polybutadiene component of ABS (also in high impact polystyrene, rubber-modified PVC, and ABS–polycarbonate blends) increases lability with regard to photo-oxidative degradation (49–51), which can result in discoloration and loss of impact. Applications involving outdoor exposure require protective measures to maintain an optimum level of performance. Light stabilizers provide some measure of protection (52,53), as illustrated by the very successful use of ABS in interior automotive trim. Colorants have a significant effect on light stability and can either increase or decrease color fastness, depending on colorant type. For extended outdoor exposure, the best protection is provided by a protective coating which can be either paint or a cap layer of a weatherable polymer such as a thermoplastic acrylic, cast acrylic, or ASA (acrylonitrile–styrene–acrylate terpolymer). A cap layer of ASA vs acrylics (PMMA) minimizes brittle surface layer effects. The cap layer is applied by coextrusion over ABS, resulting in a laminate sheet which can be thermoformed into parts providing a favorable balance of cost and part performance that includes excellent weatherability.

The photodegradation of ABS typically occurs in the outermost layer (54,55). Impact loss upon irradiation is due to embrittlement of the rubber and possibly scission of the grafted SAN (49,56). Appearance changes such as yellowing are caused by chromophore formation in both the polybutadiene and SAN components (49,57). Mechanisms describing the photo-oxidative degradation of ABS have been proposed (51,52,58). Oxidation studies with singlet oxygen have shown that initial attack on ABS occurs on the polybutadiene component (59). Weathering studies have been conducted using artificial (60,61) and outdoor exposure (60) conditions. Light wavelength dependence has been studied, and photodegradation of the polybutadiene component has been reported to be primarily initiated by wavelengths below 350 nm (62) but can extend into the visible region (63). For discoloration, photochemical yellowing is caused primarily by wavelengths between 300 and 360 nm, and maximum bleaching of yellow colored species is reported to occur in the 475- to 485-nm region (62). For the above reasons, any spectral difference between accelerated aging and actual exposure could lead to a lack of correlation, affecting predictive capability by accelerated techniques. Xenon arc is preferred vs other test methods (eg, carbon arc, HPUV) because of the closer simulation of the spectral distribution of sunlight by Xenon arc if the appropriate filter combination is used. Oxidative degradation induced by processing may also affect photosensitivity (49,64). A comparative study on the weathering of ABS and other acrylic-based plastics has shown that elastomer type and SAN phase composition are two key factors affecting both color and impact retention (65).

Test methods that have been used to determine the effects of light aging on embrittlement of ABS include Izod impact, Charpy impact, flexural tests, falling dart, and dynamic mechanical measurements. Because photodegradation occurs only on the outer surface and the interior of the sample remains essentially unaffected, a pendulum type of notched impact will not be sensitive to changes in surface embrittlement. Falling dart types of testing increase sensitivity to surface changes; the use of a high speed puncture test has been described for determining the effect of outdoor exposure on crack-initiation energy values for ABS (65).

Flammability. The general-purpose grades are usually recognized as 94 HB according to the requirements of Underwriters' Laboratories UL94. Flame-retardant (FR) grades (V0, V1, and V2) are also available which meet Underwriters' UL 94/94 5V and Canadian Standards Association (CSA) requirements. Flame retardancy is typically achieved by utilizing halogenated additives in combination with antimony oxide or by alloys with PVC or PC (66–68). A wide variety of brominated flame retardants have been used in ABS with tetrabromobisphenol-A (TBBPA) and brominated epoxy oligomers (BEOs), currently in widespread use. Both are melt-blendable and can be well dispersed on most commercial equipment. TBBPA is very cost effective, providing excellent flame retardancy and good flow properties; however, products formulated with TBBPA generally have poorer light stability and a lower heat-deflection temperature. Although TBBPA exhibits low thermal stability, processing is usually not an issue if recommended guidelines are followed. Flame-retardant ABS grades formulated with BEOs are preferred if reduced color shift upon light exposure is required.

Polymerization

All manufacturing processes for ABS involve the polymerization of styrene and acrylonitrile monomers in the presence of an elastomer (typically polybutadiene or a butadiene copolymer) to produce SAN that has been chemically bonded or "grafted" to the rubber component termed the "substrate."

Rubber Chemistry. The rubber substrate is typically produced by the free-radical polymerization of butadiene. The radical source can be provided by either thermal decomposition or oxidation–reduction (redox) systems. The primary product is primarily 1,4-polybutadiene with some 1,2-polybutadiene, which contains a pendent vinyl group. Cross-linking of polymer occurs at high conversion through abstraction of reactive allylic sites or by copolymerization through double bonds (especially the double bonds in the more sterically accessibly pendent vinyl groups). Rubber cross-linking is controlled by the use of chain-transfer agents and the concentration and type of the intiator used; the reaction can also be affected by chain transfer to emulsifiers. For emulsion ABS, the rubber is typically both produced and subsequently used for grafting as a latex.

Graft Chemistry. Grafting of styrene and acrylonitrile onto a rubber substrate is the essence of the ABS process. Grafting is a free-radical process initiated by the abstraction of allylic hydrogens on the rubber substrate or by copolymerization through double bonds that are pendent or internal in the rubber substrate, as illustrated in Figure 5 (69). Initiator level and type affects the extent of grafting (69–75) with oxyradicals yielding a higher degree of grafting than carbon radicals because of higher rates of abstraction from the rubber substrate. Chain-transfer agents are also used in controlling overall degree of grafting and graft molecular weight.

Ungrafted SAN is formed concurrently with grafted SAN, with the ratio controlled by factors that include temperature, chain-transfer agent, pendent vinyl content of rubber, initiator level, and initiator type (69–77). As previously described, occlusions of SAN can also form within the rubber particles with the mass process leading to significantly higher occlusion levels than the emulsion

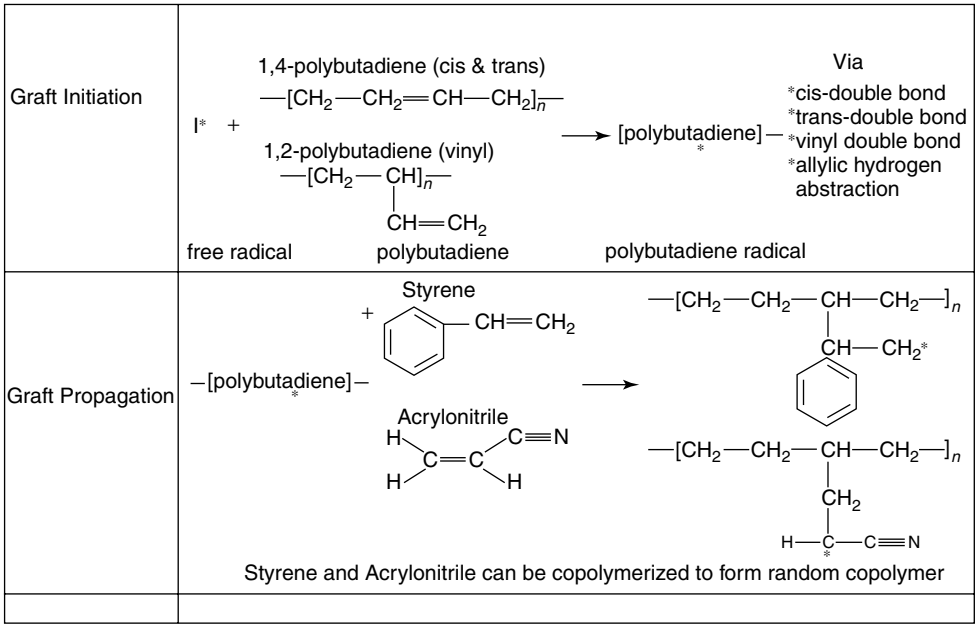

Fig. 5. Mechanisms of graft SAN formation.

process (78,79). In the mass process, block copolymers of styrene and butadiene can be added to obtain unusual particle morphologies (eg, coil, rod, capsule, cellular) (78).

Emulsion Process. The emulsion process for making ABS has been commercially practiced since the early 1950s. Its advantage is the capability of producing ABS with a wide range of compositions, particularly higher rubber contents than are possible with other processes. Mixing and transfer of the heat of reaction in an emulsion polymerization is achieved more easily than in the mass polymerization process because of the low viscosity and good thermal properties of the water phase. The energy requirements for the emulsion process are generally higher because of the energy usage in the polymer recovery area. The emulsion polymerization process is typically a two-stage reaction process (80,81), as illustrated in Figure 6.

In the first stage, a rubber substrate, primarily composed of polybutadiene, is made using an emulsion polymerization process. The desired particle size of the rubber is either obtained by direct growth during polymerization or by an agglomeration process subsequent to polymerization. In a second-stage reaction, styrene and acrylonitrile are grafted onto the rubber substrate by emulsion polymerization. After the graft reaction is complete, the polymer can be recovered from the graft latex and compounded into a final pellet product (81–86).

Rubber Substrate Process. The rubber substrate can be made by a variety of different reaction processes including batch, semi-batch, and continuous (87). Butadiene monomer is primarily used in the substrate reaction, but comonomers such as styrene and acrylonitrile are common (84,85). The amount

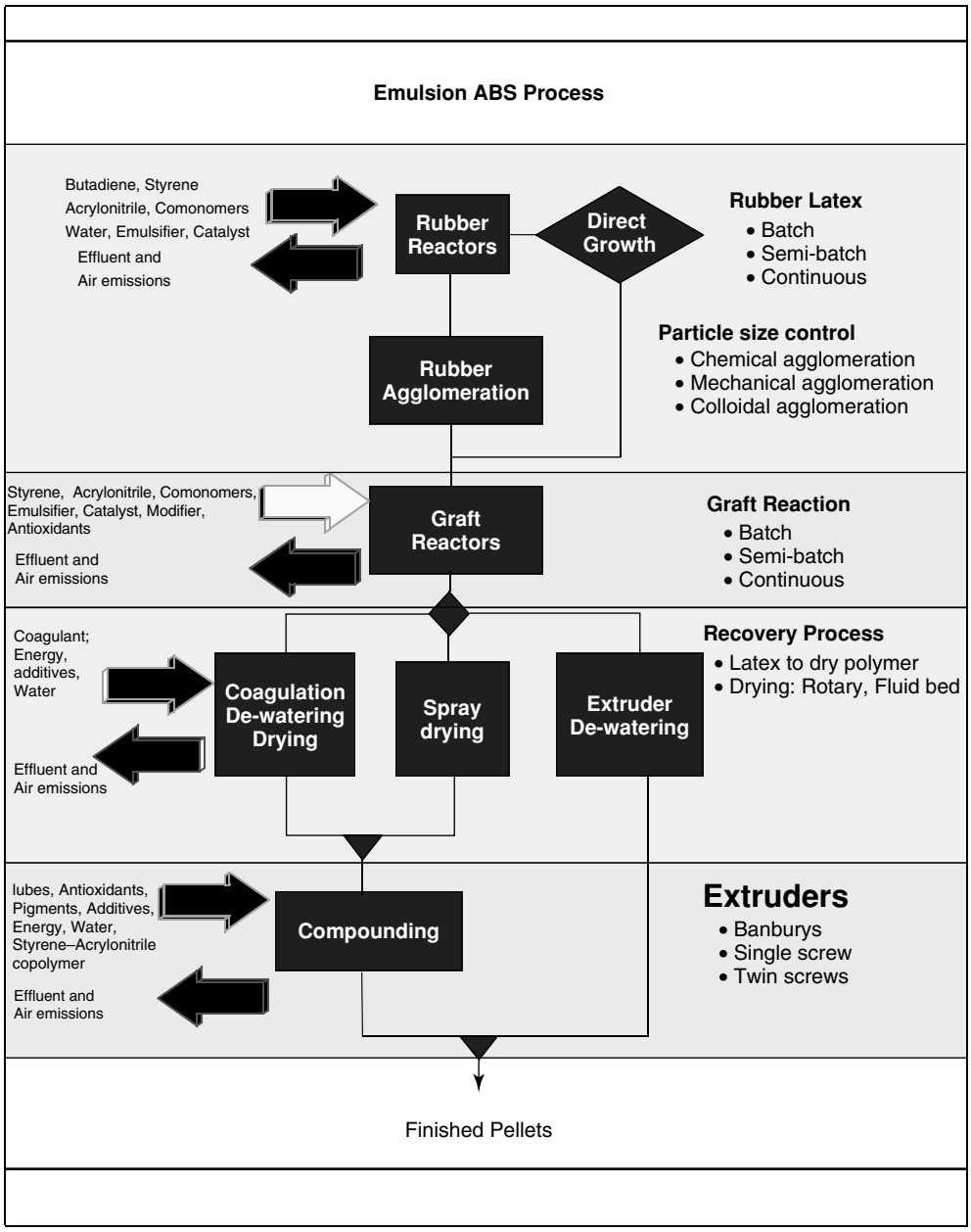

Fig. 6. Emulsion ABS process.

and type of comonomer employed will affect the glass transition of the rubber substrate and, thereby, influence the impact properties of the ABS polymer. Oxidation–reduction systems (eg, hydrogen peroxide and iron) or thermal initiators (eg, potassium persulfate or azobisisobutyronitrile) are used to initiate polymerization. Cross-link density is controlled by type and level of initiator, type and

level of chain-transfer agent, reaction temperature, degree of conversion, or by the addition of comonomers. It is important to note that the graft process also can affect the cross-link density of the rubber. Various surfactant types can be employed to emulsify the monomer and stabilize the latex particles. Standard fatty acid soaps and derivatives are the most common emulsifiers employed; however, detergents such as sodium dobenzyl sulfonate and sodium lauryl sulfate can also be used. The use of nonionic surfactants has been reported (88). The "soap-free" emulsion polymerization of butadiene is possible using reactive surfactants (89), functional monomers such as acrylic acid (90), or high levels of potassium persulfate (91). The incorporation of surfactants into the polymer backbone provides the advantage of minimizing low molecular by-products in the final polymer that could result in mold buildup or juicing.

The incorporation of comonomers into the rubber substrate can be useful in achieving specialized performance of the final ABS polymer, such as adjusting the refractive index of the rubber phase to better match the continuous SAN phase to achieve a clear or more translucent ABS product (92). The incorporation of polymerizable antioxidants or uv stabilizers has also been reported (93). Typically, these modifications increase the cost of ABS and are only employed for specialized applications.

Reactor productivity can be effected by various factors including initiator type, latex particle size, monomer purity, chain-transfer agents, and reaction temperature (87). As previously described, rubber particle size and distribution are important factors controlling the final properties of the ABS polymer. Large particles can be obtained by direct growth in the reactor, but much longer reaction times are needed. Comonomers such as AN can be added to speed the reaction rate and achieve relatively large particles in less time (94,95). Productivity can also be improved by the use of antifouling agents to minimize buildup of polymer on reactor heat-transfer surfaces (96–98). These antifouling agents improve heat transfer and minimize the time the reactor is down for cleaning.

Graft Process. Grafted SAN is critical to achieving effective dispersion of the rubber in the matrix phase, with key factors being SAN composition and rubber particle surface coverage. The composition of the grafted SAN depends on the monomer-feed composition and the monomer reactivity ratio. The composition of the polymer formed will equal the feed at the azeotropic composition, which occurs at ~3/1 mass ratio of styrene-to-acrylonitrile (80,88), and compositional drift will occur at monomer feed compositions other than the azeotropic concentration. Note that in aqueous systems, the difference in water phase solubility of acrylonitrile vs styrene can also perturb monomer concentrations at the reaction site and, thus, affect compositional drift. Polymerization techniques such as continuous vs batch processes and controlling pump rates can be used to control compositional drift (99–105). Surface coverage is controlled by rubber particle surface area and is effected by factors including initiator type, monomer feed to rubber level, and chain-transfer agents.

Resin Recovery Process. Typically, the polymer is recovered by the addition of coagulants which destabilize the ABS latex. Different coagulants are used depending on the surfactant. Thus, strong and weak acids work well with fatty acid soaps, and metal salts are used with acid stable soaps (106). The use of nonionic coagulants has also been reported (107,108). Acrylic latices have been

used to control the coagulation process and obtain a narrow resin particle-size distribution (109).

Once coagulated, the resulting slurry can then be filtered or centrifuged to recover wet ABS resin, which is then dried to a low moisture content. A variety of dryers can be used for ABS, including tray, fluid bed, and rotary kiln-type dryers. Other methods of recovery have been employed such as spray drying (110) and extruder dewatering (111). Spray drying allows for good control of the final particle size of the resin, but uses a significant amount of energy in the drying process. In extruder dewatering, the latex is either directly fed into the extruder or is first coagulated and then fed into the extruder. Extruder dewatering allows for more efficient stripping and recovery of unreacted monomer than standard drying processes.

Air and Water Treatment. The emulsion process exerts a greater demand on wastewater treatment than other processes (suspension or mass) because of the quantity of water used, and air emissions may be higher because of the types of process equipment employed. Recent federal and state EPA regulations governing air emission from ABS facilities affect the level of styrene, acrylonitrile, butadiene, and other volatile organic compounds that can be emitted into the air or sent to wastewater treatment facilities. In some cases, effluent water can be recycled and reused, but ultimately the water must be discharged, requiring treatment of the water prior to discharge. Air emissions from an emulsion ABS process can be reduced by improving the conversion of the monomers (112), the installation of equipment to strip and recover monomers, or the installation of end-of-pipe controls. End-of-pipe controls such as regenerative catalytic oxidation, regenerative thermal oxidation, fixed and fluid bed carbon absorption, and biofiltration are viable means of addressing air emission issues (113).

Mass Polymerization Process. In the mass (114–122) ABS process, the polymerization is conducted in a monomer medium rather than in water, usually employing a series of two or more continuous reactors. The rubber used in this process is most commonly a solution polymerized linear polybutadiene (or copolymer containing sytrene), although some mass processes utilize emulsion-polymerized ABS with a high rubber content for the rubber component (123). If a linear rubber is used, a solution of the rubber in the monomers is prepared for feeding to the reactor system. If emulsion ABS is used as the source of rubber, a dispersion of the ABS in the monomers is usually prepared after the water has been removed from the ABS latex.

In the mass process (124) using linear rubber, the rubber initially dissolved in the monomer mixture will phase separate, forming discrete rubber particles as SAN polymerization procedes. This process is referred to as phase inversion since the continuous phase shifts from rubber to SAN during the course of polymerization. Special reactor designs are used to control the phase inversion portion of the reaction (115,117–120). By controlling the shear rate in the reactor, the rubber particle size can be modified to optimize properties. Grafting of some of the SAN onto the rubber particles occurs as in the emulsion process. Typically, the mass-produced rubber particles are larger than those of emulsion-based ABS and contain much larger internal occlusions of SAN. The reaction recipe can include polymerization initiators, chain-transfer agents, and other additives. Diluents are sometimes used to reduce the viscosity of the monomer and polymer mixture to

facilitate processing at high conversion. The product from the reactor system is devolatilized to remove the unreacted monomers and is then pelletized. Equipment used for devolatilization includes single- and twin-screw extruders and flash and thin film/strand evaporators. Unreacted monomers are recovered and recycled back to the reactors to improve the process yield.

The mass ABS process was originally adapted from the mass polystyrene process (125). Mass produced ABS typically has very good unpigmented color and is usually somewhat more translucent because of the large rubber phase particle size and low rubber content. Increased translucency can reduce the concentration of colorants required. The extent of rubber incorporation is limited to approximately 20% because of viscosity limitations in the process; however, the mass-produced grafted rubber can be more efficient (on an equal percent rubber basis) at impact modification than emulsion-grafted rubber because of the presence of high occlusion levels in the rubber phase. The surface gloss of the mass-produced ABS is generally lower than that of emulsion ABS because of the presence of the larger rubber particles, but recent advances provide additional flexibility to achieve higher gloss (115–119).

Suspension Process. The suspension process utilizes a mass (126) or emulsion reaction (127,128) to produce a partially converted mixture of polymer and monomer and then employs a batch suspension process (129) to complete the polymerization. When the conversion of the monomers is approximately 15–30% complete, the mixture of polymer and unreacted monomers is suspended in water with the introduction of a suspending agent. The reaction is continued until a high degree of monomer conversion is attained and then unreacted monomers are stripped from the product before the slurry is centrifuged and dried, producing product in the form of small beads. The morphology and properties of the mass suspension product are similar to those of the mass-polymerized product. The suspension process retains some of the process advantages of the water-based emulsion process, such as lower viscosity in the reactor and good heat removal capability.

Compounding. ABS either is sold as an unpigmented product, in which case the customer may add pigments during the forming process, or it is colored by the manufacturer prior to sale. Much of the ABS produced by the mass process is sold unpigmented; however, precolored resins provide advantages in color consistency. If colorants, lubricants, fire retardants, glass fibers, stabilizers, or alloying resins are added to the product, a compounding operation is required. ABS can be compounded on a range of equipment, including batch and continuous melt mixers, and both single- and twin-screw extruders. The device must provide sufficient dispersive and distributive mixing dependent on formulation ingredients for successful compounding, and low work or low shear counterrotating twin-screw extruders as used in PVC are not recommended. In the compounding step, more than one type of ABS may be employed (ie, emulsion and mass-produced) to obtain an optimum balance of properties for a specific application. Products can also be made in the compounding process by combining emulsion ABS having a high rubber content with mass- or suspension-polymerized SAN.

Analysis. Analytical investigations may be undertaken to identify the presence of an ABS polymer, characterize the polymer, or identify nonpolymeric

ingredients. Fourier transform infrared (ftir) spectroscopy is the method of choice to identify the presence of an ABS polymer and determine the ABS ratio of the composite polymer (130,131). Confirmation of the presence of rubber domains is achieved by electron microscopy. Comparison with available physical property data serves to increase confidence in the identification or indicate the presence of unexpected structural features. Identification of ABS by pyrolysis gas chromatography (132) and dsc (133) has also been reported. Detailed compositional and molecular weight analyses involve determining the percentage of grafted rubber; determining the molecular weight and distribution of the grafted SAN and the ungrafted SAN; and determining compositional data on the grafted rubber, the grafted SAN, and the ungrafted SAN. This information is provided by a combination of phase-separation and instrumental techniques. Separation of the ungrafted SAN from the graft rubber is accomplished by ultracentrifugation of ABS dispersions (134,135), which causes sedimentation of the grafted rubber. Cleavage of the grafted SAN from the elastomer is achieved using oxidizing agents such as ozone [10028-15-6] (135,136), potassium permanganate [7722-64-7] (137), or osmium tetroxide [20816-12-0] with *tert*-butyl-hydroperoxide [75-91-2] (138). Chromatographic and spectroscopic analyses of the isolated fractions provide structural data on the grafted and ungrafted SAN components (139). Information on the microstructure of the rubber is provided by analysis of the cleavage products derived from the substrate (135,137). The extraction of ungrafted rubber has also been reported (140). Additional information on elastomer and SAN microstructure is provided by ^{13}C nmr analysis (141). Rubber particle composition may be inferred from glass-transition data provided by thermal or mechanochemical analysis. Rubber particle morphology as obtained by transmission or scanning electron microscopy (142) is indicative of the ABS manufacturing process (78) (see Fig. 1).

The isolation and/or identification of nonpolymerics has been described, including analyses for residual monomers (131,143,144) and additives (131,145–147). The determination of localized concentrations of additives within the phases of ABS has been reported; the partitioning of various additives between the elastomeric and thermoplastic phases of ABS has been shown to correlate with solubility parameter values (48).

Processing

Good thermal stability plus shear thinning allow wide flexibility in viscosity control for a variety of processing methods. ABS exhibits non-Newtonian viscosity behavior. For example, raising the shear rate one decade from 100/s to 1000/s (typical in-mold shear rates) reduces the viscosity by 75% on a general-purpose injection-molding grade. Viscosity can also be reduced by raising melt temperature; typically increasing the melt temperature 20–30°C within the allowable processing range reduces the melt viscosity by about 30%. ABS can be processed by all the techniques used for other thermoplastics: compression and Injection Molding, Extrusion, calendering, and Blow Molding. Clean, undegraded regrind can be reprocessed in most applications (plating excepted), usually at 20% with

virgin ABS. Post-processing operations include cold forming; thermoforming; metal plating; painting; hot stamping; ultrasonic, spin, and vibrational welding; and adhesive bonding.

Material Handling and Drying. Although uncompounded powders are available from some suppliers, most ABS is sold in compounded pellet form. The pellets are either precolored or natural to be used for in-house coloring using dry or liquid colorants or color concentrates. These pellets have a variety of shapes including diced cubes, square and cylindrical strands, and spheroids. The shape and size affect several aspects of material handling such as bulk density, feeding of screws, and Drying. Very small particles called fines can be present as a carryover from the pelletizing step or transferring operations; these tend to congregate at points of static charge buildup. Certain additives can be used to control static charges on pellets (148).

ABS is mildly hygroscopic. The moisture diffuses into the pellet and moisture content is a reversible function of relative humidity. At 50% relative humidity, typical equilibrium moisture levels can be between 0.3 and 0.6% depending on the particular grade of ABS. In very humid situations moisture content can be double this value. Although there is no evidence that this moisture causes degradation during processing, drying is required to prevent voids and splay (149) and achieve optimum surface appearance. Drying down to 0.1% is usually sufficient for general-purpose injection molding and 0.05% for critical applications such as plating. For nonvented extrusion and blow-molding operations a maximum of 0.02% is required for optimum surface appearance.

Desiccant hot air hopper dryers are recommended, preferably mounted on the processing equipment. Tray driers are not recommended, but if used the pellet bed should be no more than 5 cm deep. Many variables affect drying rates (150,151); the pellet temperature has a stronger effect than the dew point. Most pellet drying problems can be a result of actual pellet temperatures being too low in the hopper. Large particles dry much more slowly than pellets, thus regrind should be protected from moisture regain. Supplier data sheets should be consulted for specific drying conditions. Several devices are available commercially for analytically determining moisture contents in ABS pellets (152–154). Alternatives to pellet drying are vented injection molding (155) and cavity-air pressurization (counterpressure) (156).

Injection Molding.

Equipment. Although plunger machines can be used, the better choice is the reciprocating screw injection machine because of better melt homogeneity. Screws with length-to-diameter ratios of 20:1 and a compression ratio of 2–3:1 are recommended. General-purpose screws vary significantly in number and depth of the metering flights; long and shallow metering zones can create melt temperature override which is particularly undesirable with FR grades of ABS. Screws with a generous transition length perform best because of better melting rate control (157). Good results have been realized with a long transition “zero-meter” screw design (158). Some comments on the performance of general-purpose and two-stage vented screws used for coloring with concentrates is given in Reference 159. Guidelines for nozzle and nonreturn valve selection as well as metallurgy are given in References 160 and 161. Gas-nitrided components should be avoided; ion-nitrided parts are acceptable.

A variety of mold types can be used: two-plate, three-plate, stack, or runnerless. Insulated runner molds are not recommended. If heated torpedoes are used with hot manifold molds, they should be made from a good grade of stainless steel and not from beryllium copper. Molds are typically made from P-20, H-13, S-7, or 420 stainless; chrome or electroless plating is recommended for use with FR grades of ABS. Mold cavities should be well vented (0.05 mm deep) to prevent gas burns. Polished, full round, or trapezoidal runners are recommended; half or quarter round runners are not. Most conventional gating techniques are acceptable (160,161). On polished molds a draft angle of 0.5° is suggested to ease part ejection; side wall texturing requires an additional 1° per 0.025 mm of texture depth. Mold shrinkage is typically in the range of 0.5–0.9% (0.005–0.009 cm/cm) depending on grade, and the shrinkage value for a given grade can vary much more widely than this because of the design of parts and molding conditions.

Processing Conditions. Certain variables should be monitored, measured, and recorded to aid in reproducibility of the desired balance of properties and appearance. The individual ABS suppliers provide data sheets and brochures specifying the range of conditions that can be used for each product. Relying on machine settings is not adequate. Identical cylinder heater settings on two machines can result in much different melt temperatures. Therefore, melt temperatures should be measured with a fast response hand pyrometer on an air shot recovered under normal screw rpm and back-pressure. Melt temperatures range from 218 to 268°C depending on the grade. Generally, the allowable melt temperature range within a grade is at least 28°C. Excessive melt temperatures cause color shift, poor gloss control, and loss of properties. Similarly, a fill rate setting of 1 cm/s ram travel will not yield the same mold filling time on two machines of different barrel size. Fill time should be measured and adjusted to meet the requirements of getting a full part, and to take advantage of shear thinning without undue shear heating and gas burns. Injection pressure should be adjusted to get a full part free of sinks and good definition of gloss or texture. Hydraulic pressures of less than 13 MPa (1900 psi) usually suffice for most moldings. Excessive pressure causes flash and can result in loss of some properties. Mold temperatures for ABS range from 27 to 66°C (60–82°C for high heat grades). The final properties of a molded part can be influenced as much by the molding as by the grade of ABS selected for the application (162). The factors in approximate descending order of importance are polymer orientation, heat history, free volume, and molded-in stress. Izod impact strength can vary severalfold as a function of melt temperature and fill rate because of orientation effects, and the response curve is ABS grade dependent (163). The effect on tensile strength is qualitatively the same, but the magnitude is in the range of 5–10%. Modulus effects are minimal. Orientation distribution in the part is very sensitive to the flow rate in the mold; therefore, fill rate and velocity-to-pressure transfer point are important variables to control (164). Dart impact is also sensitive to molding variables, and orientation and thermal history can also be key factors (165). Heat-deflection temperature can be influenced by packing pressure (166) because of free volume considerations (167). The orientation on the very surface of the part results from an extensionally stretching melt front and can have deleterious effects on electro-plate adhesion and paintability. A phenomenon called the mold-surface effect, which involves grooving the nonappearance half of

the mold, can be employed to reduce unwanted surface orientation on the noncorresponding part surface (168–170). Other information regarding the influence of processing conditions on part quality are given in References 171–175.

Part Design. For optimum economics and production cycle time, wall thicknesses for ABS parts should be the minimum necessary to satisfy service strength requirements. The typical design range is 0.08–0.32 cm, although parts outside this range have been successfully molded. A key principle that guides design is avoiding stress concentrators such as notches and sharp edges. Changes in wall thickness should be gradual, sharp corners should be avoided, and generous radii (25% of the wall thickness) used at wall intersections with ribs and bosses. To avoid sinks, rib thickness should be between 50 and 75% of the nominal wall. Part-strength at weld lines can be diminished; thus, welds should be avoided if possible or at least placed in noncritical areas of the part (176). Because of polymer orientation, properties such as impact strength vary from point to point on the same part and with respect to the flow direction (162). Locations of highest Izod impact strength can be points of lowest dart impact strength because of the degree and direction of orientation. ABS suppliers can provide assistance with design of parts upon inquiry and through design manuals (177). There are a number of special considerations when designing parts for metal plating to optimize the plating process, plate deposition uniformity, and final part quality (178). ABS parts can also be designed for solid–solid or solid–foam co-injection molding (179) and for gas-assisted-injection molding (180) (see INJECTION MOLDING).

Extrusion.

Equipment. Since moisture removal is even more critical with extrusion than injection molding, desiccant hot-air hopper drying of the pellets to 0.02% moisture is essential for optimum properties and appearance. The extruder requirements are essentially the same for pipe, profile, or sheet. Two-stage vented extruders are preferred since the improved melting control and volatile removal can provide higher rates and better surface appearance. Barrels are typically 24:1 minimum L/D for single-stage units and 24 or 36:1 for two-stage vented units. The screws are typically 2:1 to 2.5:1 compression ratio and single lead, full flighted with a 17.7° helix angle. Screen packs (20–40 mesh = 840–420 μm) are recommended.

For sheet, streamlined coat-hanger type dies are preferred over the straight manifold type. Typically, three highly polished and temperature controlled rolls are used to provide a smooth sheet surface and control thickness (181). Special embossing rolls can be substituted as the middle roll to impart a pattern to the upper surface of the sheet. ABS and non-ABS films can be fed into the polishing rolls to provide laminates for special applications, eg, for improved weatherability, chemical resistance, or as decoration. Two rubber pull rolls, speed synchronized with the polishing rolls, are located far enough downstream to allow sufficient cooling of the sheet; finally, the sheet goes into a shear for cutting into lengths for shipping.

Pipe can be sized using internal mandrels with air pressure contained by a downstream plug or externally using a vacuum bushing and tank. Cooling can be done by immersion, cascade, or mist. Water temperatures of 41–49°C at the sizing zone reduce stresses. Foamcore pipe has increased in market acceptance significantly over the last few years, and cooling unit lengths must be longer than for solid pipe. Drawdown should not exceed 10–15%.

Profile dies can be flat plates or the streamline type. Flat-plate dies are easy to build and inexpensive but can have dead spots that cause hang-up, polymer degradation, and shutdowns for cleaning. Streamlined, chrome-plated dies are more expensive and complicated to build but provide for higher rates and long runs. The land length choice represents a tradeoff; long lands give better quality profile and shape retention but have high pressure drops that affect throughput. Land length to wall thickness ratios are typically 10:1. Drawdown can be used to compensate for die swell but should not exceed 25% to minimize orientation. Sizing jigs vary in complexity depending on profile design; water mist, fog, or air cooling can be used. The latter gives more precise sizing. Also, water immersion vacuum sizing can be used. Accurate, infinitely adjustable speed control is important to the takeoff end equipment to guarantee dimensional control of the profile.

With sheet or pipe, multilayer coextrusion can be used. Solid outer-solid core coextrusion can place an ABS grade on the outside that has special attributes such as color, dullness, chemical resistance, static dissipation, or fire-retardancy over a core ABS that is less expensive or even regrind. Composites can be created in which the core optimizes desired physical properties such as modulus, whereas the outer layer optimizes surface considerations not inherent in the core material. Solid outer-foam core can provide composites with significant reductions in specific gravity (0.7). Dry blowing agents can be "dusted" onto the pellets or liquid agents injected into the first transition section of the extruder.

Extrusion processing conditions vary depending on the ABS grade and application; vendor bulletins should be consulted for details. Information for assistance in troubleshooting extrusion problems can be found in Reference 182 (see EXTRUSION).

Calendering. The rheological characteristics of the sheet extrusion grades of ABS easily adapt them to calendering to produce film from 0.12 to 0.8 mm thick for vacuum forming or as laminates for sheet. The advantages of this process over extrusion are the capability for thinner gauge product and quick turnaround for short runs.

Blow Molding. Although ABS has been blow molded for over 20 years, this processing method has been gaining popularity recently for a variety of applications (183). Better blow-molding grades of ABS are being provided by tailoring the composition and rheological characteristics specifically to the process. While existing polyolefin equipment can often be easily modified and adjusted to mold ABS, there are some key requirements that require attention.

Pellet predrying is required down to 0.02–0.03% moisture. High shear polyolefin screws must be replaced with low shear 2.0:1 to 2.5:1 screws with L/D ratios of 20:1 to 24:1 to keep the melt temperature in the 193–221°C optimum range. The land length of the tooling can be reduced to 3:1 to 5:1 because ABS shows less die swell; this also helps to reduce the melt pressure resulting from the higher viscosity. The accumulator tooling should be streamlined to reduce hang-up and improve re-knit, and be capable of handling the higher pressures required with large programmed parisons. Mold temperatures of 77–88°C provide good surface finish. It is recommended that the material vendor be consulted to confirm equipment capability and provide safety and processing information (184) (see BLOW MOLDING).

Secondary Operations.

Thermoforming. ABS is a versatile thermoforming material. Forming techniques in use are positive and negative mold vacuum forming, bubble and plug assist, snapback and single- or twin-sheet pressure forming (185). It is easy to thermoform ABS over the wide temperature range of 120–190°C. As-extruded sheet should be wrapped to prevent scuffing and moisture pickup. Predrying sheet that has been exposed to humid air prevents surface defects; usually 1–3 h at 70–80°C suffices. Thick sheet should be heated slowly to prevent surface degradation and provide time for the core temperature to reach the value needed for good formability. Relatively inexpensive tooling can be made from wood, plaster, epoxies, thermoset materials, or metals. Tools should have a draft angle of 2° to 3° on male molds and 0.5° to 1° on female molds. More draft may be needed on textured molds. Vacuum hole diameters should not exceed 50% of the sheet thickness. Mold design should allow for 0.003–0.008 cm/cm mold shrinkage; exact values depend on mold configuration, the material grade, and forming conditions. Maximum depth of draw is usually limited to part width in simple forming, but more sophisticated forming techniques or relaxed wall uniformity requirements can allow greater draw ratios. Some definitions for draw ratios are given in Reference 186. Pressure forming, with well-designed tools, can make parts approaching the appearance and detailing obtained by injection molding. Additional information on pressure forming is given in Reference 187 (see THERMOFORMING).

Cold Forming. Some ABS grades have ductility and toughness such that sheet can be cold formed from blanks 0.13–6.4 mm thick using standard metalworking techniques. Up to 45% diameter reduction is possible on the first draw; subsequent redraws can yield 35%. Either aqueous or nonaqueous lubrication is required. More details are available in Reference 188.

Other Operations.

Metallizing. ABS can be metallized by electroplating, vacuum deposition, and sputtering. Electroplating (qv) produces the most robust coating; progress is being made on some of the environmental concerns associated with the chemicals involved by the development of a modified chemistry. An advantage to sputtering is that any metal can be used, but wear resistance is not as good as with electroplating. Attention must be paid to the molding and handling of the ABS parts since contamination can affect plate adhesion, and surface defects are magnified after plating. Also, certain aspects of part design become more important with plating; these are covered in References 169 and 178.

Fastening, Bonding, and Joining. Often parts can be molded with various snap-fit designs (189) and bosses to receive rivets or self-tapping screws. Thermal-welding techniques that are easily adaptable to ABS are spin welding (190), hot plate welding, hot gas welding, induction welding, ultrasonic welding, and vibrational welding (191,192). ABS can also be nailed, stapled, and riveted. There are a variety of adhesives and solvent cements for bonding ABS to itself or other materials such as wood, glass, and metals; for more information, contact the material or adhesives suppliers. Joining ABS with materials of different coefficients of thermal expansion requires special considerations when wide temperature extremes are encountered. An excellent review of joining methods for plastics is given in Reference 193.

Table 2. Markets for ABS Plastics by Region in 1999, 10^6 lb

Market	United States and Canada	Western Europe	Japan	Total	%
Transportation	374	397	132	903	21
Electrical[a]	501	569	415	1485	34
Miscellaneous[b]	869	457	679	2005	46
Total	1744	1423	1226	4393	100

[a]Electrical includes consumer electronics, business equipment, and appliances.
[b]Miscellaneous includes construction, pipe, consumer, and others.

Applications

Its broad property balance and wide processing window has allowed ABS to become the largest selling engineering thermoplastic. ABS enjoys a unique position as a "bridge" polymer between commodity plastics and other higher performance engineering thermoplastics. Table 2 summarizes estimates for 1999 regional consumption of ABS resins by major use (194). In 1999 the single largest market for ABS resins worldwide was transportation. Uses are numerous and include both interior and exterior applications. Interior injection-molded applications account for the greatest volume. General-purpose and high heat grades have been developed for automotive instrument panels, consoles, door post covers, and other interior trim parts. ABS resins are considered by many the preferred material for components situated above the "waistline" of the car. Exterior applications include radiator grilles, headlight housings, and extruded/thermoformed fascias for large trucks. ABS plating grades also account for significant ABS sales and include applications such as knobs, light bezels, mirror housings, grilles, and decorative trim. Appliances were the second largest market segment for ABS. The majority of this consumption was for major appliances; extruded/thermoformed door and tank liners lead the way. Other applications in the appliance market include injection-molded housings for kitchen appliances, power tools, vacuum sweepers, sewing machines, and hair dryers. Transparent ABS grades are commonly used in refrigerator crisper trays, vacuum sweeper dirt cups, and other applications requiring premium aesthetics.

A large "value-added" market for ABS is business machines and other electrical and electronic equipment. Although general-purpose injection-molding grades meet the needs of applications such as telephones and ink jet printer covers, significant growth exists in more demanding FR applications such as computer housings and displays.

An emerging application base for ABS products has been in consumer applications requiring differentiation through aesthetic appeal vs mechanical performance. A wide range of options featuring inherent aesthetic looks such as metalic, sparkle, metamerism, or even thermochromatic color change can be found in products ranging from computers to telephones.

Pipe and fittings remain a significant market for ABS, particularly in North America. ABS foam core technology allows ABS resin to compete effectively with PVC in the primary drain-waste and vent pipe market.

Table 3. Worldwide Capacity for ABS Plastics 1994–2000 by Region, 10^3 t

Region	1994	1995	1996	1997	1998	1999	2000
Western Europe	841	838	865	882	1000	1000	990
Eastern Europe	80	80	81	81	82	82	82
Africa	0	0	0	0	0	0	0
North America	931	894	894	934	1083	1098	1098
Latin America	128	115	127	129	126	230	267
Middle East	0	0	0	0	0	0	0
Asia-Pacific	2130	2535	3158	3292	3712	3857	3977
Total	*4110*	*4462*	*5125*	*5318*	*6003*	*6267*	*6414*

Table 4. World Capacity of Leading ABS Producers

Producer	2000 Capacity, 10^3 t	Largest producer in
GE Plastics	855	North America
Bayer	766	Europe
Chi Mei Industrial	1120	Pacific

Other uses of ABS include consumer and industrial applications such as luggage, toys, medical devices, furniture, shower stalls, and bathroom fixtures.

Economic Aspects

Capacity. Estimated ABS capacity worldwide in 2000 is given in Table 3 (195). Accurate ABS capacity figures are difficult to obtain because significant production capability is considered "swing" and can be used to manufacture polystyrene or SAN as well as ABS. From a regional standpoint, Asia-Pacific has the largest ABS nameplate production capability at 3977 t. The United States has approximately 17% of the world's capacity at 1068 t. Most suppliers have multiple facilities with the largest producers regionally being GE in North America, Bayer in Europe, and Chi Mei in the Pacific. As shown in Table 4, these three producers account for almost 50% of the world's capacity (195).

Table 5. U.S. Unit Sales Values for ABS Resins

Year	Value, $/kg	Year	Value, $/kg
1986	1.56	1993	1.83
1987	1.68	1994	1.87
1988	1.93	1995	2.03
1989	2.03	1996	1.86
1990	1.95	1997	1.67
1991	1.92	1998	1.48
1992	1.86	1999	1.76* est.

Price. The price history of ABS in the United States is presented in Table 5 for the period from 1986 to 1998 (196). The cyclical nature of prices during this period reflects both the cyclical nature of key feedstocks (197–199) and the increased global capacity available. The change also represents the changing mix of ABS resins and blends toward higher value, higher performance applications. Since late 1999, prices have risen appreciably because of dramatic increases in raw material feedstocks and stronger global demand.

Although ABS resins have a long history by industry standards, the products are anything but mature. ABS resins and blends are, and are expected to remain, the engineering thermoplastics of choice for a wide array of markets.

BIBLIOGRAPHY

"Acrylonitrile–Butadiene–Styrene Copolymers" in *EPST* 1st ed., Vol. 1, pp. 436–444, by A. Lebovits, Gaylord Associates, Inc., "Acrylonitrile–Butadiene–Styrene Polymers" in *EPST* 2nd ed., Vol. 1, pp. 388–426, by D. M. Kulich, P. D. Kelley, and John E. Pace, Borg-Warner Chemicals, Inc.

1. D. J. Buckley, *Toughening Mechanisms in the High Strain Rate Deformation of Rubber-Modified Polymer Glasses*, Ph.D. Thesis, Cornell University, 1993.
2. R. A. Bubeck and co-workers, *J. Mater. Sci.* **26**, 6249 (1991).
3. P. Y. B. Jay, T. Shinmura, and K. Konishi, *J. Mater. Sci. Lett.* **19**, 2800 (1973).
4. A. Lazzeri and C. B. Bucknall, *J. Mater. Sci.* **28**, 6799 (1993).
5. G. F. Giaconi and co-workers, *Polymer* **39**, 6315 (1998).
6. A. Donald and E. J. Kramer, *J. Mater. Sci.* **17**, 1756 (1982).
7. S. K. Gaggar, *ASTM STP 936, American Chemical Society for Testing and Materials*, Philadelphia, Pa., p. 236.
8. J. F. Fellers and B. F. Kee, *J. Appl. Polym. Sci.* **18**, 2355 (1974).
9. G. E. Molau, *Polym. Lett.* **3**, 1007 (1964).
10. E. Kim, E. J. Kramer, and P. D. Garrett, *Polymer* **36**, 2427 (1995).
11. A. Zosel, *Rheol Acta* **11**, 229 (1972).
12. H. Munstedt, *Polym. Eng. Sci.* **21**, 259 (1981).
13. Y. Aoki and K. Nakayama, *Polym. J.* **14**, 951 (1982).
14. Y. Aoki, *Macromolecules* **20**, 2208 (1987).
15. Y. Aoki, *J. Non-Newtonian Fluid Mech.* **22**, 91 (1986).
16. M. G. Huguet and T. R. Paxton, *Colloidal and Morphological Behavior of Block and Graft Copolymers*, Plenum Press, New York, 1971, pp. 183–192.
17. T. Masuda and co-workers, *Pure Appl. Chem.* **56**, 1457 (1984).
18. A. Casale, A. Moroni, and C. Spreafico, *Copolymers, Polyblends, and Composites* (Adv. in Chem. Ser. No. 142), American Chemical Society, Washington, D.C., 1975, p. 172.
19. L. L. Blyler Jr., *Polym. Eng. Sci.* **14**, 806 (1974).
20. A. J. Poslinski and P. R. Oehler, *SPE Tech. Pap.* **42**, 470 (1996).
21. R. D. Leaversuch, *Mod. Plast.* **66**(1), 77 (1989).
22. D. M. Kulich, P. D. Kelley, and J. E. Pace, in J. I. Kroschwitz, ed., *Encyclopedia of Polymer Science and Engineering*, 2nd ed., Vol. **1**, Wiley-Interscience, New York, 1985, p. 396.
23. F. M. Smith, *Manufacture of Plastics*, Vol. **1**, Reinhold Publishing Corp., New York, 1964, p. 443.
24. D. L. Fulkner, *Polym. Eng. Sci.* **24**, 1174 (1984).

25. J. M. Heaps, *Rubber Plast. Age* 967 (1968).
26. T. H. Rogers and R. B. Roennau, *Chem. Eng. Progress* **62**(11), 94 (1966).
27. A. Casale and O. Salvatore, *Polym. Eng. Sci.* **15**, 286 (1975).
28. W. I. Congdon, H. E. Bair, and S. K. Khanna, *Org. Coatings Plast. Chem.* **40**, 739 (1979).
29. M. L. Heckaman, *Soc. Plast. Eng. Tech. Pap.* **18**, 512 (1972).
30. B. D. Gesner, *J. Appl. Polym. Sci.* **9**, 3701 (1965).
31. P. G. Kelleher, *J. Appl. Polym. Sci.* **10**, 843 (1966).
32. J. Shimada, *J. Appl. Polym. Sci.* **12**, 655 (1968).
33. M. D. Wolkowicz and S. Gaggar, *Polym. Eng. Sci.* **21**, 571 (1981).
34. P. So and L. J. Broutman, *Polym. Eng. Sci.* **22**, 888 (1982).
35. B. D. Gesner, *SPE J.* **25**, 73 (1969).
36. J. Kovarova, L. Rosik, and J. Pospisil, *Polym. Mater. Sci. Eng.* **58**, 215 (1988).
37. F. Gugumus, in G. Scott, ed., *Developments in Polymer Stabilization*, Vol. **8**, Elsevier, New York, 1987, p. 243.
38. D. M. Chang, *Org. Coatings Plast. Chem.* **44**, 347 (1981).
39. M. G. Wygoski, *Polym. Eng. Sci.* **16**, 265 (1976).
40. L. Zlatkevich, in P. Klemchuk, ed., *Polymer Stabilization and Degradation* (ACS Symp. Ser. No. 280), American Chemical Society, Washington, D.C., 1985, Chapt. "27".
41. L. Zlatkevich, *J. Polym. Sci., Polym. Phys. Ed.* **25**, 2207 (1987).
42. B. Gilg, H. Muller, and K. Schwarzenbach, Paper presented at *Advances in Stabilization and Controlled Degradation of Polymers*, New Paltz, N.Y., June 1982.
43. J. Shimada, K. Kabuki, and M. Ando, *Rev. Electr. Commun. Lab.* **20**, 564 (1972).
44. N. J. Earhart, Paper presented at the *Additives '98: International Conference and Exhibition*, 1998, p. 1.
45. F. Gugumus, in G. Scott, ed., *Developments in Polymer Stabilization*, Vol. **1**, Elsevier Applied Science Publishers, Ltd., London 1979, p. 319.
46. G. Scott, *Developments in Polymer Stabilization*, Vol. **4**, Elsevier Applied Science Publishers, Ltd., London, 1981, p. 181.
47. Eur. Pat. 0109008 and (May 23, 1984), J. C. Wozny (to Borg-Warner Corp.).
48. D. M. Kulich and M. D. Wolkowicz, *Rubber-Toughened Plastics* (Adv. in Chem. Ser. No. 222), American Chemical Society, Washington, D.C., 1989, p. 329.
49. G. Scott and M. Tahan, *Eur Polym. J.* **13**, 981 (1977).
50. M. Tahan, *Weathering of Plastics and Rubber, International Symposium of the Institute of Electrical Engineers*, London, June 1976, Chamelon Press, Ltd., London, 1976, p. A2.1.
51. J. B. Adeniyi, *Eur Polym. J.* **20**, 291 (1984).
52. J. Shimada and K. Kabuki, *J. Appl. Polym. Sci.* **12**, 671 (1968).
53. T. Kurumada, H. Ohsawa, and T. Yamazaki, *Polym. Degrad. Stab.* **19**, 263 (1987).
54. E. Priebe, P. Simak, and G. Stange, *Kunststoffe* **62**, 105 (1972).
55. T. Hirai, *Jpn. Plast.* 23 (Oct. 1970).
56. M. Ghaemy and G. Scott, *Polym. Degrad. Stab.* **3**, 233 (1981).
57. R. D. Deanin, I. S. Rabinovic, and A. Llompart, *Multicomponent Polymer Systems* (Adv. in Chem. Ser. No. 99), American Chemical Society, Washington, D.C., 1971, p. 229.
58. X. Jouan and J. L. Gardette, *J. Polym. Sci., Part A* **29**, 685 (1991).
59. T. Kurumada, H. Ohsawa, and T. Yamazaki, *Polym. Degrad. Stab.* **19**, 263 (1987).
60. A. Davis and D. Gordon, *J. Appl. Polym. Sci.* **18**, 1159 (1974).
61. P. G. Kelleher, D. J. Boyle, and R. J. Miner, *Mod. Plast.* 189 (Sept. 1969).
62. N. D. Searle, M. L. Maecker, and L. F. Crewdson, *J. Polym. Sci., Part A* **27**, 1341 (1989).
63. X. Jouan and J. L. Gardette, *Polym. Degrad. Stab.* **36**, 91 (1992).

64. J. B. Adeniyi and E. G. Kolawole, *Eur. Polym. J.* **20**, 43 (1984).
65. D. M. Kulich and S. K. Gaggar, *Polymer Durability* (Adv. in Chem. Ser. No. 249), American Chemical Society, Washington, D.C., 1996, p. 483.
66. P. Roma, M. P. Luda, and G. Camino, *Polym. Degrad. Stab.* **64**, 497 (1999).
67. J. G. Uhlmann and co-workers, *Plast. Compounding* 8 (May/June 1993).
68. I. Finberg, Y. Bar Yaakov, and P. Georlette, *Polym. Degrad. Stab.* **64**, 465 (1999).
69. R. A. Hayes and S. Futamura, *J. Polym. Sci., Polym. Chem. Ed.* **19**, 985 (1981).
70. A. Brydon, G. M. Burnett, and C. G. Cameron, *J. Polym. Sci., Polym. Chem. Ed.* **12**, 1011 (1974).
71. P. W. Allen, G. Ayrey, and C. G. Moore, *J. Polym. Sci.* **36**, 55 (1959).
72. J. L. Locatelli and G. Riess, *Angew. Makromol. Chem.* **32**, 117 (1973).
73. N. J. Huang and D. C. Sundberg, *J. Polym. Sci., Polym. Chem. Ed.* **33**, 2551 (1995).
74. L. V. Zamoiskaya and co-workers, *Vysokomol. Soedin. Ser. A* **40**, 557 (1998).
75. C. S. Chern and G. W. Pehlein, *J. Polym. Sci., Polym. Chem. Ed.* **28**, 3073 (1990).
76. G. Reiss and J. L. Locatelli, in Ref. 18, p. 186.
77. B. Chauvel and J. C. Daniel, in Ref. 18, p. 159.
78. A. Echte, in Ref. 48, p. 15.
79. E. Beati, M. Pegoraro, and E. Pedemonte, *Angew. Makrom. Chem.* **149**, 55 (1987).
80. G. Odian, *Principles of Polymerization*, McGraw-Hill, Inc., New York, 1970, Chapt. "4".
81. P. J. Flory, *Principles of Polymer Chemistry*, Cornell University Press, Ithaca, N.Y., 1953, pp. 203–217.
82. A. M. Aerdts, S. J. Theelen, and T. M. Smith, *Polymer* **35**, 1648 (1994).
83. R. Kuhn and co-workers, *Colloid Polym. Sci.* **271**, 133 (1993).
84. Jpn. Pat. 09286827 (Nov. 4, 1997), Y. Ii and Y. Nakai (to Mitsubishi Rayon Co.).
85. Jpn. Pat. 01259015 (Oct. 16, 1989), J. Sugiura and co-workers (to Mitsubishi Monsanto Chemical Co.).
86. U.S. Pat. 2,820,773 (Jan. 21, 1958), C. W. Childers and C. F. Fisk (to United States Rubber Co.).
87. U.S. Pat. 19970630 (1997), V. Lowry (to General Electric Co.).
88. E. S. Daniels and co-workers, *J. Appl. Polym. Sci.* **41**, 2463 (1990).
89. Jpn. Pat. 09296015 (Nov. 18, 1997), H. Kitayama, Y. Ishikawa, and M. Nomura (to Kao Corp.).
90. H. S. Chung and co-workers, *Komu Hakhoechi* **28**, 267 (1993).
91. H. S. Chung and Y. J. Shin, *Kongop Hwahak* **4**, 284 (1993).
92. Eur. Pat. 712894 (Apr. 2, 1997), V. J. Kuruganti, S. K. Gaggar, and R. A. St Jean (to General Electric Co.).
93. Eur. Pat. 479725 (Apr. 26, 1995), B. Gilg and co-workers (to Ciba Geigy).
94. Jpn. Pat. 05017506 (Jan. 26, 1993), A. Shichizawa and S. Ozawa (to Asahi Chemical Ind.).
95. Jpn. Pat. 05017508 (Jan. 26, 1993), A. Shichizawa and S. Ozawa (to Asahi Chemical Ind.).
96. Jpn. Pat. 04266902 (Sept. 22, 1992), M. Watanabe and co-workers (to Shin-Etsu Chemical Ind. Co.).
97. Eur. Pat. 496349 (Apr. 10, 1996), M. Watanabe and co-workers (to Shin-Etsu Chemical Ind. Co.).
98. Eur. Pat. 466141 (Nov. 8, 1995), M. Watanabe, S. Ueno, and M. Usuki (to Shin-Etsu Chemical Ind. Co.).
99. J. L. Locatelli and G. Riess, *Angew. Makromol. Chem.* **27**, 201 (1972).
100. C. F. Parsons and E. L. Suck Jr., *Multicomponent Polymer Systems* (Adv. in Chem. Ser. No. 99), American Chemical Society, Washington, D.C., 1971, p. 340.
101. J. Stabenow and F. Haaf, *Angew. Makromol. Chem.* **29/30**, 1 (1973).

102. J. L. Locatelli and G. Riess, *J. Polym. Sci., Polym. Chem. Ed.* **2**, 3309 (1973).
103. J. L. Locatelli and G. Riess, *Angew. Makromol. Chem.* **32**, 101 (1973).
104. P. Mathey and J. Guillot, *Polymer* **32**, 934 (1991).
105. R. Born and co-workers, *Dechema Mongr.* **134**, 409–418 (1998). 6th International Workshop on Polymer Reaction Engineering.
106. Jpn. Pat. 08027306 (Jan. 30, 1996), M. Motai and co-workers (to Japan Synthetic Rubber Co.).
107. Jpn. Pat. 03026705 (Feb. 5, 1991), M. Tsutsumi and M. Shidara (to Hitachi Chemical Co.).
108. Jpn. Pat. 08016126 (Feb. 21, 1996), H. Hayashi, T. Maruyama, and O. Murai (to Kao Corp.).
109. Jpn. Pat. 05163359 (June 29, 1993), F. Suzuki and co-workers (to Mitsubishi Rayon Co.).
110. Eur. Pat. 527605 (Feb 17, 1993), M. C. Will (to Rohm and Haas Co.).
111. A. K. Ghosh and J. Lindt, *J. Appl. Polym. Sci.* **39**, 1553 (1990).
112. U.S. Pat. 3991136 (1976), William Dalton (to Monsanto Chemical Co.).
113. W. P. Flanagan, V. Lowry, T. E. Ludovico, A. P. Togna, and W. J. Fucich, *AICHE 1998 Annual Meeting, Session 16: Clean Air Technologies*, AICHE Publication, New York, 1998.
114. K. R. Sharma, *Polym. Mater. Sci. Eng.* **77**, 656 (1997).
115. U.S. Pat. 05569709 (Oct. 29, 1996), C. Y. Sue and co-workers (to General Electric Co.).
116. U.S. Pat. 05551859 (Sep. 3, 1996), J. E. Cantrill and T. R. Doyle (to Novacor Chemicals International).
117. U.S. Pat. 05550186 (Aug. 27, 1996), J. E. Cantrill and T. R. Doyle (to Novacor Chemicals International).
118. U.S. Pat. 055514750 (May. 7, 1996), J. E. Cantrill and T. R. Doyle (to Novacor Chemicals International).
119. U.S. Pat. 05414045 (May. 9, 1995), C. Y. Sue and co-workers (to General Electric Co.).
120. U.S. Pat. 04415708 (Nov. 15, 1983), S. Matsumura, and co-workers (to Kanegafuchi Kagaku Kogyo Kabushiki Kaisha).
121. U.S. Pat. 04239863 (Dec. 16, 1980), C. Bredeweg (to The Dow Chemical Company.).
122. U.S. Pat. 03945976 (Mar. 23, 1976), J. L. McCurdy and N. Stein (to Standard Oil Co.).
123. U.S. Pat. 3,950,455 (Apr. 13, 1976), T. Okamoto and co-workers (to Toray Industries, Inc.).
124. U.S. Pat. 3,660,535 (May 2, 1972), C. R. Finch and J. E. Knutzsch (to The Dow Chemical Company).
125. U.S. Pat. 2,694,692 (Nov. 16, 1954), J. L. Amos, J. L. McCurdy, and O. R. McIntire (to The Dow Chemical Company).
126. U.S. Pat. 3,515,692 (June 2, 1970), F. E. Carrock and K. W. Doak (to Dart Industries, Inc.).
127. U.S. Pat. 1700011 (Dec. 23, 1991), A. Z. Zumer and co-workers (to USSR).
128. U.S. Pat. 04151128 (Apr. 24, 1979), A. J. Ackerman and F. E. Carrock (to Mobil Oil Corp.).
129. F. Rodriguez, *Principles of Polymer Systems*, McGraw-Hill, Inc., New York, 1970, Chapt. "5".
130. J. Haslam, H. A. Willis, and D. C. M. Squirrell, *Identification and Analysis of Plastics*, 2nd ed., Heyden Book Co., Inc., Philadelphia, Pa., 1980, Chapt. "8".
131. J. C. Cobbler and G. E. Stobbe, in F. D. Snell and L. S. Ettre, eds., *Encyclopedia of Industrial Chemical Analysis*, Vol. **18**, Wiley-Interscience, New York, 1973, p. 332.
132. T. Okumoto and T. Tadaoki, *Nippon Kagaku Kaishi* **1**, 71 (1972).

133. K. Sircar and T. Lamond, *Thermochim. Acta* **7**, 287 (1973).
134. B. D. Gesner, *J. Polym. Sci., Part A* **3**, 3825 (1965).
135. L. D. Moore, W. W. Moyer, and W. J. Frazer, *Appl. Polym. Symp.* **7**, 67 (1968).
136. J. Tsurugi, T. Fukumoto, and K. Ogawa, *Chem. High Polym. (Tokyo)* **25**, 116 (1968).
137. H. Shuster, M. Hoffmann, and K. Dinges, *Angew. Makrom. Chem.* **9**, 35 (1969).
138. D. Kranz, K. Dinges, and P. Wendling, *Angew. Makrom. Chem.* **51**, 25 (1976).
139. D. Kranz, H. V. Pohl, and H. Baumann, *Angew. Makrom. Chem.* **26**, 67 (1972).
140. R. R. Turner, D. W. Carlson, and A. G. Altenau, *J. Elastomer Plast.* **6**, 94 (1974).
141. L. W. Jelinski and co-workers, *J. Polym. Sci., Polym. Chem. Ed.* **20**, 3285 (1982).
142. V. G. Kampf and H. Shuster, *Angew. Makrom. Chem.* **14**, 111 (1970).
143. D. Simpson, *Br. Plast.* 78 (1968).
144. L. I. Petrova and co-workers, *Gig. Sanit.* **37**, 62 (1972).
145. T. R. Crompton, *Chemical Analysis of Additives in Plastics*, Pergamon Press, New York, 1971.
146. N. E. Skelly, J. D. Graham, and Z. Iskandarani, *Polym. Mater. Sci. Eng.* **59**, 23 (1988).
147. R. Yoda, *Bunseki* **1**, 29 (1984).
148. R. J. Pierce and J. W. Bozzelli, Paper presented at the *45th Annual Technical Conference of the Society of Plastics Engineers*, May 1987, p. 19.
149. L. W. Fritch, Paper presented at the *33rd Annual Technical Conference of the Society of Plastics Engineers*, May 1975, p. 70.
150. L. W. Fritch, *Plast. Technol.* 69 (1980).
151. *Cycolac Brand ABS Pellet Drying*, Technical Publication SR-601A, GE Plastics, 1989.
152. J. W. Bozzelli, B. J. Furches, and S. L. Janiki, *Mod. Plast.* 7 (1988).
153. *Product Bulletin: Computrac Vapor Pro Manual, Arizona Instrument, Tempe, Ariz.*, 2001.
154. *Product Bulletin Mark 2 User Manual 0-2094*, Omnimark Instrument Corp., Tempe, Ariz., 1999.
155. B. Miller, *Plast. World* 51 (1987).
156. H. Lord, Paper presented at the *36th Annual Technical Conference of the Society of Plastics Engineers*, May 1978, p. 83.
157. R. E. Nunn, *Injection Molding Handbook*, Van Nostrand Reinhold Co., New York, 1986, Chapt. "3".
158. B. Miller, *Plast. World* **40**(3), 34 (1982).
159. B. Furches and J. Bozzelli, Paper presented at the *45th Annual Technical Conference of the Society of Plastics Engineers*, May 1987, p. 6.
160. *Cycolac Brand ABS Resin Injection Molding*, Technical Publication CYC-400, GE Plastics, Pittsfield, Mass., 1990.
161. *Molding Flame Retardent ABS*, Technical Publication P-408, GE Plastics, Pittsfield, Mass., 1989.
162. L. W. Fritch, in Ref. 157, Chapt. "19".
163. L. W. Fritch, Paper presented at the *45th Annual Technical Conference of the Society of Plastics Engineers*, May 1987, p. 218.
164. L. W. Fritch, *Plast. Eng.* 43 (1989).
165. L. W. Fritch, Paper presented at the *40th Annual Technical Conference of the Society of Plastics Engineers*, May 1982, p. 332.
166. L. W. Fritch, Paper presented at the *5th Pacific Area Technical Conference of the Society of Plastics Engineers*, Feb. 1980.

167. S. Gaggar and J. Wilson, Paper presented at the *40th Annual Technical Conference of the Society of Plastics Engineers*, May 1982, p. 157.
168. L. W. Fritch, Paper presented at the *37th Annual Technical Conference of the Society of Plastics Engineers*, May 1979, p. 15.
169. L. W. Fritch, *Prod. Finish. Cincinnati* **48**(5), 42 (1984).
170. L. W. Fritch, *Plast. Machin. Equip.* 43 (1988).
171. R. M. Criens and H. Mosle, Paper presented at the *42nd Annual Technical Conference of the Society of Plastics Engineers*, May 1984, p. 587.
172. J. W. Bozzelli and P. A. Tiffany, Paper presented at the *44th Annual Technical Conference of the Society of Plastics Engineers*, May 1986, p. 120.
173. U. Wolfel and G. Menges, Paper presented at the *45th Annual Technical Conference of the Society of Plastics Engineers*, May 1987, p. 292.
174. S. M. Janosz, Paper presented at the *45th Annual Technical Conference of the Society of Plastics Engineers*, May 1987, p. 323.
175. H. Cox and C. Mentzer, *Polym. Eng. Sci.* **26**, 488 (1986).
176. G. Brewer, Paper presented at the *45th Annual Technical Conference of the Society of Plastics Engineers*, May 1987, p. 252.
177. *Cycolac Brand ABS Resin Design Guide*, Technical Publication CYC-350, GE Plastics, Pittsfield, Mass., 1990.
178. *Cycolac Brand ABS Electroplating*, Technical Publication 402, GE Plastics, Pittsfield, Mass., 1990.
179. M. Snyder, *Plast. Machin. Equip.* 50 (1988).
180. K. C. Rusch, Paper presented at the *45th Annual Technical Conference of the Society of Plastics Engineers*, May 1987, p. 1014.
181. W. Virginski, Paper presented at the *46th Annual Technical Conference of the Society of Plastics Engineers*, May 1988, p. 205.
182. J. L. Throne, *Technology of Thermoforming*, Hanser Publishers, New York, 1996), Chapts. "8" and "10".
183. L. E. Ferguson and R. J. Brinkmann, Paper presented at the *45th Annual Technical Conference of the Society of Plastics Engineers*, May 1987, p. 866.
184. *Cycolac Brand ABS—General Purpose Blow Molding Grades*, Technical Publication SR-616, GE Plastics, Pittsfield, Mass., 1989.
185. *Thermoforming Cycolac Brand ABS*, Technical Publication P-406, GE Plastics, Pittsfield, Mass., 1989.
186. J. L. Throne, Paper presented at the *45th Annual Technical Conference of the Society of Plastics Engineers*, May 1987, p. 412.
187. N. Nichols and G. Kraynak, *Plast. Technol.* 73 (1987).
188. R. Royer, Paper presented at the *Regional Conference of the Society of Plastics Engineers*, Quebec Section, 1968, p. 43.
189. G. Trantina and M. Minnicheli, Paper presented at the *45th Annual Technical Conference of the Society of Plastics Engineers*, May 1987, p. 438.
190. T. L. La Bounty, Paper presented at the *43rd Annual Technical Conference of the Society of Plastics Engineers*, May 1985, p. 855.
191. *Cycolac Brand ABS Resin—Assembly Techniques*, Technical Publication CYC-352, GE Plastics, Pittsfield, Mass., 1990.
192. H. Potente and H. Kaiser, Paper presented at the *47th Annual Technical Conference of the Society of Plastics Engineers*, May 1989, p. 464.
193. V. K. Stokes, Paper presented at the *47th Annual Technical Conference of the Society of Plastics Engineers*, May 1989, p. 442.
194. *Monthly Petrochemical and Plastics Analysis*, 9 (Sept. 1999).
195. *International Trader Publications*, ABS Global Capacity, issued July, 2000.
196. *Modern Plastics*, **77**(2), 74–79 (Feb. 2000).

197. *Chemical Economics Handbook*, SRI International, Menlo Park, Calif., 1989, 580.0180D.
198. *World Petrochemicals*, SRI International, Menlo Park, Calif., 1990, WORL 2-16.
199. *Synthetic Organic Chemicals*, United States Production and Sales, USITC Publication, 1989.

D. M. KULICH
S. K. GAGGAR
V. LOWRY
R. STEPIEN
GE Plastics, Technology Center

ADDITIVES

Introduction

Plastics additives are typically organic molecules that are added to polymers in small amounts (typically 0.1–5.0 wt%) during manufacture, processing, or converting so as to improve the inherent properties of the polymer resin. Additives can be categorized in three major segments: polymer modifiers, performance enhancers, and processing aids. Pigments and Colorants are not included in this overview. Antiozonants, accelerators, and vulcanizing agents, used in large volumes in elastomers, are also excluded (see RUBBER CHEMICALS). The global market for plastics additives in 1998 has been estimated to be of the order of $15–16 billion in value and 7–8 million tons in volume (1). Poly(vinyl chloride) (PVC) and polyolefins are the largest consumers of additives and drive the growth rates of 4–5% on average.

Polymer modifiers, accounting for about half of the total value (4.5 million tons globally in 1999), are added primarily to alter the physical and mechanical properties of the plastic. These include plasticizers, foaming (blowing) agents, coupling agents, impact modifiers, organic peroxides, and nucleating/clarifying agents. Plasticizers, used primarily in flexible PVC, are the highest volume additives (see PLASTICIZERS). Coupling agents are among the fastest growing additives (6–7%) in this class (see SILANE COUPLING AGENTS).

Performance enhancers are added to plastics to provide functionality not inherent to polymer itself. These include flame retardants (FRs), Heat Stabilizers for PVC, Antioxidants, light stabilizers, biocides, and Antistatic Agents. Performance enhancers for 40% of the total global market for additives are led by FRs with a total value of $2 billion. Among performance enhancers, light stabilizers show above average growth rates of 6–7% (2) (see UV STABILIZERS).

Encyclopedia of Polymer Science and Technology. Copyright John Wiley & Sons, Inc. All rights reserved.

Processing aids are typically surface-active agents that are added by the plastics converters/transformers to improve throughput and alter the surface properties of the finished article. Additives in this class include lubricants, slip agents, antiblocks, and mold-release agents (see RELEASE AGENTS).

A key driver of change and new product development in the plastics additives markets is a host of environmental concerns. This is seen most dramatically in PVC where concerns over the use of heavy-metal heat stabilizers based on lead have led to a widespread conversion to tin-based materials and even to nonmetallic stabilizers. The widely used phthalate-based Plasticizers for flexible PVC have come under fire because of concerns over their potential adverse effects on the human reproductive systems. Concerns over the potential for brominated FRs to form dioxins are fueling the development of new halogen-free systems.

Plastics additives are used extensively in food packaging and as such are regulated by the U.S. Food and Drug Administration (FDA) (and related international agencies) as indirect food additives. Regulation by the FDA of a new additive requires submission of toxicity, as well as migration data from the polymer in question into a variety of food stimulants so as to calculate estimated daily intake. The level of migration and anticipated annual usage determines the extent of toxicity testing that is required. Information on the petition process for obtaining regulations as well as a directory of all indirect food additives can be obtained through the FDA website www.fda.gov.

Additives are incorporated into polymer matrixes by a variety of methods and at various points in the manufacturing process. Polymer producers typically incorporate additives as single components or as blends of two or more additives during the pelletization/isolation step. Converters and transformers often introduce additives as a concentrate or masterbatch. *Concentrate is a mixture* is a mixture of an additive dissolved in a polymer resin carrier at fairly high (10–30%) concentrations. A *masterbatch* is a blend of additives and often pigments in a resin carrier designed for a specific end-use application.

Modifiers

Plasticizers. Plasticizers, through their use in flexible PVC, are the largest volume polymer additives used in plastics. Flexible PVC accounts for nearly 90% of the volume of plasticizers used in plastics. Plasticizers are added at very high loadings (up to 80%) depending on the degree of flexibility required. Plasticizers are added to inherently hard thermoplastics to increase the flexibility, softness, and/or extensibility. In addition, secondary benefits of improved processability, greater impact resistance, and higher ductility can often be achieved. Plasticizers are often used as carriers for pigments and are the liquid vehicle for PVC plastisols. Plasticizers are predominately esters produced through the reaction of an acid or anhydride with a linear or branched alcohol (3).

Dialkyl phthalates produced by the reaction of phthalic anhydride [85-44-9] with alcohols varying in chain length from C_4 to C_{11} with 2-ethyl-1-hexanol [104-76-7] and 1-octanol [111-87-5] typically used, are the most commonly used plasticizers. While somewhat interchangeable, performance properties such as low temperature flexibility, volatility, processability, and extractability are governed

by chain length and degree of branching. For example, in interior automotive PVC applications, the octyl phthalates have been replaced by isodecyl phthalates because of their lower volatility and thereby enhanced fogging resistance.

The remaining plasticizers are more specialty in nature. Aliphatics are typically 2-ethylhexyl esters of dibasic acids, such as glutarates, adipates, or sebacates. The primary use of aliphatics is when low temperature flexibility and crack resistance is required. When very low volatility and low migration is required, the plasticizers of choice are based on esters of trimellitic anhydride [552-30-7]. A typical application for mellitates is in PVC wire and cable jacketing, which requires excellent long-term heat aging properties and extraction resistance. For particularly demanding performance applications, dibasic acids are polymerized with diols to produce low molecular weight polymeric plasticizers. Esters of phosphorus oxychloride [10025-87-3], the phosphate esters, are typically used as FRs and also impart plasticizing properties. A final class are the epoxies, with epoxidized soybean oil [8013-07-8] (ESBO) being the most common (epoxies based on tall oils and linseed oil are also available). While primarily added as secondary thermal stabilizers in PVC because of their ability to scavenge HCl generated during processing, as plasticizers they exhibit excellent extraction resistance and low migration.

Typically the large producers of plasticizers are backward integrated into either alcohol and phthalic anhydride or both. The key suppliers of the commodity plasticizers in North America are ExxonMobil (Jayflex), BASF (Pluronic), Eastman (Eastman), and Aristech (PX). About 2.5 billion pounds of plasticizer are consumed in North America.

Foaming (Blowing) Agents. *Chemical blowing agents* are inorganic or organic additives that produce a foamed structure. They are used extensively in PVC but also in polyethylene (PE), polypropylene (PP), and polystyrene (PS) to improve properties and appearance (insulation against heat and noise, better stiffness, removal of sink marks in injection-molded parts, and improved electrical properties) as well as to reduce weight. Chemical-blowing agents can be classified as either physical or chemical. They are typically added via a concentrate or masterbatch. The total market for blowing agents in North America is 6800 tons (4,5).

Physical blowing agents are volatile liquids or compressed gasses that are dissolved in the polymer and change state during processing to form a cellular structure. Chemical blowing agents (CBAs) decompose thermally during processing to liberate gasses that form a foamed product. Organic CBAs typically are solid hydrazine derivatives that generate nitrogen in an exothermic reaction. Most common is azodicarbonamide [123-77-3], which in pure or modified form accounts for up to 80% of all CBAs. It begins to decompose at 390°F. Other types are the sulfonyl hydrazides {most common is 4,4′-oxybis(benzenesulfonyl hydrazide) [80-51-3] which is used for low temperature applications} and *p*-toluene semicarbazides {most common is *p*-toluenesulfonylsemicarbazide [10396-10-8] which is used in high temperature applications such as acrylonitrile–butadiene–styrene (ABS), poly(phenylene oxide) (PPO), nylon, and high impact polystyrene (HIPS)}. High gas yields and pressures for exothermic CBAs make them useful in applications such as cross-linked PE and extruded products. Uniroyal Chemical (Celogen, Expandex) is the major producer of these products in North America. Endothermic

CBAs are based on blends of inorganic carbonates and polycarbonic acids. Proper combination of these materials allows for operating temperature ranges of 150–300°C. A common commercial system is based on citric acid [77-92-9] and sodium bicarbonate [144-55-8]. Endothermic CBAs generally produce a lower gas yield providing foams with smaller cell structure than exothermic CBAs do. Clariant (Hydrocerol) is the leading supplier of endothermic CBAs.

Coupling Agents. Coupling agents promote adhesion between polymers and inorganic fillers by forming stable chemical bonds between the organic matrix and the surface of the filler. The highest usage of coupling agents is in the treatment of glass fibers for use in thermosets such as epoxies and polyesters. Other fillers include clay, silica, mica, wollastonite, calcium carbonate and aluminum trihydrate (ATH).

The most common type of coupling agent is the organosilanes. Silanes have the general structure $RSi(OR')_3$, where R is a functionalized organic group that binds to the polymer matrix (ie, amino, epoxy, acrylate, or vinyl) and R′ is typically methyl or ethyl. The methoxy or ethoxy groups hydrolyze to silanols which react with surface hydroxyl groups on the inorganic fillers to form oxane bonds. The result is improved mechanical or electrical properties. Amino silanes are typically used for epoxy and phenolic resins, epoxy silanes for epoxy resins, and methacrylate silanes with unsaturated polyesters. Fillers are typically pretreated with an aqueous dispersion of silane at levels of 0.2–0.75%. The treated fillers are then reacted with the polymer matrix during compounding. The silane improves wetting during the compounding process, thereby reducing the surface tension of the organic–inorganic interface for better dispersion. The filled compound has much improved moisture resistance. Dow Corning, Crompton, and Degussa-Huels (Sivento) are major suppliers of silanes in North America with an estimated market value of $70–100 million.

In addition to silanes, a variety of organometallics (primarily titanates, but also zirconates, aluminates, and zircoaluminates) are used as coupling agents, although in significantly lower volumes. While mechanistically similar, titanates are more versatile than silanes because they can react with a broader range of fillers (ie, calcium carbonate). However, they are more susceptible to hydrolysis. Titanates are often used as dispersing agents for fillers in polyolefins by reducing the surface energy of the filler, resulting in better impact strength, lower melt viscosity, and better aged mechanical properties. DuPont and Kenrich are the primary suppliers of organometallics.

A specialty class of coupling agent are the maleated polyolefins (6). The pendant maleic anhydride unit reacts with surface hydroxyl groups (or siloxy group in the case of pretreated fillers) while the polymeric portion cocrystallizes with the polymer matrix. Their main applications are in glass-filled PP composites and in non-halogenated FR wire and cable applications. The addition of 1–2% maleated PP can improve the tensile strength of a 30% glass-filled PP by up to 40%. In FR applications, 4% maleated PE in a PE/EVA (polyethylene/ethylene–vinyl acetate) blend containing 65% ATH gives up to three times improvement in elongation. The maleic anhydride reacts with the basic inorganic FR, fillers, ATH, and magnesium hydroxide. Maleated polyolefins are marketed in North America by DuPont (Fusabond) and Uniroyal (Polybond).

Organic Peroxides. Organic peroxides are used in the plastics industry to catalyze polymerization reactions or to modify the properties of polymers (7,8). On the polymerization side, peroxides are used as initiators for PVC, low density polyethylene (LDPE), PS, and acrylics. As modifiers of existing polymers, peroxides are used for the curing of unsaturated polyester resins, as cross-linkers of PE, silicones, and a variety of ethylene-based elastomers (9) and to break down the molecular weight of PP in a process known as *visbreaking* or *controlled rheology* (10). Peroxides function through the thermal decomposition of the unstable peroxide bond to generate two free radicals. The reactivity of the peroxide is modified by altering the organic substituents attached to the peroxide or through the use of coadditive promotors. The reactivity of the peroxide is defined by the *10-h half-life temperature*, or the temperature at which one-half of the peroxide decomposes in a 10-h period. The lower the 10-h half-life temperature, the more reactive the peroxide. Organic peroxides fall into seven basic groupings depending on the organic substituent. These are dialkyl peroxides, diacyl peroxides, hydroperoxides, ketone peroxides, peroxydicarbonates, peroxyesters, and peroxyketals. The following table categorizes organic peroxide by grouping and chemical process:

The choice of organic peroxide used for initiating polymerizations is dictated by the polymerization temperature used to produce the polymer. The low temperatures used for PVC polymerization, for example, dictate the use of organic peroxides with low 10-h half-life temperatures. For the higher polymerization temperatures used for LDPE, an organic peroxide with a higher 10-h half-life temperature may be used. When used as polymerization catalysts, organic peroxides are typically used in the 0.1–0.5% range. Approximately half of all organic peroxides are used in the various polymerization processes.

Unsaturated polyesters are produced through the cross-linking of low molecular weight polyester resins and comonomers such as styrene in the presence of 1.0–2.5% based on resin weight. Fillers, pigments, and reinforcements such as glass fiber are often added as well. Depending on the cure temperature, promotors are often used. For room-temperature cures and resin-transfer molding, organic cobalt and copper promotors are added to the ketone peroxides, which are typically used. Unsaturated polyester resin production is the largest single application of organic peroxides, accounting for 30–40% of total consumption.

For the cross-linking of ethylene-based polymers for applications such as wire and cable jacketing and tubings, peroxides are added during compounding/processing at levels of 0.2–0.4%. In the visbreaking of controlled-rheology PP, to reduce the molecular weight and melt viscosity of the polymer, similar levels are used. Controlled-rheology PP is particulary common for fiber and extrusion grades. When peroxides are used together with other additives, particularly antioxidants, a careful balance of concentrations must be chosen since the radicals formed during thermal decomposition can react with the other additives, lowering the effective concentrations of each.

Key suppliers of organic peroxides in North America include Akzo Nobel (Trigonox, Perkadox), LaPorte, and AtoFina (Luperox).

Impact Modifiers. Impact modifiers function by absorbing the impact energy and dissipating it in a nondestructive fashion. Typically elastomers, they are added to a wide range of thermoplastic materials at levels up to

20%. The major types of impact modifiers are acrylics, styrenics including methacrylate–butadiene–styrene (MBS) copolymers and Acrylonitrile-Butadiene-Styrene Polymers, chlorinated polyethylene (CPE), EVA copolymers, and the ethylene–propylene copolymers and terpolymers (EPR and EPDM respectively). The major market for impact modifiers is in PVC, although they are used in a wide range of other polymers such as polyolefins and engineering polymers.

MBS is the highest volume of the styrenic types. These terpolymers consist of an elastomeric core with a hard outer shell, which provide good impact resistance together with excellent processability. Typically used in transparent PVC packaging because of its good clarity, its market growth has slowed as PET and polyolefins have replaced PVC in packaging applications. Because of poor weatherability owing to the butadiene component, outdoor applications are limited. Kaneka Texas and Rohm & Haas are the major producers.

ABS is used in a variety of resins with PVC again being the major market. Like MBS, ABS suffers from poor weatherability and is therefore useful in outdoor applications only when a uv-resistant capstock is applied. GE Specialty Chemicals is the leading producer in North America.

Acrylics are the fastest growing impact modifiers because of their usage in exterior PVC siding and profile. While they function in the same way as MBS and ABS, the graft phase is based on butyl or ethylhexyl acrylates which are far more uv-stable than butadiene. Rohm & Haas and AtoFina are the major producers in North America.

EPDM and EPR are used to modify polyolefins, primarily in the automotive industry. The largest volume is in automotive PP bumpers. This application is gradually being replaced by impact-resistant polymers produced by metallocene technology, providing better performance and economics. DuPont Dow and Exxon are leading producers in North America. When used with plastics such as nylon, PET, and PBT, the EPDM and EPR are often modified with a functionalized monomer to allow them to react with the plastic. Additionally, the shell of a core-shell modifier can also be modified to include a reactive group. Suppliers of functionalized modifiers include Rohm & Haas, AtoFina, Shell, and Exxon.

CPE is again most widely used in PVC, although it does find applications in polyolefins. It can only be used in opaque applications but it does have excellent weatherability, making it useful for PVC pipe, siding, and profiles. DuPont Dow is the leading producer in North America.

Nucleating/Clarifying Agents. Materials added to semicrystalline plastics prior to processing and fabrication, which affect the rate of cystallization and spherulite size, are referred to as *nucleating agents*. These are typically insoluble or immiscible materials which provide sites for crystal formation. The main benefit for the addition of nucleating agents is improved cycle time during injection molding. When the addition of nucleators decreases the size of the crystallites to less than the wavelength of visible light, these agents are referred to as *clarifying agents* because they reduce haze and improve transparency (11).

For nucleation of nylon and PP, sodium benzoate [532-32-1] is the traditional material of choice. Use levels are of the order of 0.1% with injection-molded packaging closures being a major application. Sodium benzoate does not impart any improvement in optical properties. Low molecular weight polyolefins, ionomers,

as well as plasticizers such as ESBO are used for nucleation of semicrystalline plastics such as PET. Modified benzylidene sorbitols dominate the market for nucleation and clarification of PP. They are used at 0.1–0.3% levels in both homo- and copolymers, with injection-molded housewares, medical devices such as syringes, and other packaging being the major applications. Metal salts of organic phosphates have also been introduced for nucleation/clarification of PP. In North America, Milliken (Millad), Ciba Specialty Chemicals (Irgaclear), and Amfine (AdekaStab North America) are key suppliers. Talc and other minerals are often used as nucleators.

Property Extenders

Antimicrobials/Biocides. Biocides are used to provide protection against mold, mildew, fungi, and bacterial growth on the surface of polymers. Since they function by being toxic to the microorganisms which cause growth, they are considered as pesticides under the Federal Insecticide, Fungicide and Rodenticide Act and as such are carefully regulated by the U.S. EPA. All end-use applications and related performance claims must be registered through the EPA and supported with toxicity, safety, handling, environmental, as well as efficacy data. Since microorganisms grow at the surface of plastics, in order to be effective biocides must migrate. Their rate of migration is closely related to their efficacy (12,13).

The primary use of biocide additives is for flexible PVC which accounts for over 70% of the total demand. While PVC is inherently resistant to microbial attack, the phthalate plasticizers are quite susceptible. Moisture contact and external factors such as uv-exposure can increase susceptibility by providing surface crazing/defects as sites for growth. Typical applications for biocide use in PVC are pool and pond liners, outdoor furniture, marine upholstery, roofing membranes, garden hoses, shower curtains, and wire and cable jacketing. Use of biocides in polyolefins is growing with applications such as children's toys and furniture, kitchen utensils, cutting boards, and trash bins. Biocides are also used in a variety of engineering polymers (PET, PA) and in PUR foams.

A variety of organic and inorganic biocides have been developed for use in plastics, including arsines, isothiazolinones, chlorinated phenols, silver, and zinc compounds. Among the arsines, 10,10′-oxybisphenoxyarsine [58-36-6] is most common and is used at an active level of 0.02–0.05%. A typical isothiazalone is 2-*n*-octyl-4-isothiazolin-3-one [26530-20-1]. These are used at levels of 0.1–0.15% and are available in a 4% concentrate in a plasticizer (either dialkylphthalate or ESBO). Zinc-2-pyridinethianol-1-oxide [13463-41-7] (commonly known as omacide or zinc omadine) and trichlorophenoxyphenol [3380-34-5] (Triclosan) are other common biocides. In North America, Morton/Rohm & Haas (Vinyzene) is the market leader in terms of volume and breadth of product line. Other key players include Akros Chemicals (Intercide), Arch Chemical, and Ferro. The global market for biocides used in plastics is of the order of 23,000 tons.

Antioxidants. Polymers may be oxidized during processing, fabrication, and end use resulting in loss of aesthetic and mechanical properties. This thermally induced autoxidation results in the formation of free radicals which will react with oxygen to form hydroperoxides. These hydroperoxides are themselves

thermally unstable and their ensuing decomposition results in chain scission, cross-linking, and the formation of chromophores. In order to inhibit the initiation of polymer oxidation and to retard the resulting destructive chemical processes Antioxidants are added during manufacture, processing, and/or during fabrication of plastic articles (14–16). The global market for antioxidants is estimated to be 227,000 tons or $1.3 billion (1) (see ANTIOXIDANTS).

Traditional antioxidants are classified as either primary or secondary types depending on their mode of action. Primary antioxidants act by trapping free radicals, usually hydroperoxy radicals, through donation of a labile hydrogen to the radical species. Secondary antioxidants interfere with the propagation steps of autoxidation by decomposing hydroperoxides to form stable, nonradical species. It is quite common for a combination of primary and secondary antioxidants to be used to provide the maximum stabilization of a plastic. Use of antioxidants in plastics is ubiquitous, since nearly all resin types require some form of stabilization in order to provide useful and durable materials.

The two most common classes of primary antioxidants are the aromatic amines and hindered phenols. Aromatic amines, such as substituted diphenylamines are extremely effective, acting as both radical chain terminators and peroxide decomposers. A major drawback of aromatic amines is their tendency to form highly discolored oxidation products during use (staining). As a result their use is restricted to applications where discoloration is not an issue, such as carbon black filled or pigmented systems. As such their major usage is in the rubber industry. In plastics a major application is black wire and cable jacketing. Flexsys (Santonox), Goodyear (Wingstay), and BF Goodrich (Agerite) are among the leading suppliers of aromatic amines. For stabilizing end-use articles, relatively high levels of amine are used—typically 0.5–1.0 wt%. When used as a storage stabilizer for polyols which in turn are used in polyurethane (PUR) manufacture, lower levels (typically 200–1000 ppm) are used. The standard primary antioxidants used in plastics are based on hindered phenols which in turm are usually based on derivatives of 2,6-di-*t*-butylphenol [128-39-2] (BHT). One of the most common phenols is 2,6-di-*t*-butyl-4-methylphenol [128-37-0] (BHT). While highly effective, it is relatively volatile and is susceptible to discoloration upon oxidation. In order to improve on the properties of BHT, a host of analogues have been developed These modifications generally involve either altering the hindering alkyl groups or changing the substituent in the 4-position. In order to improve on the volatility of BHT, antioxidants with two, three, and four hindered phenols linked together are available and commonly used. Hindered phenols are effective both during polymer processing and during end use. Typically they are used in combination with a secondary antioxidant to maximize their effectiveness during high temperature processing and to minimize color formation resulting from the overoxidation of the phenol. Use levels of 0.1–0.5% are common. Hindered phenols are available from a number of producers, with Ciba Specialty Chemicals (Irganox), Great Lakes Chemical (Anox, Lowinox), and Cytec (Cyanox) being key suppliers in North America. Recently Vitamin E (α-tocopherol) [10191-41-0], a high molecular weight but extremely reactive phenol, has found niche use primarily in food-contact applications because to its effectiveness at low levels (100–200 ppm) and its "green" image. Its major limitation is its tendency to form highly discoloring chromophores upon oxidation. While primarily used to provide

uv-stability, hindered-amine light stabilizers (HALS) can be used as antioxidants when use temperatures are below 135°C. The primary benefit of HALS when used as an antioxidant is that unlike aromatic amines or hindered phenols, their oxidation products are colorless. Since they do not provide high temperature stability, they must be used in conjunction with phosphites or some other melt-processing stabilizer.

Secondary antioxidants generally fall into two classes: the organophosphites and thioesters. Organophosphites are typically trivalent arylphosphites which react with hydroperoxides in the polymer to generate a pentavalent phosphate and a nonreactive alcohol. Phosphites are effective at the high temperatures used in polymer processing but do not provide any stabilization during end- use. As such they are nearly always used with hindered phenols in practical applications. Trisnonylphenylphosphite [26523-78-4] is commonly used but is slowly being replaced by more complex arylphosphites with improved hydrolytic stability. Typical use levels are in the range of 500–1500 ppm. Ciba (Irgafos), GE Specialty Chemicals (Ultranox), and Clariant (Sandostab) are major suppliers. Thioesters are derivatives of 2,2′-thiobispropionic acid [5811-50-7], the most common being the lauryl esters, dilaurylthiodipropionate [128-28-4], and stearyl esters, distearylthiodipropionate [693-36-7]. In contast to the arylphosphites, thioesters are active at the lower end-use temperature range 125–150°C and are often used in combination with hindered phenols to stabilize polyolefins for under-the-hood applications. They are not active as melt-processing stabilizers. The primary drawback of thioesters is poor organoleptic properties, which limit their use in food-contact applications. Typical use levels are in the range of 1.0–1.5%. Cytec (Cyanox) and Crompton (Argus) are major suppliers in North America.

Newer developments (17) have focused on higher performing stabilizers which can be used at low levels with enhanced ancillary properties such as low color and odor. Dialkylhydroxylamines used in combination with HALS provide an excellent, low color stabilization system for PP fibers. Arylbenzofuranones have been shown to boost the performance of traditional hindered phenol/phosphite stabilization systems at use levels of 150 ppm.

Antistats. As a result of their low electrical conductivity (surface resistivity in the order of $10^{15} - 10^{17}$ Ω/sq), plastics are known for their ability to accumulate electrostatic charges. The static charge can be generated during processing, transportation, handling, or final use, and typically occurs because of friction between the plastic and another material. The build up of static charge leads to a number of undesirable properties such as dust/dirt buildup, solids buildup on walls of plastic containers during filling, clinging effects during fabrication or conversion of films, destruction of electronic parts packaged in plastic materials, and ignition of vapors or particulates. A number of approaches have been developed to address these problems including topically applied antistatic additives, carbon black and other conductive fillers, intrinsically conductive polymers, and the classical migratory additives such as ethoxylated amines and glycerol monostearates (18). The total market for antistats in North America is estimated to be $30 million. Polyolefins, styrenics, and PVC consume the majority of Antistatic Agents.

For nondurable applications, topical, external antistats can be applied to the finished plastic article through dipping or spraying of the part. The most

common type is the quaternary ammonium salts or "quats," which are typically applied as a water or alcohol solution. Since these materials are easily removed during handling or use, they are only effective for relatively short duration. For more durable applications, internal antistats added during compounding have been developed. The classical systems have a lipophilic tail and a hydrophobic head which migrates to the polymer surface to form a moisture-absorbing layer allowing for static dissipation. These systems rely on migration of the additive and sufficient humidity to form the moisture layer. The most common type of migratory antistat is the nonionics, essentially surfactants. This class is dominated by the ethoxylated fatty alkylamines and the ethoxylated alkylamides. These antistats are effective at lower loadings (<2%), require at least 50% relative humidity, have an induction time before being active, can ultimately be wiped or washed from the surface affecting permanence, and can have adverse surface effects such as plate-out and poor printability. To achieve the optimum blend of performance characteristics (permanence vs fast induction) blends of fast and slow migrators are typically used. Key suppliers of migratory antistats in North America are Ciba SC (Atmer), Akzo (Armostat), and Crompton (Kemamine).

In order to improve on the performance of the classical migratory antistats with respect to permanence and humidity sensitivity, a number of newer approaches have been developed. These include hydrophilic polymers, inherently conductive polymers, and conductive fillers. The most common ICPs are based on polyaniline, a highly conjugated polymer which is converted to a cationic salt with an organic acid. The relatively high cost has relegated these materials to niche applications. Fillers such as carbon black and nickel-coated graphite have good permanence but can affect mechanical properties and are highly colored. Finally, the hydrophilic polymers are the most rapidly growing of the permanent technologies. These are based typically on polyether/polyamide block copolymers and develop a conductive network when used at 10–30% loadings. These types of permanent antistats are available from Atofina (Pebax) and Ciba (Irgastat). Typical applications are in business machines such as fax and copier parts, typically HIPS and ABS (see ANTISTATIC AGENTS).

Flame Retardants. Added to plastics to inhibit ignition and retard the spread of flame, mechanistically, flame retardants (FRs) can be categorized as one of the following (19,20):

(1) **Char formers:**

Typically phosphorus-based organic compounds which when burned provide a physical and insulating barrier between the flame and the fuel or polymer

(2) **Heat absorbers:**

such as ATH or magnesium hydroxide which decompose at high temperature to generate water which in turn removes heat from the system through evaporation. Additionally they form glassy oxide barrier layers.

(3) **Radical sources:**

typically brominated or chlorinated hydrocarbons; they act by interfering with the radical-chain mechanism occurring in the gas phase. High energy hydroxyl and oxygen radicals formed during the chain-branching phase of combustion are trapped in the gas phase and replaced by much lower energy halogen radicals.

(4) **Antimony synergists:**

antimony trioxide [1309-64-4] which shows no FR activity on its own, synergizes with halogen-containing compounds through the formation of antimony trichloride.

By chemical class, FRs can be categorized as follows.

Brominated Hydrocarbons. Accounting for the highest dollar value, these consist of additives such as decabromodiphenyloxide [1163-19-5] and tetrabromobishphenol A [79-94-7] and derivatives. These products are used in engineering resins primarily (HIPS, ABS, and PC) for the business machine market. Typically they are used with antimony oxide [1309-64-4] as a synergist in a ratio of 3:1 respectively. Major suppliers of brominated FRs are Great Lakes Chemical Co. (GLCC), Albemarle (Saytex), and Dead Sea Bromine.

Chlorinated Hydrocarbons. The chlorinated paraffins are used as FRs/plasticizers for PVC, in PUR foams, and in certain elastomeric materials. Dover Chemical (Chlorez) is a key supplier. Dechlorane [2385-85-5] (Occidental) has its main application in polyolefin wire and cable jacketing. A reactive type, chlorendic acid and anhydride chlorendic [115-28-6] (Occidental) is used primarily in unsaturated polyester. Typically the chlorinated compounds can also be used with antimony synergists.

Phosphate Esters. The phosphate esters can be subdivided into halogenated and non-halogenated versions. Halogenated phosphate esters are used almost exclusively in PUR foams. Rhodia (Antiblaze) and Akzo Nobel (Fyrol) are key suppliers. The non-halogenated phosphate esters are primarily aryl esters and are used in engineering plastics. They are widely used in lubricants and as plasticizers in PVC. Rhodia, GLCC, and Akzo Nobel are the key producers.

Antimony. Antimony trioxide is the primary product but sodium antimonate and antimony pentoxide are also used to a minor extent. Antimony compounds are used as synergists with halogens, with GLCC (Anzon) and Occidental (Laurel) as the major producers.

Aluminum Trihydrate. Since aluminum trihydrate (ATH) [21645-51-2] begins to decompose at relatively low temperature, it can only be used in polymers which can be processed at temperatures not exceeding 200°C for long periods of time (polyolefins, acrylics, unsaturated phosphate esters, and PVC. When higher temperature processing is required, magnesium hydroxide can be substituted. It is used at very high loading levels (60 wt% or greater). These high loadings can

have a detrimental effect on physical properties. Major producers are Alcoa, Alcan, and Martinswerke (Lonza).

FRs are a greater than $2 billion global business (1), with bromine-based products accounting for nearly half of the value, followed by phosphate esters.

Heat Stabilizers. Chlorinated polymers, primarily PVC, decompose during processing to liberate HCl via dehyrochlorination reactions. The liberated HCl catalyzes the dehydrochlorination leading to rapid discoloration, embrittlement, and loss of mechanical properties. Primary Heat Stabilizers act by trapping the liberated HCl and also by reacting with labile chlorines on the polymer chain formed during polymerization (eg, allylic chlorines) (21). There are three major types of primary heat stabilizers: lead compounds, mixed metal salts, and organotins. Major producers in North America include Crompton/Witco (Mark), AtoFina (Thermolite), Rohm & Haas/Morton (Advastab), Ferro (Synpron, Thermcheck), Akcros (Akcrostab), and Baerlocher (Baerostab). The total market in North America is 110,000 tons or $500 million. Globally the heat stabilizer market is valued at $1.8 billion and 500,000 t (1).

Lead Compounds. These may be either organic or inorganic with dibasic lead stearates and phthalates, tribasic lead sulfate, and dibasic lead phosphite and carbonate as common examples. Their primary usage is in wire and cable insulation because of their nonconductive properties due to the water insolubility of the lead chloride which is produced during thermal processing. Once extensively used in a wide variety of applications, they have largely been replaced by mixed metals and tins because of intense regulatory pressure. Only in wire and cable have lead compounds persisted since no suitable technical replacement is available despite significant R&D activity. The major producer in North America is the Hammond Group (Halstab).

Mixed Metal Salts (or Soaps). These consist of Ba/Cd salts (once the most widely used because of their effectiveness but now declining owing to regulatory pressure), Ba/Zn, and Ca/Zn salts. The efficacy of these "mixed metal salts" as thermal stabilizers follows that order. Mainly used in flexible or semirigid PVC, they are available in solid and liquid versions. Solids are typically salts of fatty acids such as stearates and laurates while liquid versions are octoate, phenolate, and neodecanoate salts. Mixed metal salts are almost always used in the presence of secondary stabilizers such as organophosphites, epoxies (eg, epoxidized soyabean oil), and β-diketones. This is particularly the case for the less active Ba and Ca/Zn. The ratio of metal salt to secondary stabilizer is typically 4:1. Mixed metal salts or soaps are available from Akros, Baerlocher, Ferro, and Rohm & Haas in North America.

Organotins. Primarily used in rigid PVC, the most widely used types are the dibutyl and octyltin mercaptides. While excellent stabilizers, they suffer from odor, staining, and poor uv-stability. Sulfur-free organotins which include the dibutyltin maleates are useful in applications requiring good weatherability such as extruded siding and profile. Methyl tins are the most active (particularly at high temperature and shear) and are favored from a toxicity and regulatory perspective. Crompton, AtoFina, and Rohm & Haas are the leading suppliers in North America.

Light Stabilizers. Most polymers degrade as a result of photo-induced oxidation so that for durable applications requiring weatherability it is necessary

to add light stabilizers. Ultraviolet induced degradation results in the loss of both aesthetic (color, gloss, clarity) as well as mechanical properties. The uv-portion of sunlight has sufficient energy to break chemical bonds in polymers resulting in the formation of free radicals. Light stabilizers interfere with these processes, slowing the harmful effects of uv-radiation (16,22,23).

Light stabilizers fall into three general classes: ultraviolet absorbers (UVAs), nickel quenchers, and HALS. While the largest consumption of light stabilizers is in polyolefins, there are significant usages in engineering resins, styrenics, PURs, and in coatings. HALS account for approximately half of the sales of light stabilizers and has approximately double the growth rates of UVAs in total. The global light stabilizer market is valued at $530 million and is growing at 6–7%/year (1).

UVAs are organic molecules that preferentially absorb uv-radiation and dissipate it in the form of heat. They are transparent in the visible region so as to not impart color and are highly photostable in order to provide long-term protection. UVAs fall into two major classes: 2-hydroxy-4-alkoxybenzophenones and substituted 2-hydroxybenzotriazoles. A wide variety of modifications have been made to these basic types to provide for enhanced ancillary properties such as reduced volatility, better polymer compatibility, and enhanced photostability. Benzophenones are widely used in PVC and polyolefins. Because of their superior performance, benzotriazoles are used in high performance resins such as PC, nylon, and acrylics. Other minor types include benzoates, salicylates, and diphenyl acrylates. More recently a high performance class based on 2-(2-hydroxyphenyl)-1,3,5-triazines have been introduced. These products have superior inherent photostability to the standard types making them suitable for applications such as automotive and construction having high weatherability requirements. Ciba Specialty Chemicals (Tinuvin, Chimassorb), Cytec (Cysasorb), and Great Lakes Chemcal (Lowilite) are the major suppliers of UVAs in North America. UVAs are added to polymers at levels of 0.2–0.5%.

Nickel quenchers such as nickel dibutyldithiocarbamate [13927-77-0] and 2,2′-thiobis-(4-octylphenolato)-*n*-butylamine nickel (II) [14516-71-3] deactivate excited chromophores which act as sensitizers for the photolysis of hydroperoxides (24). Once widely used in pp fibers, they have been replaced almost entirely by HALS. Because of their high resistance to pesticides used in greenhouses, these products are widely used in PE agrofilm applications. Their usage is gradually declining, however, because of concerns over the toxicity of nickel. Cytec remains the leading producer of nickel quenchers.

The other important light stabilizers, the HALS, are based on substituted 2,2,4,4-tetramethylpiperidines. During initial light exposure, HALS are converted to nitroxyl radicals which are effective scavengers of the free radicals formed during weathering. A wide range of variations of HALS are available to optimize volatility and migration and to minimize interaction with other additives. For example, high molecular weight HALS have been developed to minimize volatility from high surface area PP fibers. Recent developments have centered on modifying the piperidine nitrogen with alkyl or alkoxy groups to reduce basicity, and hence interaction with other additives such as FRs, thioester antioxidants, and environmental agents such as pesticides and acid rain. HALS major application is in polyolefins but they are also used extensively in styrenics and acrylics. Typical use levels are from 0.15 to 0.3%. Ciba Specialty Chemicals and Cytec are the major

producers in North America, with Great Lakes Chemical and Clariant (Sanduvor) significant on a global basis.

Because HALS and UVAs function via different mechanisms, they are often used together for synergistic performance and optimum weatherability.

Processing Aids

Lubricants. Lubricants are added to polymers during processing to improve their flow characteristics. While primarily acting as processing aids to reduce energy consumption and enhance the surface properties of extruded articles, they provide additional benefits in terms of mold release, improved antistatic properties, and better pigment dispersion. These additives act either "internally" as friction modifiers between polymer chains to decrease melt viscosity or "externally" by coating or treating the metal surfaces of the processing equipment, thereby reducing the friction at the polymer–metal interface. A wide variety of chemical classes of lubricants are available, including metal stearates, fatty amides, fatty acid and glyceral esters, waxes of various types, and flouropolymers. Depending on the application, many of these exhibit both external and internal lubricating properties (25,26).

Metal stearates, including predominately calcium stearate as well as zinc stearate, are the most widely used lubricants. In PVC calendering and extrusion, the stearates provide heat stabilizing effects as well as act as an internal lubricant. In polyolefins, stearates act as external lubricants as well as deactivators of catalyst residues. Ferro (Synpro, Petrac), Baerlocher (Hydense), and Crompton (Witco) are the major producers of metal stearates in North America.

Fatty amides provide multifunctionality, acting both as external lubricants and as slip agents and antiblocks. Primary amides such as oleamide [301-02-0], erucamide [112-84-5], and stearamide [1309-64-4] are primarily used as slip and mold-release agents for polyolefins. The higher molecular weight ethylene bisstearamide is used as a lubricant in both rigid and flexible PVC and in engineering polymers such as polyacetal, nylon, and ABS. Croda (Crodamide) is a major supplier of amides in North Amercia.

Fatty alcohols are used primarily in rigid PVC where their excellent compatibility makes them useful where clarity is important Fatty acids, represented by stearic acid, find some use in calendered and blow-molded PVC. Fatty esters, such as glycerolmonostearate [31566-31-1], function as either internal or external lubricants depending on molecular weight (compatibility). Again, PVC is the primary substrate but PC, PS, and PUR can be processed with these materials.

Polyethylene and paraffin waxes are used widely as external lubricants for PVC because of their high level of incompatibility. They are often used in combination with calcium stearate in unplasticized PVC pipe formulations. Honeywell (A-C Wax), Petrolite (Baker Petrolite), and Clariant (Hoechst Wax) are leading suppliers of waxes.

Fluoropolymers, a small but high value type of external lubricant/processing aid, are based on tetrafluoroethylene (27). These materials form monomolecular layers on metal surfaces and are primarily used in PE-blown film applications to

reduce "shark-skin" and gels. These materials are growing rapidly as the use of metallocene PE resins increases, which is more difficult to process than conventional resins. DuPont Dow (Viton), 3M/Dyneon (Dynamar), and AtoFina (Kynar) supply these types of lubricants.

Slip/Antiblock Agents. Slips and antiblocks are used primarly in PE films to modify the inherent self-adhesion which causes the film layers to stick together. In the case of antiblocks, inorganic particles such as silk, talc, and diatomite (processed diatomaceous earth) are added at the compounding step to form a roughness at the surface which prevents the films from sticking (28). Slip agents, primarily migratory fatty acid amides, are added to provide a lubricity or reduced coefficient of friction at the surface, allowing a plastic film to slide over itself or another plastic (29). Erucamide [112-84-5], a C-22 fatty amide, is the most widely used slip agent because of its slower migration rate and better thermal stability than the stearamides and oleamides, accounting for over half of the total consumption. In North America, the major suppliers of slip agents are Akzo Nobel (Armoslip), Crompton (Kemamide), Croda (Crodamide), and Ciba Specialty Chemicals (Atmer SA). In polyolefin films a combination of slip and antiblock agents are used to impart desirable surface properties in such consumer applications as packaging and garbage and other bags.

BIBLIOGRAPHY

1. *Chem. Eng. News* 21 (Dec. 4, 2000).
2. *Chem. Mark. Rep.* 7 (June 19, 2000).
3. *Modern Plastics Encyclopedia '99*, **75**(12), C-27.
4. H. Hurnik, in H. Zweifel, ed., *Plastics Additives Handbook*, 5th ed., Carl Hanser Verlag, Munich, 2001, p. 699.
5. *Modern Plastics Encyclopedia'99*, **75**(12), C-16 (1998).
6. *Modern Plastics Encyclopedia'99*, **75**(12), C-12 (1998).
7. *Modern Plastics Encyclopedia'99*, **75**(12), C-25 (1998).
8. D. Munteanu, in Ref. 4, p. 725.
9. M. Lazar, R. Rado, and J. Rychly, *Adv. Polym. Sci.* **95**, 149–197 (1990).
10. A. H. Hogt, J. Meijer, and J. Jelenic, in S. Al-Malaika, ed., *Reactive Modifiers for Polymers*, Blackie Academic & Professional, London, 1997, pp. 84–132.
11. J. Kurja and N. Mehl, in Ref. 4, p. 949.
12. D. Ochs, in Ref. 4, p. 647.
13. *Modern Plastics Encyclopedia'99*, **75**(12), p. C-3.
14. K. Swartzenbach and co-workers, in Ref 4, p. 1.
15. J. Salamone, ed., *Polymeric Materials Encyclopedia*, CRC Press, Cleveland, Ohio, 1996, p. 306.
16. H. Zweifel, *Stabilization of Polymeric Materials*, Springer-Verlag, Berlin, 1998, pp. 71–106.
17. R. King III, in *SPE Antec Conference Proceedings*, New York, 1999.
18. N. Ergenc and R. Todesco, in *Addcon World Proceedings*, Basle, Switzerland, 2000.
19. J. Green, *J. Fire Sci.* **15**, 52–67 (1997).
20. P. Rankin, in Ref. 4, p. 681.
21. B. Bacalogulu and co-workers, in Ref. 4, p. 427.
22. Ref. 15, p. 3616.

23. F. Gugumus, in Ref. 4, p. 141.
24. J. Chien and W. Conner, *J. Am. Chem. Soc.* **90**, 101 (1968).
25. E. Richter, in Ref. 4, p. 511.
26. *Modern Plastics Encyclopedia'99*, **75**(12), p. C-23.
27. S. Amos and co-workers, Ref. 4, p. 553.
28. F. Kromminga and G. Van Esche, in Ref. 4, p. 585.
29. F. Wylin, in Ref. 4, p. 601.

RICHARD THOMAS
Ciba Specialty Chemicals

ADHESION

Definition of Adhesion and Adhesive Joint

Adhesion is the attraction between two different condensed phases when they are in contact. Attractive forces range in magnitude from strong chemical bonds (≈25–100 kcal/mol) to much weaker physical forces, known as van der Waals interactions. An adhesive joint is a structure usually consisting of two bodies (adherends, substrates), which are held together by adhesion. The bodies may be directly bonded to each other, or coupled by an adhesive layer. The science of adhesion is multidisciplinary and can be divided into two parts: one dealing with surfaces and interfaces and the other with the fracture of adhesive joints. The former is largely concerned with bond formation and predicting attractive forces and energies, whereas the latter deals with test methods to measure joint strength.

One of the most important findings in adhesion science is that the *mechanical* energy required to fracture an adhesive joint (so-called *work of detachment* or *interfacial fracture energy*) is larger than the *intrinsic* interaction energy holding the joint together. The latter is a reversible quantity—equal to the *minimum* energy needed to disrupt an interface or the energy gained upon forming it. However, in general, the fracture of an adhesive joint is not a reversible process. When a joint is loaded, only some of the input mechanical energy is available (stored) to disrupt the interface and the rest is converted (dissipated) into increased molecular motion (heat). Additional input energy is required to attain sufficient elastic energy at the interface to disrupt it. Thus, bulk energy dissipation augments joint strength and causes the mechanical work of detachment to be larger than the interfacial interaction energy.

To judge the intrinsic adhesion at an interface by the measured fracture energy may be misleading. For example, if an adhesive is modified by adding fillers

Encyclopedia of Polymer Science and Technology. Copyright John Wiley & Sons, Inc. All rights reserved.

or tackifiers, and the modified adhesive gives a higher fracture energy than the unmodified one, it is tempting to conclude that intrinsic adhesion has been enhanced. But, by adding filler, the bulk properties of the adhesive are also modified and the improved performance may reflect merely a higher dissipation of mechanical energy within the adhesive layer.

Adhesion is important in many technologies (eg, adhesives, coatings, composites) and usually involves bringing solid and liquid surfaces, or two liquid surfaces, into contact. This article begins by considering characteristics of solid and liquid surfaces and then proceeds to discuss their contact to form interfaces and interphases. Next, the various types of adhesive bonds are discussed as well as the thermodynamics of adhesion. This is followed by a section on surface treatments to enhance the bondability of plastics and metals, and one dealing with the special case of elastomer tack. Two final parts deal with test methods to measure joint strengths and a discussion of the relationship between joint fracture energy and intrinsic adhesion.

Surfaces

Solids. Nearly all solid surfaces are rough at dimensions of a few nanometers. They may contain asperities, pores, projections, depressions, etc. In addition, surface regions of solids generally have different compositions than their bulk. All metals that have been exposed to the atmosphere have an oxide layer on them (1). The thickness of the oxide depends on the nature of the metal and the environment. Some metals, eg, aluminum and titanium, form thin, tough, tenaciously adhering oxides, which passivate the surface and prevent continued oxidation. Others, like iron, have oxides which continue to grow, especially in a humid environment.

In practice, metal oxides are covered with organic molecules and water adsorbed from the atmosphere (2). Other common sources of surface contamination are residual processing oils and lubricants. Another source of surface species is from the bulk. For example, iron containing only 10 ppm of carbon has been shown to form a carbon-rich structure on its surface upon heating or straining. In addition to carbon, other species, including sulfur, nitrogen, boron, and oxygen, have been shown to diffuse from the interior of metals to their surfaces (1).

It is also common for polymeric compounds to form surface regions with compositions different from the bulk material, by selective diffusion of components. This process is termed *blooming* when the surface component is solid, and *bleeding* if it is liquid. Sulfur and fatty acid blooms can inhibit adhesion in rubber laminates (3). Laser desorption mass spectroscopy has been employed to identify surface species on vulcanized rubber (4). X-ray scattering methods for the study of polymer surfaces and interfaces have been reviewed (5). Other surface analysis techniques commonly used with polymers include attenuated total reflectance (6–8), electron microprobe (9), Auger electron spectroscopy (10), x-ray photoelectron spectroscopy (11), and scanning probe microscopic methods (12). Overviews on polymer surface analysis have been published (13,14).

Liquids. Consider a pool of a simple, pure, low molecular weight liquid. Its molecules are mobile and diffusing about. Molecules in the bulk of the liquid interact with other molecules in all directions, while those at the surface

experience a net attraction tending to pull them toward the interior. This causes surface molecules, on average, to be at greater spacing than bulk molecules and possess greater free energy. This gives rise to a surface tension, as the liquid behaves as if it has an elastic skin. Moreover, since nature seeks to minimize free energy, a volume of liquid in the absence of other forces takes a spherical shape to minimize the number of surface molecules. At constant temperature and pressure, the increase in Gibbs free energy accompanying a unit area increase in surface area of a liquid is, by definition, its surface tension γ. Alternatively, γ may be viewed as the force per unit length, tending to contract the surface and cause a liquid to resist spreading.

Real adhesive liquids are often complex mixtures, and, like solids, may have surface compositions different from their bulk. In addition, practical adhesive liquids are often reactive and/or polymeric.

Interfaces, Interphases, and Weak Boundary Layers

Schematically, Figure 1 shows two "real" materials, say A and B, that are composed of molecular components a_i and b_i, respectively. These are located in the bulk (a_{ib}, b_{ib}), at the surface (a_{is}, b_{is}), and/or within the near surface region (a_{in}, b_{in}). Upon contacting A and B under ambient conditions, the *interface*, defined as the locus of interactions between the two materials, initially involves the surface species on each and any entrapped air. In general, the interface will not be continuous at first. Entrapped air and surface rugosity prevent immediate, full molecular contact, although applied pressure can speed interface formation. With time, depending on the particular system, the region between the two bulk materials, the so-called *interphase*, changes. Along with increased molecular contact, diffusion of surface and near-surface species can change the composition and structure of the interface and interphase. For example, the interface may thicken by interdiffusion and chemical reactions may occur. (Specific examples are considered later.) If the interphase contains a mechanically weak layer (weak boundary layer), it may be the site of fracture when the adhesive joint is loaded. Weak boundary layers (WBLs) may originate on or near the surface of materials before they are contacted, or they may develop *in situ* during the dynamic conditions of contact.

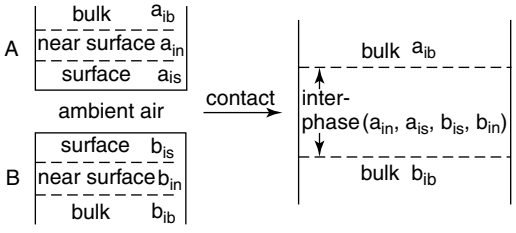

Fig. 1. Two hypothetical "real" materials A and B: (**a**) prior to contact and (**b**) after contact. Surface and near surface components form the interphase, which contains the interface(s) as well as (gradient) compositions and structures different from the bulk materials. In general, the interphase is quite complex. See text for further description.

To provide a strong joint, the *structural* components, ie, those responsible for the cohesive strengths of A and B, must interact well at the final interface, and a WBL must not be present. WBLs may be removed prior to bonding or be disrupted by diffusion during bonding.

After an adhesive contacts a solid substrate, it is normally necessary to convert it to a hardened state (setting) so that the joint will be capable of supporting stress. However, since setting severely reduces the molecular mobility required to achieve true contact and good bond formation, it should not take place too quickly. Many weak adhesive joints can be traced to rapid setting before sufficient interface formation. Setting of adhesives can occur by physical or chemical means. In order to minimize internal stresses in a joint, there should not be a large change in volume of the adhesive during solidification, and the thermal expansion coefficients of the adhesive and adherends should be similar. This is especially important when the solid adhesive has a high modulus. Furthermore, joints with plane interfaces have been suggested (15) to be more sensitive to adhesive shrinkage than are joints made with complex, high surface area adherends. Solvent-based adhesives experience the most shrinkage during setting compared to those which harden by cooling (hot melt) or by chemical reaction (usually thermosets). The fact that epoxy resins shrink only about 3% upon setting is one reason for their good performance. Another advantage of epoxy solidification reactions compared to many other condensation polymerizations is that no small molecules, eg, water, which can interfere with bonding, are created during setting. Polyurethane reactions are also favorable in this regard.

Some inorganic substances adhere exceptionally well because they expand upon freezing. For example, ice will adhere to almost any surface, even those not wetted well by water (16). When water freezes in a depression in a solid surface, expansion causes it to lock against the sides of the depression and form a strong joint. Attempts (17,18) have been made to develop organic adhesives, based on ring opening polymerizations, that expand upon setting.

Bond Classification

When two different materials are contacted, a complete description of the interaction between them requires understanding the number, type, and distribution of bonds formed. This depends on surface topography and the extent of molecular mixing between the materials. In the following subsections, we classify various types of adhesive bonds. It is beyond the intent of this article to consider all the detailed possibilities, which become apparent from the previous discussion of interface and interphase complexity. Rather, we primarily discuss relatively simple systems, from which general principles may be gleaned.

Adsorption on Planar Substrates. The simplest type of adhesive bond occurs when a liquid is contacted with a planar solid with which it is totally immiscible and into which it cannot diffuse. Bonding is limited to physical and/or chemical adsorption at specific sites on the substrate surface. A sharp and planar interface is formed. This is the usual situation when an organic adhesive adheres to a very smooth inorganic substrate. The time-dependent process during which interfacial bonds form is called *wetting*. In general, it involves an increase in the

number of interactions (more actual contact area) and/or a change in the type of interactions.

Surface species can be a hindrance to wetting. Many polar substrates such as glasses or metals, which have been exposed to ambient air, have several molecular layers of adsorbed moisture on them. Wetting is expected to be speeded if the liquid readily solubilizes surface moisture. Perhaps this is one role of polar groups in a typical adhesive. Certainly an adhesive that is completely incapable of displacing or solubilizing surface moisture (or other surface contaminants) would find it difficult, if not impossible, to attain molecular contact with the actual substrate. Furthermore, air entrapped during contact may slow wetting.

Adsorption on Substrates with Complex Surface Topography. As in the previous case, the substrate is completely immiscible with the liquid adhesive, so that adhesive–substrate interactions are limited to adsorption at surface sites. However, the substrate surface topography is now rough and complex. The interface is still two-dimensional and sharp, but now has the complex shape of the substrate surface. Because of pores, depressions, and/or asperities, there are many more surface sites available to interact with an adhesive as compared to a planar substrate. Thus, if the adhesive has sufficient mobility and the wetting forces are high enough, the extent of adhesion may be increased by surface roughening. On the other hand, very viscous adhesives may form relatively few interactions with roughened substrates, especially if the (wetting) time from adhesive application to solidification (setting) is short.

Another consequence of a complex topography is mechanical interlocking between the adhesive and substrate. This is analogous to fastening with a "hook" and "eye" or with Velcro®, where a resistance to separation is present without intrinsic adhesion. Of course, joint strength is improved if both mechanical interlocking and intrinsic adhesion are operative. Mechanical interlocking plays an important role in bonding wood, textiles, and paper because of their finely divided and porous nature. In addition, many metals and plastics are etched before bonding so that the adhesive can penetrate and lock into them. When mechanical interlocking is substantial, the region around the interface forms a composite interlayer within the interphase.

Interdiffusion. When two polymers are contacted, the interface will not be two-dimensional, but rather will become a region (volume) consisting of interdiffused molecules from each material (19,20). The thickness of this interlayer depends on the thermodynamic compatibility of the materials, the contact time, and molecular diffusion rates. Molecular interdiffusion is quite different from mechanical interlocking. The former is analogous to a homogeneous solution and involves interpenetration at the molecular level, whereas in the latter case, analogous to a heterogeneous mixture, the bulk adhesive flows into and around surface features of the substrate that are much larger than molecules. Interdiffusion increases the number of interactions among dissimilar chains, and, if the interdiffused distance is sufficient, interchain entanglements develop. Reviews on polymer interdiffusion have been written (21,22).

When two incompatible polymeric melts A and B are contacted, the equilibrium interface width a_I is dependent on the Flory–Huggins interaction parameter χ and the molecular weights of each polymer. A mean field approach has been used (23,24) to predict that a_I is given by

$$a_I = \frac{2b}{\sqrt{\chi \cdot c}} \frac{1}{\sqrt{1 - 2\ln 2\left(\frac{1}{\chi N_A} + \frac{1}{\chi N_B}\right)}} \quad (1)$$

where b is the statistical segment chain length, and N_A and N_B are the degrees of polymerization of A and B, respectively. The parameter $c = 6$, when a_I is small compared to the chain radius of gyration, R_g, while $c = 9$ in the limit $a_I \gg R_g$ (25). Neutron reflectivity experiments (26,27) have established the validity of Helfand's mean field approach.

When two pieces of the same material are contacted, their bonding is termed *autohesion* (or *self-bonding*) (19). This has also been called *healing* (28). Using reptation theory (29), chain interdiffusion across the original contact junction has been analyzed. The crossing density, which is the number of times the interdiffusing molecules intersect the contact plane per unit area after a time t, has been calculated (30,31) as has the average interpenetration distance (28,32–34). Both measures of healing are predicted to be proportional to $t^{1/2}$. Furthermore, for polybutadienes with different vinyl contents it has been shown that the tensile strengths of autohesion increase linearly with $t^{1/2}$ (see Fig. 2) before reaching plateau values (35). Further discussion of autohesion is delayed until a later section, in which pressure-sensitive tack and time/temperature effects are also considered.

Effect of Interdiffusion on Joint Strength. The joint strength of a thermodynamically compatible adherend pair [poly(methyl methacrylate) and poly(vinyl chloride)] has been found to be quite high, while that for an incompatible pair [poly(butyl methacrylate) and poly(vinyl chloride)] was low (36). Furthermore, using electron microscopy, it was shown that the interfacial thickness for the compatible pair was about 0.1 μm, whereas the incompatible pair formed a much sharper interface, too narrow to be determined experimentally. In principle,

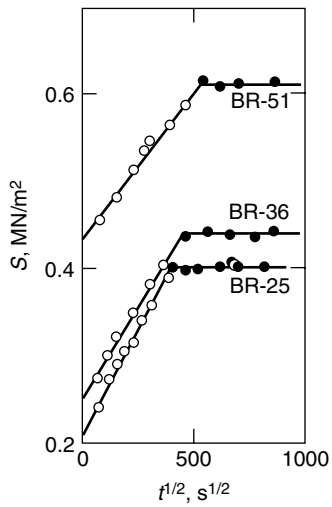

Fig. 2. Development of tensile strength S of autohesion with time of contact for different types of polybutadiene (35) ($MN/m^2 = MPa$). To convert MN/m^2 to psi, multiply by 145.

compatible polymer pairs will form an interface thickness that will continue to increase as long as the adherend molecules remain mobile. On the other hand, the equilibrium width of the interface between incompatible polymers is typically in the range of 2–50 nm (37).

The effect of interdiffusion on the autohesion of rubbery adherends has been studied using a peeling geometry (38). Two layers, each composed of a butyl rubber network and miscible, unattached (non-network) polyisobutylene (PIB) chains, were contacted for 14 h at 60°C. The PIB chains were free to diffuse through the butyl network and across the contact junction. Joints were peeled apart over a wide range of rates and temperatures, and peel energies G were superposed to form a mastercurve covering eight decades of reduced rate. At intermediate peel rates, G was about 10 times the value obtained for a butyl network control containing no PIB. However, at both sufficiently low and high reduced rates, autohesion was little affected by PIB. The behavior at low rates was attributed to ready disentanglement of interdiffused PIB molecules from the network, while, at high rates, it was proposed that interdiffused molecules had little influence on joint strength, because they broke during separation rather than disentangling. The authors hypothesized that disentanglement of interdiffused PIB chains takes place at intermediate rates, with substantial viscous energy expended in the process.

Ellipsometry (39) has been used to determine the interface thickness between layers of poly(methyl methacrylate) (PMMA) and poly(styrene-*co*-acrylonitrile) (SAN) contacted at 130°C. PMMA and SAN are miscible when the SAN contains 9.5–33 wt% acrylonitrile, but they are immiscible outside this composition range. Figure 3 shows interfacial thicknesses for both miscible and immiscible cases. The interface thickness for the miscible pair grows linearly with $t^{1/2}$. On the other hand, the interfacial thickness for the immiscible pair quickly reaches a value of about 20 nm and remains constant even after contacting for 12 h above T_g. Figure 4 shows tensile strengths of adhesion (normalized with respect to the tensile strength of the weaker SAN) for the compatible adherends plotted against the square root of the interface thickness. The data are linear and a surprisingly high

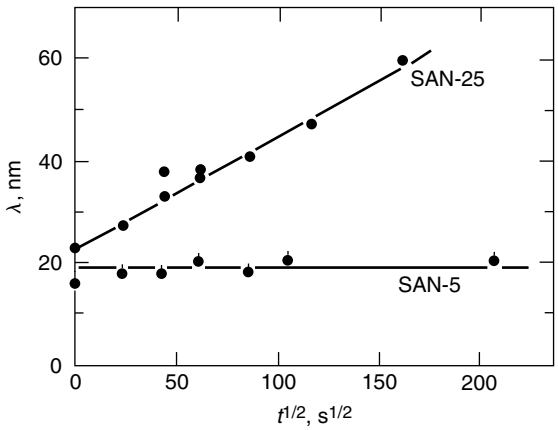

Fig. 3. Interface thickness after various contact times for miscible (PMMA/SAN-25) and immiscible (PMMA/SAN-5) pairs (39).

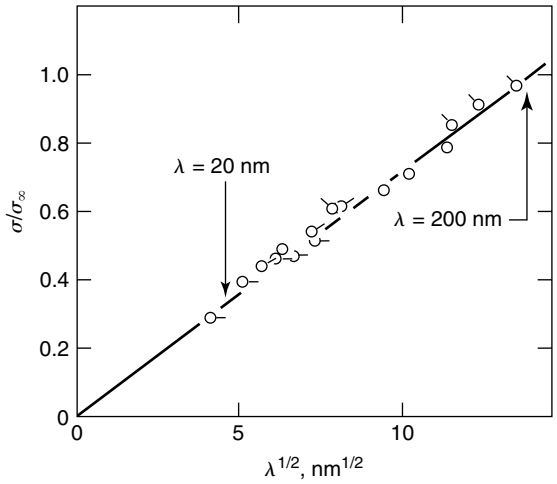

Fig. 4. Normalized strength of PMMA/SAN joints as a function of interface thickness (39).

interface width of about 200 nm is necessary for the joint strength to reach the tensile strength of the SAN.

Autohesion between two uncross-linked layers of polybutadiene has been studied (40). The self-diffusion coefficient was measured using small-angle neutron scattering, and T-peel specimens were used to determine joint strengths. The contact time required to reach the cohesive strength was 3 orders of magnitude greater than the time required for a diffusion distance equal to the chain radius of gyration. The authors speculated that low autohesion, even with significant interdiffusion, was due to different diffusion rates of branched and linear chains within the polybutadiene. Branched chains were proposed to impart increased bond strength, but have suppressed interdiffusion. Therefore, during the early stages of contact, the interdiffusion layer is rich in linear chains, resulting in lower strength. A much longer time is required for branched chains to interdiffuse and for the joint to obtain the full cohesive strength. There appears to be a difference in structure between bulk chains and the interdiffused layer during the initial stage of healing.

Forward recoil spectroscopy has been employed to determine interdiffusion widths for the autohesion of a polyimide film (41). In addition, fracture energies G were measured by T-peel testing. When a_I was less than 20 nm, G was so low ($<$10 J/m^2) that it was difficult to measure. At larger extents of interdiffusion, G increased linearly with a_I. Again, an unexpectedly large interdiffusion distance of at least 200 nm was required before complete healing was attained.

Adhesion between the nearly compatible pair, polystyrene and poly(*p*-methyl styrene), has been investigated (42). Variations in annealing temperature and molecular weight were used to change interface widths, which were measured by neutron reflectivity. Fracture energies, determined using double cantilever beam test-pieces, increased linearly from about 100 to 450 J/m^2 as a_I increased from 9 to 11 nm. The large, fourfold increase in G over this rather narrow range of a_I was

attributed to increased energy dissipation with the onset of sufficient interchain entanglements to induce crazing.

Bonding Involving Diffusion and Chemical Reaction. A number of technologically important adhesive bonds are formed by contacting materials which have components that diffuse to the interfacial region and chemically react. The strength of the reaction product and its interaction with each material controls joint strength. The generality and success of the approach will be demonstrated by discussing industrially important examples involving polymer/polymer, polymer/inorganic glass, and polymer/metal bonding.

Nitrile Rubber/Polypropylene. Nitrile rubber (NBR), a copolymer of butadiene and acrylonitrile, is quite incompatible with polypropylene (PP) and forms a very weak bond when contacted with it. As a result, a blend of these two polymers, prepared by melt mixing, produces a heterogeneous material that processes poorly and has very low strength and extensibility. Adhesion between the phases can be increased by adding to the blend a small amount of two reactive components: a telechelic, amine-functionalized NBR oligomer and an anhydride-terminated PP (43). These materials react *in situ* to form an NBR/PP block copolymer, which is thought to locate at the interface and increase bonding between the NBR and PP phases. The modified blend processes easily and has excellent strength. A similar methodology has been used to promote bonding between nitrile rubber and butyl rubber (44). An analogue of this approach is interfacial polymerization (45), in which immiscible phases (aqueous and organic) containing reactive components (diamine and diacid chloride) are contacted and polymer forms at the interface (so-called nylon-rope trick). Similarly, immiscible polymers may contain certain reactive components which can diffuse to the interface and form a product that increases adhesion between phases.

Adhesion between immiscible polymers has also been increased by using already prepared block or graft copolymers composed of segments of each polymer. In one approach (46), the copolymer is added to one or both of the adherends before contacting them. However, here, the copolymer may itself phase separate *away* from the interface. In another approach (47), the copolymer is spun-coated sparingly on one of the adherends to assure its presence at the interface.

In general, a third component, "technological compatibilizer," may couple phases in different ways. The compatibilizer may

(1) phase separate, at least in part, as a distinct layer *between* the two phases. In this case, the cohesive strength of the layer and its interaction with each phase are important;
(2) locate at the interface and form a "monolayer" or less coverage. In this case, the degree to which the compatibilizer alters the bonding between phases will depend on its concentration at the interface and the extent to which it is entangled and/or linked to each phase;
(3) dissolve in each phase and increase the thermodynamic compatibility between the phases, thereby causing the interface to thicken.

The compatibilizer may not be *directly* involved in improving interphase bonding, but rather cause the molecules of each phase to interdiffuse more

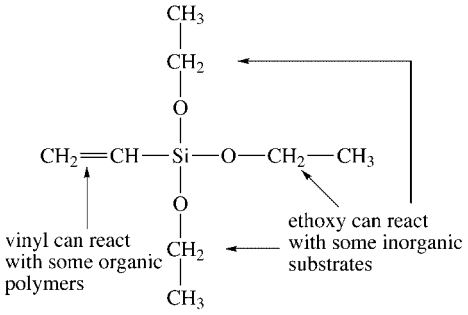

Fig. 5. Vinyltriethoxysilane coupling agent.

extensively. (Analogous behavior is known with small molecules. For example, an immiscible mixture of water and benzene forms one phase upon the addition of methanol.) This mechanism may explain the increased adhesive tack and cured adhesion of dissimilar elastomers containing certain tackifier resins and so-called bonding agents.

Silane Coupling Agents. Silane coupling agents are very effective in promoting the adhesion of various polymers to inorganic glasses and are widely used in composites as well as joined structures (48–50). Silanes may be directly applied to substrates or may be added to a polymer prior to bonding. In the latter case, the silane diffuses to the glass–polymer interface and reacts as discussed next.

Silane coupling agents have four functional groups as shown in Figure 5. The three alkyloxy groups undergo hydrolysis to become silanols, which are capable of reacting with glass or self-condensing to form a polysiloxane. The fourth functional group reacts with the polymer. Thus, an *in situ* polysiloxane layer forms between the glass and polymer and couples them together. Table 1 gives several types of silane coupling agents and some polymers commonly used with them.

Brass/Rubber. When rubber containing sulfur curatives is pressed into contact with brass (typical alloy ~65% copper, 35% zinc) and then vulcanized, copper diffuses to the brass surface and reacts with sulfur to form cuprous sulfide (51). This interlayer grows outward from the brass surface, strongly interlocking into the rubber phase (52,53). Again, diffusion to an interface and *in situ* reaction to form a "coupling" interlayer is employed to provide bonding. Joint strength can

Table 1. Silane Coupling Agents

Type	Formula	Used With
Vinyl triethoxysilane	$CH_2{=}CHSi(OCH_2CH_3)_3$	Cross-linked polyethylene, thermosetting polyester, diene elastomers
γ-Glycidoxypropyl trimethoxy silane	$CH_2OCHCH_2O(CH_2)_3Si(OCH_3)_3$	Epoxy, urethane, poly(vinyl chloride), phenolic
γ-Aminopropyl triethoxysilane	$NH_2CH_2CH_2CH_2Si(OCH_2CH_3)_3$	Epoxy, melamine, nylon, polycarbonate, polyimide
γ-Mercaptopropyl trimethoxysilane	$HSCH_2CH_2CH_2Si(OCH_3)_3$	Epichlorohydrin, urethane, polyvinylchloride

be very high, and, because of this, steel cords used to reinforce tires are brass-plated.

Thermodynamics of Adhesion

Contact Angle. The degree to which a liquid wets a solid is measured by the contact angle θ (Fig. 6). When $\theta = 0$, the liquid spreads freely over the surface and is said to completely wet it. This occurs when the molecular attraction between the liquid and solid molecules is greater than that between similar liquid molecules (54). Surface tensions are related to the contact angle by an expression from equilibrium considerations (55):

$$\gamma_{sv} = \gamma_{sl} + \gamma_{lv}\cos\theta \tag{2}$$

where γ_{sv} is the solid–vapor surface tension, γ_{sl} is the solid–liquid interfacial tension, and γ_{lv} is the liquid–vapor surface tension.

The surface tension γ_{sv} of a solid that has adsorbed a layer of vapor is generally less than that of the solid in vacuo γ_s and this reduction is termed the spreading pressure π_s:

$$\pi_s = \gamma_s - \gamma_{sv} \tag{3}$$

However, liquid surface tension is little affected by the vapor phase so that $\gamma_{lv} \approx \gamma_l$.

Whether or not a given liquid will wet a solid surface depends on the surface tension of both substances. The ability of a liquid to wet a solid is often described by the spreading coefficient S_{sl}:

$$S_{sl} = \gamma_{sv} - \gamma_{sl} - \gamma_{lv} \tag{4}$$

A large positive S_{sl} implies that a liquid will spontaneously wet the solid. A negative S_{sl} indicates incomplete wetting and $\theta > 0$.

A widely used method for determining γ_s was developed using contact angle measurements (56). A plot of $\cos\theta$ against surface tensions for a homologous series of liquids can be extrapolated to give a critical surface tension γ_c at which

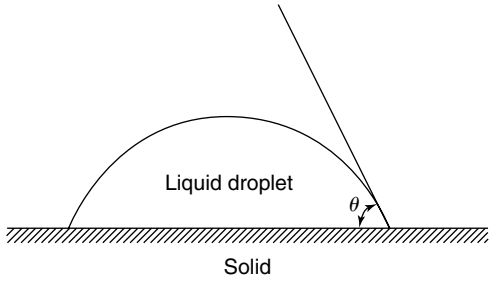

Fig. 6. Contact angle of a liquid droplet on a planar solid surface.

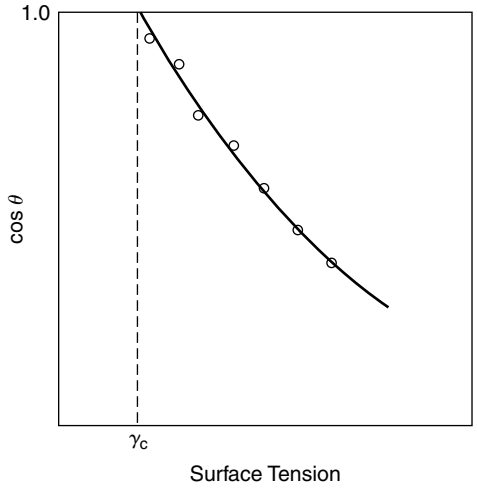

Fig. 7. Zisman plot for a particular solid surface and a homologous series of liquids.

cos $\theta = 1$; such a plot is shown in Figure 7. Any liquid with a surface tension less than γ_c completely wets the solid surface. γ_c has been taken as an approximate measure of γ_s. It should be noted, however, that the value of γ_c is generally dependent on the particular series of liquids used to determine it. A series of polar liquids, such as alcohols, will give a higher γ_c than a series, such as simple hydrocarbons, which interacts less strongly with the same surface (57).

Thermodynamic Work of Adhesion. If a liquid is placed on a solid surface with which it has no interaction, then the interfacial tension between them is simply the sum of the surface tensions of the liquid and the solid. However, in all real systems, there are at least van der Waals attractions between the molecules of the liquid and those of the solid. This interaction decreases the interfacial tension so that $\gamma_{sl} < \gamma_l + \gamma_s$. The extent of the decrease is a direct measure of the interfacial attraction, and is termed the thermodynamic work of adhesion W_a:

$$W_a = \gamma_l + \gamma_s - \gamma_{sl} \tag{5}$$

This expression, first given by Dupré (58), states that the reversible work W_a of separating a liquid and a solid in vacuo must be equal to the free energy change of the system. (In wetting phenomena, the surface free energies are given directly by the surface tensions.)

Another expression relates γ_{sl} to the individual surface tensions of the liquid and solid (59):

$$\gamma_{sl} = \gamma_s + \gamma_l - 2\phi^{(\gamma_s\gamma_l)}1/2 \tag{6}$$

The last term represents the reduction in interfacial tension owing to molecular attraction between the liquid and solid. The term ϕ is defined by

$$\phi = \frac{W_a}{(W_{cl}W_{cs})^{1/2}} \tag{7}$$

where W_{cl} and W_{cs} are the work of cohesion of the liquid and solid, respectively, ie, the thermodynamically reversible work required to create a unit area of new surface in each material. For simple interfaces, ϕ is approximately unity, but for systems in which there are different types of intermolecular force in the two substances, ϕ may be appreciably less than unity.

By combining equations (2),(3), and (6), an expression for γ_s is obtained:

$$\gamma_s = \frac{[\gamma_{lv}(1+\cos\theta)+\pi_s]^2}{4\phi^2\gamma_{lv}} \tag{8}$$

If $\pi_s \approx 0$, as has been suggested for high energy liquids on low energy surfaces (60,61) then equation (8) reduces to

$$\gamma_s = \frac{\gamma_{lv}(1+\cos\theta)^2}{4\phi^2} \tag{9}$$

From the preceding discussion, as $\theta \to 0$, then $\gamma_{1v} \to \gamma_c$ (Zisman plot). Substituting this condition into equation (9), it is found that

$$\gamma_c = \phi^2\gamma_s \tag{10}$$

Thus, γ_c is predicted to be approximately equal to γ_s only when $\phi \approx 1$, ie, for simple interfaces for which

$$\gamma_s = \frac{\gamma_{1v}(1+\cos\theta)^2}{4\phi^2}$$

When γ_s and γ_l have values appropriate to simple nonpolar substances, about 25 mJ/m^2, W_a is only about 50 mJ/m^2, or less. The work for detaching one adhering substance from another has been found to be much larger than this, in the range 1 J/m^2 to 10 kJ/m^2. Thus, other contributions to the mechanical strength, from dissipative processes within the joint, greatly outweigh the intrinsic adhesion. Nevertheless, dissipative contributions depend upon the intrinsic adhesion, and in some instances, they are directly proportional to its magnitude (62,63). If there is no affinity between the adherends, there is certainly no mechanical strength of an adhesive bond.

Surface Treatment

In order to obtain a strong and durable adhesive joint, the surfaces of adherends are often treated before bonding. In general, these treatments alter the surface region in one or more of the following ways: removal of a weak boundary layer, change in surface topography, change in chemical nature of the surface, or modification of the physical structure of the surface.

Polyolefins, Polyester.

Corona Discharge. The material is exposed to a corona discharge, usually in air and at atmospheric pressure. Polyethylene treated in this way experiences surface oxidation (64). Figure 8 gives xps spectra for a treated surface of low density polyethylene. The appearance of the O 1s peak indicates the formation of

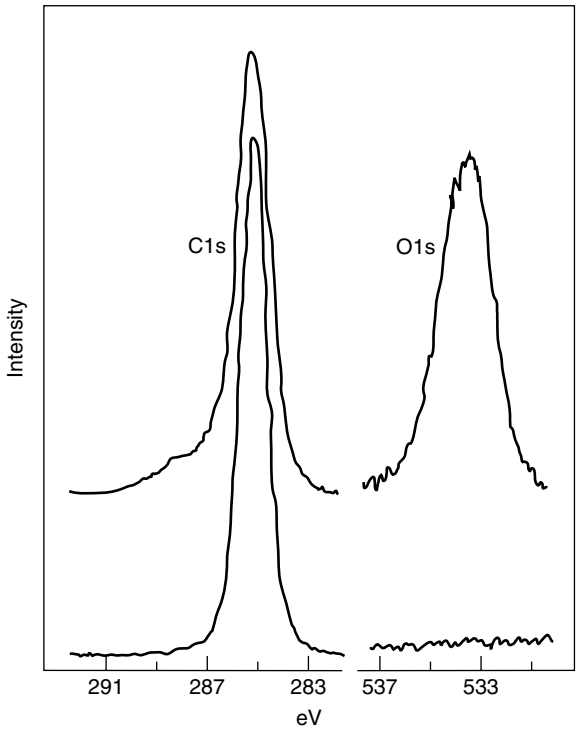

Fig. 8. ESCA spectra of low density polyethylene before (lower curve) and after (upper curve) treatment with a corona discharge (64).

surface oxidation products. These are capable of dipolar or even perhaps acid–base interactions with polar adhesives. In addition, there is fine-scale roughening of the surface (65). This indicates that the corona has degraded and removed portions of the surface in a nonuniform way. Since polyethylene has both crystalline and amorphous regions, it is likely that the corona selectively attacks the more vulnerable amorphous regions. The enhanced bonding of polar adhesives to corona-treated polyethylene is attributed both to the increase in surface roughness and to an increase in surface energy. Only a small degree of oxidation is needed to markedly increase the adhesion of polyethylene to an epoxy adhesive. Oxidation not only increases the *specific energy* of interaction with the epoxy, but also increases the *number* of interactions because of more interdiffusion. Thus, bonding is enhanced autocatalytically by surface oxidation.

The wettability, and hence ability to bond, of oxidized polyethylene decreases quickly upon heating it to 85°C (66). Apparently, oxygen-containing groups in the surface spontaneously turn inward toward the bulk of the sample, so that the surface energy of the material is reduced and the hydrocarbon character of the surface is increased. At room temperature, the loss of bondability is slower since the chains have less mobility for this redistribution.

Acid Etching. Chromic acid is used to treat polyolefins before bonding. This causes selective removal of portions of the surface region and hence surface

roughening (67). In addition, hydroxyl, carbonyl, carboxylic acid, and sulfonic acid groups are introduced (68). Bond strengths of epoxy adhesives are dramatically improved after short exposure to a chromic acid etch solution, and quickly become comparable to the cohesive strength of the polyolefin substrate. As with corona discharge treatment, the increase in joint strength after acid etching is attributed both to the introduction of polar groups and to the increased surface roughness. Extended treatment times are detrimental to joint strength because extensively etched polymer becomes a weak boundary layer.

Flame treatment. Polyester and polyethylene films are commonly exposed to flame treatment to increase bondability. Here, an oxidizing flame briefly ($\sim$0.01–0.1 s) impinges on the surface (69,70). XPS analysis (71) has shown that amide surface groups are generated, as well as typical oxidation functionality. Flame-treated films maintain bondability better than those that have been given corona treatment. Moreover, for all types of treatment, it is best to bond surfaces as soon as possible after treatment.

Surface Grafting. Rather than allowing the active species formed at a surface to simply combine with ambient oxygen, it is possible to have a reactive monomer present and form grafts to a surface. In one study (72), radicals and ions were created in a polyethylene surface by irradiation with γ rays in the presence of vinyl acetate monomer. The resulting polyethylene–vinyl acetate graft showed excellent bonding with an epoxy adhesive. Other researchers (73) have grafted acrylic acid onto polyethylene using electron beam irradiation. Adhesion to aluminum was increased about 10-fold.

Fluorocarbon Polymers. Fluorocarbon polymers require treatment with powerful etchants before they can be strongly bonded. Metallic sodium dissolved in either a mixture of naphthalene and tetrahydrofuran, or in liquid ammonia, is effective (74,75). These reagents reduce the polymer surface by defluorination (76). Initially, the surface is discolored, and it will form a carbonaceous black residue if treatment is continued too long. XPS analyses have shown the presence of unsaturation, and carbonyl and carboxyl functionality after treatment (76). Wettability and joint strengths are dramatically improved. Care must be taken not to treat the polymer too long, since substantial degradation of the surface region would generate a weak boundary layer and lower joint strength.

An interesting technique to improve the bonding of an epoxy adhesive to polytetrafluoroethylene (PTFE) has been demonstrated (77,78). Two adherends are abraded in the presence of liquid adhesive. These are then brought into contact and the adhesive allowed to set. The shear strength of the joint is about seven times that obtained if the adherends are abraded in air before applying the adhesive. Presumably, when abrasion is carried out in the presence of the adhesive, active species are created in the PTFE surface as a result of chain rupture and they react directly with the adhesive. When abrasion takes place in air, these species may decay away before the adhesive is applied.

Metals. A metal that has been exposed to air invariably forms an oxide layer on its surface. This oxide layer may be intrinsically weak or it may adhere poorly to the underlying metal, leading to weak adhesive joints in either case. Furthermore, usually there are organic contaminants present on the surface, ie, residual lubricants from the manufacturing process or substances adsorbed from the atmosphere. In order to prepare a metal surface for bonding, etching

techniques have been developed that remove both the surface contaminant and the existing oxide layer. Under controlled conditions, a new oxide layer is then formed, which is strong and adheres firmly to the underlying metal.

Chemical etching removes some of the underlying metal as well. The metal near the surface may have quite a different physical structure from the bulk as a result of the particular process used in forming. For example, if the surface was created by a cutting action, then the metal near the cutting blade, now the surface region, is subjected to high stresses that can cause local yielding and plastic deformation. Because the state of deformation of the surface material influences its reactivity with oxygen, the oxide formed is different from that which would have formed on a strain-free surface. Also, the structure of the deformed surface varies because of the inevitable nonuniformity in local deformations during cutting. After removing the irregular oxide layer by etching, a new oxide with improved uniformity and strength can be formed in a controlled way.

Aluminum. The treatment of aluminum to enhance bonding has received considerable attention because of the widespread use of aluminum/epoxy bonds in aircraft. It is a relatively simple matter to prepare an aluminum substrate so that it will initially bond tenaciously to epoxy adhesives. An aluminum/epoxy lap-shear joint in which the aluminum has been degreased and grit-blasted before bonding is so strong that it fails within the epoxy layer when stressed (79). However, upon modest exposure to a moist environment, bond strength falls and the locus of failure changes to the interfacial region. The decrease in strength is more rapid if the adhesive joint is also stressed while exposed to moisture (80). (The accelerated action of an environmental degradant caused by stress is an important general phenomenon in materials science and has been called mechano-chemical degradation.) The oxide (Al_2O_3) on aluminum may change into the hydroxide (AlOOH), boehmite, on exposure to a humid atmosphere (81). Boehmite is weaker than the original oxide and adheres less strongly to the aluminum beneath it. This leads to the decrease in joint strength upon exposure to moisture (82–84). Auger electron spectroscopic analysis of joints broken after exposure to high humidity has shown that fracture occurs at or near the boehmite–metal interface (84).

Both the physical structure of the oxide and its resistance to moisture can be changed by special surface treatments. One treatment is the Forest Products Laboratory (FPL) process (85). This consists of degreasing, alkaline cleaning, and etching in a solution containing $Na_2Cr_2O_7{\cdot}2H_2O$, H_2SO_4, and H_2O in a 1:10:30 ratio by weight. Specimens are then thoroughly rinsed and air-dried. Joints made from FPL-etched aluminum bonded with epoxy adhesives are much more resistant to degradation by moisture compared to joints made with unmodified aluminum. Part of the increase in durability is attributed to the physical structure of the oxide layer, which consists of a uniform layer about 5 nm thick with long oxide spikes (ca 40 nm) protruding outward (86). It is proposed that the adhesive can flow around the protrusions, thereby increasing the area of interaction between the oxide and the adhesive, and also providing mechanical interlocking.

A further enhancement in aluminum/epoxy joint durability in a moist environment is obtained by anodizing the aluminum after FPL treatment (80). Typically, samples are anodized for several minutes in an aqueous solution of phosphoric acid (phosphoric acid anodization or PAA) before rinsing and drying in warm air. The process produces a thin, uniform oxide layer near the bulk metal and a

much thicker (400 nm) porous layer on top of it (86). This upper layer is much thicker than that formed using the FPL process alone, and, in addition, after PAA a monolayer of $AlPO_4$ is present on top of the Al_2O_3 (87). The high durability of joints containing PAA-treated aluminum is again attributed, at least in part, to the microporosity of the oxide layer into which the adhesive may flow and solidify. Water molecules that diffuse to the interfacial region and therefore swell the adhesive within the pores may actually cause it to press more firmly against the cell wall and tend to enhance joint strength. An additional mechanism that may confer high durability on joints containing PAA-treated aluminum is the resistance to moisture provided by the $AlPO_4$ top layer. This will protect the oxide and delay the formation of the undesirable hydration product, boehmite (87).

Copper. The bonding of polyethylene to copper provides another example of the importance of oxide topography on joint strength (88,89). If copper is first cathodically cleaned or chemically polished, then polyethylene adheres rather poorly. However, if copper is given a wet oxidation treatment with sodium chloride, sodium hydroxide, and sodium phosphate solution before bonding, then polyethylene adheres tenaciously. In the former cases, the oxide layer is rather smooth and uniform, whereas the latter treatment produces a thick, black dendritic oxide that adheres strongly to polyethylene by mechanical interlocking. The bond strength is enhanced by plastic deformation of the composite interlayer, consisting of the fibrous oxide embedded in polyethylene, which interlinks the bulk copper and polyethylene (90).

Steel. Not all metal adherends require chemical surface treatments in order to optimize joint durability. With mild steel, removal of soluble contaminants by vapor degreasing followed by grinding or grit blasting is sufficient (91). However, the freshly created surface of steel is very reactive and reoxidizes almost instantly. It will continue to oxidize, especially in the presence of moisture, eventually forming a visible rust. The treated surface must be coated with a primer or adhesive before the oxide layer becomes too thick, otherwise joint strength and durability will be poor (92).

Tack

Some rubbery materials adhere firmly to themselves (autohesive tack or autohesion) or to a different surface (adhesive tack) after brief contact under light pressure. They have a liquid character which results in rapid bond formation, yet, without setting, they resist detachment like a solid, ie, they are *str*ong and so*ft*. (Tacky substances are "stroft," like toilet paper.) Typically, adhesive tack involves bonding to a hard substrate and interdiffusion is absent or minimal. Adsorption is the principal mechanism of adhesion. On the other hand, autohesion involves both molecular contact and interdiffusion. Autohesion is important in the manufacture of articles, such as tires, which are built by laminating rubbery components.

Adhesive Tack. Adhesives that exhibit adhesive tack are often called *pressure-sensitive* adhesives (PSAs), since joint strengths depend on the pressure applied during bonding. In practice, PSAs are usually carried on a backing; tapes and labels are examples. In order to secure rapid wetting on common surfaces, a PSA must have a creep compliance after 1 s greater than about 10^{-6} m^2/N

(93). When the compliance is greater than this value, the forces of attraction between molecules of the adhesive and substrate are sufficient to pull the adhesive into intimate contact with the substrate surface, even when that surface is irregular on a microscopic scale. Furthermore, in order to provide a strong joint, a PSA should have a long yield plateau followed by hardening at large strains. Yielding blunts the separation front, reduces stresses, and therefore inhibits detachment. Strain-hardening prevents continued flow and easy rupture of the adhesive. This distinguishes a good PSA from a simple liquid. Both may readily attain molecular contact, but although liquids easily flow apart at low stresses, suitable elastomeric formulations will resist relatively large tensile stresses before rupturing. Some elastomers are self-strengthening upon deforming, by virtue of the steric regularity of their molecules, which allows them to rapidly crystallize on stretching. Since this mechanism is inactive at low strains, it imparts strength without hindering wetting. Natural rubber strain-crystallizes and is widely used in pressure-sensitive adhesive formulations.

Thus, in brief, a successful pressure-sensitive adhesive not only has low resistance to small strain deformation in order to facilitate wetting, but also it can resist large strains without flowing apart easily. Certain neat elastomers such as acrylate-based PSAs possess these features and are intrinsically tacky without additives. Other PSAs are formulated by diluting high molecular weight rubbers with special resins called tackifiers.

Tackifiers. *Tackifiers* are solid resins added to elastomers to improve pressure-sensitive adhesion. They generally have molecular weights in the 500–2000 range, with broad molecular weight distributions. Tackifiers are glassy, with softening points varying from 50 to 150°C, and they often have limited compatibility with the elastomer to which they are added (94,95). Common tackifiers include rosin derivatives, coumarone-indene resins, terpene oligomers, aliphatic petroleum resins, and alkyl-modified phenolics (96). In order to impart tack to an elastomer, a substantial portion of the tackifier must dissolve in the elastomer, thereby reducing entanglements and softening it, without excessive weakening. This requires control of the molecular weight of the tackifier. If it is too high, the tackifier becomes an incompatible filler—stiffening and strengthening, but preventing rapid wetting. On the other hand, if molecular weight is too low, the tackifier becomes a low T_g liquid and acts as a plasticizing solvent. In addition, tackifiers in PSAs have been reported to have marginal compatibility with the elastomer, often resulting in migration of some tackifier to the surface (97).

The effect of adding tackifiers on the rheological properties of elastomers has been investigated (98–100), and the results are instructive in understanding how a tackifier functions. Figure 9 shows a plot of the shear storage modulus G' of natural rubber with and without a tackifying resin (98). When the resin is present, the resistance to deformation is reduced at low rates, ie, lower G'. This results from a reduction in the rubber entanglement density and facilitates wetting on contact. At the same time, when measuring the strength of the bond at higher rates of deformation, the modulus G' is high, reflective of the tackifier's high T_g, and the material is stronger. This behavior can be contrasted with the effects of adding a filler or a simple plasticizer. A filler would increase G' over the entire range of rates of deformation, leading to difficulties in bond formation. A simple plasticizer unduly lowers the cohesive strength of an adhesive, so that, at

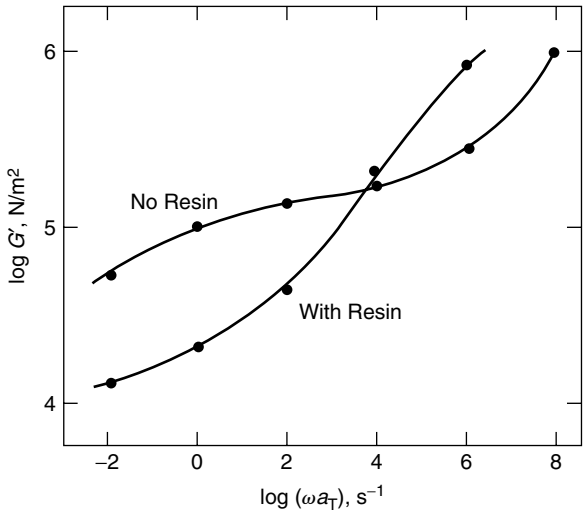

Fig. 9. Effect of a tackifier on the dynamic modulus G' of natural rubber as a function of reduced deformation frequency ωa_T (98). To convert N/m^2 to psi, multiply by 1.45×10^{-4}.

high dilution, a plasticized rubber is very weak. In contrast, a highly tackified rubber, though soft, nonetheless resists easy fracture (97).

Rate and Temperature Effects. Pressure-sensitive adhesives are soft elastomeric semisolids. Their peel strength depends strongly upon the rate of peel and the test temperature, as shown for a simple model system in Figure 10 (101). At low rates, the peel force increases with rate, and failure takes place entirely within the adhesive layer, which fails by flowing apart. The peel strength is primarily a measure of the work of extending a viscoelastic liquid to the point of rupture. Although the local stress required to disentangle the molecules at low rates is

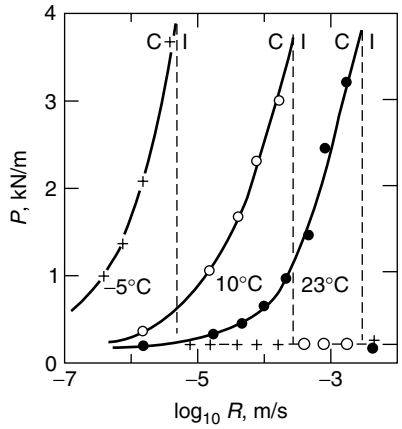

Fig. 10. Peel–force vs. rate of peeling for an elastomeric layer adhering to a polyester film. *C* and *I* denote cohesive and interfacial failure modes, respectively (101). To convert kN/m to ppi, divide by 0.175.

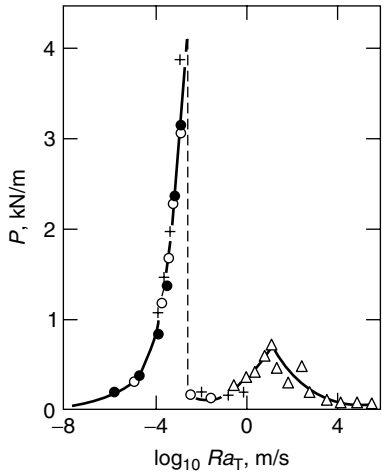

Fig. 11. Results from Figure 10 replotted against the reduced rate of peeling at 23°C, obtained by WLF time–temperature superposition (101). To convert kN/m to ppi, divide by 0.175.

relatively small, the work expended in ductile flow is large and the peel force, which measures the work of separation, is correspondingly high. At a critical rate of peel, which increases as test temperature increases, an abrupt transition takes place to interfacial fracture between the adhesive and substrate. This transition occurs when the rate of deformation of the adhesive layer at the peeling front becomes so high that the adhesive molecules do not disentangle and flow apart like a liquid. Instead, the molecules remain intertwined and respond like an elastic solid. In the elastic state, the work of separation is expended nearer to the interface, and is relatively small.

The rate of peel and test temperature at which the abrupt transition occurs are directly dependent upon the rate of Brownian motion of molecular segments. Simple viscoelastic adhesives therefore obey the WLF rate–temperature equivalence (102). Applying this principle to the data in Figure 10 results in the mastercurve shown in Figure 11. Thus, it is possible to predict the rate dependence of the peel strength over a wide range of peel rates, using only limited data obtained over a narrow range of rates at various temperatures.

Autohesive Tack (Autohesion). For two layers of the same elastomer to resist separation after being brought into brief contact, the basic criteria already outlined for adhesive tack must be satisfied. The two surfaces must come into intimate molecular contact and the materials themselves must resist high stresses without flowing apart. However, there is an important difference between the two types of tack. Pressure-sensitive adhesives based on hydrocarbon rubbers *always* contain substantial amounts (∼50% or more) of tackifier to allow them to readily achieve wetting. As discussed earlier, this is attributed to the need for the adhesive to be sufficiently compliant so that it will be quickly "pulled" by adsorption forces into intimate molecular contact with common hard substrates. Neat hydrocarbon rubbers exhibit very little adhesive tack, but they can exhibit very strong autohesion. For example, unmodified natural rubber is a poor pressure-sensitive

adhesive, but its autohesion is high. When interdiffusion is active, a high resistance to separation develops quickly in spite of relatively low compliance. Although interdiffusion cannot occur until molecular contact has been established, it appears that interdiffusion somehow speeds molecular contact. This apparent paradox is addressed next.

When two layers of the same elastomer are pressed together, molecular contact is not generally complete, but develops in a progressive manner. Thus, after a brief contact time t, some microscopic areas may not have achieved molecular contact and other areas will have achieved intimate contact at times varying from 0 to t. The overall bond strength, then, is the sum of many interactions of varying magnitude at the contact sites, together with interfacial defects (noncontacted regions). As t increases, the defects "close-up." Perhaps, interdiffusion at contact sites can speed the closing-up of interfacial defects around them.

Finally, it should be noted that the barriers to molecular contact may be different for adhesive tack and autohesion. Surface impurities, eg, from bloom, may readily redissolve into the bulk elastomer during autohesive bonding. On the other hand, impurities on common substrates, such as surface moisture, may not be readily displaced by an adhesive that is too stiff. Molecular mobility and microscopic flow are expected to aid displacement of impurities.

Molecular Weight. The effect of molecular weight on the autohesion and cohesive strength of natural rubber (NR) is shown in Figure 12 (103). As the molecular weight is increased, the cohesive strength rises because of a greater number of molecular entanglements per chain. On the other hand, the autohesion after a given contact time passes through a broad maximum with increasing molecular weight. At the lowest molecular weights, contact and interdiffusion are rapid. (*Relative autohesion*, defined as autohesion divided by cohesive strength, is unity.) Still, the autohesion is low because of the poor cohesive strength. At the highest molecular weights, both contact and diffusion are slow owing to restricted molecular mobility. Thus, the autohesion again is low. Qualitatively, similar results are found for other elastomers.

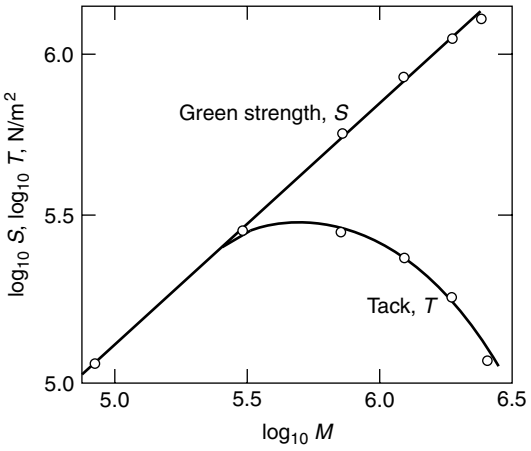

Fig. 12. Tensile strengths of autohesion (tack T) and cohesion (green strength S) of natural rubber as a function of molecular weight M (103).

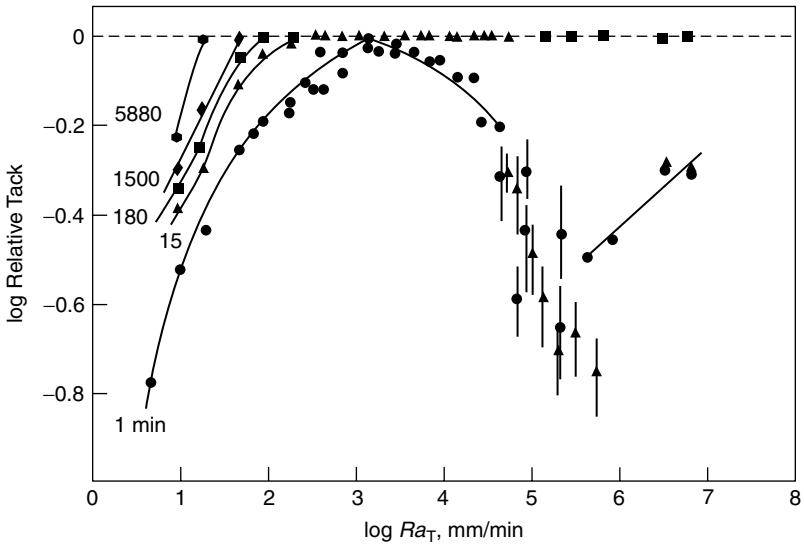

Fig. 13. Mastercurves of relative tack of an SBR versus reduced test rate at 23°C for various contact times, given in minutes for each curve. Ends of vertical lines are extreme values when failure was stick-slip (104).

Dried NR latex has very high molecular weight and low autohesion. However, NR undergoes molecular scission upon mastication and moderate amounts of milling improve autohesion as the molecular weight is reduced (Fig. 12). However, the cohesive strength, and hence, maximum achievable autohesion, becomes low after prolonged milling. Other elastomers, eg, styrene–butadiene rubber (SBR), are less susceptible to shear degradation, and autohesion is less altered by mastication. Nonetheless, shearing conditions used to prepare specimens for testing of autohesion should be well controlled.

Rate and Temperature Effects. Like adhesive tack, autohesion of elastomers is strongly dependent on test rate and temperature. Furthermore, as shown in Figure 13 for the T-peel autohesion of a cold emulsion SBR, relative autohesion P_r (for a given time and pressure of contact) is not unique, but it too depends markedly on test conditions (104).

Figure 13 is a mastercurve of relative autohesion after various contact times versus reduced test rate Ra_T at 23°C. The dotted line, log $P_r = 0$, ie, $P_r = 1$, is the maximum value that relative autohesion can attain. When data lie on this line, tack is equal to the cohesive strength, ie, the joint is as strong as the fully healed one. Of course, if healing were complete, data for all Ra_T would fall on the dotted line. Remarkably, as seen in Figure 13 and discussed below a tack joint may behave as if it was fully healed at certain Ra_T ($P_r = 1$), even though healing is actually quite incomplete ($P_r \ll 1$ at other Ra_T).

After 1 min of contact, $P_r \ll 1$ at the lowest test rates. Clearly, healing is incomplete. However, P_r increases with rate and reaches a value of one at a reduced test rate of about 1.6 m/min [log Ra_T (mm/min) ≈ 3.2]. At higher rates, P_r decreases to a minimum and the peel response becomes stick-slip. (Ends of the vertical lines

in Fig. 13 are extremes of P_r when the peel force oscillates in a regular stick-slip manner.) Thereafter, P_r increases again at the highest peel rates. As contact time is increased, the range of reduced rates where $P_r = 1$ broadens, but even after 100 h of contact, the junction is not fully healed, since, at the lowest test rate, P_r is still less than one. This is probably indicative of a very high molecular weight fraction in this cold-emulsion SBR, with an extremely slow interdiffusion rate. Nonetheless, after just 1 min of contact, the junction behaves as though it were fully healed under certain test conditions. At slow test speeds, substantial interdiffusion is required to attain a high value of P_r, whereas it appears that only limited interdiffusion is sufficient to give $P_r = 1$ at somewhat higher rates.

For contact times of 1 or 15 min, P_r increases with rate to a value of one, then decreases markedly and the failure becomes stick-slip. It has been hypothesized that this decrease is associated with the presence of small, non-contacted regions or interfacial flaws, which act as stress-raisers, when the elastomer is deformed at sufficiently high rate. If this is correct, then the abrupt decrease in P_r at high rates should be eliminated when the contact time and pressure are sufficient to cause the disappearance of these "defects." Indeed, after 180 min of contact, the decrease in P_r at high rates no longer occurs. After P_r becomes unity at some critical rate, it retains this value at all higher rates. Furthermore, if, after 180 min of contact, the contact pressure is removed while further healing proceeds, then the autohesion increases as if the pressure had been maintained for the entire contact period. However, for contact times less than 15 min, if pressure is removed for an interval during the contact period then autohesion is reduced. It appears that full molecular contact of surface elastomeric chains takes place between 15 and 180 min of contact. Then, autohesion becomes independent of pressure, since interdiffusion rates are insensitive to light pressures. With full contact, P_r remains equal to one at high rates and there is no stick-slip region where P_r falls off.

There has been disagreement in the literature whether molecular contact is sufficient to give high autohesion or whether substantial chain interpenetration is required (105). The previous results indicate that the answer may depend on the test rate and temperature. At high rates, complete, intimate molecular content may be sufficient, whereas molecular interdiffusion becomes relatively more important when the debonding rate is low.

Relating Joint Fracture Energy to Intrinsic Adhesion

In an earlier section, it was noted that the mechanical fracture energy G per unit of bonded area is greater, sometimes by several orders of magnitude, than the interfacial interaction energy holding the joint together. This section discusses this important feature in more detail.

Many basic studies attempting to relate fracture energy and intrinsic adhesion have involved the detachment of lightly cross-linked elastomers, usually over a broad range of test rates and temperatures. Work expended irreversibly in stressing these joints up to the point of failure is included in the total work of detachment. To focus attention on interfacial bonding it is therefore necessary to minimize any dissipative processes in the adherends. A simple cross-linked

elastomer can no longer flow like a liquid, but it is still not perfectly elastic because of internal friction between moving molecular segments. However, internal losses can be minimized by raising test temperature, so that molecular Brownian motion is more rapid, and by detaching the adhering layer at very low speeds. Under these "threshold" conditions the adhering layer is almost perfectly elastic, and the minimum fracture energy G_0 is determined.

In some simple cases of an amorphous elastomeric network adhered to a hard substrate, it has been found (62,106,107) that the fracture energy obeys the following equation:

$$G = G_0[1 + \phi(Ra_T)] \tag{11}$$

where ϕ is a quantity reflective of bulk energy losses, and dependent on test rate R and temperature T through the WLF factor a_T. ϕ has been related to an elastomer's loss modulus (108). For cross-linked rubbery materials, if the locus of failure stays the same, ϕ generally increases as the test rate is increased and tends to zero as Ra_T becomes sufficiently low. The (total) detachment fracture energy must also be equal to the sum of the ways in which energy is expended during fracture (109):

$$G = G_0 + H \tag{12}$$

where H is the hysteretic energy loss per unit area as a result of irreversible deformation in the *bulk* of the bonded components. Combining these two equations it is seen that

$$H = G_o\phi(Ra_T) \tag{13}$$

so that it is implicit in equation (11) that bulk energy losses depend directly on G_0.

Gent and Schulz (62) demonstrated that detachment energy was the product of an intrinsic strength and a loss function dependent on molecular mobility. Peeling of a cross-linked SBR from a polyester substrate was carried out at various rates both in air and in several wetting liquids. Values of G were equal to W_a (which had been determined from wetting experiments) times a much larger dissipative factor. Using a similar, lightly cross-linked SBR, the tensile fracture energy to separate the elastomer from various plastic substrates that had different surface energies was measured (106,107). In accord with equation (11), double-log plots of fracture energy versus reduced rate were parallel.

Although equation (11) is obeyed for certain cases of simple rubbers bonded to hard substrates, deviations from this relationship have been reported (110–112). One reason is that G_0 itself may sometimes be rate dependent (38,112,113). Furthermore, bulk dissipative losses may not be proportional to intrinsic adhesion, especially for joints containing components which can yield during fracture (112).

Next, we consider the relationship between G_0, the minimum mechanical energy required to disrupt an interface, and W_a, the equilibrium, thermodynamic work of adhesion. Firstly, however, we discuss the corresponding quantities for the *cohesive* fracture of a lightly cross-linked rubber. These are G_{0c}, the threshold tearing energy (114), and W_c, the reversible fracture energy of the bonds

acting across the cohesive fracture plane. Values of G_{0c} are of the order of 50 J/m^2 (0.024 ft·lbf/in.^{2}) (115,116). This value is much greater than W_c, which is calculated to be only about 2 J/m^2 (0.001 ft·lbf/in.^{2}). Thus, the minimum mechanical energy to fracture an elastomeric network is about 25 times that needed to (chemically) dissociate the carbon–carbon bonds crossing the fracture plane. The reason for this is that even under threshold conditions, in order to break just one backbone bond in a network chain, it is necessary to stretch all of the bonds in the chain essentially to their breaking point. Energy is not only expended in breaking bonds, but it is also lost within the broken, recoiling network strands. This idea was first proposed by Lake and Thomas (117). In mechanical rupture of a (strong) covalent network, the minimum dimension in which energy is expended away from the fracture plane is equal to the distance between cross-link points. On the other hand, cleaving bonds chemically does not require deformation and hence involves the minimum amount of energy to create new surface.

Although the Lake and Thomas analysis was carried out for cohesive fracture, the principles have been found to apply to the peeling detachment of a cross-linked polybutadiene layer bonded to glass (110). The amount of interfacial bonding was varied in a systematic way by changing the proportions of vinyltriethoxysilane and ethyltriethoxysilane used to treat a glass surface. Vinyltriethoxysilane is capable of forming covalent bonds with polybutadiene during free-radical cross-linking (118), whereas ethyltriethoxysilane is unreactive and interacts with the elastomer only by relatively weak van der Waals forces. The amount of interfacial covalent bonding between the elastomer and the glass surface was thus varied from only van der Waals forces, when ethyltriethoxysilane was used alone, to increasing amounts of interfacial chemical bonding, as increasing proportions of vinyltriethoxysilane were used. The detachment work was found to increase steadily with the amount of interfacial chemical bonding. Furthermore, values of G_0 were about 20–30 times higher than the calculated W_a. For instance, when the glass was treated with ethyltriethoxysilane, G_0 was 1.5 J/m^2, whereas the thermodynamic work of adhesion calculated from the surface energies of the treated glass and the elastomer was only about 0.05 J/m^2. Similarly, for glass treated with vinyltriethoxysilane, G_0 approached the threshold cohesive fracture energy of the elastomer, about 50 J/m^2, about 25 times greater than the calculated value for rupture of a plane of C—C bonds.

Andrews and Kinloch (106,107) also determined fracture energies for a lightly cross-linked elastomer bonded to various substrates. However, unlike Ahagon and Gent (110), they found approximate agreement between G_0 and W_a. The discrepancy in the two cases may be related to differences in test geometry. Andrews and Kinloch employed a cleavage mode, whereas peeling, which requires more severe bending, was used by Ahagon and Gent.

An easier way to measure G_0 for weakly adhering soft elastomers is the JKR (Johnson, Kendall, Roberts) technique (119,120), which usually involves contacting a hemispherical cap of elastomer with a planar substrate. Contact mechanics are employed to relate contact area to intrinsic adhesion. Using the JKR technique, a value of G_0 has been obtained of 0.12 J/m^2, about a factor of 2 higher than the expected work of adhesion (121). In other works (122,123) JKR experiments have been employed to determine threshold adhesion energies as low as 0.05 J/m^2.

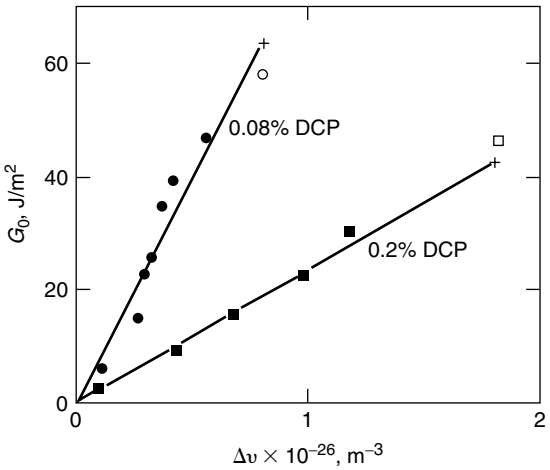

Fig. 14. Threshold work of detachment as a function of interfacial cross-link density for an elastomer (DCP = dicumyl peroxide) (124). To convert J/m^2 to lbf/in., divide by 175.

In other experiments (124) the density $\Delta\upsilon$ of chemical bonds between two layers of the same elastomer was varied by partially cross-linking the layers before contacting them and completing the cure. In Figure 14, G_0 is plotted against the increase $\Delta\upsilon$ in cross-linking while the two sheets were in contact. $\Delta\upsilon$ is a measure of the amount of interfacial bonding. As can be seen, the threshold work of detachment increased in direct proportion to $\Delta\upsilon$, up to the measured tear energy of the elastomer, denoted by crosses. Thus, there appears to be a direct relation between the mechanical strength, ie, work of detachment, obtained under threshold conditions and the density of chemical bonds at the interface.

However, it is noteworthy that the bond strengths for sheets prepared with more cross-linking agent were lower than those prepared with a smaller amount. The joints were weaker in adhesion (o and □) and weaker in tearing in the fully bonded state (+). This again points to the importance of the length of the molecular strands between cross-links. When the strands are long, they contain a large number of bonds that must be highly stressed in order to break or detach one of them. Thus, when the material is highly cross-linked and the molecular strands are short, then it is also less extensible and weaker.

The theoretical relation for the threshold bond strength (117,125), supported by the experimental results, is

$$G_0 = 1.0(C_\infty U/a^{1/2})L^{3/2}\Delta\upsilon \tag{14}$$

where C_∞ is the characteristic ratio of the molecule, generally lying between 2 and 10, a is the length of a C—C bond, U is its dissociation energy, and L is the contour length of the molecular strand between interlinks. Note that the strand length L is as important as the number $\Delta\upsilon$ of connecting strands in determining the strength of interlinked layers.

Strength of Adhesives and Joints

Fracture Mechanics of Simple Joints. In general, the strength of an adhesive joint is a function of the mode of loading and the dimensions and elastic properties of the bonded components, as well as the intrinsic strength of the interface. Fracture mechanics is used to relate the breaking load to these factors. One criterion for fracture assumes that a characteristic amount of energy is required to break apart the interface. Originally proposed for the brittle fracture of elastic solids (126), an energy criterion for fracture has been successfully applied to highly elastic materials (127), to materials that become locally dissipative (128,129), and to the separation of two adhering solids (130–142). An alternative criterion for fracture assumes that a critical *stress* is set up at the site of fracture (143). The two criteria are fundamentally equivalent, but energy calculations are often easier to perform.

In applying either criterion to predict the fracture of an adhesive bond, it is, in most cases, necessary to identify an initial failure site, usually a flaw at the interface. Failure is then assumed to take place by growth of this initial debond until the joint is completely broken. When an energy criterion is adopted for fracture, an energy balance is formulated in which changes in the strain energy of the joint and in the potential energy of the loading device when the debond grows by a small amount are equated to the work required for detachment. Strain energy is supplied by a loading device and stored in the deformable material. It is expended at failure in two ways: in supplying the work of fracture or detachment, and in deforming material that was previously undeformed or deformed less. By equating the energy made available to that required, the magnitude of the stored strain energy at the moment of fracture is deduced, and hence the breaking stress σ_b.

Modes of Failure.

Peeling. The peel test is particularly simple to analyze because the elastic energy of the deformed adherends does not change much as peeling proceeds. Most adhering layers do not stretch significantly under peel forces, and the amount of material subjected to bending does not alter. Thus, for flexible and inextensible adherends, the work of detachment is provided directly by the loading device. For peeling at 90° (Figure 15a), the peel force P per unit width is given by

$$P = G_a \tag{15}$$

where G_a denotes the work of detachment per unit area of interface. For peeling at 180° (Figure 15b),

$$P = G_a/2 \tag{16}$$

(The factor of 2 arises in this case because the point of loading moves through twice the distance of the detachment front.)

The contribution of plastic yielding to the measured peel force has been analyzed for an elastic–plastic adherend (144,145). If the adherend has a thickness greater than about $6EG_a/\sigma_y^2$, where σ_y is the yield stress, then no plastic deformation occurs and the peel force is unaffected. But if the adherend is thinner

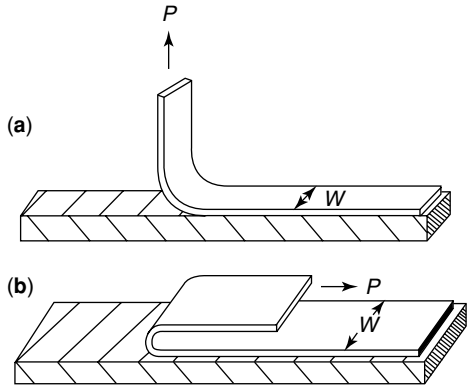

Fig. 15. Peel tests: (a) 90°; (b) 180°.

than this, it undergoes plastic deformation during peeling. The dissipated energy is provided directly by the peel force, which increases by a factor of up to about 3. However, for much thinner adherends the peel force falls again because now there is less material undergoing plastic deformation and less energy dissipated. Thus, the peel force is higher for adhesives that are capable of dissipating large amounts of energy during detachment, and for thicker adhesive layers, since this provides a greater volume of material in which dissipation occurs.

Lap Shear. Two simple examples of failure in lap shear are considered here. In the first, the adhering layer itself is elastic and stretchable (Fig. 16). The detachment force, applied parallel to the bond plane, stretches the detached layer and uses energy in doing so. For a linearly elastic layer, the relationship between the detachment force P per unit width and the work G_a of detachment per unit of bonded area is

$$P^2 = 2tEG_a \tag{17}$$

where E is Young's modulus of elasticity in tension for the detaching layer and t is its thickness (137). The corresponding tensile stress σ_b in the detaching layer is

$$\sigma_b^2 = 2EG_a/t \tag{18}$$

We note that equation (18) does not contain the size of the debonded zone. Shearing detachment is therefore predicted to take place at a constant force that depends on the elastic modulus and thickness of the adhering layer but not on the length

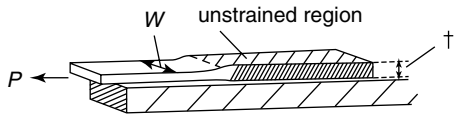

Fig. 16. Detachment of an adhering layer by a force parallel to the interface.

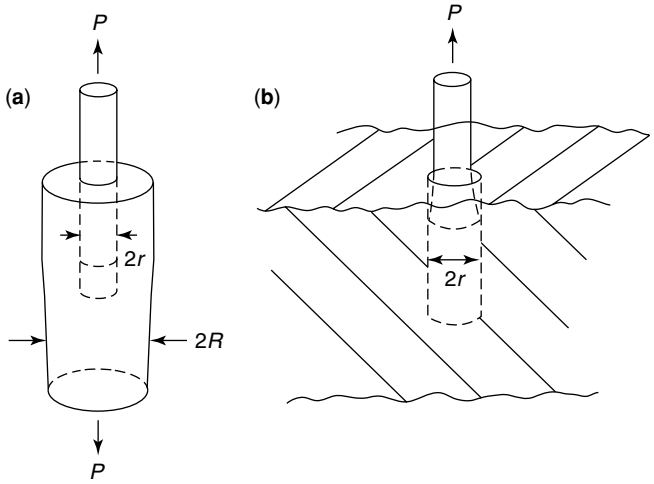

Fig. 17. Pullout of (**a**), an inextensible rod from an elastic cylinder and (**b**) an elastic rod from an inextensible block.

of the bonded region or on the extent of debonding. These features have been verified experimentally for adhering elastomeric layers (137), and the theory has been extended to deal with short overlaps, when bending deformations become important (137), with adherends of unequal thickness (137), and with prestressed layers (146). The success of a simple energy criterion for detachment confirms its general validity.

Pullout of Inextensible Fibers. By applying the same principle of energy conservation during detachment, it can be shown (141) that the pullout force P for an inextensible fiber of radius r embedded in a cylindrical elastic block of radius R (Fig. 17a) is given by

$$P^2 = 4\pi^2 R^2 r E G_a \tag{19}$$

When a bonded elastic cylinder of radius r is pulled out from a cylindrical cavity (Fig. 17b), then the pullout force is also given by equation (19) in the special form (142)

$$P^2 = 4\pi^2 r^3 E G_a \tag{20}$$

Experimental results with rubber cylinders have confirmed the general validity of equations (19) and (20). Measurements of failure loads in compression and torsion and in the presence of friction at the interface have been successfully analyzed in the same way (142). Moreover, a transition from pullout to fracture is expected when the strength of adhesion G_a is relatively large compared to G_c. The transition takes place at a critical ratio of the diameter of the embedded fiber to the diameter of the elastic cylinder in which it is embedded (147). An analysis along these lines also accounts for the brittleness of well-bonded laminar

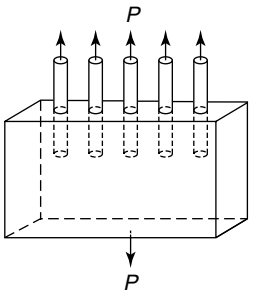

Fig. 18. Pullout of n fibers simultaneously from an elastic block.

composites compared to weakly bonded ones (138). Thus, again, energy considerations account for the principal features of the strength of adhesive joints.

When a number n of fibers are embedded in a single block of elastomer and they are all pulled together (Fig. 18), then the work required for detachment is obviously larger than for a single fiber by a factor of n. The strain energy stored within the block must therefore be larger than before, by a factor of n, and the total force applied for pullout must be increased by a factor of $n^{1/2}$. Thus, energy considerations immediately lead to the surprising conclusion that the total force required to pull out n fibers simultaneously from a single elastic block will increase in proportion to $n^{1/2}$. This prediction has been verified experimentally for 1–10 cords embedded in a rubber block (141). This is a striking example of the success of simple energy calculations in accounting for important features of the strength of joints and structures.

Shear Failure of an Adhesive Layer. Another type of shear failure occurs in a thin adhesive layer that is bonded and sheared between two rigid adherends (Fig. 19). Assuming that the adhesive is an elastic solid, the condition for growth of a debond that is long compared to the adhesive thickness t is (148)

$$G_a = tW \tag{21}$$

where W is the strain energy stored by the shear deformation, per unit volume. Thus, a thinner adhesive layer with higher elastic modulus will be more resistant to growth of a debond. However, the relation for short debonds is more complex. Initially, the value of G_a falls as the debond grows and the rate of debonding therefore slows, but when the debond length approaches t, G_a rises again to reach the value given by equation (21).

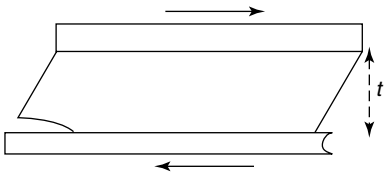

Fig. 19. Debonding in simple shear.

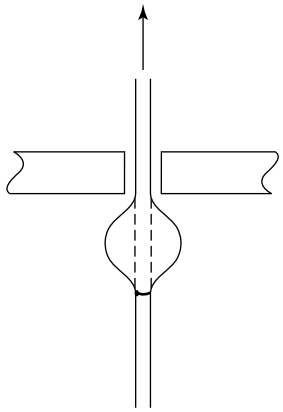

Fig. 20. Shearing a resin droplet from a fiber.

Other Shear Tests. A common test method for examining the strength of bonds between a resin and a fiber is the microdroplet test (149), shown in Figure 20. A droplet of resin about 20 μm in diameter is applied to a single fiber and then stripped away by pulling the fiber through a narrow aperture. Originally, the stripping force divided by the total bond area was regarded as the failure stress in shear. Later, the microdroplet test was reevaluated using the concepts of fracture mechanics and the stripping force was reinterpreted in terms of the fracture energy required for growth of an initial debond (150–152). It has recently been found necessary to take into account the effects of friction between the fiber and the resin droplet after debonding (153).

Another test method for resin–fiber bond strength employs a single fiber embedded within a long resin bar (154). As the bar is stretched, the less-extensible fiber breaks into smaller and smaller fragments with a final mean length of l_c. Originally, l_c was interpreted in terms of a characteristic failure stress σ_s of the resin–fiber bond in shear (155):

$$\sigma_s = \sigma_f(r/2l_c) \tag{22}$$

where r is the fiber radius and σf is its breaking stress in tension. Attempts have been made to reinterpret the repeated fractures of the fiber in terms of the energy required for both debonding and frictional sliding (156,157).

Tensile Detachment from a Rigid Plane. For a circular debonded patch at the interface between a half-space of an elastic material and a rigid substrate (Fig. 21), the applied stress σ_b sufficient to cause growth of the debond is (158)

$$\sigma_b^2 = 2\pi EG_a/3r \tag{23}$$

The same result is obtained for a pressurized debond, ie, a blister, of radius r at the interface between an elastic half-space and a rigid plane (159) because a tensile stress σ_b applied at infinity is equivalent to a pressure σ_b applied to the inner surface of the debonded region if the material is incompressible in bulk, as is assumed here.

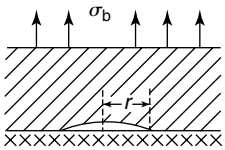

Fig. 21. Penny-shaped debond in a butt tensile test geometry.

Detachment from a Spherical Inclusion. A relation analogous to equation (23) has been deduced for the applied stress required to detach an elastic matrix from a rigid spherical inclusion (Fig. 22). The relation obtained is (140)

$$\sigma_b^2 = 4\pi EG_a/3r\sin 2\theta \tag{24}$$

where r now denotes the radius of the inclusion and 2θ denotes the angle subtended by an initially debonded patch located in the most favorable position for growth, ie, in the direction of the applied tensile stress (Fig. 22).

It is clear that σ_b will be extremely large for inclusions of small radius r, even if the level of adhesion, represented by G_a, is relatively small, only of the order of magnitude of van der Waals attractions. For example, when E is assumed to be 2 MPa, representative of soft elastomers, and G_a is given the relatively low value of 10 J/m^2, then the critical applied stress for detachment is predicted to reach a magnitude similar to E when the radius of the inclusion is reduced to about 20 μm, even if the initially debonded zone is as large as feasible, $\theta = 45^\circ$. These considerations appear to account for some features of reinforcement of elastomers by particulate fillers Fillers (140).

It is noteworthy that equation (24) predicts a decrease in detachment stress as the radius of the spherical inclusion is increased. This trend is in striking contrast to the result for a single fiber (eq. (19)), where the pullout force is predicted to increase as the radius of the inclusion is increased. Both trends are predicted

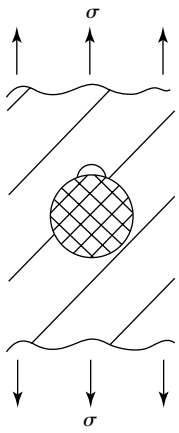

Fig. 22. Detachment from a rigid spherical inclusion.

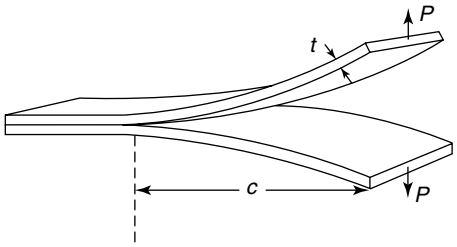

Fig. 23. Cleavage separation of two adhering plates.

by the theoretical analysis, and both are confirmed by experiment (141,160). The surface area to be debonded and the energy required to debond are both greater for fibers of larger diameter and, as a result, the pullout force is increased. For spherical inclusions, on the other hand, the amount of highly stressed material in the vicinity of the debond, which provides the energy needed for propagating the debond in this case, also increases with the size of the inclusion. The highly stressed volume grows in proportion to r^3, whereas the area to be debonded only grows in proportion to r^2. In consequence, it is easier to propagate a debond on a larger inclusion than on a smaller one.

Fracture Mechanics for Bonds between Relatively Stiff, Elastic Adherends. Two test methods are now discussed that are particularly convenient for use with relatively stiff adherends. They are denoted cleavage failure and torsional failure. At first sight, a cleavage experiment, shown in Figure 23, resembles simple peeling but the mechanics of separation are quite different. In peeling, the peeled strip is long and flexible, and bends around into alignment with the peel force, as sketched in Figure 15. In a cleavage experiment, on the other hand, the bonded plates are relatively stiff so that they do not deform greatly under the cleavage force (Fig. 23). They bend only slightly so that the cleavage force continues to act effectively at right angles to the plane of the plates, even when the separation distance c is fairly long.

In peeling, the strain energy due to bending the peeled strips does not change as peeling proceeds, because the degree of bending remains constant. Therefore, elastic strain energy does not feature in the relation between work of peeling and work of detachment, equations (15) and (16). On the other hand, in cleavage the bending energy stored in the separated portions of the plates is a function not only of the applied force P but also of the debonded length c. Thus, as debonding proceeds and the debonded length increases, the plates, regarded as long elastic cantilevers, become more compliant. When the corresponding change in strain energy is taken into account, the following relation is obtained between peel force P per unit width and work G_a of detachment:

$$P^2 = Et^3 G_a / 12c^2 \tag{25}$$

Note that the cleavage force P required to propagate the debond decreases continuously as the debond propagates. If, on the other hand, a constant deflection δ is imposed, then the energy available for debonding is given by

$$G = 3Et^3\delta^2/c^4 \tag{26}$$

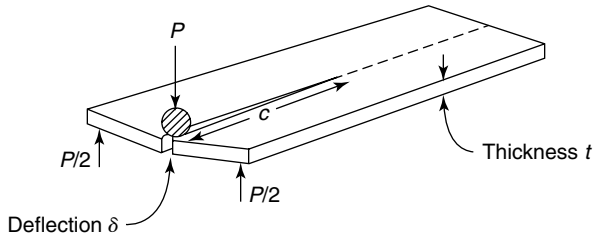

Fig. 24. Propagating a debond between two adhering plates by torsional loading (161, 162).

which decreases strongly as the debond length c increases. Thus, the initial debond will grow until there is no longer a sufficient amount of stored elastic energy to propagate it. This is an attractive feature of cleavage experiments: they can be employed to study the minimum (threshold) strength of the joint.

However, it is experimentally inconvenient to measure the debond length continuously as the debond grows, in order to calculate the energy available for debonding from equation (25) or (26). Another experimental arrangement has been proposed for stiff adherends that does not have this disadvantage. It is sketched in Figure 24. Two plates are adhered together partway along their narrow edges and the unbonded portions are twisted by a load P applied at one end point of the common interface. As the debond is forced to propagate, the debonded portions of the plates increase in length and in torsional compliance, in direct proportion to the distance c debonded. This feature leads to a fracture force P that is, in principle, independent of the distance c debonded (161):

$$P^2 = 2G_a t/C' \tag{27}$$

where C' denotes the torsional compliance of a unit length of the debonded portions of the adhering plates and t is the thickness of the bond itself. Note that the value of C' can be determined from the slope of the linear relation between deflection and applied load before the initial debond starts to propagate. This test technique has also been modified using a pulley arrangement to apply torsional deflections of much greater magnitude (162).

Because the fracture force P is, in principle, constant, it will only fluctuate if the bond strength itself is variable. Thus variations in the fracture force can be directly associated with variations in the strength of adhesion.

Both of the test techniques considered in this section depend on the adherends being linearly elastic. If this is not the case, then the relations given (eq. (26) and (27)) no longer apply. (This is the case for all of the relations given in this chapter: the adherends are assumed to be perfectly elastic so that energy expended in deforming them is available for fracture.) However, it is sometimes possible to bond fully elastic backing plates (eg, of spring steel) to the adherends under study and thus to convert plastic or yielding adherends into effectively elastic ones.

ACKNOWLEDGMENT

Funding for the preparation of this article was provided by the D'Ianni Research Endowment.

BIBLIOGRAPHY

"Adhesion and Bonding" in *EPST* 1st ed., Vol. 1, pp. 445–502 and pp. 538–550, by W. A. Zisman, U.S. Naval Research Laboratory; J. J. Bikerman, Massachusetts Institute of Technology; I. Skeist, Skeist Laboratories, Inc.; and R. F. Blomquist, Forest Products Laboratory, U.S. Department of Agriculture; "Adhesion" in *EPSE* 2nd ed., Vol. 1, pp. 476–518, by A. N. Gent and G. R. Hamed, The University of Akron.

1. D. H. Buckley, *Surface Effects in Adhesion, Friction, Wear, and Lubrication*, New York, Elsevier Scientific Publishing Co., 1981.
2. K. L. Mittal, ed., *Surface Contamination: Genesis, Detection, and Control*, Vols. **1** and **2**, Plenum Press, New York, 1979.
3. G. R. Hamed, *Rubber Chem. Technol.* **54**, 576 (1981).
4. W. H. Waddell and co-workers, *Rubber Chem. Technol.* **64**, 622 (1991).
5. M. D. Foster, *Crit. Rev. Anal. Chem.* **24**, 179 (1993).
6. C. M. Paralusz, *J. Coll. Interface Sci.* **47**, 719 (1974).
7. A. E. Tshmel, V. I. Vettegren, and V. M. Zoloturev, *J. Macromol. Sci., B: Phys.* **21**, 243 (1982).
8. R. S. Whitehouse, P. J. C. Counsell, and C. Lewis, *Polymer* **17**, 699 (1976).
9. I. M. Stewart, in J. L. McCall and W. Mueller, eds., *Microstructural Analysis: Tools and Techniques*, Plenum Press, New York, 1973, pp. 281–285.
10. G. E. Riach and R. E. Weber, *Handbook of Auger Electron Spectroscopy*, 2nd ed., Physical Electronic Industries, Eden Prairie, Minn., 1976.
11. T. A. Carlson, *Photoelectron and Auger Spectroscopy*, Plenum Press, New York, 1975.
12. A. A. Galuska, R. R. Pouleter, and K. O. McElrath, *Surf. Interface Anal.* **25**, 418 (1997).
13. G. Gillberg, *J. Adhesn.* **21**, 129 (1987).
14. T. P. Russell, *Annu. Rev. Mater. Sci.* **21**, 249 (1991).
15. Y. Kobatake, and Y. Inoue, *Appl. Sci. Res. A* **7**, 53 (1958).
16. J. J. Bikerman, *The Science of Adhesive Joints*, Academic Press, New York, 1968.
17. W. J. Bailey, Z. Ni, and S. R. Wu, *J. Polym. Sci., Polym. Chem. Ed.* **20**, 3021 (1982).
18. W. J. Bailey, *Polym. J.* **17**, 85 (1985).
19. S. S. Voyutskii, *Autohesion and Adhesion of High Polymers*, Wiley-Interscience, New York, 1963.
20. S. S. Voyutskii, *Rubber Chem. Technol.* **33**, 748 (1960).
21. J. Klein, *Science* **250**, 640 (1990).
22. E. Jabbari and N. A. Peppas, *J. Macromol. Sci., C: Rev. Macromol. Chem. Phys.* **34**, 205 (1994).
23. E. Helfand and Y. Tagami, *J. Chem. Phys.* **56**, 3592 (1972).
24. D. Broseta and co-workers, *Macromolecules* **23**, 132 (1990).
25. S. H. Anastasiadis, I. Gancarz, and J. T. Koberstein, *Macromolecules* **21**, 2980 (1988).
26. S. H. Anastasiadis and co-workers, *J. Chem. Phys.* **92**, 5677 (1990).
27. D. W. Schubert and co-workers, *Macromolecules* **28**, 2519 (1995).
28. R. P. Wool and K. M. O'Connor, *J. Appl. Phys.* **52**, 5953 (1981).
29. P. G. deGennes, *J. Chem. Phys.* **55**, 572 (1971).
30. S. Prager and M. Tirrell, *J. Chem. Phys.* **75**, 5194 (1981).

31. D. B. Adolf, S. Prager, and M. Tirrell, *J. Chem. Phys.* **79**, 7015 (1983).
32. R. P. Wool and K. M. O'Connor, *J. Polym. Sci., Polym. Lett. Ed.* **20**, 7 (1982).
33. R. P. Wool, *Polym. Prepr. (Am. Chem. Soc., Div. Polym. Chem.)* **23**, 62 (1982).
34. Y. H. Kim and R. P. Wool, *Macromolecules* **16**, 1115 (1983).
35. L. Bothe and G. Rehage, *Rubber Chem. Technol.* **55**, 1308 (1982).
36. S. S. Voyutskii, *J. Adhesn.* **3**, 69 (1971).
37. M. Stamm and D. W. Schubert, *Annu. Rev. Mater. Sci.* **25**, 325 (1995).
38. M. D. Ellul and A. N. Gent, *J. Polym. Sci., Polym. Phys. Ed.* **22**, 1953 (1984).
39. S. Yukioka, K. Nagato, and T. Inoue, *Polymer* **33**, 1171 (1992).
40. C. M. Roland and G. G. Böhm, *Macromolecules* **18**, 1310 (1985).
41. H. R. Brown and co-workers, *Polymer* **29**, 1807 (1988).
42. R. Schnell, M. Stamm, and C. Creton, *Macromolecules* **31**, 2284 (1998).
43. A. Y. Coran and R. Patel, *Rubber Chem. Technol.* **56**, 1045 (1983).
44. M. H. Chung and G. R. Hamed, *Rubber Chem. Technol.* **62**, 367 (1989).
45. G. Odian, *Principles of Polymerization*, McGraw-Hill, New York, 1970, pp. 91–93.
46. G. E. Molau, *J. Polym. Sci., Part A* **3**, 4235 (1965).
47. H. R. Brown, *Annu. Rev. Mater. Sci.* **21**, 463 (1991).
48. E. P. Plueddemann, *Silane Coupling Agents*, Plenum Press, New York, 1982.
49. B. Arkles, *Chemtech* **7**, 766 (1977).
50. M. R. Rosen, *J. Coatings Technol.* **50**, 70 (1978).
51. S. Buchan, *Rubber to Metal Bonding*, Crosby, Lockwood, and Sons, Ltd., London, 1948.
52. W. J. van Ooij, *Rubber Chem. Technol.* **52**, 605 (1979).
53. G. R. Hamed and R. Paul, *Rubber Chem. Technol.* **70**, 541 (1997).
54. F. W. Fowkes, in R. L. Patrick, ed., *Treatise on Adhesion and Adhesives*, Marcel Dekker, Inc., New York, 1967.
55. T. Young, *Philos. Trans. R. Soc. London* **95**, 65 (1805).
56. W. A. Zisman and H. W. Fox, *J. Colloid Sci.* **5**, 514 (1950).
57. J. R. Dann, *J. Colloid Interface Sci.* **32**, 302, 321 (1970).
58. A. Dupré, *Théorie Mécanique de la Chaleur*, Gauthier-Villars, Paris, 1869, p. 369.
59. R. J. Good and L. A. Girifalco, *J. Phys. Chem.* **64**, 561 (1960).
60. F. M. Fowkes, *Ind. Eng. Chem.* **56**, 40 (1964).
61. D. P. Graham, *Ind. Eng. Chem.* **57**, 4387 (1965).
62. A. N. Gent and J. Schultz, *J. Adhesn.* **3**, 281 (1972).
63. E. H. Andrews and A. J. Kinloch, *Proc. R. Soc. London, Ser. A* **332**, 401 (1973).
64. D. Briggs, *J. Adhesn.* **13**, 287 (1982).
65. C. Y. Kim and D. A. I. Goring, *J. Appl. Polym. Sci.* **15**, 1357 (1971).
66. A. Baszkin, M. Nishino, and L. Ter-Minassian-Saraga, *J. Colloid Interface Sci.* **54**, 317 (1976).
67. J. Shield, *Adhesives Handbook*, Butterworth Publishers, Ltd., London, 1970.
68. D. Briggs, D. M. Brewis, and M. B. Konieczo, *J. Mater. Sci.* **11**, 1270 (1976).
69. D. M. Brewis and D. Briggs, *Polymer* **22**, 7 (1981).
70. U.S. Pat. 2632921 (Mar. 31, 1953), W. H. Kreidl.
71. D. Briggs, D. M. Brewis, and M. B. Konieczko, *J. Mater. Sci.* **14**, 1344 (1979).
72. S. Yamakawa, F. Yamamoto, and Y. Kato, *Macromolecules* **9**, 754 (1976).
73. J. Schultz, A. Carré, and C. Mazeau, *Int. J. Adhesn. Adhesv.* **4**, 163 (1984).
74. R. H. Dahm, D. J. Barker, and D. M. Brewis, in K. W. Allen, ed., *Adhesion-4*, Applied Science Publishers, London, 1980, p. 215.
75. E. R. Nelson, T. J. Kilduff, and A. A. Benderly, *Ind. Eng. Chem.* **50**, 329 (1958).
76. D. W. Dwight and W. M. Riggs, *J. Colloid Interface Sci.* **47**, 650 (1974).
77. C. H. Lerchenthal, M. Brenman, and N. Yitshaq, *J. Polym. Sci., Polym. Chem. Ed.* **13**, 737 (1975).

78. C. H. Lerchenthal and M. Brenman, *Polym. Eng. Sci.* **16**, 747 (1976).
79. A. J. Kinloch, *J. Adhesn.* **10**, 193 (1979).
80. J. D. Minford, *J. Appl. Polym. Sci., Appl. Polym. Symp.* **32**, 91 (1977).
81. A. Pattnaik and J. D. Meakin, *J. Appl. Polym. Sci., Appl. Polym. Symp.* **32**, 145 (1977).
82. K. E. Weber and G. R. Johnston, *SAMPE* **6**, 16 (1974).
83. W. T. McCarvill and J. P. Bell, *J. Adhesn.* **6**, 185 (1974).
84. G. D. Davis and J. D. Venables, in A. J. Kinloch, ed., *Durability of Structural Adhesives*, Applied Science Publishers, London, 1983, pp. 43–84.
85. H. W. Eickner and W. E. Schowalter, A Study of Methods for Preparing Clad 24S-T3 Aluminum Alloy Sheet Surfaces for Adhesive Bonding, `Report No. 1813`, Forest Products Laboratory, May 1950.
86. J. D. Venables and co-workers, *Appl. Surf. Sci.* **3**, 88 (1979).
87. G. D. Davis and co-workers, *J. Mater. Sci.* **17**, 1807 (1982).
88. J. R. G. Evans and D. E. Packham, *J. Adhesn.* **10**, 177 (1979).
89. J. R. G. Evans and D. E. Packham, *J. Adhesn.* **10**, 39 (1979).
90. D. E. Packham, in K. L. Mittal, ed., *Adhesion Aspects of Polymeric Coatings*, Plenum Press, New York, 1983.
91. W. Brockmann, in Ref. 84, p. 281.
92. M. Gettings and A. J. Kinloch, *J. Mater. Sci.* **12**, 2049 (1977).
93. C. A. Dahlquist, in Adhesion Fundamentals and Practice (A Report of an International Conference held at the University of Nottingham, U.K., Sept. 20–22, 1966), Gordon and Breach Science Publishers, New York, 1969, p. 143.
94. C. W. Hock, *J. Polym. Sci., Part C* **3**, 139 (1963).
95. K. Kamagata and co-workers, *J. Appl. Polym. Sci.* **15**, 483 (1971).
96. G. R. Hamed, *Rubber Chem. Technol.* **54**, 576 (1981).
97. G. R. Hamed and G. D. Roberts, *J. Adhesn.* **47**, 95 (1994).
98. D. W. Aubrey and M. Sherriff, *J. Polym. Sci. Chem. Ed.* **16**, 2631 (1978).
99. G. Kraus, K. W. Rollman, and R. A. Gray, *J. Adhesn.* **10**, 221 (1979).
100. M. Sherriff, R. W. Knibbs, and P. G. Langley, *J. Appl. Polym. Sci.* **17**, 3423 (1973).
101. A. N. Gent and R. P. Petrich, *Proc. R. Soc. London, Ser. A* **310**, 433 (1969).
102. M. L. Williams, R. F. Landel, and J. D. Ferry, *J. Am. Chem. Soc.* **77**, 3701 (1955).
103. W. G. Forbes and L. A. McLeod, *Trans. Inst. Rubber Ind.* **30**(5), 154 (1958).
104. G. R. Hamed and C. H. Shieh, *Rubber Chem. Technol.* **58**, 1038 (1985).
105. J. N. Anand, *J. Adhesn.* **5**, 265 (1973).
106. E. H. Andrews and A. J. Kinloch, *Proc. R. Soc. London, Ser. A* **332**, 385 (1973).
107. E. H. Andrews and A. J. Kinloch, *Proc. R. Soc. London, Ser. A* **332**, 401 (1973).
108. D. Maugis, *J. Adhesn.* **23**, 61 (1987).
109. G. R. Hamed, in R. L. Patrick, ed., *Treatise on Adhesion and Adhesives*, Vol. **6**, Marcel Dekker, Inc., New York, 1989, pp. 33–54, Chap. "2".
110. A. Ahagon and A. N. Gent, *J. Polym. Sci.* **13**, 1285 (1975).
111. A. N. Gent and S. M. Lai, *J. Polym. Sci., Part B: Polym. Phys.* **32**, 1543 (1994).
112. G. R. Hamed and F. C. Liu, *Rubber Chem. Technol.* **75**, 1036 (1984).
113. H. R. Brown, *Annu. Rev. Mater. Sci.* **21**, 463 (1991).
114. G. J. Lake and P. B. Lindley, *J. Appl. Polym. Sci.* **9**, 1233 (1965).
115. H. K. Mueller and W. G. Knauss, *Trans. Soc. Rheol.* **15**, 217 (1971).
116. A. Ahagon and A. N. Gent, *J. Polym. Sci.* **13**, 1903 (1975).
117. G. J. Lake and A. G. Thomas, *Proc. R. Soc. London Ser. A* **300**, 108 (1967).
118. A. N. Gent and E. C. Hsu, *Macromolecules* **7**, 993 (1974).
119. K. L. Johnson, K. Kendall, and A. D. Roberts, *Proc. R. Soc. London, Ser. A* **324**, 301 (1971).
120. A. Falsafi and co-workers, *J. Rheol.* **41**, 1349 (1997).
121. H. R. Brown, *Macromolecules* **26**, 1666 (1993).

122. M. K. Chaudhury and G. M. Whitesides, *Langmuir* **7**, 1013 (1991).
123. V. Mangipudi and co-workers, *Macromol. Symp.* **102**, 131 (1996).
124. R. J. Chang and A. N. Gent, *J. Polym. Sci., Polym. Phys. Ed.* **19**, 1619 (1981).
125. H. Chun and A. N. Gent, *J. Polym. Sci., Part B: Polym Phys.* **34**, 2223 (1996).
126. A. A. Griffith, *Philos. Trans. R. Soc. London, Ser. A* **221**, 162 (1920).
127. R. S. Rivlin and A. G. Thomas, *J. Polym. Sci.* **10**, 291 (1953).
128. G. R. Irwin, *Trans. Am. Soc. Met.* **40**, 147 (1948).
129. E. Orowan, *Rep. Prog. Phys.* **12**, 185 (1949).
130. E. J. Ripling, S. Mostovoy, and R. L. Patrick, *Mater. Res. Stand.* **4**, 129 (1964).
131. B. M. Malyshev and R. L. Salganik, *Int. J. Fract. Mech.* **1**, 114 (1965).
132. T. Hata, M. Gamo, and Y. Doi, *Kobunshi Kagaku* **22**, 152 (1965).
133. M. L. Williams, in *Proceedings of the 5th U.S. National Congress on Applied Mechanics*, Minneapolis, June 1966, ASME, New York, 1966, p. 451.
134. A. N. Gent and A. J. Kinloch, *J. Polym. Sci., Part A2* **9**, 659 (1971).
135. E. H. Andrews and A. J. Kinloch, *Proc. R. Soc. London, Ser. A* **332**, 385 (1973).
136. K. Kendall, *J. Phys. D: Appl. Phys.* **4**, 1186 (1971).
137. K. Kendall, *J. Phys. D: Appl. Phys.* **8**, 512 (1975).
138. K. Kendall, *Proc. R. Soc. London, Ser. A* **344**, 287 (1975).
139. K. Kendall, *J. Mater. Sci.* **11**, 638 (1966).
140. A. N. Gent, *J. Mater. Sci.* **15**, 2884 (1980).
141. A. N. Gent and co-workers, *J. Mater. Sci.* **16**, 949 (1981).
142. A. N. Gent and O. H. Yeoh, *J. Mater. Sci.* **17**, 1713 (1982).
143. G. R. Irwin, *Appl. Mater. Res.* **3**, 65 (1964).
144. A. N. Gent and G. R. Hamed, *J. Appl. Polym. Sci.* **21**, 2817 (1977).
145. A. J. Kinloch, C. C. Lau, and J. G. Williams, *Int. J. Fract.* **66**, 45 (1994).
146. K. Kendall, *J. Phys. D: Appl. Phys.* **8**, 1722 (1975).
147. A. N. Gent and C. Wang, *J. Mater. Sci.* **28**, 2494 (1993).
148. P. B. Lindley and S. C. Teo, *Plast. Rubber: Mater. Appl.* **4**(1), 29 (1979).
149. B. Miller, P. Muri, and L. Rebenfeld, *Comp. Sci. Technol.* **28**, 17 (1987).
150. C. T. Chou and L. S. Penn, *J. Adhesn.* **36**, 125 (1991).
151. K. R. Jiang and L. S. Penn, *Comp. Sci. Technol.* **45**, 89 (1992).
152. R. J. Scheer and J. A. Nairn, *J. Adhesn.* **53**, 45 (1995).
153. C.-H. Liu and J. A. Nairn, *Int. J. Adhesn. Adhesv.* **19**, 59 (1999).
154. L. T. Drzal, M. J. Rich, and P. F. Lloyd, *J. Adhesn.* **16**, 1 (1982).
155. G. A. Cooper and A. Kelly, *J. Mech. Phys. Solids* **15**, 279 (1967).
156. A. N. Gent and G. L. Liu, *J.Mater. Sci.* **26**, 2467 (1991).
157. A. N. Gent and co-workers, *J. Mater. Sci.* **31**, 1707 (1996).
158. V. I. Mossakovskii and M. T. Rybka, *PMM* **28**, 1061 (1964); *J. Appl. Math. Mech.* **28**, 1277 (1964).
159. M. L. Williams, *J. Appl. Polym. Sci.* **13**, 29 (1969).
160. A. N. Gent and B. Park, *J. Mater. Sci.* **19**, 1947 (1984).
161. J. O. Outwater and D. J. Gerry, *J. Adhesn.* **1**, 290 (1969).
162. K. Cho and A. N. Gent, *Int. J. Fract.* **28**, 239 (1985).

GENERAL REFERENCES

S. Wu, *Polymer Interface and Adhesion*, Marcel Dekker, Inc., New York, 1982.
A. J. Kinloch, *Adhesion and Adhesives—Science and Technology*, Chapman and Hall, New York, 1987.
E. P. Plueddemann, *Silane Coupling Agents*, 2nd ed., Plenum Press, New York, 1991.

D. Satas, ed., *Handbook of Pressure-Sensitive Adhesive Technology*, 2nd ed., Van Nostrand Reinhold Co., Inc., New York, 1989.
K. L. Mittal and A. Pizzi, eds., *Handbook of Adhesive Technology*, Marcel Dekker, Inc., New York, 1994.
R. P. Wool, *Polymer Interfaces: Structure and Strength*, Hanser, New York, 1995.
A. V. Pocius, *Adhesion and Adhesives Technology: An Introduction*, Hanser, New York, 1997.

A. N. GENT
G. R. HAMED
The University of Akron

ADHESIVE COMPOUNDS

Introduction

An adhesive is a material that is used to join two objects through nonmechanical means. It is placed between the objects, which usually are called *adherends* when part of a test piece or *substrates* when part of an assembly, to create an adhesive joint. Although some adhesives form joints that nearly immediately are as strong as they will be in actual use, other adhesives require further operations for the adhesive joint to reach its full strength. Adhesives can be made in several different physical forms, and the form of a given adhesive will define the possible methods of its application to the substrate.

An adhesive is comprised of a base chemical or a combination of chemicals which define its general chemical class. Most adhesives contain a curing agent or catalyst that will cause an increase in the molecular weight of the system and frequently the formation of a polymeric network. Nearly all adhesives also contain additives or modifiers which fine tune the adhesive and may significantly influence its behavior before and after formation of the adhesive joint. These additives include solvents, plasticizers, tackifiers, fillers, pigments, toughening agents, coupling agents, stabilizers, and so on. Additives or modifiers increasingly are chosen for their ability to provide more than one benefit, for example, a pigment may not only color but may also reinforce an adhesive. In some cases, the process used to combine these diverse ingredients will strongly influence the properties of an adhesive. Although inorganic adhesives do exist, this article will be restricted to organic polymeric adhesives.

Consumers, designers, and engineers generally choose between adhesive bonding and mechanical or thermal methods when deciding how to join one object to another. Mechanical methods utilize bolts, screws, and rivets. Thermal methods include welding, soldering, and brazing. Adhesive bonding is the obvious choice

Encyclopedia of Polymer Science and Technology. Copyright John Wiley & Sons, Inc. All rights reserved.

for joining in cases in which the substrate is thin and relatively weak, for example, paper, or strong but relatively brittle, for example, glass. Use of adhesives in these situations avoids formation of stress concentration points and possible damage to the substrates. Even where the substrates will bear mechanical fastening, the geometry of certain parts sometimes makes welding or bolting more costly if not entirely impossible, as in the case of the aluminum honeycombs used in aerospace structures or tube-to-tube joining used in motor vehicle frame construction. Because they are usually applied so as to cover the entire joined surface in a continuous rather than point-by-point fashion, adhesives can provide a measure of environmental protection and mechanical reinforcement or stiffening well beyond the capabilities of mechanical fasteners. Stresses in adhesive joints are distributed over a relatively large area, which generally increases the mechanical and cosmetic integrity of joined parts. The energy damping capability of many polymeric adhesives contributes a mechanical damping component to joints that can increase their toughness and impact resistance. Adhesives are a great help in reducing the weight of structures because they add little weight and can facilitate the use of thinner substrates. Joining of dissimilar materials for reasons of economics, weight, or performance is frequently accomplished using adhesive bonding, providing properties already mentioned as well as electrical and thermal insulation, protection against galvanic corrosion, and acoustic damping. In some cases, adhesives are used in conjunction with joining methods such as welding and riveting, via weld bonding and rivet bonding, respectively, in order to maximize stiffness, strength, and fatigue resistance of joints.

Where an adhesive is the obvious choice, it is often the least expensive choice as well. In industrial situations where the performance expected of the adhesive is high and broad and its cost is that of a specialty rather than a commodity material, it is common to see users take a systems approach to make the best choice of joining method or the best choice of adhesive, if adhesive bonding is seen to be the best joining method. The systems approach to choosing adhesives goes well beyond comparing the cost per gallon of adhesives. It considers the number of parts to be joined, the time and cost constraints of assembly, spatial limitations, the need for substrate surface cleaning or preparation, the cost of all application, fixturing, and curing equipment, environmental and safety requirements, disposal costs, and, finally, part performance and lifetime.

Market Economics

In 1996, the global adhesive and sealant industry was estimated to have a size of about 7.5 million metric tons. The monetary value of this volume was considered to be about US$20.0 billion (1). The value of the market was estimated to be $28.0 billion in 1998 led by North America with a 33% share followed by Europe (30%), the Far East (19%), and the rest of the world (18%) (2). By 2002, the same marketplace is expected to grow to 16.7 million metric tons (3). Adhesives make up over 80% of the adhesives and sealants market. It has been estimated that the global use of adhesives will continue to grow annually by 3–4% from 2000 through 2005, but for some types of adhesives and for some markets, the growth could be much larger.

In the United States, the adhesive and sealants business was producing about US$1 billion from sales in 1972. By 1999, the U.S. adhesive business was estimated to be nearly 6.9 million tons in size with an approximate value of US$9.5 billion. The size of the U.S. adhesive market is anticipated to grow to 7.9 million tons by 2004 (4). The largest markets for adhesives in the United States are construction, primary wood bonding, textiles, and packaging. Markets that command some of the highest prices for adhesives include dental, aerospace, and microelectronics.

The late 1990s were marked by significant numbers of consolidations and partnerships in the adhesive industry that are expected to continue into the twenty-first century. In 1999, only seven companies produced 49% of the adhesives sold in the world (5). The remainder of the adhesive industry is highly fragmented; in the United States alone, there are about 500 adhesive companies. North American and European adhesive companies have partnered to serve the global operations of automotive OEMs expecting worldwide service. Several companies have formed joint ventures in the People's Republic of China (6) in anticipation of large market growth in that country. Such arrangements are expected to increase in number as makers of adhesives accelerate their pursuit of greater market share and opportunities in the most lucrative markets. Concurrently with these changes, many large resin suppliers have spun off their adhesive resin operations into new companies or sold off their adhesive raw materials divisions to established companies. An active adhesive formulator must keep track of raw materials sources and be prepared to trace older materials to their new sources.

The adhesives industry has been affected by environmental and regulatory concerns regarding health and safety issues of adhesive ingredients, use of solvents, and other issues. Less than 5% of the adhesives used in the United States in 1999 contained organic solvents. The use of adhesives with solvents is decreasing by about 2% annually. All other adhesives are waterborne or contain no carrier solvent. Recycling of adhesives has become more important as paper recycling has become very common, and the quality of recycled paper depends in part on the nature of adhesive residues present in recycle feedstock (7). Historically, certain adhesives have been based on natural products such as starch, natural rubber, and animal glue, and many adhesives still use as modifiers various tree-based rosins and terpenes, but there has been a strong shift away from naturally derived adhesives. Between 1972 and projected out to 2003, the value of U.S. adhesives made of synthetic resin and rubbers will have increased almost eight times while the value of U.S. adhesives made from natural bases will have increased only about five times (8). In the 1920s, nearly all primary wood bonding was done with adhesives produced from natural products (9). By the 1970s, that need was filled almost entirely by synthetic adhesives. As the price of crude oil rises and oil reserves dwindle, there is increasing interest in making more adhesives from renewable resources (10).

Principles of Adhesives and Adhesive Formulation

An adhesive is designed to perform certain functions. These functions are common to all adhesives, but the details as they relate to a given ultimate use can vary considerably.

First, the adhesive must be able to be conveniently applied to the substrate using a manual or mechanized method of application. Second, the adhesive must wet the surface to which it is applied. Third, the adhesive must achieve a permanently solid state via evaporation of a solvent, removal of pressure, a drop in temperature, or the occurrence of chemical reaction. The conversion must occur within a time period amenable to the use of the bonded part. Fourth, before it is put into service, the adhesively bonded part must have been provided with a bond that is strong enough to resist normally imposed stresses. The stresses normally imposed on a sealed envelope are very different from those imposed on a tiled wall or a bonded vehicle frame. Fifth, the adhesive must maintain the bond through the joint's functional lifetime, withstanding all environments to which the joint is normally exposed.

Methods of Adhesive Application. Until the twentieth century, adhesives and sealants were applied by hand using fingers, sticks, trowels, brushes, spatulas, shovels, and similar implements. These tools are still used by many do-it-yourselfers, craftspeople, and construction workers. Other relatively simple means of applying adhesives involve the use of squeeze bottles, spray cans, rollers, and squeeze tubes. Manual and pneumatic guns are often used to dispense adhesives, sealants, and caulks. For this type of application, the adhesive is supplied in a plastic cartridge to which can be affixed a tip or applicator to help control the shape and size of the adhesive bead as it is expelled. The adhesive is expressed from the cartridge by pressurization of a sealing piston. Such guns can be used to dispense two-part adhesive systems as well as one-parts, which are commonly called 2K and 1K adhesives, respectively, probably in reference to the German *komponent*. In the case of 2K adhesives, a mixing nozzle will be attached to the cartridge. This device consists of a tube and an inserted mixing element through which the two parts of the adhesive flow in a tortuous path, folding over on each other and becoming well mixed. For low volume applications in the industrial sector, 2K epoxy adhesives are often supplied in double-barreled plastic cartridges for application using manual or pneumatic dispensing guns.

High volume applications of adhesives generally dispense adhesives out of containers having volumes up to at least 1135 L (300 gal). Through proper choice of pump design and material choice, bulk dispensing is possible for both liquid and high viscosity paste adhesives whether 1K or 2K (11,12). For some industries, dispensing guns will be handheld and manually operated. In the automotive industry, hem flange adhesives, cosmetic sealers, antiflutter sealants, gap-filling adhesives, and other viscous materials are dispensed in high volumes using computer-controlled guns mounted on robot arms which zip about a part in a few seconds to lay down dollops or linear beads of adhesive or sealant. Gun-robot coordination must be precise. To lay down enough but not too much adhesive in a well-defined area in a controlled fashion, adhesive dispensing companies provide extrusion, spray, streaming, and swirling patterns of adhesive delivery. The adhesive is sometimes heated to lower its viscosity.

Hot-melt adhesives are also dispensed using guns. Hobbyists and do-it-yourselfers use small electric handheld guns into which they insert the adhesive sticks. The gun heats the adhesive, and the operator squeezes a trigger to dispense it. High volume dispensing systems for hot-melts generally include a stirred melting tank and a hot pumping system that delivers the adhesive to the application

device, which may be a spray gun, a roller, a brush, or a film die. Application methods include rotating pick-up wheels, transfer from a hot bar, and release from extrusion heads facilitated by spring ball valves (13).

The invention of pressure-sensitive tapes in the early 1930s provided a novel means of delivering an adhesive where it was needed. Adhesive tapes were first sold as rolls in boxes or cans and were unrolled by hand to be cut with scissors or a blade. This was followed by the design of tape dispensers that range from single-use, all-plastic disposables, to sand-weighted desk-top models fitted with metal blades, and on to the semiautomated dispensers used at large packing plants. Recent advances include dispensers of pre-cut adhesive strips that can be worn on one's wrist and the development of hand-tearable tapes. Solid curable adhesive films are available in roll, strip, and pre-cut forms of various shapes and thicknesses, with or without liners. These are typically somewhat tacky and are generally hand-applied.

Bond Formation. Adhesion science has established several mechanisms by which adhesion will occur. These are sometimes referred to as theories of adhesion, and they represent a means of explaining adhesion phenomena and increasingly provide guiding principles by which adhesion can be predicted to some extent and controlled to a larger extent. These theories are covered in most general texts on adhesives and adhesion science, many of which point out specific examples relevant to the scope of the text, for example, aerospace aluminum bonding or wood bonding. The theories of adhesion include the following:

(1) Electrostatic theory
(2) Diffusion theory
(3) Mechanical interlocking theory
(4) Acid–base theory or specific adhesion/interaction theory
(5) Covalent bonding theory

Regardless of which theory or theories are manifest in an adhesive bond, establishing an adhesive bond requires that first there be sufficient contact between the adhesive and the substrate. This can be accomplished only if the adhesive intimately wets the substrate. Although there are many types of adhesives, in order to form this necessary contact each must flow under the influence of gravity, pressure, heat, or presence of a solvent to wet any asperities on the substrate surface. This wetting is necessary for establishment of a bond, but it is ordinarily insufficient for establishment of the strongest or most durable bond. (Conversely, the area of contact may be controlled to minimize adhesion.) Adhesion science, one of the most interdisciplinary of all sciences, has established several tenets for wettability which are applicable to adhesives, coatings, and other substances whose adherability is of interest. The first is that the surface energy of the wetting material will ideally be lower than that of the substrate. Methods for establishing surface energies of liquids are well established, and tabulations of such data are readily available. Obtaining the surface energy of a solid is somewhat more problematic, but methods do exist, most based on the determination of critical surface tension from measurement of contact angles made by various liquids, and these have been

shown to have merit on a fundamental basis. Any surface roughness or surface contaminants will greatly influence the results of such measurements; however, the methods used are valuable in characterizing the wettability of ceramics and polymers, which generally have smooth surfaces.

The bulk properties of the adhesive and its ability to effect the transfer of stress across the adhesive–adherend interface will strongly dictate the measured strength of the bond, often described in terms of *practical adhesion*. The durability of the bond will be governed by the physical and chemical nature of the interfacial region formed, aptly called the *interphase*. The failure of a bond is usually characterized as being *adhesive* in the case where the failure is between the adhesive and the substrate and *cohesive* where the failure is within the adhesive. Failure may also be *mixed* mode, and other subtleties of the failure mode should be noted during testing or in the field. If surface analysis will be carried out to determine details of failure, failed bonds should be closed until that analysis can be performed.

Ideally the adhesive formulator will have at least a rudimentary knowledge about substrates, be they metals, ceramics, or polymeric materials. Whenever possible, testing of adhesives should be done on the same material being used in practice. If this is not possible, a nominally identical substitute should be used. The surface of the substrate should be what it will be in use. The state of that surface will affect adhesive wet-out, interfacial area, stress distribution, and the likelihood of chemical reaction. It is highly recommended that surfaces be as clean as possible, and it is often recommended that surface treatments be used. The most basic of all surface treatments is cleaning.

Simple cleaning methods include blowing away debris with canned or filtered air, wiping with a dry cloth or a cloth wet with ethanol, cleaning with a water-based citrus cleaner and rinsing with distilled water, and dipping in methyl ethyl ketone or petroleum ether and drying with a clean cloth. Vapor degreasing is used when the volume of parts to be cleaned can justify its installation. Until the early 1990s, chlorinated solvents were used widely for degreasing, but health and environmental concerns have shifted interest to other organic solvents and aqueous degreasers. Other environmentally acceptable cleaning methods that have been investigated include grit blasting, ultrahigh water jetting (14), and excimer laser treatments (15–17).

In some cases, cleaning of a surface is not sufficient for adequate bond formation. For metal bonding, this is especially true in situations where the adhesive joint will undergo exposure to severe environmental conditions such as moisture, salt spray, and high temperatures. The coupling of these environments with mechanical stresses can lead to failures at loads much lower than those at which the same joint would fail in a milder environment. In these situations, it is common to use a wet chemical surface treatment which removes all surface contamination as well as any poorly adhering oxides and converts the newly exposed surface to a durable oxide, preferably with a texture that encourages mechanical interlocking with an applied adhesive. Pretreatments for aluminum have been the subject of considerable research (18). In partnership with adhesive suppliers, aerospace users of aluminum have advanced the state of the aluminum-bonding art on a continuous basis for many years and often use the steps of alkaline cleaning,

phosphoric acid anodizing, and application of epoxy–phenolic primers to prepare aluminum for bonding. For industries in which failure may have less devastating results, organosilanes, sol–gel coatings, and gas plasmas have become the basis of a number of surface treatments.

Polymeric materials often present significant challenges to adhesive bonding. This is particularly true when bonding polymers with low surface energies such as polyethylene, polypropylene, and polytetrafluoroethylene; however, it is also true for bonding high surface energy polymers such as poly(ethylene terephthalate). Reliable wet chemical treatments continue to be used for plastics, but dry chemical treatments are well established as primers for adhesive bonding. These treatments include corona discharge, plasma, flame, and excimer laser.

Cleaning methods chosen should remove rather than redistribute contamination. Some methods which are ostensibly meant to clean may also contribute something in the way of a surface treatment via chemical or physical changes of a substrate. Methods which treat a surface chemically often also change surface texture, coupling roughness and chemical surface modification and making it difficult to separate their independent effects. Microscopic surface texturing can favorably enhance adhesion.

Adhesive users should not assume that meticulous cleaning and costly surface treatments will always be needed to ensure reliable adhesive bonding; however, as in all adhesive applications, the better the user understands what the adhesive must do, the more readily the need for cleaning and surface treatments can be assessed. Cleaning and surface treatment of substrates is not always economically feasible nor is it necessarily environmentally desirable. There have been considerable advances with respect to pressure-sensitive and structural adhesives which form strong durable bonds on oily metals and untreated plastics.

Adhesive Testing. The lifetime of an adhesive includes shipping and compounding of its components, storage and shipping of the adhesive in its final form, application to a surface or surfaces, service use, and a number of methods of disposal along the way and at its end. Adhesive raw materials are tested for certain characteristics at their source and then tested to some minimum standard by the adhesive manufacturer at the manufacturing site. The manufacture of adhesives is either a bulk or continuous process, as appropriate to the form and type of adhesive. After manufacture, there is testing to known standards based on customer and manufacturer requirements. Tests done on the as-manufactured adhesive include both bulk tests of the adhesive which are relevant to its handling and dispensing and tests of the adhesive as a bonding agent. Even before any of this testing occurs, there will often have been extensive laboratory testing of the adhesive to customer specifications, only a very small part of which is repeated on each lot subsequent to manufacturing. In bulk testing of both cured and uncured adhesives, attention to detail is of paramount importance. Consistency of preparation and test conditions can have a profound effect on final results, which are increasingly subjected to statistical analysis during development and through various manufacturing processes.

A variety of standardized tests have been published for adhesive testing. The American Society for Testing and Materials (ASTM), the Technical Association of the Pulp and Paper Industry (TAPPI), the Society of Automotive Engineers (SAE), the Pressure Sensitive Tape Council (PSTC), and the International Organization

for Standardization (ISO) have developed and published many different tests of interest to the technical community. Many academic and corporate libraries have bound collections of these standards. One can search the standard titles at each organization's website, respectively: www.astm.org, www.tappi.org, www.sae.org, www.pstc.org, and www.iso.ch. These organizations and their volunteer working committees actively update existing methods, standardize new methods, and obsolete older methods no longer in wide use. Additional standards are also published by or available from other professional organizations as well as specific companies and institutions. One will find that similar tests have been published by more than one organization or by the same organization; it is therefore useful to consult the source closest to one's interests and to review all applicable methods to find the one closest to one's needs. Variation from these standard methods, which is not uncommon, should be noted whenever reporting results from a given test. In cases where a specific test has not been published, these standards often provide help in developing needed tests. Numerous tests are also described in the open technical literature.

Bulk Testing. The chemical fingerprint, identity of, or contaminants present in bulk uncured adhesives can be obtained by any of the chemical tests routinely performed on other chemicals, including Fourier-transform infrared spectroscopy, mass spectrometry, and elemental analysis. Many adhesives are tested for their water or solvent content using weight loss or expansion tests or one of the analytical methods available. Percent solids are sometimes determined using mass measurements made before and after treatment in an ashing furnace. Volatile organic content is measured using weight loss tests done under relevant conditions. Measurement of the flow properties of adhesives is very important. Rheological tests include simple empirical tests that measure quantities such as the time needed to flow a certain volume a certain distance down an inclined plane or through a pressurized orifice, rotating-spindle tests that determine the relative viscosity of a liquid, and more advanced methods using cone-and-plate and parallel-plate methods that directly measure viscosity, yield stress, and flow activation energy at a variety of shear rates and temperatures. Density of paste adhesives can be measured using calibrated pycnometers. Thicknesses of solid adhesives, tapes, and related products can be measured manually or with methods such as x-ray fluorescence. Qualitative tests performed on adhesives include those addressing color, odor, consistency, foreign particulates, separation, and skinning. Shelf-life tests of bulk adhesives generally track how one or more of these many adhesive characteristics changes with time and temperature.

Testing of cured adhesives in the bulk state has become more widespread because of increasing use of adhesives in engineered structures. Concurrently, modelling of adhesive joints has become more commonplace, and for such work, measurement of the bulk mechanical and solid fracture properties in a variety of modes is essential. Developers of adhesives are also increasingly aware that testing of cured adhesives in the bulk state can provide information relevant to their performance in bonded joints.

Tests in common use for bulk characterization of adhesives include ASTM D816, *Standard Test Methods for Rubber Cements*; SAE J1524, *Method of Viscosity Test for Automotive Type Adhesives, Sealers, and Deadeners*; ASTM D638, *Standard Test Method for Tensile Properties of Plastics*; ASTM D3983, *Standard*

Test Method for Measuring Strength and Shear Modulus of Nonrigid Adhesives by the Thick-Adherend Tensile-Lap Specimen; and ASTM D2979, *Standard Test Method for Pressure-Sensitive Tack of Adhesives Using an Inverted Probe Machine*.

Adhesive Bond Testing. Practical adhesion is quantified in terms of the force or energy per unit area needed to separate a bonded joint. The most commonly used bonded joint configurations are the asymmetric and symmetric overlap shear and 90° and 180° peel. Many special or use-specific adhesive joint tests are also done. Adhesive tests based on fracture mechanics are increasingly used for their relevance to engineering design. Commonly used adhesive bond tests include ASTM D1002, *Test Method for Apparent Shear Strength of Single-Lap-Joint Adhesively Bonded Metal Specimens by Tension Loading (Metal-to-Metal)*; ASTM D2095, *Standard Test Method for Tensile Strength of Adhesives by Means of Bar and Rod Specimen*; ASTM D950, *Standard Test Method for Impact Strength of Adhesive Bonds*; ASTM D1780, *Standard Practice for Conducting Creep Tests of Metal-to-Metal Adhesives*; ASTM D2294-96, *Standard Test Method for Creep Properties of Adhesives in Shear by Tension Loading (Metal-to-Metal)*; ASTM D1876, *Standard Test Method for Peel Resistance of Adhesives (T-Peel Test)*; and ASTM D3330/D3330M, *Standard Test Method for Peel Adhesion of Pressure-Sensitive Tape*.

The testing of adhesives for their initial bonding characteristics makes up but one portion of adhesive testing. Testing of adhesive bonds under sustained mechanical loads and aggressive environments (moisture, heat, salt spray, saline soaks, solvent soaks, etc) comprises a significant part of testing. Repeated cycling of adhesive bonds through three or more environments, with or without a sustained load, is widely used although there is not always as much a strong scientific basis for the design of such test regimens as there is an experience base that suggests that such tests are predictive. Impact and dynamic or fatigue testing of adhesive bonds have become important components of adhesive testing.

Classification of Adhesives

There are many ways to classify adhesives. These include chemical class, joint strength, bulk modulus, physical form, ultimate use, general market, method of application, and price. Another classification scheme involves considering the activation of an adhesive and the driving force for its change from a liquid-like system to a solid-like system. Each of these methods of classification provides a framework within which to understand adhesives.

The primary chemical classes from which adhesives are made include epoxies, acrylics, phenolics, urethanes, natural and synthetic elastomers, amino resins, silicones, polyesters, polyamides, aromatic polyheterocyclics, and the various natural products such as carbohydrates and their derivatives as well as plant- and animal-based proteins. Chemical class was once a relatively clean differentiator of adhesives, but so many adhesives now are hybrids, designed to take advantage of specific attributes of more than one chemical class or type of material. Hybridization can be accomplished by incorporating into an adhesive a nonreactive resin of a different chemical class; adding another type of reactive monomer, oligomer,

or polymer; or chemically modifying an oligomer or polymer prior to adhesive compounding.

The measured overlap shear strength or peel strength of an adhesive joint is sometimes used to classify adhesives. The choice of substrate is a key element of such a comparison, certain aluminums or steels being most commonly chosen as standards, but glass, polyolefins, and other substrates are also used. Pressure-sensitive adhesives will be found at the low end of the bond strength spectrum, and structural adhesives will be found at the high end. In the middle will be found materials that are strong but not necessarily structural in nature; these are often called semistructural adhesives. Many sealants are strongly adherent, and some of these are referred to as adhesive sealants.

Market is a useful category for those interested in the buying and selling of adhesives, but market-based categories can be very broad. Construction adhesives, for example, include joint compound, carpet glues, ceramic and vinyl tile adhesives, a variety of wood-bonding adhesives, and double-sided foam tapes for hanging architectural glass. Although the adhesives used in some of these product categories are relatively standardized, there are many choices in other product categories. Similar breadth and depth would be encountered among adhesives used in the automotive, medical, and electronics industries. Within each of these market areas and most other market areas there will be found both commodity and specialty adhesives.

Most of those who develop adhesive compositions consider the form and ultimate use of an adhesive to be the most useful categories because these guide and direct adhesive development. The ability of the adhesive formulator to satisfy an end use will be very much related to the completeness of the information available concerning performance attributes required or expected. Price is a category of immense interest to the adhesive developer as it helps to define the raw materials from which the formulator may choose. The adhesive development team often must work closely with the customer to learn what is really needed from an adhesive.

Forms and Types of Adhesives

As supplied, adhesives can be found in the form of low viscosity liquids, viscous pastes, thin or thick films, semisolids, or solids. Before application to a substrate, an adhesive need not be sticky or otherwise particularly adherent. A distinct exception is the pressure-sensitive adhesive (PSA), which is inherently tacky when first made. Such an adhesive is applied as a thin film with or without a backing, the combination of the adhesive and the backing defining an adhesive tape. The PSA remains throughout its useful lifetime essentially the same material it was when first made. All other forms and types of adhesives undergo a transformation which is central to their function as an adhesive. This transformation is usually carried out through imposition of time, heat, or radiation, either actively or passively.

By loss of liquid, an adhesive applied as a true solution or a dispersion of solids will dry through loss of water or another solvent, leaving behind a film of adhesive. A reactive adhesive system will form internal chemical bonds through

the process of cross-linking, chemical reaction that joins dissimilar long-chain molecules, or polymerization, chemical reaction that joins similar monomer units. Solid adhesives are heated in order to be applied and then on cooling become functional adhesives. The transformation from a liquid, paste, or semi-solid to a functional adhesive is loosely termed *curing*. Additional general terms that refer to this transformation include *setting up* and *hardening*. Adhesives may also cure in stages. The first stage of curing is sometimes referred to as the B stage, and adhesives which have undergone some level of precure in their manufacture are often said to have been *B-staged*. For many adhesive applications, the ability of an adhesive to gel, precure, or develop green strength or handling strength is a key characteristic, being most important for parts which will be bonded and then transported to the next step in their processing. *Adhesives* are referred to as such before and after cure.

Pressure-Sensitive Adhesives. Pressure-sensitive adhesives (PSAs) are inherently and permanently soft, sticky materials that exhibit instant adhesion or tack with very little pressure to surfaces to which they are applied. The level of adhesion may build with time and be surprisingly high. PSAs generally have a high cohesive strength and often can be removed from substrates without leaving a residue. Some applications take advantage of a PSA's ability to quickly form a strong bond and under stress, force failure elsewhere in a system, an attribute used to advantage in tamper-proof packaging and price stickers. At the other end of the spectrum lie PSAs that can be repeatedly repositioned. The primary characteristics used to describe the performance of PSAs are tack, adhesion strength in peel, and resistance to shear forces.

PSAs can be sold in bulk or solution for later coating by product manufacturers. Most PSAs, however, are sold as components of tapes or labels. PSAs are also used to make protective or masking films, some of which also function as conventional tape products. PSAs are sold in the form of aerosol sprays for graphic arts work. Tape products join one object to another, as when one wraps a gift, seals a box, or puts up a notice. They consist of a film or web carrier coated on one or both sides with a PSA. The carrier is usually a paper or synthetic polymer made in the form of a solid or a foamed film. It is a key component of the tape. Such a construction is usually slit and wrapped on itself to form rolls of adhesive tape from which sections of the desired length can be removed. A release coating is sometimes added to the backside of the tape backing so that the tape can be removed from the roll cleanly, easily, and quietly without splitting the adhesive from the backing. Double-sided tapes that have no release liner effect release through opposite pairing of chemically different adhesives which are chemically incompatible or through use of adhesives of different levels of cross-linking which are physically incompatible. There also may be a primer on one or both sides of the tape carrier to ensure better adhesion of the PSA or the release coating. Some tapes are sold with release liners that must be removed after the tape is taken off its roll. Tapes can be applied manually or via mechanized tape dispensers for packaging, splicing, and other applications. Labels are sold with the PSA already present for their attachment to a variety of surfaces. Transfer tapes are PSAs that are provided on a liner from which the adhesive film can be transferred to another surface. PSAs that are effectively sticky hot-melt adhesives can be applied

in discrete lines, dots, or other shapes using manual and automated equipment. The convenience and adaptability of PSAs has gained them wide use in diverse applications in virtually every market served by adhesives.

Many PSA compositions contain a base elastomeric resin and a tackifier, which enhances the ability of the adhesive to instantly bond as well as its bond strength. The elastomer may be useful without cross-linking but will often require either chemical or physical cross-linking for establishment of sufficient cohesive strength. Heat or uv or radiation is usually the activator of the cross-linking, and suitable catalysts are used, their choice depending on the base resin. Small amounts of epoxy or hydroxy functionality are sometimes added to allow uv cures if the base resins are not themselves uv-curable. Electron beam curing has received attention but tends to be more costly than uv curing. Elastomers used as the primary or base resin in tackified multicomponent PSAs include natural rubber, polybutadiene, polyorganosiloxanes, styrene–butadiene rubber, carboxylated styrene–butadiene rubber, polyisobutylene, butyl rubber, halogenated butyl rubber, and block polymers based on styrene with isoprene, butadiene, ethylene–propylene, or ethylene–butylene. Any of these resins may be blended with each other to alter or optimize properties. Polychloroprene, *cis*-polyisoprene, and some waxes are rarely used as the main components in PSAs but have found some use as modifiers. Natural rubber grafted with methyl methacrylate, styrene–acrylonitrile copolymers, and other elastomers have been found useful as components of primers for PSA products. Polymers which can be useful as PSAs without tackification but may be modified beneficially with their addition include poly(alkyl acrylate) homopolymers and copolymers, polyvinylethers, and amorphous polyolefins. Comonomers useful for acrylate PSAs include acrylic acid, methacrylic acid, lauryl acrylate, and itaconic acid.

Much of the art of making PSAs rests in the choice of tackifier and the balance between base resins and tackifiers, of which there are numerous choices (19). Tackifiers commonly used with natural rubber, butyl rubber, and polyacrylates include rosins and rosin derivatives manufactured from pine tree gums. The styrenic block polymer base resins respond well to tackification with aliphatic and partially aromatic materials miscible with their continuous nonstyrenic phase or phases. Materials useful as PSA tackifiers have a lower molecular weight than the base resin. They are useful because they lower the modulus of the bulk adhesive in the rubbery region of the modulus–temperature spectrum, that is, above the glass-transition temperature. Tackifiers also tend to raise the glass-transition temperature of the system. Tackifiers which react with PSA resins have been introduced to counteract tendencies of tackifiers to migrate, bloom, or volatilize; these kinds of tackifiers are based on isocyanato-reactive or vinyl functional groups (20). Plasticizers are mentioned somewhat synonymously with tackifiers as modifiers for PSAs, but their use is recommended cautiously as any improvements they provide in tack can be quickly offset by losses in strength if the glass-transition temperature of the material is lowered too much.

Silicone PSAs are blends or reaction products of the combination of a polyorganosiloxane, such as poly(dimethyl siloxane) or its copolymers with diphenylsiloxane or methylphenyl siloxane, with a polysiloxane resin, which is largely inorganic. Pendant vinyl groups may also be incorporated into silicone PSAs,

making cross-linking possible with peroxide and other kinds of cures. These kinds of PSAs are most often tackified with additional silicone gums and siloxane resins of varying molecular weight. The silicone PSAs are unique in their resistance of temperatures up to 400°C; performance at elevated temperatures can be optimized using the siloxane resins and rare earth or transition-metal esters (21) (see PRESSURE SENSITIVE ADHESIVES).

The large bulk of PSAs are coated onto continuous webs or films to make pressure-sensitive tapes, labels, and so on. While many PSAs continue to be coated out of organic solvents, many have been converted to water-based formulations or are extruded as hot-melt adhesives, which upon cooling retain their tack. Aqueous emulsions of carboxylated styrene–butadiene and various acrylate copolymers are among the most useful as bases for water-based PSAs. The complexity of latex chemistry introduces additives such as chain-transfer agents and defoamers (22) into some emulsion-based PSAs. Proper coating of these kinds of PSAs can require addition of thickening agents based on water-soluble polymers. Other additives that may be found in PSAs include cross-linking agents, catalysts, heat stabilizers, antioxidants, photoinitiators, depolymerizers (or peptizers), and various fillers. Reinforcing agents such as phenolics and higher molecular weight relatives of the tackifiers are sometimes added to improve cohesive strength. As made, PSAs are generally colorless or off-white in appearance but are sometimes pigmented for color adjustment or become pigmented through addition of a colored filler such as titanium dioxide, talc, or silver.

Hot-Melt Adhesives. Hot-melt adhesives are solid adhesives that are heated to a molten liquid state for application to substrates, applied hot, and then cooled, quickly setting up a bond. The largest uses of hot-melt adhesives are in packaging, bookbinding, disposable paper products, wood bonding, shoemaking, and textile binding. The advantages of hot-melt adhesives include their easy handling in solid form, almost indefinite shelf life, generally nonvolatile nature, and, most importantly, ability to form bonds quickly without supplementary processing. They are considered friendly to the environment and are expected to see expanded use on a worldwide basis as the market continues to move away from solvent-based adhesives. The disadvantages of hot-melts lie in their tendency to damage substrates which cannot withstand their application temperatures, limited high temperature properties, and only moderate strength.

Application temperatures typically used for hot-melts range from about 65–220°C. Although the industry still refers to most temperature-sensitive adhesives as hot-melts, one will see references to warm-melt adhesives that soften at about 121°C and cool-melt adhesives that soften below about 100°C, but these terms are somewhat arbitrarily applied. Decreases in the application temperatures for hot-melts have lessened safety concerns associated with this type of adhesive. While most hot-melts are supplied as sticks or pellets, they are also produced as flat films or sheets, rolls, fibrous nonwovens, powders, strings, bulk masses, or dots or lines on liners.

Hot-melts generally are based on one or more thermoplastic resins. The largest portion of commercial hot-melt adhesives has for many years been based on ethylene–vinyl acetate copolymers having a vinyl acetate content of about 20–40%. The styrenic block polymers which are thermoplastic elastomers also make up a large portion of hot-melts. Other resins that have been found useful as bases

for hot-melts are synthetic elastomers, ethylene–ethyl acrylate copolymers, amorphous polyolefins, branched polyethylenes, polypropylene, polybutene-1, phenoxy resins, polyamides, polyesters, and polyurethanes. Combinations of these resins allows for property and cost adjustments. Tackifiers and plasticizers are commonly added to hot-melts to improve their flow and adhesion to substrates. Examples include synthetic hydrocarbons, natural terpenes, rosins, and various phthalates. Polybutene is occasionally used as the base resin for hot-melts having good cold flow and high wet-out characteristics, but it may also be used as a flexibilizer or plasticizer. Waxes are important hot-melt ingredients, lowering melt viscosity and improving wet out of the substrate. Reactive tackifiers exist to address migration. The polyamide, polyester, and polyurethane hot-melts are often classed separately from the other resins on which hot-melts are based. All are the result of condensation reactions, and they are frequently used with few additives, their properties instead being adjusted by changing the starting ingredients of the polymers. They may, however, contain additives that make them better suited to specific uses. Adhesives based on these polymers are considered to deliver higher performance by virtue of better high temperature resistance and higher strength and may provide better adhesion to polar substrates than the other largely hydrocarbon hot-melt adhesives (23).

Conventional hot-melt adhesives cool to set and do not chemically cross-link. Such systems have an open time of a few seconds to a few minutes. The need for more heat-stable adhesives and stronger bond strengths has driven the development of reactive hot-melts which undergo cross-linking. These are primarily based on polyurethane hot-melts with residual isocyanate groups that react with water after application to form a thermoset adhesive material. Water is provided by the surrounding air and substrate. Cure of these hot-melts is nearly complete within 24 h, but time for full cure will depend on temperature and ambient and substrate moisture content. An extension of the water-activated isocyanate cross-linking reaction is found in the use of polyurethanes which have been silylated to provide active hydrogens for reaction with residual isocyanates in polyurethanes (24). The acceptance of reactive polyurethane hot-melts has led to development of reactive block polymer and acrylate hot-melts which rely on radiation cure through activation of epoxy or vinyl groups (25,26); these are used primarily as PSAs.

Hot-melt adhesives are usually clear, off-white, white, or amber. Colored versions are available for nonbonding decorative use, for example, arts and crafts. Good color retention with heat aging is an important feature of a heat-stable hot-melt system, and antioxidants and heat-stabilizers are common ingredients in hot-melt adhesives. Photoinitiators are frequently present when uv or other radiation curing will be used. Other useful additives include fillers and reinforcing agents. When there is some lack of cohesiveness in blends of base resins, compatibilizers may be used to improve the apparent miscibility of these resins (27). Hot-melts can be based on either amorphous or semicrystalline resins. Particularly in the case of semicrystalline resins, the rate of cooling can dramatically affect adhesion to a substrate (28). To control the development of crystallinity, nucleating agents may be added to formulations based on crystallizable polymers such as polyesters.

Solution Adhesives. Adhesives delivered out of solutions are typically used for joining large areas destined for nonstructural or semistructural service.

The solution may be made with an organic solvent or with water or may be an aqueous dispersion. It is important that the liquid carrier have some means of escaping from the bondline in order for the proper bond strength to develop. It should be appreciated that many PSAs are made by casting out of liquids, but when put into use as components of tapes or labels, these adhesives are soft solids containing virtually no liquid.

Solvent-Based Solution Adhesives. Contact adhesives, activatable dry-film adhesives, and solvent-weld adhesives make up the solvent-based adhesives. Contact adhesives are solutions of high polymers which are applied to all surfaces to be joined via spray or brush, allowed to dry partially, and then given time under pressure to allow the adhesive layers to fuse. Heat is sometimes used to increase tack or accelerate drying. These adhesives are commonly used to join wood veneers to wood bases, synthetic laminates to particleboard countertops, and paper products to other materials. The major dry-film adhesive is solvent-applied natural rubber, which is unique in its ability to adhere to itself without tackification and useful for self-sealing envelopes and similar employment. After being coated on to paper or another substrate, dry-film adhesives must be wiped or sprayed with a liquid to regain their adhesiveness; the activating liquid now is nearly always water. Solvent-weld adhesives are used to join plastic parts such as PVC piping. The adhesive is usually a solution of PVC or chlorinated PVC that is applied to the outer surface of the pipe and the inner surface of a connector piece that are joined firmly together before the solvent has evaporated.

The most widely used contact adhesive is a solution of polychloroprene or modified polychloroprene in solvent blends of aromatic hydrocarbons, aliphatic hydrocarbons, esters, or ketones, for example, toluene–hexane–acetone. Viscosity, dry time needed before bonding, bond strength, and price are affected by the solvent. Using various combinations of the isomeric forms of polymerized 2-chlorobutadiene permits a fine-tuning of the crystallization rate of the dissolved polymer as the solvent evaporates. The polychloroprene may also be modified by the incorporation of methacrylic acid or mercaptans. Metal oxides (MgO and ZnO) that scavenge acids are often part of polychloroprene adhesives and also may act as cross-linking agents. Oxygen scavengers such as butylated hydroxytoluene (BHT) [128-37-0] or naphthylamines [25168-10-9] are added to prevent dehydrochlorination. To build initial handling strength, the solvent-based polychloroprene contact adhesives may be modified with alkyl phenolics, terpene phenolics, or phenolic-modified rosin esters, the first of these being the most effective and least deleterious (29). Chlorinated rubbers are sometimes added to these adhesives to improve their adhesion to plasticized PVC and other plastics. Added just before adhesive application, isocyanates are useful in modification of polychloroprene contact adhesives, reacting perhaps through hydrolysis of the pendant allylic groups present from the small number of 1,2 isomeric segments (30). The remainder of the solvent-based contact adhesives are comprised of polyurethane, SBR, styrene–butadiene–styrene block polymers, butadiene–acrylonitrile rubber, natural rubber, or various acrylic or vinyl resins in suitable solvents.

Water-Based Solution Adhesives. Solution adhesives based on water dispersions and aqueous emulsions are steadily gaining in use largely at the expense of solvent-based adhesives. These are rarely true solutions, with the exception of the viscosity modifiers often used to adjust flow characteristics. Dispersions

of polyurethanes in water find use in bonding of plastic sheets and films, cloth, shoe parts, foams, PVC veneers, and carpets. Other water-dispersible resins can be added to the polyurethane dispersion to lower costs and modify performance characteristics. The largest group of water-dispersed or water-dissolved adhesives are made of natural products, which are covered separately. At one time, vegetable gums were used widely as water-activatable adhesives, but poly(vinyl alcohol) has replaced them in envelope sealing and similar areas.

Poly(vinyl acetate) emulsions, the basis of the ubiquitous household white glues, are among the most familiar water-based adhesives. These are widely used for paper and wood bonding. They contain a substantial percentage of vinyl alcohol content, formed via partial hydrolysis from the vinyl acetate homopolymer as vinyl alcohol itself is not a stable molecule. Such latices are stabilized through the use of surfactants, one choice being well-hydrolyzed poly(vinyl acetate). After application to the substrate, latex adhesives cure by the evaporation of water accompanied by the coalescence of the latex particles. On the porous substrates with which these are most frequently used, the water exits the bondline through the substrate as well as the adhesive, preventing voiding or foaming which might weaken the bond. Subtle changes in properties can be engineered through the use of other comonomers or the use of liquid plasticizers. Glyoxal [107-22-2] or other cross-linking agents can be added to poly(vinyl acetate) latex adhesives to combat creep (31).

Polychloroprene latex adhesives have been available for many years. They are stable at pH values between about 10 and 12. The latex particles are usually lightly cross-linked. Except for the substitution of water for the organic solvent, the ingredients in these kinds of adhesives are similar to those found in their solvent-based counterparts. Terpene–phenolics are particularly effective as tackifiers for contact adhesives based on polychoroprene latices but rosin acids, rosin esters, hydrocarbons, and coumarone–indenes are also useful, particularly where heat-assisted bonding is not possible. Dehydrochlorination leading to acid generation is particularly possible with the water-based polychloroprene adhesives. Like other water-based adhesives, these may require addition of biocides or preservatives to prevent the breeding of microorganisms (32).

Structural Adhesives. Structural adhesives are designed to bond structural materials. Nearly any adhesive giving shear strengths in excess of about 7 MPa (about 1000 psi) may be called a structural adhesive. Structural adhesives are generally the first choice when bonding metal, wood, and high strength composites to construct a load-bearing structure. Bonds formed with structural adhesives cannot be reversed without damaging one or the other substrate. They are the only kind of adhesive that might be expected to be able to sustain a significant percentage of its initial failure load in a hot and humid or hot and dry environment. Any one of these descriptors names structural adhesives the strongest and most permanent type of adhesive. For good reason, they are sometimes referred to as engineering adhesives. The strength and permanence of structural adhesives is largely achieved using reactive adhesives, a term which has become something of a synonym for structural adhesives. Epoxies are the most widely used class of structural adhesive chemistry, but acrylates, urethanes, phenolics, and other classes have been used to great advantage, and the combination of these different chemical classes to create hybrid adhesives propagates the best virtues of each.

Reactive adhesive systems which are arguably not always considered structural adhesives but are conveniently grouped here are also reviewed in this section.

Epoxy Resins. Epoxy resins have a long and distinguished record as structural adhesives. Their use dates to 1950 or earlier, and their utility for adhesives was recognized upon their development. Most epoxy adhesives are resins based on what is commonly known as the diglycidyl ether of bisphenol A (DGEBPA). These resins are based on the reaction of 4,4′-isopropylidene diphenol (bisphenol A) [80-05-7], $C_{15}H_{16}O_2$, and epichlorohydrin [106-89-8], C_3H_5ClO. The molecular weight of the commercial difunctional resins formed by this reaction will vary with the molar ratio of the reactants. At a molecular weight of about 400 or less, these resins are viscous liquids which are immensely useful in epoxy adhesives. Commercially viable solid resins based on DGEBPA have molecular weights ranging up to about 4000. Many epoxy adhesives will also contain a small amount of an epoxy diluent having low viscosity and a more flexible structure; this resin adjusts the flow of the system and also helps to wet out the fillers that are usually present.

A wide variety of epoxy resins are commercially available: monofunctional or polyfunctional, aliphatic, cyclic, or aromatic. Brominated epoxies may be useful where flammability is a concern. An oxirane functionality is all that is needed to make an epoxy resin, and structural adhesives are only one of over a dozen different uses for epoxy resins. Many epoxy resins on the market will not necessarily be suitable for adhesives, but their availability does expand the choices available for adhesive formulators. The specialty epoxy resins developed specifically for adhesive use sometimes will be more costly than the DGEBPA resins but may provide the basis for a specialty adhesive that can meet a unique need and therefore command a proportionally higher price. Examples of these are epoxy-functional dimer acids, urethanes, and various elastomers.

Epoxy resins based on DGEBPA usually are quite stable at temperatures up to 200°C. Curing agents, sometimes called hardeners, must be added to the epoxy so as to cause cross-linking and chain extension to occur and a bond to form. Certain types of curing agents will be favored over others for each of the three types of epoxy structural adhesives: one-part (1K) epoxy paste adhesives, 2K epoxy paste adhesives, and 1K epoxy film adhesives. The strained oxirane ring is reactive with functional groups having either nucleophilic (basic) or electrophilic (acidic) character. Acid anhydrides, carboxylic groups, and hydroxyl groups react very slowly with the oxirane ring and are usually used with catalysts that accelerate their reaction with epoxies. Those groups which readily react without catalysts but often benefit from their use include amines and mercaptans. Both the epoxy resin and the curative package (curing agent plus catalyst) will influence final cure speed.

One-part (1K) paste adhesives usually consist of a DGEBPA resin, a reactive diluent, and latent curing agents that are insoluble with the resin at room temperature but dissolve at elevated temperatures to trigger cure. These kinds of adhesives are in use in the aerospace, automotive, and electronics industries. Dicyanodiamide or dicyandiamide [461-58-5], $C_2H_4N_4$, is the most frequently mentioned latent curing agent for cures occurring in the range of 170–180°C; practitioners refer to this material as *dicy*. Also useful in this range are metal-complexed imidazoles, complexes of Lewis acids (eg, boron trifluoride with amines), and diaminodiphenylsulfone. Cure temperature can be lowered by

using micronized dicyanodiamide ground to a particle size of 5–15 μm. Cure can be accelerated by use of aromatic tertiary amines, imidazole derivatives, and epoxy resin adducts with tertiary and other amines. Substituted ureas such as Monuron [150-68-5], $C_9H_{11}ClN_2O$, and nonchlorinated substituted ureas such as 3-phenyl-1,1-dimethylurea [101-42-8], $C_9H_{12}N_2O$, have also found use as accelerators in 1K epoxy adhesives. Dihydrazides offer a range of melting points depending on structure, their cure temperatures with epoxies beginning as low as 100–110°C. Adducts of dicyanodiamide which melt at temperatures in the 115–120°C range are available. Accelerated 1K epoxies show faster cures once heated but suffer from decreased shelf lives; after manufacture, they are usually stored in refrigerators or preferably freezers although this is usually impractical for drum quantities. For these same reasons, their manufacture is carried out at temperatures well below their activation temperatures and at low shear rates to avoid viscous heating.

The low viscosity two-part (2K) epoxy adhesives sold in hardware stores as 5-min epoxies are based on cure with polymercaptans regulated with amines to control worklife. The human nose can sense some mercaptans in air at the ppb level, making them valuable as gas odorants, but they are tremendously useful as curing agents, particularly when used in thin films as for adhesives. Their low toxicity is also an advantage. Capcure 3-800 [101359-87-9] is a commonly found polymercaptan. Low odor polymercaptans have been developed which combine strategies of odor masking, odor counteracting, and absorbency to stabilize polymercaptans, reducing the level of odor by about 75% (33). Higher molecular weight versions of the polymercaptans are useful as the base resins of polysulfide sealants, which are sometimes categorized as adhesives. In full formulation, the polysulfide base resins are blended with curing agents such as manganese dioxide or sodium perborate, accelerators or retarders, fillers, plasticizers, thixotropes, adhesion promoters, and pigments (34). These materials are used primarily in the construction and aerospace industries.

Many useful 2K epoxies utilize curing agents that are the reaction products of amines of low molecular weight with fatty acids. These are variously known as polyamidoamines, polyamides, and amidoamines and sold in a range of molecular weights under trade names such as Versamid and Ancamide. The fatty acid portion of these amines gives them larger bulk than the lower molecular weight amine curing agents, which facilitates formulation of adhesives having mix ratios closer to 1:1 by volume, which is of benefit for both packaging and off-ratio tolerance. Curing with polyamidoamines generally produces relatively flexible adhesives having good chemical resistance. Because they typically cure slowly, they are frequently used in combination with other amines such as diethylenetriamine (DETA), triethylenetriamine (TETA), tetraethylenepentamine, aminoethylpiperazine, modified imidazolines, and oligomeric amine-terminated polyethers. Some of the amines in this group are used as sole curing agents, and others, such as DETA and TETA, are used as epoxy adducts to reduce toxicity and increase stability. Aromatic amines, although useful for epoxy resin composite matrices, find little use in epoxy adhesives.

Another family of curing agents is based on substituted phenols such as tris(dimethylamino)phenol [31194-38-4], $C_{12}H_{21}N_3O$, and tris[(dimethylamino)methyl]phenol [90-72-2], $C_{15}H_{27}N_3O$. These tertiary amines

can produce rather brittle adhesives if used as sole curing agents, but are valuable as accelerators for other amines. They act as catalysts for dicarboxylic acid anhydride cures. Amines are also useful as accelerators for the oxirane–alcohol reaction, which is sluggish at room temperature but with catalysis will proceed above 120°C. Imidazoles are also generally useful as catalysts or cocuring accelerators for epoxy reactions with amines, hydroxyls, and thiols. Organic and inorganic salts sometimes find use in epoxy adhesives, coatings, and encapsulating compounds. Acid catalysts such as boron trifluoride–amine complexes find some use in epoxy adhesives but tend to require long cures, even at elevated temperatures, which normally works against their use in adhesives. Epoxy resins react slowly with acid anhydride curing agents but can be accelerated with acids or bases, imidazoles being used most often; however, anhydrides are not often used as curing agents in epoxy adhesives.

Epoxy film adhesives are 1K adhesives in film form. They are formulated much like 1K paste adhesives but often contain solid epoxy resins and additional resins that provide binding properties. These may be partially cured (B-staged) to provide a more dimensionally stable film. Epoxy film adhesives have been widely used in the aerospace industry where their relative stability accommodates the long build times needed for aircraft manufacture. Their cured properties can be outstanding in terms of strength, toughness, and durability. They can be supplied in film form and cut to size or provided as tapes in convenient slit widths. They may be made to be tacky using rubber resins and other mild tackifiers or they may be dry. Film adhesives of a more aggressive pressure-sensitive character have been developed by coating or laminating with pressure-sensitive formulations or formulating such that the bulk adhesive (35) is a PSA in its own right but can be cured to a semistructural or structural strength. Epoxy film adhesives based on thermoplastic polyamide resins are very tough when cured but can be susceptible to moisture absorption.

In addition to resins and curing agents, epoxy adhesives will contain many functional additives and modifiers. Flexibilizers and toughenersuch as polysulfides, epoxidized fatty acids, epoxidized polybutadiene, and amine- and carboxy-terminated acrylonitrile butadiene polymers react with the epoxy network. Flexibilizers remain in phase with the epoxy while toughenersypically phase separate to form domains, the result producing a tougher adhesive with more or less strength reduction relative to an unmodified system. Particulate toughenersay also be added to epoxy adhesives. These include core-shell resins, functionalized elastomeric particles, and ground reclaimed rubber. Positive aspects of structural adhesives based on epoxy resins include good adhesion to many substrates, no emission of volatiles upon cure, low shrinkage, and a broad formulating range based on a history of use dating to the 1940s. The lack of outgassing allows most curing to be done at ambient pressure although clamping till cure is standard protocol for any adhesive bonding operation. Shrinkage can be further decreased with use of appropriate fillers, harder fillers by some reports providing the lowest shrinkage.

Acrylics. Historically, acrylics offer several useful characteristics as structural adhesives. Most well known is their relatively high speed of reaction via free-radical polymerization. The details of their reaction provide a useful division

of the different classes of acrylic structural adhesives into redox-activated adhesives, encompassing both anaerobic acrylics and nonaerobic structural acrylics, and Polycyanoacrylates. These will be considered in turn.

Oxygen inhibits the polymerization of acrylic monomers to a useful extent, and its exclusion kicks off polymerization of monomeric acrylates. Early versions of anaerobic acrylics relied solely on this mode of initiation and polymerization, containing little besides acrylate monomers and diacrylic esters (36). Later it was found that if hydroperoxides were incorporated into the acrylic monomer, small amounts of free metal ions from metal substrates could help to create free radicals that initiated polymerization of the acrylate monomers. Only small amounts of metal ions are needed, iron, nickel, zinc, and copper being some of those of major industrial interest. Even though a major alloying element, for example, aluminum, may not be capable of helping to generate free radicals via the redox reaction, minor alloying elements, such as copper, may be available which can act in this capacity. The speed of reaction is limited by the ability of the metal ion to reduce the peroxide. Free-radical initiators used in anaerobic acrylics have included cumene hydroperoxide, *t*-butyl hydroperoxide, and potassium persulfate [7727-21-1], $K_2S_2O_8$. Other useful initiators for this cure are combinations of saccharin [81-07-2] with aromatic amines such as *N*,*N*′-diisopropyl-*p*-toluidine [24544-09-0] or 1-acetyl-2-phenylhydrazine [114-83-0]; such combinations were originally thought to be accelerators useful only with peroxide initiators until it was found that they were themselves initiators (37). Various accelerators can be used with initiators to hasten cure of these adhesives; classes of compounds useful as accelerators include cyclic peroxides, amine oxides, sulfonamides, and triazines (38).

A key ingredient in anaerobic acrylic adhesives is the acrylate monomer or monomers. These include primarily acrylic acid and methacrylic acid and their many and various esters such as lauryl acrylate, cyclohexyl methacrylate, methyl methacrylate, hydroxyalkyl methacrylates, and tetrahydrofurfuryl methacrylate. These monomers vary in their volatility, reactivity, and cost, the less volatile monomers forming the basis of low odor acrylic adhesives. In addition to the monomer acrylates, there generally is also present a diacrylate which acts as a cross-linker, the alkyl glycol dimethacrylates being widely used in this function. Other ingredients used in these adhesives include stabilizers or polymerization inhibitors such as phenols or quinones, chelating agents that snatch up trace metals to prolong shelf life, and various modifiers such as inert fillers, inorganic and polymeric thickeners, elastomers to improve toughness, and bismaleimides that improve high temperature performance (39).

The low viscosities and good wetting properties of these adhesives allow them to penetrate and flow in tight spaces. This is taken advantage of in many of their uses. Threadlocking and sealing are primary applications. When applied to the threads of bolts or pipes, to flanges, and to other tight-fitting machine parts which are later screwed into or pressed against a mating surface, the adhesive cures because of the exclusion of air and the formation of free radicals via the reaction of metal ions with the initiator. Other applications include bonding of optical fibers, impregnation of porous parts, crimp-bonding of electrical parts, and fastening of press-fit parts. Anaerobic adhesives are one-part adhesives, usually packaged in

small oxygen-permeable plastic containers which have not been entirely filled, this arrangement providing a sufficient supply polymerization-inhibiting oxygen to ensure good shelf life.

The non-aerobic structural acrylic adhesives are two-part adhesive systems. They are generally less oxygen-inhibited than the non-aerobic acrylics and do not rely on metal surface activation in the same way as the anaerobics. These adhesives are very similar in formulation to the non-aerobics, each borrowing technology from the other as it has developed. Lower oxygen sensitivity is accomplished through higher concentrations of accelerators and initiators. The accelerators and initiators are usually redox couples such as the commonly used hydroperoxide/amine–aldehyde condensates (oxidant/reductant), which react to form alkoxy radicals. The most widely used condensate is a polymeric resin [9003-37-6]. Produced by reaction of *n*-butyraldehyde [123-72-8] with aniline [62-53-3]. This material has a complex structure, the major component and active ingredient apparently being dihydropyridine [27790-75-6] (40). Another common redox couple is based on hydroperoxide coupled with an alkyl aromatic amine such as *N*,*N*-dimethylaniline [121-69-7]. A number of 2K acrylic formulations include metals, metal oxides, or metal salts (41).

The 2K non-aerobic acrylic adhesives can be used in any of three ways. The first is as a no-mix two-part, the use of which involves applying a thin layer of accelerator (in dilute solution) to one mating surface, flashing off the solvent, applying the adhesive to the second mating surface, and joining the two surfaces. It is perhaps a poor choice of terms, but the accelerator contains the initiator (eg, peroxide) or may contain a redox couple. As long as the bondline thickness is no more than about 500 μm (0.020 in.) for one-side activation or about 1000 μm for two-side activation, cure is expected to be adequate. 2K acrylics which are meant to be mixed before application utilize a different kind of accelerator that contains the catalyst system in a carrier resin such as an epoxy and perhaps a diluent. These can be used in a fashion similar to the no-mix adhesives, but this approach may not produce optimal properties. Typically, the 2K acrylics are made by mixing the accelerator into the one-part acrylics and immediately applying this mixture to the substrate. Volume mix ratios will range from about 2:1 to about 20:1. Additional ingredients commonly found in these compositions include various elastomeric polymeric toughenersuch as chlorosulfonated polyethylene, butadiene–acrylonitrile elastomers, and polyurethane acrylates. These toughenersare usually incorporated into the adhesives by dissolution in the acrylic monomers, creating adhesives sometimes referred to as second-generation acrylics. Their development by DuPont (42) and others marked the entry of acrylic structural adhesives into a large number of new applications.

Because of their high reactivity, these 2K acrylic adhesives are used in many situations where fast ambient cure is important. Since the incorporation of the redox couple catalysts, acrylic adhesives have advanced their use on metals as well as plastics, woods, and ceramic substrates. As a class, they tend to be fairly accommodating of oily metal and unprepared plastics and composites. Offensive odors often accompany the common forms that use the less expensive lower alkyl acrylates. Colors of these materials are clear, off-white, white, and amber. They are not often intentionally pigmented, although they may be tinted by functional metal additives or aluminum powders.

A very important class of acrylic adhesives, the cyanoacrylates are distinguished by their relative simplicity of formulation and their nearly instant bonding properties. The name recognition of "super glue" surpasses that of nearly any commercial adhesive though it is now known by a variety of other ungenericized trademarks. First discovered in the 1940s during World War II, cyanoacrylates were rediscovered and first truly appreciated in the 1950s and brought to the market in 1958. Then as now they were largely based on ethyl and methyl cyanoacrylate. Other monomers of interest have been the isopropyl, butyl, allyl, ethoxyethyl, methoxyethyl, methoxypropyl, and fluoroalkyl esters (see POLYCYANOACRYLATES).

Cyanoacrylate adhesives cure by polymerizing anionically. They are catalyzed by mild nucleophiles (bases), such as an OH^- ion, which can readily be found in small quantities on many surfaces. Strong acids, found in many woods and acid-treated metals, can inhibit polymerization. As long as the adhesive film thickness is as low as possible, that is, practically zero, sufficient catalyst provided by the substrate will be available, hence the usual directive to apply the adhesive sparingly and to avoid using it as a void filler or to bond porous surfaces. Bond thicknesses higher than about 13 μm (0.005 in.) are not recommended unless appropriate surface activators are used. As the conversion to a cured adhesive is a polymerization, it passes through and is subject to the same stages as any addition polymerization: initiation, propagation, chain transfer, and chain termination. Like the anaerobic adhesives, these adhesives are conveniently initiated by coating onto surfaces suitable initiators such as alcohols, epoxides, various amines, caffeine, and other heterocyclic compounds (43). Compositions may also incorporate accelerators as well as inhibitors, the latter usually being either phenolics designed to inhibit premature polymerization because of heat or light or anionic polymerization inhibitors consisting of sulfur dioxide, other acid gases, or complexes of sulfur dioxide with organic or inorganic compounds. Normally quite brittle, cyanoacrylate adhesives can be flexibilized using monomers having longer alkyl side chains (2-octyl cyanoacrylate) or by incorporating plasticizers such as acetyl tributyl citrate (44). Various approaches have been taken to toughening the cyanoacrylates (45). As uncross-linked thermoplastic adhesives, the cyanoacrylates begin to soften and flow at about 80°C and will also depolymerize. Their durability in hot moist environments is considered to be poor, especially on metals. This has been addressed through introduction of difunctional or bifunctional cross-linkers, addition of heat-resistant adhesion promoters, and various other strategies aimed at improving moisture resistance. The last important component of the cyanoacrylate adhesive is the thickener, which is usually polymeric in nature.

Cyanoacrylates have long been known to be effective adhesives for human skin and other soft human tissues. They are effective when used for sutureless wound closures and hemorrhage prevention, the butyl cyanoacrylate being most widely used (46) based on a good balance between biodegradability and inflammatory response. Flexibilizers as well as aids to biodegradation are added to make these more suitable for tissue bonding. In everyday use, the outstanding capability of cyanoacrylate adhesives to instantly bond human skin is seen as a negative feature. Skin-adhesion inhibitors that have been found useful include alkanols, carboxylic acid esters (47), and copolymers of maleic acid, vinyl chloride, and vinyl

acetate (48). These slow the adhesive's reaction rates against human skin or at least lower adhesion to it.

Urethanes. The core of a urethane adhesive is an isocyanate compound (see POLYURETHANES). Isocyanates react with a variety of functional groups having active hydrogens to generate a variety of linkages which give the resulting polymers their names. These include reaction with alcohols to form urethanes [R—NH—CO—O—R′], with amines to form ureas [R—NH—CO—NH—R′], with thiols to form thiocarbamates [R—NH —CO—S—R′], with amides to form acylureas [R—NH —CO—N(R′)—CO—R″], with urethanes to form allophanates [R—NH—CO—N(R′)—CO—O—R″], and with ureas to form biurets [R—NH—CO—N(R′)—CO—NH—R″]. Isocyanates can also react with water, generating carbon dioxide through the degradation of the unstable carbamic acid [R—NH—COOH]. This last reaction is the basis for the making of polyurethane foams. To a great extent, what is classified as urethane chemistry encompasses the entire chemistry available to isocyanates (see ISOCYANATE-DERIVED POLYMERS).

Most polyurethane structural adhesives are two-part systems based on the reactions of isocyanates and polyisocyanates with oligomers or polymers having at least two hydroxyl groups, which are generically referred to as diols or polyols. Although part of many earlier adhesive formulations, toluene diisocyanate (TDI) is now decreasing in use while use of diphenylmethane diisocyanate (MDI) is growing. Other common diisocyanates include 1,6-hexamethylene diisocyanate (HMDI or HDI) and isophorone diisocyanate (IPDI). Also available are the modified MDIs, multifunctional isocyanates often termed polyisocyanates, polymeric polyisocyanates, and isocyanate-capped oligomers which are often referred to as urethane prepolymers (49). Materials now available which have very low monomeric isocyanate content are expected to bring about increased use of urethanes in adhesives (50). Hydroxyl-functional materials useful in urethane adhesives have molecular weights between about 500 and 3000 and functionalities between 2 and 3. The base oligomer is usually a polyester, polyether, polycarbonate, or polydiene such as polybutadiene. Cross-linked polyurethanes can be made with the use of trifunctional isocyanates and triols or through reactions of urethanes with urethanes, ureas, or isocyanates to yield the trimer isocyanurate.

In many cases, as polyurethanes are formed, long-chain and short-chain diols alternate along the chain to form segments which are either "soft" or "hard." On a microscope scale, the soft and hard segments coexist in a domain morphology characteristic of what are known as segmented polyurethanes. The very good impact and fatigue resistance of polyurethanes is attributed to this phase-separated microstructure. Because it is the integral component of the soft segment, the particular diol or polyol chosen will greatly influence the rubbery and impact-resistance properties of the polyurethane. Likewise, the isocyanate chosen will strongly influence the strength, modulus, and hardness of the polyurethane. The domain morphology of segmented polyurethanes is most pronounced for systems containing no chemical cross-linking. In contrast to most adhesive systems, low levels of cross-linking tend to degrade the properties of polyurethane adhesives because of disruption of the domain morphology.

Because isocyanates react with so many different organic functional groups and can also react with water, which is found nearly everywhere, catalysts are

very important for the control of isocyanate reactions. Many of the catalysts used may push one reaction over another, but they do not necessarily entirely block unwanted reactions. Tertiary amines, principally bis(dimethylaminoethyl)ether, are frequently used to promote the isocyanate–water reaction, producing a blowing or foaming that generally would not be desirable for adhesives. Compounds that drive the isocyanate–hydroxyl action without substantially encouraging the isocyanate–water reaction include organometallic complexes such as dibutyltin dilaurate and stannous octoate. At temperatures higher than 100°C, urethanes and ureas will react with isocyanates to form the allophanates and biurets described previously, but above 130°C, these groups will decompose. Dimerization of isocyanates to form uretidiones is catalyzed by bases such as trialkylphosphines, pyridines, and tertiary amines. Formation of the trimer of isocyanates, isocyanurates, is favored through use of phosphines, amines, and various metal salts such as potassium acetate.

One-part urethane adhesives have been used for many years as high performance sealants. In this capacity they provide a useful combination of strength, flexibility, and elastic recovery. As adhesives, these systems have limited use unless formulated to overcome their inherent disadvantages. One-part polyurethane adhesives are typically moisture-cured and rely on a multistep reaction sequence as follows: isocyanate reacts with water to form carbamic acid, the unstable carbamic acid loses carbon dioxide and generates an amine, the amine reacts with additional isocyanate to form a urea, and the urea reacts with additional isocyanate to form a biuret, which includes a cross-link. Unless it diffuses out of the system, the CO_2 can cause foaming. Formulators learn to minimize the isocyanate content (%NCO) of a system in order to balance cure speed with foam control. Cure speeds—and foaming rates—of these systems decrease from the outside in and vary with the amount of atmospheric moisture in the air, which changes hourly and seasonally.

A different kind of moisture-activated 1K urethane adhesive utilizes a moisture-activated curing agent such as oxazolidine (51). Oxazolidines are formed by dehydration and subsequent ring closure of aminoalcohols by aldehydes or ketones. When the presence of water causes that reaction to reverse, hydroxyl and amine groups are formed. These react readily and directly with isocyanates. Monooxazolidines are useful primarily as water scavengers, but bisoxazolidines can participate in the curing reactions of urethane adhesives.

More sophisticated 1K urethane adhesives use blocked isocyanates along with polyol curing agents. Useful blocking compounds include phenols, malonates, methylethylketoxime, and caprolactam. These react with isocyanates, but at high temperatures or in the presence of strong nucleophiles, the reaction reverses, freeing the isocyanate. Such systems do not rely on water for reaction, nor do they suffer from the detriments of CO_2 generation, but they do require heat for cure. Another approach to a stable 1K urethane is to use a solid polyol, such as pentaerythritol, that melts at elevated temperatures and then reacts with the isocyanate (52). Other schemes for 1K urethanes have been described (53).

As a class, urethane adhesives have somewhat poorer thermooxidative and moisture resistance than acrylic and epoxy structural adhesives. This has historically limited their expansion into certain areas of use. A 2K adhesive having the ability to survive automotive paint oven temperatures, which run as high as 205°C,

uses polyols with high percentages of hydroxyl groups, an acrylonitrile-grafted triol, a phosphorus adhesion promoter, and a DABCO trimerization catalyst (54). 1K adhesives made with blocked isocyanates tend to be unable to withstand high temperatures because of volatility of the blocking agents, and other approaches are also unsatisfactory for high temperature stability. Use of micronized dicyanodiamide as a latent catalyst and curing agent for isocyanates has produced 1K urethane adhesives showing some capability to tolerate heating to well over 250°C while bonding well to fiber-reinforced plastic (FRP) (55). Sensitivity to hydrolysis has been another of the historic disadvantages of traditional urethane structural adhesives.

Two-part polyurethane adhesives will usually contain fillers and may contain pigments that facilitate visual qualitative off-ratio mixing detection. To increase cure speed, polyamines are sometimes added to the polyol curative, which also contains the catalysts. In addition to their primary ingredients, one-part moisture-curing urethane adhesives will typically contain fillers and perhaps pigments. Arguably the largest user of urethane structural adhesives is the transportation industry, which uses urethane structural adhesives for bonding of automotive parts made of sheet molding compound, FRP, and reinforced reaction injection molding composites and plastics. One-part urethanes are widely used for bonding of windshields to automotive vehicle frames. Although 1K urethanes are not conventionally considered to be structural in nature, automotive engineers hold that the windshield is part of the primary structure of the vehicle, conferring on these one-part urethanes the status of a structural adhesive. Wood bonding is another significant market for polyurethane structural adhesives.

As a group, polyurethane structural adhesives produce bond strengths on the lower end of the strength scale for structural adhesives, but their high flexibility, usually strong peel strength, and generally good impact and fatigue resistance recommend their use when these characteristics are important. A variety of adhesives have been developed which incorporate polyurethanes into acrylic or epoxy structural adhesives (56–59). Inclusion is done through use of isocyanate-functional ingredients or polyurethanes end-capped with a nonisocyanato functional group. The broad reactivity of isocyanates offers many other options for hybridization.

Phenolics. Phenolic Resins were the basis of the first synthetic structural adhesives. They are formed by the reaction of phenol [108-95-2], C_6H_6O, and formaldehyde [50-00-0], CH_2O. There are two types of phenolic resins, resoles and novolaks (or novolacs), the former being comprised of methylol-terminated resins and the latter of phenol-terminated resins. Resoles result from use of basic reaction conditions and an excess of formaldehyde and will cure via self-condensation at 100–200°C with loss of water. Novolaks are produced using acidic reaction conditions and formaldehyde/phenol molar ratios of 0.5–0.8, and they require addition of a curing agent for cure. Hexamethylenetetramine [100-97-0], $C_6H_{12}N_4$, is a widely used novolak curing agent. Resoles and novolaks are sometimes referred to as one-step and two-step resins, respectively.

Formulators can choose from a variety of commercially available phenolic compounds, including, in addition to phenol itself, the isomers of cresol, the isomers of xylenol, resorcinol, catechol, hydroquinone, bisphenol A, and various alkylphenols. Formaldehyde is usually used as the second major component, but acetaldehyde, furfuraldehyde, and paraformaldehyde (the polymer of

formaldehyde) have been used sometimes alone and sometimes along with formaldehyde. The reactions of these various components are complex but have been elucidated by painstaking research (60).

Like epoxies, the phenolics are very brittle unless modified by toughening. The first successful toughening were poly(vinyl formal) resins which were added as a powder sprinkled over a layer of resole phenolic applied out of solution. These Redux adhesives were the first toughened thermoset adhesives and were the basis of the first durable adhesive bonding technology for aerospace aluminum in the 1940s and 1950s. These were superseded in the 1960s by film adhesives formed from liquid phenolics filled with poly(vinyl formal) powders. Other toughening followed: poly(vinyl butyral), nitrile rubbers, polyamides, acrylics, neoprenes, and urethanes. Epoxy–phenolics are important hybrid adhesives and offer an immensely useful combination of strength, toughness, durability, and heat resistance. Phenolic structural adhesives as a class of materials are highly resistant to most chemicals.

Phenolic adhesives are found as powders, liquids, pastes, and supported and unsupported films. Among the pastes, both 1K and 2K systems are available. Fillers are commonly used in paste adhesives. Support of film adhesives is provided by glass, cotton fabric, nylon, or polyester scrims. The novolaks are almost exclusively powders in pure form, but the resoles often are found as liquids. The resole systems are usually cured at temperatures exceeding 170°C. The condensation cure of the resole phenolics systems requires that they be cured under high pressures to minimize evolution of bubbles from water vapor. This is usually done in autoclaves or hot presses at pressures of about 200 to nearly 1400 kPa (29–203 psi) (61). Cure times range from 1 to 4 h depending on temperature. The cure conditions required for the resole phenolic adhesives have limited their use, and to a great extent they as well as the relatively brittle novolak phenolics have been displaced by epoxies for aerospace aluminum bonding applications for which they were once the first choice. Nitrile–phenolic adhesives have a long history of use not only in aerospace applications but also in automotive applications such as the bonding of brake linings and the friction materials used in transmissions. Resole phenolic resin adhesives are widely used in the making of plywood and particleboard as both binders and for laminating of veneers; resorcinol is frequently used along with phenol or as the sole hydroxyl compound. In wood bonding, the porosity of the wood allows escape of the water vapor generated during curing of the adhesive and is believed to facilitate mechanical anchoring of the adhesive in the wood. Phenolics are also widely used as foundry resins for making sand-shell molds.

Urea–Formaldehyde and Related Adhesives. Urea–formaldehydes (UF) are the most significant members of the class of materials known as the Amino Resins or aminopolymers. These are the polymeric condensation products of the reaction of aldehydes with amines or amides. A molar excess of formaldehyde is used, and this along with the temperature and the pH dictate the properties of the final product. The initial reactions of urea and formaldehyde to form mono- and dimethylolureas can be catalyzed by either acids or bases, but the final condensation reactions will proceed only under acid conditions. These adhesives are widely used to make plywood and particleboard in processes utilizing heated hydraulic presses with multiple outlets for water vapor release. Temperatures up to 200°C

may be used. UF adhesives in the first use contain hardeners composed of ammonium chloride or ammonium sulfate solutions or mixtures of urea and ammonium chloride plus fillers such as grain and wood flours. Particleboard adhesives, which are really binders, contain similar hardening agents, a worklife extender (ammonia solution), insecticides, wax emulsions, and fire-retarders. The slow hydrolysis of the methylenebisurea [13547-17-6], $NH_2CONHCH_2NHCONH_2$, has been linked to the slow release of formaldehyde from UF adhesives (62). The wood industry has been under increasing pressure to reduce and eliminate unreacted and evolved formaldehyde from these products and has made great efforts to do so. Melamine–formaldehyde (MF) and the less expensive melamine–urea–formaldehyde (MUF) resins are the bases of high performing wood-bonding adhesives. Their resistance to water is superior to that of the UF resins, but their higher cost has limited their use. The urea in the MUF resins decreases the cost of the MF resins. Uses of these are similar to those for the UF resins with the addition of paper-laminates for wood panels. Melamine reacts more easily with formaldehyde than does urea, making possible full methylolation of melamine (63). Condensation of methylolated melamine with formaldehyde does occur under both acidic and slightly alkaline conditions, but acid catalysts or compounds generating acids are usually used in MF adhesives. Compounds such as acetoguanamine, ε-caprolactam, and *p*-toluenesulfonamide are often added to combat inherent brittleness and decrease stiffness. Ammonium salts are useful in making bulk wood products, but laminates can be adversely affected by these compounds; a complex of morpholine and *p*-toluenesulfonic acid is one hardener employed for this particular kind of MUF or MF adhesive. Defoamers and judicious amounts of release or wetting agents may also be used.

High Performance Adhesives. A number of adhesive needs exist which require resistance to very high temperatures and other environmental stressors such as certain gases, solvents, radiation, and mechanical loads. The upper temperature limits of the most durable epoxy and phenolic adhesives lie between about 200 and 250°C. The aerospace industry requires adhesives that are resistant to temperatures of nearly 400°C for hundreds of hours or about 150°C for much longer times. Heterocyclic polymers such as polyimides and polyquinoxalines have been the basis of most heat-resistant adhesives. Microelectronics adhesives sometimes also must deal with high heat, but they must also conduct heat away from heat-sensitive parts. This has been the inevitable result of increasing miniaturization. Epoxies continue to be the basis of many microelectronics adhesives, but adhesives based on stiff-chained thermoplastic resins such as polyethersulfone and polyetheretherketone have made some inroads. Electrical conductivity is most commonly enhanced with silver flake or powder, but nickel, copper, and metal-coated metals are also being used in this function (64). Thermal conductivity is usually adjusted through incorporation of aluminum, aluminum nitride, or other metals or ceramics (65).

Adhesives made from Natural Products. The first adhesives developed by humans were based on naturally available materials such as bone, blood, milk, minerals, and vegetable matter. Beginning with the commercial development of Baekeland's phenolic resin adhesives by the General Bakelite Co. around 1910, synthetic adhesives began to replace natural product adhesives for existing applications. The use of adhesives by industry began to grow and diversify over the

ensuing decades. In certain industries, among them furniture, food, bookbinding, and textiles, adhesives based on natural products continue to be used to a significant extent. These adhesives can be divided into those based on proteins, carbohydrates, and natural rubbers or oils. Historically, *glue* is a term used to refer to adhesives made from animal matter or vegetable-based protein.

Protein-Based Adhesives. The protein sources for these adhesives include mammals, fish, milk, soybeans, and blood. Animal and fish parts that yield useful proteins include hides, skins, bones, and collagen from cartilage and connective tissues. Most animal proteins are extracted using water and vary considerably in molecular weight, amino acid sequence, and inorganic impurities. For those proteins that are not already soluble in water, such as collagen, solubilization is accomplished by imposition of heat, pressure, or, most commonly, addition of acids or alkalis. Final molecular weights are in the range of 10,000–250,000 (66). Following solubilization, the protein solution is boiled down and dried to a final moisture content of 10–15%. Milk and cheese yield the relatively simple mixture of proteins called casein [9000-71-9]. Proteins are extracted from milk through direct acidification following decreaming and may also be generated through fermentation of lactose by bacteria to create lactic acid. Blood is almost entirely made up of proteins and after spray drying to remove water, can be stored for an extended period of time. Soybeans are important sources of both proteins and triglyceride oils. Proteins for adhesives are obtained from harvested soybeans by extracting or pressing out oils and then heating the remaining matter no higher than 70°C lest its alkaline solubility be compromised. Soybean meal is approximately 45–55% protein, the balance consisting of carbohydrates (∼30%) and ash (67).

Proteins are highly susceptible to changes in their structure through changes in pH, and the process of denaturation used when necessary to unfold protein molecules and break down their molecular weight to effect solubilization must only go far enough to obtain those effects but not deteriorate their adhesive qualities. Additional acids and bases are used in preparation of working adhesives made from proteins. Formulations of protein-based adhesives, in general, include the dried protein, water, an alkali compound which helps dispersion, and a hydrocarbon oil defoamer. Hydrated lime and sodium silicate solutions are usually added to modulate viscosity and to improve water resistance. Plasticizers are sometimes added as are fillers, biocides, preservatives, and fungicides. Protein-based adhesives are widely used for bonding of porous substrates such as wood, and as water is removed from the adhesive by absorption, air drying, and the optional application of heat, the proteins become fully denatured and the adhesive is set. A variety of denaturing and curing agents or cross-linkers can be used with protein-based adhesives, including hexamethylenetetramine, carbon disulfide [75-15-0], thiourea [62-56-6], dimethylolurea, and various metal salts. Blood glues may contain aldehydes and alkaline phenol–formaldehydes as cross-linkers. Although very strong, protein-based adhesives have been largely restricted to nonstructural interior wood-bonding applications and other uses where their susceptibility to water and moisture do not jeopardize their stability, and the use of the various cross-linkers is targeted primarily at improving their water resistance. The most water-resistant protein-based adhesives are the blood or blood-soybean blends, but even they are not fully weatherproof. Casein or casein–soybean blends are next in line, and soybean and animal hide glues exhibit the least water

resistance. The use of blood and casein adhesives is limited by the low yield of adhesive-grade dried blood from drying processes and the lack of appreciable suppliers of casein in the United States alongside a large number of diverse global sources. There has been a strong push from the soybean industry to have soy products more widely accepted in various industrial uses, but considerable work remains to be done in this area. Protein-based fibrin sealants have been the subject of considerable interest as medical adhesives and are considered by some to have many advantages when compared to cyanoacrylates and other types of adhesives (68), but their development has been limited because of human blood contamination issues.

Carbohydrate-Based Adhesives. Carbohydrates are available from a wide variety of plants, the shells of marine crustaceans, and bacteria. The raw adhesive materials obtained from these sources include cellulose, starch, and gum. Cellulose [9004-34-6] is a semicrystalline polymeric form of glucose having a molecular weight of less than 1000 to nearly 30,000. It is present in plant matter at a level between about 30 and 90%. Like some of the naturally occurring proteins, cellulose must be chemically treated in order to be used as an adhesive. Reaction of its hydroxyl groups is used to convert cellulose to cellulose esters and ethers. Important cellulose esters include cellulose nitrate, cellulose propionate, cellulose butyrate, cellulose acetate propionate, and cellulose acetate butyrate (69). The most important cellulose ethers include carboxymethylcellulose, ethylcellulose, methylcellulose, and hydroxyethylcellulose. The cellulose adhesives are film formers having a thermoplastic nature. A typical adhesive formulation includes a few percent of the cellulose, less than a percent each of a plasticizer and a natural protein, and the great balance of water or another solvent. Methylcellulose is the basis of a common nonstaining water-based wallpaper adhesive. Celluloses are very effective aqueous solution thickeners and are sometimes used in that capacity, so their solubility is limited by viscosity increases. Starches are the most significant class of carbohydrate adhesives. The source of the basic materials is broad and includes corn, wheat, rice, and potatoes as well as seeds, fruits, and roots from which starch is isolated by hot water leaching. Starch is a naturally occurring polymer of glucose. It occurs for the most part in either of two forms or something intermediate between the forms: amylose [9005-82-7], which is highly linear and has a degree of polymerization of 500–700, and amylopectin [9037-22-3], which is branched and has a degree of polymerization of about 1500–2000. Starch is also semicrystalline in nature, and its tightly packed granules must be opened to make it suitable for adhesive use. This is accomplished through heating, oxidation, or alkali or acid treatment. Colloidal suspensions of starches can be made by heating in water, but these have a tendency to solidify on cooling. Treatment with an alkali such as sodium hydroxide can lower the gelation temperature. Treatment with a mineral acid plus heat followed by neutralization with a base degrades the amorphous regions of the starch granule but does not disturb the crystalline regions, allowing a higher percentage of solids to be used in making an aqueous solution called a thin-boiling starch. Oxidation with alkaline hypochlorite produces a material similar to acid-treated starch but having better tack and adhesive properties. Dry roasting of starch in the presence of an acid catalyst produces dextrin [9004-53-9], which ranges in color from white to yellow to dark brown and shows different tendencies to repolymerize depending on the temperatures, times, and

catalyst concentrations used. Additives used in dextrin adhesives include tackifiers such as borax [1303-96-4], viscosity stabilizers, fillers, plasticizers, defoamers, and preservatives. Formaldehyde-precondensates and other compounds are added to improve water resistance. Starch-based adhesives are used in corrugated cardboard, paper bags, paper or paperboard laminates, carton sealing, tube winding, and remoistenable adhesives. Gums are naturally occurring polysaccharides obtained from various plants or microorganisms and usually prepared as adhesives by dispersion in either hot or cold water. Although they find use in applications similar to those mentioned for starches, they are more often found as additives in synthetic adhesives in which they act as rheology modifiers.

Other Nature-Based Adhesives. The use of natural rubber, an important adhesive component obtained from the rubber tree, is discussed under the section on Pressure-Sensitive Adhesives. Tannins are polymeric polyphenols isolated as one of two products from the bark of conifers and deciduous trees. Lignin is widely available as a waste material from pulp mills and has a complex structure. Tannin-based adhesives have attained some level of success in the marketplace. Despite considerable interest in and work toward more commercial use of lignins in adhesives for wood bonding, they have not yet succeeded in capturing market share. A vinyl-functionalized sugar has been developed for use in products including, most prominently, adhesives (70). Modification of sugars to make liquid epoxy resins has also been accomplished (71). Use of whey and whey by-products as adhesive components has been investigated (72). Modification of natural materials to make polyols and diisocyanates has been pursued in both the United States and the United Kingdom (73,74). It can be expected that additional plant-based monomers and polymers will be developed as the chemical industry comes to terms with the limited supply and rising costs of petrochemicals, making "green adhesives" a not-uncommon reality in the not-too-distant future (75).

Direct Bonding

Strictly speaking, direct bonding does not include the use of conventional adhesives or seemingly any adhesive at all. However, the joining of two extremely smooth solid surfaces into a spontaneous bond requires careful preparation and surface treatment which reflect the sophisticated use of chemistry, physics, and engineering. Practitioners of direct bonding consider its gluelessness to be a considerable benefit within its primary areas of applications, optics, electronics, and semiconductors, which benefit from minimal or no contamination (76). Such bonds are also considered jointless because of the atomic distances between the joined surfaces. The most prominent use of direct bonding may be wafer bonding, a key part of the silicon-on-insulator technology behind the making of integrated circuits, that is, computer chips (77). Another important use of direct bonding is construction of waveguides for optical devices.

The inclusion of direct bonding among a list of adhesive types reflects the supposition that conventional adhesives of any composition are useful because they compensate for the shortcomings of most surfaces one might wish to join. Indeed, if smooth enough, even polytetrafluoroethylene will adhere to itself. In the case of what is called stiction, direct bonding is not seen as desirable, and steps

are taken to prevent it from occurring (78). Redesign can be used to avoid material contact altogether. Surfaces can be roughened on a fine scale using chemical treatments.

Adhesive Formulation and Design

A 1999 compilation of chemicals used in adhesives listed 6300 materials (79), but the total number of compounds available for adhesive formulating is well in excess of this figure. Formulators of adhesives are in constant search of unique adhesive ingredients and their unusual combinations in order to satisfy the ever-increasing needs of their customers. In the interests of competition, many vendors of adhesive raw materials continue to protect the proprietary nature of their products by providing coded product names, a practice which though entirely understandable runs contrary to the need for the educated formulator to know the chemistry and structure of raw materials rather than relying on vague descriptions of the effects of a raw material in some standard formulation on some standard substrate.

Formulating adhesives is both a skill and an art. The novice formulator will find it invaluable to seek out other formulators in the same organization and learn from them as much as possible or at least whatever their time and patience allow. Maintaining such relationships over time can provide great benefit to the beginner as well as the veteran formulator, who will soon start learning from the former novice. The written and electronic literature of many vendors of adhesive raw materials includes information on formulating, including starting formulations. To the extent possible, one can also consult with vendor technical staff. The open technical literature, encompassing technical and trade journals, conference proceedings, and patents, provides considerable information on formulations, and its age should not discourage one from reading it as there is much to be learned from the older literature. The literature on nonadhesive polymer-based products, such as coatings, molding plastics, and composite matrix materials, may prove helpful in describing interesting raw materials not commonly used in adhesives. Likewise, components commonly used in one class of adhesives may be found to be useful in modifying adhesives of another class. The best teacher of formulating is experience, that is, trial and error.

Adhesive formulation involves more than the combining of various raw materials. The formulator must be a multidimensional technical professional able to juggle several different fields of science and engineering, legal issues, environmental considerations, computer hardware and software, and business concerns. It is not unusual to create a remarkable adhesive only to find that a key ingredient is unstable or too expensive for the intended market or poses unacceptable health and safety risks. Some customers have lists of ingredients which will not be allowed in items sold to them. Government entities require increasingly stricter labeling of adhesives and other chemical products, the requirements varying from country to country.

Better tools for adhesive formulation have been developed with the onset of the personal computer and computer workstations. These include software for design of experiments, databases used to track endless variations in adhesive recipes, mixtures design software for faster product optimization, and simple and

complex spreadsheets used to determine cost at the front end of development. Online searching of and access to the scientific and patent literature as well as the information on business trends and supplier's products available on the Internet have made information gathering easier. Adhesive development accelerates more each year, and the savvy formulator must keep pace.

BIBLIOGRAPHY

"Adhesive Compositions" in *EPST* 1st ed., Vol. 1, pp. 482–502, by I. Skeist, Skeist Laboratories, Inc.; "Adhesive Compositions" in *SPST* 1st ed., Suppl. Vol. 2, pp. 1–19, by I. Skeist and J. Miron, Skeist Laboratories, Inc.; in *EPSE* 2nd ed., Vol. 1, pp. 547–577, by S. C. Temin, The Kendall Co.

1. *The Global Adhesive and Sealant Industry: An Executive Market Trend Analysis*, 2nd ed., CHEM Research GmbH and DPNA International, Frankfurt, Germany, 1997, p. 12.
2. *U.S. Industry & Trade Outlook 2000*, McGraw-Hill, New York, p. 11-11.
3. *Adhesives Age* **42**(3), 9 (1999).
4. *Adhesives, VII*, Skeist Inc., Whippany, N. J., 2000, p. 24.
5. J. Talmage, *Adhesives & Sealants Ind.* **7**(10), 20 (Dec. 2000/Jan 2001).
6. L. H. Lee, L. Shi-Duo, and W. Zhi-Lu, *Proc. 19th Annu. Meet. Adhes. Soc.*, 1996, pp. 371–374.
7. H. Onusseit, *Adhesives & Sealants Ind.* **7**(7), 24–28 (2000).
8. *SBI Market Profile: Adhesives and Sealants*, FIND/SVP, Inc., New York, 1998, p. 18.
9. A. L. Lambuth, in R. W. Hemingway, A. H. Conner, and S. J. Branham, eds., ACS Symp. Ser., Vol. **385**: *Adhesives from Renewable Resources*, American Chemical Society, Washington, D.C., 1989, Chap. 1 pp. 1–10.
10. C. W. Paul, M. L. Sharak, M. Blumenthal, *Adhesives Age* **42**(7), 34–40 (1999).
11. E. Schlucker, in G. Vetter, ed., *Dosing Handbook*, Elsevier, Oxford, 1998, Chapt. 28.
12. P. Dreier, *Adhesives Age* **39**(7), 32–41 (1996).
13. D. M. Brewis, in D. E. Packham, ed., *Handbook of Adhesion*, Longman Scientific & Technical, Essex, England, 1992, pp. 234–235.
14. R. F. Schmid, *Mater. Perform.* **37**(5), 39–42 (1998).
15. H. Dodiuk, A. Buchman, M. Rotel, J. Zahavi, Int. Congr. Adhes. Sci. Technol., Invited Pap., 1st, Meeting Date 1995, 387–405 (1998); *Chem. Abstr.* **131**, 171182 (1999).
16. H. W. Bergmann and co-workers, *Appl. Surf. Sci.* **86**, 259–265 (1995).
17. T. E. Lizotte, and T. R. Okeefe, Proc. SPIE-Int. Soc. Opt. Eng., 2703 (Lasers as Tools for Manufacturing of Durable Goods and Microelectronics), 1996, pp. 279–287.
18. G. W. Critchlow, D. M. Brewis, *Int. J. Adhes. Adhes.* **16**, 255–275 (1996).
19. I. Benedek and L. J. Heymans, *Pressure-Sensitive Adhesives Technology*, Marcel Dekker, New York, 1997, pp. 142–145. Chap. 5 of this work is a good general reference on PSA compositions.
20. Jpn. Pat. 2000256639 A2 (Sept. 9, 2000), N. Watanabe, J. Nakamura, and Y. Mashimo, (to Toyo Ink Mfg. Co., Ltd.); U.S. Pat. 5,130,375 (July 14, 1992), M. M. Bernard and S. S. Plamthottam (to Avery Dennison Corp.).
21. S. B. Lin, in M. R. Tant, J. W. Connell, and H. L. N. McManus, eds., ACS Symp. Ser., Vol. 603: *High-Temperature Properties and Applications of Polymeric Materials*, American Chemical Society, Washington, D.C., 1995, Chap. 3, pp. 37–51.
22. A. J. DeFusco, K. C. Sehgal, D. R. Bassett, in J. M. Asua, ed., *Polymeric Dispersions: Principles and Applications*, Kluwer Academic Publishers, the Netherlands, 1997, pp. 379–396.

23. A. Hardy, *Synthetic Adhesives and Sealants, Critical Reports on Applied Chemistry*, John Wiley & Sons, Chichester, England, 1987, Vol. **16**, pp. 31–58.
24. M. Huang and co-workers, *Adhesive Technol.* **15**(2), 20–25 (1998); H. Mack, *Adhesives Age* **43**(8), 28–33 (2000).
25. M. Dupont, *J. Adhesive and Sealant Council* 229–241 (1997).
26. Jpn. Pat. 11140410 A2 (May 25, 1999), Y. Nagai and Y. Ikegami (to Mistubishi Rayon Co., Ltd.).
27. J. Piglowski, M. Trelinska-Wlazlak, and B. Paszak, *J. Macromol. Sci., Part B: Phys.* **38**, 515–525 (1999).
28. S. Ghosh, D. Khastgir, and A. K. Bhowmick, *J. Adhes. Sci. Technol.* **14**, 529–543 (2000).
29. R. S. Whitehouse, in W. C. Wake, ed., *Synthetic Adhesives and Sealants, Critical Reports on Applied Chemistry*, John Wiley & Sons, Chichester, England, 1987, Vol. **16**, pp. 1–30.
30. J. Comyn, *Adhesion Science*, The Royal Society of Chemistry, Cambridge, England, 1997, p. 56.
31. Ref. 30, p. 62.
32. P. L. Wood, *Adhesive Technol.* **15**(2), 8–11 (1998).
33. C. Frihart, A. Natesh, and U. Nagorny, *Adhesives and Sealants Ind.* **8**(1), 26–29 (2001).
34. E. A. Peterson and A. D. Yazujian, *Adhesives Age* **30**(6), 6–7 (1987).
35. Eur. Pat. Appl. (2000), A. Pahl (to Lohmann GmbH & Co).
36. W. C. Wake, *Adhesion and the Formulation of Adhesives*, Applied Science Publishers Ltd., London, 1976, p. 188.
37. C. W. Boeder, in S. R. Hartshorn, ed., *Structural Adhesives*, Plenum Press, New York, 1986, Chapt. 5 pp. 225–226.
38. Ref. 37, pp. 228–229.
39. Ref. 37, p. 231.
40. Ref. 37, p. 238.
41. U.S. Pat. 4,855,001 (Aug. 8, 1989), D. J. Damico and R. M. Bennett (to Lord Corp.); U.S. Pat. 4,857,131 (Aug. 15, 1989), D. J. Damico, K. W. Mushrush, and R. M. Bennett (to Lord Corp.); Jpn. Pat. 07109442 A2 (Apr. 25, 1995), T. Fujisawa and O. Hara (to Three Bond Co. Ltd.); Eur. Pat. Appl. 540098 A1 (May 5, 1993), V. DiRuocco, L. Gila, and F. Garbassi (Ministero dell'Universita e della Ricerca Scientifica e Tecnologica).
42. U.S. Pat. 3,890,407 (June 17, 1975), P. C. Briggs and L. C. Muschiatti (to E. I. Du Pont de Nemours & Co., Inc.).
43. G. H. Millet, in Ref. 37, Chapt. 6, pp. 262–263.
44. U.S. Pat. 5,981,621 (Nov. 9, 1999), J. G. Clark and J. C. Leung (Closure Medical Corp.).
45. Ref. 43, pp. 276–278.
46. A. C. Roberts, *Adhesive Technol*. **15**(2), 4, 6 (1998).
47. Ger. Pat. 4317886 (Dec. 2, 1993), S. Takahaski and co-workers (to Toagosei Chemical Industry Co., Ltd.).
48. U.S. Pat. 4,444,933 (Apr. 24, 1984), P. S. Columbus and J. Anderson (to Borden, Inc.).
49. See, for example, Internet address www.pu.bayer.com/pu.cfm? show=3000 for product literature from Bayer Corp. (www.pu.bayer.com) and Internet address www.basf.de/en/dispersionen/products/industrial˙coating/polyisocyanates/ for product literature from BASF Corp. Many raw materials for urethane adhesives will be found in product literature for raw materials for coatings because of the relatively larger market size for urethane coatings.
50. S. R. Hartshorn and K. C. Frisch Jr., Proc. 25th Anniv. Symp. of the Polymer Institute (Univ. of Detroit), Technomic Publishing Co., Inc., Lancaster, U.K., 1994, pp. 1–10.
51. N. Weeks, *Adhesive Technol*. **17**(3), 19 (2000).

52. U.S. Pat. 4,390,678 (June 28, 1983), S. B. LaBelle and J. E. Hagquist (to H. B. Fuller Co.).
53. B. H. Edwards, in Ref. 37, Chapt. 4, pp. 197–200.
54. E. G. Melby, in K. C. Frisch and D. Klempner, eds. *Advances in Urethane Science and Technology*, Technomic Publishing Co., Inc., Lancaster, U.K., 1998. Vol. **14**, pp. 317–319.
55. Ref. 54, pp. 319–325.
56. U.S. Pat. 3,525,779 (Aug. 25, 1970), J. M. Hawkins (to The Dow Chemical Company).
57. J. A. Clarke, *J. Adhesion* **3**, 295–306 (1972).
58. U.S. Pat. 5,232,996 (Aug. 3, 1993), D. N. Shah and T. H. Dawdy (to Lord Corp.).
59. U.S. Pat. 5,278,257 (Jan. 11, 1994), R. Mulhaupt and co-workers (to Ciba-Geigy Corp.).
60. J. Robins, in Ref. 37, Chapt. 2.
61. A. Higgins, *Int. J. Adhes*. **20**, 367–376 (2000).
62. A. Pizzi, *Advanced Wood Adhesives Technology*, Marcel Dekker, Inc., New York, 1994, p. 21.
63. Ref. 62, p. 68 and Ref. 1 therein.
64. S. K. Kang and S. Purushothaman, *J. Electron. Mater*. **28**, 1314–1318 (1999).
65. K. Gilleo and P. Ongley, *Microelectronics Int.* **16**(2), 34–38 (1999).
66. R. Vabrik and co-workers, *Prog. Rubber Plast. Technol.* **15**(1), 28–46 (1999).
67. A. L. Lambuth, in A. Pizzi and K. L. Mittal, eds., *Handbook of Adhesive Technology*, Marcel Dekker, Inc., New York, 1994, Chap. 13.
68. D. H. Sierra, *J. Biomater. Appl.* **7**, 309–52 (1993).
69. M. G. D. Bauman and A. H. Conner, in Ref. 67, Chapt. 15.
70. S. Bloembergen, Ian J. McLennan, and C. S. Schmaltz, *Adhesive Technol.* **16**(3), 10–13 (1999).
71. J. Suszkiw, *Agricultural Res.* **47**(6), 22 (1999).
72. T. Viswanathan, in Ref. 9, Chap. 28.
73. M. S. Holfinger and co-workers, *J. Appl. Polym. Sci.* **49**, 337–344 (1993).
74. J. L. Stanford, R. H. Still, J. L. Cawse, and M. J. Donnelly, in Ref. 9, Chapt. 30.
75. C. W. Paul, M. L. Sharak, and M. Blumenthal, *Adhesives Age* **42**(7), 34–40 (1999).
76. J. Haisma and co-workers, *Applied Optics* **33**, 1154–1169 (1994).
77. C. A. Desmond-Colinge and U. Gosele, *MRS Bulletin* **23**(12), 30–34 (1998).
78. N. Tas and co-workers, *J. Micromechanics and Microengineering* **6**, 385–97 (1996).
79. M. Ash and I. Ash, *Handbook of Adhesive Chemicals and Compounding Ingredients*, Synapse Information Resources, Endicott, New York, 1999.

GENERAL REFERENCES

A. V. Pocius, "Adhesives" in *Kirk-Othmer Encyclopedia of Chemical Technology*, 4th ed., Vol. **1**, (1991).

J. Johnston, *Pressure Sensitive Adhesive Tapes: A Guide to their Function, Design, Manufacture, and Use*, Pressure Sensitive Tape Council, Northbrook, Ill., 2000.

I. Benedek, *Development and Manufacture of Pressure-Sensitive Products*, Marcel Dekker, New York, 1999.

A. Pizzi, *Advanced Wood Adhesive Technology*, Marcel Dekker, New York, 1994.

S. R. Hartshorn, ed., *Structural Adhesives: Chemistry and Technology*, Plenum Press, New York, 1986.

A. Pizzi and K. L. Mittal, *Handbook of Adhesive Technology*, Marcel Dekker, New York, 1994.

W. C. Wake, *Adhesion and the Formulation of Adhesives*, Applied Science Publishers, London, 1976.
A. V. Pocius, *Adhesion and Adhesives Technology: An Introduction*, Hanser Publishers, Munich, 1997.
K. J. Saunders, *Organic Polymer Chemistry*, Chapman and Hall, London, 1973.
G. Wypych, *Handbook of Fillers*, 2nd ed., ChemTec Publishers, Toronto, 1999. May be referenced under the name Jerzy Wypych.
McCutcheon's Functional Materials, North American edition, McCutcheon's Division, Manufacturing Confectioner Publishing Co., Glen Rock, N.J., multivolume, published annually. An International edition is also published annually.

E. M. YORKGITIS
3M Company

AGING, PHYSICAL

Introduction

All glasses, including polymeric glasses, undergo a process known as physical aging or structural recovery. The origin of physical aging can be understood on a macroscopic level by examining the volume versus temperature path of an amorphous polymer, as shown in Figure 1. On cooling from the liquid state, the amorphous material does not crystallize because of kinetic or steric constraints and its volume decreases along the equilibrium density line. As the volume decreases, the molecular mobility also decreases. At the glass temperature or glass-transition temperature (T_g), the molecular mobility is such that the material can no longer maintain equilibrium density on the time scale of cooling and the material deviates from the equilibrium line onto the glass line. Although the glass temperature is often reported as a single number, its value depends on the cooling rate; faster cooling rates giving higher T_g values and higher glass lines. Independent of which glass line the material is on, the glass is not at equilibrium. Physical aging, which is also called structural recovery particularly when the evolution of thermodynamic variables is being referred to, is shown by the downward arrow in Figure 1 at aging temperature T_a.

The driving force for physical aging is the attempt to achieve equilibrium density through configurational rearrangements on a molecular scale. Corresponding to these changes on the molecular scale, we observe a decrease in volume, a decrease in enthalpy, an increase in modulus, and an increase in brittleness. The time scale for physical aging (ie, the time required to reach equilibrium) can be as short as several hundred seconds at aging temperatures in the vicinity of the nominal T_g and increases to years or millennia as the temperature decreases. According to the Gibbs and DiMarzio theory of the glass temperature (1–3), there

Encyclopedia of Polymer Science and Technology. Copyright John Wiley & Sons, Inc. All rights reserved.

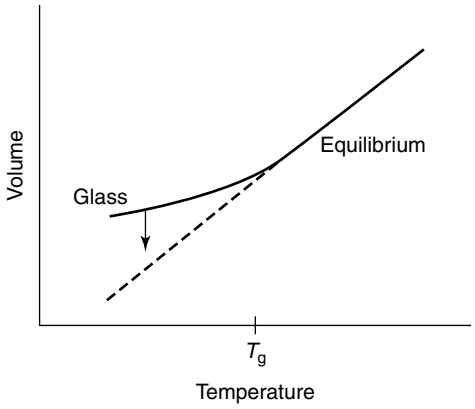

Fig. 1. Schematic of volume vs temperature for an amorphous glass-forming material. The arrow shows the evolution of volume from the nonequilibrium glass line to the equilibrium line during structural recovery.

is an underlying thermodynamic transition, often associated with the Kauzmann temperature 52°C below T_g (4).

Physical aging and structural recovery are reversible phenomena. There is no change in chemical structure during physical aging. The changes in physical and mechanical properties that accompany structural recovery are caused by the densification associated with the approach to equilibrium. The changes can be erased by heating the material above the glass temperature to a temperature where the material is again at equilibrium. Cooling the material from the equilibrium state will result in reestablishment of the glass. This reversibility is often exploited in physical aging research as is mentioned later in this article.

The importance of structural recovery and physical aging lies in the changes in material properties that accompany the phenomena. These changes can in many instances adversely affect performance and lifetime. Consequently, structural recovery and physical aging impact the design, processing, and performance of polymers in many applications, including, but not limited to, aerospace and automotive applications, xerographic applications, and glass-to-metal seals (5). In addition to the practical effects of physical aging, an understanding of glasses and the effects associated with structural recovery is important from a fundamental scientific viewpoint. In fact, Nobel laureate P. W. Anderson claimed that the glass transition was one of the greatest unsolved problems of condensed matter physics (6). Although the basic phenomenology associated with glasses is known and models exist which describe structural recovery and physical aging, researchers are not yet able to predict a priori experimental observations.

In this article on physical aging, the phenomena associated with structural recovery and physical aging are described, starting with discussion of volume recovery, enthalpy recovery, viscoelastic properties, and failure. There are more in-depth reviews of the phenomena and models associated with the glass transition (7) and enthalpy recovery (8). See also GLASS TRANSITION, AMORPHOUS POLYMERS, and VISCOELASTICITY.

Volume Recovery

The decrease in volume during physical aging is specifically known as *volume recovery* or *volume relaxation*. Volume recovery experiments include down-jump, up-jump, and memory experiments. The results of these experiments, which are shown and discussed later, demonstrate that structural recovery is both nonlinear, nonexponential and path-dependent.

The simplest volume recovery experiment performed is the down-jump. In this experiment, a material initially above T_g and at equilibrium is subjected to a temperature down-jump to an aging temperature T_a below T_g. The isothermal evolution of volume at T_a, as indicated by the downward arrow in Figure 1, is monitored with time via length or volume dilatometry. Figure 2 shows typical data replotted from Kovacs data (9) for a series of aging temperatures for poly(vinyl acetate). These curves, called intrinsic isotherms, are plotted as the relative departure from equilibrium δ versus the logarithm of time, with δ defined as

$$\delta = \frac{v - v_\infty}{v_\infty} \tag{1}$$

where v is the volume at a specific aging time and v_∞ is the volume at equilibrium density. The relative departure from equilibrium has a nonexponential shape and approaches zero asymptotically at long times as equilibrium is attained. As might be expected, the times required to reach equilibrium increase as the aging temperature decreases.

The total change in delta during aging depends on the magnitude of the temperature jump and is related to the initial departure from equilibrium (δ_0):

$$\delta_0 = \Delta\alpha\,(T_{fo} - T_a) \tag{2}$$

where $\Delta\alpha$ is the difference in thermal expansivities between the liquid and glass ($=\alpha_l - \alpha_g$, where subscripts l and g refer to the liquid or equilibrium and glassy regimes, respectively). T_{fo} is the initial fictive temperature and it equals the value of the glass temperature associated with the rate of the quench to T_a. A more general definition of T_f is given later. For a perfect quench, T_{fo} is equal to the temperature at which the quench was made, although experimentally this is never the case. Although Figure 2 shows that Kovacs plotted his original data versus $(t - t_i)$ where t_i is the time at which the quench was initiated, modeling work (10) has indicated that this is incorrect. For capillary dilatometers (10), taking time zero at the beginning of the quench resulted in insignificant error in the data on a logarithmic time scale compared to the results of a perfect quench for times greater than approximately two times the thermal equilibration time. Hence, data should be plotted versus time, with time zero being the time at which the quench is initiated. This is in agreement to Struik's earlier suggestion (11).

The total change of volume during volume recovery is small, generally being smaller than 1%, ie, the change in δ is generally less than 10×10^{-3}. For example, for the data shown in Figure 2, the volume changed approximately 0.05% at the highest temperature and 0.5% at the lowest temperature. These changes,

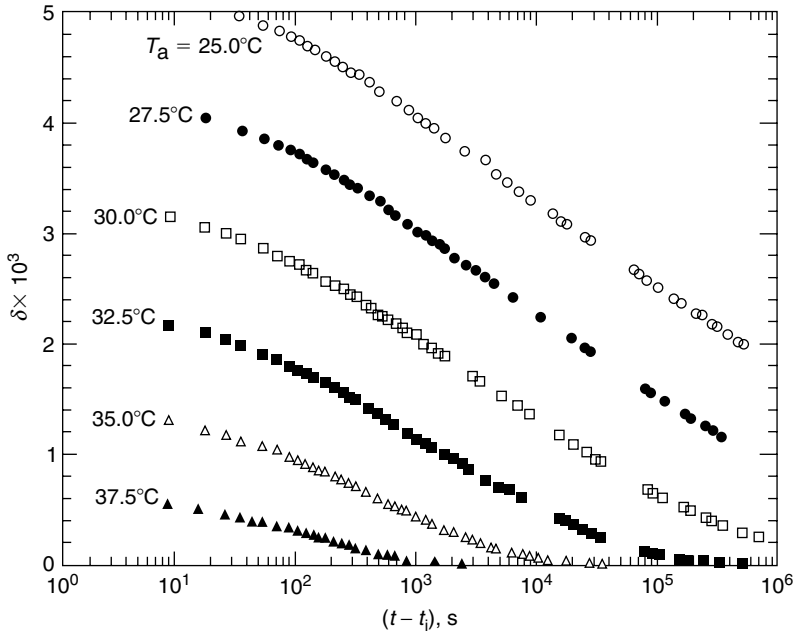

Fig. 2. Intrinsic isotherms for poly(vinyl acetate) from the data sets of Kovacs (replotted after Ref. 9). The departure from equilibrium is plotted vs time after thermal equilibration. Down-jumps were performed from 40°C to various isothermal aging temperatures ranging from 37.5 to 25°C.

in themselves, are not significant for dimensional stability in most applications. However, the associated changes in mechanical properties, and in particular in failure modes, can be significant in practical applications as is discussed later. It is noted that measurement of volume changes of this order indicates the need for high precision in the measurements. Resolution to 2×10^{-5} cm^3/g is desired and can be achieved with both traditional and automated capillary dilatometers. One source of noise in the measurements is the temperature fluctuations in the bath; preferably these fluctuations should be of the order of ± 0.01 K or less.

In addition to the down-jump volume recovery experiments, up-jumps can also be performed. In the up-jump experiment, the material is first equilibrated at a temperature T_i below T_g. It is then subjected to an up-jump in temperature to an aging temperature which may or may not be below the nominal glass temperature. During aging, the volume now increases with time as the material attempts to achieve equilibrium density. Kovacs' data (published originally in Ref. 12) for an up-jump to a single aging temperature after equilibration at the temperatures indicated are shown in Figure 3 for poly(vinyl acetate). Also shown in Figure 3 are the results of down-jumps to the same aging temperature from several initial temperatures.

The data in Figure 3 demonstrate what is known as the asymmetry of approach. For the same magnitude jump, the up-jump response is delayed relative to the down-jump and the time required to reach equilibrium is longer. The asymmetry of approach is considered to be a manifestation of the nonlinearity of the

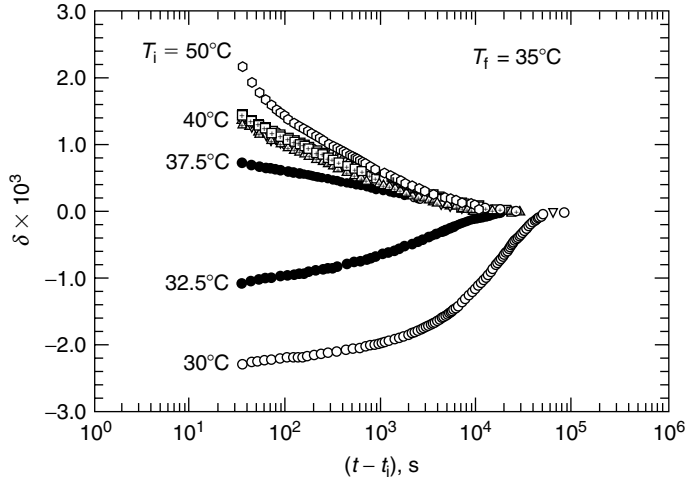

Fig. 3. The asymmetry of approach for poly(vinyl acetate) from the data sets of Kovacs and first published in Reference 12. The isothermal aging temperature is 35°C. Down-jumps and up-jumps were initiated at the temperatures T_i as shown.

relaxation process as was first recognized by Tool (13). In other words, the rate of volume recovery depends on some characteristic relaxation time (τ), which in turn depends on the instantaneous volume, which in turn depends on the rate of volume change (after Ref. 14):

$$v \rightarrow \tau \rightarrow \left(\frac{\partial v}{\partial t}\right)_{T_a} \tag{3}$$

Hence, the down-jump response is autoretarded on a logarithmic time scale with the characteristic relaxation time increasing with the time of aging, whereas the up-jump response is autoaccelerated with the characteristic relaxation time decreasing with the time of aging. For a small enough temperature jump, the response would be linear. In the linear case, the relaxation time would not change during the recovery, and the down-jump and up-jump responses would be mirror images.

The third type of volume recovery experiment, termed the memory or crossover experiment, demonstrates that the relaxation behavior is dependent on the prior thermal history of the material. In this experiment, the material is aged partially into equilibrium at temperature T_1 and then heated to a temperature T_a where the volume initially lies on the equilibrium line. Because the volume departure from equilibrium at T_a is initially zero, no evolution of volume might be expected. However, the observation is that the volume increases away from equilibrium and then decreases back to equilibrium. The thermal history involved in the memory experiment is depicted schematically in Figure 4. The experimental results of Kovacs for poly(vinyl acetate) (PVAc) (9) are shown in Figure 5 for several T_1, in addition to the down-jump response. The memory experiment is attributable to a distribution of relaxation times; for example, if at T_1 the fastest relaxing regions reached equilibrium density by the time the jump

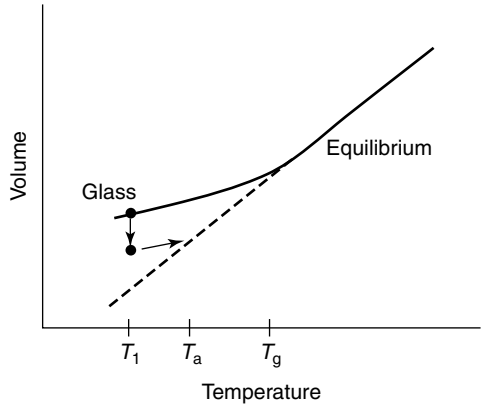

Fig. 4. Schematic of the memory experiment for volume (or enthalpy). The material is aged at T_1 such that the material is initially at equilibrium at T_a following an up-jump from T_1 to the final aging temperature T_a.

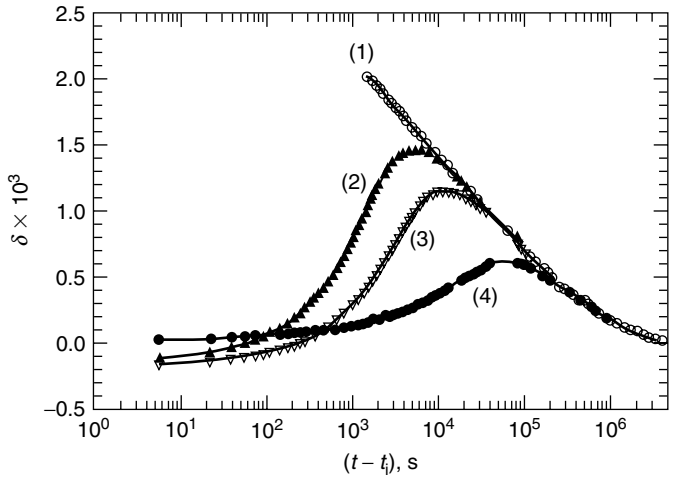

Fig. 5. Isothermal volume relaxation of poly(vinyl acetate) data of Kovacs (replotted after Ref. 9) showing the results of memory experiments. Sample 1 shows the response at 30°C after a quench from 40°C. For samples 2, 3, and 4, the material was initially quenched from 40°C and held at T_1 for a time t_1 before jumping up to T_a of 30°C. Sample 2: $T_1 = 10$°C for $t_1 = 160$ h; Sample 3: $T_1 = 15$°C for $t_1 = 140$ h; Sample 4: $T_1 = 25$ °C for $t_1 = 90$ h.

to T_a was made whereas the slowest regions had not, then at T_a the fast regions would expand to get to their equilibrium volume at this higher temperature resulting in the increase in volume away from equilibrium, and at longer times, the slowest regions would finally contract to their equilibrium density returning the material to equilibrium volume. Whether this picture is physically correct or not is unclear. However, it is clear that a single exponential relaxation function cannot reproduce the memory effect.

The majority of volume recovery experiments performed to date have been carried out close to the glass transition. The temperature range near T_g is convenient because the entire relaxation is accessible and equilibrium is attainable in reasonable times. However, glass-forming materials are often used deep in the glassy state. It is unclear whether extrapolation of volume recovery rates to temperatures far below T_g is valid. Recent work (15) on polycarbonate (PC) suggests otherwise. At low aging temperatures, volume recovery appeared to be higher than expected (15). In addition, there was a sharp transition from a slow rate of volume recovery to a much faster aging rate at 10^7 s. The observations have been confirmed qualitatively for polycarbonate but not for polystyrene (PS) (16). The significance of these results and whether current models of structural recovery can predict them is not yet clear.

Enthalpy Recovery

The decrease in enthalpy during physical aging is specifically called *enthalpy recovery* or *enthalpy relaxation*. The enthalpic response of a glass is similar to the volumetric response in that the enthalpy decreases after a down-jump in temperature. The most common way to measure enthalpy relaxation is with differential scanning calorimetry (dsc). However, the evolution of enthalpy cannot be measured *in situ* using dsc because of the small amount of heat given off and the long time scales over which the relaxation occurs. Consequently, the change in enthalpy because of aging is measured after aging for specified times. An explanation of the approach is shown schematically in Figures 6a and b. Enthalpy versus temperature is shown in Figure 6a. The diagram looks similar to that of volume versus temperature. At high temperatures the material is at equilibrium. During cooling from equilibrium, the enthalpy decreases and the molecular mobility of the material decreases. At the glass temperature (T_g), the material is no longer able to maintain equilibrium within the time scale of cooling, and the enthalpy departs from the equilibrium line and moves onto the glass line. The solid curve shows the behavior on cooling. On heating, the dashed curve is observed for an unaged glass, ie, a glass in which no relaxation occurred isothermally in the glassy state or during heating. Some small hysteresis in the vicinity of T_g is observed between the cooling and heating traces. On the other hand, the dash–dot line shows the behavior on heating of an aged glass. Since the aged glass has lower molecular mobility (corresponding to its increased density), the enthalpy often overshoots the equilibrium line during heating such that the rapid increase to equilibrium occurs at a temperature considerably above the glass temperature, as shown. The corresponding heat flow (P) or apparent heat capacity (C_p) for the aged and unaged glasses is shown in Figure 6b. For the unaged material, there is an endothermic step change in the heat flow at T_g (often with a small degree of overshoot). For the aged glass, on the other hand, a significant annealing peak or endothermic overshoot is observed. The difference between the area under the unaged and aged materials is the difference in enthalpy between the glass lines for the unaged and aged glasses (ΔH_a). In traditional dsc, ΔH_a is obtained by performing a temperature scan for an aged glass to obtain the aged response, then quenching the material at a given rate (generally the same rate that was used during the

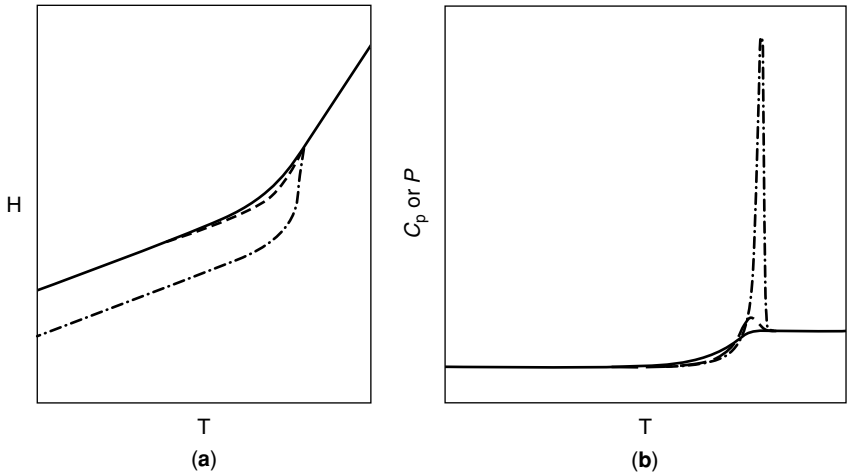

Fig. 6. (**a**) Schematic of enthalpy vs temperature. The solid line shows the response on cooling from the equilibrium state, whereas the dashed line shows the heating curve for an "unaged" glass in which there is a small hysteresis effect. The dash–dot line shows the heating curve for an "aged" glass; (**b**) Schematic of heat capacity vs temperature. The solid line shows the response on cooling from the equilibrium state, whereas the dashed line shows the heating curve for an "unaged" glass showing a small overshoot at the nominal glass temperature. The dash–dot line shows the large annealing peak observed in the heating curve for an "aged" glass.

down-jump to T_a), and performing a second temperature scan without aging the material to obtain the unaged response (17). Early suggestions that ΔH_a could also be obtained from the nonreversing heat flow using one heating scan with temperature-modulated dsc (18–20) have been shown to not be valid (21,22).

The results of typical dsc heating scans after isothermal aging are shown in Figure 7 for poly(ether imide) (PEI) for various aging times (23). In this case, one sample was used for all experiments, and isothermal aging was performed in the dsc itself. It is noted that if isothermal aging is performed in the dsc, isothermal calibration of the instrument must be performed.

As shown in Figure 7, as the time of aging increases, the overshoot peak temperature shifts to higher temperatures because of the increase in the relaxation time with aging. The area under the peak also increases. When equilibrium is reached, both the peak temperatures and the areas under the peaks stop evolving. Figure 8 shows the evolution of the departure of equilibrium for enthalpy versus the logarithm of time for poly(ether imide) for selected aging temperatures replotted from the data presented in Reference 23. The departure from equilibrium for enthalpy is defined as

$$\delta = \Delta H_{a\infty} - \Delta H_a \tag{4}$$

where $\Delta H_{a\infty}$ is the change in enthalpy at equilibrium. Each data point represents the average of three points. The intrinsic isotherms for enthalpy recovery are analogous to those for volume recovery. The times required to reach equilibrium increase as the aging temperature decreases and the initial departure

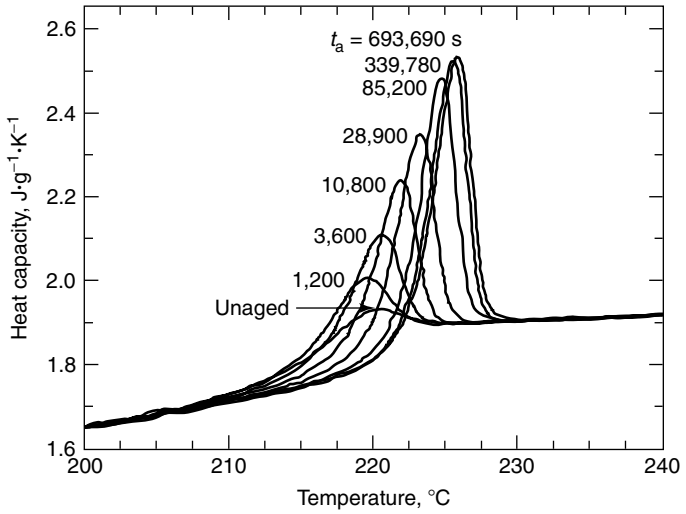

Fig. 7. DSC scans of heat capacity vs temperature for poly(ether imide) after isothermal physical aging at 201.3°C for the various aging times indicated. Scans were made on heating at 10°C/min. The data were corrected to agree with absolute C_p measurements in the liquid state. Data are replotted from Ref. 23.

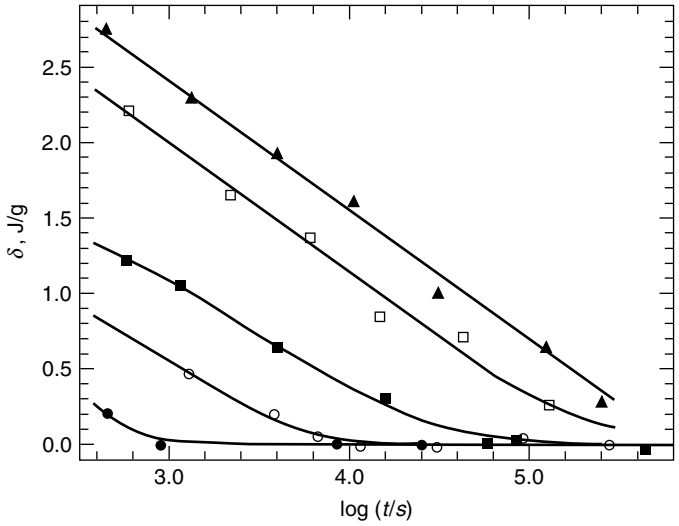

Fig. 8. Relative departure from equilibrium for enthalpy ($\Delta H_\infty - \Delta H_a$) vs the logarithm of aging time for poly(ether imide). Data are replotted from Ref. 23. T_a (°C) = (▲) 201.3, (□) 202.5, (■) 206.3, (○) 207.5, and (●) 211.3.

from equilibrium also increases as the aging temperature decreases. For a perfect quench, the initial departure from equilibrium for enthalpy (δ_0) depends on the magnitude of the temperature jump through the difference in heat capacity in the liquid $\Delta C_p = C_{pl} - C_{pg}$:

$$\delta_0 = \Delta C_p (T_{fo} - T_a) \tag{5}$$

where T_{fo} is the initial fictive temperature for the enthalpy down-jump and equals the glass temperature associated with the cooling rate used in the quench.

The asymmetry of approach and the memory effect should be observable for enthalpy although the dsc is not convenient for making such measurements. Enthalpy relaxation has been measured *in situ* using an adiabatic calorimeter in isothermal mode and asymmetry of approach data has been obtained by Oguni and co-workers (24,25). An inherent problem with adiabatic calorimetry, however, is the difficulty of the measurements, the large thermal equilibration time, and the drift of the instrument for long-time measurements. It should also be noted that the analysis performed by Oguni et al. on their asymmetry of approach data (24,25) neglected the concept of nonlinearity. The interpretation of their data must be viewed with skepticism for this reason.

Evolution of the Viscoelastic Properties

Corresponding to the changes in volume and enthalpy observed following a temperature down-jump from equilibrium, the viscoelastic properties are also observed to evolve. Changes in the dynamic mechanical properties with time of aging below the glass temperature were first reported in 1963 by Kovacs et al. for poly(vinyl acetate) (26). Subsequently, Struik published his thesis in 1978 in which periodic creep measurements were used to follow the effects of physical aging on the creep compliance (14). Figure 9 is a schematic of the stress, strain, and temperature history for the periodic creep experiment after a down-jump in temperature. The experiment consists of quenching the sample from above T_g to an aging temperature T_a below T_g and applying a load at approximately equal logarithmic increments of aging time (14). Hence, there are two time scales in the experiment: the aging or elapsed time (t_e) which begins at the moment of the quench (but often is taken as the time at which the sample reaches T_a) and the

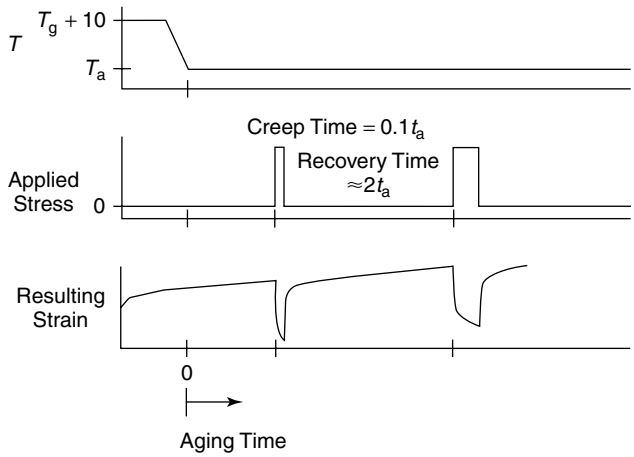

Fig. 9. Schematic of the creep experiment for monitoring physical aging.

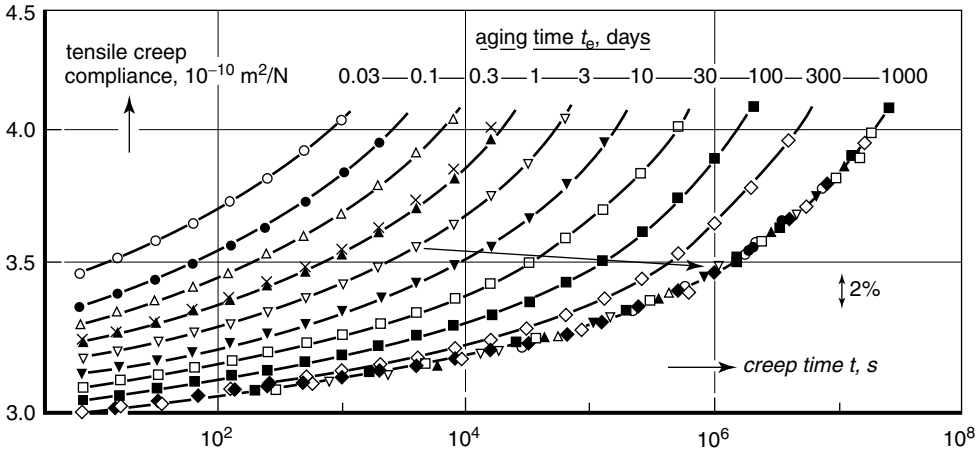

Fig. 10. Small-strain tensile creep curves for rigid poly(vinyl chloride) quenched from 90°C to 20°C and aged at 20 ± 0.1°C for a period of 4 years. The *x*-axis is the creep time. The times above the curves indicate the aging times at which each individual creep experiment was performed. The reduced curve was obtained by shifting the data to the longest aging time response as indicated by the arrow. The data are from Ref. 14, courtesy of L. C. E. Strvik.

creep time (t) which begins at the moment of loading. Creep times are generally performed for less than 10% of the aging time (0.1 t_e) in order to ensure that no appreciable aging occurs during the creep test. Hence, the creep response measured is a "snap shot" of the viscoelastic response at that particular aging time. The time between creep tests generally doubles or triples, allowing sufficient time for creep recovery; the time between measurements should be long enough that the strain change due to creep recovery from one loading is negligible compared to the subsequent loading. The time-dependent viscoelastic response to an up-jump is measured in a similar fashion. Small stresses are used to ensure that the viscoelastic response is linear.

Figure 10 shows the evolution of the creep compliance for poly(vinyl chloride) at 20°C over the course of four years (14). The T_g for poly(vinyl chloride) is around 70°C and so the aging temperature is approximately 50°C below T_g. As the material ages, the creep curves march to longer and longer times, indicating an increase in the characteristic relaxation time as aging progresses. If equilibrium were reached, the response would become independent of aging time (27). In sequential stress relaxation experiments, small strains rather than small stresses can similarly be used to probe the effect of aging on the viscoelastic response. In general, the creep or stress relaxation response due to the applied load or strain is the data analyzed in these experiments as indicated by the creep curves shown in Figure 10. A continuous test data method has recently been suggested, which involves analyzing both load and unload responses for the periodic creep experiment (28). This analysis can potentially yield a more accurate model of the mechanical response (since significantly more data is analyzed); however, the fact that in very few instrumental set-ups the load is actually zero in the unload portion of the experiment must be accounted for.

Time-aging time superposition can generally be used to reduce the curves by shifting them horizontally to superpose. A small vertical shift is sometimes needed as indicated by the slight downward slope of the arrow in Figure 10. The reduced curve is shown at the longest aging time in Figure 10. Struik has maintained that satisfactory time-aging time reduction of data infers that the structural–rheological simplicity is maintained, ie, the retardation spectrum shifts to longer times without a change in shape (14). Time-aging time superpositions have also been performed for poly(vinyl chloride), poly(methyl methacrylate) (PMMA), and polycarbonate creep data obtained by Read and co-workers over fourteen decades in time using several experimental techniques, and the satisfactory reduction of that data in the α-transition region has been interpreted as an indication of structural–rheological simplicity (29–31). On the other hand, Roe and Millman it was found that time-aging time superposition did not work for a polysytrene sample aged for several months at temperatures significantly below T_g and this was attributed to alteration of the shape of the relaxation time spectrum (32). It should be clear that a lack of time-aging time superposition indicates breakdown of structural–rheological simplicity. However, whether time-aging time superposition is sufficient to prove structural–rheological simplicity is less obvious. In order to clarify this point the concepts of time–temperature and time-aging time superpositions are briefly reviewed.

Reduction of linear viscoelastic data is based on the principles of time–temperature and time-aging time superpositions. The principle of time–temperature superposition is widely used to reduce creep or stress relaxation curves obtained at equilibrium density (33,34). The principle implies thermorheological simplicity, ie, the shape of the relaxation time spectrum does not change with temperature although the spectrum shifts to shorter times at higher temperatures. It has been demonstrated, however, that even for what was considered an ideal system, polyisobutylene, time–temperature superposition is not strictly observed (35). In addition, the ability to perform time–temperature superposition should be considered a necessary but not sufficient requirement for thermorheological simplicity because the relatively small experimental time scales over which data is usually obtained, coupled with the uncertainty in the data, leave open the possibility that time–temperature superposition is at best only a good approximation of the behavior over a large time scale. Indeed, it has been shown that although time–temperature superposition appears to be an empirically successful data reduction method for stress relaxation of semicrystalline polypropylene, the reduced stress relaxation curve is not consistent with dynamic mechanical data, and hence cannot be used to predict long-term viscoelastic performance (36). For a more in-depth discussion of time–temperature superposition, the reader is referred to the article on Viscoelasticity.

It is suggested that time-aging time superposition should similarly be considered a necessary but not sufficient requirement for structural–rheological simplicity, particularly since the basis for both shift factors is not well understood. The time-dependent compliance can often be described by

$$J(t) = J_g + J_d\psi(t) + t/\eta \tag{6}$$

where $J(t)$ is the time-dependent creep compliance, J_g refers to the glassy (zero time) compliance, and t is the time of creep. The viscous term (t/η) in equation (6),

where η is viscosity, is generally negligible during physical aging due to the high viscosity of the glass although this is not always the case as is discussed later. J_d in equation (6) is equal to $J_s - J_g$, where J_s is the steady state compliance which is equal to the long-time limiting value of the recoverable compliance for a non-cross-linked system. $\psi(t)$ is the normalized memory function for the compliance, and it goes from $\psi(0) = 0.0$ to $\psi(\infty) = 1.0$. The normalized memory function can often be described using the generalized Kohlrausch–William–Watts (KWW) (37,38) or stretched exponential function:

$$\psi(t) = 1 - e^{-(t/\tau)^{\beta}} \tag{7}$$

Equation (7) is also only valid for a short-term creep experiment in which the time of creep is short relative to the time scale of aging such that the characteristic relaxation time is constant. It is noted that the relaxation function of equation (7) has the correct limits and differs from the Kohlrausch compliance function ($J = J_s\, e^{(t/\tau)\beta}$) which was suggested initially by Struik (14) and which is not physically meaningful at long times (28).

The horizontal and vertical shift factors for reduction of two aging creep curves are defined as

$$\log a_{te} \equiv \log t_{ref} - \log t_1 \tag{8}$$

$$\log b_{te} \equiv \log J(t_{ref}) - \log J(t_1) \tag{9}$$

where $J(t_{ref})$ is the creep compliance at creep time t_{ref} on the reference curve (generally the curve obtained at longest aging times) to which all other curves are being shifted. $J(t_1)$ is the creep compliance at time t_1 which will be shifted to J(t_{ref}) and t_{ref}. By definition, the shift factors cannot depend on the creep time at which the shift is performed (ie, on the value of t_{ref}) since for a valid reduced curve the shift factors must be the same for all times along a given creep curve. For structural–rheological simplicity (eg, β = constant in eq. 7), the shift factors are given by those that Struik has reported (14):

$$a_{te} = \tau_{ref}/\tau_1 \tag{10}$$

$$b_{te} = J_{s_{ref}}/J_{s_1} \tag{11}$$

It should be noted that in addition to the criteria of structural–rheological simplicity, equation (11) is valid only when the glassy compliance J_g is negligible relative to the steady-state compliance.

Similarly, the stress relaxation modulus can often be described using the stretched exponential function:

$$G(t) = G_e + \left(G_g - G_e\right) e^{-(t/\tau)^{\beta}} \tag{12}$$

where G_g is the glass (or zero time) value of the modulus and G_e is the equilibrium (long-time) value of the modulus. For viscoelastic liquids, G_e is zero. For structural–rheological simplicity, the horizontal shift factor is given by equation (10) and the vertical shift factor is given by the following for viscoelastic liquids (39):

$$b_{te} = \frac{G_{g_{ref}}}{G_{g_1}} \tag{13}$$

When structural–rheological simplicity does not hold and, for example, β in equation (7) changes with physical aging, exact reduction of the creep or stress relaxation curves cannot be accomplished. However, it is estimated by the author that a change in the KWW β parameter of approximately 5–10% would result in a deviation of the logarithm of the aging time shift factor ($\log a_{te}$) of ± 0.05 over two decades in time scale. Scatter in reduced curves of this order of magnitude is often observed because of the scatter in the creep or stress relaxation data (23,39,40). Researchers have not systematically looked for such small deviations in their reduced curves.

In addition, structural–rheological simplicity might not be expected to be perfectly valid since the breadth of the relaxation time distribution is known to change with temperature at equilibrium (41,42) and along the glass line (43). Following a down-jump then, the breadth of the relaxation time distribution at equilibrium may be expected to differ between the initial and final temperatures and part of this change might be expected to occur during physical aging (as opposed to during the quench). A change in β with aging time of the order of 0.01–0.02 for polystyrene close to T_g has been inferred Recently by Ediger et al. (44). Based on the estimation above, such a change appears to be consistent with the majority of creep data in the literature (especially since researchers are not looking for such small deviations from superposition). For example, in a previous work on polycarbonate by McKenna (40) the value of β was observed to be invariant with aging time over the time scales investigated (up to 18 h for temperatures from 111°C below to 6°C below the nominal glass temperature). However, the error in β based on the error in the fit was reported to range from 4 to 7% at 70°C. In addition for two data sets at 135°C, β values equaled 0.47 ± 0.04 and 0.43 ± 0.02 at the longest aging time when a free fit was allowed (45). The point is that small systematic deviations in β may not be easily observable. The ability to obtain time-aging time superposition does not necessarily indicate that the shape of the spectrum is not changing with aging time.

According to equation (11), the vertical shift factor is suggested to be due to changes in the steady-state compliance, J_s, during physical aging. Such changes would arise if the steady-state compliance were temperature-dependent. J_s has been found to be independent of temperature in the range from 1.2 T_g to 2.0 T_g for several amorphous polymers (46,47). However, in the vicinity of T_g, J_s decreases with decreasing temperature for low molecular weight polystyrenes. (47) In the same work, J_s was predicted to also decrease for polystyrenes of higher molecular weight based on free volume arguments (47). This would suggest that in a down-jump experiment, J_s should decrease with aging time with the result that the vertical shift factors should be negative. Negative vertical shift factors are generally the case although two cases for positive shifts have been reported (14). However, positive vertical shift factors seem not to have a theoretical basis based on all measurements made to date on J_s.

In order to measure how the steady-state creep compliance and viscosity evolved during physical aging, a new interrupted creep experiment has been developed by plazek and co-workers (48). This experiment consists of applying a

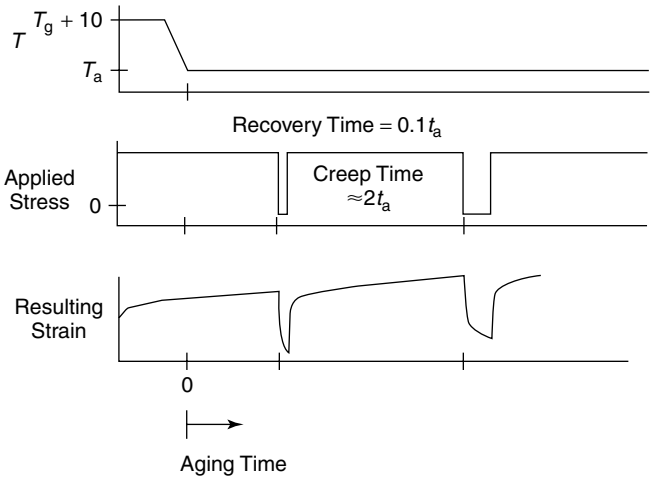

Fig. 11. A schematic of the intermittent creep experiment developed by Bernatz, Giri, Simon, and Plazek (Ref. 48).

constant load above T_g for a time long enough to reach steady state. Once in steady state, the material is quenched to the aging temperature T_a while maintaining the constant load. Successive creep-recovery measurements are made at logarithmic time increments. A schematic of the experiment for a temperature down-jump is shown in Figure 11. The rate of creep is monitored until the first creep-recovery measurement when the load is removed. After the first test, the load is reapplied and the creep rate is again monitored to ensure that adequate time has passed before the next measurement. The length of each creep-recovery measurement and the time between subsequent measurements follows the Struik protocol (14) for conventional or periodic creep experiments. The viscosity can be obtained as a function of aging time from the steady-state creep (or quasi steady-state creep for materials in which the steady-state creep compliance is temperature-dependent). The evolution of the steady-state compliance with aging time can be calculated from the horizontal shift factor (assuming β is constant, which should only be considered a first approximation):

$$a_{te} = \frac{\tau_{ref}}{\tau_1} = \frac{\eta_{ref} J_{s_{ref}}}{\eta_1 J_{s_1}} \tag{14}$$

Interpretation of the data from the interrupted creep experiment is based on the assumption that once the material reaches steady-state creep, a change in temperature will not disturb this condition if J_s is independent of temperature. Work by Leaderman on polyisobutylene above on T_g (49), as well as Plazek's work on 1,3,5-tri-α-naphthylbenzene (48), indicates this to be the case. Using the interrupted creep test, the evolution of both J_s and η for a polystyrene of 3400 molecular weight have been measured (48). This work confirms that for materials with temperature-dependent J_s, J_s will decrease during physical aging. The interrupted creep experiment may also make it possible to experimentally verify the relationship between the vertical shift factors and J_s.

Effects of Physical Aging on Failure

The most important effect of physical aging, from a practical standpoint, may well be its impact on failure and material lifetime. Physical aging has been found to cause transformation from ductile to brittle failure in many polymers, including poly(ethylene terephthalate) (50–52), polycarbonate (53–55), poly(ether imide) (56), and poly(phenylene oxide) (PPO) (57). In general, physical aging results in a decrease in the time to failure (58), as well as an increase in the yield stress and a decrease in the strain to break (50–57,59–66). A decrease in the impact fracture energy is also generally observed (63,66–69).

The effects of physical aging on craze growth are less clear. It has been found that craze breakdown and ultimate failure are accelerated by physical aging (61) in spite of the fact that the times to craze increase (61,62). However, other researchers found no effect of physical aging on the craze growth rates in polystyrene–polybutadiene diblock copolymers (70) and in polycarbonate (71). Complicating the picture, a transition from a high to low craze growth rate regime at long aging times for low aging temperatures in a styrene–acrylonitrile copolymer has been observed (72). The transition occurred over a narrow aging time window, with craze growth being relatively independent of aging time on either side of the transition. Higher aging temperatures showed only the low craze growth rate regime, leading to speculation that the transition occurred at aging times too short to be measured.

The effects of physical aging on fatigue crack propagation are even less well-documented than the effects on ultimate properties and crazing. Results seem to indicate that fatigue crack propagation depends very little on the degree of physical aging (69,73). The reason for this is suggested to be due to yielding occurring in the plastic zone (73). This is consistent with the fact that the lower yield stress which corresponds to the onset of generalized plastic flow has been observed to also be little affected by physical aging (60).

The Effect of Large Stresses on Physical Aging: Rejuvenation

The effect of large stresses on physical aging are controversial and not completely resolved. The term rejuvenation was coined by McKenna and Kovacs (74) to describe the observation that the aging time shift factor required to superpose large deformation responses was smaller than that required to superpose small deformation responses for the same thermal history. Strvik and others have interpreted this data as erasure of the previous aging by deformation-induced free volume (14,75–79). Other researchers have invoked rejuvenation to explain various observations (64,80). However, McKenna et al. have shown that although mechanical stimuli do induce a short-time volume response, the underlying volume relaxation is unperturbed by the deformation (81). This is contrary to what would be expected if rejuvenation were the case. In addition, it was found that the time required to reach equilibrium at temperatures near T_g was independent of the applied stress, suggesting that large stresses do not cause erasure of aging (82). It has been argued that the rejuvenation response is simply a result of nonlinear viscoelasticity, ie, the large deformation response is affected less by volume

(or enthalpy) changes than in the linear viscoelastic case (83,84). In fact, using the nonlinear viscoelastic Bernstin–Kearsley–Zapas (BKZ) constitutive equation (85) which includes an aging clock that depends upon the deformation magnitude, the rejuvenation response can be reproduced quantitatively without invoking any type of deformation-induced "erasure" effect (86).

There are two alternatives to the rejuvenation hypothesis: mechanical–structural decoupling which much of McKenna's work suggests (86,87) and the accelerated aging hypothesis suggested some time ago by Sternstein (88). There is some recent evidence of mechanically enhanced aging of polycarbonate (PC) at room temperature (89). Although consistent with Sternstein's ideas (88), more work is needed to directly test the accelerated aging hypothesis. It is important that this be done, however, in the context of nonlinear viscoelasticity.

Relative Time Scales for Relaxation of Different Properties

There are a number of reports in the literature on the relative time scales of relaxation for different properties (10,23,32,64,65,80,87,90–101) Table 1 summarizes experimental results on polymeric glasses. For nonpolymeric materials, Scherer (102) has summarized the relative values of characteristic equilibrium relaxation times obtained by Moynihan through modeling the relaxation behavior of various properties of low molecular weight glasses, as well as the experimental results of Rekhson on volume and stress relaxation of low molecular weight glasses. The results shown in Table 1 are seemingly contradictory at first glance, with some researchers finding that the time scales are the same for different properties and some groups finding that they differ. The time scale for relaxation is defined differently by different researchers. It has been suggested (10,23,99) that the time required to reach equilibrium may be the best measure of the relaxation time scale in spite of the fact that the relaxation response approaches equilibrium asymptotically. Most of the results reported in Table 1 reflect the relative approach to equilibrium for different properties. The rate of approach can differ for different properties because of differences in thermal history in different measurements and also because of differences in the sensitivity of the properties to the molecular changes associated with physical aging. This is the case even when the time required to reach equilibrium is the same (10,99). Hence, the assertion that the time required to reach equilibrium (rather than some characteristic relaxation time based on the shape of the relaxation response) is the appropriate time scale. McKenna et al. investigated the times required to reach equilibrium, and their results suggested that the relative time scales for stress relaxation and volume recovery depend on the physical aging temperature and the magnitude and direction of the jump from equilibrium to the aging temperature (87,90). On the other hand, the early results of Simon and co-workers on poly(ether imide) indicated that the time required to reach equilibrium for volume, enthalpy, and creep were identical (23,99). Subsequent experiments on polystyrene found that time scales to reach equilibrium were again the same for volume and enthalpy at temperatures where equilibrium was reached (10). However, model extrapolations to lower temperatures indicate that the relaxation times for enthalpy diverge from those of volume, and are shorter. The divergence might be dismissed as being due to problems

Table 1. Relative Time Scales for Evolution of Various Properties During Structural Recovery for Polymers

Material	Experiments	Findings	Reference
DGEBA[a]/PPO	Volume recovery and evolution of stress relaxation (up- and down-jumps)	Times to reach equilibrium differ: volume is faster in up-jump, slower in down-jump relative to mechanical property.	87,90
DGEBA[a]/DDS[b]	Volume recovery (up- and down-jumps) and creep (equilibrium)	Shift factors for data reduction are the same.	91
PS	Volume and enthalpy recovery	Times to reach equilibrium are the same near T_g; model calculations predict times to reach equilibrium differ: enthalpy faster than volume.	10
PS	Volume and enthalpy recovery (up- and down-jumps)	Rates of approach to equilibrium are related by a constant for volume and enthalpy.	92
PS	Volume and enthalpy recovery (double temperature jumps)	Times to reach maximum differ: volume is slower than enthalpy.	93
PS	Enthalpy recovery, and room temperature creep evolution (down-jumps)	Times to reach equilibrium differ: enthalpy is faster than mechanical property.	32
PS	Volume and enthalpy recovery (after cooling under pressure)	Times to reach specified percent recovery differ: volume is faster relative to enthalpy.	95
PMMA	Volume and enthalpy recovery (after cooling under pressure)	Times to reach specified percent recovery differ: volume is slower relative to enthalpy.	95
PMMA	Volume and enthalpy recovery, and dynamic mechanical analysis (down-jumps)	Decay functions differ: enthalpy is fastest, followed by volume, followed by mechanical property.	96
PMMA	Enthalpy recovery, and stress relaxation (down-jumps)	Model parameters for enthalpy relaxation comparable to experimental stress relaxation times.	97
PVAc	Volume and enthalpy recovery (down-jumps), dynamic mechanical analysis and dielectric analysis (equilibrium)	Equilibrium relaxation times obtained from modeling data differ: largest for enthalpy, smallest for mechanical property.	94
PVAc	Volume and enthalpy recovery (down-jumps)	Effective retardation times differ: smaller for volume relative to enthalpy.	98

Table 1. (Continued)

Material	Experiments	Findings	Reference
PVAc	Volume and dynamic mechanical analysis (up- and down-jumps)	Relaxation time from fit is smaller for volume than mechanical property on down-jump; activation energy is larger for volume.	80
PVAc	Volume, enthalpy recovery, and stress relaxation (down-jumps)	Mechanical property reaches equilibrium while volume and enthalpy are still evolving.	100,101
PEI	Enthalpy and volume recovery and creep evolution (down-jumps)	Times to reach equilibrium are the same but volume relaxes faster initially relative to enthalpy.	23,99
PC	Enthalpy recovery, creep, and yield (down-jumps)	Rate of change of enthalpy and creep are different; equilibrium is not reached.	64
PI	Enthalpy recovery and creep evolution (down-jumps)	Relaxation times from fit of data are longer for enthalpy than for creep.	65

[a]DGEBA: diglycidyl ether of bisphenol A.
[b]DDS.: 4,4′-diamino diphenyl sulfone.

with the model (see later on the TNM model and problems associated therewith), if it were not for the fact that our most recent data on the glass former selenium appears to show the divergence for temperatures at which equilibrium was reached (103). Figure 12 shows the times required to reach equilibrium as a function of the distance from the glass temperature (with T_g defined at 0.2°C/min) for polystyrene, poly(ether imide), and selenium. The selenium data is offset from the polystyrene and poly(ether imide) data because the temperature dependence of the times required to reach equilibrium differs. The symbols are the measured times required to reach equilibrium, whereas the dashed lines are the times required to reach equilibrium based on extrapolations using the Tool–Narayanaswamy–Moynihan (TNM) model for polystyrene and using a linear extrapolation for selenium (which is expected to give a lower bound for the time required to reach equilibrium). At temperatures in the vicinity of T_g all three properties appear to come to equilibrium at the same time within the scatter of the data. At lower temperatures, the times required to reach equilibrium appear to diverge for the various properties, with enthalpy reaching equilibrium before volume and creep. The divergence appears to occur closer to T_g for selenium than for polystyrene. Although the origin of the divergence in time scales is not known, it appears that this general framework is consistent for the three materials which we have studied and with the other data in the literature. We note that other researchers (80) have claimed a difference in activation energies for the characteristic relaxation time obtained from a fit of the stretched exponential to the relaxation data, resulting in a picture similar to what we observe but for the characteristic relaxation time. The two pictures are consistent; the primary difference is that we suggest that the

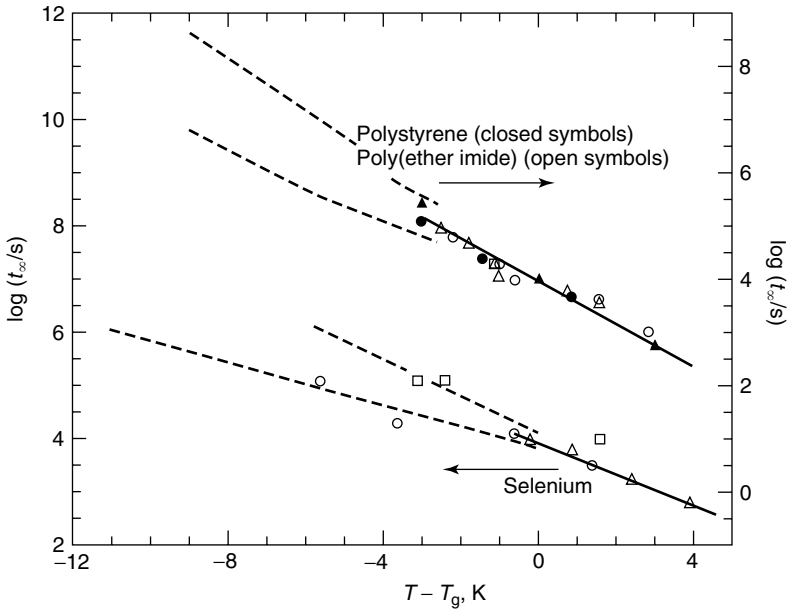

Fig. 12. The times required to reach equilibrium for polystyrene, poly(ether imide), and selenium vs the departure from T_g, where T_g is defined as the value obtained dilatometrically on cooling at 2°C/min. Data are replotted from Refs. 10, 23, 99, and 103 ▲ & △ Volume, □ Creep, and ● & ○ Enthalpy.

time required to reach equilibrium is a better parameter of the time scale because it is less influenced by magnitude of the temperature jump and the resulting shape of the relaxation response.

Temperature Dependence of the Relaxation Time at Equilibrium

The temperature dependence of the characteristic relaxation time is described by the (Williams–Landell–Ferry) (WLF) equation (104), or the equivalent Vogel–Tammann–Hesse–Fulcher (VTHF) (105–107) expression. These equations are valid from the nominal glass temperature to approximately 100–150°C above T_g. Far above the glass temperature, the temperature dependence decreases and becomes Arrhenius or follows a different WLF dependence (108). The temperature dependence of the relaxation time along the glass line below T_g is known to deviate from WLF behavior and follows what appears to be Arrhenius temperature dependence with a very low activation energy (14). What is not as well-known, however, is that below the glass temperature, the temperature dependence of the equilibrium relaxation time also appears to deviate from the WLF relationship with a lower apparent activation energy than expected based on extrapolation of the WLF equation.

The first convincing data depicting the change from WLF to an Arrhenius-type temperature dependence for the equilibrium relaxation time at T_g is the work

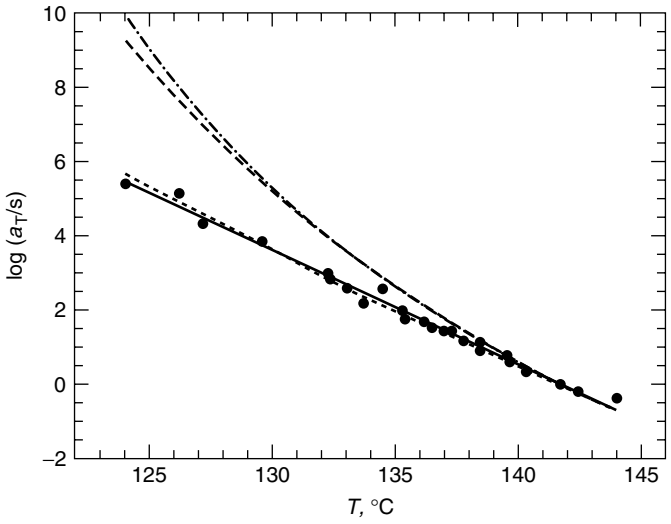

Fig. 13. The temperature dependence of the shift factors for stress relaxation of polycarbonate obtained at equilibrium. The data shows a significant deviation from the expected WLF temperature dependence; the dashed and dash–dot lines are the "universal" WLF temperature dependence and that which fits the polycarbonate data above T_g. The data are replotted from the data of Ref. 39. —●— Experimental data and linear fit, — — — WLF ($C_1 = 17.44$, $C_2 = 51.66$ K, $T_{ref} = 142^\circ$ C), – · – · – WLF ($C_1 = 14.42$, $C_2 = 43.97$ K, $T_{ref} = 142^\circ$ C), and ------- WLF ($C_1 = 49.71$ $C_2 = 174.6$ K, $T_{ref} = 142^\circ$ C).

on polycarbonate by O'Connell and McKenna in which equilibrium was reached at temperatures 17°C below the nominal glass temperature (109). This data is shown in Figure 13. Similar results were found for polystyrene (10). Similar behavior might be interpreted from earlier works on various organic liquids (110,111), although it is not clear in the early work that the measurements reported are all equilibrium measurements or that the reported Vogel fits are correct since in one case (111) T_∞ was very near T_g. Recent theoretical work by Di Marzio and Yang (112) predicts a change in the temperature dependence of the equilibrium relaxation time at T_g from WLF-type dependence to an Arrhenius temperature dependence. The non-WLF temperature dependence below T_g for the equilibrium state has major implications for modeling and predicting the effects of structural recovery, especially for aging deep in the glassy state, since knowledge of the value of the relaxation time at equilibrium is critical for accurate predictions.

Physical Aging in Semicrystalline Polymers

The effects of structural recovery are not limited to fully amorphous materials. In semicrystalline polymers, the amorphous regions physically age in a similar manner to the process in fully amorphous materials. Obviously, however, the change in properties will be only a fraction of that found in fully amorphous materials since the amount of amorphous material makes up only a fraction of the

semicrystalline material. One difference between aging in semicrystalline materials and fully amorphous materials, however, is the temperature range over which physical aging is observed. In amorphous materials, aging occurs only below the time or frequency dependent glass temperature, whereas in semicrystalline materials, physical aging has been observed at temperatures above the nominal T_g (14,113–118). The explanation is that the crystalline domains constrain the glass in the vicinity of the crystallite, increasing its T_g, and thereby increasing the temperatures at which physical aging is observed (113–116). However, above T_g secondary crystallization and/or crystal reorganization can take place. Results for physical aging of syndiotactic polystyrene above T_g suggest that in contrast to many semicrystalline polymers, the recrystallization phenomenon is the primary mechanism for physical aging above T_g (118).

Modeling Structural Recovery

Models of structural recovery include the Kovacs–Aklonis–Hutchinson–Ramos (KAHR) model (119), Moynihan's model (120), and Ngai's coupling model (121). These models are based on work done originally by Narayanaswamy (122), incorporating the ideas of Tool (13). The models of structural recovery reflect the nonlinear and nonexponential effects observed experimentally. The historical development of these equations has been detailed (7,8); only a brief description follows. The KAHR formulation (119), which is written in terms of a departure from equilibrium δ rather than in terms of T_f, is conceptually easier to use when the full three-dimensional PVT surface is considered:

$$\delta = \int_0^t \frac{d\delta}{dt} \exp\left[-\left(\int_{t'}^t \frac{dt''}{\tau} \right)^{\beta} \right] dt' \tag{15}$$

where for volume the departure from equilibrium is given by the definition in equation (1), whereas for enthalpy, the definition in equation (4) is used. τ is known as the characteristic relaxation time (although it is actually a retardation time), β is the nonexpontiality or stretching parameter, and $d\delta/dt$ is the rate of change of δ in arbitrary pressure or temperature histories:

$$\frac{d\delta}{dt} = \left(\frac{\partial \delta}{\partial P} \right)_T \frac{dP}{dt} + \left(\frac{\partial \delta}{\partial T} \right)_P \frac{dT}{dt} \tag{16}$$

For the case of isobaric temperature jumps or isothermal pressure jumps, these equations revert to the KAHR equations for volume recovery using $(d\delta/dP)_T = -\Delta\kappa$ and $(d\delta/dT)_P = \Delta\alpha$. $\Delta\kappa$ is the difference in the compressibilities of the liquid and glass at T_g. For enthalpy recovery, $(d\delta/dP)_T = VT\Delta\alpha$ and $(d\delta/dT)_P = \Delta C_p$.

The nonexponentiality of the structural recovery process is described by the nonexponentiality parameter β in equation (15); the history dependence is accounted for by the integral of the reduced time (dt/τ); and the nonlinearity is incorporated into the model by allowing the characteristic relaxation time τ

to be a function of temperature, pressure, and structure, the latter of which is often characterized by the fictive temperature (T_f), the fictive pressure (P_f), or the departure from equilibrium (δ). The fictive temperature is defined as the temperature at which a material would reach equilibrium if heated (or cooled) along the glass line. It is related to δ at constant pressure through the difference between the liquid and glass thermal expansion coefficients ($\Delta\alpha$) for volume and through the difference between the liquid and glass heat capacities (ΔCp) for enthalpy:

$$T_f = T_a + \frac{\delta}{\Delta\alpha} \quad \text{for volume recovery} \tag{17}$$

$$T_f = T_a + \frac{\delta}{\Delta C_P} \quad \text{for volume recovery} \tag{18}$$

Hence, at equilibrium, the fictive temperature is equal to the aging temperature. The fictive pressure has an analogous definition with respect to glass and liquid lines in pressure space.

Various phenomenological equations have been used to describe the dependence of the characteristic relaxation time on temperature and structure and sometimes pressure, including the TNM equation (120), equations derived by Hodge (123) and Scherer (124), both based on the approach of Adam and Gibbs (125), the KAHR and similar equations (119,126), equations based on free volume, and several others (127,128). The essential idea in all of these equations is that the characteristic relaxation time depends on the instantaneous state of the material (ie, temperature, pressure, and some measure of structure—volume, δ, T_f, and/or P_f). The most widely used form is the TNM equation for isobaric structural recovery:

$$\ln \tau_0 = \ln A + \frac{x\Delta h}{T} - \frac{(1-x)\,\Delta h^*}{T_f} \tag{19}$$

where x partitions the effects of temperature and structure and determines the degree of nonlinearity, and $\Delta h*$ and A are constants. Although this equation is unable to describe the observed WLF (104) or the equivalent VTHF (105–107) temperature dependence in the equilibrium limit when $T_f = T$, it is often thought to be a valid approximation to the narrow range of temperature over which data is modeled. Although this may be the case for modeling isothermal structural relaxation data, this assumption is suspect for modeling dsc temperature scans. To accurately model the poly(ether imide) data shown in Figure 8, the dependence of the characteristic relaxation time is needed as a function of structure and temperature from 201°C (where aging took place) to 230°C where the enthalpy overshoot returns to the baseline. The linear approximation of equation (19) is not valid over this temperature range above T_g (207°C) where the WLF equation is valid, let alone below T_g where the temperature dependence of the equilibrium relaxation time is expected to change (10,109). Consistent with the fact that equation (19)

is not a valid representation over the range of temperatures of interest when modeling dsc temperature scans, Schick and co-workers (129) have recently found that description of the loss and storage heat capacity obtained from slow temperature-modulated dsc cooling scans could only be done well by using an equation based on Adam and Gibbs which is consistent with WLF behavior above T_g.

There are unresolved issues pertaining to the models, including an apparent dependence of model parameters on thermal history and an inability to predict structural recovery for deep quenches (5,7,8,130–138). Simple fixes have been found not to resolve these problems (5,133,136,138,139). To make rational improvements to the models and to determine what "essential ingredients" (140) are needed to predict structural recovery, systematic investigation of model assumptions is now needed. The basic assumptions underlying current models of structural recovery include (*1*) thermorheological simplicity, (*2*) structural–rheological simplicity, (*3*) the assumption that the placement of the relaxation time spectrum on the time scale (ie, the mobility) depends only on the instantaneous state of the glass, and (*4*) the assumption that the relationship between glassy structure and temperature and pressure history can be described using Boltzmann superposition in a way that is analogous to viscoelasticity.

In contrast to the KAHR, TNM, and Ngai models of structural recovery, which were developed based on extending the formalism developed for viscoelasticity and an understanding of the relationship between the volume (or enthalpy) relaxation kinetics and the volume (or enthalpy), the thermoviscoelastic model developed in Caruther's group at Purdue (141) is based on Coleman's thermodynamic theory, also known as rational mechanics (142,143). It is one of the first advances in the development of equations to describe structural recovery to appear in about 20 years (144). Caruther's model begins with a free energy functional which is differentiated to obtain the time- and path-dependent nonequilibrium thermodynamic functions. The thermoviscoelastic constitutive model is the only theory which can qualitatively describe structural recovery, yield in tension and compression, multiaxial yield, nonlinear creep and stress relaxation, and constant rate of cooling isobaric studies with a single set of material parameters which can be independently obtained (145). The model is covered in detail in the Viscoelasticity article of this encylopedia.

Of particular importance to structural recovery models is the idea that the apparent mobility may depend on the temperature/pressure/stress path rather than on the instantaneous state of the material. This differs from all of the phenomenological equations for the characteristic relaxation time, including equation (19), which are presently used in other models of structural recovery. The dependence of the relaxation on the unique state has been investigated by Strvik (146), and although it was claimed that the relaxation time only appeared to depend on the instantaneous volume, there is considerable scatter in the data and the relationship appears to depend not only on the final aging temperature but also on the sample history (ie, the magnitude of down- and double-temperature jumps). The scatter may be due to the measurements of volume and relative relaxation time being made in separate instruments such that the thermal history of the samples were not identical. Alternatively, it may be an indication of a more complicated

relationship between the characteristic relaxation time and the instantaneous state as Caruther's model suggests.

Current Challenges in Physical Aging Research

One of the greatest unsolved challenges in physical aging research is understanding the relationship between the evolution of various properties, including failure, and the ability to predict time-dependent properties from limited data over, for example, the lifetime of a material. We are not at the point yet where we can predict changes in thermodynamic properties from one another, let along predict mechanical behavior from thermodynamic variables. Issues such as whether spectral shape changes during physical aging, how to correctly incorporate nonlinearity into the models of structural recovery, and how many ordering parameters exist are also not resolved.

Part of our problem lies in the absence of a universally accepted theory of the glass transition itself. For this reason, the interpretation and modeling of experimental results takes place within a weak theoretical framework. It is important that the fundamental questions associated with the glass transition be addressed, including, but not limited to, the assumptions underlying the Adam–Gibbs theory, the ability to calculate the configurational entropy, and the existence or lack thereof of an underlying thermodynamic glass transition.

BIBLIOGRAPHY

"Aging, Physical" in *EPSE* 2nd ed., Vol. 1, pp. 595–611, by L. C. E. Struik, Plastics and Rubber Research Institute.

1. J. H. Gibbs, *J. Chem. Phys.* **25**, 185 (1956).
2. J. H. Gibbs and E. A. DiMarzio, *J. Chem. Phys.* **28**, 807 (1958).
3. E. A. DiMarzio and J. H. Gibbs, *J. Chem. Phys.* **28**, 807 (1958).
4. W. Kauzmann, *Chem. Rev.* **43**, 219 (1948).
5. I. A. Hodge, *Science* **267**, 1945 (1995).
6. P. W. Anderson, *Science* **247**, 1616 (1995).
7. G. B. McKenna, in C. Booth and C. Price, eds., *Comprehensive Polymer Science*, Vol. **12**: Polymer Properties, Pergamon, Oxford, 1989, pp. 311–362.
8. I. M. Hodge, *J. Non-Cryst. Solids* **169**, 211 (1994).
9. A. J. Kovacs, *Fortschr. Hochpolym.-Forsch* **3**, 394 (1964).
10. S. L. Simon, J. W. Sobieski, and D. J. Plazek, *Polymer* **42**, 2555–2567 (2001).
11. L. C. E. Struik, *Polymer* **28**, 1869 (1987).
12. G. B. McKenna and co-workers, *Polymer* **40**, 5183 (1999).
13. A. Q. Tool, *J. Am. Ceram. Soc.* **29**, 240 (1946).
14. L. C. E. Struik, *Physical Aging in Amorphous Polymers and Other Materials*, Elsevier Scientific, New York, 1978.
15. R. Wimberger-Friedl and J. G. de Bruin, *Macromolecules* **29**, 4992 (1996).
16. C. G. Robertson and G. L. Wilkes, *Macromolecules* **33**, 3954 (2000).
17. S. E. B. Petrie, *J. Polym. Sci., Part A* **2, 10**, 1255 (1972).
18. M. Reading, *Trends Polym. Sci.* **1**, 248–253 (1993).
19. M. Reading, D. Elliott, and V. L. Hill, *J. Therm. Anal.* **40**, 949 (1993).

20. G. S. Gill, S. R. Sauerbrunn, and M. Reading, *J. Therm. Anal.* **40**, 931 (1993).
21. S. L. Simon and G. B. McKenna, *Thermochem. Acta* **307**(1), 1 (1997).
22. S. L. Simon and G. B. McKenna, *Thermochim. Acta* **348**, 77–89 (2000).
23. I. Echeverria, P.-C. Su, S. L. Simon, and D. J. Plazek, *J. Polym. Sci., B: Polym. Phys.* **33**, 2457 (1995).
24. H. Fujimori and M. Oguni, *J. Non-Cryst. Solids* **601**, 172–174 (1994).
25. H. Fujimori, H. Fujita, and M. Oguni, *Bull. Chem. Soc. Jpn.* **68**, 44 (1995).
26. A. J. Kovacs, R. A. Stratton, and J. D. Ferry, *J. Phys. Chem.* **67**, 152 (1963).
27. A. Lee and G. B. McKenna, *Polymer* **29**, 1812 (1988).
28. R. D. Bradshaw and L. C. Brinson, *Polym. Eng. Sci.* **39**, 211 (1999).
29. B. E. Read, *J. Non-Cryst. Solids* **408**, 131–133 (1991).
30. B. E. Read, G. D. Dean, P. E. Tomlins, and J. L. Lesniarek-Hamid, *Polymer* **33**, 2689 (1992).
31. P. E. Tomlins, B. E. Read, and G. D. Dean, *Polymer* **35**, 4376 (1994).
32. R. J. Roe and G. M. Millman, *Polym. Eng. Sci.* **23**, 318 (1983).
33. H. Leaderman, *Elastic and Creep Properties of Filamentous Materials*, Textile Foundation, Washington, D.C., 1943.
34. J. D. Ferry, *Viscoelastic Properties of Polymers*, 3rd ed., John Wiley & Sons, Inc., New York, 1980.
35. D. J. Plazek, *J. Rheol.* **40**, 987 (1996).
36. F.-J. Wortmann and K. V. Schulz, *Polymer* **36**, 1611 (1995).
37. F. Kolrausch, *Pogg. Ann. Phys.* **12**, 393 (1847).
38. G. Williams and D. C. Watts, *Trans. Faraday Soc.* **66**, 80 (1970).
39. P. A. O'Connell and G. B. McKenna, *J. Chem. Phys.* **110**, 11054 (1999).
40. R. D. Bradshaw and L. C. Brinson, *Polym. Eng. Sci.* **37**(1), 31 (1997).
41. D. B. Hall, A. Dhinojwala, and J. M. Torkelson, *Phys. Rev. Lett.* **79**(1), 103 (1997).
42. C. Y. Wang and M. D. Ediger, *Macromolecules* **30**, 4770 (1997).
43. P. A. O'Connell and G. B. McKenna, *Polym. Eng. Sci.* **37**, 1485 (1997).
44. C. T. Thurau and M. D. Ediger, Paper presentation N18.009, American Physical Society, March Meeting, 2001.
45. Paul O'Connell and Gregory B. McKenna, *private communication*, 2001.
46. D. J. Plazek and A. J. Chelko Jr., *Polymer* **18**, 15 (1977).
47. D. J. Plazek and V. M. O'Rourke, *J. Polym. Sci. Part A-2* **9** 209 (1971).
48. K. M. Bernatz, L. Giri, S. L. Simon, and D. J. Plazek, *J. Chem. Phys.* **111**, 2235 (1999).
49. H. Leaderman, R. G. Smith, and R. W. Jones, *J. Polym. Sci.* **14**, 47 (1954).
50. S. E. B. Petrie, *J. Macromol. Sci., Phys. Ed.* **12**, 225 (1976).
51. M. R. Tant and G. L. Wilkes, *J. Appl. Polym. Sci.* **26**, 2813 (1981).
52. A. Aref-Azar, F. Biddlestone, J. N. Hay, and R. N. Haward, *Polymer* **24**, 1245 (1983).
53. J. H. Golden, B. L. Hammant, and E. A. Hazell, *J. Appl. Polym. Sci.* **11**, 1571 (1967).
54. D. G. Legrand, *J. Appl. Polym. Sci.* **13**, 2129 (1969).
55. J. R. Flick and S. E. B. Petrie, *Proc. Second Symp. Macromolecules*, Vol. **10**, 1978, p. 145.
56. A. B. Brennan and F. Feller III, *J. Rheol.* **39**, 453 (1995).
57. A. C.-M. Yang, R. C. Wang, and J. H. Lin, *Polymer* **37**, 5751 (1996).
58. J. M. Crissman and G. B. McKenna, *J. Polym. Sci., Part B: Polym. Phys.* **28**, 1463 (1990).
59. Z. H. Ophir, J. A. Emerson, and G. L. Wilkes, *J. Appl. Phys.* **49**, 5032 (1978).
60. C. G'Sell and G. B. McKenna, *Polymer* **33**, 2103 (1992).
61. J. C. Arnold, *J. Polym. Sci., Part B: Polym. Phys. Ed.* **31**, 1451 (1993).

62. G. M. Gusler and G. B. McKenna, *Polym. Eng. Sci.* **37**(9), 1442 (1997).
63. C.-H. Lin and J. A. Nairn, *Polym. Eng. Sci.* **38**(1), 186 (1998).
64. J. M. Hutchinson, S. Smith, B. Horne, and G. M. Gourlay, *Macromolecules* **32**, 5057 (1999).
65. C. G. Robertson, J. E. Monat, and G. L. Wilkes, *J. Polym. Sci., Part B: Polym. Phys.* **37**, 1931 (1999).
66. W. Liu, J. Shen, F. Lu, and M. Xu, *J. Appl. Polym. Sci.* **78**, 1275 (2000).
67. R. M. Mininni, R. S. Moore, J. R. Flick, and S. E. B. Petrie, *J. Macromol. Sci., Part B: Phys.* **8**, 342 (1973).
68. G. B. McKenna, J. M. Crissman, and A. Lee, *Polym. Prepr.* **29**, 128 (1988).
69. J. A. Manson, R. W. Hertzberg, S. L. Kim, and W. C. Wu, in R. D. Deanin and A. M. Crugnola, eds., *Toughness and Brittleness of Plastics (Advances in Chemistry Series No. 154)*, American Chemical Society, Washington, D.C., 1976, p. 146.
70. J. A. DiCorletto and R. E. Cohen, *Polymer* **29**, 1245 (1988).
71. N. Verheulpen-Heymans, *J. Mater. Sci.* **11**, 1003 (1976).
72. M. Delin and G. B. McKenna, *Mech. Time-Dep. Mater.* **4**, 231 (2000).
73. J. A. Manson, in *Encylcopedia of Polymer Science and Engineering*, Vol. **7**, John Wiley & Sons, Inc., New York, 1987, pp. 378–453.
74. G. B. McKenna and A. J. Kovacs, *Polym. Eng. Sci.* **24**, 1138 (1984).
75. L. C. E. Struik, *Polymer* **38**, 4053 (1997).
76. T. Ricco and T. L. Smith, *Polymer* **25**, 1979 (1985).
77. T. L. Smith, G. Levita, and W. K. Moonan, *J. Polym. Sci., Part B: Polym. Phys.* **26**, 875 (1988).
78. A. F. Yee, R. J. Bankert, K. L. Ngai, and R. W. Rendell, *J. Polym. Sci., Part B: Polym. Phys.* **26**, 2463 (1988).
79. M. Utz, P. G. Debenedetti, and F. H. Stillinger, *Phys. Rev. Lett.* **84**, 1471 (2000).
80. M. Delin, R. W. Rychwalski, J. Kubat, C. Klason, and J. M. Itotchinson, *Polym. Eng. Sci.* **36**, 2955 (1996).
81. M. M. Santore, R. S. Duran, and G. B. McKenna, *Polymer* **32**, 2377 (1991).
82. A. Lee and G. B. McKenna, *Polym. Eng. Sci.* **30**, 431 (1990).
83. G. B. McKenna and L. J. Zapas, *J. Polym. Sci., Polym. Phys. Ed.* **23**, 1647 (1985).
84. G. B. McKenna and L. J. Zapas, *Polym. Eng. Sci.* **26**, 725 (1986).
85. B. E. Bernstein, A. Kearsley, and L. J. Zapas, *Trans. Soc. Rheol.* **7**, 391 (1963).
86. W. K. Waldron, G. B. McKenna, and M. M. Santore, *J. Rheol.* **39**, 471 (1995).
87. G. B. McKenna, Y. Leterrier, and C. R. Schultheisz, *Polym. Eng. Sci.* **35**, 403 (1995).
88. F. A. Myers, F. C. Cama, and S. S. Sternstein, *Ann. N.Y. Acad. Sci.* **279**, 94 (1976).
89. D. M. Colucci, P. A. O'Connell, and G. B. McKenna, *Polym. Eng. Sci.* **37**, 1469 (1997).
90. G. B. McKenna, C. R. Schultheisz, and Y. Leterrier, in *Proc. 9th Int'l Conf. on Deformation Yield and Fracture of Polymers*, Cambridge, U.K., 1994, pp. 31/1–31/4.
91. C. A. Bero and D. J. Plazek, *J. Polym. Sci., B: Polym. Phys.* **29**, 39 (1991).
92. E. F. Oleinik, *Polym. J.* **19**(1), 105 (1987).
93. K. Adachi and T. Kotaka, *Polymer J.* **14**, 959 (1982).
94. H. Sasabe and C. T. Moynihan, *J. Polym. Sci., B: Polym Phys.* **16**, 1447 (1978).
95. A. Weitz and B. Wunderlich, *J. Polym. Sci., Polym. Phys.* **12**, 2473 (1974).
96. J. Perez, J. Y. Cavaille, R. D. Calleja, J. L. G. Ribelles, M. M. Pradas, and A. R. Grevs, *Makromol. Chem.* **192**, 2141 (1991).
97. J. Mijovic and T. Ho, *Polymer* **34**, 3865 (1993)
98. J. M. G. Cowie, S. Elliott, R. Ferguson, and R. Simha, *Polym. Commun.* **28**, 298 (1987).
99. S. L. Simon, D. J. Plazek, J. W. Sobieski, and E. T. McGregor, *J. Polym. Sci., Part B: Polym. Phys.* **35**, 929 (1997).

100. J. M. G. Cowie, S. Harris, and I. J. McEwen, *Macromolecules* **31**, 2611 (1998).
101. J. M. G. Cowie, R. Ferguson, S. Harris, and I. J. McEwen, *Polymer* **39**, 4393 (1998).
102. G. W. Scherer, *Relaxation in Glass and Composites*, John Wiley and Sons, Inc., New York, 1986.
103. I. Echeverria, P. Kolek, S. L. Simon, and D. J. Plazek, to be submitted.
104. M. L. Williams, R. F. Landell, and J. D. Ferry, *J. Am. Chem. Soc.* **77**, 3701 (1955).
105. H. Vogel, *Phys. Z.* **22**, 645 (1921).
106. G. Tammann and G. Hesse, Z. Anorg. *Allg. Chem.* **156**, 245 (1926).
107. G. S. Fulcher, *J. Am. Chem. Soc.* **8**, 339, 789 (1925).
108. F. Stickel, E. Fischer, and R. Richert, *J. Chem. Phys.* **104**, 2043 (1996).
109. P. A. O'Connell and G. B. McKenna, *J. Chem. Phys.* **110**, 11054 (1999).
110. W. T. Laughlin and D. R. Uhlmann, *J. Phys. Chem.* **76**, 2317 (1972).
111. M. Cukierman, J. W. Lane, and D. R. Uhlmann, *J. Chem. Phys.* **59**, 3639 (1973).
112. E. A. Di Marzio and A. J. M. Yang, *J. Res. Natl. Inst. Stand. Tech.* **102**(2), 135 (1997).
113. L. C. E. Struik, *Polymer* **28**, 1521 (1987).
114. L. C. E. Struik, *Polymer* **28**, 1534 (1987).
115. L. C. E. Struik, *Polymer* **30**, 799 (1989).
116. L. C. E. Struik, *Polymer* **30**, 815 (1989).
117. I. Spinu and G. B. McKenna, *Polym. Eng. Sci.* **32**, 1808 (1994).
118. J. Beckmann, G. B. McKenna, B. G. Landes, D. H. Bank, and R. A. Bubeck, *Polym. Eng. Sci.* **37**, 1459 (1997).
119. A. J. Kovacs, J. J. Aklonis, J. M. Hutchinson, and A. R. Ramos, *J. Polym. Sci., Polym. Phys. Ed.* **17**, 1097 (1979).
120. C. T. Moynihan, P. B. Macedo, C. J. Montrose, P. K. Gupta, M. A. DeBolt, J. F. Dill, B. E. Dom, P. W. Drake, A. J. Esteal, P. B. Elterman, R. P. Moeller, H. Sasabe, and J. A. Wilder, *Ann. N. Y. Acad. Sci.* **15**, 279 (1976).
121. K. L. Ngai, *Comments Solid State Phys.* **9**, 127 (1979).
122. O. S. Narayanaswamy, *J. Am. Ceram. Soc.* **54**, 491 (1971).
123. I. M. Hodge, *Macromolecules* **20**, 2897 (1988).
124. G. W. Scherer, *J. Am. Cer. Soc.* **67**, 504 (1984).
125. G. Adam and J. H. Gibbs, *J. Chem. Phys.* **43**(1), 139 (1965).
126. A. R. Ramos, A. J. Kovacs, J. M. O'Reilly, J. J. Tribone, and J. Greener, *J. Phys. Sci., Polym. Phys. Ed.* **26**, 501 (1988).
127. J. J. Tribone, J. M. O'Reilly, and J. Greener, *J. Polym. Sci., Part B: Polym. Phys.* **27**, 837 (1989).
128. K. D. Pae and K. Vijayan, *Polymer* **29**, 405 (1988).
129. S. Weyer, M. Merzlyakov, and C. Schick, *Thermochim. Acta*, **85**, 377 (2001).
130. C. T. Moynihan, S. N. Crichton, and S. M. Opalka, *J. Non-Cryst. Solids* **420**, 131–133 (1991).
131. C. T. Moynihan, *Rev. Mineral* **32**, 1 (1995).
132. G. B. McKenna and C. A. Angell, *J. Non-Cryst. Solids* **528**, 133–133 (1991).
133. G. W. Scherer, *J. Am. Ceram. Soc.* **69**, 374 (1986).
134. I. M. Hodge and G. S. Huvard, *Macromolecules* **16**, 371 (1983).
135. J. M. O'Reilly and I. M. Hodge, *J. Non-Cryst. Solids* **451**, 131–133 (1991).
136. S. L. Simon, *Macromolecules* **30**, 4056 (1997).
137. G. Medvedev and J. M. Caruthers, Paper SL7, presented at the *Society of Rheology 71st Annual Meeting*, Madison, Wis., Oct. 17–21, 1999.
138. S. Rekhson and J.-P. Ducroux, in L. D. Pye, W. C. La Course, and H. J. Stevens, eds., *The Physics of Non-Crystalline Solids*, Taylor and Francis, London, 1992, p. 315.
139. C. T. Moynihan, oral presentation at Int. Conf. on Relaxations in Complex Systems, Crete, June 1990; see also Ref. 5 for details.

140. G. B. McKenna, *J. Res. Natl. Inst. Stand. Tech.* **99**(2) 169 (1994).
141. S. R. Lustig, R. M. Shay Jr., and J. M. Caruthers, *J. Rheol.* **40**(1), 69 (1996).
142. B. D. Coleman, *Arch. Ration. Mech. Anal.* **17**, 1 (1964).
143. B. D. Coleman, *Arch. Ration. Mech. Anal.* **17**, 230 (1964).
144. G. B. McKenna and S. L. Simon, in S. Z. D. Cheng, ed., *Handbook of Thermal Analysis and Calorimetry*, Vol. **3**, Elsevier, Amsterdam, in press.
145. D. M. Colucci, Ph.D. Thesis, *The Effect of Temperature and Deformation on the Relaxation Behavior in the Glass Transition Region* Purdue University, 1995.
146. L. C. E. Struik, *Polymer* **29**, 1347 (1988).

SINDEE L. SIMON
Texas Tech University

ALKYD RESINS

Introduction

Although no longer the largest volume vehicles in coatings, alkyds still are of major importance. Alkyds are prepared from polyols, dibasic acids, and fatty acids. They are polyesters, but in the coatings field the term polyester is reserved for "oil-free polyesters." The term *alkyd* is derived from *alc*ohol and a*cid*. Alkyds tend to be lower in cost than most other vehicles and tend to give coatings that exhibit fewer film defects during application. However, durability of alkyd films, especially outdoors, tends to be poorer than films from acrylics, polyesters, and polyurethanes.

There are several types of alkyds. One classification is into *oxidizing* and *nonoxidizing* types. Oxidizing alkyds cross-link by the same mechanism as drying oils. Nonoxidizing alkyds are used as polymeric plasticizers or as hydroxy-functional resins, which are cross-linked by melamine–formaldehyde (MF), by urea–formaldehyde (UF) resins, or by isocyanate cross-linkers. A second classification is based on the ratio of monobasic fatty acids to dibasic acids utilized in their preparation. The terminology used was adapted from terminology used to classify varnishes. Varnishes with high ratios of oil to resin were called *long oil varnishes*; those with a lower ratio, *medium oil varnishes*; and those with an even lower ratio, *short oil varnishes*. Oil length of an alkyd is calculated by dividing the amount of "oil" in the final alkyd by the total weight of the alkyd solids, expressed as a percentage, as shown in equation (1). The amount of oil is defined as the triglyceride equivalent to the amount of fatty acids in the alkyd. The 1.04 factor in equation (2) converts the weight of fatty acids to the corresponding weight of triglyceride oil. Alkyds with oil lengths greater than 60 are *long oil alkyds*; those with oil lengths from 40 to 60, *medium oil alkyds*, and those with oil lengths less

Encyclopedia of Polymer Science and Technology. Copyright John Wiley & Sons, Inc. All rights reserved.

than 40, *short oil alkyds*. There is some variation in the dividing lines between these classes in the literature.

$$\text{Oil Length} = \frac{\text{Weight of Oil}}{\text{Weight of Alkyd} - \text{Water Evolved}} \times 100 \quad (1)$$

$$\text{Oil Length} = \frac{1.04 \times \text{Weight of Fatty Acids}}{\text{Weight of Alkyd} - \text{Water Evolved}} \times 100 \quad (2)$$

Another classification is *unmodified* or *modified alkyds*. Modified alkyds contain other monomers in addition to polyols, polybasic acids, and fatty acids. Examples are styrenated alkyds and silicone alkyds. Since they are closely related to alkyd resins, uralkyds and epoxy esters are also discussed.

Oxidizing Alkyds

Oxidizing alkyds can be considered as synthetic drying oils. They are polyesters of one or more polyols, one or more dibasic acids, and fatty acids from one or more drying or semidrying oils.

Film Formation. Most of the studies of the chemistry of cross-linking have been with drying oils and not the alkyds derived from them, but the mechanisms are applicable to both. Films exposed to air undergo autoxidative cross-linking. In nonconjugated unsaturated oils, the active group initiating drying is the diallylic group (—CH=CHCH$_2$CH=CH—) from esters of (*Z*,*Z*)-9,12-octadecadienoic acid [60-33-3] (linoleic acid) and (*Z*,*Z*,*Z*)-9,12,15-octadecatrienoic acid [463-40-1] (linolenic acid). They have one and two diallylic groups per molecule, respectively. Drying is related to the average number of diallylic groups per molecule. If this number is greater than about 2.2, the oil is a drying oil and if it is moderately below 2.2, the oil is a semidrying oil; there is no sharp dividing line between semidrying oils and nondrying oils. Since diallylic groups are the sites for cross-linking, it is convenient to relate the average number of such groups per molecule to the number average functionality $\bar{f}_n$ of the triglyceride or synthetic drying oil. It is probable that some of the sites are involved in more than one cross-linking reaction.

The methylene groups are activated by their allylic relationship to two double bonds and are much more reactive than methylene groups allylic to only one double bond. The $\bar{f}_n$ of a typical linseed oil is 3.6; it is a drying oil. The $\bar{f}_n$ of a typical soybean oil is 2.07; it is a semidrying oil. The higher the $\bar{f}_n$ of a drying oil, the more rapidly a solvent-resistant, cross-linked film forms on exposure to air.

The reactions taking place during drying are complex. Cross-linked films form from linseed oil in the following stages: (*1*) an induction period during which naturally present antioxidants (mainly tocopherols) are consumed, (*2*) a period of rapid oxygen uptake with a weight gain of about 10% (ftir shows an increase in hydroperoxides and appearance of conjugated dienes during this stage), and (*3*) a complex sequence of autocatalytic reactions in which hydroperoxides are consumed and cross-linked film is formed. In one study, steps 1, 2, and 3 were

far along in 4, 10, and 50 h, respectively, when catalyzed by a drier (1). Cleavage reactions to form low molecular weight by-products also occur during the latter stages of film formation. Slow continuing cleavage and cross-linking reactions through the lifetime of the film lead to embrittlement, discoloration, and slow formation of volatile by-products. Oils with significant quantities of fatty acids with three double bonds, such as linolenic acid, discolor to a particularly marked degree.

When a film is applied, initially naturally present hydroperoxides decompose to form free radicals. At first, these highly reactive free radicals react mainly with the antioxidant, but as the antioxidant is consumed, the free radicals react with other compounds. Hydrogens on methylene groups between double bonds are particularly susceptible to abstraction, yielding a resonance-stabilized free radical that reacts with oxygen to give predominantly conjugated peroxy free radicals. The peroxy free radicals can abstract hydrogens from other methylene groups between double bonds to form additional hydroperoxides and generate free radicals. Thus, a chain reaction is established, resulting in autoxidation. At least part of the cross-linking occurs by radical–radical combination reactions forming C—C, ether, and peroxide bonds. These reactions correspond to termination by combination reactions in free-radical chain-growth polymerization. Reactions analogous to the addition step in chain-growth polymerization could also produce cross-links.

Studies of the reactions of ethyl linoleate with oxygen in the presence of driers by ^{1}H and ^{13}C nmr showed that the predominant cross-linking reactions were those that formed ether and peroxy cross-links (2,3). Mass spectroscopic studies showed that only about 5% of the cross-links were new C—C bonds (2). Substantial levels of epoxy groups were detected in the reaction mixture, rising to a maximum in about 5 days and virtually disappearing in 100 days; it is suggested that epoxy groups may react with carboxyl groups to form ester cross-links.

Rearrangement and cleavage of hydroperoxides to aldehydes and ketones, among other products, lead to low molecular weight by-products. The characteristic odor of oil and alkyd paints during drying is attributable to such volatile by-products, as well as to the odor of organic solvents. Undesirable odor has been a factor motivating replacement of oil and alkyds in paints with latex, particularly for interior applications. The reactions leading to these odors have been extensively studied in connection with flavor changes of vegetable cooking oils (4). Aldehydes have been shown to be major by-products from the catalyzed autoxidation and from curing of drying-oil-modified alkyd resins (2,5). It has also been shown that C_9 acid esters remain in the nonvolatile reaction mixture (5).

Dried films, especially of oils with three double bonds, yellow with aging. The yellow color bleaches significantly when exposed to light; hence, yellowing is most severe when films are covered, such as by a picture hanging on a wall. The reactions leading to color are complex and are not fully understood. Yellowing has been shown to result from incorporation of nitrogen compounds and is markedly increased by exposure to ammonia. It has been proposed that ammonia reacts with 1,4-diketones formed in autoxidation to yield pyrroles, which oxidize to yield highly colored products (6).

The rates at which uncatalyzed nonconjugated drying oils dry are slow. Many years ago, it was found that metal salts (driers) catalyze drying. The most widely used driers are oil-soluble cobalt, manganese, lead, zirconium, and calcium salts of

octanoic or naphthenic acids. Salts of other metals, including rare earths, are also used. Cobalt and manganese salts, so-called top driers or surface driers, primarily catalyze drying at the film surface. Lead and zirconium salts catalyze drying throughout the film and are called through driers. The surface-drying catalysis by cobalt and manganese salts results from the catalysis of hydroperoxide decomposition. The cobalt cycles between the two oxidation states. The activity of through driers has not been adequately explained.

Combinations of metal salts are almost always used. Mixtures of lead with cobalt and/or manganese are particularly effective, but as a result of toxicity control regulations, lead driers can no longer be used in consumer paints sold in interstate commerce in the United States. Combinations of cobalt and/or manganese with zirconium, frequently with calcium, are commonly used. Calcium does not undergo redox reactions; it has been suggested that it may promote drying by preferentially adsorbing on pigment surfaces, minimizing adsorption of active driers. The amounts of driers needed are system specific. Their use should be kept to the minimum possible level, since they not only catalyze drying but also catalyze the reactions that cause post-drying embrittlement, discoloration, and cleavage.

Oils containing conjugated double bonds, such as tung oil, dry more rapidly than any nonconjugated drying oil. Free-radical polymerization of the conjugated diene systems can lead to chain-growth polymerization, rather than just a combination of free radicals to form cross-links. High degrees of polymerization are unlikely because of the high concentration of abstractable hydrogens acting as chain-transfer agents. However, the free radicals formed by chain transfer also yield cross-links. In general, the water and alkali resistance of films derived from conjugated oils are superior, presumably because more of the cross-links are stable carbon–carbon bonds. However, since the (*E*,*Z*,*E*)-9,11,13-octadecatrienoic acid [506-23-0] (α-eleostearic acid) in tung oil has three double bonds, discoloration on baking and aging is severe.

The most commonly used polyol in preparing alkyds is 1,2,3-propanetriol [56-81-5] (glycerol), the most commonly used dibasic acid is 1,3-isobenzofurandione [85-44-9] (phthalic anhydride) (PA), and a widely used oil is soybean oil. Let us consider a simple, idealized example of the alkyd prepared from 1 mol of PA, 2 mol of glycerol, and 4 mol of soybean fatty acids. A typical fatty acid composition data for soybean oil is as follows: saturated fatty acids [hexadecanoic acid [57-10-3] (palmitic acid) and octadecanoic acid [57-11-4] (stearic acid)], 15%; (*Z*)-9-octadecenoic acid [112-80-1] (oleic acid), 25%; linoleic acid, 51%; and linolenic acid, 9%. Any oil with an $\bar{f}_n$ higher than 2.2 is a drying oil. Although soybean oil is a semidrying oil, this alkyd would have an $\bar{f}_n$ of 2.76 per molecule and, therefore, would dry to a solid film. The alkyd would form a solvent-resistant film in about the same time as a 2,2-bis(hydroxymethyl)-1,3-pentanediol [115-77-5] (pentaerythritol), ester of soybean fatty acids, since they have the same $\bar{f}_n$. However, the alkyd would form a tack-free film faster because the rigid aromatic rings from PA increases the T_g of the film.

If the mole ratio of PA to glycerol were 2 to 3, 5 mol of soybean fatty acid could be esterified to yield an alkyd with an $\bar{f}_n$ of 3.45. This alkyd would cross-link more rapidly than the 1:2:4 mole ratio alkyd and would also form tack-free films even faster because the ratio of aromatic rings to long aliphatic chains would be 2:5 instead of 1:4. As the ratio of PA to glycerol is increased further, the average

functionality for autoxidation increases and the T_g after solvent evaporation increases because of the increasing ratio of aromatic to long aliphatic chains. For both reasons, films dry faster.

A theoretical alkyd prepared from 1 mol each of glycerol, PA, and fatty acid would have an oil length of about 60. However, if one were to try to prepare such an alkyd, the resin would gel prior to complete reaction. Gelation would result from reaction of a sufficient number of trifunctional glycerol molecules with three difunctional PA molecules to form cross-linked polymer molecules, swollen with partially reacted components. Gelation can be avoided by using a sufficient excess of glycerol to reduce the extent of cross-linking. When the reaction is carried to near completion with excess glycerol, there are few unreacted carboxylic acid groups, but many unreacted hydroxyl groups.

There have been many attempts, none fully successful, to calculate the ratios of functional groups and the extent of reaction that can be reached without encountering gelation. The problem is complex. The reactivity of the hydroxyl groups can be different; for example, glycerol contains both primary and secondary alcohol groups. Under esterification conditions, polyol molecules can self-condense to form ethers and, in some cases, can dehydrate to form volatile aldehydes. Reactivity of the carboxylic acids also varies. The rate of formation of the first ester from a cyclic anhydride is more rapid than formation of the second ester. Aliphatic acids esterify more rapidly than aromatic acids. Polyunsaturated fatty acids and their esters can dimerize or oligomerize to form cross-links. The dimers form by a mechanism similar to that encountered in the drying of the oils. Of the many papers in the field, that by Blackinton recognizes the complexities best (7). In addition to the above complexities, particular emphasis is placed on the extent of formation of cyclic compounds by intramolecular esterification reactions. Equations have been developed that permit calculation of ratios of ingredients theoretically needed to prepare an alkyd of any desired oil length, number-average molecular weight, and hydroxy content (8). Just like in other equations, the important effect of dimerization of fatty acids is not included as a factor in these equations. In practice, alkyd resin formulators have found that the mole ratio of dibasic acid to polyol should be less than 1 to avoid gelation. How much less than 1 depends on many variables.

For medium oil alkyds, the ratio of dibasic acid to polyol is not generally changed much relative to alkyds with an oil length of about 60, but the fatty acid content is reduced to the extent desired. This results in a larger excess of hydroxyl groups in the final alkyd. It is commonly said that as the oil length of an oxidizing alkyd is reduced below 60, the drying time decreases to a minimum at an oil length of about 50. However, this conventional wisdom must be viewed cautiously. The ratio of aromatic rings to aliphatic chains continues to increase, increasing T_g after the solvent evaporates from the film tending to shorten the time to form a tack-free film. However, at the same molecular weight, the number of fatty acid ester groups per molecule decreases as the oil length decreases below 60, since more hydroxyl groups are left unesterified. Therefore, the time required to achieve sufficient cross-linking for solvent resistance increases.

Long oil alkyds are soluble in aliphatic hydrocarbon solvents. As the oil length decreases, mixtures of aliphatic and aromatic solvents are required, and oil lengths below about 50 require aromatic solvents, which are more expensive than

aliphatics. The viscosity of solutions of long oil alkyds, especially of those with oil lengths below 65, is higher in aliphatic than in aromatic solvents; in medium oil alkyds, which require mixtures of aliphatic and aromatic solvents, viscosity decreases as the proportion of aromatic solvents increases. In former days, and to some extent still today, it was considered desirable to use a solvent mixture that gave the highest possible viscosity; then, at application viscosity, the solids were lower and the raw material cost per unit volume was less. Accordingly, alkyds were designed to have high dilutability with aliphatic solvents. This was false economy, but it was a common practice and is still being practiced to some extent. Increasingly, the emphasis is on reducing volatile organic compounds (VOC) and so the question becomes how to design alkyds with low solvent requirements rather than high dilutability potential. Furthermore, the aromatic solvents are on the hazardous air pollutants (HAP) list. High solids alkyds are discussed in a later section.

Monobasic Acid Selection. Drying alkyds can be made with fatty acids from semidrying oils, since the $\bar{f}_n$ can be well above 2.2. For alkyds made by the monoglyceride process, soybean oil is used in the largest volume. Soybean oil is economical and supplies are dependable because it is a large-scale agricultural commodity; alkyd production takes only a few percent of the world supply. For alkyds made by the fatty acid process, tall oil fatty acids (TOFA) are more economical than soybean fatty acids. Both soybean oil and TOFA contain roughly 40–60% linoleic acid and significant amounts of linolenic acid. White coatings containing linolenic acid esters gradually turn yellow. Premium cost "nonyellowing" alkyds are made with safflower or sunflower oils, which are high in linoleic acid but contain very little linolenic acid.

Applications in which fast drying and high cross-link density are important require alkyds made with drying oils. The rate of oxidative cross-linking is affected by the functionality of the drying oils used. At the same oil length and molecular weight, the time required to achieve a specific degree of cross-linking decreases as the average number of diallylic groups ($\bar{f}_n$) increases. Linseed long oil alkyds therefore cross-link more rapidly than soybean long oil alkyds. The effect is especially large in very long oil alkyds and less noticeable in alkyds with oil lengths around 60, where $\bar{f}_n$ is very high even with soybean oil and the effect of further increase in functionality by using linseed oil is small. Because of the large fraction of esters of fatty acids with three double bonds in linseed alkyds, their color and color retention are poorer than that of soybean alkyds. Tung oil based alkyds, because of the high proportion of esters with three conjugated double bonds, dry still faster. Tung oil alkyds also exhibit a high degree of yellowing. Dehydrated castor alkyds have fairly good color retention, since they contain only a small proportion of esters of fatty acids with three double bonds; they are used primarily in baking coatings.

Drying oils and drying oil fatty acids undergo dimerization at elevated temperatures. Dimerization occurs concurrently with esterification during alkyd synthesis; it generates difunctional acids, increasing the mole ratio of dibasic acids to polyol. The rate of dimerization is faster with drying oils having a higher average number of diallylic groups per molecule and with those having conjugated double bonds. Thus, the molecular weight, and therefore viscosity of an alkyd made with the same ratio of reactants, depends on the fatty acid composition. The higher the

degree of unsaturation, the higher the viscosity because of the greater extent of dimerization. Linseed alkyds have higher viscosities than soybean alkyds made with the same monomer ratios under the same conditions. The effect is particularly marked with tung oil. It is difficult to prepare straight tung alkyds because of the risk of gelation; commonly, mixed linseed–tung alkyds are used when high oxidative cross-linking functionality is desired.

A critical factor involved in the choice of fatty acid is cost. Drying oils are agricultural products and, hence, tend to be volatile in price. By far, the major use of many vegetable oils is for foods. Depending upon relative prices, one drying oil is often substituted for another in certain alkyds. By adjusting for functionality differences, substitutions can frequently be made without significant changes in properties.

Fatty acids are not the only monobasic acids used in making alkyds. Benzoic acid is also used, especially to esterify some of the excess hydroxyl groups remaining in the preparation of medium oil alkyds. The benzoic acid [65-85-0] increases the ratio of aromatic to aliphatic chains in the alkyd, thus contributing to a higher T_g of the solvent-free alkyd and more rapid formation of a tack-free film. At the same time, the reduction in the free hydroxyl content may somewhat reduce water sensitivity of the dried films. Rosin can also be used in the same fashion. Although rosin is not an aromatic acid, its polynuclear ring structure is rigid enough to increase T_g. If the critical requirement in drying is rapid development of solvent resistance, such benzoic acid and rosin modifications do not serve the purpose; they only reduce tack-free time. Frequently, benzoic acid-modified alkyds are called chain-stopped alkyds. The implication of the terminology is that the benzoic acid stops chain growth. This is not the case; the benzoic acid simply esterifies hydroxyl groups that would not have been esterified if the benzoic acid were absent. The effect on degree of polymerization is negligible.

Polyol Selection. Glycerol is the most widely used polyol because it is present in naturally occurring oils from which alkyds are commonly synthesized. The next most widely used polyol is pentaerythritol. In order to avoid gelation, the tetrafunctionality of pentaerythritol must be taken into account when replacing glycerol with pentaerythritol. If the substitution is made on a mole basis, rather than an equivalent basis, chances for gelation are minimized. As mentioned earlier, the ratio of moles of dibasic acid to polyol should be less than 1, and generally, a slightly lower mole ratio is required with pentaerythritol than with glycerol. At the same mole ratio of dibasic acid to polyol, more moles of fatty acid can be esterified with pentaerythritol. Hence, in long oil alkyds, the average functionality for cross-linking is higher, and the time to reach a given degree of solvent resistance is shorter for a pentaerythritol alkyd as compared to a glycerol alkyd. Because off this difference, one must be careful in comparing oil lengths of glycerol and pentaerythritol alkyds.

When pentaerythritol is synthesized, 2,2′-[oxybis(methylene)]-bis[2-hydroxymethyl)-1,3-propanediol [126-58-9] (dipentaerythritol) and 2,2-bis{[3-hydroxy-2,2-bis(hydroxymethyl)propoxy]methyl}1,3-propanediol [78-24-0] (tripentaerythritol) are by-products, and commercial pentaerythritol contains some of these higher polyols. Consequently, care must be exercised in changing sources of pentaerythritol, since the amount of the higher polyols may differ. Because

of the very high functionality, dipentaerythritol and tripentaerythritol (F = 6 and 8, respectively) are useful in making fast drying low molecular weight alkyds.

To reduce cost, it is sometimes desirable to use mixtures of pentaerythritol and 1,2-ethanediol [107-21-1] (ethylene glycol) or 1,3-propanediol (propylene glycol). A 1:1 mole ratio of tetra- and difunctional polyols gives an average functionality of 3, corresponding to glycerol. The corresponding alkyds can be expected to be similar, but not identical. 2-Ethyl-2-(hydroxymethyl-1,3-propanediol [77-99-6] (trimethylolpropane, TMP) can also be used, but the rate of esterification is slower than with glycerol. Although all of TMP's alcohol groups are primary, they are somewhat sterically hindered by the neopentyl structure (9). Trimethylolpropane, however, gives a narrower molecular weight distribution, which provides alkyds with a somewhat lower viscosity than the comparable glycerol-based alkyd. A kinetic study demonstrated that esterification of one or two of the hydroxyl groups of TMP has little effect on the rate constant for esterification of the third hydroxyl group (9). It can be speculated that pentaerythritol behaves similarly.

Dibasic Acid Selection. Dibasic acids used to prepare alkyds are usually aromatic. Their rigid aromatic rings increase the T_g of the resin. Cycloaliphatic anhydrides, such as hexahydrophthalic anhydride, are also used. While they are not as rigid as aromatic rings, the cycloaliphatic rings also increase T_g.

By far, the most widely used dibasic acid is phthalic anhydride (PA). It has the advantage that the first esterification reaction proceeds rapidly by opening the anhydride ring. The amount of water evolved is lower, which also reduces reaction time. The relatively low melting point (the pure compound melts at 131°C) is desirable, since the crystals melt and dissolve readily in the reaction mixture. In large-scale manufacturing, molten PA is used, which reduces packaging, shipping, and handling costs.

The next most widely used dibasic acid is 1,3-benzenedicarboxylic acid [121-91-5] (isophthalic acid, IPA). Esters of IPA are more resistant to hydrolysis than are those of PA in the pH range of 4–8, the most important range for exterior durability. On the other hand, under more alkaline conditions esters of phthalic acid are more resistant to hydrolysis than isophthalic esters. The raw material cost for IPA is not particularly different from PA (even after adjusting for the extra mole of water that is lost), but the manufacturing cost is higher. The high melting point of IPA (330°C) leads to problems getting it to dissolve in the reaction mixture so that it can react. High temperatures are required for longer times than with PA; hence more dimerization of fatty acids occurs with IPA resulting in higher viscosity. The longer time at higher temperature also leads to greater extents of side reactions of the polyol components (11). Thus, when substituting IPA for PA, one must use a lower mole ratio of IPA to polyol in order to make an alkyd of similar viscosity.

2,5-Furandione [108-31-6] (maleic anhydride) is sometimes used with PA to give faster drying alkyds with little color. Aliphatic acids, such as 1,6-hexanedioic acid [124-04-9] (adipic acid), are sometimes used as partial replacements for PA to give more flexible films.

Chlorinated dibasic acids, such as 3,4,5,6,7,7-hexachloroendomethylene-1,2,3,6-tetrahydrophthalic anhydride (chlorendic acid), are used in making alkyds for fire-retardant coatings (12).

High Solids Oxidizing Alkyds. The need to minimize VOC emissions has led to efforts to increase solids content of alkyd resin coatings. Since xylene is on the HAP list, its use is being reduced. Some increase in solids can be realized by a change of solvents. Aliphatic (and to a somewhat lesser degree, aromatic) hydrocarbon solvents promote intermolecular hydrogen bonding, especially between carboxylic acids, but also between hydroxyl groups, thereby increasing viscosity. Use of at least some hydrogen-bond acceptor solvent, such as an ester or ketone, or hydrogen-bond acceptor–donor solvent such as an alcohol, gives a significant reduction in viscosity at equal solids.

The molecular weight of conventional alkyds is usually greater than 50,000. Solids can be increased by decreasing molecular weight, which is easily accomplished by decreasing the dibasic acid to polyol ratio. Alkyds with solids in the range of 60–80% are commercially available with molecular weights in the range of 12,000–20,000 (13). High solids alkyds tend to have lower functionality for crosslinking and a lower ratio of aromatic to aliphatic chains. Both changes increase the time for drying. There is also a decrease in branching with the higher hydroxyl excess.

The effect of longer oil length on functionality can be minimized by using drying oils with higher average functionality. Use of oils containing linolenic or α-eleostearic acid is limited by their tendency to discolor. One can use safflower oil, which has a higher linoleic acid content and less linolenic acid than soybean oil. Proprietary fatty acids with 78% linoleic acid are commercially available. Early hardness of the films can be improved by using some benzoic acid to esterify part of the free hydroxy groups. As noted earlier, the rigid rings of benzoic acid increase T_g to increase hardness after solvent evaporation.

Different drier combinations are recommended for use with high solids alkyds. A study of a variety of driers and drier combinations with high solids coatings has been published (14). Cobalt, neodymium, aluminum, and barium carboxylic acid salts were of particular interest. Performance was enhanced by adding bipyridyl as an accelerator. The author reports that the best drier system was 0.04% Co, 0.3% Nd with 0.07% bipyridyl (percentages based on the vehicle solids). Reference 15 reports studies of mechanisms of action of cobalt and mixed cobalt/zirconium driers.

Using optimized resins, good quality air dry and baking alkyd coatings can be formulated with VOC levels of 280–350 g/L of coating. A 250-g/L level is attainable only with some sacrifice of application and film properties; still lower limits of permissible VOC are projected.

Solids can be increased by making resins with narrower molecular weight distributions. For example, one can add a transesterification catalyst near the end of the alkyd cook; this gives more uniform molecular weight and a lower viscosity product. To study the effect of molecular weight distribution, model alkyds with very narrow molecular weight distribution were synthesized by using dicyclohexylcarbodiimide, which allows low temperature esterification (9). With the same ratio of reactants, the number-average molecular weight and polydispersity were lower than that of the conventional alkyd control. These differences resulted from less dimerization through reactions of the double bond systems of the fatty acids and avoidance of self-etherification of polyol in the low temperature preparation. It was found that the solids could be 2–10% higher

than with the conventionally prepared alkyd of the same raw material composition. The model alkyds dried more rapidly, but their film properties, especially impact resistance, were inferior to those obtained with control resins with the usual broad molecular weight distribution (16). Conventionally prepared TMP alkyds had lower molecular weights and viscosities than the glycerol alkyds. This difference may result from less self-etherification of TMP as compared to glycerol.

High solids alkyds for baking applications have been made using tripentaerythritol. The high functionality obtained using this polyol ($F = 8$) gives alkyds that cross-link as rapidly as shorter oil length, higher viscosity glycerol alkyds (17). However, for air dry applications, the lower aromatic to aliphatic ratio lengthens the tack-free time. Presumably, progress could be made using a high functionality polyol with some combination of phthalic and benzoic acid, together with fatty acids with as high functionality fatty acids as possible. The cost of such an alkyd would be high.

Another approach to high solids alkyds is to use reactive diluents in place of part of the solvent. The idea is to have a component of lower molecular weight and much lower viscosity than the alkyd resin, which reacts with the alkyd during drying, and so it is not part of the VOC emissions. The use of reactive diluents is reviewed in Reference 18; 2,7-octadienyl maleate and fumarate are reported to be particularly effective. The use of diethers prepared from conjugated linoleic gives faster drying reactive diluents (19).

Several other types of reactive diluents have been used to formulate high solids alkyd coatings. Polyfunctional acrylate monomers (eg, trimethylolpropane trimethacrylate) have been used in force dry coatings (coatings designed to be cured in the range of 60–80°C) (20). Another example is use of dicyclopentadienyloxyethyl methacrylate [70191-60-5] as a reactive diluent (21). It is difunctional because of the easily abstractable allylic hydrogen on the dicyclopentadiene ring structure and the methacrylate double bond. The compound coreacts with drying oil groups in the alkyd. Mixed acrylic and drying oil fatty acid amides of hexa(aminomethoxymethyl)melamine have been recommended as reactive diluents (22,23). They contain high functionalities of $>NCH_2NHCOCH{=}CH_2$ and $>NCH_2NHCOC_{17}H_x$ moieties and promote fast drying. A recent patent discloses use of a reactive diluent prepared by reacting drying oil fatty acids with excess dipentaerythritol and then with 3-isocyanato-1-isocyanatomethyl-1,3,3-trimethylcyclohexane [4098-71-9] (isophorone diisocyanate) (24).

Waterborne Alkyds

As with almost all other resin classes, work has been done to make alkyd resins for coatings that can be reduced with water. One approach that has been more extensively studied in Europe than in the United States is the use of alkyd emulsions (25,26). The emulsions are stabilized with surfactants and can be prepared with little, if any, volatile solvent. Some problems limit use of alkyd emulsions (27). Coatings prepared using alkyd emulsion loose dry time on storage because of absorption of cobalt drier on the surface of pigments and precipitation of cobalt hydroxide. Best results were obtained with a combination of cobalt neodecanoate

and 2,2′-bipyridyl. It was shown that the surfactant tends to bloom to the surface of films formed from emulsions of long oil alkyds, washing a dry film tends to leave pits in the film showing a hexagonal pattern.

It is common to add a few percent of an alkyd-surfactant blend to latex paints to improve adhesion to chalky surfaces and, in some cases, to improve adhesion to metals. It is important to use alkyds that are as resistant as possible to hydrolysis. Hybrid alkyd–acrylic latices have been prepared by dissolving an oxidizing alkyd in the monomers used in emulsion polymerization, yielding a latex with an alkyd grafted on the acrylic polymer (28,29). Nonyellowing waterborne alkyds based on rosin–fatty acid modified acrylic latices have been reported (30).

Another approach has been to make alkyds with an acid number in the range of 50, using secondary alcohols or ether alcohols as solvents. The acid groups are neutralized with ammonia or an amine. The resultant solution can be diluted with water to form a dispersion of solvent swollen aggregates in water. Molecular weight can be higher than in the case of high solids alkyd because the major factor affecting viscosity at application solids is the volume fraction of internal phase of the dispersion rather than the molecular weight of the polymer. Use of primary alcohol solvents should be avoided because they can more readily transesterify with the alkyd during resin production and storage, leading to reduction in molecular weight and $\bar{f}_n$ (31). Hydrolytic stability can be a problem with water-reducible alkyds. If the carboxylic acid groups are half esters from PA or 1,3-dihydro-1,3-dioxo-5-isobenzofurancarboxylic acid [552-30-7] (trimellitic acid anhydride), the hydrolytic stability will be poor and probably inadequate for paints that require a shelf life of more than a few months. Because of the anchimeric effect of the neighboring carboxylic acid group, such esters are relatively easily hydrolyzed. As hydrolysis occurs, the solubilizing acid salt is detached from the resin molecules, and the aqueous dispersion loses stability. A more satisfactory way to introduce free carboxylic acid groups is by reacting a completed alkyd with maleic anhydride. Part of the maleic anhydride adds to the unsaturated fatty acid esters. The anhydride groups are then hydrolyzed with amine and water to give the desired carboxylate salt groups, which are attached to resin molecules with C—C bonds and cannot be hydrolyzed off. There is still a hydrolytic stability problem with the alkyd backbone, but hydrolysis does not result in destabilization of the dispersion. Similarly, acrylated fatty acids can be used to synthesize water-reducible alkyds with improved hydrolytic stability (32). Another approach to improving package stability is to react some of the free hydroxyl groups of an alkyd with isophorone diisocyanate and 3-hydroxy-2-(hydroxymethyl)-2-methylpropanoic acid [4767-03-7] (dimethylolpropionic acid, DMPA) (33) or with 1,3-bis(2,2-dimethyl-2-isocyanato)benzene (tetramethylxylylene diisocyanate) and DMPA (34).

After the film is applied, the water, solvent, and amine evaporate, and the film cross-links by autoxidation. Since there are a fairly large number of residual carboxylic acid groups left in the cross-linked binder, the water resistance and particularly the alkali resistance of the films are reduced, but are still satisfactory for some applications (35). Early water resistance can be a problem if, for example, a freshly painted surface is rained on before all the amine has evaporated from the film. Commonly, ammonia is used as the neutralizing amine because it is

assumed that ammonia volatilizes faster than any other amine. This assumption is not necessarily valid; if the T_g of the alkyd film is sufficiently high before all of the amine has volatilized, loss of amine becomes controlled by diffusion rate. The rate of diffusion of amine through the carboxylic acid-functional film is affected by the base strength of the amine. A less basic amine, such as morpholine, may leave the film at a faster rate than ammonia even though its volatility is considerably lower.

Modified Alkyds

Oxidizing alkyds have been modified by reacting with a variety of other components; vinyl-modified, silicone-modified, phenolic-modified, and polyamide-modified alkyds are the most common examples.

Oxidizing alkyds can be modified by reaction with vinyl monomers. The most widely used monomers are ethenylbenzene [100-42-5] (styrene), 1-ethenyl-2-methylbenzene (vinyl toluene), and 2-methyl-2-propenoic acid methyl ester (methyl methacrylate), but essentially any vinyl monomer can be reacted in the presence of an alkyd to give a modified alkyd. Methyl methacrylate imparts better heat and weather resistance than styrene but at higher cost.

In making styrenated alkyds, an oxidizing alkyd is prepared in the usual way and cooled to about 130°C in the reactor; then styrene and a free-radical initiator such as dibenzoyl peroxide [94-36-0] (benzoyl peroxide) are added. The resulting free-radical chain process leads to a variety of reactions, including formation of low molecular weight homopolymer of styrene, grafting of polystyrene onto the alkyd, and dimerization of alkyd molecules. The reaction is generally carried out at about 130°C, which favors decomposition of benzoyl peroxide to form phenyl free radicals; phenyl radicals have a high tendency to abstract hydrogen, which favors grafting. After the reaction is complete, the resin is diluted with solvent. The ratio of alkyd to styrene can be varied over a wide range; commonly 50% alkyd and 50% styrene is used. The ratio of aromatic rings to aliphatic chains is greatly increased, and as a result, the T_g of styrenated alkyd films is higher and tack-free time is shorter. Styrenated alkyds give a dry film in 1 h or less versus 4–6 h for the counterpart nonstyrenated alkyd. However, the average functionality for oxidative cross-linking is reduced, not just by dilution with styrene, but also because the free-radical reactions involved in the styrenation consume some activated methylene groups. As a result, the time required to develop solvent resistance is longer than for the counterpart alkyd. The fast drying and low cost make styrenated alkyds very attractive for some applications, but in other cases, the longer time required for cross-linking is more critical, in which case styrenated alkyds are not appropriate.

Styrenated alkyd vehicles are often used for air dry primers. One must be careful to apply top coat almost immediately or not until after the film has had ample time to cross-link. During the intermediate time interval, application of top coat is likely to cause nonuniform swelling of the primer, leading to what is called lifting of the primer. The result of lifting is the development of wrinkled areas in the surface of the dried film. End users who are accustomed to using alkyd

primers, which do not give a hard film until a significant degree of cross-linking has occurred, are particularly likely to encounter problems of lifting if they switch to styrenated alkyd primers.

Silicone resins have exceptional exterior durability but are expensive. Silicone modification of alkyd resins improves their exterior durability. The earliest approach was simply to add a silicone resin to an alkyd resin in the reactor at the end of the alkyd cook. While some covalent bonds between silicone resin and alkyd might form, probably most of the silicone resin simply dissolves in the alkyd. Exterior durability of silicone-modified alkyd coatings is significantly better than unmodified alkyd coatings. The improvement in durability is roughly proportional to the amount of added silicone resin; 30% silicone resin is a common degree of modification. Further improvements in exterior durability are obtained by coreacting a silicone intermediate during synthesis of the alkyd. Such intermediates react readily with free hydroxyl groups of the alkyd resin. Silicone resins designed for this purpose may contain higher alkyl, as well as methyl and phenyl, groups to improve compatibility. Alkyd coatings modified with high phenylsilicone resins are reported to have greater thermoplasticity, faster air drying, and higher solubility than high methylsilicone modified alkyds. These differences result in the higher rigidity of the aromatic rings, which leads to a solid film at an earlier stage of cross-linking. Less cross-linking in the phenylsilicone-modified coatings makes them more thermoplastic and soluble. Since IPA-based alkyd resins have better exterior durability than PA alkyds, they are generally used as the alkyd component. Silicone-modified alkyds are used mainly in outdoor air dry coatings for which application is expensive (eg, in a top coat for steel petroleum storage tanks).

Phenolic-modified alkyds are made by heating the alkyd with a low molecular weight resole phenolic resin based on *p*-alkylphenols. Presumably, the methylol groups on the phenols react with some of the unsaturated groups of the alkyd to form chroman structures. The resins give harder films with improved water and chemical resistance as compared to the unmodified alkyd.

Polyamide-modified alkyds are used as thixotropic agents to increase the low shear viscosity of alkyd resin based paints. Typically, about 10% of a polyamide resin made from diamines such as 1,2-ethanediamine (ethylenediamine) with dimer acids is reacted with an alkyd resin. High solids thixotropic alkyds based on polyamides made with aromatic diamines have been developed, which give superior performance in high solids alkyd coatings (36).

Nonoxidizing Alkyds

Certain low molecular weight short-medium and short oil alkyds are compatible with such polymers as nitrocellulose and thermoplastic polyacrylates. Therefore, such alkyds can be used as plasticizers for these polymers. They have the advantage over monomeric plasticizers (eg, dibutyl or dioctyl phthalate) in that they do not volatilize appreciably when films are baked. It is generally not desirable to use oxidizing alkyds, which would cross-link and lead to embrittlement of the films, especially on exterior exposure. Therefore, nondrying oil fatty acids (or oils) are used in the preparation of alkyds for such applications. For exterior acrylic

lacquers, nonanoic acid (pelargonic acid) alkyds combine excellent resistance to photodegradation with good compatibility with the thermoplastic acrylic resins. An interesting sidelight on terminology is that these pelargonic alkyds have been called *polyesters* rather than alkyds because the word *polyester* connotes higher quality than the word *alkyd*. Castor-oil-derived alkyds are particularly appropriate for nitrocellulose lacquers for interior applications, since the hydroxyl groups on the 12-hydroxy-(*Z*)-9-octadecenoic acid [141-22-0] (ricinoleic acid) promote compatibility.

All alkyds, particularly short-medium oil and short oil alkyds, are made with a large excess of hydroxyl groups to avoid gelation. These hydroxyl groups can be cross-linked with MF resins or with polyisocyanates. In some cases, relatively small amounts of MF resin are used to supplement the cross-linking during baking of medium oil oxidizing alkyds. To achieve compatibility, butylated MF resins are used. Such coatings provide somewhat better durability and faster curing than alkyd resins alone, with little increase in cost. The important advantage of relative freedom from film defects common to alkyd coatings can be retained. However, the high levels of unsaturation remaining in the cured films reduce resistance to discoloration on overbake and exterior exposure and cause loss of gloss and embrittlement on exterior exposure. These difficulties can be reduced by using nondrying oils with minimal levels of unsaturated fatty acids. Coconut oil has been widely used; its performance can be further enhanced by hydrogenation of the small amount of unsaturated acids present in it.

Since isophthalic (IPA) esters are more stable to hydrolysis in the pH range of 4–8 than phthalate esters, the highest performance exterior alkyd-MF enamels use nonoxidizing IPA alkyds. Exterior durability of such coatings is satisfactory for automobile top coats with opaque pigmentation. The films have an appearance of greater depth than that of acrylic-MF coatings. The films are perceived to be thicker than films of acrylic-MF coatings of comparable thickness and pigmentation. However, for many applications, alkyd-MF coatings have been replaced with acrylic-MF or polyester-MF coatings to improve the overall balance of film properties.

Synthesis of Alkyd Resins

Various synthetic procedures, each with many variables, are used to produce alkyd resins; the general reference and References 37 and 38 provide useful reviews of manufacturing procedures. Alkyds can be made directly from oils or by using free fatty acids as raw materials.

Synthesis from Oils or Fatty Acids.

Monoglyceride Process. In the case of glycerol alkyds, it would be absurd to first saponify an oil to obtain fatty acids and glycerol, and then reesterify the same groups in a different combination. Rather, the oil is first reacted with sufficient glycerol to give the total desired glycerol content, including the glycerol in the oil. Since PA is not soluble in the oil, but is soluble in the glycerol, transesterification of oil with glycerol must be carried out as a separate step before the PA is added; otherwise, glyceryl phthalate gel particles would form early in the process. This two-stage procedure is often called the monoglyceride process.

The transesterification reaction is run at 230–250°C in the presence of a catalyst; many catalysts have been used. Before the strict regulation of lead in coatings, litharge (PbO) was widely used; the residual transesterification catalyst also acted as a drier. Examples of catalysts now used in the United States are tetraisopropyl titanate, lithium hydroxide, and lithium ricinoleate. The reaction is run under an inert atmosphere such as CO_2 or N_2 to minimize discoloration and dimerization of drying oils. Rather than using glycerol, the transesterification can also be carried out with higher functionality polyols such as pentaerythritol.

While the process is called the monoglyceride process, the transesterification reaction actually results in a mixture of unreacted glycerol, monoglycerides, diglycerides, and unconverted drying oil. The composition depends on the ratio of glycerol to oil and on catalyst, time, and temperature. In general, the reaction is not taken to equilibrium. At some relatively arbitrary point, the PA is added, beginning the second stage. The viscosity and properties of the alkyd can be affected by the extent of reaction before the PA addition. While many tests have been devised to evaluate the extent of transesterification, none is very general because the starting ratio of glycerol to oil varies over a considerable range, depending on the oil length of the alkyd being made. (In calculating the mole ratio of dibasic acid to polyol, the glycerol already esterified in the oil must also be counted.) A useful empirical test is to follow the solubility of molten PA in the reaction mixture. This test has the advantage that it is directly related to a major requirement that must be met. In the first stage, it is common to transesterify the oil with pentaerythritol to obtain mixed partial esters. The second stage, esterification of the monoglyceride with PA, is carried out at a temperature of 220–255°C.

Fatty Acid Process. It is often desirable to base an alkyd on a polyol (eg, pentaerythritol) other than glycerol. In this case, fatty acids must be used instead of oils, and the process can be performed in a single step with reduced time in the reactor. Any drying, semidrying, or nondrying oil can be saponified to yield fatty acids, but the cost of separating fatty acids from the reaction mixture increases the cost of the alkyd. A more economical alternative is to use TOFA, which have the advantage that they are produced as fatty acids. Tall oil fatty acid composition is fairly similar to that of soybean fatty acids. Specially refined tall oils with higher linoleic acid content are available, as are other grades that have been treated with alkaline catalysts to isomerize the double bonds partially to conjugated structures. Generally, when fatty acids are used, the polyol, fatty acids, and dibasic acid are all added at the start of the reaction, and the esterification of both aliphatic and aromatic acids is carried out simultaneously in the range of 220–255°C.

Process Variations. Esterification is a reversible reaction; therefore, an important factor affecting the rate of esterification is the rate of removal of water from the reactor. Most alkyds are produced using a reflux solvent, such as xylene, to promote the removal of water by azeotroping. Since the reaction is run at a temperature far above the boiling point of xylene, less than 5% of xylene is used. The amount is dependent on the reactor and is set empirically such that there is enough to reflux vigorously, but not so much as to cause flooding of the condenser. Some of the xylene is distilled off along with the water; water is separated and xylene is returned to the reactor. The presence of solvent is desirable for other reasons: vapor serves as an inert atmosphere, reducing the amount of inert gas

needed, and the solvent serves to avoid accumulation of sublimed solid monomers, mainly PA, in the reflux condenser.

Reaction time is affected by reaction temperature. Higher temperatures obviously accelerate the reaction. If the reaction is carried too far, there is a major risk of gelation. There are economic advantages to short reaction times. Operating costs are reduced, and the shorter times permit more batches of alkyd to be produced in a year, increasing capacity without capital investment in more reactors. Therefore, it is desirable to operate at as high a temperature as possible without risking gelation.

A critical aspect of alkyd synthesis is deciding when the reaction is completed. Disappearance of carboxylic acid is followed by titration to determine acid number, and increase in molecular weight is followed by viscosity. Determination of acid number and viscosity both take some time. Meanwhile, in the reactor, the reaction is continuing. After it is decided that the extent of reaction is sufficient, the reaction mixture must be dropped into a larger tank containing solvent. When a 40,000-L batch of alkyd is being made, a significant time is required to get the resin out of the reactor into the reducing tank; meanwhile, the reaction is continuing. The decision to start dropping the batch must be made so that the acid number and viscosity of the batch will be right after the continuing reaction that occurs between the time of sampling, determination of acid number and viscosity, and discharging of the reactor. The time for these determinations becomes the rate-controlling step in production. If they can be done rapidly enough, the reaction can be carried out at 240°C or even higher without overshooting the target acid number and viscosity. On the other hand, if the control tests are done slowly, it may be necessary to run the reaction at only 220°C, which may require 2 h or more of additional reaction time. Automatic titration instruments permit rapid determination of acid number and so the usual limit on time required is viscosity determination. While attempts have been made to use viscosity of the resin at reaction temperature to monitor change in molecular weight, the dependence of viscosity on molecular weight at that high temperature is not sensitive enough to be very useful. The viscosity must be determined on a solution at some lower standard temperature. Since viscosity depends strongly on solution concentration and temperature, these variables must be carefully controlled.

In alkyd production, viscosity is commonly determined using Gardner bubble tubes. The cook is continued until the viscosity is high enough so that by the time the resin batch is dropped into the solvent and the batch cooled, its viscosity will be what is called for in the specification. This means starting to discharge the reactor when the test sample is at some lower viscosity. It is not possible to generalize how large this difference should be; it depends on the specific alkyd composition, the temperature at which the reaction is being run, the time required to do the determination, the time required to empty the reactor, and so on. Viscosities can be determined more rapidly using a cone and plate viscometer than with bubble tubes; the very small sample required for a cone and plate viscometer can be cooled and equilibrated at the measurement temperature more quickly.

Many variables affect the acid number and viscosity of alkyds. One is the ratio of reactants: The closer the ratio of moles of dibasic acid to polyol approaches 1, the higher the molecular weight of the backbone of the resin, but also the greater the likelihood of gelation. A useful rule of thumb for a starting point is to

use a mole ratio of 0.95. The final ratio is determined by adjustments such that the combination of acid number and solution viscosity come out at the desired levels. The greater the ratio of hydroxyl groups to carboxylic acid groups, the faster the acid groups are reduced to a low level. The degree of completion of the reaction is an important factor controlling the viscosity, as well as the acid number. It is usually desirable to have a low acid number, typically in the range of 5–10.

The composition of the fatty acids is a major factor affecting the viscosity, and compositions of an oil or grade of TOFA can be expected to vary somewhat from lot to lot. Dimerization and oligomerization of the unsaturated fatty acids occur in the same temperature range at which the esterification is carried out. Fatty acids with conjugated double bonds dimerize more rapidly than those with nonconjugated bonds, and dimerization rates increase with the level of unsaturation. At the same ratio of phthalic to polyol to fatty acids, alkyds of the same acid number and solution concentration will increase in viscosity in the order soybean < linseed < tung.

Some volatilization of polyol, PA, and fatty acids out of the reactor will occur depending on the design of the reactor, the rate of reflux of the azeotroping solvent, the rate of inert gas flow, and the reaction temperature, among other variables; the amount and ratio of these losses affect the viscosity at the standard acid number. The exact ratio of reactants must be established in the reactor that is actually used for synthesis. Since gelation can occur if the ratio of dibasic acid to polyol is too high, it is better not to put all the PA into the reactor in the beginning. If the viscosity is too low when the acid number is getting down near the standard, more PA can easily be added. The amount of PA held back can be reduced as experience is gained cooking a particular alkyd in a particular reactor.

Side reactions can affect the viscosity–acid number relationship. Glycerol and other polyols form ethers to some degree during the reaction. Glycerol can also form acrolein by successive dehydrations. When these reactions occur, the mole ratio of dibasic acid to polyol increases and the number of hydroxyl groups decreases; therefore, at the same acid number, the molecular weight will be higher. Excessively high viscosity and even gelation can result. Ether formation is catalyzed by strong protonic acids; therefore, it is desirable to avoid them as catalysts for the esterification. Monobutyltin oxide has been used as an esterification catalyst; presumably, it does not significantly catalyze ether formation. As noted earlier, pentaerythritol and TMP seem less vulnerable than glycerol to undesirable side reactions such as ether formation, and glycerol is the only polyol that can decompose to form acrolein. A hydroxyl group on one end of a growing polyester chain can react with a carboxylic acid group on another end of the same molecule, leading to ring formation. Transesterification of chain linkages can have the same result. Since cyclization reactions reduce chain length, their net effect is to reduce viscosity.

Many alkyd resins have broad, uneven molecular weight distributions. It has been shown that even modest changes in reaction conditions can cause large differences in molecular weight distribution, which can have significant effects on final film properties (39). In many alkyds, very small gel particles (microgels) are formed. It has been shown that these microgels play an important role in giving greater strength properties to final films (39). Process changes that may make

the alkyd more uniform may be undesirable. For example, allowing glycerolysis to approach equilibrium before addition of PA and using transesterification catalysts in the final stages of esterification both favor narrower molecular weight distributions and lower viscosities, but films made from the more uniform alkyds may exhibit inferior mechanical properties.

Urethane Derivatives

Uralkyds are also called urethane alkyds or urethane oils. They are alkyd resins in which a diisocyanate, usually 2,4(6)-toluene diisocyanate [584-84-9] (TDI), has fully or partly replaced the PA usually used in the preparation of alkyds. One transesterifies a drying oil with a polyol such as glycerol or pentaerythritol to make a monoglyceride (see section Synthesis from Oils or Fatty Acids) and reacts it with some PA (if desired) and then with somewhat less diisocyanate than the equivalent amount of N=C=O based on the free OH content. To assure that no N=C=O groups remain unreacted, methyl alcohol is added at the end of the process. Just like alkyds, uralkyds dry faster than the drying oil from which they were made, since they have a higher average functionality (more activated diallylic groups per average molecule). The rigidity of the TDI aromatic rings also speeds up the drying by increasing the T_g of the resin.

Two principal advantages of uralkyd over alkyd coatings are superior abrasion resistance and resistance to hydrolysis. Disadvantages are inferior color retention (when aromatic isocyanates used) of the films, higher viscosity of resin solutions at the same percent solids, and higher cost. Uralkyds made with aliphatic diisocyanates have better color retention, but are more expensive and have lower T_g. The largest use of uralkyds is in architectural coatings. Many so-called varnishes sold to the consumer today are based on uralkyds; they are not really varnishes in the original sense of the word. They are used as transparent coatings for furniture, woodwork, and floors: applications in which good abrasion resistance is important. Since they are generally made with aromatic isocyanates, they tend to turn yellow and then light brown with age; yellowing is acceptable in clear varnishes, but would be a substantial drawback in light-colored pigmented paints.

Water-reducible polyunsaturated acid substituted aqueous polyurethane dispersions are also being used (40). They can be made by reacting a diisocyanate with a polyol, monoglyceride of a drying oil, and dimethylolpropionic acid. The carboxylic acid groups are neutralized with a tertiary amine and dispersed in water. If aliphatic isocyanates are used, good color retention can be obtained. They are much more resistant to hydrolysis than conventional alkyd resins. Films also have excellent abrasion resistance. Cost can be reduced by blending in 10–20% of acrylic latex.

Epoxy Esters

Bisphenol A (BPA) epoxy resins can be converted to what are commonly called epoxy esters by reacting with fatty acids. Drying or semidrying oil fatty acids are used so that the products cross-link by autoxidation. The epoxy groups undergo

a ring-opening reaction with carboxylic acids to generate an ester and a hydroxyl group. These hydroxyl groups, as well as the hydroxyl groups originally present on the epoxy resin, can esterify with fatty acids. They are generally made by starting with a low molecular weight epoxy resin (ie, the standard liquid resin, $n = 0.13$) and extending with 4,4′-(1-methylethylidene)bisphenol [80-05-7] (BPA) by the advancement process to the desired molecular weight. Off-specification epoxy resin is often used to reduce cost. The fatty acids are added to the molten, hot resin, and the esterification reaction is continued until the acid number is low, usually less than 7 mg of KOH per gram of resin. In the esterification reaction with fatty acids, the average number of sites for reaction is the n value, corresponding to the number of hydroxyl groups on the resin, plus twice the number of epoxy groups. The esterification is carried out at high temperatures (220–240°C). The rate of esterification slows as the concentration of hydroxyl groups diminishes, and side reactions occur, especially dimerization of the drying oil fatty acids (or their esters). It is not practical to esterify more than about 90% of the potential hydroxyl groups, including those from ring opening the epoxy groups. The lower useful limit of the extent of esterification is about 50%. This is required to ensure sufficient fatty acid groups for oxidative cross-linking.

Tall oil fatty acids are commonly used because of their low cost. Linseed fatty acids give faster cross-linking coatings because of higher average functionality. However, their viscosity is higher because of the greater extent of dimerization during esterification, and their cost is higher. For still faster cross-linking, part of the linseed fatty acids can be replaced with tung fatty acids, but the viscosity and cost are still higher. The color of epoxy esters from linseed and linseed–tung fatty acids is darker than the tall oil esters. Dehydrated castor oil fatty acids give faster curing epoxy esters for baked coatings. The rate of formation of a dry film from epoxy esters depends on two factors: the average number of diallylic groups $\bar{f}_n$ and the ratio of aromatic rings to long aliphatic chains. The $\bar{f}_n$ can be maximized by using higher molecular weight BPA epoxy resin and by using enough fatty acid to react with a large fraction of the epoxy and hydroxyl groups. The ratio of aromatic rings to fatty acids can be maximized by using high molecular weight epoxy resin and esterifying a smaller fraction of epoxy and hydroxyl groups.

Epoxy esters are used in coatings in which adhesion to metal is important. While the reasons are not completely understood, it is common for epoxy coatings, including epoxy esters, to have good adhesion to metals and to retain adhesion after exposure of the coated metal to high humidity, a critical factor in corrosion protection. A distinct advantage of epoxy esters over alkyd resins is their greater resistance to hydrolysis and saponification. The backbone of alkyds is held together with esters from PA and the polyol, whereas in epoxy esters, the backbone is held together with C—C and ether bonds. Of course, the fatty acids are bonded to the backbone with ester groups in both cases, but the fraction of polymer bonds in a dry film subject to hydrolysis is substantially lower in the case of epoxy esters. On the other hand, exterior durability of epoxy ester coatings is poor, as is the case with all films made with BPA epoxy resins. As a result of these advantages and disadvantages, the major uses for epoxy resins are in primers for metal and in can coatings, such as for crowns (bottle caps), in which the important requirements are adhesion and hydrolytic stability. In baking primers, it is sometimes desirable

to supplement the cross-linking through oxidation by including a small amount of MF resin in the formulation to cross-link with part of the free hydroxyl groups on the epoxy ester.

Epoxy ester resins with good exterior durability (better than alkyds) can be prepared by reacting epoxy-functional acrylic copolymers (made with glycidyl methacrylate) with fatty acids. The product is an acrylic resin with multiple fatty acid ester side chains. By appropriate selection of acrylate ester comonomers and molecular weight, the T_g of the resin can be designed so that a tack-free film is obtained by solvent evaporation; then the coating cross-links by autoxidation. For an application like repainting an automobile at ambient temperatures, the cross-linking can proceed relatively slowly and need not be catalyzed by metal salt driers. The rate of cross-linking is slower without driers, but exterior durability is better.

Epoxy esters can also be made water-reducible. The most widely used water-reducible epoxy esters have been made by reacting maleic anhydride with epoxy esters prepared from dehydrated castor oil fatty acids. Subsequent addition of a tertiary amine, such as 2-(dimethylamino)ethanol [108-01-0], in water results in ring opening of the anhydride to give amine salts. Like other water-reducible resins, these resins are not soluble in water but form a dispersion of resin aggregates swollen with water and solvent in an aqueous continuous phase. The hydrolytic stability of these epoxy esters is better than corresponding alkyds and sufficient for use in electrodeposition primers until anionic primers were replaced by cationic primers. Water-reducible epoxy esters are still used in spray applied baking primers and primer-surfacers. They are also used in dip coating primers in which nonflammability is an advantage. Their performance equals that of solvent-soluble epoxy ester primers.

Uses

In 1997, the U. S. consumption of alkyds was approximately 310,000 t and projected use in 5 years is estimated to be 280,000–290,000 t (41). Coatings are the largest market with use in 1997 of approximately 250,000 t (42). European and Japanese consumption of alkyd coating resins in 1996 has been reported to be 360,000 and 110,000 t, respectively (42). Use of alkyds has been declining at about 2% a year and is projected to decline further as they are replaced with resins with higher performance and lower volatile emissions. Higher solids alkyds have been replacing conventional solids alkyds. In 1997, about 81,000 ton with solids of 50–60% and 16,000 tons of greater than 60% were used in the United States in comparison with 150,000 t of alkyds with lower than 50% solids. Only 10,000 t of waterborne alkyds were used (41).

The principal advantages of alkyds are low cost, low toxicity, and low surface tension. The low surface tension permits wetting of most surfaces including oily steel. Also the low surface tension minimizes application defects such as cratering. The principal limitations are generally poorer exterior durability and corrosion protection than alternative coating resins. While high solids and waterborne alkyd

resins are manufactured, their properties are generally somewhat inferior to conventional solvent-borne alkyds.

The largest use for alkyds in coatings is in architectural paints, particularly in gloss enamels for application by contractors. Contractors tend to prefer alkyd enamels over latex enamels because coverage can be achieved with a single coat. Also, alkyd paints can be applied at low temperatures whereas latex paints can only be applied at temperatures above about 5°C. The do-it-yourself market is served primarily with latex paints because of ease of cleanup and lesser odor. While initial gloss of alkyd enamels is higher than of latex enamels, the latex enamels exhibit far superior gloss retention in exterior applications. Alkyd primers provide better adhesion to chalky surfaces than most latex paints. The next largest use is in aerosol paints.

The largest use of alkyds in industrial applications is in general industrial coatings for such applications as machinery and metal furniture. Significant amounts are used with UF resins in coatings for wood furniture. Alkyd resin/chlorinated rubber based coatings are used in traffic paints, but use is decreasing because of high VOC content. An approach to overcoming this problem is the use of solvent-free alkyds in hot melt traffic paints (43). Some alkyds are still used in refinish paints for automobiles since they give high gloss coatings with a minimum of polishing. An example of recent work in formulating refinish coatings is preparing an alkyd by reacting tris(hydroxyethyl)isocyanurate with drying oil fatty acids and formulating with trimethylolpropane trimethacrylate as a reactive diluent (44).

About 39,000 t of uralkyds were used in the United States in 1997 (41). The largest use for uralkyds is as the vehicle for so-called urethane varnishes for the do-it-yourself market. The abrasion resistance of such coatings is greatly superior to that obtained with conventional varnishes or alkyd resins. Epoxy esters give coatings with markedly superior corrosion protection as compared with alkyd resins while retaining the advantage of low surface tension. However, as with any BPA epoxy system, exterior durability is poor. They are used primarily in primers for steel and in flexible coatings such as for metal crowns. Maleated epoxy esters give primers with equivalent properties of solvent-borne epoxy ester coatings and are widely used in formulating waterborne primers for steel.

Noncoatings applications include foundry core binders and printing inks, especially lithographic inks.

BIBLIOGRAPHY

"Alkyd Resins" in *EPST* 1st ed., Vol. 1, pp. 663–734, by R. G. Mraz and R. P. Silver, Hercules Powder Co.; "Alkyd Resins" in *EPSE* 2nd ed., Vol. 1, pp. 644–679, by H. J. Lanson, Lan Chem Corp.

1. J. H. Hartshorn, *J. Coat. Technol.* **54**(687), 53 (1982).
2. W. J. Muizebelt and co-workers, *J. Coat. Technol.* **70**(876), 83 (1998).
3. N. A. R. Falla, *J. Coat. Technol.* **64**(815), 55 (1992).
4. E. N. Frankel, *Prog. Lipid Res.* **19**, 1 (1980).
5. R. A. Hancock, N. J. Leeves, and P. F. Nicks, *Prog. Org. Coat.* **17**, 321, 337 (1989).

6. T. L. T. Robey and S. M. Rybicka, Paper No. 217, Paint Research Station Technical Papers, Vol. 13, No. 1, 1962, p. 2.
7. R. J. Blackinton, *J. Paint Technol.* **39**(513), 606 (1967).
8. T. A. Misev, *Prog. Org. Coat.* **21**, 79 (1992).
9. S. L. Kangas and F. N. Jones, *J. Coat. Technol.* **59**(744), 89 (1987).
10. R. Bacaloglu and co-workers, *Angew. Makromol. Chem.* **164**, 1 (1988).
11. R. Brown, H. Ashjian, and W. Levine, *Off. Digest* **33**, 539 (1961).
12. Tech. Bull. No. 524-5, Velsicol Chemical Corp., Chicago, Ill.
13. D. Ryer, *Paint Coat. Ind.* **14**(1), 76 (1998).
14. R. W. Hein, *J. Coat. Technol.* **71**(898), 21 (1999).
15. J. Mallegol, J. Lemaire, and J.-L. Gardette, *Prog. Org. Coat.* **39**, 107 (2000).
16. S. L. Kangas and F. N. Jones, *J. Coat. Technol.* **59**(744), 99 (1987).
17. U.S. Pat. 2577770 (1951), P. Kass and Z. W. Wicks Jr. (to Interchemical Corp.).
18. K. H. Zabel and co-workers, *Prog. Org. Coat.* **35**, 255 (1999).
19. W. J. Muizebelt and co-workers, *Prog. Org. Coat.* **40**, 121 (2000).
20. E. Levine, in *Proc. Water-Borne Higher-Solids Coat. Symp., New Orleans*, 1977, p. 155.
21. D. B. Larson and W. D. Emmons, *J. Coat. Technol.* **55**(702), 49 (1983).
22. Tech. Bull., Resimene AM-300 and AM-325, Monsanto Chemical Co. (now Solutia, Inc.), St. Louis, Mo., Jan. 1986.
23. U.S. Pat. 4293461 (1981), W. F. Strazik, J. O. Santer, and J. R. LeBlanc [to Monsanto Chemical Co. (now Solutia, Inc.)].
24. U.S. Pat. 6075088 (2000), J. Braeken. (to Fina Research, S.A.).
25. G. Osterberg and co-workers, *Prog. Org. Coat.* **24**, 281 (1994); G. Ostberg and B. Bergenstahl, *J. Coat. Technol.* **68**(858), 39 (1996).
26. A. Hofland, in J. E. Glass, ed., *Technology for Waterborne Coatings*, American Chemical Society, Washington, D.C., 1997, p. 183.
27. P. K. Weissenborn and A. Motiejauskaite, *Prog. Org. Coat.* **40**, 253 (2000).
28. T. Nabuurs, R. A. Baijards, and A. L. Germna, *Prog. Org. Coat.* **27**, 163 (1996).
29. J. W. Gooch, S. T. Wang, F. J. Schork, and G. W. Poehlein, in *Proc. Waterborne, High Solids, Powder Coat. Symp.*, New Orleans, 1997, p. 366.
30. W. S. Sisson and R. J. Shah, in *Proc. Waterborne, High Solids, Powder Coat. Symp.*, New Orleans, 2001, pp. 329–336.
31. C. J. Bouboulis, in *Proc. Water-Borne Higher-Solids Coat. Symp.*, New Orleans, 1982, p. 18.
32. B. Zuchert and H. Biemann, *Farg och Lack Scandinavia*, (2) 9 (1993); W. Weger, *Fitture e Vernici* B **66**(9), 25 (1990).
33. U.S. Pat. 5004779 (1991), H. Blum and co-workers (to Bayer Aktiengesellschaft).
34. U.S. Pat. 6187384 (2001), G. Wilke, D. Grapatin, and H.-P. Rink (to BASF Coatings AG).
35. R. Hurley and F. Buona, *J. Coat. Technol.* **54**(694), 55 (1982).
36. P. J. Bakker and co-workers, in *Proc. Water-borne High-Solids, Powder Coat. Symp.*, New Orleans, 2001, pp. 439–453.
37. J. Kaska and F. Lesek, *Prog. Org. Coat.* **19**, 283 (1991).
38. Anonymous, *The Chemistry and Processing of Alkyd Resins*, Monsanto Chemical Co. (now Solutia, Inc.), St. Louis, Mo., 1962.
39. J. Kumanotani, H. Hironori, and H. Masuda, *Adv. Org. Coat. Sci. Tech. Ser.* **6**, 35 (1984).
40. W. Liu, S. Wang, and T. Rende, in *Western Coat. Symp.*, Reno, Nev., 1999.
41. *Coatings VI*, Skeist Inc., Whippany, N.J., 1998, pp. 805–826.
42. E. Connolly, E. Anderson, and Y. Sakuma, *Alkyd/Polyester Surface Coatings*, SRI International, Pasadena, Calif., 1998.

43. U.S. Pat. 6011085 (2000), B. A. Maxwell and co-workers (to Eastman Chemical Co.).
44. U.S. Pat. 6083312 (2000), G. L. Bajc (to BASF Corp.).

GENERAL REFERENCE

T. C. Patton, *Alkyd Resin Technology*, John Wiley & Sons, Inc., New York, 1962.

ZENO W. WICKS JR.
Louisville, Kentucky

AMINO RESINS AND PLASTICS

Introduction

Amino resins are thermosetting polymers made by combining an aldehyde with a compound containing an amino ($-NH_2$) group. Urea–formaldehyde (U/F) accounts for over 80% of amino resins; melamine–formaldehyde accounts for most of the rest. Other aldehydes and other amino compounds are used to a very minor extent. The first commercially important amino resin appeared about 1930, or some 20 years after the introduction of phenol–formaldehyde resins and plastics (see PHENOLIC RESINS).

The principal attractions of amino resins and plastics are water solubility before curing, which allows easy application to and with many other materials, colorlessness, which allows unlimited colorability with dyes and pigments, excellent solvent resistance in the cured state, outstanding hardness and abrasion resistance, and good heat resistance. Limitations of these materials include release of formaldehyde during cure and, in some cases, such as in foamed insulation, after cure, and poor outdoor weatherability for urea moldings. Repeated cycling of wet and dry conditions causes surface cracks. Melamine moldings have relatively good outdoor weatherability.

Amino resins are manufactured throughout the industrialized world to provide a wide variety of useful products. Adhesive Compounds, representing the largest single market, are used to make plywood, chipboard, and sawdust board. Other types are used to make laminated wood beams, parquet flooring, and for furniture assembly.

Some amino resins are used as additives to modify the properties of other materials. For example, a small amount of amino resin added to textile fabric imparts the familiar wash-and-wear qualities to shirts and dresses. Automobile tires are strengthened by amino resins which improve the adhesion of rubber to

Encyclopedia of Polymer Science and Technology. Copyright John Wiley & Sons, Inc. All rights reserved.

tire cord. A racing sailboat may have a better chance to win because the sails of Dacron (Du Pont) polyester have been treated with an amino resin (1). Amino resins can improve the strength of paper even when it is wet. Molding compounds based on amino resins are used for parts of electrical devices, bottle and jar caps, molded plastic dinnerware, and buttons.

Amino resins are also often used for the cure of other resins, such as Alkyd Resins, and reactive acrylic polymers. These polymer systems may contain 5–50% of the amino resin and are commonly used in the flexible backings found on carpets and draperies, as well as in protective surface coatings, particularly the durable baked enamels of appliances, automobiles, etc.

The term *amino resin* is usually applied to the broad class of materials regardless of application, whereas the term *aminoplast* or sometimes *amino plastic* is more commonly applied to thermosetting molding compounds based on amino resins. Amino plastics and resins have been in use since 1920s. Compared with other segments of the plastics industry, they are mature products, and their growth rate is only about half of that of the plastics industry as a whole. They account for about 3% of the U.S. plastics and resins production.

History. The basic chemistry of amino resins was established as early as 1908 (2), but the first commercial product, a molding compound, was patented in England (3) only in 1925. It was based on a resin made from an equimolar mixture of urea and thiourea and reinforced with purified cellulose fiber and was trademarked Beetle (indicating it could "beat all" others). Patent rights were acquired by the American Cyanamid Company along with the Beetle trademark, and by 1930 a similar molding compound was being marketed in the United States. The new product was hard and not easily stained and was available in light, translucent colors; furthermore, it had no objectionable phenolic odor. The use of thiourea improved gloss and water resistance, but stained the steel molds. As amino resin technology progressed the amount of thiourea in the formulation could be reduced and finally eliminated altogether.

In the early 1920s, experimentation with urea–formaldehyde resins [9011-05-6] in Germany (4) and Austria (5,6) led to the discovery that these resins might be cast into beautiful clear transparent sheets, and it was proposed that this new synthetic material might serve as an organic glass (5,6). In fact, an experimental product called Pollopas was introduced, but lack of sufficient water resistance prevented commercialization. Melamine–formaldehyde resin [9003-08-1] does have better water resistance but the market for synthetic glass was taken over by new thermoplastic materials such as polystyrene and poly(methyl methacrylate) (see METHACRYLIC ESTER POLYMERS; STYRENE POLYMERS).

Melamine resins were introduced about 10 years after the Beetle molding compound. They were very similar to those based on urea but had superior qualities. Henkel in Germany was issued a patent for a melamine resin in 1936 (7). Melamine resins rapidly supplanted urea resins and were soon used in molding, laminating, and bonding formulations, as well as for textile and paper treatments. The remarkable stability of the symmetrical triazine ring made these products resistant to chemical change once the resin had been cured to the insoluble, crosslinked state.

Prior to the rapid expansion of thermoplastics following World War II, amino plastics served a broad range of applications in molding, laminating, and bonding.

As the newer and more versatile thermoplastic materials moved into these markets, aminos became more and more restricted to applications demanding some specific property best offered by the thermosetting amino resins. Current sales patterns are very specific. Urea molding powders find application in moldings for electrical devices and in closures for jars and bottles. Melamine molding compound is used principally for molded plastic dinnerware. Urea resins have retained their use in electrical-wiring devices because of good electrical properties, good heat resistance, and an availability of colors not obtainable with phenolics. Urea–formaldehyde resins are useful as closures because of their excellent resistance to oils, fats, and waxes often found in cosmetics, and their availability in a broad range of colors. Melamine plastic is used for molded dinnerware primarily because of outstanding hardness, water resistance, and stain resistance. Melamine–formaldehyde is the hardest commercial plastic material.

Aminoplasts and other thermosetting plastics are molded by an automatic injection-molding process similar to that used for thermoplastics, but with an important difference (8). Instead of being plasticized in a hot cylinder and then injected into a much cooler mold cavity, the thermosets are plasticized in a warm cylinder and then injected into a hot mold cavity where the chemical reaction of cure sets the resin to the solid state. The process is best applied to relatively small moldings. Melamine plastic dinnerware is still molded by standard compression-molding techniques. The great advantage of injection molding is that it reduces costs by eliminating manual labor, thereby placing the amino resins in a better position to compete with thermoplastics (see INJECTION MOLDING).

The future for amino resins and plastics seems secure because they can provide qualities that are not easily obtained in other ways. New developments will probably be in the areas of more highly specialized materials for treating textiles, paper, etc, and for use with other resins in the formulation of surface coatings, where a small amount of an amino resin can significantly increase the value of a more basic material. Additionally, since amino resins contain a large proportion of nitrogen, a widely abundant element, they may be in a better position to compete with other plastics as raw materials based on carbon compounds become more costly.

Raw Materials

Most amino resins are based on the reaction of formaldehyde [50-00-0] with urea [57-13-6] [1] or melamine [108-78-1] (2).

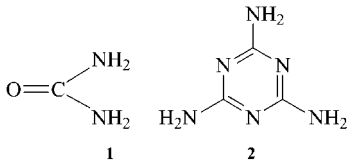

1 2

Although formaldehyde will combine with many other amines, amides, and aminotriazines to form useful products, only a few are used and are of minor

importance compared with products based on urea and melamine. Benzoguanamine [91-76-9] [3], for example, is used in amino resins for coatings because it provides excellent resistance to laundry detergent, a definite advantage in coatings for automatic washing machines. Dihydroxyethylene urea [3720-97-6] [4] is used for making amino resins that provide wash-and-wear properties in clothing. Glycoluril [496-46-8] (5) resins provide coatings with high film flexibility.

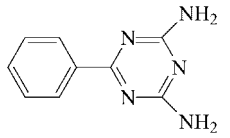

3

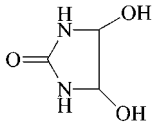

4

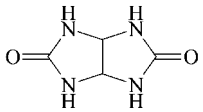

5

Aniline–formaldehyde resins were once quite important because of their excellent electrical properties, but their markets have been taken over by newer thermoplastic materials. Nevertheless, some aniline resins are still used as modifiers for other resins. Acrylamide occupies a unique position in the amino resins field since it not only contains a formaldehyde reactive site, but also a polymerizable double bond. Thus it forms a bridge between the formaldehyde condensation polymers and the versatile vinyl polymers and copolymers (see ACRYLAMIDE POLYMERS).

In the sense that formaldehyde can supply a methylene link between two molecules, it is difunctional. Each amino group has two replaceable hydrogens that can react with formaldehyde; hence, it also is difunctional. Since the amino compounds commonly used for making amino resins, urea, and melamine contain two and three amino groups, they are polyfunctional and react with formaldehyde to form three-dimensional, cross-linked polymer structures. Compounds with a single amino group such as aniline or toluenesulfonamide can usually react with formaldehyde to form only linear polymer chains. However, in the presence of an acid catalyst at higher temperatures, the aromatic ring of aniline may react with formaldehyde to produce a cross-linked polymer.

Urea. Urea (carbamide), CH_4N_2O, is the most important building block for amino resins because urea–formaldehyde is the largest selling amino resin, and urea is the raw material for melamine, the amino compound used in the next largest selling-type of amino resin. Urea is also used to make a variety of other amino compounds, such as ethyleneurea, and other cyclic derivatives used for amino resins for treating textiles. They are discussed later.

Urea is soluble in water, and the crystalline solid is somewhat hygroscopic, tending to cake when exposed to a humid atmosphere. For this reason, urea is frequently *pelletized* or *prilled* (formed into little beads) to avoid caking and making it easy to handle.

Only about 10% of the total urea production is used for amino resins, which thus appear to have a secure source of low cost raw material. Urea is made by the reaction of carbon dioxide and ammonia at high temperature and pressure to yield a mixture of urea and ammonium carbamate; the latter is recycled.

$$CO_2 + 2\,NH_3 \longrightarrow NH_2CONH_2 + H_2O \rightleftharpoons H_2NCOONH_4$$

Melamine. Melamine (cyanurotriamide 2,4,6-triamino-*s*-triazine), $C_3H_6N_6$, is a white crystalline solid, melting at approximately 350°C with vaporization, only slightly soluble in water. The commercial product, recrystallized grade, is at least 99% pure. Melamine was synthesized early in the development of organic chemistry, but it remained of theoretical interest until it was found to be a useful constituent of amino resins. Melamine was first made commercially from dicyandiamide [461-58-5] is now made from urea, a much cheaper starting material (9–12).

Urea is dehydrated to cyanamide which trimerizes to melamine in an atmosphere of ammonia to suppress the formation of deamination products. The ammonium carbamate [1111-78-0] also formed is recycled and converted to urea. For this reason the manufacture of melamine is usually integrated with much larger facilities making ammonia and urea.

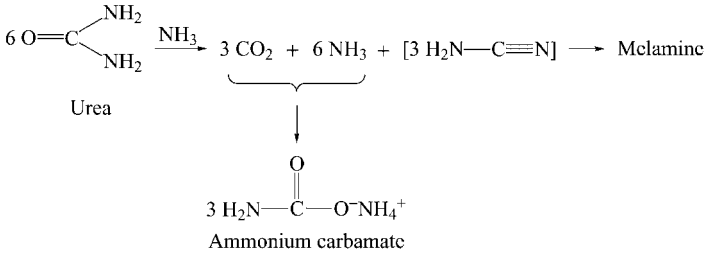

Since melamine resins are derived from urea, they are more costly and are therefore restricted to applications requiring superior performance. Essentially all of the melamine produced is used for making amino resins and plastics.

Formaldehyde. Pure formaldehyde, CH_2O, is a colorless, pungent smelling reactive gas. The commercial product is handled either as solid polymer, paraformaldehyde (13), or in aqueous or alcoholic solutions. Marketed under the trade name Formcel, solutions in methanol, *n*-butanol, and isobutyl alcohol are widely used for making alcohol-modified urea and melamine resins for surface coatings and treating textiles.

Aqueous formaldehyde, known as formalin is usually 37 wt% formaldehyde, although more concentrated solutions are available. Formalin is the general-purpose formaldehyde of commerce supplied unstabilized or methanol-stabilized. The latter may be stored at room temperature without precipitation of solid formaldehyde polymers because it contains 5–10% methyl alcohol. The uninhibited type must be maintained at a temperature of at least 32°C to prevent the separation of solid formaldehyde polymers. Large quantities are often supplied in more concentrated solutions. Formalin at 44, 50, or even 56% may be used to

reduce shipping costs and improve manufacturing efficiency. Heated storage tanks must be used. For example, formalin containing 50% formaldehyde must be kept at a temperature of 55°C to avoid precipitation. Formaldehyde solutions stabilized with urea are used (14), and various other stabilizers have been proposed (15,16). With urea-stabilized formaldehyde the user need only adjust the U/F ratio by adding more urea to produce a urea resin solution ready for use.

Paraformaldehyde [30525-89-4] is a mixture of polyoxymethylene glycols, $HO(CH_2O)_nH$, with n from 8 to as much as 100. It is commercially available as a powder (95%) and as flake (91%). The remainder is a mixture of water and methanol. Paraformaldehyde is an unstable polymer that easily regenerates formaldehyde in solution. Under alkaline conditions, the chains depolymerize from the ends, whereas in acid solution the chains are randomly cleaved (17). Paraformaldehyde is often used when the presence of a large amount of water should be avoided as in the preparation of alkylated amino resins for coatings. Formaldehyde may also exist in the form of the cyclic trimer trioxane [110-88-3]. This is a fairly stable compound that does not easily release formaldehyde; hence, it is not used as a source of formaldehyde for making amino resins.

Approximately 25% of the formaldehyde produced in the United States is used in the manufacture of amino resins and plastics.

Other Materials. Benzoguanamine and acetoguanamine may be used in place of melamine to achieve greater solubility in organic solvents and greater chemical resistance. Aniline and toluenesulfonamide react with formaldehyde to form thermoplastic resins. They are not used alone, but rather as Plasticizers for other resins including melamine and urea–formaldehyde. The plasticizer may be made separately or formed in situ during preparation of the primary resin.

Acrylamide [79-06-1] is an interesting monomer for use with amino resins; the vinyl group is active in free-radical-catalyzed addition polymerizations, whereas the—NH_2 group is active in condensations with formaldehyde. Many patents describe methods of making cross-linked polymers with acrylamide by taking advantage of both vinyl polymerization and condensation with formaldehyde. For example, acrylamide reacts readily with formaldehyde to form *N*-methylolacrylamide [924-42-5], which gives the corresponding with isobutyl alcohol.

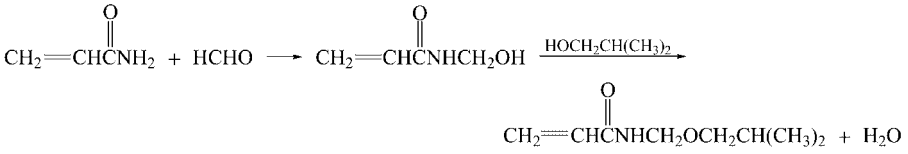

This compound is soluble in most organic solvents and may be easily copolymerized with other vinyl monomers to introduce reactive side groups on the polymer chain (18). Such reactive polymer chains may then be used to modify other polymers including other amino resins. It may be desirable to produce the cross-links first. Thus, *N*-methylolacrylamide can react with more acrylamide to produce methylenebisacrylamide, a tetrafunctional vinyl monomer.

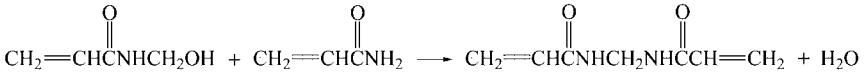

Chemistry of Resin Formation

The first step in the formation of resins and plastics from formaldehyde and amino compounds is the addition of formaldehyde to introduce the hydroxymethyl group, known as *methylolation* or *hydroxymethylation*:

$$R{-}NH_2 + HCHO \longrightarrow R{-}NH{-}CH_2OH$$

The second step is a condensation reaction that involves the linking together of monomer units with the liberation of water to form a dimer, a polymer chain, or a vast network. This is usually referred to as *methylene bridge formation*, *polymerization*, *resinification*, or simply *cure*, and is illustrated in the following equation:

$$RNH{-}CH_2OH + H_2NR \longrightarrow RNH{-}CH_2{-}NHR + H_2O$$

Success in making and using amino resins largely depends on the precise control of these two chemical reactions. Consequently, these reactions have been much studied (19–30).

The first reaction, the addition of formaldehyde to the amino compound, is catalyzed by either acids or bases. Hence, it takes place over the entire pH range. The second reaction joins the amino units with methylene links and is catalyzed only by acids. The rates of these reactions have been studied over a broad range of pH (28). The results are presented in Figure 1.

The same study also examined some of the subsequent reactions involved in the formation of more complex U/F condensation products. Rate constants for these reactions at 35°C are shown in Table 1.

The methylol compounds produced by these reactions are relatively stable under neutral or alkaline conditions, but undergo condensation, forming polymeric products under acidic conditions. Consequently, the first step in making an amino plastic is usually carried out under alkaline conditions. The amino compound and formaldehyde are combined and form a stable resin intermediate that may be used as an adhesive or combined with filler to make a molding compound. The second step is the addition of an acidic substance to catalyze the curing reaction, often with the application of heat to cure the amino resin to the solid cross-linked state. In this reaction, the methylol group is probably protonated and a molecule

Table 1. Urea–Formaldehyde (U/F) Reaction Rate Constants

Reaction at 35°C and pH 4.0	k, L/(mol·s)
$U + F \rightarrow U/F$	4.4×10^{-4}
$U/F + U \rightarrow U{-}CH_2{-}U$	3.3×10^{-4}
$U/F + U/F \rightarrow U{-}CH_2{-}U/F$	0.85×10^{-4}
$U/F_2 + U/F \rightarrow FU{-}CH_2{-}U/F$	0.5×10^{-4}
$U/F_2 + U/F_2 \rightarrow FU{-}CH_2{-}U/F_2$	$<3 \times 10^{-6}$

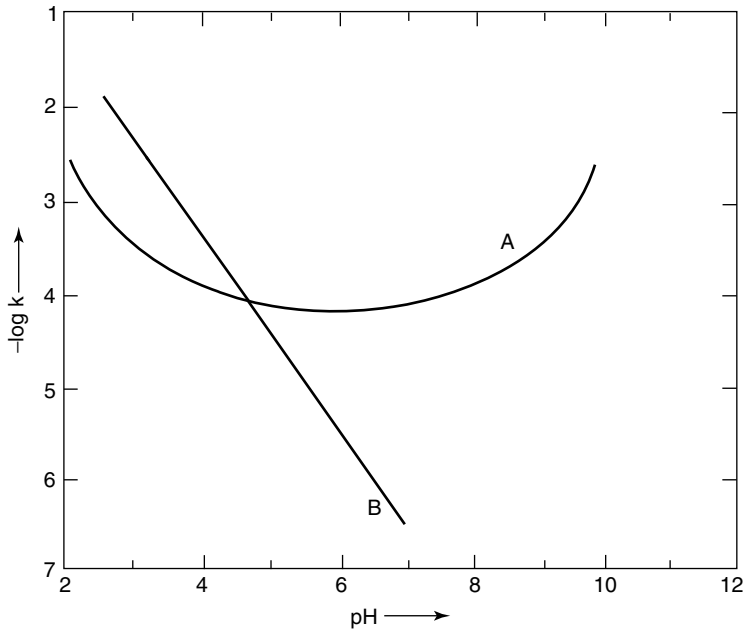

Fig. 1. Influence of pH on (**A**) the addition reaction of urea and formaldehyde (1:1), and (**B**) the condensation of methylolurea with the amino hydrogen of a neighboring urea molecule. Temperature = 35°C; 0.1 *M* aq. [Full View].

of water lost, giving the intermediate carbonium–imonium ion. This then reacts with an amino group to form a methylene link.

$$RNHCH_2OH + H^+ \rightleftharpoons RNHCH_2\overset{+}{O}H_2$$

$$RNHCH_2\overset{+}{O}H_2 \rightleftharpoons RNH\overset{+}{C}H_2 + H_2O$$

$$RN\overset{+}{H}CH_2 + H_2NR' \rightleftharpoons RNHCH_2H_2\overset{+}{N}R'$$

$$RNHCH_2H_2\overset{+}{N}R' \rightleftharpoons RNHCH_2HNR' + H^+$$

In addition to the two main reactions, ie, methylolation and condensation, there are a number of other reactions important for the manufacture and uses of amino resins. For example, two methylol groups may combine to produce a dimethylene ether linkage and liberate a molecule of water:

$$2\ RNHCH_2OH \rightleftharpoons RNHCH_2{-}O{-}CH_2NHR + H_2O$$

The dimethylene ether so formed is less stable than the diamino–methylene bridge and may rearrange to form a methylene link and liberate a molecule of formaldehyde.

$$RNH{-}CH_2O{-}CH_2NHR \longrightarrow RNH{-}CH_2{-}NHR + HCHO$$

The simple methylol compounds and the low molecular weight polymers obtained from urea and melamine are soluble in water and quite suitable for the manufacture of adhesives, molding compounds, and some kinds of textile treating resins. However, amino resins for coating applications require compatibility with the film-forming Alkyd Resins or copolymer resins with which they must react. Furthermore, even where compatible, the free methylol compounds are often too reactive and unstable for use in a coating-resin formulation that may have to be stored for some time before use. Reaction of the free methylol groups with an alcohol to convert them to alkoxy methyl groups solves both problems.

The replacement of the hydrogen of the methylol compound with an alkyl group renders the compound much more soluble in organic solvents and more stable. This reaction is also catalyzed by acids and usually carried out in the presence of considerable excess alcohol to suppress the competing self-condensation reaction. After neutralization of the acid catalyst, the excess alcohol may be stripped or left as a solvent for the amino resin.

The mechanism of the alkylation reaction is similar to curing. The methylol group becomes protonated and dissociates to form a carbonium ion intermediate which may react with alcohol to produce an alkoxymethyl group or with water to revert to the starting material. The amount of water in the reaction mixture should be kept to a minimum since the relative amounts of alcohol and water determine the final equilibrium.

Another way of achieving the desired compatibility with organic solvents is to employ an amino compound having an organic solubilizing group in the molecule, such as benzoguanamine. With one of the $-NH_2$ groups of melamine replaced with a phenyl group, benzoguanamine–formaldehyde resins [26160-89-4] have some degree of oil solubility even without additives. Nevertheless, benzoguanamine-formaldehyde resins are generally modified with alcohols to provide a still greater range of compatibility with solvent-based surface coatings. Benzoguanamine resins provide a high degree of detergent resistance, together with good ductility and excellent adhesion to metal.

Displacement of a volatile with a nonvolatile alcohol is an important reaction for curing paint films with amino cross-linkers and amino resins on textile fabrics or paper. Following is an example of a methoxymethyl group on an amino resin reacting with a hydroxyl group of a polymer chain:

$$RNHCH_2OCH_3 + HOCH_2{-}\underline{\S} \longrightarrow RNHCH_2OCH_2{-}\underline{\S} + CH_3OH$$

A troublesome side reaction encountered in the manufacture and use of amino resins is the conversion of formaldehyde to formic acid. Often the reaction mixture of amino compound and formaldehyde must be heated under alkaline conditions. This favors a Cannizzaro reaction in which two molecules of formaldehyde interact to yield one molecule of methanol and one of formic acid.

$$2\,HCHO + H_2O \longrightarrow CH_3OH + HCOOH$$

Unless this reaction is controlled, the solution may become sufficiently acidic to catalyze the condensation reaction causing abnormally high viscosity or premature gelation of the resin solution.

Manufacture

Precise control of the course, speed, and extent of the reaction is essential for successful manufacture. Important factors are mole ratio of reactants, catalyst (pH of reaction mixture), and reaction time and temperature. Amino resins are usually made by a batch process. The formaldehyde and other reactants are charged to a kettle, the pH adjusted, and the charge heated. Often the pH of the formaldehyde is adjusted before adding the other reactants. Aqueous formaldehyde is most convenient to handle and lowest in cost.

In general, conditions for the first part of the reaction are selected to favor the formation of methylol compounds. After addition of the reactants, the conditions may be adjusted to control the polymerization. The reaction may be stopped to give a stable syrup. This could be an adhesive or laminating resin and might be blended with filler to make a molding compound. It might also be an intermediate for the manufacture of a more complicated product, such as an alkylated amino resin, for use with other polymers in coatings.

The flow sheet (Fig. 2) illustrates the manufacture of amino resin syrups, cellulose-filled molding compounds, and spray-dried resins.

In the manufacture of amino resins every effort is made to recover and recycle the raw materials. However, there may be some loss of formaldehyde, methanol, or other solvent as tanks and reactors are vented. Some formaldehyde, solvents, and alcohols are also evolved in the curing of paint films and the curing of adhesives and resins applied to textiles and paper. The amount of material evolved in curing the resins may be so small that it may be difficult to justify the installation of complex recovery equipment. However, in the development of new resins for coatings and for treating textiles and paper, emphasis is being placed on those compositions that evolve a minimum of by-products on curing. The moist amino resin adhesive absorbs the high frequency radiation more readily than dry wood, thereby concentrating the heat in the glue line where it is needed. Hot pressing may be conducted in a hydraulic press comprising a large number of steam-heated platens, usually 5 cm thick. Pressures usually range from 1 to 2 MPa (150–300 psi). Hot-press temperatures for urea and melamine–urea are usually 115–132°C.

In plywood production with ureas, the spread veneers should be pressed as soon as possible. The time between spreading and pressing, usually called assembly time, should never exceed 1 h. With some formulations, the permissible assembly time may be no longer than 15 min. Melamine formulations and uncatalyzed melamine–urea combinations, however, can be spread and stored for as much as a week before use.

Ureas are not satisfactory for prolonged water immersion or for continuous exposure to warm and excessively humid conditions, although they are fairly resistant to normal humidity. Somewhat more durable bonds are obtained by heat

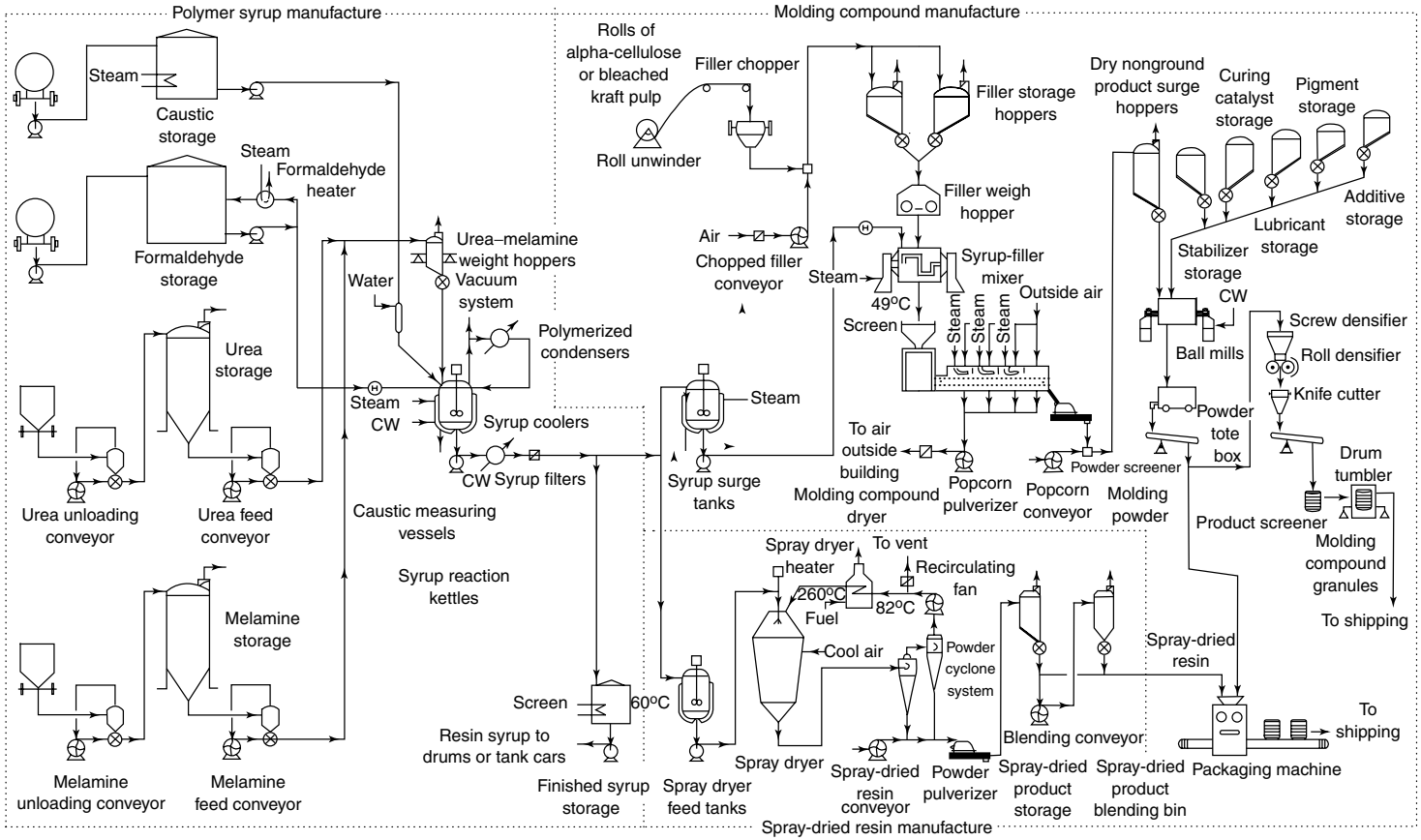

Fig. 2. Urea–formaldehyde and melamine–formaldehyde resin manufacture. CW: cold water. Courtesy of Stanford Research Institute.

setting. Ureas can be extended with wheat or rye flour, using as much as 150 parts flour to 100 parts dry resin. The extended glue still retains a fair degree of moisture resistance. Melamine resins have excellent water resistance, but cannot be cured at room temperature. Durable laminated wood beams used in building construction usually employ microwave technology for heat curing.

Continuous production of urea–formaldehyde resins has been described in many patents. In a typical example, urea and formaldehyde are combined and the solution pumped through a multistage unit. Temperature and pH are controlled at each stage to achieve the appropriate degree of polymerization. The product is then concentrated in a continuous evaporator to about 60–65% solids (31).

Laminating Resins

Phenolic and melamine resins are both used in the manufacture of decorative laminated plastic sheets for counters and tabletops. The phenolic is functional, being used in the backing or support sheets, whereas the melamine resin performs both decorative and functional roles in the print sheet and the protective overlay. Hardness, transparency, stain resistance, and freedom from discoloration are essential, in addition to a long-lasting working surface. Transparency is achieved because the refractive index of cured melamine-formaldehyde resin approaches that of the cellulose fibers and thus there is little scattering of light. Low cost and good mechanical properties are provided by the phenolic backing layers. In this instance, the combination of phenolic and amino resins achieves an objective that neither would normally be capable of performing alone. Developments in modified melamine resins have contributed to commercialization of premium priced through-color decorative laminates in which the dark color phenolic backing layers are replaced by color layers matching the full range of surface colors.

Phenolic resins are generally used in alcoholic solution, whereas melamine resins are best handled in water or water–alcohol mixtures. The paper or cloth web is passed through a dip tank containing resin solution, adjusted for pickup on squeeze rolls, and then passed through a heated drying oven. Once dried, the treated paper or cloth is fairly stable and, if stored in a cool place, it may be kept for several weeks or months before pressing into laminated plastic sheets.

A melamine laminating resin used to saturate the print and overlay papers of a typical decorative laminate might contain 2 mol of formaldehyde for 2 mol of melamine. In order to inhibit crystallization of methylol melamines, the reaction is continued until about one-fourth of the reaction product has been converted to low molecular weight polymer. A simple determination of free formaldehyde may be used to follow the first stage of the reaction, and the buildup of polymer in the reaction mixture may be followed by cloud-point dilution or viscosity tests.

A particularly interesting and useful test is run at high dilution. One or two drops of resin are added to a test tube half full of water. A cloudy streak as the drop sinks through the water indicates that the resin has advanced to the point where the highest molecular weight fraction of polymer is no longer soluble in water at that particular temperature. At this high dilution, the proportion of water to resin is not critical; hence the only measurement needed is the temperature of the water. The temperature at or below which the drops give a white streak is known

as the *hydrophobe temperature*. This test is particularly useful with melamine resins.

Laminates are pressed in steam-heated, multiple-opening presses. Each opening may contain a book of as many as 10 laminates pressed against polished steel plates. Curing conditions are 20–30 min at about 150°C under a pressure of about 6900 kPa (1000 psi).

Molding Compounds

Molding was the first big application for amino resins, although molding compounds are more complex than either laminating resins or adhesives. A simple amino resin molding compound might be made by combining melamine with 37% formalin in the ratio of 2 mol of formaldehyde/1 mol of melamine at neutral or slightly alkaline pH and a temperature of 60°C. The reaction should be continued until some polymeric product has been formed to inhibit crystallization of dimethylolmelamine upon cooling. When the proper reaction stage has been reached, the resin syrup is pumped to a dough mixer where it is combined with alpha-cellulose pulp, approximately one part of cellulose to each three parts of resin solids. The wet, spongy mass formed in the dough mixer is then spread on trays where it is combined with alpha-cellulose in a humidity-controlled oven to produce a hard, brittle popcorn-like intermediate. This material may be coarsely ground and sent to storage. To make the molding material, the cellulose–melamine resin intermediate is combined in a ball mill with a suitable catalyst, stabilizer, colorants, and mold lubricants. The materials must be ground for several hours to achieve the uniform fine dispersion needed to get the desired decorative appearance in the molded article. The molding compound may be used as a powder or it may be compacted under heat and pressure to a granular product that is easier to handle (32). A urea molding compound might be made in much the same way using a resin made with 1.3–1.5 mol of formaldehyde/1.0 mol of urea.

Amino molding compounds can be compression-, injection-, or transfer-molded. Urea molding compound has found wide use and acceptance in the electrical surface wiring device industry. Typical applications are circuit breakers, switches, wall plates, and duplex outlets. Urea is also used in closures, stove hardware, buttons, and small housings. Melamine molding compound is used primarily in dinnerware applications for both domestic and institutional use. It is also used in electrical-wiring devices, ashtrays, buttons, and housings.

The emergence of a new amino application is rare at this point in its relatively long life, but one such application has appeared and is growing rapidly. Because of the relative hardness of both urea and melamine moldings, a unique use has been developed for small, granular-sized particles of cut up molded articles. It is the employment of a pressurized stream of plastic particles to remove paint without damaging the surface beneath, and can be compared with a sandblasting operation. This procedure is gaining wide acceptance by both commercial airlines and the military for the refinishing of painted surfaces. It does not harm the substrate and eliminates the use of chemicals formerly used in stripping paint.

To speedup the molding process, the required amount of molding powder or granules is often pressed into a block and prewarmed before placing it in the mold.

Rapid and uniform heating is accomplished in a high frequency preheater, essentially an industrial microwave oven. The prewarmed block is then transferred to the hot mold, pressed into shape, and cured.

Production of decorated melamine plastic dinner plates makes use of molding and laminating techniques. The pattern is printed on the same type of paper used for the protective overlay of decorative laminates, treated with melamine resin and dried, and then cut into disks of the appropriate size.

To make a decorated plate, the mold is opened shortly after the main charge of molding compound has been pressed into shape, the decorative foil is laid in the mold on top of the partially cured plate, printed side down, and the mold closed again to complete the curing process. The melamine-treated foil is thus fused to the molded plate and, as with the decorative laminate, the overlay becomes transparent so that the printed design shows through yet is protected by the film of cured resin.

The excellent electrical properties, hardness, heat resistance, and strength of melamine resins make them useful for a variety of industrial applications. Some representative properties of amino resin molding compounds, including the industrial-grade melamines, are listed in Table 2.

Coatings

Cured amino resins are far too brittle to be used alone as surface coatings for metal or wood substrates, but in combination with other film formers (alkyds, polyesters, acrylics, epoxies) a wide range of acceptable performance properties can be achieved. These combination binder coating formulations cure rapidly at slightly elevated temperatures, making them well-suited for industrial baking applications. The amino resin content in the formulation is typically in the range of 10–50% of the total binder solids.

A wide selection of amino resin compositions is commercially available. They are all alkylated to some extent in order to provide compatibility with the other film formers, and formulation stability. They vary not only in the type of amine (melamine, urea, benzoguanamine, and glycoluril) used, but also in the concentration of combined formaldehyde, and the type and concentration of alkylation alcohol (*n*-butanol, isobutyl alcohol, and methanol).

On curing, amino resins not only react with the nucleophilic sites (hydroxyl, carboxyl, amide) on the other film formers in the formulation, but also self-condense to some extent. Highly alkylated amino resins have less tendency to self-condense (33,34) and are therefore effective cross-linking agents, but may require the addition of a strong acid catalyst to obtain acceptable cure even at bake temperatures of 120–177°C.

Amino resins based on urea have advantages in low temperature cure response and low cost. However, they are not as stable to uv radiation as melamine resins, and have poorer heat resistance; therefore, they have been successful primarily in interior wood finishes. Melamine resins, on the other hand, are uv stable, have excellent heat resistance, film hardness, and chemical resistance. They therefore dominate amino resin usage in OEM automotive coatings, general metals finishes, container coatings (both interior and exterior), and prefinished metal

Table 2. Typical Properties of Filled Amino Resin Molding Compounds

Property	ASTM or UL test	Urea	Melamine		
		Alpha-cellulose	Alpha-cellulose	Macerated Fabric	Glass fiber
Physical					
Specific gravity	D792	1.47–1.52	1.47–1.52	1.5	1.8–2.0
Water absorption, 24 h, 3.2 mm thick, %	D570	0.48	0.1–0.6	0.3–0.6	0.09–0.21
Mechanical					
Tensile strength, MPa[a]	D638	38–48	48–90	55–69	35–70
Elongation, %	D638	0.5–1.0	0.6–0.9	0.6–0.8	
Tensile modulus, GPa[b]	D638	9–9.7	9.3	9.7–11	16.5
Hardness, Rockwell M	D785	110–120	120	120	115
Flexural strength, MPa[a]	D790	70–124	83–104	83–104	90–165
Flexural modulus, GPa[b]	D7900	9.7–10.3	7.6	9.7	16.5
Impact strength, J/m[c] of notch	D256	14–18	13–19	32–53	32–1000
Thermal					
Thermal conductivity, 10^{-4} W/(m·K)	C177	42.3	29.3–42.3	44.3	48.1
Coefficient of thermal expansion, 10^{-5} cm/(cm·°C)	D696	2.2–3.6	2.0–5.7	2.5–2.8	1.5–1.7
Deflection temperature at 1.8 MPa,[a] °C	D648	130	182	154	204
Flammability class	UL-94	VO[d]	VO[d]		VO
Continuous no-load service temperature, °C		77[e]	99[e]	121	149–204
Electrical					
Dielectric strength, V/0.00254 cm	D149				
Short time, 3.2 mm thick		330–370	270–300	250–350	170–300
Step by step		220–250	240–270	200–300	170–240
Dielectric constant, 22.8°C	D150				
At 60 Hz		7.7–7.9	8.4–9.4	7.6–12.6	9.7–11.1
At 10^3 Hz			7.8–9.2	7.1–7.8	
Dissipation factor, 22.8°C	D150				
At 60 Hz		0.034–0.043	0.030–0.083	0.07–0.34	0.14–0.23
At 10^3 Hz			0.015–0.036	0.03–0.05	
Volume resistivity, 22.8°C, 50% rh, Ω·cm	D257	$0.5–5.0 \times 10^{11}$	$0.8–2.0 \times 10^{12}$	$1.0–3.0 \times 10^{11}$	$0.9–2.0 \times 10^{11}$
Arc resistance, s	D495	80–100	125–136	122–128	180–186

[a]To convert MPa to psi, multiply by 145.
[b]To convert GPa to psi, multiply by 145,000.
[c]To convert J/m to ft·lbf/in., divide by 53.38.
[d]Applies to specimens thicker than 1.6 mm.
[e]Based on no color change.

applications. Glycoluril resins have also found use in prefinished metal, primarily because of their high film flexibility properties. Unalkylated glycoluril resins are unique in that they are stable under slightly acidic conditions and have therefore found use in low temperature cure waterborne finishes. Benzoguanamine resins have historically been successful in appliance finishes because of their superior chemical resistance and specifically their detergent resistance. However, they have both poor uv resistance and economics, which have limited their use in other application areas.

When first introduced to the coatings industry, amino resin compositions were partially butylated and relatively polymeric in nature, with degrees of polymerization of 4–6. However, the dominant amino resin in today's industrial coating is based on a highly methylated, highly monomeric (degrees of polymerization of 1.4–2.6) melamine cross-linking agent. Variations of extent of methylolation and methylation exist along with a number of co-ethers, where the melamine molecule is both methylated and either *n*-butylated or isobutylated. This type of composition dominates because it best addresses the pollution (low volatile organic compounds) and performance requirements of today's industrial finishes (see COATINGS).

Methylation provides fast cure response, improved exterior exposure, high weight retention on curing, and suitability for both solvent and waterborne systems. Waterborne systems, in most instances, provide lower pollution than solvent-based formulations. High monomer content reduces the viscosity of the amino resin, again lowering pollution particularly when used in solvent-based systems, and also improves film flexibility and recoat adhesion. When some butylation is included as part of the alkylation, the viscosity of the amino resin is lowered, thereby lowering pollution (of the formulated coating), improving recoat adhesion, and improving wetting and flow characteristics. An amino resin is usually selected on the basis of specific performance properties required or performance to be emphasized.

Stability in storage is an important property for coating systems containing amino resins. If the amino resin undergoes self-condensation or reacts at room temperature with the alkyd or other film-forming polymer, the system may become too viscous or thicken to a gel which can no longer be used for coating. Alkyds usually contain sufficient free carboxyl groups to catalyze the curing reaction when the coating is baked, but this may also cause the paint to thicken in storage. Partial neutralization of the acid groups with an amine can greatly improve storage stability yet allow the film to cure when baked, since much of the amine is vaporized with the solvent during the baking process. 2-Amino-2-methyl-1-propanol [124-68-5], triethylamine [121-44-8], and dimethylaminoethanol [108-01-1] are commonly used as stabilizers. Alcohols as solvent also improve storage stability. Catalyst addition just before the coating is to be applied permits rapid curing and avoids the problem of storage stability. A strong acid soluble in organic solvents such as *p*-toluenesulfonic acid is very effective and may be partially neutralized with an amine to avoid premature reaction.

A butylated urea–formaldehyde resin for use in the formulation of fast-curing baking enamels might be made beginning with the charge: urea (1 mol), paraformaldehyde (2.12 mol), and butanol (1.50 mol). Triethanolamine is added to make the solution alkaline (about 1% of the weight of the urea), and the mixture is refluxed until the paraformaldehyde is dissolved. Phthalic anhydride is added to

give a pH of 4.0, and the water removed by azeotropic distillation until the batch temperature reaches 117°C. Cooling and dilution with solvent is done until the desired solids content is reached (35).

A highly methylated melamine–formaldehyde resin for cross-linking with little or no self-condensation might be made as follows (36). A solution of formaldehyde in methyl alcohol is charged to a reaction kettle and adjusted to a pH of 9.0–9.5 using sodium hydroxide. Melamine is then added to give a ratio of 1 mol of melamine/6.5 mol of formaldehyde, and the mixture is refluxed for 1.5 h. The reaction is then cooled to 35°C, and more methanol added to bring the ratio of methanol per mole of melamine up to 11. With the batch temperature at 35°C, enough sulfuric acid is added to reduce the pH to 1. After holding the reaction mixture at this temperature and pH for 1 h, the batch is neutralized with 50% NaOH and the excess methanol stripped to give a product containing 60% solids, which is then clarified by filtration. A highly methylated resin, such as this, may be used in water-based (37) or solvent-type coatings. It might also be used to provide crease resistance to cotton fabric.

The principal problems facing amino resins in the industrial coatings of the 1990s are formaldehyde emission and low temperature cure performance. Significant progress has been made in reducing the residual free formaldehyde in the amino resin, but formaldehyde generation on baking must still be addressed. Concerning low temperature cure performance, emphasis is being placed on catalyst selection. Amino resins cure at bake temperatures as low as 71–82°C, but at these bake temperatures they require high concentrations of acid catalyst, which negatively affect hydrolysis resistance or water sensitivity of the cured film. The development of improved catalysts is the most promising solution to low temperature cure performance enhancement.

Textile Finishes

Most amino resins used commercially for finishing textile fabrics are methylolated derivatives of urea or melamine. Although these products are usually monomeric, they may contain some polymer by-product.

Amino resins react with cellulosic fibers and change their physical properties. They do not react with synthetic fibers, such as nylon, polyester, or acrylics, but may self-condense on the surface. This results in a change in the stiffness or resiliency of the fiber. Partially polymerized amino resins of such molecular size that prevents them from penetrating the amorphous portion of cellulose also tend to increase the stiffness or resiliency of cellulose fibers.

Monomeric amino resins react predominantly with the primary hydroxyls of the cellulose, thereby replacing weak hydrogen bonds with strong covalent bonds, which leads to an increase in fiber elasticity. When an untreated cotton fiber is stretched or deformed by bending, as in forming a crease or wrinkle, the relatively weak hydrogen bonds are broken and then re-form to hold the fiber in its new position. The covalent bonds that are formed when adjacent cellulose chains are cross-linked with an amino resin are five to six times stronger than the hydrogen bonds. Covalent bonds are not broken when the fiber is stretched or otherwise deformed. Consequently, the fiber tends to return to its original condition when

the strain is removed. This increased elasticity is manifested in two important ways:

(1) When a cotton fabric is cross-linked while it is held flat, the fabric tends to return to its flat condition after it has been wrinkled during use or during laundering. Garments made from this type of fabric are known as wash-and-wear, minimum care, or no-iron.
(2) A pair of pants that is pressed to form a crease and then cross-linked tends to maintain the crease through wearing and laundering. This type of garment is called *durable-press* or *permanent press*.

This increased elasticity is always accompanied by a decrease in strength of the cellulose fiber, which occurs even though weak hydrogen bonds are replaced by stronger covalent bonds. The loss of strength is not caused by hydrolytic damage to the cellulose. If the cross-linking agent is removed by acid hydrolysis for example, the fiber will regain most, if not all, of its original strength. The loss in strength is believed to be due to intramolecular reaction of the amino resin along the cellulose chain to displace a larger number of hydrogen bonds, resulting in a net loss in strength. The intramolecular and intermolecular reactions (cross-linking) both occur at the same time.

Although there are many different amino resins used for textile finishing, all of them impart about the same degree of increase in elasticity when applied on an equal molar basis. Elasticity can be measured by determining the recovery from wrinkling. Although all these products impart about the same degree of improvement in elasticity, they also may impart many other desirable or undesirable properties to the fabric. The development of amino resins for textile finishing has been aimed toward maximizing the desirable properties and minimizing the undesirable ones. Most of the resins and reactants used in today's textile market are based on urea as a starting material. However, the chemistry differs considerably from that employed in early textile-finishing operations.

The first amino resins used commercially on textiles were the so-called urea–formaldehyde resins, dimethylolurea [140-95-4] [6], or its mixtures with monomethylolurea [1000-82-4].

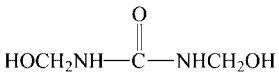

6

Their performance falls short of most present finishes, particularly in durability, resistance to chlorine-containing bleaches, and formaldehyde release, and they are not used much today. Both urea and formaldehyde are relatively inexpensive, and manufacture is simple; ie, 1–2 mol of formaldehyde as an aqueous solution reacts with 1 mol of urea under mildly alkaline conditions at slightly elevated temperatures.

Since the methylolurea monomers have limited water solubility (about 30%), they were usually marketed in dispersed form as soft pastes containing 55–65% active ingredient in order to decrease container and shipping costs. By

increasing the temperature and using slightly acidic conditions, dimethylolureas can be made as a series of short polymers that have infinite water solubility and can be marketed at concentrations as high as 85%. However, because these result in increased fabric stiffness, they cannot be used interchangeably with the monomeric materials. Both forms polymerize readily in storage and, unless kept under refrigeration, become water insoluble within a few weeks at ambient temperatures.

To overcome stability and water solubility problems, methylolurea resins are frequently alkylated to block the reactive hydroxyl groups. For reasons of economy the alkylating agent is usually methanol. In this process, 2 mol of aqueous formaldehyde reacts with 1 mol of urea under alkaline conditions to form dimethylolurea. Excess methanol is then added, and the reaction continued under acidic conditions to form methoxymethylurea. Both methylol groups can be methylated by maintaining low concentrations of water and using a large excess of methanol; however, methylation of only one of the methylol groups is sufficient to provide adequate shelf-life and water solubility. Upon completion of the methylation reaction, the resin is adjusted to pH 7–10, and excess methanol and water are removed by distillation under reduced pressure to provide syrups of 50–80% active ingredients.

Like methylolureas, cyclic ureas are based on reactions between urea and formaldehyde; however, the amino resin is cyclic rather than linear. Many cyclic urea resins have been used in textile-finishing processes, particularly to achieve wrinkle resistance and shrinkage control, but the ones described below are the most commercially important. They are all in use today to greater or lesser extents, depending on specific end requirements.

Ethyleneurea Resins. One of the most widely used resins during the 1950s and 1960s was based on dimethylolethyleneurea [136-84-5] [1,3-bis(hydroxymethyl)-2-imidazolidinone], commonly known as ethyleneurea resin. Ethyleneurea resin [28906-87-8] is most conveniently prepared from urea, ethylenediamine, and formaldehyde. 2-Imidazolidinone [120-93-4] [7] (ethyleneurea) is first prepared by the reaction of excess ethylenediamine [107-15-3] with urea (38) in an aqueous medium at about 116°C.

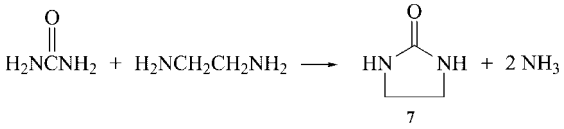

7

A fractionating column is required for the removal of ammonia and recycle of ethylenediamine. The molten product (mp 133°C) is then run into ice water to give a solution that is methylolated with 37% aqueous formaldehyde to form dimethylolethyleneurea [8].

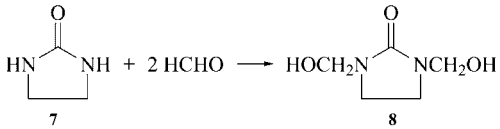

7 8

The resin, generally a 50% solution in water, has excellent shelf-life and is stable to hydrolysis and polymerization.

Propylene Urea Resins. Similar to the product from ethyleneurea [7], dimethylolpropyleneurea [3270-74-4] [9] 1,3-bis(hydroxymethyl)tetrahydro-2-(1*H*)-pyrimidinone] is the basis of propyleneurea–formaldehyde resin [65405-39-2]. Its preparation is from urea, 1,3-diaminopropane [109-76-2], and formaldehyde.

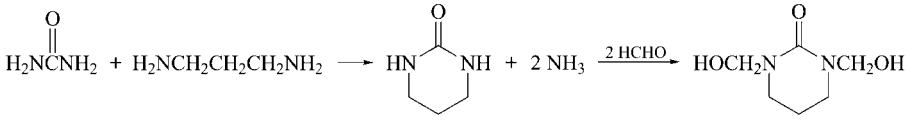

9

This resin was temporarily accepted, primarily because of its improved resistance to acid washes. However, the relatively high cost of the diamine precluded widespread commercial acceptance.

Triazone. Triazone is the common name for the class of compounds corresponding to the dimethylol derivatives of tetrahydro-5-alkyl-*s*-triazone [10]. They can be made readily and cheaply from urea, formaldehyde, and a primary aliphatic amine. A wide variety of amines may be used to form the six-membered ring (39); however, for reasons of cost and odor, hydroxyethylamine (monoethanolamine) is used preferentially. Since the presence of straight-chain methylolureas causes no deleterious effects to the fabric finish, the triazones typically are prepared with less than the stoichiometric quantity of the amine. This results not only in a less costly resin but also in improved performance (40).

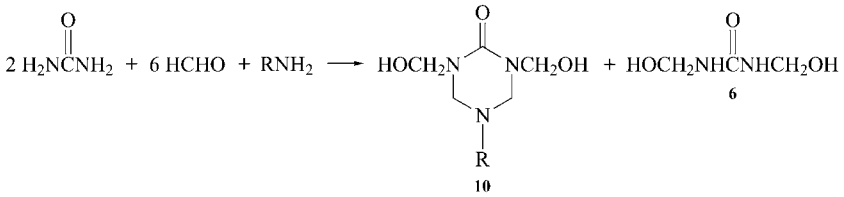

10 **6**

The resin is simply prepared by heating the components together. Usually the urea and formaldehyde are first charged to the kettle and heated under alkaline conditions to give a mixture of polymethylolureas, followed by the slow addition of the amine with continued heating to form the cyclic compound. The order of addition can be varied as can the molar ratios so as to yield a range of chain-ring compound ratios. The commercial resin is usually sold as a 50% solids solution in water.

Uron Resins. In the textile industry, the term uron resin *uron resin* usually refers to the mixture of a minor amount of melamine resin and so-called uron, which in turn is predominantly *N,N′*-bis(methoxymethyl)uron [7388-44-5] [11] plus 15–25% methylated urea–formaldehyde resins, a by-product. *N,N′*-bis(methoxymethyl)uron was first isolated and described in 1936 (41), but was commercialized only in 1960. It is manufactured (42) by the reaction of 4 mol of formaldehyde with 1 mol of urea at 60°C under highly alkaline conditions to form

tetramethylolurea [2787-01-1] [12]. After concentration under reduced pressure to remove water, excess methanol is charged and the reaction continued under acidic conditions at ambient temperatures to close the ring and methylate the hydroxymethyl groups. After filtration to remove the precipitated salts, the methanolic solution is concentrated to recover excess methanol. The product (75–85% pure) is then mixed with a methylated melamine–formaldehyde resin to reduce fabric strength losses in the presence of chlorine, and diluted with water to 50–75% solids. Uron resins do not find significant use today because of the greater amounts of formaldehyde released from fabric treated with these resins.

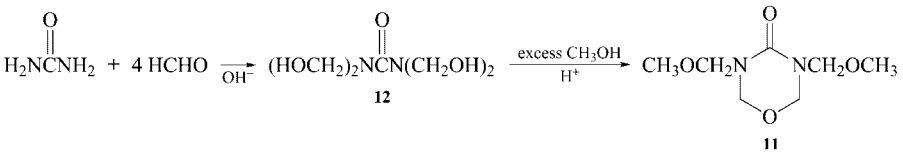

12 11

Glyoxal Resins. Since the late 1960s, glyoxal resins have dominated the textile-finish market for use as wrinkle-recovery, wash-and-wear, and durable-press agents. These resins are based on 1,3-bis(hydroxymethyl)-4,5-dihydroxy-2-imidazolidinone, commonly called dimethyloldihydroxyethyleneurea [1854-26-8] (DMDHEU) [13]. Several methods of preparation are described in the literature (43). On a commercial scale, DMDHEU can be prepared inexpensively at high purity by a one-kettle process (44): 1 mol of urea, 1 mol of glyoxal [107-22-2] as 40% solution, and 2 mol of formaldehyde in aqueous solution are charged to the reaction vessel. The pH is adjusted to 7.5–9.5 and the mixture heated at 60–70°C. The reaction is nearly stoichiometric; excess reagent is not necessary.

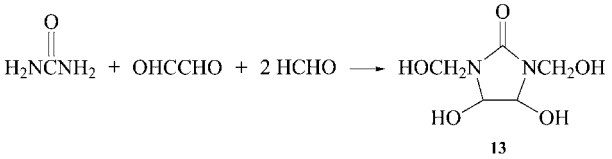

13

Glyoxal resins are generally sold at 45% solids solutions in water. Resin usage for crease-resistant fabrics had increased to well over 60×10^6 kg by 1974 and over half of this was DMDHEU for durable-press garments. In the early 1980s glyoxal resins modified with diethylene glycol [111-46-6] became prominent in the marketplace. These products are either simple mixtures of diethylene glycol and DMDHEU in water solution or the reaction product of diethylene glycol and DMDHEU. Rarely, ethylene glycol has been used in place of diethylene glycol. The diethylene glycol-modified DMDHEU products have the advantage of releasing significantly less formaldehyde from the finished fabric after resin curing than from fabric treated with DMDHEU. On the other hand, durable-press performance and shrinkage control are somewhat less with the glycol-modified resins.

A less important glyoxal resin is tetramethylolglycoluril [5395-50-6] [14] (tetramethylolacetylenediurea) produced by the reaction of 1 mol of glyoxal with 2 mol of urea and 4 mol of formaldehyde.

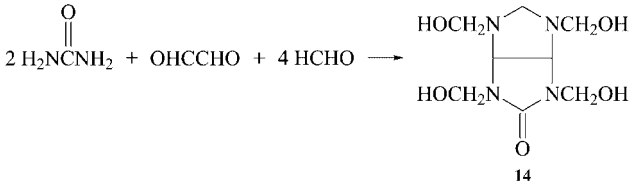

14

This resin was most popular in Europe, partly because of its lower requirements of glyoxal. However, because of increased availability and lower glyoxal costs plus certain application weaknesses, it has been generally replaced by DMDHEU.

Melamine–Formaldehyde Resins. The most versatile textile-finishing resins are the melamine–formaldehyde resins. They provide wash-and-wear properties to cellulosic fabrics, and enhance the wash durability of flame-retardant finishes. Butylated melamine–formaldehyde resins of the type used in surface coatings may be used in textile printing-ink formulations. A typical textile melamine resin is the dimethyl ether of trimethylolmelamine [1852-22-8], which can be prepared as follows:

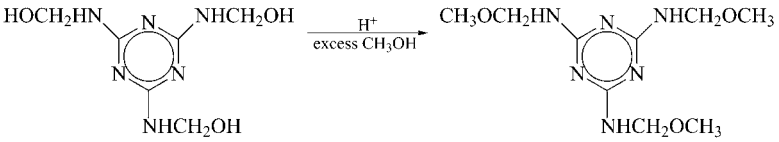

Under alkaline conditions, 3 mol of formaldehyde react with 1 mol of melamine at elevated temperatures. Since water interferes with the methylation, methylolation is carried out in methanol with paraformaldehyde and by simply adjusting the pH to about 4 with continued heating. After alkylation is complete the pH is adjusted to 8–10, and excess methanol is distilled under reduced pressure. The resulting syrup contains about 80% solids.

Miscellaneous Resins. Much less important than the melamine–formaldehyde and urea–formaldehyde resins are the methylol carbamates. They are urea derivatives since they are made from urea and an alcohol.

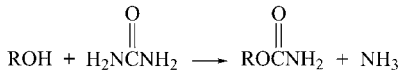

(R can vary from methyl to a monoalkyl ether of ethylene glycol). Temperatures in excess of 140°C are required to complete the reaction and pressurized equipment is used for alcohols boiling below this temperature; provision must be made for venting ammonia without loss of alcohol. The reaction is straightforward and, in the case of the monomethyl ether of ethylene glycol [109-86-4], can be carried out at atmospheric pressure using stoichiometric quantities of urea and alcohol (45). Methylolation with aqueous formaldehyde is carried out at 70–90°C under alkaline conditions. The excess formaldehyde needed for complete dimethylolation remains in the resin and prevents more extensive usage because of formaldehyde odor problems in the mill.

Other amino resins used in the textile industry for rather specific properties have included the methylol derivatives of acrylamide (46), hydantoin [461-79-3] (47), and dicyandiamide (48).

Textiles are finished with amino resins in four steps. The fabric is (*1*) passed through a solution containing the chemicals, (*2*) through squeeze rolls (padding) to remove excess solution, (*3*) dried, and (*4*) heated (cured) to bond the chemicals with the cellulose or to polymerize them on the fabric surface.

The solution (pad bath) contains one or more of the amino resins described above, a catalyst, and other additives such as a softener, a stiffening agent, or a water repellant. The catalyst may be an ammonium or metal salt, eg, magnesium chloride or zinc nitrate. Synthetic fabrics, such as nylon or polyester, are treated with amino resins to obtain a stiff finish. Cotton or rayon fabrics or blends with synthetic fibers are treated with amino resins to obtain shrinkage control and a durable-press finish.

Normally, fabrics are treated in the sequence outlined above. The temperature of the drying unit is 100–110°C and the temperature of the curing unit can vary between 120 and 200°C but usually ranges from 150 to 180°C. The higher temperatures are employed to polymerize the resins on synthetic fabrics and at the same time to heat-set the fibers. Temperatures up to 180°C are used to allow the amino resins to react with cellulosic fibers alone or blended with synthetic fibers. The fabric is held flat but with minimum tension during drying and curing, and always tends to become flat when creased or wrinkled during use or laundering. The resin-treated cellulose absorbs less water and swells less than untreated cellulose. This reduced swelling along with little or no tension induced during drying minimizes shrinkage during laundering.

The steps followed in the precure are repeated in the postcure process, except that after the drying step the goods are shipped to a garment manufacturer who makes garments, presses them into the desired shape with creases or pleats, and then cures the amino resin on the completed garment. It is important that the amino resins used in the postcure process should (*1*) not react with the fabric before it has been fashioned into a garment, and (*2*) release a minimum amount of formaldehyde into the atmosphere, especially while the goods are in storage or during the cutting and sewing operations. These requirements are met, at present, with the diethylene glycol-modified DMDHEU resin.

Tire Cord. Melamine resins are also used to improve the adhesion of rubber to reinforcing cord in tires. Textile cord is normally coated with a latex dip solution composed of a vinylpyridine–styrene–butadiene latex rubber containing resorcinol–formaldehyde resin. The dip coat is cured prior to use. The dip coat improves the adhesion of the textile cord to rubber. Further improvement in adhesion is provided by adding resorcinol and hexa(methoxymethyl)melamine [3089-11-0] (HMMM) to the rubber compound which is in contact with the textile cord. The HMMM resin and resorcinol cross-link during rubber vulcanization and cure to form an interpenetrating polymer within the rubber matrix, which strengthens or reinforces the rubber and increases adhesion to the textile cord. Brass-coated steel cord is also widely used in tires for reinforcement. Steel belts and bead wire are common applications. Again, HMMM resins and resorcinol [108-46-3] are used in the rubber compound which is in contact with the steel cord so as to reinforce

the rubber and increase the adhesion of the rubber to the steel cord. This use of melamine resins is described in the patent literature (49).

Amino Resins in the Paper Industry

Paper is a material of tremendous versatility and utility, prepared from a renewable resource. It may be made soft or stiff, dense or porous, absorbent or water repellent, textured or smooth. Some of the versatility originates with the fibers, which may vary from short and supple to long and stiff, but the contribution of chemicals should not be underestimated.

Amino resins are used by the paper industry in large volume for a variety of applications. The resins are divided into two classes according to the mode of application. Resins added to the fiber slurry before the sheet is formed are called wet-end additives and are used to improve wet and dry strength and stiffness. Resins applied to the surface of formed paper or board, almost invariably together with other additives, are used to improve the water resistance of coatings, the sag resistance in ceiling tiles, and the scuff resistance in cartons and labels.

The requirements for the two types of resins are very different. Wet-end additives are used in dilute fiber slurries in small amounts. After the sheet is formed, most of the water is drained away and some of the remaining water is pressed out of the sheet before it is dried. The amino resin must be retained (absorbed) on the surface of the cellulose fibers so that it will not be washed away. On a typical paper machine, fiber concentration in the headbox would be about 1%. If the amount of wet-strength resin used is 1% of the weight of the fiber, the concentration of resin in the headbox would be only 0.01%. If no mechanism for attaching the resin to the fiber is provided, only a trace of the resin added to the slurry would be retained in the finished sheet. Good retention is achieved with the amino resin by making the resin cationic. Since the cellulose surface is anionic because of the carboxylic acid groups present, the cationic charge on the resin makes it substantive with the fiber leading to good retention of the resin when applied in the wet-end. Resins for application to the surface of preformed paper are not required to be substantive to cellulose and they may be formulated for adhesion, cure rate, viscosity, compatibility with other materials, etc, without concern for retention.

The integrity of a paper sheet is dependent on the hydrogen bonds which form between the fine structures of cellulose fibers during the pressing and drying operations (see CELLULOSE). The bonds between hydroxyls of neighboring fibers are very strong when the paper is dry, but are severely weakened as soon as the paper becomes wet. Bonding between the hydroxyls of cellulose and water is as energetic as bonding between two cellulose hydroxyls. As a consequence, ordinary paper loses most of its strength when it is wet or exposed to very high humidity. The sheet loses its stiffness and bursting, tensile and tearing strength.

Many materials have been used over the years in an effort to correct this weakness in paper. If water can be prevented from reaching the sites of the bonding by sizing or coating the sheet, then a measure of wet strength may be attained.

Water molecules are so small and cellulose and so hydrophilic that this solution usually affords only temporary protection. Formaldehyde, glyoxal, polyethylenimine, and, more recently, derivatized starch (50) and derivatized cationic polyacrylamide resins (51) have been used to provide temporary wet strength. The first two materials must be applied to the formed paper, but the other materials are substantive to the fiber and may be used as wet-end additives. Carboxymethylcellulose–calcium chloride and locust-bean gum–borax are examples of two-component systems applied separately to paper that were used to a limited extent before the advent of the amino resins. Today three major types of wet-strength resins are used in papermaking: polyamide–polyamine resins cross-linked with epichlorohydrin (52) are used in neutral to alkaline papers; cationic polyacrylamide resins cross-linked with glyoxal are used for acid to neutral papers; and melamine–formaldehyde resins are used for acid papers.

During the 30-year period following the introduction of synthetic wet-strength additives to papermaking in 1942, most paper was made at acid pH. Low molecular weight (or even monomeric) trimethylolmelamine [1017-56-7], when dissolved in the proper amount of dilute acid and aged, polymerizes to a colloidal polymer that is retained well by almost all types of papermaking fiber, and produces high wet strength under the mild curing conditions easily attained on a paper machine (53,54). This resin, introduced by American Cyanamid in 1942, is still extensively used when rapid cure, high wet strength, and good dry strength are important in acid paper. Some processing improvements have been made, including a report (55) describing the formation of a stable melamine resin acid colloid using formic and phosphoric acids. The chemistry of this reaction is quite interesting.

Melamine–formaldehyde acts as an amine when dissolved in dilute acid, usually HCl. During polymerization, between 20 and 80 monomeric units combine to form a polymer of colloidal dimensions (6–30 nm) with the elimination of water and HCl (56,57). The development of cationicity is associated with the loss of HCl, since a unit of charge on the polymer is generated for every mole of acid lost, and the pH decreases steadily during the polymerization. In a typical formulation at 12% solids at room temperature, polymerization is complete in about 3 h. The initially colorless solution develops a light blue haze and shows a strong Tyndall effect.

Such a colloidal sol is highly substantive to all papermaking fibers, kraft, sulfite, groundwood, and soda. For its successful use in paper mills, the pH must be kept low, both to prevent precipitation of the resin in an unusable form and to promote curing of the resin; and the concentration of sulfates in the white water on the paper machine must not be allowed to exceed 100 ppm, again because the resin is precipitated in an inactive form by high concentrations of sulfates. High sulfate concentrations may build up in mills using large amounts of alum for setting size or sulfuric acid for controlling pH.

The problem of sulfate sensitivity was solved by adding formaldehyde to the aged colloid, which improved wet-strength efficiency and reduced sensitivity to sulfates (58). Later, equivalent results were obtained by adding the extra formaldehyde before the colloid was aged. The additional formaldehyde acts like an acid during the aging process and, unless compensated for by a reduction in the amount of acid charged, lowers the pH to a point where polymerization to the

Table 3. Formulations for Regular and HE Colloid Resins

	Regular MF_3	HE MF_8
Water, 20 ± 10°C, kg	412.0	330.8
HCl, 20° Bé, kg (1.16 g/mL), kg	17.7	14.1
Formaldehyde, 37%, kg		84.8
Trimethylolmelamine, kg	45.4	45.4
Total	*475.1*	*475.1*

colloids is inhibited. The high efficiency (HE) resins have been used in mills with sulfate concentrations so high that use of regular trimethylolmelamine (MF_3) colloids would be uneconomical. Sulfate tolerance is a function of the amount of extra formaldehyde present. For best cost-performance, a family of HE colloids is necessary with composition varying from MF_4, for moderate sulfate concentrations, to MF_9, for very high sulfates.

Formulations for regular and HE colloids are shown in Table 3 (59). The materials are added, in the order listed, to a 454-L (120-gal) tank provided with good agitation and ventilation. Formaldehyde fumes are evolved even from the regular colloid. The colloids develop only after aging and freshly prepared solutions are ineffective for producing wet strength. Stability of the colloids depends on temperature and concentration. Colloids at 10–12% are stable at room temperature for at least 1 week; stability may be extended by dilution after the colloids have aged properly.

Both regular and HE colloids increase the wet strength of paper primarily by increasing adhesion between fibers; the strength of the individual fiber itself is unaffected (60). The resin appears to improve the adhesion between the fibers, whether they are wet or dry, by forming bonds that are unaffected by water. The excess formaldehyde in the HE colloid appears to function by increasing the amount of formaldehyde bound in the colloid (59). The regular colloid, starting with about 3 mol of formaldehyde/1 mol of melamine, has about 2 mol bound in the colloid and 1 mol free. By mass action, the additional formaldehyde increases the amount of bound formaldehyde in the colloid. When an HE colloid is dialyzed or stored at very low concentrations (0.05%), it loses the extra bound formaldehyde and behaves as a regular colloid.

The first urea–formaldehyde resins used to any extent as wet-strength agents were anionic polymers made by the reaction of a urea resin with sodium bisulfite ($NaHSO_3$) (61). Attempts to use nonionic urea–formaldehyde polymers were unsuccessful; the neutral charge on the polymer made it unsubstantive to fiber resulting in lack of retention. The sulfomethyl group introduced by reaction with $NaHSO_3$ gave the polymers strong anionicity, but substantivity was largely restricted to unbleached kraft pulp. Lignin residues probably provided sites for absorption of the polymer. The use of alum as a mordant was essential, since both the resin and the fiber were anionic. The reaction of bisulfite with the urea–formaldehyde polymer may be represented as

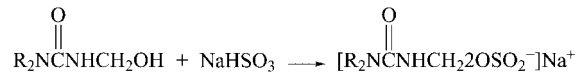

In 1945, cationic urea resins were introduced and quickly supplanted the anionic resins, since they could be used with any type of pulp (62). Although they have now become commodities, their use in the industry has been steadily declining as the shift toward neutral and alkaline papermaking continues. They are commonly made by the reaction of urea and formaldehyde with one or more polyethylene–polyamines. The structure of these resins is very complicated and has not been determined. Ammonia is evolved during the reaction, probably according to the following:

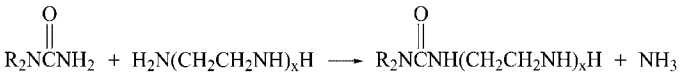

Formaldehyde may react with the active hydrogens on both the urea and amine groups and therefore the polymer is probably highly branched. The amount of formaldehyde (2–4 mol/1 mol urea), the amount and type of polyamine (10–15%), and resin concentration are variable and hundreds of patents have been issued throughout the world. Generally, the urea, formaldehyde, polyamine, and water react at 80–100°C. The reaction may be carried out in two steps, with an initial methylolation at alkaline pH, followed by condensation to the desired degree at acidic pH, or the entire reaction may be carried out under acidic conditions (63). The product is generally a syrup with 25–35% solids and is stable for up to 3 months.

The cationic urea resins are added to paper pulp preferably after all major refining operations have taken place. The pH on the paper machine must be acidic for reasonable rates of cure of the resin. Urea resins do not cure as rapidly as melamine–formaldehyde resins and the wet strength produced is not as resistant to hydrolysis. Furthermore, the resins are not retained as well as the melamine resins. On a resin-retained basis, however, their efficiency is as good. The lower retention of the urea–formaldehyde resins is due to their polydisperse molecular weight distribution. High molecular weight species are strongly absorbed on the fibers and are large enough to bridge two fibers. Low molecular weight species are not retained as well because of fewer charge sites. Attempts to improve the performance of urea–formaldehyde resins by fractionating the syrups by salt or solvent precipitation, or selective freezing or dialysis have been technically successful but economically impractical. The process for production of resins is sufficiently simple so that some paper mills have set up their own production units. With captive production, resins with higher molecular weights and lower stability may be tolerated.

The recovery of fiber from *broke* (off-specification paper or trim produced in the paper mill) is complicated by high levels of urea–formaldehyde and melamine–formaldehyde wet-strength resin. The urea resins present a lesser problem than the melamine resins because they cure slower and are not as resistant to hydrolysis. Broke from either resin treatment may be reclaimed by hot acidic repulping. Even the melamine resin is hydrolyzed rapidly under acidic conditions at high temperature. The cellulose is far more resistant and is not harmed if the acid is neutralized as soon as repulping is complete.

The TAPPI monograph (64) is an excellent source of additional information on technical and economic aspects of wet strength. An informative overview of the chemistry and mechanisms involved in wet strength chemistry can be found in Reference 65.

Wet-strength applications account for the majority of amino resin sales to the paper industry but substantial volumes are sold for coating applications. The largest use is to improve the resistance of starch–clay coatings to dampness. In offset printing, which is becoming ever more important in the graphic arts, the printing paper is exposed to both ink and water. If the coating lifts from the paper and transfers to the plate, it causes smears and forces a shutdown for cleaning. A wide variety of materials have been added to the coatings to improve wet-rub resistance, including casein, soya protein, poly(vinyl acetate), styrene–butadiene latices, glyoxal–urea resins, and amino resins. Paper coatings are applied at as high a solids content as possible to ease the problem of drying. Retention is not a problem since the resin is applied to a preformed sheet. The important characteristics for coating resins are high solids at low viscosity, high cure rates, and high wet-rub efficiency. Urea and melamine resins or mixtures are sold as high solids syrups or dry powders. They are used with starch-pigment coatings with acidic catalysts or with starch-pigment–casein (or protein) coatings usually without catalysts. The syrups are frequently methylated for solubility and stability at high solids. All of the resins are of intrinsically low molecular weight to reduce viscosity for ease of handling (see COATINGS).

Closely allied to resins for treating paper are the resins used to treat regenerated cellulose film (cellophane) which does not have good water resistance unless it is coated with nitrocellulose or poly(vinylidene chloride). Adhesion of the waterproofing coating to the cellophane film is achieved by first treating the cellophane with an amino resin. The cellophane film is passed through a dip tank containing about 1% of a melamine–formaldehyde acid colloid type of resin. Some glycerol may also be present in the resin solution to act as a plasticizer. Resins for this purpose are referred to as *anchoring agents*.

Other Uses

Water-soluble melamine–formaldehyde resins are used in the tanning of leather in combination with the usual tanning agents. By first treating the hides with a melamine–formaldehyde resin, the leather is made more receptive to other tanning agents and the finished product has a lighter color. The amino resin is often referred to as a *plumping agent* because it makes the finished leather firmer and fuller.

Urea–formaldehyde resins are also used in the manufacture of foams. The resin solution containing an acid catalyst and a surface-active agent is foamed with air and cured. The open-cell type of foam absorbs water readily and is soft enough so that the stems of flowers can be easily processed into it. These features make the urea resin foam ideal for supporting floral displays. Urea–formaldehyde resin may also be foamed in place. A special nozzle brings the resin, catalyst, and foaming agent together. Air pressure is used to deposit the foam where it is desired,

eg, within the outside walls of older houses to provide insulation. This application might be expected to grow as energy costs increase, if undesirable odors can be controlled.

Urea–formaldehyde resins are also used as the binder for the sand cores used in the molds for casting hollow metal shapes. The amino resin is mixed with moist sand and formed into the desired shape of the core. After drying and curing, the core is assembled into the mold and the molten metal poured in. Although the cured amino resin is strong enough to hold the core together while the hot metal is solidifying, it decomposes on longer heating. Later, the loose sand may be poured out of the hollow casting and recovered.

Regulatory Concerns

Both urea– and melamine–formaldehyde resins are of low toxicity. In the uncured state, the amino resin contains some free formaldehyde that could be objectionable. However, uncured resins have a very unpleasant taste that would discourage ingestion of more than trace amounts. The molded plastic or the cured resin on textiles or paper may be considered nontoxic. Combustion or thermal decomposition of the cured resins can evolve toxic gases, such as formaldehyde, hydrogen cyanide, and oxides of nitrogen.

Melamine–formaldehyde resins may be used in paper which contacts aqueous and fatty foods according to 21 CFR 121.181.30. However, because a lower PEL has been established by OSHA, some mills are looking for alternatives. Approaches toward achieving lower formaldehyde levels in the resins have been reported (66,67); the efficacy of these systems needs to be established. Although alternative resins are available, significant changes in the papermaking operation would be required in order for them to be used effectively.

Economic Aspects

Japan produces more amino resin than any other country; the United States is next, with the Commonwealth of Independent States, (CIS) France, the United Kingdom, and Germany following.

Many large chemical companies produce amino resins and the raw materials needed, ie, formaldehyde, urea, and melamine. Some companies may buy raw materials to produce amino resins for use in their own products, such as plywood, chipboard, paper, textiles, or paints, and may also find it profitable to market these resins to smaller companies. The technology is highly developed and sales must be supported by adequate technical service to select the correct resin and see that it is applied under the best conditions.

During the past 10 years (the 1990s) there has been considerable changes in the suppliers of amino resins as a result of acquisitions, spin-offs, and withdrawal of some of the smaller companies from the business. The following is a representative list of those currently in the business: Badische Aniline and Soda-Fabrik (BASF), Ludwigshafen, Germany; Berger International Chemicals, Newcastle upon Tyne, England; Borden Chemical Division, Columbus, Ohio; Casella

Farbwerk Mainkur AG, Frankfurt-Fechenheim, Germany; Cuyahoga Plastics, Cleveland, Ohio; Cytec Industries, West Patterson, N.J.; DSM Coating Resins, Zwolle, Holland; Dainippon Ink, Ltd., Tokyo, Japan; Dynamic-Nobel, AG, Troisdorf-Koln, Germany; Fiberite Corp., Winona, Minn.; Georgia-Pacific Corp., Atlanta Ga.; Gulf Adhesives, Lansdale, Pa.; Hitachi Chemical Co., Ltd., Tokyo, Japan; Matsushita Electric Works, Ltd., Osaka, Japan; McWhorter Technologies, Carpentersville, Ill. (Division of Eastmen Chemical Co., Kingspot, Tenn.); Melamine Chemicals, Donaldson, La. (Division of Borden Chemical, Columbus, OH); Mitsui-Toatsu Chemicals Ltd., Tokyo, Japan; Mitsui-Cytec, Ltd., Tokyo, Japan; Montedison SpA, Milan, Italy; Pacific Resins, Tacoma, Wash.; Perstorp AB, Perstorp, Sweden; Perstorp Compounds, Inc., Florence, Mass.; Reichhold Chemicals, White Plains, N.Y. (Division of Dainippon Ink, Tokyo, Japan); Solutia, Inc., St. Louis, Mo.; Sumitomo Ltd., Tokyo, Japan; Vianova Resins GmbH & Co., Wiesbaden, Germany (Division of Solutia, St. Louis, Mo.).

BIBLIOGRAPHY

"Amino Resins" in *EPST* 1st ed., Vol. 2, pp. 1–94, by G. Widmer, Ciba, AG; in *EPSE* 2nd ed., Vol. 1, pp. 752–789 by I. H. Updegraff, American Cyanamid Co.

1. R. Bainbridge, *Sail* **8**(1), 142 (1977).
2. A. Einhorn and A. Hamburger, *Ber. Dtsch. Chem. Ges.* **41**, 24 (1908).
3. Brit. Pats. 248,477 (Dec. 5, 1924), 258,950 (July 1, 1925), and 266,028 (Nov. 5, 1925), E. C. Rossiter (all to British Cyanides Co., Ltd.).
4. Brit. Pats. 187,605 (Oct. 17, 1922), 202,651 (Aug. 17, 1923), 208,761 (Sept. 20, 1922), H. Goldschmidt and O. Neuss.
5. Brit. Pats. 171,096 (Nov. 1, 1921), 181,014 (May 20, 1922), 193,420 (Feb. 17, 1923), 201,906 (July 23, 1923), 206,512 (July 23, 1923), 213,567 (Mar. 31, 1923), 238,904 (Aug. 25, 1924), 270,840 (Oct. 1, 1924), 248,729 (Mar. 3, 1925), F. Pollak.
6. U.S. Pat. 1,460,606 (July 3, 1923), K. Ripper.
7. Ger. Pat. 647,303 (July 6, 1937), Brit. Pat. 455,008 (Oct. 12, 1936), W. Hentrich and R. Köhler (both to Henkel and Co., GmbH).
8. R. Rager, *Mod. Plast.* **49**(4), 67 (1972).
9. E. Drechsel, *J. Prakt. Chem. [2]* **13**, 330 (1876).
10. U.S. Pat. 2,727,037 (Dec. 13, 1955), C. A. Hochwalt (to Monsanto Chemical Co.).
11. Ger. Pat. 1,812,120 (June 11, 1970), D. Fromm and co-workers (to Badische Anilin und Soda-Fabrik AG).
12. P. Ellwood, *Chem. Eng.* **77**(23), 101 (1970).
13. J. F. Walker, Formaldehyde, American Chemical Society Monograph, No. 159, 3rd ed., Reinhold Publishing Corp., New York, 1964.
14. U.F. Concentrate-85, Technical Bulletin, Allied Chemical Corp., New York, 1985.
15. U.S. Pat. 3,129,226 (Apr. 14, 1964), G. K. Cleek and A. Sadle (to Allied Chemical Corp.).
16. U.S. Pat. 3,458,464 (July 29, 1969), D. S. Shriver and E. J. Bara (to Allied Chemical Corp.).
17. Ref. 13, p. 151.
18. *N*-(iso-butoxymethyl) acrylamide, Technical Bulletin PRC 126, American Cyanamid Co., Wayne, N.J., Feb. 1976.
19. M. Gordon, A. Halliwell, and T. Wilson, *J. Appl. Polym. Sci.* **10**, 1153 (1966).
20. J. W. Aldersley and co-workers *Polymer* **9**, 345 (1968).

21. I. H. Anderson, M. Cawley, and W. Steedman, *Br. Polym. J.* **1**, 24 (1969).
22. K. Sato, *Bull. Chem. Soc. Jpn.* **40**, 724 (1967). (in English).
23. K. Sato and T. Naito, *Polym. J.* **5**, 144 (1973).
24. K. Sato and Y. Abe, *J. Polym. Sci., Polym. Chem. Ed.* **13**, 263 (1975).
25. V. A. Shenai and J. M. Manjeshwar, *J. Appl. Polym. Sci.* **18**, 1407 (1974).
26. A. Berge, S. Gudmundsen, and J. Ugelstad, *Eur. Polym. J.* **5**, 171 (1969).
27. A. Berge, B. Kvaeven, and J. Ugelstad, *Eur. Polym. J.* **6**, 981 (1970).
28. J. I. DeJong and J. DeJonge, *Recl. Trav. Chim.* **71**, 643, 661, 890 (1952); *Recl. Trav. Chim.* **72**, 88, 139, 202, 207, 213, 1027 (1953).
29. R. Steele, *J. Appl. Polym. Sci.* **4**, 45 (1960).
30. G. A. Crowe and C. C. Lynch, *J. Am. Chem. Soc.* **70**, 3795 (1948); *J. Am. Chem. Soc.* **71**, 3731 (1949); *J. Am. Chem. Soc.* **72**, 3622 (1950).
31. Brit. Pat. 829,953 (Mar. 9, 1960), E. Elbel.
32. U.S. Pats. 3,007,885 (Nov. 7, 1961), 3,114,930 (Dec. 24, 1963), W. N. Oldham, N. A. Granito, and B. Kerfoot (to both American Cyanamid Co.).
33. U.S. Pat. 3,661,819 (May 9, 1972), J. N. Koral and M. Petschel Jr., (to American Cyanamid Co.).
34. U.S. Pat. 3,803,095 (Apr. 9, 1974), L. J. Calbo and J. N. Koral (to American Cyanamid Co.).
35. W. Lindlaw, The Preparation of Butylated Urea—Formaldehyde and Butylated Melamine Formaldehyde Resins Using Celanese Formcel and Celanese Paraformaldehyde, Technical Bulletin, Celanese Chemical Co., New York, Table XIIA.
36. Technical Bulletin S-23-8, 1967, Supplement to Technical Bulletin S-23-8, Celanese Chemical Co., New York, 1968, Example VIII.
37. W. J. Blank and W. L. Hensley, *J. Paint Technol.* **46**, 46 (1974).
38. U.S. Pat. 2,517,750 (Aug. 8, 1950), A. L. Wilson (to Union Carbide and Carbon Corp.).
39. U.S. Pat. 2,304,624 (Dec. 8, 1942), W. J. Burke (to E. I. du Pont de Nemours & Co., Inc.).
40. U.S. Pat. 3,324,062 (June 6, 1967), G. S. Y. Poon (to Dan River Mills, Inc.).
41. H. Kadowaki *Bull. Chem. Soc. Jpn.* **11**, 248 (1936).
42. U.S. Pat. 3,089,859 (May 14, 1963), T. Oshima (to Sumitomo Chemical Co., Ltd.).
43. U.S. Pats. 2,731,472 (Jan. 17, 1956), 2,764,573 (Sept. 25, 1956), B. V. Reibnitz and co-workers (both to Badische Anilin-und Soda-Fabrik); U.S. Pat. 2,876,062 (Mar. 3, 1959), E. Torke (to Phrix-Werke AG).
44. U.S. Pat. 3,487,088 (Dec. 30, 1969), K. H. Remley (to American Cyanamid Co.).
45. U.S. Pat. 3,524,876 (Aug. 18, 1970), J. E. Gregson (to Dan River Mills, Inc.).
46. U.S. Pat. 3,658,458 (Apr. 25, 1972), D. J. Gale (to Deering Milliken Research Corp.).
47. U.S. Pats. 2,602,017 and 2,602,018; (July 1, 1952), L. Beer.
48. C. Hasegawa, *J. Soc. Chem. Ind. Jpn.* **45**, 416 (1942).
49. U.S. Pat. 3,212,955 (Oct. 19, 1965), S. Kaizerman (to American Cyanamid Co.).
50. U.S. Pat. 4,741,804 (May 3, 1988), D. B. Solarek and co-workers (to National Starch and Chemical Corp.).
51. U.S. Pat. 4,605,702 (Aug. 12, 1986), G. J. Guerro, R. J. Proverb, and R. F. Tarvin (to American Cyanamid Co.).
52. U.S. Pats. 2,926,116 and 2,926,154; (Feb. 23, 1960), G. L. Keim, (both to Hercules Powder Co.).
53. U.S. Pat. 2,345,543 (Mar. 28, 1944), H. P. Wohnsiedler and W. M. Thomas (to American Cyanamid Co.).
54. C. G. Landes and C. S. Maxwell, *Pap. Trade J.* **121**(6), 37 (1945).
55. Ger. Pat. 2,332,046 (Jan. 23, 1975), W. Guender and G. Reuss (to Badische Anilin-und Soda-Fabrik AG).
56. J. K. Dixon, G. L. M. Christopher, and D. J. Salley, *Pap. Trade J.* **127**(20), 49 (1948).
57. *Unpublished data*, American Cyanamid Co.

58. U.S. Pat. 2,559,220 (July 3, 1951), C. S. Maxwell and C. G. Landes (to American Cyanamid Co.).
59. C. S. Maxwell and R. R. House, *TAPPI* **44**, 370 (1961).
60. D. J. Salley and A. F. Blockman, *Pap. Trade J.* **121**(6), 41 (1945).
61. U.S. Pat. 2,407,599 (Sept. 10, 1946), R. W. Auten and J. L. Rainey (to Resinous Products and Chemical Co.).
62. U.S. Pat. 2,742,450 (Apr. 17, 1956), R. S. Yost and R. W. Auten (to Rohm and Haas Co.).
63. U.S. Pat. 2,683,134 (July 6, 1954), J. B. Davidson and E. J. Romatowski (to Allied Chemical and Dye Corp.).
64. J. P. Weidner, ed., *Wet Strength in Paper and Paper Board*, Monograph Series, No. 29, Technical Association of Pulp and Paper Industry, New York, 1965.
65. K. W. Britt, in J. P. Casey, ed., *Pulp and Paper*, Vol. **III**, John Wiley & Sons, Inc., New York, 1981, Chapt. 18.
66. W. Kamutzki, *Ind. Carta* **26**, 297 (1988).
67. W. Kamutzki, *Kunstharz-Nachr.* **24**, 9 (1987).

LAURENCE L. WILLIAMS
Cytec Industries

AMORPHOUS POLYMERS. See Volume 5.

ANTIFOAMING AGENTS

Introduction

The control or elimination of the foam that occurs in many industrial processes is a vital factor in their efficient operation. Additives for this purpose are the largest single category of process aids used in the chemical industry (1). They are used in low concentration to achieve this effect and are known variously as defoamers, antifoaming agents, foam inhibitors, foam suppressants, air release agents, and foam control agents. Defoaming implies breaking a preexisting foam, whereas antifoaming or foam inhibition indicates prevention of the formation of that foam. Such distinctions call for different product features. A defoamer is expected to exhibit rapid knockdown of a foam, whereas longevity of action might be the key requirement in many antifoam applications. Despite these varying performance features, many applications require both preventive and control functions, and in practice the same types of materials are used for both antifoaming and defoaming. For this reason, the general term *defoamers*, as used in this article, is meant to encompass all product types and degrees of action encountered with such process aids. The topic is sometimes known as chemical or physicochemical foam control as opposed to thermal and mechanical foam control approaches, such as centrifuging or spraying of the foam or the use of ultrasound, which are not covered here.

Many industries rely on the efficient and economical use of defoamers both as a process aid in product manufacture and to increase the quality of the finished product in its subsequent application. The most obvious use of defoamers

Encyclopedia of Polymer Science and Technology. Copyright John Wiley & Sons, Inc. All rights reserved.

as process aids is to increase holding capacity of vessels and improve efficiency of distillation or evaporation equipment. They are also used to improve filtration, dewatering, washing, and drainage of suspensions, mixtures, or slurries. Examples of industrial operations that benefit in these ways from the use of defoamers include oil well pumping; gas scrubbing at petrochemical plants; polymer and chemical synthesis and processing, particularly in monomer stripping; textile dyeing and finishing; leather processing; paint and adhesive manufacture; phosphoric acid production; control of wastewater and sewage; food preparation, notably the refining of sugar; the brewing of beer; and penicillin production by fermentation. Among the finished products that are improved in quality or efficacy by the proper inclusion of defoamers are lubricants, particularly cooling lubricants in metal working; diesel fuel, hydraulic and heat-transfer fluids; paints and other coatings; adhesives; inks; detergents; and antiflatulence tablets.

The use of vegetable and mineral oils as defoamers has been known for a long time. However, most modern defoamers are complex, formulated specialty chemicals, whose composition is often proprietary. Numerous reviews of the field have appeared since the previous edition of this article, notably the comprehensive book on the subject by Garrett (2). Other useful reviews include some on foam control principles (3–5), coatings applications (6), and silicones (7,8). Companies involved in the production of defoamers range from large, basic polymer producers to small regional formulators. In addition to control of foam and associated features such as rate of foam knockdown and the persistence of the effects, other frequently needed application requirements of these specialty materials include adequate shelf life, absence of adverse effects on and by the products being treated, ease of handling, lack of toxicity to manufacturing personnel and users, environmental acceptability, and cost-effectiveness. Defoamers range from relatively inexpensive mineral oils to costly fluorinated polymers. However, it is not the cost per kilogram of defoamer that matters, but rather the cost per unit produced using this processing aid that does. Another factor that strongly influences the choice of a specific defoamer is its ancillary surface properties such as wetting, dispersion, and leveling.

Defoamer Components

Modern defoamers contain numerous ingredients to meet the diverse product requirements for which they are formulated, including a variety of active ingredients in both the solid and liquid states and numerous ancillary agents such as emulsifiers, spreading agents, thickeners, preservatives, carrier oils, compatibilizers, solvents, and water. Not all defoamers contain all classes of components; some complex formulations contain several different materials in a particular category.

Active Ingredients. These are the components of the formulation that do the actual foam control work. Traditionally, defoamers were single-component liquids or homogeneous solutions of vegetable or mineral oils, but nowadays hydrophobic solids are the most effective active ingredients.

Liquid-Phase Components. The four most common liquid-phase components found in defoamers are hydrocarbons, polyethers, silicones, and fluorocarbons.

Many hydrocarbon fluids such as kerosene and other paraffinic and naphthenic mineral oils and vegetable oils such as linseed oil [8001-26-1], corn oil, soybean oil [8001-22-7], peanut oil, tall oil [8000-26-4], and castor oil [8001-79-4] are used as defoamers. Liquid fatty alcohols, acids and esters from other sources, and poly(alkylene oxide) derivatives of oils such as ethoxylated rosin oil [68140-17-0] are also used. Organic phosphates are valuable defoamers and have particular utility in latex paint applications. Another important class of hydrocarbon-based defoamer is the acetylenic glycols (9), such as 2,4,7,9-tetramethyl-5-decyne-4, 7-diol which are widely used in water-based coatings, agricultural chemicals, and other areas where excellent wetting is needed.

Among other organic polymers that have been proposed as foam control agents are polyisobutylene [9003-27-4], poly(alkyl acrylates), polyalkylene polyamines, and polyalkyleneimines. Poly(alkylene oxide) homopolymers and copolymers are frequently encountered in liquid-phase antifoam components. For example, copolymers [106392-12-5] of poly(ethylene oxide) and poly(propylene oxide) are used to reduce foam in the acid–gas scrubbing process (10). High molecular weight adducts of propylene oxide and polyhydric alcohols such as glycerol [56-81-5] and pentaerythritol [115-77-5] have also been reported to have useful antifoaming properties (11). Sometimes the polyether is mixed with other liquids, eg, poly(propylene oxide) [25322-69-4] and polydimethylsiloxane (PDMS) [9016-00-6]; sometimes the two materials are copolymerized.

Silicone oils are particularly effective antifoaming agents in nonaqueous systems because of their low surface tension and incompatibility. Polydimethylsiloxane (PDMS) is the most important silicone and is widely used in products for the petroleum industry, where its good thermal stability is very advantageous (12). Other useful silicone defoamers are polytrifluoropropylmethylsiloxanes [25791-89-3] and other fluorosilicones, which are very effective in nonaqueous foaming systems such as organic solvents and crude hydrocarbon stocks. Fluorocarbons are the most expensive class of antifoam fluid. Fluorocarbon oils and fluorine-containing amides such as the *N*-(alkylamino-trimethylene)perfluorooctanamides are used as antifoaming additives to lubricants and jet fuels (13).

Solid-Phase Components. Dispersed solids are vital ingredients in commercial antifoam formulations. Much of the current theory on antifoaming mechanism ascribes the active defoaming action to this dispersed solid phase with the liquid phase primarily a carrier fluid, active only in the sense that it must be surface-active in order to carry the solid particles into the foam films and cause destabilization. For example, PDMS, despite its considerable effectiveness in nonaqueous systems, shows little foam-inhibiting activity in aqueous surfactant solutions. It is only when compounded with hydrophobic silica [7631-86-9] to give the so-called silicone antifoam compounds that highly effective aqueous defoamers result. The three main solid-phase component classes are hydrocarbons, silicones, and fluorocarbons.

A variety of waxy hydrophobic hydrocarbon-based solid phases are used including fatty acid amides and sulfonamides, hydrocarbon waxes such as montan wax [8002-53-7], and solid fatty acids and esters. The amides are particularly important commercially. One example is the use of ethylenediamine distearamide [110-30-5] as a component of latex paint and paper pulp black liquor defoamer (14). Hydrocarbon-based polymers are also used as the solid components of

antifoaming compositions; examples include polyethylene [9002-88-4], poly(vinyl chloride) [9002-86-2], and polymeric ion-exchange resins.

In most cases, these active defoaming components are insoluble in the defoamer formulation as well as in the foaming media, but there are cases which function by the cloud-point mechanism (15). These products are soluble at low temperature and precipitate when the temperature is raised. When precipitated, these defoamer-surfactants function as defoamers; when dissolved, they may act as foam stabilizers. Examples of this type are the block polymers of poly(ethylene oxide) and poly(propylene oxide) and other low HLB (hydrophilic–lipophilic balance) nonionic surfactants. The use of soluble foam control agents has increased in recent years (7).

Pure silicone solids, such as silicone resins, are used in defoamer formulations, but the key material in this category is surface-treated silica, made hydrophobic by treatment with a silicone polymer or silane monomer. The development of these hydrophobic silicas (16) is widely acknowledged as one of the most significant advances in antifoam technology. They are used with a considerable variety of liquid components including hydrocarbons, polyethers, and silicones. The three most common ways of preparing the hydrophobic silica are to spray the silica with silicone oil and heat at 250–350°C, to treat with organochlorosilane vapors in an autoclave, and to disperse the silica in a silicone oil at elevated temperatures. Hydrophobic silica can also be produced by treatment with alcohols, fatty amines, and hydrocarbon waxes. The application of hydrophobic silica formulations as antifoaming agents has been reviewed with an emphasis on mechanism and use in textile dyeing (17).

Fluorocarbon solids are rare in defoamer compositions, presumably on account of their cost. Solid fluorine-containing fatty alcohols and amides are known. The most familiar fluorocarbon solid is polytetrafluoroethylene [9002-84-0]. It is not very effective in conventional hydrocarbon oil defoamer formulations because the particles aggregate strongly together, but in lower surface tension fluids such as silicone and fluorocarbon oils, the powdered polytetrafluoroethylene particles are much better dispersed and its performance is better (18).

Ancillary Agents.

Surface-Active Materials. The active defoamer components are necessarily surface active materials, but this ancillary category covers the surfactants that are often incorporated in the formulation for other effects such as emulsification or to enhance dispersion. Emulsifiers are essential in the common oil-in-water emulsion systems, but they are also required where mixtures of active liquid components are used. For example, specialized oil-in-oil emulsifiers are needed in defoamers based on silicone/polyether mixtures. oil-in-water emulsifiers are incorporated in some defoamers even when the final product contains no water. This is to promote emulsification (self-emulsifiable) or dispersion into aqueous foaming systems. These additives increase the speed of foam decay by promoting rapid dispersion of the defoamer throughout the foaming media. Examples of emulsifying agents used in defoamer compositions are fatty acid esters and metallic soaps of fatty acids; fatty alcohols and sulfonates, sulfates, and sulfosuccinates; sorbitan esters; ethoxylated products such as ethoxylated octyl or nonylphenols; and silicone-polyether copolymers.

Carriers. The function of a carrier is to provide an easily handleable, readily dispersible system for delivering the active defoamer components to the foaming

system and also to tie the complex defoamer formulation together, ie, coupling agents, compatibilizers, or solubilizers. Sometimes the carrier is used simply as an extender to lower the cost of the final product. Many of the low viscosity organic solvents that are used also exhibit some antifoaming properties in cases where they are both insoluble and of lower surface tension than the medium to which they are applied. Any of the usual paraffinic, naphthenic, aromatic, chlorinated, or oxygenated organic solvents can be used, but aliphatic hydrocarbons are the most common. Water is often used as a carrier fluid. In these cases, the defoamer product is typically an oil-in-water emulsion. With growing concern over unrecovered solvents, this has become a preferred type of defoamer formulation. Such products usually require preservatives to prevent bacterial spoilage in storage.

Sometimes the defoamer is required in a solid form, for example, to be suitable for incorporation into a low-sudsing detergent powder or agricultural chemical composition. Water soluble inorganic sorbent carriers such as sodium sulfate [7757-82-6], sodium carbonate [497-19-8], or sodium tripolyphosphate [7758-29-4] are used, as well as organic polymers such as methylcellulose [9004-67-5]. Sometimes the particles are further encapsulated with a coating that preserves the integrity of the defoamer formulation in storage with the detergents but allows disruption on contact with water in the wash process. When both the antifoam and the solid support are food-grade materials, they can also be used in food processing, brewing, and pharmaceutical applications.

Commercial Sources

The defoamer market is large and very specialized; suppliers differ markedly in orientation and in range of product lines. Some suppliers are large, international polymer producers with a basic manufacturing capability for the specific type of defoamer material they supply, whereas others are small, often regional, formulators who focus on the concerns of particular industries. The diversity of manufacture, supplier, product type, and application makes it impossible to present a comprehensive listing of commercial sources. Some compilations (19) are a useful source of available products. Table 1 shows significant defoamer suppliers (over five listings) in this compilation, together with one or two of their associated trade names.

Defoaming Theory

Foams are thermodynamically unstable. To understand how defoamers operate, the various mechanisms that enable foams to persist must first be examined. There are four main explanations for foam stability: (*1*) surface elasticity; (*2*) viscous drainage retardation effects; (*3*) reduced gas diffusion between bubbles; and (*4*) other thin-film stabilization effects from the interaction of the opposite surfaces of the films.

The stability of a single foam film can be explained by the Gibbs elasticity E, which results from the reduction in equilibrium surface concentration of adsorbed surfactant molecules when the film is extended (20). This produces an increase in equilibrium surface tension that acts as a restoring force. The Gibbs elasticity

Table 1. Commercial Defoamer Examples

Supplier	Trade name
Air Products and Chemicals, Inc.	Surfynol
Akzo Nobel Chemicals, Inc.	Propomeen
Ashland Chemical Co.	Drewplus
BASF Corp.	Mazu, Pluronic
Calgene Chemical, Inc.	Calgene Antifoam
Creanova, Inc.	Serdas
Clariant Corp.	Antimussol, Fluowet
Dow Corning Corp.	Dow Corning Antifoam
GE Co.	AF
Graden Chemical Co., Inc.	Rexfoam
Harcros Chemicals, Inc.	Harcros Antifoam
Henkel Corp.	Foamaster
Huntsman Corp.	Jeffox
ICI Surfactants	Synperonic
Lambent Technologies, Inc.	Lambent
Olin Corp.	Poly-Tergent
OSi Specialties, a Crompton Business	Sag
Patco Defoamers Additives	Patcote
Rhone-Poulenc Corp.	Fleetcol, Foamex
Ross Chemical, Inc.	Foam Blast
Taylor Chemical Co., Inc.	Taylor Antifoam
Trans-Chemco, Inc.	Trans
Troy Corp.	Troykyd Defoamer
Ultra Additives, Inc.	Dee Fo, Foam Ban

is given by equation (1) where σ is surface tension and A is surface area of the film.

$$E = 2A\mathrm{d}\sigma/\mathrm{d}A \tag{1}$$

In a foam where the films are interconnected, the related time-dependent Marangoni effect is more relevant. A similar restoring force to expansion results because of transient decreases in surface concentration (increases in surface tension) caused by the finite rate of surfactant adsorption at the surface. Such nonequilibrium surface tension effects are best described in terms of dilatational moduli. The complex dilatational modulus ε^* of a single surface is defined in the same way as the Gibbs elasticity as in equation (2) (the factor 2 is halved as only one surface is considered).

$$\varepsilon^* = A\mathrm{d}\sigma/\mathrm{d}A \tag{2}$$

In a dilatational experiment, where the surface is periodically expanded and contracted, ε^* is a function of the angular frequency (ω) of the dilatation

Table 2. Dilatational Elasticities and Viscosities of Crude Oil at 1 MHz[a]

Crude oil	Additive[b] identity	Additive viscosity, mm^2/s (= cST)	ε_d, mN/m (=dyn/cm)	η_d, mNs/m^2[c]
North Sea	None		1.34	153
	PDMS	12,500	0.69	90
	PDMS	60,000	0.51	33
	SK3556		0.99	87
Middle East	None		1.63	105
	PDMS	60,000	1.19	53
	FC 740		4.36	377

[a]Ref. 22.
[b]Concentration = 1 ppm.
[c]mNs/m^2 = mPa·s (=cP).

as in equation (3) where ε_d is the dilatational elasticity and η_d the dilatational viscosity.

$$\varepsilon^*(i\omega) = |\varepsilon|\cos\theta + i|\varepsilon|\sin\theta = \varepsilon_d(\omega) + \omega\eta_d(\omega) \tag{3}$$

A stable foam possesses both a high surface dilatational viscosity and elasticity (21). In principle, defoamers should reduce these properties. Ideally a spread duplex film, one thick enough to have two definite surfaces enclosing a bulk phase, should eliminate dilatational effects because the surface tension of an insoluble, one-component layer does not depend on its thickness. This effect has been verified (22). Silicone antifoams reduce both the surface dilatational elasticity and viscosity of crude oils as illustrated in Table 2. The PDMS materials are Dow Corning Ltd. polydimethylsiloxane fluids, SK 3556 is a Th. Goldschmidt Ltd. silicone oil, and FC 740 is a 3M Co. Ltd. fluorocarbon profoaming surfactant.

Both high bulk and surface shear viscosity delay film thinning and stretching deformations that precede bubble bursting. The development of ordered structures in the surface region can also have a stabilizing effect. Liquid crystalline phases in foam films enhance stability (23). In water-surfactant-fatty alcohol systems the alcohol components may serve as a foam stabilizer or a foam breaker, depending on concentration (23). Alcohol/surfactant ratios less than that corresponding to the liquid crystalline phase enhance film stability; higher ratios produced by contact with alcohol droplets disrupt this phase and cause film instability. Liquid-phase defoamer components may dilute or destroy such stabilizing phases or they may simply contribute lower surface shear viscosities than the foam stabilizing surfactant (profoamer). For example, the very low surface shear viscosity of PDMS (24) is often cited as a contributing factor to its effectiveness in defoamer compositions. On the other hand, too rigid a surface will also be prone to rupture. Thus, dilatational moduli that are too high will also result in foam instability, as in the case of diesel fuel antifoaming with a fluorosilicone antifoam agent (25).

Reduced gas diffusion between bubbles delays collapse by retarding bubble-size changes and the resulting mechanical stresses. Consequently, single films persist longer than the corresponding foam, but it seems to be a minor factor in

practical defoaming situations. The same is true of other thin-film stabilization effects from the interaction of the opposite surfaces of the film. These comprise both electric double-layer repulsion for ionic surfactants and entropic repulsion of polymer chains in the surface for nonionic materials. These effects are of paramount importance in determining the stability of very thin (less than 10 nm) films, but in practice the real challenge is usually to defoam films of at least several hundred nanometers in thickness where such effects have not begun to be significant.

All these mechanisms except high bulk viscosity require a stabilizer in the surface layers of foam films. Accordingly, most theories of antifoaming are based on the replacement or modification of these surface-active stabilizers. This requires defoamers to be yet more surface active; most antifoam oils have surface tensions in the 20–30 mN/m range, whereas most organic surfactant solutions and other aqueous foaming media have surface tensions between 30 and 50 mN/m. This is illustrated in Table 3.

Table 3. Surface Tensions of Surfactants and Defoamers

Material	CAS registry number	Surface tension,[a] mN/m (=dyn/cm)	Temperature, °C	References
Surfactants				
Sodium lauryl sulfate ($C_{12}H_{25}SO_4^-Na^+$)	[151-21-3]	39.5	25	26
Sodium 12-butoxydodecyl sulfate ($C_4H_9OC_{12}H_{24}SO_4^-Na^+$)	[3694-71-1]	44.0	25	26
Lauryl pyridinium bromide ($C_{12}H_{25}C_5H_5N^+Br^-$)	[104-73-4]	41.2	30	26
$C_{12}H_{25}(OC_2H_4)_nOH$[b]	[9002-92-0]	36.3	23	26
para-t-$C_8H_{17}C_6H_4(OC_2H_4)_nOH$[c]	[9036-19-5]	33.5	25	26
Surfactant/defoamer				
Surfynol 104[d]		31.4	25	9
Pluronic L62[e]		42.8	25	27
Defoamers				
Poly(oxypropylene)[f]		31.2	22	28
Polydimethysiloxane[g]		20.2	20	28
Kerosene	[8008-20-6]	27.5	29	29
Mineral oil (MWP paraffin)	[8020-83-5]	28.8	20	30
Corn oil	[8001-30-7]	33.4	20	31
Peanut oil	[8002-03-7]	35.5	20	31
Tributyl phosphate	[126-73-8]	25.1	20	32

[a]Surfactant values are at the critical micelle concentration (CMC) in aqueous solution; surfactant/defoamer values are at 0.1% concentration in aqueous solution.
[b]Lauryl end-capped polyoxyethylene.
[c]Polyoxyethylene end-capped with substituted phenyl group.
[d]Surfynol 104 is an acetylenic glycol, 2,4,7,9-tetramethyl-5-decyne-4,7-diol [126-86-3], marketed by Air Products and Chemicals, Inc.
[e]Pluronic L62 is a poly(oxyethylene)–poly(oxypropylene)–poly(oxyethylene) copolymer marketed by BASF AG.
[f]Mol wt: 3000.
[g]Mol wt: 3900.

In addition to having a lower surface energy than the foaming medium, defoamers must be insoluble in that medium, but also readily dispersible in it. There are five basic processes involved in the rupture of foam films by defoamers (7): entering, spreading, bridging, dewetting, and rupture.

The entering and spreading processes are governed by the entering coefficient E and the spreading coefficient S defined in equations (4) and (5), respectively (7), where σ_f is the surface tension of the foaming medium, σ_a the surface tension of the defoamer, and σ_{af} the interfacial tension between them.

$$E = \sigma_f + \sigma_{sf} - \sigma_a \tag{4}$$

$$S = \sigma_f - \sigma_{sf} - \sigma_a \tag{5}$$

The lower the value of σ_a, the more likely it is that E and S are positive, indicating a thermodynamic tendency for the processes to occur.

The displacement of the foam stabilizer and the mechanical disruption caused by these processes is sufficient to explain the function of defoamers which consist only of insoluble liquids such as silicone fluids used in the defoaming of crude oil. However, practical experience shows that blends of hydrophobic solids dispersed in the insoluble oil are generally necessary to control aggressive foaming, particularly in aqueous foam systems. Materials such as hydrophobic silica (17) or high melting point hydrocarbon amides such as ethylenediamine distearamide are notably effective. As an antifoam particle in a foam film approaches the air interface, an unsymmetrical thin film, known as a pseudoemulsion film (33), forms between the antifoam particle and the air phase. This psuedoemulsion film has a high stability in strongly foaming aqueous systems. Introduction of the hydrophobic particle into the oil drops destabilizes the pseudoemulsion film.

In such systems, bridging and dewetting effects are crucial to the defoaming mechanism. Once a defoamer particle such as hydrophobic silica has entered into a foam lamella, only then can it bridge the film. Subsequent dewetting of the particle by the foam film can then cause collapse by causing a small hole to form in the film. This hole rapidly expands, driven by surface tension effects, resulting in rupture of the film (34). The mechanical shock of this event can help propagate the defoaming action. For complete dewetting to occur, the contact angle must be greater than 90°, a requirement for defoamer action that has been well correlated for silicone-treated silica in hydrocarbon oil (35). Such dewetting helps thin the film and promote instability, and is particularly effective when sizes are such that the particle occupies both surfaces of the film. In this bridged situation, if the contact angle is large enough, a capillary pressure drop that pushes liquid away from the particle is developed (34). This flow results in migration of the air–liquid–solid interfaces toward each other until they meet and the film ruptures as it pinches off the particle. This concept offers an explanation for observed particle size and shape effects (2,18). Cinephotomicrographic studies are consistent with these dewetting ideas (36).

Debate continues about the detailed mechanisms of antifoaming by these synergistic combinations of insoluble oils and hydrophobic particles. These dewetting ideas imply that the hydrophobic particles become detached from the carrier

fluid. This separation accounts for the familiar experience of performance of antifoam compositions diminishing with time. Further additions of defoamer are needed to maintain effective foam control. Adsorption of antifoam components on other available surfaces, particularly in systems containing suspended solids, mutual saturation of foamer and defoamer changing the spreading and dewetting pressures, and coalescence of antifoam emulsions also contribute to this progressive loss of effectiveness. It has recently been demonstrated that exhausted or deactivated oil/silica defoamers segregate into two distinct populations of globules (silica-free and silica-enriched), neither of them being active defoamers (37). In addition, the spread oil layer disappears from the foam solution surface. The defoamer can be reactivated by addition of fresh oil without silica (37) which allows the entering and spreading mechanisms to function again, carrying in particles which can then bridge and dewet. Another interesting aspect of the dewetting/bridging action is its location. Most researchers explain the defoaming action in the foam films, although others (38) claim it occurs in the plateau borders of the foam. This theory can account for the fact that the typical size of antifoam drops (3–50 μm) is much larger than a typical foam lamella thickness, and also that smaller antifoam droplets are ineffective foam breakers.

Applications

The main industries and broad product groups that utilize defoamers are indicated by the subheadings in this section. These examples illustrate the wide variety of defoamer applications. Other application areas worthy of mention are agriculture and medical, particularly the use of antiflatulence tablets.

Adhesives and Sealants. Most industrial adhesives contain surface-active components and additives, and air entrainment during their mechanical application can significantly reduce joint strength. Defoamers are usually formulated into adhesives to protect users against such difficulties. Additional benefits such as improved uniformity of products, increased throughput, and reduced labor costs can also result from the use of defoamers during adhesive application. The footwear and nonwoven fabric industries are extensive users of defoamers in this way.

Chemical Processing. Agitation, distillation, and pressure differences are commonplace in many chemical processes. These are conducive to foam formation, and even when the plant design minimizes these problems it is still often necessary to employ defoamers. A review of this field (39) lists numerous problems encountered with unwanted foam in chemical processes: increased cost of coping with safety hazards from slippery floors, corrosive residues or flammable liquids; interference with process instruments, pumps, etc; slow drainage of liquids from products being dried; product rejection due to incompletely filled containers; reduced capacity in vats; premature failure in bearings and other mechanical devices because of loss of lubrication; separation and segregation of critical process ingredients; and perceived negative environmental impact and poor community relations on discharge.

Cleaning Compounds. A growth area for defoamers is in the formulation of low-foaming detergents and cleaners. This is in response to automation of

cleaning equipment and the need to operate it optimally. Changes in detergent composition and washing machine design have also had a significant impact on the need for foam control in this application (40). Incorporating defoamers in detergents in such a way that the low-foaming property does not drift with storage time is a considerable challenge. The antifoam composition has to survive storage with the surfactants, builders, bleaches, and other auxiliary agents, and yet function properly as soon as the detergent is added to the wash water. The solution is to prevent the defoamer from migrating within the detergent powder matrix such that the droplet size of the defoamer released into the wash water is the same regardless of storage conditions. Numerous patent examples of the four general ways in which this can be achieved have been provided (41): encapsulation in a water-soluble or water-dispersible wax, adsorption onto a carrier prior to wax coating, microencapsulation with film-forming polymers, and adsorption onto specially prepared inorganic salts.

Construction. Polymer dispersions in cements, mortars, and plastics are being increasingly used in the construction industry (11). Their plasticizing effect allows reduced amounts of water to be used, and they also confer strength and adhesion benefits in certain situations. The emulsifiers and dispersants used in these products can cause air entrainment problems with a detrimental effect on the ultimate stability of the construction. Powdered defoamers that can be directly added to the cement are commonly used. They are usually high surface area, highly absorbent inorganic fillers that have been treated with liquid defoamer compositions, similar to the products used in low-foaming detergents. Another approach to this problem is for the latex manufacturers to formulate low-foaming polymer dispersions with appropriate defoamers having good long-term stability.

Fermentation Processes. The efficient production of penicillin, yeasts, and single-celled protein by fermentation requires defoamers to control gas evolution during the reaction. Animal fats such as lard [61789-99-9] were formerly used as a combined defoamer and nutrient, but now more effective proprietary products are usually employed. Defoamer application technology has also improved. For example, in modern yeast production facilities, the defoamers are introduced by means of automatic electrode-activated devices. One concern in the use of defoamers in fermentation processes is the potential fouling of membranes during downstream Ultrafiltration. Silicone antifoams (42) seem less troubled by this problem than other materials.

Fertilizers. The fertilizer industry for many years has used tall oil fatty acids for the production of phosphoric acid [7664-38-2] by the digestion of phosphate-containing rocks with sulfuric acid. Carbon dioxide is liberated and presents a difficult, highly acidic foaming problem. Formulated products, many of which continue to contain tall oil fatty acids but which also contain emulsifiers and wetting agents such as dioctyl sodium sulfosuccinate [577-11-7], which greatly increase their effectiveness, are now used. Partially wetted gypsum particles contribute to the foam stabilization, and it is the modification of the gypsum wettability by these wetting agents that makes them so effective in this application.

Food and Beverages. Defoamer applications in the food and beverage industry include uses in both the preparation and processing of foodstuffs and in the cleaning and disinfecting of containers. Poly(alkylene oxide)-based defoamers

have played an important role in satisfying the foam control demands of this industry (43). The sugar beet industry is a prolific user of defoamers. This is now a fully mechanized automated procedure. The sugar is extracted with hot water, treated with limewater and carbon dioxide, filtered, and the filtrate subjected to evaporation. Foaming occurs in many of these steps. Another food processing area with considerable foam problems is the production of chips, fries, mashed potatoes, and potato starch. Proteins, starch, and other natural products in potatoes cause troublesome foams in wash baths. Beers and wines are also produced with the aid of defoamers. They permit more efficient use of vats and containers, and permit more controllable bottling procedures. The growth in returnable bottles and the widespread use of automated mechanical cleaning equipment has increased use of defoamers in this industry. They can be used directly or incorporated in low-foaming cleaning agents. It is important to note that foams occurring in food processing are generally stabilized by surface-active macromolecules, such as proteins or starch, instead of the more usual small-molecule surfactants, and this is reflected in the composition of defoamer products for these applications.

Leather. Almost every stage in leather processing, from the initial rawhide preparation, through tanning and dyeing and other finishing treatments, has the potential for causing foaming difficulties. Many of the preparations used in these steps contain wetting agents and other surfactants, or are applied in the form of emulsions or dispersions. The trend, as with many other defoamer applications, is to formulate the defoamer into the treatment product rather than deal with numerous optimized defoamers at each of the several processing steps.

Metal Working. The metal working industry encounters considerable foaming problems with the cutting oils and coolants that are sprayed onto the tool–workpiece interface to provide cooling, controlled lubrication, corrosion protection, and increased tool life. These coolants are provided as mineral oil/emulsifier concentrates that are diluted with water by the user. For many years, this industry tolerated the foam difficulty in its many milling, drilling, grinding, rolling, and drawing operations, but now uses defoamers such as formulated silicones and dispersions of fatty amides in mineral oils. Calcium soaps are also used as foam inhibitors in coolants. They are formed as a finely divided suspension of insoluble particles when the soaps present in the cooling lubricant concentrate react with hardening agents added to the dilution water.

Oil and Petrochemicals. There are a variety of uses for defoamers in oil recovery. They are used in some of the materials used in oil extraction, such as in drilling muds and cement lining, and also directly with the crude oil itself. In its natural state, crude oil contains dissolved gases held by high reservoir pressure. When this live crude oil is extracted and passed into the low pressure environment of a gas–oil separator, the dissolved gases are liberated and can cause troublesome foam that leads to oil losses via the gas stream and downstream equipment damage (44). Foaming is a problem in other petrochemical operations including distillation, cracking, coking, and asphalt processing. Defoamers are also used in the downstream petroleum market in lubricating oils and diesel fuel. The areas involving the application of oil and petrochemicals and the area of coatings(discussed below), are ones where not only the elimination of foam is important, but also the elimination of individual bubbles. This problem of deaeration

can only be dealt with using specifically designed products. Foam control agents can break foam lamellae once they are formed between bubbles but the defoamer generally cannot remove or accelerate the movement of individual air bubbles.

Coatings. Foam problems occur both during the preparation of paints and coatings and in their application. The use of ball mills and other equipment for pigment dispersion provides ideal conditions for mixing in air, and the presence of surfactants in the formulations assures considerable persistence of the foams that are generated. These problems may be controlled during manufacture by mechanical means, but a defoamer is almost always required for foam control during application since application methods vary considerably, for example, roller, brush, dip, or spray methods. The proper choice and minimum use of surfactants such as dispersants, flow agents, and wetting agents can minimize but not eliminate the use of defoamers to prevent surface defects during application such as cratering, pinholes, fisheyes, and orange peel. In addition to the final dried film appearance, the defoamer must not detract from other properties such as color acceptance, gloss, and adhesion.

Polymers. Foam is often a particular problem in the production of polymers. There are numerous situations where foam can reduce the production capacities of vats and vessels and cause problems in pumps, meters, and other equipment, particularly distillation and evaporation equipment. Foam is frequently a problem when stripping off a monomer from a polymer. Examples are in the production of styrene–butadiene [9003-55-8] and acrylonitrile–butadiene [9003-18-3] rubber latices. These latices are stabilized by surfactants that greatly contribute to foaming difficulties. Another problem foam area is in the stripping of unreacted monomer from poly(vinyl chloride) suspensions. In this process, vinyl chloride [75-01-4], a gas at room temperature, is liquefied by pressure, emulsified in water with surfactants and catalysts, and heated to bring about polymerization. The recovery of unpolymerized monomer by distillation from this mixture produces a severe foaming problem.

Pulp and Paper. The critical and troublesome foam problems of this industry have led the way in the use of defoamers. It is the world's biggest single user of defoaming agents (45). Early use of large amounts of kerosene or fuel oil has given way for ecological and cleanliness reasons to much more effective formulated defoamers. Foams are encountered at every stage from pulping, through paper fabrication and coating, to printing. A variety of wastewater streams are generated that are very prone to foaming because of the presence of dissolved soaps. Specific defoamer products are often tailored for each different stream. The so-called black-liquor defoamers were the first hydrophobic silica in hydrocarbon oil products that were then extended to other industries. The use of these defoamers has allowed some Kraft pulp mills to exceed original designed capacity.

Textiles. Defoamers are required in the jet dyeing of textiles (17). This process, which is mainly used with polyester fibers, is carried out at elevated temperature and pressure, and involves pumped recirculation of the dyeing medium from the reservoir through the jets. When the operation is complete and the pressure released, severe foaming can result in the absence of an effective defoamer. Foam control is needed in other dyeing processes also (17), such as continuous dyeing and beck dyeing. For example, in the dyeing of knitted fabrics of textured

polyester fibers, foaming of the dye liquor can cause the material to float, resulting in uneven application of the dye. Various surfactant mixtures are used in this area and bring additional benefits such as wetting and solubilization as well as foam control. Acetylenic glycols are very useful in this context (9). Dyeing is only one of several steps where foaming can cause difficulties with fiber processing. Defoamer may be required when any size or finish is applied to a textile material. One example is the pretreatment step in the processing of cotton. The fabric is exposed to strongly alkaline sodium hydroxide and anionic surfactant solution. Phosphate ester defoamers are much used in this application. Textile operations are also notorious for their wastewater foam problems.

Wastewater Treatment. Defoamers are used extensively to treat wastewater in many municipal and industrial treatment facilities and also in mining and mineral processing. Benefits are aesthetic, environmental, and economic. Aeration basins are rid of unsightly, troublesome foam, and water and energy are conserved by allowing more efficient use of mechanical equipment. Most foaming problems occur either at the biological treatment step or the effluent discharge step (46). Aeration is necessary in biological treatments to allow microorganisms to breathe, but the agitation produces foam. Defoamers that do not disrupt this process must be selected. Some of the upstream processes may depend on foaming and other surface-active phenomena such as flotation and flocculation steps, and care must also be taken to use defoamers that do not interfere with these processes if treated streams are recycled. Effluent foam discharge is illegal in some countries including the United States where the EPA prohibits discharge of floatable materials in the effluent stream (46).

Economic Aspects

Accurate information on the size of the defoamer market is impossible to obtain. There are too many types of materials and suppliers involved. Particularly for the more common oils and surfactants, defoaming is a very small part of their total usage, and no public information is available on what fraction of manufacturers' sales is in the area of foam control. Even for more expensive materials such as the poly(alkylene oxide) block copolymers, there is no way of distinguishing between their use as defoamers and other significant surfactant uses such as de-emulsifiers.

In 1993 the Encyclopedia estimate for a market for defoamers of all types was 150,000–170,000 t per year in the United States, with the rest of the world slightly exceeding that amount. The principal use area of pulp and paper accounts for between a third (47) and a half (45) of this usage. With modest growth in some markets offset by improvements in efficiency in others, the 1993 estimate remains an adequate one for 2000. No typical selling price for defoamers can be quoted because of the wide diversity of active materials and product types. The cheapest unformulated defoamer types cost as little as $0.6/kg in bulk quantities, whereas some custom-tailored defoamers cost over $5.0/kg. Usages vary from less than 0.1 kg of defoamer per ton of product to over 2.0 kg/ton of product, and it is not the unit cost of the defoamer that matters but the cost per unit of product produced that does. It often occurs that the controlled use of a relatively expensive

defoamer results in a lower cost per unit of product than use of an inexpensive defoamer.

Test Methods

The ultimate test of a defoamer is an actual field trial, and occasionally this is the only testing carried out. More usually some laboratory-scale evaluation of several different products is conducted before a recommendation is made for a suitable, economical defoamer for a specific application. Although suppliers have their chosen standard foaming surfactants, it is usual to work with the potential customer's foaming medium. Often, this work is done at the plant site to obtain fresh foaming liquors. Establishing that a given defoamer is effective in a particular application is only part of the testing required. The absence of any adverse effect on the final product and the manufacturing and use environments must also be determined. In addition, to be marketable the defoamer must be cost-effective and convenient and easy to handle for the customer. A useful account of the practical selection of defoamers has been given (39).

There are many laboratory methods for testing the relative merits of one defoamer against another. It is a simple matter to measure foam height as a function of time to compare the performance of various foam surfactants and defoamers. Unfortunately, this simplicity has led to a wide variety of methods and conditions used with no standard procedure that would make the measurement of foaminess as characteristic of a solution as its surface tension or viscosity. It has been suggested that the time an average bubble remains entrapped in the foam Σ is such a quantity (48), but few workers in the defoamer industry have adopted this proposal. One reason for this is that the measurement is not practical with strongly foaming materials, the steady-state foam height being very high and hard to reach. Nishioka et al. (49) describe dynamic methods for measuring Σ in their review of fundamental methods for measuring foam stability. They also observe that the decay of static foam is measured, most fundamentally, by the change with time in the size distribution of bubbles in a foam. This can be done by photomicroscopy of flash-frozen samples, a method that although somewhat tedious, is recommended for periodic confirmation of other less direct methods whenever possible. In practice, a wide variety of simpler methods are used that generally fall into one of five main categories:

(1) **Pneumatic methods.**

Gas introduction is controlled by injection through capillary tubes, sintered-glass spargers, diffuser stones, and the like.

(2) **Dynamic methods.**

This is a subdivision of the pneumatic class; foam heights or volumes are monitored while the gas continues to produce bubbles.

(3) **Shaking methods.**

Agitation is the easiest way of producing foam, but the results are very dependent on the details of the shaking procedure. Foam height, or for more viscous fluids specific gravity changes, are usually measured.

(4) **Pour methods.**

The liquid is poured or drained from one vessel into another. This approach is best limited to foams produced from dissolved gases in the liquid.

(5) **Stirring and blending methods.**

Like shaking methods, these are very dependent on procedural and equipment details, but they are simple to use and are widely employed for comparative purposes.

This diversity of test methods is reflected in ASTM recommendations (50). Pour (D1173-53 [reapproved 1986]), shaking (D3601-88), and blending (D3519-88) methods are suggested for aqueous solutions. Pneumatic methods are recommended for lubricating oils (D892-89) and engine coolants (D1881-86). Despite their omission by ASTM, dynamic methods are probably the most satisfactory for defoamer evaluation (12,41). The foaming solution is usually recirculated through a vertical cylinder where foam heights can be measured as a function of time. In such a device, a steady state can be achieved with a given foamer system and defoamer metered in at selected concentrations. The test enables various important defoamer characteristics to be measured such as the knockdown time, the time taken to collapse a preformed foam, and the persistence or hold-down time, the time taken for the foam to recover to some agreed level such as half its original height (defoamer half-life).

Health and Safety Factors

Defoamers are usually added at low bulk concentrations ranging from a few to a thousand parts per million of the foaming medium. Often the health risk posed by such additives is negligible compared to that of the material being defoamed. Such is the case in the defoaming of asphalt (qv) and phosphoric acid. Sometimes a specific defoamer type/foaming medium combination presents a particular problem and, so the supplier should always be involved in defoamer selection. Examples are the increase in flammability of polyester textiles with free PDMS (17), and the possibility that mineral oil antifoams may contain precursors that form dioxins in bleached pulp after chlorination (51). Health and safety concerns arise primarily in applications in the food and drug industries. Defoamers can be incorporated directly into these products, as in the production of sugar from sugar beets or in the

defoaming of fats for frying potato products, and indirectly, as in the manufacture of paper or plastic packaging materials.

U.S. government regulations governing the use of additives such as defoamers in food and drugs are listed in the Code of Federal Regulations (CFR). Title 21 contains the rules established by the Food and Drug Administration; Title 40 covers those that are the concern of the Environmental Protection Agency. For example, part 173.340 of Title 21 deals with defoamers that may be safely used in processing foods, whereas Part 180.1001 of Title 40 lists those materials exempt from the requirement of tolerance levels in pesticide chemicals, including defoamers used therein. Other parts of Title 21 that cover defoamer uses include 176.200 on coatings and 176.210 on the manufacture of paper and paperboard. One defoamer is also used as an active drug ingredient—the antiflatulent silicone, Simethicone [8050-81-5]. Such use is regulated by the FDA under part 332 of Title 21. Regulations are subject to change and the CFR is revised at least once each calendar year. It is also kept up-to-date by the individual issues of the *Federal Register*, a daily government publication.

Although the intent may be the same, the details of regulatory practice differ in other countries, and a multitude of regulations exist worldwide. Under the auspices of the Joint Expert Committee on Food Additives of the FAO–WHO, efforts are being made to establish international guidelines. However, given the changing regulatory climate, the differences in practice between countries, and the wide range and regional differences of antifoam components available, the best advice for those interested in health and safety aspects of defoamers is to contact the producers directly. Their skill and experience are the best defenses against safety hazards associated with the use of defoamers.

BIBLIOGRAPHY

"Antifoaming Agents" in *EPST* 1st ed., Vol. 2 pp. 164–171, by L. A. Rauner Dow Corning Corp.; "Antifoaming Agents" in *EPSE* 2nd ed., Vol. 2, pp. 59–73, by M. J. Owen, Dow Corning Corp.

1. K. J. Bryon, *Crit. Rep. Appl. Chem.* **30**, 133 (1990).
2. P. R. Garrett, *Defoaming: Theory and Industrial Applications* (Surfactant Sci. Ser., Vol. **45**), Marcel Dekker, Inc., New York, 1993.
3. D. T. Wasan and S. P. Christiano, in K. S. Birdi, ed., *Handbook of Surface and Colloid Chemistry*, CRC Press, Inc., Boca Raton, Fla., 1997, p. 179.
4. S. Ross, *Colloids Surf., A* **118**, 187 (1996).
5. R. Aveyard and J. H. Clint, *Curr. Opin. Colloid Interface Sci.* **1**, 764 (1996).
6. R. A. Reinhardt and co-workers, *J. Coat. Technol.* **70**, 157 (1998).
7. R. M. Hill and K. C. Fey, in R. M. Hill, ed., *Surfactant Sci. Ser., Vol. 86: Silicone Surfactants*, Marcel Dekker, Inc., New York, 1999, pp. 159–180.
8. R. D. Kulkarni, E. D. Goddard, and P. Chander, in R. K. Prud'homme and S. A. Khan, eds., *Surfactant Sci. Ser., Vol. 57: Foams*, Marcel Dekker, Inc., New York, 1996, pp. 555–180.
9. N. F. Chinoy, S. W. Dean Jr., and R. Derby, The Role of Acetylenic Glycols in the Growth of Water-Based Coatings, Air Products Technical Paper 120–313, Air Products and Chemicals, Inc., Allentown, Pa., 1979.

10. U.S. Pat. 4208385 (June 17, 1980), M. L. Robbins and E. R. Ernst (to Exxon Research and Engineering Co.).
11. R. Hofer and co-workers, in B. Elvers, J. F. Rounsaville, and G. Schulz, eds., *Ullman's Encyclopedia of Industrial Chemistry*, 5th ed., Vol. **A11**, VCH Publishers, New York, 1988, pp. 465–490.
12. U.S. Pat. 4082690 (Apr. 4, 1978), K. W. Farminer (to Dow Corning Corp.).
13. U.S. Pat. 2933382 (Apr. 19, 1960), F. M. Fowkes and F. G. Bollo (to Shell Oil Co.).
14. U.S. Pat. 3951853 (Apr. 20, 1976), D. W. Suwala (to Diamond Shamrock Co.).
15. Z. Nemeth, G. Racz, and K. Koczo, *J. Colloid Interface Sci.* **207**, 386 (1998).
16. U.S. Pat. 3076768 (Feb. 5, 1963), F. J. Boylan (to Hercules Powder Co.).
17. R. E. Patterson, *Text, Chem. Color.* **17**(9), 181 (1985).
18. P. R. Garrett, *J. Colloid Interface Sci.* **69**, 107 (1979).
19. *McCutcheon's Functional Materials Directory*, North American and International Editions, MC Publishing Co., Glen Rock, N.J., 1998.
20. J. W. Gibbs, *Collected Works*, Vol. **1**, Longman-Green and Co., New York, 1928, p. 300.
21. A. Prins and M. Van den Tempel, in *Proc. IVth Int. Congr. Surface Active Substances*, Brussels, Vol. 2, 1964, p. 1119.
22. I. C. Callaghan and co-workers, *Colloids Surf.* **8**, 17 (1983).
23. H. Saito and S. Friberg, *Pramana* (1st Suppl.), 537 (1975).
24. S. Hard and R. D. Neuman, *J. Colloid Interface Sci.* **120**, 15 (1987).
25. C. B. McKendrick, S. J. Smith, and P. A. Stevenson, *Colloids Surf.* **52**, 47 (1991).
26. M. J. Rosen, *Surfactants and Interfacial Phenomena*, John Wiley & Sons, Inc., New York, 1978, p. 164.
27. I. R. Schmolka, in M. J. Schick, ed., *Nonionic Surfactants*, Marcel Dekker, Inc., New York, 1966, p. 309.
28. S. Wu, in J. Brandrup and E. H. Immergut, eds., *Polymer Handbook*, 3rd ed., John Wiley & Sons, Inc., New York, 1989, p. VI/411.
29. M. Sato, *Proc. Japan Acad.* **31**, 713 (1955).
30. Z. Rymuza, *J. Colloid Interface Sci.* **112**, 221 (1986).
31. A. Halpern, *J. Phys. Colloid Chem.* **53**, 895 (1949).
32. A. I. Vogel and P. M. Cowan, *J. Chem. Soc.* 16 (1943).
33. D. T. Wasan, K. Koczo, and A. D. Nikolov, in L. L. Schramm, ed., *Foams: Fundamentals and Applications in the Petroleum Industry* (Adv. Chem. Ser., Vol. 242), American Chemical Society, Washington, D.C., 1994, pp. 47–114.
34. G. C. Frye and J. C. Berg, *J. Colloid Interface Sci.* **127**, 222 (1989).
35. I. A. Lichtman, V. S. Sinka, and D. W. Evans, *Assoc. Mex. Tec. Ind. Cel. Papel. Bol.* **15**, 26 (1975).
36. A. Dippenaar, *Int. J. Miner. Process.* **9**, 1 (1982).
37. N. D. Denkov and co-workers, *Langmuir* **16**, 2515 (2000).
38. K. Koczo, J. K. Koczone, and D. T. Wasan, *J. Colloid Interface Sci.* **166**, 225 (1994).
39. J. McGee, *Chem. Eng.* **96**(4), 131 (1989).
40. H. Ferch and W. Leonhardt, in P. R. Garrett, ed., *Defoaming: Theory and Industrial Applications* (Surfactant Sci. Ser. Vol. 45), Marcel Dekker, Inc., New York, 1993, pp. 221–268.
41. G. C. Sawicki, *J. Am. Oil Chem. Soc.* **65**, 1013 (1988).
42. W. C. McGregor, J. F. Weaver, and S. P. Tansey, *Biotechnol. Bioeng.* **31**(4), 385 (1988).
43. T. G. Blease, J. G. Evans, L. Hughes, and P. Loll, in Ref. 40, pp. 299–323.
44. I. C. Callaghan and co-workers, *Spec. Publ. Roy. Soc. Chem.* **59** (Ind. Appl. Surfactants), 48–57 (1988).
45. S. L. Allen, L. H. Allen, and T. H. Flaherty, in Ref. 40, pp. 151–175.

46. D. J. Avery, *Pollut. Eng.* **21**(10), 113 (1989).
47. A. Shanley, *Chem. Eng.* **104**(10), 75 (1997).
48. J. J. Bikerman, *Foams*, Springer-Verlag, New York, 1973.
49. G. M. Nishioka, S. Ross, and R. E. Kornbrekke, in Ref. 8, pp. 275–285.
50. *Annual Book of ASTM Standards*, American Society of Testing and Materials, Easton, Md., 1990.
51. G. C. Sawicki and J. W. White, *Chemspec Europe '89 BACS Symposium*, Manchester, U.K., 1989.

MICHAEL J. OWEN
Dow Corning Corporation

ANTIOZONANTS. See RUBBER CHEMICALS.

ATOMIC FORCE MICROSCOPY

Introduction

From their early beginnings in thermoset resins to the breakthrough thermoplastics of the mid-twentieth century and the liquid crystalline materials and other high performance materials of the 1970s to the present, polymers have established key roles in all sectors of human endeavor. From transportation to construction, microelectronics, and packaging, use of polymeric materials contributes to prosperity and performance. Development of new polymers for use as stand-alone materials, polymer solutions, blends, or composites is at the core of macromolecular science. It is in this arena where the disciplinary efforts of synthesis, structure, properties, and performance hybridize into a tetrahedral coordination of interdisciplinary research and engineering. While confirmation of chemical fidelity is highly advanced, the ability for structure and property determination at submicrometer scales is lacking. Most recently, the advantages of Nanocomposites are becoming clear (1) and this trend will continue only to the extent of the ability to characterize these new materials. Moreover, processing of polymer materials is critical to device performance, and affects the microstructure of semicrystalline castings as well as the nanostructure of mechanically strained or drawn films (2). The atomic force microscope enables characterization of these materials and therefore the development of more new materials.

The microscope is an invaluable tool to the materials scientist. There are two quantities that enable microscopy: contrast and resolution. Sensitivity is not inherently an issue in microscopy: signal level is not limiting because it is now possible to count single photons and electrons. Contrast and resolution determine one's ability to see at all scales. Contrast is the ability to measure changes in signal with a detector. The detector can be your eye, a CCD camera, or an

Encyclopedia of Polymer Science and Technology. Copyright John Wiley & Sons, Inc. All rights reserved.

electronic amplifier. The contrast of the signal can be from intensity changes, spectral changes, phase differences, scattering of electrons or ions, transmission of tunneling electrons, or force on an atom from a probe, amongst others. Without contrast there can never be resolving power. Resolution is defined as the smallest distance between two points in a sample, that one can detect as a change in signal. There are two modes to operate a microscope. The difference between far-field detection mode and near-field detection mode is that in the former the detector is "far" away from the signal source. When the source-to-detector distance is several times the wavelength of the signal, the system displays its wave character and is therefore subject to the diffraction limit of light. This is a fundamental limit and is a result of Heisenberg's uncertainty principle (3), which is of course a result of one of the postulates of quantum mechanics. Near-field detection does not require wave propagation of the signal. Therefore, resolution is determined by the size of the probe or pinhole detecting the signal. To increase the resolving power of the microscope, the tip of the probe needs to be smaller. This is the concept that drives the maturing area of scanning probe microscopy and is what makes the scanning tunneling microscope and atomic force microscope so powerful.

Since the development of the scanning tunneling microscope (stm) in 1982 by Binnig and Rohrer (4) (Recipients of the 1986 Nobel Prize in Physics for this discovery), the capabilities of microscopy in general have been pushed to previously unrealizable capabilities. The enhanced resolving power of the stm is attributed to the special contrast mechanism it employs. An stm operates in the near-field detection mode and is therefore not limited by diffraction as described above. In fact, only the interaction area of a local probe with the sample determines the limit of its resolution. This interaction area is actually difficult to access and strongly depends on the experimental method and the sample under study. The contrast mechanism of the stm is due to changes in the local density of electronic states at the sample. This results in a position sensitive quantum mechanical tunneling current flowing between the metal stm tip and the electrically conducting sample. Polymers, in general, are not good conductors and are therefore not typically examined with an stm. Fortunately the concepts and the technology of the stm have been applied to many other contrast mechanisms. This class of scanning probe microscope (spm) has revolutionized surface science and has enabled a nanotechnology already yielding useful new advanced materials.

Various contrast mechanisms have been deployed toward studies of materials and polymers. In general, any physicochemical signal that can be measured by a probe or through an aperture can be developed into an spm, where the resolution of the subsequent microscope is governed by the sample-to-probe distance dependence of the measured signal. Specifically the "P" in spm can be replaced by "near-field optical" (5) or "capacitance" (6,7) or "magnetic force" (8) or "thermal" (9) or "acoustic" (10) or "electron spin resonance" (11) or "nuclear magnetic resonance" (12) or "thermovoltage" (13–16). Other variants are too numerous to be inclusive. The late 1980s to early 1990s can be thought of as the renaissance period of spm inventions.

Microscopy of polymer surfaces and their high spatial resolution analysis is accomplished typically with the atomic force microscope (afm) used in various modes of operation. The contrast mechanism of the afm is the interatomic forces between the scanning probe and the sample's surface. The forces are measured

easily and result from the mean pairwise potential energies of the interacting atoms. Extracting the exact form of the potential energy versus tip-to-sample position is difficult with regard to the microscopic detail. However, it is generally described by a steep attractive interaction followed by a very steep repulsive interaction at closer separation. It is the shortness of range of this interaction energy that enables the near atomic resolution commonly provided by the afm.

Analysis

Synthesis and processing are integrally important when designing for the properties and performance of a polymer system. Bulk characterization of the system is often not enough to predict, control, and maintain desired system performance when surface interactions and particle incorporation are significantly involved. The discovery, development, and optimization of new polymeric systems (eg, composites, films, or fibers) often require ensembles of analytical investigation; no one technique is enough. The cohort of surface analytical techniques is voluminous and not appropriately reviewed here (17). It is, however, important to realize that the spatial resolution of an analysis is both technique- and sample-dependent. Atomic force microscopes are versatile analytical tools. They excel at topographic characterization of surfaces. Moreover, they can be used to probe the identity of chemical constituents at a surface and the mechanical properties of the near-surface region, both with high spatial resolution.

Imaging. Mechanical design and control of the afm is now mature. Early in its development there were some design constraints similar to all models (7,18–24). Notably, reduction of environmental noise, sharpness of the tip-probe asperity, and sensitivity of the force transducer are the most critical design elements. By far, the most commercially successful afm design is based on the laser-diode optical lever (24) coupled to an integrated micromachined Si or SiN cantilever and tip (25), as illustrated in Figure 1. There are several limitations to the resolving power of an afm; noise being one of the more benign and easily removed. Since the tip is not infinitely sharp and the tip or samples are not infinitely hard (ie, they have measurable Young's moduli), the resultant micrograph will be a convolution of the chemical, physical, and topographic properties of the entire system. This is a very important point since an artifact is only realized in hindsight.

For the idealized case of hard materials, an extremely small/sharp tip and a relatively flat sample, the principal concern is tip–sample convolution artifacts (26). Typical, commercially available afm probes have tips with radii of curvature of the order of 30 nm and with varying aspect ratios. As the topographical relief of the surface increases so must the aspect ratio of the tip. A common artifact found in samples of high relief is that the sample is actually imaging the shape of the tip instead of the converse. Since the quality of a tip varies with manufacturability and with use, overinterpretation of image structure without knowledge of tip-shape is ill-advised. A second common artifact, for the idealized sample, is observed when there is significant thermal drift, and nanometer spatial resolution is desired. Polymers have large coefficients of thermal expansion (eg, several hundred ppm/°C). Image acquisition with the afm is accomplished by raster scanning the probe across the sample. The scanner displaces the probe relative to the

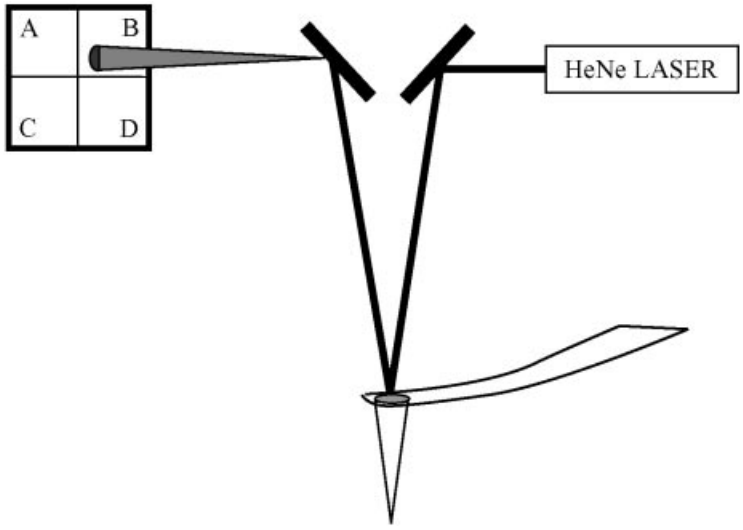

Fig. 1. Commercial afm design.

sample, one line at a time. Each line is typically scanned at a rate of many hundreds of nanometers per second in the "fast-scan" direction. After the scanner repositions the probe to the beginning of the first line, it steps down the "slow-scan" direction. This process is linear and slow. Therefore, any thermal drift will be convoluted mainly with the slow-scan direction. The effect will be to distort the image. This artifact is corrected for by subtracting out thermal drift (assuming it is constant) or by rotating the scan direction by 90°. Another common misinterpretation of afm images occurs when periodic structure is being investigated. In general, any periodic structure that is either parallel to or perpendicular to the scanning direction should never be believed. Sinusoidal noise in any number of the system's components will look like periodic structure perpendicular to the scan direction. Since the noise will most likely be out of phase with the scanning frequency, the image will appear to have a "crystalline" structure. Rotating the scan direction will not change the image. Also, spm data should not be accepted as true unless it has been reproduced at several scan speeds, several scan dimensions, a couple of scan directions, and in several areas of the sample. An afm is very powerful and can be made to generate any possible image, regardless of its validity.

There are several operating modes where the afm can generate microscopic contrast. These various modes can help deconvolute topographic relief from chemical and mechanical surface inhomogeneity. Topographic information is most precisely obtained in "contact" mode where the afm probe is very close to the sample and interacts with the repulsive potential energy of the surface. This is arguably the point at which the probe "touches" the sample. As long as the cantilever force transducer is significantly softer than the material being scanned over, such that excessive (force)/(contact area), that is pressure, does not perturb the sample, the afm will accurately trace the surface. This is an idealized situation since there will always be some deformation of the polymer surface by the probe even at static,

zero applied force F conditions. The perturbed contact area of radius a is described in the Johnson–Kendal–Roberts (JKR) (27) theory of adhesion mechanics as

$$a^3 = \frac{R}{K}\left[F + 3\pi R W_{\text{tip-sample}} + \sqrt{6\pi R W_{\text{tip-sample}} F + \left(3\pi R W_{\text{tip-sample}}\right)^2}\right]$$

where R is the mean radius of curvature of the tip and sample, $W_{\text{tip-sample}}$ is the tip–sample surface energy, and K is the weight averaged elastic moduli (28). For typical polymer systems, this result would predict a "contact" radius of 1–2 nm even for zero applied force. This seems to preclude atomic resolution with the afm; however, the JKR theory does break down at these small length scales. The afm can resolve atoms on "soft" materials, but it is difficult. Nanometer scale spatial resolution is more easily obtained, and in general, the resolution is inversely proportional to a material's elastic moduli.

While in contact mode, the user can collect both sample height and probe force information as the probe scans across the surface. In feedback mode (or height mode), the afm tries to maintain a constant applied force by driving together or retracting apart the tip from the sample as the probe is scanned. Ideally this would follow the topography of the sample, as the force would remain constant. This "height mode" has two advantages over the "force mode" with the feedback control turned off. Since the system is trying to keep a constant force, it is less likely to damage soft polymer surfaces having significant topographic relief. Moreover, the height mode provides a direct measure of the sample's topography. When the afm is operated in force mode (still addressed as contact afm), the probe-to-sample distance is not changed rapidly with varying topography. Therefore, as the tip travels over higher areas of the sample, the interatomic forces increase, resulting in the upward bending of the probe's cantilever. This mode has the advantages of allowing high scanning speeds and providing images with less noise and scanning artifacts. These come at the expense of not being able to acquire accurate and direct height measurements of the sample, and there is the possibility of more damage by the tip onto the polymer surface than when running in height mode. If only qualitative microscopy is required, force mode is the more useful technique.

An afm cantilever is flexible in several directions (29); it can be bent up and down to measure vertical displacement of a sample and it can be torqued about its long axis because of the moment applied to the end of the scanning tip. Because of the phenomena of friction and Newton's third law, there will be a measurable force applied to the tip, which is perpendicular to the load force applied normal to the sample. While the probe is scanning, this results in the twisting of the cantilever. Modern afms detect the reflection of a diode-laser from the end of the cantilever onto a position sensitive four-quadrant photodetector. The laser spot deflection is illustrated in Figure 2. The total laser power on the detector is the sum of the signal from each quadrant, $T = A + B + C + D$. Changes in sample height will cause the cantilever to deflect up or down, and the signal is recorded as $\delta H = [(A + B) - (C + D)]/T$. Simultaneously the cantilever may twist because of the frictional drag on the tip as it is pulled over the sample. The torque will deflect the laser beam horizontally and the "friction" signal is recorded as $\delta f = [(A + C) - (B + D)]/T$. Since friction is related to both surface chemistry and surface roughness, the two signals may not be independent. Variations in surface

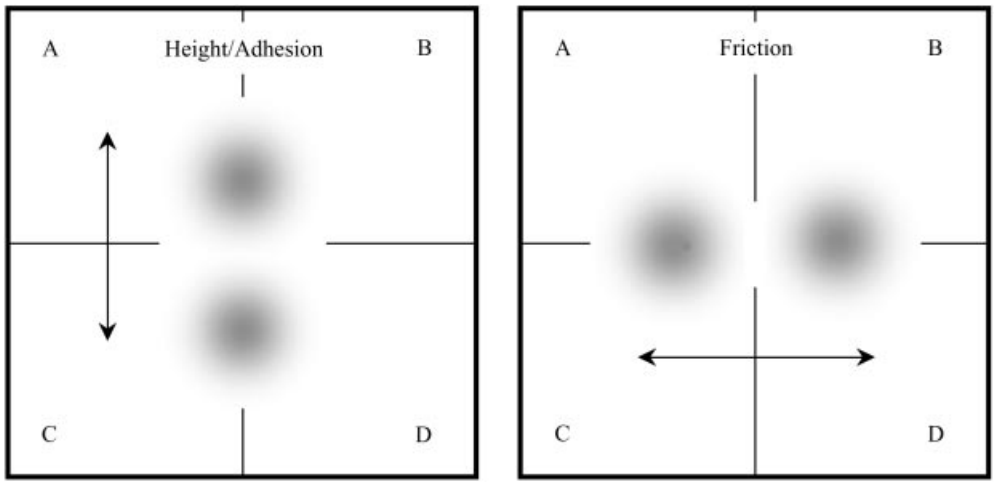

Fig. 2. Laser spot deflection.

composition are easily detected in force mode, whereas the topography signal may not detect any change in the surface character (30–33). Although differences in surface composition are sought with friction mode afm, friction forces can be dominated by the near-surface yield strength of the polymer and by any adsorbed water vapor forming a meniscus at the tip–sample contact (33).

By chemically modifying the surface of the tip with self-assembled monolayers of alkanethiols, the surface free energy and therefore the frictional drag on the system can be reduced. This technique has been used to obtain superior images of biaxially oriented PET films that are typically degraded by standard contact afm (34). Friction force studies provide another viable contrast mechanism for high spatial resolution microscopy of inhomogeneous polymer surfaces. However, it is very difficult to get absolute friction forces and thereby the coefficient of friction. Relative changes in frictional drag are measurable and aesthetic. Chemical modification of afm tips used in friction mode defines another category of "chemical force" microscopy. Selecting the terminal group at the surface of the tip (ie, making it more hydrophilic or hydrophobic) enhances the contrast of friction studies on chemically inhomogeneous surfaces (35). Even when there is no apparent change in topography, chemical force microscopy can define nanometer scale domains on polymer surfaces. Since friction is an energy dispersion phenomenon, we expect variations with surface temperature. In fact, scanning friction microscopy can be used to measure the viscoelastic properties of the near-surface region of poly(ethylene terephthalate), poly(methyl methacrylate), and polystyrene (PET, PMMA and PS, respectively) (32). As the temperature of a polymer surface increases, there are more available energy modes to dissipate the energy absorbed during the tip sliding process. These modes are intrinsic to the chemical composition near the surface.

Contact mode afm inherently damages soft materials. This is useful when trying to study wear resistance; however, it is deleterious to image quality and surface processing studies. Alternatively, the afm can interact with the attractive

potential energy, just above the surface and therefore not "touch" the surface or be dragged across it during a scan. The attractive force microscope was developed early in the evolution of the spm (19) explicitly to minimize sample perturbation from the scanning probe. It is difficult to maintain a stable mechanical system when the tip is being held a few nanometers away from and being attracted to the surface. Thermal fluctuations, scanning irregularities, sample inhomogeneity, and most importantly, capillarity affects from adsorbed water layers all contribute to this instability where the tip suddenly and unintentionally snaps onto the surface. To improve the attractive force mode, stiffer cantilevers were used. For contact afm of polymer surfaces, the softest cantilever that gives reliable scanning should be used. However, for noncontact mode, system stability requires that the force constant of the cantilever be greater than the force gradient $\partial F/\partial z$ felt by the tip near the surface, which gets larger as tip–sample separation z decreases. Moreover, lateral resolution decreases rapidly with increasing separation. For these and other mechanical design criterion, very high force constant ($k > 100$ N/m) cantilevers should be used. The trade-off in using stiff levers is that they do not deflect enough to detect the already small tip-surface forces (Recall Hook's law for a spring, $F = kz$). Various techniques were deployed to increase the sensitivity of the stiffer systems. Of these ac detection schemes, the most sensitive was heterodyne interferometry (8,23).

AC detection techniques in afm are similar in that they all oscillate the cantilever by driving the damped spring system with a sinusoidal input. The amplitude of oscillation of the free "undamped" probe A_0 is frequency dependent and reaches a maximum at its resonance frequency $\omega_0 = \sqrt{k/\mu}$ where μ is the effective mass of the probe. When the cantilever is very far from the surface, the undamped tip oscillation lags behind the sinusoidal driving signal by 90°. As the probe is brought closer to the surface, the attractive van der Waals forces pull down on the tip during the approach phase of the oscillation. This drag damps out the amplitude of oscillation by changing the effective mass of the cantilever, thereby moving the system off resonance with the driving frequency. Since the amplitude change is very sensitive to the average tip–sample separation, it can then be used to generate sample contrast and be deployed as a feedback mechanism to track sample topography. The principal disadvantage of this technique is the loss in lateral resolution because of the more gentle slope of the potential energy versus distance curve at these necessarily larger separations.

A significant advance in the development of "noncontact" afm is a new "tapping mode" afm (tmafm) (36,37). The required equipment for tmafm is similar to that for attractive force afm; however, the amplitude of oscillation A_0 is set to be much larger (typically >20 nm vs <5 nm for attractive force mode). Because of the larger amplitude, there is more energy stored in the cantilever as it accelerates away from the surface, thereby reducing the sticking instability discussed above. TMAFM actually intermittently "touches" the sample and the repulsive portion of the interatomic potential therefore affecting its motion, whereas noncontact afm involves only the attractive portion (38,39). As the oscillating tip is brought closer to the sample and starts to tap the surface, the system undergoes a transition from attractive mode to tapping mode and the "damped" oscillation amplitude decreases linearly and sensitively with average tip-surface separation. Again, this decrease in amplitude is used as a set point for feedback control of the

probe. Interatomic potential functions rise very steeply in the repulsive regime. Since the tmafm tip contacts the surface at each oscillation (>10,000 samples per second), the lateral resolution found in contact mode afm is regained or surpassed (40). As with contact mode, tmafm can also operate in liquids (40,41) although interpretation of the images is less clear because of the mechanical response of the fluid. To reduce friction-induced surface damage from contact mode afm, samples and probes are typically immersed in a liquid, which reduces the attractive capillarity force loading the tip onto the sample. With tmafm the tip contacts the sample for a very small percentage of the time and the repulsive forces at contact are still as small, or smaller, than those found in contact afm. Since the tip is most likely not contacting the surface when the probe is scanned laterally, there will be no frictional drag, effectively eliminating friction-induced damage. TMAFM has solved many of the damage and scanning artifact issues present in afm imaging of soft materials (eg, polymers, monolayers, and biological materials). Tapping mode is far superior to other afm modes for imaging and is currently the recommended state of the art. A good example of tmafm is illustrated in Figure 3 where the height and phase mode images of gelatin films on polystyrene (PS) and on mica are examined (42).

Mechanical Analysis. In addition to the wonderful imaging capabilities of afm, the tip–cantilever system can be used to extract mechanical properties of soft surfaces with the highest of spatial resolution. Since the mechanical behavior of bulk material can be dominated by the properties of the microstructure, aggregation, and domain segregation, analysis of these at length scales smaller than the surface inhomogeneity is critical for advanced materials design and characterization. Essentially, by "pushing" on the surface with the probe, one can extract a form of the Young's modulus (compliance), degree of plastic deformation, scratch and wear resistance, and the tribology of the viscoelastic nature of polymer surfaces. There are three ways to extract a relative Young's modulus E. The most accurate, easy to interpret but time-consuming method to get E (or something that looks like compliance) is with force–distance curves (FCs). As illustrated in Figure 4, the force on the cantilever is measured as a function tip–sample distance for a polystyrene/poly(vinyl methyl ether) (PS/PVME) blend (31). Initially, the tip is far from the surface and is driven toward the sample. In general this is a relative displacement; either the tip or sample is moved (typically the sample is moved, not the tip). As the tip experiences the attractive forces near the surface (mainly because of capillarity if the sample is exposed to air) it is deflected downward, toward the surface. To get accurate mechanical properties, each afm probe must be calibrated to determine its force constant (they vary greatly from designed specification) and the radius of curvature R of the tip. With knowledge of k, cantilever deflections are converted to actual forces. As the tip is driven further toward the sample the resultant force gradient exceeds the value of k; therefore, the system becomes mechanically unstable and snap to contact the surface. Once in contact with the surface and interacting with repulsive forces, further driving of the tip toward the sample results in both the upward deflection of the cantilever, p, and the downward elastic deformation of the sample, s, where the total displacement is $z = p + s$. To extract Young's modulus of soft samples (significantly softer than the afm tip material), FC contact data are fit to $F(z) = k[z - F(h)^{2/3}\left(D^2/R\right)^{1/3}]$, where $D = 3(1 - \nu^2)/(4E)$ and ν is Poisson's ratio (43). In general, the elastic

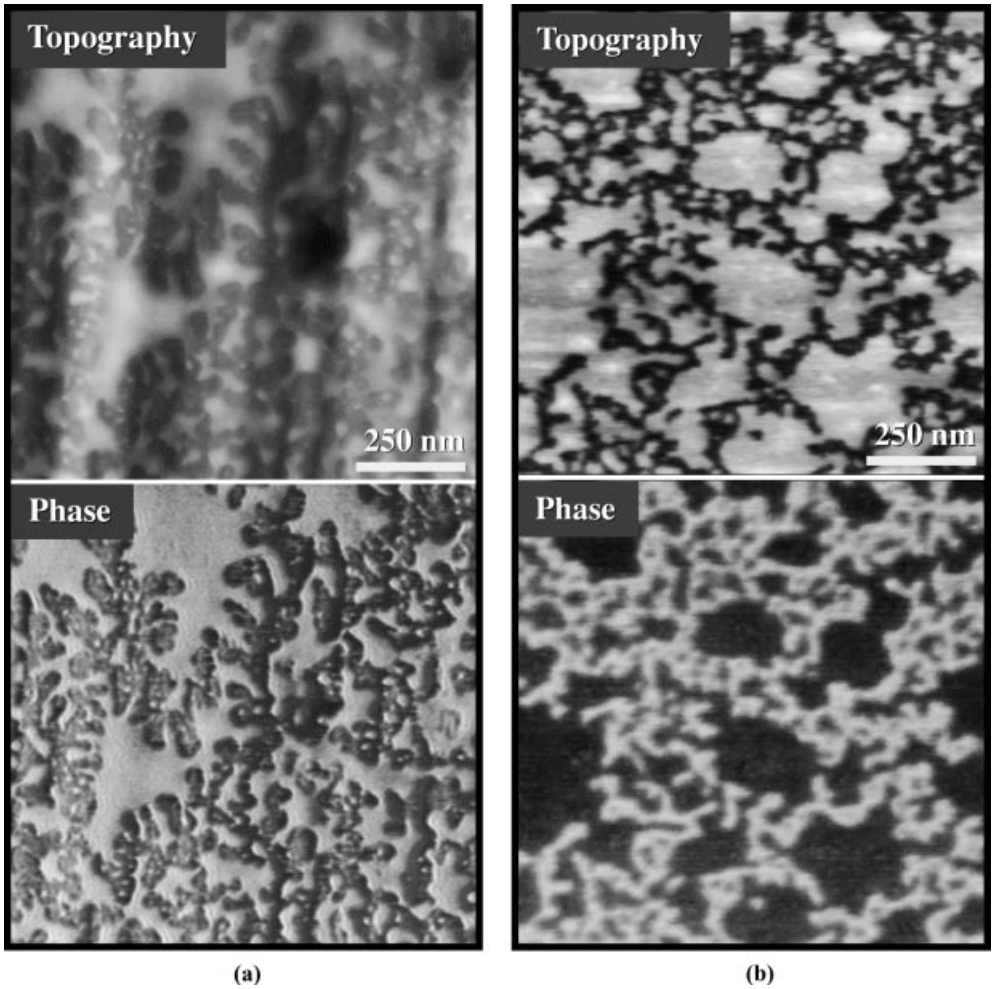

Fig. 3. Examples of tmafm. Reprinted from Ref. 42, Copyright (1998), with permission from Excerpta Media Inc.

modulus is proportional to the magnitude of the slope of the FC contact data. For soft materials there is typically an hysteresis observed during the retraction of the tip from the sample. This hysteresis is more pronounced for softer materials because of the longer relaxation time of compliant polymer films. As the tip is retracted further, still it does not release itself from the surface at the same distance where it snapped into contact initially. Adhesive interactions hold the tip onto the surface until the cantilever-induced force exceeds the adhesive force, which is related to the surface energies, the contact area, and surface roughness, and it subsequently snaps away back to its original undamped state. The difference between the force at the snap to contact point and the adhesive force has been shown to correlate with observed frictional forces (31). This is naively counterintuitive since adhesive interactions are parallel with load direction, and friction is measured perpendicular to the load; they should be uncoupled. Obviously friction

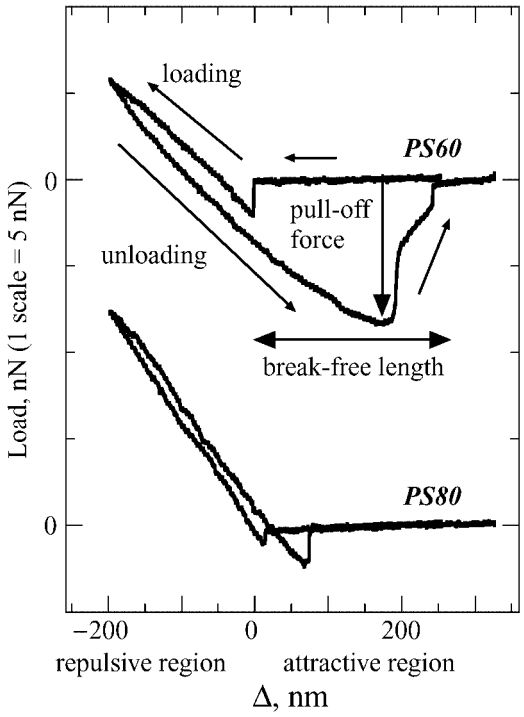

Fig. 4. Force–distance curve for a polymer blend. Reprinted from Ref. 31, Copyright (2000), with permission from AIP.

on soft materials deforms the surface and the tip pulls on the material as the surface yields.

Although FCs are useful and they can be quantitative, they are time-consuming, especially if one is mapping out the surface at each pixel (>10,000 FCs). A faster, and more convenient to visualize, method to obtain rheological information is with "force modulation" microscopy (fmm). This is a contact mode afm experiment where the sample's height is modulated by a sinusoidal signal. This is similar to tmafm except that the sample is driven while the tip remains in contact and that the oscillation frequency for fmm is an order of magnitude lower. As the tip is scanned laterally, both its height and its oscillation amplitude are recorded, where more compliant materials will absorb more energy, damping out the tip's oscillation (44,45). It can also be useful to measure the dynamic mechanical (DMA) properties of the near-surface region (see DYNAMIC MECHANICAL PROPERTIES). Polymers are typically characterized by DMA to yield frequency-dependent behavior. This technique is coupled to an afm by sweeping the oscillation frequency of the fmm experiment. By disabling the slow-scan direction and incrementing the oscillation frequency after each fast-scan line, an fmm amplitude versus position and frequency map is generated (44).

Since fmm is a contact mode technique it subjects the sample's surface to possibly destructive lateral forces as the tip scans. A less destructive alternative is to operate in the tapping-mode regime (46). Changes in mechanical properties

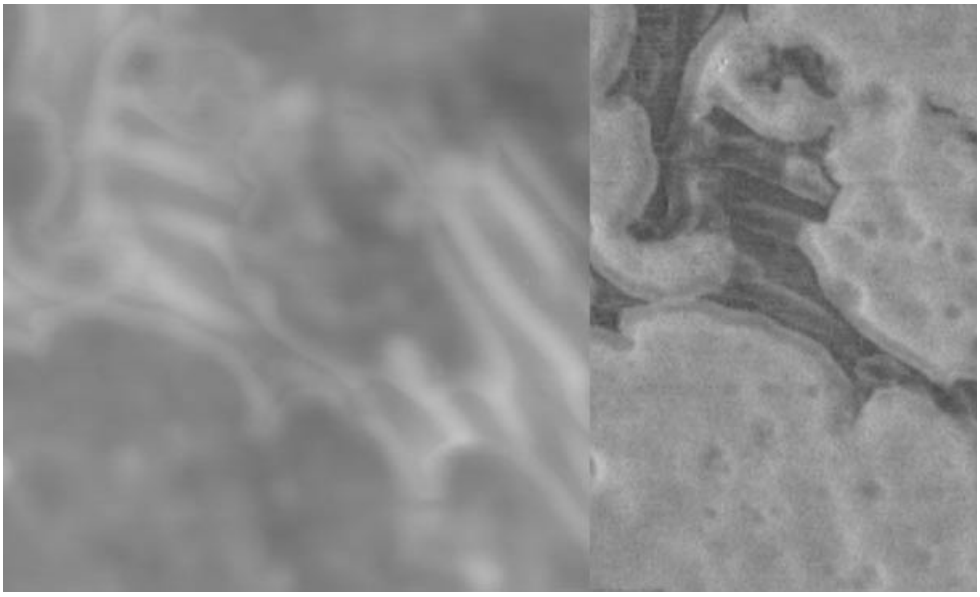

Fig. 5. Example of phase imaging for a polymer blend. Reprinted from Ref. 48, Copyright (1999), with permission from AIP.

near the surface will alter both the tip's amplitude of oscillation in tmafm and also the phase shift between the probe and the oscillating signal driving its vibration. This phase angle, ϕ, is sensitive to the oscillation frequency driving the probe and will lead or lag by $\pm 90^{\circ}$ on either side of the resonant frequency of the free cantilever. For a given frequency and driving amplitude the phase shift will increase or decrease as the compliance of the material changes. Currently this technique is limited to qualitative imaging. Since there is a reversal in contrast as experimental parameters of the tapping tip change, it is difficult to quantify these observations. However, because of the ease at which the phase images are acquired and the nondestructive nature of tmafm, this technique is now prevalent and found on all modern afm instrumentation (47). A clear demonstration of the qualitative advantage provided by phase imaging is shown in Figure 5, which compares the height (right) and phase (left) images of a doped polyanaline/cellulose acetate blend (48).

Much effort has been directed toward minimizing damage on the surface because of the scanning probes. This implies that it is quite easy to use the afm for studies of indentation and wear as illustrated in Figure 6 where a nano-scratch into a poly(ether ether ketone)(PEEK) matrix shows its relative poor wear resistance as compared to graphite (49). Using the stiff cantilevers required for tmafm, while in contact mode, softer polymer surfaces and their resultant composite systems can be plastically deformed and scratched. Indentation studies (ie, Vickers Hardness testing) are obtained by simply pushing harder than usual during an FC. With the stiffer probe pushing on the elastically deforming sample, it will eventually reach the polymer's yield strength. At this point the sample will plastically deform, leaving a tip-shaped indentation as the probe is pulled away from

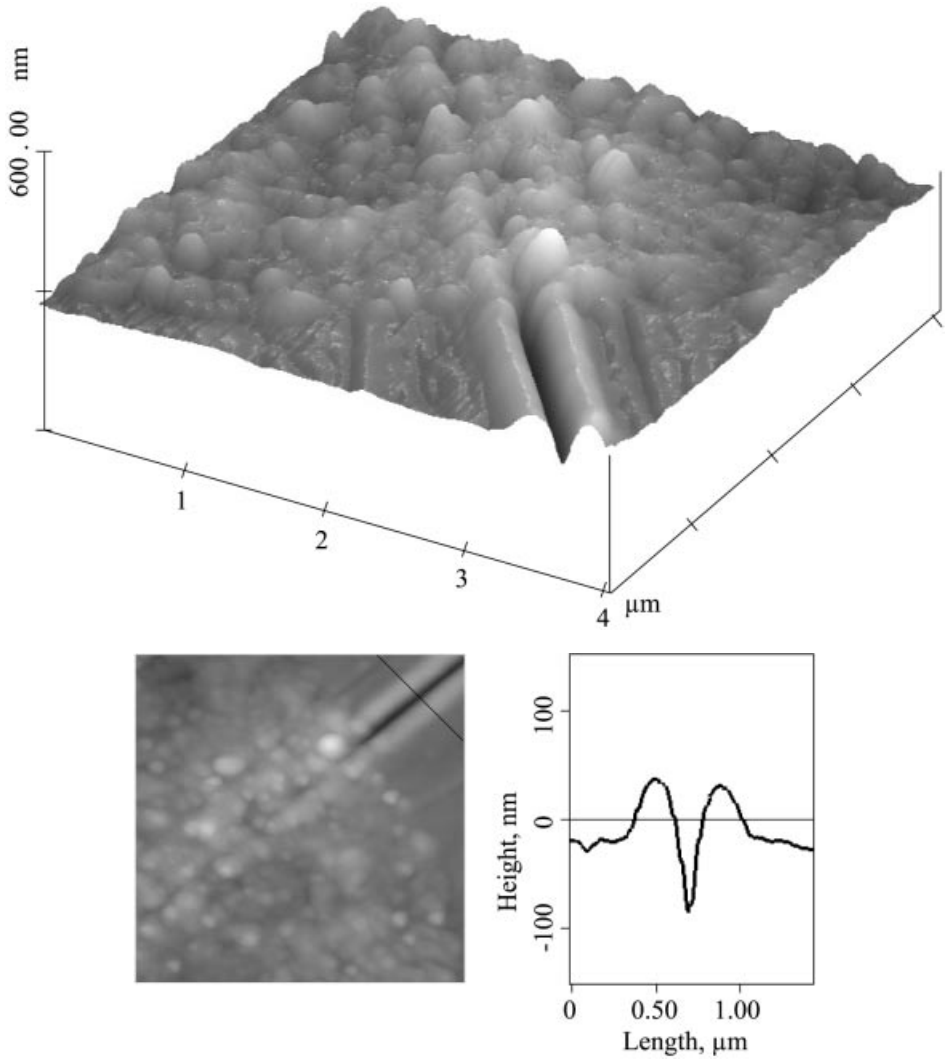

Fig. 6. Nanoscratching of a PEEK matrix sample. Reprinted from Ref. 49 (Fig. 3), Copyright (1999), with kind permission from Kluwer Academic Publishers.

the sample (50). After the indentation is formed, the same afm tip is used to scan over the new topography of the surface. Typical results exhibit a tip-shaped pit surrounded by pushed-up material. Since the elastic modulus of a standard tip is several hundred times larger than that for typical soft polymers, it can be assumed that most of the deformation is confined to the sample and that the shape of the tip is not deleteriously affected. Young's moduli and the materials tensile yield stress are extracted by modeling the contact and deformation geometry using Hertzian mechanics. The principles of nanotribology have been extensively reviewed elsewhere (51). More interesting still is the afm's ability to measure wear resistance with nanometers resolution. The contact area of the tip dragging across the sample, typically 10–100 nm, limits the spatial resolution of wear

resistance studies. Using appropriate software, the afm probe is directed across the surface to scratch out a pattern. Wear resistance versus scratch speed and tool pressure can be very useful when designing polymer blends and/or composites where low compliance and low adhesion are materials trade-offs and need to be optimized (49). This method has also been considered for pattern transfer applications. By scratching through thin, soft layers of a protective coating with the afm tip, a desired pattern can be lithographically transferred to the underlying substrate. Although direct write techniques are unacceptably inefficient, they do show promise for some limited ultrahigh resolution applications (52).

Developing Techniques. During the unloading segment of an FC on soft polymers, the tip pulls off of the surface and typically snaps back to its free position. Occasionally, however, the tip retracts in several steps, or sometimes pulls away such that the force versus distance curve is only mildly sloped. These observations are a result of polymer chain interaction with the tip (53). Material adsorbs to the afm tip during the compression and requires time to untangle itself from the chains on the substrate during pull-off (31). This phenomenon has shed light on another outstanding capability of the afm: its ability to perform single-molecule force studies. By properly functionalization of an afm tip and appropriate surface preparation, individual long-chain molecules can be manipulated and extended, again revolutionizing polymer mechanics and dynamics. Studies have yielded single-molecule force versus extension curves of poly(vinyl alcohol) (PVA) (54), polysaccharides (55,56), poly(acrylic acid) (57), and biological polymers as well (58). A typical single-molecule FC is shown in Figure 7, where a single PVA

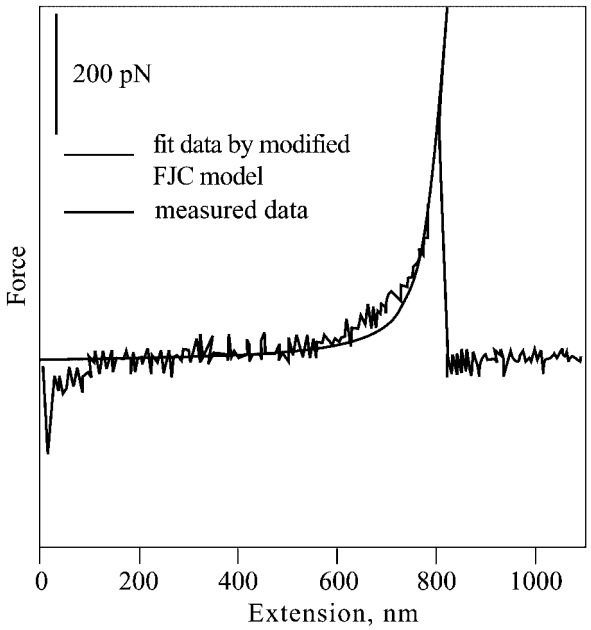

Fig. 7. A single-molecule force–distance curve for PVA. Reprinted from Ref. 54, Copyright © 1998, John Wiley & Sons, Inc.

chain is extended by an afm probe, and these data are modeled well by a freely jointed chain up to the force that causes bond rupture (54). Common to many of these studies is an apparent conformational change of the polymer strand as it is extended, followed by conversion to a significantly stiffer "crystalline" strand and then finally by bond scission. As the dimensions of nanostructured polymeric materials are reduced, single-molecule mechanics should directly correlate with these processed devices. It can be expected that the promise of chemistry's molecular fidelity finally enables true structure–function relationships for condensed materials in the near future.

In addition to imaging and mechanical analysis, researchers are now pursuing thermal analysis microscopy of polymer surfaces. Although this area is developing rapidly and has been well reviewed (59), only the state-of-the art available on commercial systems will be presented here. At the heart of scanning thermal microscopy (sthm) is the heat transfer process at the tip–sample "contact." Variations in heat transfer result in appropriate signal contrast where lateral resolution is limited by variations in thermal conductivity. Although thermal noise is quite low and signal sensitivity high, it is doubtful that the sthm will ever attain subnanometer resolution. Resolution of thermal contrast of approximately 100 nm is now common. There are several modes of operation, but typically a thermocouple or thermister is integrated into an afm probe where the tip of the temperature transducer is also the scanning tip. The system operates in contact mode and either the sample or the tip is heated. AC detection of an oscillating temperature increases signal sensitivity. This is most easily achieved by modulating the output power of a laser incident on the system. If the spectral absorption of the sample is spatially inhomogeneous, this too can be measured by scanning the wavelength of the light source at each, or some, of the scanning positions on the surface (60,61).

A more useful probe for sthm is the resistive wire (62). Instead of heating the sample and measuring the temperature with the tip, the tip itself is heated and its temperature is measured, via changes in its electrical resistance. Changes in local thermal conductivity of the sample will result in changes of the tip's temperature for a constant power through the wire. Dissipation of heat at the tip–sample "contact" and through inhomogeneous samples is convoluted, making quantitative measurements poorly understood. Thermal inhomogeneity in a polymer film can be laterally across and or longitudinally through the sample. Since the thermal diffusion length of a typical polymer is of the order of a micron, nanoscale calorimetry will approach a fundamental limit. However, micron-resolved thermal conductivity of domains in a poly(vinyl chloride)/polybutadiene (PVC/PBD) polymer blend have been clearly demonstrated in the literature (63). This type of microscopy can be more relevant on composites where fine tuning of thermal and mechanical properties is desired.

In addition to thermal conductivity, modifications of the sthm can yield thermal capacity or more specifically differential scanning calorimetry (dsc). Instead of heating the resistive wire with a constant power, its temperature is modulated with an ac current. The resultant amplitude and phase shift of the wire's temperature is measured with a lock-in-amplifier. Simultaneously, the temperature of the tip and sample are ramped up slowly so as to measure the change in heat dissipation per change in temperature, dq/dT. This measure is, of course, related to the local heat capacity of the sample and is correlated with expected phase

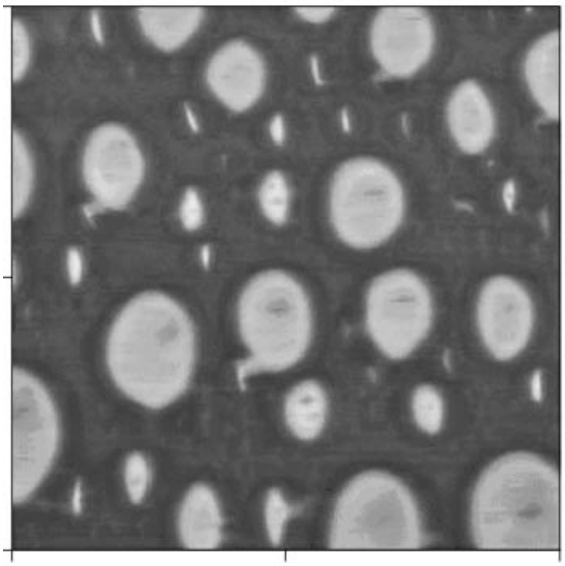

Fig. 8. A sthm scan of a PVC/PBD blend. Reprinted from Ref. 63, Copyright (1996), with permission from AIP.

transitions of the material. Plotting the first derivative of the phase shift versus sample temperature looks very similar to the bulk DSC as shown in Figure 8 for a sample of thermally quenched PET (63). Variations of glass-transition temperatures in micrometetr-sized domains could be critical as device dimensions shrink.

Since the afm is peerless at measuring vertical expansion, and the ac sthm can measure temperature, it should be possible to extract coefficients of thermal expansion (CTE) on thin films, which is nearly impossible with conventional thermal mechanical analysis (TMA). By modulating the sample's temperature the longitudinal composite expansion can be measured by the deflection of the sthm cantilever as the probe scans the sample (64). These capabilities are critically important when developing multilayered thin-film materials. Expansion of PMMA film insulating a gold interconnect line is measured and illustrated in Figure 9 (64). These data show that the theoretically expected expansion deviates from those observed, implying that this additional thermal fatigue could lead to premature device failure.

As mentioned above, the spm is mostly limited to sampling the near-surface region of a polymer system. A new technique based on tmafm has been developed to enable volume imaging with the spm. This study tracked a series of height and phase images of a styrene–butadiene–styrene (SBS) triblock polymer microdomain as the surface was being removed 7.5 nm at a time with a plasma etcher. These data are illustrated in Figure 10 (65).

Prior to the development of the spm, and all its derivatives, scaling of physical properties from the macroscopic to the nanoscopic was speculative at best. "Experiments are the only means of knowledge at our disposal. The rest is poetry and imagination" (Max Plank). The afm has opened the door of exploration into the varied complexities of advanced polymeric materials. In the following,

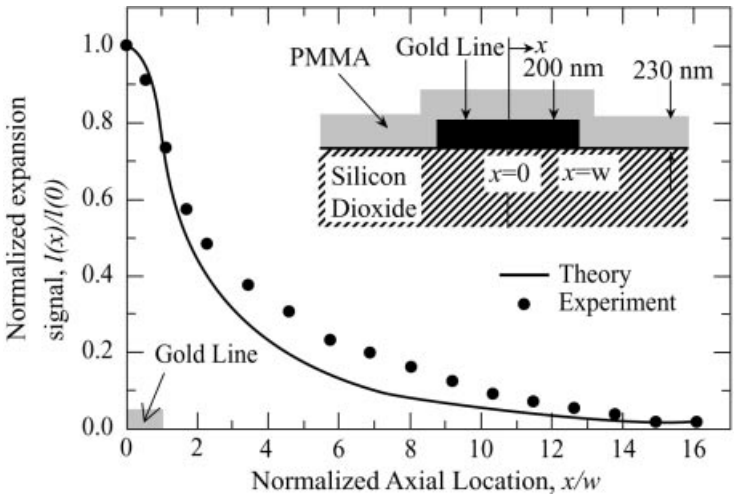

Fig. 9. A sthm scan of a multilayer device construction. Reprinted from Ref. 64, Copyright (1998), with permission from AIP.

observations on various molecular systems and the surface characteristics intrinsic to them and their processing are discussed.

Systems

LB Films. Use of Langmuir–Blodgett (LB) film techniques have been shown to be an effective method for producing thin layers of materials for thermomechanical evaluation. Morphological description of such samples by afm has been used with success in a wide range of polymer systems. Individual chains of phthalocyaninepolysiloxane shish kabob molecules were deposited on metal nanoelectrodes using LB techniques (mixed with isopentyl cellulose) and then dispersed on the surface of an LB trough. The deposition surface was dipped into the dispersion to deposit the polymer mixture. The authors demonstrated that the structures of these semiconductive polymers are not disturbed by raised patterns on the electrode (66). Polystyrene/poly(ethylene oxide) (PS/PEO) diblock copolymers of differing fractional compositions were used to produce LB films. Polystyrene aggregates were observed to accumulate on the surface of the films; the features of these aggregates were directly proportional to the PS content in the starting diblock copolymer. Hence, by manipulation of the starting polymer, controlled patterning of the film surface could be accomplished without use of any lithographic methods (67) (see LANGMUIR–BLODGETT FILMS).

Changes in the environment in which polymer LB films are produced can result in significant structural changes of the deposited materials. LB films of poly(γ-benzyl-L-glutamate) produced from a number of solvents were imaged. Solvent polarity strongly influenced the self-assembly process and is manifest as thickness and height variations of individual fibers (which formed on the mica substrate), and in the lateral globular dimensions of the polymer absorbed from

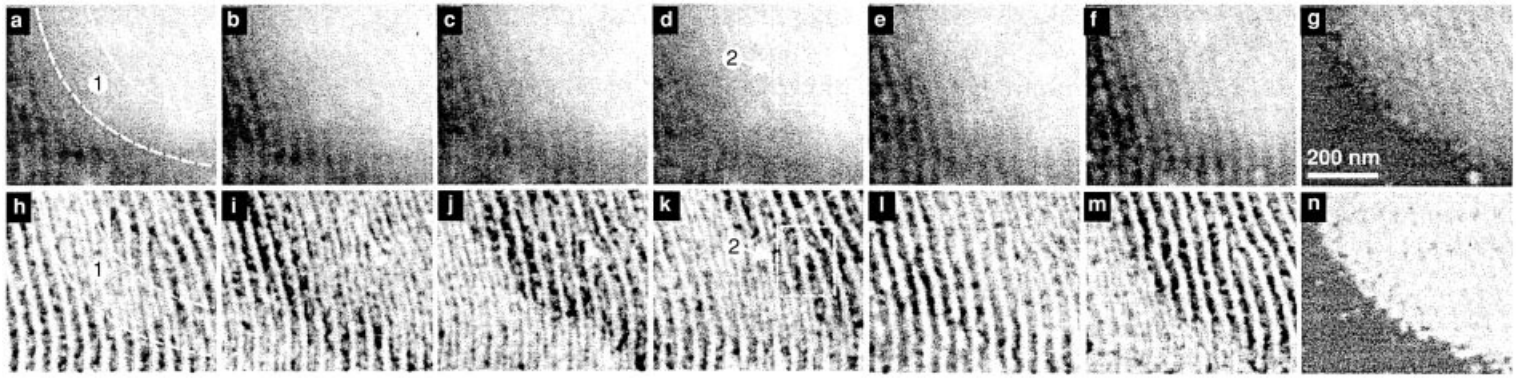

Fig. 10. TMAFM study of an SBS triblock polymer, as its surface was removed. Reprinted from Ref. 65, Copyright (2000) by the American Physical Society.

dilute solution. AFM allowed for the quantification of these structural differences, and was used to suggest a mechanism for self-assembly of polymer chains into fibrils (68). Varying the pH at which LB films of poly(linoleic acid) were produced resulted in major morphological changes within the deposited film. Tapping mode afm shows spherical particles lacking any regular pattern when depositing from a subphase solution with a pH of 6.0. As the pH is increased to 6.3 and 6.6, increasing organization into a network structure was observed. At pH 6.9, much of this structure was observed to be absent; it is at this pH that a step change in chemical reactivity of the polymer film is observed as well. Therefore, this method allows for a correlation between film structure and chemical properties (69).

Morphological differences in LB films result from small compositional changes in the polymers used, and from the difference in processing between LB and freestanding thick films. Formation of LB films from salts produced from polyamic acid and a variety of alkylamines were examined by afm. Unique morphologies were obtained, as the chemical structure of the amine was varied (70). The structure of LB films of polyaniline (PA) was shown by afm to possess preferential orientation, but with much lower levels of porosity than which had been previously observed within freestanding films. Increases of surface roughness in LB films were observed by afm when the ratio of low molecular weight PA to cadmium stearate in the subphase solution was increased, while domain sizes varied inversely with organic content (71). Varying the side chains of poly(*N*-alkyl acrylamides) was also demonstrated to produce major differences in morphologies in LB films. When decyl side chains were incorporated into the polymer film, these groups were observed to adopt random orientations. Increasing the chain lengths to octadecyl resulted in highly ordered two-dimensional crystals that were imaged by afm (72).

Monolayers (Self-Assembly of Oligomers). The degree of ordering, which results from molecular self-assembly of polymer systems, is readily ascertained using afm. Thin layers of an acetylenic phospholipid were demonstrated by afm to self-assemble into lamellar structures when cast as thin films. Uv polymerization of these films produced polymers with well-packed structures (73). Alternating layers of positively charged poly(diallyldimethylammonium chloride) and negatively charged montmorillonite clay were self-assembled onto various substrates. AFM was used to quantify the smoothing of initial surface roughness with each successful layer assembled to the surface, and to develop a representation of how clay platelets and polymer chains associate in layers (74). AFM imaging was used to determine the morphologies of nitro-containing diazoresin, as a function of deposition time, and of bilayer and multilayer assemblies of the diazoresin and poly(sodium *p*-styrene sulfonate). Flat, stable multilayer structures were demonstrated upon uv-irradiation (which resulted in replacement of the diazo group with C—C bonds between layers of polymers), and regular structures were shown to be maintained (75).

Biopolymers. Ranging from individual chains of deoxyribonucleic acid (DNA) to the "high performance" fibers produced by spiders for their use as draglines, afm has been used to provide insights into biopolymers, much as it has for synthetic systems (see POLYNUCLEOTIDES; SILK).

Solutions of single- and double-stranded DNA (as well as several synthetic polymers) were electrosprayed onto a mica surface and imaged. Each polymer

could be generated and analyzed in globular or fibrillar forms, depending on conditions of the electrospray processing of the solutions. Increasing polymer concentration in the water solutions led to formation of the globular structures. Changes in electrode potential used in the electrospraying was shown to also play a role in the morphology of the biopolymer (76).

Both stretched and unstretched silk threads from the Black Widow spider were imaged. Two types of fibers were observed within the threads (thicker, 300 nm in diameter, oriented parallel to the thread axis; thinner, 10–100 nm fibrils oriented across the thread axis). With increasing strain, mean fiber and fibril diameters were found to decrease and fibrils aligned themselves more closely with the thread axis. The authors were able to relate these structural features to models of secondary and tertiary structure and organization in spider silk (77).

Thermosets. Structure determination in thermoset polymer systems can at times be problematic because of their relative insolubilities and large molecular weights. Direct observation of structural details by afm has been advantageous for such systems, describing both inherent material properties as well as the impact of processing steps on final structure properties.

The role of processing of thermosets in determining ultimate polymer structure is well studied using afm. The morphological structures of fibers and films produced from segmented Polyimides were shown to match closely those predicted by molecular modeling (Fig. 11). In these systems, two-dimensional arrays of ordered polymer chain backbones were observed. For fibers, the polymer chain backbones were found to be oriented at a definite angle with respect to the fiber machine axis, where this angle is hypothesized to be due to differential shrinkage of the core and surface of the fiber during solvent removal and heat treatment of the fibers (78). AFM imaging of carbon fibers revealed extrusion lines, as well as the presence of "dirt" inclusions. A correlation between the concentration of these particles and the strength of the fibers was observed, providing a structural basis for optimizing the fiber-making process (79).

Inherent polymer morphologies have been determined using afm imaging. This technique was used to discover a parallel-rod structure on the surface of fluorinated polyimide films produced by vapor deposition polymerization; these structural details were not apparent by scanning electron microscopy (sem). When spin-cast films of the same polymer were imaged, a rough structure lacking the rod-like morphology was observed. The authors concluded that the parallel-rod morphology resulted from both polymer–polymer and polymer–substrate interactions (80). Cleaved surfaces of the polyacetylene poly(2,4-hexadiyne-1,6-diol bis(*p*-toluene sulphonate)) were imaged, revealing *bc*- and *ab*-planes consistent with the crystal structure of the polymer. An overall zig-zag morphology, with step heights corresponding to one polymer chain's width, was resolved clearly. Substituents on one side of the polymer backbone were observed to stick out diagonally from the surface, while other side chains were observed to be located underneath the substituents of a neighboring polymer chain (81). Thermoset epoxy resins modified with nanoclays were imaged using phase contrast afm. These images showed interlayer distances that were noticeably smaller than those measured by wide-angle x-ray scattering (waxs); the authors speculate that the mechanical deformation of the clay silicate layers by the afm tip may be the cause of this discrepancy, challenging the notion that the clays serve as rigid reinforcing layers in the composite (82).

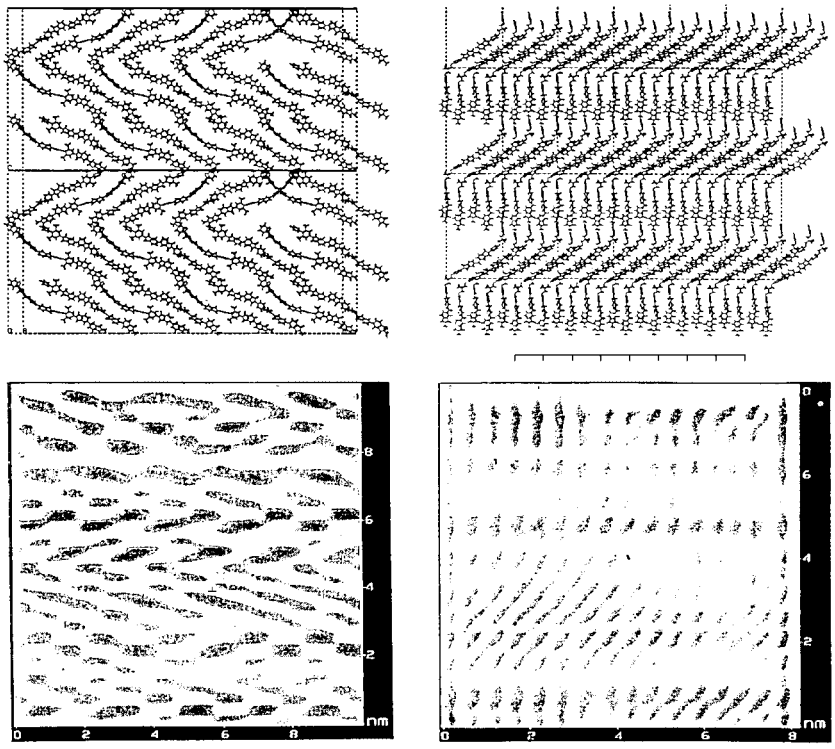

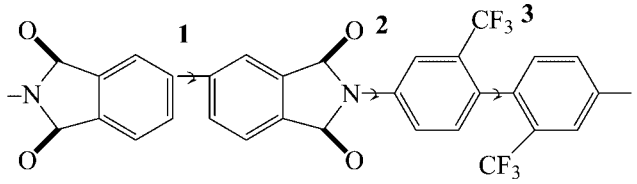

BPDA-PFMB (3,3 ,4,4 -biphenyltetracarboxylic dianhydride + 2,2 -bis(trifluoromethyl) 4,4 -diaminobiphenyl)

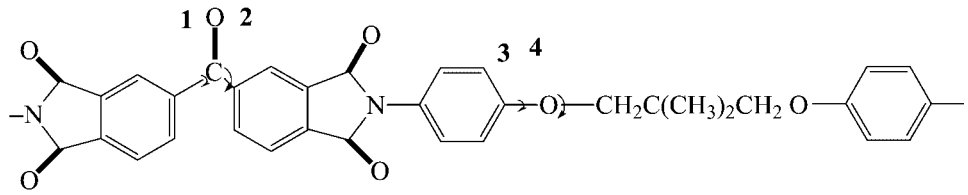

BTDA (1,3-bis(4-aminophenoxy)-2,2-dimethylpropane + 3,3 ,4,4 -benzophenontetracarboxylic dianhydride)

Fig. 11. Morphology of segmented polyimide structures. Reprinted from Ref. 78 (Figs. 1c, 1f, 3 and Scheme 3), Copyright (1992), with permission from Springer-Verlag.

Chemical modifications of thermoset resins have been documented, using afm as an analytical tool. Ion beam modification of polyimide surfaces were imaged in contact mode, which showed a reduction in surface roughness with increasing irradiation, and generation of a graphitic structure in the degraded polymer (83).

Thermoplastics. The largest body of afm structural studies to date in the area of organic polymers has probed the details of commodity thermoplastic materials. Within this work, both support and extension of knowledge gained by other techniques, such as electron microscopy, as well as new insights into the structure–property differences which result from melt processing and/or thermal treatment have been gained. Specifics of thermoplastic surfaces, important in controlling transport and adhesion phenomena, have also richly benefited from afm studies. Structural studies of combinations of these thermoplastics is discussed later.

Polyethylene. AFM imaging of thermoplastics has been widely used to corroborate and expand knowledge obtained using other structural methods, such as x-ray crystallography and electron microscopy. Direct observation of folded chain lamellar crystals of polyethylene (PE) was provided by afm. Spacings appropriate for the (known crystallographic) orthorhombic unit cell, and for the monoclinic unit cell that can be produced by mechanical deformation, were observed (84) as were boundaries between regions of differently oriented folded chains (85) (see ETHYLENE POLYMERS, HDPE).

Cold extruded PE was imaged at scales ranging from 700 nm $\times$ 700 nm down to atomic scale resolution. Fibrillar morphology was observed for uniaxially oriented materials, with microfibrils in the 20–90 nm range, aligned with the extrusion axis. Individual polymer chains and extended chains were also observed (86).

Extruded high density polyethylene (HDPE) pipe was cooled on the outside with water, while the internal surface was allowed to cool in ambient air. As a result of this cooling gradient during fabrication, a range of crystal structures could be anticipated. AFM imaging of sections across the pipe confirmed major morphological differences that arose from the differential cooling. At all locations, spherulitic structures were observed, but spherulite size, band period, and lamellae thickness increased within the pipe from the cooled to uncooled sides (Table 1) (87).

Polypropylene and Polystyrene. As with PE, afm has yielded important structural details for the different grades of polypropylene (PP) and Polystyrene (PS). Syndiotactic polystyrene (sPS) was imaged (Fig. 12), showing a spherulitic

Table 1. Morphological Differences Arising from Differential Cooling of HDPE

Imaged area	Spherulite size, μm	Band period, nm
Cooled edge	2–3	400–500
Intermediate	4–5	800–900
Middle	6–8	1000–1100
Intermediate	8.5–10.5	1200–1400
Uncooled edge	10–13	1600–2000

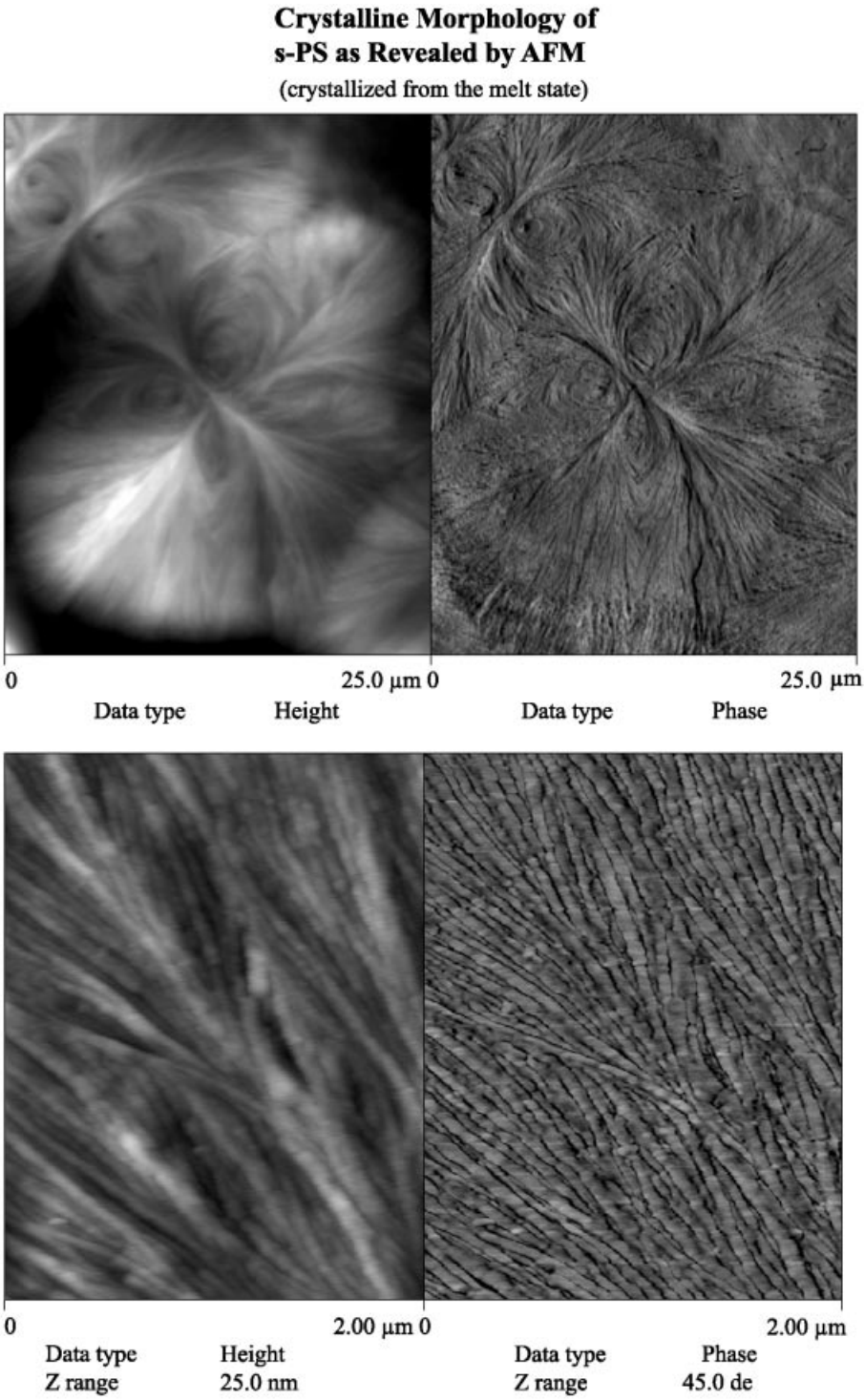

Fig. 12. Structural details of sPS. From Ref. 89, courtesy of Prof. S. Nazarenko.

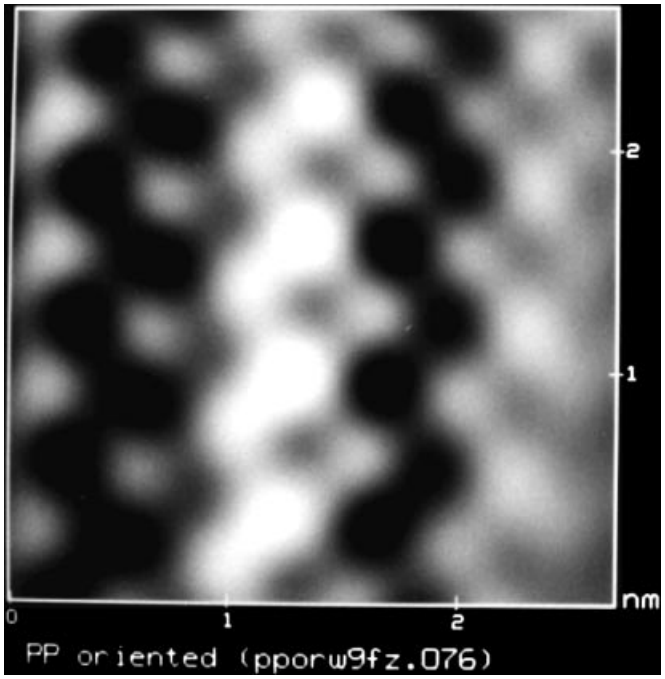

Fig. 13. Detailed structure of iPP. Reprinted from Ref. 91, Copyright (1994), with permission from Elsevier.

structure consistent with prior sem work. The radially arranged fibrils in the spherulites were shown to consist of small lamellar crystals. The observed spherulites were also twisted. Epitaxial crystallization of sPP on *p*-terphenyl created a laminar structure, such that the lamellae stand on end, with an average thickness of 20 nm (88). Similar structural details have been observed for syndiotactic polypropylene (sPP) (89).

Uniaxially oriented isotactic polypropylene (iPP) was imaged using afm, showing microfibrils and macromolecules. Fibrils with an average diameter of 150 nm were observed. Individual polymer chains with 1.17 nm chain–chain distance were seen. The authors propose that the (110) crystal plane was being resolved with this work (90). Other workers, who were able to clearly resolve right- and left-handed helices (Fig. 13) with pendant methyl groups visible, accomplished atomic scale resolution of iPP (91).

The metastable β-phase of iPP was imaged in another study, where epitaxial crystallization was found to result in a biaxial orientation that could not be achieved mechanically because of the $\beta \rightarrow \alpha$ transition that occurs during orientation. A lateral periodicity of 1.9 nm was found in the (110) face, corresponding to the distance between three chains, and is indicative of the frustrated packing of the β-phase of iPP. Variability in the image suggested the possibility of two distinct frustrated phases existing in the samples (92).

The effects of processing conditions on polymer structure have been demonstrated clearly using afm images of PP. Polypropylene fibers spun using three

different processes, gravity spinning, melt spinning, and melt blowing, were imaged by afm, and the structures resulting from each of these different processing methods compared. The surface of gravity-spun PP was found to be entirely covered with spherulites consisting of polycrystalline aggregates formed from a radiating array. Each branch of the spherulites were composed of lamellae and are connected by regions of amorphous material, consistent with general lack of orientation along the fiber axis. Similar structures were observed for melt-blown PP fibers. Analysis of images showed that spherulite diameter versus fiber diameter for melt-blown and gravity-spun fibers are correlated, which is very useful for developing polymer processors. The intercept of this correlation line is related to the amount of amorphous material in the polymer, and the slope to the number of spherulites that can fit along the circumference of the fiber. For the melt-spun fibers, no spherulites were observed. Spherulites generally grow on nonmoving surfaces since the transfer of stress to the growing threadline leads instead to the also well-known shish kabob structure in this case, consistent with polymers crystallized under strain (93).

Thermoplastic Polyesters. The effect of substrate structure upon applied polymer layer morphology was well illustrated with a thermoplastic polyester. Poly(ethylene terephthalate) films were formed on the surface of oriented poly(tetrafluoroethylene) (PTFE) and on silicon surfaces. The PTFE surface was characterized by ridges 0.1–0.2 μm wide, running parallel to the PTFE draw direction. The silicon wafer showed regular, two-dimensional roughness features. When PET film was overlaid on these two surfaces, its morphology was surface-induced. PET applied directly to the silicon wafer exhibited random, two-dimensional roughness, whereas the PET applied to the oriented PTFE surface aligned itself in parallel ribbons approximating the PTFE structure (94).

Specific chemical structures have been reported when near atomic scale resolution is obtained. When PET surfaces were imaged down to the nanometer scale, triads of roughly circular structures, 0.29 nm in diameter, corresponding to the expected size of terephthalate phenyl groups were observed (Fig. 14). The authors propose that the structures may indeed be terephthalate phenyl groups in the polymer (95).

Insights into the chemical properties of polyesters have also been obtained using afm imaging as a tool. The diffusion/deposition of oligomers to the surface of PET copolyesters was demonstrated by imaging hard nodules on the polyester surfaces as a function of copolymer composition. The frequency of these hard nodules observed by afm correlated with the levels of oligomer that could be solvent-extracted from the copolymers (96).

Other Thermoplastics. Polyoxymethylene (POM) was imaged by afm, revealing oriented polymer chains parallel with the machine axis of sample extrusion (Fig. 15). Atomic scale resolution of the chains demonstrated the helical nature of the polymer chains. Long-range correlation between polymer chains was observed as well (97). Imaging of extended chain crystals of POM closely matched molecular models for this material, allowing for the molecular packing and order in the extended chain crystal to be well understood. The authors were able to describe the polymer chain orientations with respect to the crystal (98).

Poly(tetrafluoroethylene) was imaged after a mechanical deposition method. Parallel rows of approximately 0.5 nm spacing were resolved (99). The PTFE

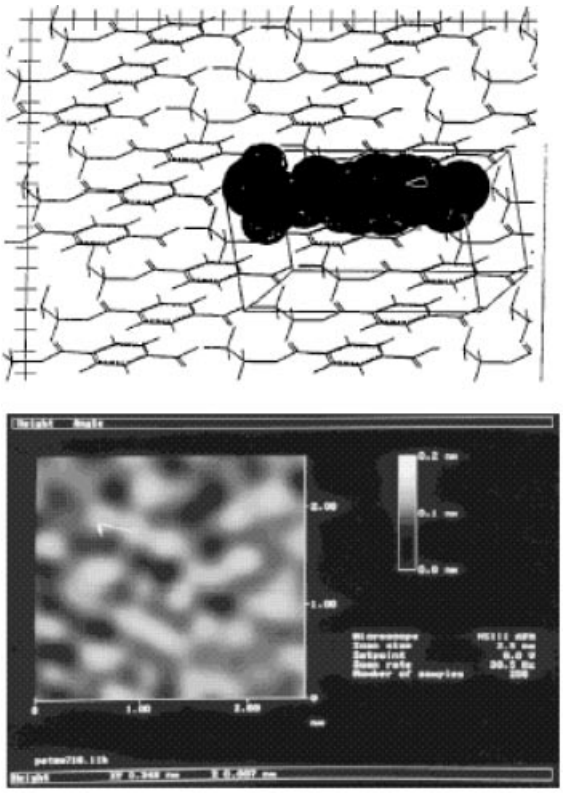

Fig. 14. Proposed atomic scale resolution in afm of PET. From Ref. 95, Copyright © (1997). Reprinted by permission of John Wiley & Sons, Inc.

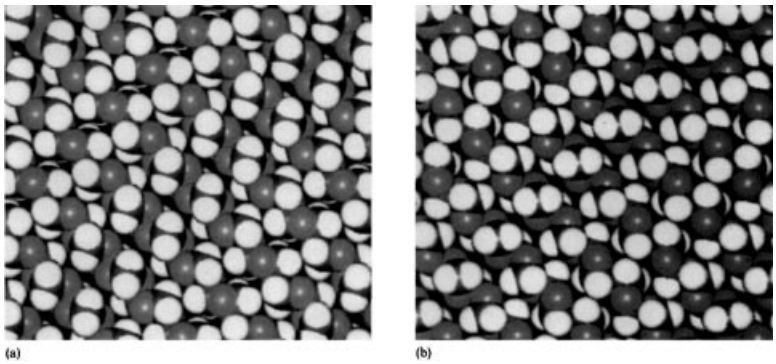

Fig. 15. Extended chain crystals of POM, showing polymer chain orientation with respect to the crystal. Reprinted from Ref. 98, Copyright (1994), with permission from Elsevier.

imaging demonstrated that because of its softness, the majority of observations with this material often are due to artifacts, rather than actual polymer structure. Operating in tapping mode, afm images of PTFE revealed structures comparable to those obtained with sem. The results of this work showed that PTFE is capable

of supporting large forces on the millisecond time scale, but is subject to creep at longer time frames (100).

Ultrahigh molecular weight polyethylene (UHMWPE) tapes were imaged under water to minimize operating repulsive forces and contact area between probe and sample. Highly regular fibular structures were obtained. Periodic contrast variations along the stretching axis were found on drawn tapes only under stronger operation forces, suggestive that these variations are a function of surface hardness, rather than of surface topology (101). Gel-drawn UHMWPE films showed bundles of microfibrils between 4 and 7 μm in diameter, depending upon the elongation, microfibrils between 0.2 and 1.2 μm in diameter, depending upon draw ratios employed, nanofibrils which form the microfibrils, and regular chain patterns on the molecular scale which correspond to the crystalline packing of the polymer chains at the surface of the nanofibrils (102).

While normally amorphous, and generally featureless on a micron scale, crystallization of polycarbonate was solvent-induced with butyl acetate, generating a disc-like spherulitic structure of ca 10 μm in diameter surrounded by an amorphous matrix. Within the spherulite, the twisted fibrils emanating from the point of nucleation were observed in these afm images, and is consistent with known lamellar growth mechanisms (103).

Liquid Crystalline Polymers. The high degree of stereoregularity associated with liquid crystalline polymer systems has been observed using afm. Effects of method of sample preparation, of post-extrusion heat treatment of the sample, and of interchain hydrogen bonding upon morphological structure have all been investigated. Lytropic poly(*p*-phenylene terephthalamide) (PPTA) was dry-jet wet-spun from sulfuric acid into a coagulant bath, and imaged as spun, after heat treatment. The authors obtained atomic scale resolution of both forms of the fibers, observing changes in periodicity in the structures resulting from the heat treatment (104,105). Thermotropic liquid crystalline polyesters were imaged (Fig. 16), showing ribbon-like fibrils; atomic-scale details of the fibril surfaces were also obtained. In polymers capable of hydrogen bonding between chains, a greater degree of chain-to-chain cohesion, which the authors propose could result from some degree of self-assembly, was observed (106).

When macromolecular cholesteric liquid crystals were imaged, a twisting of molecular orientation, which translated into a periodic lamellar structure in the materials, was found. Good agreement between afm and tem (transmission electron microscopy) was obtained in determining the widths of the lamellae. When the same polymer was processed from an isotropic solution, a homogeneous and nodular structure, lacking the periodicity of the cholesteric structure, was obtained (107).

Hyperbranched Polymers and Dendrimers. The rapid growth of knowledge in the area of Hyperbranched Polymers and dendrimers has been aided by the direct observation of large-scale structure from afm (see DENDRONIZED POLYMERS). Workers in this area have observed the nature of growth and distribution of polymeric branches as a function of both the chemical structure of the materials as well as that of surfaces on which the materials are grown. Further control of such structures, by introduction of additional, space-filling materials, has been observed by afm, as has general structural features of these complex polymers. Hyperbranched polyacrylic acid (PAA) films were imaged and it was found that

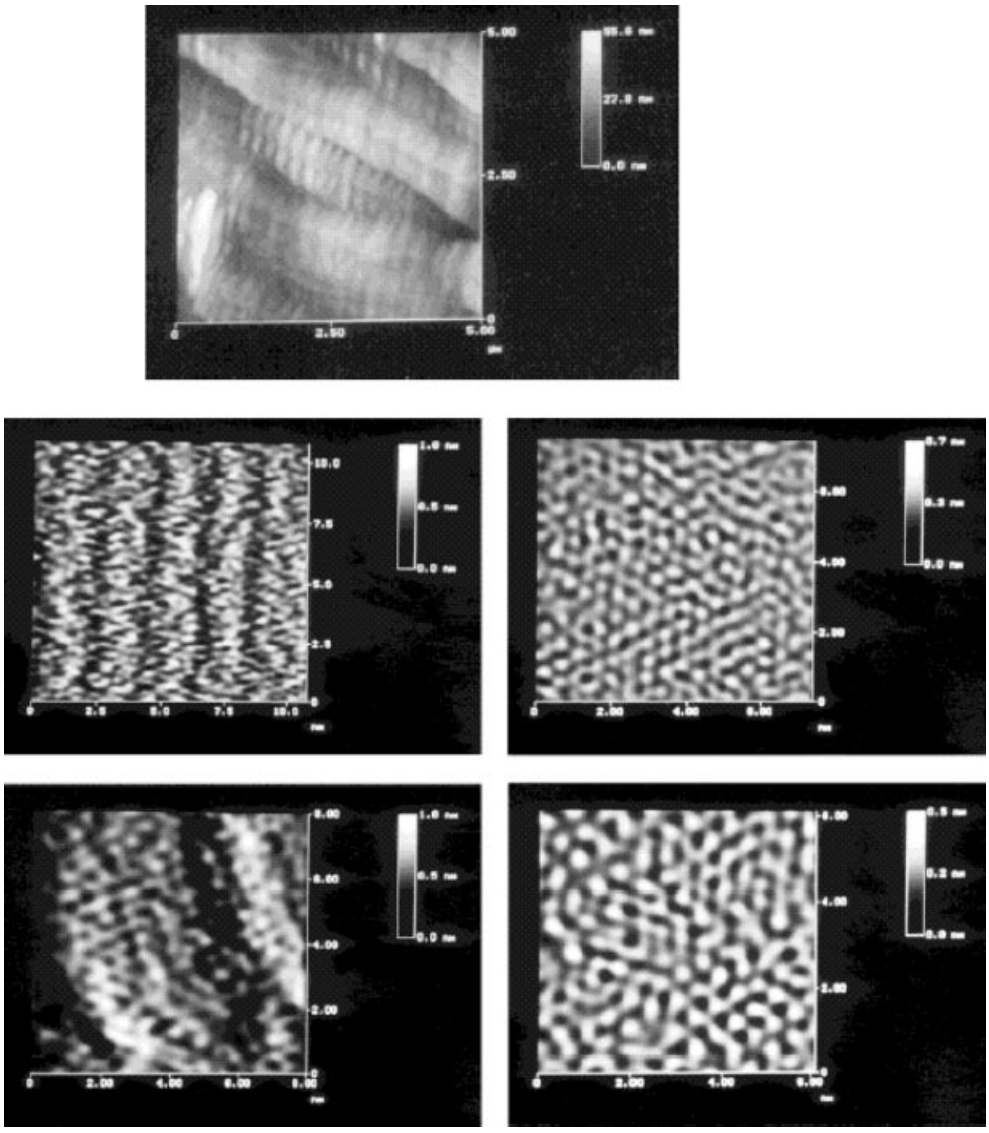

Fig. 16. An afm of a thermotropic liquid crystalline polymer, showing details of fibrillar structure. From Ref. 106, Copyright © (1999). Reprinted by permission of John Wiley & Sons, Inc.

rms roughness declined as one progressed from zero to three dendrimer "generations," and then increased monotonically up through generation six when bonded to a rough gold substrate. When a smooth gold substrate was used, increasing roughness was observed starting with the first generation of hyperbranched PAA. The authors attributed this phenomenon to a sequential masking of roughness in the nonsmooth starting gold substrate through three generations. However, once a uniform surface smoothness is established, the dendrimer could then be randomly deposited on that surface, where subsequent layers would favor deposition

at those sites which contain the highest chain ends to bond to, and hence, increasing roughness is developed. With the smooth substrate, the first generation would be deposited randomly, and each successive generation of hyperbranched polymer favors addition to those areas containing high concentrations of acidic polymer chain ends, thereby increasing roughness with each added generation (108). Polyimidoamine starburst dendimers were similarly adsorbed on Au(111) surfaces. The relatively deformable fourth generation dendrimer, and the larger, more spherical and more rigid eighth generation dendrimer were tested. Directly adhered to the gold surface, the individual fourth generation dendrimers were shorter than those of the eighth generation material. Pretreating the gold surface with hexadecane thiol, which occupies surface space, led to growth of pillars of dendrimers on unoccupied surface sites, which could be imaged with afm (109). Diaminobutane dendrimers bearing outer layers of ferrocene were imaged. Circular features were seen that are thought to correspond to individual dendrimer units (110). Dendronized PS was imaged with afm, showing multilayer films made of densely packed nanorods. The cylindrical dendrimers were grouped in domains in which they are kept parallel to each other, with a periodicity of approximately 5 nm (88).

Filled Composites. Use of afm in characterizing filled composite materials has ranged from determination of composite morphology as a function of fabrication method to examination of the morphological effects of the reinforcing agent upon the matrix resin, and static and dynamic mechanical properties of the composites.

Poly(hydroxybenzoic acid)/copolyesterether elastomer microcomposites were imaged and it was shown that time and the solvent used to make the composite result in different morphologies. When solvents with high affinities for the elastomer were used, the resultant composite showed uniform dispersion of that material. With poor solvents, the elastomer was observed to aggregate into nonuniform aggregates (111).

Sheet molding compound thermoset materials were imaged by afm; it was found that fiber reinforcement, as much as 1 μm under the surface, had an effect on surface morphology (112). AFM scratch tests conducted on carbon fiber-reinforced PEEK/PTFE blends demonstrated that reinforcing carbon fibers are harder and more scratch-resistant than graphite or the matrix resins (113). Styrene–butadiene rubber (SBR) vulcanizates containing carbon black were imaged under conditions of different levels of extension (0–700%). The authors found that filler particles tend to align in the force field into string-like arrays; surface cracks develop between these filler arrays, and may play an important role in crack propagation (114).

Microporous Membranes. Microporous membranes pose two separate opportunities for afm to contribute structural knowledge of these materials. The technique is of course capable of describing the polymeric structures on scales ranging from micrometers down to tenths of nanometers, but is also able to describe the nature of the pores which modify the transport properties of membranes.

Nafion® perfluorinated sulfonic acid polymer was imaged, showing a nodular structure with 45-nm spherical domains, which in turn contained 11-nm spherical grains. Interstitial "pores" in the polymer were found to contain lower densities of polymer, but were not completely void. The authors showed that a nonuniform

distribution of the grains, with wide and deep rifts, occur when the polymer is swelled with tributyl phosphate (115).

Polysulfone membranes were imaged and the microstructure and microporosity characterized. Through this work, it was determined that two different modes of phase separation existed during the formation of the membrane. Hence, the specific details of membrane processing were shown to influence morphology and final performance of the product (116). Linear and branched aromatic polyamide membranes were imaged by both afm and field-emission sem. The sem work established molecular structure/morphological relationships, while the afm was used to determine the surface roughness of the membranes. A strong correlation between molecular structure and roughness was determined, with meta- substituted molecules giving rougher, less regular structures. Correlations between this surface roughness and water permeability were determined as well, providing the authors with a molecular structure to polymer morphology to membrane performance working model (117).

Polymer Blends, IPNs, Latexes, and Block Copolymers. When two or more dissimilar materials are combined in the absence of covalent bonds, as is the case for polymer blends, interpenetrating polymer networks (IPNs) and latices, or through direct chemical bonds, as with block and Graft copolymers, a number of important questions are raised that can be addressed by afm. The bulk morphology of these molecular combinations, as well as the specific chemical interactions within and between species, can provide important guidance for the design of improved materials. Variations in structural and mechanical properties of the blends and copolymer components, which result from the combining of materials or from some environmental force, which the materials are exposed to, again are important information for designers of such materials.

Blends. Blends of iPP with poly(styrene)-*block*-poly(ethylene-*co*-1-butene) were prepared under various conditions and imaged by afm, where macrophase separation because of incompatibility of the components was observed (Fig. 17). The degree of phase segregation was shown to be dependent on the thermal history of the sample (118). Blends of iPP and different poly(ethylene-butene) (PEB) copolymers were imaged. The authors found that iPP and PEB containing 88% butene were miscible, and PEB containing <88% butene were partially to totally immiscible, and polybutene (100% butene) was partially miscible. So, there is a narrow window of miscibility for these blends (119).

Thin films of blended deuterated polystyrene (dPS) and poly(vinyl methyl ether) (PVME) were imaged as a function of the dPS:PVME ratio. Near the critical composition of 35% dPS, an undulating, spinodal-like structure was observed, whereas for compositions away from the critical mixture ratio, regular mounds or holes (ϕdPS $< \phi_{crit}$ and ϕdPS $> \phi_{crit}$, respectively) were present. These variations were assigned to surface tension effects (120). Blends of PBD, SBR, isobutylene-brominated *p*-methylstyrene, PP, PE, natural rubber, and isoprene–styrene–isoprene block rubbers were imaged (Fig. 18). Stiff, styrenic phases and rubbery core–shell phases were evident as the authors utilized force-modulated afm to determine detailed microstructure of blends, including those with fillers such as carbon-black and silica (121).

Incompatible PS/PMMA/PVP [poly(2-vinyl pyridine)] blend films were imaged. Combining afm and selective dissolution of the film surface, the

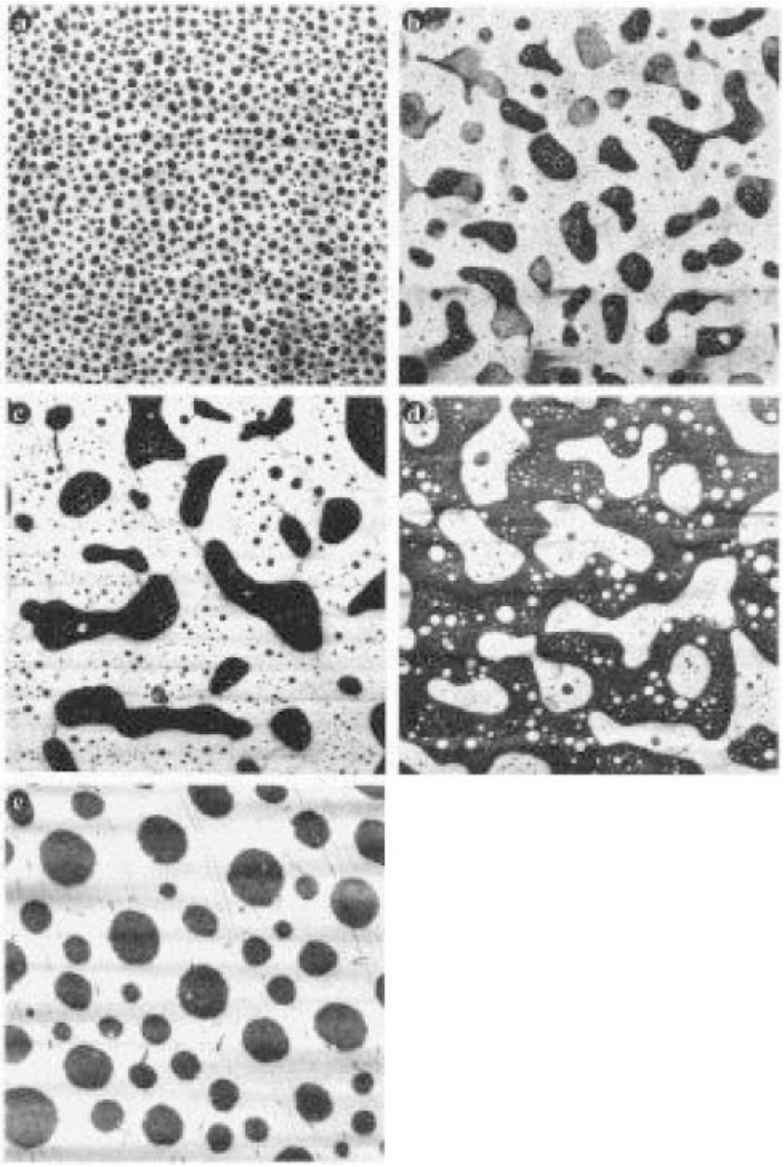

Fig. 17. Phase separation of incompatible blends of iPP and PEB, as a function of thermal history. Reprinted with permission from Ref. 118. Copyright (1998) American Chemical Society.

compositional distribution of polymers was determined. The PMMA was observed to act as a compatibilizer for the more incompatible PS and PVP domains, preventing the formation of high energy interfaces. Molecular simulation for a ternary blend of polymers with distinctly different surface energies closely models the observed morphology (122). Tapping mode imaging of triblock PS–PE–PBD and iPP showed the boundary between the materials to act as a nucleating agent,

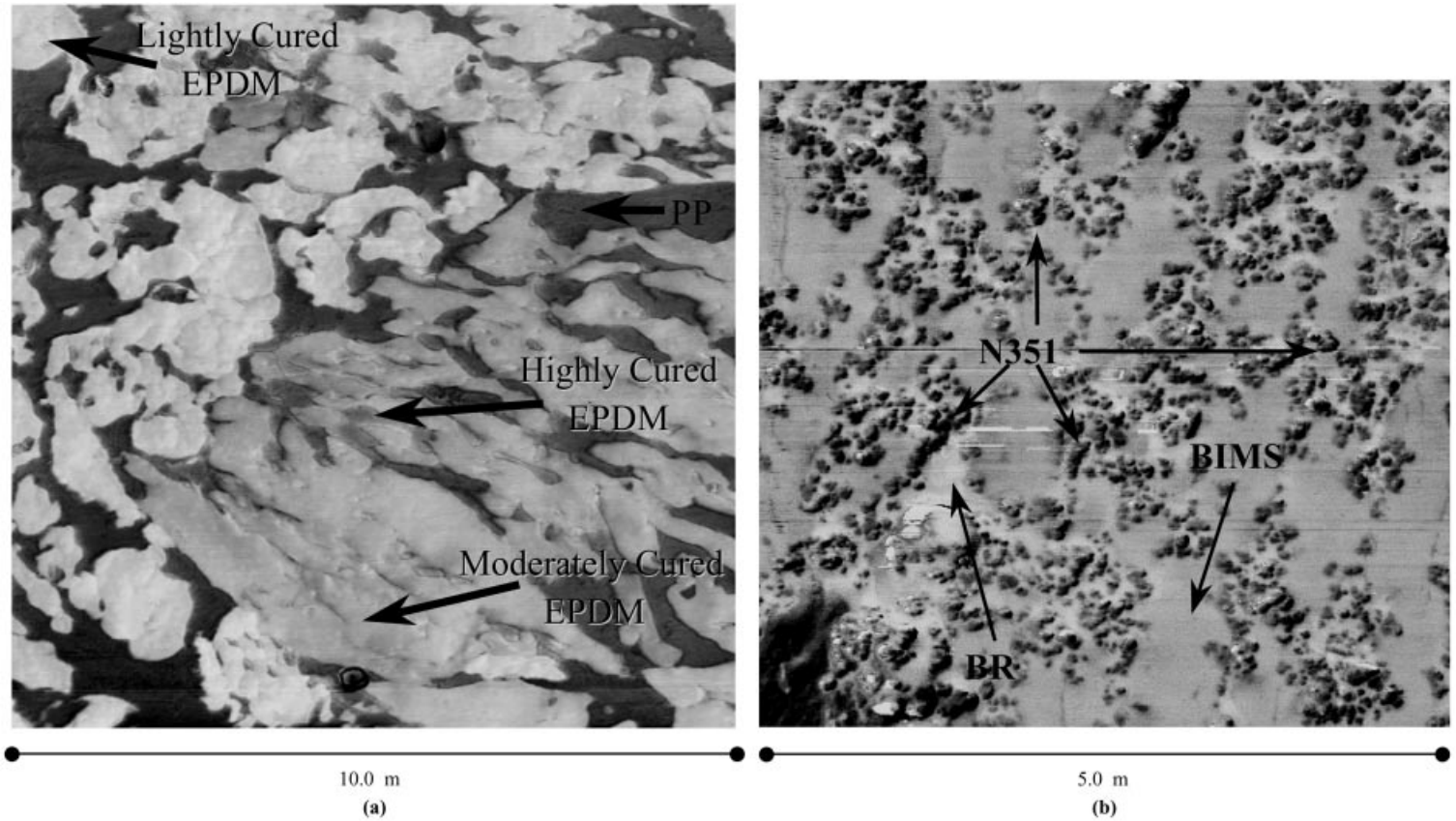

Fig. 18. Phases present in filled polymer blends. From Ref. 121, Copyright © 1997. John Wiley & Sons Limited. Reproduced with permission.

where iPP lamellae grew primarily in a direction perpendicular to the interface (123). Blends of acrylonitrile–butadiene (AB) rubber and ethylene–propylene–diene (EPD) rubber were shown to be incompatible without and compatible with a compatibilizer, such as chlorinated PE. The change in phase morphology with added compatibilizer was shown clearly by afm (124). Blends of conductive PA with plasticized cellulose acetate (CA) were imaged. The fibrillar structure of the PA in the amorphous CA matrix was evident and was correlated to electrical properties of the composite (125). Blends of poly(vinylidine difluoride) (PVDF) and PMMA or PVA were made and imaged, showing that different crystalline phases of the PVDF could be stabilized and therefore preferentially selected for use in blends with different amorphous polymers (126).

IPN. Interpenetrating networks of unsaturated polyester propylene glycol/maleic anhydride/phthalic anhydride (PG/MA/PAH) and polyurethane (PU) were imaged across a range of compositions. The afm image of unsaturated polyester was flat and featureless; however, with addition of 20% PU, phase separation of the polymers was observed. With increasing PU content, surface roughness and heterogeneity increased, whereas PU was preferentially dispersed on the surface of the matrix in clumps or circular plates of widely varying sizes (127).

Latexes. Poly(butyl acrylate)/poly(methyl methacrylate) (PBA/PMMA) core/shell latex particles were imaged. Contact mode afm was inappropriate because of excessive roughness and the associated artifacts typical to these types of experiments. However, in tapping mode, core/shells of varying compositions were imaged nicely. At 90/10 PBA/PMMA, the core is partially covered by PMMA and at 80/20, the PMMA microbeads are joined together into subparticles. At a 70/30 ratio, the subparticles merge into an intact shell (128). Tapping mode afm of perfluorooctylethyl methacrylate/poly(butylmethylacrylate) (PFMA/PBMA) latex blends showed that a film of PBMA was formed containing dispersed PFMA nanoparticles (65°C). Annealing to 100°C caused accumulation of PFMA at the surface of the film (129).

The morphology of rubber latex formation was followed as a function of time during the maturation of prevulcanization, and morphological features were shown to correlate with cross-link densities. Inhomogeneous latex particles cross-linked on the surface with uncross-linked cores were obtained during this process. It is proposed that these hard-shell/soft core structures coalesce to form the characteristic dimpled surface films (130).

Block Copolymers. The phase-separated diblock copolymer of PS–PMMA was imaged by afm during annealing. Cylinders of PMMA were observed parallel to the plane of the sample film. The evolution of defects in the structure was followed as a function of annealing time, thus giving insights into mobility and structural changes (131). Phase-separated diblocks of polyparaphenylene–poly(methyl methacrylate) (PPP/PMMA) were imaged over a range of compositions. With increasing PPP concentrations, stripes or lamellae emerged within the images. The width of these stripes was interpreted to correspond to that of the PPP in the copolymer (132) (see BLOCK COPOLYMERS).

Triblock poly(styrene-*block*-ethylene/butylene-*block*-styrene) was imaged giving a repeating series of hills and valleys. The surface area fraction of the hills increased with PS content in the copolymer. The local stiffness of the hills was higher than that of the valleys, measured by force versus displacement curves

generated with the afm probe. The authors conclude that the hills are PS and the valleys are ethylene/butylene (133). Triblock PS–PBD–PMMA was imaged showing the PS/PMMA lamellae to be mainly oriented perpendicular to the observed surface. PBD-spheroids (approximately 14 nm in diameter) are separated at the lamellar PS/PMMA interfaces. The microstructure is explained on the basis of surface energies (88).

Random block copolyamide-ethers (hard–soft block elastomers) were imaged, showing that thicker films contain much larger crystals of the hard block segments than those obtained with thin films (30-nm films had crystals of approximately 7 nm $\times$ 50–100 nm; 20-μm films had crystals of about 12 nm $\times$ 200 nm). Further analysis also suggested that within the thicker films, more soft-segment is available at the surface compared to the thinner films (134).

Hybrid Organic-Inorganic Polymers. Hybrid organic–inorganic polymers, typically produced by sol–gel inorganic polymerization–derivatization of organic polymers, are materials currently under investigation for a wide range of industrial, consumer, and military applications. With regard to afm imaging, such materials represent the combination of studies of organic polymer systems, and of inorganic polymers, most often for heterogeneous catalysts. For these emerging hybrid materials, afm has been shown to be able to discriminate between organic and inorganic phases, and to describe the boundary regions therein.

Nanophase-segregated morphologies of linear, sulfonated polystyrene–polyisobutylene–polystyrene triblock copolymers were demonstrated to act as templates for directing *in situ* sol–gel polymerizations of tetraethylorthosilicate (TEOS) around PS regions using domain-specific solvents and certain counterions. Suitable cations in conjunction with a solvent that swells only the PS domains allowed for hydrolyzed TEOS monomers to migrate to targeted ionic domains where sol–gel reactions occur. The morphology of these organic–inorganic hybrids consisted of rod-like, silicate-containing PS domains having inter-rod distances of tens of nanometers (Fig. 19). The rods were structured in essentially parallel arrays in micron-sized "grains" as is shown in the afm image (135,136). Poly(methyl methacrylate)–silica hybrid materials, prepared by sol–gel chemistry, were imaged. Fracture surfaces of optically transparent hybrids were found to exhibit very low levels of roughness, suggesting that the organic and inorganic phases are not separated, whereas the translucent variants showed significant roughness (suggestive of phase separation) (137). Poly(tetramethylene oxide)–silica hybrid materials were also prepared by sol–gel chemistry. Semi-IPNs were then produced from these materials and poly(methacrylic acid). Imaging of these revealed microphase-separated polysilicate domains (138). Similar polysilicate domains have been observed with poly(vinyl pyrrolidone)–silica hybrids (139). Silicate glass fibers, used in the reinforcement of organic polymers, were imaged (*1*) without any treatment, (*2*) with organosilane coupling agent treatment only, and (*3*) with complete emulsion-based fiber-sizing complexes. The untreated fibers were relatively smooth. Addition of a coupling agent only resulted in a rougher surface because segments of the coupling agent were torn from the glass fiber when individual fibers were separated from one another. Treatment with the complete fiber-sizing emulsions result in largely homogeneous surfaces that were smoother than those of the starting glass fibers (140). Ladder-like polyvinylsiloxane polymers were imaged, with the highly regular, two-dimensional network structure

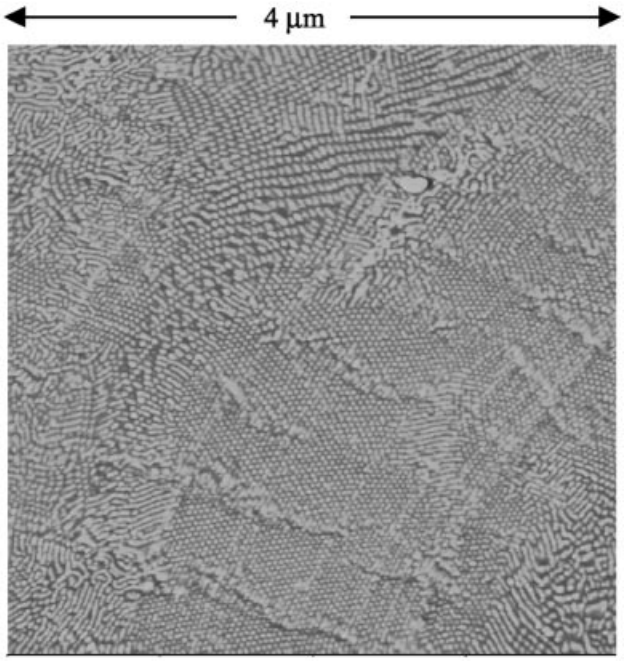

Fig. 19. Morphology of a hybrid silicate-PS molecular composite. From Ref. 135, courtesy of Prof. K. Mauritz.

clearly resolved by afm. Three-dimensional nanotubular structures from these polymers, and supermolecular structures resulting from these nanotubes, were also imaged (141).

Gels. The relative softness of most gels exacerbates the problems associated with the use of a mechanical force-based probe in determining morphology and structure. Such structural details are often scarce, given the high functionality associated with many gels. Thus, both a technical challenge and a suitable reward are associated with the use of afm with polymeric gels.

Poly(*N*-isopropylacrylamide) (PIPA) gels in water were imaged. The thickness of the gel-constrained sample geometry, cross-linking density, and osmotic pressure were all demonstrated to play a role in the observed structure. The surface microstructure, as well as the nanometer scale structure, was associated with the gel-phase transition, and there is potential, through this understanding, to control gel domain sizes. As cross-linking density was increased, the amplitude (in the afm) due to sponge-like domains is less clear. The authors hypothesize that the cross-links create local imperfections in the swelled structure (142–144).

Independently synthesized gel microspheres of PIPA were incorporated into PIPA matrix networks at the time of gelation. AFM imaging of these networks was used to visualize the microspheres, quantifying their degree of swelling as a function of temperature changes under constrained geometry. The authors found that this response was sensitive to the level of gel microspheres present in the macrogel; when a sufficient level of microspheres were present in the system, aggregation into three-dimensional domains of microspheres was observed (145).

Surface Characteristics

Roughness. Given that afm is a surface topographical technique, it should not be surprising that this method can be used to quantify the roughness of polymer surfaces, giving insights into irregularities inherent in the polymer, or resultant from chemical or mechanical action on the polymer, or from heterogeneous additives.

Surface roughness of biaxially oriented PET magnetic tape with and without metal oxide particles exhibited features down to 1 nm, including some attributed to the manufacturing process (a degree of alignment of magnetic particles along the machine axis of the films that exceeds statistical behavior). Magnetic particles, 1 μm $\times$ 0.1 μm, were observed and the surface roughness was fitted to a fractal geometry. The starting PET film surface was shown to be relatively flat and featureless at this length scale. The features observed by afm were not discernable by a noncontact optical profiler (146).

Surface roughness of PS and PS/PVME blend thin films before and after rubbing with velour cloth were measured and correlated with angle-dependent total-reflection x-ray fluorescence (TXRF). The TXRF failed to discern polymer surface changes because of rubbing, although it did characterize the underlying nickel substrate. On the other hand, afm revealed anisotropic grooves and ridges for the rubbed PS film, and isotropic, sinusoidal roughness for the rubbed blend. The anisotropy of the blend was said to be typical of phase-separated blends. Similar rms roughness of 6.1 nm and peak to peak distances of 170 nm were observed for the rubbed samples (147).

Morphology and Polymer Orientation. Morphology of polymer systems can be indicated by surface afm measurements. Of great interest in this area is the study of phase-segregated blends, blocks, and partially crystallized materials. Recently, the interpenetration of poly(butylenes succinate) lamella with the spherulites of the poly(vinylidene chloride-*co*-vinyl chloride) blend was determined by afm (148). Significant morphological changes occur in diacetylene LB films upon the addition of polyallylamine to the subphase during LB deposition (149). This addition was shown to produce microfibular structures in the resultant film consisting of "fingerprint" like features. Morphologically interesting phase segregation of phthalocyaninato-polysiloxane with poly(isobutylvinyl ether) have been measured with contact mode afm (150).

The morphology of polymer surfaces can also be influnced by electrostatics, rubbing and stretching of the materials. Polydiacetylene nanocrystals (151) and ferroelectric liquid crystalline elastomers (152,153) have been observed by afm. The morphology of these thin films yield interesting photoreactive and photoresponsive behavior. These morphologies are also affected by the rubbing (154) or stretching (153) of the materials. Understanding of molecular alignment is critical for liquid crystal display technology using polymer networks as the active matrix.

Adhesion. As mentioned previously, the afm force transducer can also be used to determine adhesion and frictional properties at surfaces. Because of the nature of afm cantilever–polymer surface interactions, it is possible to modify the cantilever tip with chemical agents, and then quantitatively probe the adhesion of these agents to the polymeric material in question. Modified afm tips were produced by attaching glass spheres to afm cantilevers. To the glass spheres,

sulfonated polysulfone was applied. The interactions between this sulfonated polysulfone and aminosilanes (which had been applied to silicon wafers) were measured using the afm. Treatment of the aminosilane with boiling water, which destroys the silane network, was shown to significantly reduce silane–polymer adhesive forces (155). Similarly, the authors showed correlation between maximum adhesive forces and silanol and sulfonic acid groups as well as mechanical entanglements (156). Adhesion between glass and HDPE or LDPE (low density polyethylene) was measured using afm. Grafting of chlorosilane-terminated PE onto the glass, to produce an amorphous interphase, was shown to enhance adhesion (157). Adhesion versus temperature was measured using afm FCs for a surface of poly(*tert*-butyl acrylate) near its glass–rubber transition (158). By studying compliance and adhesion, these authors concluded that the activation energy for molecular relaxation was the same for bulk versus free surface measurements. This indicates that afm surface measurements are accurate and useful measures of molecular scale viscoelasticity, and that when the surface properties do differ from the bulk then the afm can characterize these properties with near molecular spatial resolution. Moreover, when applied to ultrathin adsorbed polymer layers, the afm can be used for "nanorheology" so as to understand molecular lubricants at this important length scale (159).

Friction. To measure the frictional characteristics of a surface, the afm is used in contact mode, where the tip is "dragged" across the surface. The frictional force induced from the load of the tip, torques the cantilever. Higher frictional forces result in higher lateral deflection of the optical lever; these relative changes in deflection can be interpreted as changes in the coefficient of friction, μ, of the sample. In contrast to bulk measurements, afm studies of friction often contradict Amonton's "law" whereas the coefficient of friction does depend on load. This is especially true for polymer systems that exhibit significant viscous flow under load such as Hydrogels. Various hydrogels were studied by afm and μ did depend on load and also correlated with measured adhesive forces indicating a molecular chain attachment and entanglement model (160).

Friction, and more significantly wear, is an exceedingly important parameter for developing advanced polymer materials that must withstand sliding contact operations. Mechanisms of friction involve intermolecular forces, molecular adhesion, subnanometer topography of the sliding contact surfaces, and the elastic and yield moduli of the near-surface region. While studying the friction and adhesion of various polymer bearings (PS, polyacetal, Tarnamid T-27, etc) against a glass-fiber loaded, polyamide composite shaft, the resultant nanometer scale afm topography was correlated with μ (161). The high spatial resolution topographs of these worn polymer surfaces enabled a far more accurate computational model of the wear process.

Often, new materials are developed from composites, or mixed polymer systems. Since friction has been shown to be a molecularly driven mechanism, a simple weighted average of the material's constituents will not yield accurate predictions of measured tribological properties. The afm as a frictional transducer has resolved the submicrometer domains of PS/PMMA blends (162). To accentuate the sensitivity of the afm probe to very small differences in surface energy and μ, the afm tip can be functionalized. Hydroxylated tips are far better at discerning these surface changes when contrasting polar versus nonpolar blend components (163).

Table 2. RMS Roughness of Polymers Before/After Acrylamide Grafting

Polymer	Rms roughness, nm Unmodified surface	Acrylamide grafted
HDPE	308	290
PET	17	15
PTFE	165	120
PI	52	44
XPA	10	6.3

Modifications. As a method capable of describing both gross polymer features and placement of individual molecules (and small groups of atoms), afm has been shown to be an important probe in relating chemical and morphological structures. At these varying levels of magnification, afm has been demonstrated to be able to discern changes in polymers, which result from chemical modification of the starting monomer material.

A series of polymers, including HDPE, PET, PTFE, PI (polyimide), and XPA (cross-linked polyaniline) were imaged before and after Argon plasma or ozone treatment and acrylamide grafting. The basic surface features of the untreated substrates were retained after grafting. In each case, the rms roughness of the surfaces was reduced, as shown in Table 2, because the acrylamide grafts covered surface features (such coverage is similar to that described for monolayer coverage of hyperbranched polymers on inorganic surfaces). A broadening of lamellar distances was also observed upon grafting, suggesting that the grafted groups push between the existing lamellae (164).

Corona treatment of iPP (both oriented and biaxially oriented) led to the generation of spherical-shaped features on the sample surface. The size of these features was correlated to the corona dose level, as were the degree of surface oxidation, and the loss of molecular weight. Peel strength also correlated with the surface morphology (165). Poly(vinyl chloride) was oxidized using both air plasma and corona discharge. Significant differences in the surface morphologies of these two oxidized materials were imaged, with the air plasma producing smaller, regular surface nodules, and the corona producing a lower number of much larger features. The authors postulate that the plasma was more effective at removing plasticizer and other additives present in PVC, whereas the corona-generated features were the result of radical chain scissions and subsequent cross-linking of the oxidized polymer chains (166). Cross-linked, unsaturated polyester resins were treated with CF_4 under plasma conditions to produce a fluorinated surface exhibiting a greater moisture barrier than the unmodified resin. Changes in the surface were imaged, showing changes from a rough to a nodular surface upon treatment (167). LDPE and HDPE were also treated with CF_4 under plasma conditions. The degree of surface modification was found to decrease with the cystallinity level of the polymers. The lamellar surface of LDPE was converted into a uniform, nanoporous structure; this change was not observed on the HDPE. In neither case did the modification have any effect beyond the surface region (168). Polyethylene was plasma-treated in the presence of allyl alcohol, to give a hydroxylated surface, followed by silation. AFM shows that the silated surfaces are

similar to one another and consist of much higher levels of graininess than with the allyl alchol or argon plasma treatments alone. Image analysis suggested to the authors that the silane coverage might be greater than a monolayer (169).

The effectiveness of different wavelengths of light at producing the photochemical cross-linking of poly(ethynyl)carbosilane fibers was probed using afm. As the light frequency was changed, the depth of photochemical products also changed. Using broadband $\lambda > 300$ nm, photochemical products were observed to a depth of 100 nm, or about 125 molecular layers. When $\lambda = 254$ nm light was used, penetration of the photochemistry to 115 nm (130 layers) was observed. This level of detail is not readily obtained using techniques such as nmr or x-ray structural analysis (170).

BIBLIOGRAPHY

1. S. D. Burnside and E. P. Giannelis, *J. Polym. Sci., Part B: Polym. Phys.* **36**, 1595–1604 (2000).
2. G. Castelein, G. Coulon, and C. G'Sell, *Polym. Eng. Sci.* **37**, 1694–1701 (1997).
3. L. S. Bartell, *J. Chem. Educ.* **62**, 192–196 (1985).
4. G. Binnig and H. Rohrer, *Helv. Phys. Acta* **55**, 726 (1982).
5. U.S. Pat. 4,604,520 (1986), W. D. Pohl (to International Business Machines Corp.)
6. J. R. Matey and J. Blanc, *J. Appl. Phys.* **57**, 1437 (1985).
7. C. C. Williams, W. P. Hough, and S. A. Rishton, *Appl. Phys. Lett.* **55**, 203–205 (1989).
8. Y. Martin and H. K. Wickramasinghe, *Appl. Phys. Lett.* **50**, 1455 (1987).
9. C. C. Williams and H. K. Wickramasinghe, *Appl. Phys. Lett.* **49**, 1587–1589 (1987).
10. K. Takata, T. Hasegawa, and S. Hosaka, *Appl. Phys. Lett.* **55**, 1781–1783 (1989).
11. Y. Manassen and co-workers, *Phys. Rev. Lett.* **62**, 2513–2534 (1989).
12. D. Rugar, C. S. Yannoni, and J. A. Sidles, *Nature* **360**, 563–566 (1992).
13. C. C. Williams and H. K. Wickramasinghe, *Nature* **344**, 317–319 (1990).
14. C. C. Williams and H. K. Wichramasinghe, *J. Vac. Sci. Technol., B* **9**, 537–539 (1991).
15. J. C. Poler, R. M. Zimmermann, and E. C. Cox, *Langmuir* **11**, 2689–2695 (1995).
16. A. Rettenberger and co-workers, *Appl. Phys. Lett.* **67**, 1217–1219 (1995).
17. A. W. Adamson and A. P. Gast, *Physical Chemistry of Surfaces*, 6th ed., John Wiley & Sons, Inc., New York, 1997, pp. 313–327.
18. D. Sarid, *Scanning Force Microscopy with Applications to Electric, Magnetic and Atomic Forces*, revised ed., Oxford University Press, New York, 1994.
19. G. Binning, C. F. Quate, and C. Gerber, *Phys. Rev. Lett.* **56**, 930 (1986).
20. G. Neubauer and co-workers, *Rev. Sci. Instrum.* **61**, 1844 (1990).
21. C. M. Mate and co-workers, *J. Vac. Sci. Technol., A* **6**, 575 (1987).
22. D. Rugar and co-workers, *Surf. Sci.* **59**, 2337 (1998).
23. Y. Martin, C. C. Williams, and H. K. Wickramasinghe, *J. Appl. Phys.* **61**, 4723 (1987).
24. D. Sarid and co-workers, *Opt. Lett.* **13**, 1057 (1988).
25. T. R. Albrecht and co-workers, *J. Vac. Sci. Technol., A* **8**, 3386–3396 (1990).
26. K. L. Westra, A. W. Mitchell, and D. J. Thompson, *J. Appl. Phys.* **74**, 3608–3610 (1993).
27. K. L. Johnson, K. Kendall, and A. D. Roberts, *Proc. R. Soc. London, Ser. A* **324**, 301–313 (1971).
28. J. Israelachvili, *Intermolecular and Surface Forces*, 2nd ed., Academic Press, London, 1992, pp. 326–329.
29. J. L. Hazel and V. V. Tsukruk, *J. Tribology* **120**, 814 (1998).

30. Z. Elkaakour and co-workers, *Phys. Rev. Lett.* **73**, 3231–3234 (1994).
31. Y. Terada and co-workers, *J. Appl. Phys.* **87**, 2803–2807 (2000).
32. J. A. Hammerschmidt, W. L. Gladfelter, and G. Haugstad, *Macromolecules* **32**, 3360–3367 (1999).
33. B. Bhushan and C. Dandavate, *J. Appl. Phys.* **87**, 1201–1210 (2000).
34. B. D. Beake and G. J. Leggett, *Polymer* **40**, 5973–5976 (1999).
35. C. D. Frisbie and co-workers, *Science* **265**, 2071–2074 (1994).
36. Q. Zhong and co-workers, *Surf. Sci. Lett.* **290**, L688–L692 (1993).
37. A. P. Quist and co-workers, *Nucl. Instr. Meth. B* **88**, 164 (1994).
38. L. Wang, *Appl. Phys. Lett.* **73**, 3781–3783 (1998).
39. H.-N. Lin, S. H. Chen, and L. J. Lee, *Rev. Sci. Instrum.* **69**, 3840–3842 (1998).
40. C. A. J. Putman and co-workers, *Appl. Phys. Lett.* **64**, 2454–2456 (1994).
41. P. K. Hansma and co-workers, *Appl. Phys. Lett.* **64**, 1738–1740 (1994).
42. X. Chen and co-workers, *Ultramicroscopy* **75**, 171–181 (1998).
43. H.-Y. Nie and co-workers, *Thin Solid Films* **273**, 143–148 (1996).
44. J. S. Jourdan and co-workers, *Langmuir* **15**, 6495–6504 (1999).
45. D. DeVecchio and B. Bhushan, *Rev. Sci. Instrum.* **68**, 4498–4505 (1997).
46. S. N. Magonov, V. B. Elings, and M.-H. Whangbo, *Surf. Sci.* **375**, L385–L391 (1997).
47. S. N. Magonov and D. H. Reneker, *Annu. Rev. Mater. Sci.* **27**, 175–222 (1997).
48. J. Planes, Y. Samson, and Y. Cheguettine, *Appl. Phys. Lett.* **75**, 1395–1397 (1999).
49. Y. Han, S. Schmitt, and K. Friedrich, *Appl. Composite Mater.* **6**, 1–18 (1999).
50. P. Lemoine and J. Mc Laughlin, *Thin Solid Films* **339**, 258–264 (1999).
51. G. V. Dedkov, *Phys. Status Solidi A* **179**, 3–75 (2000).
52. S. Xu and G.-Y. Liu, *Langmuir* **13**, 127–129 (1997).
53. E. Zhulina, G. C. Walker, and A. C. Balazs, *Langmuir* **14**, 4615–4622 (1998).
54. H. Li and co-workers, *Macromol. Rapid Commun.* **19**, 609–611 (1998).
55. M. Rief, P. Schultz-Vanheyden, and H. E. Gaub, in N. García, M. Nieto-Vesperinas, and H. E. Gaub, eds., *Nanoscale Science and Technology*, Kluwer Academic Publishers, Dordrecht, 1998, pp. 41–47.
56. H. Li and co-workers, *Chem. Phys. Lett.* **305**, 197–201 (1999).
57. H. Li and co-workers, *Langmuir* **15**, 2120–2124 (1999).
58. M. Rief and co-workers, *Science* **276**, 1109–1112 (1997).
59. A. Majumdar, *Annu. Rev. Mater. Sci.* **29**, 505–585 (1999).
60. L. M. Walpita, J. M. R. Weaver, and H. K. Wickramasinghe, *Nature* **342**, 783–785 (1989).
61. M. Nonnenmacher and H. K. Wichramasinghe, *Ultramicroscopy* **42**, 351–354 (1992).
62. A. Hammiche and co-workers, *Rev. Sci. Instrum.* **67**, 4268–4273 (1996).
63. A. Hammiche and co-workers, *J. Vac. Sci. Technol., B* **14**, 1486–1491 (1996).
64. J. Varesi and A. Majumdar, *Appl. Phys. Lett.* **72**, 37–39 (1998).
65. R. Magerle, *Phys. Rev. Lett.* **85**, 2749–2752 (2000).
66. S. J. Tans and co-workers, *J. Vac. Sci. Technol., B* **15**, 586–589 (1997).
67. S. M. Baker and co-workers, *Macromolecules* **33**, 5432–5436 (2000).
68. V. Kitaev, K. Schillen, and E. Kumacheva, *J. Polym. Sci., Part B* **36**, 1567–1577 (1998).
69. T. J. S. Viitala and co-workers, *J. Chem. Soc., Faraday Trans.* **93**, 3185–3190 (1997).
70. S. Yokoyama, M. Kakimoto, and Y. Imai, *Synthetic Metals* **81**, 265–270 (1996).
71. A. Riul Jr. and co-workers, *Synthetic Metals* **101**, 830–831 (1999).
72. P. Qian and co-workers, *Thin Solid Films* **349**, 250–253 (1999).
73. G. Wang and R. I. Hollingsworth, *Langmuir* **15**, 3062–3069 (1999).
74. N. A. Kotov and co-workers, *J. Am. Chem. Soc.* **119**, 6821–6832 (1997).
75. J. Chen and co-workers, *Langmuir* **15**, 7208–7212 (1999).
76. V. N. Morozov, T. Y. Morozova, and N. R. Kallenbach, *Int. J. Mass Spectrom.* **178**, 143–159 (1998).

77. S. A. C. Gould and co-workers, *Int. J. Biol. Macromol.* **24**, 151–157 (1999).
78. R. Patil, V. V. Tsukruk, and D. H. Reneker, *Polym. Bull.* **29**, 557–563 (1992).
79. I. Jangchud and co-workers, *Adv. Mater. Process* **7**, 33 (1995).
80. Y. Y. Maruo, Y. Andoh, and S. Sasaki, *J. Vac. Sci. Technol., A* **11**, 2590–2596 (1993).
81. H. Yamada and co-workers, *Appl. Surf. Sci.* **65/66**, 366–370 (1993).
82. C. Zilg, R. Mulhaupt, and J. Finter, *Macromol. Chem. Phys.* **200**, 661–670 (1999).
83. V. Svorcik and co-workers, *Nucl. Instrum. Methods Phys. Res., Sect. B* **122**, 663–667 (1997).
84. R. Patil and D. H. Reneker, *Polymer* **35**, 1909–1914 (1994).
85. R. Patil and co-workers, *Polym. Commun.* **31**, 455–457 (1990).
86. S. N. Magonov and co-workers, *Polym. Bull.* **25**, 689–694 (1991).
87. D. Trifonova and co-workers, *J. Appl. Polym. Sci.* **66**, 515–523 (1997).
88. W. Stocker, *Recent Res. Dev. Macromol. Res.* **3**, 505–518 (1998).
89. S. Nazarenko, *Unpublished data*.
90. D. Snetivy, J. E. Guillet, and G. J. Vancso, *Polymer* **34**, 429–431 (1993).
91. D. Snetivy and G. J. Vancso, *Polymer* **35**, 461–467 (1994).
92. W. Stocker and co-workers, *Macromolecules* **31**, 807–814 (1998).
93. A. De Rovere, R. L. Shambaugh, and E. A. O'Rear, *J. Appl. Polym. Sci.* **77**, 1921–1937 (2000).
94. N. W. Hays and co-workers, *Polymer* **37**, 523–526 (1996).
95. S. A. C. Gould, D. A. Schiraldi, and M. L. Occelli, *J. Appl. Polym. Sci.* **65**, 1237–1243 (1997).
96. D. A. Schiraldi, S. A. C. Gould, and M. L. Occelli, *J. Appl. Polym. Sci.* **80**, 750–762. (2001)
97. D. Snetivy and G. J. Vancso, *Macromolecules* **25**, 3320–3322 (1992).
98. D. Snetivy and G. J. Vancso, *Colloids Surf., A: Physicochemical Eng. Aspects* **87**, 257–262 (1994).
99. H. Hansma and co-workers, *Polymer* **33**, 634–639 (1992).
100. A. J. Howard, R. R. Rye, and J. E. Houston, *J. Appl. Phys.* **79**, 1885–1890 (1996).
101. A. Wawkuschewski and co-workers, *Polym. Bull.* **31**, 699–705 (1993).
102. S. N. Magonov and co-workers, *Macromolecules* **26**, 1380–1386 (1993).
103. H. E. Harron and co-workers, *J. Polym. Sci., Part B* **34**, 173–180 (1996).
104. D. Snetivy, G. J. Vancso, and G. C. Rutledge, *Macromolecules* **25**, 7037–7042 (1992).
105. G. C. Rutledge, D. Snetivy, and G. J. Vancso, in S. H. Cohen, M. T. Bray, and M. L. Lightbody, eds., *Atomic Force Microscopy/Scanning Tunneling Microscopy*, Plenum Press, New York, 1994, pp. 251–263.
106. S. A. C. Gould and co-workers, *J. Appl. Polym. Sci.* **74**, 2243–2254 (1999).
107. Y. Huang, Y. Q. Yang, and J. Petermann, *Polymer* **22**, 5301–5306 (1998).
108. W. M. Lackowski, *Adv. Mater.* **11**, 1368–1371 (1999).
109. A. Hierlemann and co-workers, *J. Am. Chem. Soc.* **120**, 5323–5324 (1998).
110. K. Takada and co-workers, *J. Am. Chem. Soc.* **119**, 10763–10773 (1997).
111. F. Tian and co-workers, *Appl. Phys. A.* **66**, S591–599 (1998).
112. C. Serre and co-workers, *J. Mater. Sci.* **34**, 4203–4208 (1999).
113. Y. Han, S. Schmitt, and K. Friedrich, *Appl. Composite Mater.* **6**, 1–18 (1999).
114. S. Maas and W. Gronski, *Rubber Chem. Technol.* **68**, 652–659 (1995).
115. A. Lehmani, S. Durand-Vidal, and P. Turq, *J. Appl. Polym. Sci.* **68**, 503–508 (1998).
116. J. Y. Kim, H. K. Lee, and S. C. Kim, *J. Membr. Sci.* **163**, 159–166 (1999).
117. S.-Y. Kwak and co-workers, *J. Polym. Sci., Part B* **37**, 1429–1440 (1999).
118. G. Bar, Y. Thomann, and M.-H. Whangbo, *Langmuir* **14**, 1219–1226 (1998).
119. Y. Thomann, *Macromolecules* **31**, 5441–5449 (1998).
120. B. D. Ermi and co-workers, *Polym. Prepr.* 606–607 (1997).

121. A. A. Galuska, R. R. Poulter, and K. O. McElrath, *Surf. Interface Anal.* **25**, 418–429 (1997).
122. S. Walheim, M. Ramstein, and U. Steiner, *Langmuir* **15**, 4828–4836 (1999).
123. Y. Thomann, H.-J. Cantow, and M.-H. Whangbo, *Appl. Phys. A.* **66**, S1233–S1236 (1998).
124. D. K. Setua and co-workers, *J. Appl. Polym. Sci.* **74**, 480–489 (1999).
125. J. Planes, Y. Samson, and Y. Cheguettine, *Appl. Phys. Lett.* **75**, 1395–1397 (1999).
126. W.-K. Lee and C.-S. Ha, *Polymer* **39**, 7131–7134 (1998).
127. M.-X. Xu and co-workers, *Mater. Chem. Phys.* **47**, 9–12 (1997).
128. F. Sommer and co-workers, *Langmuir* **11**, 440–448 (1995).
129. R. F. Linemann and co-workers, *Macromolecules* **32**, 1715–1721 (1999).
130. C. C. Ho and M. C. Khew, *Langmuir* **15**, 6208–6219 (1999).
131. J. Hahm and co-workers, *J. Chem. Phys.* **109**, 10111–10114 (1998).
132. R. Lazzaroni and co-workers, *Synthetic Metals* **102**, 1279–1282 (1999).
133. M. Motomatsu, W. Mizutani, and H. Tokumoto, *Polymer* **38**, 1779–1785 (1997).
134. B. B. Sauer, R. S. McLean, and R. R. Thomas, *Polym. Int.* **49**, 449–452 (2000).
135. D. A. Mountz and co-workers, *Polym. Prepr.* **39**, 383 (1998).
136. D. A. Reuschle and co-workers, *Polym. Prepr.* **40**, 892 (1999).
137. Y. Wei and co-workers, *Chem. Mater.* **10**, 769–772 (1998).
138. A. B. Brennan and T. M. Miller, *Mater. Res. Soc. Symp. Proc.* **435**, 155–164 (1996).
139. M. Toki and co-workers, *Polym. Bull.* **29**, 653–660 (1992).
140. A. El Achari and co-workers, *Textile Res. J.* **66**, 483–490 (1996).
141. C. F. Zhu and co-workers, *J. Mater. Sci.* **14**, 1084–1090 (1999).
142. A. Suzuki, M. Yamazaki, and Y. Kobiki, *J. Chem. Phys.* **104**, 1751–1757 (1996).
143. A. Suzuki and co-workers, *Macromolecules* **30**, 2350–2354 (1997).
144. Y. Kobiki and A. Suzuki, *Int. J. Adhesion Adhesives* **19**, 411–416 (1999).
145. H. Suzuki and A. Suzuki, *Colloids Surf. A: Physicochemical Eng. Aspects* **153**, 487–493 (1999).
146. P. I. Oden and co-workers, *J. Tribology* **114**, 666–674 (1992).
147. W. L. Wu and W. E. Wallace, *J. Vac. Sci. Technol., B* **16**, 1958–1963 (1998).
148. Y. Terada, T. Ikehara, and T. Nishi, *Polym. J.* **32**, 900–903 (2000).
149. H. Tachibana and co-workers, *Polymer* **42**, 1995–2000 (2001).
150. S. Yamamoto, Y. Tsujii, and T. Fukuda, *Polymer* **42**, 2007–2013 (2001).
151. J. A. He and co-workers, *J. Phys. Chem. B* **103**, 11050–11056 (1999).
152. H. M. Brodowsky and co-workers, *J. Macromol. Sci., Phys.* **B38**, 593–601 (1999).
153. H. M. Brodowsky and co-workers, *Ferroelectrics* **243**, 115–123 (2000).
154. L. Cui and co-workers, *Mol. Cryst. Liq. Cryst. Sci. Technol., Sect. A* **333**, 135–144 (1999).
155. R. L. Orefice and A. Brennan, *Polimeros: Ciencia e Tecnologia* 82–89 (1998).
156. R. L. Orefice and A. Brennan, *Mater. Res.* **1**, 19–28 (1998).
157. J. Duchet and co-workers, *Macromolecules* **31**, 8264–8272 (1998).
158. O. K. C. Tsui and co-workers, *Macromolecules* **33**, 4198–4204 (2000).
159. S. M. Notley, V. S. J. Craig, and S. Biggs, *Microsc. Microanal.* **6**, 121–128 (2000).
160. J. P. Gong and co-workers, *Chin. J. Polym. Sci.* **18**, 271–275 (2000).
161. Z. Rymuza and co-workers, *Wear* **238**, 56–69 (2000).
162. C. Ton-That and co-workers, *Polymer* **42**, 1121–1129 (2001).
163. C. Ton-That, D. O. H. Teare, and R. H. Bradley, *Chem. Mater.* **12**, 2106–2111 (2000).
164. F. C. Loh and co-workers, *J. Vac. Sci. Technol., B* **14**, 1611–1620 (1996).
165. R. M. Overney and co-workers, *Appl. Surf. Sci.* **64**, 197–203 (1993).
166. V. S. Joss and C. Kiely, in J. M. Rodenburg, ed., *Electron Microscopy and Analysis 1997* (Inst. Phys. Conf. Ser. No. 153, Section 6), Institute of Physics Publishing, Bristol, 1997, pp. 217–220.

167. S. Marais and co-workers, *Surf. Coat. Technol.* **122**, 247–259 (1999).
168. M. B. Olde Riekerink and co-workers, *Langmuir* **15**, 4847–4856 (1999).
169. B. M. Wickson and J. L. Brash, *Colloids Surf. A: Physicochemical Eng. Aspects* **156**, 201–213 (1999).
170. H. Mostafavi and co-workers, *Adv. Mater.* **7**, 576–578 (1995).

D. A. SCHIRALDI
KoSa
J. C. POLER
University of North Carolina

BIOTECHNOLOGY APPLICATIONS

Introduction

The most important components of living cell, proteins, carbohydrates, and nucleic acids are polymers. Even lipids, which have lower molecular weights, can be regarded as methylene oligomers that have a polymerization degree of around 20. Nature uses polymers as constructive elements and parts of complicated cell machinery. The salient feature of functional biopolymers is their all-or-nothing or at least highly nonlinear response to external stimuli. Small changes happen in response to varying parameters until the critical point is reached; then a transition occurs in the narrow range of the varied parameter, and after the transition is completed, there is no significant further response of the system. Such nonlinear response of biopolymers is warranted by highly cooperative interactions. Despite the weakness of each particular interaction in a separate monomer unit, these interactions, when summed through hundreds and thousands of monomer units, provide significant driving forces for the processes in such systems.

Not surprisingly, understanding the mechanism of cooperative interactions in biopolymers has opened the floodgates for attempts to mimic the cooperative behavior of biopolymers in synthetic systems. Recent decades witnessed the appearance of synthetic functional polymers, which respond in some desired way to a change in temperature, pH, electric or magnetic fields, or some other parameters. These polymers were nicknamed stimuli-responsive. The name "smart polymers" was coined because of the similarity of the stimuli-responsive polymers to biopolymers (1). Nature has always striven for smart solutions in creating life. The goal of scientists is to mimic biological processes, and therefore understand them better, and also to create novel species and invent new processes.

Encyclopedia of Polymer Science and Technology. Copyright John Wiley & Sons, Inc. All rights reserved.

Applications of polymers in biotechnology and medicine are discussed in this article. The highly nonlinear response of smart polymers to small changes in the external medium is of critical importance for the successful functioning of a system. Most applications of polymers in biotechnology and medicine include biorecognition and/or biocatalysis, which take place principally in aqueous solutions. Thus, only water-compatible smart polymers are considered; smart polymers in organic solvents or water/organic solvent mixtures are beyond the scope of the article. The systems discussed in the article are based on either soluble/insoluble transition of smart polymers in aqueous solution or on the conformational transition of macromolecules physically attached or chemically grafted to the surface. Systems that have covalently cross-linked networks of macromolecules, called hydrogels, are not considered (see HYDROGELS).

One could define *smart polymers* used in biotechnology and medicine as macromolecules that undergo fast and reversible changes from hydrophilic to hydrophobic microstructure triggered by small changes in their environments. These microscopic changes are apparent at the macroscopic level as precipitate formation in solutions of smart polymers or changes in the wettability of a surface to which a smart polymer is grafted. The changes are reversible, and the system returns to its initial state when the trigger is removed.

Polymers Used in Biotechnology and Medicine

The highly nonlinear transitions in smart polymers are driven by different factors, for example, neutralization of charged groups by either a pH shift (2) or the addition of an oppositely charged polymer (3), changes in the efficiency of hydrogen bonding and an increase in temperature or ionic strength (4), and critical phenomena in hydrogels and interpenetrating polymer networks (5). The polymer systems that have highly nonlinear response can be divided into three general groups: pH-sensitive polymers, thermosensitive polymers, and reversibly cross-linked networks.

pH-Sensitive Polymers. The first group of smart polymers consists of polymers whose transition between the soluble and insoluble state is created by decreasing the net charge of the polymer molecule. The net charge can be decreased by changing the pH to neutralize the charges on the macromolecule and hence to reduce the hydrophilicity (increase the hydrophobicity) of the macromolecule. Copolymers of methyl methacrylate (hydrophobic part) and methacrylic acid (hydrophilic at high pH when carboxy groups are deprotonated but more hydrophobic when carboxy groups are protonated) precipitate from aqueous solutions by acidification to pH around 5, and copolymers of methyl methacrylate (hydrophobic part) with dimethylaminoethyl methacrylate (hydrophilic at low pH when amino groups are protonated but more hydrophobic when amino groups are deprotonated) are soluble at low pH but precipitate in slightly alkaline conditions (6) (see METHACRYLIC ESTER POLYMERS). Hydrophobically modified cellulose derivatives that have pending carboxy groups, for example, hydroxypropyl methyl cellulose acetate succinate, are also soluble in basic conditions but precipitate in slightly acidic media (7).

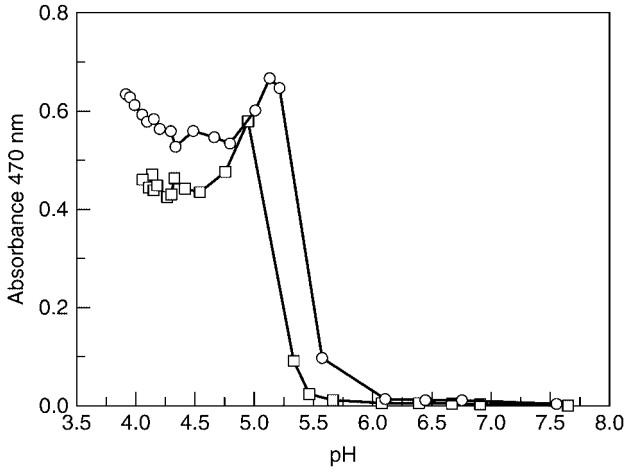

Fig. 1. pH-induced precipitation of a random copolymer of methacrylic acid and methacrylate (commercialized as Eudragit S 100 by Röhm Pharma GMBH, Weiterstadt, Germany) (open squares) and *p*-amino-phenyl-α-D-glucopyranoside-modified copolymer (open circles) measured as turbidity at 470 nm. Some decrease in turbidity at lower pH values is caused by flocculation and sedimentation of the polymer precipitate. Redrawn from Ref. 8.

The pH-induced precipitation of smart polymers is very sharp and usually requires a change in pH of not more than 0.2–0.3 units (Fig. 1). When some carboxy groups are used to couple a biorecognition element, for example, noncharged sugar, the increased hydrophobicity of the copolymer results in precipitation at a higher pH (8). The copolymerization of *N*-acryloyl sulfametazine with *N*,*N*-dimethylacrylamide results in a pH-sensitive polymer whose reversible transition is in the physiological range of pH 7.0–7.5 (9) (see ACRYLAMIDE POLYMERS).

The charges on the macromolecule can also be neutralized by adding an efficient counterion, for example, a low molecular weight counterion or a polymer molecule of opposite charges. The latter systems are combined under the name of polycomplexes. The cooperative nature of interaction between two polymers of opposite charges makes polycomplexes very sensitive to changes in pH or ionic strength (10). The complex formed by poly(methacrylic acid) (polyanion) and poly(*N*-ethyl-4-vinyl-pyridinium bromide) (polycation) undergoes reversible precipitation from aqueous solution at any desired pH value in the range 4.5–6.5 that depends on the ionic strength and polycation/polyanion ratio in the complex (Fig. 2) (11). Polyelectrolyte complexes formed by poly(ethylene imine) and poly(acrylic acid) undergo soluble–insoluble transition in an even broader pH range of 3–11 (12).

The pH of the transition of pH-sensitive polymers such as poly(methyl methacrylate-*co*-methacrylic acid) or poly (*N*-acryloyl sulfametazine-*co*-*N*,*N*-dimethylacrylamide) is strictly fixed for the given composition of comonomers. Thus, a new polymer should be synthesized for each desired pH value. The advantage of polyelectrolyte complexes is that by using only two different polymers and mixing them in different ratios, reversible precipitation can be achieved at any desired pH value in a rather broad pH range (see POLYELECTROLYTES).

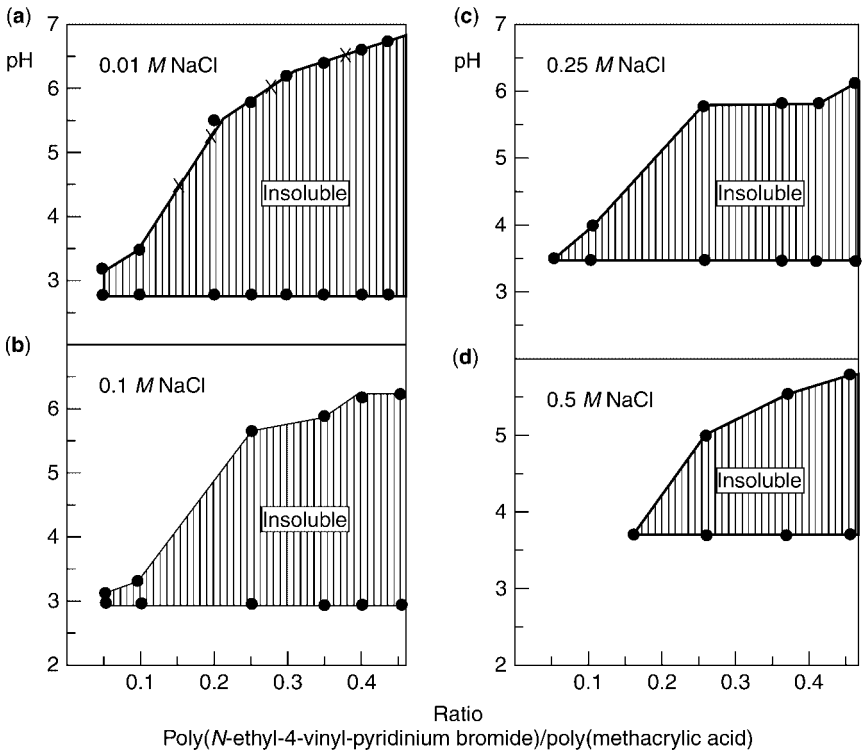

Fig. 2. Phase diagram for the polyelectrolyte complex formed by poly(*N*-ethyl-4-vinyl-pyridinium bromide) (polymerization degree 530) and poly(methacrylic acid) (polymerization degree 1830). The dots (represent pH values at which the turbidity of the polymer solutions was first observed at 470 nm. Ionic strength was 0.01 *M* NaCl (**a**), 0.1 *M* NaCl (**b**), 0.25 *M* NaCl (**c**), and 0.5 *M* NaCl (**d**). Dashed area represents pH/composition range where the complex is insoluble. Reproduced from Ref. 11 with permission.

Thermosensitive Polymers. The reversible solubility of thermosensitive polymers is caused by changes in the hydrophobic–hydrophilic balance of uncharged polymers induced by increasing temperature or ionic strength. Uncharged polymers are soluble in water because of hydrogen bonding with water molecules. The efficiency of hydrogen bonding lessens as temperature increases. The phase separation of a polymer occurs when the efficiency of hydrogen bonding becomes insufficient for the solubility of macromolecule.

When the temperature of an aqueous solution of a polymer is raised above a certain critical temperature (which is often referred to as the transition temperature, lower critical solution temperature (LCST), or "cloud point"), phase separation takes place. An aqueous phase that contains practically no polymer and a polymer-enriched phase are formed. Both phases can be easily separated by decanting, centrifugation, or filtration. The temperature of the phase transitions depends on the polymer concentration and molecular weight (Fig. 3) (13,14). The phase separation is completely reversible, and the polymer dissolves in water when the temperature is reduced below the transition temperature.

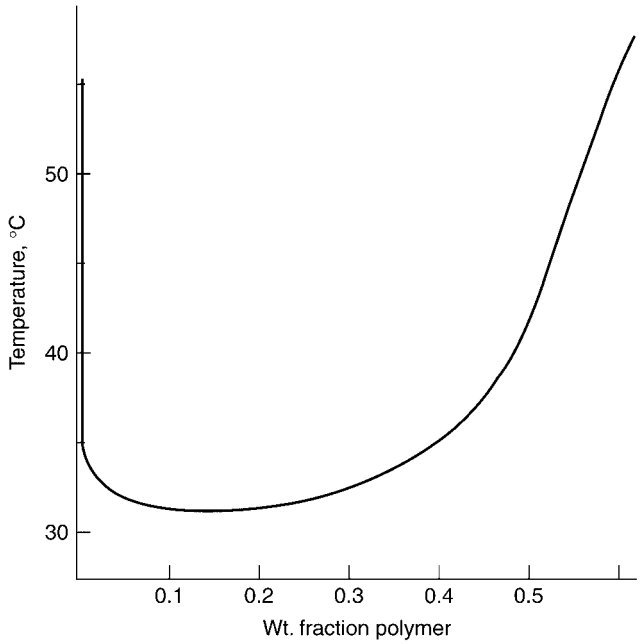

Fig. 3. Phase diagram for poly(NIPAAM) in aqueous solution. The area under the binodal curve presents the range of temperatures/polymer concentrations for homogeneous solution. Separation into polymer-enriched and polymer-depleted phases takes place for any polymer concentration/temperature above the binodal curve. Reproduced from Ref. 14 with permission.

Two groups of thermosensitive smart polymers are most widely studied and used:

(1) Poly(*N*-alkyl substituted acrylamides) and the most well-known of them, poly(*N*-isopropyl acrylamide) (poly(NIPAAM)), whose transition temperature is 32°C (14), and
(2) Poly(*N*-vinylalkylamides) such as poly(*N*-vinylisobutyramide) whose transition temperature is 39°C (15) or poly(*N*-vinyl caprolactam) whose transition temperature is 32–33°C (depending on the molecular weight of the polymer) (13)

A variety of polymers that have different transition temperatures from 4–5°C for poly(*N*-vinyl piperidine) to 100°C for poly(ethylene glycol) are available at present (16).

pH-Sensitive smart polymers usually contain carboxy or amino groups that can be used for covalent coupling of biorecognition or biocatalytic elements (ligands). Thermosensitive polymers, on the contrary, do not have inherent reactive groups which could be used for ligand coupling. Thus, copolymers that contain reactive groups can be synthesized. *N*-Acryloylhydroxysuccinimide (17) or glycidyl methacrylate (18) have often been used as active comonomers in copolymerization with NIPAAM, allowing further coupling of amino-group-containing ligands

to the synthesized copolymers. The use of an initiator of polymerization (19) or chain-transfer agent (20) that has an active group results in a polymer modified only at the end of the macromolecule. An alternative strategy is to incorporate a polymerizable double bond into the ligand, for example, by modification with acryoyl group, and then to copolymerize the modified ligand with NIPAAM (21,22).

An increase in the hydrophilicity of the polymer-accompanied incorporation of hydrophilic comonomers or coupling to hydrophilic ligands increases the transition temperature, whereas hydrophobic comonomers and ligands have the opposite effect (4). The pH-induced change in ligand hydrophobicity could have a dramatic effect on the thermoseparation of the ligand–polymer conjugate. A copolymer of NIPAAM and vinyl imidazole precipitates at about 35°C at pH 8 where imidazole moieties are noncharged and relatively hydrophobic, but no precipitation occurs even when heating the polymer solution to 80°C at pH 6 where imidazole groups are protonated and very hydrophilic (23).

Ligand–ligand interactions in a ligand–polymer conjugate also have a significant effect on the thermoseparation. The precipitation temperature for the previously mentioned copolymers of NIPAAM and vinyl imidazole increases as the imidazole content in the copolymer increases. On the contrary, the precipitation temperature decreases as the increase of imidazole content increases, when the polymer forms a Cu(II) complex (23). Each Cu(II) ion interacts with two to three imidazole groups to cross-link the segments of the polymer molecule (24). The restricted mobility of the polymer segments results in a lower precipitation temperature.

Block copolymers that have a thermosensitive "smart" part that consists of poly(NIPAAM) form reversible gels on an increase in temperature, whereas random copolymers separate from aqueous solutions by forming a concentrated polymer phase (25). Thus, the properties of polymers that are important for biotechnological and medical applications could be controlled by the composition of comonomers and also by the polymer architecture.

The phase transition of thermosensitive polymers at increased temperature results from hydrophobic interactions between polymer molecules. Because hydrophobic interactions are promoted by high salt concentrations, the addition of salts shifts the cloud point to lower temperatures. When the transition temperature is below room temperature, polymer precipitation is achieved by the addition of salt, without any heating. The addition of organic solvents, detergents, and chaotropic agents increases the transition temperature because these compounds deteriorate hydrophobic interactions.

Reversibly Cross-Linked Polymer Networks. Systems that have reversible noncovalent cross-linking of separate polymer molecules into a polymer network belong to the third group of smart polymers. When formed, reversibly cross-linked polymers either precipitate or form a physical gel. Polymers that have sugar ligands cross-linked by lectins with multibinding sites (26) and boronate-polyols (27–29) are the most widely used systems of this type. The reversible response in these systems is achieved by addition/removal of a low molecular weight analogue of the polymer. For example, small sugars added at high concentrations compete with sugar-containing polymers for binding to lectin and destroy intrapolymer cross-links that result in disengagement of the network.

Heterogeneous Systems Using Smart Polymers. A solid surface acquires new properties when modified by adsorption or chemical grafting of polymers. Smart polymer, that have terminal (only single-point) or random (multipoint) attachment possible could be covalently coupled to the respective active groups on the surface (30). Single-point attachment could also be achieved by covalent modification of the surface using an initiator of polymerization and then carrying out polymerization of monomers in the solution that surrounds the support. The growth of polymer chains occurs only at the sites where initiator was coupled (31). Alternatively, the solid support is irradiated by light (32) or a plasma beam (33) when monomer is in the surrounding solution. Active radical sites on the surface, which appear as a result of irradiation, initiate the growth of polymer macromolecules. As a rule, irradiation methods give a higher density of grafted polymer, but polymerization is less controlled as in covalent coupling or using a covalently coupled initiator. Irradiation, especially at high monomer concentrations, could produce a cross-linked polymer gel attached to the solid support (34).

A separate group of smart polymers is represented by particulate systems. Liposomes that reversibly precipitate on salt addition and removal were prepared from a synthetic phospholipid that had a diacetylene moiety in the hydrophobic chain and an amino group in the hydrophilic head of the phospholipid, followed by polymerization of diacetylene bonds (35). Latices composed of thermosensitive polymers or a layer of thermosensitive polymer at the surface represent another example of insoluble but reversibly suspended particulate systems that respond to increasing/decreasing temperature (31).

Applications Overview

There are numerous potential applications for polymers in biotechnology and medicine. The main commercial application of polymers is the production of "smart" pills where the (aside from medical plastics) polymer shell protects the pill from the harmful action of the stomach contents but allows the pill to dissolve in the intestine. There is not yet any other product on the market that applies smart polymers, but the interest in these applications is growing in both the academic community and industry. The following applications are considered in this article:

(1) smart pills that have an enteric coating
(2) smart polymers for affinity precipitation of proteins
(3) aqueous two-phase polymer systems formed by smart polymers and their application for protein purification
(4) smart surfaces for mild detachment of cultivated mammalian cells
(5) smart chromatographic matrices that respond to temperature
(6) smart polymers for controlled porosity of systems – "chemical valve"
(7) liposomes with triggered release of their contents

(8) smart polymers for bioanalytical applications
(9) reversibly soluble biocatalysts

Smart Pills That Have an Enteric Coating. Peroral introduction of medical preparations is the most convenient method compared to subcutaneous or intravenous injection and even to nasal sprays or eye droplets. The absorption of a swallowed pill takes place predominantly in the intestine and to reach the intestine the medicine must pass unharmed through the stomach that has a very low pH value of 1.4 and abundant hydrolytic enzymes that can degrade a broad variety of chemical structures. Many medicines are susceptible to damage in the stomach environment. The ideal condition for peroral introduction is to have a smart pill, which is insoluble in the stomach and hence passes through the stomach unaffected but easily dissolves at the higher pH in the intestine where the medicine is absorbed. Smart polymers provide the solution. Hydrophobic polymers such as poly(methyl methacrylate) or hydrophobically modified celluloses are insoluble in water per se, but the introduction of carboxy groups (either by partial hydrolysis of ester groups in methyl methacrylate or modification of cellulose HO groups by dicarboxylic acids such as succinic or phthalic acid) endows the polymers with pH-dependent solubility. The pill covered by a shell of such a polymer (enteric coating) is insoluble at low pH when the carboxy groups are protonated and uncharged, but is easily soluble at a pH above 6 when carboxy groups are protonated and charged. Industrially produced polymers for enteric coating belong to two main groups, synthetic copolymers of methyl methacrylate and methacrylic acid and modified derivatives of cellulose, a natural polymer (Table 1). The first group of polymers is used mainly by European and U.S. manufacturers, and the second group is more popular in Japan.

Table 1. Industrially Manufactured Polymers for Producing Smart Pills

Polymer	Trade name	Manufacturer	Country
Poly(methacrylic acid-*co*-methyl methacrylate) 1:1 monomer ratio, MW 135,000	Eudragit L	Röhm Pharma GmBH	United States, Germany
Poly(methacrylic acid-*co*-methyl methacrylate) 1:2 monomer ratio, MW 135,000	Eudragit S	Röhm Pharma GmBH	United States, Germany
Carboxymethylcellulose	CMEC	Freund Sangyo Co., Ltd.	Japan
Cellulose acetate phthalate	CAP	Wako Pure Chemicals Ltd.	Japan
Hydroxypropylmethyl cellulose phthalate	HP-50, HP-55	Shin-Etsu Chemical Co., Ltd.	Japan
Hydroxypropylmethyl cellulose acetate succinate	ASM, AS-H	Shin-Etsu Chemical Co., Ltd.	Japan
Poly(diethylaminoethyl methacrylate-*co*-methyl methacrylate) MW 150,000	Eudragit E	Röhm Pharma GmBH	United States, Germany

Whenever the charge-bearing comonomer has an amino group instead of a carboxy group, the solubility of the polymer acquires opposite pH-dependence. The polymer is soluble at low pH values but insoluble in neutral and alkaline media. Poly(diethylaminoethyl methacrylate-*co*-methyl methacrylate) (commercialized as Eudragit E) is an example of such a polymer. The shell that is composed of this polymer protects the tablet against dissolution in the neutral saliva, and the mouth is not affected by the unpleasant taste of bitter medicine, but the polymer dissolves readily in the stomach.

Bioseparation Applications

Affinity Precipitation. All bioseparation processes include three stages: preferential partitioning of target substance and impurities between two phases (liquid–liquid or liquid–solid), mechanical separation of the phases (eg, separation of the stationary and mobile phases in a chromatographic column), and recovery of the target substance from the enriched phase. Because smart polymers can undergo phase transitions, they could facilitate the second and the third stages of bioseparation processes.

The ability of smart polymers to form *in situ* heterogeneous systems is exploited in affinity precipitation (Fig. 4). The technique is based on using a conjugate of a smart polymer that has a covalently coupled biorecognition moiety, that is, a ligand specific for a target protein. The conjugate forms a complex with

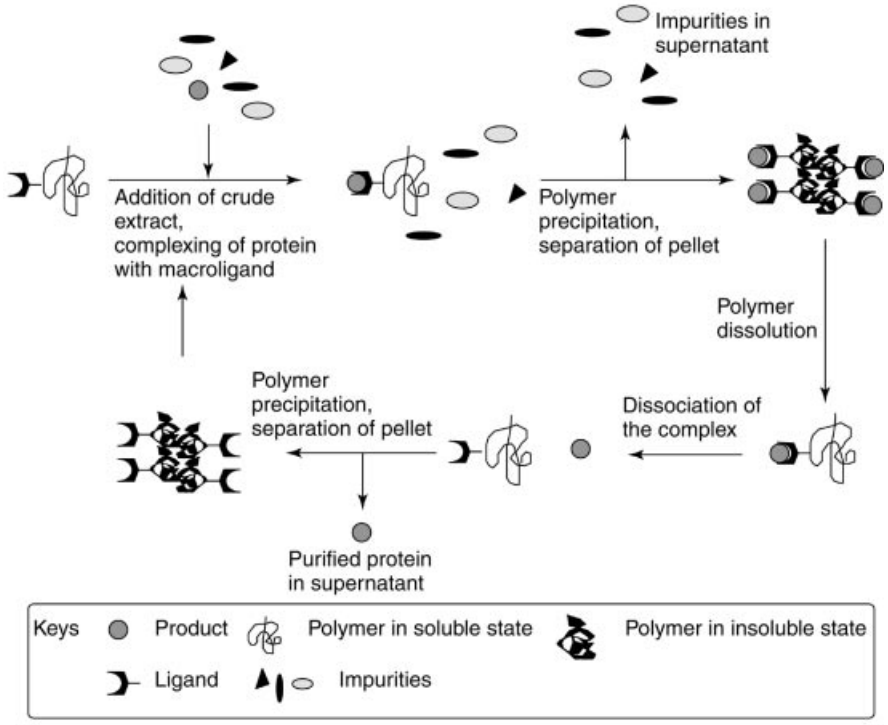

Fig. 4. Schematic of affinity precipitation technique for protein purification.

the target protein but not with the other proteins in the crude extract. Phase separation of the complex is triggered by small changes in the environment, resulting in transition of the polymer backbone into an insoluble state. The target protein specifically coprecipitates with the smart polymer, and the impurities in the crude extract remain in solution. Then, the target protein is either eluted from the insoluble macroligand–protein complex or the precipitate is dissolved. The protein is dissociated from the macroligand, and the ligand–polymer conjugate is precipitated again. Now without the protein that remains in the supernatant in purified form. A variety of different ligands such as triazine dyes, sugars, protease inhibitors, antibodies, nucleotides, double- or single-stranded DNA, and chelated metal ions were successfully used for affinity precipitation (36). After elution of the target protein the ligand–polymer conjugate could be recovered and used in the next purification cycle (37).

Triazine dyes, robust affinity ligands for many nucleotide-dependent enzymes, were successfully used in conjugates with the pH-sensitive copolymer of methacrylic acid and methyl methacrylate which precipitates when pH decreases (Eudragit S 100) for purification of dehydrogenases from various sources by affinity precipitation (38,39). Sugar ligands constitute another attractive alternative and have been used in combination with Eudragit S 100 for bioseparation of lectins (40). Restriction endonuclease Hind III was successfully isolated using the thermosensitive conjugate of poly(NIPAAM) with phage λ DNA (21). Human IgG was specifically precipitated with a conjugate of protein A and galactomannan. Galactomannan polymer was reversibly precipitated by adding tetraborate (41).

The efficient precipitation of Cu(II)-loaded poly(*N*-vinylimidazole-*co*-NIPAAM) by high salt concentrations at mild temperature is very convenient for metal affinity precipitation of proteins that have inherent histidine residues at the surface or for recombinant proteins artificially provided with histidine tags (usually four to six residues). High salt concentration does not interfere with protein–metal ion–chelate interaction, and, on the other hand, it reduces the possibility of nonspecific binding of foreign proteins to the polymer both in solution and when precipitated (23). The flexibility of polymer chains in solution allows several imidazole ligands on a polymer molecule to come close enough to interact with the same Cu(II) ion and thus to provide sufficient strength of polymer–Cu(II) interactions to purify a variety of histidine-containing proteins (37).

Polyelectrolyte complexes that have pH-dependent solubility were successfully used in different bioseparation procedures. When an antigen, inactivated glyceraldehyde-3-phosphate dehydrogenase, from rabbit was covalently coupled to a polycation, the resulting complex was used to purify monoclonal antibodies specific toward inactivated glyceraldehyde-3-phosphate dehydrogenase (11). The successful affinity precipitation of antibodies using glyceraldehyde-3-phosphate dehydrogenase bound to a polyelectrolyte complex indicates that the ligand is exposed to the solution. This fact was used to develop a new method for producing monovalent Fab fragments of antibodies. Traditionally, Fab fragments are produced by proteolytic digestion of antibodies in solution followed by isolation of Fab fragments. In the case of monoclonal antibodies against inactivated subunits of glyceraldehyde-3-phosphate dehydrogenase, digestion with papain resulted in significant damage of binding sites of the Fab fragment. Proteolysis of monoclonal antibodies in the presence of the antigen–polycation conjugate followed by (*1*)

precipitation induced by adding polyanion, poly(methacrylic acid), and a pH shift from 7.3 to 6.5, and (*2*) elution at pH 3.0 that resulted in 90% immunologically competent Fab fragments. Moreover, the papain concentration required for proteolysis was 10 times less for antibodies bound to the antigen–polycation conjugate compared to that for free antibodies in solution (42). Active glyceraldehyde-3-phosphate dehydrogenase from rabbit muscle was separated from the inactivated enzyme by using monoclonal antibodies specific for the inactivated enzyme covalently coupled to the polyanion component of the polyelectrolyte complex. This system can be regarded as a simplified model of chaperone action in living cells that assist in separating active protein molecules from misfolded ones (43).

Apart from specific interactions between a target protein and a ligand–polymer conjugate, nonspecific interactions of protein impurities with the polymer backbone could take place. The nonspecific interactions limit the efficiency of the affinity precipitation technique, and significant efforts were made to reduce these interactions. The advantage of polyelectrolyte complexes as carriers for affinity precipitation is low nonspecific coprecipitation of proteins when the polymer undergoes a soluble–insoluble transition (10).

Smart particles capable of reversible transition between aggregated and dispersed states were used for affinity precipitation of proteins. Thermosensitive (44) or pH-sensitive latices (45) or salt-sensitive liposomes that have polymerized membranes (35) are examples of such systems.

Two elements are required for successful affinity precipitation. The backbone of a smart polymer provides precipitation at the desired conditions (temperature, pH, ionic strength), and the biorecognition element is responsible for selective binding of the protein of interest. By proper choice of a smart polymer, precipitation could be achieved practically at any desired pH or temperature. For example, poly(*N*-acryloylpiperidine) terminally modified with maltose has an extremely low critical temperature (soluble below 4°C and completely insoluble above 8°C) and was used to purify thermolabile α-glucosidase (46).

Partitioning in Aqueous Polymer Two-Phase Systems. Two aqueous polymer solutions become mutually incompatible when the threshold concentrations of polymers are exceeded. Both of the polymer phases formed contain about 90% water and hence present a very friendly environment for proteins and other biomolecules. Proteins partition selectively between two phases depending on their size, charge, hydrophobicity, nature, and the concentration of the phase-forming polymers. The partitioning could also be directed by adding some salt or coupling an affinity ligand specific for a given protein to one of the phase-forming polymers (47). The selective partitioning of proteins between the two phases formed has proven to be an efficient tool for purifying proteins and some low molecular weight substances. The main problem of the method—how to separate the target protein from the phase-forming polymer—has not yet been completely solved. Smart polymers provide an elegant solution to this problem—simple precipitation of the phase-forming polymer leaves protein in the supernatant (Fig. 5): (*1*) the crude protein extract is mixed with the aqueous two-phase polymer system, and the conditions are selected so that the protein of interest partitions into a phase formed by a smart polymer (for example by coupling affinity ligand to the smart polymer), and the impurities concentrate in the other phase; (*2*) the phases are separated mechanically and the phase formed by the smart polymer is

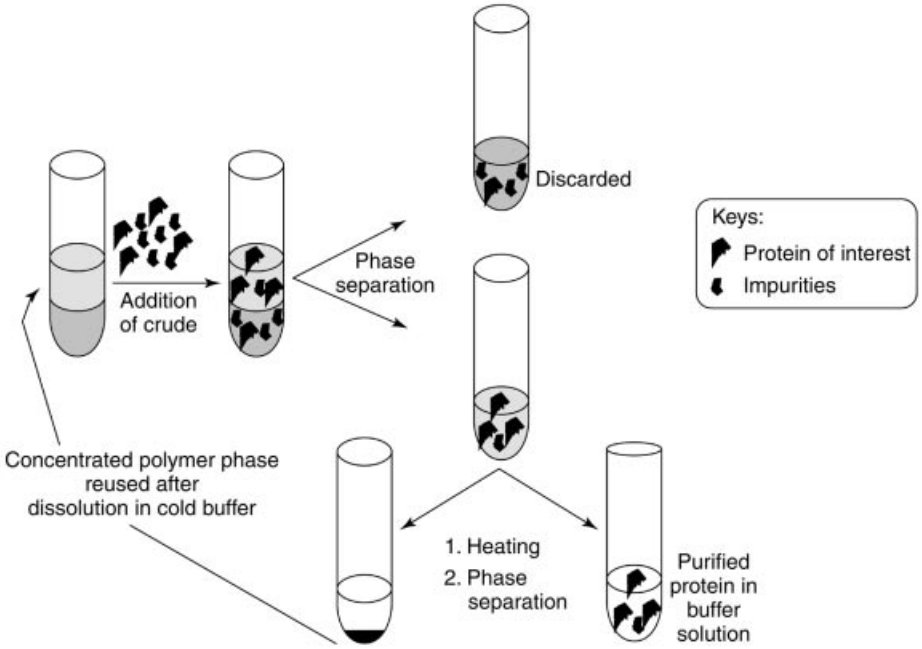

Fig. 5. Schematic presentation of protein partitioning in aqueous two-phase polymer system formed by a smart (thermosensitive) polymer. Reproduced from Ref. 140 with permission.

subjected to conditions (pH or temperature) where the polymer undergoes phase separation; and (*3*) two new phases are formed, a polymer-enriched phase of high polymer and low water concentration, which contains practically no protein, and a polymer-depleted aqueous phase that contains most of the purified protein and minute amounts of the polymer left after phase separation.

pH-Sensitive acrylic copolymers (48) or thermoresponsive polymers, poly(ethylene oxide-*co*-propylene oxide) (49,50) or poly(*N*-vinyl caprolactam-*co*-vinyl imidazole) (51), form two-phase systems with relatively hydrophilic polymers such as dextran or modified starch and have been successfully used for protein purification. The pH- or thermoprecipitated polymer in contrast to dextran could be regenerated by dissolution at a lower temperature or by changing pH. Quite recently, an aqueous two-phase polymer system was developed where both phase-forming polymers, poly(*N*-isopropylacrylamide-*co*-vinyl imidazole) and poly(ethylene oxide-*co*-propylene oxide) end modified by hydrophobic $C_{14}H_{29}$ groups, are thermoresponsive and could be recycled (52).

Smart Surfaces

Cell Detachment. The driving force behind phase separation of smart polymers is a sharp increase in hydrophobicity after a small change in

environmental conditions. The hydrophobic "collapsed" polymer aggregates form a separate phase. When grafted to the surface, macromolecules of the smart polymer cannot aggregate, but the conformational transition from the hydrophilic to the hydrophobic state endows the surface with regulated hydrophobicity: the surface is hydrophilic when the smart polymer is in the expanded "soluble" conformation and hydrophobic when the polymer is in the collapsed "insoluble" conformation. The change of hydrophobicity of the surface by grafted poly(*N*-isopropylacrylamide) was demonstrated by contact angle measurements (53) and water absorbency (54) (see SURFACE PROPERTIES).

The transition temperature for adsorbed (presumably via multipoint attachment) poly(NIPAAM) molecules is lower than that in bulk solution, and the properties of the layer of collapsed macromolecules formed above the transition temperature depend strongly on the speed by which the temperature increases. At a low speed of temperature increase, the "liquid-like" polymer layer is formed, whereas at high speeds, the polymer layer has more "solid-like" properties (55). When cooling, the collapsed polymer molecules return to the initial loopy adsorbed conformation via transitional extended conformation. The relaxation process for the extended-to-loopy adsorbed conformational transition occurs slowly and depends on the temperature obeying an Arrhenius law. Kinetic constraints, it is proposed, play an important role in this transition (56).

The change of surface properties from hydrophobic above the critical temperature of the polymer grafted to hydrophilic below it has been successfully used for detaching mammalian cells. Mammalian cells are normally cultivated on a hydrophobic solid substrate and are detached from the substrate by protease treatment, which often damages the cells by hydrolyzing various membrane-associated protein molecules. The poly(NIPAAM)-grafted surface is hydrophobic at 37°C because this temperature is above the critical temperature for the grafted polymer and those cells that are growing well on it. A decrease in temperature results in transition of the surface to the hydrophilic state, where the cells can be easily detached from the solid substrate without any damage. Poly(NIPAAM) was grafted to polystyrene culture dishes using an electron beam. Bovine hepatocytes, cells that are highly sensitive to enzymatic treatment, were cultivated for 2 days at 37°C and detached by incubation at 4°C for 1 h. Nearly 100% of the hepatocytes was detached and recovered from the poly(NIPAAM)-grafted dishes by low temperature treatment, whereas only about 8% of the cells was detached from the control dish (57). The technique has been extended to different cell types (58,59). It is noteworthy that hepatocytes recovered by cooling retained their native form, had numerous bulges and dips, and attached well to the hydrophobic surface again, for example, when the temperature was increased above the conformational transition of poly(NIPAAM). On the contrary, enzyme-treated cells had a smooth outer surface and had lost their ability to attach to the surface. Thus, cells recovered by a temperature shift from poly(NIPAAM)-grafted surfaces have an intact structure and maintain normal cell functions (58).

The molecular machinery involved in cell-surface detachment was investigated using temperature-responsive surfaces (60). Poly(NIPAAM)-grafted and nongrafted surfaces showed no difference in attachment, spreading, growth, confluent cell density, or morphology of bovine aortic endothelial cells at 37°C. Stress fibers, peripheral bands, and focal contacts were established in similar ways.

When the temperature was decreased to 20°C, the cells grown on poly(NIPAAM)-grafted support lost their flattened morphology and acquired a rounded appearance similar to that of cells immediately after plating. Mild agitation makes the cells float free from the surface without a trypsin treatment. Neither changes in cell morphology nor cell detachment occurred on ungrafted surfaces. Sodium azide, an ATP synthesis inhibitor, and genistein, a tyrosine kinase inhibitor, suppressed changes in cell morphology and cell detachment, whereas cycloheximide, a protein synthesis inhibitor, slightly enhanced cell detachment. Phalloidin, an actin filament stabilizer, and its depolymerizer, cytochalasin D, also inhibited cell detachment. These findings suggest that cell detachment from grafted surfaces is mediated by intracellular signal transduction and reorganization of the cytoskeleton, rather than by a simple change in the "stickiness" of the cells to the surface when the hydrophobicity of the surface is changed.

One could imagine producing artificial organs using temperature-induced detachment of cells. Artificial skin could be produced as the cells are detached from the support not as a suspension (the usual result of protease-induced detachment) but preserving their intercellular contacts. Fibroblasts were cultured on the poly(NIPAAM)-collagen support until the cells completely covered the surface at 37°C, followed by a decrease in temperature to about 15°C. The sheets of fibroblasts detached from the dish and within about 15 min floated in the culture medium (57). The detached cells could be transplanted to another culture surface without functional and structural changes (34). Grafting of poly(NIPPAM) onto a polystyrene surface by photolithographic technique creates a special pattern on the surface, and by decreasing temperature, cultured mouse fibroblast STO cells are detached only from the surface area on which poly(NIPAAM) was grafted (61). Lithographed films of smart polymer present supports for controlled interactions of cells with surfaces and can direct the attachment and spreading of cells (62). One could envisage producing artificial cell assemblies of complex architecture using this technique.

Temperature-Controlled Chromatography. Surfaces that have thermoresponsive hydrophobic/properties have been used in chromatography. HPLC columns with grafted poly(NIPAAM) have been used for separating steroids (63) and drugs (64). The chromatographic retention and resolution of the solutes was strongly dependent on temperature and increased as temperature increased from 5 to 50°C, whereas the reference column packed with nonmodified silica displayed much shorter retention times that decreased as temperature decreased. Hydrophobic interactions dominate in retaining solutes at higher temperature, and the preferential retention of hydrogen-bond acceptors was observed at low temperatures. The effect of temperature increase on the retention behavior of solutes separated on the poly(NIPAAM)-grafted silica chromatographic matrix was similar to the addition of methanol to the mobile phase at constant temperature (65).

The temperature response of the poly(NIPAAM)-silica matrices depends drastically on the architecture of the grafted polymer molecules. Surface wettability changes dramatically as temperature changes across the range 32–35°C (corresponding to the phase-transition temperature for NIPAAM in aqueous media) for surfaces where poly(NIPAAM) is terminally grafted either directly to the surface or to the looped chain copolymer of NIPAAM and *N*-acryloylhydroxysuccinimide which was initially coupled to the surface. The wettability changes for the

loop-grafted surface itself were relatively large but had a slightly lower transition temperature (~27°C). The restricted conformational transitions for multipoint grafted macromolecules are probably the reason for the reduced transition temperature. The largest surface free energy changes among three surfaces was observed for the combination of both loops and terminally grafted chains (30).

Introduction of a hydrophobic comonomer, butyl methacrylate, in the polymer resulted in a decreased transition temperature of about 20°C. Retention of steroids in poly(NIPAAM-*co*-butyl methacrylate)-grafted columns increases as column temperature increases. The capacity factors for steroids on the copolymer-modified silica beads was much larger than that on poly(NIPAAM)-grafted columns. The effect of temperature on steroid retention on poly(NIPAAM-*co*-butyl methacrylate)-grafted stationary phases was more pronounced compared to supports modified with poly(NIPAAM). Furthermore, retention times for steroids increased remarkably as the butyl methacrylate content increased in the copolymer. The temperature-responsive elution of steroids was strongly affected by the hydrophobicity of the grafted polymer chains on silica surfaces (63).

The mixture of polypeptides, consisting of 21–30 amino acid residues (insulin chain A, β-endorphin fragment 1–27, and insulin chain B) could not be separated at 5°C (below the transition temperature) on copolymer-grafted matrix. At this temperature, the copolymer is in an extended hydrophilic conformation that results in decreased interactions with peptides and hence short retention times insufficient to resolve them. The mixture has been easily separated at 30°C, when the copolymer is collapsed, hydrophobic interactions are more pronounced, and retention times are sufficiently long for resolving polypeptides (66). Large protein molecules such as immunoglobulin G demonstrate less pronounced changes in adsorption above and below the transition temperature. Only about 20% of the protein adsorbed on poly(NIPAAM)-grafted silica at 37°C (above the LCST) were eluted after decreasing temperature to 24°C (below the transition temperature) (67). Quantitative elution of proteins adsorbed on the matrix via hydrophobic interactions has not yet been demonstrated, although protein adsorption on poly(NIPAAM)-grafted matrices could be somewhat controlled by a temperature shift. A successful strategy for temperature-controlled protein chromatography proved to be a combination of temperature-responsive polymeric grafts and biorecognition element, for example, affinity ligands (see CHROMATOGRAPHY, AFFINITY).

The access of the protein molecules to the ligands on the surface of the matrix is affected by the transition of the polymer macromolecule grafted or attached to the chromatographic matrix. Triazine dyes, for example, Cibacron Blue, are often used as ligands for dye-affinity chromatography of various nucleotide-dependent enzymes (68). Poly(*N*-vinyl caprolactam), a thermoresponsive polymer whose critical temperature is about 35°C interacts efficiently with triazine dyes. Polymer molecules of a molecular weight of 40,000 are capable of binding up to seven to eight dye molecules, and hence, the polymer binds via multipoint interaction to the dye ligands available on the chromatographic matrix. At elevated temperature, polymer molecules are in a compact globule conformation that can bind only to a few ligands on the matrix. Lactate dehydrogenase, an enzyme from porcine muscle, has good access to the ligands that are not occupied by the polymer and binds to the column. Poly(*N*-vinyl caprolactam) macromolecules undergo transition to

a more expanded coil conformation as temperature decreases. Now, the polymer molecules interact with more ligands and begin to compete with the bound enzyme for the ligands. Finally, the bound enzyme is displaced by the expanded polymer chains. The temperature-induced elution was quantitative, and was the first reported in the literature when temperature change was used as the only eluting factor without any changes in buffer composition (69). Small changes in temperature, as the only eluting factor, are quite promising because there is no need in this case to separate the target protein from an eluent, usually a competing nucleotide or high salt concentration in dye-affinity chromatography.

Controlled Porosity, "Chemical Valve". Environmentally controlled change in macromolecular size from a compact hydrophobic globule to an expanded hydrophilic coil is exploited when smart polymers are used in systems of environmentally controlled porosity, so-called chemical valves. When a smart polymer is grafted to the surface of the pores in a porous membrane or chromatographic matrix, the transition in the macromolecule affects the total free volume of the pores available for the solvent and hence presents a means to regulate the porosity of the system (see MEMBRANE TECHNOLOGY).

Membranes of pH-sensitive permeability were constructed by grafting smart polymers such as poly(methacrylic acid) (70), poly(benzyl glutamate), poly(2-ethylacrylic acid) (71), poly(4-vinylpyridine) (72), which change their conformation in response to pH. Thermosensitive chemical valves have been developed by grafting poly(*N*-acryloylpyrrolidine), poly(*N*-*n*-propylacrylamide), or poly(acryloylpiperidine) (73); poly(NIPAAM) alone (33,74); or in copolymers with poly(methacrylic acid) (74) inside the pores. For example, grafted molecules of poly(benzyl glutamate) at high pH are charged and are in extended conformation. The efficient pore size is reduced, and the flow through the membrane is low ("off-state" of the membrane). As pH decreases, the macromolecules are protonated, lose their charge, and adopt a compact conformation. The efficient pore size and hence the flow through the membrane increases ("on-state" of the membrane) (71). The fluxes of bigger molecules (dextrans of molecular weights 4400–50,600) across a temperature-sensitive, poly(NIPAAM)-grafted membrane were effectively controlled by temperature, environmental ionic strength, and degree of grafting of the membrane, while the flux of smaller molecules such as mannitol was not affected by temperature even at high degree of membrane grafting (75). The on-off permeability ratio for different molecules (water, Cl^- ion, choline, insulin, and albumin) ranged between 3 and 10 and increased as molecular weight increased (76). An even more abrupt change of the on-off permeability ratio was observed for a membrane that had narrow pores formed by heavy ion beams when poly(NIPAAM) or poly(acryloyl-L-proline methyl ester) was grafted (77).

Different stimuli could trigger the transition of the smart polymer making it possible to produce membranes whose permeabilities respond to these stimuli. When a copolymer of NIPAAM with triphenylmethane leucocianide was grafted to the membrane, it acquired photosensitivity—uv irradiation increases permeation through the membrane (78). Fully reversible, pH-switchable permselectivity for both cationic and anionic redox-active probe molecules was achieved by depositing composite films formed from multilayers of amine-terminated dendrimers and poly(maleic anhydride-*co*-methylvinyl ether) on gold-coated silicon (79).

When the smart polymer is grafted inside the pores of the chromatographic matrix for gel permeation chromatography, the transition of grafted macromolecules regulates the pore size and, as a result, the elution profile of substances of different molecular weights. As the temperature is raised, the substances are eluted progressively earlier indicating shrinking of the pores of the hydrogel beads composed of cross-linked poly(acrylamide-*co*-NIPAAM) (80) or porous polymer beads with grafted poly(NIPAAM) (81).

When using a specific biorecognition element, which recognizes specific substances and translates the signal into a change of physicochemical properties, for example, pH, a smart membrane that changes its permeability in response to particular substances can be constructed. Specific insulin release in response to increasing glucose concentration, that is, an artificial pancreas, presents an everlasting challenge to bioengineers. One of the potential solutions is a "chemical valve" (Fig. 6). The enzyme, glucose oxidase, was used as a biorecognition element,

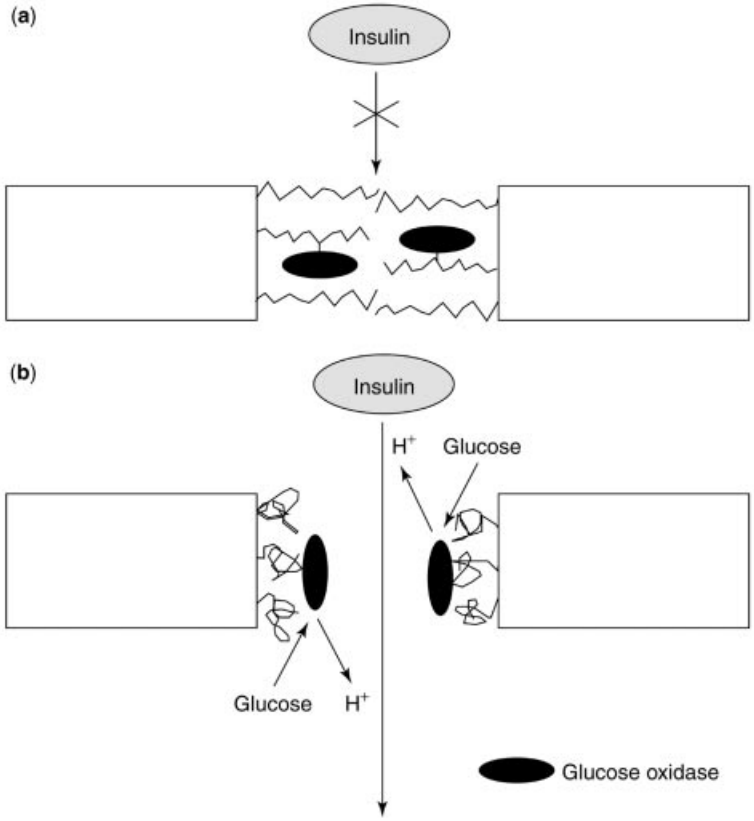

Fig. 6. Schematic of a "chemical valve." Glucose oxidase is immobilized on a pH-responsive polyacrylic acid grafted onto a porous polycarbonate membrane: (**a**) poly(acrylic acid) is in an expanded conformation that blocks insulin transport; (**b**) the oxidation of glucose is accompanied by a decrease in pH and the transition of poly(acrylic cid) into a compact conformation that results in opening of the pores and transport of insulin. Redrawn from Ref. 82.

capable of specific oxidation of glucose accompanied by a decrease in pH. The enzyme was immobilized on pH-responsive poly(acrylic acid) graft on a porous polycarbonate membrane. In neutral conditions, polymer chains are densely charged and have extended conformation that prevents insulin transport through the membrane by blocking the pores. Under exposure to glucose, the pH drops as the result of glucose oxidation by the immobilized enzyme, the polymer chains adopt a more compact conformation that diminishes the blockage of the pores, and insulin is transported through the membrane (82). Systems such as this could be used for efficient drug delivery that responds to the needs of the organism. A membrane that consists of poly(2-hydrohyethyl acrylate-*co*-*N*,*N*-diethylaminomethacrylate-*co*-4-trimethylsilylstyrene) undergoes a sharp transition from a shrunken state at pH 6.3 to a swollen state at pH 6.15. The transition between the two states changes the membrane permeability to insulin 42-fold. Copolymer capsules that contain glucose oxidase and insulin increase insulin release fivefold in response to 0.2 *M* glucose. After glucose removal, the rate of insulin release falls back to the initial value (83).

Alternatively, reversible cross-linking of polymer macromolecules could be used to control the porosity in a system. Two polymers, poly(*m*-acrylamidophenylboronic acid-*co*-vinylpyrrolidinone) and poly(vinyl alcohol) form a gel because of strong interactions between boronate groups and the hydroxy groups of poly(vinyl alcohol). When a low molecular weight polyalcohol such as glucose is added to the gel, it competes with poly(vinyl alcohol) for boronate groups. The boronate–poly(vinyl alcohol) complex changes to a boronate–glucose complex that results in eventual dissolution of the gel (84). In addition to a glucose oxidase-based artificial pancreas, the boronate–poly(vinyl alcohol) system has been used for constructing glucose-sensitive systems for insulin delivery (29,85–87). The glucose-induced transition from a gel to a sol state drastically increases the release of insulin from the gel. The reversible response to glucose has also been designed using another glucose-sensitive biorecognition element, Concanavalin A, a protein that contains four sites that can bind glucose. Polymers that have glucose groups in the side chain, such as poly(vinylpyrrolidinone-*co*-allylglucose) (26) or poly(glucosyloxyethyl methacrylate) (88), are reversibly cross-linked by Concanavalin A and form a gel. The addition of glucose results in displacing the glucose-bearing polymer from the complex with Concanavalin A and dissolving the gel.

Reversible gel-formation of thermosensitive block copolymers in response to temperature could be utilized in different applications. Poly(NIPAAM) block copolymers with poly(ethylene oxide) which undergo a temperature-induced reversible gel–sol transition were patented as the basis for cosmetics such as depilatories and bleaching agents (89). The copolymer solution is liquid at room temperature and easily applied to the skin where it forms a gel within 1 min. Commercially available ethyl(hydroxyethyl)celluloses that have cloud points of 65–70°C have been used as redeposition agents in washing powders. Adsorption of the precipitated polymer on the laundry during the initial rinsing period counteracts readsorption of dirt when the detergent is diluted (90).

Liposomes That Trigger Release of the Contents. When a smart polymer is attached somehow to a lipid membrane, the transition in the macromolecule affects the properties of the membrane and renders the system sensitive to

environmental changes. To attach a smart polymer to a lipid membrane, a suitable "anchor" which could be incorporated in the membrane should be introduced into the macromolecule. This could be achieved by copolymerizing poly(NIPAAM) with comonomers that have large hydrophobic tails such as *N*,*N*-didodecylacrylamide (91), using a lipophilic radical initiator (92), modifying copolymers (93) or polymers that have terminally active groups (94) with a phospholipid. Alternatively, smart polymers have been covalently coupled to the active groups in the hydrophilic heads of the membrane-forming lipid (95).

Interesting and practically relevant materials for studying the behavior of smart polymers attached to lipid membranes are liposomes, self-assembled 50–200 nm vesicles that have one or more (phospho)lipid bilayers which encapsulate a fraction of the solvent. Liposomes are stable in aqueous suspension because of the repulsive forces that appear when two liposomes approach each other. Liposomes are widely used for drug delivery and in cosmetics (96).

The results of a temperature-induced conformational transition of a smart polymer on the liposomal surface depend significantly on the fluidity of the liposomal membrane. When the membrane is in a fluid state at temperatures both above and below the polymer transition temperature, the collapse of the polymer molecule forces anchor groups to move closer together by lateral diffusion within the membrane. The compact globules of collapsed polymer cover only a small part of the liposomal surface. Such liposomes have a low tendency to aggregate because the most of their surface is not covered by the polymer. Naked surfaces contribute to the repulsion between liposomes. On the other hand, when the liposomal membrane is in a solid state at temperatures both above and below the polymer transition temperature, the lateral diffusion of anchor groups is impossible, and the collapsed polymer cannot adopt a compact globule conformation but spreads over most of the liposomal surface (97). Liposomes whose surfaces are covered to a large degree by a collapsed polymer repel each other less efficiently than intact liposomes. The stability of a liposomal suspension is thereby decreased, and aggregation and fusion of liposomes takes place, which is often accompanied by the release of the liposomal content into the surrounding medium (98).

When the liposomal membrane is perturbed by the conformational transition of the polymer, both the aggregation tendency and liposomal permeability for incorporated substances are affected. Poly(ethacrylic acid) undergoes a transition from an expanded to a compact conformation in the physiological pH range of 7.4–6.5 (99). The pH-induced transition of poly(ethacrylic acid) covalently coupled to the surface of liposomes formed from phosphatidylcholine results in liposomal reorganization into more compact micelles and concomitant release of the liposomal content into the external medium. The temperature-induced transition of poly(NIPAAM-*co*-*N*,*N*-didocecylacrylamide) (100) or poly(NIPAAM-*co*-octadecylacrylate) (101), incorporated into the liposomal membrane, enhanced the release of the fluorescent marker, calcein, encapsulated in copolymer-coated liposomes. Liposomes hardly release any marker at temperatures below 32°C (the polymer transition temperature), whereas the liposomal content is released completely within less than a minute at 40°C. To increase the speed of liposomal response to temperature change, the smart polymer was attached to the outer and inner sides of the lipid membrane. The polymer bound only to the outer surface if the liposomes were treated with the polymer after liposomal formation. When

the liposomes were formed directly from the lipid–polymer mixture, the polymer was present on both sides of the liposomal membrane (91).

Changes of liposomal surface properties caused by polymer collapse affect liposomal interaction with cells. Liposomes modified by a pH-sensitive polymer, partially succinilated poly(glycidol), deliver calcein into cultured kidney cells of the African green monkey more efficiently compared to liposomes not treated with the polymer (102). Polymeric micelles formed by smart polymers and liposomes modified by smart polymers could be used for targeted drug delivery. Polymeric micelles have been prepared from amphiphilic block copolymers of styrene (forming a hydrophobic core) and NIPAAM (forming a thermosensitive outer shell). The polymeric micelles were very stable in aqueous media and had long blood circulation because of small diameter, unimodal size distribution (24 ± 4 nm), and, a low critical micellar concentration of around 10 μg/mL. At temperatures above the polymer transition temperature (32°C), the polymer chains that form an outer shell collapse, become more hydrophobic, and allow aggregation between micelles and favoring binding interactions with the surface of cell membranes. Thus, hydrophobic molecules incorporated into the micelles are delivered into the cell membranes. These micelles are capable of site-specific delivery of drugs to the sites as temperature changes, for example, to inflammation sites of increased temperature (103).

Bioanalytical Applications

Because smart polymers can recognize small changes in environmental properties and respond to them in a pronounced way, they could be used directly as sensors of these changes, for example, a series of polymer solutions that have different LCSTs could be used as a simple thermometer. As salts promote hydrophobic interactions and decrease the LCST, the polymer system could "sense" the salt concentration needed to decrease the LCST below room temperature. A poly(NIPAAM)-based system that can sense NaCl concentrations above 1.5% was patented (104). The response of the polymer is controlled by a balance of hydrophilic and hydrophobic interactions in the macromolecule. Using a recognition element that can sense external stimuli and translate the signal into the changes of the hydrophilic/balance of the smart polymer, the resulting system presents a sensor for the stimulus. If the conjugate of a smart polymer and a recognition element has a transition temperature T_1 in the absence and T_2 in the presence of stimuli, fixing the temperature T in the range $T_1 < T < T_2$ allows achieving the transition of a smart polymer isothermally by the external stimulus (105). An example of such a sensor was constructed using trans–cis isomerization of the azobenzene chromophore when irradiated by uv light. The transition is accomplished by an increase in the dipole moment of azobenzene from 0.5 D (for the trans-form) to 3.1 D (for the cis-form) and hence a significant decrease of hydrophobicity. Irradiation with uv light results in increasing the LCST from 19.4 to 26.0°C for the conjugate of the chromophore with poly(NIPAAM). The solution of the conjugate is turbid at $19.4°C < T < 26.0°C$, but when irradiated, the conjugate dissolves because the cis-form is below the LCST at this temperature. The system responds to uv light by transition from a turbid to transparent solution. The termination of uv irradiation results in a slow return

of the system to its initial turbid state (105). A few other light-sensitive systems were proposed that use different chromophores: triarylmethylcyanide (106) and leuconitriles (107).

The hydrophobicity of the recognition molecule was also changed by chemical signals. Poly(NIPAAM) containing 11.6 mol% of crown ether 9 has a LCST of 31.5°C in the absence of Na^+ or K^+ ions, 32°C in the presence of Na^+, and 38.9°C in the presence of K^+. Thus, the introduction of both Na^+ and K^+ ions leads to the dissolution of the insoluble polymer at that temperature. At 37°C, this effect is achieved only by K^+ ions (108).

From better understanding of ligand–host interactions and development of new highly selective binding pairs (eg, by using combinatorial libraries to find ligands of high affinity for particular biomolecules), one could expect that smart polymer systems will be used as "signal amplifiers" to visualize a physicochemical event, which takes place in a recognition element, by a pronounced change in the system—conversion of a transparent solution into a turbid one or vice versa.

Antibody–antigen interactions present nearly ideal analytical selectivity and sensitivity developed by nature. Not surprisingly, they are increasingly used for a broad variety of bioanalytical applications. Different analytical formats have been developed. The common feature of most of them is the requirement for separating an antibody–antigen complex from a nonbound antibody or antigen. Traditionally, the separation is achieved by coupling one of the components of antibody–antigen pair to a solid support. The binding step is followed by washing nonbound material. Interactions of the soluble partner of the binding pair with the partner coupled to the support are often accompanied by undesired diffusional limitations, and hence, incubation times of several hours are required for analysis. Because smart polymers can undergo transition from the soluble to the insoluble state, they allow combining the advantages of homogeneous binding and, after the phase transition of the smart polymer has taken place, easy separation of the polymer precipitate from the supernatant. The essential features of an immunoassay that uses smart polymers (named PRECIPIA) are as follows. The covalent conjugate of poly(NIPAAM) with monoclonal antibodies to the κ-chain of human immunoglobulin G (IgG) are incubated for 1 h at room temperature (below the LCST of the conjugate), and the IgG solution is analyzed. Then plain poly(NIPAAM) (to facilitate thermoprecipitation of polymer–antibody conjugates) and fluorescently labeled monoclonal antibodies to the γ-chain of human IgG are added. The temperature is raised to 45°C, the precipitated polymer is separated by centrifugation, and fluorescence is measured in the supernatant (109). Immunoassay systems that use temperature-induced precipitation of poly(NIPAAM) conjugates with monoclonal antibodies are not inferior in sensitivity to the traditional heterogeneous immunoassay methods, but because the antigen–antibody interaction takes place in solution, the incubation can be shortened to about 1 h (110,111). The limitations of PRECIPIA as an immunoassay technique are essentially the same as those of affinity precipitation, namely, nonspecific coprecipitation of analyzed protein when poly(NIPAAM) precipitates. Polyelectrolyte complexes that have a low degree of nonspecific protein coprecipitation have also been successfully used as reversibly soluble carriers for PRECIPIA-type immunoassays (112). The conjugate of antibody and polyanion poly(methacrylic acid) binds to the antigen within a few minutes, and the polymer hardly exerts

any effect on the rate of antigen–antibody binding. Subsequent addition of a polycation, poly(*N*-ethyl-4-vinyl-pyridinium bromide) in conditions where the polyelectrolyte is insoluble, results in quantitative precipitation of the antibody–polymer conjugate within 1 min. The total assay time is less than 15 min (10).

In principle, PRECIPIA-type immunoassays could be used for simultaneous assay of different analytes in one sample, provided that conjugates specific toward these analytes are coupled covalently to different smart polymers that have different precipitating conditions, for example, precipitation of one conjugate by adding a polymeric counterion, followed by thermoprecipitation of the second conjugate by increasing temperature.

Reversibly Soluble Biocatalysts

The transition between the soluble and insoluble state of stimuli-responsive polymers has been used to develop reversibly soluble biocatalysts. A reversibly soluble biocatalyst catalyzes an enzymatic reaction in a soluble state and hence could be used in reactions of insoluble or poorly soluble substrates/products. As soon as the reaction is completed and the products are separated, the conditions (pH, temperature) are changed to promote precipitation of the biocatalyst. The precipitated biocatalyst is separated and can be used in the next cycle after dissolution. The reversibly soluble biocatalyst acquires the advantages of immobilized enzymes (ease of separation from the reaction mixture after the reaction is completed and the possibility for biocatalyst recovery and repeated use in many reaction cycles) but at the same time overcomes the disadvantages of enzymes immobilized onto solid matrices such as diffusional limitations and the impossibility of using them in reactions of insoluble substrates or products.

Biocatalysts that are reversibly soluble as a function of pH have been obtained by the covalent coupling of lysozyme to alginate (113); of trypsin to poly(acrolein-*co*-acrylic acid) (114); and of cellulase (115), amylase (115); α-chymotrypsin, and papain (116) to poly(methyl methacrylate-*co*-methacrylic acid). A reversibly soluble cofactor has been produced by the covalent binding of NAD to alginate (117). Reversibly soluble α-chymotrypsin, penicillin acylase, and alcohol dehydrogenase were produced by coupling to the polycation component of polyelectrolyte complexes formed by poly(methacrylic acid) and poly(*N*-ethyl-4-vinyl-pyridinium bromide) (118).

Biocatalysts that are reversibly soluble as a function of temperature have been obtained by the covalent coupling of α-chymotrypsin and penicillin acylase to a partially hydrolyzed poly(*N*-vinyl caprolactam) (119) and of trypsin (120), alkaline phosphatase (121), α-chymotrypsin (122), and thermolysin (123,124) to NIPAAM copolymers that contain active groups suitable for covalent coupling of biomolecules. Lipase was coupled to a graft copolymer composed of NIPAAM grafts on a poly(acrylamide-*co*-acrylic acid) copolymer (125). No significant differences in biocatalytic properties were found for α-amylase coupled to poly(NIPAAM) via single-point or multipoint mode. Both enzyme preparations demonstrated increased thermostability and the absence of diffusional limitation when hydrolyzing starch, a high molecular weight substrate (126). The temperature of a protein–ligand interaction was controlled by site-directed coupling of terminally modified

poly(NIPAAM) to a specifically constructed site (close to a biotin binding site) on a genetically modified streptavidin (127).

Biocatalysts which are reversibly soluble as a function of Ca^{2+} concentration were produced by covalent coupling of phosphoglyceromutase, enolase, peroxidase, and pyruvate kinase to α_{s1}-casein. The enzyme casein conjugates are soluble at a Ca^{2+} concentration below 20 mM but precipitate completely at a Ca^{2+} concentration above 50 mM. The precipitate redissolves when EDTA, a strong Ca^{2+}-binding agent, is added (128).

The reversible flocculation of latices has been used to produce thermosensitive reversibly soluble (more precisely reversibly dispersible) biocatalysts using trypsin (129), papain (130), and α-amylase (131). Latices sensitive to a magnetic field have been used to immobilize trypsin and β-galactosidase (132). Liposomes that have a polymerized membrane reversibly aggregate on changing salt concentration and have been used to immobilize α-chymotrypsin (133).

The most attractive application of reversibly soluble biocatalysts is repeated use in a reaction which is difficult or even impossible to carry out using enzymes immobilized onto insoluble matrices, for example, hydrolysis of water-insoluble phlorizidin (134); hydrolysis of high molecular weight substrates such as casein (123,130) and starch (115); hydrolysis of insoluble substrates such as cellulose (135) and raw starch (corn flour) (7,134,136–138); production of insoluble products such as peptide, benzyloxycarbonyl-L-tyrosyl-N^{ω}-nitro-L-arginine (116), and phenylglycine (139).

The hydrolytic cleavage of corn flour to glucose is an example of successfully using a reversibly soluble biocatalyst, amylase coupled to poly(methyl methacrylate-*co*-methacrylic acid), in an industrially interesting process (136). The reaction product of the process (glucose) inhibits the hydrolysis. The use of a reversibly soluble biocatalyst improves the efficiency of the hydrolysis which is carried out at pH 5, at which the amylase–polymer conjugate is soluble. After every 24 h, the pH is reduced to 3.5, the unhydrolyzed solid residue and the precipitated conjugate are separated by centrifugation, the conjugate is resuspended in a fresh portion of the substrate at pH 5, and the hydrolysis is continued. The conversion achieved after five cycles is 67%, and the activity of the amylase after the fifth cycle was 96% of the initial value (136).

BIBLIOGRAPHY

1. R. Dagani, *Chem. Eng. News* pp. 30–33 (1995).
2. H. Brønsted and J. Kopecek, in R. S. Harland and R. K. Prud'homme, eds., *Polyelectrolyte Gels. Properties, Preparation, and Applications*, American Chemical Society, Washington, D.C., 1992, pp. 285–304.
3. V. A. Kabanov, *Polym. Sci.* **36**, 143–156 (1994).
4. H. G. Schild, *Prog. Polym. Sci.* **17**, 163–249 (1992).
5. E. Y. Kramarenko and A. R. Khokhlov, *Polym. Gels Networks* **6**, 46–56 (1998).
6. *Eudragit, Röhm Pharma GMBH Information Materials*, 1993.
7. K. Hoshino and co-workers, *J. Chem. Eng. Jpn.* **30**, 30–37 (1997).
8. E. Linné-Larsson and B. Mattiasson, *Biotechnol. Tech.* **8**, 51–56 (1994).
9. S. Y. Park and Y. H. Bae, *Macromol. Rapid Commun.* **20**, 269–273 (1999).

10. V. A. Izumrudov, I. Yu. Galaev, and B. Mattiasson, *Bioseparation* **7**, 207–220 (1999).
11. M. B. Dainiak and co-workers, *Bioseparation* **7**, 231–240 (1999).
12. U. Dissing and B. Mattiasson, *J. Biotechnol.* **52**, 1–10 (1996).
13. A. A. Tager and co-workers, *Colloid Polym. Sci.* **271** (1993).
14. M. Heskins and J. E. Guillet, *J. Macromol. Sci., Chem. A* **2**, 1441–1455 (1968).
15. K. Suwa and co-workers, *J. Polym. Sci., Part A: Polym. Chem.* **35**, 3087–3094 (1997).
16. I. Yu. Galaev and B. Mattiasson, *Enzyme Microb. Technol.* **15**, 354–366 (1993).
17. F. Liu and co-workers, *Biotechnol. Appl. Biochem.* **21**, 257–264 (1995).
18. S. Mori, Y. Nakata, and H. Endo, *Protein Expression Purif.* **5**, 151–156 (1994).
19. F. M. Winnik and co-workers, *Macromolecules* **25**, 1876–1880 (1992).
20. G. Chen and A. S. Hoffman, *Nature* **373**, 49–52 (1995).
21. M. Maeda and co-workers, *Reactive Functional Polym.* **21**, 27–35 (1993).
22. D. Umeno, T. Mori, and M. Maeda, *Chem. Commun.* 1433–1434 (1998).
23. B. Mattiasson, A. Kumar, and I. Yu. Galaev, *J. Mol. Recognition* **11**, 211–216 (1998).
24. A. Kumar, I. Yu. Galaev, and B. Mattiasson, *Biotechnol. Bioeng.* **59**, 695–704 (1998).
25. A. Durand and D. Hourdet, *Polymer* **40**, 4941–4951 (1999).
26. S. J. Lee and K. Park, *J. Mol. Recognition* **9**, 549–557 (1997).
27. K.-Y. A. Wu and K. D. Wisecarver, *Biotechnol. Bioeng.* **39**, 447–449 (1992).
28. E. Kokufuta and S. Matsukawa, *Macromolecules* **28**, 3474–3475 (1995).
29. S. Kitano and co-workers, in Proc. 1st Int. Conf. Intelligent Mater., Lancaster, U.K., 1993, pp. 383–388.
30. T. Yakushiji and co-workers, *Langmuir* **14**, 4657–4662 (1998).
31. H. Kawaguchi, *Front. Biomed. Biotechnol.* **3**, 157–168 (1996).
32. H. Kubota and N. Shiobara, *Reactive Functional Polym.* **37**, 219–224 (1998).
33. Y. M. Lee and J. K. Shim, *Polymer* **38**, 1227–1232 (1997).
34. H. A. VonRecum and co-workers, *J. Biomed. Mater. Res.* **40**, 631–639 (1998).
35. Y. Sun and co-workers, *Biotechnol. Bioeng.* **47**, 20–25 (1995).
36. I. Yu. Galaev, M. N. Gupta, and B. Mattiasson, *CHEMTECH* 19–25 (1996).
37. A. Kumar, I. Yu. Galaev, and B. Mattiasson, *Bioseparation* **7**, 185–194 (1999).
38. D. Guoqiang and co-workers, *Biotechnol. Prog.* **11**, 187–193 (1995).
39. D. Guoqiang and co-workers, *Bioseparation* **5**, 339–350 (1995).
40. E. Linné-Larsson, I. Yu. Galaev, and B. Mattiasson, *Bioseparation* **6**, 283–291 (1996).
41. A. P. Bradshaw and R. J. Sturgeon, *Biotechnol Tech.* **4**, 67–71 (1990).
42. M. B. Dainiak and co-workers, *Anal. Biochem.* **277**, 58–66 (2000).
43. M. B. Dainiak and co-workers, *Biochim. Biophys. Acta* **1381**, 279–285 (1998).
44. A. Kondo, T. Kaneko, and K. Higashitani, *Biotechnol. Bioeng.* **44**, 1–6 (1994).
45. C. S. Chen and co-workers, *Colloids Surf., B* **6**, 37–49 (1996).
46. K. Hoshino and co-workers, *Biotechnol. Bioeng.* **60**, 568–579 (1998).
47. P.-Å. Albertson, *Partition of Cell Particles and Macromolecules*. John Wiley & Sons, Inc., New York, 1986.
48. P. Hughes and C. R. Lowe, *Enzyme Microb. Technol.* **10**, 115–122 (1988).
49. G. Johansson and F. Tjerneld, in G. Street, ed., *Highly Selective Separations in Biotechnology*, Blackie Academic & Professional, London, 1994, pp. 55–85.
50. M. Lu and co-workers, *J. Chromatogr., B* **680**, 65–70 (1996).
51. T. T. Franko and co-workers, *Biotechnol. Tech.* **11**, 231–235 (1997).
52. J. Persson and co-workers, *Bioseparation* **9**, 105–116 (2000).

53. Y. G. Takei and co-workers, *Macromolecules* **27**, 6163–6166 (1994).
54. T. Kondo and co-workers, *J. Appl. Polym. Sci.* **67**, 2057–2064 (1998).
55. F.-J. Schmitt and co-workers, *Langmuir* **14**, 2838–2845 (1998).
56. P. W. Zhu and D. H. Napper, *J. Phys. Chem. B* **101**, 3155–3160 (1997).
57. N. Yamada and co-workers, *Makromol. Chem., Rapid Commun.* **11**, 571–576 (1990).
58. T. Okano and co-workers, *Biomaterials* **16**, 297–303 (1995).
59. T. Okano and co-workers, *J. Controlled Release* **36**, 125–133 (1995).
60. M. Yamato and co-workers, *J. Biomed. Mater. Res.* **44**, 44–52 (1999).
61. Y. Ito and co-workers, *Langmuir* **13**, 2756–2759 (1997).
62. T. Bohanon and co-workers, *J. Biomater. Sci. Polym. ed.* **8**, 19–39 (1996).
63. H. Kanazawa and co-workers, *Anal. Chem.* **69**, 823–830 (1997).
64. K. Hosoya and co-workers, *Anal. Chem.* **67**, 1907–1911 (1995).
65. H. Go and co-workers, *Anal. Chem.* **70**, 4086–4093 (1998).
66. H. Kanazawa, Y. Matsushima, and T. Okano, *Trends Anal. Chem.* **17**, 435–440 (1998).
67. H. Yoshioka and co-workers, *Polym. Adv. Technol.* **6**, 418–420 (1995).
68. B. Mattiasson and I. Yu. Galaev, in P. A. Millner, ed., *High Resolution Chromatography*, Oxford University Press, Oxford, 1996, pp. 153–190.
69. I. Yu. Galaev, C. Warrol, and B. Mattiasson, *J. Chromatogr., A* **684**, 37–43 (1994).
70. Y. Ito, Y. S. Park, and Y. Imanishi, *Macromol. Rapid Commun.* **18**, 221–224 (1997).
71. Y. Ito and co-workers, *J. Am. Chem. Soc.* **119**, 1619–1623 (1997).
72. Y. Okahata, K. Ozaki, and T. Seki, *J. Chem. Soc., Chem. Commun.* 519–521 (1984).
73. Y. Okahata, H. Noguchi, and T. Seki, *Macromolecules* **19**, 493–494 (1986).
74. T. Nonaka, K. Hashimoto, and S. Kurihara, *J. Appl. Polym. Sci.* **66**, 209–216 (1997).
75. S. Akerman and co-workers, *Int. J. Pharm.* **164**, 29–36 (1998).
76. R. Spohr and co-workers, *J. Controlled Release* **50**, 1–11 (1998).
77. H. Omichi and co-workers, *Nucl. Instrum. Methods Phys. Res., Sect. B* **131**, 350–356 (1997).
78. S. Kurihara, Y. Ueno, and T. Nonaka, *J. Appl. Polym. Sci.* **67**, 1931–1937 (1998).
79. Y. Liu and co-workers, *J. Am. Chem. Soc.* **119**, 8720–8721 (1997).
80. T. G. Park and A. S. Hoffman, *Biotechnol. Prog.* **10**, 82–86 (1994).
81. K. Hosoya and co-workers, *Macromolecules* **27**, 3973–3976 (1994).
82. Y. Imanishi and Y. Ito, *Pure Appl. Chem.* **67**, 2015–2021 (1995).
83. K. Ishihara and K. Matsui, *J. Polym. Sci., Polym. Lett. Ed.* **24**, 413–417 (1986).
84. S. Kitano and co-workers, *Makromol. Chem., Rapid Commun.* **12**, 227–233 (1991).
85. K. Kataoka and co-workers, *J. Am. Chem. Soc.* **120**, 12694–12695 (1998).
86. S. Kitano and co-workers, *J. Controlled Release* **19**, 162–170 (1992).
87. D. Shiino and co-workers, *J. Controlled Release* **28**, 317–319 (1994).
88. K. Nakamae and co-workers, *J. Biomater. Sci. Polymer Ed.* **6**, 79–90 (1994).
89. Jpn. Kokai Tokkyo Koho JP 09227329 A2 (Sept. 2, 1997), Y. Mori, M. Yoshioka, and T. Mukoyama (to M and M Kenkyusho K. K.).
90. K. Lindell, Doctoral Thesis, Lund University, Sweden, 1996.
91. H. Hayashi, K. Kono, and T. Takagishi, *Bioconjugate Chem.* **10**, 412–418 (1999).

92. H. Ringsdorf, J. Simon, and F. M. Winnik, in P. L. Dubin and P. Tong, eds., *Colloid-Polymer Intercations. Particulate, Amphiphilic, and Biological Surfaces*, American Chemical Society, Washington D.C., 1993, pp. 216–240.
93. X. S. Wu, A. S. Hoffman, and P. Yager, *Polymer* **33**, 4659–4662 (1992).
94. K. Kono and co-workers, *Biochim. Biophys. Acta* **1416**, 239–250 (1999).
95. D. A. Tirrell, in J. Kost, ed., *Pulsed and Self-Regulated Drug Delivery*, CRC Press, Boca Raton Fla., 1990, pp. 110–116.
96. D. D. Lasic, *Trends Biotechnol.* **16**, 307–321 (1998).
97. H. Ringsdorf, J. Venzmer, and F. M. Winnik, *Angew. Chem., Int. Ed. Engl.* **30**, 315–318 (1991).
98. H. Hayashi, K. Kono, and T. Takagishi, *Bioconjugate Chem.* **9**, 382–389 (1998).
99. S. Sugaj and co-workers, *Colloid Polym. Chem.* **261**, 159–165 (1983).
100. K. Kono and co-workers, *J. Controlled Release* **59**, 63–75 (1999).
101. H. Hayashi, K. Kono, and T. Takagishi, *Biochim. Biophys. Acta* **1280**, 127–134 (1996).
102. K. Kono, T. Igawa, and T. Takagishi, *Biochim. Biophys. Acta.* **1325**, 143–154 (1997).
103. S. Cammas and co-workers, *J. Controlled Release* **48**, 157–164 (1997).
104. Jpn. Kokai Tokkyo Koho JP 63206653 A2 (Aug. 25, 1988), Y. Tomita (to Canan K. K.).
105. M. Irie, in K. Dusek, ed., *Responsive Gels: Volume Transitions II*, Springer-Verlag, Berlin, 1993, pp. 50–65.
106. R. Kröger, H. Menzel, and M. L. Hallensleben, *Macromol. Chem. Phys.* **195**, 2291–2298 (1994).
107. A. Mamada and co-workers, *Macromolecules* **23**, 157–1519 (1990).
108. M. Irie, Y. Misumi, and T. Tanaka, *Polymer* **34**, 4531–4535 (1993).
109. N. Monji and A. S. Hoffman, *Appl. Biochem. Biotechnol.* **14**, 107–120 (1987).
110. Q.-Z. Zhu and co-workers, *Anal. Chim. Acta* **375**, 177–185 (1998).
111. Y. G. Takei and co-workers, *Bioconjugate Chem.* **5**, 577–5582 (1994).
112. B. B. Dzantiev and co-workers, *Dokl. Biochem. (in Russian)* **342**, 549–552 (1995).
113. M. Charles, R. W. Coughlin, and F. X. Hasselberger, *Biotechnol. Bioeng.* **16**, 1553–1556 (1974).
114. E. VanLeemputten and M. Horisberger, *Biotechnol. Bioeng.* **18**, 587–590 (1976).
115. M. Taniguchi and co-workers, *J. Chem. Eng. Jpn.* **22**, 313–314 (1989).
116. M. Fujimura, T. Mori, and T. Tosa, *Biotechnol. Bioeng.* **29**, 747–752 (1987).
117. R. W. Coughlin, M. Aizawa, and M. Charles, *Biotechnol. Bioeng.* **18**, 199–208 (1976).
118. A. L. Margolin and co-workers, *Biotechnol. Bioeng.* **24**, 237–240 (1982).
119. Y. E. Kirsh and co-workers, *Biotechnology (Russian)* (2), 184–189 (1987).
120. H. Lee and T. G. Park, *Biotechnol. Prog.* **14**, 508–516 (1999).
121. A. L. Nguyen and J. H. T. Luong, *Biotechnol. Bioeng.* **34**, 1186–1190 (1989).
122. J.-P. Chen, *J. Chem. Technol. Biotechnol.* **73**, 137–143 (1995).
123. F. Liu, G. Tao, and R. Zhuo, *Polym. J.* **25**, 561–567 (1993).
124. K. Hoshino and co-workers, *J. Ferment. Bioeng.* **83**, 246–252 (1997).
125. S. Takeuchi and co-workers, *Makromol. Chem.* **194**, 1991–1999 (1993).
126. J.-P. Chen, D.-H. Chu, and Y.-M. Sun, *J. Chem. Technol. Biotechnol.* **69**, 421–428 (1997).
127. P. S. Stayton and co-workers, *Nature* **378**, 472–474 (1995).
128. K. Okumura and co-workers, *Agric. Biol. Chem.* **48**, 2435–2440 (1984).
129. H. Kitano, C. Yan, and K. Nakamura, *Makromol. Chem.* **192**, 2915–2923 (1991).
130. A. Kondo and co-workers, *J. Ferment. Bioeng.* **78**, 241–245 (1994).

131. T. Kondo, T. Urabe, and K. Yoshinaga, *Colloids Surf., A* **109**, 129–136 (1996).
132. A. Kondo and H. Fukuda, *J. Ferment. Bioeng.* **84**, 337–341 (1997).
133. Y. Sun and co-workers, *Appl. Biochem. Biotechnol.* **56**, 331–339 (1996).
134. K. Hoshino and co-workers, *J. Ferment. Bioeng.* **82**, 253–258 (1996).
135. M. Taniguchi, M. Kobayashi, and M. Fujii, *Biotechnol. Bioeng.* **34**, 1092–1097 (1989).
136. K. Hoshino and co-workers, *J. Chem. Eng. Jpn.* **22**, 54–59 (1989).
137. K. Hoshino and co-workers, *Agric. Biol. Chem.* **53**, 1961–1967 (1989).
138. K. Hoshino and co-workers, *J. Ferment. Bioeng.* **69**, 228–233 (1990).
139. Yu. V. Galaev, *Prikl. Bioxim. Mikrobiol.* **30**, 167–170 (1994).
140. I. Yu. Galaev and B. Mattiasson, *Trends Biotechnol.* **17**, 335–340 (1999).

I. YU. GALAEV
B. MATTIASSON
Lund University

BLOCK COPOLYMERS, TERNARY TRIBLOCK

Introduction

Self-assembly of matter (or the formation of superstructures by means of noncovalent bonds) is a fascinating field of research. The formation of crystals and liquid crystals by atoms or molecules is just one example. Also within a larger molecule with a lot of conformational freedom, such as a polyamide chain or a protein, certain conformations are stabilized by secondary interactions, such as hydrogen bonds, which is essential for their properties (eg, mechanical properties of polyamides and functional properties of proteins). Secondary interactions in supramolecular structures play an important role for many processes in living cells (1). Various aspects of self-assembly have been presented in books (2–4) and in a recent review (5). This article deals with the self-assembly (or self-organization) of synthetic macromolecules, namely block copolymers, principally terning triblocks (see BLOCK COPOLYMERS).

Synthetic polymeric materials have gained increasing importance in the last couple of decades. The task of polymer chemistry has always been to design polymeric materials for certain applications and with time, a number of monomers has become very important commercially. There is an ongoing research in the area of new monomers for the design of polymers with special properties, and the environmental problems related to new chemicals are also receiving increasing attention. Because the development of new monomers as well as the up-scaled production of the corresponding polymers is rather expensive and time-consuming, other strategies to obtain polymeric materials with well-defined properties are important.

The combination of different polymers into composites or blends can provide materials with desirable properties, and many successful examples have been

Encyclopedia of Polymer Science and Technology. Copyright John Wiley & Sons, Inc. All rights reserved.

reported (6). However, because of thermodynamics most blends of polymers turn out to be phase-separated, since the free-energy contribution by the gain of mixing entropy for long-chain molecules is very small as compared to free-energy contribution by even slight repulsive interactions between the segments (as expressed by the Flory–Huggins–Staverman parameter χ) of different chains, because χ multiplied by the usually large degree of polymerization, N, yields a dominating positive mixing enthalpy between dissimilar chains (7). The length scale of this phase separation is typically much larger than the length of the polymer chains; *macro*phase separation is discussed later. The tendency to phase-separate thereby depends not only on the thermodynamics, but also to a large extent on the processing, ie, kinetic parameters such as viscosity, for example. Also, an initially homogeneous blend can phase-separate after a temperature change via spinodal decomposition or via a nucleation and growth process (8). The size of the domains and the mechanical strength of their interface are some of the important parameters determining the properties of the final product.

In order to obtain fine-disperse phase-separated blends, compatibilizers can be added, which self-assemble at the interface between the incompatible blend components and prevent the blend from macrophase separation. Such compatibilizers consist of at least two parts: one is compatible with one of the blend components, and the other part is compatible with the other blend component. Thus, block copolymers composed of at least two different blocks are suitable for such applications (9–11). Because of the connectivity of their blocks, these materials undergo a *micro*phase separation when their blocks segregate from each other. Besides their use as compatibilizers in polymer blends, block copolymers have also a wide range of other applications. Examples are their use as viscosity modifiers (12), surfactants (13), light-emitting devices (14), or photonic crystals on optical length scales (15,16). Block copolymers have also been used as templates for designing novel ceramic structures (17,18) and as hosts for colloidal metals (19). The formation of vesicular structures in solution also makes block copolymers interesting as carriers of drugs or for cosmetic applications (20). Thermoplastic elastomers based on hard and soft blocks are prominent examples, where block copolymers have also received importance as bulk materials (9,21). Among multiblock copolymers with hard and soft segments polycondensates such as polyester-urethanes, polyether-urethanes, or polyester-amides should be mentioned. Also thermoplastic elastomers based on poly(butylene terephthalate) as hard segments and poly(ethylene oxide)-*block*-poly(ethylene-*co*-butylene)-*block*-poly(ethylene oxide) triblock copolymers as soft segments have been reported (22).

For the synthesis of block copolymers the reader is refered to a previous article in this series (23) and some other works describing the application of various controlled polymerization techniques for their synthesis, such as anionic polymerization (24–26), cationic polymerization (27,28), controlled radical polymerization (29,30), as well as combinations of various techniques (31–34). Synthetic procedures for star copolymers have been reviewed (35). The first synthesis of a heteroarm star terpolymer with three immiscible blocks has been described in Reference 36.

In this paragraph, some references concerning a few important aspects of block copolymers are given, which are not discussed further in this contribution. Crystallization within microdomains and the interplay between crystallization

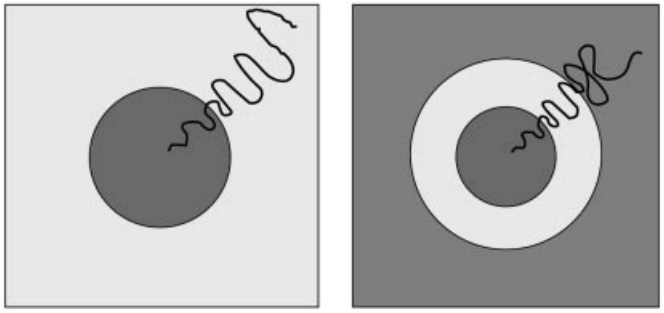

Fig. 1. Schemes of a chain in a cylindrical morphology of a diblock copolymer (left) and a core–shell cylindrical morphology of a ternary triblock copolymer (right).

and morphology formation is an ongoing topic since the beginning of research on di- and triblock copolymers (23,37–42). Also block copolymers with liquid crystalline blocks are investigated (43,44). Block copolymers in solution can form a variety of superstructures such as micelles, rods, vesicles (20,23,45–50), and tubular aggregates (51). At higher block copolymer concentrations lyotropic liquid crystalline phases can be found (52,53). Macroscopic alignment of block copolymers by mechanical (54–62) or electrical fields (63–67), orientation via directional crystallization (68), or orientation by evaporation of a solvent (69,70) are other interesting topics. However, to cover all these different aspects is beyond the scope of this contribution. There are reviews on the phase behavior (71) and dynamics (72) of diblock copolymers available. An overview of the research mainly done in the field of diblock copolymers is given in Reference 73. Here focus is mainly on the morphological behavior of ternary block copolymers consisting of amorphous blocks and their blends with other block copolymers in the bulk state.

As mentioned before, because of the connectivity of different blocks, block copolymers can only undergo a microphase separation when the different blocks become incompatible with each other (74,75). As an example, Figure 1 shows the cross section of a cylindrical diblock copolymer and a core–shell cylindrical triblock copolymer.

There are basically two different contributions to the free energy of a given microphase-separated block copolymer. On one hand the system tends to minimize the interface between connected blocks, and on the other hand the conformational entropy tends to a random coil conformation of the blocks, leading to a weak segregation between the blocks. As a result, a morphology with an interface larger than the minimal one is formed between the blocks. In contrast with polymer blends, chemically well-defined block copolymers self-assemble into regular crystal-like lattices when microphase separation occurs (as shown in Figs. 2 and 3 for diblock and triblock copolymers) (76).

The lattice sizes of block copolymer morphologies being typically in the range of approximately 10–100 nm, transmission and scanning electron microscopy (tem, sem) (77,78), scanning force microscopy (sfm) (79), and small angle x-ray (80,81) or neutron scattering (82) (saxs, sans) in many cases are powerful tools to investigate the morphology of these materials.

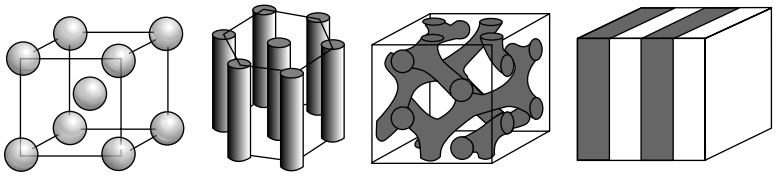

Fig. 2. Microphase-separated morphologies of diblock copolymers. From left to right: spheres, cylinders, double gyroid, lamellae. From Ref. 76. Copyright (2000) Wiley-VCH Verlag GmbH.

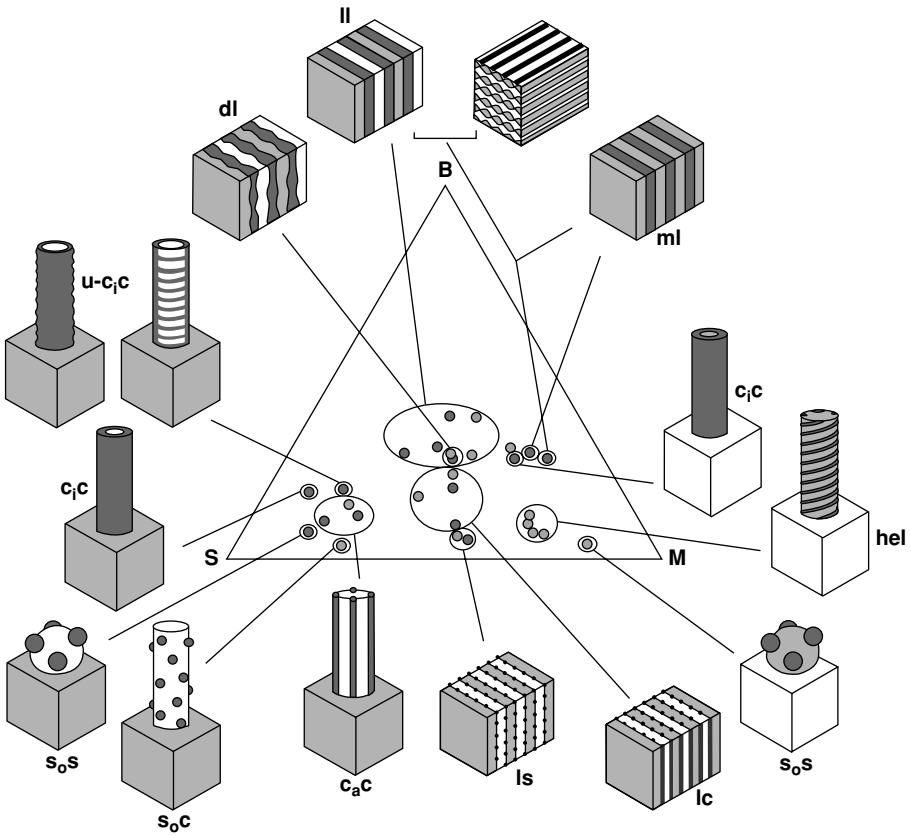

Fig. 3. Microphase-separated morphologies on the example of polystyrene-*block*-polybutadiene-*block*-poly(methyl methacrylate) (SBM) triblock copolymers (OsO_4, see Table 1). From Ref. 76. Copyright (2000) Wiley-VCH Verlag GmbH.

The aim of this contribution is to access the extremely rich phase behavior of ternary block and star copolymers by asking the following questions:

(1) How does the composition influence the morphology of ABC terpolymers?
(2) How does the chain topology influence the morphological behavior of ABC terpolymers?

Table 1. Colors of Different Components in Bright-Field TEM Images Used in the Morphological Schemes[a]

Polymer	OsO_4	RuO_4	OsO_4/CH_3I
Polystyrene	w	b	w
Polybutadiene	b		b
Polyisoprene	b		b
Poly(methyl methacrylate)	w	w	w
Poly(*tert*-butyl methacrylate)	w	w	w
Poly(cyclohexyl methacrylate)	w	w	w
Poly(methacrylic acid)	w	w	w
Poly(ethylene-*stat*-butylene)	w/g	w/g	
Poly(ethylene-*alt*-propylene)	w/g	w/g	
Poly(2-vinylpyridine)	w		g

[a] w: white, g: grey, b: black.

(3) What happens when one or two blocks of an ABC triblock copolymer are chemically modified?

(4) How does blending of ABC triblock copolymers with other block copolymers affect their morphological properties?

These questions are discussed in the sections after the next one, where first some theoretical basics are given to understand the thermodynamics of block copolymers.

The nomenclature of the block copolymers is as follows: $A_xB_yC_z{}^M$ is a block copolymer composed of the blocks A, B, and C, where subscripts denote the weight fraction (%) and M is the number-averaged overall molecular weight (kg/mol). Heteroarm star terpolymers are indicated by an asterisk ($A_xB_yC_z{}^{M*}$). The morphological schemes are presented in such a way that the typical colors found in tem images of correspondingly stained samples are used (Table 1).

Theoretical Descriptions of Block Copolymer Morphologies

Before going further into a discussion of the morphological behavior of these materials, consider the driving forces for the formation of such morphologies in some more detail. It is not intended to give a complete description of the theoretical efforts undertaken to describe this fascinating class of materials, but only to shed some light onto basic ideas of different theoretical approaches. The first focus is on diblock copolymers before switching to linear ternary triblock copolymers. The assumptions used for those materials can also be transferred to block copolymers of other topologies, although this leads to more complicated expressions.

There are two different limiting situations found in microphase-separated block copolymers. In the so-called weak segregation limit (WSL), a broad smeared interface separates neighboring microdomains; ie, there is a smooth transition of the composition across the domain boundary. On the contrary, within the so-called strong segregation limit (SSL), there is a sharp interface separating the domains and therefore an abrupt change of the composition across the domain boundary. The two situations are schematically shown in Figure 4 (83).

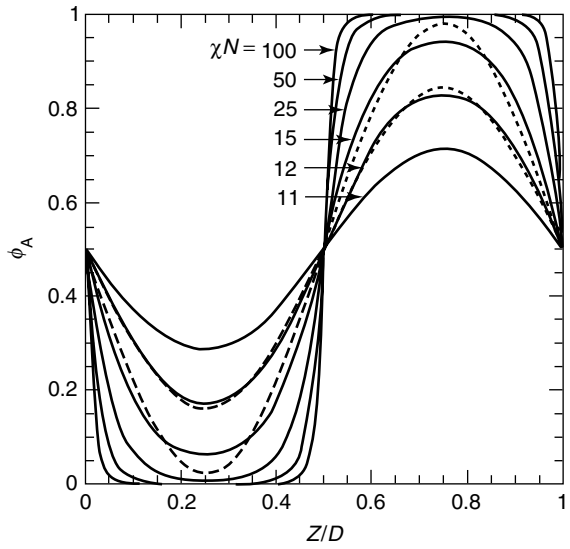

Fig. 4. Composition profile of a diblock copolymer across the domain boundary for various degrees of incompatibility. Reprinted with permission from Ref. 83. Copyright (1996) American Chemical Society.

First consider the SSL for a diblock copolymer. Here the follwing contributions to the free energy of n block copolymer chains are considered: the interfacial energy F_{int} originating from the interfacial tension γ between the incompatible blocks and the elastic contributions of the different blocks, F_{el}.

$$\begin{aligned}\frac{F}{nk_{\text{B}}T} &= F_{\text{el}}^{\text{A}}+F_{\text{el}}^{\text{B}}+F_{\text{int}} \\ &= \alpha^{\text{A}}\left(\frac{R}{aN^{1/2}}\right)^2+\alpha^{\text{B}}\left(\frac{R}{aN^{1/2}}\right)^2+\beta\,(\chi N)^{1/2}\left(\frac{R}{aN^{1/2}}\right)^{-1}\end{aligned} \tag{1}$$

The coefficients $\alpha^{\text{A,B}}$ corresponding to the elastic contributions and β corresponding to the interfacial contribution to the free energy are dependent on the morphology. R is the characteristic domain radius, and a is the statistic segment length (Kuhn length). For simplicity it is assumed that all blocks have similar statistical segment lengths. Different segment lengths of the blocks have also been treated theoretically and lead to asymmetric phase diagrams (84). For spheres, cylinders, their coronas, and for lamellae of AB diblock and ABA triblock copolymers, expressions for the free energy have been given (75,85).

While the interfacial tension ($\gamma \propto \chi^{1/2}$) (86) leads to a minimization of the interface between adjacent blocks, the conformational entropy of the different blocks favors a larger interface. As a compromise, there is an interface larger than the minimal one and the conformations of the blocks are reduced; ie, the blocks are stretched to a certain extent, leading to an elastic energy.

The minimum free energy for a given morphology is found by optimizing the radius of the domain, R, from the condition $\partial F/\partial R = 0$:

$$\frac{F}{nk_{\mathrm{B}}T} = \frac{3}{2}\left[2\left(\alpha^{\mathrm{A}} + \alpha^{\mathrm{B}}\right)\beta^2\chi N\right]^{1/3} \tag{2}$$

For the disordered state it is just the enthalpic part similar to the Flory–Huggins–Staverman free energy of polymer blends:

$$\begin{gathered}\frac{F}{nk_{\mathrm{B}}T} = \chi N f\left(1-f\right) \\ f = \phi_{\mathrm{A}}(r) \\ \sum_i \phi_i(r) = 1\end{gathered} \tag{3}$$

where f is the space-averaged volume fraction of component A and the system is considered to be incompressible. It should be noted that there are ongoing discussions on the influence of the junction point between blocks and the end groups on the interaction parameter, which is found to differ between blends of A and B homopolymers on one side and the corresponding AB block copolymer (87). However, this point is left out of this discussion, since it does not change the picture from a qualitative viewpoint.

The WSL approach for the description of the order–disorder transition, ie, the transition between the microphase-separated block copolymer and the disordered melt, where the two blocks mix with each other, has been developed (74,88,89) using the random phase approximation. This transition is often called the microphase separation transition (MST), and T_{ODT} is the temperature at which the order–disorder transition occurs. In this picture the system is described by a so-called order parameter, which is related to the space-dependent volume fraction or segment density of one of the components, say, component A. Again, the system is considered to be incompressible. The order parameter is then given by the deviation of the local segment density from the mean composition value.

$$\delta\phi_{\mathrm{A}}(r) = \phi_{\mathrm{A}}(r) - f \tag{4}$$

While in the disordered state the order parameter vanishes, it takes finite values in the ordered phases. The Fourier transform of the pair correlation function of the order parameter

$$\begin{gathered}S(q) = \int_{-\infty}^{\infty} S(r-r')^{-2\pi q(r-r')}\mathrm{d}(r-r') \\ S(r-r') = \frac{1}{k_{\mathrm{B}}T}\delta\phi_{\mathrm{A}}(r)\delta\phi_{\mathrm{A}}(r')\end{gathered} \tag{5}$$

is called the structure function and is directly related to the scattering intensity observed by saxs or sans. For the structure function of diblock copolymers in the disordered state

$$\begin{gathered}\frac{S(x) = N}{F(x,f) - 2\chi N} \\ x = q^2R_{\mathrm{g}}^2 = q^2\frac{Na^2}{6}\end{gathered} \tag{6}$$

where $\boldsymbol{q}$ is the scattering vector ($q = 4\pi/\lambda \sin\theta$, λ is the wavelength of the radiation within the sample, and 2Θ is the scattering angle) and a is the Kuhn length of the repeating units. R_g is the radius of gyration of the macromolecule.

$$F(x,f) = \frac{g(1,x)}{g(f,x)g(1-f,x) - \frac{1}{4}\left[g(1,x) - g(f,x) - g(1-f,x)\right]^2} \tag{7}$$

where $g(f, x)$ are the correlation functions of ideal noninteracting chains, which can be described by Debye functions:

$$g(f,x) = \frac{2}{x^2}\left(e^{-fx} - 1 + fx\right) \tag{8}$$

The maximum intensity occurs at

$$x^* = \left(q^* R_g\right)^2 = 3.873 \tag{9}$$

and diverges for a symmetric diblock copolymer ($f = 0.5$) at a critical value of $(\chi N)_{crit} = 10.495$

$$\left[1/S(x^*)\right]_{crit} = 0 \tag{10}$$

For the symmetric diblock copolymer a second-order transition between lamellar and disordered phase was predicted, while at all other compositions a first-order transition between disordered state and a body-centered cubic phase of spherical domains formed by the minority component was predicted, which changes into hexagonally packed cylinders and finally into lamellae upon further increasing χN. It has already been noted by Leibler's that his approach does not include fluctuation effects, which become important for finite degrees of polymerization (74). Fredrickson and Helfand accounted for this problem by modifying Leibler's theory in the following way (90):

$$S(x) = \frac{N}{\varepsilon + F(x,f) - F(x^*,f)} \tag{11}$$

At the MST for a symmetric diblock copolymer the correction parameter is $\varepsilon = 8.1114\, N^{-1/3}$ and $(\chi N)_{trans} = 10.495 + 41.022\, N^{-1/3}$.

As a consequence, the structure factor no longer diverges at the MST, but reaches a finite value, leading to a first-order phase transition also for the symmetric diblock copolymer. Moreover, there is a finite composition region where a direct transition between disordered and lamellar phase is predicted and the fluctuation effects disappear for infinite large N. However, it has been noted that the fluctuation corrections are only valid for $N > 10^4$ (90).

$$\left[\frac{S(x^*)}{N}\right]_{max} = 0.12328 N^{1/3} \tag{12}$$

Figure 5 shows the structure factor from both mean-field theory (Leibler) and the fluctuation correction (Fredrickson–Helfand) for a symmetric diblock

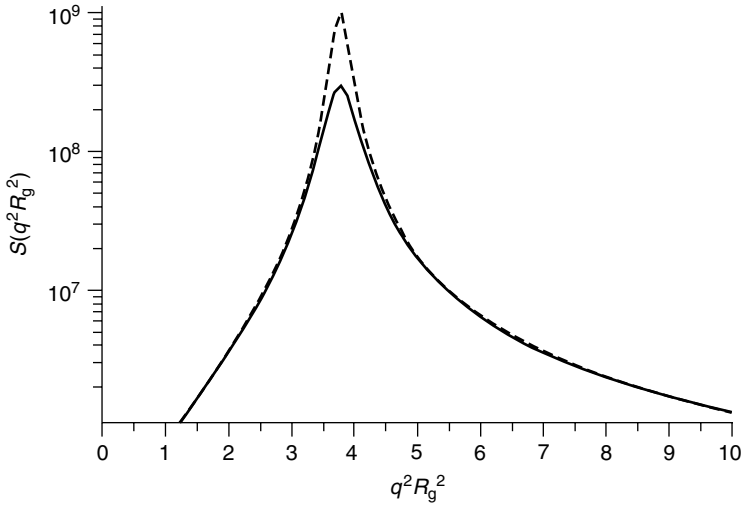

Fig. 5. Structure factor following from different theories. Note that the structure factor following Leibler's theory at $\chi N = 10.495$ would diverge. - - - - - Leibler ($\chi N = 10.49$); ——— Fredrickson–Helfand ($\chi N = 10.495 + 41.022\, N^{1/3}$).

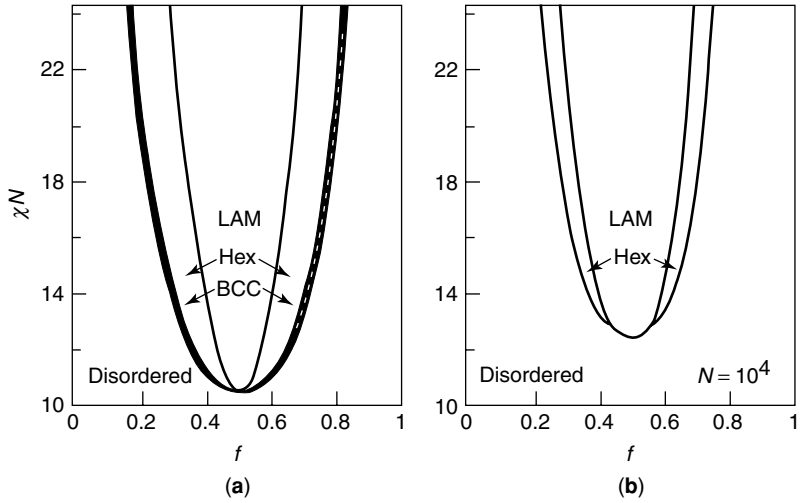

Fig. 6. Phase diagram of a diblock copolymer according to Leibler's theory (left) and including fluctuation corrections according to Fredrickson and Helfand (right). From Ref. 91. Copyright (1990) American Institute of Physics.

copolymer with $N = 10^7$ and $f = 0.5$. The phase diagrams taking into account lamellar, cylindrical, and spherical morphologies besides the disordered state were calculated and are shown in Figure 6 (91).

For these calculations the order parameter of the system was developed as a function of characteristic wave vectors, which correspond to the scattering vectors of reflections observable in a scattering experiment. These phase diagrams considered only the classical microphase morphologies (spheres, cylinders, lamellae), which are characterized by interfaces with a constant mean curvature H:

$$H(r) \equiv \frac{1}{2}(C_1 + C_2) \tag{13}$$

Here C_1 and C_2 are the two principal curvatures characterizing the shape of the interface at the location **r**. To be more precise, H is only constant for lamellae, while curved interfaces always show certain deviations from the idealized shape. For example, the cross section of cylinders is deformed hexagonally for matching the entropic requirements of the matrix-forming block: to fill space homogeneously and to avoid dissimilar stretching of different matrix blocks, the core cylinder has to be deformed to allow for almost similar distances between the interface and the borderline of the Wigner–Seitz cell ($L_1 = L_2$; see Fig. 7) (92). The deviation from the ideal symmetry of the core domain increases upon decrease of the matrix-forming block and increasing segregation.

Also nonclassical morphologies are discussed in the vicinity of the hexagonal and lamellar phase, which show a nonconstant mean curvature, even for the

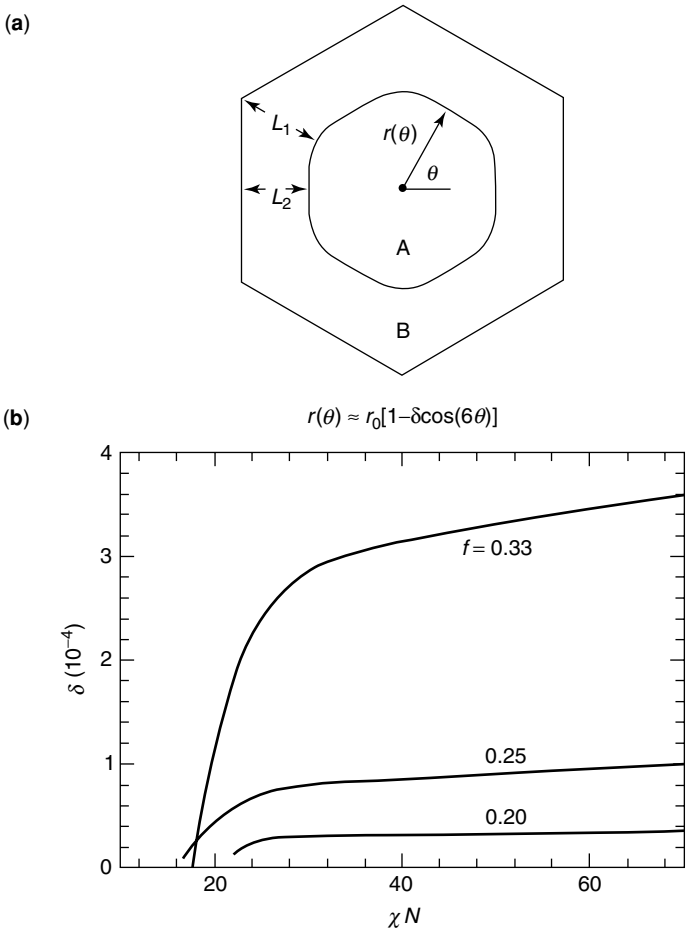

Fig. 7. (**a**) Nonconstant mean curvature of a cylindrical morphology. (**b**) The deviation from constant mean curvature δ as a function of incompatibility for various compositions. From Ref. 92. Copyright (1997) American Institute of Physics.

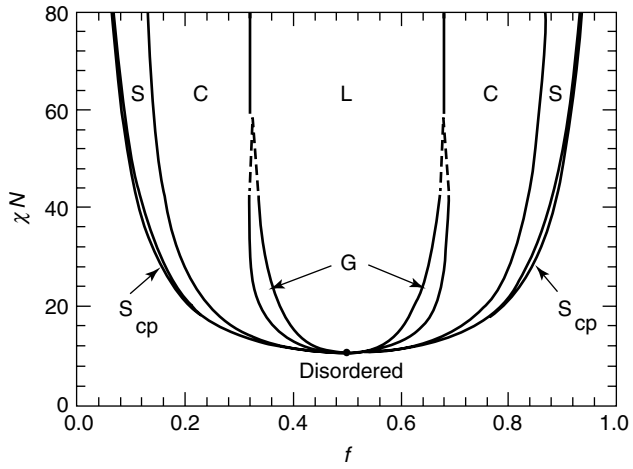

Fig. 8. Phase diagram of a diblock copolymer following from SCFT assuming similar segment lengths of both blocks. S_{cp}: spheres arranged on a face-centered cubic lattice, S: spheres arranged on a body-centered cubic lattice, C: hexagonally packed cylinders, G: double gyroid, L: lamellae. From Ref. 92. Copyright (1997) American Institute of Physics.

ideal case (large matrix-forming block). These are the double gyroid, the double diamond, and the hexagonally perforated lamellae (92). The double gyroid morphology was investigated theoretically by different groups in the WSL (93,94). This particular morphology belongs to a whole class of structures, the free energies of which differ only slightly and have not been distinguished experimentally so far (95,96). Only the double gyroid is considered to be a stable morphology, while the other two are metastable, as follows from self-consistent field theory (SCFT) calculations (92,97). The SCFT has also been used to cover the bridge between the WSL and the SSL leading to the phase diagram shown in Figure 8 (92).

Within the SCFT, the free energy is described by contributions of the internal energy U and entropy contributions by the junction points and the different blocks S_J and $S_{A,B}$, respectively (92).

$$F = U - T(S_J + S_A + S_B) \tag{14}$$

with

$$\begin{aligned}
\frac{U}{nk_BT} &= \frac{\chi N}{V}\int \mathrm{d}r\,\phi_A(r)\,\phi_B(r) \\
-\frac{S_J}{nk_B} &= \frac{1}{V}\int \mathrm{d}r\,\rho_J(r)\ln\rho_J(r) \\
-\frac{S_A}{nk_B} &= -\frac{1}{V}\int \mathrm{d}r\left[\rho_J(r)\ln q(r,f) + W_A(r)\,\phi_A(r)\right] \\
-\frac{S_B}{nk_B} &= -\frac{1}{V}\int \mathrm{d}r\left[\rho_J(r)\ln q^+(r,f) + W_B(r)\,\phi_B(r)\right]
\end{aligned} \tag{15}$$

where V is the overall volume of n block copolymers, ρ_J is the junction point density, q and q^+ are the partition functions of the A and B blocks which are influenced

by the fields W_A and W_B, respectively. Within the SSL, different contributions can be assigned to the quantities defined before. For ordered states these are

$$\frac{U}{nk_BT} \approx \frac{F_{int}}{2};\ -\frac{S_J}{nk_B} \approx 0;\ -\frac{S_A}{nk_B} \approx F_{el}^A + \frac{F_{int}}{4};\ \frac{S_B}{nk_B} \approx F_{el}^B + \frac{F_{int}}{4} \tag{16}$$

and for the disordered state it was given before (eq. 3).

Also binary block copolymers of other topologies have been studied. For symmetric ABA triblock copolymers in the WSL, a critical value of $\chi N = 18$ was determined (98), and this result was confirmed in works dealing with ABA triblock copolymers having arbitrary ratios between the two endblocks (99,100). The phase behavior of multiblock copolymers was studied by SCFT for asymmetric segment lengths also. Higher values for the critical value of χN were found here too (101). For heteroarm star copolymers with the same number of arms of both species A_nB_n, a symmetric phase diagram with a critical value of $\chi N = 10.5$ was obtained (99). Starblock copolymers $(AB)_n$ for various n and also for asymmetric segment lengths showed a lower value for critical χN by SCFT as compared to AB diblock copolymers (102). Heteroarm star copolymers with different numbers of arms A_nB_m $(m \neq n)$ (89,103–105) have also been described theoretically.

While the phase behavior of amorphous binary block copolymers, in particular diblock copolymers, has been investigated for a long time and most of the fundamental problems seem to be explored, ternary triblock copolymers, especially linear and star terpolymers have been addressed to a much lower extent (106). In contrast to the morphology of AB diblock copolymers, which is mainly determined by one interaction parameter χ and one independent composition variable such as the volume fraction ϕ_A, the morphology of ternary triblock copolymers is mostly determined by three interaction parameters χ_{AB}, χ_{BC}, χ_{AC} and two independent composition variables ϕ_A, ϕ_B. Because of the larger number of independent parameters, it is not surprising that ternary triblock copolymers show a huge variety of morphologies. The SCFT has also been used for symmetric ABC triblock copolymers $(\phi_A = \phi_C)$ (107). It was shown that a gyroid morphology with interpenetrating A and C tripod networks in a B matrix is more stable than a corresponding diamond lattice with interpenetrating A and C tetrapod networks in a B matrix. For such triblock copolymers, tetragonally packed A and C cylinders in a B matrix, as well as cubic lattices of spheres, were also described. The core–shell double gyroid morphology was described by this method, too (108).

With the exception of the cocontinuous morphologies, which are stable (in the case of gyroids) or metastable in a weak or intermediate segregation regime, the strong segregation theory gives qualitatively a good understanding of various morphologies, and therefore, it is often used for complictaed structures found in ABC triblock copolymers. In comparison to SCFT, it is much less intensive in terms of numerical calculations. In the following, the focus is on descriptions of the free energy of ABC triblock copolymers within the SSL.

If R_B is used as the characteristic dimension of the morphology (R_B being the half diameter of the B domain), F_{int} and F_{el} can be written as (109)

$$\begin{aligned} F_{int} &= \frac{N_B v_B}{R_B} K_{int} \\ F_{el} &= \frac{R_B^2}{N_B} K_{el} \end{aligned} \tag{17}$$

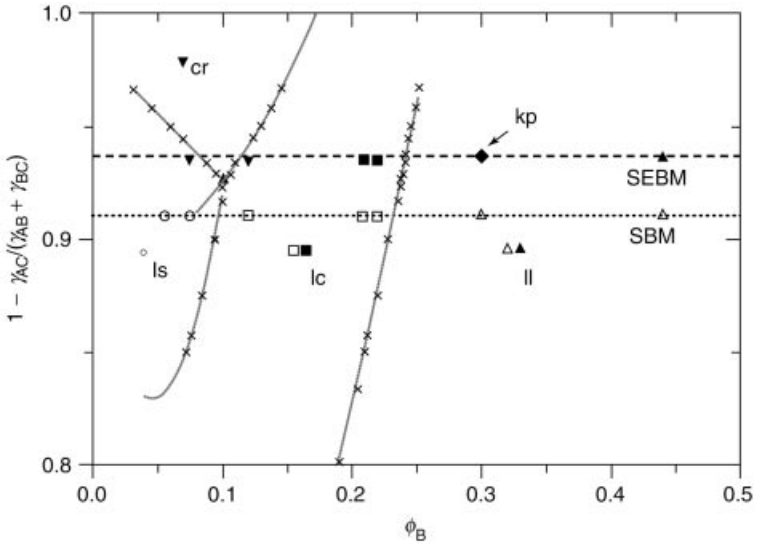

Fig. 9. Phase diagram of symmetric ABC triblock copolymers with $\phi_A = \phi_C$. cr: cylinder–ring morphology, kp: knitting pattern morphology, ls: lamellae–sphere morphology, lc: lamellae–cylinder morphology, ll: lamellae morphology. From Ref. 110. Copyright (1996) Wiley-VCH Verlag GmbH. Morphological schemes are given in Figures 3 and, 23.

where K_{int} and K_{el} are constants characterizing a particular morphology and $N_B v_B$ is the volume occupied by the B block. Upon minimization of the free energy with respect to R_B ($\partial F/\partial R_B \equiv 0$), the minimized free energy of the morphology per chain is obtained (109):

$$F = \frac{3}{2}\left(2N_B K_{el}\right)^{1/3}\left(v_B K_{int}\right)^{2/3} \tag{18}$$

Expressions for K_{int} and K_{el} have been given for various lamellar and cylindrical morphologies.

Figures 9 and 10 show transition lines between different lamellar (109,110) and cylindrical (111) morphologies of polystyrene-*block*-polybutadiene-*block*-poly(methyl methacrylate) (SBM) triblock copolymers and their hydrogenated analogues, polystyrene-*block*-poly(ethylene-*co*-butylene)-*block*-poly(methyl methacrylate) (SEBM) triblock copolymers.

Arguments based on such type of description of the free energy were also used for block copolymers showing no long-range order of A and C cylinders in a B matrix (112), as well as the stability of a spherical morphology, where one outer block forms a sphere in the matrix of the other outer block and the middle block forms either spheres on the interface or a shell (113). The free energies of ABC triblock copolymers within the SSL were also discussed by other groups (114–117).

When comparing ABC triblock with AC diblock copolymers, it is interesting to investigate the influence of the middle block on the miscibility of the two outer blocks; ie, the miscibility of A and C in an ABC triblock copolymer differs from the miscibility of these two blocks in an AC diblock copolymer. In order to answer

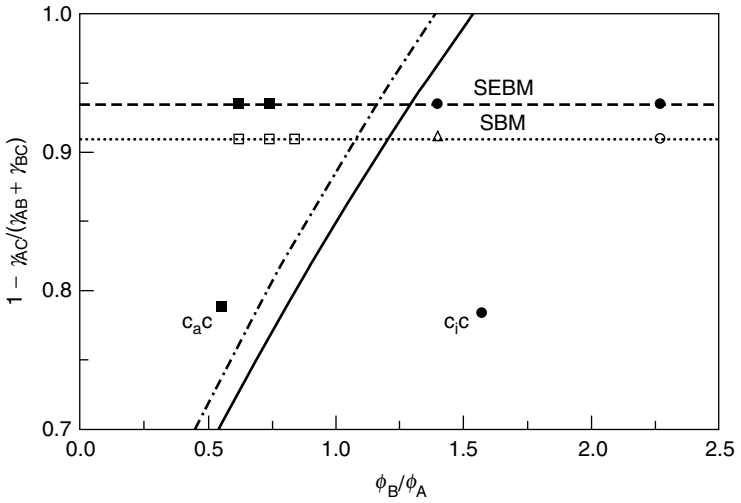

Fig. 10. Morphological transition lines between c_ac (cylinder at cylinder) and c_ic (cylinder in cylinder) morphologies for $\phi_C = 0.7$ (——) and $\phi_C = 0.6$ (.....) in comparison with experimental results on SBM and SEBM triblock copolymers. Δ indicates a core–shell morphology with an undulated shell. From Ref. 111 Copyright (1997) Wiley-VCH Verlag GmbH. Morphological schemes are given in Figure 3.

this question, the phase diagram of a diblock copolymer was calculated in the SSL by setting the free energy of a microphase-separated morphology equal to the free energy of the homogeneuos phase (118). From these calculations the volume fractions where spheres transform into cylinders and cylinders into lamellae were obtained in good agreement with experimental data on diblock copolymers. Also the critical value of the product χN, where a symmetric lamellar diblock copolymer transforms into the disordered phase, was obtained in good agreement with the weak segregation theory (74). Terms accounting for mixing energy have to be included when two of the three blocks of an ABC triblock copolymer become miscible with each other. Here a system with a strongly incompatible middle block and two less incompatible endblocks (χ_{AB}, $\chi_{BC} > \chi_{AC}$) is considered. For a given repulsive interaction $\chi_{AC}N_{AC}$ between the two outer blocks, their miscibility should be enhanced as compared to the corresponding AC diblock copolymer. One reason is a gain of conformational entropy for the middle block, since the confinements for the localization of the block junction points become similar to an ABA triblock copolymer; ie, both junction points can be localized anywhere on the surface of the middle block domain rather than being restricted to the part of the interface which connects B with A domains or B with C domains, respectively (Fig. 11).

Besides the introduction of an enthalpic contribution, the elastic energy terms of the spheres or cylinders located at lamellar interfaces have to be changed in the corresponding expressions for spheres or cylinders in a diblock copolymer. For a lamellar B block, there is no gain of conformational entropy upon mixing of the A and C blocks within this simple model. In addition the mixing entropy of the junction points S_J at the AB and BC interfaces has to be considered as another

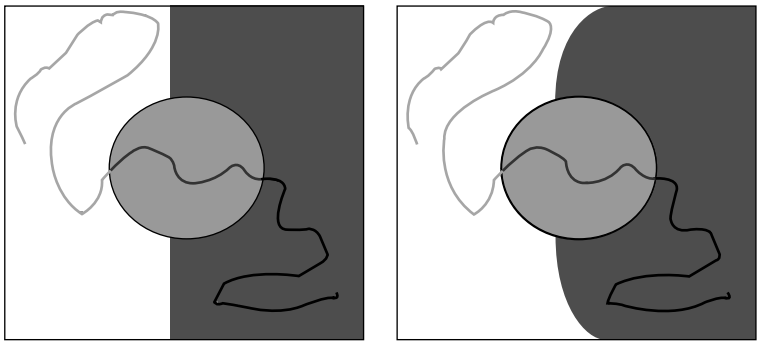

Fig. 11. ABC triblock copolymer with a demixed (left) and mixed (right) corona around the B domain.

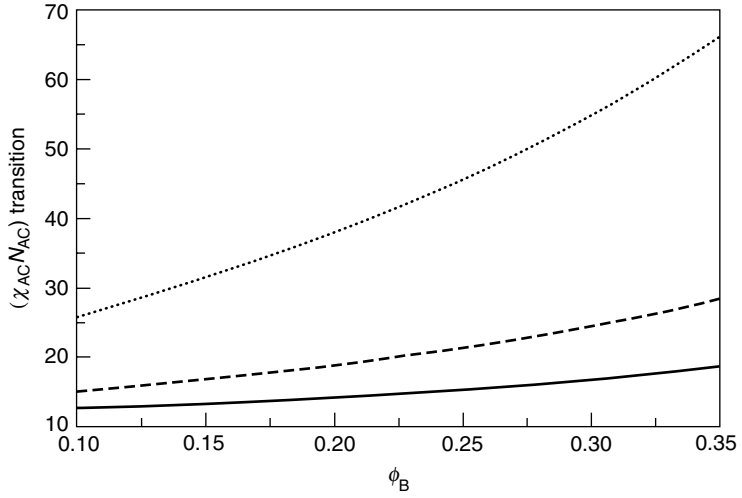

Fig. 12. Critical degree of incomaptibility between the endblocks of a symmetric ABC triblock copolymer ($\phi_A = \phi_C$) as a function of middle block content. $\chi_{AC}/(\chi_{AB} + \chi_{BC})$ with $\chi_{AB} = \chi_{BC}$: ——— 0.5; ..... 0.1; ..... 0.01. From Ref. 118. Copyright (1996) Springer-Verlag GmbH & Co. KG.

reason for enhancing miscibility of the two outer blocks. This can be expressed by (118)

$$\frac{S_J}{nk_B} = -\frac{f_A}{f_A+f_C}\ln\left(\frac{f_A}{f_A+f_C}\right) - \frac{f_C}{f_A+f_C}\ln\left(\frac{f_C}{f_A+f_C}\right) \tag{19}$$

Comparing the free energies of two morphologies with mixed or demixed A and C domains allows the calculation of the critical value of $\chi_{AC}N_{AC}$ for the order–order transition between these two morphologies. As an example, $\chi_{AC}N_{AC}$ of the transition between a morphology of B cylinders in a mixed AC matrix and a morphology of B cylinders at a lamellar AC interface (lc-morphology) is shown in Figure 12 (118).

The enhanced miscibility of the outer blocks is reflected by the larger critical value of $\chi_{AC}N_{AC}$ as compared to $\chi N = 10.495$ for a symmetric AC diblock copolymer. Qualitatively, these results on the influence of a short but strongly interacting middle block on the miscibility behavior of the two outer blocks were confirmed by a theoretical investigation within a weak segregation approach (119) and stimulated new experiments on the order–disorder transition of an ABC triblock copolymer (120).

All these approaches still suffer from the principal problem that in order to calculate the free energy of a morphology its corresponding symmetry needs to be put into the calculation. In other words, a new morphology can never be predicted from calculations of this type. In principle, Monte Carlo simulations could overcome this problem but have limitations due to finite size effects (121). An SCFT has been proposed without assuming a symmetry by solving self-consistent equations in real space in order to find the minimum of the free energy (122). An approximate free-energy functional has been minimized using an arbitrary unit cell, where both the local volume fraction and the unit cell can vary (123). Especially the possibility for the unit cell to vary during the minimization procedure avoids the occurrence of strain energy contributions, which would lead to another (wrong) equilibrium structure. In that approach the free energy is given as a function of the order parameters $\delta\phi_\alpha$, with α corresponding to the different blocks A, B, ...:

$$\begin{aligned} F\{[\delta\phi_\alpha(r)]\} &= F_{ref} + \Delta F \\ F_{ref} &= \frac{nk_BT}{V}\sum_\alpha \int dr \left(\frac{\phi_\alpha(r)}{f_\alpha}\ln\phi_\alpha(r)\right) \\ \Delta F &\cong \frac{nk_BT}{2}\sum_{\alpha,\beta,q\neq 0} S^{-1}_{\alpha\beta}(q)\,\delta\phi_\alpha(q)\,\delta\phi_\beta(-q) - F_{ref} \\ \delta\phi_\alpha(q) &= \frac{1}{V}\int dr\,[\delta\phi_\alpha(r)\exp(-iqr)] \end{aligned} \tag{20}$$

The structure factor $S_{\alpha\beta}$ is taken from Leibler's work. The following minimizations are then carried out simultaneously:

$$\begin{aligned} \left[\frac{\partial F}{\partial \delta\phi_\alpha(n_s)}\right] &= 0 \\ \left[\frac{\partial F}{\partial D_s}\right] &= 0 \end{aligned} \tag{21}$$

where s stands for the Cartesian coordinates x, y, z, and n_s is an integer number of the periodicity D_s in direction s. This approach was first demonstrated on examples of linear and star ABC block copolymers (123).

Influence of the Composition on the Morphology of ABC Terpolymers

In most of the experimental research carried out in this field so far, the phase behavior of linear ABC triblock copolymers was investigated as a function of

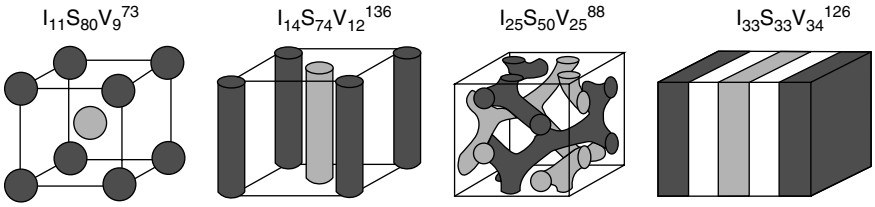

Fig. 13. Different morphologies found for symmetric ISV triblock copolymers with strongly incompatible endblocks (OsO_4/CH_3I, see Table 1).

composition for given sets of monomers (109,111,113,124). The core–shell morphologies in ABC triblock copolymers were first reported in Reference 125. A scheme for the dependence of the morphologies on composition for ABC triblock copolymers has also been proposed, where spherical, cylindrical, and lamellar morphologies were considered (125). For lower ratios of ϕ_B/ϕ_A, core–shell spheres and core–shell cylinders with a C matrix, and lamellae of all three components were proposed, while at larger ratios of ϕ_B/ϕ_A, the A component forms many little spheres within a B sphere surrounded by C matrix or, in the case for lamellae, A forms spheres within a B lamella. Some of these morphologies were found by this group in polystyrene-*block*-polyisoprene-*block*-poly(methyl methacrylate) (SIM) triblock copolymers. Polystyrene-*block*-polyisoprene-*block*-poly(4-vinylbenzyl)dimethylamine triblock copolymers have been reported, where a strong influence of the casting solvent on the morphology of the investigated films was found (126). A systematic study on polyisoprene-*block*-polystyrene-*block*-poly(2-vinylpyridine) (ISV) triblock copolymers has been presented, with $\phi_I \approx \phi_V$. Starting from $\phi_I \approx \phi_V \approx \phi_S$ and then increasing ϕ_S, they obtained lamellae, cylinders of both I and V arranged on a tetragonal lattice, and finally I and V spheres on a cubic lattice (Fig. 13) (124). Between the lamellar and cylindrical region also, a cocontinuous morphology was found, which was assigned to an ordered tricocontinuos double diamond structure (OTDD), in which one of the tetrapod lattices is formed by I and the other one by V, separated by the S matrix. However, a few years later the OTDD was ruled out (107), as it happened to the corresponding ordered bicontinuous double dimaond lattice (OBDD) discussed for binary block copolymers before (92). Instead of the OBDD the double gyroid structure was found to fit all experimental data for binary block copolymers, where two tripod-lattices of the minority component interpenetrate each other. In the ISV triblock copolymer with gyroid morphology, one tripod is formed by I while the other is formed by V and S separates them from each other (Fig. 13).

Stadler's work in the field of linear ABC triblock copolymers based on polystyrene (S), polybutadiene (B), and poly(methyl methacrylate) (M) led to the discovery of a number of new morphologies (110–113,127–130). The initial studies dealt with systems where the volume fractions of the outer blocks, ϕ_S and ϕ_M, were kept approximately equal. However, in contrast to Matsushita's work, the volume fraction of the outer blocks were kept large while ϕ_B was decreased, and only lamellar morphologies were obtained, where between the S and M lamellae B spheres (ls), B cylinders (lc), or a B lamella (ll) was embedded with increasing ϕ_B (Fig. 14).

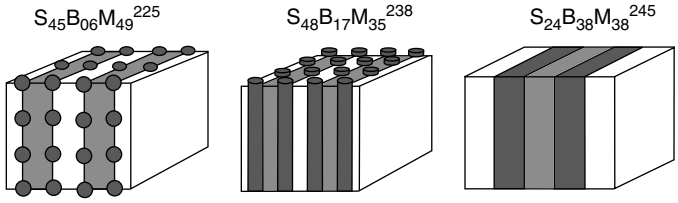

Fig. 14. Lamellar morphologies found in symmetric SBM triblock copolymers (OsO_4, see Table 1).

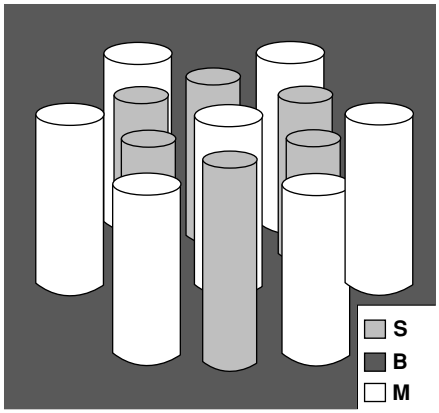

Fig. 15. Hexagonally arranged microphase-separated S and M cylinders of an SBM triblock copolymer (OsO_4, see Table 1). Reprinted with permission from Ref. 130. Copyright (1998) American Chemical Society.

An increase of ϕ_B also leads to morphologies with cylindrical domains of the endblocks. However, because of the smaller repulsion between S and M as compared to I and V of Matsushita's system, microphase separation was not complete between the different endblocks. Using a special solvent mixture, a novel hexagonal morphology was found, where both endblocks are arranged on a hexagonal lattice (Fig. 15) (130).

A symmetric linear polystyrene-*block*-poly((4-vinylbenzyl)dimethylamine)-*block*-polyisoprene triblock copolymer (131) showed a morphology with the same symmetry when cast from a particular solvent. This example underlines the influence of the preparation conditions on the bulk morphology of block copolymers. Since this type of morphology is found in coexistence with other morphologies, it might be a physically pinned nonequilibrium structure. In some ABC heteroarm star terpolymers long-range ordered structures with the same symmetry are observed, indicating that in those cases this structure is an equilibrium structure owing to the other chain topology (compare with the right scheme in Fig. 17).

Among the most spectacular morphologies found in these systems was a helical morphology (111,129), where the middle block forms helices around a cylinder formed by one endblock while the other endblock forms the matrix. This morphology is inherently noncentrosymmetric; however, no favored orientation was observed. It belongs to a whole group of morphologies with spheres or cylinders

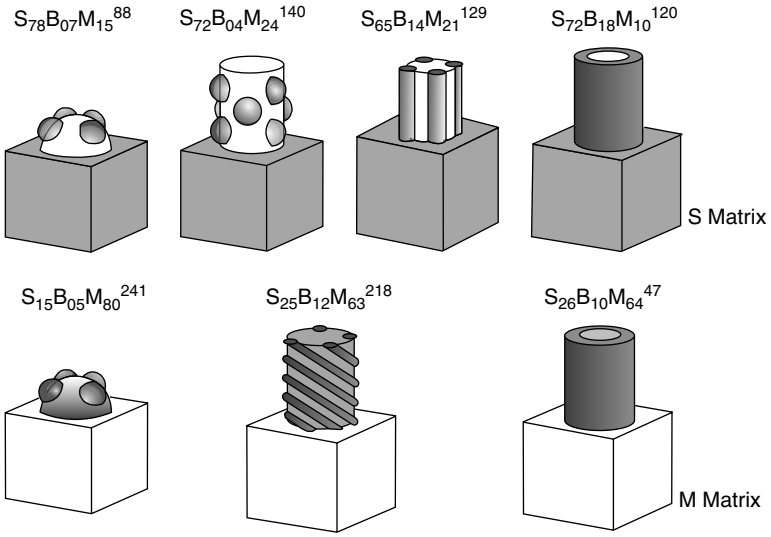

Fig. 16. Various spherical and cylindrical morphologies found in SBM triblock copolymers (OsO_4, see Table 1).

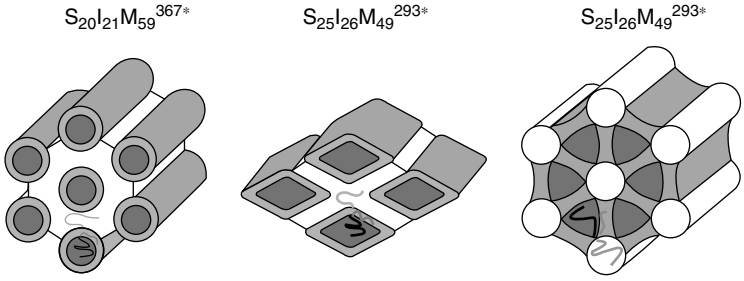

Fig. 17. Various cylindrical morphologies found in SIM heteroarm star terpolymers (OsO_4, see Table 1).

formed by one outer block in a matrix of the other outer block, with the middle block forming spherical, helical, cylindrical domains, or a shell around the core cylinder (Fig. 16) (111).

It is interesting to note that both the "sphere on sphere"(s_os) and the "cylinder in cylinder"(c_ic) morphologies were found with S and with M matrix, while the other morphologies shown in Figure 16 were found only with S or M matrix so far.

Much less work has been reported on ABC heteroarm star copolymers because of their rather difficult synthesis. Among the different publications in this field there are only a few dealing with a systematic investigation of the morphology in dependence of composition (132–135). An interesting problem of this chain topology is the location of the junction point. While in linear block copolymers junction points of incompatible blocks are more or less confined to a two-dimensional interface (depending on the degree of segregation), in incompatible ABC heteroarm star terpolymers the junction point is expected to be located along a line (one-dimensional). Of course, this means a strong entropic confinement and

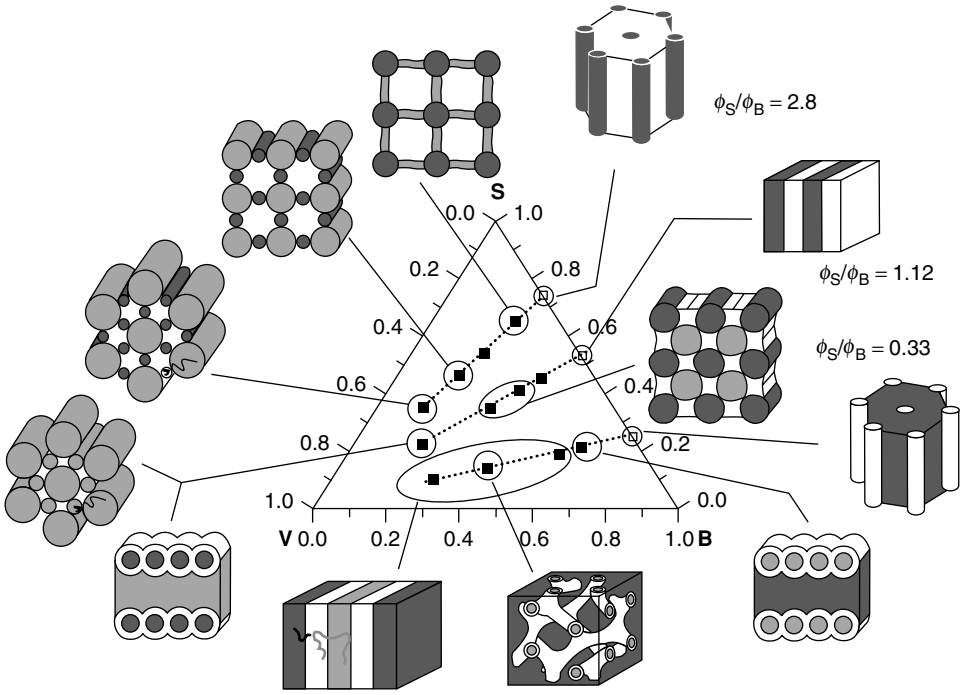

Fig. 18. Microphase-separated morphologies on the example of polystyrene-*arm*-polybutadiene-*arm*-poly(2-vinylpyridine) (SBV) heteroarm star terpolymers (OsO_4/CH_3I, see Table 1).

it may lead to a certain degree of mixing in the neighborhood of the junction point in order to reduce the stretching energy of the confined arms. For heteroarm star terpolymers of polystyrene (S), polyisoprene (I), and poly(methyl methacrylate) (M), three types of morphologies were described (133,134) (Fig. 17).

For systems with $\phi_S \approx \phi_I < \phi_M$, hexagonally packed core–shell cylinders were found when $\phi_M > 0.5$ (Fig. 17, left). For smaller volume fractions of M, tetragonally deformed core–shell cylinders were formed, where because of the short matrix-forming M block the interface adopts a nonconstant mean curvature (Fig. 17, middle). In these systems S forms a shell around the I cylinders, since $\chi_{SM} < \chi_{SI} \ll \chi_{IM}$. The S shell indicates that the junction points are not located on lines in these morphologies. Finally, systems with approximately similar amounts of all three constituents form a cylindrical morphology with a hexagonal symmetry and interfaces with nonconstant mean curvatures (Fig. 17, right). Here the junction points seem to be located along lines. A way to favor their location on lines is to use components with a stronger incompatibility. In another study SBV heteroarm star terpolymers were investigated. Because of the synthetic route, series of polymers with a constant ratio between S and B and just varying amount of V could be obtained (135). In this system the repulsive interactions are stronger as compared to the SIM system and related in the following way: $\chi_{SB} \approx \chi_{SV} \ll \chi_{BV}$. Figure 18 shows three rows of morphologies obtained for the volume ratios $\phi_S/\phi_B = 2.8$, 1.12, and 0.33 from the corresponding SB diblock copolymers, respectively.

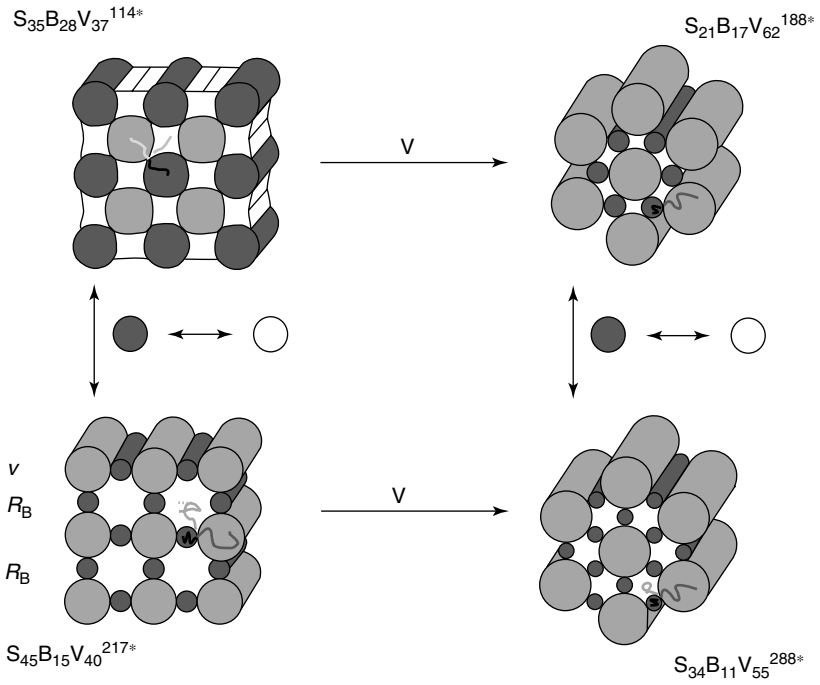

Fig. 19. Tetragonal (left column) and hexagonal morphologies (right column) of SBV heteroarm star terpolymers. The two lines are different by the symmetry positions of the B and S domains (OsO_4/CH_3I, see Table 1).

In the first two series ($\phi_S/\phi_B = 2.8$ and 1.12) mostly cylindrical morphologies are obtained, where because of the strong incompatibility between B and V these domains have a very small contact area, while the interfaces between S and B as well as between S and V are larger. These cylindrical morphologies allow the following crude consideration, as pictured in Figure 19: in tetragonally packed systems on the left side it is possible to exchange the symmetry positions of S and B by changing their relative composition (ie, the "coordination number" of the corresponding neighboring domains is exchanged). The same is true for the hexagonally packed systems on the right side. These hexagonal morphologies have the same symmetry as the symmetric SIM heteroarm star terpolymer (134). (Fig. 17, right) and the linear ABC triblock copolymers discussed in connection with Figure 15.

A similar comparison holds for the lamellae-like morphologies shown in Figure 20, where basically B and V exchange their symmetry properties when exchanging their volume fractions. However, it should be kept in mind that $S_{21}B_{17}V_{62}^{188*}$ shows two coexisting morphologies (compare with Fig. 18).

In the morphologies shown in Figure 20 as well as in the lamellar and core–shell double gyroid morphologies (136) shown at the bottom of Figure 18, the S blocks always separate the B from the V domains. Thus, in these morphologies the junction point is by no means restricted on a one-dimensional location, but it is distributed in the S domains.

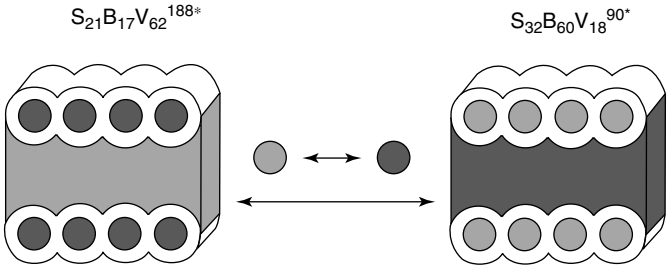

Fig. 20. Lamellar morphologies of two SBV heteroarm star terpolymers, which differ by the symmetry positions of the B and V domains (OsO_4/CH_3I, see Table 1).

Influence of the Chain Topology on the Phase Behavior of ABC Terpolymers

In this section the question of how the morphology is influenced by changing the block sequence for a given overall composition in linear ternary block copolymers is discussed. At the end of this section linear block copolymers are compared with their heteroarm star terpolymer analogues.

For a given composition and set of three monomers, the controlling factor is the interaction parameters χ_{AB}, χ_{BC}, and χ_{AC} between the middle and the two outer blocks. The latter interaction parameter plays a role only if the volume fraction of the middle block, ϕ_B, is so small that a direct interface between both outer blocks could become favorable because of a larger conformational entropy.

A core–shell cylindrical morphology with a nonconstant mean curvature of an SIV block copolymer with similar amounts of all three blocks has been reported (137). For a similar system with reversed block sequence (ISV), a lamellar morphology was found (124). Recently a systematic comparison of SBV and BSV triblock copolymers was reported (138). While the interaction parameters between the middle and the two outer blocks are comparable with each other in ISV and BSV triblock copolymers, this is not the case for SIV and SBV triblock copolymers. In the latter the much larger repulsive interaction between B (or I) and V as compared to the interaction between B (or I) and S leads to the systems' tendency to form a small interface between B (or I) and V, while the interface between B (or I) and S may be larger. So this type of triblock copolymers can form morphologies with curved interfaces (such as core–shell cylinders and core–shell double gyroids) at compositions where the corresponding BSV (or ISV) triblock copolymers form lamellae. The formation of lamellae for the latter copolymers is favored, since the repulsive interactions between S and B (or I) and between S and V are comparable and strong, while the repulsion between B (or I) and V is very strong. Note that the lamellar interface is the smallest possible interface between blocks. Figure 21 shows the different morphologies found for SBV and BSV triblock copolymers of Reference 138.

To some extent SBM triblock copolymers behave similar to BSV triblock copolymers. Since the interactions between B and S on one side and between B and M on the other side are comparable and strong, but the repulsive interactions

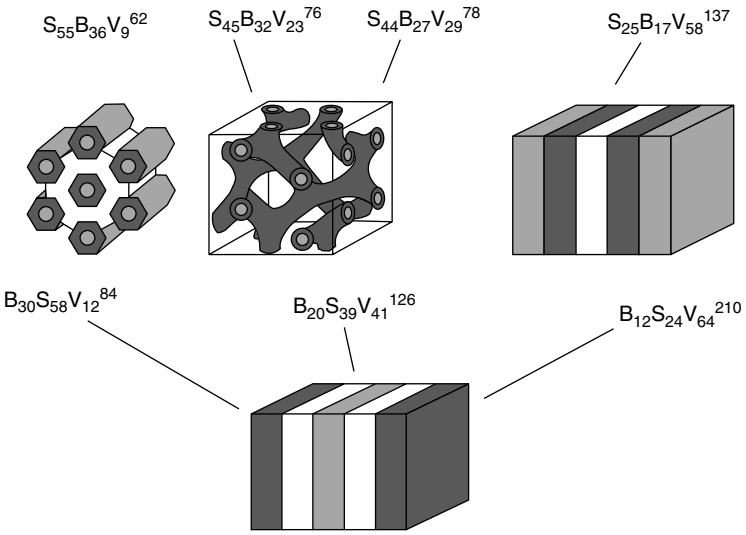

Fig. 21. Influence of the block sequence on the morphology in SBV and BSV triblock copolymers (OsO_4/CH_3I, see Table 1).

between S and M are weak, a system with similar volume fractions of S and M ($\phi_S \approx \phi_M > 0.3$) forms lamellae with B forming either a separating lamella between them ($\phi_B \approx 0.3$), or cylinders ($\phi_B \approx 0.17$) or spheres ($\phi_B \approx 0.06$) for smaller volume fractions of B, which leads to a direct interface between the S and M domains (Fig. 14). By the appearance of a direct A/C interface these block copolymers differ from the BSV system. The morphologies of BSM triblock copolymers are comparable to the morphologies observed in SBV triblock copolymers. While an SBM system composed of equal amounts of the three components forms lamellae, the corresponding BSM triblock copolymer cast from chloroform forms core–shell double gyroids (in coexistence with lamellar regions), which again is due to the dissimilarity of the interactions between the middle block and the two outer blocks (76,138). A further reason for the formation of the core–shell double gyroid morphology in this case may be the slight selectivity of chloroform for the M block. As discussed before, the solvent also plays an important role in the formation of the final morphology on block copolymers cast from solution (131). A solvent with lower polarity, such as toluene, leads to a more disordered morphology, while a more polar solvent, such as butanon (methyl ethyl ketone), results in a morphology of B cylinders in a matrix of S and M. Here the B domains precipitate first from the solution, while S and especially M are still swollen to a larger degree by the solvent (139).

Finally the morphologies of ternary linear block copolymers and heteroarm star terpolymers are compared. Here systems containing I or B are also compared, since these two polymers show rather similar interactions toward the other blocks (see Table 2 for solubility parameters). Figure 22 shows in the left column symmetrically composed SIM heteroarm star terpolymers (134) and linear BSM and SBM triblock copolymers (76). In the right column corresponding SBV (135) and SIV (144) heteroarm star terpolymers are compared with their linear compositional

Table 2. Solubility Parameters δ for Estimation of Interaction Parameters $\chi \propto (\delta_i - \delta_j)^2$ [a]

	Solubility parameter at room temperature[b] δ, $(MPa)^{1/2}$
Polymer	
Polystyrene	18.5
Poly(1,2-butadiene)	17.4
Poly(2-vinylpyridine)	20.4[c]
Poly(1,4-isoprene)	16.8
Poly(methyl methacrylate)	19.0
Poly(*tert*-butyl methacrylate)	18.0
Poly(cyclohexyl methacrylate)	18.2
Poly(methacrylic acid)	21.9
Poly(ethylene-*co*-butylene)	19.1 (27°C), 17.4 (121°C)[d]
Poly(ethylene-*alt*-propylene)	18.4 (27°C), 17.0 (121°C)[d]
Solvent	
Tetrahydrofuran	18.6
Chloroform	19.0
Toluene	18.2
Butanone[e]	18.5

[a]Note that this approach cannot account for negative χ parameters (attractive interactions). Solubility parameters found from different sources may vary significantly.
[b]Refs. 140 and 141.
[c]Ref. 142.
[d]Ref. 143.
[e]Butanone = methyl ethyl betone.

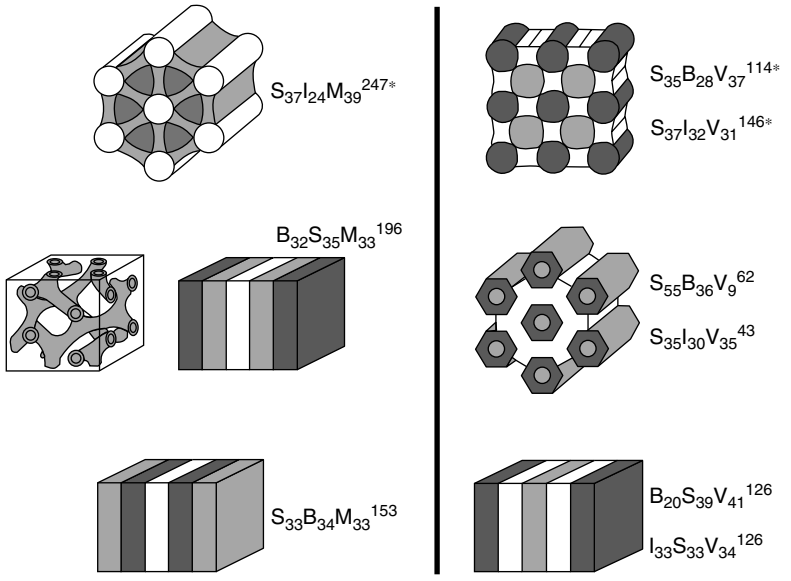

Fig. 22. Influence of the chain topology on the morphology in SBM and SIM terpolymers (left column; OsO_4, see Table 1). Influence of the chain topology on the morphology in SBV and SIV terpolymers (right column; OsO_4/CH_3I, see Table 1).

analogues (124,137,138). In all systems the thermodynamically most unfavorable interaction leads to the smallest interface of that particular system, ie, between I (or B) and M (left column) and between I (or B) and V (right column). The lower incompatibility between S and M as compared to between that between S and V leads to a larger interface in the SIM star terpolymer, which forms a hexagonal morphology. The similar interactions between S and I (B) and between S and V lead to an SBV and SIV star terpolymer with a tetragonal morphology, where the interfacial areas between S and the other two blocks are of approximately similar size. For the linear block copolymers the stronger repulsive interactions between B (I) and V as compared to those between B and S leads to a stronger curvature (cylinders) for SBV and SIV triblock copoylmers, while the corresponding BSM triblock copolymer shows coexisting core–shell double gyroids and lamellae. Finally, the triblock copolymers with approximately similar interactions between the middle and the two endblocks lead to lamellae. This discussion neglects the possible influences by different segment lengths of the different components, which might lead to different entropic contributions of the different blocks, even if they have the same volume fractions. However, the differences of the segment lengths are small for these monomers.

Morphological Changes Induced by Chemical Modification of Linear ABC Triblock Copolymers

The relative change of the χ parameters between the middle block and the two outer blocks of ABC triblock copolymers can induce morphological changes without induction of miscibility between the outer blocks. Among the previous works on SBM triblock copolymers there were three examples where a morphological change was observed after hydrogenation of the B middle block to poly(ethylene-*co*-butylene) (EB) (Fig. 23). In two cases an SBM triblock copolymer with B spheres (109) or cylinders (145) at a lamellar interface between S and M after hydrogenation transformed into a hexagonal morphology of S cylinders surrounded by EB rings in an M matrix. The other example was the "knitting pattern" morphology (kp-morphology), which was formed after hydrogenation of a slightly asymmetrically composed lamellar SBM triblock copolymer (ll-morphology) (110). The composition range of the kp-morphology has been investigated in more detail later, and from those investigations, where the preparation conditions were also carefully studied, it is now assumed that the kp-morphology is metastable (146). This morphology was observed only in samples cast from chloroform solutions, while the samples cast from toluene formed distorted lamellae. While chloroform is a good solvent for S, B, and M, it is not a good solvent for EB; this fact leads to a segregation of EB domains from the solution, which are embedded in highly swollen S and M domains. On the other hand, toluene is a better solvent for EB than for M, which could be the reason for the formation of distorted lamellae in films cast from this solvent.

Another type of polymer analogous reaction has been applied in order to modify triblock copolymers. Polystyrene-*block*-polybutadiene-*block*-poly(*tert*-butyl methacrylate) (SBT) triblock copolymers were transformed to SBA triblock copolymers [A: poly(methacrylic acid)] by saponification of the T block (147). Both

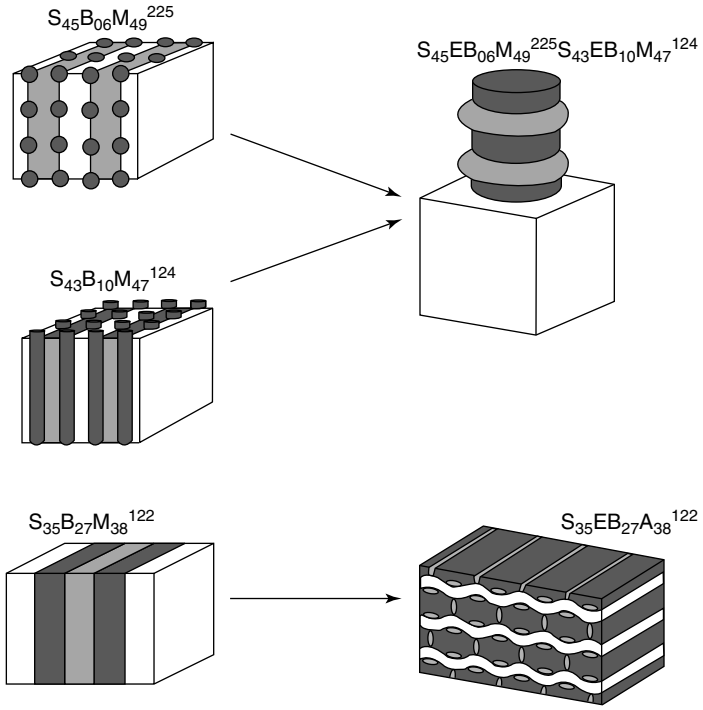

Fig. 23. Morphological changes induced via hydrogenation in SBM triblock copolymers. SBM: OsO_4, see Table 1; SEBM: RuO_4, see Table 1.

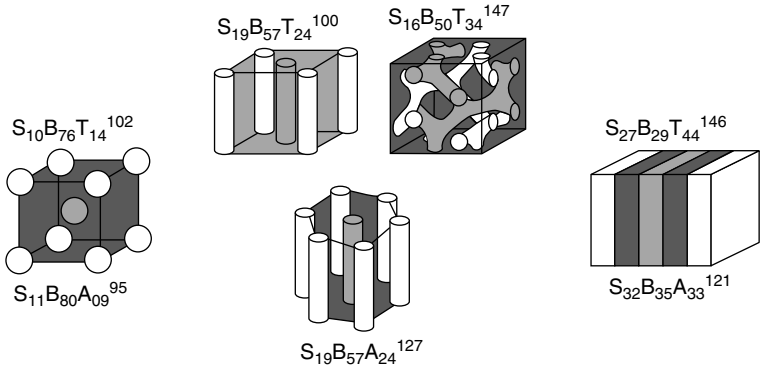

Fig. 24. Morphologies of SBT and SBA triblock copolymers.

systems are characterized by strong incompatibilities between all components. Figure 24 shows the morphologies of corresponding SBT and SBA triblock copolymers with slightly asymmetric endblocks, $\phi_S \approx \phi_{T,A}$. While the SBT triblock copolymers adopt the same morphologies already discussed for the ISV triblock copolymers with $\phi_I = \phi_V$, the SBA triblock copolymers show a different behavior. For increasing B content the morphology changes from lamellae to the same hexagonal motif for an SBM triblock copolymer (130). Upon further increase of the B

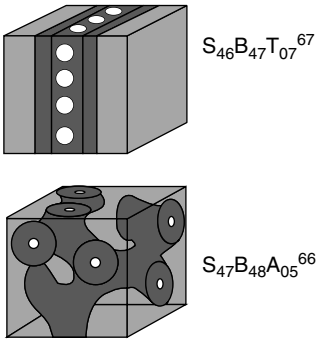

Fig. 25. Morphologies of an SBT and an SBA triblock copolymer with a short third block.

content, a lamellar structure is obtained, where B lamellae may alternate with lamellae being composed of S and A cylinders. However, the morphology of that polymer is not well characterized and therefore not shown in Figure 24. It turns out that $S_{19}B_{57}A_{24}{}^{127}$ (the product of the saponified $S_{16}B_{50}T_{34}{}^{147}$) corresponds to $S_{19}B_{57}T_{24}{}^{100}$ in terms of the mass fractions. Further increase of B then finally leads to a morphology where both endblocks form spheres, as does the corresponding SBT.

For an SBT triblock copolymer with $\phi_S = \phi_B$ and a very short T block, a lamellar structure is observed, where T spheres are embedded within the B lamellae. The corresponding SBA triblock copolymer forms a gyroid morphology, where the increased repulsive interaction between A and B (as compared to between T and B) may explain the behavior (Fig. 25). The change from a lamellar-like to a gyroid morphology can be interpreted as a decrease of incompatibility between the two major blocks S and B, which is driven by changing the interaction of a short endblock. It has been predicted that a strongly interacting endblock can also modify the order–disorder transition of the attached diblock copolymer in such a way that the region of the disordered phase is increased (119). As mentioned for the kp-morphology, in these systems also the selectivity of the solvent could explain the morphological transitions. A block has the lowest solubility and therefore may segregate as the first block from the solution.

In another work, the ls-morphology was used as a host for transition-metal complexes, which should be located selectively in the B domains (148). While the hydrogenation mentioned before was a quantitative polymer-analogous reaction, it was assumed that only a slight modification of the B domains with transition-metal complexes (based on Pd and Fe, respectively) would not lead to any change of the morphology. However, the morphology was changed in a dramatic way. While the complexation of a few percent of the B units with $PdCl_x$ led to a double gyroid morphology, complexation of a few percent of the B units with $Fe(CO)_3$ led to a cylindrical morphology. Like in the unmodified triblock copolymer, in both modified block copolymers the middle block forms spherical objects at the interface between the outer blocks. An explanation for this behavior is the induction of curvature of the interface between the two outer blocks by the fact that the middle block domain centered on the lamellar interface approximately along its equatorial plane in the SBM triblock copolymer moves out of that plane after chemical modification

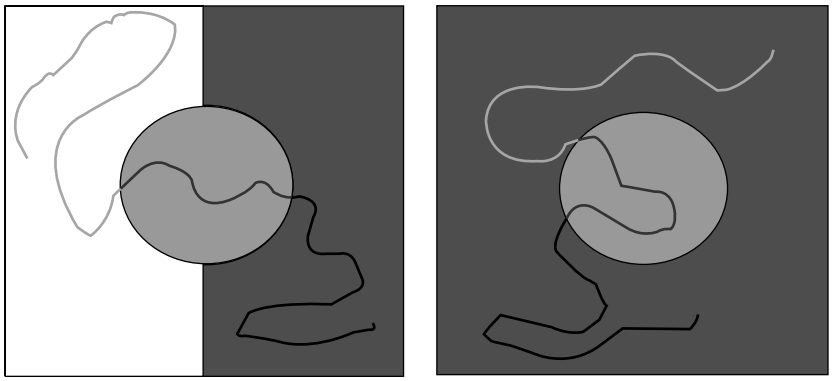

Fig. 26. Change of curvature in $S_{45}B_6M_{49}$[225] by modification of the middle block with a transition-metal complex.

(Fig. 26). This should be due to a change of the relative incompatibilities between the middle and the two outer blocks, which in turn leads to a change of the balance between the elastic energy contributions of the different blocks and the interface between them. Neglecting the small middle block, the overall morphology in this system changes from lamellae via double gyroid to a cylindrical morphology; although in terms of the outer blocks the system is composed almost symmetrically. Such behavior is unknown for amorphous diblock copolymers, where the corresponding morphologies are stable only at different compositions at a given temperature. Thus, an increasing asymmetry of the interactions between middle and outer blocks of a triblock copolymer with similar sized outer blocks and a short middle block leads to an increasing interfacial curvature driving the system from a lamellar morphology to curved morphologies; ie, the outer blocks become less incompatible with each other because of the changed balance between entropic and enthalpic contributions (Fig. 27). This behavior seems to agree qualitatively with the theoretical estimations discussed before (118,119).

Up to this point, morphological changes due to chemical changes have been presented. In the last part of this section discussion turns to a system, in which rather weak incompatibilities also play a role, which can be reduced sufficiently in order to achieve miscibility between the corresponding blocks by increasing the temperature. This system is composed of a symmetric diblock copolymer attached to a stronger incompatible third block of varying length. The chosen

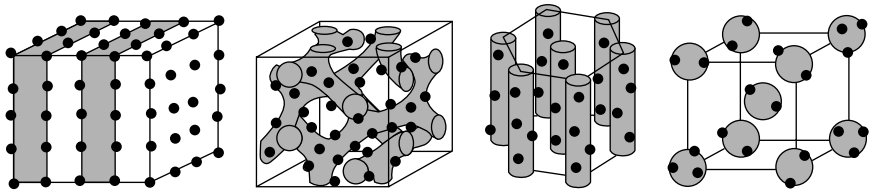

Fig. 27. Increasing curvature of the interface between the grey A and white C domains of an ABC triblock copolymer for increasing asymmetric interactions of the black B domains.

example consists of poly(ethylene-*alt*-propylene)-*block*-poly(ethylene-*co*-butylene)-*block*-polystyrene (EPEBS), which was obtained after hydrogenation of IBS triblock copolymers. This system was chosen because the order–disorder transition of EPEB diblock copolymers had been widely investigated before (149). It is well known that I and B homopolymers form single-phase blends with each other up to very large degrees of polymerization (150). Thus the corresponding IB diblock copolymers form disordered melts as well. While the IBS triblock copolymers behave like microphase-separated diblock copolymers with the compatible I and B blocks forming one microdomain and S forming the other one at low temperatures, at higher temperatures the order–disorder transition occurs and all three blocks form a disordered phase. This was monitored by dynamic mechanical spectroscopy (151). Especially the appearance of master curves in plots of the storage versus the loss modulus served as an indicator of the formation of the homogeneous disordered phase (152). This technique was also applied to EPEB diblock and the corresponding EPEBS triblock copolymers (153). While the order–disorder transitions of the EPEB diblock copolymers could be determined by this method, the order–order transition related to the onset of miscibility between these two blocks in the EPEBS triblock copolymer could not be resolved. A system with a short S block located in spherical domains (as proven by tem), $EP_{50}EB_{44}S_6$[48], showed an order–disorder transition around 70°C, which could be confirmed by the disappearance of the maximum in the saxs curve at that temperature. It is not obvious whether this system undergoes a phase transition from three microphase-separated domains into one homogeneous phase, or whether there is another order–order transition prior to the order–disorder transition. Because of the lack of sufficient electron density contrast between the two elastomeric blocks EP and EB, saxs only monitors EP and EB together in contrast to S. A system with a larger S block, $EP_{46}EB_{38}S_{16}$[74], shows rhombohedrally packed S cylinders at room temperature. At elevated temperatures a phase transition to a system with hexagonally packed S cylinders occurs. This indicates a mixing of the two elastomeric blocks at significantly larger temperatures as compared to the order–disorder transition of the corresponding EPEB diblock copolymer (order–disorder transition < 20°C), and hence the conclusion that the grafting of a diblock copolymer to an incompatible surface leads to an increase of its order–disorder transition. This can be explained by the fact that the system cannot gain as much entropy as a free diblock copolymer because of the fixed end of one block (EB) at the interface with the immiscible third block (S). Moreover, the penetration of the EP block into the EB domain necessarily leads to an increase of the interface between S and the mixed elastomeric domain, which results in an increase of interfacial energy, unless a temperature-induced reduction of the interfacial tension compensates this enthalpic hindrance.

Comparing the morphologies of the IBS and EPEBS triblock copolymers, a shift from the disordered state toward the lamellae upon hydrogenation could be observed. This is shown in Figure 28. Upon hydrogenation of the two elastomeric blocks they become incompatible (or less compatible), which changes the conformation of the elastomeric corona around the microphase-separated S domains. The appearance of a new interface (even if it is not sharp) confines the junction point between the elastomeric blocks, and as a result of the repulsive interaction the interfacial area tends to get reduced, in order to reduce the number of

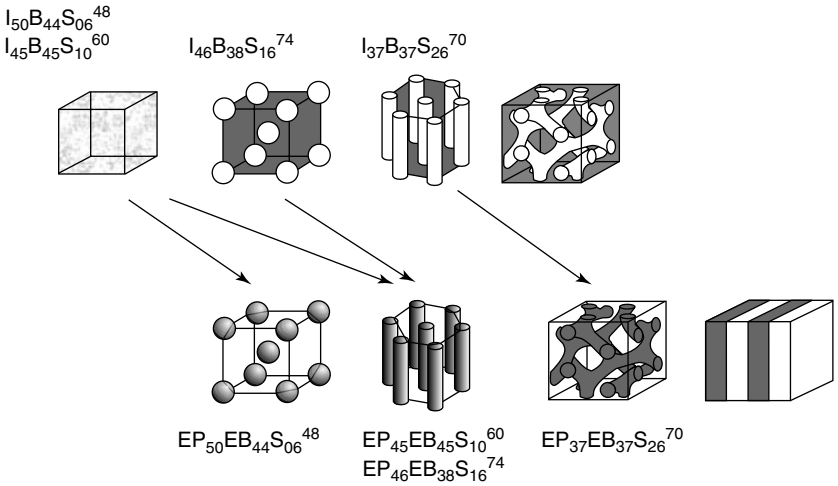

Fig. 28. Change of the morphologies of IBS triblock copolymers via hydrogenation to EPEBS triblock copolymers.

contacts between dissimilar segments. This leads to a stretching which reduces the curvature of the interface toward the S domains. For simplicity in Figure 28 the morphologies are shown as obtained from tem and saxs. Both methods cannot distinguish between the two elastomeric blocks, but distinguish only S from the I, B or EP, EB, respectively.

Blends of ABC Triblock Copolymers with Other Block Copolymers

Three articles of this encyclopedia consider only the morphological behavior of pure block copolymers in their bulk state by changing their topology or the thermodynamic properties of their blocks. Another interesting possibility to control block copolymer morphologies is given by blending block copolymers with other polymers or block copolymers. It is well known that free polymer chains can penetrate into grafted polymer chains under certain conditions (154). A block located at the interface of a microphase-separated block copolymer can be considered as a grafted chain. For chemically similar chains penetration is possible, when the free chains are shorter than the grafted chains. In such a case the gain of mixing entropy (or translational entropy of the free chains) is larger than the reduction of conformational entropy of the grafted chains induced by the chain stretching accompanied by mixing (Fig. 29).

The stretching in a grafted chain (or polymer brush) is a function of the distance to the interface. While close to the interface the stretching may be very large (depending on the interfacial tension), it vanishes at the surface of the polymer brush, where the chain approaches a random coil conformation. A certain interpenetration of similar chains always occurs when brushes with chemically similar chains are in contact with each other, as it is in the case of microphase-separated block copolymers in the bulk state. Since the interpenetration in these cases occurs

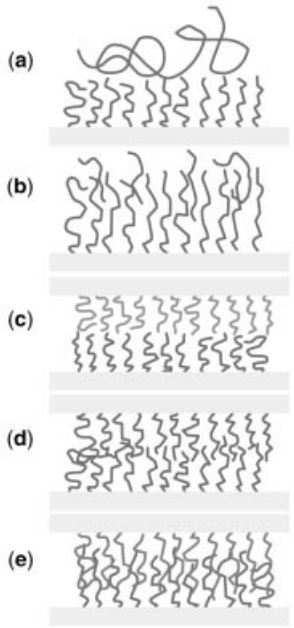

Fig. 29. Different situations of polymer brushes in contact with free chains or other polymer brushes. (**a**) Dry brush: long free chain cannot interpenetrate the brush; (**b**) Wet brush: short free chain interpenetrates brush; (**c**) $\chi > 0$: no interpenetration, phase separation; (**d**) $\chi = 0$: some interpenetration; (**e**) $\chi < 0$: stronger interpenetration.

between chemically similar chains, the driving force of this chain interpenetration is of pure entropic origin. While interpenetration will be suppressed when the interactions between different brushes are repulsive, attractive interactions will enhance the interpenetration (Fig. 29). This latter effect was used, for example, when compatibilizing blends of two polymers with a diblock (10) or triblock (11) copolymer, where each of the outer blocks shows selective attractive interactions to one of the other blend components.

Blends of microphase-separated binary block copolymers, mainly diblock copolymers, have been investigated for a long time (155). Blends of diblock copolymers were used to determine the stability region of the double gyroid morphology, which exists in a relatively narrow composition window in the weak and intermediate segregation regimes for binary block copolymers (156). In all these blends and also in blends of an AB diblock copolymer with an A homopolymer (157), only those morphologies were found which were similar to the morphologies found for a diblock copolymer with the same or slightly different overall composition; ie, no qualitatively different morphologies exist in these systems. A more dramatic effect has been reported in Reference 158, in which blends of different starblock copolymers, which all contained 25% S, were investigated. For some of these blends a lamellar morphology was found, which is very different from the stability region of the lamellar phase in diblock copolymers (158). Also an investigation of blends composed of SI diblock copolymers with various molecular weights and

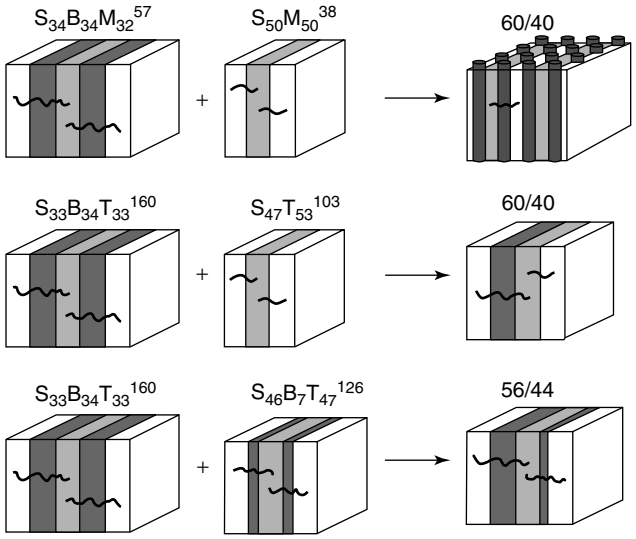

Fig. 30. Scheme of blends of various lamellar ABC and AC block copolymers forming the "cylinder at lamellar interface" and "noncentrosymmetric lamellae." Weight ratios of the blends are indicated in the figure (OsO_4, see Table 1).

various compositions showed a significant shift of the stability regions of different morphologies (159), which could be explained by a change of the interfacial curvature of the large block copolymer by swelling with the small diblock copolymer (160). In comparison, blending of ABC triblock copolymers with other block copolymers (ABC, AC) turned out to generate also new morphologies with symmetries not accessible in pure ABC or AC systems.

An idea proposed for periodic noncentrosymmetric layers in order to obtain longitudinal ferroelectric smectics was to use a structural sequence of α–β–γ–α (161). While ABC triblock copolymers self-assemble in a centrosymmetric way, ie, $\cdots$ABC CBA ABC$\cdots$, the idea of Reimund Stadler was to blend lamellar ABC with AC block copolymers to get a structure with the sequence $\cdots$ABC CA ABC$\cdots$, which is noncentrosymmetric (76,162,163). The initial attempts toward such a morphology were carried out on lamellar SBM and SM block copolymers (163). However, no composition and no molecular weights of components of such blends were found where the desired morphology was formed. Either macrophase separation between the pure triblock and diblock copolymers occurred for large molecular weights ($M_{SBM} \approx 150$ kg/mol, $M_{SM} \approx 100$ kg/mol) or a centrosymmetric superlattice was formed, where the B blocks were located in cylinders in a lamellar matrix of S and M (like lc-morphology) (Fig. 30).

From that result it was concluded that the repulsive interaction between the two outer blocks need to be increased, in order to force the system to suppress direct interfaces between the two outer blocks of the triblock copolymer. In the blend the effective volume fraction of the middle block is decreased by the swelling of the two outer blocks of the triblock copolymer by the corresponding blocks of the diblock copolymer. Thus a system is required where all three components form

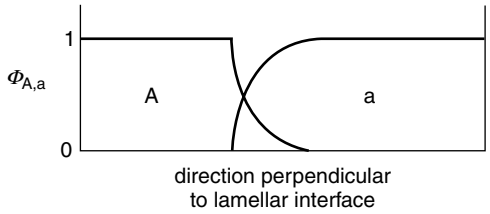

Fig. 31. Concentration profile of asymmetric interpenetration in a mixed lamella of A and a blocks from ABC and ac block copolymers.

lamellae, even for small volume fractions of the middle block. This is true for SBT. The blend of an SBT and ST block copolymer in fact formed the desired periodic noncentrosymmetric lamellar superlattice (Fig. 30) (76,162,163).

The driving force for the formation of such an arrangement has been discussed (164), and it was shown that the different stretching of the S and T blocks of the two block copolymers should be the reason for the formation of mixed domains for the two types of S and T blocks, respectively. The more stretched chains of the diblock copolymer can reduce their stretching when mixing with the corresponding less stretched chains of the triblock copolymer. This different degrees of stretching lead to an asymmetric concentration profile of A blocks coming from a diblock copolymer (a) and a triblock copolymer (A) (Fig. 31).

The best condition for ABC and ac block copolymers with $N_A = N_C = N_{ABC}$ and $N_a = N_c = N_{ac}$ to form a periodic noncentrosymmetric lamellar superlattice was found (164) to be

$$\left(\frac{X_{ac}}{X_{ABC}}\right)^3 = \frac{2N_{ac}^4}{N_{ABC}^3\,(N_{ABC} + N_B/\kappa)}\,\frac{\gamma_{ac}}{\gamma_{ABC}} \tag{22}$$

with $X = N\Sigma a/v$ (N is the degree of polymerization of the block, Σ is the interfacial area per chain, a is the segmental length, v is the monomeric volume, κ is a coefficient of the elastic energy in the order of unity, and $\gamma_{AB} = \gamma_{BC} = \gamma_{ABC}$). For a symmetric triblock copolymer ($N_B = N_{ABC}$) the best conditions for the formation of alternating triblock and diblock lamellae (periodic noncentrosymmetric lamellae) is with $X_{ac} = X_{ABC}$:

$$\frac{N_{ABC}}{N_{ac}} = \left(\frac{\gamma_{ac}}{\gamma_{ABC}}\right)^{1/4} \tag{23}$$

It is difficult to compare this formula quantitatively with the experimental results because the values of the interfacial tensions are not known to a high level of certainty. The solubility parameter of T reported in literature does not differ very much from B (Table 2). This would indicate a vanishing surface tension betwen B and T in the SBT triblock copolymer but is in contradiction with the microphase separation experimentally found in BT diblock copolymers.

The energy reduction of the diblock chains is higher than the increase of elastic energy of the triblock chains, leading to an overall reduction of the free

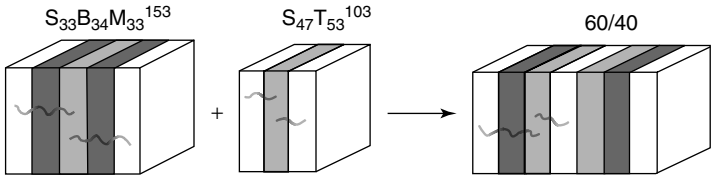

Fig. 32. Scheme of a blend of SBM and ST in a weight fraction of 60/40 forming periodic double lamellae (OsO_4, see Table 1).

energy of the system. Following this idea, a periodic noncentrosymmetric lamellar structure could also be generated when blending two SBT triblock copolymers with very different sizes of the middle blocks but similar lengths of the outer blocks (Fig. 30) (76). The different length of the middle block leads to different interfacial areas between the middle block and the outer blocks. As a result, the degree of chain stretching of the outer blocks is different in a similar way as discussed for the blend of SBT with ST. The noncentrosymmetric blend of two SBT triblock copolymers offers the possibility to introduce different functionalities into the two different B domains via chemical modifications of the two SBT triblock copolymers prior to their mixing.

While noncentrosymmetric superstructures can be obtained in blends of ABC and AC under favorable conditions, it may be expected that centrosymmetric double lamellar superstructures can be obtained in blends of ABC with AD, where D is incompatible with all other blocks. Such a structure is shown in Figure 32 and was obtained for a blend of lamellar SBM and ST block copolymers, while a corresponding blend of SBT with SM macrophase-separated (139). A similar structure was found for a blend of a lamellae-forming SBT triblock copolymer with a symmetric poly(2-vinylpyridine)-*block*-poly(cyclohexyl methacrylate) (VC) diblock copolymer, in which S and C form a mixed lamellar domain because of attractive interactions (165).

Blending of two SBM triblock copolymers which are also different in their middle block molecular weights (one forms the ll-morphology and the other forms the lc-morphology) leads to the kp-morphology (Fig. 33) (76,166). This again is an example that blending of block copolymers may lead to morphologies which are not observed for one of the pure components at any composition. Note that the kp-morphology was only observed for certain SEBM triblock copolymers, but it was never found in the non-hydrogenated SBM triblock copolymers (167). While there are indications that the kp-morphology is only metastable for SBM triblock copolymers, this is still an open question for the block copolymer blend (166).

Another type of block copolymer blends consisted of ABC and BC block copolymers. Here a situation can be imagined where the BC diblock chains align parallel to the BC blocks of the triblock chains, which leads to an increase of the effective volume fractions of B and C with respect to A. Blending of lamellar SBM with BM block copolymers of similar block sizes leads to core–shell morphologies. Depending on the blend ratio core–shell cylinders or core–shell double gyroid morphologies can be obtained, with S forming the core domains (76,168). Also coexistence of the different morphologies can be observed (see Table 2 of Ref. 168). For

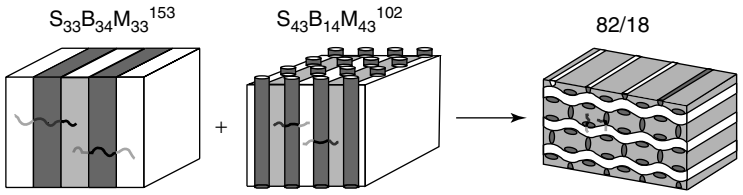

Fig. 33. Schemes two SBM triblock copolymers forming the kp-morphology in a blend with weight fractions of 82/18 (OsO_4, see Table 1).

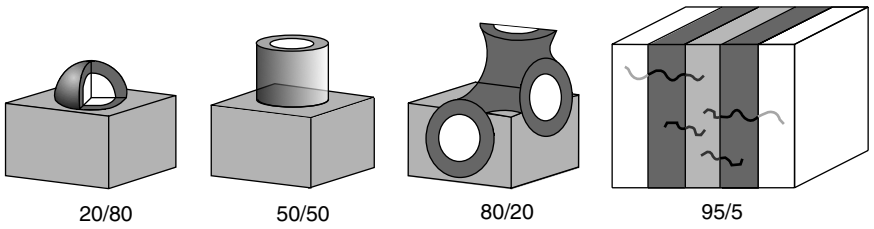

Fig. 34. Schemes of the core–shell analogues of diblock copolymer morphologies in a blend of $S_{33}B_{34}T_{33}^{160}$ and $S_{69}B_{31}^{71}$ block copolymers, with increasing weight fraction of the triblock copolymer from left to right (OsO_4, see Table 1).

comparison, blends of symmetric $S_{33}B_{34}M_{33}^{153}$ with symmetric $S_{49}B_{51}^{87}$ block copolymers show macrophase separation (76). Reducing the molecular weight of B of the SB diblock copolymer again leads to miscible blends of $S_{33}B_{34}M_{33}^{153}$ and $S_{69}B_{31}^{71}$. Depending on the blend ratio, either a morphology with S cylinders surrounded by four B cylinders in an M matrix (50/50, c_ac-morphology; see Figs. 3 and 16: there the locations of S and M are reversed) or an lc-morphology is observed for smaller amounts of diblock copolymer (80/20) (76).

With increasing amount of triblock copolymer, blends of lamellar SBT triblock copolymers with the asymmetric SB diblock copolymer form core–shell spheres, core–shell cylinders, core–shell double gyroids, and lamellae (Fig. 34). T forms the core domains in these morphologies, which can be considered as core–shell analogues of the well-known diblock copolymer morphologies (76).

In the blends of triblock and diblock copolymers presented so far only lamellae-forming triblock copolymers were used. Thus, the blend morphologies showed an increasing curvature of the interfaces with increasing amount of diblock copolymer (from lamellae toward core–shell spheres). As discussed before, the symmetrically composed $B_{32}S_{35}M_{33}^{196}$ triblock copolymer forms a core–shell double-gyroid morphology with B cores as a result of the asymmetric interactions between the middle and the two outer blocks. Adding a symmetric $S_{49}B_{51}^{87}$ diblock copolymer of comparable block lengths reverses the interfacial curvature: depending on the relative composition, lamellae or the inverted core–shell double gyroid morphology with M cores and S shells are formed (76) (Fig. 35).

Thus, blends of SBM with BM and BSM with SB (all blocks being of comparable size) form mixed superstructures, while the blend of SBM with SB macrophase-separates. The formation of mixed lamellar superstructures of ABC and AB block

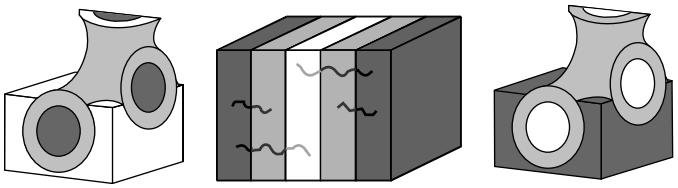

Fig. 35. Schemes of blends of $B_{32}S_{35}M_{33}$[196] with $S_{49}B_{51}$[87] with increasing weight fraction of SB from left to right (OsO_4, see Table 1).

copolymers in the SSL has been investigated (169,170). The chemical potential of the diblock copolymer in the mixed superstructure and in the pure state was compared in order to determine an approximate critical molar fraction of the triblock copolymer, q^*_{appr}, below which further diblock copolymers cannot be incorporated into the triblock copolymer domains. For the case where the A and B blocks of the diblock copolymer are shorter than the corresponding blocks of the triblock copolymer ($N_a < N_A$, $N_b < N_B$), the following critical composition is obtained:

$$q^*_{appr} = \left(\frac{\gamma_{BC}}{\gamma_{AB}} \frac{Y_a + Y_b}{Y_A + Y_B + Y_C - Y_a - Y_b} \right)^{1/3} \tag{24}$$

with $Y = Nv^{5/3}/a$ [N is the degree of polymerization of the block, v is the monomer volume, and a is the segmental length (Kuhn length)]. The critical composition becomes larger when the block lengths of the diblock and triblock copolymers are similar; ie, the incorporation of diblock copolymer chains becomes less favorable, which is in qualitative agreement with the experimental results:

$$q^*_{appr} = \left(\frac{\gamma_{BC}}{\gamma_{AB}} \frac{Y_A + Y_B}{Y_C} \right)^{1/3} \tag{25}$$

where $Y_A = Y_a$ and $Y_B = Y_b$.

Thus, the incorporation of diblock chains into triblock lamellae is favorable for a system with similar block lengths under the condition that the interfacial tension within the AB diblock copolymer is larger than the interfacial tension of the BC interface in the ABC triblock copolymer:

$$\frac{\gamma_{AB}}{\gamma_{BC}} > 1 \tag{26}$$

Other mixed superstructures were not considered in detail, but it is obvious that they may become stable with respect to mixed lamellae or macrophase separation at blend compositions with even larger amounts of the diblock copolymer.

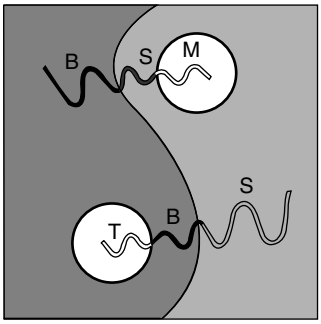

Fig. 36. Scheme of the tetracontinuous gyroid morphology in a blend of $B_{32}S_{35}M_{33}{}^{196}$ and $S_{33}B_{34}T_{33}{}^{160}$ at a ratio of the weight fractions of 50/50 (OsO_4, see Table 1). From Ref. 76. Copyright (2000) Wiley-VCH Verlag GmbH.

The concept of parallel alignment of the diblock copolymer chains with the corresponding blocks of the triblock copolymer was also extended to blends of two triblock copolymers. In a blend of $B_{32}S_{35}M_{33}{}^{196}$ and $S_{33}B_{34}T_{33}{}^{160}$ with comparable lengths of all blocks, a sequence of domains such as $\cdots$MSBTBSM$\cdots$ can be expected. In fact, such sequence is observed besides domains containing the pure components. Both S and B form a single gyroid interface dividing half of the unit cell (Fig. 36) (76) which was not observed in any system before. Both M and T form core gyroids in the S and B shells, respectively (76). In comparison to the tricontinuous double gyroid morphology of two components in diblock copolymers and the pentacontinuous core–shell double gyroid morphology of three components in triblock copolymers or block copolymer blends, this morphology shows a tetracontinuous gyroid morphology of four components. These cocontinuous morphologies have recently attracted stronger interest as possible candidates for membrane materials or for photonic applications (16).

The preparation of blends of microphase-separated block copolymers, which self-assemble in common superstructures, is easier as compared to mixed homopolymer or random copolymer blends. The latter often macrophase-separate during processing (for example during evaporation of a common solvent). This is due to a selectivity of the solvent–polymer interactions in favor of one of the blend components. This problem is present to a much lesser extent in blends of block copolymers where at least one of the blocks is chemically similar in both block copolymers and thus the selectivity problem in many cases is less important. In some cases, however, macrophase separation is observed at intermediate length scales. Systems where the incompatibility between SI and S(I-*stat*-EP) diblock copolymers was adjusted by the degree of hydrogenation of the latter one have been reported (171). Different structures were observed depending on whether first microphase separation between S and I or I-*stat*-EP, or the macrophase separation between the different elastomeric components, occurred leading to so-called macrophase separation within microphase separation. Blends of lamellar SBM (ll- or lc-morphology) with the analogous SEBM triblock copolymers both show a macrophase separation, where the S and M lamellae are continuous across both block copolymer domains, but the B and EB domains are well separated from each

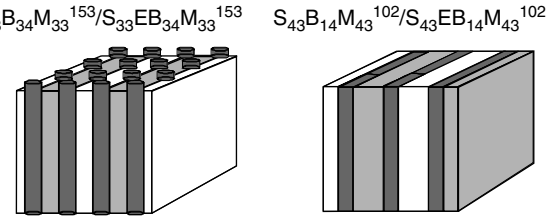

Fig. 37. Macrophase separation in blends of morphologically similar SBM and SEBM triblock copolymers: macrophase separation of cylindrical (left) and lamellar middle block domains (right) (OsO_4, see Table 1).

other (Fig. 37) (76). The control of macrophase separation in such block copolymer blends is thus a further way to design morphologies in these materials.

BIBLIOGRAPHY

1. G. Ebert, in C. Elschenbroich, F. Hensel, and H. Hopf, eds., *Biopolymere*, Teubner Studienbücher Chemie, B. G. Teubner, Stuttgart, Germany, 1993.
2. F. Vögtle, in C. Elschenbroich, F. Hensel, and H. Hopf, eds., *Supramolekulare Chemie*, Teubner Studienbücher Chemie, B. G. Teubner, Stuttgart, Germany, 1989.
3. J.-M. Lehn, *Supramolecular Chemistry—Concepts and Perspectives*, VCH, Weinheim, 1995.
4. A. Ciferri, ed., *Supramolecular Polymers*, Marcel Dekker, Inc., New York, 2000.
5. C. Tschierske, *Annu. Rep. Prog. Chem., Sect. C* **97**, 191 (2001).
6. L. A. Utracki, *Polymer Alloys and Blends*, Hanser, Munich, 1989.
7. G. Beaucage, R. S. Stein, and R. Koningsveld, *Macromolecules* **26**, 1603 (1993).
8. K. Binder, *Adv. Polym. Sci.* **112**, 181 (1994).
9. N. R. Legge, G. Holden, and H. E. Schroeder, eds., *Thermoplastic Elastomers*, Hanser, New York, 1987.
10. C. Auschra, R. Stadler, and I. Voigt-Martin, *Polymer* **34**, 2094 (1993).
11. C. Auschra and R. Stadler, *Macromolecules* **26**, 6364 (1993).
12. M. J. Folkes, ed., *Processing, Structure and Properties of Block Copolymers*, Elsevier, New York, 1985.
13. V. M. Nace, ed., *Nonionic Surfactants: Polyoxyalkylene Block Copolymers*, Marcel Dekker, Inc., New York, 1996.
14. Y. Heischkel and H.-W. Schmidt, *Macromol. Chem. Phys.* **199**, 869 (1998).
15. Y. Fink and co-workers, *IEEE J. Lightwave Technol.* **17**, 1963 (1999).
16. E. L. Thomas, *Science* **286**, 1307 (1999).
17. M. Templin and co-workers, *Science* **278**, 1795 (1997).
18. E. Krämer and co-workers, *Langmuir* **14**, 2027 (1998).
19. J. P. Spatz, A. Roescher, and M. Möller, *Adv. Mater.* **8**, 337 (1996).
20. L. Luo and A. Eisenberg, *J. Am. Chem. Soc.* **123**, 1012 (2001).
21. R. J. Spontak and N. P. Patel, *Curr. Opin. Colloid Interf. Sci.* **5**, 334 (2000).
22. H. Schmalz and co-workers, *Macromolecules* **34**, 795 (2001).
23. G. Riess, G. Hurtrez, and P. Bahadur, in J. I. Kroschwitz, ed., *Encyclopedia of Polymer Science and Engineering*, Vol. **2**, Wiley-Interscience, New York, 1985, p. 324.
24. M. Szwarc, *J. Polym. Sci., Polym. Chem.* **36**, IX (1998).
25. C. Auschra and R. Stadler, *Polym. Bull.* **30**, 257 (1993).

26. C. Neumann, V. Abetz, and R. Stadler, *Polym. Bull.* **36**, 43 (1996).
27. N. Mougin, P. Rempp, and Y. Gnanou, *Makromol. Chem.* **194**, 2553 (1993).
28. Y. C. Bae, and R. Faust, *Macromolecules* **31**, 2480 (1998).
29. D. A. Shipp, J.-L. Wang, and K. Matyjaszewski, *Macromolecules* **31**, 8005 (1998).
30. K. A. Davis and K. Matyjaszewski, *Macromolecules* **34**, 2101 (2001).
31. E. Yoshida and A. Sugita, *J. Polym. Sci., Polym. Chem.* **36**, 2059 (1998).
32. E. Ruckenstein and H. Zhang, *Macromolecules* **31**, 2977 (1998).
33. J. Feldthusen, B. Iván, and A. H. E. Müller, *Macromolecules* **31**, 578, (1998).
34. K. Loos and R. Stadler, *Macromolecules* **30**, 7641 (1997).
35. N. Hadjichristidis, *J. Polym. Sci., Part A: Polym. Chem.* **37**, 857 (1999).
36. T. Fujimoto and co-workers, *Polymer* **33**, 2208 (1992).
37. G. Floudas and co-workers, *Macromolecules* **31**, 7279 (1998).
38. V. Balsamo, F. von Gyldenfeldt, and R. Stadler, *Macromolecules* **32**, 1226 (1999).
39. C. Park and co-workers, *Macromolecules* **33**, 7931 (2000).
40. H. Schmalz and co-workers, *Polym. Mater. Sci. Eng.* **85**, 478 (2001).
41. H. Schmalz and co-workers, *Macromolecules* **34**, 8720 (2001).
42. M. L. Arnal and co-workers, *Macomolecules* **34**, 7973 (2001).
43. J. Adams and W. Gronski, *Makromol. Chem., Rapid Commun.* **10**, 553 (1989).
44. G. Mao and co-workers, *Macromolecules* **30**, 2556 (1997).
45. M. Shibayama, T. Hashimoto, and H. Kawai, *Macromolecules* **16**, 16 (1983).
46. K. Yu and A. Eisenberg, *Macromolecules* **29**, 6359 (1996).
47. K. Yu, L. Zhang, and A. Eisenberg, *Langmuir* **12**, 5980 (1996).
48. G.-E. Yu and A. Eisenberg, *Macromolecules* **31**, 5546 (1998).
49. R. Bieringer, V. Abetz, and A. H. E. Müller, *EPJE* **5**, 5 2001.
50. R. Erhardt and co-workers, *Macromolecules* **34**, 1069 (2001).
51. K. Yu, and A. Eisenberg, *Macromolecules* **31**, 3509 (1998).
52. P. Alexandridis, U. Olsson, and B. Lindman, *Langmuir* **13**, 23 (1997).
53. I. W. Hamley, *Curr. Opin. Colloid Interface Sci.* **5**, 342 (2000).
54. R. J. Albalak and E. L. Thomas, *J. Polym. Sci., Polym. Phys. Ed.* **31**, 37 (1993).
55. C. C. Honeker and E. L. Thomas, *Chem. Mater.* **8**, 1702 (1996).
56. S. Brinkmann and co-workers, *Kautsch. Gummi Kunstst.* **52**, 806 (1999).
57. J. Sänger and co-workers, *Macromolecules* **30**, 7621 (1997).
58. M. E. Vigild and co-workers, *Macromolecules* **34**, 951 (2001).
59. U. Wiesner, *Macromol. Chem. Phys.* **198**, 3319 (1997).
60. Z.-R. Chen and J. A. Kornfield, *Polymer* **39**, 4679 (1998).
61. Z.-R. Chen and co-workers, *Macromolecules* **30**, 7096 (1997).
62. H. Leist, K. Geiger, and U. Wiesner, *Macromolecules* **32**, 1315 (1999).
63. J. Le Meur and co-workers, *J. Phys., Colloq.* **32**, C5a-301 (1971).
64. K. Amundson and co-workers, *Macromolecules* **26**, 2698 (1993).
65. P. Mansky and co-workers, *Macromolecules* **31**, 4399 (1998).
66. T. Thurn-Albrecht and co-workers, *Adv. Mater.* **12**, 787 (2000).
67. A. Böker and co-workers, *Macromolecules* **35**, 1319 (2002).
68. C. De Rosa and co-workers, *Nature* **405**, 433 (2000).
69. F. Annighöfer, and W. Gronski, *Makromol. Chem., Rapid Commun.* **4**, 123 (1983).
70. K. Fukunaga and co-workers, *Macromolecules* **33**, 947 (2000).
71. F. S. Bates and G. H. Fredrickson, *Annu. Rev. Phys. Chem.* **41**, 525 (1990).
72. G. H. Fredrickson and F. S. Bates, *Annu. Rev. Mater. Sci.* **26**, 501 (1996).
73. I. W. Hamley, *The Physics of Block Copolymers*, Oxford University Press, Oxford, 1998.

74. L. Leibler, *Macromolecules* **13**, 1602 (1980).
75. A. N. Semenov, *Sov. Phys. JETP* **61**, 733 (1985).
76. V. Abetz, and T. Goldacker, *Macromol. Rapid Commun.* **21**, 16 (2000).
77. S. L. Flegler, J. W. Heckman, and L. L. Klomparens, *Elektronenmikroskopie: Grundlagen, Methoden, Anwendunge*, Spektrum Akademischer Verlag, Heidelberg, Germany, 1995.
78. E. L. Thomas, in J. I. Kroschwitz, ed., *Encyclopedia of Polymer Science and Engineering*, 2nd ed., Vol. **5**, Wiley-Interscience, New York, 1996.
79. S. N. Magonov and D. H. Reneker, *Annu. Rev. Mater. Sci.* **27**, 175 (1997).
80. O. Glatter and O. Kratky, *Small Angle X-ray Scattering*, Academic Press, New York, 1981.
81. R.-J. Roe, in J. I. Kroschwitz, ed., *Encyclopedia of Polymer Science and Engineering*, 2nd ed., Vol. **17**, Wiley-Interscience, New York, 1989.
82. J. S. Higgins and H. C. Benoît, *Polymers and Neutron Scattering*, Clarendon Press, Oxford, 1994.
83. M. W. Matsen and F. S. Bates, *Macromolecules* **29**, 1091 (1996).
84. M. W. Matsen and M. Schick, *Macromolecules* **27**, 4014 (1994).
85. L. Leibler, *Makromol. Chem., Macromol. Symp.* **16**, 1 (1988).
86. E. Helfand and Z. R. Wasserman, *Macromolecules* **9**, 879 (1976).
87. H. Frielinghaus and co-workers, *Macromolecules* **34**, 1096 (2001).
88. I. Ya. *Erukhimovich, Polym. Sci. U.S.S.R.* **24**, 2223 (1982).
89. I. Ya. *Erukhimovich, Polym. Sci. U.S.S.R.* **24**, 2232 (1982).
90. G. H. Fredrickson, and E. Helfand, *J. Chem. Phys.* **87**, 697 (1987).
91. F. S. Bates, J. H. Rosedale, and G. H. Fredrickson, *J. Chem. Phys.* **92**, 6255 (1990).
92. M. W. Matsen and F. S. Bates, *J. Chem. Phys.* **106**, 2436 (1997).
93. I. Ya. Erukhimovich, *JETP Lett.* **63**, 460 (1996).
94. S. T. Milner and P. T. Olmsted, *J. Phys. II* **7**, 249 (1997).
95. K. Grosse-Brauckmann, *J. Colloid Interface Sci.* **187**, 418 (1997).
96. W. Gozdz and R. Holyst, *Macromol. Theory Simul.* **5**, 321 (1996).
97. M. W. Matsen and M. Schick, *Phys. Rev. Lett.* **72**, 2660 (1994).
98. A. M. Mayes and M. Olvera de la Cruz. *J. Chem. Phys.* **91**, 7228 (1989).
99. A. V. Dobrynin and I. Ya. Erukhimovich, *Vysokomol. Soedin.* **32B**, 663 (1990).
100. A. V. Dobrynin and I. Ya. Erukhimovich, *Macromolecules* **26**, 276 (1993).
101. M. W. Matsen and M. Schick, *Macromolecules* **27**, 7157 (1994).
102. M. W. Matsen and M. Schick, *Macromolecules* **27**, 6761 (1994).
103. M. Olvera de la Cruz and I. C. Sanchez, *Macromolecules* **19**, 2501 (1986).
104. M. W. Matsen and M. Schick, *Macromolecules* **27**, 6761 (1994).
105. V. Grayer and co-workers, *Macromolecules* **33**, 6330 (2000).
106. F. S. Bates and G. H. Frederickson, *Phys. Today* **52**, 32 (1999).
107. M. W. Matsen, *J. Chem. Phys.* **108**, 785 (1998).
108. T. A. Shefelbine and co-workers, *J. Am. Chem. Soc.* **121**, 8457 (1999).
109. R. Stadler and co-workers, *Macromolecules* **28**, 3080 (1995).
110. U. Breiner, U. Krappe, and R. Stadler, *Macromol. Rapid Commun.* **17**, 567 (1996).
111. U. Breiner and co-workers, *Macromol. Chem. Phys.* **198**, 1051 (1997).
112. K. Jung, V. Abetz, and R. Stadler, *Macromolecules* **29**, 1076 (1996).
113. U. Breiner and co-workers, *Polym. Bull.* **40**, 219 (1998).
114. L. Kane and R. J. Spontak, *Macromolecules* **27**, 663 (1994).
115. Yu. V. Lyatskaya, and T. M. Birshtein, *Polymer* **36**, 975 (1995).
116. S. Phan and G. H. Fredrickson, *Macromolecules* **31**, 59, (1998).
117. W. Zheng and Z.-G. Wang, *Macromolecules* **28**, 7215 (1995).

118. V. Abetz, R. Stadler, and L. Leibler, *Polym. Bull.* **37**, 135 (1996).
119. I. Erukhimovich, V. Abetz, and R. Stadler, *Macromolecules* **30**, 7435 (1997).
120. S. Pispas, G. Floudas, and N. Hadjichristidis, *Macromolecules* **32**, 9074 (1999).
121. K. Binder, in A. Abe and co-workers, eds., *Advances in Polymer Science*, Vol. **112**, Springer-Verlag, Berlin, 1994.
122. F. Drolet and G. H. Fredrickson, *Phys. Rev. Lett.* **83**, 4317 (1999).
123. Y. Bohbot-Raviv and Z.-G. Wang, *Phys. Rev. Lett.* **85**, 3428 (2000).
124. Y. Mogi and co-workers, *Macromolecules* **27**, 6755 (1994).
125. G. Riess, M. Schlienger, and S. Marti, *J. Macromol. Sci. Part B* **17**, 355 (1980).
126. Y. Isono and co-workers, *Macromolecules* **16**, 5 (1983).
127. C. Auschra and R. Stadler, *Macromolecules* **26**, 2171 (1993).
128. C. Auschra, J. Beckmann, and R. Stadler, *Macromol. Rapid Commun.* **15**, 67 (1994).
129. U. Krappe, R. Stadler, and I.-G. Voigt-Martin, *Macromolecules* **28**, 4458 (1995).
130. S. Brinkmann, R. Stadler, and E. L. Thomas, *Macromolecules* **31**, 6566 (1998).
131. Y. Matsushita and co-workers, *Macromolecules* **16**, 10 (1983).
132. S. Okamoto and co-workers, *Polymer* **38**, 5275 (1997).
133. S. Sioula, N. Hadjichristidis, and E. L. Thomas, *Macromolecules* **31**, 5272 (1998).
134. S. Sioula, N. Hadjichristidis, and E. L. Thomas, *Macromolecules* **31**, 8429 (1998).
135. H. Hückstädt, A. Göpfert, and V. Abetz, *Macromol. Chem. Phys.* **201**, 296 (2000).
136. H. Hückstädt and co-workers, *Macromolecules* **33**, 3757 (2000).
137. S. P. Gido and co-workers, *Macromolecules* **26**, 2636 (1993).
138. H. Hückstädt, A. Göpfert, and V. Abetz, *Polymer* **41**, 9089 (2000).
139. T. Goldacker, *Doctoral Thesis, Bayreuth*, 1999.
140. A. F. Barton, *CRC Handbook of Polymer Liquid Interaction Parameters and Solubility Parameters*, CRC Press, Boca Raton, Fla., 1990.
141. J. Brandrup and E. H. Immergut, *Polymer Handbook*, 3rd ed., Wiley, New York, 1989.
142. R. L. Lescanec, L. J. Fetters, and E. L. Thomas, *Macromolecules* **31**, 1680 (1998).
143. R. Krishnamoorti and co-workers, *Macromolecules* **27**, 3073 (1994).
144. V. Abetz, Ternäre Triblockcopolymere mit sternförmiger Topologie, in *AiF Forschungsberichte 1998*, 1998 p. 222.
145. U. Breiner, *Doctoral Thesis, Universität Mainz*, 1996.
146. H. Ott, V. Abetz, and V. Altstädt, *Macromolecules* **34**, 2121 (2001).
147. V. Abetz, K. Markgraf, and V. Rebizant, *Macromol. Symp.* **177**, 139 (2002).
148. L. Bronstein and co-workers, *Polym. Bull.* **39**, 361 (1997).
149. J. H. Rosedale and co-workers, *Macromolecules* **28**, 1429 (1995).
150. C. M. Roland and C. A. Trask, *Macromolecules* **22**, 256 (1989).
151. C. Neumann, V. Abetz, and R. Stadler, *Colloid Polym. Sci.* **276**, 19 (1998).
152. C. D. Han, D. M. Baek, and J. K. Kim, *Macromolecules* **23**, 561 (1990).
153. C. Neumann and co-workers, *Macromolecules* **31**, 2493 (1998).
154. T. A. Witten, L. Leibler, and P. A. Pincus, *Macromolecules* **23**, 824 (1990).
155. G. Hadziioannou and A. Skoulios, *Macromolecules* **15**, 267 (1982).
156. M. F. Schulz and co-workers, *Phys. Rev. Lett.* **73**, 86 (1994).
157. K. I. Winey, E. L. Thomas, and L. J. Fetters, *Macromolecules* **25**, 422 (1992).
158. G. Kraus, L. M. Fodor, and K. W. Rollman, *Adv. Chem. Ser.* **176**, 227 (1979).
159. F. Court and T. Hashimoto, *Macromolecules* **34**, 2536 (2001).
160. A.-C. Shi and J. Noolandi, *Macromolecules* **28**, 3103 (1995).
161. R. G. Petschek and K. M. Wiefling, *Phys. Rev. Lett.* **59**, 343 (1987).
162. T. Goldacker and co-workers, *Nature* **398**, 137 (1999).
163. T. Goldacker, V. Abetz, and R. Stadler, *Macromol. Symp.* **149**, 93 (2000).
164. L. Leibler, C. Gay, and I. Ya. Erukhimovich, *Europhys. Lett.* **46**, 549 (1999).

165. K. Markgraf and V. Abetz, www.e-Polymers.org 15 (2001).
166. T. Goldacker and V. Abetz, *Macromol. Rapid Commun.* **20**, 415 (1999).
167. H. Ott, V. Abetz, and V. Altstädt, *Macromolecules* **34**, 2121 (2001).
168. T. Goldacker and V. Abetz, *Macromolecules* **32**, 5165 (1999).
169. T. M. Birshtein and co-workers, *Macromol. Theory Simul.* **8**, 151 (1999).
170. T. M. Birshtein, A. Polotsky, and V. Abetz, *Macromol. Theory Simul.* **10**, 700 (2001).
171. K. Kimishima, H. Jinnai, and T. Hashimoto, *Macromolecules* **32**, 2585 (1999).

VOLKER ABETZ
Universität Bayreuth

BLOWING AGENTS. See CELLULAR MATERIALS.

BLOCK COPOLYMERS

Introduction

Block copolymers are useful in many applications where a number of different polymers are connected together to yield a material with hybrid properties. For example, thermoplastic elastomers are block copolymers containing a rubbery matrix (polybutadiene or polyisoprene) containing glassy hard domains (often polystyrene). The block copolymer, a kind of polymer alloy, behaves as a rubber at ambient conditions, but can be molded at high temperatures because of the presence of the glassy domains that act as physical cross-links. In solution, attachment of a water-soluble polymer to an insoluble polymer leads to the formation of micelles in amphiphilic block copolymers. The presence of micelles leads to structural and flow characteristics of the polymer in solution, that differ from either parent polymer.

A block copolymer molecule contains two or more polymer chains attached at their ends. Linear block copolymers comprise two or more polymer chains in sequence, whereas a starblock copolymer comprises more than two linear block copolymers attached at a common branch point. Polymers containing at least three homopolymers attached at a common branching point have been termed *mixed arm block copolymers*, although they can also be viewed as multigraft copolymers (see GRAFT COPOLYMERS).

In this article, block copolymers prepared by controlled polymerization methods only are considered, primarily di- and triblock copolymers. Multiblock copolymers such as poly(urethanes) and poly(urethane-ureas) prepared by condensation polymerization are not discussed (see POLYURETHANES (PUR)). Although these materials do exhibit microphase separation, it is only short range in spatial extent due to the high polydispersity of the polymers.

Encyclopedia of Polymer Science and Technology. Copyright John Wiley & Sons, Inc. All rights reserved.

A standard notation for block copolymers is becoming accepted, whereby X-*b*-Y denotes a diblock copolymer of polymer X and polymer Y. However, sometimes the *b* is replaced by the full term *block*, or alternatively is omitted, and the diblock denoted X–Y.

A number of texts covering general aspects of block copolymer science and engineering have appeared in the last 30 years eg, References 1 and 2. More recently specialized reviews have appeared on block copolymer melts and block copolymer solutions, and these are cited in appropriate following sections. The burgeoning interest in block copolymers is illustrated by contributions covering various aspects of the subject in a review journal (3) and in an edited book (4).

Since the last edition of the Encyclopedia there have been many advances in the field of block copolymer science and engineering, including new synthesis methods, developments in the understanding of phase behavior, and the investigation of structure and dynamics in thin films. Many of these advances are likely to lead soon to novel applications.

Synthesis

The main techniques for synthesis of block copolymers in research laboratories around the world are presently anionic polymerization and living polymerization, cationic and radical. The older technique of anionic polymerization is still used widely in the industrial manufacture of block copolymers. Cationic polymerization may be used to polymerize monomers that cannot be polymerized anionically, although it is used for only a limited range of monomers. A summary of block copolymer synthesis techniques has been provided (5).

Anionic Polymerization. Anionic polymerization (qv) is a well-established method for the synthesis of tailored block copolymers. The first anionic polymerizations of block copolymers were conducted as early as 1956 (6). To prepare well-defined polymers, the technique is demanding, requiring high purity starting reagents and the use of high vacuum procedures to prevent accidental termination due to the presence of impurities. In the laboratory, it is possible to achieve polydispersities $M_w/M_n < 1.05$ via anionic polymerization. However, the method is also used industrially to prepare several important classes of block copolymers including SBS-type thermoplastic elastomers (S = polystyrene, B = polybutadiene) and polyoxyethylene-*b*-polyoxypropylene-*b*-polyoxyethylene Pluronic amphiphilic copolymers (4). There are a number of reviews that cover the application of anionic polymerization to block copolymers (7–11). Recent advances have mainly been directed toward the synthesis of block copolymers with exotic architectures, such as mixed arm stars (12–14), H-shaped copolymers (12), and ring-shaped (cyclic) block copolymers (15). All of these require the careful choice of multifunctional initiators (see BLOCK COPOLYMERS, TERNARY TRIBLOCKS; DENDRONIZED POLYMERS; HYPERBRANCHED POLYMERS).

Living Radical Polymerization. Undoubtedly the main advance in block copolymer synthesis in the last decade has been the development of techniques of living radical polymerization (sometimes termed controlled radical polymerization). The principle of controlled radical polymerization methods is to establish a dynamic equilibrium between a small fraction of growing free radicals and a

large majority of dormant species. Generated free radicals propagate and terminate as in conventional radical polymerization, although the presence of only a small fraction of radicals prevents premature termination. Among living polymerization methods, atom transfer radical polymerization (ATRP) has been used most extensively to synthesize block copolymers. Here, the radicals are generated through a reversible redox process catalyzed by a transition-metal complex that undergoes a one-electron oxidation with the abstraction of a halogen atom from the dormant species. The ATRP method, and its application to the synthesis of block copolymers, has recently been reviewed (16).

ATRP has been used to prepare AB diblock, ABA triblock, and most recently ABC triblock copolymers (17). To date, the technique has been used to create block copolymers based on polystyrene and various polyacrylates (16). However, it is possible to synthesize a so-called macroinitiator by other polymerization mechanisms (anionic, cationic, etc), and use this in the ATRP of vinyl monomers. Examples, such as the anionic polymerization of PEO macroinitiators for ATRP synthesis of polyethylene oxide/polystyrene block copolymers, are discussed in Reference 16.

Other Methods. Sequential living cationic polymerization is primarily used to prepare block copolymers containing a vinyl ether block, or polyisobutylene (18–20). It can also be coupled with other techniques (18,20). However the range of monomers that may be polymerized by this method is comparatively limited and consequently living cationic polymerization is only used in prescribed circumstances.

Ring-opening metathesis polymerization has also been exploited to build blocks from cyclic olefins, especially polynorbornene (5). The development of ring-opening metathesis polymerization for block copolymer synthesis has recently been facilitated by the introduction of functional group tolerant metathesis catalysts (21).

Block Copolymer Melts

The interest in the phase behavior of block copolymer melts stems from microphase separation of polymers that leads to nanoscale-ordered morphologies. This subject has been reviewed extensively (1,22–24). The identification of the structure of bicontinuous phases has only recently been confirmed, and this, together with major advances in the theoretical understanding of block copolymers, means that the most up-to-date reviews should be consulted (1,24). The dynamics of block copolymer melts, in particular rheological behavior, and studies of chain diffusion via light scattering and nmr techniques have also been the focus of several reviews (1,25,26).

The phase behavior of block copolymer melts is, to a first approximation, represented in a morphology diagram in terms of χN and f (1). Here f is the volume fraction of one block and χ is the Flory–Huggins interaction parameter, which is inversely proportional to temperature, that reflects the interaction energy between different segments. The configurational entropy contribution to the Gibbs energy is proportional to N, the degree of polymerization. When the product χN exceeds a critical value $(\chi N)_{\mathrm{ODT}}$ (ODT = order–disorder transition), the block copolymer microphase separates into a periodically ordered structure, with a

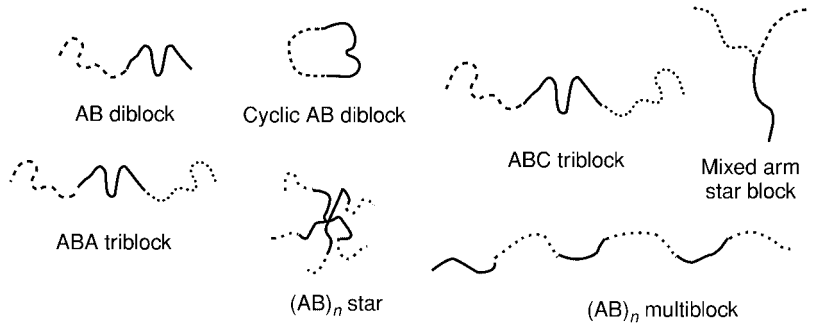

Fig. 1. Block copolymer architectures.

length scale ~5–500 nm. The structure that is formed depends on the copolymer architecture and composition (1) (see Fig. 1). For diblock copolymers, a lamellar (lam) phase is observed for symmetric diblocks ($f = 0.5$), whereas more asymmetric diblocks form hexagonal-packed cylinder (hex) or body-centered cubic (bcc) spherical structures. A complex bicontinuous cubic gyroid (gyr) (space group $Ia\bar{3}d$) phase has also been identified (27,28) for block copolymers between the lam and hex phases near the ODT, and a hexagonal-perforated layer (HPL) phase has been found to be metastable in this region (29–31). A useful compilation is available of studies on the morphology of block copolymers of various chemistries (32).

The main techniques for investigating block copolymer microstructures are transmission electron microscopy and small-angle x-ray or neutron scattering. Transmission electron microscopy provides direct visual images of the structure, albeit over a small area of the sample. Usually samples are stained using the vapors from a solution of a heavy metal acid (OsO_4 or RuO_4) to increase the contrast for electrons between domains (33). Small-angle scattering probes the structure over the whole sample volume, giving a diffraction pattern. The positions of the reflections in the diffraction pattern can be indexed to identify the symmetry of the phase (1,22). The preparation method can have a dramatic influence on the apparent morphology, for example whether solvent casting or melt processing is performed. Numerous cases of mistaken identification of "equilibrium phases" have appeared in the literature, when the phase was simply an artifact. For instance, different morphologies were obtained by varying the preparation conditions for a polyolefin diblock (34). In other cases, phases such as HPL have been observed (29) which although reproducible, have turned out to be only long-lived metastable phases, ultimately transforming to the equilibrium gyr phase (30,31). The ODT in block copolymers can be located by a number of methods—from discontinuities in the dynamic shear modulus (35–37) or small-angle scattering peak shape (38,39) or from calorimetry measurements (40).

To establish relationships between different block copolymer phase diagrams and also to facilitate comparison with theory, it is necessary to specify parameters in addition to χN and f. First, asymmetry of the conformation of the copolymer breaks the symmetry of the phase diagram about $f = 0.5$. For AB diblocks, conformational asymmetry is quantified using the "asymmetry parameter" $\varepsilon = (b_A{}^2/v_A)/(b_B{}^2/v_B)$ (41,42), where b_J is the segment length for block J and v_J is the segment volume. Composition fluctuations also modify the phase diagram, and

this has been accounted for theoretically by the Ginzburg parameter $\bar{N} = Nb^6\rho^2$, where ρ is the number density of chains (43,44). The extent of segregation of block copolymers depends on the magnitude of χN. For small χN, close to the ODT (up to $\chi N = 12$ for symmetric diblocks for which $\chi N_{\mathrm{ODT}} = 10.495$), the composition profile (density of either component) is approximately sinusoidal. This is termed the weak segregation limit. At much larger values of χN ($\chi N > \sim 100$), the components are strongly segregated and each domain is almost pure, with a narrow interphase between them. This is the strong segregation limit.

The first theories for block copolymers were introduced for the strong segregation limit (SSL) and the essential physical principles underlying phase behavior in the SSL were established in the early 1970s (1). Most notably, Helfand and coworkers (45–47) developed the self-consistent field (SCF) theory, thus permitting the calculation of free energies, composition profiles, and chain conformations. In the SCF theory, the external mean fields acting on a polymer chain are calculated self-consistently with the composition profile. The theory of Leibler (48) describes block copolymers in the weak segregation limit. It employs a Landau–Ginzburg approach to analyze the free energy, which is expanded with reference to the average composition profile. The free energy coefficients are computed within the random phase approximation. Weak segregation limit theory can be extended to allow for thermal composition fluctuations. This changes the mean field prediction of a second-order phase transition for a symmetric diblock copolymer to a first-order transition. This effect for block copolymers has been studied, and it was shown that composition fluctuations, incorporated via the renormalization method of Brazovskii, lead to a "finite size effect," where the phase diagram depends on $\bar{N}$ (43). A powerful new method to solve the SCF equations for block copolymers has been applied to analyze the ordering of many types of block copolymer in bulk and in thin films (49–52). The strong and weak segregation limits are spanned, as well as the intermediate regime where the other methods do not apply. This implementation of SCF theory predicts phase diagrams and other quantities such as domain spacings, in good agreement with experiment, and represents an impressive state of the art for modeling the ordering of soft materials. Accurate liquid state theories have also been used to model block copolymer melts (53,54), although they are hard to implement and consequently the method is often regrettably overlooked (1). Recently, a method has been developed to directly simulate field theories for polymers without introducing approximations such as mean field approaches and perturbation expansions (55). This technique holds much promise for examining the thermodynamics of block copolymers in the limit of low molecular weight where approximate methods such as mean field theory or renormalization techniques break down.

A phase diagram computed using self-consistent mean field theory (49,51) is shown in Figure 2. The figure shows the generic sequence of phases accessed just below the ODT temperature for diblock copolymers of different compositions. The features of phase diagrams for particular systems are different in detail, but qualitatively they are similar, and well accounted for by SCF theory.

The phase behavior of ABC triblocks is much richer (24) than that of two-component diblocks or triblocks, as expected because multiple interaction parameters (χ_{AB}, χ_{AC}, and χ_{BC}) result from the presence of a distinct third block.

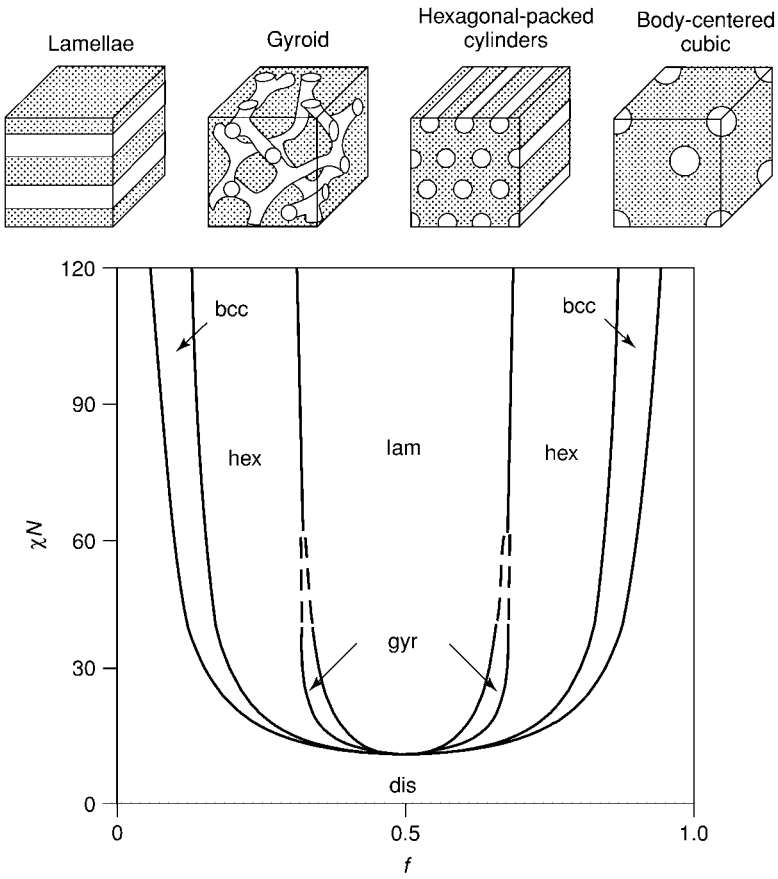

Fig. 2. Phase diagram for a conformationally symmetric diblock copolymer, calculated using SCF theory (49,51), along with illustrations of the equilibrium morphologies. In the phase diagram, regions of stability of disordered (dis), lamellar (lam), gyroid (gyr), hexagonal (hex), and body-centered cubic (bcc) phases are indicated.

Summaries of work on ABC triblock morphologies have appeared (1,56) and these systems are considered separately elsewhere in this encyclopedia (see BLOCK COPOLYMERS, TERNARY TRIBLOCKS). Because of the large number of possible morphologies, theorists are presently working to predict the phase behavior of these copolymers by using methods that do not require a priori knowledge of the space group symmetries of trial structures (57,58).

During processing block copolymers are subjected to flow. For example thermoplastic elastomers formed by polystyrene-*b*-polybutadiene-*b*-polystyrene (SBS) triblock copolymers, are molded by extrusion (see ELASTOMERS, THERMOPLASTIC). This leads to alignment of microphase-separated structures. This was investigated in the early 1970s by Keller and co-workers (22,59) who obtained transmission electron micrographs from highly oriented specimens of Kraton SBS copolymers following extrusion. Examples are included in Figure 3. Work on the effect of flow on block copolymer melts has been reviewed (1,25,61,62). Because of the

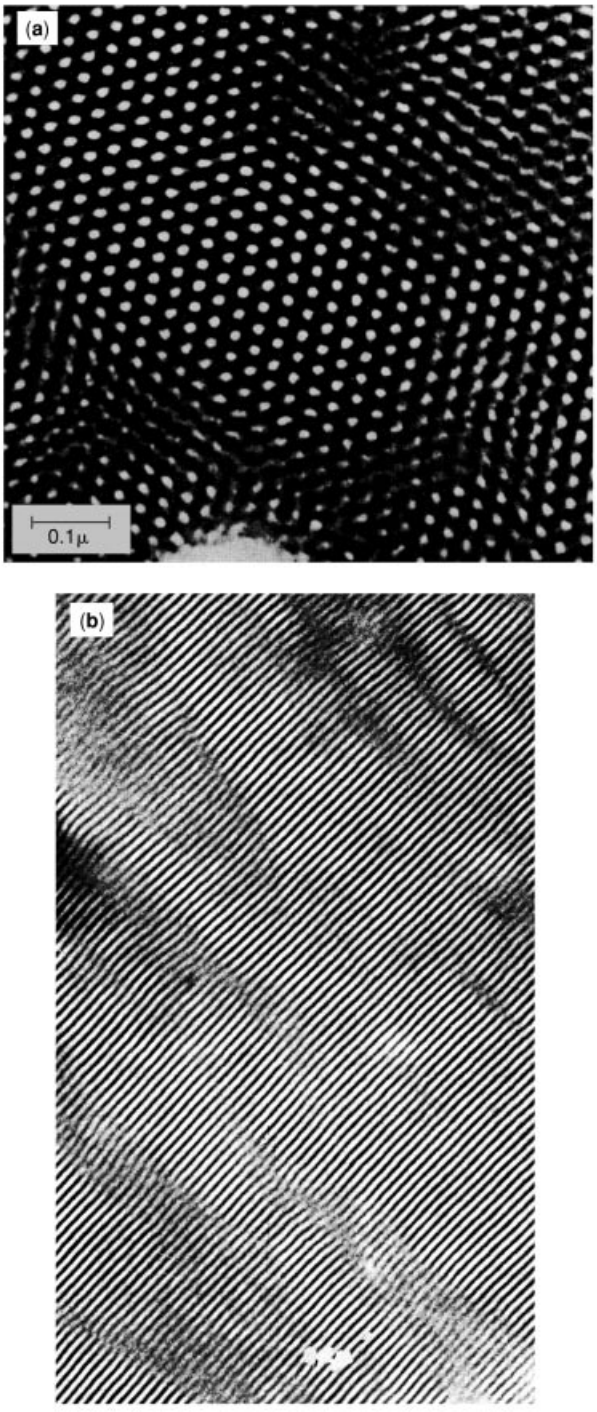

Fig. 3. Transmission electron micrographs from a hexagonal-packed cylinder structure subjected to flow during high temperature extrusion. The sample was a PS–PB–PS tribock (Kraton D1102) (60). (**a**) Perpendicular to the extrusion direction, (**b**) a parallel section.

convenience and well-defined nature of the shear geometry, most model studies have exploited this type of flow. The application of shear leads to orientation of block copolymer microstructures at sufficiently high shear rates and/or strain amplitudes (in the case of oscillatory shear). Depending on shear conditions and temperature, different orientations of a morphology with respect to the shear plane can be accessed. This has been particularly well studied for the lamellar phase where so-called parallel (lamellar normal along shear gradient direction) and perpendicular (lamellar normal along the neutral direction) orientations have been observed (63). Distinct orientation states of hexagonal and cubic phases have also been investigated, details being provided elsewhere (62). The ability to generate distinct macroscopic orientation states of block copolymers by shear is important in future applications of block copolymers where alignment will be important (reinforced composites, optoelectronic materials, and separation media). Shear also influences thermodynamics, since the ODT shifts upwards on increasing shear rate because the ordered phase is stabilized under shear (64,65).

The phase behavior of rod–coil block copolymers is already known to be much richer than that of coil–coil block copolymers, because the rod block can orient into liquid crystal structures (1). The rod block may be analogous to a biomacromolecule; for example, poly(benzyl glutamates) (66,67) and poly(peptides) (68) forming helical rod-like blocks have been incorporated in block copolymers. Possible applications of these materials arising from their biocompatibility are evident.

Block Copolymer Films

Microphase separation by block copolymers in thin films has been investigated from several perspectives. First, the physics of self-assembly in confined soft materials can be studied using model block copolymer materials for which reliable mean field statistical mechanical theories have been developed (69). Second, interest has expanded due to potential exciting applications that exploit self-organization to fabricate high density data storage media (70), to lithographically pattern semiconductors with ultrasmall feature sizes (71,72), or to prepare ultrafine filters or membranes (73). Research in this field is growing at a rapid pace, and the field has not been reviewed since 1998 (1,74), since when many new developments have occurred.

Block copolymer films can be prepared by the spin-coating technique, where drops of a solution of the polymer in a volatile organic solvent are deposited on a spinning solid substrate (often silicon wafers are used because of their uniform flatness). The polymer film spreads by centrifugal forces, and the volatile solvent is rapidly driven off. With care, the method can give films with a low surface roughness over areas of square millimeters. The film thickness can be controlled through the spin speed, the concentration of the block copolymer solution, or the volatility of the solvent, which also influences the surface roughness (75). Dip coating is another reliable method for fabricating uniform thin films (76). Whatever the deposition technique, if the surface energy of block copolymer is much greater than that of the substrate, dewetting will occur. The mechanism of dewetting has been investigated (77–79).

In thin films, the lamellae formed by symmetric block copolymers can orient either parallel or perpendicular to the substrate. A number of possible arrangements of the lamellae are possible, depending on the surface energies of the blocks and that of the substrate, and whether the film is confined at one or both surfaces. These are illustrated in Figure 4. In the case that a different block

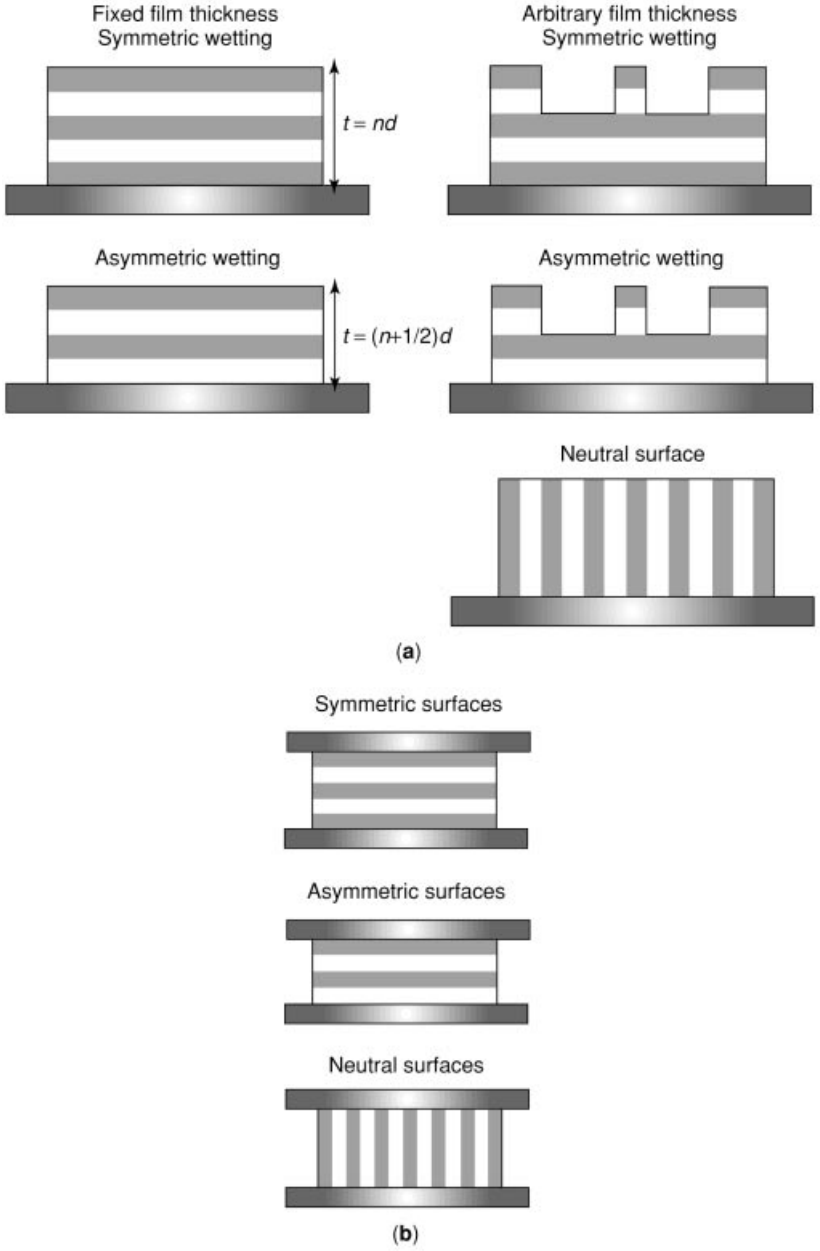

Fig. 4. Possible configurations of lamellae in block copolymer films: (**a**) confined at one surface and (**b**) confined at both surfaces.

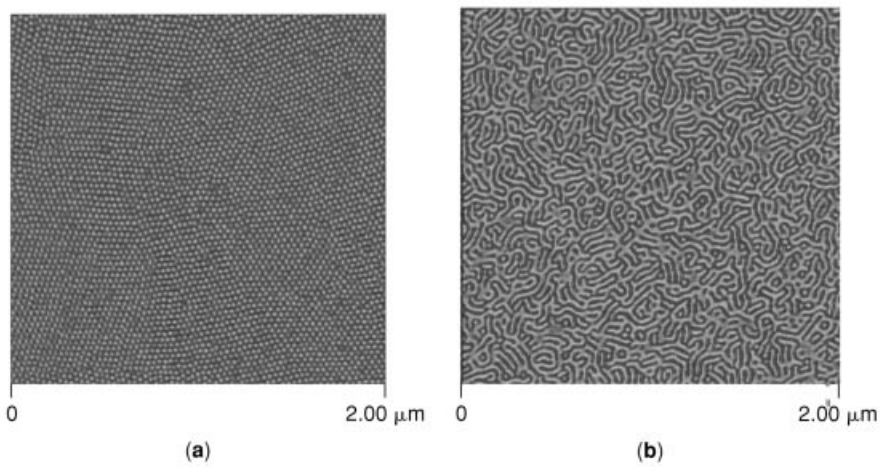

Fig. 5. Hexagonal and stripe patterns observed via atomic force microscopy (Tapping Mode). Phase contrast images of (a) polystyrene-*b*-poly(ethylene-*co*-butylene)-*b*-polystyrene, Kraton G1657 and (b) Kraton G1650 (82).

preferentially wets the interfaces with substrate and air, wetting is asymmetric and a uniform film has a thickness $(n+\frac{1}{2})d$. If the initial film thickness is not equal to $(n+\frac{1}{2})d$, then islands or holes (quantized steps of height d) form to conserve volume (80). In addition to leading to distinct orientations, confinement of block copolymers can change the thermodynamics of ordering, in particular surface-induced ordering persists above the bulk ODT (81).

Asymmetric block copolymers which form hexagonal or cubic-packed spherical morphologies in the bulk, form stripe or circular domain patterns in two dimensions, as illustrated in Figure 5. The stripe pattern results from cylinders lying parallel to the substrate, and a circular domain surface pattern occurs when cylinders are oriented perpendicular to the substrate, or for spheres at the surface. Bicontinuous structures cannot exist in two dimensions; therefore the gyroid phase is suppressed in thin films. More complex multiple stripe and multiple circular domain structures can be formed at the surface of ABC triblocks (83). Nanostructures in block copolymer films can be oriented using electric fields (if the difference in dielectric permittivity is sufficient), which will be important in applications where parallel stripe (84) or perpendicular cylinder configurations (85) are desired.

The morphology of block copolymers on patterned substrates has attracted recent experimental (86,87) and theoretical (88–90) attention. It has been shown that block copolymer stripes are commensurate with striped substrates if the mismatch in the two length scales is not too large.

The surface morphology of block copolymer films can be investigated by atomic force microscopy. The ordering perpendicular to the substrate can be probed by secondary ion mass spectroscopy or specular neutron or x-ray reflectivity. Suitably etched or sectioned samples can be examined by transmission electron microscopy. Islands or holes can have dimensions of micrometers, and consequently may be observed using optical microscopy.

Theory for block copolymer films has largely focused on the ordering of lamellae as a function of film thickness. Many studies have used brush theories for block copolymers in the SSL (91,92), although SCF theory has also been employed (69,89,93). Theory for weakly segregated block copolymers has been applied to analyze surface-induced order above and below the bulk ODT of a lamellar phase (94) and surface-induced layering in a hexagonal block copolymer film (95). Computer simulations using the dynamic self-consistent mean field method have predicted a range of "perforated lamellar" morphologies (96).

Block Copolymers in Solution

In a solvent, block copolymer phase behavior is controlled by the interaction between the segments of the polymers and the solvent molecules as well as the interaction between the segments of the two blocks. If the solvent is unfavorable for one block, this can lead to micelle formation in dilute solution. The phase behavior of concentrated solutions can be mapped onto that of block copolymer melts (97). Lamellar, hexagonal-packed cylinder, micellar cubic, and bicontinuous cubic structures have all been observed (these are all lyotropic liquid crystal phases, similar to those observed for nonionic surfactants). This is illustrated by representative phase diagrams for Pluronic triblocks in Figure 6.

The main classes of block copolymer examined in solution are those based on polyoxyethylene, which is water soluble and is the basis of most amphiphilic block

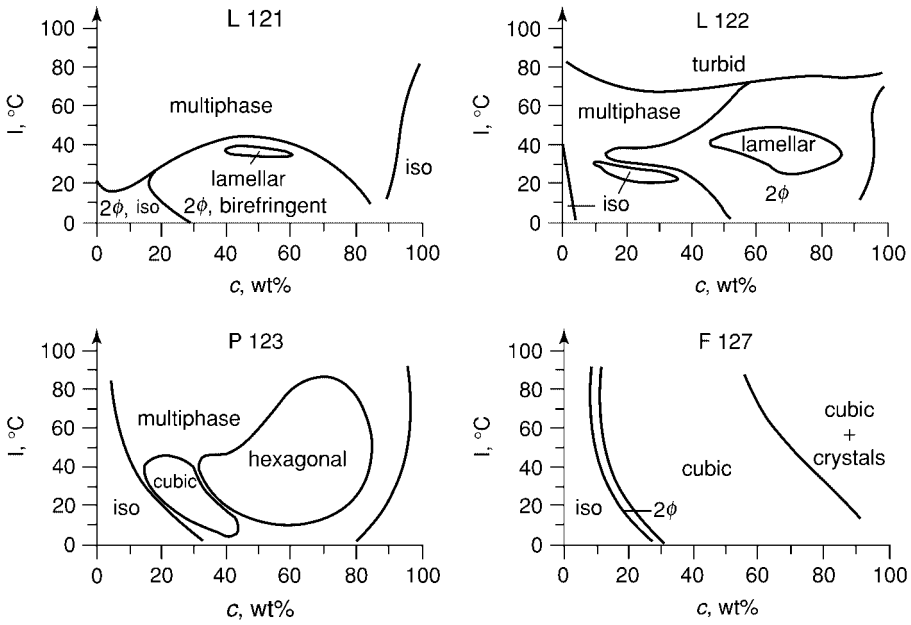

Fig. 6. Phase diagrams in water of $E_mP_nE_m$ (E = polyoxyethylene, P = polyoxypropylene) Pluronics with $n = 69$ and $m = 4$ (Pluronic L121), $m = 11$ (Pluronic L122), $m = 20$ (Pluronic P123) and $m = 99$ (Pluronic F127) (98). Two phase regians are denoted 2ϕ.

copolymers, and styrenic block copolymers in organic solvents. Selected studies on these systems up to 1998 have been summarized (1). Polyoxyethylene-based block copolymers include those of polyoxyethylene (E) with polyoxypropylene (P), especially EPE triblocks (commercial name: Pluronic or Synperonic), which are widely used commercially as surfactants in detergents and personal care products (99), and also in pharmaceutical applications, especially drug delivery (100–102). A number of edited books on water-soluble polymers cover applications of block copolymers (103–108). Related copolymers include those with a polyoxybutylene hydrophobic block (109,110). Work on styrenic block copolymers in organic solvents has also been reviewed (1,111). Block copolymers containing a polyelectrolyte chain have attracted attention from a number of research teams [(112,113) and references therein], copolymers containing a well-studied polyelectrolyte such as poly(styrene sulfonate) (114) or a polyacrylate (112) often being chosen.

Like surfactants, block copolymers form micelles above a critical concentration. The critical micelle concentration can be located by a variety of techniques (115), the most commonly used being surface tensiometry where the *critical micelle concentration* is located as the point at which the surface tension becomes essentially independent of concentration. The primary methods to determine micelle size and shape are light scattering and small-angle x-ray or neutron scattering. The thermodynamic radius (from the thermodynamic volume which is one eighth of the excluded volume) of micelles can be obtained from static light scattering experiments using the Carnahan–Starling equation for hard spheres to the Debye function (110). This procedure can be used in place of Zimm plots when the angular dependence of the scattered intensity is weak, which is usually the case for block copolymer micelles, which are much smaller than the wavelength of light (110). Static light scattering also provides the association number (from the micellar mass) and the second virial coefficient (1,110,116). Dynamic light scattering provides the hydrodynamic radius from the mode corresponding to micellar diffusion obtained from the intensity distribution of relaxation times [usually obtained from analysis of the intensity autocorrelation function using the program CONTIN (117)]. The Stokes–Einstein equation can then be used to calculate the hydrodynamic radius from the diffusion coefficient (1,110). Small-angle x-ray scattering or neutron scattering can be used to extract information on intra- and inter-micellar ordering (1). Neutron scattering has the advantage compared to x-ray scattering that the contrast between different parts of the system (eg, within the micelle or between the micelle and the solvent) can be varied by selective deuteration of solvent and/or one of the blocks. In dilute solution, only intramicellar structure contributes to the scattered intensity (the so-called form factor) and this can be modeled to provide information on micelle size and shape. The simplest model is that of a uniform hard sphere (118), although more sophisticated models are usually required for high quality data fitting (118–121). The intermicellar structure factor dominates at higher concentrations. It can be analyzed using the hard sphere model (118,122,123) to give information on the micellar radius and the micellar volume fraction. Where attractive interactions between micelles are significant, these also influence the structure factor and this can be modeled using the “sticky sphere” approximation (120).

A diverse range of theoretical approaches have been employed to analyze the structure of block copolymer micelles, and for micelle formation (1). The first models were based on scaling relationships for polymer "brushes" and give predictions for the dependence of micelle dimensions on the size of the blocks, as well as the association number of the micelle. A "brush" theory by Leibler and coworkers enables the calculation of the size and number of chains in a micelle and its free energy of formation (124). The fraction of copolymer chains aggregating into micelles can also be obtained. Self-consistent field theory was first applied to predict the critical micelle concentration of a diblock in a homopolymer matrix, and then applied to block copolymers in solution (1). The lattice implementation of SCF theory has been applied to analyze the dimensions of micelles for specific (Pluronic) block copolymers (125).

In addition to applications as surfactants and in personal care products, block copolymer micelles have been extensively investigated as nanoparticles for solubilizing active agents for drug delivery (100,101,126,127), or as "nanoreactors" for the production of inorganic nanoparticles, eg, of metals with potential applications in catalysis (128,129). An alternative approach is to form vesicles (bilayers wrapped round into a spherical shell) (130,131). These may be cross-linked or polymerized to form hollow shell nanoparticles (132–134).

At higher concentrations, block copolymers in solution form a variety of lyotropic mesophases (1,135–138). Because such phases possess a finite yield stress and so usually do not flow under their own weight, these are often termed gels. However, it must be emphasized that the gel properties result from the ordered microstructure rather than any cross-links between polymer chains as in a conventional polymer gel. The symmetry of the ordered phase formed largely depends on the interfacial curvature, as for conventional amphiphiles (115); however, the phase behavior can also be understood by mapping it onto that for block copolymer melts (97). Shear can be used to orient block copolymer gels as for block copolymer melts. The effects of shear on lyotropic lamellar, hexagonal-packed cylindrical micellar, and cubic micellar phases have all been investigated (135,139,140). Large amplitude oscillatory shear or high shear rate steady shear both lead to macroscopic orientation of the structures. In the case of cubic phases in particular, the flow mechanisms are complex, as is the rheological behavior with interesting nonlinear effects such as plateaus in the flow curve (141,142).

Theory for the phase behavior of block copolymers in semidilute or concentrated solution is less advanced than that for melts or dilute solutions because of the complexity of interactions between polymer and solvent. The two main methods developed have been (*1*) SCF theory for density profiles and domain spacings and (*2*) weak segregation limit calculations of the shift in ODT temperature with changing concentration. An overview of both approaches can be found elsewhere (1). SCF theory calculations have produced phase diagrams for specific Pluronic copolymers in aqueous solution that are in remarkably good agreement with those observed experimentally (143,144). Simulations using the dynamic density functional theory (commercially available as the Mesodyn module of Cerius^2 from Accelerys) have also yielded surprisingly accurate predictions for the sequence of phases obtained on varying concentration (145).

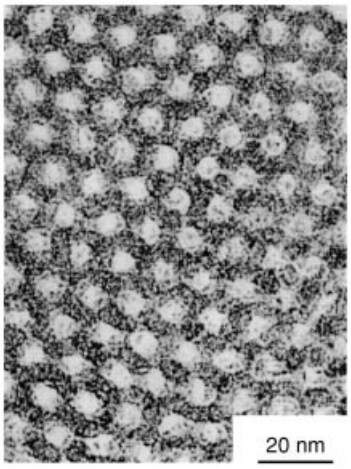

Fig. 7. Transmission electron micrograph of calcined silica structure templated using an acidic solution of Pluronic poly(oxyethylene)-*b*-poly(oxypropylene)-*b*-poly(oxyethylene) triblock. From Ref. 212.

Lyotropic block copolymer mesophases can be used to template inorganic materials such as silica (146,147), thus producing materials with a high internal surface area that could be useful in catalysts or separation technology. Figure 7 shows a transmission electron micrograph of hexagonal mesoporous silica, templated using a Pluronic block copolymer.

Crystallization in Block Copolymers

In semicrystalline block copolymers, the presence of a noncrystalline block enables modification of the mechanical and structural properties compared to a crystalline homopolymer, through introduction of a rubbery or glassy component. Crystallization in homopolymers leads to an extended conformation, or to *kinetically controlled* chain folding. In block copolymers, on the other hand, *equilibrium* chain folding can occur, the equilibrium number of folds being controlled by the size of the second, noncrystallizable block. The structure of block copolymers following crystallization has been reviewed (1,149) (see SEMICRYSTALLINE POLYMERS).

The most important crystallizable block copolymers are those containing polyethylene (PE) or poly(ethylene oxide) (PEO) (systematic name polyoxyethylene). Polyethylene in block copolymers is prepared by anionic polymerization of poly(1,4-butadiene) (1,4-PB), followed by hydrogenation, and has a melting point in the range 100–110°C. This synthesis method leads to ethyl branches in the copolymer, with on average 2–3 branches per 100 repeats. These branches induce lengths for folded chains which are set by the branch density and not by the thermodynamics of crystallization. The melting temperature of PEO in block copolymers is generally lower than that of PEO homopolymer (melting temperature $T_m =$ 76°C for high molecular weight samples). In contrast to PE prepared by hydrogenation of 1,4-PB, there is no chain branching in these copolymers and the fold

length depends on the crystallization procedure. Molecules with 1, 2, 3, . . . folds can be obtained by varying the crystallization protocol (quench depth, annealing time, etc). Crystallization has been investigated for other block copolymers, in particular those containing poly(ε-caprolactone) (PCL) ($T_m = 57^\circ$C). The morphology in block copolymers where both blocks are crystallizable has also been investigated. It has been found that co-crystallization occurs in diblock copolymers, in contrast to blends of crystallizing homopolymers (150). However, one block can influence the crystallization of another as shown by studies on polystyrene-*b*-polyethylene-*b*-poly(ε-caprolactone) ABC triblocks (151). A suppression of the crystallization temperature of the poly(ε-caprolactone) block was noted when the polyethylene block crystals were annealed before crystallization of PCL at lower temperatures (151), this effect being termed "antinucleation."

It is now firmly established that confinement of crystalline stems has a profound influence on crystallization in block copolymers. Confinement can result from the presence of glassy domains or simply strong segregation between domains. In contrast crystallization can overwhelm microphase separation when a sample is cooled from a weakly segregated or homogeneous melt (152–154). The lamellar crystallites can then nucleate and grow heterogeneously to produce spherulites (152,155), whereas these are not observed when crystallization is confined to spheres or cylinders.

Crystallization confined by glassy blocks leads to a drastic slow down in crystallization kinetics and a reduction in the corresponding Avrami exponent (156,157). Poly(ethylene) crystallites in a strongly segregated diblock have been observed to nucleate homogeneously within the PE spheres, leading to first-order kinetics, ie, exponential growth in the degree of crystallinity (158). Confined crystallization was first observed for a lamellar phase with glassy lamellae (159,160), and later in cylinders confined in a glassy matrix (161). Crystallization of the PE matrix in the inverse structure (ie, a phase containing rubbery or glassy cylinders) occurs without disrupting the melt microstructure (162).

Chain folds can exist in equilibrium in block copolymers, in contrast to homopolymers, because of the finite cross-sections of the blocks at the lamellar interface, which have to be matched if space is to be filled at normal densities. The equilibrium fold diagram has been mapped out for PEO-based block copolymers in the melt (163) and in solution (164). Nonequilibrium states of highly folded chains can also be trapped kinetically (164,165).

The orientation of crystalline stems in block copolymers depends on the morphology of the structure and the crystallization protocol. A parallel orientation of PE stems with respect to a lamellar interface was reported for a series of polyethylene-*b*-polyethylethylene diblocks (166), and a similar orientation was later reported (159,160) for a series of PE-containing diblocks based on simultaneous small-angle x-ray scattering/wide-angle x-ray scattering (saxs/waxs) experiments, as shown in Figure 8. SAXS on aligned specimens gives the lamellar orientation, whereas WAXS provides information on unit cell orientation. Samples may be aligned in the melt, for example using large amplitude oscillatory shear (159,167). In constrast to these studies showing parallel stem orientation, a perpendicular orientation of PE stems was proposed in a series of polyolefin diblocks (152). Again using the combination of saxs and waxs, it was found that PE stems generally orient perpendicular to the cylinder axis, although tilted stems were

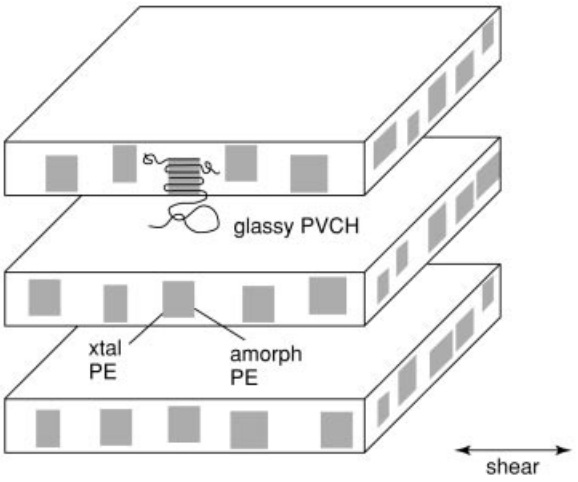

Fig. 8. Model for confined crystallization in a lamellar phase formed by a polyethylene-*b*-poly(vinylcyclohexane) diblock (159).

observed when crystallization was confined by strong segregation or by a glassy matrix (168). These apparently conflicting observations of parallel and perpendicular stem orientations can be rationalized when it is recognized that in both orientations the *b* axis of the PE crystals is the fast growth direction—in the lamellar plane and along the cylinder axis, respectively. Recently, the orientation of PE stems in a PS-*b*-PEO diblock forming a lamellar phase was investigated using saxs and waxs (167). Four regimes were identified: (*1*) A random stem orientation for a deep quench into liquid nitrogen, (*2*) stems parallel to lamellae for a crystallization temperature $-50^{\circ}\mathrm{C} \leq T_c \leq -10^{\circ}\mathrm{C}$, (*3*) stems inclined with respect to lamellae for $-5^{\circ}\mathrm{C} \leq T_c \leq -30^{\circ}\mathrm{C}$, and (*4*) stems perpendicular to lamellae for $T_c \geq 35^{\circ}\mathrm{C}$. For PEO cylinders formed in a PS–PEO diblock, the parallel orientation of stems was not observed, although the states (*1*), (*3*), and (*4*) were confirmed (169). These conclusions were supported by a separate study of the correlation lengths (apparent crystallite sizes) obtained from SAXS for different crystal orientations (170). In this report it was also noted that it is the initial growth stage that determines the final crystal orientation in nanoconfined lamellae rather than the primary nucleation step. Crystal orientation and changes in lamellar thickness of a related diblock were examined in a companion paper, in which the change in the crystallization kinetics for confined and unconfined crystallization were deduced from Avrami plots of the degree of crystallinity (171).

Theories for semicrystalline block copolymers are able to provide predictions for the scaling of amorphous and crystal layer thickness with chain length (1,149). A brush-type theory was developed by DiMarzio and co-workers (172) and an SCF theory by Whitmore and Noolandi (173). The latter approach predicts a scaling for the overall domain spacing $d \sim NN_a^{-5/12}$ (where N is the total degree of polymerization and N_a is that of the amorphous block) which is in good agreement with experimental results (174), as detailed elsewhere (1,149). Approaches used for crystallization in homopolymers may be used to calculate the change in melting temperature due to finite crystal thickness (Thompson–Gibbs equation)

and lamellar crystal surface energies (Flory–Vrij theory), and also growth rates (kinetic nucleation theory). Details can be obtained from Reference 1.

The morphology of thin films of crystallized block copolymers can be probed most conveniently at the microscopic scale by atomic force microscopy, whereas spherulites can be observed optically. Crystallization in thin films of PE-*b*-PEO diblocks has recently been investigated (175,176). For a diblock containing 45% PEO, parallel lamellae were observed in the melt but lamellae oriented perpendicular to the substrate upon crystallization at a large undercooling were observed using Atomic (Force) Microscopy (176). This was ascribed to a kinetically trapped state of chain-folded PEO crystals. However, ultimately the morphology evolved into the equilibrium parallel one, which was also observed for three other diblocks with a higher PEO content (176). Films of these copolymers were characterized by islands and holes at the surface because of an incommensurability between the film thickness and an integral number of lamellae, as discussed earlier. The island and hole structure was retained upon crystallization, although craters and cracks appeared in the lamellae. Within craters, terracing of lamellar steps was observed, from which the lamellar thickness could be extracted. Terracing of crystal lamellae oriented parallel to the substrate was also reported for a PEO-*b*-PBO diblock and a PEO-*b*-PBO-*b*-PEO triblock, probed by AFM (177). In this work a comparison of the lamellar thickness was also made with the domain spacing obtained from saxs and a model of tilted chains was proposed (fully extended for the diblock, once folded for the triblock). However, this is not in agreement with recent simultaneous saxs/waxs results that indicate PEO chains oriented perpendicular to lamellae in a PEO-*b*-PBO diblock (178).

Blends Containing Block Copolymers

In blends of block copolymer with homopolymer, there is an interplay between macrophase separation (due to the presence of homopolymer) and microphase separation (of the block copolymer). Which effect predominates depends on the relative lengths of the polymers and on the composition of the blend.

Macrophase separation can be detected by light scattering or via turbidity measurements of the cloud point since macrophase separation leads to structures with a length scale comparable to the wavelength of light. Regions of macrophase and microphase separation can also be distinguished by transmission electron microscopy or via small-angle scattering techniques. Microphase separation leads to a scattering peak at a finite wavenumber q, whereas macrophase separation is characterized by $q = 0$. The segregation of block copolymers to the interface between polymers in a blend can be determined in bulk from small-angle scattering experiments or transmission electron microscopy. In thin films, neutron reflectivity, forward recoil spectroscopy, and nuclear reaction analysis have been used to obtain volume fraction profiles, which quantify the selective segregation of block copolymers to interfaces.

An important application of block copolymers is as compatibilizers of otherwise immiscible homopolymers. There are a number of useful reviews of work in this area (179–182). The morphology of blends of polymers with block copolymer and theories for this have been reviewed (1). The influence of added homopolymer

on block copolymer structure has also been investigated, as have binary blends of block copolymers, and these systems are also considered in this section.

Blends of Block Copolymer with One Homopolymer. Block copolymers can solubilize homopolymers up to a certain amount, beyond which phase separation occurs. This ability to continuously swell block copolymer microstructures is the basis of a number of potential and actual applications in optoelectronics where the periodicity of the block copolymer structure is extended up to 0.1–1 μm which corresponds to wavelengths for reflection or guiding of light. The limit for macrophase separation in blends of block copolymer with homopolymer depends on the relative chain lengths, ie, on $\alpha = N_{Ah}/N_{Ac}$, where N_{Ah} is the degree of polymerization of the homopolymer (A) and N_{Ac} is the degree of polymerization of the same component of the copolymer. Work by two groups (183–186) has led to the identification of three regimes (1). If $\alpha < 1$, the homopolymer tends to be selectively solubilized in the A domain of the microphase-separated block copolymer, and is weakly segregated toward the domain center. If $\alpha \approx 1$, the homopolymer is still selectively solubilized in the A microdomains. However, it does not significantly swell the A block chains and tends to be more localized in the middle of the A microdomains. If $\alpha > 1$, macrophase separation occurs, with domains of microphase-separated copolymer in the homopolymer matrix. A transmission electron micrograph of the structure formed by a phase-separated lamellar diblock is shown in Figure 9.

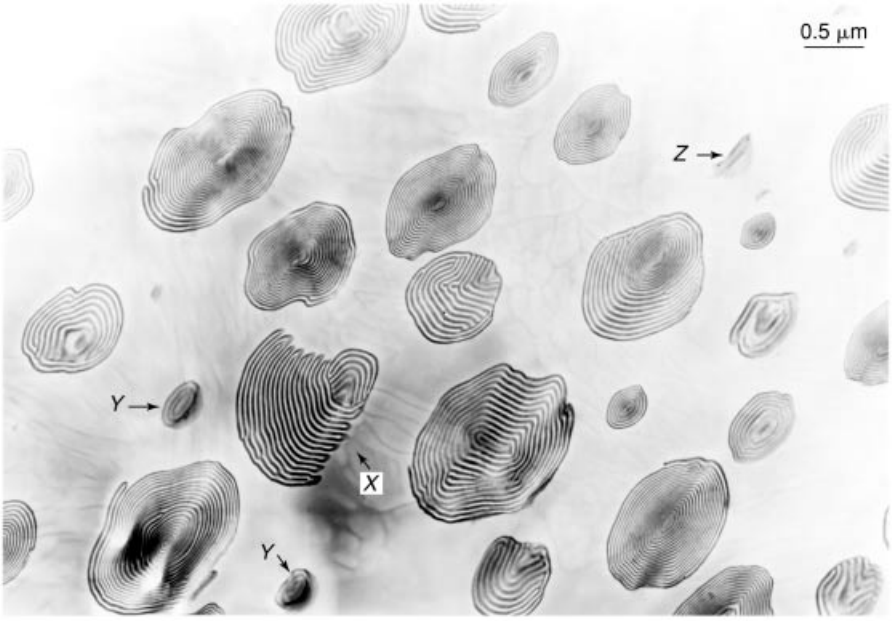

Fig. 9. Electron micrograph showing macrophase separation of domains of microphase-separated polystyrene-*b*-polyisoprene block copolymer (M_n = 100 kg/mol, $f_{PS} = 0.46$) in a PS homopolymer (M_n = 580 kg/mol) matrix (187).

Another important aspect of adding homopolymer to a block copolymer is the ability to change morphology (without synthesis of additional polymers). Furthermore, morphologies that are absent for neat diblocks such as bicontinuous cubic "double diamond" or HPL phases have been predicted in blends with homopolymers (188), although not yet observed. Transitions in morphology induced by addition of homopolymer are reviewed elsewhere (1), where a list of experimental studies on these systems can also be found.

Blends of Block Copolymer with Two Homopolymers. The ability of block copolymers to act as compatibilizers is now established. However, a debate has occurred in the literature as to whether block copolymers are more effective compatibilizers that random copolymers. For example, it has been reported that polystyrene/poly(2-vinylpyridine) random copolymers act to compatibilize the parent homopolymers (189), but that random polystyrene/poly(methyl methacrylate) copolymers are much less effective than corresponding block copolymers (190). The key appears to be the blockiness of the copolymer, which is much higher for the latter (191). Theory suggests that compositional polydispersity is also important for effective compatibilization (191,192). It leads to a greater gradation in composition across the interface, and consequently a lower configurational entropy of the homopolymers (192). In practice, polymers are compatibilized during melt processing. Then kinetic quantities such as the rate of diffusion of the copolymers to the interface and the shear rate are important. It has been shown that the coalescence of polymer droplets is inhibited by diffusion of block copolymers (193). The molar mass must be low enough so that diffusion occurs rapidly but not too low to prevent entanglements at the interface. On the other hand, copolymers with a molar mass that is too high get stuck in micelles.

Block copolymers act as compatibilizers by reducing the interfacial tension between homopolymers. Recent work shows that block copolymers can reduce the interfacial tension between homopolymers to the extent that polymeric microemulsions can be formed where the copolymer forms a continuous film between spatially continuous homopolymer domains (194–196). A transmission electron micrograph of a microemulsion formed in a blend of two polyolefins and the corresponding symmetric diblock is shown in Figure 10. A bicontinuous microemulsion forms in the mixture composition range where mean field theory predicts a Lifshitz point (197). A *Lifshitz point* is defined as the point along the line of critical phase transitions at which macro- and microphase branches meet (1). The observation of a microemulsion shows that mean field theory breaks down owing to the existence of thermal composition fluctuations. Although a theory for these composition fluctuations has not yet been developed, it has been shown that some properties of the microemulsion (elastic constants, composition profiles) can be modeled using an approach where the effective interaction between copolymer monolayers is computed (192,198,199). Both SCF and SSL theories have been employed (199). The effect of shear on polymeric microemulsions has recently been investigated, and it was shown that macrophase separation can be induced at sufficiently high shear rates (200). The connection between microemulsions formed by block copolymers and those containing conventional amphiphiles (which can be used to stabilize oil/water mixtures) has been emphasized (195,201) because of the importance of this aspect of block copolymer phase behavior to applications.

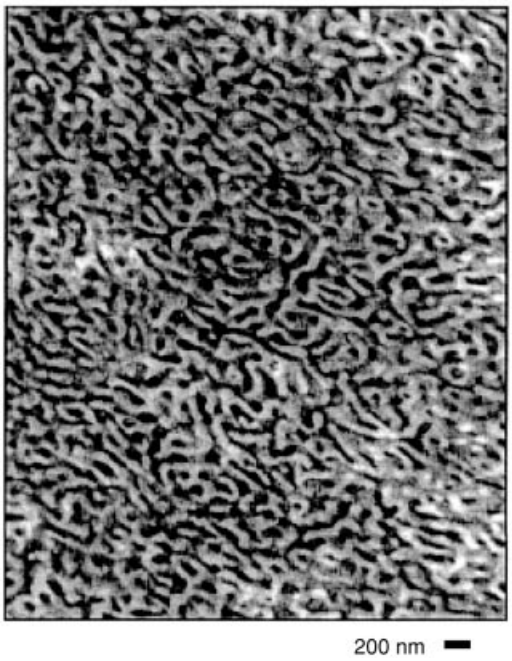

Fig. 10. Transmission electron micrograph of a microemulsion formed in a ternary blend of polyethylene, poly(ethylene–propylene), and a symmetric diblock of these two polymers. From Ref. 195.

Blends of Block Copolymers. Macro- versus microphase separation in blends of block copolymers has been investigated in particular for blends of polystyrene-*b*-polyisoprene diblock copolymers (202–206). Writing the ratio of molecular weights as $\delta = N_1/N_2$, it was found that blends of lamellar diblocks are miscible for $\delta < 5$, whereas for $\delta > 5$, the mixtures are only partially miscible (202,205). The same limiting value of δ was obtained using SCF calculations (207). The miscibility of pairs of asymmetric diblocks with the same (203) or complementary (203,204,208) compositions has also been investigated. By blending complementary diblocks (ie, those with composition f and 1-f), it is possible to induce a lamellar phase even for mixtures of asymmetric diblocks forming cylinder phases when pure (203,208). Blends of diblocks with similar compositions and molecular weights can be used to map the phase diagram by interpolation in the composition range spanned (146). By blending, the synthesis requirements to obtain a full phase diagram are reduced. The validity of this so-called single-component approximation has been tested using SCF theory. It was found that phase boundaries in the (f_1, f_2) plane (where f_1 and f_2 are the compositions of the two diblocks) map onto those of the corresponding pure diblock, if f_1 and f_2 do not differ too much (209,210). In the case that either f_1 or f_2 becomes close to zero or unity, this approximation completely breaks down (210). Thus, the one-component approximation is useful, although evidently the phase diagram of binary blends will contain biphasic regions.

Motivated by the possibility to prepare "exotic morphologies" exhibited by ABC triblocks (Block Copolymers, Ternary Triblocks) just by blending diblocks, researchers have investigated phase diagrams of strongly interacting AB and BC diblocks where the common B block is polyisoprene and the other two blocks are polystyrene and poly(ethylene oxide) (211,212). Although exotic phases were not found, regions of miscibility and immiscibility were mapped out. The phase diagrams obtained were in surprisingly good agreement with the predictions of a simple random phase approximation calculation of the spinodals (213).

BIBLIOGRAPHY

"Block and Graft Copolymers" in *EPST* 1st ed., Vol. 2, pp. 485–528, by R. J. Ceresa, W. R. Grace & Co.; Suppl. Vol. 2, pp. 129–158, by M. Matzner, L. M. Robeson, and A. Noshay, Union Carbide Corp., and J. E. McGrath, Virginia Polytechnic Institute and State University; "Block Copolymers" in *EPSE* 2nd ed., Vol. 2, pp. 324–434, by G. Riess and G. Hurtrez, Ecole Nationale Superieure de Chimie de Mulhouse, and P. Bahadur, Sourth Gujurat University.

1. I. W. Hamley, *The Physics of Block Copolymers*, Oxford University Press, Oxford, 1998.
2. I. Goodman, ed., *Developments in Block Copolymers*, Vol. **1**, Applied Science, London, 1982; *Developments in Block Copolymers*, Vol. **2**, Elsevier Applied Science, London, 1985.
3. P. Alexandridis and J. F. Holzwarth, *Curr. Opin. Colloid Interface Sci.* **5**, 312 (2000).
4. I. W. Hamley, ed., *Developments in Block Copolymer Science and Technology*, John Wiley & Sons, Inc., New York, in preparation.
5. M. Hillmyer, *Curr. Opin. Sol. Stat. Mater. Sci.* **4**, 559 (1999).
6. M. Scwarc, M. Levy, and R. Milkovich, *J. Am. Chem. Soc.* **78**, 2656 (1956).
7. R. N. Young, R. P. Quirk, and L. J. Fetters, *Adv. Polym. Sci.* **56**, 1 (1985).
8. P. Rempp, E. Franta, and J. Herz, *Adv. Polym. Sci.* **86**, 147 (1989).
9. M. van Beylen and co-workers, *Adv. Polym. Sci.* **86**, 89 (1989).
10. H. L. Hsieh and R. P. Quirk, *Anionic Polymerization: Principles and Practical Applications*, Marcel Dekker, Inc., New York, 1996.
11. N. Hadjichristidis and co-workers, *J. Polym. Sci., Part A: Polym. Chem.* **38**, 3211 (2000).
12. M. Pitsikalis and co-workers, *Adv. Polym. Sci.* **135**, 1 (1998).
13. N. Hadjichristidis, *J. Polym. Sci., Part A: Polym. Chem.* **37**, 857 (1999).
14. N. Hadjichristidis and co-workers, *Adv. Polym. Sci.* **142**, 71 (1999).
15. Z.-G. Yan and co-workers, *Makromol. Chem., Rapid Commun.* **14**, 725 (1993).
16. K. Matyjaszewski and J. Xia, *Chem. Rev.* **101**, 2921 (2001).
17. K. A. Davis and K. Matyjaszewski, *Macromolecules* **34**, 2101 (2001).
18. J. P. Kennedy and E. Maréchal, *Carbocationic Polymerization*, John Wiley & Sons, Inc., New York, 1982.
19. J. P. Kennedy and B. Ivan, *Designed Polymers by Carbocationic Macromolecular Engineering: Theory and Practice*, Hanser, Munich, 1992.
20. M. Sawamoto and M. Kamigaito, in J. R. Ebdon and G. C. Eastmond, eds., *New Methods of Polymer Synthesis*, Vol. **2**, Blackie, London, 1995.
21. S. T. Nguyen and co-workers, *J. Am. Chem. Soc.* **114**, 3975 (1992).
22. M. J. Folkes and A. Keller, in R. N. Haward, eds., *The Physics of Glassy Polymers*, Applied Science, London, 1973, p. 548.
23. F. S. Bates and G. H. Fredrickson, *Ann. Rev. Phys. Chem.* **41**, 525 (1990).

24. F. S. Bates and G. H. Fredrickson, *Phys. Today* **52**, 32 (Feb. 1999).
25. G. H. Fredrickson and F. S. Bates, *Annu. Rev. Mater. Sci.* **26**, 501 (1996).
26. R. H. Colby, *Curr. Opin. Colloid Interface Sci.* **1**, 454 (1996).
27. D. A. Hajduk and co-workers, *Macromolecules* **27**, 4063 (1994).
28. S. Förster and co-workers, *Macromolecules* **27**, 6922 (1994).
29. I. W. Hamley and co-workers, *Macromolecules* **26**, 5959 (1993).
30. D. A. Hajduk and co-workers, *Macromolecules* **30**, 3788 (1997).
31. M. E. Vigild and co-workers, *Macromolecules* **31**, 5702 (1998).
32. M. F. Schulz and F. S. Bates, in J. E. Mark, ed., *Physical Properties of Polymers Handbook*, American Institute of Physics, Woodbury, N.Y., 1996, p. 427.
33. K. Kato, *J. Electron Microsc. (Japan)* **14**, 220 (1965).
34. P. M. Lipic, F. S. Bates, and M. W. Matsen, *J. Polym. Sci., Part B: Polym. Phys.* **37**, 2229 (2001).
35. F. S. Bates, J. H. Rosedale, and G. H. Fredrickson, *J. Chem. Phys.* **92**, 6255 (1990).
36. J. H. Rosedale and F. S. Bates, *Macromolecules* **23**, 2329 (1990).
37. C. D. Han and co-workers, *Macromolecules* **28**, 5043 (1995).
38. S. M. Mai and co-workers, *Macromolecules* **29**, 6212 (1996).
39. N. Sakamoto and T. Hashimoto, *Macromolecules* **28**, 6825 (1995).
40. V. P. Voronov and co-workers, *Macromolecules* **30**, 6674 (1997).
41. E. Helfand and A. M. Sapse, *J. Chem. Phys.* **62**, 1327 (1975).
42. F. S. Bates and G. H. Fredrickson, *Macromolecules* **27**, 1065 (1994).
43. G. H. Fredrickson and E. Helfand, *J. Chem. Phys.* **87**, 697 (1987).
44. G. H. Fredrickson and K. Binder, *J. Chem. Phys.* **91**, 7265 (1989).
45. E. Helfand, *Macromolecules* **8**, 552 (1975).
46. E. Helfand and Z. R. Wasserman, *Macromolecules* **9**, 879 (1976).
47. E. Helfand and Z. R. Wasserman, in I. Goodman, ed., *Developments in Block Copolymers 1*, Applied Science, London, 1982, p. 99.
48. L. Leibler, *Macromolecules* **13**, 1602 (1980).
49. M. W. Matsen and M. Schick, *Phys. Rev. Lett.* **72**, 2660 (1994).
50. M. W. Matsen and M. Schick, *Curr. Opin. Colloid Interface Sci.* **1**, 329 (1996).
51. M. W. Matsen and F. S. Bates, *Macromolecules* **29**, 1091 (1996).
52. M. W. Matsen, *J. Phys., Condens. Matt.* **14**, R21 (2002)
53. E. F. David and K. S. Schweizer, *J. Chem. Phys.* **100**, 7767 (1994).
54. E. F. David and K. S. Schweizer, *J. Chem. Phys.* **100**, 7784 (1994).
55. V. Ganesan and G. H. Fredrickson, *Europhys. Lett.* **55**, 814 (2001).
56. A. J. Ryan and I. W. Hamley, in R. N. Haward and R. J. Young, eds., *The Physics of Glassy Polymers*, Chapman and Hall, London, 1997.
57. F. Drolet and G. H. Fredrickson, *Phys. Rev. Lett.* **83**, 4317 (1999).
58. Y. Bohbot-Raviv and Z.-G. Wang, *Phys. Rev. Lett.* **85**, 3428 (2000).
59. A. Keller, E. Pedemonte, and F. M. Willmouth, *Nature* **225**, 538 (1970).
60. J. Dlugosz, A. Keller, and E. Pedemonte, *Kolloid Z. Z. Polym.* **242**, 1125 (1970).
61. C. C. Honeker and E. L. Thomas, *Chem. Mater.* **8**, 1702 (1996).
62. I. W. Hamley, *J. Phys.: Condens. Matter.* **13**, R643 (2001).
63. K. A. Koppi and co-workers, *J. Phys. France II* **2**, 1941 (1992).
64. K. A. Koppi, M. Tirrell, and F. S. Bates, *Phys. Rev. Lett.* **70**, 1449 (1993).
65. K. Almdal and co-workers, *J. Phys. France II* **6**, 617 (1996).
66. A. Nakajima and co-workers, *Macromolecules* **12**, 840 (1979).
67. A. Nakajima, K. Kugo, and T. Hayashi, *Macromolecules* **12**, 844 (1979).
68. J. J. L. M. Cornelissen and co-workers, *Science* **280**, 1427 (1998).
69. M. W. Matsen, *J. Chem. Phys.* **106**, 7781 (1997).
70. K. Liu and co-workers, *Phys. Rev. B* **63**, 060403(R) (2001).
71. M. Park and co-workers, *Science* **276**, 1401 (1997).

72. C. Harrison and co-workers, *J. Vacuum Sci. Technol. B* **16**, 544 (1998).
73. G. Widawski, M. Rawiso, and B. François, *Nature* **369**, 387 (1994).
74. M. W. Matsen, *Curr. Opin. Colloid Interface Sci.* **3**, 40 (1998).
75. K. E. Strawhecker and co-workers, *Macromolecules* **34**, 4669 (2001).
76. A. Böker, A. H. E. Müller, and G. Krausch, *Macromolecules* **34**, 7477 (2001).
77. I. W. Hamley and co-workers, *J. Colloid Interface Sci.* **209**, 255 (1999).
78. R. Limary and P. F. Green, *Langmuir* **15**, 5617 (1999).
79. P. Müller-Buschbaum, J. S. Gutmann, and M. Stamm, *Phys. Chem., Chem. Phys.* **1**, 3857 (1999).
80. D. Ausserré and co-workers, *J. Phys. France* **51**, 2571 (1990).
81. S. H. Anastasiadis and co-workers, *Phys. Rev. Lett.* **62**, 1852 (1989).
82. S. Collins, T. Mykhaylyk, and I. W. Hamley, unpublished work, 2002.
83. N. Rehse and co-workers, *Phys. Rev. Lett.* **87**, 035505 (2001).
84. T. L. Morkved and co-workers, *Science* **273**, 931 (1996).
85. T. Thurn-Albrecht and co-workers, *Science* **290**, 2126 (2000).
86. L. Rockford and co-workers, *Phys. Rev. Lett.* **82**, 2602 (1999).
87. X. M. Yang and co-workers, *Macromolecules* **33**, 9575 (2000).
88. G. G. Pereira and D. R. M. Williams, *Europhys. Lett.* **44**, 302 (1998).
89. D. Petera and M. Muthukumar, *J. Chem. Phys.* **109**, 5101 (1998).
90. Y. Tsori and D. Andelman, *Europhys. Lett.* **53**, 722 (2001).
91. M. S. Turner, *Phys. Rev. Lett.* **69**, 1788 (1992).
92. D. G. Walton and co-workers, *Macromolecules* **27**, 6225 (1994).
93. G. T. Pickett and A. C. Balazs, *Macromolecules* **30**, 3097 (1997).
94. G. H. Fredrickson, *Macromolecules* **20**, 2535 (1987).
95. M. S. Turner, M. Rubinstein, and C. M. Marques, *Macromolecules* **27**, 4986 (1994).
96. H. P. Huinink and co-workers, *Macromolecules* **34**, 5325 (2001).
97. K. J. Hanley, T. P. Lodge, and C.-I. Huang, *Macromolecules* **33**, 5918 (2000).
98. G. Wanka, H. Hoffmann, and W. Ulbricht, *Macromolecules* **27**, 4145 (1994).
99. J. E. Glass, ed., *Water-Soluble polymers: Beauty with Performance*, Vol. **213**, American Chemical Society, Washington, D.C., 1986.
100. I. R. Schmolka, in P. J. Tarcha, ed., *Polymers for Controlled Drug Delivery*, CRC Press, Boston, 1991.
101. M. W. Edens, in Ref. 106, p. 185.
102. M. Malmsten, in Ref. 107, p. 319.
103. P. Molyneux, *Water-Soluble Synthetic Polymers: Properties and Behavior*, CRC Press, Boca Raton, Fla., 1983.
104. S. W. Shalaby, C. L. McCormick, and G. B. Butler, eds., *Water-Soluble Polymers. Synthesis, Solution Properties and Applications*, Vol. **467**, American Chemical Society, Washington, D.C., 1991.
105. J. E. Glass, ed., *Hydrophilic Polymers: Performance with Environmental Acceptability*, Vol. **248**, American Chemical Society, Washington, D.C., 1996.
106. V. N. Nace, ed., *Nonionic Surfactants. Polyoxyalkylene Block Copolymers*, Vol. **60**, Marcel Dekker, Inc., New York, 1996.
107. P. Alexandridis and B. Lindman, eds., *Amphiphilic Block Copolymers: Self-Assembly and Applications*, Elsevier, Amsterdam, 2000.
108. J. E. Glass, ed., *Associative Polymers in Aqueous Media*, Vol. **765**, American Chemical Society, Washington, D.C., 2000.
109. C. Booth, G.-E. Yu, and V. M. Nace, in Ref. 107, p. 57.
110. C. Booth and D. Attwood, *Macromol. Rapid Commun.* **21**, 501 (2000).
111. Z. Tuzar and P. Kratochvil, in E. Matijevic, ed., *Surface and Colloid Science*, Vol. **15**, Plenum, New York, 1993, p. 1.

112. L. Zhang and co-workers, in Ref. 107, p. 87.
113. K. Szczubialka, K. Ishikawa, and Y. Morishima, *Langmuir* **16**, 2083 (2000).
114. P. Guenoun and co-workers, *Eur. Phys. J. B* **1**, 77 (1998).
115. I. W. Hamley, *Introduction to Soft Matter*, John Wiley & Sons, Inc., Chichester, 2000.
116. Z. Tuzar and P. Kratochvil, in W. Brown, ed., *Light Scattering—Principles and Development*, Oxford University Press, Oxford, 1996, p. 327.
117. S. W. Provencher, *Makromol. Chem.* **180**, 201 (1979).
118. J. S. Pedersen, *Adv. Colloid Interface Sci.* **70**, 171 (1997).
119. J. S. Pedersen and M. C. Gerstenberg, *Macromolecules* **29**, 1363 (1996).
120. Y. Liu, S.-H. Chen, and J. S. Huang, *Macromolecules* **31**, 2236 (1998).
121. J. S. Pedersen, *Curr. Opin. Colloid Interface Sci.* **4**, 190 (1999).
122. N. W. Ashcroft and J. Lekner, *Phys. Rev.* **145**, 83 (1966).
123. K. Mortensen and J. S. Pedersen, *Macromolecules* **26**, 805 (1993).
124. L. Leibler, H. Orland, and J. C. Wheeler, *J. Chem. Phys.* **79**, 3550 (1983).
125. P. Linse, *Macromolecules* **26**, 4437 (1993).
126. J. Zipfel and co-workers, *Langmuir* **15**, 2599 (1999).
127. T. Riley and co-workers, *Langmuir* **17**, 3168 (2001).
128. M. V. Seregina and co-workers, *Chem. Mater.* **9**, 923 (1997).
129. L. M. Bronstein and co-workers, *Langmuir* **15**, 6256 (1999).
130. L. Zhang, K. Yu, and A. Eisenberg, *Science* **272**, 1777 (1996).
131. L. Luo and A. Eisenberg, *J. Am. Chem. Soc.* **123**, 1012 (2001).
132. S. Stewart and G. Liu, *Chem. Mater.* **11**, 1048 (1999).
133. B. M. Discher and co-workers, *Science* **284**, 1143 (1999).
134. C. Nardin and co-workers, *Langmuir* **16**, 1035 (2000).
135. K. Mortensen, *Curr. Opin. Colloid Interface Sci.* **3**, 12 (1998).
136. P. Alexandridis, U. Olsson, and B. Lindman, *Langmuir* **14**, 2627 (1998).
137. P. Alexandridis and R. J. Spontak, *Curr. Opin. Colloid Interface Sci.* **4**, 130 (1999).
138. K. Mortensen, *Coll. Surf. A* **183–185**, 277 (2001).
139. I. W. Hamley, *Curr. Opin. Colloid Interface Sci.* **5**, 342 (2000).
140. I. W. Hamley, *Phil. Trans. R. Soc. Lond.* **359**, 1017 (2001).
141. E. Eiser and co-workers, *Phys. Rev. E* **61**, 6759 (2000).
142. P. Holmqvist and co-workers, *Coll. Surf. A* **196**, 39 (2002).
143. J. Noolandi, A.-C. Shi, and P. Linse, *Macromolecules* **29**, 5907 (1996).
144. M. Svensson, P. Alexandridis, and P. Linse, *Macromolecules* **32**, 637 (1999).
145. B. A. C. van Vlimmeren and co-workers, *Macromolecules* **32**, 646 (1999).
146. J. Zhao, B. Majumdar and co-workers, *Macromolecules* **29**, 1204 (1996).
147. P. Kipkemboi and co-workers, *Langmuir* **17**, 5394 (2001).
148. D. Zhao and co-workers, *Science* **279**, 548 (1998).
149. I. W. Hamley, *Adv. Polym. Sci.* **148**, 113 (1999).
150. S. Nojima, M. Ono, and T. Ashida, *Polym. J.* **24**, 1271 (1992).
151. V. Balsamo, A. J. Müller, and R. Stadler, *Macromolecules* **31**, 7756 (1998).
152. P. Rangarajan, R. A. Register, and L. J. Fetters, *Macromolecules* **26**, 4640 (1993).
153. P. Rangarajan and co-workers, *Macromolecules* **28**, 1422 (1995).
154. A. J. Ryan and co-workers, *Macromolecules* **28**, 3860 (1995).
155. V. Balsamo and co-workers, *Macromolecules*, Submitted.
156. I. W. Hamley and co-workers, *Polymer* **39**, 1429 (1998).
157. T. Shiomi and co-workers, *Polymer* **42**, 4997 (2001).
158. Y.-L. Loo, R. A. Register, and A. J. Ryan, *Phys. Rev. Lett.* **84**, 4120 (2000).

159. I. W. Hamley and co-workers, *Macromolecules* **29**, 8835 (1996).
160. I. W. Hamley and co-workers, *Polymer* **37**, 4425 (1996).
161. D. J. Quiram and co-workers, *Macromolecules* **30**, 8338 (1997).
162. Y.-L. Loo, R. A. Register, and D. H. Adamson, *Macromolecules* **33**, 8361 (2000).
163. S.-M. Mai and co-workers, *Macromolecules* **30**, 8392 (1997).
164. M. Gervais and B. Gallot, *Makromol. Chem.* **171**, 157 (1973).
165. A. J. Ryan and co-workers, *Macromolecules* **30**, 1723 (1997).
166. K. C. Douzinas and R. E. Cohen, *Macromolecules* **25**, 5030 (1992).
167. L. Zhu and co-workers, *J. Am. Chem. Soc.* **122**, 5957 (2000).
168. D. J. Quiram, R. A. Register, and G. R. Marchand, *Macromolecules* **30**, 4551 (1997).
169. P. Huang and co-workers, *Macromolecules* **34**, 6649 (2001).
170. L. Zhu and co-workers, *Macromolecules* **34**, 1244 (2001).
171. L. Zhu and co-workers, *Polymer* **42**, 5829 (2001).
172. E. A. DiMarzio, C. M. Guttman, and J. D. Hoffman, *Macromolecules* **13**, 1194 (1980).
173. M. D. Whitmore and J. Noolandi, *Macromolecules* **21**, 1482 (1988).
174. S. Nojima, S. Yamamoto, and T. Ashida, *Polym. J.* **27**, 673 (1995).
175. G. Reiter and co-workers, *Phys. Rev. Lett.* **83**, 3844 (1999).
176. G. Reiter and co-workers, *Euro. Phys. J. E* **2**, 319 (2000).
177. I. W. Hamley and co-workers, *Polymer* **39**, 3321 (1998).
178. J. P. A. Fairclough and co-workers, *J. Chem. Phys.* **114**, 5425 (2001).
179. D. R. Paul and S. Newman, eds., *Polymer Blends*, Academic Press, London, 1978.
180. M. J. Folkes and P. S. Hope, eds., *Polymeric Blends and Alloys*, Blackie, London, 1993.
181. S. Datta and D. J. Lohse, *Polymeric Compatibilizers: Uses and Benefits in Polymer Blends*, Hanser, Munich, 1996.
182. L. A. Utracki, *Commercial Polymer Blends*, Chapman and Hall, London, 1998.
183. H. Hasegawa and T. Hashimoto, in S. L. Aggarwal and S. Russo eds., *Comprehensive Polymer Science. Second Supplement*, Pergamon Press, London, 1996, p. 497.
184. K. I. Winey, E. L. Thomas, and L. J. Fetters, *Macromolecules* **24**, 6182 (1991).
185. K. I. Winey, *MRS Symp. Proc.* **248**, 365 (1992).
186. K. I. Winey, E. L. Thomas, and E. L. Fetters, *Macromolecules* **25**, 2645 (1992).
187. S. Koizumi, H. Hasegawa, and T. Hashimoto, *Macromolecules* **27**, 6532 (1994).
188. M. W. Matsen, *Phys. Rev. Lett.* **74**, 4225 (1995).
189. C.-A. Dai and co-workers, *Phys. Rev. Lett.* **73**, 2472 (1994).
190. M. Sikka and co-workers, *Macromolecules* **30**, 445 (1997).
191. M. D. Dadmun, *Macromolecules* **33**, 9122 (2000).
192. R. B. Thompson and M. W. Matsen, *Phys. Rev. Lett.* **85**, 670 (2000).
193. C. W. Macosko and co-workers, *Macromolecules* **29**, 5590 (1996).
194. F. S. Bates and co-workers, *Phys. Rev. Lett.* **79**, 849 (1997).
195. M. A. Hillmyer and co-workers, *J. Phys. Chem. B* **103**, 4814 (1999).
196. J. H. Lee and co-workers, *Macromolecules* **34**, 6557 (2001).
197. F. S. Bates and co-workers, *Phys. Rev. Lett.* **75**, 4429 (1995).
198. M. W. Matsen, *J. Chem. Phys.* **110**, 4658 (1999).
199. R. B. Thompson and M. W. Matsen, *J. Chem. Phys.* **112**, 6863 (2000).
200. K. Krishnan and co-workers, *Phys. Rev. Lett.* **87**, 098301 (2001).
201. T. L. Morkved and co-workers, *J. Chem. Phys.* **114**, 7247 (2001).
202. T. Hashimoto and co-workers, *Macromolecules* **26**, 2895 (1993).
203. S. Koizumi, H. Hasegawa, and T. Hashimoto, *Macromolecules* **27**, 4371 (1994).
204. D. Yamaguchi and co-workers, *Macromolecules* **34**, 1707 (2001).

205. D. Yamaguchi and T. Hashimoto, *Macromolecules* **34**, 6495 (2001).
206. D. Yamaguchi, H. Hasegawa, and T. Hashimoto, *Macromolecules* **34**, 6506 (2001).
207. M. W. Matsen, *J. Chem. Phys.* **103**, 3268 (1995).
208. A. D. Vilesov and co-workers, *Macromol. Chem. Phys.* **195**, 2317 (1994).
209. A.-C. Shi and J. Noolandi, *Macromolecules* **28**, 3103 (1995).
210. M. W. Matsen and F. S. Bates, *Macromolecules* **28**, 7298 (1995).
211. H. Frielinghaus and co-workers, *Europhys. Lett.* **53**, 680 (2001).
212. H. Frielinghaus and co-workers, *Macromolecules* **34**, 4907 (2001).
213. P. D. Olmsted and I. W. Hamley, *Europhys. Lett.* **45**, 83 (1999).

I. W. HAMLEY
University of Leeds

BLOW MOLDING

Introduction

Blow molding is defined as a plastic process whereby a thermoplastic material is heated to its forming temperature, which is below that of the plastic materials being used; at its melting point it is made to form a hollow tube called a parison or preform. This heated homogeneous plastic material is then placed between two female molds that are cooled through some medium. The two female molds close on the heated parison or preform and a gas, usually air, enters via an open end of the parison via a blow pin or needle; the gas is blown into the closed female mold halves, taking the shape of the internal female closed mold, allow to cool, and is then sent out through an exhaust. The two female molds are then separated and the cooled, shaped hollow part is then ejected or allowed to drop out for the cycle to repeat.

In the first attempt over 100 years ago, to blow-mold hollow objects, two sheets of cellulose nitrate were clamped between two female mold halves. Steam injected between the sheets softened the material, sealed the edges, and expanded the heated sheets to form the inside shape of the two female mold halves. The high flammability of cellulose nitrate, however, limited the usefulness of this technique.

In the early 1930s, more suitable materials, such as cellulose acetate and polystyrene (PS), were developed; these led to the introduction, by Plax Corp. and Owens-Illinois, of automated equipment based on glass-blowing techniques. Unfortunately, the high cost and poor performance of these materials discouraged rapid development; they offered no advantage over the glass bottles. Finally, the introduction of low density polyethylene (LDPE) in the mid-1940s provided the advantage of squeezability, which glass could not match.

Encyclopedia of Polymer Science and Technology. Copyright John Wiley & Sons, Inc. All rights reserved.

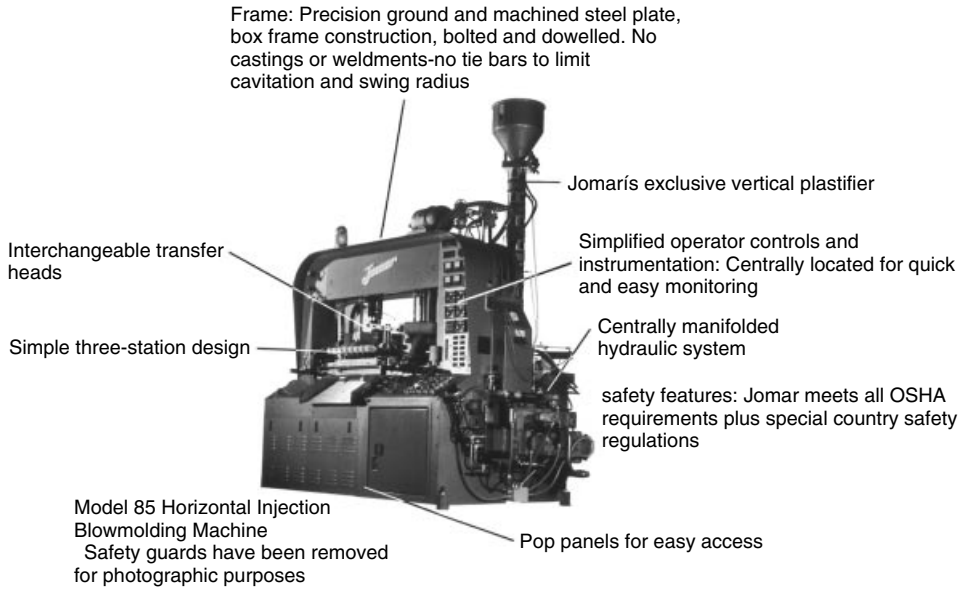

Fig. 1. Three-station injection blow-molding machine utilizing a vertical screw produced by Jomar, Pleasantville, N.J., U.S.A.

The first item to use LDPE was an underarm deodorant named Stoppette; the bottle was blow molded by the Plax Corp. In the first year, over 5 million units were sold and the blow-molding industry was born.

In the early 1950s, high density polyethylene (HDPE) was developed and today blow molding is the largest user of HDPE, which is the largest volume thermoplastic produced in the world, with over a billion pounds produced worldwide.

Blow molding, until the last few years, was the main plastic process utilized to produce a hollow object. In the past few years, other plastic processes, such as rotational molding and twin sheet thermoforming, have evolved with technical achievements and plastic raw materials improvements to where today, they can compete with blow molding for many uses as toys, gasoline tanks, holding tanks, etc.

The injection blow-molding (IBM) machines shown in Figures 1 and 2, even though produced by different injection blow-molding machinery manufacturers, can use tooling designed for either machine with slight mold design changes because of the bolt pattern or the platens used by each independent IBM machinery producer. There is no standard bolt pattern in the blow-molding industry for mounting the necessary tooling in the machines.

Resins

Most thermoplastic resins in use in the plastics industry can be blow-molded. Naturally, several resins are the leaders. HDPE is used in over 57% of the blow-molding market. In the year 2000, there was over 7021 million pounds of HDPE produced domestically. Poly(ethylene terephthalate) (PET) follows with over 33%

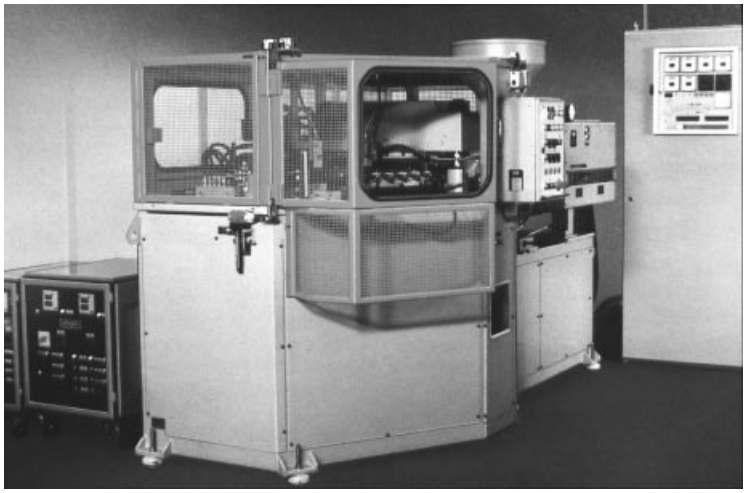

Fig. 2. Three-station injection blow-molding machine utilizing a horizontal reciprocating screw produced by Bekum, Berlin, Germany.

of the blow-molding market. In the year 2000, there was over 1720 million pounds of PET produced domestically.

Thus, these two plastic resins are used in slightly over 90% of the blow-molding industry. All the other thermoplastic resins such as polypropylene (PP), polystyrene (PS), poly(vinyl chloride) (PVC), acrylic–butadiene–styrene (ABS), acetal, polycarbonate (PC), low density polyethylene (LDPE), polysulfone, and others, all combine for the other uses in the approximate 10% blow-molded industry.

Examples would be gallon milk containers (HDPE), soft drinks (PET), gasoline tanks (HDPE), detergents, bleach, household chemicals (HDPE), automotive interiors (PP and ABS), mascara containers (ABS, PVC, HDPE), gas tanks for small yard mowers (nylon) to familiarize the reader with various markets. Naturally, the choice of resin used is based on performance, cost, barrier, availability, cleanliness, processing, transparency, and strength. The fastest growing markets at present are the automotive gasoline tanks, the 55-gallon drums (both HDPE) and the 20-oz soft drink products, the pint milk bottle (both PET). The beer market is just starting with specialty marketing.

Processes

There are three main processes used by the blow-molding industry to supply containers and hollow products to the blow-molding market: injection blow molding, extrusion blow molding, and stretch blow molding.

Generally, injection blow molding is used for small bottles and parts less than 500 mL in volume. The process is scrap-free, with extremely accurate control of weight and neck finish. However, part proportions are limited and the method is impractical for containers with handles and tooling costs are relatively high.

Extrusion blow molding, the most common process, is used for bottles or parts 250 mL in volume or larger. Tanks as large as 1040 L (275 gal) weighing

Table 1. Injection Blow Versus Extrusion Blow

Injection blow	Extrusion blow
Injection molded neck finish	Blown neck finish or calibrated neck finish
Scrap free	Must trim off tail and moilles
No pinch mark	Pinch mark which can be an area of the container for failure
Fast cycles for high output	Slower cycle
Tool cost relatively expensive	Tool cost relative low with use of aluminum molds
No handle ware	Handle ware of many sizes and shapes
Excellent surface finish or texture	Good surface area or texture
No die lines	Possible die lines due to extrusion of parison
Ease of automation for decorating and packing	Automation may be cumbersome and use large floor space
Small floor space	Greater floor space utilized

120 kg (265 lb) have been blow-molded; tooling is less expensive, and part proportions are not severely limited. Containers with handles and off-set necks are easily fabricated. On the other hand, flash or scrap resin must be trimmed from each part and recycled. Operator skill is more crucial to the control of part weight and quality. The two processes are compared in Table 1.

Stretch blow molding is used for bottles between 237 L (8 oz) and 2 L (67.6 oz) in size, and occasionally as large as 25 L (6.6 gal). The molecular biaxial orientation of certain resins enhances stiffness, impact, and barrier performance, and permits weight reduction.

Injection Blow Molding

In injection blow molding, melted plastic resin is injected into a parison cavity and around a core rod. This test-tube-shaped parison, while still hot, is transferred on the core rod to the bottle blow-mold cavity. Air is then passed through the core rod, expanding the parison against the cavity, which, in turn, cools the part.

Early injection blow-molding two-position techniques used adaptations of standard injection-molding equipment fitted with special tooling. The Piotrowski method used a 180° rotating arbor with two sets of core rods and one set of parison and bottle cavities. The Farkas, Moslo, and Gussoni methods used an alternating shuttle with two sets of core rods, one set of parison cavities, and two sets of bottle cavities. The difficulty with these methods was that the injection-mold and blow-mold stations stood idle while the finished parts were removed. In 1961 in Italy, Gussoni developed the three-position method, which used a horizontal 120° indexing head with split-mold parison and bottle cavities and three sets of core rods. The third station was intended for removal of the part, and the parison- and bottle-molding phases were completed simultaneously. A special machine was required, and by the late 1960s, this technique was perfected; it is the principal system used today. A layout of the standard three-station machine is seen in Figure 3.

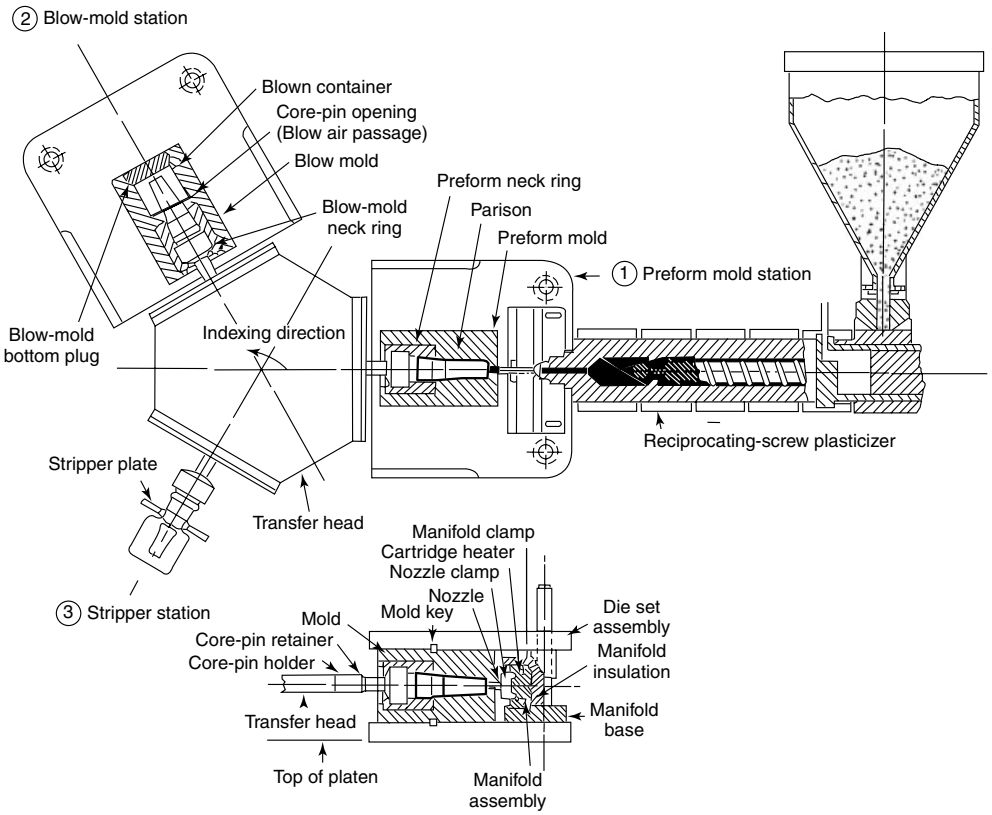

Fig. 3. A typical three-station injection blow-molding machine. Courtesy of Rainville Operation, Hoover Universal, Inc.

The three-position injection blow molding machine was upgraded to have four stations through companies as Larson Mardon Wheaton, Bekum, and Uniloy Milacron. The addition of the fourth station allowed for faster cycle times since the rotating table containing the core rods only indexed 90° instead of 120° as on the third station. The addition of fourth station was placed after the eject station and prior to the injection station. This additional station also could be used as a safety station to ensure the core rods were free of any debris. This station could also be used for in-mold decoration and also for conditioning the core rods prior to moving to the inject station to have a parison injection molding onto each core rod. The four-station machine is depicted in Figure 4.

One of the main features one should always be cognizant of is the dry cycle time of the machine. The *dry cycle time* is the time that it takes to open the clamp, raise the rotating table, index to the next station, drop the rotating table into position, and close the clamp or mold halves. There is no processing during the dry cycle. Processing time will add to the dry cycle time. Normally, on a three-station machine, the dry cycle time will vary from 2.8 to 3.5 s. On a four-station machine the dry cycle may range from 1.8 to 2.6. s. Larson Mardon Wheaton has taken this a step farther by designing and building their own all-electric machine. Their new all-electric four-station machine can dry cycle from 1.1 to 1.8 s depending

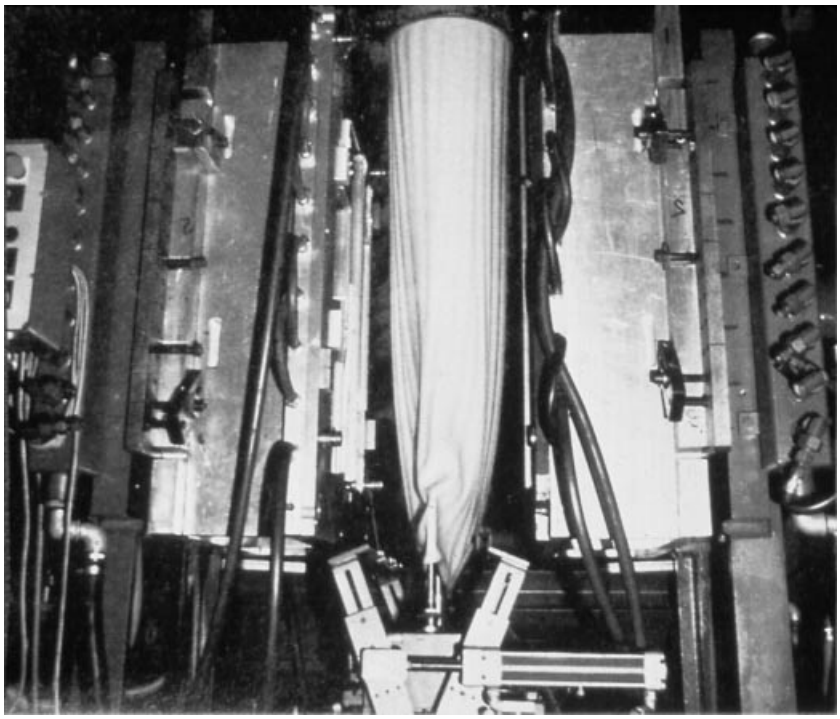

Fig. 4. Four-station layout.

on the size of the machine, whether it be a 15 or 180 ton. The tonnage relates to the clamp tonnage at the inject station plus the addition of the blow-mold clamp station. The injection station utilizes the greater tonnage. For example, a Larson Mardon Wheaton four-station may have 150 ton at the inject station and 30 ton at the blow-mold station. Together, the machine is rated at 180 ton. The Uniloy Rainville (85-3) three-station machine has 68-ton clamp at the injection station and 17-ton clamp at the blow-mold station, which added together to be the 85-ton machine. Figure 5 is a typical time or cycle sequence for an injection blow-molding machine.

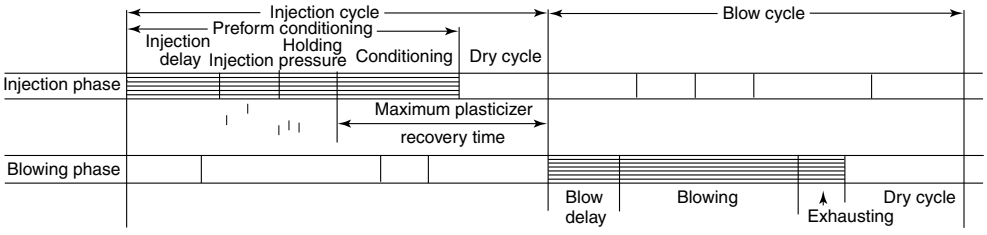

Fig. 5. Time sequence of injection blow molding. Courtesy of Rainville Operation, Hoover Universal, Inc.

Injection blow-molding machines are manufactured by Uniloy Milacron, JOMAR, Nissei, and Bekum for sale in the blow-molding industry. Several companies produce and use their own as Larson Mardon Wheaton and Captive Plastics and are not offered for sale. Injection blow-molding is normally considered when the container to be produced is 8 ounce (0.24 L) or under. The advantages and disadvantages of injection blow molding when compared to extrusion blow molding are listed in Table 1.

Injection Blow-Mold Tooling

Injection blow-molding requires two molds: one for molding the preform or parison, and the other for molding the bottle. The preform mold consists of the preform cavity, injection nozzle, neck-ring insert, and core-rod assembly. The blow mold consists of the bottle cavity, neck-ring insert, and bottom-plug insert (see Figs. 6–10).

The preform cavity design is governed by four basic rules or constraints. The first rule concerns the core-rod or cavity length-to-diameter ratio, which ideally approximates 10:1 or less. This ratio is frequently based on the overall height and the neck-finish diameter of the bottle. It ensures a minimum of core-rod deflection from injection pressures, which, in turn, provides uniform wall distribution and heat. Higher ratios have been used, but often require sliding pins to momentarily center the end of the core rod during the injection phase.

The second rule concerns the ratio of preform size to maximum bottle size, ie, blow-up ratio, which ideally is 3:1 or less. Most often, it is based on the maximum bottle diameter, width, or depth, and the neck-finish diameter. Maintaining this ratio provides uniform and consistent bottle cross-sectional wall distribution. If

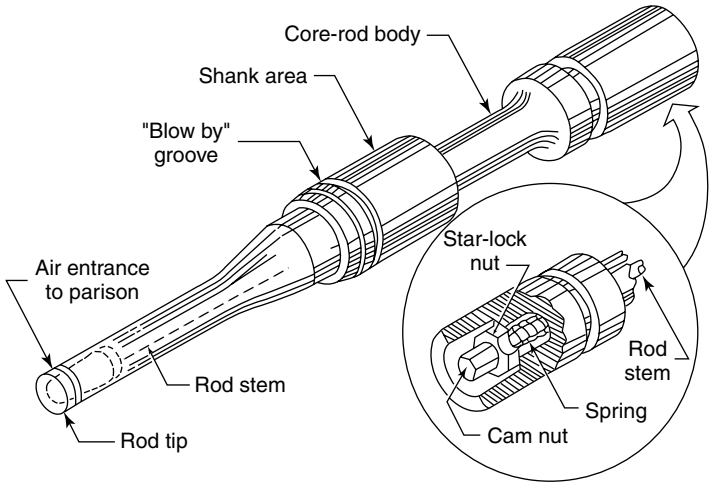

Fig. 6. Typical bottom-blow core rod and its principal elements. The core-rod tip mechanism that closes the air passage during the parison-injection cycle is shown enlarged at right (17). Courtesy of Plastic Engineering.

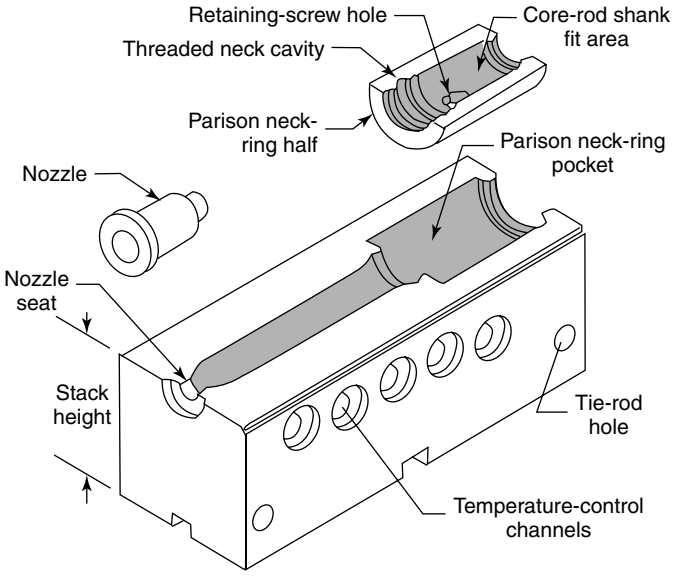

Fig. 7. Exploded view of one-half of a parison-mold cavity, with nozzle and neck-ring details.

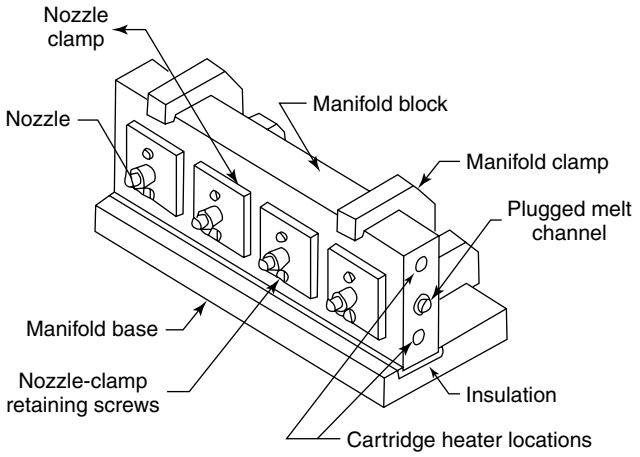

Fig. 8. Injection manifold for injection molding of parisons. Individual nozzles are clamped to the manifold block, which houses a hot runner for the melt.

the ratio is higher, the parison tends to float around during expansion, which therefore increases the chances of an eccentric wall distribution.

The third rule concerns the parison wall thickness, ideally between 2 and 5 mm. A wall thicker than 6 mm is difficult to temperature-condition and may act unpredictably during expansion. A wall less than 2-mm thick may also act unpredictably. For a given weight, a thin wall also increases the projected area, and thus possibly exceeds the capacity of the press.

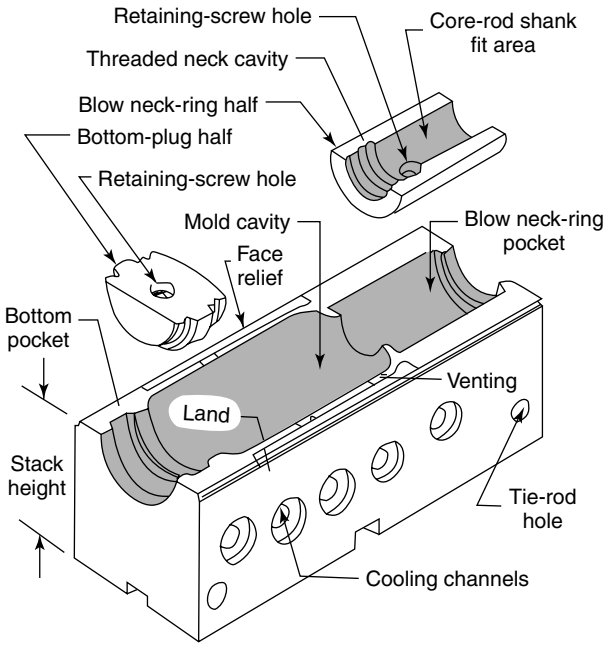

Fig. 9. Exploded view of one-half of an injection blow mold, with details of bottom plug and neck ring.

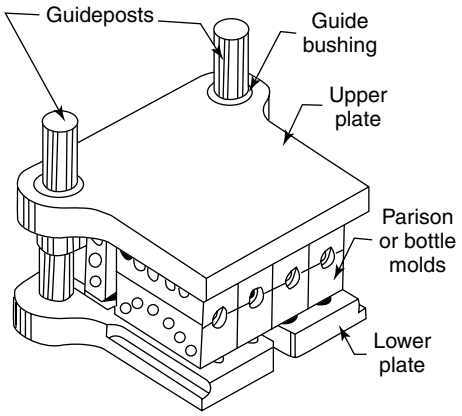

Fig. 10. Die set for manufacturing position and alignment of injection blow-mold cavities.

An important advantage of injection blow molding is the diametrical and longitudinal programming of the parison by shaping the parison mold cavity or core rod, or both. This is particularly important with oval bottles and leads to the fourth rule: in an annular cross-section, the heaviest area should not be more than 30% thicker than the lightest area. Generally, the shaping is done in the cavity and the core rod is round. With a higher ratio, the selective fill of material during the injection phase causes a vertical weld line in the bottle. Avoiding this

condition, in turn, restricts the bottle ovality to 2:1, that is, the width should not exceed two times the depth.

In multiple-cavity arrangements, each parison cavity is fitted with an injection nozzle of decreasing sizes. Material flow through the injection manifold is balanced, thus allowing each cavity to be filled at an equal rate.

The neck-ring insert has four functions: (*1*) it forms the finish or threaded neck section of the bottle; (*2*) because it is an insert, it provides a relatively low cost, easy method to change the size or style of the finish; (*3*) it firmly centers and locates the core rod in the parison cavity; and (*4*) it provides venting and a thermal break.

During the process, the neck-finish area of the parison must be cooled to retain its shape; the remainder of the parison is kept hot for later expansion in the bottle cavity. Depending on the plastic molding material, the temperature of the parison is between 65 and 135°C. The neck-ring insert is at times cooled as low as 5°C. The water lines for both the cavity and the neck-ring are usually drilled as closely together as possible, perpendicular to the cavity axis. The water flows from one cavity to the next.

The core-rod assembly also have four functions: (*1*) it forms the interior of the preform; (*2*) it supports the parison or the bottle during transfer; (*3*) it supplies the valve where air enters to expand the parison (the valve is located in the shoulder area or the tip, depending on the shape of the bottle or the ratio of the core-rod length to diameter; wide-mouth bottles, ie, core rods with low length-to-diameter ratios, are usually equipped with a shoulder valve); and (*4*) it has a "blow by" groove. This annular groove, located near the seating shank, 0.1–0.25 mm deep, is needed to seal the parison to prevent excessive air loss during blowing and to eliminate elastic retraction of the parison during the transfer between cavities.

Various materials are used to construct the parison cavity and core rods. For nonrigid polyolefin resins, the parison cavity is made of prehardened P-20 tool steel with a hardness of 31–35 HRC. For rigid resins, the parison cavity is made of A-2 tool steel, air hardened to 52–54 HRC. The neck-ring insert for most resins is made of A-2 tool steel. The core rod, for greater strength, is made of L-6 tool steel, hardened to 52–54 HRC. In all cases, the cavity surfaces are highly polished and chromium-plated, except for the neck-ring insert for polyolefin resins, which is occasionally sandblasted with a No. 120 grit.

The cavity defines the final shape of the bottle. The only design constraint is that the cavity width should not exceed two times the depth. To compensate for resin shrinkage after molding, the cavity dimensions are slightly enlarged. Specific shrinkage rates vary with the resin type and process conditions. For nonrigid polyolefin resins, shrinkage is between 1.6 and 2.0%; for rigid resins, 0.5% shrinkage is added. Slightly higher rates are usually applied to the heavier neck-finish dimension than to the body.

Vents are placed along the mold-parting surface to allow the escape of trapped air between the expanding parison and the cavity. If these are too deep, an objectionable mark is left on the bottle. Because an air pressure of 1 MPa (145 psi) is used in injection blow molding, these vents are kept less than 0.05-mm deep.

The neck-ring insert is used in the bottle cavity in a manner similar to its use in the parison cavity, although they are not identical. The thread diameter dimensions in the bottle cavity are 0.05–0.25 mm larger than in the parison cavity.

Unlike the parison neck-ring, the bottle neck-ring does not form the finish detail, but only secures the already-formed neck. The additional size provides clearance, reducing the change of distortion.

The bottom-plug insert forms the bottom or push-up area of the container; in some molds, this insert must be retractable. Generally, the push-up of polyolefin bottles can be stripped without side action if the height is less than 5 mm. With rigid resins, this height is reduced to 0.8 mm. When side action is required, an air cylinder, cam, or spring mechanism is used.

Aluminum, steel, or beryllium–copper is used for the bottle cavity and neck ring. For polyolefin resins, aluminum No. 7075, as well as QC-7, is used. The surface is usually finished with No. 120-grit sandblast, which increases the venting of trapped air. For rigid resins, A-2 tool steel air-hardened to 52–54 HRC is used. The surface finish is highly polished with chromium plating. Cast beryllium-copper is often used for minute detail. As with the parison cavity, water lines are drilled as closely together as possible, perpendicular to the cavity axis.

The parison and bottle molds are mounted onto a die set, which is then mounted to the platens of the injection blow molder. Keyways in two directions, on the upper and lower platens, are used to precisely position the cavities. Guideposts and bushings maintain precise alignment between the plates. To speed the operation, the entire die set or mold assembly is exchanged during a job change. It is considered false economy to reuse the die set with another mold set.

Injection blow-mold tooling must be designed for very precise tolerances, with dimensions often held to ± 0.015 mm, otherwise bottle quality will be inconsistent. For example, the core rods must be located closely fore and aft, and left and right of centerline of the parison and bottle cavities. If too tight, the mold could be damaged or the assembly might bind. If too loose, resin could flash around the shank area of the core rod, or the core rod could shift sideways, causing uneven wall distribution. In addition, many parts and sections of the mold setup must fit together and be interchangeable. Several core rods must fit the pocket of the parison or bottle cavities. These core rods are stacked alongside each other on a face bar. Clearly, the need for precision is the most crucial factor in the high cost of injection blow-mold tooling. However, once properly assembled, the injection blow-mold process can provide high yield and trouble-free production. Additional tooling for setup of the injection blow-molding machine would include the stripper plate (see Figs. 11 and 12) for stripping the formed containers from the core rods. The stripper consists of a stripper base and a stripper plate plus the screws and washers. On most machines the stripper is able to rotate 90° downward to

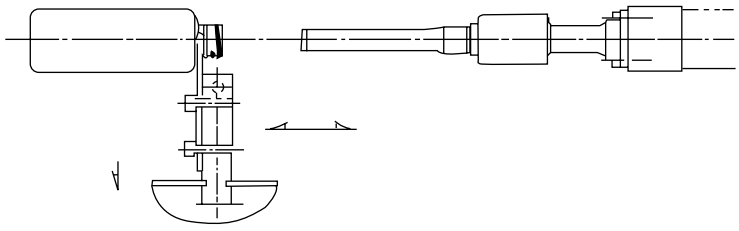

Fig. 11. Stripper action.

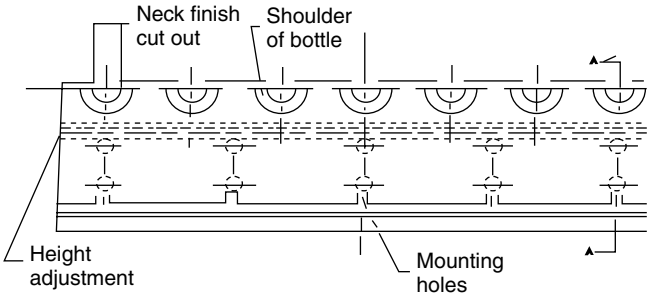

Fig. 12. Stripper plate.

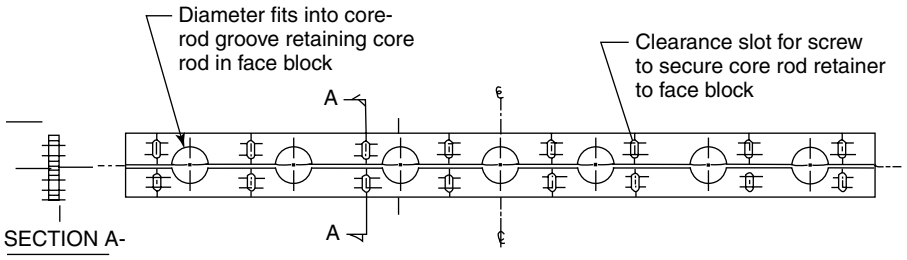

Fig. 13. Face bar.

deposit the product onto a conveyor, etc. We refer to this stripper as a stripper/tipper.

Figure 11 shows the blown bottle being ejected with the stripper moving out, and once the bottle is dropped into a container or on a conveyor belt, the stripper returns for the next cycle. Figure 13 shows a face bar which mounts to the rotating table (three-station machine requires three face bars and a four-station machine requires four face bars) to hold the core rods.

Figure 14 shows the retainers that fit over the rear shank of the core rod and hold the core rod in place on the face bar. In some instances, possibly because of core rod damage it may be necessary to use a face block plug. However, the manifold also has to be plugged for this same cavity.

By reviewing all the tooling essential for injection blow-molding, one can easily understand why it is more expensive than the extrusion blow-molding process. However, the injection blow-molding process yields a process that produces scrap-free, high volume containers that have the best neck finish dimensions and details in the blow-molding industry. Roll-on-deodorant containers are evidence of this statement.

Troubleshooting Injection Blow Molding. Injection blow-molding is no different than any other plastic process as to troubleshooting the process. One should first analyze as to what you feel is the problem and then approach the problem systematically. In approaching the problem, you should only make one change at a time and after the change, provide adequate time for the change you made to show its effect.

Below is a list of items or problems that are some-what common in the injection blow-molding process with possible solutions to the happening. The list is a

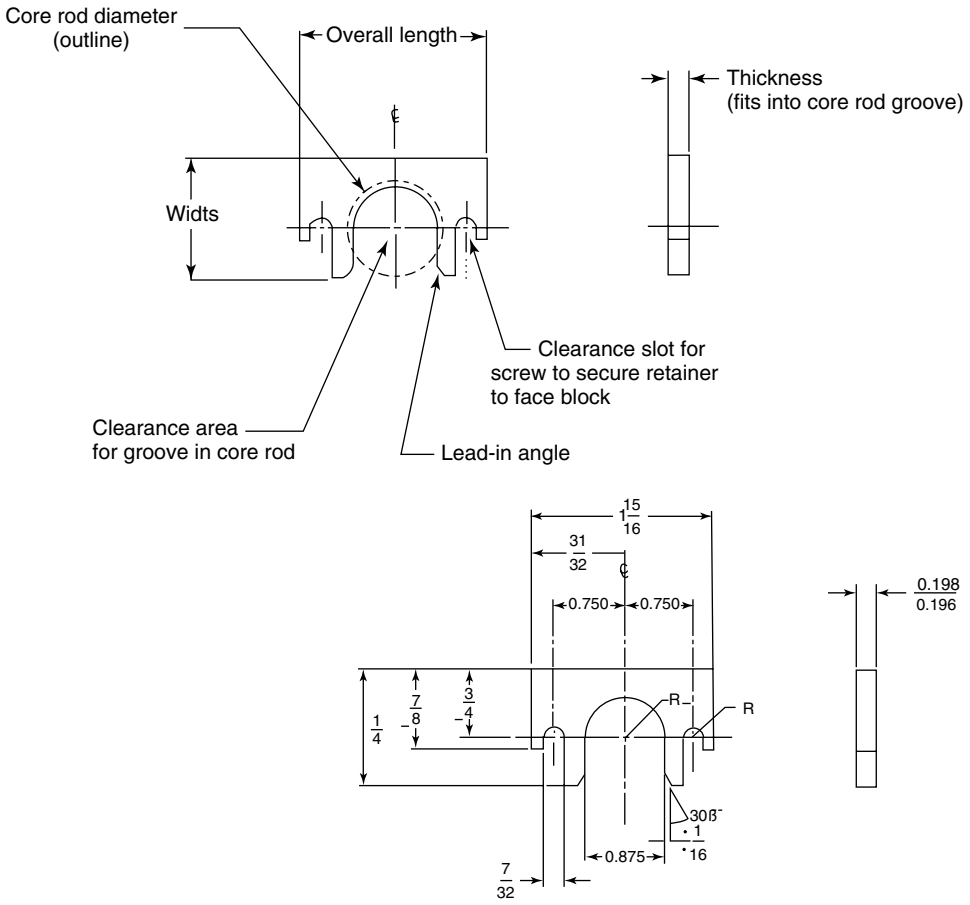

Fig. 14. Core-rod retainer.

guide and is not inclusive as machines and materials change along with controls. Always keep in mind, your injection-molding parisons and if you make a good parison, you should make a quality container.

Problem	Solution
Short shots	Out of material in the barrel
	Hopper out of material
	Material is budging
	Material slide not open
	Material too cold
	Secondary gates dirty or not large enough
	Inadequate venting
	Shot size not adequate
Sink marks in parison	Material not homogeneous
	Not adequate packing time or pressure
	Inadequate venting

Problem	Solution
Streaks in parison	Mold dirty
	Regrind or material fines
	Cavity damaged
	Melt not homogeneous
	Injection pressure too high or too fast
Stringing of gate of parison	Melt temperature is too high in secondary nozzle or manifold
	Secondary gate too large
Parison stuck to core rod	Melt temperature too hot
	Parison mold coolant not adequate or at proper temperature
	Core rod cooling not adequate
Parison tip too large to compress	Reduce land in secondary gate
	Move secondary nozzle in toward the parison
	Reduce land in end cap on spherical nozzles
Product torn	Lower gate temperature
	Check core rods
	Check nozzle seats
	Check parting line of parison and blow mold
	Add injection time
	Replace nozzle
Weak spot in center of product	Lower gate temperature
	Check parison body temperature
	Lower parison body temperature
	Add more injection time and pack time
	Lower injection pressure
	Decrease back pressure
Heavy section in product	Raise gate temperature
	Decrease core rod cooling
	Raise temperature in parison body
Push up not consistent	Increase blow time
	Increase blow pressure
	Increase bottom plug cooling
	Reduce gate temperature
	Add core rod tip cooling
	Lengthen cycle time
	Check vents
Rocker bottoms	Flash
	Vent
	Improper cooling
	Mold dirty
	Increase cycle time
	Check exhaust-possibly add exhaust time
	Check core rod openings
Bottom folds	Increase blow pressure
	Check core rod openings
	Reduce injection pressure
	Increase temperature in parison mold at fold location

Problem	Solution
Surface finish	Dirty molds
	Venting
	Material not homogeneous
	Temperature of parison too cold
	Increase blow pressure
	Increase cycle time
Dips in finish	Parison not packed
	Vents
	Neck rings too cold
	Increase pack time
Cracked necks	Raise melt temperature
	Increase parison neck ring temperature
	Retainer grooves on core rod too deep
Cocked necks	Increase blow pressure
	Increase blow time
	Check bottom plug movement
	Increase cooling on blow mold products body
Shrinkage	Increase blow time
	Decrease blow mold temperature
	Increase pack pressure
	Increase pack time
	Lower parison mold temperature
Flash	Melt too hot
	Injection pressure too high
	Molds not flat
	Vents too deep
	Clamp not adequate
	Platens not aligned
	Mold damaged
Parison sag (parison parting line and blow mold parting line do not overlap)	Decrease melt temperature
	Redo parison cooling lines for more balance
	Venting
	Add packing pressure
	Melt not homogeneous
	Check for nozzle uniform flow
Nozzle freeze-off	Contamination
	Damaged nozzle
	Temperature too low
	Manifold dirty
	Thermocouple malfunctioning
Stripping	Decrease blow time
	Retainer grooves too deep
	Increase pressure to stripper
	Lubricate stripper
	Check core rods for damage
Weld lines	Raise manifold temperature
	Raise parison mold temperature
	Raise injection pressure

Problem	Solution
Parting line	Increase pack time Increase secondary nozzle opening Molds damaged Molds not aligned Molds not flat Clamp pressure inadequate

Setup for Injection Blow Tooling. When doing a setup, whether it be for injection molding, blow molding, or extrusion, one should always strive to do the setup so that there are areas that can be used if needed in the process. Short cuts should not be taken in doing your setup.

In setting up the injection parison mold, a separate cooling line should be used for the neck rings, the parison end cap, and the zone immediately above the end cap. The temperature of the parison that is going to be blown needs to be controlled as uniformly as possible. If core-rod cooling is utilized, then a separate cooling unit should be utilized for the core rods.

In the blow mold, a separate cooling line should be used on the neck rings, the bottom plug, and the containers body.

It is recommended that all secondary nozzles from the manifold to the parison injection mold have a smooth bore so no material can be stagnant or hung up, nor be sheared. Each secondary nozzle should have its own heater band and thermocouple control. The manifold should have two deep well thermocouples that are averaged together to ensure that the manifold maintains an even melt temperature.

It is a good idea to have all the die sets nickel-coated plus the water lines. This will prevent rust within the die sets, which leads to pitting of the machine platen. This also prevents rust and mineral deposits from forming in the mold water lines.

The future of injection blow-molding will see a 3–5% growth. The machines will be redesigned to be all-electric based on the all-electric injection machines. The shortage of electrical power and its rising costs will force machine producers plus their customers to reduce energy use and costs. It is well documented that the all-electric injection machines reduce energy use by 30–35%, thus injection blow will follow the injection-molding machine lead into this industry.

Extrusion Blow-Molding

In extrusion blow molding, homogeneous melted thermoplastic resin is extruded as a tube into the air. This tube, called a parison, is captured between two mold halves that are of the female type. Gas usually air, enters as the female molds are closed, either through a blow pin or needle, and expands the homogeneous melted thermoplastic into the female mold halves, taking design of whatever is cut into the two female mold halves, alllowed to cool, then the gas is exhausted, the molds

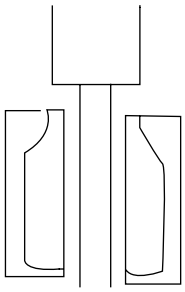

Fig. 15. Extrusion blow-molding process.

open, and exits the cooled desired product. Unlike injection blow molding, this process produces flash or trim off, that has to be trimmed and reclaimed. This excess is formed when the heated parison is pinched together at the bottom and top of this heated hollow tube. In some cases, there can be flash or trim on the entire periphera of the product to be formed (ie, automotive gasoline tanks) (See Fig. 15).

There are basically two different machines offered in the extrusion blow-molding industry. They are intermittent and continuous.

In continuous extrusion blow molding, the extruder or plastifier is running continuously and forming a parison continuously. The continuous extrusion provides the most homogeneous heated parison as the heated thermoplastic material is moving constantly with the least amount of residence time on the heated thermoplastic material. This method is employed to produce containers as on Bekum & Kautex; shuttle blow-molding machines such and on large industrial machines

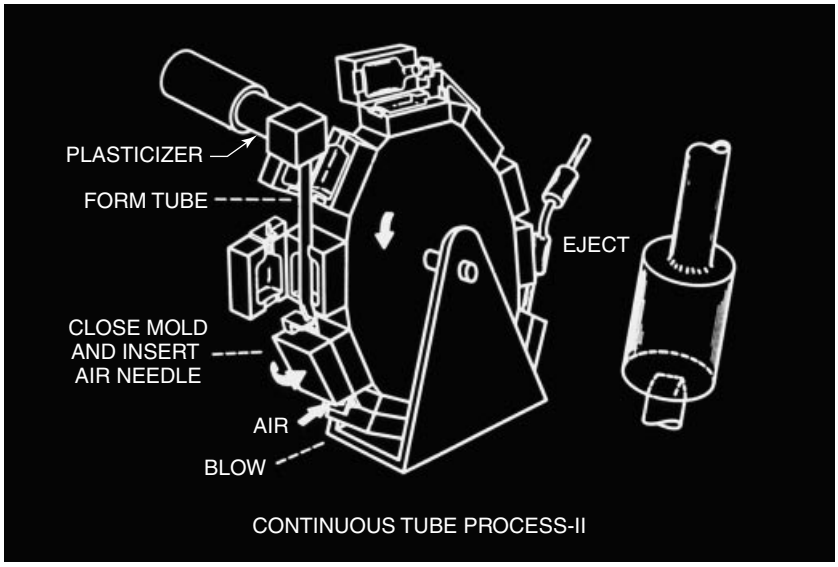

Fig. 16. Schematic of a rotary or wheel machine with continuous extrusion of the parison. Number of blow molds depends on size of wheel diameter and extruder size for output.

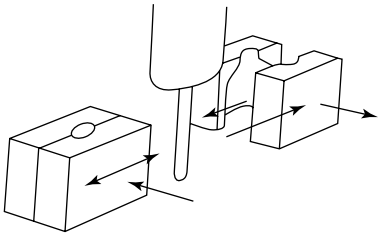

Fig. 17. Depicts a continuous extruded parison with blow molds that shuttle right or left, cut the parison, capture the cut parison in the closed blow mold and move right or left to blow the container.

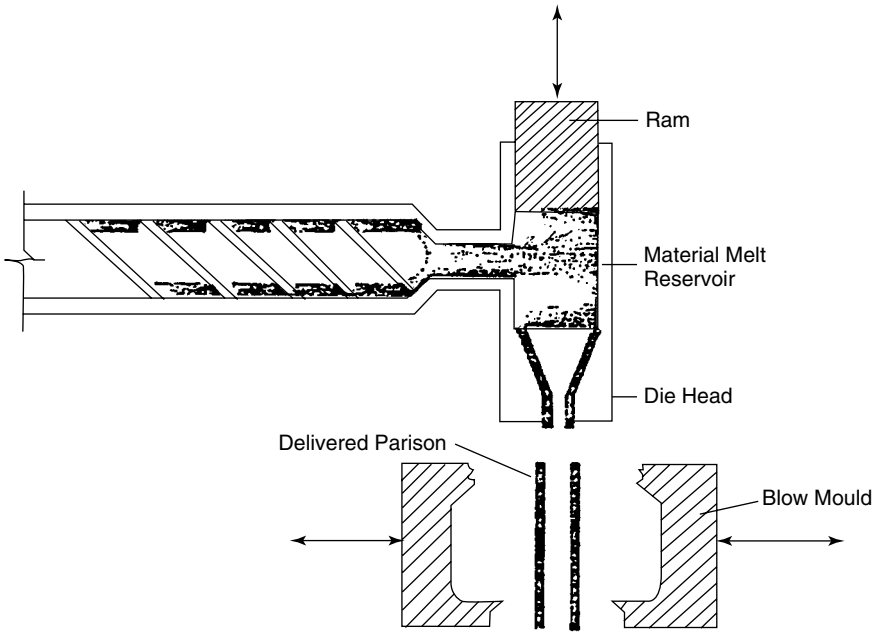

Fig. 18. Intermittent extrusion blow molding.

such as wheels produced by Uniloy Milacron, Plastipak, Graham & Owens Brockway. It is also used by Bekum, Kautex, Wilmington, Uniloy Milacron, Graham, Davis Standard, and Jackson Machinery to produce containers such as automotive gasoline tanks, holding tanks, 55-gal drums (see Figs. 16 and 17).

A reciprocating screw extrusion blow-molding machine sketch is shown in Figure 18. This is the process where the parison is extruded, then the blow molds cut the parisons and close, and the containers are then blown. Only after the blow molds open and the blown containers exit the machine is the parison once again extruded (see Fig. 18).

In intermittent extrusion blow molding, the parison is formed immediately after the blow-molded product is removed from the blow mold in most machines. In some large machines, the parison is cut and closed within the blow mold and then

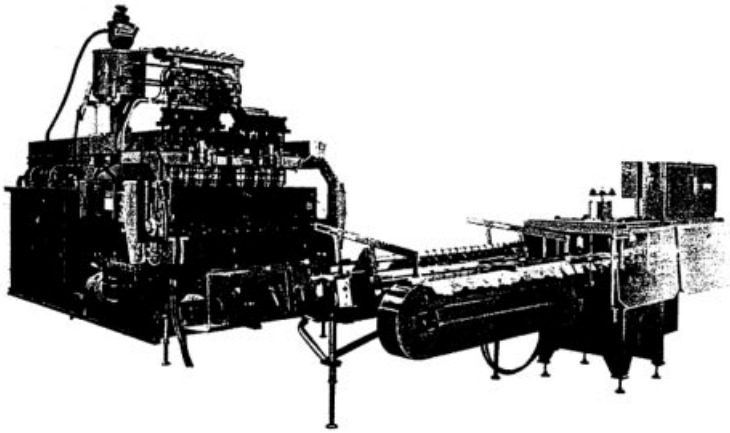

Fig. 19. Uniloy 350R2 8-head intermittent extrusion blow molder for the manufacture of 2-L (0.5-gal) milk bottles with handles. Production rates of over 65 bottles/min have been achieved; also shown is the flash trimmer. Courtesy of Hoover Universal, Inc..

the blow mold moves out from under the parison head tooling to allow another parison to be formed. Because of the stop and start of the parison, this method is normally not employed to use heat-sensitive materials, such as PVC. It is more suitable for heat-stable materials, such as HDPE, and ABS. Examples are gallon milk containers, automotive ducts, 5-gal water containers (polycarbonate).

The intermittent process utilizes a reciprocating-screw plastifier. After the parison is formed, the screw moves back (or recovers) accumulating new homogeneous melt in front of its tip. Once the blow mold exits the product, the signal is given for the plastifier to form a new parison. The screw will then move forward as a ram forcing the plastic melt through the extrusion head forming the next parison. At present, up to 12 parisons can be formed simultaneously. A reciprocating screw extrusion blow molder for a dairy bottle is shown in Figure 19.

Another modification is the ram-accumulator method, although no longer in widespread use. It is intended for parts weighing 2 kg or more. This system, much like the reciprocating-screw method, is used to extrude quickly heavy parisons that might sag or be deformed by their own weight. The accumulator is a reservoir mounted alongside the extruder. A piston or plunger pushes the melt through the extrusion head. In this method, unlike the reciprocating-screw process, melt that enters the reservoir first is last to leave. As a result, melt history of the resin is not uniform.

The accumulator head (see Fig. 20) has replaced the ram accumulator in its application for heavy parts. The tubular reservoir is a part of the extrusion head itself. Plastic melt that enters the head first is first to leave. A tubular plunger quickly extrudes the melt from the head annulus with a low, uniform pressure, which helps reduce the stresses found in other systems.

Related to extrusion blow molding is the extrusion-molded neck process (see Fig. 21). Still used by Owens-Illinois, this proprietary process can be traced to glass-blowing technology. In an unusual approach, the neck of the bottle is injection-molded and the bottle body is extrusion blow-molded. The two halves of

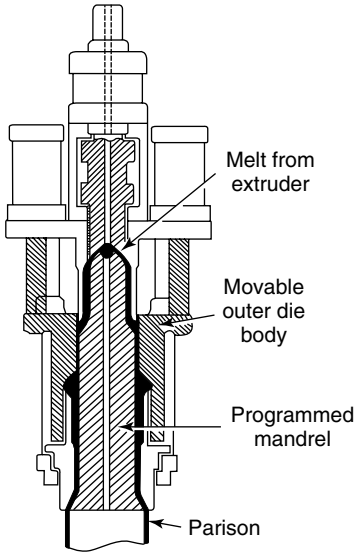

Fig. 20. Typical accumulator head.

the neck-finish cavity or neck ring are mounted to an actuating-head assembly, which intermeshes with the two halves of the blow-mold cavity. The process cycle begins with the main-body mold cavity open and the neck-ring cavity closed. The actuating-head assembly moves downward to contact the extrusion die head. When in position, extrusion pressure fills the neck section with plastic melt. After holding for 1–2 s, the head assembly moves upward while the parison is extruded. When the head assembly reaches the top of its stroke, the blow-mold cavity closes on the parison. The remaining steps of flash pinch-off, blowing, and part removal follow conventional techniques. Although the production cycle is somewhat slow, the process offers the advantages of an accurately molded neck and of a parison held at both ends. The other advantage is that only tail scrap is to be reground whereas in standard extrusion, both neck and tail scrap are to be reground.

Preference for a specific type and manufacturer of a blow-molding machine is based on experience, exposure to specific extrusion blow-molding methods, and different manufacturer equipment.

There are many blow-molding machine manufacturers, and choice should be based on the following criteria: cost, energy usage, floor space, reliability, output, service, manufacturer's reputation, controls–user friendly, cleanliness, world class design, height, maintenance, options available, dry cycle time, mold open and mold close time, and CFM usable per cycle with gauge and reservoir.

On any extrusion blow-molding machine, the buyer or user should know or test to have answers to the following:

(1) pound per hour output – actual
(2) plastifier – $\frac{L}{D}$ barrel

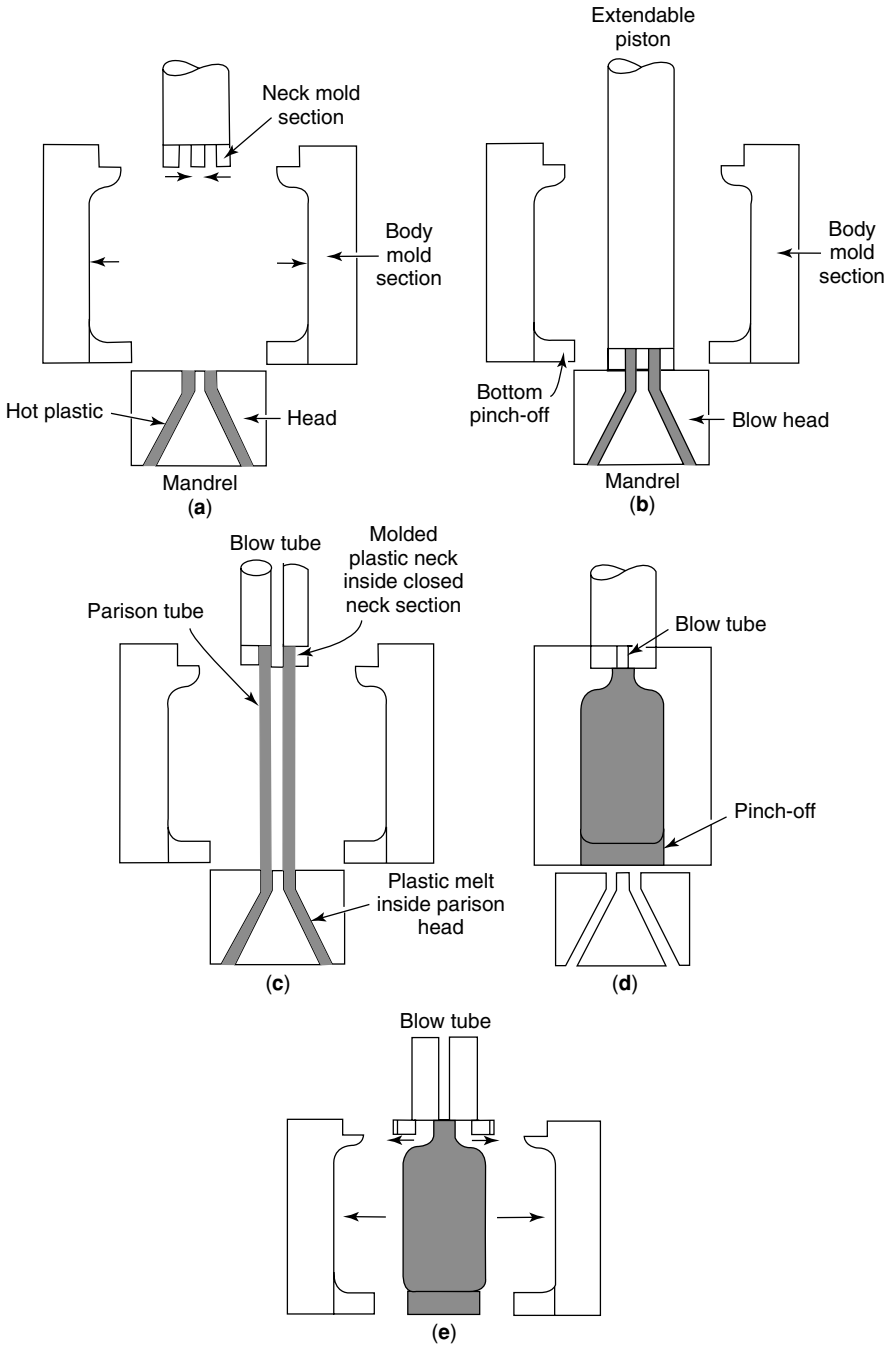

Fig. 21. Extrusion-molded neck blow-molding process. (a) Body section open, neck section closed, neck section retracted; (b) neck section extended to mate with parison nozzle (plastic fills neck section); (c) neck section retracted with parison tube attached; (d) body section closed, making pinch-off (parison blown to body sidewalls); (e) body molds open, neck molds open, bottle about to be ejected.

(3) compression ratio of the screw
(4) what type of screw—general-purpose, barrier screw or specific to one type resin
(5) barrel heating or cooling
(6) number of zones for heating the barrel
(7) location of the thermocouples
(8) Is there an extrudate temperature readout? Where is it located?
(9) Does it have a grooved feed throat on the barrel?
(10) Are the heater bands rotated so there is not an area on the barrel or head tooling that could have a cold area due to all the heater band endings aligned?
(11) Is accumulator type first in, first out or first in, last out.
(12) Is the tooling converging or diverging
(13) Is the head tooling center-fed or side-fed?
(14) How many points can be programmed rising the parison programmer?
(15) Can the blow molds be mounted safely and quickly?
(16) Can the clamp tonnage be adjusted for large or small blow molds?
(17) How is the parison cut?
(18) Is coextrusion possible?

In any extrusion blow-molding process, there is off-fall or trim that has to be reclaimed. How a production plant handles their off-fall or trim can make a difference as to profit or loss. Use of regrind, as well as the use of color additives and lubricants, will have a major effect on parisons repeatability.

The screw of the plastifier is designed to pick-up pellets (virgin pellets), not chopped and screened chop of the resin. In grinding, a uniform ground chop is not achieved. You and up with strings, fines, and various chopped sizes of plastic. Thus, the feed hopper of the machine is being fed a different bulk density because of the grinding, the virgin, and the colorant additive, all being of different sizes. The plastifier is nothing more than a pump and with a different bulk density being fed to the screw, the plastic melt has a differential of pressures within its melt stream causing short and long parisons, excessive sag, black specks, streaks, gels, and different die smells, and the result is poor efficiency.

Fines are in the virgin resin as received. Fines are generated when any plastic is ground in a grinder. Fines do not melt at the same melting temperature as the virgin resin nor the regrind. Their molecular weight is different. Fines should always be eliminated. They can clog the dryers, cause streaks, black specks, star bursts, and tear drops in the parison and in the blown product. A separating type grinder should be used in the regrind area. It is also good practice to pass your virgin plastic material through a fine eliminator system as it is being fed to the machine hopper.

Any blender should be checked for accuracy of delivery. Weigh blenders are preferred in today's blow-molding plants.

Formulas. In extrusion blow-molding, there are some definite formulas you should be aware of and use.

The blow up ratio (BUR) is defined as the blow mold diameter (product) divided by the parison outer diameter.

$$\text{BUR} = \frac{\text{Inside largest diameter inside blow mold}}{\text{parison outer diameter}}$$

Generally, this value is between 1.5 and 3; however, it can be up to 7 in unusual cases.

The amount of stretching a parison is subjected to is a function of the part size and configuration in relation to the parison size and orientation. In general, this can be expressed as follows:

$$\text{Average part thickness} = \frac{\text{parison surface area} \times \text{parison thickness}}{\text{product surface area}}$$

High blow pressure, greater than 60 psi, is necessary to achieve a good surface finish on the product, to pick up the mold detail, and to ensure the material is against the blow-mold surface to be cooled. Low blow pressure will increase the shrinkage of the product and will increase the cycle time since the mold cooling is not being utilized effectively. With some resins, such as polypropylene, a pressure of 100 psi has been found to be very satisfactory. However, the new procedure is to use low pressure of 80–120 psi and once the product is formed, then use high pressure of air (220–250 psi). Lower cycle times are achieved and an improved product is formed.

In PET stretch blow molding, single-stage machines, such as the Nissei, use a maximum pressure of 300 psi. In the two-stage method for PET, two-stage blow air is used. The low blow pressure would be approximately 220–250 psi and high blow pressure as high as 650 psi is used. Thus, the back plates and the blow mold must withstand these blow pressures and clamp closing forces.

Clamp Tonnage Required.

The required clamp tonnage is the sum of the blow pressure tonnage and pinch-off tonnage required with a 25% safety factor calculated as follows:

Production part projected area (IN^2) $\times$ Blow pressure $\times$ 1.25 $\div$ 2000 lb/ton = Blow pressure tonnage required with a 25% safety factor.

Pinch-off area (IN^2) (length $\times$ width) $\times$ pressure (lb/IN^2) $\times$ 1.25 $\div$ 20,000 lb/ton = Pinch-off tonnage required with a 25% safety factor.

Approximate pinch-off pounds per inch (ppi) for specific resins: PVC, 400/500; HDPE, 600–700; PP, 700–800; and PC, 1000.

Units. There is no uniform rating by the machinery manufacturers for clamp tonnage units nor is there a uniform use of nomenclature. One might see U.S. tons listed followed by KN and both are listed. Sometimes the multiplier is 10, so a 42 ton clamp will also show as 420KN. Other times a clamp will show 67 tons and 600KN which means a multiplier of 8.95 was used. Also, sometimes the U.S. tons are also given in metric eg, Cincinnati Milacron does this. The best conversion would be to rate in U.S. and metric tons with the U.S. tons being divided by 1.1 to yield metric tons.

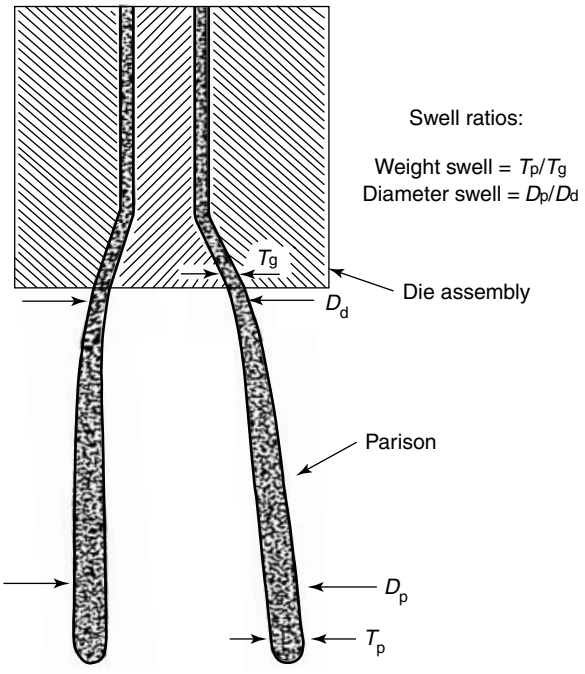

Fig. 22. Swelling behavior of viscoelastic material in parison formation.

Die/Weight Swell. The extrudate will swell as it exits the die. The swelling behavior is a result of the elastic component of the resin's flow. It is quite possible to measure the resins swell as it exits the die and to use this to ascertain the tooling sizes, and to determine if the resins can be used in producing the product.

There is also a weight swell of the resin and this is a result of the temperature, length of parison, speed of parison, drop, hang time of the parison, and the hot melt strength of the resin to be used. Swell ratios are defined in Figure 22.

Heat Extraction Load. The heat extraction load or the amount of heat to be removed from the product must be determined. This is important, as the amount of heat taken out by the blow mold must be known if the process is to be economically predictable. The amount of heat to be removed, Q, is determined by the material's temperature and the amount of plastic being delivered to the mold. It is calculated as follows:

$$Q = Cm\Delta t$$

where, Q is the total change desired during molding (J), C is the specific heat (J/g·°C) of the plastic material being processed, m is the amount (g) of plastic per hour to be cooled, and $\Delta t = (T_0 - T_f)$ is the initial plastic parison temperature into the mold minus final (demolding) temperature of the plastic (°C). As an example, for determining the heat load for a typical mold, the following data are used:

(1) C, specific heat for polyethylene = 2.5 J/g·°C.
(2) m, amount of PE to be cooled = 32 shots/h × 8.5 kg/shot × 0.80 shot reduction length = 218 kg/h

(3) T_0, parison temperature = 215.6°C (420°F).
(4) T_f, demolding temperature = 37.8°C (100°F).
(5) Δt, material temperature change = $T_0 - T_f = 215.6 - 37.8 = 177.8$°C

Thus,

$$Q = Cm\Delta t$$
$$= (2.3)(218{,}000)(177.8)$$
$$= 89\,\text{MJ}(84{,}440\,\text{BTU/h per mold, avg})$$

Assume 75% efficiency for heat transfer between chilled water and PE. Then,

$$\text{Cooling required} = \frac{119\,\text{MJ}}{0.75}(112{,}600\text{BTU/h})$$

With polyolefins, it is frequently desirable to run the molds as cold as possible, 4.5–15.5°C or lower. Condensation or moisture on the mold can cause outside surface defects when mold cooling temperatures are below dew point. To reduce or eliminate these, either the mold heat transfer fluid temperature can be increased, or it is possible with recently developed techniques to dehumidify the immediate blowing area to eliminate the condensation and maintain good surface appearance at a fast cycle. Effective dehumidification systems can be installed on existing equipment very satisfactorily, permitting ready access to the blow area while providing the dehumidification necessary to prevent condensation. Savings of 20–30 % have been reported through the use of this system.

Utilization of existing water temperatures in plants can be supplemented to improve cooling conditions through the use of turbulent flow of fluid through the mold channels. Depending upon the channel sizes, the greater the volume and the higher the pressure of the fluid put through the channels, the greater is the heat transfer. A turbulent flow wipes the side walls of the channels, permitting better heat transfer than that obtained with laminar flow of the fluid through the channels. This laminar flow characteristic tends to have reduced heat transfer at the channel circumference, whereas a turbulent flow enables more heat to be removed quicker with higher fluid temperatures, which also reduces the possibility of condensation.

A large-capacity temperature control unit (eg, with 2–7.5 HP pumping capacity, depending on the mold and channel sizes) can not only provide the desire turbulent flow, but can also assist in maintaining uniformity of control throughout the mold on an automatic basis. Production reports indicate that temperature variations of no more than 0.6–1.1°C are readily obtained with this approach, even with intricate molds.

To determine the proper flow for each mold, the Reynolds number should be determined. The Reynolds number ($N = DVP/M$, where D is pipe diameter, V is fluid velocity, P is fluid density, and M is fluid viscosity) is a nondimensional parameter used to determine the nature of the flow along surfaces. Numbers between 2100 represent laminar flow, numbers from 2100 to 3000 represent transitional flow, and numbers above 5000 represent turbulent flow.

The cooling time of parts is related to the wall thickness of the part. Tests on HDPE bottles have shown that wall thickness increases of 50% can increase the required cooling time as much as 200%. This increase of time is necessary to prevent warpage and to control shrinkage of the final product outside the molding cycle.

Because of the broad range of material, and part sizes, specific sizes and location of channels can be subjected to debate. To avoid this it would be better to state that channels should be as large as possible to provide high velocity flow for good heat transfer. They should be located approximately 0.5 in. from mold surface, depending upon mold size. These factors are highly desirable to ensure proper circulation through the work area to heat and cool the mold as rapidly as possible.

A roughened cavity surface is very helpful in blow-molding PE to assist in the movement of trapped air to the mold vents and to improve heat transfer rates.

Water, with its excellent heat transfer characteristics, is used primarily as the heat transfer medium for polyolefin blow-molding, but for the newer engineering resins a synthetic heat transfer fluid that operates up to temperatures of 121–149°C or more at low pressure is highly desirable because of the safety factor. Because the heat transfer characteristics of the synthetic fluid are not as effective as water, care must be exercised to use proper fluids in a safe manner to obtain as efficient production cycles as possible. Compromises sometimes are necessary, depending upon the required temperatures.

The most common material used for blow molds is aluminum. Aluminum has good conductivity, is lightweight, and has low mold costs. In considering the thermal conductivity, as measured in calories per square centimeter per centimeter per degree centigrade per second (cal/cm^2·cm·C·s) [or collecting terms, calories/(s·cm·°C)], aluminum has a thermoconductivity of 0.37, beryllium–copper 0.21 to 0.61, Kirksite 0.25, and steel 0.12–0.14. (In SI units of W/m·K the values are Al, 155; Be–Cu 88–255; Kirlisite, 105; and steel, 50–59). Aluminum is soft, however, and to protect against wear to specific points in the molds, steel or beryllium–copper inserts are used in production applications. The introduction of dissimilar materials, no matter how closely they are machined and mated, affects the heat transfer characteristic of the molds. Kirksite is less frequently used for inserts because of its weight and mass.

Metals Used in Blow Molds

Predominately, the choice of raw material for the main body of a blow mold is a high grade aluminum such as QC-7 or Alumnel 89.

With today's CADAM and CNC equipment, the blow-mold industry is producing large blow molds via machining rather than cast aluminum (Table 2). However, there are some industries that because of the blow-mold cost and short run volumes rely solely on cast aluminum blow molds. They also live with the problem of aluminum pinch-offs, rather than insert steel or beryllium–copper.

Aluminum is approximately eight times better in conductivity than steel. In some cases, blow molds are (for PVC or for inserts or cams) made of stainless steel (420,430).

Table 2. Some Metal Properties

Metal	Cast/cut	Upper cm^3	Durability	Resistance to PVC	Heat conductivity
Zinc	Cast	4.24	Fair	None	0.0017
Aluminum 70/75T6	Cut	1.60	Good	Fair	0.002
Aluminum	Cast	[a]	Fair (−)	Fair (−)	[a]
Brass	Cut	4.98	Good	Fair (+)	0.0015
Beryllium-copper	Cut	5.24	Very good	Very good	0.004
Beryllium-copper	Cast	5.24	Very good	Very good	0.004
Stainless steel 300	Cut	4.75	Fair	Very good	0.0006
Stainless steel 400	H.T. cut	4.75	Good	Fair	0.0003

[a]Depends on density of casting.

Pinch-offs can be produced from BeCu, Ampcoloy 940, or steel. S-7 are preferred for pinch-offs and 54–56 Rc for long life.

Shrinkage

Because molding is executed with a melt which is then solidified, shrinkage and warpage are experienced with most materials. Higher crystallinity polymers have higher shrinkage values (Table 3). Shrinkage is dependent upon the wall thickness because of the different cooling rates. The cycle time to cure the product will be what it takes to cool the thickest wall section. Cooling of a plastic part consists of three separate transfer mechanisms:

(1) Conduction of heat in wall of part
(2) Conduction of heat in mold wall
(3) Convective transfer of heat in cooling fluid

Step 1 is dependent upon resin type, temperature, and wall thickness. Step 2 depends upon the mold material's thermal properties, porosity, and mold/cooling

Table 3. Shrinkage and Other Properties of Some Common Blow-Molding Materials

Polymer	Shrinkage,[a] %	Linear coefficient of thermal expansion, $(10^{-4}\ K^{-1})$	Specific Volume, cm^3/g (at 20°C)
LDPE	1.2–2	2.3 (20°C)	1.09
HDPE	1.5–3	2.0 (20°C)	1.05
Polyacetal	1–3	1.3	0.7–0.71
PP	1.2–2.2	1.6	1.10
PS	0.5–0.7	0.7–0.8	0.89–0.95
PVC	0.5–0.7	0.8	0.81

[a]Measured on an axially symmetrical test bottle with an average wall thickness of 0.7–1 mm, by method of R. Holzmann, Kautex-Werke, Hangelar.

layout geometry. Some thermal properties of selected resins are shown in Table 3. Step 3 can be optimized with regard to temperature, fluid flow rate, and prevention of scale formation on the liquid side. The cooling rate of most processes is limited more by the rate of conduction within the plastic than by the rate of conduction in the mold. The cycle time of a part is usually strongly dependent on its wall thickness.

Venting

All blow molds have to be vented. The air that first occupied the product area must escape more rapidly than the rate at which the hot plastic is blown to fill the product area within the closed blow mold. This is known as venting.

In some cases it is very hard to ascertain that improper venting is the production problem that is keeping consistent quality parts from being produced in each cycle. Olefins will show burn signs and in some cases, carbon residue on the blown product, if the venting is really insufficient. There may be no burning of the plastic evident; however, the part produced just does not totally reproduce the blow-molding surface. In blow molding styrene and particularly PET, the resin will cool and just quit stretching since the compressed air, due to it being trapped, results in higher pressure than what is inside the heated parison or preform.

Well-designed molds are vented, as entrapped air in the mold prevents good contact between the parison and the mold cavity surface. When air entrapment occurs, the surface of the blown part is rough and pitted in appearance. A rough surface on a shampoo bottle, for example, is undesirable because it can interfere with the quality of decoration and can detract from the overall appearance. Molds are easily vented by means of their parting line, with face vents and with small holes. A typical mold parting line venting system is shown in Figure 23.

The venting is incorporated only in one mold half. This type of venting can be used on all sizes of molds. When certain areas of the mold cavity are prone to trap air, core vents as shown in Figure 24 can be used.

Venting in the mold cavity should be anticipated in the mold design and layout of the cooling channels so that provisions can be made for their locations.

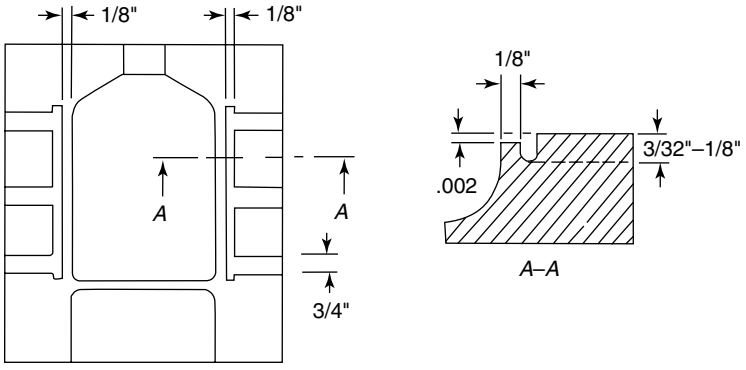

Fig. 23. Parting line venting.

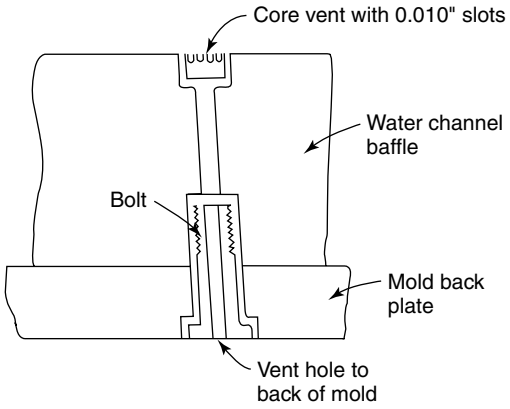

Fig. 24. Core venting.

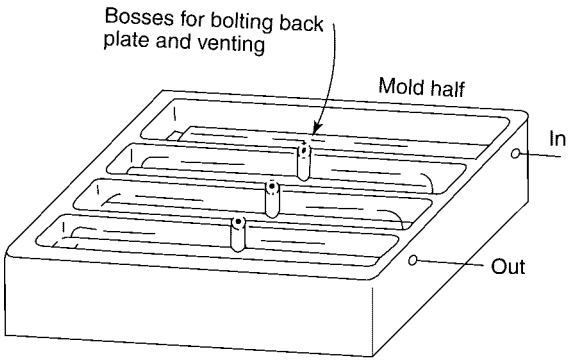

Fig. 25. Location of vents in baffles.

For the cast mold, the cooling channel baffles can be located over areas to be vented, as shown in Figure 25.

The vent opening will pass through a boss in the baffle to the back or outside of the mold. In machined molds, care must be taken so that vents miss the drilled cooling channels. When core vents cannot be used because the slots mark on the blown part will show, small drilled holes can be used. The effect of the size of hole on the surface of the part is shown in Figure 26.

If the hole is too large, a protrusion will be formed; if it is too small, a dimple will be formed on the part. Venting also can be incorporated in molds that are made in sections. A 76–250 μm (3–10-mil) gap between the two sections with venting to the outside of the mold is a very effective vent. For small containers, a 5–7.6 μm (0.2- to 0.3-mil) opening is used, and up to a 250μm (10-mil) opening has been used on large parts such as a 20-gal garbage container.

The mold cavity surface has an important bearing on mold venting and on the surface of the molded part. For PEs and PPs, a roughened mold-cavity surface is necessary for the smoothest surface. Grit blasting with 0.25–0.17 mm (60–80 mesh) grit for bottle molds and 0.59–0.42 mm (30–40 mesh) grit for larger molds is

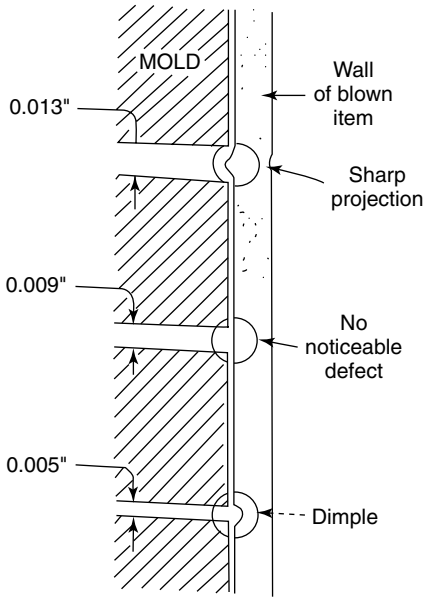

Fig. 26. Effect of vent hole size on part surface.

a common practice. The clear plastics such as PVC and styrene require a polished mold cavity for the best surface. A grit-blasted surface will reproduce on some clear plastics, an effect that is not normally desirable.

The pinch-off areas pinch the ends of the plastic parison and seal the edges together when the mold closes. These surfaces are subject to more wear than any other part of the mold. The high-heat-conductive metals preferred for blowing molds, such as aluminum and copper alloys, generally are less wear-resistant than steel. Steel inserts often are used for the pinch-off areas of the molds. An additional advantage of pinch-off inserts is that they can be made replaceable in the event of wear or damage. A neck pinch-off insert is sketched in Figure 27.

Generally, in volume production, pinch-off inserts are made of hard steel with the other portions of the blow mold produced from a nonferrous metal. The

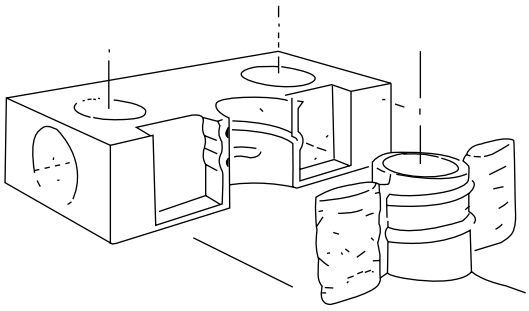

Fig. 27. Replaceable neck insert pinch-off.

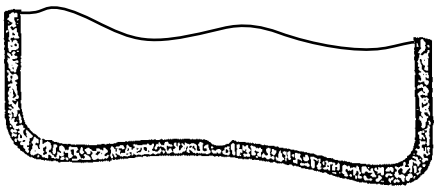

Fig. 28. Poor weld line (weak) pinch-off had knife edge; relief angle was either too large or too small.

pinch-off edge should not be similar to a knife edge, or it will tend to act as a cutter and will yield a "V" groove where the tail or pinch-off area of the parison is forced to bond (See Fig. 28).

The parts of the mold that weld the ends, and sometimes the interior portions, of the parison together, and also cut it or facilitate its removal are called the pinch-offs. Pinch-offs design has an important effect on the success of a blow-molding product because the weld seams are usually the weakest parts of the container. The pinch-off must be designed to maximize the strength of the blown product in this area. The results of a pinch-off optimization study for various grades of olefins are listed in Table 4 and also in Figure 29. A quality type pinch-off is depicted in Figure 30.

In bottle blow molds, there will be a hardened steel insert with a land of 0.076–0.13 mm (0.003–0.005 in.), a relief angle of 20° with a total depth of 0.76 mm (0.030 in.) measured from the inside bottom of the blow mold, and then a 45° cut to the bottom of the relief section in the pinch-off area. Normally, the total of this relief section will be 90% of the parison wall thickness to be pinched (see Fig. 31). This design will also minimize residual flash. It is best to design the pinch land at 0.25–0.4 mm (0.010–0.015 in.) and have metal to remove, if the pinch is not adequate.

Many different designs have been used in the pinch-relief sections. Two typical ones are shown in Figure 32. Design A is probably the one most widely used. In some instances, however, where the mold must pinch on a relatively thin portion of the parison and next to this pinching edge the parison must expand a large amount, the plastic will thin down and may even leave a hole on the parting line. This defect is sometimes seen near the finger hole on containers having handles. To prevent thin sections and holes, Design B is sometimes employed. The shallower angle of 20° has a tendency to force plastic to the inside of the blown

Table 4. Optimization Study Results for Various Grades of Olefins

Container volume (V), L	Pocket Opening Angel, (a), deg	Welding edge width b, mm	Pocket Width, (c), mm
≤1	30	0.6–1	2d
1–30	30	1–3	2d
30–250	30	3–5	1d–1.5d
250–2000	30	5–7	1d–1.5d

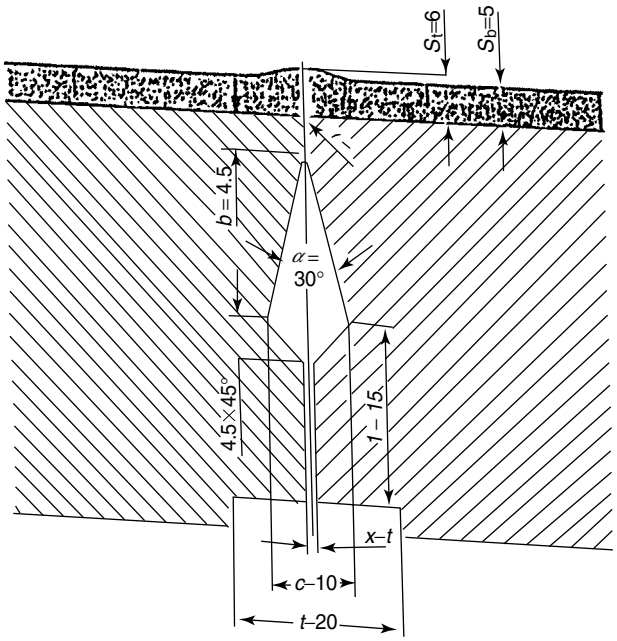

Fig. 29. Optimized mold base for a 60-L can be made from HMW-HDPE. Dimensions are defined in Table 4. Courtesy of Hoechst AG.

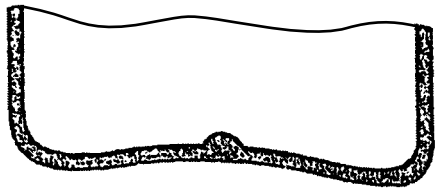

Fig. 30. Good weld line.

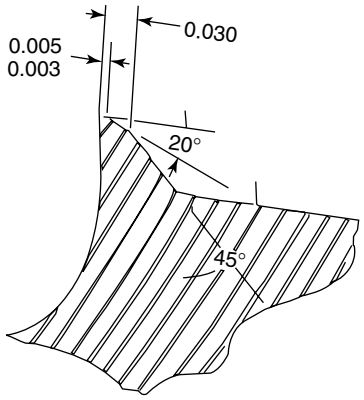

Fig. 31. Design often used to minimize residual flash.

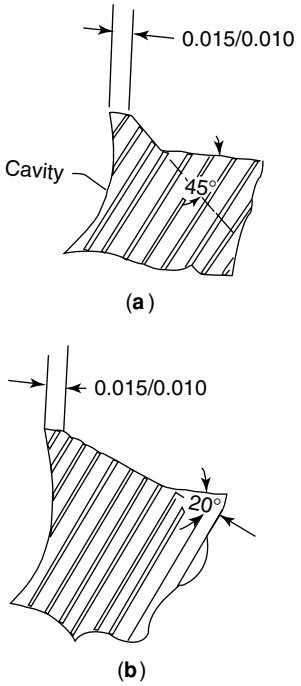

Fig. 32. Pinch-relief section designs.

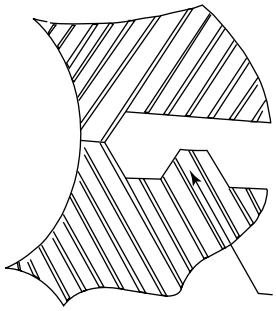

Fig. 33. Dam or restriction used to increase wall thickness on some designs. Arrow points to restriction.

part and increase the wall thickness at the parting line rather than pushing the excess material back into the pinch relief. Another method used for increasing the wall thickness at the parting line employs a restriction or dam in the pinch relief similar to that shown in Figure 33. The pinch-off must be designed to maximize the strength of the weld. Some different types of pinch-off designs are shown in Figure 34.

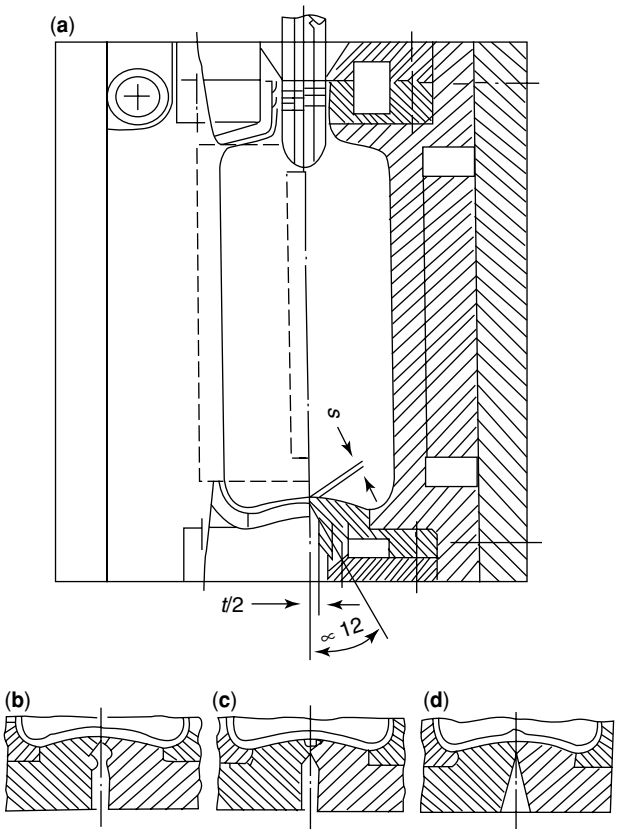

Fig. 34. Design of welding edges and pinch-off pockets. *s*, welding edge width;, opening angle of pinch-off pocket; *t*, width of pinch-off pocket. Courtesy of Hoechst AG.

Troubleshooting Extrusion Blow Molding

Problem	Suggested solution
Low gloss	Increase material temperature
	Increase mold temperature
	Improve mold venting
	Increase air pressure
	Increase air blowing rate
Excessive cycle	Decrease material temperature
	Decrease mold temperature
	Decrease part wall thickness
	Improve mold coring
	Increase material density
	Increase air pressure
	Increase melt index (with decreased stock temperature)

Problem	Suggested solution
Die lines	Clean the die
	Smooth and polish the die
	Increase mold temperature
	Increase air pressure
	Increase air blowing rate
	Increase purge time when changing materials
	Improve die streamlining
Low bottle weight	Increase due to mandrel clearance
	Decrease material temperature
	Increase extrusion speed
	Decrease extrusion die temperature
Surface roughness	Increase stock temperature
	Decrease extrusion speed
	Increase die temperature
	Improve die streamlining
Weak pinch	Adjust material temperature
	Increase pinch blade land width
	Decrease rate of mold closing
Parison curl	Adjust and center die-parison curls toward thin area
	Improve die and head heat uniformity
	Dirty die head
Wall thickness non-uniform	
vertically sag	Decrease material temperature
	Increase extrusion speed or accumulator ram pressure
	Lower melt index
	Increase material density
circumferentially	Decrease blow-up ratio
	Improve head and die heat uniformity
	Adjust and center the die
Excessive thinning at parting line	Decrease wall thickness, or make more uniform
	Decrease mold temperature
	Increase air pressure
	Decrease material temperature
	Decrease density
	Improve mold coring
Excessive shrinkage	Increase material temperature
	Decrease mold temperature
	Increase air pressure
	Decrease material temperature
	Decrease density
	Improve mold coring
Excessive parison swell	Increase material temperature
	Increase die temperature
	Decrease extrusion speed
	Increase melt index
	Reduce die size
Doughnut formation	Wait for mandrel temperature to reach die temperature
	Clean the lower surface of the die

Problem	Suggested solution
Warped top and bottom	Slow the cycle
	Decrease mold temperature
	Decrease stock temperature
	Decrease part weight
	Improve mold coringJ
Variable bottle weight	Finer extruder screen pack
	Increase screw cooling
	Raise rear extruder heats
	Decrease extruder rate

Coextrusion

A growing trend in extrusion blow molding is to coextrude parisons that contain up to seven layers of different materials. However, as of this time, coextrusion is limited to machines that only use one (1) parison as on a wheel and the continuous-type machine. Since the different materials combine in the head tooling (see Fig. 35), the use of manifolds for multiple cavity is not feasible, nor are accumulator machines (see COEXTRUSION).

Coextrusion blow-molding machines are very expensive and demand skilled operators. Coextrusion is used to produce containers having a view stripe and more recently for 55-gal drums and the plastic gasoline tanks that are in passenger cars, sport utility vehicles, or pick-up trucks. The plastic gasoline tanks are produced from a coextruded parison that contains six layers of different resins. For example, HDPE/adhesive/EVOH/adhesive/regrind/HDPE (see Fig. 35).

Major companies are finding that they can coextrude parisons that not only make use of their regrind, but also use less color additive. It is very feasible to extrude a virgin layer with no color additive on the inside of the

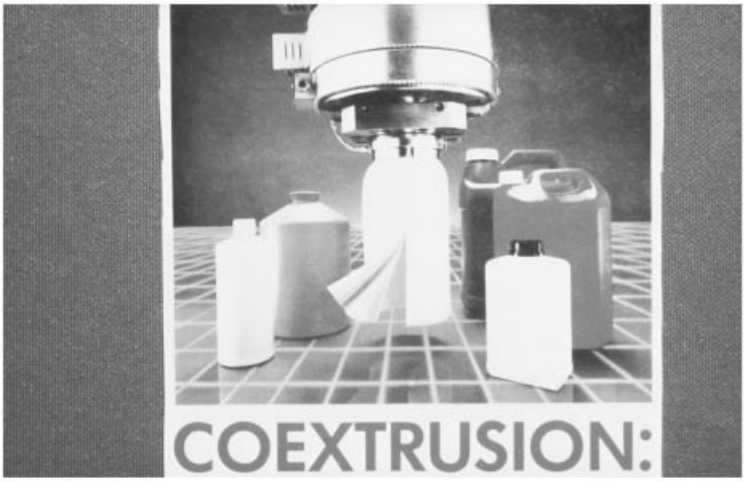

Fig. 35. Coextrusion head.

parison that is against the product to be packaged. The second layer is for the off-fall or regrind. The outer layer would be virgin with color additive, which would make up a three-layer coextruded parison. A six- or seven- layer coextruded parison may be HDPE/adhesive/EVOH/adhesive/regrind/virgin or HDPE/regrind/adhesive/EVOH/adhesive/regrind/virgin as examples.

Stretch Blow Molding

For stretch blow molding, mainly PET, PVC, PP, and PAN are used. In this process, based on the crystallization behavior of the resin, a parison or preform is temperature-conditioned and then rapidly stretched and cooled. For best results, the resin must be conditioned, stretched, and oriented just above the glass-transition temperature. At this point, the resin can be moved without the risk of crystallization (see Figs. 36 and 37).

Stretch blow molding is the most significant development since the development of the two piece can. This process improves produce performance, such as bottle-impact strength, cold strength, transparency, surface gloss, stiffness, and gas barrier. The bottles are lighter and less costly, and products that otherwise would not be suitable can be packaged. The process uses injection-molded, extruded, or extrusion blow-molded parisons in one or two steps.

In the one-step method, parison production, stretching, and blowing take place in the same machine. In the two-step method, the parison is produced separately from stretching and blowing. The main advantage of the one-step approach

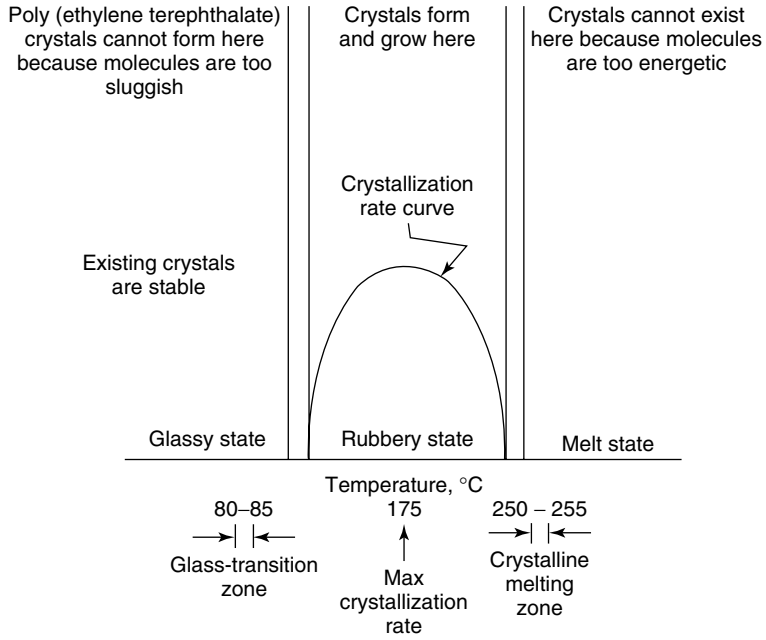

Fig. 36. Molders' diagram of crystallization behavior (8). Courtesy of the Society of Plastics Engineers.

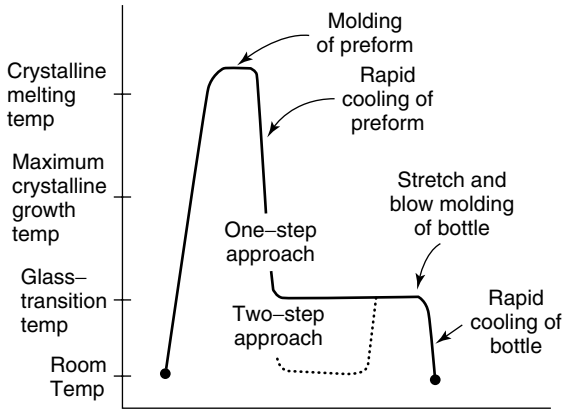

Fig. 37. Basic stretch blow mold process. Courtesy of Jerome S. Schaul.

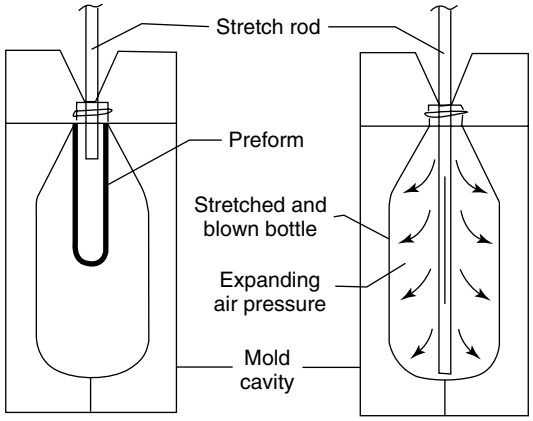

Fig. 38. A temperature-conditioned preform is inserted into the blow-mold cavity and is rapidly stretched. A rod is often used to stretch the preform in the axial direction, and air pressure to stretch the preform in the radial direction.

is the savings in energy as the parison is rapidly cooled to the stretch temperature. In the two-step approach, the parison is cooled to room temperature and reheated to the stretch temperature (see Fig. 38). On the other hand, production in the two-step method is more efficient, and a minor breakdown in one of the steps does not stop the other. The optimum balance of design vs output is also easier to achieve with the two-step approach. Limits on parison production, for example, do not force a compromise in parison design to achieve higher bottle production. For optimum performance, each bottle design has a unique parison-design and temperature-conditioning requirement which may or may not fit, for optimum productivity, the assumptions used in the design of the one-step equipment, which are virtually the same.

In the two-step method, the parison is injection-molded in a separate machine, sorted, and placed in an oven for temperature conditioning and blow molding. A rod is used inside the parison, in combination with high air pressure,

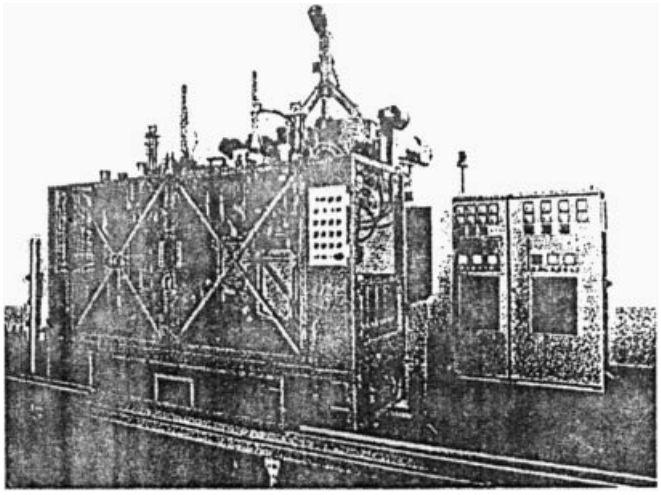

Fig. 39. Bekum BM04D continuous extrusion blow molder for the manufacture of biaxially oriented PVC bottles. Production rate for 1-L bottle is 2000 per h; maximum bottle size is 2 L. Courtesy of Bekum Plastic Machinery, Inc.

to complete the stretch (see Fig. 38). Injection stretch blow molding is commonly used for PET resin.

The extruded parison stretch process can use either the one- or two-step method. In the former, a parison is extruded and fed directly into an oven for conditioning. After conditioning, the parison is cut into lengths. Mechanical fingers grab both ends and stretch the parison. The two mold halves close, whereupon air pressure expands the stretched parison against the mold cavity. In the two-step method, the extruded tube is cooled and cut to length. Later, the cut tubes are placed in an oven for conditioning. This technique is used mainly for PP, and occasionally for PVC.

With the extrusion blow stretch process, the parison is shaped and temperature-conditioned in a preform cavity in the same way a bottle is extrusion blow-molded. From this preform cavity, the parison is transferred to the bottle cavity where a rod and air pressure combine to stretch and expand the resin. PVC is most often stretch blow-molded with this process. Although the one-step method is the most common (see Fig. 39), a two-step technique, in the same fashion as the others, is feasible.

PET is the second largest volume resin used in the blow-molding industry. HDPE is first, with a 57% share of the blow-molding market today. PET has 33% of the blow-molding market and is growing. Thus, all the other resins combine for 10% of the blow-molding market.

As stated previously, stretch blow molding impacts clarity, top load strength, drop impact resistance, improved barrier, and will allow approximately 15% or greater reduction in material usage for the same size container.

In stretch blow molding, there are two ratios that multiply together to provide the blow up ratio BUR. In extrusion blow molding, there is only the hoop ratio (that is the blow-up ratio). In stretch blow molding there is the hoop that is multiplied by the axial ratio. Thus, BUR = Hoop ratio $\times$ axial ratio.

The hoop ratio is the most important. If the product to be packaged is pressurized as soft drinks, carbonated water, and beer, the hoop ratio should be at least 10 or higher. The *hoop ratio* is defined as the ratio of the largest inside diameter (D_1) of the blown article to the inside diameter (D_2) of the parison or preform.

The *axial ratio* is also very important as this provides vertical strength, material distribution, improved barrier, and allows for raw material savings. Usually, the axial ratio should be at least 1.7 with greater than 2 preferred. The *axial ratio* is defined as the axial length (A_1) where the actual axial stretch is initiated in the preform measured to the inside bottom of the bottle to be produced divided by the axial length (A_2) of the preform as it is measured from the point where stretching is initiated to the inside bottom of the preform.

The BUR is used to determine the wall thickness that would be necessary in the precursor or preform. If the BUR is 10, and the desired minimum wall thickness is 0.38 mm, then the BUR $\times$ the desired wall thickness, would indicate that the minimum wall thickness in the preform should be 3.8 mm since the thickness will be expanding 10 times. The total BUR is equal to the hoop ratio times the axial ratio.

To check if the orientation is correct, a dog bone can be cut from the stretch blow-molded PET container and a tensile test conducted on an Instron or similar machine. A dog bone shape is cut in the hoop direction and one is cut in the axial direction. PET has a base strength of approximately 46 MPa (6700 psi). If the hoop ratio is 5, then in the container in the hoop direction, the tensile strength should be approximately 231 MPa (33,500 psi). If the axial ratio is 2, then the tensile strength in the vertical direction would approximately be 92 MPa (13,400 psi).

In order to achieve these results, the stretch blow molding has to be performed when the heated preform's body is within the orientation window for the polymer that is to be stretch blow-molded. A list of the orientation temperatures for specific polymers follows:

Material	Orientation temperature, °C
PP	128
PAN	124
POM	160
PVC	100
PET	95
PS	150

It is important to note that each polymer listed has specific stretch ratios and if exceeded the polymer will fail.

Material	Stretch ratio	Orientation temperature range, °C
PET	16/1	90–115
PVC	7/1	99–110
PAN or AN	12/1	115–127
PP	6/1	127–138
PS (Crystal)	12/1	143–160

Table 5. Gas and Water Vapor Barrier Properties of Glass-Clear Resins

Polymer	O_2[a]	CO_2[b]	Water[c]
Oriented PVC via extrusion blow molding (high impact)	9.0	16.5	0.7
Oriented PET	11.1	22.2	1.5
Oriented PVC via extrusion blow molding (normal impact)	9.6	5.2	1.1
Nonoriented PVC via extrusion blow molding (high impact)	12.2	35.7	1.5
Nitrile	1.1	1.3	4.4
PC	215.0	400.0	9.0

[a] cc/mL/24 h/atm/100 in.^{2}/73°F.
[b] g/mL/24 h/atm/100 in.^{2}/100°F, 90% RH.
[c] Test results provided by Occidental Chemical Corp.

Stretch blow-molded containers of AN, PVC, and PET may have an average wall thickness of 0.23–0.64 mm (0.009–0.025 in.) Normal blow molding would call for an average wall thickness of 0.46–0.5 mm (0.018–0.020 in).

As noted, each polymer has a temperature at which the heated preform or parison should be stretch blow-molded to achieve maximum orientation properties. Each polymer exhibits its own natural stretch ratio. Orientation of polymers is a study by itself, and there are references to in-depth study of specific polymers (13) (see also, FILMS, ORIENTATION).

Table 5 depicts barrier properties of several stretch orientable polymers and their barrier improvements obtainable through stretch blow molding (see BARRIER POLYMERS).

PET has grown in its use because of several properties possessed by this polymer which no other stretch blow-molded polymer possesses. PET has what is referred to as self-leveling. Since PET work hardens similar to a metal, as it stretches out, the material stretching becomes stronger than the material next to it and so it waits until the material next to it stretches and becomes stronger. Thus, the term *self-leveling*. No other polymer possesses this feature. All the other polymers behave as bubble gum when they are being blow-molded.

Another unique property of PET is that it can be heat set. Heat set is achieved by either of two methods. Normally, a PET stretch blow-molded container cannot be subjected to heat above approximately 54°C (130°F) because of distortion. This relates to the fact that the glass transition of PET is approximately 68–71°C (155–160°F).

However, this can be altered by inducing the PET stretch blow-molded container to become more crystalline. A quality 2-L PET soda container will have approximately 14–22% crystallinity. This crystallinity is induced by heating the preform and through the orientation. To increase the crystallinity within the wall of the container, the container may be blow-molded in a hot blow mold in the range of 124–155°C, with the bottom plug or push up at approximately 68–88°C. When produced in a hot blow mold, the crystallinity with in the wall of the stretch blow-molded container can be increased to be in the range of 28–32%. There is a loss in orientation because of blowing in a hot blow mold. The heat set stretch blow-molded container is tested fresh. It is filled with hot water to the top of the finish at a temperature of 90°C. It cannot distort nor shrink greater than 2% when dimensions are checked before and after the hot fill test. This ensures the container will pack a 85°C hot fill product such as juice and sport drinks. An aged container

over 24 hours is checked using 85°C hot water. There are many other quality assurance tests performed and produces such as Schmalbach Lubeca, Graham, Ball Corp, and Crown Cork & Seal have their own test procedures.

Other Blow-Molding Operations

Many related operations have been used to improve blow molding, eg, in-mold labeling, fluorination of surface, and internal cooling.

In-Mold Labeling. A label with a heat-activated adhesive is automatically placed into the mold cavity and held by a vacuum. The expanding hot parison activates the adhesive to create a strong bond.

Some of the advantages of the process include a stiffer, stronger structure, bottle-weight reduction, improved label appearance, elimination of high speed complex labeling equipment, and varied package opportunities. Bottle weight is often reduced without impairing performance. The strong bond improves label appearance by eliminating blisters and wrinkles. The pick-and-place mechanism used to place the label into the mold cavity, although somewhat complex, is often simpler than using high speed equipment for labeling on the filling line. New package-design opportunities are created with the possibility of placing the label closer to or around the bottle edges, which could further increase strength.

However, with in-mold labeling, production efficiency can suffer from the slower cycle and the complexities of the process. The scrap is more valuable and costly to reclaim. Very high production runs are required to justify the investment.

Fluorination. Fluorination surface treatment improves the resistance of PE to nonpolar solvents. A barrier is created by the chemical reaction of the fluorine and the PE, which forms a thin (20–40 mm) fluorocarbon layer on the bottle surface. Two systems are available. The in-process system uses fluorine as a part of the parison expand gas in the blowing operation. A barrier layer is created only on the inside. In the post-treatment system, bottles are placed in a chamber filled with fluorine, and a barrier layer forms on both inside and outside surfaces.

This surface treatment allows low cost blow-molded PE bottles to be used for paint, paint thinner, lighter fluid, polishes, cleaning solvents, cosmetics, toiletries, etc, and higher cost resins or coextrusion processes are not always necessary. For floorination to be effective, the parison temperature must be greater than 195°C.

Internal Cooling. Normally, a blow-molded part is cooled externally by the mold cavity, forcing heat to travel through the entire wall thickness. With the poor thermal conductivity of plastic resins, molding-cycle times of heavy parts can be lengthy. Internal cooling systems are designed to speed mold cooling, thus reducing costs by removing some heat from the inside. Three basic systems have been developed: liquefied gas, supercold air with water vapor, and air-exchange methods.

In the liquefied-gas system, liquid carbon dioxide or nitrogen is atomized through a nozzle in the blow pint into the bottle immediately after the parison has been expanded. The liquid quickly vaporizes, removing heat, and exhausts at the end of the cycle. This method has increased production rates by 25–35%. A disadvantage is the cost of the liquefied gas. If consumption is not precisely controlled, the cost saving is small.

The supercold-air system with water vapor is similar. A stream of very dry, subzero air expands the parison, circulating through the bottle and exhaust.

Immediately after the parison has expanded, a fine mist of water is injected into the cold air stream and turns into snow. As the snow circulates through the container, it melts and vaporizes. At the end of the molding cycle, the water mist is stopped, permitting the circulating air to dry the interior before the mold is opened and the article is removed. Production rates can be improved as much as 50%.

The air-exchange system is far simpler. Here, plant air, after the parison has been expanded, is circulated through the bottle and is exhausted continuously. Differential pressure inside the bottle is maintained at 550 kPa (80 psi) to keep the parison in contact with the mold cavity. Production rates, however, are increased by only 10–15%.

More expensive internal cooling systems are often not justifiable with today's equipment because most blow-molding machines do not have the additional extruder capacity to support the high production rate. This is particularly true for the heavier bottles that would benefit most. As a result, only the low cost air-exchange systems have been accepted.

With the exception of larger industrial blow molds cast from aluminum (typically No. A356), most extrusion blow molds today are cut from No. 7075 or No. 6061 aluminum or from No. 165 or No. 25 beryllium-copper. The latter is corrosion-resistant and very hard, making it the choice for PVC blow molding. However, compared with aluminum, it weighs about three times as much, costs about six times as much per cubic centimeter, and requires about one-third more time to machine. In addition, thermal conductivity is slightly lower (see Table 6). For polyolefin blow molding, some mold makers combine the materials by inserting beryllium-copper into the pinch-off area of an aluminum cavity, thus gaining a lightweight, easy-to-manufacture mold with excellent thermal conductivity and hard pinch-off areas.

Table 6. Blow-Mold Tool Materials

Material	Hardness[a]	Tensile strength, MPa[b]	Thermal conductivity, W/m·K
Aluminum			
No. A356	BHN-80	255	151
No. 6061	BHN-95	275	168
No. 7075	BHN-150	460	105
Beryllium-copper			
No. 25 and 165	HRC-30 BHN-285	930	105
Steel			
No. O-1 and A-2	HRC-52-60 BHN-530-650	2000	35
No. P-20	HRC-32 BHN-298	1000	37

[a]HRC: Rockwell hardness (C scale); BHN: Brinell.
[b]To convert Mpa to psi, multiply by 145.

Unlike injection blow molds, which are mounted onto a die set, extrusion blow molds are fitted with hardened-steel guide pins and bushings to ensure that the two mold halves are perfectly matched. Dies, mandrels, blow-pin cutting sleeves, and neck-ring striker plates are made from tool steel hardened to 56–58 HRC.

Guidelines. Guidelines have been mentioned throughout this article in the form of process and tooling limitations, such as parison blow-up ratios, ovality ratios, tooling sizes, and so forth. Product design begins with a clear understanding of process.

Most blow-molded articles perform better with rounded, slanted, and tapered surfaces. Square or flat surfaces with sharp corners are undesirable. Wall thickness can vary considerably from side panels to corners. Corners become thin and weak, heavy side panels thick and distorted. Flat panels are not uniform and flat shoulders offer little strength. Highlight accent lines should be "dull" with a radius of 1.5 mm or more. If they are sharper, the parison does not penetrate, and trapped air marks result along the edge.

The blow-up ratio of 4:1 for extrusion blow-molded bottles or parts is considered a maximum. This applies overall and to separate sections as well. For example, bottle handles that are deeper than they are wide across the mold-parting face are difficult to mold and are often thin and weak.

Ribs do not always stiffen. Blow-molded ribs often increase surface area and reduce wall thickness, creating a flexible-bellow or accordion effect. Flexing may affect "hinge" points. Proper design prevents this.

Designers must be familiar with bottle-performance tests. The Society of the Plastics Industry has recommended 21 standard practices; the most important are vertical compression or top-load strength, drop-impact resistance, product compatibility and permeability, closure torque, and top-load stress-crack resistance.

Blow-molding process conditions can influence not only bottle dimensions, but also bottle volume. HDPE bottles shrink, with 80–90% of the shrinkage taking place in the first 24 h. Lighter-weight bottles use less plastic for a given capacity and bulge more. A 4-L bottle weighing 5 g less increases about 12 mL in volume—5 mL for the plastic and 7 mL for bulge. Shorter cycle times, lower parison-expansion air pressure, and lower melt and mold temperatures reduce bottle volume. Storage temperature is very important. After 10 days, bottles stored at 60°C change more than bottles stored at 20°C.

The guidelines will continue to change with the use of the computer with CAD flow analysis, blow simulation, and new talent in the industry. The future is bright.

BIBLIOGRAPHY

"Blow Molding" in *EPST* 1st ed., Vol. 9, pp. 84–118, by G. E. Pickering, Arthur D. Little, Inc.;

"Blow Molding" in *EPSE* 2nd ed., Vol. 2, pp. 447–478, by C. Irwin, Hoover Universal, Inc.

1. G. P. Kovach, in E. C. Bernhardt, ed., *Processing of Thermoplastic Materials*, R. E. Krieger Publishing Co., Inc., Huntington, N.Y., 1959, pp. 511–522, (reprinted 1974).
2. R. Holzmann, *Kunststoffe* **69**, 704 (1979).
3. K. Stoeckhert, *Ind. Prod. Eng.* **4**, 62 (1980).

4. K. J. Presswood, in *Oriented PVC Bottles; Process Description and Influence of Biaxial Orientation on Selected Properties, 39th Annual Technical Conference,* May 1981, Society of Plastics Engineers, Inc., Brookfield Center, Conn., pp. 718–721.
5. R. J. Abramo, in *Fundamentals of Injection Blow Molding, 37th Annual Technical Conference*, May 1979, Society of Plastics Engineers, Inc., Brookfield Center, Conn., pp. 264–267.
6. H. G. Fritz, *Kunststoffe* **71**, 687 (1981).
7. R. W. Saumsigle, in *The Three "E" System of Blow Molding Displacement Blow Molding, 39th Annual Technical Conference*, May 1981, Society of Plastics Engineers, Inc., Brookfield Center, Conn., pp. 727–728.
8. J. S. Schaul, in *38th Annual Technical Conference*, Society of Plastics Engineers, Inc., Brookfield Center, Conn., 1980.
9. S. Date, in *Co-Pak Multilayer Plastic Containers, 5th Annual International Conference on Oriented Plastic Containers*, Mar. 1981, Ryder Associates, Inc., pp. 37–48.
10. *Package Eng.* 64 (Nov. 1981).
11. E. Jummrich, *Ind. Prod. Eng.* **2**, 180, 184, 185 (1981).
12. L. B. Ryder, *Plast. Eng.* 22 (Jan. 1980).
13. L. B. Ryder, *Plast. Eng.* 32 (May 1975).
14. S. Collins, *Plast. Mach. Equip.* 15 (May 1983).
15. R. A. Barr, in *Screw Design for Blow Molding, 39th Annual Technical Conference*, May 1981, Society of Plastics Engineers, Inc., SPE, Brookfield Center, Conn., pp. 734–735.
16. J. Sneller, *Mod. Plast. Int.* 48 (Mar. 1982).
17. J. R. Dreps, *Plast. Eng.* 34 (Jan. 1975).
18. D. Boes, *Kunststoffe* **72**(1, 7 (1982).
19. B. T. Morgan, N. R. Wilson, and D. L. Peters, in J. Agranoff, ed., *Modern Plastics Encyclopedia*, Vol. **46**, No. 10A McGraw-Hill, Inc., New York, 1969/1970, p. 525.
20. N. Lee, ed., *Handbook of Blow Molding*, Society of Plastics Engineers.
21. S. L. Belcher, ed., *Practical Extrusion Blow Molding*, Marcel Dekker, New York.
22. S. L. Belcher, M. Berins, ed., in *Plastics Engineering Handbook of the Society of Plastics Industry*, Chapt. "12", pp. 341–382.
23. S. L. Belcher, *Comprehensive Polymer Science, Vol. 7, Specialty Polymers and Polymer Processing*, Pergamon Press, Oxford, Chapt. "15", pp. 489–514.
24. S. A. Jabarin, *Plastics Encyclopedia Orientation of PET and Other Polymers*, University of Toledo, Toledo, Ohio.

GENERAL REFERENCES

Glossary of Plastic Bottle Terminology, Plastic Bottle Institute of The Society of The Plastics Industry, New York, 1980.
Operator's Guide: Controlling Shrinkage of HDPE Bottles, The Dow Chemical, Co., Midland, Mich., 1979.
W. W. Bainbridge and B. Heise, in *Design and Construction of Extrusion Blow Molds, National Symposium—Plastics Molds/Dies*, Oct. 1977, Society of Plastics Engineers, Inc., Palisades Section, Brookfield Center, Conn. SPE Design RETEC 21–1.
C. C. Davis Jr., *Materials for Plastics Molds and Dies, National Symposium—Plastic Molds/Dies*, Oct. 1977, Society of Plastics Engineers, Inc., Palisades Section, Brookfield Center, Conn. SPE Design Retec, 1–1.
R. D. DeLong, *Injection Blow Mold, Design and Construction, National Symposium—Plastic Molds/Dies*, Oct. 1977, Society of Plastics Engineers, Inc., Palisades Section, Brookfield Center, Conn. SPE; Design Retec, 22–1.

J. R. Dreps, *Plast. Eng.* 32 (Feb. 1975).
M. Hoffmann, *Plast. Technol.* 67 (Apr. 1982).
C. Irwin, *Plast. Mach. Equip.* 57 (Sept. 1980).
W. Kuelling and L. Monaco, *Plast. Technol.* 40 (June 1975).
B. Miller, *Plast. World* **30**, 87 (July 1983).
D. L. Peters, *Plast. Eng.* 21 (Oct. 1982).
J. Szajna, *Food Drug Packag*. 14 (May 1983).

SAM BELCHER
Consultant

CHITIN AND CHITOSAN

Introduction

Chitin is a structural polysaccharide widely found in nature. Chitin occurs as highly ordered microfibrils in many species, in a variety of arrangements, from diatom spines to cell wall components of many fungi and yeast. It is also a principal component in the exoskeleton of insects and marine invertebrates such as *Arthropoda* and *Mollusca*. Chitin is a homopolymer of 1-4 linked 2-acetamido-2-deoxy-β-D-glucopyranose, although some of the glucopyranose residues are deacetylated and occur as 2-amino-2-deoxy-β-D-glucopyranose. When chitin is deacetylated to about 50% of the free amine form, it is referred to as chitosan. Figure 1 indicates the copolymeric nature of this material. Chitosan is rarely found in nature but does occur in dimorphic fungi such as *Mucor rouxii* wherein it is formed by the action of a deacetylase enzyme on chitin. Most chitosan is obtained by the chemical or enzymatic treatment of chitin obtained from the shell of commercially harvested *Arthropoda*, such as shrimp and crab.

Chitin was first isolated from mushroom tissue and named "fungine" in 1811 by Braconnot, a French botanist. A similar material was isolated by Odier from insect exoskeleton, which he termed "chitine" (1). Chitin is considered the second most plentiful biomaterial, following cellulose. The annual production of chitin biomass has been estimated at 1×10^{13} kg worldwide (2). This has led to considerable scientific and technological interest in chitin and chitosan. Chitosan has become the preferred commercial form of this material as it is more tractable than chitin. Chitin is insoluble in most common solvents, whereas chitosan dissolves in many common aqueous acidic solutions. Chitosan has found applications in many primary industries such as agriculture, paper, textiles, and wastewater

Encyclopedia of Polymer Science and Technology. Copyright John Wiley & Sons, Inc. All rights reserved.

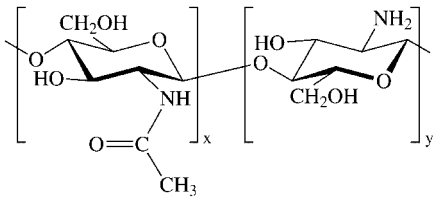

Fig. 1. The chemical structure of chitin and chitosan, a copolymer of the N-acetyl sugar and the amino sugar. Chitin occurs as mostly the "x" or N-acetyl form. Chitosan occurs as the "y" or amino form.

treatment. Chitosan is also under study for medical and pharmaceutical uses. It has also become a popular nutritional dietary additive (3).

Biosynthesis

The synthesis of any polysaccharide involves the addition of an activated monomeric sugar to the end of a growing polysaccharide chain by an enzyme mediated mechanism (4). In higher plants, algae, and photosynthetic bacteria (autotrophic organisms), polysaccharides are produced by a reductive metabolic pathway beginning with water, carbon dioxide, and light. In nonphotosynthetic bacteria, lower plants, fungi, and animals (heterotrophic organisms), they are synthesized from ingested foods. Chitin synthase catalyzes the polymerization of activated *N*-acetyl-glucosamine monomer (5,6).

Most studies of chitin synthesis and microfibril assembly have involved easily cultured unicellular fungi, protists, and algae, which have simple biochemical pathways. Insect and fungi chitin biosyntheses have been perceived as a route to the development of new pesticides as well as for monitoring the environmental impact of these biocides in crustacea (4). Post-polymerization deacetylation by chitin deacetylase converts chitin to chitosan in nature (7). The completion of the biological cycle is accomplished with chitinases and chitosanases, which ultimately degrade chitin and chitosan to their corresponding sugars (8–10).

Chitin and chitosan occur in a wide range of disparate organisms (Table 1). In crustaceans and insects most of the biosynthesis of chitin occurs in the layer of epidermal cells lying just under the cuticle (exoskeleton). Chitin usually occurs in the presence of other cellular materials such as glucans, proteins, and calcium carbonate. One of the purest forms of chitin is the spike of some centric diatoms, such as *Thalassiosira fluviatilis* (5). Some algae also produce a 100% N-acetylated chitin (17). Chitosan is always obtained by the action of a deacetylase on chitin. Figure 2 illustrates the high degree of organization found in native chitin microfibrils.

In animals, chitin biosynthesis begins with glucose. Glucose is phosphorylated, aminated, N-acetylated, and then converted to *N*-acetyl-uridine diphosphate (UDP)-glucosamine. Chitin is polymerized by the activated monomer *N*-acetyl-UDP-glucosamine. The polymerization is driven by the scission of the phosphoester bond. A similar pathway is involved in fungi. The gene fragments

Table 1. Sources of Chitin and Chitosan

Source structure	Type	Reference
Chitin		
Insects		
Cuticle	α-Chitin	11
Ovipositors	α-Chitin	12
Beetle cocoon	γ-Chitin	13
Crustaceans		
Crab shell	α-Chitin	6
Shrimp shell	α-Chitin	14
Squid		
Ommastrephes pen	β-Chitin	15
Loligo stomach wall	γ-Chitin	16
Centric Diatoms		
Thalassiosira fluviatilis	β-Chitin (100% N-acetylated)	5
Algae	α-Chitin	17
Fungi		
Mucor rouxi	α-Chitin	18
Aspergillis nidulans	α-Chitin	19
Fungi		
Mucor rouxi	60–92% deacetylated	20
Deacetylated chitin		
Shrimp shell	M_w up to 1.6×10^6 Da.	21

coding for chitin synthase have been sequenced for many fungi and classified (23). Chitin synthase is an integral membrane protein. It is oriented such that its carboxyl terminus is exposed to the cytoplasmic side of the membrane (24).

Chitin deacetylase catalyzes the hydrolysis of the *N*-acetyl group in chitin. A chitin deacetylase has been purified from *M. rouxii* and identified as a high mannose glycoprotein requiring (at minimum) a tetramer of chitin sugars for catalysis (7). Chitin deacetylase is found outside the plasma membrane and is associated with the nascent chitin chains during fungal chitin biosynthesis. Chitin deacetylation may also be a fungal defense mechanism, as chitosan is more resistant to plant chitinase defense mechanisms.

Isolation

Chitin and chitosan rarely occur in a pure, easily isolated form. A substantial effort has been made to develop chemical, mechanical, and enzymatic methods to obtain purified materials (25). The usual method of obtaining chitin involves the chemical treatment of shell fish wastes from the crab and shrimp industries. The first step is to demineralize the shell with dilute hydrochloric acid at room temperature. This is followed with a deproteinization step with warm dilute caustic. This yields a partially deacetylated chitin, which may then be further deacetylated to chitosan. Figure 3 shows the underlying chitin matrix in the crab shell and its microfibrillar

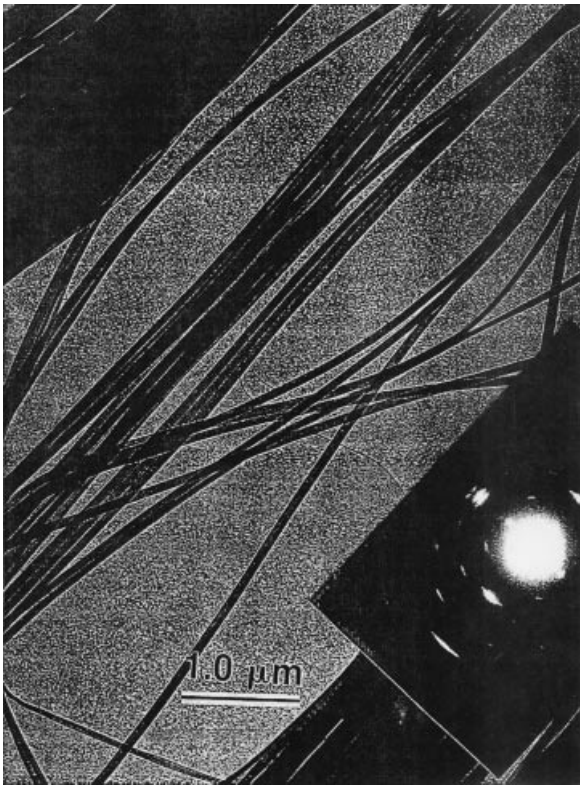

Fig. 2. Chitin usually occurs in the form of microfibrils in many organisms. Shown here are β-chitin microfibrils from *Tevnia jerichonana*, a deep sea hydrothermal vent worm. The insert is a typical electron diffractogram oriented with respect to the bundle. The image was obtained by transmission electron microscopy (TEM) after protein removal (22). Reproduced with permission.

structure. This chitin is termed α-chitin because of its crystal structure (see next section). Treatment of this chitin with 50% NaOH for 1–3 h at 120°C gives a 70% deacetylated chitin (chitosan), which is soluble in many dilute acids. Repeating this step can give deacetylation values up to 98%.

A more reactive form of chitin is obtained from squid pens (15). This β-chitin (see next section) is easily isolated and has a looser chain packing in the crystal, accounting for its higher reactivity and solubility in formic acid. The isolation of β-chitin is accomplished by first washing the squid pens in 1 *M* HCl for 12 h, followed by a 12-h treatment with 2 *M* NaOH. The final step is to heat the pens at 100°C for 4 h in fresh 2 *M* NaOH. This procedure yields 35% chitin from the mass of the pens. The degree of acetylation may be up to 92%.

Properties

Physical. Chitin occurs naturally as one of three crystalline forms, known as α-, β-, and γ-chitin. The unit cell parameters, determined by x-ray diffraction,

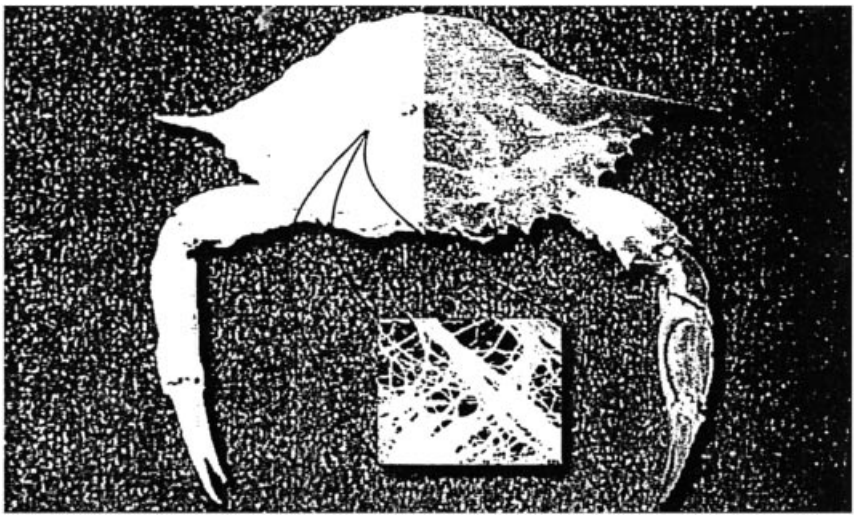

Fig. 3. Chitin and chitosan are commonly isolated from the shells of crab and shrimp. On the right-hand side is the original, cooked crab shell. On the left-hand side is the underlying matrix of chitin, after the proteins and minerals have been removed. Chitin is biosynthesized as an ordered assembly of chains yielding microfibrils, which are seen in the scanning electron micrograph insert. The scale bar in the insert is 2000 nm.

are given in Table 2. The α- and γ-chitin forms are defined as antiparallel stack unit cell structures. The β-form is similar to Cellulose I and assigned a parallel stack structure (16). Chitin is mostly found as either the α- or β-form. The α-form has a strong, three-dimensional hydrogen bond network, which makes the swelling and dissolution of α-chitin difficult. The β-form lacks hydrogen bonding between the stacked planes of the parallel chitin chains. This allows for the easy formation of hydrates and accounts for the higher reactivity of the β-chitin.

Chitosan is also found in different crystalline or polymorphic forms. The unit cell dimensions for these different forms are shown in Table 2. They are obtained by different processing conditions. Chitosan is not usually found completely deacetylated; hence, it has some of the characteristics of a random copolymer. When the deacetylation of the chitin is less than 90%, the crystallization is hindered, and the chitosan has a lower degree of crystallinity than the original chitin.

Table 2. Unit Cell Parameters for Chitin and Chitosan

			Unit cell parameters			
Form	Source	Density, g/cm^3	a, nm	b, nm	c, nm	Reference
α-Chitin	Lobster tendon	1.46	0.474	1.886	1.032	26
β-Chitin	Diatom spines	1.46	0.485	0.926	1.038	27
γ-Chitin	Loligo stomach	1.47	0.47	2.84	1.03	16
Chitosan I	Shrimp shell	1.23	0.776	1.091	1.03	28
Chitosan II	Shrimp shell	1.18	0.44	1.00	1.03	29

The two polymeric characteristics that are the most important for chitin/chitosan solubility are the degree of deacetylation and the molecular weight. Chitin is insoluble in most solvent systems. Chitosan, having at least 50% of its repeat groups deacetylated, is soluble in aqueous acidic solution existing as a randomly coiled cationic polyelectrolyte. Chitin and chitosan have an extensive hydrogen bonded network in the solid state, requiring solvents which either induce interchain repulsions or disturb intermolecular hydrogen bonding for dissolution.

Protonation of the amine group found in the deacetylated repeat units of chitosan provides a means of introducing interchain coulombic repulsions promoting dissolution. Highly deacetylated chitosan, having a pK_a of approximately 6.5, requires a pH lower than 6 for complete dissolution. However, with increasing acetyl content the pK_a of residual amine groups increases and is believed to approach a value slightly greater than 7.5 (29). As a result of this pK_a shift, chitosan with a degree of deacetylation of 50% is soluble in neutral water. Upon further increases in acetyl content, the interpolymeric attractions dominate, and the material (chitin) is insoluble in water with the addition of acid despite the protonation of accessible amine groups. Chitosan is not soluble in diprotic acids such as sulfuric acid. The divalent sulfate anion facilitates interchain ionic attractions preventing dissolution and forming ionic cross-links.

Chitin is soluble in *N*,*N*-dimethylacetamide–5% LiCl, *N*-methyl-2-pyrrolidone–5% LiCl, and mixtures of trichloroacetic acid with chlorinated hydrocarbons (ie, chlorinated methanes and ethanes) (30). Generally, the solubilities of chitin and chitosan decrease with increases in molecular weight. Oligomers of chitin and chitosan with a degree of polymerization of 8 or less are water soluble regardless of pH. Many derivatives of chitin and chitosan, which have wide solubility characteristics, have been synthesized.

Chemical. A large number of chitin and chitosan derivatives have been synthesized through modification of the primary (C-6) and secondary (C-3) hydroxyl groups present on each repeat unit, including amine (C-2) functionality existing on deacetylated units (31). Reactions typical of hydroxyl and amine groups (such as acylations with acid chlorides and anhydrides) including urethane and urea formation respectively, are feasible with isocyanates. The primary amine can be quaternized by alkyl iodides or converted to an imine with a variety of aldehydes and ketones that can subsequently be reduced to an N-alkylated derivative. Chitin and chitosan are reactive with a variety of alkyl chlorides after treatment with concentrated NaOH. Important derivatives such as carboxymethylated chitin and chitosan are commonly produced in this manner with the addition of sodium chloroacetate.

Chitin and chitosan have been chemically modified by graft copolymerization using a variety of monomers ("grafting from") and telechelic polymers ("grafting onto"). *"Grafting from" techniques* have predominantly utilized either a free-radical mechanism with vinyl monomers such as styrene, methyl methacrylate, methyl acrylate, acrylic acid, and acrylamide, or a ring-opening mechanism (initiated by free amine groups) with D,L-alanine and γ-methyl L-glutamate *N*-carboxyanhydrides (32). Vinyl grafting has been initiated with techniques involving the ceric ion (Ce^{4+}), Fenton's reagent (Fe^{2+}/H_2O_2), and γ-irradiation. *"Grafting onto"* methods have bonded poly(ethylene glycol) (33) or poly(2-methyl-2-oxazoline) (34) chain ends to the trunk polymer. For example, poly(ethylene glycol)

was synthesized with an activated carboxylic acid chain end capable of forming an amide linkage with free amine groups along the chitin/chitosan backbone. The range of possible chitin and chitosan modifications, using either lower molecular weight reagents or graft copolymerizations, allows modification of chitin and chitosan solubility, miscibility with other materials, conductivity, and moisture absorbency.

Biological. A wide range of hydrolytic enzymes lead to the biodegradability of chitin and chitosan. Within an organism, directed degradation by chitinases are involved in fungal autolysis and the molting of arthropod cuticle. Other chitinases are abundantly secreted into the environments of plants and microbes as part of their defense and feeding mechanisms. In bacteria, chitinases play a role in nutrition and parasitism. The major groups of enzymes degrading chitin and chitosan have been classified and described (4,8–10). Many studies have also utilized lysozyme, an easily obtainable hydrolytic enzyme, found in the lymphoid system of vertebrates. Lysozyme shows hydrolytic activity over a range of deacetylation values for chitin and chitosan.

Generally, the complete hydrolysis of chitin to *N*-acetyl-glucosamine requires the consecutive action of two chitinase enzymes. These are frequently found together in plant and animal species as well as bacteria and fungi. Usually, the chitin is degraded to oligosaccharides and *N*,*N*′-diacetylchitobiose by endochitinase enzymes. Chitobiases then hydrolyze these products to monomeric *N*-acetyl-glucosamine. Exochitinases, which directly degrade chitin to chitobiose, are also known. The same is also found for chitosanases.

In arthropods, synthesis and degradation of chitin occurs at different stages of the molting cycle and is hormonally controlled. During the molt, the rate of chitin synthesis is slowed by molting hormones (ecdysteroids) that also stimulate the production of chitinases. Many animals and marine microorganisms have a high digestive capacity for chitin. In seawater, the presence of secreted chitinases from microorganisms leads to the near total degradation of crustacean chitin in shallow water sediments within 4 months in temperate regions.

Processing

Chitin is usually obtained as a powder or a flake upon isolation from crab shell, fungi, or algae. Further processing is difficult because of the lack of simple solvents for chitin. However, chitosan is easily solubilized and formed into shaped articles such as films (membranes), fibers, and gel microspheres (30,35). Chitosan is conveniently dissolved in an aqueous 5 vol% acetic acid solution, in the form of a cationic polyelectrolyte. This ability to develop basic properties in solution gives chitosan its uniqueness among common polysaccharides. Chitin and chitosan are also easily treated with acids and hydrolytic enzymes to yield useful sugars and oligomers.

Economic Aspects

A worldwide industry has developed around the production and uses of chitin and chitosan. Shrimp and crab shell wastes pose local waste disposal problems

in many areas. The seasonal harvesting of these crustacea has created problems for an economic, year-round chemical production of chitin and chitosan, in some regions though. In the United States, there are several producers who manufacture and import chitosan. These include Vanson, Inc., DCV, Inc., Biopolymer Engineering, Inc., and Marine Polymer Technologies. There are also industries manufacturing chitin and chitosan in many countries in almost every continent. In particular, Japan, China, and Norway have well-established companies. Chitin and chitosan are still in the stage of a speciality chemical and is sold mostly in the form of chitosan powder, at $25–50/kg, depending on purity. The primary uses are in the water treatment, paper, and agricultural industries. It is also sold as a dietary additive worldwide. Speciality producers offer very pure chitin and chitosan derived from algae and squid pen. These are primarily employed in biomedical research and biomedical products.

Specifications and Analytical Methods

Chitin and chitosan are natural products, commercially available from many sources as mentioned previously. It is usually found in the presence of proteins, calcium carbonate, and perhaps other polysaccharides. Thus, its quality ranges from crude extracts to high purity material. Many of the properties of chitin and chitosan are dependent on the degree of deacetylation. The distribution of *N*-acetyl groups in these polymers is also expected to have an influence on the properties.

Most spectroscopic and titration methods have been employed to determine these values and were listed by Rathke (36). The structural differences between chitin polymorphs have been studied by nmr and ir (37,38). Conductometric titrations have been confirmed by solid state nmr to be an accurate but easy method to determine the degree of deacetylation of chitosan (39).

The molecular weight and its distribution are also important. Commercial chitosan samples may have molecular weights up to 4×10^6 Da. The Mark Houwink equation $[\eta] = kM_v{}^a$ is used to obtain a viscosity average molecular weight. However, the values of k and a are most likely functions of the degree of deacetylation (21). Gel permeation chromatography is also suited for the determination of chitosan molecular weight and polydispersity (21).

Health and Safety Factors

The benefits of chitosan as a dietary fiber have been recognized (3,40,41). Chitin and chitosan have very low toxicity. Studies on the oral administration of chitosan indicates that it may have beneficial actions on osteoarthrosis, body weight control, and the lowering of blood plasma cholesterol levels. Chitosan's complexation with bile acids helps block the absorption of lipids. Both materials have been granted approval for different food additive uses for humans and animals in several countries. The corresponding sugars of these polysaccharides, glucosamine, and *N*-acetyl-glucosamine are also of interest. In many circumstances it is these sugars which have the observed biological activity. Tissue and animal studies

indicate that chitin and chitosan promote wound healing and increase immune response, but these claims need to be validated by human clinical trials. Certain medical precautions should be observed, however, with long-term ingestion of high doses of chitosan to avoid potential adverse metabolic effects (3).

Uses

Chitin is mainly used as a powder and as a precursor to chitosan. However, the unusual aminopolysaccharide structure of chitosan has led to many potential applications. The ease of processing chitosan into shaped articles, coupled with its ease of chemical derivatization, makes it a versatile material. The specificity of chitin and chitosan's structure is also important for many biological applications involving the binding and purification of many proteins.

Chitin and chitosan have potential in agricultural applications because of their ability to increase crop yields. The presence of chitosan appears to enhance plant reproduction (42), and coating seeds with chitin/chitosan activates the secretion of plant chitinases into the environment providing extra protection from harmful pests.

Incorporating chitin and chitosan into different aspects of the food industry has received considerable attention (43). The antibacterial and antifungal properties of chitin and chitosan have potential in reducing the amount of synthetic food preservatives. N,O-carboxymethylated chitosan, a water soluble derivative, has also been found to possess antifungal activity. The most probable means of application are either through packaging wraps or directly as food coatings. Chitin and chitosan films are improvements to synthetic wraps as a result of the reduction in oxygen permeability and increased moisture transfer. Chitosan films have also decreased the level of browning in physically damaged fruits.

In regard to nutritional value, chitin and chitosan oligomers have been observed to lower cholesterol and exhibit antitumor activity. "Fat-blockers" containing chitosan are currently on the market (40). The amine groups along the polymer backbone form carboxylate-protonated amine complexes with fats which are subsequently excreted from the body because of chitosan's lack of digestibility in humans.

Chitosan has potential applications in various wastewater treatments (44). Chitosan is a natural chelating polymer as a result of the amine group (C-2) and the adjacent hydroxyl group (C-3), and thus could be used to remove transition metal ions from wastewater streams. Some important factors that affect the level of ion removal are the degree of deacetylation, pH, and surface area of the chitosan substrate. Since protons compete for amine sites, the metal ions can be removed from the chitosan backbone by lowering the pH. Chitosan beads cross-linked with gluteraldehyde appear to be a more practical physical form because of its lack of solubility at low pH and its higher surface area.

Chitosan can be used as a flocculating agent for food processing streams. Having a partial positive charge in water, chitosan can break down food particles comprised of a protein-based colloidal suspension possessing a partial negative charge. Suspended solids can be coagulated by chitosan, collected, and used as a protein source for animal feed.

Anionic dyes can be removed from textile effluent streams at acidic pH with chitosan through protonated amine complexation with anionic dye sites. Phenols are common waste products in paper processing. Application of mushroom enzyme tyrosinase to the stream specifically converts phenols into quinones, which can subsequently be absorbed by chitosan. Toxic polychlorinated biphenols (PCBs), commonly used in plastic processing and lubricants, are a significant source of water contamination. Although the nature of the interaction is not currently known, chitosan treatment shows potential in lowering PCB concentrations.

Research on the use of chitosan for drug delivery indicates promise in oral, parenteral, transdermal, ocular, and nasal applications (45). Generally, chitosan has low toxicity with excellent mucoadhesion properties. Cross-linked chitosan has potential in tablet form because of its low solubility in the stomach. The same effect can be obtained by incorporating hydrophobic coatings on chitosan microspheres. Chitosan gels and films exhibit sustained release of various drugs useful for wound dressings and colon treatments. Many other examples of drug delivery applications of chitosan have been reviewed (46), and chitosan peroral peptide delivery systems have been described (47). Other pharmaceutical applications of chitosan and the mechanisms of action for various *in vitro* and *in vivo* models have been outlined and discussed (48).

The direct application of chitin and chitosan to wounds stimulates several different physiological activities (49). The presence of chitin and chitosan on the wound surface stimulates macrophage activity for the secretion of lysozyme and human chitinase, enzymes which breakdown chitin-based pathogens to prevent infection. The chitin/chitosan present in the wound dressing is thus simultaneously hydrolyzed to chitooligomers, which further stimulate collagen deposition and other macrophage functions, namely nitric oxide and tumor necrosis factor production.

Hemodialysis utilizes film and hollow fiber membranes to remove solutes and water from patients suffering from kidney failures. The excellent fiber and film forming properties of chitosan have led to many studies on its use for this purpose (30,50). Chitosan may be blended with other polymers to give permeability control and to improve blood compatibility.

BIBLIOGRAPHY

"Chitin" in *EPST* 1st ed., Vol. 3, pp. 695–705, by J. Conrad; in *EPST* 2nd ed., Vol. 3, pp. 430–441, by R. A. Muzzaarelli.

1. C. Jeuniaux, *Adv. Chitin Sci.* **1**, 1 (1996).
2. C. Jeuniaux and M. F. Voss-Foucart, *Biochem. Syst. Ecol.* **19**(5), 347 (1991).
3. S. Koide, *Nutr. Res.* **18**(6), 1091 (1998).
4. S. Salmon and S. M. Hudson, *J.M.S., Part C: Rev. Macromol. Chem. Phys.* **37**(2), 199 (1997).
5. R. Smucker, *Biochem. Syst. Ecol.* **19**(5), 357 (1991).
6. R. A. Muzzaarelli, *Chitin*, Pergamon Press, New York, 1977.
7. D. Kafetzopoulos, A. Martinou, and V. Bouriotis, *Proc. Natl. Acad. Sci.* USA, **90**, 2564 (1993).
8. D. Somashekar and R. Joseph, *Bioresource Tech.* **55**, 35 (1996).
9. K. J. Kramer and S. Muthukrishnan, *Insect Biochem. Mol. Biol.* **27**(11), 887 (1997).

10. R. Patil, V. Ghormade, and M. Deshpande, *Enzyme Microb. Technol.* **26**, 473 (2000).
11. A. Retnakaran, in R. Muzzarelli, C. Jeuniaux, and G. Gooday, eds., *Chitin in Nature and Technology*, Plenum Press, New York, 1986, p. 147.
12. M. Giraud-Guille, H. Chanzy, and R. Vuong, *J. Struct. Biol.* **103**, 232 (1990).
13. K. Rudall and W. Kenchington, *Biol. Rev.* **49**, 597 (1973).
14. K. Kurita, T. Sannan, and Y. Iwakura, *Makromol. Chem.* **178**, 3197 (1997).
15. K. Kurita and co-workers, *J. Polym. Sci., Polym. Chem.* **31**, 485 (1993).
16. A. Walton and J. Blackwell, *Biopolymers*, Academic Press, New York, 1973.
17. U.S. Pat. 5622834 (1997), J. Vournakis, Marine Polymer Tech., Inc.
18. S. Bartnicki-Garcia, in G. Skjak-Braek, T. Anthonsen, and P. Sandford, eds., *Chitin and Chitosan: Sources, Chemistry, Biochemistry, Physical Properties and Applications*, Elsevier Applied Science, New York, 1989.
19. F. Reyes, M. Martinex, J. Caltyud, and R. Lahoz, in R. Muzzarelli, C. Jeuniaux, and G. Gooday, eds., *Chitin in Nature and Technology*, Plenum Press, New York, 1986, p. 99.
20. S. Arcidiacono and D. Kaplan, *Biotech. Bioeng.* **39**, 281 (1992).
21. J. Knaul and co-workers, *Can. J. Chem.* **76**, 1699 (1998).
22. G. Gaill and co-workers, *J. Struct. Biol.* **109**, 116 (1992).
23. A. Bowen and co-workers, *Proc. Natl. Acad. Sci.* USA, **89**, 519 (1992).
24. S. Machida and M. Saito, *J. Biol. Chem.* **268**, 1702 (1993).
25. S. Hudson and C. Smith, in D. Kaplan, ed., *Biopolymers from Renewable Resources*, Springer, New York, 1998, p. 99.
26. R. Minke and J. Blackwell, *J. Mol. Biol.* **120**, 167 (1978).
27. K. Gardner and J. Blackwell, *Biopolymers*. **14**, 1581 (1975).
28. R. J. Samuels, *J. Polym. Sci., Polym. Phys. Ed.* **19**, 1081 (1981).
29. A. Domard, *Adv. Chitin Sci.* **3**, 24 (1998).
30. T. Rathke and S. Hudson, *J.M.S., Part C: Rev. Macromol. Chem. Phys.* **34**, 375 (1994).
31. G. A. F. Roberts, *Chitin Chemistry*, MacMillan Press, London, 1992.
32. K. Kurita, in M. F. A. Goosen, ed., *Applications of Chitin and Chitosan*, Technomic, Lancaster, 1997, p. 297.
33. T. Ouchi, H. Nishizawa, and Y. Ohya, *Polymer* **39**(21), 5171 (1998).
34. K. Aoi, A. Takasu, and M. Okada, *Macromolecules* **30**, 6134 (1997).
35. K. Yao and co-workers, *J.M.S., Part C: Rev. Macromol. Chem. Phys.* **35**, 155 (1995).
36. T. Rathke and S. Hudson, *J. Polym. Sci., Polym. Chem. Ed.* **31**, 749 (1993).
37. B. Focher and co-workers, *Carbohydr. Polym.* **17**, 97 (1992).
38. M. Takai and co-workers, in W. Glasser and H. Hatakeyama, eds., ACS Symp. Ser., Amer. Chem. Soc., Vol. **489**: *Viscosity of Biomaterials*, Washington, D.C., 1992, p. 38.
39. L. Raymond, F. Morin, and R. Marchessault, *Carbohydr. Res.* **246**, 331 (1993).
40. I. Furda and C. Brine, eds., Adv. Exper. Med. & Bio. Ser., Vol. **270**: *New Developments in Dietary Fiber*, Plenum, New York, 1990.
41. R. A. A. Muzzarelli, *Adv. Chitin Sci.* **4**, 212 (2000).
42. R. A. A. Muzzarelli and C. Muzzarelli, in B. A. Stankiexicz and P. F. van Bergen, eds., ACS Symp. Ser., Vol. **707**: *Nitrogen-Containing Macromolecules in the Bio- and Geosphere*, Amererican Chemical Society, Washington, D.C., 1998, p. 148.
43. F. Shahidi, J. K. V. Arachchi, and Y. Jeon, *Trends Food Sci. Technol.* **10**, 37 (1999).
44. H. K. No and S. P. Meyers, *Rev. Environ. Contam. Toxicol.* **163**, 1 (2000).
45. W. Paul and C. P. Sharma, *S.T.P. Pharma Sci.* **10**(1), 5 (2000).

46. O. Felt, P. Buri, and R. Gurny, *Drug Dev. Ind. Pharm.* **24**(11), 979 (1998).
47. A. Schnurch, *Int. J. Pharm.* **194**, 1 (2000).
48. V. Dodane and V. Vilivalam, *Pharm. Sci. Tech. Today* **1**(6), 246 (1998).
49. R. A. A. Muzzarelli, *Cell. Mol. Life Sci.* **53**, 131 (1997).
50. D. Singh and A. Ray, *J.M.S., Part C: Rev. Macromol. Chem. Phys.* **40**(1), 69 (2000).

SAMUEL M. HUDSON
DAVID W. JENKINS
North Carolina State University

CHLOROSULFONATED POLYETHYLENE.

See ETHYLENE POLYMERS, CHLOROSULFONATED.

CHLOROTRIFLUOROETHYLENE POLYMERS.

See FLUOROCARBON ELASTOMERS.

CHROMATOGRAPHY, AFFINITY

Introduction

One of the most important developments in enzymology has been the introduction of a rapid and highly efficient means of protein purification utilizing the highly selective ability of enzymes to recognize certain biological compounds or their analogues. This technique, termed *affinity chromatography*, involves the immobilization of an appropriate ligand in such a way that the enzyme is still capable of recognizing and binding to the immobilized form of the ligand, whereas "contaminating proteins" have no such recognition. Virtually hundreds of proteins have been purified in this way, using a wide variety of bioligands immobilized in a matrix; enzyme inhibitors, coenzymes, antibodies, and even other enzymes may be useful bioligands in the purification of a particular protein (1). A classification of the types of affinity chromatography is as follows (2):

Bioselective adsorption is the process where the affinity is based on biologically relevant binding. It includes group-specific ligands, eg, lectins and nucleotide cofactors (NAD, AMP), and specific ligands, eg, certain less common cofactors (vitamin B_{12}), receptor proteins, and antibodies as used in immunosorbents.

Chemiselective adsorption is the process where the affinity is based on chemically defined nonbiological interactions. It includes hydrophobic chromatography, ion-exchange chromatography, covalent chromatography (active thiols, Hg^{2+}, etc), and borate complexes.

The basic application of affinity chromatography involves several steps, as illustrated in Figure 1. First, the necessary affinity-chromatographic packing, or bioselective adsorbent, as it may be more appropriately termed, is synthesized. Next, a cell-free extract containing the desired enzyme is prepared. This extract is freed of any endogenous substrate or biomolecule that might compete with the

Encyclopedia of Polymer Science and Technology. Copyright John Wiley & Sons, Inc. All rights reserved.

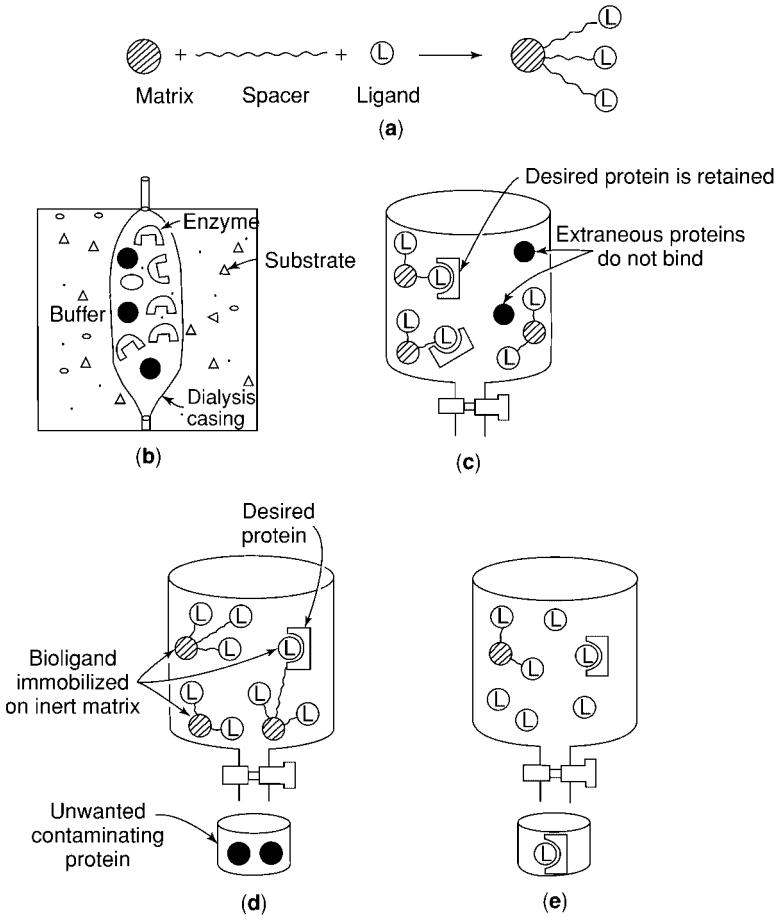

Fig. 1. The steps of affinity chromatography: (**a**) A bioligand is immobilized; (**b**) A crude extract is prepared and freed from endogenous substrate; (**c**) The substrate-free extract is applied to the chromatographic packing of immobilized bioligand from step (**a**); (**d**) Unwanted protein is removed by washing; and (**e**) The desired protein is eluted, possibly with a soluble bioligand (2).

enzyme for the adsorbent. This is normally achieved by dialysis or enzyme precipitation. The crude extract is applied to the column, and contaminating proteins, which ideally have no affinity for the column under the conditions employed, are removed by washing. The protein to be purified remains bound to the column because of its affinity for the immobilized ligand. It is subsequently removed by eluting the column with a solution of the free ligand. Alternatively the enzyme may be eluted by altering the chromatographic conditions, ie, pH, ionic strength, dielectric constant, etc, in such a way that the enzyme no longer retains its affinity for the immobilized ligand.

Efficient purification by affinity chromatography depends on the nature of the ligand, the methods used in the preparation of the chromatographic packing,

the type of inert matrix, and the methods for both attaching the ligand to the matrix and eluting the enzyme from the bioselective adsorbent. Nonspecific adsorption of proteins, which can be defined as the retention of proteins by some general factor, eg, ion exchange, hydrophobic interactions, and charge-transfer complexation, may cause a large variety of proteins to be nonspecifically retained.

Finally, it must be decided whether affinity chromatography is employed primarily for purification or primarily as a method for studying enzyme–substrate interaction. The choice of the final system to be used is governed by the nature of the application.

Matrices

The selection of an appropriate inert matrix is of great importance and depends on the type of separation desired. Large columns, or those employed under high pressure, require beads with high mechanical stability. Affinity purification as a final step following a long series of conventional procedures requires a small column. When affinity chromatography is employed in the last stages of purification as a "polishing" step, high yields of the valuable partially purified enzyme are especially important. Even a small percentage of nonspecific adsorption or protein denaturation on the column would limit the usefulness of the procedure. For this reason a hydrophilic, nonionic matrix with little capacity for nonspecific adsorption is essential.

Nonspecific adsorption must not occur in the "derivatized" matrix, even though the untreated matrix might have considerable nonspecific adsorption. For example, virgin glass adsorbs enzymes in an active form, yet dextran-coated glass or glass treated with hydrophilic silanes exhibits little or no adsorption (4) of ribonuclease and other proteins.

In high performance liquid affinity chromatography (hplac), a rapidly growing technique, the matrix must be mechanically stable and capable of sustaining very high pressures. High pressure chromatography resins of the Trisacryl or TSK-type may supplement the silica-based hplac matrices. Several activated resin forms are commercially available (Pierce Chemical Co., Rockford, Ill.).

The most widely used matrix is beaded agarose, a common gel-permeation chromatography packing used chiefly because of the hydrophilicity of the underivatized matrix (5). It might be thought that derivatized agarose would not have more nonspecific adsorption than its untreated counterpart. However, this is not the case, and this observation confirms that it is the derivatized chromatographic packing, and not the matrix, that must possess the appropriate properties for a bioselective adsorbent.

In addition to mechanical stability and nonspecific adsorption, the chemical stability and ease of derivatization of the matrix must be considered. Agarose provides the least nonspecific adsorption, fair chemical stability, and a rather poor and often limiting mechanical stability whereas controlled-pore glass provides the greatest mechanical stability and ease of derivatization, with acceptable capacity but often with unacceptable amounts pf nonspecific adsorption.

Other matrices have certain advantages and disadvantages for specific applications. Regenerated cellulose, polyacrylamide, and cross-linked dextrans generally yield high capacity adsorbents as defined chemically, ie, the amount of ligand bound per gram, but often much of their surface is not available to large macromolecules; thus the effective capacity, ie, the amount of ligand accessible to a particular enzyme, is generally low. In other words, many of the ligands are buried in the matrix in such a way so as to be inaccessible to the enzyme.

Agarose. This material is among the most useful matrices for affinity chromatography. It is a linear polysaccharide containing alternating residues of D-galactose and 3,6-anhydro-L-galactose (6).

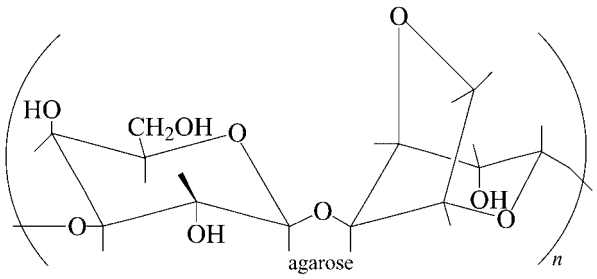

Agarose is prepared by mixing a hot aqueous solution of specially purified agar (2–6%) with an organic solvent, eg mineral oil, and a small amount of detergent. The aqueous solution is mixed rapidly with the organic phase to form droplets that, upon cooling, form agarose beads (7). These beads are fragile even to the touch. Cross-linking with epichlorohydrin increases their strength but decreases porosity.

The agar base, and thus agarose, is a naturally occurring polysaccharide with many ionic residues, chiefly carboxylate and sulfate, which are removed by hydrolysis and reduction. Commercial agarose beads contain up to 0.37% sulfur (8), indicating the presence of a significant number of ionic groups in commercial agarose.

Agarose also presents other problems: It lacks thermal stability, cannot be dried or frozen readily, and shrinks and swells upon changes of ionic strength or dielectric constant of the medium, especially in the presence of organic solvents. Thus, commercial agarose is completely soluble in dimethyl sulfoxide at 100°C or in 4 *M* sodium iodide, whereas agarose cross-linked with epichlorohydrin is essentially unaffected under the same condition (<1% soluble) (8).

Agarose is frequently used as the cyanogen bromide derivative. This activated matrix reacts with proteins and other molecules with amino groups (5,9–11) and covalently couples them to the agarose surface.

The most serious problem encountered with agarose is the formation of an unstable isourea function from the reaction of cyanogen bromide-activated agarose with primary amines. This isourea forms a positively charged derivative:

Activation:

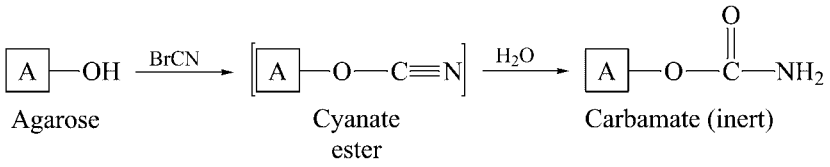

Coupling:

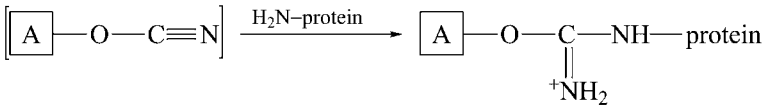

Until 1973 the ionogenic nature of cyanogen bromide-activated agarose was not known, and many early investigations using this method must be examined closely. Furthermore, it should be noted that cyanogen bromide is toxic and presents an explosion hazard when impure.

Derivatized agarose often possesses ion-exchange properties in addition to, if not in place of, bioselective adsorption. In many instances it is suspected that what was hitherto thought to be a purification based on bioselective adsorption, or affinity chromatography, was in reality a specifically tailored ion-exchange chromatography, which may or may not have given better results than classical ion-exchange methods (12).

Even though there is some question about the mode of action of some bioselective adsorbents based on cyanogen bromide activation, enzymes can be purified by ligands coupled to cyanogen bromide-activated agarose. However, there are many methods for derivatizing agarose that are not ionogenic. Coupling can be employed by means of bifunctional reagents, including bisoxiranes, eg, 1,4-bis(2,3-epoxypropoxy)butane, and diphenyl sulfone (13). The reactions of bisoxiranes are shown below:

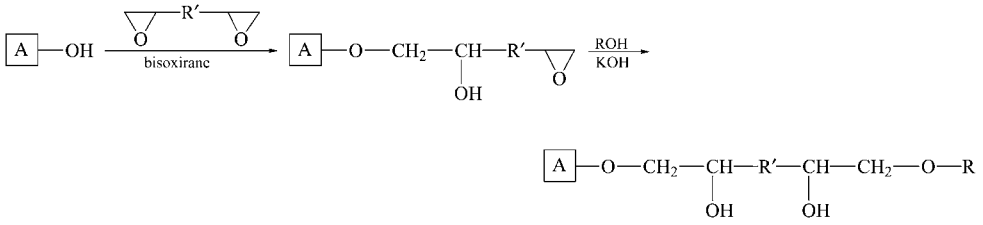

where R is the ligand to be attached to the agarose.

Other activation methods are performed with carbonyldiimidazole or tresyl chloride (14); both yield uncharged materials. Coupling with carbonyldiimidazole (CDI) is very rapid, but the bond formed, a substituted carbamate, is not as stable as the secondary amine formed with the slower tresyl chloride.

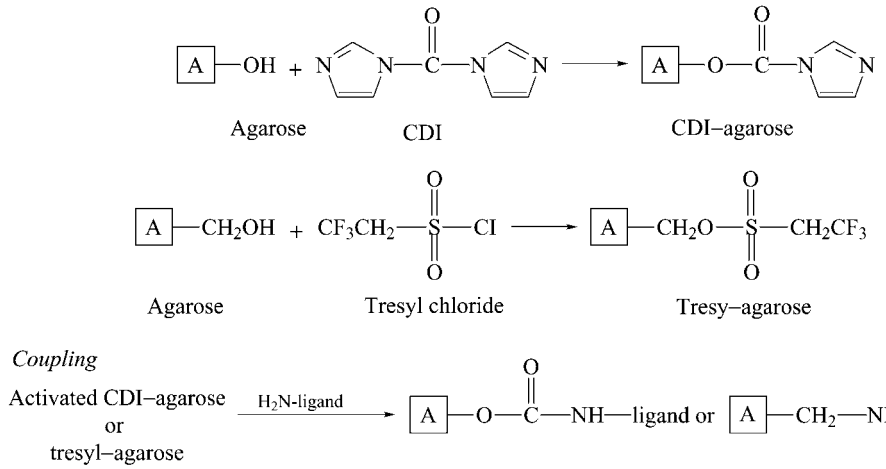

A group of activation reagents similar to CDI have been developed in Israel (11). They resemble phosgene and produce immobilized enzymes with bonds identical to those produced by CDI. One of their advantages is that *p*-nitrophenyl chloroformate can be used to prepare an activated matrix that has the property of releasing the yellow *p*-nitrophenol anion as coupling occurs, thereby permitting one to easily monitor the reaction visually:

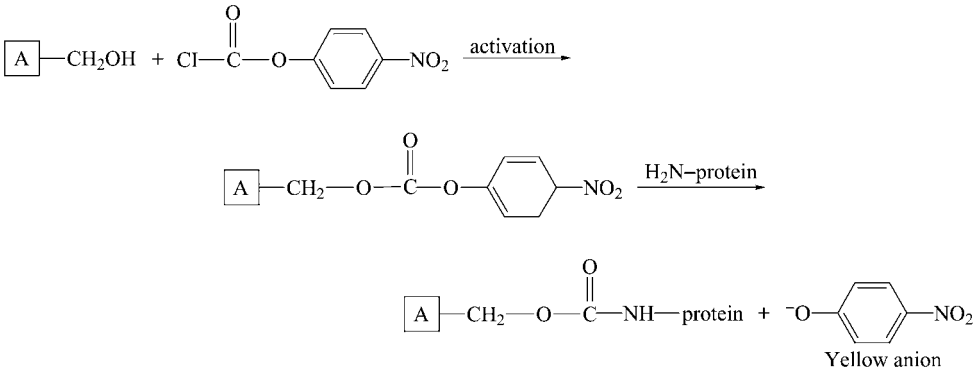

Controlled-Pore Glass. Many bioselective adsorption separations can be performed on columns of porous glass with excellent results (2).

Controlled-pore glass was developed when it was discovered that borosilicate glass heated to 700–800°C separates into borate and silicate phases (15,16). The borate phase is removed by an acid etching process, leaving a porous 96% silica network. These pores, ca 4.5 nm in diameter, can be enlarged by additional alkali etching to produce porous silica beads with nominal pore diameters of 4.5–2500 nm. The pore distribution (±10%) is the most uniform of any porous chromatographic support. Controlled-pore glass with pore diameters above 250 nm are generally too friable for chromatographic application, although large-pore-diameter glass, up to about 400 nm, has been employed.

Another type of inorganic matrix that is similar to controlled-pore glass but considerably less expensive can be prepared by fusing inorganic compounds such as finely pulverized silica and zirconium oxide to form a porous body. Although the pore distribution is less uniform, the surface composition is almost uniform; in the case of silica, the surface is nearly 100% silica. Controlled-pore

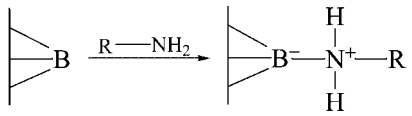

glass is 96+% silica, but alkali leeching facilitates the migration of boron to the surface, which may in fact contain as much as 30% boron (15). The numerous boron Lewis acid sites that result may adsorb ammonia or nucleophiles such as protein amines to yield positively charged centers, both of which lead to nonspecific adsorption

Early synthetic procedures for preparing glass for affinity chromatography or enzyme immobilization involved refluxing γ-aminopropyltriethoxysilane with the beads (17) under various conditions; the beads were coated with multiple layers of silane, which were not as stable as desired. A more stable layer is obtained by employing aqueous silanization at pH 3.75 and 75°C (17). Nonetheless, aminoalkyl glass, or any other silanized glass material, is unstable in aqueous solution at pH values much above 7. Similar materials prepared from zirconium oxides are, conversely, stable in base and labile in acid.

Some derivatives of aminopropyl glass exhibit nonspecific adsorption in certain enzyme preparations, others do not (18). Nonspecific adsorption is minimized by coating the glass with glycidoxypropyltrimethoxysilane, followed by appropriate treatments to yield a highly stable glass with a hydrophilic surface because of the presence of hydroxyl groups in the coating. This surface can be further derivatized in a manner similar to that used for agarose, although the same reservation expressed above for cyanogen bromide activation of agarose, namely its ionogenic nature, applies to glycidoxy controlled-pore glass.

β-Galactosidase has been purified from cell-free extracts of *Aspergillus niger* (19) by using a bioselective adsorbent consisting of the inhibitor β-aminophenyl-β-D-thiogalactose coupled to controlled-pore glass by means of an amide linkage using a soluble carbodiimide as the coupling reagent. However, the same matrix prepared with aniline as a ligand in place of the inhibitor results in a substantial purification of β-galactosidase (20). The aniline-modified material has a capacity 75% of that containing the bound inhibitor and produces β-galactosidase with about 50% of the specific activity of that produced with the affinity packing consisting of inhibitor-controlled-pore glass. A combination of ionic and hydrophobic forces results in a reasonably selective adsorbent whose function is not totally based upon enzyme-active site–inhibitor interaction. The exact nature of the interactions are not known.

Deoxyribonucleic acid (DNA) and ribonucleic acid (RNA) polymerases have been separated and purified on DNA-glass columns, effecting more rapid purification than affinity chromatography on DNA–cellulose (21,22). The DNA is coupled

to aminopropyl glass beads, using the method for covalent coupling of DNA to cellulose with a soluble carbodiimmide as the coupling reagent (23).

Silica and porous glass can be used as matrices for hplac (24–26). In this technique, where mechanical stability under pressure is critical and pH changes are transient, porous silica matrices are useful.

Cellulose. A widely used DNA affinity-chromatography procedure (21) depends upon the physical trapping of DNA fibers in a mesh of cellulose fibers. The DNA–cellulose is prepared by drying DNA and cellulose together in an appropriate buffer, followed by washing the untrapped DNA. However, as one might expect from a method involving physical trapping, DNA slowly elutes.

Bulk cellulose is a poor affinity-chromatographic matrix; its principal advantage is its low cost. This is rarely an overriding consideration since the enzymes to be purified are usually expensive. Cellulose was employed in 1953 in one of the earliest affinity-chromatography separations, where tyrosinase was purified on a column of aromatic cellulose ethers (27). Currently, cellulose (28) or related polysaccharides (29) are used in a number of applications as a bioselective adsorbent including DNA–cellulose for the purification of DNA-binding proteins.

Polyacrylamide. Polyacrylamide is familiar to most biochemists, since it serves as the support for polyacrylamide gel electrophoresis and a medium for gel-permeation chromatography (see also ACRYLAMIDE POLYMERS).

For the latter purpose, preformed spherical beads, Biogel-P, are available from Bio-Rad Laboratories, Richmond, California. These beads are hydrophilic and chemically stable and have a uniform pore diameter and mesh size. These desired traits, and the fact that the polyacrylamide beads are readily derivatized, suggest that it should be an excellent affinity-chromatographic support. In fact, it is not often used because the beads are not sufficiently porous to permit proteins to have access to ligands bound within the beads. The lack of normal porosity for polyacrylamide beads is aggravated by the shrinkage of the gel occurring upon derivatization. As a result, the effective capacity of polyacrylamide gel is very low for all except the smallest enzymes.

Several derivatives of polyacrylamide have been formulated that have the capacity for much larger pore sizes and less shrinkage upon derivatization. Trisacryl, a product of LKB–IBF, is the polyamide of Tris, tris(hydroxymethyl)aminomethane, and acrylic acid. It is a promising matrix material that can be derivatized by all of the methods available for agarose but with far greater mechanical stability. Czechoslovakian investigators have prepared other hydrophilic gels based on hydroxyalkylmethacrylates (30). These supports exhibit increased porosity, with exclusion limits of up to a molecular weight of 10^8.

An interesting application of polyacrylamide has been in the technique of affinity electrophoresis, where enzymes are purified on a support medium containing an immobilized bioselective adsorbent (31). This technique has two advantages over affinity chromatography: A highly porous polyacrylamide can be employed because the material does not assume a spherical form but is cast in a glass or plastic supporting-gel tube; and the separation of two or more substances with similar affinity for the same ligand is greatly increased since charge and gel-permeation effects, as well as bioselective adsorption, contribute to the migration of proteins. Phytohemagglutinins have been purified by electrophoresis on acrylamide-derived gels prepared from alkenyl-*O*-glycosides and a

bisacrylamide (32). The phytohemagglutinins have also been separated by bioselective adsorption chromatography with a similar glycoside-containing polyacrylamide gel derivative (32).

Other Matrices. A large number of other matrices have been employed, including starch (33), cross-linked dextrins (34,35), a vinyl maleimide polymer (36), chitin (37), mannan (38), and insolubilized proteins (39). The number of potential matrices is almost limitless, and most of the matrices used for immobilization of enzymes have potential application in bioselective adsorption. Among these are nylon (40), metal oxides (41), maleic anhydride–ethylene co-polymers (42), and polystyrene derivatives (43). Few of these have been used because of their potential for nonspecific adsorption either by charge, as with the metal oxides, or by hydrophobic interactions (as would be the case with polystyrene). The derivatized matrix must be free of nonspecific adsorption. Proper derivatization can eliminate nonspecific adsorption or, as with cyanogen bromide activation, create nonspecific adsorption in matrices having no prior nonspecific adsorption properties.

Ligands

The ligand to be immobilized can be an inhibitor, a substrate, substrate analogue, coenzyme, or any other biomolecule with an affinity for a specific site (active site, allosteric site, membrane-binding site, etc) on the protein to be purified. Such biomolecules are usually small (mol wt 500), although macromolecules have been successfully employed, eg, with the purification of soybean trypsin inhibitor on immobilized trypsin as a bioselective adsorbent. The precise type of ligand for any purification is dictated by the nature of the enzyme and the aim of the investigation.

The ligand must have sufficient affinity for the enzyme being purified to retain it on the ligand–matrix complex (44). In addition, the bioselective adsorption of the enzyme to the ligand must exceed the nonspecific adsorption of the proteins to the matrix under the conditions of the preparation. Even under optimum conditions, some nonspecific adsorption is certain to occur. Enzyme adsorption is due to a bioselective component and heterologous, nonspecific factors (45).

By altering the chromatographic conditions, eg, ionic strength, pH, and dielectric constant, the ability of the enzyme to be specifically adsorbed is enhanced and/or the nonspecific adsorption is decreased. For example, the bioselective affinity of lipoamide dehydrogenase on propyllipoamide glass has been shown to increase with the addition of 10% acetone to the aqueous enzyme solution.

A good example of the use of an organic solvent in the elution buffers to eliminate nonspecific binding is the purification of lactate dehydrogenase on N^6-(6-aminohexyl)-AMP-agarose (46). When lactate dehydrogenase is purified on this bioselective adsorbent, yields of only 60% are obtained by elution with the reduced form (NADH) of nicotinamide adenine dinucleotide (NAD^+). Addition of ethylene glycol, and thus further alteration of the dielectric constant of the elution buffer, was shown to change the conformation of the enzyme, thus lowering its affinity for the immobilized (NAD^+) analogue. The enzyme was eluted from the column with buffers containing about 43% ethylene glycol, with a recovery of about 45% of the activity.

The corollary to the requirement of a sufficiently large ligand–enzyme attraction or binding energy for enzyme retention is that the enzyme–ligand binding must be loose enough to permit dissociation of the enzyme from the column under appropriate conditions. Such binding can be so tight that enzyme dissociation is extremely difficult. For example, uterine estradiol-receptor proteins can be removed from serum or uterine cellular extracts by exposure to estradiol coupled to various matrices, eg, cellulose, glass, agarose, or a vinyl maleimide polymer (36,44,47,48), but estradiol-receptor protein is not eluted from the bioselective adsorbent by an appropriate method, eg, elution with free estradiol, changes in pH or ionic strength, or even the use of mild denaturants. Normal affinity chromatography is precluded by the inability to elute the purified enzyme-immobilized enzyme complex. Purification can be successful using estradiol immobilized on agarose by an azo linkage. Uterine cell extracts are applied to this column and unbound proteins are removed. The estradiol-receptor protein–adsorbent complex is then treated with hydrosulfite to cleave the azo linkage between the agarose and the coupled estradiol, and the resulting estradiol-receptor complex is freed of estradiol by extensive dialysis.

Attachment. Numerous methods of attachment of ligands or spacer arms to the appropriate matrix are given in References 44 and 49–52. Attachment must be performed in such a way that few charged, ionogenic, or hydrophobic residues remain after derivatization. This fact has only recently been appreciated, and therefore must be kept in mind when reviewing the earlier literature. Cyanogen bromide or bisoxiranes can be employed in reactions similar to those shown earlier for matrix activation. Other methods include azo coupling (51), ester formation (51,52), and amide formation (52).

Azo coupling

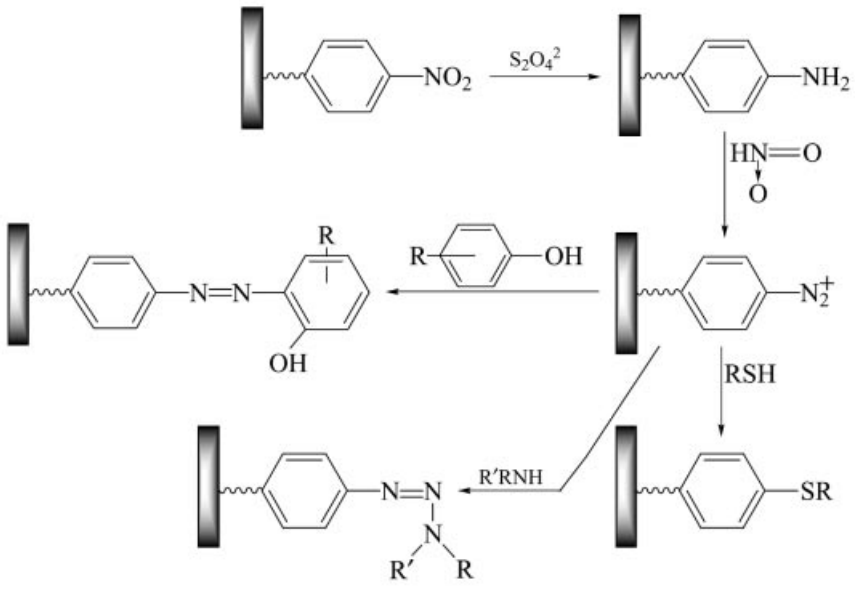

Ester formation

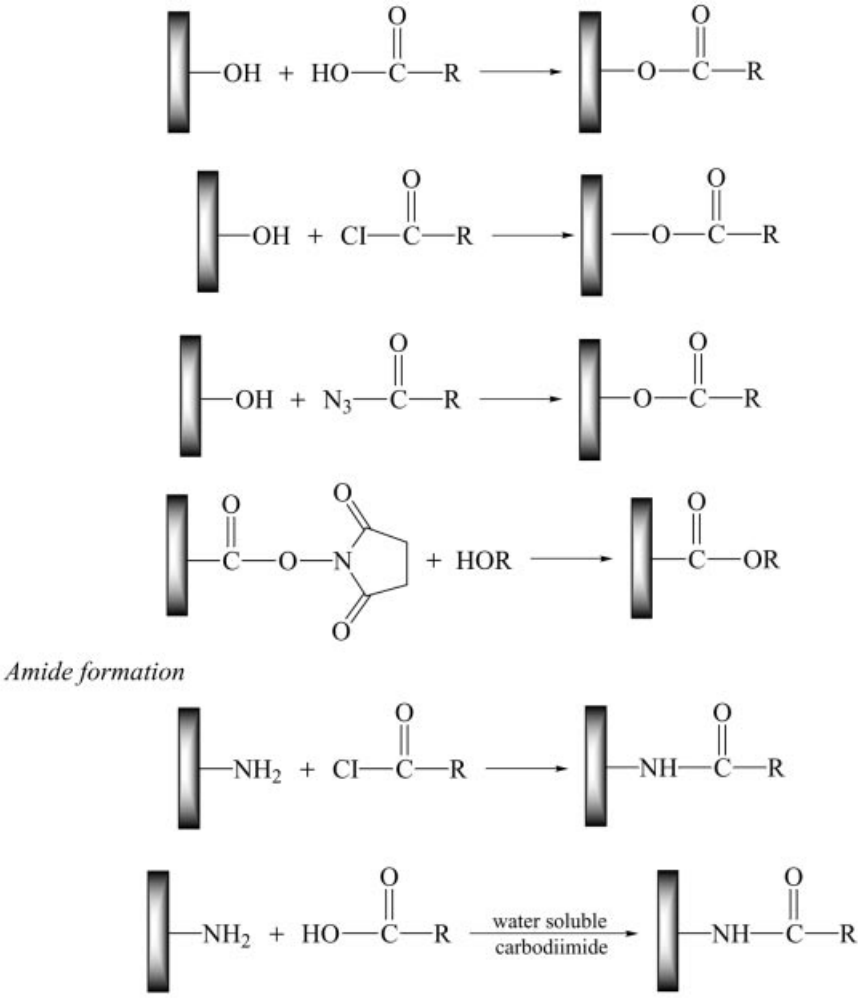

Spacer Arms between Matrix and Ligand. Although a ligand may be directly attached to an activated matrix, an intervening organic group usually serves as the point of attachment and/or as a "spacer" or "arm" to separate the ligand from the matrix. For example, when a series of eight agarose–insulin complexes were used for the purification of insulin-receptor protein, the derivative with the longest spacer arm was the most effective (53). Similarly, guanine deaminase was not retained by the inhibitor, 9-phenyl-guanine, when it was bound directly to cyanogen bromide-activated agarose, whereas it is retained when the affinity packing contains a—OCH_2CH_2—spacer arm between the ligand and the matrix (54).

The spacer arm positions the ligand a certain distance from the matrix in order to reduce steric interference from the matrix (see Figs. 2a and 2b). Occasionally a spacer arm may interfere with the bioselective adsorption process because hydrophobic ligands fold back (Fig. 2c).

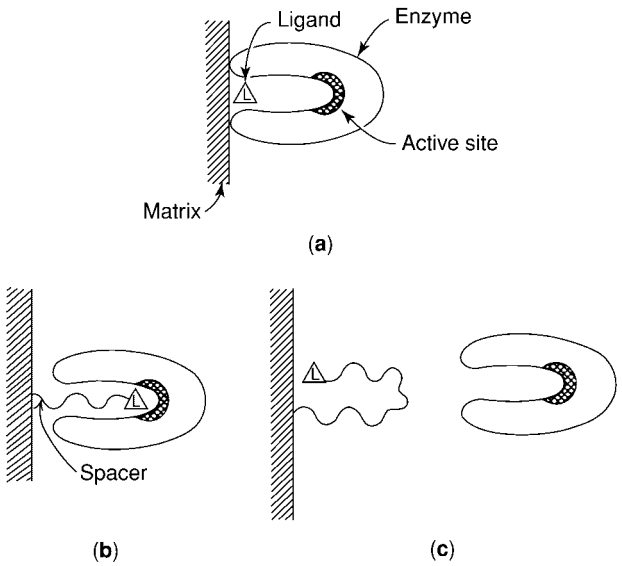

Fig. 2. (**a**) Direct ligand attachment, little or no ligand–enzyme interaction; (**b**) Ligand attachment through a spacer molecule, true ligand–enzyme interaction; and (**c**) Spacer arm too long, the effective distance of ligand from matrix is too short to permit adequate ligand–enzyme interaction.

Spacers are not always needed, and if possible, should not be incorporated in the packing since they can contribute to nonspecific adsorption. Early investigators often ignored spacer–enzyme interactions, and many results are obscured by the ion-exchange effect of spacers. Ion-exchange has been observed when neuraminidase is purified on a column of *p*-aminophenyloxamic acid coupled to agarose. Neuraminidase was initially reported to be retained (55) and specifically eluted from such a column at pH 5.5, but it has since been shown that these preparations yield neuraminidase contaminated with hemagglutinin, hemolysin, and phospholipase C (56). If the purification is performed at pH 7.5, only the sialidase is retained by the column. This suggests strongly that chiefly ion exchange is operating at pH 5.5; at pH 7.5 bioselective adsorption predominates.

On the other hand, the use of long hydrophobic side chains as spacers may lead to nonspecific hydrophobic protein–spacer interactions. These observations show that the spacer, as all other components of the system, must have minimal interaction with protein molecules. They also demonstrate that appropriate controls are required to demonstrate that the chromatographic separation is solely a result of bioselective adsorption.

Hydrophobic Chromatography. The observation that affinity chromatography separations were attributed chiefly to hydrophobic interaction between the spacers and one or more enzymes (57) stimulated the development of so-called hydrophobic chromatography (58). Similar to ion exchange, hydrophobic chromatography depends upon chemiselective adsorption, in this case hydrophobic interaction between the enzyme and an alkyl or aromatic arm bound to an agarose matrix. Affinity chromatography on such materials frequently

yields active enzyme preparations in cases where conventional ion-exchange chromatography results in substantial, if not total, enzyme denaturation. Thus, α-isopropylmalate isomerase was purified in the presence of high concentrations of ammonium sulfate and glycerol, both of which stabilize the enzyme (59). The glycerol serves to weaken the affinity of the enzyme for the matrix, whereas ammonium sulfate increases binding.

Applications

Applications of affinity chromatography include (60)

(1) Protein purification
   a. Enzymes
   b. Antibodies and antigens
   c. Binding or receptor proteins
   d. Complementary proteins
   e. Repressor proteins
(2) Separative procedures
   a. Cells and viruses
   b. Denatured and chemically modified proteins from native proteins
   c. Nucleic acids and nucleotides
(3) Concentration of dilute protein solutions
(4) Storage of otherwise unstable proteins in immobilized form
(5) Investigation of kinetic sequences and mechanisms
(6) Medical applications
   a. Extracorporeal adsorbents
   b. Immunoassays

The most spectacular applications of affinity chromatography are in therapeutic and clinical uses. For example, immunoadsorption chromatography has been used to treat familial hypercholesterolemia (61) by passing the hypercholesterolemic blood through an extracorporeal shunt consisting of a blood cell separator and, on the plasma side, an immunosorbent column containing antibodies to plasma low density lipoprotein (LDL), and finally back to the blood supply.

Because elevated blood cholesterol concentrations, which cause heart attacks in the victims, are directly related to high LDL levels, the removal of LDL-cholesterol in the extracorporeal shunt effects considerable relief from hypercholesterolemia. After saturation, the immunosorbent anti-LDL column is removed from the extracorporeal shunt and regenerated by elution of the LDL with glycine–HCl buffer at pH 3.0 (see Fig. 3).

Other important clinical applications include solid-phase (heterogeneous) immunoassays (62). These are widely used in therapeutic drug monitoring, pregnancy testing, and allergy testing, among others, as well as in research.

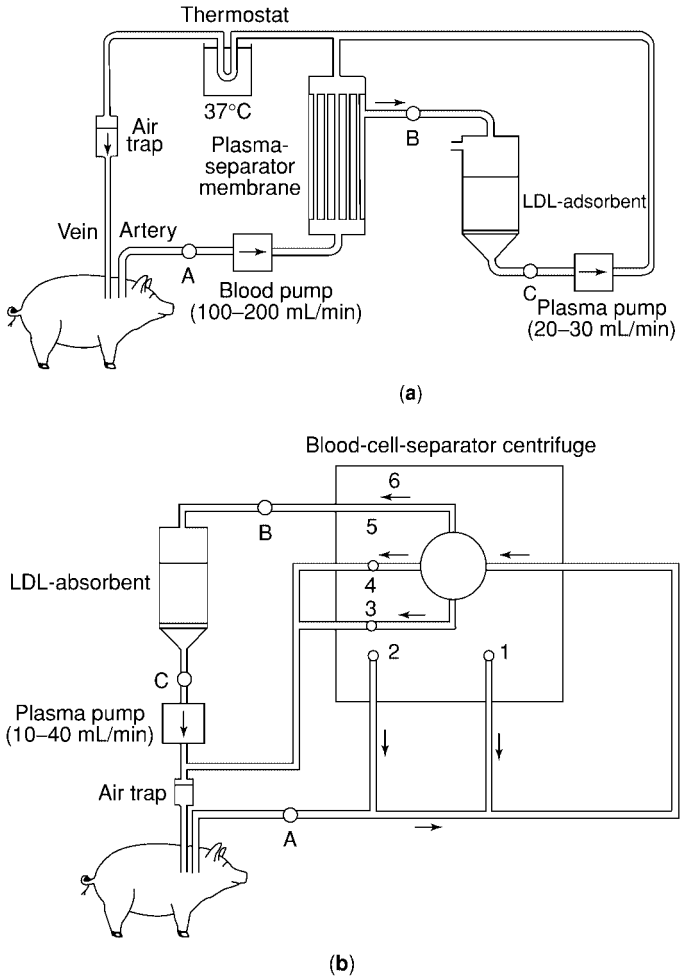

Fig. 3. Plasma-separator-membrane system and LDL adsorbent (**a**) and the continuous-flow blood-cell-separator centrifuge and immunoadsorbent column (**b**) in the arteriovenous shunt. Samples were derived from the flow system at A, B, and C in time intervals of 40 min. Pumps of the blood-cell-separator centrifuge (**b**): 1, citrate anticoagulant (1–3 mL/min); 2, heparin (1 mL/min, 80,000 units/L of saline); 3, leukocytes; 4, erythrocytes (10–40 mL/min); 5, plasma (10–40 mL/min); 6, lubrication (1 mL/min, 2000 units of heparin/L of saline) (51).

The largest single application of affinity chromatography is the purification of enzymes and other proteins. As the biotechnological revolution has proceeded, the demand for new DNA-related enzymes has increased. Many of these are only available by means of DNA-affinity chromatography. For example, thermophilic DNA-ligase can be purified (63) from *Thermus thermophilus*, using DNA–cellulose chromatography as the key step. This enzyme, unlike many classical DNA ligases, is extremely heat stable and withstands 37°C for 1 week and 65°C for 2 days. This is only one of hundreds, if not thousands, of enzymes prepared by means of affinity chromatography that have been commercialized or have commercial potential.

An area of growing importance is the purification of fusion proteins produced by fusing the coding sequence for a desired protein with a second sequence, or "tag," engineered for the future purification of the fusion product. Usually a unique sequence is inserted between these two such that the desired protein can readily be cleaved from the tag using a very selective protease.

While many such tag sequences exist, the most popular is a poly-6-histidine that readily binds via a chemiselective process to an immobilized metal ion chelating column or "IMAC" (64,65).

Excellent examples are the purification of recombinant chloramphenicol acetyltransferase, dihydrofloate reductase, and green fluorescent protein, each one of which was fused to a natural polyhistidine tag consisting of a 19 amino acid sequence from lactate dehydrogenase (66). All three fusion proteins were purified on a Co^{2+}-carboxymethylaspartate agarose "Superflow." The latter is synthesized from Superflow agarose, which is one of the new generation highly cross-linked matrices produced for commercial high flow rates and high dynamic capacities. Purities greater than 95% could be obtained with yields greater than 75%.

The enzyme β-galactosidase was purified directly from crude cell extracts using expanded bed chromatography on another second generation matrix, Ni^{2+} loaded streamline chelating resin. The natural histidine content of the enzyme permitted the enzyme to be recovered in almost 90% yield and 5.95-fold purification from a crude unclarified cell extract (67).

β-Galactosidase, the enzyme missing in Gaucher's disease, has been the subject of numerous affinity-chromatographic preparations, both because of its clinical importance and its potential use in the food industry. Reports on β-galactosidase purification by affinity chromatography have been obscured because a weak inhibitor, *p*-aminophenyl-β-D-thiogalactose, was used as ligand in many of the earlier studies. These purifications of this enzyme using this inhibitor occur through a combination of ion-exchange and hydrophobic chromatography (12,57). For example, β-galactosidase was purified on alkyl amine-glass coupled to *p*-aminophenyl-β-D-thiogalactose via malonic and azelaic spacer arms (20). With a control column containing aniline coupled to the controlled-pore glass in the same way as the inhibitor, significant purification of the enzyme was obtained. Similar results were found with aniline, or the inhibitor *p*-aminophenyl-β-D-thiogalactose, coupled to agarose or glass by means of an anilide or azo linkage.

A growing tendency in affinity chromatography is to utilize combinatorial libraries and phage display techniques to identify new ligands for protein purification.

For example, the recombinant human insulin precursor protein, M13, has been purified by using a biomimetic ligand produced using a combinatorial system (68). Initially the x-ray structure of the protein was used to design a ligand that putatively would bind to a known portion of the protein sequence. This was followed by combinatorial synthesis of a group of ligands similar to the designed ligand based on the reaction of various amines with cyanuric acid (trichlorotriazine) bound through one of its reactive chlorine residues to amino agarose. The amines reacted sequentially with the remaining reactive chlorine residues, yielding completely substituted triazines bound to agarose. When these were screened for their M13 protein binding ability, the result was an affinity matrix used to purify the protein to over 95% purity with a recovery above 90%.

Similarly small protein ligands have been created by selection from randomized Protein A receptor domain using phage display selection techniques from about a 40-million-member library (69). The selected peptides, termed *affibodies*, were so stable that the peptides, immobilized on HiTrap NHS Sepharose, could be repetitively sanitized by treatment with 0.5 *M* sodium hydroxide.

Lastly, affinity chromatography has been utilized as a basic research tool to study proteins and enzymes. In one such study heparin–agarose was used to purify the heparin–binding domain of platelet thrombospondin (70). The thrombospondin was first purified from outdated blood platelets using successive affinity chromatography on heparin–agarose and gelatin–agarose. The purified enzyme was then partially proteolytically digested with thermolysin or plasmin. The lysate was chromatographed on heparin–agarose to yield purified heparin-binding fragments.

Similarly, the dissociation constant of staphlococcal nuclease was determined for free and matrix-bound thymidine-3′-(*p*-aminophenylphosphate)- 5′-phosphate, a competitive inhibitor of staphlococcal nuclease (71). The dissociation constant for the soluble ligand that was determined by using quantitative affinity chromatography closely correlated with the value determined by traditional techniques. An affinity chromatographic method was used for kinetic studies of lactate dehydrogenase (72). The enzyme was applied to a bioselective matrix consisting of oxamate covalently coupled to agarose in the presence or absence of the reduced form (NADH) of NAD. With NADH present at concentrations of 10^{-2} *M* or higher, the enzyme was retained, but when NADH was removed from the elution buffer, the enzyme was eluted. This confirms the previous hypothesis of a compulsory-ordered mechanism for lactate dehydrogenase, that is, a mechanism in which NADH binding must precede substrate binding. Further studies using the same procedure demonstrated that the nicotinamide portion, but not the adenosine portion, of NADH was needed for the substrate–enzyme interaction.

Immobilized Biochemicals. Immobilized biomolecules, or bioreagents, are being synthesized in increasing numbers. For example, dihydroxyboryl cellulose has been employed to purify and study sugars and nucleic acids. Aminopropyl glass and its *p*-phenylene diisocyanate derivative have been employed as a support for solid-phase Edman degradation of peptides (73). Enormous advances including the synthesis of an active enzyme, ribonuclease A (74), have been made in the synthesis of peptides by the Merrifield solid-phase method.

A mild reducing agent, the dihydrolipoyl derivative of aminopropyl glass, has been employed for the reduction of various protein and peptide disulfides (18). An immobilized mild oxidizing reagent has also been prepared by the azo coupling of methylene blue to porous glass (75). This reagent photolytically catalyzes the formation of singlet oxygen, which in turn oxidizes protein methionyl, tyrosyl, and tryptophenyl residues. Under certain conditions this can be limited to the oxidation of methionine. When lysozyme, for example, is photo-oxidized in the presence of methylene blue in 84% acetic acid, only 5% of the activity is retained (76). This reduction results from the oxidation of one protein methionine to methionine sulfoxide, a process that is reversed by reducing the enzyme methionine sulfoxide with thiols, thus restoring 85% of the original activity.

Numerous other examples of both bioselective adsorption and the use of immobilized biomolecules have been reported. Many new applications can be anticipated in the near future.

BIBLIOGRAPHY

"Affinity Chromatography" in *EPST* 1st ed., Suppl. Vol. 2, pp. 19–38, by W. H. Scouten, Sr., Bucknell University; "Chromatography, Affinity", in *EPSE* 2nd ed., Vol. 3, pp. 531–548; by W. H. Scouten, Baylor University.

1. J. Turkova, *Bioaffinity Chromatography*, 2nd ed., Elsevier, Amsterdam, 1993.
2. W. H. Scouten, ed., *Solid Phase Biochemistry*, Wiley-Interscience, New York, 1983, p. 1.
3. W. H. Scouten, *Affinity Chromatography*, Wiley-Interscience, New York, 1981, includes detailed discussion of techniques.
4. *Pierce Reviews*, Pierce Chemical Co., Rockford, Ill., Jan. 1975.
5. J. Porath and co-workers, *J. Chromatogr.* **86**, 53 (1973).
6. T. Låås, *J. Chromatogr.* **111**, 373 (1975).
7. C. Araki, *Bull. Chem. Soc. Jpn.* **29**, 543 (1966).
8. J. Porath, *Biochimie* **55**, 943 (1973).
9. R. Axen, J. Porath, and S. Ernback, *Nature (London)* **214**, 1302 (1967).
10. J. Kohn and M. Wilchek, in Ref. 1, p. 599.
11. J. Kohn and M. Wilchek, *Anal. Biochem.* **115**, 375 (1981).
12. A. H. Nishikawa and P. Bailon, *Arch. Biochem. Biophys.* **168**, 576 (1975).
13. L. Sundberg and J. Porath, *J. Chromatogr.* **90**, 87 (1974).
14. K. Nilsson and K. Mosbach, *Biochem. Biophys. Res. Commun.* **102**, 449 (1981).
15. W. J. Haller, *Chem. Phys.* **42**, 686 (1961).
16. H. H. Weetall and A. M. Filbert, in W. B. Jakoby and M. Wilchek, eds., *Methods in Enzymology*, Vol. **34**, Academic Press, Inc., New York, 1974, p. 59.
17. W. Haller, *Nature* **206**, 693 (1965).
18. W. H. Scouten, *Chem. Phys.* **42**, 288 (1961).
19. J. H. Woychik and M. V. Wondolowski, *Biochim. Biophys. Acta* **289**, 347 (1972).
20. G. Baum, *J. Chromatogr.* **104**, 105 (1975).
21. B. M. Alberts and co-workers, *Cold Spring Harbor Symp. Quant. Biol.* **30**, 289 (1968).
22. R. M. Litman, *J. Biol. Chem.* **243**, 6222 (1968).
23. M. S. Poonian, A. J. Schlabach, and A. Weissbach, *Biochemistry* **10**, 424 (1971).
24. S. Ohlson and co-workers, *FEBS Lett.* **93**, 5 (1978).
25. P. O. Larsson and co-workers, in C. Giddings and co-workers, eds., *Advances in Chromatography*, Vol. **21**, Marcel Dekker, Inc., New York, 1983, p. 41.
26. S. Ohlson and M. Glad, in I. Chaiken, M. Wilchek, and I. Parikh, eds., *Affinity Chromatography and Biological Recognition*, Academic Press, Inc., New York, 1983, p. 241.
27. L. S. Lerman, *Proc. Natl. Acad. Sci. U.S.A.* **39**, 232 (1953).
28. J. R. Uren, *Biochim. Biophys. Acta* **236**, 67 (1971); G. W. Jameson and D. T. Elmore, *Biochem. J.* **124**, 66 (1974).
29. D. Rickwood, *Biochim. Biophys. Acta* **269**, 47 (1972).
30. J. Turkova, *J. Chromatogr.* **91**, 267 (1974).
31. V. Horejsi and J. Kocourek, *Biochim. Biophys. Acta* **336**, 338 (1974).
32. V. Horejsi and J. Kocourek, *Biochim. Biophys. Acta* **297**, 346 (1973).
33. P. Cuatrecasas, *Nature* **228**, 1327 (1970).
34. L. Eldjarn and E. Jellum, *Acta Chem. Scand.* **17**, 2610 (1963).

35. R. Axen and J. Porath, *Nature* **210**, 367 (1966).
36. B. Vonderharar and G. C. Mueller, *Biochim. Biophys. Acta* **176**, 626 (1969).
37. T. Imoto and K. Yagishita, *Agric. Biol. Chem.* **37**, 1191 (1973).
38. J. Sandula and L. Kuniak, *J. Chromatogr.* **91**, 293 (1975).
39. S. Tomino and K. Paigen, *The Lactose Operon, Cold Spring Harbor Symposium*, Cold Spring Harbor, New York, 1970, p. 233.
40. W. E. Hornby and H. Filipusson, *Biochim. Biophys. Acta* **220**, 343 (1970).
41. H. H. Weetall and L. S. Hersh, *Biochim. Biophys. Acta* **206**, 54 (1970).
42. H. Fritz and co-workers, *Angew. Chem.* **78**, 775 (1966).
43. W. Ledingham and W. Hornby, *FEBS Lett.* **5**, 118 (1969).
44. P. Cuatrecasas and C. B. Anfinsen, *Annu. Rev. Biochem.* **40**, 259 (1971).
45. Ref. 2, p. 44.
46. C. R. Lowe and K. Mosbach, *Eur. J. Biochem.* **52**, 99 (1975).
47. E. V. Jensen, E. P. De Sombro, and P. W. Jungblut, in L. Martini, F. Frascini, and M. Motta, eds., *Hormonal Steroids*, Excerpta Median Foundation, Amsterdam, 1967, p. 492.
48. H. Truong and co-workers, *FEBS Lett.* **35**, 289 (1973).
49. P. Cuatrecasas, in G. R. Stark, ed., *Biochemical Aspects of Reactions on Solid Supports*, Academic Press, Inc., New York, 1971, p. 79.
50. P. Cuatrecasas, *Agric. Food Chem.* **19**, 600 (1971).
51. H. H. Weetall, *Sep. Purif. Methods* **2**, 199 (1973).
52. W. B. Jakoby and M. Wilchek, *Methods in Enzymology*, Vol. **34**, Academic Press, Inc., New York, 1974.
53. P. Cuatrecasas, *Proc. Natl. Acad. Sci. U.S.A.* **69**, 1277 (1972).
54. B. R. Baker and H. U. Siebeneick, *J. Med. Chem.* **14**, 799 (1974).
55. P. Cuatrecasas and G. Illiano, *Biochem. Biophys. Res. Commun.* **44**, 178 (1971).
56. J. I. Rood and R. G. Wilkinson, *Biochim. Biophys. Acta* **334**, 168 (1974).
57. B. H. J. Hofstee, *Biochem. Biophys. Res. Commun.* **50**, 751 (1973).
58. B. H. J. Hofstee, *Enzyme Technol. Dig.* **2**, 90 (1974); S. Shaltiel and Z. Er-el, *Proc. Natl. Acad. Sci. U.S.A.* **70**, 778 (1973); Z. Er-el, Y. Zaidenzaig, and S. Shaltiel, *Biochem. Biophys. Res. Commun.* **49**, 383 (1972).
59. R. Bigelis and H. E. Umbarger, *J. Biol. Chem.* **250**, 4315 (1975).
60. C. R. Lowe and P. D. G. Dean, *Affinity Chromatography*, John Wiley & Sons, Inc., London, 1974.
61. W. Stoffel and T. Demant, *Proc. Natl. Acad. Sci. U.S.A.* **78**, 611 (1981).
62. M. Oellich, in H. U. Bergmeyer, ed., *Methods of Enzymates Analyses*, 3rd ed., Vol. **I**, Verlog Chemie, Weinheim, Germany, 1983, p. 233.
63. M. Takahashi, E. Yamagushi, and T. Uchida, *J. Biol. Chem.* **259**, 10041 (1984).
64. L. Kagedal, in J.-C. Janson and L. Ryden, eds., *Protein Purification*, 2nd ed., Wiley-Liss, New York, 1998, p. 311.
65. J. Portah and co-workers, *Nature (London)* **258**, 598 (1975).
66. S. F. Teng and co-workers, *J. Chromatogr. B* **740**, 1 (2000)
67. R. H. Clemmitt and H. A. Chase, *J. Chromatogr., A* **874**, 27 (2000)
68. K. Sproule and co-workers, *J. Chromatogr., B* **740**, 17 (2000)
69. K. Nord and co-workers, *J. Biotechnol.* **80**, 45 (2000)
70. V. V. Dixit and co-workers, *J. Biol. Chem.* **259**, 10100 (1984).
71. B. M. Dunn and I. M. Chaiken, *Biochemistry* **14**, 2343 (1975).
72. P. O'Carra and S. Barry, *FEBS Lett.* **21**, 281 (1972).
73. E. Wachter and co-workers, *FEBS Lett.* **35**, 97 (1973).
74. R. B. Merrifield, *J. Am. Chem. Soc.* **85**, 2149 (1963).
75. C. Lewis and W. H. Scouten, *J. Chem. Educ.* **53**, 395 (1976).
76. G. Jori, G. Galiazzo, and E. Scoffone, *Biochemistry* **8**, 2868 (1969).

GENERAL REFERENCES

Refs. 1, 3, 4, 8, 46–54, and 63 are also good general references. Ref. 1 has an excellent detailed discussion of techniques

A. H. Nishikawa, in W. H. Scouten, ed., Solid Phase Biochemistry: Analytical and Synthetic Aspects (*Chemical Analysis: A Series of Monographs on Analytical Chemistry and its Applications*), Wiley–Interscience, New York, 1983, p. 17.
W. H. Scouten, *Am. Lab.* **6**, 23 (1974).
C. R. Lowe, *Introduction to Affinity Chromatography*, Elsevier, Amsterdam, 1979.

WILLIAM H. SCOUTEN
University of Texas

CHROMATOGRAPHY, HPLC

Introduction

High performance liquid chromatography (hplc) is a powerful tool for characterization of synthetic and natural polymers by separating individual fractions by molecular weight, chemical composition, functional groups, etc. It is also used for isolation and purification of biopolymers and analysis of additives in complex polymer formulations. As in any chromatographic technique, separation occurs due to thermodynamic partitioning between the sample components in the mobile and stationary phases. In hplc, this process takes place in solution inside a chromatographic column packed with inorganic (usually, silica-based) or organic (synthetic resin, such as polystyrene–divinyl benzene and acrylic-based) porous particles, capable of resisting the high pressure created by a moving liquid (mobile phase) mechanically pumped through the column. Depending on application, isocratic (constant mobile phase composition) or gradient (variable composition) modes of separation can be employed, which significantly extends the capabilities of the technique.

Column liquid chromatography has been used for more than 60 years for analytical and preparative separations of polymers. Baker–Williams Fractionation, introduced in the mid-1950s, employed both temperature and solvent gradients to separate polymer fractions according to solubility through multiple precipitation–redissolution steps. This technique has been significantly improved in the last two decades and is still used for fractionation of synthetic copolymers and polymer blends under the term high performance precipitation liquid chromatography (hpplc). Dramatic changes in instrumentation and column preparation for liquid chromatography in 1970s, as well as better understanding of the mechanisms of separation, had a dramatic impact on polymer separation approaches.

Encyclopedia of Polymer Science and Technology. Copyright John Wiley & Sons, Inc. All rights reserved.

Thus, a new technique Chromatography, SEC (a.k.a. gel-permeation chromatography for organic solutions or gel-filtration chromatography for aqueous mobile phases) emerged at that time as a premier method for molecular weight distribution (MWD) determination of synthetic and natural polymers. Since the early 1970s, sec as well as traditional types of hplc (reversed-phase, ion-exchange, hydrophobic-interaction, and affinity chromatography) have been widely used for analysis of proteins and other biopolymers. For two decades, normal- and reversed-phase chromatography have attracted significant interest as methods of separation of synthetic copolymers and polymer blends by chemical composition. Two-dimensional hplc techniques (also called chromatographic cross-fractionation) have been used for most complete polymer characterization in recent years. Thus, consequently coupling two different modes of chromatographic separation can result in determination of both molecular weight and chemical composition distributions of synthetic copolymers.

Instrumentation for HPLC

Each contemporary hplc instrument consists of a pump for solvent delivery, an injector device for sample introduction, column(s) for sample separation, detector(s) for visualization of the separated components (solutes), and a computer for system control and data acquisition and reduction, as depicted in Figure 1. Precise temperature control of columns and some other parts of a chromatographic system becomes an important prerequisite for a successful separation.

Solvent Delivery. The function of the solvent delivery system is to deliver the mobile phase (eluent) through the chromatograph, accurately and reproducibly. The most popular are reciprocating-piston pumps, usually with two

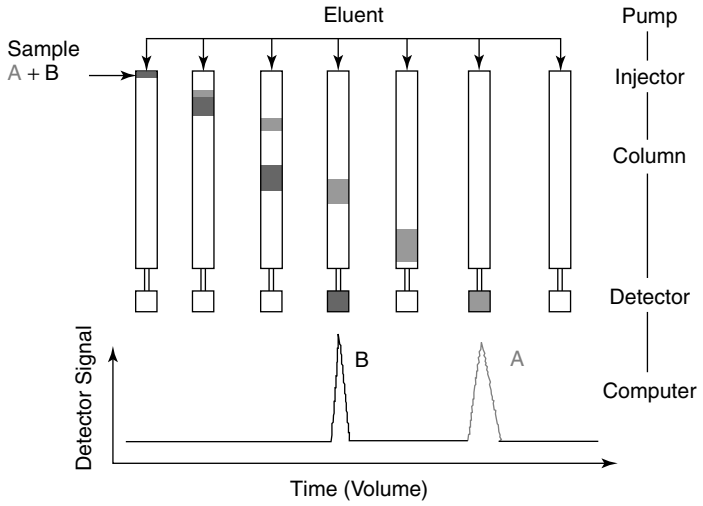

Fig. 1. Schematic presentation of separation of two components, A and B. Reprinted from Ref. 1 with permission.

pump heads containing two sets of moving parts: the check valves and seal-piston assembly. For analytical chromatography, such pumps can deliver liquid at a flow rate from 100 μL/min up to 10 mL/min. Microscale capillary chromatography needs syringe (positive displacement) pumps with capability to produce a flow rate as low as 1 μL/min, while preparative chromatography utilizes flow rates up to 50 mL/min. Gradient pumping system is capable of delivering more than one solvent during an analysis with variable mobile phase composition. The blending of the solvents can occur in one of two ways: high pressure mixing or low pressure mixing. In the former case the solvents are mixing on the injector side, while in the latter case the mixing takes place at atmospheric pressure and a single high pressure solvent delivery system is used to pump the mixture.

Accurate and reproducible eluent flow rate and composition are important prerequisites for successful separation and detection. This is achieved in contemporary "intelligent" pumps through completely independent, digitally controlled piston drives. The sophisticated, software-driven mechanism produces pulse-free eluent delivery, compensates for changes in eluent viscosity, and automatically purges any gaseous mobile phase, thereby enhancing performance for both isocratic and gradient applications (2). The quality of solvents affects the accuracy of flow and baseline noise. On-line solvent filtering and degassing become the necessary elements of any commercial hplc system.

Sample Introduction. To minimize the dispersion and broadening of peaks, sample solution must be injected as a sharp plug with minimal interruption of flow. Typically, two-position six-port valves are used for sample injection, which may be operated manually or automatically (such as in an autosampler, where the sample is introduced from a sample vial held in an injection station). While the general intention is to keep the injection volume as small as possible, the limits are imposed by column dimensions, the sensitivity of detectors, and the nature of separation. An additional factor is the concentration of the analyte, which for high molecular weight species may often be selected very low to reduce solution viscosity and avoid intermolecular interaction.

Stationary and Mobile Phases. Chromatographic columns provide the means for polymer fractionation or separating mixtures into components. The selectivity, capacity, and efficiency of the columns are all affected by the nature of the packing material. Most modern hplc packings are porous spherical microparticles with 3- to 10-μm size. The efficiency of a column increases with decreasing particle size, but so does the backpressure, which usually cannot exceed 27.2 MPa (4000 psi) on traditional instruments. The use of new generation of ultra-high pressure chromatographs with backpressure up to 690 MPa (100,000 psi) can potentially reduce the particle size up to 1 μm or lower. In general, silica-based columns can withstand higher pressure as compared with resin-based columns.

Pores (mean diameter usually from 6 to 100 nm) play a crucial role in hplc, as they provide the surface where retention and hence separation occur. The chemical structure of the surface determines the thermodynamic "environment" for the analyte in thin surface layer (stationary phase) and in such a way determines the mechanism of retention. Flexible macromolecules approaching the internal surface of a solid particle change their spatial conformations because of steric interaction, which plays an important role in any mode of polymer chromatography. This interaction restricts the fluctuation motion of a macromolecule, decreases its

conformation entropy, and effectively reduces the retention. In sec, where particles with inert surface are used and the size of macromolecules is comparable with the internal pore diameter, steric interaction is dominant and separation occurs according to size of macromolecules. All other modes of polymer chromatography also exploit enthalpic (attraction) specific interactions between macromolecules and the functional groups on the surface. For this reason they are often lumped together as interaction polymer chromatography (ipc). The name "adsorption polymer chromatography" is also used because the size of macromolecules usually far exceeds the size of the surface functional groups participating in interaction, and retention has the adsorption mechanism.

The nonsteric interactions in ipc depend on the chemical structure of the analyte, and also on nature of stationary and mobile phases. In normal- or reversed-phase hplc, neutral solutes are separated on the basis of their polarity. In the former case, polar stationary phases are employed (eg, bare silica with polar silanol groups) and less polar mobile phases based on nonpolar hydrocarbons are used for elution of the analytes. Solvent selectivity is controlled by adding a small amount of a more polar solvent, such as 2-propanol or acetonitrile or other additives with large dipole moments (methylene chloride and 1,2-dichloroethane), proton donors (chloroform, ethyl acetate, and water), or proton acceptors (alcohols, ethers, and amines). Correspondingly, the more polar the solute, the greater is its retention on the column, yet increasing the polarity of the mobile phase results in decreased solute retention.

The opposite situation takes place for reversed-phase separation, when nonpolar stationary phase is accompanied by a polar mobile phase, typically water, to which a less polar solvent such as acetonitrile or methanol is added, and solvent selectivity is controlled by the nature and amount of the added solvent. As a result, a decrease in the polarity of the mobile phase leads to a decrease in solute retention. Many organic polymers are not soluble in water, and other polar solvents can be used. Thus, the combination of acetonitrile as an initial solvent with addition of tetrahydrofuran (THF) can be used in reversed-phase separation of many styrene-based copolymers and acrylic polymers. Modern reversed-phase chromatography typically refers to the use of chemically bonded stationary phases, where functional groups, such as alkyl ($-CH_3$, $-C_4H_9$, $-C_8H_{17}$, and $-C_{18}H_{37}$) groups, phenyl ($-C_6H_5$) groups, cyano [$-(CH_2)_3CN$] groups, and amino [$-(CH_2)_3NH_2$)] groups, are bonded to the silica. Note that some of these bonded packings, such as those with cyano- and amino-groups, as well as diol groups [$-(CH_2)_3OCH_2CH(OH)CH_2OH$], can also be used in normal-phase separations, as they contain moderately polar moieties. The same stationary phases are also used for separation of biomolecules in hydrophobic-interaction chromatography. Weak nonionic interactions between hydrophobic portions of proteins and nonpolar moieties of the stationary phase have an entropic nature and are highly sensitive to salt concentration in a totally aqueous, buffered mobile phase of high ionic strength.

In ion-exchange chromatography, the ionic species, such as proteins or synthetic polyelectrolytes, are separated on the basis of differences in electric charge. The stationary phases with ionic groups (fixed ions) are employed, and the mechanism of retention is the electrostatic attraction of ionic solutes in solution to opposite charged ions (anions or cations) on the stationary phase support. The stationary phase for ion-exchange chromatography is called ion exchanger and

is classified as an anion-exchange material when the fixed ion carries a positive charge, and as a cation exchanger in the opposite case. There are strong and weak ion exchangers depending on the pH range over which the stationary phase can retain the charge on the fixed ion. Acrylic-based copolymers treated with an appropriate reagent to produce the desired functional group are the most used ion exchanger because of wider pH range (pH 1–13) and higher ion-exchange capacity as compared with silica-based columns (pH 2–8). Eluents for ion-exchange chromatography are aqueous solutions of salts with small addition of organic solvent. Selectivity in the separation of polyelectrolytes may be varied by changing either the pH of the mobile phase or the nature or concentration of the displacing (competing) ions.

Chromatography, SEC is used for the separation of biomolecules on the basis of the lock-and-key mechanism prevalent in biological systems.

Detectors. When separated macromolecules leave the column, they are detected by one or more on-line electrical devices with signals proportional to the concentration of the analyte. In all hplc detectors, the eluent flows through a measuring cell, where the change of a physical or chemical property with elution time is detected. Each monitored trace represents a chromatogram: a set of chromatographic peaks separated by baseline regions. The sensitivity (the ratio of peak height to the sample concentration), signal-to-noise ratio (the amount of signal visible above the baseline noise), as well as linear dynamic range (maximum linear response divided by the detector noise) are the most important characteristics of any detector.

Ultraviolet (uv) absorption photometers capable of absorbing light at a selected wavelength (in the range 190–350 nm for uv detectors, or 190–700 nm for uv/Visible detectors) are the most popular detectors in hplc of both synthetic and biological polymers. In case of proteins, wavelengths that are typically monitored include the regions of absorbance of peptide bonds (210–220 nm), and tyrosine and tryptophan side chains (ca 280 nm). Many synthetic polymers also contain chromophoric groups. Variable-wavelength and photodiode array detectors have the advantage that more than one wavelength can be monitored during a single run. Photodiode array detectors allow for simultaneous measurement of an entire uv spectrum at any point of the chromatogram, which can aid in peak identification. Among other selective (solute property) detectors used in hplc of polymers are fluorescence and IR photometers. For example, fluorescence detectors can provide higher sensitivity, as well as greater selectivity, in the detection of proteins containing tyrosine and tryptophan residues that have intrinsic fluorescence. Both types of detectors are limited to certain mobile phases. A good alternative is off-line coupling of ftir to hplc system using an evaporative interface (3). In such a system, the eluent is sprayed onto a Germanium disc, which can be transferred to any ftir spectrometer to yield the full spectrum information over any peak of the chromatogram. The same principle is applied also to the matrix-assisted laser desorption/ionization mass spectrometer, which otherwise is difficult to couple to the hplc system (4).

A few universal (bulk property) detectors are of frequent use in hplc of polymers. Refractive index detector is limited to isocratic elution and is utilized primarily in sec. The same is true for the recently introduced density detector based on mechanical oscillator principle (B. Trathnigg in Ref. 4). Evaporative light

scattering detector (ELSD) becomes very popular in nonaqueous gradient elution of synthetic copolymers and polymer blends (3). The eluent is nebulized, and the solvent is evaporated from the droplets. Each droplet containing nonvolatile material will form a particle, which scatters the light while crossing a light beam. This detector has significant advantages over the uv detector for ability to work with aliphatic polymers without chromophore groups, and also for its applicability to practically any mobile phase which does not contain a nonvolatile buffer. Despite these obvious merits, ELSD cannot be considered as an ultimate choice for quantitation because of nonlinear concentration response, which depends on numerous factors such as chemical nature of the sample including its molar mass and chemical composition, the eluent composition, viscosity and surface tension, and operating conditions. Coupling ELSD to another detector can help to solve these problems with quantitation.

The quadrupole mass spectrometers, single-quadrupole (MS) or triple-quadrupole (MS–MS), have proved to be the detectors of choice for interfacing with chromatographs. The resulting combinations LC–MS or LC–MS–MS have become very popular among protein scientists. Soft ionization methods, such as electrospray ionization and matrix-assisted laser desorption, are used extensively for biopolymers and some ionic synthetic polymers (5). The interface usually requires the use of very low flow rates (below 10 μL/min) and therefore necessitates capillary chromatographic equipment, or a sample splitter. Miniaturization of separation with laboratory-on-a-chip technology and microfluidics with nanoscale columns can additionally improve the compatibility of column chromatography with mass spectrometry detection.

In addition to the widespread use of mass spectrometry as a detection technique, scientists report investigations of other spectroscopic techniques such as nuclear magnetic resonance (nmr) and inductively coupled plasma mass spectrometry. These emerging technologies in a few years may have a major impact as on-line detection methods for characterizing both synthetic and biological polymers. Miniaturization of separation makes these detectors more feasible for on-line coupling. Using internal reflectance spectroscopy to study molecular interactions at phase surfaces has helped researchers to understand retention mechanisms and to confirm or expand chromatographic data.

Data Treatment. The traditional hplc method involves two types of data analysis: qualitative (peak identification) and quantitative (determining the analyte concentration). Both analyses require specific data manipulations, such as matching retention times, peak integration and peak calibration. The use of spectroscopic detectors (photodiode array, ftir, and mass spectrometry) suggests additional mathematical procedures because of the necessity to manipulate with uv-, ftir-, and MS-spectra and corresponding library matching (6). Most commercial chromatographic software packages contain necessary functionalities and can be applied to hplc of proteins, peptides, and DNAs. The characterization of other natural and all synthetic polymers is a much more difficult problem, which includes calculating the distributions of different macromolecular parameters, such as molecular mass, chemical composition, branching frequency and end group functionality, from raw chromatograms. This involves additional calibration procedures (column calibration), calculation of statistical moments of distributions, etc. Two-dimensional chromatographic cross-fractionation of synthetic copolymers

requires the construction of two-dimensional distributions to characterize the copolymer heterogeneity (7).

Retention Mechanism and Modes of Separation

Isocratic Elution. Contrary to sec, where any nonsteric effects are undesirable and suppressed, week nonsteric adsorption interactions between a solute and a stationary phase play a dominant role in ipc. The best way to demonstrate the difference between size-exclusion and interaction (adsorption) modes of polymer separation is to use the so-called molecular weight calibration curves (log M vs V, where M is the molecular weight, and V is the elution volume) depicted in Figure 2. The set of narrow polydispersity polystyrene samples with molecular weights from several hundred up to million were subjected to isocratic elution on the reversed-phase column (silica bonded with octadecyl chains) with different acetonitrile/tetrahydrofuran (ACN/THF) mixtures as eluents. THF is less polar than ACN (polarity parameters 4.0 and 5.8, respectively). Pure THF completely suppresses nonpolar interactions between polystyrene and alkyl chains on silica, and conventional sec behavior is obtained, that is, elution time increases with decreasing molar mass of the sample. The separation occurs within pore volume $V_P = V_T - V_0$, where V_T is the liquid volume inside the column and V_0 is the interstitial volume between particles. The steric interactions prevail until the amount of ACN in the mobile phase reaches ca. 50%. After that, a completely reversed retention behavior is obtained, which is typical for the adsorption mode of separation, when retention volume V_R exceeds V_T. At 45 and lower % THF, retention

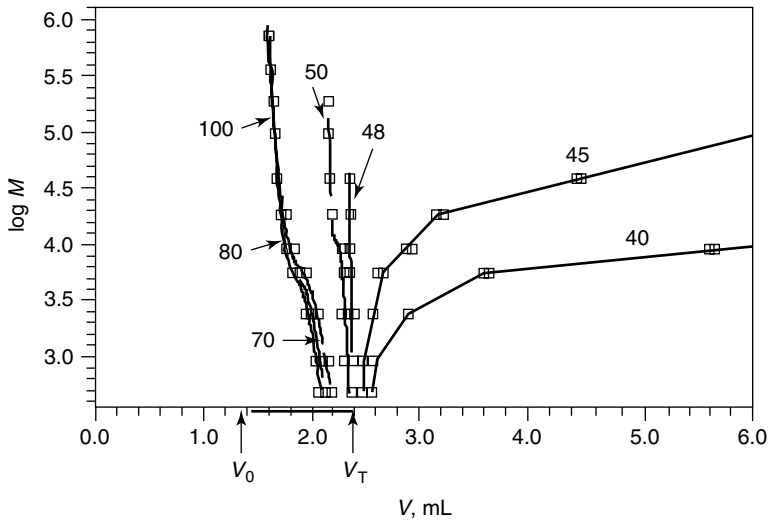

Fig. 2. Transition from size-exclusion to adsorption mode for isocratic elution of polystyrene samples with low polydispersity. Column: Nova-Pak C_{18} (Waters Corporation, USA), mobile phase: THF/ACN mixtures (numbers on the graph represent vol% THF), 1 mL/min, detector: ELSD Model 500 (Alltech Corp.).

dramatically increases with molecular weight and becomes extremely sensitive to the eluent composition, so that high molecular weight fractions are practically irreversibly retained by the column. For this reason, the IPC separation of high molecular weight polymers is usually performed in gradient mode.

It is important to note the elution at 48% THF: Retention becomes completely independent of molecular mass, and all fractions elute with the column's liquid volume V_T. At this transition point, which is termed critical point of adsorption (CPA), entropy driven size-exclusion effects are completely compensated by enthalpic adsorption interactions. Although both types of interaction strongly depend on molecular weight, this mutual compensation phenomenon leads to molecular weight independent retention at CPA. This phenomenon allows for practical implementation of isocratic polymer separation other than sec. Thus, because of chromatographic "invisibility" of a main polymer chain, effective separation of telechelic polymers based on types of end-groups can be performed (Ref. 7, p. 125). The same principle is applied for isocratic separation of some block copolymers (Ref. 7, p. 151).

The isocratic separation at CPA requires very careful control of chromatographic conditions, such as the quality of stationary phase, mobile phase composition, and temperature, because of high sensitivity of retention to these parameters, especially for polymers with high molecular weight. Another limitation of the techniques is associated with the dynamic effects. The success of separation depends on the ability of all macromolecules to penetrate all pores (the same way as the solvent molecules). But small diffusion coefficients and steric restrictions make the equilibration time for large macromolecules and narrow pores unreasonably long. Because of this, the use of isocratic separation at CPA is practicable only when the internal pore diameter exceeds the size of macromolecules in solution.

Gradient Elution. In gradient mode, the elution strength of the mobile phase is gradually increased within the chromatographic run to facilitate the elution of strongly retained compounds. This is especially important for high molecular weight polymers that otherwise are practically irreversibly retained by the column in the adsorption mode. Such gradient can be performed by changing the chemical composition, ionic strength or pH of the eluent, or even temperature. In protein separation, the salt gradient is used in both hydrophobic-interaction and ion-exchange chromatographies. During the chromatographic run, the salt concentration is decreased in the former case and increased in the latter one.

Typical reversed-phase gradient elution of synthetic polymers is demonstrated in Figure 3 for the same set of polystyrene samples as in Figure 2. The increase in eluent strength is achieved by linear increase of the concentration of less polar THF in the mobile phase that allows the elution of all polystyrenes within 8 min. The elution of lower molecular weight samples (below 10,000 Da) occurs in the adsorption mode at low content of THF in the mobile phase, and strongly depends on molecular weight. Excellent resolution for polystyrene oligomers in this mode allows one to distinguish between fractions with different end groups (double peaks on the chromatograms). In contrast, all higher molecular weight polystyrenes have practically the same elution volume, which coincides with the volume where eluent reaches its CPA (48% THF). The principle that gradient elution of high molecular weight polymers occurs at CPA has been introduced

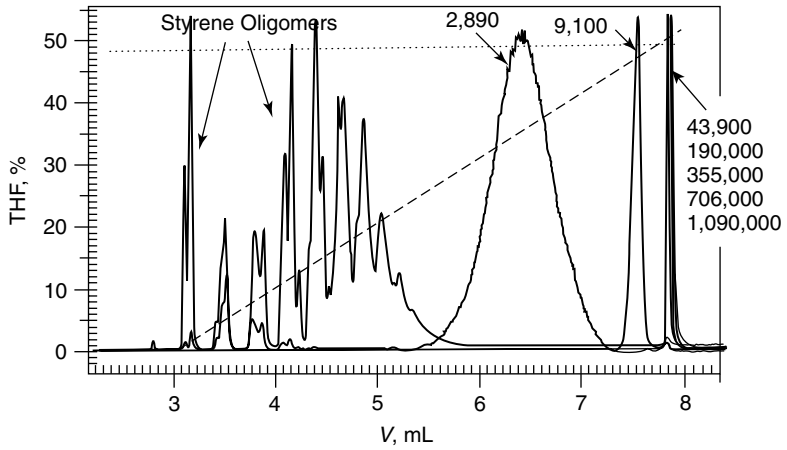

Fig. 3. Gradient elution of polystyrene samples from Figure 1. The same chromatographic system and conditions as in Figure 1, except eluent gradient: 100% ACN to 100% THF over 10 min (dashed line). Numbers on the graph: molecular weights of individual polystyrenes. Broken line: critical point of adsorption (48% THF).

recently (8). It provides the basis for gradient separation of copolymers and polymer blends by chemical composition. Each compositionally homogeneous fraction of a copolymer or a polymer blend elutes at its own CPA independently of molecular weight. By this means, gradient elution produces the chemical composition distribution of copolymers and polymer blends.

In general, gradient elution is a much more versatile technique for polymer separation as compared with isocratic elution at CPA Pore and particle sizes and hence dynamic effects do not impose such significant restrictions. Macromolecules do not need to penetrate the entire pore volume, and elution at CPA is achieved when their size exceeds the pore diameter. Gradient run allows for a sample precipitation on the frit or inlet of the column, when starting eluent is a nonsolvent for the polymer. This is a rather common situation because the solubility window for many polymers is relatively narrow, and the eluent with a poor elution strength often has a poor thermodynamic quality. This is true even for some proteins (membrane proteins or collagen), which can precipitate at the intermediate stage of the gradient separation. However, the elution of different components of a polymer sample still follows the rules of gradient separation described in the previous paragraph as soon as all polymer fractions are redissolved and adsorbed by the column during the chromatographic run. Only if macromolecules elute without any adsorption interactions immediately after redissolution, as in hpplc, the separation based solely on polymer solubility occurs. In this case, retention always strongly depends on molecular weight and concentration of the sample (9).

Multidimensional Separation. In some cases, a single separation step is not enough to complete the analysis of biological or synthetic polymers. In this case, coupling two or more different modes of separation involving column-switching mechanism is widely used in multidimensional polymer

chromatography. This approach provides the opportunity to simplify complex mixtures before their characterization by spectroscopic techniques, especially LC–MS and LC–MS–MS. A typical example is the combination of ion-exchange or size-exclusion separation with reversed-phase chromatography in protein purification (10). Gradient or isocratic elution at CPA followed or preceded by size-exclusion separation is often used in chromatographic cross-fractionation of synthetic polymers (11). The use of ipc as a first step is a more feasible way to achieve the true two-dimensional characterization of copolymers or polymers with functional groups, because it allows for molecular weight independent separation by chemical composition or by other structural differences in macromolecules. Size of macromolecules in each compositionally homogeneous fraction obtained after the first separation, is directly related to molecular weight thereof, and the following size-exclusion separation of all these fractions can complete the cross-fractionation.

The coupling of two modes of polymer separation can be achieved off-line or on-line. In the former case fractions from one chromatographic system are transferred to another system manually, in the second one, automatically, when the eluent from the first instrument flows through the injection valve of the second instrument. The most sophisticated automatic two-dimensional chromatographic systems employ two six-port valves or one eight- or even ten-port injection valve (10). Two storage loops make it possible to collect fractions continuously without losses. The proper coordination of the flow rates in consecutive chromatographic steps is an important feature of any automated system. Thus, in chromatographic cross-fractionation, the collection time of one hplc fraction should coincide with the analysis time in the following sec step (Ref. 7, p. 198).

Theory of Polymer Chromatography

Thermodynamic Treatment. Each component of a polymer sample injected in the chromatographic system can be characterized by its retention volume V_R, ie, the volume of solvent that passes through the column from the time of sample injection to the detection of the corresponding peak. To eliminate the variability of retention caused by operational variance of the flow rate, mobile phase, or other parameters, the normalized quantity $k = (V_R - V_T)/V_T$ (capacity factor) is often used instead of V_R. The resolution of the chromatographic system, ie, its ability to discriminate between individual macromolecules, depends on the selectivity of separation, which is described by the ratio of corresponding capacity factors.

The basic assumption in any chromatographic theory is that retention is determined by the thermodynamic factors. In such a way, mobile and stationary phases are interpreted as true thermodynamic phases with volumes V_M and V_S, respectively, so that retention volume depends on the partition (distribution) equilibrium coefficient K of the solute in these two phases: $V_R = V_M + KV_S$. By definition, all enthalpic and entropic interactions between the macromolecules and the chromatographic surface occur in the stationary phase. If the size of macromolecules in solution is comparable with the internal diameter of pores, the entire pore volume represents the stationary phase, $V_S = V_P$, yet the mobile phase is formed by the interstitial volume only, $V_M = V_0$. This is not always the case for

gradient separation of peptide or proteins, when the pore diameter usually far exceeds the size of compact macromolecules, and practically the entire liquid volume, $V_T = V_0 + V_P$, represents the mobile phase.

The role of thermodynamic theory is to relate the distribution coefficient K (or free energy change due to solute sorption on the stationary phase) to the parameters describing the configurational and conformational structure of a macromolecule (such as molecular weight, chemical composition and shape), as well as temperature, pore geometry, mobile phase composition, etc. These parameters determine the entropy of steric interaction and the energy of multipoint nonsteric interactions between the macromolecule and the surface, and in this way affect the retention.

Construction of a universal thermodynamic model for chromatographic separation of proteins and other biological polymers is hardly probable because of the complexity of chemical and spatial structure of such macromolecules, which can undergo a diversity of conformational transitions during separation. Even for small peptides composed of 5–15 amino acids, which are assumed to exist in solution as a random coil, amino acid identity and position, as well as peptide sequence, all play an extremely important role in retention. Nevertheless, semiquantitative approaches applied to specific modes of separation often allow for understanding the mechanism of separation, as well as the effect of operating parameters such as salt type and concentration, temperature, nature of packing material, organic modifiers, and pH. Examples are the solvophobic (12) and preferential interaction (13) theories applied to hydrophobic interaction and reversed-phase chromatography of proteins (14). Several useful retention models exist in ion-chromatography, where the equilibria, which govern ion-exchange separations, are generally well understood (1).

In the case of synthetic polymers, a simple continuous random-flight model of a flexible polymer chain allows for quantitative consideration of the chromatographic process in a rather general way (15). The theory provides a simple analytical expression for the distribution constant K of a macromolecule penetrating the slit-like or cylindrical pore and interacting with its walls, in terms of macromolecule and pore sizes, and a segment energy of nonsteric interactions between the macromolecule and stationary phase. Depending on the mobile phase composition, the competition between steric (repulsive) and nonsteric (attractive) interactions may produce either size-exclusion, $K<1$, or adsorption, $K>1$, modes of separations, yet the intermediate condition, $K=1$, represents the critical mode of adsorption, where both types of interaction counterbalance each other (see Fig. 2).

Present models of gradient elution (16) assume that migration in gradient mode occurs in the same way as for isocratic elution. That is, given the dependence of K on eluent composition, which changes during the mobile phase gradient, one can calculate the gradient elution volume for gradients with various slopes and shapes using the well-known mass-balance integral equation (17). The results of such calculations applied to gradient separation of polymer homologous series can explain (8) the peculiarities depicted in Figure 3. Thus, the combination of molecular–statistical theory of dilute polymer solutions in confined (porous) media with conventional chromatographic theory produces a valuable tool in elucidating the polymer chromatography (8). Recent extension (18) of the concept

on copolymers and stationary phases with heterogeneous surface (which actually is inherent in most if not all of available sorbents) significantly improves the feasibility of the theory for separation of complex polymer formulations.

Dynamic effects. Besides the thermodynamically driven selectivity, the resolution of the chromatographic system depends also on dynamic (kinetic) factors that determine the efficiency of separation. These factors cause the broadening of the chromatographic peaks so that even peaks from individual compounds such as proteins have a finite width. For polydisperse polymers this chromatographic peak broadening (or bandspreading) is usually hidden by the overall polymer distribution, but still can produce erroneous results if no correction has been made to compensate for this effect.

The major contributor to peak broadening in polymer chromatography is a "stagnant" mobile phase mass transfer, that is, kinetics hindrance due to penetration of macromolecules into the pores of the support packings. The molecular diffusion is the only way for macromolecules to reach the internal surface of pores, whereas the migration in interstitial volume is governed by the convection mechanism. The effect of bandspreading tends to diminish with the ratio of characteristic times of these two processes, $t_D = L^2/D$ (L is the average length of pores, D is a solute diffusion coefficient), and $t_0 = V_0/F$ (F is the flow rate). The diffusion coefficient of macromolecules inside pores drops rapidly as molecular weight increases, and so does peak broadening. As the length of an individual pore is usually comparable with the size of a particle [exception is perfusive particles, which contain very broad flow-through pores with only shallow diffusive pores and are mostly used in preparative chromatography 19], the most popular solution to date for minimizing the problem in biological applications is the use of small porous particles of 2–5 μm so that the depth of the stagnant pools is not excessive (20). It is significant that in gradient separation of synthetic polymers the internal surface area is not so important, and separation usually takes place only at the inlet of very narrow pores, which significantly reduces the dynamic effects.

Applications

Separation of Biological Polymers. The development of wide-pore bonded-phase packings has dramatically affected the separation of biopolymers in the life sciences and biotechnology (21). Nevertheless, several factors should be taken into account in selecting the optimum mechanism of separation for a specific application. Reversed-phase chromatography is the most popular mode for separation of peptides because of exceptional selectivity and resolution. But in case of proteins, hydrophobic interaction is often the method of choice because of the much milder effect on solute conformation. Many proteins are denatured by acids or organic solvents, as well as by the alkyl chain of the bonded phase, the usual constituents of the reversed-phase separation (22). These conformational transitions may cause additional chromatographic problems, such as peak broadening, multiple peaks, poor sample recovery, and ghosting, if the conformational transition time is of the same order as the migration time (23). Hydrophobic interaction chromatography as well as ion-exchange chromatography have been

predominantly used to analyze proteins, nucleic acids, and other biological macromolecules when maintenance of the three-dimensional structure is a primary concern (24).

With the human genome now sequenced (primarily by capillary electrophoresis technology), scientists are turning their attention to proteomics. The term *proteome* has been introduced to define the full complement of proteins in a cell. It also requires a description of the localization, concentration, and multisubunit association of each of these proteins (25). The multidimensional hplc with automated column switching technology can successfully complement the more conventional approaches to protein separation, such as two-dimensional gel electrophoresis, which usually involve many manual steps and are not conducive to high throughput applications.

Separation of Synthetic Polymers. Interest in interaction polymer chromatography as a technique complementary to sec for characterization of synthetic polymers and polymer blends has quickened in recent years. The principle difference between these two methods is depicted in Figures 4 and 5, where three polymers with close average molecular weights, as well as the equimolar blend of these polymers were subjected to isocratic size-exclusion and gradient reversed-phase separations, respectively. In the first case (Fig. 4), only molecular weight information is available from the chromatograms, the result of second separation (Fig. 5) reveals the individual components, ie, chemical composition of the blend. This way, many statistical, block and graft copolymers and blends were fractionated by chemical compositions in gradient mode on both

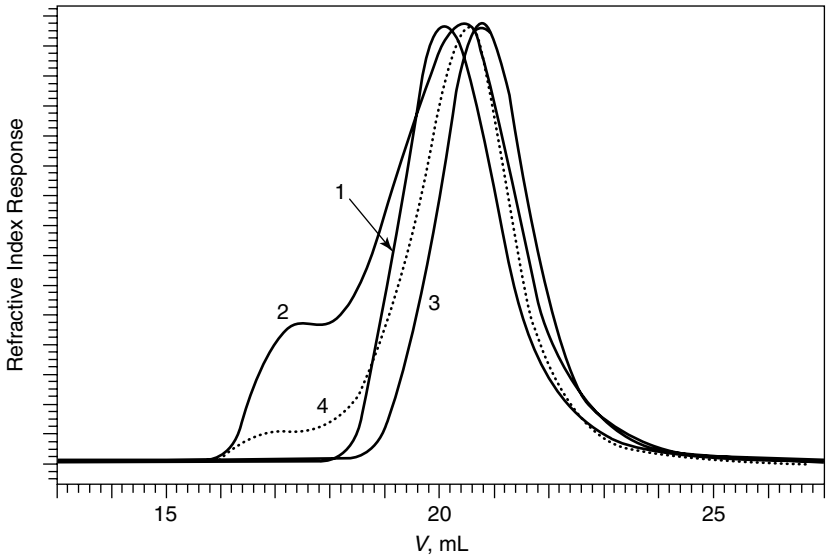

Fig. 4. Size-exclusion chromatograms of polystyrene (1), styrene–butadiene statistical copolymer (2), styrene–acrylonitrile statistical copolymer (3), and equimolar mixture of them (4, dotted line). Columns: 3 HR Styragel (Waters Corp.), mobile phase: THF, 1 mL/min, detector: refractometer model 2410 (Waters Corp.).

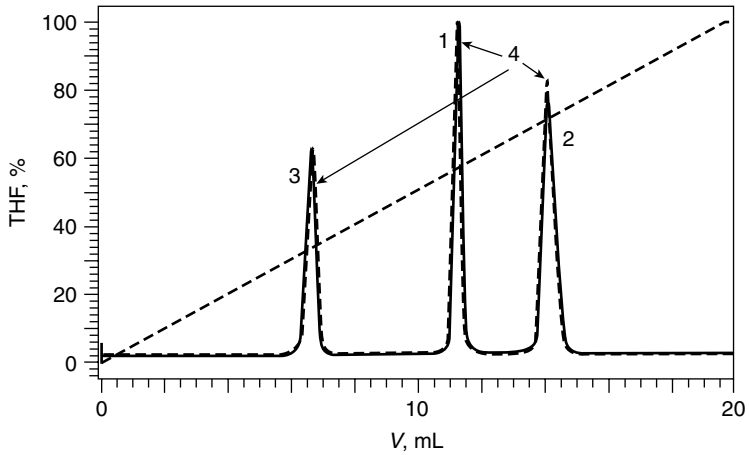

Fig. 5. Gradient reversed-phase elution of the same polymers as in Figure 3. Column: SymmetryShield C_8 (Waters Corp.), mobile phase: 100% ACN to 100% THF over 20 min (dashed line), 1 mL/min, detector: ELSD Model 500 (Alltech Corp.).

normal- and reversed-phase columns, without any practical limitations on the molecular weight of polymers [see reviews in Refs. 7, 11 (chapt. 9), and 26–29]. On the other hand, several reported (7) isocratic separations of block copolymers at CPA were limited by the oligomeric range of molecular weights. Many recent publications deal with two-dimensional characterization of copolymers, where the molecular weight independent separation is achieved by ipc as the first step (7,30,31).

To summarize briefly, in spite of solid age, hplc of polymers remains the workhorse of the biotechnology and chemical industries, and at the same time presents a fruitful field for future development and improvement.

BIBLIOGRAPHY

"Chromatography" in *EPSE* 1st ed., Vol. 3, pp. 731–745, by P. M. Kamath and L. Wild, U.S. Industrial Chemicals Co.; "Chromatography" in *EPSE* 2nd ed., Vol. 3, pp. 491–531, by J. F. Johnson, The University of Connecticut at Storrs.

1. P. R. Haddad and P. E. Jackson, *Ion Chromatography: Principles and Applications*, Elsevier, New York, 1990, Chapt. "5". Journal of Chromatography Library, Vol. **46**.
2. J. B. Li, J. Morawski, *Liq. Chromatogr. / Gas Chromatogr.* **16**, 468 (1998).
3. P. C. Cheung, S. T. Balke, and T. C. Schunk, in T. Provder, H. G. Barth, and M. W. Urban, eds., *Chromatographic Characterization of Polymers: Hyphenated and Multidimensional Techniques*, American Chemical Society, Washington, D.C., 1995.
4. J. L. Dwyer, in T. Provder, ed., *Chromatography of Polymers: Hyphenated and Multidimensional Techniques*, American Chemical Society, Washington, D.C., 1999. ACS Symposium Series 731.
5. S. A. Carr and co-workers, *Anal. Chem.* **63**, 2802 (1991).

6. A. Weston and P. R. Brown, *hplc and CE: Principles and Practice*, Academic Press, San Diego, Calif., 1997, p. 220.
7. H. Pasch and B. Trathnigg, *hplc of Polymers*, Springer, Berlin, 1998, Chapt. "7".
8. Y. Brun, *J. Liq. Chromatogr. Relat. Technol.* **22**, 3067–3090 (1999).
9. D. W. Armstrong and R. E. Boehm, *J. Chromatogr. Sci.* **22**, 378 (1984).
10. H. J. Cortes and L. D. Rothman, in H. J. Cortes, ed., *Multidimensional Chromatography: Techniques and Applications*, Marcel Dekker, Inc., New York, 1990. Chromatographic Science Series 50.
11. G. Glöckner, *Gradient hplc of Copolymers and Chromatographic Cross-Fractionation*, Springer, Berlin, 1991, p. 148.
12. C. F. Poole and S. K. Poole, *Chromatography Today*, Elsevier, New York, 1991.
13. S. L. Wu, K. Benedek, and B. L. Karger, *J. Chromatogr.* **359**, 3 (1986).
14. M. I. Aguilar and M. T. W. Hearn, in M. T. W. Hearn, ed., *hplc of Proteins, Peptides and Polynucleotides*, VCH Publishers, New York, 1991.
15. A. A. Gorbunov and A. M. Skvortsov, *Adv. Colloid Interface Sci.* **62**, 31–108 (1995).
16. J. Jandera and J. Churacek, *Gradient Elution in Column Liquid Chromatography—Theory and Practice*, Elsevier, Amsterdam, 1985.
17. L. R. Snyder and M. A. Stadalius, in C. Horvath, ed., *High-Performance Liquid Chromatography: Advances and Perspective*, Vol. **4**, Academic Press, Inc., Orlando, Fla., 1986, p. 195.
18. Y. Brun, *J. Liq. Chromatogr. Relat. Technol.* **22**, 3027–3065 (1999).
19. N. B. Afeyan and co-workers, *J. Chromatogr.* **519**, 1 (1990).
20. R. L. Cunico, K. M. Gooding, and T. Wehr, *Basic hplc and CE of Biomolecules*, Bay Bioanalytical Laboratory, Richmond, Calif., 1998, p. 23.
21. K. M. Gooding and F. E. Regnier, *hplc of Biological Macromolecules: Methods and Applications*, Marcel Dekker, Inc., New York, 1990.
22. F. E. Regnier, *Science* **238**, 319 (1987).
23. A. Sadana, *Bioseparation of Proteins: Unfolding/Folding and Validations*, Academic Press, Inc., San Diego, Calif., 1998, Chapt. "5".
24. M. T. W. Hearn, in S. Ahuja, ed., *Handbook of Bioseparations*, Vol. **2**, Academic Press, Inc., San Diego, 2000.
25. M. R. Wilkins, K. I. Williams, R. D. Appel, and D. F. Hochstrasser, eds., *Proteome Research: New Frontier in Functional Genomics*, Springer-Verlag, New York, 1997.
26. S. Mori, in Ref. 3.
27. T. C. Chunk, *J. Chromatogr. A* **656**, 591–615 (1993).
28. S. Teramachi, in D. Berek, ed., Chromatography of Polymers (special issue), *Macromol. Symp.* **110**, 217 (1996).
29. H. Sato, K. Ogino, T. Darwint, and I. Kiyokawa, in Ref. 28.
30. P. Kilz, R.-P. Kruger, H. Much, and G. Schulz, in Ref. 3.
31. B. Trathnigg, M. Kollroser, M. Parth, and S. Roblreiter, in T. Provder, ed., *Chromatography of Polymers: Hyphenated and Multidimensional Techniques*, American Chemical Society, Washington, D.C., 1999.

GENERAL REFERENCES

Refs. 6 and 19 are recommended as introductory material to hplc of biopolymers.
Refs. 14 and 20 deal critically with all aspects of hplc of biological molecules.

Refs. 23 and M. Kastner, ed., *Protein Liquid Chromatography, Elsevier, Amsterdam, 2000, J. Chrom. Library, Vol 61, reflect the current state of the art in protein chromatography*.
U. D, Neue, *hplc Columns: Theory, Technology, and Practice, Wiley-VCH, Inc., New York, 1997, in-depth review of column technology*.
Refs. 7 and 11 reflect the current state of hplc of synthetic polymers.
Refs. 1, 8, and 17 deal with theoretical aspects of polymer chromatography.

YEFIM BRUN
Waters Corporation

CHROMATOGRAPHY, SIZE EXCLUSION

Introduction

A polymeric product contains chains of varying lengths because of the statistical nature of polymerization processes. All synthetic polymers, and many natural polymers, have a molecular weight distribution (MWD), which may be represented by the differential weight distribution $w(M)$ as a function of molecular weight M (1). From the normalized distribution $w(M)$, the number-, viscosity-, and weight-average molecular weights, M_n, M_v, and M_w respectively, are calculated from the relations

$$M_n = 1/\left(1/M\right) w\,(M)\ \mathrm{d}M \tag{1}$$

$$M_v^a = M^a w\,(M)\ \mathrm{d}M \tag{2}$$

$$M_w = M w\,(M)\ \mathrm{d}M \tag{3}$$

Here, a is the exponent in the Mark–Houwink dilute solution viscosity equation

$$[\eta] = K M_v^a \tag{4}$$

where $[\eta]$ is the intrinsic viscosity (dL/g) and K is a constant. Higher moments of the distribution curve may also be used to derive the z and $z+1$ average molecular weights (1) (Molecular weight determination (GPC, osmometry)).

Various methods are available for the determination of average molecular weight (2), but the three averages in equations 1–3 cannot define a distribution

Encyclopedia of Polymer Science and Technology. Copyright John Wiley & Sons, Inc. All rights reserved.

within a polymer having many components. The polydispersity defined as M_w/M_n can provide an indication of the width of the MWD, but does not disclose distribution shape. Two polymers may have the same average molecular weight but quite different MWD. However, measurement of a specific average molecular weight is quite useful for correlation with polymerization kinetics and with a range of solution and bulk properties. Inevitably, attention was therefore directed to polymer fractionation as a means of determining MWD (see FRACTIONATION). The classical experiment is preparative fractionation from which a cumulative weight distribution $I(M)$, and hence $w(M)$, is calculated from the weights and average molecular weights of the isolated fractions. By the mid-1960s, a range of fractionation methods was available (3,4), but the limitations of most of these were well recognized. In particular, for polymer fractionations relying on the molecular weight dependence of polymer solubility, the experimental methods were inefficient, tedious, and time consuming.

Size exclusion chromatography (SEC) is now established as the most popular and convenient method for analytical polymer fractionation. Reliable and reproducible chromatograms are obtained in relatively short time (elution < 1 h), permitting routine characterization and effective application to quality control. In retrospect, it is perhaps surprising that SEC as a characterization method was not established earlier. The characteristic separation of short chains having elution times higher than those of long chains had been reported by a number of workers in the published literature between 1935 and 1958 (5). The major advance by Porath and Flodin (6) provided effective demonstration that polymers may be separated by the size dependence of the degree of solute penetration into a porous packing. Their technique was named gel filtration (GF) involving cross-linked dextran gels, which are soft and highly swollen networks for separations of water-soluble polymers. The description of analytical gel permeation chromatography (GPC) by Moore (7), and the subsequent availability of commercial instrumentation (8), attracted widespread interest. Moore made two important contributions. First, he prepared versatile porous cross-linked polystyrene/divinylbenzene (PS/DVB) gel particles covering a wide range of pore diameters for separations of synthetic polymers in organic media. These rigid gels (particle diameter d_p exceeding 50 μm) had good mechanical stability and were packed in columns (length 120 cm) which could be operated at high pressures and fast flow rates. The second contribution was the direct coupling of an on-line refractometer to the GPC column (or columns) in order to measure continuously the concentration of the polymer in the eluent. A chromatogram as recorded by a differential refractive index (DRI) detector is thus a record of molecular size distribution as a function of elution (or retention) time (or volume), and so the recovery and characterization of fractions were avoided.

Initial work in GPC focused on the conversion of a chromatogram to an accurate MWD. Column calibration methodologies were developed, and concentration detectors based on infrared (IR) and ultraviolet (UV) spectrophotometers and on evaporative light scattering were introduced. It was not until 1979 that a suitable reference book became available (9), by which time the term SEC had become widely accepted. The main advance during this decade was to identify conditions for high performance separations. The advantages of microparticulate rigid gels (particle diameter ~ 10 μm) were demonstrated, resulting in the use of short

columns (30 cm) so that elution times were much reduced. In the next 10 years up to 1990, instrumentation for multiangle laser-light scattering and differential viscometry appeared. These molecular size detectors, which generate on-line molecular weight data as a function of elution time, may be coupled to the SEC column system, and in conjunction with an on-line concentration detector permit the computation of MWD and average molecular weights. Examples of these advances are detailed in several books (10–12). The principles, practice, and applications of SEC are emphasized here, and further details on these and other aspects can be found in two recent books (13,14).

Principles of SEC

The resolution of solute molecules in a complex mixture by a chromatographic method depends on two types of processes. *The separation process* in the stationary phase controls the differential migration of the molecules, and in the SEC case includes all the mechanisms that may determine the permeation of molecules in the column packing. *The dispersion process*, which generally consists of at least two mechanisms, determines the band broadening of one type of molecule, and this broadening is influenced by molecular diffusion and column packing. In the determination of MWD and average molecular weights by SEC, an important part of data interpretation is the establishment of a correct calibration relation between the molecular weight M of a polymer and retention volume V_R. An understanding of the separation process is necessary because of the prevalent use of universal calibration methods, which assume that SEC separations are controlled solely by an exclusion mechanism. An understanding of the dispersion process is also required because the experimental chromatogram will always correspond to a distribution of molecular weights, which is too broad because of band broadening of all components in a polymer. Experimental conditions have to be chosen to minimize chromatogram broadening in order to optimize accuracy of molecular weight data and to obtain high resolution separations of low polymers, prepolymers, and small molecules.

Separation Mechanism. The basic separation mechanism in SEC assumes that the column packing is "inert," and interactive mechanisms that might contribute to retention behavior are neglected. The size exclusion mechanism is dependent on solute access to pore volume within gel particles determined by pore size distribution and solute size. Consequently, all solute molecules are eluted within one column solvent volume, corresponding to the sum of the interstitial (or void) volume V_0 of solvent between porous gel particles, defined as the volume of the mobile phase, and the volume V_i of solvent within the porous gel particles, defined as the volume of the stationary phase. Retention is given by the equation

$$V_R = V_0 + K_{SEC} V_i \tag{5}$$

where the distribution coefficient K_{SEC} represents the fraction of stationary phase solvent that is accessible to the solute. For very large molecules, the value of K_{SEC} will be zero at the exclusion limit because the sizes of these molecules prohibit solute diffusion into the gel pores. Very small molecules, on the other hand, have

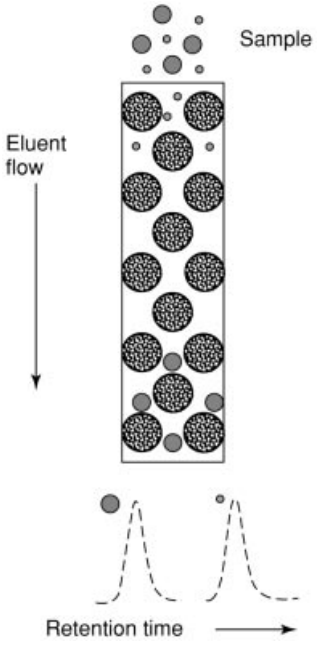

Fig. 1. Simple representation of the separation mechanism in SEC, showing larger molecules eluting faster than smaller molecules.

total access to both stationary and mobile phases, ie, K_{SEC} is unity at the permeation limit. As the chromatographic column is washed with solvent, the large molecules are eluted first, followed by solutes of decreasing size, which penetrate an increasing fraction of the solvent within gel particles. These observations are illustrated in Figures 1 and 2.

Practical separations with a porous column packing in SEC are performed close to equilibrium conditions. Elutions are performed at flow rates around 1 mL/min when V_R is independent of flow rate. Although many theoretical models have been proposed for polymer separations in SEC, thermodynamic treatments provide a sound representation of separation behavior. For a separation operating at equilibrium conditions, the standard free-energy change ΔG^0 for the transfer of solute molecules from the mobile phase to the stationary phase at constant temperature T is related to K_{SEC} by

$$\Delta G^0 = \Delta H^0 - T\Delta S^0 = -RT \ln K_{SEC} \tag{6}$$

where R is the gas constant and ΔH^0 and ΔS^0 are the standard enthalpy and entropy differences between the phases, respectively. Thermodynamic theories for SEC (15–18) calculate the pore volume accessible to a solute of given size in solution in terms of pore size for various models of pore shape. Such a treatment may be regarded as an excluded volume problem in which small solutes are permitted close approach to a pore surface whereas larger solutes have a larger exclusion

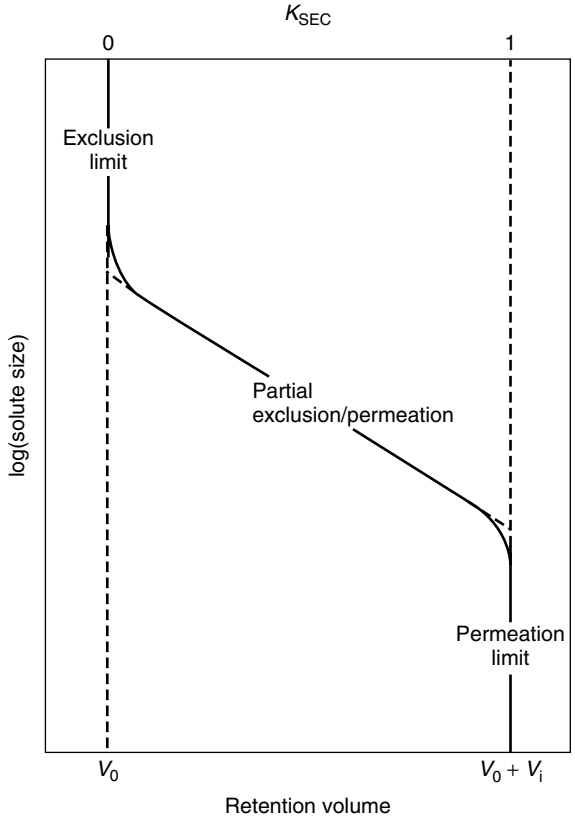

Fig. 2. Calibration curve for a size exclusion mechanism, presuming an inert column packing.

zone. Presuming that the pore surface is indeed inert, then ΔH^0 will be zero and the distribution coefficient is defined by

$$K_{SEC} = \exp(\Delta S^0/R) \tag{7}$$

Therefore, K_{SEC} is considered to be the fraction of accessible solute arrangements within the porous packing to those within the mobile phase, and represents loss in conformational entropy on solute transfer to a pore. Thermodynamic theories demonstrate for various solute types, namely sphere, rod, and random coil, and various pore geometries, such as lamellar and cylindrical shapes, that K_{SEC} for polymer separations may be generalized in terms of the relation

$$K_{SEC} = \exp(-sL_p/2) \tag{8}$$

where L_p is the mean external length or molecular projection, eg, L_p is equal to the diameter D of a sphere, and s is the surface area per unit pore volume. These treatments of size exclusion therefore suggest that for a column containing a given packing a characteristic molecular parameter L_p will represent the behavior of all solutes.

Equilibrium theories therefore predict that the behavior of all polymers can be represented by a universal size parameter. Benoit and co-workers (19) showed that solute size should be the hydrodynamic volume V_h of a polymer molecule in solution defined by Einstein's equation

$$V_h = 40[\eta]M/N_0 \tag{9}$$

where N_0 is Avogadro's number (see Fig. 2). It follows that a plot of $\log [\eta]M$ vs V_R should be a universal calibration plot for all polymers, and many experimental studies of a wide range of polymer-solvent-packing combinations have been performed, confirming the validity of this approach (20). Consequently, a molecular weight calibration curve for one polymer may be calculated from a calibration curve established with polymer standards. The calibrations are related by the expression

$$\log M_p - \log M_{ps} = \log [\eta]_{ps}/[\eta]_p \tag{10}$$

where p refers to the polymer and ps to an experimental study with well-characterized standards having narrow MWD.

Separations of polymers in organic media with cross-linked PS/DVB gels are generally performed with an eluent which is a good solvent for polystyrene. As long as this eluent is also a good solvent for a polymer, then interactive mechanisms are relatively unimportant compared with size exclusion, and it is reasonable to presume that ΔH^0 is about zero for separations with cross-linked PS/DVB gels. However, there are combinations of polymer and eluent, dependent on the polarities of these components and good/poor solvency of the eluent, for which plots of $\log [\eta]M$ vs V_R are displaced to high V_R, indicating the presence of a secondary mechanism such as adsorption (21). Thus, it is possible to conceive of columns of cross-linked PS/DVB gels operating by two limiting mechanisms dominated by size exclusion on the one hand (entropic effect) and by adsorption on the other (enthalpic effect). These two limiting behaviors could be controlled by adjusting the mobile phase, and could be represented by the retention equation

$$V_R = V_0 + K_{SEC}V_i + K_{ads}s_{ads} \tag{11}$$

where K_{ads} is the distribution coefficient for the adsorption mechanism and s_{ads} is an equivalent volume related to the available surface area for the eluting polymer. Therefore, a column will function solely in the adsorption mode for $K_{SEC} = 0$ and $K_{SEC} = 1$, although the appropriate value of s_{ads} for the stationary phase for each limiting case will need to be defined in equation 11.

When there is a mixed mechanism consisting of a primary mechanism, which is size exclusion, ie $0 < K_{SEC} < 1$, and a secondary interaction mechanism, then retention can be defined by (22,23)

$$V_R = V_0 + K_{SEC}K_pV_i \tag{12}$$

where K_p is the distribution coefficient for polymer–gel interactions. Therefore, equations 5 and 12 are identical for $K_p = 1.0$. Consequently, it can be suggested that values of K_p are given by

$$K_p = \exp\left(-\Delta H^0/RT\right) \tag{13}$$

Equation 12 has been shown to be a reasonable representation of a mixed mechanism for polymers in organic media separating on cross-linked PS/DVB gels (21,22).

Water-based polymers have aqueous solubility based on hydrophilic functionalities and/or ionic groups, and are likely to contain hydrophobic segments. Because aqueous separations require the column packing to have a polar surface, with or without ionic groups, a range of polymer–substrate interactions may occur, giving rise to various secondary retention mechanisms. For example, separations may involve ion exchange, ion exclusion, ion inclusion, intramolecular interaction, and adsorption (to include hydrogen bonding and hydrophobic interactions) (12,14). To establish the validity of universal calibration for water-based polymers, the choice of aqueous SEC system requires considerable care. For anionic polyelectrolytes separating on inorganic packings, conditions involving addition of electrolyte to the mobile phase have been established in order to minimize intrachain interactions and interactions between ionic groups on the polyelectrolyte and charges on the surface of the column packing. However, this methodology fails for cationic polyelectrolytes requiring modified inorganic packings with bonded phases. Alternatively, polymer-based packings may be preferred because by analogy with GF matrices rigid macroporous polymeric gels may be much less susceptible to secondary interaction effects. The absence of charged sites may result in a tendency toward hydrophobic interactions, in which case it may be necessary to introduce an organic modifier such as methanol or glycerol to the mobile phase. In practice, the choice of composition of an aqueous mobile phase for a specific polymer with a column packing may not be straightforward, and a balance between the need to increase ionic strength to reduce ionic interactions and to lower electrolyte concentration to limit hydrophobic interactions may have to be determined. Guidelines for minimizing secondary interactions for water-based polymers for a polymer-based packing are provided in Table 1.

Dispersion Mechanisms. A measure of the efficiency of a chromatographic column is the plate number N. Various procedures exist for calculating N from an experimental chromatogram (9), and equation 14 is commonly utilized

$$N = 5.54(V_R/W_{0.5})^2 \tag{14}$$

where V_R is computed from the point of application of the solution of polymer into the column to the appearance of the peak height maximum of the chromatogram and $W_{0.5}$ is the width of the chromatogram at half height. This procedure assumes that the chromatogram is symmetrical corresponding to a normal error (or Gaussian) function. The plate number is a popular way of measuring column efficiency, and a typical microparticulate packing with $d_p \sim 10$ μm will generate a value $N > 30{,}000$ plates/m for a solute eluting at $V_R = V_0 + V_i$.

Table 1. Secondary Interactions in Aqueous SEC

Type	Symptom	Action
Ionic exclusion	Peaks elute early, maybe before SEC exclusion limit	Modify eluent, addition of salt, and/or pH adjustment
Ionic adsorption	Peaks elute late, maybe after SEC permeation limit, peak tailing or no peaks detected	Modify eluent, addition of salt, and/or pH adjustment
Ionic inclusion	Peak at total permeation due to salt even though samples prepared in eluent	Recognize salt peak, do not include in sample integration
Hydrophobic adsorption	Peaks elute late, maybe after SEC permeation limit, peak tailing or no peaks detected	Modify eluent, addition of organic modifier (check column compatibility)

If a polymer sample contains several species of very different sizes, then peaks for each monodisperse species will be obtained when $W_{0.5}$ is minimized. However, because of the SEC elution volume range defined by $0 < K_{SEC} < 1.0$, high efficiency columns are required for high resolution separations. It can be estimated that an SEC column operating at 40,000 plates/m has a maximum resolution of 40 peaks (24). For the case of two monodisperse solutes 1 and 2 having different sizes, column resolution R_s is given by

$$R_s = 2\,(V_{R2} - V_{R1})\,/\,(W_1 + W_2) \tag{15}$$

where V_{R2} and V_{R1} are retention volumes and W_1 and W_2 are peak widths at the base of a chromatogram. The numerator in equation 15 will depend on separation power, which is inversely proportional to the slope D_2 of the plot of log M vs V_R defined by

$$\log M = D_1 - D_2 V_R \tag{16}$$

The values of D_1 and D_2 will depend on the pore size distribution of the packing, gel capacity, ie pore volume, and on column length L, and these parameters need to be optimized to increase separation power, and therefore peak resolution. Variables influencing the denominator in equation 15 are discussed in connection with equation 19.

The definition of R_s can be extended by considering molecular weight differences, in terms of the slope D_2 as defined by equation 16. It follows that a general measure of SEC resolution may be developed (9), and the specific resolution R_{sp} was proposed

$$R_{sp} = 0.576/\,(D_2\sigma) \tag{17}$$

where σ is the standard deviation of a Gaussian peak with $4\sigma = W_1 = W_2$ and will vary with M. In practice, important parameters are D_2, L, d_p, and σ, chosen so that R_{sp} exceeds unity. Examples of column performance data are

Table 2. Column Performance Parameters

Column type	Exclusion limit (PS equivalent)	Efficiency,[a] plates/m	σ,[b] mL	D_2[c]	R_{sp}[d]
PLgel 20 μm MIXED-A	40,000,000	15,100	0.204	1.155	1.061
PLgel 10 μm MIXED-B	10,000,000	34,200	0.166	1.138	1.703
PLgel 5 μm MIXED-C	2,000,000	47,600	0.115	0.915	2.376
PLgel 5 μm MIXED-D	400,000	50,100	0.115	0.737	2.949
PLgel 3 μm MIXED-E	30,000	96,000	0.106	0.605	3.898

[a]Determined using toluene as test probe.
[b]Determined using narrow PS standard, $M_{peak} = 9200$.
[c]Determined using narrow PS standards.
[d]Determined using $0.25/(D_2\sigma)$.

presented in Table 2 for a range of column types operating at an eluent flow rate of 1 mL/min.

Theoretical interpretations of column efficiency consider dispersion mechanisms of solutes in the mobile and stationary phases. These mechanisms influence the dependence of the height equivalent to a theoretical plate, or just plate height H, on the linear flow velocity u of the eluent. The value of H may be determined from an experimental separation from the equation

$$H = L/N \tag{18}$$

The basic concepts for general chromatographic separations (25) can be applied to SEC (9). For separations of polymers, it was proposed that only two column dispersion terms influence H (26,27), namely eddy diffusion in the mobile phase and mass transfer in the stationary phase. The expression for H for a permeating monodisperse high polymer is

$$H = 2\lambda d_p + \left[r\left(1-r\right)ud_p^2/30D_s\right] \tag{19}$$

where λ is a constant (close to unity) characteristic of the packing, r is the retention ratio defined by V_0/V_R, and D_s is the diffusion coefficient of the solute in the stationary phase. Column dispersion by eddy diffusion, represented by the first term in equation 19, arises because solute molecules reside in different streamlines with reference to their proximity to particles of the column packing. Column dispersion by mass transfer, represented by the second term in equation 19, arises because at any instant a fraction of the molecules will be within the porous column packing and are left behind by the remaining fraction in the mobile phase.

Equation 19 identifies the experimental variables that have to be considered in optimizing separations for reduced chromatogram broadening for high polymers and for improved resolution of peaks for low polymers and small molecules. The two column dispersion terms clearly demonstrate how lowering d_p will maximize column efficiency. For low polymers the mass transfer term will not be too significant because D_s is high, so that fast separations may be performed with little loss in efficiency. Larger polymers that have lower values of D_s will have higher mass transfer dispersion. Therefore, a much more significant rise in H as u increases

will be observed as molecular weight increases, and so high speed separations for high polymers will operate with considerable broadening of a chromatogram.

These predictions can be compared with experimental studies of polystyrene standards (26,27). However, all synthetic polymers will have an MWD, and it is necessary to include a polydispersity contribution to the experimental value of H. This is achieved by extending equation 19 to include a third term, presuming that the permeating polymer has a logarithmic normal distribution for the MWD. With this addition it is observed that equation 19 provides a good representation of experimental results for plots of H vs u.

In practice, a polydisperse polymer having a range of solute sizes generates an SEC chromatogram which may be considered as a collection of a large number of overlapping Gaussian peaks. Because of dispersion mechanisms, the tails of the chromatogram result from broadening alone and so the computed $w(M)$ distribution is broader than the true MWD. Various correction methods have been proposed to transform the experimental chromatogram into an MWD (4). However, it is not necessarily easy to achieve reliable corrected chromatograms before calculating a $w(M)$ distribution. The alternative approach is to reduce the level of column dispersion in order to minimize broadening of a chromatogram for a polydisperse polymer, according to the parameters in equation 19. If the optimum separations can be achieved, then calculations of broadening corrections can be omitted.

SEC Column Technology

SEC column packing materials, based on porous particles of a variety of substrates, are commercially available from a large number of suppliers (13). In the field of organic-soluble, mainly synthetic, polymers, column technology was initially developed using both porous silica and porous PS/DVB particles as the stationary phase. Although in the early days, columns of porous silica emerged as popular candidates, mainly because silica was well established in liquid chromatography (LC), the production of very highly cross-linked PS/DVB particles with well-controlled pore size and particle size distribution, and excellent temperature and mechanical stability, led to their dominance in the field, which continues today (28). The continued refinement of PS/DVB particle technology has produced smaller particle size packings (typically 5–10 μm), resulting in more efficient columns and subsequent reductions in analysis times to typically 20–40 min. Recent years have heralded the emergence of 3 μm columns exhibiting extremely high efficiency (>80,000 plates/m), which have particular application in the very low molecular weight SEC separation range, competing with other types of LC for the resolution of small molecules (29).

Columns for aqueous SEC have also been developed based on porous silica and porous polymeric stationary phases. Columns of silica have excelled in the field of monodisperse biopolymer separations (eg proteins and peptides) offering very specific pore size distributions and small particle size for high resolution. High performance packings, consisting of rigid hydrophilic polymeric particles, were introduced in the early 1980s and offered considerable improvements in both column efficiency and chemical and mechanical stability compared to the

early GF columns of soft polymeric networks. The continued development of high performance, hydrophilic stationary phases has expanded the use of SEC for the characterization of synthetic water-soluble polymers as they exhibit a much larger separation range and better linearity of calibration curves, and much lower adsorption effects compared to silica packings. In light of environmental issues, the requirement to produce water-soluble polymers has in recent years significantly increased the level of interest in aqueous SEC.

SEC column packing materials are generally represented by a characteristic calibration curve produced using a series of polymer standards. Typical calibration curves for individual pore size columns, as illustrated in Figures 3a and 4 for SEC columns with organic and aqueous eluents respectively, exhibit a

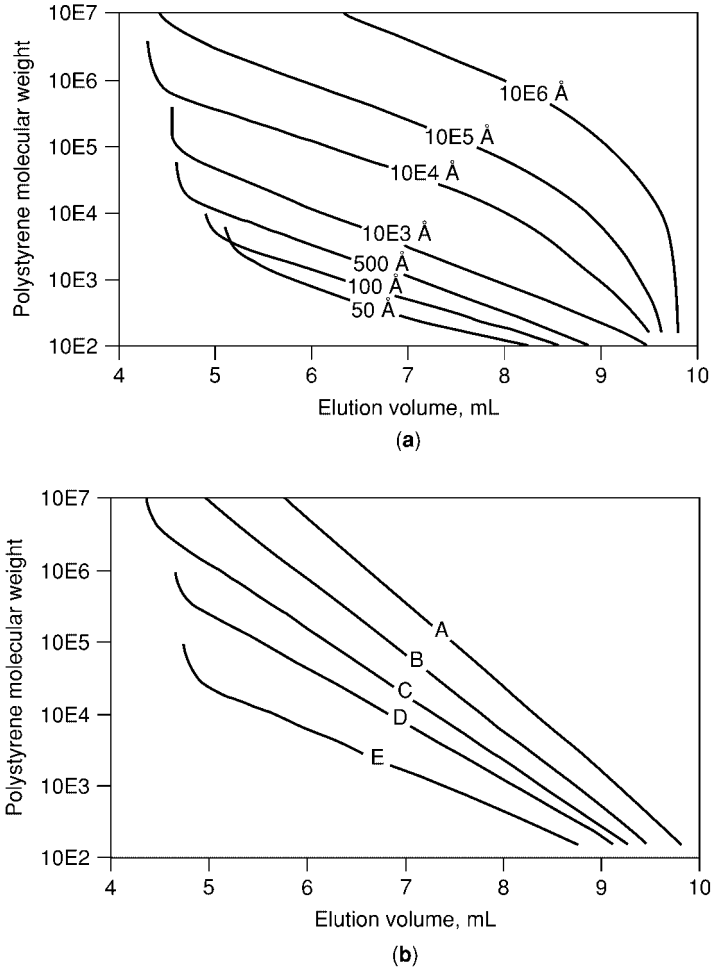

Fig. 3. Calibration curves for columns of PLgel for organic SEC at ambient temperature: (**a**) a range of individual pore size columns designated 50 Å to 10E6 Å, (**b**) a range of mixed gel columns designated A to E. Eluent: THF, flow rate: 1 mL/min, calibrants: polystyrene standards.

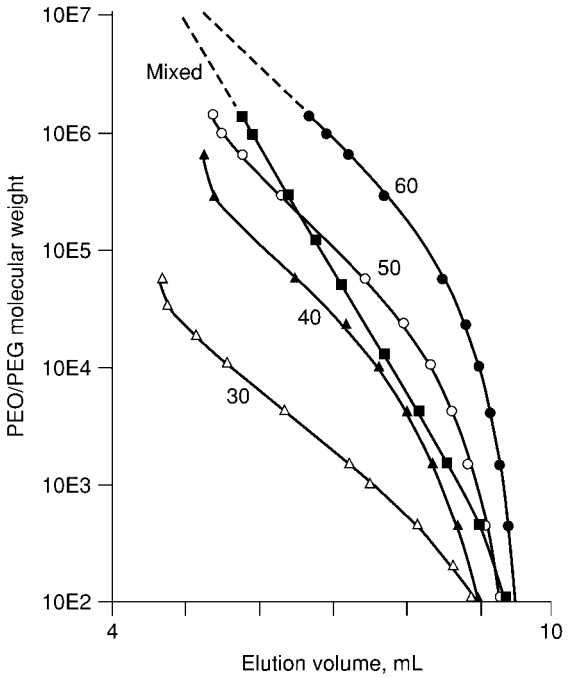

Fig. 4. Calibration curves for columns of PLaquagel-OH, designated 30 (△), 40 (▲), 50 (○), 60 (●), and Mixed (■), for aqueous SEC at ambient temperature. Eluent: water, flow rate: 1 mL/min, calibrants: poly(ethylene oxide/glycol) standards.

reasonably linear region spanning 1–2 decades in molecular weight, which defines the optimum resolving range of that type of packing material. Most commercial polymers exhibit a broad MWD demanding a very wide resolving range. Traditionally, this was achieved using combinations of several different individual pore size columns, but nowadays the use of mixed gel columns (where a homogeneous blend of individual pore size media is packed into the columns) is widespread (30). This approach provides a linear calibration curve (as illustrated in Fig. 3b and 4) over a specified molecular weight range, simplifies column selection, and minimizes replacement stock.

Typical column dimensions for SEC are length of 25–30 cm and internal diameter of 7–8 mm. SEC is normally a multicolumn technique and sets of two to five columns are used routinely. It is a requirement that the column technology should provide widespread solvent compatibility and good mechanical strength for durability across a wide range of applications.

Eluent Selection

The primary consideration in eluent selection is that the polymer must be fully dissolved for SEC analysis. A diverse range of organic solvents can be used for SEC, covering a wide range of polarity from hydrocarbons through to alcohols.

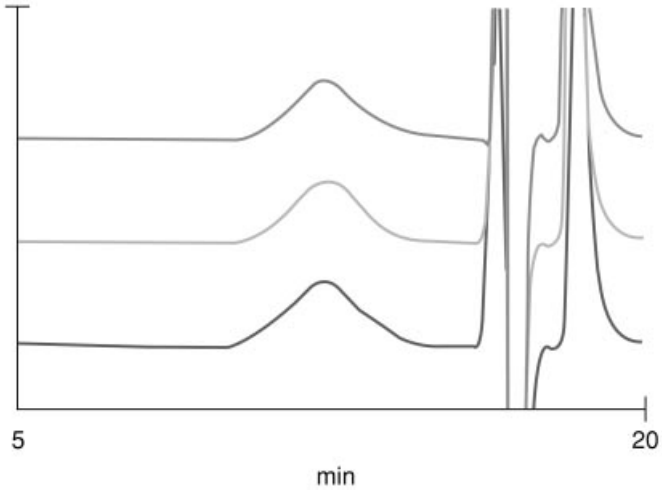

Fig. 5. Aqueous SEC analysis of three samples of chitosan at ambient temperature. Columns: 2 × PLaquagel-OH MIXED 8 μm 300 × 7.5 mm, eluent: 0.5 *M* $NaNO_3$/0.01 *M* NaH_2PO_4/pH 2, flow rate: 1 mL/min, detector: DRI.

The physical characteristics of the organic solvent selected must be taken into consideration with respect to detection, for instance, the refractive index of the solvent if DRI is to be used, or the UV or IR spectrum of the solvent if spectrophotometric detection at a given wavelength is to be employed. Furthermore, the viscosity of the eluent is important; if it is relatively high, then the SEC separation may need to be carried out at elevated temperature in order to reduce the eluent viscosity, thus decreasing column operating pressure and improving mass transfer. In aqueous SEC, many water-soluble polymers contain charged species or relatively hydrophobic groups which are likely to give rise to sample-column packing interactions in the SEC separation. Such nonsize exclusion behavior as shown in Table 1 must be suppressed if SEC is to be used for determination of MWD, and this can be achieved by modification of the eluent. Water containing salts and buffers successfully inhibit ionic interactions and the addition of a minor volume of organic solvent (eg methanol) is used to suppress hydrophobic interactions between the polymer and the column packing material. A typical aqueous SEC separation is illustrated in Figure 5.

Instrumentation

An SEC system consists of a solvent reservoir, an isocratic pump to deliver the eluent, an injection system to introduce the sample without interrupting the eluent flow, SEC columns to perform the fractionation, a detector which, in its simplest form, detects the concentration of the solute, and a form of data logging to record detector response as a function of elution time (11).

Pumping/Injection Systems. Because of the dependence of the technique on the precise measurement of elution volume, the pumping system must

be capable of delivering eluent at a constant volumetric flow rate, independent of back pressure or temperature. The accuracy of the flow rate at which the solvent is delivered is less important than the consistency, since very small variations in flow rate can cause large errors if SEC is to be used for characterization of MWD. Beyond the limits of acceptable pump performance, it is common practice to inject an internal standard or marker such that corrections for flow rate variation can be made to improve repeatability of results. When viscosity and light scattering detectors are employed in the SEC experiment, it is also preferable for the pumping system to exhibit minimal pulsations in pressure through the system so as to improve detector baseline stability.

A two position injection valve, either manually or automatically actuated, is usually employed for SEC, as for other forms of LC. The injection loop volume should be minimized in order to avoid chromatogram broadening as a result of dispersion in the injector. This is particularly the case when using SEC columns packed with very small particles, where the column efficiency is very high. However, in the case of solutions of medium to high molecular weight polymer, attempts to increase detector response by increasing sample concentration should be avoided as the increase in solution viscosity may result in a change in elution volume and additional dispersion as a result of viscous streaming. In these cases, it is necessary to increase the injector loop volume rather than increase the solute concentration if additional detector response is required. As a rule of thumb, an injection volume of 50 μL per column length of 30 cm in SEC is deemed to be a good compromise between minimal dispersion and maximum detector response.

Concentration Detectors. In the simplest SEC system, the concentration of the sample eluting from the columns must be measured via some appropriate form of detector. The most commonly used type of concentration detector is the DRI detector in which the difference in refractive index between pure solvent and the eluent flowing from the separating columns is measured. The response from the DRI detector is proportional to concentration, assuming that the specific refractive index increment (dn/dc) for the eluting polymer is constant. Because short chain polymers might have a molecular weight dependent dn/dc, a correction for the measured DRI response might have to be considered. In the case of heterogeneous samples (eg block copolymers and formulated materials), where the dn/dc for different components may vary as a function of elution volume, DRI may not be the most appropriate choice of concentration detector. DRI detectors are very sensitive to fluctuations in temperature and pressure, and baseline stability can be problematic if the system is not well conditioned. However, this type of detector does have broad general application and is relatively low in cost.

Detectors operating on the principle of absorption of incident UV or IR radiation are also used in SEC. These detectors rely on the polymer containing functional groups that give rise to specific absorption at the wavelength of the incident radiation and therefore are limited to certain applications where the polymer contains a UV chromophore or has a characteristic IR absorption band. Furthermore, the extensive use of a diverse range of organic solvents for SEC can restrict the use of UV or IR detectors as the background absorption from the solvent itself can be significant enough to mask out any contribution from the sample itself. Both UV

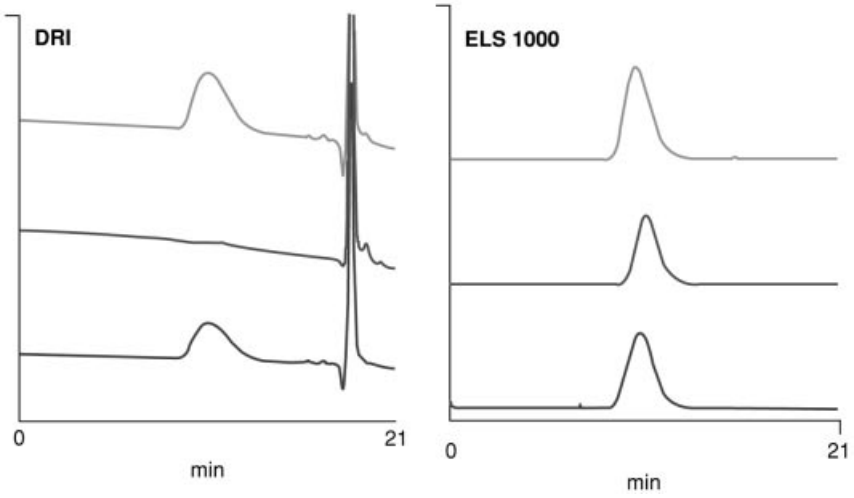

Fig. 6. Comparison of detector responses for DRI and ELSD in the analysis of PS (top), PDMS (middle), and PS/PDMS blend (bottom) at ambient temperature. Columns: 2 × PLgel 5 μm MIXED-C 300 × 7.5 mm, eluent: THF, flow rate: 1 mL/min.

and IR detectors can be useful for the characterization of copolymers using dual detection, as the wavelength of the detector can be tuned to respond specifically to one moiety.

The evaporative light scattering detector (ELSD) has found increasing application in SEC over the last decade or so. In this device, the eluent stream is mixed with an inert nebulizer gas to form a continuous stream of droplets that pass through an evaporation chamber where the volatile solvent is driven off leaving a plume of solute particles. The concentration of solute is determined by the amount of light obscured by the particles as they pass through the optical chamber of the device. This detector is often referred to as more "universal" than the others mentioned above, since it does not rely on the characteristics of the solute and is less affected by the choice of eluent. This is graphically illustrated in Figure 6, which compares detector outputs from DRI and ELSD for the analysis of a blend of polystyrene (PS) and polydimethylsiloxane (PDMS) using tetrahydrofuran (THF) as eluent. In this case, there is a reasonable difference in refractive index between the THF and PS, giving a positive peak response. However, PDMS is isorefractive with THF and no peak is detected by DRI; hence the PS/PDMS blend results in a chromatogram that reflects only the PS portion of the sample. However, in the case of the ELSD, where eluent is evaporated, all solutes result in a positive response and the chromatograms of PS, PDMS, and the blend are suitable for quantification purposes.

Molecular Weight Sensitive Detectors. Light scattering and viscometry are two classical techniques routinely applied to the characterization of polymers in solution (2). When operated in a flow through mode, so-called molecular weight sensitive detectors can be combined with the SEC separation to provide direct measurement of molecular weight (light scattering) or a property related

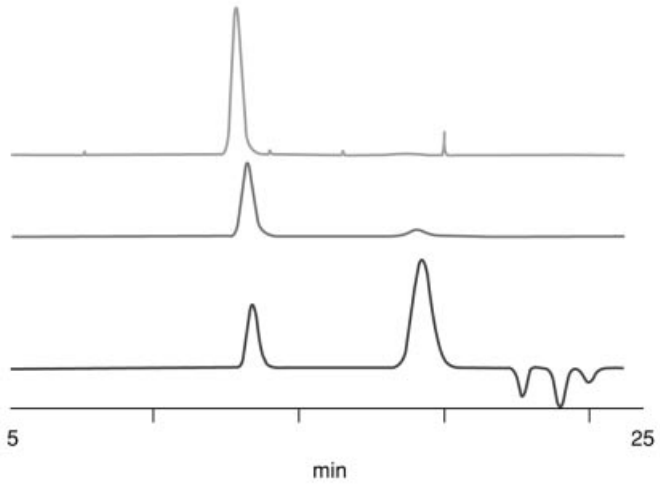

Fig. 7. Comparison of detector sensitivity for DRI (bottom), viscosity (middle), and light scattering (top) for two narrow PS standards (M_{peak} 186,000 and 1260). Columns: 2 × PLgel 5 μm MIXED-C 300 × 7.5 mm, eluent: THF, flow rate: 1 mL/min, temperature: 40°C.

to molecular weight (intrinsic viscosity), providing more accurate determination of molecular weight as well as facilitating the study of polymer architecture. The molecular weight sensitivity of such detectors compared to a conventional DRI concentration detector is illustrated in Figure 7.

In light scattering measurements, the intensity of scattered light from the polymer is expressed in terms of the excess *Rayleigh factor* R_θ, which is defined as the scattering intensity of the polymer solution to the scattering intensity of the solvent at a given angle θ. In practice for an SEC detector, R_θ is the measured response above the baseline, that is the detector output when there is no sample in the eluent exiting from the column. The general light scattering equation

$$R_\theta = cM_w(dn/dc)^2K \tag{20}$$

is applicable to on-line SEC measurements, where c is the polymer concentration and K is an optical constant.

SEC detectors are available with single, dual, and multiple angles at which the light scattering measurements are made and in each case the data treatment will vary slightly to accommodate the number of angles. In all cases the light scattering detector is used to determine the M_w of each fraction of the polymer as it elutes from the column, and by making a direct measurement of molecular weight, precludes the necessity to perform a column calibration. In order to calculate MWD, the concentration of each fraction must also be determined, and thus it is necessary to employ a concentration detector (usually DRI) as well as the light scattering detector in the SEC system. The sensitivity of light scattering detectors generally falls rapidly below around $M_w = 10{,}000$. However, below this limit the choice of solvent may be manipulated in order to increase dn/dc for a given polymer type and also the solute concentration for low molecular weight

polymers can generally be increased with no deterioration in chromatographic performance.

Viscometric detectors generally consist of one or more precision manufactured stainless steel capillaries through which the eluent from the SEC column flows and across which a pressure differential can be measured. Therefore, according to Poiseuille's law

$$P = \frac{8L\eta \mathrm{F}}{Pr^4} \tag{21}$$

where L and r are the length and radius of the capillary, F is the flow rate, and P is the pressure drop measured across the capillary. The specific viscosity (η_{sp}) of a polymer solution passing through the detector can be determined as a function of elution volume or time. Once again, an additional concentration detector is required in order to precisely determine the concentration of each eluting fraction such that a value of $[\eta]$ can be determined according to

$$[\eta] = \eta_{sp}/c \qquad (\text{when } c \text{ approaches zero}) \tag{22}$$

The measurement of $[\eta]$, also abbreviated IV, permits the determination of molecular weight of the polymer under investigation according to the principle of universal calibration, using hydrodynamic volume as defined in equation 9 as long as this polymer type is eluting by a size exclusion mechanism.

Conventional SEC calibration curves derived using different polymer types will yield polymer specific calibration plots of log M versus retention time as illustrated in Figure 8a. However, if an on-line viscometer is employed to measure $[\eta]$ directly, then the universal calibration plot of log $[\eta]M$ versus retention time will hold for any polymer type so long as the separation mechanism is based on size exclusion only, as illustrated in Figure 8b. Thus, having constructed a universal calibration using well-characterized polymer standards, any type of polymer can be analyzed, and by measuring $[\eta]$ on-line after the separation, the molecular weight of each eluting fraction can be obtained from the universal calibration plot.

In addition to the measurement of molecular weight, both light scattering and viscosity detectors permit the study of polymer architecture, eg branching. Figure 9 shows a series of typical Mark–Houwink plots for polyethylene samples derived from triple detector data (ie DRI, light scattering, and viscosity). A linear unbranched polyethylene results in a straight line plot where the slope and intercept equal the Mark–Houwink constants a and log K respectively. If the polyethylene is branched, the branched polymer will have relatively higher segment density compared to a linear polymer of equivalent molecular weight, resulting in a decrease in intrinsic viscosity. The ratio of the intrinsic viscosity of the branched polymer compared to a linear analogue will be dependent on the degree of polymer branching. Previous reference to concentration detectors for samples having compositional heterogeneity indicates that careful selection of a single

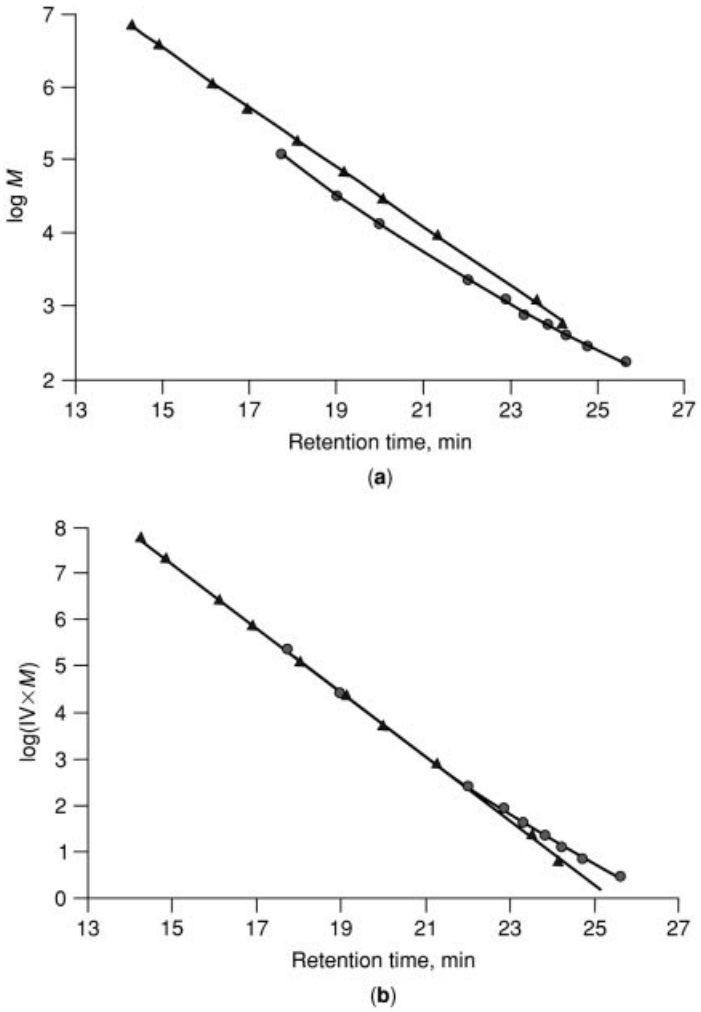

Fig. 8. Comparison of (**a**) conventional SEC calibration and (**b**) universal calibration, generated for polystyrene and polyethylene standards. Columns: 3 × PLgel 10 μm MIXED-B 300 × 7.5 mm, eluent: TCB, flow rate: 1 mL/min, temperature: 160°C. ▲ Polystyrene; ● polyethylene.

detector or dual detectors, together with light scattering or viscometric detectors, will be necessary for characterizing specific copolymers and blends.

Data Treatment

A primary application of SEC is for the determination of MWD (31). In this approach the raw data chromatogram obtained as output from the concentration detector is divided into a number of time slices of equal width, as shown in Figure 10.

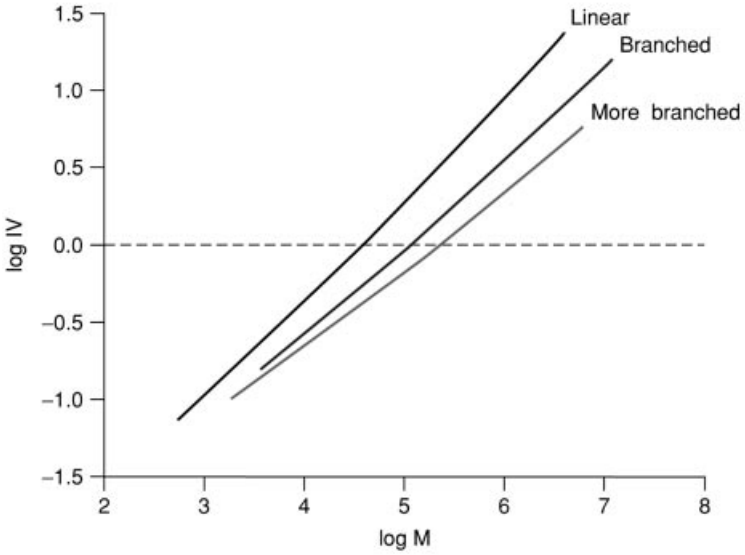

Fig. 9. Mark–Houwink plot from SEC with triple detection indicating linear polyethylene and polyethylenes with increasing degree of branching.

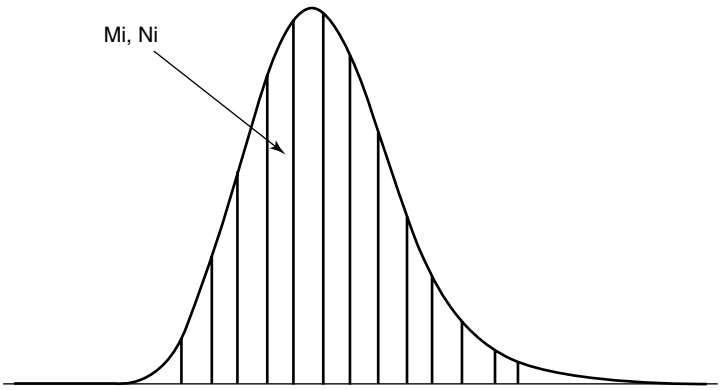

Fig. 10. Chromatogram from SEC indicating time slices for data manipulation.

For polydisperse samples the number of time slices must be selected in order that the computed average molecular weights will be unaffected by the number of time slices used. Since the introduction of high capacity computers with modern SEC software, this is nowadays not a limitation for samples with narrow and broad distributions. An average molecular weight is assigned to each time slice and it is *assumed* for computational purposes that each time slice is *monodisperse* in molecular weight. A table is constructed with one row assigned to each time slice i and containing values for retention volume, area A_i, cumulative area, molecular weight M_i, A_i/M_i, and $A_i \times M_i$. The area of each slice is assumed to represent the

mole fraction N_i (or number fraction) of each mondisperse species in Figure 10. The moments of the distribution, and hence the average molecular weights, can then be calculated:

$$\text{Number average } M_n = \frac{\sum A_i}{\sum A_i / M_i} \tag{23}$$

$$\text{Weight average } M_w = \frac{\sum A_i M_i}{\sum A_i} \tag{24}$$

$$z \text{ average } M_z = \frac{\sum A_i M_i^2}{\sum A_i M_i} \tag{25}$$

When light scattering detection is employed, M_i can be measured instantaneously for each slice in the chromatogram.

Calibration Methods. In the absence of a light scattering detector, the calculation of MWD and average molecular weights from an experimental chromatogram necessitates the determination of the relationship

$$\log M = f(V_R) \tag{26}$$

or, for a constant flow rate through the system

$$\log M = f(t_R) \tag{27}$$

where t_R is retention time. Thus, a value of molecular weight can be assigned to each eluting slice based on its retention time or volume, and the MWD can be calculated. To achieve this, the column set used for the analysis must be calibrated, most commonly using a series of narrow polydispersity, well-defined polymer standards to establish the relationship. Narrow polydispersity standards, where M_w/M_n is typically less than 1.1, are available in a reasonably wide range of polymer types for both organic and aqueous SEC, for example, polystyrene, poly(methyl methacrylate), poly(ethylene oxide), and polysaccharide. Such standards must be characterized using a combination of techniques including SEC, since it is the peak molecular weight of the standard (M_{peak}) that should be plotted against peak retention time. Because of the relatively high efficiency of modern SEC columns and the narrow polydispersity of the calibrants, several standards are usually chromatographed together to save time, as illustrated in the upper part of Figure 11. This gives a conventional SEC calibration curve relating molecular weight to retention time for that specific polymeric calibrant type, as shown in the lower part of Figure 11, and in the application of this curve any molecular weight values calculated for unknown polymer samples must be quoted as relative values.

If narrow polydispersity polymer standards are not available for the polymer type under investigation, a calibration can still be established by applying the principle of universal calibration. For a chromatographic system containing a

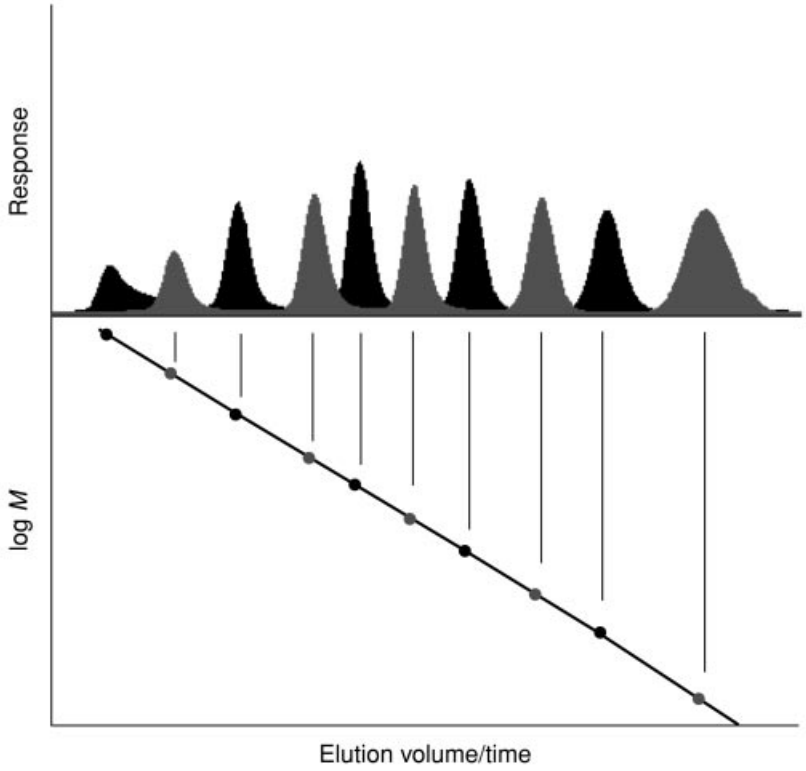

Fig. 11. Separation of narrow polymer standards of low polydispersity, and subsequent SEC calibration plot.

viscosity detector, an on-line measurement of intrinsic viscosity can be determined for any polymer type, and hence be converted to a calibration of log M_p against V_R according to equation 10. Alternatively, this approach can be modified by incorporating constants from the Mark–Houwink relation represented by equation 4, and by rearranging equation 10 it can be shown that

$$\log M_p = \left[\left(1+a_{ps}\right) / \left(1+a_p\right) \right] \log M_{ps} + \left[1/\left(1+a_p\right)\right] \log \left(K_{ps}/K_p\right) \qquad (28)$$

Values for the Mark–Houwink parameters K and a have been tabulated (14), and should be utilized where the solvent and temperature are appropriate. If only a value for M_n for a sample is required, then the method proposed by Goldwasser (32) can be applicable. This method requires the establishment of a universal calibration curve in conjunction with a viscometric detector without the need for a concentration detector or Mark–Houwink constants.

Software packages include calibration methods based on well-characterized reference materials with an MWD that may be somewhat broader than a narrow standard or with polydispersities exceeding 1.5. For calibrants with $M_w/M_n < 1.5$,

M_{peak} is close to M_w or M_v, which can be used in plotting the calibration curve, whereas for $M_w/M_n > 1.5$ search methods are required to generate a calibration curve over the range of M for the reference material (20).

BIBLIOGRAPHY

"Chromatography" in *EPST* Ist ed., Vol. 3, pp. 731–745, by P. M. Kamath and L. Wild, U.S. Industrial Chemicals, Co.; "Chromatography" in *EPSE* 2nd ed., Vol. 3, pp. 491–531, by J. F. Johnson, The University of Connecticut at Storrs.

1. L. H. Peebles, *Molecular Weight Distributions in Polymers*, Wiley-Interscience, New York, 1971.
2. A. R. Cooper, ed., *Determination of Molecular Weight*, Wiley-Interscience, New York, 1989.
3. M. J. R. Cantow, ed., *Polymer Fractionation*, Academic Press, New York, 1967.
4. L. H. Tung, ed., *Fractionation of Synthetic Polymers: Principles and Practices*, Marcel Dekker, Inc., New York, 1977.
5. J. V. Dawkins, in R. Epton, ed., *Chromatography of Synthetic and Biological Polymers*, Vol. **1**, Ellis Horwood Limited, Chichester, U.K., 1978, p. 30.
6. J. Porath and P. Flodin, *Nature (London)* **183**, 1657 (1959).
7. J. C. Moore, *J. Polym. Sci., Part A* **2**, 835 (1964).
8. L. E. Maley, *J. Polym. Sci., Part C* **8**, 253 (1965).
9. W. W. Yau, J. J. Kirkland, and D. D. Bly, *Modern Size-Exclusion Liquid Chromatography*, Wiley-Interscience, New York, 1979.
10. J. Janca, ed., *Steric Exclusion Liquid Chromatography of Polymers*, Marcel Dekker, Inc., New York, 1984.
11. B. J. Hunt and S. R. Holding, eds., *Size Exclusion Chromatography*, Blackie, Glasgow, U.K., 1989.
12. P. L. Dubin, ed., *Aqueous Size Exclusion Chromatography*, Elsevier Science, Amsterdam, 1988.
13. C.-S. Wu, ed., *Handbook of Size Exclusion Chromatography*, Marcel Dekker, Inc., New York, 1995.
14. S. Mori and H. G. Barth, *Size Exclusion Chromatography*, Springer, Berlin, 1999.
15. E. F. Casassa, *J. Phys. Chem.* **75**, 3929 (1971).
16. J. C. Giddings, E. Kucera, C. P. Russell, and M. N. Myers, *J. Phys. Chem.* **72**, 4397 (1968).
17. M. E. Van Kreveld and N. Van Der Hoed, *J. Chromatogr.* **83**, 111 (1973).
18. E. F. Casassa, *Macromolecules* **9**, 182 (1976).
19. Z. Grubisic, P. Rempp, and H. Benoit, *J. Polym. Sci., Polym. Lett. Ed.* **5**, 753 (1967).
20. J. V. Dawkins, in J. Janca, ed., *Steric Exclusion Liquid Chromatography of Polymers*, Marcel Dekker, Inc., New York, 1984, pp. 53–116.
21. C. M. Gomez, R. Garcia, I. Recalde, A. Codoner, and A. Campos, *Int. J. Polym. Anal. Character.* **6**, 365 (2001).
22. J. V. Dawkins and M. Hemming, *Makromol. Chem.* **176**, 1795 (1975).
23. J. V. Dawkins, *J. Polym. Sci., Polym. Chem. Ed.* **14**, 569 (1976).
24. J. C. Giddings, *Anal. Chem.* **39**, 1027 (1967).
25. J. C. Giddings, *Dynamics of Chromatography, Part 1: Principles and Theory*, Marcel Dekker, Inc., New York, 1965.
26. J. V. Dawkins and G. Yeadon, *Faraday Symp.* **15**, 127 (1980).
27. J. V. Dawkins and G. Yeadon, *J. Chromatogr.* **206**, 215 (1981).

28. E. Meehan, in Ref. 13, pp. 25–46.
29. E. Meehan, *LC-GC Int.* **5**(11), 32 (1992).
30. S. R. Holding and E. Meehan, Rapra Review Report 83, Rapra Technology Ltd., Shawbury, U.K., 1995.
31. S. T. Balke, *Quantitative Column Liquid Chromatography*, Elsevier Science, Amsterdam, 1984.
32. J. M. Goldwasser, *Am. Chem. Soc. Symp. Ser.* **521**, 243 1993.

JOHN V. DAWKINS
Loughborough University
ELIZABETH MEEHAN
Polymer Laboratories Limited

COATING METHODS, SURVEY

Introduction

Coating process technology is in widespread use because there are few single materials that are suitable for the intended final use without treating the surface (1–7) to meet all the functional needs and requirements of the product. The modification is accomplished by applying a coating or series of coatings to the material—the substrate—to improve its performance and make it more suitable for use, or to give it different characteristics. The coating process is defined here as replacing the air at a substrate with a new material—the coating.

Typical coatings are the paints and the diverse surface coatings used to protect houses, bridges, appliances, automobiles, etc. These coatings protect the surface from corrosion and degradation, and may provide other functional advantages such as making the materials waterproof or flameproof, and improving the appearance. Adhesives are applied to paper or plastic to produce labels and tapes for a variety of uses. A thin layer of adhesive is coated onto paper to produce self-sticking note pads. Glass windows are coated with a variety of materials to make them stronger and to control light penetration into the structure. High energy lithium batteries contain coated structures. Plastic food wrap has layers to reduce oxygen penetration and retain moisture for the product to retain its freshness. Packaging materials for electronic products are coated with antistatic compounds to protect the sensitive components. Other important coated products are photographic films for medical, industrial, graphic arts, and consumer use; optical and magnetic media for audio and visual use data storage; printing plates; and glossy paper for magazines.

Encyclopedia of Polymer Science and Technology. Copyright John Wiley & Sons, Inc. All rights reserved.

Several industries are based on coating process technology. Printing itself is a coating process, and much of the paper used in the printing industry had previously been coated to improve its gloss, strength, and ink acceptability. Lithographic printing plates for printing presses are photosensitive coatings on aluminum. Photographic film, itself a coated product, is used to expose the plates, set the type, and prepare the printed pictures. The entertainment industry uses magnetic tape, silver halide film, and coated optical disks to record the material for distribution to the consumer. The electronics industry uses coated products such as photoresist films to fabricate circuit boards and to add functionality to the circuit boards. The computer industry stores information on coated magnetic structures such as hard drives and floppy disks.

Coating Machines

The basic steps in continuously producing a coated structure are

(1) preparing the coating solution or dispersion
(2) unwinding the roll of substrate
(3) transporting it through the coater
(4) applying the coating from a solvent, or as a liquid to be cross-linked, or from the vapor
(5) drying or solidifying the coating
(6) winding the final coated roll
(7) converting the product to the final size and shape needed

Other operations that are often used are

(1) surface treatment of the substrate to improve adhesion
(2) cleaning of the substrate prior to coating, to reduce contamination
(3) lamination, where a protective cover sheet is added to the coating structure.

Different types of machinery are used to produce coated products. Depending on the substrate, they can be web coaters, sheet coaters, and coaters for nonflat applications. Web coaters, the most prevalent, coat onto continuous webs of material. Magnetic tapes, window films, wallpaper; barrier coatings for plastic films, and many printed goods are all produced using this process. A typical web coater with all the process steps is shown in Figure 1.

These machines are commercially available in sizes from pilot coaters using narrow webs, 6–24 in. wide, and running at low speeds, 10–50 ft/min, to production machines using wide webs, over 5 ft wide and coating at 500–5000 ft/min. A typical pilot coater is shown in Figure 2.

Sheet coaters are available to coat individual sheets. Many printing operations and all copying machines are sheet-fed. Sheet coaters are also used as laboratory coaters to develop new products where many different solutions need to be coated and only small volumes of sample are available. These methods use a variety of devices such as draw-down blades, dies, or wire-wound rods to spread

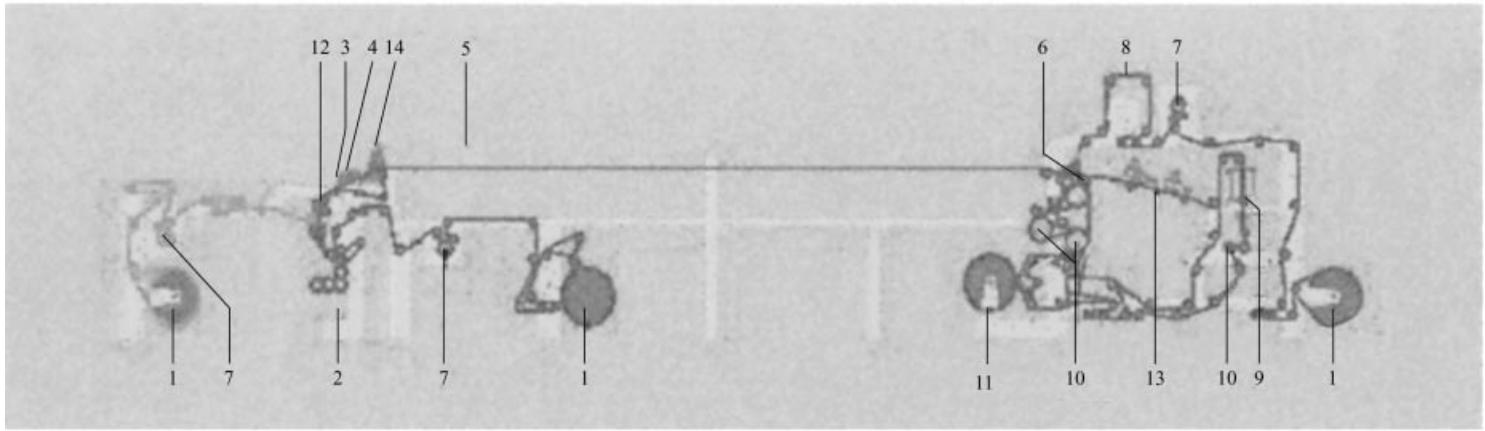

1. Unwinder
2. Coating unit
3. Infrared lamp (short wave)
4. Infrared lamp (medium wave)
5. Air floatation dryer
6. Dry laminating station
7. Corona station
8. Edge guide unit
9. Remoisturising station
10. Cooling station
11. Rewinder
12. Wet laminating station
13. Uv curing unit
14. Curtain coater

Fig. 1. Coating line showing components. Courtesy of Polytype America Corp.

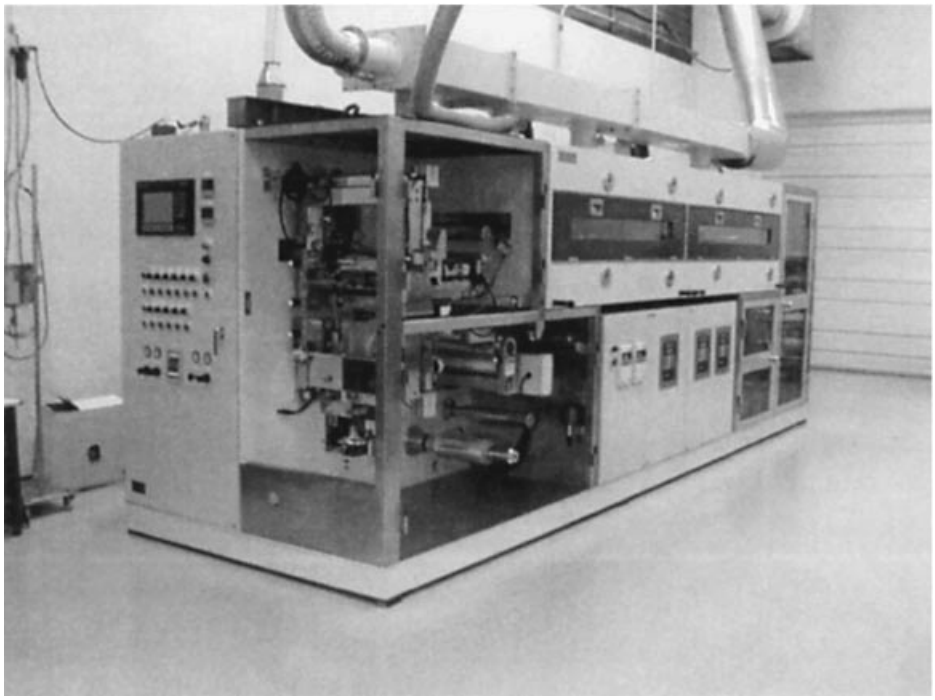

Fig. 2. Pilot coater. Courtesy of Texmax, Inc.

a uniform layer of solution across the web. Most applicators can provide wet coverages of 0.2–50 mil (5–1270 μm). Spray coaters may also be used to coat sheets. The coated webs or sheets are then dried by ambient air or in an oven. Laboratory automated sheet coaters are available. These give better reproducibility and control but are more expensive than hand applicators. They can be coupled to feed directly into dryers, with the temperature and residence time controlled, as shown in Figure 3.

Fig. 3. Laboratory bench-top coater. Courtesy of Werner Mathis.

In nonweb applications the coating is applied to a specific part at the end of the fabrication process. The part is usually three-dimensional and of varying shape. Automobiles, appliances, and steel structures all have the coating applied to the individual items as they are being built. It should be noted that many smaller steel items are made from prepainted sheet steel.

Coating Processes

The application of a liquid to a traveling web or substrate is accomplished by one of the many coating methods. Widely used commercial coating methods are reverse roll, wire-wound or Mayer rod, direct and offset gravure, slot die, blade, hot melt, curtain, knife over roll, extrusion, air knife, spray, rotary screen, multilayer slide, coextrusion, meniscus, comma and microgravure coaters (based on analysis of methods reported by coaters in various trade sources). Each of these has many designs and hardware arrangements leading to many specific coating configurations. Powder coating is covered in the article Coating Methods, Powder Technology.

The choice of the method depends on the nature of the support to be coated, the rheology of the coating fluid, the solvent, the wet-coating weight or coverage desired, the needed coating uniformity, the desired coating width and speed; the number of layers to be coated simultaneously, cost considerations, environmental considerations, and whether the coating is to be continuous or intermittent.

The method should be chosen based on the specific requirements. Often a method is selected based on the availability of a specific coating applicator, even though it may not be the best choice. All applicators can apply a coating at some conditions. Much time and money can be wasted by trying to make the product by a process that is not suitable. The coating window may be too narrow at the conditions selected, or it may be impossible to ever obtain a quality coating. The successful process will provide defect-free film over a wide range of conditions. A process that works well at low speeds in the laboratory may not be appropriate for a manufacturing plant coating at high speeds, and conversely, a high speed coating process may not be appropriate for laboratory trials.

The first step in the selection proces is to establish the requirements for the product to be coated. These requirements are then matched with the capabilites of the process and the best methods are evaluated experimentally to determine the one to use. Some of the basic characteristics of the principal coating processes are listed in Table 1.

The processes are grouped according to the principle used to control the coverage or coating weight of the coating and its resulting uniformity. We have three groupings, but there are no generally accepted definitions of the terminology we use: self-metered, premetered and hybrid. Self-metered processes are those in which the coverage is a function of the liquid properties and the system geometry, the web speed, the roll speeds, and any doctoring device. Examples are dip coating in which viscosity and web-speed control coverage, and blade and air knife coating in which excess is applied and then removed. Premetered processes deliver a set flow rate of solution per unit width to the applicator and all the material is transferred to the web. If a smooth coating is obtained then the coverage is fixed.

Table 1. Summary of Coating Methods[a]

Process	Viscosity, mPa·s (=cP)	No. of layers	Wet thickness, μm	Coating accuracy, %	Max. speed, m/min
Self-metered					
Rod	20–1000	1	5–50	10	250
Dip	20–1000	1	5–100	10	150
Forward roll	20–1000	1	10–200	8	150
Reverse roll	100–50,000	1	5–400	5	400
Air knife	5–500	1	2–40	5	500
Knife over roll	100–50,000	1	25–750	10	150
Blade	500–40,000	1	25–750	7	1500
Premetered					
Slot	5–20,000	1–3	15–250	2	500
Extrusion	50,000–5,000,000	1–3	15–750	5	700
Slide	5–500	1–18	15–250	2	300
Curtain	5–500	1–18	2–500	2	300
Hybrid					
Gravure, direct	1–5000	1	1–25	2	700
Gravure, offset	100–50,000	1	5–400	5	300
Microgravure	1–4000	1	1–40	2	100

[a]Values given are only guidelines.

Hybrid processes use features of both self- and premetered coating to achieve coating weight control. Gravure is an example of this method. The cell transfer determines coverage but doctoring is used to remove excess fluid from the gravure cylinder.

In most coating operations a single layer is coated. When more than one layer must be applied one can make multiple passes, or use tandem coaters where the next layer is applied at another coating station immediately following the dryer section for the previous layer, or a multilayer coating station can be used. Slot, extrusion, slide, and curtain coaters are used to apply multiple layers simultaneously. Slide and curtain coaters can apply an unlimited number of layers simultaneously, whereas slot coaters are limited by the complexity of the die internals and extrusion coaters by the ability of the combining adapter, ahead of the extrusion die, to handle many layers.

The precision or uniformity of the coating is very important for some products such as photographic or magnetic coatings. Some processes are better suited for precise control of coverage. When properly designed, slot, slide, curtain, gravure, and reverse-roll coaters are able to maintain coverage uniformity to within 2%. In many of the other coating processes the coverage control may be only 10%. Table 1 lists generally accepted attainable control.

The substrates or support coated on include paper and paper board, cellophane, poly(ethylene terephthalate), poly(ethylene naphthalate), polyethylene, polypropylene, polystyrene, poly(vinyl chloride), poly(vinyl fluoride), poly(vinylidene fluoride), polyimide, metal foils, woven and nonwoven fabrics, fibers, and metal coils. The surfaces of these supports can be impervious as in plastic films, or there may be a pore structure such as in paper. Primer coatings

may be applied to seal these pores to give a uniform surface for the coating and to improve adhesion. The surfaces can also be modified with surface treatments such as flame treatment, plasma treatment, or corona discharge. These treatments increase the surface energy, thereby improving wetability and adhesion.

The web coating process can be used for intermittent coatings, such as in the printing process and to form coated batteries, as well as for the more common continuous coatings such as photographic films. In general, there is an ideal coater arrangement for any given product. However, most coating machines produce many different products and coating thickness and the machine is therefore usually a compromise made for the several applications.

Limits of Coatability. In any coating process there is a maximum coating speed above which coating does not occur. At higher speeds air is entrained, resulting in many bubbles in the coating, or in ribs and finally rivulets, or in wet and dry patches. In slot coating below a critical speed, to coat thinner often means to coat slower. Above the critical speed the minimum thickness depends only on the gap. Above some higher speed a coating cannot be made (5). Using bead vacuum, thinner coatings can be obtained. Similar effects were found in slide coating, except the critical speed is never reached (6). The maximum coating speed in slide coating for thick coatings, where no bead vacuum or electrostatic assist is used, is identical to the velocity of air entrainment for a tape plunging into a pool of coating fluid. Lower viscosity liquids can be coated faster and thinner. Polymer solutions can be coated at higher speeds than Newtonian liquids. These phenomena have been explained in terms of a balance of forces acting on the coating bead, ie, the coating liquid in the region where it first makes contact with the web (7). Stabilizing forces are mainly bead vacuum or electrostatic assist, if used. The destabilizing forces are primarily the drag force on the coating liquid and the momentum of the air film carried along by the web. Thus, with no bead vacuum or electrostatic assist, there is a net destabilizing force which is balanced by the cohesive strength of the liquid. Limits of coatability occur in all coating operations but under different conditions in each process. A good description of the window of coatability in slot coating can be found in Reference 8.

The air entrainment velocity for plunging tapes does not depend on the wettability of the surface, but does increase with surface roughness (9,10). Presumably the rough surface lets air that would otherwise be entrained escape in the valleys between the peaks that are covered with coating liquid (11). In the converting industry, which involves coatings on rough and porous paper surfaces, much higher (up to 25 m/s) coating speeds can be attained than in photographic coatings on smooth plastic films. Although the wettability itself plays little or no role in coatability, it does play an extremely important role in coating. On a nonwetting surface, immediately after coating, the fluid will dewet and ball up into distinct islands.

Knife and Blade Coatings. Knife and blade coatings are in many ways similar. In both cases the knife or the blade doctors off excess coating that has been put on the web. Knives are usually held perpendicular to the web, whereas blades are usually tilted so that they form an acute angle with the incoming web. Typically blades are thin, only 0.2–0.5 mm thick, and can be rigid or flexible (of spring steel). Knives are thicker and are always rigid. Blades, being thinner, wear faster and have to be changed relatively often, perhaps two to four times a

day. Blades are always pressed against the web, which is supported by a backing roll either made of chrome-plated steel or rubber-covered. Knives may be pressed against web on a rubber-covered backing roll; they may be pressed against the unsupported web which is held taut by the tension in the web; or they may be held at a fixed gap from the web that is supported by a backing roll.

The ends of the knives can be square, beveled or rounded. If the end is square and parallel to the web, if the upstream face is perpendicular to the web, and if there is a fixed gap between the end of the knife and the web, then the wet coverage is exactly one-half the gap. On the other hand, if there is a low angle in a converging section of the knife or of the blade, leading up to a tight gap as there is for many knives and for all bent blades, then strong hydrodynamic forces build up and tend to lift the knife or blade away from the web. This forces more fluid under the knife or blade, so that the coated thickness is greater than half the gap.

In all cases of knife and blade coatings, except in knife coating at a fixed gap, a rigid member and a flexible member are pressed together. The flexible member can deflect to allow for nonuniformities in the web. In knife coating and beveled blade coating, the knife or blade is rigid, and the unsupported web or the web on a rubber-covered roll is flexible. In bent blade coating the blade is flexible and the web on the roll is rigid or relatively rigid as in the case of a rubber-covered roll. Knife coating against unsupported web is more difficult to control than the other knife- and blade-coating techniques because, here, the web tension is a very important variable.

The simplest and least expensive, but still effective, coating method is knife coating, either against a backing roll or on unsupported web. Coating against a backing roll is more accurate, as it is independent of web tension. The knife, held perpendicular to the web, acts as a doctor blade and removes excess coating liquid. The coating can be applied by any convenient method, such as with an applicator roll, or by pumping the fluid into a pool formed by the web, the knife, and two end dams. The control of the coverage is by proper positioning of the knife. The unsupported knife shown in Figure 4a is used for coating open fabric webs where coating penetration is desired or cannot be prevented. A full width endless belt can be used to support a weak web and pull it through the knife area without tearing so as to overcome the drag of the knife.

The knife over roll coater (Fig. 4b) is probably the most common of the knife coaters. It is simple and compact. The driven back-up roll may be precision-made

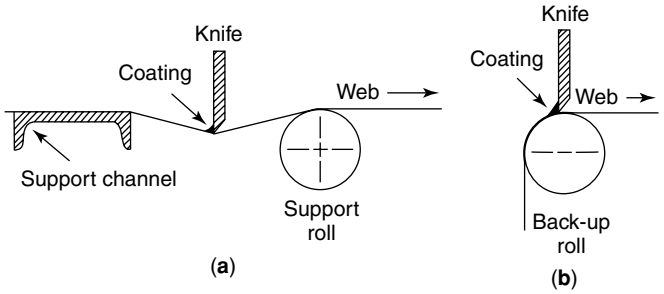

Fig. 4. (**a**) Unsupported knife; (**b**) knife over roll.

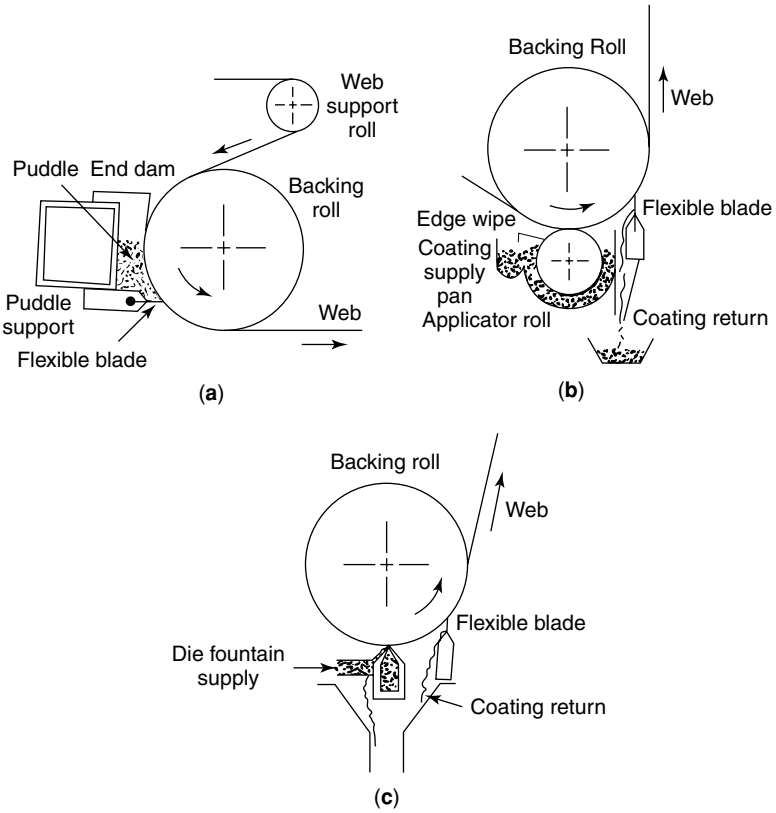

Fig. 5. (**a**) Puddle coater; (**b**) roll applicator blade coater; (**c**) fountain blade coater.

and chrome-plated, having a controlled gap between the web and the knife. The backing roll may also be rubber-covered, the knife pressing against the web. Here the coating weight is determined by the pressure against the knife. Higher pressures give lower coating weights.

Knife coaters can apply high coverages, up to 2.5-mm wet, and can handle high viscosities, up to 100,000 mPa·s (=cP). They tend to level rough surfaces rather than give a uniform coverage, a characteristic that can be desirable or not depending on the needs of the finished coating. Streaks and scratches are hard to avoid, especially using high viscosity liquids.

Blade Coating. Flexible blade coaters can be used either with a downward moving web, as shown in Figure 5a, or with an upward moving web, as shown in Figure 5b. As with knife coaters there are many ways of feeding the metering blade. A puddle behind the blade is shown in Figure 5a, a forward turning applicator roll in Figure 5b, and a slot applicator or die fountain in Figure 5c. Jet fountains, where the coating liquid spurts out to the web 25–50 mm away, are occasionally used.

Blade coaters are commonly used on pigmented coatings. They have the unique feature of troweling in the low areas in a paper web, thus producing a coated surface that has excellent smoothness and printing qualities. The backing

roll is usually covered with resilient material and is driven at the same speed as the web to stabilize the web and draw it past the blade. A replaceable blade is rigidly clamped at one end and the unsupported end is forced against the substrate. The wet coverage is adjusted by varying blade thickness, the blade angle, and the force pushing the blade against the substrate. The force on the blade can be obtained by various means: a rubber tube between the blade and a rigid member can be inflated with varying air pressures or the blade holder can be rotated so as to apply a greater or lesser force at the tip, while keeping constant the angle the blade tip makes with the web.

As the force on the blade increases, and as the force is concentrated at the blade tip, the wet coverage decreases rapidly. However, further increases in force bend the blade and a larger area of the blade presses the liquid against the web. Increasing the loading of the blade then causes the tip to lift up and the coverage now increases. At further increases in load the coverage again decreases.

The beveled blade coater uses a rigid blade held at an angle of 40–55° to the web. The end of the blade is parallel to the substrate and pressed against it. If initially the end of the blade is not parallel to the web, it soon is as a result of abrasion by the pigmented fluid. When the loading on the blade increases, the wet coverage decreases. With the same force but using a thicker blade, the pressure, or force per unit area, on the coating fluid between the blade and the web decreases and the coverage increases.

In the rod–blade coater unit, a rod is mounted at the end of the blade. This coater behaves more like the beveled blade coater than a flexible blade coater.

Two-Blade Coaters. In order to coat both sides of a web simultaneously, two flexible blade coaters can be used back-to-back, ie, with both blades pressing against each other and the web between them. The web usually travels vertically upward. Different coatings can be applied on each side of the web. The blades tend to be thinner and more flexible than the standard blades and the angle to the web is lower. The web has to have sufficient tensile strength to be pulled through the nip.

Simultaneous coatings can also be made with one flexible blade against the web on the roll, where the web moves downward. On one side the coating fluid is supplied to a puddle in front of the blade, and on the other side the fluid is carried into the nip by the roll. Edge dams between the web and the blade and between the web and the roll keep the fluid contained. The roll may rotate faster than the web. Figure 6 shows a version where the fluid on the roll side is supplied by a transfer roll.

Air-Knife Coater. The air-knife coater is a versatile coating process in use for a wide range of products. A coating pan and roll are used to apply the coating solution and then an air knife is positioned after the pan to regulate the final wet-coating weight by applying a focused jet of air to the web. The excess solution is collected in an overflow pan and can be either recirculated and used again or scrapped. The air knife can function either in the precision or in the squeegee mode. These give very different types of coating and performance characteristics, although the same name is used for both processes.

In the precision mode, the air knife uses low pressures and doctors off some of the coating to control the coating weight and to level the surface to give a uniform coating of reasonable quality. The coating weight is a function of web

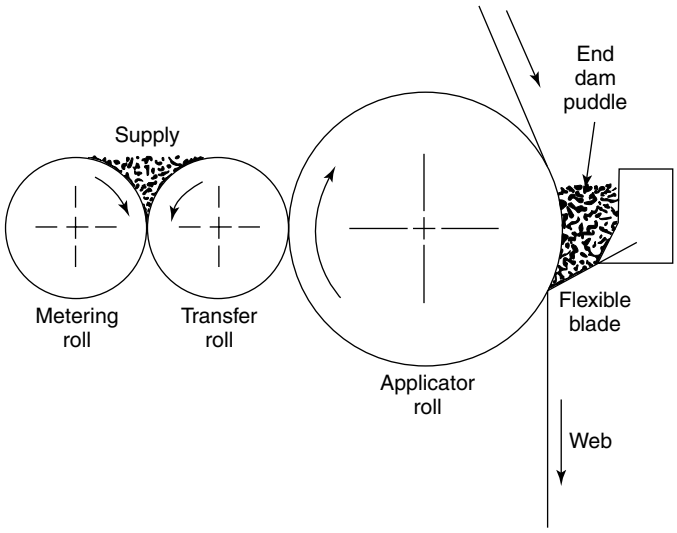

Fig. 6. Billblade with transfer rolls.

speed, viscosity of solution, surface tension, and air-knife pressure. This precision mode has been used to coat photographic films where the air velocities are 13–130 m/min and air pressures are 50–2500 Pa (0.2–10 in. of water) to give 1- to 200-μm wet thickness.

In the squeegee mode, the air knife operates at much higher pressures and coating speeds than in the precision mode and effectively doctors off the majority of the coating. This process is used for porous supports, such as paper, where the coating is absorbed into the voids. After the air knife, which effectively functions as a leveling device, the coating solids remain in the voids and in a thin surface layer.

The advantages of the air-knife process are low initial cost, versatility for coating a variety of webs and solutions, ease of changing and maintaining the coating, and the good coating quality. The disadvantages are the noise and contamination problems created by the air stream and the resulting spray, solution viscosity limitations, a somewhat restricted coating weight range, and the high cost to operate the air blowers.

Wire-Wound Rod Coating. The wire-wound rod coater shown in Figure 7, called a Mayer rod, meters off excess applied coating solution. The rod is often rotated to increase its life by causing even wear and to prevent particles from getting caught under the rod and causing streaks. Normal rotation is in the reverse direction to the web travel. The wire size controls the coating weight. As the rod has an undulating surface because of the wire, one would expect the coating to have a similar unevenness. However, the down-web lines that form are frequently spaced at other than the wire diameter and are due to ribbing. If the solution is not self-leveling, a smoothing rod may be used to smooth out the surface. Rod coaters are best used with low viscosity liquids.

From the geometry of the wire-wound rod, one would expect the wet thickness to be 10.7% of the wire diameter. It is frequently less. It has been shown that with

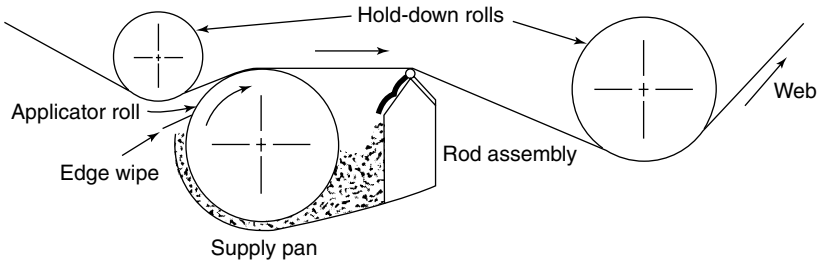

Fig. 7. Wire-wound rod coater.

increasing load on the rod the wet thickness decreases to about 7% of the wire diameter (11).

Rod coaters are commonly used for low solids, low viscosity coatings such as those used to coat adhesives and barrier layers on poly(vinylidene chloride) carbon paper and silicone release papers. Coating weights range from 1.5–10 g/m^2, and speeds are as high as 300 m/min. The wire-wound rod can be held against unsupported web, as shown in Figure 6, or against a backing roll. When used against unsupported web the web tension affects the coverage. Coating rods are compact, simple, and inexpensive, but wear rapidly when used with abrasive fluids.

Roll Coating.

Meniscus or Bead-Roll Coater. One of the simplest and most widely used coaters is the meniscus or bead-roll coater (Fig. 8). In this process the web passes over a backup roll that is just above the liquid level in a pan. A meniscus or coating bead is formed between the web and the coating solution by raising the pan, and the solution transfers to the web. The coverage is determined by the viscosity of the solution and the coating speed. The pan design is very critical and a variety of configurations are available. The coating speed is very slow, only about 10 m/min on low viscosity liquids. High quality optical coatings may be produced. These coaters have also been used for adhesives.

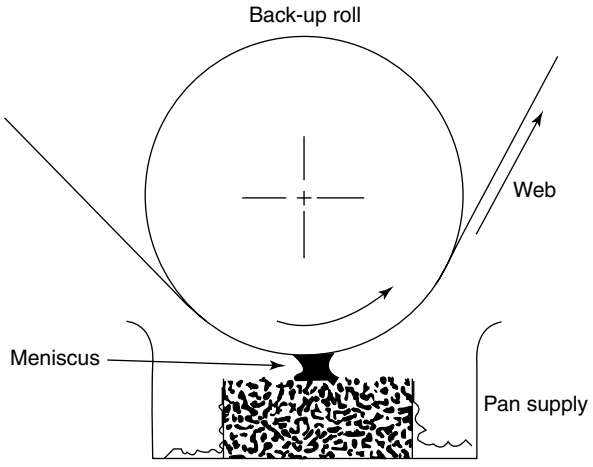

Fig. 8. Pan-type Meniscus coater.

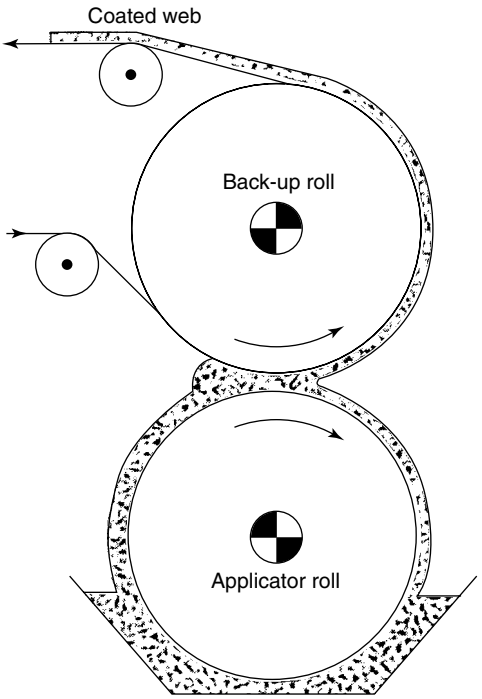

Fig. 9. Two-roll forward-roll coater (12).

Kiss Coaters. In kiss coating fluid is transferred from a rotating applicator roll, called a kiss roll, to unsupported web. There are many types of kiss coaters. The kiss roll can turn in the direction of the web or in the reverse direction, but usually operates in the web direction. Kiss coaters are tension sensitive and are often used to apply excess coating prior to a metering device.

Forward-Roll Coaters. In forward-roll coating the web passes between two rolls rotating in the same direction, the applicator roll and the backing roll. The applicator roll drags fluid into the nip, as shown in Figure 9 (12). The fluid exiting the nip splits in two, with some adhering to the web and some to the applicator roll. One might expect that if both rolls are rotating at the same surface speeds, then the fluid between them should move at that same speed and the flow rate per unit width through the nip, q, would equal the product of the surface speed, U, and the gap in the nip, G. Actually it is more than this because of the buildup of pressure as the fluid approaches the nip, which produces a greater flow. The dimensionless flow rate γ is defined as the ratio of the actual flow rate per unit width to GU, the "expected" value, or

$$\gamma = \frac{q}{GU}$$

where U is now the average surface speed of the two rolls. The dimensionless flow rate is approximately equal to 1.3 to 0.5, depending upon conditions.

Each roll carries away some of the flow. The ratio of film thickness on the two rolls, t_2/t_1, depends on the speed ratio, and for Newtonian fluids is

$$t_2/t_1 = (U_2/U_1)^{0.65}$$

where the subscript 1 corresponds to the web and the subscript 2 to the applicator roll. The total flow through the gap per unit width, q, is equal to the sum of the flow on the web, t_1U_1, and that on the exit side of the applicator roll, t_2U_2. With shear-thinning fluids, when the roll speeds differ the split is more symmetrical than the equation indicates.

In forward-roll coating it is fairly common to have an instability called *ribbing*, where the coating thickness varies sinusoidally across the web and the coating looks as if a giant comb were dragged down the wet coating. Ribbing occurs when the *capillary number*, Ca, the ratio of viscous to surface forces, exceeds a certain value, depending on the gap-to-diameter ratio. The capillary number is

$$Ca = \eta U/\sigma$$

where U is the average surface speed of the two rolls, η is the viscosity of the coating fluid, and σ is the surface tension.

It is very difficult to avoid ribbing in forward-roll coating. When the fluid is not self-leveling, a smoothing bar is often used to smooth out the ribs. It has been found that a fine wire or thread stretched across the gap exit and touching the liquid eliminates ribbing (10).

Reverse-Roll Coating. Reverse-roll coating is an extremely versatile coating method and can give a very uniform, defect-free coating (12–1200 μm thick) at a very wide range of coating speeds, using coating fluids with viscosities ranging from low to extremely high. In reverse-roll coating, the coating fluid is applied to the applicator roll by any of a number of techniques, such as having the applicator roll rotate in a pan of fluid, using a fountain roll or a fountain or slot die. The excess fluid is then metered off by a reverse-turning metering roll and the remaining fluid is completely transferred to the web traveling in the reverse direction. Two of the many possible configurations are shown in Figure 10.

All the flow remaining on the applicator roll after it rotates past the metering roll is transferred to the web; therefore it is important to know what this flow is. The thickness of the metered coating on the applicator roll, t_a, is found to be a function of the gap, of the ratio of the speed of the metering roll to that of the applicator roll, and of the capillary number based on the applicator roll speed (Fig. 11).

In reverse-roll coating, as in forward-roll coating, instabilities can form. However, it is possible to obtain defect-free coatings at high coating speeds. Sometimes increasing the speed can lead to a smooth coating when a ribbing condition is present.

Another defect, called cascade or seashore, can form in reverse-roll coating. This defect is caused by the entrapment of air under certain conditions and can appear in the metered flow on the applicator roll. An operability diagram, showing the region of stable flow as well as the regions where these defects form, is given in Figure 12 for two gaps. The region where stable coatings can be made is at

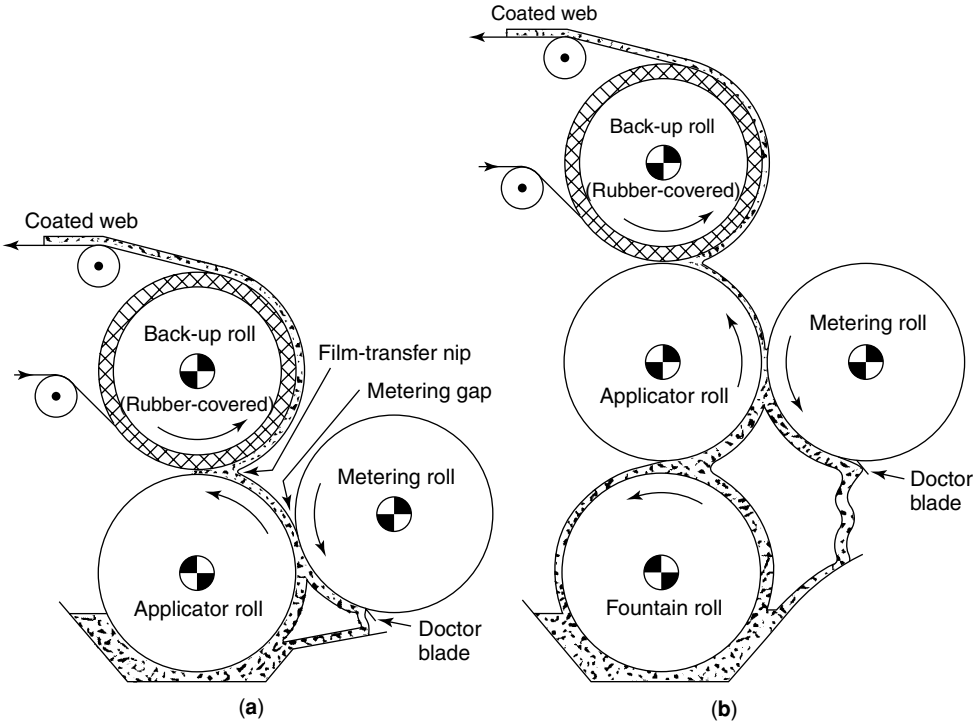

Fig. 10. Pan-fed reverse-roll coaters: (**a**) three roll; (**b**) four roll (12).

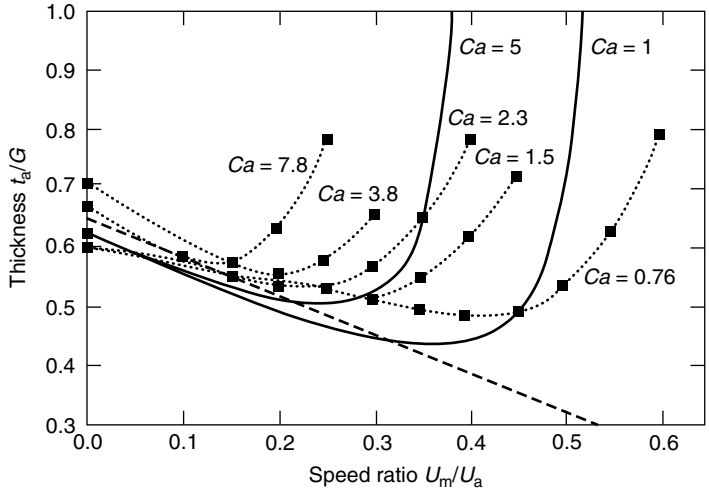

Fig. 11. Reverse-roll, metered film thickness on the applicator roll divided by gap, t_a/G, as a function of the ratio of the metering roll speed U_m to applicator roll speed U_a for various capillary numbers based on U_a. (—) represents theoretical values; (· · ·) experimental ones; and (- - -) is the lubrication model (12).

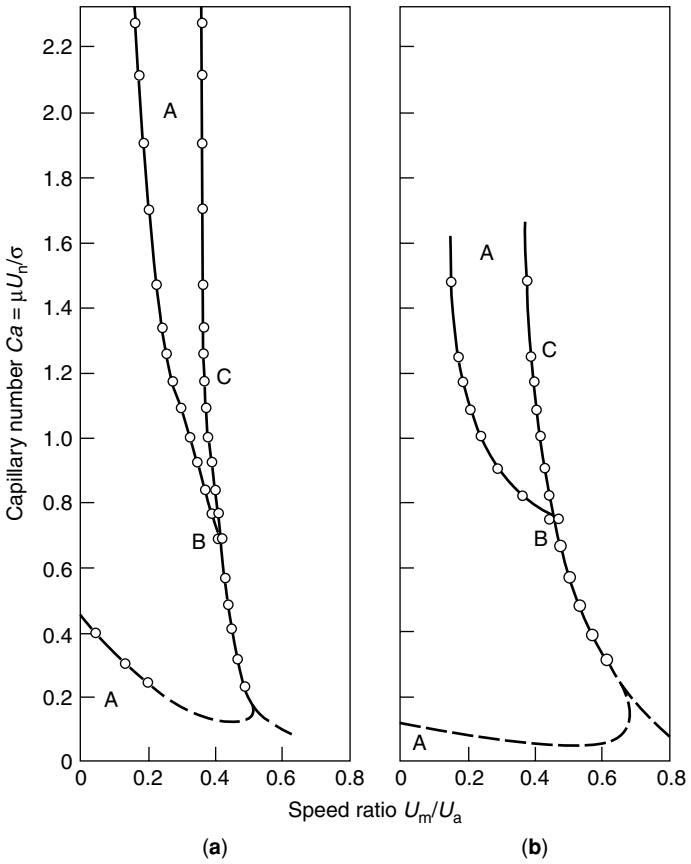

Fig. 12. Operability diagram for reverse-roll coating, where A represents a stable coatings area; B, ribbing; and C, cascade; for (**a**) a gap $G = 750$ μm and (**b**) a gap $G = 250$ μm (12).

high capillary numbers, ie, at high speeds. There is also a stable region at very low speeds, but low speeds are not usually desirable. The principal advantage of reverse-roll coating is that conditions can be adjusted to give a stable, defect-free coating at high coating speeds. Using precision bearings, reverse-roll coaters can lay down as uniform a coating as any coating process, about $\pm 2\%$.

Gravure Coating. Gravure coating is an accurate way of coating thin (1- to 25-μm wet coverage) layers of low [10–5000 mPa·s (=cP)] viscosity liquids. The coating liquid is picked up by a patterned chrome-plated roll, the excess doctored off and the liquid transferred from the filled cells to the web. Figure 13 illustrates two types of gravure coaters. In direct gravure the liquid is transferred directly from the gravure roll to the web. In offset gravure the liquid in the cells is first transferred to a rubber-covered offset roll before the final transfer to the web. In reverse gravure the gravure roll or the offset roll turns in the reverse direction with respect to the web. In differential gravure the forward rotating gravure cylinder runs at a different speed than the backing or impression roll. However, the web does not have to be held against a backing or impression roll; it can also be

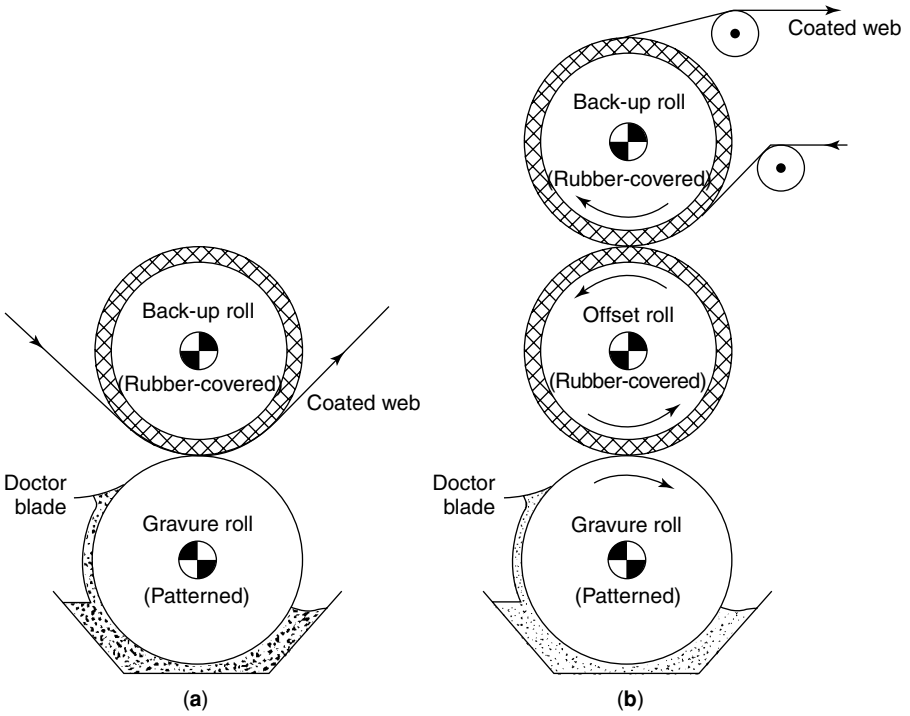

Fig. 13. Gravure coaters (**a**) direct; (**b**) offset (12).

unsupported, as in kiss coating. The coating liquid can be applied to the gravure roll by a number of methods, not just by the pan-fed system illustrated.

The three common cell patterns for the gravure cylinder are illustrated in Figure 14. The pyramidal and quadrangular cells are similar, except that the quadrangular has a flat, not a pointed, bottom in order to empty easier. The trihelical pattern consists of continuous grooves spiraling around the roll, usually at a 45° angle. The volume factor is the total cell volume per unit area, and has units of height, typically ranging from 4 to 300 μm. The fraction of the cell volume that transfers varies greatly, depending on the system. With high impression roll pressures, about 58% of the cell volume normally transfers. The cell pitch or count is the number of cells per centimeter measured perpendicular to the pattern and usually ranges from 4 to 160 cm^{-1}. The pattern is made by mechanical engraving, chemical etching, electromechanical engraving, or laser etching.

After the gravure cylinder is coated with coating liquid, the excess is doctored off, normally using a 01- to 0.4-mm spring steel blade. Usually the doctor blade makes a 55–70° angle with the incoming gravure roll surface and is oscillated 6–50 mm to give even wear and to dislodge dirt that could cause streaks. A reverse-angle doctor blade can also be used. It often makes an angle of 65–90° with the exiting surface. This blade does not have to be loaded against the cylinder face because fluid forces press the blade against the surface, and so the reverse blade can be made of softer materials, such as bronze or plastic. There is no need to oscillate

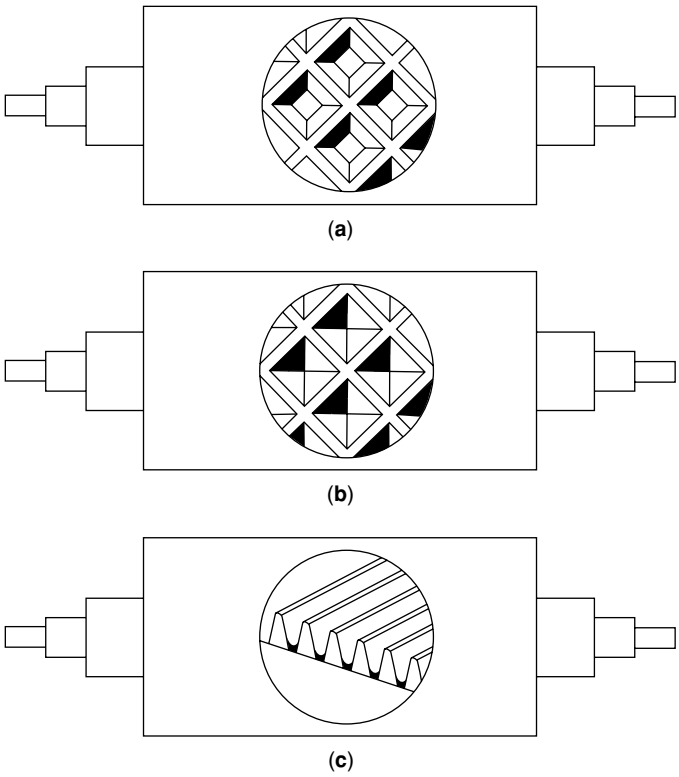

Fig. 14. Common cell patterns in gravure coating: (**a**) quadrangle; (**b**) pyramid; and (**c**) trihelical (2).

this blade because in this position it cannot trap dirt; however, the standard blade is felt to do a better job of doctoring.

As with the flexible-blade coater, a softer doctor blade or one having a lower loading and an almost smooth cylinder with a shallow pattern allows excess liquid to pass through. A stiff, highly loaded blade against a cylinder having a large volume factor (cell volume per unit area) wipes the surface clean. The gravure roll has to be heavily loaded against the backup or impression roll in order to achieve good transfer to the web. The usual force is about 2000–20,000 N/m.

The most important factor in determining the transfer or web pickup is the gravure pattern design. The cell pitch controls the stability of web pickup. The leveling of the coating can be a problem. Large spacing between cells often results in printing of the cell pattern, rather than a uniform coating. Reverse and differential gravure tend to give better leveling. A smoothing bar can also be used.

A very useful new gravure coating technique is the Micro-gravure™ technique, which was introduced in the early 1990s. It is intended for low coating weight products on light gauge films for imaging, electronics, packaging, batteries, and other specialty applications. The unique features are the use of small diameter rolls, 20–50 mm versus 150–300 mm for conventional gravure. This results in a small stable bead, which when combined with reverse application gives very good quality and a low coating weight. A typical configuration is shown in Figure 15.

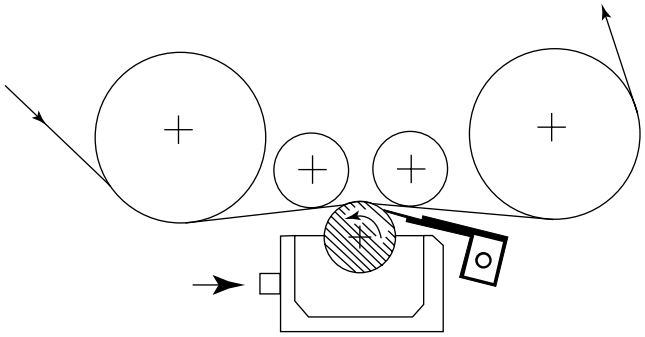

Fig. 15. Side view sketch of Micro-Gravure™ coating head. Courtesy of Yasui-Seikei.

Dip Coating. Dip coating is one of the oldest coating methods in use. Using continuous webs, the web passes under an applicator roll partially submerged in a pan of the coating fluid. The web is thus actually dipped into the coating solution. A doctor blade may be used to remove excess fluid if a reduction in the wet coating weight is desired. Otherwise the coverage is determined by coating speed and the characteristics of the liquid. The coverage increases with increasing viscosity and coating speed. Surface tension has a relatively small effect.

Dip coating is very commonly used for coating continuous objects that are not flat, such as fibers and for irregularly shaped discrete objects. Drops of coating at the bottom of dip-coated articles may be removed by applying electrostatic forces as the article is moved along a conveyor.

Extrusion. Extrusion coating and slot coating are in principle very similar. In extrusion coating a high viscosity material, often a polymer melt, is forced out of the slot of the coating die onto a substrate where it is cooled to form a solid coating. As can be seen in Figure 16a, the highly viscous liquid does not wet the lips of the die. Similarly in slot coating, a relatively low viscosity liquid, usually under several thousand mPa·s (=cP), often a polymer solution, is forced out of the slot and onto the web. In slot coating the coating liquid does wet the lips of the die, as shown in Figure 16b. Some engineers use the terms slot coating and extrusion coating interchangeably.

Extrusion coating is often used in food packaging where vapor and oxygen barriers are required and heat sealability is desired. The expanding food packaging industry is the direct result of packaging improvements that can be attained from improving the surface and physical characteristics of a flexible web by extrusion coating.

Because of the high viscosities involved in extrusion coating, the coating die and the auxiliary equipment are massive. An extruder is needed to heat and melt the thermoplastic polymer, the die is heated by electric heaters, and the die also contains adjusting bolts every 10 cm or so across the width that control the lip openings to try and obtain a uniform cross-web coverage. Internal choker bars controlled by bolts may also be used to adjust the uniformity. The bolts may be computer controlled. There may also be a laminating station to combine the plastic sheet with a substrate and to cool the laminate. The plastic may leave the die at about 175°C and may be about 0.5 mm thick. It is then elongated by

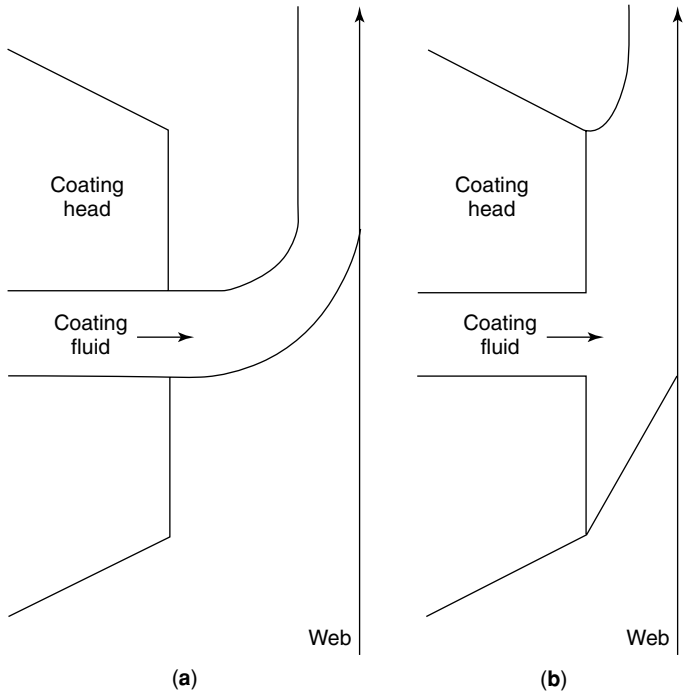

Fig. 16. Comparison of (**a**) extrusion coating and (**b**) slot coating.

the pulling effect of the faster-moving substrate which it joins in the pressure nip in the laminating section. The elongation reduces the width of the extruded film by perhaps 2–6 cm and reduces film thickness to approximately 12–25 μm before it makes contact with the substrate.

Good temperature control of the plastic and pressure control ahead of the coating die is important to the success of the coating. Variations in temperature lead to irregularities in the coating thickness both in the machine direction and across the web. Thickness variations in the cross-web direction can be reduced by adjusting the slot opening via the adjusting bolts and use of choker bars. The extruded film width is adjustable by external deckles to block off the exit of the die. In the laminator the nip helps to promote bonding, before chilling the molten plastic. The driven chill roll is chromium or nickel plated and can have a mirror, matte or an embossed surface. Once the extruded film passes through the laminating nip, it takes on the finish of the chill roll. The chill roll is 60–90 cm in diameter with perhaps a 120° wrap and utilizes refrigerated water to reduce the film temperature to about 65°C before the film is stripped. To improve adhesion of the extruded film to the substrate, adhesion-promoting "primers" are usually applied to the web before the laminator. Priming can be electrostatic (corona treatment), chemical, or in the form of ozone treatment. Coating weights are controlled by the line and extruder speeds, but in many cases the chill roll capacity limits the maximum thickness that can be obtained. Extrusion coating lines operate at speeds up to 1000 m/min and can apply 10–30 g/m^2 of coating.

Slot Coating. Slot coating (Fig. 16b) involves a relatively low viscosity fluid, under perhaps 10,000 mPa·s (=cP) and uses much simpler equipment than extrusion coating. An ordinary pump or a pressurized vessel feeds the fluid through a flow meter and control valve to the coating die, which often operates at room temperature. If heating is required, water flowing through internal channels is usually adequate. Because of the simple rheologies of the fluids, the die can be designed to give uniform flow across the width with no adjustments. In fact, an adjustable die should be avoided. It is not difficult to design the die to give uniform flow, but it is very difficult to make the exactly correct adjustments. Because the viscosity is relatively low the pressures within the die are also relatively low, and the die can be much less massive than an extrusion die and still withstand the spreading forces.

Normally the web is supported by the backing roll in slot coating. However, for very thin coatings, under about 15-μm wet, the gap between the coating lips and the web becomes very tight, under about 100 μm, and the system becomes difficult to control and operate. The runout of the bearings can become a significant fraction of the gap. Dirt can hang up in the gap to cause streaks. If the web contacts the coating die the web can tear, causing a shutdown of the operation. Coating against unsupported or tensioned web should be used for very thin coatings. In this case web tension becomes an important variable.

In slot coating, bead vacuum is often used to increase the window of coatability, that is to allow thinner coatings and perhaps to allow coatings at higher speeds. A vacuum box is placed under the coating die and a vacuum of up to about 1000 Pa (4 in. of water) is pulled by a vacuum fan. Higher vacuums may be needed for higher viscosity liquids. There should be a tight vacuum seal against the sides or ends of the rotating backing roll, but no rubbing contact where the web enters the vacuum chamber in order to prevent scratches. The air in the vacuum chamber can resonate as in a musical instrument. These pressure fluctuations can cause chatter at wide gaps. The air leakage should be kept as small as possible to reduce the amplitude of the pressure fluctuations.

Curtain Coating. Curtain coating is used to deliver coating liquid in a falling sheet or curtain to the substrate, which moves through the curtain at the coating speed. In one version a slot coating head is aimed downward and the coating emerges as a falling film or sheet as seen in Figure 17. The curtain thickness is controlled by the feed rate and by precise adjustments of the slot opening. The vertical distance of the coating die above the substrate can be adjusted. The falling curtain is protected from stray air movements by transparent enclosure sheets. Coating thicknesses as low as 12 μm are possible when coating with lacquers or with low viscosity wax melts, and are as low as 20 μm with hot-melt compositions of higher viscosity. There is no problem in obtaining heavier coating coverages.

Air-bubble entrapment may occur in the case of a gravity-applied continuous coating over an impermeable substrate. Bubbles may also be caused by moisture vaporization from the substrate. Remelting of the coating may minimize the bubble defects. Curtain-coating equipment of this design is capable of operation at substrate speeds up to 500 m/min.

Curtain-coating equipment is also available in which the falling curtain is generated by overflow from an open weir. The coating is delivered to the open weir uniformly across its width by a pipe having diffuser jet openings. As the coating

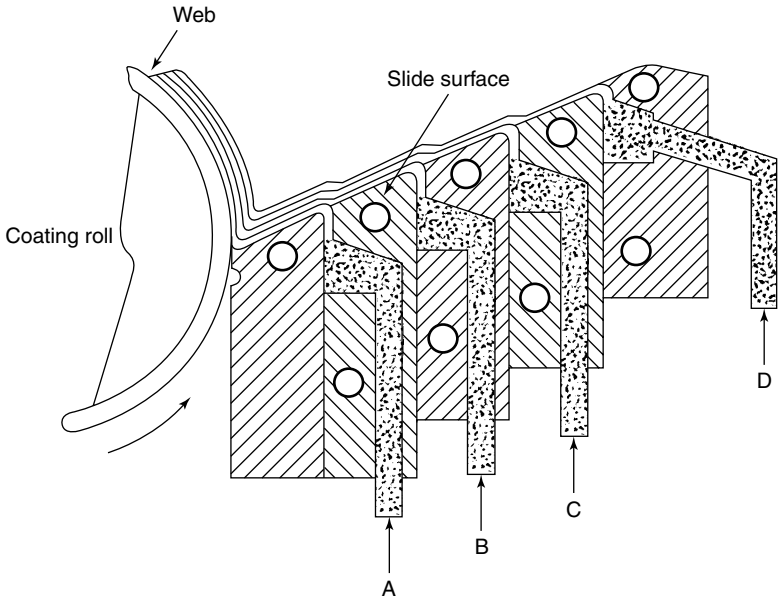

Fig. 17. A slide coater where A, B, C, and D correspond to the inlets for the liquids for layers 1, 2, 3, and the top layer, respectively (8,13).

overflows the low side of the weir, it travels down a short flat skirt before dropping. The thickness of the falling curtain is adjusted by precise control of the rate of delivery of coating to the weir. Hot-melt coatings can also be applied by the open weir, as in the slot die. Because there is no close restriction to flow as in the slot die, the open weir does not tend to form scratches or coating streaks because of crusting or coating hang-up in the slot opening. When applying hot-melt coating formulations the coating supply is held in a reservoir at a temperature that does not thermally degrade the material during its residence. The coating is brought to this temperature using heat exchangers as it is pumped to the weir. Weir-type equipment is recommended for operation at substrate speeds up to 400 m/min. The coating fluid not carried away on the coated surface falls into a collection trough for recirculation.

Curtain coating is adaptable for coating irregularly sized sheets such as slotted cut-out corrugated carton blanks or sheets of plywood, as well as for continuous substrates. Coatings may also be applied to uneven geometric shapes such as blocks. The principal limitation of curtain coating is that a high flow rate of about 0.5–1.5 $cm^3/(s \cdot cm$ width) is needed to maintain an intact curtain. Usually about double this minimum is desirable. Thus, to obtain a thin coating, high coating speeds are required. Curtain coating is inherently a high speed process and the curtain will not form at low speeds or flow rates.

Multilayer Methods

Slide Coating. Slide coating is the primary method for simultaneously coating a multilayer structure. A slide coater, illustrated in Figure 17, can coat an

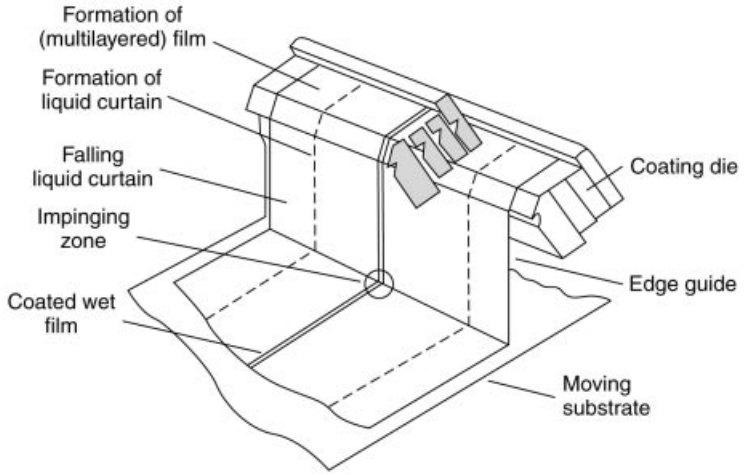

Fig. 18. Curtain-coating apparatus (13).

unlimited number of top layers, 18 or more, simultaneously. Each layer flows out onto the slide yet does not mix with the other layers as they all flow together down the slide, across the gap, and onto the web, all in laminar motion. Slide coating is extensively used in coating photographic films and papers, both color and black and white. In color films, nine or more layers are coated simultaneously.

Instabilities can form on the slide in the form of interfacial waves, which may disturb the desired laminar flow and cause mixing. The closer the physical properties of all the layers are, the closer the system resembles a single layer in which internal waves do not form. The densities of the individual layers are always reasonably close to each other, and are usually not subject to control. The viscosities of adjacent layers should generally not vary by too much (14). It has been suggested that to avoid these waves the ratio of the viscosity of a layer to that of the adjacent lower layer should be more than 0.7 and less than 1.5 or 2 (15). However, if the ratio is above 10, waves again do not form. The bottom layer should have the lowest viscosity to reduce drag forces and allow higher coating speeds.

As with slot coating, a slight vacuum (up to 1 kPa for the usual low viscosity fluids) under the coating bead aids in coating by allowing thinner coatings and higher coating speeds. The bottom edge of the slide should be sharp and have a small radius of curvature, no more than about 50 μm or so, to pin the bottom meniscus and reduce the chance of cross-web barring or chatter.

Precision Multilayer Curtain. A variation of curtain coating can also be used to produce multilayer coatings. A slide is used to generate the multilayer structure which then flows over an added lip of the die to form a curtain. Edge guides are used to prevent the curtain from necking in because of surface tension. For precision coating the curtain has to be completely uniform across the width. Precision multilayer curtain coating is used to coat color photographic materials. This is illustrated in Figure 18. In most precision coatings the curtain is narrower than the web.

Slot Coating. Multiple layers can be coated simultaneously from a slot-coating die with multiple slots. The layers come together in the coating bead to form the final coating. Multiple layers in slot coating work well, but the die internals are complicated, especially when more than two layers are involved. This technique is particularly useful for coating of organic solvent systems, since the enclosed bead minimizes evaporation.

Extrusion Coating. In the most popular method of multilayer extrusion coating, the several layers come together before the coating die in a combining adapter or block, and then exit as one stream into the extrusion die (see EXTRUSION). The extrusion die is a standard single layer die, except that the feed port is rectangular to match the dimensions of the rectangular sandwich formed in the combining adapter. The separate layers remain distinct in the combining adapter and in the die. As long as the viscosity ratios are no greater than about 3:1 under processing conditions, the layer uniformity should be acceptable.

Multilayer extrusion provides the unique capability of producing layers of different resins to give superior functional properties. For example, an inexpensive resin can be used as the core of a three-ply extrudate, the outer plies being more expensive but also much thinner than if extruded alone (see COEXTRUSION).

Discrete Surface-Coating Methods

A variety of coating techniques are available to coat surfaces which are planar and have irregular surfaces.

Spray Coating. Coatings may be applied by spraying the coating material onto the object to be coated, which may be irregularly shaped with compound curves and with sharp edges. Many coating powders of suitable dielectric constant may be electrically polarized so that the powders are attracted to a grounded or oppositely charged surface. The object may then be heated to fuse the powders into a continuous film.

Dip Coating. The dip-coating technique described for webs can also be used to coat discrete surfaces such as toys and automotive parts. The item to be coated is suspended from a conveyor and dipped into the coating solution. The item is then removed; the coating drains and then levels to give the desired coverage. The object is then dried or cured in an oven.

Spin Coating. Spin coating is used to produce a thin uniform coating on discrete supports. In this process the coating fluid, usually a colloidal suspension, is placed on a horizontal substrate which rests on a rotating platform. The speed of the platform is increased to the desired level, which can be as high as 10,000 rpm. Centrifugal forces drive much of the coating off the support, leaving a thin, uniform film behind. In addition, the coating is drying during the process and as a result the viscosity increases, resistance to flow occurs, and a level thin coating is left. The coating chamber can provide hot air to the coating to dry or cure the remaining film. Additional coatings of different coating materials can be applied to develop a multilayer structure. This process is used to coat structures such as photomasks, magnetic disks, optical coatings, and a variety of layered products in the microelectronics industry.

Vacuum Deposition Techniques. Thin coatings are applied to a variety of substrates for use on semiconductors, ceramics, and electrooptical devices, using a wide variety of vacuum deposition techniques. Vacuum deposition is a rapidly advancing area of coating technology. In these processes the support to be coated is placed in a vacuum chamber which contains the coating material. Typically the coating material is a metal such as aluminum, gold, or tungsten. A high vacuum is then pulled; electrical energy or an electron beam is applied to heat the metal which evaporates off to deposit on the substrate. In sputtering, an ion beam is used to knock off atoms of the metal at lower temperatures. Individual supports, such as a target to be examined in a scanning electron microscope, or a continuous web, such as in making metallized poly(ethylene terephthalate), can be used. The coatings can be continuous, or patterns or electrical circuits can be made if the support is masked.

There are several vacuum processes such as physical vapor deposition, chemical vapor deposition, sputtering, and anodic vacuum arc deposition. Materials other than metals, such as tetraethylorthosilicate, silane, and titanium aluminum nitride, can also be applied.

Patch Coating

It is sometimes necessary to coat patches of material on a web, such as coating the anode and cathode in batteries and in fuel cell membranes (Fig. 19). With these products an uncoated border is required around the coating to prevent a short circuit. Gravure coating is well suited for this purpose because the desired pattern can be etched into the gravure cylinder. Slot-coating techniques are also used (16). With slot coating there is the problem, however, of nonuniform coverage at the start and end of the patch, and the thicker edges along the sides. The start and end problems may be minimized by carefully controlling the flow with pumps and valves.

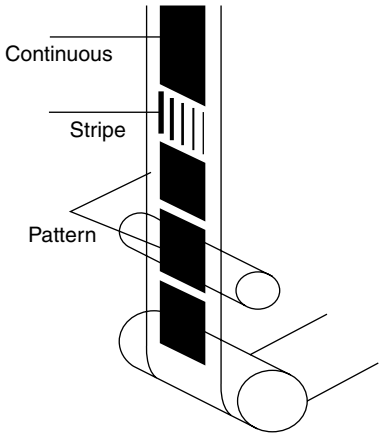

Fig. 19. Patch coating.

Coating Process Mechanisms

One of the principal advances in the coating process area in the 1980–1990s was the development of techniques to understand and define basic coatings mechanisms. This has led to improved quality and a wider range of utility for most coating techniques. This has involved the computer modeling of the coating process and the development of visualization techniques to actually see the flows in the coating process. The flow patterns predicted by the computer models can be verified by the visualization techniques.

Free surfaces and interfaces make the physics of coating flow systems extremely difficult to model by classical mathematical methods. As a result, coater designs and parameter ranges for defect-free coating have traditionally been determined through expensive and time-consuming statistical experimentation. Therefore coating developed largely as an art rather than a science. The ability to model the coating process by using modern methods of numerical and functional analysis, and to explain many of the complex mechanisms of coating instabilities and the resulting defects, is thus refreshing.

The most successful models are based on the finite element method. The flow is discretized into small subregions (elements) and mass and force balances are applied at each node. The result is a large system of equations, the solution of which usually gives the velocity and pressure of the coating liquid in each element and the location of the unknown free surfaces. The smaller the elements, the more the equations, which are often in the range from 10,000 to upwards of 100,000.

It is now possible to simulate steady transversely uniform flows of Newtonian or non-Newtonian liquids by using commercially available software packages such as FIDAP, NEKTON, FLUENT, PHOENICS, and POLYFLOW. Using these codes it is possible to locate regions of flow recirculation that may cause coating defects as a result of the increased residence time of solution. The free-surface handling capabilities of currently available commercial codes are limited to relatively simple steady flows and the transient response to specified transversely uniform disturbances. For a steady uniform flow to exist in nature, however, it should be able to recover from all small disturbances, such as building vibrations and the molecular fluctuations that are always present. Flow instabilities resulting in defects such as ribbing cannot be predicted by commercial software. Using more advanced methods developed first at the University of Minnesota and now in widespread use (17–20), it is now possible to predict most coating flow instabilities including bead break-up, flooding, cross-web barring (chatter), down-web ribbing, and diagonal chatter. It is also possible to follow the longtime development of the resulting defects and to explore parameter ranges of stable, defect-free operation (coating windows) at a fraction of the cost of the actual physical experiments. In a computer model the geometry can be quickly changed without having to construct expensive new parts. Considerable time and cost savings can be realized by optimizing coating systems computationally.

Experimental techniques to visualize flows have been extensively used to define fluid flow in pipes and air flow over lift and control surface of airplanes. More recently this technology has been applied to the coating process and it is now possible to visualize the flow streamlines (15,21). The dimensions of the flow field are small, and the flow patterns both along the flow and inside the flow are important. Specialized techniques involve generating small hydrogen bubbles

using fine electrodes and injecting dyes in the regions of interest; optical sectioning is then required to observe and to photograph these flows.

A stereo zoom microscope having a very small depth of field and a clear window on the side of the applicator is employed. Fiber optic cables may be used for remote viewing. Accurate control of the light level and position is needed to reduce reflections that may mask the details of the flow field. The microscope is focused at varying points and flow nonuniformities are recorded. Using this technique, air entrainment, flow recirculation in the bead, curtain-coating formation, and the teapot effect have all been visualized for many types of slot, slide, and curtain coatings. This information leads to an improved understanding of the coating process. The same technology can also be applied to many other types of coating.

Drying and Solidification

The coating solution after application is in the liquid state and must be solidified. For coating with solvents, including water, this is brought about by removing the solvent, ie, drying. The drying process after the application of the coating is as important as the coating process itself. The properties of the coating are not complete until solidification has occurred. The coated film or web is transported through the dryer where the properties of the coating can either be enhanced or deteriorated by the drying process. Drying of coatings involves the removal of the inert inactive solvent used to suspend, dissolve, or disperse the active ingredients of the coating, which include polymeric binder, pigments, dyes, slip agents, hardener, coating aids, etc. Coating solvents range from the easy-to-handle water to flammable and toxic organic materials. Drying must occur without adversely affecting the coating formulation while maintaining the desired physical uniformity of the coating.

For polymer melts and for certain materials that gel on cooling, such as gelatin solutions, the temperature is lowered to solidify the coatings. With gelatin gels drying is still necessary. Similar hardware can be used for both heating and evaporation and for cooling, since they are both heat transfer devices.

While drying is a physical process involving only solvent removal, solidification can occur by cross-linking liquid monomer or liquid low molecular weight polymer. This can be accelerated by catalysts or can be accomplished by an electron-beam or uv radiation. This cross-linking process is called *curing*. Material coated from solution often also undergoes curing to improve the physical properties of the dried coating. Thus both curing and drying may occur in the dryer. This takes place with aqueous gelatin coatings which are cured using aldehyde cross-linkers. The cross-linking starts in the dryer.

The dryer provides heat to volatilize the solvent and a means to carry the solvent away from the coating. Efficient hardware is used to minimize energy costs. The dryers may be equipped with the appropriate pollution abatement devices to meet both OSHA and EPA standards. Dryers commonly use hot air both to provide heat and to carry away the solvent. The air may be heated by steam or by heat exchange with flue gases. Flue gases from the combustion of natural gas may be used directly in place of hot air. Infrared radiant energy from gas combustion or electric resistance heaters is sometimes used. Conduction heat transfer from heated

drums is also used. The choice depends on availability of supply, the temperature range desired, and costs. Dryers can also use other sources of energy such as microwaves or radio-frequency waves. However, air is still needed to carry off the evaporating solvent. Radiant energy tends to be more expensive and is only used in special circumstances. If the coating can react with oxygen or if the solvents are flammable, inert gases such as nitrogen may be used in place of the air.

Because the evaporation of the solvent is an endothermic process, heat must be supplied to the system through conduction, convection, radiation, or a combination of these methods. The total energy flux into a unit area of coating, q_t, is the sum of the fluxes resulting from conduction, convection, and radiation.

Although heat transfer by conduction from heated drums is used extensively in the paper industry, convective heat transfer is very popular and used in most coating operations. Here the main focus is on convective heat transfer.

The rate of convective heating can be estimated as

$$q_{\text{convection}} = hA\Delta t$$

where A is the area (m^2), h is the heat-transfer coefficient [$W/(m^2 \cdot K)$], q is the rate of heat transfer (W), and Δt is the temperature difference between the hot gas and the coating (K).

The heat-transfer coefficient is a key property of the dryer. It is controlled by the nozzle geometry and spacing, the distance from the web, and the velocity of the air. The evaporation rate is the rate at which heat is supplied for evaporation (heat also goes into heating the coating and the web) divided by the latent heat of vaporization of the solvent.

Air Impingement Dryers. Air impingement dryers, the most widely used for drying coated webs, basically consist of a heat source and heat exchangers (unless hot flue gas from combustion of natural gas is used), fans to move the air, ducts and nozzles or air delivery devices positioned close to the web, and solvent removal ducts. If all the air is recirculated, then equipment to remove solvent from the air is also provided. Figure 20 shows a typical dryer. In addition, there are controls for the air temperature and the air velocity from the nozzles and, in some cases, for the solvent level in the drying air. There may also be controls to keep the solvent concentration well below the lower explosive unit. Dryers often have separate sections or zones where the air temperature and velocity (and perhaps solvent level) can be controlled independently.

The dryer must also transport the web through the dryer using a combination of driven and idler rolls. The web path can be either horizontal or vertical, or, with the appropriate web-turning devices, fold back upon itself to conserve space. The idler rolls in single-sided dryers should be spaced so that there is enough wrap for the web to turn the rolls, and the coating should be kept within the effective area of the nozzles. Sometimes the web slips on the idler rolls and gets scratched. To prevent this the idler rolls can be driven by tendency drives which have two sets of bearings. The axle is driven at approximately the speed of the web, and the roll idles at this speed on a separate set of bearings. The driven web then easily brings the roll to the exact speed of the web. Tendency drives are needed for light webs. Typically the web should be within six to seven nozzle slot widths of the impingement nozzles.

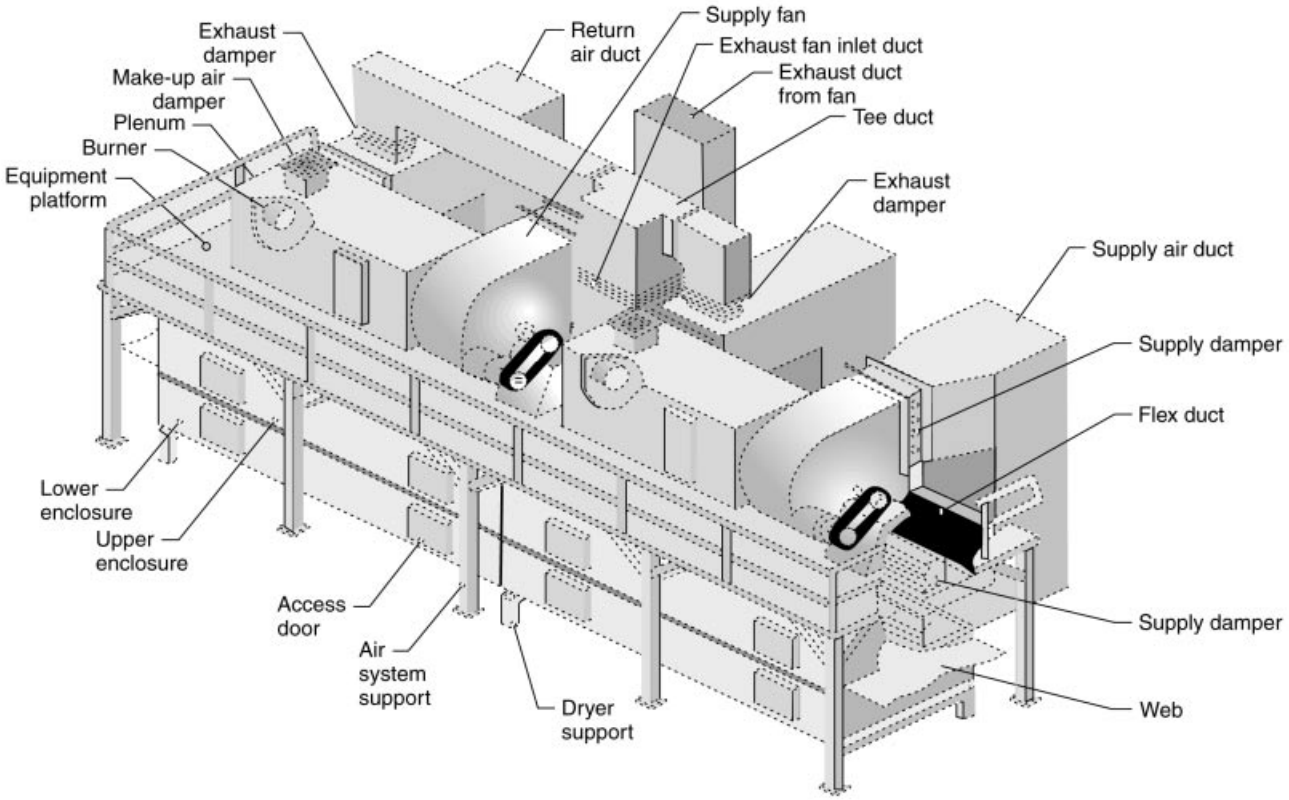

Fig. 20. Dryer components of a top mounted air system dryer. Courtesy of MEGTEC Systems.

In these single-sided dryers, the air impinges only on the coated side, heating and drying from that side only. The air can be delivered to the web from plenums with slots, with holes, or from specially designed nozzles. In a basic configuration the nozzles and idler rolls are contained in insulated boxes to minimize heat losses, solvent escape, and noise. The efficiency of the dryers depends on the heat transfer coefficient, the air usage, the temperatures used, and the solvent level. Wet coatings flow easily and the drying air should not disturb them.

The two-sided or floater dryer is now most often used. In this configuration the roll transport system in the dryer is replaced with air nozzles on the back side of the web so that the air transports and supports the web as well as heating and drying it from both sides. When impervious webs are used, while the heating is from both sides, the drying is only from the coated side. The two-sided heat transfer results in higher drying rates and thus shorter dryers, while eliminating problems of scratching from the idler rolls. However, more air is used.

Two types of floater nozzles are currently in use. One, based on the Bernoulli principle, is used in the airfoil flotation nozzles in which the air flows from the nozzle parallel to the web and the high velocities create a reduced pressure, which attracts the web while keeping it from touching the nozzles. The other uses the Coanda effect to create a flotation nozzle where the air is focused and follows the contours of surface of the air bar chamber, thus creating a pressure pad which supports the web, as shown in Figure 21.

Air flotation dryers have excellent heat-transfer coefficients, give very uniform drying across the web, and give excellent web stability. They can be used for a wide range of web types and tensions, and tend to be quieter, and thus pose less noise problems than the higher velocity single-sided dryers. Floater dryers are totally enclosed and compact so that they are clean and cause less dirt defects in the coating.

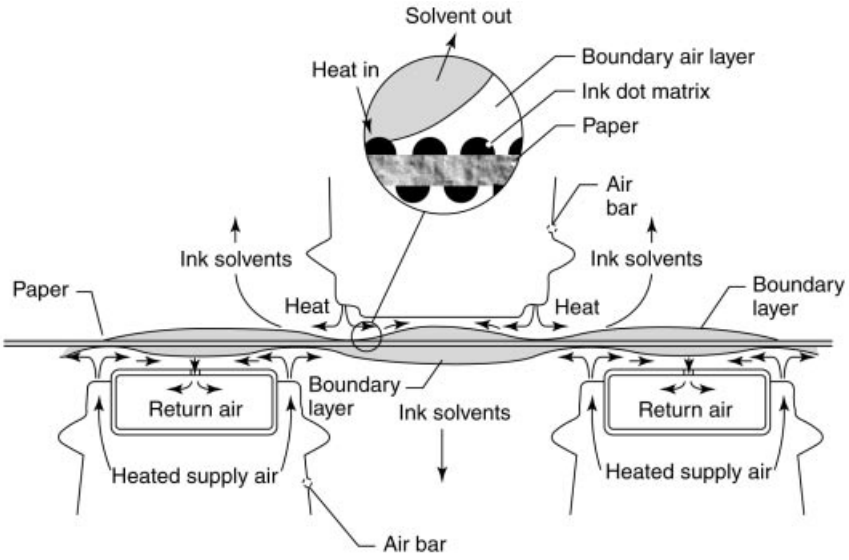

Fig. 21. Coanda effect air bars. Courtesy of MEGTEC Systems.

Single-sided dryer air velocities are 150–600 m/s, giving heat-transfer coefficients of 30–140 W/(m^2·K). Floater dryers operate at slightly lower (150–500 m/s) slot velocities, and have higher [50–275 W/(m^2·K)] heat-transfer coefficients based on the same single-sided web area.

Contact or Conduction Dryers. Coatings on webs, as well as sheets of newly formed paper, can be dried by direct contact with the surface of a hot drum. The drum is usually heated by steam. Here conduction is used to transfer the heat. Air still has to be supplied to carry away the solvent vapors. Drums can also be used to rapidly cool warm extruded films, to increase the viscosity, and to solidify the film.

Radiation Drying. Infrared or microwave radiation can supply concentrated energy to the web to evaporate the solvent, but air must still be used to carry away the solvent. These techniques provide a high heat input over short distances. Often Infrared is used in conjunction with convection dryers. It is often used at the start of drying to rapidly solidfy the coating, with the balance of drying done in convection oven. This can be cost efficient. Infrared heaters can be placed between the air nozzles. This increases the drying rate and thus the production rate without increasing the length of the dryer, and without requiring additonal air handling systems. Use of Infrared heating is most effective in the first sections of the dryer, in the constant rate period, where the coating is coolest and most of the added heat, including that by Infrared radiation, goes to evaporate the solvent. In the falling rate period in most cases the drying rate is the rate of diffusion of the solvent to the surface, which is influenced only by the temperature. Infrared heating can only raise the temperature faster, which usually has just a minor effect.

Pollution Control. The solvent removed during drying is frequently a pollutant and the exhaust air must be treated to ensure that it meets government standards before being discharged to the atmosphere. The two basic approaches to treating the air are to recover the solvent for reuse and to convert it by burning to compounds which can safely be discharged. The basic solvent recovery systems involve condensation or adsorption in a charcoal bed. After recovery the solvent needs to be purified before reuse. For combustion of the exhaust sovent both thermal and catalytic systems are used. Pollution control systems are an essential part of the drying process and are available from dryer manufacturers. One should reduce the amount of volatile solvents in the coating process by coating as concentrated a coating fluid as possible. One should also investigate changing to a water-based system.

Modeling Convection Drying. Models of the drying process have been developed to estimate whether a particular coating can dry under the conditions of an available dryer. These models can be run on personal computers.

To model convection drying in the constant rate period both the heat transfer to the coated web and the mass transfer from the coating must be considered. The heat-transfer coefficient can be taken as proportional to the 0.78 power of the air velocity or to the 0.39 power of the pressure difference between the air in the plenum and the ambient pressure at the coating. The improvement in heat-transfer coefficients in dryers since the 1900s is shown in Figure 22. The mass-transfer coefficient for solvent to the air stream is related to the heat-transfer coefficient by the Chilton–Colburn analogy (23,24):

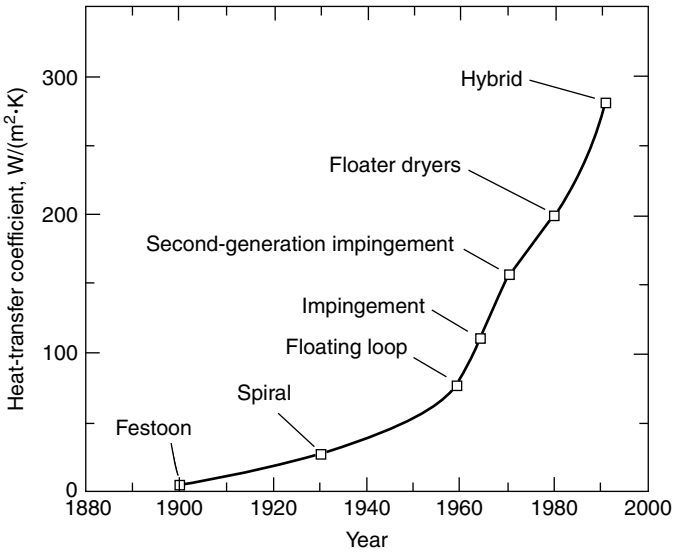

Fig. 22. Improvement in dryer heat-transfer coefficients over time (22). To convert W/(m^2·K) to Btu/(h·ft^2·°F), multiply by 0.176.

$$\frac{h}{\rho c_p k_m} = N_{Le}^{2/3}$$

where c_p is the heat capacity of the air [J/(kg·K)], h is the heat transfer-coefficient [W/(m^2·K)], k_m is the mass-transfer coefficient {kg/[s·m^2·(kg/m^3)]}, N_{Le} is the Lewis number, equal to the thermal diffusivity of the air divided by the mass diffusivity of solvent vapors in the air, and ρ is the density of the air (kg/m^3).

The total heat transfer to the coated web is then equated to the heat consumed by the evaporating solvent and the heat used in heating the web and the coating. This allows calculation of the temperature of the coated web (14,25). For single-sided drying, the equilibrium constant rate web temperature is the wet-bulb temperature of the air for that particular solvent. In the constant rate period of drying the coating behaves as if it were a pool of solvent. When dry patches appear on the surface, the rate of drying decreases and the falling rate period begins.

Modeling the falling rate period is more difficult, because the drying rate then depends on the mechanisms occurring within the coating. In coating on impervious webs the rate-limiting process is diffusion; in porous coatings and coatings on porous paper it may be capillary action. In aqueous coatings most of the drying occurs in the constant rate period; for organic solvent systems most of the drying occurs in the falling rate period, to the extent that in some cases the constant rate period is over before the coated web enters the dryer. In the falling rate period all the solvent that reaches the surface evaporates; thus the rate of diffusion to the surface is the rate of evaporation (if diffusion is the transport mechanism).

The higher the air temperature, the more rapid the drying. However, there are temperature limitations both for the web and for the coating. Plastic films should not be heated above their glass-transition temperature (the softening

Table 2. Coating Process Shear Rates

	Shear rate, s^{-1}
Coating	
Dip	10–100
Roll, reverse	1,000–100,000
Roll, forward	10–1,000
Spray	1,000–10,000
Slide	3,000–120,000
Gravure, reverse	40,000–1,000,000
Gravure, forward	10–1,000
Slot die	3,000–100,000
Curtain	10,000–1,000,000
Blade	20–40,000
Ancillary operations	
Simple mixing	0–100
High shear mixing	1,000–100.000
Measurement	
Brookfield	1–100
Haake	1–20,000
Cannon-Fenske glass	1–100

point) to prevent distortion and stretching. The coatings themselves may have a maximum temperature above which the coating may degrade. Many photographic coatings, for example, should not be heated above about 50°C.

Rheology. Rheology is the science of deformation and flow of matter. Because the coating process creates shear and extensional stresses in the coating fluid, the rheological properties of coating liquids are important factors in the selection and successful running of a coating operation. The coating hardware exposes the coating solution to a wide range of shear rates (Table 2). As a first approximation, the extensional rates would be of the same order as the shear rates. Shear and extension affect the properties of the solution. Therefore, the rheological properties, the deformation and flow under stress, are important factors in the selection and successful running of a coating operation.

The shear or dynamic viscosity is the ratio of shear stress to shear rate, and measures the resistance of the fluid to flow while undergoing shear. The common unit of viscosity is centipoise (cP). One cP is the same as 1 mPa·s. A high viscosity solution flows slowly. The shear rate is the rate of change of velocity with distance in the direction perpendicular to flow and can be crudely approximated by the coating speed divided by a coating gap. In coating flows it can reach values over 10^5 s^{-1}. In simple or Newtonian fluids the viscosity is a constant and does not change with shear rate. However, it is not constant in dilute polymer solutions, where the shape of the polymer molecules distort with shear. The spherical shape of a random coil becomes elongated in the direction of flow and so offers less resistance to flow. Thus the viscosity decreases with shear rate. At very low shear rates, such that the shape of the molecules has not yet changed, the viscosity is constant at its zero shear value. At high shear rates where the molecules are fully elongated, such that they cannot offer less resistance with increasing shear, the viscosity is again constant, now at its infinite shear value (assuming the molecule

is not destroyed by the mechanical forces). Almost all coating fluids contain dissolved polymers and are shear thinning.

Extensional or stretching flows are also very important in coating. The extensional viscosity is the ratio to the tensile stress in the fluid to the extension rate. Fluids can support a tensile stress when they are in motion. If you put a finger in a jar of honey and withdraw it, a strand of honey will be carried along by the finger. If you stop moving the finger the honey will fall back in the jar. But while in motion the honey will be in tension. With Newtonian fluids the extensional viscosity is three times the shear viscosity. When polymer solutions are stretched slowly, the molecules can relax, disentangle, and slip past each other. At higher extension rates they do not have time to relax and disentangle, and the extensional viscosity increases. This aids the coating process, and polymer solutions are easier to coat than Newtonian fluids of the same low shear viscosity.

The extensional thickening of polymer solutions is one form of viscoelastic behavior. This ability to support a tensile stress can also be demonstrated in a tubeless syphon with dilute aqueous solutions of polymers such as polyacrylamide or polyethylene oxide. If you suck up solution with a medicine dropper attached to a water aspirator and then lift the dropper out of the solution, the solution will still be sucked up. In shear, viscoelastic fluids develop normal stresses, which causes rod climbing on a rotating shaft, as opposed to the vortex and depressed surfaces that form with Newtonian liquids. Polymer solutions and semiliquid polymers exhibit other viscoelastic behaviors, where, on short time scales, they behave as elastic solids. "Silly putty," a childrens toy, can be formed into a ball and will slowly turn into a puddle if left on a flat surface. But if dropped to the floor it bounces.

Concentrated dispersions may be shear thickening, as opposed to the shear thinning of dilute polymer solutions. Some materials, such as latex paints, tend to form a structure. As the structure breaks down with shearing action, the viscosity decreases. Such materials are thixotropic. Some fluids have a yield stress. A thorough characterization of the rheology may require a number of different measurements.

Surface Forces. Because fresh surface is created during coating, surface forces are involved. These are normally expressed as surface tension, in dyn/cm, which is identical to mN/m. Surface tension is identical to surface energy, expressed as erg/cm^2 or mJ/m^2. Whether we call it surface tension or surface energy is a matter of personal preference. Surface tension gives rise to a higher pressure on the concave side of a curved interface; thus the pressure on the inside of a drop is higher than on the outside. This higher pressure is called capillary pressure. It can be used to explain the shape of some coating beads.

In coating, the coating fluid should spread out on the support. For this to occur the surface tension of the fluid should be low and the surface energy of the support should be high. The contact angle in a drop of fluid on the surface, between the surface of the support and the surface of the fluid measured through the fluid, is a measure of the ability of the fluid to wet the surface. This contact angle should be low.

The surface energy of the support may be increased by oxidizing it, such as in a flame (flame treatment) or in an electrical discharge (corona treatment). Flame treatment is permanent, but for many polymers corona treatment is labile—after a matter of hours or days the surface energy decreases toward its original value.

Because of this, corona treatment is done in-line, before the coating stand. High energy coatings may be applied to the support, such as the subbing often used on supports for photographic coatings.

The surface tension of a fluid containing surfactants varies with the age of the surface. As surfactant diffuses to the surface it lowers the surface tension; fresh surfaces have the higher surface tension of the solvent. The time for the surface to reach equilibrium varies from a number of milliseconds to several hours, depending on the system. The surface tension as a function of time is called the dynamic surface tension.

Similarly, the contact angle of a fluid on a support depends on whether the fluid is stationary or is moving, and at what speed. The contact angle for a stationary drop is lowest; as one coats faster in a coating operation the dynamic contact angle increases. When the coating speed increases to the point where the dynamic contact angle is 180°, air will be entrained and one can no longer coat.

Commercial Availability. All of the many types of coaters and dryers discussed herein are commercially available from many different vendors. These vendors usually have pilot facilities so that new coating and drying techniques can be easily tested. Contract coating companies, specializing only in coating, also exist.

BIBLIOGRAPHY

"Coating Methods, Survey" in *EPST* 1st ed., Vol. 3, pp. 765–807, by D. G. Higgins, Waldron-Hartig Division, Midland-Ross Corp. "Coating Methods, Roll Coating" in *EPSE*, 2nd ed., Vol. 3, pp. 553–567, by R. T. Scharenberg, Consultant; "Coating Methods, Spray Coating" in EPSE, 2nd ed., Vol. 3, pp. 567–575, by K. J. Coeling and T. J. Bublick, The De Vilbiss Co.

1. E. D. Cohen and E. B. Gutoff, eds., *Modern Coating and Drying Technology*, Wiley-VCH, New York, 1992, pp. 64, 67, 83, 89, 92, 105, 120.
2. D. Satas, ed., *Web Processing and Converting Technology and Equipment*, Van Nostrand Reinhold Co., Inc., New York, 1984, pp. 32, 44.
3. D. Satas, ed., *Coatings Technology Handbook*, Marcel Dekker, Inc., New York, 1991.
4. H. L. Weiss, *Coating and Laminating Machines*, Converting Technology Co., Milwaukee, Wis., 1977.
5. E. D. Cohen and E. B. Gutoff, *Coating and Drying Defects: Troubleshooting Operating Problems*, John Wiley and Sons, Inc., New York, 1995.
6. S. F. Kistler and P. M. Schweizer, *Liquid Film Coating*, Chapman & Hall, London 1997.
7. R. J. Stokes and D. Fennell Evans, *Fundamentals of Interfacial Engineering*, Wiley-VCH, New York, 1997.
8. E. B. Gutoff and C. E. Kendrick, *AIChE J.* **33**, 141–145 (1987).
9. R. A. Buonopane, E. B. Gutoff, and M. M. I. Rimore, *AIChE J.* **32**, 682–683 (1986).
10. T. Hasegawa and K. Sorimachi, *AIChE J.* **39**, 935–945 (1993).
11. R. Hanumanthu, S. J. Gardner, and L. E. Scriven, Paper 7a presented at the *AIChE Spring National Meeting*, Atlanta, Ga., Apr. 17–21, 1994.
12. D. J. Coyle, in Ref. 1, pp. 63–109.
13. U.S. Pat. 2,761,410 (Sept. 4, 1956), J. A. Mercier and co-workers (to Eastman Kodak).
14. E. B. Gutoff, *Chem. Eng. Prog.* **87**(1), 73–79 (Feb. 1991).
15. L. E. Scriven and W. J. Suzynski, *Chem. Eng. Prog.* **86**(9), 24–29 (Sept. 1990).
16. U.S. Pat. 5,360,629 (Nov. 1, 1995), T. M. Milbourn and J. J. Barth, (to Minnesota Mining and Manufacturing Co.).
17. K. N. Christodoulou and L. E. Scriven, *J. Sci. Comput.* **3**, 355–406 (1988).

18. K. N. Christodoulou, S. F. Kistler, and P. R. Schunk, in Ref. 6, pp. 297–366.
19. L. E. Scriven, Paper presented at *AIChE Spring Meeting*, Atlanta, Ga., Mar. 1984.
20. L. E. Sartor, Slot Coating: Fluid Mechanics and Die Design, Ph.D. dissertation, University of Minnesota, 1990.
21. P. M. Schweizer, *J. Fluid Mech.* **193**, 285–302 (1988).
22. E. D. Cohen, in Ref. 1, pp. 267–296.
23. T. H. Chilton and A. P. Colburn, *Ind. Eng. Chem.* **26**, 1183 (1934).
24. R. H. Perry and C. H. Chilton, eds., *Chemical Engineers' Handbook*, 5th ed., McGraw-Hill, New York, 1973, p. 12–2.
25. S. F. Kistler and L. E. Scriven, Paper presented at *AIChE Spring Meeting*, Orlando, Fla., Mar. 1982.

EDWARD D. COHEN
Technical Consultant
EDGAR B. GUTOFF
Consulting Chemical Engineer

COATINGS

Introduction

Coatings are ubiquitous in an industrialized society. U.S. shipments of coatings in 1999 were about 5.7×10^6 m^3, having a value of $18 billion (1). Coatings are used for decorative, protective, and/or a functional purpose on many kinds of surfaces. The low gloss paint on the ceiling of a room is used for decoration, but it also diffuses light. The coating on the outside of an automobile adds beauty to it and also protects it from rusting. The coating on the inside of a beer can protects the beer from the can; in soft drink cans, the interior coating protects the can from the beverage. Other coatings reduce growth of barnacles on ship bottoms, protect optical fibers against abrasion, and so on.

Traditionally, coatings changed slowly in an evolutionary response to new performance requirements and competitive pressures. An important reason for the slow rate of change was the difficulty in predicting product performance. In recent years, there has been increasing research on understanding the basic relationships between composition and performance to permit more rapid responses to the needs for change. Since about 1965, the pace of technical change has increased. A major reason for change has been to reduce VOC (volatile organic compound) emissions. Other factors are the cost of energy for heating curing ovens requiring lower temperature curing, increasingly stringent regulations of the use of potentially toxic materials, and increased performance requirements.

Various approaches to meet the new requirements, particularly to reduce VOC emissions, are being pursued. The use of waterborne coatings has increased substantially and has surpassed solventborne in volume. Latex paints have been used for many years in architectural coatings. These coatings have had less solvent than traditional solventborne paints but still contained significant amounts

Encyclopedia of Polymer Science and Technology. Copyright John Wiley & Sons, Inc. All rights reserved.

of solvent. Low solvent and solvent-free latex paints are being introduced. Use of waterborne industrial coatings has been dramatically expanded. Solventborne coatings are still used but solvent levels are being reduced. In many applications, high solids coatings have been successfully adopted. Research is currently directed to making solvent-free coatings. A growth area has been the use of powder coatings for industrial purposes. In many applications, use of powder coatings permits complete elimination of solvent emissions. Radiation curable coatings, particularly uv-cured coatings, have also grown particularly for clear coatings on heat-sensitive substrates. They are solvent free and very low levels of energy are required for curing.

Film Formation

Most coatings are applied as liquids and converted to solid films after application. Powder coatings are applied as solid particles, fused to a liquid, then forming a solid film. Almost all the polymers used in coatings are amorphous and the term solid has no absolute meaning. A useful definition of a solid film is that it does not flow significantly under the pressures to which it is subjected during testing or use. A film can be defined as solid under a set of conditions by stating the minimum viscosity at which flow is observable in the specified time interval. For example, it is reported that a film is dry-to-touch if the viscosity is greater than about 10^6 mPa·s (2). A film resists blocking when two coated surfaces are put against each other for 2 s under a mass per unit area of 1.4 kg·cm^{-3} (20 psi), when the viscosity is greater than 10^{10} mPa·s.

A way to form films is to dissolve a polymer in solvent(s) at a concentration needed for application, apply the coating, and allow the solvent to evaporate. In the first stage of solvent evaporation, the rate of evaporation is essentially independent of the presence of the polymer. As solvent evaporates, viscosity increases, T_g increases, free volume decreases, and the rate of loss of solvent becomes dependent on how rapidly solvent molecules can diffuse to the surface of a film. If a film is formed at 25°C from a solution of a polymer that, when solvent free, has a T_g greater than 25°C, the film retains considerable solvent even though it is a hard "dry" film.

Less solvent is needed for a coating based on solutions of lower molecular weight thermosetting resins. After application, the solvent evaporates, and chemical reactions cause cross-linking. The number-average functionality $\bar{f}_n$ has to be over 2, and the amount of monofunctional resin should be minimal for good properties. A problem with thermosetting systems is the relationship between stability during storage and time and temperature required to cure a film after application. Generally, it is desirable to store a coating for many months without a significant increase in viscosity. After application, one would like to have the cross-linking reaction proceed rapidly at the lowest possible temperature. Reaction rates depend on concentration and are reduced by dilution with solvent and increase as solvent evaporates; cross-linking in the applied film after solvent evaporation is initially faster than during storage. As formulations shift to higher solids, there are higher concentrations of functional groups, and there is greater difficulty in formulating storage-stable coatings. To minimize the temperature required for curing while

maintaining adequate storage stability, it is desirable to select cross-linking reactions for which the rate depends strongly on temperature. Arrhenius equations have been used to calculate what orders of magnitude of E_a and A are required to permit various combinations of storage times and curing temperatures (3). Such calculations show that to formulate a coating stable for 6 months at 30°C, the calculated kinetic parameters become unreasonable if cure is desired in 30 min below about 120°C. No known chemical reactions have a combination of E_a and A that would have a lower cure temperature while maintaining a 6-month stability. More reactive combinations can be used in two package (2K) coatings, in which one package contains a resin with one of the reactive groups and the second package contains the component with the other reactive group. The packages are mixed shortly before use. 2K coatings are used commercially on a large scale. 2K coatings have the analogous problem of pot life—the time after the two packages are mixed that the viscosity stays low enough for application.

Design of stable coatings that cure at lower temperatures or shorter times must be based on factors other than kinetics. Several approaches are used, including use of blocked reactants or catalysts where the blocking group volatilizes with heat, moisture, or oxygen curing; use of a volatile inhibitor; use of a cross-linking reaction that is a reversible condensation reaction involving loss of a volatile reaction product with some of the monofunctional volatile reactant used as solvent; use of a reactant that undergoes a phase change over a narrow temperature range; and uv curing.

Another consideration is the effect of the availability of free volume on reaction rates and reaction completion. If the diffusion rate is greater than the reaction rate, the reaction will be kinetically controlled. If the diffusion rate is slow compared to the kinetic reaction rate, the rate of the reaction will be mobility controlled. If the temperature is well below T_g, the free volume is so limited that the polymer chain motions needed to bring unreacted groups close together are very slow, and reaction virtually ceases. Since cross-linking starts with low molecular weight components, T_g increases as the reaction proceeds. If the initial reaction temperature is well below the T_g of the solvent-free coating, little or no reaction can occur after solvent evaporation and a "dry" film forms merely as a result of solvent evaporation, without much cross-linking. The result is a weak, brittle film. Mobility control is less likely in baking coatings because the final T_g of the film is below the baking temperature. In powder coatings, mobility control of reaction can be a limitation, since the initial T_g of the reactants has to be over 50°C so that the powder will not sinter during storage. The effect of variables on mobility control of reaction rates has been studied (4).

Dispersions of insoluble polymer particles form films by coalescence of the particles. The largest volume of such coatings use latexes as a binder. The lowest temperature at which coalescence occurs to form a continuous film is called its *minimum film-formation temperature* (MFFT). A major factor controlling MFFT is the T_g of the polymer particles. The MFFT of latex particles can be affected by water, which can act as a plasticizer (5). Most latex paints contain volatile plasticizers, coalescing solvents, to reduce MFFT. The mechanism of film formation from latexes has been extensively studied; the papers in References 6–9 review various theories associated with it. Film formation occurs by three overlapping steps: evaporation of water and water-soluble solvents that leads to a close packed

layer of latex particles; deformation of the particles leading to a continuous, but weak, film; and interdiffusion, a slow process in which the polymer molecules cross the particle boundaries and entangle, strengthening the film. A review paper discusses factors affecting development of cohesive strength of films from latex particles (10). The extent of coalescence has been studied by small-angle neutron scattering, direct energy transfer of particles labeled with fluorescent dyes, and scanning probe microscopy. Coalescing solvents have been necessary to formulate latex coatings to form films at low temperatures while resisting blocking at higher temperatures. Environmental regulations are limiting permissible emissions of VOC. See section on Latexes for discussion.

Flow

Flow properties control application and appearance of films. In brush application of paint, flow properties govern settling of pigment during storage, how much paint is picked up on the brush, film thickness applied, and leveling and sagging of the film. Reference 11 reviews flow of coatings. (see also RHEOOPTICAL MEASUREMENT)

Viscosity of Solutions. The viscosity of liquids depends on free volume availability. When a stress is applied, movement to relieve the stress is favored, and the liquid flows through free volume holes. Temperature dependence of viscosity for low molecular weight resins and their solutions has been shown to fit a Williams–Landel–Ferry (WLF) equation, equations (1), (12,13).

$$\ln \eta = 27.6 - \frac{A(T - T_g)}{B + (T - T_g)} \tag{1}$$

Generally, in designing resins lower T_g will lead to a lower viscosity of the resins and their solutions. Exceptions have been reported for some high solids acrylic resins made with a comonomer that has a bulky group, such as isobornyl methacrylate (14), have low viscosities at high solids even though they have high T_g values.

Equations have been proposed to express the relationships between concentration and viscosity of resin solutions. Equation (2), in which w_r is weight fraction resin and the k's are constants, has been shown to fit over a wide range of concentrations (12). Over narrower ranges of concentration, a simpler equation, equation (3), gives reasonable fits with the experimental data.

$$\ln \eta_r = \frac{w_r}{k_1 - k_2 w_r + k_3 w_r^2} \tag{2}$$

$$\ln \eta_r = \frac{w_r}{k_1 - k_2 w_r} \tag{3}$$

Log of viscosity of narrow average molecular weight resins dissolved in good solvents increases with the square root of molecular weight in the range of viscosities between about 0.01 and 10 Pa·s (12,15). In poor solvent–resin combinations, clusters of resin molecules form, and viscosity is higher. In solutions in good

solvents, flow is generally Newtonian. In many cases, flow of more concentrated resin "solutions" in poor solvents is non-Newtonian because shear can break up or distort resin clusters. Intermolecular hydrogen bonding between carboxylic acid-functional resin molecules is particularly strong and solvent effects on the viscosity of acid-substituted resins are large (16).

Viscosity of Liquids with Dispersed Phases. When a small amount of a dispersed phase is present, there is only a small effect on viscosity; as the volume of dispersed phase increases, there is a sharply increasing effect. When the system becomes closely packed with particles, viscosity approaches infinity. Equation (4) shows the effects of variables on viscosity, where η_e is the viscosity of the continuous or external phase, K_E is a shape constant, V_i is the volume fraction of internal phase, and ϕ is the packing factor.

$$\ln \eta = \ln \eta_e + \frac{K_E V_i}{1 - V_i/\phi} \tag{4}$$

The *packing factor* is the maximum volume fraction of internal phase when the particles are randomly close-packed and external phase just fills all the interstices between the particles. The shape constant K_E for spheres is 2.5. Many of the particles in coatings are spheres or are close to being spheres. For uniform diameter spheres, the value of ϕ is 0.637 and is independent of particle size. The packing factor depends strongly on particle size distribution: the broader the particle size distribution, the higher the packing factor. Figure 1 shows a plot of a typical dispersion (17).

The viscosity of dispersions of nonrigid particles does not follow equation (4). When a shear stress is applied to such a dispersion (eg, an emulsion), the particles can distort. When the particles are distorted, the shape constant changes to a lower value and the packing factor increases (18); both changes lead to a decrease in viscosity. Such systems are thixotropic since, depending on the difference between the viscosities of the internal and external phases, there is time dependency of the distortion of the particles and, hence, a decrease in viscosity as a function of time at a given shear rate. Time dependency can be studied using viscoelastic deformation analysis (19). The viscosity of dispersions is also affected by particle–particle interactions. If clusters of particles form, the viscosity of the dispersion increases; if the clusters separate when shear is exerted, the viscosity drops. Examples of such shear thinning systems are flocculated pigment dispersions.

Extensional Flow. Another mode of flow encountered in coating application is extensional flow. When a fiber passes through a spinneret, the mode is shear flow. The fiber is pulled after leaving the spinneret, extending the fiber. The flow is extensional flow, and the resistance to flow is extensional viscosity. The symbol used for extensional viscosity is $\eta*$. In Newtonian fluids, $\eta*/\eta = 3$. Extensional flow in coating application is encountered when applying coatings by direct roll coating. In the nip, the coating is under pressure; as the coating comes out of the nip, the roller is moving up away from the film, and flow is extensional. As the film stretches, it splits; small imbalances of pressures lead to variations in the timing of film splitting. If the extensional viscosity is relatively low, the film splits quickly, leaving a ridged film. However, with higher extensional viscosity, fibers grow; longer fibers tend to split in two places, resulting in formation of droplets, which

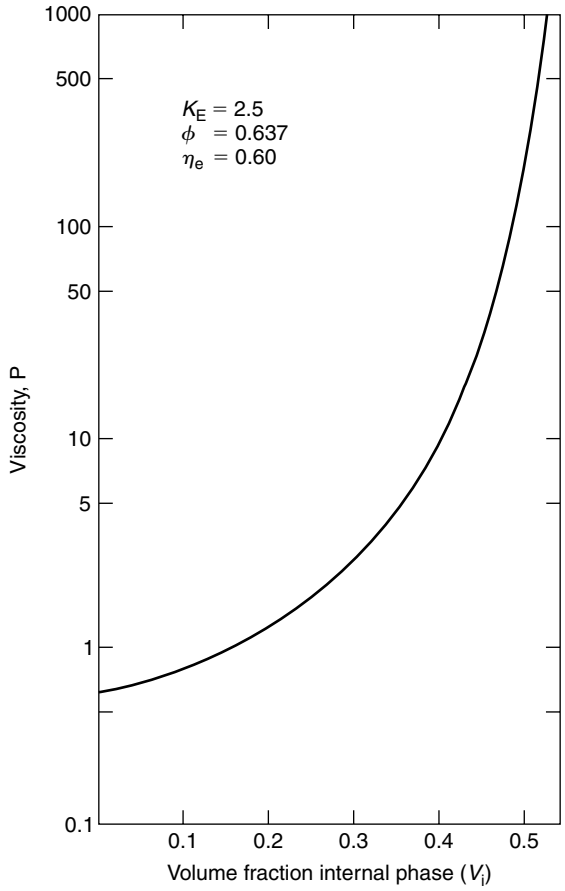

Fig. 1. The effect of increasing volume fraction of noninteracting spherical particles on the viscosity of a dispersion. From Ref. 17, with permission.

are thrown out into the air. This is called *misting* or *spattering*,. Reference 17 discusses the relationship of variables and extensional viscosity effects in roll coating.

Extensional flow can also be encountered in spray application. If, for example, a solution of a thermoplastic acrylic resin with $\bar{M}_w$ above about 100,000 is sprayed, instead of droplets coming out of a spray gun orifice, fibers emerge. The "strength" of the solution is high enough for the stream of coating to stay as a fiber rather than to form droplets. Reference 21 discusses extensional viscosity phenomena in spray application.

Mechanical Properties

Coating films should withstand use without damage. The coating on the outside of an automobile should not break when hit by a piece of flying gravel. The coating on

the outside of a beer can must not abrade when cans rub against each other during shipment. The coating on wood furniture should not crack when the wood expands and contracts as a result of changing temperatures or swelling and shrinkage from changes in moisture content of the wood. The coating on aluminum siding must be flexible enough for fabrication of the siding and resist scratching during installation on a house. A methodology for considering the factors involved in service life prediction has been given (22). A monograph (23) discusses problems of predicting service lives and proposes reliability theory methodology for database collection and analysis.

Basic Mechanical Properties. Understanding relationships between composition and basic mechanical properties of films can provide a basis for more intelligent formulation. Reference 24 is a good review paper. In ideal elastic deformation a material elongates under a tensile stress in direct proportion to the stress applied. When the stress is released, the material returns to its original dimensions essentially instantaneously. An ideal viscous material elongates when a stress is applied in direct proportion to the stress, but does not return to its original dimensions when the stress is released. Almost all coating films are viscoelastic—they exhibit intermediate behavior. Figure 2 shows a schematic plot of the results of a stress–strain test, in which a coating film is elongated (strain) at a constant rate and the resulting stress is recorded as percent elongation. The ratio of stress to strain is the *modulus*. In the initial part of this plot, modulus is independent of strain. However, as strain increases, the modulus depends on the strain. The end of the curve signifies that the sample has broken. This point is defined in two ways: *elongation-at-break*, a measure of how much strain is withstood before breaking; and the *tensile strength*, a measure of the stress when the sample breaks. The area under the curve represents the work-to-break (energy per unit volume). Commonly, as shown in Figure 2, at an intermediate strain, the stress required for further elongation decreases. The maximum stress at that point is called the *yield point*. Yield point can be designated in two ways: elongation-at-yield and yield strength.

Elastic deformation is almost independent of time and temperature. Viscous flow is time and temperature dependent; the flow continues as long as a stress is applied. Viscoelastic deformation is dependent on the temperature and the rate at which a stress is applied. If the rate of application of stress is rapid, the response can be primarily elastic; if the rate of application of stress is low, the viscous component of the response increases and the elastic response is lower. Similarly, if the temperature is low, the response can be primarily elastic; at a higher temperature, the viscous response is greater.

Stress–strain analysis can also be done dynamically by using instruments that apply an oscillating strain. The stress and strain vary according to sine waves. Stress and phase angle difference between applied strain and resultant measured stress are determined. For an ideal elastic material, the maximums and minimums occur at the same angles and the phase shift is 0°. For a Newtonian fluid, there would be a phase shift of 90°. Viscoelastic materials show an intermediate response. If the elastic component is high, the phase shift δ is small; if the elastic component is low compared to the viscous component, the phase shift is large. The phase shift, along with the maximum applied strain ε_0 and the maximum measured stress σ_0, is used to calculate the dynamic properties. Storage modulus E'

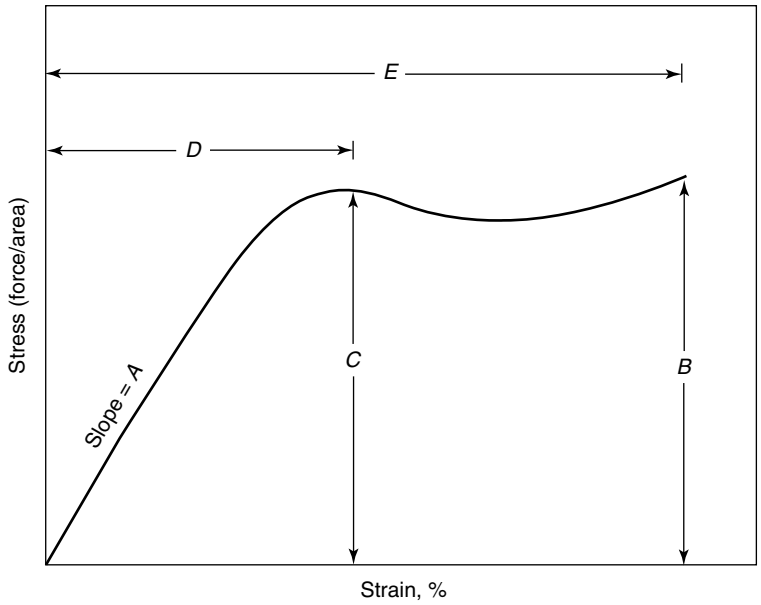

Fig. 2. Stress–strain plot. A is initial modulus, B is elongation-to-break, C is yield strength, D is elongation-to-break, and E is tensile strength. From Ref. 25, with permission.

is a measure of elastic response: $E' = (\sigma_0 \cos \delta)/\varepsilon_0$. Loss modulus E'' is a measure of the viscous response: $E'' = (\sigma_0 \sin \delta)/\varepsilon_0$. The square of the total modulus equals the sum of the squares of the storage and loss moduli. The ratio E''/E' is called loss tangent, since all of the terms cancel except the ratio $\sin \delta/\cos \delta$, corresponding to the tangent of an angle, $\tan \delta$, commonly called tan delta.

Dynamic mechanical analysis (qv) has the advantage over stress–strain studies that the elastic and viscous components of modulus can be separated. The higher the frequency of oscillation, the greater the elastic response and the smaller the phase angle; the lower the frequency, the greater the viscous response and the larger the phase angle. Generally, it is possible to run experiments over a range of frequencies in dynamic tests wider than the range of rates of application of stress possible in linear stress–strain experiments. Dynamic testing can be done over a wider range of temperatures and rates of heating. In dynamic tests, it is not possible to determine tensile-at-break, elongation-at-break, or work-to-break, since the sample must remain unbroken.

Formability and Flexibility. Many coated products are subjected to mechanical forces either to make a product, as in forming bottle caps or metal siding, or in use, as when a piece of gravel strikes the surface of a car with sufficient force to deform the steel substrate. To avoid film cracking, the elongation-at-break must be greater than the extension of the film. Cross-linked coatings have low elongations-at-break when below T_g. The T_g of cross-linked polymers depends on structure of the segments between cross-links, cross-link density (XLD), amount of dangling chain ends, and the extent of cyclization of the backbone (26).

The relationship between XLD and modulus for melamine–formaldehyde (MF) cross-linked films has been shown (27). As shown in equation (5), in which

ν_e is XLD expressed as the number of moles of elastically effective network chains per cubic centimeter of film. Since E'' is low at temperatures well above T_g, $E \approx E'$. XLD can also be calculated from the extent of swelling of a film by solvent. While cross-linked films do not dissolve in solvent, solvent dissolves in a cross-linked film. As cross-links get closer together the extent of swelling decreases. Equation (5) can be used to predict the storage modulus above T_g from the XLD.

$$E = 3\nu_e RT (T \gg T_g) \tag{5}$$

Properties are affected by the extent to which cross-linking has been carried to completion. Incomplete reaction leads to lower XLD and, hence, lower storage modulus above T_g. The extent of reaction can be followed by determining storage modulus as a function of time (28). Thus, one can, at least in theory, design a cross-linked network to have a desired storage modulus above T_g by selecting an appropriate ratio of reactants of appropriate functionality.

An additional factor that can affect the mechanical properties of polymeric materials is the breadth of the T_g transition region (29). The same effect can be seen in tan delta plots, which exhibit various breadths. Broad tan δ peaks are frequently associated with heterogeneous polymeric materials. Blends of different thermoplastic resins often display two distinct T_g's because of phase separation. Other blends of thermoplastics have a single, often broad, T_g, when phase separation is indistinct. For thermosetting polymers, the T_g transition region is generally broader than for thermoplastics. Breadth of the distribution of chain lengths between cross-links is a factor, and blends of thermosetting resins such as acrylics and polyesters often display a single, broad T_g transition. As a rule, materials with broad and/or multiple T_g's have better impact resistance than comparable polymers with a sharp, single T_g.

When a cross-linked film on a metal substrate is deformed by fabrication, it is held in the deformed state by the metal substrate. As a result, there is a stress within the film, acting to pull the film off the substrate. Stress within films can also arise during the last stages of solvent loss and/or cross-linking of films (30). It is common for coatings to become less flexible as time goes on. Particularly in air-dried coatings, loss of the last of the solvent may be slow. If the cross-linking reaction was not complete, the reaction may continue, decreasing flexibility. Another possible factor with baked films is densification. If a coating is heated above its T_g and then cooled rapidly, the density is commonly found to be lower than if the sample had been cooled slowly (31). During rapid cooling, more and/or larger free-volume holes are frozen into the matrix. On storage, the molecules slowly move and free volume decreases, causing densification; it is also called *physical aging*. To achieve the desired properties of baked films, some minimum time at a temperature is required, but overbaking can lead to excessive cross-linking. There is a cure window, and within this set of time and temperature satisfactory properties are obtained. High solids acrylic/MF coatings have narrower cure windows than conventional solids coatings.

Abrasion and Mar Resistance. *Abrasion* is the wearing away of a surface; *marring* is a disturbance of a surface that alters its appearance (see WEAR). A study of the mechanical properties of a series of floor coatings with known wear life concluded that work-to-break values best represented the relative wear lives

(32,33). Studies of automobile clear coats have shown that wear resistance increases as energy-to-break of films increases (34). Wear tends to increase as the angle of application of stress decreases. Urethane coatings generally exhibit superior abrasion resistance combined with solvent resistance. This combination of properties may result from the presence of intersegment hydrogen bonds in addition to the covalent bonds. At low levels of stress, hydrogen bonds act like cross-links, reducing swelling on exposure to solvent. At higher levels of stress, the hydrogen bonds dissociate, permitting the molecules to extend without rupturing covalent bonds. When the stress is released, the molecules relax and new hydrogen bonds form. Urethanes are used as wear layers for flooring, as well as topcoats in aerospace applications, where this combination of properties is desirable.

The coefficient of friction of a coating can affect abrasion resistance. Abrasion of the coating on the exterior of beer cans during shipment can be minimized by incorporation of a small amount of incompatible wax or fluorosurfactant in the coating. Another variable is surface contact area. Incorporation of a small amount of a small particle size SiO_2 pigment in a thin silicone coating applied to plastic eyeglasses reduces abrasion. The pigment particles reduce contact area, permitting the glasses to slide more easily over a surface.

Marring is a near-surface phenomenon; even scratches less than 0.5 μm deep can degrade appearance. Marring is a main problem with automobile clear topcoats. In going through automatic car washes, the surfaces of some clear coats are visibly marred and lose gloss (35). Mar resistance is a requirement in coatings for floors and for transparent plastics. The physics of marring is complex; various models have been proposed to describe what happens to a viscoelastic material when a hard object is drawn over its surface. Plastic deformation and fracture lead to marring. The responses can be quantitatively measured by scanning probe microscopy (36). In general, MF cross-linked acrylic clear coats are more resistant to marring than isocyanate cross-linked coatings, but MF cross-linked coatings have poorer environmental etch resistance. Coatings can be made hard enough so that the marring object does not penetrate into the surface, or they can be made elastic enough to bounce back after the marring stress is removed. If the hardness strategy is chosen, the coating must have a minimum hardness; however, such coatings may fail by fracture. Film flexibility is an important factor influencing fracture resistance (37). Maximum mar resistance results from coatings having as high a yield stress as possible without being brittle; high yield stress minimizes plastic flow and avoidance of brittleness minimizes fracture (38). Reference 38 provides a review of the relation of bulk mechanical properties of coatings to mar resistance.

Test Methods. Field applications on a small scale and under especially stringent conditions accelerate possible failure. Traffic paints are tested by painting stripes across the lanes of traffic instead of parallel to traffic flow. Automobiles are driven on torture tracks with stretches of gravel, through water, under different climatic conditions. Sample packs of canned goods are made; the linings are examined for failure and the contents evaluated for flavor after storage.

Many tests have been developed to simulate use conditions in the laboratory. An example is a gravelometer to evaluate resistance of coatings to chipping of automotive coatings when struck by flying gravel. Pieces of standard shot are

propelled at the coated surface by compressed air under standard conditions. The tests have been standardized by comparison to a range of actual results and give reasonably good predictions of actual performance. A more sophisticated instrument, a precision paint collider, which permits variations in angle and velocity of impact and temperature, has been described (39).

Many empirical tests are used to test coatings. In most cases, they are more appropriate for quality control than performance prediction. ASTM tests of importance to the coatings field are in Volumes 06.01, 06.02, and 06.03: *Paint—Tests for Formulated Products and Applied Coatings*. Many people believe the tests are more precise than they proved to be in ASTM round robin tests (40). An excellent reference book is the *Paint and Coating Testing Manual* (*Gardner-Sward Handbook*) (41). It gives descriptions of test methods and summaries of each main class of properties.

Exterior Durability

The primary ways of degradation on exterior exposure are photoinitiated oxidation and hydrolysis resulting from exposure to sunlight, air, and water.

Photointitiated Oxidative Degradation. Exterior coatings should exclude resin components that absorb uv radiation at wavelengths longer than 290 nm or that are readily oxidized. Photoinitiated oxidation of polymers proceeds by a chain reaction. Absorption of uv produces highly energetic photoexcited states that undergo bond cleavage to yield free radicals that undergo a chain reaction with O_2 (autoxidation), leading to polymer degradation. Functional groups in a coating that promote hydrogen abstraction by free radicals should be minimized. Aromatic groups with directly attached heteroatoms, as in aromatic urethanes and bisphenol A (BPA) epoxies, absorb uv above 290 nm and undergo direct photocleavage to yield free radicals that participate in oxidative degradation.

Ultraviolet absorbers and antioxidants are used to stabilize films. Reference 42 reviews photostabilization and thermal stabilization of coatings. A uv absorber converts uv energy into thermal energy. One cannot eliminate uv absorption by the resin by adding a uv absorber; it reduces absorption by the binder to slow the rate of photodegradation reactions. Since absorption increases as the path length increases, uv absorbers are most effective in protecting the lower parts of a film or substrate (eg, a base coat, wood, or plastic under a clear top coat containing an absorber) and least effective in protecting at the air interface. A uv absorber should have very high absorption of uv radiation from 290 through 380 nm and no absorption above 380 nm. Substituted 2-hydroxybenzophenones, 2-(2-hydroxyphenyl)-2*H*-benztriazoles, are the most used uv stabilizers. A requirement of a uv stabilizer is permanence. There can be physical loss by vaporization, leaching, or migration and/or chemical loss by photochemical reactions of the stabilizer. If a uv stabilizer has even a small vapor pressure, it slowly volatilizes. Longer term physical permanence may be achieved by using oligomeric photostabilizers or polymer-bound stabilizers.

Antioxidants are classified into two groups: preventive and chain-breaking antioxidants. Preventive antioxidants include peroxide decomposers, which reduce hydroperoxides to harmless products. Examples are sulfides and phosphites

that are oxidized to sulfoxides and phosphates. Metal complexing agents are preventive antioxidants that tie up transition metal ions present as contaminants that catalyze conversion of hydroperoxides into radicals. The most widely used chain-breaking antioxidants are hindered amine light stabilizers (HALS)—amines with two methyl groups on each of the two alpha carbons; most are derivatives of 2,2,6,6-tetramethylpiperidine, as shown in general formula (**1**). They act as free-radical traps to break the photoxidation chain reaction (43).

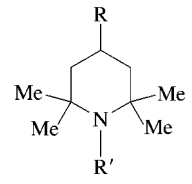

(R′ = H, alkyl, alkanoyl, alkoxy)

1

HALS derivatives undergo photoxidative conversion into nitroxyl radicals ($R_2NO\cdot$) that react with carbon-centered radicals by disproportionation and combination to yield corresponding hydroxylamines and ethers. The hydroxylamines and ethers, in turn, react with peroxy radicals to regenerate nitroxyl radicals. HALS derivatives interfere with propagation steps involving both carbon-centered and peroxy radicals in autoxidation. A variety of HALS compounds are available. The "R" in general formula (**1**) is often a diester group that joins two piperidine rings; this increases molecular weight, decreasing volatility. The first commercial HALS compounds had R′ = H. Later versions with R′ = alkyl exhibit better long-term stability. Both of these types are basic and interfere with acid-catalyzed cross-linking reactions, such as with MF resins. Hydroxylamine ethers (R′ = OR″) such as an octyl ether is a HALS with low basicity that converts rapidly to nitroxyl free radicals (44). HALS compounds, especially with R′ = H, can accelerate degradation of polycarbonate plastics. Combinations of uv absorbers and HALS compounds act synergistically (45). Ultraviolet absorbers are inefficient at protecting the outer surface of a film; HALS compounds effectively scavenge free radicals at the surface. Analysis of films after exterior exposure shows that significant amounts of HALS derivatives remain after 2 years of black box Florida exterior exposure. With clear coat–base coat finishes, a major mode of failure is delamination between topcoats and base coat, primer, or plastic substrate (46). Application of sufficient film thickness and proper choice of uv stabilizers and HALS are needed to avoid delamination.

Many pigments absorb uv radiation. The strongest uv absorber known is fine particle-size carbon black. Many carbon blacks have structures with multiple aromatic rings and, in some cases, phenol groups on the pigment surface. Such black pigments are both uv absorbers and antioxidants. Coatings of thickness 50 μm pigmented with fine particle size, transparent iron oxide pigment absorb virtually all radiation below about 420 nm (47). It is useful in wood stains, since the pigmented transparent coating protects the wood from photodegradation.

TiO_2 absorbs uv strongly, but it can accelerate photodegradation of films, causing chalking of coatings—degradation of the organic binder and exposure of unbound pigment particles on the film surface that rub off easily. Degradation

of the binder is enhanced by interaction of photoexcited TiO_2 with oxygen and water to yield oxidants (48). Anatase TiO_2 is more active in promoting oxidative degradation than rutile TiO_2. The photoactivity of TiO_2 pigments is reduced by coating the pigment particles with a thin layer of silica and/or alumina. Chalking reduces gloss, since the film becomes rougher. In paints containing both TiO_2 and color pigments, chalking results in color changes as a result of the gloss loss; the higher surface reflectance of the low gloss films gives weaker colors. However, loss of gloss does not necessarily correlate with ease of chalking (49). Initial gloss loss in some TiO_2 pigmented coatings results from film shrinkage, which, in some cases, is greater with more resistant grades of TiO_2.

Hydrolytic Degradation. A general ordering of groups subject to hydrolysis is esters > ureas > urethanes ≫ ethers, but activated ethers in MF cross-linked hydroxy-functional resins, are more reactive than ureas and urethanes. The tendency to hydrolyze can be reduced by steric hindrance, for example, by alkyl groups in the vicinity of the susceptible groups, such as esters. The lower the water solubility of the diacid or diol used to make a polyester, the greater the resistance to hydrolysis (50). Phthalate esters are more readily hydrolyzed under acidic conditions than isophthalate esters. Hydrolysis of polyesters results in backbone degradation. Backbones of (meth)acrylic resins are resistant to hydrolysis, since the linkages are carbon–carbon bonds.

Base coat–clear coat finishes for automobiles are subject to environmental etching. Small spots appear in the clear coat surface in a warm climate with acidic rain. The spots are uneven, shallow depressions from hydrolytic erosion of resin in the area of a droplet of acidic water. Several factors are involved in differences in resistance to environmental etching (51). Since urethane linkages are more resistant to acid hydrolysis than the activated ether cross-links obtained with MF resins, generally urethane–polyol clear coats are less susceptible to environmental etching. Temperature, T_g, and surface tension are also important.

Silicone coatings are subject to hydrolysis at cross-linked sites, where silicon is attached to three oxygens (52,53). The reaction is reversible, and cross-links can hydrolyze and reform. If a silicone-modified acrylic coating is exposed to water over long periods or is used in a climate with very high humidity, the coating softens. MF resin as a supplemental cross-linker minimizes the problem.

Other Modes of Failure. When paint is applied to wood, it must be able to withstand the elongation that results from the uneven expansion of wood grain when it absorbs moisture. A problem of exterior, oil-based house paints on wood siding is *blistering*. The blistering results from accumulation of water in the wood beneath the paint layer. The vapor pressure of the water increases with heating by the sun, and blisters form to relieve the pressure. Since latex paints have higher moisture vapor permeability than oil-based paints, the water vapor can pass through a latex paint film. The high moisture vapor permeability of latex paint films can lead to failures of other types. If calcium carbonate fillers are used in an exterior latex paint, frosting can occur. Water and carbon dioxide permeate into the film, dissolving calcium carbonate by forming soluble calcium bicarbonate, which diffuses out of the film. At the surface, the calcium bicarbonate is converted back to a deposit of calcium carbonate.

Dirt retention can be a problem with exterior gloss latex paints. Latex paints must be designed to coalesce at relatively low application temperatures.

At warmer temperatures, soot and dirt particles that land on the paint surface cannot be washed off by rain. Dirt pickup is less for paints formulated with higher T_g polymers (54).

Testing. No test is available that reliably predicts the exterior durability of coatings, partly due to the wide variety of environments and application conditions (see WEATHERING). The limitations of accelerated tests, the need for data based on actual field experience, and methods of building a database are described in Reference 23. Use of reliability theory using statistical distribution functions of material, process, and exposure parameters for predicting exterior durability of automotive coatings has been recommended (46). Reference 55 reviews various test methods.

The most reliable accelerated tests are outdoor fence exposures of coated panels carried out in several locations with different environments. Reference 56 reviews testing of exposed panels. Southern Florida has a subtropical climate with high humidity, temperature, and sunshine level. Arizona has more hours of sunshine per year and a higher average daily high temperature, but lower humidity. The differences between exposure conditions in Florida and Arizona have been reviewed (57). Test specimens are examined periodically. Part of the coating is cleaned for comparison. Ease of cleaning, change in gloss, change in color, degree of chalking, and gross film failures are reported. Film degradation is accelerated using black box exposure. Panels are mounted at 5° to the horizontal on black boxes. Increase in the temperature of the coating accelerates degradation. The temperature increase and the extent of acceleration vary from coating to coating with color.

Results can be obtained in shorter times by using Fresnel reflectors to concentrate sunlight on test panels. High intensity is achieved by reflecting sunlight from moving mirrors that follow the sun to maintain a position perpendicular to the sun's direct beam radiation (57). They enhance the intensity of sunlight on the panel surfaces by a factor of 8 over direct exposure; it is said to accelerate degradation rates 4–16 times the rate for nonaccelerated exposure.

Chemical changes begin before physical changes become evident. Studies of chemical changes help determine the mechanism of failure, providing a basis for formulating more resistant coatings. References 44 and 58 provide reviews of various approaches. Electron spin resonance (esr) spectrometry can monitor changes in free-radical concentrations within a coating. The rate of disappearance of stable nitroxyl radicals has been correlated with loss of gloss in long-term Florida exposure (45). Use of ESR spectrometry to monitor the rate of disappearance of nitroxyl radicals in acrylic/MF coatings allows calculation of photoinitiation rates (PR) of free-radical formation, which were found to correlate with rates of gloss loss (GLR): $\mathrm{GLR} \propto (\mathrm{PR})^{1/2}$. Photoinitiation rates have been used to evaluate experimental conditions for the synthesis of acrylic polyols on the exterior durability of the acrylic/MF coating (59). Electron spin resonance spectrometry has been used to study photostability of coating films by determination of free-radical concentration after uv irradiation of films at a temperature of 140 K, well below T_g (59). Fourier transform infrared (ftir) spectroscopy is used to follow chemical changes on a surface (60). Photoacoustic-ftir spectroscopy; has also been used; it has the advantages that the sample does not have to be removed from the substrate and the film can be analyzed at different depths within a film (61).

Many laboratory devices for accelerating degradation are available. See Reference 62 for descriptions of various devices and their advantages and disadvantages. They expose panels to uv sources with different wavelength distributions and the panels are subjected to cycles of water spray (or high humidity). Although these tests are widely used, results frequently do not correlate with actual exposure results. The predictive value of accelerated weathering with artificial light sources is particularly questionable when a light source includes wavelengths less than 290 nm. Variability of performance of the test instruments can also be a problem, especially when comparing results from laboratory to laboratory (63). An evaluation of accelerated weathering devices for a polyester–urethane coating, using photoacoustic-ftir spectroscopy, concluded that none of the conventional devices were suitable (64). Many examples of reversals of results comparing coatings with known exterior durability with laboratory tests have been found. Stabilizer loss by volatilization may be insignificant in an accelerated test, but very important over the long time periods of actual use.

Adhesion

Adhesion is an essential characteristic of most coatings. A coatings formulator thinks how hard is it to remove the coating? But, a physical chemist thinks of the work required to separate the interface. The latter is only one aspect of the former. Removal of a coating requires breaking or cutting through the coating and pushing the coating out of the way, as well as separating the coating from the substrate.

With a very smooth interface between coating and substrate, the only forces holding the substrate and coating together are the interfacial attractive forces. With a rough surface on a microscopic scale, the contact area between the coating and the rough substrate is larger than the geometric area and penetration of coating into undercuts adds mechanical strength. Surface roughness can be a disadvantage; if the coating does not completely penetrate into the microscopic pores and crevices in the surface, dovetail effects are not realized, and interfacial contact area can be smaller than the geometric area. The viscosity of the continuous phase of the coating is a significant factor controlling penetration. Coatings with low viscosity external phases, slow evaporating solvents, and slow cross-linking rates give better adhesion. Because of the drop in viscosity by heat, baked coatings give better adhesion than do air-dried coatings. Viscosity of resin solutions increases with molecular weight; one would expect that lower molecular weight resins would provide superior adhesion. This hypothesis has been confirmed in the case of epoxy resin coatings on steel (65).

Internal stresses act to reduce adhesion; less external force is required to disrupt the adhesive bond. As film formation proceeds, T_g rises and free volume is reduced; the film becomes fixed in unstable conformations, and internal stress increases (66). The stress can build up sufficiently so that spontaneous delamination occurs (67). Stresses also result from volume expansions, such as swelling of films by exposure to high humidity (67) or water immersion (68). As the rate of cross-linking increases, stresses increase, since less time is available for

polymer relaxation to occur. An extreme example is uv curing of acrylated resins by free-radical polymerization in a fraction of a second.

Nonuniform curing, film defects, and imperfections in the film, can lead to localized stresses that can lead to fractural failure (69). Stress applied to that part of the film concentrates at an imperfection, increasing the probability of forming a crack; the crack propagates to the coating–substrate interface, leading to delamination. Pigment particles with sharp crystal corners and air bubbles are examples of potential sites for concentration of stresses. On the other hand, incorporation of particles of rubber may lead to dissipation of stresses.

Wetting is a significant factor in adhesion. If a coating does not spread spontaneously over a substrate surface so that there is intermolecular contact between the substrate surface and the coating, there will be no contribution to adhesion. The relationships between wetting and adhesion have been extensively studied (70). A liquid spreads spontaneously on a substrate if the surface tension of the liquid is lower than the surface free energy of the solid. Additives with single polar groups and long hydrocarbon chains in coatings can result in poor adhesion since they get preferentially absorbed on a metal surface, resulting in poor adhesion between the coating and a monolayer of additive. An example is the poor adhesion to steel that results from use of dodecylbenzenesulfonic acid [27176-87-0] as catalyst. Adhesion of latex films can be affected by a layer of surfactant forming at the interface between the coating and the substrate (71).

The metal and its surface characteristics affect adhesion; Reference 72 is a review of metal surface characteristics, cleaning, and treatments. The surface tension of a clean metal surface is higher than that of any potential coating. Oils and soluble salts must be removed from the surface. Steel surfaces are generally given a metal phosphate conversion treatment. The resulting mesh of crystals on the surface of the steel increases the interfacial area for interaction, and the hydrogen-bond interactions between the phosphate crystals and the resin molecules are stronger than those between the steel surface and the resin molecules. The last rinse has contained a low concentration of chromic acid to protect against corrosion. Because of the toxic risks of hexavalent chromium, replacements for the chromate rinse are being sought. Over zinc phosphate, a rinse of 0.5% trimethoxymethylsilane with H_2ZrF_6 at pH of about 4 is reported to give better performance than a chromic acid rinse (73). Plasma polymerization of trimethylsilane on the surface of cold-rolled steel provides corrosion protection (74). Also, plasma polymerization of hexamethyldisiloxane in the presence of oxygen is under investigation (75). Bis(trisilylalkoxy)alkanes are being investigated to treat the surface of steel to increase adhesion (76). Clean steel is rinsed with water, and then the wet steel is dipped first in an aqueous solution of bis(trimethoxysilyl)ethane (BTSE) and then in an aqueous solution of a reactive silane. The BTSE reacts with water and hydroxyl groups on the steel and silanols from other molecules of BTSE to give a water-resistant anchor to the steel. The reactive silane reacts with other silanol groups from the BTSE, and the reactive group can react with a coating binder.

For many applications, aluminum requires no treatment other than cleaning. If there will be exposure to salt, surface treatment is necessary. Most treatments for aluminum have been chromate treatments. See Reference 72 for further discussion. In the past several years, many chrome- and cyanide-free proprietary

aluminum conversion coatings have been developed with equivalent performance to chrome coatings. Electrodeposited cerium oxide conversion coats show promise (77).

To provide greater protection against corrosion, steel coated with zinc is widely used in construction and automobiles. There can be large variations in adhesion, depending on the condition of the zinc layer of the galvanized steel. If zinc-coated steel has been exposed to rain or high humidity, surface oxidation leads to formation of ZnO, $Zn(OH)_2$, and $ZnCO_3$; they are basic and somewhat soluble in water. It is important to use saponification-resistant resins in primers for galvanized steel. Reference 78 reviews coating of galvanized steel. Treating the surface of galvanized steel with a solution of zirconium nitrate, followed by treatment with *N*-aminoethylaminopropyltrimethoxysilane, is reported to be a good pretreatment for galvanized steel for coil coating (79).

The surface of clean steel is not iron; rather, hydrated iron oxides are present as a monolayer (80). Adhesion to this surface is promoted by developing hydrogen bonds between groups on the resin molecules and the oxide and hydroxide groups on the surface of the steel. Adhesion is promoted by using resins having multiple hydrogen-bond donor and acceptor groups. Best results are obtained with hydrogen-bond donor groups are scattered along a resin chain. Adsorption of resin molecules occurs with loops and tails sticking up from the surface so that some of the polar groups are adsorbed on the surface and some on the loops and tails, where they interact with the rest of the coating. BPA epoxy resins and their derivatives commonly provide excellent adhesion to steel. These resins have hydroxyl and ether groups along the chain, which can provide for interactions with both the steel surface and the other molecules in the coating. The backbone consists of alternating flexible 1,3-glyceryl ether and rigid BPA groups; the combination provides the flexibility necessary to permit multiple adsorption of hydroxyl groups on the surface of the steel, along with rigidity to prevent adsorption of all of the hydroxyl groups. References 65 and 81 discuss effects of variations in epoxy resin composition on adhesion. Amine and phosphate groups on the resin particularly improve adhesion in the presence of water.

Surface analysis is useful in understanding factors affecting adhesion. The surfaces of steels have been studied by Auger analysis. In some cold-rolled steels organic compounds become imbedded in the surface of the steel during coil annealing. If this happens, it becomes difficult to apply high quality phosphate conversion treatments on the steel (82). X-ray photoelectron spectroscopy (xps) is used to study the surface of steel from which a coating has been removed and the underside of the coating that was in contact with the steel. The site of failure occurred can be identified—that is, whether failure was between the steel and the coating or between the main body of the coating and a monolayer of material on the surface of the steel. Other valuable analytical procedures for thin surface layers are attenuated total reflectance (atr) and ftir spectroscopies.

Stronger interactions with the substrate surface are possible by forming covalent bonds. Reactive silanes enhance adhesion of coatings to glass (83). In an epoxy-amine coating for glass, one can add 3-aminopropyltrimethoxysilane. The trimethoxysilyl group reacts with silanol groups on the surface of the glass to generate siloxane bonds. The trimethoxysilyl groups also react with water to produce silanol groups that react with remaining methoxysilyl groups to generate

polysiloxane groups at the glass surface. The terminal amine groups react with epoxy groups in the resin so that the coating is multiply bonded to the surface of the glass. Resins with acetoacetic ester substituents can coordinate with ferric salts. Reports indicate improvement in adhesion and corrosion protection (84).

With many plastics there is a problem wetting the surface with a coating. Wetting can be affected by mold release agents on a molded plastic part. Polyolefins have low surface free energies. Adhesion to polyolefins generally requires treatment of the surface to increase its surface free energy. Oxidation of the surface generates polar groups that increase surface free energy and provide hydrogen-bond acceptor and donor groups for interaction with coating resin molecules. A variety of processes are used to treat the surface (85,86). The surfaces can be oxidized by flame treatment; corona discharge or chemical oxidizing treatments are effective. Adhesion to untreated polyolefins can be assisted by applying a thin tie coat of a low solids solution of a chlorinated polyolefin or chlorinated rubber. The various approaches and results of various types of surface analysis have been reviewed (85). See Reference 87 for further discussion of surface treatments.

Curing at a temperature above the T_g of the plastic enhances adhesion by migration of resin molecules into the surface of the plastic. In some cases, heating the plastic substrate above its T_g is not feasible because the plastic substrate undergoes heat distortion. Solvents in the coating that are soluble in the plastic can enhance adhesion by lowering its T_g. The solvents should evaporate slowly to permit time for penetration to occur. Fast evaporating solvents, such as acetone, can cause crazing of thermoplastics, such as polystyrene and poly(methyl methacrylate). *Crazing* is the development of many minute surface cracks.

Adhesion to other coatings, intercoat adhesion, requires the surface tension of the coating to be lower than the surface free energy of the substrate coating. Polar groups in both coatings permit hydrogen bonding; in the case of thermosetting coatings, covalent bonding enhances intercoat adhesion. Curing temperatures above T_g, use of compatible resins, and solvents in the coating that can swell the substrate coating enhance intercoat adhesion. Coatings with lower XLD are more swollen by solvents. Sometimes, one can undercure the primer thus having a lower XLD when the topcoat is applied. Cure of the primer is completed when the topcoat is cured.

Primers with low gloss have rougher surfaces and are easier to adhere to. When possible, increasing the pigment loading of a primer above critical pigment volume concentration (CPVC) facilitates adhesion of a topcoat. Above CPVC, the dry film contains pores; when a topcoat is applied, vehicle from the topcoat penetrated into the pores, giving a mechanical anchor.

Testing. Formulators use a penknife to see how hard it is to scrape a coating from a substrate. While a penknife in the hand of an experienced person can be a valuable tool, there is no good way of assigning a numerical value to the results. A variety of methods for evaluating the adhesion of coatings have been investigated (88). None are very satisfactory. The most useful is a direct pull test. A rod is fastened perpendicular to the upper surface of the coated sample with an adhesive. The panel is fastened to a support with a perpendicular rod on its back and an Instron Tester is used to measure the tensile force to pull the coating off the substrate. A potential complication is cohesive failure of the coating; no information on adhesion is obtained. One must exercise caution in interpreting the results

even when the sample appears to have failed adhesively at the substrate–coating interface. Sometimes, when no coating can be seen on the substrate surface after the test, there is a monolayer of material from the coating left on the substrate surface. Surface analysis is useful in determining the locale of failure and the identity of the adsorbed material. Fairly often, there is a combination of adhesive and cohesive failure when an initial crack propagates down to the interface. See Reference 88 for discussion of the effect of variables on test results.

Adhesion can be affected by the angle of application of stress. An instrument called STATRAM II has been devised to combine a normal load and lateral traction to measure friction induced damage (89). Optical measurements are combined with measurements of total energy consumed during the scraping process. The test has been used to study delamination of coatings when plastic automobile bumpers rub together or scrape against solid objects. In many cases, cohesive failure of the plastic occurred near the surface of thermoplastic olefin (TPO), rather than adhesive failure between the coating and the substrate. Composition of coatings, especially solvents, can affect the structure of the upper layer of the plastic.

The most widely used test is the crosshatch test. Using a device with 11 sharp blades, a scratch mark pattern is made across the sample, followed by a second set cut perpendicular to the first. A strip of pressure-sensitive adhesive tape is pressed over the pattern of squares and pulled off. The test distinguishes between samples having poor adhesion and those having fairly good adhesion, but is not very useful in distinguishing among higher levels of adhesion. See Reference 88 for discussion of the variables affecting the test.

Corrosion Protection by Coatings

Steel corrodes by electrochemical reactions. In the presence of oxygen, at anodic areas ferric ions and at cathodic areas hydroxyl ions are formed. Aluminum generally corrodes more slowly than steel because of a dense, coherent layer of aluminum oxide. However, aluminum corrodes more rapidly than iron under either highly acidic or basic conditions. Also, salt affects the corrosion of aluminum more than it affects the corrosion of iron. Galvanized steel is protected since zinc acts as a sacrificial anode and a barrier preventing water and oxygen from reaching the steel surface.

Corrosion Protection by Intact Films. Coatings can be effective barriers to protect steel when a coating can be applied to cover all of the surface and remains intact in service. An important factor is wet adhesion. If water displaces the film, corrosion starts generating ions, giving an osmotic cell under the film (90). Osmotic pressure provides force to remove more coating from the substrate. Amine and phosphate groups are particularly effective polar substituents for promoting wet adhesion. Epoxy phosphates have been used to enhance the adhesion of epoxy coatings on steel (81). Primers made with saponification-resistant vehicles give better corrosion protection than primers made with vehicles that saponify readily (91).

Low water and oxygen permeability increase corrosion protection. Many factors affect permeability of coating films to water and oxygen (92). Coatings with a T_g above the temperature at which corrosion protection is desired reduce

permeability. The higher T_g values of baked coatings is another factor in their superior corrosion protection. Higher XLD leads to lower permeability. Permeability is affected by the solubility of water in a film. Water solubility in halogenated polymers is low; hence vinyl chloride and vinylidene chloride copolymers and chlorinated rubber are often used in formulating topcoats for corrosion resistance. The effect of pigmentation and other variables is reviewed in Reference 93. Water permeability decreases as pigment volume concentration (PVC) (up to CPVC) increases. Pigments with platelet shaped particles reduce permeability rates when they are aligned parallel to the coating surface (94). Leafing aluminum is frequently used. A Monte Carlo simulation model of the effect of several variables on diffusion through pigmented coatings has been devised (95).

Corrosion Protection by Nonintact Films. In many end uses, there will be breaks in the films. Then it is desirable to design coatings to suppress electrochemical reactions. If there are gouges through the film down to bare metal, and wet adhesion is not adequate, water creeps under the coating, and the coating comes loose from the metal over a wider area. Poor hydrolytic stability exacerbates the situation.

Passivating pigments form a barrier layer over anodic areas. The pigments must have some minimum solubility; however, if the solubility is too high, the pigment leaches out of the coating film too rapidly. Red lead [1314-41-6] in oil primers is used for air-dry application over rusty, oily steel. Toxic hazards of red lead restrict its use and regulations can be expected to prohibit its use. The utility of chromate pigments for passivation is well established. Chromate ions must be in aqueous solution. Zinc yellow [85497-55-8] pigment has been widely used in primers. Strontium chromate is sometimes used in primers, especially latex paint primers. Soluble chromates are human carcinogens. They must be handled with appropriate caution. In some countries, their use has been prohibited and prohibition worldwide is probable in the future. Basic zinc and zinc–calcium molybdates, barium metaborate, zinc phosphate, and calcium and barium phosphosilicates, and borosilicates are examples of replacement pigments (96).

Zinc-rich primers contain high levels (over 80 wt%) of powdered zinc. Zinc content exceeds CPVC to assure electrical contact between the zinc particles and with the steel. The film is porous, permitting water to enter, and thus completing the electrical circuit. The zinc serves as a sacrificial anode, and zinc hydroxide is generated in the pores. Vehicles for zinc-rich primers must be saponification resistant. Epoxy resins are used in organic primers. However, the most widely used vehicles are tetraethylorthosilicate (silicic acid tetraethyl ester) [78-10-4] and oligomers derived from it by partial hydrolysis. Alcohol is used as the principal solvent to maintain package stability. After application, the alcohol evaporates, and water from the air completes the hydrolysis of the oligomer to yield a film of polysilicic acid, partially converted to zinc salts. Waterborne zinc-rich primers have been developed using sodium, potassium, and/or lithium silicate solutions in water as the vehicle.

Evaluation and Testing. There is no laboratory test available to predict corrosion protection performance of a new coating system. Suppliers and end users of coatings for such applications as bridges, ships, chemical plants, and automobiles have collected data correlating performance of different systems over many years. These data provide a basis for selection of current coatings

systems for particular applications and insight into how new coatings could be formulated.

Panels are exposed on ocean beaches. The difficulties in such tests are discussed in Reference 97. The steel used is a critical variable (98). Film thickness, evenness of application, flash-off time, baking time and temperature, and many other variables affect performance. Results obtained with laboratory panels can be quite different than results with actual production products. It is desirable to paint test sections on ships, bridges, and chemical storage tanks, and observe their condition over the years.

Since wet adhesion is critical for corrosion protection, techniques for studying wet adhesion can be useful. Electrochemical impedance spectroscopy (eis) is used to study coatings on steel. Many papers (99,100) are available, covering various applications of eis. When a coating film begins to delaminate, there is an increase in apparent capacitance. The rate of increase of capacitance is proportional to the amount of area delaminated by wet adhesion loss. Onset of delamination can be determined by eis studies (101). Results of eis tests are subject to considerable variation (102). Other problems with eis are discussed in Reference 103.

There have been many attempts to develop laboratory tests to predict corrosion protection by coatings. The most widely used test is the salt spray test (ASTM method B117-95). Coated steel panels are scribed through the coating and hung in a chamber with a mist of 5% salt solution at 100% RH at 35°C. The scribe is examined to see how far from the scribe mark the coating is undercut. It has been repeatedly shown that there is little correlation between salt spray tests and actual performance of coatings (104,105). Since with intact films the first failure is blister formation, so humidity resistance tests are widely used (ASTM method D2247-94). They give comparisons of wet adhesion. Alternating high and low humidity causes faster blistering than continuous exposure to high humidity. A large number of humidity cycling tests have been described, involving repeated immersion in warm water and removal for several hours. Prohesion test has been reported to correlate better with actual performance than the standard salt spray test (106); however, other results show poor correlation (107). Another cycling test is the Society of Automotive Engineers test (SAE J-2334).

Resins and Cross-linkers

Latexes. A *latex* is a dispersion of polymer particles in water. Molecular weights of polymers prepared by emulsion polymerization are generally high; $\bar{M}_w$ of 1,000,000 or higher is common. The molecular weight does not affect the viscosity of the latex. Latex viscosity is governed by the viscosity of the medium in which the polymer particles are dispersed, by the volume fraction of particles, and by their packing factor. Latexes are used as the vehicle in a majority of architectural coatings. A growing part of the original equipment manufacture (OEM) product and special purpose coatings markets is latex based.

Acrylic latexes are used for exterior paints because of their resistance to photodegradation and hydrolytic stability. Acrylic latex paints are useful for alkaline substrates such as masonry and galvanized metal. Acrylic and styrene–acrylic

latexes are being used increasingly for industrial maintenance coatings. Acrylic latexes are finding increasing interest for kitchen cabinet finishes and for OEM automotive applications.

Latex paint formulations include coalescing solvents; VOC regulations require use of less coalescing solvent. Various modifications in preparation of latexes have been suggested for reduction of coalescent (108–110). A promising approach is use of thermosetting latexes. A low T_g thermosetting latex permits coalescence without addition of a coalescing solvent. After film formation, cross-linking increases modulus to give block resistance. If a significant degree of cross-linking occurs before application, coalescence will be adversely affected. Hydroxy-functional latexes can be formulated with MF resins or a water-dispersible polyisocyanate for wood and maintenance coatings (111). Carboxylic acid-functional latexes can be cross-linked with carbodiimides (112), or polyfunctional aziridines (113). *m*-Isopropenyl-α,α-dimethylbenzyl isocyanate (TMI) [1-(1-isocyanato-1-methylethyl)-3-(1-methylethenyl)benzene] [2094-99-7] reacts slowly with water and can be used to make thermosetting latexes (114).

Other thermosetting latexes cross-link at room temperature and are storage stable. Carboxylic acid-functional latexes can be cross-linked with β-(3,4-epoxycyclohexyl)ethyltriethoxysilane (115). A combination of amine-functional and epoxy-functional latexes gives stable one package coatings (116). A latex with allylic substitution cross-links on exposure to air (117). Hybrid alkyd/acrylic latexes are prepared by dissolving an oxidizing alkyd in the monomers used in emulsion polymerization (118). Stable thermosetting latexes can be prepared using triisobutoxysilylpropyl methacrylate as a comonomer (115).

Vinyl acetate (VAc) (acetic acid ethenyl ester) [108-05-4] is less expensive than (meth)acrylate monomers. VAc latexes are inferior to acrylic latexes in photochemical stability and resistance to hydrolysis and are used in flat wall paints. Reference 119 discusses use of a variety of vinyl esters in latexes. The polymers are more hydrophobic than VAc homopolymers and have superior hydrolytic stability and scrub resistance. Reference 120 reports the advantages of using vinyl versatate in both VAc and acrylic copolymers.

Amino Resins. Melamine (1,3,5-triazine-2,4,6-triamine) [108-78-1] is reacted with formaldehyde [50-00-0] and alcohols to make melamine–formaldehyde (MF) resins, the most widely used cross-linkers for baked coatings. The ethers groups are activated toward nucleophilic substitution by the neighboring N. Hydroxyl, carboxylic acid, urethane, and phenols with an unsubstituted ortho position react (see AMINO RESINS).

A variety of MF resins are made with differences in the ratio of functional groups, the alcohol, and the degree of polymerization, $\bar{P}$. MF resins are classified into two broad classes: I and II. Class I resins are made with relatively high ratios of formaldehyde to melamine, and most of the nitrogens have two alkoxymethyl substituents. All the resins contain some oligomers; the lowest viscosity ones have high hexamethoxymethylmelamine (HMMM) contents. Class I resins tend to provide tougher films than Class II. Strong acid catalysts are required. Class II resins are made with smaller ratios of formaldehyde to melamine, and many of the nitrogens have only one substituent. The predominant reactive group present in Class II resins is $-NHCH_2OR$. They yield cross-linked films at temperatures lower than that for Class I resins and are catalyzed by weak acids. Some grades of

TiO_2 lead to loss of catalyst activity. Silicon dioxide treated TiO_2 is preferable to aluminum oxide treated TiO_2.

Hydroxy-functional acrylic and polyester resins are most commonly cross-linked by MF resins. The hydroxyl groups of polyols react either by transetherification with the activated alkoxymethyl groups or by etherification with methylol groups of MF resins to form new ether cross-links. The reactions are reversible, but are driven toward cross-linking by volatilization of the monofunctional alcohol or water produced. Rates of reaction with hydroxyl groups depend on the structure of the polyol and the MF resin, the type and amount of catalyst, and the temperature. The rates of development of solvent resistance and film hardness when a fractionated Class I resin with about 95% HMMM was used to cross-link polyester resins made with cyclohexanedimethanol (CHDM) (1,4-dimthylolcyclohexane) [27193-25-5], neopentyl glycol (NPG) (2,2-dimethyl-1,3-propanediol) [126-30-7], and hexylene glycol (HG) (1,6-hexanediol) have been reported (121). CHDM polyesters are most reactive, NPG polyesters are a close second, and HG polyesters are least reactive. During acid-catalyzed cross-linking with polyols, reactions between MF resin molecules also occur. These self-condensation reactions form methylene and dimethylene ether bridges. Both self- and cocondensation reactions contribute to the film properties. With strong acid catalysis, the apparent rate at which Class I resins react with most polyols by cocondensation is faster than by self-condensation. With Class II resins, the rates of cocondensation and self-condensation are similar. In high solids coatings in which the hydroxy equivalent weight is high and the average functionality of the polyol is low, curing is sensitive to variations in cure temperature and time, that is cure window (122). Carboxylic acid-functional resins react with MF resins to form ester derivatives; the reaction is slower than with hydroxyl groups.

Stability is somewhat improved by addition of small quantities of amines. Class II resins generally give poorer package stability than Class I resins. Primary or secondary amines, which react with formaldehyde, should not be used with Class II resins. Use of monofunctional alcohol as part of the solvent extends the storage stability. It is desirable to utilize the same alcohol that is used to synthesize the MF resin. If a different alcohol is used, undesirable changes may occur; if 1-butanol [71-36-3] is used in the solvent with a methoxymethylmelamine resin, the cure response gradually becomes slower as the proportion of butyl ether increases.

Benzoguanamine (6-phenyl-1,3,5-triazine-2,4-diamine) [91-76-9] is used to make benzoguanamine-formaldehyde (BF) resins that give cross-linked films with greater resistance to alkali and alkaline detergents than MF resins. Exterior durability of BF-based coatings is poorer. BF resins are used for applications such as washing machines and dishwashers.

Urea–formaldehyde (UF) resins are made with different ratios of formaldehyde to urea and different alcohols. UF resins are the most economical and most reactive amino resins. With sufficient acid catalyst, coatings formulated with UF resins cure at ambient or mildly elevated temperatures. The coatings have poor exterior durability. UF resins are used in coatings for temperature-sensitive substrates, such as wood furniture, paneling, and cabinetry.

Glycoluril (tetrahydroimidazo[4,5-*d*]imidazol-2,5-(1*H*, 3*H*)-dione) [496-46-8] reacts with formaldehyde and alcohols to form glycoluril–formaldehyde (GF) resins (123). The tetramethyl ether resin is used as a cross-linker in powder

coatings. In solution coatings, ethyl and butyl ethers are used. GF resin coatings have greater flexibility than MF coatings; they are used in applications such as coil coatings and can coatings. GF resins evolve less formaldehyde during cure. GF cross-linked polyols are more resistant to hydrolysis under acidic conditions than MF cross-linked polyols.

Binders Based on Isocyanates. Isocyanates react with any active hydrogen compound. The largest use of polyisocyanates is as cross-linkers for hydroxy-functional acrylic and polyester resins to make urethane coatings. The high reactivity permits ambient or low temperature curing. Because of the intermolecular hydrogen bonding, polyurethanes generally have good abrasion resistance (see ISOCYANATE–DERIVED POLYMERS; URETHANE COATINGS).

Isocyanates react with water to yield ureas and CO_2. Isocyanates react with amines to give urea derivatives. Reaction of most amines is too rapid for use in coatings; however, hindered diamines with lower reactivity have been developed. Polyaspartic esters are used in very high solids coatings (124). Reaction with ketimines and aldimines gives a mixture of a urea from hydrolysis of the ketimine or aldimine and a cyclic unsaturated urea. Aldimines are less reactive with water than ketimines and so a higher ratio of the direct reaction product is obtained. They are used in high solids 2K coatings (124).

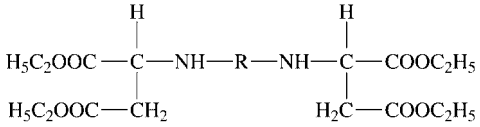

The aromatic diisocyanates most widely used in coatings are bis(4-isocyanatophenyl)methane (MDI) [101-68-8] and toluene diisocyanate (TDI) (2,4-diisocyanato-1-methylbenzene) [584-84-9]. MDI is used in making polyurethanes such as in electrodeposition primers. TDI is used to make cross-linkers such as a low molecular weight trimethylolpropane (TMP) [2-ethyl-2-(hydroxymethyl)-1,3-propanediol] [77-99-6] derivative. The higher molecular weight minimizes toxic hazards and the higher functionality increases the rate of cure. Aromatic isocyanate based coatings turn yellow on exposure. The principal aliphatic isocyanates used are 1,6-hexamethylene diisocyanate (HDI) (1,6-isocyanatohexane) [822-06-0], bis(4-isocyanatocyclohexyl)methane (H_{12}MDI) [5124-30-1], and isophorone diisocyanate (IPDI) [(5-isocyanatomethyl)-1,3,3-trimethylcyclohexane] [4098-1-9]. To reduce toxic hazard and increase functionality, HDI is converted to HDI biuret or HDI isocyanurate. The linear hydrocarbon chain gives flexible coatings. IPDI is used primarily as the isocyanurate derivative; the cyclic structure gives more rigid coatings.

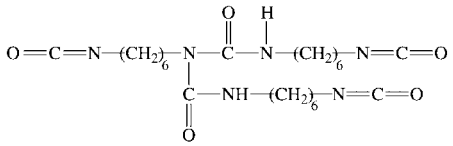

HDI-Biuret

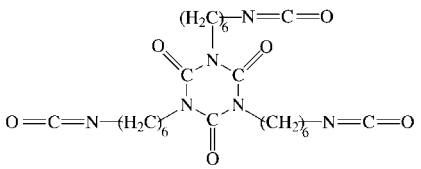

HDI- Isocyanurate

Specialty isocyanates such as tetramethyl-*m*-xylidene diisocyanate (TMXDI) [2778-42-9] and TMI are used in smaller volumes. They have aromatic rings, but give color retention and exterior durability equivalent to aliphatic isocyanates. Since the isocyanato group is on a tertiary carbon, the reactivity is lower than that of less sterically hindered aliphatic isocyanates. TMXDI is offered as a low molecular weight prepolymer with TMP. TMI is used as a comonomer with acrylic esters to make 2000–4000 molecular weight copolymers with 40–50 mol% TMI; thus each molecule has several isocyanate groups (125).

Reaction of isocyanates with alcohols is catalyzed by tertiary amines, metal salts and chelates, organometallic compounds, acids, and urethanes. The most widely used catalysts for reaction with hydroxyl groups are diazabicyclo[2.2.2]octane (DABCO) and dibutyltin dilaurate (DBTDL) [dibutylbis[1-(oxododecyl)oxy]stannate] [77-58-7]. Combinations of DABCO and DBTDL act synergistically. With tin catalysts, the reactivity of aliphatic isocyanates is similar to that of aromatic isocyanates. Carboxylic acids inhibit catalysis by organotin compounds; volatile acids are used to increase pot life without affecting cure rate. Reaction of amines and imines with isocyanates is catalyzed by carboxylic acids and water; since organotin compounds complex with acids, they decrease reactivity (124). CO_2 generated by reaction with water can reduce gloss or result in bubbling. It is desirable to use catalysts such as zirconium acetoacetate $Zr(AcAc)_4$ in waterborne coatings that selectively catalyze reaction with hydroxyl groups (126).

The largest volume of urethane coatings is 2K coatings. One package contains the polyol (or other coreactant), pigments, solvents, catalyst(s), and additives; the other contains the polyisocyanate and moisture-free solvents. The principal reaction is formation of urethane cross-links; some urea cross-links result from reaction with water. Urethane coatings for maintenance paint applications are generally cured at ambient temperatures; those for automobile refinishing and aircraft applications are cured at ambient or modestly elevated temperatures. A N=C=O/OH ratio of 1.1:1 usually gives better film performance than a 1:1 ratio since part of the N=C=O reacts with water to give urea cross-links. Aircraft coatings are often formulated with N=C=O/OH ratios as high as 2:1 to have longer pot life. If very fast cure at relatively low temperatures is needed, reactive coreactants and/or high catalyst levels are used and applied using spray equipment, in which the two packages are fed to a spray gun by proportioning pumps and mixed inside the gun just before they are sprayed.

Blocked isocyanates permit making coatings that are stable at ambient temperature; when baked, the monofunctional blocking agent is volatilized and the coreactant is cross-linked. An extensive review of blocked isocyanates, their reactions, and uses is available (127). The blocking agents most widely used are phenols, oximes, alcohols, ε-caprolactam (hexahydro-2*H*-azepin-2-one) [105-60-2], 3,5-dimethylpyrazole, 1,2,4-triazole, and diethyl malonate (propanedioic acid diethyl ester) [105-53-3]. A variety of catalysts are used: DBTDL is most widely used but many other catalysts have also been used. Bismuth tris(2-ethyl hexanoate) has been particularly recommended (128). In electrodeposition primers, DBTDL has insufficient hydrolytic stability, and tributyltin oxide is an example of an alternate catalyst (129). Cyclic amidines, such as 1,5-diazabicyclo[4.3.0]non-5-ene, are reported to be superior catalysts for use with uretdione cross-linkers in powder coatings (130).

Phenols are used as blocking agents in wire coatings. Phenol blocked isocyanates react with amines at room temperature. They are used as flexibilizing reactive additives in amine cured epoxy coatings (131).

Methyl ethyl ketone oxime (MEKO) (2-butanone oxime) [96-29-7] blocked isocyanates are more reactive than phenols. One package coatings formulated with hydroxy-functional resins cure in 30 min at 130°C. In automotive clear coats, MEKO leads to yellowing. Use of a combination of 3,5-dimethylpyrazole and 1,2,4-triazole has been recommended for clear coats that are non-yellowing (132).

The largest volume coatings with blocked isocyanates are cationic electrodeposition primers. They must be stable in water indefinitely; 2-ethylhexanol blocked isocyanates give the necessary hydrolytic stability. Many other blocking agents have been used to reduce cure temperatures; butoxyethoxyethanol is an example (133).

Diethyl malonate blocked diisocyanates cross-link polyols at 120°C for 30 min. The reaction with alcohols does not yield urethanes, rather transesterification occurs (134), and reaction with amines yields amides, not ureas. Storage-stable coatings can be formulated by using monofunctional alcohol in the solvent (135). Clear coats for automobiles that have both excellent environmental etch and abrasion resistance have been formulated with a combination of a hydroxy-functional acrylic resin, malonic ester blocked HDI and IPDI trimers, and an MF resin (136).

Blocked isocyanates are used in powder coatings with hydroxy-functional resins. ε-Caprolactam blocked IPDI isocyanurate has been the principal reactant. Use of caprolactam is decreasing because of the high temperatures required for curing and oven buildup. Polyol derivatives of IPDI uretdione are being increasingly used since, with cyclic amidine catalysts, they permit curing at lower temperatures than caprolactam and no volatile blocking agent is released (137).

Polyurethane moisture curing coatings cross-link by reaction of isocyanates with atmospheric water. They use isocyanate-terminated resins made from hydroxy-terminated polyesters by reacting the hydroxyl groups with excess diisocyanate. Cure rates depend on the water content of the air. At high humidity and temperature, cure is rapid, but the carbon dioxide released by the reaction of isocyanate with water can be trapped as bubbles, especially in thick films. See Reference 138 for discussion of the effects of temperature and humidity and other application considerations. Moisture curing urethane coatings are used for applications such as floor coatings, for which abrasion resistance and hydrolytic stability are important.

A variety of waterborne polyurethane systems have been investigated (139). Polyurethane dispersion resins (PUD) are polymers dispersed in water; both high molecular weight thermoplastic and lower molecular weight resins with reactive functional groups are available. The high molecular weight polymers are used in coatings similarly to the use of latexes. Since urethanes hydrogen bond strongly with water, they are plasticized permitting film formation with higher T_g polymers than acrylic latexes (140). They also exhibit superior abrasion resistance. hydroxy-functional PUDs can be cross-linked with MF resins or blocked isocyanates. MEKO blocked isocyanates are used with water-reducible anionic acrylic or polyester resins.

Waterborne 2K coatings have been developed. Bayer Corporation was awarded a Presidential Green Award in 2000. Waterborne 2K coatings have limited pot life. In solventborne coatings, pot life can be determined by monitoring viscosity increases; in waterborne 2K coatings, viscosity does not change as reactions occur, since the change in viscosity occurs inside aggregate particles without affecting the bulk viscosity. Coalescence is inhibited if there is too much reaction before volatiles are evaporated. Since isocyanates also react with water, an excess of isocyanate is usually required. The reaction with water results in formation of CO_2, which can lead to blistering, especially as thicker films are applied. Since TMXDI reacts more slowly with water than other isocyanates, it can be used to cross-link water-reducible acrylic resins with lower NCO/OH ratios (141). Polyisocyanate can be mixed in a water-reduced coreactant just before spraying. Spray equipment has been designed to provide in line intensive mixing of the two components (142). Hydrophilically modified polyisocyanates made by reacting a fraction of the —NCO groups of a polyisocyanate with a polyglycolmonoether are more easily mixed (143).

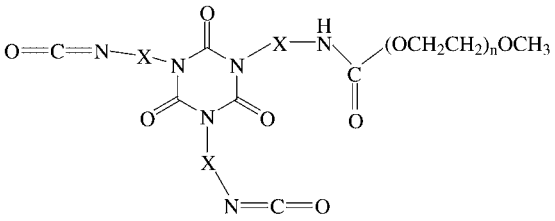

Hydrophilically modified polyisocyanate

Epoxy Resins. The largest volume epoxy resins are made by reacting BPA [4,4′-(1-methylethylethylidene)bisphenol] [80-05-7] with epichlorohydrin (ECH). The resins are represented by the following general formula, where the molar ratio of ECH to BPA determines the average n value.

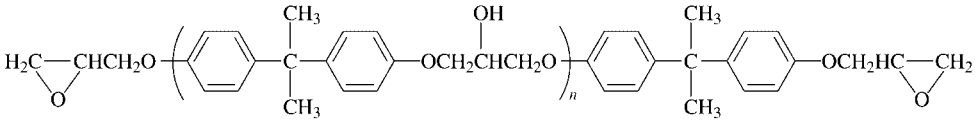

Bisphenol A epoxy resins

Resins are available, having average n values from 1.3 to 16. Viscosity increases with molecular weight. Above an average n value of 2, the resins are amorphous solids with increasing T_g. Because of side reactions, commercial resins have an $\bar{f}_n$ less than 2, commonly about 1.9. BPA epoxy resins are used in coatings in which excellent adhesion and corrosion resistance are required. A limitation of their use is poor exterior durability. Epoxy resins are also prepared by reaction of ECH with novolak phenolic resins. The resulting novolak epoxy resins have $\bar{f}_n$ of 2.2–5.5 (see EPOXY RESINS).

Epoxy-functional acrylic resins are made by using glycidyl methacrylate (GMA) as a comonomer. Epoxidized soy and linseed oils are used in making

acrylate derivatives for uv-cured resins and thermal cationic cure resins. Also available are low molecular weight cycloaliphatic diepoxy compounds such as 3,4-epoxycyclohexylmethyl 3′,4′-epoxy-4-cyclohexylcarboxylate (**2**). They are used as reactive diluents in cationic coatings and as cross-linking agents for polyols, carboxylic acids, and anhydrides.

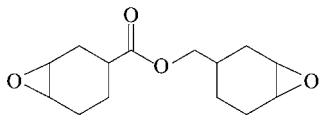

2

Epoxy groups react at ambient temperatures with primary amines to form secondary amines and with secondary amines to form tertiary amines. Aliphatic amines are more reactive than aromatic amines. The reaction is catalyzed by water, alcohols, tertiary amines, and phenols. Reactivity is high enough to require 2K coatings. Pot life is limited to a few hours and coatings take about a week to cure at ambient temperature. Several factors control pot life, including reactive group concentrations; the structural effects of amine, epoxy, and solvents; the equivalent and molecular weights; and $\bar{f}_n$ of the reactants. As the molecular weight of a BPA epoxy resin is increased, the number of equivalents per liter of epoxy groups decreases; therefore, the reaction rate is slower. Higher solids coatings have shorter pot lives.

Many amines such as diethylenetriamine (DETA) [*N*-(2-aminoethyl)-1,2-ethanediamine] [111-40-0] are toxic. Low molecular weight diamines have the disadvantages of low equivalent weights and viscosities, which increases the risk of error in mixing stoichiometric amounts in 2K coatings and the difference in viscosity between the DETA and epoxy resin makes uniform mixing difficult. Amine adducts, BPA epoxy ($n = 0.13$) reacted with an excess of a multifunctional amine, have higher equivalent weight and lower toxic hazard. Amine Mannich bases, prepared by reacting a methylolphenol with excess polyamine, give faster curing (144). Although the functionality of the amine is reduced, the phenolic hydroxyl accelerates the epoxy/amine reaction. Another approach is to react a multifunctional amine with aliphatic mono- or dicarboxylic acids to form amine-terminated polyamides. Dimer fatty acids are widely used; they are complex mixtures, predominately C_{36} dicarboxylic acids, made by acid-catalyzed dimerization of unsaturated C_{18} fatty acids.

BPA epoxy resins and polyamides are mutually soluble in the solvents used in epoxy-amine coatings, but most are not compatible in the absence of solvents. As solvent evaporates, phase separation can occur, resulting in a rough surface, called *graininess*. Graininess can be avoided by allowing the coating to stand for an hour after the two packages are mixed. *Blushing* is the appearance of a grayish, greasy deposit on the surface of films, and incomplete surface cure. Low temperature, high humidity conditions increase the probability of blushing. Blushing decreases gloss, increases yellowing, gives poor recoatability, and may interfere with intercoat adhesion. Blushing results from formation of carbamate salts of amine by reaction with CO_2 and water (145). As with graininess, it is

often possible to minimize blushing by mixing the epoxy and amine components an hour before application.

Waterborne epoxy amine coatings are made using emulsifying agents in either or both the amine and the epoxy package. Proprietary "self-emulsifiable" epoxy resins and polyamides are available; properties approaching those of solventborne coatings can be achieved (146). Nitroalkanes form salts of amines; the salt groups stabilize epoxy-amine emulsions and allow the system to be reduced with water (147). After application, the nitroalkane solvent evaporates, freeing the amine.

BPA epoxy resins can be cross-linked with phenolic resins; both resole and novolak phenolic resins are used. The reaction is acid catalyzed. The coatings require baking, and package stability is relatively limited. Package stability is enhanced with etherified resole resins. Increased solids and high functionality are reported using butoxymethylolated BPA as the phenolic resin (148). Unpigmented epoxy-phenolic coatings are used as linings for beverage cans and for some types of food cans. Concern has been raised because of the possible endocrine disruption by free BPA, an estrogen mimic. Studies are underway to determine whether trace amounts of BPA are extracted in food or beverage cans from BPA epoxy containing can linings (149).

Carboxylic acids are cross-linkers for epoxy coatings. The literature has been reviewed in Reference 150. Reaction of a carboxylic acid and an epoxy group yields a hydroxy ester. GMA copolymers and cycloaliphatic epoxides such as 2 react more rapidly than BPA epoxies. Tertiary amines catalyze the reaction of carboxylic acids with epoxies. Triphenylphosphine is reported to be a particularly effective catalyst. With triphenylphosphine catalysis and an excess of epoxy groups, coatings can be formulated that cross-link at 25°C (151). Cyclic anhydrides are also used. See Reference 151 for a review of the literature. Reaction of anhydrides with epoxy resins can occur initially with the epoxy resin hydroxyl groups, yielding esters and carboxylic acids. The resulting carboxylic acid groups then react with epoxy groups.

Cycloaliphatic epoxies serve as cross-linking agents for polyols for films baked at 120°C. Waterborne coatings are made with caprolactone polyols and (**2**), with diethylammonium triflate as a blocked catalyst (152).

BPA epoxy resins can be cross-linked by reaction of their hydroxyl groups with MF and UF resins are used. Amine salts of a sulfonic acid are used as latent catalysts. Polyisocyanates also cross-link the hydroxyl groups of epoxy resins.

Epoxy resins undergo homopolymerization to polyethers with very strong protic acids. Acid precursors are most commonly used as initiators. There are two types: blocked acids that undergo thermal decomposition to give the free acid, and photoinitiators that release acid on exposure to uv. Suitable super acids are trifluoromethylsulfonic acid (triflic acid) (F_3CSO_3H) and hexafluorophosphoric acid (HPF_6). Only super acids are effective for homopolymerization of epoxies. Homopolymerization with α,α-dimethylbenzylpyridinium hexafluoroantimoniate as a blocked catalyst permits curing of a GMA copolymer at 120°C using (**2**) as a reactive diluent while retaining adequate pot life (153).

A large-scale use of epoxy resins is to make acrylic graft copolymers for interior linings of beverage cans (154). A solution of a BPA epoxy resin in a glycol ether solvent is reacted with ethyl acrylate (2-propenoic acid ethyl ester)

[140-88-5], styrene (ethenylbenzene) [100-42-5], and methacrylic acid (2-methyl-2-propenoic acid) using benzoyl peroxide (dibenzoyl peroxide) [94-36-0] as initiator to make a graft copolymer. The resin is neutralized with an amine such as 2-dimethylaminoethanol (DMAE) [108-01-0]. Class I MF resin is added as a cross-linker, and the system is diluted with water. Sometimes, a latex is blended with the dispersion to reduce cost.

Acrylic Resins. Acrylic resins are used as the primary binder in a wide variety of industrial coatings (see ACRYLIC ESTER POLYMERS). Their main advantages are photostability and resistance to hydrolysis. Hydroxy-functional thermosetting acrylic resins (TSA) are copolymers of nonfunctional monomers with a hydroxy-functional monomer such as 2-hydroxyethyl methacrylate (HEMA) (2-methyl-2-propenoic acid 2-hydroxyethyl ester) [868-77-9]. They are cross-linked with MF resins or polyisocyanates. An increase in solids became necessary to meet lower VOC emission requirements. The amount of non- or monofunctional resin must be kept to a very low fraction. Molecules with no hydroxyl groups would either volatilize or remain in the film as plasticizers. Molecules with one hydroxyl group terminate cross-linking reactions, leaving loose ends in the coating. Statistical methods have been used to calculate the proportions of nonfunctional molecules that would be formed during random copolymerization of monomer mixtures with differing monomer ratios to different molecular weights and molecular weight distributions (155). Esters of bulky alcohols, such as isobornyl methacrylate, as comonomers that can combine relatively low viscosity and high T_g are used (14). For most purposes the upper limit of solids that gives good properties is 45–50% NVV (nonvolatile volume). Solids can be increased by blending acrylic polyols with other low viscosity polyols, such as polyesters (156).

Carboxylic acid-functional acrylic resins are cross-linked with epoxy resins. Epoxy-functional acrylics are made using GMA as a comonomer. Such resins have been recommended for powder clear coats for automobiles (157,158). They can be cross-linked with dicarboxylic acids, such as dodecanoic acid or with carboxylic acid-functional acrylic resins. Isocyanato-functional acrylics can be prepared by copolymerizing TMI with acrylates (159); they can be cross-linked with polyols or hydroxy-functional acrylic resins. They can also be reacted with hydroxypropylcarbamate to yield carbamate-functional acrylic resins (160). Carbamate-functional acrylics can be cross-linked with Class I MF resins to give films with better environmental etch resistance than MF cross-linked hydroxy-functional acrylics while retaining the advantage of mar resistance. Carbamate-functional acrylics can also be prepared by reacting acrylic resins with urea. Trialkoxysilyl-functional acrylics can be prepared using a trialkoxysilylalkyl methacrylate as a comonomer (161). Clear coats made with them are cross-linked by moisture in the air.

VOC emissions can be reduced using water-reducible hydroxy- and carboxylic acid-functional TSA resins with acid numbers of 40–60. Solutions of amine salts of these resins in organic solvents diluted with water form stable dispersions of polymer aggregates swollen by solvent and water. In preparing a coating an amine, such as DMAE, is added; then other coating components (pigments, MF resin, sulfonic acid catalyst) are dispersed or dissolved in this solution and before application the coating is diluted with water.

The morphology of water-reducible TSA dispersions has been studied fairly extensively (162,163). The change in viscosity with dilution of amine salts of

water-reducible resins is abnormal. Initially the viscosity decreases rapidly then rises again to a peak before falling sharply to application viscosity. At application viscosity they have solids in the range of 20–30% NVW (nonvolatile weight). The height of the peak in the dilution curve is dependent on the resin and formulation, and the systems are highly shear thinning in the peak region. Another abnormality of water-reducible resins is that their pH is over 7 (commonly 8.5–9.5), even though less than the theoretical amount of amine necessary to neutralize the carboxylic acid is used (163).

Class I methyl MF resins are the most commonly used cross-linkers. Various types and amounts of amine can be used (164–166). Generally, less than the stoichiometric amount of amine is used. The lower the amine content, the lower the viscosity of the fully diluted systems. For any resin–amine combination, there is a minimum amount of amine required to give a stable dispersion at application viscosity, that is, to prevent macrophase separation. The viscosity is sensitive to amine content. The structure of the amine affects application solids, stability, and cure rate. DMAE is widely used but N-alkylmorpholines and 2,2-dimethylaminopropanol permit faster curing. The amine also affects on wrinkling during curing (164).

Polyester Resins. Polyesters for coatings are low molecular weight, amorphous, and branched, with functional groups for cross-linking. Most of the polyesters are hydroxy-terminated polyesters. They are cross-linked with MF resins or polyisocyanates. Carboxylic acid-terminated polyesters cross-linked with epoxy resins, MF resins, or 2-hydroxyalkylamides are used. In general terms, thermosetting polyesters give coatings with better adhesion to metal substrates and better impact resistance than TSAs. On the other hand, TSAs give coatings with superior water resistance and exterior durability.

Most hydroxy-terminated polyesters are made by coesterifying two polyols (a diol and a triol) and two diacids (an aliphatic dibasic acid and an aromatic dicarboxylic acid or its anhydride). The ratio of moles of dibasic acid to polyol must be less than 1 so as to give terminal hydroxyl groups and avoid gelation. Molecular weight is controlled by this ratio; the smaller the ratio, the lower the molecular weight. The molecular weight distribution $\bar{M}_n$, and $\bar{f}_n$ are all controlled by the diol-to-triol ratio. The ratio of aromatic to aliphatic dibasic acids controls T_g of the resin.

Polyols are selected on the basis of cost, rate of esterification, stability during high temperature processing, functionality, and hydrolytic stability of their esters. The most widely used diol is NPG, and the most widely used triol is TMP. A comparison of results of testing films of coatings made with a series of polyesters from several polyols is given in Reference 167. Coatings based on CHDM polyesters cross-linked with MF resins showed the best hydrolytic stability.

Aromatic acid esters hydrolyze more slowly than aliphatic esters. Esters of phthalic acid are more easily hydrolyzed than esters of isophthalic acid (IPA) (1,3-benzenedicarboxylic acid) [121-91-5]. Adipic acid (1,6-hexanedioic acid) [124-04-9] is the most widely used aliphatic dibasic acid. Dimer acids made by dimerization of drying oil fatty acids are also used.

Viscosity of polyester solutions depends on several variables: molecular weight, molecular weight distribution, T_g of the resin, and the number of functional groups per molecule. Intermolecular hydrogen bonding can be minimized by using hydrogen-bond acceptor solvents such as ketones. Synthesis of low

molecular weight polyesters with two or more hydroxyl groups on all of the molecules is relatively easy. Usually, an $\bar{f}_n$ of between two and three hydroxyl groups per molecule is used. A difunctional polyester with a narrow molecular weight distribution and an $\bar{M}_n$ of 425 is commercially available (168). Low viscosity polyester diols and triols prepared by reacting caprolactone (2-oxepanone) [502-44-3] with a polyols are available (169). These types of resins are useful in blends to increase the solids content of higher molecular weight polyester or acrylic based coatings. They are often called *reactive diluents*.

Polyesters with both hydroxyls and carboxylic acids as terminal groups are used in waterborne coatings. When reduced with water, they have abnormal viscosity dilution curves similar to those described for water-reducible acrylic resins. The most widely used are made by reacting a hydroxy-functional resin with trimellitic anhydride (TMA) (1,3-dihydro-1,3dioxo-5-isobenzofurane carboxylic acid) [552-30-7] to esterify a fraction of the hydroxyl groups, generating two carboxyl groups at each site. The ester group of partially esterified TMA is subject to hydrolysis because of the anchimeric effect of the adjacent carboxylic acid group. water-reducible polyesters are used in applications for which good storage stability and hydrolytic stability are not important, such as industrial coatings with a fast turnover.

Hydrolysis can be minimized by making powdered solid polyesters. An example of such a solid polyester is made from IPA, adipic acid, NPG, CHDM, hydrogenated BPA, and TMA (170). The resin is powdered and stored until a coating is to be made; then, it is stirred into a hot aqueous solution of DMAE to form a dispersion.

Water-thinnable polyester coatings have been formulated with low molecular weight oligomeric hydroxy-terminated polyesters (171). Up to about 20% of water dissolves in a polyester-Class I MF resin binder, reducing the viscosity to about half. This permits making solvent-free coatings.

Polyester resins for powder coating are brittle solids with a relatively high T_g (50–60°C) and so the powder coating does not sinter during storage. Terephthalic acid (TPA) and NPG are used as the principal monomers with smaller amounts of other monomers to increase $\bar{f}_n$ and to reduce T_g to the desired level. Both hydroxy- and carboxy-terminated polyesters are used. The former are most commonly cross-linked with blocked isocyanates and the latter with epoxy resins. Other cross-linkers include 2-hydroxyalkylamides and tetramethoxymethylglycoluril.

Alkyd Resins. Alkyds are synthetic drying oils (see chapter on *Drying Oils* in Reference 172) prepared from polyols, dibasic acids, and fatty acids. Alkyd Resins are lower in cost than most other vehicles and give coatings that exhibit fewer film defects during application. However, durability of alkyds is poorer than acrylics and polyesters. Oxidizing alkyds cross-link by autoxidation. Nonoxidizing alkyds are used as polymeric plasticizers or as hydroxy-functional resins, which are cross-linked by MF resins. Alkyds are classified by oil length calculated by dividing the amount of "oil" in the final alkyd by the total weight of the alkyd solids, expressed as a percentage. Alkyds with oil lengths greater than 60 are long oil alkyds; those with oil lengths from 40 to 60, medium oil alkyds; and those with oil lengths less than 40, short oil alkyds (see ALKYD RESINS).

Oxidizing alkyds are polyesters of a polyol, a dibasic acid, and drying or semidrying oil fatty acids. The rate of cross-linking increases as the number of methylene groups between two double bonds, $\bar{f}_n$, is increased, reaching a

maximum at an oil length of 60. The rate of drying also increases as the ratio of aromatic rings to long aliphatic chains increases. When the reaction is carried to near completion with excess polyol, there are few unreacted carboxylic acid groups, but many unreacted hydroxyl groups. Soybean oil and tall oil fatty acids are most often used. Dehydrated castor alkyds have fairly good color retention; they are used primarily in baking coatings.

Glycerol is the most widely used polyol because it is present in natural oils. The next most widely used is pentaerythritol (PE). At the same mole ratio of dibasic acid to polyol, more moles of fatty acid can be esterified with PE and f_n is higher.

The most widely used dibasic acid is phthalic anhydride (PA) (1,3-isobenzofurandione) [85-44-0]. The rigid aromatic rings increase the T_g of the resin. The first esterification reaction proceeds rapidly by opening the anhydride ring. The amount of water evolved is low, which also reduces reaction time. The next most widely used dibasic acid is IPA. Esters of IPA are more resistant to hydrolysis than are those of PA in the pH range of 4–8, the most important range for exterior durability.

Reduction of VOC emissions has led to efforts to increase solids content of alkyd resin coatings. Since xylene is on the hazardous air pollutants (HAP) list, its use is being reduced. Some increase in solids can be obtained by a change of solvents. Hydrocarbon solvents promote intermolecular hydrogen bonding, especially between carboxylic acids, increasing viscosity. Including some 1-butanol in the solvent gives a significant reduction in viscosity at equal solids. Decrease in molecular weight increases solids. However, making a significant reduction in VOC by this route gives an alkyd with lower functionality for cross-linking and a lower ratio of aromatic to aliphatic chains. Both changes increase the time for drying. The effect of longer oil length on functionality can be minimized by using drying oils with higher average functionality, such as safflower oil. Proprietary fatty acids with 78% linoleic acid are commercially available. Increasing the concentration of driers accelerates not only drying but also embrittlement. One can add a transesterification catalyst near the end of the alkyd cook; this gives more uniform molecular weight and a lower viscosity product, but film properties, especially impact resistance, are inferior to those obtained without transesterification catalyst. Reactive diluents have much lower viscosity than the alkyd resin and react with the alkyd during drying, reducing VOC. The use of reactive diluents is reviewed in Reference 173; 2,7-octadienyl maleate and fumarate are reported to be particularly effective.

Alkyd emulsions are used in Europe and to a lesser degree in the United States (174). The emulsions are stabilized with surfactants and can be prepared with little, if any, volatile solvent. It is common to add a few percent of an alkyd–surfactant blend to latex paints to improve adhesion to chalky surfaces and, in some cases, to improve adhesion to metals.

Oxidizing alkyds can be modified by reaction with styrene. In making styrenated alkyds, an oxidizing alkyd is prepared in the usual way and cooled to about 130°C in the reactor; then styrene and a free-radical initiator such as benzoyl peroxide are added. The ratio of alkyd to styrene can be varied; commonly 50% alkyd and 50% styrene is used. The ratio of aromatic rings to aliphatic chains is increased, and as a result, the T_g of styrenated alkyds give a “dry” film in 1 h

or less versus 4–6 h for the counterpart nonstyrenated alkyd. However, the average functionality for oxidative cross-linking is reduced because the free-radical reactions involved in the styrenation consume some activated methylene groups. As a result, the time required to develop solvent resistance is longer than for the counterpart alkyd. Styrenated alkyd vehicles are often used for air-dried primers. The topcoat must be applied almost immediately or not until after the film has had ample time to cross-link. During the intermediate time interval, application of topcoat is likely to cause nonuniform swelling of the primer, leading to lifting of the primer. The result of lifting is the development of wrinkled areas in the surface of the dried film.

Short-medium oil and short oil alkyds are made with a large excess of hydroxyl groups to avoid gelation. The hydroxyl groups can be cross-linked with MF resins. The advantage of relative freedom from film defects common to alkyd coatings is retained. Nondrying oils with minimal levels of unsaturated fatty acids are used to maximize exterior durability and color retention. Since IPA esters are more stable to hydrolysis in the pH range of 4–8 than phthalate esters, the highest performance exterior alkyd-MF enamels use nonoxidizing IPA alkyds.

Uralkyds. Uralkyds are alkyd resins in which a diisocyanate, usually TDI or MDI, replaces PA. One transesterifies a drying oil with a polyol to make a "monoglyceride" and reacts it with somewhat less diisocyanate than the equivalent amount of isocyanate. Like alkyds, uralkyds dry faster than the drying oil from which they are made, since they have a higher $\% \bar{f}_n$ and the rigidity of the aromatic rings. Two principal advantages of uralkyd over alkyd coatings are superior abrasion resistance and resistance to hydrolysis. Disadvantages are inferior color retention of the films, higher viscosity of resin solutions at the same percent solids, and higher cost. The largest use of uralkyds is in so-called varnishes. They are used as transparent coatings for furniture, woodwork, and floors ie, applications in which good abrasion resistance is important.

Epoxy Esters. BPA epoxy resins are converted to epoxy esters by reacting with fatty acids. It is not practical to esterify more than about 90% of the potential hydroxyl groups, including those from ring opening the epoxy groups. The lower useful limit of the extent of esterification is about 50%, to ensure sufficient fatty acid groups for oxidative cross-linking. Tall oil fatty acids are commonly used because of their low cost. Dehydrated castor oil fatty acids give faster curing epoxy esters for baked coatings. Epoxy esters are used in coatings in which adhesion to metal is important. Epoxy esters have good adhesion to metals and retain adhesion even after exposure of the coated metal to high humidity. An advantage of epoxy esters over alkyd resins is their greater resistance to hydrolysis and saponification. Exterior durability of epoxy ester coatings is poor.

Epoxy esters can also be made water-reducible by reacting maleic anhydride (2,5-furandione) [108-31-6] with epoxy esters prepared from dehydrated castor oil fatty acids. Addition of a tertiary amine opens the anhydride to give amine salts. Like other water-reducible resins, these resins are not soluble in water, but form a dispersion of resin aggregates swollen with water and solvent in an aqueous continuous phase. They are used in baking primers and primer-surfacers.

Phenolic Resins. Although their importance has waned, phenolic resins still have significant uses. Resole phenolics useful in coatings applications are

made by reacting monosubstituted phenols and mixtures of them with phenol with more than 1 mol of formaldehyde. They are methylol-terminated; the substituted phenols reduce cross-link density. There are two groups: alcohol-soluble, heat-reactive phenolics and oil-soluble, heat-reactive phenolics. Alcohol-soluble resole phenolics are used with an acid catalyst in interior can coatings and tank linings. To enhance flexibility and adhesion, they can be blended with low molecular weight poly(vinyl butyral). They are also blended with epoxy resins in thermosetting coatings for applications such as primers and can coatings. Oil-soluble resole phenolics are prepared by reacting a para-substituted phenol, such as *p*-phenylphenol. They are solid, linear resins with terminal methylol groups. They are used to make varnishes with drying oils.

The package stability of alcohol-soluble resole resins and their compatibility with epoxy resins can be improved by partial conversion of the methylol groups to ethers. Allyl ethers have been used with epoxy resins in interior can coatings. Low molecular weight butyl ethers are used with acid catalysts to cross-link epoxy resins and other hydroxy-substituted resins, by etherification and transetherification reactions (148).

Novolak phenolics are made with acid catalysts and ortho- or para-substituted phenols. Molecular weight is controlled by the molar ratio of phenol and formaldehyde, which is always greater than 1. The terminal phenol groups are not metholylated. Alcohol-soluble novolak phenolics derived from *o*- or *p*-cresol are used to make novolak epoxy resins. Oil-soluble novolak phenolics made with a substituted phenol, such as *p*-phenylphenol, are used with drying oils to make varnishes, such as marine spar varnish (see PHENOLIC RESINS).

Silicon Derivatives. Three classes of organic silicon derivatives are used in coatings: Silicones, reactive silanes, and orthosilicates.

Silicones are polymers with backbones consisting of —[$Si(R)_2$—O]— repeating units. They are prepared by reacting chlorosilanes with water to form silanols that condense to form siloxanes. Silicone oils made from dimethyldichlorosilane and methyltrichlorosilane are used as additives to reduce surface tension. Chemically modified silicone fluids, such as polysiloxane/polyether block copolymers, with broader ranges of compatibility have been described (175).

Polymerization of a mixture of mono-, di-, and trichlorosilanes results in a silicone resin with some unreacted hydroxyl groups. Silicone resins cross-link in 1 h at 225°C with catalysts such as zinc octanoate. The cross-linking process is reversible; hence, silicone films are sensitive to water. Ammonia and amines are especially destructive to such films (176). The coatings are repellent to liquid water, but permeable to water vapor. Most silicone resins are copolymers of methyl- and phenyl-substituted monomers; properties depend on the phenyl-to-methyl ratio. The rate of the cross-linking reaction is faster with high-methyl-substituted silicone resins. The uv resistance of high-methyl silicone resins is greater than high-phenyl ones. The exterior durability of silicone coatings is better than that of other coatings except highly fluorinated polymers (177). Coatings from methylsilicone resins have low temperature flexibility superior to those from phenylsilicones and to most other organic coatings.

High-phenyl silicones are superior to high-methyl silicones for applications requiring high temperature resistance, and far superior to other organic coatings except certain fluoropolymers. When silicones are thermally decomposed the

product is silicon dioxide, which, although brittle, can serve as a temperature-resistant coating binder. Chimney paints are made from silicone resins pigmented with aluminum flake for use at over 500°C for years. At the high service temperature, the organic substituents burn off, leaving behind a film of the aluminum pigment in a matrix of silicone dioxide, possibly with some aluminum silicate. See Reference 177 for discussion of coatings with varying heat resistance.

High solids silicone resins have been made available, which cure either by directly using zinc octonoate catalysts or by cross-linking with trialkoxysilanes using a titanate catalyst (178). Waterborne silicone resins have also been developed; one approach is to emulsify a silicone resin in water (179).

Silicone-modified alkyds are made by coreacting a silicone intermediate during synthesis of the alkyd. Silicone intermediates are low molecular weight silicone resins; frequently with the hydroxyl groups converted to methoxy groups, they react with free hydroxyl groups on the alkyd. Exterior durability of silicone-modified alkyd coatings is significantly better than unmodified alkyd coatings. The improvement in durability is roughly proportional to the amount of added silicone resin; 30% silicone resin is a common degree of modification. Silicone-modified alkyds are used mainly in outdoor air-dried coatings such as topcoats for steel petroleum storage tanks. Silicone-modified polyester and acrylic resins are used in baking coatings, especially in coil coatings for metal siding. See Reference 177 for examples of formulations and preparation of silicone-modified resins.

Waterborne silicone resins can be prepared from water-reducible acrylic and polyester resins. Also, acrylic latexes prepared with hydroxyethyl (meth)acrylate as a comonomer can be modified with silicone intermediates (178).

Reactive silanes are silanes with a substituted alkyl group and a trialkoxysilyl group. They are used in coatings in several ways; review papers are given in Reference 180. Resins with multiple trialkoxysilyl groups can be used as binders for moisture-cure coatings. For example, an isocyanate-terminated resin can be reacted with 3-aminopropyltriethoxysilane to give a resin with terminal triethoxysilyl groups. Coatings made using such resins cross-link to a polymer network after application and exposure to humid air. Part of the solvent used is ethyl alcohol, which permits reasonable pot life in the presence of water. They do not form CO_2, which can lead to film imperfections in moisture cure urethanes.

Trialkoxysilyl acrylic resins are made with a trialkoxysilylalkyl methacrylate as a comonomer (181). Coatings cure on exposure to atmospheric moisture; the reaction is catalyzed with organotin compounds or organic acids. The coatings have excellent exterior durability, resistance to environmental etching and marring, and adhesion to aluminum. Automotive clear coats are being made by combining trialkoxysilylalkyl- and hydroxy-functional acrylic resins with MF resins or blocked isocyanates (182).

Trialkoxysilylated acrylic and vinyl acetate latexes can be prepared using 3-methacryloxypropyltriisobutoxysilane as a comonomer in emulsion polymerization (115). Coatings are reported to have superior adhesion, as well as high chemical, solvent, and mar resistance.

Use of various silanes for treatment of metal surfaces is discussed in the section on Corrosion Protection.

Halogenated Resins. Halogenated polymers have low water permeability. They are used in topcoats for corrosion protection. Some are sufficiently soluble

in polyolefin plastics, and therefore they are used in tie coats to provide adhesion for topcoats. Thermoplastic vinyl chloride copolymers were formerly used on a large scale but are being phased out because of high VOC.

Dispersion grade vinyl chloride copolymers with high molecular weights are used in high solids plastisol coatings. Plastisols are polymer particles dispersed in a plasticizer. Since the T_g of the polymer is well above room temperature and polymer is partially crystalline, the polymer does not dissolve in the plasticizer at room temperature. When a plastisol is heated, the polymer dissolves in the plasticizer and the particles coalesce to a molten state. When cooled, the product is a plastic consisting of a homogeneous solution. The viscosity is reduced by addition of solvents that dissolve the plasticizer without swelling the polymer particles. Solids at application viscosities are 80% or more. A variety of stabilizing agents are used, including organotin esters such as dibutyl tin dilaurate; barium, cadmium, and strontium soaps; maleates; and oxirane compounds.

Chlorinated rubber is used in topcoats for heavy duty maintenance paints because of its low water permeability. It is also used in tie coats on polyolefin plastics. Chlorinated rubber dehydrochlorinates and requires stabilizers similar to those used with PVC. Some metal salts, especially those of iron, tend to promote degradation of chlorinated rubber and so it degrades when applied over rusty steel. Chlorinated ethylene/vinyl acetate copolymers have been developed that can be used to replace chlorinated rubber in at least some applications (183).

Polytetrafluoroethylene (PTFE) has the greatest exterior durability and heat resistance of any polymer used in coatings. However, PTFE is insoluble in solvents, and its fusion temperature is so high that coating uses are limited to applications in which the substrate can withstand high temperatures. Aqueous dispersions of PTFE are used to coat the interior of chemical processing equipment and cookware. After application, the polymer particles are sintered at temperatures as high as 425°C. PTFE has such a low surface free energy that it is not wet by either water or oils. Since its fusion temperature is lower, poly(vinylidene fluoride) (PVDF) can be used in additional applications. PVDF is used in coil coatings as a plastisol-like dispersion in a solution of acrylic resin (184). The fusion temperature of the films is reported to be 245°C. The exterior durability is outstanding but only low gloss coatings are possible. Copolymers of vinylidene fluoride (VDF) are also being used in powder coatings.

Fluorinated copolymers with functional groups such as hydroxyl groups can be cross-linked after application. Copolymers of VDF with a hydroxy-functional monomer cross-linked with a polyisocyanate give coatings with superior wet adhesion and corrosion as compared with PVDF homopolymer (185). Halofluoroethylene (CF_2=CFX)/vinyl ether copolymers have been used on steel building panels and in clear coats for automobiles (186). Vinyl ethers and CF_2=CFX form alternating polymers; functional groups can be introduced by copolymerizing hydroxy-substituted vinyl ether comonomers. Copolymers with hydroxyl groups can be cross-linked with MF resins or polyisocyanates.

Other Binders. Unsaturated polyester resins are maleic acid-containing polyesters dissolved in styrene. The resin/styrene solution is cross-linked using free-radical initiators. The polymerization is oxygen inhibited. Inhibition is minimized by incorporating some insoluble semicrystalline paraffin wax. The wax layer results in a relatively uneven, low gloss surface, suitable for some applications.

Oxygen inhibition can be minimized using coreactants that have allyl groups with styrene–unsaturated polyesters (187). Waterborne unsaturated polyester resins are prepared by reacting 2 mol of maleic anhydride with 1 mol of a mixture of low molecular weight polyalkylene glycols and diols. The resulting partial ester is further esterified with 2 mol of trimethylolpropane diallyl ether (188). Unsaturated polyester/styrene resins can be used in uv-cured coatings. A photoinitiator generates free radicals on exposure to uv radiation. High intensity radiation sources are used, which generate very large numbers of free radicals sufficiently rapidly at the surface, so that the oxygen in the air at the surface is depleted.

Gel coats are pigmented unsaturated polyester–styrene coatings; they are sprayed on the inside of a mold surface. The gel coat is then sprayed with glass fiber-loaded unsaturated polyester–styrene compound and then covered with plastic film. Many glass-reinforced plastic objects, ranging from prefabricated shower stalls to boat hulls, are made this way. Unsaturated polyesters made using neopentyl glycol, MA, and isophthalic acid provide better gloss retention than those made from propylene glycol and PA.

Various types of nitrocellulose are made, and the grade used in coatings is RS (Regular Solubility) grade with a percent nitrogen of 11.8–12.3. To reduce the handling hazard, nitrocellulose is shipped wet with ethyl or isopropyl alcohol. While nitrocellulose is not soluble in alcohol, it is soluble in mixtures of ketones and esters with alcohols and hydrocarbons. Several molecular weight grades are available. Use has dropped substantially because of the high VOC of NC lacquers; the principal remaining use is in wood finishing. These lacquers have relatively low solids but continue to be used to a significant, if decreasing, extent because they enhance the appearance of wood grain to a greater extent than any other coating. Increasingly stringent VOC emission regulations can be expected to force further reductions in use of nitrocellulose.

Acrylated oligomers are prepared from a variety of starting oligomers. Acrylated urethane oligomers tend to give coatings with a good combination of hardness and elasticity, and epoxy resin derivatives tend to give coatings with good toughness, chemical resistance, and adhesion. Any polyol or hydroxy-terminated oligomer can be reacted with excess diisocyanate to yield an isocyanate-terminated oligomer, which is reacted with hydroxyethyl acrylate to yield an acrylated urethane oligomer. The oxirane groups of epoxy resins are reacted with acrylic acid, with triphenylphosphine as a catalyst. Epoxidized soybean or linseed oil also react with acrylic acid to give lower T_g oligomers with higher functionality.

2-Hydroxyalkylamides esterify more rapidly than simple alcohols. Polyfunctional 2-hydroxyalkylamides (eg, the tetrafunctional hydroxyalkylamide derived from aminolysis of dimethyl adipate with diisopropanolamine) are cross-linkers for carboxylic acid-functional acrylic or polyester resins (189). The properties of coatings obtained by cross-linking carboxylic acid-functional acrylic resins with hydroxyalkylamides compare favorably with those obtained using MF resins as cross-linkers with the same resins. An advantage relative to MF cross-linkers is the absence of formaldehyde, which is emitted in low concentrations when MF-based coatings are baked. The cross-linking reaction is not catalyzed by acid. See Reference 190 for discussion of the mechanism of esterification. Tetra-*N*,*N*,*N*′,*N*′-(2-hydroxyethyl)adipamide is a solid used in powder coatings (191).

Acetoacetoxy-functional acrylic solution resins can be made by copolymerizing acetoacetoxyethyl methacrylate (AAEM) with other acrylate monomers (192,193). hydroxy-functional resins can be reacted with diketene or transesterified with methyl acetoacetate to form acetoacetylated resins. MF resins react with acetoacetate groups in the presence of an acid catalyst somewhat slower than with hydroxyl groups (192). There are indications of improved wet adhesion, perhaps resulting from chelating interactions with the surface of the steel. Isocyanates also react with acetoacetate groups; the cure rate is slower than with hydroxyl groups, but pot life is longer. Polyacrylates (eg,TMP triacrylate) [37275-47-1] undergo Michael reactions with acetoacetate groups at ambient temperatures, with the formic acid salt of 1,8-diazabicyclo[5.4.0]undec-7-ene as a blocked catalyst (193). Ketimines give tautomeric ketimine–eneamine cross-links that interact strongly with metal surfaces (194). A primer is reported to give excellent adhesion and corrosion resistance when applied to an aircraft grade aluminum alloy with a chromate-free pretreatment.

Polyfunctional aziridines are used as cross-linkers. Polyaziridines are skin irritants, and some individuals may become sensitized. Mutagenicity of polyaziridines is controversial; however, dilution by coating vehicles reduces their possible toxic effects (195). Polyaziridines, such as the addition product of 3 mol of aziridine to 1 mol of trimethylolpropane triacrylate, react with polyfunctional carboxylic acids to form 2-aminoester cross-links. The main uses are to cross-link carboxylic acid groups on latexes and waterborne polyurethanes. Reaction with the carboxylic acid is much faster than the reaction of the aziridine groups with water, pot lives are 48–72 h. Additional cross-linker can be added to restore reactivity.

Polycarbodiimides react with carboxylic acid and slowly enough with water so that they can be used in waterborne systems. The product of the reaction with a carboxylic acid is an *N*-acylurea. Polycarbodiimides cross-link carboxylic acid-functional resins, including aqueous polyurethane dispersions and latexes (196, 197). Cross-linking occurs within several days at ambient temperature and faster with heat.

Solvents

Most coatings contain volatile material that evaporates during application and film formation. They reduce viscosity for application and control viscosity changes during application and film formation. Selection of volatile components affects popping, sagging, and leveling and can affect adhesion, corrosion protection, and exterior durability. For a more extensive discussion see chapter on *Solvents* in Reference 172. Air pollution regulations have limited solvent usage and will become more restrictive. Most solvents used in coatings are controlled except acetone. Also some solvents are on the HAP list and there will be increasing pressure to reduce these emissions.

Solvents are selected using the general rule that like dissolves like. Three-dimensional solubility parameters are used when a change of solvent combination is required by cost changes, new toxicity information, etc. Solvents have a marked effect on the viscosity of resin solutions (see the section on Flow for discussion).

The rate at which evaporation occurs affects the time required to convert a coating to a dry film, and the appearance and physical properties of the final film. The rate of evaporation of a solvent is affected by four variables: temperature, vapor pressure, surface-to-volume ratio, and rate of air flow over the surface. When a coating is applied by a spray gun, it is atomized to small particles as it comes out of the orifice of the gun; thus, evaporation is rapid because the ratio of surface to volume is high. Rate of solvent depends on film thickness; the fraction of solvent present in a 50-μm film after a given time is greater than that remaining in a 25-μm film. The rate of air flow over the surface is a factor because the rate of evaporation depends on the partial pressure of the solvent vapor in the air at the surface. Spraying a coating with an air spray gun results in more loss of solvent than with an airless gun. Air flow effects cause nonuniform evaporation from coated objects; solvent evaporates more rapidly near the edges of a coated panel than from its center. RH has little effect on the evaporation rates of most solvents; however, it has a significant effect on the evaporation rate of water.

Rates of evaporation of solvents are related to the evaporation rate of *n*-butyl acetate [123-86-4]. Determination of relative evaporation rates requires measurement under standardized conditions. A study by Rocklin illustrates the effects of changes in conditions on relative evaporation rates (198).

When formulating baking coatings for spray application, it is common to use a mixture of fast and very slow evaporating solvents. A significant fraction of the fast evaporating solvent evaporates before the spray droplets reach the object being coated, raising viscosity and reducing the tendency of the coating to sag, while the slow evaporating solvent keeps the viscosity low enough to promote leveling and to minimize the probability of popping when the coated object is put into a baking oven.

Except in high solids coatings, the resin or other coating components have little effect on initial rate of solvent evaporation when coating films are applied. However, as solvent loss from a coating continues, a stage is reached at which the rate of evaporation slows sharply. As the viscosity of the remaining coating increases, availability of free volume decreases, and the rate of solvent loss becomes dependent on the rate of diffusion of solvent through the film to the surface, rather than on the rate of evaporation from the surface. The solids level at which the transition from evaporation rate control to diffusion rate control occurs varies widely, but is often in the 40–60% NVV range. If the T_g of the resin is sufficiently higher than the temperature of the film, the rate of solvent loss will, in time, approach zero. Years after films have been formed, there will still be residual solvent left in the film. The smaller the size of the solvent molecule, the greater its chance of finding sufficiently large free-volume holes. Even though its relative evaporation rate is higher, cyclohexane is retained in films to a greater degree than toluene because cyclohexane is bulkier. Equations have been developed that model the effect of solvent size on diffusion based on free volume of polymers (199). Solvents evaporate more slowly from high solids coatings, making it more difficult to control their sagging (see section on Sagging for discussion).

Volatile Loss from Waterborne Coatings. RH during application and drying of the coatings has a major effect on rates of volatile loss from waterborne coatings. Limited levels of organic solvents are used to modify evaporation rates; however, future regulations can be expected to reduce the levels permitted.

Evaporation of water from a drying latex paint film resembles first-stage drying throughout most of the process; it is controlled by temperature, humidity, evaporative cooling, and rate of air flow over the surface (200). After most of the water has left, evaporation slows as a result of coalescence of a surface layer through which water must diffuse. In latex paints that are to be applied by brush or roller, it is desirable to retard the development of a partially coalesced surface layer to permit lapping of wet paint on wet paint. This generally requires the presence of some slow evaporating solvent, such as propylene glycol. The presence of this solvent does not affect the initial rate of water loss, but does slow down the development of a surface skin (201). The presence of such a water-soluble solvent also facilitates the loss of coalescing solvent.

In coatings formulated water-reducible resins, the relative evaporation rate of water and solvent is affected by RH. Rocklin studied azeotropy in speeding up water/solvent evaporation in humid air (202). For example, at 40% RH, the time required for evaporation of 90% of a 20 wt% solution of 2-butoxyethanol [111-76-2] in water is 1820 s compared with 2290 s for water alone. The relative evaporation rate E of water at 0–5% RH and an air temperature of 25°C is 0.31, but at 100% RH it is 0. If a solution of 2-butoxyethanol ($E = 0.077$) in water evaporates at low RH, water evaporates more rapidly, and the remaining solution becomes enriched in 2-butoxyethanol. At high RH, 2-butoxyethanol evaporates more rapidly, and the remaining solution becomes enriched in water. At an intermediate RH, the relative evaporation rates of water and 2-butoxyethanol are equal and the composition of the remaining solution is constant. This RH is the critical relative humidity (CRH) (203). The CRH for 2-butoxyethanol solutions in water is estimated at about 80%. CRH is different in coatings; for example, CRH is 65% for 10.6 wt% (based on volatile components) 2-butoxyethanol in a coating (204). The high heat capacity and heat of vaporization of water also affect the evaporation rates of water and water-solvent blends in an oven. For example, the times for 99% weight loss of 2-butoxyethanol (bp 171°C), water, and a 26:74 blend of 2-butoxyethanol/water in a TGA when room temperature samples were put into the furnace at 150°C were 2, 2.6, and 2.5 min, respectively (205). The higher heat of vaporization of water (2260 $J \cdot g^{-1}$ at its boiling point) compared to 2-butoxyethanol (373 $J \cdot g^{-1}$ at its boiling point) slowed the rate of heating of the water and water-solvent blend enough to more than offset the expected evaporation rates based on boiling points. Such effects can be critical in controlling sagging and popping of waterborne coatings.

Water can also serve to reduce viscosity of oligomers with hydrogen-bond interactions. It has been shown that up to 20% (depending on the formulation) water can dissolve in solvent-free coatings (171).

Other Properties. Flammability depends on structure and vapor pressure. There is an upper and a lower level of vapor concentration that limits flammability or explosion. The most common cause for fires in coating factories has been static electricity. Solvent flowing out of one tank and into another tank by gravity picks up enough electrostatic charge to cause a spark; all equipment used in handling solvents and solvent-containing mixtures should be electrically grounded. There are two main types of flammability tests: open cup and closed cup; both measure a *flash point*, the minimum temperature at which solvent can be ignited by a hot wire. ASTM specifies standard conditions for both tests.

Generally, open-cup testers give results more appropriate for indicating degree of hazard of a mixture when exposed to air, as during a spill. The closed-cup flash point more nearly describes the fire hazard of a liquid enclosed in a container. U.S. Department of Transportation regulations for shipment of flammable liquids are based on closed-cup tests. Transportation costs can be substantially affected by flash points of the material being shipped. A discussion of the factors affecting flash points, including molecular interactions in blends, is given in Reference 206. Predictions of closed-cup flash points for mixed solvents can be made by computer program that requires only flash points and molecular structures of the pure components (207,208).

Density can be an important variable. Most solvents are sold on a weight basis but critical cost is the cost per unit volume. Most U.S. air pollution regulations are based on weight of solvent per unit volume of coating, which also favors use of low density solvents in formulations.

Electrostatic spraying requires control of the conductivity of the coating. The conductivity of hydrocarbon solvents is too low to permit pickup of adequate electrostatic charge. Alcohols, nitroparaffins, and amines are common solvents or additives to increase conductivity. The conductivity of waterborne coatings poses problems, such as the need to insulate the spray apparatus and relatively fast loss of charge from spray droplets.

Surface tension is a factor influencing solvent selection. Solvents affect the surface tension of coatings, which can have important effects on the flow behavior of coatings during application, as discussed in the section on Film Defects. Since surface tensions depend on temperature and concentration of resins in solution, solvent volatility can have a large effect on the development of surface tension differentials.

Toxicity and Air Pollution Regulations. All solvents are toxic at some level of exposure. The greatest potential risk comes from inhalation. Acute toxicity data indicate the level of single doses that can be injurious or lethal, and is important in cases of accidental ingestion or spills. The level of exposure that is safe for people exposed 8 h a day for long periods of time is used to set the upper concentration limits in a spray booth. Exposure over periods of years to low levels of some solvents increase the risk of cancer. For solvents that may be carcinogenic, very low levels of permissible exposure are set. The levels are frequently too low to be controlled by economically feasible methods. For example, benzene has not been used in coatings for many years for this reason. A common difficulty is to know what the level of exposure will be. Reference 209 describes an approach to assessing possible exposures when retail consumers apply coatings in a room.

In 1990 the U.S. Congress listed HAP whose use is to be reduced (210). Among those of importance in the coatings field are methyl ethyl ketone (MEK) (2-butanone) [78-93-3], methyl isobutyl ketone (MIBK), *n*-hexane, toluene, xylene, methanol, ethylene glycol, and ethers of ethylene glycol. The EPA Hazardous Air Pollutants Strategic Implementation Plan describes regulatory efforts (211). The first step was a voluntary program aimed at reducing emissions of 17 chemicals, including MEK, MIBK, toluene, and xylene, by 50% (of 1988 levels) by 1995. Mandatory HAP limits are included in EPA's Unified Air Toxics Regulations,

issued for all major categories of coatings users in 1995–1999; for an example, see Reference 212. A group of solvent producers has petitioned for removal of 2-butoxyethanol, MEK, and MIBK from the HAP list.

U.S. VOC regulations treat solvents (except water, acetone, CO_2, certain silicone fluids, and fluorinated solvents) as equally undesirable. Removal of methyl acetate and *t*-butyl acetate from the list has been requested. The EPA assessed the most advanced technology for each end use and established maximum VOC guidelines for major applications. During the 1990s, the EPA guidelines ranged from 0.23 to 0.52 $kg \cdot L^{-1}$ (1.9–4.3 $lb \cdot gal^{-1}$) for most major industrial coating operations (213). Tighter EPA guidelines are expected. EPA standards can be obtained on the internet (214).

In establishing future regulations, there is a difference of opinion as to whether all solvents should be considered as equally undesirable in the atmosphere as they are now. The present approach is simpler to enforce. However, it may well be that using less reactive solvents to replace more reactive ones would be advantageous by allowing at least some opportunity for dissipation in the atmosphere to minimize the probability of local excess ozone concentrations. In Europe, some regulations are based on the photochemical ozone concentration potential (POCP) of individual solvents. Reference 215 provides a list of POCP values and examples of reformulation of solvents to minimize POCP emissions.

An approach to VOC reduction is use of supercritical carbon dioxide as a component in a solvent mixture (216). The critical temperature and pressure of CO_2 are 31.3°C and 7.4 MPa (72.9 atm), respectively. Below that temperature and above that pressure, CO_2 is a supercritical fluid. Under these conditions, solvency properties of CO_2 are similar to aromatic hydrocarbons. A very high solids coating and supercritical CO_2 are metered into a proportioning spray gun in such a ratio as to reduce the viscosity to the level needed for proper atomization. Airless spray guns are used; it has been found that the rapid evaporation of the CO_2 as the coating leaves the orifice of the spray gun assists atomization. VOC emission reductions of 50% or more have been reported.

VOC emissions can be substantially affected by transfer efficiency in spraying coatings. When a coating is sprayed, only a part of the coating is actually applied to the object being coated. Transfer efficiency is the percentage of coating used actually applied to the product. As the transfer efficiency increases, the VOC emissions decrease. Transfer efficiency depends on many variables, particularly the type of spray equipment utilized. In some cases, regulations have been established, setting a lower limit on transfer efficiency.

In some cases, it is feasible to recover the solvent used in coatings. Solvent recovery is desirable, but feasibility is limited by low solvent concentration in the air stream, needed to stay below the lower explosive limits. VOC emissions can also be minimized by incineration. The effluent solvent-laden air stream is heated in the presence of a catalyst to a temperature high enough to burn the solvent. As with solvent recovery, this approach is feasible only when solvent concentrations are relatively high. Incineration has been found to be particularly applicable in coil coating. Most of the solvent is released in the baking oven; part of the effluent air from the baking oven is recirculated back into the oven. The amount of such recirculation is limited so that the solvent content does not approach the lower explosive limit. The balance of the effluent air is fed to the gas burners that heat

the oven. The solvent in the air is burned along with the gas; the fuel value of the solvent reduces the gas requirement.

The VOC emitted by a coating is not easily determined. Solvent can be retained in films for very long periods of time. In latex paints, coalescing solvents are used that are only slowly released from the coating. In cross-linking coatings, volatile by-products may be generated by the reaction. For example, MF cross-linking leads to the evolution of a molecule of volatile alcohol for each cocondensation reaction, and in self-condensation reactions, there can be emission of alcohol, formaldehyde, and methylal. The amount released depends on curing conditions and the amount of catalyst used. On the other hand, when slow evaporating glycol ether solvents are used in an MF cross-linking system, some of the glycol ether reacts with the MF resin and is not emitted. Amines used in "solubilizing" water-reducible coatings volatilize to different extents, depending on conditions and amine structure. With high solids 2K coatings, the amount of volatile material is affected by the time between mixing and application. Very high solids coatings use low molecular weight oligomers; particularly when baked, some oligomer may volatilize. Thus, in many cases, only approximations of potential VOC emissions can be calculated, even when the formulation of a coating is known.

It would be desirable to have a standard method for determining VOC. However, there is little agreement as to what that standard method should be. Methods for determination of VOC are available in Reference 210. Methods for determining VOC of waterborne coatings is made difficult because of the need to determine water content. A modified Karl Fischer method in which the water in a coating is azeotropically distilled before titration is most accurate and convenient (217).

Color and Appearance

Color and gloss are important to the decorative aspects of the use of coatings and, sometimes, to the functional aspects of their use. Color has three components: an observer, a light source, and an object. If a surface is very smooth, it has a high gloss; if it is rough on a scale below the ability of the eye to resolve the roughness, it has a low gloss. Color and gloss interact; changing either changes the other. Reference 218 is a monograph covering color and appearance.

Interactions of Light Sources and Observer. Color depends on the interaction of three factors: light source, object, and observer. If any factor changes, the color changes. If an object is observed under a light source with the energy distribution of a tungsten light bulb and shifts to a different illuminant, the color changes. If the chemical composition of the colorants in two coatings are the same, their reflectance spectra are identical, and the coatings match under any light source. Two coatings with different colorant compositions and different reflectance spectra can have the same color under a certain light source. However, such a pair will not match under light sources with different energy distributions. This phenomenon is called *metamerism*. In a spectral match, the two panels change color with a new light source, but it is the same change in both cases. In a metameric pair, the color is the same with one light source; the colors of both panels also change when the light source is changed, but the extent of change is different between the two panels.

Hiding. With coatings that do not completely hide the substrate, color is affected by reflectance of light through the film, reaching the substrate. Hiding increases as film thickness increases and as light scattering increases, that is, hiding is affected by the refractive index differences, particle sizes, and concentrations of scattering pigments present. Hiding increases as absorption increases. Black pigments, which have high absorption coefficients for all wavelengths, are particularly effective. Surface roughness increases hiding; a larger part of the light is reflected at the top surface, reducing the differences of reflection resulting from differences in the substrate to which a coating is applied. Preparation of a transparent coating requires that there is no light scattering within the film; therefore, the particle size of pigment particles must be very small. There are quality control tests that compare hiding of batches of the same or similar coatings, but no test is available that can provide an absolute measure of hiding (219).

Metallic and Interference Colors. Metallic coatings are widely used on automobiles. They are made with transparent colorants with nonleafing aluminum pigment. They exhibit shifts in color as a function of viewing angle. Regular high gloss paints exhibit dark colors when a panel is looked at from relatively small viewing angles and light colors when a panel is observed from large angles of view. Metallic coatings are lighter in color when viewed near the normal angle (the face color) and darker when viewed from a larger angle (the flop color). The surface must be smooth (high gloss) with no light scattering from the resin or color pigment dispersion, and the aluminum flake particles be aligned parallel to the surface of the film.

Pigments that produce colors by interference are also used in automotive coatings. Pearlescent pigments are mica flakes on which thin films of TiO_2 or iron oxide have been deposited, serving to give interference reflection of light striking the pigment surface. The hues of the coatings vary with angles of illumination and viewing. Another type of interference color pigment is composite flakes with a center layer of opaque metal sandwiched between two clear layers and thin layers of metal so that the flakes are semitransparent. Color is also affected by the angle of illumination and viewing, since the path length of light through the layers depends on the angles of illumination and viewing (220).

Color Systems. The human eye can discriminate thousands of colors. However, it is difficult for a person to tell another person what colors he/she sees. Two types of color systems are used: one that uses color samples and one that identifies colors mathematically. The visual color system used in the United States is the Munsell Color System with color chips, classified in a three-dimensional system. The dimensions of the Munsell System are hue, value, and chroma. The color chips have equal visual differences between pairs of adjacent chips. The light source must be specified. Surface roughness affects color, and so comparisons have to be made at equal gloss levels. Two sets of Munsell chips are available: one with high gloss and the other with low gloss.

The mathematical color system is the CIE Color System based on mathematical descriptions of light sources, objects, and a standard observer. Light sources are specified by their relative energy distributions, objects are specified by their reflectance (or transmission) spectra, and the observer is specified by the CIE standard human observer tables. For color analysis, the light reflected (or transmitted) from (or through) an object is measured with a spectrophotometer. The

CIE system permits accurate representation of all colors; however, mathematical differences are not visually uniform. For further discussion of color systems, see Reference 218.

Color Matching. Many pigmented coatings are color matched. The customer chooses a color for a product and a coating formulator is given a sample to match the color. Before starting the initial laboratory color match, the color matcher needs certain information:

(1) **Metamerism.**

Is a spectral (nonmetameric) match possible (using the same colorants)? If not, any match will be metameric. If the customer has been using a coating made with one or more pigments containing lead compounds and wants a lead-free coating, only a metameric match is possible.

(2) **Light sources.**

If the match is to be metameric, the customer and supplier must agree on the light source(s) under which the color is to be evaluated.

(3) **Gloss and texture.**

The color of a coating depends on its gloss and texture. Some of the light reaching the eye of an observer is reflected from the surface of the film and some from within the film. The color seen by the observer depends on the ratio of the two types of reflected light. At most angles of viewing, more light is reflected from the surface of a low gloss coating than from the surface of a high gloss coating. It is impossible to match the colors of a low gloss and high gloss coating at all angles of viewing.

(4) **Color properties.**

Colorants that meet the performance requirements have to be chosen. Does the coating need to have exterior durability, resistance to solvents, resistance to chemicals such as acids and bases, resistance to heat, or meet some regulation for possible toxicity?

(5) **Film thickness and substrate.**

Since in many cases, the coating will not completely hide the substrate, the color of the substrate and film thickness affect the color of the coating.

(6) **Baking schedule.**

Since the color of many resins and some pigments are affected by heating at high temperatures, color of a coating can be affected by the time and temperature of baking.

(7) **Tolerance.**

How close a color match is needed? Coatings for exterior siding or automobile topcoats require very close color matches. For many others, close matching is unnecessary. Overly tight tolerances raise cost without performance benefits. For coatings that are going to be produced over time with many repeat batches, the most appropriate way to set color tolerances is to have an agreed on set of limit panels.

It is desirable to use four pigments to make the original match. This provides the four degrees of freedom necessary to move in any direction in three-dimensional color space. In visual color matching, color matchers look at the sample to be matched, and from their experience select a combination of pigment dispersions that they think will permit matching the color. Computerized instrumental color matching is replacing visual color matching. Computer programs can be used to select colorants and their ratio, both to match original color in the laboratory and to provide information as to the amount of the different pigment dispersions to be added in the factory so as to match production batches. Establishing such a program requires a major effort to set up the database. The reflectance values are measured at 16 wavelengths. See Reference 218 for discussion of pigment databases. Discussion of computer color matching is beyond the scope of this article; see References 218 and 221 for reviews of computer color matching. Matching of metallic and pearlescent colors has been difficult to computerize because the colors have to match at multiple angles. Measurement of metallic and pearlescent coatings is the topic of ongoing research between instrument manufacturers, coating suppliers, and users with the ASTM; Reference 222 summarizes the approaches.

Gloss. Gloss is a complex phenomenon; for discussions of gloss see References 223 and 224. Individuals frequently disagree on gloss difference. Partly because of the difficulty of visual assessment, progress in developing useful mathematical treatments or measurements of gloss has been limited.

There are several types of gloss. *Specular gloss*, a high gloss surface reflects a large fraction of the light at the specular angle. Lower gloss surfaces reflect a larger fraction at nonspecular angles. When considering gloss, people visually compare the amount of light reflected at the specular angle with the amounts reflected at other angles. If the contrast in reflection is high, gloss is said to be high. The fraction of light reflected at a surface increases as the angle of illumination increases. Surface reflection at the specular angle increases as the refractive index of an object increases. If a surface is rough on a microscale, the angle of incidence of a beam of light is not the same as the geometric angle of the surface with

the light beam. Light is reflected at specular angles between the light beam and individual rough facets of a surface. If a surface has many small facets oriented at all possible angles, a beam of light is reflected in all directions. Such a surface is a diffuse reflector and has a low gloss.

Related to specular gloss is *distinctness-of-image (DOI) gloss*. A perfect specular reflector is a perfect mirror. If a surface has perfect diffuse reflection, no mirror image can be seen. At intermediate stages, the image is more and more blurred as the ratio of specular to diffuse reflection decreases. Often one sees both blurring and distortion.

Sheen refers to reflection of light when a low gloss coating is viewed from near a grazing angle. A high gloss coating reflects a high fraction of light whose angle is near grazing. Reflection from most low gloss surfaces is low at a grazing angle. A low gloss coating is said to have a high sheen if there is significant reflection at a grazing angle.

Haze affects gloss. When light enters a hazy film, it is scattered to some degree, causing some diffuse reflection. The contrast between the fractions of light reflected at specular and nonspecular angles is reduced.

The principal factor controlling gloss of coatings is pigmentation. Roughness of the surface varies with the ratio of PVC to the CPVC in the dry film. Reference 225 discusses the effect of pigmentation on gloss as solvent evaporates. In solventborne, high gloss coatings, the pigment concentration in the top micrometer or so of a dry film contains little, if any, pigment. This layer results from motions within a film as solvent evaporates. Convection currents are set up in the film, and resin solution and dispersed pigment particles move freely. As solvent evaporates, viscosity of the film increases, and movement of pigment particles is slowed. Movement of resin solution continues longer and so the top surface contains little pigment.

Particle size of the pigment affects gloss; if aggregates of pigment are not broken up in the dispersion process, gloss will be lower. Flocculated pigment systems have a lower CPVC, and so at the same PVC there will usually be lower gloss. However, since large particles stop moving before small ones, flocculated particles will stop moving sooner than well stabilized ones, which can lead to increased gloss in low PVC coatings. Reference 226 discuss effects of pigment particle size and clear layer thickness on specular gloss.

In some coatings, it is desirable to have a low gloss, but still a high degree of transparency. This is accomplished using a small quantity of very fine particle size silicon dioxide as a pigment. The combination of small particle size and low refractive index difference results in minimal light scattering as long as concentration is low. When solvent evaporates from such a lacquer, the SiO_2 particles keep moving until the viscosity of the surface of the film becomes high. The result is a higher than average concentration of pigment at the top of the film, reducing gloss at relatively low PVC.

Latex coatings generally have lower gloss than solventborne coatings. Latex coatings have both resin and pigment particles as dispersed phases. During drying of a latex paint film, there is not the same separation to give a pigment-free thin layer at the top of the film as in a solvent coating. Latexes with smaller particle size give somewhat higher gloss films than larger particle size latexes. Pigment-free dry films of many latexes are hazy, reducing gloss.

Gloss can change during the life of an applied film. In some cases, the surface of the film embrittles and then cracks as the film expands and contracts. Generally, this mechanical failure is progressive, and after initial loss of gloss, there is film erosion. In other cases, especially clear coats, erosion occurs first, and loss of gloss is only evident after erosion is deep enough to cause protrusion of pigment particles of the base coat. Erosion of binder in pigmented films can proceed to a stage in which pigment particles are freed from binder on the surface and rub off easily; this phenomenon is called *chalking*. Chalky surfaces have lower gloss and the color changes to a lighter color. Loss of gloss can also result from loss of volatile components after a film is exposed, causing film shrinkage and increased surface roughness (227). An excellent review of durability and gloss has been given in Reference 227.

No fully satisfactory method for measuring gloss is available, and no satisfactory rating scale for visual observation of gloss has been developed. While all people will agree as to which film is glossier if the gloss difference is large, they frequently disagree in ranking if the difference is small. Specular gloss meters are widely used, but correspondence between meter readings and visual comparisons is limited. The aperture of the slit in a gloss meter is about 2° whereas the limit of resolution of a human eye is about 0.0005° of arc. A gloss meter is, therefore, less sensitive to DOI than the eye. The distance between the aperture and a panel is fixed in a gloss meter, whereas a person can view a panel from any distance. The most widely used gloss meters measure response only at the specular angle. Those mostly used in the coatings industry make measurements at angles of incidence and viewing of 20°, 60°, and 85°. One must use the standard that has been calibrated at the selected angle. Black and white standards are available. Reflection at the specular angle is not the same from a white and a black standard with equal surface roughness because the white pigment scatters light. Normally, one first measures at 60°. If the reading is over 70, readings should be made at 20° since the precision is higher nearer the midpoint of the meter reading. It is common to read low gloss panels at both 60° and 85°. Readings at 85° may have a relationship to sheen. Readings are reproducible on carefully calibrated instruments to ±2 gloss units. This is a high percentage of error in the low gloss range.

There is confusion as to what the numbers mean. They are *not* the percentage of light reflected at the surface. They are closer to being the percentage of light reflected at that angle compared to the reading that would be obtained if a perfectly smooth surface were measured. The total reflection from a black matte surface is much higher at most angles of illumination and viewing than that from a high gloss black surface. Meter readings are lower for the same panel when the setting is 20° as compared to 60° (228). The instruments can be used for quality control comparisons of lots of the same or very similar coatings and for following loss of gloss on aging. For specification purposes other than quality control, specular gloss meters are not appropriate, and one must rely on standard visual panels.

DOI meters use the sample as a mirror. The reflection of a grid on the surface of the panel is compared visually to a set of photographic standards ranging from a nearly perfect mirror reflection to a blurred image in which the grid cannot be detected. One reports the comparison of the degree of blurring and also a qualitative statement about distortion. Correspondence with visual assessment in

the high gloss range is better than with specular gloss meters, but DOI tends to be insensitive to small differences in the low gloss range. Instruments are available to make comparisons based on optical density.

New instruments with linear diode array detectors permit multiple measurements of light reflected at small angle increments without using an aperture in front of the detector (229). Computerized instruments make multiple measurements of reflectance from small areas (approximately 100-μm diameter) over a 10-cm^2 area. This permits separation of the reflection from micro- and macroroughness, thus giving a numerical rating for gloss and a separate measurement of macro roughness, such as orange peel or texture.

Pigment Dispersion

Pigments are manufactured with a particle size distribution that gives the best compromise of properties, but the particles become cemented together into aggregates during processing. Breaking these aggregates and forming stable dispersions of optimally sized pigment particles is a critical process. Making dispersions involves three aspects: wetting, separation, and stabilization.

Dispersions in Organic Media. Wetting is essential for pigment dispersion. Wetting requires that the surface tension of the vehicle be lower than the surface free energy of the pigment. In organic media this is the case for all inorganic and most organic pigments. There can be important differences in the rate of wetting. When a dry pigment is added to a vehicle to make a mill base, it tends to clump up in clusters of pigment aggregates. For wetting to occur, the vehicle must penetrate through these clusters and into the pigment aggregates. The rate of wetting is dominantly controlled by the viscosity of the vehicle.

Processes are designed to separate pigment aggregates into individual crystals without grinding crystals to smaller particle size. Many different types of machinery are used to carry out the separation stage. Dispersion machines apply a shear stress to the aggregates suspended in the vehicle. If the aggregates are easily separated, the machinery only needs to be able to exert a small shear stress. If aggregates require a relatively large force for separation, then machinery that can apply a higher shear stress is required. Pigment manufacturers have been increasingly successful in processing and surface-treating pigments so that their aggregates are relatively easily separated. The available shear rate for a dispersion machine is set by its design. The formulator must select appropriate dispersion machinery that can transfer sufficient shear stress to the aggregates and formulate a mill base for its efficient use. Discussion of such machinery is beyond the scope of this article. Several types of machines have been discussed in Reference 230, and detailed engineering information is available from machinery manufacturers. Reference 231 deals more fundamentally with engineering aspects of some dispersion methods.

Stabilization is usually the key to making good pigment dispersions. If the dispersion is not stabilized, the pigment particles will be attracted to each other and undergo flocculation. Flocculation is a type of aggregation, but the aggregates formed are not cemented together like the aggregates in the dry pigment powder.

Flocculation can be reversed by applying relatively low levels of shear stress. Flocculation is almost always undesirable.

There are two mechanisms for stabilization: charge repulsion and entropic repulsion. In charge repulsion, particles with like electrostatic charges repel each other. In organic media, entropic repulsion is the more important stabilizing mechanism. The repelling effect of layers of adsorbed material on the surface of the particles of a dispersion prevents the particles from getting close enough together for flocculation to occur. In many dispersions of pigments in organic media, the adsorbed layer consists of resin molecules swollen with solvent. The particles are in rapid, random (Brownian) motion. As they approach each other, their adsorbed layers become crowded; there is a reduction in the number of possible conformations of molecules of resin and associated solvent in the adsorbed layers. The resulting decrease in disorder constitutes a reduction in entropy. Reduction in entropy corresponds to an increase in energy and requires force; hence, resistance to reduction in entropy leads to repulsion.

Much of our understanding of entropic stabilization of pigment dispersions comes from the seminal work of Rehacek (232). A technique has been discussed to determine the thickness and composition of the adsorbed layer on the surface of a pigment dispersed in a resin solution. It has been found that if the adsorbed layer thickness of resin plus solvent is less than 9–10 nm, the dispersion is not stable (232–234). With monofunctional surfactants, the adsorbed layer can be thinner and still protect against flocculation. It has been shown that an adsorbed layer thickness of 4.5 nm of surfactant and associated solvent was adequate (235). In contrast to the adsorbed layer of resin, which is nonuniform in thickness, the surfactant layer is comparatively uniform, and so it does not have to be as thick to provide stabilization.

Absorption plots deviate from linearity at low values of resin concentration. This results from competition between resin and solvent adsorption that depends on both the relative affinity of resin and solvent molecules for the pigment surface and the concentration of resin. At low concentrations, both solvent and resin are adsorbed on the particle surface and so the average layer thickness is insufficient to prevent flocculation. Below the start of the linear section of the curve, the low shear viscosities of the dispersions are higher than those above it, separation of pigment during centrifugation is more rapid, and the bulk of the centrifugate formed is greater. This behavior shows flocculation below the critical concentration.

With resins having several adsorption sites, the largest single factor controlling adsorbed layer thickness is molecular weight. The adsorbed layer thickness on TiO_2 dispersed in a series of BPA epoxy resins in MEK, increased from 7 to 25 nm as the molecular weight of the epoxy resin increased (233). With the lowest molecular weight resin, the layer thickness of 7 nm was insufficient. Dispersions in solutions of the higher molecular weight resins were stable. Adsorbed layer thickness is also affected by the pigment surface. A TiO_2 surface treated with alumina forms a more stable dispersion than a TiO_2 surface treated with silica in the same long oil alkyd solution (236). It was proposed that the adsorbed layer is more compact on the silica-treated TiO_2. Resin molecules that have multiple adsorbing groups have an advantage in competition with solvent molecules, but if the solvent interacts strongly with the pigment surface and the resin only interacts

weakly, the more numerous solvent molecules will "win" the contest. If the ratio of resin to solvent is just sufficient to allow adequate adsorption of resin to stabilize the dispersion, addition of more of the same solvent shifts the equilibrium, displacing part of the resin and reducing the average adsorbed layer thickness below the critical level for stabilization. The dispersion is said to have been subjected to solvent shock.

It is frequently difficult to make stable pigment dispersions in high solids coatings. Increasing the solids of organic solution coatings requires decreasing the molecular weight of the resins and reducing the number of functional groups per molecule. The low molecular weight results in thinner adsorbed layers of resin and associated solvent molecules. The reduced number of functional groups per resin molecule decreases the probability of the adsorption of resin molecules. Surfactants have been designed that are so strongly adsorbed on a pigment that, little excess over the amount sufficient to saturate the pigment surface area is needed to stabilize a dispersion. For example, phthalocyanine blue modified by covalently attaching long aliphatic side chains has been used as a surfactant with phthalocyanine blue pigment; the phthalocyanine end of the molecules of surfactant in effect joins the crystal structure of the surface of the pigment particles so that little, if any, is in solution (235). Special dispersing aids called *hyperdispersants* have been designed. The design parameters have been described in Reference 237. The most effective class of dispersant has a polar end with several functional groups and a less polar tail of sufficient length to provide for a surface layer that is at least 10 nm thick. See Reference 238 for a further review of the use of hyperdispersants.

The combination of resin (and/or dispersant), solvent, and pigment, used to make a pigment dispersion, is called a *mill base*. Higher pigment loading gives more efficient production; high loadings are possible when the viscosity of the vehicle (solvent plus resin) used in the mill base is low. Low viscosity also gives faster wetting. For maximum pigment loading, it is desirable to use the minimum concentration of resin solution that provides stability. The Daniel flow point method gives an estimate of the appropriate resin concentration to be used with a particular pigment (230).

Dispersions in Aqueous Media. Dispersion of pigments in aqueous media involves the same factors as in organic media. However, the surface tension of water is high and so there is more likely to be a problem in wetting the surface of pigment particles. In some cases, water interacts strongly with the surface of pigments; therefore, the functional groups on the stabilizers have to interact more strongly with the pigment surface to compete with water. Also, many aqueous dispersions are in latex paints, and so the systems have to be designed such that stabilization of the latex dispersion and the pigment dispersion do not adversely affect each other.

Inorganic pigments such as TiO_2, iron oxide, and most inert pigments have highly polar surfaces, and so there is no problem with wetting them with water. Most organic pigments require a surfactant to wet the surfaces. Some organic pigments are surface treated with adherent layers of inorganic oxides to provide a polar surface that is more easily wet by water. In contrast to dispersions in organic media, stabilization by charge repulsion can be a principal mechanism in aqueous media. Stability of the dispersions depends on pH, since pH affects surface charges. For any combination of pigment, dispersing agent, and water, there is a

pH at which the surface charge is 0; this pH is called the *isoelectric point* (*iep*). At *iep*, there is no charge repulsion; above *iep*, the surface is negatively charged; and below *iep*, it is positively charged. The stability of dispersions is at a minimum at *iep* $\pm$ 1 pH unit (239). The *iep* value for pigments varies, for example, 4.8 for kaolin clay and 9 for $CaCO_3$.

Entropic stabilization can also be effective. A study of stabilization of aqueous TiO_2 dispersions by anionic and nonionic surfactants concluded that a high molecular weight nonionic copolymer provided the greatest resistance to flocculation both in the dispersion and during drying of a gloss latex paint film (240). Since stabilization resulted from entropic stabilization it was not affected by changes in pH. Block copolymers with hydrophobic and hydrophilic segments made by group transfer polymerization have been recommended for stabilization of aqueous dispersions of a range of organic pigments (241).

Most latex paint formulations contain several pigments and several surfactants. The *iep* of the various pigments are different, which complicates the problem of charge stabilization. Commonly, mixtures of surfactants are used. Anionic surfactants are frequently used as one component. Polymeric anionic surfactants (such as salts of acrylic copolymers in which acrylic acid and hydroxyethyl acrylate are used as comonomers) provide salt groups for strong adsorption on the polar surface of the pigment and hydroxyl groups for interaction with the aqueous phase; nonpolar intermediate sections add adsorbed layer thickness. Polymeric surfactants are less likely to lead to performance problems in the final films than monomeric surfactants. Nonionic surfactants are frequently used along with an anionic surfactant. It is common to also add potassium tripolyphosphate, the basicity of which may assure that the pH is above the *iep* of all pigments.

Evaluation of Degree of Dispersion. Assessment of degree of dispersion is a critical need for establishing original formulations, optimizing processing methods, for quality control. Differences in degree of dispersion come from two factors: incompleteness of separation of the original aggregates into individual crystals and flocculation after separation. An effective evaluation method is by determination of tinting strength in comparison to a standard. One can check for flocculation by pouring some of the tint mix on a plate and rubbing the wet coating with a finger. If the color changes, the dispersion is flocculated. Well-stabilized dispersions have Newtonian flow properties. If a dispersion is shear thinning (and does not contain a component designed to make it shear thinning), it is flocculated. A further method of assessing pigment dispersion is by settling or centrifugation. The rate of settling is governed by particle size and difference in density of the dispersed phase from the medium. A well-separated, well-stabilized dispersion centrifuges slowly, but when settling is complete the amount of sediment is small. A well-separated but poorly stabilized dispersion settles quickly to a bulky sediment. If the pigment settles or centrifuges relatively quickly to a compact layer, the separation step is incomplete. The degree of flocculation can be calculated from rates of centrifugation (235).

One can also examine the dispersion with a microscope; one must exercise caution in preparing the samples for examination. In general, it is necessary to dilute the sample. If the sample is diluted with solvent, there is a possibility of flocculation. Electron microscope studies of the surfaces of etched dry coating films can be useful for assessing variations in dispersion (242). Flocculation gradient

technique is an accurate method for quantitative study of the degree of pigment dispersion in both liquid coatings and dry films. The method was originally developed to study TiO_2 dispersions (243). The extent of scattering of 2500-nm ir radiation by a film as a function of film thickness is measured. A plot of backscatter against film thickness gives a straight line whose gradient increases with increasing flocculation. The technique has proven useful in evaluation of flocculation of other pigments (244).

The most widely used method of testing for fineness of grind is the Hegman drawdown gauge. A sample of dispersion is placed on the steel block before the zero reading and drawn down by a steel bar scraper. One then lifts the block up and quickly looks across the drawdown sample to see at which graduation one can start to see particles projecting or streaks caused by particles being dragged along. It is said that the higher the scale reading, the "better" the dispersion. The device is not capable of measuring degree of dispersion. A major problem in making satisfactory dispersions is avoiding flocculation, but the gauge cannot detect flocculation. The particle sizes of properly dispersed pigments are small compared to the depth of the groove on the gauge. The depth on some gauges ranges from 0 to 10 mil (250 μm) in graduation units of 1.25 mil (approx 30 μm). TiO_2 pigment particles have an average size of about 0.23 μm. Aggregates of a large number of particles would escape detection. Many color pigment particles are even smaller and carbon black particles can be as small as 5 nm. It has been shown that in TiO_2 dispersions approximately 0.1% of the total pigmentation of a coating was responsible for an unacceptable fineness of grind rating (245).

Pigment Volume Relationships

Coatings formulators often work with weight relationships, but volume relationships are generally more important. A series of performance variables have been viewed to be a function of the PVC, the volume percent of pigment in a dry film (246). It has been found that many properties of films change abruptly at some PVC as the PVC is increased in a series of formulations. This PVC has been designated as CPVC. Also, *CPVC* has been defined as that pigment volume concentration where there is just sufficient binder to provide a complete adsorbed layer on the pigment surfaces and fill all the interstices between the particles in a close-packed system. Below CPVC, the pigment particles are not close-packed and binder occupies the "excess" volume in the film. Above CPVC, the pigment particles are close packed, but there is not enough binder to occupy all the volume between the particles, resulting in voids in the film. Slightly above CPVC, the voids are air bubbles in the film, but as PVC increases, the voids interconnect and film porosity increases sharply. When films are prepared from coatings with PVC near CPVC, there may not be uniform distribution of pigment through the dry film, and so parts of the film may be above CPVC and other parts below CPVC (247). Some properties start to change as soon as PVC increases so there are air voids in films, and other properties change when the PVC is sufficiently greater than CPVC and so the film begins to be porous. Coatings with flocculated pigment clusters result in films with nonuniform distribution of pigment particles, and

CPVC with flocculated pigments is lower than the CPVC with the same pigment combination that is not flocculated.

There is a controversy about the applicability of CPVC to latex paints. Reference 248 includes a review of the literature. The effect of PVC on hiding of latex paints showed that CPVC was lower in latex paint than in solvent-based paint made with the same pigment composition (249). It has been recommended that the term latex CPVC (LCPVC) be used (230). Although CPVC is approximately independent of the binder in solventborne paints, LCPVC varies with the latex and some other components of latex paints. LCPVC increases as the particle size of the latex decreases, as the T_g of the latex polymer decreases, and concentration of coalescing agent increases. A quantitative study of the effect of latex particle size on CPVC using a series of monodisperse vinyl acetate/butyl acrylate latexes with TiO_2 pigment showed that CPVC depended on the ratio of the number of latex and pigment particles and the ratio of their diameters (248). A simulation program using particle size distributions of latex and pigment and a measure of the deformability of latex particles has been developed to predict the CPVC of simple latex paints (250).

As PVC is increased in a series of coatings made with the same pigments and binders, density increases to a maximum when PVC equals CPVC and then decreases. Above CPVC the lower density of air reduces the film density. Tensile strength generally increases with PVC to a maximum at CPVC but then decreases above CPVC. Below CPVC, the pigment particles serve as reinforcing particles and increase the strength. Above CPVC, air voids weaken the film; abrasion and scrub resistances of films drop above CPVC. Stain resistance decreases above CPVC, since staining liquids can penetrate into pores. A single coat of a coating with PVC above CPVC to steel exposes the panel to humidity and rapid rusting occurs. An alkyd-based coating with PVC above CPVC to a wood substrate is less likely to blister than with a similar coating with PVC below CPVC as a result of the porosity of films above CPVC. Gloss is related to PVC. In general, unpigmented films have high gloss. The initial (low) percentage of pigment has little effect on gloss, but above a PVC of 6–9, gloss drops until PVC approaches CPVC. It is almost always desirable to make primers with a high PVC, since the rougher, low gloss surface gives better intercoat adhesion than a smooth, glossy surface. It is sometimes desirable to design a primer with PVC greater than CPVC. Adhesion of a topcoat to such a primer is enhanced by mechanical interlocking resulting from penetration of vehicle from the topcoat into pores of the primer. Many of the pores in the primer are filled with binder from the topcoat, which increases the PVC of the topcoat, resulting in loss of gloss. Such a primer is said to have poor enamel hold out. The primer PVC should be only enough higher than CPVC to provide adhesion to minimize loss of gloss of the topcoat.

PVC affects hiding; as pigmentation increases, hiding generally increases. Initially, hiding increases rapidly, but then levels off. In the case of rutile TiO_2 hiding goes through a maximum, gradually decreases with further increase in PVC, and then increases above CPVC. This increase in hiding above CPVC results from air voids left in the film when PVC is above CPVC. The refractive index of air (1.0) is less than that of the binder (approx 1.5) and so there is light scattering by the air interfaces in addition to interfaces between pigment and binder. Owing to the high cost of TiO_2, coatings are not generally formulated with a PVC of

TiO_2 greater than about 18% since incremental hiding at higher PVC is not cost efficient. (This value is dependent on the actual TiO_2 content of the TiO_2 pigment and on the stability of the TiO_2 dispersion.) In high PVC coatings, lower cost inert pigments are used to occupy additional volume. The scattering efficiency of TiO_2 is affected by the particle size of the inert pigments used with it (251). Inclusion of some inert pigment with a particle size smaller than that of TiO_2 (ie, less than 0.2 μm) increases the efficiency by acting as a so-called *spacer* for the TiO_2 particles. The increase in hiding above CPVC can be useful. Hiding of ceiling paints can be improved by formulating above CPVC. This permits hiding with one coat, which is particularly desirable in ceiling paints. The stain and scrub resistances of the paint are inferior to similar paints with PVC; less than CPVC; they are not important in ceiling paints. Tinting strengths of white coatings increase as the PVC of a series of coatings is increased beyond CPVC. The air voids above CPVC increase light scattering so that a colored paint dries with a lighter color than one with the same amount of color pigment but with a PVC below CPVC.

For any application, there is a ratio of PVC to CPVC most appropriate for the combination of properties needed. Once this ratio has been established, changes in pigment combinations for that application should be made such that this PVC/CPVC ratio is maintained. This concept is developed in detail in Reference 252.

There are large variations in CPVC, depending on the pigment or pigment combination in a coating and the extent, if any, of pigment flocculation. With the same pigment composition, the smaller the particle size, the lower the CPVC. The ratio of surface area to volume is greater for smaller particle size pigments; hence, a higher fraction of binder is adsorbed on the surface of the smaller pigment particles and the volume of pigment in a close-packed final film is smaller. CPVC depends on particle size distribution; the broader the distribution, the higher the CPVC, since broader particle size distribution of spherical, dispersed-phase systems increases packing factor. In low gloss coatings, the least expensive component of the dry film is inert pigment; to minimize cost, it is desirable to maximize inert pigment content by using inert pigments with a broad particle size distribution.

Pigment dispersion affects CPVC; CPVC of films from coatings in which the pigment is flocculated are lower than CPVC from corresponding coatings with nonflocculated pigment. Films prepared from coatings with flocculated pigment clusters have less uniform distribution of pigment, and hence, are more likely to have portions where there are local high concentrations of pigment. In one example, it is reported that CPVC decreased from 43 to 28 with increasing flocculation (253).

CPVC has been determined by many different procedures. Tinting strength is one of the most widely used. A series of white paints with increasing PVC are prepared and tinted with the same ratio of color to white pigment. Above CPVC, the white tinting strength of the coating increases because of the "white" air bubbles above CPVC. Since the density of most pigments is higher than that of binders and the density of air is lower, density maximizes at CPVC. The CPVC can be determined by filtering a coating and measuring the volume of the pigment filter cake. CPVC for a pigment or pigment combination can be calculated from oil absorption (OA), provided the OA value is based on a nonflocculated dispersion. The definitions of both OA and CPVC are based on close-packed systems with just

sufficient binder to adsorb on the pigment surfaces and fill the interstices between the pigment particles. OA is expressed as g of linseed oil per 100 g pigment; CPVC is expressed as mL of pigment per 100 mL of film. OA and CPVC are approximately independent of the binder, provided the pigment particles are not flocculated. OA values determined by a mixing rheometer, such as a Brabender Plastometer, are preferable. Although the CPVC for individual pigments can be calculated from OAs, CPVC values of pigment combinations cannot be calculated from these values alone, since differences in particle size distribution with pigment combinations affect the packing factor. The most successful equations use OA values, densities, and average particle sizes of the individual pigments (254). The equations assume that the particles are spheres, a fair assumption for many, but not all, pigments. Calculated values correspond reasonably well to experimentally determined CPVC values.

Film Defects

Many kinds of defects can develop in a film during or after application. Reference 255 is a monograph about film defects.

Leveling. The most widely studied leveling problem has been leveling of brush marks. It has been proposed that the driving force for leveling is surface tension (256). The formulator has little control over the variables except viscosity. The Orchard model (256) provides satisfactory correlation between experimental data and predictions when the liquid film has Newtonian flow properties and sufficiently low volatility such that viscosity does not change. In most cases, viscosity changes due to solvent evaporation and the equation is not applicable. It has also been proposed that surface tension differential is the principal driving force for leveling in coatings with volatile solvents (257). Wet film thickness in valleys of brush marks is less than in the ridges; when the same amount of solvent evaporates per unit area of surface, the fraction of solvent that evaporates in the valleys is larger than that in the ridges. As a result, the surface tension in the valleys is higher than that in the ridges and surface tension differential flow drives coating from the ridges into the valleys. The extent of the flow driven by surface tension differential depends on the rate of evaporation of the solvent. Solvent evaporation and leveling of water-reducible coatings has been studied (258), and it has also been shown that the forces driving leveling depend on the solvent in the formulation. Equations have been developed that model the drying process through the changes in surface tension differentials and changes in viscosity during solvent evaporation (259).

In spray application, surface roughness is called *orange peel*, which consists of bumps surrounded by valleys. Orange peel is encountered when spraying coatings that have solvents with high evaporation rates. Leveling of sprayed films can often be improved by addition of small amounts of silicone fluid that reduces surface tension. An explanation for the phenomenon has been provided (260). When one sprays a lacquer, initially the surface is fairly smooth and then orange peel grows. It has been proposed that the growth of orange peel results from a surface tension differential driven flow. The last atomized spray particles to arrive on the wet lacquer surface have traveled for a longer distance between the spray gun

and the surface, and hence, have lost more solvent, have a higher resin concentration and, therefore, a higher surface tension than the main bulk of the wet film. The lower surface tension wet lacquer flows up the sides of these last particles to minimize overall surface free energy. With the silicone fluid, the surface tension of the wet lacquer surface and the surface tension of the last atomized particles are uniformly low; there is no differential to promote growth of orange peel.

Electrostatically sprayed coatings are likely to show surface roughness. It has been suggested that the greater surface roughness results from arrival of the last charged particles on a coated surface that is quite well electrically insulated from the ground. These later arrivals may retain their charges sufficiently long to repel each other and thereby reduce the opportunity for leveling. It has also been suggested that when coatings are applied by high speed bell electrostatic spray guns, differentials in the pigment concentration within the spray droplets may result from the centrifugal forces (261). These pigment concentration differentials lead to rougher surfaces and reduction in gloss of the final films.

Leveling problems are particularly severe with latex paints. Latex paints, in general, exhibit a shear thinning and rapid recovery of viscosity after exposure to high shear rates. Because of their higher dispersed phase content, the viscosity of latex paints changes more rapidly with loss of volatile materials than the viscosity of solventborne paints. The leveling is primarily surface tension driven, since surfactants give low surface tension to latex paints, which is almost unchanged as water evaporates.

Sagging. When a wet coating is applied to a vertical surface, gravity causes it to flow downward (*sagging*). Sagging increases with increasing film thickness and decreases with increasing viscosity. The commonly used test is a sag-index blade. A drawdown, which is a series of stripes of coating of various thickness, is made on a chart and placed in a vertical position. Sag resistance is rated by observing the thickest stripe that does not sag down to the next stripe. For research purposes, a more sophisticated method, the sag balance, has been developed (262).

In spray-applied solvent solution coatings, sagging can generally be minimized while achieving adequate leveling by a combination of proper use of the spray gun and control of the rate of evaporation of solvents. Sagging of high solids solventborne coatings is more difficult to control than with conventional solids coatings. While other factors may be involved, less solvent evaporates while atomized droplets are traveling between a spray gun and the object being coated (263). A factor is the colligative effect of the lower mole fractions of solvent(s) in a high solids coatings. While this effect slows solvent evaporation from a high solids coating, it is not large enough to account for the large differences in solvent loss that have been reported. High solids coatings may undergo transition from first-stage to second-stage solvent loss with relatively little solvent loss as compared to conventional coatings (17). T_g of the solution in a high solids coatings changes more rapidly with concentration, and hence, reaches a stage of free-volume limitation of solvent loss after only a little loss of solvent. It has been found that high solids polyesters are formulated at concentrations above the transition concentration where solvent loss rate becomes diffusion controlled (264). It has also been found that the transition points occur at higher solids with linear molecules such as *n*-octane [111-65-9] versus isooctane (2,2,4-trimethylpentane)

[540-84-1], and *n*-butyl acetate [123-86-4] as compared to isobutyl acetate [105-46-4].

It is necessary to make the systems thixotropic. For example, dispersions of fine particle size SiO_2, precipitated SiO_2, bentonite clay treated with a quaternary ammonium compound, or polyamide gels can be added to impart thixotropy. The problem of sagging in high solids automotive metallic coatings can be particularly severe. Even a small degree of sagging is very evident in a metallic coating, since it affects the orientation of the metal flakes. Use of SiO_2 to impart thixotropy is undesirable, since even the low scattering efficiency of SiO_2 is enough to reduce color flop in the coatings. Acrylic microgels have been developed that impart thixotropic flow using the swollen gel particles (265). In the final film, the index of refraction of the polymer from the microgel is nearly identical with that of the cross-linked acrylic binder polymer so that light scattering does not interfere with color flop. Reference 266 discusses the rheological properties of the systems.

Hot spraying helps control sagging. The coating cools on striking the object and the viscosity increase reduces sagging. Use of CO_2 under supercritical conditions is helpful in controlling sagging, since the CO_2 flashes off almost instantaneously when the coating leaves the orifice of the spray gun, increasing viscosity. High speed electrostatic bell application permits application of coatings at higher viscosity, which helps control sagging.

Crawling, Cratering, and Related Defects. If a coating is applied to a substrate that has a lower surface free energy, the coating will not wet the substrate. The mechanical forces involved in application spread the coating on the substrate surface, but since the surface is not wetted, surface tension forces tend to draw the liquid coating toward a spherical shape. Meanwhile, solvent is evaporating, and viscosity is increasing and flow stops, resulting in uneven film thickness with areas having little, if any, coating adjoining areas of excessive film thickness. This behavior is called *crawling*. Crawling can result from applying a coating to steel with oil contamination on the surface. It is especially common in coating plastics. Crawling can also result from the presence of surfactant-type molecules in the coating, that can orient rapidly on a highly polar substrate surface. Even though the surface tension of the coating is lower than the surface free energy of the substrate, it could be higher than the surface free energy of the substrate after a surfactant in the coating orients on the substrate surface. If one adds excess silicone fluid to a coating to correct a problem such as orange peel, small droplets of insoluble fractions of the poly(dimethylsiloxane) can migrate to the substrate surface and spread on it, and the film crawls. Higher molecular weight fractions of poly(dimethylsiloxane) are insoluble in many coating formulations (175). Modified silicone fluids, such as polysiloxane–polyether block copolymers, have been developed, which are compatible with a wider variety of coatings and are less likely to cause undesirable side effects. The effect of a series of additives on crawling and other film defects has been reported (267).

Cratering is the appearance of small round defects that look somewhat like volcanic craters on the surface of coatings. Cratering results from a small particle or droplet of low surface tension contaminant, which lands on the wet surface of a freshly applied film (260). Some of the low surface tension material dissolves in the adjacent film, creating a localized surface tension differential. This low surface tension part of the film flows away from the particle to cover the

surrounding higher surface tension liquid coating. Loss of solvent increases viscosity flow, leading to formation of a characteristic crest around the pit of the crater. The user applying the coating should minimize the probability of low surface tension contaminants arriving on the wet coating surface. Spraying lubricating oils or silicone fluids on or near the conveyor causes craters. Presence of some contaminating particles cannot be avoided, and so coatings must be designed to minimize the probability of cratering. Lower surface tension coatings are less likely to form craters. Alkyd coatings have low surface tensions and seldom give cratering problems. In general, polyester coatings are more likely to give cratering problems than acrylic coatings. Additives can be used to minimize cratering. Small amounts of silicone fluid generally eliminate cratering; excess silicone must be avoided. Octyl acrylate copolymer additives usually reduce cratering. A comparison of effects of additives on the control of defects such as cratering is available (268).

In roll coating tin plate sheets, the coated sheets are passed on to warm wickets that carry the sheets through an oven. In some cases, one can see a pattern of the wicket as a thin area on the final coated sheet. The heat transfer to the sheet is fastest where it is leaning against the metal wicket. The surface tension of the liquid coating on the opposite side drops locally because of the higher temperature. This lower surface tension material flows toward the higher surface tension surrounding coating. In spraying flat sheets as solvent evaporates the coating is thickest at the edges and just in from the edge the coating is thinner than average. Solvent evaporates most rapidly from the coating near the edge, where the air flow is greatest. This leads to an increase in resin concentration at the edge and to a lower temperature. Both factors increase the surface tension there, causing the lower surface tension coating adjacent to the edge to flow out to the edge to cover the higher surface tension coating. Surface tension differential driven flow can also result when overspray from spraying a coating lands on the wet surface of a different coating. If the overspray has lower surface tension than the wet surface, cratering occurs. If the overspray has high surface tension compared to the wet film, local orange peeling results.

Floating and Flooding. Floating is most evident in coatings pigmented with two pigments. A light blue gloss enamel panel can show a mottled pattern of darker blue lines on a lighter blue background. With a different light blue coating, the color pattern might be reversed. These effects result from pigment segregations that occur as a result of convection current flows driven by surface tension differentials while a film is drying. Rapid loss of solvent from a film during drying leads to considerable turbulence. Convection patterns are established whereby coating material flows up from lower layers of the film and circulates back down into the film. The flow patterns are roughly circular, but as they expand, they encounter other flow patterns and the convection currents are compressed. As solvent evaporation continues, viscosity increases and it becomes more difficult for the pigment particles to move. The smallest particle size, lowest density particles continue moving longest. The segregated pattern of floating results. Floating is particularly likely to occur if one pigment is flocculated and the other is a nonflocculated dispersion of fine particle size. If, in a light blue coating, the white pigment is flocculated and the blue is not, one will find darker blue lines on a lighter blue background. If the blue one is flocculated and not the white, there will be lighter blue lines on a darker blue background. Floating can occur

without flocculation using a combination of pigments with very different particle sizes and densities. When a fine particle size carbon black and TiO_2 are used to make a gray coating, the particle size of the TiO_2 is several times that of the carbon black and TiO_2 has about a fourfold higher density. A larger particle size black, such as lamp black, can be used to make a gray with a lower probability of floating. As with other flow phenomena driven by surface tension differentials, floating can be prevented by adding a small amount of a silicone fluid.

In flooding the color of the surface is uniform, but different than should have been obtained from the pigment combination used. One might have a uniform gray coating, but a darker gray than that expected from the ratio of black to white pigments. The extent of flooding can vary with the conditions encountered during application, leading to different colors on articles coated with the same coating. Flooding results from surface enrichment by one or more of the pigments in the coating. The stratification is thought to occur as a result of different rates of pigment settling within the film, which are caused by differences in pigment density and size or flocculation of one of the pigments. Flooding is accentuated by thick films, low vehicle viscosity, and low evaporation rate solvents. The remedies are to avoid flocculation and low density fine particle size pigments.

Wrinkling. A wrinkled coating shriveled or wrinkled into many small hills and valleys. Some wrinkle patterns are so fine that to the unaided eye, the film appears to have low gloss rather than to look wrinkled. However, under magnification, the surface can be seen to be glossy but wrinkled. In other cases, the wrinkle patterns are broad or bold and are readily visible. Wrinkling results when the surface of a film becomes high in viscosity while the bottom of the film is still relatively fluid. It can result from rapid solvent loss from the surface, followed by later solvent loss from the lower layers. It can also result from more rapid cross-linking at the surface of the film than in the lower layers of the film. Subsequent solvent loss or cure in the lower layers results in shrinkage, which pulls the surface layer into a wrinkled pattern. Wrinkling is more apt to occur with thick films than with thin films because the possibility of different reaction rates and differential solvent loss within the film increases with thickness.

Wrinkling can occur in uv curing of pigmented acrylate coatings with free-radical photoinitiators. High concentrations of photoinitiator are required to compete with absorption by the pigment. Penetration of uv through the film is reduced by absorption by the pigment as well as by the photoinitiator. There is rapid cross-linking at the surface and slower cross-linking in the lower layers of the film, resulting in wrinkling. Wrinkling is likely to be more severe if the curing is done in an inert atmosphere rather than in air. In the latter case, the cure differential is reduced by oxygen inhibition of surface cure. uv curing of pigmented cationic coatings, which are not air inhibited, is even more prone to surface wrinkling.

Popping. *Popping* is the formation of broken bubbles at the surface of a film that do not flow out. Popping results from rapid loss of solvent at the surface of a film during initial flash off. When the coated object is put into an oven, solvent volatilizes in the lower layers of the film, creating bubbles that do not readily pass through the high viscosity surface. As the temperature increases further, the bubbles expand, finally bursting through the top layer, resulting in popping. The viscosity of the film meanwhile has increased enough so that the coating cannot flow together to heal the eruption. Popping can also result from entrapment of

air bubbles in a coating. Popping can result from solvent that remains in primer coats when the topcoat is applied. In coating plastics, solvents can dissolve in the plastic and then cause popping when a coating is applied over the plastic and then baked. Another potential cause of popping is evolution of volatile by-products of cross-linking.

Popping can be minimized by spraying more slowly in more passes, by longer flash-off times before the object is put into the oven, and by zoning the oven so that the first stages are relatively low in temperature. The probability of popping can also be reduced by having a slow evaporating, good solvent in the solvent mixture. This tends to keep the surface viscosity low enough for bubbles to pass through and heal before the viscosity at the surface becomes too high. Popping can be particularly severe with water-reducible baking enamels because of slow loss of water during baking, especially with high T_g resins. In contrast to increased probability of popping with higher T_g water-reducible coatings, popping is more likely to occur with lower T_g latex polymers. Coalescence of the surface before the water has completely evaporated is more likely with a lower T_g latex.

Foaming. During manufacture and application, a coating is subjected to agitation and mixing with air, creating the opportunity for foam formation. In formulating a latex paint, an important criterion in selecting surfactants and water-soluble polymers as thickeners is their effect on foam stabilization (269). Acetylene glycol surfactants, such as 2,4,7,9-tetramethyl-5-decyne-4,7-diol, are reported to be effective surfactants that do not increase the viscosity of the surface of bubbles as much as surfactants such as alkylphenol ethoxylates (270).

A variety of additives can be used to break foam bubbles. Most depend on creating surface tension differential driven flow on the surface of bubbles. Silicone fluids are effective in breaking a variety of foams, since their surface tension is low compared to almost any foam surface. Small particle size hydrophobic SiO_2 can also act as a defoamer and/or a carrier for active defoaming agents (270). Also, a small amount of immiscible hydrocarbon will often reduce foaming of an aqueous coating. Several companies sell lines of proprietary antifoam products and offer test kits with small samples of their products. The formulator evaluates the antifoam products in a coating with foaming problems to find one that overcomes the problem. While it is possible to predict which additive will break a foam in a relatively simple system, such predictions are difficult for latex paints because of the variety of components that could potentially be at the foam interface. The combination of surfactants, wetting agents, water-soluble polymers, and antifoam can be critical.

BIBLIOGRAPHY

"Surface Coatings" in *EPST* 1st ed., Vol. 13, pp. 486–533, by P. R. Buechler, K. J. Quinn & Co., Inc., and D. Cannell, The Sherwin-Williams Co.; "Coatings" in *EPSE* 2nd ed., Vol. 3, pp. 615–675, by J. H. Lowell, Consultant, and "Coatings" in *EPSE* 2nd ed., Suppl. Vol., pp. 53–122, by Z. W. Wicks, Jr., North Dakota State University.

1. A. H. Tullo, *Chem. Eng. News* **78**(41), 19 (2000).
2. H. Burrell, *Off. Dig. Fed. Soc. Paint Technol.* **34**(445), 131 (1962).
3. S. P. Pappas and L. W. Hill, *J. Coat. Technol.* **53**(675), 43 (1981).

4. K. Dusek and I. Havlicek, *Prog. Org. Coat.* **22**, 145 (1993).
5. F. Lin and D. J. Meier, *Prog. Org. Coat.* **29**, 139 (1996).
6. T. Provder, M. A. Winnik, and M. W. Urban, eds., *Film Formation in Waterborne Coatings*, American Chemical Society, Washington, D.C., 1996. ACS Symposium Series, Vol. **648**.
7. K. L. Hoy, *J. Coat. Technol.* **68**(853), 33 (1996).
8. G. A. Vandezande and A. Rudin, *J. Coat. Technol.* **68**(860), 63 (1996).
9. M. A. Winnik, in P. A. Lovell and M. S. El-Aasser, eds., *Emulsion Polymerization and Emulsion Polymers*, John Wiley and Sons, Inc., New York, 1997, pp. 467–518.
10. E. S. Daniels and A. Klein, *Prog. Org. Coat.* **19**, 359 (1991).
11. C. K. Schoff, *Rheology*, Federation of Societies for Coatings Technology, Blue Bell, Pa., 1991.
12. Z. W. Wicks Jr. and co-workers, *J. Coat. Technol.* **57**(725), 51 (1985).
13. F. N. Jones, *J. Coat. Technol.* **68**(852), 25 (1996); S. Haseebuddin, K. V. S. N. Raju, and M. Yaseen, *Prog. Org. Coat.* **30**, 25 (1997).
14. A. J. Wright, *Eur. Coat. J.* **32**, 696 (1996).
15. P. R. Sperry and A. Mercurio, *ACS Coat. Plast. Chem. Prepr.* **43**, 427 (1978).
16. M. A. Sherwin, J. V. Koleske, and R. A. Taller, *J. Coat. Technol.* **53**(683), 35 (1981).
17. L. W. Hill and Z. W. Wicks Jr., *Prog. Org. Coat.* **10**, 55 (1982).
18. D. A. R. Jones, B. Leary, and D. V. Boger, *J. Colloid Interface Sci.* **150**(1), 84 (1992).
19. L. J. Boggs, M. Rivers, and S. G. Bike, *J. Coat. Technol.* **68**(855), 63 (1996); R. D. Hester and D. R. Squire Jr., *J. Coat. Technol.* **69**(864), 109 (1997).
20. D. A. Soules, R. H. Fernando, and J. E. Glass, *J. Rheol.* **32**, 181 (1988).
21. D. A. Soules, G. P. Dinga, and J. E. Glass, in J. E. Glass, ed., *Polymers as Rheology Modifiers*, American Chemical Society, Washington, D.C., 1991, pp. 322–332.
22. R. A. Dickie, *J. Coat. Technol.* **64**(809), 61 (1992).
23. J. W. Martin, S. C. Saunders, F. L. Floyd, and J. P. Wineburg, *Methodologies for Predicting Service Lives of Coating Systems*, Federation of Societies for Coatings Technology, Blue Bell, Pa., 1996.
24. L. W. Hill, in Ref. 41, p. 534.
25. L. W. Hill, *Mechanical Properties of Coatings*, Federation of Societies for Coatings Technology, Blue Bell, Pa., 1987.
26. H. Stutz, K.-H. Illers, and J. Mertes, *J. Polym. Sci., Part B: Polym. Phys.* **28**, 1483 (1990).
27. L. W. Hill, *J. Coat. Technol.* **64**(808), 29 (1992).
28. D. J. Skrovanek, *Prog. Org. Coat.* **18**, 89 (1990).
29. M. B. Roller, *J. Coat. Technol.* **54**(691), 33 (1982).
30. D. Y. Perera and P. Schutyser, *FATIPEC Congress Book*, Vol. **I**, 1994, p. 25.
31. P. J. Greidanus, *FATIPEC Congress Book*, Vol. **I**, 1988, p. 485.
32. R. M. Evans, in R. R. Myers and J. S. Long, eds., *Treatise on Coatings*, Vol. **2**, Part I, Marcel Dekker, Inc., New York, 1969, pp. 13–190.
33. R. M. Evans and J. Fogel, *J. Coat. Technol.* **47**(639), 50 (1977).
34. K. L. Rutherford and co-workers, *Wear* **203/204**, 325 (1997).
35. T. Hamada and co-workers, *Prog. Org. Coat.* **30**, 271 (1997).
36. F. N. Jones and co-workers, *Prog. Org. Coat.* **34**, 119 (1998).
37. B. V. Gregorovich and I. Hazan, *Prog. Org. Coat.* **24**, 131 (1994).
38. J. L. Courter, *J. Coat. Technol.* **69**(866), 57 (1997).
39. R. A. Ryntz, A. C. Ramamurthy, and J. W. Holubka, *J. Coat. Technol.* **67**(842), 23 (1995).
40. R. D. Athey Jr., *Amer. Paint Coat. J.* 38 (Dec. 7, 1992).

41. J. V. Koleske, ed., *Paint and Coating Testing Manual*, 14th ed., ASTM, Philadelphia, 1995.
42. A. Valet, *Light Stabilizers for Paints*, translated by M. S. Welling, Vincentz, Hannover, Germany, 1997.
43. D. J. Carlsson, J. P. T. Jensen, and D. M. Wiles, *Makromol. Chem.* **8**(Suppl.), 79 (1984).
44. D. R. Bauer, *J. Coat. Technol.* **66**(835), 57 (1994).
45. J. L. Gerlock and co-workers, *J. Coat. Technol.* **57**(722), 37 (1985).
46. D. R. Bauer, *J. Coat. Technol.* **69**(864), 85 (1997).
47. R. F. Sharrock, *J. Coat. Technol.* **62**(789), 125 (1990).
48. H. G. Voelz, G. Kaempf, H. G. Fitzky, and A. Klaeren, in S. P. Pappas and F. H. Winslow, eds., *Photodegradation and Photostabilization of Coatings*, American Chemical Society, Washington, D.C., 1981, pp. 163–182. ACS Symposium Series, Vol. **151**.
49. J. H. Braun and D. P. Cobranchi, *J. Coat. Technol.* **67**(851), 55 (1995).
50. T. E. Jones and J. M. McCarthy, *J. Coat. Technol.* **67**(844), 57 (1995).
51. P. Betz and A. Bartelt, *Prog. Org. Coat.* **22**, 27 (1993); B. V. Gregorovich and I. Hazan, *Prog. Org. Coat.* **24**, 131 (1994).
52. L. H. Brown, in R. R. Myers and J. S. Long, eds., *Treatise on Coatings*, Vol. **I**, Part III, Marcel Dekker, Inc., New York, 1972, pp. 536–563.
53. S. P. Pappas and R. L. Just, *J. Polym. Sci., Polym. Chem. Ed.* **18**, 527 (1980).
54. A. Smith and O. Wagner, *J. Coat. Technol.* **68**(862), 37 (1996).
55. B. W. Johnson and R. McIntyre, *Prog. Org. Coat.* **27**, 95 (1996).
56. L. S. Hicks and M. J. Crewdson, in Ref. 41, p. 619.
57. J. L. Martin, in *Proc. Adv. Coat. Technol. Conf. Eng. Soc.*, Society of Automotive Engineeers, Detroit, Mich., 1991, p. 219.
58. B. W. Johnson and R. McIntyre, *Prog. Org. Coat.* **27**, 95 (1996).
59. J. L. Gerlock and co-workers, *Prog. Org. Coat.* **15**, 197 (1987).
60. R. M. Fischer, W. D. Ketola, and W. P. Murray, *Prog. Org. Coat.* **19**, 151 (1991).
61. D. R. Bauer, D. F. Mielewski, and J. L. Gerlock, *Polym. Degrad. Stab.* **38**, 57 (1992).
62. V. D. Sherbondy, in Ref. 41, p. 643.
63. R. M. Fischer, W. D. Ketola, and W. P. Murray, *Prog. Org. Coat.* **19**, 165 (1991).
64. D. R. Bauer, M. C. P. Peck, and R. O. Carter III, *J. Coat. Technol.* **59**(755), 103 (1987).
65. P. S. Sheih and J. L. Massingill, *J. Coat. Technol.* **62**(781), 25 (1990).
66. D. Y. Perrera and D. Van den Eynden, *J. Coat. Technol.* **59**(748), 55 (1987).
67. D. Y. Perera, *Prog. Org. Coat.* **28**, 21 (1996).
68. O. Negele and W. Funke, *Prog. Org. Coat.* **28**, 285 (1995).
69. V. E. Basin, *Prog. Org. Coat.* **12**, 213 (1984).
70. W. A. Zisman, *J. Coat. Technol.* **44**(564), 42 (1972).
71. J. Y. Charmeau, E. Kientz, and Y. Holl, *Prog. Org. Coat.* **27**, 87 (1996).
72. B. M. Perfetti, *Metal Surface Characteristics Affecting Organic Coatings*, Federation of Societies for Coatings Technology, Blue Bell, Pa., 1994.
73. N. Tang, W. I. Van Ooij, and G. Gorecki, *Prog. Org. Coat.* **30**, 255 (1997).
74. T. J. Lin and co-workers, *Prog. Org. Chem.* **31**, 351 (1997).
75. C. Vautrin-Ul and co-workers, *Prog. Org. Coat.* **38**, 9 (2000).
76. W. J. van Ooij and T. Child, *Chemtech* 26 (Feb. 1998).
77. J. O. Stoffer and co-workers, in *Proc. Waterborne High-Solids Powder Coat. Symp.*, New Orleans, La., 1999, pp. 20–34.
78. S. Maeda, *Prog. Org. Coat.* **28**, 227 (1996).
79. M. F. Montemor and co-workers, *Prog. Org. Coat.* **38**, 17 (2000).
80. G. Reinhard, *Prog. Org. Coat.* **15**, 125 (1987).

81. J. L. Massingill and co-workers, *J. Coat. Technol.* **62**(781), 31 (1990).
82. S. Maeda, *J. Coat. Technol.* **55**(707), 43 (1983).
83. E. P. Pluddemann, *Prog. Org. Coat.* **11**, 297 (1983).
84. F. D. Rector, W. W. Blount, and D. R. Leonard, *J. Coat. Technol.* **61**(771), 31 (1989).
85. R. A. Ryntz, *Polym. Mat. Sci. Eng.* **67**, 119 (1992).
86. J. M. Lane and D. J. Hourston, *Prog. Org. Coat.* **21**, 269 (1993).
87. R. A. Ryntz, *Painting of Plastics*, Federation of Societies for Coatings Technology, Blue Bell, Pa., 1994.
88. G. L. Nelson, in Ref. 41, pp. 513–524.
89. A. C. Ramamurthy and co-workers, *Wear* **203/204**, 350 (1997); D. J. Mihora and A. C. Ramamurthy, *Wear* **203/204**, 362 (1997).
90. W. Funke, *J. Coat. Technol.* **55**(705), 31 (1983); W. Funke, *J. Oil Colour Chem. Assoc.* **68**, 229 (1985); W. Funke, *Farbe Lack* **93**, 721 (1987).
91. J. W. Holubka and R. A. Dickie, *J. Coat. Technol.* **56**(714), 43 (1984).
92. N. L. Thomas, *Prog. Org. Coat.* **19**, 101 (1991).
93. G. K. van der Wel and O. C. G. Adan, *Prog. Org. Coat.* **37**, 1 (1999).
94. B. Bieganska, M. Zubielewicz, and E. Smieszek, *Prog. Org. Coat.* **16**, 219 (1988).
95. D. P. Bentz and T. Nguyen, *J. Coat. Technol.* **62**(783), 57 (1990).
96. A. Smith, *Inorganic Primer Pigments*, Federation of Societies for Coatings Technology, Blue Bell, Pa., 1988.
97. T. S. Lee and K. L. Money, *Mater. Perform.* **23**, 28 (1984).
98. R. G. Groseclose, C. M. Frey, and F. L. Floyd, *J. Coat. Technol.* **56**(714), 31 (1984).
99. J. R. Scully, Electrochemical Impedance Spectroscopy for Evaluation of Organic Coating Deterioration and Underfilm Corrosion—A State of the Art Technical Review, Report No. DTNSRDC/SME-86/006, D. W. Taylor Naval Ship Research and Development Center, Bethesda, Md., 1986
100. U. Rammelt and G. Reinhard, *Prog Org. Coat.* **21**, 205 (1991).
101. E. P. M. van Westing and co-workers, *Prog. Org. Coat.* **23**, 89 (1993).
102. W. S. Tait, *J. Coat. Technol.* **66**(834), 59 (1994).
103. H. J. Prause and W. Funke, *Farbe Lack* **101**, 96 (1995).
104. R. Athey and co-workers, *J. Coat. Technol.* **57**(726), 71 (1985); J. Mazia, *Met. Finish.* **75**(5), 77 (1977); R. D. Wyvill, *Met. Finish.* **80**(1), 21 (1982).
105. W. Funke, in H. Leidheiser Jr., ed., *Corrosion Control by Coatings*, Science Press, Princeton, N.J., 1979, pp. 35–45.
106. R. L. Howard, S. B. Lyon, and J. D. Scantlebury, *Prog. Org. Coat.* **37**, 91 (1999).
107. E. Almeida, D. Santos, and J. Uruchurtu, *Prog. Org. Coat.* **37**, 131 (1999).
108. D. R. Bassett and K. L. Hoy, in D. R. Bassett and A. E. Hamielec, eds., *ACS Symposium Series 165*, American Chemical Society, Washington, D.C., 1981, p. 371.
109. M. A. Winnik and J. Feng, *J. Coat. Technol.* **68**(852), 39 (1996).
110. S. A. Eckersley and B. J. Helmer, *J. Coat. Technol.* **69**(864), 97 (1997).
111. A. Trapani and co-workers, *Pitture Vernici Eur.* **71**(9), 14 (1995).
112. J. W. Taylor and D. W. Bassett, in J. E. Glass, ed., *Technology for Waterborne Coatings*, American Chemical Society, Washington, D.C., 1997, p. 137.
113. G. Pollano, *Polym. Mater. Sci. Eng.* **77–73**, (1996).
114. Y. Inaba, E. S. Daniels, and M. S. El-Aasser, *J. Coat. Technol.* **66**(833), 63 (1994).
115. M. J. Chen and co-workers, *J. Coat. Technol.* **69**(875), 49 (1997).
116. J. M. Geurts, J. J. G. S. van Es, and A. L. German, *Prog. Org. Coat.* **29**, 107 (1996).

117. G. Monaghan, *Polym. Mater. Sci. Eng.* **76**, 178 (1997); M. J. Collins, J. W. Taylor, and R. A. Martin, *Polym. Mater. Sci. Eng.* **76**, 172 (1997).
118. T. Nabuurs, R. A. Baijards, and A. L. German, *Prog. Org. Coat.* **27**, 163 (1996).
119. R. A. Prior and co-workers, *Prog. Org. Coat.* **29**, 209 (1996).
120. F. Decocq, D. Heymans, M. Slinckx, S. Spanhove, and C. Nootens, in *Proc. Waterborne High-Solids Powder Coat Symp.*, New Orleans, La., 1997, p. 168.
121. G. Chu and F. N. Jones, *J. Coat. Technol.* **65**(819), 43 (1993).
122. D. R. Bauer and R. A. Dickie, *J. Coat. Technol.* **54**(685), 57 (1982).
123. G. G. Parekh, *J. Coat. Technol.* **51**(658), 101 (1979).
124. D. A. Wicks and P. E. Yeske, *Prog. Org. Coat.* **30**, 265 (1997).
125. U.S. Pat. 5254651 (1993), V. Alexanian, R. G. Lees, and D. E. Fiori [to American Cyanamid Corp. (now Cytec Industries)].
126. J. Blank, Z. A. He, and E. T. Hessell, *Prog. Org. Coat.* **35**, 19 (1999).
127. D. A. Wicks and Z. W. Wicks Jr., *Prog. Org. Coat., Part A* **36**, 148 (1999); *Part B*, **41**, 1 (2001).
128. W. J. Blank, Z. A. He, and M. E. Picci, *Polym. Mater. Sci. Eng.* **79**, 399 (1998).
129. U.S. Pat. 5356529 (1993), V. Eswarakrishnan, R. R. Zwack, and E. R. Coleridge (to PPC Industries, Inc.).
130. K. P. Yonek, H.-U. Meier-Westhues, U. Freudenberg, and H.-J. Laas, in *Proc. Waterborne High-Solids Powder Coat. Symp.*, New Orleans, La., 1998, p. 43.
131. K.-H. Hentschel, *Eur. Coat. J.* (3) 188 (1988).
132. U.S. Pat. 5596064 (1997), E. Koenig and Th. Engebert (to Bayer Aktiengesellschaft).
133. U.S. Pat. 5908910 (1999), A. Gam (to E. T. du Pont de Nemours & Co., Inc.).
134. Z. W. Wicks Jr. and B. W. Kostyk, *J. Coat. Technol.* **49**(634), 77 (1977).
135. U.S. Pat. 4518522 (1985), P. H. Markusch, R. G. Kelso, and P. D. Schmitt [to Mobay Chemical Corp. (now Bayer Corporation)].
136. U.S. Pat. 5516559 (1996), U. Rockrath, G. Wigger, and U. Poth (to BASF Lachet Farben).
137. R. M. Guida, *Modern Paint Coat.* 34 (July 1996).
138. G. Gardner, *J. Protective Coat. Linings* 81 (Feb. 1996).
139. J. C. Padget, *J. Coat. Technol.* **66**(839), 89 (1994).
140. R. Satguru and co-workers, *J. Coat. Technol.* **66**(830), 47 (1994).
141. D. E. Fiori, *Prog. Org. Coat.* **32**, 65 (1997).
142. M. Dvorchak and H. Bui, in *Proc. Waterborne High-Solids Powder Coat. Symp.*, New Orleans, La., 1998, p. 80.
143. M. J. Dvorchak, H. Casselmann, S. X. Feng, M. W. Shaffer, and P. C. Yu, in *Proc. Waterborne High-Solids Powder Coat. Symp.*, New Orleans, La., 1999, pp. 142–155.
144. D. J. Weinmann, K. Dangayach, and C. Smith, *J. Coat. Technol.* **68**(863), 29 (1996).
145. R. W. Tess, in C. A. May, ed., *Epoxy Resins—Chemistry and Technology*, Marcel Dekker, Inc., New York, 1988, p. 743.
146. A. Wegmann, *J. Coat. Technol.* **65**(827), 27 (1993).
147. R. Albers, in *Proc. Waterborne High-Solids Coat. Symp.*, New Orleans, La., 1983, pp. 130–143.
148. Santolink EP 560, Technical Bulletin, Monsanto Chemical Co. (now Solutia, Inc.), 1990.
149. S. R. Howe, L. Borodinsky, R. S. Lyon, *J. Coat. Technol.* **70**(877), 69 (1998); R. J. Wingender, P. Niketas, and C. K. Switala, *J. Coat. Technol.* **70**(877), 75 (1998).
150. M. Ooka and H. Ozawa, *Prog. Org. Coat.* **23**, 325 (1994).
151. M. D. Shalati, J. R. Babjak, R. M. Harris, and W. P. Yang, in *Proc. Int. Conf. Coat. Sci. Technol.*, Athens, 1990, p. 525
152. R. F. Eaton and K. T. Lamb, *J. Coat. Technol.* **68**(860), 49 (1996).

153. S. Nakano and T. Endo, *Prog. Org. Coat.* **28**, 143 (1996).
154. J. T. K. Woo and A. Toman, *Polym. Mater. Sci. Eng.* **65**, 323 (1991).
155. K. O'Driscoll, *J. Coat. Technol.* **57**(705), 57 (1983).
156. K. Okadaa, K. Yamaguchi, and H. Takeda, *Prog. Org. Coat.* **34**, 169 (1998).
157. J. C. Kenny, T. Ueno, and K. Tsutsui, *J. Coat. Technol.* **68**(855), 35 (1996).
158. T. Agawa and E. D. Dumain, in *Proc. Waterborne High-Solids Powder Coat. Symp.*, New Orleans, La., 1997, p. 342.
159. U.S. Pat. 5254651 (1993), A. Vazken, R. G. Lees, and D. E. Fiori [to American Cyanamid Company (now Cytec Industries)].
160. U.S. Pats. 5356669 (1994), J. W. Rehfuss and D. L. St. Aubin; 5605965 (1997), J. W. Rehfuss and D. L. St. Aubin (to PPC Industries, Inc.).
161. R. P.-T. Chung and D. H. Solomon, *Prog. Org. Coat.* **21**, 227 (1992).
162. Z. W. Wicks Jr., E. A. Anderson, and W. J. Culhane, *J. Coat. Technol.* **54**(688), 57 (1982).
163. L. W. Hill and Z. W. Wicks Jr., *Prog. Org. Coat.* **8**, 161 (1980).
164. Z. W. Wicks Jr., and G. F. Chen, *J. Coat. Technol.* **50**(638), 39 (1978).
165. P. E. Ferrell and co-workers, *J. Coat Technol.* **67**(851), 63 (1995).
166. L. W. Hill, P. E. Ferrell, and J. J. Gummeson, in Ref. 6, p. 235.
167. D. J. Golob, T. A. Odom Jr., and R. W. Whitson, *Polym. Mater. Sci. Eng.* **63**, 826 (1990).
168. L. J. Calbo, in *Proc. Waterborne High-Solids Coat. Symp.*, New Orleans, La., 1986, p. 356.
169. TONE Polyols, Technical Bulletin, Speciality Polymers and Composites Division, Union Carbide Corp., 1986.
170. R. Engelhardt, in *Proc. Waterborne High-Solids Powder Coat. Symp.*, New Orleans, La., 1996, p. 408.
171. F. N. Jones, *J. Coat. Technol.* **68**(852), 25 (1996).
172. Z. W. Wicks Jr., F. N. Jones, and S. P. Pappas, *Organic Coatings*, 2nd ed., Wiley-Interscience, New York, 1999.
173. K. H. Zabel and co-workers, *Prog. Org. Coat.* **35**, 255 (1999).
174. G. Osterberg and co-workers, *Prog. Org. Coat.* **24**, 281 (1994); G. Ostberg, and B. Bergenstahl, *J. Coat. Technol.* **68**(858) 39 (1996).
175. F. Fink and co-workers, *J. Coat. Technol.* **62**(791), 47 (1990).
176. S. P. Pappas and R. L. Just, *J. Polym. Sci. Polym Ed.* **18**, 527 (1980); Y.-C. Hsiao, L. W. Hill, and S. P. Pappas, *J. Appl. Polym. Sci.* **19**, 2817 (1975).
177. W. A. Finzel and H. L. Vincent, *Silicones in Coatings*, Federation of Societies for Coatings Technology, Blue Bell, Pa., 1996.
178. W. A. Finzel, *J. Coat. Technol.* **64**(809), 47 (1992).
179. T. Laubender, in *Proc. Int. Conf. Water-Borne Coat.*, Milan, 1992. Paper No. 21.
180. V. A. Ogarev and S. L. Selector, *Prog. Org. Coat.* **21**, 135 (1992); G. L. Witucki, *J. Coat. Technol.* **65**(822), 57 (1993).
181. M. Ooka, and H. Ozawa, *Prog. Org. Coat.* **23**, 325 (1993); H. Furukawa and co-workers, *Prog. Org. Coat.* **24**, 81 (1994).
182. J. D. Nordstrom, in *Proc. Waterborne, High-Solids Powder Coat. Symp.*, New Orleans, La., 1995, p. 192.
183. Hypalon CP Chlorinated Polyolefins, Technical Bulletin, E. I. du Pont de Nemours & Co. Inc., Wilmington, Del., 1989.
184. J. E. Gaske, *Coil Coatings*, Federation of Societies for Coatings Technology, Blue Bell, Pa., 1987.
185. A. Barbucci and co-workers, *Prog. Org. Coat.* **29**, 7 (1996).
186. S. Munekata, *Prog. Org. Coat.* **16**, 113 (1988).

187. H.-J. Traenckner and H. U. Pohl, *Angew. Makromol. Chem.* **108**, 61 (1982).
188. M. J. Dvorchak, and B. H. Riberi, *J. Coat. Technol.* **64**(808), 43 (1992).
189. J. Lomax and G. F. Swift, *J. Coat. Technol.* **50**(643), 49 (1978).
190. Z. W. Wicks Jr., M. R. Appelt, and J. C. Soleim, *J. Coat. Technol.* **57**(726), 51 (1985).
191. A. Mercurio, in *Proc. Int. Conf. Org. Coat*, Athens, 1990, p. 235.
192. F. D. Rector, W. W. Blount, and D. R. Leonard, *J. Coat. Technol.* **61**(771), 31 (1989); J. S. Witzeman, W. D. Nottingham, and F. D. Rector, *J. Coat. Technol.* **62**(789), 101 (1990).
193. T. Li and J. C. Graham, *J. Coat. Technol.* **65**(821), 64 (1993).
194. K. H. Zabel and co-workers, *Prog. Org. Coat.* **34**, 236 (1998).
195. G. Pollano, *Polym. Mater. Sci. Eng.* **77**, 383 (1997).
196. J. W. Taylor, and D. R. Bassett, in Ref. 112, ACS Symposium Series, Vol. **663**, p. 137.
197. *Ucarlink® Crosslinkers, Technical Bulletin UC-350, Union Carbide Corp., Danbury, Conn., 1994*.
198. A. L. Rocklin, *J. Coat. Technol.* **48**(622), 45 (1976).
199. J. S. Vrentas, C. M. Vrentas, and N. Faridi, *Macromolecules* **29**, 3272 (1996).
200. S. G. Croll, *J. Coat. Technol.* **59**, (751), 81 (1987).
201. D. A. Sullivan, *J. Paint Technol.* **47**(610), 60 (1975).
202. A. L. Rocklin, *J. Coat. Technol.* **58**(732), 61 (1986).
203. P. W. Dillon. *J. Coat. Technol.* **49**(634), 38 (1977).
204. L. B. Brandenburger and L. W. Hill, *J. Coat. Technol.* **51**(659), 57 (1979).
205. B. C. Watson, and Z. W. Wicks Jr., *J. Coat. Technol.* **55**(698), 59 (1983).
206. W. H. Ellis, *J. Coat. Technol.* **48**(614), 45 (1976).
207. D. T. Wu, S. Lonsinger, and J. A. Klein, *FATIPEC Congress Book*, Vol. **IV**, 1988, p. 227.
208. J. L. McGovern, *J. Coat. Technol.* **64**(810), 33–39 (1992).
209. R. L. Smith, L. J. Culver, and S. L. Hillman, *J. Coat. Technol.* **59**(747), 21 (1987).
210. J. J. Brezinski, in J. V. Koleske, ed., *Paint and Coating Testing Manual*, 14th ed., ASTM, Philadelphia, 1995, pp. 3–14.
211. *U.S. EPA, Hazardous Air Pollutants Strategic Implementation Plan, http://www.epa.gov/ttn/uatw/happlan.html, 1997.*
212. *U.S. EPA, Final Air Toxics Regulation for Wood Furniture Manufacturing Operations, http://www.epa.gov/ttn/utaw/fswood.html, 1995.*
213. J. J. Brezinski, ed., *Manual on Determination of Volatile Compounds in Paints, Inks, and Related Coating Products*, 2nd. ed., ASTM, Philadelphia, 1993. ASTM Manual Series: **MNL 4**.
214. *U.S. EPA, Final Revisions to the Ozone and Particulate Matter Air Quality Standards, http://www.epa.gov/oar/oaqps/ozpmbro/current.htm*, 1997.
215. R. Atkinson, *Atmospheric Environment* **24A**, 1 (1990).
216. K. A. Nielsen and co-workers, *Polym Mater. Sci. Eng.* **70**, 170 (1990).
217. V. C. Jenkins and co-workers, *J. Coat. Technol.* **67**(841), 53 (1995).
218. P. E. Pierce and R. T. Marcus, *Color and Appearance*, Federation of Societies for Coatings Technology, Blue Bell, Pa., 1994.
219. E. Cremer, *Prog. Org. Chem.* **9**, 241 (1981).
220. F. J. Droll, *Paint Coat. Ind.* 54 (Feb. 1998).
221. D. C. Rich. *J. Coat. Technol.* **67**(840), 53 (1995).
222. A. B. J. Rodrigues, *ASTM Standardization News* 98 (Oct. 1995).
223. U. Zorll, *Prog. Org. Coat.* **1**, 113 (1972).
224. H. K. Hammond III and G. Kigle-Boeckler, in Ref. 41, pp. 470–480.
225. J. H. Braun, *J. Coat. Technol.* **63**(799), 43 (1991).

226. H. Braun and D. P. Fields, *J. Coat. Technol.* **66**(828), 93 (1994).
227. J. H. Braun and D. P. Cobranchi, *J. Coat. Technol.* **67**(851), 55 (1995).
228. H.-J. Freier, *Farbe Lack* **73**, 316 (1967).
229. K. B. Smith, *Surface Coat. Int.* **80**, 573 (1997).
230. T. C. Patton, *Paint Flow and Pigment Dispersion*, 2nd. ed., Wiley-Interscience, New York, 1979.
231. J. Winkler, E. Klinke, and L. Dulog, *J. Coat. Technol.* **59**(754), 35 (1987); J. Winkler and co-workers, *J. Coat. Technol.* **59**(754), 45 (1987); J. Winkler and L. Dulog, *J. Coat. Technol.* **59**(754), 55 (1987).
232. K. Rehacek, *Ind. Eng. Chem. Prod. Res. Dev.* **15**, 75 (1976).
233. A. Saarnak, *J. Oil Colour Chem. Assoc.* **62**, 455 (1979).
234. L. Dulog and O. Schnitz, in *Proc. FATIPEC Congress*, Vol. II, 1984, p. 409.
235. R. B. McKay, in *Proc. Int. Conf. Org. Coat. Technol.*, Athens, 1980, p. 499.
236. A. Brisson and A. Haber, *J. Coat. Technol.* **63**(794), 59 (1991).
237. H. L. Jakubauskas, *J. Coat. Technol.* **58**(736), 71 (1986).
238. J. D. Schofield, *J. Oil Colour Chem. Assoc.* **74**, 204 (1991).
239. W. H. Morrison Jr., *J. Coat. Technol.* **57**(721), 55 (1985).
240. J. Clayton, *Surface Coat. Int.* **94**, 414, (1997).
241. H. J. Spinelli, *Prog. Org. Coat.* **27**, 255 (1996).
242. A. Brisson, G. L'Esperance, and M. Caron, *J. Coat. Technol.* **63**(801), 111 (1991).
243. G. Balfour and M. J. Hird, *J. Oil Colour Chem. Assoc.* **58**, 331 (1975).
244. J. E. Hall and co-workers *J. Coat. Technol.* **60**(756), 49 (1988); J. E. Hall, R. Bordeleau, and A. Brisson, *J. Coat. Technol.* **61**(770), 73 (1989).
245. R. R. Blakely, in *Proc. FATIPEC Congress*, 1972, p. 187.
246. W. K. Asbeck and M. Van Loo, *Ind. Eng. Chem.* **41**, 1470 (1949).
247. G. P. Bierwagen and co-workers, *Prog. Org. Coat.* **35**, 1 (1999).
248. G. del Rio and A. Rudin, *Prog. Org. Coat.* **28**, 259 (1996).
249. F. Anwari and co-workers, *J. Coat. Technol.* **62**(786), 43 (1990).
250. G. T. Nolan and P. E. Kavanaugh, *J. Coat. Technol.* **42**(850), 37 (1995).
251. J. Temperley and co-workers, *J. Coat. Technol.* **64**(809), 33 (1992).
252. G. P. Bierwagen and T. K. Hay, *Prog. Org. Coat.* **3**, 281 (1975).
253. W. K. Asbeck, *J. Coat. Technol.* **64**(806), 47 (1992).
254. G. P. Bierwagen, *J. Paint Technol.* **44**(574), 46 (1972); C. R. Hegedus, and A. T. Eng, *J. Coat. Technol.* **60**(767), 77 (1988).
255. P. E. Pierce and C. K. Schoff, *Coating Film Defects*, Federation of Societies for Coatings Technology, Blue Bell, Pa., 1988.
256. S. E. Orchard, *Appl. Sci. Res. A* **11**, 451 (1962).
257. W. S. Overdiep, *Prog. Org. Coat.* **14**, 159 (1986).
258. S. Kojima and T. Moriga, *Polym. Eng. Sci.* **35**, 1098 (1995).
259. S. K. Wilson, *Surface Coat. Int.* **80**, 162 (1997).
260. F. J. Hahn, *J. Paint Technol.* **43**(562), 58 (1971).
261. K. Tachi, C. Okuda, and K. Yamada, *J. Coat. Technol.* **62**(791), 19 (1990).
262. W. S. Overdiep, *Prog. Org. Coat.* **14**, 1 (1986).
263. S. H. Wu, *J. Appl. Polym Sci.* **22**, 2769 (1978); D. R. Bauer and L. M. Briggs, *J. Coat. Technol.* **56**(716), 87 (1984).
264. W. H. Ellis, *J. Coat. Technol.* **53**(696), 63 (1983).
265. U.S. Pat. 4290932 (1981), H. J. Wright, D. P. Leonard, and R. A. Etzell (to Cook Paint & Varnish Co.).
266. S. Ishikura, K. Ishii, and R. Midzuguchi, *Prog. Org. Coat.* **15**, 373 (1988).
267. R. Berndimaier and co-workers, *J. Coat. Technol.* **62**(790), 37 (1990).
268. L. R. Waelde and co-workers, *J. Coat. Technol.* **66**(836), 107 (1994).

269. J. Schwartz and S. V. Bogar, *J. Coat. Technol.* **67**(840), 21 (1995).
270. W. Heilin, O. Klocker, and J. Adams, *J. Coat. Technol.* **66**(829), 47 (1994).

GENERAL REFERENCES

Z. W. Wicks Jr., F. N. Jones, and S. P. Pappas, *Organic Coatings: Science and Technology*, 2nd ed., Wiley-Interscience, New York, 1999.
Monograph series published by The Federation of Societies for Coatings Technology, Blue Bell, Pa. A continuing series with coverage of many aspects of coatings.

ZENO W. WICKS JR.
Consultant Louisville, Kentucky

COEXTRUSION

Introduction

Multilayer coextrusion of thermoplastic film and sheet has developed into an important plastic fabrication process, providing large growth opportunities for the plastics industry. Coextruded multilayer plastics are challenging such traditional materials as metals, glass, paper, and textiles.

The attraction of coextrusion is both economic and technical. It is a single-step process starting with two or more plastic materials that are simultaneously extruded and shaped in a single die to form a multilayer sheet or film. Thus, coextrusion avoids the costs and complexities of conventional multistep lamination and coating processes, where individual plies must be made separately, primed, coated, and laminated. Coextrusion readily allows manufacture of products with layers thinner than can be made and handled as an individual ply. Consequently, only the necessary thickness of a high performance polymer is used to meet a particular specification of the product. In fact, coextrusion has been used commercially to manufacture unique films consisting of hundreds of layers with individual layer thicknesses less than 100 nm (1). It is difficult to imagine another practical method of manufacturing these microlayer structures.

Layers may be used to place colors, bury recycle, screen uv radiation, provide barrier properties, minimize die-face buildup, and to control film-surface properties, for example. Additives, such as antiblock, antislip, and antistatic agents, can be placed in specific layer positions. High melt strength layers can carry low melt strength materials during fabrication.

The largest market for coextruded films and sheets is in packaging applications, eg, two- or three-layer films for trash bags or five- to nine-layer structures for flexible and semirigid packages. As many as five different polymers may be used

Encyclopedia of Polymer Science and Technology. Copyright John Wiley & Sons, Inc. All rights reserved.

to obtain heat sealability, barrier, chemical resistance, toughness, formability, and aesthetics. Coextrusion is also suitable for applying thin multilayer films as coatings on substrates (2). Growing applications for coextrusion are in automotive, construction, appliance, and food packaging markets (see PACKAGING, FLEXIBLE; BARRIER POLYMERS).

Methods of Coextrusion

Coextruded films are produced by a tubular-blown film process and a flat-die, chill-roll casting process. Capital and operating costs for blown-film vs cast-film coextrusion lines are strongly dependent on product mix and utilization. Equipment suppliers provide comparative economic evaluations for specific products. Practical cast-film equipment has been discussed previously (3). Coextrusion dies are unique. Extruders used before the die and take-away equipment used afterwards are standard equipment for single-layer film manufacture of blown or cast film (see EXTRUSION).

Tubular-Blown Film Process. This process is more flexible with regard to the permissible polymer viscosity mismatch, control of film orientation balance in the transverse and machine directions through blow-up ratio, and easy randomization of film-thickness variations. Production rates are limited by flow rates per circumferential length of die (pressure drop) and cooling rates (heat transfer).

Casting Process. The flat-die, chill-roll, cast-film process is more suitable for high volume production on dedicated lines because of higher output rates obtained by wide dies and more efficient cooling on chill rolls. Cast films usually have better clarity than blown films because of rapid quenching, but uniaxial orientation can cause the film to split in the machine direction for some structures.

Coextrusion Dies

Tubular-Blown Film Dies (Circular Dies). Tubular coextrusion dies were the earliest dies used to make multilayer plastic film. Successful design requires formation of uniform concentric layers in the annular die land formed by the mandrel and adjustable or nonadjustable outer die ring. Early designs included center-fed dies that had the mandrel supported by a spider (4). Feedports arranged a concentric melt stream that was pierced by the mandrel as it flowed to the die exit, forming annular layers. Limitations of this early design were discontinuity and nonuniformity caused by spider-induced weld lines in the layers.

Another early design used stacks of toroidal distribution manifolds, so that as flow proceeded to the die exit, concentric layers were extruded on one another sequentially (5). The number of layers could be varied by changing the number of toroidal manifolds in the stack. The crosshead design of this die eliminated the spider support of the mandrel with its attendant weld-line problem.

The design most commonly used today is the multimanifold spiral mandrel tubular-blown film die (Fig. 1a). This die consists of several concentric manifolds, one within the other. The manifolds are supported and secured through the base of the die. Each manifold consists of a flow channel that spirals around the mandrel,

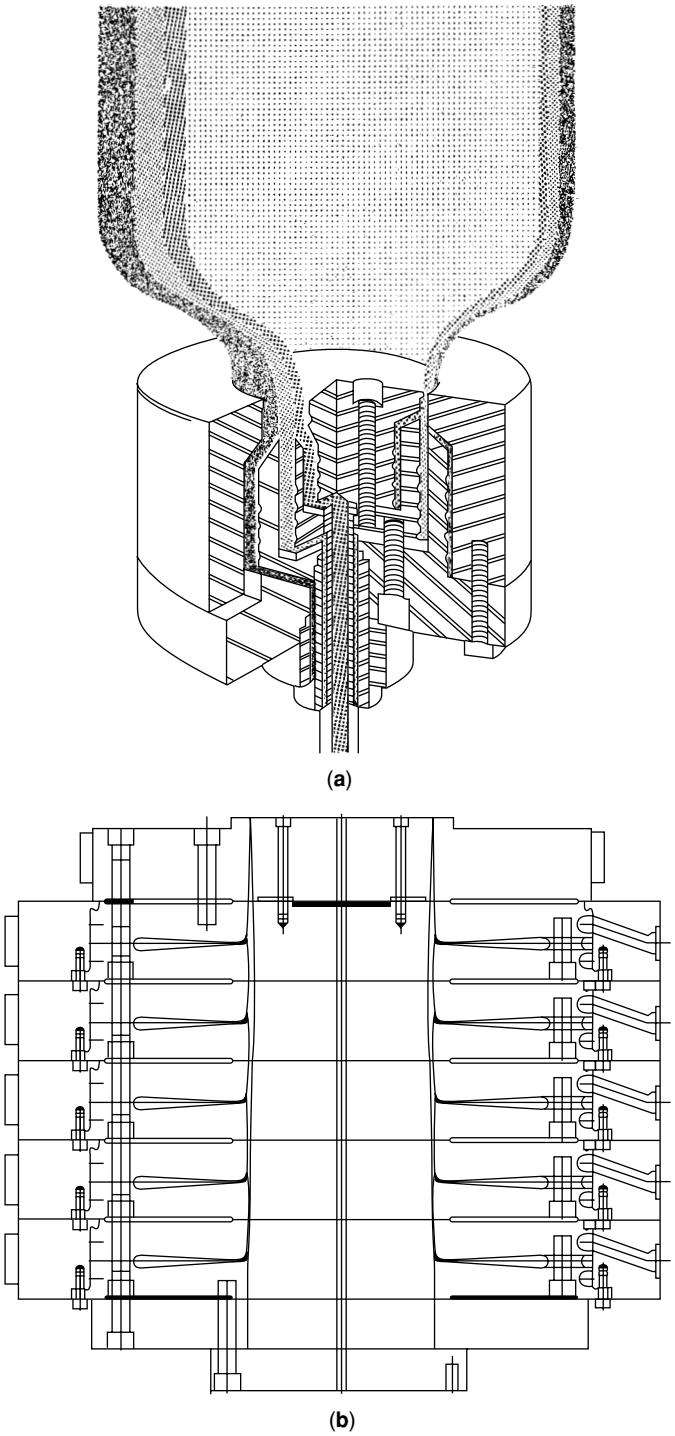

Fig. 1. (**a**) A three-layer blown film die and (**b**) a stackable blown film die.

allowing polymer to flow down the channel or leak across a land area to the next channel. This flow pattern smoothes out the flow of the polymer and minimizes any weld lines in the final film. While early designs were limited to two or three layers, dies containing seven or more layers are now offered commercially.

These dies must achieve uniform concentric flow of all layers because it is impractical to provide circumferential thickness adjustment for each layer. Most polymers are non-Newtonian, and polymer viscosity usually decreases with shear rate. Thus, rheological data obtained at the intended extrusion temperature and shear rate are needed to size manifolds and channels for layer uniformity and minimum pressure drop. Frequently, spiral mandrel manifolds, common in single-layer dies, are used to improve circumferential distribution. A well-designed spiral mandrel manifold can be helpful, but streamlining is necessary to minimize stagnation, residence time, and purging. A manifold design is only optimum for a particular polymer. Employing a polymer with significantly different properties may require a different manifold insert in the die in order to obtain satisfactory layer distribution.

Most tubular-blown film lines are designed for oscillation of the die or winder to randomize film thickness variations at the windup and avoid buildup of gauge bands, which can cause problems with film flatness. More layers complicate bearing and sealing systems in an oscillating die, but designs have now been refined to employ new sealing materials that minimize polymer leakage. New designs incorporate temperature control of individual annular manifolds to permit coextrusion of thermally sensitive polymers.

Another style of tubular-blown film die is the stackable plate die (Fig. 1b). In this style of die, each layer is spread uniformly and formed into a tube in a single plate. Plates are then stacked on top of each other and the layers are added sequentially. This style of die is becoming popular for specific applications since the number of layers can be adjusted by simply changing the number of plates in the die.

Tubular coextrusion dies are expensive, and care must be taken when disassembling and reassembling them to clean or change parts. Discussions of additional practical design, maintenance, and operating considerations have appeared (6–10).

Flat Dies (Slit Dies). Flat dies, also called slit dies because the orifice is a wide rectangular opening, are used in chill-roll, cast-film coextrusion. These dies are used almost exclusively for multilayer coextrusion with sheet thickness $>254\ \mu$m, as well as in coextrusion coating processes (2), where a multilayer web is extrusion-coated onto a substrate such as paperboard, aluminum foil, plastic foam, or textiles.

Another commercial application for flat-die coextrusion is biaxially oriented multilayer films (11) made with the tentering process to improve mechanical properties. Tentered film is biaxially oriented by stretching in the longitudinal and transverse direction, either sequentially or simultaneously, at uniform optimum temperature. In sequential stretching, the multilayer extrudate is cooled to a suitable orientation temperature on a first set of rolls and then stretched in the machine direction between a second set of rolls which is driven faster than the first set. The uniaxially stretched film then enters a tentering frame, which has traveling clips that clamp the edge of the film. The clips are mounted on two

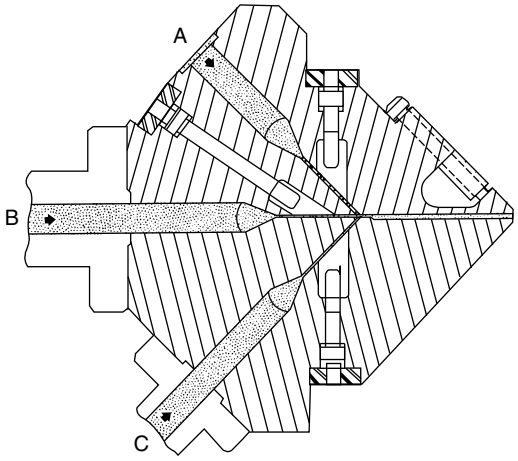

Fig. 2. Cross-sectional view of three-layer internal-combining multimanifold flat film or sheet die.

tracks that diverge inside a temperature-controlled oven increasing film width to provide transverse stretch. The film is then heat set and cooled. Simultaneous tentering frames are also used which feature accelerating clips that stretch the film longitudinally as they diverge transversely.

Two basic die types used in flat-die coextrusion systems are multimanifold dies and the feedblock/single-manifold die. A hybrid combines feedblocks with a multimanifold die.

Multimanifold Dies. For each layer, these dies have individual manifolds that extend the full width of the die. Each manifold is designed to distribute its polymer layer uniformly before combining with other layers outside the die (external combining) or inside the die before the final die land (internal combining).

External-combining dies are typically limited to two-layer coextrusion because two slit orifices must be individually adjusted with die-lip adjusting bolts. The webs are combined at the roll nip.

In principle, internal-combining dies are similar to multimanifold-tubular-coextrusion dies, except that the manifolds are flat (Fig. 2). With these dies, it is possible to regulate flow across the width by profiling an adjustable restrictor bar in each manifold to help obtain uniform distribution. However, wide dies require numerous adjusting bolts on each layer manifold along with die-lip adjustment to control final thickness; this can make them difficult to operate. Multimanifold dies have been sold, capable of coextruding five and six layers; they are expensive and require skilled operators. The principal advantage of multimanifold dies is the ability to coextrude polymers with very different viscosities since each layer is spread independently prior to combining.

A significant disadvantage of wide multimanifold dies is difficulty in coextruding very thin layers, such as thin cap (surface) layers, or thin adhesive (tie) layers used to bond two dissimilar polymers. Often these thin layers represent only 1 or 2% of the total structure thickness and are therefore extruded at a relatively low rate. With wide dies it is difficult to obtain uniformity when extrusion

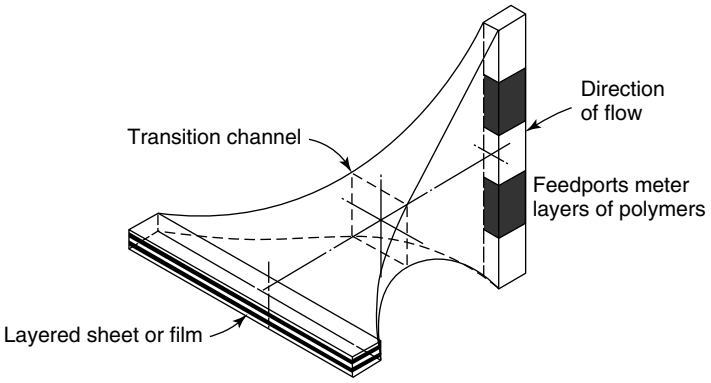

Fig. 3. The principle of the feedblock for coextruding multilayer film or sheet. Number of layers is equal to number of feedports.

rate per width is very low. Also, it is difficult to coextrude thermally- sensitive polymers such as poly(vinyl chloride) (PVC) and poly(vinylidene chloride) copolymers (PVDC) in wide dies because slow-moving material near the walls greatly increases residence time and thermal exposure.

Feedblock/Single-Manifold Dies. The feedblock method of flat-die coextrusion, originally developed and patented by The Dow Chemical Company, uses a feedblock before a conventional single-manifold die (12,13). A layered melt stream, which is prearranged ahead of the die inlet by the feedblock is extended to the width of the die as it is reduced in thickness (Fig. 3). Polymer melts from each extruder can be subdivided into as many layers as desired in the final product. Feedports arrange metered layers in required sequence and thickness proportions. A commercial feedblock/single-manifold die system is shown in Figure 4. Modular feedblock design similar to that illustrated can be used to change the number, sequence, or thickness distribution of layers by changing a flow programming module in the feedblock. Programming modules consist of machined flow channels designed to subdivide and direct flow of each material to specific locations and proportions required by the product.

The shape of the multilayer melt stream entering the die inlet can be round, square, or rectangular, as long as the feedblock is properly designed to deliver the layers to the die with constant composition (14). Some feedblock suppliers prefer round die entry design for ease of machining or retrofitting to old dies. Others prefer square or rectangular die entries for ease of design and minimization of shape change as the layer interfaces are extended to the rectangular die orifice. A thermally sensitive polymer can be encapsulated by stable polymers so that it does not contact the die walls, thus reducing residence time.

The fact that the multilayer stream at the die inlet is narrow (∼2.5–10 cm) compared to die width makes it relatively easy to meter thin surface or adhesive layers.

The versatility of the feedblock has made it the most popular flat-die coextrusion method. Large numbers of layers may be coextruded, layer structure may be readily altered with interchangeable modules, and thermally sensitive

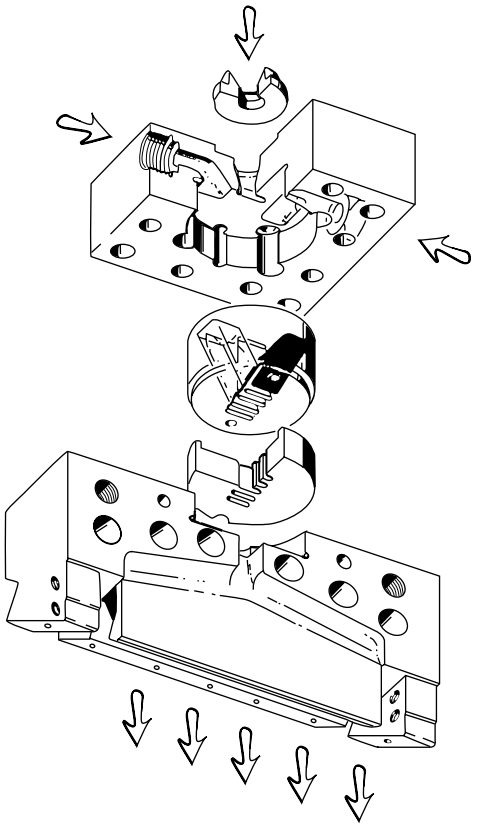

Fig. 4. Exploded view of modular feedblock and single-manifold die for three polymers forming a five-layer coextrusion.

polymers may be protected by encapsulation. It is estimated that over 95% of flat-die coextrusion systems use a feedblock.

One limitation of feedblocks is that polymer viscosities must be matched fairly closely because the combined melt stream must spread uniformly within the die. Severe viscosity mismatch results in nonuniform layers; the lower viscosity material tends to flow to the die edges. A crude rule of thumb is that polymer viscosities must be matched within a factor of 3 or 4, which is a reasonably broad range for many commercially important coextrusions. Layer uniformity may be adjusted by varying melt temperature within limits dictated by heat transfer. Increasing temperature decreases viscosity, and material moves from the center to the edges; decreasing temperature has the opposite effect. Typically, the individual polymer melt temperatures differ by as much as 30–60°C. Beyond that, heat transfer tends to nullify further adjustment by temperature variation.

Often polymers are intentionally selected with a mismatch in viscosities to avoid flow instabilities. Viscosity mismatch of a factor of 10 or more may be necessary. Layer nonuniformity expected with the mismatch is compensated by using shaped feedport geometry; that is, the layers are introduced into the die nonuniformly so that uneven flow within the die results in a satisfactorily uniform

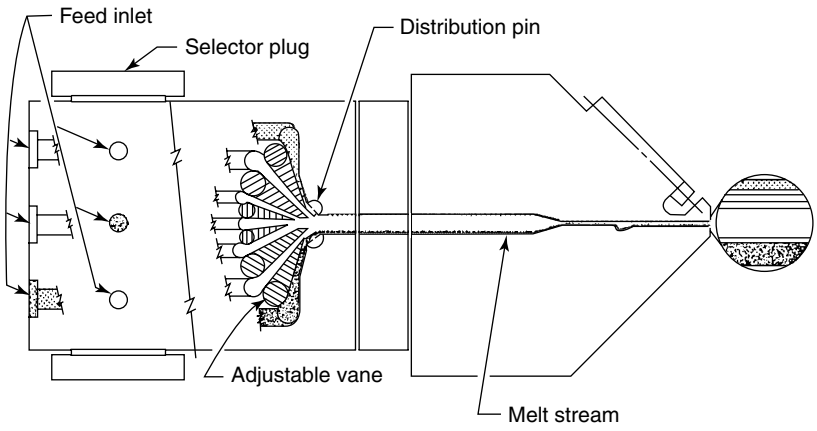

Fig. 5. Feedblock with movable vane partitions that adjust positions for different polymer viscosities and/or layer-flow rates.

final distribution. Considerable art has been developed to extend the range of viscosity mismatch that can be accommodated in a feedblock system by using compensating feedport geometry.

Some feedblocks are reportedly capable of coextruding polymers with viscosity mismatch of 100 or more (15). This style of feedblock has movable vanes that partition individual layers prior to combining (Fig. 5). The vanes may be freely floating, automatically seeking their equilibrium position on the basis of flow rates and viscosities. This self-adjusting feature can accommodate wide ranges in relative flow rates and viscosities while maintaining layer uniformity in the final product. The vanes may be rotated manually and locked into a nonequilibrium position to adjust uniformity further. Often distribution pins are used, or the vanes are profiled to compensate for nonuniform layers.

Combined Feedblock/Multimanifold Dies. Combinations of feedblocks and a multimanifold die are also used commercially. The multimanifold die can incorporate the same design principles as the feedblock, ie, vanes separating individual manifolds within the die. In a sense, the multimanifold die is a wide feedblock. A feedblock may be attached to one or more manifold inlets, as shown in Figure 6. With this system, polymers with widely different polymer viscosities and processing temperatures may be coextruded. A very viscous or high temperature polymer may be extruded through one or more die manifolds, while a thermally sensitive or much lower viscosity polymer is coextruded with adhesive layers through a feedblock feeding another manifold. Combining of all layers occurs prior to the final die land.

Rheological Considerations

Polymer rheology information is critical for designing coextrusion dies and feedblocks. The flow characteristics of the polymer must be considered when selecting materials for coextruded products (see RHEOLOGY).

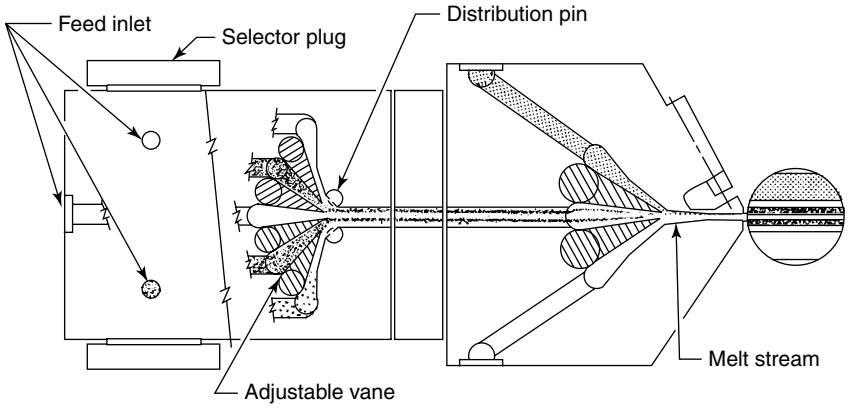

Fig. 6. Combination feedblock and multimanifold die system. Feedblock feeds center-die manifold.

The best designed die or feedblock does not necessarily ensure a commercially acceptable product. Layered melt streams flowing through a coextrusion die can become unstable leading to layer nonuniformities and even intermixing of layers under certain conditions. The causes of these instabilities are related to non-Newtonian flow properties of polymers and viscoelastic interactions.

Viscosities of non-Newtonian polymers are dependent on extrusion temperature and shear rate, both of which may vary within the coextrusion die. The shear rate dependence is further complicated in that it is determined by the position and thickness of a polymer layer in the melt stream. A polymer used as a thin surface layer in a coextruded product experiences higher shear rate than it would if it were positioned as a central core layer. There are several types of flow instabilities that have been observed in coextrusion.

Interface Distortion from Viscosity Mismatch. The importance of viscosity matching for layer uniformity was first studied in capillary flow of two polymers in bicomponent fiber production (16–19). Two polymers introduced side by side into a round tube experience interfacial distortion during flow if the viscosities are mismatched. The lower viscosity polymer migrates to regions of highest shear (at the wall) and tends to encapsulate the higher viscosity polymer. It is possible for the low viscosity polymer to encapsulate the higher viscosity polymer totally. Nature seeks the path of least resistance. The degree of interfacial distortion due to viscosity mismatch depends on the extent of viscosity difference, shear rate, and residence time.

Layer nonuniformities in feedblock fed flat dies occur for the same reason when there is a large enough viscosity mismatch. Low viscosity polymer migrates to wet the die wall. For unencapsulated layers, this migration starts in the die manifold as the layered stream spreads, resulting in increased layer thickness for low viscosity polymer at the edges of the film or sheet. If unencapsulated low viscosity polymer is a core layer, it not only becomes thicker at the edges but may even wrap around higher viscosity skin layers at the film edges.

Tubular-blown- film dies are more tolerant of viscosity mismatch because the layers are arranged concentrically, ie, there are no ends. Since streamlines

cannot cross each other, further migration cannot occur. However, good die design is required to obtain concentric layers.

Interface Distortion from Viscoelasticity. While matching the viscosities of adjacent layers has proven to be very important, the effect of polymer viscoelasticity on layer thickness uniformity is also important (20–24).

It has been shown that polymers that are comparatively high in elasticity produce secondary flows normal to the primary flow direction in a die that can distort the layer interface. This effect becomes more pronounced as the width of a flat die increases. Appropriate shaping of the die channels can minimize the effect of layer interface distortion due to elastic effects.

Coextruding a structure that contains layers of polymers with low and high levels of elasticity can cause interface distortion because of the differences in elasticity between the layers in flat dies. The effect is typically not observed in tubular dies.

Flow Instability. Interface distortion causes thickness nonuniformities, but the interface remains smooth. Other instabilities result in irregular interfaces and even layer intermixing in severe cases. These instabilities are related to viscoelasticity in non-Newtonian polymers. At low output rates, low amplitude waviness of the interface is observed, which is barely noticeable to the eye and may not interfere with the functionality of the multilayer film. At higher output rates, the layer distortion becomes more severe. If a large amplitude waveform develops in the flowing multilayer stream within the die, the velocity gradient can carry the crest forward and convert it into a fold. Multiple folding results in an extremely jumbled, intermixed interface. This type of instability has been observed in tubular-blown film dies, multimanifold dies, and feedblock/single-manifold dies.

This instability develops in the die land, and its onset can be correlated with a critical interfacial shear stress for a particular polymer system (2). The most important variables influencing this instability are skin-layer viscosity, skin-to-core thickness ratio, total extrusion rate, and die gap. Although the interfacial shear stress does not cause instability, elasticity is related to shear stress, and interfacial stress is used to correlate variables for a particular system.

Interfacial instability in a number of coextruded polymer systems has been experimentally correlated with viscosity ratios and elasticity ratios (25), and a simplified rheology review has been given (26).

This type of interfacial instability can be reduced or eliminated by increasing skin-layer thickness, increasing die gap, reducing total rate, or decreasing skin-layer polymer viscosity. These methods may be used singly or in combination. These remedies reduce interfacial shear stress, and stable flow results when it is below the critical stress for the polymer system being coextruded. Most often skin-layer polymer viscosity is decreased. In feedblock coextrusion the resultant viscosity mismatch imposed by this remedy can cause variations in layer thickness as discussed earlier. Shaped skin layer feedslots are then used to compensate.

Other types of instabilities may exist, for example, a problem has been observed in feedblock coextrusion of axisymmetric sheet (27). A wavy interface is also characteristic of this instability, but the wave pattern is more regular when viewed from the surface. The instability originates in the die, well ahead of the die land, and internal die geometry influences both the severity and pattern. For a given die geometry, the severity of instability increases with structure asymmetry and some polymers are more susceptible to unstable flow than others.

It has been suggested that this type of instability may be related to the extensional rheological properties of the polymers used in the coextruded structure (28).

No complete predictive theory exists for these complicated rheological interactions, but the accumulated experience of polymer producers, equipment suppliers, and experienced fabricators provides guidance in polymer selection.

Polymers for Coextruded Films

Polymers are chosen for individual layers to achieve special combinations of properties, eg, mechanical strength and stiffness, gas and water-vapor barrier, oil and grease barrier, heat seal, hot tack, Adhesion, optics, formability, machinability, and economics. Individual layers may be pure polymers or blends, sometimes with regrind or recycled scrap. The polymer layers are often formulated with color, antislip, antiblock, antistats, processing aids, fillers, biocides, oxygen scavengers, antifogs, flame retardants, nucleating agents, and stabilizer additives to enhance layer characteristics (29–35) (see ADDITIVES). Adhesive polymers are used as tie layers to bond dissimilar polymers that do not normally adhere to each other (see ADHESIVE COMPOUNDS).

Common polymers used in coextrusion applications are listed below with their abbreviations:

Name	Abbreviation
Low density polyethylene	LDPE
Medium density polyethylene	MDPE
High density polyethylene	HDPE
High molecular weight, high density polyethylene	HMW-HDPE
Linear low density polyethylene	LLDPE
Ultralow density polyethylene	ULDPE
Polyolefin plastomer	POP
Ethylene–styrene interpolymer	ESI
Ethylene–vinyl acetate	EVA
Ethylene–acrylic acid	EAA
Ethylene–methyl acrylate	EMA
Ethylene–ethyl acrylate	EEA
Cyclic olefin copolymer	COC
Ethylene–*n*-butyl acrylate	EnBA
Ethylene–methacrylic acid copolymer	EMAA
Ethylene–methacrylic acid salts	Ionomer
Ethylene–vinyl alcohol	EVOH
Poly(vinyl alcohol)	PVOH
Polyamide	PA
Poly(vinyl chloride)	PVC
Poly(vinylidene chloride) copolymers	PVDC
Polypropylene	PP
Polybutylene	PB
Poly(ethylene terepthalate)	PET
Glycol modified polyester	PETG
Poly(ethylene napthalate)	PEN

Name	Abbreviation
Poly(methyl methacrylate)	PMMA
Poly(hydroxyaminoether)	PHAE
Polycarbonate	PC
Polystyrene	PS
High impact polystyrene	HIPS
Acrylonitrile–methyl acrylate copolymer	AN/MA
Acrylonitrile copolymers	AN
Acrylonitrile–butadiene–styrene polymers	ABS
Styrene–butadiene block copolymer	SB

See ETHYLENE POLYMERS, LDPE; ETHYLENE POLYMERS, HDPE; ETHYLENE POLYMERS, LLDPE; VINYL ALCOHOL POLYMERS; VINYL CHLORIDE POLYMERS; VINYLIDENE CHLORIDE POLYMERS (PVDC); POLYAMIDES, PLASTICS; POLYESTERS, THERMOPLASTIC; PROPYLENE POLYMERS (PP); METHACRYLIC ESTER POLYMERS; ACRYLONITRILE POLYMERS; STYRENE POLYMERS (PS); IONOMERS.

An individual polymer usually can provide several functions, but selection for each layer is determined by the key property that the polymer can contribute to the total film for a specific application.

Mechanical Properties. The coextruded film must have adequate tensile and impact strength, tear resistance, elongation, and puncture resistance for package integrity. LDPE, LLDPE, POP, HDPE, PP, nylon, ionomer, and EAA are typical resins used for toughness. Significant catalyst development has resulted in various forms of polyethylene copolymers. Ziegler–Natta catalysts produce linear copolymers with a broad short-chain branch distribution and a broad molecular weight distribution. Metallocene catalysts produce copolymers with a more homogeneous comonomer distribution and a narrower molecular weight distribution. Constrained geometry catalysts produce copolymers with a small but significant amount of long-chain branching, in addition to any short-chain branching from the comonomer, as well as with a more homogeneous comonomer distribution and a narrower molecular weight distribution. Metallocene and constrained geometry catalysts allow higher levels of comonomer and molecular tailoring for specific properties. In general, metallocene and constrained geometry catalysts have better optical properties, ESCR, impact strength, puncture strength, and tensile strength than Ziegler–Natta catalyst polymers. The lower density copolymers made possible with metallocene and constrained geometry catalysts, POP, demonstrate enhanced breathability for controlled atmosphere packaging applications. The lower density resins also have lower melting points and may be used as heat seal resins with good hot tack and seal integrity, allowing them to be substituted for EVA or ionomers. The open sites of the metallocene and constrained geometry catalysts also allow the copolymerization of different comonomers such as styrene and norbornene with ethylene. Metallocene technology has also been used for the manufacture of isotactic PP, syndiotactic PP, copolymers of PP with other olefins, and syndiotactic PS (36–45).

Most published film data is derived from monolayer film and as a first approximation, tensile strength of a coextruded film may be estimated from the percentage of each polymer present in the film according to the law of mixtures,

ie, the summation of the tensile strength per unit thickness of each layer, multiplied by its thickness, divided by total thickness. However, layer interactions can greatly influence mechanical behavior of composites. Favorable (synergistic) interactions provide mutual interlayer reinforcement (46,47), and the composite acquires better mechanical properties than expected from summation of the components as a blend (48–52). For example, when a normally brittle polymer layer is sandwiched between ductile layers which can inhibit crack propagation, the brittle layer may undergo greater deformation than is possible for it as an unsupported free film.

Unfavorable layer interactions can lead to mutual interlayer destruction, ie, failure in one layer leads to premature failure in normally ductile layers, causing catastrophic failure of an entire composite. In this case, the cracked layer acts as a notch to localize stress concentration in adjacent layers.

Layer multiplying enables structures with hundreds or thousands of layers to be produced. A layered melt stream from a feedblock is fed through layer multipliers. In each multiplier, the initial melt stream is divided vertically in two, spread horizontally, and then recombined, resulting in a doubling of the initial number of layers. Improved physical properties, mechanical, optical, barrier, and electronic, have been demonstrated. Synergistic combinations of the properties of the component polymers have also been reported. The failure mechanism of microlayered PC/SAN structures can be controlled, with layer thicknesses in the micron range demonstrating improved toughness and impact relative to conventional blends. Microlayering can also produce structures with aligned platelet fillers, demonstrating anisotropic physical, barrier, and electrical properties. Breathable films with high water vapor transition rates and good mechanical properties are obtained with a microlayered filled polypropylene/polyethylene oxide system. A number of companies have commercialized microlayer structures with unique optical properties. These structures have from 100 to 500 layers and total thickness from 1 to 2.5 mil. These films can be tuned to reflect or transmit different segments of the visible or near ir portions of the electromagnetic spectrum. Applications range from iridescent decorative films for packaging and labeling to metal free films that specularly reflect up to 98% of visible light from any incident angle for electronic display enhancement. Microlayer structures, with the ability to control the interface/volume ratio, have also been used for fundamental interdiffusion and adhesion studies (53–59).

Molecular orientation is another important factor influencing mechanical properties of coextruded films (11). Biaxial orientation can greatly improve film strength. However, uniaxial or highly unbalanced orientation causes poor transverse properties, which result in easy splitting of coextruded films in the machine direction. This tendency may occur even when a relatively thin layer responds to unidirectional orientation and propagates failure to thicker adjacent layers.

Therefore, although law of mixture calculations for multilayer films may be used for an approximate estimate of strength, it is inadequate for predicting layer interactions and ultimate film performance.

Mechanical properties measured on coextruded films include the effect of orientation during processing, as well as polymer–layer interactions. Optimization of film properties by plotting property against percentage composition of polymer combinations yields the most comprehensive picture of film performance.

Table 1. Oxygen Permeabilities

Resin[a]	$\frac{\text{nmol}}{\text{m}\cdot\text{s}\cdot\text{GPa}}$	$\frac{\text{mL}\cdot\text{mil}}{\text{m}^2\cdot\text{d}\cdot\text{atm}}$	$\frac{\text{mL}\cdot\text{mil}}{100\text{in}^2\cdot\text{d}\cdot\text{atm}}$
EVOH	0.04	0.3	0.02[b]
PVDC	0.3	2.3	0.15
Nitrile barrier resin	1.6	12.4	0.8
Nylon-6	5.2	40.3	2.6
Polyester	7	54	3.5
Rigid PVC	10–40	78–310	5–20
Polypropylene	300	2300	150.0
HDPE	300	2300	150.0
PS	700	5400	350.0
LDPE	840	6500	420.0

[a] See listed abbreviations in "Polymers for Coextruded Films" section.
[b] Dry only.

Gas-Barrier Properties. Coextruded films are often used to provide a barrier to gases (oxygen, nitrogen, and carbon dioxide) and water vapor in packaging applications. PVDC, EVOH, acrylonitrile, nylon, PVC, and PET provide varying degrees of barrier to gases, flavor and aroma components, and organic fractions (60,61). A variety of nylon polymers are available including nylon-6, nylon-6,6, nylon-11, nylon-12, amorphous nylon, and MXD-6 (62) (see POLYAMIDES, PLASTICS). Coextruded films with liquid crystalline copolymers as well as with PCTFE have been reported (63–65). Poly(hydroxyaminoether) thermoplastics for barrier packaging have recently been commercialized (66). Table 1 gives comparative oxygen permeabilities for several plastics based on 25.4-μm thickness at 23°C. Various aspects of film barriers have been reviewed (67–70) (see BARRIER POLYMERS).

At steady state, gas-transmission rate through a given layer is inversely proportional to its thickness. The total transmission rate through a multilayer film may be calculated by treating the contribution of each layer as resistances in series (71). For many coextruded films the overall transmission rate is controlled by the high barrier layer, ie, the layer with lowest transmission rate. Gas-transmission rates through polymers increase with temperature. Some polymers, such as EVOH, are moisture-sensitive, and oxygen-transmission rate increases with relative humidity. Therefore, application of coextruded barrier films to packaging requires knowledge of the package environment during filling, processing, shipping, and storage. Data comparing EVOH and PVDC suggest an aggregate oxygen exposure index to evaluate barrier coextrusions under varying environmental conditions (72).

Inadequate understanding of product barrier requirements poses a package-design problem in predicting adequate shelf life from gas-transmission data.

Langmuir kinetic theory has been discussed for prediction of barrier requirements (73), but packagers still must rely on extensive shelf life testing of individual food products in candidate barrier films.

Table 2 gives water vapor transmission rates for several polymers. The ranking of polymers for water vapor transmission is different from ranking them for

Table 2. Water Vapor Transmission Rates

Resin[a,b]	$\frac{\mu mol}{m^2 \cdot s}$	$\frac{g}{h \cdot m^2}$	$\frac{g}{100 in.^2 \cdot d}$
PVDC	1–1.5	0.065–0.097	0.1–0.15
PP	2.5	0.16	0.25
HDPE	3–4	0.23	0.3–0.4
LDPE	10–15	0.81	1.0–1.5
polyester	10–13	0.8	1.0–1.3
rigid PVC	9–51	0.6–3.3	0.9–5.1
nitrile barrier resin	50	3.2	5.0
PS	70–100	4.5–6.5	7.0–10.0
EVOH	130	8.4	13.0
nylon	160–220	10.3–14.2	16–22

[a] 25.4-μm (1 mil) film at 37.8°C and 90% rh.
[b] See listed abbreviations in "Polymers for Coextruded Films" section.

oxygen transmission. LDPE, HDPE, and PP are economical barrier polymers to water vapor. PVDC is one of the few polymers that provide an excellent barrier to both oxygen and water vapor.

Barriers to aromas and flavors are very important in packaging and cannot be predicted from common gas-barrier data. Nylon has a good aroma barrier for certain snack-food packaging (74). Flavor scalping is also important in some applications.

Oil and Grease Barrier. Oils and grease must be retained in the packaged product for product quality and must not degrade the package, its printing, or customer appeal. Nylon, EAA, and ionomers are good oil- and grease-barrier materials.

Adhesion. Successful combination of coextruded film layers has been described in terms of rheological compatibility, surface tension and melt viscosity at processing temperature, interfacial behavior at the surfaces between layers, chemical interaction between two combined materials, crystallinity, and shear compatibility between components of the composite (67). Critical factors in layer bonding are polymer functionality (chemical composition), melt temperature, time in contact at temperature, viscosity of the joining layers, layer thickness, thermal stability, orientation, quench rate, and moisture sensitivity.

No comprehensive theory exists for predicting interlayer adhesion in coextrusion (see ADHESION). Most knowledge comes from trial-and-error testing that has led to qualitative rating charts for polymer adhesion such as the one shown in Table 3. Polymer or copolymer functionality plays a strong role. Polar polymers tend to adhere to each other; adhesion is difficult between nonpolar polymers. Some polymers form covalent bonds in addition to H-bonding, acid–base, ionic, and dipole–dipole interactions (75–78).

Tie layers are used to adhere incompatible layers of dissimilar polymers. EVA, EMA, EAA, EEA, EnBA, SB, and ionomer are frequently used copolymers. The importance of tie layers for coextrusion has led material suppliers to develop new chemically modified polymers for specific applications. Tie layers also contribute physical properties, optics water barrier, modulus, thermal resistance,

Table 3. Qualitative Degree of Adhesion Between Resins[a,b]

	Olefins			Styrenes						Vinyl			Miscellaneous						Adhesives				
Material	LDPE	HDPE	PP	Low impact PS	Medium impact PS	High impact PS	Crystal PS	ABS[c]	ABS	Rigid PVC	Flexible PVC	Vinylidene chloride–vinyl chloride copolymer	Polycarbonate	Polyurethane	Acrylic	Nitriles	Nylon–6	EAA	EVA	Ionomers	SBS[d]	CPE[e]
Olefins																							
LDPE	G	G	P	P	P	P	P	P	P	P	P	P	P	F	P	P	P	G	G	G	G	G
HDPE	G	G	P	P	P	P	P	P	P	P	P	P	P	F	P	P	P	G	G	G	G	G
PP	P	P	G	P	P	P	P	P	P	P	P	P	P	F	P	P	P	G	G	P	G	G
Styrenes																							
Low impact PS	P	P	P	G	G	G	G	G	P	P	P	P	P	F	P	P	P	P	G	P	G	F
Medium impact PS	P	P	P	G	G	G	G	G	P	P	P	P	X	F	P	P	P	P	G	P	G	F
High impact PS	P	P	P	G	G	G	G	G	P	P	P	P	X	F	P	P	P	P	G	P	G	F
Crystal PS	P	P	P	G	G	G	G	G	P	P	P	P	X	F	P	P	P	P	G	P	G	F
ABS[c]	P	P	P	G	G	G	G	G	G	G	G	G	X	F	G	P	P	P	G	P	G	G
ABS	P	P	P	P	P	P	P	G	G	G	G	G	X	F	G	P	P	P	G	P	G	G
Vinyl																							
Rigid PVC	P	P	P	P	P	P	P	G	G	G	G	F	U	G	G	P	U	P	G	P	G	G
Flexible PVC	P	P	P	P	P	P	P	G	G	G	G	F	U	G	G	P	U	P	G	P	G	G
Vinylidene chloride–vinyl chloride copolymer	P	P	P	P	P	P	P	G	G	F	F	G	U	G	G	X	P	P	G	P	G	G
Miscellaneous																							
Polycarbonate	P	P	P	P	X	X	X	X	X	U	U	U	G	X	G	P	X	X	X	X	X	X
Polyurethane	F	F	F	F	F	F	F	F	F	G	G	G	X	G	X	P	X	F	G	X	F	G
Acrylic	P	P	P	P	P	P	P	G	G	G	G	G	G	X	G	P	X	X	X	X	X	F
Nitriles	P	P	P	P	P	P	P	P	P	P	P	X	P	P	P	G	P	P	F	X	F	X
Nylon-6	P	P	P	P	P	P	P	P	P	U	U	P	X	X	X	P	G	G	P	G	P	X
Adhesives																							
EAA	G	G	G	P	P	P	P	P	P	P	P	P	X	F	X	P	G	G	G	G	F	G
EVA	G	G	G	G	G	G	G	G	G	G	G	G	X	G	X	F	P	G	G	X	G	G
Ionomers	G	G	P	P	P	P	P	P	P	P	P	P	X	X	X	X	G	G	X	G	X	G
SBS[d]	G	G	G	G	G	G	G	G	G	G	G	G	X	F	X	F	P	F	G	X	G	G
CPE[e]	G	G	G	F	F	F	F	G	G	G	G	G	X	G	F	X	X	G	G	G	G	G

[a] Key: G = good; F = fair; P = poor; X = unknown; U = undesirable for coextrusion.
[b] See listed abbreviations in "Polymers for Coextruded Films" section.
[c] Less than 20% acrylonitrile content.
[d] Styrene–butadiene–styrene.
[e] Chlorinated polyethylene.

and toughness. Examples include a family of Plexar resins by Equistar (79), a series of CXA resins by DuPont (80), and Mitsui's Admer adhesive resins. Greater development of extrudable adhesive polymers is expected.

Heat Seal. Heat sealability characteristics of a structure are controlled by the outer surface layers and the type of seal geometry used to form a package. Heat-seal layers must fuse and adhere to themselves and other layers. Seal strength, heat-seal temperature range, and sealability through contaminants (81) are important to high fabrication rates and package integrity. LDPE, POP, EVA (82), EAA (83), ionomer (84), and LLDPE are common seal-layer materials. LDPE is the standard multiple-purpose layer, whereas EVA has outstanding low temperature seal and seal range. EVA is frequently coextruded with HDPE to prevent the puckering that occurs when HDPE is heated to its softening point to form a heat seal. The higher softening temperature of HDPE allows use of hotter heat-seal bars. EAA, POP, and ionomers are strong and seal through contaminants (85–87). A resin's hot tack, ie, the ability of a molten seal to resist separating force,

determines the rate at which the polymer can be sealed. LDPE, LLDPE, POP, EVA, EAA, and ionomer are materials of choice.

Machinability. Packaging films must run through printing presses and package-forming machinery without marring, hang-up, wandering, or deformation. Combinations of LDPE, PP, and PET are selected for structure-fabrication needs. PC is being investigated as a high modulus layer that can provide toughness without orientation and compete with oriented PET.

Optical Properties. Many packages need sparkling clarity to display their contents (see OPTICAL PROPERTIES). Other packages have printing over nearly all of the surface area or the product must be protected from uv radiation. White, brown, and black pigmented layers are combined to protect light-sensitive products.

The gloss and haze of a coextruded structure are modified by particular layers in the structure. The total haze exhibited by a film depends on the surface haze and the internal film haze. Placing a high haze layer on the inside of a film and low haze layers on the outside surfaces improves the haze of the buried material. The outside layer controls the gloss. Modification of haze gloss may be obtained with processing conditions, processing aids, nucleating agents, and other additives. In the case of cast films, a polished roll gives a high gloss, low haze film with tack. A matte chill roll produces a dull surface.

High Temperature Dimensional Stability. Dimensional stability at elevated temperatures is important in high temperature filling, sterilization applications, and microwave oven lidding. Resistance to physical deformation under load is linked to physical distortion of the part or package. HDPE, PP, nylon, and PET are suitable for high temperature applications. Coextrusion of PC with barrier polymers is being developed for high temperature barrier packaging (88).

Economics. An advantage of coextrusion is the capability of combining layers of high performance resins with low cost resin layers to produce high performance/low cost composite structures. The use of recycled and scrap resins in buried layers further improves economy. Multilayer extrusion economic considerations have been calculated (89). The effect of recycle on film properties, eg, tensile strength, impact, and elongation, depends on the degree of compatibility of polymers in the recycle layer. Often the tie-layer polymer acts as a compatibilizer for recycle. Recycle of incompatible polymers with different refractive indexes usually causes haziness and cannot be used when excellent optical properties are required.

Aesthetics. Coextruded layers may be colored for appearance, light screening, or coding. White is used as a printing background or a cleanliness layer adjacent to the product. Colors are used to designate sterile and nonsterile surfaces; black and brown screen uv light. Coextruded film composed of over 100 layers of alternating materials with different refractive indexes produces a vivid iridescence used in decorative applications (1,90). If gloss is essential, a thin surface layer of a high gloss polymer can be coextruded to give the package sparkle for marketing appeal.

Formability. Materials with a broad softening range, such as PS and PC, can be thermoformed into deep-draw package shapes. Crystalline polymers, eg, HDPE and PP, are more difficult to thermoform, but solid-phase forming processes below the melting point are possible. Multilayer semirigid barrier containers are made by Shell's Solid Phase Pressure Forming Process and the patented Dow

Scrapless Forming Process (91–94) that is being developed by Cincinnati Milacron. An advantage of the latter process is that round containers may be made from square blanks cut from sheet without the trim scrap normally associated with sheet forming.

Applications

Flexible packaging is important in several markets. Stand-up pouches have grown significantly in the pet foods and agricultural chemical markets. In 2002, food packaging will be over half of the $9.7 billion converter sales in flexible packaging. Case ready meats, growing at 21% annually through 2002, is the fastest growing segment of the perishables market. Structures include clear antifog lidding material, high barrier films, and high abuse shrink films. High or moderate barrier materials will exhibit a 5% growth rate in flexible foodservice pouches. Dry foods markets include snacks and candy, cereals, pet food, and coffee, all of which are growing approximately 5% annually. Consumer and industrial markets include healthcare packaging growing (6% annual growth), medical disposables (8% annual growth), agricultural packaging (4% annual growth), and palletizing and unitizing (9% annual growth) (95–99). Future developments are expected to focus on high barrier coextruded films for longer shelf life and better control of product quality. Products now packaged in conventional materials such as glass and metal will be packaged in more efficient coextruded materials.

Structure design requires careful selection and planning because of the multitude of possible choices regarding material combinations, layer placement, layer thickness, etc. Often a coextruded film is further processed by lamination and coating into more complex structures to meet specific product application requirements. Theoretical design and product testing must be combined to yield the most efficient film structure for a specific application. Table 4 shows common designs that have evolved for the principal markets (100–102).

Agricultural films for mulch, greenhouse, and fumigation is illustrative. Films have been developed to capture a specific portion of the light spectrum. Films that absorb or block certain ir wavelengths and films with a specific color designed for a particular crop have been developed. Solarization films generate heat, raise soil temperature, and sterilize the soil. Light stabilizers are added to extend the life of greenhouse films on one hand while other films have been developed to minimize disposal costs at the end of the growing season. Coextruded barrier films that have 1000 times the methyl bromide barrier of a monolayer polyethylene film are also available (103).

Commercial applications for coextruded multilayer sheet began later than for films, but volume has been growing rapidly and now exceeds that of films. The largest use of coextruded sheet is in thermoformed semirigid containers. The earliest applications were two- and three-layer sheet of similar polymers, such as PS two-color drinking cups, disposable dinnerware, and dairy tubs for cottage cheese and margarine. These dairy containers had a thin gloss layer of crystal PS coextruded on HIPS for marketing appeal. Because the layers were compatible in these easily thermoformed structures, problems with trim-scrap recycle were minimal. The disposable containers were usually coextruded as three layers with

Table 4. Film Structures for Principal Markets

Markets	Typical structures[a]
Trash bags	LDPE/LLDPE/LDPE
Waste disposal	LDPE/LLDPE
	EVA/LLDPE
	LLDPE
	LLDPE/LDPE + regrind
	HDPE/regrind/LLDPE
Stretch film	LDPE/LLDPE/LDPE
	EVA/LLDPE/EVA
	LDPE/LLDPE
	LDPE/LLDPE + regrind/LDPE
Shrink Film	EVA/LLDPE/EVA
Tray wrap	LDPE/EAA
Meat packaging	
Primal, subprimal packaging	EVA/PVDC/EVA
	EVA/PVDC/EVA/ionomer
	Nylon/adhesive/EVA
	Nylon/ionomer
Bacon/luncheon/weiners	Nylon/EVA/ionomer
Flexible, formed web	Nylon/PVDC/adhesive/EVA–ionomer
	Nylon/adhesive/EVOH/adhesive/ionomer
	PVC/PVDC/EVA
	Nylon/EVOH/EVA/ionomer
Flexible, nonformed webs	PET/adhesive/EVA–ionomer
	PP/adhesive/EVA–ionomer
	PVC/PVDC/EVA
Rigid formed web	AN, MA/adhesive/EVA–ionomer
	PETG[b]/adhesive/EVA–ionomer
Cooked ham	Nylon/adhesive/ionomer
	PP/adhesive/nylon/adhesive/ionomer
Poultry	
Individual bags	LDPE/EVA
	HDPE/EVA
	HDPE/ionomer
Bulk barrier bag	EVA/HDPE/LDPE/ionomer
	HDPE/EVA
	HDPE/ionomer + PVDC coating
Snack foods	OPP, white LDPE, white HDPE/EVA–ionomer
	HDPE/adhesive/nylon/EVA
	HDPE/EVA–ionomer blend
	HDPE/ionomer/EVA
	HDPE/ionomer/nylon/ionomer
	White HDPE/brown HDPE/EVA
Cookies/crackers, bakery	HDPE/EVA
	HDPE/HDPE/EVA
	HDPE/MDPE/EVA
	PP/adhesive/EVA

Table 4. (Continued)

Markets	Typical structures[a]
Cereals	
Low barrier	HDPE/EVA
	HDPE/HDPE/EVA
	HDPE/HDPE/EVA–ionomer blend
Medium barrier	HDPE/adhesive/EVOH/adhesive/EVA
	HDPE/adhesive/nylon/adhesive/EVA
Cheese	PP/PE
	Nylon, PVDC, LDPE/ionomer
	LDPE/PVDC/LDPE/ionomer
	EVA/PVDC/EVA
	LDPE/PVDC/LDPE/adhesive/EVA
Frozen food	EVA/white LDPE/EVA
	EVA/white LLDPE/EVA
	PET/adhesive/LDPE–ionomer
Heavy-duty bags	LDPE/PVDC/LDPE
Shipping bags	LDPE/EVA
	LDPE/LLDPE/EVA
	LDPE/HDPE/EVA
	LDPE/LLDPE
	Chlorinated PE/EVA
	White LDPE/black MDPE–EVA
Medical	White LDPE/colored LDPE
	White ionomer/LDPE/colored EVA
	Plexar/nylon/LDPE/Plexar/nylon/Plexar
	PET/LDPE
	Nylon/LDPE
	LDPE/PVDC/LDPE

[a]See listed abbreviations in "Polymers forCoextruded Films" section.
[b]Poly(ethylene glycol-co-cyclohexane-1,4-dimethanol terephthalate).

mixed-color scrap as a buried layer. The marketing appeal and ease of fabrication of coextruded semirigid containers quickly saturated those market applications. The principal growth area is in high barrier, semirigid food packages for long shelf life applications in competition with metal and glass for unrefrigerated storage. These advanced coextruded structures were developed in Europe during the 1970s and combine as many as five dissimilar polymers into six- to -nine layer structures (Fig. 7). A relatively thin barrier layer is coextruded with one or more bulk structural layers of HDPE, PP, or HIPS to provide package strength and rigidity. Often a thin surface layer as the interior of the package provides heat sealability for the lid stock to the container flange. In other applications, a hermetic seal is made by double seaming a metal can end onto the plastic container body. Adhesive layers bond the barrier layer to the structural layers. Often a pigmented, light barrier layer is included as an inner layer for food products that are sensitive to uv light.

Early European applications for barrier sheet were in form-fill-seal (FFS) packaging of soft cheese, fruit drinks, jams, jellies, and condiments, and high temperature-short time sterilized milk. FFS packaging (where roll stock is

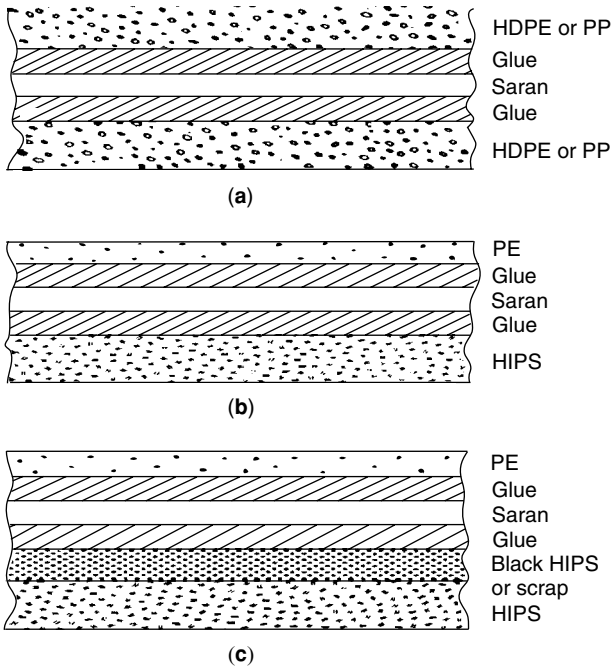

Fig. 7. Typical coextruded sheet structures used for barrier food packaging. Functional properties: (**a**) retortability, high oxygen and moisture barrier (three extruders); (**b**) heat sealability, oxygen and moisture barrier, low taste and odor transfer, thermoformability (four extruders); (**c**) oxygen and moisture barrier, uv light protection, heat sealability, thermoformability (five extruders).

converted into packages, filled with product, and sealed in the customers plant) minimizes scrap recycle. Round FFS packages have square heat-seal flanges so that most of the material is used in the package. However, the desire to use round preformed containers and to make more economical use of materials has stimulated recycling of multilayer scrap of dissimilar materials as a buried core layer. Sometimes this recycle layer is a black, pigmented uv barrier layer.

Selection of the bulk structural layers to be coextruded with the barrier polymer layer depends on package strength requirements, rigidity at minimal wall thickness, and package temperatures during product filling, thermal processing, and storage. In many FFS packaging applications, the food product is filled at ambient or low temperatures (74°C), and HIPS is chosen for its modulus and ease of forming. Most FFS machines are designed to form HIPS.

Products requiring higher fill temperatures have layers of HDPE or PP. Heat-sterilized containers heated up to 121°C employ PP, although HDPE can be used for retort temperatures up to about 112°C. HDPE has better low temperature impact properties than PP, which may be important in distribution and warehousing. HDPE and PP are more difficult to thermoform than HIPS; PP usually undergoes solid phase forming. Fillers are sometimes added to improve polyolefin stiffness and formability.

An alternative to high temperature retort sterilization of shelf-stable foods in the package is aseptic packaging in which a sterile food is packaged in a commercially sterile environment. In one technique the container is sterilized with a hydrogen peroxide solution before it is filled and sealed in a safe environment. A second technique, invented by the French company, ERCA, and licensed to Continental Packaging, uses a novel sacrificial layer to provide a sterile package interior. Continental's FFS machine, the Conoffast System, has the forming and filling stations in a safe environment. Roll stock of coextruded PP/PE/tie/PVDC/tie/black HIPS/HIPS is fed into the machine where the PP layer is separated, exposing a sterile PS layer. The barrier sheet is formed, filled, and then sealed with a second sacrificial-layer lid stock.

Formed multilayer barrier packages, eg, trays, bowls, and cans from coextruded PP/PVDC/ PP, are being developed for soups and entrees that can be stored at ambient temperatures and heated to serving temperature in a microwave oven. Coextrusions of high performance, high temperature polymers, such as polyetherimide and polysulfone, for dual-oven containers capable of withstanding conventional bake-oven temperatures of 204–232°C are being tested.

In addition to packaging markets, sheet coextrusion is applied in construction, recreational vehicle, and sanitaryware markets where weatherable or chemically resistant layers are coextruded with low cost polymers.

Continuing development of coextruded film and sheet structures from combinations of high performance polymers with low cost polymers and improved adhesive resins will expand the market opportunities for plastics in competition with other materials. Easy combination of many layers and a better understanding of synergistic behavior in multilayer film and sheet will also lead to new applications.

BIBLIOGRAPHY

"Films, Multilayer" in *EPSE* 2nd ed., Vol. 7, pp. 106–127, by W. J. Schrenk and E. W. Veagey, The Dow Chemical Company.

1. W. J. Schrenk and J. Pinsky, in *Tappi Paper Synthetics Proceedings*, 1976, pp. 141–145.
2. G. L. Wooddell, in *Tappi Paper Synthetics Proceedings*, 1980, pp. 119–127.
3. D. Djordjevic, in *Tappi/PLC Conference Proceedings*, 1984, pp. 67–75.
4. U.S. Pat. 3,223,761 (Apr. 30, 1962), G. E. Raley (to Union Carbide Corp.).
5. U.S. Pat. 3,308,508 (Mar. 14, 1967), W. J. Schrenk (to The Dow Chemical Company).
6. A. Toporek, in *Tappi Coextrusion Seminar*, 1983, pp. 23–28.
7. W. P. Wright, in *Tappi Coextrusion Seminar*, 1983, pp. 29–35.
8. M. Tanella, in *Tappi Coextrusion Seminar*, 1983, pp. 37–46.
9. J. E. Snell, in *Tappi Paper Synthetics Proceedings*, 1983, pp. 439–450.
10. R. Hessenbruch, in *Tappi/PLC Conference Proceedings*, 1984, pp. 85–94.
11. J. P. McCaul and J. J. Hohaman, in *Tappi/PLC Conference Proceedings*, 1984, pp. 633–636.
12. U.S. Pat. 3,557,265 (Jan. 19, 1971), D. Chisholm and W. J. Schrenk (to The Dow Chemical Company).
13. W. J. Schrenk, *Plast. Eng.* **30**, 65 (Mar. 1974).
14. L. M. Thomka and W. J. Schrenk, *Mod. Plast.* **49**, 62 (Apr. 1972).
15. Chemical Week Publishing, LLC, *Mod. Plast.* **60**(28), 22 (Aug. 1983).
16. J. H. Southern and R. L. Ballman, in D. C. Bogue, M. Yamamoto, and J. L. White, eds., *U.S. Jpn. Semin. Polym. Process. Rheol.; Appl. Polym. Symp.* **20**, 175 (1973).
17. J. L. White and co-workers, *J. Appl. Polym. Sci.* **16**, 1313 (1972).

18. C. D. Han *J. Appl. Polym. Sci.* **17**, 1289 (1973).
19. A. E. Everage Jr., *Trans. Soc. Rheol.* **17**, 629, (1973).
20. J. Dooley K. S. Hyun, and K. R. Hughes, *Polym. Eng. Sci.* **38**(7), 1060 (July 1998).
21. J. Dooley, and B. T. Hilton, *Plast. Eng.* **50**(2), 25 (Feb. 1994).
22. J. Dooley and L. Dietsche, *Plast. Eng.* **52**(4), 37 (Apr. 1996).
23. B. Debbaut and co-workers, *J. Non-Newtonian Fluid Mech.* **69**(23), 255 (Apr. 1997).
24. B. Debbaut and J. Dooley, *J. Rheol.* **43**(6), 1525 (Nov./Dec. 1999).
25. C. D. Han, Y. J. Kim, and H. B. Chin, *Polym. Eng. Rev.* **4**, 3 (July 1984).
26. M. A. Arvedson, in *Tappi/PLC Conference Proceedings*, 1984, pp. 513–519.
27. W. J. Schrenk and S. A. Marcus, in *Tappi/PLC Conference Proceedings*, 1984, pp. 627–631.
28. R. Ramanathan and co-workers, *SPE-ANTEC Tech. Pap.* **42**, 224 (1996).
29. S. C. Pahuja, Tappi CA Rep (1978).
30. Chemical Week Publishing, LLC, *Mod. Plast.* **77**(5), 5 (2000).
31. Chemical Week Publishing, LLC, *Mod. Plast.* **76**(10), 73 (1999).
32. J. Edenbaum, *Plastic Additives and Modifiers Handbook*, Van Nostrand Reinhold Co., Inc., New York, 1992
33. J. T. Lutz, *Thermoplastic Polymer Additives*, Marcel Dekker, Inc., New York, 2001.
34. G. M. Giacoletto, in *Tappi 1999 Polymers Laminations & Coatings Conference*, 1999, p. 79.
35. J. Turick, *Film Extrusion Manual, Tappi Press*, 1992, p. 611.
36. K. G. Schurzky, in *Tappi/PLC Conference Proceedings*, 1984, pp. 7–10.
37. E. W. Veazey, T. L. Barnette, and T. J. Pate, *Plast. Eng.* **40**(9), 33 (Sept. 1984).
38. E. W. Veazey, in *SPE/ANTEC Conference Proceedings*, 1984, pp. 26–29.
39. P. S. Chum, W. J. Kruper, and M. J. Guest, *Adv. Mat.* **12**(23), 1759 (2000).
40. J. J. Wooster, in *Tappi 1999 Polymers, Laminations & Coatings Conference*, 1999, p. 619.
41. A. J. Peacock, *Handbook of Polyethylene*, Marcel Dekker, Inc., New York, 2000.
42. G. M. Benedikt and B. L. Goodall, *Metallocene Catalyzed Polymers*, Plastics Design Library, 1998.
43. C. Vasile and R. B. Seymour, *Handbook of Polyolefins*, Marcel Dekker, Inc., New York, 1993.
44. E. M. Moore, *Polypropylene Handbook: Polymerization, Characterization, Properties, Processing, Applications*, Hanser Publishers, Munich, 1996.
45. J. Karger-Kocsis, *Polypropylene Structure, Blends and Composites*, Chapman & Hall, London, 1995.
46. W. J. Schrenk and T. Alfrey, *Polym. Eng. Sci.* **9**, 393 (1969).
47. H. E. Stanley, in *SPE Coextrusion RETEC*, 1981, pp. 161–171.
48. J. Taylor and J. J. Baik, in *Tappi 1999 Polymers, Laminations & Coatings Conference*, 1999, p. 993.
49. F. Martinez, G. E. Mazuera, and D. R. Parikh *J. Plast. Film Sheeting* **6**(1), 44 (1990).
50. V. Patel, S. Mehta, S. A. Orroth, and S. P. McCarthy, in *SPE 1999 ANTEC*, 1999, p. 391.
51. C. M. Beagan, C. M. McNally and W. R. Murphy, in *SPE 1998 ANTEC*, 1998, p. 128.
52. D. Acierno, F. P. LaMantia and G. Titomanlio, *Acta Polym.* **37**(1112), 695 (1986).
53. J. Im and W. J. Schrenk, *Plast. Film Sheeting* **4**(2), 104 (1988).
54. C. Mueller and co-workers, *J. Appl. Polym Sci.* **78**(4), 816 (2000).
55. J. Kerns and co-workers, *Macromol. Symp.* **147**, 15 (1999).
56. S. Nazarenko, A. Hiltner and E. Baer *J. Mater. Sci.* **34**, 1461 (1999).
57. E. Baer, D. Jarus, and A. Hiltner, SPE 1999 *Antec*, 1999, p. 3947.
58. J. C. Van Der Hoeven, R. Wimberger-Friedl, and H. E. H. Meijer, *Polym. Eng. Sci.* **41**(1), 32 (2001).
59. M. F. Weber and co-workers, *J. Sci.* **287**, 2451 (2000).

60. T. Iwanami and Y. Hirari, in *Tappi Paper Synthetics Proceedings*, 1982, pp. 339–346.
61. R. C. Adam and S. J. Warsala, in *Tappi Paper Synthetics Proceedings*, 1984, pp. 79–82.
62. M. I. Kohan, *Nylon Plastics Handbook*, Hanser Gardner Publications, Inc., Cincinnati, Ohio, 1995.
63. S. Kenig, A. Ophir, F. Wiener, and M. Omer, in *SPE 2000 ANTEC*, 2000, p. 438.
64. R. Lusigna, in *Tappi 1998 Polymers, Laminations & Coatings Conference*, 1998, p. 889.
65. *Mod. Plas. Int.* **29**(11), 90 (1999).
66. J. E. White and co-workers, *Adv. Mat.* **12**(23), 1791 (2000).
67. C. Kirkland, *Plast. Technol.* 58 (Feb. 1983).
68. L. B. Ryder, *Plast. Eng.* 41 (May 1984).
69. G. Mahajan and S. Arnold, in *Tappi/PLC Conference Proceedings*, 1984, pp. 561–573.
70. S. J. Waisala and J. J. Hoffman, in *Tappi/PLC Conference Proceedings*, 1984, pp. 79–85.
71. W. J. Schrenk and T. Alfrey, in D. R. Paul and S. Newman, eds., *Polymer Blends*, Academic Press, New York, 1978, Chapt. "15".
72. S. A. Marcus and P. T. Delassus, in *Proceedings on Future-Pak '84, Second International Ryder Conference on Packaging Innovations*, Dec. 3–5, 1984.
73. L. J. Bonis, in *Tappi/PLC Conference Proceedings*, 1984, pp. 319–328.
74. Tappi PLC, *Pap. Film Foil Converter* **59**, 2 (Feb. 1985).
75. J. Villalpana-Olmos, S. Sanchez-Valdes, and I. G. Yanez-Flores, *Polym. Eng. Sci.* **19**(9), 1597 (1999).
76. G. W. Kamykowski and S. Goto, in *Tappi 1996 Polymers, Laminations & Coatings Conference*, 1996, p. 197.
77. B. A. Morris, *Tappi J.*, **107** (Aug. 1992).
78. M. G. Botros, in *Tappi 1995 Polymers, Laminations & Coatings Conference*, 1995, p. 331.
79. M. Shida and co-workers, in *Tappi Paper Synthetics Proceedings*, 1976. pp. 133–140.
80. J. E. Guillotte and K. Y. Wright Jr., Tappi Coex Coating and Film Report, 1983, pp. 129–137.
81. R. T. Van Ness, in *Tappi Paper Synthetics Proceedings*, 1978, pp. 293–299.
82. R. A. L. Eidman, in *Tappi Paper Synthetics Proceedings*, 1978, pp. 161–168.
83. D. M. Naeger, in *Tappi Paper Synthetics Proceedings*, 1983, pp. 1–10.
84. W. L. Strum, in *Tappi Paper Synthetics Proceedings*, 1983, pp. 11–17.
85. M. F. Simpson and J. L. Presa, *J. Plast. Film Sheeting* **13**, 159 (1997).
86. J. R. De Garavilla *Tappi J.* **78**(6), 191 (1995).
87. L. K. Mergenhagen and N. F. Whiteman, in *Tappi 1993 Polymers, Laminations & Coatings Conference*, 1993, 569.
88. J. M. Mihalic and L. E. Baccaco, in *Tappi Coextrusion Seminar*, 1983, pp. 103–128.
89. C. P. Finch, in *SPE Coextrusion RETEC*, Chicago, 1981, pp. 103–128.
90. W. Schrenk and co-workers, *Int. Polym. Process.* **6**(3), 255 (1991).
91. U.S. Pat. 3,739,052 (Aug. 11, 1970), R. E. Ayers, K. J. Cleerman, and W. J. Schrenk (to The Dow Chemical Company).
92. U.S. Pat. 3,947,204 (Mar. 30, 1976), R. E. Ayers, K. J. Cleerman, and W. J. Schrenk (to The Dow Chemical Company).
93. U.S. Pat. 3,995,763 (Dec. 7, 1976), R. E. Ayers, K. J. Cleerman, and W. J. Schrenk (to The Dow Chemical Company).
94. U.S. Pat. 4,005,967 (Feb. 1, 1977), R. E. Ayers, K. J. cleerman, and W. J. Schrenk (to The Dow Chemical Company).
95. K. Huston, *Pap. Film Foil Converter* (Apr. 2000).
96. S. B. Marks, in *Tappi 1998 Polymers, Laminations & Coatings Conference*, 1998, p. 325.

97. R. W. Halle, in *Tappi 1998 Polymers, Laminations & Coatings Conference*, 1998, p. 285.
98. T. Clark, *Pap. Film & Foil Converter*, (Nov. 1996).
99. P. M. German, in *Tappi 1998 Polymers, Laminations & Coatings Conference*, 1998, p. 311.
100. J. Osborn, *Plastic Films Technology & Packaging Applications*, Technomic Publishing Co., Inc., Lancaster, Pa. 1992.
101. K. M. Finlayson, *Plastic Film Technology*, Technonmic Publishing Co., Inc., 1993.
102. R. J. Hernandez, S. E. M. Selke, and J. D. Culter *Plastics Packaging*, Hanser Gardner Publications, Inc., Cincinnati, Ohio, 2000.
103. Chemical Week Publishing, LLC, *Mod. Plast.* **76**(7), 60 (1999).

JOSEPH DOOLEY
HARVEY TUNG
The Dow Chemical Company

COLORANTS

Introduction

Colorants for plastics can be grouped into two broad categories: pigments and dyes. Pigments are organic or inorganic colored, white, or black materials. They are nearly insoluble in plastic. Dyes are intended to dissolve or go into solution in a given polymer. Physical forms for dyes and pigments can range from dry prills or powder to liquids. These forms can be used as is or can be preincorporated into compatible dispersions. The colorant supplier or concentrate supplier can manufacture predispersions. A concentrate supplier usually adds additional value-added steps such as additive packages and color matching.

The main considerations when selecting colorants usually include dispersion, migration resistance, heat stability, light stability, and cost. All are dynamic and change with concentration of the colorant, processing conditions, part thickness, and additives. Similarly, changes in properties can be expected for a single pigment type depending on supplier.

Dispersion

Dispersion relates mainly to pigment. The pigment manufacturing process usually leaves a variety of particle sizes and distributions. Primary particles are true single crystals of pigment. Nonetheless, aggregates and agglomerates are also present. These are single pigment particles that are joined together. To provide good color strength and physical properties these particles must be separated. Use of wetting agents combined with shear is the key to agglomerate and aggregate reduction.

Encyclopedia of Polymer Science and Technology. Copyright John Wiley & Sons, Inc. All rights reserved.

Migration. Migration refers to dissolved portions of a dye or pigment bleeding or blooming (1). Simply, the color is transported to the surface and can be wiped off or imparts unwanted color to an adjoining part. Dyes should be thoroughly evaluated, as they are naturally soluble. A pigments' tendency to migrate increases with the processing temperatures. When pigments are being used at the thresholds of their heat stability and/or at very low levels, caution should be observed. Plasticizers are known to facilitate migration; therefore plasticized poly(vinyl chloride) (PVC) is a good medium for evaluation.

Thermal Stability. Thermal stability of a colorant is important as thermoplastics have different melt processing temperatures and thermosets have different cure temperatures. Color changes in a pigmented or dyed polymer system usually originate from one of the following mechanisms: *Thermal decomposition* – degradation occurs if a pigment is processed above its decomposition temperature. This can be rapid as in the case of pyrazolone, Pigment Red 38; it totally decomposes at 218°C and turns brown. Decomposition can also be a slow gradual process as in the case of some quinacridones. They decompose slowly at 300–350°C. *Chemical substitution* – it is less common but can occur. In PVC some of the azomethine pigments can shift color rapidly at temperature above 160°C. The copper complex can be substituted by atoms from barium/cadmium and lead stabilizers. *Crystal shift* – polymorphous materials may undergo crystal phase transitions. Phthalo blue is a classic example. The alpha crystal can convert back to the more stable beta crystal. *Particle size or crystal growth* – pigment particles can grow in a hot solvent. As they grow a decrease in chroma and tinting strength can be observed. *Solubility* – a pigment if processed at higher than recommended temperature range can fully or partially dissolve. The fugitive material will generally change color and reduce the other properties of the colorant.

Light Stability and Weatherfastness. *Light stability and weatherfastness* are defined by the ability of a pigment or dye, in plastic, to retain its color upon exposure to sunlight and/or atmospheric impacts. If the polymer is not correctly stabilized for uv it will degrade at a rate that may negate the colorants performance. Conversely, uv stabilizers cannot greatly improve the stability of a colorant that has poor fastness properties. Lightfastness and weatherfastness are largely dependent on the particle size of a colorant. This is understandable as the job of a colorant is to absorb and reflect light. Failure of the pigment in most cases is not abrupt. A darkening of color occurs when used in masstone, and a loss of chroma and strength can be observed in the tint. The color changes layer by layer.

Cost. The broad spectrum cost for colorants is from $6.00 to $200.00/kg. Accordingly cost is as important as the above properties. Color matching and color formulation is critical. An effective colorant package should meet the needs of the application, provide a slight safety factor but not significantly exceed the properties required. As with most things, "you get what you pay for." This is also true for colorants. In most cases, the better the properties the higher the price. When comparing colorants for value, do not focus on the price alone, as this method can be misleading. Focus on the strength or amount needed for a specific application, ie "value in use."

As in many raw materials there can be large differences in properties among a pigment type. A single supplier can have a variety of Pigment Blue 15:3s. The product line can cover a range of transparency, dispersions, heat stabilities, cost,

FDA approval, shade, and physical forms. By factoring in those Pigment Blue 15:3s offered by a multitude of other suppliers the number can grow exponentially. There are many varieties of each pigment type that is discussed.

FDA Colorants. Because of the large amount of pigment used in packaging, house wares, and food-processing equipment, a colorants impact on health and safety should be considered. The U.S. Federal Government by way of the Food and Drug Administration (FDA) regulates food additives. Pigments that are used to color materials that come in contact with food are deemed to be indirect additives (2). This is based on the assumption that the pigment will extract from the plastic article and become part of the food. The FDA has published a list of sanctioned colorants. The list was introduced in Title 21 of CFR 178.3297 "Colorants for Polymers" and 175.300 for resinous and polymeric coatings. CFR 178.2600 may also be of interest when dealing with rubber articles. In very general terms, the pigments listed in these articles are suitable as components for plastic products used in producing, manufacturing, packaging, transporting, or holding food. In recent years the FDA has added new colorants or expanded usage of previously listed colorants. Some have limitations in regard to a colorants percentage and the resin to be incorporated. Current FDA regulations should be referenced for details.

Inorganic Pigments

Whites.

Titanium Dioxide. Titanium dioxide is the most common white of choice and by weight; it is actually the most widely used pigment. Product selection can be difficult as the variety can be staggering. Focus on particle size and surface coating during the selection process. Particle sizes usually range from 0.20 to 0.35 μm. Most plastic grades are manufactured to minimize reactivity. Reactive sites are masked with surface coatings of alumina, silica, and silicone fluid. This process increases dispersion and improves weatherability.

Titanium dioxide has a high Mohs' hardness and is very abrasive. Its outstanding importance is due to its light scattering properties, its FDA approval, and excellent properties. Its large particle size provides ease of dispersion, excellent heat stability, migration resistance, and lightfastness at a typical cost of less than $2.00/kg. Titanium dioxide is used in nearly all plastics to provide pastels and to adjust colors. The opacity is valued for ascetics and its ability to absorb uv radiation. In fiber, titanium dioxide pigments provide a matte finish that eliminates the undesirable oily appearance caused by translucence. *Rutile* titanium dioxide is the first choice for most plastic applications. The shade is slightly yellow. If desired, very small amounts of blue or violet can be used to provide a cooler white. *Anatase* titanium dioxide is less yellow, not highly recommended for outdoor use, blocks less uv radiation and is generally more reactive.

Zinc Sulfide. Zinc sulfide pigments were developed in 1850. They still have some use in plastic because they are less abrasive and can have a smaller particle size. However, after the introduction of titanium dioxide in the 1950s they have continually lost market share.

Zinc Oxide. Zinc oxide has lost importance as a pigment but is noteworthy for its use as an activator for accelerating vulcanization in rubber (3).

Carbon Black. Carbon blacks are not only valued as colorants but for the functional benefits they provide. They improve weatherability of plastics by blocking ultraviolet, visible, and infrared radiation. They can act as free-radical traps and provide a wide range of electrical properties. Fineness, structure, porosity, and surface chemistry are properties used in selection of a carbon black. Typical particle size is from 18 to 80 nm. Keep this in mind when considering loading levels. It can require a large quantity of resin to wet out the pigment.

For practical purposes there are two basic types of carbon black, channel and furnace. Burning enriched natural gas makes *channel black*. Channel black has become nearly obsolete with increased natural gas prices. They still find some use in plastics for FDA and special applications. *Furnace black* is produced by thermal decomposition of feedstock oil for petroleum refineries. Channel black has been all but replaced by furnace black.

Iron Oxide. Iron oxide pigments find value in plastics as they are nontoxic, chemically stable, and low in cost, and are offered in a variety of shades. They can be naturally occurring, *natural iron oxides*, or they can be synthesized, *synthetic iron oxides*. There are four basic types and thus four colors of iron oxide pigments, yellow, red, brown, and black. Synthetic iron oxides are much purer, have better tinting strength, and vary less in composition. As a consequence, they have nearly replaced natural iron oxides. Natural iron oxides still find use in cellulose and phenolics. In cases where black is required at low levels, iron oxide is often the pigment of choice. It has much lower strength than carbon black whereby larger amounts can be used. This allows for a more homogenous mixture and contributes less in weighing errors. Red, yellow, and brown can be used in most plastics. They have good durability but are dull. Use caution with the yellow (ferric hydrate) as water can be driven at temperatures above 175°C and shift the color red.

Chromium Oxide Green. Chromium oxide green is a dull olive green. It has excellent heat and weatherfastness. Its large particle size offers easy dispersion. Its reflectance is similar to that of chlorophyll, making it suitable for camouflage (3). However, its lack of tint strength and other suitable colorants in this color space exclude it from significant use.

Iron Blue. Iron Blue or Pigment Blue 27 has replaced the older names of Paris blue, Prussian blue, Berlin blue, and Toning blue, etc. It is ferric ammonium ferrocyanide [$FeNH_4Fe(CN)_6$]. It finds little use in plastics at present. It is mixed with chrome yellow to form chrome green. Chrome green offers a low cost opaque green that finds some use in polyethylene film. Caution should be used as it has little alkali resistance.

Ultramarine Pigments. Ultramarine pigments are a complex of aluminum sulfosilicate. *Pigment Blue 29* is most common though; *Pigment Violet 15* and pink *Pigment Red 259* are also available. The blue can be used in almost any polymer; the pink and violet have maximum processing temperatures of 200°C. All have poor acid resistance. Surface-treated grades do provide better acid resistance and dispersion. They do not promote shrinking or warpage and are approved worldwide for coloring of food-contact plastics. The most popular is blue. Blue has its uses in plastics but is now often replaced by phthalocyanines that have 10 times the tint strength.

Mixed Metal Oxides. The term MMO (mixed metal oxides) denotes a pigment that crystallizes in a stable oxide lattice. They are manufactured by heating combinations of metal salts to temperatures of 800–1400°C. They are regarded as solid solutions and so some prefer to call them "complex inorganic color pigments." The following are some of the colors produced: Cobalt blue – *Pigment Blue 28* ($CoAl_2O_4$) and *Pigment Blue 36* ($Co(Al,Cr)_2O_4$), cobalt green – *Pigment Green 50* ($(Co,Ni,Zn)_2TiO_4$), zinc iron brown – *Pigment Yellow 119* ($ZnFeO_4$), spinel black – *Pigment Black 28* ($Cu(Cr,Mn)_2O_4$) and *Pigment Black 22* ($Cu(Fe,Cr)_2O_4$). nickel rutile yellow – *Pigment Yellow 53* and chromium rutile yellow – *Pigment Brown 24* are commonly referred to as titanates.

Compared with organic pigments they lack clean hues and tinting strength. Compared with most inorganics they are considered expensive and hard to disperse. Nonetheless, they are indispensable in high heat applications and their weatherfastness and chemical resistance are outstanding. Use in engineering resins for automotive interior and under-the-hood application is common. MMOs are also important tools for coloring rigid PVC siding.

Lead Chromates and Lead Molybdates. Lead chromates and lead molybdates are characterized by their bright hues and good opacity. The pigments of importance are chrome yellow – *Pigment Yellow 34* and molybdate red and orange – *Pigment Red 104*. Because of the toxicity of lead and hexavalent chromium these pigments are forbidden from many uses. As a result, formulation into plastic has declined at a considerable rate. They are susceptible to acids, alkalis, and hydrogen sulfide. Surface treating of the pigments improves the weathering, chemical resistance, and heat stability. They are readily blended with each other and are often shaded with quinacridones to provide a variety of colors. Environmental regulations have caused a significant downturn in use. They are/have been replaced by high performance inorganic pigments where applicable.

Cadmium Pigments. Among the inorganic pigments, cadmium pigments are known for their bright shades. Their physical properties allow their use in most plastics. They are very heat stable, weatherfast, chemical resistant, and easy to incorporate. They also show good dimensional stability in large injection molded parts. These pigments are sensitive to overgrinding. The colors range from yellow through maroon (yellow, orange, red, bordeaux).

The pigments are cadmium sulfides and selenides. These raw materials are precipitated, dried, and calcined at 600°C (3). They usually undergo a dilute acid wash to remove impurities. Cadmium orange (*Pigment Orange* 20) is pure cadmium sulfide. Cadmium yellow (*Pigment Yellow 35*) is cadmium sulfide mixed with crystals of zinc cadmium sulfide. Cadmium red (*Pigment Red 108*) is produced in similar fashion to the yellow. Selenium powder is added to obtain the desired shade. The maroon is manufactured in the same manner as the red, selenium replacing the sulfur, at 50 mol% the shade shifts to a maroon.

Lithapones are coprecipitates with up to 60% barium sulfate. The lithapones are offered in the full color range and provide slightly better dispersion and value in use. Also available are a variety of mercury cadmiums in shades of orange, red, and maroon. They contain mercuric sulfide to replace a quantity of selenium. The advantage is slightly better economics and heat stability. Shortages of raw materials have caused increases in the price of cadmiums. Environmental

regulations have also caused a significant downturn in use. They are/have been replaced by high performance organics (eg, perylene, quinacridone, and azo condensation pigments).

Special Effect Pigments

Pearlescents. Pearlescent, nacreous, or interference pigments are designed to simulate the natural luster of pearls. Simply put, pearlescents are constructed of various layers of platy particles with differing indices of refraction. The *index of refraction* is the degree to which light slows and is bent as it passes through a substance (eg, prism). Numerous effects can be achieved by altering the incident light via reflection, refraction, and transmission.

Natural pearlesence (Guanine) is produced from the scales of herring and Atlantic salmon caught in cold waters. It does not find much use in plastics as it is more fragile, expensive, and is only available in a paste. *Bismuth oxychloride* is produced by precipitating platelet crystals from an aqueous solution of $BiCl_3$ via hydrolysis. Bismuth oxychloride pigment is the closest to natural pearl but is fragile and has relatively poor light stability.

Oxide-coated micas are produced by precipitating a metal oxide onto the surface of refined mica. Titanated micas are produced by precipitating a layer of TiO_2 from an aqueous solution of titanium tetrachloride onto a refined mica substrate. The titanium precipitates as the hydrate that is in turn converted to the oxide by calcinations at 800°C. They offer a wide range of colors, good light stability, and are generally low cost. The factors that affect luster and color are particle size, mica quality and color, and TiO_2 layer thickness. The larger particles offer more luster and transparency. The smaller particles offer more of a satin finish. The iridescent titanated micas that are produced by increasing the thickness of the TiO_2 layers are called *interference colors*. Two-tone and intensified versions of these interference colors can be produced by the addition of absorption colors. Using an absorption color that is the same as the interference color will produce a deeper colored TCM (titanium dioxide-coated mica). Using an absorption color that is different from the interference color will produce a TCM with two-tone flop effect. In a "two-tone flop effect" the color will change to two distinctly different colors when observed at different angles.

When using any of the pearls, care must be taken during incorporation. The pigment has to be wet-out but care must be taken to keep from breaking down the particles. Try to avoid twin-screw extruders unless you use a downstream feed port. If using a banburry try avoiding long cycles. This is one of a few products where mold design should be considered in the product-engineering phase as controlling flow and weld lines may be required. A variety of colors and effects can be achieved with these pearl pigments. Varying the combination and loading of pearls and traditional pigments are common practice.

Over 95% of pearls used in plastics are oxide-coated micas. The major application for plastics is polyolefin packaging. Recent interest in mass coloration for automotive parts could spur the already strong growth rate of pearls.

Metallic Pigments. Plastics can be given a metallic appearance by incorporation of very thin platelets of aluminum, aluminum–bronze, zinc, copper, and

copper–zinc alloys. The metal effect is caused by the reflection of light at the pigment surface. Larger pigment particles increase reflectance and hence brilliance. A large particle also increases *flop* (color change when viewing at an angle).

Grinding aluminum powder produces aluminum pigments. Wet milling does this best as aluminum powder forms explosive mixtures with air. The pigment suspension is usually sieved, filtered, and vacuum-dried in the case of products for plastics. Copper, gold, and bronze pigments (powdered copper–zinc alloys) are produced by dry milling. Copper is produced using 100% copper. A variety of gold shades can be achieved by adding up to 25% zinc.

Unlike most pigments used in plastics, metallics may agglomerate after a shelf life of 1 year. Proper dispersion is important. In organic colorants the objective is to deagglomerate by use of shear. However, use of high shear will tear, ball up, or fold the metallics. This will change their color and hiding power. Avoid high intensity mixers or add pigment at the end of the cycle at low speeds. Try to avoid twin-screw extruders unless you use a downstream feed port. Plate-out on calendering rollers and extruder screws have been reported. Flakes with a polymer surface treatment may reduce or eliminate the problem. Controlling flow and weld lines should be considered in mold design.

Fluorescent Pigments. There are three basic types of fluorescent pigments: A thermoplastic pigment based on a polyamide resin, a thermoplastic pigment based on a polyester resin matrix, and a pigment based on a blend of polyester and polyamide resin.

Fluorescent pigments are based on dyes that not only absorb some visible light, but also photons of higher energy form from the invisible uv region of the electromagnetic spectrum. The dyes used for the red pigments are members of the rhodamine family. The yellows are typically members of the coumarin family. There are no blue or green fluorescent dyes. These colors are achieved by blending phthalocyanines green with fluorescent yellow and phthalocyanines blue with optical brightener respectively.

The compatibility and heat stability of the pigments is important. Polyamides exhibit the highest degree of heat stability, but lack good compatibility in polyolefin. Polyester resins have excellent compatibility in olefin but lack good heat resistance. The polyester/polyamide hybrid has good heat stability and good compatibility. All lack good light stability.

Plate-out is an area of concern when processing concentrate or molding parts. At higher temperatures the components of a fluorescent pigment can undergo sublimation. The colored material will be deposited on the barrels and molds. Plate-out can be reduced by a number of methods. The combined use of absorbent agents such as barium sulfate and reactive agents such as titanate coupling agents can greatly reduce or eliminate plate-out.

Organic Pigments

Azo Pigments. Many of the red, yellow, and orange pigments used in plastics are classified as azo pigments. This classification is attributed to the fact that they contain the azo chromophore (—N=N—). Further subdivisions of azo pigment are possible. They can be labeled as metallized or nonmetallized; the

latter are most common in plastics. Manufacture of a metallized azo pigment involves four basic steps:

(1) *Diazotization*: reacting a primary aromatic amine with nitrous acid that was formed *in situ* by reacting sodium nitrite with hydrochloric acid; this forms a diazonium salt. Some common primary amines are Tobias acid, C acid, 4B acid, 2B acid, and anthranilic acid.
(2) *Coupling*: the diazonium salt is coupled to form the pigment. Common couplers are β- napthol and BON. This forms an azo dye or very unstable pigment.
(3) *Metallization*: the azo dye is precipitated as a metallized salt such as calcium, manganese, strontium, or barium. This is accomplished in the presence of anionic groups. Consequently, the sulfonic or carboxylic acid on the dye can react with metals to form an insoluble pigment.
(4) *Washing*: the suspension is then filtered and washed. This removes any unwanted impurities.

Figure 1 is an example of the process of manufacture for a metallized azo pigment, barium lithol red (**1**). Reaction with a metal salt causes the azo dye to precipitate, forming an insoluble metallized azo pigment. Most nonmetallized reds contain no anionic groups.

Azo pigments are the perfect workhorse pigments for non-high performance applications. Overall, azo pigments are low cost and have excellent tinting

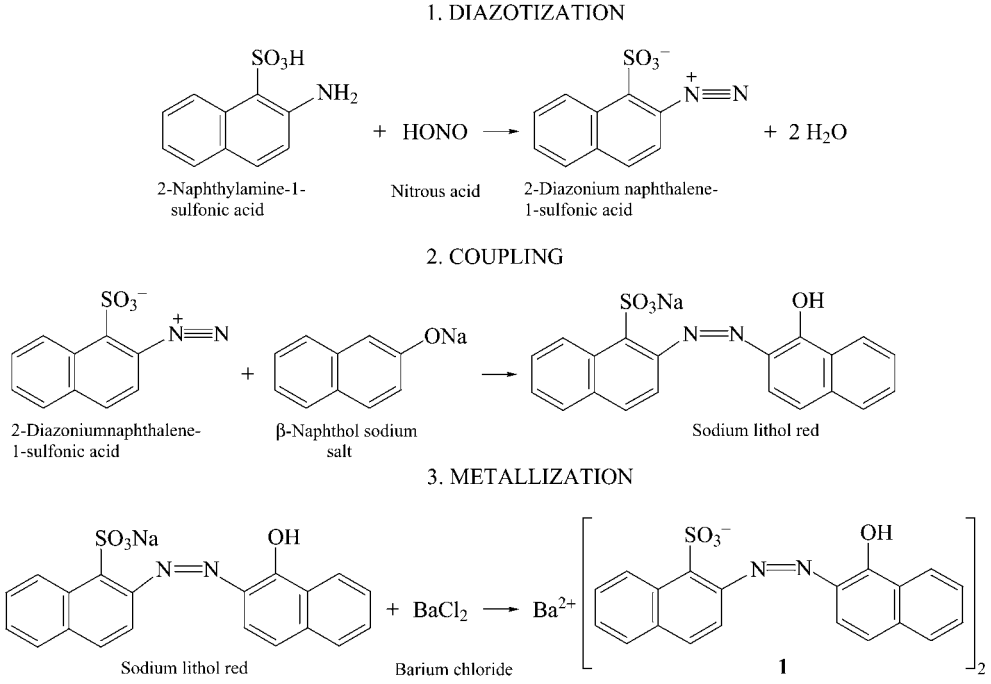

Fig. 1. Lithol red manufacture.

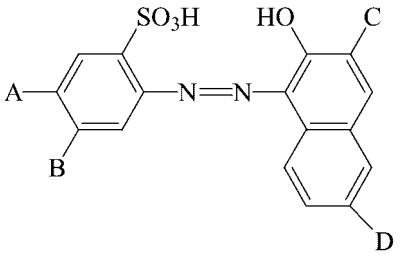

Fig. 2. A generalized representation of several red, orange, and yellow pigments. PigmentRed48.1(BariumSalt)(A = CH_3,B = Cl,C = COOH) (2); Pigment Red48.2 (Calcium Salt)(A = CH_3,B = Cl,C = COOH) (3); Pigment Red53.1(Barium Salt) (A = Cl,B = CH_3,C = H) (4); Pigment Orange46(Barium Salt)(A = Cl,B = C_2H_5,C = H) (5); PigmentRed57.1(CalciumSalt)(A = CH_3,B = H,C = COOH). (6)

strength. They have fair to good dispersion, migration, and light and heat stability properties. The following review will be focused on the most commonly used azos, as there are more azos than time for discussion allows.

Metallized Azo Reds, Oranges, and Yellows. *Pigment Red 48:1* (**2**) – Barium 2B is a strong, very yellow shade pigment with heat stability up to 260°C. Lightfastness rates a 3 on the 1–8 blue-wool scale. It has good dispersion and is used in almost all thermoplastics, excluding the engineering polymers. It has good migration in PVC systems.

Pigment Red 48:2 (**3**) – Calcium 2B is the counterpart to Barium 2B. It fills color space for a formulator by offering a clean, strong, and economical blue shade red. Physical properties are similar to Barium 2B although the Calcium 2B has slightly better light stability.

Pigment Red 53:1 (**4**) – Red Lake C is almost identical in shade to Barium 2B. Its slightly better heat stability of 288°C allows its use in ABS (acrylonitrile–butadiene–styrene) where lightfastness is not important. Caution should be used in plasticized PVC since migration can occur.

Pigment Red 57:1 (**6**) – Calcium Lithol Rubine is bluer than Ca 2B, with slightly inferior fastness properties. In Europe it replaces Ca 2B as the blue shade red of choice.

Pigment Red 60:1 – Pigment Scarlet is unique as it is laked using barium chloride and alumina hydrate. The shade is not the typical yellow shade usually offered by a Barium Lake. It is bluer, tends to be weaker but has much better physical properties than the 2Bs. Heat stability of 300°C and midrange light stability offers a pigment with properties between those of high performance pigments and the above-mentioned azos.

Pigment Orange 46 (**5**) – Clarion Red offers a brighter and yellower shade of Red Lake C. Properties are similar and caution should be used in plasticized PVC since migration can occur.

Monoazo yellow pigment lakes (Fig. 3) are synthesized by first adding the diazotizedamine to the coupler. This dye is then precipitated as an insoluble metal salt. Ordinarily they have large particle size for an organic. This offers good opacity, heat stability, and dispersion. However, the tinting strength in application is one-half that of a diarylide yellow. Major applications are low to medium

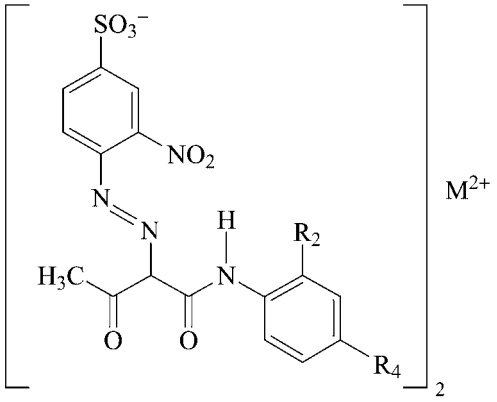

CI name	CI constitution no.	R_2	R_4	M	Shade
P.Y. 62:1(**7**)	13940:1	CH_3	H	Ca	Yellow
P.Y. 168 (**8**)	13960	Cl	H	Ca	Greenish yellow

Fig. 3. Monoazo yellow pigment takels.

performance film, fiber, and injection-molded products in olefins. They also exhibit good migration resistance in PVC. They are often used in applications in which diarylide yellows are unacceptable. *Pigment Yellow 62* (**7**) is the most common red shade yellow and Pigment *Yellow 168* (**8**) is its counterpart on the green side.

Naphthol Red. *Pigment Red 170* (Napthol red) is offered in a transparent and opaque version. Pigment's particle size of crystal form controls the opacity. The opaque version has a larger particle size. It is yellower in masstone and has better heat and light stability. Napthol red finds use in some low cost exterior applications (eg, coolers) as they have better light stability as compared with metallized azo reds.

Disazo Yellow and Red. Diarylide yellows use dichlorobenzidine (DCB) as a difunctional amine. The coupler changes, as can be seen by the generic name AAOT, AAMX, AAA, etc; hence it is the coupler that imparts the differences seen in the pigment (see Fig. 4).

Pound-per-pound, diarylide yellows cannot be out-performed for value in use. They are used in low temperature olefin and PVC application. Caution is required in plasticized PVC as migration is possible. The amine DCB is suspected to release at temperatures above 200°C in polyolefins. This is an area where discussion with your pigment supplier is recommended.

Pigment Yellow 12 (**9**) – AAA Yellow is a medium-to-red shade yellow with low heat stability. Pigment Yellow 12 finds use in rubber. Heat stability is generally too low for olefins. *Pigment Yellow 13* (**10**) – AAMX Yellow is a medium-to-red shade yellow with good opacity. *Pigment Yellow 14* (**11**) – AAOT Yellow is a very opaque medium shade yellow. *Pigment Yellow 17* (**12**) – AAOA Yellow is a slightly transparent green shade yellow. *Pigment Yellow 83* (**13**) – AADMCA Yellow is a very red shade yellow with slightly better properties than the other diarylides.

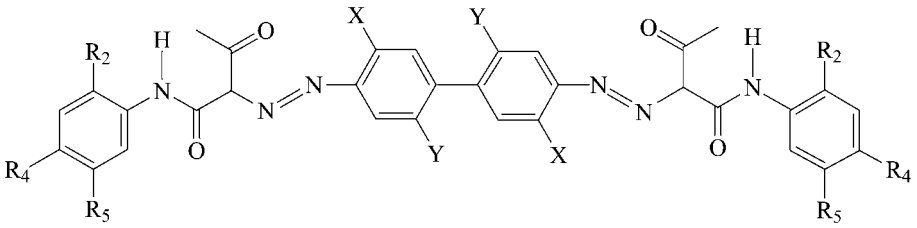

CI name	CI constitution no.	X	Y	R_2	R_4	R_5	Shade
P.Y. 12 **(9)**	21090	Cl	H	H	H	H	Yellow
P.Y. 13 **(10)**	21100	Cl	H	CH_3	CH_3	H	Yellow
P.Y. 14 **(11)**	21095	Cl	H	CH_3	H	H	Yellow
P.Y. 17 **(12)**	21105	Cl	H	OCH_3	H	H	Greenish yellow
P.Y. 83 **(13)**	21108	Cl	H	OCH_3	Cl	OCH_3	Reddish yellow

Fig. 4. Disazo yellows and reds.

Pigment Red 38 – Pyrazolone red is ideal for rubber and other low heat applications. The bright clean red masstone quickly shifts to brown or black at temperatures above 218°C. Alkali resistance is excellent. Pyrazolone red is FDA approved for use in rubber. *Pigment Orange 13* and *Pigment Orange 34* are also disazopyrazolones that find use in rubber or low temperature olefin applications. Pigment Orange 34 is slightly redder than Pigment Orange 13.

Benzimidazolone Yellow and Orange Pigments. Benzimidazolone pigments contain 5-aminobenzimidazolone group (Fig. 5). This group is common to all the pigments and hence the name. They are a very important group of pigments for plastics despite their high cost. They are not as clean and strong as diarylides. Nevertheless, they find use in a variety of applications as they have excellent lightfastness, heat stability, and migration resistance. Dispersion is fair. Some specific grades are FDA approved and others are considered low warp.

Pigment Yellow 154 (**14**) is medium-to-green shade with select codes having some FDA approval. Nevertheless, most usage is in PVC. This is due to its bleed resistance being excellent and its heat stability of 200°C being too low to find much use in olefins. *Pigment Yellow 151* (**15**) is somewhat greener than Pigment Yellow 154 (**16**) and has better heat stability (260°C). It is often used with phthalo green to provide a very yellow but stable green. *Pigment Yellow 180* (**17**) is a medium shade with select codes having some FDA approval and low warp qualities. It is stable up to 290°C in olefins and is useful in coloring engineering resins. It does not show migration in PVC. *Pigment Yellow 181* (**18**) is very red. Its heat stability is good in polyolefins and most engineering resins; however, Pigment Yellow 181 is not recommended for use in nylon. Select codes have

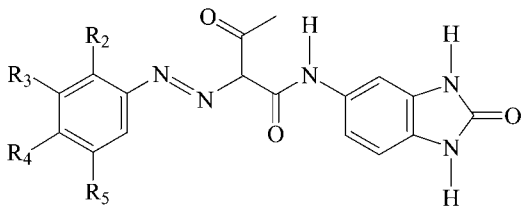

CI name	CI constitution no.	R_2	R_3	R_4	R_5	Shade
P.Y. 120 **(14)**	11783	H	$COOCH_3$	H	COO CH_3	Yellow
P.Y. 151 **(15)**	13980	COOH	H	H	H	Greenish yellow
P.Y. 154 **(16)**	11781	CF_3	H	H	H	Greenish yellow
P.Y. 180 **(17)**	21290	*a*	H	H	H	Greenish yellow
P.Y. 181 **(18)**	11777	H	H	*b*	H	Reddish yellow
P.O. 36 **(19)**	11780	NO_2	H	Cl	H	Orange

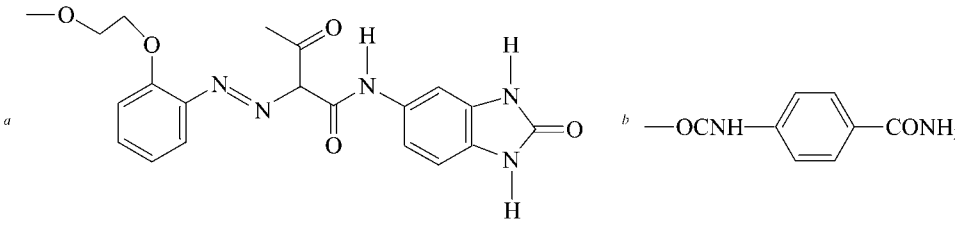

Fig. 5. Benzimidazolone pigments.

restricted FDA approval. *Pigment Orange 36* (**19**) is a reddish shade orange with very good lightfastness properties. It finds most of its use in plastisols and PVC since its heat stability is 220°C, much lower than that of the other benzimidazolones. It is often used with carbon black to create lightfast shades of organic browns.

Disazo Condensation Pigments. Disazo condensation pigments (Fig. 6) represent a multistep approach to disazo chemistry. For disazo pigments of the diarylide types both the amino groups of the DCB are diazotized simultaneously, followed by reaction with two equivalents of coupler, to form the pigment. In the category of condensation pigments the disazo components are coupled to afford monoazo carboxylic acids. In a separate stage these are converted to their respective acid chlorides. The condensation pigment then forms, in the final stage, when two equivalents of an acid chloride react with one equivalent of an appropriate diamine (**22**). By selecting the amines in the coupling or diamines in the condensation a variety of pigments can be made. The high molecular weight of these products brightens the shade and increases stability.

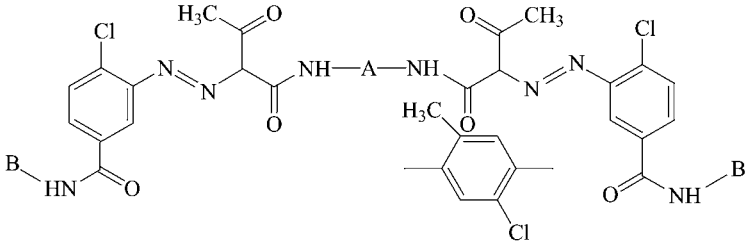

Structure A	Structure B	Shade	CI name	CI constitution no.
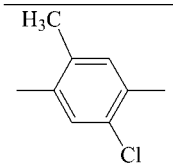	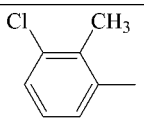	Yellow	P.Y. 93 (**20**)	20710
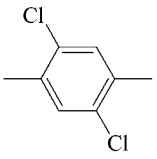	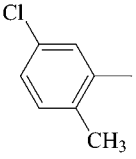	Reddish yellow	P.Y. 95 (**21**)	20034

Fig. 6. Disazo condensation pigments.

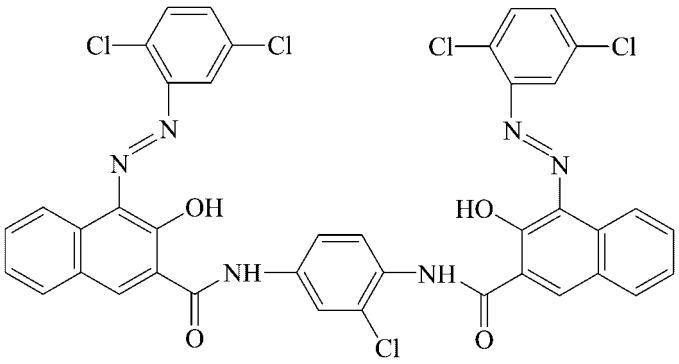

(**22**)

Because of the complex manufacturing process, azo condensations are expensive when compared with most organic pigments. The result is they are only used in high performance applications, the majority of that being polypropylene and polyacrylonitrile fiber. They have replaced lead and cadmium pigments where toxicity was an issue. All physical properties are excellent but shrinkage in large molded parts can be an issue. There are three important pigments for use in plastics. They are *Pigment Yellow 93* (**20**), a medium-to-green shade yellow, *Pigment Yellow 95* (**21**), a red shade yellow, and *Pigment Red 144* (**22**), a medium shade red (its CI number is 20735). Select codes of Pigment Yellow 95 have restricted FDA approval.

Miscellaneous Yellows.

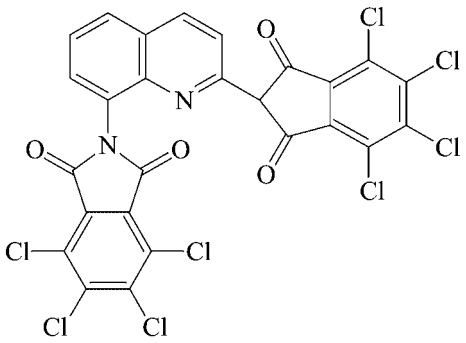

(**23**)

Pigment Yellow 138 (**23**) is a quinophthalone. It is considered slightly more opaque and weaker in tint than some of the other high performance yellows. It has good light and heat stability. The pigment is known to nucleate, which can lead to shrinkage in large parts. Select codes have restricted FDA approval.

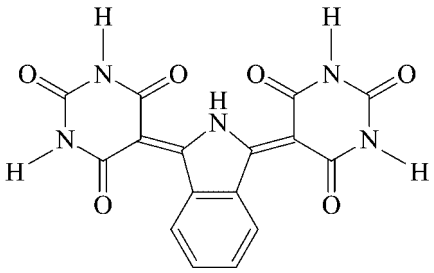

(**24**)

Pigment Yellow 139 (**24**) is a methine-type isoindoline that has a red shade.

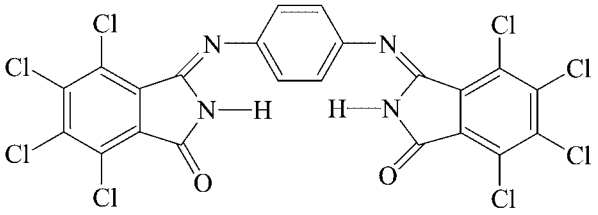

(**25**)

Pigment Yellow 110 (**25**) is an azo methine-type tetrachloroisoindolinone that has a very red shade. Pigment Yellow 110 is hard to disperse and transparent. Its good performance in PVC, heat stability in olefins of 270°C, generally good lightfastness, and the fact that select codes are FDA approved, make it worth mentioning (1).

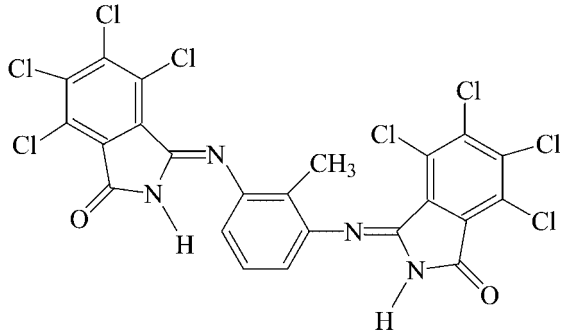

(**26**)

Pigment Yellow 109 (**26**) is an azo methine-type tetrachloroisoindolinone. It has overall good properties and is considered a green shade yellow.

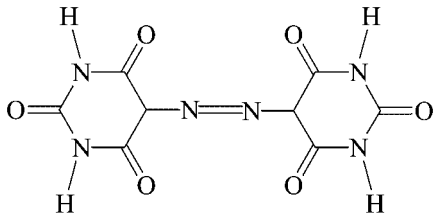

(**27**)

Pigment Yellow 150 (**27**) (Pyrimidine Yellow) is an azo/nickel complex. Its color is dull and it lacks tinting strength. It finds its importance in a good stable yellow for fiber applications. It can react with zinc sulfide.

Phthalocyanine Pigments. Presently, phthalocyanine blue and green are the most important organic pigments being used in plastics. They have bright clean shades and their physical properties are excellent. Lightfastness and weatherfastness are of automotive quality. Most can be used in all but the highest processing temperature resins. They are very high in tint strength and have excellent value in use. They are sold in high volumes and most domestic sources are FDA approved. Shrinkage in large molded parts can be an issue.

Phthalocyanines are planar molecules that comprise four isoindole moieties connected by four nitrogen atoms. This forms a 16-membered ring with the central atom being copper. Manufacture of the crude pigment is relatively straightforward (Fig. 7). Phthalic anhydride reacts with urea to form a compound that reacts at 190°C with copper salts. Molybdates and vanadates are often used as catalysts for this condensation reaction (4). This process produces crude pigment. Chemically replacing the hydrogen in the phthalo blue (**28**) with chlorine results in Pigment Green 7. Replacement of the hydrogen with bromine results in production of the yellower, Pigment Green 36.

The crude of all of these phthalos has a very large particle size and needs to be conditioned in order to make it pigmentary. Conditioning can be completed using several processes: *Salt attrition* – The crude is ground in a ball mill or a double-arm

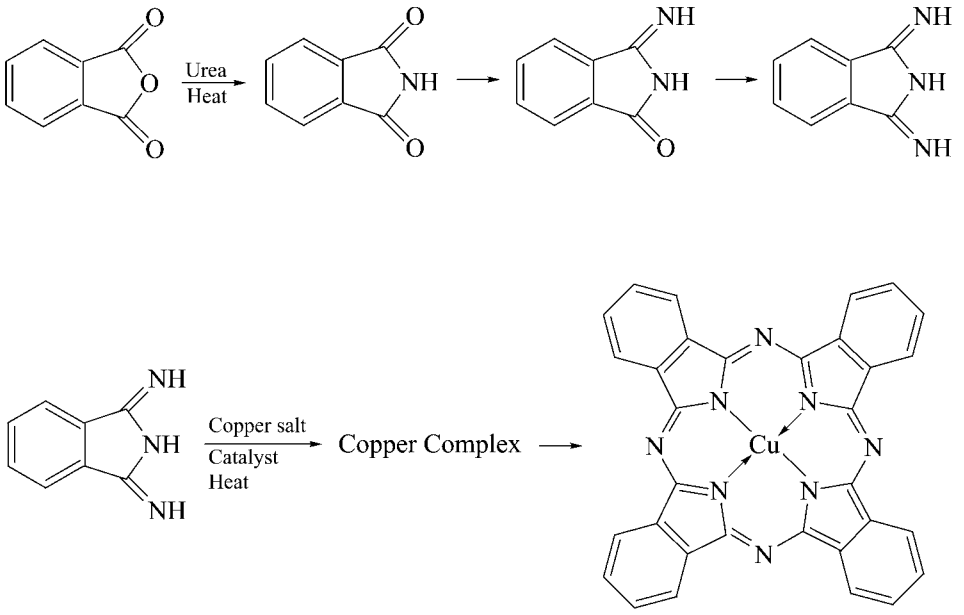

28

Fig. 7.

mixer in the presence of salt and optionally a solvent such as diethylene glycol. This provides the green shade beta crystal in the case of blue crude. *Solvent free attrition* – The crude is ground in a ball mill in the presence of a large excess of salt, excluding the solvent; this is used exclusively for production of red shade or alpha crystal blue. *Acid pasting* – The crude is dissolved in a large excess of concentrated sulfuric acid, then reprecipitated by drown-out in iced water. *Acid swelling* – The crude is treated with a smaller amount of concentrated sulfuric acid than used in acid pasting technique. This acid-swelled paste is added to iced water to precipitate the pigment.

Phthalocyanine Blue Pigment. Phthalocyanine blue pigment (**28**) exhibits polymorphism. Although chemically the same, changes in crystal shape change the color and properties. The beta phase or green shade is more inherently stable. The alpha shade or red shade will readily convert back to the more stable green shade if not stabilized. Current methods of stabilization are essentially proprietary. They offer added heat stability and resistance to flocculation in coatings applications. Light stability remains consistent for the different crystals phases.

Pigment Blue 15 is a nonstabilized alpha crystal. It has a strong red shade and finds use in low temperature applications like rubber and PVC. Heat stability becomes a problem above 230°C.

Pigment Blue 15:1 is a stabilized or noncrystallizing alpha or red shade. Because of differing types and qualities of additives, heat stability can range from 275 to 300°C. Red shade blues are stabilized by additives or by the

addition of up to one molecule of chlorine. The chlorinated version is slightly greener in a tint and has a jet masstone as compared with the additive-stabilized Pigment Blue 15:1. In recent years, a semi-Cl version has become popular. It is a midshade and has good heat stability. Pigment Blue 15:2 is a noncrystallizing, nonflocculating red shade. It does not find much use in typical thermoplastics. Its design is for resistance to flocculation and is used in some plastisol, acrylic, and liquid color application. Heat stability is equal to that of Pigment Blue 15:1.

Pigment Blue 15:3 is a nonstabilized beta shade or green shade blue. The more stable beta phase crystal does not require an additive to stabilize it for heat resistance. It has heat stability up to 290°C. It is applicable for and used in almost all thermoplastics.

Pigment Blue 15:4 is a noncrystallizing, nonflocculating beta or green shade blue. Its original design was for coatings application. In spite of this, the additive used for flocculation provides excellent heat stability and accordingly Pigment Blue 15:4 finds use in very high temperature applications. Pigment Blue 15:4 often finds use in place of Pigment Blue 15:3 in engineering polymers.

Phthalocyanine Green Pigment. Phthalocyanine green demonstrates the good overall properties of phthalo blue, differing from blue in that it is not a polymorph (4). Pigment Green 7 is recognized as being more stable than its phthalo blue counterpart. This is largely due to the stabilizing factor of chlorine or bromine or both. Heat stability is the area of most improvement over blue. *Pigment Green 7* is offered in medium to blue shades of green. *Pigment Green 36* is much yellower than Pigment Green 7.

Quinacridone Pigment. Quinacridone pigments fill an important need in the coloring of plastics. They are the high performance counterparts to azo red pigments. They cover a key color space, from bright red to violet. They are exceptionally strong but can be difficult to disperse because of its especially small particle size. A few suppliers offer predispersion that limits loss through dusting and provide additional dispersion and strength, as a result, increasing their value in use. They have excellent fastness properties. They can be used in olefins for everything from packaging to fiber applications. They are also used in acrylonitrile, nylon-6, and polyester fiber. Some varieties find use in engineering resins. Quinacridones are also the pigment of choice for automotive interior and vinyl applications. Most have some FDA approval. Pigment Violet 19 is polymorphic and has two basic crystals. The beta crystal is a violet whereas the gamma crystal is a yellow shade red. The beta crystal is most stable.

Quinacridone pigments are made by the use of two different but similar processes. They involve either the oxidation of dihydroquinacridone or the cyclization of 2,5-diarylaminoterephthalic acid. Both processes require a condensation of diethyl succinylsuccinate with an aromatic amine to form the 2,5-diarylamino-3,6-dihydroterephthalic acid diester. The diester is converted to dihydroquinacridone during ring closure at high temperatures. Subsequent conditioning leads to a quinacridone with the desired morphology. Use of 2,5-dianilinoterephthalic acid yields Pigment Violet 19 (**29**). Use of 2,5-ditoluidinoterephthalic acid yields the 2,9-dimethylquinacridone, Pigment Red 122. Use of 2,5-diparachloroanilinoterephthalic acid yields the dichloroquinacridone, Pigment Red 202 (4).

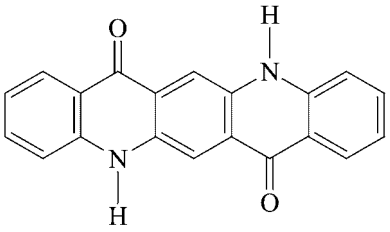

(**29**)

Pigment Violet 19 (Violet) (**29**) can have a variety of shades and properties. This diversity is largely dependent on the particle size and manufacturing processes. The beta crystal provides a clean violet shade. Most have FDA approval and can find use in FDA applications using extrusion coating, injection molding, and film processes. Its excellent lightfastness and heat stability make it useful in most melt-dyed fiber. Some solubility issues exist when used at very low loadings in engineering resins.

Pigment Violet 19 (Red) is also offered with variety of properties and comes in a variety of shades and opacities. The more opaque have better lightfastness and heat stability and the more transparent have excellent tinting strength. Some recently developed products can offer both. The particle size and particle size distribution are mainly responsible for the variety of products offered. Most grades are FDA approved.

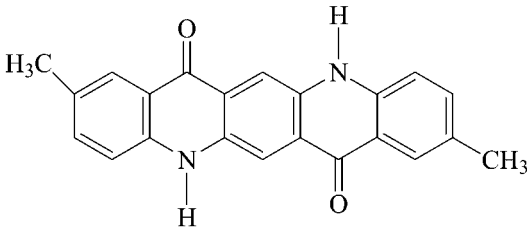

(**30**)

Pigment Red 122 (**30**) is the dimethylquinacridone. It is a magenta shade and is typically thought of as having better fastness properties than of the unsubstituted types. It is used in all of the above-mentioned plastic applications. Some grades are FDA approved.

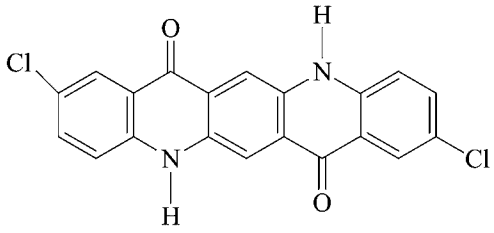

(**31**)

Pigment Red 202 (**31**) is a *dichloroquinacridone*. It is also a magenta shade and is similar in properties and uses to Pigment Red 122. Pigment Red 202 was typically offered in a hard to disperse and opaque coatings grade. New, easy dispersing, high tinting strength grades are now available. Red 202 is unique in that it is the least soluble of the quinacridones. Therefore, the majority of its use is in engineering resins and other high performance applications.

Perylene Pigments.

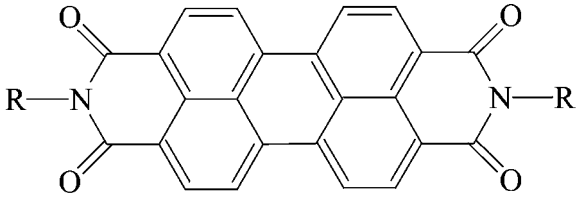

(**32**)

Perylene pigments are similar to quinacridones, given that they find use in high performance applications. Of perylenes, only three types are actively used for coloring plastics. They are Pigment Red 179 (**32**) (R=methyl), Pigment Red 149, and Pigment Violet 29 (**32**) (R=H). They are unique as compared with quinacridones in that the majority of the pigment not consumed in automotive coatings is used to color fiber. Caution should be exercised when perylenes are used in olefins that are stabilized with HALS (Hindered Amine Light Stabilizers) UV Stabilizers. At high pigment levels the stabilizers can be inactivated upon exposure to light. Perylenes are used to a lesser degree in PVC for automotive interiors.

Perylenes are chemically diimides of perylene tetracarboxylic acid. The shade change is dependent on the substitution of the imide nitrogen (4).

Pigment Red 149 is a clean, medium shade red. It exhibits high tinting strength and is very transparent. Its small particle size can cause shrinkage in large molded parts. Interestingly, its influence on shrinkage decreases with increasing temperatures. Superior migration resistance in plasticizers allows use of all types of vinyl. Pigment Red 149 can endure processing in polycarbonate because of its heat stability of 320°C. Pigment Red 149 is also used to color unsaturated polyester and other cast resins (1). *Pigment Red 179* is perylene maroon. It is a very blue shade that is very dirty and brown looking at high loadings. Most common usage is in fiber as tinted and low percentage masstone colors. At these levels it is a clean, reddish-maroon color. It is thermochromic and will change color during processing only to return to original color as it cools. *Pigment Violet 29*, a very blue shade violet, appears black at high pigment concentration. Pigment Violet 29 finds use in fiber; however, volumes are much lower than those for Pigment Red 179.

Dioxazine Pigment.

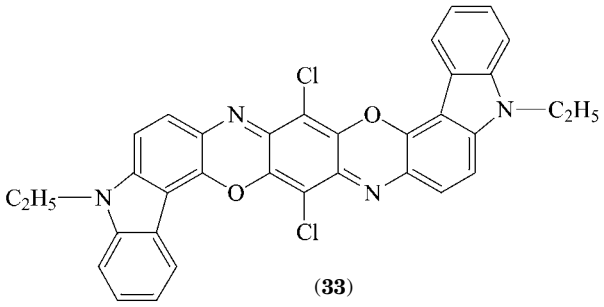

(**33**)

Dioxazine violet or *Pigment Violet 23* (**33**) can be used in most plastics excluding engineering resins. It is very strong in tint and can look black in masstones at normal levels. It finds most use in olefins and PVC. It is often used at low levels with TiO_2 to provide a clean pastel violet. In fiber, carbazole is often added in small quantities to blue to provide a clean red shade blue. Another use is in combination with blue as a bluing agent for whites. Use caution as decomposition can occur if processing above 250°C. Pigment Violet 23 has also exhibited solubility issues when used at very low levels. Lightfastness also requires attention since it can swing from 8 (excellent) to 3 (poor) on the blue-wool scale as pigment loadings are decreased. Carbazole dioxazine violet is manufactured by reacting chloranil with 2 mol of aminoethylcarbazole followed by oxidative cyclization.

Diketopyrrolo Pyrrole Pigment. *Pigment Red 254* is a new arrival when compared with most of the other pigments mentioned. It is offered in several different shades of medium red. The tint reductions are somewhat bluish red. Pigment Red 254 offers good color strength and has excellent fastness properties. For economic reasons it is often combined with less expensive napthols and quinacridones. This provides both a variety of shades and properties while reducing the expense of the formula.

FD&C Food Lakes. FD&C lake pigments are vital to the plastics industry. They are certified by U.S. Government specifications to be of a purity and composition that allow their use as a direct food additive and colorant for certain drug and cosmetic applications. This certification makes them the pigment of choice for medical or food packaging applications (5,6). They have heat stability in the area of 250°C. Limited light stability and poor tinting strength excludes them from use in areas where their certification is not required.

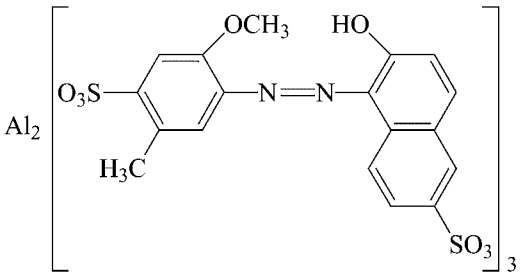

(**34**)

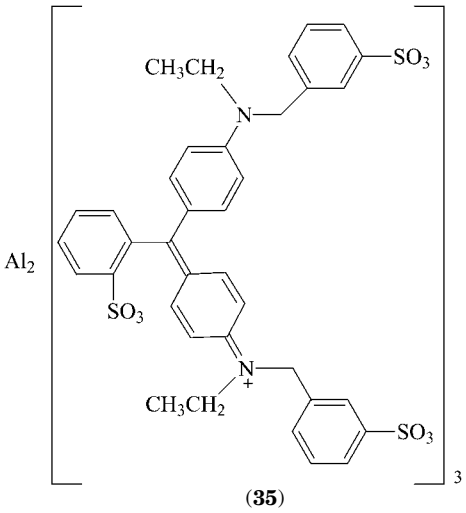

(**35**)

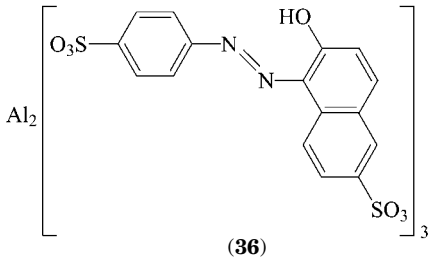

(**36**)

Manufacture of the food lakes requires the precipitation of food-certified dyes onto the surface of aluminum hydrate. The water of hydration present is to some extent driven off during incorporation into the plastic. Vented equipment is recommended. Over 90% of their use in plastics is in olefins for food-packaging applications. The colors available are FD&C Red 40 (**34**), FD&C Blue 1 (**35**), FD&C Yellow 5, and FD&C Yellow 6 (**36**).

Dyes. Dyes similar to pigments are listed according to their class, generic name, and Color Index (CI) name and number. The dyes are essential; without them, many transparent effects in plastics could not be achieved. Dyes are soluble in plastic, and therefore more transparent by nature than pigments. Dyes are known for poor lightfastness in tinted application. This is not as great a concern in masstone or transparent parts as failure occurs on the surface, and the color beneath is unaffected.

Dyes should be avoided in plasticized PVC and olefins because they tend to migrate. Plasticizers solubilize the dyes making them fugitive. In olefins, the dyes lack an affinity for aliphatic hydrocarbons and consequently migrate to the surface. Migration testing is a standard procedure unless the dye is proven in the polymer system.

Azo Dyes. Azo dyes contain the structure —N=N— similar as referred to in the Azo Pigment section. They are available in a wide range of colors. Their main uses are coloring transparent, rigid PVC, polystyrene, phenolics, and poly(methyl methacrylate). The most commonly used azo dyes are Solvent Reds 1, 24, and 26,

Solvent Yellows 14 and 72, and Solvent Black 3. Acid Orange 7 and 8, and Acid Yellow 36 find most use in phenolic resins (7) (**37**, **38**).

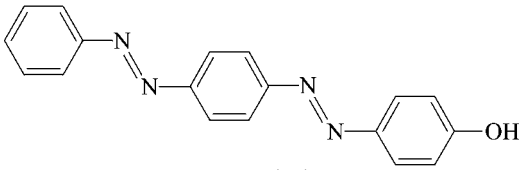

(**37**)

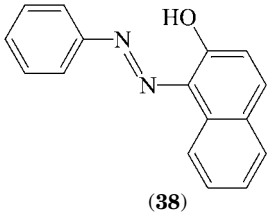

(**38**)

Anthraquinone Dyes. Anthraquinone dyes have much better heat and light stability when compared with azos. This does not come without a cost. In spite of this, it greatly expands the potential for use in exterior application. The most commonly used are *Solvent Red 111*, *Solvent Violet 13* and *3*, *Solvent Blue 12* and *59*, and *Solvent Green 3*. Usage is expanded to ABS and polycarbonate. Most recognize Solvent Red 111 for its use in automobile taillights made with poly(methyl methacrylate). Again, the acid types are mainly for phenolics. They are *Acid Blue 24* and *Acid Green 25*.

Xanthene Dyes. Xanthene dyes are an important class since they offer brilliant and fluorescent colors. Conversely they are only fair to good in heat and light stability. Useful xanthene dyes are Basic Violet 10, a fluorescent, Solvent Green 4, Acid Red 52, Basic Red 1, and Solvent Orange 63.

Azine Dyes. Azine dyes include nigrosine and induline. They have excellent heat and lightfastness. They produce very jet blacks, which are not achievable with carbon black. Nigrosenes, Solvent Black 5, and Solvent Black 7 are the largest volume dyes used in the plastics industry. Solvent *Black 5* is alcohol soluble and can be used in coloring ABS, phenolics, and polypropylene. Solvent Black 7 has higher tint strength than Black 5. Its low electrical transmission properties make it very desirable for coloring phenolic resin often used in electrical components (7).

BIBLIOGRAPHY

"Colorants" in *EPSE*, 2nd ed., Vol. 3, pp. 746–758, by T. G. Webber, Consultant.

1. W. Herbst and K. Hunger, *Industrial Organic Pigments*, VCH, Weinheim, 1993.
2. R. J. Hernandez, S. E. M. Selke, and J. D. Culter, *Plastics Packaging*, Hanser, Munich, 2000.
3. G. Buxbaum, *Industrial Inorganic Pigments*, VCH, Weinheim, 1993.
4. P. A. Lewis, *Organic Pigments*, 2nd ed., FSCT, Pennsylvania, 1995, p. 24.
5. D. Marmion, "Colorants for Foods, Drugs, and Cosmetics," in *Kirk Encyclopedia of Chemical Technology*, 4th ed., Vol. **6**, John Wiley & Sons, Inc., New York, p. 918. (Both print and online version available.)

6. D. M. Marmion, *Handbook of U.S. Colorants, Foods, Drugs, Cosmetics, and Medical Devices*, John Wiley & Sons, Inc., New York, 1991.
7. T. G. Webber, *Coloring of Plastics*, Wiley-Interscience, New York, 1979.

GENERAL REFERENCES

"Colorants for Plastics," in *Kirk Encyclopedia of Chemical Technology*, 4th ed., Vol. **6**, John Wiley & Sons, Inc., New York, pp. 944–965.
Society of Plastics Engineers, Color and Appearance Division, RETEC Papers 1994.
Society of Plastics Engineers, Color and Appearance Division, RETEC Papers 1998.
R. Harris, *Coloring Technology for Plastics*, Plastics Design Library, Norwich, 1999.

SCOTT HEITZMAN
Sun Chemical Corporation

COLORING PROCESSES

Introduction

Coloration of plastic materials is accomplished by depositing a colorant on the surface of the plastic part or incorporating the colorant into the plastic itself. Standard coating, dyeing, and printing techniques are used for surface coloration (see COATING METHODS, POWDER TECHNOLOGY; COATING METHODS, SURVEY). This article deals with colorants that are incorporated into the plastic.

The three basic forms of colorants used in plastics are raw pigments or dyes, color concentrates, and color compounds. Dyes and pigments are typically dry powders. Some pigment suppliers also offer single pigment dispersions containing only pigment and polymer. These products offer increased color strength, dispersion, and ease of use. Dyes and pigments are sold into many different levels of the supply chain.

Pigments and Dyes. The largest volume of raw pigment and dye is supplied to color houses that provide value-added products and services to molders and extruders. In turn the extruders and molders manufacture colored parts, bottles, and fibers. Some of the raw pigments and dyes are incorporated directly into finished parts via molding and extrusion; however, this is not common.

Color Concentrate. Color concentrate or masterbatch consists of a carrier resin that is highly loaded with colorants and additives. It is designed to match a reference colored sample when let down or reduced at a specified ratio, ie 25:1, 50:1 (resin/concentrate). When let down, the concentrate colors the resin as required.

Color Compound. A color compound is a system of colorants, additives, and resin that requires no letdown or addition of materials. It is ready to be processed into finished parts via molding or extrusion. A compound can be colored with dry pigment and dye or color concentrate.

Encyclopedia of Polymer Science and Technology. Copyright John Wiley & Sons, Inc. All rights reserved.

Color Houses

Color houses offer expertise in coloring of plastics. Whether a compounder or a concentrate house, they provide a high level of service to their customers. They supply a colorant and resin system that will match both the shade desired and the physical properties needed for the life of a product.

The physical form of the compound or concentrate and equipment used in manufacturing colored plastic objects can vary. Color houses can provide liquid, powdered, or pelletized systems that can be converted using all types of equipment (media mills, extruders, continuous mixers). The functions and equipment typical of a color house are detailed in the following.

Color Labs. Color matching is a complicated art and/or science. Color matchers must balance the designers' aesthetic desires with the engineers' required physical properties. This is not always an easy task. It is often difficult to achieve the color and physical properties in the desired resin. Interaction between designers and engineers provides a forum for selecting colorants and end part colors based on economics and/or performance. This improves the ability to achieve a good and reproducible color match.

Color labs are outfitted with laboratory size equipment that simulates the larger machines used for production internally and by their customers. Typical processing equipment found in the lab are small extruders, two-roll mills, banburry mills, and media mills. Small rotational, injection and blow molding machines are used to duplicate the customers' process. Instruments and computers are required for testing physical properties and color. Most labs have a computer-controlled color measuring system and a light booth to evaluate color. The spectrophotometer with computer is initially used to assist in colorant formulation and later as a quality control (QC) tool to provide certification of the quality of match to standard. The light booth provides a standardized set of conditions to visually observe color and appearance.

Product literature, provided by the pigment supplier, is kept in the color lab for reference. General information regarding cost, compatibility, FDA approval, heat stability, lightfastness, and migration resistance is used for initial colorant selection. Laboratory quantities of a large variety of colorants are kept on hand. The samples are required for physical testing, QC adjustment evaluation, and color matching.

The color lab is usually divided into two parts: color development and quality control. The color development group works closely with the sales and marketing departments. Anything, from a competitive color concentrate to bottles, films, or injection-molded parts, can be submitted to the lab for color-matching. Pantone® books or chips and other color standards are also used to specify or select targets. Specifications regarding resin, letdown ratios, weatherfastness, and price are typically submitted with the target.

In the next step, a starting formulation of colorants, additives, and resin is developed. The computer generates formulas on the basis of a database of known spectral curves of colorants. The formulas are reviewed to ensure that colorants meet heat stability, weatherfastness, and migration and chemical resistance requirements, at a cost that is competitive. Lab samples are produced, evaluated, and submitted to the customer for approval. The customer can be internal or

external. Internal, if they are manufacturing an end use product, or external, if the concentrate or compound is sold to a molder or extruder.

The QC group is focused on the evaluation of the color concentrate or compound made in the plant. Grab samples are taken during the production run. The samples (molded chips, film, fiber) are prepared and evaluated versus standards. If required, adjustments are made to fine-tune color and properties.

Incorporation of Colorants. There are a variety of points in the manufacturing process for the introduction of colorants. All involve similar steps: premixing, dispersion, and letdown. Colorants, and more specifically pigments, require more attention than other additives that can be incorporated simultaneously, eg plasticizers, antioxidants, flame retardants, fillers, and impact modifiers. This is true as the manufacturing process of pigments results in different particle sizes and particle size distributions. Primary particles (true single crystals of pigment) are uniform in size, shape, and distribution but they can combine to form aggregates and agglomerates. Aggregates and agglomerates are usually created during the drying of the pigment. The water is evaporated and the crystals come in contact with one another. Van der Waal, electrostatic, magnetic forces, and, at times, atomic bonding are responsible. Aggregates are primary pigment crystals randomly joined at their surfaces. Their interior surfaces are not available to polymer or plasticizers, and aggregates as a result are difficult to separate. Agglomerates are primary crystals joined at corners or edges with interior surfaces available. They are more readily dispersed than aggregates.

The finer the dispersion and the better the incorporation, the lower is the impact on a polymer's performance. Properties like impact and tensile strength are lowered when agglomerates or aggregates are present. Surface problems such as specks in film and injection-molded parts are also a result of poor dispersion. Poor incorporation can lead to other typical color problems of low strength and inconsistency. Processing issues such as screen pack plugging and low throughput can also be avoided if a robust process is employed.

A robust process includes several steps: wetting the pigment surfaces, breaking down aggregates, and agglomerates, and distribution of the particles in the resin. The methods to accomplish this are numerous. In general, a premix is made and milled or extruded and then is let down and extruded, calendered, or molded into a final part. Many of the processes and equipments are used in more than one phase of the coloring process.

Mixing

Mixing is usually the first step in the manufacturing of a color concentrate or compound. The goal of mixing is to achieve a homogeneous blend of polymer and colorants. In a dry or liquid mix, pigments are not fully dispersed. Remaining agglomerates preclude direct use in thin cross-section parts like film and fiber. The agglomerates are less of a problem in thick cross-section parts like injection-molded containers. In any case the undeveloped pigment provides economic motivation to process further.

High Shear Mixing Dry Powders and Resin. High shear mixing is required for achieving fiber and film quality dispersion. The shear impacts the pigment particle onto the surface of the resin and waxes. The air on the surface is

partially displaced and thus the pigment is easier to "wet out" (break down) in the dispersion phase of processing. Powdered resin and waxes are included as carriers for the colorants in this step.

High shear mixing is accomplished in a Henschel® or Hobart® type mixer. These equipment manufacturers are known throughout the food and plastic industries for jacketed kettle-type mixers with high speed impellers. The rotors have a mixing speed of up to 3600 rpm revolutions per minute. Most blends are run on low speed to slowly mix the ingredients and then at high speed to homogenize. A good vortex is required. A charge of no more than 80% of the mixer's capacity is good practice. Mixers of this type can also be used to completely flux or melt the resin and incapsulate the colorants.

Low Shear Mixing of Powders and Resin. Low shear mixing is suitable for easier dispersing inorganic pigments. These pigments have a large particle size and are in turn easy to de-agglomerate. Low shear mixing is preferred for pearlescents and metallics as these products can be destroyed in high shear environments. Dyes are suitable for low shear mixing, as they only need to be distributed evenly throughout the polymer.

Low shear mixing can be accomplished with anything from a drum tumbler to a variety of planetary mixers. Planetary mixers have low speed screws or paddles that mix the ingredients in the bin or hopper. A charge of no more than 80% of the mixer's capacity is good practice.

Mixing Liquids. Carriers like mineral oil and plastisol are typical. Mineral oil is used in a variety of liquid color application. Plastisols find use in calendered and slush-molded PVC applications. The process provides good mixing but a low level of dispersion. Some of these blends are suitable for end-use applications. Most are milled to provide a higher quality of dispersion.

A spindle or cowles mixer is used to mix colorants into liquids. The spindle is equipped with a sawtooth blade. The blade turns at 1000–5000 ft/s. Average mixing time is an hour.

Flushing. The Sigma blade mixer is used almost exclusively by pigment manufacturers. It is often referred to as a "flusher." It is named after the flush process, used by pigment manufacturers to incorporate pigment into a polymer. The goal of the process is to take the pigment while in its aqueous phase and transfer it into a plasticizer or polymer. Under temperature and shear, the pigment has a higher affinity for the polymer than water. The pigment migrates, into the polymer and the water is "flushed" (displaced) to the surface and poured off. The lid on the mixer is closed to pull vacuum and the dispersion is dried at an elevated temperature. It is allowed to cool and is cryogenically ground.

This process avoids drying of the pigment during its manufacture and thus there is no opportunity to form the "hard to disperse" agglomerates. The outcome is a highly loaded, up to 60%, pigment dispersion. It is nondusting, has excellent dispersion, and offers high throughput rates.

Concentrate houses utilize these products as single pigment concentrates or mix them with other flushes and traditional pigments to make high quality color matches for film and fiber. Flushing is also used to increase the pigment concentration in a typical dry color concentrate. With its high loading and low molecular weight carrier, flushing aids wetting of the dry color while at the same time increasing the pigment loading.

Dispersion Methods for Liquids

Milling is used to disperse pigment that is incorporated into a premix. The term "milling" is generally reserved for liquid or paste systems. There are several types of mills used to fully disperse pigment into polymer. Three-roll mills, media mills, and ball mills are the most common. They are used in making color dispersions for cast acrylics, epoxies, and plastisols.

Viscosity is the key to a good grind and/or dispersion in liquid systems. The colorant's loading and surface area are important factors. In general, higher loadings of low surface area pigment and lower loadings of a high surface area pigment are desired for a good grind. High surface area pigments can cause vehicle demand problems. Low viscosity mixes may run with little shear.

Three-Roll Mill. The three-roll mill was designed for the ink industry in order to incorporate pigment into liquid carriers. Its main use in plastics is for the manufacture of high quality plastisol dispersions and liquid colors. The typical pigment levels for these concentrates range from 25 to 50%. The pigment level is largely dependent on its surface area and the customer's requirements.

The mill is configured as a series of three rollers horizontally positioned. They are separated only by a small nip, which can be opened or closed to control the level of shear. The premix is milled and agglomerates are reduced as it is passed through the nip from roller to roller. The finished paste is scraped off the front roll. Several passes may be required to obtain a desired level of dispersion. The viscous paste is packed out in buckets.

Media Mill. The media mill, formerly designed for the ink and paint industries, is used in plastics, for the manufacture of liquid color or paste dispersions. Suitable ink or paint grade colorants along with dispersion aides are useful in solving viscosity and flocculation problems. Buehler, Netzch, and Schold are a few of the manufacturers of media mills. A premix is pumped through a cavity containing steel, ceramic, or glass shot. A variety of shot sizes are used. An impeller agitates the shot and the impact reduces agglomerate size.

Dispersion Methods and Equipment for Solids

Two-Roll Mills. Two-roll mills are key to making high quality PVC and rubber concentrates. These mills are easily cleaned. The batch process is ideal for producing small volumes; thus, a variety of colors and materials can be run without much equipment down time.

The two-roll mill rollers are parallel and horizontally mounted. The speeds and directions of rotation are different. The gap or nip between rolls can be controlled. Heat is applied or can be developed by friction. The dry premix is forced down through the gap and allowed to form a band or sheet on one of the rollers. There is little mixing, and so the banded material is usually cut and reintroduced manually to promote mixing (1). Leaving the material on the mill for a longer period of time can maximize dispersion. On occasion, the majority of the resin is added separately and allowed to band. The colorant blend is then slowly added. This can help contain the pigments and additives. The powders quickly stick to the banded resin and are incorporated as the material passes through the nip.

Banburry Mixer. The Banburry mixer is most often used to produce highly loaded concentrates for olefins and PVC. The process can be used with or without a premix. A premix is recommended when making highly loaded concentrates and/or using high surface area pigments.

The Banburry mixer is an internal, high shear compounder. Two cylindrical cavities intersect at an open feed throat that can be closed after the Banburry mixer is charged. Two intermeshing helical rotors turn at high rpm inside the cavities. A pneumatic ram seals the cavity for processing. Most are jacketed so they can be heated or cooled. Most are run cool, using shear to generate the heat to flux or melt the ingredients to form the concentrate. The fluxed material is unloaded via trapdoors in the bottom of the mixing chamber. The mix or molten mass can be fed either into an extruder and pelletized or onto a two-roll mill and sheeted out. Colors changes are rapid as the equipment is nearly self-cleaning.

Continuous Mixer. A continuous mixer is similar to a Banburry mixer but it offers the advantage of a continuous process. Residence time can be controlled by the size of the discharge unit and/or the feed rates. The continuous mixer is known for its ability to produce high volume but tends to lack in the quality of dispersion achieved in a Banburry mixer.

Extrusion

Plastics processing operations often include extrusion (see EXTRUSION).

Single Screw Extruders. The single screw extruder is the workhorse of the plastics industry. It is used to incorporate color into concentrates and compounds. It is also used to extrude rods, pipe, sheeting, film, siding, and other profiles.

An extruder consists of a hopper, a heated barrel, a screw, and a die. The hopper is used to flood-feed the colorant and plastic premix into the feed section of the screw. An alternative to flood-feeding is to starve-feed the screw by metering in a controlled flow of material. Metering is not required for a single screw and has been found to have no impact on pigment dispersion.

The feed section of the barrel can be cooled. The barrel can be heated at different temperature in different zones. The feed section of the screw is designed to convey the resin into the heated barrel, where melting takes place. The next zone is commonly referred to as the transition or compression section. The screw flights are smaller and decrease in size. External heating and heat from friction cause the melting to take place. The polymer melt is then conveyed, under pressure from the screw rotation, to the mixing and metering zones. Most extruders have a screen pack in front of the die to filter undispersed materials and trap contaminants. Typical downstream equipment consists of die face or strand pelletizing. Die face pelletizers are selected for high output extruders and “hard to run” materials.

Twin Screw Extrusion. Twin screw extruders provide more mixing and dispersion energy. In general they are more versatile as they are manufactured using segmented barrels. The different sections can be vented or used as a port to “side stuff” product into the melt stream. The length can also be changed with respect to the segments. Twin screw extruders have two screws mounted side by side. The flights of one screw are intermeshing with the grooves in the other screw. Screw designs are similar to those in a single screw extruder in that different areas

of the screws provide different functions. They differ in that they are usually modular and can be changed for a specific process or material. Screw elements are placed on a spline, as required. The elements can be for conveying, dispersing, mixing, devolatilizing, and kneading. A volumetric or gravimetric feeding system is required for a twin screw, as this type of extruder needs to be starve-fed.

Molding

Coloring may take place during a molding process.

Injection Molding. Injection molding is the process of forcing molten plastic into a mold where it is to be formed. Similar to extrusion, the process begins with delivery of the plastic to the feed hopper. The plastic is usually pelletized and is normally added directly or fed into a hopper. The hopper flood-feeds the resin directly into the feed throat. The barrel is heated and temperature profiles are established, similar to extrusion. The screw is unique in that it can move both forward and backward. As the screw turns, melted polymer is forced to the front of the barrel. It is held in place by a check valve. The pressure of the melt forces the screw backward in the barrel. When the desired shot size is reached the screw stops rotating. The valve is opened and the screw is driven forward. The plastic is forced through a nozzle into the closed mold. The melt is held under pressure by the cushion of polymer in the barrel. This allows the melt to completely fill or "pack" the mold. The mold itself is held under great pressure. After the part is allowed to cool, it is ejected. The screw starts to turn and feed fresh polymer into the barrel and the process begins again.

The screw and molding machine itself are designed for distributive mixing, and not dispersive mixing. Color concentrate is typically used for this reason. There is not enough shear to break down the agglomerates and aggregates of dry pigments. Dispersion problems and low value in use preclude dry pigment from most applications. Also, not many molders want to manage the color-matching process. By using precolored compounds or color concentrates, the color aspects are simplified and focus can be placed on molding.

Precompounded color contains all the needed ingredients required for the molded parts. It is simply added to the hopper and molded. Compounds are used when an excellent shot-to-shot consistency is required.

Concentrates require a letdown before molding. On the dry side, a typical letdown ratio is 25:1, or 25 parts of polymer mixed with 1 part of color concentrate. Viscosities or melt index of the polymers should be as alike as possible for the best mixing and color incorporation. The letdown ratio can be adjusted to achieve better economics or dispersion.

Higher the loadings lower are the conversion charges for the concentrate, and the better the economics. Lower the letdown ratio less colored pellets required, resulting in a lower probability of good mixing and color consistency.

On the liquid side, the color is let down in the feed section just above the screw or is introduced directly into the barrel. Here it quickly mixes with the polymer as it starts to soften. The liquid color is metered at a specified feed rate. This rate can be adjusted if required.

Applications for injection molding are numerous, and all but a few are colored. A few end uses are plastic containers and lids for the packaging industry, parts and components for toys, automobiles, electronics, appliances, etc.

Blow Molding. Blow molding is a process that utilizes internal air pressure to force the polymer outwards into a clamshell mold. This technique is a very practical way of molding hollow parts. Bottles for packaging are the main application; however, parts as large as plastic drums and garbage cans are made. The two types of blow molding are extrusion and injection blow molding.

Color is incorporated using the same processes as in injection molding. Pelletized and liquid color concentrate are let down into virgin resin. For injection blow molding the color is incorporated during the molding of the preform. In extrusion blow molding the color is extruded into the polymer, forming the bubble of polymer or parison. Some colorants are known to plate out and stain the mold and/or blow pin. Formulations using proper pigments and additives can prevent this occurrence. The down time required to clean the mold and blow pin is usually found unacceptable.

Extrusion Blow Molding. This is simple and economical. It can produce a variety of shapes, with fairly good control over wall thickness. The process is multistep. In the first step an extrusion of a tube of partially molten polymer is extruded down into a mold area. Then, the two halves of the mold close in on the tube of polymer. This cuts it from the extruder and captures the bubble of polymer inside. A blow pin (a hollow tube) is inserted and air is blown into the mold. The air forces the parison to fill the cavity (2). The flash or excess is then cut from the container ground and recycled when possible.

Injection Blow Molding. This is a two-step process. The first step is injection-molding a preform to be used in place of the parison in extrusion blow molding. Next the preform is placed into the blow mold. The preform can be soft, coming straight from injection molding, or it may require preheating. This is dependent on the type of process involved. The second step is the introduction of air through a core rod that is inserted into the throat of the bottle or part. Air pressures are higher than those used in extrusion blow molding.

Rotational Molding. The process of rotational molding is ideal for creating hollow parts. Polyethylene is the most common polymer used in rotational molding. Powdered plastic is introduced into a clamshell mold. Color and additives, usually a micro-pulverized blend, are added and the mold is closed. The mold is then rotated. The powder is distributed to the mold's surface by the centrifugal force. The mold is heated and a melt skin forms on the mold's surface. Spinning continues as the mold is allowed to cool. The mold is then opened, the part removed, and the process starts again.

Lack of mixing or shear makes the type of concentrate supplied to the rotational molder unique. Typical color concentrates, in the pelletized form, is ineffective for rotational molding. The pellets lack adequate surface to melt in and color a part. Commonly all colorants and additives are blended and micro-pulverized by a concentrate house. Pigment strength achieved by micro-pulverizing is not equal to that of an extruded concentrate. The molder simply adds the blend at the time the mold is filled. This ensures that the required color is achieved.

Fiber

Most fibers are created by forcing molten polymer through a spinneret to form continuous strands of polymer. This is typically accomplished using an extruder

or gear pump. A spinneret is a die that has one to several hundred holes. The tiny holes are sensitive to corrosion and clogging. Prefiltering of the molten polymer and frequent preventive maintenance to the die and filler are required. The polymer emerges in a semisolid state and solidifies in a process called spinning. This process is not the same as the "spinning" in the textile industry, where staple fibers are twisted into yarn.

Stretching and orientation is the last step. The fibers can be stretched or "drawn" while solidifying or after they have hardened. Drawing orients the molecular chains along the major axis of the fiber. This creates a much stronger yarn.

Most olefins are colored by adding color concentrates to the polymer melt during extrusion (solution-dyeing, mass-coloration, pigmentation). Other synthetic fibers are spun without color and dyed later. However, pigmentation is increasing because of the lower cost and better fastness properties. Pigmentation of nylon and polyester is experiencing rapid growth. No additional process water is required and no effluents are produced, as is the case in dye systems. Inventory flexibility is reduced with pigmented fibers.

Coloration can also be added in the condensation process before polymerization. In the case of polyester, this can mean the colorants are exposed to temperatures reaching 290°C for 5–6 h. Only a few high performance pigments can withstand these conditions.

The methods of spinning are (*a*) Melt, (*b*) Wet, and (*c*) Dry (3).

Melt Spinning. This is used with thermoplastics like polypropylene, polyamide, and polyesters. The polymer is blended with dry, pelletized concentrate or flush containing the additives required to color and stabilize the fiber. The mix is extruded and forced through a screen pack to remove agglomerates. The polymer is then pressed through spinnerets. The small strands of polymer descend vertically through a cooling chamber and are stretched and wound. The fibers can be spun in different shapes (round, pentagonal, octagonal, etc) to achieve a variety of appearances and properties.

Excellent dispersion is needed where pigments are used. After processing, remaining pigment agglomerates must not exceed 5 μm. Larger particles (pigments or additives) can lower the tensile strength and often cause failure as the fiber is stretched. With this in mind, dry pigment should be avoided. Pigment preparations, flushes or concentrates, are required.

Wet Spinning. This is used to spin a filtered viscous polymer that has been dissolved in a solvent. The spinnerets are submerged and the fibers are forced into a chemical coagulation bath. The filaments precipitate from solution and solidify. This is termed wet spinning as the fibers are formed in a chemical bath. Acrylic, rayon, and spandex are produced with this type of spinning.

In wet spinning a pigment's heat stability is of less concern than in melt spinning, but solvent resistance is required.

Dry Spinning. In dry spinning, the polymer is dissolved in a solvent, filtered, and forced through spinnerets. The fibers are then, by use of vacuum, pulled through an oxygen-free heated chamber. The polymer solidifies as the solvent evaporates. The filaments do not come in contact with a liquid and thus there is no need for drying. Solvent recovery is easy. Acetate, acrylic, and spandex fibers can be produced using dry spinning.

BIBLIOGRAPHY

1. T. G. Webber, *Coloring of Plastics*, Wiley-Interscience, New York, 1979W.
2. R. J. Hernandez, S. E. M. Selke, and J. D. Culter, *Plastics Packaging*, Hanser, Munich, 2000.
3. H. K. Hunger, *Industrial Organic Pigments*, VCH, Weinheim, 1993.

GENERAL REFERENCES

Society of Plastics Engineers, Color and Appearance Division, RETEC Papers 1994.

SCOTT HEITZMAN
Sun Chemical

COMPOSITES, FABRICATION

Introduction

In the last half of the twentieth century, the processes used for fabrication of parts made from composite materials evolved from operations relying on manual labor to manufacture by automated equipment controlled from sophisticated microprocessor systems. Early pioneers combined fiber and resin raw materials and formed them into a finished structure by hand lay-up or spray-up on open molds. The parts were cured at ambient temperature.

As the value of fiber-reinforced polymers became apparent and accepted in electrical applications, recreation products, and corrosive environments, these synthetic materials began to penetrate virtually every other market worldwide, from automotive and marine to primary structural elements of aircraft and bridges. Such widespread growth in product applications mandated corresponding growth in materials technology, design approaches, and fabrication processes.

For convenience, terms frequently encountered in composite fabrication are defined below:

Angle of winding (wind angle)	The angle the roving band is laid with respect to the mandrel axis of rotation
Closed-end vessels	Parts that have much smaller diameters or totally closed domes at the ends
Debulking	A process in which air is squeezed out of a prepreg laminate in order to promote adhesion
Doff	Roving package
Fiber payout	Transfer of rovings from delivery system to product line

Encyclopedia of Polymer Science and Technology. Copyright John Wiley & Sons, Inc. All rights reserved.

Overtravel	The additional carriage or eye travel beyond the ends of the part mandrel that is necessary to provide laydown of the fiber mandrel
Mat	Chopped or random reinforcement material cut to the contour of a mold, usually impregnated with resin just before or during the molding process
Peel ply	The outside expendable layer of a laminate, which is removed to improve bonding of additional layers
Prepregs	Reinforcements in the form of a cloth impregnated with thermosetting resin advanced in cure only through the B-stage. The term also covers fabrics such as jute and rayon, which have been impregnated with a thermoplastic resin, eg, vinyl or ABS
Roving	A form of reinforcing fiber glass comprised of 8–120 (and usually 60) single strands gathered into a bundle, and treated with a coupling agent to promote adhesion of the glass to the plastic matrix
Tape	A form of reinforcement similar to mat and broad goods, cut in 7.5- to 30-cm widths, and of flexible consistency for laying onto a mold. Tapes are generally prepregs and are supplied with backing paper to prevent loss of integrity prior to use
Tow	Term used instead of roving to designate fiber strands when referring to graphite or boron reinforcements in the fiber strand form
Wet systems	Composite fabrication processes and equipment that incorporate reinforcement impregnation as part of the process, just before the raw material die entry or mold contact

Product and Machine Design

Before a fabrication process can be determined for producing a new product, and production equipment designed and built, the designer must know something about the product. In the formative years of composites fabrication, traditional procedures allowed each discipline to proceed independently, with little consultation between design and manufacturing. The result has too often been equipment that did not operate efficiently. Product and process optimization are only achieved through cooperative design, planning, and manufacturing.

An integrated approach is necessary to achieve the best results in product automation and economics. Cooperative effort among all disciplines is required from the start of a project.

Although it is not necessary for the machine designer to be familiar with every detail of manufacture, it is important to have certain basic data, such as environment, load paths, throughput rates, economic constraints, and configuration information.

Structural analysis is recommended to determine specific property requirements of the product application. Hybrid materials—for example, combining carbon fiber with glass fiber in areas of high stress—can often satisfy strength and

weight specifications at reasonable cost. An over-designed composite part that uses more material or higher cost materials than necessary cannot compete with wood, steel, and other established materials. However, a well-designed part can be commercially competitive, especially when installation, maintenance, and life-cycle costs are considered.

In general, the resin matrix of a composite product provides corrosion and weather resistance and other physical characteristics, and the reinforcing fiber imparts strength characteristics such as stiffness and impact resistance.

Fiber type, form, and orientation (fiber architecture) comprise the main considerations when choosing reinforcements. In a part that will be carrying little or no structure loads, chopped or continuous strand mat with random fiber orientation is sufficient. However, in a part that will see primary or secondary structural loads, fiber orientation is critical and departures from the optimum can result in drastic property reduction. Fiber architecture can be tailored for specific requirements, with parallel longitudinal (0°) strands carrying tension loads, circumferential (90°) strands providing compression and impact strength, and helical (commonly $\pm 33^\circ$ or $\pm 45^\circ$) strands handling torque stresses. This design principle is comparable to the way that civil engineers use steel-reinforcing bar in a concrete structure.

Responding to the challenge of achieving optimum fiber architectures, material producers have devised innovative braided, woven and nonwoven, and stitched fabrics that are being used today even in bridge decks, beams, and other primary structural elements.

The difficulty of making complex arrangements to direct oriented fibers into automated equipment is the primary reason why hand lay-up and other labor-intensive processes are still prevalent in the composite industry. However, this is not to say that complex arrangements are impossible; fiber architecture in nearly every conceivable configuration has been achieved on automated equipment. Appropriate design and arrangement of supply spools and folding tooling for pultrusion equipment, multiaxis controls on filament-winding and tape-placement equipment, and other devices make complex laminate schedules feasible.

The most common composite-reinforcing materials are fiber glass, carbon fibers, aromatic polyamide (aramid), and boron. The term composite is used throughout to include glass fibers and other so-called advanced composite materials (see COMPOSITE MATERIALS & COMPOSITE MATERIALS, FIBER-MATRIX INTERPHASES). Reinforcement selection is based on intended usage, and property values established for these materials can be used as guidelines. Although most machines accommodate all reinforcements, designers who know the type of reinforcement to be used can take unique characteristics such as high modulus into consideration.

In addition to the common roving strands, raw material is available in many other forms, such as preimpregnated (prepreg) and wet systems, mats (paper and nonwovens), woven specialties with knit and braided reinforcement, multiple-ply broad goods, core materials as they apply to automation, fillers, extenders, and additives (films, coatings, plating, etc). The characteristics of the reinforcement must be familiar to the machine designer.

Matrix selection is another important design consideration; resin chemistry can accommodate nearly every conceivable product application. Running speed,

cure rates, and final properties vary widely with resin, catalyst, additive, and fillers. Advance consultation with the supplier is recommended.

In addition to wet systems, where reinforcements are resin-coated during the process, more convenient prepregs are available that can be used for many applications. Suppliers assist in the selection of preimpregnated materials, which are available as unidirectional, woven, and nonwoven tape, tow, mat, and so forth.

Although thermosets are the standard composite matrices, recent advances in thermoplastic technology may change this situation.

The diversity of products that can be fabricated on automated equipment is fast expanding as suppliers increase the flexibility of raw materials, and designers and manufacturers gain experience with integrated designs.

Methods and Processes

Open contact molding in one-sided molds, typically spray-up and hand lay-up, is still common for fabricating large nonstructural parts such as boat hulls, recreational vehicle panels, and bathware. To reduce emissions of volatile organic compounds (VOCs) during processing, vacuum-assisted resin transfer molding (VARTM) systems can be used, which cover even very large parts with a vacuum bag before resin is applied (see Figs. 1 and 2).

However, VARTM systems are still highly labor-intensive, and as the industry matured, it sought to develop methods and processes that reduce labor and increase production rates.

Fig. 1. Very large parts can be produced by the patented Seaman Composites Resin Infusion Molding Process (SCRIMP), in which dry reinforcements are vacuum bagged before thermoset resin is introduced into the lay-up. Courtesy Hardcore Composites, New Castle, Del.

Fig. 2. One-piece bridge deck made by SCRIMP process. Courtesy Hardcore Composites, New Castle, Del.

An early move toward automation and mass production was the invention of preform machines that sprayed chopped-glass strands onto a three-dimensional air screen that approximated the shape to be molded. The preformed glass mat was placed in a matched metal die in a compression molding press and liquid resin was added to form the product. Today, resin transfer molding (RTM) and resin injection molding (RIM) preform die-molding processes are used to mass-produce small and mid-size parts with two finished sides, notably automobile bodies, truck cabs, and even small boat shells.

Recent variations on preform technology include prefabricated preforms that are replacing wood as stringers for framing boat hulls (1). The preformed stringers are installed in an open hull mold, wet-out and co-cured with the hull skin laminate. In another development, prefabricated panels in a structural sandwich configuration can be purchased as a custom "kit" to build an original boat design (2). And in the late 1990s, a process was patented that lays up an entire boat hull preform, injects resin to wet-out the part, and compression molds the whole hull (with two finished sides) in matched composite molds (3) (see Figs. 3 and 4).

Sheet molding compounds (SMCs) that sandwich chopped fiber glass between two layers of resin paste are also used extensively to compression mold parts for the electrical, transportation, and other high volume industries. Automakers are exploring the use of carbon-fiber-reinforced SMC for body panels and other exterior parts because of the material's high strength and stiffness-to-weight ratio (4).

Bulk molding compounds (BMCs) are used for injection molding, which is a fast, high volume closed process. A BMC is a thermoset resin formulation containing 15–20% chopped fiber glass. A metered measure of the thick compound is dropped into the injection-molding machine and is forced by a ram or screw-type plunger through the machine's heated barrel. The compound liquefies as it

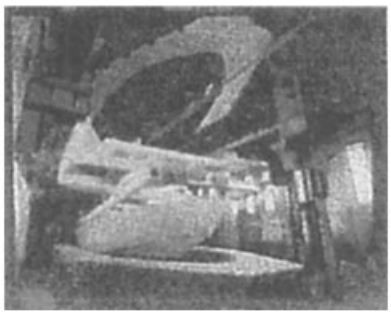

Fig. 3. One piece boat hull, 6.4 m long is pulled fully cured from female half of matched composite molds. Courtesy of VEC Technology, Greenville, Penn.

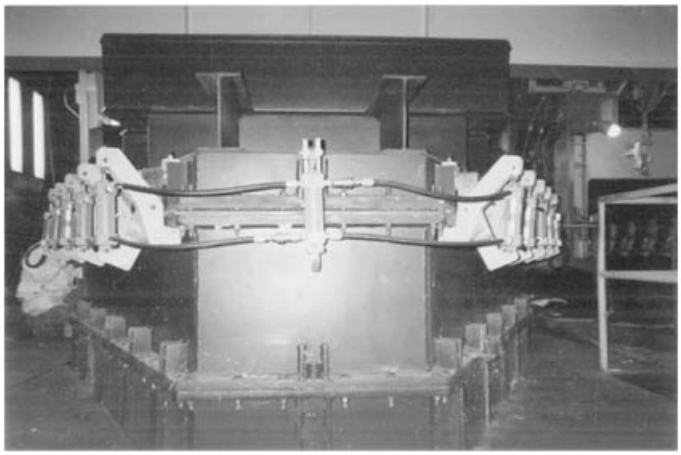

Fig. 4. Matched composite molds are locked together between steel housings in patented thermoset-injection-molding-type process to produce an entire boat hull. Courtesy of VEC Technology, Greenville, Penn.

approaches its cure temperature and the liquid flows along channels into forming cavities in the mold, where it quickly cures. Nearly 2000 small parts can be produced per hour.

A thermoplastic version of BMCs, long fiber-reinforced thermoplastics (LFRT) are gaining ground in the automotive market because of their superior impact resistance and recyclability compared to that of thermoset compounds. Another significant advantage is that thermoplastics emit no VOCs during processing and so do not require the expensive environmental equipment and procedures required for fabricating thermoset parts. LFRT compounds can be processed by "plasticising" equipment in a process similar to injection molding, using a reciprocating screw extruder to move the material forward under low pressure, with low shear. This heats and "plasticates" the material, melting and mixing the compound. The screw pushes the hot charge out and drops it onto a cold tool, where it solidifies in the mold. The screw then retracts to pick up another charge. The material flows easily and so large parts can be made on smaller presses and at

Fig. 5. Twintex (Vetrotex) long fiber reinforced thermoplastic (LFRT) fabric—made by commingling woven fiber glass with polypropylene fibers—is preformed for manufacture of automotive bumper beams. Courtesy of Plastic Omnium, Paris.

lower pressure than other compression-molding systems such as SMCs. In a recent LFRT innovation, a commingled fiber glass and polypropylene woven fabric has been developed (see Fig. 5). In one successful product application, the fabric is being used to produce high volume, low weight structural bumper beams in Europe and the United States (5).

While many of these are automated methods and processes with economic advantage in high and low volume production, in most cases they produce nonstructural or semistructural parts using chopped or randomly oriented fibers. To meet the needs of the burgeoning infrastructure market for composite primary structures, fully automated and controlled processes using continuous fiber reinforcements must be used.

Pultrusion. The pultrusion process makes structural profiles of any shape continuously from composite materials (6–9), just as they would be extruded in aluminum. It is a one-step process that converts raw stock into finished product at rates up to 4.5 m/min.

Reinforcements are drawn into the system, impregnated with resin, and simultaneously formed and cured in a heated die; radio frequency or induction energy can be used to supplement curing (10–12).

The graphs shown in Figures 6, 7, 8, 9 illustrate the heat–pressure–time (line speed) interactions taking place inside a 90-cm long die during curing (13). The temperature profiles of Figure 6 show that the die temperature must be lower at the inlet to prevent pre-gel, and also at the exit to prevent hot-cracking. Preheating permits a more gradual die heat profile and avoids skinning. As can be seen from Figure 7, superimposing material temperature on the die heat profile shows inversion of the heat–flux relationship. First, the material absorbs heat from the die, then the die cools the cured profile. In Figure 8, material viscosity

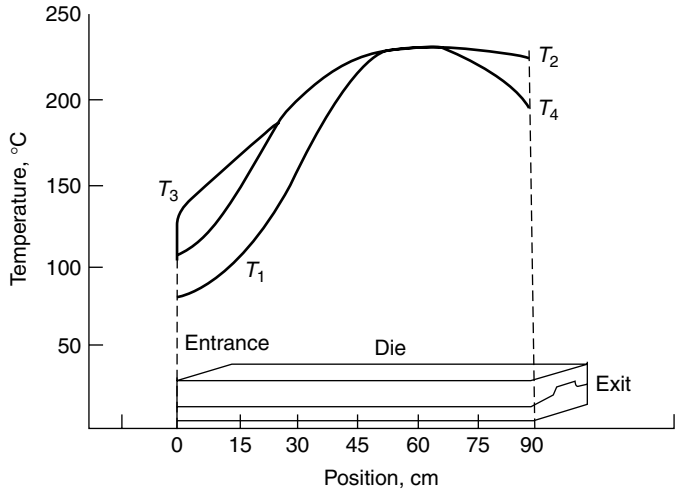

Fig. 6. Die temperature profiles. T_1, start-up; T_2, steady-state; T_3, with preheat; and T_4, cool-down.

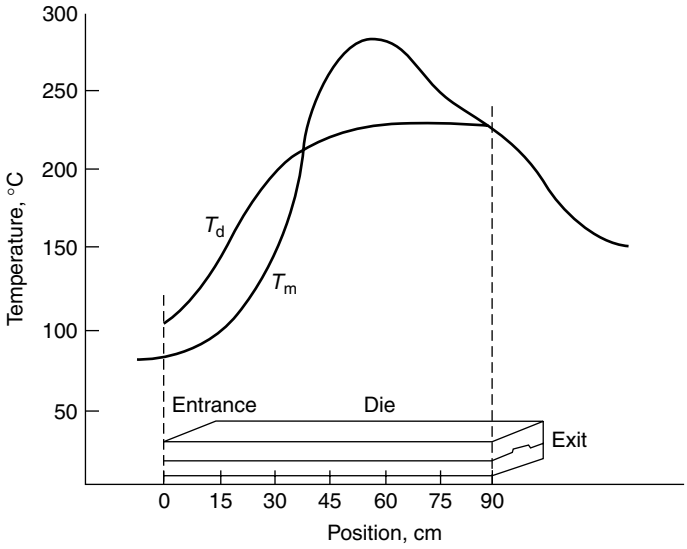

Fig. 7. Die (T_d) and material (T_m) temperatures.

is superimposed on temperature curves. Viscosity at the die inlet must be high enough to prevent porosity formation inside the die.

Pultrusion Machines. A typical pultrusion machine is shown in Figure 10. Reinforcements are impregnated by one of the available devices, in this case a pass-through-type wet-out tank, before passing through squeeze-out bushings. All the energy required to cure the resin system can be supplied by a radio frequency (r-f) generator. The process is run fast enough to bring the material into

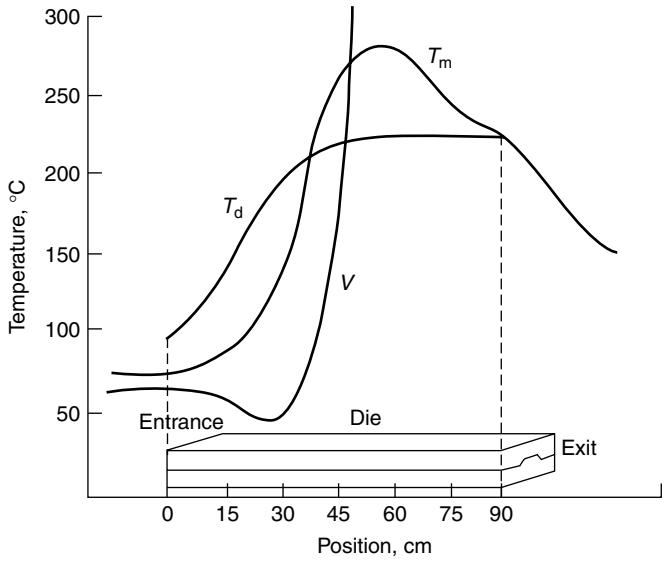

Fig. 8. Viscosity and temperature. V, viscosity; T_d, die temperature; and T_m, material temperature.

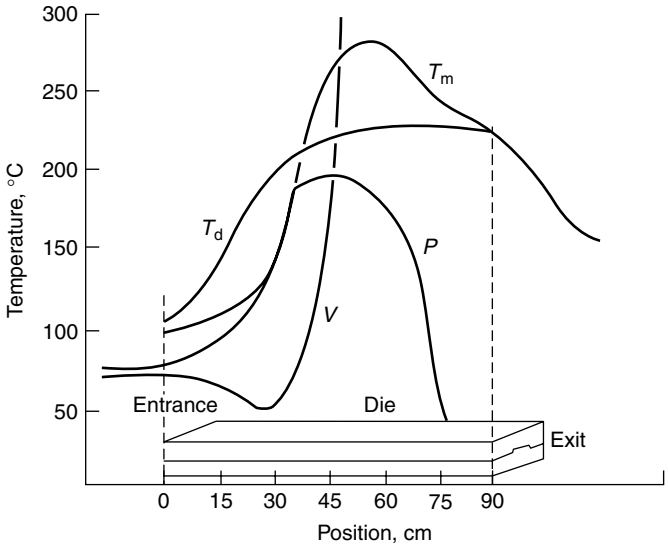

Fig. 9. Pressure, viscosity, and temperature. P, pressure; V, viscosity; T_d, die temperature; and T_m, material temperature.

the forming die just before gelation. The die, 75–120 cm long, is heated to prevent it from becoming a heat sink that would draw heat from the package. The cured product leaving the die proceeds downstream through the pullers, which gives rise to the term pultrusion. Unlike extrusion, in which the material is forced through a die with pressure, pultrusion pulls material through the die. As the stock leaves

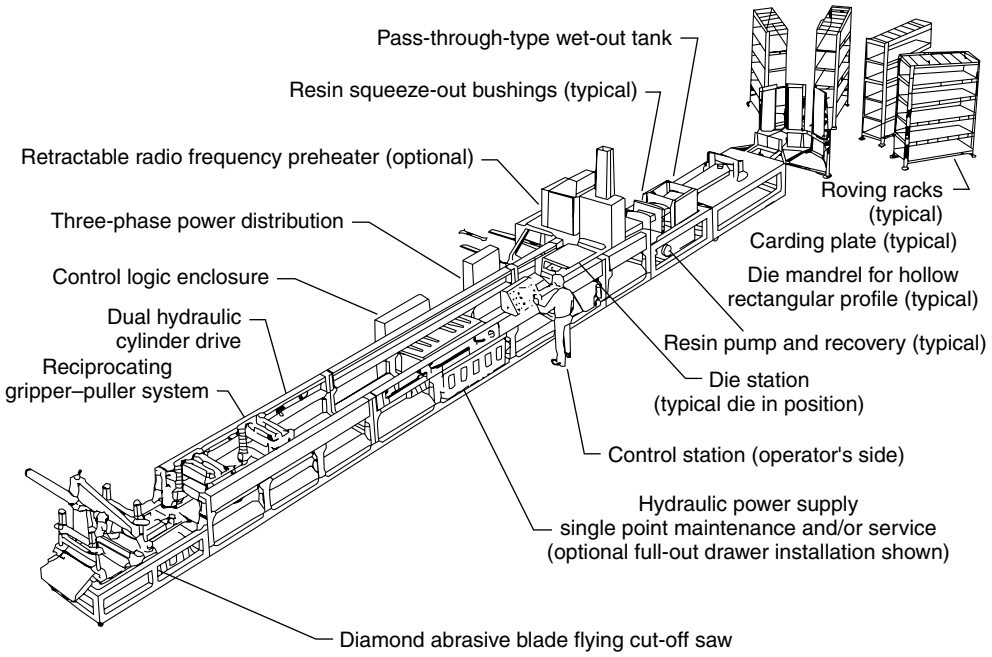

Fig. 10. Typical pultrusion machine.

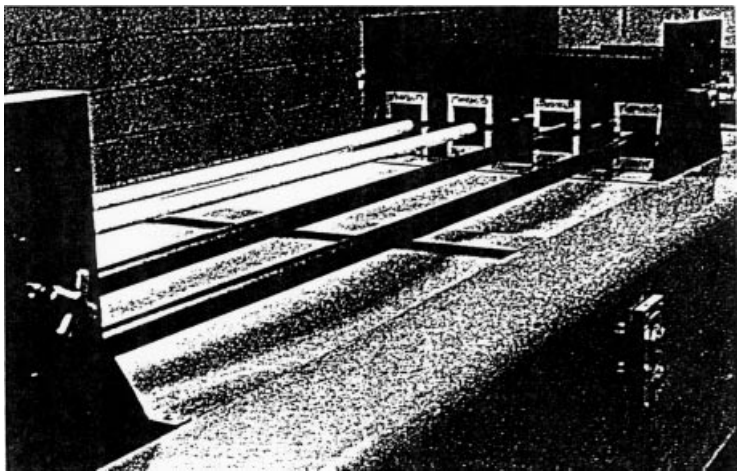

Fig. 11. Reciprocating clamp-puller system. Courtesy of Pultrusion Technology, Inc.

the pulling mechanism, a flying saw cuts it to length. Reciprocating clamp-puller systems with multistream capability, such as the equipment shown in Figure 11, are commonly employed.

Product center-line control is an often overlooked but necessary feature in pultrusion processing. This control can be conveniently provided by hydraulic jackscrews, which can change the height of the bottom platen (see Fig. 12).

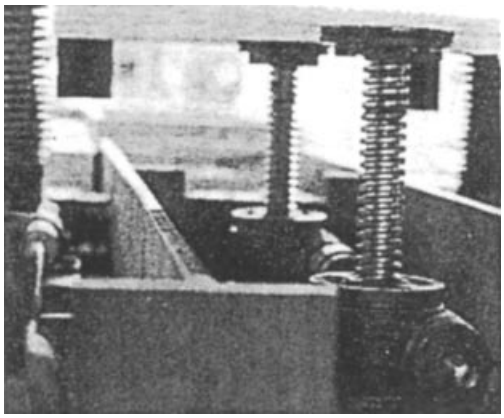

Fig. 12. Product center-line control. Courtesy of Pultrusion Technology, Inc.

Center-line control can also be obtained by shimming of tools on the bottom platen. Center-line height must be compatible with the height of the cutoff saw.

The trend in the United States to reduce air pollution has driven pultrusion manufacturers to reduce styrene emissions by enclosing the resin tank. This led to the development of the so-called injection die pultrusion, in which dry reinforcements are pulled into a heated die and resin is continuously injected through special ports directly into the closed die (14). An added benefit is that the dry preform retains its fiber orientation better than a wet package as it enters the die, and the die retains the fibers in position during resin injection. The result is reported to be a stronger part with more reliable and repeatable structural integrity.

Capacity. The capacity of pultrusion equipment is steadily increasing and the future market for pultruded product may be in profiles much larger than anything possible with traditional materials such as aluminum or rolled steel sizes. The Goldsworthy Pulmaster is designed to produce profiles up to 90 cm wide and 60 cm high.

The potential of automated composite fabrication is further illustrated by the pultrusion of residential building panels up to 2.6 m wide and 10–15 cm deep, with internal ribbing. A full-length panel can be tilted up on a building in any desired length, limited only by available means of transportation. Such large panels can be made because pultrusion is not a pressure operation, and size is limited only by the size of surrounding structure. Competitive processes, such as the steel rolling and aluminum extrusion, require very high pressures, and sizes are correspondingly limited.

Very large profiles are difficult to cut off. To reach the center of a 90 cm $\times$ 60 cm profile, a diamond saw, 19 m in diameter, is required. For the 90 cm $\times$ 45 cm capacity machine, two saws are used.

Fiber Orientation. Contrary to common belief, pultrusion is not limited to unidirectional reinforcements, but can bring reinforcing fibers into the profile in any needed orientation.

The development of inline winding wheels, which wrap roving around formed packages before they enter the die, and other material in-feed equipment enables

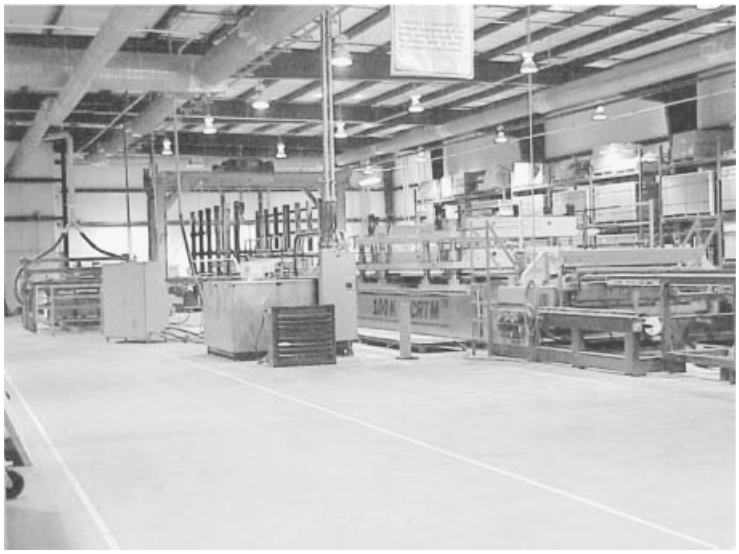

Fig. 13. Clean injection die pultrusion process and equipment is producing structural elements such as beams for bridge decks and one-piece 224-cm by 297-cm floor panels for semitruck cab and sleeper. Courtesy of Glasforms Inc.

pultrusion of fibrous reinforcements in virtually every axial orientation. Fiber forms from continuous strand mat to sophisticated stitched, multiaxial fabrics are being pultruded in both conventional and injection die processes. These systems have produced primary structure for load-bearing building panels, transmission towers, bridge decks, and even bridge beams (see Figs. 13, 14, 15).

Square tubing is made on the equipment shown in Figure 16, which includes longitudinal reinforcement of pure roving, three plies of random continuous fiber mat for omni-directional plies, and a circumferential overwind. Random mat is fed into a folding shoe that convolutely folds the mat around the mandrel, while longitudinal fiber is brought in from supply racks and the circumferential ply is applied by the rotating wheel.

Nearly any construction can be achieved. Tooling fabricated for round tubing with 6.25-mm wall starts with an inside ply of polyester wall mat, a ply of random glass fiber, and a ply of longitudinal fibers. Because of the thickness of the wall, this package is taken through an impregnating bushing; two additional plies of random glass mat are added, and the package wrapped with plies of pure circumferentials by a winding wheel. Another ply of random mat is added, following which a $+45^\circ$ ply and a -45° ply are added by large winding wheels. Another impregnating bushing wets out this last group of plies. The package then enters the r-f system, where the energy is introduced. More plies can be added. The product proceeds through the pullers in the usual manner.

Production Rate. Throughput speed depends largely on the resin system. A vinyl ester system at 1.2–1.5 m/min is used for the round tubing. Polyester and vinyl ester systems have been developed that permit a production rate of ca 4.5 m/min with pure unidirectional reinforcement. However, when an off-axis

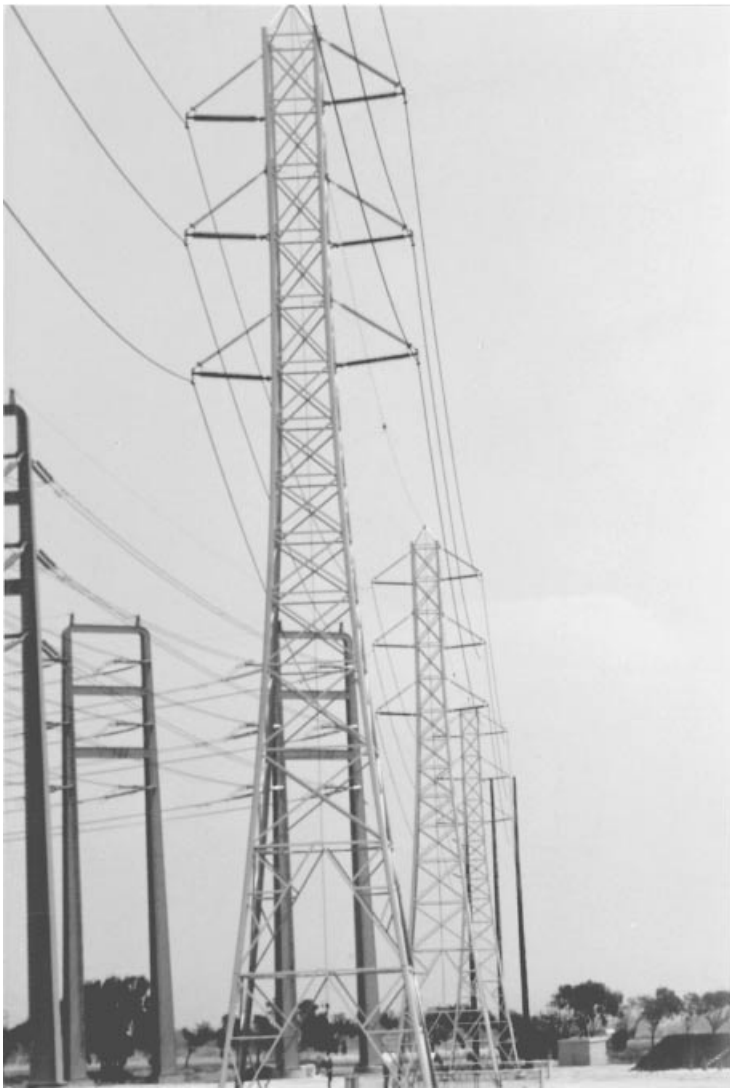

Fig. 14. Composite transmission towers energized at Southern Calif. Edison power generation station; the entire tower was constructed from pultruded structural elements. Courtesy of Goldsworthy & Assoc.

reinforcement such as mat is added, viscous shear forces increase exponentially with velocity, and at speeds of 2–3 m/min the reinforcements tear.

Radio-frequency heat is recommended only for glass-reinforced stock. For graphite or conductive fiber reinforcement, inductive heating is applied. The mass can be instantly heated through by one of these techniques.

Curved Configuration. Since there is no way to bend pultrusions after curing, curved pultrusion must be made in the desired configuration. The roving is drawn off supply racks in the usual manner, impregnated, passed through an r-f

Fig. 15. Pultruded transmission tower elements are joined by patented fastenerless interlocking system. Courtesy of Goldsworthy & Assoc.

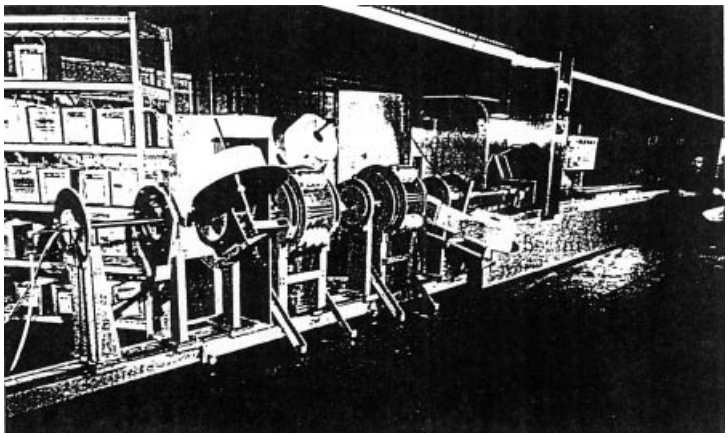

Fig. 16. Pultrusion machine tooled for square tubing. Courtesy of Goldsworthy Engineering Inc.

generator, and brought between a fixed and a rotating die. The preheated stock is pulled through the system by a curved die located on the face of a rotating curved quadrant, pulling the part continuously through the orifice formed by the fixed and rotating dies (15). Goldsworthy Engineering developed this curved pultrusion process and built prototype equipment for NASA for making graphite hat-section stiffener rings for the space shuttle.

Filament Winding. Filament winding allows control of fiber volume and orientation, utilizing continuous filaments, thereby maximizing laminate strength. The reinforcement, its alignment, and the resin matrix are determined during the design, according to process requirements. The winding process

parameters can be calculated from the product geometry and the wind angle for each layer. The angle of rotation required through certain portions of the mandrel is calculated, and circuit pattern, band width, and the number of circuits needed are determined. This is an iterative process; several variables are interdependent. After test winds, winding parameters are often changed; this process is repeated to give full optimization.

Nongeodesic winding, though more complex, utilizes the same theory. A friction factor is introduced into the fiber-path motion function, allowing the winding to be located out of its geodesic pattern; the matrix resists side slip. Tension and resin viscosity greatly influence the degree and speed of winding such patterns without resorting to mechanical resistance to side slippage.

Traditionally, the pattern was based on the fiber tension; winding proceeded along geodesic paths irrespective of structure. Innovative filament-placement techniques, however, deviate widely from the geodesic path, and may lead to winding of very complex structures.

This innovative technique was made possible by two developments: computer control and the winding on nonuniform mandrel surfaces. For instance, it would be possible in one operation to wind an aircraft fuselage with interruptions to the pure geodesic path such as doublers around doors and transparencies.

Filament winding was originally used to fabricate tanks and pipes; early equipment consisted of little more than converted lathes, with a reciprocating feed eye winding a helical pattern onto a rotating mandrel. This created the impression that helical winding of pipes and tanks is necessary, when in fact, other winding patterns are equally effective.

Winding can be accomplished on a horizontal (Figs. 17 and 18) or vertical (Fig. 19) tooling face. Employment of mechanical or computer-controlled filament-winding machines depends on equipment cost, part geometry, and usage, ie, dedicated to a single task or adaptable for a broad range. Capital equipment costs are significantly lower for mechanical machines, which, however, require time-consuming calculations and hardware changes.

If large quantities of simple parts are to be produced, a mechanical winding machine offers advantages. Programming consists of coordinating the motion

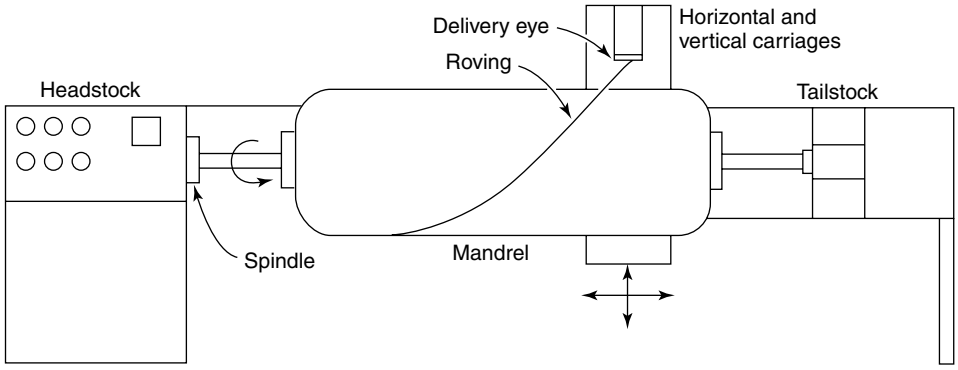

Fig. 17. Horizontal filament winding machine. Courtesy of Engineering Technology, Inc.

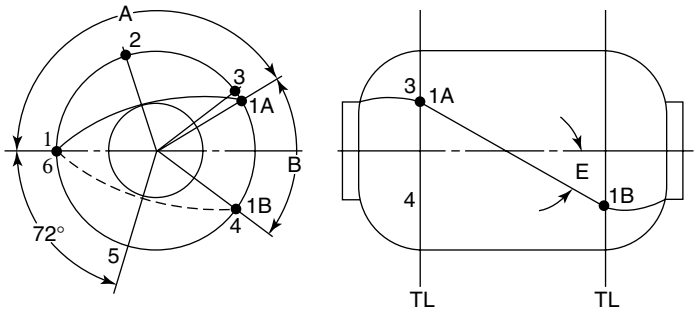

Fig. 18. Helical winding pattern. Courtesy of Engineering Technology, Inc.

between spindle and carriage by selecting a drive-gear ratio and determining the carriage drive sprocket and chain length.

Computerized programmable equipment is usually more cost effective where a variety of parts are to be produced or where part configuration is complex, such as a wind turbine blade. Sophisticated software for filament winding such as FGX Windows developed by Entec Composite Machines (Salt Lake City, Utah) allows the manufacturer to create patterns to wrap a pressure vessel, as an example, before winding begins. Filling in a simple menu defines the part geometry, and the computer uses this database to calculate a fiber path for the part and establish the

(1) wind angle throughout the path,
(2) friction values, which indicate if the fiber might slip anywhere on the part,
(3) thickness buildup on the part, and
(4) data to help with the analysis of the composite part.

It can also set band advance parameters. Small changes in the fiber path often drastically modify the way the fiber is distributed over the mandrel surface and a band advance module makes it easier to control these changes. By changing the band advance parameters in the computer, the operator can see what the result will be before winding begins. Winding simulations show how the final winding pattern will look on the part.

Equipment. A typical early filament-winding machine with rudimentary computer controls is the lathe-type winder illustrated in Figure 20, utilizing rotating mandrel and traversing carriage.

Another type is known as the orbital, or racetrack winder, where the winding heads move completely around the mandrel, as shown in Figure 21. It is used primarily for rocket motor cases and where polar winding is desired; high speed is attainable.

In the tumble-type winder (Fig. 22), the mandrel is tumbled end over end during a polar wind, whereas the feed eye is traversed and the mandrel rotated in the normal lathe-type fashion for helical or circumferential winds. This type is widely used for high volume commercial products such as water-softener tanks and pool filter tanks.

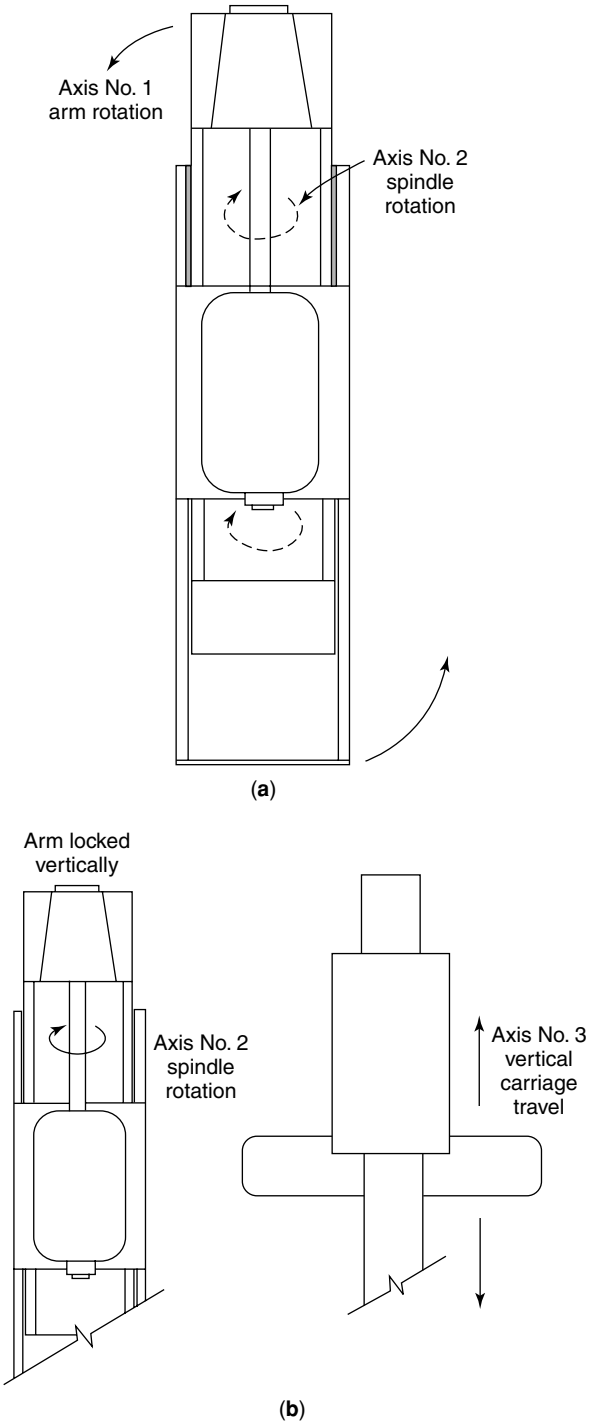

Fig. 19. Winding on a vertical mandrel; (a) longitudinal; (b) circumferential. Courtesy of Engineering Technology, Inc.

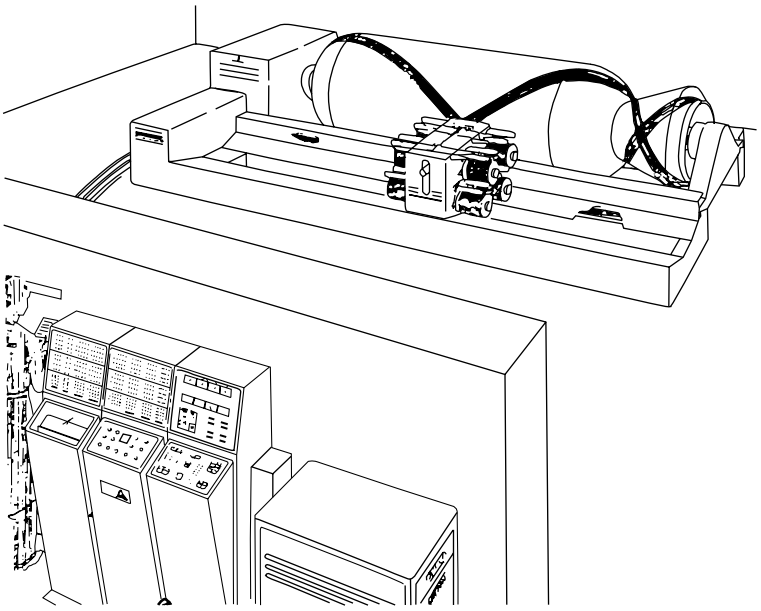

Fig. 20. Typical lathe-type filament-winding machine.

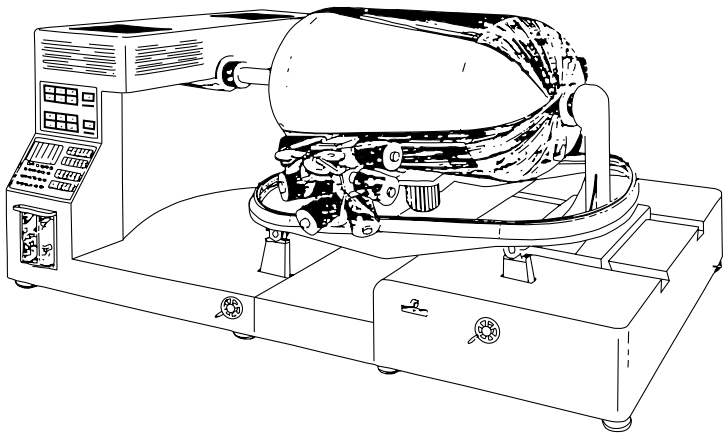

Fig. 21. Typical racetrack-type filament-winding machine.

Whirling-arm filament winding is illustrated in Figures 23 and 24. Polar wind is accomplished by means of the C-shaped arm, which supplies filaments from feed eyes at both extremities. While whirling on its horizontal axis, the arm winds on the polar axis of the mandrel, which is circumferentially indexed at appropriate intervals. During polar wind, the horizontal winding arm is retracted;

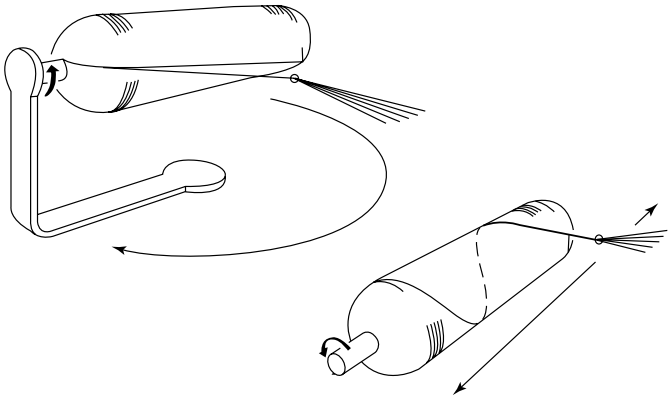

Fig. 22. Tumble-type winder.

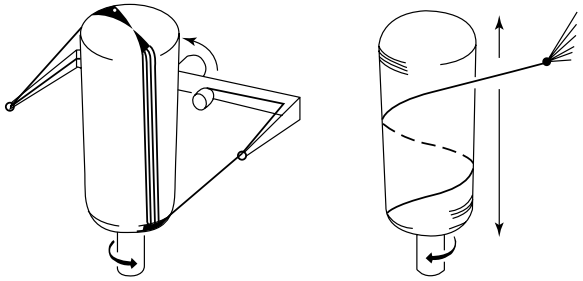

Fig. 23. Whirling-arm-type winder.

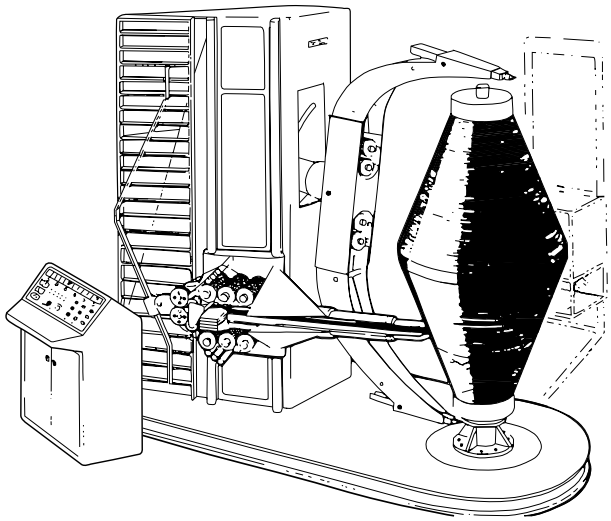

Fig. 24. Typical whirling-arm-type filament-winding machine.

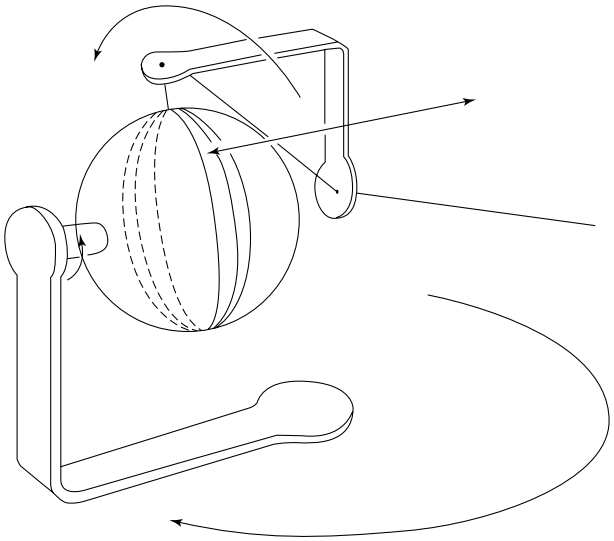

Fig. 25. Spherical winder.

when the polar wind is completed, the horizontal arm extends and reciprocates vertically to effect helical or circumferential winds while the mandrel rotates.

Although filament winding is most commonly employed on curved surfaces of rotation, it is also possible to wind on flat-sided surfaces. A flat-sided whirling-arm winding machine was built in the early 1960s for winding high strength instrument cases (16). All six faces of the tool had to be wound, and rather than using normal support mandrels, the tool was flipped into position by means of hydraulically operated tables.

Spherical winding is most difficult (Fig. 25). Before the advent of the computer, most machines were digitally controlled.

Contact-type balls, such as basketballs, volleyballs, and soccer balls, are filament wound. Although a totally random wind must be effected, it must be controlled; because it is necessary to wind all over the ball, there is no way of holding onto it or driving it. The required controlled random pattern can be obtained by suspending the rubber bladder on an air column and changing product rotational speed and thereby direction of wind by air jetting the column.

In a ring winder (Fig. 26), the winding head rotates around and traverses a passive mandrel. This type originated for the filament winding of massive structures, for example, a 45-m windmill blade. It is clearly a formidable task to support and rotate such a structure. The ring-winder design allows the mandrel to remain passive while the rotating ring-feed-eye assembly reciprocates along its length, laying a helical pattern. Steady rests stationed along the length of the part are hydraulically lowered by the carriage and raised behind it.

Tape Laying. Tape-laying equipment utilizes an automated tape-laying head to place the tape contiguously on a pattern table or mold in such a way

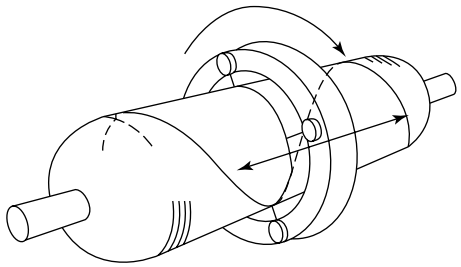

Fig. 26. Ring-type winder.

that each tape lies within a specified distance of any previous tape course with no overlap. Precise sequential-layer orientation (cross-plying) is mandatory for strength; taper can be achieved by step-back buildup (17). The raw materials used at present are graphite, aramid fiber, or glass reinforcements in the form of unidirectional or woven tape. Widths range from 2.5 to 30 cm. The tape is usually impregnated with an epoxy-based resin system.

Early automated tape laying imitated manual operations to lay 7.5-cm unidirectional tape on a flat table. All manufacturers at first produced 7.5-cm tape, and tape-laying machines were built accordingly. Tape sizes were then extended to 15 and 30 cm, then back to 2.5 cm. Today most machines have two heads: one for 2.5-cm, and another for 15-cm tape.

This progress resulted from the fact that if tape of any width is laid over a compound curvature, one edge of the tape travels farther than the other. Hand lay-up in the manufacture of aircraft structures established the tradition of using unidirectional tape for flat patterns, which in most cases were draped in the tooling to form simple curved parts. As the need to produce parts with compound curvature became apparent, manual methods were adapted to machinery, although they usually incorporate guided adjustments that the machine does not imitate, leaving ripples at the long edge.

A typical early tape-laying head is illustrated in Figure 27. As this device was built without computer control, optical devices were utilized to sense the edge of the tool, accelerate machine motion, set shear to the right angle, and trim the tape (17). At that time, the head was usually built separately and then attached to an existing machine. For example, a head built by Goldsworthy Engineering was used by Lockheed with a profiler as the host machine; the lay-up is trimmed after the machine is in place.

The first machine to use 30-cm tape fabricated weapon bay doors for the B1 bomber. A government contract limited the expenditure by the prime contractor (Rockwell), but without any sacrifice in accuracy. Requirements were met by a manually operated machine with automatic width indexing, with other motions initiated by the operator.

Computer Control. The Army's desire to test an all-purpose, multiaxis tape placement machine led to the next step forward, an automatic machine built in 1974 for helicopter rotor blades for the Army Aviation Systems Command (AVSCOM) (19). This was the first 6-axis minicomputer-controlled tape-laying

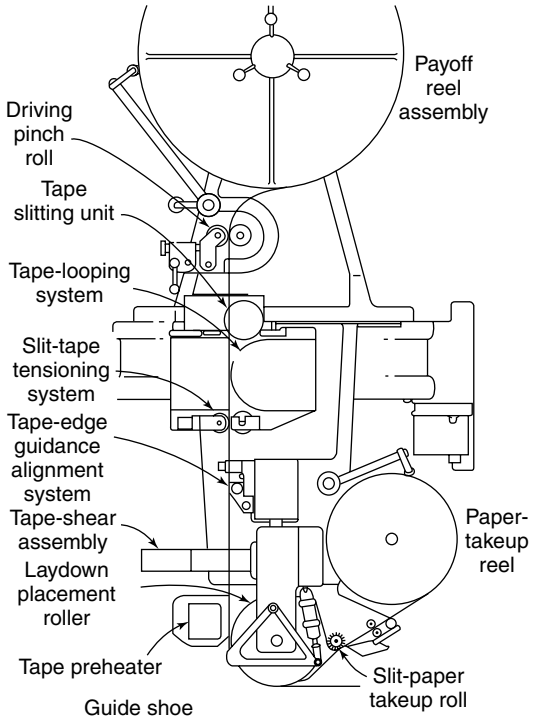

Fig. 27. Typical early tape-placement head.

machine. The entire gantry, including the *Y*-axis structure, was built from composites. At first, army personnel strenuously objected because of the established use of iron machine tools. However, an essential element of tape-laying machines is rapid *X*-axis travel, and it was vital to control the structure at the desired speeds. The composite gantry provided this capability.

The machine was actually an 8-axis machine, with two steady rests to support the blade tooling. Extreme compound curvatures existed in the transition area between the air-foil section of the blade and the hub section. For conformity with these extreme compound curvatures, the tape head had the capability of splitting the 7.5-cm tape into 24 individually tensioned 0.31-cm tapes.

In the first composite blade to be laid up, the spar was built up on the machine, honeycomb put in place to form the section of the blade aft of the spar, and the skin wound over it. In effect, this structure became a mandrel in place.

This machine was an excellent tool for developing the techniques of spar making, skin lay-ups, and attachment of helicopter rotor blades; it pointed the way to specialty production machinery (see Figs. 28 and 29).

Production Design. These machines were adequate in the airframe industry for prototypes and testing, but large structural components require production tape-laying machines. These presented certain problems, of which the most pressing was that the tape, lacking integrity, must be guided by the backing paper. If

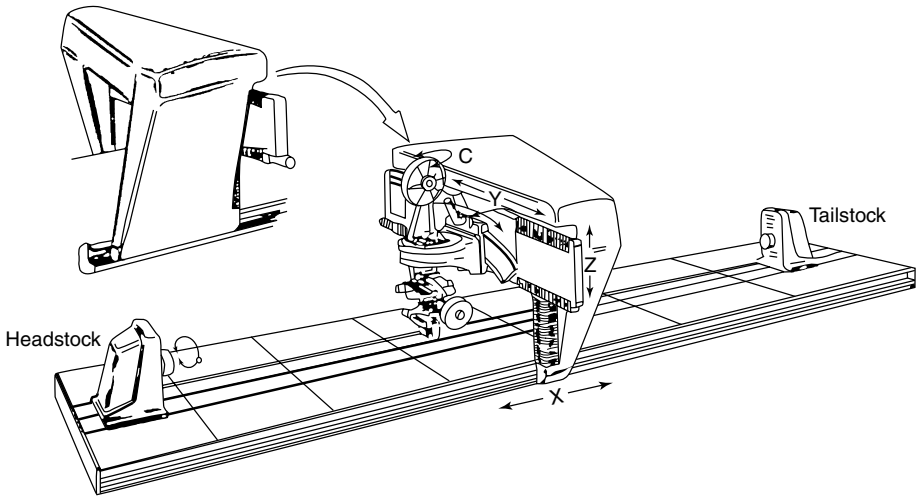

Fig. 28. Original 8-axis automated tape lay-up system (ATLAS). Courtesy of Goldsworthy Engineering, Inc.

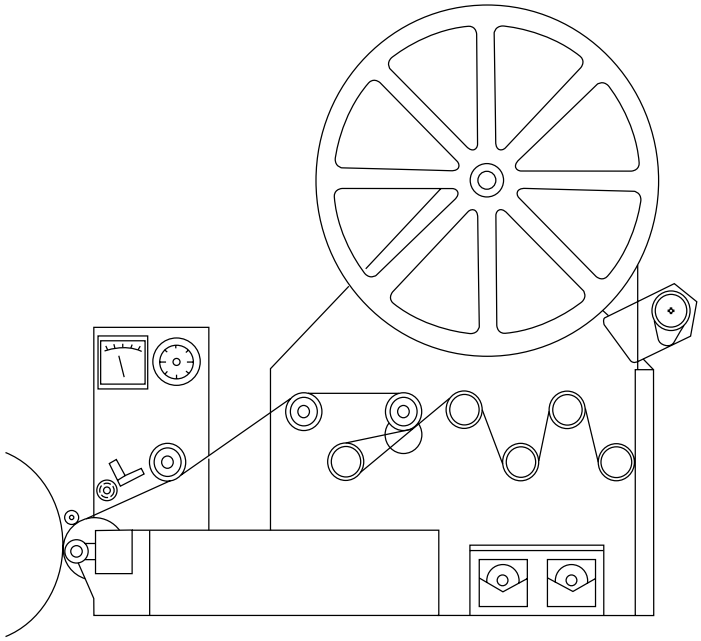

Fig. 29. Tape-wrapping head. Courtesy of Cincinnati Milacron, Inc.

tape and paper are separated, tape control is therefore lost. It follows that a device is required that will shear the tape to the proper trim angles without shearing the backing paper. A number of devices were developed to perform this difficult task; their success rate has been about 93%. Unfortunately, a 7% failure rate is

disastrous since even one uncut filament destroys the integrity of the entire system by pulling it up when the head lifts; the damage must be repaired manually before resuming production. In other words, even a low failure rate destroys the automated functioning of the machine.

High angle cuts present a similar problem. The long tapering tail on one side of the cut needs to be pressed down, and the other side picked up.

To overcome these and other difficulties, Goldsworthy Engineering developed a two-phase system (Fig. 30): tape preparation is accomplished in phase I, and lay-up in phase II.

In the preparation phase designated ACCESS (Advanced Composite Cassette Edit–Shear System), the supply spool is interfaced with CAD system software specific to the part to be produced. The material from the supply spool is measured, cut lengthwise, angled on both ends, and transferred to new backing paper in order to be spaced to compensate for long tails. Defective material is removed. Voids, cut failure, and high angle problems during lay-down are thus eliminated. The cut tape on its new backing paper is rewound on a new supply spool, and the "composite cassette" installed on the tape-laying machine for the second lay-up phase of the system. The second phase is termed ATLAS II (Automated Tape Lay-up System, second version).

This ACCESS/ATLAS II system offers several important advantages: 100% shear dependability, properly spaced tails, preinspected and edited tape, and elimination of all waste motion from the tape-laying machine. The result is higher production rates.

However, the most important feature of the ACCESS/ATLAS II is that it is the only tape lay-up machine that will lay compound contours. The reason it can do this is that the ACCESS system cuts the tape lengthwise into narrow strips. As the ATLAS machine dispenses the cut tape from the cassette along the contour of the tool, both edges of the tape travel the exact same distance. This contrasts sharply with standard tape-laying where typically 3-in. to 12-in. wide patterns are laid down; as the tape follows the contour of the tool, the tape edges must travel unequal distances, creating folds and wrinkles in the tape.

The only other alternative for automated lay-up of compound curvatures is fiber placement, which lays individual tows on the part.

Fiber Placement. Fiber placement machines can separately dispense, cut, and restart each tow during placement on the mandrel.

Cincinnati Machine (Cincinnati, Ohio), Automated Dynamics (Schenectadm, New York), Ingersoll Milling Machine (Rockford, Illinois), and other machine manufacturers are building multiaxis fiber-placement systems for building complicated parts and primary structures in a wide range of sizes. Computer numerical controls (CNC) on Cincinnati's Viper Fiber Placement System steer thermoset prepreg tow and slit tape over curves and into hollows to make a variety of complicated shapes for such things as engine inlet ducts, cowlings, side-skin panels, small fuselage sections, and spars for rotor blades and rotor grips on helicopters (see Figs. 31 and 32).

Pulforming. The curved-pultrusion process developed for the NASA shuttle stiffener rings led to so-called pulforming. In this process, as in pultrusion, primary reinforcing fibers are drawn through a tank for resin impregnation and then through a die. Pulforming may be curved or straight with machines that

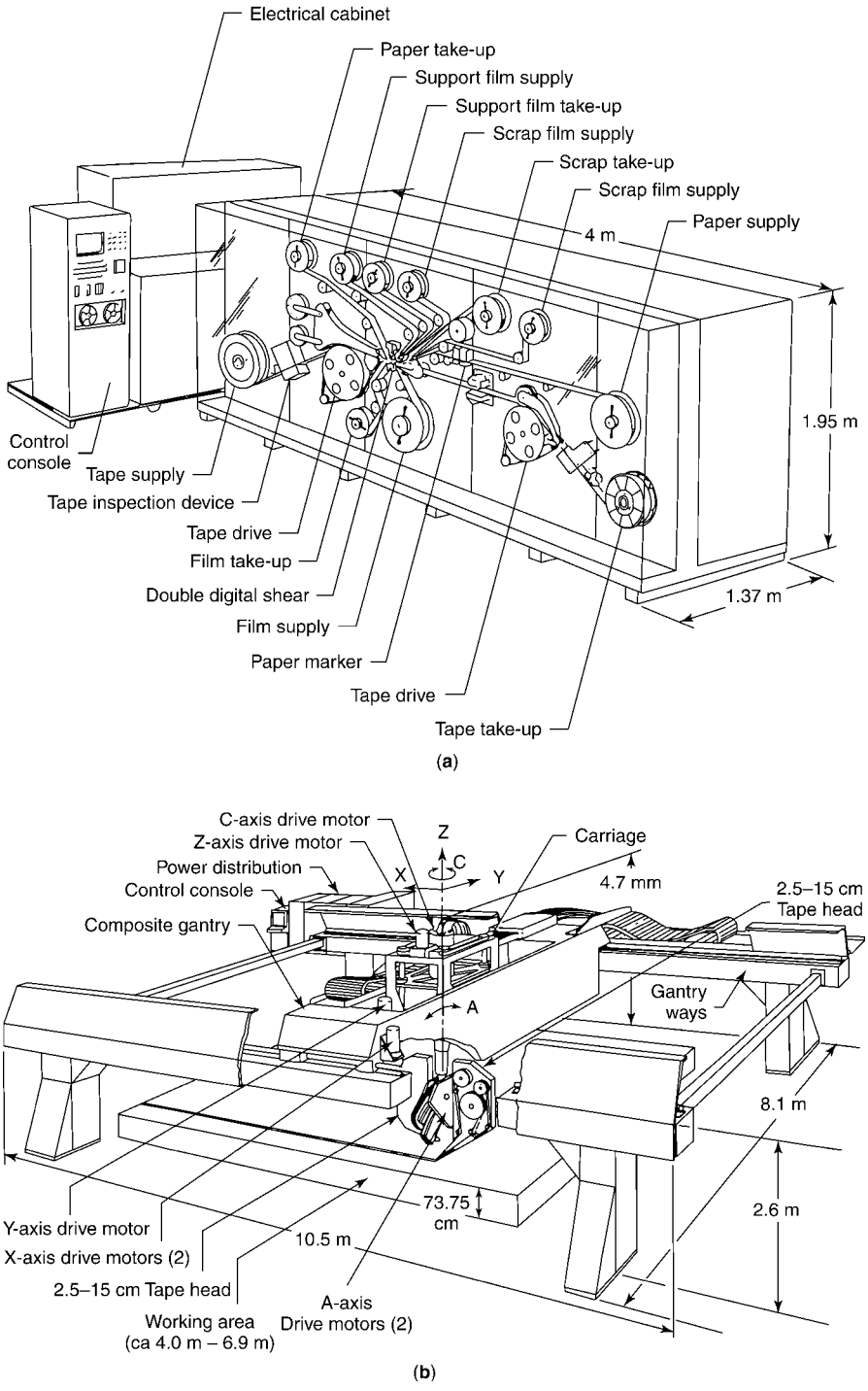

Fig. 30. Two-phase tape-laying system. (a) Phase I: tape preparation machine, ACCESS (Advanced Composite Cassette Edit–Shear System); (b) Phase II: tape-laying machine, ATLAS II (Automated Tape Lay-up System, second version). Travel: X, 7.28 m; Y, 4.08 m; Z, 4.8 m; C, $\pm 200^\circ$; and A, $\pm 30^\circ$. Courtesy of Goldsworthy Engineering, Inc.

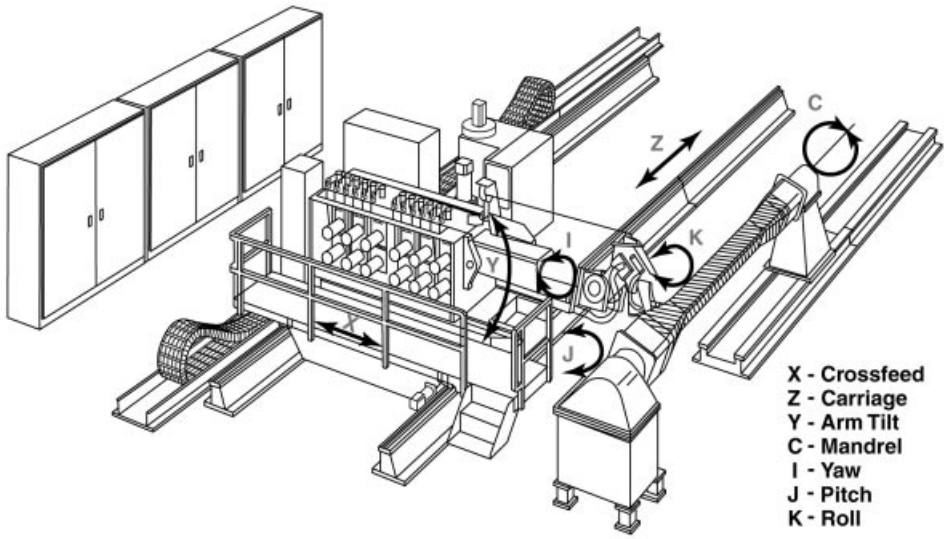

Fig. 31. Seven axes of motion on fiber-placement system can steer prepreg tow or slit tape around compound-curvature shapes to make highly contoured parts. Courtesy of Cincinnati Machine.

Fig. 32. CNC Viper fiber-placement system lays individual tows on a mandrel, shown here making a helicopter rotor blade spar at Bell Helicopter Textron (Fort Worth, Tex.). Courtesy of Cincinnati Machine and Bell Helicopter.

produce profiles of changing volume and changing shape or constant volume and changing shape.

Changing Volume and Shape. An example is the composite hammer handle made continuously on straight pulforming equipment (20). Volume is changed

as follows: a BMC in the form of extruded rope on a supply spool is fed through a monitoring device that measures length to provide the desired volume. The length is cut and crimped around a single traveling roving strand at uniform intervals. The result resembles a string of beads proceeding downstream. A blivet press traveling at line speed forms the BMC pieces into the shape of the changing volume. Further downstream, all primary reinforcing fibers come together to encapsulate the center fiber with the formed BMC. Film is convolutely folded and ultrasonically welded around the package, creating a roll, which passes through a shrink tunnel; this tightens the film to produce a very controlled package.

The package next enters a split female die, which travels at line speed downstream and is closed with a C-press, which injects the die into a belt-clamping system that butts a whole stream of the dies together. The dies are heated as they traverse the clamping area; when they reach the end, the dies open, releasing cured stock, and return to the upstream C-press end of the die section. Operation is thus effected continuously. The part is cut to length with a flying saw.

Constant Volume and Changing Shape. The automatic machine pictured in Figure 33 was developed to make automotive leaf springs (21,22). Reinforcing materials from supply racks pass through an impregnating tank, are heated in an r-f generator, and enter the die cavity, which is at the convergence of a

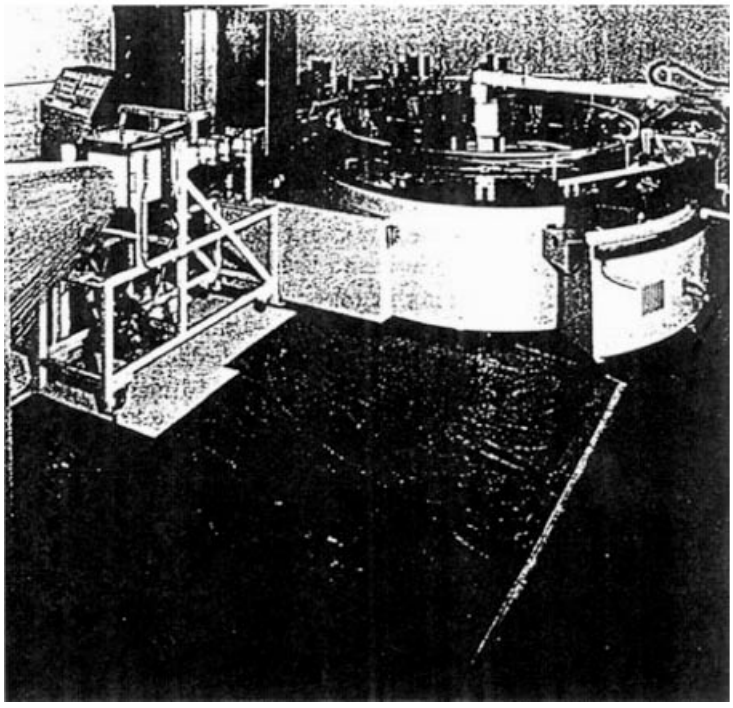

Fig. 33. Pulformer curved pultrusion machine; constant volume–changing shape. Courtesy of Goldsworthy Engineering, Inc.

stainless-steel belt and the rotating die. The die cavity is in the shape of the spring to be produced. The stainless-steel belt is clamped to the die face and runs continuously with it, thereby closing the fourth side of the die. Curing of the part is finished along that belt; it is then peeled out of the die cavity and guided into the path of the flying saw. At present, such machines are controlled by standard switch and relay logic; future machines will utilize programmable controllers. Production rate, depending on specific configuration, is approximately two springs per minute. Springs produced by pulforming are much cheaper than steel springs.

Specialty Machines. Machinery can usually be designed to accommodate any reinforcing fiber and resin system on the market today. Since the goal is the lowest possible cost, the industry usually employs roving or tow as the cheapest raw material, and thermoset polyesters and vinyl ester resins, rather than epoxies, for the highest running rates.

Most of the machines described here are flexible as to fibrous form; however, very high modulus fibers, such as carbon graphite, can create problems. If designers know that high modulus fibers are to be used on prospective equipment, they can plan accordingly.

The specialty machinery described below was designed for a variety of applications and demonstrates the flexibility of automated composite production equipment.

Plywood. Composite-faced plywood equipment for the truck and container industry continuously applies a bidirectional glass facing to both sides of standard plywood (3 m × 1.2 m), producing an endless laminate-faced plywood panel 3 m wide. An automatic saw cuts it to the desired length, the standard being 12 m × 3 m (23–25).

The plywood is stacked at the entrance of the machine, where it is automatically elevated, separated, and butted at the edges, then driven into the system. Cross-ply glass is applied with a large winding wheel, holding about 80 doffs of roving, which rotates around the plywood as it proceeds at a controlled rate. Longitudinal rovings are added by feeding roving through carding racks above and below the product stream just ahead of an opposed belt laminator. Resin is poured onto the upper and lower surfaces of the product just upstream of the longitudinal roving contact point, wetting cross and longitudinal fiber as it enters the opposed belt laminator. The package proceeds through the laminator and is cured, trimmed, and cut to length.

Sporting Goods. A continuous-taper tube-winding machine is used to manufacture graphite–epoxy golf clubs (26). Stock is filament wound using ten stacked winding wheels; speed is individually controlled in such a way that angle of wind and tape can be varied for production of flexible or stiff shafts. Steel mandrels are centerless ground to the taper requirement; the small end of one mandrel is indexed into the large end of the other, and the mandrels can pass continuously through the machine.

Insulation. A reinforced foam machine designed for McDonnell Douglas may be the most complex automated composite fabrication equipment ever built (27). Its purpose was to produce a 70 cm × 22.5 cm three-dimensionally reinforced, urethane foam log continuously, to be used for insulating tankers transporting liquefied natural gas. This equipment probably holds a record number of ends of reinforcing material handled on a single machine. A supply rack feeds 3500 ends

of glass fibers into the system for X and Y reinforcement; additional creels in the center section supply 1500 ends of *Z*-direction fiber.

Military Equipment. Filament-winding machines are used to wind wet filament on 155-mm artillery projectiles, five shells at a time on a 3-min cycle. The steel casings are automatically loaded horizontally onto a continuous chain- and spud-conveyor system. The casings are oriented vertically under a row of winding heads, which move into position for winding and then withdraw. At the next station the filament is severed, while the conveyor brings a new bank of shells into position. The wound shells are cured in an r-f oven and removed at the end of the machine.

During the Vietnam war, a machine was designed to transport water, gas, and jet fuels to the front. Rolled steel or aluminum tanks were bulky, awkward, and required seam welding, a skilled operation. A pultrusion machine was installed in a standard 12-m highway trailer, and a composite tank constructed on-site (28).

After the foundation was poured, a continuously pultruded tongue-and-groove profile resembling hardwood flooring was produced in the length required for the tank wall (ca 1560 m). An unusual feature was that two streams of two-sided, bondable Tedlar were fed in with glass roving reinforcements, to create an impermeable barrier. The profile was fed into an erection machine that wound and zippered it continuously together while injecting epoxy bonding. With unskilled labor, the prototype tank (6 m in diameter and 3 m high) was erected in about 4.5h and then grouted into the foundation.

Under the auspices of the Air Force Materials Laboratory, Air Force Wright Aeronautical Laboratories (AFWAL), several primary airframe manufacturers such as Grumman Dynamics have spent several years in research and development of automated integrated composite laminating centers, commonly termed "factory of the future."

Grumman's integrated laminating center (ILC), for example, fills the need for more fully automated fabrication of gently contoured composite structures from unidirectional tape (29). Elimination of manual operation significantly cuts costs of airframe components such as the 56-ply covers of the F-14A horizontal stabilizer (utilizing 7.5-cm wide boron–epoxy tape), and hybrid boron graphite–epoxy B-1 stabilizers. In the late 1970s, Grumman teamed with AFWAL to develop mechanized equipment for fabricating severely contoured, integrally stiffened, complex structures for high performance aircraft. For the Automated Integrated Manufacturing System (AIMS) (Fig. 34), three modules were integrated with the ILC, ie, a contour ply handler, broad-goods prepreg dispenser, and trans-laminar stitcher. Computerized air-passage contour database; computerized detail design of flat ply patterns, templates, and curing tools; and computer-generated nesting pattern for automatic laser trimming are included.

Automotive Applications. Another example of low cost production is provided by a machine continuously manufacturing automotive drive shafts. A hybrid drive shaft is produced with glass fiber in the $\pm 45^{\circ}$ directions to take torsional loads and graphite as longitudinal fiber for stiffness. An endless stream of mandrels is fed through the machine; steel end fittings are inserted and later welded to universal joint spiders. Winding wheels apply glass fiber, and longitudinal graphite fibers are fed in at the next station. Circumferential fibers are added last. The mass is cured by induction heating.

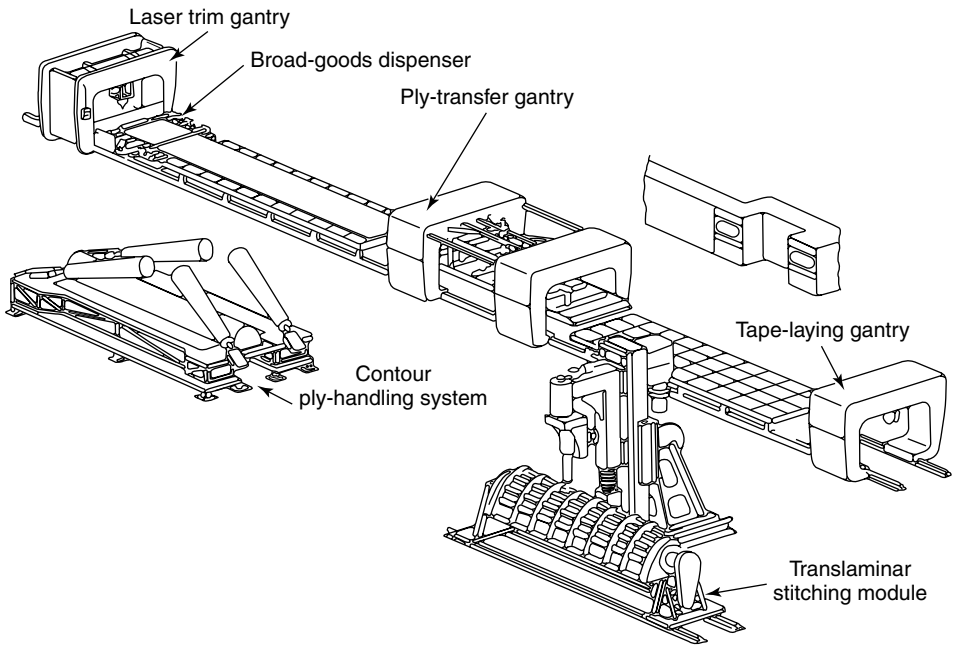

Fig. 34. Factory of the future: Grumman's Automated Integrated Manufacturing System (AIMS). Courtesy of Grumman Aerospace Corp.

Other automotive applications include pulformed leaf springs, bumpers, door frames, and others.

Aircraft. A "pin winder" built for Bell Helicopter for making blade spars is shown in Figure 35. Carrying impregnated S-glass, the carriage moves along the tooling bed, rotating 180° at each end. The beam is computer-controlled for vertical *Z*-axis motion; the feed eye moves in a plane but any path is possible.

Interest has recently grown in the fabrication of structural aircraft components from composites, but it must be understood that neither economic nor performance benefits are realized by designing a metal airplane and building it from composites.

A 2.4-m full-scale test section of a geodesic aircraft fuselage is shown in Figure 36. The entire fuselage section is filament wound. Although during World War II thousands of Wellington bombers were built with geodesic structures, they are troublesome with metal. However, a geodesic pattern is probably the simplest design for composite aircraft structures. By a straightforward procedure, the structure is wound first, and then the skin. The test section shown in Figure 36 was for a pressurized airplane, and therefore required bulkheads at both ends; these usually create severe stress problems. Problems also arise in the filament winding of end sections. They were solved by winding across the pressure bulkhead and keeping it in tension with the structure being stiffened. The wound skin was cured in a female die to form aerodynamic surfaces. A peel ply was wound with the skin in the geodesic pattern, leaving a clean surface after stripping. Both

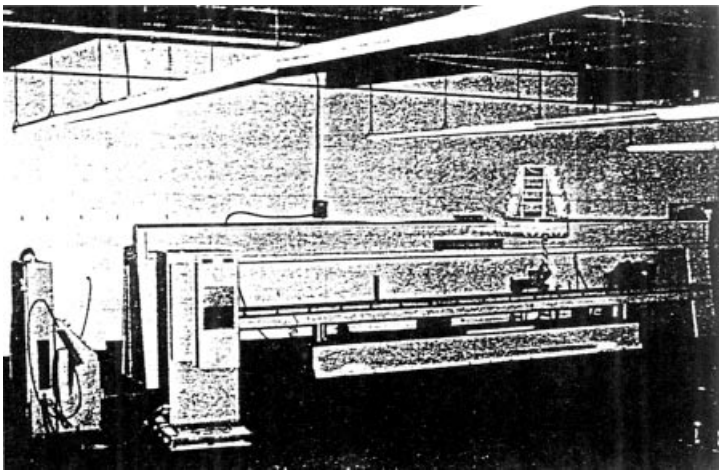

Fig. 35. Helicopter spar "pin winder." Courtesy of Goldsworthy Engineering, Inc.

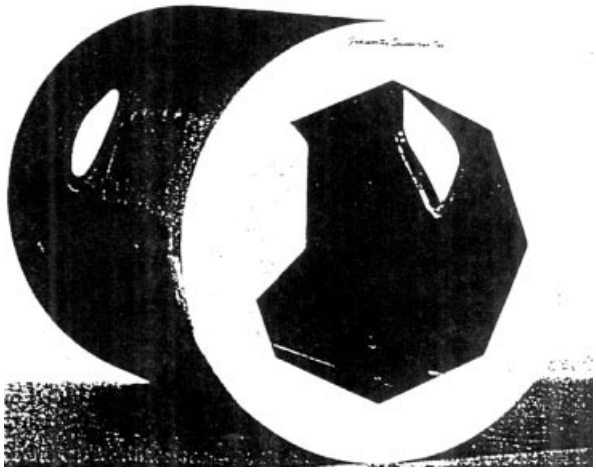

Fig. 36. Geodesic aircraft fuselage. Courtesy of Goldsworthy Engineering, Inc.

diamond and round windows were wound into the test section, the former because they were compatible with the geodesic structure.

Composites in Orbit. A ribbon-forming machine was developed for the NASA SSPS (satellite solar power system) program (Fig. 37). The $0 + 45 - 45 - 0$ graphite–thermoplastic matrix ribbon formed would be installed in a cassette in a machine in the cargo bay of the space shuttle. In orbit, the machine would process the ribbon into a triangular truss beam (see Fig. 38). The graphite-reinforced, polysulfone matrix ribbon is formed and welded into the triangular closed beam. The intercostals are continuously wound or welded on the beam to form a truss. Prototype equipment was built in the Goldsworthy Engineering laboratory, and a triangular truss beam is on display at NASA Huntsville, Alabama.

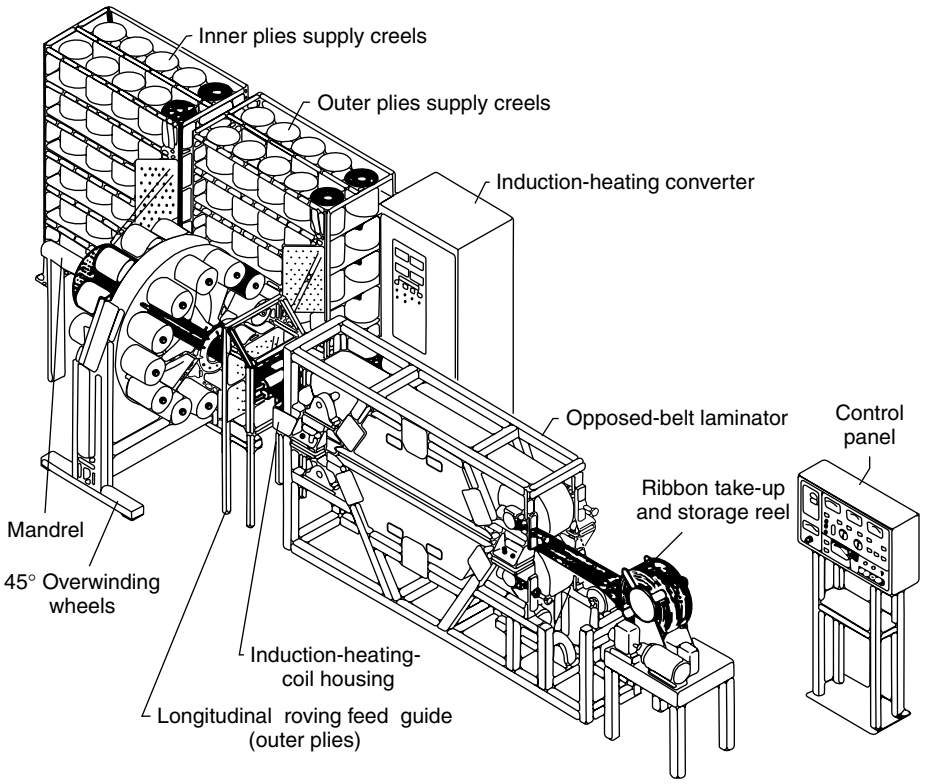

Fig. 37. Earthbound ribbon-forming beam machine; thermoplastic matrix-graphite fiber $(0 + 45 - 45 - 0)$.

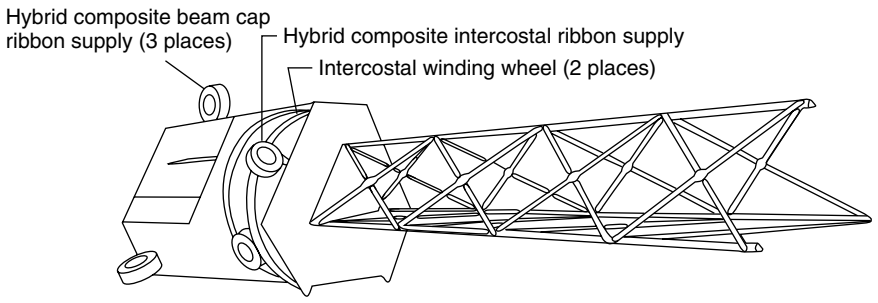

Fig. 38. Beam machine: continuously wound and welded intercostal version.

Thermoplastics. Thermoplastic matrix composites represent a new and intensively researched area. They offer promise in significantly improved properties and faster processing, as well as reduced cost in most cases.

Thermoplastic matrices, by definition, require no cure cycle. They are heated until they flow or permanently deform, pushed into their new shape, and cooled. Elimination of cure cycles reduces processing cycle times.

Compression molding and filament winding are already commercially viable and production processes and equipment are in service, manufacturing a variety of parts such as automotive bumper beams and sports equipment, notably basketball backboards, and snowboards.

Continuous processes such as pultrusion still represent a challenge to processors because the very high melt viscosities of thermoplastic matrices, compared to the low thermoset viscosities, limit the throughput rate severely as high hydraulic shear forces are generated in the dies and forming tools. These forces can damage the reinforcement and generate high pull loads unless line speeds are kept to a few centimeters per minute.

However, fluidized bed powder matrix application and derivative processes may solve these problems. Ideally, processors would like to see a material with the properties of polyetheretherketones (peek), poly(acrylene sulfides) (qv), polysulfones, and similar engineering thermoplastics with melt viscosities below 1 Pa·s (=cP).

Other processes like tape laying also show great promise in the application of thermoplastic matrices. Present tape-laying operations, even when machine performed, require several "debulk" cycles plus the normal multihour cure cycle. Capability for heating under pressure and debulking may make it possible to have a complete trim-ready wing skin at the end of the lay-up operation, without debulk or cure cycles.

Clearly the potential here, both in the tougher, higher temperature physical properties available from thermoplastics, and in the near instantaneous processing, will increase research and investment in thermoplastic matrix-processing of composites. It is possible that in 10–20 years thermoplastics will be the dominant form of matrix. Much depends both on the progress of research and applications and the competitive response of the thermoset manufacturers (18).

Standards and Specifications

Specifications and standards pertaining to reinforced plastics-composites fall into one of the following classifications (30):

(1) Standards developed and published primarily by ASTM and ANSI committees.
(2) Codes set by users such as building officials, American Petroleum Institute (API), American Water Works Association (AWWA), etc.
(3) Design data generated by commercial and government research.

Table 1 is a guide to the major organizations that write standards for composites and the agencies that specify those standards in codes and handbooks, shown by composite markets and product applications.

Table 1. Guide to Organizations and Agencies that Specify Standards for Composites in Codes and Handbooks

Market	Major product applications	Standards[a] in Codes and Handbooks: Major organizations	Standards[a] in Codes and Handbooks: Major governing agencies (US)
Housing construction	Bathware	ANSI, ASTM	International Code Council (ICC, incl. ICBO, BOCA & SBCCI)
Infrastructure construction	Highway	ACI, AASHTO, ACPA[b]	AASHTO, State DOTs, U.S. Army Corps of Engineers
	Pilings	ASTM, ACI, PCI[c], AWPI[d], AISC[e]	AASHTO, PCI FHWA, DOTs, ACI, U.S. Army Corps of Engineers, other government agency handbooks
	Power/utility	ASCE, ANSI, NEMA, IEEE	Individual power/utility companies, EPRI
Corrosion-resistance	Pipe and tank in chemical plants, petroleum refineries, and wastewater facilities	ASTM, API, NACE, AWWA, ANSI, ASME, UL	Chemical Plant And Petroleum Refinery Code. Local regulations. AWWA controls building codes for drainage pipes & underground water pipes.
Electrical	Line tools	ASTM, NEMA, IEEE	OSHA
	Cable trays	ASTM, UL, NEMA, IEEE	Uniform Building Code
Automotive	Exterior structural & nonstructural body panels, interior, under-the-hood	SAE, ASTM, ISO, DIN (Germany)	OEMs

[a]Standards, test methods, recommendations, industry specifications.
[b]American Concrete Pavement Assoc., Skokie, Ill.
[c]Precast/Prestressed Concrete Institute, Chicago.
[d]American Wood Preservers Institute, Fairfax, Va.
[e]American Institute of Steel Construction, Chicago.

Economic Aspects

The composites industry has usually been perceived as providing specialty parts at premium prices. Today, however, composites are being reclassified from "specialty" to "commodity" industry. The growth of composite product development has resulted in lower prices without loss of properties, such as light weight, high stiffness, and corrosion resistance. Composites are now often cheaper than traditional materials—especially when installation costs, maintenance costs, and life cycle are factored in—and may become the economic barometer of the country, similar to steel in an earlier era.

This change is accelerated in times of energy crises, which typically results in a sharp price increase of traditional materials. Energy requirements are given in Table 2. In general, those for composite materials and processing are lower than those for steel and aluminum.

Table 2. Energy Requirements for Traditional Raw Materials and Composites[a]

Material	MJ/kg[b]
Traditional metals	
Steel, sheet	29
Aluminum sheet	175
Die cast	90
Glass fiber	
Roving	43
Chopped strand mat	52
Chopped strands	44
Woven roving	46
Yarn	63
Resins	
Polyester	92
Epoxy	167
Phenolic	82
Polyamide	190
Polycarbonate	146
Composite compounding	
BMC[c], 18% glass–52% filler	44
SMC[d], 30% glass–35% filler	54
Polyamide–30% glass	153
Polycarbonate–30% glass	126
Polypropylene–30% glass	107
Composite products	
Contact-molded	82
Sprayed-up	80
Hot-press-molded	88
SMC	60
Pultruded	58
Filament-wound	80

[a] Ref. 31.
[b] To convert J to cal, divide by 4.184.
[c] Bulk-molding compound.
[d] Sheet-molding compound.

Cost Savings Example. Leaf springs provide a clear example of cost savings that are possible with composites. Composite springs weigh only a fifth as much as steel and perform far better. In a fatigue test, a steel spring fails at 35,000–50,000 cycles, whereas the composite spring survives 500,000 or even 5×10^6 cycles with no sign of failure. The cost savings extend beyond material cost to weight reduction and every aspect of production and performance. For example, the steel spring requires skilled labor in a multiple-step process, whereas the composite spring is made on automatic machinery.

Environmental Advantages. With respect to expensive safety and pollution-control devices, composites have a marked advantage. A steel-spring plant presents a variety of hazards and serious pollution problems, whereas composites fabrication is conducted at a console. Emissions of styrene and other VOCs have been significantly reduced through closed processing and improved resin chemistries and take-off systems that vent remaining EPA allowable emissions outside the plant.

Quality Assurance Techniques

Quality assurance techniques for composite products fall into two categories: process control and product evaluation.

Raw material control is, of course, critical to all manufacturing processes and is assumed in this article.

This type of manufacturing confronts problems not found elsewhere, such as process variables and determining the size and degree of a fault area in large composite pieces. Still another problem is that faults in composite materials do not propagate as in more traditional materials and are harder to locate. As a result, in-process quality assurance is of much greater importance than in traditional manufacturing. Some defects can be corrected while the process is under way; others can be detected only in the end product and therefore corrective action must wait until another cycle (see also COMPOSITES, TESTING).

A recently patented system that holds promise for nondestructive evaluation of a composite product is the Reverse Geometry X-ray from Digiray Corp. in Danville, Calif.(see Fig. 39). RGX is a motionless, portable system of computed tomography that relays a digital image through layers of a composite structure directly into a computer. As an example, the system can inspect aircraft, spacecraft, and aerospace structures without the costly removal of wings, helicopter, or wind-tunnel blades. Digital recording media replaces expensive x-ray photographic film and the system is said to eliminate the "fogging" of the image that is typical of conventional x-ray technology.

One of the most important features of digital inspection is speed. Because everything is done digitally there is no need to develop plates like in the old days. The result is that inspections which used to take days now only take hours. Also for record-keeping, everything is stored digitally and can be retrieved and shared at any time during the life of the component.

Traditional methods of inspection are summarized below.

Tape-Laying Process. The automated tape-laying process assumes the correct size, angle of cut, material constituency, and order of progression on the

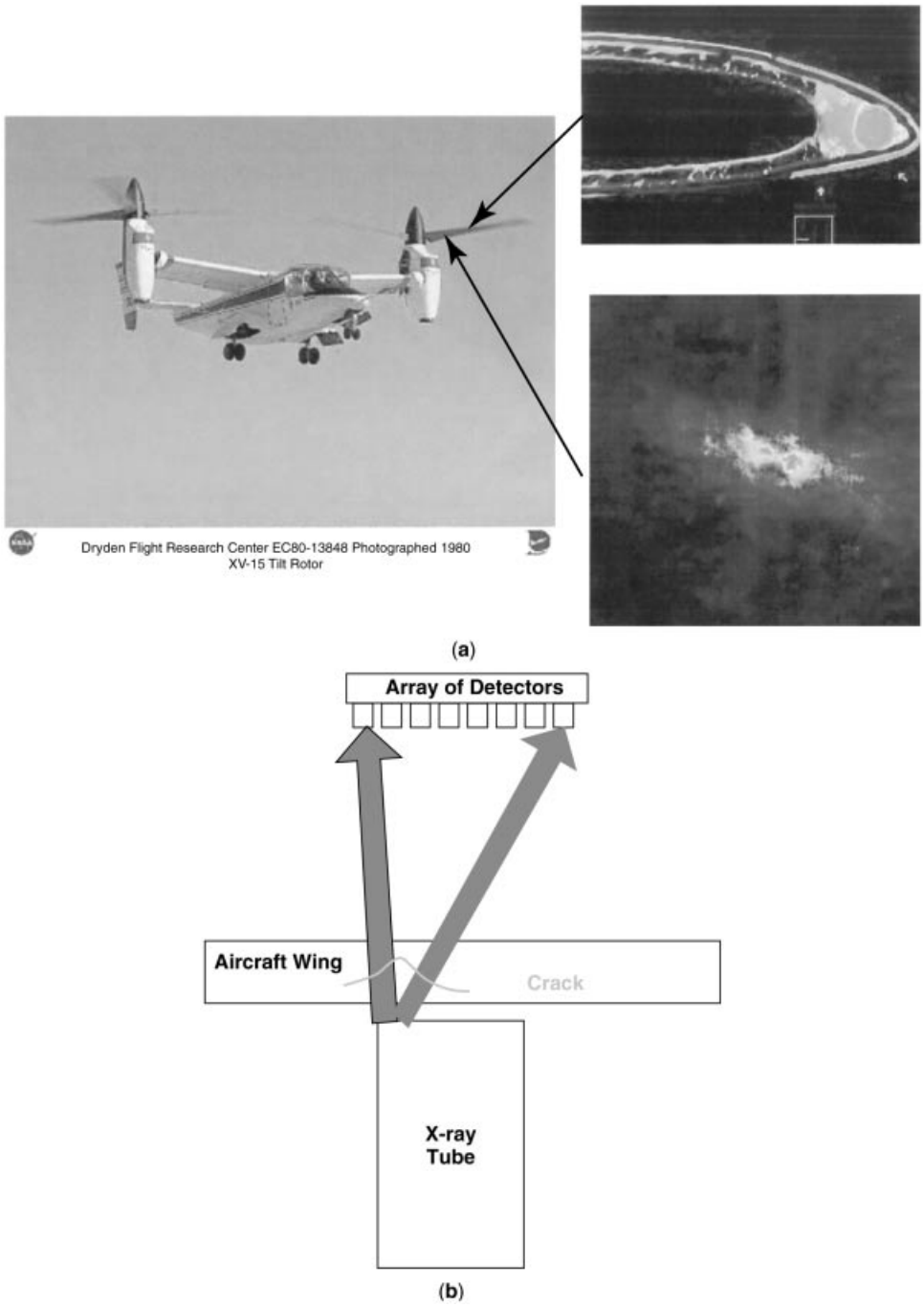

Fig. 39. Digiray Reverse Geometry x-ray technology (Source: Digiray). (**a**) Impact damage on the rotor blades of XV-15 tiltrotor (experimental development vehicle for V-22); (**b**) Schematic of setup for scan through a wingbox; (**c**) Hardware setup on wingbox of Boeing 707.

(c)

Fig. 39. (Continued)

roll of the prepreg tape supplied by a programmed tape magazine. It can be termed an intermediate process, since the product is moved to another process center for thermal development of properties.

Defects in orientation, tape width, length, ply thickness, angle of cut, or smoothness are found mainly by visual inspection. An extremely high accuracy and control are required of the tape supply magazine and its programming.

Detection of defects is easier after thermal processing. Pressure and temperature must be monitored closely, usually by self-correcting mechanisms and without manual adjustment. After thermal processing, the part may be subjected to appropriate nondestructive testing, as described later.

The size, complexity, and value of the processed part may limit testing to "on-site" techniques. Thorough visual inspection usually reveals significant surface defects, such as porosity, scratches, deficiency or surplus of resin, tape misorientation, and wrinkles.

Hardness of peripheral regions should be tested. The impressions or indentations made by instruments such as the Barcol tester are considered destructive testing, although many materials recover fully.

Separate specimens are used for destructive analysis and evaluation with regard to fiber fraction, void content, porosity, and mechanical properties.

Pultrusion. In contrast to tape laying, pultrusion requires almost continuous monitoring to ensure continuous flow and optimum product properties. Curing of the resin matrix is critical, ie, gelation must be reached before the stock leaves the curing die. The degree of cure is checked by dielectric inspection. As marginal conditions are discovered, heating corrections to ensure gelation and continuity of flow through the dies can be made. This is true for polyesters and even more for epoxy resins, which require more time to gel.

The mandatory visual inspection can detect discoloration, crazing, surface fractures, pitting, bubbles, porosity, voids, finish inconsistencies, and surplus or deficiency of resin.

The pultruded part is evaluated by ultrasonic C-scan or ir scanning. Uniform fiber dispersion and even coating by the matrix resin are the main requirements.

Pulforming. Pulforming resembles pultrusion, except that the products can be straight or curved and may have constant volume and changing shape or changing volume and shape.

During pulforming, complications due to changes in cross-sectional shape and volume of the developing part require that close attention be paid to shrink rate and surface uniformity. The proper timing of resin gelation with respect to entry into the pulforming dies is determined by dielectric inspection of the degree of cure.

The surface is inspected visually during processing, but as in pultrusion, ultrasonic C-scan or ir scanning are valuable techniques. Uniform dispersion of the fibers and evenness of the resin coating are essential.

Both pultrusion and pulforming may benefit from inspection by flash x-ray or cineradiography, with associated good visual display.

Filament Winding. In filament winding, many factors influence the product, including mandrel stiffness and surface finish, winding speed, resin precure, filament alignment and tension, and temperature control.

The three winding methods include wet winding, in which the roving passes from a spool through the impregnating bath and onto the mandrel; dry winding with preimpregnated B-staged roving fed directly onto a heated mandrel or first through a softening oven; and postimpregnation, in which the roving is dry wound onto the mandrel and the resin applied by brushing, pressure, or vacuum. All methods require close control of fiber and resin properties.

The filaments are applied to the mandrel by circumferential or helical winding; both require uniform filament tension, even resin coating, correct filament patterns, and temperature control throughout.

The importance of inspection during winding may be reduced by computerized control. Visual inspection can detect filament out of position and uneven resin distribution, indicating variation in tension.

With the completion of filament winding, the testing of the wound and cured part encounters other difficulties. The correlation of standard test results with final performance poses a major problem. Since the filaments are wound in a curve, tensile tests of detached specimens are not directly relatable to material requirements. Recently, special test specimens have been developed for use with standard ASTM methods.

Nondestructive tests applicable to filament-wound parts include ultrasonic C-scan and radiographic and visual inspection.

Advantages and disadvantages of nondestructive methods are given in Table 3.

Outlook. Continuous-flow processes, eg, for composite pipe, are adequately controlled by continuous scanning. With the improvement of such systems as ir scanning and cineradiography and self-correcting loop-feedback controls, continuous processing machines will gain in scope. For noncontinuous processes,

Table 3. Nondestructive Test Methods for Wound Filaments

Method	Advantages	Disadvantages
Penetrant inspection	Good detection of defects or discontinuities open to the surface	No graphic record in normal operation
	Familiarity and reliability	Not always portable
Holographic interferometry	Good definition of material integrity, especially subsurface	Expensive
	Good graphic record	Not always applicable
		Not portable
Radiographic inspection	Good definition of material integrity, surface, and subsurface	Radiation hazard
	Good graphic record Detects almost every type of defect	Time-consuming
		Expensive
		Not always portable
Ultrasonic C-scan	Good definition of material integrity, surface, and subsurface	Expensive
	Choice of techniques for specific applications	Requires liquid coupling agent that is not always practical
		Not always portable
Visual, aided or unaided	Convenient	No graphic record
	Inexpensive	Limited to surface conditions
	Wide scope	
Infrared scanning	As accurate as ultrasonic techniques	Still under development as standard equipment
	Good graphic record	
	Portable	
	No coupling agent required	
Dielectric inspection	Can determine degree of cure on moving material	Still under development as standard equipment

functional design criteria obtained from field use may facilitate the control of low volume composite products. Automated composite-fabrication systems and their quality control methods are at the frontiers of composite technology.

BIBLIOGRAPHY

"Composites, Fabrication" in *EPSE* 2nd ed., Vol. 4, pp. 1–36, by W. B. Goldsworthy, Goldsworthy Engineering, Inc.

1. D. K. Dawson, *Composites Technol.* 20–28 (Jan./Feb. 1999).
2. D. K. Dawson, *Composites Technol.* 40–42 (Nov./Dec. 1999).
3. D. K. Dawson, *Composites Technol.* 34–37 (Nov./Dec. 2000).
4. Richard Stewart, *Composites Technol.* 22–26 (Jan./Feb. 2001).
5. D. K. Dawson, *Composites Technol.* 33–36 (Sept./Oct. 2000).
6. U.S. Pat. 2,871,911 (Feb. 3, 1959), W. B. Goldsworthy (to Glastrusions, Inc.).
7. U.S. Pat. 2,990,091 (June 27, 1961), W. B. Goldsworthy (to Glastrusions, Inc.).
8. U.S. Pat. 3,556,888 (Jan. 19, 1971), W. B. Goldsworthy (to Glastrusions, Inc.).
9. U.S. Pat. 3,684,622 (Aug. 15, 1972), W. B. Goldsworthy (to Glastrusions, Inc.).
10. U.S. Pat. 3,674,601 (July 4, 1972), W. B. Goldsworthy (to Glastrusions, Inc.).
11. U.S. Pat. 3,793,108 (Feb. 19, 1974), W. B. Goldsworthy (to Glastrusions, Inc.).
12. U.S. Pat. 3,960,629 (June 1, 1976), W. B. Goldsworthy (to Glastrusions, Inc.).
13. J. E. Sumerak and J. D. Martin, *Plast. Technol.* (Feb. 1983).
14. D. K. Dawson, *Adv. Composites Bull.* 6–7 (Feb. 2001).
15. U.S. Pat. 3,873,399 (Mar. 25, 1975), W. B. Goldsworthy (to Goldsworthy Engineering, Inc.).
16. U.S. Pats. 3,701,489 (Oct. 31, 1972), 3,740,285 (June 19, 1973), and 3,783,637 (June 12, 1973), W. B. Goldsworthy (to Goldsworthy Engineering, Inc.).
17. E. E. Hardesty, Paper presented at the *SAMPE 15th National Conference*, Los Angeles, Calif., Apr. 1969, Society of Aerospace Materials and Process Engineers, Covina, Calif., 1969.
18. W. B. Goldsworthy, *Plast. World* (Aug. 1984).
19. E. E. Hardesty, *Composites* (Nov. 1972).
20. U.S. Pat. 4,462,946 (July 31, 1984), W. B. Goldsworthy (to Goldsworthy Engineering, Inc.).
21. U.S. Pat. 4,440,593 (Apr. 3, 1984) and 4,469,541 (Sept. 4, 1984), W. B. Goldsworthy (to Goldsworthy Engineering, Inc.).
22. U.S. Trademark 1,187,389 (Pulformer) (Jan. 26, 1982), W. B. Goldsworthy (to Goldsworthy Engineering, Inc.).
23. U.S. Pat. 3,801,407 (Apr. 2, 1974), W. B. Goldsworthy (to Goldsworthy Engineering, Inc.).
24. U.S. Pat. 4,402,778 (Sept. 6, 1983), W. B. Goldsworthy (to Goldsworthy Engineering, Inc.).
25. U.S. Pat. 4,420,359 (Dec. 13, 1983), W. B. Goldsworthy (to Goldsworthy Engineering, Inc.).
26. U.S. Pat. 4,125,423 (Nov. 14, 1978), W. B. Goldsworthy (to Goldsworthy Engineering, Inc.).
27. U.S. Pat. 4,032,383 (June 28, 1977), W. B. Goldsworthy and H. E. Karlson (to McDonnel Douglas).
28. U.S. Pat. 3,966,533 (June 29, 1976), W. B. Goldsworthy (to Goldsworthy Engineering, Inc.).
29. *Automated Integrated Manufacturing System: Cost-cutting Composite Fabrication for*

the '80s, Materials Laboratory, Air Force Wright Aeronautical Laboratories (AFWAL), Dayton, Ohio, and Gruman Aerospace Corp., Midgeville, Ga., 1978.
30. J. McDermott, Paper presented at the *36th Annual Conference of the SPI*, RP/C Institute, Feb. 16–20, 1981, The Society of the Plastics Industry, Inc., New York, 1981.
31. *Energy Content of Reinforced Plastics Materials*, International Reinforced Plastics Industry (IRPI), London, Nov. 1981.

W. BRANDT GOLDSWORTHY
DONNA DAWSON
W. Brandt Goldsworthy & Associates

COMPOUNDING. See PROCESSING.

COMPUTER CONTROLLED PROCESSING. See PROCESS AUTOMATION.

CRITICAL PHASE POLYMERIZATIONS

Introduction

A supercritical fluid (SCF) can be defined as a substance or mixture which has both a temperature and pressure that exceed its critical temperature (T_c) and critical pressure (P_c), and a density at or above its critical density (1) (Fig. 1). Near this critical point, the density, transport properties (such as diffusivity and viscosity), and other physical properties (such as dielectric constant and solvent strength) can be varied in a continuum from gas-like to liquid-like, with relatively small changes in temperature or pressure. The tunability of SCFs makes them very attractive as solvents for polymerization reactions.

The first example of polymerization in an SCF and the most commercially significant till this time is the high pressure synthesis of low density polyethylene (PE) (2). In this process, ethylene from a recycle stream and a makeup source are compressed to 250 MPa (2500 bar) in a tubular reactor at 250°C. The free-radical reaction is initiated with either peroxide or traces of oxygen. The polymer produced has an average molecular weight higher than 100,000 g/mol that is soluble in the ethylene monomer at the process conditions. Polyethylene is precipitated and collected in a separator downstream of the reactor section by reducing the pressure of the solution to 35 MPa (350 bar), thus changing the solvent quality of ethylene.

In an effort to reduce emission of volatile organic compounds, to completely phase out the use of chlorofluorocarbons (CFCs), and to reduce the generation of aqueous waste streams generated in the polymer industry, scientists have turned to the use of supercritical carbon dioxide ($scCO_2$). In the 1990s, CO_2 has proven to be a suitable alternative solvent for critical phase polymerization reactions (3). It has an easily accessible critical point with a T_c of 31.1°C and a P_c of 7.38 MPa

Encyclopedia of Polymer Science and Technology. Copyright John Wiley & Sons, Inc. All rights reserved.

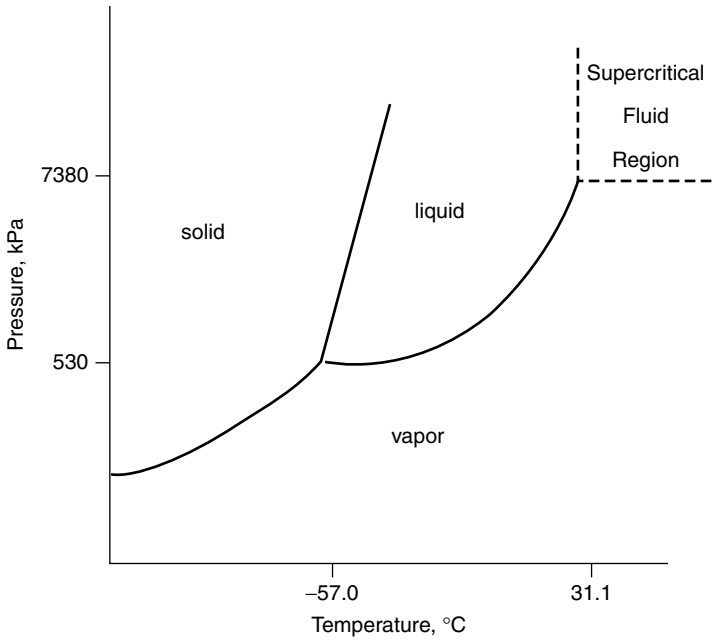

Fig. 1. Supercritical fluid phase diagram. To convert kPa to bar, divide by 100.

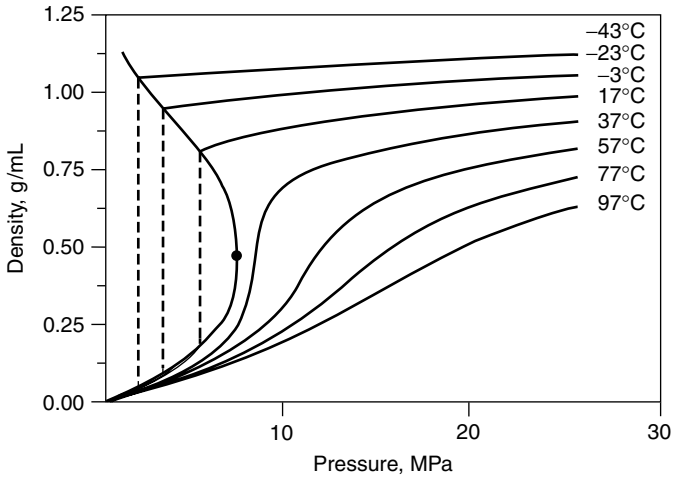

Fig. 2. CO_2 density profile. To convert MPa to psi, multiply by 145.

(73.8 bar) (4). Within this region, scCO_2 exists as a low viscosity medium with a tunable density (Fig. 2). It is nontoxic, nonflammable, relatively inexpensive, naturally abundant, and generally regarded as safe. Because CO_2 is an ambient gas, it can be separated from the polymer by depressurizing the reaction vessel, resulting in a dry polymer product. CO_2 is also inert toward free radicals and cations, which lessens chain-transfer reactions. These aspects make CO_2 very attractive

for use in synthesis of industrially important polymers. Numerous examples exist of both chain-growth and step-growth polymerizations using CO_2 as a reaction medium. This article focuses on the utilization of liquid and scCO_2 as a reaction medium for polymer synthesis.

Knowledge of two important issues is important when CO_2 is used as a polymerization solvent: solubility and plasticization. CO_2 is a nonpolar solvent and should generally dissolve anything that dissolves in hexane. This concept is valid for many low molar mass compounds that have appreciable vapor pressures; however, it fails in the case of polymers that have negligible vapor pressures (5). In fact, the only polymers that show good solubility in CO_2 under mild conditions [$<100^{\circ}$C, <35 MPa (<350 bar)] are amorphous fluoropolymers, siloxanes (6,7), and polyether carbonates (8). CO_2 has a very low polarizability per unit volume (27.6×10^{-25} cm^3) (9) and a low dielectric constant (1.01–1.67) (10), making its solvating power similar to that of a fluorocarbon oil. Because of structural symmetry, CO_2 lacks a dipole moment; however, it does have a strong quadrapole moment that contributes to its solubility parameter. This quadrapole moment along with the Lewis acidity of CO_2 allows it to participate in specific solute–solvent interactions that allow certain polymers to have enhanced solubilities in CO_2. Experiments conducted using Fourier transform infrared spectroscopy reveals that CO_2 is capable of having Lewis acid–base type interactions with polymers that have electron-donating functional groups such as carbonyls (11). Amorphous fluoropolymers have an especially high solubility that is attributed to specific interactions such as the formation of weak CO_2–fluoropolymer complexes or favored clustering of the CO_2 near the more polar C—F bonds of the polymer. High resolution ^{1}H and ^{19}F nmr studies confirm that such interactions do exist, thus causing magnetic shielding of the fluorine nuclei (12,13).

The unique solubility characteristics of CO_2 limit the types of polymerization techniques that can be successfully employed. While amorphous fluoropolymers may be synthesized homogeneously in CO_2, most other polymers are insoluble in CO_2 and must be made via heterogeneous processes such as precipitation, dispersion, and emulsion techniques or via mass polymerizations swollen by CO_2.

The plasticization of polymers by CO_2, which causes a decrease in the glass-transition temperature (T_g) of the polymer, is another important feature that must be taken into account. This plasticization facilitates the occurrence of important effects that are essential to polymer synthesis. Plasticization of the polymer allows enhanced diffusion of monomer and initiator into the polymer phase which often results in increased polymerization rates in heterogeneous polymerizations, removal of residual monomer, solvent, or catalyst from the polymer, and the formation of blends by polymerization within a CO_2-swollen host polymer. An important emerging issue is the role that CO_2 plays in manipulating the loci of reactants such as monomer/comonomer/initiator partition coefficients. Each of these topics is discussed in this chapter.

Chain-Growth Polymerizations in CO_2

Homogeneous Polymerizations. Fluoropolymers are used in many technologically demanding applications because of their balance of high

performance properties. Several significant impediments to the synthesis of commercially important fluoropolymers exist including their general insolubility in most solvents, the undesirable effect of chain transfer of fluoroolefin radicals to most hydrogen-containing solvents (hence the extensive use of CFC solvents), and their high hydrophobicity (which necessitates the use of specially fluorinated surfactants when synthesized in water). Preparing these amorphous low melting materials in $scCO_2$ can circumvent the environmental concerns for CFCs and can avoid the ensemble of problems associated with their synthesis in water. The feasibility of utilizing liquid and $scCO_2$ as a solvent for homogeneous solution polymerization of high molar mass amorphous fluoropolymers by using thermal free-radical initiation has been demonstrated (14–16). Several fluorinated acrylates have been polymerized using this methodology to give high yields of polymer. For example, poly(1,1-dihydroperfluoroctyl acrylate) (PFOA) (50 w/v) was polymerized using 2,2′-azobis(isobutyronitrile) (AIBN) as the initiator at 59.4°C and 20.7 MPa (207 bar) CO_2 for 48 h (eq. (1)).

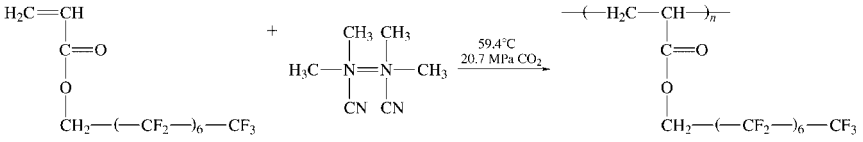

(1)

The results from a uv spectroscopy study revealed that the decomposition rate of AIBN in CO_2 is 2.5 times slower than those observed in more viscous solvents (15). This was attributed to the difference in dielectric constants of the solvents. In contrast, higher initiator efficiencies were observed in CO_2, relative to other solvents, as a result of a decreased solvent cage effect in the supercritical phase due to the inherently low solvent viscosity. Other fluorinated acrylates, methacrylates, and perfluoroalkyl derivatized styrenes have been homogeneously polymerized or copolymerized in CO_2 (17–19). The free-radical propagation kinetics of styrene, methyl methacrylate, and butyl methacrylate in CO_2 has been evaluated using a pulsed laser polymerization (PLP) (20–22). The propagation rate was found to be slightly lower than that in the bulk, which indicates that CO_2 does not interfere with the chain-growth process. Homogeneous free-radical polymerizations have also been used to synthesize telomers of 1,1-difluoroethylene (23). The perfluoroalkyl iodides prepared in this manner had both controlled molecular weights and relatively narrow molecular weight distributions.

Precipitation Polymerizations. A variety of polymers have been synthesized in CO_2 by free-radical precipitation polymerization. In the earliest studies, the free-radical polymerization of ethylene in CO_2 using either gamma radiation or AIBN initiation was investigated (24–26). Other patents (27,28) disclosed the polymerization of several vinyl hydrocarbon monomers in liquid and $scCO_2$. Homopolymers of vinyl chloride, acrylonitrile, acrylic acid, vinyl acetate, 2-hydroxyethylacrylate, and some *N*-vinylcarboxamides as well as PS/PMMA and PVC/PVAc random copolymers have been made. The polymerization reactions resulted in polymers with gravimetric yields ranging from 15 to 97% and viscosity average molecular weights (M_v) ranging from 1.2×10^4 to 1.6×10^6 g/mol depending on the monomer and the reaction conditions used. More recently, the free-radical polymerization of high molecular weight poly(acrylic acid)

($M_n = 1.5 \times 10^5$ g/mol) has been achieved in $scCO_2$ despite the fact that the polymer precipitates from solution at molecular weights greater than 1000 g/mol (29,30). The molecular weight of the polymer could be controlled by either adding ethyl mercaptan as a chain-transfer agent or by manipulating the temperature and pressure parameters for the reaction. High performance fluoropolymers have also been synthesized in CO_2 by free-radical precipitation polymerization. Homo- and copolymers of tetrafluoroethylene (TFE) have generated particular interest, since it was discovered that TFE can be handled more safely as a mixture with CO_2 (31). In 1995, homopolymerizations (32) of TFE and copolymerizations (33,34) of TFE with hexafluoropropylene (HFP) or perfluoropropyl vinyl ether (PPVE) yielding high molecular weight polymers ($>10^6$ g/mol) in good yield were reported. Copolymerization of TFE and perfluoroalkyl vinyl ether monomers in CO_2 occurs with virtually no β-scission, implying that propagation of terminal vinyl ether-containing radicals is more favorable in CO_2 than in traditional solvents. A system for the continuous polymerization of various monomers in $scCO_2$ has been developed (35). Continuous precipitation polymerization of vinylidene fluoride and acrylic acid can occur in an intensely agitated continuous stirred tank reactor (CSTR). Rates of polymerization of vinylidene fluoride in the CSTR are significantly higher than the average rates of batch polymerization, under similar conditions. CO_2 has also been employed as a solvent in precipitation polymerizations of cross-linked polymers, using high levels of divinylbenzene cross-linker (36). The AIBN-initiated reactions were performed at 65°C for 12 h in 31 MPa (310 bar) CO_2 and yielded spherical particles without the use of surfactants. Multifunctional monomers such as trimethylolpropane trimethacrylate and ethylene glycol dimethacrylate were also investigated (37). These reactions produced well-defined polymer monoliths with pore diameters ranging from 20 to 8000 nm (see the "Porous Polymer Synthesis" section). A clear advantage to the use of CO_2 in each of these precipitation reactions is that the products are easily isolated from the depressurized reaction vessels as dry, solvent-free materials.

Dispersion and Emulsion Polymerizations. The relative insolubility of many industrially important polymers in $scCO_2$ necessitates the use of heterogeneous polymerization techniques conducted with added stabilizers. Conventional heterogeneous dispersion polymerizations of unsaturated monomers are performed in either aqueous or organic dispersing media, with the addition of interfacially active agents to stabilize the colloidal dispersion that forms (38,39). Successful stabilization of the polymer colloid during polymerization results in the formation of high molar mass polymers with high rates of polymerization. A similar analogy applies to dispersion polymerization in CO_2 where stabilization can be accomplished with the aid of nonionic homopolymers, block copolymers, and reactive macromonomer surfactants (40) (Fig. 3). Typically, a free-radical dispersion polymerization in $scCO_2$ starts as a one-phase, homogeneous system such that both the monomer and the polymerization initiator are soluble in the polymerization medium. As the reaction progresses, the resulting growing polymer phase separates into primary particles that are stabilized by amphiphilic materials so as to prevent particle flocculation and aggregation. Polymer colloids produced by dispersion polymerizations in CO_2 are usually stabilized by a steric mechanism as compared with an electrostatic mechanism that is common to colloidal stabilization in aqueous environments because of the low dielectric constant of CO_2. Steric stabilization of a colloidal dispersion is usually imparted by

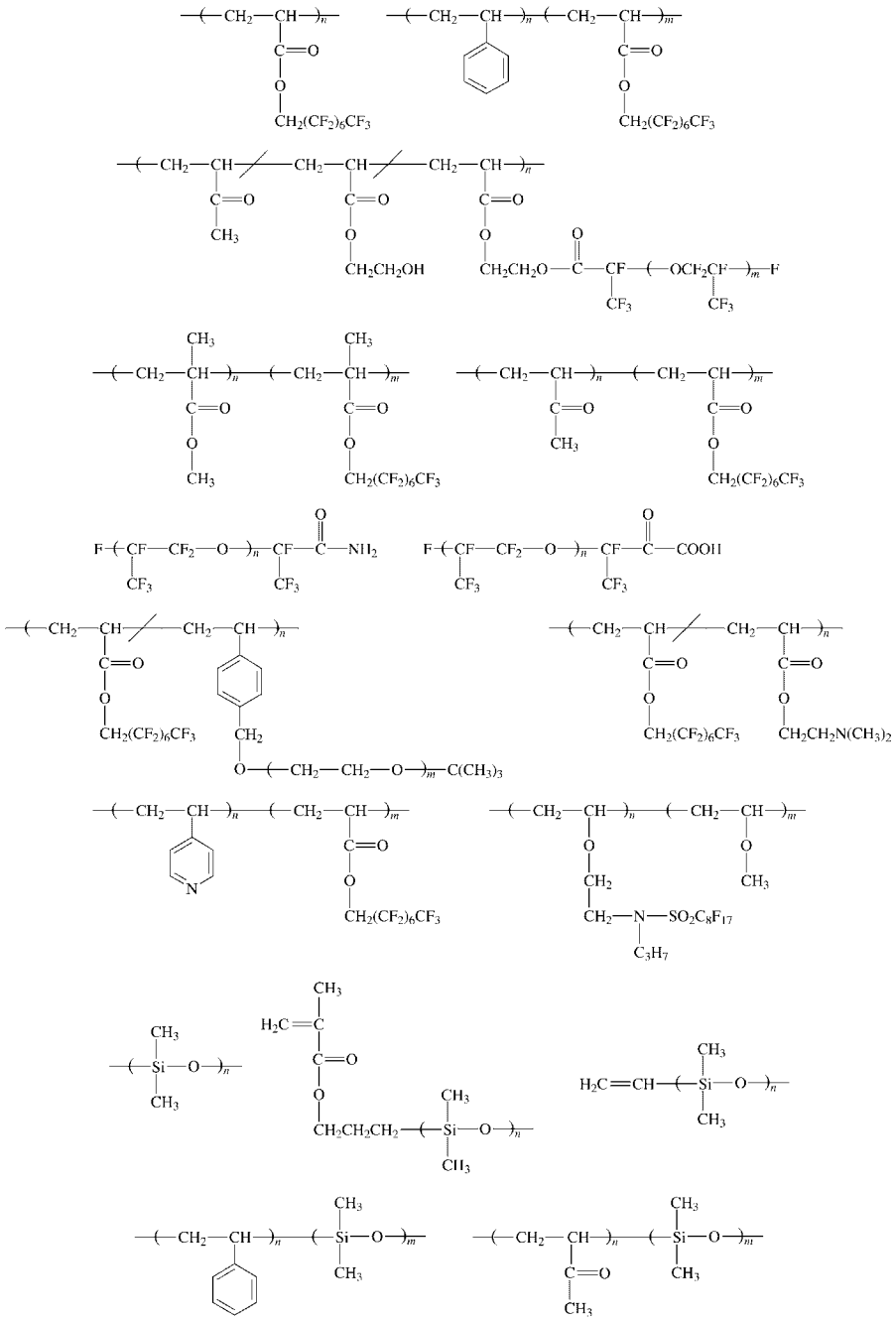

Fig. 3. Surfactants for CO_2.

amphiphilic macromolecules that become adsorbed onto the surface of the dispersed phase. These macromolecules contain an anchoring segment that attaches to the particle usually by physical adsorption and stabilizing moieties that are soluble in the continuous phase. The stabilizer prevents aggregation of particles by coating the surface of each particle and imparting long-range repulsions between them.

A substantial number of studies on the dispersion polymerization of lipophilic monomers in CO_2 have focused on methyl methacrylate (MMA). The first success in this area exploited the amphiphilic nature of the homopolymer PFOA as a stabilizer (40) (eq. (2)).

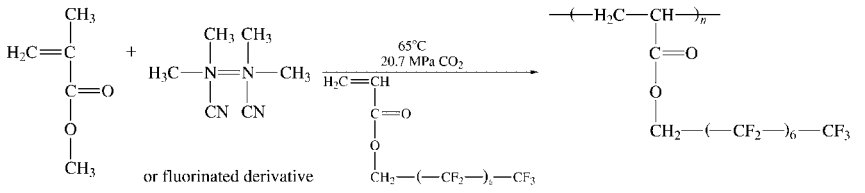

(2)

MMA was polymerized heterogeneously to very high conversions (>90%) and high degrees of polymerization (>3000 g/mol) in $scCO_2$. These polymerizations were conducted at 65°C and 20.7 MPa (207 bar) CO_2 with AIBN or fluorinated derivatives of AIBN as initiators and PFOA ($M_n = 1.1 \times 10^4$ or 2.0×10^5 g/mol) as the surfactant. The reactions resulted in kinetically stable dispersions of micrometer-sized particles with a narrow size distribution. In contrast, reactions that were performed without PFOA as a stabilizer resulted in precipitated polymer with an unstructured, nonspherical morphology. Several other monomers were also polymerized by dispersion polymerization methods in CO_2 (Table 1).

Table 1. Summary of Dispersion and Emulsion Polymerizations in CO_2

Monomer(s)	Stabilizers	Reference
Acrylamide	Amide end-capped PFPE	41
2,6-Dimethylphenylene oxide	PFOA, PFOA-based random copolymers, PS-*b*-PFOA	42
Divinylbenzene and ethylvinylbenzene	Fluorinated methacrylate–PMMA block copolymer	37
Methyl methacrylate	PFOA	40,43,44
	PDMS macromonomer	(45,46)–(47)
	Fluorinated graft or block copolymers	48
Styrene	PFOA, PS-*b*-PFOA	49
	PDMS, PS-*b*-PDMS	50
	FVE-*b*-MVE	51
	Carboxylic acid terminated PFPE	52
Vinyl acetate	PFOA, PDMS, PDMS macromonomer, PVAc-b-PDMS and PVAc-b-PFOA	53
Vinyl acetate and ethylene	PDMS, PVAc-*b*-PFOA	53
1-Vinyl-2-pryrrolidinone	PFOA	54
Acrylonitrile	PFOA, PS-*b*-PFOA	55

Typical emulsion polymerizations utilize oil-soluble monomers dispersed in an aqueous media with a water-soluble initiator, whereas "inverse" emulsions employ water-soluble monomers dispersed in an organic medium containing an oil-soluble initiator. The insoluble polymer particles that result from these reactions are stabilized as colloids in solution by repulsive forces imparted by a small molecule ionic surfactant and/or an amphiphilic macromolecular stabilizer (56,57). These reactions produce high molecular weight, spherical polymer particles with sizes typically smaller than 1 μm. Since most common monomers are highly soluble in CO_2, there are very few examples of CO_2-based emulsion polymerizations. However, acrylamide is a rare example of a vinyl monomer that has a low solubility in CO_2 at moderate temperatures and pressures. The AIBN-initiated water-in-oil or "inverse" emulsion polymerization of acrylamide has been attempted at 65°C in 35.2 MPa (352 bar) CO_2 (41,58) (eq. (3)).

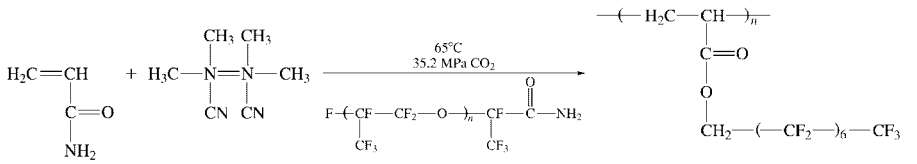

(3)

Reactions performed with an amide end-capped perfluoropolyether (PFPE) appeared to form a milky-white latex, but produced polymers with conversions and molecular weights similar to those polymers precipitated in reactions without a stabilizer. More inverse emulsion studies are expected with the utilization of surfactants that have the ability to form water in CO_2 microemulsions. Several researchers have demonstrated that various amphiphilic surfactants like the graft copolymer PFOA-*g*-PEO (59), an ammonium carboxylate PFPE $[(OCF_2\text{-}CF(CF_3))_n(OCF_2)_m]OCF_2COO^-NH_4^+$ (60), and the hybrid hydrocarbon–fluorocarbon $C_7F_{15}CH(OSO_3^-Na^+)C_7H_{15}$ (61) are able to stabilize water-in-CO_2 microemulsions. In principle, these same surfactants could be used to form microemulsions of water and water-soluble monomers in CO_2 for inverse emulsion polymerizations.

***In Situ* Synthesis of Polymer Blends.** The ability of $scCO_2$ to plasticize most polymers enables the synthesis of polymer blends that are not easily accessible by other methods. Supercritical CO_2 can be used to swell a CO_2-insoluble polymer matrix and subsequently infuse CO_2-soluble monomers and initiators into the matrix for polymerization. In one system, poly(chlorotrifluorethylene) (PCTFE), poly(4-methyl-1-pentene) (PMP), high density polyethylene (HDPE), nylon-6,6-poly(oxymethylene), and bisphenol A polycarbonate (PC) were each swollen with CO_2 and infused with styrene monomer and either AIBN or *tert*-butyl perbenzoate initiators (62,63). Polymerization was thermally initiated within the polymer matrix either in the presence of CO_2 or N_2 to generate a polymer blend. Mass uptakes of up to 118% based on the original mass of the polymer were observed. In the case of PCTFE, extraction of polystyrene from the matrix and subsequent gpc analysis showed high molecular weight polymer ($M_n > 1 \times 10^5$ g/mol) in the blend. Transmission electron microscopy and energy dispersive x-ray analysis were used to demonstrate that the polystyrene exists as discrete phase-segregated regions

throughout the matrix polymer. Thermal analysis results revealed that radical grafting reactions are not significant. Other materials including PS/PE composites (64) and FEP/PS blends (65) can be synthesized by related routes. In a similar study this strategy has been used as a route to polymer surface modification. Styrene (with and without various cross-linkers) was infused into three polymer substrates (PTFE, PCTFE, and FEP), polymerized, and subsequently sulfonated in order to provide surface modified semi-interpenetrating networks (66). An increase in wettability of the modified fluoropolymer matrices was shown using water contact angle measurements.

Cationic Polymerizations. Homogeneous and heterogeneous cationic polymerizations of various monomers in liquid and $scCO_2$ have been performed (Table 2). Several different catalyst systems were employed in these polymerizations, all of which proved to be effective. The early experiments conducted using monomers such as isobutylene (67) and formaldehyde (70–72) normally resulted in a low yield of low molecular weight products. Nonetheless, proof of concept for the use of CO_2 as an effective solvent for cationic chain-growth reactions was achieved. Other polymers based on different substituted alkenes (73), vinyl ethers (74,75) (eq. (4)), and oxetanes (75) (eq. (5)) have been synthesized.

Table 2. Summary of Cationic Polymerizations in CO_2[a]

Monomer (s)	Catalyst System	Reference
Isobutylene	$AlBr_3$/ethyl bromide (cosolvent)	67
	$TiCl_4$/isopropyl chloride	67
	2-(2,4,4-trimethylpentyl) chloride (TMPSCl)/$TiCl_4$/methyl chloride	68
Isobutylene/styrene	TMPSCl/$TiCl_4$/methyl chloride	69
Ethyl vinyl ether	$SnCl_4$ or BF_3-$O(C_2H_5)_2$	28
Formaldehyde	Acetic acid or trifluoroacetic acid	70,71–72
3-Methyl-1-butene	Water/$AlCl_3$/methyl chloride	73
4-Methyl-1-pentene	Water/$AlCl_3$/methyl chloride	73
Isobutyl vinyl ether (IBVE)	Acetic acid adduct of IBVE	74,75
	$C_2H_5AlCl_2$	
	$C_2H_5OOCCH_3$ (Lewis base deactivator)	
2-(*N*-propyl-*N*-perfluorooctyl-sulfonamide ethyl vinyl ether (FVE)	Acetic acid adduct of FVE	74,75
	$C_2H_5AlCl_2/C_2H_5OOCCH_3$	
Bis(ethoxymethyl)oxetane	BH_3-THF/NaOH[b]	76
3-Methyl-3′[1,1-dihydrohepta-fluorobutoxy)methyl]-oxetane	BH_3-THF/NaOH	76
FVE/methyl vinyl ether	Acetic acid adduct of FVE $C_2H_5AlCl_2$/ $C_2H_5OOCCH_3$	76
Styrene	$TiCl_4$[c]	77

[a] reactions are homogeneous unless noted.
[b] heterogeneous precipitation reaction.
[c] heterogeneous dispersion reaction.

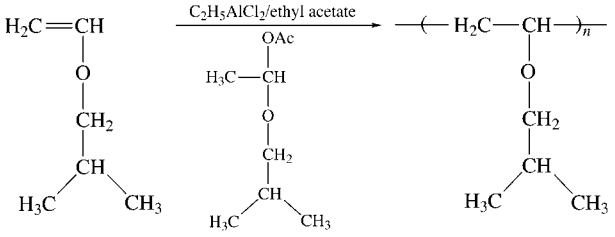

(4)

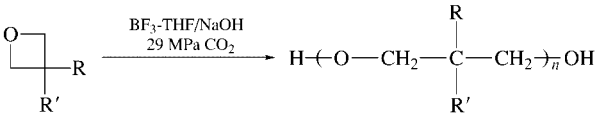

R = R′ = $-CH_2OCH_2CH_3$ or R = $-CH_3$; R′ = $-CH_2OCH_2CF_2CF_2CF_3$ (5)

Fast reaction kinetics generated by the high reactivity of carbocations is a major benefit in cationic polymerizations. However, this same reactivity leads to unwanted side reactions such as chain transfer to monomer and early chain termination by abstraction of acidic hydrogen atoms beta to the carbocation. CO_2 has several features that make it a suitable solvent for cationic polymerization reactions. It is relatively inert toward the carbocationic propagating species and is not incorporated into the polymer backbone (75). CO_2 as a solvent mimics the typical nonpolar solvents that are conventionally used by affecting the equilibrium between contact pairs and solvent-separated pairs. This in turn affects the activation energy for chain transfer and termination reactions. To minimize the limitations of cationic polymerizations, lower reaction temperatures (typically -70°C to -30°C) as well as controlled polymerization techniques are used. Living cationic polymerization methods that involve the stabilization of the cationic propagating species with a nucleophilic counterion or an added Lewis base have been developed and allow well-defined polymer and block copolymers to be prepared (75).

Transition-Metal-Catalyzed Polymerizations. Metal-catalyzed polymerizations (76) have been performed in scCO_2 (77,78). The ring-opening metathesis polymerization (ROMP) of norbornene has been performed with CO_2 and CO_2/methanol mixtures using a $Ru(H_2O)_6(O_3SC_6H_4CH_3\text{-}p)_2$ catalyst as the initiator (78) (eq. (6)).

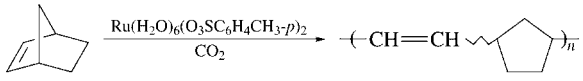

(6)

These reactions were carried out at 65°C and 6–34.5 MPa (60–345 bar) CO_2 and yielded polymers with conversions, molecular weights, PDIs, and polymer microstructures similar to those obtained in other solvent systems. Addition of methanol as a cosolvent to the polymerization medium accomplished several things: it enabled the ruthenium catalyst that was insoluble in neat CO_2 to be solubilized in the CO_2/monomer mixture; it allowed for increased rates of

polymerization yielding similar conversions in a shorter period of time compared to polymerizations done in pure CO_2; and it strongly affected the cis–trans ratio of the polymer microstructure by favoring the trans carbene propagating species (76,79). Both a ruthenium-based Grubbs catalyst (80) and a molybdenum-based Shrock catalyst (81) have shown even greater activity in the ROMP of norbornene, producing high molecular weight polymer (10^5–10^6 g/mol) in good yields (up to 97%) at milder reaction conditions [25–45°C and 11 MPa (110 bar) CO_2]. The ruthenium catalyst was also used to polymerize cis-cyclooctene in 50% yield and a molecular weight of 10^5 g/mol.

An insoluble rhodium catalyst [(nbd)Rh(acac)] has been used to synthesize polyphenylacetylene in the presence of liquid and $scCO_2$ (82). The catalyst is solubilized in the reaction mixture by addition of a perfluoroalkyl-substituted triphenylphosphine ligand. Polyphenylactylene formed in good yields (60–75%) had a molecular weight of about 4×10^4 g/mol for THF soluble fractions, and molecular weight distributions in the range of 8–10.

A number of metal-catalyzed polymerizations have utilized CO_2 as both a solvent and as a reagent in the reactions. Precipitation copolymerization of either propylene oxide (83) or cyclohexene oxide (84) with CO_2 in $scCO_2$ has been catalyzed using heterogeneous zinc catalysts. Copolymerizations of CO_2 and propylene oxide formed PCs with a molecular weight of about 10^4 g/mol and incorporation of CO_2 at greater than 90% (eq. (7)). A small percentage of propylene carbonate by-product was also observed.

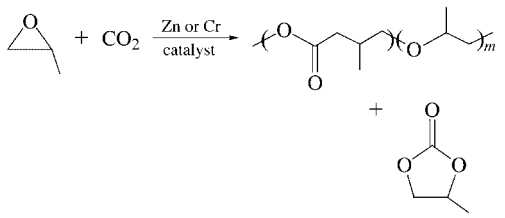

(7)

The cyclohexene oxide reactions yielded polymers with $M_w = 3.8 \times 10^5$ g/mol and 91% CO_2 incorporation. Catalyst efficiencies for these two systems were low to average (3–400 g of polymer per gram of Zn), possibly because of the insolubility of the zinc complexes in the CO_2/monomer mixture (85). Molecular weight distributions were also very broad (PDI = 2.4–27). A partially fluorinated porphyrin complex was found to be soluble in CO_2, and CO_2/monomer mixtures catalyzed the polymerization of cyclohexene oxide and CO_2 (in the presence of a base) forming polymer in good yields with high degrees of carbonate linkages (90–97%) (86). This system demonstrated substantially higher catalyst efficiencies (up to 3900 g of polymer per gram of Cr) than other systems and very narrow molecular weight distributions (PDI < 1.4).

Thermal Ring-Opening Polymerization. The thermal ring-opening polymerization of a silicone-bridged [1]-ferroceneophane in $scCO_2$ was performed at 20.7 MPa (207 bar) and 75–130°C (87) (eq. (8)). The polymer molecular weights were of the same order of magnitude as the polymers prepared by the solvent-free methods, but were uniformly lower ($M_w = 2.87 \times 10^5$ vs 5.2×10^5 g/mol).

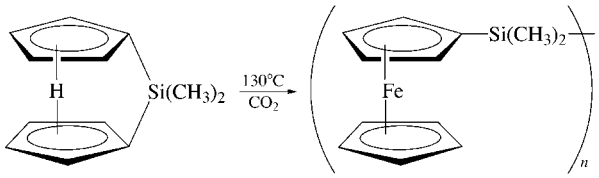

(8)

In addition to the lower molecular weights, the PDIs of the polymers made in CO_2 were broader (3.0–5.1 vs 1.5). Increasing the monomer concentration by 75% for the same reaction increased the M_w of the polymer to 5.9 × 105 g/mol and decreased the PDI to 2. This synthesis represents a comprehensible way to make organometallic polymers from highly strained precursors without dealing with the limitations imposed by melt-phase (88,89) or polycondensation routes (90).

Step-Growth Polymerizations in CO_2

Melt-Phase Condensation Polymerizations. Many condensation polymerizations are performed in the melt phase to produce high molecular weight material without the need for organic solvents. These polycondensation reactions are driven by the removal of small molecule condensates such as water, methanol, and phenol. Current industrial processes require high temperatures and high vacuum to allow the removal of the condensate molecule from the polymer melt phase. The drawback to this method is that the high molecular weight polymers produced have high viscosities that make polymer processing difficult and costly, as well as limit the molecular weight of the polymer. CO_2 is capable of acting as a plasticizing agent for the polymer melt phase, thus increasing the free volume of the melt and decreasing the viscosity of the melt for greater processability. Using CO_2 also facilitates the driving force for polycondensation reactions. Plasticization of the polymer melt phase provides a greater surface area for condensate removal, and solubilization of the small molecule condensate in CO_2 assists in carrying it out of the reactor. This enhancement in condensate removal results in greater mobility of chain ends, leading to higher reaction rates and higher molecular weight products. This strategy has been pioneered by DeSimone to synthesize polymers by step-growth methods, including polycarbonates, polyesters, and polyamides.

Melt polymerization of bisphenols (bisphenol A, bisphenol P, bisphenol AF, and bisphenol Z) with diphenyl carbonate in CO_2 with several catalysts have been achieved (91,92). Polymers with number-average molecular weights ranging from 2.2×10^3 to 1.1×10^4 g/mol ($M_w = 4.5 \times 10^3$ to 2.7×10^4) were obtained over a range of reaction temperatures (180–250°C) and CO_2 pressures [20.7–24.1 MPa (207–241 bar)]. Reaction conditions were chosen to ensure efficient removal of solubilized condensate (phenol) without extracting the reactants (diphenyl carbonate). Polycarbonate synthesis from bisphenol A and diphenyl carbonate catalyzed by tetraphenylphosphonium tetraphenyl borate were also performed in $scCO_2$ (93) (eq. (9)).

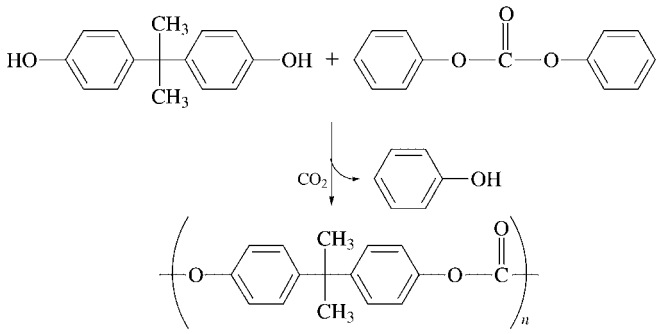

(9)

Polymers with high molecular weights (M_n up to 1.3×10^4 g/mol) were obtained at 270°C and 29.6 MPa (296 bar) CO_2. In this technique a slight excess of diphenyl carbonate is required because of monomer extraction. Supercritical CO_2 has also been used to induce crystallization of PC prepolymer beads for solid-state polymerization (94). The amorphous PC beads ($M_w = 2500$ g/mol) were rendered 19% crystalline by treatment with $scCO_2$ and were subsequently polymerized at temperatures from 180 to 240°C yielding polymers with molecular weights as high as 1.4×10^4 g/mol.

Poly(ethylene terephthalate) (PET) is commonly prepared by melt-phase polycondensation reactions. Bis(hydroxyethyl) terephthalate (BHET) was converted to PET under a variable flow (2–10 mL/min) of CO_2 at 20.7 MPa (207 bar) (95). Molecular weights were obtained over the range 3×10^3 to 6.3×10^3 g/mol and increased significantly with flow rate and/or reaction time. These values are low compared to normal molecular weights obtained in commercial processes (approx. 2×10^4 g/mol) and may be attributed to the decreased solubility of the ethylene glycol condensate in CO_2 compared with phenol in the polycarbonate system.

Polyamides have also been synthesized in the melt phase in the presence of CO_2 by the nylon salt route (96). A 1:1 salt of hexamethylenediamine and adipic acid was heated at 220°C for 2 h and then at 280°C for 3 h in 20.7 MPa (207 bar) CO_2 producing nylon-6,6 with molecular weights up to 2.45×10^4 g/mol.

Oxidative Coupling. The synthesis of polypyrrole, an organic conducting polymer known for its good thermal stability, has been extended to SFCs. Polypyrrole was synthesized in supercritical fluoroform and in $scCO_2$ from pyrrole that is generated *in situ* by decarboxylation of 2-carboxypyrrole and a chemical oxidant [either $FeCl_3$ or $Fe(CF_3SO_3^-)_3$] (97). $Fe(CF_3SO_3^-)_3$ was more soluble in CO_2 and gave higher yields compared to $FeCl_3$ (50–60% vs. 87% yield). These yields are still lower than those obtained from control reactions run in toluene (92%). Unlike the globular structure normally obtained when polypyrrole is prepared in traditional solvents, these polymers possess a different morphology with fibers ranging from 100 to 200 nm in diameter and several micrometers long.

Poly(2,6-dimethylphenylene oxide) (PPO) is synthesized via oxidative coupling in a CO_2 continuous phase (43). The reactions proceed at 34.5 MPa (345 bar) and at either room temperature or 40°C for 20 h using a CuBr/amine/O_2 catalyst system (eq. (10)). PPO with yields as high as 83% and Mn up to 1.7×10^4 g/mol were precipitated. Small molecule amines (pyridine and dimethylethylamine) and CO_2-soluble polymeric amines (block copolymers of FOA and either 4-vinylpyridine or DMAEA) were used in the reaction.

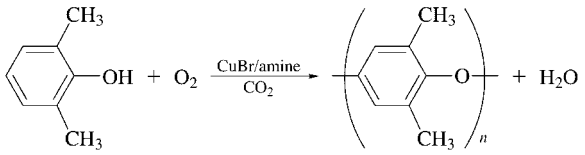

(10)

The pyridine proved to be the most effective amine for the system. Although the polymeric amines produced milky white latexes and served to stabilize the PPO as a colloid, no increase in yields or molecular weight associated with dispersion polymerizations were observed.

Porous Polymer Synthesis. Supercritical CO_2 is an attractive solvent for the preparation of porous polymers since conventional processes often require large volumes of "porogenic" organic solvents that tend to become trapped in the polymer matrix. Microcellular polyurethane foams have been synthesized in $scCO_2$ by treating a range of diisocyanates with various propylene oxide and ethylene oxide polyols (98). Phase separation was found to lead to the generation of a polymer-rich phase and a CO_2-rich phase that became porous upon removal of CO_2. Another example of the synthesis of porous polymers is the direct formation of aerogels by sol–gel polymerization of alkoxysilanes in $scCO_2$ (99). A "water-free" sol–gel polymerization technique is utilized in order to account for the low miscibility of water and CO_2 (100). In this technique, alkoxysilanes such as tetramethoxysilane (TMOS) and 1,4-bis-(triethoxysilyl) benzene (BESP) can react with anhydrous formic acid at 35–40°C in the presence of 41 MPa (410 bar) $scCO_2$ for up to 12 h. Opaque white silica aerogels were obtained in nearly quantitative yields (after aging for 12–18 h). The silica gels contained pores larger than those found in gels made in traditional solvents and had interconnected particles 100–200 nm in diameter. Surface areas of silica gels (260–308 m^2/g) were similar to gels formed in ethanol or formic acid. BESP aerogels had surface areas lower than those prepared by aqueous sol–gel polymerizations in organic solvents (471–586 m^2/g vs 1000–1600 m^2/g) (101). A technique has been developed that exploits the selation of CO_2 to form well-defined macroporous materials based on acrylate monomers (IOZ) and by using suspension polymerization methods (103).

Conclusion

The many examples cited in this article suggest that CO_2 is a viable alternative solvent for numerous polymerizations. The use of CO_2 provides not only environmental advantages over traditional solvents but also performance advantages. And its tunable properties allow it to be used as a continuous phase in a variety of both step-growth and chain-growth polymerization techniques with control heretofore unattainable with conventional solvents. The rapid growth of CO_2 technology in the past ten years has provided fundamental knowledge that will undoubtedly enable the preparation of more advanced materials in the future.

BIBLIOGRAPHY

1. J. A. Darr and M. Poliakoff, *Chem. Rev.* **99**, 565 (1999).
2. K. M. Scholsky, *J. Supercrit. Fluids* **6**, 103 (1993).
3. A. I. Cooper, *J. Mater. Chem.* **10**, 207 (2000); J. L. Kendall and co-workers, *Chem. Rev.* **99**, 543 (1999).

4. E. L. Quinn and C. L. Jones, *Carbon Dioxide*, Reinhold Publishing Corp., New York, 1936.
5. J. A. Hyatt, *J. Org. Chem.* **49**, 5097 (1984).
6. M. A. McHugh and V. J. Krukonis, *Supercritical Fluid Extraction: Principles and Practice*, 2nd ed., Butterworth-Heineman, Stoneham, 1993.
7. P. E. Jessop and W. Leitner, eds., *Chemical Synthesis Using Supercritical Fluids*, Wiley-VCH, Weinheim, 1999.
8. T. Sarbu, T. Styranec, and E. J. Beckman, *Nature* **405**, 165 (2000).
9. R. C. Reid, J. M. Praunsnitz, and B. E. Poling, *The Properties of Gases and Liquids*, 4th ed., McGraw-Hill Book Co., Inc., New York, 1987.
10. F. G. Keyes and J. G. Kirkwood, *Phys. Rev.* **36**, 754 (1930).
11. S. G. Kazarian and co-workers, *J. Am. Chem. Soc.* **118**, 1729 (1996).
12. A. Dardin and co-workers, *Macromolecules* **30**, 3593 (1997).
13. A. Dardin, J. M. DeSimone, and E. T. Samulski, *J. Phys. Chem. B* **102**, 1775 (1998).
14. J. M. DeSimone, Z. Guan, and C. S. Elsbernd, *Science* **257**, 945 (1992).
15. Z. Guan and co-workers, *Macromolecules* **26**, 2663 (1993).
16. Int. Pat. Appl. PCT/US 93/01626 (1993), J. M. DeSimone.
17. Z. Guan and co-workers, *Polym. Prepr. (Am. Chem. Soc., Div. Polym. Chem.)* **34**, 329 (1993).
18. K. K. Kapellen, C. D. Mistele, and J. M. DeSimone, *Polym. Prepr. (Am. Chem. Soc. Div. Polym. Mater. Sci. Eng.)* **74**, 256 (1996).
19. M. Shaw, J. Ryan, and C. Erkey, *Abstr. Pap. Am. Chem. Soc.* **214**, 243 (1997).
20. A. M. van Herk and co-workers, *Macromolecules* **30**, 4780 (1997).
21. M. A. Quadir and co-workers, *Macromolecules* **31**, 6481 (1998).
22. S. Beuermann and co-workers, *Macromol. Chem. Phys.* **199**, 1209 (1998).
23. J. R. Combes, Z. Guan, and J. M. DeSimone, *Macromolecules* **27**, 865 (1994).
24. M. Hagiwara and co-workers, *J. Polym. Sci., Part A-1* **6**, 603 (1968).
25. M. Hagiwara and co-workers, *J. Polym. Sci., Part A-1* **6**, 609 (1968).
26. U.S. Pat. 3471463 (1969), T. Kagiya and co-workers.
27. Fr. Pat. 1524533 (1968) (Sumitomo Chemical Co.).
28. U.S. Pat. 3522228 (1970), K. Fukui and co-workers.
29. T. J. Romack, E. E. Maury, and J. M. DeSimone, *Macromolecules* **28**, 912 (1995).
30. H. Q. Hu and co-workers, *Acta Polym. Sinica* 740 (1998).
31. U.S. Pat. 5345013 (1994), D. J. Van Bramer, M. B. Shiflett, and A. Yokozeki.
32. T. J. Romack, B. E. Kipp, and J. M. DeSimone, *Macromolecules* **28**, 8432 (1995).
33. T. J. Romack and J. M. DeSimone, *Macromolecules* **28**, 8429 (1995).
34. J. P. DeYoung, T. J. Romack, and J. M. DeSimone, *Polym. Prepr. (Am. Chem. Soc., Div. Polym. Chem.)* **38**, 424 (1997).
35. P. A. Carpentier and co-workers, *Macromolecules* **32**, 5973 (1999).
36. A. I. Cooper, W. P. Hems, and A. B. Holmes, *Macromol. Rapid Commun.* **19**, 353 (1998).
37. A. I. Cooper, W. P. Hems, and A. B. Holmes, *Macromolecules* **32**, 2156 (1999).
38. K. E. J. Barret, *Dispersion Polymerization in Organic Media*, John Wiley & Sons Inc., New York, 1975
39. E. D. Sudol, in J. M. Asua, ed., *Polymeric Dispersions: Principles and Applications*, Vol. **335**, Kluwer Academic Press: Boston, Mass. 1997, pp. 141–153.
40. J. M. DeSimone and co-workers, *Science* **265**, 356 (1994).
41. F. A. Adamsky and E. J. Beckman, *Macromolecules* **27**, 312 (1994).
42. K. K. Kapellen, C. D. Mistelle, and J. M. DeSimone, *Macromolecules* **29**, 495 (1996).
43. Y. L. Hsiao and co-workers, *Macromolecules* **28**, 8159 (1995).
44. Y. L. Hsiao and J. M. DeSimone, *J. Polym. Sci., Part A: Polym. Chem.* **35**, 2009 (1997).
45. K. A. Shaffer and co-workers, *Macromolecules* **29**, 2704 (1996).
46. M. L. O'Neill and co-workers, *Macromolecules* **31**, 2848 (1998).
47. M. L. O'Neill and co-workers, *Macromolecules* **31**, 2838 (1998).

48. C. Lepilleur and E. J. Beckman, *Macromolecules* **30**, 745 (1997).
49. D. A. Canelas, D. E. Betts, and J. M. DeSimone, *Macromolecules* **29**, 2818 (1996).
50. D. A. Canelas and J. M. DeSimone, *Macromolecules* **30**, 5673 (1997).
51. M. R. Clarke, J. L. Kendall, and J. M. DeSimone, *Macromolecules* **30**, 6011 (1997).
52. P. Christian and S. M. Howdle, *Macromolecules* **33**, 237 (2000).
53. D. A. Canelas and co-workers, *Macromolecules* **31**, 6794 (1998).
54. T. Carson, J. Lizotte, and J. M. DeSimone, *Macromolecules*, **33**, 1917–1920 2000.
55. H. Shiho and J. M. DeSimone, *Macromolecules*, **33**, 1565–1569 2000.
56. D. C. Blackley, *Emulsion Polymerization*, John Wiley & Sons, Inc., New York, 1975.
57. R. G. Gilbert, *Emulsion Polymerization: A Mechanistic Approach*, Academic Press, London, 1995.
58. F. A. Adamsky and E. J. Beckman, *Macromolecules* **27**, 523 (1994).
59. E. E. Maury and co-workers, *Polym. Prepr. (Am. Chem. Soc., Div. Polym. Chem.)* **6**, 205 (1993).
60. K. P. Johnston and co-workers, *Science* **271**, 624 (1996).
61. K. Harrison and co-workers, *Langmuir* **10**, 3536 (1994).
62. J. J. Watkins and T. J. McCarthy, *Macromolecules* **27**, 4845 (1994).
63. J. J. Watkins and T. J. McCarthy, *Macromolecules* **28**, 4067 (1995).
64. E. Kung, A. J. Lesser, and T. J. McCarthy, *Macromolecules* **31**, 4160 (1997).
65. K. A. Arora, A. J. Lesser, and T. J. McCarthy, *Macromolecules* **32**, 2562 (1999).
66. P. Rajagopalan and T. J. McCarthy, *Macromolecules* **31**, 4791 (1998).
67. R. Biddulph and P. Plesch, *J. Chem. Soc.* 3913 (1960).
68. T. Perneker and J. P. Kennedy, *Polym. Bull.* **32**, 537 (1994).
69. U.S. Pat. 5376744 (1994), J. P. Kennedy and T. Pernecker.
70. H. Yokota and co-workers, *J. Polym. Sci., Part A-1* **42**, 1412 (1969).
71. T. Pernecker, G. Deak, and J. P. Kennedy, *Macromol. Rep. A* **32**, 969 (1995).
72. M. R. Clarke and J. M. DeSimone, *Polym. Prepr. (Am. Chem. Soc., Div. Polym. Chem.)* **35**, 482 (1994).
73. M. R. Clarke and J. M. DeSimone, *Macromolecules* **28**, 3002 (1995).
74. T. Higashimura, M. Sawamoto, and M. Miyamoto, *Macromolecules* **17**, 265 (1984).
75. M. R. Clarke, J. L. Kendall, and J. M. DeSimone, *Macromolecules* **30**, 6011 (1997).
76. S. T. Nguyen, R. H. Grubbs, and J. W. Ziller, *J. Am. Chem. Soc.* **115**, 9858 (1993).
77. C. D. Mistle, H. H. Thorp, and J. M. DeSimone, *J. Macromol. Sci., A: Pure Appl. Chem.* **33**, 953 (1996).
78. J. G. Hamilton and co-workers, *Macromolecules* **31**, 4387 (1998).
79. P. Schwab and co-workers, *Angew. Chem. Int. Ed. Engl.* **34**, 2039 (1995).
80. P. Schwab, R. H. Grubbs, and J. W. Ziller, *J. Am. Chem. Soc.* **118**, 100 (1996).
81. R. R. Schrock and co-workers, *J. Am Chem. Soc.* **112**, 3875 (1990).
82. H. Hori, C. Six, and W. Lietner, *Macromolecules* **32**, 3178 (1999).
83. D. J. Darensbourg, N. W. Stafford, and T. Katsurao, *J. Mol. Cat. A: Chem.* **104**, L1–L4 (1995).
84. D. J. Darensbourg and M. W. Holtcamp, *Macromolecules* **28**, 7577 (1995).
85. D. J. Darnsbourg and M. W. Holtcamp, *Coord. Chem. Rev.* **153**, 155 (1996).
86. S. A. Mang and co-workers, *Macromolecules*, in press.
87. P. Christrian and co-workers, *Polym. Prepr.* **8**, 434 (1997).
88. C. U. Pittman and S. Yukihiko, *Chem. Lett.* 383 (1975).
89. D. A. Foucher, B. Z. Tang, and I. Manners, *J. Am. Chem. Soc.* **114**, 6246 (1992).
90. E. W. Neuse and L. Bednarik, *Macromolecules* **12**, 187 (1979).
91. P. G. Odell and G. K. Hamer, *Polym. Prepr.* **38**, 470 (1997).
92. U.S. Pat. 5698665 (1997), P. G. Odell.
93. S. M. Gross and co-workers, *Macromolecules* **31**, 25, 9090 (1998).
94. S. M. Gross and co-workers, *Macromolecules* **32**, 3167 (1999).
95. A. L. Burke, G. Maier, and J. M. DeSimone, *Polym. Mater. Sci. Eng.* **74**, 248 (1996).

CYCLOHEXANEDIMETHANOL POLYESTERS

Introduction

1,4-Cyclohexanedimethanol (CHDM) is an important commercial cycloaliphatic diol that is used in a variety of important commercial polyesters. It is produced by the catalytic hydrogenation of dimethyl terephthalate (DMT) (1). CHDM can exist as the cis or trans isomer; however, most commercial high volume production CHDM is a mixture of isomers with an approximately 70/30 trans/cis ratio. This isomer ratio plays an important role in determining the final properties of polyesters containing CHDM by influencing the ability of chains to pack efficiently. Structure **1**, trans (axial, axial) enchainment, and structure **2**, cis enchainment, schematically illustrate the differences in these structures. Most CHDM containing polyesters are based on the 70/30 (trans/cis) mixture and the stereochemistry of CHDM is maintained during the polycondensation.

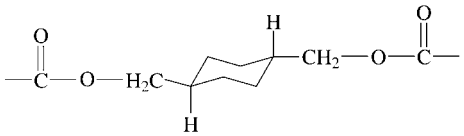

1

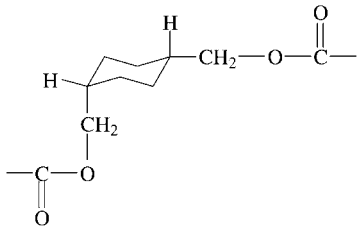

2

Encyclopedia of Polymer Science and Technology. Copyright John Wiley & Sons, Inc. All rights reserved.

The amount of CHDM incorporation as a comonomer also has a large effect on the crystalline nature of the backbone since it is so dissimilar in size and shape to other common diols (2). Poly(ethylene terephthalate) (PET) containing low levels of CHDM (less than 5 mol%) has enjoyed widespread use in stretch blow molded carbonated soft drink containers, where the CHDM modifies strain hardening during stretching, which therefore serves to widen the processing window. When incorporated into a terephthalic acid (TPA) based polyester at higher levels, the absolute level of CHDM can regulate whether the polyester is a high melting crystalline material or a tough clear amorphous composition. In general, when CHDM is copolymerized with other aliphatic diols with common diacids such as TPA, it increases the T_g of the backbone as well as rendering the backbone more resistant to hydrolysis. The flexible character of the CHDM unit is also known to impart enhanced impact and toughness to polyesters. The origin of these effects has been studied and a recent report correlates these properties to secondary relaxation modes arising from the CHDM structure (3).

The most important commercial polyesters containing CHDM are based on TPA and ethylene glycol (EG). Isophthalic acid (IPA) can also be used as a comonomer with TPA. The polyester of CHDM with TPA is poly(1,4-cyclohexylenedimethylene terephthalate) (PCT), which melts at 300°C. When this structure is modified with an acid such as IPA, the abbreviation PCTA (acid-modified PCT) is used. PCT polyesters with glycol modification of up to 50 mol% EG are abbreviated as PCTGs. Likewise, PET polyesters with up to 50% CHDM content are called PETGs. The abbreviations of PETG, PCTG, and PCTA are generally reserved for compositions that contain enough of the comonomer to render the backbone slow to crystallize or amorphous. This article discusses the chemical characteristics and properties of the important commercial crystalline and amorphous examples of polyesters based on CHDM.

Crystalline Polymers Based on CHDM

The primary crystalline polymer based on CHDM is the terephthalate, PCT. PCT was originally developed for fiber applications but has since found wider utility as a reinforced polymer for injection molding and (when copolymerized with a small amount of IPA) as a material for crystallized food packaging trays. The key property of PCT, which sets it apart from other thermoplastic polyesters in these latter applications, is melting point.

When made with the normal 70/30 trans/cis CHDM isomer ratio, the melting point of PCT is about 290°C. The melting point varies substantially with isomer ratio, however, as shown in Table 1 (4).

Table 1. Effect of trans/cis Isomer Ratio on Melting Point of PCT

% trans	T_m, °C
100	315
70	290
50	275
0	250

For comparison, the melting point of poly(butylene terephthalate) (PBT) is 225°C and that of PET is in the range of 250–260°C.

Crystallization of PCT is relatively rapid, but because of its higher T_g (90°C) the maximum rate of crystallization occurs at a higher temperature than is typical of other crystalline polymers such as PET (T_g about 70°C) or PBT (T_g about 35°C).

The bulky in-chain CHDM moiety results in several other important differences between PCT and crystallizable polyesters such as PET. The amorphous density is significantly lower, 1.195 g/cm^3 for PCT compared to 1.334 g/cm^3 for PET. PCT also exhibits a strong sub-T_g molecular relaxation, which results in a relatively low modulus at room temperature (155 MPa vs 240 MPa for PET) and improved toughness in the amorphous state. As an example of the latter phenomenon, the notched Izod impact strength of amorphous PCT is greater than 1000 J/m, while that of amorphous PET is less than 100 J/m.

The CHDM isomer ratio also has an effect on gas barrier properties, with better barrier properties resulting from higher cis levels. Because of the higher local free volume contributed by the CHDM structure, the diffusivity through PCT is generally higher than that through denser structures like PET (5). However, the magnitude of this effect is strongly dependent on the isomer ratio, as shown in Table 2. A recent patent (6) discloses that PCT with a 93/7 cis/trans ratio containing 50% 2,6-naphthalene dicarboxylic acid has a permeability of 2.68 (cm^3·mil)/(100 in.^{2} · 24 h · atm).

Preparation of PCT is best accomplished from DMT using standard transesterification catalysts such as titanium compounds. Because of the high melting point of the polymer, final polyesterification temperatures must be high (greater than 300°C at typical commercial trans/cis ratios) (7). PCT prepared in the melt phase can be crystallized and then solid phase polymerized to obtain even higher molecular weights.

If PCT is modified with relatively high levels of comonomer, substantially amorphous materials result (as described later). However, it is possible to maintain crystallinity at lower levels of modification. For example, replacing up to about 10 mol% of the terephthalate units with isophthalate results in a polymer with reasonable crystallization rates and ultimate degrees of crystallinity.

One might expect that replacing the terephthalate unit in PCT with naphthalene dicarboxylate would make an interesting high temperature polymer. This polymer cannot be successfully prepared, however, because its melting point is above its degradation temperature. Reduction of the melting point by

Table 2. Effect of cis Isomer Content on Gas Barrier Properties of PCT

% cis CHDM	Oxygen permeability, nmol/(m·s·GPa)[a]
93	30
46	62
26	80

[a] To convert nmol/(m·s·GPa) to (cm^3·mil)/(100 in.^{2}·24 h·atm), divide by 2.

copolymerization (for example either with terephthalic acid or isophthalic acid) eliminates this problem (8).

Crystalline polyesters from CHDM and aliphatic diacids are possible, but generally are of little interest because of low melting points and low glass-transition temperatures. Cyclic aliphatic diacids offer some potentially attractive possibilities since the melting points are not so depressed. For example, the polyester of CHDM with the high trans isomer of 1,4-cyclohexane dicarboxylic acid has a melting point similar to that of PBT (7).

Processing of Crystalline PCT-Based Polymers. Melt processing of the high-melting PCT-type polymers must be done carefully, owing to a relatively small window between the melting point and the temperature at which degradation rates become significant. The degradation is both thermal and hydrolytic in nature. While it may be argued that the PCT structure is inherently more hydrolytically stable than other polyesters such as PET, the higher processing temperature compensates by accelerating the rate. Thus drying of the polymer or formulation before processing is recommended. Dessicant drying at temperatures up to about 125°C is commonly used.

Degradation results in color formation, loss of molecular weight, and deterioration of critical mechanical properties such as toughness.

Injection Molding Applications. PCT forms the basis of a family of reinforced, crystalline plastics for injection molding. As mentioned previously, the high melting point of the polymer is a key property, as this results in high heat-deflection temperatures (HDT) in glass-fiber-reinforced formulations. Good toughness, flow into the mold, and rapid crystallization are also important attributes in these applications.

Formulations for injection molding typically contain 30–40 wt% glass fiber or a mixture of glass fiber and mineral filler. Stabilization packages to improve processing stability and additives to enhance crystallization rate are also incorporated. These products may or may not be flame-retarded, depending on the application area, with HDTs ranging from about 250°C to about 260°C. This level of heat resistance makes PCT-based plastics suitable for high temperature applications such as electronic connectors, where high soldering temperatures are encountered. Typical competitive materials in this market include poly(phenylene sulfide), with an HDT of about 260°C, and high temperature polyamides, with HDTs in the range of 270–280°C. Other properties of a typical 30% glass-reinforced, flame-retarded grade of PCT are shown in Table 3.

Table 3. Properties of 30% Glass-Reinforced Flame-Retarded PCT

Specific gravity	1.63
Tensile strength, MPa[a]	120
Tensile elongation, %	2
Flexural modulus, MPa[a]	9600
Notched Izod impact, J/m[b]	90
HDT, 1.82 MPa, °C	255
UL Subject 94 flammability	V0

[a]To convert MPa to psi, multiply by 145.
[b]To convert J/m to ft·lbf/in., divide by 53.38.

Flame-retarded grades are widely used for various computer connectors and circuit board components. Representative applications are edge card connectors, grid arrays, and memory modules. Non-flame-retarded grades find use in automotive (under the hood) applications, typically connectors and related parts. As higher temperature soldering techniques become more common in the automotive industry, the use of high temperature plastics such as PCT is expected to increase.

It is also possible to formulate unreinforced PCT with crystallization aids and tougheners to provide a material similar in some respects to supertough nylon. PCT provides advantages in dimensional stability and lower moisture sensitivity compared to the polyamide-based products.

Extrusion Applications. A well-established application for extruded unreinforced PCT (copolymerized with isophthalate) is in the preparation of crystallized, thermoformed trays for foods. Crystallized PET is widely used for this application, but where higher temperature performance is needed the PCT-based polymer may be chosen. Such trays are formed from extruded sheet, using a hot mold to promote crystallization. Isophthalate-modified PCT polymers are approved by the Food and Drug Administration for high temperature food contact use.

The good hydrolytic stability of PCT-based polymers leads to applications for monofilament in paper machine belts. Monofilament is extruded from high molecular weight polymer, drawn, and crystallized, then woven into a screen. Such belts are found in the drying section of paper machines, where there is a combination of high moisture and high temperature. Because of their hydrolytic stability, PCT-based polymers provide much longer service life in this application than PET-based.

Amorphous Polyesters, CHDM-Modified PET and PCT

The size and shape of CHDM render it as an effective diol for modifying crystallinity in polyesters. The decrease in crystallization rates for low levels of CHDM incorporation into PET is shown in Figure 1, where the half-times (measured by dsc) for crystallization vs temperature in the melt are plotted. When copolymerized with EG and TPA, the middle composition ranges, from approximately 70/30 CHDM/EG to 20/80 CHDM/EG, have very slow crystallization rates and do not show crystallization peaks when scanned by dsc at 20°C/min and thus are amorphous polyesters. These compositions can be processed into clear, transparent sheets and molded articles.

As the composition is varied from a PETG composition to a PCTG composition, several general property trends are noted. These are illustrated in the schematic in Figure 2.

Increasing CHDM level leads to an increase in toughness, as measured by impact and increasing elongation-to-break values, a decrease in tensile modulus, and increases in T_g and HDT. A comparison of the physical and mechanical properties for a PETG composition of approximately 70 EG/30 CHDM and a PCTG composition of approximately 60 CHDM/40 EG is shown in Table 4.

Preparation of Amorphous PETGs and PCTGs. In general, amorphous PETG and PCTG polyesters can be made by standard melt-phase polycondensation processes, starting either with DMT or TPA. One significant difference

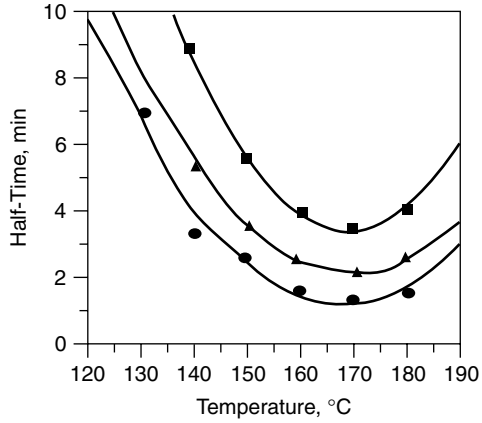

Fig. 1. Plot of crystallization half-time in minutes as determined by dsc versus temperature in degree Celsius. ● PET; ▲ PET–1.5% CHDM; ■ PET–3.5% CHDM.

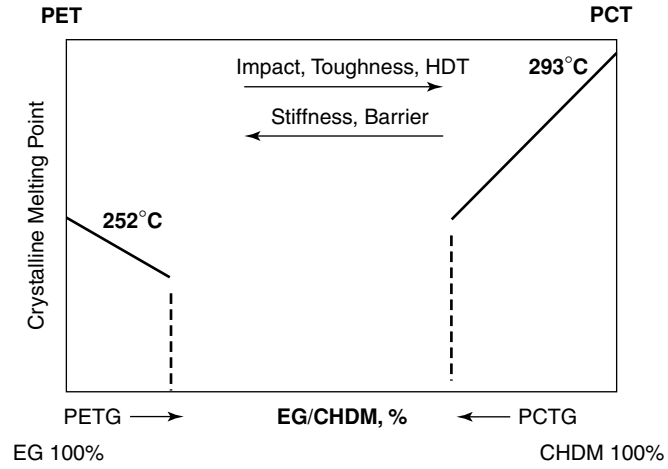

Fig. 2. Schematic showing the general properties and amorphous regions for PETG and PCTG polyesters.

in the preparation of amorphous copolyesters compared to crystalline copolyesters is the need to achieve the required degree of polymerization directly in the melt-phase process. Crystalline polyesters are readily solid-state polymerized to high degrees of polymerization, thus avoiding any problem with melt viscosity in the large-scale finishing reactors used for the melt-phase processes. However, the slow crystallization rates for amorphous copolyesters prohibit converting to a crystalline state, which is required to avoid the fusing of pellets or powders used in the solid-state processes.

Processing and Applications of PETGs and PCTGs. The amorphous nature of both PETG and PCTG permits them to be processed into clear transparent sheets and articles. PETG has found large volume application in extruded

Table 4. Physical Property Comparison of Amorphous PETG, PCTG, and PCTA

Property	PETG	PCTG	PCTA
Specific gravity	1.27	1.23	1.20
Thermal properties[a]			
T_g, °C	81	84	88
HDT			
0.455 MPa	70	74	75
1.82 MPa	64	65	65
Tensile properties[a]			
Stress @ yield, MPa	50	45	47
Stress @ break, MPa	28	52	51
Elongation @ yield, %	4.3	5	5
Elongation @ break, %	110	330	300
Flexural properties[a]			
Flexural modulus, MPa	2100	1900	1800
Flexural yield strength, MPa	70	66	69
Izod impact strength[b,c]			
Notched @ 23°C, J/m	101	NB	80
Unnotched @ 23°C, J/m	NB	NB	NB
Notched @ −40°C, J/m	37	64	40
Unnotched @ −40°C, J/m	NB	NB	NB

[a]To convert MPa to psi, multiply by 145.
[b]To convert J/m to ft·lbf/in., divide by 53.38.
[c]NB = no break.

heavy gauge sheet products, blister packages, etc. It offers better toughness than acrylic-based sheet products and better chemical resistance than polycarbonate products (9). The higher CHDM-containing copolyesters are often preferred for applications in medical devices where resistance to lipid solutions and property retention after gamma and ethylene oxide sterilization are important (9).

Acid-Modified PET and PCT Amorphous Copolyesters. Some of the performance benefits of PCT vs PET include improved toughness, hydrolysis resistance, electrical properties, color, and clarity. However, because of the high melting point of PCT (typically ∼290°C), this polyester must be processed at temperatures in excess of 300°C. This results in a very narrow processing range for PCT in order to avoid degradation (10). Incorporation of relatively low levels of a modifying diacid, such as IPA, into PCT yields PCTA compositions which are less crystalline and have lower melting points but which retain the good toughness characteristics and other beneficial properties of PCT. As the isophthalate level in the PCTA is increased, the melting point decreases and the processing window increases. IPA is also used in low levels as a modifier for PET. It provides a slight improvement in barrier properties and also allows for a slightly lower processing temperature. Higher levels of IPA modification of PET can further improve the barrier properties but lead to significant loss of toughness and heat resistance of molded containers. In contrast, PCT can be modified using high levels of IPA to yield PCTA compositions with outstanding properties. Above about 20% isophthalate incorporation, the poly(1,4-cyclohexylenedimethylene terephthalate-*co*-isophthalate) copolyesters are tough, amorphous thermoplastics, which are easy

to process. These amorphous materials can be processed at 230–280°C, much lower than the temperatures in excess of 300°C required for unmodified PCT. They can be injection molded to form tough, transparent parts and can be extruded into sheet, pipe, and profiles as well. The properties of a typical amorphous PCTA which has a composition of about 70 mol% TPA and 30 mol% IPA are shown in Table 4 and are very similar to those of amorphous PETG and PCTG. One advantage of amorphous PCTA compositions over analogous amorphous PETG and PCTG materials (with EG as the modifier) arises from the superior hydrolysis resistance of the PCTA. This manifests itself in the ability to melt process the PCTA with minimal or no drying, whereas PETG and PCTG require more extensive drying to avoid excessive loss in molecular weight during processing (11). Acids other than IPA have been investigated as modifiers for PCT and have been shown to give different performance attributes; however, no other PCTA compositions are commercially available.

BIBLIOGRAPHY

1. E. V. Martin and C. J. Kibler, in H. F. Mark, S. M. Atlas, and E. Cernia, eds., *Man-Made Fiber Science and Technology*, Vol. **3**, Interscience Publishers, a division of John Wiley and Sons, Inc., N.Y., 1968, pp. 83–134.
2. R. M. Schuylken Jr., R. B. Boy Jr., and R. H. Cox, *J. Polym. Sci., Part C* (6), 17 (1964).
3. L. P. Chen, A. F. Yee, and E. J. Moskala, *Macromolecules* **32**, 5944 (1999).
4. C. J. Kibler, A. Bell, and J. G. Smith, *J. Polym. Sci., Part A* **2**, 2115 (1964).
5. R. R. Light and R. W. Seymour, *Polym. Eng. Sci.* **22**(14) 857 (1982).
6. U.S. Pat. 5552512 (Sept. 3, 1996), B. J. Sublett (to Eastman Chemical Co.).
7. U.S. Pat. 2901466 (Aug. 25, 1959), C. J. Kibler, A. Bell, and J. G. Smith (to Eastman Kodak Co.).
8. D. C. Hoffman and T. J. Pecorini, *Polym. Prepr. (Am. Chem. Soc., Div. Polym. Chem.)* **40**(1) 572 (1999).
9. H. Yang, E. Moskala, and M. Jones, *J. Appl. Med. Polym.* **3**(2), 50 (1999).
10. J. R. Caldwell, W. J. Jackson Jr., and T. F. Gray Jr., in H. Mark, ed., *Encyclopedia of Polymer Science and Technology*, Suppl. 1, 1976, p. 444.
11. U.S. Pat. 56546715 (Aug. 12, 1997), J. P. Dickerson and co-workers (to Eastman Chemical Co.).

S. RICHARD TURNER
ROBERT W. SEYMOUR
THOMAS W. SMITH
Eastman Chemical Company

DENDRONIZED POLYMERS

Introduction

Practically all dendrimers (1–5) known today have cores with a few functional groups to which the corresponding number of dendrons (dendritic wedges) are attached. The fact that these dendrons are connected to one another by a small, almost dot-like molecule results in considerable steric congestion around the core. This congestion is a unique structural feature and has led one to view dendrimers, specifically those of high generation, as molecular boxes or containers (6,7) and as entities that assume a spherical shape to which a "surface" can be assigned. The term surface may, of course, only be applied with care. Since their discovery some 20 years ago, dendritic macromolecules have stimulated an almost explosive research effort and many synthetic, analytical, and application-related issues have been addressed (1–5). Even industrially applicable syntheses were developed (8–11). During this stormy process, research has virtually exclusively focused on dendrimers with small cores, in spite of a U.S. patent entitled "Rod-like Dendrimer" in 1987 (12,13). There the dendrimers are like (**1**) with polymeric cores and are proposed as being useful in the production of molecular composites and as crystallinity modifiers for polymeric materials. It took some years more before first (published) steps were undertaken to obtain these dendrimers (14,15). It is immediately apparent that they not only complement dendrimers with small cores under structural aspects but as a consequence of the structural differences they should also have unique properties. A simple reason for this slow development may be that in the beginning of dendrimer research spherical dendrimers were simply considered a more appropriate and perhaps more important target. As judged by the increasing number of publications, this view is presently undergoing a rapid modification. Another reason may be seen in a reluctance to begin

Encyclopedia of Polymer Science and Technology. Copyright John Wiley & Sons, Inc. All rights reserved.

working on a seemingly more complex area than small core dendrimers where chemists are already being confronted with considerable synthetic and analytical difficulty.

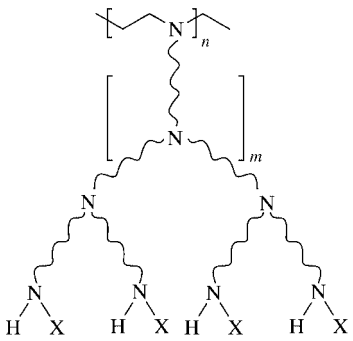

X = H, X = $CH_2CH_2CO_2^{\ominus}$ $Na^{\oplus}$

1

This article tries to draw a comprehensive picture of what has been done in the field of dendrimers with polymeric cores, putting emphasis on synthetic issues, on accurate molecular weight determination, and, finally, on the aggregation behavior of these intriguing macromolecules both in the bulk and at solid and fluid interfaces. First attempts to manipulate individualized dendronized polymers on surfaces are also described. The article starts with a small chapter summarizing some of the ideas why these make up a challenging project and where these unusual molecules are expected to have impact on the natural sciences.

The macromolecules treated here may be considered as either dendrimers with polymeric cores or alternatively dendronized polymers (or polymers with appendent dendrons) depending on whether one sees them from the vantage point of an organic or macromolecular chemist (Fig. 1). The first view is somewhat puzzling, because dendrimers are normally considered monodisperse, which they certainly are not (16), whereas polymeric dendrimers are intrinsically polydisperse. At best the polymeric core may have a narrow molecular weight distribution. Not considered here are polymers which do not carry dendrons at every repeat unit (r.u.) but at a few ones only, eg, at both termini (17–22), as well as works on

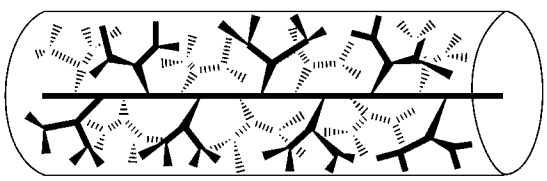

Fig. 1. Design of a dendronized polymer whose dendritic layer is so densely packed around the backbone that it is stretched out and a molecular cylinder with a "surface" is generated.

surface coatings with dendrons or hyperbranched molecules (23–28). The references to dendrimers with dot-like cores are kept at a minimum and the reader is referred to pertinent reviews, monographs (1–5,29), and other articles. Reviews on dendronized polymers are available (30–32). Attempts to stiffen polymer chains by attaching flexible, straight oligomers to each repeat unit which lead to the interesting class of bottle-brush-like polymers (33–41) are not covered in this article because of space limitations.

Dendronized Polymers

Dendronized polymers are formally comb polymers (42), with the combs' teeth being dendrons. What makes them so unique that one does not normally refer to them as such? Mainly it is the complex interplay of dendron size, distance between dendrons, and backbone flexibility/rigidity, together with several interactions (eg, dendron/dendron, dendron/backbone, solvent/dendron). All these factors sum up to a slower decrease of density on going from the interior to the exterior than in common comb polymers where the teeth are linear chains. This unusual density profile, which for spherically shaped dendrimers has been controversially discussed (43–46), leads to new and rather fascinating properties of otherwise conventional polymers. The first issue to mention here is their shape and its dependence on the substitution with dendrons. Depending on the dendrons' structure, size, and attachment density along the backbone, conventional polymer backbones such as polyacrylate or polystyrene can attain conformations all the way from random-coil to fully stretched linear: A flexible, cooked spaghetti-like polymer can be converted into a rigid (high bending modulus) rod just by proper substitution with large dendrons. This stiffening of the backbone is caused by steric repulsion between the pendent dendrons. For this reason the whole matter is referred to as shape-control by implementation of steric strain. In this sense steric strain may be compared to hydrogen bonding and π,π-stacking as the main shape-determining factors in proteins or DNA. In the extreme case, which will be described later, the dendritic layer around the polymer backbone is so dense that a macromolecule can turn into a molecular cylinder with defined dimensions: Its length is determined by the degree of polymerization and its diameter is roughly two times the dendron extension. In this case the dendrons spread away from each other to keep steric repulsion between them at a minimum.

Dendronized polymers can, however, also be designed so that there is an attractive interaction between dendrons that leads to shape control. This requires two features: (*1*) dendrons with mesogenic properties and (*2*) their loose attachment to the backbone which leaves the dendrons sufficient freedom to find the optimum packing. This kind of shape control driven by the dendrons' mesogenic properties can lead to highly ordered materials in the solid state as will be described later.

Let us come back to rigid polymers with a tightly packed dendritic layer around the backbone. What is the importance of such cylindrical objects (Fig. 2 and 3). Contrary to conventional polymers, their diameter is of the order of a few nanometers rather than tenths of a nanometer. As a consequence, the rigidity is so high that the persistence length of an individual chain can be a few tens of

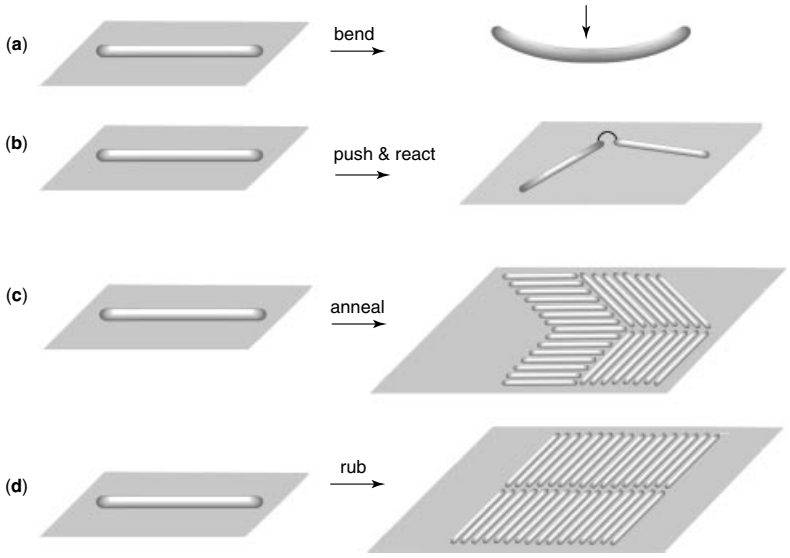

Fig. 2. Characterization, manipulation, and assembly of rigid dendronized polymers: (**a**) determination of bending moduli of individual macromolecules in dependence of factors like nature of backbone, generation of the attached dendrons, and the dendrons' molecular structure; (**b**) manipulation of individualized macromolecules on surfaces in order to use them for covalent nanoconstructions, eg, by inducing linkages photochemically; (**C**) Self-assembly of ordered arrays; and (**d**) generation of large oriented areas by rubbing or one-dimensional flow for applications, eg, in polarizers, polarized emitters, or as templates in LC-applications.

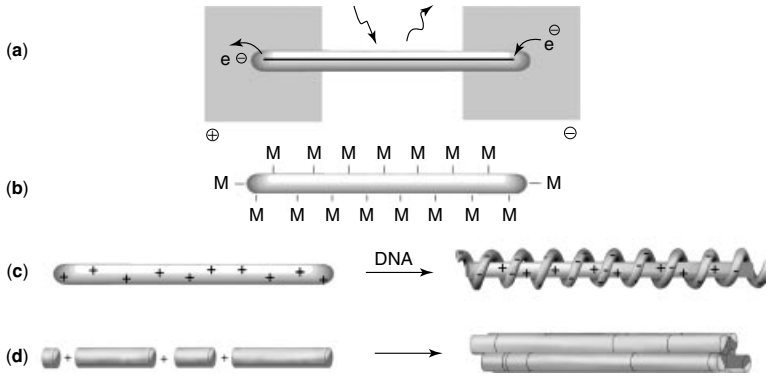

Fig. 3. Further potential applications of rigid dendronized polymers: (**a**) Use of conjugated polymers with dendritic shells for photoluminescence or charge carrier transport. The black line indicates a conjugated backbone. (**b**) Usage as nanometer-sized supports for catalysis when surface charged with catalytically active centers (m). (**c**) Generation of hybrid materials by, eg, wrapping of positively charged dendronized polymers with DNA, which is a negatively charged polyelectrolyte. (**d**) Amphiphiles with a lengthwise segregation of the polar and nonpolar domains (left) should possibly self-aggregate into supercylinders (right) which during growth can accept amphiphiles of different lengths and nevertheless be monodisperse regarding the diameter.

nanometers. Thus, exceptionally high bending moduli can be expected, despite the fact that the polymers are still single stranded (Fig. 2a). Dendritic rods could therefore potentially be used for constructions on the nanometer scale very much like an architect builds frames for houses, bridges, etc from plywood (Fig. 2b). The first steps in this direction would be to isolate individual rods, determine their dimensions, and move them about. The high modulus results in a strong tendency of these rods to form large ordered two-dimensional arrays in which the individual rods are packed parallely to each other like tree trunks of a raft, the only difference being that the dendritic trunks have a length distribution (Fig. 2c). Please note that the designs in this figure do not account for this. Rubbing or one dimensional flow may be used to orient the rods over large areas (Fig. 2d). Such large parallel-ordered arrays of nanometer scale objects on surfaces are interesting for a number of applications, eg, as polarizers, polarized emitters, or orienting surfaces in liquid crystal displays. Shielding comes into play when the backbones are electrically conducting or when they fluoresce (Fig. 3a). In the former case dendritic cylinders can be used to contribute to the important question of charge transport along an individual molecular wire. Because of their rigidity and the mere size, single cylinders could be placed between nano electrodes, the current be measured and correlated with one and only one molecular wire (Fig. 3a). The dendritic layer would just act as an insulating shell which, at the same time, provides some mechanical stiffness, a relevant issue for device fabrication. Insulation by dendritic layers can also help prevent fluorescence quenching in bulk phase, since conjugated backbones have a strong tendency to aggregate, which almost automatically results in quenching. Indeed, this spoils the potential utility of conjugated polymers as light emitters. Finally, the dendritic layer could possibly be used to harvest and channel energy to the backbone.

Apropos tree trunks and cylindrical surface: This may also be a starting point to think about dendritic rods as supports with defined curvatures to which catalytically active components could be attached (Fig. 3b). In a way, cylinders of the size discussed here bridge the gap between homogeneous and heterogeneous catalysis. They may combine the respective advantages of both. Attachment of catalytically active groups to the surface at more or less constant distances may well provide candidates, eg, for applications in flow reactors. Spherically shaped dendrimers equipped with transition-metal complexes have already been successfully employed for such purposes (47–50).

The fact that the tobacco mosaic virus also has a cylindrical shape at first glance may appear as a somewhat artificial link to the biosciences, but this striking similarity may nevertheless help initiate thought about the potential biological importance of dendritic rods and derivatives thereof. Spherically shaped dendrimers have already been used as gene vectors. Positively charged poly(amido amine) (PAMAM) dendrimers (51), for example, render DNA more compact through coulombic interactions, which facilitates cell membrane transfection (52,53). First experiments indicate a similar aggregation behavior between the cylinders' positive surface charges and the negatively charged phosphates of DNA (Fig. 3c). This could influence endocytosis and endosome formation, which are important matters during transfection.

Another important application of dendritic cylinders is as amphiphiles. Common amphiphiles like dodecylsulfonate can form micelles, bilayers, and other

interesting and sometimes even commercially relevant supramolecular aggregates (54). These amphiphiles normally are a few nanometers long and have diameters of a few tenths of a nanometer. If it were possible to decorate the surface of a dendronized polymer with one hydrophilic and one hydrophobic block segregated perpendicularly to the backbone, giant amphiphiles would result, which may lead to a big jump in the size of the corresponding aggregates. Alternatively, if it were possible to decorate the cylinders not cross- but lengthwise, the resulting amphiphiles (Fig. 3d) would have the unique polarity distribution of some ion channel membrane proteins and could be used for coatings to switch surface polarities to their opposite, or for various applications as colloids. These latter amphiphiles should also exhibit a rather unique aggregation behavior in which a defined number of linear sequences of the individual amphiphilic constituents (Fig. 3d, left), regardless of their respective chain length, form an indefinitely long super cylinder with monodisperse diameter (Fig. 3d, right). Such aggregates would exhibit an unprecedented mechanical stiffness when compared with the many known cylindrical self-aggregates from small (tenth of nanometer) amphiphiles (55).

Last but not least, the issues of synthesis and structural analysis ought to be mentioned. Before entering into all the exciting options mentioned above, dendronized polymers need to be synthesized and sufficiently characterized on both the organic chemistry and polymer level. Without going into details the main synthetic problems include (*1*) steric repulsion and thus incomplete reactions, (*2*) autocatalytic decomposition of sensitive dendrons because of their exceptionally high functional group density, (*3*) high molar mass and sometimes high molar mass difference of reactants which makes it difficult to meet correct stoichiometry, and (*4*) purification of high molar mass reactants. These factors may appear almost trivial but can brew together to a seething mixture which renders a controlled synthesis quite an endeavor and challenge. Additionally, the size of the molecules involved makes the tools of organic chemistry absolutely insufficient. Additional methods like small-angle neutron scattering (sans), scanning force microscopy (sfm), x-ray diffraction (qv), matrix-assisted laser desorption ionization time of flight (MALDI-TOF) mass spectrometry need to be employed to really prove what one proposes to have.

Synthesis

There are two principally different synthetic routes to dendronized polymers (Fig. 4). In the first, the polymer which becomes the core in the final product serves as starting material. Its anchor groups are used to convergently attach a dense sequence of dendrons (attach-to route, route A). In the second, monomers already carrying dendrons are subjected to polymerization or polycondensation (macromonomer route, route B). The intrinsic problems of both routes become more serious and limiting, the more sterically demanding the dendrons are. An obviously critical issue associated with route A is achieving complete coverage of the backbone anchor groups with dendrons. Even if a very efficient coupling chemistry is available, a large dendron excess may be required to drive the reaction to completion. This excess may, in turn, make it difficult to purify the product. If

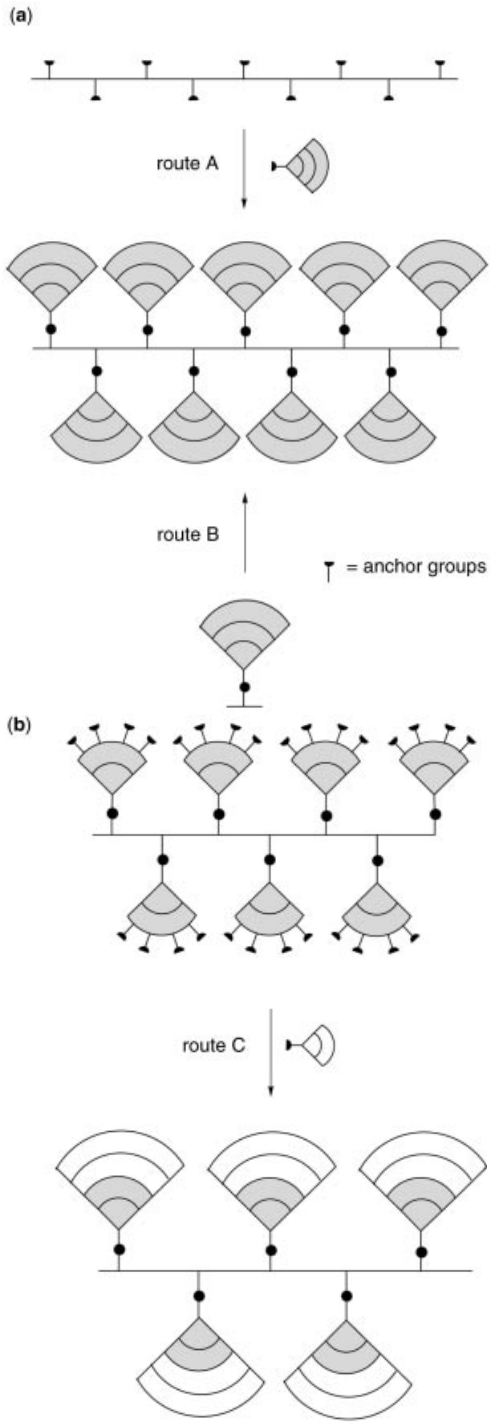

Fig. 4. Routes A and B (**a**) and C (**b**) to dendronized polymers. They may be referred to as attach-to route (A), macromonomer route (B), and mixed route (C). The dendrons shown are of generation 3 (routes A and B) and generation 2 and 4 respectively (route C).

large dendrons are to be attached, steric hindrance also comes into play for two reasons: (*1*) the shielding of unreacted anchor groups on the backbone by dendrons already attached in close proximity and (*2*) the dendron's conformation, which may lead to a self-shielding of the functional group at the focal point through which the attachment ought to take place. Both factors lead to a decrease in the rate of attachment, if they do not suppress the process entirely. This decrease of rate can favor side reactions which may not just involve themselves or the solvent but also the already attached dendrons.

The problems associated with route B also have something to do with steric hindrance. Here the critical point is the steric demand of both monomer and chain end. Incoming monomer will only be connected to the chain end if steric hindrance is not too high. Otherwise this process will be slowed or even rendered impossible. Depending on the kind of polyreaction applied, this may lead to termination of the reactive chain end and/or to side reactions of the monomer, like loss of coupling functionality as in some polycondensations or auto-initiation specifically in radical polymerizations. From this discussion it can be extracted that the basic problems for both routes are incomplete coverage (route A) and low molecular weight dendronized polymer (route B). Of course, intermediate solutions may also be applicable and have actually been developed to some ripeness during the last 3–4 years. If for some reason, eg, a fourth generation macromonomer does not polymerize (which in fact is normally the case) and the alternative attempt to attach a G4 dendron to a polymer also does not work (which is so in all reported cases), route C may offer the solution. Here a polymer which already carries second or third generation dendrons is converted to a higher generation one by attaching a second or first generation dendron. This of course requires the existence of functional groups at the surface of the starting polymer and the availability of a very efficient attachment chemistry whose efficiency must be quanti fiable.

Besides synthetic hurdles there are also analytical ones. Dendronized polymers tend to have repeat units with considerable molecular weight. Repeat units with 1, 2, or even 3 kDa are no exception. Such high molar masses sometimes render structural characterization difficult because the proportion of backbone to dendron atoms becomes so unfavorable that nmr spectroscopy reaches its limits. For example, sometimes the degree of attachment (coverage) simply cannot be determined with sufficient accuracy because the signal intensity of the unreacted anchor groups is too weak for comparison with reference signals in the spectrum. The nmr characterization may occasionally be further complicated by large differences in the relaxation times of backbone and dendron nuclei. Thus, nmr signal integrals are rendered unreliable if a sufficient pulse delay time is not applied. Another problem with dendronized polymers is their molar mass determination. Gel permeation chromatography (gpc) is a quick and easy method to roughly estimate the molar mass of a polymer (56). This estimation can only be reasonably used as long as the hydrodynamic volumina of the polymer under consideration and the polymer used for calibration purposes, typically polystyrene, are in the same range. The hydrodynamic volume of dendronized polymers strongly deviates, however, from parent polystyrene, and gpc results should be treated with care. Additionally, facile aggregation of these dendrimers is sometimes encountered, which leads to further complications. Other methods of molar mass

determination like light scattering have to be used and measures taken to avoid aggregation.

Looking back over what has happened regarding synthesis of dendronized polymers since 1992, when work (14,15) began in this field, one has to arrive at the conclusion that the attach-to route (route A) is inferior to the alternative macromonomer approach (route B). There is no reported route A case in which a complete coverage of a polymeric core with dendrons of higher generation than G2 was achieved. Additionally the polymeric cores used [mostly of the poly(*para*-phenylene) (PPP)-type] did not have very high molar masses. For route B, however, many high molar mass G2 cases, a few G3 ones, and a low molar mass G4 case are known. Furthermore, a high molar mass G4 polymer was reported recently. Since the mixed solution (route C) also has proven to be a successful alternative in certain situations, this article concentrates on route B and gives some insight into what has been accomplished along the lines of route C. For a treatment of route A representatives, however, the reader is referred to a pertinent review (30).

Overview of Macromonomer Approach. Synthesis of dendronized polymers from macromonomers (route B) has been developed broadly in recent years. A reason for this is the advantage that polymers, if they can be obtained at all by this method, necessarily carry the predetermined number of dendrons at the backbone. The above questions of dendron perfection and coverage degree in divergent and convergent syntheses do not play a role. This only holds true, of course, if the dendrons are compatible with the polymerization conditions and do not degrade, a prerequisite which is fulfilled in many of the cases reported. The polymerization procedures used may be divided into (*a*) radically initiated and transition-metal catalyzed chain-growth and (*b*) step-growth polymerizations (polycondensations). Figure 5 gives an overview of the macromonomers' structures reported to date and groups them into the subclasses *a* and *b* depending on the respective type of polyreaction. Fréchet-type dendrons (57) are drawn in an abbreviated form, which is explained in Figure 6. Monomers are polymerized by radical polymerization [**2** (15), **3** (58), **4** (59), **5** (60), **6** (61), **7** (62), **8** (63), **9** (64), **10** (61), **11** (55), and **12** (65)], insertion polymerization [**13** (66)], ring-opening metathesis polymerization (ROMP) (67) [**14** (68,69)], Suzuki polycondensation (SPC) (70,71) with **17** [**15** (72) and **16** (73)] and **24** [**20** (74), **21** (75), **22** (76), and **23** (76)], polyaddition with **19** under polyurethane formation [**18** (77)], Heck coupling of **25** with **26** (78,79), Sonogashira/Hagihara-type coupling of **27** with **28** (80), and, finally, Yamamoto reaction of **29** (81). Dendronized oligomers with enediine repeat units were also prepared (82).

Some features of the dendronized polymers obtained from the macromonomers of Table 1 will become important later in this article and are therefore emphasized in the following: (*1*) Most of the macromonomers carry G1 or G2 dendrons. Exceptions are only (**12**) (G3), (**16**) (G3), (**18**) (G3 and G4), (**23**) (G4), (**25**) (G3), and (**27**) (G3 and G4); (*2*) Many dendrons are of the benzyl ether type whose terminal phenyl rings are either unsubstituted or have one to three long alkoxy or fluoroalkoxy chains. The corresponding polymers are important for a variety of reasons but are unreasonable candidates, of course, whenever chemical modification becomes an issue; (*3*) This is where dendrons (**7**), (**8**), (**10**), (**11**), and potentially also (**13**) come into play which carry protected

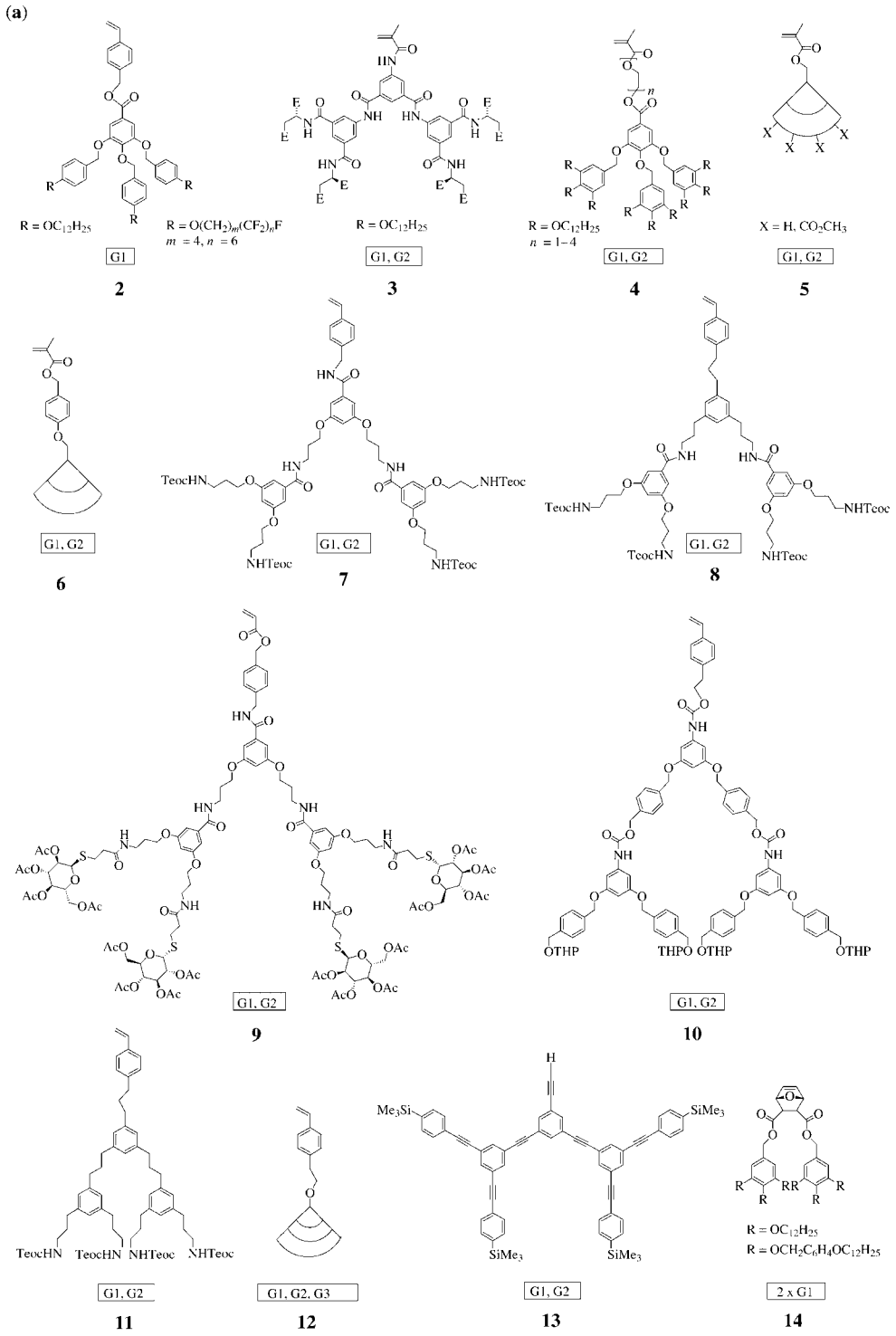

Fig. 5. Structures of macromonomers to obtain dendronized polymers by chain-growth (**a**) and step-growth procedures (**b**).

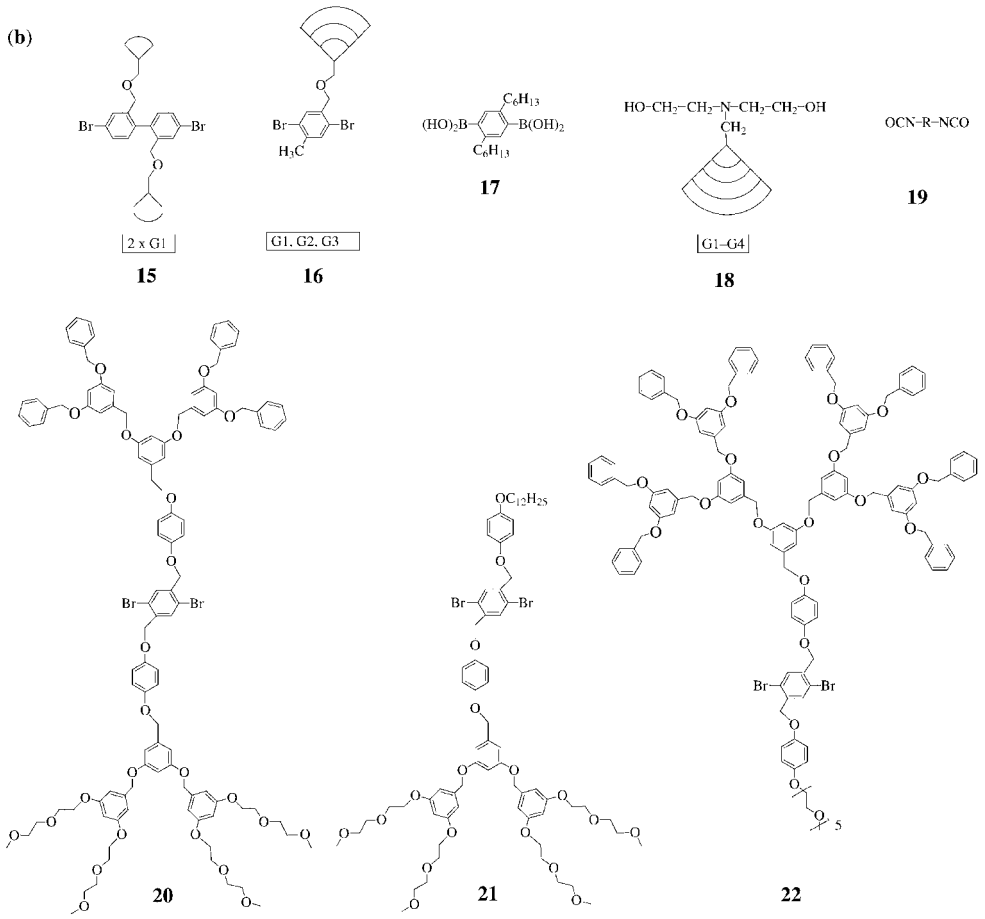

Fig. 5. (Continued)

functional groups [hydroxy, amino, trimethylsilyl (TMS)] in the periphery. The corresponding polymers are the starting point for the important aspect of surface modification; and finally (*4*) dendron (**8**) (G2) has one nonpolar and two polar branching units, and dendron (**11**) (G2) is completely nonpolar except for its terminal protected amine groups. These structural features stay in context with considerations regarding dendronized polymers with specific polarity patterns which will become an important matter in future but will not be discussed in this article.

Monomer (**23**) (G4) requires a special comment: The attempt to subject this G4 monomer to SPC met with a trivial but nonetheless serious synthetic difficulty (76) which is typical for related polycondensations in which two monomers with grossly different molar masses are to be reacted with one another in the strictly required exact 1:1 stoichiometry. The molar mass difference between the two components (**23**) and (**24**) is so considerable (**23**: 3540 g/mol; **24**: 246 g/mol) that it is difficult to meet in practice this requirement. For that purpose, monomer

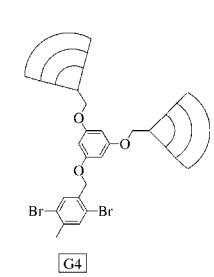

23

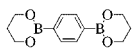

24

26

28

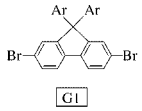

29

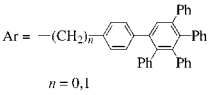

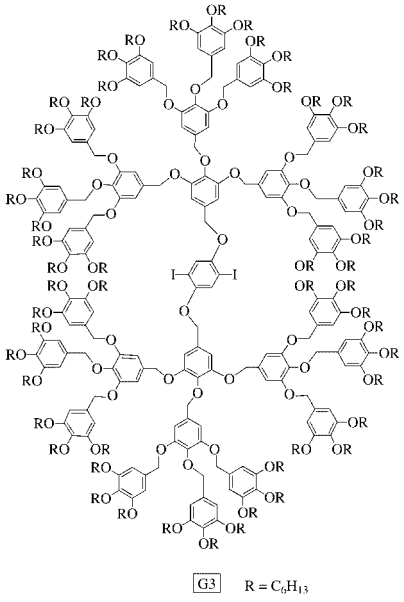

25

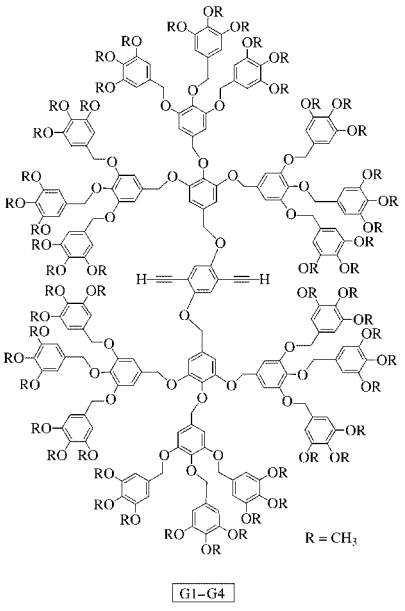

27

Fig. 5. (Continued)

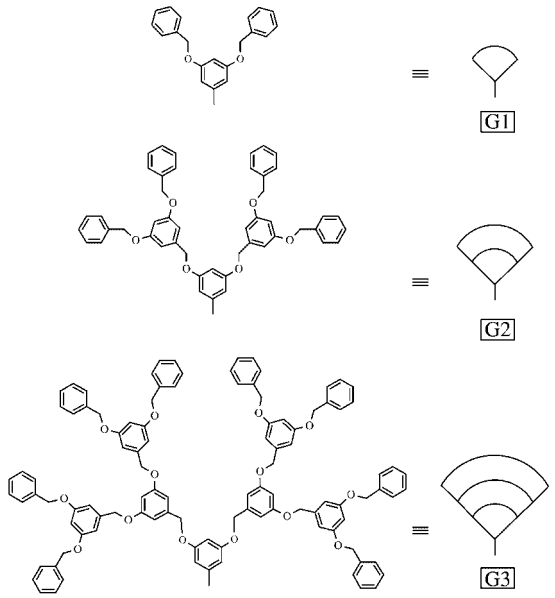

Fig. 6. Fréchet-type dendrons G1-G3 and their cartoon-like representations.

(**23**) was prepared on the 20-g scale as analytically pure material. This enabled one to do SPC on a relatively large scale ensuring sufficient stoichiometry control. In a series of optimization experiments, conditions were finally found which gave the corresponding polymer **P23/24** (G4) with $P_n = 25$ and $P_w = 125$ according to gpc on the gram scale (76). Presently, fractions of this material with $P_n = 10$, 75, 150, and 300 (gpc) are being investigated by sans in order to determine their true molar mass. Though it is still unclear as to what the actual molar mass of this polymer is, this data clearly shows that SPC works even for sterically enormously loaded G4 monomers. This is in contrast to vinyl-type macromonomers. No such

Table 1. Molar Masses of Dendronized Polymers P7 and P12 Determined by gpc and sans

	$M_w \times 10^{-3}$		
Polymer	(gpc)[a]	(sans)	M_w (sans)/M_w (gpc)
P7 (G1)	277	437[b]	1.6
P7 (G2)	84	275[b]	3.3
P12 (G1)	178	276[c]	1.6
(**P12 (G3)**)	710	2530[c]	3.6
(**P12 (G3)**)	59	233[c]	3.9

[a] In THF.
[b] In CD_3OD.
[c] In C_6D_6.

monomer carrying a G4 dendron has yet been found to undergo radically initiated polymerization.

Finally, it should be pointed out that apart from common organic reactions, the concentration of the reaction medium plays an absolutely important role in the polymerization of vinyl macromonomers. This may go as far as that below certain (very high) concentrations polymerization is not only slowed down but rather rendered impossible. This matter has been treated in some detail (33,34,55).

Route C and Cylinder "Surface" Modification. Both the "mixed" route (route C) and controlled surface modifications of dendritic nanorods are challenging goals for synthesis and many application related issues. The former allows to increase the dendritic layer around a backbone whenever needed and other synthetic routes (A and B) fail. The latter is an important option to engineer properties in various directions by attaching to one and the same polymer the different groups considered relevant for a certain application. For both cases it is obviously necessary to have accessible surface functions to which either another dendritic fragment or the modifying groups can be attached. Some experiments along these lines have been undertaken. The essential steps are

(1) Synthesis of monomers with protected functional groups in the periphery. The protection is required for compatibility with the polymerization conditions.
(2) Polymerization of these monomers and complete deprotection of the peripheral functional groups of the resulting polymer. The resulting deprotected polymer needs to be soluble.
(3) Derivatization of the deprotected polymer with the desired dendritic or other functional units.

Step *1* has been solved at least for up to generation 2. Monomers (**7**), (**8**), (**10**), and (**11**) in Figure 5 are good examples. These monomers have all been polymerized to the corresponding high molar mass materials **P7**, **P8**, **P10**, and **P11** (step *2*) and their functional groups deprotected. For the use of the somewhat uncommon trimethylsilyl(ethyloxy)carbonyl (Teoc) protecting group, see Reference 62. Figure 7 shows ^{1}H nmr spectra of monomer (**7**) (G2), the corresponding polymer **P7** (G2), and its deprotected counterpart. The deprotection can obviously be driven to completion. This aspect has also been quantified for many G3 and even G4 polymers, and deprotection was found to be virtually 100% in all cases. This is important because the remaining protected functional groups are an integral part of the polymer and cannot be removed by purification as in common organic chemistry. Step *3* has mainly been developed for the "mixed" route even though the knowledge gained here should be fully transferable to all kinds of surface modifications. Figure 8 shows an example in which high molar mass polymer **P11** (G2) was first converted into its G3 analog (polymer **A**) by deprotection of its Teoc protected amine groups with trifluoro acetic acid and subsequent reaction of the amines with the active ester G1 dendron **30**. Polymer **A** was then subjected to the same sequence of deprotection (to give **B**) and dendronization with (**30**) to give polymer **C**. The degree of deprotection was determined by

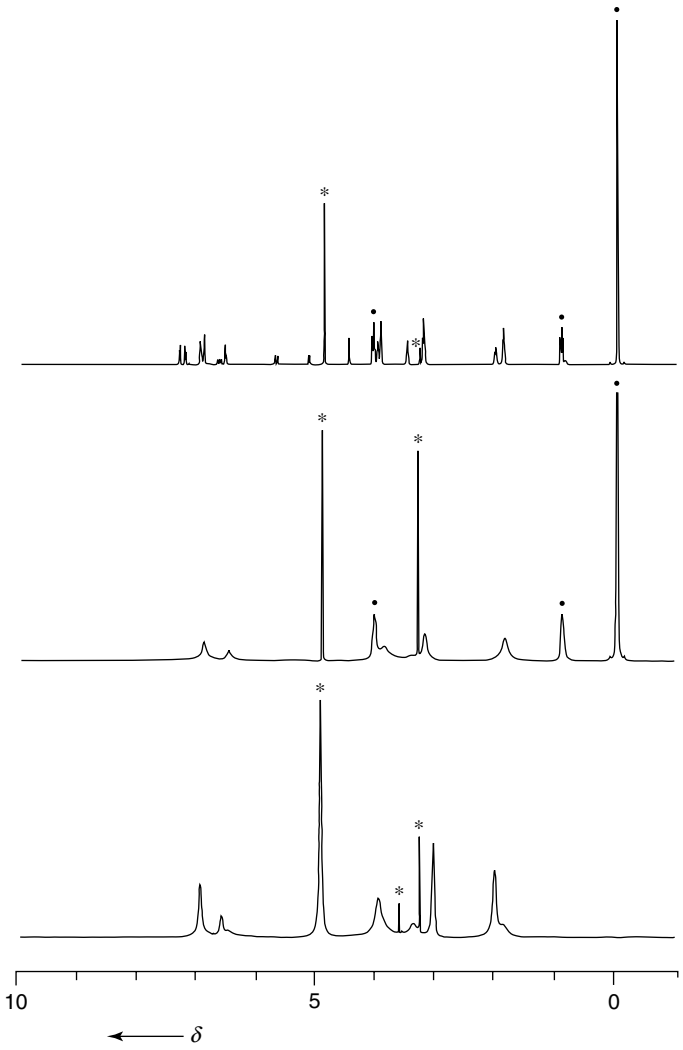

Fig. 7. ^{1}H nmr spectra of monomer (**7**) (G2), the corresponding polymer **P7** (G2), and its deprotected counterpart (from top to bottom) to illustrate the structure control during polymerization and the degree to which deprotection of the polymer can be achieved. Signals of the Teoc protecting group (full dots) and the solvent are marked (asterix).

rigorous application of 500-MHz nmr spectroscopy and that of the dendronization by applying Sanger's reagent, 2,4-dinitrofluorobenzene, and quantitative uv absorbance measurements. This reagent upon reaction with amines gives intensely yellow derivatives whose formation can be accurately quantified when its uv absorbance is compared with model compounds. Under broadly varied conditions and with the help of control experiments it was made sure that each amine group of polymer **B** which had not reacted with the G1 dendron (**30**) had in fact done so with the Sanger reagent (83). With a series of experiments it was proven that the

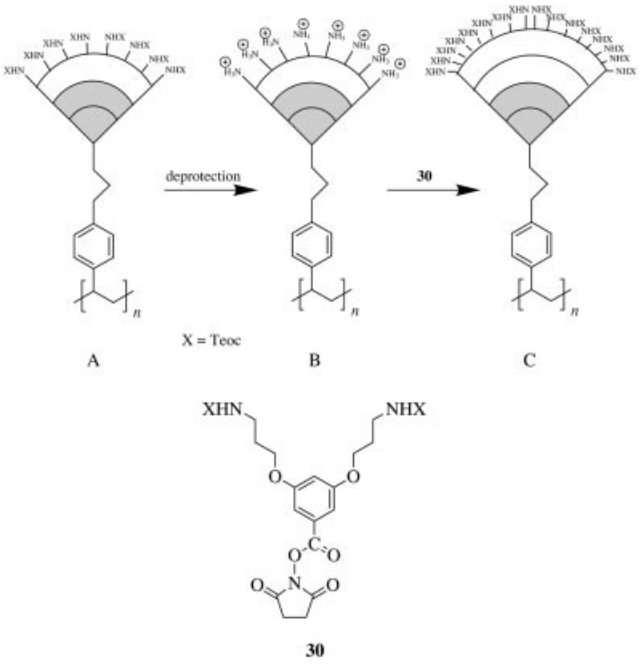

Fig. 8. Route C used to convert a third generation dendronized polymer (**A**) with terminal amine groups into the corresponding fourth generation derivative **C**. The sequence involves complete deprotection of **A**'s protected amine termini and reaction of the resulting polyelectrolyte **B** with the first generation dendron (**30**). Compound (**30**) has an active ester focal point functionality which proved to react extremely efficiently with polymer **B**'s amines.

conversions of the dendronization of **B** furnishing polymer **C**, whose structure is given in detail, can easily be driven beyond 99.3% (84).

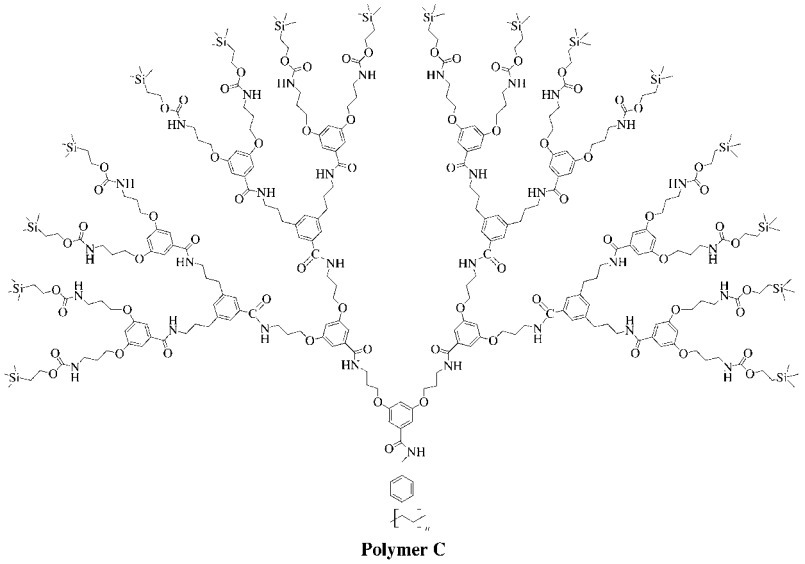

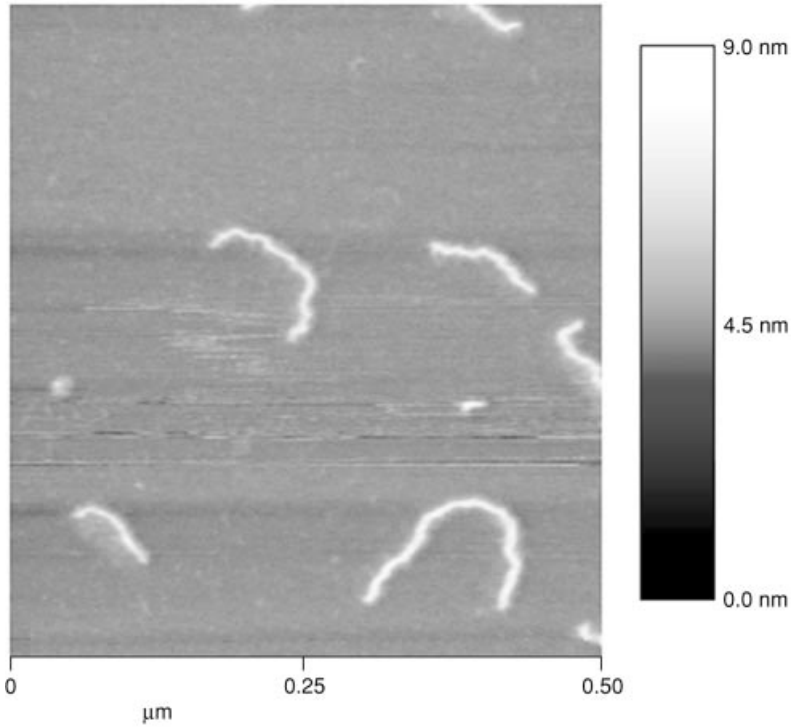

Fig. 9. Tapping mode sfm height image of a G4 polystyrene (**C**) on mica to visualize the length of individual chains.

These very high conversions were found for high molar mass polymers **A** which had degrees of polymerization between approximately 400 and 800. Figure 9 illustrates this point by showing a tapping mode sfm image of polymer **C** on mica. Even though a statistical evaluation of the length is not yet available, it can be seen that some chains reach considerable lengths of up to 250 nm. This equals 1000 r.u.'s assuming the backbone attains an all-trans zigzag conformation, which may not even be the case. This astounding result not only underlines the effectiveness of the route C dendronization protocol but also shows the power of amide formation between surface amines and activated ester components like (**30**). This latter aspect opens an avenue to all kinds of surface modifications based on this chemistry. All what is required is to use active esters which carry sugars, amino acids, catalytically active sites, etc. An alternative way to get to modified dendronized polymers is to polymerize modified dendronized monomers, for example, monomer (**9**) (G1 and G2) which gives sugar-coated polymer **P9** (64).

Molar Mass Determination. In practically all cases the molar masses of dendronized polymers were obtained from gpc versus polystyrene standard. As pointed out above, this is not an appropriate method for such polymers. The values reported (32,40,85) should therefore be treated at best as rough guesses (see below) and a direct comparison of different polymers is impossible. This refers also to polymers with the same backbone but different generation dendrons. Despite the

importance of an accurate molar mass determination of dendronized polymers, a systematic study on this matter is not yet available. The most extended one is one where gpc molar mass of five polymers obtained from monomers (**7**) (G1), (**7**) (G2), (**12**) (G1), (**12**) (G2), and (**12**) (G3) are compared with those obtained from sans (86). Both fractions and representative samples of these polymers were employed. Table 1 summarizes the results. In all cases the sans data are higher than those from gpc and the factor by which gpc underestimates the real molar masses varies between 1.6 and 3.9. A qualitative explanation for this finding is to be seen in the much larger mass per unit length of dendronized polymers than the calibration standard polystyrene. The true molar mass should therefore be higher than the gpc molar mass. There is, however, an opposing effect which has to do with the chain stiffening of the polymer chain imposed by the spatially demanding substituents. This leads to an increased hydrodynamic volume, causing the gpc molar mass to become larger than the actual one. For the cases of Table 1, the latter effect obviously does not overcompensate the former. Whether this will still be the case even for polymers with G4 substituents awaits to be seen. The sans measurements also revealed that polymer (**12**) (G3) is a rigid rod whose persistence length is of the order of the contour length.

The degree of polymerization (P_n) of polymer **P16/17 (G3)**, a representative of a step-growth polymer (Fig. 5b) obtained from monomers (**16**) (G3) and (**17**), was also investigated carefully in order to learn about the effectiveness of step-growth procedures [here SPC (70,71)] in the case of sterically demanding monomers. Its P_n could not be directly determined because of unsurmountable problems with aggregation. Through some chemical modification, however, an average $P_n = 110$ was finally obtained. According to Carother's equation (87), this P_n results when each coupling step proceeds with a conversion of 99.1%. From a synthetic point of view, this result is truly remarkable. It shows the enormous potential of SPC even for cases where steric congestion is considerable.

Some Aspects of the Molecular Structure. As discussed above, one objective for research of dendronized polymers was to use the decoration with dendrons as a means to stiffen the backbone to the point that it is fully stretched linear. This should be reached when the appendent individual dendrons are evenly distributed around the backbone and tightly packed at van der Waals distance. This fully stretched conformation will also be reached, of course, at a somewhat less tight situation, provided solvent molecules are sucked into the dendritic layer through osmotic effects. Both cases lead to a rigid rod with a cylindrical envelope; however, only in the first case this shape would be practically independent from the surrounding medium, whereas in the second, the dendritic layer would collapse under conditions where the solvent diffuses out (eg, in vacuum). The question of tightness of packing is an essential one for synthesis. Generally speaking, the synthesis becomes more difficult, the less spatial mobility the reaction partners have to attain the mechanistically required relative conformation in the transition state of the reaction (here, growth step). To evaluate the feasibility of a certain polymerization on grounds of sterics, it would be ideal to have a detailed picture of the spatial changes around the reaction center on going along the reaction coordinate. Since it is practically impossible to obtain this with a reasonable amount of computational effort, only some molecular dynamics (MD) calculations of final products were performed. Additionally, some polymers were visualized by

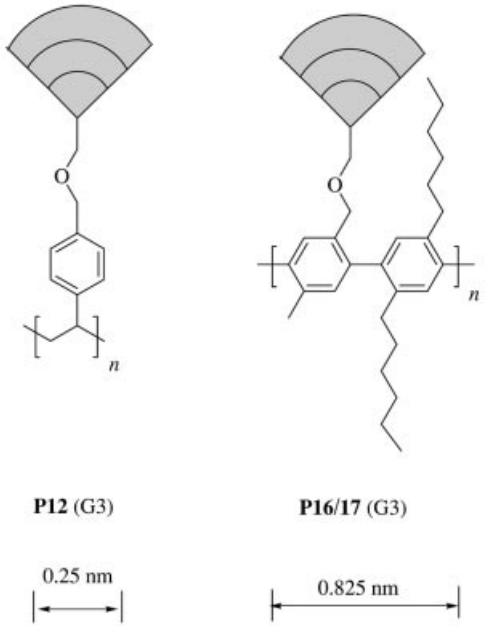

Fig. 10. The lengths of repeat units of polymers **P12 (G3)** (0.25 nm) and **P16/17 (G3)** (0.825 nm) to qualitatively assess the average distance between attached dendrons.

computer-generated 3-D images in order to help the synthetic chemist to assess whether or not a macromonomer undergoes polymerization.

MD simulations were performed in vacuo with polymers **P12 (G3)** (88) and **P16/17 (G3)** (89), which carry both of the same G3 dendrons but differ by the average distance between the dendrons' anchor groups [**P12 (G3)**: 0.25 nm, **P16/17 (G3)**: 0.825 nm] and the flexibility of the backbone (Fig. 10). Unfortunately, solvent molecules could not be considered because of the enormous number of atoms already contained in the polymers. Figure 11 shows the minimum conformations obtained. While the dendritic layer of **P12 (G3)** is quite compact, that of **P16/17 (G3)** is much more open and loose. The diameters of **P12 (G3)** and **P16/17 (G3)** are on average approximately 4.4 nm and 2–4 nm, respectively. This difference in compactness is certainly to a large extent due to the difference of the average distance of the dendrons' anchor groups at the backbones, but the backbones' different stiffnesses also play a role here. While the contour length of **P16/17 (G3)** of the starting conformation upon equilibration remains practically constant, that of **P12 (G3)** is reduced by some 30% when the minimum conformation is reached. This shows that the dense appearance of the latter polymer can be partially attributed to some backbone coiling. It is reasonable to assume that it is exactly this small space still available which rendered the polymerizations feasible. Considerations regarding preaggregation of polymerizable dendrons into ordered cylindrical arrays prior to polymerization through the aggregate (85) do not seem to be applicable here.

Figure 12 shows computer-generated structures of **P16/17** (G1) through **P16/17** (G4). Though these structures are not fully energy minimized, it is quite

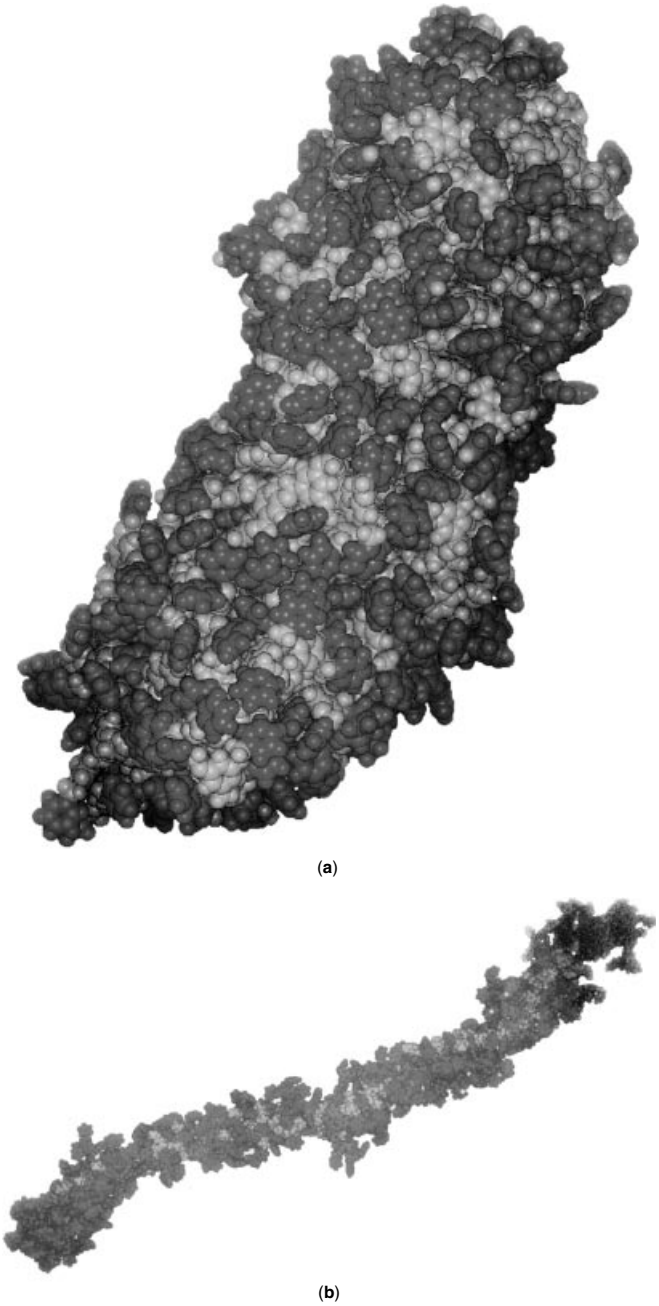

Fig. 11. Molecular dynamics (MD) simulations of dendronized polymers **P12 (G3)** (**a**) and **P16/17 (G3)** (**b**). **P12 (G3)** has 50 r.u's and the structure shown was obtained after 300 ps. End-to-end distance 9.1 nm, average diameter 4.4 ($\pm$0.2) nm. The backbone atoms are kept in *yellow*, the terminal benzene rings in *red*, all other atoms in *green*. **P16/17 (G3)** has 40 r.u.'s and a contour length of 33 nm. The backbone and the hexyl chain atoms are in *yellow*, the terminal benzene rings in *red*, and all other atoms in *green*. The diameter fluctuates between approximately 2 and 4 nm.

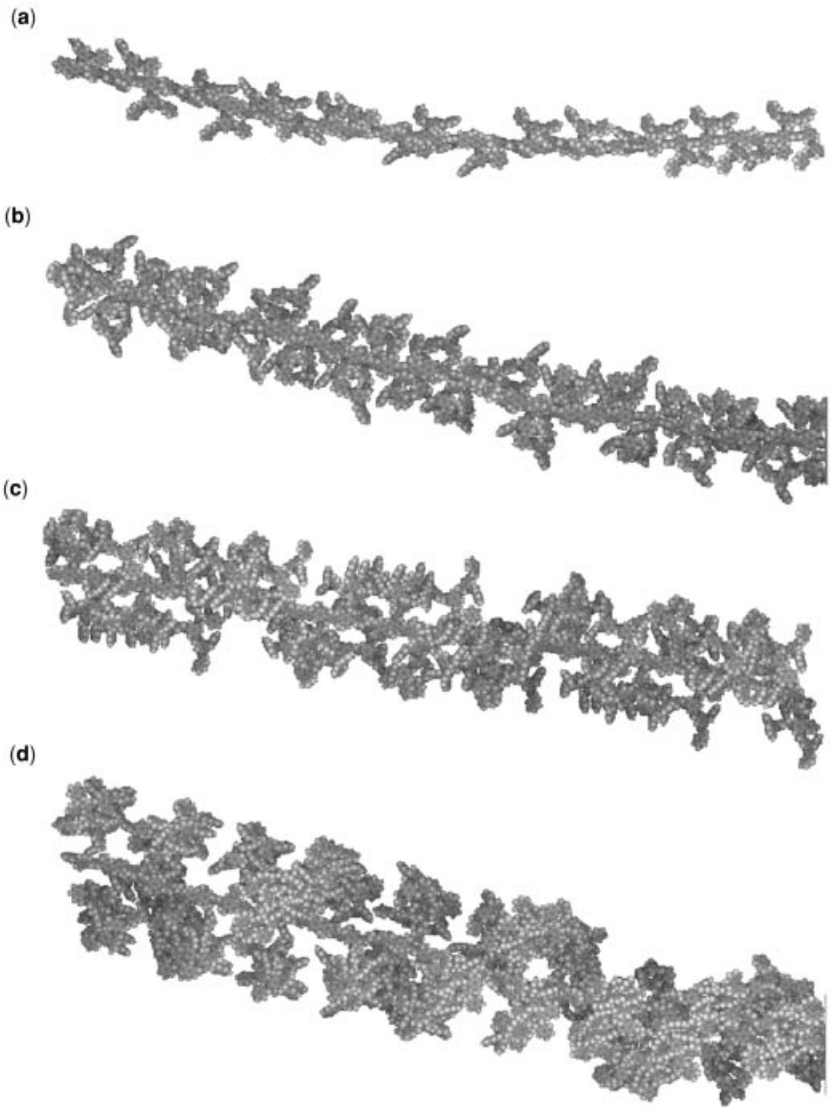

Fig. 12. Computer-generated images of dendronized polymers **P16/17** (G1) to **P16/17** (G4) (**a**–**d**).

obvious that there is space between consecutive dendrons even for the G4 case. This space, together with the surprisingly successful polymerization of monomer (**16**) (G3) supported the idea to also try SPC with monomer (**16**) (G4).

Behavior in the Bulk

The bulk properties have been investigated for polymers **P2** (G1 and G2) (59), **P4** (G2) (59,90) (**P2**, **P4**: R = $OC_{12}H_{25}$), **P18/19** (G4) (77), and **P25/26** (78). All four

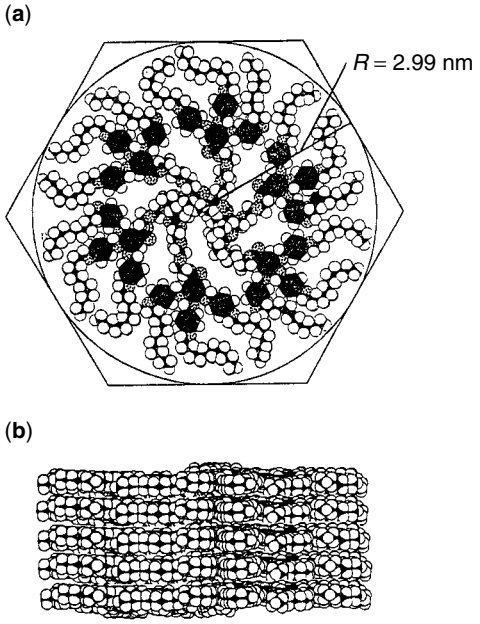

Fig. 13. Schematic representation of a supramolecular cylinder of dendronized polymer **P2** (G1) (R = $OC_{12}H_{25}$, $n = 3$) in the Θ_h mesophase: (**a**) top view of a cylinder containing 6 repeat units in a stratum with the alkyl tails melted to match the average column radius determined by x-ray scattering experiments, (**b**) side view of a cylinder containing 30 repeat units of the polymer assembled with melted alkyl tails. Reproduced with permission from Ref. 15.

structures have flexible backbones with a noncompact sequence of dendrons. In the first two cases and in the last one, the dendrons have liquid crystalline properties, whereas in the third they do not. Polymer **P2** (G1) self-assembles into a tubular supramolecular structure exhibiting enantiotropic columnar hexagonal (Θh) phases. These phases are characterized by differential scanning calorimetry, wide-angle and small-angle x-ray scattering, thermal optical polarized microscopy, and molecular modeling (15). The structure model proposes the stratum of the column to be formed by the backbone and the linking segments melted and segregated in the center of the column and their melted dendrons radiating toward the column periphery (Figs. 13 and 14). When a second generation dendron is used as in **P2** (G2) and **P4** (G2), an additional interesting feature is observed (59). As the degree of polymerization increases, the dendrimer's shape shifts from spherical to cylindrical. This is accompanied by the backbone going from random-coil to the extended conformation. This phenomenon provides the unique possibility for molecular engineering of polymer shapes, backbone conformation, and properties and is a way to show the interplay and impact of the above-mentioned interactions. Spherical and extended architectures of these dendrimers are basically proven by x-ray diffraction and can also be visualized by an sfm investigation using bilayers on a mica substrate. For a G1 polymer with closely related structure (not shown), a second columnar liquid crystalline phase was observed (90). For a polymer coated

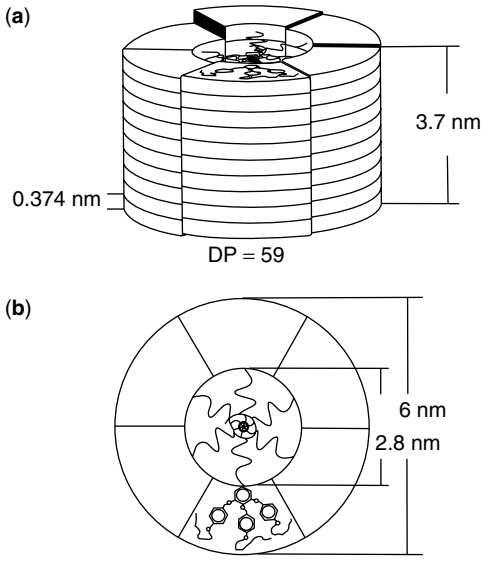

Fig. 14. An idealized representation of the supramolecular cylinder self-assembled from a single chain of dendronized polymer **P2** (G1) (R = $OC_{12}H_{25}$, $n = 3$) in the hexagonal columnar phase, assuming one single backbone per cylinder, drawn to proportion with existing data: (**a**) a tilted side view, (**b**) top view. Reproduced with permission from Ref. 15.

with two tapered units per side chain (not shown), a hexagonal columnar liquid crystalline superlattice was observed (91).

Though polymer **P18/19** (G4) does not show any liquid crystallinity, it nevertheless forms supramolecular structures in the bulk (77). This was concluded from x-ray diffraction patterns obtained from Si plates coated with this polymer and monomer (**18**), respectively. A series of Bragg peaks for the polymer showed the existence of an ordered structure. Based on MD calculations and additional small-angle x-ray scattering experiments, this structure was proposed to be body-centered cubic.

Polymer **P25/26** self-orders in solvent-cast films, with the backbones parallel to the substrate and a strong solvent dependence of the degree of ordering (78). Spacings of 2.2–2.6 nm are observed by x-ray diffraction, indicating interdigitation of the dendritic side chains. **P25/26** also forms thermotropic nematic liquid crystalline phases. With optical microscopy, Schlieren textures are observed for thin films cast from solution.

Assembly and Manipulation at Surfaces

Dendronized polymers can self-assemble on surfaces into highly ordered layers, which renders them into a material attractive for various applications. The assembly process can be investigated on the molecular scale using the sfm. In addition, the sfm may be used to manipulate single macromolecules on solid substrates in order to generate assemblies, which would not form spontaneously.

The behavior of the dendronized polymers at interfaces is determined not only by intra- and intermolecular forces but also by interfacial forces. The latter (92) include the van der Waals force, which is important on the nanometer scale and which is due to the difference in the dielectric properties of the two adjacent phases. This force is always attractive, and therefore favors a high molecular segment density at the interface, which in turn favors 2-D crystallization, since crystals exhibit usually higher densities than less ordered phases. Counteracting is the influence of entropy: Immobilizing flexible molecules in 2-D crystals at interfaces reduces entropy, since the molecules lose both translational as well as conformational entropy. For the adsorption from a liquid mixture, this favors the adsorption of the *largest* molecules, since the loss of translational entropy is counted per particle, wherear the van der Waals energy gained is proportional to the mass. Entropy effects also favor the adsorption of the most *rigid* molecules, since they lose the least conformational entropy. As a result, the large and rigid rods will be preferably adsorbed from a liquid molecular mixture. In addition, there are short-range chemical forces, which are specific for the particular chemical species at the interface and may be attractive or repulsive. Well-known consequences of these forces are epitaxial layering on crystalline substrates and the ordering of amphiphilic molecules at the water–air interface. Moreover, there are electrostatic forces for charged species.

In the following, the behavior of two classes of dendronized polymers at interfaces will be discussed: those with one type of dendrons (homophilic systems) and others with a hydrophobic and a hydrophilic dendron at each repeat unit (amphiphilic systems).

Homophilic Systems. Dendronized polymers can be observed by sfm either in ordered ultrathin films or as individual molecules on solid supports. SFM (93,94) is a powerful tool for investigating morphology, molecular packing, and molecular dynamics at surfaces with a resolution on the molecular scale. Both, synthetic and biological polymers (87,95,96) as well as spherical dendrimers have been studied (97–99). Of particular interest for rather soft organic materials is the operation in the "intermittent contact" or "tapping" mode (94), which minimizes sample wear during imaging.

Ultrathin layers of homophilic dendrimers can be prepared by solution casting (slow layer formation) or spin coating (fast layer formation) from organic solvents. SFM images of **P12 (G3)** were obtained for thin (in the range of 20–30 nm) solution casted layers on highly oriented pyrolytic graphite (HOPG) (Fig. 15) (88). They reveal a remarkably high degree of order: One observes domains which consist of periodic arrays of rows (Fig. 2c) with a periodicity of $D = 5.0 \pm 0.5$ nm. For comparison, MD simulations (Fig. 5a) and sans measurements reveal rod diameters of $D = 4.4 \pm 0.2$ nm and $D = 5.1 \pm 0.5$ nm, respectively. These numbers are very similar to the distances between the rows, suggesting that the rows can be attributed to molecules, which are predominantly oriented parallel to the surface. They are grouped in anisotropic domains, whose sizes vary between 20 and 200 nm (parallel to the director axis) and between 20 and 100 nm (perpendicular to the director axis). However, a reliable correlation of individual chain lengths with domain size is not possible, since, despite the high resolution of the image, only the chain ends at the grain boundaries can be clearly identified, while those in the interior may be obscured if two dendrimers with the same director axis

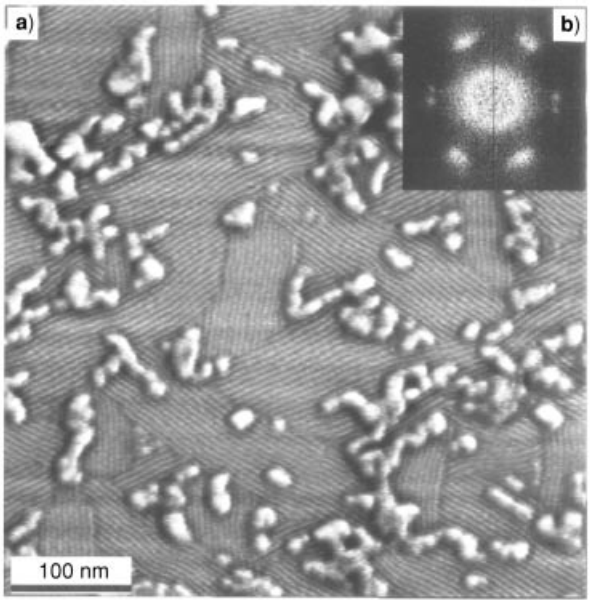

Fig. 15. Tapping mode phase contrast sfm image of an ultrathin layer of **P12 (G3)** on highly oriented pyrolytic graphite (HOPG) (50). The rows are attributed to molecules, which are predominantly oriented parallel to the surface as well as to each other. Their orientation within the surface plane reflects also the threefold symmetry of the substrate, as indicated by the Fourier-Transform in the inset.

are in tight contact and oscillate somewhat along this axis (88). Large-scale sfm images show that the films exhibit terraces with height differences δh between adjacent terraces of 4.2 ± 0.2 nm. This is close to 5.0 nm $\times$ cos $30^\circ = 4.3$ nm, which one would expect for a model of closely packed cylinders of a diameter of 5 nm (Fig. 16).

Interestingly, the different domains in Figure 13 exhibit three molecular orientations at $60^\circ \pm 8^\circ$ relative to each other, indicating that even in a layer of a thickness of the order of five monolayers, the top layer reflects the threefold symmetry of the graphite substrate. While this symmetry is stable in time, reorientations by 120° do occur. The case of a similar dendronized polymer, **P16/17 (G3)**, is demonstrated in Figure 17 (89).

The results described above show that the ultrathin layers of the described dendronized polymers offer the possibility to orient the polymeric backbones along substrate axes, and to access molecular dimensions in arrays by sfm imaging. In order to follow the assembly process on the molecular scale, it is desirable to prepare submonolayers with isolated single molecules on the surface. A convenient preparation for this is spin-coating HOPG from a dilute solution. SFM images of **P14** (2$\times$G1) (100–102) (Fig. 18a) reveal single molecules stretched out on the surface with sharp kinks of typically 120°, which reflect again the symmetry of the substrate. The sharpness of the kinks indicates that this polymer is quite flexible. Upon annealing, compact monolayer islands can form (Fig. 18b), revealing that the flexibility of the chains allows the formation of very sharp bends. SFM images

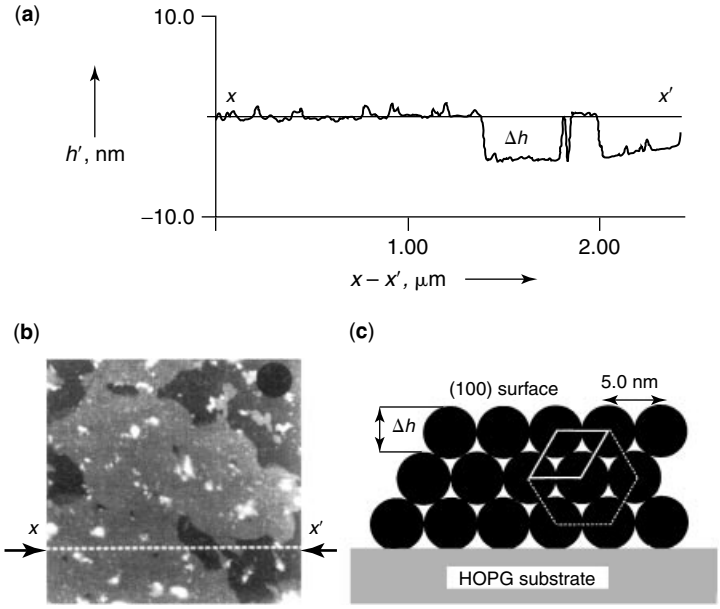

Fig. 16. Tapping mode sfm of ultrathin films of **P12 (G3)** on HOPG and a packing model (97). (**a**) Cross-sectional profile along x-x′ as indicated in (**b**). The height difference between adjacent terraces has the dimension of a monolayer ($\Delta h = 4.2 \pm 0.2$ nm), (b) Large-scale ($2.4 \times 2.4\ \mu m^2$) sfm image of molecular terraces, (c) Schematic model of close-packed molecularly defined cylinders in ultrathin films of **P12 (G3)** on HOPG. From Ref. 88.

may also be used to determine the distributions of contour lengths. They revealed that **P14** (2×G1), ie, a polymer with a spatially not very demanding side group, appeared to be at least two times shorter than the contour length as expected on the basis of size exclusion chromatography and static light scattering. This was attributed to a disordered helix-like conformation of the polymeric backbone, and can be contrasted to the case of **P4** (G1) with a spatially more demanding side group, whose contour lengths agreed fairly well with the expectation (100–102). On one hand, it shows that bulky dendrons force the backbone into extension. On the other hand, there is a degree of freedom for less bulky dendrons, namely the conformation of the flexible polymer backbone, which may be used to control the contour length of the dendronized polymer (eg, by contraction through helix formation).

Polymers at surfaces may also be manipulated with the sfm (Fig. 2). An example for the manipulation of dendronized polymers by rubbing (Fig. 2d) with the sfm is shown in Figure 19, which has been obtained as follows: First a rather low molecular weight fraction (of the order of 10 r.u.'s on average according to gpc with polystyrene standard) of **P16/17** (G4) was spin-coated to give a monolayer on HOPG. The result is an apparently disordered surface. Scanning with the sfm tip, however, orients the molecules almost prefectly uniformly in the whole scan window which can be 1 μm^2 or more (104), limited apparently only by the domain size of the underlying HOPG, which is typically of the order of 10 μm, but can also vary.

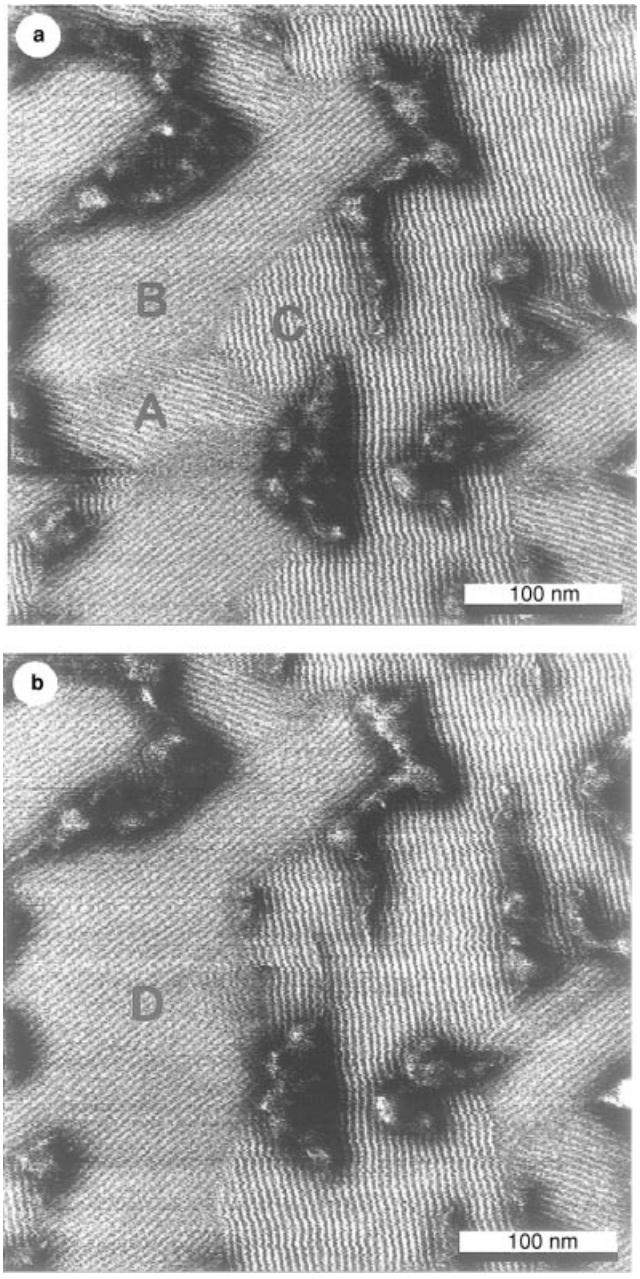

Fig. 17. Tapping mode phase contrast sfm images of an ultrathin film of **P16/17 (G3)** on HOPG (89). The rows are again attributed to molecules, which are predominantly oriented parallel to the surface as well as to each other. Their orientation within the surface plane reflects also the threefold symmetry of the substrate (three molecular orientations denoted A, B, and C in panel **a**). Images (**a**) and (**b**) have been recorded at the same position at an interval of 10 min. Domain A reorients in the same direction as domain B, resulting in a new domain D.

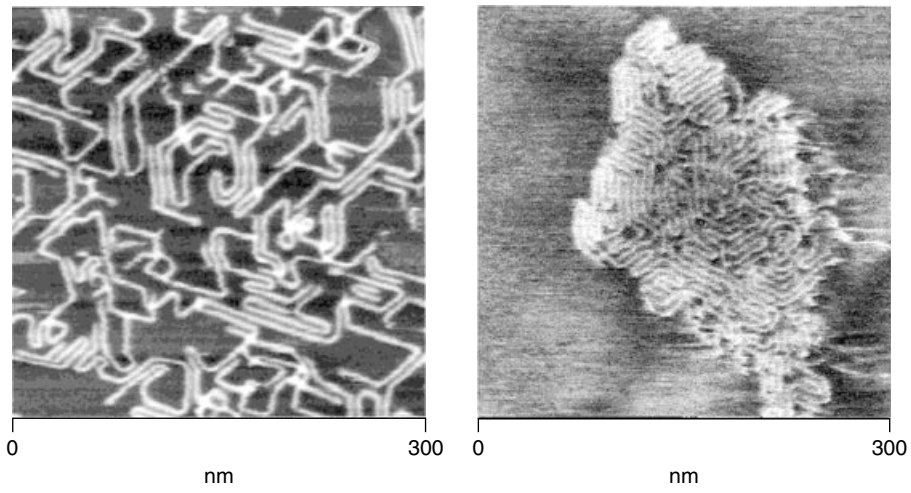

Fig. 18. Tapping mode sfm height images of **P14** (2×G1) with a theoretical $P_n = 100$ on HOPG prepared by spin casting from a solution in THF (102): (**a**) as prepared, (**b**) after annealing at 100°C for 24 h. The molecular orientations reflect the symmetry of the substrate; the molecules are flexible enough to let them be frequently bent by 120°. The strong tendency for the single molecule to align along lattice axes of the substrate has been attributed to the orientation of the pendent alkyl chains (103). Upon annealing, compact, domains are formed.

But not only layers can be manipulated by the sfm tip, also single macromolecules can be moved across the surface (Fig. 2b). Figure 20 (left) shows an sfm image of **P7** (G2) with two C12 chains per terminal amine group (not shown) on HOPG. The alkyl chains cause the backbones again to orient preferentially according to the threefold symmetry of the substrate, and the flexibility of the backbone allows sharp kinks to form. Figure 18b shows the same area after one molecule has been moved to the left by sliding the sfm tip at stronger interaction with the substrate along a path indicated by the red arrow. The image reveals that the macromolecule also bent because of its flexibility.

Such manipulations should be better defined for polymers with higher rigidity. Since Coulomb-charges along the backbone should stiffen the macromolecule, polyelectrolytes, similar to the polymers with bulky dendrons **P12 (G3)** and **P16/17** (G4), should be promising candidates to manipulate them one by one with the sfm tip, and to determine single molecule properties, like persistence lengths and Young's or bending moduli (Fig. 2a).

Amphiphilic Systems. Amphiphilic dendronized polymers may lead to amphiphilic cylinders which, depending on the surrounding medium, could segregate lengthwise into two different halves (Figs. 3d, Fig. 21). This structural motif is rather unique. In nature it can be found in some ion channel membrane proteins, which means that amphiphilically dendronized polymers are of interest as models for such proteins (105–108). They may also serve as novel and giant constituents of self-aggregated assemblies and should show interesting behavior at interfaces. A good candidate is a dendronized polymer, whose repeating units are equipped with two sterically demanding substituents, one of which being hydrophobic and

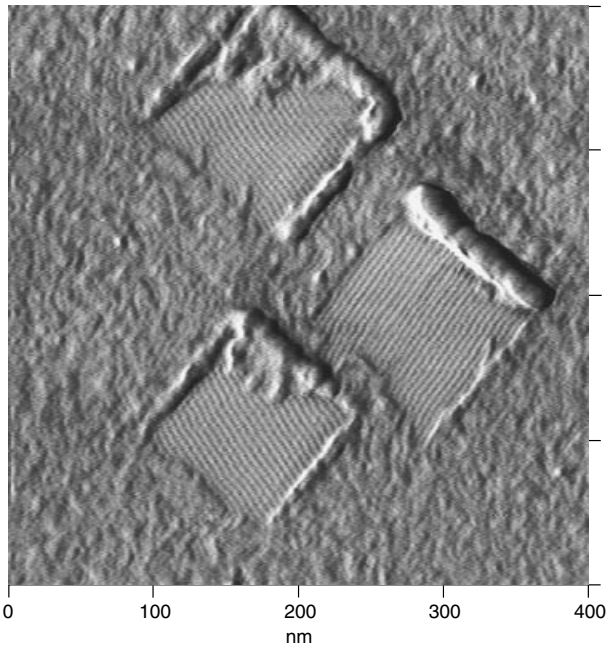

Fig. 19. Tapping mode phase contrast sfm image of a monolayer of oligomeric **P23/24** (G4) after scanning three areas with the sfm (104). It reveals that upon scanning the molecules are perfectly oriented along one of the three symmetry axes of the substrate.

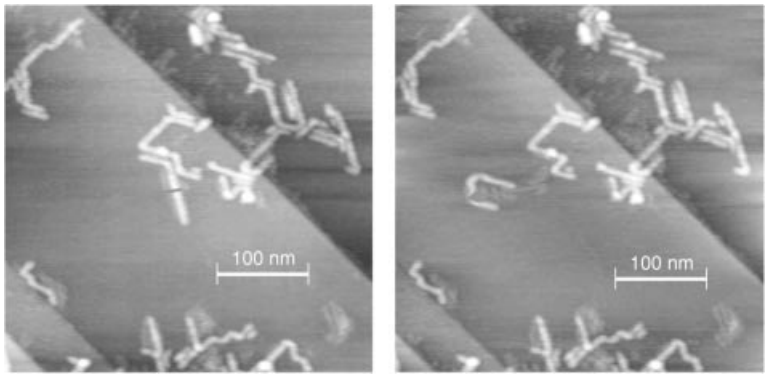

Fig. 20. Manipulation of individualized **P7** (G2) with two C12 chains per terminal amine group on HOPG by switching from an sfm tapping mode imaging modus to manipulation by approaching the tip to the sample and moving along the path of the red arrow. (**a**) image before and (**b**) image after manipulation. From Ref. 104.

the other hydrophilic (62). This area was entered with three differently equipped PPPs **P20/24**, **P21/24**, and **P22/24**, which differ in the relative spatial demand of their polar and nonpolar substituents.

There are different ways to prepare ultrathin layers from amphiphilic polymers: One is to form Langmuir monolayers at the water–air interface followed by

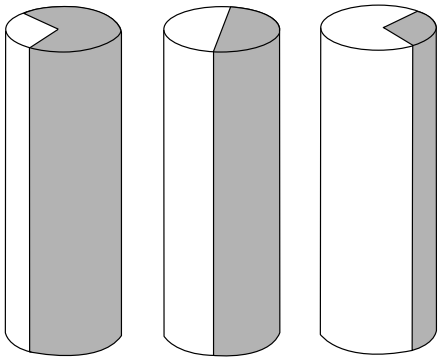

Fig. 21. Representations of amphiphilically equipped dendritic cylinders with varying spatial demands of polar and nonpolar domains. The lengthwise segregation of these domains is interesting for surface modifications and for attaining unprecedented aggregates in solution.

transfer to solid substrates using the Langmuir–Blodgett technique. Another is spin coating as for the homophilic systems.

Amphiphilic dendron-based molecules have been investigated at the air–water interface and stable Langmuir monolayers were found for some of these systems (109–114). In one study (115), the behavior of the hydrophobic Fréchet-type dendrons (Fig. 6) carrying hydrophilic ethyleneoxy (EO) chains at their focal point was studied at this interface by systematically varying the dendron size (G3 to G5) and chain length. Longer hydrophilic chains increased the stability of the Langmuir films for G3 and G4 by roughly 3.1 and 4.1 mN/m (=dyn/cm), respectively, per additional EO unit. On going from the lower to the higher generations, the shape of the dendrons changes from vertically elongated to more flat. The collapse pressures ranged from approximately 6 mN/m for G3 with one EO group to 25 mN/m for G3 with six EO groups.

Langmuir monolayers of monomer 20 and polymer **P20/24** have been prepared at the air–water interface (74), exhibiting surface pressure-area isotherms at room temperature, which reveal stable monolayers. The monolayers of 20 exhibit very good reversibility for compression, decompression, and repeating cycles, with an area per molecule of about 0.73 nm^2 per molecule at 20 mN/m. This is consistent with a monolayer structure, in which the four EO chains per water-soluble dendron are close-packed and oriented perpendicularly to the monolayer, thereby defining a minimum area per molecule. In comparison, polymer **P20/24** exhibits a 10% larger area per repeat unit (0.82 nm^2/r.u.) upon the first compression with a hysteresis in the first decompression and a shift to a more reversible isotherm, and a smaller area per repeat unit in the second cycle (0.77 nm^2/r.u.). The good agreement between the areas per molecule of monomer (**20**) and per repeat unit of polymer **P20/24** indicates a structure of the polymer monolayer, in which the rod-like polymer molecules are oriented with their long axes within the monolayer plane and close-packed. Moreover, the hydrophylic ethyleneoxide chains are on that side of the polymer which faces the water subphase, while the more hydrophobic dendron faces the air side of the polymer. This picture is supported by a control experiment using a closely related polymer in which the hydrophilic

dendron of **P20/24** is replaced by another G2 Fréchet dendron (structure not shown). Under the same conditions this polymer does not form a stable monolayer at the air–water interface.

Also, polymers **P21/24** and **P22/24** with their corresponding monomers (**21**) and (**22**) were investigated at the air–water interface (75). Except **P22/24** they all form stable monolayers on the Langmuir trough, which can be transferred by the Langmuir–Blodgett (LB) technique to mica. While the transferred films of (**21**) and (**22**) are unstable, **P21/24** forms stable, rather smooth monolayers, whose morphology remains unchanged for at least a week. The fact that both monomers are stable on water but not on mica reflects the discrepancy of the space demand of the hydrophilic and hydrophobic parts. Since the polymer **P21/24** is stable on mica, the covalent attachment of the amphiphilic repeat units can stabilize an LB-layer. On the other hand, the fact that **P22/24** does not form a stable monolayer, not even on water, indicates that this polymer with its amphiphilic misbalance does not behave like an amphiphile under these conditions.

A quantitative comparison of the collapse pressures of the Curtis–Hawker amphiphiles (114) with the ones described here cannot be made. There are substantial structural differences even if this comparison is restricted to the monomers (**20**), (**21**), (**22**). Additionally, the Curtis–Hawker amphiphiles have EO chains with terminal (polar) hydroxy functions whereas the monomers have (non-polar) methoxy groups instead. The collapse pressures are, however, in a similar range.

Usually, no molecular scale resolution sfm images were obtained for the LB-layers, contrary to the analogous homophilic systems prepared by spin coating. Therefore, spin coating has been employed as an alternative preparation method for the amphiphilic systems also (104). Figure 22 displays an sfm image of a

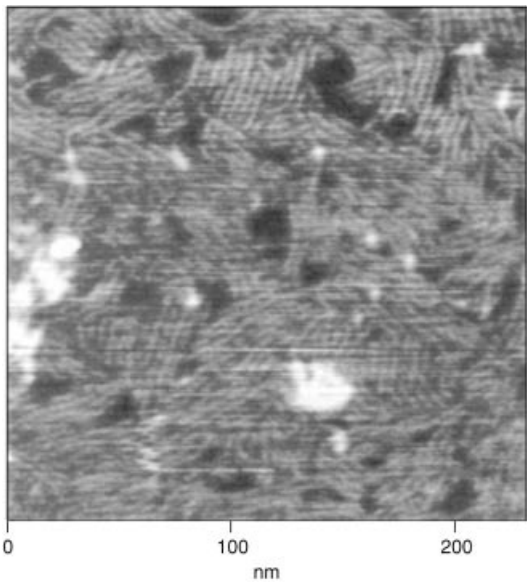

Fig. 22. Molecular resolution tapping mode sfm height image of spin-coated amphiphiles **P20/24** on HOPG. From Ref. 104.

spin-coated monolayer of **P20/24** on HOPG, which reveals rather straight rods. Again, their orientation within the plane is not random but it reflects the threefold symmetry of the substrate. Within the experimental error, the length distribution of the rods agrees with their determination by size exclusion chromatography. However, the distance between the rods is 4.4 ± 0.5 nm, which is larger than what one would expect for close-packed molecules. A possible explanation is a well-defined aggregation of the amphiphilic rods, eg, into dimers, which exhibit hydrophobic surfaces in contact with both the rather hydrophobic substrate and the ambient.

Optical Properties

Dendronized polymers may exhibit interesting optical and electrical properties which should at least be briefly mentioned here. Poly(phenyleneethynylene)s are among the few conjugated polymers which are interesting candidates for blue light-emitting diodes (116,117). A problem which hampers the use of these polymers in commercial devices is luminescence quenching of the excited state because of intimate contact between the backbones. Wrapping of such a backbone by a dendritic layer, which itself does not quench the luminescence, can be a solution (80). Over a wide concentration range, the quantum yield of the luminescence of **P27/28** (G4) was nearly 100%, contrary to the case of **P27/28** (G3 or G2) where it drops below 40% (Fig. 23). Additionally, upon 278-nm excitation of the dendritic substituents of **P27/28** (G4) in tetrahydrofuran (THF), the observed fluorescence was 11 times more intense than that of the lower generation analogs under identical conditions. In this case, the dendritic layer harvests the uv photons, channels them to the backbone which then emits with high efficiency in the blue Light-emitting diode.

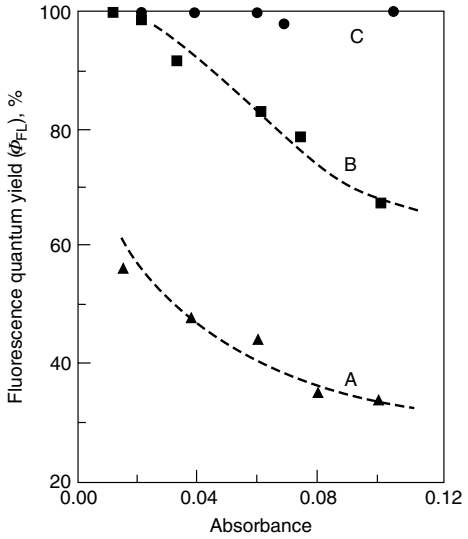

Fig. 23. Fluorescence quantum yields of **P27/28** (G2) (A), **P27/28** (G3) (B), **P27/28** (G4) (C) upon excitation of the conjugated backbone in THF with absorbances of 0.01–0.1 at the excitation wavelength $\lambda = 425$ nm under Ar at 20 °C. From Ref. 80.

The same idea of isolating active backbones from one another and, thus, exploiting their intrinsic undisturbed properties, were also followed (78,79,81). In Reference 81, polymers **P29** ($n = 0,1$) were prepared and it was shown that the attachment of bulky substituents does not influence the electronic characteristics of the backbone. No increase of the dihedral angle between consecutive repeat units was observed. The emission maximum ($\lambda_{exc.} = 380$ nm) of a drop-casted film of **P29** ($n = 1$) was virtually unchanged and no sign of aggregation behavior was found. **P29** ($n = 1$) was incorporated into a device which produces blue emission with an onset voltage below 4 V. On very similar experiments with **P25/26**, an enhancement in solid-state photoluminescence by a factor of 4 because of the intermolecular separation of the chromophores by the attached dendrons was found (78,79).

Summary and Outlook

High molecular weight dendronized polymers are synthetically accessible. If certain prerequisites are taken into account, even the sterically demanding macromonomers (**12**) (G3), (**16**) (G3), and (**23**) (G4) can be employed, which widens the scope of both radically initiated polymerizations as well as Suzuki polycondensation. The successful synthesis of polymers like **P12 (G3)**, **P23/24** (G4), and **C** (G4) allows investigation of the impact of the dendritic decoration on the backbones' coiling behavior and addresses the important question of whether or not steric congestion can be used as a tool to force molecules into a certain shape, which is more or less independent of the surrounding medium (in solution, adsorbed on surfaces, spread at solid–liquid interfaces, and in the solid state). SFM and sans measurements as well as MD simulations reveal that, eg, polymer **P12 (G3)** is quite stiff and can be viewed as a cylindrically shaped molecular object with a defined diameter of approximately 5 nm and a persistence length on the length scale

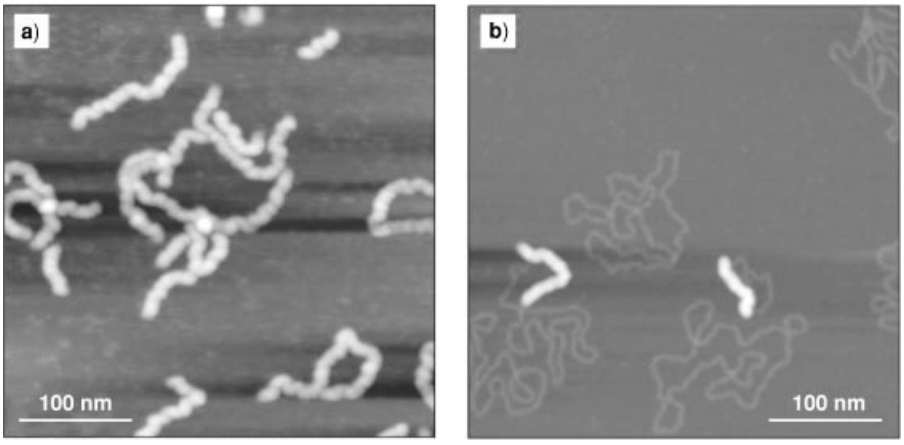

Fig. 24. Tapping mode sfm height images of (**a**) unprotected and quaternized (charged!) polymer **C** (G4) on mica and (**b**) the same when complexed with plasmid DNA. The brighter and wider features in (**b**) are attributed to the aggregate between the two oppositely charged polyelectrolytes while the other features represent neat DNA. From Ref. 118.

of a few tenths of a nanometer. One may even be inclined to assign a "surface" to this polymer. Driven by the idea of generating molecular nanoobjects with functional surfaces just by polymerizing appropriately equipped monomers, first steps were made to decorate these surfaces with both functional and polar/nonpolar groups in order to engineer properties and explore possible fields of application. Research on nano-objects of the described kind is a truly interdisciplinary enterprise, and progress depends upon tight cooperation between synthetic chemists, experimental physicists, and theoreticians. Some future directions will be (*1*) to develop synthesis to the point where several rigid objects with various surface functionalities are available and their length distributions are somewhat better under control, (*2*) to isolate individual very rigid cylinders on surfaces and determine quantitatively molecular properties like bending moduli, (*3*) to move them about on surfaces for patterning and construction purposes, and (*4*) to start investigations into their properties along the lines described under "Dendronized Polymers." Figure 24 gives, as an example, a taste of what is presently being investigated in the directions indicated in Fig. 3c. Complex formation of the kind described here is possible. Figure 24a shows an sfm image of unprotected and quaternized (positively charged) polymer **C** (G4) spin-coated on mica. Figure 24b shows the same polymer complexed with (negatively charged) DNA after complexation in solution and subsequently spin-coated on mica. The image reveals both neat DNA and complexes of the dendronized polymer with DNA, which are a little thicker than the neat polymer (118).

BIBLIOGRAPHY

"Dendritic Polymers" in *EPSE* 2nd ed., Index Volume, pp. 46–92, by D. A. Tomalia, D. M. Hedstrand, and L. R. Wilson, The Dow Chemical Company.

1. G. R. Newkome, C. N. Moorefield, and F. Vögtle, *Dendritic Molecules—Concepts, Syntheses, Perspectives*, VCH, Weinheim, Germany, 1996.
2. D. K. Smith and F. Diederich, *Chem. Eur. J.* **4**, 1353 (1998).
3. H. Frey, C. Lach, and K. Lorenz, *Adv. Mater.* **10**, 279 (1999).
4. C. Gorman, *Adv. Mater.* **10**, 295 (1999).
5. A. W. Bosman, H. M. Janssen, and E. W. Meijer, *Chem. Rev.* **99**, 1665 (1999).
6. J. F. G. A. Jansen, E. M. M. de Brabander-van den Berg, and E. W. Meijer, *Science* **266**, 1226 (1994).
7. J. F. G. A. Jansen, E. W. Meijer, and E. M. M. de Brabander-van den Berg, *J. Am. Chem. Soc.* **117**, 4417 (1995).
8. D. A. Tomalia and co-workers, *Polym. J. (Tokyo)* **17**, 117 (1985).
9. D. A. Tomalia and co-workers, *Macromolecules* **19**, 2466 (1986).
10. E. M. M. de Brabander-van den Berg and E. W. Meijer, *Angew. Chem. Int. Ed. Engl.* **32**, 1308 (1993).
11. C. Wörner and R. Mülhaupt, *Angew. Chem. Int. Ed. Engl.* **32**, 1306 (1993).
12. U.S. Pat. 4,694,064 (1987), D. A. Tomalia and P. M. Kirchhoff (to The Dow Chemical Company).
13. R. Yin and co-workers, *J. Am. Chem. Soc.* **120**, 2678 (1998).
14. R. Freudenberger and co-workers, *Polymer* **35**, 4496 (1994).
15. V. Percec and co-workers, *J. Chem. Soc., Perkin Trans. 1* 2799 (1993).
16. J. C. Hummelen, J. L. J. van Dongen, and E. W. Meijer, *Chem. Eur. J.* **3**, 1489 (1997).
17. I. Gitsov, K. L. Wooley, and J. M. J. Fréchet, *Angew. Chem. Int. Ed. Engl.* **31**, 1200 (1992).

18. I. Gitsov and J. M. J. Fréchet, *Macromolecules* **27**, 7309 (1993).
19. C. J. Hawker and J. M. J. Fréchet, *Polymer* **33**, 1507 (1992).
20. T. Kawaguchi and J. S. Moore, *Polym. Prepr. (Am. Chem. Soc., Div. Polym. Chem.)* **35**(2), 872 (1994).
21. M. A. Fox, *Chem. Mater.* **10**, 860 (1998).
22. G. Klaerner, R. D. Miller, and C. J. Hawker, *Am. Chem. Soc. Polym. Prepr.* **39**, 1006 (1998).
23. M. L. Bruening and co-workers, *Langmuir* **13**, 770 (1997).
24. V. Swali and co-workers, *J. Org. Chem.* **62**, 4902 (1997).
25. Z. Bo and co-workers, *Chem. Lett.* 1197 (1998).
26. L. Zhang and co-workers, *Thin Solid Films* **221**, 327 (1998).
27. R. F. Peez and co-workers, *Langmuir* **14**, 4232 (1998).
28. D. E. Bergbreiter, G. Tao, and A. M. Kippenberger, *Org. Lett.* **2**, 2853 (2000).
29. M. Fischer and F. Vögtle, *Angew. Chem. Int. Ed. Engl.* **38**, 884 (1999).
30. A. D. Schlüter, *Top. Curr. Chem.* **197**, 165 (1998).
31. H. Frey, *Angew. Chem. Int. Ed. Engl.* **37**, 2193 (1998).
32. A. D. Schlüter and J. P. Rabe, *Angew. Chem. Int. Ed.* **39**, 864 (2000).
33. Y. Tsukahara and co-workers, *Macromolecules* **23**, 5201 (1990).
34. M. Wintermantel and co-workers, *Macromolecules*, **29**, 978 (1996).
35. P. Dziezok and co-workers, *Angew. Chem. Int. Ed. Engl.* **36**, 2812 (1997).
36. S. S. Sheiko and co-workers, *Langmuir*, **13**, 5368 (1997).
37. M. Gerle and co-workers, *Macromolecules* **32**, 2629 (1999).
38. R. Djalali and co-workers, *Macromol. Rapid Commun.* **20**, 444 (1999).
39. I. Wataoka and co-workers, *Macromolecules*, **32**, 1816 (1999).
40. K. Ito and S. Kawaguchi, *Adv. Polym. Sci.* **142**, 128 (1999).
41. K. Fischer and M. Schmidt, *Macromol. Rapid Commun.* **22**, 787 (2001).
42. H.-G. Elias, *Makromoleküle*, 5th ed., Hüthig&Wepf, Basel, 1990, pp. 43, 628.
43. R. G. deGennes and H. J. Hervet, *Phys. Lett. (Paris)* **44**, 351 (1983).
44. R. L. Lescanec and M. Muthukumar, *Macromolecules* **23**, 2280 (1990).
45. D. Pötschke and co-workers, *Macromolecules* **32**, 4079 (1999).
46. D. Pötschke and co-workers, *Macromol. Chem. Phys.* **201**, 330 (2000).
47. J. W. J. Knappen and co-workers, *Nature* **372**, 659 (1994).
48. N. Brinkmann and co-workers, *J. Catal.* **183**, 163 (1999).
49. N. J. Hovestad and co-workers, *Angew. Chem. Int. Ed. Engl.* **38**, 1655 (1999).
50. G. Van Koten and co-workers, *J. Am. Chem. Soc.* **122**, 12112 (2000).
51. D. A. Tomalia, A. M. Naylor, and W. A. Goddard, III, *Angew. Chem. Int. Ed. Engl.* **29**, 138 (1990).
52. J. F. Kukowska-Catallo and co-workers, *Proc. Natl. Acad. Sci. USA* **93**, 4897 (1996).
53. M. X. Tang, C. T. Redemann, and F. C. Szoka, *Bioconjugate Chem.* **7**, 703 (1996).
54. J.-H. Fuhrhop and J. Köning, in J. F. Stoddart, ed., *Supramolecular Chemistry*, Royal Society of Chemistry, London, 1994.
55. L. Shu and A. D. Schlüter, *Macromolecules* **33**, 4321 (2000).
56. W. W. Yan, J. J. Kirkland, and D. D. Bly *Modern Size-Exclusion Chromatography*, John Wiley & Sons, Inc., New York 1979.
57. J. M. J. Fréchet, K. L. Wooley, and C. J. Hawker, *J. Am. Chem. Soc.* **113**, 4252 (1991).
58. G. Draheim and H. Ritter, *Macromol. Chem. Phys.* **196**, 2211 (1995).
59. V. Percec and co-workers, *Nature* **391**, 161 (1998).
60. Y. M. Chen, C. F. Chen, W. H. Liu, and F. Xi, *Macromol. Rapid Commun.* **17**, 401 (1996).
61. I. Neubert and co-workers, *Acta Polym.* **47**, 455 (1996).
62. I. Neubert and A. D. Schlüter, *Macromolecules* **31**, 9372 (1998).
63. L. Shu and A. D. Schlüter, *Macromol. Chem. Phys.* **201**, 239 (2000).
64. A. Zistler, S. Koch, and A. D. Schlüter, *J. Chem. Soc., Perkin Trans. 1* 501 (1999).

65. I. Neubert, E. Amoulong-Kirstein, and A. D. Schlüter, *Macromol. Rapid Commun.* **17**, 517 (1996).
66. T. Kaneko and co-workers, *Macromolecules* **30**, 3118 (1997).
67. K. J. Ivin, *Olefin Metathesis*, Academic Press, London, 1983.
68. V. Percec and co-workers, *Macromolecules* **29**, 1464 (1996).
69. V. Percec and D. Schlueter, *Macromolecules* **30**, 5783 (1997).
70. A. D. Schlüter and G. Wegner, *Acta Polym.* **44**, 59 (1993).
71. A. D. Schlüter, *J. Polym. Sci., Polym. Chem.* **39**, 1533 (2001).
72. W. Claussen, N. Schulte, and A. D. Schlüter, *Macromol. Rapid Commun.* **16**, 89 (1995).
73. B. Karakaya and co-workers, *J. Am. Chem. Soc.* **119**, 3296 (1997).
74. Z. Bo, J. P. Rabe, and A. D. Schlüter, *Angew. Chem. Int. Ed. Engl.* **38**, 2370 (1999).
75. Z. Bo and co-workers, *Macromolecules* **33**, 2688 (2000).
76. Z. Bo and A. D. Schlüter, *Chem. Eur. J.* **6**, 3235 (2000).
77. S. Jahromi and co-workers, *J. Am. Chem. Soc.* **120**, 9753 (1998).
78. Z. Bao, K. R. Amundson, and A. J. Lovinger, *Macromolecules* **31**, 8647 (1998).
79. R. Jakubiak, Z. Bao, and L. Rothberg, *Synth. Met.* **114**, 61 (2000).
80. T. Sato, D.-L. Jiang, and T. Aida, *J. Am. Chem. Soc.* **121**, 10658–10659 (1999).
81. S. Setayesh and co-workers, *J. Am. Chem. Soc.*, **123**, 946 (2001).
82. A. P. H. J. Schenning and co-workers, *Chem. Commun.* 1013 (1998).
83. L. Shu and A. D. Schlüter, submitted.
84. L. Shu and co-workers, *Polym. Mater. Sci. Eng.*, **84**, 744 (2001).
85. V. Percec, C.-H. Ahn, and B. Barboin, *J. Am. Chem. Soc.* **119**, 12978 (1997).
86. S. Förster and co-workers, *Macromolecules* **32**, 4042 (1999).
87. J. M. G. Cowie, *Polymers: Chemistry & Physics of Modern Materials*, International Textbook Comp. Ltd., Bucks, U.K., 1973.
88. W. Stocker and co-workers, *Adv. Mater.* **10**, 793 (1998).
89. W. Stocker and co-workers, *J. Am. Chem. Soc.* **120**, 7691 (1998).
90. S. N. Chvalun and co-workers, *Acta Polym.* **50**, 51 (1999).
91. V. Percec and co-workers, *Chem. Eur. J.* **5**, 1070 (1999).
92. J. N. Israelachvili, *Intermolecular and Surface Forces*, Academic Press, London, 1985.
93. G. Binnig, C. F. Quate, and C. Gerber, *Phys. Rev. Lett.* **56**, 930 (1986).
94. Q. Zhong, D. Innis, and V. Elings, *Surf. Sci.* **290**, 688 (1993).
95. H. G. Hansma and co-workers, *Science* **256**, 1180 (1992).
96. S. J. Tans and co-workers, *Synth. Met.* **84**, 733 (1997).
97. S. S. Sheiko and co-workers, *Macromol. Rapid Commun.* **17**(5), 283 (1996).
98. S. S. Sheiko and co-workers, *Langmuir* **13**, 4172 (1997).
99. M. C. Coen and co-workers, *Macromolecules* **29**, 8069 (1996).
100. S. A. Prokhorova and co-workers, *Macromol. Rapid Commun.* **19**, 359 (1998).
101. S. A. Prokhorova and co-workers, *Macromolecules* **32**, 2653 (1999).
102. S. A. Prokhorova and co-workers, *Langmuir* **16**, 6862 (2000).
103. J. P. Rabe and S. Buchholz, *Science* **253**, 424 (1991).
104. J. Barner, Kraftmikroskopische Untersuchung mesoskopisch strukturierter Polymeroberflächen, Diploma Thesis, Department of Physics, Humboldt University Berlin, 1999; J. Barner and co-workers, *Europhysics Conference Abstracts, European Conference on Macromolecular Physics*, Supplement 23H, 1999.
105. F. Zeng and S. C. Zimmermann, *Chem. Rev.* **97**, 1681 (1997).
106. A. P. H. J. Schenning, C. Elissen-Roman, J.-W. Weener, M. W. P. L. Baars, S. J. van der Gaast, and E. W. Meijer, *J. Am. Chem. Soc.* **120**, 8199 (1998).
107. For non-dendronized polymers with a similar polarity pattern, see: H. M. Janssen, E. Peeters, M. F. van Zundert, M. H. P. van Genderen, and E. W. Meijer, *Macromolecules* **30**, 8113 (1997).
108. T. Bjornholm and co-workers, *J. Am. Chem. Soc.* **120**, 7643 (1998).
109. Y. Sayed-Sweet and co-workers, *J. Mater. Chem.* **7**, 1199 (1997).

110. O. Karthaus, K. Ijiro, and M. Shimomura, *Langmuir* **12**, 6714 (1996).
111. J. C. M. van Hest and co-workers, *Chem. Eur. J.* **2**, 1616 (1996).
112. F. Cardullo and co-workers, *Langmuir* **14**, 1955 (1998).
113. P. M. Saville and co-workers, *J. Phys. Chem.* **99**, 8283 (1995).
114. Z. Bo and co-workers, *Polym. Bull.* **38**, 257 (1997).
115. J. P. Kampf and co-workers, *Langmuir* **15**, 227 (1999).
116. A. Kraft, A. C. Grimsdale, and A. B. Holmes, *Angew. Chem.* **110**, 416 (1998).
117. R. H. Friend and co-workers, *Nature* **397**, 121 (1999).
118. I. Goessl and co-workers, in preparation.

A. DIETER SCHLÜTER
Freie Universität Berlin
JÜRGEN P. RABE
Humboldt-Universität zu Berlin

DENTAL APPLICATIONS

Introduction

The dental industry has taken great advantage of polymer science to design materials. Materials used in the oral cavity or external prostheses have very specific requirements, ie, these materials must have physical, chemical, biological, and aesthetic requirements, not always fulfilled by currently available materials. A host of requirements must often be met, including adequate strength, resilience, wear or abrasion resistance, dimensional stability for both fabrication and use, translucency or transparency to provide a match of the natural tissue replaced, good color stability, resistance to the oral environment, show tissue tolerance and low toxicity, and exhibit ease of fabrication into a needed dental device. Since few resins fulfill all the mentioned requirements, the search for improved dental materials has been limited to a few classes of polymeric materials. The various types of monomers and polymers used in dentistry are discussed, along with brief attention given to new areas of promise for preparing better materials.

The largest volume of polymeric materials used in dentistry is in prosthetic applications. Polymeric materials are also important in operative dentistry, being used to produce composite resins, dental cements, adhesives, cavity liners, and as a protective sealant for pits and fissures. Elastomers are employed as impression materials. Resilient prosthetic devices are often fabricated to restore external soft-tissue defects. Mouth protectors are fabricated to prevent injury to teeth, as well as prevent head and neck injuries. Other polymer applications include fabricating patterns for metal castings and partial denture frameworks, impression trays, orthodontic and periodontal devices, space maintainers, bite plates, cleft palate obdurators, and oral implants. Polymeric materials may also be used to fabricate an artificial tongue, when disease results in its loss.

Encyclopedia of Polymer Science and Technology. Copyright John Wiley & Sons, Inc. All rights reserved.

The discovery of vulcanized rubber in 1839 gave rise to the first polymeric dentures, followed by celluloid dentures about 1870, and subsequent use of vinyl chloride copolymers, phenol–formaldehyde resins, and polystyrene. Acrylic-based resins gained rapid acceptance after 1937, and are being greatly used today. Their main disadvantages are related to shrinkage because of the free-radical polymerization of methyl methacrylate, poor abrasion resistance, and fracture toughness. Other polymers, such as epoxy resins, polystyrene, polyesters, polycarbonates, polysulfones, vinyls, silicones, polysulfides, and polyethers, have been explored or used to some degree.

The various dental polymers discussed in this article include impression materials, dentures and denture liners, artificial teeth, crown and bridge materials, mouth protectors, maxillofacial materials, restoratives (consisting of glass polyalkenoates or glass-ionomers and composites), adhesives, and sealants. Specifications and standards for dental materials are also briefly mentioned in the text.

Impression/Duplicating Materials

Impressions must accurately show the dimensions, surface detail, and relationship of teeth and soft oral tissues. Materials used to accomplish this task include rigid gels of the reversible hydrogen-bonding type, irreversible alginate hydrocolloids, and elastomers such as silicones, polysulfides, and polyethers. Duplicates of original casts, used to fabricate partial or complete dentures, are made from duplicating materials.

Agar (Reversible Hydrocolloids). Agar, a galactose sulfate or mucopolysaccharide (sulfonic acid ester of a galactan complex), is a long-chain polymer having a molecular weight of about 150,000. The material forms a colloid with water, with the solutions being liquid at $\geq 70^{\circ}$C and setting to a gel at 30–50°C. Strong hydrogen bonding causes the molecule to form a helical structure, which uncoils on heating. On cooling, the gel forms and reproduces the shape of the oral tissues. These materials can be used several times, but prolonged heating causes degradation. While agar is the main constituent, it is by no means the main constitutent by weight. For example, a typical formulation consists of about 85.5% water, 12.5% agar, 1.7% potassium sulfate, 0.1% alkyl benzoate, and trace amount of pigments. Fillers, such as zinc oxide and a hard wax or clay, are often used to modify the formulations. Borax or calcium metaborate may be used to control the pH, increase viscosity, toughness, and resiliency. These materials were developed to make accurate impressions, even of undercut areas. The agar used in duplicating uses has a composition similar to the agar impression material, but with a higher water content. ANSI/ADA Specifications No. 11 (1997) applies to agar-based impression materials.

Alginates (Irreversible Hydrocolloids). The reactive component in these materials is the sodium or potassium salt of anhydro-*o*-D-mannuronic acid (alginic acid), isolated from brown seaweed (algae). A typical formulation consists of about 18% sodium or potassium alginate, 14% calcium sulfate dihydrate, 2% sodium phosphate, 10% potassium sulfate, 56% diatomaceous earth filler, and 4% sodium silicofluoride. When mixed with controlled amounts of water, the soluble

hydrocolloid is converted to insoluble calcium alginate, ie, and an acid–base reaction leads to matrix cross-linking. In the sol–gel conversion, calcium cations form salt-bridges with the carboxylate anions, forming ionic cross-linking. The material can only be used once. The addition of sodium tripolyphosphate or tetrasodium pyrophosphate retards rapid precipitation of gel. Addition of a fluorosilicate completes the precipitation of the insoluble alginate, after adequate working time has elapsed. Besides diatomaceous earth filler, zinc oxide may be used to improve strength and yield a material with a smooth, nontacky surface. Alginates, used most frequently to make impressions, are inexpensive, easy to manipulate, and comfortable for the patient. But, alginates deteriorate rapidly on storage at $\geq 50^{\circ}$C and once set they must be kept in 100% relative humidity to prevent shrinkage. In addition, they are the least accurate of the impression materials. Both reversible and irreversible hydrocolloids have been used at the same time in a laminating technique. ANSI/ADA Specification No. 18 (1992) sets the requirements for fast and slow setting alginate impression materials.

Synthetic Elastomers. Synthetic elastomers, such as polysulfides, silicone, and polyethers, exhibit much better dimensional stability than the hydrocolloids. They are mainly used in crown and bridge applications or for impressions of dentate patients. These polymers are used at a temperature above their glass-transition temperature (T_g). The viscosity of the materials used is influenced by both the working temperature above T_g and the length of the polymer chains, as well as by fillers and other additives. The formulated materials are liquids or pastes at room temperature, which transform into a solid by covalent bonding between the long-chain molecules. The process of forming chemical bonds creates a three-dimensional organic matrix. The chemistry of the impression materials is described separately, followed by a brief comparison of their properties. ANSI/ADA Specification No. 19 (1982) sets requirements for the elastomeric-type impression materials.

Polysulfides. The starting materials have molecular weights of about 2000–4000 and can be formulated to yield a wide range of physical and chemical properties. In the two-component (paste) system, the base material is a viscous polysulfide liquid prepolymer having terminal and pendant mercaptan (SH) groups, such as a Thiokol LP-2 rubber, commonly called thiols (see Fig. 1). Titanium dioxide (TiO_2), calcium sulfate, calcium carbonate, silica, or alumina is used as fillers, to extend, reinforce, or harden the product. Dibutyl phthalate, tricresyl phosphate, or tributyl citrate is added as modifiers or diluents to improve mixing and flow properties. The paste may also contain sulfur and oleic or stearic acid, which act as a retarder to control the set. The SH groups are oxidized by lead dioxide or copper hydroxide supplied as a separate part of the formulation. When the accelerator (oxidizer) is added to the base (polysulfide) paste an exothermic reaction occurs, bringing about a 3–5°C rise in temperature, depending on the

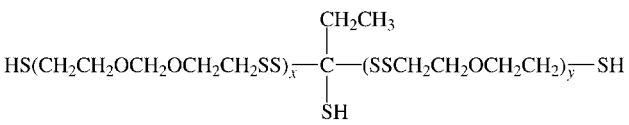

Fig. 1. Polysulfide oligomer.

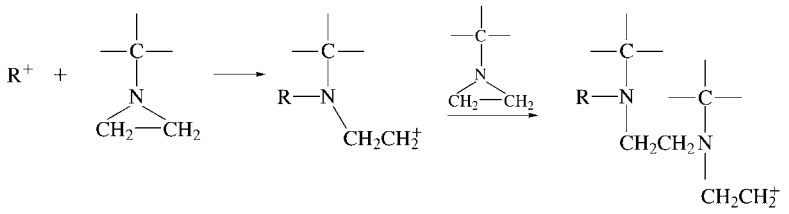

Fig. 2. Polyether impression material reaction.

amount of sulfur used. The exothermic reaction is accompanied by a rapid increase of molecular weight and elimination of water, caused by formation of the chain-extending and cross-linking —S—S— bonds. Besides being sticky and having a disagreeable odor, polysulfides [$R(SH)_x$] are difficult to mix and exhibit relatively poor elastic recovery when stressed. In undercut areas, they may not provide accurate reproduction of oral structures. When properly used they exhibit good tear resistance and acceptable stability.

Polyethers. These impression materials were developed in Germany in the 1960s. The reactive oligomer used is a polyether having cyclic imine (ethyleneimine) residues, which undergo ring opening and subsequent cross-linking via a cationic initiator, as shown in Figure 2. The two-part formulation contains the imine functionalized polyether, silicate filler, and a glycol ether plasticizer as one paste, and the cationic initiator (such as an alkylester of benzene sulfonic acid), a silicate filler, and a plasticizer as the second paste (1). Adding a polyester diluent or thinner controls the rheological properties and working time. Mixing is moderately easy and dimensional changes in air are low (<0.1%) over several hours, as no products are released during curing. The elastic recovery and reproduction of detail are excellent. These materials have a much higher modulus of elasticity than silicones or polysulfides, making them more difficult to remove from the mouth. Polyether impression materials tear readily and have an equilibrium water sorption of about 14%. Dimensional stability in water is poor, necessitating storage in a dry environment.

Silicones. Two types of silicones are used in impression materials: addition (Fig. 3) and condensation (hydrosilylation) (Fig. 4). Both are based on using poly(dimethylsiloxane), with the two having different end groups and different curing mechanisms. Addition siloxanes are a two-paste system, with one paste

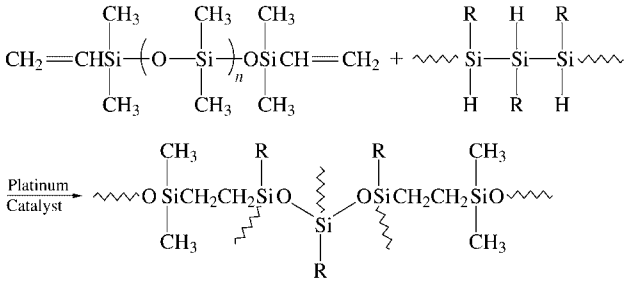

Fig. 3. Addition silicone structure/reaction.

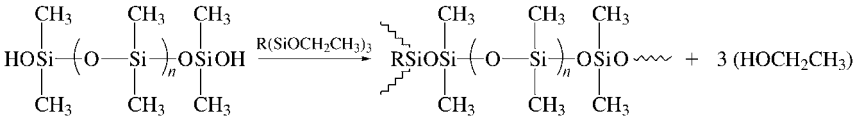

Fig. 4. Condensation silicone structure/reaction.

containing a low molecular weight silicone having terminal vinyl groups (Fig. 3) and reinforcing filler and the other paste consisting of the hydrogen-terminated silanol oligomer, filler, and chloroplatinic acid catalyst. Mixing the pastes gives a cross-linked elastomer. No volatiles are given off during polymerization—a definite advantage—compared to the condensation type, which eliminates ethyl alcohol.

The condensation-type silicone impression materials are based on hydroxyl-terminated poly(dimethylsiloxane), ie, viscous liquids of structure (Fig. 4). Colloidal silica or micronized metal oxides, having 5–10 μm particle size, are added to prepare a paste which is cross-linked with an alkyl silicate containing 50% ethoxy groups, such as tetraethyl orthosilicate (TEOS). Organic tin activators, such as stannous octoate or dibutyltin dilaurate (2), are used at the 1–2% level.

The chief uses of silicone impression materials are for crown and fixed partial dentures. These systems may be used in a wide range of impression techniques. They are relatively easy to mix, producing high tensile strength materials having good elastic properties, along with permanent-set values of about 1% at 40% strain. But, they tear at relatively low extension.

Communicable diseases have caused concern in handling of impression materials, meaning impressions are not generally accepted by dental laboratories unless they are disinfected. However, disinfection must be accomplished without distorting the impression. Reversible and irreversible hydrocolloids, as well as polyether impressions, should be avoided if they are to be disinfected, since they lack the required stability. A guide for disinfecting impression materials may be found in the ADA Council on Dental Materials, Equipment and Instruments (COMEI, 1988 and 1992).

Impression Materials Merits. Elastomeric impression materials reproduce surface details very accurately, provided low viscosity formulations are used. Since these materials are generally hydrophobic, they will not properly wet out the surface of the tooth with saliva present. Contact angle studies of water on the elastomeric impression surfaces for polyether, polysulfide, and addition silicones show angles of 49.3°, 82.1°, and 98.2°, respectively, indicating that polyethers work best where saliva cannot be excluded. The setting process for polysulfides is highly susceptible to temperature and humidity, influencing working and setting times. Condensation silicones may also show erratic setting, because of inadequate mixing and possibly some hydrolysis of TEOS. The setting behavior of addition silicones and polyethers is the most consistent. Condensation silicones are dimensionally less stable than polysulfides, addition silicones, or polyethers. The contraction or shrinkage of condensation silicones, upon cooling from mouth temperature (37°C) to room temperature, is ca 0.35%, compared to 0.20% for the polysulfides. This shrinkage is essentially caused by release of alcohol generated

during the condensation reaction. However, condensation silicones are cleaner to handle than polysulfides (3).

Elastomer Thermal and Mechanical Properties. Comparing stiffness of the polysulfide (PS), condensation silicone (CS), addition silicone (AS), and the polyether (PE) elastomeric impressions, the ranking would be as follows: PS < CS < AS < PE. The permanent set or resistance to deformation on removal would be as follows: PS > PE > CS > AS. Tear strength would be approximated as follows: PS $\ggg$ PE > AS and CS. Polymerization shrinkage for the elastomers is of the order PE = AS < PS < CS. The materials may thermally contract on removal from the oral cavity, with PE = 320, PS = 270, and AS = CS = 200 ppm/°C.

Denture Resins/Prosthetic Materials

A variety of polymeric materials have been studied or used for preparing dentures, including epoxy resins, cellulose nitrate, rubber or vulcanite, phenol–formaldehyde, vinyl acrylics, polystyrene, polycarbonates, and polysulfones, but acrylics have become the materials of choice. It happens that compression-molded, cross-linked acrylic dentures are as dimensionally stable and useful as the dentures made with special resins (4).

Denture wearers demand an accurate fit and natural appearance. The fit is very important, since chewing efficiency of artificial dentures is substantially lower than that of natural teeth. Besides being easy to fabricate, an ideal denture material would have high strength, stiffness, hardness, and toughness, ie, be fracture resistant, have low density, good dimensional stability, show resistance to oral fluids, have an absence of odor or taste, be resistant to bacterial growth, have good thermal conductivity, show good retention to other polymers, porcelain, and metals, be radiopaque, be easy to repair, easy to clean, have good storage life, and be inexpensive to make. Significant challenges remain to produce the ideal denture material.

To achieve needed comfort, dentures must be custom-made. To form the customized denture, in which the artificial teeth are embedded, a wax pattern is used. The wax pattern is inserted in a plaster or dental stone in a split mold flask. After removal of the wax, the surface of the resulting mold cavity is painted with a separating medium, usually an aqueous alginate solution, followed by the addition of the acrylic resin. The separating medium aids in removal of the cured acrylic from the mold.

Acrylic denture materials are made by free-radical (addition) polymerization, using methyl methacrylate (MMA) monomer. In the process, the MMA becomes poly(methyl methacrylate) (PMMA). The resins are available in either heat- or cold-cured formulations. A cross-linking monomer, such as ethylene glycol (Fig. 5)

Fig. 5. Dimethacrylate monomers/reactive diluents. EGDMA (R = CH_2CH_2); DEGDMA (R = $CH_2CH_2OCH_2CH_2$); TEGDMA (R = $CH_2CH_2OCH_2CH_2OCH_2CH_2$).

or diethylene glycol dimethacrylate (Fig. 5), is included with the MMA mixture to improve the mechanical properties. The dimethacrylates are covalently bonded at various points along the PMMA chains, forming a cross-linked matrix. Visible light-cured versions have also become available, with the chemistry akin to that of composite restoratives.

Heat-Cured Methacrylate Formulations. These resins consist of granular PMMA powder blended with liquid MMA, along with a cross-linking monomer, as shown in Figure 5 (EGDMA or DEGDMA). After mixing and heating, the monomer–polymer dough forms a rigid plastic. The powder component is mostly granules of PMMA, along with benzoyl peroxide initiator (BPO, 0.5–1%), titanium/zinc oxide pigments and opacifiers, dibutyl phthalate plasticizer, and acrylic- or nylon-type reinforcing fibers. The liquid component contains the inhibited MMA, along with a cross-linker (Fig. 5, DEGDMA). The blends, normally consisting of about two to three parts of PMMA and one part of monomer by volume, are packed with pressure into the mold, having the properly positioned teeth. The MMA is normally inhibited with the methyl ether of hydroquinone (MEHQ) or butylated hydroxytoluene (BHT). Small amounts of other acrylic monomers, plasticizers, and 1–5% of a cross-linking agent may be employed. The polymeric granules may also have methyl acrylate in the backbone or be plasticized by ethyl or butyl methacrylate or ethyl acrylate to increase solubility in the monomer syrup. Particle size and molecular weight distribution of the PMMA controls the solubility of the polymer and the working consistency of the mixture. Traces of poly(acrylic acid) or soluble starch suspension agents may remain in the polymer, preventing wetting of the beads by the monomer. The residual initiator content of the polymer beads may be at the level to obviate the need of further BPO to be added to the mix.

Most dentures are fabricated from the heat-cured formulations with the polymerization rate increasing directly with temperature, proportional to the square root of the initiator concentration. The half-life temperature ($t_{1/2}$, °C) for BPO at 72°C is 10 h (5). The customary curing cycle of the fully mixed powder/liquid blend is about 90 min at 65°C. Post-curing is usually done at 100°C for 60 min so as to produce a more fully cured denture with low porosity. After cooling, the denture is separated from the embedding material, trimmed, and polished. Red fibrous materials and beads of varying translucency are added in small amounts prior to curing so as to simulate the appearance fo natural oral-tissue.

Autopolymerizing Resins. Room temperature (RT) curing, initiated by a suitable redox (oxidizer–reducer) combination, is a simple modification of the heat-cured formulations. In such formulations tertiary aromatic amines, such as *N*,*N*-dihydroxyethyl-*p*-toluidine or *p*-*N*,*N*-dimethylaminophenethanol (6), are added at about the 0.3–0.8% level to the monomer, which is subsequently blended with a polymer containing 2% BPO. The rate and degree of polymerization depends on both the type and concentration of initiator (BPO) and activator (amine), as well as the particle size of the PMMA powder. Techniques for preparing the molding are very similar to the procedure described for heat-cured dentures. In this procedure, the freshly mixed monomer–polymer blends are more limited in use because of the handling characteristics of the formulations, ie, the polymerization is slightly delayed upon mixing. The rise in temperature depends on the mass of material and the powder/liquid (P/L) ratio used. Since polymerization occurs from inner to

outer portions of the mass, temperatures within the bulk portion of the casting are higher than those at the surface. The cured dentures are usually not very porous, since monomer evaporation is limited. The bulk of the polymerization takes place within 30–45 min, but may continue for hours. The denture flask is therefore held under pressure for several hours so as to ensure complete curing. Room-temperature cured materials usually contains about 3–5% free monomer, compared with only 0.2–0.5% found in heat-cured materials. Thus, this method of curing is not as efficient as the heat-cured process, since the product produced has less cross-linking density and a lower T_g than the heat-cured materials. The latter factors also make these RT-cured materials more susceptible to creep, eventually creating distortion in the denture. The larger the amounts of free monomer present in the final product, the greater the propensity for warpage to occur. Materials generated by using amines in the curing have poorer color stability upon aging. Blue dye, a ultraviolet absorber (7), may be added to the formulation to mask color shift. Production of high dimensional accuracy is one of the main advantages of RT-cured resins, resulting from lower curing temperature leading to reduction of stresses in the matrix. Differences between thermal expansion of the denture resin and the plaster mold may result in undesired dimensional changes when the mold is subjected to a wide temperature range during processing. Dentures cured at RT have better dimensional accuracy (8,9) than heat-cured dentures. However, both are clinically acceptable.

Low Viscosity, Chemically Cured Resins. The pour and cure acrylic resins are blends of high molecular weight polymer powder mixed with monomer and other additives to achieve a pourable viscosity. The mixture is usually poured through sprues into a hydrocolloid-based mold, with polymerization conducted under pressure for about 30 min at RT (10). This procedure for preparing dentures is inferior to heat- and cold-cured acrylics. However, it is an excellent technique for denture duplication. Polymerization shrinkage is a problem for this type of system, possibly causing posterior teeth to be displaced in the resilient mold and out of the desired occlusal pattern (11). Methods have been developed to improve the latter, by increasing the bond of acrylics to denture teeth (12). This technique requires great attention to detail in order to produce clinically acceptable prostheses.

Visible Light-cured Resins. Employing high intensity visible (blue) light to bring about free-radical polymerization (curing) of the denture resins holds great promise (13). A photopolymerizable formulation in this case could consist of a urethane dimethacrylate–acrylic polymer combination, reinforced with a microfine silica filler. Thus, the materials produced have more in common with a composite restorative material than with the commonly used denture-based resins. The matrix produced is a highly cross-linked acrylic, having an interpenetrating polymer network (IPN)-type structure. MMA is not used in the urethane dimethacrylate (Fig. 8) cross-linked IPN matrix, filled with colloidal silica and acrylic polymer beads. Akin to composite restoratives, the formulation makes use of the camphorquinone–*tert*-amine initiator system. With the exception of brittleness, the cured materials have properties as good or better as the denture materials made by the methods described earlier. This technique shows good potential for expanded use.

Mixing/Working Properties. For denture resins certain aspects are important to note. First, great care needs to be taken to use the correct P/L ratios,

usually about 2.0/1.0 wt% or 1.6:1.0 vol%. Too much powder will result in underwetting of the beads, leading to production of a weak structure. Conversely, too much monomer will produce excessive shrinkage. All ingredients must be thoroughly mixed to achieve the best results. A separating medium must be used to prevent adhesion of the resin to the mold surface. Control of porosity and prevention of processing stress are also two areas of concern. Polymerization shrinkage and escape of volatiles can generate porosity.

Concerning shrinkage, volume reduction of about 20% for the monomer is minimized by using polymer (PMMA) powder, cutting shrinkage to about 5–8%. It is very important that this contraction is not translated into the high linear-type contraction, which on the basis of volumetric shrinkage should be about 1.5–2.0%, but is actually in the range of about 0.20–0.5%. The observed change is probably due to thermal contraction, caused by temperature changes, and not to actual polymerization shrinkage. The resin becomes very rigid once the temperature of the reaction descends below the T_g of the material, at which point the curing contraction will have essentially been completed. From this point onwards thermal contraction contributes to dimensional changes of the denture material. Because of the latter, cold-cured dentures should have a better fit, since the processing temperature is considerably lower, ca 60°C, compared to heat-cured dentures at ca 100°C. Thus, it is very important to pack the viscous mix in the mold in sufficient quantity to create pressure, facilitating removal of voids and helping to cut down on curing contraction. In all systems, polymerization generates an exotherm, which might elevate to the point of causing monomer vaporization and creating porosity. Thus, temperatures of cure should be controlled to avoid gaseous porosity and pressure maintained to eliminate contraction porosity. Dimensional changes also give rise to internal stress, which if allowed to relax may lead to warpage, crazing, and distortion of the denture. The use of acrylic teeth, rather than porcelain teeth, eliminates differential shrinkage, helping to reduce strain. Craze development is another problem that may develop in dentures as a result of strain relief, polishing, presence of alcohol, and differential contraction due to the type of teeth used. Cross-linking helps reduce craze formation. A brief summary of the denture materials' properties is shown in Table 1.

Biocompatability. PMMA is highly biocompatible, with very few patients showing any type of allergic reaction. Adverse reactions are usually caused by leachable monomers. Cold-cured formulations may be a problem, since they tend to have more residual, free monomer. Post-curing of the denture helps lower free monomer content, but may also cause some denture distortion.

Dimensional and Mechanical Properties. Even though the denture is placed on soft tissues, there is still great need for the denture to have dimensional stability. The denture must fit as accurately as possible to promote retention of the denture to the mucosa. As shown in Table 1, there is a considerable variation in mechanical properties, depending on composition, processing technique, and environment factors. Room-temperature cured resins have lower strength and stiffness, with about the same elastic modulus as heat-cured materials. Polymerization shrinkage of the monomer–polymer dough is about 6–7%. Linear shrinkage is about 0.5% across the posterior aspect, under normal denture processing. Water sorption, about 1–2 wt%, partially compensates for the shrinkage. Linear shrinkage of 0.3–0.4% is clinically insignificant, since the tissue on which the

Table 1. Physical Properties of Denture-Based Materials[a]

Property	Poly(methyl methacrylate)	Vinyl acrylics
Compressive strength MPa[b]	76	70–76
Tensile strength, MPa[b]	48–62	51–60
Flexural strength, MPa[b]	83–117	69–110
Elastic modulus, MPa[b]	3.8×10^3	2.3×10^3
Elongation, %	1–2	7–10
Impact strength, N·m[c]	1050	3150
Transverse strength, MPa[b]	41–55	41–55
Knoop hardness (KHN)	15–23	14–20
Coefficient of linear thermal expansion per °C	81×10^{-6}	71×10^{-6}
Heat-distortion temp., °C	160–195	130–170
Polymerization shrinkage[d], %	6–7	6–7
Water sorption, 24 h, %	0.3–0.4	0.07–0.4

[a]Partially taken from Ref. 14.
[b]To convert MPa to psi, multiply by 145.
[c]To convert N·m to ft·lbf, multiply by 0.74.
[d]Linear shrinkage of commercial dentures is ca. 0. 12–0.97%.

denture rests adjusts to such changes (14,15). Some cross-linked resins contain 2-hydroxyethyl methacrylate (HEMA), which promotes higher water sorption, lowering dimensional stability. Fillers reduce the thermal expansion of the dentures, providing higher impact strength. However, they are difficult to polish, tend to stain, and may collect debris and imbibe bacteria at the surface.

It has been clearly shown that radiopaque materials are needed (16,17) for visualization of aspirated or swallowed denture fragments. This is accomplished with additives such as barium sulfate, barium fluoride, barium or bismuth glasses, and halogenated organic compounds. The physical properties of the materials are significantly affected by large quantities of these additives. ANSI/ADA specifications or requirements for radiopaque materials for denture-based polymers have been described (18).

While commercial denture materials are reasonably strong and show good flexibility, improved fracture resistance and fatigue strength are still sought. Seeking to improve such things as fracture toughness, impact and transverse strength, tensile strength, etc, various types of fiber (glass, carbon, Kevlar, and polyethylene) reinforcement have been found to significantly improve many of the aforementioned properties (19). Glass fiber reinforced composite resins have also been introduced as a replacement for metal framework in crown and bridges or fixed partial dentures as per recent clinical studies (20). Yet, research is still needed to develop improved materials, pointed toward reducing the need for denture repair (21). ANSI/ADA Specification No. 12 sets the requirements for denture-based Resins.

Polymeric Teeth for Dentures. Acrylic resin denture teeth were introduced in the late 1930s. About 60% of all preformed artificial teeth used in dentures, at least in the United States are produced from acrylics or vinyl acrylic resins. The chemistry used is based on the well-known MMA polymerization

technology. Poor wear, crazing, blanching, fracturing, etc, found in earlier acrylic teeth, has been overcome by better methods of fabrication, improved formulations, and use of higher cross-linking density. The molding technique for preparing the teeth must be highly controlled, with respect to particle size, molecular weight, and residual initiator. Further, the mix flow properties and curing cycle must be highly controlled. Mechanical retention serves, to some degree, to anchor the teeth in the chemically activated denture-based resins. However, a combination of mechanical and chemical bonding is used to retain the teeth (22).

Polycarbonates and polyslfones have also been explored for producing molded teeth. Compositions containing very finely dispersed spheres of pyrogenic silica as reinforcing fillers, urethane dimethacrylate (Fig. 8) resin, highly cross-linked IPNs, and the fabrication of layered teeth with an exterior made up of a 2,2-bis-*p*(2′-hydroxy-3′-methacryloxypropoxy)-phenylpropane (BisGMA)-based resin have also been explored (23). All formulations employ pigments to provide a natural appearance. Other additives/modifiers are also used to achieve a more natural appearance.

Acrylic teeth, with compressive strength of 76 MPa (11,000 psi), abrasion resistance, elastic modulus of 2700 MPa (3.9×10^5 in.$^{-2}$), elastic limit of 55 MPa (8000 psi), Knoop hardness (KHN) range of 18–20 kg/mm^2, and good abrasion resistance, have physical properties which are lower than those of metal alloys used for dentures and those of human enamel or dentin. For example, dentin and enamel have an ultimate compressive strength of 297 and 384 MPa, respectively, and ultimate tensile strength of 105.5 and 10.3 MPa, respectively. Furthermore, the low modulus of elasticity in plastic teeth reduces the clicking sound often exhibited by denture wearers. Compared to porcelain teeth, acrylic teeth have less resistance to creep, higher water sorption, greater fracture toughness, better resistance to thermal shock, and bond to the denture base. In contrast, porcelain teeth display better dimensional stability and increased wear resistance. A study of plastic teeth opposite plastic teeth or opposite smooth porcelain teeth has been published (24). Plastic teeth are covered by ANSI/ADA Specification No. 15.

Denture Repair Resins. Fractured dentures are readily repaired with materials similar to the RT- or cold-cured denture resins. Repairs are achieved with little to no dimensional change. However, the strength of the repaired denture may be substantially less than the original prosthesis (25). ANSI/ADA Specification No. 13 (1999) sets the requirements for cold-cured repair resins.

Denture Liner Materials. There are three groups of these materials: hard and soft liners and tissue conditioners. It is often necessary to refit the denture because of the changes in the denture-bearing tissue. To meet this need a hard relining material can be employed, using an RT- or cold-cured acrylic resin at the dentist's office, or by sending the denture to a laboratory to be repaired with a heat-cured acrylic resin. Soft liners weaken the strength of the heat-cured resins, since they can reduce the thickness of the denture base and allow diffusion of monomer or solvent into the base. The cold-cured formulations are basically of two types: a two part PMMA powder blended with MMA monomer, containing the plasticizer di-*n*-butyl phthalate or poly(ethyl methacrylate), PEMA powder, blended with liquid butyl methacrylate (BMA) monomer. The BPO–amine redox initiator system is used for curing. The use of PEMA and BMA works best where

the patients may be sensitive to PMMA or MMA. However, the use of PEMA and BMA creates a liner with a lower T_g, which may create dimensional problems. The liners must show good adhesion to the denture, allow recovery from deformation, provide a good cushioning effect, have good wetability, be relatively resistant to oral fluids, not support bacterial growth, not impair denture function, and be easily cleaned. At present, a material awaits discovery for fulfilling all of these requirements. Polyphosphazine fluoroelastomers have been formulated and cured with peroxides (26), showing that systems may be found to eliminate some of the deficiencies found in currently available liners.

Soft liners were developed to eliminate the use of MMA directly against soft tissue. Also, there are patients who are not able to tolerate a hard relining surface, even though the denture fits well. The soft liner is more comfortable and provides a means of absorbing masticatory forces via the highly resilient material placed between the denture and the soft oral tissue. In addition, soft liners may be used to reduce tissue inflammation caused by worn out or ill-fitting dentures. Polymers with a T_g slightly above the mouth temperature exhibit a rubbery behavior in the oral cavity. A variety of materials have a T_g low enough to be useful as soft liners, including silicones and acrylics. PMMA is also useful when plasticized to obtain the required T_g. Fortunately, acrylic monomers are available which produce polymers with a wide range of T_g, starting with PMMA at 105°C, PEMA at 65°C, and poly(*n*-butyl methacrylate) (PBMA) at 20°C. They are all useful for producing soft liners. The soft liners are generally supplied as powder-liquid kits or ready-to-use sheets. Materials currently available are usually plasticized acrylics. All formulations contain fairly high molecular weight acrylate or methacrylate polymers or copolymers, derived from ethyl, *n*-propyl, *n*-butyl, etc, monomers and a liquid or solvent, such as ethyl alcohol or ethyl acetate, a plasticizer, such as dibutyl phthalate, and a polymerizable monomer. The T_g of the material is set to $\leq$47°C. The materials adhere well to denture-based resins. But, they have poor elasticity and harden upon aging because of the loss of the plasticizer (27–30). More hydrophilic liners have been formulated by using HEMA or other copolymers (28). However, HEMA-based resins may soften and swell excessively due to water sorption, leading to undersirable functional changes.

Silicone liners are similar in composition to the previously described elastomeric impression materials, which are produced by condensation polymerization. Systems for the relining application may be either a one-component system, which cures in the presence of moisture or heat, or a two-component system, containing base and catalyst. Both types generally have poor adhesion to the denture surface, and can readily support bacterial growth.

Tissue Conditioners. These products alleviate discomfort from soft-tissue injury or inflammation. Tissue conditioners are soft materials applied temporarily to the denture fitting surface, allowing better distribution of stress. They exhibit viscous flow under pressure, forming a very soft cushion between the hard denture and the soft tissue. In terms of softness, the material must not be too soft or flow to the extent that it will be displaced from between the denture and the mucosa. These materials may consist of PEMA powder mixed with a solvent (such as ethyl alcohol) and a plazticizer (such as *n*-butyl phthalate and *n*-butyl glycolate) (31,32). The alcohol swells the PEMA beads, rapidly promoting diffusion of the plasticizer into the polymer, yielding a plasticized gel. Alcohol and plasticizer are

slowly leached out from the applied gel, which may cause the material to become too rigid. The liner must be replaced every few days to retain properties, until the patients supporting tissues return to normal state.

Crown and Bridge Temporary Resins. Materials used in this area are usually based on methyl or ethyl methacrylates and BisGMA-acrylics mixtures (20), or even an ethyleneimine-terminated monomer (33). The formulations are supplied as a two-component paste, composed of monomers and polymerization initiator. Used for interim tooth coverage, these materials are not as strong as other acrylics. However, they exhibit good flow, low exotherm, and low curing shrinkage. They maintain the correct biting relationship, stop teeth drifting, and protect the prepared tooth against fracture, while waiting for the permanent prosthesis to be delivered.

Polymeric materials are also used for fixing veneers on crown and bridges. Polymers used for this application include acrylics, vinyl acrylics, and dimethacrylates, as well as silica- or quartz-microfilled composites. After placing on the metallic substrates of the prostheses, the materials are heat or light cured. These materials are easy to fabricate, and can be readily matched to the color of the tooth structure. The acrylic facings have poor adhesion to the metals, being retained only by curing the monomers into mechanical undercuts designed into the metal substrate. They have less mechanical strength, less color stability, poorer abrasion, etc, than normal dental composites, along with deforming more under bruxism. With the advent of porcelain fused to metal crowns and bridges, restoratives with polymeric veneers are less frequently used.

Mouth Protectors. The widespread growth of contact sports has accelerated the use of mouth guards (34,35). Guards may be produced from natural rubber, poly(vinyl chloride), poly(vinyl acetate-*co*-ethylene), or polyurethane materials. Customized guards are often fabricated from poly(vinyl acetate-*co*-ethylene) blanks, soft acrylic dough, liquid rubber latex, polyurethane, and laminated thermoplastic (36,37). Over the counter protectors usually fit poorly, in contrast to dimensionally stable and comfortable, customized mouth protectors.

Maxillofacial Prosthetic Materials

A large number of polymers, including latexes, vinyl plastisols, silicone elastomers (heat or RT vulcanized), and polyurethanes, may be formulated into materials for facial prostheses (38–41). The materials should be biocompatible, easy to fabricate, easy to clean, feel like real skin, translucent, stable to heat, light, and cleaning solutions, and sufficiently resilient to prevent tearing. It should be possible to modify the formulation to match skin color. No material meets all these requirements.

Latexes. These materials do not have the strength and color stability to be very useful for this application. In addition, they may cause an allergic reaction. However, a recent terpolymer derived from *n*-butyl acrylate, MMA, and methyl methacrylamide, can be formulated with colorants to provide a superior latex, compared to earlier materials.

Vinyl Plastisols. These materials have some utility in maxillofacial prostheses. The formulations are viscous liquids, made up of small vinyl particles dispersed in a plasticizer, along with colorants. They are heated to generate the

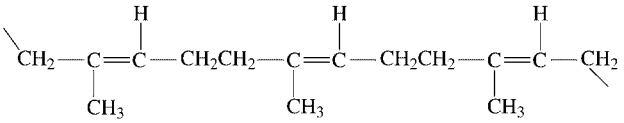

Fig. 6. Gutta-percha structure.

desired materials. The loss of plasticizer and lack of stability decreases the use of these materials.

Silicones. These materials have some only recently been used to produce maxillofacial prostheses. Both the RT- and heat-vulcanized materials may be used. Heat-vulcanized formulations are supplied as a semisolid or putty-like material, which requires the addition of colorants. The molded material is cured under pressure at 180°C/30 min. The heat-cured materials exhibit better strength and color stability than the RT-cured materials.

Polyurethanes. This is the most recent material used in maxillofacial applications. Fabrication requires accurate proportioning of the components. The isocyanate and polyol are blended, placed in a suitable mold, and allowed to cure at room temperature. Colorants and other additives are also used in the formulations. Even though the fabricated prosthesis has a natural feel and appearance, the final product is still relatively unstable.

Root-Canal Sealants

A variety of materials have been used to hermetically seal the root canal, preventing ingression of oral fluids into the canal. One natural material used is gutta-percha (Fig. 6), a rubber obtained from the Taban tree. This material has been used in endodontics for over a hundred years. Rubbers are polymers of 2-methyl-1,3-butadiene (isoprene), having two possible conformations, ie, a cis and trans form, with the trans form being gutta-percha. These rubbers are hardened by vulcanization, achieved by blending and heating with a few percent of sulfur, which causes cross-linking. A typical formulation used in a root canal has about 19–22% gutta-percha, 59–75% zinc oxide filler, 1–17% heavy metal salts, and 14% wax plasticizer. The material softens at about 60–65°C and melts in the vicinity of 100°C, providing a temperature range to soften, deform, and condense the material into the prepared root-canal space. Other materials used for endodontically treated, fractured teeth are based on zinc oxide-eugenol, epoxy resin, polyvinyl resin, calcium hydroxide resin based formulations, and glass-ionomers formulations.

Other Uses

Patterns for gold-inlay castings can be prepared from acrylics. Castings made this way are not superior to castings produced from a wax pattern, accounting for the lack of interest in this technique. Some dental laboratories use epoxy die

materials for fabrication of casts. Autopolymerizing resin formulations are used to make custom impression trays, with such resins containing substantial quantities of fillers to increase the rigidity of the materials. PMMA or other thermoplastics are used to prepare occlusal night guards. Other areas of dentistry make extensive use of polymers in retainers, splints, temporary space maintainers, and bite plates.

Restorative Materials

Filling Materials. Resins used to formulate dental composites/restoratives were initially derived from the free-radical polymerization of doughs made from PMMA beads blended with MMA monomer (42–46). Many studies have focused on improving these materials, by addition of cross-linking monomers and reinforcing fillers (45), with much of the early work done at the National Bureau of Standards. Earlier, the polymer industry had previously shown that epoxy resins, based on bisphenol A, were excellent matrix resins for a variety of composites. However, epoxies exhibited poor ambient polymerization characteristics under conditions useful in the oral cavity. Knowing the latter, as well as the need to have a new monomer which would be both free-radical polymerizable with less shrinkage in composites, Bowen (47,48) made the discovery that the diepoxide derived from bisphenol A and epichlorohydrin could be treated with methacrylic acid to form a unique hybrid monomer, well known today as BisGMA (45,47,48). Alternatively, the BisGMA monomer may also be produced by reaction of bisphenol A with 2 mol of glycidyl methacrylate. The synthetic path to the bulky, thermosetting dimethacrylate, BisGMA, launched a new era for development of composites used in dentistry. BisGMA (Fig. 7) has two chiral carbon atoms (denoted by an asterisk) with the dimethacrylate diastereomers helping to make the BisGMA mixture a viscous syrup. Compared with the PMMA–MMA doughs, the BisGMA-based formulations, combined with inorganic reinforcing fillers and suitable polymerization initiators, made available composite fillings with lower polymerization shrinkage, improved mechanical properties, reduced water sorption, a more attractive coefficient of thermal expansion, better esthetics, and more acceptable biocompatibility (44,45). A good review of dental composite resins has been published (49).

Dental Composite Restoratives. Polymeric restoratives have three major components: an organic resin matrix, an inorganic filler modified with a coupling agent, and a suitable polymerization initiator system. The formulation used to produce the organic matrix, or continuous phase, is made up of free-radical polymerizable monomers. The monomer mostly used in the formulations for both anterior and posterior resins is BisGMA (Fig. 7), or alternatively formulated with

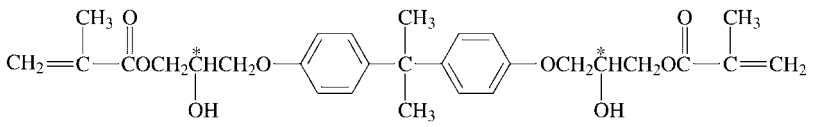

Fig. 7. BisGMA structure(s).

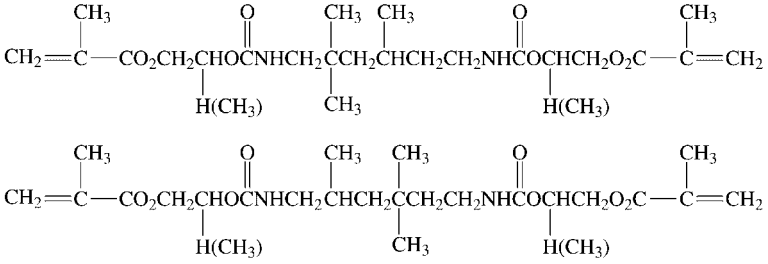

Fig. 8. Monomers structures in urethane dimethacrylate mixture.

a urethane dimethacrylate monomer (Fig. 8). A variety of fillers may be used to make up the reinforcing phase. Fillers may consist of silanized quartz, glass or various ceramics, with silanization affording the coupling mechanism. A prepolymerized resin containing pyrogenic silica may also be used to reduce polymerization shrinkage. Various polymerization initiators or activator–initiator combinations are known to be useful to achieve curing. Inhibitors are required to prevent polymerization during storage. Sealants used in dentistry have similar compositions, but are more lightly filled or possibly unfilled. Composites used in dentistry can come in various forms, ie, a one- or two-part formulation, a uniform paste, a powder–liquid, a paste–liquid, or a paste–paste formulation.

Polymerization. Methacrylate-based restoratives are free radical not radicals polymerized by redox systems or photochemically by visible light, using photoinitiators or photoinitiator–photosensitizer combinations with only the visible light range (400–500 nm) allowed for curing. Redox initiation systems may consist of such things as BPO/*tert*-amines, hydroperoxides-thioureas, peroxides with ascorbic acid or derivatives, and BPO/*tert*-amine with synergistic promoters, eg, polythiols (4,50–52). A commonly used combination for redox use is the BPO/*N*,*N*-dihydroxyethoxy-*p*-toluidine system. The combination of α-diketones, such as camphorquinone (CQ), with a tertiary amine, such as *N*,*N*-dimethylaminoethyl methacrylate (DMAEMA) (52), are particularly useful for visible light-curing (VLC) (53,54). With light activation, CQ and DMAEMA form an "exciplex" with the "exciplex" subsequently producing a DMAEMA-based radical, which initiates the polymerization. VLC resins provide the dentist a significant control over the restorative hardening process. Further, the porosity and surface tackiness, owing to air inhibition, are lower in the VLC-cured materials compared with that of the redox formulations. But, properly mixed redox formulations polymerize much more uniformly, especially in areas of great bulk, compared to the VLC formulations. When using VLC systems to fill deep cavities, a layering technique must be used to ensure adequate polymerization.

Monomers or Matrix Phase. Although BisGMA is widely used in commercial dental composites, other types of dimethacrylates have also been studied or developed for use as alternatives to BisGMA (55–76). Because of the high viscosity of BisGMA, a variety of dimethacrylates have been found to be useful as reactive diluents or polymerizable modifiers to provide suitable viscosities for high filler loading, with diethylene glycol and triethylene glycol dimethacrylates (Fig. 5) being good examples. Studies on the kinetics and the nature of the network

formation in the dimethacrylate polymerizations have been given significant attention (77–83), with the types of monomers used and the degree of carbon–carbon double bond conversion achieved determining the T_g obtained (49). There is growing interest in varying the polymerization stages, ie, using a "soft start" stage, as a way to improve the resin properties.

Resins have also been designed to utilize multifunctional methacrylate prepolymers, derived from the chain-extending reaction of BisGMA with a diisocyanate, such as 1,6-hexamethylene diisocyanate, combined with a diluent monomer (64,65). Incorporating urethane residues in the matrix, which enhances toughness, gained great acceptance in Europe, with an example being the monomer derived from the reaction of HEMA with a branched aliphatic diisocyanate (Fig. 8).

Many experimental dimethacrylates have been explored for reduction of shrinkage and water sorption in composites, seeking to improve such things as dimensional stability, creep resistance, fracture toughness, wear resistance (66,84–95). The goal is to formulate a better alternative to the commonly used amalgam. Some of these have been prepared from nonhydroxylated homologues of BisGMA, having lower viscosity (66). In one case, a multimethacrylate prepared from esterification of a low molecular weight styrene–allyl alcohol copolymer was shown useful in reducing shrinkage or polymerization contraction stress in BisGMA/TEGDMA neat resin blends (96,97).

A variety of fluorine-containing monomers and polymers have been prepared and examined to produce hydrophobic dental composites with low water sorption, high contact angles, reduced margin leakage, and resistance to surface staining (67–73). One such formulation consisted of 75 wt% octafluoro-1,1,5-trihydropentyl methacrylate and 25 wt% of a nonhydroxylated homologue of BisGMA (66–68). But, the polymerization shrinkage and strength deficiencies were not improved. Also, the volatility of the nonbulky fluorinated-monomer component was a problem. In contrast, a stronger hydrophobic composite was prepared from a low surface-energy matrix resin consisting mainly of a highly fluorinated multifunctional methacrylate prepolymer, ie, PFMA (70–73,98). The viscosity of this formulation was comparable to that of BisGMA, along with solubility in a variety of diluent monomers. The dimethacrylate derivative of a fluorinated triethylene glycol, having low viscosity, was recently examined as a reactive diluent, showing some promise to improve the performance properties of an ethoxylated bisphenol A dimethacrylate (BisEMA)-based composite (99–101).

Elimination of polymerization shrinkage has been under study for some time (74,75). In the early work, a blend of a BisGMA-based resin and a solid spiroorthocarbonate (SOC), which also polymerizes by a free-radical, ring-opening mechanism, was cured to give thermosets with very low volume shrinkage (75). Following the latter study, a great variety of compositions have been designed for ring opening, expanding polymerizations, focused on eliminating or reducing the shrinkage as well as improving the physical and mechanical properties of composites. The focus has mainly been on SOC and SOC-type monomers with epoxy resins (102–113). This concept has not, to date, produced marketable dental restoratives.

More recently, the possible use of liquid crystalline monomers (114), hyperbranched polymers (115,116), inorganic–organic hybrid monomers (117–120), and sol–gel technology (121) has started to be examined for preparing improved

composites. The use of multimethacrylate substituted hyperbranched polymers looks to be a particular attractive path to explore for generating composites with significantly lower shrinkage, since low viscosity, high molecular weight entities can be formulated into the monomer–polymer mixture. Also, the *in situ* generation of a nanocomposite, where the inorganic component is truly distributed at the molecular level in the cured composite, may satisfy the great need for preparing restoratives with both low shrinkage and significantly improved wear resistance.

Reinforcement Phases. After introduction of quartz filler in the late 1950s, many types of reinforcing fillers have been studied or used in dental composites. In addition to quartz, fused or colloidal silica, and other inorganic fillers, finely divided, organic prepolymenized composite particles are also useful as a dispersed phase. This is especially true for microfilled and hybrid composites (122–124). Fillers serve to increase hardness and compressive strength, and significantly reduce shrinkage of the restoratives. Filler technology has brought many improvements to currently used composites. But, in order for the composites to have acceptable mechanical properties, it is critical for the resin matrix and filler to have a strong interfacial bond. A breakdown at the interface, followed by load application, will not allow the stresses developed to be effectively distributed throughout the material. Bonding is achieved by the use of coupling agents, incorporated into the formulation at the surface of the filler. Vigorous efforts have been focused on maximizing filler volume or obtaining highly loaded composites, which exhibit much better stress-bearing capability.

Physical Properties. Table 2 shows some physical properties of unfilled (neat) resins and filled composites. Microfilled composites generally have inferior properties compared to conventional or the more recent hybrid restoratives, with

Table 2. Physical Properties of Resin Restoratives

Property	Unfilled PMMA	Microfilled composite	Conventional and filled hybrid composite
Inorganic content[a], wt%		33–51	70–80
Compressive strength, MPa[b]	55–78	225–350	250–400
Knoop hardness (KHN)	15	5–30	50–60
Tensile strength, MPa[b]	14–28	30–55	50–90
Modulus of elasticity, GPa[c]	1.9–2.3	3.2–6.0	8.0–20.0
Linear coefficient of thermal expansion, 10^{-6} °C	92	50–70	20–40
Water sorption, mg/cm^2	1.70–2.03	0.94–2.20	0.50–0.70
Polymerization shrinkage, vol%	5.2–8.0	1.0–1.8	1.2–5.3
Thermal conductivity[d,e] W/(m·K)	2.4	6.3–8.4	1.5–4.0

[a]The volume (weight) of the filled systems varies from about 30 to 77% (50–85%). Traditional, small particle filled, micro-filled, and hybrid composites have fillers ranging in size, respectively, from 8–12, 1–5, 0.04–0.4, to 0.6–1.0 μm.
[b]To convert MPa to psi, multiply by 145.
[c]To convert GPa to psi, multiply by 145,000.
[d]Thermal conductivity of enamel and dentin, respectively, is 0.87 and 0.59 W/(m·K).
[e]Composite restoratives are good insulators.

the exception of polishability. By definition, hybrids (blends) have a combination of colloidal and fine particles as filler, at approximately 60–65 vol% with the fillers ranging in size from 8–12, 1–5, 0.04–0.4, to 0.6–1.0 μm. The higher volume ratio of polymer to inorganic filler, ie, low filler content, of the microfilled resins leads to lower modulus of elasticity, greater thermal dimensional changes, less resistance to indentation, and higher water sorption. Requirements for dental composites are covered by ANSI/ADA Specification No. 27.

Dental Cements. Polymeric matrices used in formulating cements are similar to those used in methacrylate-based composites and sealants. BisGMA or some other dimethacrylate is blended with monomers such as MMA, along with fillers and other additives, to make the formulated adhesive useful in the oral cavity. They may be of the VLC type and/or chemically cured type. They may also contain additives such as inorganic fluoride salts, which may result in reducing recurrent decay.

Polyelectrolyte-Based Restoratives. Alginates, previously described under Impression Materials, were the first ionic polymers to be employed in dental applications. But, polyelectrolytes derived from poly(acrylic acid), various co- and terpolymers of acrylic acid, and other alkenoic acids (ie, itaconic acid and maleic acid) are used in aqueous solutions for formulating polyelectrolyte-based cements. These materials are also known as *glass polyalkenoates* or more commonly *glass-ionomers* (GIs) (125–135). Several articles present the chemistry associated with GIs (136–139). Cements based on glass ionomers adhere well to enamel but only weakly to dentin.

Glass Polyalkenoate Cements. Polyalkenoate cements, which evolved from the zinc phosphate cements, were formulated with an organic polyacid and subsequently called zinc polyacrylate cements (127). Zinc oxide was the basic powder component, with smaller amounts of magnesium or tin oxide and, optionally, small quantities of silica, calcium hydroxide, stannous fluoride, and other salts. The acid component was an aqueous solution of poly(acrylic acid), having about 30–50% solids, with the polymer having an average molecular weight of 30,000–50,000. Copolymers of acrylic and other alkenoic acids, eg, itaconic, maleic, and aconitic acids, were subsequently used to make shelf stable aqueous solutions with lower viscosity, providing a cement with better properties. A series of acid–base reactions brings about hardening or setting of the cements, with ionic-type cross-linking achieved by the ionized carboxylate groups forming a complex (salt-bridge) with the divalent metal cations, producing a highly, ionically cross-linked, hydrophilic matrix. Free powder embedded in the stiff polymeric hydrogel or matrix acts as a normal reinforcing agent. Other types of additives are incorporated into the formulations to improve certain properties. Cements of this type, which have an opaque appearance due to the high concentration of zinc oxide, adhere well to tooth structure and base metals, enabling them to be used as bases under permanent fillings and to cement prefabricated restorations and orthodontic appliances. The properties of various cements are given in Table 2. A family of non-aqueous polycarboxylate cements may also be formulated, with such systems displaying excellent hydrophobic and energy-absorbing properties. Chain-extending, acid-base reactions of dimer and trimer acids with various basic powders may be used (140). The water-based cements are covered by ANSI/ADA Specification No. 96 (1994).

Table 3. Physical Properties of Resin Restoratives

Property	Unfilled PMMA	Microfilled composite	Conventional and filled hybrid composite
Inorganic content, wt%		33.2–50.9	70.4–80.2
Compressive strength, MPa[a]	55–76	221–330	127–350
Tensile strength, MPa[a]	14–28	28–56	28–63
Modulus of elasticity, GPa[b]	2.3	3.2–5.0	7.1–16.2
Linear coefficient of thermal expansion, 10^{-6} °C	92	46–70	25–40
Water sorption, mg/cm^2	2.03	0.94–2.20	0.13–0.74
Polymerization shrinkage, vol%	5.2–8.0	1.9–5.8	1.2–5.3
Thermal conductivity, W/(m·K)	2.4	6.3–8.4	10.5–13.8

[a]To convert MPa to psi, multiply by 145.
[b]To convert GPa to psi, multiply by 145,000.

More translucent glass polyalkenoate- or polyelectrolyte-based cements (GI) were developed by using similar aqueous solutions of polyacids, such as poly(acrylic acid), poly(acrylic acid-*co*-itaconic acid), poly(acrylic acid-*co*-maleic acid), etc, and ion-leachable calcium fluoro aluminosilicate type glass powders (126,128,135). The matrix in this conventional-type GI is formed by acid-base reactions involving the di- (Ca^{2+}) and trivalent ($A1^{3+}$) cations, binding carboxylate groups in ionic cross-links (salt-bridges), producing a stiff hydrogel into which partially reacted glass particles are embedded (136–138). Glass-ionomers, similar to the zinc polycarboxylate cements, exhibit good adhesion properties. Glass-ionomer cements may be used as a cosmetic filling materials and for the repair of cervical erosions because of good adhesion and semitranslucent nature. In the area of mechanical strength, GI-based cements are superior to zinc phosphate and zinc polycarboxylate, approaching the dental silicate cements in compressive strength and modulus of elasticity (Table 3). Other polyelectrolytes have also been explored as polymeric acids for formulating GIs, with poly(vinyl phosphonic acid) being an example (141,142). The vinyl phosphonic acid polymer formulations were too acidic to allow suitable working and setting times (142). Experimental cements have also been described for taking advantage of the reaction of an aqueous solution of phytic acid and myoinositol hexakisphosphate with zinc oxide or alumino-silicate glass powders (143). In such a formulation, a polyelectrolyte network matrix is formed by ionic chain extension and cross-linking reactions involving leachable multivalent cations and the organophosphoric acid groups.

Acrylic acid copolymers were recently modified with *N*-acryloyl- or *N*-methacryl-oylamino acids, such as *N*-methacryloyl-glutamic acid (MGA), providing a possible path to improved, conventional GIs (144–148). The copolymers studied had the carboxylic acid groups tethered at various distance off the copolymer backbone, with the acid groups having a range of pK_a or dissociation constants (149,150). The AA—IA—MGA copolymer having an 8:1:1 monomers ratio looked particularly attractive to use in formulating conventional GIs, as shown by statistically designed experiments. The study showed that an 8:1:1 (AA:IA:MGA)

copolymer gave the highest compressive strength (148). Raman spectroscopy studies showed that tethering the acid groups various distances off the copolymer backbone influences the level of salt-bridge formation (149). This type of modification was also shown to enhance the adhesion of the GI to tooth structure, improve fracture toughness, and enhance fluoride release. All the improvements were attributed to greater availability of the carboxylic acid groups to ionize and form salt-bridges. The copolymers with pendant amino acid residues have also been developed for preparing VLC formulations (146,150).

The monomer *N*-vinylpyrrolidinone (NVP), 1-vinyl-2pyrrolidinone, has been explored for modification of poly(acrylic acid-*co*-itaconic acid), providing a path to new polyelectrolytes for formulating GIs (151–155). For these copolymers, the optimum monomer ratios and molecular weights, to give good mechanical properties, were determined by statistical design of experiments. Formulations containing NVP residues were also developed for VLC applications. Clearly, new polyelectrolytes can be prepared for formulating improved GIs.

VLC Glass-Ionomers. Presently, the GI formulations used in the United States are either the free-radical, VLC, redox initiated, or a combination of VLC and redox initiation types (128,136–139). These are water-soluble polylectrolytes having both pendant carboxylic acid groups and free-radical polymerizable moieties, such as methacrylate residues. These hybrid-type formulations, which are more composite-like, are also referred to as resin modified glass-ionomers (RMGIs) (138,156–158). The two-component formulations, with one being an aqueous solution of the polyelectrolyte (acidic polymer), initiators, and reactive monomers and the second the basic glass powder consisting of calcium fluoro-aluminosilicate, are mixed, placed in the cavity, and exposed to visible light. Hardening occurs in two ways: formation of a free-radically cross-linked organic matrix and salt-bridge formation. A combined VLC, redox, and salt-bridge reaction in the same formulation appears to work best (157,158). The VLC GIs are less technique sensitive, cure in shorter time, may be finished at the time of placement, are more plastic in nature, have better adhesion to tooth structure, and reduce microleakage better than the conventional GI formulations (159). All in all, the RMGI modifications made the GI family of restoratives significantly stronger than the conventional GIs, leading to recommendations that these materials could be used in Class V and Classes I and II restorations in primary teeth.

Compomers. Glass-ionomers have evolved along with composite resin technology to produce a new family of materials for restoratives, now commonly called *compomers* (160–166). To some degree, compomers offer the advantages of both GI and composites in one material. Starting from the first resin modified cements (160,161) work, compomers were first introduced to the market in 1995. The term polyacid modified composite more readily describes the chemistry of compomers. These formulations consist of an organic and an inorganic phase, with the inorganic phase having some level of fluoride-containing, basic or reactive glass particles. The organic phase also contains carboxylic acid functionalized monomers and initiators. On exposure to light, free-radical polymerization occurs to give the cured resins. Water sorption of the cured organic matrix facilitates an acid-base reaction, bringing about further hardening due to formation of some ionic-type cross-linking. Water diffusion also facilitates the release of fluoride ions to the tooth structure. The physico-mechanical properties of GIs, compomers, and

composite restoratives have recently been compared (167), with this and other efforts showing that the mechanical properties of compomers, as well as their resistance to wear, are significantly better than both conventional- and VLC-type GIs. The compressive strength and diametral tensile strength for compomers is in the range 280–460 MPa and 52–62 MPa, respectively, with polymerization shrinkage in the range of 2.0–3.0%, and the coefficient of thermal expansion (ppm/°C) being in the range 12–41. The reported coefficient of thermal expansion for coronal tooth structure is about 11 ppm/°C. Clearly, research on compomers suggests that there are still others ways to be discovered for improving the handling characteristics and compensating for polymerization shrinkage in the design of dental restoratives.

Sealants

A variety of sealants have been explored or developed (168), with many people having one or more applications of a sealant. Sealants are vital for promotion of adhesion, which significantly reduces caries formation (169–177). Pit and fissure sealants are covered under the American Dental Association (ADA) Acceptance Program. These materials are used to seal high caries-susceptible pits and fissures of the deciduous and permanent molars, and also to seal microspaces between the tooth and restorative materials, enabling these materials to adhere firmly both to prepared cavity walls and to other restoratives. They provide dental pulp protection and protection from secondary caries formation.

Most dental sealants are resinous materials derived from free-radical polymerizable monomers, but GI dental cements (discussed earlier) also have some use as sealants. Sealing with resinous materials or GIs is part of modern preventive technology, where the sealants used for this purpose are called *preventive dental sealants* (PDS). Dental caries that occur around restorations are called secondary caries. Sealing the microspaces with adhesive resinous materials is effective in controlling secondary caries; here we call these adhesive materials the *restorative dental sealants*.

A brief history and state-of-the-art ion enamel and dentin bonding was published in 1995 (178). Recent advancements in synthetic chemistry and polymer science of dental sealants are now briefly reviewed or discussed, including those designed for various clinical uses, directed toward prolonging the lifetime service of natural teeth.

Preventive dental sealants, used to seal the susceptible areas of teeth, are classified into pit and fissure sealants and smooth surface sealants. From a material science perspective, pit and fissure sealants can be further classified into resin sealants and GI cements. Preventive dental sealants are usually placed onto molar teeth of young children who are at high risk for caries development.

Pit and Fissure Sealants. Resin sealants consist of a free-radical polymerizable monomer mixture, having a viscosity low enough to penetrate easily into narrow pits and fissures, capable of being cured to a hard and durable sealing material. BisGMA, urethane dimethacrylate, and other methacrylates are very popular as monomers for resin sealants, along with other monomers, to lower

mixture viscosity to enhance penetration ability, which is interesting to note. The highly active, anerobically cured cyanoacrylate monomers have also been evaluated for sealant applications (179). Etchants, such as phosphoric acid, citric acid, or other acidic solutions, are applied to the enamel pit or fissure area prior to application of the sealant, to provide the required tooth bonding to the nonadhesive resin (179–181). This so-called *acid etching* changes the enamel surface to a microrugged structure, which fosters better penetration of the sealant into the fissure and results in stronger adhesion between the sealant and the tooth surface (182). Acidic monomers have been developed for use in the sealant formulations to further enhance the penetration and adhesion. Polymerization of the sealants is initiated chemically with BPO/amine or sulfinate (redox combinations) or visible (blue) light irradiation, where the formulation contains CQ as the photosensitizer. These sealants may be one- or two-component formulations. One-component, photopolymerizable sealants can be cured very rapidly (<60s) by exposure to visible light, with two-component, self-curing sealants taking significantly longer time to harden or cure after mixing (183).

Glass-ionomer cements, where the chemistry was described earlier in the text, are widely used as sealants. Uses of this type of hydrogel (184) vary with the dental treatment, where low viscosity pastes, which exhibit fast setting, characterize the cements for pit and fissure sealing. In this process a glass powder and an aqueous polymer solution are mixed in given proportions and packed into pits and fissures without prior acid etching of the tooth surfaces. The cement paste cures within a short time through the salt-bridge formation between poly(acrylic acid) (185), or acrylic acid copolymers with maleic and itaconic acids (6), and Ca^{2+} and Al^{3+} cations leaching out from the glass powder. Poly(acrylic acid) undergoes ionic interaction with calcium ions on the enamel surface, producing bond strengths of 2–4 MPa. Fluoride ion released from these compositions helps prevent caries formation, improving the acid resistance of surrounding dental enamel (186).

Smooth surface sealants are used to prevent bacteria, staining, and physical damage to susceptible teeth. Cured sealants are directly exposed to the oral conditions, and therefore strong adhesion to enamel and dentin, good physical properties, good wear resistance, chemical stability, biological stability, and thin-film formation are required. Glass-ionomer cements fail to meet these requirements because of insufficient physical properties. Instead, highly cross-linked resin sealants, reinforced with ultrafine silica particles, are used.

Shear bond strengths of composite restoratives on enamel, etched with 30–40% phosphoric acid solutions are typically in the range of 18–25 MPa (182). In comparison, bonding to dentin is a much tougher challenge because of its organic constituents, fluid-filled tubules, and intrinsic compositional variation (187). However, substantial progress has been made to facilitate minimal invasive restorative therapy, by design of new bonding techniques/agents. First, it was discovered that resin penetration into the acid etched (conditioned) dentin, which is critical to achieve good bonding, is influenced by dentinal conditions (moist or dry) and by the type of solution used (188,189). There is great correlation of the bond strength received with the permeability and dentin penetration depth (189–191). The elusive goal, not yet totally reached, is to have a simplified application

method for a dentin bonding system which will produce a very durable bond with total elimination of future microleakage (192–194). Composite resin polymerization shrinkage is the main reason for marginal gaps and stress at interfaces, leading to microleakage (192,195). Thermo- and load-cycling studies are essential for determining or predicting the dentin-restoration bond longevity (196,197). Apart from using simple acid etching, the evolutionary development of surface-active comonomers with both hydrophilic and hydrophobic moieties, as part of the primer system, has made a very significant impact on improving bonding to dentin (198–201). The work on self-etching primers, to improve the understanding of what it takes to bond well to dentin, also played a very important role in the design of improved dentin bonding systems (202–206). For specific information on some of the most recent, commercial enamel and dentin bonding systems, see literature on Excite (Ivoclar AG or Vivident), Single Bond (3M Dental Products), One Step (BISCO), Prime Bond (Dentsply/DeTrey), and Optibond Solo (Kerr Sybron).

Dental Restorative Sealants. Dental amalgams are mixed and condensed into molar teeth cavities, hardened by the amalgamation process. The amalgam has no chemical interaction with the cavity wall, and irregular microspaces are produced along the interface between them. Amalgam sealant and amalgam bonding agents are used to seal the microspace and control the incidence of secondary caries around the amalgam restoration. Chemical composition of this sealant or bonding agent may be as follows: a monomer such as diethylene glycol dimethacrylate (Fig. 5) or a comonomer such as methacryloxyethyl phthalate (MEP). Other formulation additives may be *tert*-butyl hydroperoxide initiator, *o*-sulfobenzimide accelerator, and hydroquinone inhibitor.

This sealant is composed of only one liquid, which remains uncured before application, but cures quickly once applied to amalgam. Because of *tert*-butyl hydroperoxide and *o*-sulfobenzimide, polymerization occurs anaerobically when it is cut off from air and it contacts the copper in the amalgam. When placed between two glass plates at 25°C, it takes more than 10 min to cure. However curing occurs within 2 min between a glass plate and the amalgam. The MEP (207) monomer is used to enhance penetration of the sealant into micro spaces and achieve adhesion to both arnalgam and tooth surface. This sealant achieves amalgam–enamel bonding by about 1.0 MPa and bonds amalgam–dentin by about 2.6 MPa without acid etching. Examples of two amalgam bonding agents illustrate the latter, brief discussion.

Amalgam Restorative Sealants. These adhesives are of two types: adhesive resin cements and bonding agents originally developed for composite restorations. One commonly used adhesive resin cement is Amalgambond (Sun Medical Co., Japan), which consists of PMMA powder and MMA monomer, containing 4-methacryloxyethyl trimellitate anhydride (4-META) and tributylborane oxide (TBB-O) as a catalyst. TBB-O is activated by the water on the surface of adherents and promotes graft polymerization of MMA onto collagen in dentin, promoting strong adhesion (201,207,208).

Panavia 21 (Kuraray Co., Japan) is an adhesive cement, characterized by the use of 10-methacryloyloxydecyl dihydrogen phosphate (MDP). This cement consists of a primer and a composite paste. The primer is a monomer solution containing MDP, which develops strong adhesion to enamel and dentin. The

cement paste is a mixture of polymerizable monomers, including MDP, and inorganic filler, with polymerization/curing caused by the catalyst BPO/*text*-amine/sulfinate. Strong adhesion to tooth substances and amalgam is achieved. Panavia has a shearbond strength, in MPa, of 20 to dentin, 37 to enamel, 15 to amalgam, and 47 to Ni–Cr alloy.

Composite Restoration Sealants. Systems used in this case consist essentially of dimethacrylate mononers, such as BisGMA, homologues of BisGMA, urethane dimethacrylate, and silanated inorganic fillers, as discussed in the section on Composite Resins. The sealants used for restorations (called *bonding agents*) are applied onto the cavity walls prior to the placement of composites and bond the two substances tightly.

Bonding Agent Chemistry. Composite bonding agents are a mixture of polymerizable monomers or a solution of monomers in volatile solvents, which cures through free-radical polymerization on the cavity walls or between cavity walls and composite restorations. Liquid monomers, such as MMA, HEMA (207,209,210), other erythritol methacrylates, and ethylene glycol dimethacrylate, exhibit strong adhesion to dry teeth. The well-known Gluma adhesive system is made up of water, HEMA, and glutaraldehyde (211). When the teeth cavity walls are wet, application of acidic monomers is common for getting reliable adhesion, even when using a water-free adhesive primer (189). Monomer composition is selected for a balance of hydrophilicity and hydrophobicity, physical properties of the cured polymers, adhesion to composite restorations, curing time, and so on. Polymerization catalysts used are similar to those for pit and fissure sealants.

Pretreatment of cavity walls with bonding agents is a must for composite restorations. A typical procedure for restoration with composites, using a light-cured bonding agent and a light-cured composite is as follows: (*1*) cavity preparation, (*2*) washing and air drying, (*3*) acid etching of the cavity wall, (*4*) application of the bonding agent and visible light irradiation, (*5*) composite restoration filling and visible light irradiation, and (*6*) finishing and polishing. Researchers have improved this procedure by using acidic monomer in the bonding agent as the acid for etching. Combining the etching and bonding agents reduces the number of steps and gives higher bonding strength to the dentin.

Dental Adhesives (For Alloys and Ceramics)

Various materials such as polymers, alloys, ceramics, and composites are used to restore or replace tooth structure. It is vitally important for these materials to be bonded securely to the tooth surface. Lack of bonding between the materials and tooth will induce secondary dental caries or restoration detachments. Recent dental adhesive techniques are based on chemo-mechanical bonding between the adhesive and adherend.

Surface conditioning before applying adhesives effectively increases the surface bonding area and enhances the strength of the bonding agent. The enamel is commonly etched with an aqueous solution of phosphoric acid or other acids. Most current enamel bonding systems employ phosphoric acid in various concentrations and viscosities as an etchant (169,170).

Casting alloys in dentistry are categorized into base metals and noble metals. Base metals include cobalt–chromium (Co–Cr), nickel–chromium (Ni–Cr), and titanium (Ti) alloys, while noble metals include gold (Au), silver (Ag), and palladium (Pd) alloys. Mechanical methods, such as air-abrading with 50–200 μm alumina, are the most common way to prepare the alloy surface. Electrolytic etching creates micro-mechanical retention on the alloy surface. Other types of surface modification include electroplating, silica coating, and ion-coating.

Dental ceramics consist mainly of metal oxides of silicon, aluminum, potassium, and sodium. Etching with an aqueous solution of hydrofluoric acid roughens the ceramic surface.

The roughened, adherend surface is treated with a primer for chemical bonding. Because the composition of dental adhesives is based on methacrylate monomers, the primers for chemical bonding also contain functional monomers. The functional monomer usually consists of a polymerizable methacrylate or vinyl group, a hydrophobic intermediate spacer, and a functional group capable of bonding to the adherend surface. Functional groups effective for bonding base metal alloys are the acid anhydride, carboxylic acid, and phosphoric acid groups. Thiol derivatives are used to prime noble metal alloys. The dental ceramic surface is primed with silane couplers activated in acids, such as carboxylic acid monomers, ferric chloride, and/or a tri-*n*-butylborane derivative (TBB) (212,213). Silane couplers are also used for surface modification of filler particles included in dental composites (214).

After surface preparation, the restorative material is bonded to the tooth structure with auto-polymerizing adhesive resin. One prerequisite for dental adhesives is an ability to cure in the mouth; that is why methacrylate-based polymer materials are used in dentistry. Initiation systems are BPO–*t* amine or TBB (201). Monomers used are MMA or bifunctional methacrylate monomers. The needed optical opacity (215,216) is achieved by various inorganic and metal compounds incorporated into the formulations.

Acid anhydride or acidic monomers, such as 4-methacryloxyethyl trimellitate anhydride (4-META), 4-methacryloxyethyl trimellate (4-MET), 4-(3-methacryloyloxypropoxy carbonyl) phthalic anhydride (MPRPA), and 4-(4-methacryloyloxybutoxycarbonyl) phthalic anhydride (MBPA), prepared by condensing hydroxyalkyl methacrylates and trimellitic anhydride acid chloride, are very important coupling agents. The phosphoric acid derivative, MDP is synthesized from methacrylic acid, 1,10-decanediol, and phosphorus oxychloride. These very useful, functional (polymerizable) monomers are added to the primer or liquid part of the adhesive.

The MMA-based adhesive system, 4-META/MMA–TBB resin formulation, has three components: initiator, monomer liquid, and powder. The initiator is partially oxidized TBB (TBB-O). The monomer liquid contains 5% 4-META in MMA. The powder is finely pulverized PMMA, with a number-average molecular weight of about 100,000. The original MMA–TBB resin without 4-META is a transparent, unfilled resin. Bonding to enamel and base metal alloys is improved by addition of 4-META monomers to the liquid part. A primer containing 0.5% 6-(4-vinylbenzyl-*n*-propyl)amino-1,3,5-triazine-2,4-dithol (VBATDT) in acetone is used to bond noble metal alloys. Mercaptan (SH) groups on the VBATDT monomer bond to noble metals and copper on the alloy surface. The ceramic surface is treated with a

two-part liquid primer before applying 4-META resin. One liquid contains 4% γ-methacryloxypropyl trimethoxysilane (γ-MPTS), while the other liquid contains 5% 4-META (or 4-MET) in MMA or 0.5% ferric chloride in ethanol. The γ-MPTS is activated by mixing with 4-META (or 4-MET) or ferric chloride to silanate the dental ceramic surface. The use of MMA polymer (PMMA)-coated titanium oxide (217) makes 4-META/MMA–TBB-O resin optically opaque.

Shear bond or tensile tests determine the dental adhesive bond strength, with thermocycling in water effectively evaluating the bond durability. The monomer VBATDT is effective for bonding Ag–Pd alloy, while 4-META is suitable for Ni–Cr alloy and titanium. For Ni–Cr alloys, the chromium content influences bond durability. Ferric chloride combined with a silane coupler significantly improves the bond strength of 4-META/MMA–TBB-O resin joined to dental porcelain.

Ceramic restoratives are often bonded directly to the tooth surface with adhesive resins, reducing the amount of healthy tooth reduction needed in clinical treatment. Resin-bonded fixed partial denture or resin-bonded ceramic restoration methods are often employed. Adhesive resins are also used for bonding orthodontic brackets, amalgam restoratives, and many other metal and ceramic materials.

BIBLIOGRAPHY

"Dental Applications" in *EPST* 1st ed., Vol. 4, pp. 727–739, by B.D. Halpern, Polysciences, Inc.; Suppl. Vol. 2, pp. 205–230, by B. D. Halpern and W. Karo, Polysciences, Inc.; National Bureau of Standards.

"Dental Applications" in *EPST* 2nd ed., Vol. 4, pp. 698–719, by G. M. Brauer and J. M. Antonucci, National Bureau of Standards.

1. M. Braden, B. E. Causton, and R. L. Clarke, *J. Dent. Res.* **51**, 889 (1972).
2. M. Braden and J. C. Elliott, *J. Dent. Res.* **45**, 1016 (1966).
3. *Dent. Advis.* **1**, 3 (1984).
4. *Dentist's Desk Reference: Materials, Instruments and Equipment*, 1st ed., American Dental Association, Chicago, Ill., 1981, p. 97.
5. O. L. Mageli and J. R. Kolczynski, *Encyclopedia of Polymer Science and Technology*, Vol. **9**, Interscience Publishers, a Division of John Wiley & Sons, Inc., New York, 1968, p. 9.
6. G. M. Brauer and H. Argentar, *Am. Chem. Soc. Symp. Ser.* **211**, 357 (1983).
7. S. Winkler, J. P. Powell, and H. R. Ortman, *Dent. Dig.* **77**, 460 (1971).
8. J. B. Woelfel, G. C. Paffenbarger, and W. T. Sweeney, *J. Am. Dent. Assoc.* **70**, 1170 (1965).
9. W. E. Mowery and co-workers, *J. Am. Dent. Assoc.* **57**, 345 (1958).
10. W. L. Shepard, *J. Prosthet. Dent.* **19**, 561 (1968).
11. J. B. Woelfel, *Dent. Clin. North Am.* **15**, 67 (1971).
12. N. W. Rupp, G. C. Paffenbarger, and R. L. Bowen, *J. Am. Dent. Assoc.* **83**, 601 (1971).
13. Dentsply TRIAD Denture System, Pamphlet 3542C, Dentsply International, York, Pa., 1983.
14. J. B. Woelfel, G. C. Paffenbarger, and W. T. Sweeney, *J. Am. Dent. Assoc.* **67**, 40 (1963).
15. B. Woelfel, G. C. Paffenbarger, and W. T. Sweeney, *J. Am. Dent Assoc.* **61**, 413 (1960).
16. H. H. Chandler, R. L. Bowen, and G. C. Paffenbarger, *J. Biomed. Mater. Res.* 245 (1971).

17. Council on Dental Materials, Instruments and Equipment, *J. Am. Dent. Assoc.* **102**, 347 (1981).
18. H. H. Chandler, R. L. Bowen, and G. C. Paffenbarger, *J. Biosmed. Mater. Res.*, **5** 335 (1971).
19. G. Uzun, N. Hersek, and T. Tincer, *J. Prosthet. Dent.* **81**, 616–620 (1999).
20. T. N. Gohring, W. H. Mormann, and F. Lutz, *J. Prosthet. Dent.* **82**, 662–668 (1999).
21. R. G. Craig, in B. R. Lang and C. C. Kelsey, eds., *International Prosthodontics Workshop on Complete Denture Occlusion*, University of Michigan Press, Ann Arbor, 1975, pp. 237–244. Sect. Report.
22. N. W. Rupp, G. C. Paffenbarger, and R. L. Bowen, *J. Am. Dent. Assoc.* **83**, 601 (1971).
23. R. J. Michl, *Quint. Int.* **3**, 29 (1978).
24. R. L. Myerson, *J. Prosthet. Dent.* **7**, 625 (1957).
25. J. W. Stanford, C. L. Burns, and G. C. Paffenbarger, *J. Am. Dent. Assoc.* **61**, 307 (1955).
26. L. Gettleman, R. J. Lebouf Jr., and H. R. Rawls, *61st Gen. Sess. Int. Assoc. J. Dent. Res.* **62**, 725 (1983) (Abstr).
27. P. S. Wright, *J. Dent.* **4**, 247 (1976).
28. W. J. O'Brien, J. Herman, and J. H. Shepherd, *J. Biomed. Mat. Res.* **6**, 15 (1972).
29. J. F. McCabe, *J. Oral Rehab.* **3**, 273 (1976).
30. E. Makila and O. Honka. *J. Oral Rehab.* **6**, 199 (1979).
31. M. Braden, *J. Dent. Res.* **49**, 145 (1970).
32. M. Braden, in J. A. von Fraunhofer, ed., *Scientific Aspects of Dental Materials*, Butterworth, Ltd., London, 1975, pp. 448–458.
33. E. Makila and O. Honka. *J. Oral Rehab.* 439–448 (1979).
34. J. C. Hickey and co-workers, *J. Am. Dent. Assoc.* **74**, 735 (1967).
35. J. M. Stenger and co-workers, *J. Am. Dent. Assoc.* **69**, 273 (1964).
36. R. E. Going, R. E. Loehman, and M. S. Chan, *J. Am. Dent. Assoc.* **89**, 132 (1974).
37. S. J. Chaeonas, A. A. Caputo, and N. K. Bakke, *62nd Gen. Sess. Int. Assoc. Dent. Res.* **63**, 1488 (1984) (Abstr).
38. A. D. Rahn and L. J. Boucher, *Maxillofacial Prosthetics: Principles and Concepts*, The Saunders Press, Philadelphia, Pa., 1970, pp. 18–30.
39. W. R. Laney, in V. A. Chalian, J. B. Drane, and S. M. Standish, eds., *Maxillofacial Prosthetics: Multidisciplinary Practice*, Williams & Wilkins Co., Baltimore, Md., 1971, pp. 1–20.
40. V. A. Chalian, in Ref. 39, pp. 279–307.
41. R. W. Phillips, P. M. Maryetis, J. J. Urban, and F. Leonard, in W. R. Laney, ed., *Maxillofacial Prosthetics*, PSG Publishing Co., Littleton, Mass., 1979, pp. 89–107.
42. G. C. Paffenbarger, L. C. Schoonover, and W. Souder, *J. Am. Dent. Assoc.* **25**, 32 (1938).
43. G. C. Paffenbarger, R. J. Nelsen, and W. T. Sweeney, *J. Am. Dent. Assoc.* **47**, 516 (1953).
44. H. D. Coy, *J. Am. Dent. Assoc.* **47**, 532 (1953).
45. R. L. Bowen, G. C. Paffenbarger, and A. L. Mullineaux, *J. Prosthet. Dent.* **20**, 426 (1968).
46. J. W. Stanford, *Dent. Clin. North Am.* **15**, 57 (1971).
47. U.S. Pat. 3066112 (Nov. 27, 1962), R. L. Bowen (to U.S. Dept. Commerce).
48. R. L. Bowen, *J. Am. Dent. Assoc.* **66**, 57 (1963).
49. A. Peutzfeldt, *Eur. J. Oral. Sci.*, **105**, 97–116 (1997).
50. U.S. Pat. 3991008 (Nov. 9, 1976), S. C. Temin and C. L. Richards (to The Kendall Co.)
51. J. M. Antonucci, C. L. Grams, and D. J. Termini, *J. Dent. Res.* **58**, 1887 (1979).
52. J. M. Antonucci, J. W. Stansbury, and D. J. Dudderar, *J. Dent. Res.* **61**, 270 (1982).
53. R. J. Kilian, in C. G. Gebelin and F. F. Koblitz, eds., *Biomedical and Dental Applications of Polymers*, Plenum Press, New York, 1981, pp. 411–417.
54. R. E. Kerby and co-workers, *J.M.S., A: Pure Appl. Chem.* **36**(9), 1227–1239 (1999).
55. J. F. Glenn, in Ref. 39, pp. 317–335.

56. B. D. Halpern and D. W. Karo, in Ref. 39, pp. 337–345.
57. J. M. Antonucci, in Ref. 39, pp. 357–371.
58. J. R. Griffith and J. C. O'Rear, in Ref. 39, pp. 373–377.
59. G. F. Cowperthwalthe, J. J. Fox, and M. A. Malloy, in Ref. 39, pp. 379–385.
60. K. Dermann, N. W. Rupp, and G. M. Brauer, *J. Dent. Res.* **61**, 1250 (1982).
61. D. M. Dulik, R. Bernier, and G. M. Brauer, *J. Dent. Res.* **60**, 983 (1981).
62. J. F. Glenn, in D. C. Smith and D. F. Williams, eds., *Biocompatibility of Dental Materials*, Vol. **I11**, CRC Press, Boca Raton, Fla., 1982, pp. 97–130.
63. U.S. Pat. 3775420 (Aug. 28, 1973), D. C. Stoffey and H. L. Lee (to Lee Pharmaceuticals).
64. U.S. Pat. 3629187 (Dec. 21, 1971), D. E. Waller (to Dentsply International, Inc.).
65. U.S. Pat. 3709866 (Jan. 9, 1973), D. E. Waller (to Dentsply International, Inc.).
66. U.S. Pat. 3810938 (July 14, 1974), W. Schmitt, R. Purrman, and P. Jochum (to ESPE FabrikPharmazeutischer Praeparate GmbH).
67. W. H. Douglas, R. G. Craig, and C. J. Chen, *J. Dent. Res.* **58**, 1981 (1979).
68. W. H. Douglas, R. G. Craig, and C. J. Chen, *J. Dent. Res.* **59**, 1507 (1980).
69. W. H. Douglas and R. G. Craig, *J. Dent. Res.* **61**, 41 (1982).
70. J. M. Antonucci and co-workers, *J. Dent. Res.* **58**, 242 (1979).
71. J. M. Antonucci and co-workers, *J. Dent. Res.* **62**, 285 (1983).
72. S. Venz, N. W. Rupp, and J. M. Antonucci, *J. Dent. Res.* **62**, 254 (1983).
73. J. M. Antonucci, S. Venz, J. W. Stansbury, and D. J. Dudderar, in Proceedings of the First Medical Plastic Conference of the Society of the Plastics Industry, Inc., New Brunswick, N. J., 1983.
74. T. Endo and W. J. Bailey, *J. Polym. Sci. Polym. Chem. Ed.* **13**, 2525 (1975).
75. V. P. Thompson, E. F. Williams, and W. J. Bailey, *J. Dent. Res.* **58**, 1522 (1979).
76. S. Anseth and co-workers, *J. Dent. Res.*, **75**, 1607–1612 (1996).
77. G. F. Cowperthwaite, F. F. Fay, and M. A. Malloy, in C. G. Gebelein and F. F. Koblitz, eds, *Biomedical and Dental Applictions of Polymers*, Plenum Press, New York, 1981, **14**, pp. 379–385.
78. G. F. Cowperthwaite, C. R. Kregg, and L. M. Higby, *Dent. Res.* **70**, 294 (1991).
79. J. W. Stansbury and co-workers, *J. Dent. Res.*, **77**, 155 (1998).
80. A. R. Kannaurpatti, and co-workers, *J. Polym. Sci., Part B: Polym. Phys.* **35**, 2297 (1997).
81. A. R. Kannurpatti and C. N. Bowman, *Macromolecules* **31**, 3311 (1998).
82. K. A. Beuchtold and C. N. Bowman, in RadTech Europe 99 Conf. Proceedings, Berlin, Germany, Nov. 1999, p. 767.
83. J. E. Elliott and C. N. Bowman, *Macromolecules*, **32**, 8621 (1999).
84. M. Kawaguchi, T. Fukushima, and T. Horibe, *Dent. Mater. J.* **7**, 176–181 (1988).
85. M. Kawaguchi, T. Fukushima, and T. Horibe, *Dent. Mater. J.* **8**, 40–45 (1989).
86. S. Kalachandra and T. W. Wilson, *Biomaterials*, **13**, 105–109 (1992).
87. S. Kalachandra and co-workers, *Polymer*, **34**(4), 778–782 (1993).
88. H. K. Shobha and co-workers, *Macromol. Symp.* **111**, 73–83 (1996).
89. S. Kalachandra and co-workers, *J. Mater. Sci.: Mater. Med.* **8**, 283–286 (1997).
90. S. Kalachandra and co-workers, *J. Mater Sci.: Mater. Med.* **8**, 465–468 (1997).
91. B. M. Culbertson and co-workers, *Polym. Adv. Technol.* **10**, 275–281 (1999).
92. A. Tiba and B. M. Culbertson, *J.M.S., A: Pure Appl. Chem.* **36**, 489–506 (1999).
93. B. M. Culbertson, J. Xu, and A. Tiba, *Polym. Adv. Technol.* **10**, 206–214 (1999).
94. B. M. Culbertson, Q. Wan, and Y. Tong, *J.M.S., A: Pure Appl. Chem.* **34**, 2405–2421 (1997).
95. A. Tiba and B. M. Culbertson, *J.M.S., A: Pure Appl. Chem.* **36**, 1209–1226 (1997).
96. B. M. Culbertson, Y. Tong, and Q. Wan, *J. Dent. Res.* **76**, 77 (1997). IADR Abstract #506.
97. J. R. Condon and J. L. Ferracane, *J. Dent. Res.* **78**, 370 (1999). IADR Abstract #2120.

98. J. M. Antonucci, J. W. Stansbury, and S. Venz, *Polym. Mater. Sci. Eng.*, **59**, 388–396 (1988).
99. G. Wang and co-workers, *J.M.S., A: Pure Appl. Chem.* **36**, 225–236 (1999).
100. G. Wang and co-workers, *J.M.S., A: Pure Appl. Chem.* **36**, 237–252 (1999).
101. G. Wang, B. M. Culbertson, and R. R. Seghi, *J.M.S., A: Pure Appl. Chem.* **36**, 373–388 (1999).
102. J. W. Stansbury and W. J. Bailey, *Polym. Mater. Sci. Eng.* **59**, 402–406 (1988).
103. J. W. Stansbury, in R. K. Sadhir and R. M. Luck, eds., *Expanding Monomers: Synthesis, Characterization and Applications*, CRC Press, Boca Raton, 1992, pp. 153–185.
104. J. W. Stansbury, *J. Dent. Res.*, **71**, 1408–1412 (1992)
105. J. W. Stansbury and J. M. Antonucci, *Dent. Mater.* **8**, 270–273 (1992).
106. U.S. Pat. 5808108 (Sept. 15, 1998), C. C. Chappelow and co-workers (Midwest Research Institute).
107. B. B. Reed, J. W. Stansbury, and J. M. Antonucci, in S. W. Shalaby, ed. *Polymers of Biological and Biomedical Significance*, American Chemical Society, pp. 84–190. Symposium Series 540, 1994.
108. J. W. Stansbury, in Ref. 107, pp. 171–183.
109. C. S. Pinzino and co-workers, *J. Dent. Res.* **76**, 41 (1997).
110. C. C. Chappelow and co-workers, *J. Dent. Res.*, **77**, 639 (1998).
111. C. S. Pinzino and co-workers, *J. Dent. Res.*, **78**, 315 (1999).
112. R. P. Chappell and co-workers, *J. Dent. Res.*, **78**, 3782 (1999).
113. F. Millich and co-workers, *J. Dent. Res.*, **77**, 603–606 (1998).
114. B. K. Norling and co-workers, *J. Dent. Res.*, **78**, 233 (1999). Abstr. # 1020.
115. Qichun Wan, Scott. R. Schricker, and Bill M. Culbertson, *ACS Polym. Prepr.* **41**(1), 101, 102 (2000).
116. Qichun Wan, Scott. R. Schricker, and Bill M. Culbertson, *ACS Polym. Prepr.* **41**(1), 155, 156 (2000).
117. J. M. Antonucci, and co-workers, *ACS Polym. Prepr.* **38**(2), 108–109 (1997).
118. J. M. Antonucci, and co-workers, *ACS Polym. Preper* **39**, 810–811 (1998).
119. J. M. Antonucci, B. O. Fowler, and J. W. Stansbury, *J. Dent. Res.*, **76**, 40 (1997).
120. Feng Gao and co-workers, *ACS Polym. Prepr.* **41**, 580–581 (2000).
121. Q. Feng and co-workers, *ACS Polym. Prepr.* **41**, 515–516 (2000).
122. R. G. Craig, *Dent. Clin. North Am.* **25**, 219 (1981).
123. F. Lutz and R. W. Phillips, *J. Prosthet. Dent.* **50**, 480 (1983).
124. Z. U. Hague and D. T. Turner, *J. Mater. Sci.* **22**, 3379–3384 (1987).
125. D. C. Smith, *Br. Dent. J.* **125**, 381 (1968).
126. A. D. Wilson and B. E. Kent, *Br. Dent. J.* **132**, 133 (1972).
127. D. C. Smith, in R. G. Craig, ed., *Dental Materials Review*, School of Dentistry, University of Michigan, Ann Arbor, 1977, pp. 52–77.
128. A. D. Wilson and S. Crisp, in L. Holiday, ed., *Ionic Polymers*, John Wiley & Sons, Inc., New York, 1975, pp. 208–260.
129. A. D. Wilson, *Chem. Soc. Rev.* **7**, 265 (1978).
130. A. D. Wilson, in Ref. 39, pp. 419–426.
131. D. Belton and S. I. Stupp, in Ref. 39, pp. 427–439.
132. D. C. Smith, in Ref. 39, Vol **11**, 1982, pp. 157–174.
133. W. D. Cook, *Biomaterials* **3**, 232 (1982).
134. W. D. Cook, *Biomaterials* **4**, 21, 85 (1983).
135. A. D. Wilson, *J. Dent. Res.* **61**, 42–47 (1982).
136. A. D. Wilson and J. W. McLean, *Glass-ionomer Cement*, Quintessence Publishing, Co., Chicago, 1988, p. 11.
137. A. D. Wilson and J. W. Nicholson, *Acid–Base Cements*, Cambridge University Press, Cambridge, U.K., 1993.

138. J. Nichloson and M. Anstice, *Trends Polym. Sci.* **2**, 272–276 (1994).
139. L. A. Linden in J. C. Salarnone, ed., *Polymeric Materials Encyclopedia*, Vol. **3**, CRC Press, Boca Raton, Fla., 1996, pp. 1854–1860.
140. J. M. Antonucci and co-workers, *J. Dent. Res.* **63**, 214 (1984).
141. J. M. Cassel and co-workers, Properties and Interactions of Oral Structures and Restorative Materials, NBSIR 81-2431, National Bureau of Standards, Washington, D.C., Dec. 1981, pp. 58–60.
142. J. Ellis and A. D. Wilson, *Polym. Int.* **24**, 221–228 (1991).
143. H. J. Prosser and co-workers, *J. Dent. Res.* **62**, 598 (1983).
144. U.S. Pat. 5369142 (Nov. 29, 1994), B. M. Culbertson and E. C. Kao (Ohio State University Research Foundation).
145. E. C. Kao, B. M. Culbertson, and D. Xie, *J. Dent. Mater.*, **12**, 44–51 (1996).
146. B. M. Culbertson, D. Xie, and A. Thakur, *Macromol. Symp.* **131**, 11–18 (1998).
147. B. M. Culbertson, D. Xie, and A. Thakur, *J.M.S., A: Pure Appl. Chem.* **36**, 681–696 (1999).
148. B. M. Culbertson and M. H. Dotrong, *J.M.S, A: Pure Appl. Chem.* **37**, 419–431 (2000).
149. Z. Ouyang and co-workers, *Appl. Spectroscopy*, **53**, 297–301 (1999).
150. B. M. Culbertson, A. Thakur, and D. Xie, *J. Dent. Res.* **76**, 76 (1997). Abst. # 497.
151. D. Xie, B. M. Culbertson, and G. Wang, *J.M.S, A: Pure Appl. Chem.* **35**, 547–561 (1998)
152. D. Xie, B. M. Culbertson, and W. M. Johnston, *J.M.S, A: Pure Appl. Chem.* **35**, 1615–1629 (1998).
153. D. Xie, B. M. Culbertson, and W. M. Johnston, *J.M.S. A: Pure Appl. Chem.* **35**, 1631–1650 (1998).
154. B. M. Culbertson, D. Xie, and W. M. Johnston, in K. O. Kavelka and C. C. McCormick, eds., *Specialty Monomers and Polymers*, 2000, pp. 222–232. ACS Symposium Series 755.
155. D. Xie and co-workers, *Dent. Mater.* **16**, 129–138 (2000).
156. J. W. McLean, J. W. Nicholson, and A. D. Wilson, *Quintessence Int.* **25**, 587–589 (1994).
157. S. B. Mitra and B. L. Kedrowski, *ACS Polym. Prepr.* **38**(2), 129–130 (1997).
158. S. B. Mitra and B. L. Kedrowski, *ACS Polym. Prepr.* **35**(2), 77–78 (1994).
159. H. M. Anstice and J. W. Nicholson, *J. Dent. Mater. Sci.: Mater. Med.* **3**, 447–451 (1992)
160. U.S. Pat. Appl. 160856 (1988), J. M. Antonucci, J. E. McKinney, and J. W. Stansbury (U.S. Government).
161. Paul D. Hammesfahr, in *Proc. 2nd Int. Symp. on Glass-Ionomers*, School of Medicine, University of Pennsylvania, Pa., June 16–19, 1994.
162. S. K. Sindhu, *Am. J. Dent.* **8**, 59–67 (1993)
163. P. D. Hammesfahr, *ACS Polym. Prepr.* **37**(2), 131–132 (1997).
164. J.-M. Meyer, M. A. Cattani-Lorente, and V. Dupuis, *Biomaterials* **19**, 529–539 (1998).
165. M. Irie and H. Nakai, *J. Dent. Mater.* **17**(1), 77–82 (1998)
166. M. A. Cattani-Lorente and co-workers, *J. Dent. Mater.* **15**, 21–32 (1999).
167. S. Gladys and co-workers, *J. Dent. Res.*, **76**, 883–894 (1997).
168. H. Lee and J. Orlowski, *J. Oral Rehab.* **6**, 97–129 (1979).
169. M. G. Buonocore, *J. Dent. Res.* **34**, 849 (1955).
170. M. G. Buonocore, W. Wileman, and F. B. Brudevold, *J. Dent. Res.* **35**, 846 (1956).
171. G. E. Boudreaux and C. B. Jerge, *J. Am. Dent. Assoc.* **92**, 383 (1979).
172. J. D. Brooks and co-workers, *J. Am. Dent. Assoc.* **98**, 42 (1979).
173. E. J. Mertz-Fairhurst, *J. Dent. Ed.* **48**, 18 (1984).
174. W. P. Rock, *J. Dent. Ed.* **48**, 27 (1984).
175. R. E. Going, *J. Dent. Ed.* **48**, 35 (1984).
176. A. J. Gwinnett, *J. Dent. Ed.* **48**, 56 (1984).
177. D. E. Smith, *J. Dent. Ed.* **48**, 103 (1984).
178. E. J. Swift, J. Perdigao, and H. O. Heymann, *Quint. Int.* **26**(2), 95–110 (1995).

179. Irmansyah, K. Wakasa and M. Yamaki, *J. Mater. Sci.: Mater. Med.* **1**, 33–37 (1990).
180. L. M. Silverstone, *J. Dent. Ed.* **48**, 107 (1984).
181. National Institutes of Health, *J. Am. Dent. Assoc.* **108**, 233 (1984).
182. B. T. Rosa and J. Perdigao, *Quint. Int.* **31**, 353–358 (2000).
183. M. R. Barrow and co-workers, *J. Dent. Res.* **73**, 522–528 (1995).
184. L.-A. Linden and J. F. Rabek, in J. C. Salamone, ed., *Polymeric Materials Encyclopedia*, CRC Press, Boca Raton, Fla., 1996, pp. 1861–1867.
185. A. D. Wilson and B. E. Kent, *Brit. Dent. J.* **132**, 122–135 (1972).
186. Y. Kadona and co-workers, *Makromol. Chem.* **182**, 273–277 (1981).
187. J. Perdigao and co-workers, *J. Dent. Res.* **3**(1), 44–55 (1994).
188. E. L. Pashley and co-workers, *Dent. Mater.* **9**, 1922 (1993).
189. F. R. Tay and co-workers, *J. Dent. Res.* **75**, 1034–1044 (1996).
190. D. H. Pashley and co-workers, *Dent. Mater.* **16**, 7–14 (2000).
191. D. H. Pashley and R. M. Carvalho, *J. Dent. Res.* **25**, 355–372 (1997).
192. D. E. Rigsby and co-workers, *Am. J. Dent.* **3**, 289–294 (1990).
193. Y. H. Tsai and co-workers, *Oper. Dent.* **15**, 53–80 (1990).
194. H. Li, M. F. Burrow, and M. J. Tyas, *Dent. Mater.* **16**, 48–56 (2000).
195. G. Soh and L. J. Henderson, *Int. J. Prosthodont.* **3**, 59–63 (1990).
196. E. C. Munksgaard, K. Itoh, and K. D. Jorgensen, *J. Dent. Res.* **64**(2), 144–146 (1985).
197. A. J. L. Carracho and co-workers, *Quint. Int.* **22**, 745–752 (1991).
198. R. L. Bowen, E. N. Cobb, and J. E. Rapson, *J. Dent. Res.* **61**, 1070 (1982).
199. R. L. Bowen, *J. Am. Dent. Assoc.* **107**, 734–736 (1983).
200. N. Nakabayashi, *Oper. Dent.* (Suppl 5), 125–130 (1992).
201. N. Nakabayashi and Y. Saimi, *J. Dent. Res.* **75**, 1706–1715 (1996).
202. H. Chigira and co-workers, *J. Dent. Res.* **73**, 1088–1095 (1994).
203. N. Nakabayashi, M. Ashizaawa, and M. Nakamura, *Quint. Int.* **23**, 135–141 (1992).
204. I. Watanabe, N. Nakabayashi, and D. H. Pashley, *J. Dent. Res.* **73**, 1212–1220 (1994).
205. G. E. Schumacher and co-workers, *J. Dent. Res.* **76**, 602–609 (1997).
206. H. Sano and co-workers, *J. Dent. Res.* **78**, 906–911 (1999).
207. A. Olmez and T. Ulusu, *Quint. Int.* **26**, 785–793 (1995).
208. S. R. Grobler and co-workers, *Quint. Int.* **31**, 501–508 (2000).
209. B. E. Causton and J. Sefton, *Br. Dent. J.* **157**, 308–311 (1989).
210. E. C. Munksgaard, M. Irie, and E. Asmussen, *J. Dent. Res.* **4**, 1409–1411 (1985).
211. A. Manabe and co-workers, *J. Dent. Res.* **70**, 1294–1298 (1991).
212. H. Matsumura and co-workers, *J. Jpn. Prosthodont. Soc.* **31**, 1494 (1987).
213. M. Maeda and co-workers, *J. Jpn. Orthodont. Soc.* **46**, 370 (1987).
214. H. Matsumura and co-workers, *Dent. Mater. J.* **6**, 135 (1987).
215. K. Yoshida and co-workers, *J. Prosthet. Dent.* **69**, 357 (1993).
216. H. Matsumura, M. Suevoshi, and M. Atsuta, *J. Dent. Res.* **71**, 2 (1992).
217. H. Matsumura and N. Nakabayashi, *J. Dent. Res.* **67**, 29–32 (1988).

GENERAL REFERENCES

K. J. Anusavice, *Phillips Science of Dental Materials*, 10th ed., The Saunders Press, Philadelphia, Pa., 1996.
R. van Noort, *Dental Materials*, 1st ed., C. V. Mosby Co., St. Louis, Mo., 1989.
W. J. O'Brien, *Dental Materials Properties and Selection*, Quintessence Publishing Co., Chicago, 1997.
R. G. Craig, ed., *Restorative Dental Materials*, 10th ed., C. V. Mosby Co., St. Louis, Mo., 1997.

C. M. Sturdevant, *The Art and Science of Operative Dentistry*, C. V. Mosby Co., St. Louis, Mo, 1997.
A. D. Wilson and J. W. McLean, *Glass-Ionomer Cement*, Quint essence Publishing Co., Chicago, 1988.
A. D. Wilson and J. W. Nicholson, *Acid–Base Cements: Their Biomedical and Industrial Applications*, Cambridge University, Cambridge, 1993.

BILL M. CULBERTSON
RONALD E. KERBY
The Ohio State University

DIACETYLENE AND TRIACETYLENE POLYMERS

Introduction

Polydiacetylene (1–5) and polytriacetylene along with polyacetylene are the only known linear conjugated polymers (6). Conjugated polymers are distinguished from traditional polymers in that they contain alternating π-bonds along the polymer backbone. This structural feature imparts useful electronic and optical properties for the development of advanced materials. The linearly conjugated polymers are distinguished from the other conjugated polymers [eg, poly(phenylene vinylene) (**1**)] because the linearly conjugated polymers do not have branch points along the network of π-bonds. Polydiacetylene (**2**), polytriacetylene (**3**), and polyacetylene (**4**) are also the first three members of a series of linearly conjugated polymers with an increasing number of alkyne groups that terminates with polycarbyne.

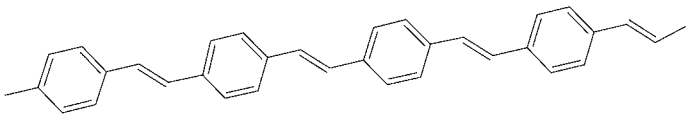

Poly(phenylene vinylene)

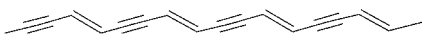

Polydiacetylene

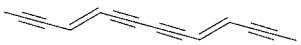

Polytriacetylene

Encyclopedia of Polymer Science and Technology. Copyright John Wiley & Sons, Inc. All rights reserved.

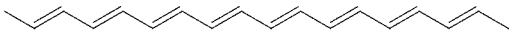

Polyacetylene

The polydiacetylenes and polytriacetylenes differ from polyacetylene because preorganization of the diacetylene and triacetylene is required for a successful polymerization (7). This remarkable observation was first recognized (8,9) in 1969 and marks the beginning of modern polydiacetylene and polytriacetylene chemistry. In a few cases, this topochemically controlled polymerization occurs from a crystal of the monomer to a crystal of the polymer, giving rare examples of macroscopic single polymer crystals (9).

The study of polydiacetylenes has been an active area of research. From 1969 there have been 3301 publications concerned with the preparation and study of polydiacetylenes, and 2713 of these have been published since 1986.

Polydiacetylenes

Preparation of the Diacetylene Monomers. Although a few interesting methods have appeared (10), the oxidative coupling of monosubstituted acetylenes, using copper salts (11,12) (Hay or Eglinton reaction conditions), continues to be the most common route to symmetrical diacetylenes (eq. 1). For unsymmetrical and symmetrical diacetylenes the Cadiot–Chodkiewicz coupling reaction, along with its modifications, has proven useful. When the traditional copper coupling methods fail, some success has been had, mediating this reaction with transition metals such as palladium (13).

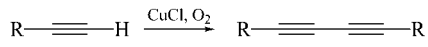

(1)

Preparation of Polydiacetylene. The preorganization for the 1,4-polymerization of diacetylenes has been discussed previously (7,14,15). Successful polymerization occurs when the diacetylenes have a translational repeat distance (d) of about 0.49 nm and an angle (π) of about 45° with respect to the translational direction and van der Waals contact (R_v) of the polydiacetylene functionalities (Fig. 1). If these structural parameters are met then the C1 and C4 carbon atoms of adjacent diacetylenes will be in a position for a topochemically controlled polymerization. Because the 0.49 nm translational repeat distance (d) of the monomer is about the same as the repeat distance in the polymer, the polymerization process can occur with little disruption of the reactant packing.

A number of diacetylenes have been reported to undergo a solid-state polymerization to give polydiacetylenes. However, one of the more exciting aspects of the diacetylene polymerization, shown in Figure 1, is the ability of some diacetylene single crystals to polymerize to give single crystals of the polymer. Although there is a difference in the quality of the x-ray data, 16 examples of polymer single crystals have been reported (16,17). Eleven of these were reported before 1986 whereas only five have been reported after this date. Given the large number (508) of diacetylenes that have been reported in the Cambridge Structural Database (CSD), only a very small percentage possess the structural parameters to undergo

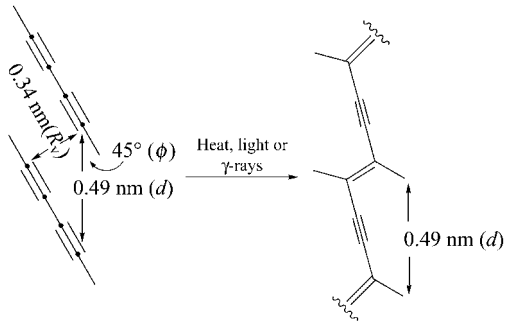

Fig. 1. Topochemical requirements for the 1,4-polymerization of diacetylenes.

a crystal-to-crystal polymerization. Clearly, diacetylenes, by themselves, show no tendency to self-assemble with the required structural parameters shown in Figure 1. The organization of diacetylenes in the solid state for a topochemically controlled polymerization would appear to be an excellent candidate for crystal engineering (18) or supramolecular synthesis. However, there has been little effort devoted to the application of crystal design methods (19) to the preparation of diacetylene crystals suitable for a topochemical polymerization.

The most critical structural parameter shown in Figure 1 is the transitional repeat distance d of the diacetylene. The ideal value for d is about 0.49 nm. This is a necessary structural parameter for a topochemically controlled polymerization. If this structural condition is achieved and the diacetylene functionalities close pack then a simple calculation demonstrates that the angle will be about 45° and the 1–4 carbons of the diyne will be in close contact.

Inspection of the known crystal-to-crystal polymerizations reveals two packing themes for establishing a d value of about 0.49 nm. The diacetylene monomers contain either an aromatic ring or amide functionality. Parallel translated aromatic rings is a common self-assembly for aromatic compounds. This assembly produces a translational repeat distance between 0.46 and 0.54 nm (20), which includes the required d of 0.49 nm. The difficulty of using the π-stacking to establish a desirable d for polymerization, in a directed supramolecular synthetic scheme, is that there are three other common assemblies of aromatic rings that are not suitable for polydiacetylene polymerizations. The π-stacking of aromatic rings is not a reliable supramolecular interaction. Nevertheless, π-stacking has been observed for the organization of diacetylenes for a topochemically controlled polymerization. One notable example that has often been studied is PTS (polyhexadiyne-1,6-diol-bis-*p*-toluene sulfonate; Fig. 2) (21).

A variation of this theme, the use of parallel translated aromatic rings as a supramolecular synthon (19), has been exploited as a possible route to the *cis*-polydiacetylene, an isomer of the *trans*-polydiacetylene shown in Figure 1. The required supramolecular structure was achieved using the benzene–hexafluorobenzene interaction (22), which stacks the aromatic rings almost on top of each other. This arrangement places the terminal carbon atoms of adjacent diynes into close contact for a polymerization to the *cis*-polydiacetylene.

Hydrogen bonded amides are commonly used by nature for supramolecular assembly. The translational repeat of amides (23) is within the range of the

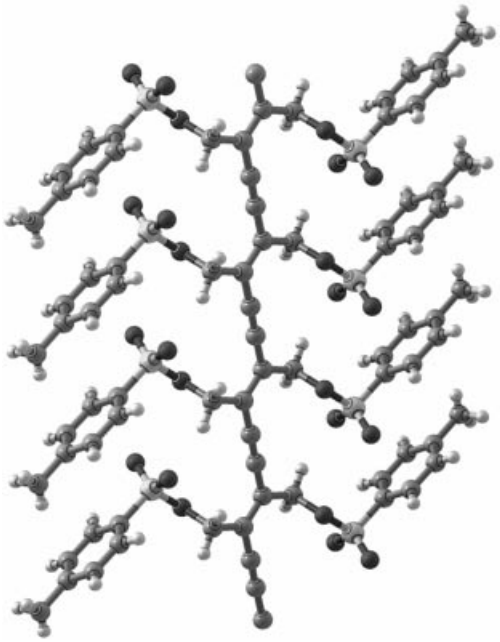

Fig. 2. Crystal structures of PTS showing the π-stacking of aromatic rings to establish the required translational distance for a topochemically controlled polymerization.

0.49 nm shown in Figure 1. This hydrogen bond motif is persistent and has often been used to organize diacetylenes for a topochemical polymerization. Because of its solubility in common organic solvents one of the better known examples of a polydiacetylene is derived from the symmetrical 4-BCMU [5,7-dodecadiyne-1,12-bis(butylcarboxymethylurethane); Fig. 3] (3). Because of the ability of the urethane functionality to self-assemble according to Figure 1 and the relative ease of synthesis (24) (Fig. 4), the poly *n*-BCMUs have been a popular class of compounds to study (25). By varying the nature of the alkyl ester, this class of potentially polymerizable diynes can be further extended (26).

It has been observed that with *N*-phenyl urethanes the conformation of the alkyl link between the diacetylene and urethanes can have an effect on the polymerization. When the alkyl group contained an even number of carbon atoms (four or six) the polymerization occurred as anticipated but failed with an odd number of carbon atoms (five). Although the association of all of these urethanes was the same, the low energy molecular conformations of this latter compound do not allow for close contact of the 1,4 atoms of adjacent diacetylenes shown in Figure 1. This observation demonstrates the importance to consider both intermolecular and intramolecular interactions in the design of a supramolecular synthetic strategy.

Polydiacetylenes with aromatic rings attached to the polymer backbone has been a challenge to synthetic chemistry. These compounds are of interest because of the known abilities of aromatic systems to interact with the delocalized π-system to produce new materials with interesting properties. For example, it has been argued that aromatic rings extend the π-system to give materials with

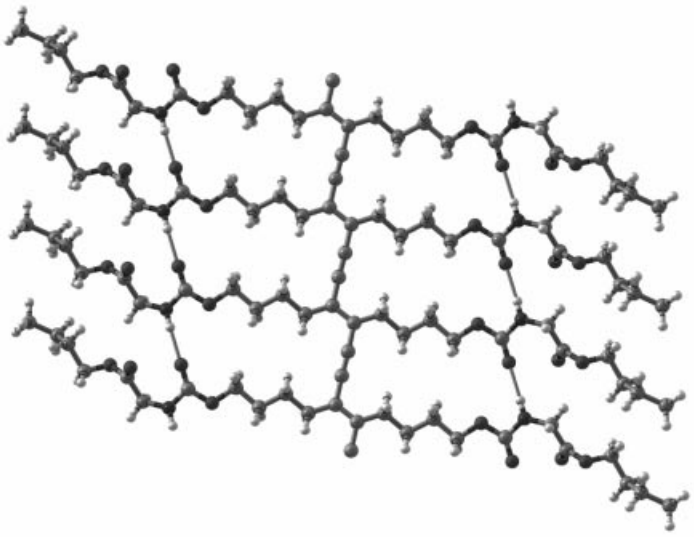

Fig. 3. Crystal structures of BCMU showing the hydrogen bonding of the carbamate functionality to establish the required translational distance for a topochemically controlled polymerization.

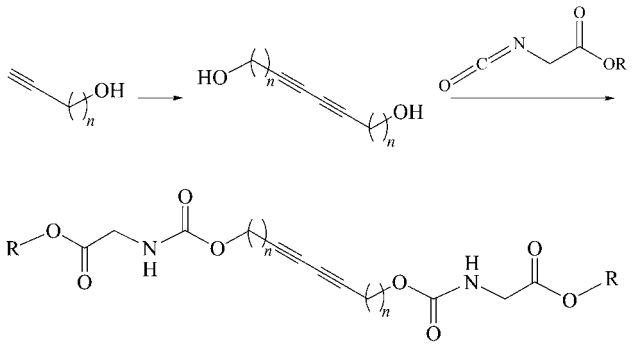

Fig. 4. Preparation of *n*-BCMUs. R = *n*-butyl.

enhanced nonlinear properties. Because of the tendency of aromatic rings to stack in parallel planes, diacetylenes with aromatic rings attached to the dialkyne functionality sometimes have favorable parameters for a topochemical polymerization (27). However, the reluctance of diaryl-substituted diacetylenes to polymerize is well known and is believed to be due to the development of unfavorable nonbonded interactions between the aromatic rings along the reaction trajectory.

In order to prepare polydiacetylenes with aromatic rings directly attached to the polymer backbone an interesting strategy has been employed. The aromatic ring is attached to one position of the diyne and a functionality for proper self-assembly (Fig. 1) is attached to the other position of the diyne. A carbamate functionality has commonly been used to provide the proper supramolecular structure (Fig. 5). Advantages of this scheme are that the reduced nonbonded interactions

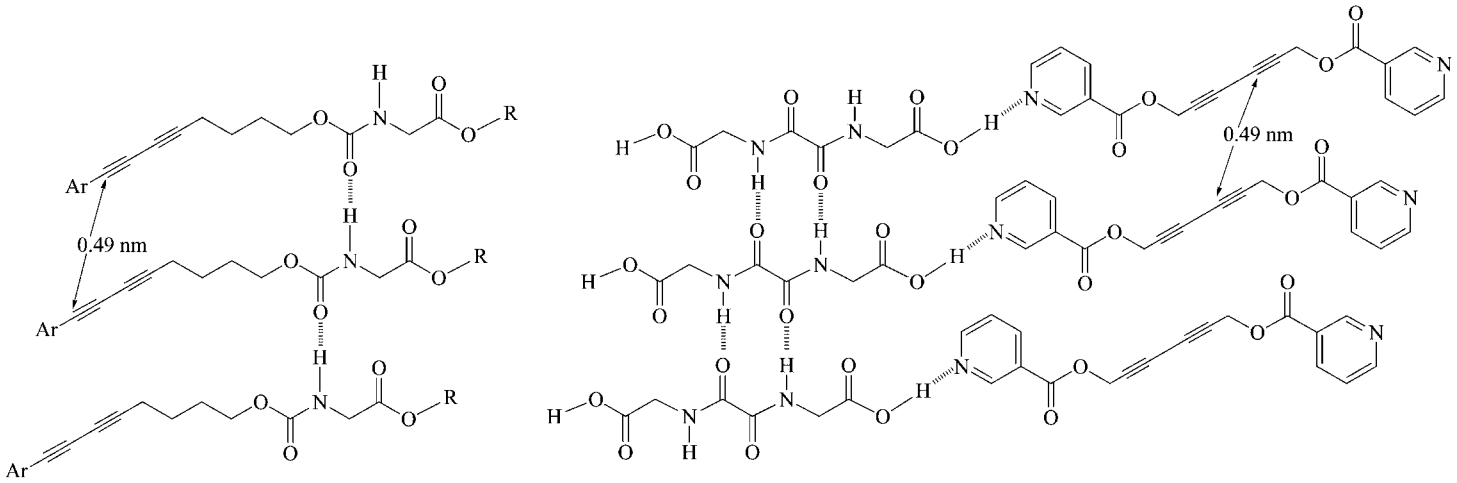

Fig. 5. The use of carbamates and host–guest chemistry to organize diacetylenes for a topochemically controlled polymerization.

between the aromatic rings will facilitate polymerization and a choice of carbamates analogous to the *n*-BCMUs may impart favorable solubility properties to the polydiacetylenes. A disadvantage of this scheme is that the molecular synthesis of the monomers becomes more tedious. This strategy has been applied to the synthesis of a number of interesting polydiacetylenes (28) and will undoubtedly continue to be important in the future.

A different but related strategy to the polymerization of diacetylenes has been to use host–guest chemistry. One molecule, the host, provides the required molecular scaffold and the other, the guest, contains the diacetylene functionality. Reliable functionalities for producing the molecular repeat distance *d* (Fig. 1) are ureas or, better, oxalamides (29). The carboxylic acid–pyridine interaction has been used to assemble the host and the guest.

The practical goal of the above studies is to prepare different polydiacetylenes with different properties. This is done by using synthetic chemistry to alter the nature of the substituents on the diacetylene monomer that can produce a polydiacetylene with different properties. A major problem with this approach is that a change in the substituent can change the solid-state packing and can produce a diacetylene without the proper structural parameters for a topochemically controlled polymerization. Rather than modifying the monomer an alternate strategy is to modify the polymer. This elegant approach has led to some new azo and tricyanovinylated polydiacetylenes with interesting properties. Postmodification of polydiacetylene polymers will undoubtedly prove to be an effective method for the production of advanced polymers.

The structural parameters required for a topochemically controlled diacetylene polymerization can be achieved by organizing the diacetylenes into layers. Advantages of layered materials are that they are anisotropic and can more readily be adapted to traditional fabrication methods than single crystals. Layered diacetylene structures can be constructed using a number of methods such as Langmuir–Blodgett films (30), membranes (31), liquid crystals (32), and SAMs (33). Layers meet the translational spacing requirement shown in Figure 1. If the head groups are spaced at about 0.49 nm and the chains containing the diacetylene functionality associate within the van der Waals radii, then the diacetylenes will be properly oriented for polymerization. Topochemically controlled diacetylene polymerization has been observed in a number of layered structures. Amphiphilic molecules frequently contain a polar, hydrogen bonding head group, such as a carboxylic acid or amide, to establish the required 0.49 nm translational spacing. If the hydrocarbon chains close pack then carbon atoms 1 and 4 of the diacetylene functionality will be in close contact for a 1,4-diacetylene polymerization.

Related to the above approach for the preparation of polydiacetylenes is the recent report of forming single polydiacetylene nanowires of 10,12-nonacosadiynoic acid on a graphite surface. The polymerization of single arrays of this diacetylene were initiated and terminated using the probe of a scanning tunneling microscope (STM). This technique has the interesting possibility of interconnecting nanostructures by using polydiacetylene nanowires (34).

The use of monolayers to achieve the supramolecular structural parameters for a topochemical polymerization is a powerful strategy that will undoubtedly prove to be useful for the preparation of sensors (35) and devices (36) that exploit the diacetylene-conjugated polymeric backbone (Fig. 6).

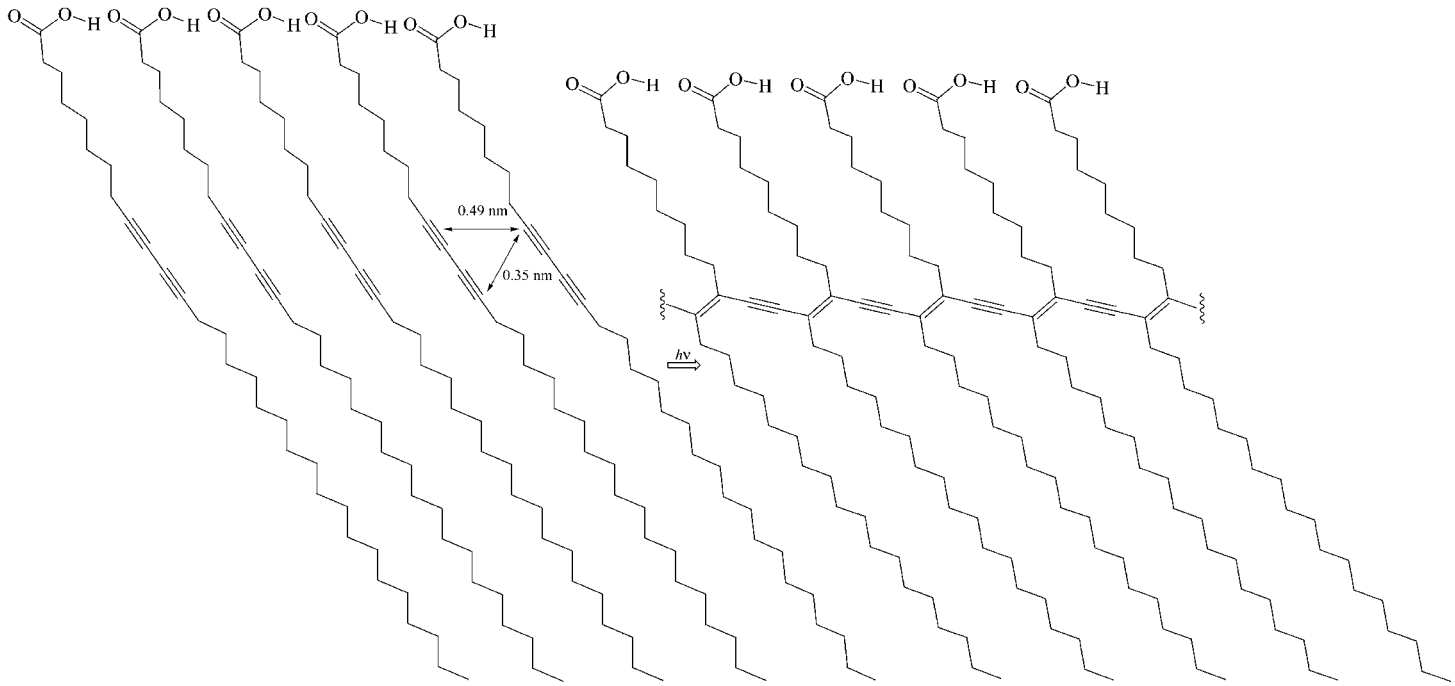

Fig. 6. A lipid monolayer with the diacetylene functionalities properly oriented for a topochemically controlled polymerization.

Properties of Polydiacetylenes. Among the interesting properties displayed by conjugated polymers such as polydiacetylenes, nonlinear optical response and electrical conductivity have attracted the most attention (37). In addition, polydiacetylenes display chromism that is induced by environmental conditions. Interestingly, the chromism (blue to red to yellow) of polydiacetylenes has been known for a long time but its orgins are still controversial (25). The color changes have generally been attributed to a decrease of the effective conjugation length of the polymer backbone. The changes in the effective conjugation length can be affected by changes in the conformation of the polymer backbone. Polymer conformational changes can be the result of a number of different actions involving polymer associations or the interactions of the substituents on the polymer backbone.

Whatever its origin, the chromism of polydiacetylenes has been the basis of interesting sensor development. Amphiphilic diacetylenes are known to form vesicles that can be polymerized to colored polydiacetylenes. If a specific ligand is attached to the vesicle then binding to receptor can induce a color change due to a conformational change of the polymer backbone (38). For example, sialic acid binds to the influenza virus lectin, hemagglutinin. A polydiacetylene liposome with sialic acid attached undergoes a color change from blue to red when exposed to the influenza virus. These impressive sensors are acting in an analogous, although primitive, manner to a biological membrane.

A robust polydiacetylene/silica composite has recently been prepared that undergoes a color change in response to thermal, chemical, and mechanical stimuli (39). This new hybrid material holds considerable promise for the fabrication of new devices.

Probably the most studied and exciting property of polydiacetylenes is their nonlinear optical properties (40). Polydiacetylenes are one-dimensional molecular quantum wires. Along the polymer backbone of the polymer the polydiacetylenes are effectively centrosymmetric and have only odd order nonlinearities such as 3. PTS has the largest known off-resonant nonlinear refractive index (41,42). This property makes the polydiacetylenes exciting candidates for the preparation of optical devices such as waveguides (43). The development of polydiacetylenes that can be deposited as oriented noncrystalline thin films would be desirable. However, an advantage of organic materials is that their properties can be fine-tuned using organic synthesis.

One of the interesting aspect of conjugated polymers is their ability to behave as electrical conductors (44) (see ELECTRICALLY-CONDUCTING POLYMERS). The metallic appearance of many polydiacetylene crystals suggests they would be good candidates as electrical conductors. However, these organic materials are insulators with conductivities less than 10^{-10}. Polyacetylene also shows low conductivity in the solid state but it is dramatically altered by doping. Because of the similarity of polydiacetylene to polyacetylene it was anticipated that doping would enhance the conductivity of polydiacetylene. Although increases in conductivity have been observed, it is not as large as has been observed for polyacetylene (4). One of the problems that appears is the inability of the dopant to penetrate the polydiacetylene materials because of their high crystallinity.

Polytriacetylenes

Preparation of the Triacetylene Monomers. Triacetylenes are most commonly prepared using the Cadiot–Chodkiewicz coupling reaction (11,12). Using this method each triple bond is added in a separate step.

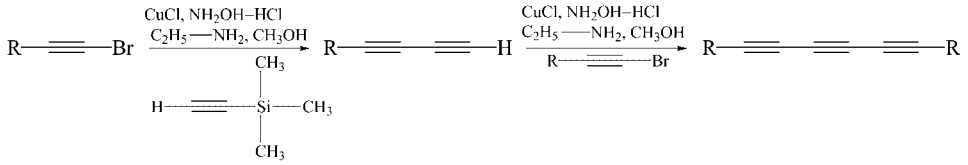

Preparation of Polytriacetylene. Soon after the early understanding of the diacetylene polymerization was reported (8,9), attempts were made to polymerize a triacetylene to produce a polytriacetylene (45). However, these early attempts as well as more recent efforts (7) were not successful. The difficulty of the topochemically controlled polymerization is the organization of the triacetylene monomer with a translational repeat distance of about 0.74 nm.

The first oligomers with the backbone structure of polytriacetylene were actually prepared by the oxidative coupling of ene diynes (Fig. 7) (46). An advantage of oligomers is that they can usually be prepared with a defined length, making them excellent models for conjugated polymers. The triacetylene oligomers prepared by oxidative coupling have been proven to be remarkably stable and are promising candidates for second hyperpolarizabilities (47).

Polytriacetylenes have recently been prepared by a topochemically controlled polymerization of a triacetylene. This was accomplished using the host–guest strategy (Fig. 8). A vinylogous amide was used to establish the required translational repeat distance and γ-rays were necessary to induce the polymerization (48).

The pyridine host can be removed from the polytriacetylene by washing with acid and the polytriacetylene can be dissolved in base. The optical and Raman spectra are in accord with those that have been observed for the oligomers.

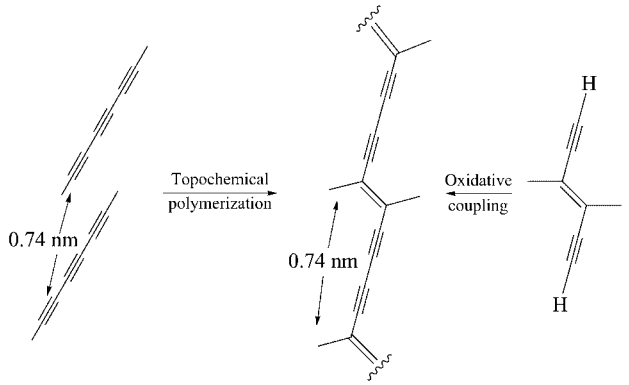

Fig. 7. Two strategies for the preparation of polytriacetylene.

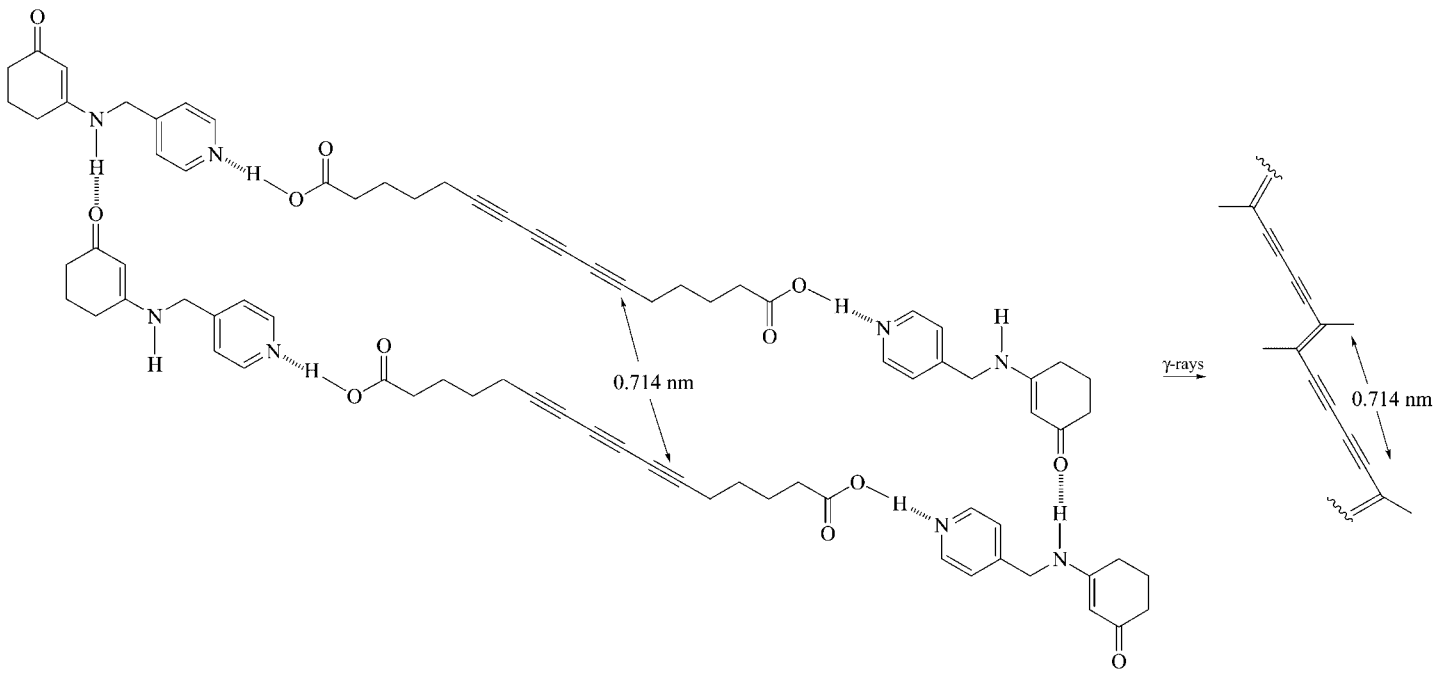

Fig. 8. The host–guest strategy for the preparation of polytriacetylenes.

Properties of Polytriacetylenes. Most of what is known about the properties of polytriacetylene has been determined from studies on the oligomers prepared by oxidative coupling of ene diynes (46). It has been determined that the effective conjugation length of the polymer is about 10 monomer units; that is, most properties of polytriacetylenes will be expressed in oligomers containing 10 monomer units. These oligomers display high environmental stability and excellent solubilities in common solvents. These properties facilitate their study and possible development into devices.

The solution optical gap for polytriacetylenes has been estimated to be $E_g =$ 2.3 eV. This is comparable to $E_g = 2.3$ eV for polydiacetylenes (49).

Their second hyperpolarizabilities (47) have been studied using third-harmonic generation and degenerate four-wave mixing. These studies suggest interesting macroscopic hyperploarizability (7) for properly prepared bulk materials.

The polydiacetylenes and the newer polytriacetylenes are clearly exciting families of conjugated polymers. Because these polymers are highly organized and their properties can be controlled by organic synthesis they offer considerable potential for the development of advanced materials. Their major disadvantage is their preparation. The preparation of a given polymer requires two major steps. Preparation of the monomers, followed by their organization in the solid state for a topochemically controlled polymerization. This latter step, the control of supramolecular structure, is particularly challenging. If the preparation of advanced materials is to ever be a rational process, it is important that the scientific community meet this challenge.

BIBLIOGRAPHY

"Diacetylene Polymers" in *EPSE* 2nd ed., Vol. 4, pp. 767–779, by R. R. Chance, Allied Corp.

1. A. Sarkar and co-workers, *J. Mater. Chem.* **10**, 819–828 (2000).
2. D. S. Chemla and J. Zyss, eds., *Nonlinear Optical Properties of Organic Molecules and Crystals*, Vol. **2**, Academic Press, Orlando, 1987, p. 3.
3. R. R. Chance, M. W. Washabaugh, and D. J. Hupe, in D. Bloor and R. R. Chance, eds., *Polydiacetylenes*, Martinus Nijhoff, Dordrecht, the Netherlands, 1985, pp. 239–256.
4. H. Shirakawa, T. Masuda, and K. Takeda, in S. Patai, ed., *The Chemistry of Triple-Bonded Functional Groups*, Supplement C2, John Wiley & Sons, Inc., New York, 1994, pp. 946–1007.
5. H.-J. Cantow, ed., *Advances in Polymer Science*, Vol. **63**, Springer-Verlag, Berlin.
6. D. T. McQuade, A. E. Pullen, and T. M. Swager, *Chem. Rev.* **100**, 2537–2574 (2000); J. Roncali, *Chem. Rev.* **97**, 173–205 (1997).
7. V. Enkelmann, *Chem. Mater.* **6**, 1337–1340 (1994).
8. G. Wegner, *Z. Naturforsch.* **24B**, 824 (1969); G. Wegner, *J. Polym. Sci, Polym. Lett. Ed.* **9**, 133 (1971).
9. G. Wegner, *Makromol. Chem.* **154**, 35 (1972).
10. J.-H. Lee, M. D. Curtis, and J. W. Kampf, *Macromolecules* **33**, 2136–2144 (2000); W. Shen, S. A. Thomas, *Org. Lett.* **2**, 2857–2860 (2000); A. Sarkar, S. H. Nakanishi, and H. Matsuda, *Helv. Chim. Acta* **82**, 138–141 (1999).
11. K. Sonogashira, in B. M. Trost, ed., *Comprehensive Organic Synthesis*, Vol. **3**, Pergamon Press, Oxford, 1991, p. 551.
12. L. Brandsma, *Preparative Acetylene Chemistry*, 2nd ed., Elsevier, Amsterdam, 1988.

13. W. Sato, H. Miyaji, and J. L. Sessler, *Tetrahedron Lett.* **41**, 6731–6736 (2000).
14. R. H. Baughman and K. C. Yee, *Macromol. Rev.* **13**, 219–239 (1978).
15. M. Schott and G. Wegner, in Ref. 2, p. 3.
16. *Cambridge Crystalographic Structural Data Base*, Version 5.21, April 2001.
17. Ref. 14, p. 24.
18. G. R. Desiraju, *Crystal Engineering: The Desigh of Organic Solids*, Elsevier, Amsterdam, 1989.
19. G. R. Desiraju, *Angew. Chem., Int. Ed. Engl.* **34**, 2311 (1995).
20. G. R. Desiraju and A. Gavezzotti, *J. Chem. Soc., Chem. Commun.* 621 (1989).
21. D Kobelt and E. F. Paulus, *Acta Crystallogr., Sect. B* **30** 232 (1974).
22. G. W. Coates and co-workers, *Angew. Chem., Int. Ed. Engl.* **36**, 248–251 (1997).
23. G. A. Jeffrey and W. Saenger, *Hydrogen Bonding in Biological Structures*, Springer-Verlag, Berlin, 1991.
24. G. N. Patel, *Polym. Pepr. (Am. Chem. Soc., Div. Polm. Chem.)* **19**, 154 (1978).
25. R. J. O. M. Hoofman and co-workers, *Macromolecules* **33**, 9289–9297 (2000).
26. R. J. O. M. Hoofman and co-workers, *Macromolecules* **34**, 474–480 (2001).
27. J.-H. Lee, M. D. Curtis, and J. W. Kampf, *Macromolecules* **33**, 2136–2144 (2000); A. Sarkar and S. S. Talwar, *J. Chem. Soc., Perkin Trans.* **1**, 4141–4146 (1998).
28. W. H. Kim and co-workers, *Macromolecules* **27**, 1819–1824 (1994); S. Shimada and co-workers, *Chem. Commun.* 1421–1422 (1997); A. Sarkar and co-workers, *Polym. Bull.* **41**, 425–431 (1998); A. Sarkar and co-workers, *Chem. Lett. (Japan)* 1073 (1998); H. Matsuzawa and co-workers, *Polym. J.* **33**, 182–189 (2001).
29. F. W. Fowler and J. W. Lauher, *J. Phys. Org. Chem.* **13**, 1–8, (2000).
30. A. S. Alekseev and co-workers, *Langmuir* **16**, 3337–3344 (2000).
31. K. Morigaki and co-workers, *Angew. Chem., Int. Ed.* **40**, 172–174 (2001).
32. W. Wang, *J. Polym. Res.* **7**, 1–6 (2000).
33. M. Cai and co-workers, *Langmuir* **15**, 1215–1222 (1999).
34. Y. Okawa and M. Aono, *Nature* **409**, 683–684 (2001).
35. S. Kolusheva and co-workers, *J. Am. Chem. Soc.* **123**, 417–422 (2001).
36. G. Wang and R. I. Hollingsworth, *Langmuir* **15**, 3062–3069 (1999).
37. H. S. Nalwa, ed., *Handook of Advanced Electronic and Photonic Materials and Devices*, Vols. **3**, **8**, **9**, **10**, Academic Press, San Diego, 2001.
38. S. Okada and co-workers, *Acc. Chem. Res.* **31**, 229–239 (1998).
39. Y. Lu and co-workers, *Nature* **410**, 913–916 (2001).
40. J. L. Brédas and co-workers, *Chem. Rev.* **94**, 243–278 (1994).
41. D. M. Krol and M. Thakur, *Appl. Phys. Lett.* **56**, 1406 (1990).
42. G. I. Stegeman and co-workers, *Nonlinear Optics* **24**, 1–17 (2000).
43. A. Boyle and W. J. Blau, in H. S. Nalwa, ed., *Handook of Advanced Electronic and Photonic Materials and Devices*, Vol. **9**, Academic Press, San Diego, 2001, pp. 309–345.
44. H. Kiess, ed., *Conjugated Conducting Polymers*, Springer, Berlin, 1992.
45. J. Kiji and co-workers, *Polymer* **14**, 433–439, (1973).
46. R. E. Martin and co-workers, *Chem. Eur. J.* **3**, 1505–1512 (1997).
47. R. E. Martin and co-workers, *Chem. Eur. J.* **6**, 4400–4412 (2000).
48. J. Xiao and co-workers, *Angew. Chem., Int. Ed.* **39**, 2132–2135 (2000).
49. J. Anthony and co-workers, *Angew. Chem., Int. Ed. Engl.* **33**, 763–766 (1994).

FRANK FOWLER
SUNY

DNA. See POLYNUCLEOTIDES.

ELASTICITY, RUBBER-LIKE

Introduction

Elasticity is the reversible stress–strain behavior by which a body resists and recovers from deformation produced by a force (1). This behavior is exhibited by rubber-like materials in a unique and extremely important manner. Unlike metals or glasses, they can undergo very large deformations without rupture (and are thus similar to liquids) and then can come back to their original shape (as do solids). This exceptional ability was investigated in 1805 (2,3), well before the concept of polymers as long-chain molecules was established in the 1920s. It was observed that a rubber gave off heat upon stretching and, when submitted to a constant load, became shorter as temperature was increased. Later, Kelvin (4) derived the thermodynamic laws of elasticity, and more careful experiments were performed by Joule (5). Many books and review papers have been published on the subject (6–36).

Deformation and Mechanical Testing

When a body is submitted to external stress or pressure, it undergoes a change in shape or volume. Mechanical testing of rubber involves application of a force to a specimen and measurement of the resultant deformation or application of a deformation and measurement of the required force. The results are expressed in terms of stress and strain and thus are independent of specimen geometry. Stress is the force f per unit original cross-sectional area A, and strain the deformation per unit original dimension. The units of stress are Newtons per square meter (N/m^2 or Pa); strain is dimensionless. The ratio of stress to strain is called the

Encyclopedia of Polymer Science and Technology. Copyright John Wiley & Sons, Inc. All rights reserved.

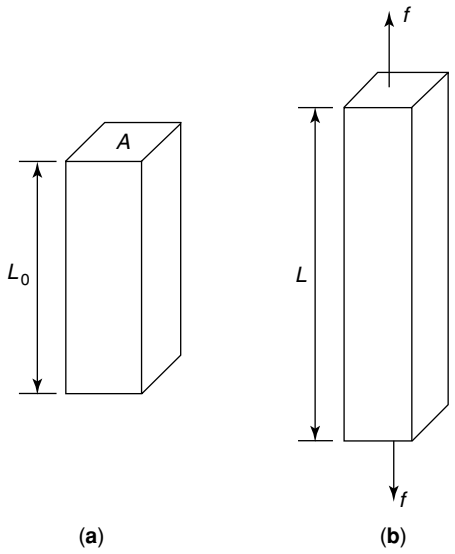

Fig. 1. Uniaxial extension of a bar-shaped sample. (a) No load; (b) tensile load. A = area; f = force; L_0 = original length; L = length.

modulus. A material is Hookean when its modulus is independent of strain (typical of a metal spring or wire); elastomers are Hookean only in the range of very small deformations.

The simplest deformations are isotropic compression under hydrostatic pressure, uniaxial extension (or compression), and simple shear. They are used to determine the bulk modulus K, Young's modulus E, and shear modulus G, respectively (37–44). Elastomer testing for commercial applications is highly dependent on the method, the conditions (eg, strain rate, temperature), and the shape of the samples. Therefore, mechanical tests have been standardized for uniformity and simplicity by the American Society for Testing and Materials (ASTM) (45).

Isotropic Compression. The volume of a sample decreases from V_0 to V when submitted to a hydrostatic pressure p. The bulk modulus is the ratio of this pressure to the volume change per unit volume $\Delta V/V_0$:

$$K = p/(\Delta V/V_0) \tag{1}$$

where $\Delta V = V_0 - V$; K is the reciprocal of the compressibility and can be determined by direct measurement of compressibility (46) or velocity of longitudinal elastic waves (sound) or by theoretical calculations (39).

Uniaxial Extension. A rubber strip of original length L_0 is stretched uniaxially to a length L, as illustrated in Figure 1. The stretch and elongation are $\Delta L = L - L_0$ and $\lambda = L/L_0$, respectively. The strain ϵ (also known as the relative deformation, linear dilation, or extension) and the elongation or extension ratio λ are related by

$$\epsilon = \Delta L/L_0 = \lambda - 1 \tag{2}$$

The lengthwise extension is in general accompanied by a transverse contraction. The ratio of the change Δw in width per unit width w_0 to the change in length per unit length is called *Poisson's ratio* (47):

$$\nu_p = (\Delta w/w_0)/(\Delta L/L_0) \tag{3}$$

Ideal rubbers and liquids deform at constant volume, for which ν_p is equal to 0.5. Poisson's ratio for real elastomers may be experimentally determined by applying extensometers in the transverse and axial directions of a sample. Approximate values of ν_p thus determined are 0.33 for glassy polymers, 0.4 for semicrystalline polymers, and 0.49 for elastomers. *Young's modulus E* is the ratio of normal stress f/A to corresponding strain ϵ:

$$E = (f/A)/\epsilon \tag{4}$$

Generally, stress–strain curves deviate markedly from a straight line, as illustrated in Figure 2. The Young's modulus at small deformation is the slope tan θ of the stress–strain curve at the origin (initial tangent modulus). It can be measured in flexure or by tensile experiments (48).

Tension testing of a vulcanized elastomer also permits the determination of the tensile strength, which is the maximum stress applied during stretching a specimen to rupture; the corresponding rupture strain is called the maximum extensibility (49–52). Typical values are given in Table 1 (14). Dumbbell and ring specimens can be used.

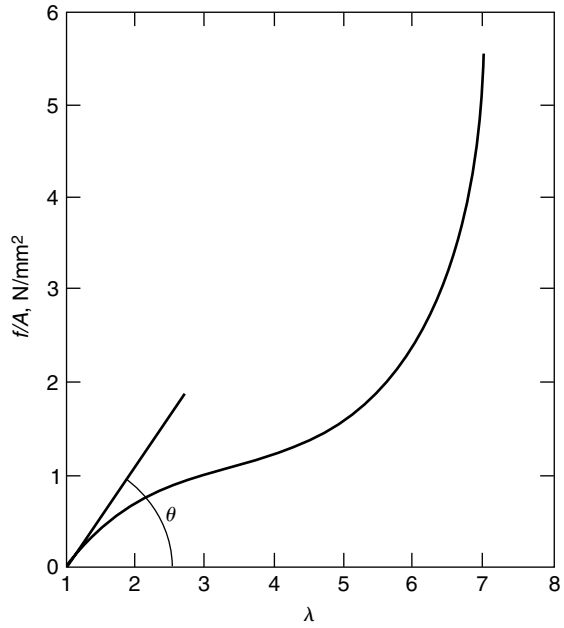

Fig. 2. Stress–strain curve of a non-Hookean solid; typical curve for an elastomer in uniaxial extension.

Table 1. Properties of a Typical Rubber, Metal, and Glass[a]

Property	Rubber	Metal	Glass
Breaking extension, %	500	Large, plastic	3
Elastic limit, %	500	2	3
Tensile strength, MN/m^2[b]	10^c	5×10^4	5×10^3

[a] Ref. 14.
[b] To convert MN/m^2 (MPa) to psi, multiply by 145.
[c] $>10^3$ if based on area at break.

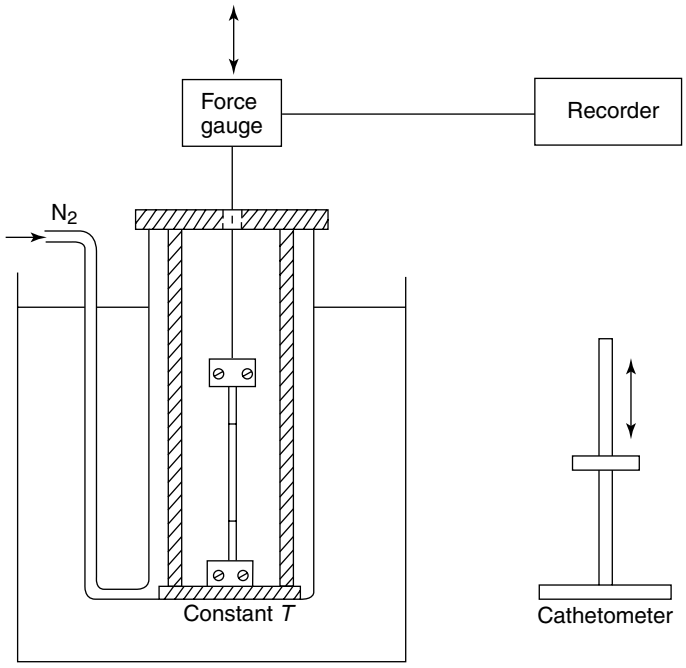

Fig. 3. Schematic diagram of a typical apparatus used to measure elastomer stress as a function of strain (21). T = Temperature.

A typical apparatus used to measure the equilibrium stress of an elongated network as a function of strain and temperature is shown in Figure 3 (21). The rubber strip is held between two clamps and maintained under a protective atmosphere of nitrogen. The sample length, required to characterize its deformation, is obtained by means of a cathetometer or traveling microscope (the central test section of the sample is delineated by ink marks applied before loading). Values of the force are obtained from a calibrated stress gauge, the output of which is displayed as a function of time on a standard recorder. Measurements are made at elastic equilibrium; the influence of temperature can also be studied. Another example of a stretching device is an automatic stress relaxometer (53).

Simple Shear. Simple shear, illustrated in Figure 4, is a deformation in which the height H and surface A of the sample are held constant. The shear

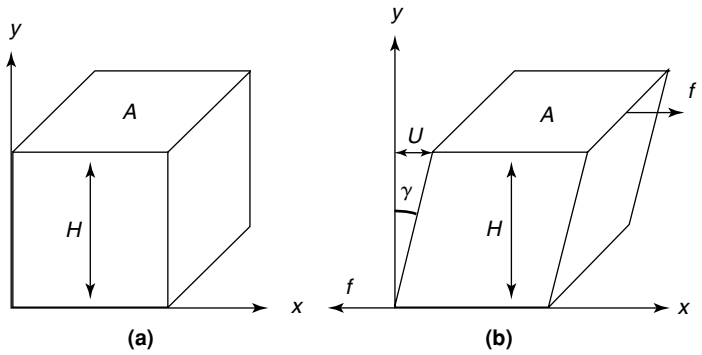

Fig. 4. Simple shear of a rectangular sample. (a) No deformation; (b) simple shear. A = area; H = height; f = force; U = linear displacement.

modulus or rigidity G is expressed by the relations

$$G = (f/A)/(U/H) = (f/A)\tan\gamma \simeq f/\gamma A \tag{5}$$

where γ is the shear strain and f/A the shear stress. As in the case of Young's modulus, the shear modulus (41,42) is a material constant if stress and strain are directly proportional. If they are not, the *shear modulus* at small deformation is employed; it is defined as the slope at the origin of the stress–strain curve. The shear modulus is generally measured on a cylindrical specimen and a tension-testing machine.

Typical values of moduli and Poisson's ratios for metals, ceramics, and polymers are given in Table 2 (39). Moduli of rubbers are strikingly low, and even those of other types of polymers are of the order of one tenth of those of metals. However, compared at equal weights, ie, ratio of modulus to density ρ, polymers (except rubbers) compare favorably.

Relationships between Moduli and Poisson's Ratio. On the basis of the theory of elasticity of isotropic solids, the moduli and Poisson's ratio are interrelated (54) as follows:

$$E = 2G(1+\nu_p) = 3K(1-2\nu_p) \tag{6}$$

For elastomers, the Poisson's ratio is nearly 0.5, and thus $E \simeq 3G$.

Conditions for Rubber-like Elasticity

Long, Highly Flexible Chains. Elastomers consist of polymeric chains which are able to alter their arrangements and extensions in space in response to an imposed stress. Only long polymeric molecules have the required exceedingly large number of available configurations.

It is necessary that all the configurations are accessible; this means that rotation must be relatively free about a significant number of the bonds joining neighboring skeletal atoms.

Table 2. Poisson's Ratio, Moduli, and Density of Metals, Ceramics, and Polymers[a]

Material	ν_p	Young's modulus E, 10^9 N/m^2[b]	Shear modulus G, 10^9 N/m^2[b]	Bulk modulus K, 10^9 N/m^2[b]	Density ρ, g/cm^3	Specific properties		
						E/ρ, 10^6 m^2/s^2	G/ρ, 10^6 m^2/s^2	K/ρ, 10^6 m^2/s^2
Metals								
Cast iron	0.27	90	35	66	7.5	12.0	4.7	8.8
Steel (mild)	0.28	220	86	166	7.8	28.0	11.0	21.0
Aluminum	0.33	70	26	70	2.7	26.0	9.6	26.0
Copper	0.35	120	44.5	134	8.9	13.5	4.5	15.0
Lead	0.43	15	5.3	36	11.0	13.6	4.8	33.0
Mercury	0.5	0	0	25	13.55	0.0	0.0	1.85
Inorganics								
Quartz	0.07	100	47	39	2.65	38.0	17.8	14.7
Vitreous silica	0.14	70	30.5	32.5	2.20	32.0	14.0	14.7
Glass	0.23	60	24.5	37	2.5	24.0	9.8	14.9
Granite	0.30	30	11.5	25	2.7	11.1	4.3	9.2
Whiskers								
Alumina		2000	1000	667	3.96	510	253	225
Carborundum		1000	500	333	3.15	315	160	106
Graphite		1000	500	333	2.25	440	220	150
Polymers								
Polystyrene	0.33	3.2	1.2	3.0	1.05	3.05	1.15	2.85
Poly(methyl Methacrylate)	0.33	4.15	1.55	4.1	1.17	3.55	1.33	3.5
Nylon-6,6	0.33	2.35	0.85	3.3	1.08	2.21	0.79	2.3
Polyethylene (low density)	0.45	1.0	0.35	3.33	0.91	1.1	0.385	3.7
Ebonite	0.39	2.7	0.97	4.1	1.15	2.35	0.86	3.6
Rubber	0.49	0.002	0.0007	0.033	0.91	0.002	0.00075	0.04
Liquids								
Water	0.5	0.0	0.0	2.0	1.0	0.0	0.0	2.0
Organic liquids	0.5	0.0	0.0	1.33	0.9	0.0	0.0	1.5

[a]Ref. 39. Courtesy of Elsevier.

[b]N/m^2 = Pa. To convert Pa to psi, multiply by 0.000145.

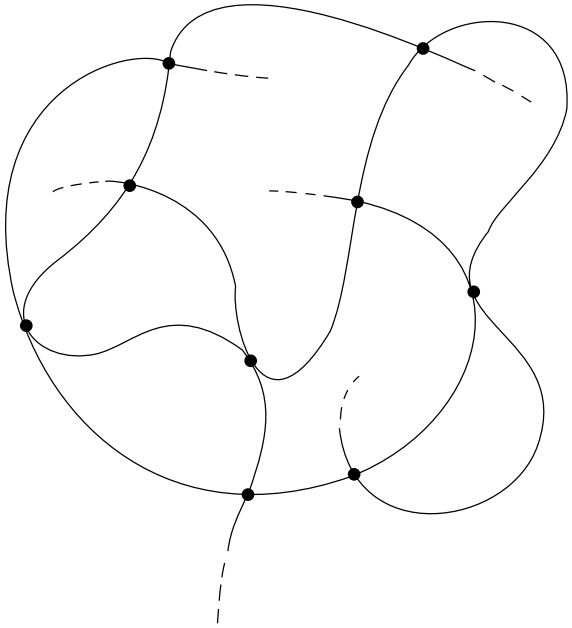

Fig. 5. Segment of an elastomeric network.

Network Structure. Chains must be joined by permanent bonds called cross-links, as illustrated in Figure 5. The network structure thus obtained is essential so as to avoid chains permanently slipping by one another, which would result in flow and thus irreversibility, ie, loss of recovery. These cross-links may be chemical bonds or physical aggregates, eg, glassy domains in multiphase block copolymers (55,56).

At the end of the cross-linking process, the topology of the mesh is composed of the different entities represented in Figure 6 (16,57–59). An elastically active junction is one joined by at least three paths to the gel network (60,61). An active chain is one terminated by an active junction at both its ends. Rubber-like elasticity is due to elastically active chains and junctions. Specifically, upon deformation the number of configurations available to a chain decreases and the resulting decrease in entropy gives rise to the retractive force.

Weak Interchain Interactions. Apart from the effects of the cross-links, the molecules must be free to move reversibly past one another, that is, the intermolecular attractions known as secondary or van der Waals forces, which exist between all molecules, must be small. Specifically, extensive crystallization should not be present, and the polymer should not be in the glassy state.

Differences between Elastomers and Metals

Elastomers and metals differ greatly with regard to deformation mechanisms (26, 62,63). Metals and minerals are formed of atoms arranged in a three-dimensional crystalline lattice, joined by powerful valence forces operating at relatively short

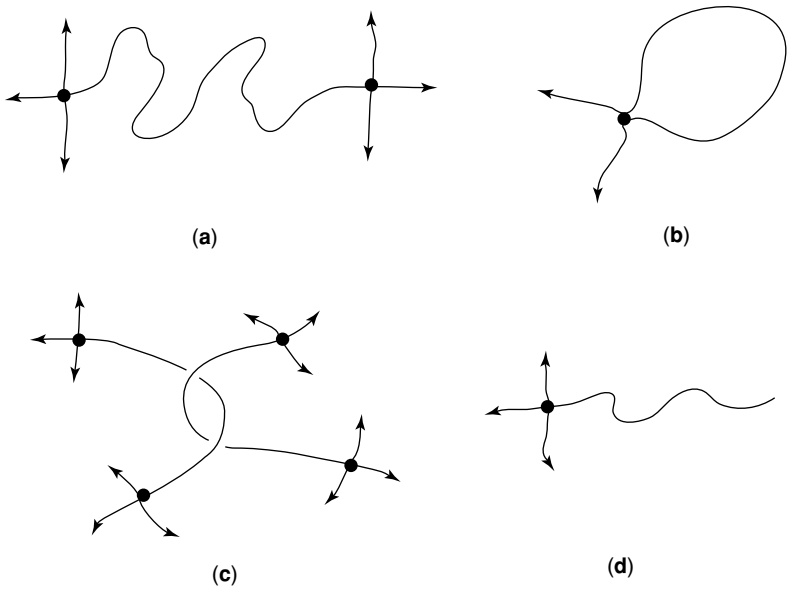

Fig. 6. Structural features of a network. (a) Elastically active chain; (b) loop; (c) trapped entanglement; (d) chain end.

range. Deformation of such materials involves changes in the interatomic distance, which requires large forces; hence the elastic modulus of these materials is very high. After a small deformation, slippage between adjacent crystals occurs at the yield point, and the deformation increases much more rapidly than the stress and becomes irreversible or plastic. The primary effect of stretching a metal short of this yield point is the increase ΔE_m in energy caused by changing the distance d of separation between metal atoms. The sample recovers its original length when the force is removed, since this process corresponds to a decrease in energy. Heating increases oscillations about the minimum of the asymmetric potential energy curve and thus causes the usual volume expansion.

Stretching of elastomers does not involve any significant changes in the interatomic distances, and therefore the forces required are considerably lower. The number of available configurations for a network chain is reduced in the deformation process. After suppression of the stress, the specimen recovers its original shape, since this corresponds to the most disordered state. Thus the retractive force arises primarily from the tendency of the system to increase its entropy toward the maximum value it had in the undeformed state. At high elongations, stress–strain curves turn upward, a behavior very unlike that of metals. The number of available configurations is drastically reduced in this region, and chains reach the limits of their extensibility. For polymers with regular structures, crystallization may also be induced. Further elongation may then require deformation of bond angles and length, which requires much larger forces.

At constant force, heating increases disorder, forcing the sample in the direction of the state of disorder it had at a lower temperature and smaller deformation. The result is therefore a decrease in length.

Extension of Elastomers and Compression of Gases

The extension of elastomers and the compression of gases are associated with a decrease in entropy. Thus, similar behavior is expected in regard to (adiabatic) deformation and heating. The work of deformation of a gas is $dW = -pdV$, where p is the pressure and V the volume. For an elastomer it is $dW = f\,dL$, where f is the force and L the length; the term $-pdV$ is not taken into account, since there is only a negligible change in rubber volume during stretching. These observations can be used to explain Gough's experiments by making use of classical thermodynamic principles (64).

Statistical Distribution of End-To-End Dimensions of a Polymer Chain

Before treating the statistical properties of a network, the statistics of a single chain must be considered, mainly to establish the relationship between the number of configurations and the deformation (12,16,65–72). A polymeric chain is constantly changing its configuration by Brownian motion. Statistical methods and idealized models permit calculation of the average properties of such a chain.

The Freely Jointed Chain. This type of idealized chain consisting of n links of length l is represented in Figure 7, where r is the end-to-end distance. When the chain is completely extended, $R = nl$. The chain may assume many configurations, each associated with an end-to-end distance r_i. In statistics, it is equivalent to consider a molecule at different times or an assembly of N molecules at the same time. An average quantity describing the assembly is the mean-square end-to-end distance $\overline{r^2}$ defined by

$$\overline{r^2} = \frac{1}{N}\sum_{i=1}^{N} r_i^2 \tag{7}$$

where r_i is the end-to-end distance of the ith chain. The vector $\boldsymbol{r}_i$ is the sum of the link vectors $\boldsymbol{I}_j$:

$$r_i = \sum_{j=1}^{n} I_j \tag{8}$$

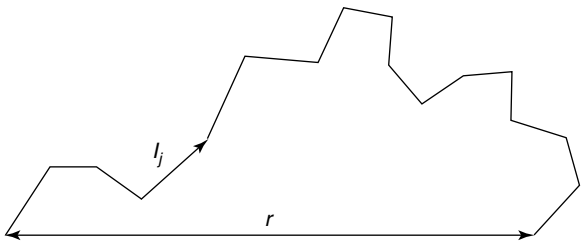

Fig. 7. Ideal chain formed with n links of length l. r = End-to-end distance, $\boldsymbol{I}_j$ = link vector.

and $r^2{}_i$ is the scalar product of r_i with itself:

$$r_i^2 = \sum_{j=1}^{n} I_j^2 + 2\sum_{k<j} I_k \cdot I_j \tag{9}$$

If the chain is assumed to be freely jointed and volumeless, any two links can assume any orientation with respect to each other. Therefore the second term of equation (9) is zero and

$$r_i^2 = nl^2 \tag{10}$$

The mean-square end-to-end distance of a freely orienting chain is deduced from equations (7) and (10) (73–76) as follows:

$$\overline{r^2} = nl^2 \tag{11}$$

Another interesting quantity is the probability that a chain has a given end-to-end distance (77–81). This is called the Gaussian distribution function

$$W(x,y,z)\mathrm{d}x\mathrm{d}y\mathrm{d}z = W(x)\mathrm{d}x\,W(y)\mathrm{d}y\,W(z)\mathrm{d}z = (b/\pi^{1/2})^3 \exp(-b^2r^2)\mathrm{d}x\mathrm{d}y\mathrm{d}z \tag{12}$$

where $r^2 = x^2 + y^2 + z^2$, and $b^2 = 3/2\overline{r^2}$. This generalization is valid only for small extensions of a relatively long chain (82). Equation (12) gives the probability that if one extremity of the vector r is fixed at the origin of the coordinates, the other lies in the volume $\mathrm{d}x\ \mathrm{d}y\ \mathrm{d}z$ centered around the point (x, y, z). What is more interesting is the probability for a chain to have its end in a spherical shell of radius r and thickness $\mathrm{d}r$ centered at the origin, irrespective of direction. This is the radial distribution

$$W(r)\mathrm{d}r = (b/\pi^{1/2})^3 \exp(-b^2r^2)4\pi r^2\mathrm{d}r \tag{13}$$

which is illustrated in Figure 8 (3). The maximum occurs at $r = (2nl^2/3)^{\frac{1}{2}}$. The mean-square end-to-end distance is the second moment of the radial distribution function

$$\overline{r^2} = \int_0^\infty r^2 W(r)\mathrm{d}r \Big/ \int_0^\infty W(r)\mathrm{d}r \tag{14}$$

which yields the result of equation (11)

$$\overline{r^2} = 3/2b^2 = nl^2 \tag{15}$$

The Gaussian distribution (eq. (12)) was obtained in the aforementioned treatment with the assumption that chains are far from their full extension. Moreover, the Gaussian distribution function predicts zero probability only for $r = \infty$ instead of for all r in excess of that for full chain extension, and does not adequately

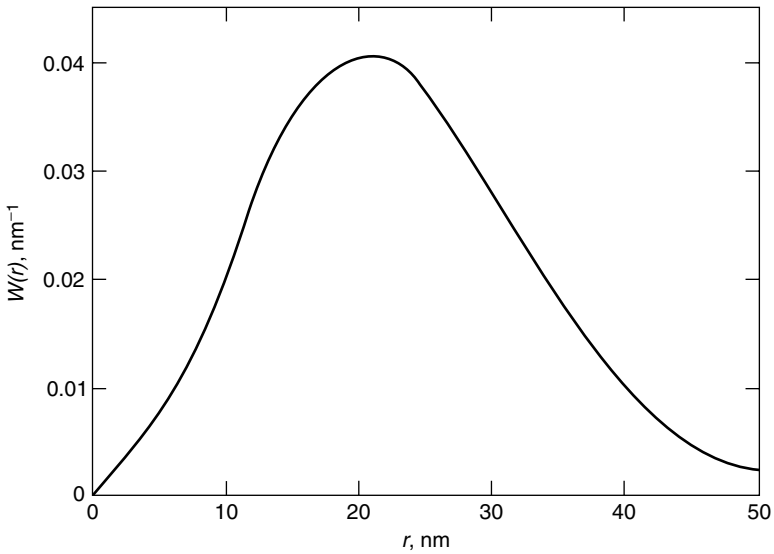

Fig. 8. Radial distribution function $W(r)$ of the chain displacement vectors for chain molecules consisting of 10^4 freely jointed segments, each of length $l = 0.25$ nm; $W(r)$ is expressed in nm^{-1} and r in nm (3). Courtesy of Cornell University Press.

take into account the significant geometric and conformational differences known to exist among different types of polymer chains (83). The distribution obtained from a more general treatment is of the more complicated form (84–86) shown as follows:

$$W(r)\mathrm{d}r = \text{const.} \times \exp\left(-\int_0^r \mathcal{L}^{-1}(r/nl)\mathrm{d}r/l \right) 4\pi r^2 \mathrm{d}r \tag{16}$$

where $\mathcal{L}^{-1}$ is the inverse Langevin function and

$$\mathcal{L}(u) = \coth u - 1/u \tag{17}$$

Equation (16) can be expanded in the series

$$W(r)\mathrm{d}r = \text{const.} \times \exp\{-n[(3/2)(r/nl)^2 + (9/20)(r/nl)^4 + (99/350)(r/nl)^6 + \cdots]\} 4\pi r^2 \mathrm{d}r \tag{18}$$

and the Gaussian distribution (eq. (13)) recovered for $r \ll nl$. A comparison of the Gaussian and inverse Langevin distributions for $n = 6$ is shown in Figure 9 (7).

Chain with Bond-Angle Restrictions. Although the chain in the aforementioned treatment was assumed to be freely jointed, a real polymer chain has fixed bond angles θ. Therefore, the second term in equation (9) is no longer zero. The scalar product of two vectors $\boldsymbol{I}_i \cdot \boldsymbol{I}_j$ is $l^2 \cos^{|j-i|}\theta$. It can be shown (9,73,74) that

$$\overline{r^2} \simeq nl^2(1 - \cos\theta)/(1 + \cos\theta) \tag{19}$$

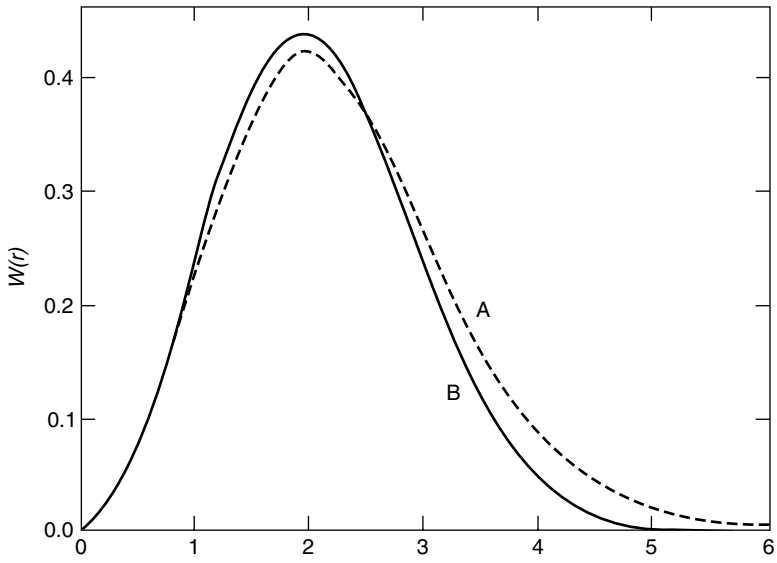

Fig. 9. Distribution function $W(r)$ for a six-link random chain, with length $l = 1$ in arbitrary units: A, Gaussian limit; B, inverse Langevin function (7). Courtesy of Oxford University Press.

In the particular case of a tetrahedrally bonded chain, $\theta = 109.5^\circ$ and $\overline{r^2} = 2nl^2$, twice the value for a freely jointed chain. Thus, a real chain is quite different from this ideal representation. Nevertheless, any flexible real chain can be represented by a simple model which is the statistical equivalent of a freely jointed chain (87,88). The two conditions are that the real and freely jointed chains have the same mean-square end-to-end distance and the same length at complete extension:

$$\overline{r^2} = \overline{r_e^2} = n_e l_e^2 \tag{20}$$

and

$$R = R_e = n_e l_e \tag{21}$$

Thus, only one model chain is equivalent to the real one, obeying the same Gaussian distribution function and composed of n_e segments of length l_e given by

$$n_e = R^2/\overline{r^2} \tag{22}$$

$$l_e = \overline{r^2}/R \tag{23}$$

Chain with Bond-Angle Restrictions and Hindered Rotations. The angle of rotation ϕ of a single bond around the axis formed by the preceding one may be restricted by steric interferences between atoms. When n is large and the average value of $\cos\phi$, ie, $\overline{\cos\phi}$, is not too close to unity, the following relationship can be established (89,90):

$$\overline{r^2} = nl^2\left(\frac{1-\cos\theta}{1+\cos\theta}\right)\left(\frac{1+\overline{\cos\phi}}{1-\overline{\cos\phi}}\right) \tag{24}$$

When the rotation is not hindered, ie, when $\overline{\cos\phi} = 0$, equation (24) is equivalent to equation (19).

The conformations of polymer chains may be generated by a Monte Carlo simulation method. The dimensions of linear chains, unperturbed by excluded-volume interactions, have been measured in various solvents by light scattering, x-ray small-angle scattering, and dilute-solution viscosity measurements. They are reported most comprehensively in the *Polymer Handbook* (91,92). A powerful tool to investigate chain conformations in unswollen and swollen melts and networks is small-angle neutron scattering (sans) (67,93–97).

The Equation of State for a Single Polymer Chain. The variation in the Helmholtz free energy is the negative of the work of deformation in isothermal elongation

$$\mathrm{d}A = -\mathrm{d}W = f\,\mathrm{d}r \tag{25}$$

with

$$\mathrm{d}A = \mathrm{d}U - T\mathrm{d}S \tag{26}$$

The tensile force f on a polymer chain for a given length r is

$$f = \left(\frac{\partial A}{\partial r}\right)_T = \left(\frac{\partial U}{\partial r}\right)_T - T\left(\frac{\partial S}{\partial r}\right)_T \tag{27}$$

In freely jointed and freely rotating model chains, no rotation is preferred; therefore, the internal energy is the same for all the conformations. Then,

$$f = -T\left(\frac{\partial S}{\partial r}\right)_T \tag{28}$$

The entropy is given by the Boltzmann relation

$$S = \mathrm{k}\ln\Omega \tag{29}$$

where k is the Boltzmann constant, and Ω, the total number of configurations available to the system, is proportional to $W(r)$ (eq. (13)). Calculation of the force gives

$$f = 2kTb^2r \tag{30}$$

$$f = 2kTr/\overline{r^2} \tag{31}$$

Thus, f is directly proportional to the absolute temperature and to r, which means the chain acts as a Hookean spring with modulus $3kT/\overline{r^2}$. The use of a non-Gaussian distribution for Ω leads to (71,85,86)

$$f = (kT/l)\mathcal{L}^{-1}(r/nl) \tag{32}$$

Classical Thermodynamics of Rubber-like Elasticity

In experiments concerning the relationships between length, temperature, and force, usually the change in force with temperature at constant length is recorded (53,98–101). It is therefore necessary to extend the thermodynamic treatment of the elasticity. Moreover, the force is not purely entropic, and the energetic contribution carries useful information on the dependence on temperature of the average end-to-end distance of the network chains in the unstrained state (21,102). It is therefore important to know how to deduce these quantities from a thermoelastic experiment.

The change in internal energy during stretching an elastic body is

$$\mathrm{d}U = \mathrm{d}Q - \mathrm{d}W \tag{33}$$

where $\mathrm{d}Q$ is the element of heat absorbed by the system and $\mathrm{d}W$ the element of work done by the system on the surroundings. In a reversible process,

$$\mathrm{d}Q = T\mathrm{d}S \tag{34}$$

where S is the entropy of the body. The work $\mathrm{d}W$ can be expressed as the sum

$$-\mathrm{d}W = -p\mathrm{d}V + f\mathrm{d}L \tag{35}$$

where p is the equilibrium external pressure, $\mathrm{d}V$ the volume dilation accompanying the elongation of the elastomer, and f the equilibrium tension. Thus,

$$\mathrm{d}U = T\mathrm{d}S - p\mathrm{d}V + f\mathrm{d}L \tag{36}$$

At constant pressure, the enthalpy change is

$$\mathrm{d}H = \mathrm{d}U + p\mathrm{d}V = T\mathrm{d}S + f\mathrm{d}L \tag{37}$$

A deformation $\mathrm{d}L$ at constant pressure and temperature induces a retractive force

$$f = \left(\frac{\partial H}{\partial L}\right)_{T,p} - T\left(\frac{\partial S}{\partial L}\right)_{T,p} \tag{38}$$

Expression 38 is one of the forms of the thermodynamic elastic equation of state. Measurements of stress at constant length as a function of temperature have been

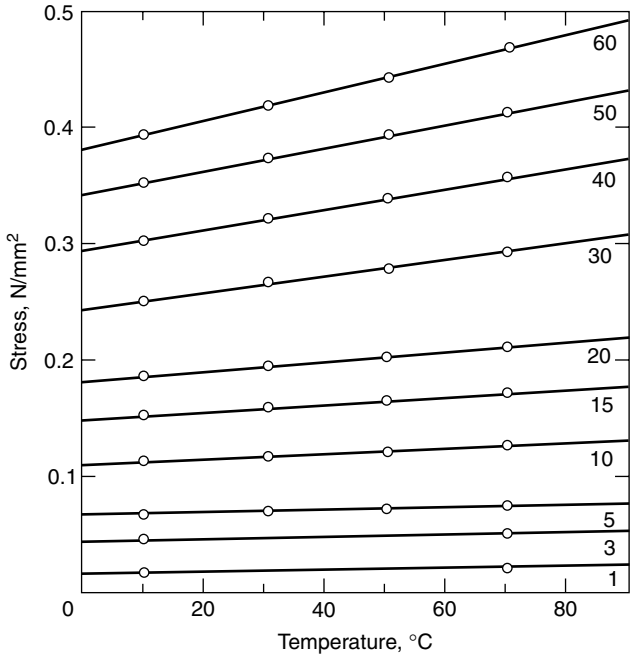

Fig. 10. Stress–temperature curves for sulfur-vulcanized natural rubber (99,103). Courtesy of the American Chemical Society.

performed (see Fig. 10) (97,103–105). All the curves appear to be straight lines; the slope increases with increasing elongation, but for very small elongations, the slopes can be negative. This phenomenon, called the thermoelastic inversion, is due to the volume expansion occurring in any elastomer. The condition of constant length does not correspond to constant elongation as well, since the sample's unstrained reference length changes with temperature. The inversion is suppressed by correction of the original length (11).

The energetic and entropic contributions to the force in the intramolecular process of stretching the chains can be obtained in experiments where there is no other energetic contribution resulting from changes in (intermolecular) van der Waals forces. Therefore, these experiments must be performed at constant volume. A basic postulate of the elasticity of amorphous polymer networks is that the stress exhibited by a strained polymer network is assumed to be entirely intramolecular in origin. That is, intermolecular interactions play no role in deformations at constant volume and composition.

An equation similar to equation (38) is obtained for the elastic force measured at constant volume:

$$f = \left(\frac{\partial U}{\partial L}\right)_{T,V} - T\left(\frac{\partial S}{\partial L}\right)_{T,V} \tag{39}$$

The variation in the Helmholtz free energy has the following expression:

$$dA = -SdT - pdV + fdL \tag{40}$$

The second derivative obtained by differentiating $(\frac{\partial A}{\partial L})_{V,T}$ with respect to T at constant V and L is identical with that obtained by differentiating $(\frac{\partial A}{\partial T})_{V,L}$ with respect to L at constant V and T:

$$-\left(\frac{\partial f}{\partial T}\right)_{V,L} = \left(\frac{\partial S}{\partial L}\right)_{V,T} \tag{41}$$

Thus, equation (39) can be written as

$$f = \left(\frac{\partial U}{\partial L}\right)_{T,V} + T\left(\frac{\partial f}{\partial T}\right)_{V,L} \tag{42}$$

The energetic and entropic components of the elastic force, f_e and f_s, respectively, are obtained from thermoelastic experiments using the following equations:

$$f_e = \left(\frac{\partial U}{\partial L}\right)_{T,V} = f - T\left(\frac{\partial f}{\partial T}\right)_{V,L} \tag{43}$$

$$f_s = -T\left(\frac{\partial S}{\partial L}\right)_{T,V} = T\left(\frac{\partial f}{\partial T}\right)_{V,L} \tag{44}$$

An example of thermoelastic data is given in Figure 11 (99). The change in entropy with elongation up to 350% is responsible for more than 90% of the total stress at room temperature, whereas the contribution of internal energy is less than 10%. Thus, the restoring force is due almost entirely to the tendency of the extended rubber molecules to return to their unperturbed, random conformational states. Above 350%, crystallization appears. This is a specific feature of stereoregular rubbers, such as natural rubber which is capable of crystallization. Data concerning most of the polymers studied in this manner are reviewed in References 21 and 106.

Statistical Treatment of Rubber-like Elasticity

A network is an ensemble of macromolecules linked together, each of them rearranging its configurations by Brownian motion. Classical thermodynamics explains the behavior of elastomers with regard to force, temperature, pressure, and volume, but does not give the relationship between the molecular structure of the network and elastic quantities such as the moduli. Therefore, statistical mechanics was introduced in the 1940s (16,86,87,107–109), and its theoretical predictions were tested (110–112). Because of the complexity of network structures, two models based on affine and phantom networks were studied. The cross-linking points

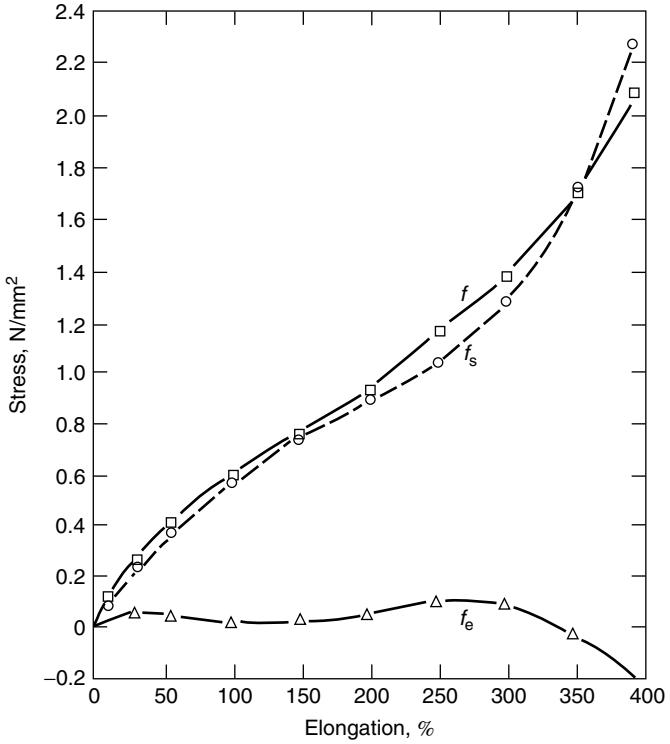

Fig. 11. Plot of the energetic (f_e) and entropic (f_s) contributions to the stress at 20°C for sulfur-vulcanized rubber (99). N/mm^2 = MPa; to convert MPa to psi, multiply by 145. Courtesy of the American Chemical Society.

of the affine network are fixed, whereas those of the phantom network can undergo fluctuations independent of their immediate surroundings. The effects of the macroscopic strain are transmitted to the chains through these junctions at which the chains are multiply joined, with the internal state of the network system specified in terms of the positions of the cross-linkages. Deformation transforms the arrangements of these points. The system is represented by the vectors $\boldsymbol{r}_i$, each of which connects the two ends of a chain. For a given end-to-end vector $\boldsymbol{r}_i$, the number of available configurations is directly proportional to the probability $W(r_i)$ or relative number of configurations. Representation of $W(r)$ by a Gaussian function according to equation (13) fails as r approaches the maximum extension r_{max}. Experimental evidence of deviations from the Gaussian theory have been reported (24,113–116) and non-Gaussian theories based on an expression for $W(r)$ similar to equation (16) have been developed (84,85,117–119). These theories have the disadvantage of containing parameters that can be determined only by comparisons between theory and experiments, specifically ν, the number density of chains in the network, and n, the number of statistical links.

The tensile force is expressed by

$$f/A_0 = (1/3)\nu kTn^{1/2}\left[\mathcal{L}^{-1}(\lambda n^{-1/2}) - \lambda^{-3/2}\mathcal{L}^{-1}(\lambda^{-1/2}n^{-1/2})\right] \tag{45}$$

where

$$\mathcal{L}^{-1}(t) = 3t + (9/5)t^3 + (297/175)t^5 + \cdots$$

and A_0 is the cross-sectional area of the unstrained sample. The number n of random links may be obtained by birefringence and stress–strain measurements, and from this result, an estimation of the number of monomer units in the equivalent-random link (of the Kuhn–Grün theory) of the polymeric chain (120). Another approach to a non-Gaussian theory utilizes information provided by rotational isomeric state theory on the spatial configurations of chain molecules (83), including most of those used in elastomeric networks. Specifically, Monte Carlo calculations (121–123) based on the rotational isomeric state approximation are used to simulate spatial configurations followed by distribution functions for the end-to-end separation r of the network chains (124).

The theory in the Gaussian limit has been refined greatly to take into account the possible fluctuations of the junction points. In these approaches, the probability of an internal state of the system is the product of the probabilities $W(r_i)$ for each chain. The entropy is deduced by the Boltzmann equation, and the free energy by equation (26). The three main assumptions introduced in the treatment of elasticity of rubber-like materials are that the intermolecular interactions between chains are independent of the configurations of these chains and thus of the extent of deformation (125,126); the chains are Gaussian, freely jointed, and volumeless; and the total number of configurations of an isotropic network is the product of the number of configurations of the individual chains.

Affine Networks. Diffusion of the junctions about their mean positions may be severely restricted by neighboring chains sharing the same region of space. The extreme case is the affine network where fluctuations are completely suppressed, and the instantaneous distribution of chain vectors is affine in the strain. The elastic free energy of deformation is then given by

$$\Delta A_{\text{el}}(\text{aff}) = (1/2)\upsilon kT(I_1 - 3) - (\upsilon - \xi)kT \ln(V/V_0) \tag{46}$$

where I_1 is the first invariant of the tensor of deformation

$$I_1 = \lambda_x^2 + \lambda_y^2 + \lambda_z^2 \tag{47}$$

The quantities λ_x, λ_y, and λ_z are the principal extension ratios, which specify the strain relative to an isotropic state of reference having volume V_0; V is the volume of the deformed specimen, and υ is the number of linear chains whose ends are joined to multifunctional junctions of any functionality $\phi > 2$. (The *functionality of a junction* is defined as the number of chains connected to it.) The cycle rank ξ (102) represents the number of chains that have to be cut to reduce the network to an acyclic structure or tree (127). The cycle rank is the difference between the number of effective chains ν and effective junctions μ of functionality $\phi > 2$:

$$\xi = \nu - \mu \tag{48}$$

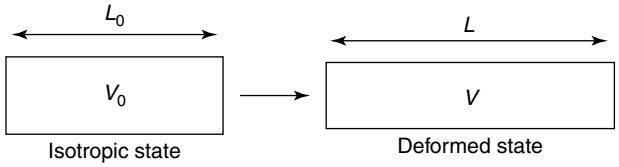

Fig. 12. Simple extension of an unswollen network prepared in the undiluted state (99). Courtesy of the American Chemical Society.

For a perfect network of functionality ϕ,

$$\xi = (1 - 2/\phi)\nu \tag{49}$$

Simple Extension. The most general case is an extension with change in sample volume, as illustrated in Figure 12. The strain along the direction of stretching is given by λ_x as

$$\lambda = \lambda_x = L/L_0 \tag{50}$$

Since the volume changes from V_0 to V,

$$\lambda_x \lambda_y \lambda_z = V/V_0 \tag{51}$$

Because there is symmetry about the x axis, $\lambda_y = \lambda_z$. Combining equations (50) and (51) leads to

$$\lambda_y = \lambda_z = (V/\lambda V_0)^{1/2} \tag{52}$$

The force f is the derivative of the free energy with respect to length; specifically,

$$f = \left(\frac{\partial \Delta A}{\partial L}\right)_{T,V} = (1/L_0)\left(\frac{\partial \Delta A}{\partial \lambda}\right)_{T,V} \tag{53}$$

Using equation (46),

$$f = (\nu kT/L_0)\left[\lambda - V/\left(V_0 \lambda^2\right)\right] \tag{54}$$

It is also possible to deduce the expression for the force as a function of the extension α measured relative to the length $L_v{}^i$ of the unstretched sample when its volume is fixed at the same volume V as occurs in the stretched state:

$$\alpha = L/L_v^i = \lambda L_0/L_v^i \tag{55}$$

and

$$L_0 = L_v^i (V/V_0)^{-1/3} \tag{56}$$

Equation (54) is then transformed to

$$f = \left(vkT/L_v^i\right)(V/V_0)^{2/3}(\alpha - 1/\alpha^2). \tag{57}$$

Energetic Contributions. Equation (57) can be used for the molecular interpretation of the ratio f_e/f. Thus, equation (43) can be rewritten as

$$f_e = f - T\left(\frac{\partial f}{\partial T}\right)_{V,L} = -fT\left(\frac{\partial \ln(f/T)}{\partial T}\right)_{V,L} \tag{58}$$

or

$$\frac{f_e}{f} = -T\left(\frac{\partial \ln(f/T)}{\partial T}\right)_{V,L} \tag{59}$$

The derivative of f at constant volume and length, thus at constant α, can be obtained from equation (57), with the result

$$f_e/f = (2/3)T(\mathrm{d}\ln V_0/\mathrm{d}T) = T\left(\mathrm{d}\ln \overline{r_0^2}/\mathrm{d}T\right) \tag{60}$$

since V_0 is the volume of the isotropic state so defined that the mean square of the magnitude of the chain vectors equals $\overline{r_0^2}$, the value for the free unperturbed chains.

The intramolecular energy changes arising from transitions of chains from one spatial configuration to another are, by equation (60), directly related to the temperature coefficient of the unperturbed dimensions. It is interesting to compare the thermoelastic results for polyethylene (128), $f_e/f = -0.45$, and poly(dimethylsiloxane) (129), $f_e/f = 0.25$. The preferred (lowest energy) conformation of the polyethylene chain is the all-trans form, since gauche states at rotational angles of $\pm 120^\circ$ cause steric repulsions between CH_2 groups (83). Since this conformation has the highest possible spatial extension, stretching a polyethylene chain requires switching some of the gauche states, which are, of course, present in the randomly coiled form, to the alternative trans states (106,130). These changes decrease the conformational energy and are the origin of the negative type of ideality represented in the experimental value of f_e/f. (This physical picture also explains the decrease in unperturbed dimensions upon increase in temperature. The additional energy causes an increase in the number of the higher energy gauche states, which are more compact than the trans ones.) The opposite behavior is observed in the case of poly(dimethylsiloxane) (26). The all-trans form is again the preferred conformation; the relatively long Si—O bonds and the unusually large Si—O—Si bond angles reduce steric repulsion in general, and the trans conformation places CH_3 side groups at distances of separation where they are strongly attractive (83,129,131). Because of the inequality of the Si—O—Si and O—Si—O bond angles, however, this conformation is of very low spatial extension. Stretching a poly(dimethylsiloxane) chain therefore requires an increase in the number of gauche states. Since these are of higher energy, this explains the fact that deviations from ideality for these networks are found to be positive (106,129,130).

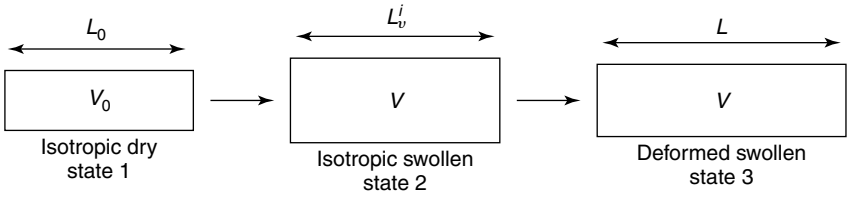

Fig. 13. Simple extension of a swollen network.

Simple Extension of Swollen Networks. The force required to deform an elastomeric sample, from state 2 to state 3 in Figure 13, is given by equation (57), in which $\alpha = L/L_v^i$ is the extension ratio for the isotropic swollen state relative to the deformed swollen state. The ratio V_0/V is the volume fraction v_2 of polymer in the swollen system, and A_0 is the cross-sectional area of the dry sample, which is generally measured before the experiment. The area of the swollen sample is given by

$$A_v^i = A_0(V/V_0)^{2/3} \tag{61}$$

Equation (56), of course, still holds, and $L_0A_0 = V_0$. In an experiment, the force f is measured as a function of elongation. Under these conditions,

$$f/A_0 = (\nu kT/L_0A_0)v_2^{-1/3}(\alpha - 1/\alpha^2) \tag{62}$$

Hence, the quantity $[f*] \equiv v_2^{1/3}/A_0(\alpha - 1/\alpha^2)$ should be a constant, independent of the degree of swelling, and be equal to $\nu kT/V_0$. As shown later $[f*]$ is commonly plotted versus $1/\alpha$ to determine deviations from theory (112,132,133).

Simple Extension of Networks Cross-linked in the Diluted State. The polymer is dissolved, cross-linked, and dried. The stress–strain measurements are carried out on the dry network, as illustrated in Figure 14. Equation (57) also holds for this case. If A_v^i is the cross-sectional area of the undeformed dry specimen, the force per unit undeformed area is

$$f/A_v^i = (\nu kT/V)(V/V_0)^{2/3}(\alpha - 1/\alpha^2) \tag{63}$$

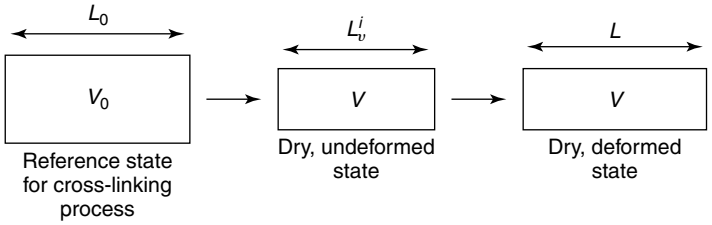

Fig. 14. Simple extension of an unswollen network cross-linked in the diluted state ($V_0 > V$).

which is $(V/V_0)^{2/3}$ times the tension of a network cross-linked in the dry state (111,134).

The Affine Shear Modulus. For $V = V_0$, equation (54) becomes

$$f/A_0 = (\nu kT/V_0)(\lambda - 1/\lambda^2) \tag{64}$$

Making use of equation (2) gives $\lambda = 1 + \epsilon$. For small values of ϵ, $\epsilon \ll 1$, equation (64) may be written as

$$f/A_0 = 3(\nu kT/V_0)\epsilon \tag{65}$$

The tensile modulus E_{aff} is three times the shear modulus G_{aff}, since Poisson's ratio for elastomers is close to 0.5. Specifically,

$$E_{\text{aff}} = 3\upsilon kT/V_0 = 3G_{\text{aff}} \tag{66}$$

and hence,

$$G_{\text{aff}} = \upsilon kT/V_0 \tag{67}$$

If υ/V_0 is the molar number density of chains [equal to ρ/M_{c} for a perfect network, where ρ is the elastomer density and M_{c} is the molecular weight between cross-link points (in g/mol)], then

$$G_{\text{aff}} = \upsilon RT/V_0 \tag{68}$$

where R is the gas constant. In the remaining material, υ is a molar quantity unless it is followed by the Boltzmann constant k.

For an affine perfect network,

$$G_{\text{aff}} = \rho RT/M_c \tag{69}$$

As a numerical example, the affine shear modulus of a perfect poly (dimethylsiloxane) tetrafunctional network of density $\rho = 0.97$ g/cm^3 and $M_{\text{c}} =$ 11,300 g/mol is $G_{\text{aff}} = 0.212 \times 10^6$ N/m^2. However, imperfections such as chain ends exist in typical networks, as illustrated in Figure 6. The following correction can be made to account for this circumstance (16). Before the cross-linking reaction, it is assumed that υ_{m} chains of length $\overline{M}_n$ are present in the melt, with $\upsilon_m = \rho/\overline{M}_n$. Each chain has two ends, thus there are $2\rho/\overline{M}_n$ chain ends. After the cross-linking process, there are υ_0 chains of length M_{c}, $\upsilon_0 = \rho/M_{\text{c}}$, along with the $2\rho/\overline{M}_n$ chain ends. Therefore the number of chains that are elastically effective is

$$\upsilon = \rho/M_{\text{c}} - 2\rho/\overline{M}_{\text{n}} = (\rho/M_{\text{c}})(1 - 2M_{\text{c}}/\overline{M}_{\text{n}}) \tag{70}$$

This correction is small for $M_c \ll \overline{M}_n$, which is frequently the case.

Phantom Networks. In this idealized model, chains may move freely through one another (135). Junctions fluctuate around their mean positions because of Brownian motion, and these fluctuations are independent of deformation. The mean square fluctuations $\overline{\Delta r^2}$ of the end-to-end distance r are related to the mean square of the end-to-end separation of the free unperturbed chains $\overline{r^2}$(102,136,137) by

$$\overline{\Delta r^2}/\overline{r^2}_0 = 2/\phi \tag{71}$$

The fluctuation range ($\overline{\Delta r^2} = \overline{r_0^2}/2$ for a tetrafunctional network) is generally quite large and of considerable importance. The instantaneous distribution of chain vectors $\boldsymbol{r}$ is not affine in the strain because it is the convolution of the distribution of the affine mean vector $\boldsymbol{r}$ with the distribution of the fluctuations $\Delta\boldsymbol{r}$, which are independent of the strain. The elastic free energy of such a network is

$$\Delta A_{\mathrm{el}}(\mathrm{ph}) = (1/2)\xi kT(I_1 - 3) = (1/2)(\nu - \mu)kT(I_1 - 3) \tag{72}$$

In simple extension, the equivalent of equation (62) is now

$$f/A_0 = (\nu - \mu)kTV_0^{-1}v_2^{-1/3}(\alpha - 1/\alpha^2) \tag{73}$$

and the shear modulus is given by

$$G_{\mathrm{ph}} = (\upsilon - \mu)RT/V_0 \tag{74}$$

For a perfect network of functionality ϕ, equation (49) holds, and therefore,

$$G_{\mathrm{ph}} = (1 - 2/\phi)\upsilon RT/V_0 \tag{75}$$

$$G_{\mathrm{ph}} = (1 - 2/\phi)\rho RT/M_{\mathrm{c}} \tag{76}$$

The relationship between affine and phantom moduli is then

$$G_{\mathrm{ph}} = (1 - 2/\phi)G_{\mathrm{aff}} \tag{77}$$

For example, G_{aff} is twice G_{ph} for a perfect tetrafunctional network.

Comparisons With Experimental Results. Stress–strain measurements in uniaxial extension can be compared with the prediction of an affine Gaussian network (eq. (64)), as illustrated in Figure 15 (113). The Gaussian relationship in the affine limit is valid only at small deformations. The best fit is obtained using $G_{\mathrm{aff}} = 0.39$ MN/m^2 (56.6 psi) (7); deviations occur when $\lambda > 1.5$. The experimental curve may nevertheless be well represented by adjusting the parameters of the non-Gaussian stress–strain relationship (eq. (45)) (84,117,138). These disagreements between experiments and the simple predictions of statistical mechanics have led some workers to develop a phenomenological theory of rubber-like elasticity.

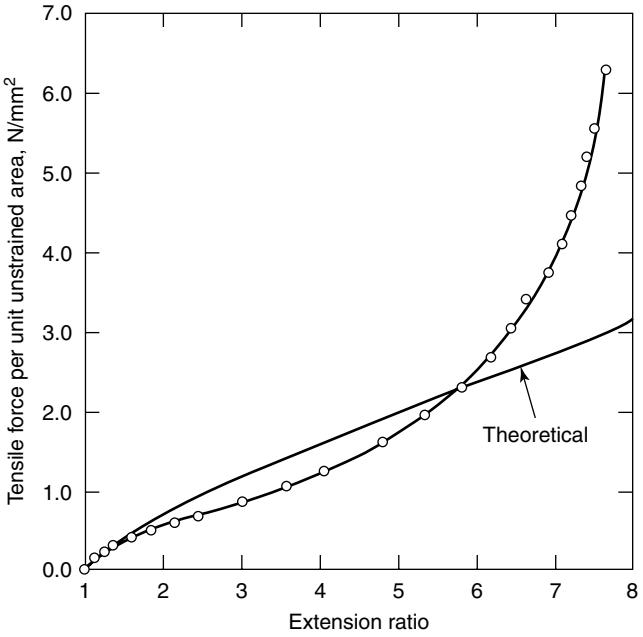

Fig. 15. Stress–strain isotherms in simple elongation; comparison of experimental curve (open circles) with theoretical prediction (eq. (64)) (113). To convert N/mm^2 to psi, multiply by 145. Courtesy of The Royal Society of Chemistry.

Phenomenological Theory. Continuum mechanics is used to describe mathematically the stress–strain relations of elastomers over a wide range in strain. This phenomenological treatment is not based on molecular concepts, but on representations of observed behavior (132,139–143). The main goal is to find an expression for the elastic energy W stored in the system (assumed to be perfectly elastic, isotropic in its undeformed state, and incompressible), analogous to the free energy of the statistical treatment. The condition of isotropy in the unstrained state requires that W be symmetrical with respect to the three principal extension ratios λ_x, λ_y, λ_z. A rotation of the material through 180°, ie, a change of sign of two of the λ_i ($i = x, y, z$), does not alter W (144). The three simplest even-powered functions satisfying these conditions are the strain invariants I_1, I_2, and I_3 defined as

$$I_1 = \lambda_x^2 + \lambda_y^2 + \lambda_z^2$$

$$I_2 = \lambda_x^2\lambda_y^2 + \lambda_y^2\lambda_z^2 + \lambda_z^2\lambda_x^2 \tag{78}$$

$$I_3 = \lambda_x^2\lambda_y^2\lambda_z^2$$

The most general form of the strain–energy function, which vanishes at zero strain, for an isotropic material is the power series

$$W = \sum_{i,j,k=0}^{\infty} C_{ijk}(I_1 - 3)^i (I_2 - 3)^j (I_3 - 1)^k \tag{79}$$

In equation (79), the experimental results obtained at sufficiently small strains are well represented with two nonzero terms, C_{100} and C_{010}:

$$W = C_{100}(I_1 - 3) + C_{010}(I_2 - 3) \tag{80}$$

In uniaxial extension, the so-called Mooney–Rivlin equation is obtained (17):

$$f\upsilon_2^{1/3}/A_0 = 2(C_1 + C_2/\alpha)(\alpha - 1/\alpha^2) \tag{81}$$

A convenient and standard way to treat stress–strain data is to plot the reduced force

$$[f*] \equiv f^* \upsilon_2^{1/3}/(\alpha - 1/\alpha^2) \tag{82}$$

versus $1/\alpha$, where $f*$ is the nominal stress f/A_0 and υ_2 the volume fraction of polymer in the network, if swollen (Fig. 16).

In this scheme, the affine and phantom networks are represented by horizontal lines (eqs. (62) and (73)) from equations $[f*] = \upsilon RT/V_0$ and $[f*] = (\upsilon - \mu)RT/V_0$, respectively. It has been reported that C_2 decreases as υ_2 decreases, whereas C_1 is approximately constant, as illustrated in Figure 16 (112). In view

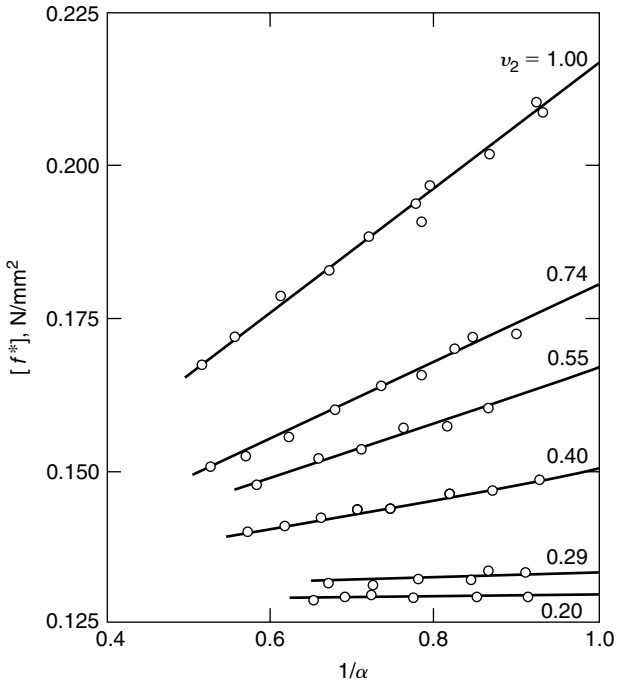

Fig. 16. Plot of $[f*]$ versus $1/\alpha$ for a natural rubber vulcanizate swollen in benzene to demonstrate the influence of υ_2 on C_2 (114). To convert N/mm^2 to psi, multiply by 145. Courtesy of The Royal Society of Chemistry.

of experimental results on swollen networks (69,114,145,146), the following form of the strain energy per unit volume of dry network is to be preferred:

$$W/V_0 = C_1(I_1 - 3) + C_2(I_2 I_3^{-1+m/2} - 3) \tag{83}$$

The reduced force can be deduced (145) as $[f*] = 2C_1 + 2C_2 v_2^{(4/3)-m} \alpha^{-1}$. The parameter C_1 of the swollen network is equal to C_1 of the dry network, whereas C_2 (swollen) is equal to C_2 (dry) $v_2^{(4/3)-m}$. Experimentally, m was found to be 0 or $\frac{1}{2}$ (145). The constant C_1 increases with the cross-linking density of the rubber (114,147), and $2C_1 + 2C_2$ is approximately the shear modulus at small deformation (148). Although there have been many attempts (149–155), a molecular explanation of C_1 and C_2 has been achieved only recently, as is described later.

The experimental error range is of great importance. A 1% error in the determination of λ has a tremendous effect on the Mooney curve when $1/\alpha > 0.9$; this part of the curve is therefore highly unreliable (156).

Statistical Theory of Real Networks. Affine and phantom networks are extreme limits. Stress–strain measurements in uniaxial extension have revealed that the behavior of real networks is between these limits. A theoretical attempt has been made to account for this dependence of $[f*]$ on $1/\alpha$ in terms of a gradual transition between the affine and phantom deformations (102,157), and a molecular theory has been formulated (102,158–161). In this model, the restrictions of junction fluctuations due to neighboring chains are represented by domains of constraints. At small deformations, the stress is enhanced relative to that exhibited by a phantom network. At large strains, or high dilation, the effects of restrictions on fluctuations vanish and the relationship of stress to strain converges to that for a phantom network. In a later theoretical refinement, the behavior of the network is taken to depend on two parameters. The most important is κ which measures the severity of entanglement constraints relative to those imposed by the phantom network. Another parameter ζ takes into account the nonaffine transformation of the domains of constraints with strain. Topological and mathematical treatment leads to the expression

$$[f*] = f_{\text{ph}}(1 + f_{\text{c}}/f_{\text{ph}}) \tag{84}$$

where f_{ph} is the usual phantom modulus and $f_{\text{c}}/f_{\text{ph}}$ is the ratio of the force due to entanglement constraints to that for the phantom network. A specific expression for $f_{\text{c}}/f_{\text{ph}}$ in uniaxial extension is

$$f_{\text{c}}/f_{\text{ph}} = (\mu/\xi)\left[\alpha K\left(\alpha_1^2\right) - \alpha^{-2} K\left(\alpha_2^2\right)\right]/(\alpha - 1/\alpha^2) \tag{85}$$

where $\alpha_1 = \alpha v_2^{-1/3}$, $\alpha_2 = \alpha^{-1/2} v_2^{-1/3}$, and μ/ξ is the ratio of the number of effective junctions to the cycle rank. For a perfect network, $\mu/\xi = 2/(\phi - 2)$. The function $K(x^2)$ is given by

$$K(x^2) = B[\dot{B}\,(B+1)^{-1} + g(\dot{g}\,B + g\,\dot{B})(gB+1)^{-1}] \tag{86}$$

with

$$g = x^2[1/\kappa + \zeta(x-1)]$$

$$\dot{g} = 1/\kappa - \zeta(1 - 3x/2)$$

$$B = (x-1)(1+x-\zeta x^2)/(1+g)^2$$

$$\dot{B} = B\left[(2x(x-1))^{-1} - 2\,\dot{g}\,(1+g)^{-1} + (1-2\zeta x)[2x(1+x-\zeta x^2)]^{-1}\right]$$

It is interesting to note that junction fluctuations increase in the direction of stretching but decrease in the direction perpendicular to it. Therefore the modulus decreases in the direction of stretching, but increases in the normal direction since the state of the network probed in this direction tends to be more nearly affine. The curve of $[f*]$ versus $1/\alpha$ is sigmoidal. The parameters κ and ζ of poly(dimethylsiloxane) networks are determined in Figure 17 (155); the intercept of the sigmoidal curves is the phantom modulus. This Flory–Erman theory has been compared successfully with such experiments in elongation and compression (155,162,162–166). It has not yet been extended to take account of limited chain extensibility or strain-induced crystallization (167).

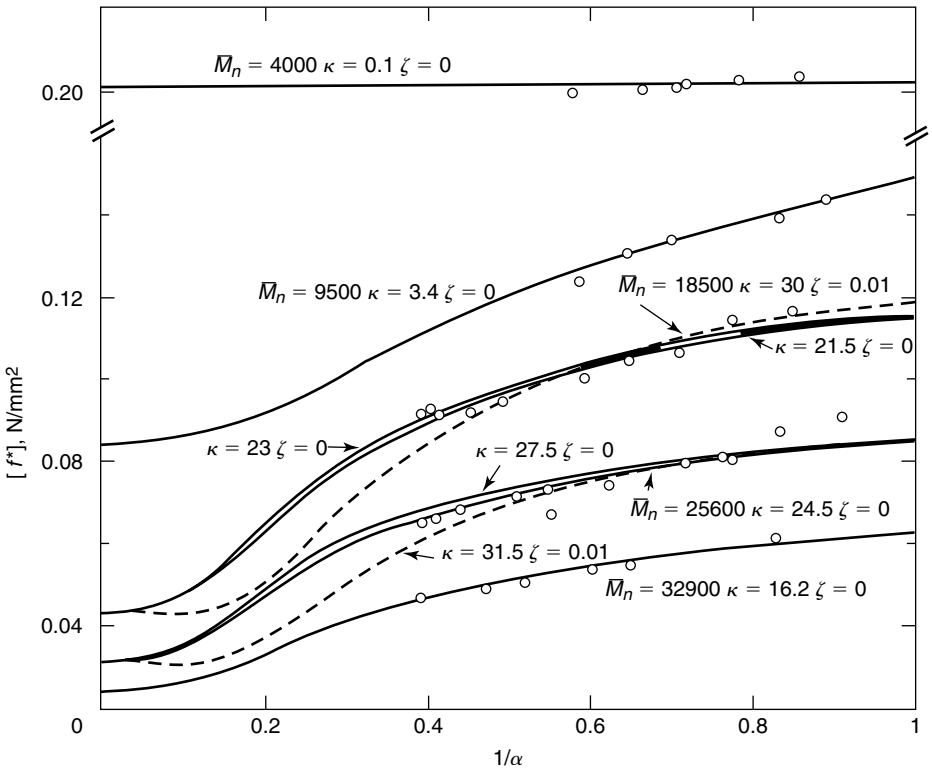

Fig. 17. Determination of the parameters κ and ζ of the Flory–Erman theory for perfect trifunctional poly(dimethylsiloxane) networks (155). To convert N/mm^2 to psi, multiply by 145. Courtesy of Springer-Verlag.

Predictions for the Parameters κ and ζ. The parameter ζ is not far from zero, which is to be expected since the surroundings of junctions cause their deformation to be nearly affine with the macroscopic strain. The primary parameter κ is defined as the ratio of the mean-square junction fluctuations in the equivalent phantom network, ie, in the absence of constraints, to the mean-square junction fluctuations about the centers of domains of entanglement constraints (in the absence of the network) in the isotropic state. Thus in a phantom network, the absence of constraints leads to $\kappa = 0$. In an affine one, the complete suppression of fluctuations is equivalent to $\kappa = \infty$. It has been proposed that κ should be proportional to the degree of interpenetration of chains and junctions (165). Since an increasing number of junctions in a volume pervaded by a chain leads to stronger constraints on these junctions, κ was taken to be

$$\kappa = I\left(\overline{r_0^2}\right)^{3/2}(\mu/V_0) \tag{87}$$

where I is a constant of proportionality, $(\overline{r_0^2})^{3/2}$ is assumed to be proportional to the volume occupied by a chain, and μ/V_0 is the number of junctions per unit volume. The mean-square unperturbed dimension $\overline{r_0^2}$ can be taken proportional to M_c (95), the molecular weight between cross-links, and μ/V_0 to M_c^{-1} for a perfect tetrafunctional network; therefore $\kappa \simeq M_c^{1/2}$ (93,155,165).

Swelling Equilibrium. The isotropic swelling of a cross-linked elastomer by a liquid has two important opposing effects: the increase in mixing entropy of the system because of the presence of the small molecules, and the decrease in configurational entropy of the network chains by dilation. Therefore, an equilibrium degree of swelling is established, which increases as the cross-linking density decreases (168–170). The free energy change ΔA for this process is usually assumed to be separable into the free energy of mixing, ΔA_m, and the elastic free energy ΔA_{el},

$$\Delta A = \Delta A_m + \Delta A_{el} \tag{88}$$

although questions have been raised with regard to this separability (171,172). The contribution ΔA_m has been calculated with the help of a lattice model (173, 174). The other contribution ΔA_{el} is given in the later Flory–Erman theory (161) by

$$\Delta A_{el} = \Delta A_{el}(\text{ph}) + \Delta A_c \tag{89}$$

where $\Delta A_{el}(\text{ph})$ is given by equation (72); ΔA_c is the additional term which accounts for the constraints and is given by

$$\Delta A_c = \mu kT/2 \sum_{i=x,y,z} \{[1 + g(\lambda_i)]B(\lambda_i) - \ln[(B(\lambda_i) + 1)(g(\lambda_i)B(\lambda_i) + 1)]\}. \tag{90}$$

The λ_i are the principal extension ratios, and g and B have been defined in equation (86).

The chemical potential of the solvent in the swollen network is

$$\mu_1 - \mu_1^0 = N\left(\frac{\partial \Delta A_{\mathrm{m}}}{\partial n_1}\right)_{T,p} + N\left(\frac{\partial \Delta A_{\mathrm{el}}}{\partial \lambda}\right)_{T,p}\left(\frac{\partial \lambda}{\partial n_1}\right)_{T,p} \tag{91}$$

where n_1 is the number of moles of solvent, and the isotropic extension ratio λ is

$$\lambda = \lambda_x = \lambda_y = \lambda_z = [(n_1 V_1 + V_0)/V_0]^{1/3} = v_2^{-1/3} \tag{92}$$

where V_1 is the molar volume of the solvent and V_0 the volume of the dry network. At swelling equilibrium, $\mu_1 = \mu_1^0$. Hence, the standard expression for ΔA_{m} (3) leads to

$$\ln(1 - v_{2m}) + v_{2m} + \chi v_{2m}^2 = -\left(\frac{\partial \Delta A_{\mathrm{el}}}{\partial \lambda}\right)_{T,p}\left(\frac{\partial \lambda}{\partial n_1}\right)_{T,p} (\mathrm{RT})^{-1} \tag{93}$$

where v_{2m} is the volume fraction of polymer at swelling equilibrium. The interaction parameter χ_1 may be determined, for example, by vapor pressure or by osmometry measurements (145,175–178). It depends on the concentration of polymer in the polymer–solvent system (175). Using the Flory–Erman expression for the elastic energy and assuming the parameter κ to be independent of swelling (isotropic swelling does not change the relative topology of the network), equation (93) (with the left-hand side abbreviated as H) becomes

$$H = -(\xi/V_0)V_1 v_{2m}^{1/3}\left[1 + (\mu/\xi)K\left(v_{2m}^{-2/3}\right)\right] \tag{94}$$

The molecular weight M_{c} between cross-links of a perfect network is then obtained by combination of equations (48),(49), and (94), with $v/V_0 = \rho/M_{\mathrm{c}}$:

$$M_{\mathrm{cr}} = (2/\phi - 1)\rho V_1 v_{2m}^{1/3}\left[1 + (\varphi/2 - 1)^{-1} K\left(V_1 v_{2m}^{-2/3}\right)\right]/H \tag{95}$$

where the subscript r is employed here for real networks.

For a network deforming affinely, $\kappa = \infty$, $K(\lambda^2) = 1 - \lambda^{-2}$, and

$$M_{\mathrm{ca}} = -\rho V_1 v_{2m}^{1/3}\left(1 - 2v_{2m}^{2/3}/\phi\right)\Big]/H \tag{96}$$

For a phantom network, $\kappa = 0$, $K(\lambda^2) = 0$, and

$$M_{\mathrm{cp}} = (2/\phi - 1)\rho V_1 v_{2m}^{1/3}/H \tag{97}$$

Determination of the Degree of Cross-linking by Stress–Strain Measurements and by Swelling Equilibrium

Characterization of network structures is often the main objective of theoretical and experimental works in the field of rubber elasticity (179–183). Simple experiments such as swelling equilibrium have been extensively used. However, most of the experimental swelling results on cross-linked polymers have been interpreted using the Flory–Rehner expression for an affinely deforming network (6,184–186).

The modern theory of real networks now permits a more accurate determination of network structures through use of equations (84),(87), and (95) (187–204). Stress–strain measurements can be analyzed as shown in Figure 17. The phantom modulus thus determined leads to ν and M_c through equations (75) and (76) (189). Swelling equilibrium data are similarly analyzed through equation (94), with the parameter κ given by equation (87) (189).

If M_c and κ have been determined previously from stress–strain measurements, then the interaction parameter χ_1 may be calculated through equation (95) (187,190).

Entanglements

Entanglements have been introduced in the later Flory–Erman theory as constraints that restrict junction fluctuations. Another viewpoint considers entanglements to act as physical cross-links, being based, in part, on the observation that linear polymers of high molecular weight exhibit a storage modulus $G'(\omega)$, which remains relatively constant over a wide range of frequencies ω (205). This plateau modulus G_N^0 is independent of chain length for long chains and is insensitive to temperature. Since it varies with the volume fraction of polymer in concentrated solutions, it could be due to pair-wise interactions between chains (20), and a universal law has been proposed for the dependence of G_N^0 on the chemical structure of the polymer (206). During the cross-linking process, some of such interactions or entanglements could be trapped in the network and act as physical junctions. This conclusion has been tested by irradiation cross-linking of already deformed networks (207–209), and then measuring the dimensional changes.

In the simplest phenomenological approach for rubber-like elasticity of trapped entanglements at small deformation (210,211), the shear modulus is taken to be the sum of two terms:

$$G = G_c + G_e T_e \tag{98}$$

where G_c is the contribution of the chemical cross-links. Taking into account the restrictions of junction fluctuations, as in the Flory theory, leads to

$$G_c = (\upsilon - h\mu)RT \tag{99}$$

in which the empirical parameter h was introduced (153). Its value, between 0 (affine) and 1 (phantom), characterizes the nature of the networks at small deformation; h can also be expressed as a function of the Flory parameters κ and ζ (155,212). The additional contribution $G_e T_e$ is said to arise from permanently trapped (interchain) entanglements in the network. The modulus G_e is thought to have a value close to G_N^0, and T_e, the "trapped entanglement factor," is the probability that all of the four directions from two randomly chosen points in the system, which may potentially contribute an entanglement, lead to the gel fraction.

The idea of entanglements acting as physical junctions was originally developed in the literature to explain deviations from the predictions for affine networks (185,213). The possibility of a contribution at equilibrium caused by trapped entanglements has been tested with model networks, ie, those prepared in such a way that the number and functionality of the cross-links are known. A

typical, highly specific reaction used for this purpose is the end-linking of functionally terminated polymer chains. Specific examples would be hydroxyl-terminated or vinyl-terminated chains of poly(dimethylsiloxane), $-[Si(CH_3)_2O]_x-$, end-linked with an organic silicate or silane (214,215). A considerable body of published data has, in fact, been interpreted as proving the existence of a trapped-entanglement contribution in this kind of network (216–222). Typically, the network characteristics, eg, number of chains and junctions, extent of cross-linking reaction p, trapped entanglement factor T_e, and effective functionality ϕ_e, were calculated by the branching theory after measurement of the network sol fraction. The main assumption of this probabilistic method is that the sol fraction, after subtraction of the amount of nonreactive species as determined by gel permeation chromatography analysis (218), is composed only of primary reactive chains (223). On the contrary, however, the sol fraction is a complicated mixture of reactive, unreactive, reacted, and unreacted molecules. For example, simulation of nonlinear polymerizations has shown that about half of the sol molecules are (reacted) cyclics (224). Their presence indicates that the value of the extent of the cross-linking reaction, formerly calculated with the assumption that the sol fraction is composed of nonreacted reagents, has to be significantly increased. As a result, many model networks can be considered as nearly perfect. This casts some doubt on the results interpreted as showing an entanglement contribution at equilibrium. If these networks are considered as perfect, such a contribution does not seem to be important (155,225). Entanglement contributions have been reported for polybutadiene (153) and ethylene–propylene copolymer (154) networks prepared by radiation-induced cross-linking. Again some doubt exists on the method used to characterize the network structure.

Molecular models treating entanglements as interstrand links that are free to slip along the strand contours have been developed (226–228) and tube models have been investigated (229,230). These approaches have been reviewed in Reference 27.

The question of entanglements is still controversial. It has been postulated (160) that an entanglement cannot be equivalent to a chemical cross-link. Contacts between a pair of entangled chains are transitory and of short duration owing to the diffusion of segments and associated time-dependent changes of configurations. Such trapped entanglements as previously described are possibly of minor importance in equilibrium stress measurements.

BIBLIOGRAPHY

"Elasticity, Rubber-like" in *EPSE* 2nd ed., Vol. 5, pp. 365–408, by J. P. Queslel and J. E. Mark, University of Cincinnati.

1. D. R. Lide, ed., *Handbook of Chemistry and Physics*, 62nd ed., CRC Press, Cleveland, Ohio, 1981–1982, p. F-91.
2. J. Gough, *Mem. Lit. Phil. Soc. Manchester 2nd Ser.* **1**, 288 (1805).
3. P. J. Flory, *Principles of Polymer Chemistry*, Cornell University Press, Ithaca, N.Y., 1953, p. 434.
4. Lord Kelvin, *Q. J. Math.* **1**, 57 (1857).
5. J. P. Joule, *Philos. Trans. R. Soc. London, Ser. A* **149**, 91 (1859).
6. Ref. 3, Chapt. "XI".

7. L. R. G. Treloar, *The Physics of Rubber Elasticity*, 3rd ed., Clarendon Press, Oxford, U.K., 1975.
8. A. V. Tobolsky, *Properties and Structure of Polymers*, John Wiley & Sons, Inc., New York, 1960.
9. F. Bueche, *Physical Properties of Polymers*, Wiley-Interscience, New York, 1962, pp. 37, 225.
10. A. R. Payne and J. R. Scott, *Engineering Design with Rubber*, MacLaren and Sons, London, 1960, p. 7.
11. D. J. Williams, *Polymer Science and Engineering*, Prentice-Hall, Englewood Cliffs, N.J., 1971, Chapt. "9".
12. A. N. Gent, B. Erman, and J. E. Mark, in J. E. Mark, B. Erman, and F. R. Eirich, eds., *Science and Technology of Rubber*, 2nd ed., Academic Press, Inc., New York, 1994, pp. 1, 189.
13. J. J. Aklonis and W. J. MacKnight, *Introduction to Polymer Viscoelasticity*, 2nd ed., John Wiley & Sons, Inc., New York, 1983, p. 102.
14. J. W. S. Hearle, *Polymers and Their Properties*, Vol. **1**, John Wiley & Sons, Inc., New York, 1982, p. 153.
15. P. Meares, *Polymers: Structure and Bulk Properties*, Van Nostrand Reinhold Co., Inc., New York, 1965, p. 160.
16. P. J. Flory, *Chem. Rev.* **35**, 51 (1944).
17. W. R. Krigbaum and R.-J. Roe, *Rubber Chem. Technol.* **38**, 1039 (1965).
18. K. Duek and W. Prins, *Adv. Polym. Sci.* **6**, 1 (1969).
19. K. J. Smith Jr. and R. J. Gaylord, *Rubber Age* **107**(6), 31 (1975).
20. W. W. Graessley, *Adv. Polym. Sci.* **16**, 1 (1974).
21. J. E. Mark, *J. Polym. Sci. Macromol. Rev.* **11**, 135 (1976).
22. R. G. C. Arridge, *Adv. Polym. Sci.* **46**, 67 (1982).
23. K. Duek, *Adv. Polym. Sci.* **44**, 164 (1982).
24. L. R. G. Treloar, *Rep. Prog. Phys.* **36**, 755 (1973).
25. J. E. Mark, *J. Educ. Mod. Mater. Sci. Eng.* **4**, 733 (1982).
26. J. E. Mark, *J. Chem. Educ.* **58**, 898 (1981).
27. B. E. Eichinger, *Ann. Rev. Phys. Chem.* **34**, 359 (1983).
28. M. C. Boyce and E. M. Arruda, *Rubber Chem. Technol.* **73**, 504 (2000).
29. K. J. Smith Jr., *Comprehensive Polymer Science*, 2nd supplement, Elsevier, Oxford, 1996.
30. O. H. Yeoh, *Comprehensive Polymer Science*, 2nd supplement, Elsevier, Oxford, 1996.
31. A. N. Gent, in A. N. Gent, ed., *Engineering with Rubber: How to Design Rubber Components*, Hanser, Munich, 1992, p. 33.
32. J. E. Mark, M. A. Sharaf, and B. Erman, in S. M. Aharoni, ed., *Synthesis, Characterization, and Theory of Polymeric Networks and Gels*, Plenum, New York, 1992.
33. A. Kloczkowski, J. E. Mark, and B. Erman, *Macromolecules* **28**, 5089 (1995).
34. J. E. Mark and B. Erman, in R. F. T. Stepto, ed., *Polymer Networks*, Blackie Academic Chapman and Hall, Glasgow, 1998.
35. B. Erman and J. E. Mark, in W. Brostow, ed., *Performance of Plastics*, Hanser, Munich, 2000.
36. J. E. Mark, in C. Carraher and C. Craver, eds., *Applied polymer Science—21st Century*, American Chemical Society, Washington, D.C., 2000.
37. R. P. Brown, *Elastomerics* **115**, 46 (1983).
38. L. E. Nielsen, *Mechanical Properties of Polymers and Composites*, Vol. **1**, Marcel Dekker, Inc., New York, 1974, pp. 5, 39.
39. D. W. van Krevelen, *Properties of Polymers: Correlations with Chemical Structure*, Elsevier, Amsterdam, 1972, p. 147.

40. F. S. Conant, in M. Morton, ed., *Rubber Technology*, Van Nostrand Reinhold Co., Inc., New York, 1973, p. 114.
41. P. G. Howgate, in C. Hepburn and R. J. W. Reynolds, eds., *Elastomers: Criteria for Engineering Design*, Applied Science, London, 1979, p. 127.
42. E. R. Praulitis, I. V. F. Viney, and D. C. Wright, in Ref. 41, p. 139.
43. Ref. 10, pp. 123, 225.
44. Ref. 15, p. 179.
45. S Standards, Rubber, Natural and Synthetic—General Test Methods, and Materialscos Part 09:01, *American Society for Testing and Materials*, Philadelphia, Pa.
46. W. K. Moonan and N. W. Tschoegl, *Macromolecules* **16**, 55 (1983).
47. O. Posfalvi, *Kautsch. Gummi Kunstst*. **35**, 940 (1982); L. M. Boiko, *Ind. Lab.* **49**, 538 (1983).
48. E. Galli, *Plast. Compounding* **5**, 14 (1982).
49. T. L. Smith, *Polym. Eng. Sci.* **17**, 129 (1977).
50. R. R. Rahalkar, C. U. Yu, and J. E. Mark, *Rubber Chem. Technol.* **51**, 45 (1978).
51. A. L. Andrady and co-workers, *J. Appl. Polym. Sci.* **26**, 1829 (1981).
52. A. J. Chompff and S. Newman, eds., *Polymer Networks: Structural and Mechanical Properties*, Plenum Press, New York, 1971, pp. 111, 193.
53. M. C. Shen, D. A. McQuarrie, and J. L. Jackson, *J. Appl. Phys.* **38**, 791 (1967).
54. Ref. 13, p. 29.
55. W. O. Murtland, *Elastomerics* **114**, 19 (1982).
56. A. Whelan and K. S. Lee, eds., *Development in Rubber Technology—3 Thermoplastic Rubbers*, Applied Science Publishers, London, 1982.
57. D. S. Pearson and W. W. Graessley, *Macromolecules* **11**, 528 (1978).
58. P. J. Flory, *Macromolecules* **15**, 99 (1982).
59. L. C. Case and R. V. Wargin, *Makromol. Chem.* **77**, 172 (1964).
60. J. Scanlan, *J. Polym. Sci.* **43**, 501 (1960).
61. L. C. Case, *J. Polym. Sci.* **45**, 397 (1960).
62. Ref. 10, p. 15.
63. Ref. 40, p. 7.
64. L. K. Nash, *Elements of Classical and Statistical Thermodynamics*, Addison-Wesley, Reading, Mass., 1970.
65. Ref. 6, p. 399.
66. Ref. 13, p. 85.
67. P. G. De Gennes, *Scaling Concepts in Polymer Physics*, Cornell University Press, Ithaca, N.Y., 1979, p. 29.
68. P. J. Flory, *Pure Appl. Chem.* **52**, 241 (1980).
69. G. Gee, *Polymer* **7**, 373 (1966).
70. A. V. Tobolsky, D. W. Carlson, and N. Indictor, *J. Polym. Sci.* **54**, 175 (1961).
71. T. L. Hill, *An Introduction to Statistical Thermodynamics*, Addison-Wesley, Reading, Mass., 1962, p. 214.
72. F. A. Bovey, *Chain Structure and Conformation of Macromolecules*, Academic Press, Inc., New York, 1982, p. 185.
73. F. T. Wall, *J. Chem. Phys.* **11**, 67 (1943).
74. H. Eyring, *Phys. Rev.* **39**, 746 (1932).
75. P. Debye, *J. Chem. Phys.* **14**, 636 (1946).
76. B. H. Zimm and W. H. Stockmayer, *J. Chem. Phys.* **17**, 1301 (1949).
77. S. Chandrasekhar, *Rev. Mod. Phys.* **15**, 1 (1943).
78. W. Kuhn, *Kolloid Z.* **68**, 2 (1934).
79. E. Guth and H. Mark, *Monatsh. Chem.* **65**, 93 (1934).
80. M. V. Volkenshtein, *Configurational Statistics of Polymeric Chains*, Wiley-Interscience, New York, 1963.

81. Ref. 13, p. 90.
82. Lord Rayleigh, *Philos. Mag.* **37**, 321 (1919).
83. P. J. Flory, *Statistical Mechanics of Chain Molecules*, Wiley-Interscience, New York, 1969.
84. M. C. Wang and E. Guth, *J. Chem. Phys.* **20**, 1144 (1952).
85. W. Kuhn and F. Grun, *Kolloid Z.* **101**, 248 (1942).
86. H. M. James and E. Guth, *J. Chem. Phys.* **11**, 470 (1943).
87. W. Kuhn, *Kolloid Z.* **76**, 256 (1936).
88. W. Kuhn, *Kolloid Z.* **87**, 3 (1939).
89. R. A. Jacobson, *J. Am. Chem. Soc.* **54**, 1513 (1932).
90. W. H. Hunter and G. H. Woollett, *J. Am. Chem. Soc.* **43**, 135 (1921).
91. J. Brandrup and E. H. Immergut, eds., *Polymer Handbook, Part IV*, Wiley-Interscience, New York, (1975), p. 1.
92. R. Ullman in J. E. Mark and J. Lal, eds., *Elastomers and Rubber Elasticity*, ACS, Washington, D.C., (1982), p. 257.
93. R. Ullman, *Macromolecules* **15**, 1395 (1982).
94. H. Benoît and co-workers, *J. Polym. Sci. Polym. Phys. Ed.* **14**, 2119 (1976).
95. M. Beltzung and co-workers, *Macromolecules* **15**, 1594 (1982).
96. M. Beltzung, J. Herz, and C. Picot, *Macromolecules* **16**, 580 (1983).
97. S. Candau, J. Bastide, and M. Delsanti, *Adv. Polym. Sci.* **44**, 27 (1982).
98. Ref. 52, pp. 23, 47.
99. R. L. Anthony, R. H. Caston, and E. Guth, *J. Phys. Chem.* **46**, 826 (1942).
100. K. J. Smith Jr., A. Greene, and A. Ciferri, *Kolloid Z.* **194**, 49 (1964).
101. U. Bianchi and E. Pedemonte, *J. Polym. Sci. Part A* **2**, 5039 (1964); G. Allen, U. Bianchi, and C. Price, *Trans. Faraday Soc. Part II* **59**, 2493 (1963); J. Bashaw and K. J. Smith Jr., *J. Polym. Sci. Part A-2* **6**, 1041 (1968); Yu. K. Godovsky, *Polymer* **22**, 75 (1981).
102. P. J. Flory, *Proc. R. Soc. London, Ser. A* **351**, 351 (1976).
103. Ref. 11, p. 261.
104. Ref. 6, p. 489.
105. Ref. 11, p. 263.
106. J. E. Mark, *Rubber Chem. Technol.* **46**, 593 (1973).
107. P. J. Flory and J. Rehner, *J. Chem. Phys.* **11**, 512, 521 (1943).
108. F. T. Wall, *J. Chem. Phys.* **10**, 485 (1942).
109. L. R. G. Treloar, *Trans. Faraday Soc.* **39**, 36, 241 (1943).
110. J. E. Mark, *J. Am. Chem. Soc.* **92**, 7252 (1970).
111. R. M. Johnson and J. E. Mark, *Macromolecules* **5**, 41 (1972).
112. C. U. Yu and J. E. Mark, *Macromolecules* **6**, 751 (1973).
113. L. R. G. Treloar, *Trans. Faraday Soc.* **40**, 59 (1944).
114. S. M. Gumbrell, L. Mullins, and R. S. Rivlin, *Trans. Faraday Soc.* **49**, 1495 (1953).
115. A. N. Gent and V. V. Vickroy, *J. Polym. Sci. Part A2* **5**, 47 (1967).
116. A. L. Andrady, M. A. Llorente, and J. E. Mark, *J. Chem. Phys.* **72**, 2282 (1980).
117. L. R. G. Treloar and G. Riding *Proc. R. Soc. London, Ser. A* **369**, 261 (1979).
118. W. Kuhn and F. Grün, *J. Polym. Sci.* **1**, 3 (1946).
119. L. R. G. Treloar, *Trans. Faraday Soc.* **43**, 277, 284 (1947).
120. R. G. Morgan and L. R. G. Treloar, *J. Polym. Sci. Part A-2* **10**, 51 (1972).
121. D. Y. Yoon and P. J. Flory, *J. Chem. Phys.* **61**, 5366 (1974).
122. P. J. Flory and V. W. C. Chang, *Macromolecules* **9**, 33 (1976).
123. J. C. Conrad and P. J. Flory, *Macromolecules* **9**, 41 (1976).
124. J. E. Mark and J. G. Curro, in R. A. Dickie and S. S. Labana, eds., *Characterization of Highly Cross-Linked Polymers*, American Chemical Society, Washington, D.C., 1983.
125. P. J. Flory, *Pure Appl. Chem. Macromol. Chem.* **33**(Suppl. 8), 1 (1973).

126. P. J. Flory, *Rubber Chem. Technol.* **41**, 641 (1968).
127. F. Harari, *Graph Theory*, Addison-Wesley, Reading, Mass., 1971.
128. A. Ciferri, C. A. J. Hoeve, and P. J. Flory, *J. Am. Chem. Soc.* **83**, 1015 (1961).
129. J. E. Mark and P. J. Flory, *J. Am. Chem. Soc.* **86**, 138 (1964).
130. J. E. Mark, *Macromol. Rev.* **11**, 135 (1976).
131. J. E. Mark, *J. Chem. Phys.* **49**, 1398 (1968).
132. M. Mooney, *J. Appl. Phys.* **11**, 582 (1940).
133. D. S. Chiu, T.-K. Su, and J. E. Mark, *Macromolecules* **10**, 1110 (1977).
134. M. A. Llorente and J. E. Mark, *J. Chem. Phys.* **71**, 682 (1979).
135. H. M. James and E. Guth, *J. Chem. Phys.* **15**, 669 (1947).
136. B. E. Eichinger, *Macromolecules*, **5**, 496 (1972).
137. W. W. Graessley, *Macromolecules* **8**, 865 (1975).
138. L. R. G. Treloar, *Trans. Faraday Soc.* **50**, 881 (1954).
139. Ref. 7, p. 211.
140. Ref. 13, p. 123.
141. P. J. Blatz, S. C. Sharda, and N. W. Tschoegl, *Trans. Soc. Rheol.* **18**, 145 (1974).
142. R. W. Ogden, *Proc. R. Soc. London, Ser. A* **326**, 565 (1972).
143. K. Tobish, *Colloid Poly. Sci.* **257**, 927 (1979).
144. R. S. Rivlin, *Philos. Trans. R. Soc., Ser. A* **241**, 379 (1948).
145. P. J. Flory and Y. Tatara, *J. Polym. Sci., Polym. Phys. Ed.* **13**, 683 (1975).
146. L. Mullins, *J. Appl. Polym. Sci.* **2**, 257 (1959).
147. J. E. Mark, *Rubber Chem. Technol.* **48**, 495 (1975).
148. B. Erman, W. Wagner, and P. J. Flory, *Macromolecules* **13**, 1554 (1980).
149. W. J. Bobear, *Rubber Chem. Technol.* **40**, 1560 (1967).
150. D. R. Brown, *J. Polym. Sci., Polym. Phys. Ed.* **20**, 1659 (1982).
151. R. L. Carpenter, O. Kramer, and J. D. Ferry, *Macromolecules* **10**, 117 (1977).
152. J. D. Ferry and H. C. Kan, *Rubber Chem. Technol.* **51**, 731 (1978).
153. L. M. Dossin and W. W. Graessley, *Macromolecules* **12**, 123 (1979).
154. D. S. Pearson and W. W. Graessley, *Macromolecules* **13**, 1001 (1980).
155. J. P. Queslel and J. E. Mark, *Adv. Polym. Sci.* **65**, 135 (1984).
156. Ref. 13, p. 126.
157. G. Ronca and G. Allegra, *J. Chem. Phys.* **63**, 4990 (1975).
158. P. J. Flory, *J. Chem. Phys.* **66**, 5720 (1977).
159. B. Erman and P. J. Flory, *J. Chem. Phys.* **68**, 5363 (1978).
160. P. J. Flory, *Polymer* **20**, 1317 (1979).
161. P. J. Flory and B. Erman, *Macromolecules* **15**, 800 (1982).
162. B. Erman and P. J. Flory, *J. Polym. Sci., Polym. Phys. Ed.* **16**, 1115 (1978).
163. H. Pak and P. J. Flory, *J. Polym. Sci., Polym. Phys. Ed.* **17**, 1845 (1979).
164. B. Erman, *J. Polym. Sci., Polym. Phys. Ed.* **19**, 829 (1981).
165. B. Erman and P. J. Flory, *Macromolecules* **15**, 806 (1982).
166. B. Erman, *J. Polym. Sci., Polym. Phys. Ed.* **21**, 893 (1983).
167. L. R. G. Treloar, *Br. Polym. J.* **14**, 121 (1982).
168. Ref. 7, p. 128.
169. J. P. Queslel and J. E. Mark, *Polym. Bull.* **10**, 119 (1983).
170. G. Rehage, *Rubber Chem. Technol.* **39**, 651 (1966).
171. R. W. Brotzman and B. E. Eichinger, *Macromolecules* **15**, 531 (1982).
172. R. W. Brotzman and B. E. Eichinger, *Macromolecules* **16**, 1131 (1983).
173. Ref. 6, pp. 495, 541.
174. P. J. Flory, *J. Chem. Phys.* **10**, 51 (1942).
175. B. E. Eichinger and P. J. Flory, *Trans. Faraday Soc.* **64**, 2035, 2053, 2061, 2066 (1968).
176. P. J. Flory and H. Daoust, *J. Polym. Sci.* **25**, 429 (1957).
177. W. R. Krigbaum and P. J. Flory, *J. Am. Chem. Soc.* **75**, 1775 (1953).

178. C. H. Baker and co-workers, *Polymer* **3**, 215 (1962).
179. B. Erman and J. E. Mark, *Structures and Properties of Rubber-like Networks*, Oxford University Press, New York, 1997.
180. J. E. Mark and B. Erman, *Rubber-like Elasticity: A Molecular Primer*, Wiley-Interscience, New York, 1988.
181. J. E. Mark and B. Erman, *Elastomeric Polymer Networks*, Prentice Hall, Englewoods Cliffs, N.J., 1992.
182. J. E. Mark and co-workers, *Physical Properties of Polymers*, American Chemical Society, Washington, D.C., 1993.
183. L. H. Sperling, *Introduction to Physical Polymer Science*, 2nd ed., Wiley-Interscience, New York, 1992.
184. L. A. Woods, *J. Res. Nat. Bur. Stand. Sect. A* **80**, 451 (1976).
185. G. C. Moore and W. F. Watson, *J. Polym. Sci.* **19**, 237 (1956).
186. B. Ellis and G. N. Welding, *Rubber Chem. Technol.* **37**, 571 (1964).
187. B. Erman and P. J. Flory, *Macromolecules* **16**, 1607 (1983).
188. J. P. Queslel and J. E. Mark, *Adv. Polym. Sci.* **71**, 229 (1985).
189. J. P. Queslel, *Rubber Chem. Technol.* **62**, 800 (1989).
190. J. P. Queslel and J. E. Mark, *Rubber Chem. Technol.* **63**, 46 (1990).
191. J. P. Queslel and J. E. Mark, *J. Chem. Phys.* **82**, 3449 (1985).
192. B. Erman and L. Monnerie, *Macromolecules* **22**, 3342 (1989).
193. J. P. Queslel and J. E. Mark, *Eur. Polym. J.* **22**, 273 (1986).
194. J. P. Queslel and L. Monnerie, *Makromol. Chem., Macromol. Symp.* **30**, 145 (1989).
195. J. P. Queslel, F. Fontaine, and L. Monnerie, *Polymer* **29**, 1086 (1988).
196. B. Erman and J. E. Mark, *Macromolecules* **20**, 2892 (1987).
197. J. P. Queslel, P. Thirion, and L. Monnerie, *Polymer* **27**, 1869 (1986).
198. L. Y. Shy and B. E. Eichinger, *Macromolecules* **19**, 2787 (1986).
199. M. A. Sharat, A. Kloczkowski, and J. E. Mark, *Comput. Theor. Polym. Sci.* **11**, 251 (2001).
200. J. P. Queslel and J. E. Mark, *J. Chem. Educ.* **64**, 491 (1987).
201. I. Bahar and B. Erman, *Macromolecules* **20**, 1696 (1987).
202. J. P. Queslel and J. E. Mark, *Polym. J.* **18**, 263 (1986).
203. M. A. Sharaf and co-workers, *Comput. Polym. Sci.* **2**, 84 (1992).
204. J. E. Mark and B. Erman, *Comput. Polym. Sci.* **5**, 37 (1995).
205. J. D. Ferry, *Viscoelastic Properties of Polymers*, 2nd ed., John Wiley & Sons, Inc., New York, 1970.
206. W. W. Graessley and S. F. Edwards, *Polymer* **22**, 1329 (1981).
207. R. L. Carpenter, H. C. Kan, and J. D. Ferry, *Polym. Eng. Sci.* **19**, 266 (1979).
208. W. Batsberg and O. Kramer, *J. Chem. Phys.* **74**, 6507 (1981).
209. S. Granick and J. D. Ferry, *Macromolecules* **16**, 39 (1983).
210. N. R. Langley, *Macromolecules* **1**, 348 (1968).
211. N. R. Langley and K. E. Polmanteer, *J. Polym. Sci., Polym. Phys. Ed.* **12**, 1023 (1974).
212. M. Gottlieb, *J. Chem. Phys.* **77**, 4783 (1982).
213. B. M. E. van der Hoff and E. J. Buckler, *J. Macromol. Sci. Chem.* **1**, 747 (1967).
214. J. E. Mark, *Rubber Chem. Technol.* **54**, 809 (1981).
215. J. E. Mark, *Adv. Polym. Sci.* **44**, 1 (1982).
216. M. Gottlieb and co-workers, *Macromolecules* **14**, 1039 (1981).
217. M. Gottlieb, C. W. Macosko, and T. C. Lepsch, *J. Polym. Sci., Polym. Phys. Ed.* **19**, 1603 (1981).
218. C. W. Macosko and G. S. Benjamin, *Pure Appl. Chem.* **53**, 1505 (1981).
219. K. O. Meyers, M. L. Bye, and E. W. Merrill, *Macromolecules* **13**, 1045 (1980).
220. K. A. Kirk and co-workers, *Macromolecules* **15**, 1123 (1982).
221. E. M. Valles and C. W. Macosko, *Macromolecules* **12**, 673 (1979).

222. E. M. Valles and C. W. Macosko, *Rubber Chem. Technol.* **49**, 1232 (1976).
223. D. R. Miller and C. W. Macosko, *Macromolecules* **9**, 206 (1976).
224. Y. K. Leung and B. E. Eichinger, *Prepr. Div. Polym. Mater.* **48**, 440 (1983).
225. J. P. Queslel and J. E. Mark, *J. Polym. Sci., Polym. Phys. Ed.* **22**, 1201 (1984).
226. W. W. Graessley and D. S. Pearson, *J. Chem. Phys.* **66**, 3363 (1977).
227. W. W. Graessley, *Adv. Polym. Sci.* **47**, 67 (1982).
228. R. C. Ball and co-workers, *Polymer* **22**, 1011 (1981).
229. R. J. Gaylord, *Polym. Bull.* **8**, 325 (1982).
230. G. Marrucci, *Macromolecules* **14**, 434 (1981).

J. P. QUESLEL
Manufacture Michelin, CERL – GPA
J. E. MARK
University of Cincinnati

ELECTRONIC PACKAGING

Introduction

Organic polymers are widely used as structural materials and as processing aids in the electronics industry. The widespread use of polymeric materials in electronics is due to the ease in which desired engineering properties can be designed into materials by the manipulation of polymer structures and formulary compositions. In addition, the wide range of fabrication processes by which polymers can be formed into finished articles and the frequently lower fabrication costs of polymers compared to metals or ceramics have contributed to ubiquitous use of polymers in electronic assemblies.

The Electronic Packaging Hierarchy. Electronic packaging is broadly defined as the physical interconnection of electronic and electromechanical components to provide an enclosed system that provides for power and signal distribution, allows heat dissipation, and protects the components from the environment (1). Efficient construction and configuration of an electronic system is obtained through the packaging hierarchy (1) shown in Figure 1.

The first level of assembly begins with assembling one or more integrated semiconductor devices or "chips," each of which may contain millions of transistors fabricated in multiple layers of active devices, insulating layers, and metal interconnection layers (2), into a discrete module or *first level package*. The goals of first level packaging are to provide reliable electrical connections between the devices on one or more chips and the external metal conductors on the package, protect the delicate chip from the environment, and provide electrical and mechanical connection to the next level of assembly. High humidity, salts, certain gases such as the oxides of nitrogen and sulfur, radiation, static electrical discharges, and mechanical shock are all common environmental stresses that are harmful to

Encyclopedia of Polymer Science and Technology. Copyright John Wiley & Sons, Inc. All rights reserved.

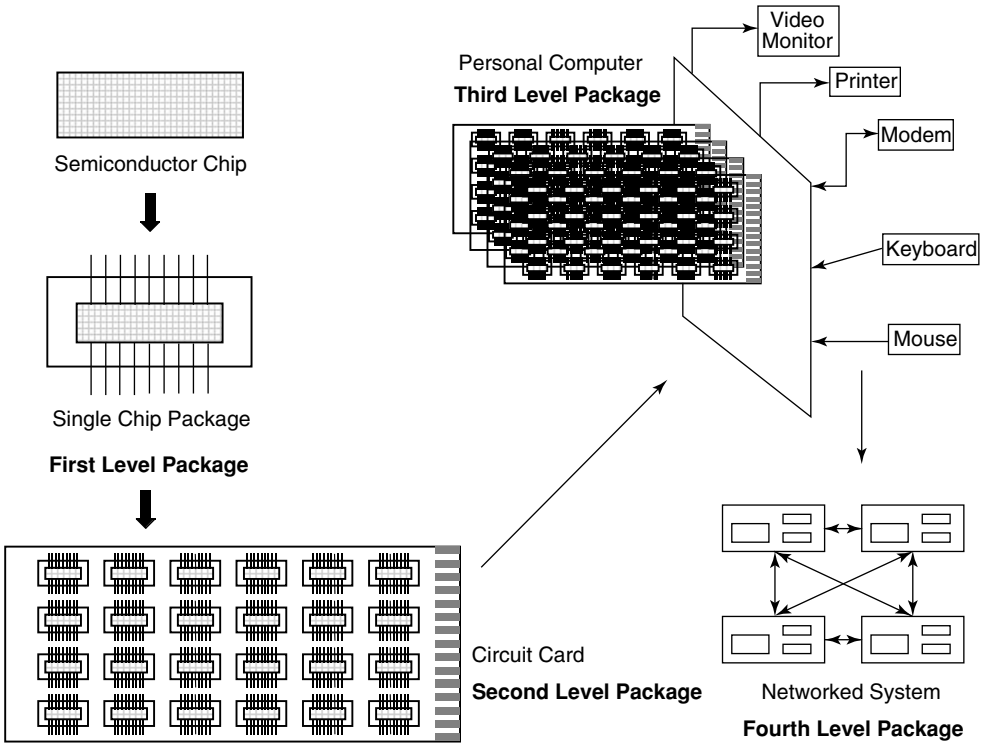

Fig. 1. The electronic packaging assembly hierarchy.

integrated circuits. First level packages are attached to a substrate or *second level package* bearing metal conductors that provide interconnections between the first level components. The most familiar example of second level packages is the ubiquitous fiber glass-epoxy laminate circuit board found in a wide range of consumer electronics and computer systems. Second level packages often have a defined, modular function such as memory cards, disk drive controller cards, and video cards. In other instances, the second level package is a system and is mounted in a protective case to produce a modular component that is used directly, for example, an automotive ignition module or the electronics of a consumer product such as a cellular telephone. A group of second level packages are frequently assembled on a larger card, termed a "motherboard" or "backplane" and the resulting assembly is housed in a cabinet or case. This assembly produces a *third level package* that provides electrical interconnection between cards and other board or cabinet mounted components such as power supplies and disk drives and provides connectivity to input devices, such as a keyboard and mouse, to output devices, such as printers and video monitors, and to input–output devices such as modems. An easily recognizable third level package is a personal computer. *Fourth level packages* are obtained through interconnection of third level systems to provide more complex systems such as the familiar office network or large mainframe computer system.

Electronic packaging makes use of a wide variety of polymer material classes to fulfill a diverse range of engineering uses. Table 1 provides a segmentation

of commonly used polymeric materials by engineering use and polymer class (3,4).

Polymers in First Level Packages

One of the most common and recognizable first level packages is the plastic dual in-line package (DIP) as shown in Figure 2. This package provides a convenient case example for further discussion of the polymers and polymer processing used in first level electronic packaging.

The sequential assembly (Fig. 3) of a DIP (1) begins by attaching the chip, which often bears a top-side polymeric passivation or *stress buffer coating*, to a metal lead frame substrate by using a *die attach adhesive* formulation. A linear array of aluminum alloy contacts or bond pads are arranged along the periphery of the chip. Typical bond pads are squares with dimensions in the 50–200 μm range and are the termini for the internal chip wiring. The bond pads are connected to contact points on the lead frame by 25–50 mm diameter gold or aluminum wire using ultrasonic, thermocompression, or thermosonic bonding (5). The wire-bonded lead frame-chip assemblies are then loaded into cavity molds and a molten, *encapsulation resin* composition is transferred into the mold under heat and pressure. Assembly is completed by applying lead finish plating, marking component identifying information on the package, singulating the packages, forming the leads into the required geometry by precision bending, and final packing for shipment to the second level package assembler. The single-chip plastic package appears in a variety of sizes and pin counts, depending upon the chip size, the number of leads required to connect the chip, and the amount of space allocated on the circuit board for the package (Fig. 4). For example, the DIP was designed for insertion into plated-through holes on a circuit board while the

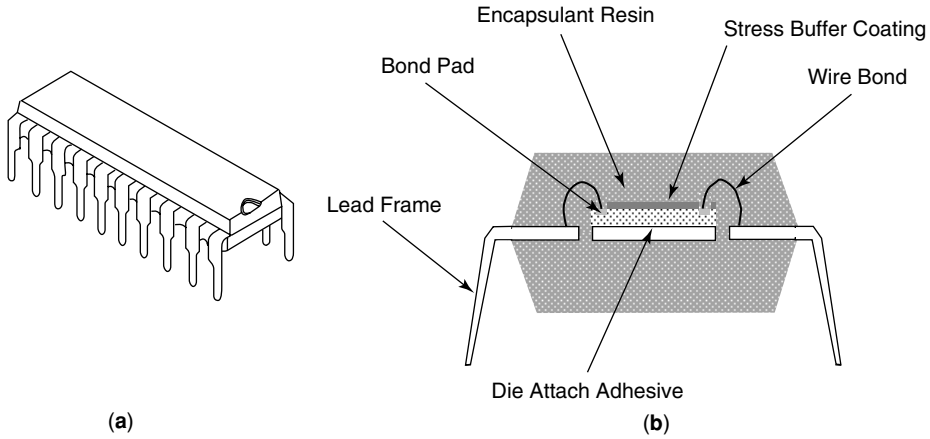

Fig. 2. (**a**) An exterior view line drawing of a DIP (1). (**b**) A schematic cross section of a DIP showing the components of construction.

Table 1. Polymeric Materials Used in Electronic Packaging Segmented by Engineering Use and Polymer Class[a]

Engineering use	Polymer class
Adhesive	Acrylic
	Epoxy silicone
	Epoxy novalac
	Epoxy bisphenol A
	Epoxy polyimide
	Epoxy polyurethane
	Polyimide
	Silicones
Encapsulation	Polyetherketone
	Polyetheretherketone
	Polysulfone
	Polyethersulfone
	Polyester
	Epoxy and filled epoxy
	Silicones and filled silicones
Substrate	Bis-maleimide triazine (BT) resin
	BT-Epoxy E-glass laminate
	Epoxy-E-glass laminate
	Polyimide-E-glass laminate
	Poly(tetrafluoroethylene)-E-glass laminate
	Polyimide-E-glass laminate
	Polyester film
	Polyimide film
	Poly(tetrafluoroethylene) film
	Polyamide film
	Poly(vinyl chloride) film
	Poly(vinyl fluoride) film
	Polyethylene film
	Polypropylene film
	Polycarbonate film
	Polysulfone film
	Poly(parabanic acid) film
	Poly(ethersulfone) film
Stress buffer coating	Poly(amide-imide)
	Poly(benzocyclobutene)–BCB
	Polybenzoxazole
	Polyimide
	RTV Silicone
Interlayer dielectric	Poly(benzocyclobutene)–BCB
	Polybenzoxazole
	Polyimide
	Poly(norbornene)
	Triazine blend resin

[a]From Refs. 3 and 4.

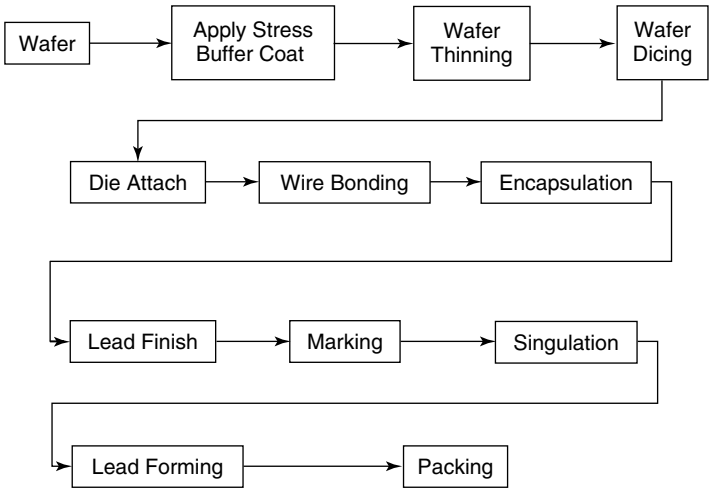

Fig. 3. Assembly sequence for plastic packages.

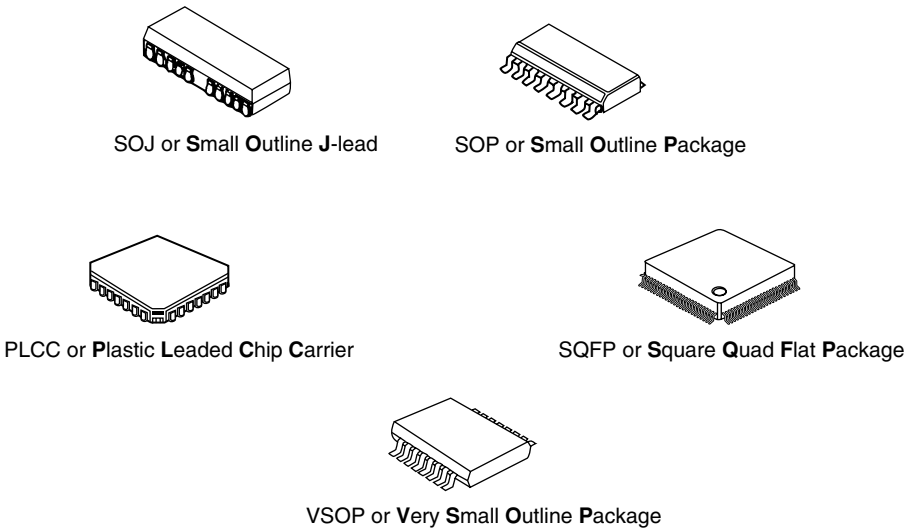

Fig. 4. Exterior view line drawings showing other types of plastic packages. From Ref. 7, with permission.

packages shown in Figure 4 were designed for surface mounting to a circuit board. Surface mounting technology, or SMT, allows internal board space to be used for routing connections and reduces the board size by eliminating the space needed for the plated-through holes. Package size reduction is a major industry trend and is driven by the space constraints imposed by personal electronic products such as cellular phones, laptop computers, and personal digital assistants. This trend has resulted in the recent development of several new package types with the

goal of obtaining package geometries that are as close as possible to the size of the chip itself. These technologies are collectively know as chip scale packaging or CSP (6).

Stress Buffer Coatings. The top or device surface of semiconductor chips is frequently coated with a polymeric passivation coating that acts as a protective stress buffer layer (Fig. 2b). While stress buffer coatings (SBCs) are applied in the last steps of the wafer fabrication process, they have been shown to provide several important benefits to packaged device yield and reliability (8–10) and are considered herein as packaging materials. The SBC protects the chip from mechanical damage during package assembly and provides a relatively soft and ductile material on the chip that prevents chip cracking from the shear stresses that occur during encapsulant molding. The SBC also provides a mechanism for distributing stress over the surface of the chip and greatly reduces chip failures due to locally high stresses. Shear stress at the chip surface can cause movement or sliding of the underlying metal lines chip, cracking in silicon oxide and silicon nitride passivation layers, and parametric shifts in the electrical characteristics of the chip (8). The incidence of stress-related failure modes are frequently higher in larger chips and packages because of the larger distances over which thermal stress can be developed. As a consequence, most current memory and logic devices use SBCs to improve the yield of packaged devices and to lower lifetime failure rates. Finally, SBCs provide a barrier to alpha-particle radiation, which can lead to soft errors (11) in the device.

Stress buffer coat films require film mechanical properties that result in strong, tough films that resist mechanical damage but are soft enough to absorb stress. Successful materials generally have an elastic modulus in the range of 2–4 GPa (290,000–580,000 psi), a yield strain of 5–10%, and a tensile failure strain of 25% or greater. The use of low modulus materials runs a risk of wire bond breakage due to creep. Film thermal stability is important in that the materials must be dimensionally stable at the process temperatures frequently required in latter process steps and must not outgas volatiles during these operations. This thermal stability requirement leads to a need for materials with a glass-transition temperature T_g of 260°C or greater, with some assembly processes requiring T_gs greater than 350°C. Silicon is a low expansion material with a coefficient of thermal expansion (CTE) of 3.2 ppm/°C. Because polymers typically have CTEs that are higher than the CTE of silicon, there is a significant CTE mismatch between the chip and the stress buffer coat, resulting in tensile coating stress that is large enough to bend or bow the chip. The extent of bow is largely determined by the thickness ratio of the coating to the chip, the magnitude of CTE mismatch, the coating thermal history, the elastic modulus of coating and substrate, and by the extent of in-plane coating shrinkage during cure (12). In general, the CTE of the SBC should be matched as closely as possible to the CTE of the package components with which it is adhered. The adhesion of the SBC to the chip must be exceptionally good so that delamination does not occur during package assembly or during the operational lifetime of the package. Finally, the SBC chemistry must promote adhesion to the encapsulating resin so that adhesion failures do not occur at the SBC–encapsulant interface.

Stress buffer coats are applied to semiconductor devices by two commonly used methods. The first method is termed “glob-top coating” and involves

dispensing a drop of polymer solution or neat resin formulation onto the chip after wire bonding. Multiheaded syringe systems that dispense material on many parts at once are commonly used for this purpose. The dispensed material is heated to cure the resin and to remove solvents. The second method is to apply the coating at the wafer level using standard wafer fabrication spin coating equipment. Materials applied at the wafer level by spin coating have largely replaced glob-top coating in the manufacture of many device types including large memory and logic devices, with small power devices remaining as the major application for drop-on coatings. This trend is due to the greater throughput of the spin coating process where hundreds of chips are processed at once on a single wafer and to the reduction in device mechanical damage that is obtained by applying the top coat prior to processing the wafers into packages.

Materials for Stress Buffer Coatings. Stress buffer coating formulations have been prepared using polymers from several classes including polyimides, polybenzoxazoles, polybenzocyclobutenes, and polysiloxanes. Polyimides are the most commonly used buffer coat materials, and commercial formulations are available from several suppliers. Polyimides offer several advantages as SBCs including high thermal stability, good dielectric properties, good chemical resistance, and excellent film mechanical properties. The adhesion of formulated polyimide materials to silicon oxide and silicon nitride is excellent as most materials feature chemical modifications designed to promote adhesion to these surfaces. Two types of modification strategies are used to improve adhesion: modification of the polymer backbone by incorporating siloxane-containing monomers or by adding adhesion-promoting additives such as aminosiloxanes. In addition, the processability of formulated polyimide products has greatly improved over the last 10 years and materials are available that have been optimized for high throughput on current semiconductor factory tool sets and process methods. Finally, commercial materials are available with low trace metal and halogen content demonstrating the maturity of the supply chain in providing electronic grade materials. As a class, polyimides have relatively high moisture absorbance which limits their use in some applications where stable dielectric properties or low tolerance for absorbed moisture are important considerations.

Structure–Property Relationships in Polyimides. Electronic polyimides are obtained from the polymerization of aromatic or aliphatic diamines with aromatic dianhydrides or derivatives of the dianhydrides. Table 2 provides selected physical properties of several structurally diverse polyimides derived from the monomer units shown in Figure 5. The thermal and mechanical properties of polyimide films are readily modified in a designed approach by selecting the dianhydride–diamine pairs needed to provide the desired film properties. An additional degree of property optimization may be obtained through the copolymerization of one or more dianhydrides with one or more diamines. In general, the selection of rigid monomers provides materials with a high modulus and high T_g and a low CTE while selection of monomers with flexible spacer groups, such as ether linkages, between the imide bearing aromatic rings provides materials with a lower modulus and lower T_g and a higher CTE, with copolymers demonstrating properties predicted by the rule of mixtures. While most aromatic polyimides are

Table 2. Thermal and Mechanical Properties of Selected Polyimides.[a]

Dianhydrides	Property	Diamines			
		ODA	pPPD	mPPD	DAPI
PMDA	T_g, °C	380–400	–	–	>400
	Modulus, GPa[b]	3	–	–	–
	CTE[c], ppm/°C	35–40	–	32	–
BPDA	T_g, °C	306	360	–	384
	Modulus, GPa	–	11	–	–
	CTE, ppm/°C	46	2.6	40	45
BTDA	T_g, °C	280	–	–	331
	Modulus, GPa	–	–	300	3.3
	CTE, ppm/°C	42.8	21	29	54
ODPA	T_g, °C	268	342	–	295
	Modulus, GPa	2.9	6.4	–	–
	CTE, ppm/°C	55	–	–	–
6-FDA	T_g, °C	285	326	297	331
	Modulus, GPa	–	–	–	–
	CTE, ppm/°C	–	–	–	55

[a] From Refs. 13–17.
[b] Tensile modulus. To convert GPa to psi, Multiply by 145,000.
[c] Coefficient of thermal expansion in units of ppm/°C.

not soluble in common solvents and must be processed using soluble precursors, solvent-soluble materials can be prepared using monomers that contain several flexible linkages, have strongly dissymmetric structures, or have bulky pendent groups.

Polyimide SBCs can be grouped into four classes based on both the chemistry of their precursors and the processing strategy used to pattern their coatings. These classes are polyamic acids, solvent-soluble polyimides, solvent-developed, photosensitive materials, and aqueous-base developed, photosensitive materials.

Polyamic Acids. Polyamic acids are commonly prepared by the step-growth polymerization of one or more aromatic dianhydrides and one or more aromatic or aliphatic diamines in *N*-methylpyrrolidinone (NMP) solvent to yield 15–25% solids solutions which are typically used without isolation of the polymer. While numerous polyamic acids have been reported in the literature (18,19), only a few are in common use in stress buffer formulations as many of the monomers reported in the literature are not available in commercial quantities. Special care must be taken to use the purest materials available so that the product is free of metallic and organic contaminants, especially surface-active materials, that may cause coating defects or lead to poor adhesion. The polymer molecular weight may be controlled by conventional methods, either by adjusting the stoichiometry of the reactants (20) or by using monofunctional anhydrides or amines to limit chain growth. Molecular weight control is of great importance because the mechanical properties and thermal stability of the cured film are functions of molecular weight (21) and because the thickness of the spin-coated film depends on both the viscosity and the solids loading of the polymer solution. The need for

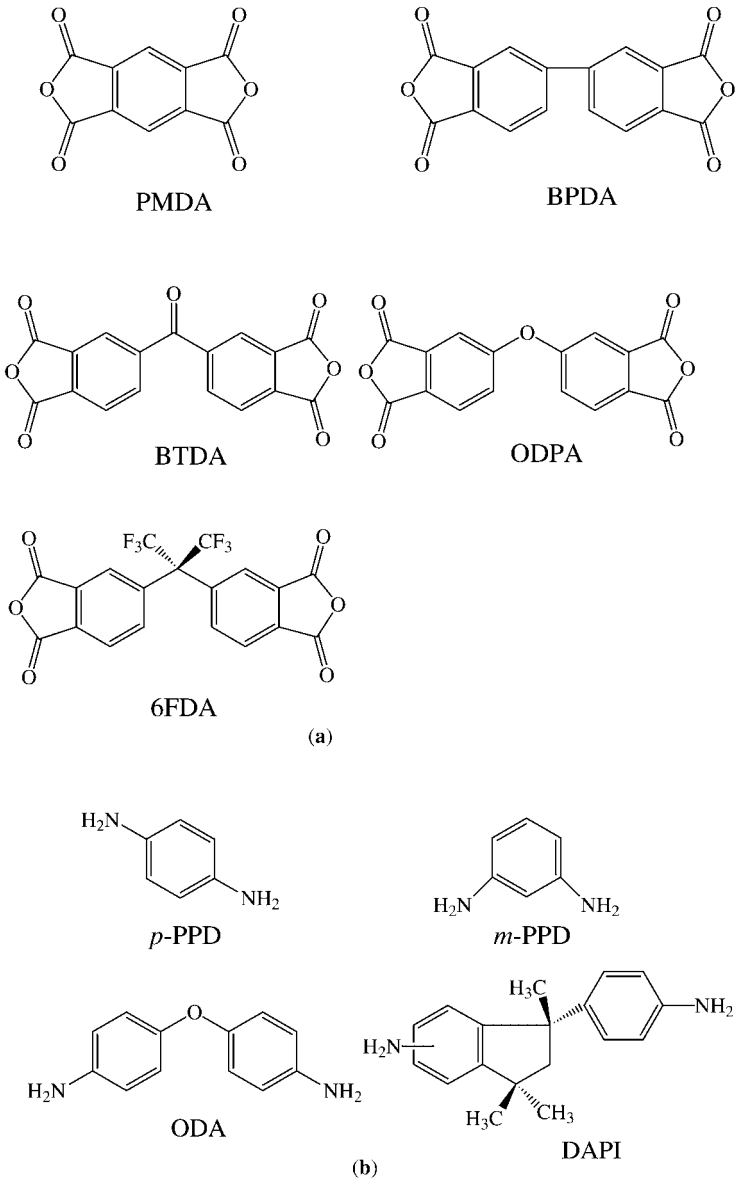

Fig. 5. The chemical structures of some common aromatic dianhydride (**a**) and aromatic diamine (**b**) monomers used in the synthesis of electronic-grade polyimides.

control of these parameters is demonstrated by Figure 6 which shows plots of spin coat film thickness vs solution solids content and the relationship between solids content and viscosity obtained from measurements on a PMDA–ODA polyamic acid solution. Prior to use, polyamic acid solutions must be filtered to remove particulate matter to prevent film defects that will cause problems in subsequent processing.

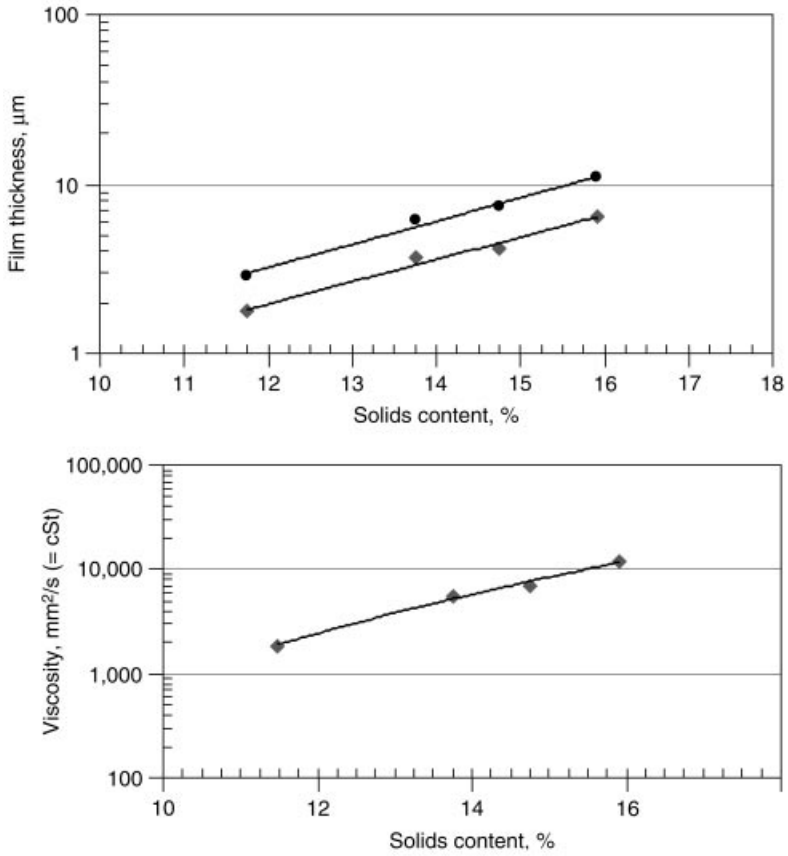

Fig. 6. (**a**) Relationship between film thickness and solution solids content. (**b**) Relationship between solution viscosity and solution solids content.▪, Cured thickness;▫, Soft baked thickness. Data are from a PMDA–ODA polyamic acid solution.

The polyamic acid film is prepared by spin-coating the solution on a wafer and then baking the wet film at 85–150°C on a hot plate to yield a tack-free film that can be handled by automated wafer handling equipment without perturbing the coating thickness. Imidization or "curing" of the polyamic acid film to form a polyimide film is completed by heating the polyamic acid to temperatures ranging from 250 to 400°C in a nitrogen atmosphere, resulting in cyclodehydration and evaporation of solvent (Fig. 7).

In order to permit wire bonding, openings must be patterned through the SBC so that metallurgical contact can be made with the aluminum pads on the device. The required openings are readily patterned in polyamic acid films using a photolithographic, bilayer patterning and base etch process (22,23) (Fig. 8). In this process, the polyamic acid solution is dispensed onto the center of a rotating silicon wafer using a metering pump. After dispensing is complete, the wafer is accelerated to a higher speed and then held at constant speed for 20–30 s. The wafer is then moved to a programmable hot plate and "soft-baked" at temperatures ranging from 85 to 150°C to yield a tack-free film with a coating thickness and etch

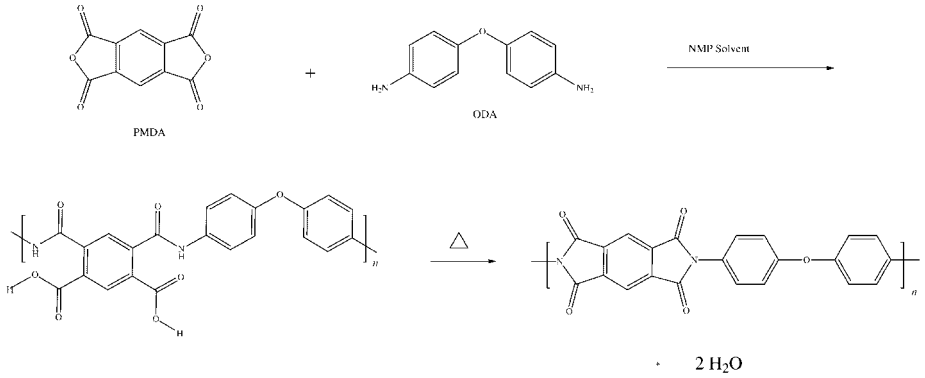

Fig. 7. Synthesis and cyclodehydration of PMDA–ODA polyamic acid to yield PMDA–ODA polyimide.

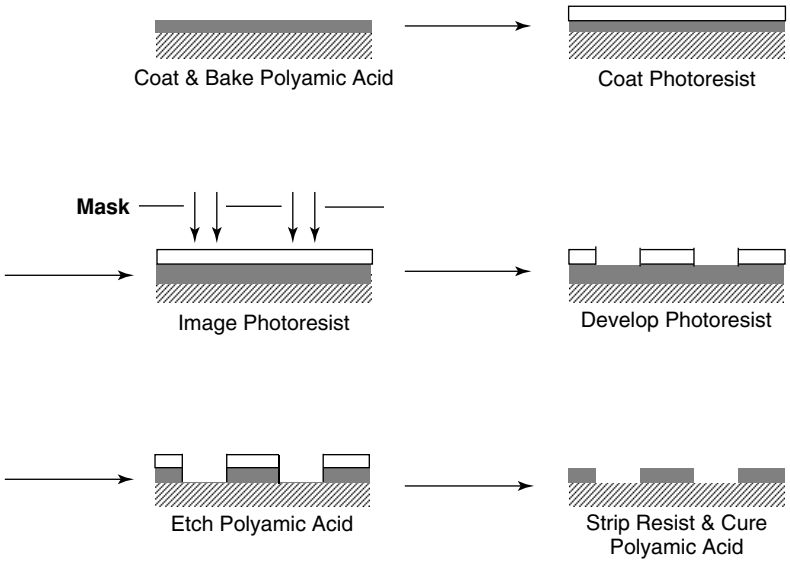

Fig. 8. Bilayer process for patterning polyamic acid films.

rate defined by the soft bake time and temperature program. This process results in a coating of defined thickness and, if the process is optimized, film thickness variation is less than 2% of the film thickness. The dried and partially imidized polyamic acid film is then coated with a resist layer formed by spin coating and baking a diazonapthaquinone-novalac photoresist film (24) on the polyamic acid film. The photoresist is imaged by exposure to uv light through a photomask (25). Treatment of the exposed resist with an aqueous hydroxide base solution such as tetramethylammonium hydroxide develops the latent resist image and yields a positive-tone relief image of the mask. The development process is then allowed to continue, resulting in an isotropic etch that transfer the resist relief image into the

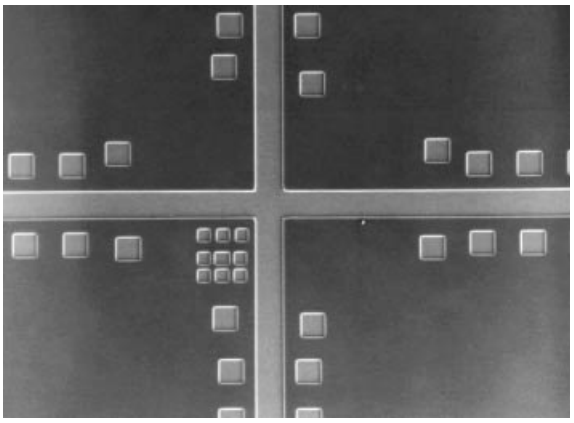

Fig. 9. A stress buffer coat pattern formed in PMDA–ODA polyamic acid using the bilayer process shown in Figure 8. Courtesy of Arch Chemicals, Inc.

polyamic acid film by solubilizing the polyamic acid through the combined effects of soluble salt formation and chain hydrolysis. Next, the photoresist film is removed by dissolving the resist in a solvent, such as acetone, that is compatible with the polyamic acid film. The process is completed by heating the film at 300–400°C, which completes the imidization reaction and removes the water of imidization and residual solvent. Figure 9 shows a photograph of a patterned film where the small square features are bond pad openings and the large open lines or "dicing streets" are formed to allow passage of the diamond saw blade used to singulate chips from the wafer without blade fouling from adhered polymer.

The polyamic acid patterning process described above has been used for many years. However, the process has several drawbacks. First, the number of process steps involved reduces process throughput, produces a significant amount of waste, and increases the possibility of process defects. Second, pattern resolution is limited to a maximum feature width that is about 50% of the polyamic acid film thickness. Third, processing polyamic acid films greater than 10 μm in thickness is difficult owing to thickness uniformity in spin-coating polyamic films to film thicknesses greater than 10 μm in one coating operation and to chipping of the resist etch mask during long etch times which causes defects in the pattern. Finally, the process etch rate is sensitive to the bake temperature and time used to set the polyamic acid film which can cause reproducibility problems in etch rate. In consequence, the dimensional tolerances of the pattern are affected resulting in a deviation, or bias, from the mask dimensions.

Electronic grade polyamic acid products are available from several supplies including Arch Chemicals, Inc., HD Microsystems, and Toray Industries. Commercial materials are generally formulated to provide reproducible coating thickness over a certain range of coating thickness or spin speeds.

Solvent-Soluble Polyimides. Materials in this class are also termed "preimidized polyimides" because the film-forming polymer is a polyimide rather than a polyimide precursor such as a polyamic acid. Thus, the curing process for these materials involves only removal of solvent. In some instances, a high

temperature post-cure above T_g can be used to cross-link the polymer and impart increased resistance to solvents. The best known examples are polyamide-imides prepared by the step condensation of 4,4′-methylenebis(phenyl isocyanate) with trimellitic acid (26), polyimide–siloxanes, and polyimides derived from trimethylphenyl diaminophenylindane (DAPI) monomers (15,27,28). Use of these materials for stress buffer applications is generally restricted to glob-top applications. However, the materials may be spin-coated and patterned using a hard mask etch process. The hard mask process is an extension of the bilayer process in which a layer of oxygen plasma etch-resistant material, such as aluminum or silicon dioxide, is coated on the cured polyimide film prior to applying the photoresist. The resist is applied and imaged as usual resulting in a positive relief image over the hard mask. Next, the hard mask is patterned using a plasma or wet chemical etchant that is selective for the hard mask material. The process is completed by transferring the pattern into the polyimide film using a oxygen reactive ion etch process followed by removal of the resist and hard mask. This process is seldom used as it is even more time consuming and expensive than the bilayer process. However, the process has an important advantage in that it can be used to define very high aspect ratio structures and it is generally applicable to a wide variety of polymers. Commercial examples of solvent-soluble polyimide include the Durimide™ 32 and Durimide™ 200 series materials (Fig. 10) available from Arch Chemicals, Inc. (29).

A compilation of commercially available nonphotosensitive stress buffer coat materials is shown in Table 3 (29–34). Table 4 provides selected physical data for some of the materials shown in Table 3.

Solvent-Developed Photosensitive Materials. Many of the limitations of the bilayer polyamic acid process have been overcome through the use of photosensitive polyimides (9). Formulated photosensitive products have been developed that result in improved process capability resulting in increased pattern resolution, improved soft bake time and temperature process latitude, and improved lithographic process latitude and throughput while maintaining desired film physical properties. Moreover, the film patterning process requires fewer steps

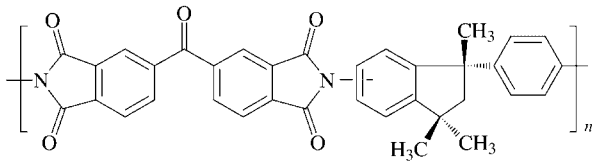

(**a**)

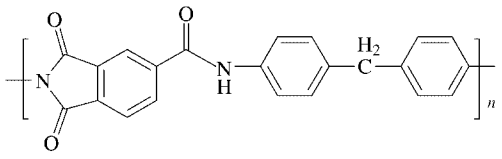

(**b**)

Fig. 10. (**a**) The structure of a solvent-soluble polyimide based on DAPI monomer. (**b**) The structure of a solvent-soluble polyamide-imide.

Table 3. Non-photosensitive Stress Buffer Coat Formulations Available from Various Suppliers

Supplier	Trade name	Product code	Comments
Arch Chemicals	Durimide[a]	32	Poly(amide-imide), AP
	Durimide	32A	Poly(amide-imide), SP
	Durimide	112A	PAA, SP, high T_g
	Durimide	114A	PAA, SP, high T_g
	Durimide	115A	PAA, SP, high T_g
	Durimide	116A	PAA, SP, high T_g
	Durimide	116	PAA, AP, high T_g
	Durimide	200	Preimidized, AP
HD Microsystems	Pyralin[a]	PI-2525	PAA, AP
	Pyralin	PI-2545	PAA, AP
	Pyralin	PI-2555	PAA, AP
	Pyralin	PI-2556	PAA, AP
	Pyralin	PI-2562	PAA, AP
	Pyralin	PI-2575	PAA, SP
	Pyralin	PI-2579B	PAA, SP
	Pyralin	PI-2610	PAA, AP, low CTE
	Pyralin	PI-2611	PAA, AP, low CTE
	Pyralin	PI-2616	PAA, AP, low CTE
	Pyralin	PI-5811	PAA, AP, low CTE
	Pyralin	PI-5878G	PAA, AP
	–	PIX-1400	PAA, SP
	–	PIX-3476	PAA, SP
	–	PIX-5200	PAA, SP
	–	PIX-5500	PAA, SP
	–	L110SX	PAA, SP, low CTE
		PIX 6400	PAA, SP
Toray	Semicofine[a]	SP-811	PAA, SP
	Semicofine	SP-341	PAA, SP
	Semicofine	SP-483	PAA, SP
	Semicofine	SP-042	PAA, SP, low CTE

[a]PAA = polyamic acid; AP = adhesion primer required; and SP = self-priming formulation, no adhesion primer required.
[b]Durimide is a trademark, and Pyralin and Semicofine are registered trademarks.

resulting in reduced costs and increased yields. Consequently, photosensitive materials are rapidly replacing polyamic acids as SBC materials.

Two approaches for the synthesis of photosensitive polyimide precursors are in common use today. The first approach was pioneered at Siemens (35–37) and is based on polyamic acid esters wherein the ester group is a radiation cross-linkable group such as 2-hydroxyethylmethacrylate (Fig. 11). Materials based on the ester chemistry are often described as "covalent-type" photosensitive polyimides. The second approach, developed by Toray Industries, involves combining a polyamic acid solution with a tertiary amine bearing radiation cross-linkable groups (38) (Fig. 12). The tertiary amine forms a salt with the polyamic acid and the resulting ionic interactions are of sufficient strength to provide solubility discrimination in the imaging process. Materials based on the amine salt chemistry

Table 4. Selected Physical Properties of Polyimide Films Derived from Nonphotosensitive Polyimide Precursors

Supplier	Product code	T_g, °C	Modulus, GPa[a]	e_b, %	CTE, ppm/°C
Arch Chemicals	32	300	3.3	56	53
	115A	370	3.3	80	32
	200	309	3.3	75	54
HD Microsystems	PI-2525	325	2.5	–	50
	PI-2545	400	1.4	–	20
	PI-2562	325	2.5	–	50
	PI-2611	360	8.5	–	5
	PIX-1400	290	3.0	–	50
	PIX-3476-4L	310	3.1	–	40
	L110SX				
Toray	SP-811	300	2.9	70	40
	SP-341	330	2.9	80	40
	SP-483	300	2.7	20	40
	SP-042	–	–	20	17

[a]To convert GPa to psi, multiply by 145,000.

are commonly referred to as "ionic-type" photosensitive polyimides (39). The ionic approach provides the additional advantages of a simple synthesis starting from polyamic acids. Material suppliers have made steady improvements during the last 15 years, resulting in formulations with improved lithographic performance and final film properties (40–42).

Following exposure to uv light, both the covalent- and ionic-type materials undergo photoinitiated radical cross-linking reactions between the ester groups. This reaction provides the differential solubility between the exposed and unexposed area of the film that is necessary for forming relief images (Fig. 13). The photoinitiated cross-linking reaction of a 2-hydroxyethyl methacrylate polyamic ester bearing a ^{13}C label at the methacrylate β-carbon has been studied using a solids nmr method (43). The nmr spectra showed that the percentage of methacrylate groups reacted varied with exposure dose and processing conditions.

Photosensitive precursor polymers are formulated in a suitable solvent such as *N*-methylpyrrolidinone or γ-butyrolactone with a radical photoinitiator and a variety of additives such as glycol acrylates to improve image contrast and photospeed; functionalized silane coupling agents to improve adhesion of silicon and silicon nitride; photosensitizers to improve photosensitivity; substituted phenolic stabilizers to improve formulation working life and storage stability; and leveling agents to improve coating quality and uniformity.

The single-layer imaging process for photosensitive polyimides is represented in Figure 14, which, in comparison to Figure 8, clearly shows the simplification of the patterning process compared to the polyamic acid etch process. Because the solubility of the exposed film is less than the solubility of the unexposed film, the relief image is a negative image of the mask. In contrast to the bilayer polyamic acid etch process, the single-layer photosensitive process readily provides images with a pattern aspect ratio of 2:1, and if care is taken, resolution can be extended to an aspect ratio of 3:1. Because of their decreased

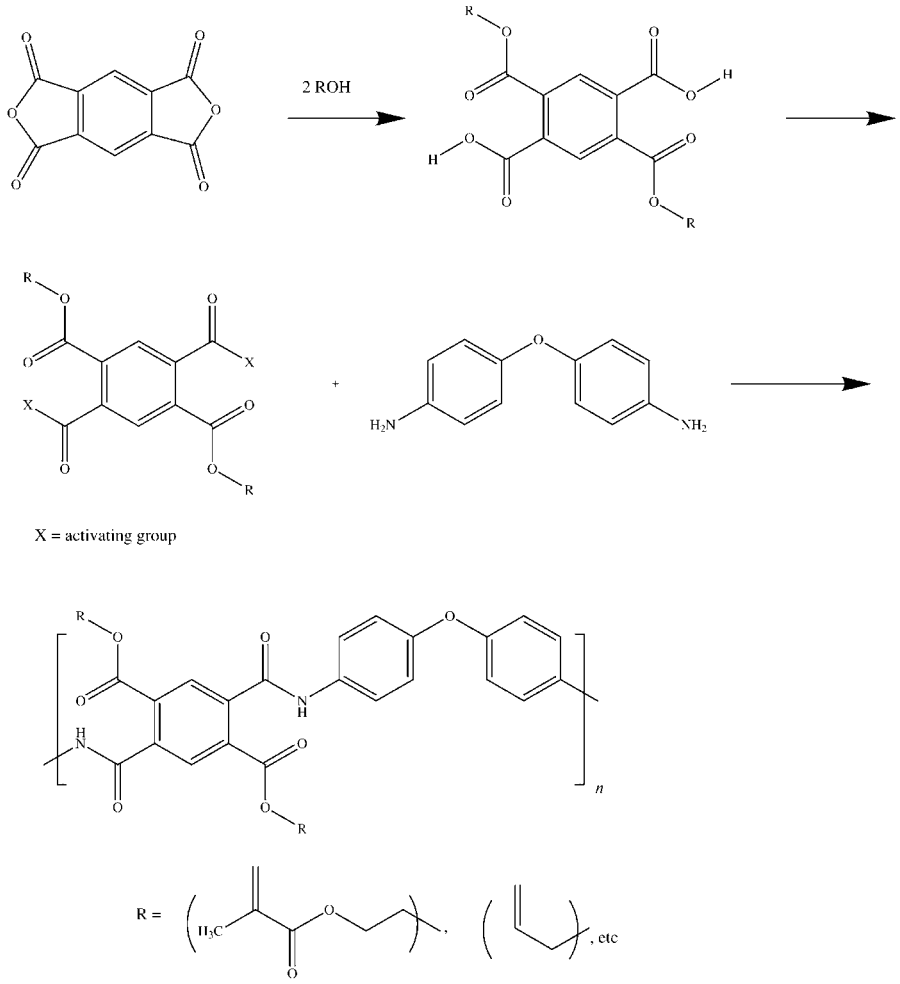

Fig. 11. Synthesis of a covalent-type photosensitive polyimide precursor based photoreactive polyamic esters.

hydrogen bonding compared to polyamic acids, photosensitive polyamic esters are particularly suited to the processing of thick films as their solutions have lower viscosities than polyamic acids at equivalent molecular weights and solids loading. Thus, high solids content solutions that are suitable for casting thick films can be formulated at viscosities suitable for spin coating. Robust patterning processes have been demonstrated in 50-μm thick films which yield 25-μm thick films after curing (44). Recently, detailed characterization studies on the lithographic process latitude of covalent-type materials processed using modern, stepper exposure tools have been reported (45,46). Figure 15 shows some examples of relief structures patterned in a photosensitive polyamic ester film. The process is completed by curing the imaged polyamic ester at 300–400°C in an inert atmosphere, which results in imidization with the loss of the photoreactive groups as volatile products (Fig. 13). The imaged film shrinks by 40–50% in thickness

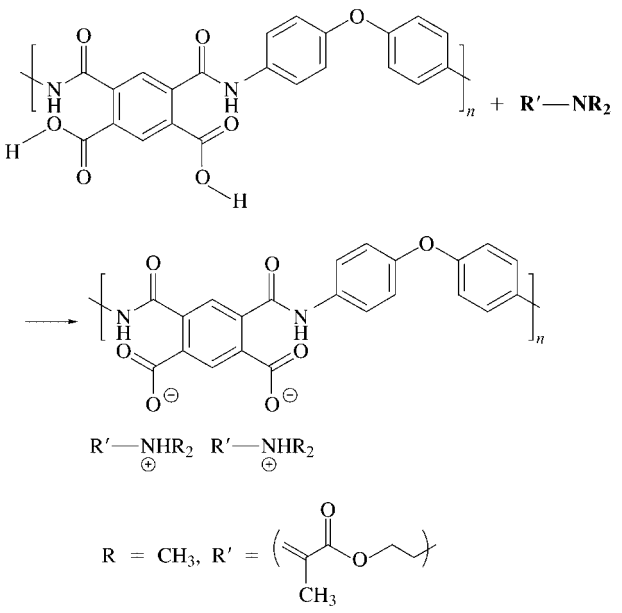

Fig. 12. Synthesis of an ionic-type photosensitive polyimide precursor based on tertiary amine-polyamic acid salts containing photoreactive groups.

during the curing process, leading to cured film aspect ratios ranging from 1.0 to 1.5.

Autophotosensitive, preimidized polyimides (Fig. 16) represent a third approach to negative tone materials and are based on the inherent photosensitivity of polyimides containing benzophenone tetracarboxylic dianhydride (BTDA) derived segments together with ortho-alkyl-substituted diamine segments (47). The photochemical basis for imaging is believed to be radical cross-linking initiated by a benzophenone ketyl radical to yield cross-linked photoproducts (48,49). The most interesting feature of these materials is that they do not require formulation with the photoinitiators, photosensitizers, contrast enhancing agents, and stabilizers commonly found in the additive packages used in the formulation of covalent- and ionic-type materials. Accordingly, films prepared from autophotosensitive materials show substantially less shrinkage during cure than do covalent or ionic materials (26). However, autophotosensitive materials have not been extensively used in SBC applications because of their low photosensitivity and long developing times as compared to covalent and ionic materials. Commercial examples of autophotosensitive materials are the Probimide® 400 series from OCG Microelectronic Materials and the Ultradel® 7500 series from Amoco.

A separate group of negative tone materials based on the thermal polymerization of benzocyclobutenes (BCB) has been developed by the Dow Chemical Co. (50,51) and have been used as SBCs (52). The chemistry is based on the *in situ* generation of reactive, ortho-quinodimethane dienes that undergo facile polymerization to form a thermoset network (Fig. 17). The physical properties of the materials can be tailored by modification of the connecting group X. One such modified

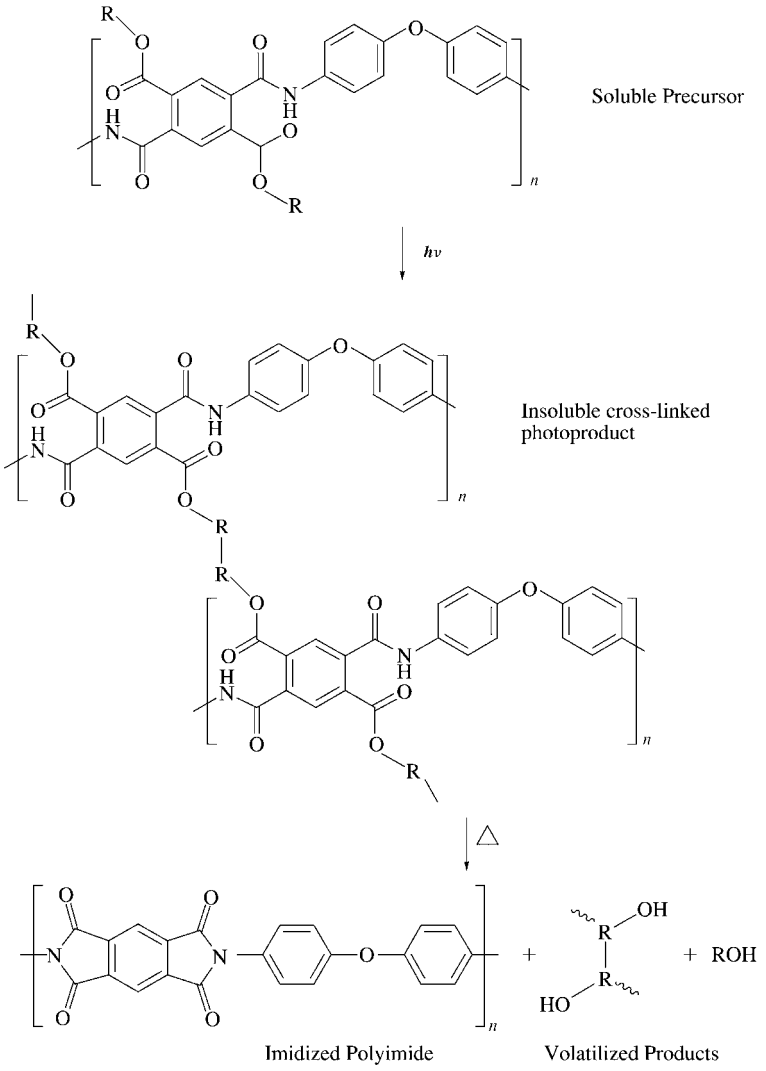

Fig. 13. Photochemical cross-linking of a covalent-type photosensitive polyimide precursor.

monomer is divinylsiloxane-bis-benzocyclobutene (DVS-bis-BCB). Photosensitive formulations are obtained by combining B-staged, or partially polymerized DVS-bis-BCB, with aromatic bisazide compounds in solvent. Such formulations can be spin-coated and are processable using the negative tone process described in Figure 14. Processing of the patterned films is completed by heating to convert the photocross-linked, B-staged film into the cured thermoset. BCB derived films have attracted much interest in electronic packaging owing to their low dielectric constants and low moisture uptake. The BCB materials are marketed under the trade name Cyclotene®.

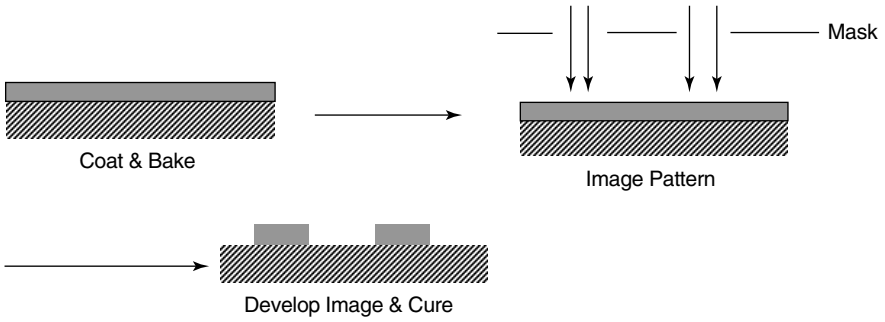

Fig. 14. Single-layer imaging process for negative tone photosensitive polyimide precursors.

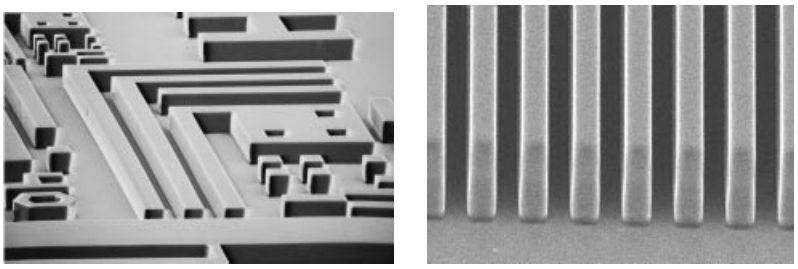

Fig. 15. Negative tone relief patterns formed in a covalent-type photosensitive polyamic ester film using the process shown in Figure 11. (**a**) Resolution test pattern showing 40 μm features in a 40-μm film, (**b**) Resolution of 5 μm lines and space patterns in a 18-μm film. Courtesy of Arch Chemicals, Inc.

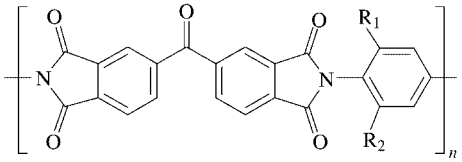

Fig. 16. The generic structure of autophotosensitive polyimides where R_1 and R_2 are alkyl groups.

Aqueous-Developed Materials. During the last 5 years, aqueous developable materials have been introduced as a new class of photosensitive SBCs. Development of these materials is an area of intense current activity and is driven by industry needs for materials with improved cost of ownership and improved compatibility with semiconductor factory process strategies and materials. One of the drawbacks of most negative tone materials is that they require organic solvents for image development. Organic solvents impose a significant cost penalty on semiconductor factories for several reasons. First, high purity, electronic grade solvents are expensive to purchase. Second, standard process equipment must be modified to allow the safe use of solvent sprays, and the modified equipment is not generally usable for other coating processes such as positive photoresists. Many factories must obtain VOC emission permits to use solvent-processed materials.

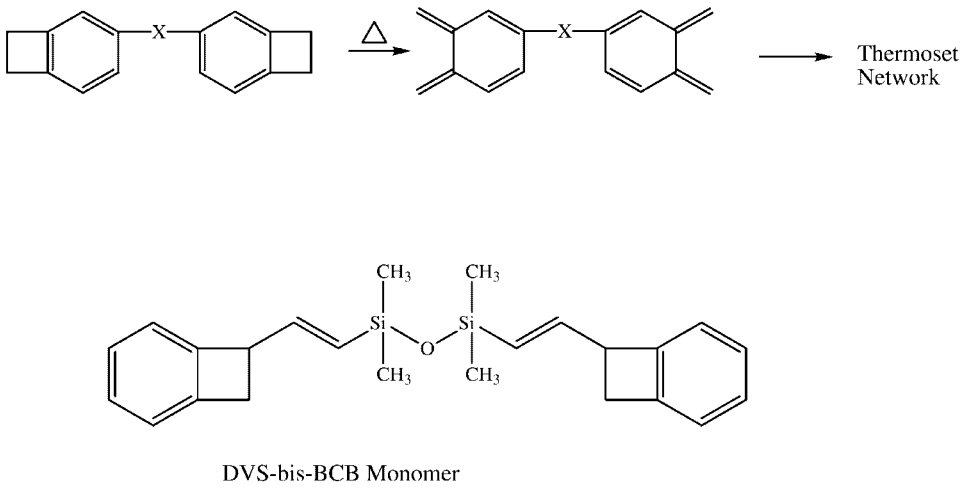

Fig. 17. The benzocylcobutene cure reaction and the structure of DVS-bis-BCB monomer.

Finally, factories must collect and segregate spent solvent waste as a separate waste stream and thus incur additional cost. These cost of ownership issues are substantially decreased through the use of aqueous, metal-ion free developers based on tetramethylammonium hydroxide which are the semiconductor industry standard for developing positive photoresists.

Both negative and positive tone aqueous developable materials have been introduced. Negative tone materials have been derived from the covalent-type polyamic ester precursors through the use of additives that enhance solubility of the unexposed film in aqueous developers (53). Positive tone materials are based on either polyamic ester precursors containing carboxylic acid (54) or phenolic oxygen substituents (55,56) or on aromatic poly(ortho-hydroxyamides) as precursors to polybenzoxazoles (57,58), a class of high temperature stable, heterocyclic polymers with thermal and mechanical film properties similar to polyimides (Fig. 18). In both approaches, the acid–base reaction of the phenolic or carboxylic

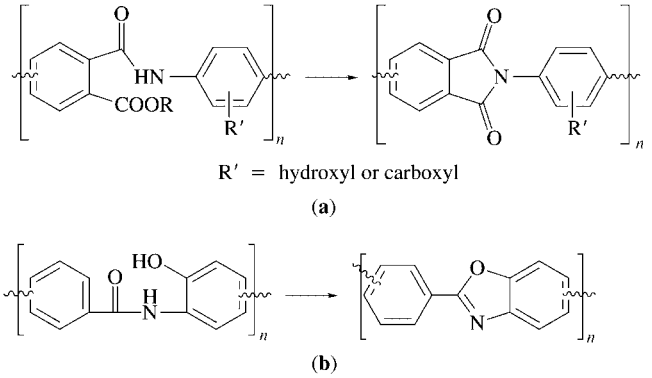

Fig. 18. Generic structures of positive tone, aqueous processable precursors for polyimide (**a**) and polybenzoxazole (**b**) based materials.

substituents with base provides the mechanism for solubilizing the precursor in an aqueous developer. When formulated with diazonaphthaquinone-containing photoactive compounds (DNQ-PACs), the resulting formulations function as positive photoresists. The DNQ-PAC inhibits the solubility of the precursor polymer in base. When the DNQ-PAC is exposed to uv light, the DNQ moeity undergoes a formal Wolff rearrangement to form a ketene as the primary photoproduct which undergoes reaction with environmental water to form an indene carboxylic acid derivative (59). The indene carboxylic acid photoproducts increase the dissolution rate of the exposed film relative to the unexposed film. Thus, the photolithographic contrast of the system is obtained from the dissolution rate difference between the unexposed and exposed films (Fig. 19). Processing this class of materials retains the cost and simplicity benefits of the single-layer process used for solvent-developed negative tone materials and adds the benefit of positive tone imaging, which results in higher image resolution and a decreased sensitivity to pattern defects due to particles on the surface of the film (60).

Commercial photosensitive SBC formulations are available from several suppliers and provide a range of materials differentiated by wavelength photosensitivity, chemistry type, and film properties. A list of commercial photosensitive SBC formulations is shown in Table 5 (29,30,32,61–63). Table 6 shows a compilation of selected film physical property data selected from those listed in Table 5.

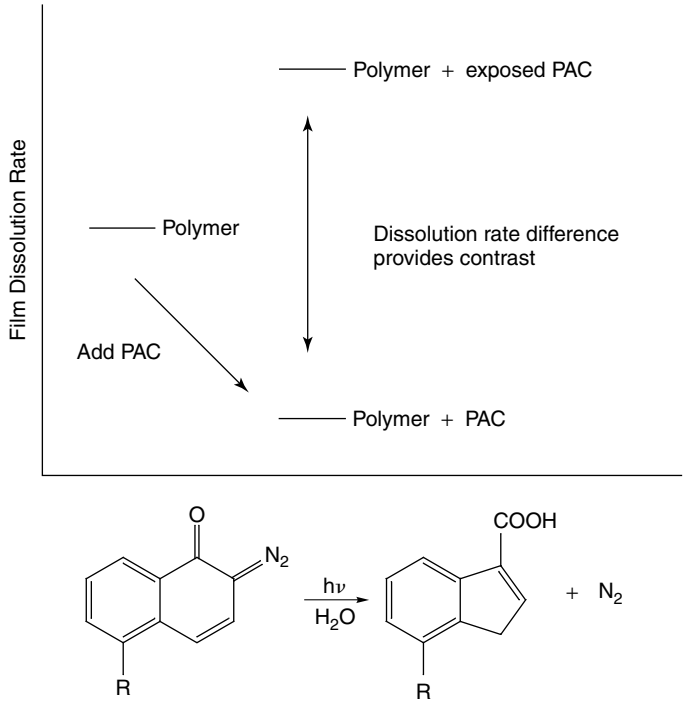

Fig. 19. Chemical basis for image contrast in positive tone buffer coat materials based on DNQ-PAC chemistry.

Table 5. Commercial Photosensitive SBC Formulations

Supplier	Trade name	Product code	Characteristics
Arch Chemicals	Durimide[a]	7800	C, N, I, BB, S, high resolution
		7520	C, N, I, BB, S, high sensitivity, thick films
		7410	C, N, I, BB, S, for reflective substrates
		7320	C, N, I, BB, S, for Cu substrate
		7000	C, N, G, BB, S, high T_g
		348	C, N, G, BB, S, thick films
		HTR3	C, N, G, BB, S, thick film plating stencil
		9000	P, G, I, BB, A
Asahi Chemical	Pimel[a]	G-7600s	C, N, G, BB, S
		I-8300s	C, N, I, BB, S
		I-8600s	C, N, I, BB, S
		TL-530s	C, N, G, BB, S
Dow Chemical	Cyclotene[a]	4024-40	I,S
	Cyclotene	4026-46	I,S
HD Microsystems		PI-2720	C, N, G, BB, S
		PI-2730	C, N, G, BB, low stress
		PI-2770	N, G, I, A
		HD-4000	C, N, I, BB, S, high T_g
		HD-8000	P, G, I, BB, A
Toray	Photoneece[a]	UR-3100E	IN, G, H, S
		UR-3800	IN, G, H, S, high sensitivity
		UR-5100FX	IN, N, G, BB, S, low stress
		UR-5400	IN, G, H, S, low stress
		BG-2400	IN, G, BB, S, low stress
		BG-7730	IN, G, BB, S, fast developing
		BG-8000	IN, I, S
		PW-1000	P, I, G, A
Sumitomo-Bakelite	Excel	CRC-8000	P, G, I, BB, A

[a]C = covalent-type photosensitive polyimide precursor; IN = ionic-type photosensitive polyimide precursor; N = negative image tone; P = positive image tone; G = sensitive to g-line (436 nm) of Hg lamp; H = sensitive to h-line (406 nm) of Hg lamp; I = sensitive to i-line (365 nm) of Hg lamp; BB = sensitive to unfiltered output of Hg lamp; S = developed using solvent mixtures; and A = developed using aqueous bases.
[b]Durimide and Pimel are trademarks, and Cyclotene and Photoneece are registered trademarks.

Die Attach Adhesives. After completion of SBC processing, the finished wafers are electrically tested and nonfunctional chips are marked for discard. It is a common occurrence that the wafer and fabrication packaging facilities are separate factories or even different companies and cassettes of wafers are routinely shipped from the wafer fabrication plant to the packaging plant for assembly. At the packaging plant, the wafers are first thinned using a grinding and polishing process that removes bulk silicon from the backside of the wafer. Substantial thickness reduction is necessary to allow assembly into the thin packages commonly used in board assembly. For example, a 200-mm wafer 725 μm thick is commonly thinned to a thickness of 250 μm and sometimes to as thin as 80 μm (64). The

Table 6. Selected Physical Properties of Stress Buffer Coat Films Derived from Photosensitive Precursors

Supplier	Product code	T_g, °C	Modulus, GPa[a]	CTE, ppm/°C	Coating stress, MPa[b]
Arch Chemicals	Durimide[c] 7500	285	2.5	55	33
	Durimide 7000	>350	2.9	27	30
	Durimide 9000	320	2.5	32	–
Asahi Chemical	G-7600s	355	3.3	40–50	40
	I-8300s	280	2.8	50	35–40
	I-8600s	–	–	50	35–40
	TL-530s	–	–	10–20	20–30
Dow Chemical	Cyclotene[c] 4000	>350	2.9	52	28–32
HD Microsystems	PI-2720	310	2.5	57	39
	PI-2730	350	4.7	16	13.5
	PI-4000	350	3.5	33	–
	HD-8000	300	2.5	47	–
Toray	UR-3100	285	3.2	40	–
	UR-5100FX	>350	4.8	20	–
	UR-5440	>350	4.2	16	–
	BG-2400	255	3.9	25	–
	BG-7730	290	3.0	45	–
	BG-8000	260	3.5	39	–
	PW-1000	290	3.0	36	–
Sumitomo-Bakelite	CRC-8000	300	2.45	55	–

[a]To convert GPa to psi, multiply by 145,000.
[b]To convert MPa to psi, multiply by 145.
[c]Durimide is a trademark and Cyclotene is a registered trademark.

SBC layer provides both protection and support during the thinning process. The thinned wafer is then mounted, with their active device side up, onto a tacky adhesive release tape fixed in a steel ring. The mounted wafer is then singulated or "diced" into chips using a high speed diamond wet saw. To allow for the cutting kerf, the blade passes between device boundaries known as "saw streets" that were established during wafer fabrication (see Fig. 9). In high volume factories, the processes of wafer thinning and singulation are highly automated assembly line operations.

After dicing, the chips are removed from the release tape using a vacuum tool, which then places the die onto the metal lead frame to which has been applied die attach adhesive material in the form of a paste or film. Most die attach adhesives in use today are formulated products based on epoxies, thermoplastic polyimides, or thermoplastics such as bismaleimides, polysulfone, polyphenylene sulfide, and polyesters. The polymers may be used separately or as blends. Die attach adhesives usually contain inorganic metal or metal oxide fillers that impart electrical and/or thermal conductivity to the adhesive bond, thus creating an electrical connection to the lead frame and improving package heat dissipation by allowing better heat transfer from the device to the lead frame. High speed, automated dispense equipment is used to dispense and place the adhesive with a

high degree of accuracy with a cycle time of 2 s per chip placement (65). The lead frames are then loaded into magazines and placed in ovens to cure the adhesive. Typical curing cycles are 1 h at 150°C for epoxy-based formulations and 30 min at 150°C followed by 30 min at 275°C for polyimide-based formulations. Rapid or "snap" curing materials are now available that can be cured in one minute and can thus allow integration of the adhesive cure process into the dispense line.

In addition to excellent adhesion, critical design considerations for die attach adhesives may be segregated into those involving processability, thermal properties, electrical properties (insulating or conductive), and thermal conductivity. The viscosity, thixotropic index, and working life are important parameters with respect to the dispense method used. Dispense methods include needle dispensing, stamping or pin transfer, and screen or stencil printing. Needle dispensing is the most common method and allows uniform deposition of material at high speeds. The glass-transition temperature, thermal stability, shear strength, modulus, and fatigue resistance of the cured adhesive determine the strength and stress characteristics of the bond. The choice of filler material determines electrical and/or thermal conductivity, and formulations are available with metallic fillers, such as silver and gold, to provide electrical conductivity, or with mineral oxides that provide thermal conductivity but are electrically insulating. Curing conditions are chosen to optimize the bond strength and physical properties of the adhesive while providing maximum efficiency of assembly. The most commonly used materials are silver-filled conductive epoxies. Because of steady improvements, manufacturers provide materials with optimized physical properties and processing characteristics. In recent years, low modulus materials have been developed for use with larger chips and great attention has been given to developing formulations with fast or "snap" cure chemistry that increase throughput through the assembly line by allowing adhesive cure to be integrated into the adhesive dispense line. A list of die attach materials and their formulation type is shown in Table 7 along with selected physical property data.

Encapsulation Resins. Encapsulation is the general process of surrounding the wire bonded chip with an electrically insulating material that protects the circuit from the environment, provides mechanical support for the chip lead frame assembly, and assists in conducting heat out of the package. Plastic encapsulation materials are in widespread use throughout the microelectronic industry and the majority of plastic packages are encapsulated using formulated epoxy molding compounds in a transfer molding process. In the molding process, lead frames are loaded into cavity molds and the mold halves are pressed together in a molding press. The molding compound charge is heated in a transfer pot until it is sufficiently soft to be transferred under pressure through the mold runners and gates into the cavities. The mold compound is then held for a short period of time in the heated mold to allow curing to proceed. The mold halves are then separated and the molded lead frames are ejected and loaded into magazines for post-curing in a batch oven for 1–4 h at 175°C. The objective of post-curing is to complete resin cure such that the optimal thermomechanical properties of the resin are obtained. Parameters that are critical to the success of the process include mold pressure, compound viscosity, transfer pressure, mold temperature, and the geometry of the mold.

Table 7. Die Attach Adhesives and Their Formulation Type with Selected Physical Property Data[a]

Supplier	Designation	Resin	Filler	Conductive[b]	T_g, °C	Thermal conductivity, W/m·K	Thixotropic index	Modulus, GPa[c]	Viscosity, m Pa·s (= cP)	Cure
Ablestik	Ablebond 71-1	Polyimide	Silver	E	240	2	2.9	3.40	14,000	Oven
	Ablebond 826-1DS	Epoxy	Silver	E	67	2	1.6	5.30	19,000	Oven
	Ablebond 8322A	–	–	E	30	0.7	5	1.63	9,000	Snap
	Abletherrm 2600L	–	–	T	70	22	4.3	3.30	7,500	Oven
	Ablebond 979-1A	–	–	E	193	2.7	2.7	3.80	3,800	Snap
	Ablebond 84-1LMISR4	Epoxy	Silver	E	120	2.5	5.6	3.94	8,000	Oven
	Ablebond 8340	–	–	E	25	1.1	5.1	0.71	9,000	Fast oven
	Ablebond 8325L	–	–	E	20	–	4.8	3.00	8,600	Fast oven
	Abletherm 2600K	–	–	T	68	20	4.3	3.67	8,100	Oven
	Ablebond 84-3J	–	–	I	87	0.5	2.5	6.10	20,000	Oven
Dexter	QMI 505MT	BMI	Silver	E	−10	2.0	4.6	0.86	10,700	Snap
	QMI 509	BMI	Silver	E	1	2.8	3.5	1.8	9,000	Snap
	QMI 518	BMI	Silver	E	−64	1.5	4.8	0.10	8,200	Snap
	QMI 534	BMI	Teflon[d]	I	−35	0.3	5.0	0.30	7,800	Snap
	QMI 5030	Resin blend	Silver	E	50	25	4.0	2.0	5,500	Oven
	Hysol[d] K0110	Epoxy	Silver	E	78	3.5	4.5	7.0	7,000	Oven or snap
	Hysol K0111	Epoxy	Silver	E	68	3.7	4.9	7.4	7,500	Oven or snap
	Hysol K0120	Epoxy	Silver	E	99	2.8	3.7	6.6	7,500	Oven or snap
Epotek	H20E	Epoxy	Silver	E	>80	29	–	–	2,700	Oven
	H20E-175	Epoxy	Silver	E	>80	1.6	–	–	3,300	Oven
	P 1011	Polyimide	Silver	E	>90	1.3	–	–	10,000	Oven
	E 3001	–	–	E	>100	2.0	–	–	3,000	Fast oven
	E 3081	–	–	E	>200	2.0	–	–	8,000	Oven
	T 6116	–	Alumina	T	92	1.5	–	–	13,000	Snap

[a]From Refs. 66–68.
[b]E = Electrically conductive; T = thermally conductive; I = insulating.
[c]To convert GPa to psi, multiply by 145,000.
[d]Teflon and Hysol are registered trademarks.

Table 8. Generic Molding Compound Composition[b]

Component	Concentration (wt% of resin)	Function	Typical agents
Epoxy resin		Binder	Epoxy cresol novalac (ECN resin)
Curing agent	Up to 60	Polymerization	Acid anhydrides, amines, phenols
Cure accelerators	<1	Catalyze cure	Amines, imidazoles, organophosphines, Lewis acids
Filler	68–80	Decrease CTE	Ground fused silica, alumina
		Increase thermal conductivity	
		Increase modulus	
		Reduce resin bleed	
		Reduce shrinkage	
		Reduce residual stress	
Flame retardant	~10	Retard flammability	Brominated epoxy, antimony trioxide
Mold-release agent	Trace	Aids in release from mold	Silicones, fluorocarbon waxes, organic acid salts
Adhesion promoter	Trace	Enhance adhesion to IC	Silanes, titanates
Coloring agent	~0.5	Reduce photonic activity	Carbon black
		Reduce device visability	
Stress-relief additives	Up to 25	Inhibit crack propagation	Silicones, acrylonitrile–butadiene elastomers, poly(butyl acrylate)
additives		Reduce crack initiation	
		Reduce CTE	

[a]From Ref. 69.

Modern epoxy molding compounds are multicomponent formulations whose exact compositions are highly proprietary. However, most materials are variations on the general composition (69) shown in Table 8. Commercial formulation are carefully formulated to provide materials that adhere strongly to all interfaces; have thermal and mechanical properties optimized to minimize stress arising from thermal expansion mismatch between the encapsulant, lead frame, and chip; have low moisture absorbance; have low shrinkage during molding; and have processing characteristics that provide for good moldability and short post-cure times.

Early resin materials used in mold compound formulations were silicones, phenolic resins, and bisphenol-A or bisphenol-F epoxies. Because of shortcomings in performance, these materials have been displaced by epoxy phenol or cresol novalac resins (ECN resins) and by the biphenyl- and tris(triphenylmethane)-type epoxies (70) (Fig. 20). The high cross-link density of ECN-based materials results in low moisture absorption rate and higher thermal stability than

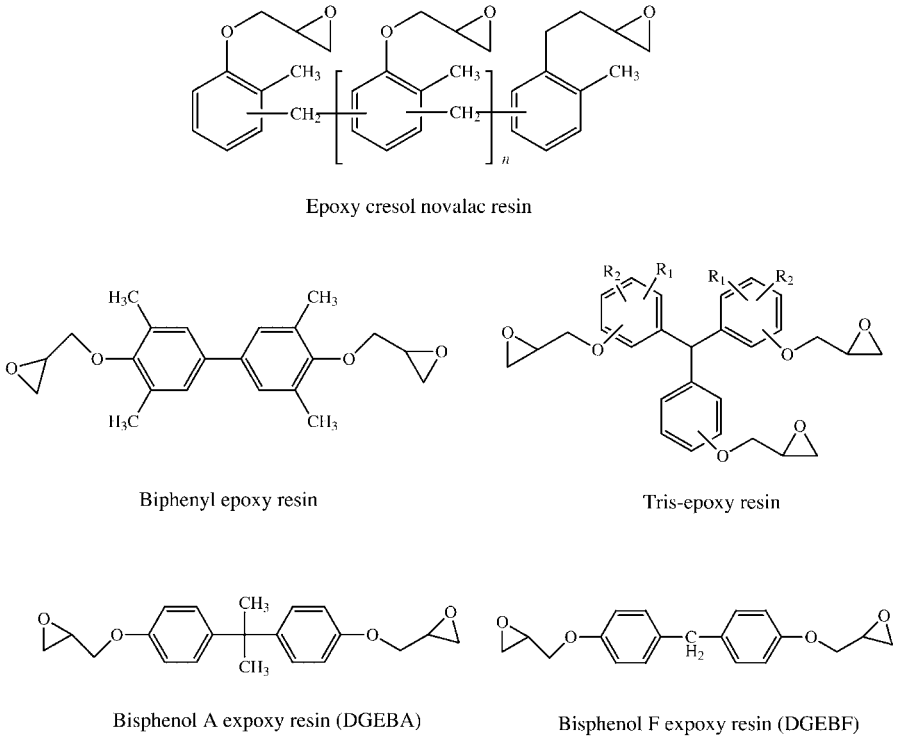

Fig. 20. General structures of epoxy resins used in semiconductor mold compounds.

bisphenol A epoxies. The choice of curing agent and cure accelerator not only determines the structure of the cured resin but also affects viscosity and reactivity. Anhydrides and amines are the most commonly used curing agents. *Accelerators* are catalysts that control the composition gel and cure times and can, as the case of Lewis acid catalysts, promote linear polymerization to form polyether linkages and thus modify the modulus of the resin by decreasing the number of network crosslinks.

Filler materials are used to modify resin properties and are essential components in obtaining desired encapsulant properties (71). The preferred filler material is ground, fused quartz which has a CTE of 0.5 ppm/°C. A silica filler loading of 68–70% reduces the CTE of the neat resin from 40–50 ppm/°C to 20–24 ppm/°C. Improved resins and spherical filler technology has allowed an increase in loading up to 85%, resulting in reduction of CTE to 10–15 ppm/°C. Decreased CTEs provide improved thermal stability and thermal-shock resistance during wide temperature fluctuations. Additional benefits of increased filler loading are increased thermal conductivity, reduced moisture absorbance, and reduced shrinkage during molding. While generally increasing the encapsulant elastic modulus, fillers decrease the flexural and tensile strength and do not usually provide significant enhancement to T_g or to package heat distortion properties. Filler size, shape, and loading determine the rheology of the molten encapsulant. Filler materials are treated with adhesion promoters to increase the adhesion of the resin to

Table 9. Selected Properties of Commercial Semiconductor Molding Compounds

Supplier	Designation	Thermal conductivity, J/cm·s·°C	T_g, °C	CTE α_1, ppm/°C	CTE α_2, ppm/°C	Flexural strength, MPa	Flexural modulus, GPa	Moisture absorption, wt%	Resin type
Dexter	Hysol[a] MG36F-25A	7.5×10^{-3}	170	19	65	138	16.6	0.43[b]	ECN
	Hysol MG46F	7.5×10^{-3}	160	17	70	131	15.2	0.47[b]	Blend
	Hysol MG52F-99B	8.4×10^{-3}	155	15		138	16.6	0.46[b]	ECN
	Hysol GR810	9.6×10^{-3}	155	11	11	118	20.5	0.28[b]	ECN
	Hysol GR8800	8.8×10^{-3}	200	10	50	107	16.9	0.39[b]	Blend
Hitachi Chemical	CEL-9120	–	135	7	–	–	26.5	0.32[c]	–
	CEL-9200	–	120	8	–	–	25.5	0.30[c]	–
	CEL 9600	–	145	7	–	–	27.5	0.23[c]	–
Nitto Denko	MP-8000A	6.7×10^{-3}	158	18	70	137	13.2	0.6[d]	ECN
	MP-8000C	8.4×10^{-3}	150	13	49	167	18.6	0.3[d]	ECN
	MP-7000	7.1×10^{-3}	125	16	65	167	16.2	0.35[e]	BP
	MP-7410TA	8.8×10^{-3}	120	8	32	177	27.0	0.17[d]	BP
	HC-100-X1	9.6×10^{-3}	160	6	25	147	27.5	0.18[d]	
Sumitomo-Bakelite (76)	EME 1100H[2]	6.7×10^{-3}	155	20	–	137	15.7	–	–
	EME 6200[2]	6.7×10^{-3}	165	18	–	127	12.7	–	–
	EME 6300H[1]	6.7×10^{-3}	168	16	65	118	12.7	0.30	–
	EME 6710[1]	6.7×10^{-3}	175	13	65	118	11.3	0.30	–

[a] Hysol is a registered trademark.
[b] After 168 h at 85°C/85% rh.
[c] After 20 h pressure cooker.
[d] After boiling 48 h.
[e] After 120 h at 85°C/85% rh.

the filler, resulting in improved encapsulant mechanical strength and decreased moisture absorption. Commonly used adhesion promoters include organosilanes and organotitanates. Stress-relief additives, such as silicones and acrylonitrile–butadiene elastomers, are often added to reduce the elastic modulus, improve toughness and flexibility, and lower the compound CTE (72). The final components added to the mold compound formulation are mold-release agents that aid in releasing the molded packages from the mold; flame retardants to reduce flammability; and coloring agents, generally carbon-black, that reduce device visibility and serve to distinguish one device type from another. Table 9 shows a listing of some commercial semiconductor molding compounds with selected physical data (73–76).

BIBLIOGRAPHY

1. E. J. Rymaszewski and R. R. Tummala, in R. Tummala and E. J. Rymaszewski, eds., *Microelectronics Packaging Handbook*, Vol. **3**, Van Nostrand Reinhold Co., Inc., New York, 1989.
2. P. Van Zandt, *Microchip Fabrication: A Practical Guide to Semiconductor Processing*, McGraw-Hill, New York, 1997.
3. M. G. Pecht and co-workers, *Electronic Packaging Materials and Their Properties*, Vol. **28**, CRC Press, Inc., Boca Raton, Fla., 1999.
4. J. H. Lau, C. P. Wong, J. L. Prince, and W. Nakayama, *Electronic Packaging: Design, Materials, Process, and Reliability*, Vol. **406**, McGraw-Hill, New York, 1998.
5. Ref. 1, pp. 537–538.
6. J. H. Lau and S. W. Ricky Lee, *Chip Scale Packaging: Design, Materials, Processes, and Applications*, McGraw-Hill, New York, 1999.
7. Ref. 1, pp. 532–534.
8. F. Shoraka, C. A. Gealer, and E. Bettez, *Semiconductor International* 110–113 (Oct., 1988).
9. K. Horie, in K. Horie and T. Yamashita, eds., *Photosensitive Polyimides: Fundamentals and Applications*, Technomic Publishing Co., Inc., Lancaster, Pa., 1995.
10. P. V. Robock and L. T. Nguyen, in R. Tummala and E. J. Rymaszewski, eds., *Microelectronics Packaging Handbook*, Vol. **540**, Van Nostrand Reinhold Co., Inc., New York, 1989.
11. Ref. 10, pp. 542–544.
12. Ref. 10, pp. 618–621.
13. Ref. 4, p. 419.
14. M. Fryd, in K. Mittal, ed., *Polyimides: Synthesis, Characterization, and Applications*, Plenum Press, New York, Vol. **1**, 1984 pp. 377–383.
15. M. J. Wusik and B. Jha, *Poly. Prepr. (Am. Chem. Soc., Div. Poly. Chem.)* 218–219, (1991) **32**(3).
16. H. H. Gibbs, *J. Appl. Polym. Sci.* **35**, 207 (1999).
17. C. Feger and H. Franke, in M. K. Ghosh and K. Mittal, eds., *Polyimides: Fundamentals and Applications*, Marcel Dekker, Inc., New York, 1996, pp. 787–788.
18. M. I. Bessonov and V. A. Zubkov, *Polyamic Acids and Polyimides: Synthesis, Transformations, and Stucture*, CRC Press, Inc., Boca Raton, Fla., 1993.
19. M. I. Bessonov, M. M. Koton, V. V. Kudryavtsev, and L. A. Laius, in W. W. Wright, ed., *Polyimides: Thermally Stable Polymers*, Consultants Bureau Division of Plenum Publishing Corp., New York, 1987.

20. W. Volksen and P. Cotts, in Ref. 14, pp. 163–169.
21. W. D. Weber and M. R. Gupta, in W. D. Weber and M. R. Gupta, eds., *Recent Advances in Polyimide Science and Technology*, Mid-Hudson Society of Plastics Engineers, 1987, pp. 214–224.
22. A. Saiki, K. Mukai, T. Nishida, H. Suzuki, and D. Makino, in K. Mittal, ed., *Polyimides: Synthesis, Characterization, and Applications*, Vol. **2**, Plenum Press, New York, 1984, pp. 826–839.
23. C. E. Diener and J. R. Susko, in Ref. 14, pp. 353–376.
24. R. Dammel, *Diazonapthoquinone Resists, SPIE-The International Society for Optical Engineering*, Bellingham, Wash., 1993.
25. L. F. Thompson, C. Grant Willson, and M. J. Bowden, *Introduction to Microlithography*, 2nd ed., American Chemical Society, Washington, D.C., 1994.
26. R. Mo, K. Schlicht, T. Maw, M. Masola, and R. Hopla, in C. Feger, M. M. Khojastek, and M. S. Htoo, eds., *Advances in Polyimide Science and Technology*, Technomic Publishing Co., Inc., Lancaster, Pa., 1993, pp. 559–570.
27. U.S. Pat. 3,856,752, (1974), J. Bateman and D. A. Gordon (to Ciba-Geigy Corp.).
28. P. Falcigno, M. Masola, D. Williams, and S. Jasne, in C. Feger, M. M. Khojasteh and J. E. McGrath, eds., *Polyimides: Materials, Chemistry, and Characterization*, Elsevier, New York, 1989, pp. 497–512.
29. *Product brochure, Durimide(TM) Polyimides for the Microelectronics Industry*, Arch Chemicals, Inc., Norwalk, Conn., 2000.
30. *Product brochure, Polyimide Coatings for Electronics*, Toray Industries, Inc., Chiba, Japan, 1999.
31. *Product brochure, PIX Series-Self Priming, Wet-Etch Polyimides*, HD Microsystems, LLC, Wilmington, Del., 2001.
32. *Product brochure, Sumiresin Excel CRC-8000*, Sumitomo-Bakelite Co., Ltd., Tokyo, 1998
33. *Product data from company website*, HD Microsystems, LLC, Wilmington, Del., 2001 (www.hclmicrosystems.com).
34. C. Czornyj and co-workers, in R. R. Tummala, E. J. Rymaszewski, and A. G. Klopfenstein, eds., *Microelectronics Packaging Handbook: Semiconductor Packaging Part II*, 2nd ed., Chapman and Hall, New York, 1997, p. 590.
35. R. Rubner, *Siemens Forsch.-u.Entwikl.-Ber.* **5**, 92 (1976).
36. R. Rubner, W. Bartel, and G. Bald, *Siemens Forsh.-u. Entwickl. -Ber.* **5**, 235 (1976).
37. H. Ahne, H. Kruger, E. Pammer, and R. Rubner, in Ref. 14, pp. 353–376.
38. N. Yoda and H. Hiramoto, *J. Macromol. Sci. Chem. A* **21**, 1641 (1984).
39. J. M. Bureau and J. P. Droguet, in Ref. 17, pp. 745–746.
40. O. Rohde, M. Riediker, and A. Schaffner, SPIE, Proceedings, Vol. 539, (*Advances in Resist Technology and Processing*), 1985, pp. 175–180.
41. R. Hopla and co-workers, in *Proceedings of The 10th International SPE Conference on Photopolymers*, Mid-Hudson Society of Plastics Engineers, 1994, pp. 463–469.
42. C. N. Lazaridis, D. K. Flattery, and W. J. Lautenberger, in *Proceedings of the 10th International SPE Conference on Photopolymers*, Mid-Hudson Society of Plastics Engineers, 1994, pp. 470–472.
43. S. A. Swanson, M. Sherwood, D. R. McKean, J. W. Labadie, and R. D. Johnson, in *Proceedings of the 10th International SPE Conference on Photopolymers*, Mid-Hudson Society of Plastics Engineers, 1994, pp. 474–482.
44. L. Peterson, D. Racicot, A. Roza, and W. Weber, *Microlithography World, Summer ed.*, Pennwell, Tulsa, Okla., 1998.

45. S. Hagen and co-workers, in *Proceedings of the 11th International SPE Conference on Photopolymers*, Mid-Hudson Society of Plastics Engineers, 1997, pp. 422–437.
46. W. W. Flack, G. E. Flores, L. Chrisensen, and G. Newman, *SPIE Proceedings*, Vol. 2726, 1996.
47. J. Pfeifer and O. Rohde, in W. D. Weber and M. R. Gupta, eds., *Recent Advances in Polyimide Science and Technology*, Mid-Hudson Society of Plastics Engineers, 1987, pp. 336–361.
48. A. A. Lin and co-workers, *Macromolecules* **21**, 1165–1169 (1988).
49. M. Ree, K. J. Chen, and G. Czornyj, *Polym. Eng. Sci.* **32**(14), 924–930 (1992).
50. Ref. 34, pp. 589–602.
51. E. W. Rytter Jr. and co-workers, in *Proceedings of 1st International Conference on Multichip Modules*, Denver, 1992, p. 394.
52. P. Garrou and co-workers, *IEEE Trans. Advanced Packaging*, Vol. **22**, 1999, p. 487.
53. U.S. Pat. 6,010,825 (Jan. 4, 2000), S. Hagen and N. Reichlin, (to Olin Microelectronic Chemicals, Inc.).
54. U.S. Pat. 5,856,065 (Jan. 12, 1999), Y. Okabe and co-workers (to Hitachi, Ltd., Hitachi Chemical Co.).
55. U.S. Pat. 6,025,113 (Feb. 15, 2000), H. Kikkawa and co-workers (to Hitachi Chemical Company, Ltd.).
56. U.S. Pat. 4,927,736 (May 22, 1990), W. H. Mueller and D. K. Khanna (to Hoescht Celanese Corp.).
57. U.S. Pat. 4,339,521 (July 13, 1982), H. Ahne, E. Kuhn, and R. Rubner (to Siemens Aktiengesellschaft).
58. R. Sezi and co-workers, in *Proceedings of the 10th International SPE Conference on Photopolymers*, Mid-Hudson Society of Plastics Engineers, 1994, pp. 444–452.
59. Ref. 24, pp. 19–24.
60. R. Sezi, G. Schmid, W. Radlik, D. Krabe, and K. Buschick, *Abstracts of the 11th International SPE Conference on Photopolymers*, SPE, 1997.
61. *Product brochure, Pyralin (R) PI2720 Processing Guidlines*, HD Microsystems, LLC, Wilmington, Del., 1998.
62. *Product brochure, PIMEL™ Photosensitive Polyimide Precursors*, Asahi Chemical Industry Co., Ltd., Tokyo, Japan, 1999.
63. *Product brochure, PI2771 Photosensitive Polyimide Process Guidelines*, HD Microsystems, LLC, Wilmington, Del., 2001.
64. J. Hintzke, *HDI Magazine*, **26** (March, 2001).
65. M. G. Pecht and L. T. Nguyen, in Ref. 34, p. 502.
66. Product brochures, Ablestik Laboratories, Rancho Dominguez, Calif., www.ablestik.com, May 2001.
67. Product brochures, Hysol® and Quantum Conductive Adhesives, Leadframe Die Attach, Dexter Electronic Materials, Industry, Calif., www.dexelec.com, May 2001.
68. Product brochures, Conductive Adhesives, Epoxy Technology, Billerica, MA, www.eopotek.com, May 2001.
69. Ref. 65, p. 408.
70. H. Rauhut, New Types of Microelectronic Epoxy Compounds, Technical Report, Dexter Electronic Materials, 1994, pp. 4–5.
71. Ref. 10, pp. 562–563.
72. Ref. 65, p. 418.
73. *Product data sheets, Dexter Electronic Materials*, Olean, N.Y. Internet web site: www.dexelec.com, Aug. 1999.

74. *Product data sheets*, Hitachi Chemical Co., America, Ltd., Santa Clara, Calif., www.hitachi-chemical.com, May 2001.
75. *Product data sheets*, Nitto-Denko America, Ltd. Fremont, Calif., www.nitto.com, May 2001.
76. *Product brochures, Ultra Low Stress Compound EME 6710 (Sept. 1989) and Super Low Stress Epoxy Molding Compound "Sumikon" EME-6300/9300 Series For VLSI"* Sumitomo-Bakelite Co., Ltd., Tokyo, Japan.

WILLIAM D. WEBER
Arch Chemicals

ELECTROOPTICAL APPLICATIONS

Introduction

The term *electrooptic* can have widely different meanings. In the broadest sense, it can imply any change produced in an optical beam by application of an electrical field from either a low frequency (dc to millimeter wave) field or another optical (micrometer wave) field. Change of the index of refraction of the material through which an optical beam is transiting can influence the (velocity of the) propagating optical beam. Such change of index of refraction can be accomplished by altering either the electron distribution or the nuclear configuration of a material. The associated optical phenomena are referred to as Kerr and Pockels effects (1–15) and have been known since the nineteenth century.

However, altering an optical beam by electrically controlled mechanical movement of a mirror (particularly as in micro-electro-mechanical-systems, MEMS) is also referred to as an electrooptic operation. Indeed, even greater confusion arises by usage of the terms electrooptic and all-optical signal processing in the telecommunications industry. Electrooptic is taken to refer to converting optical signals to electrical signals, carrying out signal processing in the electrical (electronic) domain, and then converting back to the optical domain. Thus, techniques such as bubble jet (Hewlett Packard/Agilent) and MEMS (Texas Instruments) optical switching at network nodes are referred to as all-optical signal processing by telecommunication engineers while an optical physicist would reserve the term all-optical switching for the dynamic Kerr phenomenon (switching of one optical beam by another).

A review of electrooptical applications in the broadest sense is out of the question. It would involve treatment of topics ranging from modulated lasers (direct modulation) to light-emitting diodes (LEDs), to liquid crystalline materials,

Encyclopedia of Polymer Science and Technology. Copyright John Wiley & Sons, Inc. All rights reserved.

not to mention MEMS, thermooptic, and bubble jet technologies currently used in telecommunications. Moreover, the literature is enormous. Over 1000 reviews and texts have appeared on the subject of liquid crystalline electrooptic materials alone. In this article, a narrow view of electrooptic phenomena, materials, and applications is taken and focus is upon the "electronic" Pockels effect, with emphasis on the phenomenon realized using polymeric or dendritic materials rather than inorganic or organic single crystals. The term *electronic* refers to changes in refractive index associated purely with electric-field-induced change of the electron distribution of a material (in contrast to changes in nuclear configuration associated with molecular reorientation). Moreover, there is a focus upon π-electron organic chromophores rigidly embedded in polymeric or dendritic supramolecular matrices. Currently, commercially utilized materials exploiting the electronic Pockels effect are inorganic crystalline materials such as lithium niobate. Although the most commercially viable organic electrooptic (defined in the broader sense) materials are liquid crystalline materials (16–58), electronic Pockels effect organic materials are receiving increased attention because of the possibility of exceptional (greater than 100 GHz) bandwidth performance. Although potential applications of such materials range from telecommunications to information processing, to defense, to transportation, and to display industries, the telecommunications and defense industries are particularly important drivers of development of electrooptic materials with greater bandwidths. Electronic Kerr materials (59–67) have the potential for even greater bandwidth and the possibility of convenient all-optical signal processing; however, to the present time electronic Kerr coefficients have not been large enough to be commercially viable for telecommunication applications. Mott–Hubbard transition-metal oxide and halide systems with charge-transfer gaps and low hydrogen-density organic materials such as the fullerenes and chromophore-containing dendrimers may hold future promise for all-optical switching at telecommunication wavelengths (eg, 1.55 μm) because of their large two-photon absorption coefficients (third-order optical nonlinearities) and their low optical loss. Inorganic Kerr materials such as titanium sapphire are currently used for mode-locked lasers and other applications.

Other reasons for heightened interest in organic electronic electrooptic materials include large electrooptic coefficients (greater than 50 picometers/volt (pm/V) at telecommunication wavelengths). Large electrooptic coefficients permit voltages from semiconductor electronics to drive electrooptic devices without the introduction of amplifiers. Amplifiers are undesirable because of their bandwidth limitations, noise figures, weight, bulk, and cost. Indeed, a major reason for increased commercial interest in organic electrooptic materials is that drive voltages of less than 1 V can be realized with simple broadband device structures (68,69). Such drive voltages permit lossless telecommunication links to be achieved and even permit realization of gain in electrical-to-optical-to-electrical signal transduction. Another attractive feature of organic electrooptic materials is facile integration with semiconductor electronics and silica fiber optics (70–74). In this article, both the state of development of organic electrooptic materials and the principles that define material performance are reviewed.

The reader is referred elsewhere for reviews of organic photorefractive materials (75–86) and of photochromic and optomechanical materials (87). Electronic electrooptic chromophores (such as charge transfer azobenzenes) have frequently

been used for such applications, but the response times of these phenomena and their conceptual basis are quite different from the phenomenon and applications discussed here. (See also CHROMOGENIC POLYMERS; LIGHT-EMITTING DIODES).

General Theoretical Principles

At the molecular level, the change in electron distribution (polarization) with application of an electrical field is given by

$$p_i = p_{0i} + \alpha_{ij}E_j + \beta_{ijk}E_jE_k + \gamma_{ijkl}E_jE_kE_l + \cdots \tag{1a}$$

where p_{0i} is the permanent polarization of the molecular site "i" and E stands for the local electric field strength. The tensors α, β, and γ are the molecular polarizability and molecular first and second hyperpolarizabilities. For macroscopic or bulk materials, the polarization equation is

$$P_i = P_{0i} + \chi^{(1)}_{ij}E_j + \chi^{(2)}_{ijk}E_jE_k + \chi^{(3)}_{ijkl}E_jE_kE_l + \cdots \tag{1b}$$

It is assumed that the electric fields in equations (1a) and (1b) have frequencies that are outside the domain of both electronic and lattice resonances of the system. If only one electric field is applied and it is in the form of a square wave pulse (of amplitude E_0), or an a-c field ($E_0 \cos \omega t$), or a d-c field (of amplitude E_0), then equations (1a) and (1b) lead to the following expression for refractive index n:

$$(1/n^2) = (1/n_0^2) + rE_0 + RE_0^2 + \cdots \tag{2}$$

where n_0 is the refractive index in the absence of the electric field. The linear and quadratic terms correspond to the Pockels and Kerr effects, respectively. The Pockels effect is observable only for noncentrosymmetric materials; the electrooptic coefficient r is related to the molecular first hyperpolarizability β and the noncentrosymmetric order parameter $\langle \cos^3 \theta \rangle$ by

$$r = 2\mathrm{Nf}(\omega)\beta\langle \cos^3\theta \rangle / n^4 \tag{3}$$

where N is the chromophore number density and $f(\omega)$ is a local field factor accounting for the dielectric nature of the medium (host material). The electrooptic coefficient r is related to the drive voltage required to effect electrical-to-optical signal transduction (with a Mach Zehnder interferometer) by

$$V_\pi = \lambda d/(n^3 \mathrm{rL}\Gamma) \tag{4}$$

V_π is the voltage required for a π phase shift of light passing through the arm of the Mach Zehnder modulator to which an electric field has been applied. The optical wavelength of the transiting light is given by λ, d is the gap between the electrodes used to apply the electric field, L is the interaction length of the

electrical and optical fields (electrode length in the simplest case), and Γ is a modal overlap integral. Equation (3) is greatly oversimplified as we have neglected the vectorial nature of the interaction of the fields, but this equation is frequently applicable to poled polymer materials.

From equations (2) and (3), it is readily seen that optimizing the drive voltage performance of electrooptic materials is a matter of optimizing β, N, and $\langle\cos^3\theta\rangle$. We shall proceed to discuss the optimization of these parameters and the status of organic electrooptic materials, but before we do this, it is important to indicate what additional material properties must be achieved for commercial viability. These can be briefly summarized as follows: (*1*) fast response time or high operational bandwidths, (*2*) low optical loss including both material loss and insertion (optical mode mismatch) loss, (*3*) good stability including thermal and photochemical stability, (*4*) good mechanical properties, (*5*) good processability and ease of integration with disparate materials such as silica fibers, semiconductors, and metals, and (*6*) low production cost. For polymers to displace alternative technologies such as modulated semiconductor lasers, lithium niobate electrooptic modulators, or gallium arsenide (GaAs) electroabsorptive modulators, they must exhibit competitive or superior performance characteristics in all material categories. Thus, in the following paragraphs, we consider auxiliary properties as well as electrooptic activity.

Electrooptic Activity

It is clear that optimizing electrooptic activity involves optimizing the molecular hyperpolarizability β of organic chromophores. Quantum mechanics has provided effective guidance for the improvement of molecular nonlinear optical (electrooptic) activity by several orders of magnitude in the past 10 years (88–97). If chromophores are aligned into a noncentrosymmetric (acentric) lattice by electric field poling and if the interactions among chromophores are neglected, then the order parameter becomes (in the high temperature approximation) $\langle\cos^3\theta\rangle = \mu F/5kT$, where μ is the chromophore dipole moment, F is the applied electric poling field felt by the chromophores, k is the Boltzmann constant, and T is the poling temperature (Kelvin). In this approximation, macroscopic electrooptic activity would be expected to increase as $\mu\beta$. As can be seen from Figure 1, $\mu\beta$ values have been systematically improved over the past decade from the value of the 1990 state-of-the-art material Disperse Red (DR). Indeed, if current chromophores could be organized into a pure chromophore lattice with perfect acentric order, $\langle\cos^3\theta\rangle = 1.0$, then electrooptic coefficients in excess of 1000 pm/V could be achieved. Such electrooptic coefficients would permit true millivolt drive voltages to be routinely employed. Such materials would greatly exceed the performance of lithium niobate ($r = 31$ pm/V, $V_\pi = 5$–6 V) and would likely displace liquid crystalline materials in applications such as spatial light modulation and optical switching. However, while the DR chromophore of Figure 1 exhibits an electrooptic coefficient of 10–15 pm/V and V_π voltages of 12–20 V, the FTC chromophore exhibits a surprising low electrooptic coefficient of 35–50 pm/V and V_π voltages of 3–5 V. Clearly, a problem existed/exists in translating large molecular electrooptic activity into usably large macroscopic electrooptic activity.

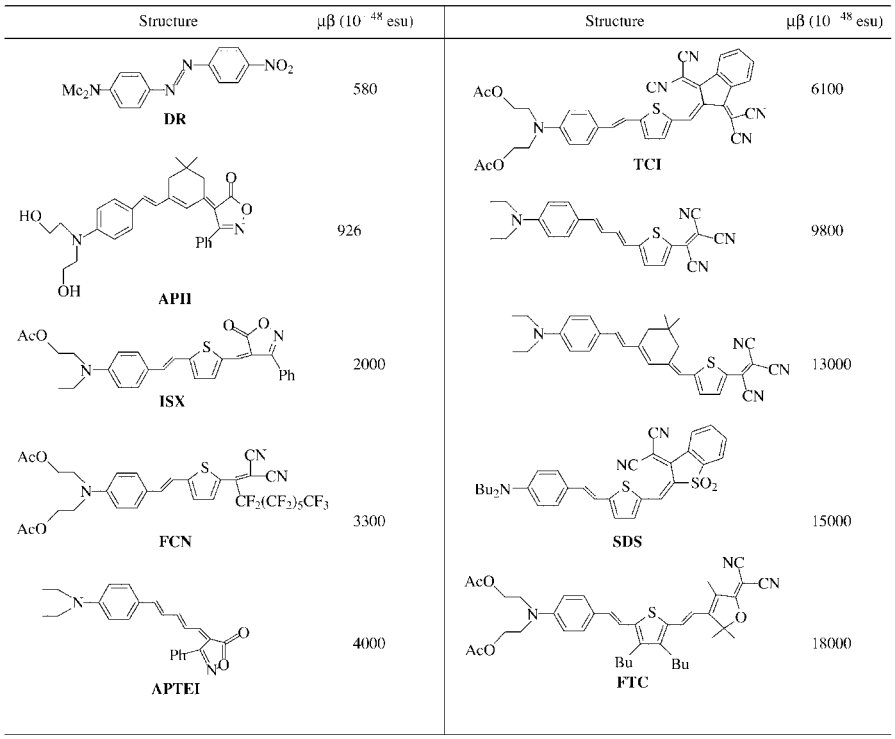

Fig. 1. The variation of $\mu\beta$ (dipole moment-first hyperpolarizability product) with chromophore structure is shown.

As is illustrated in Figure 2, the problem is now understood to derive from intermolecular electrostatic interactions among chromophores opposing the poling field in introducing the acentric order required for electrooptic activity (68,98–102). The same interactions oppose introduction of acentric order by sequential synthesis, self-assembly techniques where surface forces are used in place of a poling field to guide the assembly of chromophores into an acentric lattice (103). In this latter case, intermolecular electrostatic interactions cause the chromophores to tip away from the normal to the surface in their assembly. The problem has been successfully modeled using both equilibrium statistical mechanical methods and kinetic Monte Carlo methods, with both approaches specifically treating the many-body, long-range, spatially anisotropic interactions among chromophores. The intermolecular electrostatic interaction potential functions of equilibrium statistical mechanical and Monte Carlo methods are found to be very similar and approximate the potential function introduced by Piekara in the 1930s (104). Theoretical calculations explain a great many additional experimentally observed features including the relatively weak dependence of maximum achievable electrooptic activity upon electric poling field strength and phenomena such as concentration and electric-field-dependent phase separation. The theoretical rationalization of the dependence of achievable electrooptic activity upon the electronic and molecular structure of chromophores and the processing conditions (applied poling field

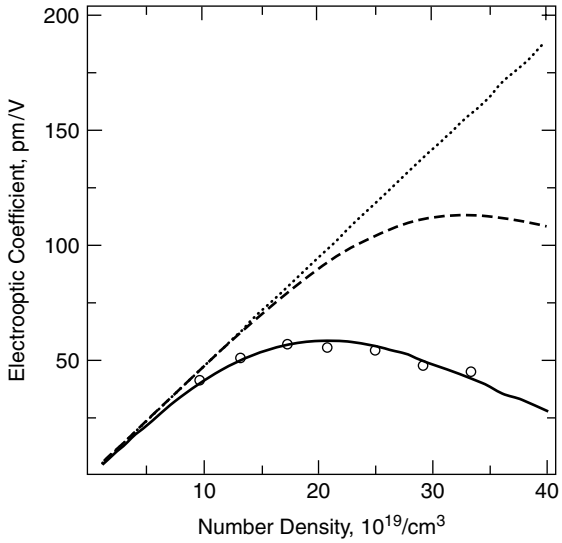

Fig. 2. The experimental and theoretically predicted dependence of electrooptic coefficient for the FTC chromophore (see Fig. 1) in poly(methyl methacrylate) (PMMA) upon chromophore number density (concentration in PMMA) is shown. Theoretical results are shown for various shape approximations and for the neglect of intermolecular electrostatic interactions (the ideal gas model). ------ Gas model; – – Sphere; —Prolate ellipsoid; ○ Experimental.

strength, dielectric constant of the host polymer matrix, chromophore concentration, temperature, etc) has provided both good and bad news. The bad news is that it will always be impossible to realize more than a fraction of the potential electrooptic activity represented by a given chromophore structure. Electrooptic coefficients of a few hundred pm/V may be obtainable, but values of 1000 pm/V or greater will be unobtainable with high dipole moment chromophores unless some other force (eg, ionic) is used to overwhelm the effect of dipole–dipole interactions. The good news is that theory provides guidance to quick optimization of electrooptic activity for a given chromophore/polymer system. The concentration (number density) of chromophores leading to maximum electrooptic activity is predicted by theory with high accuracy. Moreover, theoretical results argue that the shape of chromophores should be altered from their normal prolate ellipsoidal shape to a more spherical shape. This is readily accomplished by adding inert substituent (alkyl or alicyclic) groups to the waist of chromophores (68). An even more promising route is that of dendrimer synthesis including dendrimer structures where more than one chromophore is incorporated into the dendrimer. Very simply, steric forces are used to prevent chromophores from achieving centric order driven by dipole–dipole interactions. An example of an early version multichromophore dendrimer, which has led to electrooptic coefficients of 60 pm/V at 1.55 μm telecommunication wavelength, is shown in Figure 3 (105).

Theoretical guidance has permitted polymeric electrooptic materials to be fabricated that exhibit electrooptic coefficients in excess of 100 pm/V (68,106) at telecommunication wavelengths. With these materials, V_π voltages of less than 1 V have been achieved. This has been, without question, a very important

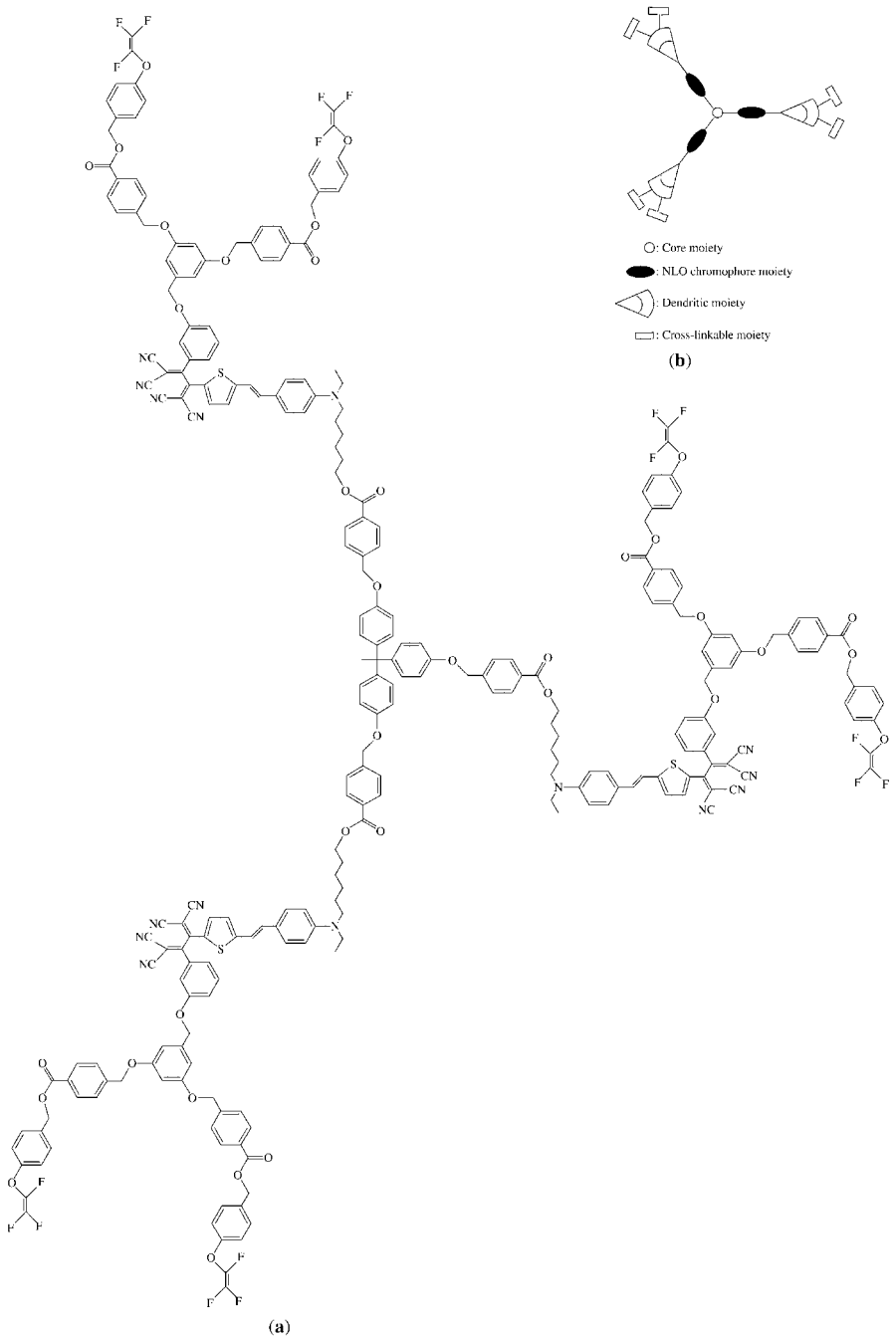

Fig. 3. (a) An early version multichromophore dendrimer (105) is shown. This cross-linkable dendrimer yields an electrooptic coefficient of 60 pm/V at 1.55 μm wavelength that is stable under testing at 85°C for 1000 h. (b) Schematic representation. $M_w = 4664$; Chromophore density: 33 wt%.

result stimulating considerable interest from both large and small companies in the telecommunications and defense fields. V_π voltages on the order of 1 V permit low cost complementary metal oxide semiconductor (CMOS) and high speed electrochemical luminescent circuits to be used without amplifiers. Moreover, such low voltages are important for the realization of transparent (low loss) communication links. Indeed, the realization of deep optical modulation with low electrical drive voltage can lead to gain in electrical-to-optical-to-electrical signal transduction. In satellite telecommunication applications, the elimination of low noise amplifiers is important for the reduction in launch weight as well as for reducing noise and cost. The practical (commercial) importance of the advances in electrooptic activity rests upon two issues: (*1*) Can electrooptic activity be further improved and by how much? (*2*) Can large electrooptic activity be achieved in conjunction with all of the other required properties? The answer to the first question is very likely positive. Indeed, it is clear that electrooptic activity will be further improved by at least another factor of 2. The answer to the second question will become clear from the following paragraphs.

Bandwidth

The bandwidth (response time or highest frequency component of data that can be handled) of devices fabricated from electrooptic materials is determined by the index of refraction n and dielectric constant ε of the materials from which the devices are fabricated. For polymeric organic electrooptic materials, $\varepsilon = n^2$ approximately. This means that low frequency electrical and high frequency optical waves propagate with the same velocities in a material. This in turn means that long interaction lengths can be employed, which leads to low drive voltage requirements. For example, 3-cm electrodes were used to achieve sub 1-V V_π values for polymeric modulators (68). For organic materials, voltage-length products are currently of the order of 1–3 V·cm. The typical index of refraction values ($n = 1.55$–1.70) and dielectric constant values ($\varepsilon = 2.4$–3.0) for polymeric organic materials have permitted electrooptic device bandwidths of 113 GHz to be demonstrated using simple device structures (107–110). Pulsed measurements establish that the intrinsic material bandwidth response is of the order of 350 GHz (essentially defined by the phase relaxation time of the π-electron system). Device bandwidth-length product values could conceivably be as high as 350 GHz·cm with polymeric organic electrooptic materials; however, the difficulty of transmitting electrical signals with frequency components above 120 GHz through metal electrodes makes this a difficult objective to achieve. The low dielectric constants of organic materials also lead to very favorable power requirements (eg, typical P_π values are on the order of 4 dB). Crystalline organic materials achieve acentric order by exploiting ionic interactions to overwhelm the chromophore π-electron dipole interactions that favor centric order. These ionic interactions lead to higher index of refraction and dielectric permittivity values, eg, 2.5 and 7.0 respectively.

For lithium niobate, dielectric constants are of the order of 28 while index of refraction is of the order of 2.2. The bandwidth-length product is 10 GHz-cm and the voltage-length product is 5 V-cm. By clever engineering (minimizing the

time spent by electrical waves in high dielectric lithium niobate), lithium niobate devices have been demonstrated to approximately 90 GHz. Commercial devices are available from Lucent with bandwidths of 30 GHz, V_π voltages of 6 V (1550 nm), insertion loss of 6 dB, and temperature stability to 70°C. The high dielectric constant of lithium niobate results in high power dissipation, ie, $P_\pi >$ 32 dB currently. While high frequency operation is possible with devices fabricated from lithium niobate, more sophisticated device engineering is required. Moreover, such bandwidth is accomplished with sacrifice of drive voltage. The high intrinsic bandwidth afforded by polymeric organic materials was early on recognized as one of the greatest advantages of such materials. The fact that the high bandwidth of organic electrooptic materials is now accompanied by low drive voltage requirements argues for the serious commercial consideration of these materials.

GaAs electroabsorptive modulators offer the possibility of high bandwidth (50 GHz) and low drive voltage (1–2 V). However, these materials exhibit substantial chirp. It is impossible to change absorption without also changing index of refraction. Moreover, GaAs devices are plagued by high insertion loss (9–12 dB). Lithium niobate modulators seem to be the currently preferred alternative to GaAs modulators for high frequency (10–30 GHz) applications.

Modulated lasers, thermooptic switches, liquid crystalline modulators, bubble jet switches, and MEMS devices suffer even greater bandwidth limitations. The introduction of wavelength division multiplexing (WDM) has taken some of the bandwidth pressure off of purely time division multiplexing (TDM) approaches to handling telecommunication throughput. However, bandwidth is likely to remain a serious issue for future telecommunication systems, and thus the bandwidth performance organic and inorganic electrooptic materials will remain an issue of active concern.

Optical Loss

One of the most attractive advantages of lithium niobate is exceptionally low optical loss (material loss of 0.2–0.4 dB/cm and device insertion loss of 3–6 dB at telecommunication wavelengths). Optical loss has been a problem with polymer materials until recently when a better understanding of factors leading to both material and insertion optical loss has permitted significant improvement in loss values (to material loss values of as low as 0.2 dB/cm and insertion loss values as low as 4 dB at telecommunication wavelengths). Material optical loss can be associated with either absorption loss or loss due to scattering. Absorption loss can arise from either (or a combination of) interband electronic absorption or C—H (or N—H, O—H) vibrational overtone absorption at 1.3 or 1.55 μm wavelengths. Wavelength-dependent interband absorption is easily assessed by techniques such as photothermal deflection spectroscopy. Appropriate chromophore design can keep optical loss due to interband absorption below 1 dB/cm even at 1.3 μm wavelength. Such loss is probably not a significant factor at 1.55 μm telecommunication wavelength. Vibrational absorption at 1.3 and 1.55 μm wavelengths is a much more serious problem. As with the production of low loss silica fiber, the answer to the problem of intrinsic optical loss is to get the hydrogen out of

the material. Without such reduction in hydrogen content, optical loss in organic materials is typically limited to approximately 1 dB/cm at 1.3 μm wavelength and somewhat higher values at 1.55 μm wavelength. With organic materials, reduction in hydrogen content typically means using partially fluorinated materials or materials constructed with functionalities, such as the cyanurate ligand, that do not contain hydrogen (when the carbon positions are substituted). Using cyanurate and fluorinated dendrons, optical loss values as low as 0.2 dB/cm have been obtained for electrooptic dendrimer materials. Fluorination of polymer materials frequently involves unwanted changes in processability; for example, changes in solubility in spin-casting solvents. Dendrimer synthesis has been demonstrated to provide a convenient means of reducing optical absorption loss without paying a price in material processability.

Scattering losses induced by processing have been a much more insidious problem in the fabrication of low loss organic waveguide structures. Scattering losses can arise from several sources. One of the most obvious is material inhomogeneity associated with spin casting. Any phase separation leads to disastrously high loss values. Strong dipole–dipole interactions among chromophores can drive phase separation. Fortunately, such interactions can be attenuated by appropriate derivatization of chromophores. Such derivatization also improves the entropy of mixing (and hence the solubility) of chromophores in spin casting solvents. Electric field poling and the concurrent cross-linking of materials to lock-in poling-induced electrooptic activity can also lead to optical loss (71,100,106,111–113). Two types of optical loss are typically associated with electric field poling. The first arises from electric-field-induced surface damage. This is simply a form of dielectric breakdown and can be avoided by keeping corona poling field strengths below damage thresholds. It is important to keep in mind that the harder (more cross-linked) the polymer lattice, the higher the damage threshold. Thus, electric field poling and lattice hardening are typically carried out using a stepped temperature/electric field protocol (71,100,112,114–116). The second type of poling-induced scattering loss is associated with introduction of inhomogeneity in the material as the result of electric field poling. Such inhomogeneity can arise from an electrophoretic effect or from poling-induced birefringence. If defects (such as dust particles) exist that are not influenced by the poling field, then poling can enhance the index difference between these defect regions and the electrooptic material leading to enhanced scattering loss (117). Lattice hardening (cross-linking) chemical reactions can also be a source of material inhomogeneity that leads to increased scattering loss. This is particularly true with thermosetting reactions such as urethane chemistry where a variety of oligomeric structures can exist and grow at different rates (111). Some of these structures can become incompatible and phase separate. Moreover, some cross-linking chemistries, such as urethane chemistry, are susceptible to atmospheric moisture. The reaction with water from the atmosphere can upset the one-to-one stoichiometry of lattice hardening reactions leading to the buildup of incompatible components and phase separation. The occasionally observed cloudy appearance of polyurethane electrooptic polymers is typically indicative of problems with atmospheric moisture. However, when sources of optical loss associated with electric field poling and lattice hardening are taken into account, optical loss values on the order of 1 dB/cm are readily obtained (71,100,106,111–113).

Optical loss can also arise from fabrication of buried channel waveguide structures by reactive ion etching (RIE) techniques and by the deposition of cladding layers where the solvent employed in spin casting the cladding layer causes solvent pitting of the electrooptic film layer. Both of these loss mechanisms can be controlled by lattice hardening of the electrooptic material and by control of processing conditions. Control of the kinetic energy of reactive ions in RIE (118,119) can keep optical loss values due to waveguide wall roughness to insignificant values (0.01 dB/cm). Cladding layers pose an unanticipated problem for the utilization of organic-electrooptic materials. While cladding materials have been utilized that make no problematic contribution to optical loss, problems in device operation can frequently be traced to cladding materials rather than to the electrooptic materials. Conducting cladding materials can be particularly problematic. In general, one wants the electrical conductivity of the cladding material to be higher than that of the electrooptic material so as to drop the poling field across the cladding layer. However, if the cladding material has significant optical loss, the penetration of the propagating optical field into the cladding layer will result in unwanted attenuation of the transiting beam. The cladding material can also undergo photochemical damage and may do so even when the electrooptic material does not show damage. This can manifest in time-dependent loss of mode confinement when no change in electrooptic modulation efficiency is observed. A more subtle problem that can arise with conducting cladding materials is that of photoconductivity (or optical power-dependent conductivity). Electrooptic chromophores are very polarizable materials and can inject charge into a conducting medium (71,112). Thus, an optical power-dependent conductivity of the cladding material can result if that material is susceptible to accepting charge and transporting that charge. Such effects are typically observed only at high power levels in devices such as high frequency oscillators based on electrooptic modulator technology. Of course, optical fields must be kept away from lossy metal electrodes. Again, if care is taken in the design and execution of device structures, loss from waveguide fabrication, cladding deposition, and electrode deposition can be kept to insignificant values, and overall active waveguide loss values of 1 dB/cm can be routinely achieved.

The greatest loss issue to be faced in the commercial implementation of organic electrooptic devices is that of mode mismatch loss when coupling silica fiber and polymeric electrooptic modulator waveguides. For 1.3 μm telecommunication wavelength operation, silica optical fiber waveguides are cylindrical with spherical cross-sectional core diameters on the order of 10 μm, while the cross-sectional shapes of polymeric electrooptic modulator waveguides are elliptical with heights of 1–2 μm. Butt coupling of such active and passive waveguides leads to optical loss on the order of 4 dB per transition. The coupling problem is readily addressed using spherical lens or tapered transitions (70,71,112,120). A tapered transition such as shown in Figure 4 reduces coupling loss to a few tenths of a decibel. Thus, total insertion losses of 4–5 dB have been obtained for polymeric materials exhibiting material loss on the order of 1 dB/cm. Tapered transition structures can be fabricated by employing offset, gray scale, and shadow ion masking techniques (70), which are to be discussed later. Such lithographic techniques are also useful for constructing sophisticated 3-D circuits (70).

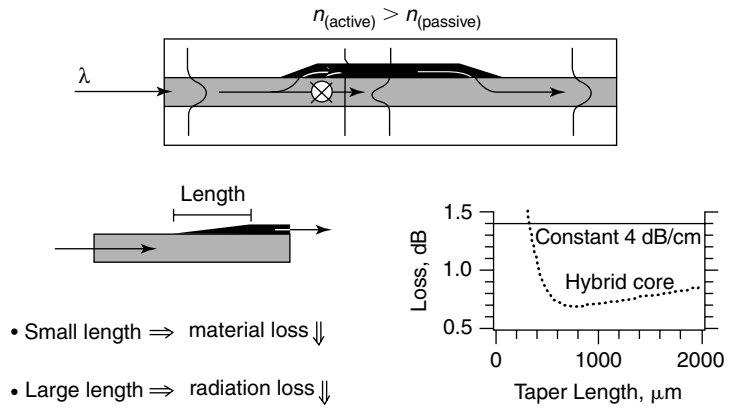

Fig. 4. A low loss polymeric electrooptic modulator transition structure is shown. The optimum taper length is defined by the trade-off between acceptable radiation loss and material loss.

Stability

For electrooptic materials (eg, liquid crystalline materials) based on index of refraction changes associated with molecular reorientation, one wants facile reorientation to permit fast switching times. Organic photorefractive materials also exhibit enhanced response when molecular reorientation contributes to observed index changes. In contrast, reorientation destroys the electric-field-poling-induced electronic electrooptic activity of chromophore-containing polymeric materials. When one speaks of thermal instability of electronic electrooptic activity for organic materials, one is referring to reorientational (molecular rotational) dynamics that destroy poling-induced acentric order. There are two general approaches to improving the stability of poling-induced order. One is to place chromophores in polymer materials, such as polyimides or polyquinolines, characterized by high glass-transition temperatures. This may be accomplished either by physically dissolving chromophores in polymers to produce composite materials or by covalently coupling chromophores to polymer lattices (71,112,121–134). The stability will be defined by both the segmental flexibility of the polymer backbone (the glass transition temperature) and the number (and positioning) of covalent bonds coupling the chromophore to the polymer lattice. The stability of poling-induced acentric chromophore order (electrooptic activity) can be readily assayed by monitoring second harmonic generation (another phenomena related to $\chi^{(2)}$) as a function of heating the sample (see Fig. 5) (135). This is a nonlinear optical analogue of thermal gravimetric analysis except that molecular reorientation rather than material decomposition accounts for the loss of second-order nonlinear optical activity. As shown in Figure 5, thermal stability of electrooptic activity is increased with cross-linking. When dynamic thermal stability is increased to temperatures such as 170°C as shown in Figure 5, then long-term stability is typically observed for periods of several thousand hours even when devices are operated at 100°C. Segmental flexibility of polymers is one of the most serious problems with relaxation

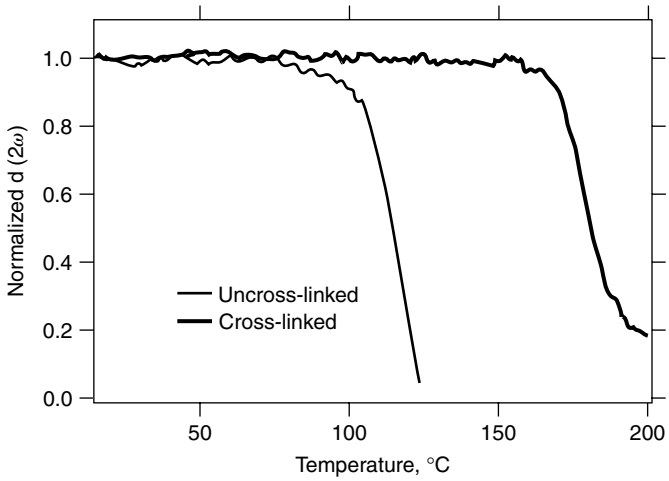

Fig. 5. Second harmonic generation is shown as a function of temperature for heating at a rate of 10°C per minute for two samples. The uncross-linked sample (chromophore is attached covalently by one end to a PMMA backbone) starts to lose second-order optical nonlinearity (acentric chromophore order) before 100°C. The cross-linked sample corresponds to both ends of the chromophore being covalently coupled to the polymer lattice. For this sample, thermally stable second-order optical nonlinearity is observed until nearly 170°C.

of poling-induced acentric order. Dendrimer materials appear to have distinct advantages for enhancing the thermal stability of poling-induced electrooptic activity. Not only can the covalent bonds and steric interactions of dendrimers hold chromophores away from each other (inhibiting centric ordering) but dendrimer structures can also oppose thermal relaxation. The dendrimer material of Figure 3 is observed to exhibit stable electrooptic activity for 1000 h at 85°C. Greater thermal stability should be achieved by greater attention to the flexibility of dendrons and by better control of cross-link density. In comparison, the thermal stability of lithium niobate devices is typically listed as 90°C while gallium arsenide devices are specified as stable to 80°C.

Preliminary studies of the stability of organic electrooptic materials to high energy (gamma ray) radiation and particles (protons) carried out by Lockheed Martin (Palo Alto) and by researchers at the Air Force Research Laboratory (Wright Patterson Air Force Base) suggest that space application of polymeric electrooptic materials should proceed without problems.

Photochemical stability is more difficult to assess. Lithium niobate is specified as having optical power handing capabilities to 250 mW while gallium arsenide is specified as having a maximum power handling capability of 30 mW. However, such power handling capability is typically specified for packaged materials where oxygen has been excluded. The photochemical stability of organic materials is dramatically affected by the presence of oxygen. Exclusion of oxygen typically improves photochemical stability by several orders of magnitude. The addition of oxygen (radical) scavengers can also improve photochemical stability (136). Photochemical stability can also improve

with lattice hardening (100) although this will depend upon the porosity of the polymer lattice, which may not always correlate simply with cross-link density. Unfortunately, controlled evaluation of photochemical stability under conditions appropriate for commercial applications have not been carried out for polymeric electrooptic materials; thus, photochemical stability remains the most serious question concerning the commercialization of organic electrooptic materials.

Mechanical Properties

Polymeric electrooptic materials have the advantage of being conformal and of exhibiting effective bonding to a variety of surfaces. Moreover, by control of cross-link density, the mechanical properties of polymeric electrooptic materials can be controlled. Electrooptic device operation can be carried out over a wide range of temperatures. Eventually, different coefficients of thermal expansion may cause delamination problems upon thermal cycling over wide temperature ranges, but such problems have not been noted to the present. A unique feature of polymeric systems is that good mechanical properties are obtained for lightweight materials. Weight is an issue in satellite telecommunication and reconnaissance systems. Regarding weight issues in satellite telecommunications and reconnaissance operations, the low drive voltage requirements of polymeric electrooptic devices permit the elimination of low noise amplifiers, which in turn results in substantial weight reduction. Thus, the weight issue is not the relative weights of lithium niobate and polymeric electrooptic materials but the relative weights of total systems fabricated from these materials. Also, the critical weight saving comes from using photonic (optical fiber) versus electrical (coaxial) cables.

Processing and Integration

Polymeric materials are amenable to facile processing by RIE (70,71,112,119,120) and photolithographic techniques (71,112,137). Use of offset, gray scale, and shadow ion lithographic masks and RIE has permitted implementation of vertical waveguide transitions and the fabrication of 3-D circuits permitting the ready integration of passive and active optical waveguide components (70,71). Polymeric electrooptic materials are also very compatible with semiconductor processing, and electrooptic circuitry has been fabricated on top of very large-scale integration (VLSI) semiconductor chips (71,112). Indeed, through use of planarizing polymers, electrooptic modulators have been vertically integrated (in high density) with VLSI chips. Integration has been accomplished without the perturbation of the performance characteristics of either electronic or optical (electrooptic) circuitry. One of the advantages of polymeric electrooptic materials is this ready integration with semiconductor electronics and the ability to fabricate a large number of modulator waveguides on a single chip. With lithium niobate, such integration is not possible and connection to electronic circuitry is typically made by wires and flip chip bonding. By use of tapered transitions and

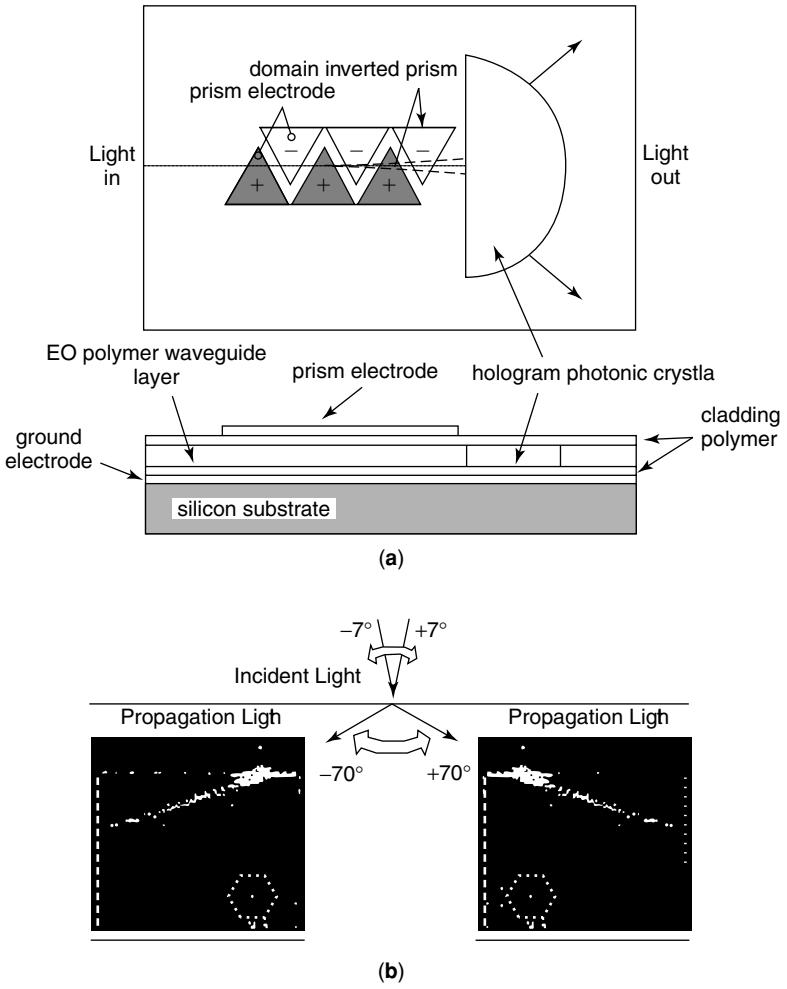

Fig. 6. Large-angle beam steering is shown for a device based on a polymeric electrooptic material (a cross-linkable version of the CLD chromophore discussed in Ref. 68). (a) EO waveguide prism introduces a small deflection angle to initialize the beam scanning. The half-circle 2-D photonic crystal region is embedded into the waveguide so that the deflection angle is "amplified" as the light passes through the crystal region. 3-D scanning can also be provided if a 3-D structure is built. (b) The experimental observation of the angle sensitivity.

spherical lens, electrooptic waveguides have been coupled to silica fiber optics. Again, coupling can be achieved in a more straightforward manner than with lithium niobate.

An example of sophisticated device development is shown in Figure 6. Large-angle (-70° to $+70^\circ$) beam steering is demonstrated by implementing a series of cascaded electrooptic prisms, which initiate beam steering and feed light into a photonic band gap lattice (138,139). The photonic band gap lattice is fabricated by holography in a photopolymer material (see Fig. 7). Beam steering is accomplished with more than an order of magnitude lower drive voltage than required using

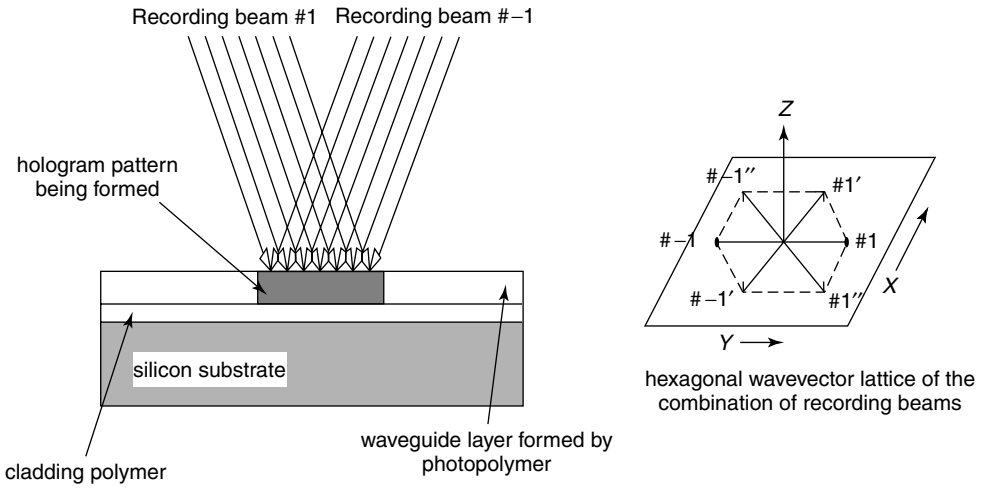

Fig. 7. The holographic production of the polymeric photonic band gap lattice used in the beam steering device of Figure 6 is shown.

lithium niobate materials. Through the cascaded prism electrodes, the deflection angle is given for steering of a TM polarized beam by

$$\theta = n_0^2 r_{33}(V/\mathrm{d})(L/h) \tag{5}$$

where L and h are the length and width of the prism array, respectively. V is the applied driving voltage and d is the electrode spacing. The electrooptic coefficient in the direction of the driving field is r_{33}, while n_0 is the voltage independent index of refraction. In the present example, L/h is approximately 80 with $L = 16$ mm and $h = 200$ μm. The model used to arrive at equation (4) is based only upon the total phase retardation across the wave front. The deflection angle thus depends only on the overall dimension of the prisms, since the accumulated phase difference across the wave front is independent of how the deflector is subdivided into individual prisms, as long as the interfaces between adjacent prisms are straight lines.

Devices

The most simple device configurations utilizing electrooptic materials are shown in Figure 8 (122). These include the Mach Zehnder and birefringent modulators and the directional coupler. As configured in Figure 8, the first two devices are amplitude modulators. A somewhat higher drive voltage is required for the birefringent modulator than for the Mach Zehnder modulator. This is because the V_π voltage of the Mach Zehnder relates directly to the principle component (r_{33}) of the electrooptic coefficient. The V_π voltage of the birefringent modulator relates to the difference between the major and minor components

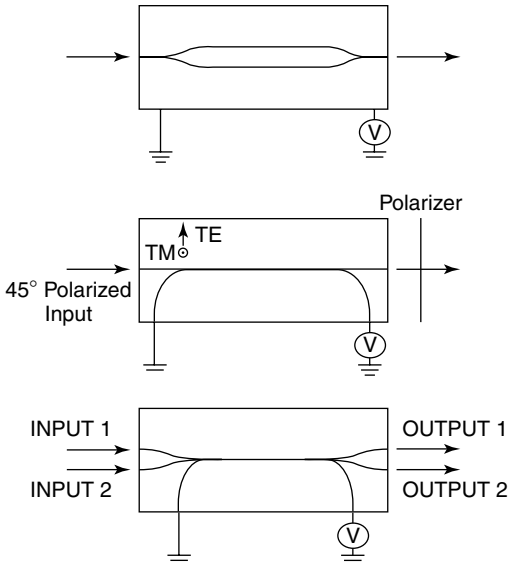

Fig. 8. Mach Zehnder interferometer (top), birefringent modulator (middle), and directional coupler (bottom) device configurations are shown.

$(n_3^3 r_{33} - n_1^3 r_{13})$. A still higher drive voltage is required for the directional coupler, and the relationship to material electrooptic activity is somewhat more complex (122).

We have already shown a large-angle spatial light modulator based upon organic electrooptic and photonic band gap materials (Figs. 6 and 7). Such beam steering without moving parts is relevant for holographic optical data storage, switching in all optical networks, advanced laser radar (ladar), photonic phased array antennas, optical sensors, and laser printers. Spatial light modulation exploiting electronic electrooptic activity has not only the advantage of greater speed but also avoids instability due to overshoot associated with the momentum of mechanical beam steering (MEMS) devices. The fact that such beam steering can be accomplished with application of driving voltages in the range of volts rather than kilovolts (as is the case for lithium niobate) is also a very attractive feature. For fiber optic switching, spatial light modulation has the advantage that a large number of fiber channels can be selectively addressed using only one electrode. Overall, electrooptic beam steering offers a simplified operating scheme, low driving voltage, high switching speed, small size, and low cost.

Ultra high bandwidth analogue-to-digital (A/D) conversion has been accomplished utilizing polymeric electrooptic materials in several different device configurations. Analogue-to-digital conversion employing a cascaded series of Mach Zehnder modulators has been discussed elsewhere (112). Analogue-to-digital conversion can also be accomplished by time stretching (140). In this application, a femtosecond pulse is stretched (by a dispersive medium) to match the length of an incoming data stream containing high frequency information. The data stream is transduced as an amplitude modulation (by a polymeric electrooptic modulator)

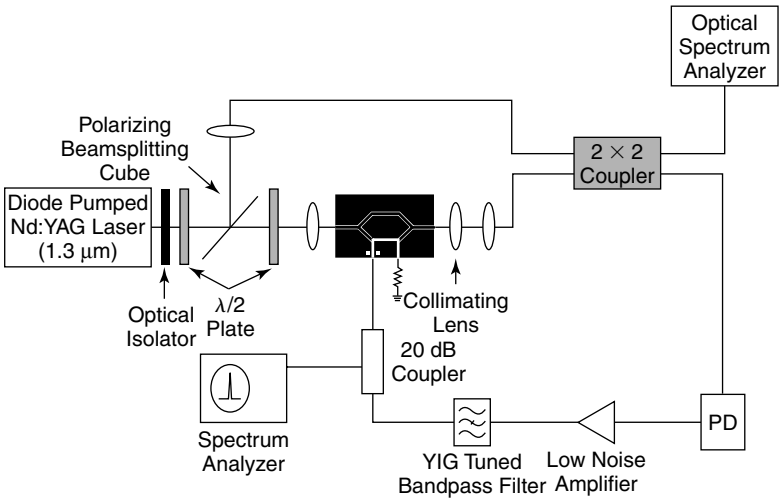

Fig. 9. A broadband, ultrastable oscillator based on polymeric electrooptic materials is shown.

onto the optical pulse. The pulse is then further time stretched to a length compatible with conventional A/D converters. The pulse is then converted to an electrical signal by a diode detector and A/D conversion is effected. Such time stretching permits A/D conversion at rates of 100 Gbit/s.

Another prototype device, which has been demonstrated by researchers at Pacific Wave, is that of a high frequency oscillator (see Fig. 9). In this oscillator, the stability of the oscillator is determined by the length (Q) of the optical circuit (loop) and can thus be very high indeed.

A variety of phased array systems have been fabricated based on polymeric electrooptic materials (141,142). One configuration is based on the photonic phase shifter shown in Figure 10. This provides a very linear phase shift as a function of control d-c voltage. Optical signals of controlled phase are thus sent to various radiating antenna elements. The optical signals are converted to radiofrequency signals by diode detectors.

High frequency (including secured communication by frequency hopping) telecommunication applications are receiving considerable attention (143). As can be seen in Table 1, the bandwidth limitation of current electronic components is the limiting factor to achieving increased bandwidth performance with polymeric electrooptic materials. In Figure 11, a device configuration capable of 130-GHz bandwidth operation is shown.

Other demonstrated prototype devices include optical gyroscopes (144), broadband acoustic spectrum analyzers (145), 1×2 Y-fed directional couplers (146) and polarization-insensitive electrooptic modulators (147,148). For long-haul telecommunication applications, it is difficult to maintain polarization control; thus, a need exists for polarization-insensitive modulators. Indeed, polarization insensitivity was one of the advantages claimed for gallium arsenide electroabsorptive modulators. By using different poling schemes, overall polarization insensitivity has been achieved for polymeric modulators (147,148).

Table 1. The Bandwidth Characteristics of Various Electrical Interfaces

Modulator type	Electrical interface	Bandwidth, GHz	Technology availability	Reliability	Cost
Traditional	K-coax	0–40	Simple, commercial	Proven	Low
M-Z modulators	V-coax	0–65	Simple, commercial	Proven	Low
	W-coax	0–110	Ongoing at TACAN	R&D	Low
	WR-15	50–75	Complicated, customer	R&D	High
	WR-10	75–110	Complicated, customer	R&D	High

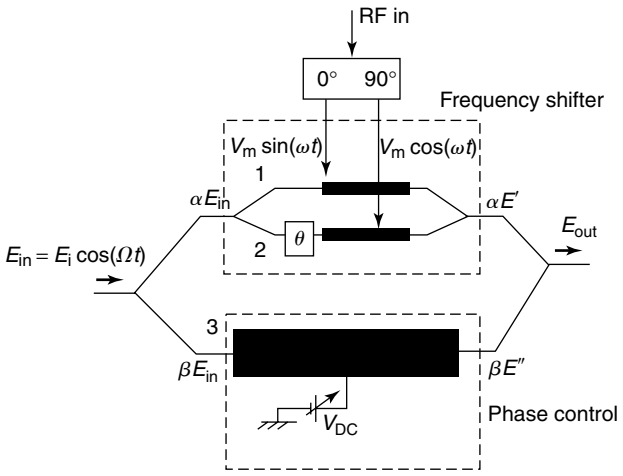

Fig. 10. A schematic representation of a photonic radiofrequency phase shifter is shown.

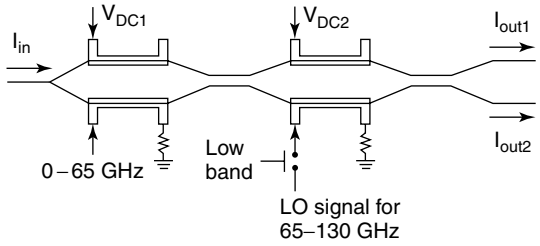

Fig. 11. A 130-GHz telecommunications device is shown.

Commercialization and Cost

As with lithium niobate, the cost of devices based on polymeric electrooptic modulators is in the packaging rather than in the materials. A Lucent lithium niobate modulator sells for approximately $6000. Polymer modulator vendors such as Pacific Wave Industries (Los Angeles, California) are quoting comparable prices. The low material cost is associated with the fact that modulator devices are thin-film

devices and a chip containing 6–100 modulators requires very little polymeric electrooptic material.

A number of small companies such as Lumera (Bothel, Washington), Pacific Wave Industries (Los Angeles, California), Radiant Research (Austin, Texas), IP-ITEK/TACAN (Carlsbad, California), KVH Industries (Tinley Park, Illinois), etc are exploring the commercialization of electrooptic devices based on polymeric materials. Lockheed Martin has pursued research in polymeric electrooptic materials for more than a decade and continues to be a leader in the field. Lucent has recently resumed research on polymeric electrooptic materials. A number of telecommunication companies including Nortel, Agilent, Cisco, and JDS-Uniphase are currently evaluating polymeric electrooptic technology to determine the viability of R&D and commercial activity in this area.

The market for inorganic electrooptic and electroabsorptive modulators is currently in the hundreds of millions of dollars per year with wait times of several months for delivery of lithium niobate modulators. The perceived need for greater bandwidth in the telecommunications industry is likely to drive demand even higher.

Future Prognosis

Provided that no unexpected problems arise that would inhibit the commercialization of polymeric electrooptic technology, the prognosis is very good. The greatest uncertainty involves whether or not organic electrooptic materials will exhibit adequate photochemical stability over many years of in-field operation. Preliminary studies suggest that exclusion of oxygen and hermetic sealing will yield devices capable of exhibiting photochemical stability over many years for exposure to optical fields at telecommunication wavelengths and powers. Almost certainly, electrooptic coefficients will continue to be improved. New and improved chromophores are being synthesized with great regularity (149). Devices operating with sub 1-V V_π values should become commonplace. Utilization of photonic band gap materials and controlled coupling to resonated structures should permit further reduction in drive voltage requirements (possibly even to microvolt levels); such reduction is, of course, at the expense of some reduction in response time (bandwidth). Low drive voltage requirements, together with high bandwidth capabilities and the ease of integration with semiconductor electronics and silica transmission fibers, should be a powerful driver for the deployment of polymeric electrooptic technology in telecommunication, defense, transportation, and display industries. However, the extent of utilization of polymer electrooptic technology in the telecommunication industries will depend upon perceived bandwidth needs. If low cost alternatives to high information throughput with reduced bandwidth requirements (such as expanded use of WDM technology) become popular, limited bandwidth technologies such as thermooptic, liquid crystalline, MEMS, and modulated laser technologies may continue to dominate sales in the telecommunications area. However, even if deployment is slow in telecommunications, defense industries should find use for the exceptional capabilities of polymeric electrooptic materials for applications such as radar, electronic counter measure, sensor, and display systems. Other

niche applications including biomedical sensors, analytical instrumentation, and high frequency test equipment are likely to develop.

The main limitation to general deployment of organic electrooptic materials is that they have been optimized to this point in time for applications at telecommunication wavelengths. Inorganic materials such as lithium niobate are still the materials of choice for applications at visible wavelengths. Such inorganic modulators are likely going to continue to dominate the laboratory market for modulators to be used with research laser systems.

Nomenclature

p_i	ith component of the molecular polarization vector in the presence of electrical fields
p_{0i}	ith component of the permanent polarization of the molecule
E	the local electric field strength
F	the local electric poling field strength
α	molecular polarizability tensor
β	molecular first hyperpolarizability tensor
γ	molecular second hyperpolarizability tensor
P_i	ith component of the bulk polarization vector in the presence of electrical fields
P_{0i}	ith component of the bulk polarization vector in the absence of external fields
V	applied voltage
$\chi^{(1)}_{ij}$	first-order electric susceptibility tensor
$\chi^{(2)}_{ijk}$	second-order electric susceptibility tensor
$\chi^{(3)}_{ijkl}$	third-order electric susceptibility tensor
n	refractive index in the presence of an applied electric field
n_0	refractive index in the absence of an applied electric field
r	Pockels coefficient or electrooptic coefficient
r_{33}	electrooptic coefficient in the direction of the applied field (principal element)
r_{13}	electrooptic coefficient orthogonal to the applied field direction (minor element)
R	Kerr factor
E_0	applied electric field amplitude
N	number density
$f(\omega)$	local field factor
$\langle\cos^3\theta\rangle$	acentric order parameter
V_π	applied voltage required to produce a phase shift of π
λ	wavelength of light
d	electrode gap
L	interaction length of electrical and optical fields in material
Γ	modal overlap integral
θ	beam deflection angle

BIBLIOGRAPHY

"Electrooptical Applications" in *EPSE* 2nd ed., Vol. 5, pp. 756–771, by M. Thakur and S. Tripathy, GTE Laboratories, Inc.

1. J. Kerr, *Phil. Mag.* **50**, 337 (1875).
2. F. Pockels, *Lehrbuch der Kristalloptic*, Teubner, Leipzig, Germany, 1906.
3. G. T. O'Konski, in N. M. Bikales, ed., *Encyclopedia of Polymer Science and Technology*, 1st ed., Wiley-Interscience, New York, Vol. **9**, 1968, p. 551.
4. B. R. Jennings, *IEE Proc.* **130**, 212 (1983).
5. C. T. O'Konski, ed., *Molecular Electrooptics*, Marcel Dekker, Inc., New York, 1976.
6. S. Krause, ed., *Molecular Electro-Optics*, Plenum Press, New York, 1980.
7. I. P. Kaminow, *An Introduction to Electrooptic Devices*, Academic Press, Inc., New York, 1974.
8. J. Wilson and J. F. B. Hawkes, *Opto-electronics, An Introduction*, Prentice-Hall, Englewood Cliffs, N.J., 1983.
9. N. Bloembergen, *Nonlinear Optics*, Benjamin, New York, 1965.
10. P. N. Prasad and D. J. Williams, *Introduction to Nonlinear Optical Effects in Molecules and Polymers*, John Wiley & Sons, Inc., New York, 1991.
11. L. R. Dalton, in J. I. Kroschwitz and M. Howe-Grant, eds., *Kirk-Othmer Encyclopedia of Chemical Technology*, Vol. **17**, John Wiley & Sons, Inc., New York, 1996, p. 287.
12. D. L. Wise, G. E. Wnek, D. J. Trantolo, T. M. Cooper, and J. D. Gresser, eds., *Electrical and Optical Polymer Systems*, Marcel Dekker, Inc., New York, 1998.
13. H. Nalwa and S. Miyata, eds., *Nonlinear Optics of Organic Molecules and Polymers*, CRC Press, Inc., Boca Raton, Fla., 1997.
14. Y. R. Shen, *Nonlinear Optics*, John Wiley & Sons, Inc., New York, 1984.
15. R. W. Boyd, *Nonlinear Optics*, Academic Press, Inc., New York, 1993.
16. T. J. Bunning and co-workers, *Annu. Rev. Mater. Sci.* **30**, 83 (2000).
17. R. Dabrowski, *Ferroelectrics* **243**, 1 (2000).
18. S.-M. Chang and co-workers, *Mater. Sci. Eng. C* **12**(1/2), 111 (2000).
19. T. Ikeda and A. Kanazawa, *Bull. Chem. Soc. Jpn.* **73**, 1715 (2000).
20. T. Fuhrmann and J. H. Wendroff, *Int. J. Polym. Mater.* **45**, 621 (2000).
21. K. M. Blackwood, *Int. J. Polym. Mater.* **45**, 585 (2000).
22. N. Boiko and V. Shibaev, *Int. J. Polym. Mater.* **45**, 533 (2000).
23. F. Simoni and O. Francescangeli, *Int. J. Polym. Mater.* **45**, 381 (2000).
24. V. Shibaev, *Int. J. Polym. Mater.* **45**, 307 (2000).
25. J. Zubia and J. E. Ecenarro, *Int. J. Polym. Mater.* **45**, 503 (2000).
26. E. Lizuka, *Int. J. Polym. Mater.* **45**, 191 (2000).
27. G. Abbate and J. M. Oton, *Adv. Mater.* **12**, 459 (2000).
28. D. A. Higgins, *Adv. Mater.* **12**, 251 (2000).
29. D. J. Broer and co-workers, *Macromol. Symp.* **154**, 1 (2000).
30. T. J. Sluckin, *Contemp. Phys.* **41**, 37 (2000).
31. R. L. Wisnieff and J. J. Ritsko, *IBM J. Res. Dev.* **44**, 409 (2000).
32. M. O'Neill and S. M. Kelly, *J. Phys. D: Appl. Phys.* **33**, R67 (2000).
33. S. R. Collinson and D. W. Duncan, *Perspect. Supramol. Chem.* 285 (1999).
34. W. A. Crossland and co-workers, *Proc. SPIE* **3955**, 70 (2000).
35. M. Hird, J. W. Goodby, and K. J. Toyne, *Proc. SPIE* **3955**, 15 (2000).
36. J. W. Goodby and co-workers, *Proc. SPIE* **3955**, 2 (2000).
37. B. L. Feringa and co-workers, *Chem. Rev.* **100**, 1789 (2000).
38. K. Ichimura, *Chem. Rev.* **100**, 1847 (2000).
39. S. Susumu, *Opt. Rev.* **6**, 471 (1999).
40. F. Bloisi and L. Vicari, *Recent Res. Dev. Macromol. Res.* **4**, 113 (1999).
41. T. Tsukada, *Springer Ser. Mater. Sci.* 7 (2000).

42. J. W. Goodby, *Curr. Opin. Solid State Mater. Sci.* **4**, 361 (1999).
43. I. C. Khoo, *J. Nonlinear Opt. Phys. Mater.* **8**, 305 (1999).
44. G. Scalia and co-workers, *Proc. SPIE* **3800**, 112 (1999).
45. R. A. Herke, M. H. Anderson, and T. G. Baur, *Proc. SPIE* **3800**, 45 (1999).
46. R. W. Sabnis, *Displays* **20**, 119 (1999).
47. S. Naemura, *Mater. Res. Soc. Symp. Proc.* **559**, 263 (1999).
48. C. C. Bowley and co-workers, *Mater. Res. Soc. Symp. Proc.* **559**, 97 (1999).
49. W. Haase, D. Ganzke, and E. P. Pozhidaev, *Mater. Res. Soc. Symp. Proc.* **559**, 15 (1999).
50. G. W. Gray and S. M. Kelly, *J. Mater. Chem.* **9**, 2037 (1999).
51. W. M. Gibbons and co-workers, *Proc. SPIE* **3635**, 32 (1999).
52. P. Palffy-Muhoray, *Phys. Prop. Liq. Cryst.* 467 (1999).
53. L. M. Blinov, *Phys. Prop. Liq. Cryst.* 375 (1999).
54. D. Dunmur and K. Toriyama, *Phys. Prop. Liq. Cryst.* 113 (1999).
55. D. Dunmur and K. Kazuhisa, *Phys. Prop. Liq. Cryst.* 102 (1999).
56. G. W. Gray, *Phys. Prop. Liq. Cryst.* 1 (1999).
57. E. Lueder, *Proc. Electrochem. Soc.* 98 (1999).
58. A. Sinha, T. A. P. Rao, and V. R. K. Murthy, *Liq. Cryst.* **27**, 191 (2000).
59. Ch. Bosshard, *Springer Ser. Opt. Sci.* 7 (2000).
60. M. Samoc, A. Samoc, and B. Luther-Davies, *Synth. Met.* **109**, 79 (2000).
61. M. Samoc and co-workers, *MCLC S&T, Sect. B.: Nonlinear Opt.* **20**, 183 (1999).
62. S. R. Marder and co-workers, *Science* **276**, 1233 (1997).
63. R. L. Nelson and R. W. Boyd, *Appl. Phys. Lett.* **74**, 2417 (1999).
64. D. R. Greve and co-workers, *Synth. Met.* **102**, 1533 (1999).
65. F. Cherioux and co-workers, *Chem. Commun.* **20**, 2083 (1999).
66. M. G. Kuzyk, *Opt. Lett.* **25**, 1183 (2000).
67. K. A. Drenser and co-workers, *J. Phys. Chem.* **103**, 2290 (1999).
68. Y. Shi and co-workers, *Science* **288**, 119 (2000).
69. Y. Shi and co-workers, *Appl. Phys. Lett.* **77**, 1 (2000).
70. S. M. Garner and co-workers, *IEEE J. Quantum Electron.* **35**, 1146 (1999).
71. L. Dalton and co-workers, *Ind. Eng. Chem. Res.* **38**, 8 (1999).
72. W. H. Steier and co-workers, *Chem. Phys.* **245**, 487 (1999).
73. R. A. Norwood and co-workers, *Proc. SPIE* **3281**, 2 (1998).
74. S. Kalluri and co-workers, *IEEE Photon. Technol. Lett.* **8**, 644 (1996).
75. B. Kipplen and co-workers, *ACS Symp. Ser.* **72**, 204 (1999).
76. R. J. Twieg and co-workers, *Mater. Res. Soc. Symp. Proc.* **561**, 119 (1999).
77. S. R. Marder and co-workers, *Nature* **388**, 845 (1997).
78. B. Kippelen and co-workers, *J. Am. Chem. Soc.* **119**, 4559 (1997).
79. B. Kippelen and co-workers, *Proc. SPIE* **3144**, 176 (1997).
80. B. Kippelen and co-workers, *Science* **279**, 54 (1998).
81. E. Hendrickx and co-workers, *Appl. Phys. Lett.* **72**, 1670 (1998).
82. Z. Peng, A. Gharavi, and L. Yu, *J. Am. Chem. Soc.* **119**, 4622 (1997).
83. W. Li and co-workers, *Adv. Mater.* **10**, 927 (1998).
84. W. E. Moerner, A. Grunnet-Jepsen, and C. L. Thompson, *Annu. Rev. Mater. Sci.* **27**, 585 (1997).
85. A. Grunnet-Jepsen and co-workers, *J. Opt. Soc. Am. B* **15**, 901 (1998).
86. A. Grunnet-Jepsen, C. L. Thompson, and W. E. Moerner, *Opt. Commun.* **145**, 145 (1998).
87. J. A. Delaire and K. Nakatani, *Chem. Rev.* **100**, 1817 (2000).
88. S. R. Marder, D. N. Beratan, and L. T. Chang, *Science* **252**, 103 (1991).
89. S. R. Marder and J. W. Perry, *Science* **263**, 1706 (1993).
90. D. R. Kanis, M. A. Ratner, and T. J. Marks, *Chem. Rev.* **94**, 195 (1994).
91. I. D. L. Albert, T. J. Marks, and M. A. Ratner, *J. Am. Chem. Soc.* **119**, 6575 (1997).

92. B. Champage and B. Kirtman, *Chem. Phys.* **245**, 211 (1999).
93. J. Lipinski and J. Bartkowiak, *Chem. Phys.* **245**, 263 (1999).
94. A. Painelli, *Chem. Phys.* **245**, 185 (1999).
95. A. K.-Y. Jen and co-workers, *Adv. Mater.* **9**, 132 (1997).
96. S. R. Marder and co-workers, *Science* **265**, 632 (1994).
97. J. L. Brédas and co-workers, *Acc. Chem. Res.* **32**, 267 (1999).
98. L. R. Dalton, A. W. Harper, and B. H. Robinson, *Proc. Natl. Acad. Sci. USA* **94**, 4842 (1997).
99. A. W. Harper and co-workers, *J. Opt. Soc. Am. B* **15**, 329 (1998).
100. L. R. Dalton and co-workers, *J. Chem. Mater.* **9**, 1905 (1999).
101. B. H. Robinson and co-workers, *Chem. Phys.* **245**, 35 (1999).
102. B. H. Robinson and L. R. Dalton, *J. Phys. Chem.* **104**, 4785 (2000).
103. W. Lin and co-workers, *J. Am. Chem. Soc.* **119**, 2205 (1997).
104. A. Piekara, *Proc. R. Soc. London A* **149**, 1 (1939).
105. H. Ma and co-workers, *J. Am. Chem. Soc.* **123**, 986 (2001).
106. L. R. Dalton, *Advances in Polymer Science*, Vol. **154**, Springer-Verlag, Heidelberg, 2001.
107. D. Chen and co-workers, *Proc. SPIE* **3006**, 314 (1997).
108. D. Chen and co-workers, *Appl. Phys. Lett.* **70**, 3335 (1997).
109. D. Chen and co-workers, *IEEE Photon. Tech. Lett.* **11**, 54 (1999).
110. A. H. Udupa and co-workers, *Electron. Lett.* **35**, 1702 (1999).
111. S. S. H. Mao and co-workers, *Chem. Mater.* **10**, 146 (1998).
112. L. R. Dalton, in D. L. Wise, G. E. Wnek, D. J. Trantolo, T. M. Cooper, and J. D. Gresser, eds., *Electrical and Optical Polymer Systems*, Marcel Dekker, Inc., New York, 1998, p. 609.
113. L. R. Dalton, *Opt. Eng.* **39**, 589 (2000).
114. S. Kalluri and co-workers, *Proc. SPIE* **2285**, 67 (1994).
115. S. Kalluri and co-workers, *Appl. Phys. Lett.* **65**, 2651 (1994).
116. H. W. Oviatt Jr. and co-workers, *Chem. Mater.* **7**, 493 (1995).
117. C. C. Teng, M. A. Mortazavi, and G. K. Boughoughian, *Appl. Phys. Lett.* **66**, 667 (1995).
118. A. Chen and co-workers, *J. Electrochem. Soc.* **143**, 3648 (1996).
119. W. H. Steier and co-workers, *Mat. Res. Soc. Symp. Proc.* **413**, 147 (1996).
120. A. Chen and co-workers, *Proc. SPIE* **3005**, 65 (1997).
121. D. M. Burland, R. D. Miller, and C. A. Walsh, *Chem. Rev.* **94**, 31 (1994).
122. L. R. Dalton and co-workers, *Adv. Mater.* **7**, 519 (1995).
123. L. R. Dalton and co-workers, *Chem. Mater.* **7**, 1060 (1995).
124. Z. Liang and co-workers, *Chem. Mater.* **7**, 941 (1995).
125. Z. Liang and co-workers, *Chem. Mater.* **7**, 1756 (1995).
126. Z. Liang and co-workers, *Chem. Mater.* **8**, 2681 (1996).
127. C. Xu and co-workers, *Macromolecules* **26**, 5303 (1993).
128. M. A. Hubbard and co-workers, *Chem. Mater.* **4**, 965 (1992).
129. J. E. Becker and co-workers, *J. Am. Chem. Soc.* **115**, 12216 (1993).
130. R. E. Harelstad and co-workers, *Mater. Res. Soc. Symp. Proc.* **328**, 637 (1994).
131. D. Yu, A. Gharavi, and L. Yu, *Macromolecules* **28**, 784 (1995).
132. D. Yu and co-workers, *ACS Symp. Ser.* **672**, 123 (1997).
133. H. Saadeh and co-workers, *Macromolecules* **30**, 5403 (1997).
134. H. Ma and co-workers, *Chem. Mater.* **11**, 2218 (1999).
135. M. W. Becker and co-workers, *Chem. Mater.* **6**, 104 (1994).
136. A. Galvan-Gonzalez and co-workers, *Appl. Phys. Lett.* **77**, 2083 (2000).
137. B. H. Cumpston and co-workers, *Nature* **398**, 51 (1999).
138. L. Sun and co-workers, *Opt. Eng.* in press; L. Sun and co-workers, *Proc. SPIE* **3950**, 98 (2000).

139. L. Sun and co-workers, *Proc. SPIE* **3632**, 134 (1999).
140. D. H. Chang and co-workers, *IEEE Photon. Tech. Lett.* **12**, 537 (2000).
141. S. S. Lee and co-workers, *IEEE Microwave and Guided Wave Lett.* **9**, 357 (1999).
142. R. Chen and co-workers, *Proc. PSAA*, in press.
143. J. H. Bechtel and co-workers, *Proc. SPIE* **4114**, 58 (2001); see also http://depts.washington.edu/eooptic (last updated 7/6/2001).
144. P. R. Ashley and J. S. Cites, *OSA Tech. Dig. Ser.* **14**, 196 (1997).
145. A. Yacoubian and co-workers, *J. Sel. Top. Quant. Elect.* **6**, 810 (2000).
146. D. An and co-workers, *Appl. Phys. Lett.* **76**, 1972 (2000).
147. A. Donval and co-workers, *J. Appl. Phys.* **87**, 3258 (2000).
148. L. Sun and co-workers, *Appl. Phys. Lett.* in press.
149. J.-M. Raimundo and co-workers, *Chem. Commun.* 1597 (2000).

LARRY R. DALTON
University of Southern California

EMULSION POLYMERIZATION. See HETEROPHASE POLYMERIZATION.

ELECTROOPTICAL APPLICATIONS

Introduction

The term *electrooptic* can have widely different meanings. In the broadest sense, it can imply any change produced in an optical beam by application of an electrical field from either a low frequency (dc to millimeter wave) field or another optical (micrometer wave) field. Change of the index of refraction of the material through which an optical beam is transiting can influence the (velocity of the) propagating optical beam. Such change of index of refraction can be accomplished by altering either the electron distribution or the nuclear configuration of a material. The associated optical phenomena are referred to as Kerr and Pockels effects (1–15) and have been known since the nineteenth century.

However, altering an optical beam by electrically controlled mechanical movement of a mirror (particularly as in micro-electro-mechanical-systems, MEMS) is also referred to as an electrooptic operation. Indeed, even greater confusion arises by usage of the terms electrooptic and all-optical signal processing in the telecommunications industry. Electrooptic is taken to refer to converting optical signals to electrical signals, carrying out signal processing in the electrical (electronic) domain, and then converting back to the optical domain. Thus, techniques such as bubble jet (Hewlett Packard/Agilent) and MEMS (Texas Instruments) optical switching at network nodes are referred to as all-optical signal processing by telecommunication engineers while an optical physicist would reserve the term all-optical switching for the dynamic Kerr phenomenon (switching of one optical beam by another).

A review of electrooptical applications in the broadest sense is out of the question. It would involve treatment of topics ranging from modulated lasers (direct modulation) to light-emitting diodes (LEDs), to liquid crystalline materials,

Encyclopedia of Polymer Science and Technology. Copyright John Wiley & Sons, Inc. All rights reserved.

not to mention MEMS, thermooptic, and bubble jet technologies currently used in telecommunications. Moreover, the literature is enormous. Over 1000 reviews and texts have appeared on the subject of liquid crystalline electrooptic materials alone. In this article, a narrow view of electrooptic phenomena, materials, and applications is taken and focus is upon the "electronic" Pockels effect, with emphasis on the phenomenon realized using polymeric or dendritic materials rather than inorganic or organic single crystals. The term *electronic* refers to changes in refractive index associated purely with electric-field-induced change of the electron distribution of a material (in contrast to changes in nuclear configuration associated with molecular reorientation). Moreover, there is a focus upon π-electron organic chromophores rigidly embedded in polymeric or dendritic supramolecular matrices. Currently, commercially utilized materials exploiting the electronic Pockels effect are inorganic crystalline materials such as lithium niobate. Although the most commercially viable organic electrooptic (defined in the broader sense) materials are liquid crystalline materials (16–58), electronic Pockels effect organic materials are receiving increased attention because of the possibility of exceptional (greater than 100 GHz) bandwidth performance. Although potential applications of such materials range from telecommunications to information processing, to defense, to transportation, and to display industries, the telecommunications and defense industries are particularly important drivers of development of electrooptic materials with greater bandwidths. Electronic Kerr materials (59–67) have the potential for even greater bandwidth and the possibility of convenient all-optical signal processing; however, to the present time electronic Kerr coefficients have not been large enough to be commercially viable for telecommunication applications. Mott–Hubbard transition-metal oxide and halide systems with charge-transfer gaps and low hydrogen-density organic materials such as the fullerenes and chromophore-containing dendrimers may hold future promise for all-optical switching at telecommunication wavelengths (eg, 1.55 μm) because of their large two-photon absorption coefficients (third-order optical nonlinearities) and their low optical loss. Inorganic Kerr materials such as titanium sapphire are currently used for mode-locked lasers and other applications.

Other reasons for heightened interest in organic electronic electrooptic materials include large electrooptic coefficients (greater than 50 picometers/volt (pm/V) at telecommunication wavelengths). Large electrooptic coefficients permit voltages from semiconductor electronics to drive electrooptic devices without the introduction of amplifiers. Amplifiers are undesirable because of their bandwidth limitations, noise figures, weight, bulk, and cost. Indeed, a major reason for increased commercial interest in organic electrooptic materials is that drive voltages of less than 1 V can be realized with simple broadband device structures (68,69). Such drive voltages permit lossless telecommunication links to be achieved and even permit realization of gain in electrical-to-optical-to-electrical signal transduction. Another attractive feature of organic electrooptic materials is facile integration with semiconductor electronics and silica fiber optics (70–74). In this article, both the state of development of organic electrooptic materials and the principles that define material performance are reviewed.

The reader is referred elsewhere for reviews of organic photorefractive materials (75–86) and of photochromic and optomechanical materials (87). Electronic electrooptic chromophores (such as charge transfer azobenzenes) have frequently

been used for such applications, but the response times of these phenomena and their conceptual basis are quite different from the phenomenon and applications discussed here. (See also CHROMOGENIC POLYMERS; LIGHT-EMITTING DIODES).

General Theoretical Principles

At the molecular level, the change in electron distribution (polarization) with application of an electrical field is given by

$$p_i = p_{0i} + \alpha_{ij}E_j + \beta_{ijk}E_jE_k + \gamma_{ijkl}E_jE_kE_l + \cdots \tag{1a}$$

where p_{0i} is the permanent polarization of the molecular site "i" and E stands for the local electric field strength. The tensors α, β, and γ are the molecular polarizability and molecular first and second hyperpolarizabilities. For macroscopic or bulk materials, the polarization equation is

$$P_i = P_{0i} + \chi^{(1)}_{ij}E_j + \chi^{(2)}_{ijk}E_jE_k + \chi^{(3)}_{ijkl}E_jE_kE_l + \cdots \tag{1b}$$

It is assumed that the electric fields in equations (1a) and (1b) have frequencies that are outside the domain of both electronic and lattice resonances of the system. If only one electric field is applied and it is in the form of a square wave pulse (of amplitude E_0), or an a-c field ($E_0 \cos \omega t$), or a d-c field (of amplitude E_0), then equations (1a) and (1b) lead to the following expression for refractive index n:

$$(1/n^2) = (1/n_0^2) + rE_0 + RE_0^2 + \cdots \tag{2}$$

where n_0 is the refractive index in the absence of the electric field. The linear and quadratic terms correspond to the Pockels and Kerr effects, respectively. The Pockels effect is observable only for noncentrosymmetric materials; the electrooptic coefficient r is related to the molecular first hyperpolarizability β and the noncentrosymmetric order parameter $\langle \cos^3 \theta \rangle$ by

$$r = 2\mathrm{Nf}(\omega)\beta\langle \cos^3\theta \rangle / n^4 \tag{3}$$

where N is the chromophore number density and $f(\omega)$ is a local field factor accounting for the dielectric nature of the medium (host material). The electrooptic coefficient r is related to the drive voltage required to effect electrical-to-optical signal transduction (with a Mach Zehnder interferometer) by

$$V_\pi = \lambda d/(n^3 \mathrm{rL}\Gamma) \tag{4}$$

V_π is the voltage required for a π phase shift of light passing through the arm of the Mach Zehnder modulator to which an electric field has been applied. The optical wavelength of the transiting light is given by λ, d is the gap between the electrodes used to apply the electric field, L is the interaction length of the

electrical and optical fields (electrode length in the simplest case), and Γ is a modal overlap integral. Equation (3) is greatly oversimplified as we have neglected the vectorial nature of the interaction of the fields, but this equation is frequently applicable to poled polymer materials.

From equations (2) and (3), it is readily seen that optimizing the drive voltage performance of electrooptic materials is a matter of optimizing β, N, and $\langle\cos^3\theta\rangle$. We shall proceed to discuss the optimization of these parameters and the status of organic electrooptic materials, but before we do this, it is important to indicate what additional material properties must be achieved for commercial viability. These can be briefly summarized as follows: (*1*) fast response time or high operational bandwidths, (*2*) low optical loss including both material loss and insertion (optical mode mismatch) loss, (*3*) good stability including thermal and photochemical stability, (*4*) good mechanical properties, (*5*) good processability and ease of integration with disparate materials such as silica fibers, semiconductors, and metals, and (*6*) low production cost. For polymers to displace alternative technologies such as modulated semiconductor lasers, lithium niobate electrooptic modulators, or gallium arsenide (GaAs) electroabsorptive modulators, they must exhibit competitive or superior performance characteristics in all material categories. Thus, in the following paragraphs, we consider auxiliary properties as well as electrooptic activity.

Electrooptic Activity

It is clear that optimizing electrooptic activity involves optimizing the molecular hyperpolarizability β of organic chromophores. Quantum mechanics has provided effective guidance for the improvement of molecular nonlinear optical (electrooptic) activity by several orders of magnitude in the past 10 years (88–97). If chromophores are aligned into a noncentrosymmetric (acentric) lattice by electric field poling and if the interactions among chromophores are neglected, then the order parameter becomes (in the high temperature approximation) $\langle\cos^3\theta\rangle = \mu F/5kT$, where μ is the chromophore dipole moment, F is the applied electric poling field felt by the chromophores, k is the Boltzmann constant, and T is the poling temperature (Kelvin). In this approximation, macroscopic electrooptic activity would be expected to increase as $\mu\beta$. As can be seen from Figure 1, $\mu\beta$ values have been systematically improved over the past decade from the value of the 1990 state-of-the-art material Disperse Red (DR). Indeed, if current chromophores could be organized into a pure chromophore lattice with perfect acentric order, $\langle\cos^3\theta\rangle = 1.0$, then electrooptic coefficients in excess of 1000 pm/V could be achieved. Such electrooptic coefficients would permit true millivolt drive voltages to be routinely employed. Such materials would greatly exceed the performance of lithium niobate ($r = 31$ pm/V, $V_\pi = 5$–6 V) and would likely displace liquid crystalline materials in applications such as spatial light modulation and optical switching. However, while the DR chromophore of Figure 1 exhibits an electrooptic coefficient of 10–15 pm/V and V_π voltages of 12–20 V, the FTC chromophore exhibits a surprising low electrooptic coefficient of 35–50 pm/V and V_π voltages of 3–5 V. Clearly, a problem existed/exists in translating large molecular electrooptic activity into usably large macroscopic electrooptic activity.

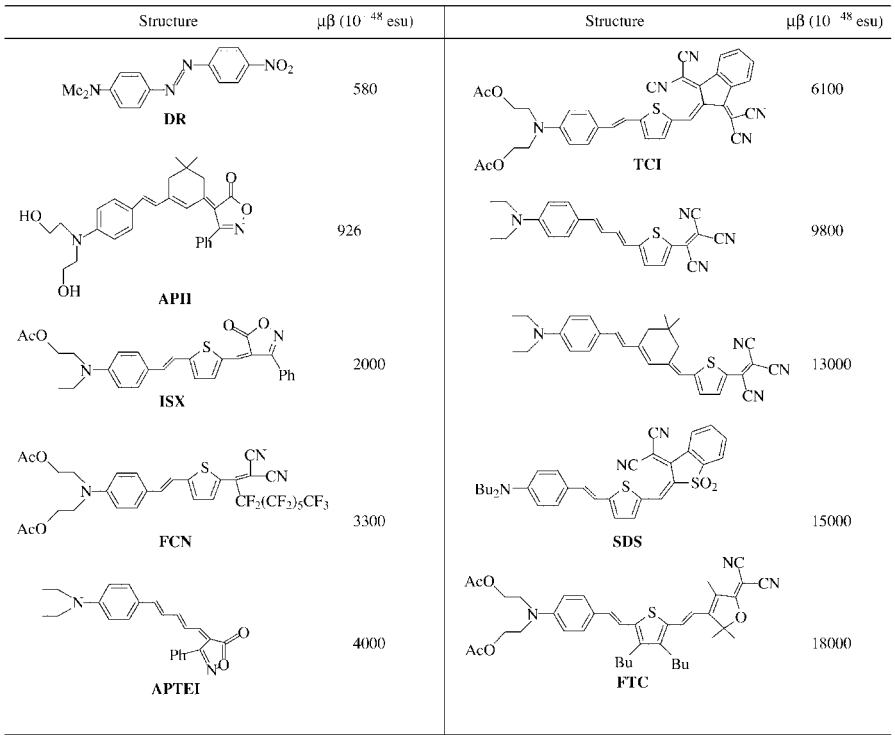

Fig. 1. The variation of $\mu\beta$ (dipole moment-first hyperpolarizability product) with chromophore structure is shown.

As is illustrated in Figure 2, the problem is now understood to derive from intermolecular electrostatic interactions among chromophores opposing the poling field in introducing the acentric order required for electrooptic activity (68,98–102). The same interactions oppose introduction of acentric order by sequential synthesis, self-assembly techniques where surface forces are used in place of a poling field to guide the assembly of chromophores into an acentric lattice (103). In this latter case, intermolecular electrostatic interactions cause the chromophores to tip away from the normal to the surface in their assembly. The problem has been successfully modeled using both equilibrium statistical mechanical methods and kinetic Monte Carlo methods, with both approaches specifically treating the many-body, long-range, spatially anisotropic interactions among chromophores. The intermolecular electrostatic interaction potential functions of equilibrium statistical mechanical and Monte Carlo methods are found to be very similar and approximate the potential function introduced by Piekara in the 1930s (104). Theoretical calculations explain a great many additional experimentally observed features including the relatively weak dependence of maximum achievable electrooptic activity upon electric poling field strength and phenomena such as concentration and electric-field-dependent phase separation. The theoretical rationalization of the dependence of achievable electrooptic activity upon the electronic and molecular structure of chromophores and the processing conditions (applied poling field

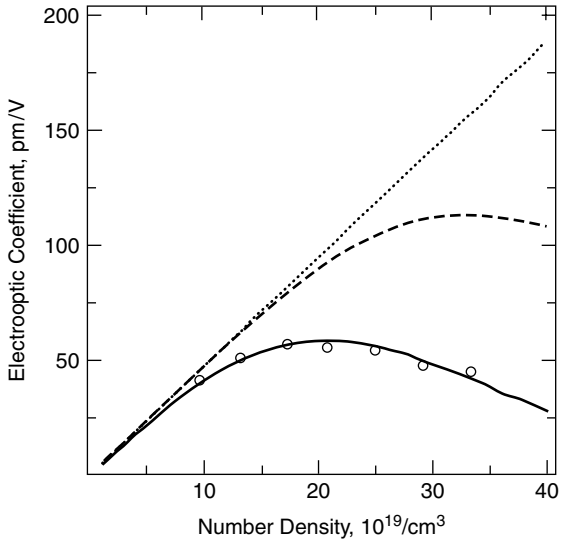

Fig. 2. The experimental and theoretically predicted dependence of electrooptic coefficient for the FTC chromophore (see Fig. 1) in poly(methyl methacrylate) (PMMA) upon chromophore number density (concentration in PMMA) is shown. Theoretical results are shown for various shape approximations and for the neglect of intermolecular electrostatic interactions (the ideal gas model). ------ Gas model; – – Sphere; —Prolate ellipsoid; ○ Experimental.

strength, dielectric constant of the host polymer matrix, chromophore concentration, temperature, etc) has provided both good and bad news. The bad news is that it will always be impossible to realize more than a fraction of the potential electrooptic activity represented by a given chromophore structure. Electrooptic coefficients of a few hundred pm/V may be obtainable, but values of 1000 pm/V or greater will be unobtainable with high dipole moment chromophores unless some other force (eg, ionic) is used to overwhelm the effect of dipole–dipole interactions. The good news is that theory provides guidance to quick optimization of electrooptic activity for a given chromophore/polymer system. The concentration (number density) of chromophores leading to maximum electrooptic activity is predicted by theory with high accuracy. Moreover, theoretical results argue that the shape of chromophores should be altered from their normal prolate ellipsoidal shape to a more spherical shape. This is readily accomplished by adding inert substituent (alkyl or alicyclic) groups to the waist of chromophores (68). An even more promising route is that of dendrimer synthesis including dendrimer structures where more than one chromophore is incorporated into the dendrimer. Very simply, steric forces are used to prevent chromophores from achieving centric order driven by dipole–dipole interactions. An example of an early version multichromophore dendrimer, which has led to electrooptic coefficients of 60 pm/V at 1.55 μm telecommunication wavelength, is shown in Figure 3 (105).

Theoretical guidance has permitted polymeric electrooptic materials to be fabricated that exhibit electrooptic coefficients in excess of 100 pm/V (68,106) at telecommunication wavelengths. With these materials, V_π voltages of less than 1 V have been achieved. This has been, without question, a very important

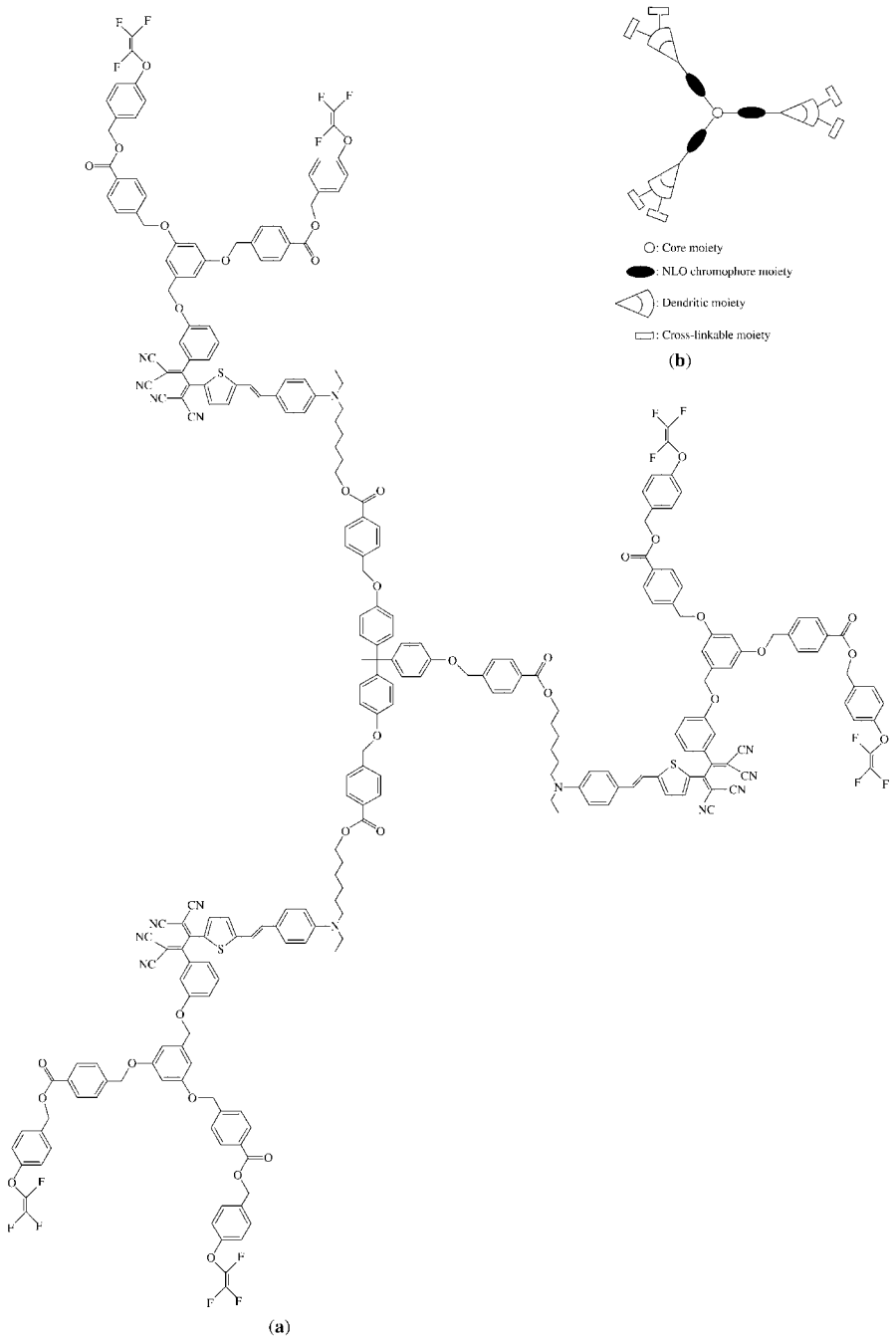

Fig. 3. (a) An early version multichromophore dendrimer (105) is shown. This cross-linkable dendrimer yields an electrooptic coefficient of 60 pm/V at 1.55 μm wavelength that is stable under testing at 85°C for 1000 h. (b) Schematic representation. $M_w = 4664$; Chromophore density: 33 wt%.

result stimulating considerable interest from both large and small companies in the telecommunications and defense fields. V_π voltages on the order of 1 V permit low cost complementary metal oxide semiconductor (CMOS) and high speed electrochemical luminescent circuits to be used without amplifiers. Moreover, such low voltages are important for the realization of transparent (low loss) communication links. Indeed, the realization of deep optical modulation with low electrical drive voltage can lead to gain in electrical-to-optical-to-electrical signal transduction. In satellite telecommunication applications, the elimination of low noise amplifiers is important for the reduction in launch weight as well as for reducing noise and cost. The practical (commercial) importance of the advances in electrooptic activity rests upon two issues: (*1*) Can electrooptic activity be further improved and by how much? (*2*) Can large electrooptic activity be achieved in conjunction with all of the other required properties? The answer to the first question is very likely positive. Indeed, it is clear that electrooptic activity will be further improved by at least another factor of 2. The answer to the second question will become clear from the following paragraphs.

Bandwidth

The bandwidth (response time or highest frequency component of data that can be handled) of devices fabricated from electrooptic materials is determined by the index of refraction n and dielectric constant ε of the materials from which the devices are fabricated. For polymeric organic electrooptic materials, $\varepsilon = n^2$ approximately. This means that low frequency electrical and high frequency optical waves propagate with the same velocities in a material. This in turn means that long interaction lengths can be employed, which leads to low drive voltage requirements. For example, 3-cm electrodes were used to achieve sub 1-V V_π values for polymeric modulators (68). For organic materials, voltage-length products are currently of the order of 1–3 V·cm. The typical index of refraction values ($n = 1.55$–1.70) and dielectric constant values ($\varepsilon = 2.4$–3.0) for polymeric organic materials have permitted electrooptic device bandwidths of 113 GHz to be demonstrated using simple device structures (107–110). Pulsed measurements establish that the intrinsic material bandwidth response is of the order of 350 GHz (essentially defined by the phase relaxation time of the π-electron system). Device bandwidth-length product values could conceivably be as high as 350 GHz·cm with polymeric organic electrooptic materials; however, the difficulty of transmitting electrical signals with frequency components above 120 GHz through metal electrodes makes this a difficult objective to achieve. The low dielectric constants of organic materials also lead to very favorable power requirements (eg, typical P_π values are on the order of 4 dB). Crystalline organic materials achieve acentric order by exploiting ionic interactions to overwhelm the chromophore π-electron dipole interactions that favor centric order. These ionic interactions lead to higher index of refraction and dielectric permittivity values, eg, 2.5 and 7.0 respectively.

For lithium niobate, dielectric constants are of the order of 28 while index of refraction is of the order of 2.2. The bandwidth-length product is 10 GHz-cm and the voltage-length product is 5 V-cm. By clever engineering (minimizing the

time spent by electrical waves in high dielectric lithium niobate), lithium niobate devices have been demonstrated to approximately 90 GHz. Commercial devices are available from Lucent with bandwidths of 30 GHz, V_π voltages of 6 V (1550 nm), insertion loss of 6 dB, and temperature stability to 70°C. The high dielectric constant of lithium niobate results in high power dissipation, ie, $P_\pi >$ 32 dB currently. While high frequency operation is possible with devices fabricated from lithium niobate, more sophisticated device engineering is required. Moreover, such bandwidth is accomplished with sacrifice of drive voltage. The high intrinsic bandwidth afforded by polymeric organic materials was early on recognized as one of the greatest advantages of such materials. The fact that the high bandwidth of organic electrooptic materials is now accompanied by low drive voltage requirements argues for the serious commercial consideration of these materials.

GaAs electroabsorptive modulators offer the possibility of high bandwidth (50 GHz) and low drive voltage (1–2 V). However, these materials exhibit substantial chirp. It is impossible to change absorption without also changing index of refraction. Moreover, GaAs devices are plagued by high insertion loss (9–12 dB). Lithium niobate modulators seem to be the currently preferred alternative to GaAs modulators for high frequency (10–30 GHz) applications.

Modulated lasers, thermooptic switches, liquid crystalline modulators, bubble jet switches, and MEMS devices suffer even greater bandwidth limitations. The introduction of wavelength division multiplexing (WDM) has taken some of the bandwidth pressure off of purely time division multiplexing (TDM) approaches to handling telecommunication throughput. However, bandwidth is likely to remain a serious issue for future telecommunication systems, and thus the bandwidth performance organic and inorganic electrooptic materials will remain an issue of active concern.

Optical Loss

One of the most attractive advantages of lithium niobate is exceptionally low optical loss (material loss of 0.2–0.4 dB/cm and device insertion loss of 3–6 dB at telecommunication wavelengths). Optical loss has been a problem with polymer materials until recently when a better understanding of factors leading to both material and insertion optical loss has permitted significant improvement in loss values (to material loss values of as low as 0.2 dB/cm and insertion loss values as low as 4 dB at telecommunication wavelengths). Material optical loss can be associated with either absorption loss or loss due to scattering. Absorption loss can arise from either (or a combination of) interband electronic absorption or C—H (or N—H, O—H) vibrational overtone absorption at 1.3 or 1.55 μm wavelengths. Wavelength-dependent interband absorption is easily assessed by techniques such as photothermal deflection spectroscopy. Appropriate chromophore design can keep optical loss due to interband absorption below 1 dB/cm even at 1.3 μm wavelength. Such loss is probably not a significant factor at 1.55 μm telecommunication wavelength. Vibrational absorption at 1.3 and 1.55 μm wavelengths is a much more serious problem. As with the production of low loss silica fiber, the answer to the problem of intrinsic optical loss is to get the hydrogen out of

the material. Without such reduction in hydrogen content, optical loss in organic materials is typically limited to approximately 1 dB/cm at 1.3 μm wavelength and somewhat higher values at 1.55 μm wavelength. With organic materials, reduction in hydrogen content typically means using partially fluorinated materials or materials constructed with functionalities, such as the cyanurate ligand, that do not contain hydrogen (when the carbon positions are substituted). Using cyanurate and fluorinated dendrons, optical loss values as low as 0.2 dB/cm have been obtained for electrooptic dendrimer materials. Fluorination of polymer materials frequently involves unwanted changes in processability; for example, changes in solubility in spin-casting solvents. Dendrimer synthesis has been demonstrated to provide a convenient means of reducing optical absorption loss without paying a price in material processability.

Scattering losses induced by processing have been a much more insidious problem in the fabrication of low loss organic waveguide structures. Scattering losses can arise from several sources. One of the most obvious is material inhomogeneity associated with spin casting. Any phase separation leads to disastrously high loss values. Strong dipole–dipole interactions among chromophores can drive phase separation. Fortunately, such interactions can be attenuated by appropriate derivatization of chromophores. Such derivatization also improves the entropy of mixing (and hence the solubility) of chromophores in spin casting solvents. Electric field poling and the concurrent cross-linking of materials to lock-in poling-induced electrooptic activity can also lead to optical loss (71,100,106,111–113). Two types of optical loss are typically associated with electric field poling. The first arises from electric-field-induced surface damage. This is simply a form of dielectric breakdown and can be avoided by keeping corona poling field strengths below damage thresholds. It is important to keep in mind that the harder (more cross-linked) the polymer lattice, the higher the damage threshold. Thus, electric field poling and lattice hardening are typically carried out using a stepped temperature/electric field protocol (71,100,112,114–116). The second type of poling-induced scattering loss is associated with introduction of inhomogeneity in the material as the result of electric field poling. Such inhomogeneity can arise from an electrophoretic effect or from poling-induced birefringence. If defects (such as dust particles) exist that are not influenced by the poling field, then poling can enhance the index difference between these defect regions and the electrooptic material leading to enhanced scattering loss (117). Lattice hardening (cross-linking) chemical reactions can also be a source of material inhomogeneity that leads to increased scattering loss. This is particularly true with thermosetting reactions such as urethane chemistry where a variety of oligomeric structures can exist and grow at different rates (111). Some of these structures can become incompatible and phase separate. Moreover, some cross-linking chemistries, such as urethane chemistry, are susceptible to atmospheric moisture. The reaction with water from the atmosphere can upset the one-to-one stoichiometry of lattice hardening reactions leading to the buildup of incompatible components and phase separation. The occasionally observed cloudy appearance of polyurethane electrooptic polymers is typically indicative of problems with atmospheric moisture. However, when sources of optical loss associated with electric field poling and lattice hardening are taken into account, optical loss values on the order of 1 dB/cm are readily obtained (71,100,106,111–113).

Optical loss can also arise from fabrication of buried channel waveguide structures by reactive ion etching (RIE) techniques and by the deposition of cladding layers where the solvent employed in spin casting the cladding layer causes solvent pitting of the electrooptic film layer. Both of these loss mechanisms can be controlled by lattice hardening of the electrooptic material and by control of processing conditions. Control of the kinetic energy of reactive ions in RIE (118,119) can keep optical loss values due to waveguide wall roughness to insignificant values (0.01 dB/cm). Cladding layers pose an unanticipated problem for the utilization of organic-electrooptic materials. While cladding materials have been utilized that make no problematic contribution to optical loss, problems in device operation can frequently be traced to cladding materials rather than to the electrooptic materials. Conducting cladding materials can be particularly problematic. In general, one wants the electrical conductivity of the cladding material to be higher than that of the electrooptic material so as to drop the poling field across the cladding layer. However, if the cladding material has significant optical loss, the penetration of the propagating optical field into the cladding layer will result in unwanted attenuation of the transiting beam. The cladding material can also undergo photochemical damage and may do so even when the electrooptic material does not show damage. This can manifest in time-dependent loss of mode confinement when no change in electrooptic modulation efficiency is observed. A more subtle problem that can arise with conducting cladding materials is that of photoconductivity (or optical power-dependent conductivity). Electrooptic chromophores are very polarizable materials and can inject charge into a conducting medium (71,112). Thus, an optical power-dependent conductivity of the cladding material can result if that material is susceptible to accepting charge and transporting that charge. Such effects are typically observed only at high power levels in devices such as high frequency oscillators based on electrooptic modulator technology. Of course, optical fields must be kept away from lossy metal electrodes. Again, if care is taken in the design and execution of device structures, loss from waveguide fabrication, cladding deposition, and electrode deposition can be kept to insignificant values, and overall active waveguide loss values of 1 dB/cm can be routinely achieved.

The greatest loss issue to be faced in the commercial implementation of organic electrooptic devices is that of mode mismatch loss when coupling silica fiber and polymeric electrooptic modulator waveguides. For 1.3 μm telecommunication wavelength operation, silica optical fiber waveguides are cylindrical with spherical cross-sectional core diameters on the order of 10 μm, while the cross-sectional shapes of polymeric electrooptic modulator waveguides are elliptical with heights of 1–2 μm. Butt coupling of such active and passive waveguides leads to optical loss on the order of 4 dB per transition. The coupling problem is readily addressed using spherical lens or tapered transitions (70,71,112,120). A tapered transition such as shown in Figure 4 reduces coupling loss to a few tenths of a decibel. Thus, total insertion losses of 4–5 dB have been obtained for polymeric materials exhibiting material loss on the order of 1 dB/cm. Tapered transition structures can be fabricated by employing offset, gray scale, and shadow ion masking techniques (70), which are to be discussed later. Such lithographic techniques are also useful for constructing sophisticated 3-D circuits (70).

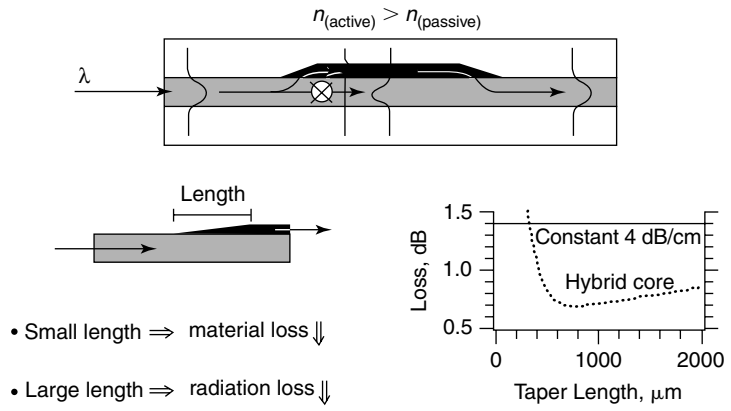

Fig. 4. A low loss polymeric electrooptic modulator transition structure is shown. The optimum taper length is defined by the trade-off between acceptable radiation loss and material loss.

Stability

For electrooptic materials (eg, liquid crystalline materials) based on index of refraction changes associated with molecular reorientation, one wants facile reorientation to permit fast switching times. Organic photorefractive materials also exhibit enhanced response when molecular reorientation contributes to observed index changes. In contrast, reorientation destroys the electric-field-poling-induced electronic electrooptic activity of chromophore-containing polymeric materials. When one speaks of thermal instability of electronic electrooptic activity for organic materials, one is referring to reorientational (molecular rotational) dynamics that destroy poling-induced acentric order. There are two general approaches to improving the stability of poling-induced order. One is to place chromophores in polymer materials, such as polyimides or polyquinolines, characterized by high glass-transition temperatures. This may be accomplished either by physically dissolving chromophores in polymers to produce composite materials or by covalently coupling chromophores to polymer lattices (71,112,121–134). The stability will be defined by both the segmental flexibility of the polymer backbone (the glass transition temperature) and the number (and positioning) of covalent bonds coupling the chromophore to the polymer lattice. The stability of poling-induced acentric chromophore order (electrooptic activity) can be readily assayed by monitoring second harmonic generation (another phenomena related to $\chi^{(2)}$) as a function of heating the sample (see Fig. 5) (135). This is a nonlinear optical analogue of thermal gravimetric analysis except that molecular reorientation rather than material decomposition accounts for the loss of second-order nonlinear optical activity. As shown in Figure 5, thermal stability of electrooptic activity is increased with cross-linking. When dynamic thermal stability is increased to temperatures such as 170°C as shown in Figure 5, then long-term stability is typically observed for periods of several thousand hours even when devices are operated at 100°C. Segmental flexibility of polymers is one of the most serious problems with relaxation

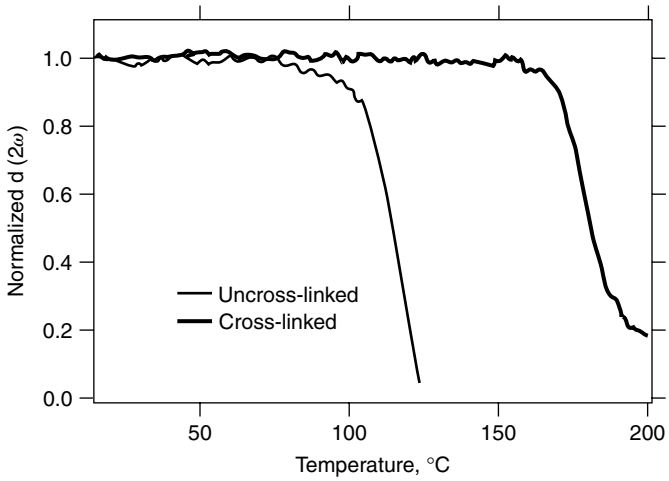

Fig. 5. Second harmonic generation is shown as a function of temperature for heating at a rate of 10°C per minute for two samples. The uncross-linked sample (chromophore is attached covalently by one end to a PMMA backbone) starts to lose second-order optical nonlinearity (acentric chromophore order) before 100°C. The cross-linked sample corresponds to both ends of the chromophore being covalently coupled to the polymer lattice. For this sample, thermally stable second-order optical nonlinearity is observed until nearly 170°C.

of poling-induced acentric order. Dendrimer materials appear to have distinct advantages for enhancing the thermal stability of poling-induced electrooptic activity. Not only can the covalent bonds and steric interactions of dendrimers hold chromophores away from each other (inhibiting centric ordering) but dendrimer structures can also oppose thermal relaxation. The dendrimer material of Figure 3 is observed to exhibit stable electrooptic activity for 1000 h at 85°C. Greater thermal stability should be achieved by greater attention to the flexibility of dendrons and by better control of cross-link density. In comparison, the thermal stability of lithium niobate devices is typically listed as 90°C while gallium arsenide devices are specified as stable to 80°C.

Preliminary studies of the stability of organic electrooptic materials to high energy (gamma ray) radiation and particles (protons) carried out by Lockheed Martin (Palo Alto) and by researchers at the Air Force Research Laboratory (Wright Patterson Air Force Base) suggest that space application of polymeric electrooptic materials should proceed without problems.

Photochemical stability is more difficult to assess. Lithium niobate is specified as having optical power handing capabilities to 250 mW while gallium arsenide is specified as having a maximum power handling capability of 30 mW. However, such power handling capability is typically specified for packaged materials where oxygen has been excluded. The photochemical stability of organic materials is dramatically affected by the presence of oxygen. Exclusion of oxygen typically improves photochemical stability by several orders of magnitude. The addition of oxygen (radical) scavengers can also improve photochemical stability (136). Photochemical stability can also improve

with lattice hardening (100) although this will depend upon the porosity of the polymer lattice, which may not always correlate simply with cross-link density. Unfortunately, controlled evaluation of photochemical stability under conditions appropriate for commercial applications have not been carried out for polymeric electrooptic materials; thus, photochemical stability remains the most serious question concerning the commercialization of organic electrooptic materials.

Mechanical Properties

Polymeric electrooptic materials have the advantage of being conformal and of exhibiting effective bonding to a variety of surfaces. Moreover, by control of cross-link density, the mechanical properties of polymeric electrooptic materials can be controlled. Electrooptic device operation can be carried out over a wide range of temperatures. Eventually, different coefficients of thermal expansion may cause delamination problems upon thermal cycling over wide temperature ranges, but such problems have not been noted to the present. A unique feature of polymeric systems is that good mechanical properties are obtained for lightweight materials. Weight is an issue in satellite telecommunication and reconnaissance systems. Regarding weight issues in satellite telecommunications and reconnaissance operations, the low drive voltage requirements of polymeric electrooptic devices permit the elimination of low noise amplifiers, which in turn results in substantial weight reduction. Thus, the weight issue is not the relative weights of lithium niobate and polymeric electrooptic materials but the relative weights of total systems fabricated from these materials. Also, the critical weight saving comes from using photonic (optical fiber) versus electrical (coaxial) cables.

Processing and Integration

Polymeric materials are amenable to facile processing by RIE (70,71,112,119,120) and photolithographic techniques (71,112,137). Use of offset, gray scale, and shadow ion lithographic masks and RIE has permitted implementation of vertical waveguide transitions and the fabrication of 3-D circuits permitting the ready integration of passive and active optical waveguide components (70,71). Polymeric electrooptic materials are also very compatible with semiconductor processing, and electrooptic circuitry has been fabricated on top of very large-scale integration (VLSI) semiconductor chips (71,112). Indeed, through use of planarizing polymers, electrooptic modulators have been vertically integrated (in high density) with VLSI chips. Integration has been accomplished without the perturbation of the performance characteristics of either electronic or optical (electrooptic) circuitry. One of the advantages of polymeric electrooptic materials is this ready integration with semiconductor electronics and the ability to fabricate a large number of modulator waveguides on a single chip. With lithium niobate, such integration is not possible and connection to electronic circuitry is typically made by wires and flip chip bonding. By use of tapered transitions and

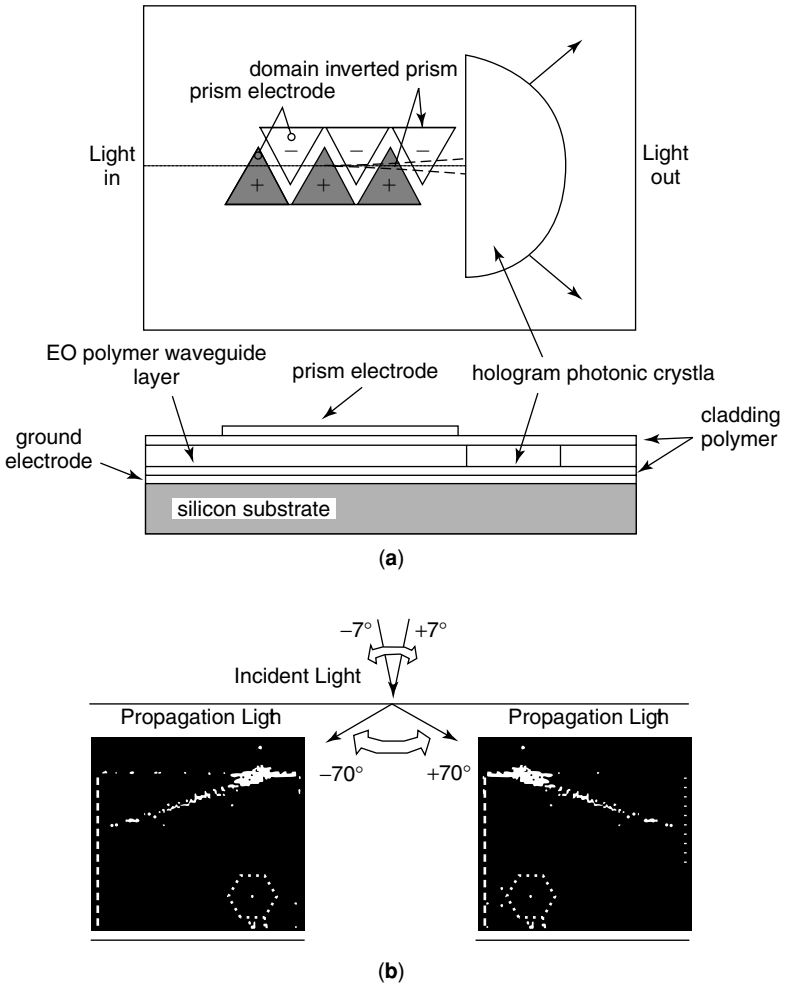

Fig. 6. Large-angle beam steering is shown for a device based on a polymeric electrooptic material (a cross-linkable version of the CLD chromophore discussed in Ref. 68). (a) EO waveguide prism introduces a small deflection angle to initialize the beam scanning. The half-circle 2-D photonic crystal region is embedded into the waveguide so that the deflection angle is "amplified" as the light passes through the crystal region. 3-D scanning can also be provided if a 3-D structure is built. (b) The experimental observation of the angle sensitivity.

spherical lens, electrooptic waveguides have been coupled to silica fiber optics. Again, coupling can be achieved in a more straightforward manner than with lithium niobate.

An example of sophisticated device development is shown in Figure 6. Large-angle (-70° to $+70^\circ$) beam steering is demonstrated by implementing a series of cascaded electrooptic prisms, which initiate beam steering and feed light into a photonic band gap lattice (138,139). The photonic band gap lattice is fabricated by holography in a photopolymer material (see Fig. 7). Beam steering is accomplished with more than an order of magnitude lower drive voltage than required using

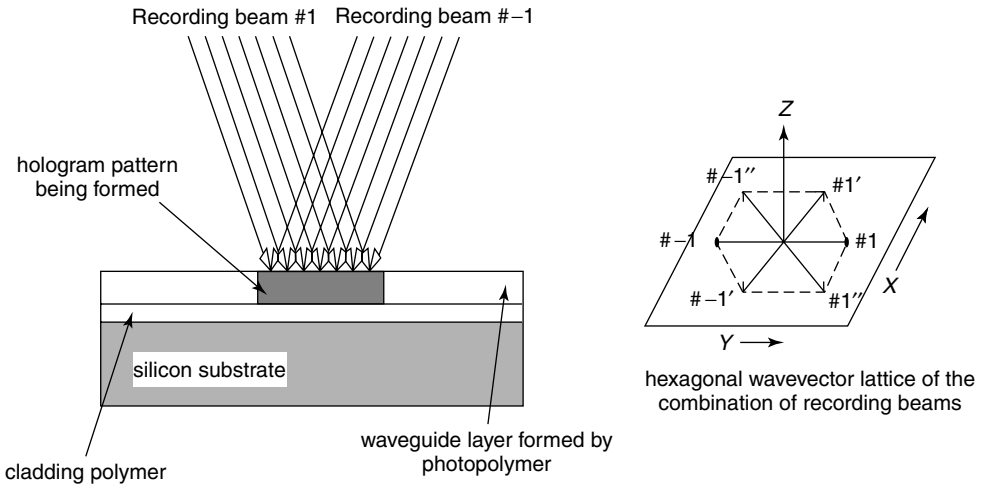

Fig. 7. The holographic production of the polymeric photonic band gap lattice used in the beam steering device of Figure 6 is shown.

lithium niobate materials. Through the cascaded prism electrodes, the deflection angle is given for steering of a TM polarized beam by

$$\theta = n_0^2 r_{33}(V/\mathrm{d})(L/h) \tag{5}$$

where L and h are the length and width of the prism array, respectively. V is the applied driving voltage and d is the electrode spacing. The electrooptic coefficient in the direction of the driving field is r_{33}, while n_0 is the voltage independent index of refraction. In the present example, L/h is approximately 80 with $L = 16$ mm and $h = 200$ μm. The model used to arrive at equation (4) is based only upon the total phase retardation across the wave front. The deflection angle thus depends only on the overall dimension of the prisms, since the accumulated phase difference across the wave front is independent of how the deflector is subdivided into individual prisms, as long as the interfaces between adjacent prisms are straight lines.

Devices

The most simple device configurations utilizing electrooptic materials are shown in Figure 8 (122). These include the Mach Zehnder and birefringent modulators and the directional coupler. As configured in Figure 8, the first two devices are amplitude modulators. A somewhat higher drive voltage is required for the birefringent modulator than for the Mach Zehnder modulator. This is because the V_π voltage of the Mach Zehnder relates directly to the principle component (r_{33}) of the electrooptic coefficient. The V_π voltage of the birefringent modulator relates to the difference between the major and minor components

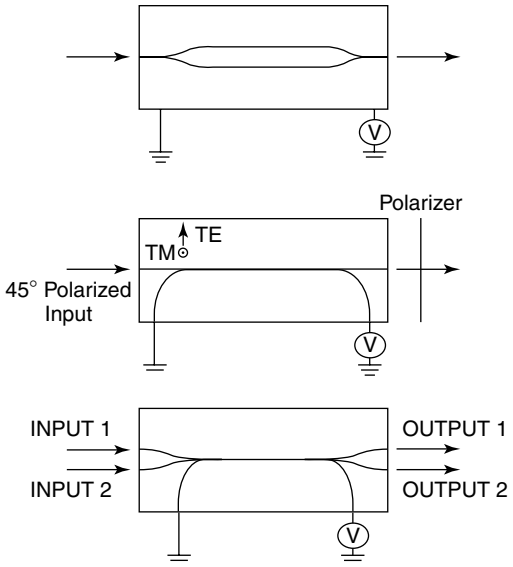

Fig. 8. Mach Zehnder interferometer (top), birefringent modulator (middle), and directional coupler (bottom) device configurations are shown.

$(n_3^3 r_{33} - n_1^3 r_{13})$. A still higher drive voltage is required for the directional coupler, and the relationship to material electrooptic activity is somewhat more complex (122).

We have already shown a large-angle spatial light modulator based upon organic electrooptic and photonic band gap materials (Figs. 6 and 7). Such beam steering without moving parts is relevant for holographic optical data storage, switching in all optical networks, advanced laser radar (ladar), photonic phased array antennas, optical sensors, and laser printers. Spatial light modulation exploiting electronic electrooptic activity has not only the advantage of greater speed but also avoids instability due to overshoot associated with the momentum of mechanical beam steering (MEMS) devices. The fact that such beam steering can be accomplished with application of driving voltages in the range of volts rather than kilovolts (as is the case for lithium niobate) is also a very attractive feature. For fiber optic switching, spatial light modulation has the advantage that a large number of fiber channels can be selectively addressed using only one electrode. Overall, electrooptic beam steering offers a simplified operating scheme, low driving voltage, high switching speed, small size, and low cost.

Ultra high bandwidth analogue-to-digital (A/D) conversion has been accomplished utilizing polymeric electrooptic materials in several different device configurations. Analogue-to-digital conversion employing a cascaded series of Mach Zehnder modulators has been discussed elsewhere (112). Analogue-to-digital conversion can also be accomplished by time stretching (140). In this application, a femtosecond pulse is stretched (by a dispersive medium) to match the length of an incoming data stream containing high frequency information. The data stream is transduced as an amplitude modulation (by a polymeric electrooptic modulator)

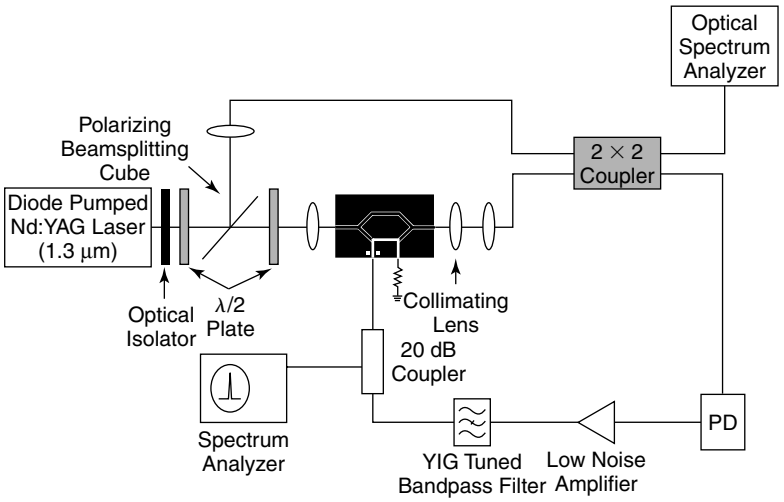

Fig. 9. A broadband, ultrastable oscillator based on polymeric electrooptic materials is shown.

onto the optical pulse. The pulse is then further time stretched to a length compatible with conventional A/D converters. The pulse is then converted to an electrical signal by a diode detector and A/D conversion is effected. Such time stretching permits A/D conversion at rates of 100 Gbit/s.

Another prototype device, which has been demonstrated by researchers at Pacific Wave, is that of a high frequency oscillator (see Fig. 9). In this oscillator, the stability of the oscillator is determined by the length (Q) of the optical circuit (loop) and can thus be very high indeed.

A variety of phased array systems have been fabricated based on polymeric electrooptic materials (141,142). One configuration is based on the photonic phase shifter shown in Figure 10. This provides a very linear phase shift as a function of control d-c voltage. Optical signals of controlled phase are thus sent to various radiating antenna elements. The optical signals are converted to radiofrequency signals by diode detectors.

High frequency (including secured communication by frequency hopping) telecommunication applications are receiving considerable attention (143). As can be seen in Table 1, the bandwidth limitation of current electronic components is the limiting factor to achieving increased bandwidth performance with polymeric electrooptic materials. In Figure 11, a device configuration capable of 130-GHz bandwidth operation is shown.

Other demonstrated prototype devices include optical gyroscopes (144), broadband acoustic spectrum analyzers (145), 1×2 Y-fed directional couplers (146) and polarization-insensitive electrooptic modulators (147,148). For long-haul telecommunication applications, it is difficult to maintain polarization control; thus, a need exists for polarization-insensitive modulators. Indeed, polarization insensitivity was one of the advantages claimed for gallium arsenide electroabsorptive modulators. By using different poling schemes, overall polarization insensitivity has been achieved for polymeric modulators (147,148).

Table 1. The Bandwidth Characteristics of Various Electrical Interfaces

Modulator type	Electrical interface	Bandwidth, GHz	Technology availability	Reliability	Cost
Traditional	K-coax	0–40	Simple, commercial	Proven	Low
M-Z modulators	V-coax	0–65	Simple, commercial	Proven	Low
	W-coax	0–110	Ongoing at TACAN	R&D	Low
	WR-15	50–75	Complicated, customer	R&D	High
	WR-10	75–110	Complicated, customer	R&D	High

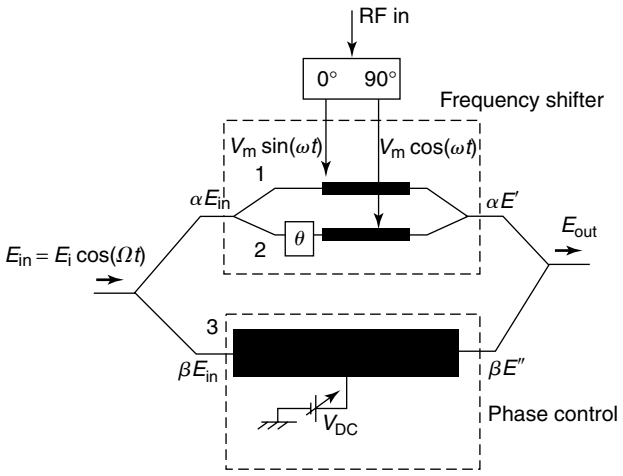

Fig. 10. A schematic representation of a photonic radiofrequency phase shifter is shown.

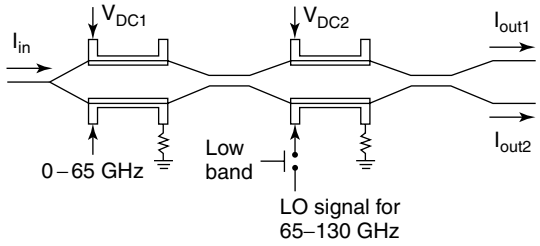

Fig. 11. A 130-GHz telecommunications device is shown.

Commercialization and Cost

As with lithium niobate, the cost of devices based on polymeric electrooptic modulators is in the packaging rather than in the materials. A Lucent lithium niobate modulator sells for approximately $6000. Polymer modulator vendors such as Pacific Wave Industries (Los Angeles, California) are quoting comparable prices. The low material cost is associated with the fact that modulator devices are thin-film

devices and a chip containing 6–100 modulators requires very little polymeric electrooptic material.

A number of small companies such as Lumera (Bothel, Washington), Pacific Wave Industries (Los Angeles, California), Radiant Research (Austin, Texas), IP-ITEK/TACAN (Carlsbad, California), KVH Industries (Tinley Park, Illinois), etc are exploring the commercialization of electrooptic devices based on polymeric materials. Lockheed Martin has pursued research in polymeric electrooptic materials for more than a decade and continues to be a leader in the field. Lucent has recently resumed research on polymeric electrooptic materials. A number of telecommunication companies including Nortel, Agilent, Cisco, and JDS-Uniphase are currently evaluating polymeric electrooptic technology to determine the viability of R&D and commercial activity in this area.

The market for inorganic electrooptic and electroabsorptive modulators is currently in the hundreds of millions of dollars per year with wait times of several months for delivery of lithium niobate modulators. The perceived need for greater bandwidth in the telecommunications industry is likely to drive demand even higher.

Future Prognosis

Provided that no unexpected problems arise that would inhibit the commercialization of polymeric electrooptic technology, the prognosis is very good. The greatest uncertainty involves whether or not organic electrooptic materials will exhibit adequate photochemical stability over many years of in-field operation. Preliminary studies suggest that exclusion of oxygen and hermetic sealing will yield devices capable of exhibiting photochemical stability over many years for exposure to optical fields at telecommunication wavelengths and powers. Almost certainly, electrooptic coefficients will continue to be improved. New and improved chromophores are being synthesized with great regularity (149). Devices operating with sub 1-V V_π values should become commonplace. Utilization of photonic band gap materials and controlled coupling to resonated structures should permit further reduction in drive voltage requirements (possibly even to microvolt levels); such reduction is, of course, at the expense of some reduction in response time (bandwidth). Low drive voltage requirements, together with high bandwidth capabilities and the ease of integration with semiconductor electronics and silica transmission fibers, should be a powerful driver for the deployment of polymeric electrooptic technology in telecommunication, defense, transportation, and display industries. However, the extent of utilization of polymer electrooptic technology in the telecommunication industries will depend upon perceived bandwidth needs. If low cost alternatives to high information throughput with reduced bandwidth requirements (such as expanded use of WDM technology) become popular, limited bandwidth technologies such as thermooptic, liquid crystalline, MEMS, and modulated laser technologies may continue to dominate sales in the telecommunications area. However, even if deployment is slow in telecommunications, defense industries should find use for the exceptional capabilities of polymeric electrooptic materials for applications such as radar, electronic counter measure, sensor, and display systems. Other

niche applications including biomedical sensors, analytical instrumentation, and high frequency test equipment are likely to develop.

The main limitation to general deployment of organic electrooptic materials is that they have been optimized to this point in time for applications at telecommunication wavelengths. Inorganic materials such as lithium niobate are still the materials of choice for applications at visible wavelengths. Such inorganic modulators are likely going to continue to dominate the laboratory market for modulators to be used with research laser systems.

Nomenclature

p_i	ith component of the molecular polarization vector in the presence of electrical fields
p_{0i}	ith component of the permanent polarization of the molecule
E	the local electric field strength
F	the local electric poling field strength
α	molecular polarizability tensor
β	molecular first hyperpolarizability tensor
γ	molecular second hyperpolarizability tensor
P_i	ith component of the bulk polarization vector in the presence of electrical fields
P_{0i}	ith component of the bulk polarization vector in the absence of external fields
V	applied voltage
$\chi^{(1)}_{ij}$	first-order electric susceptibility tensor
$\chi^{(2)}_{ijk}$	second-order electric susceptibility tensor
$\chi^{(3)}_{ijkl}$	third-order electric susceptibility tensor
n	refractive index in the presence of an applied electric field
n_0	refractive index in the absence of an applied electric field
r	Pockels coefficient or electrooptic coefficient
r_{33}	electrooptic coefficient in the direction of the applied field (principal element)
r_{13}	electrooptic coefficient orthogonal to the applied field direction (minor element)
R	Kerr factor
E_0	applied electric field amplitude
N	number density
$f(\omega)$	local field factor
$\langle\cos^3\theta\rangle$	acentric order parameter
V_π	applied voltage required to produce a phase shift of π
λ	wavelength of light
d	electrode gap
L	interaction length of electrical and optical fields in material
Γ	modal overlap integral
θ	beam deflection angle

BIBLIOGRAPHY

"Electrooptical Applications" in *EPSE* 2nd ed., Vol. 5, pp. 756–771, by M. Thakur and S. Tripathy, GTE Laboratories, Inc.

1. J. Kerr, *Phil. Mag.* **50**, 337 (1875).
2. F. Pockels, *Lehrbuch der Kristalloptic*, Teubner, Leipzig, Germany, 1906.
3. G. T. O'Konski, in N. M. Bikales, ed., *Encyclopedia of Polymer Science and Technology*, 1st ed., Wiley-Interscience, New York, Vol. **9**, 1968, p. 551.
4. B. R. Jennings, *IEE Proc.* **130**, 212 (1983).
5. C. T. O'Konski, ed., *Molecular Electrooptics*, Marcel Dekker, Inc., New York, 1976.
6. S. Krause, ed., *Molecular Electro-Optics*, Plenum Press, New York, 1980.
7. I. P. Kaminow, *An Introduction to Electrooptic Devices*, Academic Press, Inc., New York, 1974.
8. J. Wilson and J. F. B. Hawkes, *Opto-electronics, An Introduction*, Prentice-Hall, Englewood Cliffs, N.J., 1983.
9. N. Bloembergen, *Nonlinear Optics*, Benjamin, New York, 1965.
10. P. N. Prasad and D. J. Williams, *Introduction to Nonlinear Optical Effects in Molecules and Polymers*, John Wiley & Sons, Inc., New York, 1991.
11. L. R. Dalton, in J. I. Kroschwitz and M. Howe-Grant, eds., *Kirk-Othmer Encyclopedia of Chemical Technology*, Vol. **17**, John Wiley & Sons, Inc., New York, 1996, p. 287.
12. D. L. Wise, G. E. Wnek, D. J. Trantolo, T. M. Cooper, and J. D. Gresser, eds., *Electrical and Optical Polymer Systems*, Marcel Dekker, Inc., New York, 1998.
13. H. Nalwa and S. Miyata, eds., *Nonlinear Optics of Organic Molecules and Polymers*, CRC Press, Inc., Boca Raton, Fla., 1997.
14. Y. R. Shen, *Nonlinear Optics*, John Wiley & Sons, Inc., New York, 1984.
15. R. W. Boyd, *Nonlinear Optics*, Academic Press, Inc., New York, 1993.
16. T. J. Bunning and co-workers, *Annu. Rev. Mater. Sci.* **30**, 83 (2000).
17. R. Dabrowski, *Ferroelectrics* **243**, 1 (2000).
18. S.-M. Chang and co-workers, *Mater. Sci. Eng. C* **12**(1/2), 111 (2000).
19. T. Ikeda and A. Kanazawa, *Bull. Chem. Soc. Jpn.* **73**, 1715 (2000).
20. T. Fuhrmann and J. H. Wendroff, *Int. J. Polym. Mater.* **45**, 621 (2000).
21. K. M. Blackwood, *Int. J. Polym. Mater.* **45**, 585 (2000).
22. N. Boiko and V. Shibaev, *Int. J. Polym. Mater.* **45**, 533 (2000).
23. F. Simoni and O. Francescangeli, *Int. J. Polym. Mater.* **45**, 381 (2000).
24. V. Shibaev, *Int. J. Polym. Mater.* **45**, 307 (2000).
25. J. Zubia and J. E. Ecenarro, *Int. J. Polym. Mater.* **45**, 503 (2000).
26. E. Lizuka, *Int. J. Polym. Mater.* **45**, 191 (2000).
27. G. Abbate and J. M. Oton, *Adv. Mater.* **12**, 459 (2000).
28. D. A. Higgins, *Adv. Mater.* **12**, 251 (2000).
29. D. J. Broer and co-workers, *Macromol. Symp.* **154**, 1 (2000).
30. T. J. Sluckin, *Contemp. Phys.* **41**, 37 (2000).
31. R. L. Wisnieff and J. J. Ritsko, *IBM J. Res. Dev.* **44**, 409 (2000).
32. M. O'Neill and S. M. Kelly, *J. Phys. D: Appl. Phys.* **33**, R67 (2000).
33. S. R. Collinson and D. W. Duncan, *Perspect. Supramol. Chem.* 285 (1999).
34. W. A. Crossland and co-workers, *Proc. SPIE* **3955**, 70 (2000).
35. M. Hird, J. W. Goodby, and K. J. Toyne, *Proc. SPIE* **3955**, 15 (2000).
36. J. W. Goodby and co-workers, *Proc. SPIE* **3955**, 2 (2000).
37. B. L. Feringa and co-workers, *Chem. Rev.* **100**, 1789 (2000).
38. K. Ichimura, *Chem. Rev.* **100**, 1847 (2000).
39. S. Susumu, *Opt. Rev.* **6**, 471 (1999).
40. F. Bloisi and L. Vicari, *Recent Res. Dev. Macromol. Res.* **4**, 113 (1999).
41. T. Tsukada, *Springer Ser. Mater. Sci.* 7 (2000).

42. J. W. Goodby, *Curr. Opin. Solid State Mater. Sci.* **4**, 361 (1999).
43. I. C. Khoo, *J. Nonlinear Opt. Phys. Mater.* **8**, 305 (1999).
44. G. Scalia and co-workers, *Proc. SPIE* **3800**, 112 (1999).
45. R. A. Herke, M. H. Anderson, and T. G. Baur, *Proc. SPIE* **3800**, 45 (1999).
46. R. W. Sabnis, *Displays* **20**, 119 (1999).
47. S. Naemura, *Mater. Res. Soc. Symp. Proc.* **559**, 263 (1999).
48. C. C. Bowley and co-workers, *Mater. Res. Soc. Symp. Proc.* **559**, 97 (1999).
49. W. Haase, D. Ganzke, and E. P. Pozhidaev, *Mater. Res. Soc. Symp. Proc.* **559**, 15 (1999).
50. G. W. Gray and S. M. Kelly, *J. Mater. Chem.* **9**, 2037 (1999).
51. W. M. Gibbons and co-workers, *Proc. SPIE* **3635**, 32 (1999).
52. P. Palffy-Muhoray, *Phys. Prop. Liq. Cryst.* 467 (1999).
53. L. M. Blinov, *Phys. Prop. Liq. Cryst.* 375 (1999).
54. D. Dunmur and K. Toriyama, *Phys. Prop. Liq. Cryst.* 113 (1999).
55. D. Dunmur and K. Kazuhisa, *Phys. Prop. Liq. Cryst.* 102 (1999).
56. G. W. Gray, *Phys. Prop. Liq. Cryst.* 1 (1999).
57. E. Lueder, *Proc. Electrochem. Soc.* 98 (1999).
58. A. Sinha, T. A. P. Rao, and V. R. K. Murthy, *Liq. Cryst.* **27**, 191 (2000).
59. Ch. Bosshard, *Springer Ser. Opt. Sci.* 7 (2000).
60. M. Samoc, A. Samoc, and B. Luther-Davies, *Synth. Met.* **109**, 79 (2000).
61. M. Samoc and co-workers, *MCLC S&T, Sect. B.: Nonlinear Opt.* **20**, 183 (1999).
62. S. R. Marder and co-workers, *Science* **276**, 1233 (1997).
63. R. L. Nelson and R. W. Boyd, *Appl. Phys. Lett.* **74**, 2417 (1999).
64. D. R. Greve and co-workers, *Synth. Met.* **102**, 1533 (1999).
65. F. Cherioux and co-workers, *Chem. Commun.* **20**, 2083 (1999).
66. M. G. Kuzyk, *Opt. Lett.* **25**, 1183 (2000).
67. K. A. Drenser and co-workers, *J. Phys. Chem.* **103**, 2290 (1999).
68. Y. Shi and co-workers, *Science* **288**, 119 (2000).
69. Y. Shi and co-workers, *Appl. Phys. Lett.* **77**, 1 (2000).
70. S. M. Garner and co-workers, *IEEE J. Quantum Electron.* **35**, 1146 (1999).
71. L. Dalton and co-workers, *Ind. Eng. Chem. Res.* **38**, 8 (1999).
72. W. H. Steier and co-workers, *Chem. Phys.* **245**, 487 (1999).
73. R. A. Norwood and co-workers, *Proc. SPIE* **3281**, 2 (1998).
74. S. Kalluri and co-workers, *IEEE Photon. Technol. Lett.* **8**, 644 (1996).
75. B. Kipplen and co-workers, *ACS Symp. Ser.* **72**, 204 (1999).
76. R. J. Twieg and co-workers, *Mater. Res. Soc. Symp. Proc.* **561**, 119 (1999).
77. S. R. Marder and co-workers, *Nature* **388**, 845 (1997).
78. B. Kippelen and co-workers, *J. Am. Chem. Soc.* **119**, 4559 (1997).
79. B. Kippelen and co-workers, *Proc. SPIE* **3144**, 176 (1997).
80. B. Kippelen and co-workers, *Science* **279**, 54 (1998).
81. E. Hendrickx and co-workers, *Appl. Phys. Lett.* **72**, 1670 (1998).
82. Z. Peng, A. Gharavi, and L. Yu, *J. Am. Chem. Soc.* **119**, 4622 (1997).
83. W. Li and co-workers, *Adv. Mater.* **10**, 927 (1998).
84. W. E. Moerner, A. Grunnet-Jepsen, and C. L. Thompson, *Annu. Rev. Mater. Sci.* **27**, 585 (1997).
85. A. Grunnet-Jepsen and co-workers, *J. Opt. Soc. Am. B* **15**, 901 (1998).
86. A. Grunnet-Jepsen, C. L. Thompson, and W. E. Moerner, *Opt. Commun.* **145**, 145 (1998).
87. J. A. Delaire and K. Nakatani, *Chem. Rev.* **100**, 1817 (2000).
88. S. R. Marder, D. N. Beratan, and L. T. Chang, *Science* **252**, 103 (1991).
89. S. R. Marder and J. W. Perry, *Science* **263**, 1706 (1993).
90. D. R. Kanis, M. A. Ratner, and T. J. Marks, *Chem. Rev.* **94**, 195 (1994).
91. I. D. L. Albert, T. J. Marks, and M. A. Ratner, *J. Am. Chem. Soc.* **119**, 6575 (1997).

92. B. Champage and B. Kirtman, *Chem. Phys.* **245**, 211 (1999).
93. J. Lipinski and J. Bartkowiak, *Chem. Phys.* **245**, 263 (1999).
94. A. Painelli, *Chem. Phys.* **245**, 185 (1999).
95. A. K.-Y. Jen and co-workers, *Adv. Mater.* **9**, 132 (1997).
96. S. R. Marder and co-workers, *Science* **265**, 632 (1994).
97. J. L. Brédas and co-workers, *Acc. Chem. Res.* **32**, 267 (1999).
98. L. R. Dalton, A. W. Harper, and B. H. Robinson, *Proc. Natl. Acad. Sci. USA* **94**, 4842 (1997).
99. A. W. Harper and co-workers, *J. Opt. Soc. Am. B* **15**, 329 (1998).
100. L. R. Dalton and co-workers, *J. Chem. Mater.* **9**, 1905 (1999).
101. B. H. Robinson and co-workers, *Chem. Phys.* **245**, 35 (1999).
102. B. H. Robinson and L. R. Dalton, *J. Phys. Chem.* **104**, 4785 (2000).
103. W. Lin and co-workers, *J. Am. Chem. Soc.* **119**, 2205 (1997).
104. A. Piekara, *Proc. R. Soc. London A* **149**, 1 (1939).
105. H. Ma and co-workers, *J. Am. Chem. Soc.* **123**, 986 (2001).
106. L. R. Dalton, *Advances in Polymer Science*, Vol. **154**, Springer-Verlag, Heidelberg, 2001.
107. D. Chen and co-workers, *Proc. SPIE* **3006**, 314 (1997).
108. D. Chen and co-workers, *Appl. Phys. Lett.* **70**, 3335 (1997).
109. D. Chen and co-workers, *IEEE Photon. Tech. Lett.* **11**, 54 (1999).
110. A. H. Udupa and co-workers, *Electron. Lett.* **35**, 1702 (1999).
111. S. S. H. Mao and co-workers, *Chem. Mater.* **10**, 146 (1998).
112. L. R. Dalton, in D. L. Wise, G. E. Wnek, D. J. Trantolo, T. M. Cooper, and J. D. Gresser, eds., *Electrical and Optical Polymer Systems*, Marcel Dekker, Inc., New York, 1998, p. 609.
113. L. R. Dalton, *Opt. Eng.* **39**, 589 (2000).
114. S. Kalluri and co-workers, *Proc. SPIE* **2285**, 67 (1994).
115. S. Kalluri and co-workers, *Appl. Phys. Lett.* **65**, 2651 (1994).
116. H. W. Oviatt Jr. and co-workers, *Chem. Mater.* **7**, 493 (1995).
117. C. C. Teng, M. A. Mortazavi, and G. K. Boughoughian, *Appl. Phys. Lett.* **66**, 667 (1995).
118. A. Chen and co-workers, *J. Electrochem. Soc.* **143**, 3648 (1996).
119. W. H. Steier and co-workers, *Mat. Res. Soc. Symp. Proc.* **413**, 147 (1996).
120. A. Chen and co-workers, *Proc. SPIE* **3005**, 65 (1997).
121. D. M. Burland, R. D. Miller, and C. A. Walsh, *Chem. Rev.* **94**, 31 (1994).
122. L. R. Dalton and co-workers, *Adv. Mater.* **7**, 519 (1995).
123. L. R. Dalton and co-workers, *Chem. Mater.* **7**, 1060 (1995).
124. Z. Liang and co-workers, *Chem. Mater.* **7**, 941 (1995).
125. Z. Liang and co-workers, *Chem. Mater.* **7**, 1756 (1995).
126. Z. Liang and co-workers, *Chem. Mater.* **8**, 2681 (1996).
127. C. Xu and co-workers, *Macromolecules* **26**, 5303 (1993).
128. M. A. Hubbard and co-workers, *Chem. Mater.* **4**, 965 (1992).
129. J. E. Becker and co-workers, *J. Am. Chem. Soc.* **115**, 12216 (1993).
130. R. E. Harelstad and co-workers, *Mater. Res. Soc. Symp. Proc.* **328**, 637 (1994).
131. D. Yu, A. Gharavi, and L. Yu, *Macromolecules* **28**, 784 (1995).
132. D. Yu and co-workers, *ACS Symp. Ser.* **672**, 123 (1997).
133. H. Saadeh and co-workers, *Macromolecules* **30**, 5403 (1997).
134. H. Ma and co-workers, *Chem. Mater.* **11**, 2218 (1999).
135. M. W. Becker and co-workers, *Chem. Mater.* **6**, 104 (1994).
136. A. Galvan-Gonzalez and co-workers, *Appl. Phys. Lett.* **77**, 2083 (2000).
137. B. H. Cumpston and co-workers, *Nature* **398**, 51 (1999).
138. L. Sun and co-workers, *Opt. Eng.* in press; L. Sun and co-workers, *Proc. SPIE* **3950**, 98 (2000).

139. L. Sun and co-workers, *Proc. SPIE* **3632**, 134 (1999).
140. D. H. Chang and co-workers, *IEEE Photon. Tech. Lett.* **12**, 537 (2000).
141. S. S. Lee and co-workers, *IEEE Microwave and Guided Wave Lett.* **9**, 357 (1999).
142. R. Chen and co-workers, *Proc. PSAA*, in press.
143. J. H. Bechtel and co-workers, *Proc. SPIE* **4114**, 58 (2001); see also http://depts.washington.edu/eooptic (last updated 7/6/2001).
144. P. R. Ashley and J. S. Cites, *OSA Tech. Dig. Ser.* **14**, 196 (1997).
145. A. Yacoubian and co-workers, *J. Sel. Top. Quant. Elect.* **6**, 810 (2000).
146. D. An and co-workers, *Appl. Phys. Lett.* **76**, 1972 (2000).
147. A. Donval and co-workers, *J. Appl. Phys.* **87**, 3258 (2000).
148. L. Sun and co-workers, *Appl. Phys. Lett.* in press.
149. J.-M. Raimundo and co-workers, *Chem. Commun.* 1597 (2000).

LARRY R. DALTON
University of Southern California

EMULSION POLYMERIZATION. See HETEROPHASE POLYMERIZATION.

ENGINEERING THERMOPLASTICS, OVERVIEW

Introduction

The development of plastic materials is one of the most successful stories of the twentieth century. In the sixties, plastics represented a small fraction of the total annual consumption of materials, but 20 years later they surpassed metallic materials (mostly iron-based) in terms of consumed volume. At the end of the century, plastics reached the astonishing total amount of 150 million metric tons produced per year. Of this amount, 70% is comprised by the so-called commodity plastics (HDPE, LDPE, PP, PVC, and PS), 11% by thermoset resins, 7% by elastomers, and 12% by engineering thermoplastics.

The definition of engineering plastics is rather arbitrary. In the last edition of this encyclopedia they were defined as *thermoplastic resins, neat or filled, which maintain dimensional stability and most mechanical properties above 100°C and below 0°C*. In such a definition, engineering plastics are obviously intended as engineering thermoplastics and the terms are used interchangeably. They encompass plastics that can be formed into parts suitable for bearing loads and able to withstand abuse in thermal environments traditionally tolerated by metals, ceramics, glass, and wood. A more general definition defines *engineering plastics* as those *high performance materials that provide a combination of high ratings for mechanical, thermal, electrical, and chemical properties*. This article adopts this latter definition, with the following three restrictions: (*1*) thermoplastics considered here are generally produced on an industrial scale; (*2*) with some exceptions, their predominant application is as solid parts or films, not fibers or cellular materials; and (*3*) sophisticated derivations of commodities, like reinforced PP, UHMWPE, etc, widely used in engineering applications are excluded. Following

Encyclopedia of Polymer Science and Technology. Copyright John Wiley & Sons, Inc. All rights reserved.

Table 1. Engineering Thermoplastics

Material	Class[a]	Morphology[b]	Acronym[c]	CASRN
C-containing polymers				
Cyclic olefin copolymers	E	A	COP, COC	[26007-43-2]
Ethylene/tetracyclododecene				
Ethylene/norbornene				
Syndiotactic polystyrene	E	C	sPS	[28325-75-9]
O-containing polymers				
Acetal resins (polyoxymethylene)	E	C	POM	[25231-38-3]
Polyesters, Thermoplastic thermoplastics	E	C		
Poly(ethylene terephthalate)			PET	[25038-59-9]
Poly(butylene terephthalate)			PBT	[24968-12-5]
Poly(ethylene naphthalate)			PEN	[25230-87-9]
Polyarylates	E	A	PAR	[39281-59-9]
Liquid crystal line polymers	HP	C	LCP	[144114-03-4]
Poly(phenylene ether)[d]	E	A	PPE	[24983-67-8]
Polycarbonates	E	A/C	PC	[25037-45-0]
Aliphatic polyketones	E	C	PK	[88995-51-1]
Poly(ether ketones)	HP	C	PEEK	[31694-16-3]
			PEK	[27380-27-4]
			PEKK	[54991-67-2]
			PEKEKK	[60015-05-6]
Acrylic resins[e]	E	A	PMMA	[9011-14-7]
Sulfur-Containing Polymers				
Poly(phenylene sulfide)[f]	HP	C	PPS	[25212-74-2]
Polysulfones	E	A	PSU	[25135-51-7]
Poly(ether sulfone)	HP	A	PES	[25667-42-9]
Poly(aryl sulfone)	HP	A	PAS	[25839-81-0]
N-containing polymers				
Styrene copolymers[g]	E	A	ABS	[9003-56-9]
			SAN	[9003-54-7]
			SMA	[9011-13-6]
Polyamides, Plastics	E	C/A	PA6,6	[32131-17-2]
			PA6,10	[9008-66-6]
			PA6,12	[24936-74-1]
			PA4,6	[50327-22-5]
			PA6	[25038-54-4]
			PA11	[25035-04.5]
			PA12	[24937-16-4]
Polyamides, Aromatic	HP	–	ArPA	[24938-64-5][h]
				[24938-60-1][i]
Polyimides	HP	A/C	PI	[25036-53-7]
Polyamide imide	HP	A	PAI	[61970-49-8]
Polyphthalamides	HP	C	PPA	[25750-23-6]
Polyetherimide	HP	A	PEI	[61128-46-9]
F-containing polymers				
Fluoropolymers[j]		C		
Poly(tetrafluoroethylene)			PTFE	[9002-84-0]
Ethylene–tetrafluoroethylene copolymer			ETFE	[25038-71-5]

Table 1. (Continued)

Material	Class[a]	Morphology[b]	Acronym[c]	CASRN
Fluorinated ethylene–propylene copolymer			FEP	[25067-11-2]
Perfluorovinylether–tetrafluoroethylene copolymer			PFA	[26655-00-5]

[a]E: engineering plastics (medium performance); HP: high performance plastics.
[b]C: crystalline; A: amorphous.
[c]Acronyms used through the text are reported.
[d]See POLYETHERS, AROMATIC.
[e]See ACRYLIC ESTER POLYMERS, METHACRYLIC ESTER POLYMERS.
[f]See POLY(ARYLENE SUFIDE)S.
[g]See ACRYLONITRILE and ACRYLONITRILE POLYMERS.
[h]Referred to poly(*p*-phenylene terephthalamide).
[i]Referred to poly(*m*-phenylene isophthalamide).
[J]See PERFLUORINATED POLYMERS, POLYTETRAFLUOROETHYLENE.

these guidelines, Table 1 was compiled; occasionally, copolymers, blends, and reinforced polymers are included. The materials have been arbitrarily grouped by considering the most representative heteroatom present in their chemical structure. These materials are discussed in general in this article and in more detail in articles devoted to the various polymers. Cross references are provided.

The selection of polymer families treated here is somewhat arbitrary. For instance, fluoropolymers are more functional materials than engineering materials, and acrylic resins suffer enough thermal instability to be considered by some authors as outside the border of engineering plastics. However, PTFE (together with some copolymers) and PMMA have been considered because of their notoriety and some specific engineering applications.

Table 1 categorizes polymeric materials as *engineering polymers* (lower performance) or *high performance polymers;* the borderline between the two groups is rather vague. Relatively good indicators for such a classification are the selling price and/or the amount produced per year. Polymers can be either amorphous or partially crystalline, depending on their molecular structure and conditions of formation of the solid phase (polymerization and/or thermal history). The amorphous or semicrystalline nature of each material is reported in Table 1 as the form predominantly used in applications. A polymer is considered semicrystalline when it develops a detectable crystalline phase upon nonaccelerating cooling of the melt (see SEMICRYSTALLINE POLYMERS; CRYSTALLIZATION KINETICS). However, in particular conditions a polymer normally crystalline appears amorphous. For example, PET, is crystalline by slow cooling of the melt, but by rapid quenching it is amorphous. Crystalline and amorphous polymers are distinguished by several different properties, and the most evident of them is light transmission: crystalline polymers are opaque, whereas amorphous polymers are transparent (see AMORPHOUS POLYMERS). Finally, Table 1 collects the acronyms which are assigned to the various polymers through the text, as well as the Chemical Abstract Service Registry Number (CASRN). In the case of polymers, the assignment of more than one CASRN to the same material is frequent.

Table 2. Relationships between Polymer Properties and Morphology

Property	Crystalline	Amorphous
Light transmission	High	None to low
Solvent resistance	High	Low
Lubricity	High	Low
Dimensional stability	High	Low
Mold shrinkage	High	Low
Resistance to dynamic fatigue	High	Low
Facility to form high strength fibers	High	None
Thermal expansion coefficient	High	Low
Melting temperature	Sharp	Absent
Dependence of properties on temperature	High	Low

In Table 2, the qualitative dependence of some properties of polymeric materials as a function of their morphological state is reported. Such properties are determined directly or indirectly by the different response of chains to solicitations (chemical, thermal, and so on) when they are in an ordered arrangement or in a random one. Totally crystalline (100%) polymers are impossible to obtain because of the unavoidable presence of chain folds; further, the crystallinity degree can change under the effect of thermal, mechanical, or chemical operations.

History of Development

The development of engineering thermoplastics began in the thirties and is still continuing. The first patent on polyamide (nylon) was obtained by Carothers in 1931. Before the second World War, acrylic and polyester resins were discovered, as well as styrene-based copolymers (ABS) and PTFE. The latter was brought to full production in 1950 as Teflon by DuPont. In the same year, polycarbonates were introduced by General Electric and acetal resins by Celanese. In the period of 1960–1980, most of the actual high performance polymers were developed, among them were polyimides, PES, PPS, PEEK, and PEI, as well as other engineering resins such as PPO and PBT. At that time, the potential of development of novel engineering plastics was overestimated, and when it was realized that the volume growth was not so fast, the introduction of new families slowed down. Several factors contributed to this change of attitude, from the growing of costs necessary for the introduction of a new material, to a lower demand of materials studied for structural applications, and finally to the competition of tailored grades of existing polymers (also commodity plastics, like PP), new blends, and reinforced materials. Furthermore, the time from the invention of a new polymer structure to the achievement of the industrial stage remained quite high (10–12 years), in spite of the experience accumulated in such processes. Thus, from an originally forecasted 25% of the whole plastics market, engineering plastics cover only 10% roughly. It remains true that the growth rate is higher than that of commodities, but this expands their total fraction only very slowly. In Figure 1, the chronological development of commercial thermoplastic polymers is sketched, taking into account commodities nearer to engineering polymers (in properties) (1,2). The figure shows that most of the engineering thermoplastics were

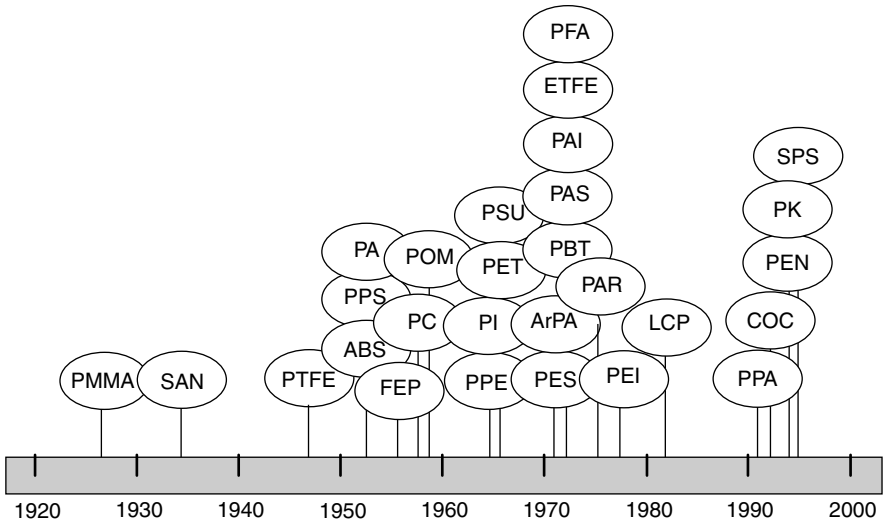

Fig. 1. The historical development of synthetic thermoplastic resins. The reported years indicate the presumed entry in the market. See Table 1 for an explanation of acronyms.

introduced industrially in the 1950–1980 period. The new flourishing in the nineties was partly enhanced by some particular events, like the development of metallocene catalysts, which rendered convenient the fabrication of new materials like sPS and COCs, and the availability of the monomer for PEN.

Table 3 reports for each polymer family the most important producers and corresponding trade names, with the aim of helping the reader to identify materials. Some books are dedicated to this task (3–5), which is complicated by ongoing mergers and selling of operations, resulting in changed connections between producers and trade names.

Properties of Thermoplastics

Some material properties are intrinsic to the chemical substance under investigation; others depend on the processing operation, which confers a shape and orientation to the material. Because some processing is often necessary to prepare testing specimens, intrinsic properties can be difficult to measure. Some properties acquire relevance only when the final article is manufactured and strictly depend on the specific use of the article. Properties have been distinguished as performance, maintenance, or aesthetic properties (1); however, this classification is extremely subjective. Herein, mainly intrinsic and processing properties are considered, divided into four conventional groups: physical, electrical, thermal, and mechanical. Several of such properties change remarkably depending on the morphology (amorphous or semicrystalline materials) or for the presence of fillers and reinforcing fibers. It is impossible to report the properties of all the grades present on the market; it was estimated that more than 5300 grades of engineering plastics were offered by producers in 1997 (6). Thus, the more representative of them are described in discussions of specific polymers. In Table 7, the most

Table 3. Producers and Trade Names of Engineering Thermoplastics

Material[a]	Trade Name	Manufacturer
COC	Topas	Ticona
	Apel	Mitsui Petrochemical
	Zeonex[b], Zeonor[c]	Nippon Zeon
	Arton	JSR
sPS	Questra	Dow
	Xarec	Idemitsu
POM	Delrin	DuPont
	Hostaform, Celcon	Ticona
	Ultraform	BASF
	Tenac	Asahi
	Iupital	Mitsubishi
PET, PBT	See Table 4	See Table 4
PAR	U-Polymer	Unitika[d]
	Durel	Ticona
LCP	Vectra	Ticona
	Xydar	BP Amoco
	Zenite	DuPont
	Summika	Sumitomo
	Siveras	Toray
PPE	PPO, Noryl[e]	GE Plastics
	Luranyl	BASF
	Vestoran	Degussa Huls
PC	Makrolon	Bayer
	Lexan	GE Plastics
	Calibre	Dow
	Iupilon	Mitsubishi
PK	Carilon	Shell
	Ketonex	BP Amoco
PEEK	Victrex	ICI
	Ketron	DSM
PEK	Stilan	Raytheon
	Hostatec	Ticona
	Kadel	BP Amoco
PEKK	Declar	DuPont
PEKEKK	Ultrapek	BASF
PEN	Koladex	ICI
	Hipertuf	Shell[f]
PMMA	Perspex, Diakon	ICI
	Plexiglas, Plexidur, Altuglas, Vedril	AtoHaas
	Acrifix	Rohm
	Vestiform	Hüls
	Paraglas, Degalan	Degussa
	Lucryl	BASF
	Sumipex	Sumitomo
PPS	Fortron	Ticona
	Ryton	Phillips
	Supec	GE Plastics
	Tedur	Bayer
	Craston	CIBA-GEIGY
	Techtron	DSM

Table 3. (Continued)

Material[a]	Trade Name	Manufacturer
PSU	Udel	BP Amoco
	Ultrason S	BASF
PES	Radel A	BP Amoco
	Ultrason E	BASF
	Victrex PES	ICI
	Astrel	Carborundum
PAS	Radel R	BP Amoco
ABS	See Table 5	See Table 5
SAN	Luran	Bayer
	Lustran	BASF
	Tyril	Dow
PA	See Table 6	See Table 6
ArPA	Nomex	DuPont
	Conex	Teijin
	Kevlar	DuPont
	Twaron	Akzo
PI	Kapton, Vespel, Avimid	DuPont
	Upilex	UBE
	Kinel, Matrimid	CIBA-GEIGY
	Apical	Allied
	Aurum	Mitsui Toatsu
	Kerimid	Nyltech
	Duratron	DSM
PAI	Torlon	BP Amoco
PPA	Amodel	BP Amoco
PEI	Ultem	GE Plastics
Fluoropolymers	Teflon, Tefzel	DuPont
	Fluon	ICI
	Hostaflon	Dyneon
	Algoflon, Hyflon	Ausimont
	Neoflon, Polyflon	Daikin
	Aflon	Asahi Glass

[a] See Table 1 for explanation of acronyms.
[b] Homopolymer.
[c] Copolymer.
[d] Commercialized by Amoco for several years under the trade name of Ardel.
[e] In blend with other polymers.
[f] Business acquired by Mossi & Ghisolfi.

representative properties are reported, together with the proper SI units and, if existing, the respective standard measurement method. Several books describe the methods in more detail (2,3,7).

Physical Properties. Physical properties include density, properties connected to their combustion tendency (flammability and oxygen index), optical properties (refractive index and yellow index), and the ability to absorb water. Density ρ, ie, the mass per unit volume, depends on the nature of atoms present in the chemical structure and the way molecules (chains) pack together. Polyolefins, composed of C and H only, have densities in the range 0.85–1; organic polymers

Table 4. Producers and Trademarks of Thermoplastic Polyesters

Producer	PET	PBT
Eastman	Ektar, Eastapak, Kodapak, Tenite, Kodar	Ektar
Allied Signal	Petra	
DuPont	Rynite, Mylar	Crastin
Dow	Lighter	
Ticona	Impet	Celanex
Hoechst	Polyclear	
Bayer		Pocan
BASF		Ultradur
GE Plastics		Valox
DSM	Arnite	Arnite
Degussa/Hüls		Vestodur
ICI	Melinar[a], Melinex[a]	
Shell		Cleartuf[b]
Nyltech	Techster	Techster
Mitsubishi		Novadur
EMS Chemie		Grilpet

[a]Business acquired by DuPont.
[b]Business acquired by Mossi & Ghisolfi.

Table 5. Producers and Trademarks of ABS Materials

Producer	Pure grade	Blend with PC	Blend with PBT	Blend with PVC	Blend with others
GE Plastice	Cycolac	Cycoloy	Cycolin	Cycovin	
Dow	Magnum	Pulse			Prevail[a]
Bayer	Lustran	Bayblend			Triax[b]
	Novodur				
EniChem	Sinkral	Koblend			
Hoechst	Cevian				
Toray	Toyolac	Toyolac			
Condea	Vista			Suprel	
Shin-A	Claradex				
Nova	Cycogel				
Schulman	Polyfabs			Polyman	

[a]With polyurethane.
[b]With PA.

containing heteroatoms rarely have densities higher than 2. Conformations and crystalline phases strongly influence density. Crystalline phases are generally more dense than amorphous phases, an average ρ_c/ρ_a ratio of 1.13 ± 0.08 has been determined (1).

The Limited Oxygen Index (LOI) test determines the minimum oxygen fraction in an oxygen/nitrogen mixture able to support combustion of a candle-light sample under specific test conditions. The LOI test is necessary but not sufficient for determining the burning behavior of polymers in real conditions. For this task, specific flammability tests have been established on an empirical basis. The most widely used test is UL94, elaborated by Underwriters Laboratories, rating the

Table 6. Producers of Aliphatic Polyamides

Company	PA 6	PA 6,6	Other PA	Trade names
AlliedSignal	Y	Y	N	Capron
Ashley Polymers	Y	Y	6, 10; 6, 12; 11; 12	Ashlene
ELF-Atochem	N	N	11; 12	Rilsan, Orgalloy
BASF	Y	Y	Y	Ultramid
Bayer	Y	Y	Y	Durethan
Nyltech	Y	N	Y	Sniamid, Technil
DuPont	Y	Y	11; 6, 12	Zytel, Minlon
DSM	Y	Y	4, 6; 6, 10	Akulon, Stanyl
Ems	Y	Y	12; 6, 12	Grilon, Grilamid, Grivory
Hüls	N	N	12; 6, 12	Vestamid, Trogamid
Mitsubishi Kasei	Y	N	N	Novamid
Radici	Y	Y	Y	Radilon
Rohdia	Y	Y	Y	Technyl
Ticona		Y		Celanese
Toray	Y	Y	6, 10	Amilan
UBE	Y	Y	Y	UBE-Nylon

ability of a material to extinguish a flame once ignited (8). In decreasing order, the UL94 degrees are V-0, V-1, V-2, and HB, based on a specific specimen thickness. Only a few high performance polymers, like polyetherimides, have been classified as inherently nonflammable (ie, V-0); other polymers can reach a good classification after the addition of specific additives, ie, flame-retardants, in the material formulation.

The refractive index n measures the deviation of light when passing through matter and is expressed as $\sin(i)/\sin(r)$, where i and r are the angles of incident light and refracted light, respectively. It is closely linked to molecular structure of polymers and contributes to their optical properties, like clarity, haze, birefringence, color, transmittance, and reflectance. Most of engineering plastics considered here are opaque and/or inherently colored, with the exceptions of PC, PMMA, and COC. For them, when used in optical applications, the yellow index (YI) is relevant. Yellow index indicates the degree of departure of an object color from colorless or from a preferred white toward yellow and is determined from spectrophotometric data.

Water absorption indicates the increase of weight of a polymer after immersion in water under specified conditions of temperature and time. Generally, it is referred to 24 h at room temperature (23°C) and is expressed as a percentage with respect to the initial weight. If water is absorbed by a polymer, drying is required before processing operations because the presence of water at high temperature results in uncontrolled degradation of the material and consequently poor performance. This is the case of PET and other polyesters. Some polymers like polyamides absorb water from air humidity and hold water molecules rather firmly by hydrogen bonding. Absorbed water causes a slow variation of properties like electrical characteristics, mechanical strength, and dimensions. For this reason, polymers or specific grades insensitive to water must be employed in moist environments.

Table 7. Properties, Units and Standard Methods of Measurement

Property	ASTM method	ISO method
Physical properties		
Density, g/mL	D792	1183
Flammability	UL94[a]	
Oxygen index (LOI), %	D2863	4589
Refractive index	D542	489
Yellowness index (YI)	D1925	
Water absorption (24 h, 23°C)		
Electrical properties		
Dielectric constant (1 MHz)	D150	
Dielectric strength (1 mm), kV/mm	D149	
Dissipation factor (1 kHz)	D150	
Volume resistivity (23°C, dry), Ω·cm	D150	
Thermal properties		
Glass-transition temperature (T_g), °C		
Melting temperature (T_m), °C		
Heat-deflection temperature (HDT) at 0.45 or 1.8 MPa, °C	D648	75
Specific heat capacity J/(kg·K)		
Thermal conductivity (23°C), W/(m·K)	C177	
Thermal expansion coefficient, K^{-1}	D696	
Upper working temperature, °C		
Mechanical properties		
Elastic modulus, GPa[b]	D638	527
Tensile strength, MPa[c]	D638	527
Flexural modulus, GPa[b]	D790	178
Flexural strength, MPa[c]	D790	178
Compressive strength, MPa[c]	D638	527
Elongation at break, %	D638	527
Notched Izod impact resistance (3.2 mm), J/m[d]	D256	180
Hardness (Rockwell M or R)	D785	2039
Friction coefficient	D1894	8295
Rheological properties		
Intrinsic viscosity, Pa·s		
Melt-flow index, g/10 min	D1238	1133

[a] UL94 is an Underwriters Laboratories method.
[b] To convert GPa to psi, multiply by 145,000.
[c] To convert MPa to psi, multiply by 145.
[d] To convert J/m to lbf·ft/in., divide by 53.38.

Electrical Properties. Electrical properties include dielectric constant, dielectric strength, dissipation factor, and volume resistivity. All of them depend on temperature and water absorption.

The (relative) dielectric constant is the ratio of the capacitance of a condenser formed by two metal electrodes separated by a suitable layer of the material considered and the same separated by dry air. The dielectric strength measures the dielectric breakdown resistance of a material under an applied voltage. The applied voltage value just before breakdown is divided by the specimen thickness. Thus, because the result depends on thickness, this value must be specified. The

dissipation factor, also called loss tangent, measures the tangent of the difference angle between 90° (ideal angle for a perfect dielectric material) and the true angle at which an alternating current leads the voltage. It is equivalent to the ratio of current dissipated into heat and current actually transmitted. The volume resistivity is the electrical resistance of a unit cube of a given material when an electrical potential is applied to two opposite faces of the cube.

Thermal Properties. Thermal properties include some transitions like melting temperature and glass transition transition temperature, the heat-deflection temperature (HDT), specific heat capacity, thermal conductivity, coefficient of thermal expansion, and upper working temperature.

The melting temperature T_m is the temperature at which a solid becomes a liquid (or, on cooling, at which a liquid solidifies). For polymeric materials, T_m is often a temperature range rather than a single value; however, its point value should represent the maximum temperature at which crystallites exist. Amorphous polymers do not exhibit a T_m. The glass-transition temperature T_g is the temperature at which a solid, rigid, and brittle polymer becomes rubbery by loosening remarkably its rigidity. Mechanical properties are also reduced at T_g, and other properties like volume, thermal expansion coefficient, and specific heat capacity change noticeably. Being kinetic in nature, T_g occurs over a temperature range (depending, for instance, on cooling rate) and is hardly visible in some polymers. HDT measures the temperature at which a specimen is deformed a specific amount (eg, 0.25 mm) under a given load (usually, 0.45 or 1.82 MPa), applied in a three-point arrangement. HDT is also called DTUL (deflection temperature under load) and should not be interpreted as a safe temperature for continuous operation (which is usually somewhat lower). The specific heat capacity represents the amount of heat necessary to increase the temperature of a unit mass of a substance by one degree. Depending on its definition at constant pressure or at constant volume, it is indicated as c_p or c_v, respectively. Thermal conductivity represents the amount of heat conducted per unit of time through a unit area of a material of unit thickness having a difference of one degree between its faces. The thermal expansion coefficient represents the change in volume (or length) accompanying a temperature unit variation and is of great importance in molding operations of plastic articles, having mold shrinkage as a practical effect. The upper working temperature is a purely empirical indication at which a given plastic can be expected to perform safely and satisfactorily. It is generally lower than HDT.

Mechanical Properties. Mechanical properties include tensile properties (modulus and strength), flexural properties (modulus and strength), compressive strength, elongation at break, impact resistance, hardness, and friction coefficient. Other relevant properties are creep and fatigue but it is difficult to find comparative data among materials.

The tensile modulus (also elastic, or Young's modulus) E is the stress-to-strain ratio within its proportional limit for a material under tensile loading (in practice, the initial slope of the stress–strain curve). The tensile strength represents the maximum tensile stress observed when the specimen is being pulled. It may or may not coincide with the ultimate strength, ie, the tensile stress at specimen failure. In tough materials it can be equal to the yield stress. The flexural modulus is the stress-to-strain ratio within its proportional limit for a material

under bending load conditions. It measures the stiffness of a material. The flexural strength is the ability of a material to flex without permanent deformation or breaking. The elongation at break is equal to tensile strength at failure multiplied by 100. It is expressed as a percent of the original length of the specimen. The impact strength (or impact resistance) represents the ability of a material to resist physical breakdown when subjected to a rapidly increasing force and is accepted as a comparison guide for toughness (see IMPACT RESISTANCE). It depends strongly on the type of test used. The most widely used test in the field of plastics is Izod; the Charpy test is less common. The Izod test requires specimens of thickness from 3.18 to 12.7 mm, preferentially notched following the test method prescriptions. A weighted pendulum arm released from a fixed height strikes the specimen in a specified way. The Izod impact energy is measured by dividing the energy lost by the pendulum (presumably absorbed by the specimen) by the specimen thickness. Hardness, defined as the resistance of a material to local deformation, is connected in a complex way to mechanical properties, elasticity, and plasticity. Hardness cannot be defined unambiguously and depends strongly on the test adopted for its determination. It is usually characterized by the combination of three parameters, ie, scratch resistance, abrasion resistance, and identation under load. For the identation test, different Shore and Rockwell scales are in use, Rockwell M and Rockwell R being the most popular for engineering plastics (2). The scale depends on the combination of load and indentor dimensions. The friction coefficient represents the resistance of surfaces of solid bodies in contact with each other to sliding or rolling. It is represented as $k = F/w$, where F is the force necessary to move one surface with respect to the other one, and w the load exerted on them.

Rheological Properties. Rheological properties (qv), describing the deformation of materials under stress and concerning their flow properties, must be considered in all processing techniques for the fabrication of plastic articles. In order to give operators necessary rheological information, melt viscosity vs shear plots are commonly included in Data Sheets provided by plastics producers. Here only a few properties connected to rheology are considered, ie, intrinsic viscosity (IV) and melt-flow index (MFI).

Intrinsic viscosity measures the capability of a polymer in solution to increase the viscosity of the solution itself. Because IV increases with molecular mass, it is an indication of this last property. The MFI (or simply melt index) measures the isothermal resistance to flow through an extrusion plastometer commonly referred to as melt indexer. Practically, the amount of matter forced by a given load to pass in 10 min through a standard die is determined. Melt-flow index can be considered as a single-point test (ie, resistance to flow at a single shear rate). Every plastics processing technology operates at a defined MFI range as follows (2): 5–100 g/10 min for injection molding, 5–20 g/10 min for rotational molding, 0.5–6 g/10 min for film extrusion, and 0.1–1 g/10 min for blow molding and profile extrusion.

Chemical Resistance. Chemical resistance is less rigidly defined than the properties discussed previously. Measurement methods include immersion in selected vapors or liquids of a test specimen, then determining the variation of mechanical properties after and before treatment. Optical properties are also considered, particularly in the case of transparent materials. The test results are generally indicated as excellent, good, fair, or poor, or are given other arbitrary

scale units. Chemical agents are chosen in order to simulate possible real situations: strong and weak acids, alkalis, saline solutions, hydrocarbons (aliphatic or aromatics), oils and greases, alcohols, aldehydes, ketones, etc. Engineering plastics are generally difficult to dissolve in most solvents. Strictly correlated to chemical resistance is weathering resistance, where a combination of a particular environment, temperature, time, and uv irradiation is considered, also with cyclic experiments.

Processing of Thermoplastics

Processing of thermoplastic materials can be classified into four main categories: extrusion, post-die processing, forming, and injection molding (9–11).

In an extruder, the polymer is melted and pumped into a shaping device called a die, through which the material is forced to assume a particular shape. The pumping action is done by a single-screw or by a twin-screw device, the configuration of which is essential for a suitable result. Extruders are very often used at the end of the polymerization reactor in order to obtain polymer pellets by chopping an extruded strand. Extruders are also currently used to mix in the proper additives for the polymer, to obtain intimately mixed polymer blends, to devolatilize the material from the monomers or solvent residues, and in some special cases as a chemical reactor (reactive extrusion). For example, polyetherimide is prepared at the industrial level by reactive extrusion. Depending on the extrusion die geometry, final articles can also be obtained, including sheets, films, pipes, rods, and profiles of various geometries (T, double T, C, and so on). Coating on wires can be done, as well as coextrusion of two or more layers.

Post-die processing includes a number of operations carried out at the exit of the extruder die in a free-surface way. Examples of such processes are fiber spinning, film blowing, and sheet forming. The shape and dimensions of the extrudate material are determined by the rheological properties of the melt, the die dimensions, the cooling conditions, and the take-up speed (relative to the extrusion rate).

Forming processes use a mold to confer the final form to the article. Blow molding is widely used in the manufacture of bottles or other containers for liquids, widely using engineering polymers like PET and PC. Essentially, an extruded cylindrical parison is inflated with a gas until it fills the mold cavity. A good equilibrium between the melt strength of the resin under low shear conditions (parison stability) and the flow properties under high shear conditions (blowing) are essential for obtaining a satisfactory result. In thermoforming, a polymer sheet is heated to a temperature above its T_g (or sometimes above T_m) and then pressed into the female part of the mold by means of a suitable plug or by vacuum pulling. Simple-shape articles such as trays can be obtained. In compression molding, an amount of polymer is heated at the proper temperature and then squeezed by means of the male part of the mold into the mold cavity.

Injection molding is the most commonly used processing technique for engineering thermoplastics. Typically, the polymer pellets are melted and the melt pulled forward by means of a screw as in extrusion, so filling a mold under appropriate pressure. The shape of the mold, the number and relative location of the injection devices, and the mold cooling rate determine, together with the intrinsic properties of the material, the final quality of the molded articles. Very complex

article shapes can be obtained by this technique. A viscosity of the resin around 10,000 Pa·s and a shear rate of 100 s^{-1} are needed for a convenient operation.

The main problem in injection molding is shrinkage, caused by the volume changes during transition from the melt to the solid. The typical shrinkage of semicrystalline polymers during processing is around 1–4%, compared to 0.2–0.8% for amorphous polymers (11). To reduce the problem, crystallinity could be maintained low, but this is to the detriment of mechanical properties. A compromise should be used. For polymers which crystallize slowly, like PET, it is preferable to allow the polymer to reach the maximum crystallization degree by the use of nucleating agents. If the shrinkage amount is different in different volume portions of the fabricated part, warpage of the part itself can be observed.

Interpolymer Competition

The properties of engineering thermoplastics span a wide range, and there are many overlapping situations among resins. To select the right polymeric material for a specific application is a hard job because the forest of commercial polymers has become so crowded. Books have appeared to guide the materials engineer in the selection of thermoplastic materials, with the help of a dedicated software (6).

Four main groups of technical considerations must be made in order to make the right choice, ie, mechanical, electrical, environmental, and appearance. In addition, two other elements are important, ie, cost and specifications (eg, imposed by a government body or by a corporation). The environmental considerations include the operating temperature, the chemical environment, the weathering exposure, and humidity degree. The appearance includes style, shape, color, transparency, and surface finish of the fabricated object. Mechanical and electrical considerations must include both short-time and long-time values, and also the effects of environment on such properties. Also, appearance can vary under service conditions. The necessary information must be provided by different actors, that is, the material supplier, the processor, the processing equipment supplier, and the product designer/producer.

Depending on the particular application, numerous properties should be considered during the selection of the best candidate. Further, every property has a different importance, and thus a different weight on the final choice. Property values reported here are representative; several of them vary over a wide range depending on several factors, like the nature and amount of fillers, the possible occurrence of copolymerization, etc. Also, some data are not available in the current literature and others are difficult to describe with just one figure. This is particularly true for rheological data reported in data sheets as flow curves viscosity vs temperature curves, etc. Similar difficulties arise for creep curves (related to long-term mechanical resistance) and shrinkage and warpage of fabricated parts, strongly dependent on the geometry and thickness of the part itself. The internet has made it easier to access data about polymer grades actually produced (Table 8).

In the final selection of the best material for the fabrication of a specific object, a compromise is generally made by choosing the material which shows an optimized balance of the most relevant properties. In addition to some particular

Table 8. WWW Sites Containing Data Sheets of Engineering Thermoplastics

URL (Uniform Resource Locator)	Information source
General	
http://matls.com/materials	MatWeb, the on-line
http://polydatabase.com/index2.htm	Information resource
Wholesalers	
http://www.boedeker.com/mguide.htm	Boedeker Plastics Inc.
http://www.goodfellow.com/static/A/start.html	Goodfellow
http://www.panpolymers.co.uk/fprodb.htm	Pan Polymers
http://members.aol.com/vpisales/tpguide.html	Venture Plastics
http://www.actech-inc.com/engmrgt.htm	Actech Inc.
http://www.plasticsandmetals.com/plastics.html	Cal Plastics and Metals
http://www.plasticeng.com/copy˙of˙plasticeng/engineeringmaterials.htm	Plastics Engineering Inc.
Producers	
http://www.dow.com/Homepage/index.html	Dow Chemicals
http://www.shellchemicals.com/home/1,1098,-1,00.html	Shell Chemicals
http://www.ticona.com/	Ticona (Celanese AG)
http://www.basf.com/	BASF
http://www.dupont.com/	DuPont
http://www.bayer.com/	Bayer
http://polymers.alliedsignal.com/	Allied Signal
http://geplastics.com/	GE Plastics
http://dsmepp.com/	DSM

properties, like transparency and the question of processability (which involves complex issues as rheology, shrinkage, and surface finishing), in most of the applications of engineering thermoplastics, the following characteristics and properties are considered: price, mechanical properties, thermal properties, electrical properties, and chemical resistance.

Price. The price of a thermoplastic resin is basically determined by the cost of preparation, which in turn strongly depends on the cost of reagents (monomers, catalysts, etc), the complexity of the manufacturing process, and the dimension of production plants. Aliphatic polyketones, for instance, are made from very cheap raw molecules as ethylene, propylene, and CO; their cost is determined by the need for expensive catalysts, based on Pd complexes, and the relatively complex production plant. On the other hand, PEN, which can easily be prepared in the same reactors used for PET, suffers from the difficult availability of its basic monomer dimethyl 2,6-naphthalene dicarboxylate. Most engineering polymers contain aromatic monomers, which are difficult to synthesize and polymerize, with slow and sophisticated mechanisms (condensation, substitution, oxidative coupling).

Roughly, commodities are priced at US$0.5–1/kg, engineering polymers in the range of US$1–5/kg, and high performance polymers the range of US$5–50/kg. The current prices fluctuate following market conditions and can be found as a price range, for most materials, in technical journals like Plastics Technology. In Figure 2, the prices of engineering thermoplastics are reported as a function of annual production volume, confirming, with a few exceptions, the inverse relationship between the two parameters. The price is reported in U.S. cents per

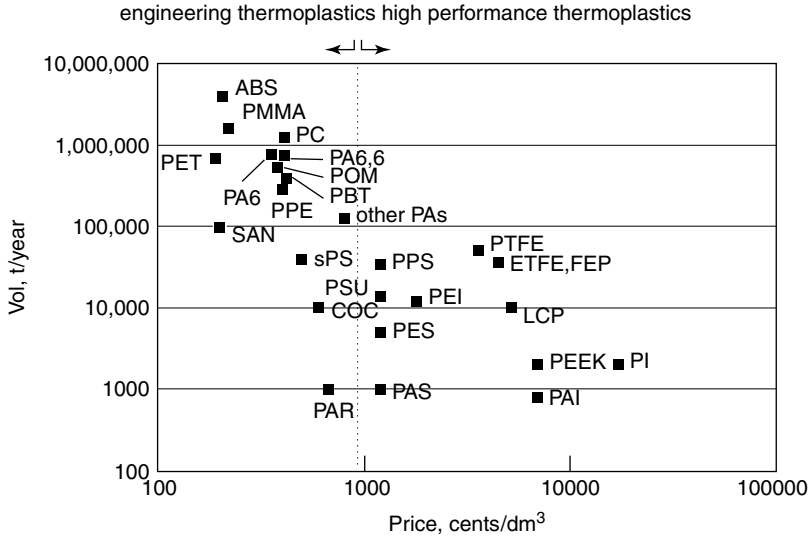

Fig. 2. Production volumes and prices for volume units for thermoplastics considered in this compilation. The dashed line represents an arbitrary border between engineering and high performance thermoplastics. In some cases, reinforced resins have been considered, ie, PPS: 10% glass fibers (GF); PSU, PA11: 30% GF; PAS: 40% GF. Acronyms are those listed in Table 1.

volume unit, more significant than the corresponding price per mass unit. The unfilled materials have a density ranging from 1.02 g/mL for COCs to 2.18 g/mL for PTFE. However, the density of most engineering thermoplastics falls around 1.15–1.45 g/cm^3. The price/volume relationship does not work when a low volume material can be produced in a captive way in a plant used also for producing a higher volume polymer. This is the case of polyarylates, some aliphatic polyamides, and polysulfones.

Mechanical, Thermal, and Electrical Properties. The most representative mechanical properties are elastic (or tensile) modulus, tensile strength, flexural modulus, and toughness. Flexural modulus is particularly interesting, because it represents the stiffness of the material; unfortunately, data are not available for all materials. However, because flexural modulus values are mostly of the same order of magnitude of tensile modulus values, the latter can be used for comparison purposes. Toughness is approximately described by Izod impact strength. Figure 3 reports elastic moduli and Izod strengths of engineering thermoplastics. Data ranges are particularly wide for toughness data. The figure shows that for any application, a wide number of combinations of stiffness and toughness is available in the field of engineering thermoplastics. Further, reinforcing practice with fibers, minerals, or other fillers is largely applied in order to enhance the mechanical and thermal properties. Most of the materials treated here are offered in the market in a large number of reinforced grades. Such a practice also influences the cost of the material, and this is particularly relevant when the cost of the matrix is higher than the cost of the filler. Figure 4 shows the increase of modulus values that can be obtained by adding glass fibers to several polymers.

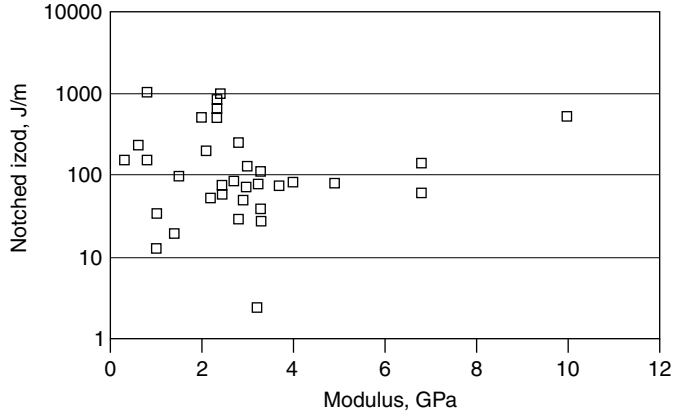

Fig. 3. Modulus vs notched Izod of engineering thermoplastics. To convert J/m to ft·lbf/in., divide by 53.38. To convert GPa to psi, multiply by 145,000.

Heat-deflection temperature does not correspond to the practical use temperature; however, it has been widely used in the plastics industry to compare the physical response of materials to temperature at a single–load level. In Figure 5, HDT vs tensile strengths at two different loads are reported. Both groups of data roughly show a proportional trend that can be ascribed to the fact that in many cases the molecular structure of the chain influences, in the same sense, the mechanical and thermal properties.

The electrical properties of engineering thermoplastics are generally excellent. In specific applications, like cable and wire coatings, electrical or electronic parts, etc, demanding values are requested. On the other side, electrical conductivity can be increased by adding particular fillers like metallic powders.

Chemical Resistance. Chemical resistance belongs to environmental considerations because the accidental or expected exposure of a material to the action of chemicals or solvents can have relevant short-and long-term influence

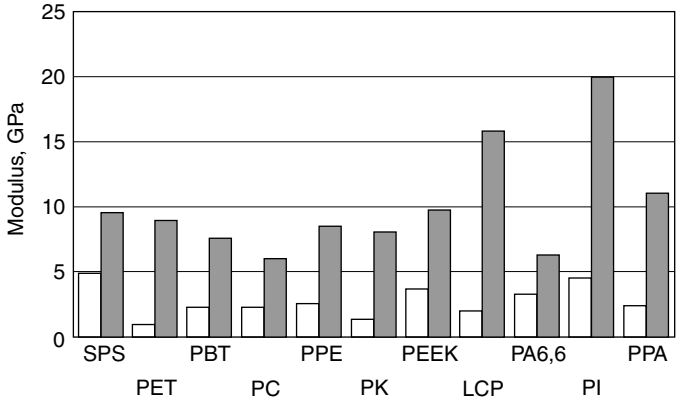

Fig. 4. Modulus increases obtained by reinforcing thermoplastic matrices with glass fibers. GF contents are at 30 wt%, but those of PC and PK are at 20 wt%. PPE values are referred to a PPE–PS blend. To convert GPa to psi, multiply by 145,000.

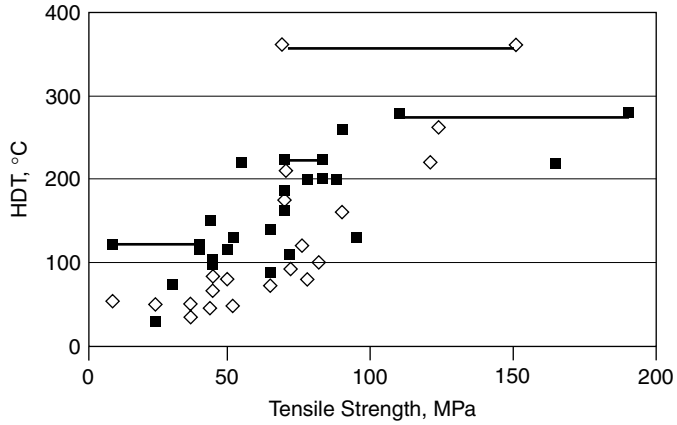

Fig. 5. Tensile strength vs HDT of engineering thermoplastics. Full squares represent HDT values obtained at 0.45 MPa, empty rhombi at 1.8 MPa. Horizontal bars between two tensile strength values represent a range. To convert MPa to psi, multiply by 145.

on the other properties. Table 9 summarizes the resistance of polymers against the most common families of chemicals and solvents. As expected, fluoropolymers show the best response against the whole range of chemicals considered. Chemical resistance values reported in the table are indicative because they can be significantly affected by exposure length and temperature. In practice, chemical resistance testing under end-use conditions is suggested.

The Future

Thermoplastic materials have now pervaded every important aspect of the human life, from food management (through packaging) to clothing (through synthetic fibers), ground and air transportation, office equipment, health (medical instruments and devices, artificial prostheses), entertainment (audio and video reproduction components), sports goods, and so on. Applications of thermoplastic materials, both commodities and engineering thermoplastics, will continue to expand at the expense of other materials like glass, metals, wood, and ceramics. Moreover, the time between the laboratory synthesis of a new polymer and its industrial production remains high (12), thus discouraging the introduction of new materials. The expected expansion of the engineering thermoplastics market is of the order of 12% per year in the next three years (13). Interestingly, the most significant threat to engineering polymers comes from some commodities, like polypropylene, which in some reinforced (but also unreinforced) grades reach the performance of some engineering materials.

More About Engineering Thermoplastics. Many of the individual resins mentioned in this overview are covered in articles devoted to them. Cross references are provided in Table 1. A list of related articles is as follows: ACETAL RESINS; ACRYLIC ESTER POLYMERS; ACRYLONITRILE AND ACRYLONITRILE POLYMERS (SAN and ABS); ETHYLENE-NORBORNENE COPOLYMERS; LIQUID CRYSTALLINE POLYMERS, MAIN-CHAIN; METHACRYLIC ESTER POLYMERS;

Table 9. Chemical Resistance of Engineering Thermoplastics

Material	Ketones	Acid		Alkali	Alcohol	Hydrocarbons (aromatic)	Greases and oil
		Dilute	Conc.				
sPS	G	G	G	G	F	G	G
POM		P	P	G	G	G	F/G
PET		G	P	G	F	G	G
PBT		G	F	G	G	G	G
PEN		G	F	G	G	G	G
PAR				F	F	F	F
LCP	G	F	G	F	G	G	G
PPE		F/G	G	F	P	F	F
PC		F/G	P	G	P	G	P
PK	G	P	G	F	G	G	G
PEEK	G	F	G	G	G	G	G
PMMA	G	F	G	F	P	P	P
PPS	G	F	G	G	G	G	G
PSU		G	G	G	P	G	P
PES		G	G	G	P	G	P
PAS		G	G	G	P	G	F
ABS		G	F		P		P
SAN		P	P	F	F	G	F
PA6,6	P	P	G	G	G	G	G
PA6	P	P	G	G	G	G	G
PA11	P/F	P	G	F	G	G	G
PA12	P/F	P	G	F	G	G	G
ArPA		F	F/G	G	G	G	G
PI	G	G	P	G	G	G	G
PAI	G	G	P	G	G	G	G
PPA	G	F	G	F	G	G	G
PEI		G	F/G		G		
F-polymers	G	G	G	G	G	G	G

[a] P: poor; F: fair; G: good.

PERFLUORINATED POLYMERS, POLYTETRAFLUOROETHYLENE; POLYAMIDES, AROMATIC; POLYAMIDES, PLASTICS; POLYARYLATES; POLY(ARYLENE SUFIDE)S; POLYCARBONATES; CYCLOHEXANEDIMETHANOL POLYESTERS; POLYESTERS, MAIN CHAIN AROMATIC; POLYESTERS, THERMOPLASTIC; POLYETHERS, AROMATIC; POLY(ETHYLENE NAPHTHANOATE); POLYIMIDES; POLYKETONES; POLY(PHENYLENE ETHER); POLYSULFONES; POLY(TRIMETHYLENE TEREPHTHALATE); RIGID ROD POLYMERS; SYNDIOTACTIC POLYSTYRENE;.

Poly(ether ketone) resins are discussed in the next section.

Poly(ether ketones)

Poly(ether ketones) include a variety of aromatic high performance polymers characterized by the presence of ether bridges and ketone groups in the main chain, linking together arylene groups. Currently, the only product manufactured worldwide is Victrex PEEK, launched by ICI in 1978 and produced annually in an

amount of about 2000 tons (14). PEEK has the following chemical structures and is believed to be produced by polycondensation of 4,4′-difluorobenzophenone and a potassium salt of bisphenol (15).

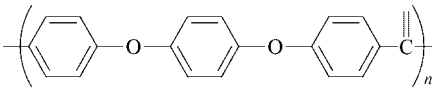

The reaction is carried out at high temperature (up to 300°C) in a high boiling solvent like diphenylsulfone. It is produced in batches, with rather high production cost. Similar products, bearing various sequences of ether and ketone groups bridging together arylene rings can be synthesized in similar ways, eg, PEK, PEKK, and PEKEKK (15). Some of these structures have been commercialized.

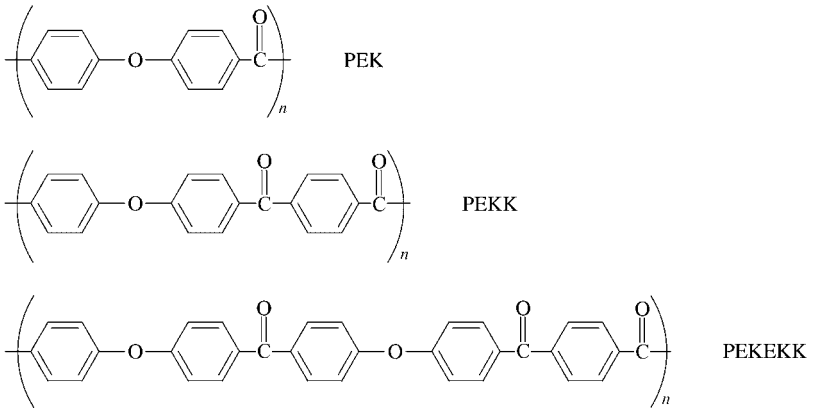

The first polymer of this group (PEK) was commercialized by Raytheon in the 1970s under the trade name Stilan. Equivalent materials were commercialized by Hoechst Celanese and Amoco, whereas PEKEKK and PEKK were commercialized by BASF and DuPont, respectively. Their T_g values are in the range of 150–165°C, and T_m values are in the range of 370–390°C. PEEK has a pale amber color and is usually semicrystalline and opaque. It has excellent thermal, mechanical, and tribological resistance and is insoluble in most solvents, with the exception of strong protonating acids like concentrated H_2SO_4 and HF. It is also soluble above 220–230°C in benzophenone and chloronaphthalene. Properties of PEEK are reported in Table 10.

A review (16) and a book (17) on the chemistry and properties of poly(ether ketones) have been published. PEEK is present in the market also in reinforced grades (glass or carbon fibers) as well as in yarns or in powder for coatings. Fibers are marketed by ICI under the trade name Zyex. PEEK found application in the transport, teletronics, and aerospace sectors, with the fabrication of injection-molded engineering components and circuit boards. PEEK materials have also found a place in medical technologies. For this purpose, their biological and toxicological safety has been certified (14).

Table 10. Properties of PEEK

Property	Neat	30% GF
Density, g/mL	1.32	1.50
Flammability	V0	V0
Oxygen index (LOI), %	35	
Water absorption (24 h, 23°C), %	0.5	0.1
Dielectric constant (10 kHz)	3.2	3.7
Dielectric strength (1 mm), kV/mm	24	
Dissipation factor (1 MHz)	0.003	0.004
Volume resistivity (23°C, dry), Ω·cm	10^{16}	10^{16}
Glass-transition temperature (T_g), °C	143	143
Melting temperature (T_m), °C	334	334
HDT		
at 0.45 MPa, °C	>260	
at 1.8 MPa, °C	160	315
Specific heat capacity, J/(kg·K)	320	
Thermal conductivity (23°C), W/(m·K)	0.25	
Thermal expansion coefficient, K^{-1}	$50–110\times10^{-6}$	
Upper working temperature, °C	250	
Elastic modulus, GPa[a]	3.7–4.4	9.7
Tensile strength, MPa[b]	70–110	156
Flexural modulus, GPa[a]	3.7	
Flexural strength, MPa[b]	170	
Elongation at break, %	50	2
Notched Izod (3.2 mm), J/m[c]	83	90
Hardness (Rockwell)	M105	

[a] To convert GPa to psi, multiply by 145,000.
[b] To convert MPa to psi, multiply by 145.
[c] To convert J/m to lbf·ft/in., divide by 53.38.

BIBLIOGRAPHY

"Engineering Plastics" in *EPSE* 2nd ed., Vol. 6, pp. 84–131, by D. C. Clagett General Electric Co.

1. D. W. Van Krevelen, *Properties of Polymers*, 3rd ed., Elsevier, Amsterdam, the Netherlands, 1990.
2. D. V. Rosato, *Rosato's Plastics Encyclopedia and Dictionary*, Hanser, Munich, 1993.
3. W. V. Titow, *Technological Dictionary of Plastics Materials*, Elsevier Science Ltd., Kidlington, Oxford, 1998.
4. Fachinformationszentrum Chemie GmbH, *Index of Polymer Trade Names (Parat)*, 2nd ed., VCH, Weinheim, 1992.
5. D. P. Bashford, *Thermoplastics Directory and Databook*, Chapman & Hall, New York, 1997.
6. C. P. MacDermott and A. V. Shenoy, *Selecting Thermoplastics for Engineering Applications*, 2nd ed., Marcel Dekker, Inc., New York, 1997.
7. J. Brandrup, E. H. Immergut, and E. A. Grubke, eds., *Polymer Handbook*, 4th ed., John Wiley & Sons, Inc., Chichester, 1999.
8. J. A. Brydson, *Plastics Materials*, 6th ed., Butterworth-Heinemann Ltd., Oxford, 1995.
9. D. G. Baird and D. I. Collias, *Polymer Processing*, John Wiley & Sons, Inc., Chichester, 1998.
10. J. M. Charrier, *Polymeric Materials and Processing*, Hanser, Munich, 1990.

11. A. N. Wilkinson and A. J. Ryan, *Polymer Processing and Structure Development*, Kluwer Academic Publishers, Dordrecht, 1998.
12. F. Garbassi, *CHEM TECH*, 48 (Oct. 1999).
13. *Chem. Week*, 37 (June 21, 2000).
14. W. Reimer and R. Weidig, *Kuntstoffe* **89**, 150 (1999).
15. T. E. Attwood and co-workers, *Polymer* **22**, 1096 (1981).
16. V. Lakshmana Rao, *J.M.S., C: Rev. Macromol. Chem. Phys.* **35**, 661 (1995).
17. G. Pritchard, *Anti-Corrosion Polymers: PEEK, PEKK and Other Polyaryls*, Rapra Technologies, Shrewsbury, 1995.

FABIO GARBASSI
RICCARDO PO
EniChem SpA Research Center

ENZYMATIC POLYMERIZATION

Introduction

Enzymes catalyze not only all *in vivo* biosynthetic reactions in living cells for maintaining "life" but also many *in vitro* reactions of natural and unnatural substrates under selected reaction conditions. Enzymatic catalysis for organic synthesis possesses advantages such as much acceleration of reaction rate, operation under mild conditions, and high stereo-, regio-, and chemoselectivities of reactions in comparison with those of chemical catalysts. Such characteristic properties have brought about an extraordinarily rapid increase in interest in the area of biotransformations (1–5).

All naturally occurring polymers are produced *in vivo* by enzymatic catalysis. Recently, *in vitro* synthesis of polymers through enzymatic catalysis ("enzymatic polymerization") has been extensively studied (6–14); highly selective polymerizations catalyzed by enzymes have been developed to produce various functional polymers in response to increasing demands of structural variation of synthetic targets for polymers in material science.

This article deals with recent advances in enzymatic polymerizations. We define *enzymatic polymerization* as "chemical polymer synthesis *in vitro* (in test tubes) via nonbiosynthetic (nonmetabolic) pathways catalyzed by an isolated enzyme." Enzymes are generally classified into six groups. Table 1 shows typical polymers produced with catalysis by respective enzymes. The target macromolecules for the enzymatic polymerization have been polysaccharides, poly(amino acid)s, polyesters, polycarbonates, polyaromatics, vinyl polymers, etc. Here, enzymatic polymerizations are described according to the polymer structure. In many cases, enzymatic polymerization enables the synthesis of polymers, which otherwise are difficult to prepare. Enzymatic polymerization often provides an environmentally

Encyclopedia of Polymer Science and Technology. Copyright John Wiley & Sons, Inc. All rights reserved.

Table 1. Classification of Enzymes and *In Vitro* Production of Typical Polymers Catalyzed by Respective Enzymes

Enzymes	Typical polymers
Oxidoreductases	Polyphenols, polyanilines, vinyl polymers
Transferases	Polysaccharides, cyclic oligosaccharides, polyesters
Hydrolases	Polysaccharides, poly(amino acid)s, polyamides, polyesters, polycarbonates
Lyases	
Isomerases	
Ligases	

benign process, where starting materials and products are within the natural material cycle; this is in the context of "green polymer chemistry" (13,14).

Polysaccharides

Polysaccharides are among the most important biopolymers as are proteins and nucleic acids in nature. They are regarded as three important families of natural biomacromolecules. As to the enzymatic polymerization for polysaccharides, hydrolases and transferases are reported to catalyze their synthetic reactions.

Hydrolases. It is generally accepted that an enzymatic reaction is virtually reversible, and hence, the equilibrium can be controlled by selecting the reaction conditions. Based on this view, hydrolases, enzymes catalyzing a bond-cleavage reaction by hydrolysis, have been developed as catalyst for the reverse reaction of hydrolysis, leading to polymer production by a bond-forming reaction (9,12).

It is believed that using a glycosidase for the glycosylation process is one of the most promising methodologies for selective construction of a glycosidic linkage under appropriate conditions, since chemical approach requires complicated procedures including a regioselective blocking and deblocking of a hydroxy group in the sugar moiety to achieve regioselectivity, and furthermore, complete stereocontrol of the glycoside bond-formation has not often been achieved by chemical catalysts.

Enzymatic formation of a glycosidic bond is realized by combined use of a glycosyl donor and a glycosyl acceptor. The former is to be activated by an enzyme to give a glycosyl-enzyme intermediate which can be attacked by a hydroxy group of the acceptor, forming a glycosidic bond between the donor and the acceptor. The repeated glycosylations are expected to produce polysaccharide molecules.

Glycosyl fluorides, sugar derivatives whose anomeric hydroxy group is replaced by a fluorine atom, are known to be recognized by glycosidases. Cellulose is one of the most important biomacromolecules, which is the most abundant organic substance on the earth (12). Thus, in 1991, the first *in vitro* synthesis of cellulose via nonbiosynthetic pathway has been achieved by an enzymatic polymerization of β-cellobiosyl fluoride as substrate for *Tricoderma viride* cellulase, an extracellular hydrolytic enzyme of cellulose (Fig. 1) (15–21). The polymerization was performed in an aqueous organic solvent in order to make the desired

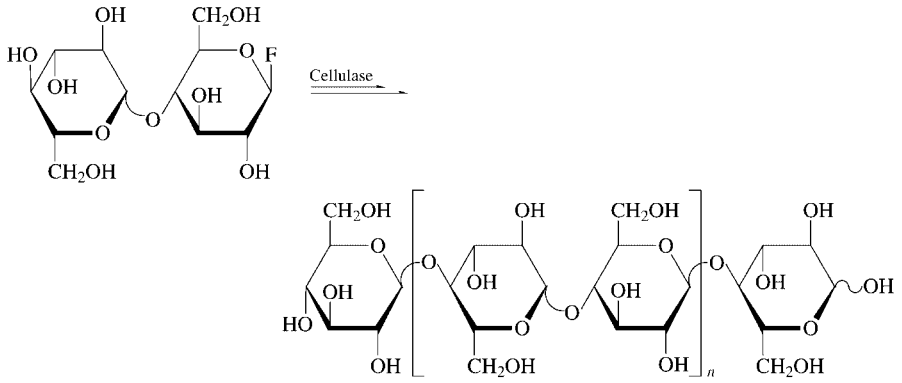

Fig. 1. *In vitro* synthesis of artificial cellulose via cellulase catalysis.

polycondensation predominant in comparison with the competitive hydrolysis reaction. A mixed solvent of acetonitrile/acetate buffer (pH 5) (5:1) gave the best results in terms of the yield of water-insoluble "artificial cellulose." The enzyme promoted transglycosylation of the cellobiosyl moiety toward the 4′-hydroxy group of another monomer eliminating hydrogen fluoride. In this polymerization, regio- and stereoselectivities were perfectly controlled.

The cellulase-catalyzed polycondensation of new cellobiosyl fluoride derivatives, 6-*O*-methyl and 6′-*O*-methyl-β-cellobiosyl fluorides, have been examined (22,23). The 6-O-methylated monomer was polymerized using the purified enzyme in a regio- and stereoselective manner to give a novel cellulose derivative having a methyl group alternatingly at the 6-position, which can never be realized by the conventional modification of natural cellulose, ie, methylation of cellulose. On the other hand, the 6′-O-methylated monomer gave a mixture of low molecular weight oligomers. The difference of the polymerization behavior can be explained by the steric repulsion between the methyl group of the monomers and the active site of the cellulase catalyst.

The process of the artificial cellulose was visually analyzed by using transmission electron microscopy (24). Cellulose formation was detected as early as 30 s after the initial stage of the reaction in the aqueous acetonitrile. The electron diffraction pattern of the product showed the typical pattern of the crystal structure of thermodynamically stable cellulose II with antiparallel orientation between each glucan chains. When the purified cellulase (39 kDa) was used, cellulose microfibrils with an electron diffraction pattern characteristic of metastable cellulose I with parallel orientation, an allomorph of natural cellulose, were first observed in an artificial process (25). Based on these results, a new concept of *choroselectivity*, selectivity concerning the relative ordering of the polymer chain direction, in polymerization chemistry has been proposed (26–28).

In some cases, the enzymatic polymerization afforded spherulites of artificial cellulose II, composed of single crystals with the molecular axis orientated perpendicular to the plane (29). Both positive- and negative-type spherulites were observed by polarization optical microscopy. By changing the reaction parameters,

the size, growth and formation/degradation rate, and number of spherulites could be controlled.

α-Amylase catalyzed the polycondensation of α-D-glucosyl fluoride in an aqueous solution to produce maltooligosaccharides (mainly pentamer) (30). α-D-Maltosyl fluoride was also polymerized by α-amylase catalyst in an aqueous methanol, yielding a maltooligosaccharide with degree of polymerization (DP) up to 7 (31). Enzymatic transglycosylation of α-D-maltosyl fluoride with a cyclodextrin using pullulanase or isoamylase as a catalyst produced a branched cyclodextrin, 6-*O*-α-maltosylcyclodextrin (32,33).

Synthetic xylan was synthesized by a cellulase-catalyzed polymerization using β-xylobiosyl fluoride as a substrate (34). The enzymatic polymerization proceeded in a perfect regio- and stereoselective manner to produce powdery artificial xylan, which is insoluble in any organic solvent. Xylan, one of the most important components of hemicellulose in plant cell walls, normally contains 4-*O*-methylglucuronic acid or L-arabinose as a minor unit in the side chain. On the other hand, the artificial xylan consists exclusively of a xylopyranose moiety connected through a $\beta(1\rightarrow4)$ glycosidic bond.

The first synthesis of a cellulose–xylan hybrid polymer, a novel polysaccharide having a glucose–xylose repeating unit, has been achieved by the xylanase-catalyzed polymerization of β-xylopyranosyl-glucopyranosyl fluoride (Fig. 2) (35, 36). Identification of the enzyme fraction promoting the polymerization showed that endoxylanase was highly efficient for production of the hybrid polymer.

Cellulase-catalyzed polycondensation of 4-thio-β-cellobiosyl fluoride produced hemithiocellodextrins having 4-thiocellobiosyl repeating units linked by $\beta(1\rightarrow4)$ oxygen linkages (37). A water-soluble oligomer with DP up to 20 was obtained in an aqueous acetonitrile.

Chitin is the most abundant organic macromolecules in the animal field found in invertebrates (12). The *in vitro* synthesis of this important biomacromolecule has been achieved for the first time by enzymatic ring-opening polyaddition of a chitobiose oxazoline monomer (Fig. 3). Chitinase, a hydrolysis enzyme of chitin, regio- and stereoselectively induced the polymerization of the monomer in a basic buffer (38–41). It is postulated that the monomer is preferable as a

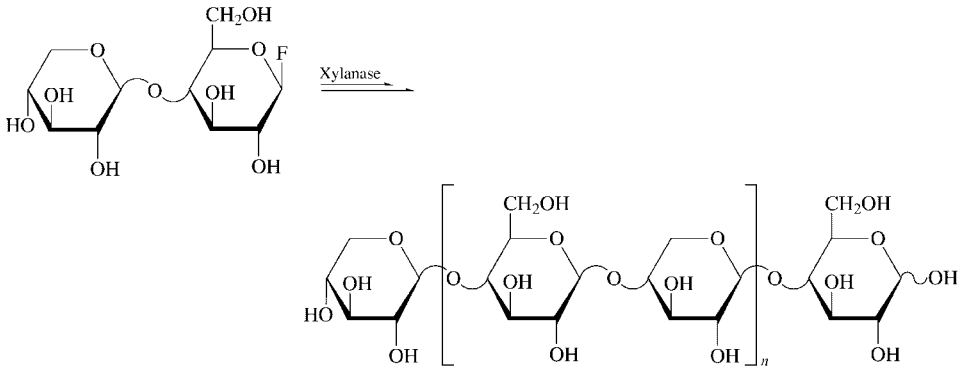

Fig. 2. Enzymatic synthesis of cellulose–xylan hybrid polymer.

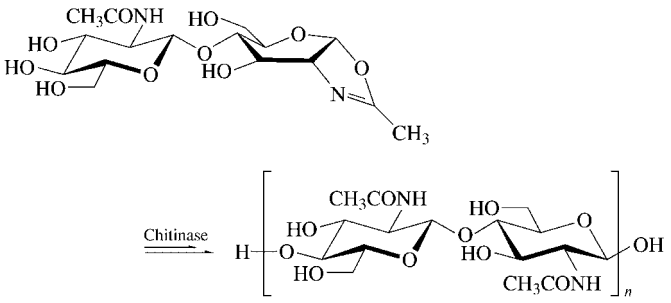

Fig. 3. *In vitro* synthesis of artificial chitin via chitinase catalysis.

substrate because it can be recognized by the active site of chitinase readily due to the oxazoline structure resembling that of the transition state of the chitin hydrolysis with chitinase as revealed by a later work (12,42). Thus, the monomer is regarded as a "transition state analogue substrate" for chitinase. From x-ray diffraction and nmr analysis, the product was found to show crystal structure of α-chitin. A oxazoline monomer from *N*-acetyl glucosamine was also polymerized at high substrate concentration to give chitooligosaccharides.

The visualization of high ordered structure formation during the enzymatic synthesis of artificial chitin has been investigated (43). Plate-like single crystals of α-chitin were first formed and gradually shaped into ribbons by the rapid growth along the a axis with the crystalline thickness being ca 10 nm. The α-chitin ribbons then aggregated to form bundle-like or dendritic assemblies as the ribbon concentration in solution increased. They grew up to spherulites by splaying and branching. This artificial chitin spherulite, in which a number of α-chitin ribbons radiated from a common center, is completely different from the helicoidal textures composed of α-chitin microfibrils known as a typical three-dimensional organization of chitin (see CHITIN and CHITOSAN).

A cellulose–chitin hybrid polymer, a nonnatural polysaccharide having a glucose unit and an *N*-acetyl glucosamine unit alternatingly in the main chain, was synthesized by chitinase-catalyzed polyaddition of a disaccharide oxazoline monomer in an aqueous solution (44).

Sugar-chain elongation from di-*N*-acetylchitobiose as initial substrate to hexamer and heptamer of chitooligosaccharide was efficiently induced through lysozyme catalysis in an acetate buffer containing 30% ammonium sulfate at 70°C. The high concentration of ammonium sulfate resulted in a remarkable increase of the hexamer and heptamer productions. In this reaction, a sugar-elongation from the dimer to trimer was the rate-limiting step in the overall process of transglycosylation (45).

Transferases. Phosphorylase catalyzes polymerization of α-D-glucose-1-phosphate in the presence of primer, leading to *in vitro* synthesis of amylose (Fig. 4) (46). By utilizing phosphorylase catalysis, various amylose derivatives such as linear-, star-, and comb-shaped amylose polymers were synthesized (47). The chain length could be controlled by a simultaneous start for all chains using a primer with a minimum length of four glucosyl residues. This method was

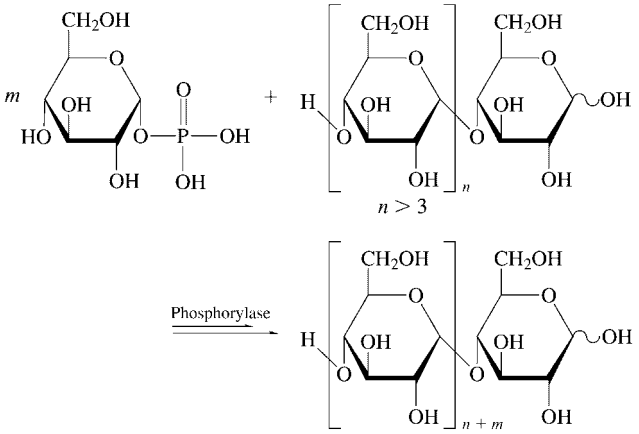

Fig. 4. Phosphorylase-catalyzed synthesis of amylose.

applied to production of styryl-type amylose macromonomer (48), amylose-*graft*-poly(dimethylsiloxane) (49), amylose-*graft*-poly(L-glutamic acid) (50), amylose-*block*-polystyrene (51), amylose-*block*-poly(ethylene oxide) (52), and amylose-containing silica gel (53,54). Amylose-polytetrahydrofuran (PTHF) inclusion complex was synthesized by the phosphorylse-catalyzed polymerization in the presence of PTHF (55).

Cyclodextrin-$\alpha(1\rightarrow4)$glucosyltransferase (CGTase) catalyzes formation of cyclodextrins from starch. By use of immobilized CGTase (silica gel support functionalized with glutardialdehyde), α-glucosyl fluoride was transformed in high yields, predominantly into cyclodextrin and maltooligomers as by-products (56). α-Maltosyl fluorides substituted at the 6- or 6′-position with H, F, Br, OCH_3, and $OCOCH_3$ have been tested as substrates for CGTase (57). Among these substrates, only 6′-*O*-CH_3 and 6′-*O*-$COCH_3$ monomers were polymerized to give the cyclic compounds, indicating that the affinity of substrates toward the catalytic site of CGTase (*Bacillus marcerans*) greatly affected the specificity of the cyclization.

Poly(amino acid)s

Biosynthesis of artificial polypeptides has been achieved by the expression of target proteins in living cells with a gene recombination technique; polypeptides with precise control of the chain length, sequence, and stereochemistry have been synthesized by genetic engineering. On the other hand, it is well known that amino acid derivatives are subjected to protease-catalyzed coupling reaction, yielding functional peptide compounds (58). In using amino acid esters as monomer, poly(amino acid)s are obtained.

Papain catalyzed the polymerization of L-methionine methyl ester hydrochloride to give water-insoluble oligomer with DP = 8–10 (59–61). The resulting water-insoluble oligomer was converted to water-soluble sulfoxide and sulfone derivatives by treatment of DMSO or hydrogen peroxide. Esters of phenylalanine,

threonine, and tyrosine were also subjected to the protease-catalyzed oligomerization (62).

Polymerization of L-glutamic acid diethyl ester hydrochloride took place in the presence of papain or α-chymotrypsin as catalyst to give the corresponding oligomer composed of 5–9 glutamic acid residues (63,64). An nmr analysis showed that the product consisted exclusively of α-peptide linkage (65). Diethyl L-aspartate was polymerized by alkanophilic protease from *Streptomyces* sp. to give poly(ethyl α,β-L-aspartate) with weight-average molecular weight (M_w) up to 3600 (66). The ratio of α-linkage was about 88%, independent of the enzyme concentration.

In order to enhance the molecular weight, protease was modified by mutation technique to show high catalytic activity in an aqueous *N*,*N*-dimethylformamide (DMF) solution. A subtilisin mutant (subtilisin 8350) derived from BPN′ (subtilisin from *Bacillus amyloliquefaciens*) via six site-specific mutation (Met 50 Phe, Gly 169 Ala, Asn 76 Asp, Gln 206 Cys, Tyr 217 Lys, and Asp 218 Ser) induced the polymerization of L-methionine methyl ester in the aqueous DMF to produce poly(methionine) with DP up to 50 (67). The increase of the molecular weight is due to the improvement of the product solubility and minimization of the enzymatic peptide cleavage under the high concentration of DMF. Another mutant (subtilisin 8397) showing higher stability in DMF, the same as 8350 except that there is no change for Tyr 217, has been applied as the catalyst for the polymerization of single amino acid, dipeptide, and tripeptide methyl esters (68).

A different type of peptide hydrolase, dipeptidyl transferase (dipeptidylpeptide hydrolase), catalyzed the polymerization of dipeptide amide in an aqueous solution. In the case of glycyl-L-phenylalaninamide, trimer was formed in 78% yield (69). The polymerization of glycyl-L-tyrosinamide produced the corresponding oligomer with DP up to 8 (70).

Protease was used as catalyst for polymer modification. Phenylalanine residues at the side chain of methacrylamide polymers were coupled with alanine *t*-butyl ester by α-chymotrypsin catalyst in water–chloroform solvent (71). Up to 35% peptide-bond formation was achieved for 7 days at room temperature. Polyamide synthesis was performed by cellulase-assisted polycondensation of chiral fluorinated compound having carboxylic acid and amino groups (72).

Polyesters

Syntheses of aliphatic polyesters by fermentation and chemical processes have been extensively studied in a viewpoint of biodegradable materials. Recently, another approach of their production has been performed by using an isolated lipase or esterase as catalyst via nonbiosynthetic pathways under mild reaction conditions. Lipase and esterase are enzymes which catalyze hydrolysis of esters in an aqueous environment in living systems. Some of them can act as a catalyst for the reverse reactions, esterifications and transesterifications, in organic media (1–5). These catalytic actions have been expanded to enzymatic synthesis of polyesters. Figure 5 represents three major reaction types of lipase-catalyzed polymerization leading to polyesters (6–14,73).

Polycondensation of Oxyacids or Their Esters

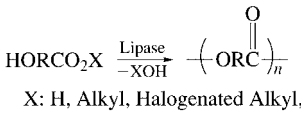

Polycondensation of Dicarboxylic Acids or Their Derivatives with Glycols

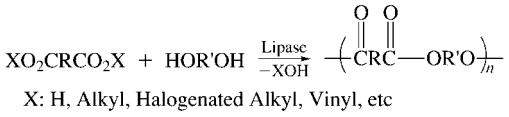

Ring-Opening Polymerization of Lactones

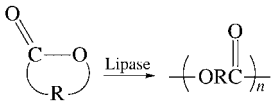

Fig. 5. Typical routes of polyester production using an isolated enzyme as catalyst.

Polymerization of Oxyacids and Their Esters.

Oxyacids. In 1985, a lipase-catalyzed polymerization of 10-hydroxydecanoic acid was reported. The monomer was polymerized in benzene using poly(ethylene glycol) (PEG)-modified lipase soluble in the medium to give an oligoester with DP more than 5 (74).

Ricinoleic acid, 12-hydroxyoctadecanoic acid, 16-hydroxyhexadecanoic acid, and 12-hydroxydecanoic acid were polymerized by lipase from *Candida cylindracea* (lipase CC) or *Chromobacterium viscosum* as a catalyst at 35°C in water, hydrocarbons, or benzene (75). The molecular weight of the polymers was ca 1×10^3. Oligomerization of ricinoleic acid proceeded in the presence of lipase CC immobilized on ceramics (76).

In the polycondensation of 10-hydroxydecanoic and 11-hydroxyundecanoic acids, a large amount of lipase CC catalyst (10 weight fold for the monomer) afforded the corresponding polyesters with relatively high molecular weight (77, 78). From the latter monomer, the polymer with M_w of 2.2×10^4 was formed in the presence of activated molecular sieves.

Porcine pancreas lipase (PPL) polymerized 3-hydroxybutyric and 12-hydroxydodecanoic acids in anhydrous hydrophobic solvents (79). The molecular weight of the polymer from the former was low (ca 500), whereas the polymerization of the latter at 75°C produced the polymer with molecular weight of 3×10^3. A cellulase-assisted polymerization of chiral fluorinated compound having carboxylic acid and phenolic groups produced the aromatic polyester (72).

Enzymatic synthesis of a methacrylamide-type polyester macromonomer was reported (80,81). In the polymerization of 12-hydroxydodecanoic acid in the presence of 11-methacryloylaminoundecanoic acid using lipase CC or *Candida antarctica* lipase (lipase CA) as catalyst, the polymerizable group was quantitatively incorporated into terminal of the polymer chain.

By using characteristic catalysis of lipase, regio- and enantioselective polymerizations of oxyacids have been achieved. Lipase CA catalyzed regioselective

polymerization of cholic acid, in which the hydroxy group at 3-position was regioselectively acylated to give the oligoester with molecular weight less than 1×10^3 (82). An optically active oligoester was obtained by the enantioselective polymerization of racemic 10-hydroxyundecanoic acid catalyzed by lipase CC. The resulting polymer was enriched in the (S) enantiomer with 60% enantiomeric excess (ee) and the (R)-enriched unreacted monomer with 33% ee was recovered (83). In the polymerization of racemic lactic acid catalyzed by lipase CA at 50°C (84), nonamer was detected in the product by MALDI-TOF mass measurement. A hplc analysis showed that the D-enantiomer possessed higher enzymatic reactivity.

Oxyacid Esters. The polymerization of ethyl glycolate using PEG-modified esterase from hog liver and lipase from *Aspergillus niger* (lipase A) gave oligo(glycolic acid) with DP up to 5 (85). PPL catalyzed the polymerization of methyl esters of 5-hydroxypentanoic and 6-hydroxyhexanoic acids (86). In the polymerization of the latter in hexane at 69°C for more than 50 days, the polymer with DP up to 100 was formed. Relationships between solvent type and polymerization behaviors were systematically investigated; hydrophobic solvents such as hydrocarbons and diisopropyl ether were suitable for the enzymatic production of high molecular weight polymer. Polycondensation of various hydroxyesters, ethyl esters of 3- and 4-hydroxybutyric acids, 5- and 6-hydroxyhexanoic acids, 5-hydroxydodecanoic acid, and 15-hydroxypentadecanoic acid, proceeded by *Pseudomonas* sp. lipase catalyst to give the corresponding polyesters with molecular weight of several thousands (87).

A symmetrical hydroxy diester, dimethyl β-hydroxyglutarate, was enantioselectively polymerized by lipase catalyst to produce a chiral oligomer (dimer or trimer) with 30–37% ee (88). The enantioselective polymerization of ε-substituted-ε-hydroxy esters took place in the presence of PPL catalyst, yielding optically active oligomers (DP < 6) (89). The enantioselectivity increased as a function of bulkiness of the monomer substituent. Optically active polyesters with molecular weight more than 1×10^3 were obtained by the copolymerization of the racemic oxyacid esters with methyl 6-hydroxyhexanoate.

Lipase-Catalyzed Polymerization of Dicarboxylic Acids or Their Derivatives. Enzymatic synthesis has been achieved via various combinations of dicarboxylic acid derivatives and glycols. As to the diacid monomer, dicarboxylic acids, activated and nonactivated esters, cyclic acid anhydrides, and polyanhydrides were enzymatically reacted with glycols under mild reaction conditions.

Dicarboxylic Acids. Immobilized *Mucor miehei* lipase (lipase MM) catalyzed polycondensation of adipic acid and 1,4-butanediol by using a horizontal two-chamber reactor in the presence of molecular sieves as dehydrating agent (90). A low dispersity polyester with DP=20 was obtained by the two-stage polymerization.

The polymerization of dicarboxylic acids and glycols proceeded by using lipase CA catalyst in a solvent-free system, despite the initial heterogeneous mixture of the substrates (91–94). The polymerization behaviors strongly depended on the chain length of both monomers (93). The polymerization under reduced pressure increased the molecular weight of polyesters. The detailed studies in the combination of adipic acid (A) and 1,4-butanediol (B) showed that the propagation took place by the reaction of the preliminary adduct (AB) with a hydroxy-terminated species (92).

For the solvent-free polycondensation, a small amount of adjuvant was effective for the polymer production when both monomers were solid at the reaction temperature (93). In the polymerization of adipic acid and 1,6-hexanediol, loss of the enzymatic activity was small during the polymerization, whereas less than half of the activity remained in using glycols with methylene chain length less than 4 (94). An attempted experiment allowed the polyester production from adipic acid and 1,6-hexanediol in 200-kg scale. This solvent-free system has a good potential as an environmentally friendly practical synthetic process of polymeric materials owing to the mild reaction conditions without using organic solvents and toxic catalysts.

A dehydration polymerization of dicarboxylic acids and glycols took place by lipase catalyst even in water (95,96). This catalysis of lipase is quite specific since a dehydration reaction in an aqueous solution is generally disfavored by water, which is in equilibrium with starting materials because of the law of mass action. Hydrophobic monomer combinations gave the polyesters in good yields.

Lipase CA catalyzed the polymerization of adipic acid and glycerol to give the oligomeric products (97). The presence of molecular sieves improved the molecular weight.

The molecular weight increase was achieved using vacuum system, which removed the resulting water molecules during the polymerization (98,99). An aliphatic polyester with M_w of 4.2×10^4 was obtained from sebacic acid and 1,4-butandiol using lipase MM catalyst in diphenyl ether at 37°C for 7 days under the reduced pressure. The molecular weight was much larger than that obtained under ambient pressure. The polymerization of isophthalic acid and 1,6-hexanediol at 70°C produced the corresponding aromatic polyesters with M_w of 5.5×10^4 (100).

Dicarboxylic Acid Diesters. Since unactivated esters, typically alkyl esters, show low reactivity toward lipase catalyst, the polycondensation with glycols was often performed under vacuum to produce polyesters of high molecular weight. Lipase MM-catalyzed polycondensation of diethyl sebacate and 1,4-butanediol under vacuum produced the polymer with M_w more than 2×10^4 (98).

There is, of course, an equilibrium between the monomers and polymer in the lipase-catalyzed polycondensation of dialkyl esters and glycols. In the lipase CC- or MM-catalyzed polymerization of dimethyl succinate and 1,6-hexanediol in toluene, adsorption of methanol by molecular sieves or elimination of methanol by nitrogen bubbling shifted the thermodynamic equilibrium (101). When dicarboxylic acid dialkyl esters and α,ω-alkylene glycols were used as monomers, cyclic oligomers were formed from any monomer combinations examined (102). The yield of the cyclics depended on the monomer structure, initial concentration of the monomers, and reaction temperature. The ring-chain equilibrium was observed and the molar distribution of the cyclic species obeyed the Jacobson–Stockmayer equation.

Activated esters of halogenated alcohols, such as 2-chloroethanol, 2,2,2-trifluoroethanol, and 2,2,2-trichloroethanol, have often been used as substrate for enzymatic synthesis of esters (4), owing to the increase of the electrophilicity (reactivity) of the acyl carbonyl and the avoidance of significant alcoholysis of the products by decreasing the nucleophilicity of the leaving alcohols.

Polymerization of bis(2,2,2-trichloroethyl) alkanediaoates with glycols proceeded by PPL catalyst in anhydrous solvents of low polarity to produce the

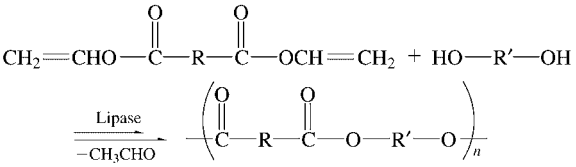

Fig. 6. Lipase-catalyzed polycondensation of divinyl esters and glycols.

polyesters with molecular weight of several thousands (103,104). The oligomer formation was observed in the polymerization of bis(2-chloroethyl) succinate and 1,4-butanediol using *Pseudomonas fluorescens* lipase (lipase PF) as catalyst (105).

Vacuum method was applied to shift the equilibrium forward by removal of the activated alcohol formed (98,99,106,107). In the polycondensation of bis(2,2,2-trifluoroethyl) sebacate and aliphatic diols, lipases CC, MM, PPL, and *Pseudomonas cepacia* lipase (lipase PC) produced the polymer with M_w more than 1×10^4. Among the enzymes examined, lipase MM showed the highest catalytic activity (106). As to solvents, diphenyl ether and veratrole were suitable for the production of the high molecular weight polyesters under vacuum. In the PPL-catalyzed reaction of bis(2,2,2-trifluoroethyl) glutarate with 1,4-butanediol, the increase of the molecular weight was attained by periodical vacuum using veratrole or 1,3-dimethoxybenzene as less-volatile solvent (107).

In lipase-catalyzed transesterifications, enol esters have been used as acyl agents (4), since the leaving unsaturated alcohol irreversibly tautomerizes to an aldehyde or a ketone, leading to the desired product in high yields. Bis(enol ester)s were reported to be much effective for the enzymatic synthesis of polyesters under mild reaction conditions (Fig. 6) (108); the polymerization of divinyl adipate and 1,4-butanediol proceeded by lipase PF at 45°C, and adipic acid and diethyl adipate did not afford the polymeric materials under the similar reaction conditions.

Various lipases (lipases CA, MM, PC, and PF) catalyzed the polycondensation of divinyl adipate or divinyl sebacate with α,ω-glycols with different chain length (109,110). A combination of divinyl adipate, 1,4-butanediol, and lipase PC afforded the polymer with number-average molecular weight (M_n) of more than 2×10^4. The polymerization behaviors of the lipase-catalyzed polymerization of divinyl adipate and 1,4-butanediol have been widely investigated (111–114). During the polymerization, the hydrolysis of the terminal vinyl ester took place, resulting in the significant limitation of the formation of the polyester with high molecular weight. A mathematical model describing the kinetics of this polymerization was proposed, which effectively predicts the composition (terminal structure) of the polyester.

Another irreversible approach was performed by using bis(2,3-butanedione monoxime) alkanedioates as diester substrate (115). The polymerization with α,ω-alkylene glycols by lipase MM produced the polymer with M_n up to 7.0×10^3.

An enantioselective polymerization of racemic substrates took place through lipase catalysis, yielding optically active oligoesters and polyesters. The polymerization of bis(2-chloroethyl) 2,5-dibromoadipate with excess of 1,6-hexanediol using lipase A catalyst produced optically active trimer and pentamer (116).

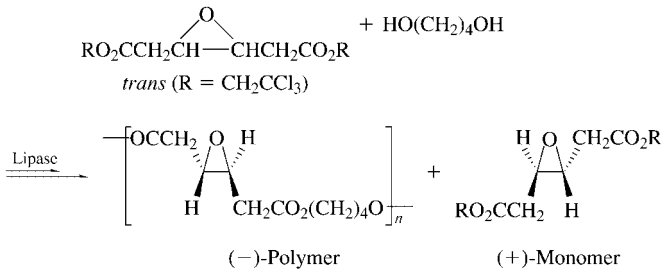

Fig. 7. Enantioselective polymerization of epoxy-containing diester with 1,4-butanediol.

PPL-catalyzed polymerization of bis(2,2,2-trichloroethyl) *trans*-3,4-epoxyadipate with 1,4-butanediol enantioselectively proceeded in anhydrous diethyl ether to give an optically active polyester with molecular weight of 5.3×10^3 (Fig. 7) (117). The molar ratio of the diester to the diol was adjusted to 2:1 so as to produce the (−) polymer with enantiomeric purity of >96%.

Polymerization of divinyl esters with triols regioselectively took place by lipase CA catalyst to give the soluble polymers with M_w of more than 1×10^4 (118,119). MALDI-TOF MS analysis confirmed the presence of a linear polyester with hydroxy substituents. An nmr analysis of the product obtained from divinyl sebacate and glycerol in bulk at 60°C showed that 1,3-diglyceride was a main unit and the branching unit (triglyceride) was contained in the resulting polymer. The regioselectivity of the acylation between primary and secondary hydroxy groups was 74:26. By choosing the reaction conditions, the polymer consisting exclusively of 1,3-acylated unit of glycerol was formed.

Lipase CA catalyzed the regioselective polymerization of sugar alcohols such as sorbitol and mannitol with divinyl sebacate to give polyesters containing sugar group in the backbone (120). Some proteases show an esterase activity, especially in their catalytic activity for regioselective acylation of sugars. By utilizing this property, protease-catalyzed synthesis of sugar-containing polyesters was demonstrated (121). Polycondensation of sucrose with bis(2,2,2-trifluoroethyl) adipate using an alkaline protease from *Bacillus* sp. as catalyst proceeded to give the polymer ($M_n=1.6\times10^3$), which was claimed to have ester linkages at the C-6 and C-1′ positions on the sucrose (Fig. 8). In using divinyl adipate as diester monomer, the molecular weight reached 1.1×10^4 (122).

Another approach of enzymatic synthesis of sugar-containing polyesters was demonstrated (123). Lipase CA-catalyzed reaction of sucrose or trehalose with an excess of divinyl adipate produced 6,6′-diacylated product having vinyl esters at both ends, which was employed as monomer in the enzymatic polycondensation with various glycols, yielding linear polyesters with M_w up to 2.2×10^4.

Unsaturated ester oligomers were synthesized by lipase-catalyzed polymerization of diesters of fumaric acid and 1,4-butanediol (124). Mild reaction conditions did not induce isomerization of the double bond to give all-trans oligomers showing crystallinity, whereas the industrial unsaturated polyester having a mixture of cis and trans double bonds is amorphous (125). The enzymatic polymerization of bis(2-chloroethyl) fumarate with xylylene glycol produced the unsaturated oligoester containing aromaticity in the backbone (126).

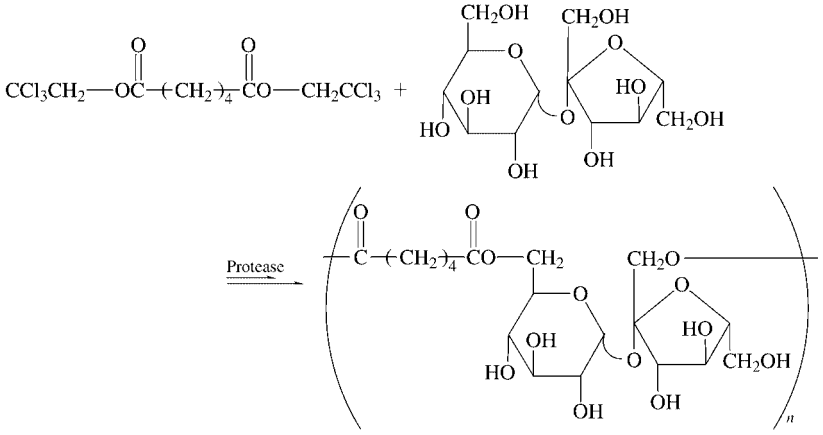

Fig. 8. Enzymatic synthesis of sucrose-containing polyester.

An unsaturated polyester possessing exclusively cis structure was synthesized by lipase CA-catalyzed polymerization of dimethyl maleate and 1,6-hexanediol in toluene (127). During the polymerization, formation of cyclic oligomers was observed. The cycles were semicrystalline, whereas the linear polymer was amorphous. In the lipase CA-catalyzed copolymerization of dimethyl maleate and dimethyl fumarate with 1,6-hexanediol, the content of the cyclization was found to mainly depend on the configuration and concentration of the monomers (128).

Polyesters containing an aromatic moiety in the backbone were synthesized by lipase CA-catalyzed polymerization of dicarboxylic acid divinyl esters and glycols under mild reaction conditions. Divinyl esters of isophthalic acid, terephthalic acid, and *p*-phenylene diacetic acid were enzymatically polymerized with α,ω-alkylene glycols to give the polymers with molecular weight of several thousands (129). Aromatic polyesters were also synthesized from methyl esters of terephthalic and isophthalic acids with 1,6-hexanediol in the presence of lipase CA (130). In using methyl isophthalate as monomer, macrocyclic compounds were formed as by-product. Protease from *Bacillus licheniformis* catalyzed the oligomerization of esters of terephthalic acid with 1,4-butanediol (131). Lipase-catalyzed synthesis of aromatic polyesters was achieved by the polymerization of divinyl esters with xylylene glycols (129,132).

Enzymatic synthesis of fluorinated polyesters was demonstrated (133). Fluorinated diols such as 2,2,3,3-tetrafluoro-1,4-butanediol and 2,2,3,3,4,4-hexafluoro-1,5-pentanediol were used as glycol substrate and polymerized with divinyl adipate using lipase CA catalyst. The enzymatic synthesis of polyester was also achieved in supercritical fluoroform solvent by the polymerization of bis(2,2,2-trichloroethyl) adipate and 1,4-butanediol (134). The molecular weight increased as a function of the pressure.

Anhydrides. Ring-opening poly(addition-condensation) of cyclic acid anhydrides with glycols proceeded through lipase catalysis (135). The polymerization of succinic anhydride with 1,8-octanediol proceeded using lipase PF catalyst at room temperature to produce the polyester with M_n of 3×10^3.

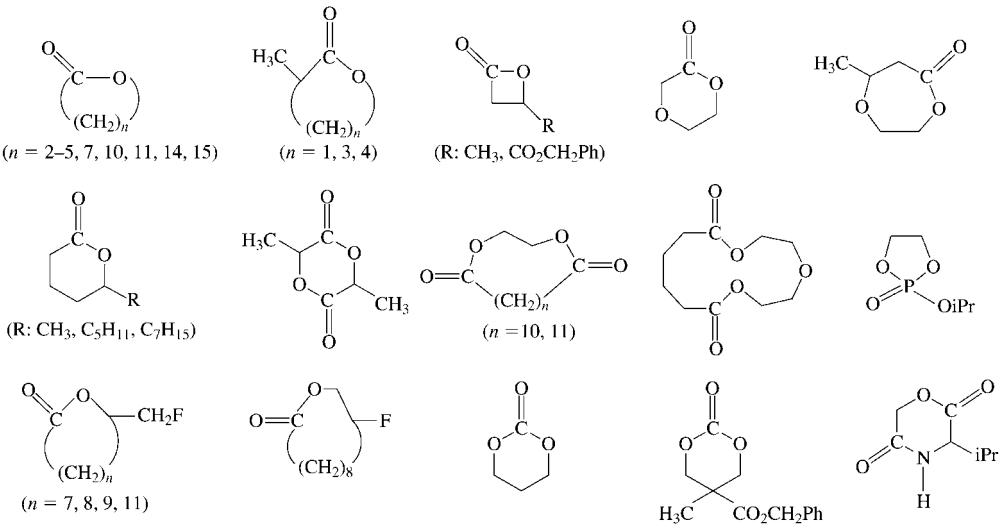

Fig. 9. Cyclic monomers polymerized by lipases.

Polyanhydrides were effective as diacid substrate for enzymatic synthesis of polyesters (136). The reaction of poly(azelaic anhydride) and 1,8-octanediol took place by lipase CA catalyst to give the corresponding polyester with molecular weight of several thousands. In the reaction of poly(azelaic anhydride) and glycerol, a highly branched polyester was obtained.

Oxiranes such as benzyl glycidate and glycidiyl phenyl ether were polymerized with succinic anhydride in the presence of PPL at 60 or 80°C (137,138). The reaction of succinic anhydride with serine residue of the lipase catalyst produces a carboxylic acid moiety, which might act as acid catalyst for ring-opening of oxirane.

Ring-Opening Polymerization of Cyclic Esters. Polyester syntheses have been achieved by enzymatic ring-opening polymerization of cyclic esters with various ring-sizes. Figure 9 summarizes cyclic monomers so far polymerized through lipase catalysis.

Lactones. Small-size (four-membered) lactone derivatives have been reported to be polymerized through lipase catalysis. The polymerization of β-propiolactone (β-PL) proceeded by using *Pseudomonas* family lipases as catalyst in bulk to give a mixture of linear and cyclic oligomers (139). By employing a very small amount of lipase CC (0.5 versus for the monomer), high molecular weight poly(β-PL) was formed (140).

Ring-opening polymerization of racemic α-methyl-β-propiolactone using lipase PC catalyst proceeded enantioselectively to produce an optically active (S)-enriched polymer (141). The highest ee value of the polymer was 0.50. An nmr analysis of the product showed that the stereoselectivity during the propagation resulted from the catalyst enantiomorphic-site control.

β-Butyrolactone (β-BL) was enzymatically polymerized to give poly(β-hydroxybutyrate) (PHB), which is a polyester produced *in vivo* by bacteria for an energy-storage substance. PPL-catalyzed polymerization of β-BL in bulk at

room temperature produced PHB with molecular weight around 1×10^3 (142). In the polymerization at high temperature (80 or 100°C), PHB with higher molecular weight was obtained by lipase CC, PF, or PPL catalyst (143,144). A significant amount of the cyclic PHB fraction was formed and the content of the cycles increased with increasing the monomer conversion. Enantioselective polymerization of β-BL was achieved by using thermophilic lipase to give (R)-enriched PHB with 20–37% ee (145).

PHB depolymerase is an enzyme catalyzing hydrolysis of PHB and its catalytic site is a serine residue, the same as lipase. The polymerization of β-BL proceeded using two types of PHB depolymerase with or without substrate-binding domains (SBD) as catalyst (146). The SBD-lacking PHB depolymerase showed higher catalytic activity.

Chemoenzymatic synthesis of biodegradable poly(malic acid) was demonstrated by lipase-catalyzed polymerization of benzyl β-malolactone, followed by the debenzylation (147). The molecular weight of poly(benzyl β-malolactone) increased by the copolymerization with a small amount of β-PL (17 mol% for the monomer) (148).

Five-membered unsubstituted lactone, γ-butyrolactone, is not polymerized by conventional chemical catalysts. However, oligomer formation from γ-butyrolactone was observed by using PPL or *Pseudomonas* sp. lipase as catalyst (87,142).

Medium size lactones, δ-valerolactone (δ-VL, six-membered) and ε-caprolactone (ε-CL, seven-membered), were subjected to lipase-catalyzed polymerizations. Lipases CC, PF, and PPL showed high catalytic activity for the polymerization of δ-VL (149,150). The molecular weight of enzymatically obtained poly(δ-VL) was relatively low (less than 2×10^3).

ε-CL was enzymatically polymerized by various lipases of different origin, lipases CA, CC, PC, PF, and PPL (86,149–157). Among them, lipase CA was the most active toward the ε-CL polymerization; a very small amount of lipase CA (less than 1 wt% for ε-CL) was enough to induce the polymerization (151). Under appropriate reaction conditions, the molecular weight reached more than 4×10^4 (157). In the lipase CA-catalyzed polymerization in organic solvents, cyclic oligomers were mainly formed, whereas the main product in the bulk polymerization was of linear structure (155).

The detailed kinetics of the ε-CL polymerization showed that termination and chain transfer did not occur and the monomer consumption followed a first-order rate law under appropriate conditions, indicating that the system provided controlled polymerizations where the molecular weight was a function of the monomer to initiator stoichiometry (152,153,156).

Effect of reaction medium has been systematically investigated in the lipase CA-catalyzed polymerization of ε-CL (157). Solvents having $\log P$ values from -1.1 to 0.49 showed low propagation rates; on the other hand, solvents with $\log P$ values from 1.9 to 4.5 efficiently induced the polymerization, leading to high molecular weight polymer. The monomer-to-solvent ratio also affected the polymerization behaviors.

Enzymatic hydrolytic degradation of poly(ε-CL) in toluene also took place using lipase CA catalyst to give oligomers with molecular weight of less than 500 (158). After the removal of the solvent from the reaction mixture, the residual

oligomer was polymerized in the presence of the same catalyst of lipase. From these data is proposed a basic concept that the degradation–polymerization could be controlled by presence or absence of the solvent, providing a new methodology of plastics recycling.

Substituted medium size lactones were polymerized by lipase catalyst. Ring-opening polymerization of α-methyl-substituted six- and seven-membered lactones (α-methyl-δ-valerolactone and α-methyl-ε-caprolactone, respectively) proceeded using lipase CA catalyst in bulk (159). As to (*R*)- and (*S*)-3-methyl-4-oxa-6-hexanolides (MOHELs), lipase PC induced the polymerization of both isomers. The apparent initial rate of the S isomer was seven times larger than that of the R isomer, suggesting that the enantioselective polymerization of MOHEL took place through lipase catalysis (160).

Poly(1,4-dioxane-2-one) is a biocompatible polymer with good flexibility and tensile strength for medical applications. Metal-free poly(1,4-dioxane-2-one) with M_w up to 4.1×10^4 was synthesized by lipase CA-catalyzed ring-opening polymerization of 1,4-dioxan-2-one (161).

Lipase-catalyzed ring-opening polymerization of nine-membered lactone, 8-octanolide (OL), has been reported (162). Lipases CA and PC showed the high catalytic activity for the polymerization.

Four unsubstituted macrolides, 11-undecanolide (12-membered, UDL) (163, 164), 12-dodecanolide (13-membered, DDL) (164,165), 15-pentadecanolide (16-membered, PDL) (163,164,166,167), and 16-hexadecanolide (17-membered) (168), were subjected to the lipase-catalyzed polymerization. An nmr analysis showed that the terminal structure of the polymer obtained in bulk was of carboxylic acid at one end and of alcohol at the other terminal.

The bulk polymerization of PDL using lipase CA or MM as catalyst produced the corresponding polyester with high molecular weight up to 3.4×10^4 (167). The polymerization behaviors (rate of the monomer consumption and molecular weight of the polymer) depended on the water content in the reaction system. Enzymatic ring-opening polymerization of macrolides (UDL, DDL, and PDL) proceeded even in an aqueous medium (169).

The enzymatic polymerization of lactones is explained by considering the following reactions as the principal reaction course (Fig. 10) (160,163,170,171). The key step is the reaction of the lactone with lipase involving the ring-opening of the lactone to give the acyl-enzyme intermediate (enzyme-activated monomer, EM). The initiation is a nucleophilic attack of water, which is probably contained in the enzyme, onto the acyl carbon of the intermediate to produce ω-hydroxycarboxylic acid ($n=1$, the shortest propagating species). In the propagation stage, the intermediate is nucleophilically attacked by the terminal hydroxyl group of a propagating polymer to produce a one-unit-more elongated polymer chain. This is a *monomer-activated mechanism* in contrast to an active chain-end mechanism, the widely known polymerization mechanism.

Macrolides have virtually no ring strain, and hence, show similar reactivities with acyclic fatty acid alkyl esters in the alkaline hydrolysis and lower anionic ring-opening polymerizability than ε-CL. However, polymerization of the macrolides using lipase PF catalyst proceeded much faster than that of ε-CL. This specific polymerizability by lipase catalyst was quantitatively evaluated by Michaelis–Menten kinetics (160,168,170–172). For unsubstituted lactones in the

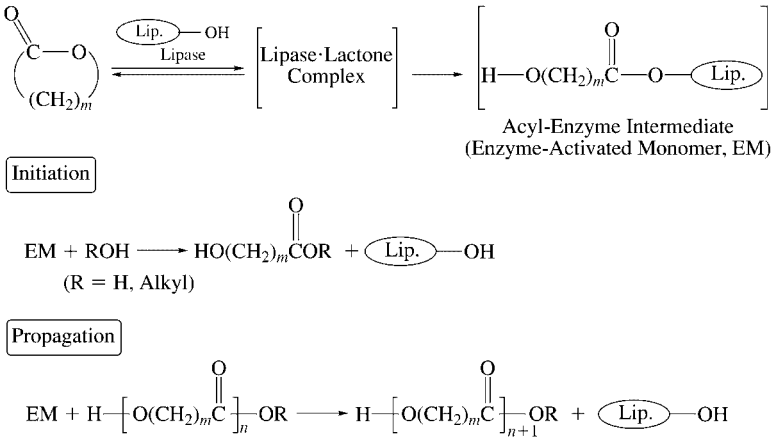

Fig. 10. Postulated mechanism of lactone polymerization catalyzed by lipase.

range of ring-size from 7 to 17, linearity was observed in the Hanes–Woolf plot for the formation of the acyl-lipase intermediate, indicating that the polymerization followed Michaelis–Menten kinetics. $V_{\max(\text{lactone})}/K_{\text{m(lactone)}}$ and $V_{\max(\text{lactone})}$ values increased as a function of the ring-size; on the other hand, $K_{\text{m(lactone)}}$ values were not so different from each other. These data imply that the enzymatic polymerizability increased as the ring-size increased, and the large polymerizability of macrolides through lipase catalysis is mainly due to the large reaction rate ($V_{\max}$), but not to the binding abilities, ie, the ring-opening reaction process of the lipase–lactone complex to the acyl-enzyme intermediate is the key step of the polymerization.

Fluorinated lactones in the ring-size from 10 to 14 were enantioselectively polymerized using lipase catalyst (173). The lipase CA-catalyzed polymerization of 10-fluorodecan-9-olide (10-membered) produced the optically active polymer with positive rotation. Interestingly, the corresponding oxyacid gave an optically inactive polyester.

Enzymatic synthesis of aliphatic ester copolymers was achieved by lipase-catalyzed polymerization of two lactones. The copolymerization of δ-VL and ε-CL catalyzed by lipase PF produced the corresponding copolymer having random structure of both units (174). In the copolymerization of OL with ε-CL or DDL, random copolyesters were also formed (162), suggesting the frequent occurrence of transesterifications between the polyesters. On the other hand, the copolymer from ε-CL and PDL was not statistically random (166).

Polyesters with high optical purity were synthesized by the lipase CA-catalyzed copolymerization of racemic β-BL with ε-CL or DDL (175). (S)-β-BL was preferentially reacted with DDL to give the (S)-enriched optically active copolymer with ee of β-BL unit = 69%. δ-CL was also enantioselectively copolymerized by the lipase catalyst to give the (R)-enriched optically active polyester with ee up to 76%.

Frequent occurrence of transesterification between polyesters chains was expanded to synthesis of random ester copolymers by the lipase-catalyzed

polymerization of lactones in the presence of poly(ε-CL) (176). Intermolecular transesterifications between poly(ε-CL) and poly(PDL) also took place through lipase catalysis.

Ester copolymers were synthesized by lipase-catalyzed copolymerization of lactones, divinyl esters, and glycols (177). The ^{13}C nmr analysis showed that the resulting product was not a mixture of homopolymers, but a copolymer derived from the monomers, indicating that two different modes of polymerization, ring-opening polymerization and polycondensation, simultaneously take place through enzyme catalysis in one pot to produce ester copolymers.

Immobilized lipase showing high catalytic activity toward the enzymatic synthesis of polyesters was demonstrated (178). Only a small amount of immobilized lipase PF adsorbed on a Celite was effective for the polymerization of lactones. The catalytic activity was further enhanced by the presence of a sugar or PEG at the immobilization. Surfactant-coated lipase efficiently catalyzed the ring-opening polymerization of lactones in organic solvents, in which the modified enzyme was soluble (179).

Enzymatic synthesis of end-functionalized polymers such as macromonomers and telechelics has been achieved by initiator and terminator methods. An alcohol could initiate the ring-opening polymerization of lactones by lipase catalyst ("initiator method"). In the lipase CA-catalyzed polymerization of DDL using 2-hydroxyethyl methacrylate as initiator, the methacryloyl group was quantitatively introduced at the polymer terminal, yielding the methacryl-type polyester macromonomer (180). In the lipase-catalyzed polymerization of ε-CL in the presence of functional alcohols (181), end-functionalized poly(ε-CL) as well as the cyclic by-product was formed.

Polyesters bearing the sugar moiety at the polymer terminal was synthesized by lipase CA-catalyzed polymerization of ε-CL in the presence of alkyl glucopyranosides (182–184). In the initiation step, the primary hydroxy group of the glucopyranoside was regioselectively acylated. Poly(ε-CL) monosubstituted first generation dendrimer was synthesized using lipase CA as catalyst. The monoacylation of the initiator took place at the initial stage (185).

Polymeric hydroxy group also initiated the enzymatic ring-opening polymerization of ε-CL (186). The polymerization was performed using thermophilic lipase as catalyst in the presence of hydroxyethyl cellulose (HEC) film to produce HEC-*graft*-poly(ε-CL) with degree of substitution from 0.10 to 0.32.

Single-step synthesis of polyester macromonomers was achieved by lipase-catalyzed polymerization of lactones in the presence of vinyl esters acting as terminator ("terminator method") (187,188). A methacryl-type poly(DDL) macromonomer was obtained using vinyl methacrylate (12.5 or 15 mol% based on DDL) and lipase PF as terminator and catalyst, respectively. By the addition of divinyl sebacate, the telechelic polyester having a carboxylic acid group at both ends was synthesized.

Cyclic Diesters. Cyclic diesters were subjected to the lipase-catalyzed ring-opening polymerization. Lactide, cyclic dimer of lactic acid, was polymerized by lipase PC in bulk at high temperature (80–130°C) to produce poly(lactic acid) with M_w up to 2.7×10^5 (189,190). Protease (proteinase K) also induced the polymerization of lactide; however, the catalytic activity was relatively low.

Ring-opening polymerization of cyclic diesters obtained from diacid and glycol, ethylene dodecanoate, ethylene tridecanoate, and 1,4,7-trioxa-cyclotridecane-8,13-dione, took place through lipase catalysis (191,192). The former two monomers were polymerized by lipase CA, PC, or PF catalyst (191). The enzyme origin affected the polymerization behaviors; the polymerization of these bislactones using lipase PC catalyst proceeded faster than that of ε-CL and DDL, whereas the reactivity of these cyclic diesters was in the middle of ε-CL and DDL in using lipase CA.

***In Vitro* PHA Polymerase-Catalyzed Polymerization to PHA.** *Alcaligenes eutrophus* has been used for industrial production of poly(hydroxyalkanoate)s (PHAs). PHA is prepared from acetyl CoA in three steps and the last step is the chain growth polymerization of hydroxyalkanoate CoA esters catalyzed by PHA polymerase, yielding PHA of high molecular weight, which has been *in vitro* examined, leading to synthesis of PHAs with well-defined structure. This synthetic process obeys the biosynthetic pathways (see POLY(3-HYDROXYALKANOATES)).

The growing polymer chain was covalently attached to a highly conserved cysteine residue (Cy319) of the polymerase (193). The granules of the precipitated polymer were quickly formed when the purified polymerase was exposed to (*R*)-hydroxybutyryl CoA (HBCoA) (194,195). The artificial PHB granules were spherical with diameters of up to 3 μm, significantly larger than the native ones.

The polymerization of the CoA monomers of (*R*)-hydroxyalkanoate was of chain growth in a living fashion; each molecule of the polymerase initiated and catalyzed the formation of one molecule of the polymer (196–198). By utilizing this property of polymerase, random and block copolyesters were synthesized. The resulting polymer had high molecular weight ($>10^6$). In the polymerization of racemic HBCoA, only the *R* monomer was polymerized. Furthermore, the presence of the *S* monomer did not reduce the polymerization rate of the *R* isomer. These data indicate that the *S* monomer does not act as competitive inhibitor for the polymerase.

Recombinant PHA synthase from *Chromatium vinosum* showed different catalytic behaviors in comparison with that of *A. eutrophus* (199). In combination of this synthase with purified propionyl-CoA transferase of *Clostridium propionicum*, a two-enzyme *in vitro* PHB biosynthesis system was established, which allowed the PHB synthesis from (*R*)-hydroxybutyric acid as substrate (200).

Hydrolase-Catalyzed Modification of Polymers. Terminal hydroxy group of poly(ε-CL) was reacted with carboxylic acids using lipase CA catalyst to give end-functionalized polyesters (181). Lipase MM catalyzed the regioselective transesterification of the terminal ester group of oligo(methyl methacrylate) with allyl alcohol (201).

The lipase-catalyzed acetylation of high molecular weight methacrylic polymers containing racemic hydroxy groups in the side chain was achieved with a maximum conversion of 40% (202,203). The optical rotation was low (up to -1.2°), suggesting a low enantioselectivity of this esterification. The enzymatic transesterification of amylose film with vinyl caprate in the isooctane solution containing solubilized subtilisin Carlsberg produced an amylose derivative regioselectively acylated at the C-6 position (204).

Enzymatic epoxidation of polybutadiene was demonstrated (205). Lipase CA catalyzed the oxidation of polybutadiene using hydrogen peroxide as oxidizing agent in the presence of acetic acid.

Polycarbonates

Polycondensation. Oligocarbonate with molecular weight of less than 1×10^3 was formed by lipase CC-catalyzed polycondensation of carbonic acid diphenyl ester with bisphenol A (206). Diethyl carbonate was polymerized with 1,4-butanediol by lipase CA catalyst (207,208). The successive two-step polymerization, the prepolymerization under ambient pressure, followed by the polymerization under vacuum (0.5 mm Hg), produced poly(tetramethylene carbonate) with M_w of more than 4×10^4.

Activated dicarbonate, 1,3-propanediol divinyl dicarbonate, was used as new monomer for enzymatic synthesis of polycarbonates (209). Lipase CA catalyzed the polymerization with α,ω-alkylene glycols under mild reaction conditions and the M_w value reached 8×10^3. Aromatic polycarbonate was enzymatically obtained from the activated dicarbonate and xylylene glycol (132).

Ring-Opening Polymerization. 1,3-Dioxan-2-one, six-membered cyclic carbonate, was polymerized in the presence of lipase catalysts (210–212). Under mild reaction conditions ($\leq$70 °C), lipase CA efficiently catalyzed the polymerization to give the corresponding polycarbonate with M_n more than 1×10^4 (211,212). No ether bond was observed in the nmr spectrum of the product, indicating that elimination of carbon dioxide did not occur during the enzymatic polymerization. The polymerization in the presence of a small amount of PPL (0.1 or 0.25 wt% for the monomer) at 100°C produced the high molecular weight polymer ($M_w = 1.6\times10^5$) (210).

The enzymatic polymerization of 5-methyl-5-benzyloxycarbonyl-1,3-dioxan-2-one produced the corresponding polycarbonate (213). Lipases PF and CA showed high catalytic activity for the polymerization. Debenzylation by catalytic hydrogenation led to the water-soluble polycarbonate with pendent carboxyl group.

Lipase CA catalyzed the polymerization of cyclic dicarbonates, cyclobis(hexamethylene carbonate) and cyclobis(diethylene glycol carbonate), to give the corresponding polycarbonates (214). The enzymatic copolymerization of cyclobis(diethylene glycol carbonate) with DDL produced a random ester-carbonate copolymer. Enzymatic synthesis of poly(ester-carbonate) was also achieved by the copolymerization of 1,3-dioxan-2-one and lactide (215). The PPL-catalyzed copolymerization at 100°C produced the copolymer with M_w higher than 2×10^4.

Besides polyesters and polycarbonates, lipase-catalyzed synthesis of polymers from cyclic monomers has been reported. 3(*S*)-Isopropylmorpholine-2,5-dione, six-membered depsipeptide, was polymerized by lipase PC and PPL catalysts to give poly(ester-amide) (216,217). High temperature (100 or 130°C) was required for the polymerization, yielding biodegradable poly(depsipeptide) with maximum $M_n = 3\times10^4$. During the polymerization, the racemization of the valine residue took place. PPL-catalyzed synthesis of poly(phosphate) was demonstrated (218). The ring-opening polymerization of ethylene isopropyl phosphate,

five-membered cyclic phosphate, took place at 40–100°C to give the polymer with molecular weight of ca 1×10^3.

Polyaromatics

In living cells, various oxidoreductases play an important role in maintaining the metabolism of living systems. So far, peroxidase containing Fe-active site, laccase containing Cu-active site, tyrosinase (polyphenol oxidase, Cu-active site), bilirubin oxidase (Cu-active site), etc, have been reported to act as catalyst for oxidative polymerization of phenol and aniline derivatives and for polymer modification via oxidative coupling.

Enzymatic Oxidative Polymerization.

Polyphenols. For enzymatic oxidative polymerization of phenol derivatives, peroxidase has been often used as catalyst. Catalytic cycle of peroxidase is shown in Figure 11. Peroxidase catalyzes decomposition of hydrogen peroxide at

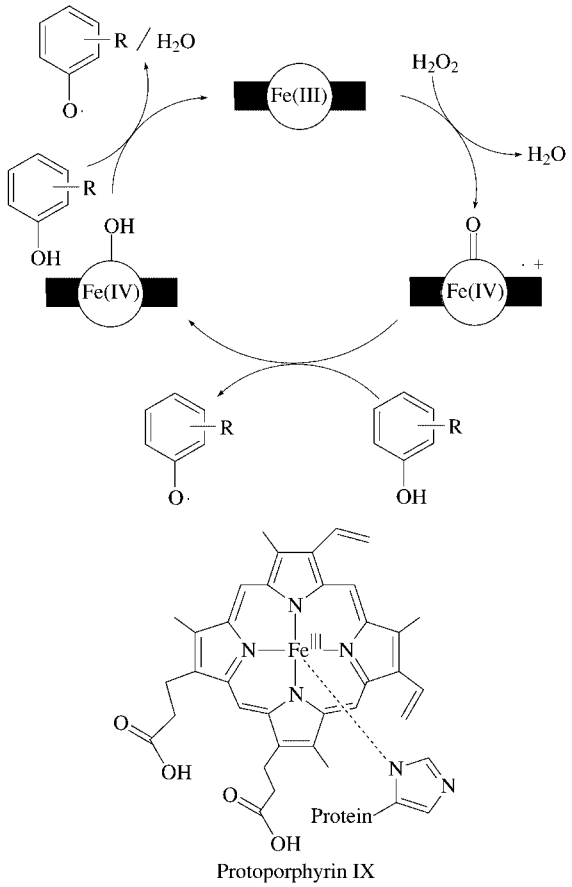

Fig. 11. Catalytic cycles of peroxidase for polymerization of phenols.

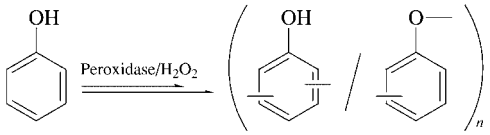

Fig. 12. Peroxidase-catalyzed oxidative polymerization of phenol.

the expense of aromatic proton donors in living cells. In some cases, the peroxidase-catalyzed oxidation of these donors, eg, phenols, yields water-insoluble polymeric materials, which had not been characterized yet.

In 1987, enzymatic synthesis of a new class of polyphenols has been first reported. An oxidative polymerization of *p*-phenylphenol using horseradish peroxidase (HRP) as catalyst was carried out in a mixture of water and water-miscible solvents such as 1,4-dioxane, acetone, DMF, and methyl formate to give powdery polymeric materials (219). The reaction medium composition greatly affected the molecular weight, and the highest molecular weight (2.6×10^4) was achieved in 85% 1,4-dioxane.

In the case of phenol, the simplest and most important phenolic compound in industrial fields, conventional polymerization catalysts afford an insoluble product with noncontrolled structure since phenol is a multifunctional monomer for oxidative polymerization. On the other hand, the peroxidase catalysis induced the polymerization in an aqueous organic solvent to give a powdery polymer consisting of phenylene and oxyphenylene units showing relatively high thermal stability (Fig. 12) (220–224). HRP and soybean peroxidase (SBP) were active as catalyst for the polymerization in the aqueous 1,4-dioxane (220–222). However, the resulting polymer showed low solubility; the polymer was partly soluble in DMF and dimethyl sulfoxide, and insoluble in other common organic solvents. The solubility was much improved by using a mixed solvent of buffer and methanol, producing the DMF-soluble polymer with molecular weight of 2100–6000 in good yields. Furthermore, the unit ratio (regioselectivity) could be controlled by changing the solvent composition; the polymer in the range of the phenylene unit from 32 to 66% was obtained (223,224).

So far, various phenol derivatives have been polymerized through peroxidase catalysis in the aqueous organic solvent (225–227). For the case of a combination of *p*-*n*-alkylphenols and HRP, the polymer yield increased as the chain length of the alkyl group increased from 1 to 5 (228,229). Polymer formation was observed in using all cresol isomers by HRP catalyst (230). The polymer was obtained in a high yield from *p*-*i*-propylphenol, whereas ortho and metaisomers were not polymerized under the similar reaction conditions. Poly(*p*-*n*-alkylphenol)s prepared in the aqueous 1,4-dioxane showed low solubility toward common organic solvents, and the molecular weight was in the range of several thousands. On the other hand, soluble oligomers with molecular weight less than 1000 were formed in using an aqueous DMF as solvent (231).

Enzymatically synthesized polyphenols showed biodegradability (232), although the degradation rate was not high. Antioxidant effects of the polymers obtained from various phenols through the enzyme catalysis were evaluated (233). Pronounced improvement for the autooxidation of tetralin was observed.

As to meta-alkyl substituted phenols, the soluble polyphenols were obtained by HRP or SBP catalyst in the aqueous methanol (234). Enzymatically synthesized poly(*m*-cresol) had glass-transition temperature (T_g) of higher than 200°C. The enzyme origin strongly influenced the polymer yield; HRP could readily polymerize the monomer having a small substituent, whereas in the case of large substituent monomers, the high yield was achieved by using SBP as catalyst.

The enzymatic reaction kinetics on the HRP-catalyzed oxidation of *p*-cresol in aqueous 1,4-dioxane or methanol showed that the catalytic turnover number and Michaelis constant were larger than those in water (235). Numerical and Monte Carlo simulations of the peroxidase-catalyzed polymerization of phenols were demonstrated (236). The simulations predicted the monomer reactivity and polymer molecular weight, leading to synthesis of polymers with specific molecular weight and index. In an aqueous 1,4-dioxane, the formation of monomer aggregate was observed (237), which might elucidate the specific polymerization behaviors in such a medium.

Effects of the monomer substituent and substituted position on the initial reaction rate in the HRP-catalyzed polymerization of substituted phenols were examined (238). Substrates with the electron-drawing group or ortho-substituted substrates showed low polymerizability. Lactoperoxidase also showed catalytic activity for the polymerization of phenols.

Four interfacial systems, micelles, reverse micelles, a biphasic, and Langmuir trough systems, have been examined for preparation of the enzymatic synthesis of polyphenols. In the polymerization in micelle solution consisting of surfactant and buffer, the obtained polymer from *p*-phenylphenol had narrow molecular weight distribution in comparison of that in the aqueous 1,4-dioxane (239).

HRP and *p*-ethylphenol were encapsulated in the reverse micelle, which was a ternary system composed of isooctane, water, and bis(2-ethylhexyl) sodium sulfosuccinate (AOT). The introduction of hydrogen peroxide into the system induced the polymerization to produce the polymer particles in the diameter range from 0.1 to 2 μm quantitatively (240–242). Similar particles were obtained by pouring the solution of enzymatically prepared polyphenol into a nonsolvent containing AOT (243).

HRP-catalyzed polymerization of *p*-alkylphenols proceeded in a biphasic system consisting of two mutually immiscible phases (isooctane and water) (226). The molecular weight increased as a function of the carbon number of the alkyl group.

Enzymatic polymerization of phenol derivatives in a monolayer form was demonstrated (241,244,245). A monolayer was formed from *p*-tetradecyloxyphenol and phenol at the air–water interface in a Langmuir trough, which was polymerized by HRP catalyst in the subphase. The polymerized film could be deposited on silicon wafer with a transfer ratio of 100% for the Y-type film. The monolayer thickness determined by Eppipsometric and AFM was 27.8 Å.

Poly(2,6-dimethyl-1,4-oxyphenylene) [poly(phenylene oxide), PPO] is widely used as high-performance engineering plastics, since the polymer has excellent chemical and physical properties, eg, a high T_g (ca 210°C) and mechanically tough property. PPO was first prepared from 2,6-dimethylphenol monomer using a copper/amine catalyst system (246,247). 2,6-Dimethylphenol was also polymerized through HRP catalysis to give the polymer consisting of exclusively 1,4-oxyphenylene unit (248). On the other hand, a small amount of Mannich-base

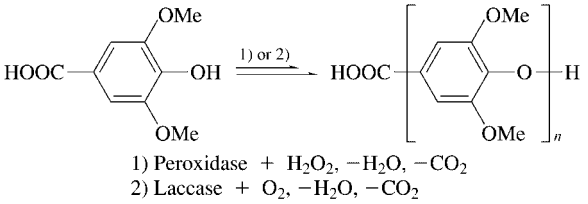

Fig. 13. Enzymatic synthesis of PPO derivative from syringic acid.

and 3,5,3′5′-tetramethyl-4,4′-diphenoquinone units are contained in commercially available PPO. The polymerization also proceeded in the presence of laccase derived from *Pycnoporus coccineus* under air without the addition of hydrogen peroxide.

HRP, SBP, and laccase catalysis induced a new type of oxidative polymerization of 4-hydroxybenzoic acid derivatives, 3,5-dimethoxy-4-hydroxybenzoic acid (syringic acid) and 3,5-dimethyl-4-hydroxybenzoic acid. The polymerization involved elimination of carbon dioxide and hydrogen from the monomer to give PPO derivatives with molecular weight up to 1.8×10^4 (Fig. 13) (110,249–251).

Polymerization of *p*-alkoxyphenols regioselectively proceeded by HRP catalyst to give PPO (252). Peroxidase-catalyzed synthesis of poly(catechol) was achieved and the iodine-labeled polymer showed low electrical conductivity in the range of 10^{-6}–10^{-9} $S\cdot cm^{-1}$ (253).

Thiol-containing polyphenol was synthesized by peroxidase-catalyzed copolymerization of *p*-hydroxythiophenol and *p*-ethylphenol in reverse micelles (254). CdS nanoparticles were attached to the copolymer to give polymer–CdS nanocomposites. By a similar procedure, polyphenol–iron oxide composites were synthesized (242). The reverse micellar system was also effective for the enzymatic synthesis of poly(2-naphthol) showing a fluorescence characteristic of the naphthol chromophore (255). nmr, ir, and uv analyses showed the formation of the polymer with quinonoid structure.

Bilirubin oxidase (BOD), a copper-containing oxidoreductase, catalyzed the oxidative polymerization of 1,5-dihydroxynaphthalene to give the polymer showing low solubility (256,257). The polymerization proceeded regioselectively to produce the polymer film having a long π-conjugated structure. This monomer was also polymerized by HRP catalyst (258). The polymerization in the presence of porous silicon (PS) wafer produced the polyphenol–PS composite showing optoelectronic properties.

Bisphenol A was polymerized by SBP catalyst to give a soluble polymer with molecular weight of several thousands in good yields (259). Interestingly, the polymer was subjected to thermal curing at 150–200°C. 4,4′-Biphenol was polymerized by HRP catalyst in an aqueous 1,4-dioxane to give the polymer showing high thermal stability (260).

The mechanistic study of the HRP-catalyzed oxidative polymerization was performed by using nmr spectroscopy (261,262). In the initial stage of the polymerization of 8-hydroxyquinoline-5-sulfonate, the oxidative coupling took place at carbons of the 2-, 4-, and 7-positions of the monomer. Polymerization and copolymerization of 8-hydroxyquinoline also took place through HRP catalysis (263).

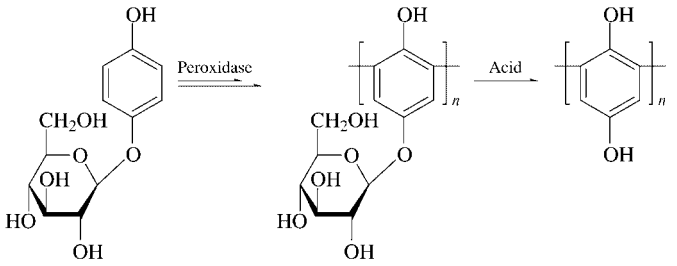

Fig. 14. Chemoenzymatic synthesis of poly(hydroquinone).

Peroxidase catalysis induced the oxidative polymerization of glucose-β-D-hydroquinone (arbutin) in a buffer to produce a water-soluble polyphenol (264). The acid treatment of the polymer led to the quantitative deglycosylation of the polymer, yielding poly(hydroquinone) soluble in polar organic solvents (Fig. 14). The resulting polymer was used as a mediator for amperometric glucose sensors (265). Another route for chemoenzymatic synthesis of poly(hydroquinone) from 4-hydroxyphenyl benzoate was demonstrated (266), whose structure was different from that obtained from arbutin. Enzymatically synthesized phenolic copolymer containing fluorophore (fluorescein or calcein) was applied as array-based metal-ion sensor (267).

A polynucleoside with unnatural polymeric backbone was synthesized by SBP-catalyzed oxidative polymerization of thymidine 5′-*p*-hydroxyphenylacetate (268). Chemoenzymatic synthesis of a new class of poly(amino acid), poly(tyrosine) containing no peptide bonds, was achieved by peroxidase-catalyzed oxidative polymerization of tyrosine ethyl esters, followed by alkaline hydrolysis (269). The amphiphile higher alkyl ester derivatives were also polymerized in micellar solution to give the polymer showing surface activity at the air–water interface (270). The polymerization was monitored by the quartz crystal microbalance (271).

HRP catalysis induced a chemoselective polymerization of a phenol derivative having methacryloyl group (272). Only the phenol moiety was polymerized without involving vinyl polymerization of methacryloyl to give a polymer having the methacryloyl group in the side chain (Fig. 15). The resulting polymer was subjected to thermal and photochemical curings (273).

A phenol with an acetylenic substituent in the meta position was also chemoselectively polymerized to give the polyphenol having the acetylenic group (274). The resulting polymer was converted to carbonized polymer in a much higher yield than enzymatically synthesized poly(*m*-cresol).

Cardanol, a main component obtained by thermal treatment of cashew nut shell liquid, is a phenol derivative mainly having the meta substituent of a C-15 unsaturated hydrocarbon chain mainly with one to three double bonds. A new cross-linkable polymer was synthesized by the SBP-catalyzed polymerization of cardanol (110,251,275). The polymerization in an aqueous acetone produced oily polymeric materials having the carbon–carbon unsaturated group in the side chain. The curing by cobalt naphthenate gave the cross-linked film with high gloss surface. The hydrogenated cardanol derivative was also oxidatively polymerized by HRP (276).

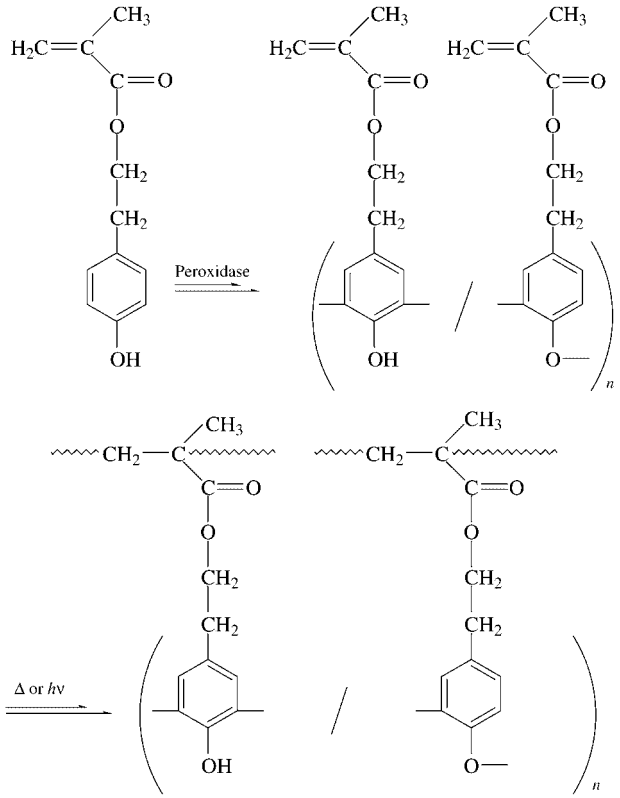

Fig. 15. Chemoselective polymerization of a phenol derivative having a methacryloyl group.

Fluorinated phenols, 3- and 4-fluorophenols and 2,6-difluorophenol, were subjected to peroxidase-catalyzed polymerization, yielding fluorine-containing polymerizations. During the polymerization, elimination of fluorine atom partly took place to give the polymer with complicated structure (277).

Morphology of the enzymatically synthesized polyphenol was controlled under the selected reaction conditions. Monodisperse polyphenol particles in the submicron range were produced by HRP-catalyzed dispersion polymerization of phenol using poly(vinyl methyl ether) as stabilizer in an aqueous 1,4-dioxane (278–280). The particle size could be controlled by the stabilizer concentration and solvent composition. Thermal treatment of these particles afforded uniform carbon particles. The particles were also formed from *m*-cresol and *p*-phenylphenol.

Bienzymatic system (glucose oxidase + HRP) was used as catalyst for the polyphenol synthesis. This system induced the polymerization of phenol in the presence of glucose without the addition of hydrogen peroxide to produce the polymer in a moderate yield (281). Hydrogen peroxide was formed *in situ* by the oxidation of glucose catalyzed by glucose oxidase, which acted as oxidizing agent for the polymerization.

In vitro synthesis of lignin, a typical phenolic biopolymer, was claimed by the HRP-catalyzed terpolymerization of lignin monomers, *p*-coumaryl alcohol, coniferyl alcohol, and sinapyl alcohol (14:80:6 mol%) in an extremely dilute aqueous solution at pH 5.5 (282). Dialysis membrane method was applied to the polymerization of coniferyl and sinapyl alcohols, yielding insoluble polymeric materials (283). In the HRP-polymerization of coniferyl alcohol in the presence of a small amount of lignin component, the molecular weight distribution became much broader than that in the absence of lignin (284).

Peroxidase-catalyzed polymerization behavior of coniferyl alcohol has been compared with that by laccase (285). Peroxidase oxidized the substrate faster than laccase in the presence of hydrogen peroxide. As to the laccase-catalyzed polymerization, the oxidation rate and reaction mechanism depended on the enzyme origin.

Enzymatic polymerization of soluble lignin fragments (lignin oligomer) was demonstrated. In the polymerization catalyzed by HRP, or polyphenol oxidase (potato), brown precipitates were formed (286). The increase of the molecular weight was observed in the laccase-catalyzed treatment of the lignin oligomer (287).

Peroxidase-catalyzed grafting of polyphenols on lignin has been attempted by HRP-catalyzed polymerization of *p*-cresol with lignin in the aqueous 1,4-dioxane or reverse micellar system. (288–290). The monomer was incorporated into lignin by the oxidative coupling between the monomer and the phenolic moiety of lignin.

Low molecular weight coal (4 kDa) was polymerized by HRP or SBP catalyst in a mixture of DMF and buffer (291). The resulting product was partly soluble in DMF and the DMF-soluble part had a larger molecular weight than that of the starting substrate.

A novel system of enzymatic polymerization, ie, a laccase-catalyzed cross-linking reaction of new "urushiol analogues" for the preparation of "artificial urushi," has been demonstrated (Fig. 16) (292,293). Single-step synthesis of the urushiol analogues was achieved by using lipase as catalyst. These compounds were cured in the presence of laccase catalyst under mild reaction conditions without the use of organic solvents to produce the cross-linked polymeric film with high gloss surface and good elastic properties. Catechol derivatives directly

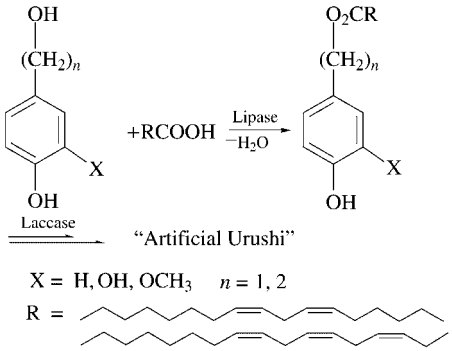

Fig. 16. Laccase-catalyzed curing of urushiol analogues to "artificial urushi."

connecting an unsaturated alkenyl group at 4-position of the catechol ring were also cured by laccase to give the cross-linked polymeric film showing ideal dynamic viscoelasticity (294).

Polyanilines. Oxidoreductases also catalyze oxidative polymerization of aromatic amines. HRP induced the polymerization of aniline. In the HRP-catalyzed polymerization under neutral conditions, the polymer with complicated structure was obtained in low yields (295). The resulting polymer showed good third-order nonlinear optical properties (296).

On the other hand, the polymerization using sulfonated polystyrene (SPS) as template produced the electroactive form of polyaniline (297–299). The resulting polymer was soluble in water and the conductivity reached 5×10^{-3} S·cm^{-1} without doping. Besides SPS, a strong acid surfactant, sodium dodecylbenzenesulfonic acid, provided suitable local template environments leading to the formation of conducting polyaniline. Aniline was also polymerized by BOD catalyst to give the polyaniline film, which was electrochemically reversible in its redox properties in acidic solution (300).

HRP-catalyzed oxidative polymerization of *o*-phenylenediamine in a mixture of 1,4-dioxane and phosphate buffer produced a soluble polymer consisting of an iminophenylene unit (301). From para and meta isomers, the polymer with well-defined structure was not obtained (302). Enzymatic polymer formation was observed from *p*-aminobenzoic acid (303), *p*-aminophenylmethylcarbitol (304), 2,5-diaminobenzenesulfonate (305), and *p*-aminochalcones (306). Cytochrome *c* catalyzed oxidation of *o*-phenylenediamine to give oligomeric products (307). Monolayer of aniline/*p*-hexadecylaniline prepared by LB technique at the air–water interface was polymerized through HRP catalysis to give polymeric monolayer (244,245).

A new class of polyaromatics was synthesized by peroxidase-catalyzed oxidative copolymerization of phenol derivatives with anilines. In case of a combination of phenol and *o*-pheneylenediamine, ftir analysis showed the formation of the corresponding copolymer (308).

Polymer Modification by Oxidoreductases. Tyrosinase (polyphenol oxidase, a copper-containing monooxygenation enzyme) was used as catalyst for modification of chitosan. The enzymatic treatment of chitosan film in the presence of tyrosinase and phenol derivatives produced a new material of chitosan derivative (309). During the reaction, unstable *o*-quinones were formed, followed by the reaction with chitosan to give the modified chitosan. In the enzymatic treatment of *p*-cresol with a low concentration of chitosan (<1%), the reaction solution was converted into a gel (310).

The similar treatment in the presence of chlorogenic acid produced the modified chitosan soluble under both acidic and basic conditions (311). On the other hand, the tyrosinase-catalyzed reaction of 3,4-dihydroxyphenylethylamine (dopamine) provided water-resistant adhesive properties to chitosan (312). A chitosan derivative modified with hydroxy or dihydroxybenzaldehyde was cross-linked by tyrosinase to give stable and self-sustaining gels (313). Phenolic moiety of a synthetic polymer, poly(*p*-hydroxystyrene), was also subjected to tyrosinase-catalyzed oxidation (314).

Peroxidase-catalyzed treatment of soy proteins (315) and wheat gliadins (316) was demonstrated, in which tyrosine residues of the protein were subjected

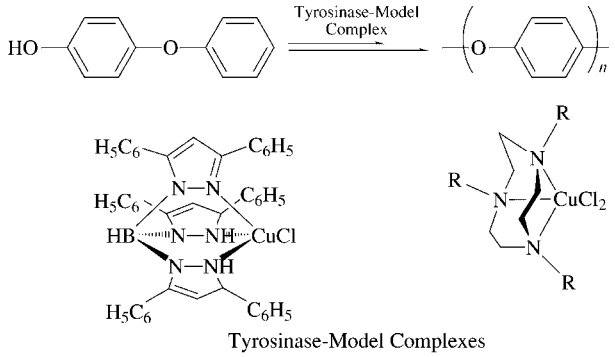

Fig. 17. Regioselective polymerization of 4-phenoxyphenol catalyzed by a tyrosinase-model complex to unsubstituted PPO.

to the enzymatic oxidative coupling, yielding a network of peptide chains. The treatment increased the tensile strength of the materials. In the oxidative polymerization of bovine pancreatic ribonuclease A catalyzed by lignin peroxidase, the coupling between tyrosine residues was confirmed (317).

Oxidative Polymerization Catalyzed by Enzyme-Model Complexes. Metal complexes containing a catalytic site of enzymes or its modified moiety have been used as catalyst for oxidative polymerizations. Regioselective oxidative polymerization of 4-phenoxyphenol was achieved by using tyrosinase model complexes as catalyst, leading to crystalline 2,6-unsubstituted PPO (318–321) (Fig. 17). The complex also catalyzed the regioselective polymerization of 2,5-dimethylphenol to give the crystalline PPO derivative with melting point higher than 300°C (322). From *o*- and *m*-cresols, polymers consisting mainly of 1,4-oxyphenylene unit were also formed (323,324).

Catalytic site of peroxidase is a heme, which is rapidly oxidized in its free form to hematin. *p*-Ethylphenol was polymerized using hematin as catalyst in an aqueous DMF (325). Iron-*N*,*N*′-ethylenebis(salicylideneamine) (Fe-salen) also can be regarded as model complex of peroxidase. Fe-salen catalyzed an oxidative polymerization of various phenols such as 2,6-dimethylphenol, bisphenol A, cardanol, and urushiol analogues (251,293,326–329). The polymerization of 2,6-difluorophenol by Fe-salen produced a crystalline fluorinated PPO derivative (330).

Vinyl Polymers

Some oxidoreductases have been reported to induce polymerization of vinyl monomers. HRP, xanthin oxidase, alcohol oxidase, chloroperoxidase, and laccase could catalyze the polymerization of acrylamide and hydroxyethyl methacrylate (331,332). Glucose oxidase mediated the initiation of vinyl polymerization in the presence of Fe^{2+} and dissolved oxygen (333).

A novel initiating system for vinyl polymerization, HRP/hydrogen peroxide/β-diketone, was demonstrated (334–336), in which the catalytic action of HRP generates carbon radical, a real initiating species, from hydrogen

peroxide and β-diketone through an oxidoreductive pathway. A combination of laccase and organic peroxide initiated the polymerization of acrylamide in the presence of lignin, yielding lignin-*graft*-polyacrylamide (337).

BIBLIOGRAPHY

1. G. M. Whitesides and C.-H. Wong, *Angew. Chem., Int. Ed. Engl.* **24**, 617 (1985).
2. J. B. Jones, *Tetrahedron* **42**, 3351 (1986).
3. A. M. Klibanov, *Acc. Chem. Res.* **23**, 114 (1990).
4. E. Santaniello and co-workers, *Chem. Rev.* **92**, 1071 (1992).
5. S. Takayama, G. J. McGarvey, and C.-H. Wong, *Chem. Soc. Rev.* **26**, 407 (1997).
6. S. Kobayashi, S. Shoda, and H. Uyama, *Adv. Polym. Sci.* **121**, 1 (1995).
7. S. Kobayashi, S. Shoda, and H. Uyama, in J. C. Salamone, ed., *The Polymeric Materials Encyclopedia*, CRC Press, Boca Raton, Fla., 1996, pp. 2102–2107.
8. H. Ritter, in R. Arshady, ed., *Desk Reference of Functional Polymers, Syntheses and Applications*, American Chemical Society, Washington, 1997, pp. 103–113.
9. S. Kobayashi, S. Shoda, and H. Uyama, in S. Kobayashi, ed., *Catalysis in Precision Polymerization*, John Wiley & Sons, Chichester, U.K., 1997, Chapt. "8".
10. R. A. Gross, D. L. Kaplan, and G. Swift, ed., *ACS Symp. Ser.* **684** (1998).
11. S. Kobayashi and H. Uyama, in A.-D. Schlüter, ed., *Materials Science and Technology, Synthesis of Polymers*, Wiley-VCH, Weinheim, 1998, Chapt. "16".
12. S. Kobayashi, *J. Polym. Sci., Polym. Chem. Ed.* **37**, 3041 (1999).
13. S. Kobayashi, *High Polym. Jpn.* **42**, 308 (1993).
14. S. Kobayashi, *High Polym. Jpn.* **48**, 124 (1999).
15. S. Kobayashi and co-workers, *J. Am. Chem. Soc.* **113**, 3079 (1991).
16. S. Kobayashi and co-workers, *Makromol. Chem., Macromol. Symp.* **54/55**, 509 (1992).
17. S. Kobayashi, S. Shoda, and K. Kashiwa, in J. F. Kennedy, G. O. Phillips, and P. A. Williams, eds., *Cellulosics: Chemical, Biochemical and Material Aspects*, Ellis Horwood, New York, 1993, pp. 23–28.
18. S. Kobayashi and S. Shoda, *Sci. Spectra* **10**, 52 (1997).
19. S. Shoda and S. Kobayashi, *Trends Polym. Sci.* **5**, 109 (1997).
20. S. Kobayashi and S. Shoda, in M. Kamachi and A. Nakamura, eds., *New Macromolecular Architecture and Functions*, Springer, Heidelberg, 1996, pp. 171–180.
21. S. Kobayashi, S. Shoda, M. J. Donnelly, and S. P. Church, in C. Bucke, ed., *Methods in Biotechnology, Vol. 10: Carbohydrate Biotechnology Protocols*, Human Press, Inc., Totowa, 1999, pp. 57–69.
22. S. Shoda and co-workers, *Macromol. Rapid Commun.* **15**, 751 (1994).
23. E. Okamoto and co-workers, *Cellulose* **4**, 161 (1997).
24. S. Kobayashi and co-workers, *Macromol. Chem. Phys.* **195**, 1319 (1994).
25. J. H. Lee, and co-workers, *Proc. Natl. Acad. Sci. USA* **91**, 7425 (1994).
26. S. Kobayashi and S. Shoda, *Int. J. Biol. Macromol.* **17**, 373 (1995).
27. S. Shoda and S. Kobayashi, *Macromol. Symp.* **99**, 179 (1995).
28. S. Kobayashi and co-workers, *J. Macromol. Sci., A: Pure Appl. Chem.* **33**, 1375 (1996).
29. S. Kobayashi and co-workers, *Biomacromolecules* **1**, 168 (2000).
30. E. J. Hehre, D. S. Genghof, and G. Okada, *Arch. Biochem. Biophys.* **142**, 382 (1971).
31. S. Kobayashi and co-workers, *Macromolecules* **25**, 3237 (1992).
32. S. Kitahata, Y. Yoshimura, and S. Okada, *Carbohyr. Res.* **159**, 303 (1987).
33. Y. Yoshimura, S. Kitahata, and S. Okada, *Carbohyr. Res.* **168**, 285 (1987).
34. S. Kobayashi, X. Wen, and S. Shoda, *Macromolecules* **29**, 2698 (1996).
35. M. Fujita, S. Shoda, and S. Kobayashi, *J. Am. Chem. Soc.* **120**, 6411 (1998).

36. S. Shoda, M. Fujita, and S. Kobayashi, *Trends Glycosci. Glycotech.* **10**, 279 (1998).
37. V. Moreau and H. Driguez, *J. Chem. Soc., Perkin Trans. 1* 525 (1996).
38. T. Kiyosada and co-workers, *Polym. Prepr. Jpn.* **44**, 660 (1995).
39. T. Kiyosada, S. Shoda, and S. Kobayashi, *Polym. Prepr. Jpn.* **44**, 1230 (1995).
40. S. Kobayashi, T. Kiyosada, and S. Shoda, *J. Am. Chem. Soc.* **118**, 13113 (1996).
41. T. Kiyosada, S. Shoda, and S. Kobayashi, *Macromol. Symp.* **132**, 415 (1998).
42. I. Tews and co-workers, *J. Am. Chem. Soc.* **119**, 7954 (1997).
43. J. Sakamoto and co-workers, *Macromolecules* **33**, 4155 (2000).
44. K. Makiguchi and co-workers, *Polym. Prepr. Jpn.* **45**, 2641 (1996).
45. T. Usui, H. Matsui, and K. Isobe, *Carbohydr. Res.* **203**, 65 (1990).
46. G. T. Cori and C. F. Cori, *J. Biol. Chem.* **135**, 733 (1940).
47. G. Ziegast and B. Pfannemüller, *Carbohydr. Res.* **160**, 185 (1987).
48. K. Kobayashi, S. Kamiya, and N. Enomoto, *Macromolecules* **29**, 8670 (1996).
49. V. von Braunühl, G. Jonas, and R. Stadler, *Macromolecules* **28**, 17 (1995).
50. S. Kamiya and K. Kobayashi, *Macromol. Chem. Phys.* **199**, 1589 (1998).
51. K. Loos and R. Stadler, *Macromolecules* **30**, 7641 (1997).
52. K. Akiyoshi and co-workers, *Macromol. Rapid Commun.* **20**, 112 (1999).
53. N. Enomoto and co-workers, *Anal. Chem.* **68**, 2798 (1996).
54. K. Loos, V. von Braunmühl, and R. Stadler, *Macromol. Rapid Commun.* **18**, 927 (1997).
55. J. Kadokawa and co-workers, *Chem. Commun.*, 449 (2001).
56. W. Treder, J. Thiem, and M. Schlingmann, *Tetrahedron Lett.* **27**, 5605 (1986).
57. S. Cottaz, C. Apparu, and H. Driguez, *J. Chem. Soc., Perkin Trans. 1* 2235 (1991).
58. W. Kullmann, *Enzymatic Peptide Synthesis*, CRC Press, Boca Raton, 1987.
59. L. A. E. Sluyterman and J. Wijdenes, *Biochim. Biophys. Acta* **289**, 194 (1972).
60. R. Jost and co-workers, *Helv. Chim. Acta* **63**, 375 (1980).
61. I. Komatsu, H. Uyama, and S. Kobayashi, *Polym. Prepr. Jpn.* **44**, 246 (1995).
62. G. Anderson and P. L. Luisi, *Helv. Chim. Acta* **62**, 488 (1979).
63. K. Aso, T. Uemura, and Y. Shiokawa, *Agric. Biol. Chem.* **52**, 2443 (1988).
64. T. Uemura and co-workers, *Agric. Biol. Chem.* **57**, 2277 (1990).
65. H. Uyama and co-workers, *Polym. Prepr. Jpn.* **45**, 217 (1996).
66. S. Matsumura and co-workers, *Macromol. Rapid Commun.* **20**, 7 (1999).
67. C.-H. Wong and co-workers, *J. Am. Chem. Soc.* **112**, 945 (1990).
68. Z. Zhong and co-workers, *J. Am. Chem. Soc.* **113**, 683 (1991).
69. J. S. Fruton and co-workers, *J. Biol. Chem.* **204**, 891 (1953).
70. C. P. Heinrich and J. S. Fruton, *Biochemistry* **7**, 3556 (1968).
71. H. Rehse and H. Ritter, *Makromol. Chem.* **189**, 529 (1988).
72. T. Kitazume, T. Sato, and T. Kobayashi, *Chem. Express* **3**, 1354 (1988).
73. S. Kobayashi and H. Uyama, in A. Steinbüchel, W. Babel, and T. Scheper, eds., *Advances in Biochemical Engineering/Biotechnology, Biopolyesters*, Springer-Verlag, Heidelberg, 2001, pp. 241–262.
74. A. Ajima and co-workers, *Biotechnol. Lett.* **7**, 303 (1985).
75. S. Matsumura and J. Takahashi, *Makromol. Chem., Rapid. Commun.* **7**, 369 (1986).
76. Y. Yoshida and co-workers, *Yukagaku* **44**, 328 (1995).
77. D. O'Hagan and N. A. Zaidi, *J. Chem. Soc., Perkin Trans 1* 2389 (1993).
78. D. O'Hagan and N. A. Zaidi, *Polymer* **35**, 3576 (1994).
79. X. Shuai and co-workers, *Eur. Polym. J.* **35**, 721 (1999).
80. K. Pavel and H. Ritter, *Makromol. Chem.* **192**, 1941 (1991).
81. O. Noll and H. Ritter, *Macromol. Rapid Commun.* **18**, 53 (1997).
82. O. Noll and H. Ritter, *Macromol. Rapid Commun.* **17**, 553 (1996).
83. D. O'Hagan and A. H. Parker, *Polym. Bull.* **41**, 519 (1998).
84. A. Szakács-Schmidt, L. Albert, and I. Kelemen-Horváth, *Biomed. Chromatogr.* **13**, 252 (1999).

85. Y. Ohya, T. Sugitou, and T. Ouchi, *J. Macromol. Sci., A: Pure. Appl. Chem.* **32**, 179 (1995).
86. D. Knani, A. L. Gutman, and D. H. Kohn, *J. Polym. Sci., Polym. Chem. Ed.* **31**, 1221 (1993).
87. H. Dong and co-workers, *Biotechnol. Lett.* **20**, 905 (1998).
88. A. L. Gutman and T. Bravdo, *J. Org. Chem.* **54**, 5645 (1989).
89. D. Knani and D. H. Kohn, *J. Polym. Sci., Polym. Chem. Ed.* **31**, 2887 (1993).
90. F. Binns and co-workers, *J. Chem. Soc., Perkin Trans 1* 899 (1993).
91. H. Uyama, K. Inada, and S. Kobayashi, *Chem. Lett.* 1285 (1998).
92. F. Binns and co-workers, *J. Polym. Sci., Polym. Chem. Ed.* **36**, 2069 (1998).
93. H. Uyama, K. Inada, and S. Kobayashi, *Polym. J.* **32**, 440 (2000).
94. F. Binns and co-workers, *J. Chem. Soc., Perkin Trans 1* 2671 (1999).
95. S. Kobayashi and co-workers, *Chem. Lett.* 105 (1997).
96. S. Suda, H. Uyama, and S. Kobayashi, *Proc. Jpn. Acad.* **75B**, 201 (1999).
97. L. E. Iglesias and co-workers, *Biotechnol. Tech.* **13**, 923 (1999).
98. Y.-Y. Linko, Z.-L. Wang, and J. Seppälä, *J. Biotechnol.* **40**, 133 (1995).
99. Y.-Y. Linko and J. Seppälä, *CHEMTECH* **26**(8), 25 (1996).
100. X. Y. Wu, Y.-Y. Linko, and J. Seppälä, *Ann. N. Y. Acad. Sci.* **864**, 399 (1998).
101. G. Mezoul and co-workers, *J. Polym. Sci., Polym. Chem. Ed.* **33**, 2691 (1995).
102. C. Berkane and co-workers, *Macromolecules* **30**, 7729 (1997).
103. J. S. Wallace and C. J. Morrow, *J. Polym. Sci., Polym. Chem. Ed.* **27**, 3271 (1989).
104. A. W. Jarvie, B. K. Samra, and A. J. Wiggett, *J. Chem. Res. (S)* 129 (1996).
105. Y.-Y. Linko, Z.-L. Wang, and J. Seppälä, *Biocatalysis* **8**, 269 (1994).
106. Y.-Y. Linko, Z.-L. Wang, and J. Seppälä, *Enzyme Microb. Technol.* **17**, 506 (1995).
107. E. M. Brazwell, D. Y. Filos, and C. J. Morrow, *J. Polym. Sci., Polym. Chem. Ed.* **33**, 89 (1995).
108. H. Uyama and S. Kobayashi, *Chem. Lett.* 1687 (1994).
109. H. Uyama, S. Yaguchi, and S. Kobayashi, *J. Polym. Sci., Polym. Chem. Ed.* **37**, 2737 (1999).
110. H. Uyama and co-workers, *ACS Symp. Ser.* **764**, 113 (2000).
111. A. K. Chaundhary, E. J. Beckman, and A. J. Russell, *Biotechnol. Bioeng.* **55**, 227 (1997).
112. A. K. Chaundhary and co-workers, *Biotechnol. Prog.* **13**, 318 (1997).
113. A. K. Chaundhary, E. J. Beckman, and A. J. Russell, *Biotechnol. Bioeng.* **59**, 428 (1998).
114. A. K. Chaundhary, E. J. Beckman, and A. J. Russell, *AIChE J.* **44**, 753 (1998).
115. V. D. Athawale and S. R. Gaonkar, *Biotechnol. Lett.* **16**, 149 (1994).
116. A. L. Margolin, J.-Y. Crenne, and A. M. Klibanov, *Tetrahedron. Lett.* **28**, 1607 (1987).
117. J. S. Wallace and C. J. Morrow, *J. Polym. Sci., Polym. Chem. Ed.* **27**, 2553 (1989).
118. B. J. Kline, E. J. Beckman, and A. J. Russell, *J. Am. Chem. Soc.* **120**, 9475 (1998).
119. H. Uyama, K. Inada, and S. Kobayashi, *Macromol. Rapid Commun.* **20**, 171 (1999).
120. H. Uyama and co-workers, *Chem. Lett.* 800 (2000).
121. D. R. Patil, D. G. Rethwisch, and J. S. Dordick, *Biotechnol. Bioeng.* **37**, 639 (1991).
122. J. S. Dordick, *Ann. N. Y. Acad. Sci.* **672**, 352 (1992).
123. O.-J. Park, D.-Y. Kim, and J. S. Dordick, *Biotechnol. Bioeng.* **70**, 208 (2000).
124. S. Geresh and Y. Gilboa, *Biotechnol. Bioeng.* **36**, 270 (1990).
125. S. Geresh and co-workers, *Polym. Engi. Sci.* **33**, 311 (1993).
126. S. Geresh and Y. Gilboa, *Biotechnol. Bioeng.* **37**, 883 (1991).
127. G. Mezoul and co-workers, *Macromol. Rapid Commun.* **16**, 613 (1995).
128. G. Mezoul and co-workers, *Macromol. Chem. Phys.* **197**, 3581 (1996).
129. H. Uyama, S. Yaguchi, and S. Kobayashi, *Polym. J.* **31**, 380 (1999).
130. G. Mezoul and co-workers, *Polym. Bull.* **36**, 541 (1996).
131. H. G. Park, H. N. Chang, and J. S. Dordick, *Biocatalysis* **11**, 263 (1994).
132. R. L. Rodney and co-workers, *Biotechnol. Bioeng.* **65**, 485 (1999).

133. A. J. Mesiano, E. J. Beckman, and A. J. Russell, *Biotechnol. Prog.* **16**, 64 (2000).
134. A. K. Chaudhary, E. J. Beckman, and A. J. Russell, *J. Am. Chem. Soc.* **117**, 3728 (1995).
135. S. Kobayashi and H. Uyama, *Makromol. Chem., Rapid Commun.* **14**, 841 (1993).
136. H. Uyama, S. Wada, and S. Kobayashi, *Chem. Lett.* 893 (1999).
137. S. Matsumura and co-workers, *Macromol. Rapid Commun.* **19**, 295 (1998).
138. S. Matsumura and co-workers, *Macromol. Symp.* **144**, 219 (1999).
139. S. Namekawa, H. Uyama, and S. Kobayashi, *Polym. J.* **28**, 730 (1996).
140. S. Matsumura and co-workers, *Biotechnol. Lett.* **18**, 1041 (1996).
141. Y. Y. Svirkin and co-workers, *Macromolecules* **29**, 4591 (1996).
142. G. A. R. Nobes, R. J. Kazlauskas, and R. H. Marchessault, *Macromolecules* **29**, 4829 (1996).
143. S. Matsumura and co-workers, *Macromolecules* **31**, 6444 (1998).
144. H. Dong and co-workers, *Ann. N. Y. Acad. Sci.* **864**, 263 (1998).
145. W. Xie and co-workers, *Macromolecules* **30**, 6997 (1997).
146. Y. Suzuki, and co-workers, *Chem. Lett.* 318 (2000).
147. S. Matsumura and co-workers, *Chem. Lett.* 795 (1996).
148. S. Matsumura, H. Beppu, and K. Toshima, *Chem. Lett.* 249 (1999).
149. H. Uyama and S. Kobayashi, *Chem. Lett.* 1149 (1993).
150. S. Kobayashi and co-workers, *Macromol. Chem. Phys.* **199**, 1729 (1998).
151. H. Uyama and co-workers, *Chem. Lett.* 1109 (1997).
152. R. T. MacDonald and co-workers, *Macromolecules* **28**, 73 (1995).
153. L. A. Henderson and co-workers, *Macromolecules* **29**, 7759 (1996).
154. H. Dong and co-workers, *J. Polym. Sci., Polym. Chem. Ed.* **37**, 1265 (1999).
155. A. Córdova and co-workers, *Polymer* **39**, 6519 (1998).
156. F. Deng and R. A. Gross, *Int. J. Biol. Macromol.* **25**, 153 (1999).
157. A. Kumar and R. A. Gross, *Biomacromolecules* **1**, 133 (2000).
158. S. Kobayashi, H. Uyama, and T. Takamoto, *Biomacromolecules* **1**, 3 (2000).
159. K. Küllmer and co-workers, *Macromol. Rapid Commun.* **19**, 127 (1998).
160. S. Kobayashi, H. Uyama, and S. Namekawa, *Polym. Degrad. Stab.* **59**, 195 (1998).
161. H. Nishida and co-workers, *J. Polym. Sci., Polym. Chem. Ed.* **38**, 1560 (2000).
162. S. Kobayashi and co-workers, *Macromolecules* **31**, 5655 (1998).
163. H. Uyama, K. Takeya, and S. Kobayashi, *Bull. Chem. Soc. Jpn.* **68**, 56 (1995).
164. H. Uyama and S. Kobayashi, in M. Yalpani, ed., *Biomedical Functions and Biotechnology of Natural and Artificial Polymers*, ATL Press, Schrewsbury, 1996, pp. 5–15.
165. H. Uyama and co-workers, *Macromolecules* **28**, 7046 (1995).
166. H. Uyama, and co-workers, *Acta Polymerica* **47**, 357 (1996).
167. K. S. Bisht and co-workers, *Macromolecules* **30**, 2705 (1997).
168. S. Namekawa, H. Uyama, and S. Kobayashi, *Proc. Jpn. Acad.* **74B**, 65 (1998).
169. S. Namekawa, H. Uyama, and S. Kobayashi, *Polym. J.* **30**, 269 (1998).
170. S. Kobayashi and H. Uyama, *Macromol. Symp.* **144**, 237 (1999).
171. S. Namekawa, H. Uyama, and S. Kobayashi, *Int. J. Biol. Macromol.* **25**, 145 (1999).
172. H. Uyama, S. Namekawa, and S. Kobayashi, *Polym. J.* **29**, 299 (1997).
173. M. Runge, D. O'Hagan, and G. Haufe, *J. Polym. Sci., Polym. Chem. Ed.* **38**, 2004 (2000).
174. H. Uyama, K. Takeya, and S. Kobayashi, *Proc. Acad. Jpn.* **69B**, 203 (1993).
175. H. Kikuchi, H. Uyama, and S. Kobayashi, *Macromolecules* **33**, 8971 (2000).
176. S. Namekawa, H. Uyama, and S. Kobayashi, *Macromol. Chem. Phys.* **202**, 801 (2001).
177. S. Namekawa, H. Uyama, and S. Kobayashi, *Biomacromolecules* **1**, 335 (2000).
178. H. Uyama and co-workers, *Chem. Lett.* 107 (1996).
179. S. Noda and co-workers, *Biotechnol. Lett.* **19**, 307 (1997).
180. H. Uyama, S. Suda, and S. Kobayashi, *Acta Polym.* **49**, 700 (1998).
181. A. Córdova, T. Iversen, and K. Hult, *Polymer* **40**, 6709 (1999).

182. K. S. Bisht, and co-workers, *J. Am. Chem. Soc.* **120**, 1363 (1998).
183. K. S. Bisht, R. A. Gross, and A. L. Cholli, *Appl. Spectrosc.* **52**, 1472 (1998).
184. A. Córdova, T. Iversen, and K. Hult, *Macromolecules* **31**, 1040 (1998).
185. A. Córdova and co-workers, *J. Am. Chem. Soc.* **120**, 13521 (1998).
186. J. Li and co-workers, *Macromolecules* **32**, 2789 (1998).
187. H. Uyama, H. Kikuchi, and S. Kobayashi, *Chem. Lett.* 1047 (1995).
188. H. Uyama, H. Kikuchi, and S. Kobayashi, *Bull. Chem. Soc. Jpn.* **70**, 1691 (1997).
189. S. Matsumura, K. Mabuchi, and K. Toshima, *Macromol. Rapid Commun.* **18**, 477 (1997).
190. S. Matsumura, K. Mabuchi, and K. Toshima, *Macromol. Symp.* **130**, 285 (1997).
191. S. Müller, H. Uyama, and S. Kobayashi, *Chem. Lett.* 1317 (1999).
192. F. Binns and A. Taylor, *Tetrahedron* **47**, 12929 (1995).
193. J. Wodzinska and co-workers, *J. Am. Chem. Soc.* **118**, 6319 (1996).
194. T. U. Gerngross and D. P. Martin, *Proc. Natl. Acad. Sci. USA* **92**, 6279 (1995).
195. G. A. R. Nobes and co-workers, *Macromol. Rapid Commun.* **21**, 77 (2000).
196. D. P. Martin, S. Zhang, L. Su, and R. W. Lenz, in A. Steinbüchel, ed., *Biochemical Principles and Mechanisms of Biosynthesis and Biodegradation of Polymers*, Wiley-VCH, Weinheim, 1999, pp. 168–175.
197. R. W. Lenz and co-workers, *Int. J. Biol. Macromol.* **25**, 55 (1999).
198. L. Su and co-workers, *Macromolecules* **33**, 229 (2000).
199. R. Jossek, R. Reichelt, and A. Steinbüchel, *Appl. Microbiol. Biotechnol.* **49**, 258 (1998).
200. R Jossek and A. Steinbüchel, *FEMS Microbiol. Lett.* **168**, 319 (1998).
201. T. Lalot, M. Brigodiot, and E. Marechal, *Polym. Bull.* **26**, 55 (1991).
202. K. Pavel and H. Ritter, *Macromol. Chem.* **193**, 323 (1992).
203. H. Ritter, *Trends Polym. Sci.* **1**, 171 (1993).
204. F. F. Bruno and co-workers, *Macromolecules* **28**, 8881 (1995).
205. A. W. P. Jarvie, N. Overton, and C. B. St Pourcain, *J. Chem. Soc., Chem. Commun.* 177 (1998).
206. D. A. Abramowicz and C. R. Keese, *Biotechnol. Bioeng.* **33**, 149 (1989).
207. S. Matsumura, S. Harai, and K. Toshima, *Proc. Jpn. Acad.* **75B**, 117 (1999).
208. S. Matsumura, S. Harai, and K. Toshima, *Macromol. Chem. Phys.* **201**, 1632 (2000).
209. R. L. Rodney and co-workers, *Biotechnol. Bioeng.* **62**, 259 (1999).
210. S. Matsumura, K. Tsukuda, and K. Toshima, *Macromolecules* **30**, 3122 (1997).
211. S. Kobayashi, H. Kikuchi, and H. Uyama, *Macromol. Rapid Commun.* **18**, 575 (1997).
212. K. S. Bisht and co-workers, *Macromolecules* **30**, 7735 (1997).
213. T. F. Al-Azemi and K. S. Bisht, *Macromolecules* **32**, 6536 (1999).
214. S. Namekawa and co-workers, *Macromol. Chem. Phys.* **201**, 261 (2000).
215. S. Matsumura, K. Tsukuda, and K. Toshima, *Int. J. Biol. Macromol.* **25**, 161 (1999).
216. Y. Feng and co-workers, *Macromol. Rapid Commun.* **20**, 88 (1999).
217. Y. Feng and co-workers, *Macromol. Chem. Phys.* **200**, 1506 (1999).
218. J. Wen and R.-X. Zhuo, *Macromol. Rapid Commun.* **19**, 641 (1998).
219. J. S. Dordick, M. A. Marletta, and A. M. Klibanov, *Biotechnol. Bioeng.* **30**, 31 (1987).
220. H. Uyama and co-workers, *Chem. Lett.* 423 (1994).
221. H. Uyama and co-workers, *Bull. Chem. Soc. Jpn.* **69**, 189 (1996).
222. H. Uyama and co-workers, *Macromol. Reports* **A 32**, 649 (1995).
223. T. Oguchi and co-workers, *Macromol. Rapid Commun.* **20**, 401 (1999).
224. T. Oguchi and co-workers, *Bull. Chem. Soc. Jpn.* **73**, 1389 (2000).
225. J. A. Akkara, K. J. Senecal, and D. L. Kaplan, *J. Polym. Sci., Polym. Chem. Ed.* **29**, 1561 (1991).
226. M. Ayyagari, J. A. Akkara, and D. L. Kaplan, *Acta Polym.* **47**, 193 (1996).
227. J. A. Akkara, D. L. Kaplan, V. T. John, and S. K. Tripathy, in Ref. 7, pp. 2115–2125.

228. H. Kurioka and co-workers, *Macromol. Rapid Commun.* **15**, 507 (1994).
229. H. Uyama and co-workers, *J. Polym. Sci., Polym. Chem. Ed.* **35**, 1453 (1997).
230. H. Uyama and co-workers, *Bull. Chem. Soc. Jpn.* **68**, 3209 (1995).
231. M. S. Ayyagari and co-workers, *Macromolecules* **28**, 5192 (1995).
232. R. Farrell and co-workers, *J. Environ. Polym. Degrad.* **6**, 115 (1998).
233. K. Asakura and co-workers, *J. Jpn. Oil Chem. Soc.* **42**, 656 (1993).
234. H. Tonami and co-workers, *Macromol. Chem. Phys.* **200**, 2365 (1999).
235. K. Ryu, D. R. Stafford, and J. S. Dordick, *ACS Symp. Ser.* **389**, 141 (1989).
236. K. Ryu and co-workers, *Biotechnol. Bioeng.* **42**, 807 (1993).
237. W. Liu and co-workers, *J. Polym. Sci., Polym. Chem. Ed.* **33**, 2339 (1995).
238. Y.-P. Xu, G.-L. Huang, and Y.-T. Yu, *Biotechnol. Bioeng.* **47**, 117 (1995).
239. W.-H. Liu and co-workers, *Ann. N. Y. Acad. Sci.* **750**, 138 (1995).
240. A. M. Rao and co-workers, *Biotechnol. Bioeng.* **41**, 531 (1993).
241. J. A. Akkara and co-workers, *Biomimetics* **2**, 331 (1994).
242. N. S. Kommareddi and co-workers, *Appl. Biochem. Biotechnol.* **51/52**, 241 (1995).
243. S. Banerjee and co-workers, *Ind. Eng. Chem. Res.* **35**, 3100 (1996).
244. F. F. Bruno and co-workers, *Ind. Eng. Chem. Res.* **34**, 4009 (1995).
245. F. F. Bruno and co-workers, *Langmuir* **11**, 889 (1995).
246. A. S. Hay and co-workers, *J. Am. Chem. Soc.* **81**, 6335 (1959).
247. A. S. Hay, *J. Polym. Sci., Polym. Chem. Ed.* **36**, 505 (1998).
248. R. Ikeda and co-workers, *Macromolecules* **29**, 8702 (1996).
249. R. Ikeda, H. Uyama, and S. Kobayashi, *Macromolecules* **29**, 3053 (1996).
250. R. Ikeda and co-workers, *Polym. International* **47**, 295 (1998).
251. H. Uyama and S. Kobayashi, *CHEMTECH* **29**(10), 22 (1999).
252. H. Kurioka, H. Uyama, and S. Kobayashi, *Polym. Prepr. Jpn.* **45**, 218 (1996).
253. S. Dubey, D. Singh, and R. A. Misra, *Enz. Microb. Technol.* **23**, 432 (1998).
254. R. Premachandran and co-workers, *Chem. Mater.* **9**, 1342 (1997).
255. R. S. Premachandran and co-workers, *Macromolecules* **29**, 6452 (1996).
256. L. Wang and co-workers, *J. Polym. Sci., Polym. Chem. Ed.* **31**, 2855 (1993).
257. M. Aizawa and L. Wang, in Ref. 7, pp. 2107–2115.
258. S. Chen and co-workers, *Ann. N.Y. Acad. Sci.* **864**, 250 (1998).
259. S. Kobayashi and co-workers, *Macromol. Chem. Phys.* **199**, 777 (1998).
260. S. Kobayashi, H. Kurioka, and H. Uyama, *Macromol. Rapid Commun.* **17**, 503 (1996).
261. K. S. Alva and co-workers, *Macromol. Rapid Commun.* **18**, 133 (1997).
262. K. S. Alva and co-workers, *J. Appl. Polym. Sci.* **70**, 1257 (1998).
263. S. Chen and co-workers, *Ann. N.Y. Acad. Sci.* **864**, 238 (1998).
264. P. Wang and co-workers, *J. Am. Chem. Soc.* **117**, 12885 (1995).
265. P. Wang and co-workers, *Polymer* **39**, 123 (1998).
266. H. Tonami and co-workers, *Macromol. Chem. Phys.* **200**, 1998 (1999).
267. J. Kim and co-workers, *Anal. Chim. Acta* **370**, 251 (1998).
268. P. Wang and J. S. Dordick, *Macromolecules* **31**, 941 (1998).
269. T. Fukuoka and co-workers, *Polym. Prepr. Jpn.* **49**, 1034 (2000).
270. R. Sarma and co-workers, *Mater. Sci. Engi.* **C4**, 189 (1996).
271. K. A. Marx, T. Zhou, and R. Sarma, *Biotechnol. Prog.* **15**, 522 (1999).
272. H. Uyama and co-workers, *Macromolecules* **31**, 554 (1998).
273. *Chem. Eng. News* **46** (Oct. 5, 1998).
274. H. Tonami and co-workers, *Biomacromolecules* **1**, 149 (2000).
275. R. Ikeda and co-workers, *Polym. J.* **32**, 589 (2000).
276. K. S. Alva and co-workers, *J. Macromol. Sci., A: Pure Appl. Chem.* **34**, 665 (1997).
277. R. Ikeda and co-workers, *J. Macromol. Sci., A: Pure Appl. Chem.* **37**, 983 (2000).
278. H. Uyama, H. Kurioka, and S. Kobayashi, *Chem. Lett.* 795 (1995).
279. H. Kurioka, H. Uyama, and S. Kobayashi, *Polym. J.* **30**, 526 (1998).

280. H. Uyama, H. Kurioka, and S. Kobayashi, *Colloids and Surfaces A: Physicochem. Eng. Aspects* **153**, 189 (1999).
281. H. Uyama, H. Kurioka, and S. Kobayashi, *Polym. J.* **27**, 190 (1997).
282. K. Freudenberg, *Science* **148**, 595 (1965).
283. M. Tanahashi and T. Higuchi, *Wood. Res.* **67**, 29 (1981).
284. S.-Y. Guan, J. Mlynár, and S. Sarkanen, *Phytochemistry* **45**, 911 (1997).
285. K. Okusa, T. Miyakoshi, and C.-L. Chen, *Horzforschung* **50**, 15 (1996).
286. O. Milstein and co-workers, *J. Biotechnol.* **30**, 37 (1993).
287. A. Guerra and co-workers, *Enz. Microb. Technol.* **26**, 315 (2000).
288. J. L. Popp, T. K. Kirk, and J. S. Dordick, *Enzyme Microb. Technol.* **13**, 964 (1991).
289. A. M. Blinkovsky and J. S. Dordick, *J. Polym. Sci., Polym. Chem. Ed.* **31**, 1839 (1993).
290. J. Liu, Y. Weiping, and T. Lo, *Electro. J. Biotechnol.* **2**, 82 (1999).
291. A. M. Blinkovsky and co-workers, *Appl. Biochem. Biotech.* **49**, 153 (1994).
292. S. Kobayashi and co-workers, *Chem. Lett.* 1214 (2000).
293. R. Ikeda and co-workers, *Proc. Acad. Jpn.* **76B**, 155 (2000).
294. M. Terada, H. Oyabu, and Y. Aso, *J. Jpn. Soc. Colour Mater.* **66**, 681 (1994).
295. J. A. Akkara, P. Salapu, and D. L. Kaplan, *Ind. J. Chem.* **31B**, 855 (1992).
296. J. A. Akkara, F. J. Aranda, D. V. G. L. N. Rao, and D. L. Kaplan, in P. N. Prasad, ed., *Frontiers of Polymers and Advanced Materials*, Plenum Press, New York, 1994, pp. 531–537.
297. L. A. Samuelson and co-workers, *Macromolecules* **31**, 4376 (1998).
298. W. Liu and co-workers, *J. Am. Chem. Soc.* **121**, 71 (1999).
299. W. Liu and co-workers, *J. Am. Chem. Soc.* **121**, 11345 (1999).
300. M. Aizawa and co-workers, *J. Biotechnol.* **14**, 301 (1990).
301. S. Kobayashi, I. Kaneko, and H. Uyama, *Chem. Lett.* 393 (1992).
302. D. Ichinose and co-workers, *J. Polym. Chem., Polym. Chem. Ed.* **36**, 2593 (1998).
303. K. S. Alva and co-workers, *Macromol. Rapid Commun.* **17**, 859 (1996).
304. E. Arias-Marín and co-workers, *Polym. Bull.* **37**, 581 (1996).
305. K. S. Alva and co-workers, *Macromolecules* **30**, 4024 (1997).
306. C. Goretzki and H. Ritter, *Macromol. Chem. Phys.* **199**, 1019 (1998).
307. Y. Zhu and co-workers, *J. Mol. Catal. B* **4**, 33 (1998).
308. H. Uyama and co-workers, *Macromol. Rep. A* **31**, 421 (1994).
309. G. F. Payne, M. V. Chaubal, and T. A. Barbari, *Polymer* **37**, 4643 (1996).
310. G. Kumar and co-workers, *Polymer* **41**, 2157 (2000).
311. G. Kumar, P. J. Smith, and G. F. Payne, *Biotechnol. Bioeng.* **63**, 154 (1999).
312. K. Yamada and co-workers, *Biomacromolecules* **1**, 252 (2000).
313. R. A. A. Muzzarelli and co-workers, *Carbohydr. Polym.* **24**, 295 (1994).
314. L. Shao and co-workers, *Enz. Microb. Technol.* **25**, 660 (1999).
315. Y. M. Stuchell and J. M. Krochta, *J. Food Sci.* **59**, 1332 (1994).
316. T. Michon and co-workers, *Biotechnol. Bioeng.* **63**, 449 (1999).
317. D. Sheng and M. H. Gold, *Eur. J. Biochem.* **259**, 626 (1999).
318. H. Higashimura and co-workers, *J. Am. Chem. Soc.* **120**, 8529 (1998).
319. H. Higashimura and co-workers, *Macromolecules* **33**, 1986 (2000).
320. H. Higashimura and co-workers, *Polym. Adv. Technol.* **11**, 733 (2000).
321. H. Higashimura and co-workers, *J. Polym. Sci., Polym. Chem. Ed.* **38**, 4792 (2000).
322. H. Higashimura and co-workers, *Macromol. Rapid Commun.* **21**, 1121 (2000).
323. H. Higashimura and co-workers, *Appl. Catal. A* **194/195**, 427 (2000).
324. H. Higashimura and co-workers, *J. Mol. Catal. A* **155**, 201 (2000).
325. J. A. Akkara and co-workers, *Macromolecules* **33**, 2377 (2000).
326. H. Tonami and co-workers, *J. Macromol. Sci., A: Pure Appl. Chem.* **36**, 719 (1999).
327. H. Tonami and co-workers, *Polym. Bull.* **42**, 125 (1999).
328. R. Ikeda and co-workers, *Macromol. Rapid Commun.* **21**, 496 (2000).

329. T. Tsujimoto and co-workers, *Chem. Lett.* 1122 (2000).
330. R. Ikeda and co-workers, *Macromolecules* **33**, 6648 (2000).
331. R. A. Derango and co-workers, *Biotechnol. Tech.* **6**, 523 (1992).
332. R. Ikeda and co-workers, *Macromol. Rapid Commun.* **19**, 423 (1998).
333. H. Iwata and co-workers, *J. Polym. Chem., Polym. Chem. Ed.* **29**, 1217 (1991).
334. O. Emery and co-workers, *J. Polym. Chem., Polym. Chem. Ed.* **35**, 3331 (1997).
335. T. Lalot, M. Brigodiot, and E. Maréchal, *Polym. Int.* **48**, 288 (1999).
336. D. Teixeira and co-workers, *Macromolecules* **32**, 70 (1999).
337. C. Mai, O. Milstein, and A. Hüttermann, *Appl. Microb. Biotechnol.* **51**, 527 (1999).

SHIRO KOBAYASHI
HIROSHI UYAMA
Kyoto University

ETHYLENE POLYMERS, CHLOROSULFONATED

Introduction

Chlorosulfonated polyethylene (CSM) [68037-39-8] describes a group of curable, halogenated olefin polymers, first introduced to the rubber industry by E. I. du Pont de Nemours and Co. in 1951 (1–5) under the trade name of Hypalon. They contain pendant chlorine and sulfonyl chloride groups and vary in consistency from soft and elastomeric to hard and plastic. The chemical structure may be represented by

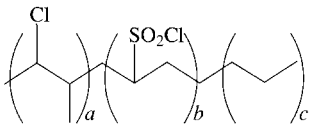

Typical ratio a::b::c = 31:1:108

Although the base resin is usually polyethylene, other base resins, ie, polypropylene (6), ethylene propylene copolymers (7), and polymers containing additional functionality (ie, vinyl acetate, acrylic or methacrylic acid, and maleic anhydride graft) have been chlorinated and chlorosulfonated commercially. This family of polymers is widely used in rubber and adhesive industries because of the valuable properties that can be achieved when properly compounded and vulcanized.

Chlorosulfonated olefin polymers may be prepared in polymer melts (8), as slurries in a nonsolvent medium (9,10), or in a fluidized bed (11), but are usually prepared by the interaction of ethylene polymers or copolymers with

Encyclopedia of Polymer Science and Technology. Copyright John Wiley & Sons, Inc. All rights reserved.

chlorosulfonating agents in a homogeneous solution. Substitution of chlorine atoms onto the polymer chains interrupts the regularity of the chain structure so that the crystalline polymer becomes semiplastic to elastomeric and eventually hard and brittle as the substitution level increases. Introduction of the sulfonyl chloride group provides a cross-linking site for vulcanization with conventional rubber technology. These polymers are known for advantages in combined heat and oil resistance compared with most other synthetic elastomers. They also offer good mechanical toughness and are superior in color retention, weatherability, flame resistance, abrasion resistance, and resistance to corrosive chemicals. In addition, it can be made to adhere well to metal and most fabric reinforcements. Chlorination of the polymer, to sufficient levels, also provides for solubility in common solvents, and the sulfonyl chloride group or other functionality offers unique advantages in specific adhesion to various substrates. This combination provides for tough, abrasion-, chemical-, and oil-resistant coatings and adhesives. The properties of these polymers vary widely with the selection of the base resin, chlorine and sulfonyl chloride content, or other functionality.

Olefin polymers containing only pendent chlorine groups may also be prepared using this procedure. The properties are very similar to those of CSMs in appearance and properties; however, the lack of sulfonyl chloride group makes them more difficult to cure and less flexible in compounding techniques.

Polymer Properties

Polyethylene. Chlorosulfonated polyethylene is one of a few examples of a class of polymers, which is formed by chemical substitution on the backbone chain of a preformed polymer. In addition, starting from one specific polyethylene, a whole new series of polymers result, whose properties depend on the degree and randomness of chlorine substitution. So, it is not surprising that the properties of the modified polymer also depend, to a large extent, on those of the precursor olefin resin.

Polyethylene is a saturated hydrocarbon and shows, in general, properties expected for high molecular weight paraffin. As such, it exhibits very low chemical reactivity at low temperatures, but impurities, such as residual catalyst fragments, may cause oxidative or free-radical attack, particularly at elevated temperatures. Oxidative attack is prevented by the addition of small amounts of antioxidants, ie, hindered phenol or alkyl phosphites. An excess of these residual antioxidants may inhibit the chlorosulfonation reaction. The structure and morphological aspects of polyethylene are tied to the synthesis technology. A large variety of synthesis processes are used in polyethylene manufacture, including high pressure polymerization in supercritical ethylene (known as “free-radical” or “high pressure” process) and solution-, slurry-, or gas-phase polymerization using Ziegler-type catalysts (known as “low pressure” or “linear” process) (12). Control of the properties is achieved by controlling molecular weight, molecular weight distribution, and density. This is accomplished by choice of catalyst, reactor configuration, and temperature profile. These structural properties are then carried over into those of the resulting chlorosulfonated polymer, since neither chain scission nor cross-linking

takes place during the chlorosulfonation process. Molecular weight and molecular weight distribution of the polymer chains then have great influence on mechanical and rheological properties of the polyethylene resin as well as the modified polymer. The average molecular weights of commercial polyethylenes may vary from about 500 for polyethylene waxes to $>10^6$ for ultrahigh molecular weight polyethylene grades.

The presence, shape, and length of side branches as well as the distribution of branches along the molecular chain also significantly modify physical properties of solid polyethylene polymers and their melts.

Depending on the catalyst system and polymerization conditions employed, a wide variation in the degree and type of chain branch is observed. In high pressure, free-radical polymerization (low density polyethylene, LDPE), these branches may be linear or branched and may vary in length from 1 to 8 (short-chain branching) or up to several thousand carbon atoms (long-chain branching). The broad molecular weight distribution in these polymers is mostly because of the varying length of chain branches. In low pressure, catalytic polymerization, polymer chains are essentially absent of branching and are termed as linear or high density polyethylene (HDPE) (13).

Alternatively, significant short-chain branching may be introduced deliberately by copolymerization of ethylene with α-olefins, ie, butene, hexene, octene, etc. Branching is controlled by the type of catalyst, α-olefin type, and composition. Metalathene polymerization catalysts give a more select distribution of branching than Ziegler catalysts. (13) These polymers are called linear low density polyethylene (LLDPE).

According to ASTM D1248, polyethylene resins are divided into various classifications based on properties. Two of the most easily measured characteristics of polyethylene are melt index and density. The density determines the type of resin and melt index determines the category. However, the shape of molecular weight distribution curve has an important bearing on the properties of both the polyethylene and the resultant chlorinated polymer. The molecular weight distribution is usually referred to as the polydispersity index or weight to number-average molecular weight ratio. Polyethylene resins are generally categorized as narrow, intermediate, or broad based on these indices, but the distribution may also be bimodal and/or skewed toward the high or low portions of the distribution curve (13). The shape function of the distribution curve may be determined by several methods; however, it is most easily determined by gel-permeation chromatography (gpc). Polydispersity index can be readily calculated from gpc data, but is also indicated by the melt flow ratio (MFR), which is the ratio of two melt indexes determined at different melt pressures. The range of MFR may vary from 25 to 150 for commercial polyethylene resins. Another term often used to describe molecular weight distribution is *stress exponent*, which is defined as the slope of the melt flow ratio curve over a specified range.

Because of its exceptional symmetry, the polyethylene molecule fits so readily into a crystalline lattice, in spite of its lack of molar cohesion, that its tendency is to crystallize into spherulite structures on relaxation rather than revert to a disordered state. However, the degree and type of chain branching that interrupts the geometrical regularity of the polyethylene molecular structure causes a local

reluctance to form crystallites so that both crystalline and amorphous regions may be present. The density of the polyethylene is a function of the degree of crystallinity. For HDPE, this crystallinity reaches levels of about 80%. The crystallinity of LLDPE is usually below 40–45% (13). So, the size, structures, and level of the crystallites for a given polymer depend on the degree, type, and uniformity of branching.

In order to convert these crystalline polymers into elastomers it is necessary to eliminate most of these areas of crystallinity. This may be accomplished by increasing the concentration of α-olefin comonomer as in the case of ethylene–propylene elastomers; however, these polymers are similar to polyethylene in chemical properties.

Chlorosulfonated Polyethylene. The process of modifying polyethylene with randomly spaced chlorine atoms represents a change in entropy conditions. Although adding chlorine to the polymer chain greatly increases its polarity and thus its molar cohesion, the increase in bulk, because of its large volume, prevents temporary chain alignment by external tension, thus reducing the entropy factor. As chlorine attachments to the chain are made, the adjacent chain segments, not held in place by crystallites, begin to exhibit rapid local Brownian motions, typical of molecules in the liquid state as may be seen in the polyethylene melt. This rapid internal Brownian movement, together with the slow external Brownian movement, or movement of entire polymer chains, due to high molecular weight, creates the captive liquid or rubbery state.

Incorporation of chlorine atoms onto the polyolefin backbone then causes sufficient molecular irregularity to break up crystalline chain segments of the base resin. As the chlorine content is increased, the crystallites gradually disappear and, eventually, the thermoplastic material becomes amorphous and behaves as an elastomer because of the inherent flexibility of the polyethylene chain. Chlorosulfonated polyethylene resins made in slurry or fluidized beds generally have a more blocky chlorine distribution, both intramolecularly and intermolecularly, so that the same degree of amorphous characteristic is not always achieved. The increase in molar cohesion, by the addition of chlorine atoms, increases the polymer solubility parameter, and thus decreases its miscibility with paraffinic and aromatic oils. So, as chlorine content of the polymer increases, resistance to swelling effect of oil increases.

The added pendant chlorine groups create intermolecular friction, due to their polar nature, binding chains together, particularly at high substitution levels, in a rigid network, reducing free volume, increasing short-range entanglement, and thereby increasing the brittle point. The glass-transition temperature (T_g), which is closely related to the brittle point, is then a function of the chlorine content ranging from -35 to -40°C at about 15–20% chlorine to $>80^\circ$C at chlorine levels above 65%. The low chlorine polymers retain some of the polyethylene crystallinity and thus yield products that are thermoplastic. At the higher chlorine substitution extremes polymer properties are achieved, which may be generally associated with relatively high temperature rigid plastic material. In between these extremes range a whole series of materials with intermediate properties, which depend on the level of chlorination and the randomness of the chlorine placement along the chain. In the range of 25–35 % chlorine, there is a series of polymers along a more random chlorination line, whose transition

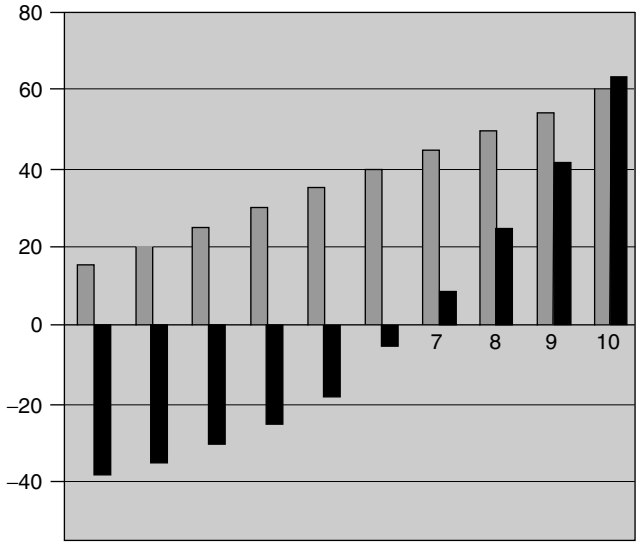

Fig. 1. Chlorine content vs T_g for CSM with random chlorine substitution. ▒ Chlorine %; ■ T_g, °C.

temperature occurs in the range of −20 to −30°C. Glass-transition temperatures in this range represent materials that behave like elastomers. The glass-transition temperature of a chlorinated polyethylene polymer may be estimated by considering that it is a copolymer of ethylene and vinyl chloride. It then follows the relationship (14)

$$T_g = \Sigma M_i T_{gi}$$

where M_i is the mole fraction of the ith component, T_g the glass-transition temperature of the copolymer in Kelvin, and T_{gi} the glass-transition temperature of the homopolymer of the ith component, ie,

$$T_g = M_1 T_{g1} + M_2 T_{g2}$$

where T_{g1} is the glass-transition temperature of polyethylene (−80°C), M_1 the mole fraction of ethylene, T_{g2} the glass-transition temperature of poly(vinyl chloride) (75°C), and M_2 the mole fraction of poly(vinyl chloride).

At higher chlorine levels, where vicinal chlorine groups may occur, one may also include a term for poly(vinylidine chloride) (T_g = 226°C). The relationship of glass-transition temperature to chlorine content for a CSM with random chlorine substitution is shown in Figure 1.

The optimum chlorine content for an amorphous elastomer is the minimum amount required to destroy the crystalline segments. This optimum level depends on the number and types of crystallites in the polyethylene precursor, the randomness of chlorine distribution along the chain, and chain-to-chain distribution. So, for HDPE, the optimum chlorine level for elastomeric properties is at about 35%

with even distribution along the chain. For low density base resin, the optimum chlorine level is about 28–30%.

The flow behavior of CSM polymers under manufacturing and finished product processing conditions is of primary practical importance in their commercial acceptance. These properties are functions of the starting polyethylene parameters and the chlorine content and distribution. For molten polymers and for elastomers, viscosities differ with deformation conditions, and elastic effects accompany the flow properties. Hence, both polymer melts and elastomers are generally viscoelastic and greatly influenced by polymer chain lengths and by the distribution of chain lengths within the whole polymer. Melt index, as described earlier, is a low average shear viscosity measurement (avg. shear rate $= 4\ s^{-1}$) measured at 190°C. It serves the polyethylene industry as an imperical measure of processing control parameters. It is not a fundamental quantity, however, and its meaning is often ambiguous, but its measurement is convenient and well entrenched in the industry as a prediction of processing characteristics. Although it is considered to be mostly responsive to the weight-average molecular weight of the polyethylene, in most cases it is not because it is measured in the non-Newtonian region of the flow curve. The shape and slope of the curve in this region are strongly effected by the molecular weight distribution and this effect can be overriding.

For the same reason of convenience and low cost, Mooney viscosity (avg. shear rate $= 1.6\ s^{-1}$), usually measured at 100°C, is an imperical control for the rubber industry. It, too, is not a fundamental quantity and is usually measured in the non-Newtonian part of the flow curve.

The Mooney viscosity of CSM is also related to the weight-average molecular weight of the starting polyethylene and the chlorine content. However, differences in molecular weight distribution, and especially in the shape function of the distribution curve, become an even more important factor in determining the final chlorosulfonated polymer bulk viscosity and shear sensitivity.

Quantitizing the effect of these parameters is difficult because of the many different possibilities in the shape function of the base resin molecular weight distribution curve. When the distribution curve is monomodal and log normal, the breadth of the molecular weight distribution is a function of the slope of a line formed by measurement of melt flow at increasing load or shear rate. Extrapolation of this slope defines a shear rate for measuring a base resin viscosity, which correlates with Mooney viscosity of the chlorinated product.

Although both base resin and chlorinated product viscosities are related to molecular weight, a higher shear rate is needed in the latter case to account for the lower measuring temperature for Mooney viscosity. Substitution of chlorine atoms onto the polymer chain increases polymer bulk and polarity, resulting in greater chain entanglement and resistance of chains to flow past one another causing viscosity increase at a predictable rate. Using these parameters, ie, extrapolated melt viscosity and chlorine content, one can predict the final product Mooney viscosity assuming log normal distribution and random chlorination (15).

$$\eta_\gamma = 3.5 + 1.06(0.56 \ln 86 + 2.66 \ln f)/f$$

$$M_v = \eta_\gamma[(-1.7 + 5.9(\%Cl)]$$

where η_γ is the polyethylene viscosity at a shear rate which corrects for measuring temperature differences between Mooney viscosity and melt index of polyethylene under standard conditions, f is the slope of melt index vs shear rate, and M_v the Mooney viscosity of the chlorinated product at 100°C.

A more general approach for a polydisperse case uses an adaptation of a model relating molecular weight distribution of the polyethylene to shear dependence. This method concerns the relationship of elastic properties of polyethylene melts to molecular weight. It postulates that bulk viscosity η_γ is a function of a specific molecular weight average $M_w{}^*$ in the same manner that zero shear viscosity is a function of weight-average molecular weight (16).

$$\eta_\gamma = K(M_w^*)_a \quad \text{when} \quad \eta_0 = K(M_w)_a$$

Where K and a are empirical constants depending on the nature of the polymer and temperature. Then,

$$M_W^* = \sum_{i=0}^{i=c-1} W_i M_I + M_c \sum_{i=c}^{\infty}$$

where W_i is the weight fraction associated with molecular weight M_i and M_c is the critical molecular weight associated with the largest polymer molecule undergoing Newtonian flow at γ, and therefore must be determined for each shear rate of interest.

For CSM, at a given chlorine content, the relationship of molecular weight to viscosity is

$$\text{Log}\,\eta(\gamma) = -13{,}8615 + 3.4\text{Log}\,M_w$$

where $\eta(\gamma)$ is the bulk viscosity of CSM at 100°C in kPa's and $M_w{}^*$ is the molecular weight average of the polyethylene used to manufacture the CSM.

To convert $\eta(\gamma)$ to CSM Mooney viscosity ($\gamma = 1.6\ s^{-1}$), $\eta(\gamma) = 1.2894 \times$ Mooney viscosity.

As expected, the viscosity of the polymer increases with increasing molecular weight. The effect diminishes, however, until a critical molecular weight is reached where chains become so long that they fail to undergo complete relaxation at a given shear rate and the additive effect on viscosity becomes negligible. Polymer chains longer than the critical molecular weight influence the whole polymer viscosity as though they were of critical molecular weight. And chain entanglements become unimportant to flow behavior if molecular weight $> M_c$. Thus, as chain length, and the weight-average molecular weight, increases in the distribution curve, its contribution to viscosity is increased until the critical molecular weight is reached. Beyond that point chains contribute to viscosity as though they were at the critical molecular weight. This gives added weight to contributions of low molecular weight fractions as confirmed by experience. This relationship gives added flexibility to design of chlorosulfonated polymers for specific application without viscosity penalties.

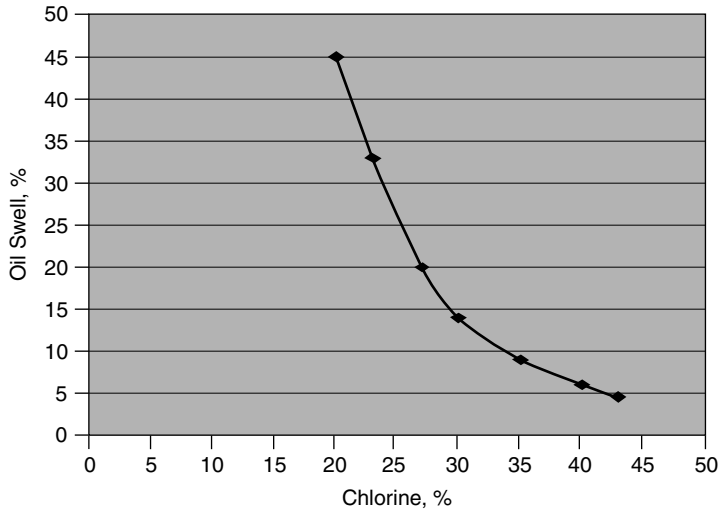

Fig. 2. General relationships of oil swell and chlorine content on a cured linear-based CSM.

To further interpret the results, the distribution curve may be divided into three segments, ie, low, medium, and high, and a polydispersity index, M_w/M_n, calculated for each segment (17).

$$M_w = \Sigma H_i M_i / \Sigma H_i \quad \text{and} \quad M_n = \Sigma H_i / \Sigma H_i M_i$$

where H is the height of the segment and M is the mass.

This model has, in fact, been found to give the most comprehensive relationship between polyethylene composition and Mooney viscosity of the resultant CSM polymer. CSM polymers are generally categorized on the basis of base resin type, ie, LDPE, HDPE, LLDPE or functionalized polyolefin, chlorine content, and Mooney viscosity.

The chlorine atoms on the polymer backbone not only provide elastomeric properties but also give useful improvement in chemical and mechanical properties. The chlorine atoms attached to the chain form centers of high cohesive energy, which prevents infusion of oil, oxygen, acids etc from reaching the main chain. Thus, oil, chemical, flame, and weather resistance improves with increasing chlorine level. Conversely, heat resistance, low temperature flexibility, and electrical resistance become poorer. When the chlorine atoms are more evenly spaced along the chain, they are more effective and, thus, more efficient. Therefore, a CSM with a homogeneous chlorine distribution would be expected to have better resistance to low temperature brittleness and oil resistance than one with blocky distribution, all other conditions being equal. Figure 2 shows the general relationships of oil swell and chlorine content on a cured linear-based CSM, made under homogeneous chlorinating conditions.

Table 1 shows a description of commercial CSM polymers produced by DuPont Dow Elastomers under the trade name of Hypalon Acsium and Hypalon CP. Toya Soda of Japan also offers similar but not all grades.

Table 1. Commercial CSM Polymers

				Polyethylene	
Hypalon type	Chlorine, %	Sulfur, %	Mooney viscosity	Melt index	Stress Exp.
From LDPE (branched)					
20	29	1.2	28	10	NA
30	43	1.3	43	100	NA
From HDPE					
45	24	1.0	37	2.5	1.44
623	24	1.0	21	14	1.72
LD-999	35	1.0	30	12	1.76
40 S	35	1.0	45	7	1.45
40	35	1.0	55	4	1.44
4085	36	1.0	90	2.5	1.25
610	35	1.0	130	0.75	1.30
48 S	43	1.0	62	14	1.76
48	43	1.0	90	17	1.28
From LLDPE					
Acsium 6367	27	1.0	45	5.0	1.30
Acsium 6932	30	1.0	60	5	1.33
Acsium 6983	90	1.0	90	0.8	1.3
From polymers containing other functional groups					
CP-770	44	2	NA	NA	NA
CP-826	28	0	NA	NA	NA

Preparation

Chlorosulfonated polyolefins are prepared by interaction of the base resin with chlorine and either sulfur dioxide (18) or sulfuryl chloride in the presence of a radical initiator (19). Sulfuryl chloride may be used alone as a chlorosulfonating agent, but must be accompanied by a catalytic amount of pyridine or other organic base. It has been proposed that the function of the organic base is to catalyze decomposition of the sulfuryl chloride molecule to form SO_2 and Cl_2. However, the chlorosulfonation rate with base-catalyzed sulfuryl chloride is 5–10 times faster than that with gaseous chlorine and sulfur dioxide. So it is possible that the mechanism is more complex. In the latter case, the ratio of sulfonyl chloride to chlorine substituted onto the polymer backbone is, to some extent, a function of the amount of organic base added. The reaction temperature (lower reaction temperatures that result in higher sulfur utilities) also affects it (19).

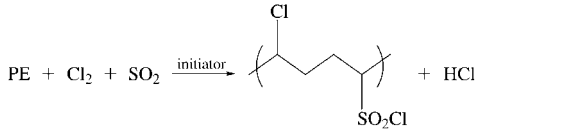

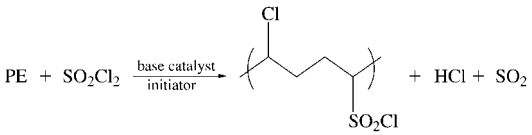

The chlorination reaction and the chlorosulfonation reaction are usually carried out simultaneously in homogeneous solution, but may be carried out in stages; that is, the resin may be partially chlorinated with elemental chlorine and then chlorosulfonated to the desired composition with a chlorosulfonating agent (20).

Many solvents have been used in laboratory preparations of CSM, eg, chloroform, chlorobenzene, trichloroethane, tetrachloroethane (21), trichlorofluoromethane, fluorobenzene (22), and carbon tetrachloride. Mixed solvents, ie, chlorobenzene and carbon tetrachloride, have also been used to achieve certain desired properties such as low temperature flexibility (23).

For practical applications, the solvent used in the reaction must dissolve the base resin and the final product, be inert to chlorination, and easily be separated from the finished product without polymer degradation. The degree of compatibility of the solvent with the base resin and the various stages of finished product may also substantially affect the chlorine distribution and thus the physical and mechanical properties of the final product.

When a highly compatible solvent is used, the solvent surrounds each segment with an "envelope" of solvating molecules, which prevents contact with other segments and other chains. The individual chain is then in a relatively elongated condition, and the solvent can flow freely around the various chain parts. When the chlorinating agent is dissolved in the solvent, equal exposure of all chains and chain segments to molecular chlorine attack is afforded and therefore a more selective chlorine distribution along the chain and between chains results.

In a solvent with poor compatibility, the chains are irregularly folded into tight coils, and considerable amounts of solvent can be immobilized by the entangled segments of the polymer. At a concentration where chains would still be separate and discrete in a good solvent, they would have associated into networks of relatively large size in a poorer solvent. These shapes and dimensions hinder attack of chlorine in hidden segments and chains, leading to a more blocky distribution of chlorine atoms substituted along the chain and among the polymer chains. In addition, as the polymer concentration is increased, chain-to-chain bridging takes place much more readily in the tightly coiled chains so that the bridged chains respond as though they are much higher in molecular weight. The rate of increase in viscosity with concentration is then distinctly greater in a poorer solvent. The higher viscosity causes the formation of larger gas bubbles during chlorine gas addition and interferes with the mass transfer of chlorine from the bubble to the main body of solution. Under this condition, a higher concentration of chlorine at the bubble interface causes overchlorination of polymer chains in that area compared to the remainder of the reaction mass. Thus, optimum conditions for a homogeneous chlorine distribution are low solution viscosity, good mixing, high reaction temperature, and a reaction solvent most compatible with the polymer.

The effect of solvent compatibility on chlorine distribution may be illustrated by comparison of reaction in fluorobenzene, an excellent solvent for both polyethylene and the chlorinated product, and in carbon tetrachloride, a poorer

solvent. Blocky chlorine distribution may be shown by comparison of ΔH values; infrared absorption at 715 and 730 cm^{-1} and by nmr determination of γ, or greater protons. Chlorinated polymers prepared in fluorobenzene show about 1/3 as many γ, or greater hydrogens as those prepared in carbon tetrachloride under the same reaction conditions, indicating more selective distribution in the former case.

In commercial solution processes, carbon tetrachloride has been the solvent of choice, in spite of its solvency limitations. It is desirable because it easily dissolves the polyolefin reactants as well as the chlorosulfonated finished product. It is also stable under reaction conditions; it is inert to chlorination and its boiling point is low enough to facilitate isolation of the polymer from solvent by evaporation at temperatures low enough to prevent decomposition of the chlorosulfonated product. In addition, it has always been readily available and reasonably priced. However, because carbon tetrachloride is toxic and a suspected carcinogen and because it is postulated that it can take part in reactions that deplete atmospheric ozone, it has been the subject of increasingly stringent controls. Consequently, the use of carbon tetrachloride on a large scale has become increasingly undesirable for both safety and environmental reasons. Its continued use requires that careful and stringent containment is maintained (24). Trichloroethane or fluorobenzene have been suggested as safe and environmentally friendly alternatives (24), but have higher boiling points, thus difficult to remove from the polymer and not completely unreactive to chlorine. Chloroform, because of its very low ozone depletion potential, is considered environmentally acceptable, but it is toxic and a suspected carcinogen and it undergoes some chlorination to carbon tetrachloride under reaction conditions. Therefore, it too requires restricted containment.

Commercial processes consist of dissolving the base resin, usually polyethylene, at a temperature above its Vicat softening point, in a glass-lined, stirred kettle, fitted with an agitator and at least one condenser. For HDPE, the dissolving temperature is at least 98°C, but dissolution rate increases with temperature. The chlorosulfonating agents together with a free-radical initiator, usually 2,2′-azobisisobutyronitrile, are added continuously during reaction. The heat of reaction, 54–145 J/g (13–35 cal/g), depending on reactants used, is removed from the reaction mass by condensing the solvent vapors and returning the cooled reflux liquid to the reaction mass. The temperature of the cooled reflux may affect composition control as it affects the solubility of sulfur dioxide, ie, lower reflux temperatures and/or reaction temperatures, at a given reaction pressure, favor higher sulfonyl chloride incorporation.

When the desired chemical composition is reached, as determined by infrared analysis, the by-product HCl and unreacted SO_2 are removed by sparging with an inert gas, ie, nitrogen, decreasing reactor pressure to atmospheric, pulling a vacuum on the system, or combinations of these. Adding a small amount of an aromatic epoxy resin then stabilizes the product. This resin reacts with residual HCl remaining in the degassed solution as well as that, which may be formed upon product storage. It also functions to prevent oxidative decomposition of the sulfonyl chloride group during storage.

The usual method for removing the solvent from the cement is by means of steam-heated drum dryers, wherein a heated solution of the polymer is introduced into the nip of rotary drum dryers and solvent is removed by evaporation. As the solvent evaporates at the drum surface, a thin film of polymer is deposited, which continues to dry as the drum rotates. The dried film is doctored from the drum surface with a knife blade; gathered into a rope and cut into small chips. It is then dusted with talc, to prevent massing, and then packaged.

Processing of Chlorosulfonated Polyethylene

As with most other elastomers, unvulcanized CSM is unsuitable for all but a few applications. In order to make useful materials having the desired processing characteristics, ultimate finished product properties, or cost control, it is usually necessary to incorporate several compounding ingredients to improve their mechanical and chemical behavior. These include vulcanizing agents, accelerators, accelerator activators, specific retarders, age resisters, processing aids, reinforcing pigments, inert fillers, coloring dyes and pigments, and other special-purpose materials, ie, blowing agents, abrasives, etc.

After the compounds have been properly mixed and shaped into blanks for molding, or calendered, extruded, or fabricated into a composite item, they must be vulcanized by one of many processes. During this vulcanization process, the polymer chains are cross-linked into three-dimensional structures, transforming the soft, weak, plastic-like material into a strong elastic product.

In most elastomers the reactive site for cross-linking is carbon–carbon double bonds either in the backbone of the polymer chain or, as in the case of EPDM elastomers, on the side chains. Vulcanization of these polymers usually involves reacting sulfur or sulfur compounds with the double bond at elevated temperatures to form sulfide or polysulfide cross-links. Metal oxides, ie, zinc oxide and organic sulfur bearing accelerators (ie, thiuram polysulfides), are added to speed up the curing process. For CSM, the major cross-linking site is the sulfonyl chloride group, which offers a variety of cross-linking reactions. The most commonly used cross-linking systems for CSM may be grouped into four general classes: sulfur donor, ionic, organic (Maleimide), and peroxide. Although they may be fundamentally different, these systems may also be viewed as the extreme end points of a broad band of possible cure recipes. Consequently, practical curing systems may incorporate various combinations of different types of vulcanizing agents offering a synergistic effect in optimizing desired properties of a given final product for a specific application.

CSM cure chemistry usually involves a cross-linking agent, an activator, an accelerator, and often an activator/retarder for processing safety. Acid acceptors must also be added to neutralize the by-products HCl and SO_2, which may evolve in the vulcanizing environment. The acid acceptors may also be involved in forming a part of the cross-linking mechanism.

The cure system most widely employed for CSM is based on sulfur and its derivatives, sometimes referred to as the sulfur or sulfur donor cure. Unlike

elastomers, ie, natural rubber, which contains unsaturation, CSM may not be cured with elemental sulfur alone, or with sulfur and a metal oxide, eg, lead oxide or magnesium oxide, even at extended cure times. However, several sulfur bearing organic compounds, eg, dipentamethylene thiuram hexasulfide ("Tetrone A"), thiuram disulfide ("Thiuram M" or "Methyl tuads"), and tetramethylthiuram disulfide ("TMTD"), have been found to give low level CSM cures when used alone. When combined with PbO or MgO, high states of cure may be achieved. Addition of finely divided elemental sulfur further enhances the state of cure. Lead compounds have become increasingly restricted in rubber stocks because of health hazards. Hydrotalcite (magnesium aluminum hydroxy carbonate) has no serious health issues and has been found to perform in the same manner as PbO in CSM compounds by trapping chlorides (25). Its use has been accepted by most of the rubber industry.

Incorporation of elemental sulfur, activated by metal oxide, into the curing recipe allows further polysulfidic cross-links through the small amount of unsaturation formed by SO_2 decomposition to further enhance the cross-link density. Benzothiazyl disulfide (MBTS) is often added in practical sulfur recipes. It functions as a retarder–activator, ie, it improves processing safety (scorch) while increasing cross-link density. The mechanism probably involves assisting in the decomposition of the polysulfide at a controlled rate. When optimum heat resistance is desired, nickel dibutyl dithiocarbamate (NBC) is often added. This material does not act as an antioxidant, which is normally added to compounds for heat aging resistance. Several mechanisms have been proposed for its effectiveness but it probably reacts with any residual sulfonyl chloride group, which survives curing conditions, causing their elimination and the formation of a stable alkyl chloride in the polymer chain. This reaction prevents further cross-linking during heat aging from the polymer radical and oxygen, which eventually causes brittleness.

The Maleimide cure of CSM is also widely used particularly when low compression set is needed along with good heat resistance. It can also give tight cures with flexible cross-links, which are important for dynamic applications. The fact that it can give heat resistance equivalent to the best mixed oxide (MgO + PbO) cures without the use of lead, and that it can be used in light colored applications has added substantially to its importance. The major disadvantage is the sensitivity of uncured compounds to moisture, causing poor bin stability. Water opens the Maleimide ring, which voids its use in the cross-links. Mixing in additional Maleimide may reactivate a stock, containing Maleimide, which has been exposed to moisture for an extended time and, therefore, rendered inactive.

The Maleimide cure system is similar to the sulfur donor system in that it involves the decomposition of the sulfonyl chloride cure site. In this case, however, the Maleimide (meta-toluene-bis-maleimide, HVA-1 or meta-phenylene-bis-maleimide, HVA-2) rather than sulfur, is involved in the cross-links, and there is no evidence of a metal ionic bond. The reaction is usually initiated with an amine involving either an amine-catalyzed decomposition of the sulfonyl chloride group or a path of radical anions. The most recently developed initiators, which have been found to give a balanced combination of

excellent processing safety and cross-link density, are a butyraldehyde/aniline condensation product (known as "Antox" special or "Vanax" AT) and *N*,*N*′-diphenylpropylene diamine (GFI), all secondary amines. These amines are antioxidants and therefore readily oxidized, which makes them less stable, particularly at elevated temperatures and in the presence of the sulfonyl chloride group (a strong oxidizing agent) and leads to decomposition. In completing the cross-linking reaction, the polymer radical, thus formed, interacts with the Maleimide.

Since SO_2 is released quantitatively in this cross-linking reaction, it is necessary to include an SO_2 absorbing ingredient in the compound. For this reason calcium hydroxide is usually added. Other SO_2 absorbers, eg, 1,3-bis (hydroxymethyl) urea, which are not too volatile, may be used as well.

Peroxide cures are used in cross-linking CSM as well as many other elastomeric and nonelastomeric polymers. It is used in CSM when very low compression set is needed along with excellent heat aging and oil resistance. Its disadvantages include limited amount and types of plasticizers, requirement of high amounts of acid acceptors, and high cure temperatures.

Hydrogen chloride, evolved at curing temperatures, inhibits the cross-linking reaction. Therefore, sufficient quantities of an acid acceptor must be added to the recipe to neutralize the HCl. Magnesium oxide is the most effective acid acceptor because it does not react with the sulfonyl chloride group to cause scorch, but its miscibility with the CSM polymer is poor. Therefore, relatively large amounts are required for an efficient cure. This increases the cost and the compound viscosity, which is already high due to the absence of plasticizer. Addition of a small amount of pentaerythratol complexes with the MgO greatly improves its solubility in the polymer mass and therefore significantly reduces the amount of MgO required.

Peroxide cures are usually temperature specific, and higher than normal curing temperatures are usually required to achieve adequate properties. Addition of a small amount of a co-agent, triallyl cyanurate or HVA-2, helps to activate the cure by forming a complex with the peroxide.

Typical vulcanizable compounds will, in addition to the curatives, contain certain plasticizers, fillers, processing aids, pigments, etc.

CSM does not crystallize upon elongation, but some reinforcement is developed through polar and hydrogen bonding effects. Thus, vulcanizates containing no filler may still develop significant tensile strength upon extension. Additional reinforcement may be achieved with certain carbon blacks and silicates. Surface reinforcing furnace blacks give the best balance of properties and are widely used as general-purpose fillers. Weathering of CSM with as little as three parts of carbon black is outstanding. Mineral fillers may be used to take advantage of CSM's nondiscoloring characteristics. Among mineral fillers, finely divided calcium carbonate gives the best heat resistance, and the best electrical properties and water resistance is obtained with calcined clay. Titanium dioxide may be used when white or pigmented end products are desired. The color of CSM products containing titanium dioxide does not fade. Flammability performance is improved by the addition of hydrated silica and alumina Table 2.

The linear low density based CSM polymers have excellent dynamic properties over a broad temperature range. The pendent alkyl groups on the linear

Table 2. Comparision of CSM Cure Systems

Compound Ingredients, phr	Sulfur donor	Maleimide	Peroxide
CSM (Hypalon 40)	100	100	100
N762 Black	35	35	
Calcium Carbonate	–	–	40
Low MW Polyethylene	3	2	–
Paraffin wax	2	2	1
Magnesium Oxide	4	–	6
Calcium Hydroxide	–	4	–
HVA-2	1	3	–
Pentaerythratol-200 mesh	3	–	3
Sulfur	1	–	–
TMTD	1	–	–
MBTS	1	–	–
Triallyl cyanurate	–	–	3
Varox powder	–	–	6
Original Properties[a]			
100% modulus, MPa[b]	6.6	6	7.5
200% modulus, MPa[b]	18.2	16	19.5
Tensile strength, MPa[b]	25.8	26.8	25
Elongation, %	340	360	300
Hardness, Shore A	73	70	76
Tear strength @ (RT) Die C, kN/m[c]	39.4	46.6	34.7
Heat-aged[d] Properties			
100% modulus, MPa[b]	10.2	9	11
200% modulus, MPa[b]	26.4	2 3	28
Tensile strength MPa[b]	27	28.3	26.5
Elongation, %	250	267	220
Compression set, 22 h @ 70 C, %	34	23	46

[a] Press cured 30 min @ 160°C.
[b] To convert MPa to psi, multiply by 145.
[c] To convert kN/m to ppi, divide by 0.175.
[d] After 7 days aging @ 120°C.

backbone reduce the crystallinity of the base resin and allow rubbery products at lower chlorine levels than linear-based polymers. High strength polymer products are produced with the heat and oil resistance near those of linear-based CSM, but with low hysteresis, high resilience, high complex modulus, low damping, and good flexibility at low temperatures. When properly compounded and cured, these resins produce tan δ values of 0.06–0.13 at 100°C, dynamic ratio (E′/tan δ) of 50–70, and a brittleness temperature of −75°C. Gehman T50 values are −30 to −40°C (26).

Economic Aspects

Production of chlorosulfonated polymers has declined somewhat in recent years because of the increased competition from polymers with similar properties.

Annual worldwide production of all products is now about 40,000 tons. The primary producer, with about 85% of world capacity, is DuPont Dow Elastomers, Inc., a joint venture of E.I. du Pont de Nemours & Co. Inc. and The Dow Chemical Co., with a single plant in the United States. The remaining capacity is provided by Toyo Soda Manufacturing Limited, with one plant in Japan. DuPont Dow Elastomers products are sold worldwide under the trade names of Hypalon, Acsium, and Hypalon CP. Products similar to several grades of Hypalon products are made by Toya Soda and sold under the trade names of CSM-CP and CSM-Ts. The material cost variability is related mostly to the petroleum costs. Prices generally range from $3 to $6 per kilogram.

Health and Safety Factors

Hypalon, Acsium, and Hypalon CP grades contain small amounts of carbon tetrachloride residue, normally <0.2%, and traces of chloroform. These chemicals are toxic and carcinogenic and carry time-weighted average exposure limits of 5 ppm. They are both regulated under the Occupational Safety and Health Act as air contaminants. These contaminants diffuse from the product at measurable rates if the product is not massed. So it is advisable to provide adequate ventilation to keep concentrations at safe levels. Toya Soda chlorosulfonated products, CSM-CP and CSM-Ts, may contain up to 0.5% trichloroethane and small amounts of tetrachloroethane. Both products contain <1% epoxy resin as stabilizer. These resins are regulated at <1% level in some European countries. Significant amounts of sulfur dioxide and hydrogen chloride as well as traces of carbon oxy sulfide (COS) may be evolved during compounding in internal mixers.

Disposal of Hypalon, Acsium, Hypalon CP, CSM- CP and CSM-Ts grades should be in an approved landfill. Incineration is not recommended because of the possible evolution of toxic gases. Additional information is available from DuPont Dow Elastomers concerning these or other potential hazards when handling Hypalon products.

Uses

CSM products are classed as specialty elastomers but enjoy use in a broad spectrum of industrial, automotive, construction, coatings and miscellaneous applications. The applications for CSM depend only in part to its combination of oil resistance and heat resistance. CSM is much more resistant to corrosive or oxidizing chemicals, including ozone, than are CR or nitrile rubbers. It is tougher than silicone and EPDM rubbers. It has good electrical insulation properties, which are not as good as EPDM but better than many other elastomers. CSM also has excellent radiation resistance needed in nuclear power applications and is also color-stable and highly weather-resistant. Good flame resistance is obtained with high chlorine grades of CSM. Chlorinated plasticizers, brominated resins, and antimony trioxide synergists are commonly used as additives. Mineral fillers,

excluding carbonates are preferred and hydrated alumna is frequently used when smoke suppression is important.

In industrial hose, CSM is particularly useful because of its combination of heat, oil, and chemical resistance and its outstanding ozone and weather resistance. It is also preferred because of the frequent need for stable bright colors. Hypalon 4085 and Hypalon 610 are often used in these applications because their high compound Mooney viscosity prevents hose collapse or "flat spotting" during curing.

In the electrical industry, CSM may be used as a protective jacketing or sheathing over elastomers having superior insulation resistance but poor weatherability. It also finds considerable usage as an integral insulator for up to 600 V. This combination of insulation resistance plus the long-term ozone resistance makes it useful for high quality applications. In these cases, the lower viscosities of LD999 and Hypalon 40 are preferred for faster and smoother extrusions.

In the automotive industry, Hypalon 40 grades are used for fuel hose, power steering hose, brake hose covers, vacuum tubing, and spark plug wire covers and boots. The new Acsium grades are finding use in high performance timing belts and accessory drive belts and in brake hose covers (26). Low permeability to moisture and refrigerants make high chlorine grades qualify for air conditioning hose and tubes. Chlorinated and chlorosulfonated maleic anhydride grafted polypropylene is used as a primer for polypropylene bumpers.

Low chlorine CSM grades, based on linear polyethylene, eg, Hypalon 45, have sufficient crystallinity to produce adequate tensile strength and elongation for uncured applications. They are generally compounded with white or light-colored pigments and calendered into film for use as unsupported membranes. Tensile strength of these sheets range from 9 to 12 MPa and Graves tear strength of the order of 50–60 kN/m. These types are also used as binders for magnetic door strips and signs because of its ability to accept very high loading and specific adhesion to magnetic metal powders, as well as its excellent weatherability.

Hypalon CP grades are similar to CSM but have additional functionality, ie, esters, acids, or maleic anhydride grafts, which set them apart for specific applications. They add value as modifiers for adhesives, coatings, and inks because of their low solution viscosity and increased solubility and compatibility. Hypalon CP 826 promotes adhesion to polypropylene and finds use as a primer coating for automobile bumpers.

A variety of miscellaneous end uses take advantages of CMS's oil resistance, colorability, and weather and ozone resistance. Grades based on LDPE find use in numerous coating applications such as awnings, gas hose, escalator handrails, and rubber boats. CSMs are also used for curb pump hose, mining cable jackets, and appliance wire jackets. Grades based on ethylene vinyl acetate polymers are used for traffic paints and marine paint.

BIBLIOGRAPHY

"Ethylene Polymers, Derivatives" in *EPST* 1st ed., Vol. 6, pp. 431–454, by P. J. Canterino, Allied Chemical Corp.; "Ethylene Polymers, Chlorosulfonated Polyethylene" in *EPSE* 2nd

ed., Vol. 6, pp. 513–521, by G. D. Andrews and Robert L. Dawson, E. I. du Pont de Nemours & Co., Inc.

1. R. R. Warner, *Rubber Age* 26–29 (May 1952).
2. R. E. Brooks, D. E. Strain, and A. M. McAlevy, *India Rubber World* 968–974 (Mar. 1953).
3. U.S. Pat. 2212786 (Aug. 27, 1940), D. M. McQueen (to E. I. du Pont de Nemours & Co., Inc.).
4. U.S. Pat. 2416016 (Feb. 18, 1947), A. M. McAlevy, D. E. Strain, and F. S. Chance (to E. I. du Pont de Nemours & Co., Inc.).
5. U.S. Pat. 2503253 (Apr. 11, 1950), M. L. Ernsberger and P. S. Pinkney (to E. I. du Pont de Nemours & Co., Inc.).
6. U.S. Pat. 2982759 (May 2, 1961), R. O. Heuse (to E. I. du Pont de Nemours & Co., Inc.).
7. U.S. Pat. 2972604 (Feb. 21, 1961), W. B. Reynolds and P. J. Canterino (Phillips Petroleum Co.).
8. U.S. Pat. 3347835 (Oct. 7, 1967), J. C. Lorenz (to E. I. du Pont de Nemours & Co., Inc.).
9. U.S. Pat. 4560731 (Dec. 24, 1985), M. R. Rifi (to Union Carbide Co.).
10. U.S. Pat. 3296222 (Nov. 20, 1970), S. Dixon and R. E. Ennis (to E. I. du Pont de Nemours & Co., Inc.).
11. U.S. Pat. 3542747 (Nov. 20, 1970) R. E. Ennis and J. W. Scott (to E. I. du Pont de Nemours & Co., Inc.).
12. R. A. V. Raff and K. W. Doak, *Crystalline Olefin Polymers*, John Wiley and Sons, Inc., New York, 1965, pp. 307–405.
13. H. V. Boenig, *Polyolefins: Structure and Properties*, Elsevier, Amsterdam, the Netherlands, 1966.
14. A. B. Peterson, *SPE Trans.* 167–175 (July 1963).
15. E. G. Brehme, Hypalon Technical Bulletin H. P. 302, E. I. du Pont de Nemours & Co., Inc.
16. B. H. Bersted, *J. Appl. Polym. Sci.* **20**, 2705 (1976).
17. P. Crouzet and co-workers, *Methode de Calcul Sur Ordinateur des Parametres d'un etalonage de Chromatographie par Permeation de Gel, Analusis, 1076, Vol. 4, No. 10*, pp. 450–455.
18. U.S. Pat. 3299014 (Apr. 15, 1967), J. Kalil (to E. I. du Pont de Nemours & Co., Inc.).
19. Jpn. Pat. 4544709 (Oct. 1, 1985), Y. Narui and co-workers (to Toya Soda Mfg. Ltd.).
20. U.S. Pat. 3314925 (Apr. 15, 1967), K. F. King (to E. I. du Pont de Nemours & Co., Inc.).
21. U.S. Pat. 4871815 (Oct. 3, 1989), T. Nakagawa and co-workers (to Toya Sota Mfg. Ltd.).
22. U.S. Pat. 5208290 (May 4, 1993), E. G. Brugel (to E. I. du Pont de Nemours & Co., Inc.).
23. T. Nakagawa, *India Rubber World* 104–111 (Jan. 1992).
24. *Code of Federal Regulations, Title 29, Government Printing Office, Washington, D.C., Parts 1910–2000.*
25. R. E. Fuller and K. S. Macturk, *Rubber and Plastics News* (Sept. 20, 1999).
26. R. E. Ennis and J. G. Pillow, *Materiaux Techniques* **78**(11/12), 17 (1990).

GENERAL REFERENCES

F. W. Billmeyer Jr., *Textbook of Polymer Science*, 2nd ed., John Wiley & Sons Inc., New York, 1971, pp. 147–149.

D. W. Van Krevlen, *Properties Of Polymers*, 2nd ed., Elsevier Scientific Publishing Co., Inc., New York, 1976, pp. 129–172.
R. F. Ohm, *Vanderbilt Rubber Handbook*, 13th ed., Vanderbilt Rubber Co., Norwalk, Conn., 1990, pp. 183–189.

ROYCE ENNIS
Consultant

ETHYLENE POLYMERS, HDPE

Introduction

Polyethylene (PE) is the most widely used plastic throughout the world, and high density PE (HDPE) is the most widely used type of PE. HDPE has generally been taken to mean the product of ethylene polymerization having density greater than about 0.935 (or 0.94). It includes ethylene homopolymers and also copolymers of ethylene and alpha-olefins such as 1-butene, 1-hexene, 1-octene, or 4-methyl-1-pentene. Other types of PE include low density PE (LDPE), made through a free-radical process, and linear low density PE (LLDPE).

An analysis of commercial usage of the world's major plastic types is shown in Table 1. In terms of amount consumed, PE dominates the other types. Table 2 lists the U.S. usage of the various types of PE. In comparison to the other types of PE, HDPE is by far the most versatile. HDPE consumption in the United States accounted for about 6.95 billion kilograms per year in 1999, or almost half of total U.S. production of all PE types. Figure 1 shows how the demand for HDPE in the United States has developed historically since its invention in 1951.

History of PE

Early Work. The history of HDPE (and polyolefins in general) actually began in the 1890s with the synthesis of "polymethylene" from the decomposition of diazomethane. Between 1897 and 1938, numerous reports of such polymers appeared in the literature (1–6). Catalysts such as unglazed china, amorphous boron, and boric acid esters were used for the decomposition. The empirical formula of such products was found to be CH_2. Later reproductions of work (3,6) established

Encyclopedia of Polymer Science and Technology. Copyright John Wiley & Sons, Inc. All rights reserved.

Table 1. Worldwide Usage of the Most Common Plastics Types

Polymer type	Share of world usage, %
PE (LDPE, EVA, LLDPE, and HDPE)	40.3
Polypropylene	21.9
PVC	21.1
Polystyrene	11.6
ABS/SAN	5.1
Total	*100*

[a]Data from Digest of Polymer Developments, Series I, Number 95, STR Publishing, Enfield, Conn., May, 2000.

Table 2. Polyolefins Usage in the United States in 1999

Polymers	Consumption in United States, 10^6 t	U.S. polyolefin consumption, %	U.S. Polyolefin consumption, %
Total PE	14.7	67.8	100
LDPE (including EVA)	3.6	16.6	24.5
LLDPE	4.1	19.1	28.2
HDPE	7.0	32.1	47.4
Total Polypropylene	7.0	32.3	
Total Polyolefins	21.7	100	

[a]Data from Digest of Polymer Developments, Series I, Number 95, STR Publishing, Enfield, Conn., May, 2000.

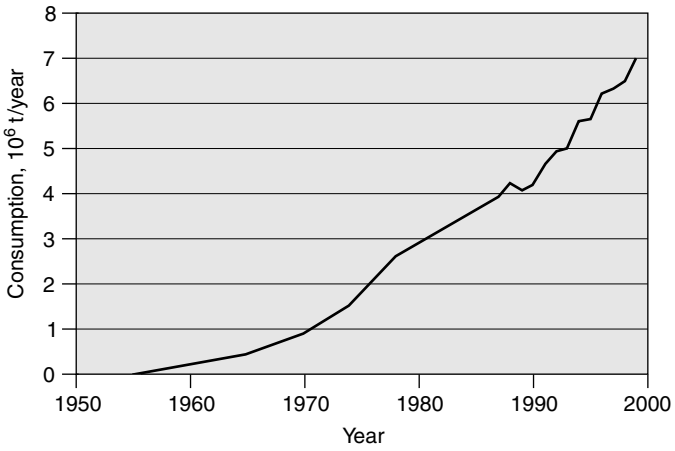

Fig. 1. HDPE consumption in the United States.

that the polymethylene thus obtained was a high molecular weight linear polymer having a melting point of 134–137°C and a density of 0.964–0.970 g/cm^3 (7). Thus, it can be stated that although no commercial use was initially made of it, HDPE was discovered long before the well-known LDPE was introduced (8,9).

In another early approach Pichler (10) and Pichler and Buffleb (11) described during 1938–1940 the preparation of high molecular weight (M_n = 23,000) polymers from the hydrogenation of carbon monoxide over ruthenium and cobalt

catalysts. The reported melting point of 132–134°C and density of 0.980 g/cm^3 indicate again that linear HDPE was obtained.

Free-Radical Process. The first commercial PE was developed by Imperial Chemical Industries from 1932 to 1938 using a free-radical process (12). Ethylene was polymerized at high pressure (142 MPa or 1400 atm) and at about 180°C. It was discovered by accident that oxygen impurity could serve as the initiator. An ICI British patent filed in 1936 (13) disclosed pressures of ca 50–300 MPa (500–3000 atm), temperatures of 100–300°C, the necessity of removing heat to control temperature, and the necessity of controlling the oxygen content of the ethylene used.

The PE produced at this time had a melting point of 115°C and a density of 0.91–0.92 g/cm^3. In 1940, Fox and Martin (14) found by infrared analysis that there were more methyl groups in the polymer than could be accounted for by the end groups of a linear chain. Thus the importance of chain branching was recognized, and subsequent studies of branching led to a better understanding of its effect on mechanical properties and polymer morphology. This material is called low density PE (LDPE) and is still in high commercial demand today. Further work on the free-radical process extended the pressure. Larcher and Pease (15) disclosed PE with densities of 0.95–0.97 g/cm^3, melting points above 127°C, and branching of less than one side chain per 200 carbon atoms.

Transition-Metal Catalysts. Today's "low pressure" catalytic processes, from which HDPE now comes, were discovered in the early 1950s. The term "low pressure" refers to operating pressures of generally 1.4–6.9 MPa (200–1000 psig), in contrast to the ICI free-radical process. Patent applications were filed by Standard Oil of Indiana (16), in 1951, by Phillips Petroleum (17) in early 1953, and by Ziegler and co-workers (18) in late 1953.

The Standard Oil patent (16) describes a supported reduced molybdenum oxide or cobalt molybdate on alumina, with the ethylene preferably contacting the catalyst in an aromatic solvent to affect the polymerization. Operating temperatures of 100–270°C were disclosed and the molecular weight could be varied from very high to low such as those of greases.

At about the same time (1951) it was discovered that supported chromium oxide catalysts would also polymerize ethylene at low pressures to produce high molecular weight polymers (17). Reaction temperatures were in the range of 60–190°C. Polymer characteristics, particularly, molecular weight and molecular weight distribution, could be varied by reactor temperature, pressure, and activation temperature of the "Phillips catalyst."

Shortly thereafter, yet another transition-metal catalyst (Ziegler catalyst) capable of polymerizing ethylene at low pressure was discovered in Germany (18). This approach used a transitional metal halide, or other complex, activated by an aluminum alkyl cocatalyst. Transition-metal compounds of Groups IVa through VIa (Ti preferred) were claimed.

Although the Standard Oil discovery came first, commercialization was slow (19,20). Three plants were eventually built between 1961 and 1971, but the process had poor economics and was soon scrapped. In contrast, the Phillips and Ziegler discoveries were both commercialized rapidly and still exist today in more advanced forms. At Phillips, the first plants were brought on stream in 1955 and 1956. However, Phillips management concluded that no one manufacturer could

develop the full market potential of the Phillips HDPE and therefore decided to license the process. By 1956, nine companies in seven countries became licensees (21–24). Ziegler also began to license his patent, following the discovery that good activity could be obtained by use of titanium halides in combination with aluminum alkyls. However, the patent included only catalyst knowledge, and each licensee had to develop a process. The first Ziegler plant was brought on stream in late 1956 by Hoechst. A second one was built in 1957 by Hercules. By 1960 U.S. production of HDPE via the Phillips process had reached over 91,000 t annually, while 32,000 t came from the Ziegler process.

Today HDPE is still made almost entirely through chromium or Ziegler systems. The two systems produce different types of polymer, which is useful for different applications. The Phillips catalyst generally produces broader molecular weight distributions than that of typical Ziegler catalysts.

Catalysts Used for HDPE Production

Chromium Catalysts. The Phillips chromium catalyst, which perhaps accounts for about half of the total HDPE production, is usually made by impregnating a chromium compound onto a porous, high surface area oxide carrier, such as silica, and then calcining it in dry air at 500–900°C (25). This latter activation step converts the chromium into a hexavalent surface chromate, or perhaps dichromate, ester. Because each Cr atom is individually attached to the surface, the support is not inert but exerts a strong influence on the polymerization behavior of the site.

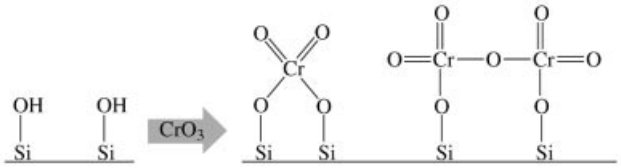

The first step in the development of polymerization activity occurs when these hexavalent surface species are then reduced by ethylene in the reactor to a lower valent active precursor, probably Cr(II) (25–28). Because Cr(VI) is tetrahedrally coordinated, and the reduced species can be octahedral, the resultant expansion of the coordination sphere creates a high level of coordinative unsaturation which plays a role in the polymerization mechanism. Thus, the reduced species chemisorbs olefin readily. However, this same trait makes the catalyst very sensitive to small levels of polar impurities in the feed streams, such as alcohols, water, amines, etc (29,30). Commercial catalysts usually contain about 1.0 wt% Cr, but only a small fraction of this, perhaps 10–20% or even less, is actually active for polymerization (25,27,30).

The second step in the development of polymerization activity is an alkylation reaction in which the first chain begins growing on the reduced chromium species. Exactly how this reaction occurs has been unclear. Several possibilities have been suggested over the years, but no clear answer has yet been established (25,31–35). Recent studies suggest that initial adsorption of olefin on Cr(II) sites may cause an oxidation to an alkylated Cr(IV) site as the active polymerization

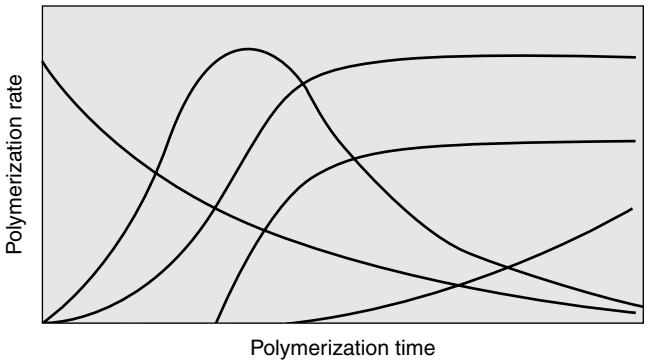

Fig. 2. Kinetic profiles of Cr-based catalysts.

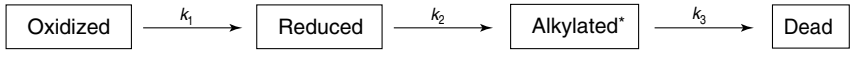

$$[C^*] = k_1 k_2 \left[\frac{e^{-k_1 t}}{(k_2 - k_1)(k_3 - k_1)} + \frac{e^{-k_2 t}}{(k_1 - k_2)(k_3 - k_2)} - \frac{e^{-k_3 t}}{(k_1 - k_3)(k_2 - k_3)} \right]$$

species (34,35). These two initial steps, reduction followed by alkylation, cause the catalyst to display an induction time. That is, the onset of polymerization occurs gradually after a delay which can last from a few minutes to over an hour depending on reaction conditions (25,27).

Alternatively, the reduction step can also be accomplished before the catalyst contacts ethylene in the reactor, by exposure to carbon monoxide at 350°C (25,27). In this case the reduced species has definitely been identified as Cr(II) (28,36–40). This catalyst behaves much like its Cr(VI)/silica parent when introduced into the reactor, producing similar polymer at similar activity in most cases. However, the onset of polymerization often occurs more rapidly when the catalyst is prereduced, since one step is omitted (25,27).

Once the polymerization reaction has developed, a decay in activity can also sometimes be observed because of a chemical instability of the active species. Thus, the kinetic profile of the polymerization reaction can be defined as a series of three consecutive reactions: (*1*) reduction, (*2*) alkylation, and (*3*) decay. Each step in the series has its own dependency on ethylene concentration, temperature, and catalyst composition. Figure 2 shows some typical kinetic profiles that are often obtained and that can be produced by varying the individual rate constants of the three steps (41).

Metal alkyl cocatalysts, such as alkyl boron, aluminum, zinc, lithium, etc, can also be added to the reactor as a way of enhancing the activity of the catalyst. Such agents act by accelerating the reduction step, by alkylating the chromium, or by scavenging minor amounts of poisons such as water and oxygen. These agents are sometimes used commercially for specific resin types, although they are not essential and in most cases are not used (41,42).

In another, less common, variation of the catalyst, lower valent organochromium compounds can be deposited onto an already calcined support to produce very active catalysts (43–51). These compounds react with surface hydroxyls to become attached to the support, often losing one or more ligands. Examples

include bisarene Cr(0), allyl Cr(II), and Cr(III), beta-stabilized alkyls of Cr(II) and Cr(IV), and biscyclopentadienyl Cr(II). The latter example has been used commercially to great extent. Such catalysts often develop activity more rapidly than the chromium oxide catalysts, being already reduced and in some cases already alkylated. The remaining organic ligands can also change the polymer obtained in certain ways.

The most common support used commercially is silica and silica–titania. However, silica–alumina, alumina, and aluminophosphates can also be used (52,53). Adding titania to the recipe enhances activity and broadens the molecular weight distribution not because the titanium itself is active, but because it influences the chromium (54). It is believed that some chromium sites become attached to the titania, which thus indirectly influences the polymerization reaction through electronic effects. Likewise, adding alumina, magnesia, boria, and other oxides have unique effects. Aluminum phosphate is particularly interesting in that it is isoelectronic and isostructural with silica, but of course the surface chemistry is quite different, containing such diverse groups as P—OH, P=O, and Al—OH (41,52,53,55). Thus, changing the support can be a way of varying polymer characteristics.

Ziegler Catalysts. Titanium chloride based Ziegler catalysts are also widely used throughout the HDPE industry. These catalysts generally produce a narrower molecular weight distribution than that obtained from chromium oxide catalysts. Figure 3 shows this typical distinction. Because of this, the Ziegler catalysts are often used for different applications compared to chromium oxide.

While chromium oxide species may vary considerably in their local environment because of the heterogeneous nature of an amorphous oxide carrier, Ziegler species are often thought to be more uniform, occupying certain places in a microcrystalline environment (56–58). Frequently, donor compounds, such as ethers,

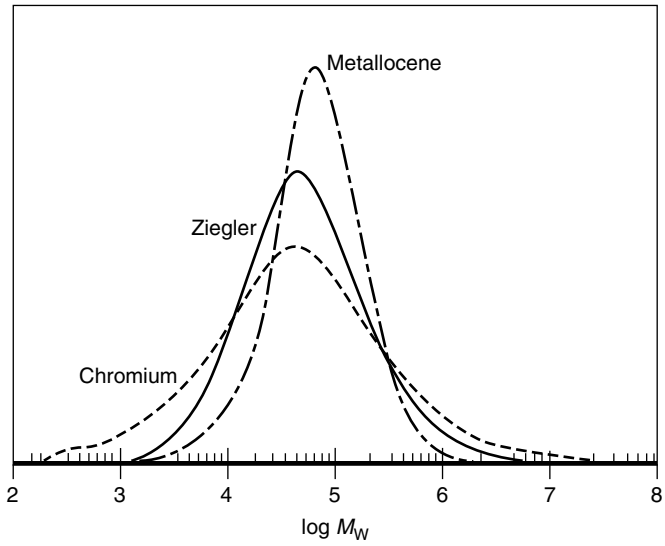

Fig. 3. Molecular weight distribution (gpc curves) of resins derived from metallocene, Ziegler, and chromium oxide based catalysts.

esters, and silane alkoxides, are added to neutralize or modify certain undesirable sites (59).

The early commercial Ziegler catalysts were based on titanium(III) chloride, often ball milled or otherwise treated to provide higher surface area. In about 1968, Hoechst introduced the so called high activity Ziegler catalysts, in which the titanium was dispersed in a magnesium chloride lattice, into which it fitted nicely (60–62). In this way the polymer yield per titanium atom was increased by 10-fold or more.

The transition-metal compound, usually a titanium(III) or titanium(IV) chloride, is transformed into the active catalytic species upon reaction with an aluminum alkyl cocatalyst. During this reaction the active metal becomes alkylated, and ethylene is inserted into the metal–alkyl bond. Often the active site is considered to be a bridging complex between the transition metal and the alkyl aluminum compound, in which one or two ligands are shared between the two metals.

In some cases, broadening has been achieved by using vanadium, zirconium, or other metal halides in the recipe, either alone or in combination with titanium (63–65). In other cases, broadening has been achieved by providing two distinctly different chemical environments for the titanium (66), or in the process by passing the Ziegler catalyst through two or more reaction zones (67).

Metallocenes and Other Single-Site Catalysts. One type of Ziegler catalyst, based on cyclopentadienyl titanium or zirconium halides (which provided only marginal activity using aluminum alkyls as cocatalysts) received an extreme enhancement in activity in the mid-1970s with the discovery of methylaluminoxane (MAO) cocatalyst (68,69). Unlike traditional aluminum alkyl cocatalysts, MAO is far more capable of ionizing the transitional metal compound (57,70–73).

$$Cp_2ZrCl_2 + CH_3Al^{2-} \longrightarrow Cp_2ZrCH_3Cl \longrightarrow Cp_2ZrCH_3{}^{+}MAO{-}Cl^{-}$$

Since that time other ionizing agents have also been developed, which are capable of activating these “metallocene” compounds (74,75).

Metallocene catalysts differ from the traditional catalysts in that the site is derived from a singular molecular species with defined ligands, unlike the heterogeneous character of chromium or Ziegler species. This accounts for the ultranarrow molecular weight distribution of the polymer obtained (see Fig. 3). Although usually described as single-site catalysts, it is nevertheless clear on closer inspection that many of these catalysts do not entirely fit the description because the ionization agent is still part of the active site. MAO, the partial hydrolysis product of trimethylaluminum, is also capable of providing a complex and varied site environment.

Metallocene catalysts are at present just entering the market in certain specialty applications, accounting for perhaps less than 1% of all HDPE sales. However, the greater degree of control offered by metallocenes, and the ability to combine different metallocenes into one catalyst, offers the ability for the first time to truly tailor polymer architecture. Thus, it seems likely that future advancements in single-site chemistry will have a profound impact on the HDPE market. The influence of metallocenes on the LLDPE market has been somewhat greater to date (see LLDPE). This has been mostly due to their ability to evenly distribute branching over the molecular weight distribution. The result has been improved film performance over traditional Ziegler systems.

Within the past 5 years, other types of new organo transitional metal compounds have also been reported, which can be activated by ionizing agents like MAO (76–78). Some of these compounds, such as Brookhart's nickel diimine complex, offer the possibility of producing highly branched ethylene homopolymers that have never before been possible from low pressure systems. Thus, although no commercial polymers are presently made from these systems, it seems likely that these new catalyst developments will have a strong influence on the future direction of HDPE markets.

Polymerization Mechanism and Reactor Control

Molecular Weight and Molecular Weight Distribution. Once an active site has been formed, through reduction and alkylation of chromium oxide species, and once polymerization has been initiated, two reactions—propagation and termination (or chain transfer)—occur simultaneously and competitively. These catalysts are not "living" systems, in which the polymer chain grows indefinitely. Rather, the length of the chain formed is determined by the rate of propagation relative to the rate of termination. On average in a commercial process, the lifetime of a chain on an active site is typically a small fraction of a second, say 0.1 s or less. Since the lifetime of the catalyst in the reactor is usually 1–2 h, this means that each site produces many chains before being discharged from the reactor.

For active chromium species on the Phillips catalyst, the rates of propagation and termination are thought to be characteristic of the local geometry and ligand field surrounding each site on the heterogeneous silica surface. Thus, different sites tend to produce polymers of different average molecular weight, and the overall molecular weight distribution of the polymer reflects the site heterogeneity of the catalyst. This connection allows the molecular weight distribution to be controlled by varying the composition and heat history of the catalyst.

The Schultz–Flory distribution has usually been considered as the simplest model for representing the molecular weight distribution expected from a polymerization catalyst (79). It assumes that each site is identical and that the probability of termination is not dependent on the length of the growing chain. Thus if the probability of propagation is considered to be p, and of termination to be $(1-p)$, then the probability of producing a chain n units long would simply be $F(n) = p^n(1-p)$. This distribution produces a breadth of molecular weight distribution, or polydispersity (weight average/number average), of 2.0. In reality, typical chromium catalysts produce much broader molecular weight distributions, with polydispersity values of 4–20. This is taken as an indication of multiple site environments on these catalysts. Indeed this is also evident by the fact that the molecular weight changes (increases) as the activity develops with time. Those sites which come on stream first produce the lowest molecular weight. Some metallocene and other single-site catalysts, however, do approach the narrow theoretical Schultz–Flory distribution of 2.0.

The propagation step, usually first order in ethylene concentration (80), is thought to occur through the insertion of coordinated ethylene into the metal–alkyl bond (56–58). Termination, or chain transfer, can occur through several different mechanisms. Two of the most common reactions are shown in Figure 4

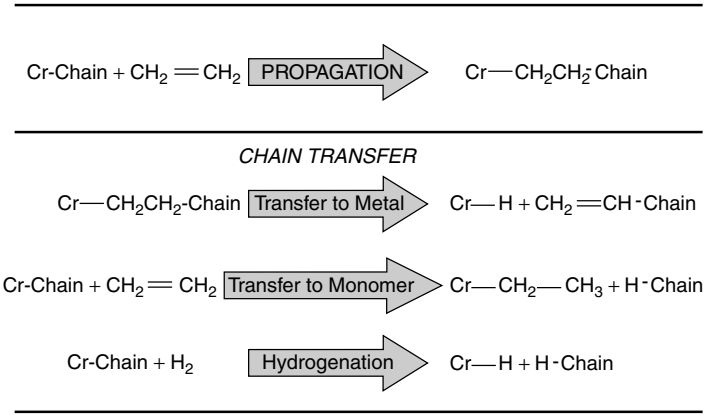

Fig. 4. Steps of polymerization.

as beta-H elimination (*1*) to monomer and (*2*) to the metal. Both reactions leave a vinyl group on one end of the chain and a methyl on the other. In the former case, the transfer step is dependent on ethylene concentration, while in the latter case it is not. On many Ziegler and metallocene catalysts the primary transfer mechanism is to monomer, so that the molecular weight is unrelated to ethylene concentration (since both propagation and transfer are first order in ethylene). However, on chromium oxide catalysts transfer to metal also becomes significant, and this fact is used to control product molecular weight during commercial manufacture. When ethylene concentration in the reactor is increased, the molecular weight also increases (25).

Hydrogen can also be added to the reactor to control molecular weight for most catalyst systems. When deuterium is used in place of hydrogen, the prominent chain end-group $-CH_2D$ is observed (27). Metallocene and Ziegler catalysts are more sensitive to hydrogen than most chromium oxide systems. In the latter case, adding hydrogen to the reactor also tends to narrow the molecular weight distribution, because the high molecular weight producing sites seem to be most sensitive. Metal alkyls can also sometimes terminate chains through alkyl exchange. Aluminum, zinc, and boron alkyls have been reported to do this for some catalyst systems. For chromium oxide catalysts there are indications that boron alkyls are particularly potent and the process may even be catalytic (81). Again, some sites seem to be more affected than others, which can be used to produce special polymer effects (82).

Fracturing. On silica supported catalysts, such as the Phillips chromium oxide system and some Ziegler catalysts, the active sites are attached to the internal surface of pore walls. Within a minute or so after polymerization begins, these pores become clogged with polymer. At this point, the silica particle begins to fracture into perhaps a billion smaller fragments because of the internal pressure created by polymer generation (25,83,84). This fracturing process only occurs on certain high porosity (and thus friable) silicas which are specially prepared for use as polymerization catalyst supports. Otherwise, fracturing does not take place and the catalyst has little or no activity. These fragments, which may be as small as 0.1 μm, then become engulfed in polymer, and unless the polymer is made in a

solution process, these subparticles are loosely held together by entwined polymer into a larger polymer particle which replicates the shape of the original catalyst particle. Each ton of catalyst produces some 2000–10,000 tons of polymer (or more) before being discharged from the reactor. Each catalyst particle thus produces a polymer particle of about the same shape, but many thousands of times its own mass. The catalyst is left in the polymer as a minor impurity.

Polymer Structure

General Structure. Commercial HDPE is a predominantly linear polymer with the chemical composition roughly of polymethylene, $(CH_2)_n$. Its name reflects the principal method of production: ethylene polymerization by transition-metal catalysts. At least one end group of each chain contains a methyl group, and depending on the method of manufacture, the other end group is also a methyl or a vinyl group. Some general properties are shown in Table 3.

The weight-average molecular weight (M_w) of typical commercial HDPE grades can vary from 20,000 to over 1,000,000, depending on the application. The molecular weight distribution of commercial HDPE polymers can range from very narrow, for metallocene derived polymers, to very broad, for grades made from chromium oxide catalysts. A convenient measure of the molecular weight breadth is the polydispersity, or the ratio of the weight-average molecular weight to the number-average molecular weight (M_w/M_n). Experimentally, the molecular weight distribution is measured by gel-permeation chromatography (gpc).

Short-Chain Branching. Although described as high density, commercial HDPE can actually vary in density from 0.975 down to 0.935. HDPE contains a crystalline phase and an amorphous phase, and the measured density directly reflects the percentage of each. Typical homopolymer is normally about 94% crystalline and has a density of 0.960–0.965. Higher densities can be achieved by low molecular weight and slow cooling.

Crystallinity is disrupted, and density therefore lowered, if branching is added to the otherwise linear polymer backbone. This is typically accomplished by copolymerizing alpha-olefins in small amounts with the ethylene. 1-Butene, 1-hexene, 1-octene, and 4-methyl-1-pentene are the comonomers most commonly used commercially, producing respectively ethyl, butyl, hexyl, and isobutyl branches. On a weight basis, comonomer is usually added in an amount less than 5% of the total composition. Figure 5 shows the relationship between density and comonomer content.

Rheology and Long-Chain Branching. Molten HDPE is a non-Newtonian fluid at temperatures of 140–200°C. Its effective viscosity is reduced sharply, up to several thousand times, when the melt-flow speed is increased. The viscosity of the polymer is also a function of its molecular weight. Non-Newtonian behavior of the melt at low shear rates allows correlation of melt viscosity with molecular weight. The reason for this behavior is disentanglement of polymer coils at high shear rate and their partial orientation in the flow direction.

By convention, the most convenient and generally accepted representation of melt viscosity is the "melt index", which is the amount of polymer flowing through a standard capillary viscosimeter at 190°C under a 2.16-kg load for 10 min (ASTM

Table 3. Properties of Three Typical Commercial HDPE Grades

Property	Test	Resin Grade		
		Injection molding	Blow molding	Film
Physical				
Melt index (2.16 kg)	ASTM D1238	33.59	0.36	0.31
High load melt index (21.6 kg)	ASTM D1238	High	34.14	23.22
Density, g/cm^3	ASTM D1505	0.9678	0.9557	0.939
Refractive Index, n_D^{25}		1.54	1.53	1.51
Molecular Weight (weight average M_w)	gpc	13,900	17,800	13,600
Molecular Weight (number average, M_n)	gpc	48,400	143,000	177,000
Polydispersity (M_w/M_n)	gpc	3.5	8.0	13.1
Weight percent hexene	C^{13} nmr	0.00	0.60	3.50
Mechanical				
Yield point, MPa[a]	ASTM D638	31.0	27.8	19.1
Tensile strength, MPa[a]	ASTM D638	31.0	23.4	29.5
Tensile Impact, kJ/m^2[b]	ASTM D638	9.0	56.8	143.6
Elongation, %	ASTM D638			
At yield point	ASTM D638	8.2	10.1	13
At break point	ASTM D638	8.2	669	745
Notched impact strength, kJ/m^2[b]	ASTM D256-84a	0.90	17.3	No Break
Flexural modulus, MPa[a]	ASTM D790-95a	1894	1375	822
Brinell hardness, MPa[a]		60–70	50–60	35–50
Hardness (Shore D)	ASTM D2240	67	62	51
Environmental stress-Condition A, h crack resistance	ASTM D1693	0	49	>1000
Condition B, h	ASTM D1693	0	29	>1000
Condition C, h	ASTM D1693	0	0	>1000
Thermal				
Melting point, °C		136	133.5	127
Brittleness temp. °C	ASTM D746		−140 to −70	
Heat resistance temp., °C		ca 122	ca 120	ca 117
Vicat softening point, °C	ASTM D1525	126	133	
Specific heat capacity, kJ/(kg·K)[c]		1.67–1.88	1.88–2.09	
Thermal conductivity, W/(m·K)		0.46–0.52	0.42–0.44	
Temp. coefficient of linear expansion			$(1–1.5) \times 10^{-4}$	
Temp. coefficient of volume expansion			$(2–3) \times 10^{-4}$	
Heat of combusion, kJ/g[c]			46.0	

Table 3. (Continued)

Property	Test	Resin Grade: Injection molding	Resin Grade: Blow molding	Resin Grade: Film
Electrical				
Dielectric constant at 1 MHz		2.3–2.4	2.2–2.4	2.0–2.3
1 kHz–1 MHz			$(2–4) \times 10^{-4}$	
1 kHz–1 MHz			$(2–4) \times 10^{-4}$	
Volume resistivity			10^{17}–10^{18}	
Surface resistivity			10^{15}	
Dielectric strength, kV/mm[d]			45–55	

[a]Data provided by D.R. Register from Phillips Petroleum Co. Polymer Testing Laboratory
[b]To convert MPa to psi· multiply by 145.
[c]To convert kJ/m^2 to ft·lbf/in.^{2}, divide by 2.1.
[d]To convert kJ to kcal, divide by 4.184.
[e]To convert kV/mm to V/mil, divide by 25.4.

Method D1238 condition 190/2). The melt index is inversely connected with molecular weight.

In addition to the so called short-chain branches (ethyl, butyl, hexyl, etc from copolymerization of alpha-olefins), many HDPE grades also contain a very small

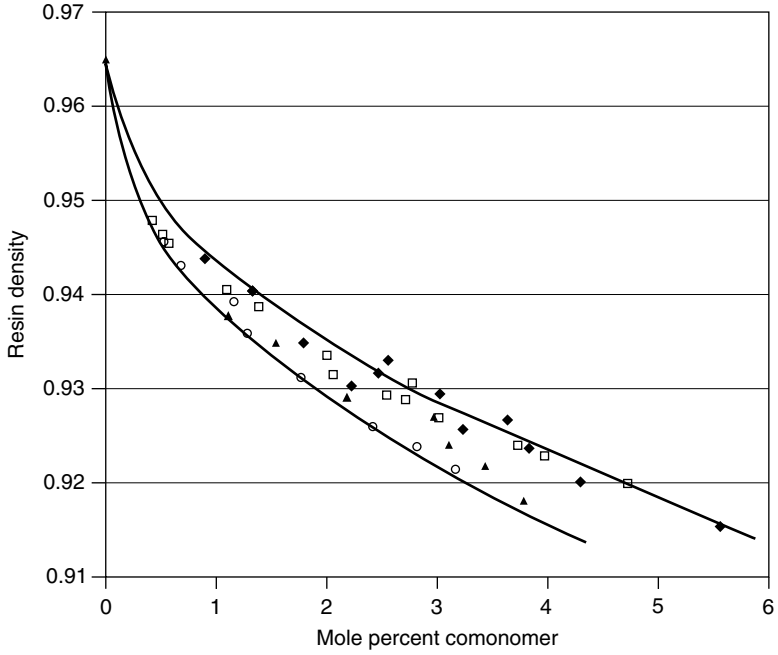

Fig. 5. Resin density vs comonomer content. ◆ 1-Butene; □ 1-hexene; ▲ 1-octene; and ○ 4-methyl pentene.

amount (perhaps less than 1 branch per 10,000 carbons) of long-chain branches. These branches are defined as being long enough to affect the rheology of the polymer, that is longer than about 130 carbons (85).

The viscosity of HDPE melt is strongly temperature dependent and can be described by an exponential dependence similar to the Arrhenius equation. The activation energy of the viscous flow of HDPE melt is usually 25–30 kJ/mol, but it increases with increasing long-chain branching (LCB) up to 40 kJ/mol, or even higher. This is one main method of determining the extent of LCB in a particular resin. Another method is to compare the measured (extrapolated) zero-shear viscosity to a value expected from a linear polymer of the same molecular weight.

Although LCB occurs infrequently in commercial HDPE, it has a profound effect when it does occur on the polymer flow behavior. Control of LCB is therefore critical in the manufacture of HDPE grades because it affects the suitability of the resin for film, blow molding, sheet, injection molding, and many other applications. Some applications require the presence of LCB, whereas in other applications it is a detriment (86,87). For example, LCB causes orientation in film, decreased die swell in blow molding, and greater melt strength in sheet, geomembranes, and blow molding. However, it also usually has a negative effect on environmental stress-crack resistance (ESCR), when compared at molecular weights to yield equivalent processing.

Long-chain branching in HDPE grades is thought to have its origin in the copolymerization of vinyl end groups. Upon termination of a chain, chromium oxide catalysts typically leave one vinyl group on one end of that chain, which can then be copolymerized into another growing chain, as shown in Figure 6 (25,88). This fact would explain why most Ziegler resins, which contain few vinyl end groups, also exhibit little LCB. The details of how this happens in a slurry process, where polymer chains crystallize out as solids as they are formed, are still debated. One thought is that chains are frozen out of solution almost instantaneously as they are formed so that reincorporation of vinyl end groups would most likely occur on a neighboring (and not the original) site as the tail of the incorporated chain is still mobile. This would explain why the degree of LCB can be controlled on a chromium oxide catalyst, by varying the chromium–chromium separation distance (ie, the chromium loading). Figure 7 shows how the activation energy of the polymer, which reflects the degree of LCB, is affected by chromium loading on the catalyst.

Other origins of LCB have also been identified. It has been observed that at the typically high molecular weight used in extrusion grade resins, LCB content is

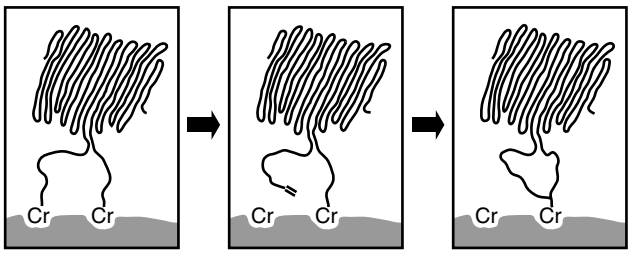

Fig. 6. Long-chain branch formation through reincorporation of vinyl end groups.

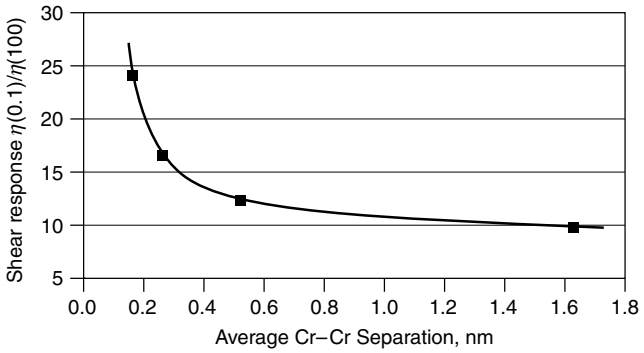

Fig. 7. Dependence of long-chain branching (as measured by shear response) on chromium loading.

highly dependent on the pore volume of the catalyst, even when the chromium site density is held constant. The effect is also seen in some silica-supported Ziegler resins of high molecular weight. When the porosity of the silica catalyst base is very low, high levels of LCB are seen in the resin. The exact reason for this behavior is unknown. One possible explanation is that long polymer chains entangled in small catalyst pores (where they were formed) of catalyst fragments resist melt flow much like true LCB, provided the relaxation time of these "knots" is longer than the relaxation time permitted by the molding process.

More recently, extreme LCB-like behavior has also been observed from certain metallocene-derived polymers (89,90). Reincorporation of vinyl end groups is again a possible method of origin. However, if true, it is hard to explain why some metallocenes are so much more potent than others at creating LCB, and why solution polymers or solution catalysts exhibit similar LCB levels to that of samples made in slurry mode. Direct activation of polymer C—H bonds by some catalysts has also been proposed as another avenue to the formation of LCB (91). "Chain walking" is known to happen on nickel-based catalysts (92) although it is unknown whether this also happens on zirconium-based systems. Recently, still another potential mechanism of LCB formation has also been advanced in this laboratory, although not proven. It is suggested that on some catalysts two alkyl chains may be simultaneously associated with one site through a bridging aluminum. If true, one chain terminated through beta-H elimination could be easily incorporated into the other on the same site as LCB (M.P. McDaniel and M.D. Jensen, Results from Phillips Petroleum Company Research Department).

Morphology. The only stable local chain conformation of HDPE at low temperature is the flat zigzag chain configuration with C—C bond length of 0.154 nm, and C—C—C bond angle of 112° (93). This local chain conformation also prevails in the melt and solution. The principal crystalline form of linear PE is orthorhombic, like the linear paraffins, with theoretical density of 1.00 g/cm^3. A second crystalline form is pseudomonoclinic with theoretical density of 0.965 g/cm^3. The former is typical of most articles made of HDPE, while the latter forms during low temperature stretching and orientation of films, and is thus always present in HDPE film. It is stable only below 50°C; annealing at 80–100°C restores the orthorhombic form.

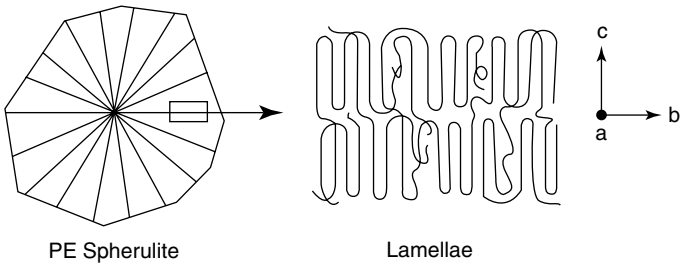

Fig. 8. Structure of HDPE spherulite.

The principal morphological units of PE crystallizing under typical conditions from the melt are spherulites, very small anisotropic spheres (ca 1–5 μm) visible under high magnification with polarizers (Fig. 8). The spherulites form as a result of a complex crystallization process of macromolecules. Their structural subunits are "rays," thin rod-like fibrils spreading in all directions from the center to the periphery and frequently branching, thus filling the spherulite body. The fibrils consist of lamellae (crystallites). Spherulites are characteristic only where HDPE crystallized slowly from the melt. In rapid crystallization, intertwined lamellae or rod-like structures are formed (94). During crystallization, polymer chains fold many times. When HDPE is crystallized from solution, this folding is tight, but when crystallized from the melt, the chain packing organization is much looser (95).

HDPE crystallizes very rapidly. Articles such as films, filaments, pipes, and injection-molded articles exhibit some degree of molecular and crystal orientation. This orientation develops either spontaneously during melt flow and crystallization, or is introduced deliberately by stretching. The degree of orientation can be measured by x-ray, polarization spectroscopy, acoustical methods, or birefringence.

When films or filaments are stretched uniaxially below the melting point, the *c*-axis of the crystals is always oriented parallel to the stretching direction, as is typical for all semicrystalline polymers. The degree of orientation increases with the stretching ratio and can approach 100% (96). A similar orientation is developed during the crystallization of a strongly oriented PE melt, such as during capillary melt flow or solid-state extrusion. Under these conditions, both crystalline and amorphous phases are nearly perfectly oriented in the flow direction (97). When a polymer melt is slightly stretched at the outset of crystallization, a condition typical in the production of blow-molded parts, the resulting solid films exhibit a significant orientation of the *a*-axis of the crystal in the machine direction (98).

Polymer Properties

Mechanical Properties. Polyethylene properties can be made to vary over a wide range, by controlling the molecular weight, the molecular weight distribution, the degree of branching, the type and placement of branching, the end group moieties, the extent of LCB, and by adding certain fillers, flow enhancers, etc. It is no surprise then that hundreds of different grades of HDPE exist for as many

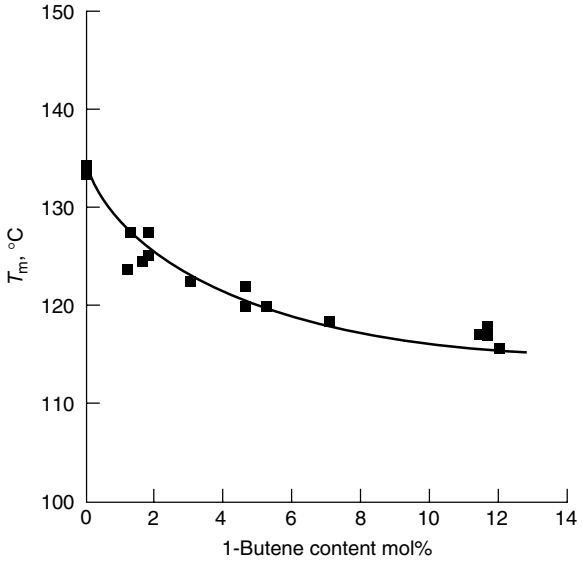

Fig. 9. Melting point of HDPE as a function of 1-butene content.

different applications, each of which require widely different properties. Such important final end-use properties include the stiffness of the polymer, the gloss or clarity, the impact, puncture or tear resistance, chemical resistance, electrical insulation properties, molding characteristics, and tensile properties, to name only a few. Table 3 lists some of the most important polymer properties for three typical commercial HDPE grades.

Measurements of highly crystallized HDPE samples give melting points of 133–138°C. The melting point is a function of both molecular weight and of branch content. In linear PE, the decrease in molecular weight from ca 1,000,000 to 40,000 is accompanied by a decrease in melting point from 137 to 128°C. The change in melting point with branch content is shown in Figure 9.

HDPE is a very good insulator and is therefore widely used for wire and cable encapsulation. Polymer density and molecular weight affect electrical properties very little. HDPE is only slightly permeable to organic compounds, both in liquid and gas phases. Permeability to water and inorganic gases is also low.

Forced elongation of an HDPE sample into a film or rod is accompanied by structural and mechanical changes (Fig. 10) At low deformations (ca 0.5% of sample length), spherulites elongate elastically. Further strain results in a partial break of bridges between crystallites in lamellae, slippage of the lamellae in rays constituting spherulites, ray splitting, and other irreversible mechanical changes. These processes can be regarded as a succession of partial "meltings" of the morphological features of HDPE under mechanical stress.

At some point, called the yield point, these transformations accumulate, causing a significant change in sample appearance. A "neck" develops, which is an area consisting of highly oriented bundles of polymer molecules. With further elongation, the initial morphological structures (spherulites, rays) are disassembled and the growth of the oriented polymer area continues. The primary mechanism

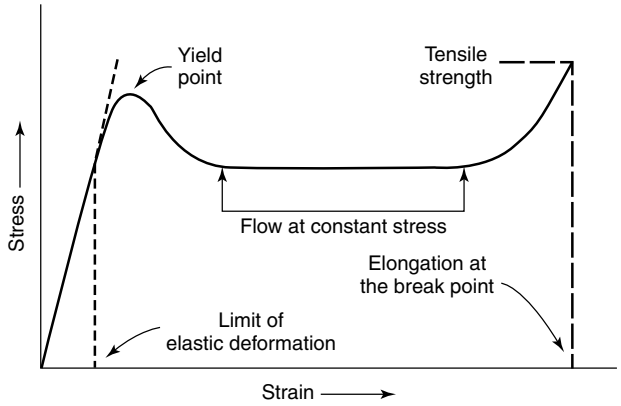

Fig. 10. Idealized stress–strain curve for HDPE.

of this transformation is slippage of lamellae with respect to one another and crystallite reorientation. This process develops in the boundary layer between the unchanged part of the sample and the neck, and continues in the neck, causing further strain. As a result, the sample elongates at nearly constant stress until all material in the samples becomes highly oriented. Subsequently, the oriented structure adsorbs additional small strain at increased stress and finally beaks. This ultimate stress is defined as the tensile strength.

Molecular weight has a large effect on this behavior. Low molecular weight HDPE is brittle and breaks at low strain (ca 10%) without neck development. In the range of 80,000–1,200,000, typical for commercial HDPE, the neck always develops. The yield point of such polymers is nearly constant. However, increasing molecular weight is accompanied by decreasing elongation at the breakpoint, from ca 1200–1500% to 200–300%, and by significant increase in tensile strength, from ca 35–40 MPa (5075–5800 psi) to ca 60 MPa (8700 psi). Finally, HDPE with molecular weight greater than 1,500,000 does not develop a neck but elongates by 200–400%. Tensile strength of such polymers is very high, ca 60–70 MPa (8700–10,150 psi).

Molecular weight also significantly affects impact strength. Low molecular weight samples are brittle, but with increasing molecular weight, impact–stress resistance can become very high.

An increase in branching reduces crystallinity and is accompanied by significant modification of mechanical characteristics. An increase in branching is accompanied by an increase in elongation at breakpoint and a significant drop in tensile strength.

It is generally accepted that the mechanical strength of a polymer sample is determined by the number of intercrystallite links, that is, polymer chains anchored in adjacent crystallites and binding them (Fig. 11). These links are the weakest elements of the polymer structure. Special developments in processing allow a significant increase in the number of the intercrystallite links. The technology employed is either low temperature (ca 100°C) extrusion of solid HDPE at high pressure [ca 200–300 MPa (29,000–43,500 psi)] or continuous casting of film from a dilute solution. Such films are highly stretched (up to 40 times), usually

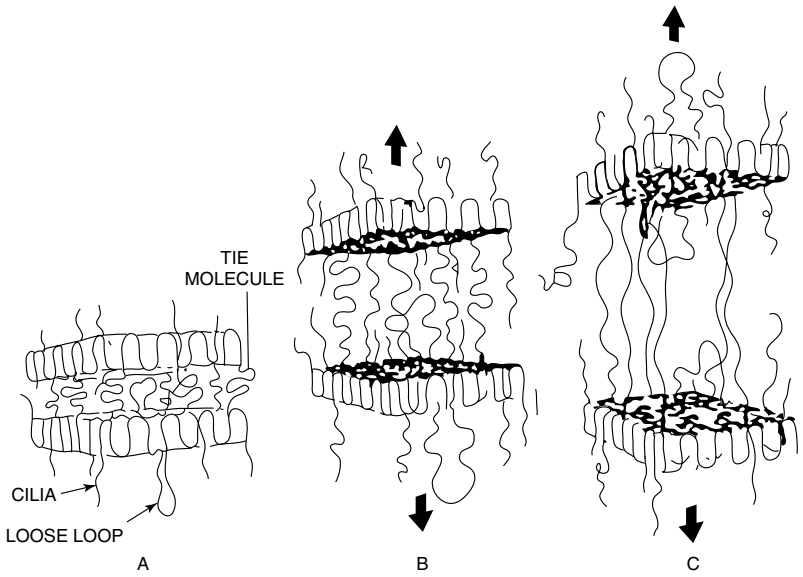

Fig. 11. Role of intercrystallite links in resin failure.

transparent, and almost perfectly oriented in both phases. They exhibit ultrahigh modulus [up to 100 GPa (1.45×10^7 psi)] and very high tensile strength of ca 500–600 MPa (72,500–87,000 psi).

One type of PE that has an increased number of intercrystallite links, and thus improved physical properties, is called bimodal polymer. These polymer grades are usually made of two components—a low molecular weight homopolymer blended with a high molecular weight branched copolymer. In this combination, having branches on the longest chains selectively places these chains in the amorphous phase, which thus increases the probability that they will function as intercrystallite links. Much of PE research today is aimed at producing more efficient methods of manufacturing such bimodal polymers.

Another important property that is influenced by molecular weight, by branching, and by intercrystallite links is load-bearing ability or resistance to creep. This property is of particular importance in applications in which the applied stress is continuous or frequent and represents an appreciable (though not necessarily large) fraction of the tensile strength. Even though the tensile strength of linear PE decreases considerably as density is decreased, the load-bearing ability of the polymer is greatly improved at densities decreasing from 0.960 to 0.950 g/cm^3. Not only is time to failure increased greatly, but deformation is decreased.

Chemical Resistance. Linear PE is predominantly saturated linear hydrocarbon, and thus in general it exhibits low chemical reactivity. High crystallinity and low permeability to most chemicals reduce the reactivity of solid HDPE even further. HDPE is stable to alkaline solutions and solutions of salts, including oxidizing agents such as $KMnO_4$ and $K_2Cr_2O_7$. It does not react with organic acids, HCl, or HF. Concentrated HNO_3 (ca 50%) does nitrate the polymer, even at room temperature.

HDPE is not soluble in any known solvent at room temperature, although several solvents (ie, xylenes) have a swelling effect. However, certain binary solution mixtures including CS_2 dissolve HDPE at as low as 30–40°C. Above 80°C HDPE dissolves in many aliphatic and aromatic hydrocarbons and their halogen-substituted derivatives. Solvents most frequently used include xylenes, tetralin, decalin, o-dichlorobenzene, 1,2,4-trichlorobenzene, and 1,2,4-trimethylbenzene. These solvents are employed for the determination of molecular weights from solution–viscosity data or by gpc.

An important measure of chemical resistance which is often used in household and industrial containers is environmental stress-crack resistance (ESCR). Many variations of the test are known and used, such as ASTM D1693, Conditions A and B. In these tests, the plastic part, a molded bar, a bottle, or a tube, etc, is placed under a standardized stress usually at elevated temperature, and exposed to a surface active agent. For example, one test uses 10% surfactant in aqueous solution at 60°C. The time needed for the sample to break is then recorded. The surfactant is thought to aid in the relaxation and disentanglement of chains.

Degradation. HDPE is relatively stable to heat because of the high bond energy of the single C—C bond. However, above about 290–300°C, chemical processes in an inert medium begin to result in breakage and cross-linking of chains. This reaction is similar to thermocracking of linear hydrocarbons. Near 500°C in an inert atmosphere, HDPE is rapidly pyrolized to a mixture of low molecular weight alkanes, alkenes, and dienes.

Oxygen is quite aggressive toward the C—H bonds of these macromolecules at the usual melt processing temperatures (200–300°C). This type of degradation is also a combination of radical reactions, resulting in a reduction of molecular weight, formation of oxygen-containing groups such as hydroxyl, carbonyl, and low molecular weight by-products such as water, aldehydes, and ketones. The initiation of oxidation can be enhanced by transition-metal impurities in the polymer from catalyst residues. For this reason it is important to achieve high activity from the catalyst, leaving only a few ppm of transition metal in the polymer. The conditions of commercial pelletization and molding favor thermooxidative degradation, and therefore oxygen is preferably excluded if possible. Protection is also nearly always afforded by the addition of an antioxidant package as well, which can include hindered phenols, phosphites, and other specialized agents added in the concentration of 0.01–1.0%.

Exposure of the molded HDPE articles to sunlight and air also attacks the polymer over time, especially at wavelengths less than 400 nm. Photooxidation resembles thermooxidation in that it is a complex chain of radical transformations. Such exterior aging of the polymer results in development of surface cracks, brittleness, changes in color, and a deterioration of mechanical and dielectrical properties. Photooxidation degradation is prevented by small amounts of light stabilizers, such as 2–4% carbon black or, for colorless articles, esters of salicylic acid or derivatives of benzotriazole or benzophone and others in the 0.1–0.5% range.

Chemical reactions of HDPE not involving oxidation include fluorination, chlorination, and sulfonation. Sometimes molded articles, such as fuel tanks, are given such a surface treatment to increase diffusional resistance.

Manufacturing Processes

Many diverse commercial technologies exist for the manufacture of HDPE, developed by many different companies worldwide. However, they can be divided into three fundamental types: (*1*) solution processes, (*2*) slurry processes, and (*3*) gas-phase processes. In recent years, hybrids and combinations of these three basic forms have also been widely used.

Solution Processes. The earliest commercial HDPE plants used a solution process in which the polymer dissolves in a hydrocarbon solvent as it is formed. Cylcohexane was commonly used as solvent at 120–150°C. Initially catalyst productivity was low, but the solution process allowed a filtration or centrifugation step in which catalyst residue could be removed. Later, as catalyst productivity improved, this step could be omitted in some processes. Low molecular weight polymers are made more easily in the solution process because of the lower solution viscosity. Although most of the earlier solution processes have been shut down due to poor economics, more recent improved designs, such as those developed by DuPont, Dow, and others, are still in production today and considered competitive (98–104).

For example, the DuPont process is reported to operate at a temperature in excess of 150°C and a pressure of about 8 MPa (1160 psi). Residence time in the reactor is short, on the order of 5–10 min and polymer concentration relatively high, up to 35% for low molecular weight grades. The sensible heat of the reaction mixture is employed to flash concentrate the solution from which the product is recovered in a devolatilizing extruder. Terminating agents and stabilizers are added in the extruder. Vapor from the flash step is condensed, cooled, and returned to the reactor. Residual hydrocarbon is removed in the extrusion step and purified for recycle to the polymerization.

The advantages of this process are a relatively small reactor and short residence time which allows fast transition between grades and easy control of some polymer properties. Because of the higher reactor temperature, higher alpha-olefins can be more easily used in the solution process than in other processes, and thus ethylene 1-octene copolymers are common from this technology. The longer side chains derived from 1-octene (versus 1-hexene or 1-butene) are thought to improve some resin properties. The solution process is also easily adaptable to multiple reactor schemes in order to tailor the molecular weight distribution.

Further development of the solution polymerization concept has led to molten PE as a medium for ethylene polymerization. Installations typically used for free-radical ethylene polymerization at high pressure are converted to accommodate catalytic ethylene polymerization. Stirred autoclaves operating at 30–200 MPa (4350–29,000 psi) and 170–350°C are convenient (105,106). Residence time is very short, typically less than 1 min.

Slurry Processes. If the hydrocarbon liquid described above is deliberately chosen to be a bad solvent for PE, and the temperature is lowered so that the polymer does not swell or melt in the hydrocarbon, the resultant process is called slurry technology because the polymer is produced as a suspended powder. In slurry systems the hydrocarbon non-solvent is called the diluent. Two major types of slurry systems are widely used throughout the worldwide HDPE industry:

(*1*) light hydrocarbon loop reactor processes and (*2*) heavier hydrocarbon stirred tank reactor processes.

Phillips Petroleum Co. originally developed the loop slurry process in the late 1950s for its chromium oxide catalyst, and Phillips has continued to develop the loop technology up to the present on an ever larger scale. The preferred diluent is isobutane, which was chosen to allow maximum reactor temperature without polymer swelling. This was necessary because the early chromium catalysts tended to produce lower melt index polymer (higher molecular weight) than optimum for the new extrusion market. Higher reaction temperatures permit higher melt index polymer to be produced. Initially, many hydrocarbon diluents were tested, and the degree of polymer swelling caused by each diluent was found to be related to the ratio of CH_3 to total carbons in the hydrocarbon (107). Thus, for example, pentane was inferior to isopentane, and neopentane, which has the highest CH_3/C ratio of any hydrocarbon, permitted the highest reactor temperature without swelling. However, isobutane, which permits a top reactor temperature of 113°C, was considered as a close second and more economical.

The choice of light diluents and high reactor temperatures also means relatively higher operating pressures. Thus a pipe-loop reactor was considered a convenient way to accommodate operating pressures of up to 5.5 MPa (800 psig). The reactor is equipped with an impeller which drives a concentrated slurry of polymer and isobutane rapidly around the jacketed loop at 5–12 m/s. Today's loop reactors can run up to 50% solids (by weight), typically in the temperature range of 80–110°C. Residence time is 0.5–1.5 h and conversion is high per pass (95–98%) (99).

The initial development of a slurry process for Ziegler-based catalysts did not face the same problems as scientists at Phillips. Since Ziegler catalysts are much more sensitive to hydrogen, molecular weight control does not rely on precise control of high reactor temperatures, as it did for the chromium oxide based loop slurry process. Therefore, lower reactor temperatures and heavier hydrocarbons were possible, and there was no need to go beyond a stirred tank. Hoechst developed the first such process, but Montedison, Mitsui, Solvay, and others have also developed similar processes.

In the Hoechst process, for example, hexane is used as the diluent (108,109). Hexane, ethylene, alpha-olefin, catalyst components, and hydrogen are continuously fed into a stirred reactor for polymerization. The slurry is then transferred into a smaller reactor for post-polymerization, after which the total charge is separated by a centrifuge into a liquid stream (which is returned to the initial reactor) and solid polymer. The wet polymer is steam-stripped from the solvent, dried, and pelletized. The stripped hexane is purified and recycled. Although stirred tanks are most common, loops can also be used in this fashion. In some schemes, a portion of the recycle diluent from the centrifuge is returned to the reactor, and a portion is fed to recycle purification for wax removal. This step removes some of the lowest molecular weight polymer, which dissolves in the diluent.

Gas-Phase Processes. Unlike solution or slurry processes, the original gas-phase polymerization processes employed no hydrocarbon diluent. Union Carbide introduced the first gas-phase technology in 1968, and other firms soon developed the approach still further, such as Naphtachimie, British Petroleum, BASF, and Amoco (110–114). In this technology, solid catalysts are used for ethylene polymerization or its copolymerization with light comonomers in the

gas phase. The system can be agitated by mechanical devices, such as horizontal paddles or screws, but more often by a gas stream of ethylene which fluidizes the PE particle bed.

A typical fluidized bed reactor has a length-to-diameter ratio of ca 7 and a disengagement zone at the top. Uniform fluidization is achieved by ethylene flow through a distribution plate at the reactor bottom, and rapid circulation is needed to remove heat. Conversion is about 2% per pass. Unreacted ethylene enters the disengagement zone, separates from the entrained polymer particles, and is filtered, cooled, compressed, and recycled. A catalyst is continuously fed to the reactor without diluent, and polymer particles are continuously removed from the bed through a system of valves. Reactor temperatures of 70–100°C are common, with pressure of 1.4–3.5 MPa (200–500 psig).

Polymerization of ethylene is quite exothermic (3.4×10^6 J/kg) and since the heat capacity of gas is much lower than that of liquid, removal of the heat of polymerization can be problematic compared to solution and slurry processes. This was usually accomplished by lowering the activity of gas-phase catalysts by say 50–75% to reduce the rate of local heat generated. To compensate, the residence time was then extended to several hours. As a result of these differences, gas-phase processes tend to have a much larger polymer inventory in the reactor. The gas-phase approach is also more rigid in its catalyst requirements. The kinetic profile of a catalyst for a gas-phase process should preferably have a steady activity lasting 2–3 h. The particle size for consistent fluidization is also sometimes important, and smaller particles are preferred for heat removal.

The fluidized bed gas-phase process offers some advantages and disadvantages compared to the slurry processes. Since there is no diluent, it makes low density resins well, without swelling. The lack of diluent also simplifies the operations and equipment to some degree. On the other hand, transitions are extremely slow and there is usually a large inventory which can greatly increase the off-specification rate during transitions. Gas-phase units are sometimes also more sensitive to poisons in the feedstocks, and more sensitive to fouling. Once a reactor has "logged," cleanup can be longer and more difficult for a gas-phase reactor.

In recent years the fluidized bed processes have been improved through the addition of liquid hydrocarbons into the polymer bed (115,116). These evaporate, adsorbing heat from the bed more effectively than gas alone, and are then condensed in the recycle stream and reused. The result of this "condensed mode" or "super condensed mode" approach is increased production rates from the same reactor, or greater tolerance for higher activity catalysts. Of course, it reverses some of the benefits of pure gas phase, since it is a step back toward hydrocarbon diluent. Nevertheless, this innovation has greatly improved operations and production of the gas-phase process, instilling new life into the technology.

Bimodal Reactor Technology. In a modification of the original stirred tank slurry process, Hoechst, Nissan, Mitsui, and others developed cascade reactor systems to make bimodal resins with improved properties (67,117,118). Under these processes, multiple reactors are aligned in series, parallel, or a combination of series and parallel, so that a Ziegler catalyst is exposed to more than one set of reaction conditions during its lifetime. In this way low molecular weight homopolymer can be produced in combination with high molecular weight copolymer, the

so-called bimodal resin combination. This technique was originally developed to counteract the limitation of Ziegler catalysts, which unaided, tend to make a narrow molecular weight distribution which is not useful for many extrusion applications. However, this type of broadening also allows the branching to be selectively placed into the high molecular weight portion of the distribution.

In later years, other reactor arrangements have also been developed to produce bimodal resins. Other variations include combining two loops in series (Solvay, Fina, and others), two gas-phase reactors in series (Union Carbide), and loop/gas phase (Borealis).

Multiple reactor processes have some advantages and disadvantages over single reactor arrangements of similar capacity. They produce some unusual resins that (at the time of this writing) cannot be exactly duplicated by any other means, such as high molecular weight film resins. However, they are also more complicated and more expensive to build and run, and they are much less flexible in what can be made. Many HDPE researchers believe that new single-site catalyst advances will eventually make bimodal reactor technology obsolete.

Commercial Applications of HDPE

Its low melting point and high chemical stability facilitate the processing of HDPE by many conventional techniques. Some of the most common applications include injection molding, blow molding, blown and cast film, pipe and tubing, and wire and cable coating. Table 4 indicates the approximate current breakdown in the United States by end use.

Injection Molding. In this technique molten HDPE is injected into a metal mold at 200–260°C and 70–140 MPa pressure (690–1380 atm). The mold is then cooled and opened and the solid article, which is now in the shape of the mold, is removed. Usually resins with a narrow molecular weight distribution are preferred

Table 4. U.S. Usage of HDPE by Application

Market	Annual usage, 10^6 t	Market share, %
Extrusion		
Film (up to 12 mil)[a]	1.06	15.6
Sheet (over 12 mil)[a]	0.35	5.1
Pipe and conduit, corrugated	0.30	4.3
Pipe and conduit, noncorrugated	0.58	8.5
Other extruded products	0.21	3.1
Rotomolding	0.07	1.0
Injection Molding	1.08	15.7
Blow Molding	2.23	32.5
Resellers and Compounders	0.85	12.4
All other uses	0.12	1.8
Total	*6.85*	*100*

[a]Reflecting usage from the first quarter, 2000. Data from Digest of Polymer Developments, Series I, Number 95, STR Publishing, Enfield, Conn., May, 2000.
1 mil = 0.025% mm.

for injection-molding applications, because broader distributions are more likely to leave orientations frozen into the articles upon cooling because of the slower relaxation time. Such frozen orientations can lead to warpage of the article upon cooling. For this reason most injection-molding resins are prepared from Ziegler catalysts. Because of the narrow molecular weight distribution, which tends to resist flow at high shear, and because of the need to completely fill sometimes intricate molds, injection-molding resins generally have lower average molecular weights than are needed for other applications. Injection-molding resins generally include the melt index range of 3–80. A wide diversity of articles are made from injection-molded HDPE including cups, pails, toys, housewares, auditorium seats and chairs, crates, food containers, etc. (see INJECTION MOLDING).

Blow Molding. Blow molded articles account for the largest single use of HDPE. The technique is used for rapid processing of large quantities of articles of relatively simple configuration, such as bottles and simple containers. A molten tube of HDPE, called a parison, is extruded through a die and then enclosed by a doubly split metal mold (Fig. 12). The parison is blown by air pressure to conform to the internal configuration of the mold into the formed article, much as glass is blown into bottles. When the melt leaves the die, it swells and the parison diameter increases, especially with HDPE of high molecular weight and at high extrusion rates (see BLOW MOLDING).

In the initial phase of blow molding, the molten tube is extruded at high pressure and rate through a small die gap and the tube thus formed is free-hanging in the mold. Thus, low viscosity at high shear is preferred to enhance extrusion, but to resist sagging in the mold, high zero-shear viscosity is preferred. Thus this combination is achieved by using broader molecular weight distribution resins of relatively high molecular weight (melt index 0.1–0.5). Chromium catalysts are ideal for producing blow-molding resins.

Another important characteristic of blow-molding resins is the degree of "parison swell" and "die swell." The former is the extent to which the molten tube tends to flare out during the extrusion step. An excessively high degree of flare can cause the tube to extend beyond the mold cavity, while too little flare can sometimes cause incomplete filling of the mold structure. Die swell is a measure of how much the tube wall expands as it exits the die under high pressure. The die gap must be adjusted to take die swell into account in order to produce the desired wall thickness. Molders prefer to set this parameter midway and not have to

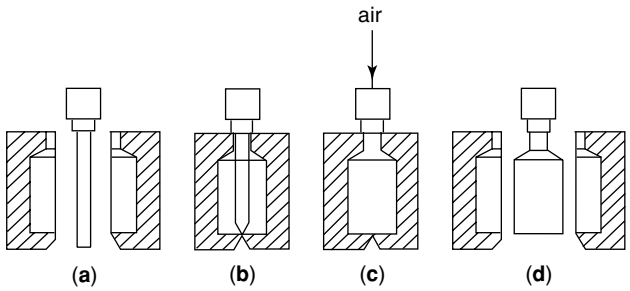

Fig. 12. HDPE blow molding processing steps: (**a**) extrusion of parison, mold is open; (**b**) mold is closed; (**c**) air is blown into parison; and (**d**) mold is opened for removal of article.

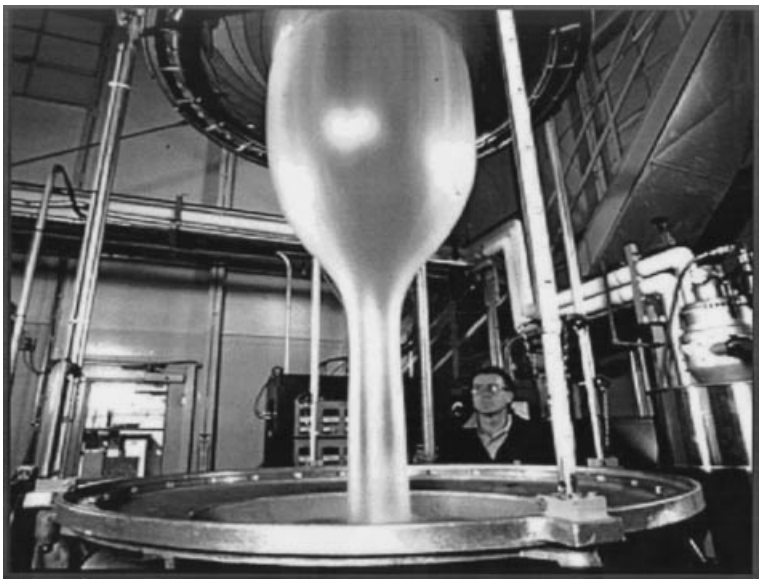

Fig. 13. HDPE film blowing.

readjust it from one resin lot to another. The degree of swell in these resins is highly influenced by the degree of LCB in the resin. A certain minimum level of LCB is required for most resins. This is another reason that chromium oxide catalysts lend themselves well to blow-molding applications. LCB content can be adjusted easily by varying chromium loading, activation temperature, or cocatalyst level.

Blow molding is widely used to form bottles for food packaging, detergents, oil, and other household materials, industrial drums, fuel tanks for automobiles, toys, and a wide assortment of other articles.

Blown Film. The impermeability, stiffness, and higher softening temperature of HPDE make it useful for certain film applications (Fig. 13). A continuous roll of blown film is produced by extrusion of HDPE melt through a die with a circular slit of ca 0.6–1.5 mm; the diameter of the ring can typically be as large as 80–100 cm. The extruded thin-walled tube rises vertically and is filled with air, thus expanding the tube to a certain size. Usually the ratio of the tube diameter to the die diameter is about 4:1, allowing for the formation of a film trunk up to 4 m in diameter. The film, 0.007–0.125 mm thick, is air-cooled and rolled. Bags can be made from the rolled hollow film tube, or it can be split into one continuous sheet for wrapping and other uses. In coextrusion, two different types of plastic are simultaneously extruded through a single die with two concentric circular slits, giving a layered film. This can be done to achieve special physical properties or permeability resistance.

Chromium-based catalysts can be used quite widely for production of HDPE film grades but some of the best HDPE films, in terms of mechanical properties and extrusion rates, are bimodal resins made from Ziegler catalysts passing through two or more reaction zones. Most recently, metallocene resins have been used to produce extremely high clarity resins, despite the high density. Applications of HDPE films include food packaging, grocery and merchant bags, and drum liners.

The thickest blown film made from HDPE, sometimes called sheeting, ranges in gauge from 0.5 to 3.0 mm and is used in geomembranes. Geomembrane blowing operations typically produce a sheet 6.9 m wide (22.5 ft), with the bubble rising eight stories into the air, weighing 2.5 tons. Geomembrane sheeting is used to protect the environment by lining pits and covering landfills. For example, sewage ponds and spillover sumps near oil and chemical storage tank areas are first lined with geomembrane to prevent seepage into the groundwater. Reservoirs to hold drinking water are also lined with geomembrane in some regions to prevent loss. Leaching pads used in mining operations, irrigation canals, evaporation ponds, and industrial waste lagoons are other applications of geomembrane. In this type of service, toughness is extremely valued to avoid penetration by rocks, tree roots, etc. Thus, high molecular weight and a significant amount of branching is preferred in the polymer. The blowing operation favors resins with high melt strength, which is imparted by high levels of LCB. Chromium catalysts are commonly used for this type of blown film.

Thermoforming. Thermoforming is a process in which the resin is extruded into flat sheets of perhaps 2–13 mm after which that sheet is softened by heat and then stamped or pulled by vacuum into a large mold. Thermoformed sheet is widely used for trays, pans, for lining the beds of pickup trucks or other vehicles, for flooring, and a wide variety of other articles. Thermoforming resins typically require stiffness, toughness, and good melt strength, all of which are achieved from chromium oxide catalysts at 0.05–0.2 melt index.

Pipe and Tubing. Pipes (diameter >1 cm) and tubing (diameter <1 cm) are produced by passing HDPE melt through a die with a circular channel, forming a thick tube. Immediately after leaving the die, the molten tube enters a vacuum calibrator, where it is forced against sizing rings and cooled. Extrusion and drawdown (ratio of the cross-sectional area of the die opening to the tube wall) are adjusted with the help of mechanical pulling devices. For pipe manufacture, die openings are large, resistance to polymer flow is low, and drawdown does not exceed 1.1. Pipes with diameter ca 1.5 m are made commercially.

HDPE pipe is used in low pressure applications for transporting potable water, gas, acids, liquid hydrocarbons, oils, salt water, and other chemicals and solvents. Long-term load bearing, or "creep," tests are essential to determine the life of PE pipe under pressure. HDPE pipe withstands pressures in short-term burst tests that are several times greater than long-term burst pressures because of the creep phenomenon. Broad molecular weight distribution resin, as obtained from chromium oxide catalysts, are ideal for most pipe applications. The introduction of superior, bimodal type, pipe resins in recent years has extended HDPE pipe applications.

Wire and Cable Insulation. Excellent electrical properties and moisture resistance make linear PE ideal for wire and cable coatings. Use includes power, communications, and control applications. Continuous coatings can be extruded directly onto wire at high speed, followed by cooling in a bath. The lubricity and high abrasion resistance of the coating aid in conduit installations. Copolymers of 0.935–0.945 g/cm^3 density and ca 1 melt index are commonly used because of the good balance of toughness, ESCR, and extrudability. Polymers of medium-to-broad molecular weight distribution are preferred because of high coating speeds

and good surface finish. Addition of about 2.5% small particle carbon black greatly increases weather resistance.

Filament. In the production of monofilament, extruded strands are quenched, reheated, then pulled to draw ratios of 10:1. The tensile strength of finished filament is 345–690 MPa (50,000–100,000 psi) due to the high degree of orientation. Cord and rope are used in sporting goods and utility purposes. Larger PE rope is used in marine applications where it has a clear advantage over nylon, since HDPE floats and does not adsorb water. Ribbon yarn, made from split film, finds applications in carpet backing, some fabrics, bags, and in binding of multiwire cable together. A large market for these products is especially found in Asia and South America. Owing to its chemical inertness, linear PE is used for monofilament gauze for tissue reinforcement in surgery. Ziegler resins are particularly well suited to these applications, although chromium oxide derived resins are also common.

Rotomolding. Larger items, such as tote boxes, fuel tanks, and water storage tanks are often made by a rotational molding operation. Usually HDPE powder or pellets are introduced into a mold cavity which is then heated and rotated evenly. As the polymer melts, it coats the inside surface of the mold uniformly. The mold is then cooled while still under rotation to prevent sagging or other imperfections. Sometimes organic peroxide is added so that upon heating the plastic, a cross-linking reaction takes place in which the molecular weight and viscosity of the plastic dramatically increases. The mold is then separated and the article removed. Tanks up to 37.8 M^3 (10,000 gal) are made in this way. Rotomolding applications require good flow under zero-shear conditions. Narrow molecular weight distribution resins, as provided by Ziegler or metallocene catalysts, are preferred for rotomolding applications.

Health and Safety of HDPE

HPDE is generally inert and lacking in any toxicity, which accounts for its widespread use in food packaging. It is also used in prosthetic devices, in surgery, hip or knee joint replacements, etc.

HDPE can present some health hazard during its combustion, pyrolysis, or during thermocutting, when smoke, fumes or toxic decomposition products can be formed. Irritation of the skin, eyes, and mucous membranes of the nose and throat are possible. In some cases this irritation has been traced to traces of acrolein or formaldehyde from thermooxidative decomposition. However, other large-scale fire testing of foamed PE under actual conditions did not reveal significant acrolein formation and demonstrated that PE presents no worse hazard than cellulosic materials. Still other studies indicate that maximum evolution of irritants occurs from smoldering combustion at 300–400°C.

BIBLIOGRAPHY

"Ethylene Polymers" in *EPST* 1st ed., Vol. 6, pp. 275–454; "Ethylene Polymers, High Density Polyethylene" in *EPSE* 2nd ed., Vol. 6, pp. 454–490, by D. L. Beach, Chevron Chemical Co., and Y. V. Kissin, Mobil Chemical Co.

1. E. Hinderman, *Dissertation*, Zurich, 1897.
2. H. von Fechman, *Ber.* **31**, 2643 (1898).
3. E. Bamberger and F. Techirner, *Ber.* **33**, 955 (1900).
4. J. Hertzig and R. Schonbach, *Monatsh. Chem.* **33**, 677 (1912).
5. H. Meerwein and W. Burneleit, *Ber.* **618**, 1840 (1928).
6. W. Werle, *Dissertation*, Marburg, 1938.
7. Phillips Petroleum Co., unpublished data, 1981; H. R. Sailors and J. P. Hogan, *J. Macromol. Sci. Chem. A* **15**(7), 1377–1402 (1981).
8. Hoberg, and K. Ziegler, *Brennstoff-Chemie* **39**, 302 (1958).
9. R. A. V. Raff and E. Lyle, in R. A. V. Raff and K. W. Doak eds., *High Polymers*, Vol. **XX**, Part I, Wiley-Interscience, New York, 1965, p. 8.
10. H. Pichler, *Brennstoff-Chemie* **19**, 226 (1938).
11. H. Pichler and H. Buffleb, *Brennstoff-Chemie* **21**(24), 285 (1940).
12. J. C. Swallows, in A. Renfraw and P. Morgan, eds., *Polythene*, 2nd ed., Interscience Publishers, New York, 1960, pp. 1–10.
13. Brit. Pat. 471590 (allowed Sept. 6, 1937), E. W. Facett and co-workers (to ICI).
14. J. J. Fox, and A. E. Martin, *Trans. Faraday Soc.* **36**, 897 (1940).
15. U.S. Pat. 2816883 (Filed 1951, Issued 1957), A. W. Larcher and D. C. Pease (to E. I. du Pont de Nemours & Co., Inc.).
16. U.S. Pat. 2692257 (Filed Apr. 28, 1951, Issued 1954), A. Zietz (to Standard Oil of Indiana).
17. Belg. Pat. 530617 (Filed Jan. 24, 1955 and in the U.S. on Jan. 27, 1953 as S.N. 333,576), J. P. Hogan and R. L. Banks (to Phillips Petroleum Co.); Aust. Pat. Appl. 864/54 (Filed Aug. 6, 1954).
18. Ger. Pat. 973626 (Filed Nov. 17, 1953 and issued Apr. 14, 1960), K. Ziegler and co-workers (to K. Ziegler); U.S. Pat. 3257332 (Filed Nov. 15, 1954 and issued June 21, 1966).
19. *Chemistry in the Economy*, American Chemical Society, Washington, D.C., 1973, p. 71.
20. E. L. D'Ouville, in Ref. 12, p. 35.
21. J. P. Hogan, in G. Ham., ed., *High Polymers, Vol. XVII*, Wiley-Interscience, New York, 1964, p. 111.
22. A. Clark and co-workers, *Ind. Eng. Chem.* **48**, 1152 (1956).
23. R. V. Jones and P. J. Boeke, *Ind. Eng. Chem.* **48**, 1155 (1956).
24. D. C. Smith, *Ind. Eng. Chem.* **48**, 1161 (1956).
25. M. P. McDaniel, *Adv. Catal.* **33**, 47–98 (1985).
26. R. Merryfield, M. P. McDaniel, and G. Parks, *J. Catal.* **77**, 348 (1982).
27. J. P. Hogan, *J. Polym. Sci., Part A-1* **8**, 2637 (1970).
28. *Inorg. Nucl. Chem.* **4**, 393 (1968); H. L. Krauss and H. Stach, *Z. Anorg. Chem.* **366**, 280 (1969).
29. M. P. McDaniel and M. E. Grayson, *J. Mol. Catal.* **65**(1/2), 139–144 (1991).
30. M. P. McDaniel and S. J. Martin. *J. Phys. Chem.* **95**, 3289 (1991).
31. C. Groeneveld and co-workers, *J. Catal.* **83**, 346 (1983).
32. H. L. Krauss and E. Hums, *Z. Naturforsch., B: Anorg. Chem., Org. Chem.* **34b**, 1628 (1979); H. L. Krauss and E. Hums, *Z. Naturforsch., B: Anorg. Chem., Org. Chem.* **35b**(7), 848 (1980); H. L. Krauss and E. Hums, *Z. Naturforsch., B: Anorg. Chem., Org. Chem.* **38b**(11), 1412 (1983).
33. H. L. Krauss, in *Symposium on the Mechanisms of Hydrocarbon Reactions*, Slofok Hungary, 1973.
34. J. A. N. Anjjou and S. L. Scott, *J. Am. Chem. Soc.* **122**(37), 8968, (2000).
35. J. A. N. Anjjou, S. L. Scott, and V. Paquet, *J. Am. Chem. Soc.* **120**(2), 415, (1998).
36. G. Ghiotti and co-workers, *J. Chem. Soc. Chem. Commun., Com.* **801**, 1032 (1979).

37. G. Ghiotti and co-workers, *J. Catal.* **80**, 249 (1983).
38. A. Zecchina and co-workers, *J. Phys. Chem.* **79**(10), 972 (1975).
39. A. Zecchina and co-workers, *J. Phys. Chem.* **79**(10), 978 (1975).
40. E. Garrone and co-workers, *J. Phys. Chem.* **79**(10), 985 (1975).
41. M. P. McDaniel and M. M. Johnson, *J. Catal.* **101**, 446–457 (1986).
42. E. A. Benham, P. D. Smith and M. P. McDaniel, *Polym. Eng. Sci. (SPE)* **28**(22), 1469–1472 (1988).
43. U.S. Pat. 3157712 (Nov. 1967), D. L. Walker and E. L. Czenkusch (to Phillips Petroleum Co.).
44. F. J. Karol and R. N. Johnson, *J. Polym. Sci., Polym. Chem. Ed.* **13**, 1607 (1975).
45. F. J. Karol, G. L. Brown, and J. M. Davison, *J. Polym. Sci., Polym. Chem. Ed.* **11**, 413 (1973).
46. F. J. Karol and co-workers, *J. Polym. Sci., Part A-1* **10**, 2621 (1972).
47. F. J. Karol and co-workers, *J. Catal.* **60**, 68 (1979).
48. U.S. Pat. 3840508 (Oct. 1974), D. G. H. Ballard and co-workers (to Imperial Chemical Industries).
49. P. D. Smith and M. P. McDaniel, *J. Polym. Sci., Polym. Chem. Ed.* **27**, 2695 (1989).
50. P. D. Smith and M. P. McDaniel, *J. Polym. Sci., Polym. Chem. Ed.* **28**, 3587 (1990).
51. M. P. McDaniel, C. H. Leigh, and S. M. Wharry, *J. Catal.* **120**, 170 (1989).
52. S. M. Wharry, S. J. Martin, and M. P. McDaniel, *J. Catal.* **115**, 463 (1989).
53. M. P. Mcaniel, C. H. Leigh, and S. M. Wharry, *J. Catal.* **120**, 170 (1989).
54. M. P. McDaniel, M. B. Welch, and M. J. Dreiling, *J. Catal.* **82**, 118 (1983).
55. T. T. P. Cheung and co-workers, *J. Catal.* **102**, 10–20 (1986).
56. F. J. Karol, *Catal. Rev. Sci. Eng.* **26**(3/4), 557 (1984).
57. G. Fink, R. Mulhaupt, and H. H. Brintzinger, *Ziegler Catalysis: Recent Scientific Innovations and Technological Improvements*, Springer-Verlag, New York, 1995.
58. J. Boor Jr., *Ziegler–Natta Catalysts and Polymerizations*, Academic Press, Inc., New York, 1979.
59. Y. V. Kissin, *Macromol. Symp.* **89**, 113 (1995).
60. Brit. Pat. 1286867 (1969), A. Mayr and co-workers (to Montedison).
61. W. A. Hewett, *J. Polym. Sci. B* **3**, 855 (1965).
62. G. A. Short, and E. C. Shokal, *J. Polym. Sci. B* **3**, 859 (1965).
63. J. L. Martin and co-workers, *Inorg. Chem.* **23**, 4589 (1984).
64. J. L. Martin and co-workers, *Inorg. Chem.* **24**, 2997 (1985).
65. H. L. Hsieh, M. P. McDaniel, J. L. Martin, P. D. Smith, and D. R. Fahey, in R. B. Seymour and T. Cheng, eds., *Advances in Polyolefins*, Plenum Publishing Corp., New York, 1987.
66. L. L. Bohm, J. Berthold, R. Franke, W. Strobel, and U. Wolfmier, in T. Keii and K. Soga, ed., *Proc. Int Symp.*, Tokyo, Japan, 4–6 July, 1985, *Proc. Int Symp.*, Elsevier, Amsterdam, 1985, p. 29.
67. L. L. Bohm, H. F. Enderle, and M. Fleissner, *Plast. Rubber Compos. Process. Appl.* **27**(1), 25 (1998).
68. W. Breslow, *Justus Liebigs Ann. Chem.* 463 (1975).
69. W. Kaminsky, *Angew. Chem.* **88**, 689 (1976).
70. M. Aulbach and F. Kuber, *Chem. Unserer Zeit* **28**, 197 (1994).
71. P. C. Mohring and N. J. Coville, *J. Organomet. Chem.* **479**, 1 (1994).
72. K. B. Sinclair and R. B. Wilson, *Chem. Ind. (London)* 857 (1994); W. Kaminsky, *Catal. Today* **20**, 257 (1994).
73. H. H. Brintzinger and co-workers, *Angew. Chem. Int. Ed. Engl.* **34**, 1143 (1995).
74. U.S. Pat. 5919983 (March, 1997), R. K. Rosen and D. D. VanderLende (to The Dow Chemical Company).
75. U.S. Pat. 6107230 (Aug. 2000), M. P. McDaniel (to Phillips Petroleum Co.).

76. B. L. Small, M. Brookhart, and A. M. A. Benett, *J. Am Chem. Soc.* **120**, 4049 (1998).
77. *Angew. Chem.* **111**, 448 (1999); G. J. P. Britovsek, V. C. Gibson, and D. F. Wass, *Angew. Chem. Int. Ed. Engl.* **38**, 428 (1999).
78. U.S. Pat. 5891963 (Apr. 6, 1999), M. S. Brookhart and co-workers (to E. I. du Pont de Nemours & Co., Inc.).
79. G. V. Schultz, *Z. Phys. Chem., Abt. B.* **30**, 379 (1935); P. J. Flory, *J. Am. Chem. Soc.* **58**, 1877 (1936).
80. A. Clark and G. C. Bailey, *J. Catal.* **2**, 230,241 (1963).
81. M. P. McDaniel and M. M. Johnson, *Macromolecules* **20**, 773 (1987).
82. U.S. Pat. 4966951, (1990), E. A. Benham, M. P. McDaniel, and F. W. Bailey (to Phillips Petroleum Co.); U.S. Pat. 4818800 (1989), M. P. McDaniel and J. N. Short (to Phillips Petroleum Co.); U.S. Pat. 4364854 (1982), M. P. McDaniel and M. M. Johnson (to Phillips Petroleum Co.).
83. M. P. McDaniel, *J. Polym. Sci. Polym. Chem. Ed.* **19**, 1967 (1981).
84. W. C. Conner and co-workers, *Stud. Surf. Sci. Catal.* **75B**, 1827–1830 (1993).
85. J. Janzen and R. H. Colby, *J. Mol. Struct.* **569**, 485–486 (1999).
86. A. M. Sukhadia, in *Soc. Plastics Eng. ANTEC Conf. Proc.*, Atlanta, Ga., 1998, p. 160.
87. A. M. Sukhadia, in *Soc. Plastics Eng. ANTEC Conf. Proc.*, Atlanta, Ga., 1998, p. 1157.
88. J. P. Hogan, *Applied Industrial Catalysis*, Vol. **1**, Academic Press, Inc., Orlando, Fla., 1983, Chapt. "6".
89. WJ. Wang and co-workers, *Macromolecules* **31**, 8677 (1998).
90. A. Malmberg and co-workers, *Macromolecules* **32**, 6687, (1999).
91. M. K. Reinking, G. Orf, and D. McFaddin, *J. Polym. Sci., Part A: Polym. Chem.* **36**, 2889 (1998).
92. V. M. Mohring and G. Fink, *Angew. Chem. Int. Ed. Engl.* **24**(11), 1001 (1985).
93. H. V. Boenig, *Polyolefins: Structure and Properties*, Elsevier, Amsterdam, 1966.
94. L. Mandelkern and co-workers, *J. Polym. Sci Polym. Lett. Ed.* **19**, 435 (1981).
95. M. Stamm, *J. Polym. Sci. Polym. Phys. Ed.* **20**, 235 (1982).
96. R. S. Stain, in B. Ke, ed., *Methods of Polymer Characterization*, Wiley-Intescience, New York, 1964.
97. A. E. Zachariades and R. S. Porter, *J. Macromol. Sci. Phys. B* **19**, 377 (1981).
98. T. Nagasawa, T. Matsumura, and T. Hochino, *Appl. Polym. Symp.* **20**, 295 (1973).
99. J. N. Short, in R. P. Quirk, ed., *Transition Metal Catalyzed Polymerizations: Alkenes and Dienes*, Harwood Academic Publishers, New York, 1983, p. 651.
100. J. P. Forsman, *Hydrocarbon Process* **51**, 132 (Nov. 1972).
101. U.S. Pat. 3644325 (Feb. 22, 1972), R. F. Roberts Jr. (to The Dow Chemical Company).
102. U.S. Pat. 4209603 (June 24, 1980), J. J. M. A. Van de Leemput (to Stamicarbon B.V.).
103. U.S. Pat. 4067822 (Jan. 10, 1978), D. E. Gessell, G. L. Dighton, and L. D. Valenzuela-Bernal (to The Dow Chemical Company).
104. *Plast. Technol.* **26**(2), 39 (1980).
105. J. P. Machon, R. Hermant, and J. P. Houzeaux, *J. Polym. Sci. Polym. Symp.* **52**, 107 (1975).
106. J. P. Machon, in Ref. 99, p. 639.
107. J. P. Hogan, D. D. Norwood, and C. A. Ayres, *Applied Polymer Symposium Vol. 36: Commodity and Engineering Plastics*, Wiley-Interscience, New York, 1982.
108. B. Diedrich, *Polym. Prepr.* **16**(1), 316 (1975).
109. H. Kreuter and B. Diedrich, *Chem. Eng.* **81**(16), 62 (1974).
110. U.S. Pat. 4011382 (1977), I. J. Levine and F. J. Karol (to Union Carbide Corp.).
111. U.S. Pat. 4003712 (1977), A. R. Miller (to Union Carbide Corp.).
112. U.S. Pat. 3965083 (1976), J. L. Jezl, E. F. Peters, and J. W. Shepard (to Standard Oil Co.).
113. U.S. Pat. 3922322 (1975), R. Dormenval, L. Havas, and P. Mangin (to Napthachimie).

114. D. M. Rasmussen, *Chem. Eng.* **79**, 104 (1972).
115. U.S. Pat. 4255542 (1981), G. L. Brown, D. F. Warner, and J. H. Byon (to Union Carbide Corp.).
116. U.S. Pat. 5352749 (Oct. 1994), M. L. DeChellis and J. R. Griffin (to Exxon Chemicals).
117. U.S. Pat. 4307209 (Dec. 22, 1981), Y. Morita and N. Kashiwa (to Mitsui Chemical).
118. U.S. Pat. 4357448 (Nov. 2, 1982), K. Tsubaki and co-workers (to Nissan Chemical).

ELIZABETH BENHAM
MAX MCDANIEL
Chevron Phillips Chemical Company

ETHYLENE POLYMERS, LDPE

Introduction

Low density polyethylene (LDPE) was the first thermoplastic polyolefin used commercially. It was discovered serendipitously in 1933 and was quickly utilized for electrical cable sheathing for radars during the war. LDPE, along with high density polyethylene (HDPE) and linerar low density polyethylene(LLDPE), offers an unparalleled combination of low cost, ease of fabrication into a variety of end uses, and balance of physical properties. Polyethylene has displaced paper, metal, wood, and other materials of construction. LDPE is unique in its polymerization process. Free-radical-initiated polymerization is used to make LDPE, as compared to transition-metal catalysis for HDPE and LLDPE. The free-radical process leads to the unique molecular structure of LDPE: large amounts of long-chain branching. The long-chain branching imparts unusual rheological behavior in both shear and extension. LDPE is used in a variety of applications, such as film, coating, molding, and wire and cable insulation. One of the reasons for its wide range of utility is its thermal stability and low toxicity.

Monomer and Comonomers for LDPE

Ethylene [74-85-1] is the monomer used to make LDPE [9002-88-4]. The predominant method of manufacture of ethylene is high temperature cracking of natural gas or crude oil. Some properties of ethylene are collected in Table 1. The principal method for the industrial preparation of ethylene is thermal cracking of hydrocarbons. Small amounts of comonomers, such as vinyl acetate [108-05-4], methyl acrylate [96-33-3], or ethyl acrylate [108-88-5], can be added to modify

Encyclopedia of Polymer Science and Technology. Copyright John Wiley & Sons, Inc. All rights reserved.

the properties of the polymer. Vinyl acetate is made by the oxidative addition of acetic acid to ethylene in the presence of a palladium catalyst. The acrylates can be commercially manufactured from acetylene, but the preferred route is by the oxidation of propylene oxide. A few of the pertinent physical properties of these monomers and more detailed descriptions of their manufacture can be found in the articles on Vinyl Acetal Polymers and Acrylic Ester Polymers and Methacrylic Ester Polymers.

Properties of LDPE

LDPE Homopolymer. LDPE, discovered by ICI in 1933 (1,2), quickly found war-time utility in high frequency cables for ground and airborne radar equipment. After the war, the balance of chemical inertness, thermal and environmental stability, ease of processing, physical properties, stiffness, and optical properties made this polyolefin polymer useful in a variety of applications. A detailed and exhaustive compilation of molecular, physical, and chemical data on LDPE can be found in the *Polymer Data Handbook* (3).

With the commercialization of HDPE in the early 1950s (see article on ETHYLENE POLYMERS, HDPE) and LLDPE in the 1960s (see article on ETHYLENE POLYMERS, LLDPE), there was cannibalization of LDPE markets and applications by these new polymers. Despite some predictions of the demise of LDPE due to the better properties and lower cost of LLDPE and HDPE, LDPE remains the resin of choice in many applications. The most unique structural difference between LDPE and HDPE/LLDPE is the presence of large amounts of long-chain branching in the molecule (Fig. 1). This branching leads to rheological and property behaviors which cannot be matched by the other polymers. Today, LDPE is still used in a variety of film, coating, wire and cable, and molding applications. The physical and extrusion properties of LDPE depend on the molecular weight, molecular weight distribution (MWD), frequency of short-chain branches, and frequency and length of the long-chain branches. Some typical molecular properties for LDPE are found in Table 1. A comparison of blown film properties between LDPE and LLDPE is

Table 1. Typical Properties of LDPE[a]

Property	Value	Method
Molecular weight	70,000–120,000	gpc
Melt index, g/10 min	0.2–50	ASTM D1238
Density at 20°C, MPa g/cm^3	0.920–0.935	ASTM D1505
Vicat softening point	80–96°C	ASTM D1525
Tensile strength, MPa[b]	9–15	ASTM D638
Tensile elongation at rupture, %	150–800	ASTM D638
Hardness, Shore D	40–60	ASTM D676
Dielectric constant @ 1 MHz	2.3	ASTM D1531
Dissipation factor @ 1 MHz	0.0001	ASTM D1531
Low temperature brittleness F_{50}, °C	< -76	ASTM D746

[a] Data supplied courtesy of Equistar Chemicals, LP.
[b] To convert MPa to psi, multiply by 145.

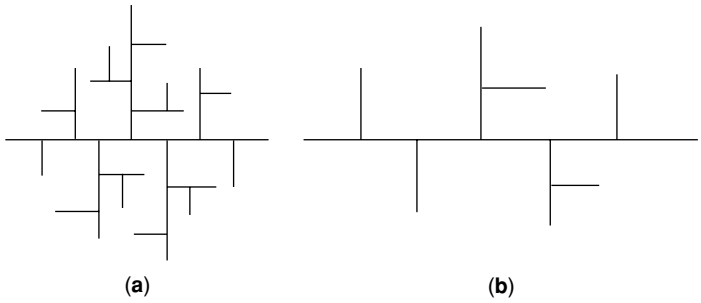

Fig. 1. Long-chain branching in fractions with M_n 200,000 from polyethylenes with melt index 1.7 and density 0.918–0.919 g/cm^3: (**a**) autoclave product with 20 long branches; (**b**) tubular product with 7 long branches. Short-chain branches are not shown.

found in Table 2. A comparison on injection-molding properties between LDPE and LLDPE is found in Table 3.

LDPE Copolymers. A variety of comonomers can be added to the polymerization of ethylene to make copolymers. The free-radical polymerization mechanism of LDPE production allows for the copolymerization of polar comonomers. At this time, the incorporation of polar comonomers is unique to LDPE. The transition metals used to catalyze HDPE and LLDPE production are generally poisoned by polar comonomers and therefore, only copolymers containing alpha-olefins like 1-butene, 1-hexene, and 1-octene can be made. Because the polar copolymers can be made only by the LDPE process, they command a premium in the market. The most common comonomers (and their corresponding copolymers) are vinyl acetate (EVA), methyl acrylate (EMA), ethyl acrylate (EEA), and acrylic acid

Table 2. Blown Film Property Comparison[a] between HP-LDPE and LLDPE

Property	ASTM test method	HP-LDPE	HP-LDPE	LLDPE	LLDPE	LLDPE
Melt index, g/10 min	D1238	2.5	0.2	1.0	1.0	1.0
Density, g/cm^3	D1505	0.921	0.923	0.918	0.918	0.918
Comonomer		None	None	Butene	Hexene	Octene
Dart drop, N/mm (=dyn/cm)	D1709	29	71	39	77	97
Puncture energy, kJ/m[b]		27	22	71	76	–
Elmendorf tear, N/mm (=dyn/cm)	D1922					
MD		62	35	54	131	143
XD		43	39	131	226	309
Tensile strength, MPa[c]	D882					
MD		20	19	35	36	45
XD		19	21	26	32	35
Haze, %	D1003	6	25	17	20	12
Gloss, 45°	D2457	70	30	53	50	60

[a]All properties measured on 38-μm film produced at a 2:1 blow-up ratio.
[b]To convert kJ/m to ft·lbf/in., multiply by 18.73.
[c]To convert MPa to psi, multiply by 145.

Table 3. Injection Molded Property Comparison of LDPE and LLDPE

Property	ASTM test method	LDPE	LDPE	LLDPE	LLDPE
Melt index, g/10 min	D1238	24	38	21	105
Density, g/cm^3	D1505	0.923	0.923	0.924	0.929
Tensile strength, MPa[a]	D638	8.3	8.9	8.3	12.5
Dishpan impact[b] at −20°C, J		12	7	41	4
Failure mode		Brittle	Brittle	Ductile	Ductile
Low temperature brittleness[c] F_{50}, °C	D746	−39	−25	< −76	−58
ESCR[d] F_{50}, h	D1693	<1	–	150	<2

[a]To convert Mpa to psi, multiply by 145.
[b]Industry test done on standard molded plastic dishpan. Parts of various weights dropped on dishpan until failure.
[c]Test method has been found useful for specification purposes, but does not necessarily indicate the lowest temperature at which the material may be used.
[d]At 50°C, 100% Igepal, no slit.

[79-10-7] (EAA). The presence of the comonomer decreases crystallinity and imparts more flexibility and softness to the final articles. Increasing levels of these comonomers imparts better adhesion to other materials. This superior adhesion of LDPE copolymers to other materials like metal, foil, cardboard, and paper is unmatched by other polyolefins and remains a unique property of LDPE. Comonomer contents as high as 20 wt% of EVA, EMA, and EEA can be used in various extrusion and molding applications. Films made from EVA, EMA, or EEA tend to have good low temperature properties and very good sealability. Because of the good sealability and broad sealing latitude, these materials are often used in coextruded structures as a seal layer. Copolymers containing acrylic or methacrylic acid have very good toughness and stress-crack resistance, but impart corrosivity to the polymer. In general, these products are used in coextruded or laminated structures. Comonomer levels from 20 to 40 wt% can also be made in the LDPE process. These copolymers are used in coating and adhesive applications.

Ionomers. Copolymers of acrylic or methacrylic acid can be converted into the sodium or zinc salts of the acids. These ionomers(qv) show strong ionic bonding, such that the properties are similar to LDPE of very high molecular weight (4). However, the ionic bonds are weakened at extrusion temperatures so that the ionomers process under similar conditions of LDPE homopolymers of normal molecular weight. Because of their polar nature, ionomers are paintable and commonly used to adhere to aluminum and metal or laminate to nylon.

Polymerization Reactors

LDPE is also known as “high pressure, low density” or HPLD, because it is exclusively made by the high pressure process. LDPE is produced under high pressures (81–276 MPa) and high temperatures (130–330°C) with a free-radical initiator, such as peroxide or oxygen. The polymerization mechanism is a free-radical

reaction that leads to the formation of long-chain branches, which can be as long as the main polymer backbone (5). The free-radical mechanism also leads to the formation of short-chain branches, typically one to five carbon atoms long (6). These short-chain branches normally seen in LDPE include 1,3-diethyl and 2-ethylhexyl side chains as well as the most common butyl branches. LDPE also contains lesser amounts of amyl branches while hexyl branches are rare. Most of the methyl branches occur when propylene is added to the reactor as a chain-transfer agent. The polymerization is carried out in tubular or stirred autoclave reactors (7).

The rate-limiting factor in LDPE production is heat removal from the reactor. The heat of polymerization of ethylene is very high, at about 3.35 kJ/g. For comparison, the heat of reaction of styrene is only about 0.657 kJ/g. There are basically two ways to dissipate the heat during the polymerization: through the walls of the reactors and by the unreacted ethylene, which is cooled and returned to the reactor. Since the LDPE polymerization occurs at very high pressures, the reactor walls must be very thick and external cooling is not very efficient. This is especially true for the autoclave reactor. The tubular reactors can benefit from cooling jackets, which is one of the factors accounting for the fact that only large tubular reactors are being built today. Older small autoclave and tubular reactors of 100–150 kta (kta $= 10^3$ t/year) cannot economically compete with new 400–500 kta low pressure "mega-reactors" being built for HDPE and LLDPE. The new high pressure tubular reactors of 350 kta, which are being installed now, will be able to compete with the HD and LLDPE units as well as offer the unique polymer properties that customers value.

In both the tubular and autoclave reactors, the control of molecular weight can be accomplished by reaction pressure, temperature, or the addition of chain-transfer agents or telogens. However, reaction pressure and temperature also affect the MWD and the amount of short- and long-chain branching. Therefore, it is desirable to use chain-transfer agents for the primary control of molecular weight so that pressure and temperature can be used for MWD and branching control.

There are subtle differences in the structure of the LDPE resins made from the tubular and autoclave reactors. The biggest difference is in the type and level of long-chain branching. As was seen in Figure 1, the autoclave reactor gives rise to shorter, more 'bushy' long-chain branching than does the tubular reactor. This is due to the higher level of backmixing in each stage of the reactor. The free radicals have more opportunity to react and terminate with other polymer molecules in the autoclave. In the tubular reactor, there is relatively little backmixing since the reaction flow is carrying the polymer down the tube as it is reacting. Therefore, once a long-chain branch is started, it is likely to continue to grow rather than interact with another polymer molecule to terminate.

The effects of these subtle differences in long-chain branching are difficult to measure (see the section on Analytical and Test Methods). Spectroscopically, the long chains are indistinguishable from the polymer backbone. The differences are also very minor in the rheology of the polymer. There are a few extrusion and physical property differences that are created by the different types of long-chain branching. Autoclave resins tend to have better see-through clarity than tubular reactors, due to the smaller spherulites formed during the crystallization process.

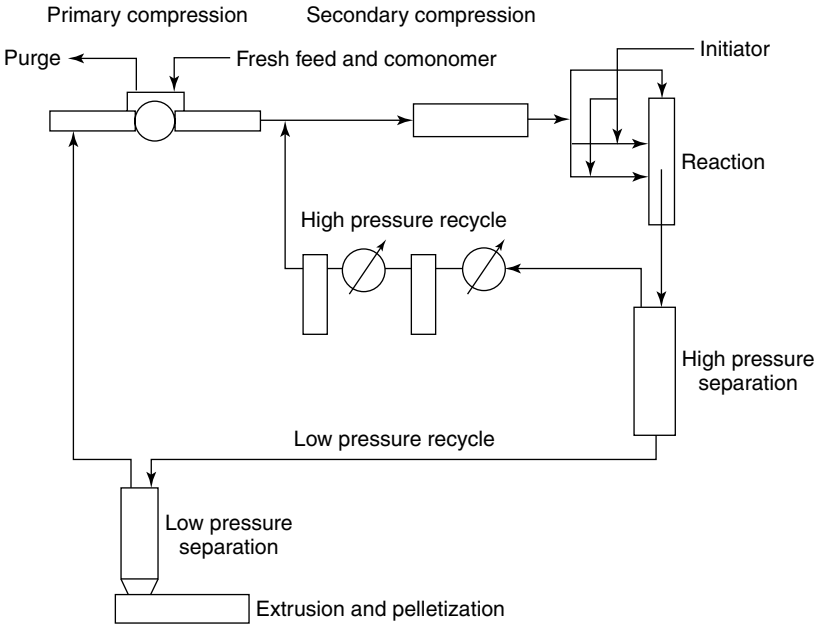

Fig. 2. Autoclave reaction process and recycle system.

Autoclave resins also exhibit better drawdown and neck-in in the extrusion coating process.

Stirred Autoclave Reactor. The stirred autoclave reactor (Fig. 2) generally has a (proprietary) stirrer running the length of a cylindrical vessel with a length to diameter ratio of 4:1 to 18:1. There are baffles in the reactor to divide it into multiple reactor zones, with independent temperature control and initiator injection points. The stirrer provides backmixing in each stage, but practically no mixing between stages. Product molecular weight, MWD, and branching are controlled by the temperatures in each zone and the placement of the initiator injection. Pressure is held constant by using a modulating valve. Because of the high pressures used, generally about 210 MPa, the reactor walls are very thick and severely limit heat removal from the vessel. Therefore, unreacted ethylene is used to remove the heat of polymerization from the reactor. This limits the conversion per pass of ethylene to about 22%. In some cases, conversion may be even lower, if unusual product characteristics are desired.

Tubular Reactor. Tubular reactors (Fig. 3) are basically long, thick-walled pipes from 0.5 to 1.5 km long, arranged as elongated coils, with cooling jackets. The use of cooling jackets allows more efficient heat removal than in the autoclave reactor and hence, higher conversion of ethylene per pass. Typical conversion rates for tubular reactors are in the 35% range. In contrast to the autoclave reactor, where reaction pressure is held constant, pressure in the tubular reactor varies. Pressure is controlled by a cycle valve that opens periodically. This generates pressure waves and surges in the reactor. These surges are actually beneficial to the process in that they help keep the walls cleaned of polymer buildup and

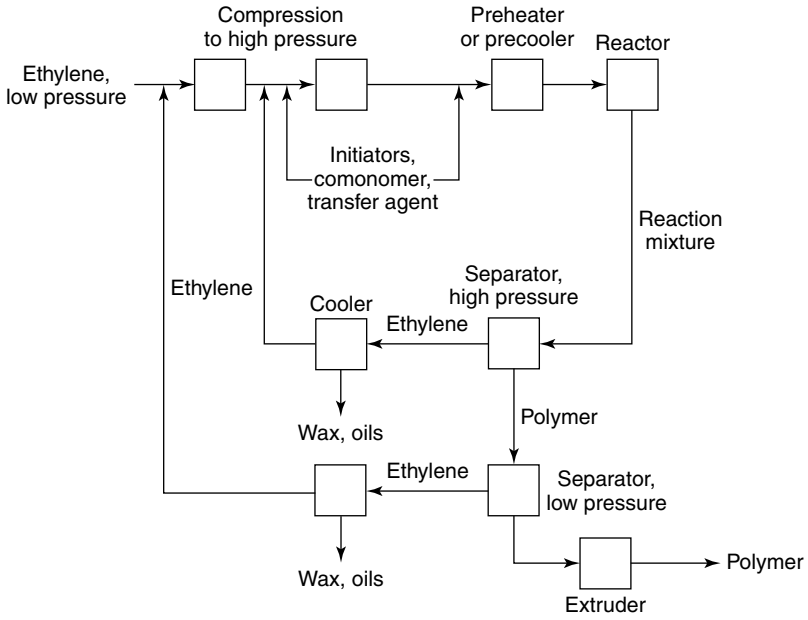

Fig. 3. Tubular reaction process.

help optimize heat transfer to the cooling jacket. Ethylene can either be added in the front or in the front with one or more additional side feed entries. Initiators, peroxide or oxygen, can also be introduced in multiple places down the tube. Thus, multiple reaction zones can be created, which can be used to control the properties of the final product.

Post Reactor Process. Since only a portion of the ethylene fed to the reactor is converted to polyethylene, recovery and recycling of the unreacted ethylene (and other monomers, if present) is necessary to improve the economics of the process. The recycle system generally comprises two sections: a high pressure separator and a low pressure separator. When the polymer first exits the reactor, it is still at very high pressures and temperatures and contains a lot of entrapped ethylene gas. The high pressure separator first partitions the polymer from the gases and low molecular weight waxes. The gases and waxes are then separated and cooled. The cool gas stream is combined with fresh feeds and fed to the secondary compressor.

Meanwhile, the polymer stream from the high pressure separator is fed to the low pressure separator. Although considerable ethylene has already been removed from this stream, further recovery is still possible. This recovered gas is fed to a multiple stage compressor to get it back to feed pressure and then fed to the secondary compressor with the gas from the high pressure separator. Small purges (less than 2%) of the feed from the multiple stage compressor may be taken to control the buildup of inert gases, such as methane and ethane.

The molten polymer coming out of the low pressure separator is then mixed with stabilizers and processing additives and fed to a pelletization process. An

extruder or a melt pump can be used to force the polymer through a die with multiple holes. The polymer strands are cut under water and the water/pellet slurry fed to a centrifugal drier. The pellets can be loaded directly into hopper cars or can be stored in silos and loaded at a later time.

Polymerization Mechanism

Initiation. A free radical is generated from the thermal decomposition of a peroxide or by an as-yet unknown mechanism in the case of oxygen. The free radical then reacts with ethylene to start a growing polymer chain.

$$I\cdot + CH_2{=}CH_2 \rightarrow I{-}CH_2{-}CH_2\cdot \tag{1}$$

$$R_i = k_i[I] \tag{2}$$

The choice of initiator is made on the basis of the type of reactor, the residence time in each zone, the desired reaction temperature, and initiator cost. A principal factor in choosing an initiator is the half-life. The longer the half-life of the initiator, the higher the degree of polymerization, but the higher the cost of the peroxide. Table 4 gives some common initiators, half-lives, and costs.

Chain Propagation. Chain propagation proceeds by radical reaction with ethylene or comonomer molecules. In the case of ethylene homopolymerization, the mechanism and kinetics are straightforward.

$$R{-}CH_2{-}CH_2\cdot + CH_2{=}CH_2 \rightarrow R{-}CH_2{-}CH_2{-}CH_2{-}CH_2\cdot \tag{3}$$

$$R_p = k_p[R\cdot]P_e \quad \text{or} \quad R_p = k_p[R\cdot][E] \tag{4}$$

where P_e is the ethylene pressure and E is ethylene.

Table 4. Peroxide Initiators for LDPE Polymerization

Peroxide	CAS No.	Half-life (1 min) temperature[a], °C	Cost[b] $/gram
t-Butyl peroxypivalate	[927-07-1]	123	
Dioctanoyl peroxide	[762-16-3]	127	
t-Butyl peroxyisobutyrate	[109-13-7]	130	
Dibenzoyl peroxide	[96-36-0]		0.084
t-Butyl peroxyisopropylcarbonate	[2372-21-6]		0.141
t-Butyl peroxybenzoate	[614-45-9]	170	0.075
Dicumyl peroxide	[80-43-3]		0.101
Di-*t*-butyl peroxide	[110-05-4]	191	0.084
t-Butyl hydroperoxide	[75-91-2]	260	0.205

[a]Refs. 8 and 9.
[b]Aldrich Catalog, 2000–2001 Edition.

When comonomers are involved, the propagation step becomes more complicated. When comonomer is present, the growing chain can react with an ethylene molecule (M_1) (eq. (5), which is the same as eq. (3) with M_1 representing the ethylene molecule) or a comonomer molecule (M_2) (eq. (6)), and those reactions may have very different rate constants. Likewise, if the growing chain does react with a comonomer, the comonomer radical end can now react with another comonomer (eq. (7)) or with ethylene (eq. (8)).

$$R{-}CH_2{-}CH_2\cdot + M_1 \rightarrow R{-}CH_2{-}CH_2{-}M_1\cdot \tag{5}$$

$$R{-}CH_2{-}CH_2\cdot + M_2 \rightarrow R{-}CH_2{-}CH_2{-}M_2\cdot \tag{6}$$

$$R{-}M_2\cdot + M_2 \rightarrow R{-}M_2{-}M_2\cdot \tag{7}$$

$$R{-}M_2\cdot + M_1 \rightarrow R{-}M_2{-}M_1\cdot \tag{8}$$

Each of these reactions has its corresponding rate reaction (eqs. (9), (10), (11), (12)).

$$R_{11} = k_{11}[R{-}M_1\cdot][M_1] \tag{9}$$

$$R_{12} = k_{12}[R{-}M_1\cdot][M_2] \tag{10}$$

$$R_{22} = k_{22}[R{-}M_2\cdot][M_2] \tag{11}$$

$$R_{21} = k_{21}[R{-}M_2\cdot][M_1] \tag{12}$$

Determining the individual propagation constants is not easy. However, if one defines reactivity ratios of the propagation constants (eqs. (13) and (14)), then the reactivity ratios can be determined by measuring the rates of disappearance of M_1 and M_2 (eq. (15)) in a controlled experiment.

$$r_1 = k_{11}/k_{12} \tag{13}$$

Table 5. Reactivity Ratios for Comonomers with Ethylene

Comonomer	r_1	r_2	Pressure, MPa[a]	Temperature, °C	Reference
Propylene	3.1 ± 0.2	0.77 ± 0.05	103–172	130–220	10, 11
1-Octene	3.1 ± 0.1	NA[b]	138	130	10, 11
Vinyl acetate	1.07 ± 0.06	1.09 ± 0.2	101	90	12, 13
Vinyl chloride	0.24 ± 0.07	3.6 ± 0.3	101	90	12, 13
Methyl acrylate	0.042 ± 0.004	5.5 ± 1.5	138	130–152	12
Methyl methacrylate	0.2	NA	207	160–220	12
Carbon monoxide	0.15	0.0	92	130	14

[a]To convert Mpa to psi, multiply by 145.
[b]NA = not available.

$$r_2 = k_{22}/k_{21} \tag{14}$$

$$\mathrm{d[M_1]/d[M_2]} = \{[\mathrm{M_1}]/[\mathrm{M_2}]\} \times \{(r_1[\mathrm{M_1}] + [\mathrm{M_2}])/([\mathrm{M_1}] + r_2[\mathrm{M_2}])\} \tag{15}$$

Between 1945 and 1970, ethylene was copolymerized with many comonomers and the reactivity ratios measured (8–12). Table 5 lists some common comonomers and their reactivity ratios.

The reactivity ratios can be used to predict how the comonomer will be distributed in the final polymer. If the product of r_1 and r_2 approaches unity, then the monomer and ethylene are randomly distributed. If r_1 equals r_2, then the concentrations of the comonomer and ethylene in the polymer is the same as their concentrations in the feed. If one reactivity ratio is higher than the other, then the copolymer contains more of that comonomer than is in the feed. If the product of r_1 and r_2 is less than one, the monomers tend to alternate along the chain. If r_1 is higher than unity, then the amount of ethylene in the copolymer is greater than in the feed. If both ratios are less than 1, then certain feed compositions yield a copolymer of the same composition. If the product of r_1 and r_2 is greater than unity, then block copolymerization is favored. This has not been established in free-radical polymerization.

For example, in Table 3, it is seen that the r_1 and r_2 ratios for EVA are nearly one. Therefore, the ethylene and EVA are randomly distributed along the polymer chain, and the concentration of EVA in the copolymer is approximately the same as in the feed.

Short- and Long-Chain Branching. LDPE is a unique polymer with respect to the high amount of long-chain branching in the polymer. The long-chain branch is a direct result of the free-radical polymerization mechanism. A free radical at the end of a growing polymer chain can abstract a hydrogen from the middle of another polymer chain. This terminates the first polymer molecule and creates a new radical growth point in the middle of the second polymer chain. This is known as intermolecular chain transfer.

$$\mathrm{R'CH_2R''} + \mathrm{R\cdot} \rightarrow \mathrm{RH} + \mathrm{R'C\cdot HR''} \tag{16}$$

$$R_{\mathrm{trp}} = k_{\mathrm{trp}}[\mathrm{R}\cdot][\mathrm{P}] \tag{17}$$

where P is the polymer.

Short-chain branching is created by intramolecular chain transfer. A free radical at the end of a growing chain can abstract a hydrogen from within the same chain (backbiting) to end up with the free radical on an internal carbon atom. When polymerization continues from that internal radical, a short alkyl branch is formed. Statistically, abstraction of the hydrogen from the fifth carbon atom back is favored, and the resulting branch is a butyl group. However, backbiting can also occur on the third, fourth, and sixth carbon atoms back, forming ethyl, propyl, and amyl branches.

$$\mathrm{RCH_2CH_2CH_2CH_2CH_2}\cdot \rightarrow \mathrm{RC}\cdot\mathrm{H{-}C_4H_9} \tag{18}$$

$$\mathrm{RC}\cdot\mathrm{H{-}C_4H_9} + \mathrm{CH_2{=}CH_2} \rightarrow (\mathrm{R})(\mathrm{C_4H_9})\mathrm{RHCH_2CH_2}\cdot \tag{19}$$

$$R_{\mathrm{b}} = k_{\mathrm{b}}[\mathrm{R}\cdot] \tag{20}$$

Termination. There are a variety of competing mechanisms by which the growth of a polymer chain can be stopped. The dominant mechanisms are determined by the polymerization conditions and the concentrations of chain-transfer agents present.

Termination by Coupling. Two growing polymer chains can react together to form one long polymer molecule or can disproportionate to form two inert chains.

$$\mathrm{R{-}CH_2{-}CH_2}\cdot + \mathrm{R{-}CH_2}\cdot \rightarrow \mathrm{R{-}CH_2{-}CH_2{-}CH_2{-}R \; or \; RCH_3 + R{-}CH{=}CH_2} \tag{21}$$

$$R_{\mathrm{t}} = k_{\mathrm{t}}[\mathrm{R}\cdot]^2 \tag{22}$$

Termination by Chain Transfer with Ethylene. The growing polymer chain can react with ethylene, and instead of the ethylene inserting into the growing chain, a radical transfer reaction can take place to form vinyl end group.

$$\mathrm{RCH_2CH_2}\cdot + \mathrm{CH_2{=}CH_2} \rightarrow \mathrm{RCH{=}CH_2} + \mathrm{CH_3CH_2}\cdot \; \mathrm{or} \; \mathrm{RCH_2CH_3} + \mathrm{CH_2{=}CH}\cdot \tag{23}$$

$$R_{\mathrm{tre}} = k_{\mathrm{tre}}[\mathrm{R}\cdot]P_{\mathrm{e}} \tag{24}$$

Termination by Chain Transfer with Chain-Transfer Agents or Solvents. Polyethylene radicals are very reactive and will react with solvents or other trace

Table 6. Common Chain-Transfer Agents and Their Constants

Agent	Transfer constant	Reference
Methane	0.0002	15
Ethane	0.0006	15
Propane	0.0030	16
Ethanol	0.0075	17
Propylene	0.0122	17
Hydrogen	0.0159	17
Acetone	0.0168	17
Isobutylene	0.021	15
2-Butene	0.038	17
1-Butene	0.047	17
Propionaldehyde	0.33	18

contaminants in the reactor to terminate one chain and begin another. Chain-transfer agents or telogens, such as propane, propylene, hydrogen, and isobutylene, can be added to the reaction to facilitate control of molecular weight.

$$RCH_2CH_2\cdot + SH \rightarrow RCH_2CH_3 + SH\cdot \tag{25}$$

$$R_{trs} = k_{trs}[R\cdot][S] \tag{26}$$

Chain-transfer constants for some common chain-transfer agents, as well as impurities found in feedstocks, are found in Table 6. As resin producers are striving to increase production rates and aim-grade polymer yield, reaction models are being used to predict polymer properties and accelerate transitions. Analytical devices are being used to measure the impurities in the incoming and recycled ethylene streams and the corresponding chain-transfer constants applied to calculate the molecular weights being made in the reactor. Therefore, these chain-transfer constants are more than just of academic interest.

Termination by β-Scission of Polymer Radicals. Internal polymer radicals, formed by either intra-or intermolecular chain transfer (see eqs. (16) and (18)), can undergo chain cleavage to form a terminated polymer chain and a new radical.

$$RCH_2C\cdot R'CH_2R'' \rightarrow R\cdot + CH_2{=}CR'CH_2R'' \text{ or } R''\cdot + RCH_2CR'{=}CH_2 \tag{27}$$

$$R_\beta = k_\beta[R\cdot] \tag{28}$$

Kinetics. The average molecular weight of LDPE can be expressed as the degree of polymerization(DP). The DP is equal to the rate of propagation (eq. (4)) divided by the sum of all the rates of termination (eqs. (22),(24),(26), and (28)).

$$DP = k_p[R\cdot]P_e/\{R_t = k_t[R\cdot]^2 + k_{tre}[R\cdot]P_e + k_{trs}[R\cdot][S] + k_\beta[R\cdot]\} \quad (29)$$

If one makes the simplifying assumption that, at steady state, the rate of initiation for a polymer radical is the same as the rate of termination (eq. (30)), then one can solve for the value of [R·].

$$k_i[I] = k_t[R\cdot]^2 \quad (30)$$

$$[R\cdot] = k_i^{1/2}[I]^{1/2}/k_t^{1/2} \quad (31)$$

Substituting for [R·] in equation (29), one gets the following:

$$DP = \{k_p P_e/k_t k_i[I]\} + \{k_P/k_{tre}\} + \{k_P P_e/k_{trs}[S]\} + \{k_P P_e/k_\beta\} \quad (32)$$

These factors can be either measured directly or calculated from other known relationships.

Processing of Polymers

LDPE can be processed by most standard plastics processes. In fact, since LDPE was the first large volume polyolefin commercialized, many plastics fabrication processes were designed around the rheological properties of LDPE. For example, blown film lines were developed to accommodate the shear thinning of LDPE during melting and extrusion and the strain hardening of LDPE in the bubble forming parts of the process (19). Therefore, when LLDPE was introduced to the film market in the late 1970s, significant retrofitting of blown film lines was necessary to handle the very different rheology of LLDPE.

Shear thinning and strain hardening are rheological phenomena that occur during extrusion and extensional deformation, respectively (20). The long-chain branching in LDPE affects these two behaviors significantly. The differences between LDPE and LLDPE in shear thinning and strain hardening are illustrated in Figures 4 and 5. *Shear thinning* is the term used to describe the flow behavior of a polymer in a melt-extrusion process. Shear thinning polymers exhibit a decrease in viscosity as the output rate is increased or as they are forced through narrower die gaps. The presence of long-chain branching, and in some cases, the broader molecular weight distribution of LDPE versus LLDPE both contribute to a greater degree of shear thinning for LDPE. The result is that under extrusion conditions, the viscosity of an LDPE resin is much lower than that of an LLDPE resin of the same molecular weight. The commonly accepted reason for the difference in melt viscosity is that the LDPE molecule, containing long-chain branches, is much more compact and 'spherical' in nature than the LLDPE molecule of the same weight. The LDPE molecules flow past each other more easily than the linear, entangled LLDPE molecules. This means that the LDPE resin will extrude at lower temperatures and requires less power per pound of resin. As a result of

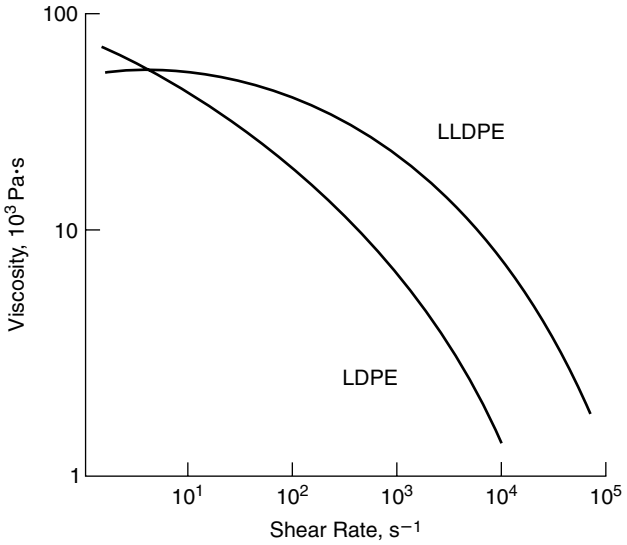

Fig. 4. Viscosity behavior under shear for LDPE and LLDPE.

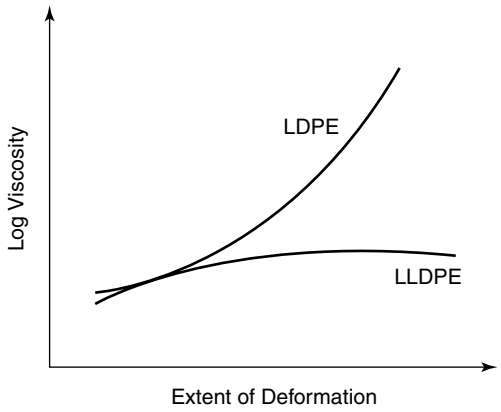

Fig. 5. Viscosity behavior under extension for LDPE and LLDPE.

this extrusion behavior, film extruders designed for LDPE were commonly underpowered for LLDPE extrusion and larger motors had to be added to convert them to efficiently extrude LLDPE.

The strain hardening effect is most clearly seen in blown film extrusion. A polymer that exhibits strain hardening will become more rigid as it is drawn to a greater extent or drawn at faster rates. An LDPE resin typically strain hardens to a greater degree than an LLDPE resin. As the polymer melt is formed into a bubble and drawn down to its final thickness, the strain hardening behavior of LDPE gives the bubble rigidity and stability to withstand the cooling air being blown on it. LLDPE, on the other hand, has a much 'softer' bubble, which is easily deformed by cooling air. The difference in extensional behavior is analogous to the

difference between pulling on a rubber band versus pulling on bubble gum. The rubber band will extend and pull, but the more you pull it, the more resistance is felt. Bubble gum can be easily pulled; it develops very little resistance to the stretching force. Because of the highly stable bubble, gauge uniformity is excellent with LDPE. On the other hand, the softer LLDPE bubble can be drawn to thinner gauges and is more forgiving of imperfections and gels that would cause the LDPE bubble to tear off or break. It is commonly accepted that the strain hardening behavior of LDPE is the result of long-chain branches.

The common methods of processing LDPE are blown and cast film extrusion and coextrusion, extrusion coating, blow molding, injection molding, rotomolding, and wire extrusion. Explanations for these processes can be found in other articles in the Encyclopedia.

Economic Aspects

Despite threats from other polyolefins, such as HDPE, LLDPE, and *m*-LLDPE, LDPE remains a viable, high volume polymer (Table 7) (21). During the 1980s, no new LDPE capacity was added because of the assumption that low cost LLDPE would replace LDPE in most applications. However, while LLDPE did displace LDPE in many areas and did absorb most of the overall growth in the North American film market, LDPE remains the resin of choice in some applications and markets (Table 8) (21,22). The overall growth of LDPE demand remains very low (0–1% annually), and there is relatively little growth in LDPE capacity. The picture for LDPE in the rest of the world is not much different in terms of growth (Table 9) (21,23,24). LLDPE took longer to be accepted by the rest of the world because the supply was mainly located in North America for several years while LDPE was locally available. LDPE is still favored in many areas of the world because of its easy film processing. In many countries, film blowing equipment is

Table 7. Comparison of Markets for LDPE, LLDPE, and HDPE (1999)[a] North America, 10^3 t

Market area	LDPE	LLDPE	HDPE
Extrusion			
Packaging film	1022	1180	164
Nonpackaging film	506	1010	753
Coating	420	13	–
Sheet	56	18	333
Pipe and extrusion	–	–	710
Injection molding	150	277	1177
Blow molding	29	9	2066
Rotomolding	58	191	65
Resellers and compounders	39	–	84
Other domestic	666	819	–
Export	707	750	718
Total	*3610*	*4268*	*6968*

[a]Ref. 21.

Table 8. Low Density PE Volumes by Market Area (1999) North America, 10^3 t

Market area	1996[a]	1997[a]	1998[b]	1999[b]
Extrusion				
Packaging film				
Food	497	459	490	502
Nonfood	416	382	328	366
Stretch/shrink	168	157	148	153
Nonpackaging film				
Carryout bags	63	49	54	56
Trash, can liners	48	29	45	55
Other	335	399	394	394
Coating	397	430	414	420
Sheet	66	59	51	56
Injection molding	135	134	128	150
Blow molding	36	31	31	29
Rotomolding	45	44	53	58
Resellers and compounders	395	392	40	39
Other domestic	–	–	702	666
Export	671	636	671	707
Total	*3580*	*3544*	*3507*	*3610*

[a]Ref. 22 (United States only).
[b]Ref. 21 (United States and Canada).

Table 9. LDPE Supply/Demand by Region, 10^3 t

	Consumption			Production
Region	1998[a]	1999[a]	2000[b]	2000[c]
North America	2,843	2,909	2,710	4,050
Western Europe	4,688	4,719	4,635	5,843
Japan	954	1,059	NA	1,355
China	1,445	1,583	1,630	714
India	238	244	254	175
All Other			7,119[c]	6,488
Global Total			*16,348*[c]	*18,625*

[a]Ref. 21.
[b]Ref. 23.
[c]Ref. 38.

old and has been designed to handle the rheology of LDPE. Substituting LLDPE causes significant production rate penalties on film lines. Many film fabricators had resorted to blends of LDPE with small amounts of LLDPE to improve film toughness without sacrificing extrusion rates.

Looking forward, continued substitution of LLDPE and HDPE for LDPE will take place. As older film extrusion equipment is replaced or retrofitted to handle LLDPE, the consumption of LDPE will decrease. The two attributes of LDPE which, as of today, have not been satisfactorily met with LLDPE are the long-chain branching and the flexibility and properties of polar comonomer

containing copolymers. But even these attributes are under attack with new technology. Some metallocene catalysts, which give very narrow molecular weight and narrow comonomer distribution LLDPE, also show the presence of long-chain branching (25). When the type and level of long-chain branching can be controlled by these catalysts, applications such as extrusion coating will be vulnerable to LLDPE substitution. Another category of new polyethylene catalysts is based on late transition metals, such as Fe and Ni. These catalyst systems give the promise of the ability to incorporate polar comonomers (26).

Pricing in the polyethylene market is extremely volatile. Because of the significant economies of scale, when new ethylene and polyethylene capacity is added, it is in very large increments. This overwhelms the regular, but modest, growth in consumption so that a large imbalance in supply versus demand occurs when the new plant starts up. When there is an overabundance of supply, prices are very low as all producers struggle to keep their facilities sold out. This condition lasts a few years until the demand catches up to the supply and prices start to rise. However, as soon as prices start increasing, new capacity is announced and the cycle starts all over. Typical low density pricing in North America will vary from US$600/ton to over US$1100/ton through the cycle (27).

Specifications and Standards

There are about 10 manufacturers of LDPE in North America. The top six include Equistar Chemicals, LP, The Dow Chemical Co., Exxon Mobil Corp., Chevron Phillips Chemical Co., DuPont, and Westlake Polymer Corp. Each company has their own trade names and specific grade slates for various applications. Data sheets and MSDSs are available from each supplier and many have them available on their web sites. A typical product data sheet will cover resin characteristics such as melt index and density, as well as 'typical' final product properties, such as film tear and tensile and impact strength. The tests will identify the ASTM test methods and the data sheet will usually have the conditions under which the test samples were made. There will also be an indication of the FDA and food contact status of the resin and the applications for which the resin is suited.

A majority of the LDPE used in North America is shipped in 82-ton rail cars. Other common forms of shipment are 18-ton bulk trucks, 500-kg boxes, and 25-kg bags. In general, no special safety labels are needed for LDPE products. In other parts of the world, the most common mode of shipment is in 25-kg bags.

Analytical and Test Methods

The most important tests for LDPE are those that measure the molecular characteristics of the resin: molecular weight, molecular weight distribution, and density. Since long-chain branching is unique to LDPE, a short description of the analytical test methods used to measure it is given. However, because of the difficulty and lack of precision of the tests, measurement of long-chain branching is not

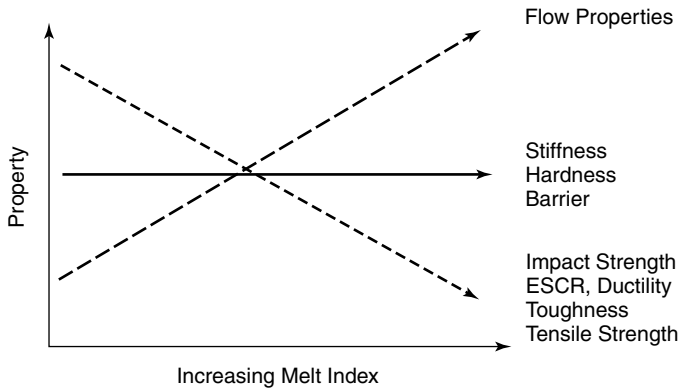

Fig. 6. Effect of molecular weight on LDPE properties.

commonly done as a quality control test. The measurement and reporting of gels, or film imperfections, are covered.

Melt Index. The melt index of a polymer is a measurement that is inversely related to molecular weight. ASTM D1238 is typically used for this test. A small amount (less than 10 g) of LDPE is melted and forced through a small orifice under constant load. The weight of polymer extruded in 10 min under 298 kPa pressure at 190°C is called the melt index. If a pressure of 2982 kPa is used, the measurement is called the flow rate (FR) or melt-flow rate (MFR). Typical LDPE melt indices range from 0.2 to over 100 g/10 min. In general, the lower melt index resins are used for film and blow molding and wire and cable applications while the higher melt index resins are used for extrusion coating and injection-molding applications. Low melt index resins have higher molecular weight than high melt index resins. The higher the molecular weight, the better the strength properties of the final products, but the more difficult the extrusion behavior (Fig. 6).

Flow Rate Ratio. The FR ratio is used as a rough estimate of the MWD of a resin. Molecular weight distribution can be measured directly by gel permeation chromatography, but this is a time-consuming, technically challenging measurement that is not commonly found in quality control laboratories. Melt-flow ratio measurements are easily done, since the MFR of a resin is the flow index of the sample divided by the melt index of the sample.

Melt-flow ratios for LDPE resins can range from very narrow [20] to very broad [100], and can be controlled by reactor conditions and reactor type. Resins with narrow MWD give stronger products but are more difficult to extrude than resins with broad MWD.

Density. ASTM D1505 is used to measure polymer density. A small sample (1–5 g) of powder or pellet is molded in a carefully prescribed manner and dropped into columns with alcohol/water gradients of different viscosities. The position of the sample in the column is compared with standards of known density, and the density of the test sample is determined.

Density is a measure of the crystallinity of the polymer. Polymer crystallinity affects such product properties as stiffness, rigidity, environmental stress-crack

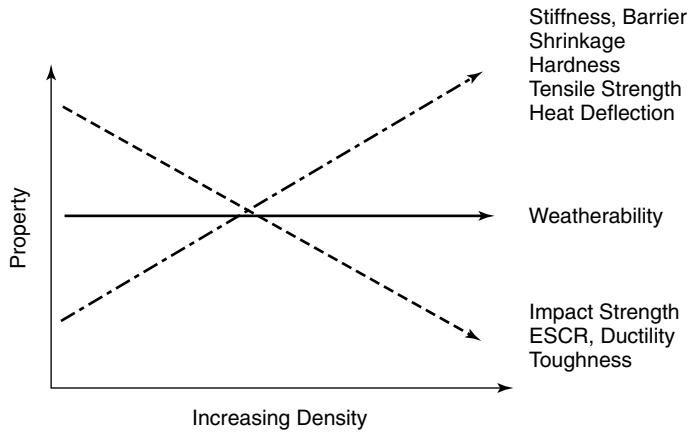

Fig. 7. Effect of density on LDPE properties.

resistance (ESCR), and barrier properties (Fig. 7). The lower the crystallinity, and hence the density, the more limp and flexible the material is. A 0.918-g/cm^3 density LDPE product has better ESCR and worse barrier properties than a product with a density of 0.930 g/cm^3.

Long-Chain Branching. The number of long-chain branches per 1000 carbon atoms on the main backbone of LDPE can range from 0.4 to over 10. Long-chain branching has been a very difficult feature to quantify. The variations in the lengths and locations and branch points for the long-chain branches make comparison of data and standardization of samples difficult. Qualitatively, the presence of long-chain branching can be surmised by looking at intrinsic viscosity as a function of molecular weight. Linear polymers give a linear response of intrinsic viscosity as a function of molecular weight. If the intrinsic viscosity of a resin with long-chain branching is plotted on this same graph, it will fall below the line for the linear polymers. However, the quantitative information on the amount and length of the long-chain branching has been difficult to extract from this method. The ^{13}C nmr analysis has been used to quantify the number of long-chain branches (28,29); however, there are some limitations to this method as well. In ^{13}C nmr, any branch longer than six carbon atoms is considered a long branch (30). Combinations of methods, such as ^{13}C nmr plus sec (size exclusion chromatography) (31,32) and sec plus intrinsic viscosity (33), are being developed to overcome the deficiencies of single-method determinations.

Gels. While gels are neither a physical property nor a reported attribute of LDPE, the gel level is a critical quality variable for LDPE film resins. Gels are physical defects which can affect the appearance, but more importantly, the performance of LDPE film. There are many forms of gels, ranging from arrowheads, pinpoint gels, black specks, and fish-eyes. Gels can be caused by many factors. Gels can be formed in the reactor by poor mixing in a reactor zone. If polymer builds up on the reactor wall, it can cross-link to form high molecular weight gels or even black specks. The compounding or pelletizing step can also cause cross-linking and gels if not cleaned and operated properly. Most resin manufacturers

will run a film quality test on LDPE resin to ensure that the gel level is low in the product before certifying it as prime material.

However, gels can be caused in the material after it has left the resin producer. Extraneous materials, like dirt, fibers, or contamination with other polymers, can occur during shipment or unloading at the fabricator. In addition, gels can be created during extrusion into film by improper film blowing conditions or inadequate maintenance and cleaning of film blowing equipment.

Gels can be analyzed by a variety of techniques to determine their origin. A simple melting point can determine if the gel is polymeric or cross-linked. Infrared spectroscopy can determine the nature of the polymer to determine if cross-contamination with another material has occurred. Conducting the melting point under a microscope can reveal if there is a solid core to the gel which might indicate a foreign contaminant. Electron microscopy can hone in on the gel and measure the presence of any metal that might indicate barrel or screw wear or totally foreign materials like bolts or nails. Because gels are an important quality issue and can be caused by a variety of mechanisms, resin producers have developed sophisticated analytical methods to identify the gels so that improvements can be made in resin production and handling to prevent them.

The reason gels are a critical quality factor with LDPE film is that they can cause problems in film extrusion and in film performance. If the gels are large enough, they can actually cause the bubble to break during the blown film process. "Bubble tear-offs" are a serious problem for the film fabricator because it causes down time and loss of product quality. If the gels are not large enough to cause problems during the extrusion process, they can still cause problems for film quality. In extrusion coating, for example, the presence of small gels in the very thin layer of polyethylene can cause pinhole leaks in the coating and destroy the barrier performance of the material. In wire and cable applications, the gel can form a weak spot in the wire coating, which will be the initiation point for electrical failure.

Health and Safety Factors

The majority of homo- and copolymer LDPE is supplied in small pellet form and is consider a material with low toxicity, low reactivity, and low flammability. However, during movement of the pellets in a conveying system, fines and dust can be created as the pellets come in contact with the piping system. If these fines build up in the system, the potential for a dust explosion exists. In addition, polyolefin powders are supplied for certain applications, such as rotomolding or coating. These polyolefin powders also pose fire and explosion safety concerns. Polyolefin dust is defined as a combustible material in the "Standard for the Prevention of Dust Explosions in the Plastics Industry" (NFPA 654). Concentrations of polyolefin powder as low as 0.02 kg/m^3 can burn, releasing sufficient heat to produce a self-propagating reaction that can result in an explosion (34). This explosive concentration is dependent on the particle size of the powder and also on the type and concentration of any additives used in the polymer. The material supplier should always be consulted for advice on handling dust and powders from LDPE.

Table 10. Low Density Resin for Film Applications[a]

Physical Properties	ASTM test method	LDPE heavy duty grades[b]	LDPE garment grade[c]
Density, g/cm^3	D1505	0.926	0.920
Melt index, g/10 min	D1238	0.25	6.5
Vinyl acetate incorporated, %		4.5	0
Vicat softening point, °C	D1525	88	85
Film properties			
Haze, %	D1003		12.0
Gloss, 45^0	D2457		50
Tensile strength @ break, MPa[d]	D882		
MD		22.1	17.3
TD		20.7	14.0
Elongation @ break, %	D882		
MD		370	225
TD		550	450
1% secant modulus, MPa[d]	D882		
MD		131	146
TD		159	166
Dart drop impact strength F_{50}, g	D 1709	320	60
Elmendorf tear strength, g	D1922		
MD		150	350
TD		250	150
Key properties		High impact strength	Good drawdown
Applications		Ice bags, frozen food, packaging	Garment bags

[a]Data courtesy of Equistar Chemicals, LP.
[b]Data obtained on film produced from Petrothene® NA 480 on an 89-mm blown film line, 203-mm die, at 221°C melt temperature, 2:1 BUR, at 51-μm thickness.
[c]Data obtained on film produced from Petrothene® NA 336 on an 89-mm blown film line, 203-mm die, at 163°C melt temperature, 1.2:1 BUR, at 32-μm thickness. Petrothene is a registered trademark of Equistar Chemicals, LP.
[d]To convert MPa to psi, multiply by 145.

Polyolefin dust is currently classified as a nuisance material. Polyolefin materials have a long history of safe use and are not thought to produce irreversible change in lung tissue or produce significant disease or toxic effects when exposure is kept under reasonable control. The Occupational Safety and Health Administration (OSHA) and the American Conference of Governmental Industrial Hygienists (ACGIH) have established permissible exposure limits of 15 and 10 mg/m^3 of air, respectively, for total nuisance dust, and 5 mg/m^3 for the respirable fraction.

Food Contact. Homopolymer LDPE is a relatively inert, nontoxic and benign polymer, which is used extensively in a variety of food contact and medical applications. Copolymers containing EEA, EMA, EVA, and other comonomers can also be used selectively in food contact applications. The resin supplier should be asked for specific information on FDA compliance for each particular resin, as the type of polymer, the amount of comonomer, and the type and level of additives

Table 11. Low Density Resin for Film Applications[a]

Physical properties	ASTM test method	LDPE clarity grades	LDPE industrial clarity grades
Density, g/cm^3	D1505	0.926	0.921
Melt index, g/10 min	D1238	1.0	2.0
Vinyl acetate incorporated, %		4.0	–
Vicat softening point, °C	D1525	90	93
Film data[b]			
Haze, %	D1003	4.0	6.0
Gloss, 45°	D2457	75	70
Tensile strength @ break, MPa[c]	D882		
MD		25.5	23.5
TD		21.4	17.3
Elongation @ Break, %	D882		
MD		340	300
TD		500	500
1% Secant Modulus, MPa[c]	D882		
MD		145	193
TD		166	221
Dart drop impact strength, F_{50}, g	D1709	100	90
Elmendorf Tear strength, g	D1922		
MD		180	380
TD		250	200
Key properties		Good clarity, excellent impact	Good processability and clarity
Applications		Bags and special film applications	Stiff liners

[a]Data courtesy of Equistar Chemicals, LP.
[b]Data obtained on film produced from Petrothene® NA 340 and NA 143 on an 89-mm blown film line, 203-mm die, at 191°C melt temperature, 2:1 BUR, at 32-μm film thickness.
[c]To convert MPa to psi, multiply by 145.

Table 12. Low Density Resin for Sheet and Profile Extrusion[a]

Typical properties	ASTM test method	LDPE resin (NA 967-000)
Density, g/cm^3	D1505	0.919
Melt index, g/10 min	D1238	1.5
Tensile strength @ break, MPa[b]	D638	10.4
Elongation @ break, %	D638	600
Low temperature brittleness F_{50}, °C	D 746	< -76
Vicat softening point, °C	D1525	90
Hardness, Shore D	D2240	51
Environmental stress-crack resistance F_{50}, h	D1693 D2561	
FDA sanction		21 CFR 177.1520
Key properties		Excellent, toughness
Applications		Sheet/profile extrusion, foamed sheet/profiles

[a]Data on Petrothene® NA 967-000, courtesy of Equistar Chemicals, LP.
[b]To convert MPa to psi, multiply by 145.

Table 13. Low Density Resin for Extrusion Coating[a]

Properties	ASTM test method	LDPE resins	
		NA 204-000	NA 206-000
Density, g/cm^3	D1505	0.918	0.918
Melt index, g/10 min	D1238	7.0	13
Nominal melt temperature range, °F		575–625	575–625
FDA sanction		21 CFR 177.1520, 176.170	21 CFR 177.1520, 176.170
Key properties		Excellent adhesion and heat seal, good neck-in, high drawdown	Formulated for high line speeds and low coating weights
Applications		General purpose flexible packaging and laminating	Sugar pouches, industrial and multi-wall bags

[a]Data on Petrothene® NA 204-000 and Petrothene® NA 206-000, courtesy of Equistar Chemicals, LP.

Table 14. Low Density Resin for Extrusion Coating[a]

Properties	ASTM test method	LDPE resins	
		NA 216-000	NA 219-000
Density, g/cm^3	D1505	0.923	0.923
Melt index, g/10 min	D1238	3.7	10
Nominal melt temperature range, °F		575–625	575–625
FDA sanction		21 CFR 177.1520, 176.170	21 CFR 177.1520
Key properties		Formulated for heavy and medium weight coatings	Formulated for high line speed, light-weight coatings
Applications		Flexible packaging, milk cartons, and food boards	Flexible packaging paperboard, and industrial papers

[a]Data on Petrothene® NA 216-000 and Petrothene® NA 219-000, courtesy of Equistar Chemicals, LP.

and stabilizers all play a part in determining the FDA compliance of a specific resin.

Environmental Impact. In recent years, there has been quite a bit of adverse publicity around the use of plastics and the impact of plastic litter on the environment. The decision of fast food restaurants to discontinue the use of expanded polystyrene clamshell hamburger containers is one example of how plastics growth and use can be changed by public opinion. Many states have considered or passed regulations specifying the amount of recycled plastic that must be incorporated into new plastic articles. This has had a direct impact on the polyethylene industry, including LDPE, because polyethylene is one of the more recyclable plastics being used today. However, the recycling effort has been

hampered by the higher cost of collecting, separating, and cleaning the polyethylene containers compared to the cost of virgin polymer.

Photo- and biodegradable plastics have been offered as possible solutions to the litter problem. LDPE copolymers containing carbon monoxide have been produced by Union Carbide Chemical and Plastics Co., Inc. (35) and The Dow Chemical Co. These photodegradable copolymers have been used to make beverage can carriers or rings but have not been widely used in other commodity applications because of the unique physical properties. Currently, the search for biodegradable LDPE has not led to a commercially successful product. Blends of LDPE and starch-like fillers improve the biodegradation of LDPE, but at a significant sacrifice of physical properties (36). A new degradable/compostable technology has been developed, such that the degradability can be triggered by heat, light, and/or stress. Products made by this technology are being currently marketed in Europe and South America (37).

Plastic pellets inadvertently lost from plastic production and warehouse facilities pose a threat to fish and wildlife. Therefore, the U.S. EPA (Environmental Protection Agency) has classified plastic pellets as "significant materials.". The finding of even one pellet in a storm water run-off without a permit is now subject to federal regulatory action with the potential for substantial fines and penalties. As a result, the plastics industry has launched Operation Clean Sweep, an initiative to prevent the accidental release of pellets into the environment. Specific recommendations for handling polyolefins to prevent resin loss into the environment have been developed by the Society for the Plastics Industry (38).

From a polymerization process standpoint, fugitive hydrocarbon emissions, mainly ethylene, are the biggest environmental concern. Much progress has been made in controlling these emissions by recovering and recycling gas from various points in the process. Using advanced process control software and better

Table 15. Low Density Copolymer Resins for Extrusion Coating[a]

Properties	ASTM test method	EVA copolymers	
		UE 652-249	UE 635-000
Melt index, g/10 min	D1238	32	9
Vinyl acetate incorporated, %	D638	19	9
Nominal melt temperature range		Not to exceed 450°F	Not to exceed 450°F
FDA sanction		21 CFR 177.1350, 175.105	21 CFR 177.1350, 175.105
Key properties		Good heat seal response, good clarity	Good heat seal response, good clarity
Applications		Formulated for cheese wrap	Coatings on PET and polypropylene film

[a]Data on Ultrathene® UE 652–249 and Ultrathene® UE 635-000, courtesy of Equistar Chemicals, LP. Ultrathene is a registered trademark of Equistar Chemicals, LP.

instrumentation, runaway reactions or "decomps" have been significantly reduced. These "decomps" are typically vented to the atmosphere and so this improved control has resulted in fewer hydrocarbons being released. On a positive side, many polymerization units capture the heat of polymerization from the reaction and use that to generate low pressure steam. This reduces the need for electrical power to run the process.

Uses

Film and Sheet. The film and sheet market is the largest application for low density polyethylene, consuming about 50% of the total North American demand (Table 8). Packaging applications include pallet and shrink wrapping, heavy-duty sacks, and food packaging. Nonpackaging applications comprise refuse bags, storage bags, agricultural film, and industrial sheeting. The film market has been the primary focus of LLDPE manufacturers, and LLDPE now accounts for over 50% of the low density film market (Table 7). At one time, garbage bags, grocery sacks, garment bags, stretch film, and food packaging films were made from 100% LDPE, but because of the outstanding physical properties of LLDPE, these markets have largely been converted to LLDPE or LLDPE-rich blends of LDPE. There are still a few film applications where LDPE remains the resin of

Table 16. Low Density Resin for Wire and Cable[a]

Property	ASTM test method	LDPE compound
Nominal unaged physical properties	D1505	0.925
Density, g/cm^3		
Melt index, g/10 min	D1238	0.2
Tensile strength @ break, MPa[b]	D638	15.9
Elongation @ break, %	D638	650
Hardness, Shore D	D2240	50
Environmental stress-crack resistance, 10% Igepal®	D1693	F_0 @ 168 h
Low temperature brittleness F_{50}, °C	D746	< -76
Nominal electrical properties		
Dielectric constant @ 1 MHz	D1531	2.36
Dissipation factor @ 1 MHz	D1531	0.00060
Volume resistivity, ω·cm	D257	2.5×10^{17}
Color		Black
Applications		Cable jacketing, line wire insulation
Specifications		ASTM D1248, Type I, class C, Category 5, Grades E5 and J3; Federal LP390C, Type III, Class L, Category 5, Grades 2–4; RUS 7CFR, 1755.390

[a]Data on PE 130 courtesy of Equistar Chemicals, LP.
[b]To convert MPa to psi, multiply by 145.

Table 17. Low Density Resin for Wire and Cable[a]

Property	ASTM test method	LDPE resin	
		NA 520-024	NA 951-080
Nominal unaged physical properties			
Density, g/cm^3	D1505	0.918	0.919
Melt index, g/10 min	D1238	0.25	2.2
Tensile strength @ break	D638		
psi		2100	1700
MPa	D638	14.5	11.7
Elongation @ break, %	D638	550	600
Hardness, Shore D	D2240	44	55
Environmental stress-crack resistance, 10% Igepal®	D1693	F_0@ 168 h	N/A
Low temperature brittleness F_{50}, °C	D746	< -76	< -76
Nominal electrical properties			
Dielectric constant @ 1 MHz	D1531	2.28	2.27
Dissipation factor @ 1 MHz	D1531	0.00010	0.00008
Volume resistivity, ω·cm	D257	1×10^{18}	2×10^{18}
Color		Natural	Natural
Applications		Primary insulation, compounding base resin	Primary insulation, coaxial and electronic cables, compounding base resin
Specifications		ASTM D1248, Type 1, Class A, Category 5, Grades E4 and E5; Federal LP390C, Type 1, Class L, Category 5, Grade 2	ASTM D1248, Type 1, Class A, Category 3, Grade E3; Federal LP390C, Type 1, Class L, Category 3, Grade 2

[a]Data on Petrothene® NA 520-024 and Petrothene® NA 951-080 courtesy of Equistar Chemicals, LP. Igepal is a registered trademark of the Rhone-Poulenc Co., Inc.

choice: shrink wrap, clarity films, etc. The advantages of LDPE in film are ease of extrusion, clarity, and low taste and odor. Typical resins used for film have melt indices from 0.2 to 6 and densities from 0.917 to 0.930 (Tables 10, 11, 12).

Extrusion Coating. In extrusion coating, LDPE is used as a thin coating on another material, such as paper, aluminum foil, paperboard, or another polymeric material. The final structure is used for snack food packaging, juice boxes, milk, or other food containers. The LDPE can serve as an adhesive, moisture barrier, seal layer, printing surface, or barrier to tearing. Typically, resins with melt indices from 4 to 10 and densities from 0.920 to 0.930 are used in this application (Tables 13, 14, 15). This is one market where LLDPE has not made significant penetration. The unique long-chain branching characteristics of LDPE, especially that produced in autoclave reactors, has not been duplicated by LLDPE manufacturers. This long-chain branching gives LDPE the combination of neck-in and drawdown necessary for successful high speed extrusion coating.

Wire and Cable. Radar sheathing cable was one of the first commercial uses for LDPE. Currently, about 10% of LDPE production is used in wire and cable applications. The cleanliness of LDPE insofar as its lack of gels or inorganic catalyst residues is a key advantage in high energy wire sheathing. The ease of extrusion is also another advantage of LDPE, as wire coating lines run at very high speeds. Many resin producers offer wire and cable resin, which has been pre-compounded with a variety of colors, including black (Table 16). Some wire and cable manufacturers prefer to add color themselves. Typical resins used for wire and cable are very similar to film resins in the melt index and density ranges employed (Table 17).

Injection Molding. This market, which includes lids, buckets, toys, freezer containers, has seen significant penetration by LLDPE. LLDPE offers advantages in product properties such that higher melt index products can be used without sacrificing product performance. The use of the higher melt indices allows the fabricator to increase production speed and reduce costs. The markets where LDPE

Table 18. Low Density Resin for Injection Molding[a]

Physical properties[b]	ASTM test method	LDPE grades	
		H-2324	NA 820-000
Density, g/cm^3	D1505	0.923	0.918
Melt index, g/10 min	D1238	24.0	2.0
Tensile strength @ break, MPa[c]	D638	8.3	11.7
Tensile strength @ yield, %	D638	1800	1500
Elongation @ yield, %	D638	13	16
1% secant modulus, MPa[c]	D790	297	255
2% secant modulus, MPa[c]	D790	221	235
Vicat softening point, °C	D1525	88	85
Hardness, Shore D	D2280	55	48
Low temperature brittleness F_{50}, °C	D746	−39	−70

[a]Data on Petrothene® H-2324 and Petrothene® NA 820-000, courtesy of Equistar Chemicals, LP.
[b]All molded properties use compression molded samples.
[c]To convert MPa to psi, multiply by 145.

Table 19. Low Density Resin for Blow Molding[a]

Typical properties	ASTM test method	LDPE homopolymer resins	
		NA 940	NA 820
ASTM Type, Class, Category	D1248	I, A, 5	I, A, 3
Density, g/cm^3	D1505	0.918	0.918
Melt index, g/10 min	D1238	0.25	2.0
Tensile strength @ break, MPa[b]	D638	14.4	9.7
Elongation @ break, %	D638	>600	>600
Flexural modulus, MPa[b]	D790	235	228
Low temperature brittleness F_{50}, °C	D746	< −76	< −76
Vicat softening point, °C	D1525	90	88
Hardness, Shore D	D2240	50	48
FDA status		21 CFR 177.1520	21 CFR 177.1520
Key properties		Good Clarity, excellent toughness, fair processability	Good Clarity, fair toughness, good processability
Applications		Flexible containers, squeeze bottles, toys	Flexible containers, squeeze bottles, toys

[a]Data on Petrothene® NA 940 and Petrothene® NA 820 courtesy of Equistar Chemicals, LP.
[b]To convert MPa to psi, multiply by 145.

is still used are those in which some clarity is desired, such as caps and closures (Table 18).

Blow Molding. HDPE is the preferred resin for blow molding because of its combination of rigidity and barrier properties. LDPE is less commonly used, but does offer advantages in applications where clarity, flexibility, and excellent ESCR are required. Typically, low melt index resins are used for blow molding applications (Table 19).

BIBLIOGRAPHY

"Ethylene Polymers" in *EPST* 1st ed., Vol. 6, pp. 275–454; "Ethylene Polymers, Low Density Polyethylene" in *EPSE* 2nd ed., Vol. 6, pp. 386–429, by Kenneth W. Doak, Consultant.

1. Brit. Pat. 471590 (Sept. 6, 1937), E. W. Fawcett and co-workers (to Imperial Chemical Industries, Ltd.).
2. U.S. Pat. 2153553 (Apr. 11, 1939), E. W. Fawcett (to ICI, Ltd.).
3. A. Prasad, in J. E. Mark, ed., *Polymer Data Handbook*, Oxford University Press, New York, 1999, p. 518.
4. H. K. Loveless, in R. Raff and K. W. Doak, ed., *Crystalline Olefins Polymers, Part II*, John Wiley & Sons, Inc., New York, 1964, p. 70.
5. P. J. Flory, *J. Am. Chem. Soc.* **59**, 241 (1937); P. J. Flory, *J. Amer. Chem. Soc.* **69**, 2893 (1947).
6. M. J. Roedel, *J. Am. Chem. Soc.* **75**, 6110 (1953).
7. K. W. Doak and A. Schrage, in R. A. V. Raff and K. W. Doak, eds., *Crystalline Olefin Polymers*, *Part 1* Wiley-Interscience, New York, 1965, Chapt. "8".

8. G. Luft, H. Bitsch, and H. Seidl, *J. Macromol. Sci. Chem*. **11**, 1089 (1977).
9. H. Siedl and G. Luft, *J. Macromol. Sci. Chem.* **15** (1), 1 (1981).
10. P. Ehrlich and G. A. Mortimer, *Adv. Polym. Sci.* **7**, 386 (1970).
11. L. Bogetich, G. A. Mortimer, and G. W. Daues, *J. Polym. Sci.* **61**, 3 (1962).
12. G. A. Mortimer, *J. Polym. Sci., Part B* **3**, 343 (1965).
13. R. D. Burkhart and N. L. Zutty, *J. Polym. Sci., Part A* **1**, 1137 (1963).
14. D. D. Coffman and co-workers, *J. Am. Chem. Soc.* **74**, 3391 (1952).
15. G. A. Mortimer, *J. Polym. Sci., Part A1* **4**, 881 (1966).
16. P. W. Tidwell and G. A. Mortimer, *J. Polym. Sci., Part A1* **8**, 1549 (1970).
17. G. A. Mortimer, *J. Polym. Sci., Part A1* **8**, 1513 (1970).
18. G. A. Mortimer, *J. Polym. Sci., Part A1* **10**, 163 (1972).
19. L. A. Utracki, *Adv. Polym. Technol.* **5**, 41 (1985).
20. J. M. Dealy and K. F. Wissbrun, *Melt Rheology and Its Role in Plastics Processing*, Van Nostrand Reinhold Co., Inc., New York, 1990.
21. *Modern Plastics* **77** (2), 74 (Feb. 2000).
22. *Modern Plastics* **75** (1), 74 (Jan. 1998).
23. *Modern Plastics* **78** (2), 42 (Feb. 2001).
24. Chem Systems, Polyolefins Planning Service, POPS 2000, Report 2: Global Commercial Analysis, Dec. 2000.
25. U.S. Pat. 5272236 (Dec. 21, 1993), S. Lai and co-workers (to The Dow Chemical Company).
26. U.S. Pat. 5866663 (Feb. 2, 1999), M. S. Brookhart and co-workers (to E. I. du Pont de Nemours & Co., Inc., and University of North Carolina).
27. *Data from Equistar Chemicals, LP.*
28. D. E. Axelson, G. C. Levy, and L. Mandelkern, *Macromolecules* **12**, 41 (1979).
29. J. C. Randall, *J.M.S. Part C: Rev. Macromol. Chem. Phys.* **29**, 201–317 (1989).
30. F. A. Bovey and co-workers, *Macromolecules* **9**, 76 (1976).
31. D. C. Bugada and A. Rudin, *J. Appl. Polym. Sci.* **33**, 87 (1987).
32. D. C. Bugada and A. Rudin, *Eur. Polym. J.* **23**, 847 (1987).
33. F. M. Mirabella Jr. and L. Wild, *Advances in Chemistry Series No. 227: Polymer Characterization: Physical Property, Spectroscopy, and Chromatographic Methods*, American Chemical Society, Washington, 1990, p. 23, Chapt. "2".
34. *Handling and Storage of Equistar Polymers, published by Equistar Chemicals, LP.*
35. Brit. Pat. 915240 (Jan. 9, 1963), G. Madgwick and co-workers (to Union Carbide Corp.)
36. F. Otey and W. Done, *in Proceedings of the Symposium on Degradation of Plastis*, Society of the Plastics Industry, Inc. Washington, D.C., June 10, 1987.
37. U.S. Pat. 5854304 (Dec. 29, 1998), R. A. Garcia and J. G. Gho (to EPI Environmental Products Inc.).
38. *Operation Clean Sweep—Pellet Loss Prevention Program, SPI, Literature Sales Department, 1801 K St., NW #600, Washington, DC 20006-1301.*

GENERAL REFERENCES

L. W. Pebsworth, *Kirk-Othmer Encyclopedia of Chemical Technology*, 4th ed., vol. **17**, Wiley-Interscience, New York, 1997, pp. 707–723.
R. A. V. Raff and J. B. Allison, *Polyethylene*, Interscience Publishers, New York, 1956.
A. Renfrew and P. Morgan, eds., *Polythene*, Interscience Publishers, New York, 1957.
H. D. Anspon, in W. M. Smith, ed., *Manufacture of Plastics*, Vol. **1**, Reinhold Publishing Corp., New York, 1964, pp. 66–193, Chapt. "2".
J. H. DuBois and F. W. John, *Plastics*, Van Nostrand Reinhold Co., Inc., New York, 1981.

T. O. J. Kresser, *Polyethylene*, Reinhold Publishing Corp., New York, 1961.
S. L. Aggarwal and O. J. Sweeting, *Chem. Rev*. **57**, 665 (1957).
W. Hollar and P. Ehrlich, *Chem. Eng. Comm*. **24**, 57–70 (1983).
D. Stoiljkovich and S. Javanovich, *Makromol. Chem.* **182**, 2811–2820 (1981).
H. Oosterwijk and H. Van Der Bend, *Akzo Chemie America Bulletin*, Initiations Seminar, New York, 1980, p. 87.

NORMA MARASCHIN
Equistar Chemicals, LP

ETHYLENE POLYMERS, LLDPE

Introduction

Linear low density polyethylene (LLDPE) was first commercialized in the late 1970s by Union Carbide and Dow Chemical. Since that first introduction, LLDPE has seen the fastest growth rate in usage of the three major polyethylene families—low density polyethylene (LDPE), LLDPE, and high density polyethylene (HDPE)—and now comprises approximately 25% of the annual production of polyethylene around the world, approaching 13 million metric tons. Conventional LLDPE differs from LDPE by having a narrower molecular weight distribution and by not containing long-chain branching. LLDPE is made by the copolymerization of ethylene and α-olefins. Significant research and development efforts were conducted throughout the 1980s to tailor LLDPE properties by controlling molecular weight distribution and comonomer distribution. In the early 1990s, the LLDPE industry was revitalized with the introduction of several new product families, including novel single-site-catalyzed very low density polyethylenes (VLDPE) called plastomers (Exxon, 1991, and Dow, 1993), super-hexene LLDPE (Mobil, 1993), and metallocene-catalyzed LLDPE(mLLDPE) for commodity applications (Exxon, 1995) (see SINGLE-SITE CATALYSTS). Work continues by resin companies around the world on new classes of LLDPE for a variety of applications.

Molecular Structure and Properties

Comonomer Type and Content. Although practically any α-olefin from C_3 to C_{20} can be used as comonomer for LLDPE, the four most commonly used are 1-butene, 1-hexene, 4-methyl-1-pentene, and 1-octene. Approximately 40% of

Encyclopedia of Polymer Science and Technology. Copyright John Wiley & Sons, Inc. All rights reserved.

Table 1. Comonomer Content and Density Ranges for Commercial LLDPE Resins

Family	Common name	Comonomer, mol%	Crystallinity, %	Density, g/cm^3
Medium density	MDPE	1–2	55–45	0.940–0.926
Low density	LLDPE	2.5–3.5	45–30	0.925–0.915
Very low/ultra low density	VLDPE/ULDPE	>4	<30	<0.915
Very low density (single-site catalyzed)	Plastomer	≤25	0–30	≤0.912

LLDPE made uses 1-hexene as comonomer, approximately 35% uses 1-butene, and approximately 25% uses 1-octene. Only a small fraction is made using 4-methyl-1-pentene. Hexene and butene copolymers are more prevalent because they are less expensive than octene and because they are commonly used in the gas-phase process, which accounts for most of the global LLDPE production. For LLDPE, density is strongly controlled by comonomer content. Conventional LLDPE basically covers the density range of 0.915–0.940. Within that density range, and also lower density ranges, there are common product family subsets. Table 1 shows comonomer content and subsequent density ranges for commercial LLDPE.

Chain Structure. LLDPE comprises linear molecules of ethylene and α-olefins and can be generally represented by the formula $-CH_2-CH_2-CH_2-CH-(C_{n-2}H_{2(n-2)+1})$, where n is the number of carbon atoms in the α-olefin. In LLDPE above 0.915 g/cm^3 density, most of the branching due to comonomer is randomly distributed along the polymer backbone, although there may be some adjacent comonomer units. Single-site-catalyzed resins have comonomer much more uniformly distributed along the polymer backbone than do conventional LLDPE resins. A conventional gas-phase hexene copolymer LLDPE at 0.918 g/cm^3 density has approximately 18 branches per thousand carbon atoms while a single-site-catalyzed gas-phase hexene copolymer LLDPE at the same density has 11–12 branches per thousand carbon atoms. In the single-site-catalyzed resins, the hexene is more randomly distributed along the backbone, shortening the average backbone sequence length for crystallization, and therefore less comonomer is needed to achieve the same density.

Most LLDPE chains have at least one methyl ($-CH_3$) group at one chain end. Other chain ends can be a methyl group from termination from chain transfer, or a vinyl group ($CH_2=CH=$) or vinylidene group ($CH_2=C\!\!<$) from termination from β-hydride transfer (1).

Generally speaking, LLDPE resins do not contain long-chain branching. However, certain families of plastomers may contain more than 0.01 long-chain branches per thousand carbons (2).

Composition. A representative schematic of the structural differences between LDPE, LLDPE, and single-site-catalyzed LLDPE is given in Figure 1.

LDPE contains a mixture of long-chain branching and short-chain branching. LLDPE contains only short-chain branching, but that branching is not uniformly distributed through the molecular weight. LLDPE made using Ziegler–Natta catalysts tends to have more comonomer in the lower molecular weight fraction and less in the high molecular weight fraction (3,4). A temperature rising elution

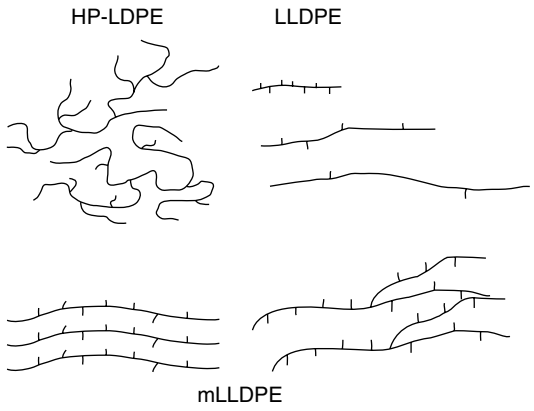

Fig. 1. Structural differences between LDPE, LLDPE, and single-site-catalyzed LLDPE.

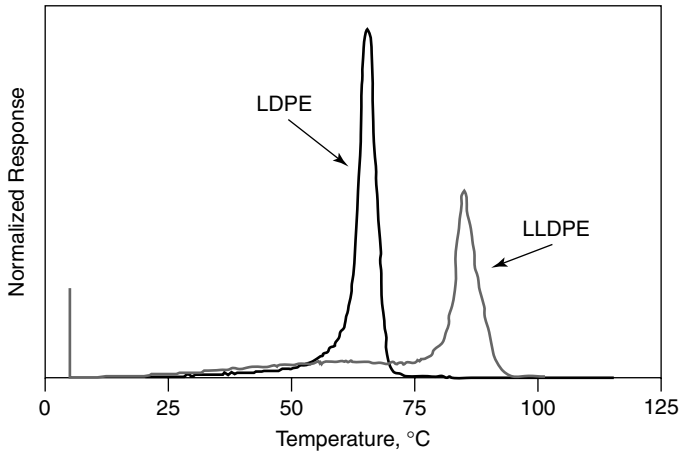

Fig. 2. LDPE and LLDPE TREF comparison.

fractionation (TREF) plot for LDPE at 0.919 g/cm^3 and LLDPE at 0.918 g/cm^3 is shown in Figure 2.

As you can see, the peak elution temperature for the LDPE is much lower and the peak is much narrower than that for the LLDPE. This indicates that the LLDPE is more compositionally heterogeneous than the LDPE.

The first commercially available single-site-catalyzed polyethylenes were very low density resins called plastomers (5,6), which had high levels of comonomer and were very homogeneous. Later, commercial commodity grade mLLDPEs were not quite as homogeneous as the plastomers, but were still more homogeneous than LLDPE (7–9). Figure 3 shows a TREF plot of an LLDPE at 0.918 g/cm^3 density and an mLLDPE at 0.917 g/cm^3 density, both produced in the gas phase. Also included is a plastomer at 0.900 g/cm^3 density produced in a slurry reactor.

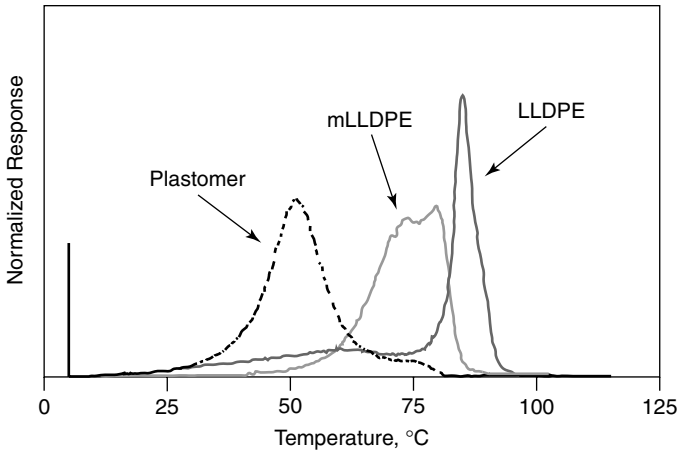

Fig. 3. TREF profiles for LLDPE, mLLDPE, and plastomer.

A polymer that has branching more uniformly distributed along the polymer backbone will have shorter sequence lengths for polymer crystallization. Shorter sequence lengths result in thinner crystals that dissolve and elute at lower temperatures than thicker crystals. The mLLDPE has a lower peak elution temperature than LLDPE at the same density, indicating that mLLDPE is more compositionally homogeneous. The plastomer has a peak elution temperature of approximately 50°C and a very narrow peak indicating that the resin is very compositionally homogeneous.

Molecular Weight. Commercially available LLDPE resins can have weight-average molecular weights from less than 20,000 to over 200,000. *Melt index*, a measure of polymer flow through a specified die for a given time, is often used as an estimator of polymer molecular weight and is inversely proportional to weight-average molecular weight. An approximate correlation of weight-average molecular weight and melt index for LLDPE is shown in Figure 4.

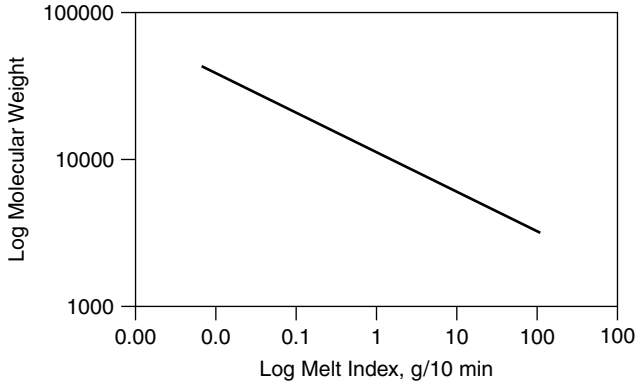

Fig. 4. Molecular weight/melt index correlation for LLDPE.

Table 2. Melt Index and Molecular Weight Data for LDPE and Several LLDPEs

Property	HP-LDPE	Gas-phase LLDPE	Gas-phase mLLDPE	Plastomer	
				Slurry	Solution
Melt index I_2, g/10 min	1.0	1.0	1.0	1.1	1.0
MIR I_{21}/I_2	60	33	17	21	31
M_n, g/mol	22,000	28,000	44,000	46,000	40,000
M_w, g/mol	104,000	107,000	102,000	99,000	82,000
PDI, M_w/M_n	4.7	3.8	2.3	2.2	2.1

Over the range shown, the relationship between molecular weight and melt index is linear but will not be completely linear over a broader range. Commercially available film grade LLDPE resins can range from 0.2 g/10 min to over 5 g/10 min melt index. Injection-molding grades vary in melt index from approximately 10 g/10 min to greater than 125 g/10 min. Table 2 shows measured molecular weights and melt-flow properties for several LDPEs and plastomers at nominal 1 g/10 min melt index.

Molecular weight distribution plots for the resins in Table 2 are given in Figures 5 and 6.

Depending on the standards used for calibration of the molecular weight fractionation technique, LLDPE has a molecular weight polydispersity index (PDI, M_w/M_n) between 3 and 4.5 with melt index ratios (MIR, I_{21}/I_2) of 20–35. LDPE has PDI usually greater than 5 and contains long-chain branching. Therefore, although the LDPE and LLDPE resins shown have similar weight-average molecular weights and melt indices, their MIR (I_{21}/I_2) values are significantly different. The higher MIR for LDPE indicates greater sensitivity to shear caused by the broader PDI and long-chain branching.

The single-site-catalyzed mLLDPE and slurry plastomers have much narrower molecular weight distributions and therefore have much lower MIR values

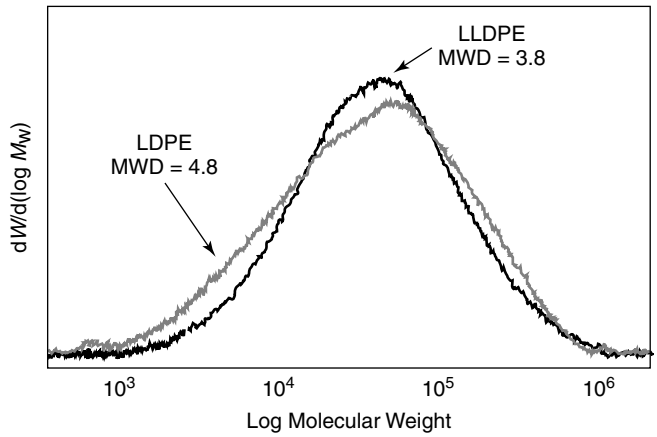

Fig. 5. Molecular weight distribution plots for LDPE and LLDPE.

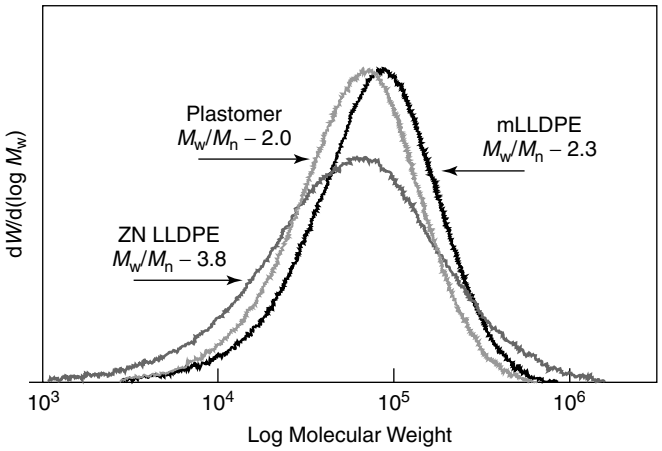

Fig. 6. Molecular weight distribution plots for LLDPE, mLLDPE, and a plastomer.

than LLDPE. The plastomer produced in solution phase has trace levels of long-chain branching that make it more sensitive to shear, giving it a higher MIR than the linear plastomer. A narrower PDI for the single-site-catalyzed resins means a smaller low molecular weight fraction commonly called hexane extractables, which can be a limiting factor for LLDPE use in food contact applications.

There is a relatively small volume of LLDPE resins made using chrome-based catalysts that have much broader PDI, 10 and higher, and MIR values of 70 and higher. Chrome-based LLDPEs are mostly used in wire and cable coatings, blow molding, and some film applications.

Chemical Properties. LLDPE is a saturated hydrocarbon and is generally unreactive. The most reactive parts of the polymer molecule are tertiary carbons at short-chain branch points and double bonds at chain ends. LLDPE is stable in alcohols, alkaline solutions, and saline solutions. It is not attacked by weak organic or inorganic acids. Reactions with concentrated sulfuric acid (H_2SO_4, >70%) at elevated temperatures can result in the formation of sulfo-compounds. LLDPE can be nitrated with concentrated nitric acid (HNO_3). Fuming nitric acid is also used in analytical techniques to etch away amorphous polyethylene. At room temperature, LLDPE is not soluble in low molecular weight solvent although very low molecular weight and very low density fractions may be extracted. At higher temperatures, LLDPE can be dissolved in certain aromatic, aliphatic, and halogenated hydrocarbons including xylenes, tetralin, decalin, and chlorobenzenes.

Physical Properties. All polyethylene above 0.86 g/cm^3 density is semicrystalline. The basic crystalline structure for most commercial LLDPE is chain-folded lamellae (Fig. 7). The body of the crystal consists of polymer backbone segments, and the surfaces are a collection of chain folds, loose cilia, and tie chains (chains incorporated into more than one crystal). When crystallized isothermally, it has been found that 95% of the lamellae in a given sample are within 5% of the same thickness (10). There is some debate over the mechanism of chain folding and of the subsequent fold loops. The most likely model includes adjacent reentry, loose adjacent reentry, and nonadjacent reentry. Short-chain branch length

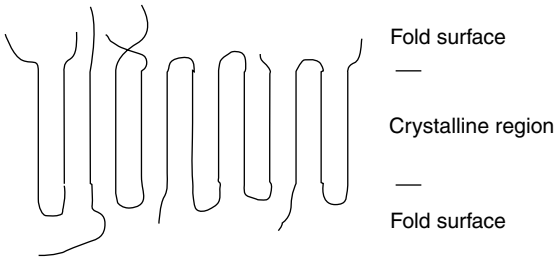

Fig. 7. Schematic of chain-folded lamellar structure.

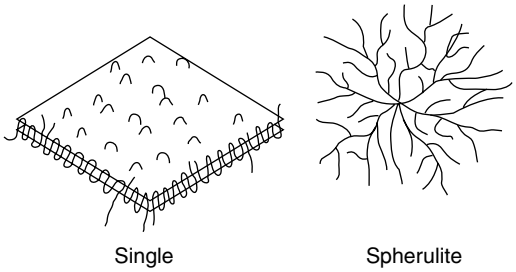

Fig. 8. Single crystal and spherulitic structures.

plays an important role in determining backbone flexibility for chain folding and subsequently fold loop size. Longer short-chain branches sterically hinder chain folding and therefore cause longer fold loops and increased numbers of tie chains. It has been found that a minimum sequence length of 14 carbons is needed for ready incorporation into a crystal lattice (11). The most stable crystalline form for polyethylene is orthorhombic with unit cell dimensions of $a = 7.42$ Å, $b = 4.94$ Å, and $c = 2.55$ Å. Research has shown that the chain axis is inclined at an angle of 30–45° to the crystal surface (12,13).

From very dilute solution ($\leq$0.1% weight or volume) single, lozenge-shaped crystals are formed (Fig. 8). They have similar relative dimensions as a sheet of paper, Angstroms thick and microns in lateral dimensions. Cooled from an unstressed melt, LLDPE forms spherulitic structures, also shown in Figure 8. Spherulites form from a defect or nucleation site and are essentially ribbon-like lamellae radiating out from a central point. They begin as sheaf-like structures and grow into spherical shapes. Regions between lamellae are amorphous chain segments and tie chains (14,15). The tie chain density between lamellae plays a dominant role in determining mechanical properties.

It is now widely accepted that LLDPE will form row nucleated, a.k.a. "shish-kebob", structures when crystallized in a melt subjected to a deviatoric stress, such as film extrusion (16–21). As given in Figure 9, a core of linear higher density polymer forms in the direction of stress (machine direction in film applications), and lamellae grow radially. Space between lamellae is filled with amorphous chain segments and tie chains. Some plastomers below 0.89 g/cm^3 density will form a fringed micellar morphology because of the very short backbone sequence length between branch points (22,23).

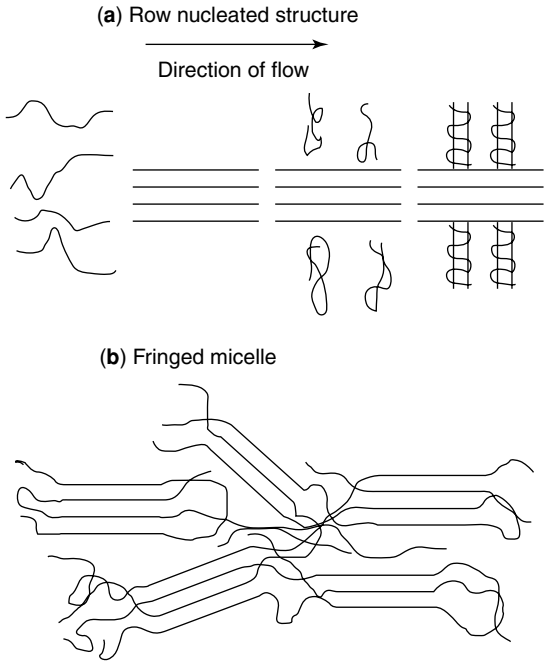

Fig. 9. (**a**) Row nucleated and (**b**) fringed micelle structures.

Polymer crystals are rarely perfect and can include chain ends, voids, and at times short-chain branches. As it is generally concluded that the ethyl branch from butene comonomers can be incorporated into the crystal lattice (24–28), this may explain why longer comonomers give LLDPEs with improved properties. Hexene and octene comonomers are more likely to produce large fold loops or tie chains that improve toughness. Quick quenching from the melt also provides less perfect crystals and may allow longer branches to be included in the crystal lattice (29).

As mentioned earlier, LLDPE has a heterogeneous composition and a higher density fraction with minimal branching. Because of this higher density fraction and its thicker crystals, the maximum melting peak in the relatively broad melting range of LLDPE usually falls between 122 and 128°C and is somewhat independent of comonomer-type. Even nonuniform VLDPE resins can have a melting point above 120°C. LDPE has thinner crystalline lamellae than LLDPE and therefore has a lower melting point as shown in the differential scanning calorimetry (dsc) profiles in Figure 10. Homopolymer LDPE usually has a melting point between 105 and 115°C.

Because of its lower melting point, LDPE has been preferred over LLDPE for many heat-sealing applications. mLLDPE and plastomers are more compositionally homogeneous than LLDPE. Shorter backbone sequence lengths for crystallization results in thinner crystalline lamellae and therefore lower melting points (Fig. 11).

mLLDPE produced in the gas phase and several produced in the slurry phase have peak melting points of 115–118°C. Plastomers have peak melting

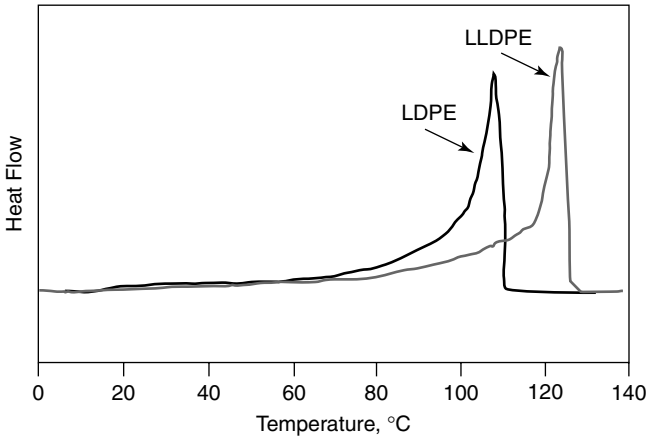

Fig. 10. The dsc melting profiles for LDPE and LLDPE.

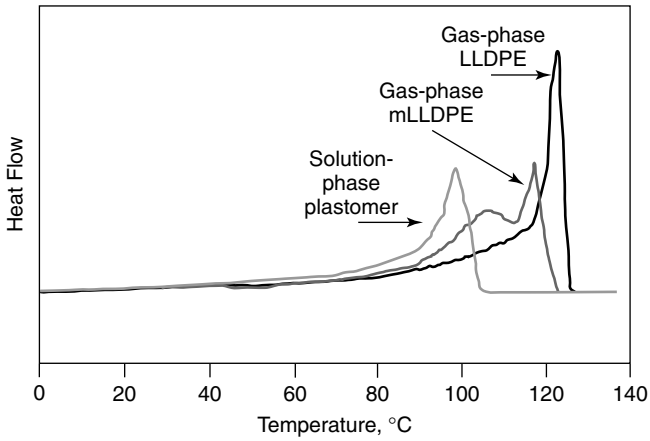

Fig. 11. The dsc melting profiles for LLDPE, mLLDPE, and a plastomer.

temperatures below 100°C. Lower melting points make single-site-catalyzed LLDPEs ideal for use as heat seal layers in many applications. Figure 12 shows heat seal strengths for LLDPE and mLLDPE, both at 0.917 g/cm^3 density, and a 0.900 g/cm^3 density plastomer produced in a high pressure reactor. All have nominal 1 g/10 min melt index. The single-site-catalyzed resins have lower seal initiation temperatures and generally have higher hot tack strengths, which allows for shorter dwell time and faster line speeds.

As with all polymers that are at least partially amorphous, polyethylene has a glass-transition temperature T_g where the transition from brittle solid to viscoelastic material occurs. There is still disagreement as to the actual T_g for polyethylene and researchers have proposed different temperatures of $-30 \pm$

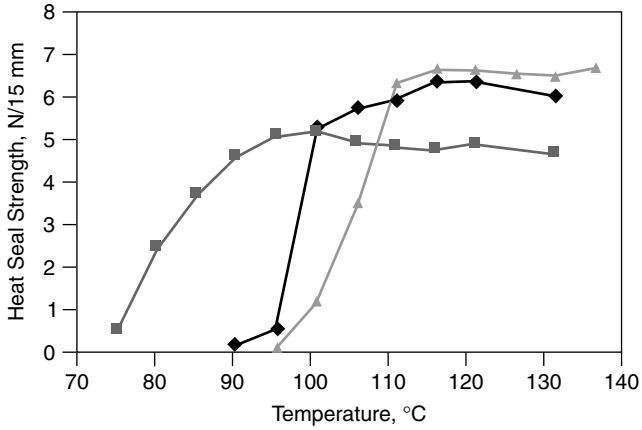

Fig. 12. Heat seal strength comparison for LLDPE, mLLDPE, and plastomer. To convert N/15 mm to ppi, divide by 2.625. –△ LLDPE–; –◇ mLLDPE–; –■ Plastomer–.

15°C (30,31), −80 ± 10°C (32), and −128 ± 5°C (33,34). Above the melting point, polyethylene is a viscous liquid.

Polyethylene has a dielectric constant of 2.3 at 1 kHz which makes it suitable for use as wire and cable housing.

Mechanical Properties

Effects of Density. Decreasing the α-olefin comonomer content increases the amount of crystallinity in LLDPE. Increasing the amount of crystallinity increases the density of the polymer and has a significant effect on polymer properties. As crystallinity increases, LLDPE becomes stiffer and in general, less tough. Table 3 shows the effect of increasing density in LLDPE blown films.

Only a seemingly small increase in density, 0.005 g/cm^3, can dramatically alter mechanical properties. Dart impact and puncture resistance are significantly reduced while tensile yield and modulus increase. For resins produced using the same catalyst and process, more crystallinity means more, larger light-scattering bodies in the film and a rougher film surface causing film haze to increase and surface gloss to decrease. At the relatively low strain rates used to test film tensile properties, density alone does not significantly affect ultimate properties such as tensile strength or elongation at break.

Effects of Comonomer and Compositional Uniformity. Table 4 shows blown film mechanical properties for an LDPE, two gas-phase LLDPEs, and one gas-phase mLLDPE, all at the same nominal melt index and density.

The first two resin columns show general film property differences between LDPE and LLDPE. LLDPE has higher tensile strength than LDPE. Modulus is higher in LLDPE resins allowing for downgauging without sacrificing stiffness. LDPE films have higher machine direction (MD) tear at low blow-up ratios (BUR) while LLDPE films have higher machine direction tear at higher BUR. Transverse

Table 3. Effects of Resin Density on Blown Film[a] Properties[b]

Property	ASTM test method	Gas-phase LLDPE	Gas-phase LLDPE
Melt index I_2, g/10 min	D1238	0.80	0.80
Density, g/cm^3	D792	0.921	0.926
Film thickness, μm		38	38
Dart impact F_{50}, g	D1709	240	210
Puncture resistance, J/mm[c]		100	50
1% secant modulus, MPa[d]			
MD	D882	180	210
TD	882	200	250
Tensile yield strength, MPa[d]			
MD	D882	10	13
TD	D882	10	14
Haze, %	D1003	10	18
Gloss, 45°	D2457	60	39

[a]Blown film with BUR = 2.5.
[b]Ref. 35.
[c]To convert J/mm to ft·lbf/in., multiply by 53.38×10^3.
[d]To convert MPa to psi, multiply by 145.

Table 4. Blown Film[a] Mechanical Properties for LDPE, LLDPE, and mLLDPE

Property	ASTM Test method	LDPE	C_4 LLDPE	C_6 LLDPE	C_6 mLLDPE
Melt index I_2, g/10 min	D1238	1.0	1.0	1.0	1.0
Density, g/cm^3		0.919	0.918	0.917	0.917
Gauge, μm		25	25	20	20
Tensile strength, MPa[b]					
MD	D882	39	46	55	66
TD	D882	26	37	42	59
1% Secant modulus, MPa[b]					
MD	D882	200	201	207	173
TD	D882	220	234	228	175
Elmendorf tear, g					
MD	D1922	170	140	255	185
TD	D1922	55	400	580	280
Dart impact, g		80	100	160	>1000
Haze, %	D1003	8	12	15	12
Gloss, 45°	D2457		50	51	47

[a]Films made at 1.8-kg/cm die circumference/h [10 lb/(hr·in.).] output rate, 2.5:1 BUR. 1.5-mm (60-mil) die gap used for LLDPE and mLLDPE, 0.76-mm (30-mil) die gap used for LDPE.
[b]To convert MPa to psi, multiply by 145.

direction (TD) tear is significantly higher in LLDPE. LLDPE has better dart impact strength than LDPE, although 0.25 g/10 min melt index LDPE will have dart impact strength approximately equal to 1 g/10 min melt index butene copolymer LLDPE. In general, LDPE has better optical properties, lower haze, and higher gloss than LLDPE. LLDPE, blended with a small amount of LDPE, 5–25 wt%, has dramatically improved optical properties. Improved mechanical properties in LLDPE are often related to microstructure, ie, increased tie chain density (36,37),

although there has been some work to suggest LLDPE contains a dispersed soft phase that leads to improved impact and fracture properties (38).

In general, as side-chain branch length increases from methyl to ethyl to butyl (C_3 to C_4 to C_6 comonomer), mechanical properties improve. While comparisons between butene and hexene copolymer LLDPEs are relatively straightforward, it is difficult to compare them with the effects of octene comonomer on properties. Butene and hexene copolymers are usually made in the gas phase while octene copolymers are usually made in solution phase. Differences in polymerization medium and catalyst can create subtle, yet significant, differences in molecular weight distribution and compositional homogeneity that make it difficult to sort out the effects of comonomer alone on mechanical properties. Generally speaking, there is little difference in mechanical properties in films made from hexene and octene copolymer LLDPEs. When produced in the same process, hexene and octene copolymer LLDPEs have nearly equivalent mechanical properties that are significantly better than those for butene copolymer LLDPE (39).

Butene copolymer LLDPE has the poorest balance of mechanical properties of the commercially available resins. Replacing even a small amount of butene comonomer with a longer α-olefin can improve toughness properties (40). A butene copolymer LLDPE and hexene copolymer LLDPE, both made in the gas phase, are compared in Table 4. Even at thinner gauge, the hexene copolymer LLDPE has improved tensile, tear, and impact properties relative to the butene copolymer LLDPE.

Also included in Table 4 is a gas-phase process hexene copolymer mLLDPE. The mLLDPE has a narrow molecular weight distribution and is more compositionally homogeneous compared to a conventional LLDPE. A narrower molecular weight distribution gives improved tensile properties but lower tear resistance. Greater compositional uniformity produces smaller crystals resulting in lower tensile modulus, significantly improved impact strength, and lower film haze.

Properties for blown films made from two different plastomers are shown in Table 5. The plastomer made in the high pressure process has better overall toughness and optical properties than the plastomer made in the solution process.

Effects of Molecular Weight and Molecular Weight Distribution. Molecular weight has the largest effect on tensile properties. Table 6 shows that for resins of equal density, higher molecular weight (lower melt index) translates into higher tensile strength. There is no major effect on yield strength or MD tear resistance, but TD tear resistance and dart impact strength are improved.

Effects of molecular weight distribution in mLLDPE have been discussed previously. Subtle changes in molecular weight distribution can also have a significant effect on LLDPE properties. Super-hexene LLDPE resins produced in the gas phase have slightly narrower molecular weight distributions, 3.5 compared to approximately 4 for conventional LLDPE, and slightly improved compositional homogeneity. The combination of molecular weight distribution and composition can lead to dart impact strengths improved over 250% and MD tear resistance improved over 30% compared to conventional LLDPE of similar melt index and density (42,43).

LLDPE resins with broad molecular weight distributions made using chrome-based catalysts find application in blown films and some molding applications (44). Because of broader molecular weight distribution, they tend to be more

Table 5. Plastomer Blown Film Properties

Property	ASTM test method	Plastomer	
		Solution	High pressure
Melt index I_2, g/10 min	D1238	1.0	1.2
MFR I_{21}/I_2		30	15
Density, g/cm^3		0.902	0.900
Comonomer		Octene	Hexene
Film thickness, μm		32	32
Tensile strength, MPa[a]			
MD	D882	77	81
TD	D882	62	77
1% Secant modulus MPa[a]			
MD	D882	73	79
TD	D882	81	83
Elmendorf tear, g			
MD	D1922	170	190
TD	D1922	470	300
Dart impact, g	D1709	1100	>1600
Haze, %	D1003	2.6	1.1

[a]To convert MPa to psi, multiply by 145.

Table 6. Effects of Molecular Weight on Cast Film[a] Properties[b]

Property	ASTM test method	C_6 LLDPE	C_6 LLDPE	C_6 LLDPE
Melt index I_2, g/10, min	D1238	2.0	2.35	3.2
Density, g/cm^3		0.917	0.917	0.917
Tensile strength @ break, MPa[c]				
MD	D882	69	67	61
TD	D882	37	34	34
Tensile strength at @ yield, MPa[c]				
MD	D882	8.3	7.4	7.9
TD	D882	7.6	7.6	7.6
Elmendorf tear, g				
MD	D1902	160	200	180
TD	D1902	920	840	770
Dart impact F_{50}, g		90	85	75

[a]Film made on 90-mm (3.5-in.) extruder at 230-m/min (750-ft/min) take-off speed, 274–300°C melt temperatures.
[b]Ref. 41.
[c]To convert MPa to psi, multiply by 145.

sensitive to orientation and therefore have less balanced properties compared to a conventional Ziegler–Natta-catalyzed LLDPE. The broad molecular weight distribution is a benefit in blow molding for having higher melt strength (for less sag) and higher environmental stress-crack resistance (ESCR) than LLDPE of similar molecular weight.

Effects of Orientation. Molecular orientation plays a significant role in determining physical performance of a finished article. In particular, film properties can be affected by processing conditions and their subsequent effects on

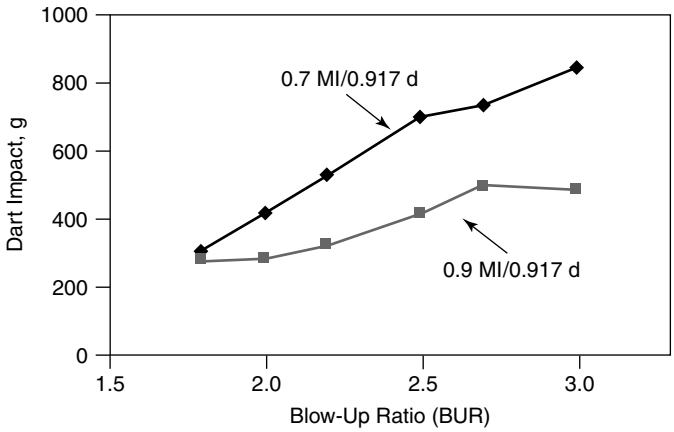

Fig. 13. Effects of blown film orientation on two LLDPEs.

molecular orientation. In general, polyethylene blown and cast films have predominant molecular orientation in the MD (41). LDPE films usually have more MD orientation than LLDPE films because of greater strain hardening behavior. Blow-up ratio (BUR) is a blown film process parameter used to control orientation. As BUR increases, molecular orientation in the MD is decreased and LLDPE blown film mechanical properties become more balanced. Impact strength is especially affected by changes in orientation. Figure 13 shows the effect of increasing BUR. In this example, output rate is held constant, BUR is increased, and line speed is reduced to maintain constant film gauge.

Catalysts for LLDPE Production

Central to the discovery and development of LLDPE has been transition-metal catalysis. However, because a given catalyst may be most useful for a different class of polyethylene or several classes, the following discussion will at times touch on other topics such as high density polyethylene (HDPE) or even polypropylene. Emphasis will be given to commercialized systems.

Almost two decades after ICI's commercialization of free-radical-polymerized LDPE in the 1930s, transition-metal catalysts proved capable to produce unbranched "linear low" density polyethylene (LLDPE) and linear "high density" polyethylene (HDPE), which had significantly different properties. Remarkably, the discovery occurred nearly simultaneously in three different research groups, using three different catalyst systems. First was Standard of Indiana's reduced molybdate on alumina catalyst in 1951 (46) followed by Phillips with chromium oxide on silica ("chromox") catalysts (47) and Ziegler's titanium chloride/alkylaluminum halide systems (48) in 1953. Only the second two were widely commercialized. This linear polyethylene is tougher than its predecessor and gave rise to entirely new markets, which are now larger globally than any other polymer. All these systems were characterized by low ethylene pressures (hundreds

of psi vs tens of thousands for HPLDPE), broadened molecular weight distributions, the absence or strong reduction of the long-chain branches characteristic of high pressure polyethylene, and the ability to incorporate α-olefins including the production of polypropylene.

The following decades saw generations of refinements to the Ziegler system, the advent of vanadium catalysts, some "single-sited," mainly for the production of ethylene–propylene–diene-modified "rubber" copolymers (EPDM), the discovery of organochromium catalysts for HDPE, and the introduction of slurry loop and gas-phase heterogeneous process technology. In the early 1980s, the field was again revolutionized by Kaminsky's discovery of the methylalumoxane (MAO) activator that led to single-site behavior and phenomenal activities for metallocene catalysts. Others, particularly Exxon and Fina, soon showed that variation of the metallocene structure leads to variation in and exquisite control of catalyst–polymer properties. While MAO has an undetermined polymeric structure, it was shown that discrete "noncoordinating" anions which could stabilize metallocene cations produced equally active catalysts. Bercaw's linked cyclopentadienylamide ligands were shown by Dow ("constrained geometry catalysts") and Exxon to give high activity when bound to titanium (see as given later). While these two catalyst systems, metallocene and "constrained geometry," long seemed unique in giving defined, single-site polyethylene, the 1990s have given rise to numerous nonmetallocene catalyst systems, some of which may be commercially viable in LLDPE applications. The uniting feature of these metal-catalyzed systems is the hypothesis that a metal–carbon bond is formed into which olefins can repeatedly insert, creating polymers by a chain-growth mechanism.

Mechanism of Metal-Catalyzed Polymerization. While the detailed mechanism of chain propagation may vary from system to system, most if not all are now believed to proceed by the Cossee–Arlman (49) mechanism in which an olefin monomer undergoes a concerted insertion into a metal–polymer chain bond via a 4-center transition state. Several fundamental steps describe the process. Initiation/Activation occurs when a metal center is transformed so that it is bonded to a group via carbon. A metal–carbon bond capable of inserting an olefin is created at the (usually cationic) metal center:

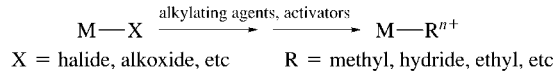

Propagation occurs when olefins insert into the metal–carbon bond, extending the chain. In the following the Cossee–Arlman transition state is shown:

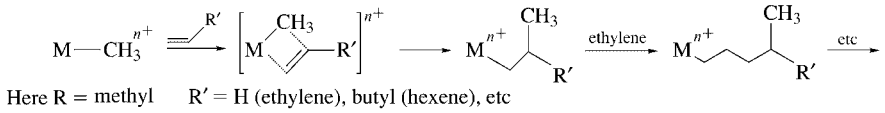

Spontaneous termination of the chain occurs when a hydrogen on the beta carbon of the chain migrates to the metal creating a metal hydride, which can reinitiate, and a chain with an unsaturated end.

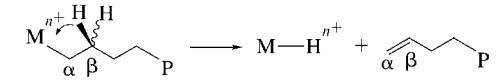

P = polymer chain

Chain transfer can occur to hydrogen, aluminum alkyls, or possibly even monomers, ending chain growth and initiating a new chain. Deactivation occurs by reaction with poisons or thermal decomposition of the catalyst center.

Standard of Indiana Catalyst. The first "low pressure" polyethylene catalyst invented (46), the Standard of Indiana catalyst system, saw relatively little commercial practice. Their 1951 patent discloses reduced molybdenum oxide or cobalt molybdate on alumina for ethylene polymerization, preferably in aromatic solvents. Later, work concerning the use of promoters was also disclosed.

Phillips Chromox Catalyst. Impregnation of chromium oxide into porous, amorphous silica–alumina followed by calcination in dry air at 400–800°C produces a precatalyst that presumably is reduced by ethylene during an induction period to form an active polymerization catalyst (47). Other supports such as silica, alumina, and titanium-modified silicas can be used and together with physical factors such as calcination temperature will control polymer properties such as molecular weight. The precatalyst can be reduced by CO to an active state. The percent of metal sites active for polymerization, their oxidation state, and their structure are the subject of debate. These so-called chromox catalysts are highly active and have been licensed extensively by Phillips for use in a slurry loop process (Fig. 14). While most commonly used to make HDPE, they can incorporate α-olefins to make LLDPE. The molecular weight distributions of the polymers are very broad with PDI > 10. The catalysts are very sensitive to air, moisture, and polar impurities.

Ziegler Catalysts. For his work in the discovery of a new class of highly active catalysts for polymerization of ethylene, propylene, and dienes, Karl Ziegler shared the 1963 Nobel Prize in Chemistry with Guilio Natta whose contributions were predominantly related to polypropylene. Today, these catalysts together with the Phillips catalyst are responsible for the majority of the world's polyethylene production. Loosely defined, Ziegler catalysts are polyethylene catalysts derived from transition-metal halides and main group metal alkyls (46,50–53). In modern

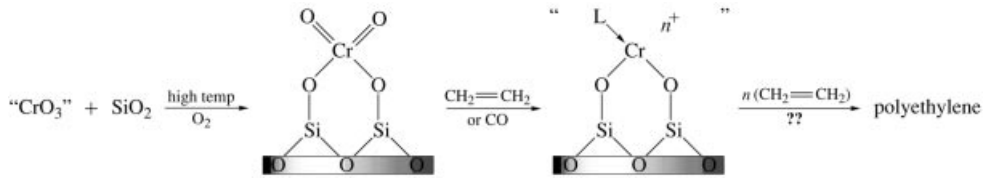

Fig. 14. Phillips' chromox catalyst. (Here "??" indicates that the actual mechanisms are as yet unknown.)

usage this generally means titanium (and sometimes vanadium) chlorides with aluminum alkyls or alkylchlorides. Numerous large research and commercialization efforts have progressed titanium-based systems through five or six generations, particularly for isospecific propylene polymerization. Most early systems used titanium halides with aluminum metal or aluminum alkylhalides to produce some form of crystalline $TiCl_3$, usually the alpha form, often with Al in the lattice. The Ti centers could be in +3, +4, and even +2 oxidation states. Aluminum alkyl cocatalyst was required for activity. In the next generation, large increases in activity were achieved by dispersing the titanium centers over crystalline $MgCl_2$, and this is now standard commercial practice. Modifiers, internal donors, external donors, and cocatalysts have been used to produce smaller $MgCl_2$ crystals, higher surface areas, poison undesired sites, control oxidation states, enhance activity, and otherwise change the catalyst performance. Silica or other porous supports are usually used to introduce the catalyst into heterogeneous processes. As with most heterogeneous systems (eg, organochrome and chromox catalysts) there are multiple active sites which may only be a fraction of the total metal centers. The exact structure and number of active sites is usually a topic of debate because of the problem of extremely active catalysts: they must be used in extremely low concentration and usually cannot be detected directly at "real world" conditions. Multiple sites lead to polyethylene chains with varying structures from chain to chain, though the typical molecular weight PDIs of 3.5–6 for Ziegler catalysts are still much narrower than the chromox catalysts. Some producers (eg, Dow and Nova) use these catalysts in solution, but most of the LLDPE volume comes from supported catalysts because of their use in the heterogeneous gas-phase processes extensively licensed by Union Carbide and British Petroleum. These catalysts are substantially less sensitive to air and moisture than chromium-based systems. Polyethylene molecular weight can be reduced by the addition of H_2, and α-olefin comonomers are copolymerized in order to lower the polymer's density.

Organochrome Catalysts. Like the Phillips chromox catalysts, the organochromium catalysts introduced by Union Carbide in the 1970s required an oxide support. Both disilyl chromates, $(R_3SiO)_2CrO_2$ (Fig. 15), and chromocenes, $(C_5H_5)_2Cr$ (Fig. 16), are believed to bond to an oxo functionality on the support ultimately leading to Cr^{2+} species. How these form the active species and its nature remain unproven. These catalysts have been licensed extensively in slurry-phase and gas-phase processes, but only for HDPE production because of negligible comonomer incorporation ability. Molecular weight distributions are broad, and hydrogen lowers molecular weight by chain transfer. These systems are very sensitive to impurities as with the Phillips catalyst.

Metallocene Catalysts. Although some commercial solution catalysts (eg, vanadium halide/alkyl aluminum EPDM systems) exhibited single-site behavior (eg, PDI = 2) earlier, metallocenes ushered in well-understood, finely tunable single-site polymerization capability on a far broader scale. Metallocenes are molecular transition-metal compounds containing the flat cyclopentadienyl ring bound "side-on" to the metal center. Shortly after their discovery in the 1950s, it was known that metallocenes could polymerize or oligomerize olefins in the presence of aluminum alkyl cocatalysts. By the 1970s, it had been found that small amounts of water increased the system's activity (48,54,55). Around this time, it was shown that unactivated, neutral Group 3 metallocenes could

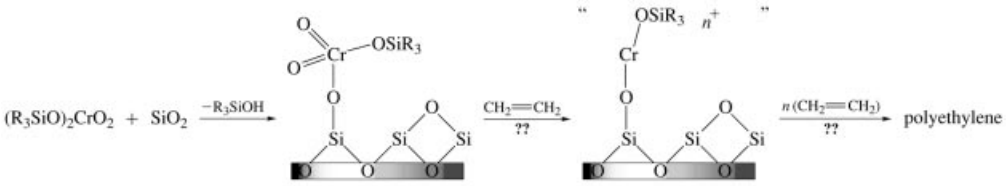

Fig. 15. Disilyl chromate catalyst. (Here "??" indicates that the actual mechanisms are as yet unknown.)

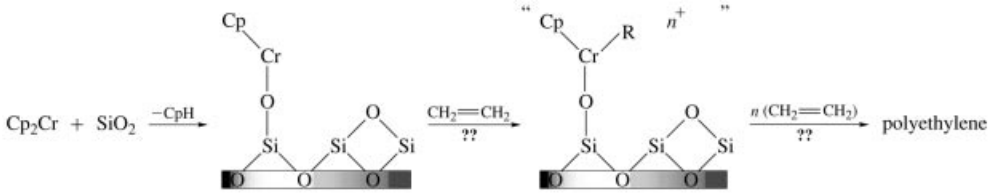

Fig. 16. Chromocene catalyst. (Here "??" indicates that the actual mechanisms are as yet unknown.)

polymerize olefins to high molecular weight with narrow molecular weight distributions (56,57). Despite these many works demonstrating most of the major characteristics of the current state-of-the-art polymerization catalysts, the critical breakthrough came in the activator.

MAO—The Kaminsky Activator and Single-Site Catalysis. In 1976, Kaminsky, Sinn, and co-workers discovered that water-treated trimethylaluminum activates metallocenes orders of magnitude better than previous systems (48,54,55,58). This finding has revolutionized this field of ethylene and α-olefin polymerization, laying the foundation upon which all further advances were built. The key activator, known as methylalumoxane (MAO), is generally formed by the reaction of less than one water with one $Al(CH_3)_3$ to create polymeric structures $(CH_3AlO)_n(Al(CH_3)_3)_n$ thought to contain chains, rings, three-dimensional cage structures, and unreacted trimethylaluminum (TMA). Typically formed in toluene, the original MAO has a tendency to form gels.

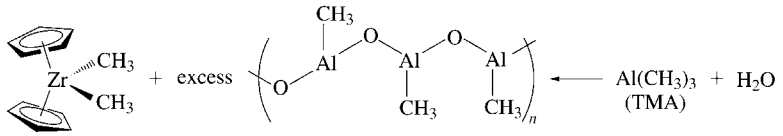

methylalumoxane, "MAO"

Versions incorporating, eg isobutyl groups (MMAO), have differing properties such as hydrocarbon solubility and less gelation. The optimal activator will vary from system to system. Despite the multisited structure of MAO, many MAO-activated metallocenes give polymers with narrow molecular weight distributions (PDI = 2.0) and narrow comonomer distributions, behavior characteristic of only a

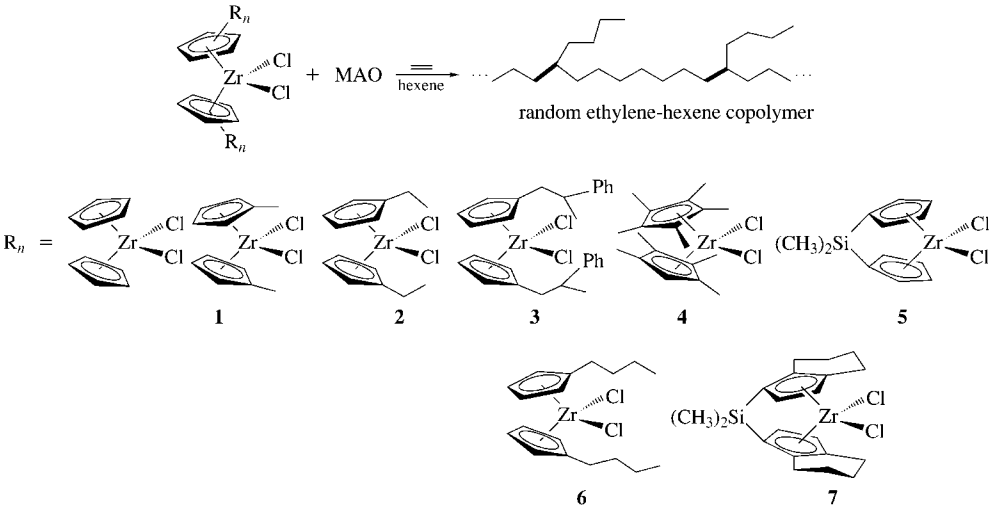

Fig. 17. Substituted metallocene catalysts. The identity of R_n controls polymer molecular weight and density, which in turn controls polymer properties. $R_n = H$ or see other examples. (**1**), (**2**), (**3**), (**4**), (**5**) from the patent (59). Many further derivatives were later disclosed, notably, (**6**) and (**7**).

single active structure. The contrast with multi-sited Ziegler and chrome systems lead to the use of single-site catalysis to describe these systems.

Metallocene Commercialization—The Significance of Substitution. The parent metallocenes used by Kaminsky and co-workers are rarely used commercially, so it is fair to say that the breakthrough was not completed until the recognition that subtle variations in the metallocene molecular structure dramatically change the catalyst performance and polymer characteristics (Fig. 17). Welborn and Ewen of Exxon lead in this discovery, leading to base patent coverage in the field (59). Patents and articles on metallocene derivatives now number into the thousands. Ewen as well as Brintzinger and Kaminsky, Spaeleck and co-workers at Hoechst, Weymouth (60,61), and many others advanced the mechanistic insights into these systems by studying tacticity control in polypropylene.

Noncoordinating Anions—Alternative, Discrete Activators. Elucidation of the nature of the active species in MAO/metallocene catalyst systems was the subject of intensive research efforts with contributions coming from many laboratories. It would be artificial to attribute credit to any one group for solving the mystery, but it was the discoveries by Jordan (62) and by Turner and Hlatky of Exxon (63) that most clearly established the current view. They demonstrated that metallocene cations possessing stable, noncoordinating anions (NCAs) such as tetraarylborates were extremely active for olefin polymerization and were single-sited in nature (Fig. 18). This strongly implied that MAO functions by abstracting an anionic ligand from a neutral metallocene to form a metallocene cation and an MAO anion. Indeed, it was shown that a neutral aryl borate could abstract a methyl group to form a metallocenium—anion pair with high activity (64). Because of the known structure of these activators vis a vis MAO, these are often referred to as discrete activators. These activators are commercially viable,

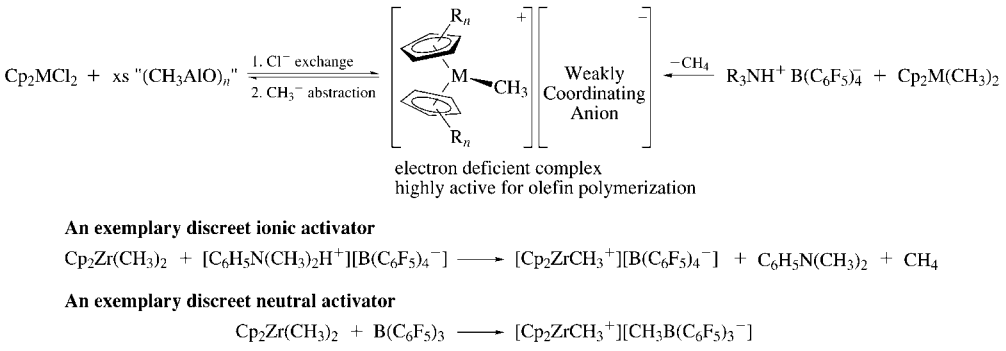

Fig. 18. Noncoordinating ionic catalysts.

often yielding greater activity than MAO with the cost advantage that large molar excesses are not needed as with MAO. Conversely, such systems are often very sensitive to impurities, whereas excess MAO acts as an impurity scavenger.

The CPSiNR Ligand for Constrained Geometry Catalysts. Biscyclopentadienylmetal complexes were not the only single-site catalysts for olefin polymerization. Monocyclopentadienyl complexes often showed activity, but generally were not competitive catalysts except when linked to a bulky amido group. Thus, Bercaw's Group 3 metal system CpSiNR ligand (**8**) was placed on titanium (**9**) by workers at Dow (65) and Exxon (66) and was found to produce very active catalysts with attractive features. The open structure leads to very good comonomer incorporation and has high molecular weight capability. Both companies filed patents in the U.S. and World offices within days of each other resulting in interferences and court actions over catalyst, activator, and polymer, which were recently settled after more than a decade. Dow proceeded with commercialization of the system dubbing them constrained geometry catalysts because of the bridge between the cyclopentadienyl and amide ligands.

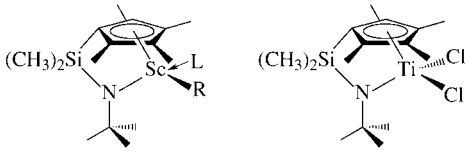

8 **9**

Commercialization of Single-Site Catalysts. In commercial practice, mono and biscyclopentadienyl (mono Cp bis Cp) catalysts show sensitivity to oxygen, water, and polar functionality more comparable to that of chrome catalysts. Depending on catalyst molecular structure, molecular weight capability and comonomer incorporation level vary over a tremendous range beyond the capabilities of other commercial catalysts. Comonomer incorporation is usually more facile and more evenly distributed throughout the chain than in the older conventional systems in addition to less chain-to-chain molecular weight and comonomer

variation. Bis Cp catalysts are very sensitive to chain termination by H_2, while mono Cp amide (constrained geometry) catalysts are more like titanium Ziegler systems in this regard. The systems are supported on silica when used in slurry-phase or gas-phase processes, and both MAO and NCA activation are practiced. Although the major components of these catalysts—metal complex, MAO, discrete activators—are inherently more expensive than conventional catalyst raw materials, volume manufacture and high activity have reduced costs to acceptable levels when combined with premiums commanded by the polymer products.

Though not well known, the commercial use of metallocenes for polymerization began in 1985 with Uniroyal's sale of "Trilene" low molecular weight polyethylene products. Exxon began production of metallocene VLDPE in a high temperature and pressure unit in 1991 under the EXACT trade name. These metallocene polymers are characterized by very narrow molecular weight and comonomer distributions, which lead to high strength and uniformity. Several years later, Dow introduced constrained-geometry-catalyst-produced polymers using a high temperature solution process to make VLDPE and LLDPE. These polymers generally emphasized easier processability relative to the bis metallocenes. Then in 1994, Exxon launched commercial metallocene products from the low pressure, low temperature, very large-scale UNIPOL™ gas-phase process. Metallocene polypropylene was introduced by Exxon and Hoechst the following year, and 1996 saw the sale by Exxon of metallocene polymers produced in slurry loop reactors. With the DuPont/Dow solution process to produce EPDM polymers, all major processes and polyethylene/polypropylene polymer types were being produced by single-site catalysts. While many commercialization announcements have been made up to 2000, relatively few producers beyond those mentioned earlier have initiated full commercial production. However, strong demand, production of specialty products like cyclic copolymers, the recent sale of single-site catalyst licenses, and the announcement of new nonmetallocene single-site catalysts suggest that these new technologies are finally coming into their own after more than a decade of development.

Other Ligand-Based or Single-Site Catalysts. The term single site is misleading because the polymers of these systems, including metallocenes, sometimes have broad molecular weight distributions indicative of multiple catalyst sites. Some prefer the term ligand-based catalysts to denote that the catalysts come from discrete molecular precursors (of exactly defined ligand sets) even though in the active system the metal complex may have been partially converted to multiple new species. The mono Cp and bis Cp complexes long seemed unique as commercially useful ligand-based catalysts, but that picture is changing. As metallocene catalysts have risen in profile during the 1990s, and MAO and discrete activators have become widely available enough, nonmetallocene ligand-based catalysts have been discovered to warrant reviews (67,68). Figure 19 depicts exemplary nonmetallocene systems, several of which may be near commercialization. Noteworthy are the nickel- and palladium-based "Versipol" catalysts of DuPont and the University of North Carolina that make hyperbanched polymers (69,70). Also, pyridyl bisimine ligand-based iron catalysts have been disclosed (71–73) and may be used in the near future for HDPE production. Nova has recently announced forthcoming products from ligand-based systems. With Stephan's titanium bisphosphaimine systems for example, they

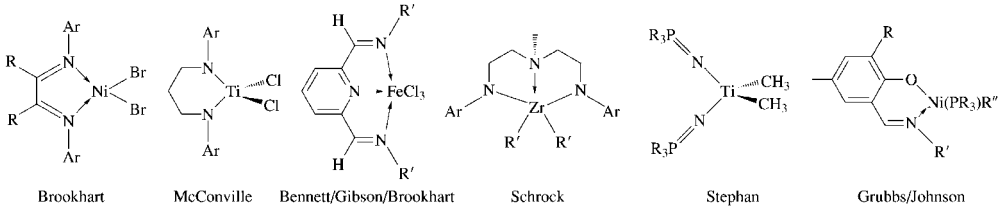

Fig. 19. Other ligand-based single-site catalysts.

collaboratively disclose performance comparable to the constrained geometry catalysts of Dow and Exxon under commercial reaction conditions (74). Given the current state of the technology, it seems very likely that advances in conventional, metallocene, and nonmetallocene catalyst systems will continue to drive LLDPE product and process performance to new levels for decades to come.

Low Pressure Manufacturing Processes and Capacities

Gas-Phase Process. The gas-phase process is considered to be the most versatile low pressure process for producing polyethylene because it can make the broadest product portfolio in terms of molecular weight and density. It had been used since the 1960s to make HDPE and in 1977, Union Carbide built the first gas-phase plant for LLDPE production. Subsequently, British Petroleum and Himont developed alternative gas-phase processes for producing LLDPE. As a result of its versatility, it is the most widely licensed technology worldwide for linear low density production. A simplified schematic of the Union Carbide Unipol process is shown in Figure 20.

In this process, purified ethylene and comonomer are continuously fed into a fluidized bed reactor. Catalyst in dry form is added directly into the bed. The gas recycle stream serves several purposes—fluidizes the polymer particles, provides polymerization raw materials, and removes heat of polymerization. Reactor temperatures are usually below 100°C to prevent resin stickiness and pressures are approximately 2 MPa (300 psi).

The gas stream fed to the bottom of the reactor is the only source of cooling for reactor temperature control. Reactor temperature is a function of polymerization rate. At one time, output rates were limited to prevent high reactor temperatures and resin stickiness. To increase cooling capacity of the gas stream and therefore increase production rates, the recycle stream can be cooled below reactant dew point forming a liquid–gas mixture that is returned to the reactor, which operates above the dew point of the recycle stream. Evaporation of liquids in the recycle stream absorbs heat from the reactor allowing for greater production rates (75). This is commonly referred to as "running in condensed mode." Nonreactive hydrocarbons such as *n*-hexane or isopentane in quantities up to approximately 30 wt% of the recycle stream can also be used as condensing agents allowing for production rates near twice design reactor capacity (76).

Residence time for polymer in the reactor can be several hours. This is one disadvantage to the gas-phase process as grade changes can take hours to

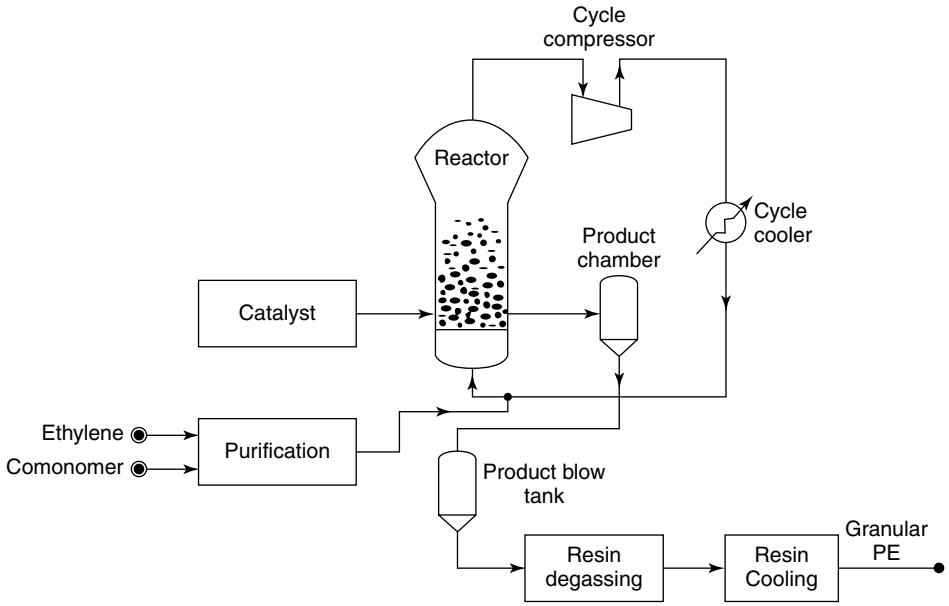

Fig. 20. Schematic of UNIPOL gas-phase polymerization process.

complete. Granular polyethylene is periodically removed from the reactor and sent via pressurized lines to a purge bin where residual catalyst is neutralized and residual monomers are removed. Resin is then conveyed to a pelleting process.

Solution Process. The solution-phase process is also very versatile. Because of short residence times in the reactor, product changes can be made in less than an hour at commercial production rates. A schematic of a solution-phase polymerization process is shown in Figure 21.

Ethylene and comonomer are purified and dissolved in a solvent. An activated catalyst is added to that solution, which is then fed to a stirred reactor. The temperature of the feed stream controls reactor temperature, which is a major determinant of polymer molecular weight. Reactor temperatures are usually 170–250°C with pressures of 4–14 MPa (500–2000 psi). The solution is then fed to a secondary, trimmer reactor where further polymerization takes place. Chelating agents are injected into the solution to neutralize active catalyst. A high pressure flash vessel is used to remove monomer and about 90% of the solvent. A secondary devolatilization step is required to completely remove solvent. Granular polymer is then conveyed for pelletization.

Two limiting factors in solution-phase polymerization are cost of operation and polymer molecular weight. Solvent recovery steps are very energy intensive and add to production costs. Also, the production of high molecular weight resins is limited because of the very high viscosity of the resultant solution. Advantages include short reactor residence time that allows for very quick product transitions (77).

Slurry Process. While the slurry polymerization process is more often associated with production of HDPE, improved catalyst technology has allowed

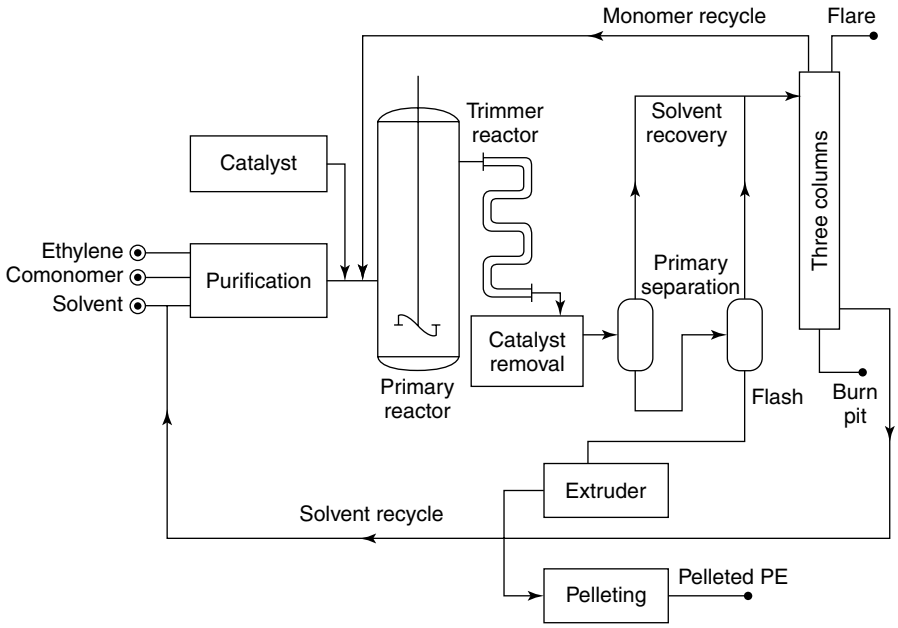

Fig. 21. Schematic of solution-phase polymerization process.

the production of LLDPE and mLLDPE resins. In the slurry process, monomer is dissolved in a diluent in which the polymer product is insoluble. Polymerization occurs below the melting point of the polymer product that forms as suspended particles. An example schematic of a slurry-phase polymerization process is shown in Figure 22.

Ethylene and comonomer are purified, then dried and fed with recycled diluent with a catalyst slurry to a double loop continuous reactor. Polymer forms as discrete particles on catalyst grains and is allowed to settle briefly at the bottom of settling legs to increase concentration from about 40% in main loop to 50–60% in the product discharge (77). Reactor temperatures are usually 70–110°C and reactor pressures are between 3 and 5 MPa (450 and 720 psi). Diluent and residual monomers are flashed off for recycle and polymer is conveyed for pelletization. Production of low density polymers was not practicable due to solubility of low density/low molecular weight polymer molecules in the diluent, but the use of chromox catalysts that produce broad molecular weight LLDPE and metallocene catalysts that produce mLLDPE have broadened the product portfolio for slurry-phase polymerization.

In order to more finely control polymer molecular architecture in LLDPE, much research and development effort has been spent on developing staged reactor technology. There are currently commercial systems in staged gas phase (Union Carbide) (78,79), staged slurry/gas phase (Borealis) (80), and staged solution phase (Nova) (81). Each of these processes allows for control of molecular weight distribution and location of comonomer, ie in high molecular weight or low molecular weight fractions.

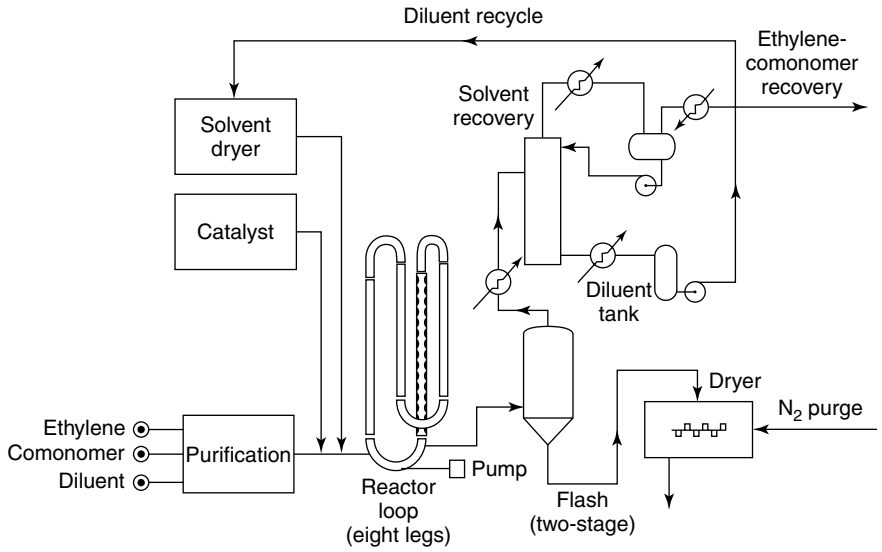

Fig. 22. Schematic of slurry-phase polymerization process.

Processing of LLDPE

Rheology. Every process used to convert LLDPE into a finished product involves melting. Therefore, polymer viscosity is a very important resin parameter that must be considered when selecting a resin for use. LLDPE melts in the normal processing range of 150–300°C exhibit non-Newtonian (shear thinning) behavior as their apparent viscosity is reduced when melt-flow speed is increased (82–85). Figure 23 shows a plot of dynamic melt viscosity for LDPE, gas-phase

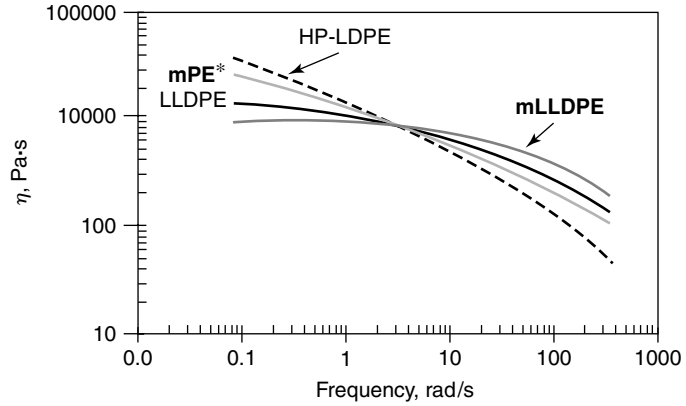

Fig. 23. Melt viscosity data for LDPE, LLDPE, and mLLDPE all normalized to1 g/10 min melt index. Also shown is new type of easy-processing metallocene-catalyzed polyethylene, mPE*. To convert Pa·s to P, multiply by 10.

LLDPE and gas-phase mLLDPE, all normalized to 1 g/10 min melt index. At very low shear rates, LDPE has the highest viscosity, caused by a broad molecular weight distribution and long-chain branching. LLDPE has a broader molecular weight distribution than mLLDPE and therefore has higher viscosity at very low shear rates. As you approach the shear rates commonly associated with extrusion, 100–1000 rad/s, those trends are reversed. The broad molecular weight distribution and long-chain branching seen in LDPE cause it to have a greater response to shear. As a result of increased shear thinning relative to LLDPE and mLLDPE, the melt viscosity of LDPE at higher shear rates is significantly lower than that of the linear resins. The LLDPE resin has lower shear viscosity than the mLLDPE because of its broader molecular weight distribution. Higher viscosities will translate to higher extrusion pressures, higher temperatures, and greater energy consumption.

Because melt viscosities for LLDPE and mLLDPE are so much greater than that for LDPE at the higher shear rates experienced during extrusion, market penetration has been limited in some applications and geographical areas where LDPE processing equipment dominates. Several resin companies are working to develop metallocene-catalyzed resins that are compositionally homogeneous but have slightly broader molecular weight distributions or trace levels of long-chain branching. This gives the resins improved mechanical properties relative to LLDPE, but with lower viscosities and easier extrudability (86–88). An example of this type of resin is shown in Figure 23. A relatively new type of metallocene-catalyzed polyethylene, here noted as mPE*, is shown to have higher melt viscosity than LLDPE at very low shear rates because of a slightly broader molecular weight distribution and trace levels of long-chain branching. Because of its broader molecular weight distribution and long-chain branching, it demonstrates greater shear thinning behavior than LLDPE allowing for use in older equipment designed for LDPE extrusion.

Figure 24 shows extensional viscometry results for 1 g/10 min melt index LDPE, LLDPE, and mLLDPE. LDPE, with its broader molecular weight

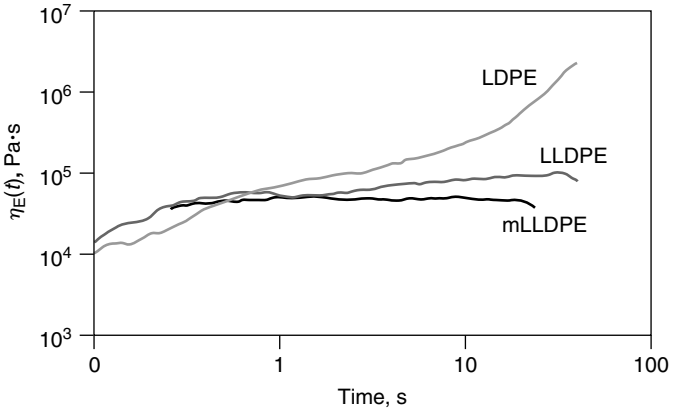

Fig. 24. Extensional rheology data for LDPE, LLDPE, and mLLDPE. To convert Pa·s to P, multiply by 10.

distribution and long-chain branching, shows appreciable strain hardening behavior relative to the linear resins. LLDPE has greater extensional viscosity than mLLDPE because of broader molecular weight distribution. Lower extensional viscosity translates to poorer bubble stability in the blown film process, but lack of strain hardening allows linear resins to be drawn down to thinner gauges than LDPE of equivalent melt index.

Film Extrusion. Approximately 77% of the LLDPE produced globally is processed into film. The most common techniques for producing film are blown film extrusion and cast film extrusion. Both involve extrusion prior to film forming.

In the extrusion process, resin pellets are gravity fed into a heated barrel. Pellets are conveyed down the barrel by a screw that first compacts and then melts the pellets through shear-induced heat. The last section of the screw, also known as the metering section, ensures a homogeneous melt and uniform output. Because of its narrower molecular weight distribution and higher shear viscosity, LLDPE extrudes differently than LDPE. At equivalent melt index, LLDPE is expected to have higher extrusion pressures and temperatures than LDPE. At equivalent temperatures and pressure, LLDPE has better pumping characteristics than LDPE, ie pounds per hour per screw rpm (89). Higher resin viscosity for LLDPE means greater power consumption than LDPE.

To compensate for extrusion differences between LDPE and LLDPE extrusion, screw designs have changed. LLDPE screws have lower compression ratios (channel depth in feed section/channel depth in metering section). Barrier screws, which have additional flights to separate the melt pool from solids bed during melting, were developed to accommodate the different melting behaviors of LLDPE. Extrusion temperatures for LLDPE range from 180 to 300°C with pressures ranging from 15 to over 40 MPa. LLDPE resins, and especially mLLDPE resins, often incorporate fluoropolymer processing aids, such as Dynamar™ products from Dyneon. Fluoropolymer processing aids coat the barrel to reduce shear and therefore pressures and temperatures, and also coat die lips to eliminate melt fracture and die lip buildup. Metallocene-catalyzed resins can be extruded on any line used by LLDPE with the understanding that there may be higher extrusion temperatures and pressures as a result of narrower molecular weight distributions in the mLLDPE compared with conventional LLDPE (90).

In blown film extrusion, molten resin is forced through an annular die. Commercial-scale diameters range from 15 to 120 cm. There are four main components to a blown film die—mandrels, inner lip, outer lip, and body. The mandrel and body distribute polymer flow around the die. Most commercial mandrels have several spirals to more uniformly distribute melt flow and minimize gauge variation (91). Die lips define the die gap. Commercial die gaps for LLDPE blown film extrusion range from 1.5 to 2.5 mm compared to die gaps for LDPE processing, which range from 0.5 to 1.0 mm. Wider die gaps are needed to eliminate melt fracture in LLDPE caused by higher viscosity. After exiting the die, the molten tube of polymer is generally pulled upward by a set of nip rolls, although in some cases it is pulled horizontally or downward. As film thickness is reduced, the tube expands because of internal bubble pressure and forms a tube of larger diameter. The ratio of final bubble diameter to initial die diameter is the BUR. Blow-up

ratios in commercial processes range from 1.5 to over 4 and are largely determined by product end use. Film cooling is aided by air rings that supply air flow around the molten tube. Because of lower extensional viscosity, LLDPE can be drawn to thinner gauges than LDPE but is more prone to bubble instabilities. Dual-lip air rings that provide Venturi-type air flows around the bubble are used to stabilize the bubble in addition to providing cooling. The tubes are drawn down to final film thicknesses of 0.007–0.25 mm. Maximum line speeds approach 240 m/min. Film rolls up to 4 m in diameter are collected on cardboard cores. Many lines have in-line converting for producing articles such as trash bags as the film is being produced.

Cast film extrusion involves extruding molten polymer through a flat die, usually with a coat-hanger design. Commercial die widths can range from 150 to over 600 cm. Die gaps for LLDPE film extrusion are 0.5–0.8 mm. The molten sheet of film is usually extruded downward, but in some cases is extruded horizontally. Within inches after exiting the die, the film is deposited onto a rotating chilled or heated roller. The roller can be polished smooth, have a matte finish, or be embossed with a repeating pattern. Film edges are usually trimmed, chopped, and refed into the system as flaky material called "fluff" or "regrind." Film gauges range from 0.007 to 0.125 mm. Film rolls up to 4 m in diameter are collected on cardboard cores. Cast film processes can be run at much higher rates (over 600 m/min) than blown film processes.

Injection Molding. LLDPE is processed by injection molding to produce complex shapes from children's toys to household containers. Polymer pellets are fed to a single-screw extruder and melted at approximately 160–240°C temperatures. The polymer melt is injected into a mold at 35–130 MPa. Higher viscosity resins, ie, higher molecular weight or narrower molecular weight distribution, will require higher pressures. Molds are usually made in two halves, one fixed and one movable. When the mold halves are together, at least one machined cavity will be formed into which molten resin is injected. Cooler mold temperatures decrease cycle time and increase toughness, but can increase molded-in stress. Higher mold temperatures produce high surface gloss. Filling times for very small molds range from 0.2 to 0.8 s and for larger, more complex molds from 3 to 6 s. After the mold is filled, it is held under pressure than cooled rapidly. Cycle time depends on polymer viscosity, density, and part requirements. LLDPE injection-molding cycle times range from 10 to 30 s (92). Plastomers can be injection molded on equipment designed for flexible polyvinyl chloride with only minor adjustments in processing conditions—colder dies, faster injection speeds, and hot runners (93).

Blow Molding. Bottles and drum liners are common LLDPE blow-molded articles. In the blow-molding process, a thick-walled tube of film called a parison is extruded vertically downward. The parison will have the correct dimensions, weight, and position relative to the mold to produce the finished product. After the parison is extruded, two mold halves with a machined cavity will close around it sealing the bottom of the tube, and the parison is then inflated by pressurized air. Air pressure is usually low, between 0.3 and 0.7 MPa. The molten resin takes the shape of the mold and is cooled to the solid state. The pressurized air is released, the mold is opened, and the part is ejected. Two areas of concern are polymer swell and melt strength. Swell is caused by shrinkage in the process direction

from elastic recovery of the melt. Melt strength of the polymer must be sufficient to support the weight of the extruded parison and prevent excessive "sag," which occurs when the parison reaches some critical length and its weight causes an abrupt increase in speed. Both parameters can be controlled by process conditions and selection of polymer molecular weight (94,95).

Rotational Molding. Rotational molding is used to produce a variety of polymer parts from small to large and from simple to complex. Instead of resin pellets, finely granulated polymer powders are used. Rotational molds are filled with the exact weight of the part to be formed. They are then heated and simultaneously rotated in two perpendicular planes. Tumbling powder sticks to the heated mold and forms a uniform coating on the interior mold surface. Rotation speeds should be relatively low to prevent strong centrifugal forces that can cause uneven thicknesses. After heating, rotation continues and the mold is cooled. The part is removed after the cooling step (96,97). The impact strength of the product is strongly dependent on the internal air temperature of the mold. Lower internal temperatures lead to inadequate sintering of articles, increased void content, and poor crystalline microstructure (98).

Extrusion. Additional extrusion applications of LLDPE include pipe, tubing, sheet, and insulated wire. Pipe and tubing are extruded through annular dies similar to blown film dies. Small diameter products, less than 10 mm, are considered to be tubing while larger diameter products are referred to as pipes (99). Sheet is produced on flat dies and is usually classified as having thickness greater than 0.254 mm. Wire coatings are made by passing a conductor through the hollow center of an annular die and coating with molten polyethylene.

Economic Aspects

LLDPE is made in every continent except Antarctica. It currently makes up approximately 25% of all polyethylene demand and has the greatest growth rate of the major product families (100) as Table 7 shows.

Usage of metallocene-catalyzed resins is predicted to grow at over 24% from 2000 to 2005 as manufacturing processes become more robust, more companies begin to produce these resins, and resin pricing becomes more competitive with commodity grades (100). Consumption in 2005 is expected to be near 3000 kton.

Table 8 shows global allocated LLDPE production capacities by country and process (101). It must be noted that capacity determination is difficult as

Table 7. Predicted Annual Growth Rates for Polyethylene[a]

	Average annual growth rate, %		
Resin	1996–2000	2000–2005	2005–2010
Polyethylene	5.5	6.0	4.7
LDPE	1.5	1.3	−0.2
LLDPE	9.4	9.3	7.3
HDPE	5.2	6.2	5.2

[a]Ref. 100.

Table 8. Global Allocated LLDPE Capacity, 10^3t[a]

Country	Gas	Solution	Slurry	Other	Total
North America					
United States	3214	1018		75	4307
Canada	769	711			1480
Latin America					
Argentina	98	21			119
Brazil	425	100			525
Venezuela		120			120
Europe					
Finland	70				70
France	420			120	540
Germany	278	166			444
Italy	200	180			380
Netherlands	120	396			516
Russia	150				150
Spain		198		99	297
Sweden	253				253
United Kingdom	100				100
Africa					
Egypt	50				50
Libya	40				40
Nigeria		160			160
South Africa	115				115
Middle East					
Iran	60				60
Kuwait	325				325
Saudi Arabia	1160				1160
Asia & Pacific					
Australia	105				105
China	683	110		77	869
India	200	286			485
Indonesia	478				478
Japan	393	120	160	383	1046
Malaysia	209				209
Pakistan		15			15
Philippines	90				90
Singapore	120				120
South Korea	468	214			682
Taiwan	180				180
Thailand	70	261			331
Totals	*10,829*	*4062*	*160*	*754*	*15,805*

[a]Ref. 101.

many processes can be used to make LLDPE and HDPE. The values shown indicate capacity used solely for LLDPE and mLLDPE production. Total LLDPE–HDPE swing capacity is approximately 25.3×10^3 kton (101). The countries with the largest LLDPE capacity are the United States, Saudi Arabia, and Japan. In the United States, LLDPE is produced by Chevron, Dow, Eastman,

Equistar, ExxonMobil, Huntsman, Montell, Phillips, Union Carbide, and Westlake. Commercial mLLDPE is available from Dow, ExxonMobil, and Phillips. Globally, it is estimated that there are eleven commercial suppliers of metallocene-catalyzed polyethylene (102).

Ethylene is produced primarily from "cracking" ethane or naphtha. Regions such as the Middle East, Western Canada, and Malaysia have cost advantages over other regions because of plentiful supply of ethane and low alternative values. Countries such as Japan and Korea have much higher ethylene production costs because of poorer plant economics (smaller scale) and expensive naphtha feedstock (82). U.S. pricing for ethylene in mid-2000 is approximately \$0.55–0.60/kg. α-Olefins are commonly produced by distillation of hydrocarbons, ethylene oligomerization, catalytic dehydrogenation of alkanes, and wax cracking. Mid-2000 U.S. pricing for butene is approximately \$0.57–0.66/kg and pricing for hexene and higher is approximately \$1.25–1.35/kg (103).

Raw materials comprise the greatest fraction of the cost to produce LLDPE. Raw materials include ethylene, α-olefin, hydrogen, catalyst, and additives. Depending on geographical region, raw materials (at cash cost) are approximately 60–75% of total production costs (100). Utilities, including power, cooling water, steam, and fuel, are approximately 5–15% of total LLDPE production costs. Overhead makes up the balance and includes physical structures, staffing, and shipping. Actual costs can vary significantly by reactor technology, environmental costs, and product mix. Frequent product or catalyst changes can significantly increase production costs by reducing the amount of prime material available for sale.

LLDPE pricing will vary according to comonomer, application, and sales volume. As of the middle of the year 2000, U.S. pricing for butene copolymer LLDPE ranged from \$0.79 to \$0.84 per kilogram for film grade resins. Hexene copolymer LLDPE film resins are \$0.06–0.09/kg higher, octene copolymer LLDPE film resins are \$0.08–0.11/kg higher, and metallocene-catalyzed volume film grades are \$0.08–0.13/kg higher. Pricing is nearly equivalent for general-purpose injection-molding grades and as much as 10% higher for lid grades. Rotomolding powders can be 50–100% greater than butene copolymer LLDPE film grades. Pricing for plastomers ranges from approximately \$1.40 to over \$2.00 per kilogram.

Shipment and Specification

In the United States, bulk resin can be delivered by rail in hopper cars in quantities of 70–100 t. Smaller bulk quantities of 15–20 t can be delivered by hopper truck. Very small quantities and samples are usually delivered in large cardboard boxes called gaylords that contain 450–650 kg of resin. Globally, much resin is packaged in 25-kg sacks.

Polyethylene is categorized by physical property for specification into groups, classes, and grades as described in ASTM D4976-98. Group 1 resins are branched and Group 2 resins are linear. Class defines density and is divided as Class 1, low density resins, from 0.910 to 0.925 g/cm^3, Class 2, medium density resins, from 0.926 to 0.940 g/cm^3, Class 3, high density resins, 0.941 to 0.960 g/cm^3, and

Class 4, high density resins, 0.961 g/cm^3 and above. Polymer melt-flow rate at 190°C using 2.16-kg weight is specified by grade. Grade 1 is a melt-flow rate of greater than 25 g/10 min, Grade 2 is greater than 10–25 g/10 min, Grade 3 is greater than 1–10 g/10 min, Grade 4 is greater than 0.4–1 g/10 min, and Grade 5 is 0.4 g/10 min or less. There are also specifications for electrical requirements, flammability requirements, weatherability requirements, and mechanical properties such as tensile strength, flexural modulus, and crack resistance, but these are not widely used in most commercial LLDPE applications.

Wire and cable resins are also categorized for color by class according to ASTM D1248-98. Class A contains no pigments, Class B contains white or black pigment, Class C contains not less than 2% carbon black, Class D is uv-resistant with colored pigment.

Analytical and Test Methods

Molecular Weight and Distribution/Rheological Properties. Methods of measuring number-average molecular weight (M_n) include ebulliometry (freezing point depression or melting point elevation), membrane osmometry, and vapor-phase osmometry. Weight-average molecular weight (M_w) can be quantified by light scattering and ultracentrifugation [M]. Both number-average and weight-average molecular weight and therefore polydispersity of LLDPE (M_w/M_n) can be measured simultaneously by high temperature gel permeation chromatography (gpc) using *o*-dichlorobenzene or 1,2,4-trichlorobenzene as solvents, ASTM D6474-99. In this method, a dilute polymer solution is passed over a porous inert material. Low molecular weight species follow a tortuous path through the system allowing the high molecular weight materials to elute first. Viscosity methods are also employed to measure molecular weight, ASTM D1601-99 and D2857-95.

Other methods for solvent fractionation are by precipitation method where a ratio of solvent and nonsolvent is incrementally adjusted from solvent-rich to nonsolvent-rich. In this technique, the higher molecular weight fractions will be precipitated first. A reverse technique is solvent gradient elution where a liquid mixture of increasing solvent power is used to remove the lowest molecular weight materials first (10).

Molten polymer flow through a specific die is often used as a quick estimation of polymer molecular weight. Such a measurement is called melt index. Melt index (also called melt-flow rate by some resin producers) for LLDPE is commonly measured according to ASTM D1238-99 using the 190/2.16 method (190°C and 2.16-kg load). Notation is shown as I_2 and this number is inversely proportional to molecular weight as long as the polydispersities of the resins compared are the same and there is no long-chain branching. A measure of polydispersity, or molecular weight distribution, can be obtained by measuring melt flow at higher stresses, 190/10 (I_{10}) or 190/21.6 (I_{21}). Ratios of the different rates, I_{21}/I_2 (known as melt index ratio, MIR) and I_{10}/I_2, correlate very well with M_w/M_n for linear polymers.

Density. LLDPE density is commonly measured using a flotation method in a density gradient column as described in ASTM D1505-98. In this technique, a glass column is filled with a liquid that provides a density gradient from top (lower density) to bottom (higher density) which is marked using calibrated glass beads. The most common liquid used for LLDPE is an isopropanol–water mixture that provides for a density range of 0.79–1.00 g/cm^3. Specimens are dropped into the column and their final resting place is then extrapolated into a resin density. One of the most important aspects of this test is sample preparation, which is done by slow cooling compression molded plaques (ASTM D1928-96). It is very important that the specimen be free of voids and have a thermal history that is consistent with prior samples for accurate comparison.

Polymer density can also be determined using ultrasonic techniques (ASTM D4883-99), and specific gravity (ASTM D792-98).

Structure and Composition. Knowing LLDPE comonomer content and distribution is an important part of predicting polymer properties. Carbon-13 nuclear magnetic resonance (nmr) is commonly employed to identify comonomer type, quantity incorporated, and distribution along the polymer backbone. ASTM D5017-96 provides for standard test method for this analysis. Branching can also be detected by infrared (ir) methods. The method described in ASTM D2238-92 (1999) quantifies methyl group absorption at 1378 cm^{-1}. Infrared analysis is also used to determine vinyl and trans unsaturation in polyethylene (ASTM D6248-98) and vinylidene unsaturation (ASTM D3124-98).

Amount of crystallinity in LLDPE can be quantified using x-ray diffraction (xrd), ir, dsc, and density. The xrd methods usually involve subtracting the amorphous contribution from the x-ray diffraction pattern. ir uses ratios of absorptions from crystalline and amorphous components. dsc uses enthalpy of fusion ΔH_f for a sample compared to the equilibrium heat of fusion ΔH_f° which for polyethylene is between 276 and 301 J/g. Percent crystallinity is given as $X = (\Delta H_f/\Delta H_f^\circ) \times 100\%$. An ASTM standard is given in D3417-99. Density measurements can also give percent crystallinity values X by using $1/\text{density} = X/d_{cr} + (1-X)/d_{am}$, where d_{cr} is usually accepted as 1.00 g/cm^3 and d_{am} is 0.852–0.862 g/cm^3.

Compositional Uniformity. Temperature rising elution fractionation is the preferred technique for measuring compositional uniformity in LLDPE and metallocene-catalyzed resins (104–110). In a typical TREF experiment, a small portion of polymer is dissolved in a heated solvent such as 1,2,4-trichlorobenzene. An inert support is added to the solution that is then cooled at a prescribed rate, eg 1.5°C/h. Polymer fractionation occurs when chains with little to no comonomer crystallize from solution at temperatures higher than those chains that contain more comonomer. After cooling, the inert support is placed in a column and a progressively heated solvent is then passed over the solvent to wash away the crystallized polymer. In this heating step, the lower density fractions, ie those with more comonomer, are eluted at lower temperatures than higher density fractions with little comonomer. Concentration of the elute is detected using an ir detector and is plotted as a function of temperature (Figs. 2 and 3). Crystallization from solution can be affected by both comonomer content and molecular weight. A light-scattering detector can be used in conjunction with the ir detector to measure molecular weight of the eluted fractions. While very informative, the process is very time and labor consuming.

Thermal methods using dsc have been developed to give somewhat the same qualitative information as TREF, but without solvent and in a less labor-intensive manner (111,112). The dsc melting profiles can be used to approximate comonomer content and distribution.

Low molecular weight, low density fractions may migrate to whatever comes into contact with the LLDPE. For food-contact applications, these materials are called hexane extractables. FDA procedure 21 CFR177.1520 calls for immersing a sample in *n*-hexane at 50°C for 2 h and measuring weight loss in the sample. For food contact during cooking, hexane extractables levels need to be below 2.6 wt% and for general noncooking contact hexane extractables levels need to be below 5.5 wt%.

Mechanical Properties of LLDPE. There are literally hundreds of test specifications written for LLDPE mechanical properties testing for all sorts of end-use applications. Since more than 60% of LLDPE consumed is used in film applications, common methods for film testing will be discussed here.

Tensile properties of thin (<1.0 mm) LLDPE films are determined using ASTM D882-97. Strips of film are pulled at controlled strain rates while load cells measure the forces required. Initial strain rates for properties such as ultimate tensile strength and elongation are usually 10 mm/(mm·min) while tensile modulus is tested at 0.1 mm/(mm·min.) ASTM D638-99 is used for thicker sheeting and molded samples from 1.0- to 14-mm thickness.

Tear properties can be determined in a variety of ways. The most common tear test is the Elmendorf test (ASTM D1922-94a). In this test, a weighted pendulum propagates a tear in a specimen. The energy lost by the pendulum while propagating the tear is related to tear strength. In another tear propagation test (ASTM D1938-94), otherwise known as a trouser-leg tear test, a tensile tester is used to propagate a tear through a specimen that resembles a pair of trousers. ASTM D1004-94a is a test method that uses a tensile tester to measure the force to initiate a tear in film. The energy required to both initiate and propagate a tear is determined using ASTM D2582-93.

Impact properties are very important in many film applications. ASTM D1709-98 is the most common technique used to determine impact resistance because of test simplicity and low equipment costs. In this test, a weighted dart with a smooth hemispherical head is dropped from a prescribed height onto a circular diaphragm of film. If the sample does not break, weight is added to the dart. If the sample breaks, weight is removed. At least 10 breaks and 10 failures are recorded to give a good statistical average. Another dart impact test, D4272-99, determines the total energy impact of a film by measuring kinetic energy loss of a dart that passes through the film.

Optical properties are important in many packaging applications. Specular gloss is a measure of the shiny appearance of films. In this test, a beam of light is reflected off of a film surface at a specified angle. It is measured using ASTM D2457-97 at three angles, 20° for high gloss films, 45° for intermediate and low gloss films, and 60° for intermediate gloss films. Film haze is a measure of film clarity. In this test (ASTM D1003-97), the wide-angle light scattering properties of a film are quantified as a percentage of light diffused.

Health and Safety

Resin manufacturers usually provide health and safety information through Material Safety Data Sheets (MSDS) that discuss resin handling and storage, toxicity, combustibility, disposal, labeling, and FDA status.

LLDPE resins are relatively inert and do not constitute hazards for skin contact and ingestion with normal handling (113,114).

Polyethylene is flammable and may give off toxic gases during combustion. Fires may be extinguished with water, carbon dioxide, or dry chemical units. Respiratory and eye protection is required for fire fighters.

Polyethylene may be disposed of by landfill or incineration. In landfill, polyethylene will not degrade unless exposed to sunlight. It is not expected to evolve gases or leechates to pollute water sources.

Most polyethylene is acceptable for use in food contact applications. In some cases of plastomers, resins containing as much as 50% comonomer are acceptable (115). FDA compliance is based mainly on levels of migratable low molecular weight, low density olefins called hexane extractables and various additive levels. A letter of compliance or other certification should be received from the appropriate resin supplier before actual use.

LLDPE Applications

Annual global production of LLDPE is approximately 13.6 million tons. Of that amount, approximately 77% is used in film applications (100). With that proportion, it is not surprising that much of the research and development that is conducted at resin suppliers is on the film market. LLDPE is supplanting LDPE in many film applications because of its improved strength properties, downgauging potential, and cost.

Film Applications. Over 3.4 billion kilograms of LLDPE were consumed in North America for film applications. Trash bags, including retail and institutional markets, is the largest North American market for LLDPE film (over 0.64 billion kilograms). Compared to LDPE, LLDPE offers better puncture resistance, tear resistance, impact, and tensile properties along with the ability to downgauge. LLDPE has better tear resistance balance and puncture resistance than HDPE. The consumer retail trash bag market has two major market thrusts: (*1*) bags with high dart impact and tear strengths but relatively low modulus and (*2*) bags with high stiffness but minimal impact and tear resistance. A significant portion of the retail market consists of blown coextrusion capabilities to meet these challenging requirements. LLDPE melt index range for this market is approximately 0.5–1 g/10 min and density range is 0.917–0.928 g/cm^3. mLLDPE resins tend to be used as layers in coextrusions or as blend components to improve the properties of less expensive resins.

Pallet wrap stretch film is the second largest North American market for LLDPE film. It consumes over 0.545 billion kilograms of LLDPE annually. Pallet wrap stretch film is used to unitize loads to prevent shifting during shipping. It is also used as a protective film and as a tamper indicator. Film

properties required for pallet wrap stretch film include high elongations, high tensile strength, high holding force, puncture resistance, tear resistance, and high cling. Stretch films must have adequate cling so that they will adhere to themselves after application to prevent unwinding and loss of holding force. The most widely used process is cast coextrusion with three, five, and seven layers now common. Approximately 40% of the stretch film capacity is produced via blown film monolayer and coextrusion. The stretch film market has two main product areas: (*1*) machine film and (*2*) handheld film. Machine film is applied by an automated unit that prestretches the film from 150 to over 300% and then applies the film under tension to a load which sits on a turntable. Handheld film is applied manually by a worker walking around a load and is usually stretched less than 200%. Common LLDPE melt indices in this market range from 1 to 4 g/10 min and most resins have a density of 0.917 or 0.918 g/cm^3. mLLDPE has made a significant market penetration in stretch film by offering improved puncture resistance and greater holding force. Blends of LLDPE and mLLDPE are used to optimize properties and reduce costs (116,117). Plastomers are being used as cling layers for consistent cling without the use of additives such as polyisobutylene.

The third largest LLDPE film application in North America is industrial liners, greater than 250 million kilograms per year. Industrial liners are used inside cans, drums, cardboard boxes and the like to prevent spillage, contamination, moisture, and ease of container reuse. Important film attributes are puncture resistance, tear strength, and tensile strength. Common LLDPE melt indices are 0.5–2 g/10 min with densities of 0.917–0.930 g/cm^3. mLLDPE finds little application here because of higher raw material costs.

Other areas where mLLDPE is making an impact are heavy-duty shipping sacks, food packaging (especially fresh produce packaging) (117–120), and breathable films for personal care use, eg diaper backsheet. Plastomers find application as modifiers in LLDPE and ULDPE to improve impact strength, low temperature toughness, and sealability (121).

ULDPE and VLDPE resins find application in low temperature applications, such as ice bags, where lower density offers greater toughness. They are also used as sealing layers, replacing low density copolymers such as vinyl acetate, and as blend components to improve toughness.

LDPE is still the preferred resin for extrusion coating. Because of the narrow molecular weight distribution of LLDPE (and also of metallocene-catalyzed polyethylenes), the resins are more difficult to extrude and have greater "neck-in" than LDPE.

Injection Molding. Injection molding is the second largest product area for LLDPE consuming approximately 8% of the global LLDPE produced. Injection-molded articles include trash cans, pails, food containers, lids, and closures. LLDPE has mechanical properties advantages over LDPE in environmental stress crack resistance, reduced warpage and shrinkage, and low temperature toughness (122). LLDPE is preferred for use over polypropylene in low temperature applications. An example of LLDPE improved properties is given in Table 9 comparing a butene copolymer LLDPE and LDPE of similar melt index and density.

Metallocene-catalyzed resins have not yet had a substantial impact on the marketplace. Primary advantages for metallocene-catalyzed resins compared to

Table 9. Comparison of LLDPE and LDPE Injection Molding Resins[a]

Property	ASTM test method	LLDPE	LDPE
Melt index I_2, g/10 min	D1238	32	37.5
Density, g/cm^3	D1505	0.925	0.923
Tensile strength @ yield, MPa[b]	D638	13.4	12.8
Tensile strength @ break, MPa[b]	D638	9.3	9.0
2% Secant modulus, MPa[b]	D790	366	186
Hardness, Shore D	D2240	55	41
Low temperature brittleness F_{50}, °C	D746	<-76	-25

[a]Ref. 123.
[b]To convert MPa to psi, multiply by 145.

Table 10. Comparison of LLDPE and HDPE Rotational Molding Resins[a]

		LLDPE		
Property	ASTM test method	Gas phase	Solution	HDPE
Melt index I_2, g/10 min	D1238	5.0	5.0	5.0
Density, g/cm^3	D1505	0.935	0.937	0.945
Flexural modulus, MPa[b]	D790	601	520	931
Tensile strength @ yield[b]	D638	17	14	21
ESCR F_{50}, h	D746	>1000	400	30

[a]Refs. (123) and (126).
[b]To convert MPa to psi, multiply by 145.

Table 11. Comparison of LDPE, LLDPE, and HDPE Blow Molding Resins[a]

Property	ASTM test method	LLDPE	LDPE	HDPE
Melt index I_2, g/10 min	D1238	0.75	0.25	0.35
Density, g/cm^3	D1505	0.934	0.918	0.954
Flexural modulus, MPa[b]	D790	578	234	1228
Low temperature Brittleness F_{50}, °C	D746	<-76	<-76	<-76
ESCR, h	D1693	>1000	NM[c]	50

[a]Ref. 123.
[b]To convert MPa to psi, multiply by 145.
[c]NM = not measured.

conventional Ziegler–Natta-catalyzed LLDPE are improved impact strength, less brittleness at higher melt indices, and less odor and taste transfer. Plastomers are seeing some use as a replacement for poly(vinyl chloride) in injection-molded articles (124). Plastomers are also used as impact modifiers in molded polypropylene automotive parts (125).

Rotational Molding and Blow Molding. Rotational molding accounts for approximately 5% of LLDPE consumption and blow molding accounts for approximately 0.5%. Rotational-molded articles include storage tanks, shipping containers, recreational equipment, and outdoor furniture. LLDPE has higher impact

resistance and stress-crack resistance than LDPE and HDPE. Table 10 lists two LLDPE resins compared to an HDPE sample. Metallocene-catalyzed resins are finding application in rotational molding primarily because of reduced cycle times, reduced energy consumption, a wider processing window (127), and greater impact strength than conventional LLDPE. Improved flexibility and stress-crack resistance make LLDPE ideal for some blow-molded bottle applications. Table 11 details the improved escr compared to HDPE.

Wire and Cable Insulation. LLDPE use in wire and cable insulation makes up approximately 1% of LLDPE consumption. Cable insulation requires flexibility, toughness, abrasion resistance, low brittleness temperature, and good dielectric properties. LLDPE offers a better balance of flexibility and toughness than LDPE or HDPE. LLDPE-coated wire and cable is used in numerous low and medium voltage applications. Metallocene-catalyzed resins are finding use in wire and cable jacketing because of improved abrasion resistance, flexibility, and low temperature toughness (125,128).

Pipe and Tubing. Extrusion of pipe and tubing accounts for a very small fraction of LLDPE consumption. LLDPE offers higher burst strength, environmental stress crack resistance, and higher heat-distortion temperature than LDPE. Plastomer grades have been used to replace plasticized polyvinyl chloride in medical tubing applications (129).

BIBLIOGRAPHY

"Ethylene Polymers" in *EPST* 1st ed., Vol. 6, pp. 275–454; "Ethylene Polymers, Linear Low Density Polyethylene" in *EPSE* 2nd ed., Vol. 6, pp. 429–454, by D. E. James, Union Carbide Corp.;

1. G. Odian, *Principles of Polymerization*, John Wiley & Sons, Inc. New York, 1981.
2. U.S. Pat. 5272236 (Dec. 13, 1993), S. Y. Lai and co-workers (to The Dow Chemical Company).
3. S. Hosoda, *Polym. J.* **20**, 383 (1988).
4. F. M. Mirabella and E. A. Ford, *J. Polym. Sci., Part B: Polym. Phys.* **25**, 777, (1987).
5. C. S. Speed, B. C. Trudell, A. K. Mehta, and F. C. Stehling, *Polyolefins VII*, Society of Plastics Engineers, Brookfield, Conn., 1991, p. 46.
6. D. Schwank, in *SPO '92*, Schotland Business Research, Skillman, N.J., 1992.
7. B. Vernyi, *Plast. News* **8** (Apr. 24, 1995).
8. M. B. Welch, S. J. Palackal, R. L. Geerts, and D. R. Fahey, in *MetCon '95*, The Catalyst Group, Spring Hill, Pa., 1995.
9. K. C. Koch, in *Antec '96*, Society of Plastics Engineers, Brookfield, Conn., 1996, p. 1879.
10. H. S. Kaufman and J. J. Falcetta, *Introduction to Polymer Science and Technology: An SPE Textbook*, John Wiley & Sons, Inc., New York, 1977, pp. 165–193.
11. D. R. Burfield and N. Kashiwa, *Makromol. Chem.* **186**, 2657 (1985).
12. W. D. Varnell, E. Ryba, and I. R. Harrison, *J. Macromol. Sci., Part B: Phys.* **26**(2), 135 (1987).
13. D. C. Bassett, and A. M. Hodge, *Proc. Roy. Soc. London, Ser. A* **377**, 25 (1981).
14. B. Wunderlich, *Macromolecular Physics*, Vol. **2**, Academic Press, Inc., New York, 1976.
15. A. Woodward, *Atlas of Polymer Morphology*, Hanser Publishers, New York, 1989.
16. I. M. Ward, *Structure and Properties of Oriented Polymers*, Science Publishers, London, 1975.

17. P. H. Lindenmeyer and S. Lustig, *J. Appl. Polym. Sci.* **9**, 227 (1965).
18. W. F. Maddams and J. E. Preedy, *J. Appl. Polym. Sci.* **22**, 2721 (1978).
19. W. F. Maddams and J. E. Preedy, *J. Appl. Polym. Sci.* **22**, 2739 (1978).
20. W. F. Maddams and J. E. Preedy, *J. Appl. Polym. Sci.* **22**, 2751 (1978).
21. D. M. Simpson and I. R. Harrison, *J. Plast. Film Sheet* **10**, 302 (1994).
22. E. Huang, S. Chum, R. Guerra, and K. Sehanobish, in *Antec '94*, Society of Plastics Engineers, Brookfield, Conn., 1994, p. 3414.
23. S. Benason and co-workers, *J. Polym. Sci., Part B: Polym. Phys.* **34**, 1301 (1996).
24. R. Alamo, R. Domsay, and L. Mandelkern, *J. Phys. Chem.* **88**, 6587 (1987).
25. E. Perez and co-workers, *Macromol.* **20**(1), 78 (1987).
26. D. C. McFadden, K. E. Russell, and E. C. Keluskey, *Polym. Comm.* **29**, 258, (1988).
27. S. Hosoda and co-workers, *Polymer* **31**, 1999 (1990).
28. L. T. Kale, T. A. Plumley, R. M. Patel, and P. Jain, in *Antec '95*, Society of Plastics Engineers, Brookfield, Conn., 1995, p. 2249.
29. J. N. Hay and X. Zhou, *Polymer* **34**, 1002, (1993).
30. G. T. Davis and R. K. Eby, *J. Appl. Phys.* **44**, 4274 (1973).
31. S. S. Chang, *J. Polym. Sci., Polym. Symp.* **43**, 43 (1973).
32. K. H. Illers, *Kolloid Z. Z. Polym.* **252**, 1 (1974).
33. F. C. Stehling and L. Mandelkern, *Macromolecules* **3**, 242 (1970).
34. P. J. Hendra, H. P. Jobic, and K. Holland-Moritz, *J. Polym. Sci., Polym. Lett. Ed.* **13**, 365 (1975).
35. *Nova Chemical Novapol Product Data Sheets.*
36. T. M. Liu and W. E. Baker, *Polym. Eng. Sci.* **32**, 944 (1992).
37. A. D. Channelll, and E. Q. Clutton, *Polymer* **33**, 4108 (1992).
38. F. M. Mirabella and co-workers, *J. Polym. Sci., Part B: Polym. Phys.* **26**, 1995 (1988).
39. Y.-M. Kim and J.-K. Park, *J. Appl. Polym. Sci.* **61**, 2315 (1996).
40. C. Lee, I. Peat, L. Wild, and P. Fernando, in *Antec '88*, Society of Plastics Engineers, Brookfield, Conn., 1988, p. 183.
41. *ExxonMobil Chemical Escorene Product Data Sheets*.
42. V. J. Crotty, V. Firdhaus, and R. O. Hagerty, *Polyolefins VIII*, Society of Plastics Engineers, Brookfield, Conn., 1993, p. 192.
43. D. M. Simpson and D. G. O'Neil, *Tappi J.* **78**(8), 170 (1995).
44. E. A. Benham, M. P. McDaniel, M. A. Smith, W. M. Whitte, and J. D. Ratzlaff, in *SPO '93*, Schotland Business Research, Skillman, N.J., 1993, p. 463.
45. D. M. Simpson, and I. R. Harrison, *J. Plast. Film Sheet* **11**, 216 (1995).
46. J. Boor, *Ziegler–Natta Catalysts and Polymerizations*, Academic Press, Inc., New York, 1979.
47. H. R. Sailors and J. P. Hogan, *Polymer News* **7**, 152 (1981).
48. G. Fink, R. Mulhaupt, and H. H. Brintzinger, *Ziegler Catalysts, Recent Scientific Innovations and Technological Improvements*, Springer-Verlag, Berlin, 1995.
49. E. J. Arlman and P. Cossee, *J. Catal.* **3**, 99 (1964).
50. R. P. Quirk, *Transition Metal Catalyzed Polymerizations, Ziegler–Natta and Metathesis Polymerizations*, Cambridge University Press, Cambridge, 1988.
51. J. C. W. Chien, *Coordination Polymerization*, Academic Press, Inc., New York, 1975.
52. F. M. McMillan, "The Chain Straighteners, Fruitful Innovation: The Discovery of Linear and Stereoregular Synthetic Polymers", Macmillan, London, 1979.
53. G. Wilkinson, *Comprehensive Organometallic Chemistry*, Vol. **3** *The Synthesis, Reactions and Structures of Organometallic Compounds*, Pergamon Press, Oxford, 1982.
54. M. Bochman, *J. Chem. Soc., Dalton Trans.* 225 (1996).
55. W. Kaminsky and H. Sinn, in *Proceedings of an International Symposium*, Springer-Verlag, Berlin, 1987.
56. Ballard and co-workers, *Chem. Commun.* 621 (1975).

57. Ballard and co-workers, *Chem. Commun.* 994 (1978).
58. W. Kaminsky and co-workers, *Angew. Chem., Int. Ed. Engl.* 630 (1976).
59. U.S. Pat. 5324800 (June 28, 1994), H. C. Welborn and J. A. Ewen (to Exxon Chemical Patents, Inc.).
60. E. W. Abel, F. G. A. Stone, and G. Wilkinson, *Comprehensive Organometallic Chemistry II, Vol. 12: A review of the Literature 1982–1994*, Pergamon Press, Oxford, 1995.
61. H. H. Brintzinger and co-workers, *Angew. Chem., Int. Ed. Engl.* **34**, 1143 (1995).
62. R. F. Jordan and co-workers, *J. Am. Chem. Soc.* **108**, 7410 (1986).
63. Eur. Pat. Appl. EP 0277004 (Aug. 3, 1988), H. M. Turner; EP0277003 (Aug. 3, 1988), H. M. Turner, G. G. Hlatky (both to Exxon Chemical Patents, Inc.).
64. X. Yang, C. L. Stern, and T. J. Marks, *J. Am. Chem. Soc.* **113**, 3623 (1991).
65. Eur. Pat. Appl. EP 0416815 (Mar. 13, 1991), J. C. Stevens and co-workers (to The Dow Chemical Company).
66. Eur. Pat. Appl. EP 0420436 (Apr. 3, 1991), J. M. Canich (to Exxon Chemical Patents, Inc.).
67. V. C. Gibson and co-workers, *Angew. Chem., Int. Ed. Engl.* **38**, 428 (1999).
68. R. Kempe, *Angew. Chem., Int. Ed. Engl.* **39**, 468 (2000).
69. M. Brookhart and co-workers, *J. Am. Chem. Soc.* **117**, 6414 (1995).
70. WO Pat. Appl. 96/23010 (Aug. 1, 1996), L. K. Johnson and co-workers (to E. I. du Pont de Nemours & Co., Inc.).
71. U.S. Pat. 5955555 (Sept. 21, 1999), A. M. A. Bennett (to E. I. du Pont de Nemours & Co., Inc.).
72. V. C. Gibson and co-workers, *J. Chem. Soc. Chem. Commun.* 849 (1998).
73. WO Pat. Appl. 99/12981 (Mar. 18, 1999), G. J. P. Britovsek and co-workers (to BP Chemicals Ltd.).
74. D. W. Stephan and co-workers, *Organometallics* **18**, 2046 (1999).
75. U.S. Pat. 4,543,399 (Sept. 24, 1985), J. M. Jenkins and co-workers (to Union Carbide Corp.).
76. U.S. Pat. 5,405,922 (Apr. 11, 1995), M. L. DeChellis, J, R. Griffin, and M. E. Muhle (to Exxon Chemical Patents, Inc.).
77. *Polyolefin Technology Update, SRI International*, July 1986.
78. *Plast. Tech.* **39**(4), 83 (1993).
79. L. M. Sherman, *Plast. Tech.* **41**(6), 36 (1995).
80. K. J. Jens, in *MetCon '99*, The Catalyst Group, Spring Hill, Pa., 1999.
81. S. Brown, in *MetCon '99*, The Catalyst Group, Spring Hill, Pa., 1999.
82. S. S. Schwatz and S. H. Goodman, *Plastic Materials and Processes*, Van Nostrand Reinhold Co., Inc., New York, 1982.
83. J. R. A. Pearson, *Mechanics of Polymer Processing*, Elsevier Applied Science Publishers, Ltd., London, 1985.
84. Z. Tadmor and C. G. Gogos, *Principles of Polymer Processing*, John Wiley & Sons, Inc., New York, 1979.
85. L. A. Utracki and B. Schlund, in *Antec '87*, Society of Plastics Engineers, Brookfield, Conn., 1987, p. 1002.
86. C. T. Lue, in *Antec '98*, Society of Plastics Engineers, Brookfield, Conn., 1998, p. 1816.
87. D. M. Simpson, P. D. Whaley, and H. T. Liu, in *SPO '97*, Schotland Business Research, Skillman, N.J., 1997 p. 257.
88. J. Lastovica, in *SPO '97*, Schotland Business Research, Skillman, N.J., 1997, p. 247.
89. S. J. Kurtz, L. S. Scarola, and J. C. Miller, in *Antec '82*, Society of Plastics Engineers, Brookfield, Conn., 1982, p. 192.
90. *Exceed Polyethylene Film Processing Facts, ExxonMobil Chemical Co.*, 1999.
91. W. W. Bode and J. Perdikoulias, *Film Extrusion Manual*, Tappi Press, Atlanta, 1992, pp. 211–230.

92. *Injection Molding Polyethylene Processing Guide*, Nova Chemicals, Alberta, Canada, 1999.
93. W. Harris and D. Moldovan, *Plast. Tech.* **41**(4), 60 (1995).
94. *Blow Molding Polyethylene Processing Guide*, Nova Chemicals, Alberta, Canada, 1999.
95. D. V. Rosato and D. V. Rosato, *Blow Molding Handbook*, Hanser Publishers, New York, 1989.
96. *Rotational Molding Polyethylene Processing Guide*, Nova Chemicals, Alberta, Canada, 1999.
97. G. L. Beall, *Rotational Molding Design Materials, Tooling, and Processing*, Hanser Publishers, Munich, 1998.
98. M. J. Oliveira, M. C. Cramez, and R. J. Crawford, in *Antec '96*, Society of Plastics Engineers, Brookfield, Conn., 1996, p. 2096.
99. C. Rauwendaal, *Polymer Extrusion*, Hanser Publishers, New York, 1986, p. 448.
100. *Global Commercial Analysis: Polyolefins Planning Service*, Chem Systems, New York, 1998.
101. *Parpinelli Tecnon, private communication*.
102. R. D. Leaversuch, *Modern Plastics* **62** (May 2000).
103. *Chemical Market Reporter*, World Wide Web Site: www.chemexpo.com.
104. S. A. Karoglanian and I. R. Harrison, *Polym. Eng. Sci.* **36**, 731 (1996).
105. L. Wild and co-workers, *J. Polym. Sci., Polym. Phys. Ed.* **20**, 441 (1982).
106. L. Wild, T. R. Ryle, and D. C. Knobeloch, *Am. Chem. Soc., Div. Polym. Chem. Polym. Prepr.* **23**, 133 (1982).
107. L. Wild and T. R. Ryle, *Am. Chem. Soc., Div. Polym. Chem. Polym. Prepr.* **18**, 182 (1977).
108. F. M. Mirabella, in *Int. GPC Symp. '87*, Itasca, Ill., 1987, p. 180.
109. P. Schouterden and co-workers, *Polymer*, **28**, 2099 (1987).
110. E. Karbashewski and co-workers, *J. Appl. Polym. Sci.* **44**, 425 (1992).
111. E. Adisson and co-workers, *Polymer* **33**, 4337 (1992).
112. F.-C. Chiu, M. Y. Keating, and S. Cheng, in *Antec '95*, Society of Plastics Engineers, Brookfield, Conn., 1995, p. 1503.
113. *Material Safety Data Sheet for Escorene LLDPE, MSDS Number 89001000, Exxon-Mobil Chemical Co., Houston, Tex*.
114. *Material Safety Data Sheet for Dowlex 2027A, MSD 002101, The Dow Chemical Company, Midland, Mich*.
115. *U.S. FDA Regulation 21 CFR 177.1520 (c) 3.2c*.
116. H. Mavridis, *Polyolefins XI*, Society of Plastics Engineers, Brookfield, Conn., 1999, p. 585.
117. D. M. Simpson and B. C. Trudell, in *MetCon '99*, The Catalyst Group, Spring Hill, Pa., 1999.
118. R. W. Halle, in *Polymers, Laminations & Coatings Conference*, TAPPI, 1998, p. 285.
119. J. H. Schut, *Plast. Tech.* **44**(10), 49 (1998).
120. G. L. Young, in *Antec '95*, Society of Plastics Engineers, Brookfield, Conn., 1995, p. 2234.
121. R. W. Halle, in *Polymers, Laminations & Coatings Conference*, TAPPI, 1995, p. 561.
122. M. A. Eddleman, in *Regional Technical Conference, S. Texas, Sec. and Thermoplastic Mat. Foams Div.*, Society of Plastics Engineers, Brookfield, Conn., 1984, p. 375.
123. *Equistar Chemicals Petrothene, Alathon, and Microthene Product Data Sheets*.
124. J. H. Schut, *Plast. Tech.* **40**(2), 19 (1994).
125. F. J. Steininger, in *SPO '93*, Schotland Business Research, Skillman, N.J., 1993, p. 271.
126. *Nova Chemicals Sclair Product Data Sheets*.

127. X. Wang, R. Crawford, A. Fatnes, and E. Harkin-Jones, in *Antec '2000*, Society of Plastics Engineers, Brookfield, Conn., 2000, p. 1326.
128. L. T. Kale, T. L. Iaccino, and K. E. Bow, in *Antec '96*, Society of Plastics Engineers, Brookfield, Conn., 1996, p. 1647.
129. D. Smock, *Plast. World* **52**(1), 16 (1994).

D. M. SIMPSON
G. A. VAUGHAN
Exxon Mobil Chemical Company

ETHYLENE–ACRYLIC ELASTOMERS

Introduction

Ethylene–acrylic is a term used to describe a family of acrylic elastomers that was first introduced commercially in 1975 under the trademark Vamac by DuPont. The original elastomer was the result of an intensive research effort to develop an oil-resistant polymer with greater heat resistance than that of nitrile or polychloroprene rubbers, at a moderate cost well below that of silicones and fluoroelastomers. Ethylene–acrylic elastomers are best known for their excellent heat and oil resistance, but they also possess a good balance of compression set resistance, flex resistance, physical strength, low temperature flexibility, and weathering resistance. Special compounded attributes include uniquely temperature-stable vibrational dampening properties and the ability to produce flame-resistant compounds with combustion products having an exceptionally low order of smoke density, toxicity, and corrosiveness. Because of this balance of properties, ethylene–acrylic elastomers have found ready acceptance in many high performance applications, especially in the automotive market (1–4).

Polymer Properties

Polymer Composition. Ethylene–acrylic elastomer terpolymers are manufactured by the addition copolymerization of ethylene [74-85-1] and methyl acrylate [96-33-3], in the presence of a small amount of an alkenoic acid to provide sites for cross-linking with diamines (5).

Encyclopedia of Polymer Science and Technology. Copyright John Wiley & Sons, Inc. All rights reserved.

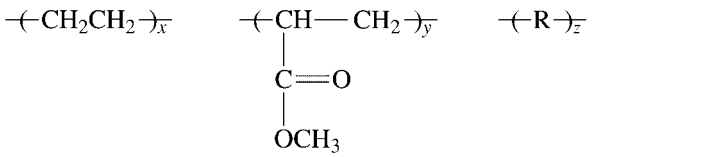

In the early 1990s, DuPont commercialized a new family of copolymers of just ethylene and methyl acrylate, which do not include a cure-site monomer. These dipolymers are cured with peroxides.

The polymerization process yields a random, amorphous terpolymer or a random, amorphous dipolymer (no cure-site monomer). The polymer backbone is fully saturated, making it highly resistant to ozone attack even in the absence of antiozonant additives. The fluid resistance and low temperature properties of ethylene–acrylic elastomers are largely a function of the methyl acrylate to ethylene ratio. As the methyl acrylate level increases, the polymer becomes more polar and has better fluid resistance to aliphatic hydrocarbon oils. Also, as the methyl acrylate level increases, the glass-transition temperature (T_g) of the polymer increases slightly. There is a trade-off between oil resistance and low temperature performance.

Commercial Forms. Four different base polymers of Vamac ethylene–acrylic elastomers are commercially available (Table 1). Until 1990, existing grades of ethylene–acrylic elastomers were based on a single-gum polymer, Vamac G, defined as a terpolymer of 55% methyl acrylate, ethylene, and a cure-site monomer (6). In 1991, a higher methyl acrylate terpolymer, Vamac GLS, was introduced. The composition of this polymer was specifically chosen because it significantly increased the oil resistance of the polymer while minimizing the loss in low temperature flexibility (7).

A new family of peroxide-cured dipolymers was introduced in 1991. The peroxide cure provides copolymers that cure faster and exhibit good compression set properties without a post-cure. The removal of the cure-site monomer has made the polymer less susceptible to attack from amine-based additives. By varying the methyl acrylate level in the dipolymer, two offerings in this family have been synthesized, Vamac D and its more oil-resistant counterpart, Vamac DLS (7).

Curing. Carboxyl cure sites are incorporated in the ethylene–acrylic terpolymer to permit cross-linking with primary diamines (1,8). Guanidines are added to accelerate the cure. If faster cure is desired for the terpolymers, one can use the combination of diamine and peroxide to approximately double the cure rate (9,10) as measured by tc(90). Dipolymers are cured only with peroxides.

Table 1. Vamac Ethylene–Acrylic Elastomer Polymers

Commercial designation	Monomers[a]	Methyl acrylate level	Type of cure system
Vamac G	E/MA/CS	Average	Amine
Vamac GLS	E/MA/CS	High	Amine
Vamac D	E/MA	Average	Peroxide
Vamac DLS	E/MA	High	Peroxide

[a]E is ethylene; MA, methyl acrylate; and CS, proprietary cure-site monomer.

Table 2. Heat Resistance Profile

Temperature of continuous exposure, °C	Approximate useful life of >50% absolute elongation
121	24 months
149	6 months
171	6 weeks
177	4 weeks
191	10 days
200	7 days

Heat Resistance and Aging Properties. The main features of ethylene–acrylic elastomers are heat (175°C by ASTM D2000) and oil resistance. At elevated temperatures, ethylene–acrylic elastomers age by an oxidative cross-linking mechanism, resulting in eventual embrittlement, rather than reversion. A general heat resistance profile is shown in Table 2.

As shown, ethylene–acrylic elastomers will function for more than 24 months at 121°C, or 6 weeks at 171°C continuous service. Exposures up to 190–200°C can be tolerated, although service life at these temperatures is measured in days rather than weeks. When immersed in service fluids, the oxidative process is often slowed down leading to longer actual service life.

Ethylene–acrylic elastomers are highly resistant to the damaging aspects of weather, ie, sun, water, oxygen, and ozone. Vulcanizates have shown little change in tensile properties and no visible signs of surface deterioration after exposure to the elements in Florida for 10 years. Samples under 20% tensile strain (static) displayed no cracks after one week's exposure to 100 ppm ozone in air, a concentration 100 times greater than is usually specified in qualifying tests.

Fluid Resistance. Ethylene–acrylic elastomers are well suited for applications requiring continuous exposure to hot aliphatic hydrocarbons, a class that includes most lubricants derived from petroleum (11). Volume swell data in Table 3 illustrate the good resistance of ethylene–acrylic elastomers to most common automotive lubricants and hydraulic fluids and to ASTM oils at elevated temperatures. The higher methyl acrylate polymer, Vamac GLS, exhibits approximately one-half the volume swell in these fluids of Vamac G. Low swell in motor oils and transmission fluids indicates usefulness for service as various seals, gaskets, and cooler hoses for transmission and engine oil and seals for wheel and crankshaft bearings. Recently, the synthetic motor oil is gaining attention because of its significantly longer service life between oil changes. Both Vamac G and Vamac GLS exhibit low volume swell and excellent retention of properties in the synthetic oils. Although resistance to water and glycol is excellent, some antifreeze-additive packages can cause excessive stiffening of the terpolymer vulcanizates. Ethylene–acrylic elastomers should not be selected for service in continuous contact with gasoline, brake fluid, highly aromatic fluids, or polar solvents such as esters and ketones.

Mechanical Properties. Typical properties of ethylene–acrylic elastomers, like those of other compounded rubbers, vary widely with formulation and also polymer grade. Among compounding ingredients, reinforcing fillers and plasticizers as well as type and amount of curing agents exert the greatest influence.

Table 3. Fluid Resistance

Medium	Time, h/Temp, °C	Volume swell, %	
		Vamac G	Vamac GLS
ASTM #1 oil	70/150	+5	+2
ASTM #2 oil	70/150	+24	+10
IRM 903 oil	70/150	+50	+25
Service fluid 105	1008/150	+22	+10
Motor oil-5W/30	168/150	+19	+9
Motor oil-5W/30	1008/150	+20	+10
Synthetic motor oil-5W/30	1008/150	+10	+4
ATF fluid	168/150	+25	+14
ATF fluid	3000/150	+32	+20
Power steering fluid	168/150	+15	+5
Fuel B	168/23	+73	+57
Kerosene	168/23	+31	
Unleaded gasoline	168/23	+68	
Water	504/100	+6	
Ethylene glycol	504/100	+4	

A typical compound based on Vamac G and Vamac GLS with pertinent vulcanizate properties is shown in Table 4. Note that while Vamac GLS has improved oil resistance versus Vamac G, its low temperature flexibility is about 2–5°C higher than that of the Vamac G compound.

Low Temperature Properties. Medium hardness compounds of average methyl acrylate, ie, Vamac G, without a plasticizer typically survive 180° flex test at −40°C. This type of performance is good for a heat-resistant polymer. Low temperature properties can be greatly enhanced by the use of ester plasticizers (12). Careful selection of the plasticizer is necessary to preserve the heat resistance performance of the polymer. At equivalent plasticizer levels, compounds made from the high methyl acrylate grades lose a few degree celsius in flexibility, compared to compounds made with the average methyl acrylate levels.

Flame Resistance and Smoke Suppression. Ethylene–acrylic elastomers are not inherently resistant to burning. Through compounding, the rate of burning can be retarded and the amount of smoke generated can be suppressed. An important feature of ethylene–acrylic elastomers is their ability to respond to the addition of hydrated alumina (13). This polymer/filler combination provides vulcanizates with good flame resistance, freedom from corrosive gases, and most importantly in many judgments, an unusually low smoke density.

Dynamic Mechanical Properties. Ethylene–acrylic elastomers have a high capacity for dampening that is uniquely insensitive to temperature changes between −10 and 160°C. Damping characteristics at room temperature, as indicated by loss tangent (tan δ), are similar to those of butyl rubber, which is noted for its damping properties. Ethylene–acrylic elastomers differ from butyl and other elastomers, however, by their ability to maintain a high loss tangent as temperature is raised to 160°C. This loss tangent remains virtually unchanged after six months aging in air at 150°C. Damping properties of ethylene–acrylic elastomers are also relatively insensitive to compound variations (14,15).

Table 4. Vulcanizate Properties of Vamac G and Vamac GLS in Black Loaded Compound[a,b]

Property	Vamac G	Vamac GLS
Physical properties at RT		
100% Modulus, MPa[c]	5.3	6.2
Tensile strength, MPa[c]	15.1	16.0
Elongation at break, %	290	273
Hardness, Durometer A	67	66
Tear die C, kN/m[d]	34	32
Low temperature properties		
Glass-transition by dsc, °C	−35	−33
Fluid resistance, 168 h at 150°C		
Volume change, %		
In ASTM #1 oil	2	−1
In SF 105	23	10
In Dexron III	28	13
Compression set, method B, plied		
70 h at 150°C	14	16
168 h at 150°C	19	14

[a]Compound parts: polymer, 100; Naugard 445 (substituted diphenylamine), 2; Armeen 18D (octadecylamine), 0.5; stearic acid, 1.5; Vanfre VAM (complex organic alkyl acid), 1.0; FEF Carbon Black (N550), 60; DIAK #1 (hexamethylenediamine carbamate), 1.5; and DOTG, 4.
[b]Press cure is 5 min at 177°C. Post-cure is 4 h at 175°C.
[c]To convert MPa to psi, multiply by 145.
[d]To convert kN/m to psi, divide by 0.175.

Processing

Mixing. Ethylene–acrylic elastomers are processed in either an internal mixer with an upside down process for large-scale production or a rubber mill for smaller scales. In either case, it is important to keep the compound as cool as possible and to avoid overmixing. Ethylene–acrylic elastomers require no breakdown period prior to addition of ingredients. Mixing cycles for a one-pass mix are short, typically 2.5–3.5 min. When compounds are mixed in a rubber mill, care should be taken to add the processing aids up front with additives. Normal mill mixing procedures are followed otherwise.

Extrusion and Calendering. Most compounds of ethylene–acrylic elastomers have low nerve and yield smooth extrusions or calendered sheets. To improve collapse resistance in hoses, compounding techniques should be used to maximize compound viscosity. This includes using a higher viscosity terpolymer, a higher structure carbon black, or fumed silica. The extruder temperatures should be kept quite low. A suggested starting temperature gradient would go from 50 to 65°C, with 75°C at the die. Extruded hose is usually vulcanized by exposure to high pressure steam in an autoclave. Other applications, such as wire insulation and jacketing, are subjected to fast, continuous, high pressure steam vulcanization. Vulcanization at atmospheric pressure produces highly porous vulcanizates and is not recommended.

Molding. Parts can be produced from ethylene–acrylic elastomers using compression, transfer, or injection-molding techniques. Because the viscosity of these polymers is usually lower than the typical rubber used in the industry, compounds of ethylene–acrylic elastomers have a tendency to trap air during molding, especially in a compression mold. This situation can be avoided with adequate venting of the mold, the use of an effective mold lubricant, the use of compounding techniques to maximize compound viscosity, good preforming techniques, and proper mold temperatures. The low viscosity of ethylene–acrylic elastomers makes them especially good for injection molding.

Mold temperatures vary between 150 and 200°C, depending on the molding methods and part size. Parts can be molded in 1.5–10 min depending on the configuration and thickness of the part, the mold temperature, and the desired state of cure at demolding. Since most ethylene–acrylic parts are post-cured, it is sometimes possible to demold partly cured articles and complete vulcanization in the post-curing oven.

Post-Curing. Whenever production techniques or economics permit, it is recommended that compounds based on terpolymer grades be post-cured for optimum properties. Relatively short press cures can be continued with an oven cure in order to develop full physical properties and maximum resistance to compression set. Various combinations of time and temperature may be used, but a cycle of 4 h at 175°C is the most common. The post-cure step increases modulus, greatly improves compression set performance, and stabilizes the initial stress–strain properties. During the post-cure step, the chemical cross-link is converted from an amide linkage to a more stable imide linkage. Peroxide-cured dipolymer compounds need not be post-cured.

Adhesion. Commercially available one- or two-coat adhesive systems produce cohesive rubber failure in bonds between ethylene–acrylic elastomer and metal (16). Adhesion to nylon, polyester, or aramid fiber cord or fabric is greatest when the cord or fabric have been treated with carboxylated nitrile rubber latex.

Additional information on processing compounds of ethylene–acrylic elastomers can be found in References 17,18–19.

Economic Aspects

The market for ethylene–acrylic elastomers was greater than 5000 t/year in 2000. The growth rate for ethylene–acrylic elastomers has been greater than 10% in the 1990s. Over 50% of ethylene–acrylic elastomers are sold in Europe.

Several new products are under development (10), including a higher viscosity terpolymer. These new products, when commercialized, will expand the serviceability of the ethylene–acrylic elastomers and also improve their processability.

Uses

The favorable balance of properties of ethylene–acrylic elastomers has gained commercial acceptance for these elastomers in a number of demanding applications, especially in the automotive industry and in wire and cable jacketing.

Approximately 80% of ethylene–acrylic elastomers are used in automotive applications with hose and tubing as the single largest end use. The recent steady increases in automobile operating temperatures make ethylene–acrylic a prime candidate for under-the-hood applications. Applications include oil and transmission seals, O-rings and gaskets, high velocity CVJ boots, spark plug boots, torsional dampers, and extruded sponges (20,21). Hose applications include transmission and engine oil cooler hoses, air conditioning hose, power steering hose, and turbo charger hose.

Industrial applications include pipe seals, hydraulic system seals, dampers for machinery and high speed printers, and motor lead wire insulation. The fact that the polymer contains no halogens along with certain unique compounding techniques for flame resistance prompts the selection of ethylene–acrylic as jacketing material on certain transportation/military electrical cables, and in floor tiles.

BIBLIOGRAPHY

"Acrylic Elastomers" in *EPST* 1st ed., Vol. 1, pp. 226–246, by P. Fram, Minnesota Mining and Manufacturing Co.; "Acrylic Elastomers, Ethylene–Acrylic Elastomers" in *EPSE* 2nd ed., Vol. 1, pp. 325–334, by J. F. Hagman and J. W. Crary, E. I. du Pont de Nemours & Co., Inc.

1. J. F. Hagman, and co-workers, *Rubber Age* **108**(5), 29, (1976).
2. R. G. Peck, Ethylene/Acrylic Elastomer—Meeting the Challenges of a Demanding Market, Bulletin EA-020.0185, DuPont Polymers, Stow, Ohio, Jan. 24, 1985.
3. T. M. Dobel, *Auto. Polym. Des.* **9**(6), 26, (1990).
4. H. J. Barager and L. C. Muschiatti, Vamac® Ethylene Acrylic Elastomers for Demanding Automotive Applications, Paper No. 189, American Chemical Society Rubber Division, Orlando, Fla., Sept. 1999.
5. U.S. Pat. 3883472 (May 13, 1975), R. N. Greene and K. J. Lewis (to E. I. du Pont de Nemours & Co., Inc.).
6. J. F. Hagman, Vamac G Gum Ethylene/Acrylic Elastomer, Bulletin E-52096, DuPont Polymers, Stow, Ohio, Sept. 1978.
7. T. M. Dobel, New Development in Ethylene/Acrylic Elastomers, Paper No. 28, American Chemical Society Rubber Division, Detroit, Mich., Oct. 1991.
8. U.S. Pat. 3904588 (Sept. 4, 1975), R. N. Greene (to E. I. du Pont de Nemours & Co., Inc.).
9. J. F. Hagman, Curing Mechanisms of Vamac, Bulletin EA-030.0684, DuPont Polymers, Stow, Ohio, 1980.
10. H. J. Barager, K. Kammerer, E. McBride, L. C. Muschiatti, and Y. T. Wu, Increased Cure Rates of Vamac® (AEM) Dipolymers and Terpolymers using Peroxides, American Chemical Society Rubber Division, Cincinnati, Ohio, Oct. 2000.
11. W. M. Stahl, Fluid Resistance of Vamac, Bulletin H-02366, DuPont Polymers, Stow, Ohio, Aug. 1988.
12. J. F. Hagman, Compounding Vamac For Low-Temperature Performance, Bulletin E-10770, DuPont Polymers, Stow, Ohio, Sept. 1978.
13. R. J. Boyce, Flame Retardance in Mineral-Filled Compounds of Vamac, Bulletin E-17762, DuPont Polymers, Stow, Ohio, Jan. 1978.
14. A. E. Hirsch and R. J. Boyce, Dynamic Properties of Ethylene/Acrylic Elastomers: A New Heat Resistant Rubber, Bulletin EA-530.604, DuPont Polymers, Stow, Ohio, May 1977.

15. A. E. Hirsch, Dynamic Characteristics of Fluoroelastomers and Ethylene/Acrylic Copolymers, Bulletin EA-530.602, DuPont Polymers, Stow, Ohio, 1980.
16. J. F. Hagman, Bonding Systems for Vamac, Bulletin E-36062, DuPont Polymers, Stow, Ohio, July 1980.
17. J. F. Hagman, Processing Vamac, Bulletin E-10755, DuPont Polymers, Stow, Ohio, Aug. 1976.
18. C. Williams, Vamac Ethylene/Acrylic Elastomer, A Survey of Properties, Compounding and Processing, Bulletin H-34753, DuPont Polymers, Stow, Ohio, Jan. 1992.
19. J. W. Crary, Ethylene/Acrylic Elastomer—Basic Principles of Compounding and Processing, Bulletin EA-030.0482, DuPont Polymers, Stow, Ohio, Apr. 1982.
20. R. G. Peck, *Auto. Eng.* **95**(7), 37 (1987).
21. R. E. Vaiden, Elastomeric Materials for Engine and Transmission Gaskets, Paper No. 920132, Society of Automotive Engineers, Detroit, Mich., Feb. 1992.

YUN-TAI WU
EDWARD MCBRIDE
E. I. du Pont de Nemours & Company, Inc.

ETHYLENE–NORBORNENE COPOLYMERS

Introduction

Copolymers made from α-olefins and cyclic olefins have been known for nearly 50 years (1,2). Ethylene–norbornene (Et–Nb) copolymers are specifically described in the patent literature as long ago as 1973 (3), with further patent filings since then (4–6). The general class of thermoplastic cyclic olefin copolymers (COCs) includes products from Mitsui Chemicals (7), Japan Synthetic Rubber (8), Nippon Zeon (9), and Ticona (10). Some of these products are manufactured by ring-opening metathesis and others by addition polymerization. Only the COCs made by Ticona, a division of Celanese AG, under the trademark Topas, are Et–Nb copolymers. These products, for which Ticona started up a 30,000-t plant in September 2000 (11), are described in this article.

Properties

Ethylene–norbornene copolymers are made by the direct addition of ethylene and norbornene, using metallocene catalysts. Although regularly alternating copolymers have been made with semicrystalline characteristics, all Et–Nb products presently available are completely amorphous random copolymers, varying only in melt flow and glass-transition temperature (T_g). The bridged ring structure of norbornene makes the resins quite stiff, and their completely amorphous nature ensures high transparency. In general, the resins are stiff, strong, glass-clear, and water-white. They have low elongation at break, negligible moisture absorption and transmission, very low dielectric loss, and low density. The glass-transition

Encyclopedia of Polymer Science and Technology. Copyright John Wiley & Sons, Inc. All rights reserved.

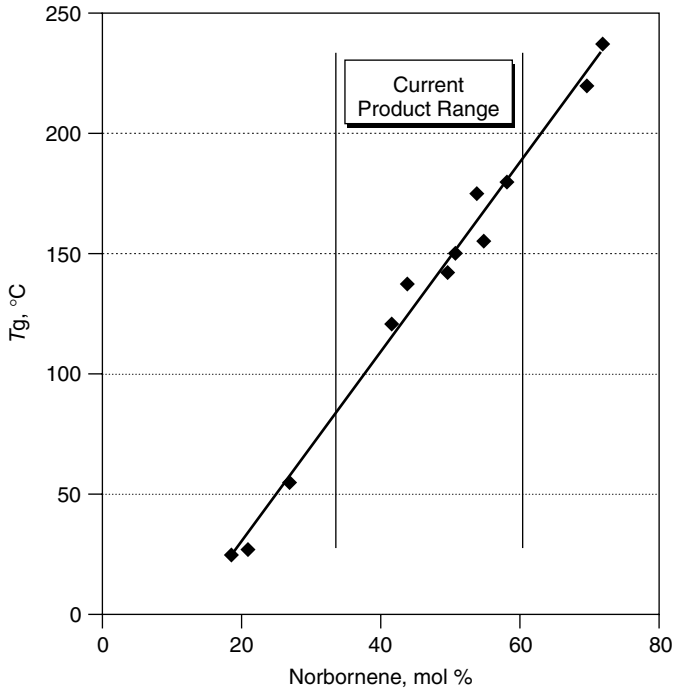

Fig. 1. Effect of norbornene content on T_g.

temperature increases linearly with norbornene content, as shown in Figure 1. The commercially available products range in T_g from about 65°C to about 180°C. Subject to some limitations, conventional thermoplastic processing methods may generally be employed with all of these products.

Because of the bulkiness of norbornene, Et–Nb copolymers remain amorphous down to very low levels of norbornene, where a clear elastomeric polymer is obtained. In the current commercial range of products, all grades on offer exhibit high rigidity, with tensile (Young's) modulus values ranging from 2600 to 3200 MPa. Specific gravity values fall in a narrow spread from 1.00 to 1.02, and light transmission is around 92%. Typical values for a range of physical properties are shown in Table 1 for the announced commercial grades of Topas COC resins (12). These materials have excellent chemical resistance to aqueous fluids (acids and bases) and many polar solvents (alcohols and ketones), but are attacked by nonpolar solvents (hexane, toluene, oleic acid, and methylene chloride) and some oils and fats. The chemical resistance of the copolymers may be summarized as follows (13).

The commercially important properties of Et–Nb copolymers include low density, high transparency and low color, high moisture barrier and low moisture absorption, low optical distortion, excellent feature replication, resistance to polar solvents, high purity, shatter resistance, good biocompatibility, extremely low dielectric loss, high temperature capability, and compatibility with polyethylenes. The resins also have the low shrinkage and warpage typical of amorphous polymers.

Table 1. Properties of Et–Nb Copolymers, Commercial Grades of Topas

Property	8007	5013	6013	6015	6017
T_g, °C	80	140	140	160	180
Melt flow (260°C), g/10 min	30	55	16	16	12
Density, g/mL	1.0	1.02	1.02	1.02	1.02
M_w (PS), g/mol	93,200	80,500	65,400	80,200	82,500
H_2O absorption, %	<0.01	<0.01	<0.01	<0.01	<0.01
Mold shrinkage, %	0.6	0.6	0.6	0.6	0.6
Tensile strength, MPa[a]	66	66	66	66	66
Elongation @ break, %	10	3	4	4	4
Tensile modulus, MPa[a]	2600	3100	3200	3200	3200
Charpy impact, kJ/m^2[b]	13	15	15	15	15
Notched Charpy impact, kJ/m^2[b]	2.6	1.7	1.7	2.0	2.0
HDT[c] @ 0.46 MPa[a], °C	75	130	130	150	170
Dielectric constant @ 1–10 kHz	2.35	2.35	2.35	2.35	2.35
Comparative tracking index, V	>600	>600	>600	>600	>600
Volume resistivity, Ω·cm	>10^{16}	>10^{16}	>10^{16}	>10^{16}	>10^{16}
Light transmission, %	92	92	92	92	92

[a] To convert MPa to psi, multiply by 145.
[b] To convert kJ/m^2 to ft·lbf/in.^{2} divide by 2.4.
[c] Heat-deflection temperature.

FDA Drug and device master file numbers respectively are DMF 12132 and MAF 1043. All grades, save only the highest temperature one, comply with U.S.P. Class VI requirements. The FDA has issued a regulation, 21 CFR 177.1520, for Et–Nb copolymers in dry food contact (14). The 80°C T_g grade complies with food contact requirements under conditions of use C through H, while the 140°C and 160°C T_g grades comply under conditions of use A through H. A Food Contact Substance Notification, FCN 000075, became effective on August 22, 2000 for the polymers in direct food contact with all food types as films, sheets, and articles made therefrom (15). The afore mentioned properties, usually in various combinations, are the drivers for current and developing applications for Et–Nb copolymers.

Manufacturing

Although, strictly speaking, Et–Nb products are copolymers of ethylene and norbornene, the manufacturing process starts with ethylene and a high purity dicyclopentadiene (DCPD) stream. The DCPD is cracked at a temperature in excess of 160°C to yield cyclopentadiene (CPD) (eq. (1)), which reacts with ethylene to give norbornene (bicyclo[2.2.1]-2-heptene) via Diels–Alder condensation (eq. (2)). Cyclopentadiene boils at 42°C, whereas norbornene melts at 47°C.

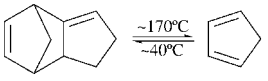

DCPD CPD (1)

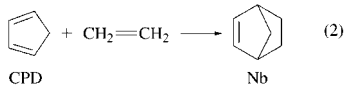

(2)

The norbornene product then reacts in solution with ethylene to form the copolymer, using a zirconium metallocene procatalyst/methylaluminoxane cocatalyst system (eq. (3)).

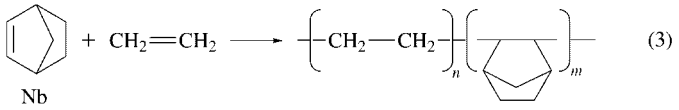

(3)

Subsequent removal of catalyst and solvent yields a very pure polymer.

Processing

Many processing methods have been employed with Et–Nb copolymers. These include injection molding, injection and coinjection blow molding, compression molding, cast film and sheet extrusion and coextrusion, blown film extrusion and coextrusion, tubing extrusion and coextrusion, extrusion compounding, film solvent casting, mono- and biaxial (tenter) orientation of film, and thermoforming of film and sheet. In co-extrusion and coinjection molding, a tie layer is normally required except for polyethylenes and high ethylene copolymers. Unless the parison is quite small, presently available polymer grades do not have sufficient melt strength for extrusion blow molding. Typical starting conditions for molding and extrusion are given in Tables 2 and 3 where the higher temperatures apply to polymers of higher T_g. For processes involving a free surface, such as extrusion or blow molding, an external processing aid should be dusted on the polymer pellets to obtain the best product esthetics. For both extrusion and molding, low compression screws are recommended. A special screw design for film extrusion is shown in Figure 2 (16). In both extrusion and molding, it is important that the forming surface be maintained near the T_g of the polymer grade being processed. For higher T_g grades, this requires oil-heated tooling for molding and oil-heated take-off rolls for film casting. Manufacture of blown films requires a shorter tower and a lower nip than those that are used in conventional olefin processing.

Post-processing assembly procedures such as lamination, machining, or diamond turning, and joining by solvent, friction, and ultrasonic bonding have all been satisfactorily demonstrated with Et–Nb copolymers. Machining lubricants should be water-based and should contain no oil. Also, relatively slow speeds and shallow cuts should be used to avoid cracking the part.

Applications

Rigid and flexible packaging are currently the leading uses for Et–Nb copolymers. This category includes both film and container applications in pharmaceutical, medical and diagnostic, and food packaging end uses. Pharmaceutical blister packaging requires high moisture barrier, transparency, and thermoformability.

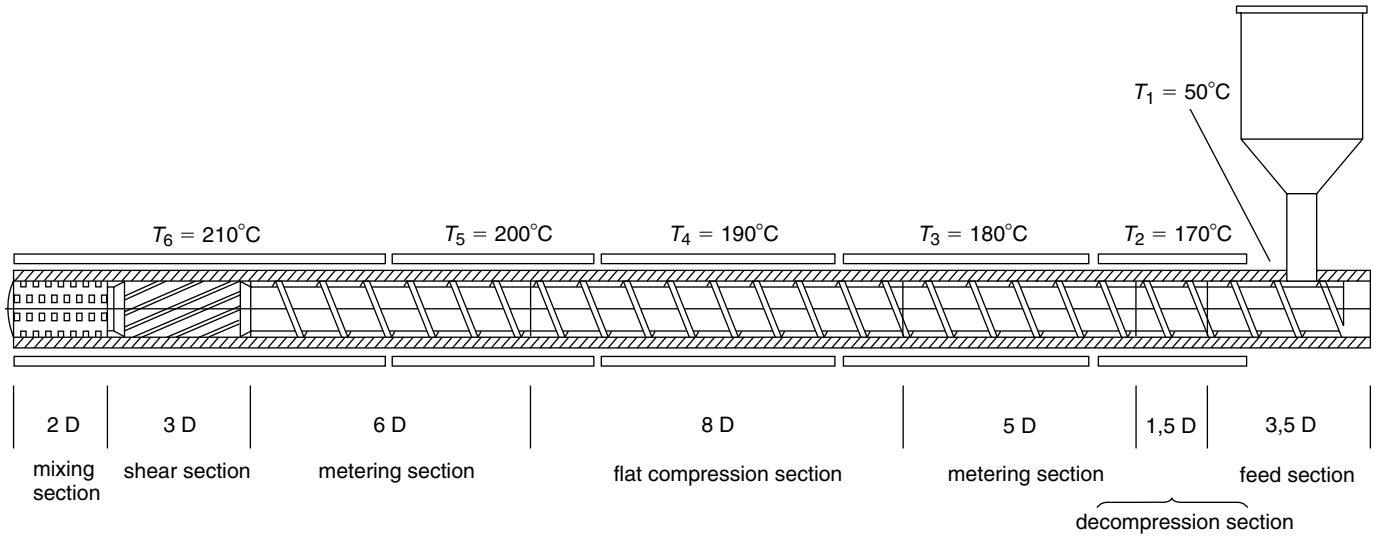

Fig. 2. Special screw design for film extrusion.

Table 2. Injection-Molding Conditions for Et–Nb Copolymers

Feed Zone	<80°C
Barrel Zone 1	230°C–270°C
Barrel Zone 2	245°C–290°C
Barrel Zone 3	260°C–300°C
Barrel Zone 4	270°C–300 °C
Nozzle	270°C–300°C
Melt	260°C–310°C
Max barrel residence	<15 min
Injection pressure	50–110 MPa[a]
Hold pressure	30–50 MPa[a]
Back pressure	0.7 MPa[a]
Screw speed	50–150 rpm
Injection speed	Moderate to fast (2–10 cm/s)
Mold temperature	110°C–150°C
Nozzle type	Open
Screw suckback	None or minimum
Cushion	Small
Screw type	Low compression
Screw turn on inject	No
Ram speed	Moderate to fast

[a]To convert MPa to psi, multiply by 145.

Table 3. Extrusion Conditions for Et–Nb Copolymers

L/D ratio	>25
Compression ratio	2.0–2.5
Casting roll	Close to HDT of polymer (50°C–70°C up to 160°C–175°C)
Feed Zone	<50°C
Zone 1	210°C–240°C up to 255°C–275°C
Zone 2	220°C–250°C up to 275°C–300°C
Zone 3	230°C–270°C up to 275°C–300°C
Zone 4	230°C–270°C up to 275°C–300°C
Die	230°C–270°C up to 275°C–300°C
Melt	230°C–270°C up to 290°C–310°C

These requirements are met with a multilayer structure containing a thicker central layer of the copolymer with thin outer layers of polypropylene (17). Such film structures are made by lamination or coextrusion, respectively using appropriate adhesive or tie layers. Other uses for these films include packaging of personal care and consumer products as in, for instance, blister bottles.

Medical and diagnostic packaging applications include syringes, vials, and tubes made by injection or injection blow molding (18,19). Here the key properties include moisture barrier, transparency, shatter resistance, bioinertness, and ability to undergo terminal steam- or gamma-sterilization. Cuvettes and micro-titer (multiwell) plates are other important diagnostic/analytical uses for the copolymers (20,21). Resistance to dimethyl sulfoxide is an important attribute in these applications, as are clarity and transparency, especially in the near uv region. Low shrinkage and dimensional stability provide the ability to mold very flat

three-dimensional structures that can be accurately and consistently positioned in automated analytical equipment.

Food packaging uses may include both mono- and multilayer films, primarily using the copolymer in a blend with polyethylene (22). Suitable blend components include low density, linear low density, and plastomer polyethylenes as well as ethylene vinyl alcohol copolymers. These blends exhibit improved stiffness, reduced friction and blocking, and improved hot tack and ultimate seal strength performance over the respective unmodified polyethylenes, with no loss, or even an improvement in clarity and oxygen permeation. Uses for the blends are in packaging of fresh-cut produce and standup pouches.

Biaxially oriented cast films have been shown to have improved mechanical properties, with modulus increased 1.5 times, tensile strength 2.5 times, and elongation 20 times (23). Films have been drawn down to about 7 μm using draw ratios between 3:1 and 4:1 in machine and transverse directions. These films can be metallized on both sides and because of their extremely low dielectric loss and higher temperature capability, can provide superior capacitor performance in a smaller package.

High transparency, low birefringence, and high Abbé number combine with low moisture absorption to make the Et–Nb copolymers extremely suitable for precision optical applications as well as more mundane uses where temperature or solvent resistance issues preclude the use of other materials such as polycarbonate or polymethyl methacrylate. Superior reproduction of surface features also makes the resins suitable for production of diffraction optics. Current applications include lenses for use in light-emitting diodes, compact disc (CD) readers, and automotive rain sensors. Light guides capable of resisting higher temperatures such as are experienced during wave soldering are another current optical application (24).

Work in the mid-nineties showed that excellent audio CDs could be made from a high flow Et–Nb copolymer. However, cycle times comparable to those obtainable with CD-grade polycarbonate were not achieved. As optical storage media standards move to higher and higher data density, renewed interest has arisen in COC resins for such applications, based on their excellent feature replication, superior birefringence, and higher transparency to the lower wavelength lasers required to read the smaller pits accurately. Et–Nb copolymers are candidates for these high data density applications (25).

The two key control parameters available in manufacture of the copolymers are T_g and molecular weight. This capability has been exploited to produce a new class of toner binder resins for electrophotographic printing (26). The new binder resins offer significant performance benefits over existing materials especially where high process speed or improved image quality is required. Control of T_g allows precise matching to the fuser temperature requirements of specific printer designs. The single-site metallocene catalysts used in manufacture of the Et–Nb resins allow a narrow molecular weight distribution with a polydispersity index (M_w/M_n) of close to 2.0. This enables undesirable oligomer content to be kept to a minimum and also facilitates design of appropriate bimodal molecular weight compositions to meet the requirements of different printing processes, especially in regard to providing a large antioffset window. The high clarity and colorlessness of the base copolymer resin provide high color fidelity in the finished print. Making toner binder resins of very low molecular weight ensures good pigment

dispersability and also facilitates grinding the finished toner into relatively uniform small and approximately spherical particles.

The Et-Nb copolymers presently on the market are all neat polymers. No compounds of these resins are commercially available at this time. However, glass-fiber-reinforced formulations have been developed (27), as have impact-modified and flame-retarded compositions (28). The glass-reinforced formulations had high flow and the ability to fill long thin sections. Complex three-dimensional parts showed very little warpage, reflecting the low shrinkage of the base resin. Reinforcement with glass fibers significantly increased notched impact strength. Improvements in tensile strength and modulus were on a par with those obtainable with polypropylene. Flame-retarded compositions were based on halogenated and nonhalogenated flame-retardant packages, and yielded both V-0 and V-2 performance.

As the unique property profiles of cyclic olefin polymers and copolymers, and particularly those of Et-Nb copolymers, become more widely known and understood, new applications and most likely, new formulations will continue to develop. This process will undoubtedly be furthered by any cost improvements obtainable via scale economies in production of the base resin, for which the U.S. developmental price in 2001 ranges between $5.70/kg and $6.60/kg at truckload quantities.

BIBLIOGRAPHY

1. U.S. Pat. 2721189 (Oct. 18, 1955), A. W. Anderson and N. G. Merckling (to E. I. du Pont de Nemours & Co., Inc.).
2. G.B. Pat. 951022 (Apr. 24, 1962) (to Montecatini Societa Generale per L'Industria Mineraria e Chimica).
3. D.D.R. Pat. 109224 (July 10, 1973), J.-P. Koinzer, U. Langbein, and E. Taeger (to VEB Leuna).
4. Eur. Pat. 0156464 (Feb. 1, 1985), H. Kajiura, H. Oda, and S. Minami (to Mitsui Petrochemical Industries, Ltd.).
5. Eur. Pat. 0283164 (Mar. 1, 1988), N. Ishimaru and co-workers (to Mitsui Petrochemical Industries, Ltd.).
6. Eur. Pat. 0407870A2 (July 4, 1990), M.-J. Brekner and co-workers (to Hoechst Aktiengesellschaft).
7. *Apel Product Bulletin, Mitsui Petrochemical Industries (undated)*.
8. Report IV-B-2, Nippon Chemtec Consulting (Dec. 1992).
9. *Zeonex Product Brochure, Nippon Zeon Co. Ltd., Jan.* 2000.
10. Topas® COC Product Bulletin, Ticona GmbH (Sept. 1997).
11. *Ticona press release* (Sept. 2000).
12. R.R. Lamonte and D. McNally, *Plastics Eng.* **56**, 6, 51 (2000).
13. D. McNally, in *New Polymer Technologies '98 Conference*, Philadelphia, Pa., 1998.
14. *Title 21, Code of Federal Regulations, 177.1520*.
15. *USFDA Food Contact Substance Notification 00075*.
16. E. Beer and W. Hatke, *Plastics Special* **6**, 1999.
17. E. Beer and K. Trombley, in *Blister-Pack 2000 Conference*, Jamesburg, NJ, May 17, 2000.
18. Schott Pharmaceutical Packaging, *American Association of Pharmaceutical Scientists Conference and Exhibition*, Philadelphia, Nov. 15, 1999.
19. *Ticona press release* (Jan 15, 2001).

20. U.S. Pat. 5910287 (June 8, 1999), P. J. Cassin and co-workers (to Aurora Biosciences Corp.).
21. U.S. Pat. 6063338 (May 16, 2000), A. A. Pham and co-workers (to Aurora Biosciences Corp.).
22. R.R. Lamonte, in *10th Worldwide Flexible Packaging Conference*, Amsterdam, Nov. 2000.
23. T. Weller, in *New Plastics '98 Conference*, London, Jan. 22, 1998.
24. *Ticona press release* (Feb. 26, 2001).
25. A. Tullo, *Chem. Eng. News* **77**, 14, 51 (2000).
26. K. Berger, T. Nakamura, and M. Bruch, in *International Conference on Digital Printing Technologies*, Vancouver, Oct. 15, 2000, pp. 623–626
27. V. Sullivan, *Glass Reinforcement of COC*, private communication, 1997.
28. T. Wehrmeister, *Flame Retardation of COC*, private communication, 1997.

DONAL MCNALLY
Ticona

EXTRUSION

Introduction

The main function of an extruder is to develop sufficient pressure in the material so as to force the material through the die. The pressure necessary to force a material through the die depends on the geometry of the die, the flow properties of the material, and the flow rate. Basically, an *extruder* is a machine capable of developing pressure. In other words, an extruder is a pump. A *plastics extruder* is a pump for plastic materials. However, this is not to be confused with a *plasticating extruder*, which is a machine that not only extrudes but also plasticates, or melts, the material. A plasticating extruder is fed with solid plastic particles and delivers a completely molten plastic to the die. On the other hand, a machine that extrudes molten plastic without melting it is called a *melt-fed extruder*.

Extruders Types

Extruders are the most common machines in the plastics processing industry. Extruders are used not only in extrusion operations, but also in most molding operations, for instance injection molding and blow molding. Essentially every plastic part has gone through an extruder at one point or another; in many cases, more than once.

Single Screw Extruders. In the plastics industry, there are three main extruder types: the screw extruder, which is the most common; the ram extruder; and the drum or disk extruder, which is the least common. In a screw extruder a screw rotates in a cylinder; the rotation of the screw creates a pumping action (see Fig. 1).

Encyclopedia of Polymer Science and Technology. Copyright John Wiley & Sons, Inc. All rights reserved.

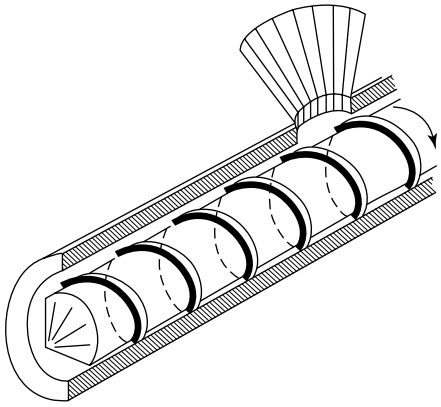

Fig. 1. A single screw extruder.

Twin Screw Extruders. A screw extruder can have one screw or more than one screw. An extruder with one screw is called a single screw extruder; it is the most common machine in the plastics processing industry. An extruder with more than one screw is called a multiscrew extruder. The most common multiscrew extruder is the twin screw extruder; it has two screws.

Co-Rotating Twin Screw Extruders. There are several types of twin screw extruders. In most twin screw extruders, the screws are located side by side. If both screws rotate in the same direction, the extruder is called a *co-rotating twin screw extruder* (see Fig. 2).

Co-rotating twin screw extruders used for compounding run at high screw speed, typically between 200 and 500 rpm. Some of the newer very high speed twin screw extruders are capable of running at speeds over 1000 rpm, as high as 1600 rpm.

Counter-Rotating Twin Screw Extruders. If the screws of a twin screw extruder rotate in opposite direction, it is called a *counter-rotating twin screw*

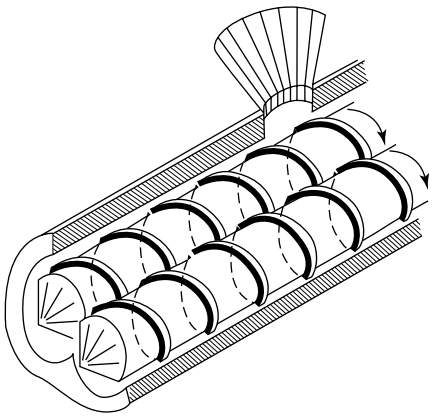

Fig. 2. A co-rotating twin screw extruder.

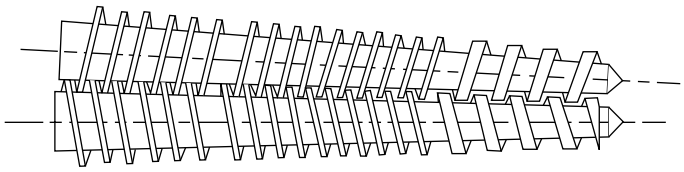

Fig. 3. Conical twin screw extruder.

extruder. Twin screw extruders can run at high or low speed, depending on the application. High speed extruders run at around 200–500 rpm and even higher; they are primarily used in compounding. Low speed extruders run at about 10–40 rpm and are used mostly in profile extrusion applications.

Most twin screw extruders for profile extrusion are counter-rotating extruders. This is because counter-rotating extruders tend to have better conveying characteristics than co-rotating extruders. Most twin screw extruders have parallel screws, but some extruders have conical screws where the screws are not parallel (see Fig. 3). Another distinguishing feature of twin screw extruders is the extent that the screws intermesh. The screws can be fully intermeshing (Fig. 4a), partially intermeshing (Fig. 4b), and nonintermeshing (Fig. 4c).

Most twin screw extruders are intermeshing. The advantage of nonintermeshing twin screw extruders is that they can have a very long length without problems with metal-to-metal contact between the screws. The *L/D* ratio can be 100:1 and higher. The *L/D* of intermeshing twin screw extruders is generally limited to values less than 60:1. A disadvantage of current nonintermeshing twin screws is that they have limited dispersive mixing capability; however, newer dispersive mixing technologies may negate this limitation (see section on The CRD Mixer and Figs. 63, 64, 65).

Ram Extruders. In a ram extruder a piston forces the material through the die (see Fig. 5). Ram extruders have very good conveying characteristics and can develop very high pressures. The drawback of ram extruders is that they have low melting capacity. Therefore, they are not used very often for normal plastics. There are some unusual plastics, however, that are often processed on a ram extruder, such as the so-called *intractable plastics* that cannot be processed on normal extruders. Examples of such plastics are PTFE and ultrahigh molecular weight (UHMW) PE. These plastics do not melt like normal plastics and are formed by sintering. Continuous products can be made on a ram extruder; the line speeds are quite low though, in the range of 25–75 cm/h (10–30 in./h).

Components of an Extruder

The Extruder Screw. The heart of the extruder is the extruder screw. This is a long cylinder with a helical flight wrapped around it (see Fig. 6). The screw is so important because conveying, heating, melting, and mixing of the plastic are mostly determined by the screw. The stability of the process and the quality of the extruded product are very much dependent on the design of the screw. The screw rotates in a cylinder that fits closely around it.

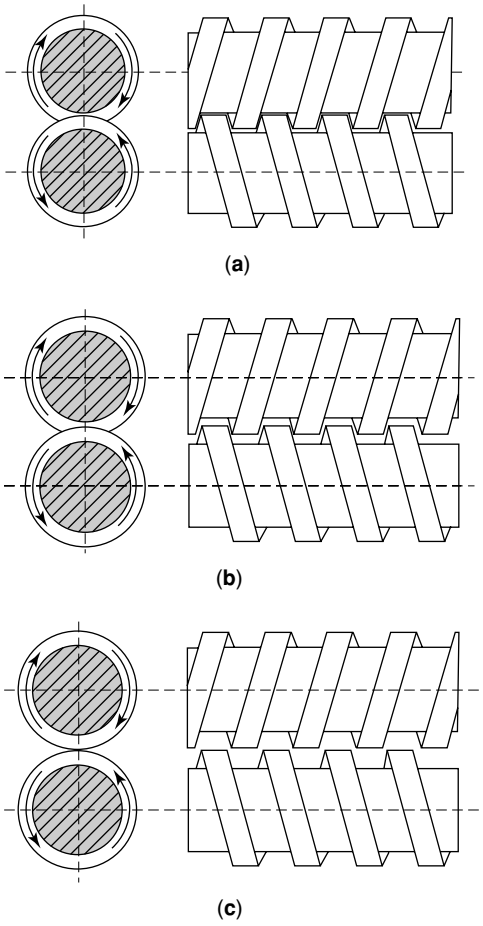

Fig. 4. Counter-rotating screws: (**a**) fully intermeshing; (**b**) partially intermeshing; and (**c**) nonintermeshing (tangential).t

The Extruder Barrel. The cylinder is called the extruder barrel. The barrel is a straight cylinder usually equipped with a bimetallic liner; this liner is a hard, integral layer with high wear resistance. In most cases, the wear resistance of the barrel should be better than that of the screw. The reason is that the screw is much easier to rebuild and replace than the barrel. Bimetallic barrels usually cannot be rebuilt.

The barrel may have a vent opening through which volatiles can be removed from the plastic (see Fig. 7), a process called *devolatilization*. An example is the removal of moisture from a hygroscopic plastic. An extruder with a vent port should use a special screw geometry to keep the plastic melt from coming out of the vent port; such a screw is called a two-stage screw (see Fig. 7).

The Feed Housing. The feed housing is connected to the barrel; it contains the feed opening through which the plastic material is introduced to the extruder. The feed throat usually has water-cooling capability because the feed

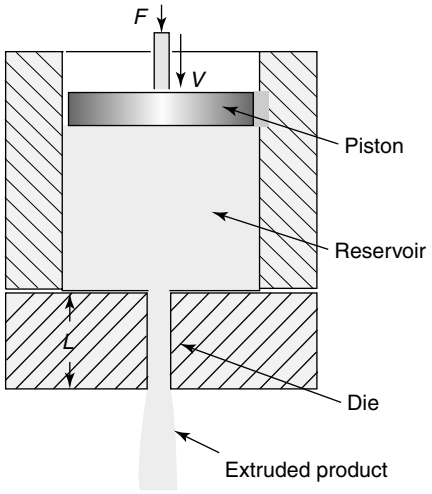

Fig. 5. Schematic of a ram extruder.

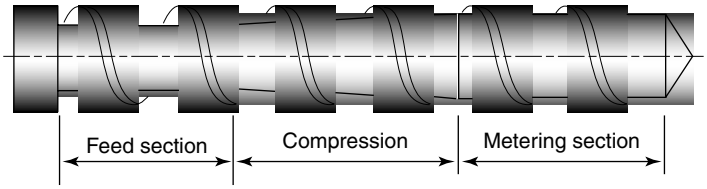

Fig. 6. A single flighted extruder screw.

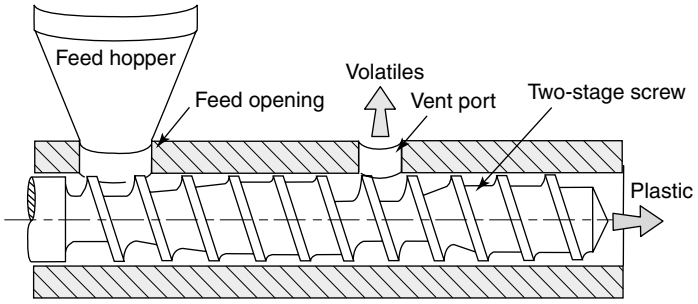

Fig. 7. A vented extruder barrel with a two-stage screw.

throat temperature is kept low enough to keep the plastic particles from sticking to the wall. To improve the intake capability of the feed throat, the feed opening can be offset as shown and have an elongated shape. The length of the feed opening should be about 1.5 times the diameter of the barrel and the width about 3/4 times the diameter, as shown in Figure 8.

Some extruders do not have a separate feed throat, but the feed opening is machined right into the extruder barrel. There are both advantages and

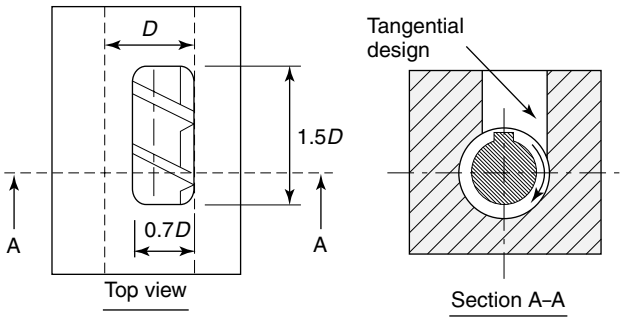

Fig. 8. Preferred geometry for feed opening in the feed throat.

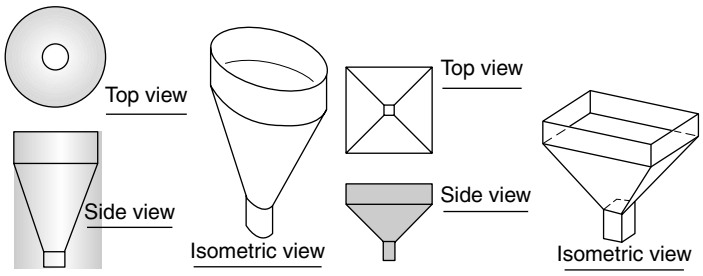

Fig. 9. Good hopper design (left) and poor hopper design (right).

disadvantages to such a setup. The advantages are lower cost, fewer parts, and no problems with alignment of the barrel to the feed throat. Disadvantages are that it is more difficult to create a thermal barrier between the hot barrel and the cold feed throat region, and good cooling of the feed throat region is more difficult.

The Feed Hopper. The feed throat is connected to the feed hopper and the extruder barrel. The feed hopper holds the plastic pellets or powder and discharges the material into the feed throat. The hopper should be designed to allow a steady flow of material through the hopper. Steady flow is best achieved with a circular hopper with a gradual transition in the conical section of the hopper (see Fig. 9). For difficult bulk materials, special devices, such as vibrating pads, stirrers, wipers, and even crammer screws, can be used to promote steady flow through the hopper so as to force the material to the discharge (see Fig. 10).

Barrel Heating and Cooling. The extruder barrel typically has both heating and cooling capability. Heating is usually done with electrical band heaters located along the length of the extruder. Induction and radiation heating are not commonly used; fluid heating is used in some rubber extrusion operations and on some older plastic extruders.

Most extruders have at least three temperature zones along the length of the barrel. Long extruders may have eight temperature zones or more. Each zone has its own heating and cooling capability and at least one temperature sensor to measure the zone temperature. The temperature is usually measured in the barrel. The die may have one or several temperature zones depending on its complexity.

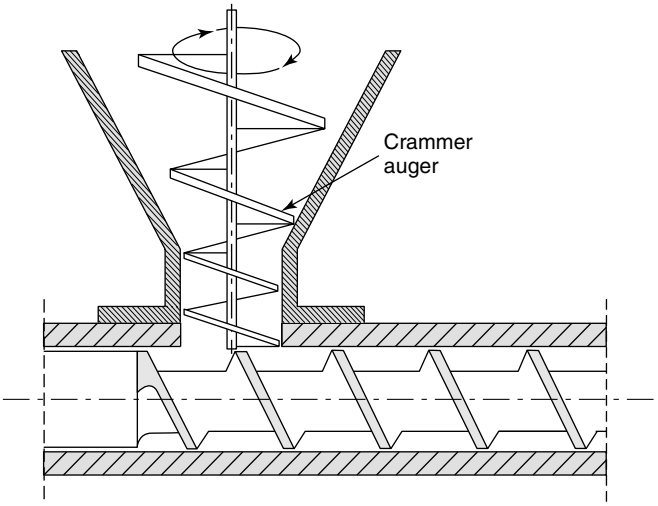

Fig. 10. Example of crammer feeder.

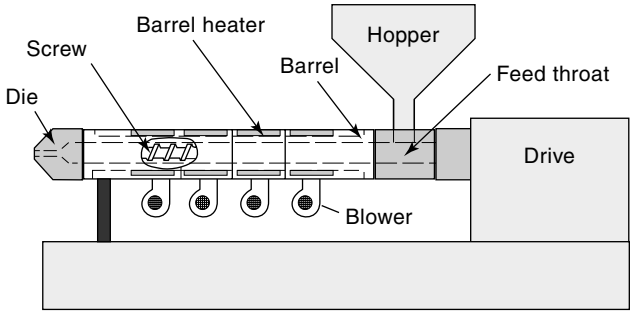

Fig. 11. Extruder with barrel heaters and blowers for cooling.

Some dies have more then 10 temperature zones. Dies have heating capability, but usually do not have cooling.

The barrel has to be cooled if the internal heat generation in the plastic raises the barrel temperatures above the set point. This is likely to occur when extruding high viscosity plastics and when running at high screw speeds. Cooling on single screw extruders is usually done with air. Blowers are placed under the extruder barrel and temperature zones are partitioned, so that one blower cools only one temperature zone (see Fig. 11).

Water cooling can be used as well, particularly if large amounts of heat must be removed. The extrusion process normally runs best when the screw supplies most of the energy needed in the process, so that little additional heating or cooling needs to be done through the barrel. As a result, air cooling is sufficient for most extrusion operations using single screw extruders. Since water cooling removes heat more quickly, it can be more difficult to maintain good temperature control

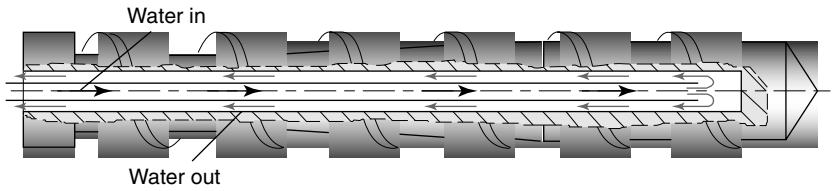

Fig. 12. Circulating a heat transfer fluid through the screw.

with water cooling. Oil cooling can be used as well; in fact, oil can be used both for heating and cooling.

With barrel cooling active, it is important to realize that even if the temperature is at its one word, the actual melt temperature is above the one word. With barrel cooling on, the heat flows from the plastic through the barrel to the outside. In this situation, the highest temperature occurs in the plastic. Even if the barrel temperature is at one word, the plastic temperature can be substantially higher. When a large amount of cooling is done in a particular part of the extruder the actual plastic temperature will be substantially above the barrel temperature set point. Therefore, barrel cooling should be minimized as much as possible.

Screw Heating and Cooling. The screw of an extruder is usually neither heated nor cooled; such a screw is called a *neutral screw*. However, it is possible to either heat or cool the screw by coring the screw (making it hollow) and circulating a heat transfer fluid through the hollow section (see Fig. 12). The screw can also be heated by a cartridge heater. The heater's electrical power has to be supplied through a slip ring assembly at the drive end of the screw. If the cartridge heater is equipped with a temperature sensor, the power to the heater can be controlled to maintain a constant temperature.

The Breaker Plate. The breaker plate is located at the end of the barrel. It is a thick metal disk with closely spaced holes.

The main purpose of the breaker plate is to support a number of screens located just ahead of the breaker plate. The other function of the breaker plate is to stop the spiraling motion of the melt as it comes off the screw. The breaker plate forces the melt to flow in a straight-line fashion into the die. It is possible to incorporate mixing capability into the breaker plate; this allows the breaker plate to act as a static mixer. Such a mixer was developed by The Madison Group in cooperation with Rauwendaal Extrusion Engineering. This mixing breaker plate (MBP) has many tapered channels that split the flow and expose the plastic melt to elongational flow. This promotes both distributive and dispersive mixing. An example of the MBP is shown in Figure 13. Different pattern can be machined into the MBP and several MBPs can be stacked together to enhance the mixing action.

The screens are used to trap contaminants so that they do not end up in the extruded product. Usually, several screens are stacked together, starting with a coarse screen, followed by increasingly finer screens, and then a coarse screen again right up against the breaker plate. The plastic melt thus flows through screens with increasingly smaller openings. The last coarse screen acts merely as a support for the finer screen. The collection of screens is called the *screen pack*.

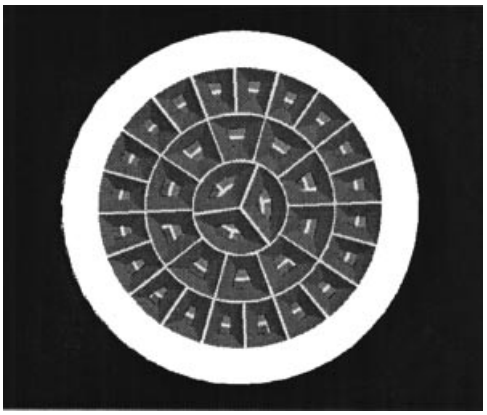

Fig. 13. Example of a mixing breaker plate.

The Screen Pack. The screen pack is not only used to trap contaminants, but in some cases the restriction of the screen pack is increased to increase mixing in the extruder. This works to some degree; however, the mixing can be improved more efficiently by adding mixing sections to the extruder screw. The most common filters are wire mesh screens. The mesh number of the screen represents the number of wires per inch (25 mm). The higher the mesh, the more wires per inch and the smaller the openings of the screen.

Figure 14 shows the relationship between the mesh value of the screen and the micron rating. The micron rating indicates what size particles the screen is able to trap. The higher the mesh, the lower the micron rating and, therefore, the

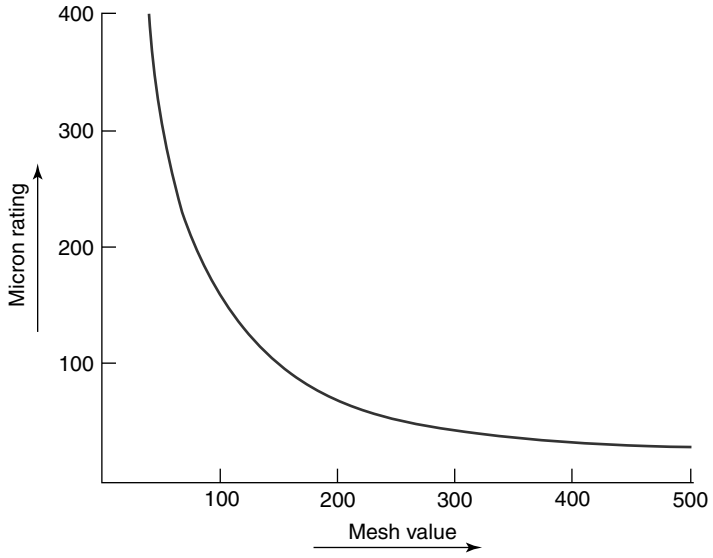

Fig. 14. The micron rating vs the mesh value for wire mesh screens.

Table 1. Comparison of Different Filter Media

	Wire mesh square weave	Wire mesh Dutch twill	Sintered metal powder	Random metal fibers
Gel capture	Poor	Fair	Good	Very good
Contaminant capacity	Fair	Good	Fair	Very good
Permeability	Very good	Poor	Fair	Good
Price	Low	Fair	High	High

finer the screen. A typical screen pack can consist of a 20-mesh screen, followed by a 40-, 60-, and 80-mesh screens, with a final 20-mesh screen for support against the breaker plate.

There are a number of different filter materials. Wire screens are the most common. Several types of wire screens are available, such as the square mesh with plain weave and the square mesh with Dutch twill. There are also depth filtration media, such as sintered metal powder and random metal fibers. Advantages and disadvantages of different filter materials are shown in Table 1.

Other filter materials used in some cases are plates with small holes and filters made up of sand. Plates with small holes are useful in filtering out coarse contaminants and, for that reason, are used for prefiltration. Sand is inexpensive and because of the large volume, sand filters can operate for long periods before they have to be changed. A drawback of sand is that the filtration action is not uniform. Also, the run-in period for sand filters can be long and the installation is complicated.

Screen Changers. In some cases, screens have to be replaced at short intervals, for instance, every 2 h. This may happen when the plastic contains a substantial level of contaminants. In such a situation, it can be advantageous to use a *screen changer*, which is a device that allows a quick change of the screens. Some screen changers allow the extruder to keep running while the screens are changed; these are called *continuous screen changers*. Screen changers are useful when pressure increases rapidly at the screens. Screen changers can be manual or automatic. In many automatic screen changers, the screens are changed when the pressure drop across the screens reaches a preset value.

There are various types of screen changers, including manual screen changers, hydraulic screen changers, semicontinuous screen changers, screen changers with a continuous moving screen, and rotary-type screen changers. Manual screen changers are used on smaller extruders, up to about 120 mm or 4.5 in. They use a slide plate design with two circular screen blocks; one is in the melt flow at all times. When the pressure builds up to a certain level, the operator uses a hand lever to insert a new screen into position. At the same time, the dirty screen is pushed out of position so that it can be removed and replaced with a clean screen pack.

Hydraulic screen changers use a hydraulic ram to push the block containing a new screen into the melt stream (see Fig. 15). They can be used with larger extruders. Semicontinuous screen changers allow the screen to be changed without stopping the melt flow. In most units, trapped air is prevented from going into the melt stream by a bleed valve. Even if the entrapped air can be eliminated

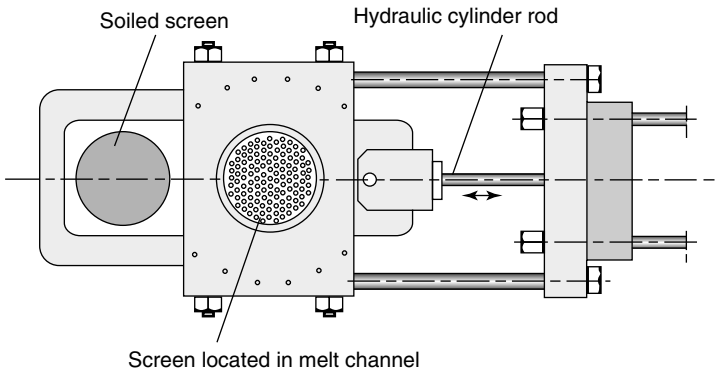

Fig. 15. Typical slide plate screen changer.

completely, there may still a pressure spike when a new screen is moved into position.

In screen changers with a continuously moving screen, a continuous band of screen material passes across the melt flow at a speed determined by the pressure difference across the screen. The rotary screen changer uses a moving wheel with 10–16 kidney-shaped cavities containing the screens. Each cavity moves slowly through the melt stream. This is similar to the continuously moving screen, except that in the rotary screen, the screen itself is not continuous because of the webs between the cavities. The webs, however, are relatively thin, so that at all times at least 90% of the channel is occupied by the screen. Rotary screen changers use separate screen inserts that are changed by the operator. The advantage of the screen changer with the continuously moving screen and the rotary screen is that pressure disturbances during screen changes are minimized.

The Extrusion Die. The die is placed at the discharge end of the extruder. Its function is to form the flowing plastic into the desired shape of the extruded product. Dies can be categorized by the shape of the product that they produce. Annular dies are used to make tubing, pipe, and wire coating. Slit dies are used to make flat film and sheet. Circular dies are used to make fiber and rod. Profile dies are used to make shapes other than annular, circular, or rectangular. Dies are also named by the product that they produce. So, we talk about tubing dies, flat film dies, blown film dies, etc.

The inlet channel of the die is usually designed to match the exit of the extruder. If the die entrance does not match the extruder exit, an adapter can be used between the extruder and the die. The three main elements of the die flow channel are the inlet channel, the manifold, and the land region (see Fig. 16).

The flow channel of the die should be designed such that the plastic melt achieves a uniform velocity across the die exit. The shape of the land region of the die corresponds to the shape of the extruded product. An example of an in-line tube or pipe die is shown in Figure 17. The material flows into the die from the extruder; then it flows around a torpedo.

The torpedo is supported by spider legs that have a streamlined shape to achieve smooth flow around the support legs. From the torpedo, the plastic melt

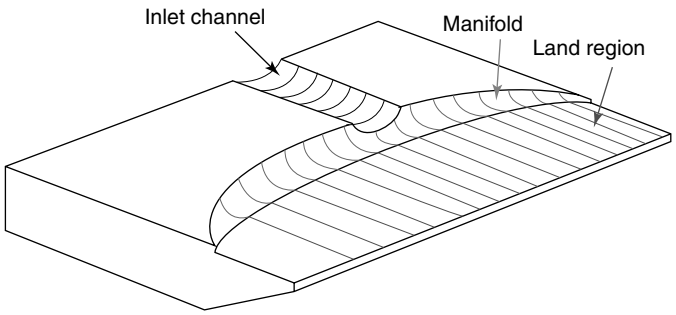

Fig. 16. The three main elements of an extrusion die.

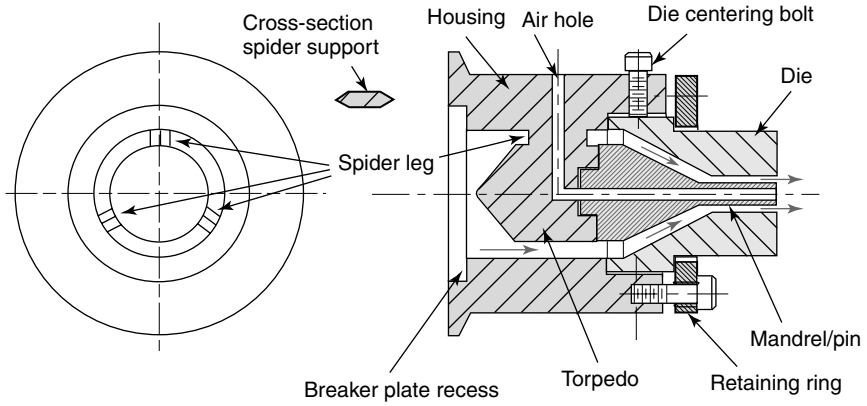

Fig. 17. Example of in-line tubing or pipe die.

flows to the tip and die where it is shaped into an annulus, so that a tube-shaped product emerges.

The size and shape of the land region are not exactly the same as the extruded product. There are several reasons for this: draw down, cooling, swelling, and relaxation. Because of the several variables affecting the size and the shape of the extruded plastic, it is often difficult to predict how exactly the size and shape of the plastic changes as it leaves the die. As a result, it is also difficult to predict how the die flow channel should be shaped to achieve the desired shape of the extruded product. This is an important reason why die design is sometimes still largely based on experience rather than on engineering calculations. With the advent of improved numerical techniques and commercial die flow analysis software, this situation is improving; however, die design is still often a trial and error process.

Coextrusion Dies. Another type of die used in the extrusion industry is the coextrusion die. This type of die is used to make a multilayered product in one step. There are two main coextrusion systems: the feed block system and the multimanifold system. In the feed block system, the different plastic melt streams are combined in a feed block and then fed into a regular single manifold extrusion die (see Fig. 18).

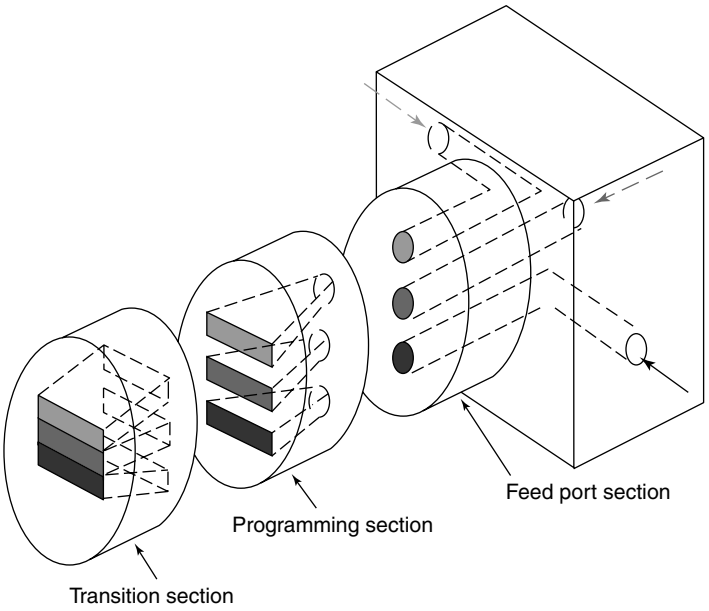

Fig. 18. Example of a feed block system.

In the multimanifold system, the different plastic melt streams enter the die separately and each material has its own manifold. The different melt streams combine close to the die exit to make the multilayered product (see Coextrusion).

The Extruder Drive. The screw drive is usually an electric motor that supplies the power to turn the screw. The nominal speed of the motor is typically around 1800 rpm, while a typical maximum screw speed is about 100 rpm. As a result, a speed reducer is needed between the motor and the screw. Various motors can be used for extruders. DC motors are most common up to the 1990s; nowadays, AC motors are starting to be used more frequently. Older extruders often use a DC brush motor with tachometer feed back. This yields a speed regulation of about 1% of full speed. One-percent regulation may be acceptable for some products, but it may not be good enough for high precision operations, such as medical tubing, particularly when the extruder operates at low speed. For example, if an extruder has a maximum screw speed of 100 rpm and a DC brush motor with tachometer feed back, the screw speed can vary as much as 1 rpm (see Table 2).

However, if the screw speed is reduced to 10 rpm, the screw speed can still vary as much as 1 rpm. This 1-rpm variation now represents 10%. Obviously, this

Table 2. Screw Speed Variation at Different Screw Speeds

Screw speed, rpm	Screw speed variation, rpm	Screw speed variation, %
100	1	1
10	1	10

would be too much for a high precision extruded product. Fortunately, nowadays we have drives with better speed control. For example, there are brushless DC drives with a speed regulation of about 0.01% of full speed. Drives with similar speed control are digital DC brush drives and variable frequency AC vector drives. Servo drives can achieve speed regulation that is considerably better than 0.001% of full speed.

Coupling between Motor and Gearbox. When we have a direct coupling between the motor and the gear reducer, we call this a *direct drive* (see Fig. 19). Some extruders have a belt transmission between the motor and the gear reducer; these are called *indirect drives* (see Fig. 20). Advantages of direct drives are no chance of slippage, energy efficiency, and fewer parts. The disadvantage of a direct drive is that it may be more difficult to change the reduction ratio. Advantages

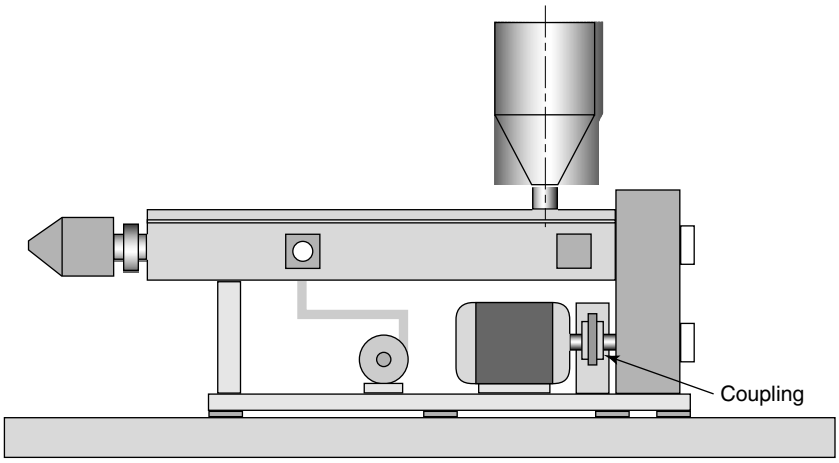

Fig. 19. Example of extruder with direct drive.

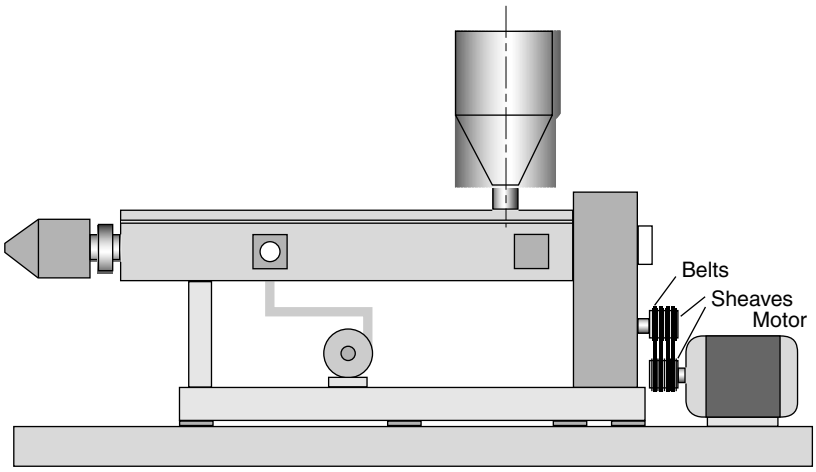

Fig. 20. Example of an extruder with indirect drive.

of indirect drives are ease of changing the reduction ratio and more freedom to position the motor. Disadvantages of indirect drives are chance of slippage, energy loss in the belts, and more parts that can wear out and fail.

Even though direct drives appear to be more attractive, many extruders are made with indirect drives. An example of an extruder with an indirect drive is shown in Figure 20.

The Speed Reducer. A speed reducer is necessary because the speed of the motor is much higher than the speed of the screw. Typical reduction ratios range from 15:1 to 20:1; they can be as low as 5:1 and as high as 40:1. The most common reducers with extruders are gear reducers using spur gears. A popular spur gear is the herringbone gear. The V-shaped tooth design practically eliminates axial loads on the gears.

Important issues with gear reducers are the reduction ratio, energy efficiency, power transmission capability, cost, and backlash of the gearbox. Backlash is basically the slop in the gears. If the screw speed is maintained at a constant value, backlash is not a big issue. However, if the screw speed is changed quickly, as is done in some advanced control schemes, then the backlash should be minimal to maintain good speed control and to avoid rapid wear of the gears.

Gear boxes can be made with a quick-change gear provision. This allows a quick and easy change of the gear ratio. A quick-change gear provision can improve the flexibility and versatility of an extruder. Changing the gear ratio on a regular gearbox is a precision job and is quite time consuming. Most gear boxes in the industry are not quick-change gear boxes.

Thrust Bearing Assembly. Thrust bearings are necessary because the extruder screw has to develop substantial pressure to overcome the flow resistance of the die. Typical diehead pressures range from 7 to 28 MPa (about 1000 to 4000 psi). The melt pressure at the end of the screw causes a thrust force on the screw, pushing it in the direction of the drive. The thrust bearings are necessary to take up the thrust load acting on the screw. A 150-mm (6-in.) extruder running at a head pressure of 35 MPa (about 5000 psi) experiences an axial thrust of about 620 kN (about 140,000 lbf). The thrust bearing assembly may be connected to the gear reducer or it may also be part of the gearbox itself.

The ability of the thrust bearings to handle the thrust load on the screw is reflected in the *B-10 life* of the thrust bearings. The B-10 life is the number of hours that 9 out of 10 identical bearings last at a certain load and speed. The B-10 life for the extruder thrust bearings is usually given at a head pressure of 35 MPa (5000 psi) and a screw speed of 100 rpm. If an extruder is operated 24 h a day, the B-10 life should be at least 100,000 h to get a useful life of more than 10 years out of the thrust bearing.

The Gear Pump. Extruders have some limitations, including the fact that high output stability is difficult to achieve. This is important in high precision extrusion operations such as fiber spinning or medical tubing extrusion. The best output variation that can be obtained in a regular extruder is about 1%. To improve the output stability, a gear pump can be added to the extruder; it is placed between the extruder and the die. The gear pump consists of two intermeshing counter-rotating gears.

Material entering the gear pump is trapped in the space between two teeth and moves forward in a circular path with the gears. At the point where the gears

start to intermesh, the plastic melt is forced out of the gears and to the discharge of the pump. The action of a gear pump is similar to that of a bucket brigade. The "buckets" are filled at one end and emptied at the other end. If each bucket has the same volume and is filled completely, precise control of the flow rate can be achieved.

The conveying of plastic melt in the gear pump is by forced conveying rather than by drag as is the case in the extruder. As a result, good output stability is easier to achieve with a gear pump than without one. Another advantage of the gear pump over the extruder is that it generates pressure more efficiently. As a result, gear pumps make sense in the following applications:

(1) high precision extrusion where the output variability must remain less than 1%
(2) operations where the extruder does not have sufficient pressure generating capability, for instance, a vented extruder that has to operate at high barrel pressure

There are some operations where the use of gear pumps can create problems. One is when a plastic containing abrasive fillers or other abrasive ingredients is extruded. This causes wears of the gear pump and reduces its pumping accuracy. Another potential problem can occur when a gear pump is used with a plastic that is susceptible to degradation. In many gear pumps, the plastic melt is used to lubricate the gears. This means that a small fraction of the plastic spends a long time in the gear pump, as much as 15 min or longer. The long residence time in the gear pump combined with the high temperatures can cause degradation.

Complete Extrusion Lines

In addition to the extruder, upstream and downstream equipment is needed to produce a useful product. The main elements of an extrusion line are resin handling system, drying system, extruder, post-shaping or calibrating device, cooling device, take-up device, and cutter or saw. The main types of extrusion lines are tubing and pipe extrusion lines, film and sheet extrusion lines, extrusion compounding lines, and profile extrusion lines. Besides these four main types there are quite a few more, such as fiber spinning lines, extrusion blow molding machines, and integrated sheet and thermoforming lines.

Tubing and Pipe Extrusion Lines. Dies for tubing and pipe were discussed earlier. Small diameter tubing (less than 10 mm) is usually made with a free extrusion process; this is a process without a sizing or calibrating unit. Large diameter tubing and pipe is made with a sizing device just downstream of the die. The purpose of the sizer or calibrator is to solidify the plastic to a thickness sufficient to transfer the stresses acting on the product while maintaining the desired shape and dimensions. The main components of a typical tubing extrusion line are shown in Figure 21.

This line does not use a sizing unit and thus, would be used for small diameter tubing. The gear pump may or may not be used depending on the precision

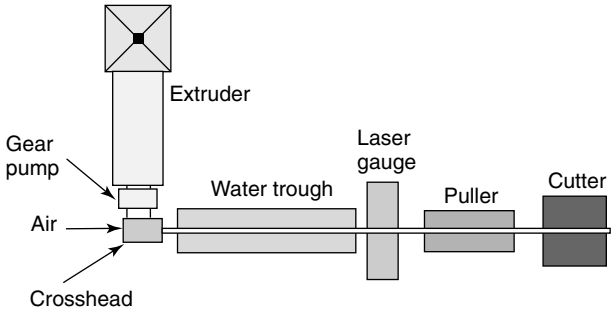

Fig. 21. Components of a typical tubing extrusion line.

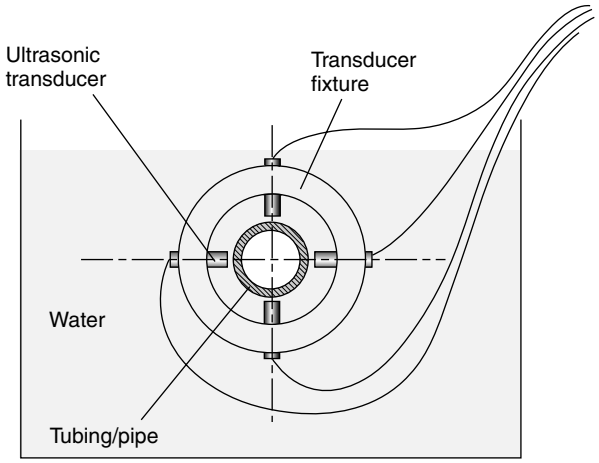

Fig. 22. Ultrasonic wall thickness gauge.

required in the extrusion process. The internal air pressure of the tubing is controlled to achieve the correct values for the outside diameter and wall thickness. The diameter is often measured with a laser gauge to allow close monitoring and control. The diameter and the wall thickness are primarily determined by the extruder output, the puller speed, and the internal air pressure. Closed loop control systems are available that automatically set the appropriate screw or gear pump speed, the puller speed, and internal air pressure. After the puller, the tubing may be cut or reeled up on a spool. In some lines, the wall thickness is measured directly; this can be done with ultrasonic sensors positioned around the circumference of the tubing or pipe as shown in Figure 22.

Film and Sheet Lines Using the Roll Stack Process. There are no significant differences between the extrusion of flat film and sheet. The main components of a sheet line are the extruder, the roll stack, the cooling section, the nip roll section, and the winder (see Fig. 23). The roll stack contains three rolls that are often referred to as polishing rolls. They are used to exert pressure on the sheet and to impart the surface conditions of the rolls to the plastic sheet. If a smooth surface is required, smooth rolls are used. If a textured surface is needed,

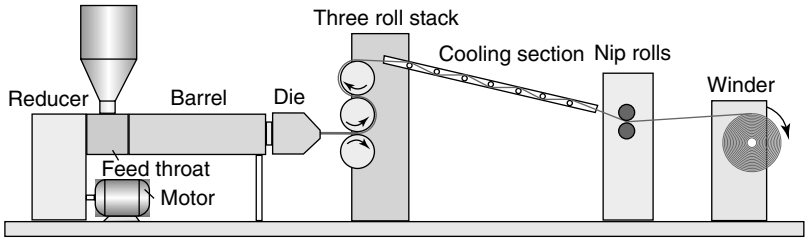

Fig. 23. Components of a sheet or flat film extrusion line.

a textured surface is used on the roll. The roll texture is the negative of the texture required on the sheet. It is possible to produce a sheet with one textured surface and the other smooth by using a smooth and textured roll next to each other.

Figure 23 shows the plastic sheet going up along the center roll and making an S-wrap around the center roll and top roll; this is called "upstack" operation. Sheet lines can also run in the "downstack" mode, where the material makes an S-wrap around the center roll and bottom roll. The rolls do not have to be in the vertical position; they can be in a horizontal position or any angle between vertical and horizontal. In fact, in some roll stacks, the angle is adjustable.

The rolls are normally cored so that the temperature of the rolls can be controlled. This is usually done with circulating hot oil. It should be possible to adjust the temperature of each roll separately. The cooling section consists of a number of rolls positioned in a frame; the sheet runs over and under the rolls to keep the sheet flat. At the end of the cooling section are the pull rolls or nip rolls; these are rubber rolls that pull the sheet from the roll stack to maintain a certain tension in the sheet. After the nip rolls, the sheet is led to the winder that rolls the sheet on a core. Many different winders are available; some winders automatically transfer the sheet to a new core when one package is full.

Film Lines Using Chill Roll Casting. Thin films are often cast on a chill roll rather than extruded into a roll stack. The main components of a cast film line are the extruder, the film die, the chill roll unit, the thickness gauging system, the surface treatment unit, and the winder.

The film is extruded downward onto the chill roll. The initial contact between the film and the chill roll is established by the use of an air knife. The air knife produces a thin stream of high velocity air across the width of the chill roll, and the air stream pushes the film against the roll surface, as shown in Figure 24.

From the chill roll unit the film is led to a thickness-gauging unit where the thickness of the sheet is measured across the width of the film. Most thickness gauges for film and sheet have a scanning measuring head that traverses across the film back and forth to measure thickness both along the length and across the width of the film.

After the thickness-gauging unit, the film passes through a surface treatment unit. Such a unit is incorporated if surface treatment of the film is required. This is usually done to improve adhesion, for instance, for a subsequent printing or laminating operation. The most important adhesion promoters are flame treatment, corona-discharge treatment, ozone treatment, and primers. From the

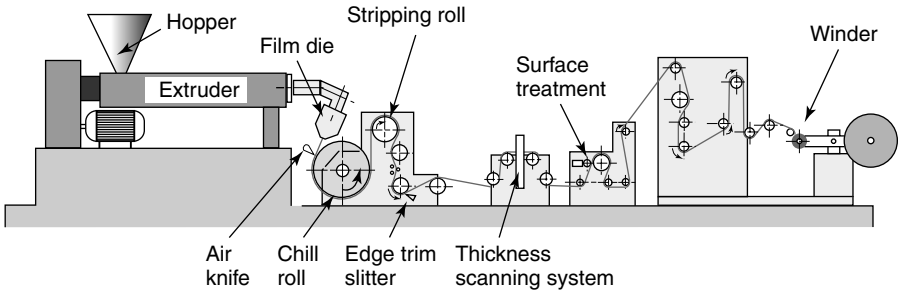

Fig. 24. Components of a cast film extrusion line

treatment unit, the film is led to the winder unit. Just as with sheet extrusion, many different types of winders are available.

Combination of Materials. The requirements of many products, particularly in packaging applications, are such that a single plastic cannot meet all of them. To meet the requirements, often two or more materials have to be combined. There are a number of techniques to combine different materials; some of the more important ones are coextrusion, coating, and lamination.

Coextrusion. *Coextrusion* is a commonly used technique to combine two or more plastics passing through a single extrusion die. There are two major coextrusion techniques: the feed block system and the multimanifold system. In the feed block system the different plastics are combined in the feed block module (see Fig. 18) and then enter into a regular extrusion die with a single inlet, manifold, and outlet.

The advantage of the feed block system is that it is simple, inexpensive, and allows many layers to be combined. The main drawback is that the flow properties of the different plastics have to be quite close to avoid interface distortion. This limits the choice of materials that can be combined through feed block coextrusion.

In the multimanifold system each plastic has its own entrance and manifold in the coextrusion die. The different melt streams are combined just before they exit the die, so that minimum interface distortion can occur. The advantage of the multimanifold system is that plastics with widely different flow properties can be combined. As a result, there is a wide choice of materials that can be combined through this extrusion technique. The disadvantage is that the design of the die is more complicated and therefore more expensive.

Figure 25 shows a multimanifold sheet or film die. This die has two inlets, two manifolds, and a single outlet. The flow of the upper layer can be adjusted by flexing the choker bar, using the adjustment nuts. The two plastics combine at the entrance to the land region; this is the last parallel section of the die flow channel. The flow in the land region can be adjusted with the flex lip adjustment bolts. These bolts are located along the width of the die exit with a spacing of about 25–40 mm (1.0–1.5 in.) and allow local adjustment of the die gap. Some newer sheet and film dies have a flexible membrane to allow adjustment of the flow. Many multimanifold dies are possible, including flat film and sheet dies, tubing and pipe dies, blown film dies, and profile dies.

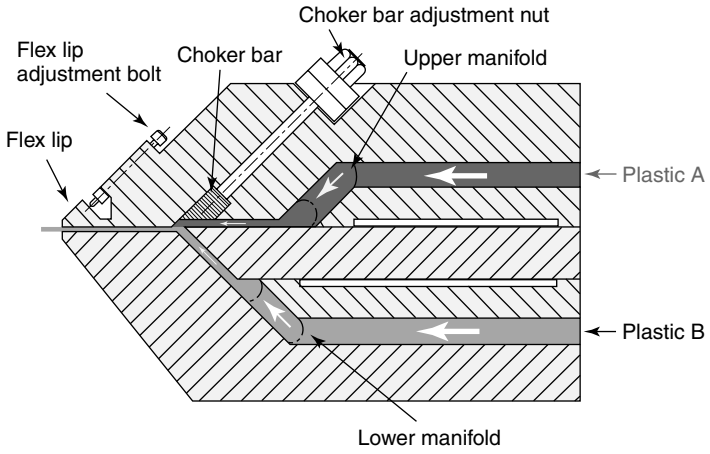

Fig. 25. Example of a multimanifold sheet die.

Extrusion Coating. In extrusion coating, a molten layer of plastic film is combined with a moving solid web or substrate. The substrate can be paper, paperboard, foil, plastic film, or fabric; the substrate can also be a multilayer product. A schematic of an extrusion coating operation is shown in Figure 26.

Extrusion Lamination. Extrusion lamination involves two or more substrates, such as paper and aluminum foil, combined by using a plastic film as the adhesive between the two substrates (see Fig. 27). The webs may be preheated or surface treated to improve bonding with the plastic film.

The extruded sheet or film can be laminated with a film on one side or both sides. The laminate can be paper, foil, mesh, or a number of other materials. With lamination many different structures of sheet or film products can be made. The laminate is unrolled from a payoff, combined with the film, and

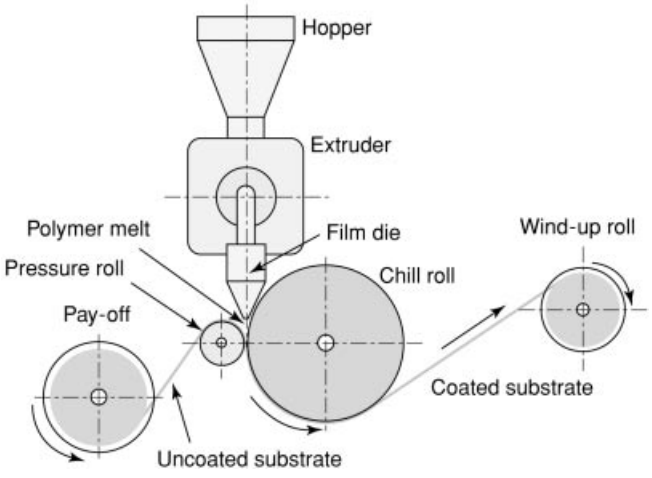

Fig. 26. Schematic of extrusion coating operation.

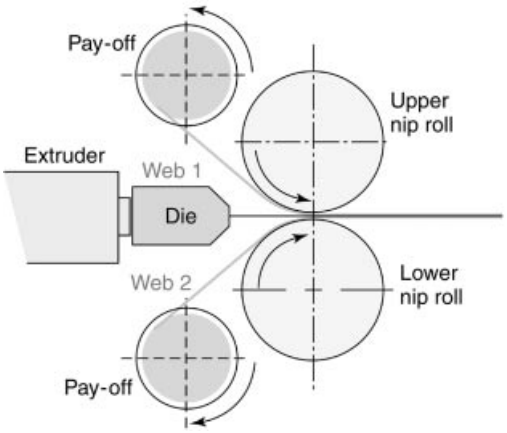

Fig. 27. Schematic of extrusion lamination.

immediately led into a set of nip rolls. After lamination, the film is handled as a regular film.

Blown Film Lines. A blown film line is quite different from a flat film line. In a blown film line, a tubular film is extruded vertically upwards as shown in Figure 28. Air is introduced to the inside of the tube; as a result, the tube expands to a bubble with a diameter larger than the diameter of the die. The ratio of the bubble diameter to the die diameter is called the *blow-up ratio*. Typical blow-up ratios used in LDPE film extrusion for packaging are in the range of 2.0–2.5:1.

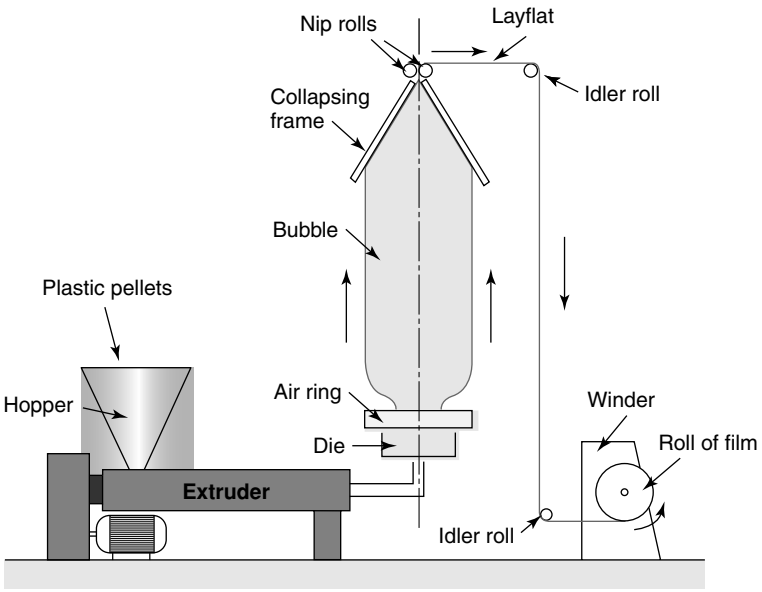

Fig. 28. Schematic of blown film line.

When the bubble has cooled sufficiently, it is flattened in a collapsing frame and pulled through a set of nip rolls to its top. From there, the layflat film is guided over several idler rollers to the winder where it is rolled up over a core.

One advantage of the blown film process is that it can produce not only tubular products (bags) but also flat film, simply by slitting open the tube. In some blown film processes the plastic is extruded downwards to produce films with special properties.

Extrusion Compounding Lines. Compounding lines come in many shapes and sizes. Compounding can be done on single screw extruders, twin screw extruders, reciprocating single screw compounders, batch internal mixers, and continuous internal mixers. The configuration of the line is determined, among other things, by the ingredients to be combined in the compounding extruder. The downstream equipment typically consists of a pelletizing system (see Fig. 29). The polymeric components are usually added through the first feed port. Fillers are often added to a downstream feed port at a point where the plastic has melted already; this arrangement reduces wear on the extruder that might be caused by the filler. High levels of filler are often added by a twin screw stuffer, particularly when the filler has a low bulk density. With high levels of filler, there is often a substantial amount of entrained air; this is removed through the vent port. The vent port is often connected to a vacuum pump; a high level of vacuum improves the removal of volatiles from the plastic.

Some pelletizers cut extruded strands cooled in a water bath; these are called strand pelletizers. Dicers cut extruded sheet rather than strands. The pellets from a dicer have a uniform cubic or octahedral shape. Other pelletizers cut the material right at the die exit; these are called die face pelletizers. These cutting systems can be dry die face pelletizers, water ring pelletizers, and under water pelletizers.

In dry die face pelletizers, the molten plastic is cut at the die face. The pellets are hurled away from the die face by the rapid motion of the cutter knives usually into a water slurry. In water ring pelletizers, the centrifugal action of the cutter hurls the pellets into a snail's cage of water whirling around the perimeter of the cutter housing. The slurry flows to a centrifugal dryer. In underwater pelletizers, the molten plastic is extruded directly into water and cut immediately by a multiple knife cutter. The die may need special heating capability to avoid die plate freeze-off. The start-up procedure for underwater pelletizers often requires careful sequencing of plastic flow, cutter rotation, and inlet water flow rate to avoid die freeze-off or agglomeration.

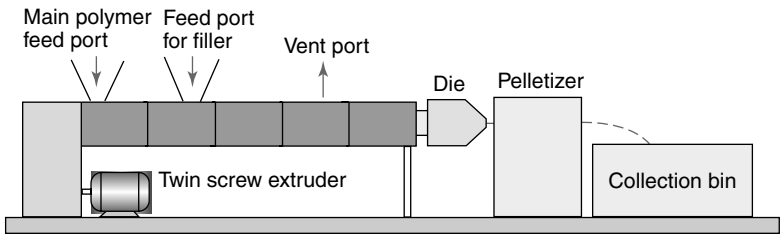

Fig. 29. Typical extrusion compounding line.

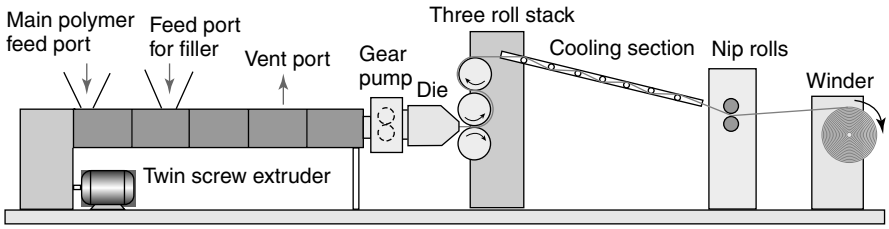

Fig. 30. Extrusion compounding line with in-line shaping.

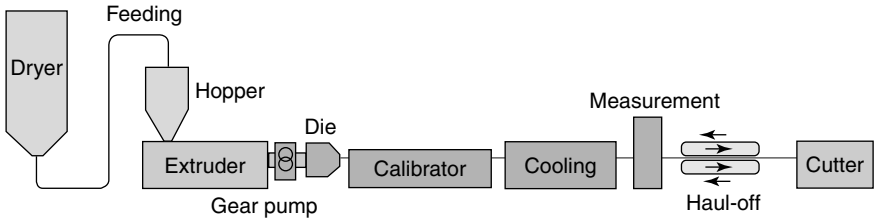

Fig. 31. Components of a profile extrusion line.

Compounding extruders can also be combined with direct forming systems downstream. In many cases, a gear pump is placed at the discharge end of the extruder to generate the diehead pressure and to control the throughput. An example of a combination compounding/sheet extrusion line is shown in Figure 30.

The plastic is introduced to the first feed port of the compounding extruder, the filler is introduced to the second feed port, and the volatiles and air entrapment are removed from the vent port. A gear pump is placed between the compounding extruder and the sheet die. The sheet is fed to a roll stack and from there it is handled as in a normal sheet line, as discussed earlier.

Profile Extrusion Lines. Many extrusion lines are used for the production of profiles. Profile lines also come in many shapes and forms. A typical extrusion line consists of an extruder, a die, a calibrating unit, a cooling unit, a measurement device, a haul-off, and a coiler or cutter or saw (see Fig. 31). A gear pump may be used if the dimensional tolerance of the extruded product is quite small. On some profile lines a film or foil is laminated to the extruded profile. Extruded profiles have an enormous range of shapes and sizes.

Extrusion Tasks: Inner Workings of an Extruder

In a plasticating extruder, a number of tasks are performed that are each critical to the proper functioning of the extruder. These tasks or functions are solids conveying, melting or plasticating, mixing, melt conveying, degassing, and shaping or forming.

Degassing is not done on all extruders; some extruders are equipped with a vent port. The vent port allows volatiles or gasses to escape from the plastic melt. Degassing is also referred to as devolatilization. The functions listed above are

interdependent. For instance, a change in the forming region affects the other functions. The forming region is the extrusion die. So, if the die temperature in lowered, this affects melt conveying, melting, mixing, solids conveying, and degassing if a vented extruder is being used.

To understand how an extruder works, it is important to know what happens in the different functional zones in an extruder. The starting and end points of each functional zone depend on the machine geometry, the plastic properties, and the operating conditions. For instance, melting starts where the plastic temperature first exceeds the melting point. This point can shift when barrel temperatures or screw speed are changed.

On the other hand, the geometrical sections of the screw are fixed by the screw geometry. The feed section is the first deep flighted section of the screw and this is where solids conveying occurs. However, the solids conveying zone may end before or after the end of the feed section. The same is true for the melting in the transition section of the screw and the melt conveying in the metering section of the screw. The boundaries of the screw sections are fixed, but the boundaries of the functional zones can shift with plastic properties and operating conditions.

Solids Conveying

Solids conveying occurs both in the feed hopper and along the first several diameters of the screw. The solids conveying in the feed hopper results from the weight of the material. The conveying mechanism at work in the hopper is called *gravity induced conveying*. The material flows down the feed hopper into the feed throat and from there, into the screw channel. The conveying along the screw results from frictional forces acting on the plastic. This conveying mechanism is called *drag induced conveying*, and is the mechanism in the solids conveying zone, the melting zone, and melt conveying zone.

Gravity Induced Conveying. The flow in the feed hopper can be quite complicated. A number of things can go wrong in this section of the machine. For instance, if the bulk material consists of small and large particles, the small particles can separate from the larger particles, causing nonuniform flow from the hopper. This, in turn, causes instabilities in the extruder resulting in output variation.

Some bulk materials are very difficult to handle; for instance, post consumer reclaim (PCR) usually has a wide particle size distribution and a low bulk density. As a result, special extruders have been developed to handle this bulk material efficiently. These machines can have larger diameters in the feed section than in the metering section; they may also use crammer feeders to achieve steady flow of material into the extruder. In some cases, a grooved feed section is used to improve the feeding of low bulk density material.

Important bulk properties are bulk density, compressibility, internal coefficient of friction, external coefficient of friction, particle size and particle size distribution, and particle shape and particle shape distribution.

The bulk density is the density of the material, including the air voids between the particles. The density of a material is the mass per unit volume. The bulk density of pelletized material is usually around 60% of the regular density.

If the bulk density is less than about 30% of the actual density, conveying the bulk solid can become quite problematic and special design features may be necessary to ensure consistent flow. The compressibility is the change in bulk density when pressure is applied. A high compressibility indicates a bulk material that compacts readily under pressure. Highly compressible materials are difficult to handle and susceptible to various flow problems in feed hoppers.

The *internal coefficient of friction* is the friction between the plastic particles themselves. The *external coefficient of friction* is the friction between the plastic particles and another surface, such as the barrel surface. For efficient conveying in the feed hopper, it is required that both the internal and external frictions should be low. For efficient conveying along the extruder screw, it is required that the barrel friction to be high and the screw friction should be low; this is discussed later.

The design of the feed hopper can have a strong effect on the flow in the hopper. This is particularly true for difficult bulk flow materials. Stagnation should be avoided in the flow through the hopper. As a result, a circular hopper is better than a hopper with a square or rectangular cross section (see under The Feed Hopper). Also, the converging region of the hopper should expose the material to a gradual compression; otherwise, unstable flow results. If the compression of the material is too rapid, the flow may stop altogether. This can happen when the bulk material is susceptible to *bridging*. This is a condition where a natural bridge is formed in the material strong enough to support the material above it. When bridging occurs, the flow can stop completely.

Various devices can be used in the feed hopper to promote steady flow. Sometimes stirrers are used to gently mix the material. The stirrer may be equipped with a blade to wipe the material off the hopper wall. This can be beneficial if the material has a tendency to stick to the wall. When the material is susceptible to bridging, vibrating pads may placed against the hopper to create a vibrating action to dislodge any bridges that could form. When the bulk material is very difficult to handle, a crammer feeder may be used. This is a conveying screw placed in the hopper that forces the material to the discharge by the rotation of the screw (see under The Feed Hopper).

A special feed hopper design to minimize flow problems was developed by Johanson (1). The geometry of this hopper transitions from a circular cross section to an oval cross section and back to a circular cross section; it is called the diamondback hopper (see Fig. 32).

The solids conveying into the extruder is also affected by the design of the feed opening. For difficult bulk flow materials, it has been found that an elongated feed opening improves feeding (see also under The Feed Housing). Also, feeding can be improved by offsetting the opening in the direction of the movement of the screw flight in the top position, as shown in the figure. By offsetting the feed opening, a more or less tangential feed opening is created that increases the action of the screw flight in pushing the feed material into the extruder barrel.

Drag Induced Conveying. Once the bulk material drops into the screw channel, it starts moving along its length as a result of frictional forces acting on the plastic. To understand conveying in screw extruders, it is important to know which frictional force is responsible for the forward movement of material and which force is holding the material back. Since the material moves forward as a

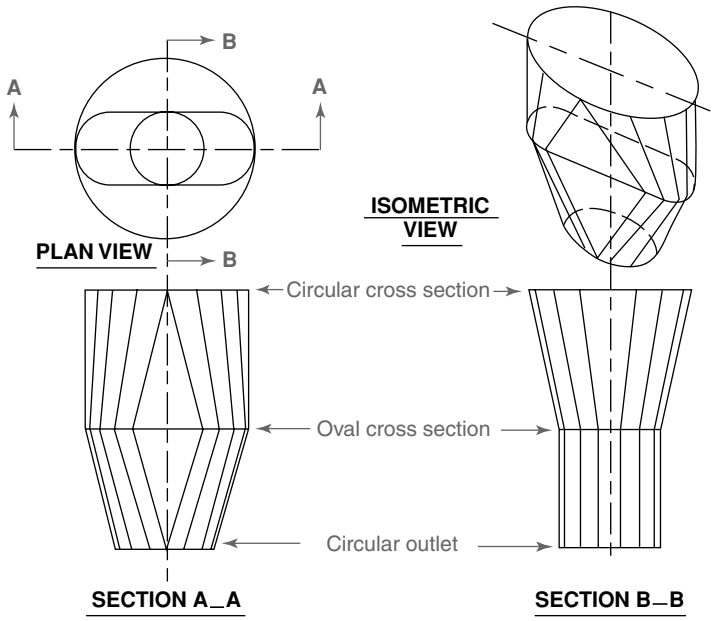

Fig. 32. The diamondback feed hopper (U.S. Pat. 4958741).

result of the rotation of the screw, it would seem that the friction between the plastic and the screw moves the material forward.

Even though this seems like a plausible argument, this is not what really happens. It is the frictional force at the barrel that is responsible for moving the material forward. To understand this, consider an extruder with a barrel coated with a zero friction material. In this case, the material drops down into the screw channel and, once in there, only moves with the screw, around and around. Without friction at the barrel, there is no forward movement of the material.

Another analogy is a rotating threaded shaft with a nut on the shaft that is free to rotate with the shaft. In this situation, the nut stays in the same position on the shaft rotating with the shaft, but not moving forward. If the nut is kept from rotating with the shaft, the nut starts to move along the length of the shaft. If the extruder screw is considered as being the threaded shaft and the plastic as being the nut on the shaft, then it becomes clear why the friction at the barrel is responsible for moving the material forward (see Fig. 33). In fact, barrel friction is a necessary condition for forward transport. If there is no barrel friction, then there can be *no* forward conveying.

Starve Feeding. Starve feeding is a method of feeding the extruder where the plastic is metered directly into the extruder at a rate below the flood feed rate. This means that the plastic drops directly into the screw channel without any buildup of plastic in the feed hopper. With starve feeding, the screw channel is partially empty in the first few diameters of the extruder. Thus, if one looks into the feed opening, one should be able to see the screw flight and part of the root of the screw.

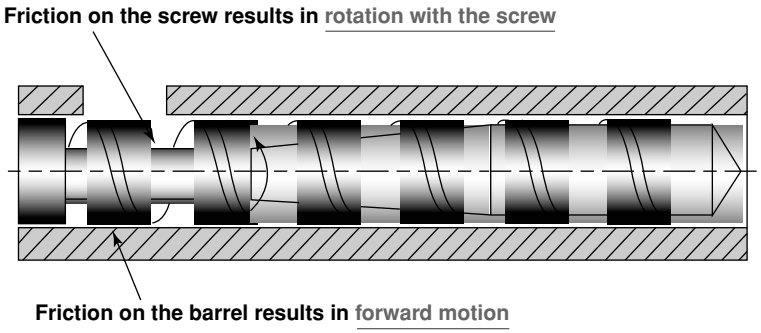

Fig. 33. Driving force and retarding force in conveying along the extruder screw.

When the screw channel is partially filled, there is no pressure development in the plastic. Without pressure development, there is very little frictional heating and mixing. In effect, starve feeding reduces the effective length of the extruder. Thus, a 25 *L*/*D* extruder might have an effective length of only 21*D* with the first four diameters partially filled with material. Starve feeding may be beneficial if the extruder is longer than necessary for the plastic being processed. However, if the length of the extruder is marginal, starve feeding most likely results in poor extruder performance.

Starve feeding is commonly used on high speed twin screw extruders; in fact, most high speed twin screw extruders run starved. Starve feeding is less commonly used with single screw extruders, because it is beneficial only in some cases. Starve feeding can be useful to reduce the motor load of the extruder, to reduce the temperature buildup in the plastic melt, and to add several ingredients simultaneously through one feed port using several feeders.

In mixing and compounding starve feeding can be very useful because it reduces the chance of agglomeration of the filler. As a result, mixing and compounding operations frequently use starve fed extruders. A number of workers have reported dramatic improvement in dispersive mixing when comparing flood fed to starve fed extruders.

Grooved Feed Extruders. The driving force for the conveying process is the frictional force at the barrel surface, as discussed earlier. The frictional force can be affected by adjusting the barrel temperature in the first one or two temperature zones. However, the effect of barrel temperature is usually small. Another method of increasing barrel friction is to machine grooves into the barrel surface; this has a strong effect on the feeding characteristics of the extruder. The grooves typically run in the axial direction, with a length of several screw diameters. The barrel around the grooved section has to be cooled to avoid plastic from melting in the grooved section; the plastic can degrade if melt collects in the grooves.

A relatively new development is the adjustable grooved feed extruder (AGFE). This extruder has a grooved feed section with a mechanism that allows adjustment of the groove depth (2). This makes it possible to adjust the solids conveying efficiency to match the characteristics of the plastic and the screw geometry. The adjustment to the grooves can be made while the extruder is running.

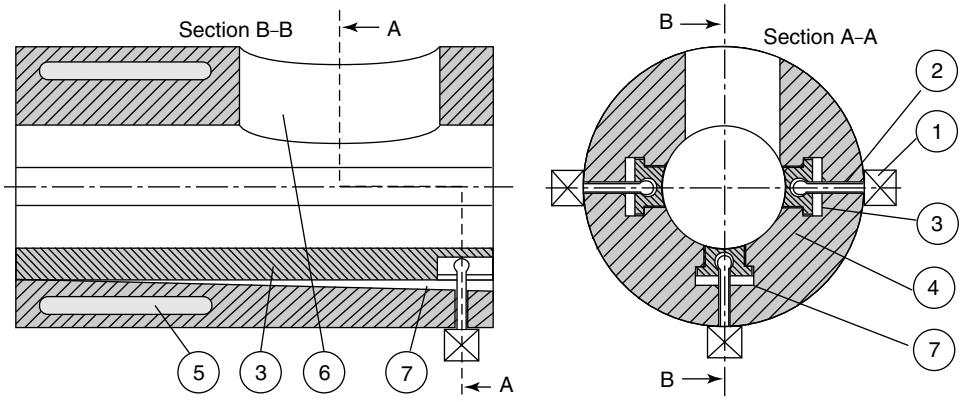

Fig. 34. Grooved feed section with adjustable groove depth.

As a result, it is possible to set the groove depth to achieve the minimum pressure fluctuation at the discharge end of the extruder. The AGFE allows a level of control and versatility not possible with conventional extruders. Figure 34 shows a schematic representation of the AGFE with the grooves shown in the zero depth position. Actuators can pull the keys into the housing to increase the groove depth. This allows continuous adjustment of the grooved depth between zero and maximum depth.

There are a number of advantages associated with grooved feed extruders, including

(1) The output of grooved feed extruders is less dependent on discharge pressure (see Fig. 35); as a result, the stability of the extrusion process tends to improve.
(2) The output of grooved feed extruders tends to be higher than that of smooth bore extruders.
(3) Grooved feed extruders allow extrusion of some very high molecular weight plastics, such as very high molecular weight PE. These materials cannot be processed on conventional smooth bore extruders.

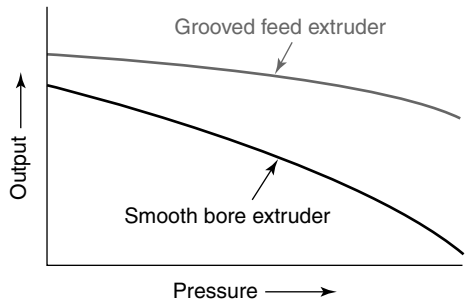

Fig. 35. Output vs discharge pressure for grooved feed vs smooth bore extruder.

With the conventional grooved feed extruder there are some disadvantages as well, such as

(1) The grooved barrel section has to be cooled well enough to avoid premature melting of the plastic in the grooves; this reduces energy efficiency and adds to the complexity of the extruder.
(2) The stresses that occur in the grooved region can be quite high, making the grooves susceptible to wear. The grooves have to be made out of a wear-resistant material to avoid high rates of wear.
(3) The pressures that occur in the grooved section can be quite high, in the range of 70–140 MPa (10,000–20,000 psi). The barrel has to be designed to withstand these high pressures.
(4) The screw design rules for grooved feed extruders are quite different from the rules for smooth bore extruders. Thus, grooved feed extruders require special screw designs. The use of conventional screw designs in grooved feed extruder can lead to a number of problems, such as overheating of the plastic and screw wear.
(5) With a grooved barrel section, the motor load increases and with it, the torsional load on the extruder screw.

It should be remembered that conveying can be improved not only by increasing the barrel friction, but also by reducing the by screw friction. This can be done by screw design, by screw temperature, and by the screw material. Screw design features that reduce screw friction are single flighted geometry (avoid multiple flights), large flight flank radius, and large helix angle. These features are illustrated in Figure 36.

Reducing screw friction can often be achieved by internal screw heating. This can be done by coring the screw and circulating a heat transfer fluid inside the screw, usually oil. Another method of heating the screw is to put a cartridge

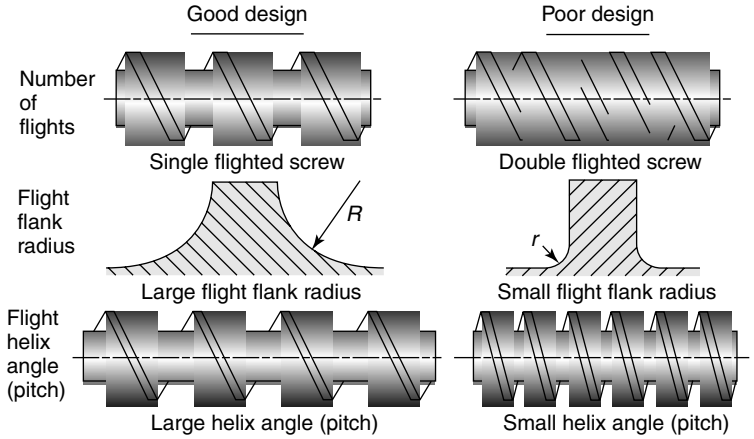

Fig. 36. Measures to reduce screw friction by screw design.

heater inside the screw. Power to the heater can be supplied through a slip-ring assembly at the shank of the screw. Finally, the surface friction of the screw can be reduced by applying a coating to the screw or a surface treatment. The following coatings and surface treatments have been used PTFE impregnated nickel plating, PTFE/chrome plating, titanium nitride, boron nitride, tungsten disulfide (WS2), and catalytic surface conversion (eg J-Tex). The advantage of a low friction coating extends beyond improved conveying along the screw. It reduces the tendency of the plastic to hang up or build up on the screw surface and makes it easier to clean the screw. These coatings can also be used for extrusion dies, particularly the inside surfaces of the die channel in contact with the plastic melt. The advantages here are reduced pressure drop in the die, improved surface quality of the extruded product, and reduced tendency of material to build up at the die exit. The last problem is often referred to as *die drool* or *beard formation*.

Melting

Melting in the extruder starts when the plastic temperature reaches the melting point. There are two types of melting that occur in screw extruders.

Contiguous Solids Melting. In the first type of melting, the solid particles are compacted and form a solid plug that spirals along the length of the screw channel. Between the solid bed and the barrel a thin melt film is located. Most of the melting occurs at the interface between the solid bed and the melt film. The newly melted material collects in the melt film, but is dragged away to the melt pool that is pushed against the active flight flank (see Fig. 37). This type of melting is called contiguous solids melting (CSM) and is most often observed in single screw extruders.

Dispersed Solids Melting. In the second type of melting, the solid particles are dispersed in a melt matrix (see Fig. 38). The solid particles decrease in size until they have melted completely. This type of melting is called dispersed solids melting (DSM) and is observed in high-speed twin screw extruders and reciprocating single screw compounding extruders. The melting in DSM is substantially more efficient than in CSM. The axial length from the start to end of melting in

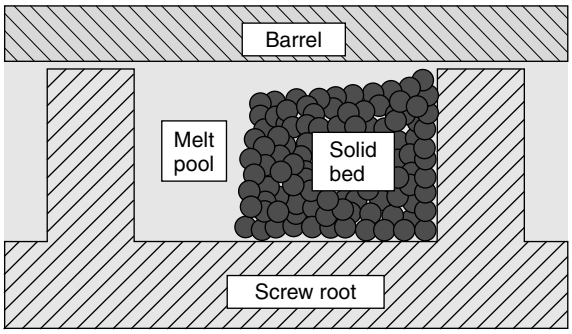

Fig. 37. Contiguous solids melting in single screw extruders.

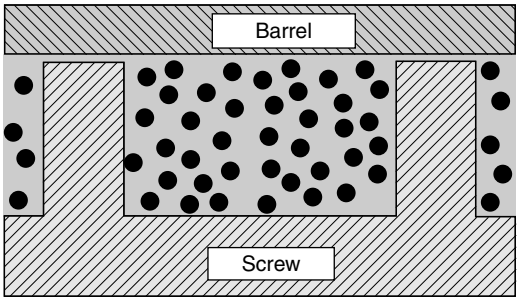

Fig. 38. Dispersed solids melting in single screw extruders.

twin screw extruders is usually about 1–2 screw diameters. On the other hand, in single screw extruders, the melting length is usually 10–15 diameters.

This is an important difference between single and twin screw extruders. In single screw extruders the solids conveying and melting zones extend about 15–20 diameters. This means in a 25 *L*/*D* extruder, there is not much length left for melt conveying, mixing, and degassing. In fact, if degassing is to be done, the extruder length is generally increased to 30–35 diameters. In a twin screw extruder, the solids conveying and melting zones may extend only 5–6 screw diameters. If the twin screw extruder is 30*D* long, it means that most of the length of the extruder is still available to do mixing, degassing, chemical reactions, etc. This makes the twin screw extruder a more versatile machine than the single screw extruder. As a result, the twin screw extruder is often the machine of choice for demanding processing tasks.

The theory of CSM melting was developed by Tadmor (3) in the early 1960s. The theory of DSM was not developed until much later (4). From the quantitative description of the CSM melting, we can determine how plastic properties, processing conditions, and screw geometry affect melting. There are two important sources of heat in the melting process. One is the heat from the barrel heaters conducted through the barrel, then through the melt film into the solid bed. The other source of heat is the viscous heating in the melt film. The amount of viscous heating is determined by the viscosity of the material and the shear rate in the melt film.

The melting mechanism in contiguous solids metting is called *drag induced melt removal*. This refers to the action in the melt film. The melted material added to the melt film is dragged away to the melt pool by the rotation of the screw. As a result, the melt film can remain thin, which is critical to maintaining a high melting rate. If the newly melted material is not dragged away, the melt film thickness will increase as melting progresses and the melting efficiency will drop off rapidly. This is why single screw extruders melt much more efficiently than ram extruders and this is why larger injection molding machines use screw extruders rather than ram extruders.

From this description of melting it is clear that the thickness of the melt film is an important parameter in the melting process. A thin melt film is important in maintaining high melting efficiency. With a thin melt film, there is high viscous

heat generation in the melt film and the barrel heat has to travel only a short distance through the melt film to reach the solid bed. The initial melt film thickness is primarily determined by the flight clearance. The larger the flight clearance, the thicker the melt film. As a result, to achieve efficient melting, it is important to keep the flight clearance small. A worn screw or barrel results in a large flight clearance, and this generally has a negative effect on melting and therefore on the overall extruder performance.

Clearly, when we increase the barrel temperature, more heat is available from the barrel heaters to melt the plastic. On the other hand, a higher barrel temperature increases the melt temperature in the melt film. This, in turn, reduces the viscosity of the melt film and the viscous heat generation. Therefore, a higher barrel temperature increases the barrel heat, but reduces viscous heat generation. If the reduction in viscous heat generation is larger than the increase in barrel heat, then the net effect is a reduction in the melting rate. This may seem somewhat counter intuitive; however, this is certainly possible when one considers that at high screw speeds, most of the heat introduced to the plastic is by viscous heating.

The helix angle of the screw flight can have a considerable effect on the melting efficiency, as shown in Figure 39. We see that the axial length required to complete melting decreases when the helix angle increases. It is interesting to see that the highest melting efficiency occurs at a helix angle of 90°. Such a helix angle may be good for melting, but it certainly would not be good for efficient conveying. Remember that a 90° helix angle means that the screw flight is parallel to the axis of the screw. Clearly, the forward conveying capability of the screw is zero when the helix angle is 90°. To achieve both good conveying and good melting we should select a helix angle that gives us not only good melting but also good conveying. Usually a helix angle in the range of 20–30° satisfies both demands.

The use of multiple flights can also improve melting, as shown in Figure 39, because the average melt film is thinner than in a single flighted screw (see Fig. 40). A drawback of multiple flights is that it reduces solids conveying and melt conveying. So, a double flighted screw may improve melting, but at the same time may cause problem in solids conveying and melt conveying. As a result,

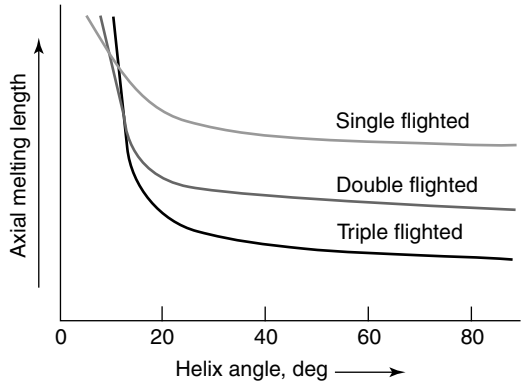

Fig. 39. The effect of the number of flights on the melting length.

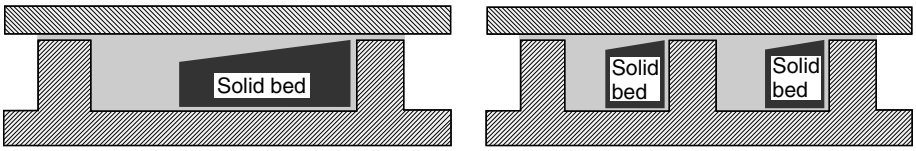

Fig. 40. Melting in a single flighted screw (left) and double flighted screw (right).

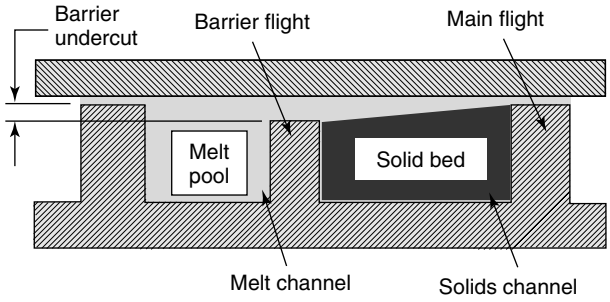

Fig. 41. Cross section of a barrier screw.

a multiflighted screw makes sense if the extrusion is clearly limited by melting capacity.

It is also important to realize that the advantage of a multiflighted screw to melting does not apply to a barrier screw. A barrier screw has two flights: a main flight and a barrier flight. The purpose of the main flight is to separate the solid material from the melted material (see Fig. 41). Thus, the barrier flight effectively separates the solid bed from the melt pool. Because the barrier screw has only one solid bed, its melting capability is about the same as a single flighted screw without a barrier flight.

One variable that affects the melting in an extruder is the temperature at which the plastic is introduced to the extruder. By preheating the plastic in the feed hopper or before, the amount of heat that has to be added to melt the plastic in the extruder is reduced and as a result, melting occurs earlier in the extruder. When it is suspected that an extrusion problem is related to melting, preheating is a method of diagnosing the problem.

The barrier screw has the following advantages:

(1) The barrier screw achieves more stable extrusion than a simple conveying screw.
(2) With a barrier screw, there is virtually no chance of unmelted material beyond the barrier section. However, this is not true for all barrier screw designs.
(3) There is a certain amount of dispersive mixing that occurs as the plastic melt flow over the barrier flight into the melt channel.

Next to these advantages, there are the following disadvantages:

(1) Barrier screws are no better in performance than nonbarrier screws designed with mixing sections.
(2) Barrier screws are more expensive than nonbarrier screws, particularly when purchased from an original equipment manufacturer (OEM).
(3) Because the solid material is restricted to the solids channel, the barrier screw is inherently more susceptible to plugging. This occurs when melting cannot keep up with the reduction in the size of the channel in the compression section of the screw, resulting in the solid material getting stuck in the screw channel. This creates a momentary obstruction to flow and leads to surging. Surging is a variation in extruder output.

Melt Conveying

Melt conveying starts when the melting is completed in the extruder. Strictly speaking, melt conveying starts when melting starts, because it is the melting zone where both solids conveying and melt conveying take place, with the amount of solid material gradually decreasing and, at the same time, the amount of melted material gradually increasing. However, the *melt conveying zone* is defined as the region where all the plastic is completely melted.

The mechanism of melt conveying is viscous drag. In other words, the viscous forces acting on the plastic melt are responsible for the forward conveying of the melt. In the melt conveying zone, the viscous force at the barrel is responsible for forward conveying, while the viscous force at the screw is a retarding force. As a result, melt conveying is improved by reducing the barrel temperature and increasing the screw temperature. Interestingly, screw heating in the melt conveying zone makes more sense than barrel heating. Internal screw heating is not used much in the extrusion industry; the obvious reason is that barrel heating is much easier than internal screw heating.

The optimum screw geometry for melt conveying can be determined from extrusion theory. The optimum helix angle is dependent only on the degree of non-Newtonian behavior of the plastic melt; it can be determined from the following expression:

$$\text{optimumhelixangle[degrees]} = 13.5 + 16.5(\text{powerlawindex})(1) \qquad (1)$$

The optimum helix angle for melt conveying decreases as the power law index decreases; in other words, when the plastic is more shear thinning. A similar expression can be derived for the optimum depth of the channel in the melt conveying zone. The optimum depth depends on the viscosity, the pressure gradient, and the power law index. When the plastic becomes more shear thinning, the channel depth should be reduced to maintain good melt conveying.

Melt Temperatures. Because of the low thermal conductivity of the plastic melts, the temperatures in the melt conveying zone can vary substantially. Local temperatures are difficult to measure because it hard to put a probe in the

screw channel while the screw is rotating. Melt temperatures can be predicted from extrusion theory using numerical techniques. A popular technique for this purpose is finite element analysis (FEA). With this technique the flow patterns and temperature distribution can be predicted.

In Figure 42 we show the temperature distribution in the screw channel by looking at a cross section of the screw channel. The temperatures are shown in colors; different colors represent different temperatures, just like the weather map on the back page of USA Today. The temperature scale is shown on the right-hand side of the figure. The lower surface of the picture is the root of the screw; the upper surface is the extruder barrel. The barrel is maintained at 175°C and the screw surface is considered insulated (adiabatic). It can be seen in the figure that the highest melt temperatures occur in the mid-region of the channel, while the outside region of the channel remains at a lower temperature.

The reason for this temperature distribution is the way the plastic melt flows along the screw channel. This flow can be illustrated by unrolling the screw channel and by looking it as a straight trough see Fig. 43 and the barrel as a flat plate.

If the flow is viewed relative to the screw, then the barrel moves in tangential direction, v_b, making an angle ϕ with the channel. Angle ϕ is the helix angle of the screw flight. A fluid element close to the barrel surface flows in the direction of the channel until it gets to the pushing side of the flight. At this point, the element moves downward and then crosses the screw channel. When the element gets to the trailing side of the flight, the element moves up again close to the barrel surface and the element starts moving in the direction of the barrel again. This pattern repeats itself numerous times as long as the regular flight geometry is maintained.

If the flow is viewed in the cross section of the screw channel (see Fig. 44), then the material moves to the pushing side of the flight at the top of the channel. This flow results from drag flow. At the bottom of the channel, the material moves toward the trailing side of the channel. This is a pressure flow resulting from the fact that the pressure at the pushing side of the flight is higher than at the trailing side of the flight. If the leakage flow through the flight clearance is negligible, the

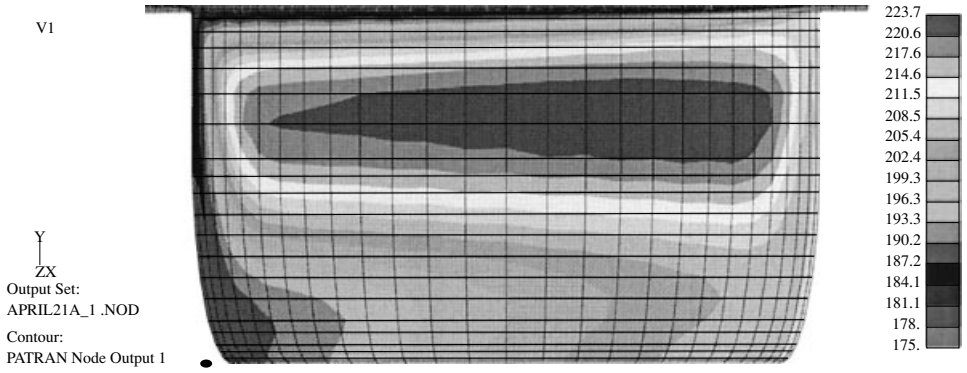

Fig. 42. Predicted melt temperatures in the screw channel.

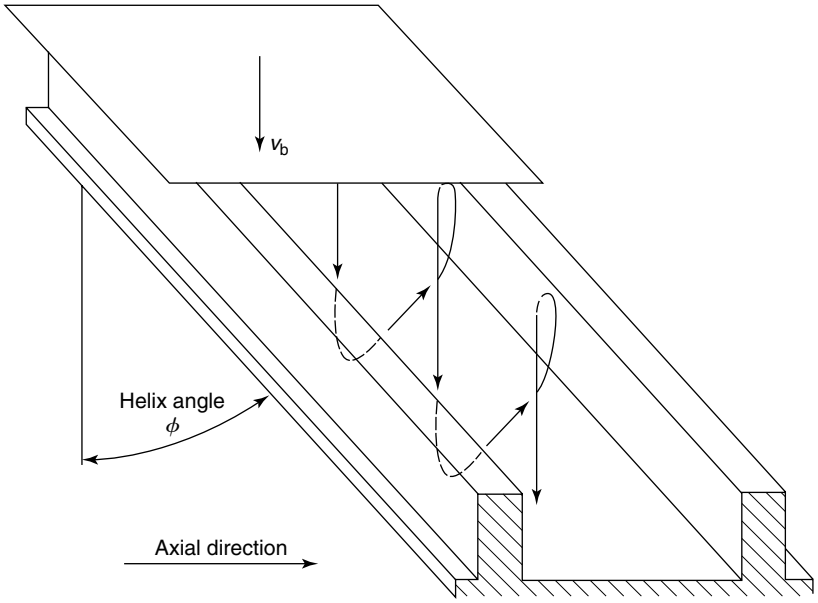

Fig. 43. Flow along the unrolled screw channel.

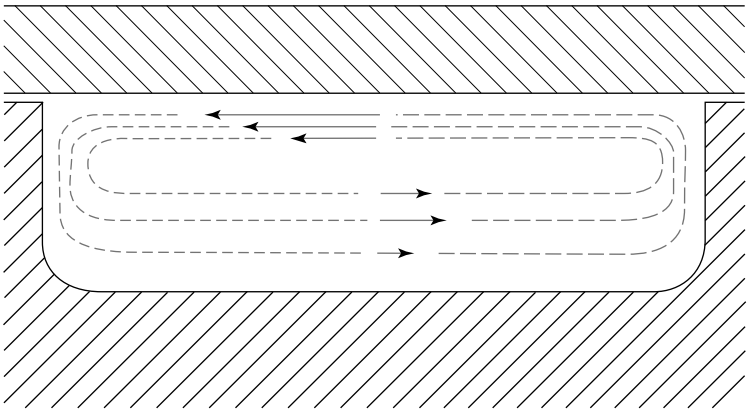

Fig. 44. Recirculating flow in the cross section of the screw channel.

amount of material flowing to the pushing flight flank is the same as the amount of material flowing to the trailing flight flank. Thus, a recirculating flow is obtained as shown in Figure 44. There are also small velocity components in the normal direction close to the flight flanks. At the pushing flight flank, the normal flow is downward, toward the root of the screw; at the trailing flight flank, the normal flow is upward, toward the barrel. The normal flow also results from pressure differences. For instance, the pressure at the top of the pushing flight flank is higher than at the bottom of the flight flank, which is why the flow is downward in this region.

The fluid is sheared as it flows along the screw channel and as a result, there is viscous heat generation in the plastic melt. The actual temperatures that occur at different points in the screw channel are determined not only by viscous heating, but also by how efficiently this heat can be removed. If the barrel is cooled, the melt flowing close to the barrel surface can exchange heat efficiently and hence cool down efficiently. When this outer layer moves along the screw surface, it remains relatively cool even if the screw is insulated.

However, the situation is quite different for the inner layer. Because this layer is trapped in the inner recirculating region, it never gets close to the barrel. As a result, this layer has very limited opportunity for removed of its heat; the outer layer of plastic melt essentially insulates the inner layer. This explains why the temperature in the inner region of the screw channel tends to be higher than in the outer region. In Figure 42, the temperature in the center region is about 60°C higher than the barrel temperature. Thus, it is clear that considerable melt temperature differences can occur in the screw channel.

If these temperature differences are carried to the end of the screw, the melt discharged into the die is not thermally homogeneous. This leads to flow problems in the die and distortion of the extruded product. It is important, therefore, to try to keep these nonuniform melt temperatures from reaching the end of the screw. The most efficient method to do this is by incorporating mixing elements into the design of the screw. Mixing sections are not only important when different plastics are mixed, but also when a single plastic is extruded so that a thermally homogeneous melt at the end of the screw is achieved.

Mixing

Mixing takes place both in the melting zone as well as the melt conveying zone of the extruder. The solid plastic typically moves in plug flow, which means that there is no relative motion between the solid plastic particles. As a result, there is little or no mixing in solids conveying. This means that complete mixing does not start until all the plastic has melted. For this reason, mixing is to be viewed only in the melt conveying zone of the extruder.

Distributive Mixing. The extent of distributive mixing can be determined from the total shear deformation of the plastic melt in the melt conveying zone. The total shear deformation is also called the *total shear strain*; it is determined by the product of the shear rate and the length of time that the fluid is exposed to the shear rate. For instance, if the plastic melt is exposed to a shear rate of $100\ s^{-1}$ for 15 s, the resulting shear strain is $100 \times 15 = 1500$. The units of shear strain are dimensionless. The shear rate is determined by the velocity profiles in the extruder.

Mixing in single screw extruders is determined mostly by the two main velocity components in the screw channel. These are the velocity in the direction of the channel (z-direction) and the velocity in the cross-channel direction (x-direction) (see Fig. 45).

There is also a velocity component in the third direction (y-direction) parallel to the flight flank. This velocity component is usually very small and therefore, can usually be neglected. The velocities in down-channel direction depend on the

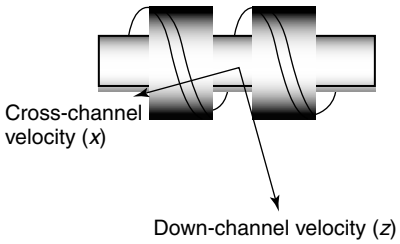

Fig. 45. The two main flow components in a single screw extruder.

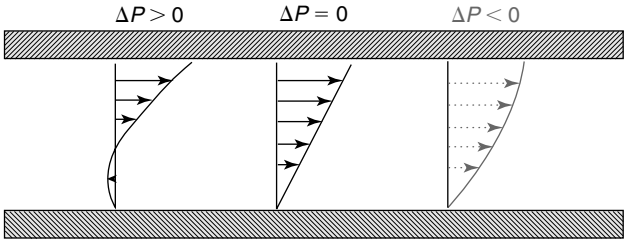

Fig. 46. Down-channel velocity profiles for three pressure conditions.

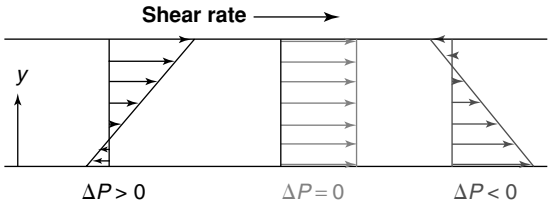

Fig. 47. Down-channel shear rates for three pressure conditions.

pressure gradient; this can be positive, zero, or negative. When the pressure gradient is positive, pressure is increasing along the melt conveying zone; when the pressure gradient is negative, pressure is decreasing along the melt conveying zone. Down-channel velocity profiles for different values of the pressure gradient are shown in Figure 46.

The cross-channel flow is shown in Figure 44. At the top of the channel, the material flows to the left by drag flow and at the bottom of the channel, the material flows to the right by pressure flow. The shear rate can be determined from the velocity profile; the shear rate is equal to the slope of the velocity profile. This slope of the velocity profile is also called the velocity gradient. From the down-channel velocities, we can determine the down-channel shear rates; these are shown in Figure 47.

When the pressure gradient is positive, the shear rates increase toward the barrel surface, when the pressure gradient is zero the shear rate is constant, and when the pressure gradient is negative the shear rates decrease toward the barrel surface. The same approach can be used to determine the cross-channel shear rate

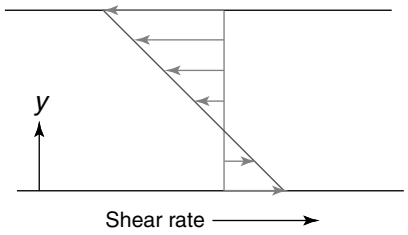

Fig. 48. Cross-channel shear rate vs normal distance.

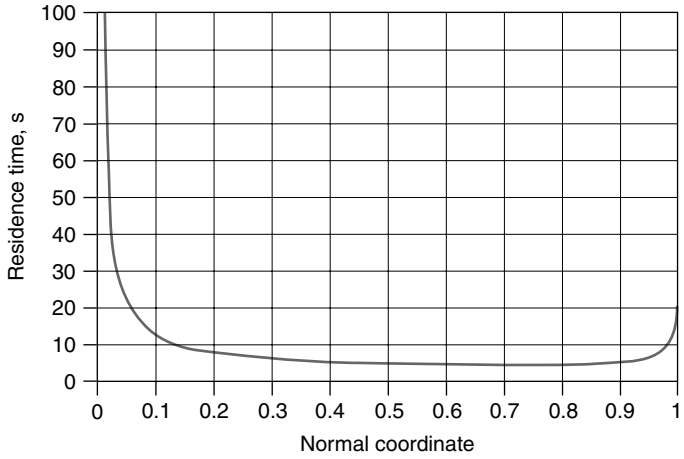

Fig. 49. Residence time vs normal distance (dimensionless).

from the cross-channel velocities. The cross-channel shear rate profile is shown in Figure 48.

In the bottom of the channel, the fluid is exposed to positive shear rates and in the top of the channel, the fluid is exposed to negative shear rates. This has important consequences for the mixing that occurs in screw extruders.

The residence time as a function of the normal distance is shown in Figure 49. The vertical axis shows the residence time $t(y)$ and the horizontal axis shows the normal distance y. The screw surface corresponds to $y=0$ and the barrel surface corresponds to $y=1$.

It is clear from this figure that fluid elements in the center region of the channel have the shortest residence time. The residence time increases toward the screw and barrel surfaces and becomes very long at the barrel and screw surfaces. From Figure 49 it is clear that particularly on the screw there is a relatively thick layer of plastic melt that has a very long residence time relative to the material in the center of the channel. Unfortunately, this increases the chance of material building up on the screw surface and causing problems with degradation.

The total cross-channel shear strain can be determined by adding the shear strain in the upper portion of the channel to that in the lower portion of the

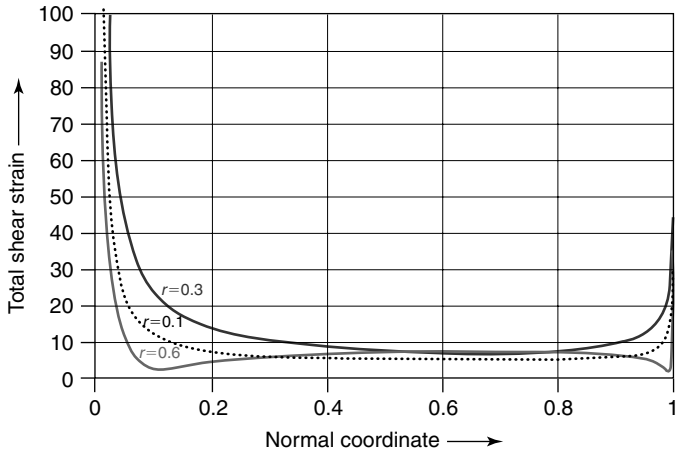

Fig. 50. Total shear strain vs normal distance (dimensionless) at various r_d values.

channel. The total down-channel shear strain can be found the same way. The total shear strain is obtained by adding the cross- and down-channel shear strains. The total shear vs normal distance for several values of the throttle ratio r_d is shown in Figure 50. The *throttle ratio* is the ratio of the pressure flow to drag flow. When $r_d = 0$, we have pure drag flow (pressure flow is zero). When $r_d = 1/3$, the drag flow is three times the pressure flow; this is a fairly common situation in single screw extruders.

The total strain depends strongly both on the normal distance and on the throttle ratio. Fluid elements close to the barrel wall experience a high level of shear strain and thus, will be well mixed. Elements further away from the wall, as well as elements close to the wall, experience a lower level of strain and will not be well mixed.

The shear strain in the center region increases with the throttle ratio. When the throttle ratio is one-third or greater, the shear strain reaches a minimum when close to the wall; this corresponds to the location where the down-channel shear strain approaches zero. Mixing is improved by increasing the throttle ratio or choking the extruder. This can be done by increasing the restriction at the end of the screw, for instance, by increasing the number of screens in the screen pack. Such an increase in mixing, however, is at the expense of output. Since reduced output increases residence time and plastic melt temperatures, there is an increased chance of degradation. Therefore, increasing the restriction of the screen pack is often not the most efficient way of improving mixing.

The nonuniform cross- and down-channel shear strains result in nonuniform mixing in the screw channel. Unfortunately, poor mixing ability is typical of single screw extruders with straight conveying screws, ie without mixing sections. The best method to really improve mixing in single screw extruders is to incorporate mixing sections. Mixing sections are also useful in reducing the large variations in melt temperature that can occur in screw extruders. If a melt with nonuniform melt temperatures is discharged into an extrusion die, several problems can occur, when affects the quality of the extruded product.

There are certain characteristics that are desirable for mixing sections in general. These are

(1) The mixing section should have minimum pressure drop, preferably by having forward pumping capability.
(2) The mixing section should have streamlined flow; dead spots should be avoided.
(3) The mixing section should wipe the barrel surface completely; thus, circumferential grooves should be avoided.
(4) The mixing section should be operator friendly; it should be easy to assemble, install, run, clean, and disassemble.
(5) The mixing section should be easy to manufacture and reasonably priced.

In addition to the general characteristics desirable for mixing sections, there are some specific characteristics important for distributive mixing:

(1) The plastic melt should be subjected to significant shear strain, and
(2) The flow should be split frequently with reorientation of the fluid elements.

Splitting and reorientation is critical to achieving efficient distributive mixing, because mixing can improve exponentially by splitting and reorientation. Distributive mixers can be divided into some main groups: cavity mixers, pin mixers, slotted flight mixers, variable channel depth mixers, and variable channel width mixers.

Based on the important characteristics of mixers we can compile the various distributive mixers and list how they perform with respect to different criteria. This is shown in Table 3; the ranking is based on a five-point system: 5 is very good, 1 is very bad.

The last column in Table 3 is the most important when it comes to distributive mixing effectiveness. The Dulmage, Saxton, CTM, TMR, and CRD all do very well in this category. The Saxton and CRD mixers combine good mixing with low cost,

Table 3. Comparison of Various Distributive Mixers[a]

Mixers	Pressure drop	Dead spots	Barrel wiped	Operator friendly	Machining cost	Shear strain	Splitting, reorientation
Pins	2	2	3	4	5	2	4
Dulmage	4	4	2	4	4	4	5
Saxton	4	4	5	4	4	4	5
CTM	1	3	2	1	1	4	5
TMR	1	3	4	3	2	4	5
CRD	4	4	5	4	3	4	5
Axon	4	4	4	4	5	4	3
Double wave	4	4	4	4	2	4	2
Pulsar	4	4	4	4	3	3	2
Strata-blend	4	3	4	4	3	3	2

[a]The ranking is based on a five-point system: 5 is very good, 1 is very bad.

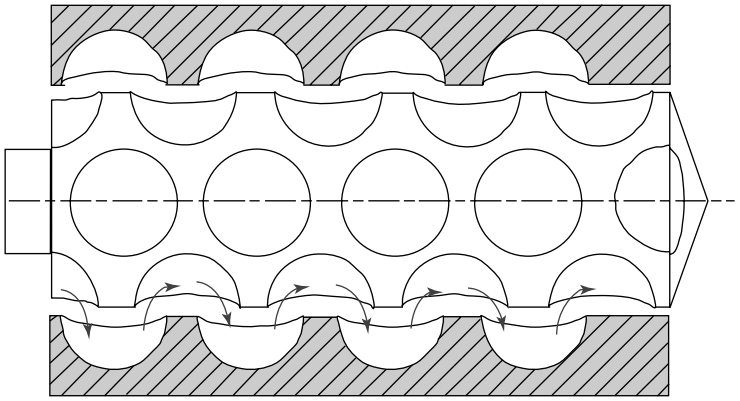

Fig. 51. Cavity transfer mixer.

good streamlining, ease of use, and low pressure drop. The CRD mixer also has dispersive mixing capability; it will be discussed in the next section.

Cavity Mixers. One of the well-known cavity mixers is the cavity transfer mixer (CTM). It consists of a screw section and a barrel section, both containing hemispherical cavities (see Fig. 51).

As the plastic melt travels through the mixer, the material is frequently cut and reoriented. This action gives the mixer good mixing capability. There are a few practical issues, however, that make the CTM a less than ideal mixer. It has no forward pumping capability; thus, the CTM is a pressure consuming mixing device that will reduce the extruder output and increase the temperature buildup in the plastic melt. With the hemispherical cavities, the streamlining is not very good; this can be a problem in product changeover and with thermally sensitive materials. Other drawbacks of the CTM are high cost, difficult installation and cleaning, and the fact that the barrel is not completely wiped during processing.

Another cavity mixer is the Twente mixing ring (TMR) developed by Semmekrot at Twente University in Enschede, the Netherlands. It is similar to the CTM, but it has a freely moving mixing ring with circular holes instead of a barrel with cavities (see Fig. 52). This removes a number of the disadvantages of the CTM; the TMR is easier to install, easier to clean, and the barrel is completely wiped.

Pin Mixers. Pin mixers have been in use for many years and come in many shapes and sizes. Often the pins are circular, but other shapes can be used as well, eg, square, rectangular, and diamond-shaped. Two examples of pin mixing sections are shown in Figure 53.

Pins achieve a moderate level of splitting and reorientation, and as a result, give a moderate improvement in mixing. One drawback of pins is that they create a restriction to flow and, thus, reduce extruder output. The greater the number of pins, the more the output goes down. Another drawback of pins is that they tend to create regions of stagnation, particularly at the corner of the pin and at the root of the screw.

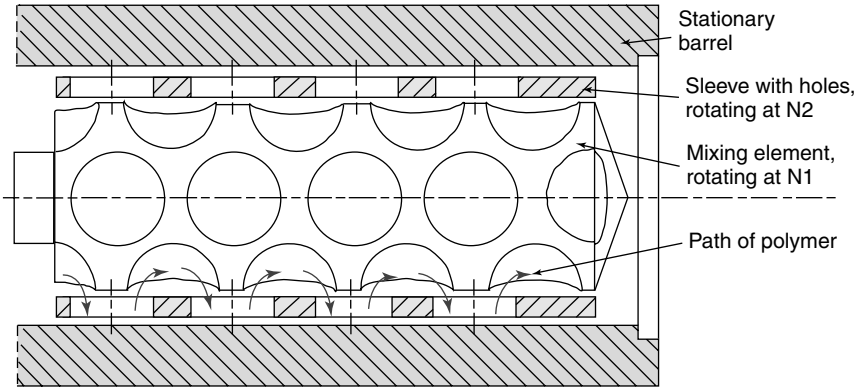

Fig. 52. Twente mixing ring, N1 > N2.

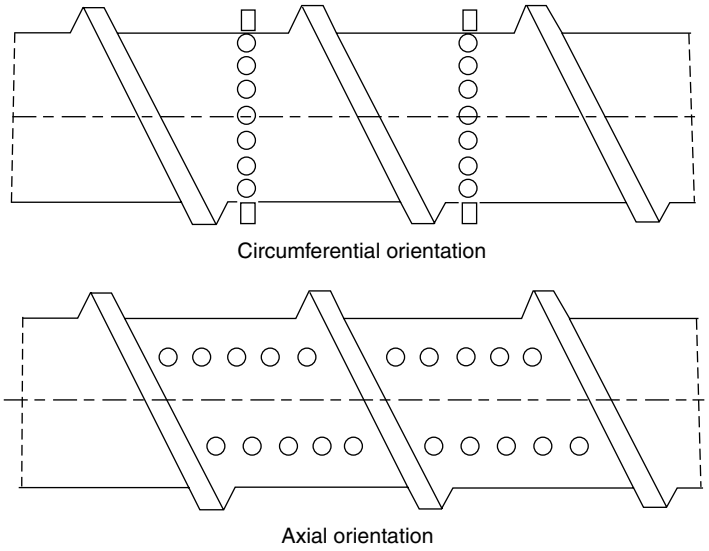

Fig. 53. Examples of pin mixing sections.

Slotted Flight Mixers. There are a great number of slotted flight mixers. Examples of slotted mixers are the Dulmage (Fig. 54) and the Saxton mixing sections (Fig. 55).

Both these mixers have frequent splitting and reorientation, resulting in effective mixing action. Because of the forward orientation of the flights, there is some forward pumping capability. Thus, good mixing can be combined with high output capability. The drawback of the Dulmage mixer is that it has circumferential slots, which means that the barrel is not completely wiped by the mixing section.

Variable Depth Mixers. In these mixers, the channel depth of the mixer is varied to obtain improved mixing. One variable depth mixer is the double wave screw (see Fig. 56).

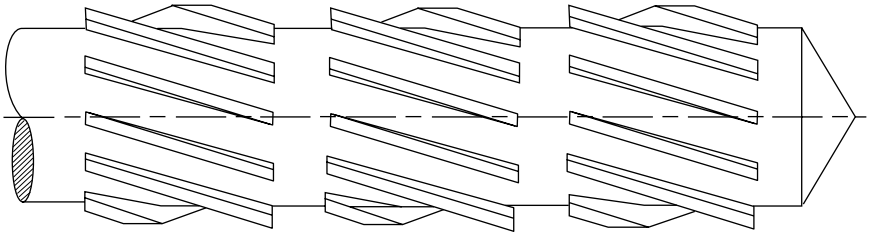

Fig. 54. The Dulmage mixing section.

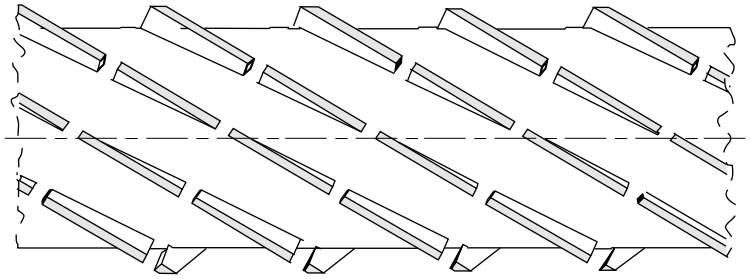

Fig. 55. The Saxton mixing section.

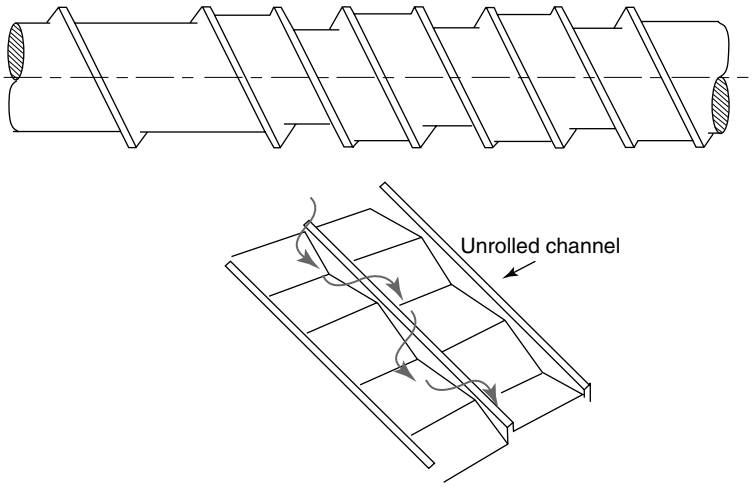

Fig. 56. Double wave screw.

The channel depth varies periodically in each channel in such a way that when one channel decreases in depth, the other increases and vice versa. In this mixer there is no strong mechanism for flow splitting and reorientation. Thus, the mixing capability of this mixer is moderate. Other variable depth mixers are the Pulsar and Strata-blend mixing sections (see Fig. 57). These do not achieve efficient flow splitting and reorientation.

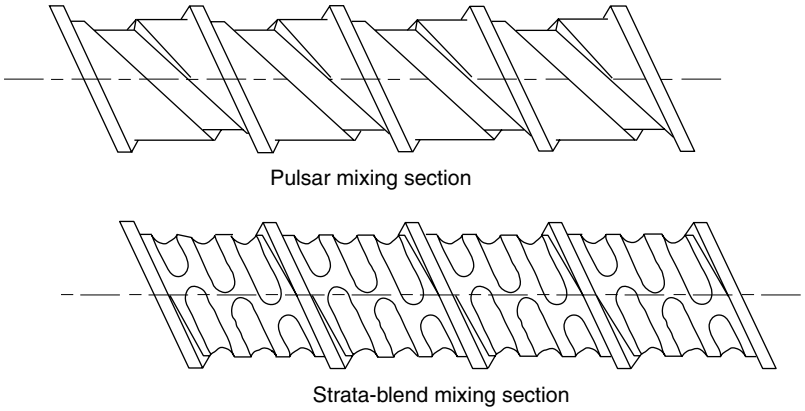

Fig. 57. Pulsar mixer and Strata-blend mixer.

Dispersive Mixing. For dispersive mixing the following characteristics are desirable:

(1) The mixing section should have a region where the material is subjected to high stresses, preferably elongational stresses.
(2) The high stress region should be designed such that the exposure to high shear stresses occurs only for a short time, while exposure to elongational stresses is maximized.
(3) All fluid elements should pass through the high stress regions many times to achieve efficient dispersive mixing action.
(4) All fluid elements should pass through the high stress regions the same number of times for uniform mixing.

A comparison of dispersive mixers is shown in Table 4; the ranking is based on a five-point system: 5 is very good, 1 is very bad.

There are several types of dispersive mixing sections: blister rings, fluted mixing sections, and planetary gear extruders.

Table 4. Comparison of Dispersive Mixers for Single Screw Extruders[a]

Mixer	Pressure drop	Dead spots	Barrel wiped	Cost	Number passes	Type of flow
Blister	1	3	2	5	1	Shear
Egan	2	5	5	4	1	Shear
LeRoy/Maddock	2	2	5	4	1	Shear
Zorro	5	5	5	3	1	Shear
Helical LeRoy	5	5	5	4	1	Shear
Planetary gear	3	5	5	2	Multiple	Shear
CRD	5	5	5	4	Multiple	Elongation

[a]The ranking is based on a five-point system: 5 is very good, 1 is very bad.

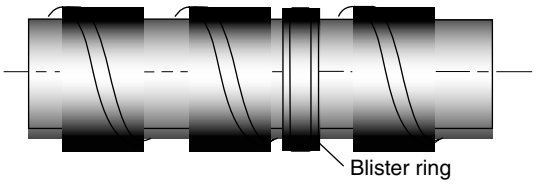

Fig. 58. Blister ring.

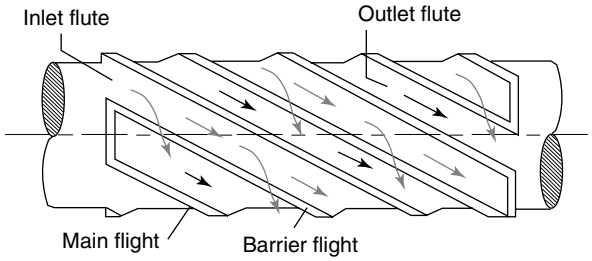

Fig. 59. Egan mixing section.

Blister Ring. The blister ring is simply a circumferential shoulder on the screw with a small clearance between the ring and the barrel (see Fig. 58). All material must flow through this small gap where it is exposed to high shear stresses. Since no forward drag flow occurs in the blister ring, relatively high pressure drops occur across the blister ring. The stress level in the gap is not uniform; therefore, the mixing action is not uniform.

Fluted Mixing Sections. These mixers have inlet and outlet flutes separated by barrier flights. For the material to exit the mixer it has to pass through the narrow gap of the barrier flights; this is where the mixing action takes place. One of the earliest fluted mixers was the Egan mixing section developed by Gregory and Street. The flutes in this mixer have a helical orientation (see Fig. 59).

Another fluted mixer is the Union Carbide mixer (UC mixer) developed by LeRoy and popularized by Maddock. It has straight flutes as shown in Figure 60. Because of the straight flutes, the LeRoy mixer has no forward pumping capability and thus, tends to have high pressure drop. It is typically machined with a ball mill; as a result, the flutes have a semicircular cross section. This tends to result in inefficient streamlining at the entry and exit of the flutes. Despite these shortcomings, the LeRoy mixer is probably the most commonly used mixer in single screw extruders.

It is important to design mixing sections to have a low pressure drop; this is particularly true for dispersive mixers. High pressure drop reduces output, increases melt temperatures, increases residence time, and increases the chance of degradation. Higher melt temperatures reduce the melt viscosity and the stresses in the melt in the mixing section. As a result, higher temperatures reduce dispersive mixing. Since high pressure drop causes high temperatures, high pressure drop should be avoided. For this reason a helical LeRoy mixer is better than the straight LeRoy mixer.

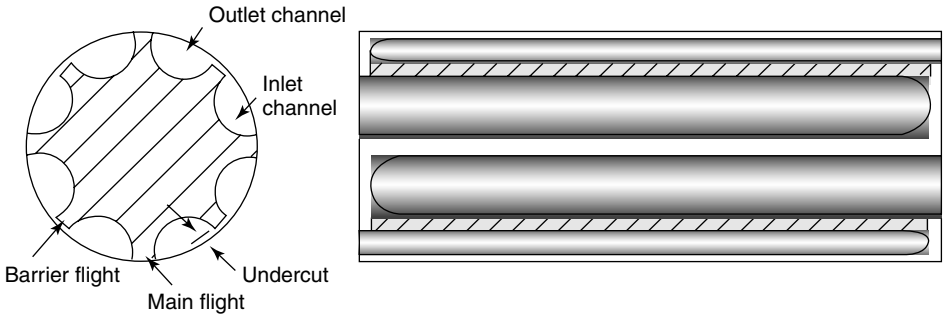

Fig. 60. LeRoy mixing section.

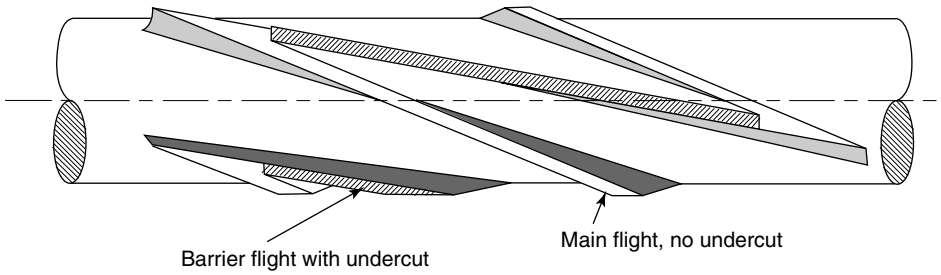

Fig. 61. Zorro mixing section.

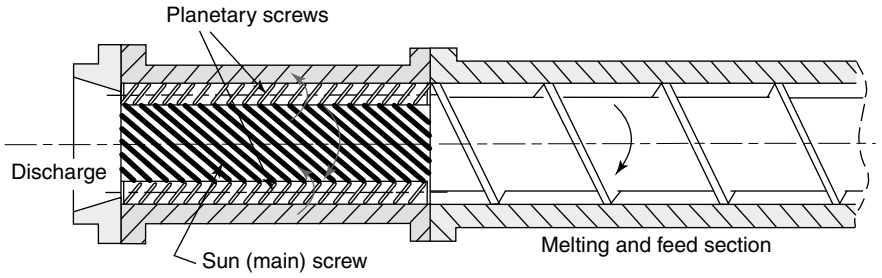

Fig. 62. Schematic of planetary gear mixer.

To promote good streamlining, the helix angle of the barrier flight can be made larger than that of the main flight. This makes the entry channel wide at the entrance and the exit channel wide at the exit. To minimize hang-up, the channels should taper to zero depth at the end of the entry channels and the start of the exit channels. A commercial version of this mixer is the Zorro mixing section (see Fig. 61).

Planetary Gear Mixers. Planetary gear mixers have six or more planetary screws that revolve around the circumference of the main screw. The planetary barrel section must have helical grooves corresponding to the helical flights on the planetary screws. The planetary barrel section is generally separate, with a flange-type connection to the other barrel section (see Fig. 62).

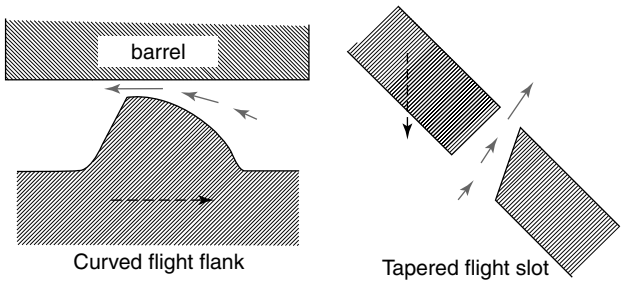

Fig. 63. Various flight geometries that form a wedge-shaped lobal region.

These machines are commonly used in Europe; they are used less in the United States. Some of the benefits of planetary gear mixers are, good homogeneity of the melt at low temperature level, uniform shear exposure, high output per screw revolution, low production cost per unit throughput, self-cleaning action for easy material change, and good dispersive and distributive mixing of various additives.

These characteristics make the planetary gear extruders well suited for processing heat-sensitive materials such as rigid and flexible PVC. They are also used to process blends (eg, PVC and ABS), plastic foams, powder coatings, epoxy, polyester, acrylic, polyurethane, chlorinated polyethylene, etc.

The CRD Mixer. Current dispersive mixers have two important drawbacks. One, they rely mostly on shear stresses to disperse materials rather than elongational stresses; dispersion is more effective in elongational flow than in shear flow. Two, the material passes over the high stress region only once. Advantages of elongational flow over shear flow are

(1) Lower viscous dissipation resulting in lower melt temperatures;
(2) Action of greater forces on agglomerates and droplets;
(3) More efficient deformation of agglomerates and droplets;
(4) Dispersion of gels in elongational flow but not in shear flow.

New mixing technology developed by Rauwendaal eliminates these disadvantages of existing dispersive mixers (5). The CRD mixer uses a slanted pushing flight flank to create a wedge-shaped lobal region, as shown in Figure 63. To create effective distributive mixing, multiple flights are used with many slots. The slots are tapered so that material flowing through the slot is accelerated and exposed to elongational deformation.

The wedge shapes create strong elongational flow. The CRD (6) mixer uses multiple mixing flights with a relatively large flight clearance to ensure that all fluid elements pass through the high stress region several times. There are also a large number of tapered slots to make sure that all fluid elements pass through the slots several times. In addition, there are two wiping flights with slots to make sure that the barrel surface is completely wiped by the mixer and to keep the mixer centered within the barrel. A picture of an actual CRD8 mixer is shown in Figure 64.

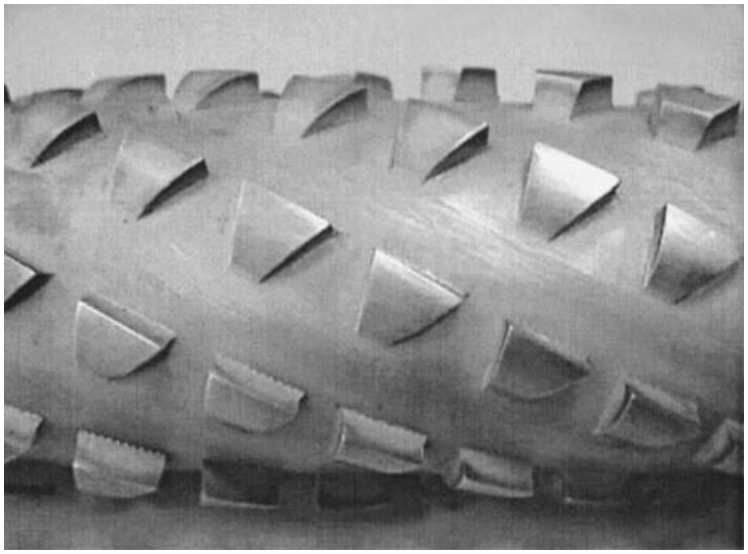

Fig. 64. CRD8 mixer with separate wiping flights. Copyright Rauwendaal Extrusion Engineering, Inc.

The mixing and wiping flights have a positive helix angle; this gives the mixing forward pumping capability. As a result, the mixer does not compromise extruder output. It also allows the mixer to be quite long. A typical length of the CRD mixer is six to eight screw diameters; this results in excellent mixing. Because of the large clearance of the mixing flights, it is necessary to use wiping flights to avoid a stagnant film at the barrel surface and improve pumping. The slots generate efficient distributive mixing in the CRD mixer to randomize the fluid elements and ensure that all elements pass through the high stress regions several times. Separate wiping flights can be avoided by incorporating wiping segments along the dispersive mixing flights.

The CRD mixer has also been applied to twin screw extruders, blow molding, and injection molding machines. A special version of the CRD mixer has been developed that combines a nonreturn valve (NRV) at the end of an injection molding screw with a CRD mixer. This CRD–NRV takes up the same space as a regular NRV, and as a result, offers a quick and convenient method to improve the mixing capability of injection molding machines. Figure 65 shows a slide-ring-type CRD–NRV; the slide ring has internal mixing pins that split the flow and accelerate the plastic melt. The conical nosepiece has tapered circular holes that cause splitting and acceleration as well. As a result, the plastic melt is exposed to three splitting, acceleration, and reorientation events as it passes through the CRD–NRV.

Even though the CRD–NRV is designed for injection molding machines the same principle can be used in conventional extruders. In this case there is no axial motion of the slide ring; however, there will still be a difference in rotational speed between the slide ring and the rest of the screw. The velocity difference will enhance the mixing action.

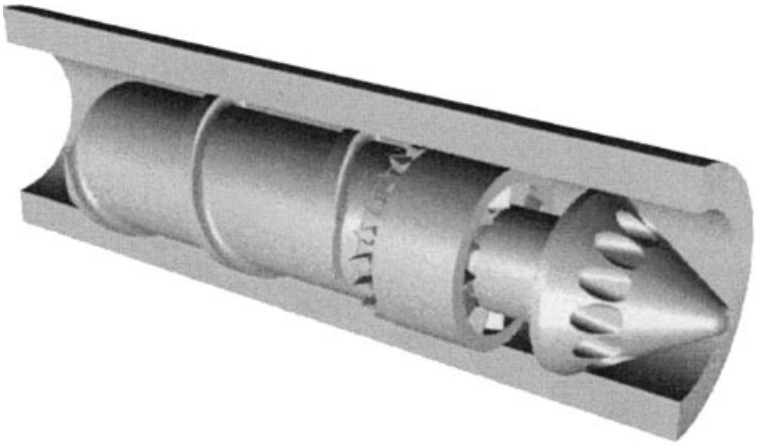

Fig. 65. CRD–NRV used in injection molding.

The following are the benefits of the CRD mixer:

(1) Better dispersive and distributive mixing than existing mixers;
(2) Reduced barrel pressure and melt temperature fluctuation resulting in better output stability and dimensional control;
(3) Reduced die lip buildup, and better and more consistent product appearance;
(4) Lower viscous dissipation and reduced power consumption resulting in lower melt temperatures (less degradation);
(5) Higher extruder output because of pumping action of the mixer; and
(6) The CRD mixer can disperse gels; shear-based mixers cannot disperse gels.

Degassing

Degassing is done on a vented extruder; this is an extruder with a vent port in the barrel. A special screw design has to be used in a vented extruder to make sure that there is a zero pressure region under the vent port. Degassing is needed when the plastic contains volatile components at a level high enough to cause problems. Generally, volatiles cause voids or surface defects in the extruded product.

Degassing is often used in extrusion of hygroscopic materials; these materials have an equilibrium moisture content higher than the level that can be tolerated in extrusion, which is about 0.1% for most plastics. For some plastics, this level is quite a bit lower. Table 5 lists hygroscopic plastics with their equilibrium moisture contents and the allowed moisture content.

With such materials we have two choices: predry the plastic or remove the moisture at the vent port. Drying plastics is usually a very slow process; it can take from 4 to 40 h. Devolatilization in the extruder is much more rapid because of the high temperatures involved. As a result, it can be advantageous to remove the moisture by venting rather than by predrying. In some cases drying and venting

Table 5. Equilibrium and Allowable Moisture Content for Various Plastics

Plastic	Equilibrium moisture content, %	Allowable moisture content, %
CA	2.2	<0.05
CAB	1.3	<0.05
ABS	1.5	<0.10
PA6	3.0	<0.10
PA66	2.8	<0.10
PC	0.19	<0.015
PBTP	0.2	<0.03
PMMA	0.8	<0.10
PAN	0.4	<0.10

are done at the same time, particulary in high output extrusion operations. Many hygroscopic plastics contain too much moisture to remove the required amount of moisture through a single vent port. In this case some predrying has to be done or an extruder can be used with two vent ports rather than one.

It should be noted that there are some hygroscopic plastics that are not good candidates for venting. Some plastics degrade rapidly when the plastic is exposed to high temperatures in the presence of moisture; an example is polyester. This moisture-induced degradation is called hydrolysis. Venting such material to remove moisture invariably results in considerable degradation of the plastic. As a result, polyester is usually dried before extrusion, rather than having the moisture removed during extrusion through the vent port. Other plastics susceptible to hydrolysis are polyamide (nylon), polycarbonate, and polyurethane.

Vented extruders require a special screw design to keep the vent port region at zero pressure; such a screw is called a two-stage screw. The zero pressure region is achieved by following a shallow metering section before the vent port with a deep flighted extraction section underneath the vent port. A short compression section and a second metering section or pump section follow this extraction section. Figure 66 shows the geometry of a two-stage extruder screw.

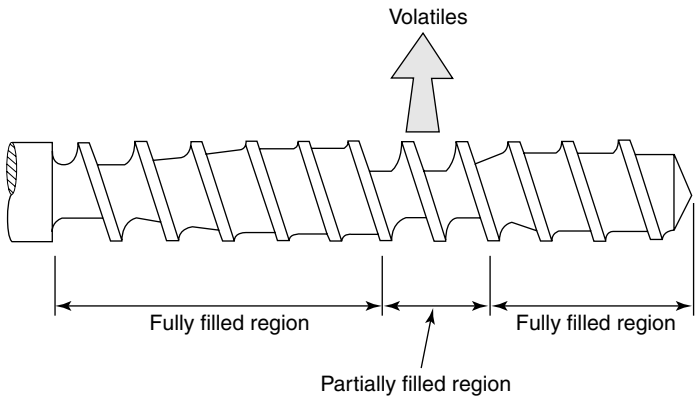

Fig. 66. A two-stage extruder screw used for devolatilization.

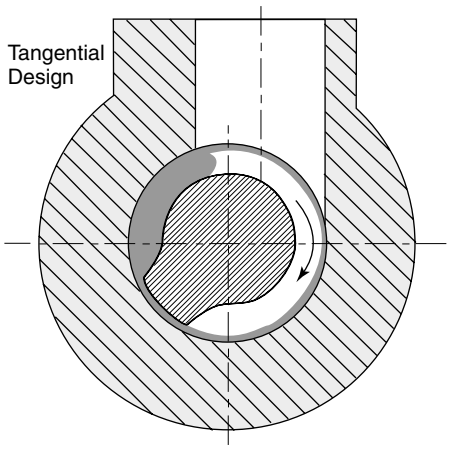

Fig. 67. Cross section of a tangential vent port region showing the rolling bank.

The feed section, the first compression section, and the first metering section make up the first stage of the screw. The extraction section, the second compression section, and the pump section make up the second stage of the screw. For the proper functioning of the screw, it is important that the conveying ability of the pump section be greater than the metering section. The metering section should be the rate controlling part of the screw; it should act as a dynamic choke. If this is the case, the extraction section of the screw is only partially filled and venting occurs properly. If this is not the case, the extraction section completely fills and molten plastic escapes through the vent port; this is referred to as vent flow.

It is critically important that the screw channel under the vent port is only partially filled with plastic; this is true for single as well as twin screw extruders. Figure 67 shows a cross section of a partially filled screw channel. The vent opening has a tangential design; this is beneficial in minimizing accumulation of plastic melt in the vent port.

There is a rolling bank of plastic melt at the leading side of the screw flight. Only when this condition is fulfilled can one be sure that no pressure is generated in the vent port region. If pressure does build up in the vent port region, the plastic melt flows out through the vent port, causing vent flow. This is a common problem in vented extruders.

Vent flow occurs when the conveying rate of the second stage cannot keep up with the first stage. This happens when the first stage is supplying more material than the second stage can handle. This condition can result from incorrect screw design. Vent flow can also occur when a high restriction die is used at the end of the extruder. The diehead pressure is generated only in the second stage of the screw because the extraction section is pressureless. As a result, a higher diehead pressure reduces the pumping capacity of the second stage while the pumping capacity of the first stage is not affected. As the diehead pressure increases, it will reach a point where the pumping capacity of the second stage decreases to that of the first stage. This is the critical diehead pressure for vent flow. If the diehead pressure increases above this value, vent flow occurs. The critical diehead pressure

for vent flow depends on the screw design, the flow properties of the plastic, and the operating conditions.

Die Forming

The shaping of the molten plastic occurs in the extrusion die. As the plastic flows through the die, it adopts the shape of the flow channel. Thus, the exit geometry of the die flow channel is shaped like the required shape of the extruded product. The exit region of the die flow channel is called the *land region*. The land region for a pipe or tubing die has an annular shape; for a flat film or sheet die, it has the shape of a slit. One of the most important objectives in die design is to distribute the melt in the flow channel such that the material exits from the die with a uniform velocity. With certain extruded shapes, it can be quite difficult to achieve a uniform exit velocity across the die.

Size and Shape Changes. The land region of the die does not have exactly the same shape and dimensions as the extruded product because there are a number of factors that change the shape and dimensions of the plastic as it emerges from the die. The main factors are drawdown, extrudate swell, cooling, and relaxation. Drawdown occurs because the take-up speed has to be higher than the velocity of the plastic at the die exit to maintain a tension in the plastic between the die and the take-up. This tension is necessary to keep the plastic from sagging. In some operations, the drawdown only reduces the size of the extrudate a few percent; in other cases, the size change can be quite large, as much as a factor of 2 or 3. Drawdown can change the shape of the product if the product has a noncircular shape.

Extrudate swell is the expansion of the plastic as it leaves the die; it is often called die swell, even though this term is not accurate; it is the material coming out of the die that swells, not the die itself! The swelling of the extrudate occurs primarily because of the elastic nature of the plastic melt. Even though plastic melts are usually considered viscous materials, they are not purely viscous but actually visco-elastic. This means that plastic melts behave both in a viscous and an elastic manner. The elastic component is responsible for most of the swelling of the extrudate. The swelling is the result of the relaxation of the strain imparted to the plastic in the die and perhaps even upstream of the die.

The swelling of the melt is determined by the die design, the flow properties of the plastic, the flow rate, the temperatures, and the drawdown between the die and the take-up. If the drawdown is large enough, there may not be any visible expansion of the material coming out of the die. In this case, the size reduction resulting from drawdown overrides the swelling of the extrudate. A problem with the swelling is that it is generally not uniform; this is illustrated in Figure 68.

With a square flow channel, swelling occurs more at the centers of the sides than in the corners. This nonuniform swelling results from the fact that the shear rates in the corners are lower than at the centers of the sides. Another reason for the distortion of the extruded product is that the flow velocities in the corners are lower than along the sides. This is illustrated in Figure 69; since the velocity field is symmetrical, only the upper left quadrant is shown.

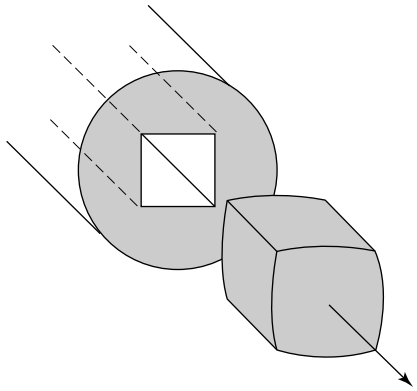

Fig. 68. Swelling of the melt coming out of a die with a square flow channel.

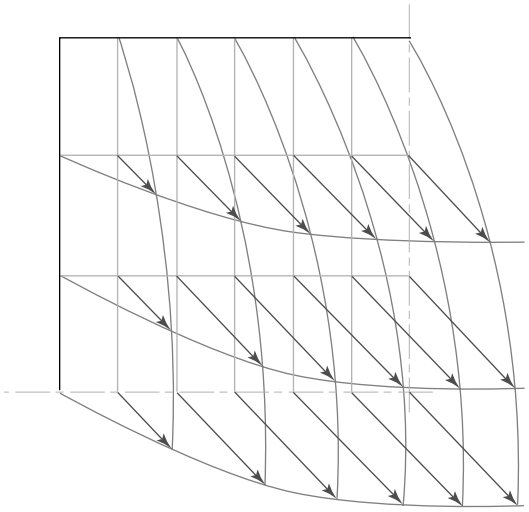

Fig. 69. Velocities in a square flow channel.

As a result, the material in the corners is drawn down more than the material along the sides. Reducing the land length in the corners can enhance flow in the corners; this is typically done by back relieving the die. An example of back relieving the corners is shown in Figure 70.

Cooling increases the density of the plastic and therefore reduces the size of the extruded product. Semicrystalline plastics shrink more upon cooling than amorphous plastics because crystalline regions have a higher density than amorphous regions. Cooling usually does not result in a uniform size reduction. In thick parts, shrink voids can form upon cooling because the outer wall cools and solidifies first. Later the inner layers cool, but they are restrained from shrinking because of the solidified outer wall. As a result, the plastic tends to shrink to the outside, leaving a shrink void in the center, as shown in Figure 71.

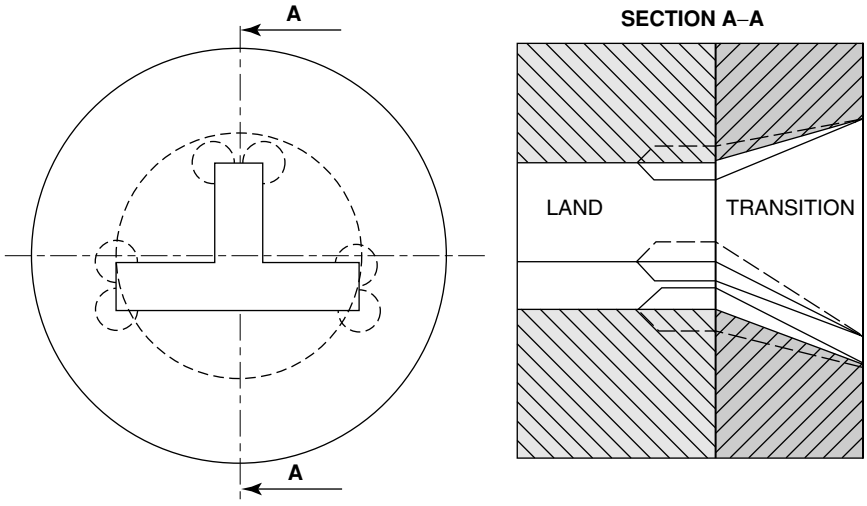

Fig. 70. An example of back relieving the corners of a T-shaped profile.

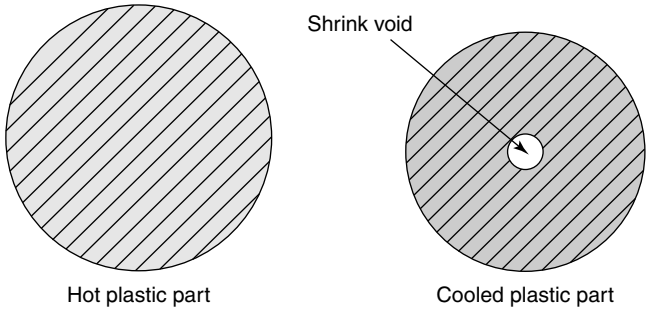

Fig. 71. Formation of a shrink void upon cooling.

Relaxation is the gradual reduction of internal stresses resulting from changes within the material. The stresses can result from the flow in and before the die. Die swell is the result of these stresses. Stresses are also induced after the die exit. The stresses resulting from drawdown are often the dominant stresses induced in the extrusion process. The relaxation processes are strongly temperature-dependent and occur rapidly at high temperatures, particularly above the melting point. At low temperatures however, relaxation occurs only slowly. If drawdown occurs at sufficiently low temperatures, the orientation can relax only partially and a high level of orientation remains in the extruded product. Several commercial processes take advantage of this, such as cold drawing of synthetic fibers.

If nonuniform stresses occur within an extruded product, relaxation of these stresses can lead to warping of the product. An example is shown in Figure 72.

The orientation in the thin legs of the profile tends to be higher than in the thick section. As a result, relaxation in the thin legs is higher than in the thick section, with a correspondingly larger reduction in length. With more length

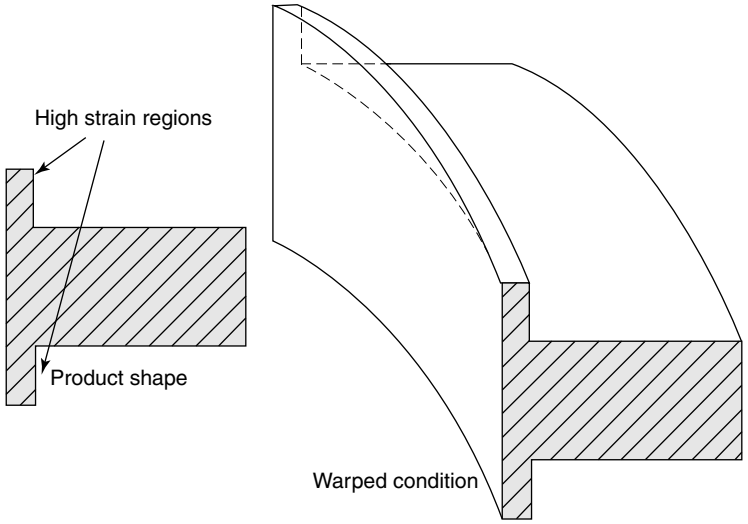

Fig. 72. Warp as a result of nonuniform relaxation in a T-profile.

reduction on the side of the legs (left side), the profile bows with the legs at the concave side as shown. The results of relaxation may not be immediately noticeable. Often the extruded profile appears perfectly straight when first produced. Warpage may not be seen until after the product has spent several days in the warehouse or worse, after it has been sitting in a customer's plant for some time.

Tubing and Pipe Dies. Extrusion dies can be categorized based on the shape of the product produced. Thus, we can distinguish annular dies, slit dies, rod dies, and profile dies. Annular dies are used to make tubing, pipe, blown film, and wire coating. Tubing is a small diameter (less than about 25-mm outside diameter) annular product; it is usually flexible. Pipe is a large diameter annular product (usually with a diameter greater than 25 mm) and is rigid in most cases. Both tubing and pipe are most often used to transport fluids; as a result, they can be exposed to substantial internal pressures. Blown film can have a very large diameter, up to 10 m (30 ft), but the wall thickness is quite small, in the range of 5–250 μm (0.002–0.010 in.). Wire coating and cable jacketing is the extrusion of a layer of plastic over a core. In wire coating, the core is conducting wire; in cable jacketing, the core is a bundle of coated wires.

Annular dies can be either in-line or crosshead. As the name implies, the entrance channel of the in-line die is in-line with the exit channel. This geometry is preferred if it is important to have uniform stresses in the extruded product. A schematic of an in-line die is shown in Figure 73.

Looking at the cross section, the melt enters from the left, then flows around the torpedo, and then though the annular space between the tip and the die. The torpedo is supported by a number of spider legs with a streamlined cross section to minimize hang-up of material. The tip is attached to the torpedo and the die is pressed against the housing by a retaining ring that is bolted against the housing.

A crosshead die is shown in Figure 74. The melt is split around the flow splitter or helicoid, then flows over a shoulder to the tip and the die. The tip is

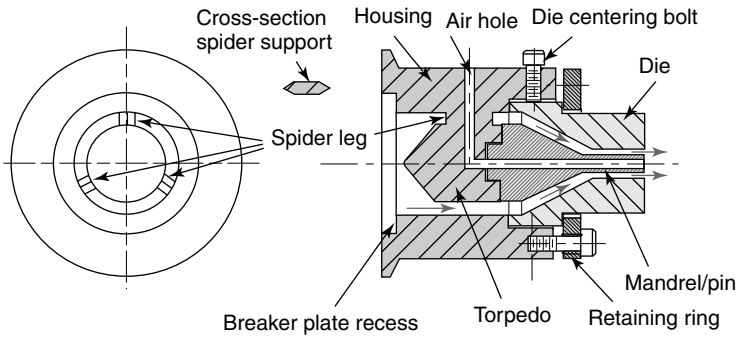

Fig. 73. Schematic of an in-line annular die.

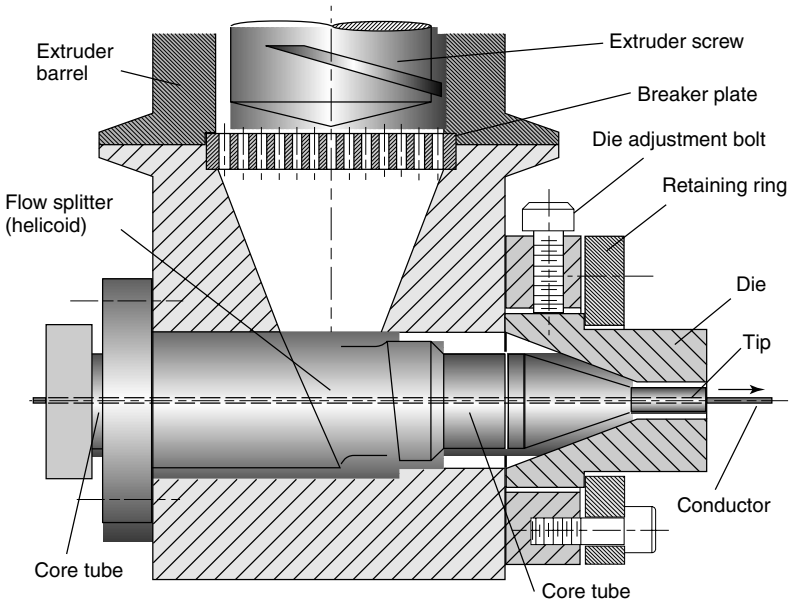

Fig. 74. Example of a crosshead die.

attached to the core tube that can be moved axially. This allows axial adjustment of the tip relative to the die. The die can be adjusted vertically and horizontally by two sets of die adjustment bolts; this allows adjustment of the concentricity of the extruded tube.

Crosshead dies are also used for wire coating. In this case, a conductor moves through the core tube and tip, often at high speed. As the conductor exits from the tip, it is coated with molten plastic in a continuous fashion. Very high line speeds can be achieved in wire coating, as high as 3000 m/min (about 10,000 ft/min).

It should be noted that the dies shown here are some simple examples of annular dies. There is an enormous variety of designs; however, at this point only the main types and features are covered. For instance, in the die assemblies shown, the die can be moved relative to a fixed tip to adjust concentricity. It is also possible to design the die assembly such that the tip can move relative to a

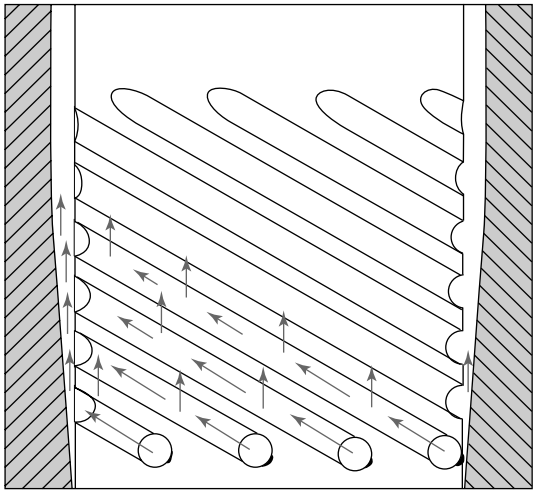

Fig. 75. Spiral mandrel die.

fixed die to adjust concentricity, for instance, by moving the core tube in the back section of the die assembly.

In some annular dies the concentricity adjustment is done automatically. In order to do this, the wall thickness has to be measured downstream of the die along the circumference of the product or in at least four positions. In most cases, the wall thickness is measured using ultrasound. Automatic adjustment is done in some pipe extrusion operations where excess material usage because of poor concentricity could be quite costly.

A special die geometry that was developed for blown film extrusion is the spiral mandrel die, shown in Figure 75. The plastic melt is usually fed through a central channel, then led through radial channels that come out in helical channels in the mandrel. The helical channels are deep initially but they gradually become shallower. At the same time the clearance between the mandrel and the housing increases. As a result, the initial flow is largely a helical flow; however, there is a gradual increase in annular leakage flow with a corresponding reduction in helical flow. At the end of the spiral mandrel section, the flow is a pure annular leakage flow.

The following are the advantages of the spiral mandrel die:

(1) Weld lines are largely eliminated.
(2) Good flow distribution is eliminated.
(3) The helical flow induces some circumferential orientation which increases the hoop strength of the extruded product.
(4) The flow through the spiral mandrel section can be readily modeled, which is helpful in design and optimization.

Even though spiral mandrel dies are primarily used in blown film, they have obvious advantages in tubing and pipe extrusion. Both tube and pipe are often

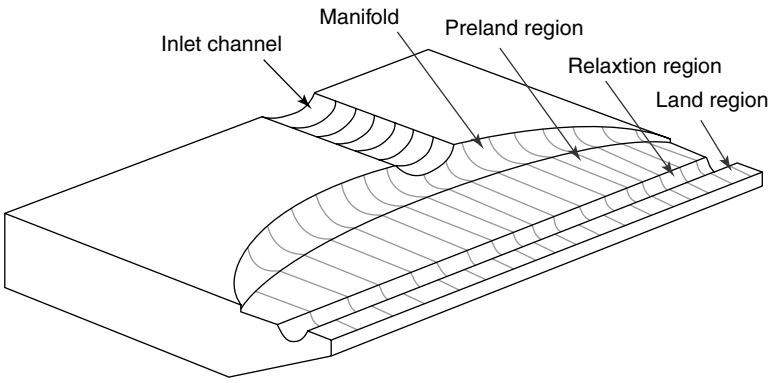

Fig. 76. Main sections of the flow channel of a flat film or sheet die.

pressurized internally in normal product use. With internal pressurization, it is important to have high hoop strength and make sure that weld lines are avoided as much as possible. Since spiral mandrel dies increase hoop strength and reduce weld line problems, they are an attractive option for almost any annular product exposed to a high internal pressure during its end-product use.

Flat Film and Sheet Dies. Dies for flat film and sheet have the same general shape, although there are many differences in the geometrical details. The main sections of the flow channel of a sheet die are the inlet channel, the manifold, the preland section, the relaxation section, and the land section. The main sections of the flow channel are shown in Figure 76.

The inlet channel connects with the discharge of the extruder on one end; on the other end it connects with the manifold section. The function of the manifold is to evenly distribute the flow from the inlet across the manifold outlet. From the manifold, the melt flows to the pre-land, through the relaxation section, and then to the land section. There are a number of different manifold designs, such as the T-die, the coat hanger die, and the horse shoe die. The T-shaped manifold of the T-die does not yield well-streamlined flow; however, the geometry works for low viscosity plastics that are not susceptible to degradation. Another advantage of the T-die is that it is not susceptible to clam shelling, which is the separation of the die lips resulting from the internal pressure of the plastic melt in the die (see Fig. 77).

The coat hanger die has a manifold shaped like a coat hanger (see Fig. 76). The manifold has a complicated shape and is not easy to design or machine. The advantage of the coat hanger manifold is that it produces streamlined flow and it is not susceptible to clam shelling. Coat hanger dies have been made in widths as large as 10 m (30 ft).

The horseshoe die has a manifold with a rectangular cross section (see Fig. 78). It can be designed such that the distribution of flow is independent of the degree of shear thinning of the plastic melt. In fact, it is the only manifold geometry that has this characteristic. The drawback is that the horseshoe die is susceptible to clam shelling. As a result, this die is not typically used for dies wider than 1 m (40 in.).

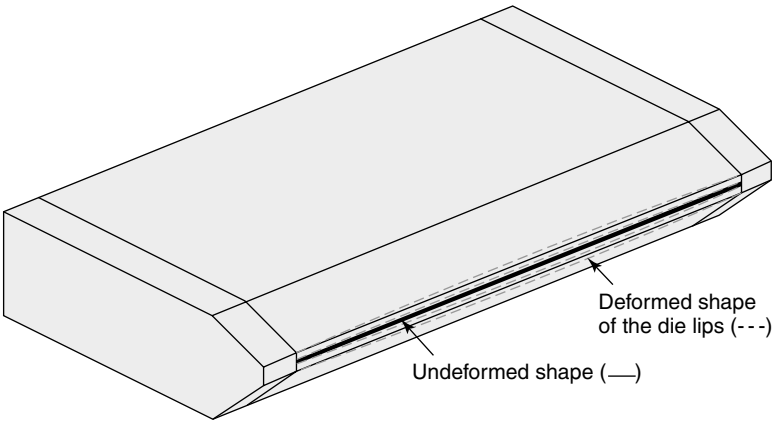

Fig. 77. Illustration of clam shelling.

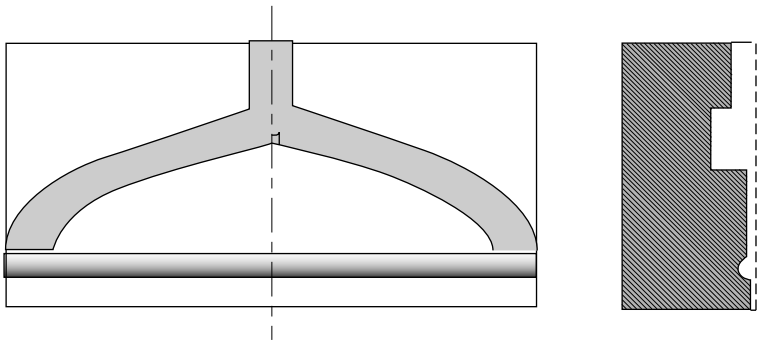

Fig. 78. Horse shoe manifold.

Profile Dies. Profile dies come in many different shapes and sizes. The term profile die is used for dies that extrude shapes other than rectangular, annular, or circular. There are two main types of profile dies: the plate die and the fully streamlined die. The plate die, shown in Figure 79, uses a plate with a cavity shaped to produce the required extruded product. This plate is attached to the end of a section with a large flow channel. The advantage of the plate die is that it is easy to make. On the other hand, the flow is not streamlined and dead spots are likely to occur.

The streamlined die, shown in Figure 80, has a flow channel that gradually changes to the exit geometry of the die. As a result, the velocities gradually increase as the plastic melt moves through the die. There is little chance of hang-up in this geometry. Therefore, the streamlined die is more appropriate for long runs and for plastics with limited thermal stability. The disadvantage of the streamlined die is that it is more difficult to manufacture and therefore more expensive.

There are many profile dies that have a geometry between the plate die and the fully streamlined die; these could be called partially streamlined dies. Because of the enormous variety of profile dies, it is not possible to cover this subject

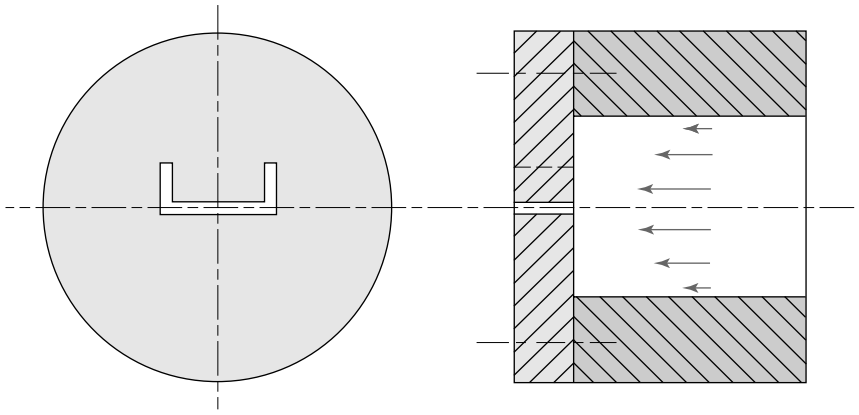

Fig. 79. Example of plate die.

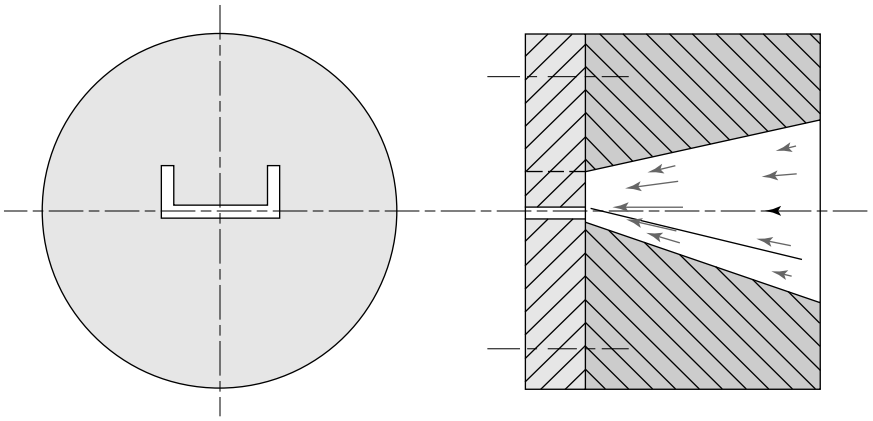

Fig. 80. Example of streamlined die.

comprehensively. For more information, the reader is referred to Michaeli's book on die design (7).

BIBLIOGRAPHY

"Melt Extrusion" in *EPST* 1st ed., Vol. 8, pp. 533–587, by R. F. Westover, Bell Telephone Laboratories, Inc.; "Extrusion" in *EPSE* 2nd ed., Vol. 6, pp. 571–631, by G. A. Kruder, Consultant.

1. J. R. Johanson, in *Pacific Paper '95*, Vancouver, B.C., Oct. 16, 1995.
2. C. Rauwendaal and J. Sikora, *Int. Polym. Process.* **XV**, 1–4 (2000).
3. Z. Tadmor, *Polym. Eng. Sci.* **6**, 185–191 (1966).
4. C. Rauwendaal, *Adv. Polym. Technol.* **15**(2), 135–144 (1996).
5. C. Rauwendaal, T. Osswald, P. Gramann, and B. Davis, in *SPE ANTEC*, 1998, pp. 277–283.

6. U.S. Pat. 5932159 (Aug. 3, 1999), C. Rauwendaal (to Rauwendaal Extrusion Engineering, Inc.).
7. W. Michaeli, *Extrusion Dies*, Hanser Verlag, Munich, 1984.

GENERAL REFERENCES

G. Schenkel, *Kunststoff Extruder-Technik*, Carl Hanser Verlag, Munich, 1963.
Z. Tadmor and I. Klein, *Engineering Principles of Plasticating Extrusion*, Van Nostrand Reinhold, New York, 1970.
H. Hermann, *Schneckenmaschinen in der Verfahrenstechnik*, Springer Verlag, Berlin, 1972.
E. Harms, *Kautschuk-Extruder*, Krausskopf Verlag, Mainz, 1974.
S. Middleman, *Fundamentals of Polymer Processing*, McGraw-Hill, New York, 1977.
Z. Tadmor and C. Cogos, *Principles of Polymer Processing*, John Wiley & Sons, Inc., New York, 1979.
W. Michaeli, *Extrusion Dies, Design and Engineering Computations*, Carl Hanser Verlag, Munich, 1984.
F. Hensen, W. Knappe, and H. Potente, eds., *Plastics Extrusion Technology*, Carl Hanser Verlag, Munich, 1988.
F. Hensen, W. Knappe, and H. Potente, eds., *Handbuch der Kunststoff-Extrusions-technik I Grundlagen*, Carl Hanser Verlag, Munich, 1989.
F. Hensen, W. Knappe, and H. Potente, eds., *Handbuch der Kunststoff-Extrusions-technik II Extrusionsanlagen*, Carl Hanser Verlag, Munich, 1989.
A. Limper, P. Barth, and F. Grajewski, *Technologie der Kautschuk-verarbeitung*, Carl Hanser Verlag, Munich, 1989.
J. White, *Twin Screw Extrusion*, Carl Hanser Verlag, Munich, 1991.
J.-F. Agassant, P. Avenas, J.-Ph. Sergent, and P. J. Carreau, *Polymer Processing, Principles and Modeling*, Carl Hanser Verlag, Munich, 1991.
M. Xanthos, ed., *Reactive Extrusion*, Carl Hanser Verlag, Munich, 1992.
C. Rauwendaal, *Polymer Extrusion*, 4th ed., Carl Hanser Verlag, Munich, 2001.
J. White, *Rubber Processing*, Carl Hanser Verlag, Munich, 1995.
A. Grefenstein, *Reaktive Extrusion und Aufbereitung*, Carl Hanser Verlag, Munich, 1996.
T. Osswald and G. Menges, *Materials Science of Polymers for Engineers*, Carl Hanser Verlag, Munich, 1996.
C. Rauwendaal, *Polymer Mixing, A Self-Study Guide*, Carl Hanser Verlag, Munich, 1998.
C. Rauwendaal, *Understanding Extrusion*, Carl Hanser Verlag, Munich, 1998.
C. Rauwendaal, *Statistical Process Control in Injection Molding and Extrusion*, Carl Hanser Verlag, Munich, 2000.
C. Rauwendaal and M. Pilar Noriega, *Troubleshooting the Extrusion Process*, Carl Hanser Verlag, Munich, 2001.
C. Rauwendaal and K. Cantor, *Extrusion Handbook*, Carl Hanser Verlag, Munich, 2001.

CHRIS RAUWENDAAL
Rauwendaal Extrusion Engineering, Inc.

FILMS, ORIENTATION

Introduction

Molecular orientation provides a wide range of improved properties for thermoplastic films. Most often, molecular orientation results in significantly higher physical properties such as tensile strength and modulus. Orientation may improve thermal properties of a film by increasing the crystallinity. Optical properties are influenced by orientation. Films with high clarity to high opacity may result from orientation. The polarization and reflective responses of films are also impacted by orientation. Enhanced electrical properties, such as increased dielectric constants or piezoelectric properties, may result from orientation. Orientation begins with a cast web suitable for stretching. This web may be stretched in one direction, two directions sequentially, or two directions simultaneously.

Cast Web Considerations

Extrudate Uniformity. The quality of the cast web has a great influence on subsequent orientation steps. While in the extruder, the polymeric melt needs to become homogeneous. Thermal gradients, poor blending of additives or polymeric blends, and entrapped gases may result in imperfections in the cast web. During orientation, these imperfections may lead to high stress concentrations and fracture of the film. Selection of the proper extrusion system, screw design, temperature profiles, venting, and homogenizing equipment will improve the orientation capability of the cast web.

Orientation of multilayer films is a common practice. The various melt streams either flow together in a feedblock prior to entering the die or in a

Encyclopedia of Polymer Science and Technology. Copyright John Wiley & Sons, Inc. All rights reserved.

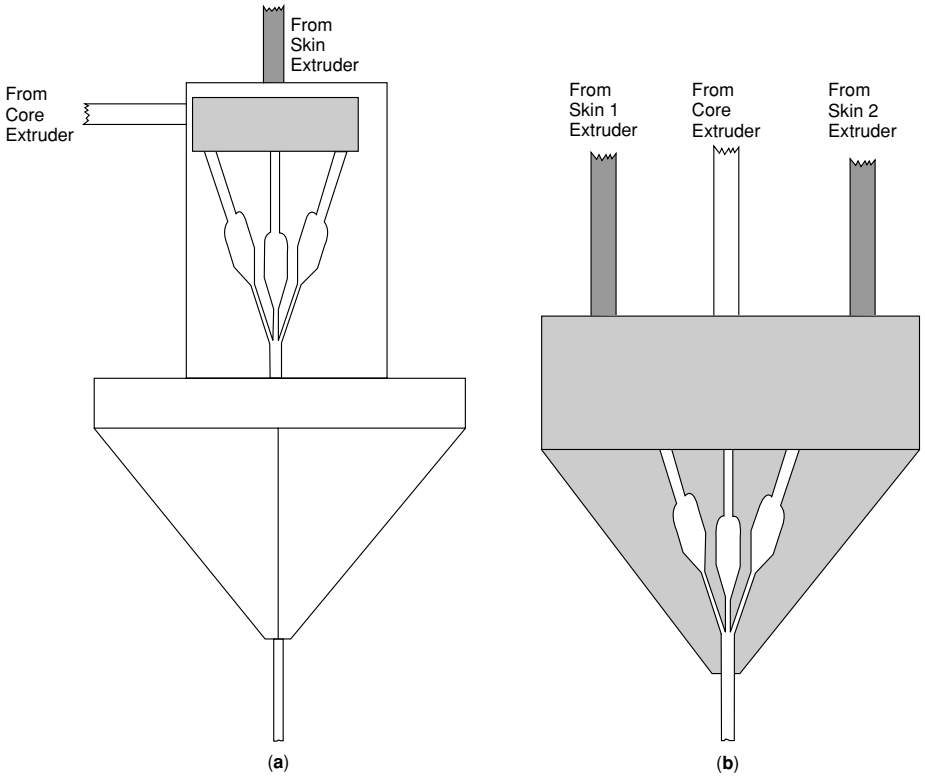

Fig. 1. (**a**) Feedblock and (**b**) die combining melt streams.

multicavity die (Fig. 1). As the layers flow together, viscosity and speed matches are critical. If the layers do not have a good match, interfacial instabilities occur. These flow effects produce minor to severe thickness variations in the extrudate. These variations are typically very localized. During the orientation process, significant stress concentration may be generated around these thickness variations, resulting in fracture of the film.

Quench. Cooling the melt to solidify the viscous extrudate is an important process parameter. Depending on the orientation process, the melt quenching process may be very different. The two primary extrudate geometries are a flat sheet and a tube. Most often, heat needs to be removed from the extrudate as quickly as possible. For semicrystalline polymers with a relatively slow crystallization kinetics, like PET, PEEK, or PPS, rapidly quenching the melt results in a molecular amorphous state. For semicrystalline polymers with a relatively fast crystallization kinetics, like polyethylene, polypropylene, or nylon 6, rapidly quenching the melt allows for the growth of smaller spherulites.

The flat sheet extrudate emerges from the die and falls on a rotating drum or continuous belt (see Fig. 2). The rotating drum or chill wheel cools the melt as quickly as possible. The internal flow design of the chill wheel must provide a uniform cooling surface to the melt. If there are zones of different temperatures, the extrudate will cool at different rates. This could lead to areas of

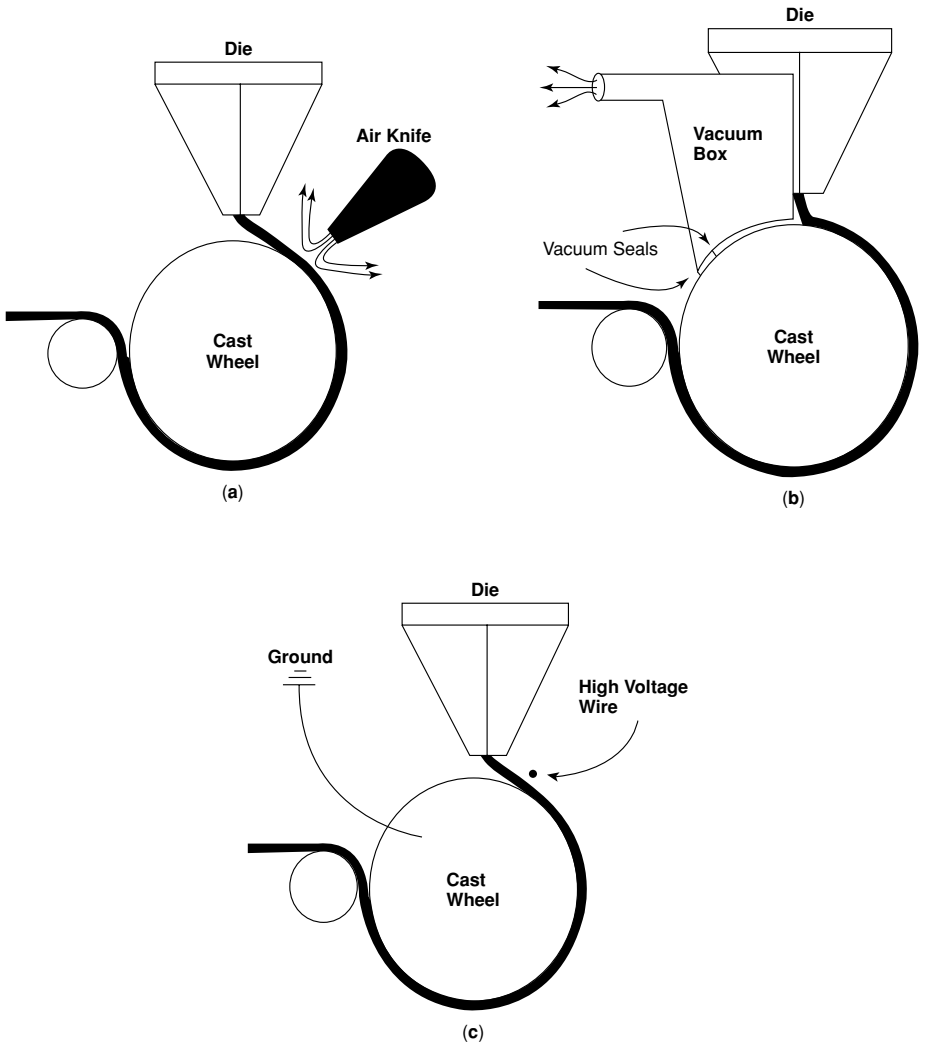

Fig. 2. (**a**) Air knife quenching, (**b**) vacuum box quench, (**c**) electrostatic pinning, (**d**) nip roll quench, and (**e**) water bath.

the cast web with different levels of crystallinity or spherulite size. The chill wheel's surface topography will impact the quench rate and smoothness of the final film.

At high line speeds found in industrial applications, air entrapment between the melt and chill wheel can greatly retard the cooling of the melt. Cooling the melt at different rates in small zones may lead to nonuniform stretching and may even result in fracture of the web during orientation. There are several methods available to improve the heat transfer from the melt into the chill wheel. A slot with high pressure air may be directed at the melt just after it hits the chill wheel. This "air knife" process presses the melt against the chill wheel to increase the heat

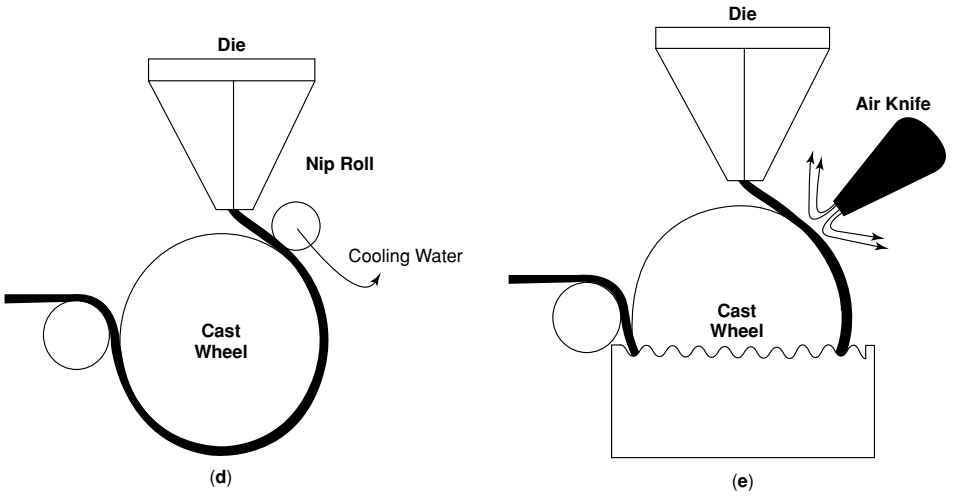

Fig. 2. (Continued)

transfer. The location, angle of incidence, and air flow are the major parameters to consider. Improper tuning of the air knife may result in a cast web with excessive flutter and resultant caliper variations. Uniform pressure or air flow across the entire melt curtain will lead to a uniform cast web.

A second method of pressing the melt against the chill wheel is through electrostatic forces (1). Passing a high voltage through a wire suspended just above the melt produces charged particles which are attracted to the ground, ie, the chill wheel. Electrostatic pinning may work better for some materials or thinner cast webs. Deposits on the wire over time will reduce its effectiveness. Continually feeding new wire will help eliminate this source of variability in the process.

A third approach to improve the heat transfer to the chill wheel is to remove the air between the melt and chill wheel. By applying a vacuum between the die and melt, a more intimate contact between the melt and chill wheel occurs. The vacuum box needs to have seals on the edge of the die in order to produce a strong enough vacuum. Uniformity of the vacuum across the melt curtain will result in a more uniformly quenched cast web. Too high a vacuum will result in the melt curtain being pulled backwards. This could result in the melt developing scratches in it by being dragged across the lip of the die. Ideally, the vacuum should be adjusted to have the melt drop straight away from the die.

A fourth method of assuring good contact to the chill wheel is to mechanically nip the melt against the chill will. This nip roll may also have to be cooled. The surface of the nip usually needs to have some flexibility in it. The cast web may not be perfectly flat and a nip roll will need to press on the entire surface of the melt. High temperature rubber sleeves on the nip roll are most often used, but these may result in producing a rough surface.

The chill wheel may also be partially submerged in a bath to provide additional cooling from the second surface of the extrudate. The flow in a water

bath must be adjusted with care. Continually circulating the water will increase the effectiveness of the quench. High pressure water jets can help keep pressure on the web against the chill wheel. These jets can also deform the surface of the cast web. If they are at the wrong angle, the web could be pulled away from the chill wheel, reducing the quench rate. If this technique is used, the chill wheel needs to be dried off by the time it rotates to the point where melt is again placed on it. If it is too wet, steam bubbles may form creating serious nonuniformities in the cast web. A nip roll or air knife has been used to accomplish the drying of the roll. Combination of both may be required in high speed operations.

When extruding a tube through an annular die there are two kinds of orientation processes available, blown film process and tubular film process. Blown film conducts the orientation in the melt state. The tube is rapidly pulled away from the die by a nip at the top of a tower. Air is pumped through the annular die to inflate the tube and to provide additional cooling. The molecular orientation produced in blown film is quite low compared to solid-state orientation. The molecules are above their melt and have very fast relaxation times. One often refers to the frost line in a blown film process. This is the point where the melt crystallizes. The polymeric web goes through a clear to hazy transition at this point. Further molecular orientation in the web in this stage of the process typically does not occur.

In the tubular film process, or double bubble process, the extruded tube encompasses a cooled mandrel and is pulled away by a nip (Fig. 3). The mandrel should not impart scratches in the tube. This first "bubble" is usually quenched as rapidly as possible for the same reasons in flat film. Controlling the air pressure inside the first bubble is another handle used to determine the quench rate. A water bath on the outside of the tube provides additional cooling of the extrudate. Water flow around the tube is very important. Too great an impingement against the melt may result in surface defects. A tube quenched in this manner will allow subsequent orientation to occur in the solid state at significantly lower temperatures, resulting in higher molecular orientation.

Melt-State Orientation—Blown Film

The blown film process, as shown in Figure 4, orients the molecules while they are in the melt state. Inflating the melt bubble provides the orientation. The air pressure in the bubble is maintained to achieve a certain "blow up ratio," the ratio of bubble diameter to the die diameter. The strain rates are relatively low and relaxation times are very fast. The subsequent molecular orientation obtained via this process falls between the high levels of orientation obtained by stretching in the solid state and very low levels obtained in standard casting operations. The orientation occurs during elongational flow of the melt. Although elongational flow is much more effective at orientation than shear flow, this process has limitations.

There are many methods to increase the amount of orientation frozen in during the blown film process. Systems have been developed to approach

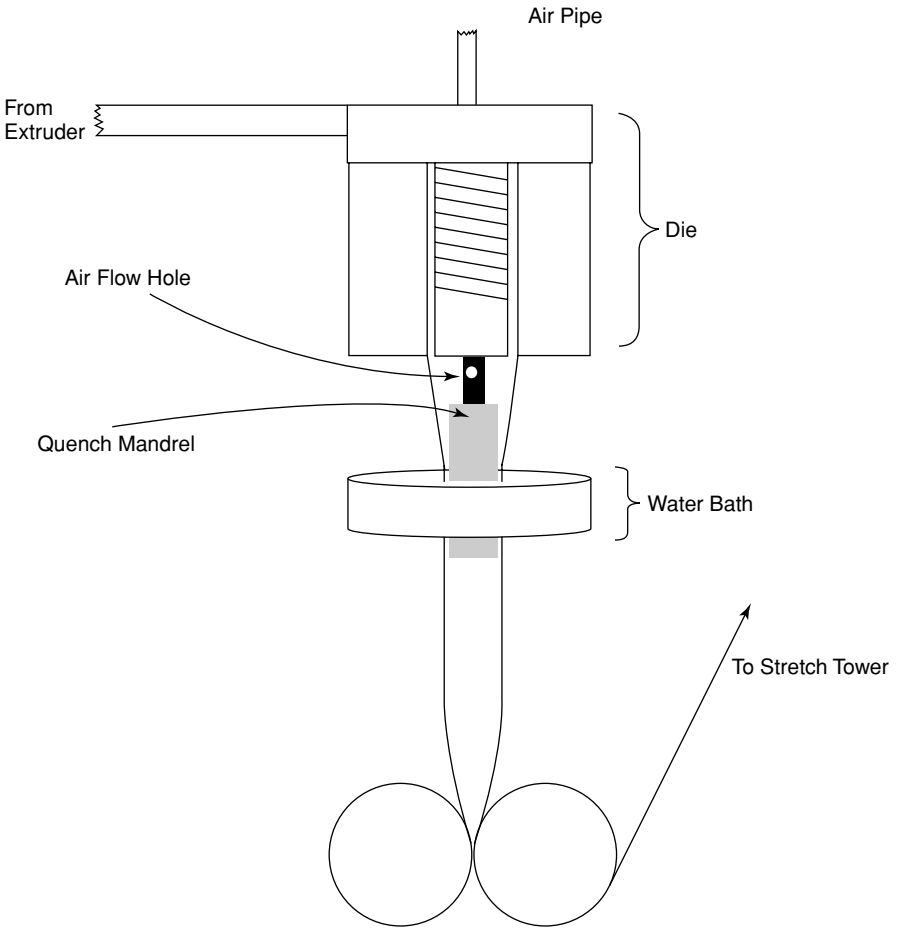

Fig. 3. Tubular film quenching.

quenching a blown film tube from both internal to the bubble and external to the bubble. The faster the quench, the greater molecular orientation is obtained. Internal devices (2,3) can cool the film preferentially, locking in molecular orientation. Externally cooling the blown film bubble in multiple stages (4–6) will allow greater orientation to occur in the tube. Operation of the primary air cooling ring has a dramatic impact on final properties (7). Attempts to separate the machine direction stretching from the transverse direction have shown some promise (8).

Choice of materials, as in any process, is a major consideration. Most resin suppliers and equipment vendors have laboratory to pilot-scale equipment that can screen various resins. Blends of similar resins can also be useful in obtaining greater orientation in the blown film process (9).

There been attempts to generate off-axis orientation in blown film. Rotation of some component of the annular die may impart diagonal orientation (10,11).

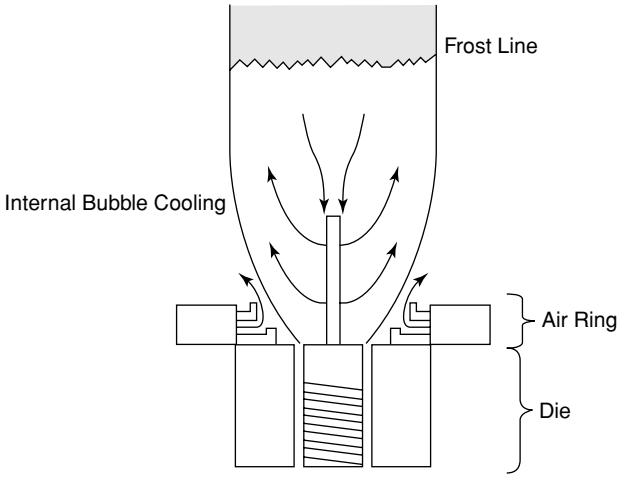

Fig. 4. Blown film process, quench air ring, and internal bubble cooling.

Solid-State Orientation—Monoaxial Orientation

Machine Direction. There are applications in which improvements in properties are required in only one direction. Most often, this high strength axis is in the machine direction (12). Equipment that stretches a film in the machine direction can be called machine direction orienter or length orienter. Uniform heating of the unoriented web is achieved by wrapping the web around a series of heated rolls. These preheat rolls need to have very smooth surfaces to ensure good heat transfer to the web and to prevent scratching the film. These rolls may be driven rolls or idler rolls. Another method to heat up the web uses ir radiation (13). It is also possible to immerse the cast web in a temperature-controlled bath to bring it up to temperature prior to orientation (14).

For a crystallized semicrystalline polymer, the web is heated to below, but near, the melting point. Amorphous polymers will only need to be heated to slightly above their glass-transition temperatures (T_g).

The web passes through an inlet nip, over the preheat rolls and enters the stretch section (Fig. 5). A high speed nip pulls the film in the machine direction. The amount of orientation in the film will be determined by the strain rate, stretch temperature, amount of stretch, and how quickly the film is cooled. Stretching between two rolls is a very high strain rate process in industrial settings, often of the order of 5000%/s. The level of orientation attainable is quite high.

Selection of the polymeric material plays an important role in the efficiency of this process. One needs to consider the molecular weight, the molecular weight distribution, and even the additive package. High loadings of some stabilizers may plate out on the equipment and interfere with consistent heat transfer.

Subsequently, a second or even more (15) machine direction stretching stations may be used. The web may have to be further heated before it is stretched a second time. This process can produce higher molecular orientation in films than

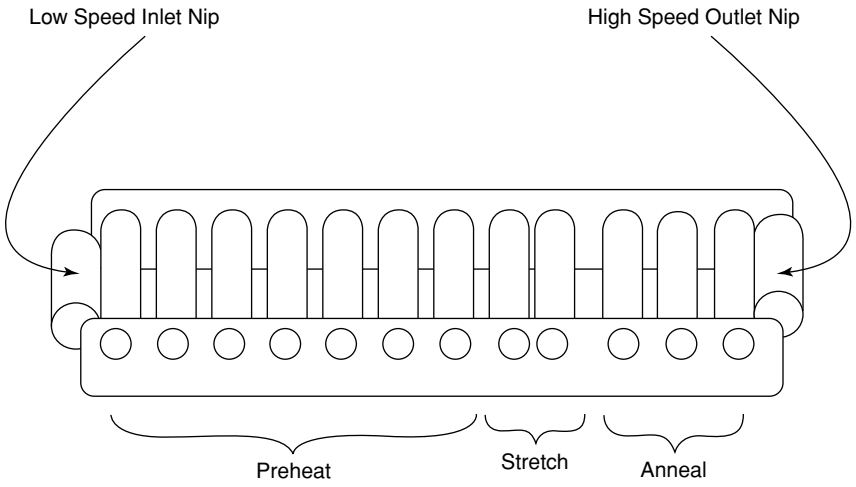

Fig. 5. Machine direction orientation unit.

a single-stage stretch. It is possible to heat-treat the stretched film at this point to allow some relaxation in the material. This will assist in maintaining greater dimensional stability as the film ages.

The width of the film reduces during the machine direction orientation. As the gap between the low speed roll and high speed roll increases, this width reduction increases. One approach to minimize the width reduction is to shorten the stretch gap. Another approach is to pin the web against the rollers with high-pressure air (16).

This machine direction stretching process is also used as the first orientation step in sequential biaxial film manufacture.

A second major machine direction orientation process involves a very high pressure nip (see Fig. 6). Input cast webs are cold-rolled or compression-rolled

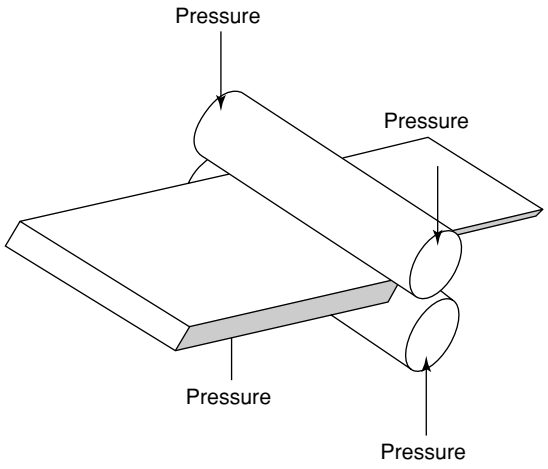

Fig. 6. Compression rolling process.

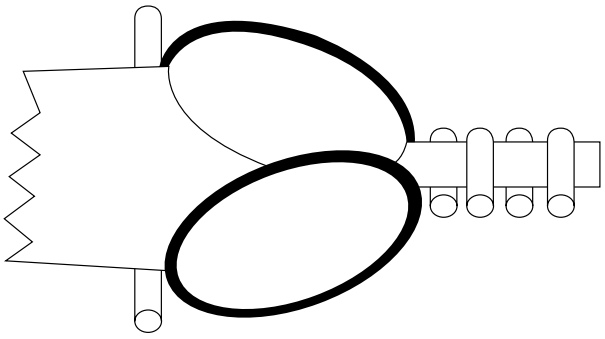

Fig. 7. Disc orienter.

to impart molecular orientation. Prior to entering the nip, a coating (17) or surface treatment (18) may be applied to the cast web. This surface treatment helps lubricate the film while in the high pressure nip. The cast web may enter the high pressure nip anywhere from room temperature to below the melt point. The temperature typically is above the glass-transition temperature of the material. Pressures on the cylinder arms can be of the order of 1,000,000 psi for some industrial applications. The thickness of the polymeric film can be reduced from 5 to 95% (19).

As with the drawing process above, it is possible to incorporate several compression rolling stages in line (20). Combination of a length orienter and a compression rolling station (21) may lead to triaxial orientation morphology. Molecular orientation from this type of process can be exceedingly high. This level of orientation leads to properties of films that are not commonly attained through standard length orientation draw stations.

Transverse Direction. In the case where the cross direction requires the improved properties, there are several ways to generate such films. Large discs (22) with a groove in the perimeter are tilted with respect to each other. At the discs' closest spacing, each edge of the web is secured to the perimeter of the divergent discs by a belt. At this point, the web must be preheated to its orientation temperature. This can be accomplished by running the web over a number of heated rolls just prior to clamping the web onto the diverging discs.

As the discs rotate, the web is stretched in the cross direction. At some point around the discs, the belt holding the web to the perimeter is peeled away and the transverse-oriented film continues down the process line (Fig. 7). If the forces required to stretch the film are quite large, this technique may not work. The film may be pulled out from under the belt.

Stretching the film only in the transverse direction may also be accomplished by using a tenter (23). The tenter process uses clips on a chain (Fig. 8). The clips grab each side of the cast web and transport the web through an oven. Once the film is heated to the orientation temperature, the rails that the chains ride on diverge. This method alone is seldom employed in practice.

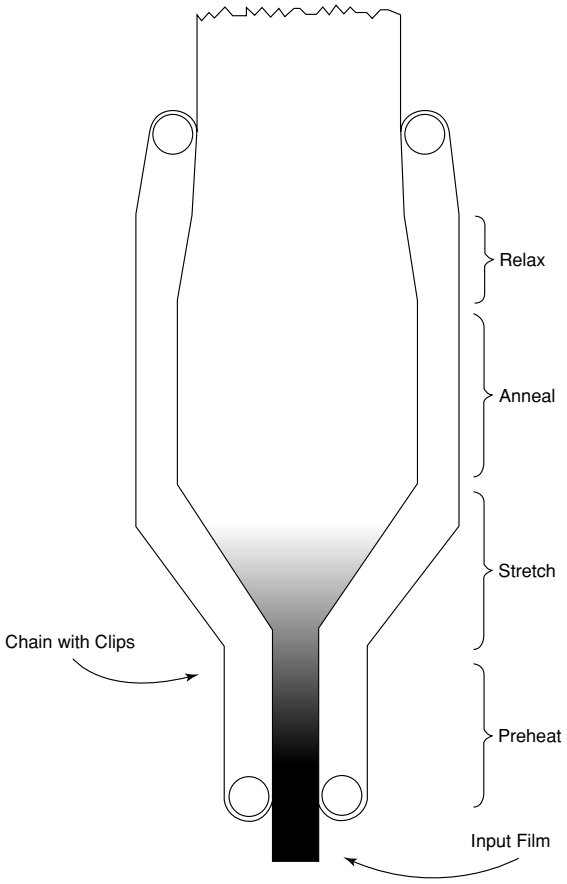

Fig. 8. Standard tenter frame.

Solid-State Orientation—Biaxial Orientation

Orienting the film in both the machine and transverse direction has produced many significant products. Biaxial orientation can be achieved in many different methods. In sequential orientation, the web is stretched first in one direction, usually the machine direction, and then in a second direction. The other main method of biaxial orientation is simultaneous biaxial stretching—stretching the film in both directions at the same time. The simultaneous orientation process has two major processes, one is based on a flat film approach and the second processes the web in a tube.

Sequential Biaxial Orientation. The standard process for sequential biaxial orientation is machine direction orientation followed by transverse orientation. This is a continuous process. The machine direction stretch occurs similar to the process described in the monoaxial section (Fig. 5). However, a second draw station is typically not present in this process. In the pure monoaxial orientation case, the process often tries to maximize the molecular orientation in the

web. This would lead to difficulties in the sequential biaxially oriented process. The orientation in this first step must be low enough such that the molecular structure of the film will support transverse direction stresses. Films stretched highly in the machine direction tend to split when pulled in the transverse direction.

The second stretch occurs in a tenter (Fig. 8). Often the temperature will need to be higher for the second stretch. A long distance in the oven is required to heat the web to the orientation temperature. The rate of divergence of the rails will impact the final properties of the film in the transverse direction. Once the stretch has been completed, the rails are often brought slightly closer together to relax the film. In this section, additional annealing may increase the crystallinity in the film for semicrystalline materials that are quenched to an amorphous state at the chill wheel.

Reversing the order of sequential stretching (24) is possible. The orientation in the first stretch is usually limited. By reversing the order, this allows the machine direction orientation to be second and hence greater than if it were done first.

A third stretching operation may also be performed. This is done to generate greater orientation in the film (25,26).

Simultaneous Biaxial Orientation. There are two predominate systems available to do this, tubular and flat film. In the tubular process (see Fig. 9), also referred to as the double bubble process, a continuous tube is extruded and quenched. Typically, an interior cooled mandrel is hung from the die inside the tube. The surface of the mandrel may greatly influence the interior surface of the tube. Care must be taken not to impart scratch lines in the melt as it is pulled down over the mandrel. Air pressure in this primary tube is very critical. The melt needs to be held out over the mandrel but not too far away. A water bath on the external side of the tube helps quench the tube rapidly. A nip pulls the tube from the die and acts to isolate the casting bubble from the air pressure in the stretching bubble (27).

Going through a nip can be very difficult for a tube. Cracks in the edge or localized stretching in the crease can negatively impact the film produced. There are several proprietary methods used to reduce this area of concern. The tube is often reinflated and transported to the top of a stretching tower. At the top of the tower, the tube is again nipped. This inlet nip again helps isolate pressures from the stretching and casting bubbles. Once through the inlet nip, the tube will descend through a heater section to the bottom of the tower.

Heaters will soften the tube and the tube is inflated with air. The initial filling of the tube with air requires good timing by the operator. As air is pumped into the expanding tube, the operator pulls the tube away faster than the top nip supplies cast tube. Once the inflated bubble reaches the bottom of the stretch tower, a second nip closes. This second nip seals the air in the tube. The second nip runs at a speed greater than the first and provides the machine direction orientation. The amount of air pumped into the tube before the second nip closes is one of the primary factors in the transverse direction stretch ratio. Other process variables that contribute to the transverse stretch ratio are the web temperature and machine direction stretch ratio. Pressure in the tube may be increased by narrowing the frame used to collapse the bubble.

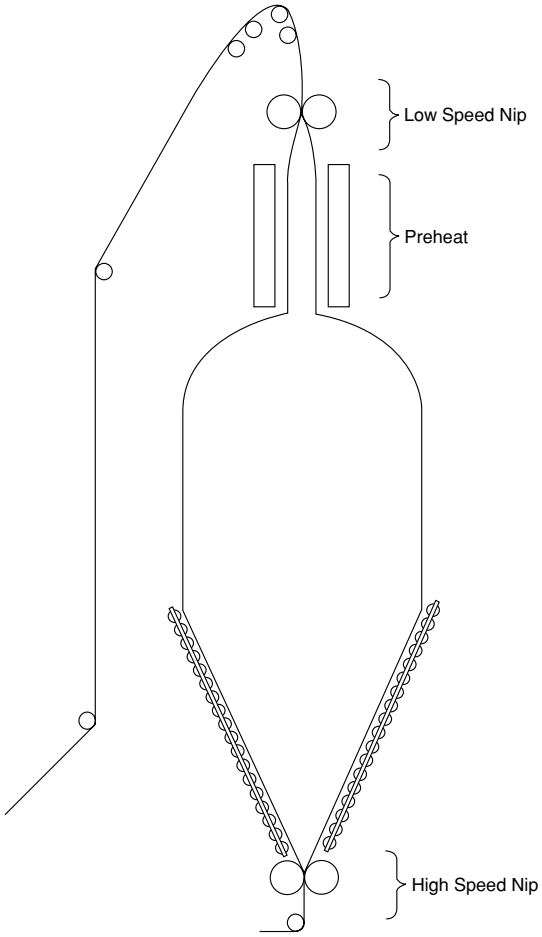

Fig. 9. Tubular orientation process.

Biaxial stretching of the tube occurs in one temperature zone, which can be limiting to the ultimate molecular orientation achieved in both directions. Another limitation to this method is gradual deflation of the stretch bubble over time. There are a few proprietary methods to maintain a constant air pressure in the stretching tube to extend the run time of this process. Continuous operation of a tubular bubble for over a week is very possible.

After the tube has been biaxially stretched, the film needs to be annealed. This process can be done in several ways (Fig. 10). The most common is to insert into the tube a set of parallel bars. These bars have air flowing out on their outer surfaces that allow the film to slide over them. These bars are in an oven or ir-heating chamber. As the tube reaches the end of the annealing zone, it is split open and sent to the winder.

Alternately, a third bubble may be inflated and passed through an oven to anneal the tubular film. This method may be preferred if excessive heat is required to anneal or crystallize the material. Shrink forces for some polymeric

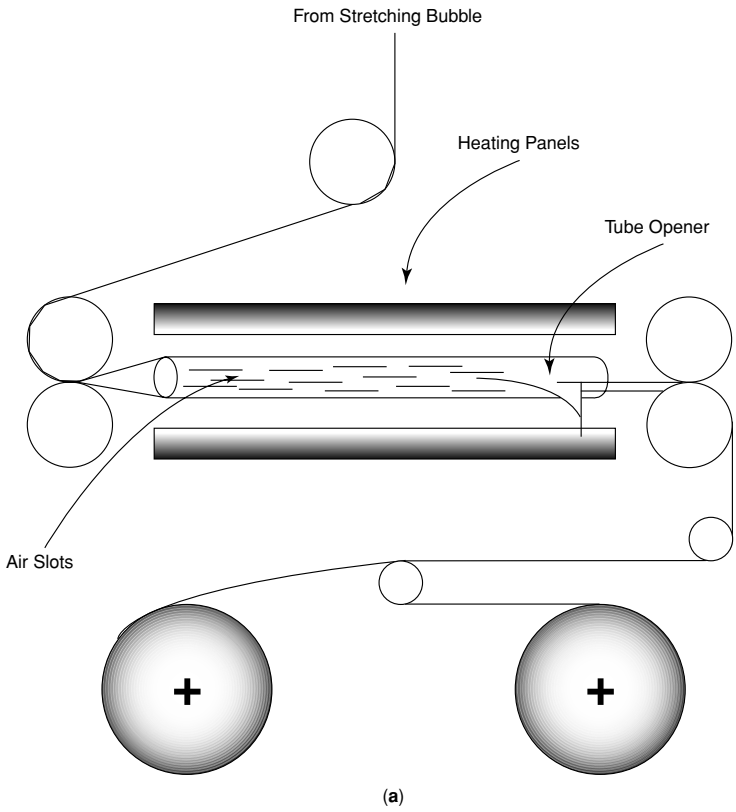

Fig. 10. Tubular annealing process: (**a**) air rails and (**b**) triple bubble.

systems may be too great to pull the tube over the annealing bars mentioned above.

One of the features of tubular film process is the roll formation obtained. It is common to rotate the tube or collapsing frame. This will distribute caliper variations in the film across the wound up roll. Soft areas and hard bands may be eliminated in the output roll with this process. This process requires low labor content as compared to larger flat film lines. As all the film is uniformly stretched, the yield of this process may be very high.

In the flat film biaxial process there are several methods available to simultaneously stretch a web (28,29). The throughput on the film line can be significantly greater with the flat film process as compared to the tubular process. With flat film processes, there is more flexibility in the temperature profile during the stretching process than that found in the tubular process. This can help attain greater levels of orientation in the film.

Common to the various processes, clips grab the edge of the cast web. These clips must allow the web to be pulled in both directions. This type of clip requires special designs as compared to the transverse direction only style clips. The geometry of the clip footprint and its surface shape are key characteristics.

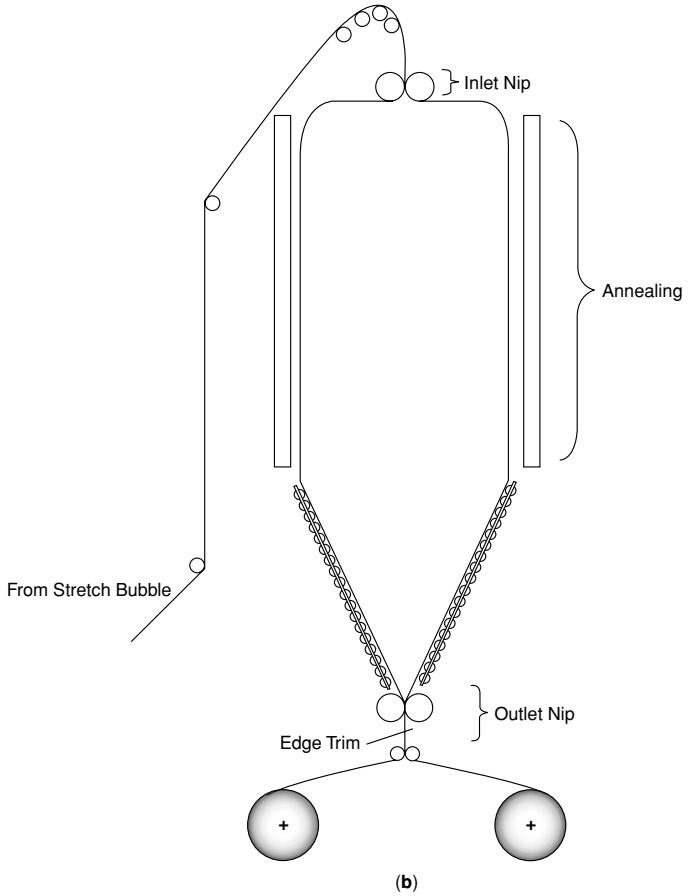

Fig. 10. (Continued)

The main difference between the flat film methods is how the clips are accelerated through the tenter. In one commercial process, the clips ride in a screw (30). As the pitch of the screw increases, the clips accelerate in the machine direction (Fig. 11). The clips may be passed from one screw to another. This type of process has large constraints on the machine direction orientation. Once the screw is machined, the machine direction stretch ratio is fixed. Changing from one screw to another can demand excessive time. A machine direction orienter prior to the inlet of the tenter oven may be used with this type of tenter (31). This permutation of this process will allow for changing the overall machine direction stretch ratio without changing the screws.

Another type of simultaneous stretching may be accomplished with a pantograph type stretching process (32). This expandable frame rides on the tenter rails (Fig. 12). The clips are initially packed close together by a drive sprocket at the entrance to the tenter oven. After transporting the web through the preheat zone, the pantograph is expanded in the machine direction at

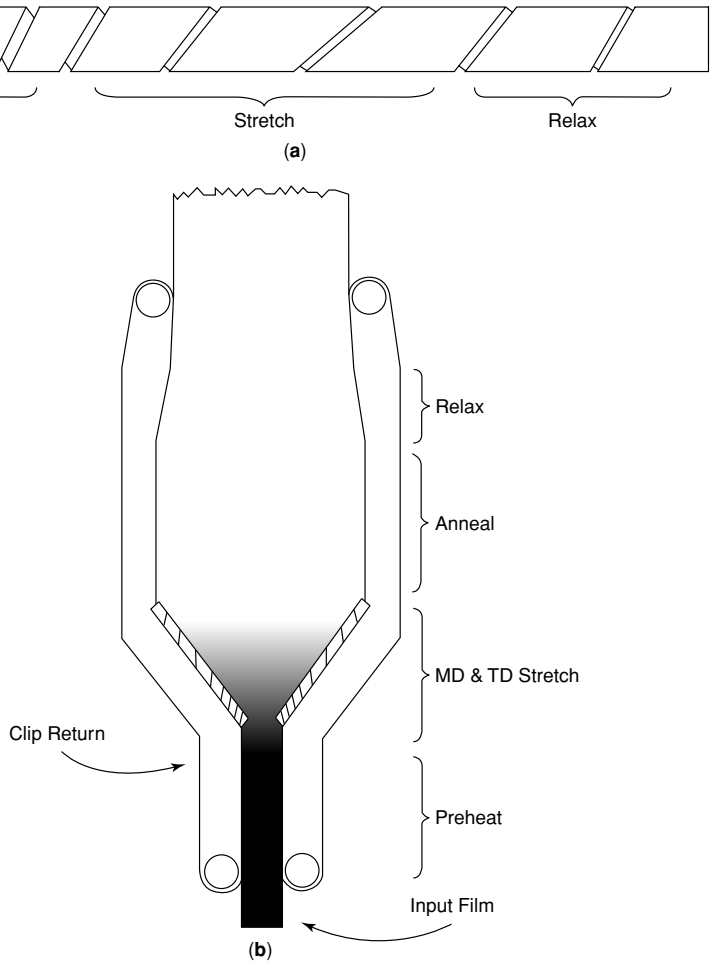

Fig. 11. Screw for screw orientation process: (**a**) stretching screw and (**b**) simultaneous biaxial tenter frame.

the same time the rails diverge. This produces a simultaneous orientation to the polymeric film. A drive sprocket at the end of the tenter maintains the separation of the clips for transport back to the tenter entrance. A third sprocket drive collapses the expanded pantograph between it and the inlet drive sprocket.

Determination of where and by how much the pantograph expands may be controlled by an additional rail or shoe that will squeeze the pantograph causing it to expand.

Most recently, a linear synchronous motor-based process (33) has been developed. The commercialized process (34) has been run successfully on several full production lines. Multilayer polyester and polyolefin films are commercially made via this latest technology. This process uses a magnetic wave to propel the

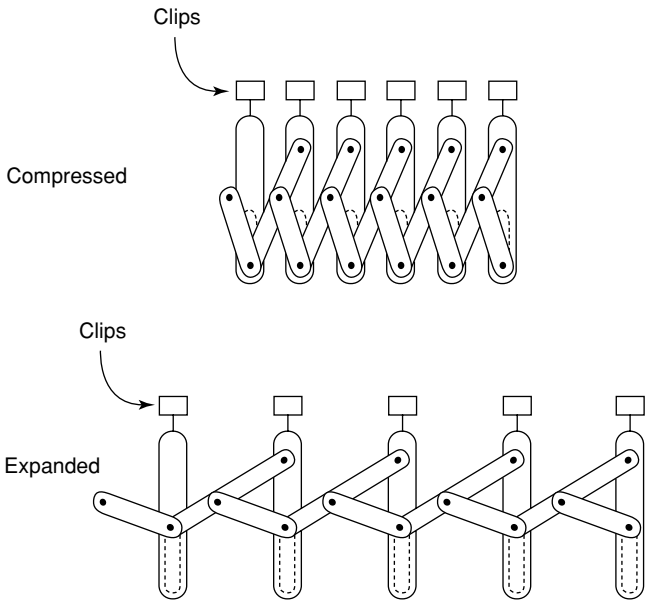

Fig. 12. Pantograph simultaneous biaxial orientation process.

clip through the oven. Once the film has been preheated, it enters the stretch section of the oven. As the rails the clips ride on diverge, the magnetic wave will accelerate the clip in the machine direction. Strain rates in the machine direction are typically of the order of 400%/s. This process allows for significant flexibility in the machine direction orientation as compared with the previous technologies.

Each clip frame assembly, as shown in Figure 13, has permanent magnets attached to its top and bottom. The linear motor consists of fixed stators. A moving magnetic wave is produced when the stator windings are energized by a three-phase electric current. This wave interacts with the magnets on the clip frame to push or pull it through the tenter (see Fig. 14). As the frequency of the power supply is changed, the speed of the magnetic wave is proportionally changed as well. Control of the ac current supply to each stator allows for programming various accelerations as well as the total amount of machine direction stretch (35). The stretch forces required by some materials or thicker webs may pose a problem for this process. If the stretch force exceeds the force the magnetic wave can impart on the clips, the clips will slip the wave. This can lead to nonuniform stretching or in the extreme case, a lack of clips at the tenter inlet.

The main feature of this type of process is the very high level of flexibility attainable in the machine direction stretch. The strain profile may be linear, exponential, logarithmic, or stepped. The amount of stretch can easily be programmed to occur in a given temperature zone in the oven. Changing the machine direction stretch ratio can easily be programmed. It takes just

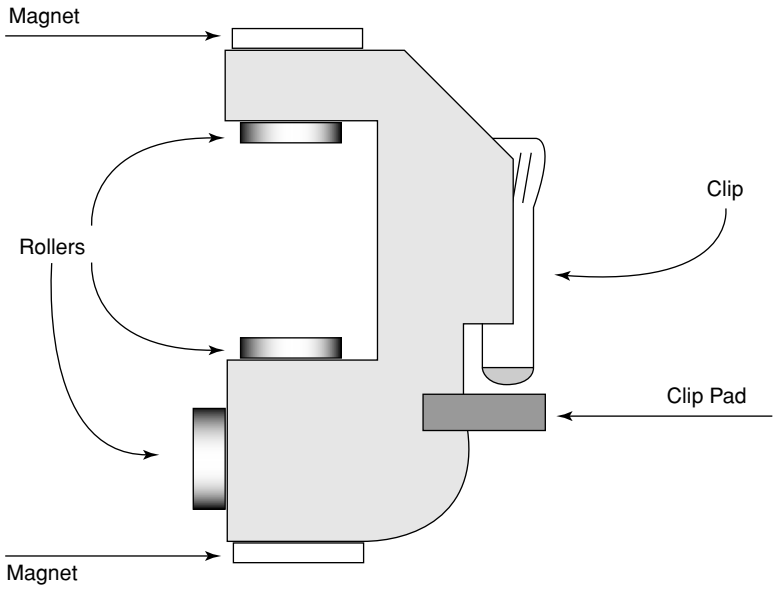

Fig. 13. Linear motor clip assembly.

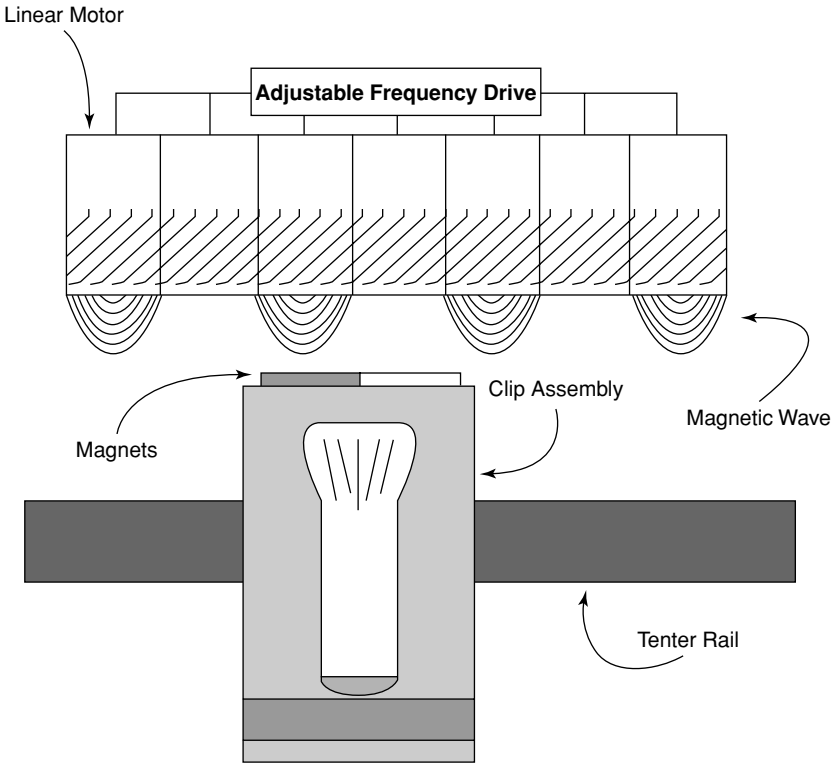

Fig. 14. Magnetic wave propulsion system.

minutes to make slight to moderate changes in the machine direction stretch profile.

A concern for these simultaneous biaxial orientation processes relates to the clips separating from each other. As the clips separate in the oven, the edge of the web between the clips tends to bow in. This can result in lower yields. At the very edge of the web, the film is oriented purely in the machine direction. The orientation in the film changes in going from the edge toward the centerline. The breadth of this transition region can be controlled with process parameters and material properties.

BIBLIOGRAPHY

1. Jpn. Pat. JP 11020004 A (1999), H. Okashiro, K. Toyoda, and K. Okubo (to Toray Industries Inc.).
2. Jpn. Pat. JP 11028764 A (1999), S. Sakai.
3. U.S. Pat. 5,891,480 (1999), J. Nowak and C. P. Schmidt (to Reifenhaeuser GmbH & Co.).
4. Ger. Pat. DE 19816119 A1 (1999), Z. Doboczky.
5. Ger. Pat. DE 29806595 U1 (1999), Z. Doboczky.
6. Eur. Pat. EP 641638 A1 (1995), T. Matsui and co-workers (to Mitsubishi Petrochemical Co. Ltd.).
7. Eur. Pat. EP 180029 A (1986), A. Bose (to Union Camp).
8. Ger. Pat. DE 4308689 C2 (1993) (to Folie Erzeugnisse GmbH).
9. U.S. Pat. 5,641,848 (1997), J. Giacobbe (to Montell North America Inc.).
10. Jpn. Pat. JP 79012507 B (1979) (to Mitsui Petrochemical Industries Co. Ltd.).
11. U.S. Pat. 5,350,471 (1994), M. Planeta.
12. Eur. Pat. EP 779144 A2 (1997), D. Busch (to Hoechst Trespaphan GmbH).
13. Jpn. Pat. JP 62087320 A (1987), Y. Kikumoto and H. Shirohige (to Teijin Ltd.).
14. Jpn. Pat. JP 4069228 A (1992), T. Arai and T. Yanagisawa (to Shinetsu Chemical Industries Co. Ltd.).
15. U.S. Pat. 4,767,578 (1988), H. Thimon (to Newtec Int.).
16. Ger. Pat. DE 3414676 A (1985), H. Stockmeyer (to Berstorff Maschbau GmbH).
17. U.S. Pat. 4,085,187 (1978), R. Jenks (to Revere Copper and Brass, Inc.).
18. U.S. Pat. 4,548,770 (1985), G. Holland (to Crown Zellerbach Corp.).
19. World Pat. WO84/02707 (1984), E. Zuscik (to Crown Zellerbach Corp.).
20. U.S. Pat. 5,695,698 (1997), A. Ajji, M. Dumoulin, and J. Dufour.
21. World Pat. WO92/04176 (1992), J. Magill (to University of Pittsburgh of the Commonwealth System of Higher Education).
22. Eur. Pat. EP 672516 A2 (1995), E. Ruscher (to Kimberly Clark Corp.).
23. U.S. Pat. 4,137,362 (1979), Y. Miki (to Nitto Electric Industries).
24. U.S. Pat. 3,271,495 (1966), L. Gronholz (to E. I. du Pont de Nemours & Co., Inc.).
25. U.S. Pat. 4,451,533 (1984), R. Wong (to Minnesota Mining and Manufacturing).
26. U.S. Pat. 4,698,261 (1987), L. Bothe (to Hoechst Aktiengesellschaft).
27. U.S. Pat. 5,891,4840 (1999), C. Schmidt (to Reifenhauser GmbH & Co.).
28. Brit. Pat. GB 2120597 (1983), H. Rottenstei (to Lindauer Dornier GmbH).
29. Eur. Pat. EP 149878 A (1985), Y. Tagami (to Toray Industries Inc.).
30. Ger. Pat. DE 2853817 A (1980), A. Hutzenlaub (to Kampf GmbH).
31. U.S. Pat. 4,330,499 (1982), F. Aufsess (to Internationale Octrooi Maatschappij B. V.).
32. Eur. Pat. EP 0149878 B1 (1987), H. Yoshimura (to Toray Industries, Inc.).
33. U.S. Pat. 3,890,421 (1975), F. Habozit (to La Cellophane).

34. World Pat. WO 8810188 A (1988), W. Hommes (to E. I. du Pont de Nemours & Co., Inc.).
35. J. Breil, *Specialty Plastic Films '98—Global Film Resins, Markets, Applications 14th Annual World Congress*, Brueckner Maschinenbau GmbH, 1998.

TOM P. HANSCHEN
3M Company

FLUOROCARBON ELASTOMERS

Introduction

Fluorocarbon elastomers are fluorine-containing, cross-linked amorphous polymers with a carbon–carbon backbone. They are designed for demanding service applications in hostile environments characterized by broad temperature ranges and contact with industrial chemicals, oils, or fuels.

Military interest in the development of fuel- and thermal-resistant elastomers for low temperature service created a need for fluorinated elastomers. In the early 1950s, the M.W. Kellogg Co., in a joint project with the U.S. Army Quartermaster Corps, and 3M Co., in a joint project with the U.S. Air Force, developed two commercial fluorocarbon elastomers. The copolymers of vinylidene fluoride (CF_2=CH_2) and chlorotrifluoroethylene (CF_2=CFCl) became available from Kellogg in 1955 under the trademark of Kel-F (1–3), and a polymer based on poly(1,1-dihydroperfluorobutyl acrylate) was marketed in 1956 as 3M brand fluororubber 1F4 (4). The poor acid-, steam-, and heat-resistance of the latter limited its commercial use (see also VINYLIDENE FLUORIDE POLYMERS).

In the late 1950s, the copolymers of vinylidene fluoride and hexafluoropropylene (CF_2=$CFCF_3$) were developed on a commercial scale by 3M (Fluorel) and by DuPont (Viton) (5–7). In the 1960s, terpolymers of vinylidene fluoride, hexafluoropropylene, and tetrafluoroethylene (CF_2=CF_2) were developed (8) and commercialized by DuPont as Viton B. At about the same time, Montedison developed copolymers of vinylidene fluoride and 1-hydropentafluoropropylene as well as terpolymers of these monomers with tetrafluoroethylene marketed as Tecnoflon polymers (9,10) (see also PERFLUORINATED POLYMERS).

Encyclopedia of Polymer Science and Technology. Copyright John Wiley & Sons, Inc. All rights reserved.

In the 1960s and 1970s, DuPont introduced polymers containing perfluoro (methyl vinyl ether), CF_2=$CFOCF_3$. With tetrafluoroethylene and a cure-site monomer, it gives a perfluoroelastomer, and when it is used as a comonomer with vinylidene fluoride and/or tetrafluoroethylene, improved low temperature properties are obtained (11,12).

Peroxide cure-site monomers, typically iodine- or bromine-containing fluorolefins, have also been polymerized with the above monomers for improved steam- and amine-resistance (13–20).

Copolymers of propylene and tetrafluoroethylene were introduced in the early 1980s by Asahi Glass Co., Japan (21–26). 3M introduced bisphenol/onium cured copolymers of vinylidene fluoride, tetrafluoroethylene, and propylene in the late 1980s (27–30).

The principal commercial fluorocarbon elastomers are given in Table 1.

Of the approximately 10,000 t consumed worldwide per year, ca 40% is used in the United States, 30% in Europe, and 20% in Japan, and 10% APAC (excl. Japan); 2000 prices were $44–$4000/kg.

Properties

The characteristics of vulcanizates prepared from commercially available fluorocarbon elastomer gumstocks are given in Table 2.

Thermal Stability. The retention of elongation after thermal aging is an indication of the thermal stability of fluorocarbon elastomers. As shown in Figure 1, fluorocarbon elastomers are far superior to hydrocarbon elastomers. A more severe test at 205°C shows that a typical molding compound retains 90% of initial elongation after 1 year. Retention of tensile strength is another important characteristic of fluorocarbon elastomers. Figure 2 demonstrates the effect of long-term heat aging on a typical O-ring compound made from vinylidene fluoride–hexafluoropropylene copolymer; 90% of the initial tensile strength is retained after

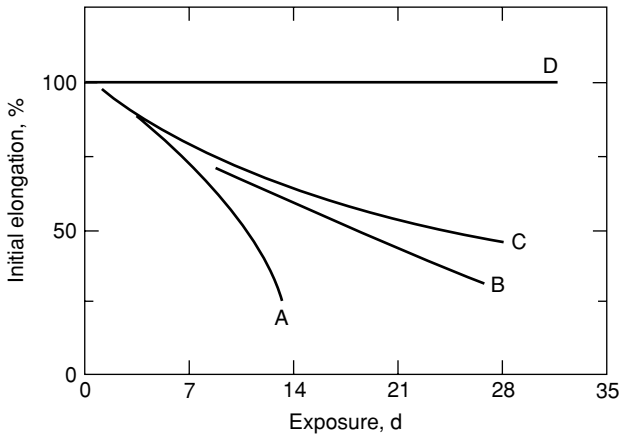

Fig. 1. Elongation retention of vulcanized elastomers at 150°C: A, nitrile; B, ethylene–propylene–diene monomer (EPDM); C, acrylate; D, fluorocarbon (31).

Table 1. Commercial Fluorocarbon Elastomers

Copolymer	Trademark	Supplier
Poly(vinylidene fluoride-*co*-hexafluoropropylene)	Dai-el	Daikin
	Dyneon	LLC[a]
	Tecnoflon	Ausimont
	Viton	DuPont Dow[b]
Poly(vinylidene fluoride-*co*-hexafluoropropylene) plus cure-site monomer	Dyneon	LLC
Poly(vinylidene fluoride-*co*-hexafluoropropylene-*co*-tetrafluoroethylene)	Dai-el	Daikin
	Dyneon	LLC
	Tecnoflon	Ausimont
	Viton	DuPont Dow
Poly(vinylidene fluoride-*co*-hexafluoropropylene-*co*-tetrafluoroethylene) plus cure-site monomer	Dai-el	Daikin
	Dyneon	LLC
	Tecnoflon	Ausimont
	Viton	DuPont Dow
Poly[vinylidene fluoride-*co*- tetrafluoroethylene-*co*-perfluoro(methyl vinyl ether)] plus cure-site monomer	Dai-el	Daikin
	Tecnoflon	Ausimont
	Viton	DuPont Dow
Poly[tetrafluoroethylene-*co*-perfluoro(methyl vinyl ether)] plus cure-site monomer	Dai-el	Daikin
	Dyneon	LLC
	Kalrez	DuPont Dow
	Tecnoflon	Ausimont
Poly(tetrafluoroethylene-*co*-propylene)	Aflas	Asahi Glass
	Dyneon	Dyneon
Poly(vinylidene fluoride-*co*-tetrafluoroethylene-*co*-propylene)	Aflas	Asahi Glass
	Aflas	Asahi Glass
	Dyneon	LLC
	Viton	DuPont Dow
	Aflas	Asahi Glass
Poly(tetrafluoroethylene-*co*-ethylene-*co*-perfluoro(methyl vinyl ether) plus cure-site monomer	Viton Extreme	DuPont Dow

[a]Wholly owned subsidiary of 3M.
[b]Joint venture between DuPont and Dow Chemical Co.

1 year at 205°C. Perfluoroelastomers [copolymers of tetrafluoroethylene and perfluoro (alkyl vinyl ethers)] are more thermally stable yet. Some of these polymers are stable up to 320°C.

Chemical Resistance. The resistance of fluorocarbon elastomer compounds to chemicals is given below:

(1) *Excellent resistance, may be used without reservation*, eg, automotive fuels and oils, hydrocarbon solvents, aircraft fuels and oils, hydraulic fluids, and certain chlorinated solvents.

Table 2. Properties of Fluoroelastomers

Property	ASTM test method	Value/description
Physical properties		
Tensile strength, MPa[a]	D412	9–20
100% modulus, MPa[a]		2–16
Elongation at break, %		100–500
Hardness, Shore A	D2240	45–95
Compression set, %	D395[b]	
70 h at 25°C		9–16
70 h at 200°C		10–30
1000 h at 200°C		50–70
Specific gravity of gumstock	D297	1.80–2.04
Low temperature flexibility,[c] °C		
T_g	E1356	0 to −30
TR10	D1329	0 to −30
Brittle point,[c] °C	D2137	−18 to −50
Thermal degradation temperature, °C	E1131	400–550
General characteristics		
Gas permeability		Very low
Flammability		Self-extinguishing or nonburning[d]
Radiation resistance		Good to fair
Abrasion resistance		Good and satisfactory for most uses
Weatherability and ozone resistance		Outstanding[e]

[a]To convert MPa to psi, multiply by 145.
[b]Method B for 5-mm O-ring.
[c]Highly dependent on material grade.
[d]When properly formulated.
[e]Unaffected after 200-h exposure to 150-ppm ozone.

(2) *Good to excellent resistance, gum and compound must be chosen with care*, eg, highly aromatic solvents, polar solvents, water and salt solutions, Aqueous acids, dilute alkaline solutions, oxidative environments, and amines.

(3) *Not recommended, to be used only with perfluoro and TFE/propylene elastomers*, eg, ammonia, strong caustic, 50% sodium hydroxide above 70°C, and, certain polar solvents, eg, low molecular weight ketones, esters, and ethers.

However, Viton Extreme (32) is resistant to ammonia, strong caustic, and certain polar solvents.

In the past 10 years fluoroelastomers containing 70–72% fluorine have been introduced. These highly fluorinated elastomers are resistant to the new oxygenated fuels now used in the automobile industry and meet the stringent permeation requirements (33–35) (see Fig. 3).

Compression-Set Resistance. Fluorocarbon elastomers are used in the sealing industry because of their resistance to compression set under extreme

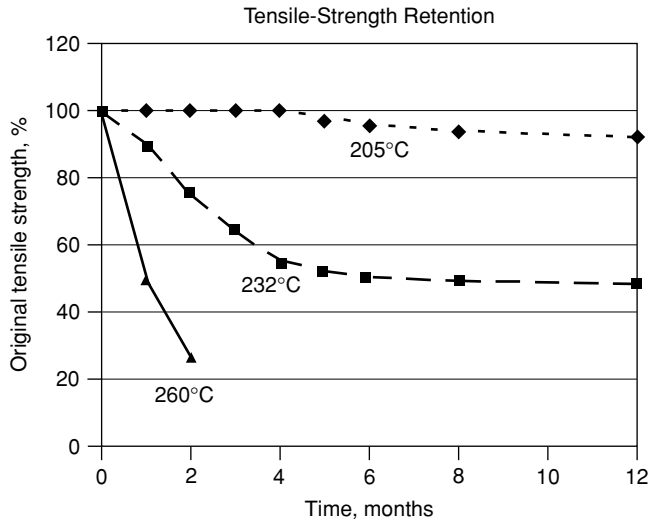

Fig. 2. Tensile-strength retention in continuous service for fluorocarbon elastomers, compound 1 (see Table 5).

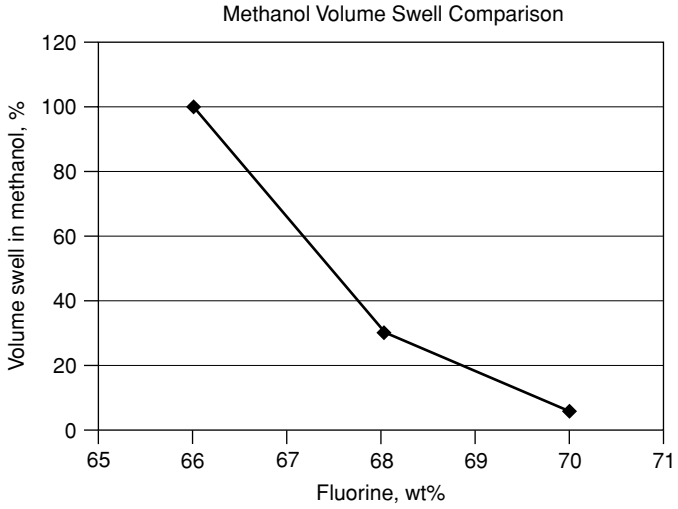

Fig. 3. The percent volume swell in methanol for 7 days at 21°C compared with the weight percent of fluorine in fluorocarbon elastomers: 66%, dipolymer of vinylidene fluoride–hexafluoropropylene; 68% and 70%, terpolymers of vinylidene fluoride–hexafluoropropylene–tetrafluoroethylene.

conditions. Plots of compression set vs time are shown in Figure 4 for compounds prepared especially for compression-set resistance (O-ring grades).

Manufacture

The elastomers listed in Table 1 are typically prepared by high pressure, free-radical, aqueous emulsion polymerization (5,8,36,37). The initiators are organic or

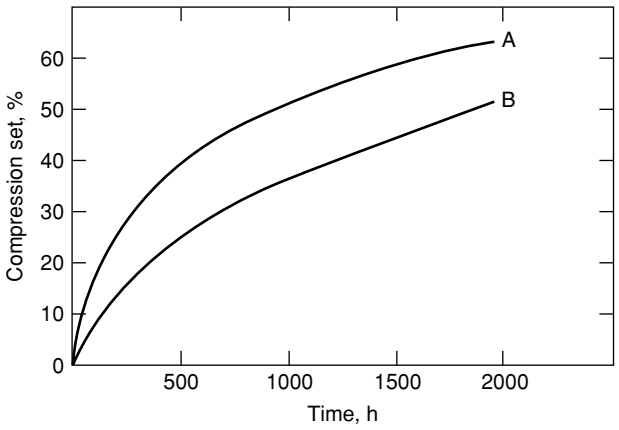

Fig. 4. Compression-set values of fluorocarbon elastomers at 200°C (ASTM D 395), 3.5-mm O-rings: A, compound 1 (see Table 5); B, compound 2 (see Table 5).

inorganic peroxy compounds, such as ammonium persulfate, and the emulsifying agent is usually a fluorinated acid soap. The temperature ranges from 30 to 125°C and the pressure from 0.35 to 10.4 MPa (50–1500 psi). The molecular weight of the polymer is controlled by the ratio of initiator to monomer or choice of chain-transfer agent, or both. Typical chain-transfer agents are ethyl acetate, methanol, acetone, diethyl malonate, and dodecylmercaptan (38–40). A typical polymerization recipe is given in Table 3.

The aqueous emulsion polymerization is conducted by batch, semicontinuous, or a continuous process (Fig. 5). In a simple batch process, all the ingredients are charged to the reactor, the temperature raised, and the polymerization run to completion.

In a semicontinuous process all the recipe ingredients are added to the reactor and the vessel is pressurized with the monomers. The reaction is started and the consumed monomers are continuously replenished in order to maintain constant reactor pressure.

In a continuous process (37), feeding of the ingredients and removal of the polymer latex are continuous. The discharge of latex from the reactor is controlled by a pressure-control or relief valve. The polymer latex is coagulated into a crumb

Table 3. Typical Fluorocarbon Elastomer Polymerization Recipe

Component	Grams
Vinylidene fluoride	61
Hexafluoropropylene	39
Diethyl malonate	0.13
Ammonium persulfate	0.35
Ammonium perfluorooctanoate	0.90
Potassium phosphate, dibasic	0.85
Water	225

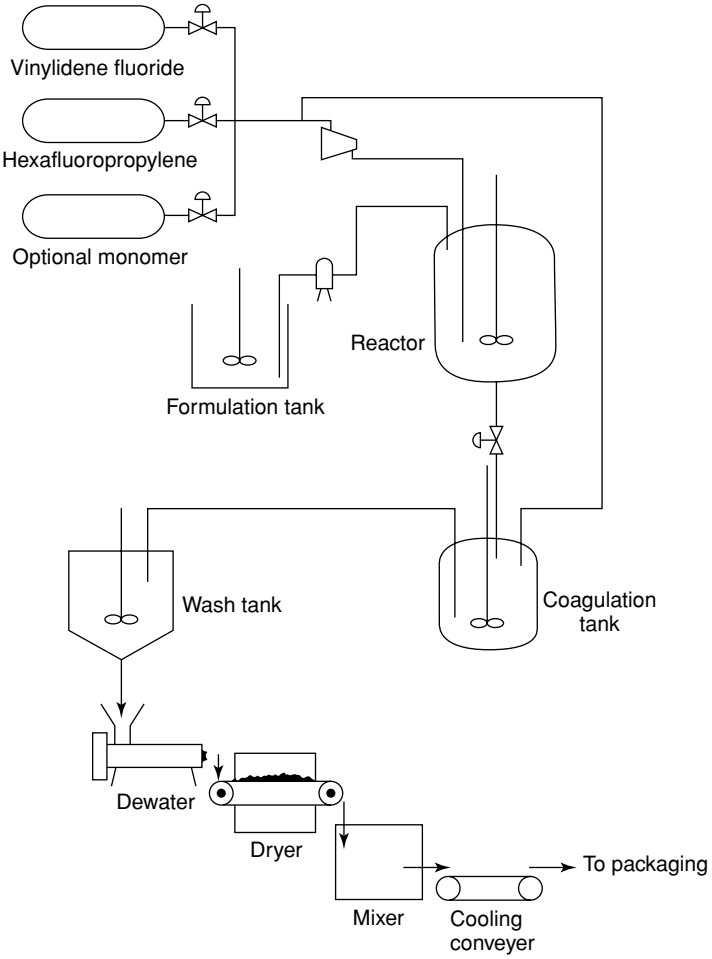

Fig. 5. Production of fluorocarbon elastomers.

by adding salt or acid, a combination of both, or by a freeze-thaw process. The crumb is washed, dewatered, and dried.

Most fluorocarbon elastomer gums contain a cure system, and, in the final step, the cure additives are incorporated in a two-roll mill, in an internal mixer, or in a mixing extruder. The cure system comprises an organic onium cure accelerator, such as triphenylbenzylphosphonium chloride, and a bisphenol cross-linking agent, such as hexafluoroisopropylidenediphenol. These cure systems improve compression-set performance and processing safety and accelerate cure cycles.

For complete formulation, reinforcing fillers and metallic oxides are added, the latter as acid acceptors (41–46). Raw gums contain no curative, and cure ingredients such as diamines, bisphenols, or peroxides (47) must be added in addition to formulation (compound) ingredients. Diamines were the first commercially important curing agents; they give good thermal resistance but poor scorch resistance. Bisphenol/onium cure systems yield very low compression set and good processing

safety. Peroxide cure systems improve steam and water resistance and give fair compression-set resistance; no water is produced during cure.

Processing

Compounding. Compared with the large number of ingredients required in a conventional rubber recipe, fluorocarbon elastomer compounding seems simple (Table 4) (see RUBBER COMPOUNDING).

O-Rings. In O-ring applications, the primary consideration is resistance to compression set. The choice of a fluorocarbon elastomer gum is based on gum viscosity, cross-link density, and cure system. Formulations are given in Table 5 (compounds 1 and 2).

Long-term compression-set resistance is described in Figure 4. Values are reduced by using gumstock of higher viscosity at comparable cross-link densities. Compression-set resistance also depends on the cure system. The bisphenol/onium cure system offers the lowest compression-set resistance, as shown in Table 6.

Table 4. Typical Fluorocarbon Elastomer Compound

Component	phr
Elastomer	100
Magnesium oxide or calcium hydroxide	6–20
Filler, reinforcing or nonreinforcing	0–60
Accelerators or curatives	0–6
Process aids	0–2

Table 5. Fluorocarbon Elastomer O-ring Compounds

	Compound 1	Compound 2
Typical formulation, phr		
Poly(vinylidene fluoride-*co*-hexafluoropropylene)		
ML[a] 1 + 10 at 121°C = 40[b]	100	
ML[a] 1 + 10 at 121°C = 100[b]		100
Hexafluoroisopropylidenediphenol	2.1	2.1
Triphenylbenzylphosphonium chloride	0.45	0.45
Magnesium oxide	3	3
Calcium hydroxide	6	6
MT Black (N-990)	30	30
Physical properties[c]		
Tensile strength, MPa[d]	15	15
Elongation at break, %	200	200
Hardness, Shore A	75	75
Compression set,[e] %	15	10
Specific gravity	1.8	1.8

[a]Mooney viscosity, large rotor.
[b]FKM 2230 and 2178 (Dyneon).
[c]Press cure, 5 min at 177°C; postcure, 24 h at 260°C.
[d]To convert MPa to psi, multiply by 145.
[e]ASTM D395, method B (O-ring) for 70 h at 200°C.

Table 6. Effect of Cure System on Processing Safety and Compression-Set Resistance

	Amine	Bisphenol	Peroxide
Formulation, phr			
Poly(vinylidene fluoride-*co*-hexafluoropropylene) plus cure-site monomer[a]			
ML[b] 1 + 10 at 121°C = 60	100	100	100
N, *N*′-Dicinnamylidene-1,6-hexanediamine	2.5		
Hexafluoroisopropylidenediphenol		2.1	
Triphenylbenzylphosphonium chloride		0.5	
Triallylisocyanurate			3.0
2,5-Dimethyl-2,5-bis-*t*-butylperoxyhexane			1.25
MT Black (N-990)	30	30	30
Magnesium oxide	15	3	
Calcium hydroxide		6	
Zinc oxide			3
Mooney scorch[c]			
Minimum	67	53	43
Time to 18-point rise, min	11	<60	37
Compression set, %	45	15	35

[a]FKM 2260 Dyneon.
[b]Mooney viscosity, large rotor.
[c]Small rotor at 121°C.
[d]ASTM D395, method B (3.5-mm O-rings) for 70 h at 200°C.

Molded Articles. In the compounding of molded articles, the most important physical property of the vulcanizate is elongation to break. Compression set is a secondary consideration. Since complex shapes are often required, compound flow is also important. These objectives are best met by using a gum with the lowest initial viscosity and a low cross-link density to permit high elongation compared with O-ring formulations.

Comparison of viscosities and properties of a molding compound (see Table 7) with an O-ring compound (see Table 5) shows differences in elongation due to lower cross-link density. Special formulations give even higher elongations and exceptionally high tear strengths in the press-cure state. Fillers (48) are of special importance for water- and acid-resistant compounds. The supplier may make specific recommendations to meet the properties required.

Extruded Articles. In an extruded article, the most important parameters are scorch safety and flow characteristics (49). The bisphenol/onium cure system provides the best scorch resistance. Gum viscosities and process aids affect flow characteristics. Typical formulations for extrusion-grade fluorocarbon elastomers are given in Table 8.

Formulation. Gum viscosity affects vulcanizate properties, especially compression set. Gums are available with Mooney viscosity (ML 1 + 10, large rotor, at 121°C) values of 0–160. A range of 20–60 gives the optimum combination of flow and physical properties. Mooney viscosity is commonly measured in a Mooney viscometer apparatus (ML = large rotor, MS = small rotor) after preheating the sample for 1 min, followed by heating at 121°C for 10 min, and then taking a reading (these values may vary). Mooney scorch (MS) is determined with a small rotor. Higher viscosities can cause excessive heat buildup during mixing,

Table 7. Fluorocarbon Elastomers for Molding

	Value
Typical formulation, phr	
Poly(vinylidene fluoride-*co*-hexafluoropropylene)[a]	100
Hexafluoroisopropylidenediphenol	1.7
Triphenylbenzylphosphonium chloride	0.4
Magnesium oxide	3
Calcium hydroxide	6
MT Black (N-990)	30
Postcure physical properties[b]	
Tensile strength, MPa[c]	14.4
Elongation at break, %	265
Hardness, Shore A	74
Compression set,[d] %	20
Specific gravity	1.8

[a]FKM 2230 (Dyneon), ML 1 + 10 at 121°C = 40.
[b]Press cure, 5 min at 177°C; postcure, 24 h at 260°C.
[c]To convert MPa to psi, multiply by 145.
[d]ASTM D395, method B (1.27-cm disk) for 70 h at 200°C.

Table 8. Fluorocarbon Elastomer Extrusion-Grade Compound

	Compound 1	Compound 2
Formulation, phr		
FKM 5830Q[a]	100	100
SRF Black (N-762)	15	
MT Black (N-990)		12
XC-72 (conductive black)		10
Magnesium oxide	3	3
Calcium hydroxide	6	5
Calcium oxide	3	6
Dibutyl sebacate		10
Physical properties[b]		
Tensile strength, MPa[c]	9.8	9.5
Elongation at break, %	380	350
Hardness, Shore A	72	72

[a]Available from Dyneon LLC.
[b]Press-cure, 45 min at 160°C.
[c]To convert MPa to psi, multiply by 145.

without improvement in physical strength. Compound viscosity depends on gum viscosity and filler type and loading. A range of 25–60, as measured by MS (121°C), is preferred.

Compound stability and safety are strongly affected by ingredients and cure systems.

The data in Table 6 clearly show the effect of cure system on scorch stability and processing, as determined by standard testing techniques (MS at 121°C). The most workable formulations are compounded with raw gums containing the bisphenol/onium cure systems. These cure systems offer maximum processibility safety.

Mixing. Fluorocarbon elastomers may be compounded by any standard rubber technique. Open mills may be used, since most commercial gums mix well, except very low viscosity gums, which stick to the rolls, and high viscosity gums, which are very tough.

Internal mixing, commonly referred to as Banbury mixing, is widely used with fluorocarbon elastomers. Gumstocks and compounds that are particularly successful fall in the viscosity ranges discussed earlier. A typical internal mix cycle takes 6–8 min with a drop temperature of 100–125°C. The formulations given in Tables 5 and 8 are both well suited to internal mixing.

Preforming. Formulations are easily preformed at cool barrel temperatures with a screw- or piston-type extruder (Barwell). Gums must be in the proper viscosity range and scorching must be avoided.

For routine calendaring operations, warm rolls (40–90°C) are recommended for optimum sheet smoothness. Process aids, such as low molecular weight polyethylene wax, are often used and sheets of 0.5- to 1.3-mm thickness are normally produced.

Molding. Compression molding is generally used to economize on material. Flow requirements are minimal and high viscosity resins may be used.

Little preforming is required for transfer molding, which is used for the production of very small parts. However, this technique often requires excessive amounts of material. Flow requirements are high, but fluorocarbon elastomers are available that can be used with this technique.

Injection molding is increasingly used in the rubber industry and fluorocarbon elastomers are well suited for this technique. Viscosity and cure rheology are very important because of high shear and fast cures (50–54). Molding at 180–200°C allows operations of 5 min or less, depending on part size.

Extrusion. Extrusion techniques are used for tubing, hose, O-ring cord, preforms, and shaped gaskets; typical extrusion conditions are 70–85°C for barrel temperature and 95–110°C for head temperature. The extruded forms are cured in a steam autoclave at 150–165°C. Special grades of peroxide–curable fluorocarbon elastomers may be vulcanized by hot air.

Postcuring. Postcuring for a period of 16–24 h at 200–260°C develops maximum physical properties, eg, tensile strength and compression-set resistance.

Specifications

Commercially available fluorocarbon elastomers meet automotive specifications in the HK section of ASTM D2000 and SAE J200. ASTM D1418 specifies designations of composition; fluorocarbon elastomers are designated FKM, FEPM, or FFKM in the case of perfluoroelastomers.

Some fluorocarbon elastomers meet the O-ring specifications, such as AMS 7276, AMS 7280A, AMS 7259, and MIL-83248 Amendment 1 Type II, Class I and II.

Certain grades and formulations are approved under the Code of Federal Regulations, 21, Food and Drugs, Part 177.2600, for articles intended for contact with food. Elastomer suppliers provide assistance in formulating for specified uses.

Test Methods; Health and Safety

The fluorocarbon elastomer raw gums are tested for Mooney viscosity (ASTM D1646) and specific gravity (ASTM D297). When compounded as described above, the stocks are tested for Mooney cure (ASTM D1646), Mooney scorch (ASTM D1646), and vulcanization characteristics (ASTM D2084 and D5289). The vulcanizates are evaluated with respect to original physical properties (ASTM D412, D2240, D1414), aged physical properties (ASTM D573), compression set (ASTM D395), and fluid aging (ASTM D471). Low temperature properties include low temperature retraction TR10 (ASTM D1329), torsional modulus (ASTM D1053), and brittle point (ASTM D2137).

Under normal handling conditions, fluorocarbon elastomers are nontoxic and nonirritating. Safe handling procedures are provided by manufacturers upon request.

Uses

About 45% of U.S. fluorocarbon elastomer consumption is in ground transportation. Typical components include engine oil seals, fuel system components such as hoses and O-rings, and drive-train seals. Growth in this area is expected to continue, considering the increased demands from higher engine temperatures, alcohol-containing fuels, and improved lubricants. Other industries include petroleum and petrochemicals, pollution control, and industrial hydraulic and pneumatic applications. These areas are more dependent upon general industrial production and overall energy demands, and will show slower growth than the automotive segment.

Consumption in Europe and Japan depends more upon the automotive industry. However, with the recent concern about acid rain, the European market is expected to show increased interest in fluorocarbon elastomers for pollution-control applications. In Japan, fluorocarbon elastomers are used for general manufacturing, eg, copiers. Petroleum applications are of little interest outside the United States. The aircraft industry uses less than 10% of the total fluorocarbon elastomer consumed.

Perfluoroelastomer parts are primarily used in the chemical processing industry and are finding increased applications in semiconductor manufacturing equipment, because of their high purity, extreme chemical inertness, and unrivaled thermal stability.

BIBLIOGRAPHY

"Fluorocarbon Elastomers" in *EPSE* 2nd ed., Vol. 7, pp. 257–269, by M. M. Lynn and Allan T. Worm, 3M Co.

1. M. E. Conroy and co-workers, *Rubber Age* **76**, 543 (1955).
2. C. B. Griffis and J. C. Montermoso, *Rubber Age* **77**, 559 (1955).
3. W. W. Jackson and D. Hale, *Rubber Age* **77**, 865 (1955).
4. F. A. Bovey and co-workers, *J. Polym. Sci.* **15**, 520 (1955).
5. U.S. Pat. 3051677 (Aug. 28, 1962), D. R. Rexford.
6. S. Dixon, D. R. Rexford, and J. S. Rugg, *Ind. Eng. Chem.* **49**, 1687 (1957).
7. J. S. Rugg and A. C. Stevenson, *Rubber Age* **82**, 102 (1957).

8. U.S. Pat. 2968649 (Jan. 17, 1961), J. P. Pailthrop and H. E. Schroeder.
9. U.S. Pat. 3331823 (July 18, 1967), D. Sianesi, G. Bernardi, and A. Regio.
10. U.S. Pat. 3335106 (Aug. 8, 1967), D. Sianesi, G. C. Bernardi, and G. Diotalleri.
11. U.S. Pat. 3235537 (Feb. 15, 1966), J. R. Albin and G. A. Gallagher.
12. Ger. Offen. 2457102 (Aug. 7, 1975), R. Baird and J. D. MacLachlan.
13. U.S. Pat. 4035565 (July 12, 1977), D. Apotheker and P. J. Krusic.
14. U.S. Pat. 4418186 (Nov. 29, 1983), M. Yamabe and co-workers.
15. A. L. Barney, G. H. Kalb, and A. A. Kahn, *Rubber Chem. Technol.* **44**, 660 (1971).
16. A. L. Barney, W. J. Keller, and N. M. Van Gulick, *J. Polym. Sci., Part A-1* **8**, 1091 (1970).
17. G. H. Kalb, A. L. Barney, and A. A. Khan, *Am. Chem. Soc. Dev. Polym. Chem.* **13**, 490 (1972).
18. S. M. Ogintz, *Lubr. Eng.* **34**, 327 (1978).
19. U.S. Pat. 4251399 (Feb. 17, 1981), M. Tomoda and Y. Ueta.
20. U.S. Pat. 4263414 (Apr. 21, 1981), A. C. West.
21. Y. Tabata, K. Ishigure, and H. Sobue, *J. Polym. Sci., Part A* **2**, 2235 (1964).
22. G. Kojima and Y. Tabata, *J. Macromol. Sci. Chem.* **5**, 1087 (1971).
23. K. Ishigure, Y. Tabata, and K. Oshima, *Macromolecules* **6**, 584 (1973).
24. G. Kojima and Y. Tabata, *J. Macromol. Sci. Chem.* **6**, 417 (1972).
25. G. Kojima, H. Kojima, and Y. Tabata, *Rubber Chem. Technol.* **50**, 403 (1977).
26. U.S. Pat. 4463144 (July 31, 1984), G. Kojima and M. Hisasue.
27. U.S. Pat. 4 882 390 (1989), W. M. Grootaert and R. E. Kolb.
28. U.S. Pat. 4 912 171 (1990), W. M. Grootaert and R. E. Kolb.
29. W. M. Grootaert, R. E. Kolb, and A. T. Worm, *Rubber Chem. Technol.* **63**, 516 (1990).
30. W. M. Grootaert, *Polymer Materials Encyclopedia*, Vol. **4**, CRC Press, Inc., Boca Raton, Fla., 1996, p. 2495.
31. J. R. Dunn and H. A. Pfisterer, *Rubber Chem. Technol.* **48**, 356 (1975).
32. U.S. Pat. 4694045 (Sept. 1987), A. L. Moore.
33. R. Mastromateo, Performance of Fuel Resistant Elastomers in Alternative Fuels, SAE Technical Paper 900195, 1990.
34. J. R. Blazer and A. L. Edmondson, Effects of Methanol Fuels on Fuel Hose Permeation, SAE Technical Paper 910106, 1991.
35. J. R. Blazer and A. M. Sohlo, Effects of Long-Term Flex Fuel Exposure on Flurocarbon Elastomers, SAE Technical Paper 900118, 1990.
36. U.S. Pat. 3845024 (Oct. 29, 1974), S. D. Weaver.
37. U.S. Pat. 3053818 (Sept. 11, 1962), F. J. Honn and S. M. Hoyt.
38. U.S. Pat. 3069401 (Dec. 18, 1962), G. A. Gallagher.
39. U.S. Pat. 3080347 (Mar. 5, 1963), C. L. Sandberg.
40. U.S. Pat. 3707529 (Dec. 26, 1972), E. K. Gladding and J. L. Nyce.
41. U.S. Pat. 3655727 (Apr. 11, 1972), K. U. Patel and J. E. Maier.
42. U.S. Pat. 3712877 (Jan. 23, 1973), K. U. Patel and J. E. Maier.
43. U.S. Pat. 3752787 (Aug. 14, 1973), M. R. deBrunner.
44. U.S. Pat. 3857807 (Dec. 31, 1974), Y. Kometani and co-workers.
45. U.S. Pat. 3864298 (Feb. 4, 1975), Y. Kometani and co-workers.
46. U.S. Pat. 3920620 (Nov. 18, 1975), C. Ceccato, S. Geri, and L. Calombo.
47. J. E. Alexander and H. Omura, *Elastomerics* **2**, 19 (1978).
48. *Compounding Fluoroelastomers*, Brochure, Dyneon, Oakdale, Minn.
49. R. Christy, *Rubber World* **184**(6), 38 (1981).
50. U.S. Pat. 5591804 (June 7, 1997) W. D. Coggio, D. H. C. Arren, and A. T. Worm.
51. U.S. Pat. 5654374 (Aug. 5, 1997) D. H. C. Arren, W. D. Coggio, and D. S. Parker.
52. U.S. Pat. 5262490 (Nov. 16, 1993) W. M. Grootaert and R. E. Kolb.
53. D. H. C. Arren, Paper presented at *Europlast*, Paris, France, Oct. 6, 1994.
54. S. Bowers, Paper presented at the *German–French Rubber Symposium*, Trier, Germany, Nov. 15, 1996 (DuPont Dow Elastomers).

GENERAL REFERENCES

J. Scheirs, ed., *Modern Fluoropolymers*, John Wiley & Sons, Inc., New York, 1997.
L. E. Crenshaw and D. L. Tabb, *The Vanderbilt Rubber Handbook*, R. T. Vanderbilt Co., New York, 1990, p. 211.
M. Morton, ed., *Rubber Technology*, Van Nostrand Reinhold Co., Inc., New York, 1973, pp. 407–439.
W. W. Schmeigel, *Makromol. Chem.* **76/77**, 39 (1979).
D. Apotheker and co-workers, *Rubber Chem. Technol.* **55**, 1004 (1982); *ACS Symp. Ser.* **260** (1984).
J. C. Salamone, *Polymeric Materials Encyclopedia*, Vol. **4**, CRC Press, Inc., Boca Raton, Fla., 1996, p. 2495.

ALLAN T. WORM
WERNER GROOTAERT
Dyneon, 3M Company

FOAMED PLASTICS. See CELLULAR MATERIALS.

FRACTOGRAPHY

Introduction

Fractography is the visualization, description, and interpretation of a fracture or a fracture surface, often in order to establish structure–property relationships. Artifact-free visualization and as accurate a description as possible are a prerequisite for interpreting a fracture surface and using it to reveal information about material properties, such as composition, deformation under load, and the failure mechanism.

The failure of a plastic part is governed by the interaction of its physicochemical structures, by the processing parameters, by the environmental conditions, such as moisture, temperature, chemical influences, and high-energy radiation, as well as by the mechanical stresses, which themselves are determined by their nature (tensile, compressive, shear, flexure), their combination and magnitude, and their rate and duration. While environmental factors may be viewed as relatively constant during the failure process, local mechanical stress changes. A description of the state of the material and the environment is offset by a visible change in the failure process over the course of time.

Any assessment of this kind of damaging process must pay special attention to these changes. It is therefore vital to find characteristics that help to interpret this process. This is the primary objective of fracture surface analysis, or fractography.

A number of standardized test methods are available for assessing the material structure and the mechanical properties of a plastic. Similarly, chemical and thermal damage, and the state of processing may be determined, eg, from an examination of the crystalline structure, of orientations, and of internal stresses. However, in contrast to fractography, these methods yield very little information about the failure process itself.

Encyclopedia of Polymer Science and Technology. Copyright John Wiley & Sons, Inc. All rights reserved.

The fractography of polymers has been based on metallurgical experiences. (References 1 and 2 and the reported review therein are documents for these roots.) Especially the analytical way of how to observe, describe, measure, and interpret a fracture surface could be adapted for and applied to polymers (3–13). However, it is necessary to take into account the more complex deformation behavior of polymers.

A fracture is an undesirable separation of a formerly whole functional element into two or more parts. The cause of the fracture may lie in wrong material selection, material defects, or the operating conditions. However, the nucleation of the fracture will begin at a minute inhomogeneity in the material. This defect can be on the surface or inside the observed part, depending on the local internal and external stress conditions leading to the failure, and may not always be in evidence.

The fracture surfaces of polymers offer many features, from which the causes may be discerned. The fracture surface often (especially with brittle materials) shows certain characteristic regions. A relatively smooth area—the so-called mirror—with the nucleating inhomogeneity in its center is due to slow-crack growth. The mirror is surrounded by a boundary called the mist, which is slightly rougher. Beyond the mist a relatively rough region of hackles is observed, finally followed by bifurcation or branching of the crack (6). The roughness increases from the center to the periphery. The smaller the stress [also the longer the time and the higher the temperature (7)], which initiated the crack, the larger is the radius of the mirror. Distinguishing the different regions can become difficult, as their geometrical extensions depend on the fracture conditions and the extent of brittle deformation behavior of the material. Therefore, depending on the micromechanical deformation mechanisms of the specific polymer under the specific loading conditions, shear bands or crazes may be observed (see also MICROMECHANICAL PROPERTIES).

Fractures propagate in different directions, either simultaneously or with a time lag. The above-mentioned boundaries deviate from circular shapes, if the propagation rate of the crack is dependent on the direction in the plane of the crack.

Optical Microscopy

A first impression of the fracture surface is obtained by conducting a macroscopic analysis with the unaided eye or a stereomicroscope. It has been suggested that the fracture diagram be annotated with arrows showing the direction of the fracture travel when fractures are being analyzed. This will yield an overall picture of complex fracture propagation (Fig. 1). In order that the object being assessed may be described objectively, no preliminary information should be available. Aspects that should be taken into account during the macroscopic analysis are summarized in Table 1.

Optical microscopy is a simple and inexpensive method to obtain the overall view of the fracture surface. By applying the reflected light mode information on the origin of the fracture, the crack propagation direction, location of arrest lines can be gained. Also, in the transmission mode, it is

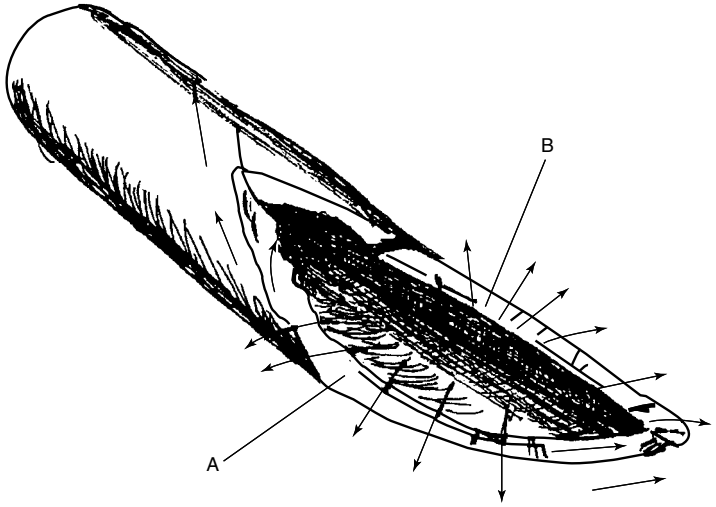

Fig. 1. Determination of fracture propagation in a pipe (original drawing by H. Klingele).

possible to reveal events and processes occurring beneath the surface, such as yield zones and damage zones at the crack tip. For further details see MICROSCOPY.

An optical microscope often has an insufficient depth of field for conducting a microscopic examination of surfaces, especially fracture surfaces. The depth of field of the optical microscope is approximately 100 times smaller than the depth of field of the scanning electron microscope (SEM) at the same magnification (14). At a magnification of 1000 the depth of field amounts to 0.5 μm for the optical microscope (15) and 50 μm for the SEM. It is for this reason, and the greater possible magnification, that the SEM is used.

A new method to overcome the disadvantage of an insufficient depth of field in conventional light microscopy is confocal scanning light microscopy (16). The different scanning techniques and light sources of this method basically have the aim to obtain several images at different heights, with only a narrow band of the surface in sharp focus, and then to combine the in-focus details of the images at different heights in one image. This partial combination of images is realized by means of computer image processing techniques.

Scanning Electron Microscopy

Polymers consist of macromolecular, chain-like base elements that are composed primarily of carbon and hydrogen. The diameter (physical sphere of influence) of a hydrogen atom is 0.24 nm and that of a carbon atom is approximately 0.38 nm. The resolution of an SEM is roughly 10 nm and that of an optical microscope is 1000 nm. Concrete visualization of atoms is therefore impossible in both cases. Not even a 0.4 nm thick and 6 μm long polyethylene chain can be visualized by

Table 1. Macroscopic Analysis (Selection)

Area	Aspects
Details of damaged part	Dimensions (eg, including section thickness)
	Design details (eg, melt accumulation, sharp edges)
	Production detail (eg, gating point)
	Coloring
	Coatings
Type of damage	Fracture, crack, deformation, corrosion, wear, discoloration... (or signs of fatigue, aging, shrinkage, distortion, creep, impact)
Extent of damage	Brittle or ductile fracture
	Length and number of cracks
	Degree of deformation
	Depth of corrosive attack or wear
Position, origin of damage	Damage at corners, edges, apertures, domes, abrupt changes in section thickness, ribs, radii, or in the gate area
	Position relative to gating point
Surface features	Mold grooves
	Grooves from machining
	Flow lines
	Crack-initiating notches, eg, through weld lines
	Surface treatment
	Thermal exposure, melt structures (partial)
	Coatings, liquid or paste-like media
	Discolorations
	Inhomogeneities
	Sink marks
	Processing traces (streaks, burner)

SEM. Individual atoms and molecules cannot be used to provide satisfactory explanations of structural and especially fracture phenomena as they are neither deformed individually nor destroyed. Failure processes therefore need to be explained in terms of the behavior of the superstructures.

In scanning electron microscopy, electrons emitted by an electron gun (primary electrons) are focused by means of Wehnelt cylinders and electromagnetic lenses onto the sample surface, which they scan line by line (Fig. 2). The secondary and back-scattered electrons emitted by the sample are captured by detectors and presented in the form of brightness modulation on, eg, a monitor. The secondary electrons come from a surface layer up to 10 nm thick, while the back-scattered electrons usually originate from deeper layers.

The imaging contrast comprises the material contrast, which varies with the atomic number of the elements in the sample; the topographical contrast, which varies with the orientation of the sample surface toward the direction of the incident primary electrons; and the orientation contrast, which varies with the relative position of the sample surface to the electron detector. While the material contrast obtained via the back-scattered electrons is of subordinate

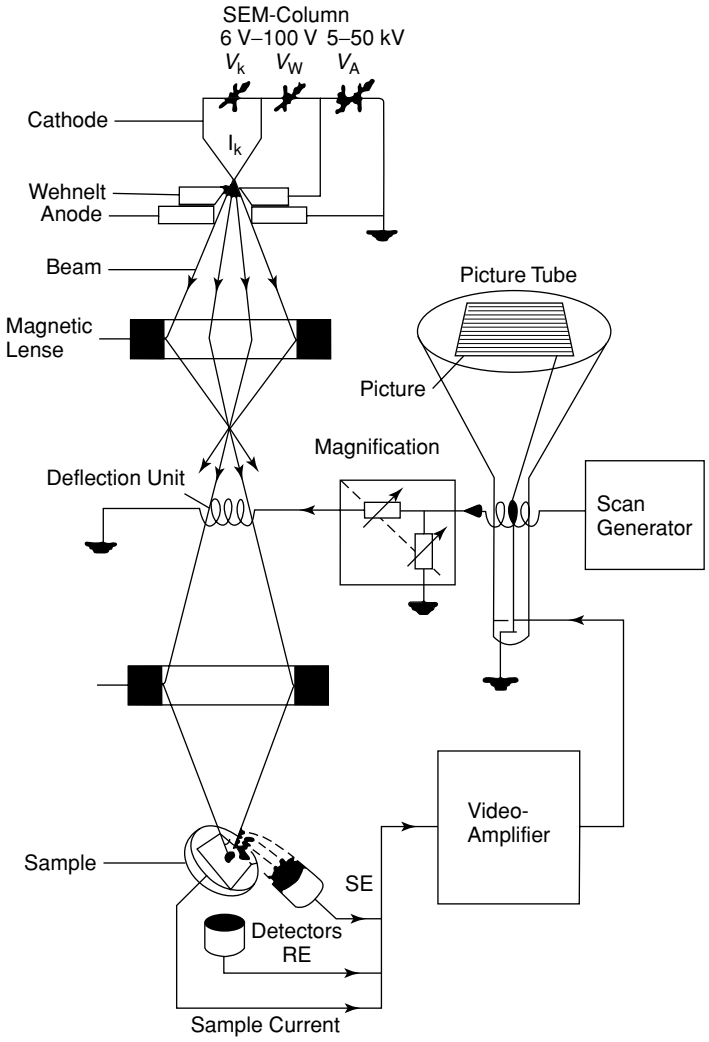

Fig. 2. Basic structure and mode of action of the scanning electron microscope.

importance in the case of pure polymers, the topographical contrast generated by the secondary electrons contributes to a brighter visualization of edges and tips, and the orientation contrast contributes to the plastic character of the SEM micrographs.

The sample surfaces, eg, fracture surfaces measuring several square millimeters, of plastics are viewed under a magnification of 20–20,000 in SEM under a vacuum. These surfaces can be recorded digitally or as a monochrome photograph.

The great depth of field evident in SEM micrographs stems primarily from the fact that an optical lens system is not necessary for building up the image. Consequently, electrons from various depths are able to reach the detector.

The detectors used for identifying materials in SEM are of the energy-dispersive and wavelength-dispersive types. However, in most cases failure analysis does not rely predominantly on the detailed knowledge of the materials contents. Similarly, for failure analysis the topographical details of the fracture surface usually do not have to be cleared up to the scale available via the atomic force microscope (see also SURFACE ANALYSIS and ATOMIC FORCE MICROSCOPY).

Sample Preparation

For optical microscopy of fracture surfaces usually little or no surface preparation is necessary. However, because plastics have poor electrical conductivity, for SEM examinations the sample surface generally needs to be coated with a conductive layer that prevents charging and heating. The energy carried into the sample can melt the polymer or vaporize low molecular contents locally and change the fracture surface irreversibly, making its interpretation impossible. On the other hand, to ensure artifact-free imaging, the applied layer itself must not have any visible structure and must be so thin that the structures on the surface are not hidden.

The surfaces under test are vacuum coated with carbon or metals. The standard equipment for this is a sputter device that ignites a glow discharge in an air or argon atmosphere at 5–20 Pa (0.05–0.2 mbar). The gas ions dislodge cathode material, which then condenses on the sample surface. The cathode is mostly made of gold, but also possible are chromium, carbon, and, because it yields a superior coating, gold–palladium. The sample itself is bonded firmly to the holder with a conductive adhesive.

Very bulky samples may be dipped in or sprayed with a metal coating. Another preparative method is to mold the sample surface, eg, in silicone rubber, and to make a replica. However, there is a possibility of artifact formation here.

Nowadays, there are so-called low-voltage scanning electron microscopes available that frequently eliminate the need to apply a conductive coating to the polymer and can permit fracture surface analyses to be performed.

While on the topic of sample preparation, it should also be mentioned that the imaging contrast of phase morphologies can be enhanced by staining the surface by means of contrasting agents, such as OsO_4 for ABS and RuO_4 for PE/PP blends, as well as by etching. Further information on these pretreatments may be found in References 17–20–21.

Classification of Fracture Modes and Examples

Load Fracture. Thermoplastics, thermosets, and elastomers deform in different ways. In the case of ductile thermoplastics, as the load increases, the tangled, thread-like macromolecules become stretched, aligned, and in some cases will glide apart. The stretched areas will recoil like a spring, and this will be most pronounced at the highly stressed fracture site, which additionally warms up on

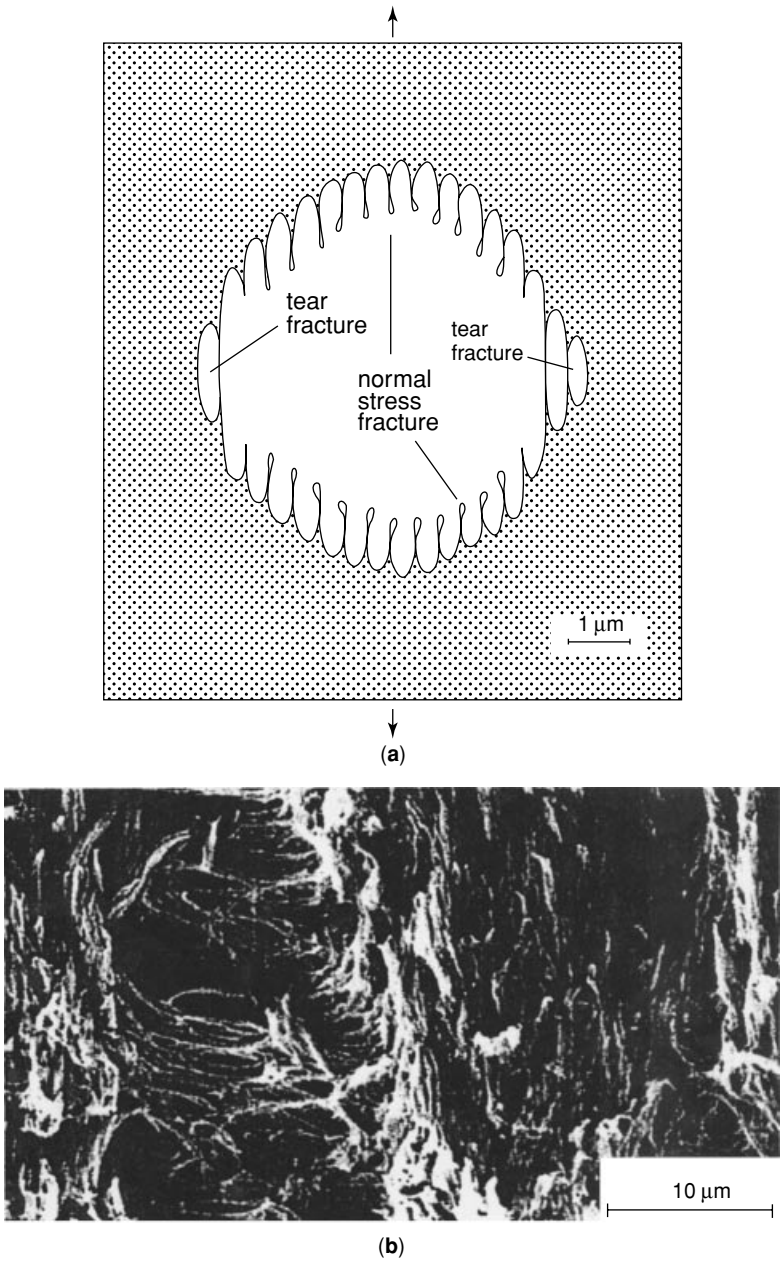

Fig. 3. Load fracture in different types of plastic. (**a**) Schematic (ductile thermoplastic); (**b**) normal stress fracture with peak formation, PA 66; (**c**) load fracture of UP with minor plastic deformation; and (**d**) load fracture of a cross-linked elastomer (rubber).

tearing. As a result, during peak-like stretching, nodular thickenings often occur at the end (Figs. 3a and 3b).

As this stretching process requires time, the deformation is dependent on the rate of loading up to fracture. Additionally, elevated temperatures facilitate

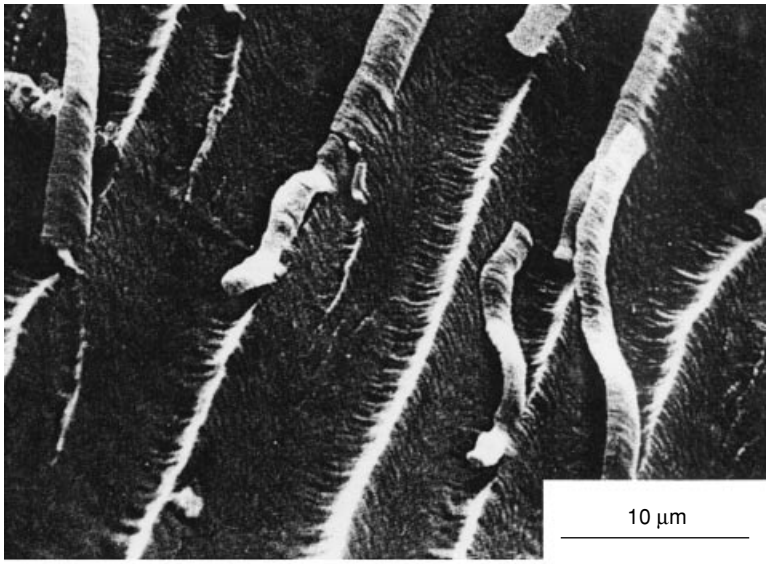

(**c**)

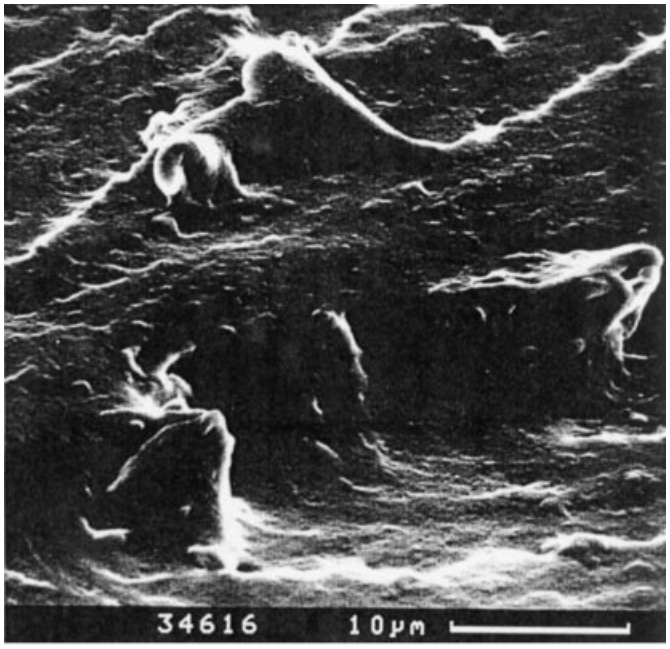

(**d**)

Fig. 3. (*Continued*)

rearrangements. When the acting stress is applied at low deformation rates and elevated temperatures, the molecules are more able to comply with it than if it occurs suddenly and at low temperatures.

With thermosets, the high degree of cross-linking of the molecules constitutes a fundamental barrier to deformation. Therefore, the elastic, completely reversible

deformation components are more predominant and the relaxing and viscous ones are less predominant than in thermoplastics. This is the reason why thermosets tend to undergo brittle fracture (Fig. 3c).

In the case of elastomers, the partially entangled macromolecules primarily undergo elastic deformation because of the low crosslinking density and the weakness of the secondary valence forces. Fracture takes the form of molecule chain fracture caused by high elongation. The permanent deformation is relatively minor, and is recognizable from the short peaks and threads. At temperatures below the glass-transition temperature of the elastomer, the secondary valence forces become stronger and the fracture comes more and more to resemble that undergone by thermosets (Fig. 3d).

Normal Stress Fracture. Stretching under external stress causes the material domains to be extended as peaks. After separation, the ends recoil quickly and form thickenings. Separation occurs perpendicularly to the tensile axis (Figs. 3a and 3b).

Tear Fracture. Normal stresses, such as flexure, that are distributed unevenly across the cross section may cause the material to tear from an external or an internal surface, eg, from a material defect. In such cases, the peaks stand at an angle in the fracture surfaces. If elongation is uniform, rims form at the crack front that remain visible in both fracture surfaces as beads with undulating crests after separation (Fig. 4). Further characteristics of tear fracture are V- and U-shaped ramps, whose tips point against the direction of fracture propagation.

Shear Fracture. Polymer failure is initiated when critical shear stresses are exceeded. Stretching at the separation faces ultimately leads to lips and peaks that on two mating fracture surfaces point toward each other. Fracture due to shear failure can only be distinguished from that due to tear fracture on two mating fracture surfaces. The separating mechanism involved is that of normal stress fracture and tear fracture, since gliding along defined crystal planes as in metals cannot occur (Fig. 5).

Crazing. *Crazing*, also called *stress cracking*, is the formation of roughly panel-like material areas that open frequently under the influence of wetting agents after an induction time has elapsed; opening is spontaneous and perpendicular to the maximum tensile stress. Unlike empty cracks, crazing involves bridging by 10- 50-nm-thick fibrils between the separation surfaces (Fig. 6). The formation of crazes is accompanied by an increase in volume (reduction in density) in contrast to the constant volume if shear yielding takes place. Crazing is not synonymous with complete failure of the molded part and may even relieve locally stressed material areas. Only as the crazing grows and then ruptures, particularly on impact stress, do cracks form.

Crazing can occur both on free surfaces and inside the work piece, and therefore is either semicircular or circular. In the case of transparent plastics, the expansion of the circle is visible to the unaided eye (stress whitening). In SEM, ruptured crazing is characterized as follows:

(1) Arc-like borders that are clearly different from residual force fracture
(2) Features of ductile fracture, ie peaks and threads

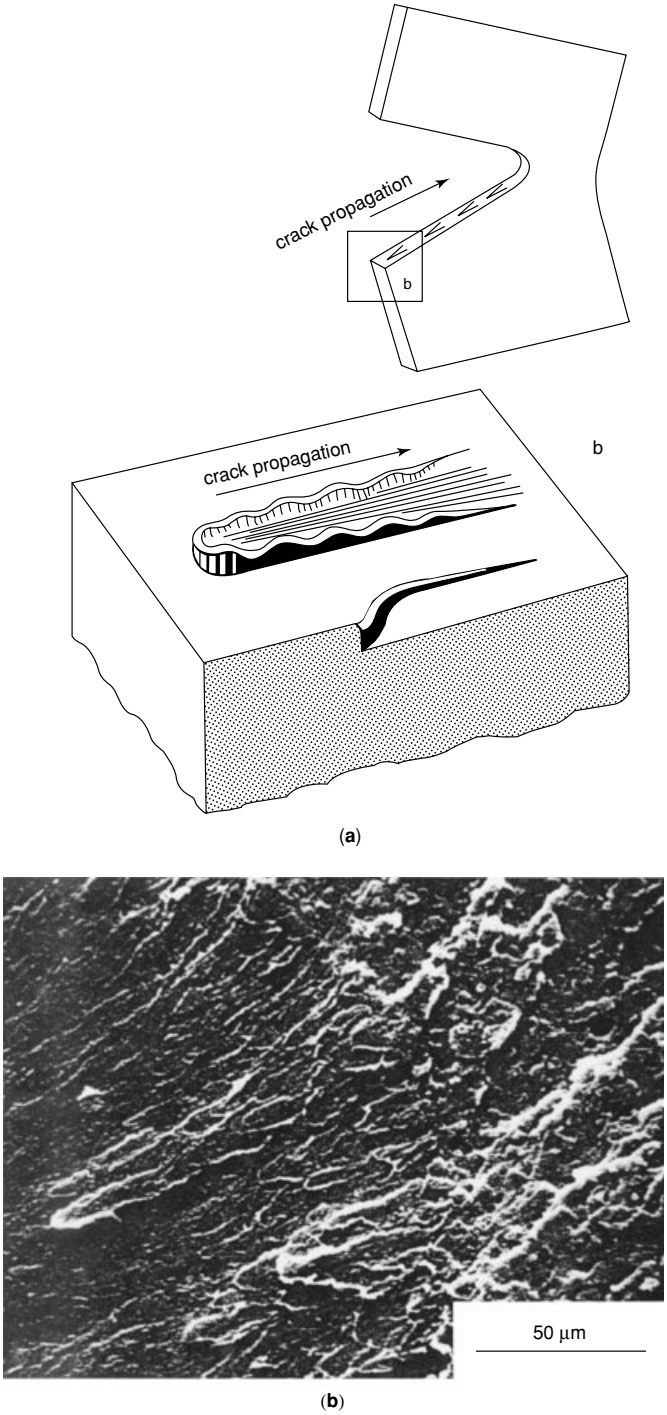

Fig. 4. Tear fractures. (**a**) U- and V-shaped ramps with rims; (**b**) V-shaped radial crack propagation in PS crazing; (**c**) tear fracture at a free film surface; and (**d**) ruptured crazing in PS with films exhibiting deformation in an otherwise low deformation fraction.

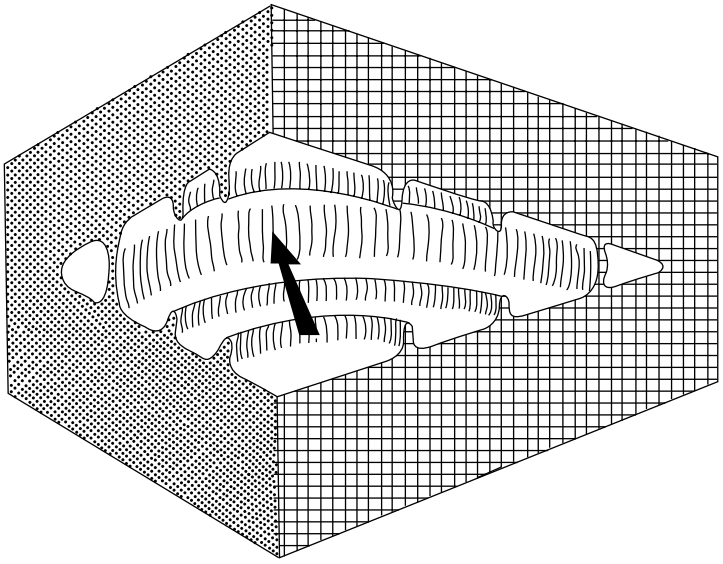

(**c**)

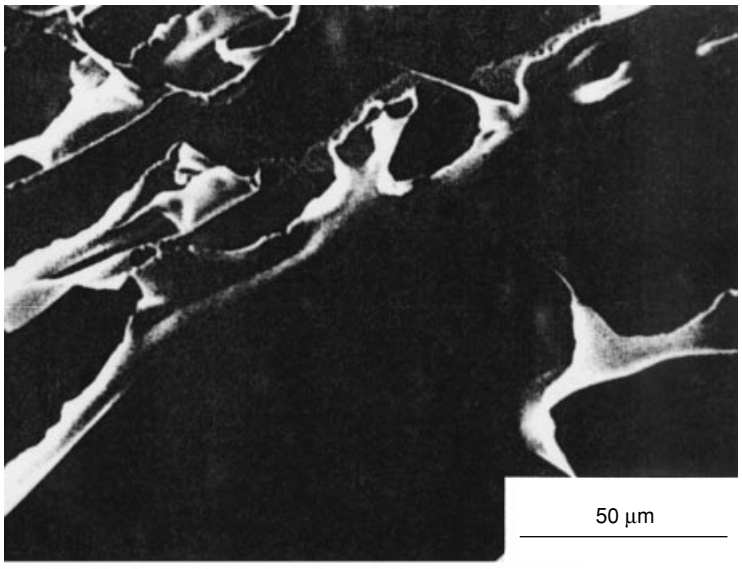

(**d**)

Fig. 4. (*Continued*)

Accordingly, crazing is the initial stage of ductile fracture. Crazing on surfaces occurs in homogeneous materials, generally as a result of continuous slow tensile stress, but not of impact stress. Consequently, it is comparable to creep failure in metals. Rubber-modified polymers also exhibit crazing following impact stress.

Ruptured crazing generally contains a central normal stress zone and a contiguous tear zone. The concentric propagation of crazing can be recognized from

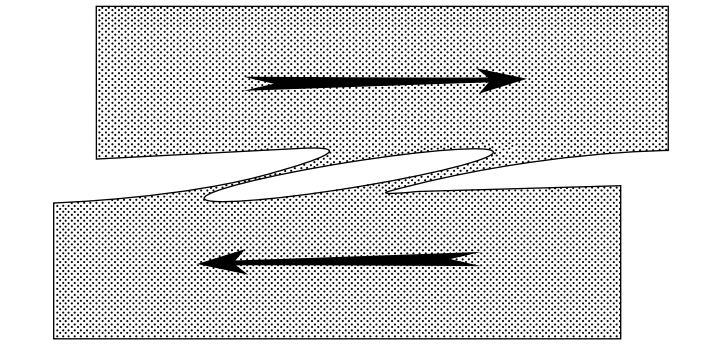

(**a**)

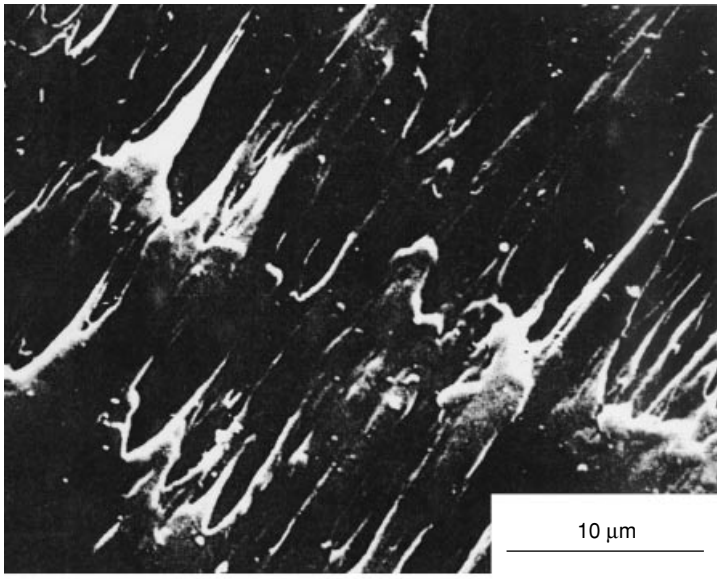

(**b**)

Fig. 5. Shear failure. (**a**) Shear failure in polymers and (**b**) shear-stretched peaks on PBT tooth flank after dry running.

V shaped markings. The chemicals which loosen secondary valence bonds, particularly solvents, reduce the tensile stress required for crazing. Crazing and environmental stress cracking are therefore frequently initiated on surfaces accessible to chemicals.

Ductile Fracture. There are two types of ductile fracture, and the deciding criterion is the length of the peak remaining in the fracture:

(1) Polymers that undergo high plastic deformation to fracture—permanent peak length $> 10\ \mu$m
(2) Polymers that undergo minor plastic deformation to fracture—permanent peak length $= 1$–$10\ \mu$m

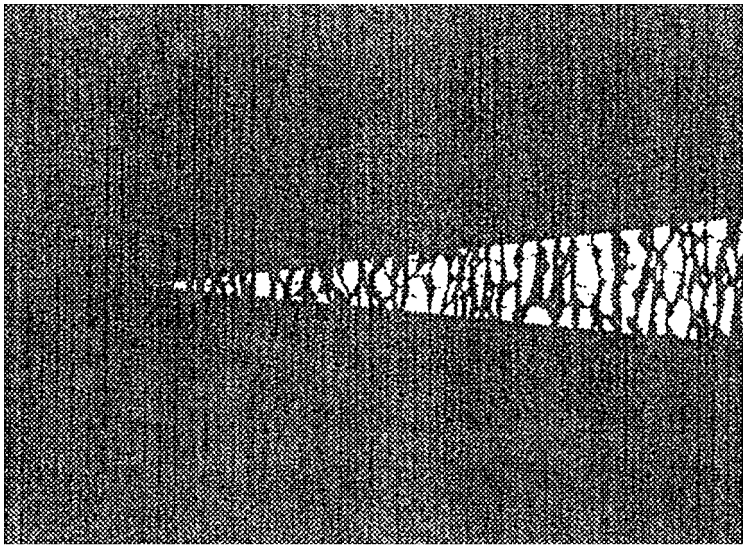

(**a**)

(**b**)

Fig. 6. Crazing. (**a**) Schematic and (**b**) normal stress peaks in fracture surface of a PP part.

According to this classification, fractures with permanent peak lengths <1 μm are brittle. Materials generally considered to be prone to high plastic deformation are: PE, PP, PA, POM, PBTP, PETP, PTFE, PC, PVC, and ABS. Polymers categorized as having poor deformation (peak length after fracture 1–10 μm) are PS, SAN, EP, and UP. In conditions that hinder deformation (high stress rate, low temperature, multiaxial stress state and foreign additives), otherwise-ductile materials may fall into this category, such as PE, PA, POM, PBTP, PTFE, PC, PVC, and ABS.

Brittle Fracture. Polymers do not exhibit brittle fracture comparable to the cleavage fracture occurring in metals with a body-centered cubic lattice structure. Even in the case of low temperature fractures, high magnification reveals films and peaks resulting from ductile deformation. To be sure, the deformations are restricted to a planar layer less than 1 μm thick. As the deformed volume is very small, this is brittle fracture in macroscopic terms. Microscopic examination reveals that the stressed 1-μm layer is distributed on both fracture faces after separation. This gives rise to oval lids or torn-open blisters, steps, and striped patterns. The edges of the microstructures are lined with fine beads and sometimes with short threads. Since the brittle fracture spreads out across the material, it leaves behind structures that permit conclusions to be made about the direction of fracture propagation. These are called *cleavage stops* and they are formed wherever the material is inhomogeneous. They cause the fracture front to divide into several fracture paths that recombine again during the course of further propagation. This explains the occurrence of step-like patterns and chips which splinter off (Fig. 7).

Fatigue Fracture. Like other materials, polymers withstand static stress more than they can withstand dynamic stress, especially the tensile stress situations. As alternating stress decreases, the number of stress cycles that can be endured increases. This results in a flattening of the fatigue endurance curve.

Vibration-Induced Creep Fracture. Genuine fatigue strength would only be feasible if the alternating load were to be absorbed purely elastically in the long term. However, this would presuppose extensive elastic behavior at the microlevel as well. At the same time, irreversible stretching processes must be expected at inhomogeneities on the surface or inside the material. These give rise to heat simultaneously, which in turn promotes the mobility of the molecule chains. This explains why a type of dynamic fatigue fracture exists in polymers which is on a par with continuous creep failure and is known as *vibration-induced creep fracture*. Owing to poor thermal conductivity, vibration-induced creep fracture also varies with frequency. High frequencies and high loads harbor the risk of local softening and even melting in the middle of the cross section. In this case, characteristics of periodic crack propagation must not be expected in the fracture surface, i.e., there are no fatigue striations (Fig. 8).

When dependable fatigue fracture characteristics such as fracture paths, fatigue striations, secondary cracks, or spherical melt voids occur, fatigue fracture may be identified. However, it is also possible that vibrational load will only leave behind load fracture features. Fatigue fracture without fatigue striations may be expected particularly in very ductile polymers, at high operating temperatures and at high alternating load frequencies. Theoretically possible is a dynamic fatigue fracture with extreme fracture constriction with point or edge-like separation.

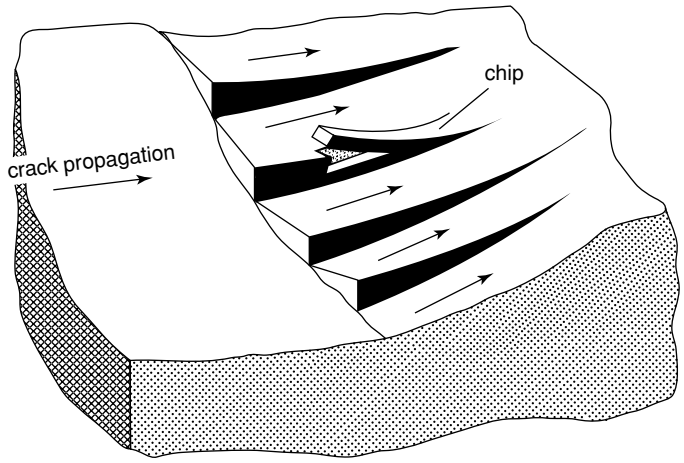

(**a**)

(**b**)

Fig. 7. Brittle fracture. (**a**) Cleavage stops, recombining fracture planes, and splintering chips and (**b**) cleavage stops in brittle fracture.

Normally, an extensively rounded crack emanating from the surface or from an internal defect will migrate through the material.

On the other hand, it is important to note that discontinuous crack growth under a static load may yield fracture surfaces, which may look quite similar to fatigue striations. To observe this phenomenon, the material has to be able to slowdown or even stop the crack propagation after the static load initiated the

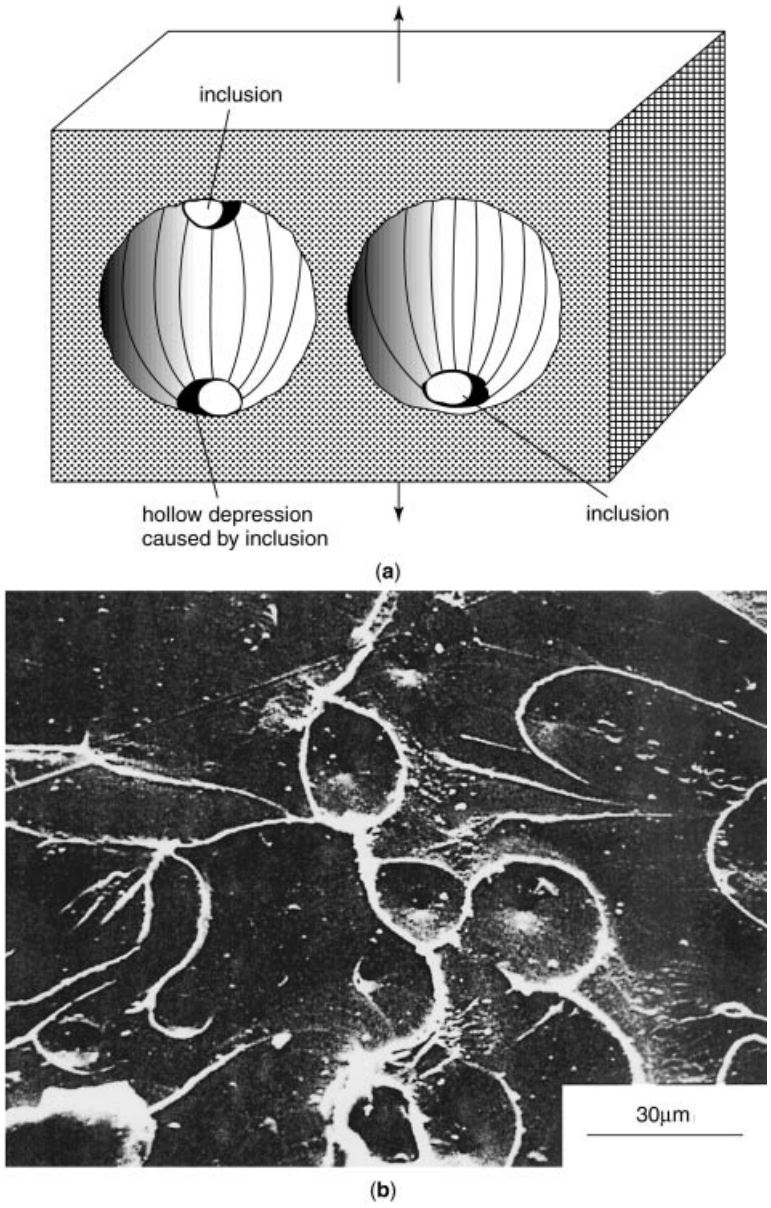

Fig. 8. Vibration-induced creep fracture. (**a**) Radially propagating dynamic fatigue fracture inside the material and (**b**) dynamic creep fracture in PS samples.

crack. Then the next tension build-up takes place until it is released in further crack growth. The varying growth rates result in varying surface roughness, which may eventually be confounded with fatigue striations.

Genuine Vibration Fracture. A genuine crack tip will form under alternating load in polymers with low deformation capability. Owing to the spatial rigidity

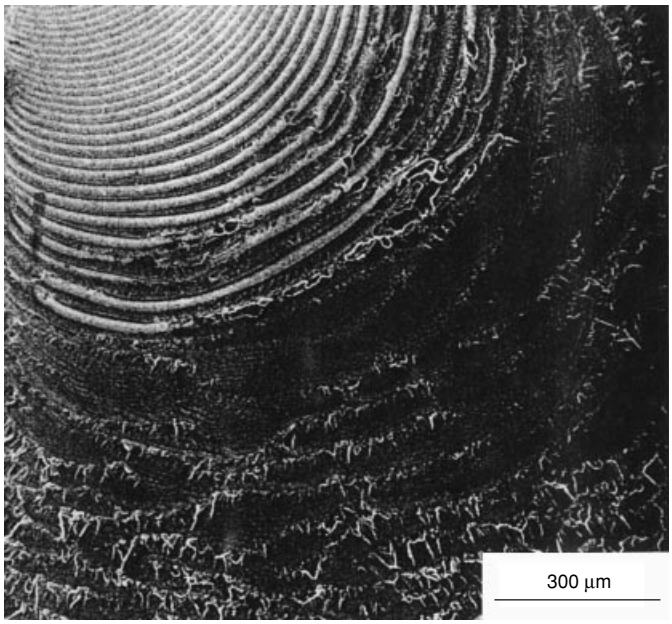

Fig. 9. Tensile fatigue striations in SAN with residual force fracture at elevated load.

of the molecule bonds, the molecule chains are severed by the crack tip after just minor stretching. A crack front with sharp notch base may form and migrate through the plastic under the alternating load. This gives rise to parallel fatigue striations. This phenomenon is dependent on the loading frequency and level as well as on the material. Genuine dynamic fatigue fracture has been observed in PC, SAN, PVC, PE, PA, and PP. Looking at the possible deformation or even separation in the crack base, it is possible to distinguish more or less ductile fatigue striations (Fig. 9).

Genuine Ductile Fatigue Fracture. Dynamic fatigue fracture may propagate on different fracture paths and expand at different times. Materials relatively easy to deform yield fold-like, rounded, cloth-like residual fractures between the fracture paths (Fig. 10). The fatigue striations too are more fold-like and rounded and the fracture plane contains exposed inclusions.

Genuine Brittle Fatigue Fracture. In polymers that are very difficult to deform, fatigue striations with very flat profiles and sharp-edged steps occur between the paths. Fatigue striations are frequently very faint and barely recognizable. When the dynamic fatigue fracture propagates in the form of a crack front, inclusions function as hindrances. Hard inclusions are surmounted by the fracture front, with the result that they become plainly visible or are masked in the fracture surface. Soft inclusions are sliced through by the sharp-edged crack root (Fig. 11). These features make brittle dynamic fatigue fracture the most similar to dynamic fatigue fracture in metals.

Influence of Chemicals—Environmental Stress Cracking. In metallurgy, *corrosive stress cracking* is the simultaneous interaction of a certain

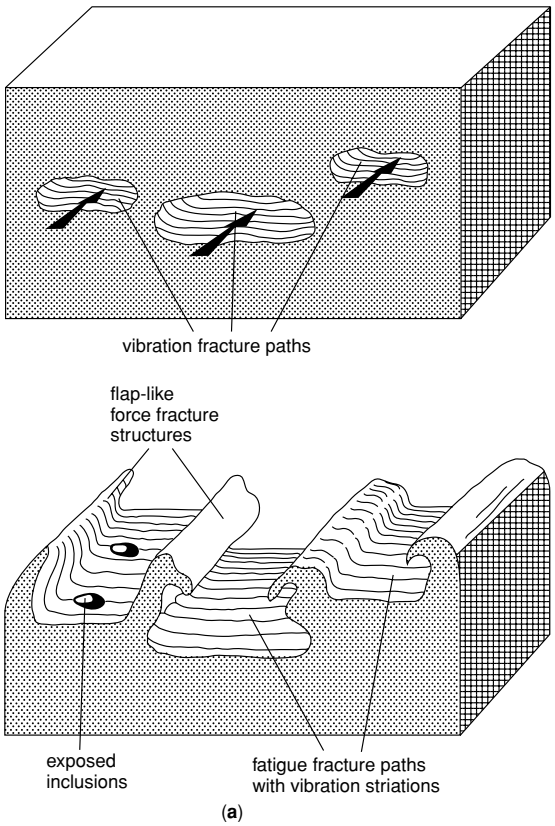

Fig. 10. Propagation of dynamic fatigue fracture in offset fracture paths with fatigue striations and cloth-like residual fractures. (**a**) Schematic and (**b**) example for nylon-6,6 (PA 66).

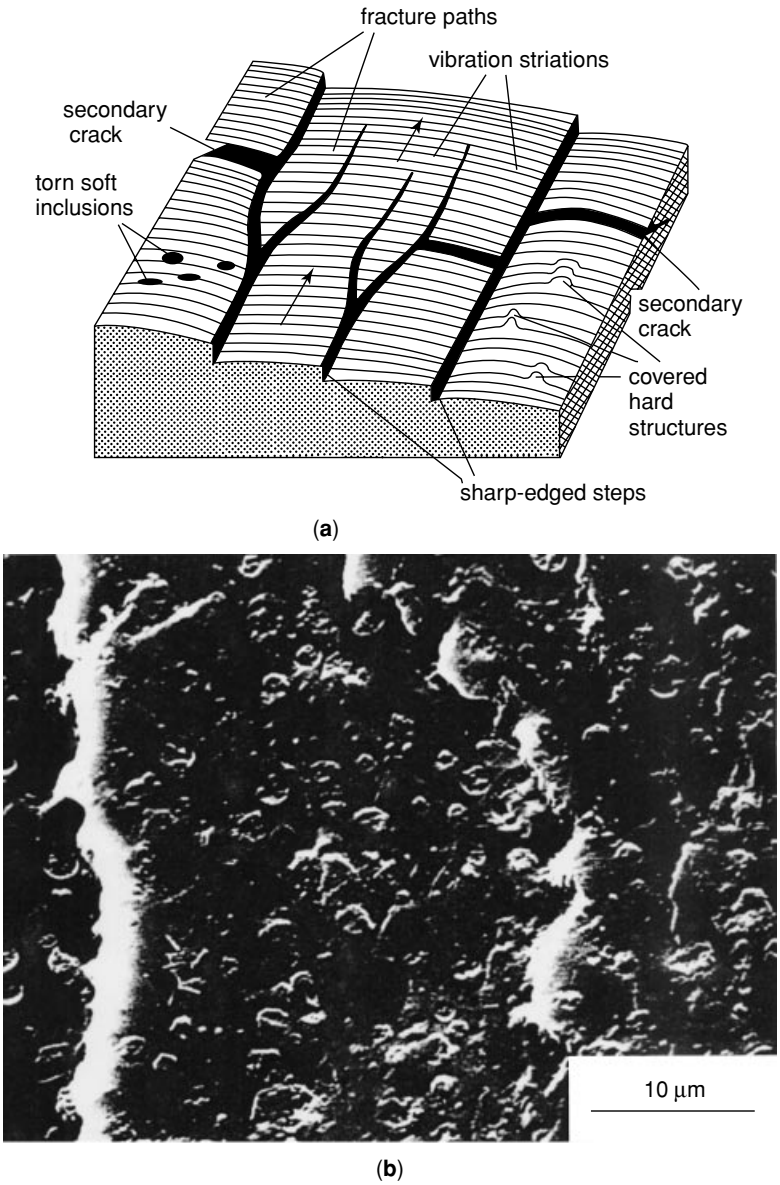

Fig. 11. Dynamic fatigue fracture in brittle polymer with sharp-edged dynamic fatigue fracture paths, fatigue striations, and secondary cracks. (**a**) Schematic (**b**) styrene–butadiene copolymer with severed butadiene spheres.

sensitive material in conjunction with a specific medium and tensile stresses. If one of these three components is absent, stress cracking does not occur. In plastics, the comparable phenomenon is usually called environmental stress cracking, especially if solvents weaken the physical intervalence forces. If a solvent will cause stress cracking in a certain polymer, it can be estimated by comparing the

solubility parameters of solvent and polymer. Equal parameters support the solubility of the solvent in the polymer. However, a prediction of the forming of environmental stress cracking only on the basis of the solubility parameters is not possible. Other factors such as viscosity of the solvent, geometric features, and processing conditions of the part, direction, and size of the load play a significant role in the formation of cracks. Also, there is the term *corrosive stress cracking*, which emphasizes the rarer chemical effect of an aggressive medium during the fracture process.

Aside from environmental stress cracking, occlusion of foreign materials into the molecule or the dissolution of certain components may bring about permanent changes in the mechanical properties. These lead to a change in deformability. An example is the initial dissolution of the crack base and thus acceleration of separation. If, under tensile stress, additional crazing occurs at the surface, it promotes ingress of the medium into the work piece (Fig. 12a). In one and the same combination of material/medium, the level of the tensile stress governs whether brittle or ductile fracture occurs.

Characteristics of genuine stress cracking are separation surfaces with feather-like propagation patterns, huge cracks at right angles to the main fracture surface, and micropeaks (0.1 μm in diameter and 0.3 μm in length).

Chemicals can weaken secondary valences and increase the deformability of the polymers. Through the inclusion of chemicals in vacancies, it is also possible, however, to hinder the mobility of the macromolecules and consequently for a loss of deformability to occur (Fig. 12b). The material becomes permanently changed and its properties differ greatly from those in the as-delivered state. This behavior must be distinguished from stress cracking in which only the simultaneous effect of tensile stress and medium causes fracture. Separation occurs after sufficient embrittlement through external stress or through internal stress, which is increased by the embrittlement.

Partial solution of the crack tip by chemicals always occurs when chemicals dissolve the material at the crack tip and thereby accelerate crack propagation.

Special Crack Causes. Apart from crack formation due primarily to loading and material, and which has just been discussed above, in fracture analysis there are always fracture characteristics that are attributable to design, processing deficiencies, or both. However, it is often not possible to definitively assign, for example, failing weld lines and voids to defects in design or processing.

Weld Lines. In unreinforced polymers, smooth fracture surfaces may be a sign of weld-line failure (Fig. 13a). This is a case of adhesive failure: the melt fronts were unable to join together in such a way that cohesive failure and the corresponding deformation in the fracture surface or different fracture planes, shown in Figure 13b, could occur.

In reinforced polymers, the orientation of the reinforcing materials often provides clues as long as the reinforcing materials are capable of aligning in the melt. This is the case with fibers. Figure 14 shows a molded part made of glass-fiber-reinforced polyamide where the fracture occurred in the knit-line area. Clearly evident are the glass fibers lying mostly parallel to the surface. If the fracture had occurred within the bulk material, glass fibers would be projecting mainly vertically from the fracture surface.

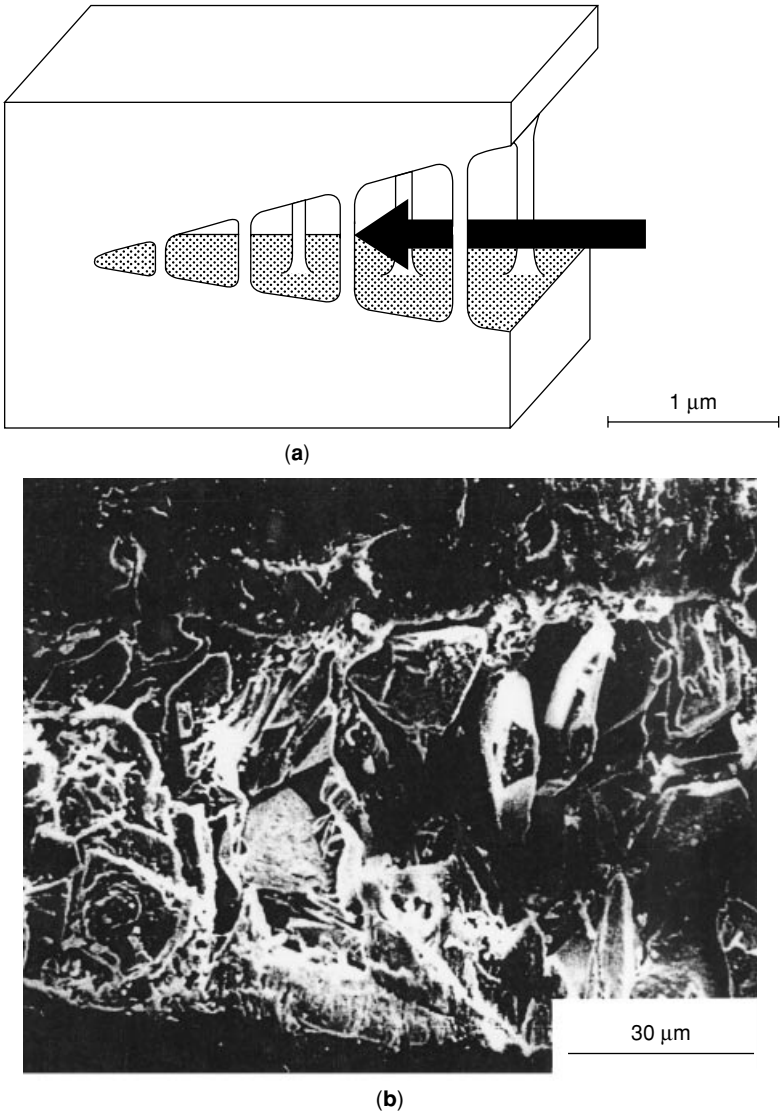

Fig. 12. Effect of chemicals. (**a**) Crazing promotes penetration of medium into inside and (**b**) ruptured crazing; NaOH has an embrittling effect on PP.

If blends are involved, the poor miscibility of most polymers with each other generally leads to a situation in which one component forms a matrix in which the other is dispersed. It is then possible that only the matrix component is found in the weld line. Proof of this can be established, where the blend composition is appropriate, by conducting comparative etching at the fractured weld-line surface and a reference fracture through the blend.

Voids and Gas Inclusions. Voids and gas inclusions are relatively easy to identify in unreinforced polymers. They constitute the only voids in the fracture

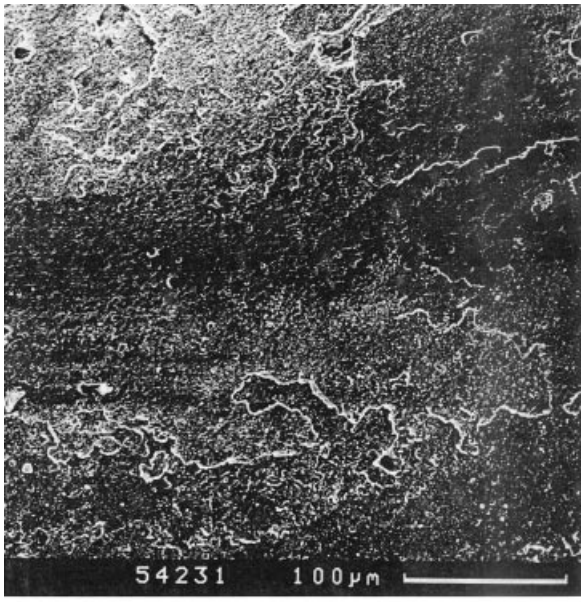

(**a**)

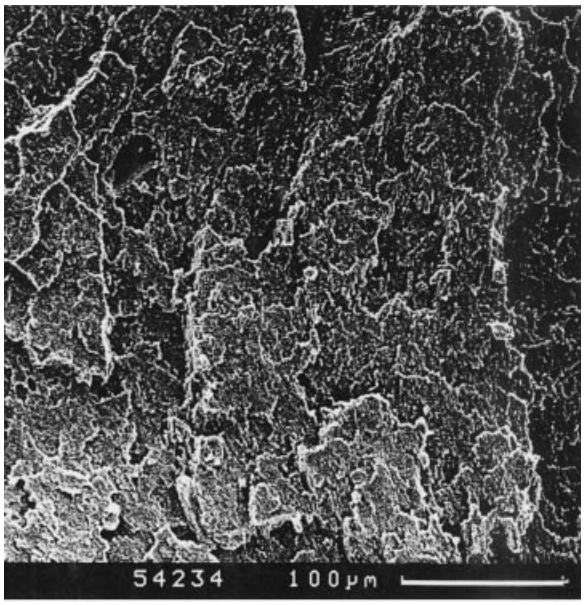

(**b**)

Fig. 13. Part made from recycled PE. (**a**) Fracture responsible for damage in weld line and (**b**) fracture due to base material.

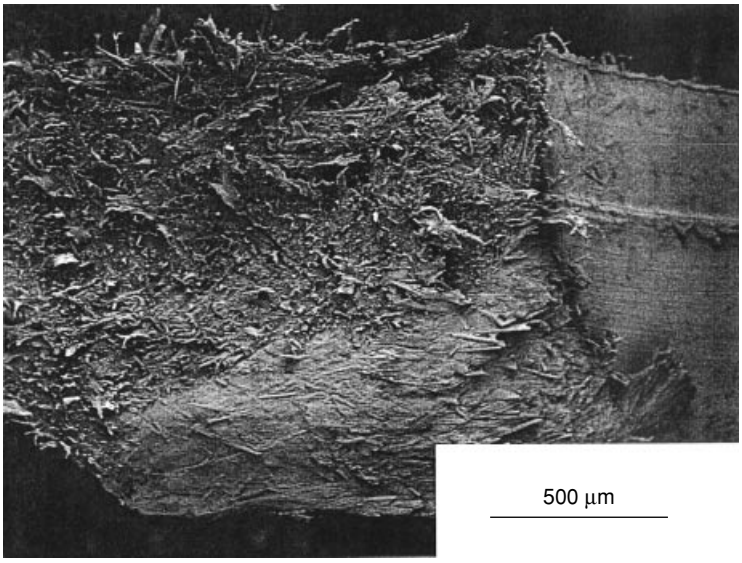

Fig. 14. Fractured knit line of a molded part made from glass-fiber-reinforced polyamide.

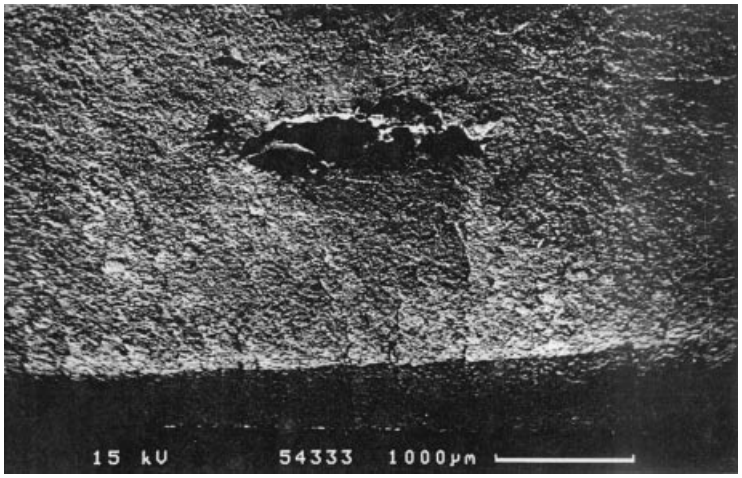

Fig. 15. Voids in a polyamide 6 molded part.

surface (Fig. 15). The situation is more difficult with filled materials as here the fillers erupt alternately from the respective opposite fracture surface, thereby leaving holes behind. As a result, confusion is possible. In such cases, however, it is often possible to classify the void by means of measurements.

Contaminants. While contaminants are an inhomogeneity in the material composition, it is not uncommon for them to originate from processing in the wider sense. In terms of fractography, inhomogeneities—especially contaminants

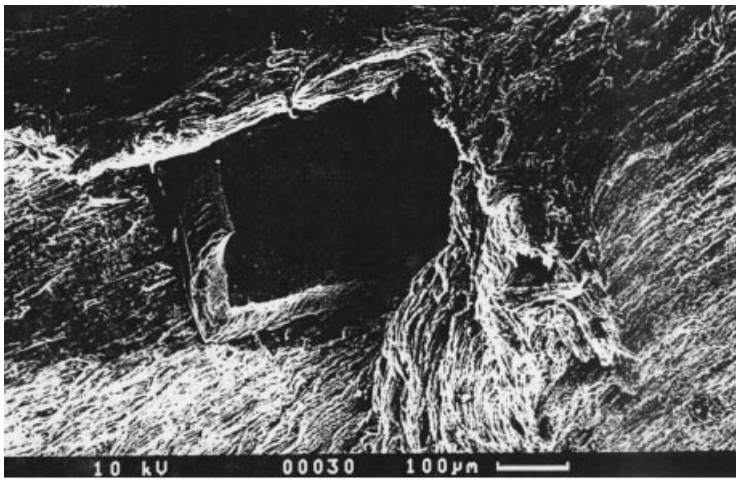

(**a**)

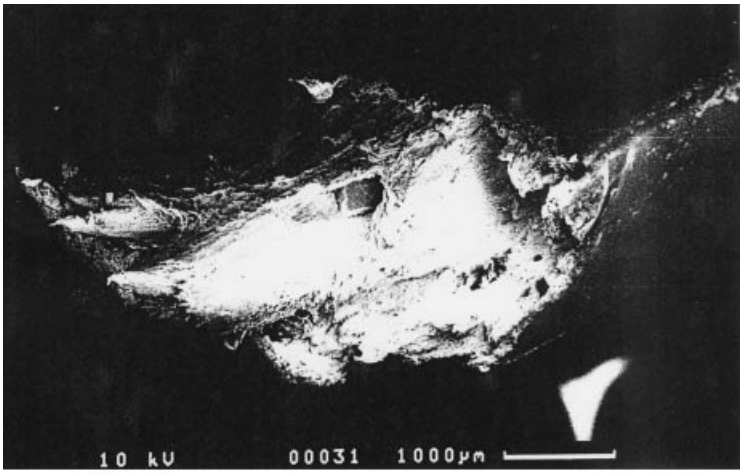

(**b**)

Fig. 16. Paint particles in the fracture surface of a molded polypropylene part.

such as paint particles—are found in the middle of fracture mirrors because they mark the cause of the crack and thus the origin of the crack (Fig. 16). On account of the different mechanical properties of the contaminant and the surrounding material, stress concentrations occur at their interface that may lead to cracking. Here, force transmission and thus adhesion between the contaminant and the matrix is of crucial importance to the stress-loading capability. With the help of energy dispersive x-ray scanning (EDX or EDS) an elemental analysis of inorganic inclusions would be possible (see SURFACE ANALYSIS).

Quantitative Evaluation of Fracture Surfaces

The objective of quantitative fractography is the quantitative description of the fracture surface in terms of parameters such as roughness, fiber orientation, phase content, and particle size distribution. Therefore different characteristics such as shape (area), size (eg length, diameter), anisotropy (orientation, direction), and distribution (spacing) of material components or topographical details are being evaluated.

The mathematical task of reconstructing the material's three-dimensional structure parameters from measured data obtained on a section of the material is called *stereology*. Different principles are used for areal, linear, and point analyses. The problem of scale is solved with a fractal approach, making the length of a curve a function of the size of the measuring device (22).

Important for the daily routine is the unchangable combination of an image with the corresponding scaling bar, so that an enlargement of the image simultaneously adopts the size of the bar. Otherwise the dimensions of topographical details cannot be evaluated correctly.

For measuring the topology of the fracture surface (i.e. roughness), direct contact profilometry, laser profilometry, or the atomic force microscopy are available (6). With the help of a coordinate system, contour maps of the fracture surface can be drawn based on roughness data or through-focus procedures for the light microscope.

An example for the use of fractography for evaluating the phase morphology of polymer blends is shown in Figure 17. The specimen, a PP with 30-wt% of a metallocene polymerized polyethylene (mPE), was fractured at −30°C. Afterwards the mPE-phase was dissolved in xylene, so that the resulting holes visualize the distribution of mPE in the PP matrix. The micrograph shows a

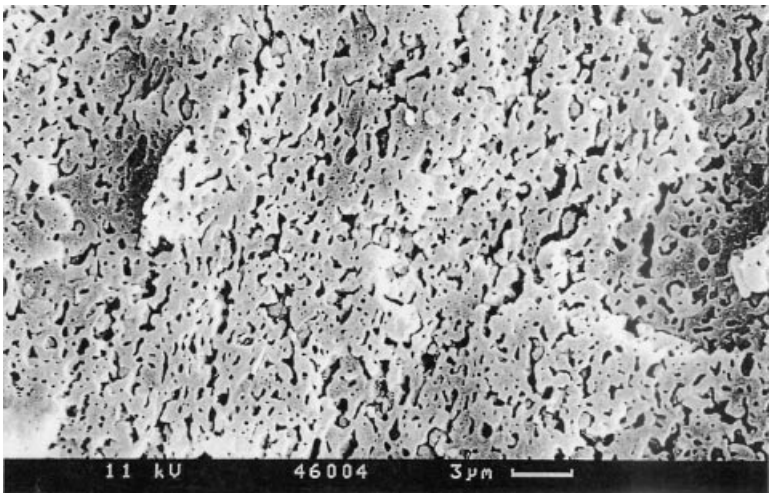

Fig. 17. Phase morphology of polypropylene with 30-wt% mPE (fractured at −30°C, mPE dissolved in xylene). From Ref. 23.

homogeneous dispersion of the minor phase. When carrying out an image analysis in order to quantify the content and phase distribution of the dispersed phase, the two-dimensional SEM picture of the three-dimensional fracture surface may not be representative enough for a good statistical value, based on stereological methods for sections. Preparing a thin section or a polished surface would be advisable.

Fractography is an indispensable tool for extending understanding of how and why a material fails. On account of its great depth of field, SEM is an essential item of equipment for fracture surface analysis. Scanning electron microscopic examination, together with the crack formation concepts (classification into fracture modes and description of their characteristics), provides an opportunity to reconstruct failure processes and to illustrate the limits to loading.

BIBLIOGRAPHY

1. G. Henry and J. Plateau, *La Microfractographie*, IRSID: Editions Métaux, 1967.
2. J. R. Davis and P. Blau, *ASM Handbook, Vol. 12: Fractography*, 2nd ed., American Society of Metals International, 1992.
3. L. Engel, H. Klingele, G. W. Ehrenstein, and H. Schaper, *Rasterelektronenmikroskopische Untersuchungen von Kunststoffschäden*, Carl Hanser Verlag, Munich, 1978.
4. L. Engel, H. Klingele, G. W. Ehrenstein, and H. Schaper, *An Atlas of Polymer Damage—Surface Examination by Scanning Electron Microscope*, Wolfe Publishing, London, 1981.
5. G. W. Ehrenstein, *Kunststoffberater* **42**(10), 23–28 (1997).
6. D. Hull, *Fractography: Observing, Measuring, and Interpreting, Fracture Surface Topography*, Cambridge University Press, Cambridge, U.K., 1999.
7. A. C. Roulin-Moloney, *Fractography and Failure Mechanisms of Polymers and Composites*, Elsevier Science Publishers, London, 1989.
8. R. Holm and B. Reinfandt, *Z. Werkstofftech.* **9**(5), 153–188 (1978).
9. G. Michler and V. Schmidt, *Plaste und Kautschuk* **34**(1), 1–6 (1987).
10. G. Michler, in H. Bethge and J. Heydenreich, eds., *Elektronenmikroskopie i.d. Festkörperphysik*, Springer-Verlag, Berlin, 1982.
11. K. Wetzig, *Materialprüfung* **39**, 200–203 (1997).
12. D. Pohl and H. Jaksch, *Materialprüfung* **37**, 412–415 (1995).
13. J. A. Sauer and C. C. Chen, *Adv. Polym. Sci.* **52/53**, 170–223 (1983).
14. P. F. Schmidt, *Praxis der Rasterelektronenmikroskopie und Mikrobereichsanalyse*, Expert-Verlag, Renningen-Malmsheim, 1994.
15. H. Beyer and H. Riesenberg, *Handbuch der Mikroskopie*, VEB Verlag Technik, Berlin, 1998.
16. A. Hall, M. Browne, and C. V. Howard, *Proc. Roy. Microscopical Soc.* **26**, 63–70 (1991).
17. K. Kato, *Polym. Eng. Sci.* **1**, 38–39 (1967).
18. H. Sano, T. Usami, and H. Nakagawa, *Polymer* **27**, 1497–1504 (1986).
19. A. Breining, G. W. Ehrenstein, and J. Varga, *Materialprüfung* **39**(3), 81–85 (1997).
20. V. Jaussent and G. W. Ehrenstein, *Praktische Metallographie* **34**, 544–554 (1997).
21. W. Wegener and R. Merkle, *Chemiefasern* **17**(4), 296–298 (1968).

22. S. L. Chan, in Ref. 7.
23. F. Raue, *Mechanisches Werkstoffverhalten von olefinkautschukmodifiziertem Polypropylen*, Ph.D. Thesis, University of Erlangen – Nuremberg, 2000.

G. W. EHRENSTEIN
F. RAUE
University of Erlangen – Nuremberg

FRACTURE

Introduction

Fracture is defined as stress-biased material disintegration through the formation of new surfaces within a body. Fracture starts out as a localized event that eventually encompasses the whole object (Fig. 1). Fracture is synonymous with rupture and breakage but not with failure. The latter term is more general and also encompasses nonmechanical breakdown through heat (thermal failure) or environmental degradation (chemical attack, irradiation).

For fracture to occur, it is generally necessary that a specimen be subjected to mechanical loads and that the resulting, initially homogeneous (viscoelastic) material deformation—which eventually would lead to creep and ductile failure—becomes heterogeneous and initiates material separation. The most likely sites for material separation are structural irregularities, growing material *defects*, or preexisting cracks. In a polymeric material, such sites are for instance given by inclusions of particles or voids, craze-like features, or cracks. Crazes and subsequently cracks extend as the material between voids and adjacent to a crack tip deforms and/or disintegrates. Depending on the nature and the extent of such deformation, breakdown occurs in quite different modes of failure: as brittle fracture by rapid crack propagation (Fig. 1), crazing, or slow crack growth, or by ductile failure (Fig. 2).

The mode of failure (of a cracked specimen) is not an inherent property of a given material in a given environment. It also depends on the loading rate and especially on the local state of stress, which is strongly influenced by the configuration of the crack itself. For this reason a mechanical analysis of a cracked, stressed body is presented first, which is based on linear and nonlinear elastic fracture mechanics.

Encyclopedia of Polymer Science and Technology. Copyright John Wiley & Sons, Inc. All rights reserved.

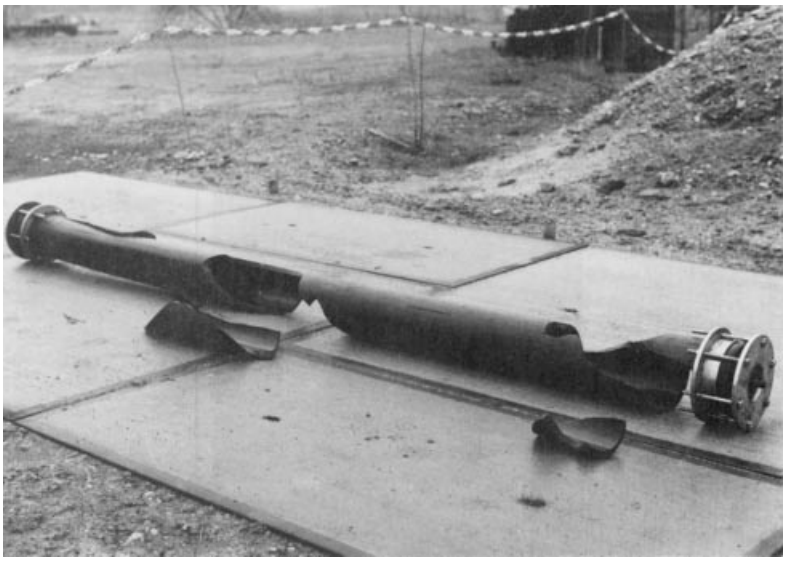

Fig. 1. Brittle fracture of a polyethylene pipe subjected to a burst test at 500 kPa (5 bar). From Ref. 1.

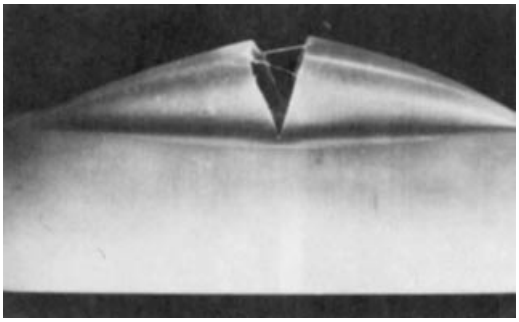

Fig. 2. Ductile failure of an internally pressurized polyethylene pipe.

Linear Elastic Fracture Mechanics

Fracture mechanics concepts describe the behavior of cracks or other defects when a body is loaded. A crack constitutes a discontinuity within a body. At the boundary of the discontinuity, very high local stresses and strains are usually observed, and in the limit of a sharp crack in an elastic body, these may theoretically be infinite or singular. Linear elastic fracture mechanics (LEFM) describes the conditions under which a crack grows or propagates, creating new surface area. LEFM assumes a globally linear elastic deformation with energy absorption confined to a very local region at the crack tip. The theory has been extended to plastically deforming materials, which undergo rate-independent, irreversible deformation. Neither of these assumptions is strictly true for polymers, since all exhibit a more

or less viscoelastic and time-dependent behavior. However, much of the behavior observed in the fracture of polymers can be described in terms of LEFM. There are two approaches to describing the condition of fracture. In the first, the *balance of energy* is discussed; energy is released from the elastically deformed specimen if the length of a crack increases, and at the same time energy is absorbed by the creation of the new crack surface area. In the second approach, the local stress field around the crack tip is considered and its intensity at fracture is characterized by some parameter, the *fracture toughness*. Fracture mechanics is a macro theory, being concerned with the overall behavior of a body. The particular material behavior is considered only in connection with fracture criteria or with the nature of the deformation processes involved. Much of the theory is thus not material specific and applies equally to all materials. When dealing with ductile polymer fracture, plasticity modifications are of value. It is possible to modify the analysis to encompass time effects; this is particularly necessary for the two extreme phenomena such as slow crack growth and dynamic or impact fracture. References 2–4–5 cover these topics in much more detail and provide an extensive bibliography.

Resistance or *R* Curve. It is a useful approach to define the toughness of a material in terms of its resistance or R curve, as shown in Figure 3. Here R is the energy per unit area necessary to produce the new fracture surface S. For a crack of length a_0 and in a plate of uniform thickness B, the incremental increase in surface area ΔS may be expressed in terms of the crack growth Δa. Any virgin material will first resist to crack-growth initiation by crack tip deformation; the development of this *process zone* is associated with a certain resistance $R = R_c$. Subsequent growth in many polymers may be described, as shown in line A, with R increasing as the crack extends. (As will be shown below, this is usually ascribed to an increase of the local plastic flow in a zone of size r_y around the crack tip). If however the extent of this zone, which represents the energy absorption, remains the same, R remains constant as shown in line B. This is so for the more brittle fractures, where the energy absorption is very local and the zone is small and very much less than a_0. For tougher materials, an increasing r_y is more likely. The plastic zone size r_y is a very important parameter, since it provides a length factor which controls the various size effects.

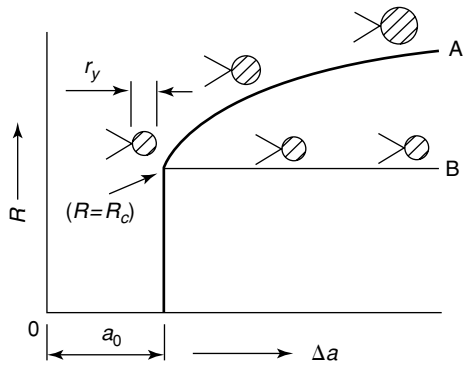

Fig. 3. The resistance or R curve. See text for significance of curves A and B.

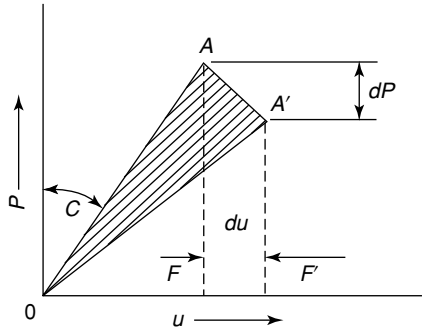

Fig. 4. Energy release during crack extension in an elastic plate shown by the shaded area.

Energy-Release Rate. As first formulated by Griffith (6), the driving force for fracture comes from the energy which is released by the growth of the crack. Such growth violates the continuity within the body and results in the final energy state being lower than the initial; the difference is released and available to overcome the crack resistance R. This is shown in Figure 4 for a linearly elastic body, in which crack growth initiates at A. The growing crack reduces the stiffness of the sample, which results in a reduction in load P and an increase in deformation (to the point A'). The initial stored energy corresponds to the area $0AF$ and that after crack growth to $0A'F'$. During crack extension, external work has been furnished, which is given by $AA'F'F$. The energy $\mathrm{d}U$ which is released by the system corresponds to the shaded area $0AA'$ and is given by

$$\mathrm{d}U = 1/2(P\mathrm{d}u - u\mathrm{d}P) \tag{1}$$

where u is the deformation in the direction of applied load.

The rate of energy release $\mathrm{d}U/B\mathrm{d}a$ is given the symbol G and expressed by

$$G = \frac{1}{B}\frac{\mathrm{d}U}{\mathrm{d}a} = \frac{1}{2}\left(P\frac{\mathrm{d}u}{\mathrm{d}a} - u\frac{\mathrm{d}P}{\mathrm{d}a}\right) \tag{2}$$

where a is the crack length. Introducing the compliance C of the body which is a function of crack length

$$C = \frac{u}{P} \tag{3}$$

we obtain

$$G = \frac{P^2}{2B}\frac{\mathrm{d}C}{\mathrm{d}a} = \frac{u^2}{2B}\frac{1}{C^2}\frac{\mathrm{d}C}{\mathrm{d}a} = \frac{U}{B}\frac{1}{C}\frac{\mathrm{d}C}{\mathrm{d}a} \tag{4}$$

Thus, G can be determined from the load and the deflection at crack extension, provided the compliance $C(a)$ is known. For any load, lines of G vs a can be plotted for a cracked body, as shown in Figure 5, together with an (arbitrary) R

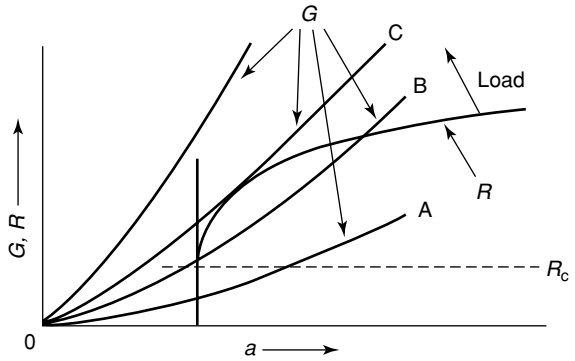

Fig. 5. Energy-release rate G and material resistance R for various loads levels.

curve. For the load of line A, there is no growth when G intersects R, but for line B there is. However, just after initiation $R > G$, which prevents immediate and unstable crack growth. The crack would grow, of course, if the load were increased. Cracks in a time-dependent material can also grow, in a stable manner, by plastic deformation at loads smaller than the breaking stress (see further below). Crack growth will be stable if

$$G = \frac{\mathrm{d}U}{B\mathrm{d}a} = R \text{ and } \frac{1}{B}\frac{\mathrm{d}G}{\mathrm{d}a} = \frac{1}{B^2}\frac{\mathrm{d}^2U}{\mathrm{d}a^2} < \frac{\mathrm{d}R}{B\mathrm{d}a} \tag{5}$$

For the tangency condition C there is a small region of stable growth (up to the tangency point), followed by instability. For a constant $R(a) = R_c$, there is no growth until $G = R_c$, and the initiation is immediately followed by unstable growth. G at initiation is usually written as G_c $(=R_c)$. An important example of fracture mechanics concerns the stability of a crack of length $2a$ in an infinitely wide sheet loaded with a constant stress σ, as shown in Figure 6.

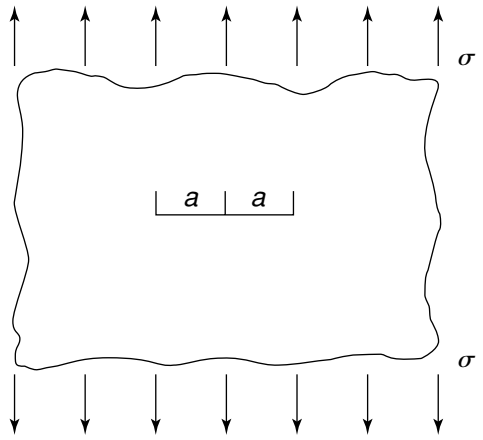

Fig. 6. The infinite sheet.

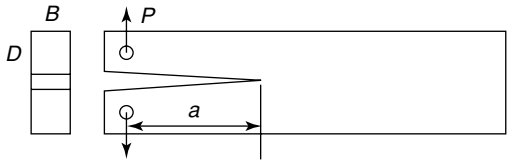

Fig. 7. The double-cantilever beam (DCB).

The energy-release rate G for the above geometry has been derived (6,7) as

$$G = \frac{\pi \sigma^2 a}{E} \tag{6}$$

where E is the Young's modulus. In a perfectly brittle material undergoing no plastic work, we have at fracture $G_c = 2\gamma = \pi\sigma^2 a/E$, where γ is the true surface work of the solid. Thus, the basic relationship of fracture mechanics is that $\sigma^2 a \approx$ constant at fracture. In this case $dR/da = 0$ and $dG/da > 0$, and the fracture is always unstable. However, this does not hold for a cracked specimen at fixed displacement.

Another important specimen geometry is the double-cantilever beam (DCB) shown in Figure 7. From beam theory,

$$C = \frac{8a^3}{EBD^3} \tag{7}$$

where B is specimen thickness and D specimen width. In practice, $C \propto an$, $n < 3$, because of rotation at the beam ends, and this empirical result is frequently used in practice. Using equations (4) and (7) we have

$$G = \frac{12P^2a^2}{EB^2D^3} = \frac{3}{16}\frac{ED^3u^2}{a^4} \tag{8}$$

Again, $G = G_c = 2\gamma$ at fracture giving load-crack length and displacement-crack length relationships at fracture, and also $dR/da = 0$. Fixed load gives $dG/da > 0$ as before, resulting in unstable growth, but for constant displacement, $dG/da < 0$ and stable growth occurs.

In principle, any body can be characterized by finding $C(a)$ by measurement or computation. Thus, by detecting crack-growth initiation, the G value at fracture, termed G_c, can be found. Subsequent stability can be described in terms of dG/da and dR/da. Some more general aspects to the analysis are also important and, in particular, the fact that G may be described for any elastic body, not necessarily linear, as

$$G = \int^s W dy \quad \text{displacement constant} \tag{9}$$

where W is the strain–energy–density function, y the coordinate normal to the crack direction, and s some closed contour taken around the crack tip. This form

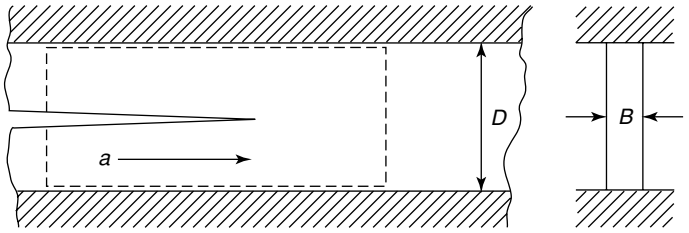

Fig. 8. The parallel strip.

is particularly useful for the analysis of nonlinear elastic systems as encountered in rubber elasticity (8). An example is a very wide parallel strip (Fig. 8) where a contour may be taken, as indicated by the broken line. The horizontal portions give no contribution since $dy = 0$, and if the vertical lines are remote from the crack tip, the part behind it has no stored energy, whereas that in front has the energy per unit volume of the uncracked strip, eg, W_0. Equation (9) then gives

$$G = W_0 D \tag{10}$$

The result is obvious, since a strip of width dx has an initial stored energy of $W_0 BD\ dx$. After fracture, this is reduced to zero by the creation of area $B\ dx$, giving the above results. Of course, W_0 may be found for any type of elastic behavior simply by loading the strip initially. This result is also true in this case even when the crack speed is high and there are no kinetic energy effects, since these must all eventually go to zero as in the static case, though it is debatable if kinetic energy is truly reversible in real systems.

Stress–Intensity Factor. The stresses around the crack tip, as shown in Figure 9, may be expressed in the form of a series:

$$\sigma = \frac{Kf(\theta)}{\sqrt{2\pi r}} + A(\theta) + B(\theta) r^{1/2} + \cdots \tag{11}$$

where f, A, B, etc, are functions of the angle θ, and r is the distance from the crack tip. As the crack tip is approached ($r \to 0$), all terms other than the first two tend to zero and the first term is dominant; $A(\theta)$ represents nonsingular stresses which can have effects, but, in general, the first singular term, which tends to ∞ as $r \to 0$ dominates. The form of the stress field is the same for all remote

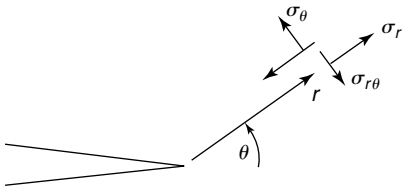

Fig. 9. Local stresses around a crack tip.

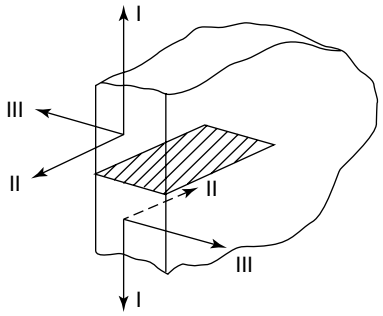

Fig. 10. Modes of loading.

loading states and is determined by $f(\theta)$. The *magnitude* of the local stresses is conveniently expressed by K, the stress–intensity factor, which is a function of the remote loading σ. K is defined as

$$K = \sigma\sqrt{2\pi r} \quad \text{as} \quad r \to 0 \quad \text{at} \quad \theta = 0 \tag{12}$$

If a characterizing parameter in the local region of the crack tip is sought, clearly σ (or strain) is not useful since it tends to infinity as $r \to 0$. However, the product $\sigma\sqrt{r}$ is finite in the local zone and for this reason K (and not σ) is taken as the local parameter characterizing the mechanical effort to which a cracked specimen is subjected. If stress intensity is the decisive parameter, fracture should occur once K attains a critical value K_c; K_c is termed fracture toughness.

It is convenient to express the loading on a crack in terms of three orthogonal components (Fig. 10), which may be super-imposed to give any loading state: Mode I, the opening mode; Mode II, the shear mode; and Mode III, the out-of-plane shear mode. An applied loading may give rise to a mixture of all three modes, which can be expressed in terms of K_I, K_{II}, and K_{III}. Mode I is the most severe and thus generally the most important; in the presence of a combination of loading modes this often results in local mode-I fracture.

For the most frequently observed modes I and II, the local stress fields may be written as (2)

$$\sigma_\theta = \frac{K_I}{\sqrt{2\pi r}}\frac{1}{2}\cos\frac{\theta}{2}(1+\cos\theta) - \frac{K_{II}}{\sqrt{2\pi r}}\frac{3}{2}\sin\frac{\theta}{2}(1+\cos\theta) \tag{13}$$

$$\sigma_r = \frac{K_I}{\sqrt{2\pi r}}\frac{1}{2}\cos\frac{\theta}{2}(3-\cos\theta) - \frac{K_{II}}{\sqrt{2\pi r}}\frac{1}{2}\sin\frac{\theta}{2}(1-3\cos\theta) \tag{14}$$

$$\sigma_{r\theta} = \frac{K_I}{\sqrt{2\pi r}}\frac{1}{2}\sin\frac{\theta}{2}(1+\cos\theta) - \frac{K_{II}}{\sqrt{2\pi r}}\frac{1}{2}\cos\frac{\theta}{2}(1-3\cos\theta) \tag{15}$$

$$K_{\mathrm{I}} = \sigma_\theta \sqrt{2\pi r} \quad \text{at} \theta = 0 \tag{16}$$

$$K_{\mathrm{II}} = \sigma_{\mathrm{r}\theta} \sqrt{2\pi r} \quad \text{at} \theta = 0 \tag{17}$$

In mode-I loading of a brittle material, fracture occurs when K_{I} attains a critical value K_{Ic}. In combined-loading modes, crack propagation is not colinear and some complications result. If in a state involving modes I and II fracture occurs by crack opening, then the crack will propagate under an angle θ_{c} (2). This angle is obtained from equation (13):

$$K_{\mathrm{Ic}} = K_{\mathrm{I}} \frac{1}{2} \cos\frac{\theta_{\mathrm{c}}}{2}(1 + \cos\theta_{\mathrm{c}}) - K_{\mathrm{II}} \frac{3}{2} \sin\frac{\theta_{\mathrm{c}}}{2}(1 + \cos\theta_{\mathrm{c}}) \tag{18}$$

and an additional condition that

$$\frac{\mathrm{d}\sigma_\theta}{\mathrm{d}\theta} = 0 \quad \text{which is equivalent to } \sigma_{\mathrm{r}\theta} = 0 \tag{19}$$

giving

$$0 = K_{\mathrm{I}} \frac{1}{2} \sin\frac{\theta_{\mathrm{c}}}{2}(1 + \cos\theta_{\mathrm{c}}) - K_{\mathrm{II}} \frac{1}{2} \cos\frac{\theta_{\mathrm{c}}}{2}(1 - 3\cos\theta_{\mathrm{c}}) \tag{20}$$

In pure mode I ($K_{\mathrm{II}} = 0$), θ_{c} is zero as expected, whereas in pure mode II ($K_{\mathrm{I}} = 0$), $\theta_{\mathrm{c}} = \cos^{-1} 1/3 = \pm 70.3^\circ$.

Relation between *G* and *K*. The local singular stress field is described by K_{I} and it is from this discontinuity that the energy is released by way of G. It is to be expected, therefore, that G and K_{I} would be related and this can be demonstrated by deriving G around a local contour (2):

$$K_{\mathrm{I}}^2 = EG \tag{21}$$

The π factor in equation (11) is introduced in the definition of K_{I} to remove any numerical constant in equation (21). There is no similar result for mode II alone or for mixed modes, since the propagation is not colinear ($\theta_{\mathrm{c}} \neq 0$) and the above result would not be valid.

Returning to the case of the infinite plate,

$$K_{\mathrm{I}}^2 = EG = \pi \sigma^2 a \tag{22}$$

If σ is measured at fracture for a given a, K_{Ic} is obtained and the fracture toughness is characterized without the need to know E, which is involved when G is used. This is of considerable benefit in the polymer field, where E is time-dependent and often uncertain. K_{Ic} may also be defined for specimens having a noninfinite geometry by means of a more general form of equation (21′):

$$K_{\mathrm{I}}^2 = Y^2(a/W)\sigma^2 a \tag{23}$$

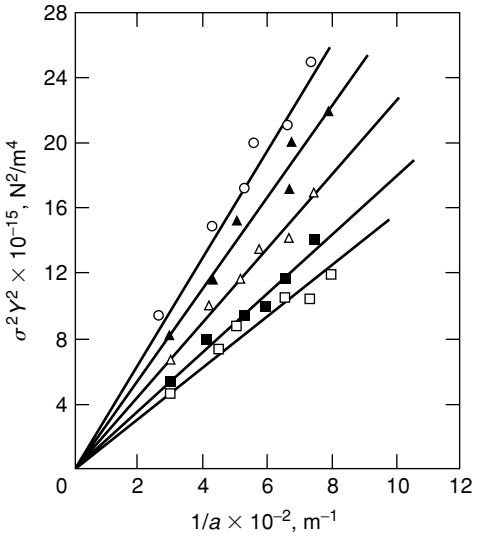

Fig. 11. Crack-initiation data. Single-edge notch bend data for polyacetal at temperatures of 20 to −60°C. The symbols represent the following temperatures: □, 20°C; ■, 0°C; △, −20°C; ▲, −40°C; ○, −60°C.

where $Y^2(a/W)$ is a calibration function [to account for the noninfinite sample geometry, it is available for most practical cases (9,10)]. For the infinite plate Y^2 is π, all other cases tend to this result for $a/W \to 0$. For a linearly elastic material it is assumed that relation 22 is valid up to fracture; a plot of σ^2Y^2 vs $1/a$ should result in a straight line passing through the origin, the slope of which is equal to ${K_{\mathrm{Ic}}}^2$. Figure 11 demonstrates that in the temperature range of $-60°\mathrm{C} < T < 20°\mathrm{C}$ polyacetal behaves in a linear elastic manner. Nonlinearity in the σ^2Y^2 vs a^{-1} graph occurs because of local plasticity and/or damage formation in the crack tip zone.

For the important compact tension geometry (Fig. 12c), K_{I} is generally expressed in terms of the applied load P:

$$K_{\mathrm{I}} = \frac{P}{B\sqrt{W}} Y(a/W) \tag{24}$$

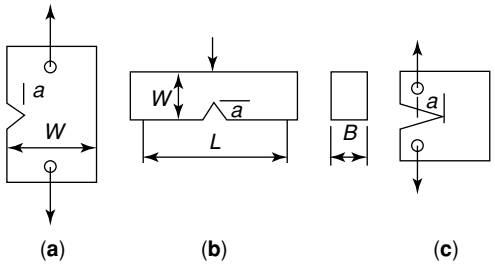

Fig. 12. Testing geometries: (**a**) single-edge notch tension (SENT), (**b**) single-edge notch three-point bending (SENB), and (**c**) compact tension (CT).

Of course, the correction function Y is another way of expressing the compliance calibrations given in equation (4); for a three-point bend test (Fig. 12b), for example, is

$$\frac{dC}{da} = \frac{9}{2}\frac{L^2}{BW^4E}Y^2a \tag{25}$$

where L is the length of the beam.

An important alternative form is the energy version of the general equation (4):

$$G = \frac{U}{BW\phi} \tag{26}$$

in which the calibration factor is expressed by

$$\phi = \frac{C}{dC/d(a/W)} = \frac{\int Y^2 x\,dx}{Y^2x} + \frac{L}{18W}\frac{1}{Y^2x} \tag{27}$$

where $x = a/W$.

Values of ϕ are available for bending (2), and G_c may be found by measuring the energy to crack initiation and via equation (25). In any test, the three parameters at fracture (a, G_c, K_c) can be measured and various combinations of E and G determined. Thus, from the load $P = u/C$ in a bending experiment, the displacement G/E is obtained by

$$\frac{G}{E} = \frac{u^2W^2}{9L^2a}\frac{1}{(\phi Y)^2} \tag{28}$$

$G/E = (\pi/4)\rho$, where ρ is the elastic tip radius of the crack under load. If all three of the above parameters are used, consistency can be checked, and in addition, E is found.

Fracture Mechanics Admitting Confined Plasticity and Viscoelasticity

Irwin Model of Plasticity and Size Effects. The elastic analysis predicts infinite stresses at the crack tip, but local yielding prevents this from happening. Irwin has modeled this situation by a small, local yielding zone surrounded by a larger, outer elastic zone (Fig. 13). For a state of plane stress ($\sigma_z = 0$) as in thin plates or at the surface of thick plates, the radius of the plastic zone r_y can be derived from equation (20) to be approximately

$$r_y \approx \frac{1}{2\pi}\left(\frac{K_{Ic}}{\sigma_y}\right)^2 \text{(planestress)} \tag{29}$$

The elastic stresses in the outer zone can be calculated from the Irwin model by assigning a fictitious length $a + r_y$ to the crack.

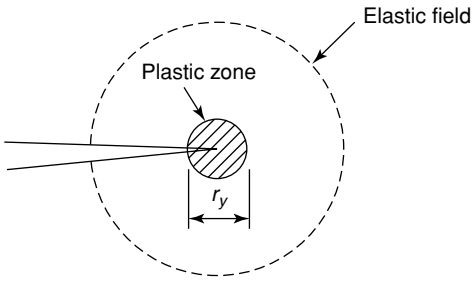

Fig. 13. Irwin model: Small plastic zone surrounded by an elastic field.

In the center of thick plates a state of plane strain is approached in which the contraction in the z direction is constrained ($e_z = 0$) and $\sigma_z = \nu(\sigma_r + \sigma_\theta)$. Because of these constraints the plastic zone radius is much smaller:

$$r_y' \approx \frac{1}{2\pi}\left(\frac{K_{Ic}}{\sigma_y}\right)^2 (1-2\nu)^2 (\text{planestrain}) \tag{30}$$

Within the plastic zone, $\nu \to 1/2$ and so the stress state tends to be equitriaxial tension $\sigma_r = \sigma_\theta = \sigma_z$, the most severe in fracture terms. In testing it is desirable to employ the most severe conditions to explore the worst case. To achieve this, the specimen dimensions (B, W) must be considerably greater than the plastic zone. This is defined by the ASTM size criterion (11) for bend testing which requires a minimum thickness:

$$\hat{B} > 2.5\left(\frac{K_{Ic}}{\sigma_y}\right)^2 \tag{31}$$

approximately equivalent to $\hat{B} > 16 r_y$. If $B < \hat{B}$ the stress state tends to be plane stress and the measured toughness values are unrealistically high.

Line Zone or Dugdale Model. In many polymers, crazes form at stress concentrations such as crack tips (12). A craze is a planar structure, which can be realistically modeled by a line zone, as shown in Figure 14. Here, microyielding at the craze boundaries is modeled by a line of elastic tractions as in the Dugdale model. There is mechanical equilibrium if the zone length is

$$r_y = \frac{\pi}{8}\left(\frac{K_{Ic}}{\sigma_y}\right)^2 \tag{32}$$

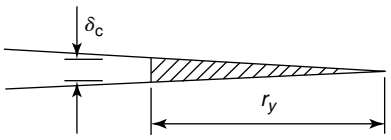

Fig. 14. The line zone model well represents single crazes.

Another useful parameter arises, since the displacement at the crack tip δ_c (in a state of plane stress) is predicted by this model as

$$\delta_c = \frac{K_{Ic}^2}{E\sigma_y} = \frac{G_c}{\sigma_y} \tag{33}$$

The critical crack tip opening displacement δ_c (CTOD) can be used as a fracture criterion. A constant δ_c is equivalent to constant K_{Ic} and G_c as used in LEFM. If δ_c remains constant outside the LEFM range, it can be used to make predictions for viscoelastic and large-scale plasticity behavior.

Viscoelastic Effects. In all the above analyses, fracture mechanics parameters were considered to be independent of time; consequently G_c (or K_{Ic}) would have to be independent of loading rate or crack speed. However, most polymers show some degree of viscoelasticity, which can have an important influence on fracture behavior. This is particularly pronounced in cross-linked elastomers. The time-dependent fracture of polymers has been reviewed repeatedly (13–15). Without going into details the pioneering work in the sixties and seventies of Williams, Barenblatt, Knauss and Müller, Retting, Williams and Marshall, and Schapery should be mentioned. These authors have extended Griffith's work to linearly viscoelastic materials. They pointed out that the work of fracture in polymers depends on the load history, that is on the rate of crack growth $\dot{a}$, and that viscoelastic creep crack growth can be described by replacing the elastic by viscoelastic moduli. In simplifying, it can be said that the time dependence of crack growth in polymers has three different origins: firstly, it is influenced by the viscoelastic behavior of the far field stresses (the energy necessary to drive the crack is released as a function of time rather than instantaneously). Secondly, there are viscous losses because of the (steady) extension of the process zone through plastic flow and/or the formation and growth of fibrils. Thirdly, cracks grow, occasionally in a discontinuous manner, because of the weakening and rupture of the material in the process zone through disentanglement, chain scission, and formation and coalescence of voids (see section on Fracture Phenomena for a discussion of these mechanisms).

It is generally a reasonable assumption that yield strain e_y and ultimate strain or crack opening displacement δ_c are relatively constant with loading rate (2,13–17), whereas the elastic modulus follows a power law in time:

$$\frac{\sigma_y}{E} = e_y \quad \text{and} \quad \frac{E}{E_0} = \left(\frac{t}{t_{0-}}\right)^{-n} \tag{34}$$

where e_y, E_0, t_0, and n are constants. If a constant δ_c criterion in the line zone model is assumed and if the time scale is related to the inverse of crack speed, a relation between $\dot{a}$ and K is obtained, which has been verified experimentally for many thermoplastic and thermosetting polymers (16–20):

$$\dot{a} = A(K_I)^{1/n} \tag{35}$$

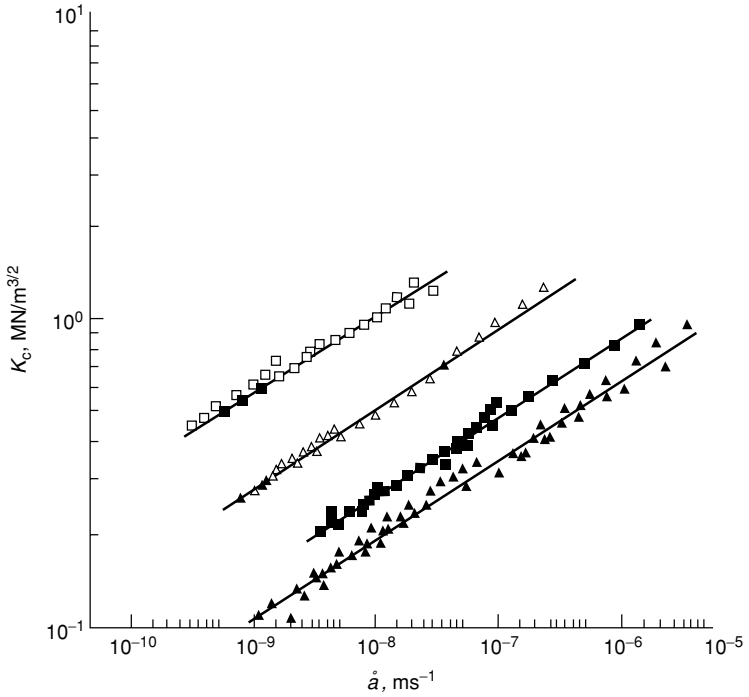

Fig. 15. K_c–$\dot{a}$ curves for polyethylene in distilled water at different temperatures. Slopes = 0.25. The symbols represent the following temperatures: □, 19°C; △, 40°C; ■, 60°C; ▲, 75°C.

This form represents a continuous relationship between K and $\dot{a}$; in a log–log plot straight lines are obtained as well illustrated by Figure 15 for polyethylene in distilled water at different temperatures.

Since it is usually convenient to measure the crack speed in a specimen in which K does not vary with a for a given load or loading rate, the double-torsion and tapered-cantilever beam tests are used (Fig. 16). In the first we have

$$K^2 = \frac{3(1+\nu)}{2}\frac{P^2 l^2}{B^2 D^3} \tag{36}$$

where l is the distance from the center of the specimen to the point of load support. For the tapered beam,

$$K^2 \approx \frac{45P^2}{B^2 D_0^3} \quad \text{for a tape angle } \alpha \approx 11^\circ \tag{37}$$

Under dead loads (constant P), K values are constant resulting in a fixed crack speed, which can be measured over a certain distance of crack growth; the K_c–$\dot{a}$ curve is then determined by changing the load. Environmental data are obtained by conducting the test with the specimen immersed in the environment.

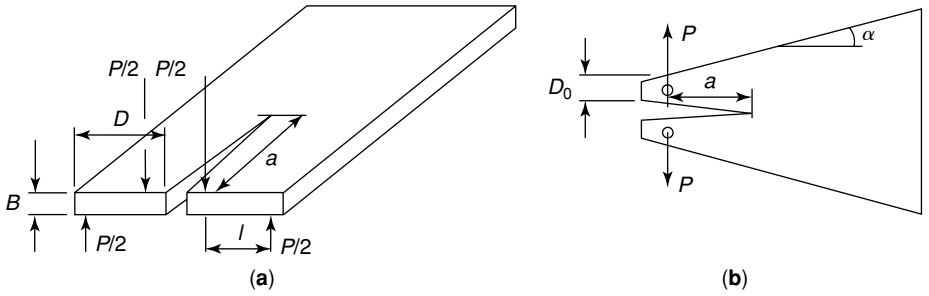

Fig. 16. Crack-growth testing geometries for constant K tests: (**a**) double tension, (**b**) tapered cantilever.

Side grooves are often used in these tests to guide the crack, with appropriate modifications made to the formula for K. Typical data for polyethylene in water are given in Figure 15.

Such data on $K_c(\dot{a})$ are of particular importance because they provide a method by which long-term failure may be predicted from much shorter-term results. The measured crack-growth rates may be integrated to predict failure times. For example, the time for a flaw of original length a_0 to grow to a length much more than a_0 is given by

$$t = t_i\left[1 + \frac{5n}{1-n}\left(\frac{a_0}{r_0}\right)\right], \quad n \ll 1 \tag{38}$$

where $r_0 = (\pi/8)\,(\delta_c/e_y)$ is the zone size, and t_i is the crack initiation time. For very small flaws, $t \sim t_i$ and very little of the life is spent in crack propagation. Such a result predicts $\sigma \propto t^{-n}$ for a constant stress test, ie, the log stress–log rupture time curve has the reverse slope of the log K–log $\dot{a}$ crack-growth line (Fig. 15). Such a behavior has been verified experimentally for a number of thermoplastic and thermosetting polymers (16–20).

Fracture Mechanics of Dissipative Materials

Plasticity Effects. In LEFM, it is assumed that the plastic-zone size r_y is very small, but because of specimen size limitations it is often difficult to take measurements under conditions where this is true. In any event, a first correction can be made by increasing the crack length a by r_y to compensate for the modification of the elastic stress field by the plastic zone. In this case, the computed toughness parameters are termed K_{eff} and G_{eff}. A schematic representation of the determination of the stress intensity factor from a compact tension test is given in Figure 17. In the case of brittle or semibrittle fracture, a straight line is obtained if P_{max} is plotted as a function of $BW^{1/2}Y[(a/W)^{1/2}]$. For a perfectly elastic material, the line passes through the origin and the slope gives K_{Ic} (eq. (23), Fig. 11). In the case of a plastically deforming material, the line will not pass through the origin. However, by introducing an appropriate effective crack length $a + r_y$ into

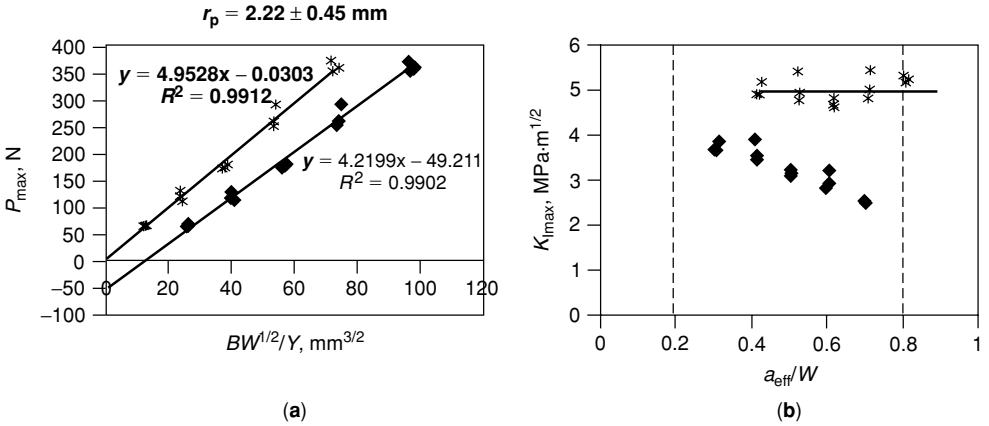

Fig. 17. (**a**) Determination of K_{Ic} for a perfectly elastic material, (**b**) Effect of introducing an appropriate effective crack length $a + r_y$ into the correction function $Y^n[((a + r_y)/W)^{1/2}]$. ◆ $r_p = 0$ mm; ✱ $r_p = 2.22$ mm. From Ref. 21.

the correction function $Y[((a + r_y)/W)^{1/2}]$, the line can be made to pass through the origin. The slope then gives the effective toughness K_{eff}. The appropriate plastic zone size r_y can be determined by iteration from equation (23) (21).

The ratio between the effective energy-release rate G_{eff} and the linear elastic value G_c is approximated by

$$\frac{J}{G} = \left[1 - \frac{1}{2}\left(\frac{\sigma}{\sigma_y}\right)^2\right]^{-1} \tag{39}$$

where $G = \pi\sigma^2 a/E$. This correction is useful for $\sigma/\sigma_y < 0.8$, and it can be seen that $G_{eff} \rightarrow G_c$ for small stresses. On the other hand, as the fully plastic condition is approached, such corrections are not satisfactory because they are very sensitive to the stress and the analysis is better couched in terms of displacement.

A simple case where this can be done is that of three-point bending, shown in Figure 18. If the ligament is fully plastic with a stress distribution as shown, the collapse load is given by

$$P = \sigma_y \frac{B}{L}(W - a)^2 \tag{40}$$

The plastic-zone work is $U_p = Pu_p$, where u_p is the displacement. The general definition of fracture toughness R, analogous to G for stable growth, may be used:

$$R = J = \frac{1}{B}\frac{dU_p}{da}, \; u_p = \text{constant} \tag{41}$$

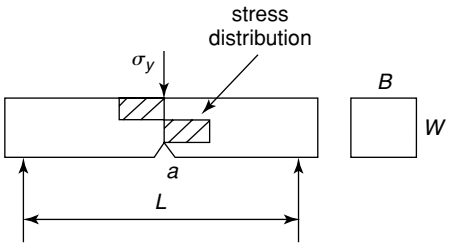

Fig. 18. Fully plastic three-point bending.

In the context of an important plastic deformation the computed toughness is termed J_c. Thus

$$J_c = \frac{2U_p}{B(W-a)} \tag{42}$$

This assumes a fully plastic ligament and ignores elastic effects but does allow J to be found in the fully plastic case. In fact, this form is true when elastic energy is included, provided that $L/W = 4$. This analysis has been widely employed for measuring the toughness of very tough materials since the stress state in the ligament is very close to plane strain for the three-point bend test. Thus, the J_c measured at crack initiation should be the same as G_c in an LEFM test. The specimens may be much smaller and the size criterion is

$$B \text{ and } (W-a) > 25\left(\frac{J_c}{\sigma_y}\right) \tag{43}$$

which is generally about a factor of 3 less than the LEFM value (11,22).

***J*-Integral.** Crack initiation in these fully plastic cases is usually followed by slow, stable growth, and it is often difficult to determine when growth has been initiated. It has been attempted to solve this problem by a procedure (22,23) in which several identical specimens with $a/W \sim 0.5$ are tested, but each is loaded to a different load-point displacement. The energy under each load-deflection curve is measured and J should be found from equation (41). Each specimen is broken open after cooling in liquid nitrogen to reveal the growth reached when the test was stopped. Growth is then plotted as a function of J and, by extrapolation to zero, J_c at initiation is obtained. However, the crack tip is often blunted considerably. This can be modeled by assuming a semicircular crack tip; the apparent blunting growth is then $\delta/2$ and this growth is given by

$$\Delta a_b = \frac{\delta}{2} = \frac{J}{2\sigma_y} \tag{44}$$

The extrapolation of the measured Δa values, which include Δa_b, should then be made to the blunting line of slope $2\sigma_y$. This is shown in Figure 19 in which A is the blunting line and B the initiation condition $J = J_c$.

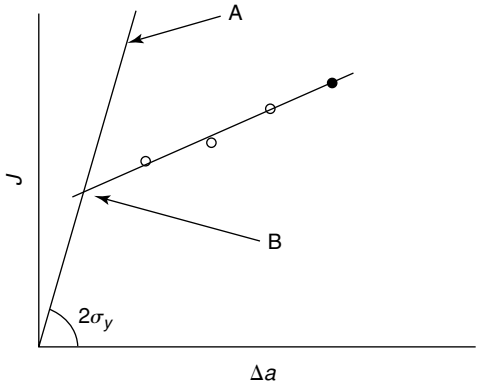

Fig. 19. Determination of J_c in a fully plastic three-point bend test, A: blunting line; B: initiation condition $J = J_c$.

Concept of Essential Work of Fracture (EWF). The EWF method was originally proposed for the evaluation of the fracture properties of thin metal sheets. In recent years, it has also been used for the characterization of the fracture behavior of tough polymers (24).

The EWF concept is based on the assumption that the total work of fracture W_f is the sum of two deformation energies W_e and W_p, dissipated in two distinct regions at the crack tip, the so-called process zone or inner fracture zone, and the outer plastic zone (Fig. 20a):

$$W_f = W_e + W_p \tag{45}$$

The energy dissipated in the process zone W_e, is related to the creation of new surfaces. It depends, therefore, on the size $A = lt$ of the surface of the zone to be fractured, where t is sample thickness and l the ligament length (see Fig. 20a). The energy W_p dissipated in the outer plastic zone depends on the volume V of that zone [proportional to the square of the ligament length and the sample thickness (24,25)]. W_e and W_p can therefore be expressed by

$$W_e = W_e A = w_e lt \tag{46}$$

$$W_p = w_p V = w_p \beta l^2 t \tag{47}$$

The quantity w_e is referred to as the specific essential work of fracture (in kJ/m^2) and the parameter w_p is called the specific nonessential or plastic work of fracture (in MJ/m^3). The factor β is dependent on the strain hardening capacity of the material, which determines the shape and extension of the plastic zone parallel to the loading direction. It is assumed that β does not vary with the ligament length (24). If this condition is met, then the force–displacement curves of specimens with different ligament lengths display the same shape. Using equations (45) and (46),

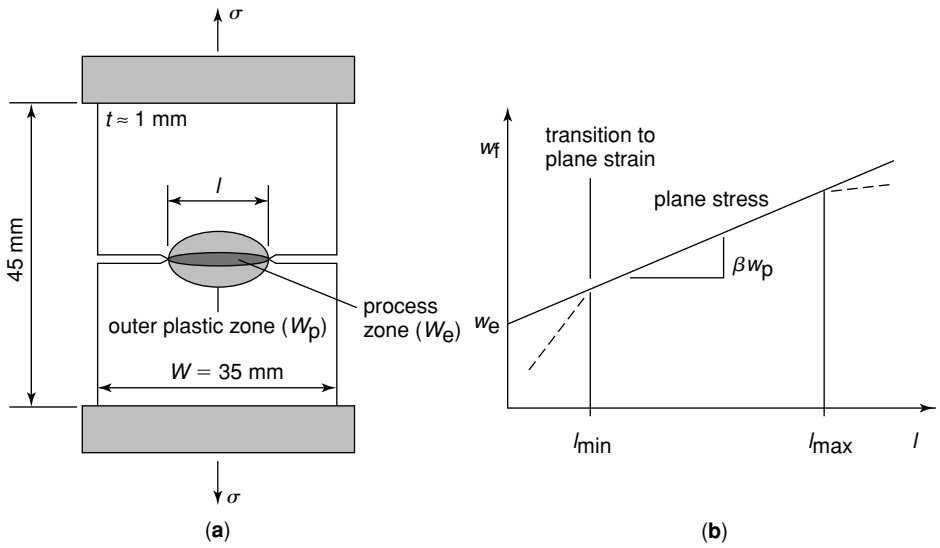

Fig. 20. (**a**) Double-edge notched tension (DENT) specimen and indication where the essential (W_e) and the nonessential work of fracture (W_p) is dissipated, (**b**) schematic EWF plot.

the total work of fracture can be expressed by

$$W_f = w_e l t + w_p \beta l^2 t \tag{48}$$

The specific work of fracture w_f is obtained by normalizing W_f:

$$w_f = \frac{W_f}{lt} = w_e + \beta w_p l \tag{49}$$

A plot of w_f versus the ligament length results in a straight line (EWF plot), as sketched in Figure 20b. The specific essential work of fracture w_e is given by the intercept of the EWF plot with the y-axis. The slope of the curve yields the plastic work term βw_p. This quantity is a geometry dependent measure of the ductility of the material since it depends on the size of the plastic zone and the specific plastic work. The essential work of fracture w_e is considered as a characteristic material parameter. For the evaluation of the EWF parameters w_e and βw_p, the European Structural Integrity Society (ESIS) protocol recommends the use of double-edge notched tension (DENT) samples. In principle, it is also possible to determine a w_e value for plane strain conditions (24). Evidently, w_e and βw_p are dependent on temperature and strain rate (21,25–27).

In order to ensure plane stress behavior, the DENT specimens must satisfy certain geometry requirements. Typically, there are two critical regimes in the EWF plot as sketched in Figure 20b. At low ligament lengths the stress state in the sample changes from plane stress to plane strain. As a result, w_f decreases more rapidly than for plane stress conditions. The ligament length corresponding to the transition from plane stress to plane strain behavior depends on the individual

polymer. The ESIS test protocol recommends for the lower limit of the ligament length a value of $l_{min} = 3t - 5t$ (24).

Samples with high ligament lengths often fail in a semibrittle manner prior to full ligament yielding owing to "edge-effects." The specific work of fracture therefore shows a negative deviation from the linear relationship. Full ligament yielding, however, is a prerequisite for the applicability of the EWF method. In order to exclude nonlinear behavior, the maximum ligament length should not exceed $l_{max} \approx W/3$ (24). This limit was proposed on the basis of previous investigations. The maximum ligament length can also be estimated from an analysis of the plastic zone size r_p at the crack tip. Nonlinear effects occur if $l > 2r_p$ (24). Usually, $W/3$ and $2r_p$ are close to each other. However, for some polymers the relationship between w_f and l remains linear beyond $l_{max} = W/3$ (22). In other words, l_{max} depends on the polymer in question.

As for the LEFM approach, the EWF data must be checked for validity. The maximum net section stress σ_{max} ($=F_{max}/lt$) in the ligament is supposed to depend very little on ligament length; it should satisfy the following relationship (24):

$$0.9\sigma_m < \sigma_{max}(l) < 1.1\sigma_m \tag{50}$$

where σ_m is the average value of the maximum net section stress σ_{max}. Data which do not satisfy equation (49) should be rejected from the determination of w_e and βw_p. Furthermore, the net section stress σ_{max} in the ligament should not exceed the theoretical stress in the ligament of DENT specimens at the onset of yielding. Under plane stress conditions the latter quantity is given by the following relation:

$$\sigma_{max} = 1.15\sigma_y \tag{51}$$

Note, it is probable that $w_e = G_c$ for the appropriate stress state.

Fracture Development

Initiation and Propagation. Most polymer objects are homogeneous on a macroscopic scale and their first response to a (gradually) applied critical load is a more or less homogeneous deformation, which eventually will turn into the different forms of ductile or brittle failure. For brittle fracture to occur the homogeneous deformation has to become localized, whereas ductile failure generally involves a more extended region (Fig. 2) and occasionally the whole specimen. Ductile deformation phenomena leading to polymer failure include yielding with and without neck formation, creep, and flow. The latter two phenomena certainly do not comply with the definition of fracture given in the introduction, since neither creep nor flow would give rise to the formation of new surfaces within the body. All these phenomena and the criteria of their initiation are discussed elsewhere in this Encyclopedia (see MECHANICAL PROPERTIES; VISCOELASTICITY). Reference will be made where appropriate since these phenomena frequently precede and/or modify subsequent brittle fracture.

The most likely sites for *crack nucleation* or *initiation* are irregularities of the polymer network or stress concentrators already present such as defects, inclusions, or surface scratches. Generally, a nucleus or a defect need to grow,

sometimes for a long time, before they reach a size sufficient to influence their own growth and to provoke eventually the instability of the loaded object. Thus, the following four stages of fracture development can be distinguished:

(1) **crack nucleation**

(or activation of an existing defect);

(2) **thermally activated extension**

in mode I the plane of crack growth is rather smooth (mirror), the rate $\dot{a}$ normally increases with crack length a and stress intensity factor K (eq. (34)), $\dot{a}$ decreases through crack tip blunting (or at constant external displacement due to the increase in compliance C, eq. (7)). Such a decrease can lead to crack arrest and also give rise to the so-called stick-slip behavior of crack propagation;

(3) **nucleation of secondary cracks**

ahead of the primary crack and thermally activated coalescence between primary and secondary crack planes leading to some roughness of the fracture surface. The rate of crack propagation can increase notably during this stage, thus its contribution to the total time under stress of a sample can mostly be neglected;

(4) **unstable crack propagation**

once K_{Ic} is reached [$G_c > R(a)$].

In Figure 21 the fracture surface of a specimen of PMMA is shown. Loaded in tension, the specimen deformed homogeneously up to 70 MPa when brittle fracture occurred. It is important to point out that even under the condition of apparently instantaneous fracture, a semicircular, mirror-like zone had grown in a stable manner to about one half of the specimen thickness (stages 2 and 3).

The specimen failed after K_{Ic} was reached. These different stages exist in most cases of tensile brittle fracture, but their duration, their relative importance, and additional structural features (Wallner lines in impact, parabolic markings due to the initiation of secondary cracks, striations in fatigue) depend on the stress–time history (19).

In order to understand and avoid (or at least, to predict correctly) a fracture event, one has to know the elementary molecular mechanisms involved in crack advance and the effect of the principal extrinsic and intrinsic variables. In the following we will discuss, therefore, the strength determining structural elements of the different polymer classes.

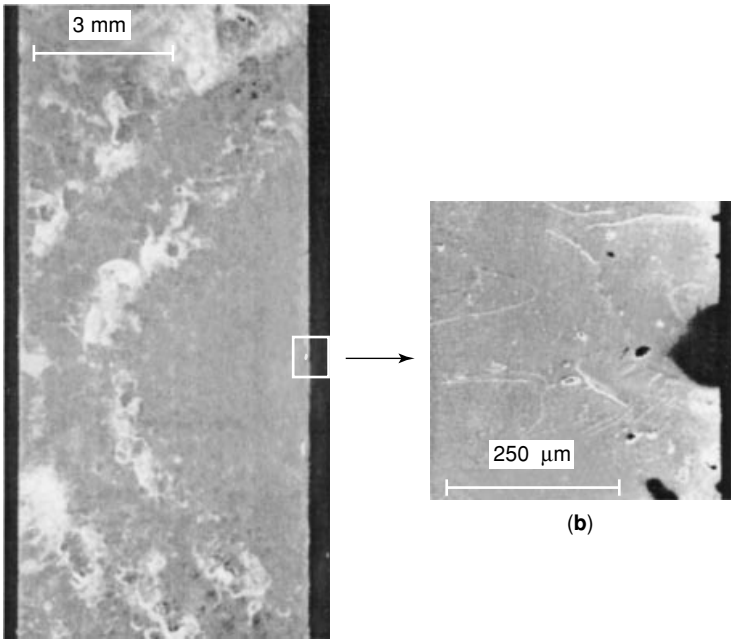

Fig. 21. Brittle fracture of a PMMA specimen loaded in tension at 23°C; (**a**) the surface shows the semicircular, thermally activated crack grown to about one half of the specimen thickness, (**b**) crack initiation at a surface defect.

Essential Elements of Polymer Structure. *Amorphous thermoplastics* are formed by randomly coiled, interpenetrated chain molecules, which cohere by weak van der Waals forces. To give tenacity to such a physical network it is indispensable that stresses are transferred by the chain backbones over long distances. This requires long, well entangled chains. The molecular weight M_w must be many times larger than the molecular weight between entanglements (M_e). And the entanglement density ν_e has been found to be a prime parameter controlling the tendency for crazing of glassy polymers (see CRAZING)) (12). Readily crazing polymers like polystyrene have a ν_e of the order of 3×10^{25} m^{-3}, whereas tough homopolymers generally have a $\nu_e > 20\times10^{25}$ m^{-3}. In fact, compiling data from literature (26,27) shows that K_{Ic} scales with $\nu_e^{1/2}$ (Fig. 22).

The same conditions concerning M_w and ν_e also apply to semicrystalline polymers (see Fig. 22). In addition, semicrystalline thermoplastics are characterized by their heterogeneous, lamellar, and frequently spherulitic structure (Fig. 23). Morphological features of particular importance for the deformation behavior include the size, morphology, and perfection of spherulites, the strength of the interspherulitic boundaries, and the physical structure of the crystalline phase. The smallest building-blocks considered here are aggregates of crystal lamellae connected by amorphous regions (Fig. 24). These latter consist of a network of nonextended entangled chains, dangling chain ends and/or loops, and more or less taut tie-molecules. Above T_g there is a pronounced difference between the

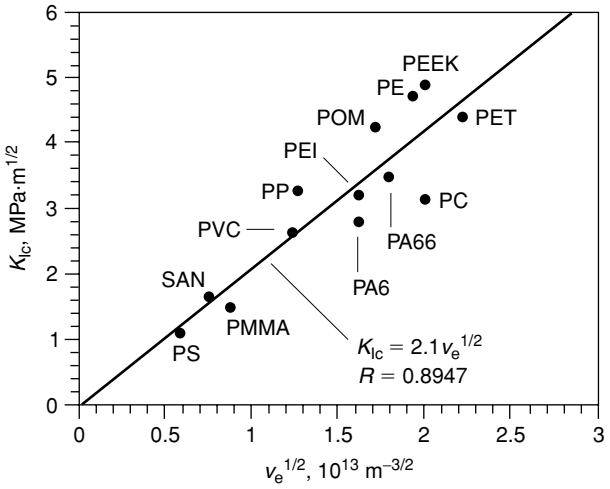

Fig. 22. Representative static plane-strain toughness values of different amorphous and semicrystalline thermoplastics as a function of the square root of the entanglement density. From Refs. 26 and 27.

Young's modulus of an amorphous region (typically very much less than 1 GPa) and that of a crystalline lamella in the chain axis direction (235 GPa for orthorhombic polyethylene and 40 GPa for helical isotactic polypropylene). Thus, the amorphous regions will account for most of the elastic and anelastic deformation. The regions oriented perpendicular to an applied (uniaxial) stress will initially mainly deform by interlamellar separation (Fig. 24c). In this case, strong hydrostatic tensions within the constrained amorphous network are created. At the same time, the tie chains become more extended and transfer locally concentrated elastic stresses to the lamellae (28). Stress relief can occur in three ways: by homogeneous deformation of the amorphous network (only possible in thin films), through void formation in the interlamellar regions involving chain scission, segmental slip and/or disentanglement (Fig. 24f) and/or through crystal plastic deformation (Figs. 24d and 24e).

Thermoplastic elastomers, blends, and filled polymers also show a superstructure consisting of different phases. These structures and their pronounced

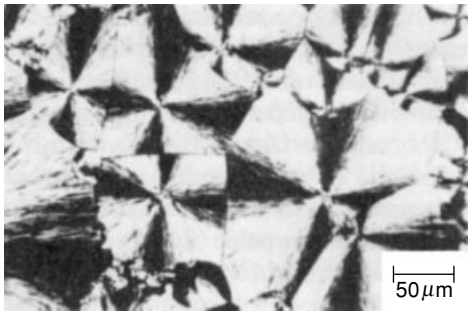

Fig. 23. Spherulitic structure of melt-crystallized polypropylene.

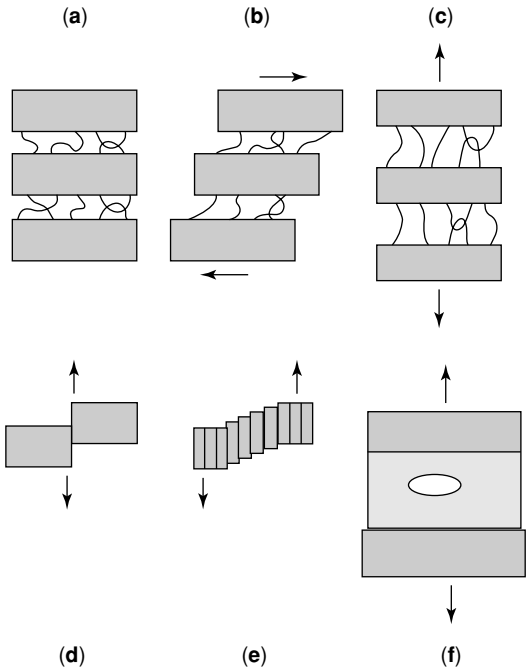

Fig. 24. Schematic representation of the possible deformation processes of a stack of crystal lamellae: (**a**) the initial state, (**b**) interlamellar shear, (**c**) interlamellar separation, (**d**) intralamellar block shear, (**e**) intralamellar fine shear (not shown: bending and rotation of lamellae), and (**f**) cavitation within the amorphous regions.

effect on the deformation mechanisms and ultimate properties will be discussed elsewhere (see ELASTOMERS, THERMOPLASTIC; POLYMER BLENDS).

Filled rubbers form a complex network of cross-linked chains connected to surface-active particles such as carbon black or amorphous silica (see CARBON BLACK). Here we will only indicate the structural features of importance in unfilled cross-linked elastomers. Two breakdown mechanisms are conceivable: the initiation and growth of a cavity in a moderately strained matrix and the accelerating, cooperative rupture of interconnected, highly loaded network chains. The second mechanism is more important under conditions, which permit the largest breaking elongation λ_{bmax} to be attained (29). In that case, the quantity λ_{bmax} is expected to be proportional to the inverse square root of the cross-link density ν_e; in fact, an increase of λ_{bmax} with $\nu_e{}^{-0.5}$ to $\nu_e{}^{-0.78}$ is found experimentally for a variety of networks. The maximum elongation λ_{bmax} is the *only* feature of large deformation behavior which depends only on network topology (29).

The structure of cross-linked resins is characterized by the average mass M_c of the segments between cross-links, their configuration and by the nature of the cross-linking agent (for instance amine-cured epoxy resin systems show distinct β-relaxations resulting in greater toughness and flexibility and in higher T_g values as compared to anhydride-cured polymers). Generally, Young's modulus in the glassy state, yield strength and the glass transition temperature increase with $1/M_c$, that is, with increasing cross-link density. On the other hand, the critical

crack opening displacement δ_c and the critical energy release rate G_{Ic} grow with M_c (30).

Deformation and Damage Mechanisms of Thermoplastic Polymers

Effect of Temperature. In the context of this article we will discuss the fracture behavior of thermoplastic polymers more extensively. When a spherulitic sample is strained, local strains within a lamellar stack will vary considerably, depending on the local Young's modulus, the relative orientation of the lamellar stack with respect to the principal stress direction, and on the intensity and relative importance of the elementary deformation and damage mechanisms. The activation energies of such mechanisms are widely different and their rates vary accordingly. The potential barrier U_{tt} for twisted translation of, eg, a CH_2-group with respect to its neighbor in a polyethylene-crystal is at room temperature 2.1 kJ/mol, whereas the energy U_s for chain scission amounts to 335 kJ/mol. The tensile deformation of HDPE at room temperature and modest rates of loading is below the yield point determined by lamellar separation, interlamellar shear, and some uncorrelated intralamellar slip [preferentially along the (100) plane]. Correlated intralamellar (coarse block) slip was observed at Hencky strains ε_H between 0.1 and 0.6, lamellar fragmentation and fibril formation at $\varepsilon_H > 0.6$, and truly plastic flow at $\varepsilon_H > 1$ (27,31–33). The considerable plastic deformation remains homogeneous under these conditions, and it leads to a highly oriented fibrillar structure which finally fractures in a fibrous manner and at very little additional deformation.

This behavior changes with decreasing temperature. The amorphous regions stiffen below T_g, conformational changes and intra-lamellar slip processes become more difficult, the overall yield is suppressed (Fig. 25F), the density of stored elastic energy increases, and the deformation becomes more and more localized. The mode of fracture is particularly influenced by the competition between *correlated intralamellar slip* and the *cavitation* within and *fibrillation* of the amorphous intercrystalline regions. The former mechanism dominates at higher temperature and modest rates of deformation and leads to extended plastic deformation, the latter giving rise to craze-like features and stress whitening. Depending on the stability of the formed craze micro fibrils the stress-whitened zones can be more or less extended. Fracture at liquid nitrogen temperature (Fig. 25A) is initiated by the scission of interlamellar tie-molecules (33).

As a second example the fracture behavior of an amorphous, unplasticized poly(vinyl chloride) (PVC) is presented (Fig. 26). At low temperatures there is no intersegmental slip, fracture stresses σ_b are high, and fracture is brittle showing a substantial variability in σ_b. This is explained by the presence of a large number of network irregularities and/or flaws of different size or severity, the most severe of which determines the fracture strength. With the onset of chain relaxation and small-scale plastic deformation, the elastic strain energy at the crack tip is reduced and possibly some local strain hardening occurs (34,35). This counterbalances the detrimental effect of a defect leading to much less scatter in the semibrittle and ductile regions (Fig. 26). Evidently, elimination of defects not only reduces the observed scatter but also increases the service life of a structure (19,36).

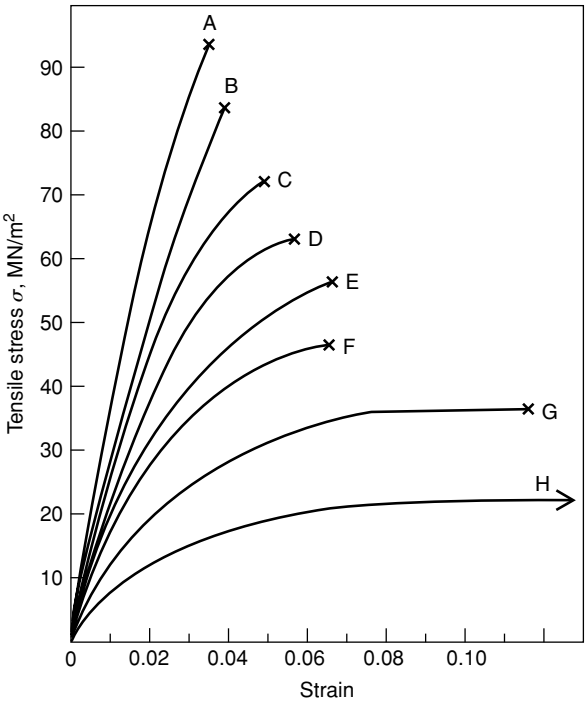

Fig. 25. Stress–strain curves of polyethylene at different temperatures: A, 93 K; B, 111 K; C, 149 K; D, 181 K; E, 216 K; F, 246 K; G, 273 K; H, 296 K. From Ref. 32.

Effect of Loading Rate. As to be expected for a viscoelastic material, increasing the rate of loading has the same effect as decreasing the temperature. As an example the behavior of a high molecular weight polypropylene (PP) is shown schematically in Figure 27. It exhibits the same deformation and fracture phenomena mentioned above, which range from extensive shear and stress whitening (at loading rates v from 0.1 to 1 mm/s) to small scale yielding and crazing (10 mm/s), multiple crazing (50 mm/s to 1 m/s), and the formation of a single craze turning into a crack (at $v = 2$–10 m/s) (26,27).

The evolution of the critical stress intensity factor of the PP homopolymer reflects perfectly well the observed stress–strain behavior. Toughness K_{Ic} decreases with the decreasing amount of plastic deformation at increasing rates of loading. This is different, though, for rubber toughened PP where the rate of cavitation of rubber particles increases with loading rate. The cavitation gives rise to local matrix plasticity and thus to an increase in K_{Ic} (Fig. 28, see also Figs. 32 and 33) (21,26,27).

Stress Transfer and Internal Main Chain Mobility. In concluding this section it can be stated that brittle fracture of a polymer occurs if two conditions are met: firstly, lateral stress transfer between segments must be efficient so as to build up a high strain energy density. And secondly, internal main chain mobility must be small since it would counteract large axial chain stresses. The competition between stress transfer and stress relaxation determines the level of stored energy (which can be reached), the damage (which is created or activated), and the

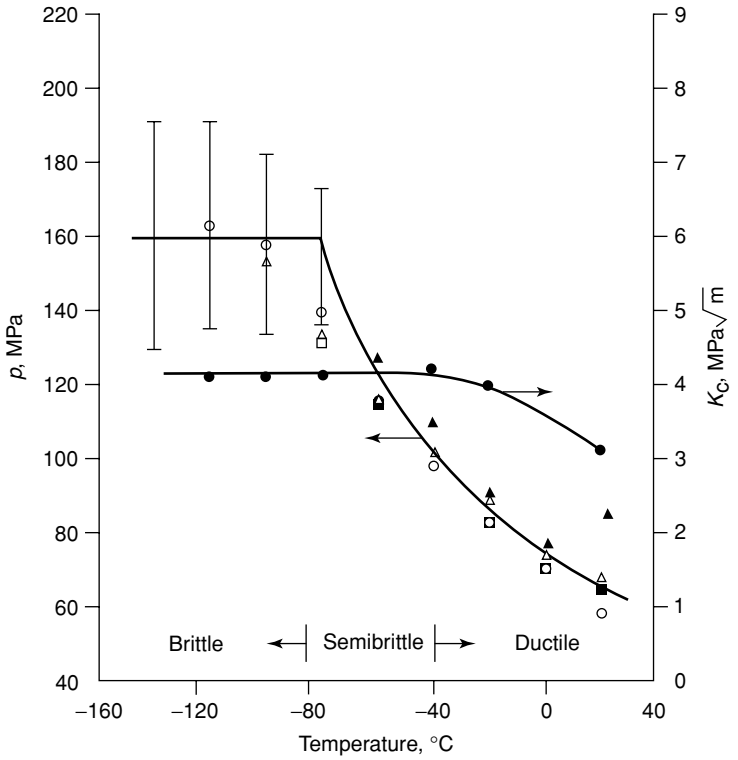

Fig. 26. Fracture stress in tension (T) or bending (three-point bending) of unplasticized PVC. The vertical bars indicate the maximum scatter band. From Refs. 34 and 35.

		Specimen width, mm	Specimen depth, mm
Tension	•	6	10
Three-point bending	△	3	12.5
	□	6	15
	▲	12.5	15
	ˆ	6	50

mode of fracture. This is convincingly shown by the brittle fracture of elastomers at liquid nitrogen temperature when the axial stresses imposed onto the chains by intersegmental shear become so important that chain scission occurs (19,37). The critical tensile stress for brittle fracture of a thermoplastic is well correlated with the level of interaction between (or packing density of) the chain backbones (19,38). On the other hand, reducing the degree of crystallinity (through quenching, introduction of chain branching, or addition of an atactic component) improves toughness at the expense of sample stiffness. This statement is corroborated by the decrease of the impact resistance rating of a homopolymer with increasing storage modulus (brittle if $E' > 4.49$ GPa, brittle if bluntly notched if $E' > 3$ GPa) (19,38). The role of chain mobility is demonstrated by the positive correlation between

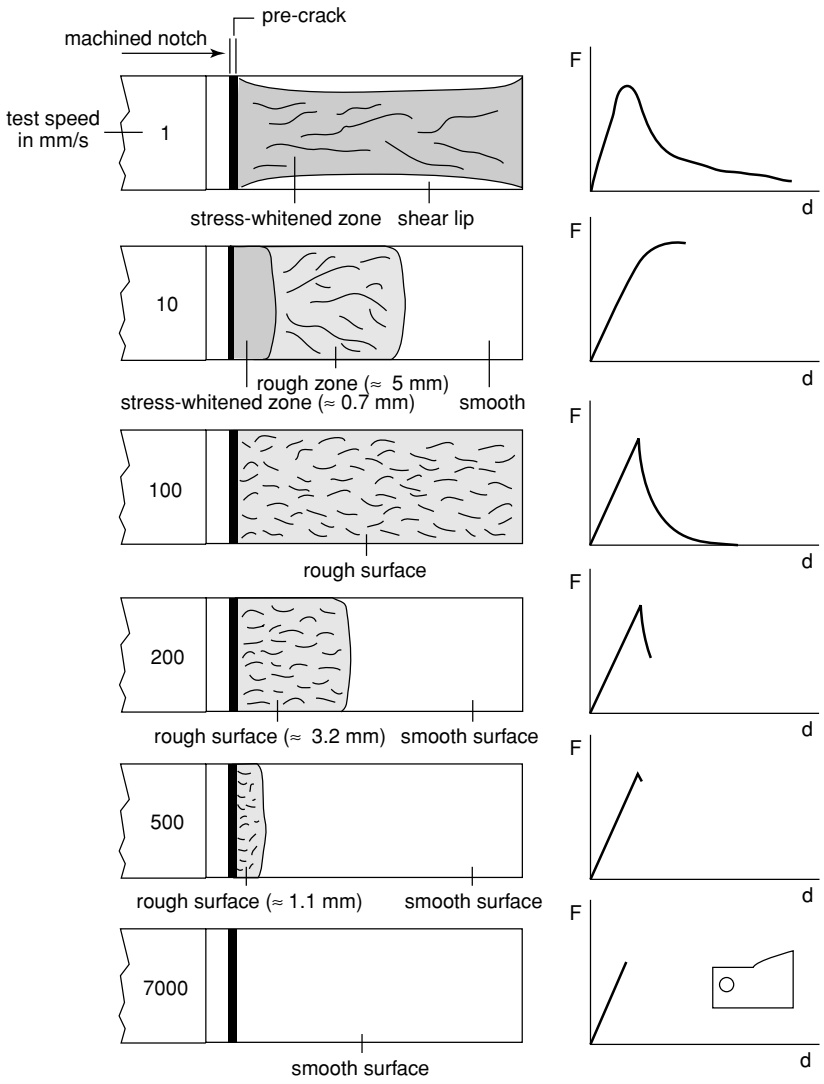

Fig. 27. The effect of loading rate on the mode of fracture of a high molecular weight PP. From Refs. 26 and 27.

polymer toughness and the β-peak intensity of tan δ (21) and by the frequent coincidence of the temperature of secondary relaxations with that of brittle–ductile transitions (19,39). The fine interplay between lateral stress transfer and chain mobility can be seen by the different craze extension modes displayed by a methyl methacrylate glutarimid copolymer strained at different temperatures (40,41). At $T < 0^\circ$C, craze tips are sharp and grow by chain scission and at $T < 50^\circ$C, stresses at the craze tip are distributed by chain slip over diffuse deformation zones, which become more confined at 80°C. Secondary crazes appear because of disentanglement, if straining is done at 130°C, and the sample deforms homogeneously above the glass transition at 145°C.

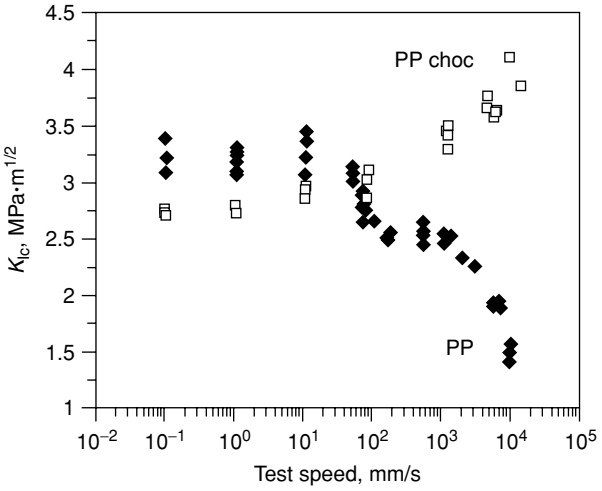

Fig. 28. The effect of loading rate on the toughness of a high molecular weight PP. From Refs. 26 and 27.

Two important modifications have to be mentioned, which permit to control stiffness and toughness of a polymer material separately: polymer orientation and reinforcement through a second phase such as core-shell particles, mineral fillers, or short fibers (see REINFORCEMENT).

Durability

All the above examples concern the more or less rapid loading of a sample up to fracture. The most frequent load histories, however, are application of a constant load at a level much below the fracture strength (see VISCOELASTICITY) or the repeated application of a (regularly or statistically) varying load (see FATIGUE). The long-term strength or durability of a polymer material depends foremost on its resistance to slow crack growth and to environmental attack.

Slow Crack Growth. Many thermoplastics exposed to constant and moderate stresses over extended periods of time, as for instance pipes under internal pressure, fail in either of two different modes, in a ductile or in an apparently brittle manner. The durability is often represented as a stress–lifetime (σ–t) diagram (Fig. 29). The simultaneous action of two failure mechanisms gives in this case rise to two different branches of the lifetime curves. At moderate stresses (above $\sim$50% of σ_y) the HDPE pipes fail in a ductile manner because of plastic instability of the creeping material (Fig. 2, which corresponds to Point 1 in Fig. 29). The ductile failures are strongly stress-activated (E_a = 307 kJ/mol) giving rise to the flat portions of the σ–t curves. Fracture at smaller stresses and after more extended time periods often occurs in an apparently brittle manner by thermally activated slow crack growth (SCG) (steep branches in Fig. 28, E_a = 181 kJ/mol). Such a crack usually initiates from a defect, mostly at a boundary (Fig. 30a); it grows by transformation of matrix material into fibrillar matter. Further growth of this craze-like feature occurs through the disentanglement and breakdown of the numerous microfibrils, which leave some traces on the (moderately plane) fracture

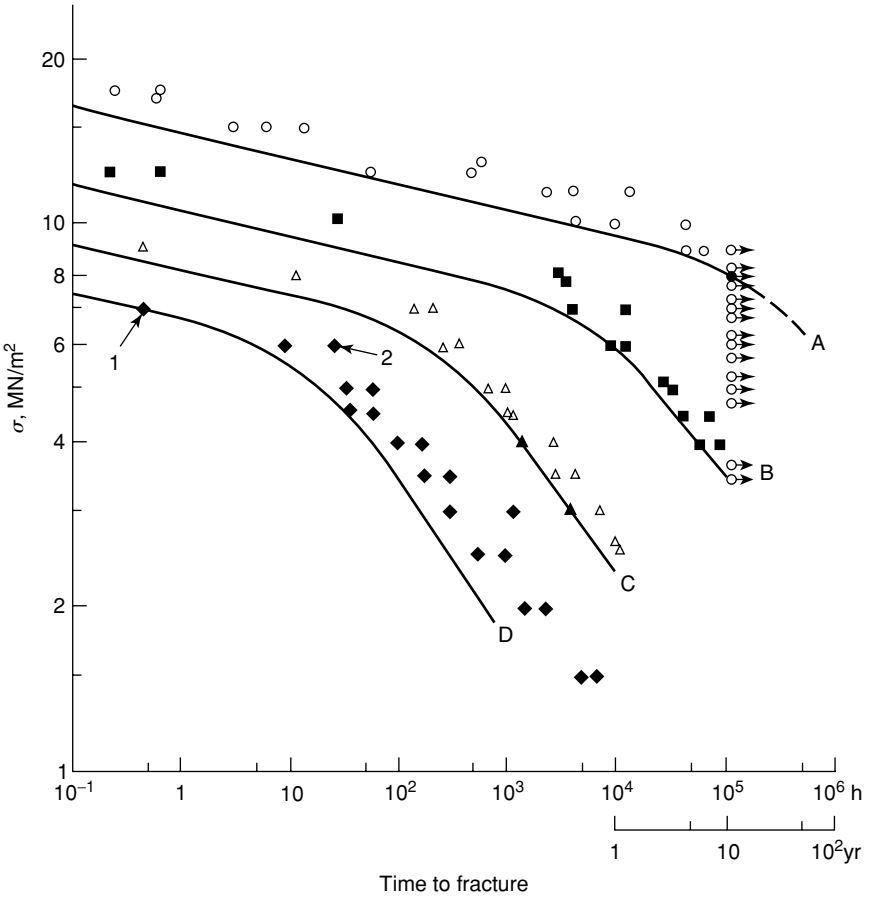

Fig. 29. Times to failure of HDPE water pipes under internal pressure p at different stresses and temperatures: A, 20°C; B, 40°C; C, 60°C; D, 80°C. 1 = ductile failure (see Fig. 2); 2 = creep crazing (see Fig. 28). Circumferential stress $\sigma = d_m/2s$, where d_m = average diameter and s = wall thickness. From Ref. 19.

zone (Fig. 30b). The temperature dependence of the two failure mechanisms—and of the transition points—follow an Arrhenius equation. The displacement with temperature of the two branches in the (σ–t) diagram is generally highly regular, so that reliable predictions may be made of the lifetime as a function of stress level by extrapolation of the steeper branch (42).

The rate $\dot{a}$ of SCG increases with the applied stress and the time-to-failure decreases. For HDPE, the rate $\dot{a}$ has been found to be proportional to K_c^4 (17; Fig. 15). The rate is reduced by all parameters, which increase the number of tie-molecules and/or make chain pull-out and disentanglement more difficult like high molecular weight and presence of short-chain branches (SCB). A dramatic increase of durability with branch density has been found (43,44). A density of 5 butyl-groups/1000°C increases the time-to-failure of linear HDPE by up to a factor of 10^4 with the resistance to SCG of an ethylene–hexene copolymer residing in those chains whose $M_w > 1.5 \times 10^5$ (44). There is an indication of a threshold

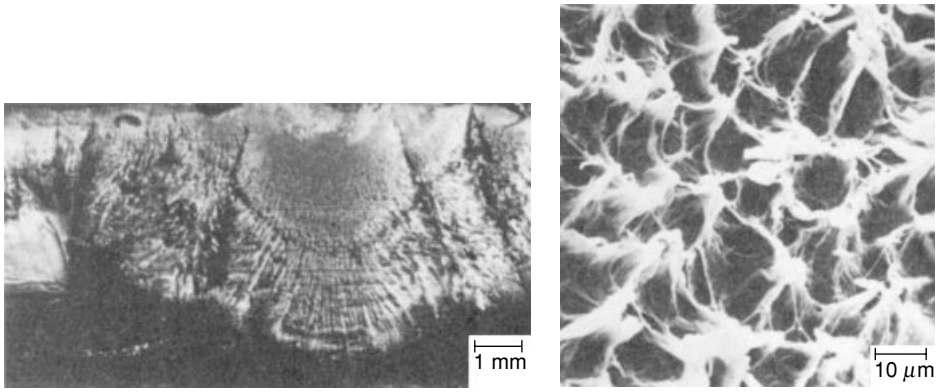

Fig. 30. (**a**) Surface of a creep craze formed in HDPE under conditions shown as point 2 in Figure 27: $\sigma_v = 6$ MN/m^2, $T = 80°$C; (**b**) Detail of the fracture surface close to the upper center of the zone which was apparently the point of creep craze initiation. From Ref. 19.

value for the hoop stress, below which defects do not develop into creep cracks (45). Under such conditions, a third and horizontal branch of the σ–t_b curve is observed (at about 3 MPa for HDPE at 80°C). SCG can be substantially reduced by cross-linking, as for instance observable in peroxy cross-linked HDPE (46).

While most studies of durability show a linear log (t_b)–log (σ) relationship, the slopes may vary depending on sample geometry, crack tip blunting, preorientation, or material degradation. Long-term studies with fully notched tensile specimens basically confirm the results of Figure 29 (47,48). This creep rupture test is a reliable and rapid method and much simpler to perform. A perfect proportionality was found (48) between the times to failure t_b in hydrostatic pipe rupture tests and the t_b in uniaxial, fully notched creep tests, the latter being 10 times faster, however. The use of a surfactant (ethylene glycol) accelerated the tests by another factor of 4 while maintaining the proportionality between the times to failure of the different (pipe) materials, thus permitting their grading. Such a possibility (to accelerate tests) is especially welcome in view of the continuous improvement of resins. In fully notched creep tests (according to ASTM F1473), an increase in lifetime (by a factor of 1.5–2) in the transition region was observed (47) when the stress was increased to such a level that ductile deformation just became the dominant mechanism. This effect, due to crack tip blunting, leads to a hook in the σ–t_b diagram (47). They also report an abnormal temperature-shifting behavior for some copolymers of ethylene with hexene or octene.

From the original concept of flow, ie, the thermally activated motion of molecules across an energy barrier, various fracture theories of solids have emerged, considering, eg, a reduction of primary and/or secondary bonds (19,49, 50). The importance of primary bonds for static strength had been deduced very early from the dependencies of sample strength on molecular weight and volume concentration of primary bonds. A more general approach, the rule of cumulative damage (51), does not explicitly specify the nature of the damage incurred during loading, but attempts to account for the influence of load history on sample

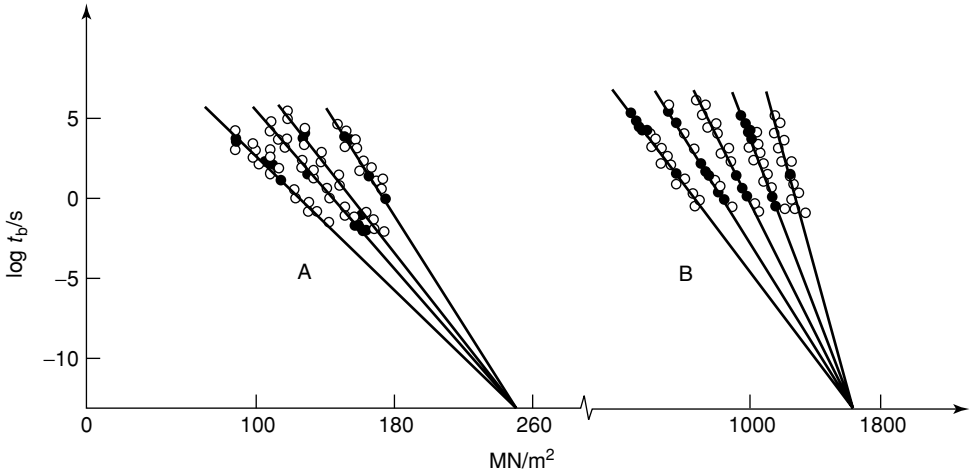

Fig. 31. Times to fracture under constant uniaxial load σ_0. A, Cellulose nitrate (CN) at temperatures of 70, 30, −10, and −50°C, reading from left to right. B, Nylon-6 at temperatures of 80, 30, 18, −60, and −110°C, reading from left to right. To convert MN/m^2 to psi, multiply by 145. From Refs. 19 and 50.

strength. The kinetic theory of fracture proposes that the "rate of local material disintegration" is proportional to $1/[t_b(\sigma_0)]$ and that fracture occurs after a critical concentration of damage has been attained:

$$t_b = t_0 \exp(U_0 - \gamma\sigma_0)/\mathrm{RT} \tag{52}$$

The three parameters involved have to be interpreted as energy of activation U_0 of breakage of some bonds (primary or secondary), as an inverse of a molecular oscillation frequency t_0, and a structure-sensitive parameter γ. Experimental data and theoretical curves according to equation (51) are given in Figure 31. At this point it should be stated again, that the durability of a polymer does not so much depend on the ultimate strength—and breakage—of the backbone chains, but on their capacity to effectively transmit stresses over long distances. This capacity suffers from low molecular weight and all chain parameters, which favor slip, pull-out, and disentanglement.

At relatively high temperatures, the lifetime is limited by a third mechanism, the oxidative degradation of the backbone chains. Such loss in mechanical strength can occur abruptly, giving rise to a vertical branch of the σ–t_b curve (26,45,46, 52). In order to retard oxidative damage, stabilizers are added to most polymers, especially to polyolefins and PVC (see DEGRADATION). The presence of a stabilizer not only has a positive effect on the time of final breakdown but it also appears to reduce the rate of SCG (45), probably by hindering the selective degradation of highly loaded tie-molecules (26,27). On the other hand, the lifetime is reduced if stabilizer is extracted from a pipe wall through contact with an active liquid. Active agents in this respect include even stagnant, deionized hot water (52). A still greater reduction in lifetime will occur in the presence of certain surface-active media or of a liquid under flow (see below).

Multiaxial Stress Criteria and Environmental Effects

Multiaxial States of Stress. Throughout this article we have indicated that failure depends on the level and on the multiaxiality of stress. The classical approach to predict safe operating conditions is based on the assumption that failure must be expected whenever the components of the stress tensor (usually the three principal stresses σ_1, σ_2, and σ_3) combine in such a way that a strategic quantity reaches a critical value C (19,53). The condition $f(\sigma_1, \sigma_2, \sigma_3) = C(T, \varepsilon)$ represents a two-dimensional failure surface in three-dimensional stress space. Such failure criteria, which are not based on fracture mechanics, describe most commonly the initiation of Crazing or Yielding. They have to be considered here for two reasons. In the first place they permit to judge whether crazing or general yielding are initiated *before* brittle fracture. Secondly, they help to predict the extent of local plastic deformation, which has a notable influence on toughness. In the following we will mention three criteria, which are applied to the shear yielding of homogeneous polymers, to craze initiation and to the formation of voids or cavities respectively.

Shear Yielding. The most widely used criterion of von Mises is based on the assumption that only the energy of distortion determines the criticality of a state of stress. It can be expressed as

$$(\tau_{\text{oct}})^2 = \frac{1}{9}[(\sigma_1 - \sigma_2)^2 + (\sigma_2 - \sigma_3)^2 + (\sigma_3 - \sigma_1)^2] < (\tau^*)^2 \tag{53}$$

where τ^* designates a critical value, which could be expressed in terms of eg, the octahedral shearing stress τ_{oct}, or the yield stress τ_{y} in pure shear. The above expression does not take into account the rigidifying effect of hydrostatic pressure. Thus, the critical octahedral shear stress should be corrected accordingly:

$$\tau_{\text{oct}} < \tau_0 - \mu p \tag{54}$$

where μ describes the sensibility of yield stress to pressure. If $p = (\sigma_1 + \sigma_2 + \sigma_3)/3$ (the hydrostatic component of the stress tensor) is positive, it designates a tension, which reduces τ_{oct}. On the other hand, application of compressive stresses or external hydrostatic pressure will increase the critical (octahedral) shear stress. This leads to a difference between the uniaxial compressive strength σ_{cb} and the uniaxial tensile strength σ_{tb}, the ratio $m = \sigma_{\text{cb}}/\sigma_{\text{tb}}$ varying between 1 and 1.45 (see YIELDING).

Craze Initiation. Although the effect of multiaxial states of stress on the brittle and ductile failure of isotropic polymers is sufficiently well represented by the above classical failure criteria, this is not the case for crazing or the failure of anisotropic polymers, ie, oriented sheets, fibers, single crystals, etc. For craze initiation we will cite the stress-bias criterion as proposed by Sternstein (54):

$$\sigma_{\text{craze}} = |\sigma_1 - \sigma_2| \geq A(T) + \frac{B(T)}{\sigma_1 + \sigma_2 + \sigma_3} \tag{55}$$

where A and B are functions of the temperature T. For uniaxial stress two elegant formulations exist, namely the relation of Kambour (55) that σ_{craze} is a linear function of the cohesive energy density (CED) times ΔT (where $\Delta T = T_g - T_{test}$), and that of Wu (56) that σ_{craze} is linearly related to the entanglement density ν_e.

Formation of Voids or Cavities. Voids or cavities are most likely formed in flexible polymers subjected to triaxial strains. It is a major mechanism to initiate heterogeneous deformation in elastomers, in the amorphous phase of semicrystalline polymers above its T_g and in elastomer-modified polymers (57). Based on these considerations, the volume strain ε_v has been used as a critical quantity (26,27,58):

$$\varepsilon_v = (1+\varepsilon_{xx})(1+\varepsilon_{yy})(1+\varepsilon_{zz}) - 1 \tag{56}$$

It is supposed that cavities (in elastomeric modifier particles) form wherever $\varepsilon_v > \varepsilon_{vc}$. The volume strain ε_v in the vicinity of a sharp crack (in the plane of the crack, for opening mode I and for small strains) can be expressed as

$$\begin{aligned} \varepsilon_v &= \frac{2K_I}{E\sqrt{2\pi r}}(1-\nu-2\nu^2)(\text{plane strain}) \\ \varepsilon_v &= \frac{2K_I}{E\sqrt{2\pi r}}(1-2\nu)(\text{plane stress}) \end{aligned} \tag{57}$$

If Poisson's ratio ν is taken to be 0.43 (as for a semicrystalline, rubber-modified polypropylene), the term in parentheses amounts to 0.20 in plane strain and to 0.14 in plane stress. This means that the critical distance where $\varepsilon_v > \varepsilon_{vc}$ is by a factor $1/\sqrt{(0.20/0.14)} = 2$ *larger* in plane strain than in plane stress. The same applies for the size of the plastic zone if matrix plastic deformation is triggered by particle cavitation. This is a remarkable result since it is exactly the opposite of what the von Mises criterion would predict.

For a rubber modified polypropylene Gensler has numerically determined the contours of the (plastic) zone where a critical volume strain of 0.4% was exceeded for deformation rates of 100 and 5800 mm/s, and for plane stress and plane strain conditions, respectively (Fig. 32) (26,27). The shape of the calculated cavitation zone corresponds reasonably well to the actual shape of the stress-whitened zone (see Fig. 33a). Under both plane stress and plane strain conditions, the size of the plastic zone increases slightly with increasing test speed. What seems to be more important, however, is the gradual change of the stress state from plane stress to plane strain, which is responsible for the significant increase of the extension h of the plastic zone with increasing testing speed (Fig. 33a). These studies confirm again the excellent correlation between the toughness K_{Ic} and the size of the plastic zone (Fig. 33b) (26,27).

Environmental Effects. Environmental parameters acting on a specimen from outside are generally classified as physical (electromagnetic radiation, particle irradiation), physicochemical (like wetting or swelling), or chemical (oxidation, other forms of chemical attack). The action of these latter parameters mostly influences the strength of a polymer through the intervening structural changes (see also DEGRADATION; RADIATION CHEMISTRY OF POLYMERS; WEATHERING). At this point a special effect, the formation of environmental stress cracks (ESC) has to

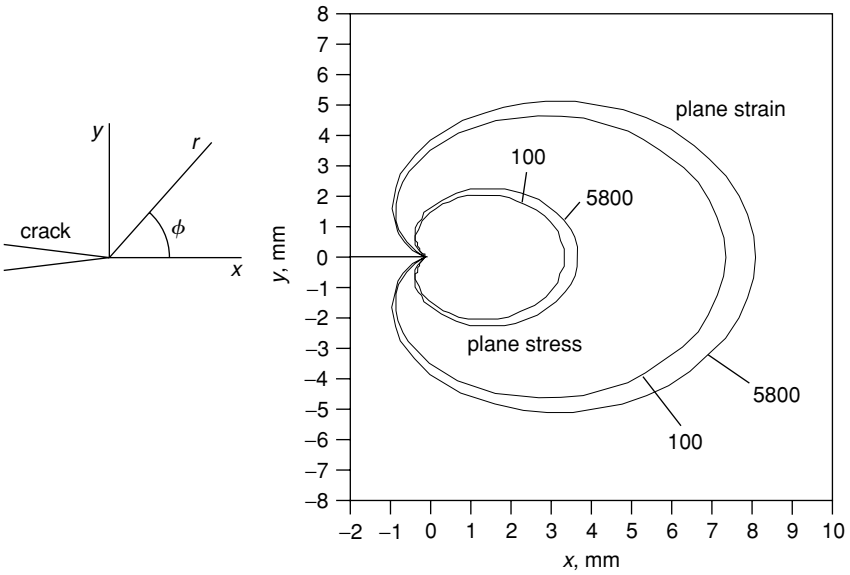

Fig. 32. Calculated shape of the plastic zone ahead of the crack tip in CT specimens of impact modified high molecular weight polypropylene as a function of test speed (100 and 5800 mm/s) and stress state. From Refs. 26 and 27.

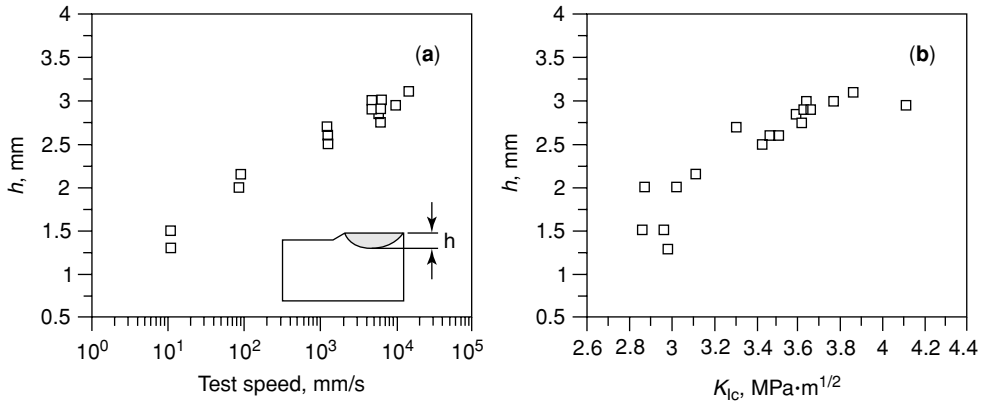

Fig. 33. Extension h of the stress-whitened zone parallel to the loading direction as a function of (**a**) the test speed and (**b**) the stress intensity factor K_{Ic}. From Refs. 26 and 27.

be discussed. Such a synergistic interaction between mechanically stressed polymers and the ambient medium is observed in many rubbers and thermoplastics in contact with sensible liquid or gaseous environments. The origin of ESC is a stress-enhanced sorption and/or diffusion of the environmental agent by the polymer, which leads to swelling and plasticization (or even degradation) of the contacted (surface) zone of the polymer. The increased local chain mobility greatly facilitates crazing and eventually cracking. The critical strain ε_c for craze initiation can be notably reduced as compared to that in air or in an inert medium

(dry crazing). For amorphous polymers, a strong correlation between ε_c and the difference $\{\delta_s - \delta_p\}$ of the solubility parameters of environment (s) and polymer (p) has been found (12,19,59). The smallest values of ε_c are usually observed for those polymer-solvent pairs where the equilibrium solubility S_v shows a maximum. The action of alcohols on PMMA, of Lewis acids and some metal salts on polyamides, and of hydrocarbons and detergents on polyolefins should be specifically mentioned (59).

Environmental agents also influence the later stages of stress cracking, ie, craze growth and breakdown, resulting in crack formation. The fracture-mechanics concept has proved to be useful to explain quantitatively the kinetics of crack growth in a liquid environment if the wetting, spreading, flow, and diffusion behavior of the liquid at the crack tip and within the capillaries opened up through the craze are taken into account. The three typical stages of environmental stress cracking are well represented by a semicrystalline polymer, LDPE in contact with a detergent (Fig. 34). Sorption starts with the application of stress, but for an incubation period (t_i) the stress-cracking agent has no, or little, apparent effect. In the following period there is a rather modest increase in durability with decreasing K_c, since at this stage SCG is strongly assisted by the action of the active liquid (Stage II, steep slope of the K_c–t_b curve). A durability threshold is only attained at a very low level of K_c (Fig. 34). On the other hand, in the absence of the stress-cracking agent the rate of SCG depends very strongly on the applied stress intensity factor K_c (eq. (34)). Thus one observes a very pronounced increase in durability if K_c is decreased from the value of the initial toughness of $K_{Ic} = 0.9\ \text{MPa} \cdot \text{m}^{1/2}$ (a rather flat K_c–t_b curve). An amorphous polymer [ABS with and without a nonionic surfactant (60)] would behave in a rather similar manner also exhibiting these three different stages.

The ESC fracture behavior of semicrystalline polymers can be understood on the basis of a stress-activated diffusion of stress-cracking agent into the interlamellar regions. Fracture at $t_b < t_i$ occurs by local drawing of the practically unplasticized sample. In the second stage ($t_b > t_i$) and at higher stresses, ESC leads to a mixed mode fracture involving large-scale plastic deformation, void

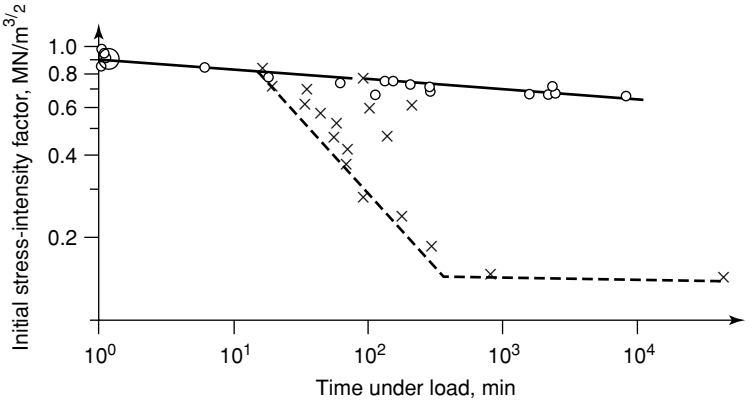

Fig. 34. Environmental crack growth: (——) in air, (———) in an active environment (detergent).

formation, and multiple cracking giving rise to a fairly rough fracture surface. In low stress ESC at $t_b \gg t_i$ fracture occurs by craze breakdown or interlamellar failure (through chain disentanglement or rupture), leaving rather smooth fracture surfaces. From this analysis it can be deduced that environmental effects are reduced through the same factors which improve the interlamellar connectivity. The excellent proportionality between the times to failure of different polymer grades in the presence and absence of a surfactant mentioned above (48) is further evidence.

Characterization and Test Methods

Fracture toughness characterization has been discussed throughout this article from different view points. It requires well-defined specimens and procedures, which have already been indicated. For convenience this information is here summarized again.

Fracture mechanics specimens:

(1) Compact tension (CT), Fig. 12
(2) Double cantilever beam (DCB), Fig. 7
(3) Double-edge notch for essential work of fracture (EWF), Fig. 20
(4) Double torsion (DT), Fig. 16
(5) Single-edge notch tension (SENT), Fig. 12
(6) Single-edge notch three point bending (SENB), Fig. 12
(7) Tapered cantilever, Fig. 16.

Fracture concepts treated in individual paragraphs:

(1) Linear elastic fracture mechanics (including the Irwin model of confined plasticity, the line-zone or Dugdale model and viscoelastic effects)
(2) Fracture mechanics of dissipative materials (including the J-integral and the Essential work of fracture concepts).
(3) Slow crack growth
(4) Multiaxial states of stress
(5) Environmental effects

For a more detailed discussion on testing methods the reader is referred to the International Standards (ASTM, ISO) and the cited comprehensive literature (2–5).

Special care has been taken to elucidate the molecular and physical background of fracture phenomena.

BIBLIOGRAPHY

"Fracture" in *EPST* 1st ed., Vol. 7, pp. 261–361; "Long-Term Phenomena," pp. 261–291, by J. B. Howard, Bell Telephone Laboratories; "Short-Term Phenomena," pp. 292–361, by P. I.

Vincent, Imperial Chemical Laboratories. "Fracture and Fatigue" in *EPST* 2nd ed., Vol. 7, pp. 328–405, "Fracture" by H. H. Kausch, Ecole Polytechnique Fédérale de Lausanne, and J. G. Williams, Imperial College of Science and Technology, London.

1. E. Gaube and W. Müller, *3R Internat.* **23**, 236 (1984).
2. J. G. Williams, *Fracture Mechanics of Polymers*, Ellis Horwood, Ltd., Chichester, U.K., 1984.
3. T. L. Anderson, *Fracture Mechanics—Fundamentals and Applications*, CRC Press, Inc., Boca Raton, Fla., 1995.
4. W. Grellmann and S. Seidler, Eds., *Deformation and Fracture Behaviour of Polymers*, Springer, Berlin, 2001.
5. J. G. Williams and A. Pavan, eds. *Fracture of Polymers, Composites and Adhesives*, Elsevier, Amsterdam, 2000.
6. A. A. Griffith, *Philos. Trans. Royal Soc. London, Ser. A* **221**, 163 (1921).
7. C. Gurney and J. Hunt, *Proc. R. Soc. London, Ser. A* **299**, 508 (1967).
8. R. S. Rivlin and A. G. Thomas, *J. Polym. Sci.* **10**, 291 (1953).
9. W. F. Brown and J. E. Srawley, *ASTM STP 410*, The American Society for Testing and Materials, Philadelphia, Pa., 1966.
10. D. P. Rooke and D. J. Cartwright, *Compendium of Stress Intensity Factors*, Her Majesty's Stationery Office (HMSO), London, 1976, p. 29.
11. *ASTM Standards 31* (1969) and *ASTM STP 463* (1970), The American Society for Testing and Materials, Philadelphia, Pa.
12. H. H. Kausch, ed., *Crazing in Polymers*, Vols. **I** and **II**, Springer-Verlag, Berlin, 1983 *Crazing in Polymers*, (Vol. **I**), 1990 (Vol. **II**). *Advances in Polymer Science*, Vol. **52/53** and Vol. **91/92**.
13. M. L. Williams, *Int. J. of Fracture Mechanics* **1**, 292 (1965).
14. W. G. Knauss, in *Proceedings of the Seventh Int. Conf. on Fracture*, Mar. 1989, Houston, Tex., p. 2683.
15. R. A. Schapery, *Int. J. Fracture* **42**, 189 (1990).
16. W. Bradley, *Mechanics of Time-Dependent Materials* **1**, 241 (1998).
17. M. K. V. Chan and J. G. Williams, *Polymer* **24**, 234 (1983).
18. N. Brown and X. Lu, *Polymer* **36**, 543 (1995).
19. H. H. Kausch, *Polymer Fracture*, 2nd ed., Springer-Verlag, Berlin, 1986.
20. W. Döll and L. Könczel, *Kunststoffe* **70**, 563 (1980).
21. C. Grein, Ph.D. No. 2341, Ecole Polytechnique Fédérale de Lausanne, Lausanne, 2001.
22. ASTM E813-97 (Standard Test Method for J_{Ic}, A Measure of Fracture Toughness), The American Society for Testing and Materials, Philadelphia, Pa., 1997, p. 802.
23. European Structural Integrity Society (ESIS) Testing Committee protocol for conducting J-crack growth resistance curve tests on plastics, in D. R. Moore, B. R. K. Blackman, P. Davies, A. Pavan, P. Reed, J. G. Williams, eds., *Experimental Methods in the Application of Fracture Mechanics Principles to the Testing of Polymers, Adhesives and Composites*, Elsevier, London, 2000, p. 140.
24. *ESIS Test protocol for essential work of fracture*, in Ref. 23, p. 188.
25. J. Karger-Kocsis, *Polym. Eng. Sci.* **36**, 203 (1996).
26. R. Gensler, Ph.D. No. 1863, Ecole Polytechnique Fédérale de Lausanne, Lausanne, 1998.
27. R. Gensler and co-workers, *Polymer* **41**, 3809 (2000).
28. H. H. Kausch and co-workers, *J. Macromol. Sci.-Phys. B* **38**, 803 (1999).
29. T. L. Smith and W. H. Chu, *J. Polym. Sci. Part A-2* **10**, 133 (1972).
30. M. Fischer, *Adv. Polym. Sci.* **100**, 313 (1992).
31. R. Hiss and co-workers, *Macromolecules* **32**, 4390 (1999).
32. X. C. Zhang, M. F. Butler, and R. E. Cameron, *Polymer* **41**, 3797 (2000).
33. N. Brown and I. M. Ward, *J. Mater. Sci.* **18**, 1405 (1983).

34. S. Hashemi, Ph.D. Thesis, Imperial College of Science and Technology, London, 1984.
35. S. Hashemi and J. G. Williams, *J. Mater. Sci.* **20**, 4202 (1985).
36. G. Sandilands and co-workers, *Polym. Commun.* **24**, 273 (1983).
37. E. H. Andrews and P. Reed, in E. J. Kramer and E. H. Andrews, eds., *Developments in Polymer Fracture*, Vol. **1**, Applied Science Publishers, Ltd., London, 1979, p. 17.
38. P. I. Vincent, *J. Appl. Phys.* **13**, 578 (1962).
39. F. Ramsteiner, *Kunststoffe* **73**, 148 (1983).
40. L. Tézé, Thèse de doctorat de l'Université P.et M. Curie, Paris, 1995.
41. C. J. G. Plummer and co-workers, *Polymer* **37**, 4299 (1996).
42. *Norme, Thermoplastic Pipes for the Transport of Fluids, ISO TR 9080* (1992).
43. N. Brown and co-workers, *Makromol. Chem., Macromol. Symp.* **41**, 55 (1991).
44. X. Lu, N. Ishikawa, and N. Brown, *J. Polym. Sci., Part B: Polym. Phys.* **34**, 1809 (1996).
45. R. W. Lang and G. Pinter, in *Eur. Conf. on Fracture 13*, San Sebastian, 2000.
46. E. Kramer and J. Koppelmann, *Kunststoffe* **73**, 714 (1983).
47. X. Lu and N. Brown, *Polymer* **38**, 5749 (1997).
48. M. Fleissner, *Polym. Eng. Sci.* **38**, 330 (1998).
49. S. Glasstone and co-workers, *The Theory of Rate Processes*, McGraw-Hill, New York, 1941.
50. S. N. Zhurkov and co-workers, *Fiz. Tverd. Tela* **13**, 2004 (1971); S. N. Zhurkov and co-workers, *Sov. Phys. Solid State* **13**, 1680 (1972); S. N. Zhurkov and co-workers, *J. Polym. Sci. Part A-2* **10**, 1509 (1972).
51. M. A. Miner, *J. Appl. Mech.* **12A**, 159 (1945).
52. U. W. Gedde and co-workers, *Polym. Eng. Sci.* **34**, 1773 (1994).
53. H. H. Kausch, N. Heymans, C. J. Plummer, and P. Decroly, *Matériaux polymères: propriétés mécaniques et physiques, principes de mise en oeuvre*, Presses Polytechniques et Universitaires Romandes, Lausanne, 2001.
54. S. S. Sternstein, L. Ongchin, and A. Silverman, *Appl. Polym. Symp.* **7**, 175 (1968).
55. R. P. Kambour, *Polym. Commun.* **24**, 292 (1983).
56. S. Wu, *Polym. Int.* **29**, 229 (1992).
57. C. Fond, A. Lobrecht, and R. Schirrer, *Int. J. Fracture* **77**, 141 (1996).
58. Y. Kayano, H. Keskkulla, and D. R. Paul, *Polymer* **39**, 821 (1998).
59. E. J. Kramer, in E. H. Andrews, ed., *Developments in Polymer Fracture*, Vol. **1**, Applied Science Publishers, Ltd., London, 1979, p. 55.
60. T. Kawaguchi and co-workers, *Polym. Eng. Sci.* **39**, 268 (1999).

HANS-HENNING KAUSCH
École Polytechnique Fédérale de Lausanne
J. G. WILLIAMS
Imperial College of Science Technology and Medicine

GLASS TRANSITION

Operational Definition

At a relatively simple-minded practical and operational (and thus theoretically nonrigorous) level of treatment, we can define (1) the *glass-transition temperature* (T_g) as the temperature at which the forces holding the distinct components of an amorphous solid together are overcome by thermally induced motions within the time scale of the experiment, so that these components are able to undergo large-scale molecular motions on this time scale, limited mainly by the inherent resistance of each component to such flow. The practical effects of the glass transition on the processing and performance characteristics of polymers are implicit in this definition.

In most polymeric as well as nonpolymeric amorphous materials, the ability to undergo large-scale molecular motions implies the freedom to flow, so that the material becomes a fluid above T_g. However, in the special class of polymers commonly described as "thermosets," covalent cross-links limit the ability to undergo large-scale deformation. Consequently, above T_g, thermosets become "elastomers" (also known as "cross-linked rubbers").

On the experimental time scale, above T_g, nonthermoset amorphous materials are viscous fluids. Their glass transitions can then be viewed as transitions, over the experimental time scale, from predominantly elastic "solid-like" to predominantly viscous "liquid-like" behavior. In fact, traditionally, the glass transition has often been identified in practical terms (not only for polymers, but also for amorphous inorganic materials) as taking place when the viscosity reaches a threshold value (most commonly taken to be 10^{13} P). The glass transition occurs in the reverse direction if the temperature is instead lowered from above to below T_g, with the material then undergoing "vitrification." Again with the

Encyclopedia of Polymer Science and Technology. Copyright John Wiley & Sons, Inc. All rights reserved.

exception of thermosets, this reverse transition upon cooling can be described as going from viscous to elastic behavior. For every glass former, there is a temperature-dependent frequency f (T), and a time scale $t(T)=1/f$ (T), such that at frequencies higher than f the system is elastic and for lower frequencies it is viscous.

In thermosets large-scale molecular motions also become possible above T_g, but these motions are limited by the cross-links that serve as topological constraints for the chain segments between them. (The chain segments between cross-links are the "distinct components" for such materials). The general operational definition given above, therefore, remains valid. However, the specimen as a whole does not and cannot undergo large-scale viscous flow. In fact, it may instead exhibit strongly elastic behavior above T_g because of the presence of the network junctions. The glass transition, therefore, involves the onset of large-scale motions (in other words, "viscous" behavior) on the molecular scale in all amorphous materials. However, on a larger length scale, in thermosets, it cannot be described as occurring between predominantly elastic and predominantly viscous behavior. In the remainder of this article, whenever the glass transition is described in terms of its effect on the viscosity in large-scale flows, it should be understood that thermosets and elastomers are being excluded from the scope of the discussion.

Experimental Methods and Modeling

Several well-established experimental methods are available to measure T_g. The tabulated data are subject to many uncertainties. These uncertainties include the use of different experimental methods, ill-characterized differences between samples in terms of their precise composition and thermal history, and the nonequilibrium (kinetic) aspect of the glass transition which introduces an inherent rate dependence. It is, therefore, best to compare T_g values by using data obtained with the same experimental method for well-characterized samples, whenever possible.

Many theories based on thermodynamic and kinetic considerations, as well as many quantitative structure–property relationships with different amounts of empiricism, have been developed for T_g as a result of decades of research. Further work along these directions can be expected to result only in incremental improvements in fundamental understanding and predictive ability. The rapidly increasing power of computational hardware and software has encouraged attempts to study the glass transition by fully atomistic or coarse-grained numerical simulations, and significant progress may be expected along this exciting new research frontier in coming years.

Practical Importance and Common Methods for Measurement

The glass transition is by far the most important one among the many transitions and relaxations (2) observed in amorphous polymers. When an amorphous polymer undergoes the glass transition, almost all of its properties that relate to its processing and/or performance change dramatically. These changes are important both in determining the processing and performance characteristics of polymers,

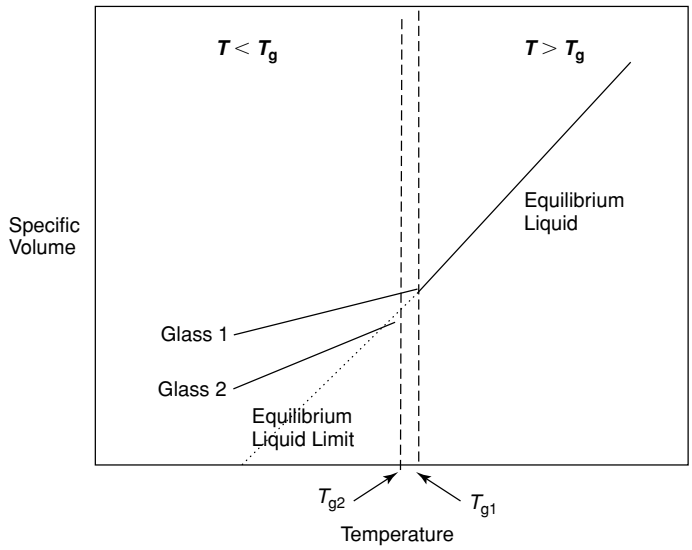

Fig. 1. Schematic illustration of temperature dependences of specific volumes of amorphous materials. This figure also illustrates the effects of the nonequilibrium nature of glass structure, which results from kinetic factors. Glass 1 and Glass 2 are specimens of the same polymer, but subjected to different thermal histories. For example, Glass 1 may have been quenched from the melt very rapidly, while Glass 2 may either have been cooled slowly or subjected to volumetric relaxation via annealing in the glassy state.

and in the selection of suitable methods for measuring the value of T_g itself. The following are some important examples of the effects of going through T_g, as well as of the common methods for measuring T_g based on these effects (1).

The temperature dependence of the specific volume (1/density) of an amorphous material is shown schematically in Figure 1. The coefficient of thermal expansion (rate of change of specific volume with temperature) increases from its value for the "glassy" polymer to its typically much larger value for the "rubbery" polymer when the temperature increases from below to above T_g. The rate of decrease of the density with increasing temperature then becomes much faster above T_g. However, unlike melting where there is a discontinuity in the specific volume itself, the specific volume is a continuous function of the temperature at T_g; only its slope changes in going through the glass transition. Figure 1 also illustrates the effects of the nonequilibrium nature of glass structure, which results from kinetic factors, as will be discussed further later in this article. The effect of T_g on the coefficient of thermal expansion enables its measurement by *dilatometry*.

The dependence of the specific heat capacity of an amorphous polymer on the temperature is shown schematically in Figure 2. The heat capacity of an amorphous polymer jumps from its value for the "solid" polymer to its significantly larger value for the "liquid" (molten or rubbery) polymer at T_g. However, unlike melting where there is a discontinuity in the enthalpy, the enthalpy is a continuous function of the temperature at T_g; only its slope changes in going through the glass transition. The effect of T_g on the heat capacity enables its measurement by *differential scanning calorimetry*, which is by far the most commonly used method to measure it.

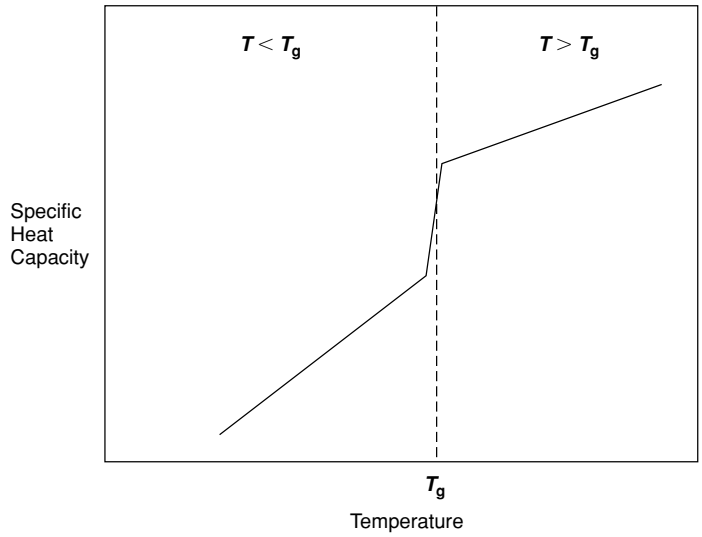

Fig. 2. Schematic illustration of temperature dependences of specific heat capacities of amorphous polymers. The heat capacity "jumps" to a much higher value over a narrow temperature range as the polymer goes through the glass transition. It increases more slowly with increasing temperature above T_g than it did below T_g.

An amorphous polymer typically "softens" drastically as its temperature is raised above T_g, so that its structural rigidity is lost. At the typical time scale of a practical observation, the key indicators of stiffness (the tensile and shear moduli), which decrease very slowly with increasing temperature below T_g, decrease rapidly over a narrow temperature range with further increase in temperature by several (sometimes up to three or even four) orders of magnitude upon traversing T_g. The typical behavior of the tensile (Young's) or shear modulus upon going through the glass transition is compared for a linear (physically entangled but not chemically cross-linked) amorphous polymer, a chemically cross-linked amorphous polymer, and a semicrystalline polymer, in the schematic drawings shown in Figure 3. [However, strictly speaking, this summary is an oversimplification. The elastic moduli for elastic frequencies are not sharp functions of T. The apparent changes are due to the change of f (T) when one works at the time scale of the experiment.] The yield stress also decreases rapidly upon traversing T_g, going to zero slightly above T_g. These changes in the mechanical properties, from "glassy" (below T_g), to "leathery" (in the immediate vicinity of T_g), to "rubbery" (above T_g), have strong implications in terms of practical applications of polymers. These changes also enable the use of mechanical testing methods to measure T_g. Among such methods, *dynamic mechanical spectroscopy*, which measures the viscoelastic characteristics of a polymer under mechanical deformation, is the most reliable and most widely utilized one.

It is worth noting that, in practice, the "heat distortion temperature" (3) is used more often than T_g in the product literature of commercial polymers as an indicator of the mechanical softening temperature. It is closely related to (usually slightly lower than) T_g for amorphous polymers.

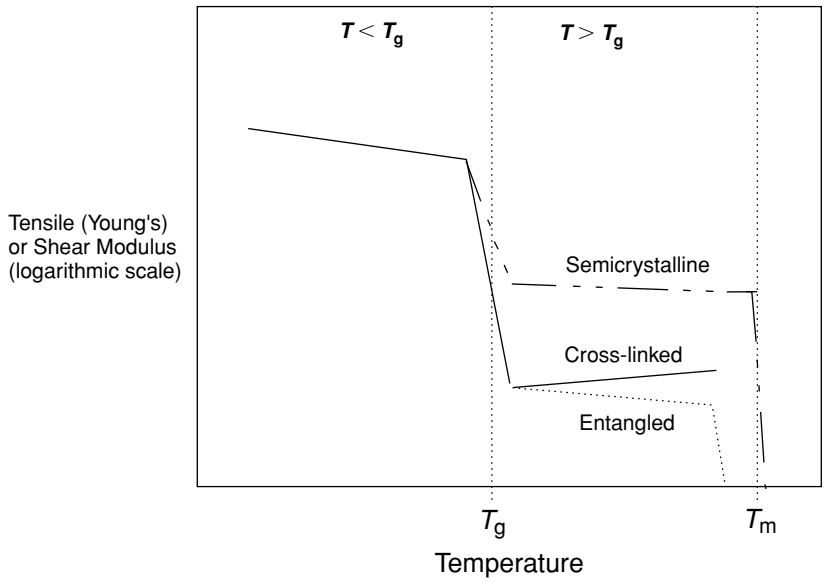

Fig. 3. Schematic illustration of typical behavior of tensile (Young's) and shear moduli upon going through the glass transition. Linear (physically entangled but not chemically cross-linked) amorphous polymers, chemically cross-linked amorphous polymers, and semicrystalline polymers are compared. These two moduli decrease slowly for $T < T_g$, and then drop rapidly over a narrow temperature range as the temperature increases above T_g. The drop may be up to 4 orders of magnitude for amorphous polymers, while it is smaller for semicrystalline polymers. The slight gradual increase in the modulus of the chemically cross-linked polymers above T_g is a result of entropic effects, as described by rubber elasticity theory, and persists until T is raised sufficiently for the polymer to undergo degradation. The gradual decrease in the modulus of a physically entangled polymer over the "rubbery plateau," followed by a precipitous drop into the "terminal zone" where the polymer becomes fluid-like, is due to increasing slippage of labile entanglement junctions. The crystallites in a semicrystalline polymer may provide a wide rubbery plateau regime if $T_m \gg T_g$, and the polymer then becomes fluid-like above T_m.

The rates of change (slopes of the curves) of many important properties (such as the refractive index, surface tension, and gas permeabilities) as a function of temperature, the value of the dielectric constant, and many other optical and electrical properties, often change considerably at T_g. These changes enable the measurement of T_g by using techniques such as *refractometry* and *dielectric relaxation spectroscopy*. Refractometry provides results which are similar to those obained from dilatometry because of the correlation between the rates of change of the specific volume and of the refractive index with temperature. Dielectric relaxation spectroscopy is based on general physical principles which are similar to those in dynamic mechanical spectroscopy, the main difference being in its use of an electrical rather than a mechanical stimulus.

In considering the methods summarized above for measuring T_g, it is important to note that, as discussed later in greater detail, the observed value of T_g can be affected significantly by kinetic factors. T_g is, therefore, dependent on the measurement rate. For example, the T_g measured by differential scanning calorimetry can be increased significantly by increasing the heating rate or by decreasing the

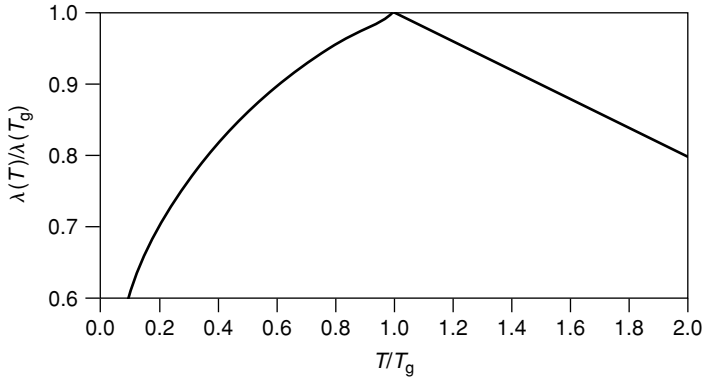

Fig. 4. Approximate form of the temperature dependence of the thermal conductivity $\lambda(T)$ of amorphous polymers, showing that it goes through its maximum value at T_g.

cooling rate during a calorimetric scan. Furthermore, the glass transition does not occur at a single sharply defined temperature but instead over a range of temperatures. There is often confusion in the literature about which point in that range (its onset, midpoint, or end) to use as the value of T_g. Similarly, the glass-transition range depends both on the rate (frequency) of measurement and on whether the specimen is being heated or cooled, in measuring T_g by dynamic mechanical spectroscopy or by dielectric relaxation spectroscopy. The typical temperature and/or frequency scanning rates used most often in different types of experiments also differ significantly. It is worth remembering, therefore, that not only are there many different methods for measuring T_g, but each method only gives a range of temperatures over which the glass transition occurs, and the T_g range measured by any one method can also vary because of the use of different testing conditions.

The thermal conductivity of a completely amorphous polymer goes through its maximum value at T_g, as illustrated in Figure 4.

The melt viscosity above T_g is typically lower than the viscosity in the glassy state below T_g by more than 10 orders of magnitude. Melt processing by techniques such as extrusion, injection molding, and compression molding requires temperatures significantly above T_g. If T_g is expressed in Kelvin, the optimum melt-processing temperature is normally at least $1.2T_g$. The general form of the dependence of the zero-shear melt viscosities η_0 of amorphous polymers as a function of the temperature is illustrated schematically in Figure 5. It is seen that η_0 has a non-Arrhenius "universal" shape for $T_g \leq T \leq 1.2T_g$, where the "reduced temperature" T/T_g roughly serves as the "corresponding states" variable. This universal behavior is lost above $1.2T_g$. The curves for different polymers separate from each other. For $T \gg 1.2T_g$, an Arrhenius-like (activated flow) regime is approached asymptotically. The activation energy in the extrapolation to the hypothetical limit of $T \to \infty$ depends on the chemical structure of the polymer.

One of the many practical uses of T_g is in characterizing polymer blends. When polymers with significantly different T_g values are blended, the effects on T_g often provide a useful indication of the extent of relative miscibility. For example, suppose that two polymers with T_g values of T_{g1} and T_{g2} (where $T_{g1} < T_{g2}$) are blended. If the blend manifests two distinct T_g values, near T_{g1} and T_{g2},

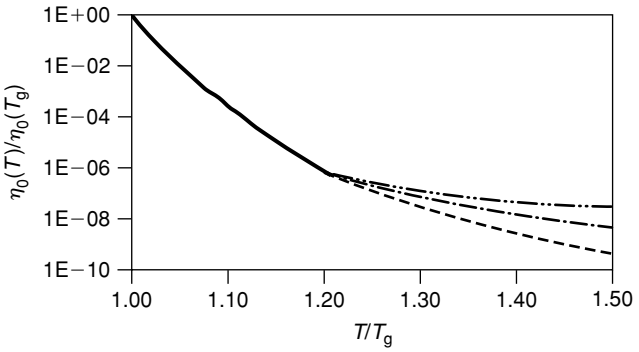

Fig. 5. Schematic illustration of general form of temperature dependence of zero-shear melt viscosities η_0 of amorphous polymers. It is seen that η_0 has a non-Arrhenius "universal" shape for $T_g \leq T \leq 1.2T_g$, where the "reduced temperature" T/T_g serves as the "corresponding states" variable. This universal behavior is lost above $1.2T_g$. The curves for different polymers separate from each other, as shown below for three polymers. For $T \gg 1.2T_g$, an Arrhenius-like (activated flow) regime is approached asymptotically. The activation energy in the extrapolation to the hypothetical limit of infinite temperature depends on the chemical structure of the polymer.

with relative intensities corresponding to the volume fractions of the components, this result usually implies that the polymers are immiscible and separated into macroscale phase domains. If the two glass transitions are broader than those observed for the individual polymers, and/or if the T_g values in the blend (T_g^{g1} and T_g^{g2}) fall between those of the polymers ($T_{g1} < T_g^{g1} < T_g^{g2} < T_{g2}$), this result usually indicates some intermixing of the polymers. If a single T_g value in the range of $T_{g1} < T_g < T_{g2}$ is observed and its position is correlated strongly with the volume fractions of the polymers, this result usually indicates that the polymers are miscible over the volume fraction range where such a single T_g value is observed. However, the use of T_g measurements to assess miscibility is subject to pitfalls, such as whether the T_g's differ sufficiently to allow resolution by a given measurement method, and whether the phase domains in a particular multiphase system are large enough for their effects on T_g to be detectable with that experimental technique (4).

Another practical use of T_g is in characterizing blends of polymers with small molecules. Over the industrially important blend composition ranges where the small molecules are dissolved in a polymeric matrix, such blends are usually referred to as *plasticized polymers*.

The glass transition also plays a major role in determining both the physical properties and the processing characteristics of semicrystalline polymers. Amorphous portions "melt" or "soften" at T_g. Crystalline portions remain "solid" up to the melting temperature T_m. (In practice, usually a semicrystalline polymer contains crystallites over a range of sizes and correspondingly a range of T_m values.) A semicrystalline polymer can be considered as a solid below T_g, as a composite consisting of solid and rubbery phases above T_g but below T_m, and as a fluid above T_m. The effect of the glass transition on the physical properties of semicrystalline polymers decreases with increasing crystallinity. Crystallization upon cooling from the

melt (from $T > T_m$) occurs over the range of $T_g < T < T_m$. Several industrially important fabrication processes (such as thermoforming, blow molding, and preparation of biaxially oriented films) take advantage of this crystallization temperature range, in manufacturing articles with the desired semicrystalline morphologies.

Thermoplastic elastomers (TPEs) (5) are multiphase polymers which behave like elastomers over a wide temperature range, but which can be melt-processed after raising the temperature sufficiently. They are used in many applications. Many TPEs are semicrystalline, with their practical use temperatures ranging from a lower limit of T_g (below which the amorphous phase solidifies so that the elastomeric behavior is lost) to an upper limit of T_m (above which the specimen becomes a viscous fluid so that its structural integrity is lost); see Figure 3. (The crystallites in such TPEs can thus be imagined to behave like meltable cross-links.) Many other TPEs are completely amorphous, with a use temperature range of T_{g1} (for lower-T_g phase) to T_{g2} (for higher T_g phase). On the other hand, certain families of thermoplastic elastomers have sharp glass transitions near room temperature and manifest reversible changes of up to 3 orders of magnitude in stiffness in going through T_g. These materials are known as *shape memory polymers* (6,7). These attributes make them ideally suited for some important specialized applications such as catheters which are rigid when handled by a surgeon outside the human body at room temperature (25°C), but flexible when inserted into the body (∼37°C).

Key Physical Aspects

Despite its apparent simplicity, the operational definition of T_g given earlier comprehends both of the key aspects of the physics of the glass transition. It states that, when a solid is heated up to T_g, it acquires enough thermal energy to be able to overcome two types of resistance to the large-scale motions of its components (1):

(1) The *cohesive forces* holding its different components together. The relevant components for the glass transition in amorphous polymers are chain segments. The cohesive forces can be quantified in terms of properties such as the cohesive energy density or the solubility parameter (square root of cohesive energy density).

(2) Attributes of the individual components (chain segments in polymers) which resist viscous flow. Resistance to the viscous flow of polymer chain segments is related to the topological and geometrical arrangement of their atoms, especially as expressed by the somewhat nebulous concept of *chain stiffness*. The glass transition occurs when there is enough freedom of motion for chain segments of up to several "statistical chain segments" (Kuhn segments) in length to be able to execute cooperative motions (8,9). As a general rule, the length of the Kuhn segment increases with increasing chain stiffness. See the two classic textbooks by Flory (10,11) for background information on statistical chain segments and on other configurational properties of polymer chains.

The effects of chain stiffness and cohesive forces on the value of T_g are different from each other. The "intrachain" effect of the stiffness of individual chain segments is generally (but not always) somewhat more important than the "interchain" effect of the cohesive (attractive) forces between different chains in determining the value of T_g.

Fundamental Theoretical Considerations

Based on the considerations summarized in previous section, it is not surprising to find that most theories of the glass transition (12–30) describe this phenomenon, either explicitly or implicitly, in terms of key physical ingredients whose values strongly depend on the chain stiffness and/or the cohesive forces. These theoretical treatments invariably treat the observed value of T_g as a kinetic (rate-dependent) manifestation of an underlying thermodynamic phenomenon. However, they differ significantly in their description of the nature of this phenomenon at a fundamental level.

Differences of opinion exist concerning the issue of whether or not the discontinuities observed at T_g in the second derivatives of the Gibbs free energy (ie, the coefficient of thermal expansion and the heat capacity) justify referring to the glass transition as a "second-order phase transition". It is important to note that the observed value of T_g is a function of the rate of measurement. For example, when the glass transition is approached from below, heating a specimen very quickly results in a higher apparent T_g than heating it very slowly. Conversely, when the glass transition is approached from above, cooling a specimen very quickly results in a lower apparent T_g than cooling it very slowly (see Fig. 1). There is, therefore, obviously, an important rate-dependent (kinetic) aspect of the glass transition. Nonetheless, it appears that the glass transition may also have an underlying fundamental thermodynamic basis. In other words, there is always a *thermodynamic equilibrium state*, defined as the state which has the lowest possible Gibbs free energy. Therefore, a thermodynamic driving force (preference for achieving as low a free energy as possible) must exist toward that equilibrium state. However, at the prevailing conditions of temperature and pressure, the approach toward that thermodynamic equilibrium state is so slow that the material seems to be "frozen" into a thermodynamically metastable glassy state. Consequently, *the consideration of the glass transition as a kinetic manifestation of an underlying thermodynamic phenomenon provides a reasonable fundamental physical framework for theories of the glass transition.*

The most essential aspects of this interplay of kinetics and thermodynamics are that (*1*) the glass transition involves freezing–defreezing phenomena, (*2*) one sees no sharp change in the parameters describing the static structure (such as the density and the structure factors) relative to the fluid after the vitrification event, and (*3*) what is a glassy material over a short time scale becomes a fluid over a sufficiently long time scale. (Sometimes, "sufficiently long" may mean millions of years, as in some geological phenomena.) The real mystery of the glass transition is in the acceleration of freezing (fragility) that makes the frequency $f(T)$ depend more strongly on the temperature than would be expected from a simple Arrhenius-type activated flow theory.

Quantitative Structure–Property Relationships

It is often important, especially in developing polymers for industrial applications, to be able to predict, rapidly, rough values for T_g as well as the probable trends between structural variants within and between polymer families. There is a long tradition of using quantitative structure–property relationships, developed by the statistical analysis of experimental data to express T_g as a function of (hopefully well-selected) compositional and structural descriptors, for such calculations. All such correlations either explicitly or implicitly attempt to account for the effects of chain stiffness and cohesive forces. One such correlation is the familiar relationship of van Krevelen (31) based on group contributions. Many other empirical correlations, which also usually express T_g as a function of quantities calculated via group contributions, have been used with limited success. A review article (32) provides detailed quantitative critical assessments, and extensive lists of the original references, for some of the best-known empirical correlations for T_g. Some of the many other interesting attempts to estimate T_g, which were not reviewed (32), include the method of Askadskii and Slonimskii (33,34), an alternative version of this method developed by Wiff and co-workers (35), and the combination of molecular modeling and group contributions in the method of Hopfinger and co-workers (36).

More recently, new quantitative structure–property relationships for T_g have been developed (1); they are based on the statistical analysis of experimental data for 320 linear (uncross-linked) polymers collected from many different sources, containing a vast variety of compositions and structural features. The T_g of the atactic form was used, whenever available, for polymers manifesting different tacticities. The T_g values of a subset of the polymers listed in this extensive tabulation are reproduced (with some minor revisions) in Table 1. (It is important to caution the reader here that these data were assembled from a wide variety of sources. Many different experimental techniques were used in obtaining these data.) The resulting relationship for T_g has the form of a weighted sum of "structural terms" mainly taking the effects of chain stiffness into account plus a term proportional to the solubility parameter δ which takes the effects of cohesive interchain interactions in an explicit manner, as shown in equation (1):

$$T_g \approx a + b\cdot\Delta + (\text{weighted sum of 13 structural terms}) \quad (1)$$

Literature data for the dependence of T_g on the number-average molecular weight (M_n) were also tabulated in Reference 1, and used to develop a quantitative structure–property relationship for the fitting parameter K_g in equation (2) (developed from considerations of free volume) where $T_{g\infty}$ is the limiting value of T_g for $M_n \rightarrow \infty$ (37). As shown for poly(ethylene terephthalate) in Figure 6 (38), T_g increases asymptotically toward $T_{g\infty}$ with increasing M_n. $T_{g\infty}$ is often larger than the commonly quoted T_g of a polymer, as measured at ordinary molecular weights. For example, $T_{g\infty} \approx 382$ K for polystyrene and $T_{g\infty} \approx 434$ K for bisphenol A polycarbonate, in comparison with the commonly quoted values of $T_g \approx 373$ K and $T_g \approx 423$ K, respectively. A subset of the data tabulated elsewhere (1) for the dependence of T_g on M_n, as fitted by using equation (2), is listed in Table 2. The final form of the resulting quantitative structure–property relationship is given by

Table 1. Glass-Transition Temperatures (T_g) of Some Polymers[a]

Polymer	T_g, K	Polymer	T_g, K
Poly(dimethyl siloxane)	152	Poly(vinyl butyral)	324
Poly(1,4-butadiene)	171	Poly(ethylene isophthalate)	324
Polyoxytetramethylene	190	Poly(ethyl methacrylate)	324
Polyisobutylene	199	Poly(*sec*-butyl methacrylate)	330
Polyisoprene	203	Poly(hexamethylene adipamide)	330
Poly(tetramethylene adipate)	205	Poly(*p*-xylylene)	333
Polyoxyethylene	206	Poly(ε-caprolactam)	335
Poly(propylene oxide)	206	Poly(ethylene terephthalate)	345
Poly(ε-caprolactone)	213	Poly(vinyl chloride)	348
Poly(decamethylene adipate)	217	Poly(vinyl alcohol)	358
Polyoxymethylene	218	Poly[oxy(*p*-phenylene)]	358
Poly(dodecyl methacrylate)	218	Poly(2-hydroxyethyl methacrylate)	359
Poly(*n*-butyl acrylate)	219	Polystyrene	373
Poly(vinyl *n*-butyl ether)	221	Phenoxy resin	373
Poly(1-hexene)	223	Poly(cyclohexyl methacrylate)	377
Polychloroprene	225	Poly(methyl methacrylate)	378
Poly(1-butene)	228	Polyacrylonitrile	378
Poly(ethylene adipate)	233	Poly(acrylic acid)	379
Poly(isobutyl acrylate)	249	Polymethacrylonitrile	393
Poly(ethyl acrylate)	251	Poly(ethylene-2,6-naphthalenedicarboxylate)	397
Poly(*n*-octyl methacrylate)	253	Poly(*p*-*t*-butyl styrene)	402
Poly(vinylidene chloride)	256	Poly(hexamethylene isophthalamide)	403
Polypropylene	266	Poly(*o*-methyl styrene)	409
Poly(*n*-hexyl methacrylate)	268	Poly(α-methyl styrene)	409
Poly(1,2-butadiene)	269	Poly(*m*-phenylene isophthalate)	411
Poly(*p*-*n*-butyl styrene)	279	Poly(*p*-vinylpyridine)	415
Poly(methyl acrylate)	281	Poly(*N*-vinylpyrrolidinone)	418
Poly(*n*-butyl methacrylate)	293	Poly(*p*-hydroxybenzoate)	420
Poly(vinyl acetate)	301	Bisphenol A polycarbonate	423
Poly(4-methyl-1-pentene)	302	Poly(*N*-vinyl carbazole)	423
Poly(12-aminododecanoic acid)	310	Poly(α-vinyl naphthalene)	432
Poly(hexamethylene sebacamide)	313	Poly(bisphenol A terephthalate)	478
Poly(10-aminodecanoic acid)	316	Poly[oxy(2,6-dimethyl-1,4-phenylene)]	482
Poly[oxy(*m*-phenylene)]	318	Poly[4,4′-diphenoxy di(4-phenylene)sulfone]	493
Poly(isobutyl methacrylate)	321	Poly(*m*-phenylene isophthalamide)	545
Poly(8-aminocaprylic acid)	324	Poly(*p*-phenylene terephthalamide)	600

[a]Data presented here are a part of literature data summarized in Ref. 1.

equation (3), which is illustrated in Figure 7. Other (more complex) relationships for the M_n dependence of T_g, which work better than equation (3) for polymers with a vinyl-type chain backbone, are also available and have been reviewed elsewhere (1).

$$T_g \approx T_{g\infty} - \frac{K_g}{M_n} \tag{2}$$

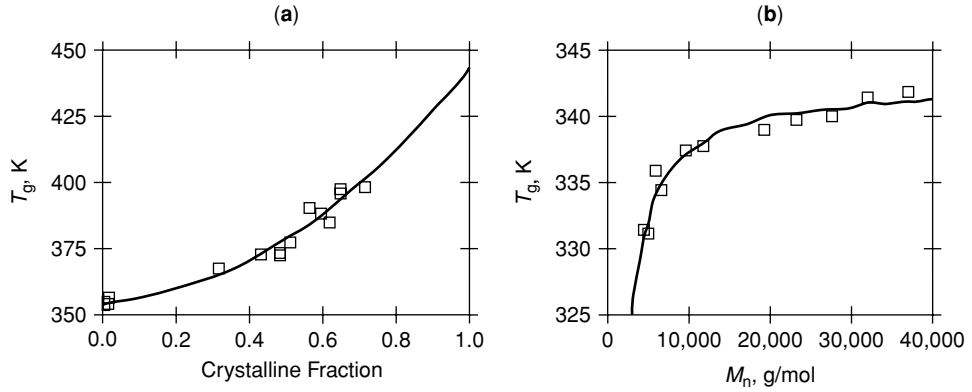

Fig. 6. Experimental data collected from the literature and empirical fits to these data, for the T_g of poly(ethylene terephthalate) (38), as a function of (a) crystalline fraction, and (b) M_n.

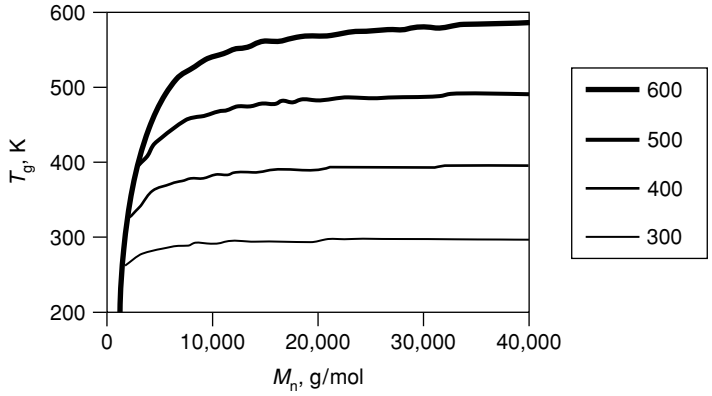

Fig. 7. Illustration of simple quantitative structure–property relationship given by equation (3) for the M_n dependence of T_g. Each curve is labeled by the value of $T_{g\infty}$, which is the limiting value of T_g for $M_n \to \infty$. More accurate relationships are also available for vinylic polymers.

$$T_g \approx T_{g\infty} - 0.002715\frac{T_{g\infty}^3}{M_n} \tag{3}$$

Many commercial polymers are cross-linked, ranging from lightly cross-linked elastomers to very densely cross-linked thermosets. The effects of crosslinking on the properties of polymers can be roughly classified as follows (40,41): (*1*) *Topological effect* caused by topological constraints introduced by cross-links on the properties. This effect is referred to simply as the *cross-linking effect* by many authors. (*2*) *Copolymerization effect* (also referred to as the *copolymer effect*) related to the change of the fractions of two or more types of repeat units with increasing cross-linking. Depending on the types of monomers involved, this effect may either strengthen or weaken the trends expected on the basis of the topological

Table 2. Dependence of T_g on M_n as fitted by the Parameter K_g of Equation (2)[a]

Polymer	K_g, 10^4 k·g/mol	$T_{g\infty}$, K
Poly(dimethyl siloxane)	0.6	150
n-Alkanes	1.2	176
Polyisoprene	1.2	207
Polybutadiene	1.2	174
Poly(ethylene adipate)	1.3	228
Poly(propylene oxide)	2.5	198
Polypropylene	3.9	266
Poly(tetramethylene terephthalate)	4.6	295
Poly(ethylene terephthalate)	5.1	342
Polyisobutylene	6.4	243
Poly(vinyl acetate)	8.9	305
Isotactic poly(methyl methacrylate)	11.0	318
Poly(glycidyl methacrylate)	11.3	350
Poly(vinyl chloride)	12.3	351
Polyacrylonitrile	14.0	371
Bisphenol A polycarbonate	18.7	434
Polystyrene	20.0	382
Atactic poly(methyl methacrylate)	21.0	388
Poly(*N*-vinyl carbazole)	22.8	500
Syndiotactic poly(methyl methacrylate)	25.6	405
Poly(*p*-methylstyrene)	26.5	384
Syndiotactic poly(α-methylstyrene)	31.0	453
Atactic poly(α-methylstyrene)	36.0	446
Poly(*p*-tert-butylstyrene)	38.5	430

[a]Data presented here are a part of literature data summarized in Ref. 1 (see Ref. 39 for a more extensive discussion) to develop a relationship for the parameter K_g in equation (2).

effect, and may even reverse them in some cases. The analysis of a large amount of experimental data collected from the literature [(1); for a more detailed discussion see (39)] led to the simple quantitative structure–property relationship given by equation (4) (illustrated in Fig. 8), where n (defined by eq. (5)) is the average number of "repeat units" between cross-links. M_c is the average molecular weight between cross-links. M is the molecular weight per repeat unit. $T_g(\infty)$ is T_g at the uncross-linked limit ($n\rightarrow\infty$). N_{rot} is a "number of rotational degrees of freedom per repeat unit" parameter.

$$T_g(n) \approx T_g(\infty)\left[1+\frac{5}{n\times N_{rot}}\right] \tag{4}$$

$$n=\frac{M_c}{M} \tag{5}$$

In many phase-separating block copolymers (especially segmented multiblock copolymers such as polyurethanes where the blocks are usually short), lowering the soft block M_n *increases* the soft phase T_g because of "cross-link-like" topological constraints imposed by hard phase domains.

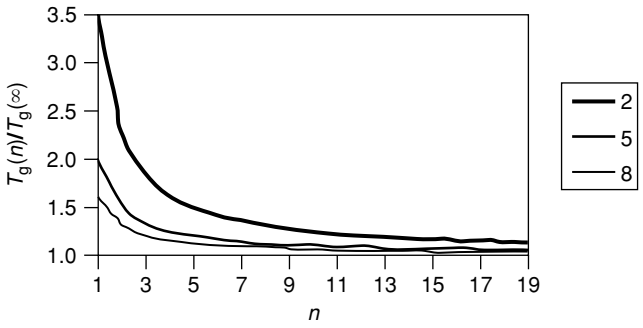

Fig. 8. Illustration of simple quantitative structure–property relationship given by equation (4) for the dependence of T_g on cross-linking. $T_g(\infty)$ is the T_g of the uncross-linked limit ($n \rightarrow \infty$, where n is the number of repeat units between cross-links). N_{rot} is a "number of rotational degrees of freedom per repeat unit" parameter. Each curve is labeled by the value of N_{rot}.

Other recently published correlative methods for predicting T_g include the "group interaction modeling" (GIM) approach of Porter (42), neural networks (43–45), genetic function algorithms (46), the CODESSA (acronym for "Comprehensive Descriptors for Structural and Statistical Analysis") method (47), the "energy, volume, mass" (EVM) approach (48,49), correlation to the results of semiempirical quantum mechanical calculations of the electronic structure of the monomer (50), and a method that combines a thermodynamic equation-of-state based on lattice fluid theory with group contributions (51).

Most theories and quantitative structure–property relationships for T_g only consider the case of a random distribution of repeat units along the polymer chains in treating copolymers. They give equations which predict a monotonic change of T_g between the T_g values of the homopolymers of the constituent repeat units, as a function of composition. However, the distribution of repeat units in a copolymer is often nonrandom. It may, for example, manifest various levels of "blockiness." Sometimes, T_g shows a nonmonotonic dependence on the composition variables, usually as a result of deviations of the repeat unit sequence from complete randomness. Some developed useful relationships correlating the T_g of a copolymer to the sequence of its repeat units have been developed (52). See also a review by Schneider (53), dealing with the deviations of T_g from simple additive relationships for copolymers and miscible polymer blends, and a review by Cowie and Arrighi (54), discussing the glass transition and sub-T_g relaxations in blends in greater depth. It should also be noted that sometimes nonmonotonic dependence of T_g on copolymer composition may arise as a result of preferential ("specific") types of nonbonded interactions (such as polar interactions and hydrogen bonding) between certain types of repeat units causing nonmonotonic composition dependence for the cohesive energy density. It has been shown that the differences between the solubility parameters (square root of the cohesive energy density) of the components of a random copolymer or a miscible blend can be correlated with the magnitude of such effects (53). In the context of experimental data for copolymers of vinylidene chloride, it has been shown how "the T_g-composition relationship is affected by four distinct structural features: the size, shape, and polarity of the comonomer unit, and the sequence distribution" (55).

It is important to note that quantitative structure–property relationships for T_g (as well as for other polymer properties) can be combined with nonlinear optimization techniques to perform "reverse engineering." These approaches involve working backwards, from a desired set of properties toward the repeat unit structures of the polymers that may give those targeted properties. See References 56–58 for some examples.

Detailed Simulations

In recent years, the rapidly increasing power of computational hardware and software has encouraged attempts to study the glass transition by fully atomistic or coarse-grained numerical simulations. Such simulations can be used to probe details of the physical processes taking place in a system at length scales, which cannot be probed by thermodynamic and kinetic theories which are based on a more "global" description of the system at larger length scales. Some of the details that can be probed by such simulations are also not accessible by any of the existing experimental techniques. Simulations have already begun producing valuable physical insights.

An objective of such work is to predict T_g by identifying the temperature at which discontinuities occur in the properties obtained directly from the results of the simulations. The results obtained thus far are insufficient to demonstrate conclusively the ability to accomplish this task routinely and reliably within computer time requirements that would be acceptable for the practical use of detailed simulations to predict T_g. The main challenge, at a fundamental level, is that the time scales involved in the glass transition are very long compared to what can currently be explored routinely in simulations on model systems large enough to represent a bulk polymer sample adequately and sufficiently fine-grained to account adequately for the effects of differences in chemical structure. Another significant challenge, at the implementation level, is the difficulty of developing potential functions (often referred to as "force fields") of sufficient quality to provide faithful representations of the properties and dynamics of the materials of interest. Significant progress is expected in coming years with further improvements in computer hardware and simulation software. It may, ultimately, become possible to use detailed simulations to predict reliably the effects of subtle variations in polymeric structure and conformation, which are very difficult to capture either with theoretical equations based on "global" thermodynamic and kinetic considerations or with empirically based relationships.

For further information, see the following four especially interesting articles:

(1) A review article (59) on the prediction of T_g by extending volume–temperature curves generated by molecular dynamics simulations to low temperatures.

(2) A study of the question of whether computer simulation can solve the challenge of understanding the glass transition and the amorphous state of matter (60).

(3) Molecular dynamics simulations of the thermal properties of ultrafine polyethylene powders (61). This study shows that, for particle diameters below 10 nm, both T_g and T_m are expected to decrease rapidly with decreasing particle diameter.

(4) Isobaric (constant pressure) and isochoric (constant volume) glass transitions in polymers were first observed for bisphenol A polycarbonate (62). A molecular dynamics study of such transitions in a model amorphous polymer has also been reported (63). This study shows that the glass transition is primarily associated with the freezing of the torsional degrees of freedom of polymer chains (related to chain stiffness), which are strongly coupled to the degree of freedom associated with the nonbonded Lennard–Jones potential (related to interchain cohesive forces).

Comprehensive List of Factors Determining T_g

Several of the most important factors determining the value of T_g have been discussed earlier:

(1) *Rate of measurement*
(2) *Structural and compositional factors*—the most fundamental of which are *chain stiffness* and interchain *cohesive forces*
(3) *Number-average molecular weight*
(4) *Cross-linking*

The following are the additional factors which affect the value of T_g:

(1) Morphological effects, and especially *crystallinity*.
   a. The presence of the rigid crystallites, and of the interphase regions ("tie molecules") between amorphous and crystalline regions, often increases T_g (1,38,64), as shown for poly(ethylene terephthalate) in Figure 6 (38). In addition, the decrease of the amorphous fraction of the polymer naturally leads to a decrease in the strength (intensity) of its amorphous relaxations, with the decrease in the strength of the glass transition at a given percent crystallinity normally being larger than the decrease in the strength of the secondary (sub-T_g) relaxations (65). The increase in T_g due to crystallinity bears some resemblance to the increase in T_g due to cross-linking, so that it can be viewed somewhat superficially to arise from the topological constraints introduced by the crystallites. This simple physical picture, however, is not entirely correct. Unlike a crosslink in an amorphous polymer, which can be viewed as a "point-like" network junction, a crystalline domain in a semicrystalline polymer can be very large, such domains can occupy a very large fraction of the total volume of the specimen, and they often transition into the amorphous phase gradually via "interphase" regions of significant thickness. It has, therefore, not yet proved to be possible to develop any simple and statistically significant general quantitative structure–property relationship for the

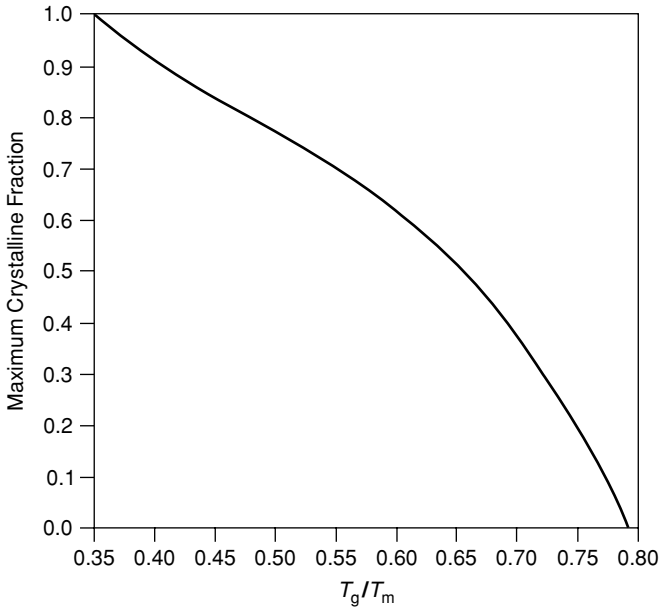

Fig. 9. Empirical relationship for maximum crystalline fraction under isothermal quiescent crystallization as a function of the ratio T_g/T_m, where the temperatures are in Kelvin.

effects of crystallinity on T_g, unlike equation (4) which works quite well in describing the effects of cross-linking.

b. While crystallinity influences T_g, T_g in turn influences the crystallization of a polymer when it is cooled down from the melt (38). The temperature at which the isothermal quiescent crystallization rate is at its maximum is roughly halfway between T_g and T_m. The maximum crystalline fraction increases with increasing T_m/T_g (with temperatures expressed in Kelvin) which can be viewed as an index for the driving force for crystallization, and thus decreases with increasing T_g/T_m as shown in Figure 9. A very important physical difference between T_g and T_m is worth noting in this context. They both depend strongly on chain stiffness and on cohesive energy density, *but* only T_m depends on how easily polymer chains can be packed into a periodic lattice. Otherwise, the T_m/T_g ratio and crystallizability would have been very similar for all polymers, instead of depending strongly on the smoothness and regularity of polymer chains.

(2) The effects of *orientation* via mechanical deformation on T_g have been reviewed (64). T_g increases in those amorphous regions of a semicrystalline polymer that are either attached to crystallites or so close to them that their chain segment mobilities are hindered because of the interference of the crystallites. On the other hand, orientation has little effect on T_g in amorphous regions far away from crystallites as well as in completely amorphous polymers.

Table 3. Glass-Transition Temperatures of Syndiotactic, Isotactic, and Atactic Polymers[a]

Polymer	T_g (syndiotactic), K	T_g (isotactic), K	T_g (atactic), K
Poly(methyl methacrylate)	433	316	378
Poly(ethyl methacrylate)	393	281	324
Poly(isopropyl methacrylate)	412	300	327
Poly(*n*-butyl methacrylate)	361	249	293
Poly(isobutyl methacrylate)	393	281	321
Poly(cyclohexyl methacrylate)	436	324	377
Poly(2-hydroxyethyl methacrylate)	377	308	359
Poly(methyl acrylate)	–	283	281
Poly(ethyl acrylate)	–	248	249
Poly(isopropyl acrylate)	270	262	267
Poly(*sec*-butyl acrylate)	–	250	251
Poly(cyclohexyl acrylate)	–	285	292
Poly(methyl α-chloroacrylate)	450	358	416
Poly(ethyl α-chloroacrylate)	393	310	366
Poly(isopropyl α-chloroacrylate)	409	341	363
Polystyrene	378	360	373
Poly(α-methyl styrene)	453	–	446
Polypropylene	269	255	267
Poly(*N*-vinyl carbazole)	549	399	423
Poly(vinyl chloride)	T_g increased with syndiotactic triad content (28–43%), and decreased with isotactic triad content (13–21%) showing lowest and highest values of 352 and 370 K, respectively, for a set of samples.		

[a]Data presented here are a part of literature data summarized in Ref. 1.

(3) *Conformational factors*. The most important conformational factor is the *tacticity* of vinyl-type polymers. A polymer such as poly(methyl methacrylate) can have quite different values of T_g, depending on whether it is isotactic, syndiotactic, or atactic. See Table 3 for a collection of literature data (1) on the effects of tacticity on T_g. A theoretical analysis of the effects of tacticity variations on T_g has been provided (52).

(4) The presence of *additives, fillers, unreacted residual monomers, and/or impurities*, whether deliberately included in the formulation of a resin, or left over as undesirable by-products of synthesis. For example, plasticizers of low molecular weight generally decrease T_g (1,19,31,66,67), as illustrated in Figure 10. On the other hand, under some conditions, T_g may increase when rigid nanoscale additives are incorporated into a polymer (64).

(5) *Thermal history*. The annealing (or "physical aging") of amorphous polymers at elevated temperatures below T_g usually increases T_g. This increase is larger for higher annealing temperatures, provided that the annealing temperature remains below T_g. It approaches an asymptotic limit as a function of time. For example, see Reference 68 for bisphenol A polycarbonate and Reference 64 for amorphous rigid poly(vinyl chloride).

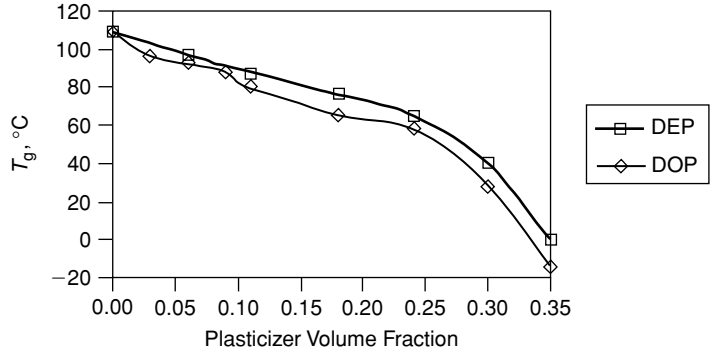

Fig. 10. Data illustrating typical effects of plasticization on T_g (67) for poly(methyl methacrylate) (obtained by polymerization of purified methyl methacrylate monomer), plasticized with diethyl phthalate (DEP) or dioctyl phthalate (DOP).

(6) *Thermal, thermooxidative, and/or photochemical degradation*. The onset of rapid degradation sometimes occurs in the temperature range of the glass transition, obscuring the distinction between the glass transition and degradation. For example, T_g values of 700 K or above, reported in the literature for some polymers with very stiff chains, are often not true T_g values, since degradation and softening take place simultaneously and inextricably.

(7) *Pressure* (P). T_g is usually measured under normal atmospheric pressure. The effect of P on T_g is rarely considered, although it may become important in processing polymers under high hydrostatic pressure. Increasing P increases T_g (19,63,64,69,70). The observed rate of change of T_g with increasing P (the derivative dT_g/dP) seems to be of the same order of magnitude for many polymers. The following examples from a tabulation of literature data (64) illustrate the typical magnitude of this effect: T_g went from (a) 100°C at atmospheric pressure (P_{atm}) to 182°C for polystyrene at P=200 MPa, (b) 103°C at P_{atm} to 121°C at P=100 MPa for poly(methyl methacrylate), (c) 75°C for poly(vinyl chloride) at P_{atm} to 89°C at P=100 MPa, and (d) 31.5°C at P_{atm} to 48.5°C at P=80 MPa for poly(vinyl acetate).

(8) *Specimen size effects*.

a. Sometimes, as in many electronics and lubrication applications, very thin polymeric films are used. The T_g values of such films can differ significantly from the bulk values for the same polymers (71–76). It was shown that T_g decreases with decreasing thickness for thin free-standing polystyrene films (71). T_g also decreases with decreasing thickness for polymers that have no specific interactions with the substrate on which they have been placed (72), as shown in Figure 11. By contrast, if strong attractive specific interactions between the polymer and the substrate restrict the mobility in the interfacial region, the behavior becomes very different and T_g may increase with decreasing thickness (73,74).

b. The surface of a polymeric specimen may behave differently from the bulk in its glass-transition behavior. For example (75), the surface T_g of a monodisperse polystyrene film was observed to be lower than the

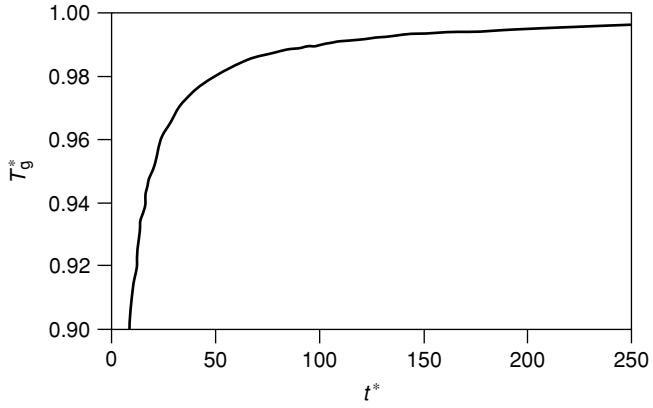

Fig. 11. "Master curve" for thickness (t) dependence of T_g of thin films of polymers that have no specific interactions with the substrate (72). The equation for the curve is $T_g* = t*/(1+t*)$; where $T_g* = T_g(t)/T_g(\text{bulk})$, T_g is in Kelvin, $t* = t/L$, and L is the statistical chain (Kuhn) segment length. By contrast, if strong specific interactions between the polymer and the substrate result in restricted interfacial region mobility, the behavior becomes very different from what is shown below and T_g may instead increase with decreasing thickness.

bulk T_g. This result was interpreted in terms of an increase in the free volume near the surface region, being induced by the preferential surface localization of chain end groups.

c. Finite specimen size, resulting from confinement within small spaces, can also affect T_g significantly. For example, it has been observed that the T_g of two glass-forming organic liquids decreased (but not as much as the decrease of T_m) when the confining controlled pore glass diameter decreased over the range of 73–4 nm (77,78).

(9) *Incorporation of ionic charges*. An ionic polymer (sometimes referred to as an "ionomer") contains both covalent and ionic bonds in its chain or network structure (79,80). Examples include metal salts of poly(acrylic acid), poly(styrene-*co*-methacrylic acid), and sulfonated polystyrene. The effect of ionic bonds on T_g somewhat resembles the effect of covalent cross-links for organic polymers, as T_g generally increases with ion concentration. However, ionic bonding is more complex than covalent cross-linking, because of the possible effects of (*1*) ionic valency, (*2*) chain stiffening induced by incorporating ionic charges along the chain backbone, (*3*) ionic aggregation, and (*4*) thermal lability of "ionic cross-links."

This long list of factors affecting T_g demonstrates that many factors not related either to the composition or to the structure of a polymer can significantly affect T_g. Some internal inconsistency, and the need to exercise judgment and to make choices, is therefore inherent in preparing any data set collected from different sources for use in developing or validating any correlative or predictive scheme for T_g. In the best of all possible worlds, one would synthesize all of the polymers which will be used in the dataset, characterize them very carefully, and

then measure their T_g's under identical test conditions. For practical reasons, however, the use of data from many different sources in examining the trends in T_g is often unavoidable.

A review article (81) provides further insights into the many factors determining T_g.

BIBLIOGRAPHY

"Glass Transition" in *EPST* 1st ed., Vol. 7 p. 461; "Glass Transition" in *EPSE* 2nd ed., Vol. 7, pp. 531–544, by R. J. Roe, University of Cincinnati.

1. J. Bicerano, *Prediction of Polymer Properties*, 2nd ed., Marcel Dekker, Inc., New York, 1996.
2. D. J. Meier, ed., *Molecular Basis of Transitions and Relaxations*, Gordon and Breach Science Publishers, London, 1978.
3. M. T. Takemori, *Polym. Eng. Sci.* **19**, 1104–1109 (1979).
4. S. Krause, in D. R. Paul and S. Newman, eds., *Polymer Blends*, Vol. **1**, Academic Press, New York, 1978, pp. 15–112.
5. G. Holden, N. R. Legge, R. P. Quirk, and H. E. Schroeder, eds., *Thermoplastic Elastomers*, 2nd ed., Hanser Publishers, Munich, 1996.
6. B. K. Kim, S. Y. Lee, and M. Xu, *Polymer* **37**, 5781–5793 (1996).
7. S. Hayashi, in K. Inoue, S. I. Y. Shen, and M. Taya, eds. *US–Japan Workshop on Smart Materials and Structures*, The Minerals, Metals and Materials Society, Warrendale, Pa., 1997, pp. 29–38.
8. V. A. Bershtein and V. M. Yegorov, *Polym. Sci. USSR* **27**, 2743–2757 (1985).
9. V. A. Bershtein, V. M. Yegorov, and Yu. A. Yemel'yanov, *Polym. Sci. USSR* **27**, 2757–2764 (1985).
10. P. J. Flory, *The Principles of Polymer Chemistry*, Cornell University Press, Ithaca, N.Y., 1953.
11. P. J. Flory, *Statistical Mechanics of Chain Molecules*, Wiley-Interscience, New York, 1969.
12. R. Zallen, *The Physics of Amorphous Solids*, John Wiley & Sons, Inc., New York, 1983.
13. J. Bicerano and D. Adler, *Pure Appl. Chem.* **59**, 101–144 (1987).
14. J. H. Gibbs and E. A. DiMarzio, *J. Chem. Phys.* **28**, 373–383 (1958).
15. E. A. DiMarzio and J. H. Gibbs, *J. Chem. Phys.* **28**, 807–813 (1958).
16. G. Adam and J. H. Gibbs, *J. Chem. Phys.* **43**, 139–146 (1965).
17. R. P. Kusy and A. R. Greenberg, *Polymer* **23**, 36–38 (1982).
18. A. R. Greenberg and R. P. Kusy, *Polymer* **24**, 513–518 (1983).
19. P. R. Couchman, *Polym. Eng. Sci.* **24**, 135–143 (1984).
20. M. Goldstein, *Ann. N.Y. Acad. Sci.* **279**, 68–77 (1976).
21. M. Goldstein, *J. Chem. Phys.* **64**, 4767–4774 (1976).
22. G. P. Johari, in B. Escaig and C. G. Sell, eds., *Plastic Deformation of Amorphous and Semicrystalline Materials*, "Les Houches Lectures, Les Editions de Physique", 1982, pp. 109–141.
23. M. H. Cohen and G. S. Grest, *Phys. Rev. B* **20**, 1077–1098 (1979).
24. G. S. Grest and M. H. Cohen, *Adv. Chem. Phys.* **48**, 455–525 (1981).
25. H. Stutz, K.-H. Illers, and J. Mertes, *J. Polym. Sci., Polym. Phys. Ed.* **28**, 1483–1498 (1990).
26. C. A. Angell, *J. Non-Cryst. Solids* **131–133**, 13–31 (1991).
27. C. A. Angell, *Science* **267**, 1924–1935 (1995).
28. C. A. Angell, *ACS Symp. Ser.* **710**, 37–52 (1998).

29. H. Sillescu, *J. Non-Cryst. Solids* **243**, 81–108 (1999).
30. G. B. McKenna and S. C. Glotzer, eds., *J. Research National Institute of Standards and Technology* **102**(2 Special Issue: 40 Years of Entropy and the Glass Transition) (Mar.–Apr. 1997).
31. D. W. van Krevelen, *Properties of Polymers*, 3rd ed., Elsevier, Amsterdam, 1990.
32. C. J. Lee, *J. Macromol. Sci., C: Rev. Macromol. Chem. Phys.* **29**, 431–560 (1989).
33. A. A. Askadskii and G. L. Slonimskii, *Polym. Sci. USSR* **13**, 2158–2160 (1971).
34. A. A. Askadskii, *Physical Properties of Polymers: Prediction and Control*, Gordon and Breach, New York, 1996.
35. D. R. Wiff, M. S. Altieri, and I. J. Goldfarb, *J. Polym. Sci., Polym. Phys. Ed.* **23**, 1165–1176 (1985).
36. A. J. Hopfinger and co-workers, *J. Polym. Sci. Polym. Phys. Ed.* **26**, 2007–2028 (1988).
37. T. G. Fox and P. J. Flory, *J. Appl. Phys.* **21**, 581–591 (1950).
38. J. Bicerano, *J. Macromol. Sci., C: Rev. Macromol. Chem. Phys.* **38**, 391–479 (1998).
39. J. Bicerano and co-workers, *J. Polym. Sci., Polym. Phys. Ed.* **34**, 2247–2259 (1996).
40. T. G. Fox and S. Loshaek, *J. Polym. Sci.* **15**, 371–390 (1955).
41. S. Loshaek, *J. Polym. Sci.* **15**, 391–404 (1955).
42. D. Porter, *Group Interaction Modelling of Polymer Properties*, Marcel Dekker, Inc., New York, 1995.
43. B. G. Sumpter and D. W. Noid, *Macromol. Theory Simul.* **3**, 363–378 (1994).
44. C. W. Ulmer II and co-workers, *Comput. Theor. Polym. Sci.* **8**, 311–321 (1998).
45. E. R. Collantes and co-workers, *Antec '97 Preprints* 2245–2248 (1997).
46. D. Rogers and A. J. Hopfinger, *J. Chem. Inf. Comput. Sci.* **34**, 854–866 (1994).
47. A. R. Katritzky and co-workers, *J. Chem. Inf. Comput. Sci.* **38**, 300–304 (1998).
48. P. Camelio and co-workers, *J. Polym. Sci., Polym. Chem. Ed.* **35**, 2579–2590 (1997).
49. P. Camelio and co-workers, *Macromolecules* **31**, 2305–2311 (1998).
50. T. T. M. Tan and B. M. Rode, *Macromol. Theory Simul.* **5**, 467–475 (1996).
51. D. Boudouris, L. Constantinou, and C. Panayiotou, *Fluid Phase Equilib.* **167**, 1–19 (2000).
52. H. Suzuki, N. Kimura, and Y. Nishio, *J. Therm. Anal.* **46**, 1011–1020 (1996).
53. H. A. Schneider, *J. Therm. Anal. Calorim.* **56**, 983–989 (1999).
54. J. M. G. Cowie and V. Arrighi, *Plast. Eng. (N.Y.)* **52** (Polymer Blends and Alloys) 81–124 (1999).
55. R. A. Wessling and co-workers, *Appl. Polym. Symp.* **24**, 83–105 (1974).
56. R. Vaidyanathan and M. El-Halwagi, *Ind. Eng. Chem. Res.* **35**, 627–634 (1996).
57. C. D. Maranas, *Ind. Eng. Chem. Res.* **35**, 3403–3414 (1996).
58. C. D. Maranas, *AIChE J.* **43**, 1250–1264 (1997).
59. R. H. Boyd, *Trends Polym. Sci.* **4**, 12–17 (1996).
60. K. Binder, *Comput. Phys. Commun.* **121/122**, 168–175 (1999).
61. K. Fukui and co-workers, *Macromol. Theory Simul.* **8**, 38–45 (1999).
62. D. M. Colucci and co-workers, *J. Polym. Sci, Polym. Phys. Ed.* **35**, 1561–1573 (1997).
63. L. Yang, D. J. Srolovitz and A. F. Yee, *J. Chem. Phys.* **110**, 7058–7069 (1999).
64. S. M. Aharoni, *Polymers for Advanced Technologies* **9**, 169–201 (1998).
65. T. Alfrey Jr. and R. F. Boyer, in Ref. 2, pp. 193–202.
66. J. K. Sears and J. R. Darby, *The Technology of Plasticizers*, John Wiley & Sons, Inc., New York, 1982.
67. S. Kalachandra and D. T. Turner, *J. Polym. Sci., Polym. Phys. Ed.* **25**, 1971–1979 (1987).
68. K. Neki and P. H. Geil, *J. Macromol. Sci., B: Phys.* **8**, 295–341 (1973).
69. R. W. Warfield and B. Hartmann, *Polymer* **23**, 1835–1837 (1982).
70. S. Saeki and co-workers, *Polymer* **33**, 577–584 (1992).
71. J. R. Dutcher, K. Dalnoki-Veress, and J. A. Forrest, *ACS Symp. Ser.* **736**, 127–139 (1999).

72. J. H. Kim, J. Jang, and W.-C. Zin, *Langmuir* **16**, 4064–4067 (2000).
73. J. L. Keddie, R. A. L. Jones, and R. A. Cory, *Faraday Discuss.* **98**, 219–230 (1994).
74. W. E. Wallace, J. H. van Zanten, and W. L. Wu, *Phys. Rev. E* **52**, R3329–R3332 (1995).
75. T. Kajiyama and co-workers, *Macromol. Symp.* **143**, 171–183 (1999).
76. J. Ral, *Curr. Opin. Colloid Interface Sci.* **4**, 153–158 (1999).
77. C. L. Jackson and G. B. McKenna, *J. Non-Cryst. Solids* **131–133**, 221–224 (1991).
78. C. L. Jackson and G. B. McKenna, *Chem. Mater.* **8**, 2128–2137 (1996).
79. L. Holliday, in L. Holliday, ed., *Ionic Polymers*, John Wiley & Sons, Inc., New York, 1975, pp. 1–68. The glass transition in ionic polymers is discussed on pages 35–46.
80. C. W. Lantman, W. J. MacKnight, and R. D. Lundberg, *Annu. Rev. Mater. Sci.* **19**, 295–317 (1989).
81. D. J. Plazek and K. L. Ngai, in J. E. Mark, ed., *Physical Properties of Polymers Handbook*, American Institute of Physics, Woodbury, N.Y., 1996, pp. 139–159.

JOZEF BICERANO
The Dow Chemical Company

HARDNESS

Introduction

Hardness H defines the resistance to local deformation of a material when indented, drilled, sawed, or abraded. It involves a complex combination of properties (elastic modulus, yield strength, strain-hardening capacity). The prevailing deformation mechanism depends upon the material and the type of tester. Hardness is either measured by (*1*) static penetration of the specimen with a standard indenter at a known force, (*2*) dynamic rebound of a standard indenter of known mass dropped from a standard height, or (*3*) scratching with a standard pointed tool under a load. The hardness tester, indenter shape, and force employed strongly influence the hardness numbers (1).

Hardness is used in identification, classification, and quality control. Hardness tests provide a rapid evaluation of variations in mechanical properties affected by changes in chemical or processing conditions, heat treatment, microstructure, and aging. Since the hardness test usually produces an insignificant permanent change in the specimen, it is considered to be a nondestructive test.

The methods commonly used in determining the *hardness* of polymers are static indentation methods. Here, the indenter penetrates the test specimen at normal incidence under the application of a known force. Typical forces range from 10^{-2} to 1 kN, leading to indentation widths of a few millimeters. The hardness is determined from the optical imaging of the residual width of indentation. Pyramidal indenters are preferred because the contact pressure is independent of the load applied and the indentation is less affected by elastic release than other indenters (1).

The *microhardness* technique is used when the specimen size is small or when a spatial map of the mechanical properties of the material within the

Encyclopedia of Polymer Science and Technology. Copyright John Wiley & Sons, Inc. All rights reserved.

micron range is required. Forces of 0.05–2 N are usually applied, yielding indentation depths in the micron range. While microhardness determined from the residual indentation is associated with the permanent plastic deformation induced in the material (see section on Basic Aspects of Indentation), microindentation testing can also provide information about the elastic properties. Indeed, the hardness to Young's modulus ratio H/E has been shown to be directly proportional to the relative depth recovery of the impression in ceramics and metals (2). Moreover, a correlation between the impression dimensions of a rhombus-based pyramidal indentation and the H/E ratio has been found for a wide variety of isotropic polymeric materials (3). In oriented polymers, the extent of elastic recovery of the imprint along the fiber axis has been correlated to Young's modulus values (4).

More recently, *ultramicrohardness* and *nanohardness* testers have been developed with the purpose to mechanically characterize near surfaces and thin films (5). Continuous load–displacement monitoring, as the indenter is driven into and withdrawn from the film, substitutes the imaging method used in conventional static indentation methods. Smaller loads can be applied ($10^{-1} - 2 \times 10^3$ mN) so that a minimum residual depth of several tens of nanometers can be achieved at best. The advantage of continuous depth-sensing recording entails a high level of precision due to automatic registering of data, thus, avoiding the error in determining the indentation size. In addition, each test gives a complete loading/unloading data cycle, rather than just a simple reading. This approach enables hardness, elastic modulus, yield strength, and the energy used during loading and unloading to be determined. In addition, the H/E ratio derived from continuous depth-sensing recording can be shown to be directly proportional to the ratio between the elastic and plastic components of indentation at peak load (6).

During the last two decades, studies of the hardness properties of polymers have evolved from topics of applied significance to fundamental studies aiming at acquiring an understanding of the structure–property relationship of polymer materials including glassy and semicrystalline polymers and copolymers, as well as polymer blends and composites (4,7,8). Figure 1 illustrates the hardness of polymer materials as compared with typical values for metals and alloys.

Basic Aspects of Indentation

Figure 2 shows the contact geometry for a pyramid indenter at zero load, at maximum load, and after unloading. The material under the indenter consists of a zone of plastic deformation (a few times the penetration depth distance) surrounded by a larger outer zone of elastic deformation. Several effects can be distinguished during the indentation process:

(1) An instant elastic recovery of the indentation depth upon load release. The loss of contact with the indenter allows for a change in the shape of the indentation.
(2) A permanent plastic deformation. Hardness is related to the irreversible deformation, measured from the diagonal of the residual impression, d.
(3) A time-dependent contribution during loading. The plastic deformation in polymers is known to be influenced by the time at which the load is held

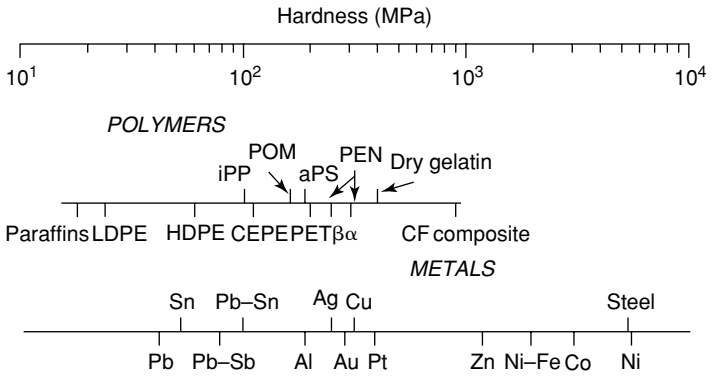

Fig. 1. Typical microhardness values of polymers compared with data for metals. LDPE, low density polyethylene; HDPE, high density polyethylene; iPP, isotactic polypropylene; CEPE, chain-extended polyethylene; POM, polyoxymethylene; aPS, atactic polystyrene; PET, poly(ethylene terephthalate); PEN, poly(ethylene naphthalene-2,6-dicarboxylate); CF composite, carbon-fiber composite. Hardness data of metals and alloys markedly depend on composition, degree of work-hardening, processing conditions, etc. For this reason, the values in Figure 1 should be considered as typical values rather than as absolute values. Most of the data for metals are taken from Ref. 1.

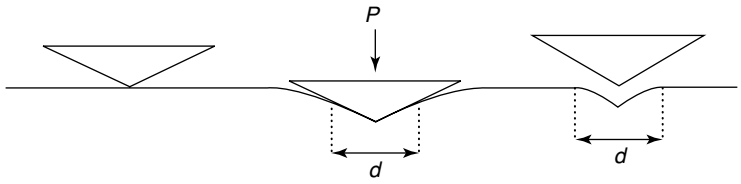

Fig. 2. Schematic illustration of the contact geometry of a pyramid indenter during a static indentation test at zero load, under load, and after load release.

(creep effect). To minimize the creep effect, indentation times of a few seconds are usually employed (4).

(4) A long delayed elastic recovery (*viscoelasticity*). The residual indentation should be measured immediately after load release in order to minimize the viscoelastic recovery of the material.

Microhardness of Polymer Glasses

The microhardness of glassy polymers decreases with increasing temperature because of thermal expansion (9). At the glass-transition temperature T_g, the onset of liquid-like motions takes place. The motions of long segments above T_g require more free volume and lead to a fast decrease of microhardness with temperature. The microhardness of several glassy polymers, measured at room temperature, has been shown to be directly proportional to its glass-transition temperature (10).

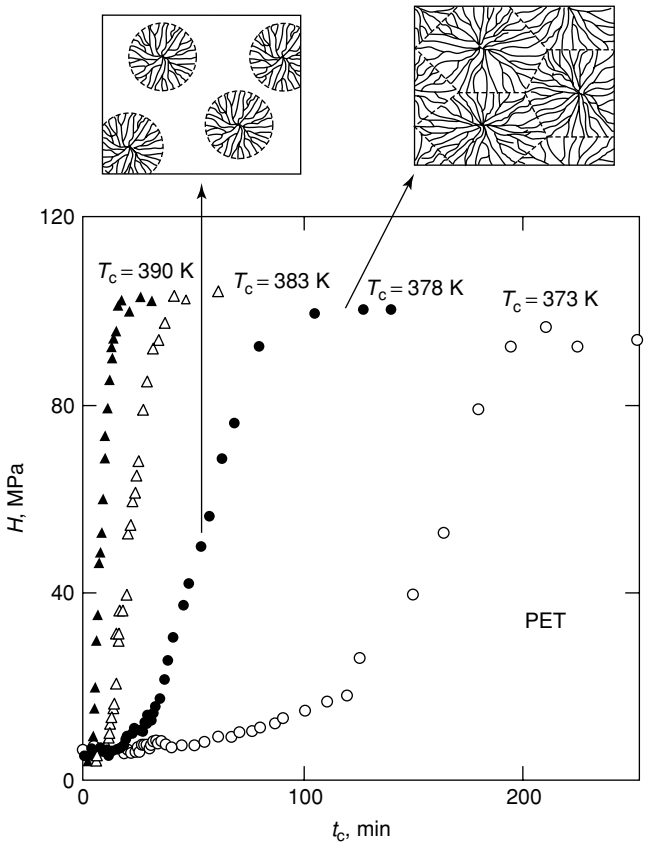

Fig. 3. Variation of microhardness for PET with crystallization time t_c for different crystallization temperatures T_c.

Structure Development: The Role of Crystallinity

Hardness has been shown to be a useful technique to detect the structural changes occurring during crystallization (11,12). Figure 3 shows the hardness variation in the course of isothermal crystallization of poly(ethylene terephthalate) (PET) at various crystallization temperatures T_c. A sigmoidal rapid hardness increase with increasing time t_c is followed by a slower hardness increase. The comparatively rapid H increase, during primary crystallization, is connected with the growth of polycrystalline aggregates (spherulites) until they impinge on each other, finally filling up the sample completely. The much slower hardening process is denoted as secondary crystallization and is related with crystal thickening and formation of new crystals. For samples crystallized from the glassy state where spherulitic growth is incomplete, H can be described as follows (12):

$$H = H_{\text{sph}}\Phi + H_a(1 - \Phi) \tag{1}$$

Here, H_{sph} is the hardness value of the spherulites, H_a is the hardness of the amorphous interspherulitic regions, and Φ is the volume fraction of

crystallized spherulites. During primary crystallization, H_{sph} remains constant and hardness is directly proportional to the volume occupied by the spherulites (12). The hardness variation in the course of isothermal crystallization of PET and poly(ethylene naphthalene-2,6-dicarboxylate) (PEN) has been shown to follow Avrami law (13,14).

For samples in which spherulitic growth is complete ($\Phi = 1$), $H = H_{sph}$ and the hardness of the material can be accounted for using (7)

$$H = H_c\alpha + H_a(1-\alpha) \tag{2}$$

Here, H_c is the hardness of the crystalline lamellae within the stacks, H_a is the hardness of the amorphous intraspherulitic material, and α is the fraction of crystalline material within the spherulites. Equation (2) is consistent with a parallel model of crystalline and amorphous regions, which has been proved to be successful in a wide variety of polymeric materials (7).

Microhardness Dependence on Nanostructure

Equation (2) suggests that the volume fraction of crystalline material controls the microhardness value of a polymer. However, it was soon recognized the large influence of the crystalline lamellar thickness l_c upon microhardness in case of chain-folded and chain-extended polyethylene (PE) (4). Based on a thermodynamic approach, the dependence of hardness on the average crystal thickness was derived (15):

$$H_c = \frac{H_c^{\infty}}{1} + (b/l_c) \tag{3}$$

Here, H_c^{∞} is the hardness of an infinitely thick crystal and b is a parameter related to the surface free energy of the crystal, σ_e, and to the energy required for plastic deformation of the crystal blocks, $\Delta h (b = 2\sigma_e/\Delta h)$.

Figure 4 shows the plot of H_c^{-1} (derived using eq. (2)) versus l_c data for poly(ethylene oxide) (PEO), crystallized at various temperatures (M_n=13,000), and chain-folded PE, annealed at 130°C for different annealing times (M_n=11,700). Using equation (3), the plot of H_c^{-1} versus l_c^{-1} yields an ordinate intercept $(H_c^{\infty})^{-1}$ and a slope b/H_c^{∞}. Values of $H_c^{\infty} = 150$ MPa and $H_c^{\infty} =$ 170 MPa are derived for PEO and PE respectively. The H_c^{∞} value for PET, PEN, poly(butylene terephthalate) (PBT), and isotactic poly(propylene) (iPP) crystals has also been reported (16–19).

It is to be noted that H_c^{∞} is intimately related to the packing of the chains in the crystals (4). Since the crystal hardness reflects the response of the intermolecular forces holding the chains within the lattice, it has been shown that the microhardness technique permits to distinguish between polymorphic modifications of the same polymer (20,21). Indeed, the study of the transition from the α to the β form in iPP confirmed that changes in H were directly related to the different crystal hardness values of each phase (20). More recently, the microhardness technique has been successfully applied to follow the reversible strain-induced polymorphic α–β transition occurring on PBT (21).

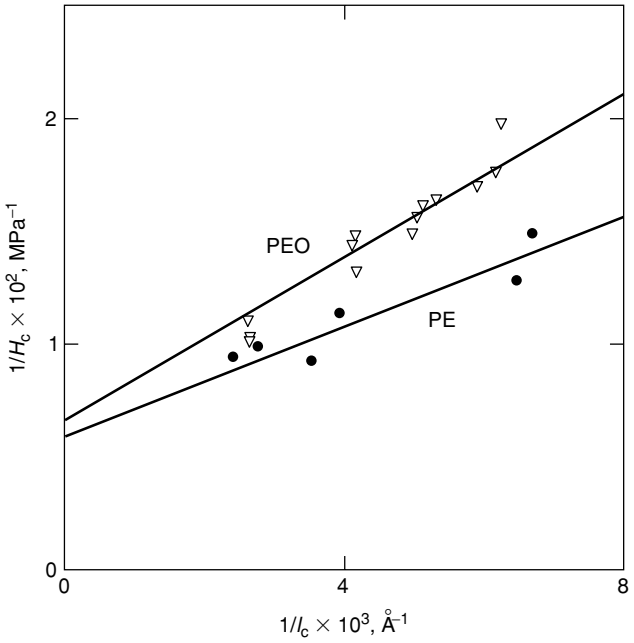

Fig. 4. Plot of reciprocal crystal hardness H_c^{-1} as a function of reciprocal crystal thickness l_c^{-1} for PEO (▽) and PE (●).

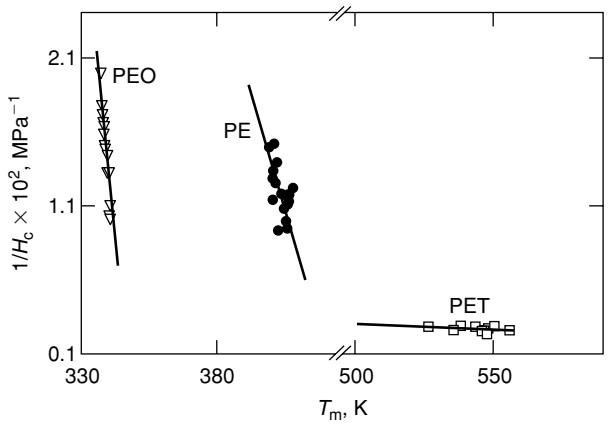

Fig. 5. Variation of H_c^{-1} with T_m for different polymeric materials: PEO (▽), PE (●), and PET (□).

Microhardness Correlation to Thermal Properties

While the hardness depression due to finite thickness lamellae is given by equation (3), Thomson–Gibbs equation accounts for the melting point depression of a crystal of thickness l_c with respect to the equilibrium melting point T_m^0 (22). It has been shown that by combination of Thomson–Gibbs equation and equation (3), the reciprocal value of the crystal hardness is directly proportional to the melting

temperature of the crystals, as seen in Figure 5, for PEO, PE, and PET. The three series of H_c^{-1} versus T_m data fit into a straight line. From these linear regressions, one can derive the T_m^0 values for each polymer, provided H_c^∞ is known or vice versa.

Creep Behavior

An important aspect concerning the indentation mechanism in polymers is the time-dependent part of the plastic deformation. Several studies on polymeric materials have shown that hardness decreases with indentation time, following a function of the form (4,23)

$$H = H_1 \Delta t^{-k} \tag{4}$$

Here, H_1 is the hardness at a given reference time $\Delta t = 1$ and k is the so-called creep constant. The creep constant is a measure of the rate at which the material flows under the indenter and can be derived from the slope of a log H versus log Δt plot. Data near $\Delta t = 0.1$ min are usually adopted as the hardness value for polymers (4). Recent research evidences the strong influence of temperature upon the k values (23). At room temperature, the k- parameter has been shown to primarily depend on l_c (23).

Correlation of Microhardness to Macroscopic Mechanical Properties

According to the classical theory of plasticity, indentation hardness for a Vickers indenter is approximately equal to three times the yield stress measured in frictionless compression, Y_c (1). However, recent data evidence that the theory fails when dealing with polymers (24). Indeed, hardness-to-compressive yield stress ratios of $H/Y_c \approx 2$ have been found for various chain-folded and chain-extended PE samples due to the nonnegligible elastic strains of the indented material (24). On the other hand, hardness-to-tensile yield stress ratios of $H/Y_t \approx 3$ have been obtained on a wide variety of PE samples, provided the strain rate of the tensile test is comparable to that employed in the hardness test (24,25).

As pointed out in the Introduction, the hardness to Young's modulus ratio may be derived from the extent of elastic recovery in the depth of a Vickers indent (2). H/E values of different polymers have also been found to be linearly related to the ratio of the lengths of the short and long diagonals of a Knoop imprint (3). The correlation between microhardness and Young's modulus has been explored on various PE samples of different morphology (24,26). It has been shown that an H-increase parallels a rise in the Young's modulus values derived from tensile testing (24,26). Furthermore, the H/E_c ratio (E_c is the Young's modulus value determined from compression testing) was shown to be the lowest for highly crystalline samples such as chain-extended PE, in agreement with an enhanced plastic behavior (24).

Microhardness of Blends

Hardness is a promising technique for the structural investigation of multicomponent blends. The hardness technique can provide information on the degree of

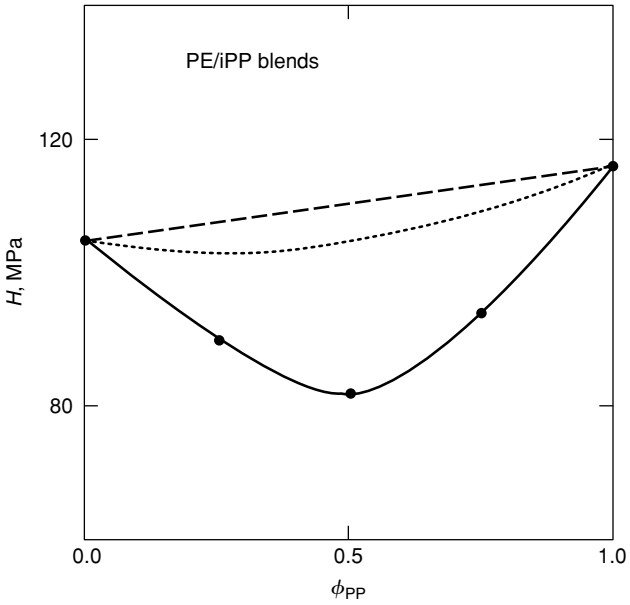

Fig. 6. Plot of microhardness of PE/iPP blended gel films as a function of the weight concentration of iPP. The dashed line follows equation (5), using the hardness values of the individual homopolymers. The dotted line is derived from the crystallinity values for each component within the blend.

interpenetration of the blend component. The case of blends of low density (LD) and high density (HD) PE is an example where the microhardness can be very well described in terms of an additive (parallel) system of two independent components, H_1 (LD) and H_2 (HD) (27):

$$H_{\text{blend}} = H_1\phi + H_2(1-\phi) \tag{5}$$

where ϕ is the fraction of LDPE component. Equation (5) emphasizes the existence of distinct H values for the two phases owing to a molecular segregation at a crystal level.

In other systems, such as in iPP/EPR, PE/iPP, and iPP/polyamide (PA) blends, a deviation from the additivity law given by equation (5) is detected (19,28,29). Figure 6 illustrates, as an example, the obtained deviation of H from the additivity law (dashed line) for PE/iPP blends, ϕ being in this case the weight fraction of polypropylene. If one takes into account the measured crystallinity values for the H_1 and H_2 components within the blends, and the H_c values of the homopolymers, then equation (5) leads to the dotted line in Figure 6. Still, the experimental data are clearly deviated from the predictions of equation (5). The low experimental H values found for the PE/iPP blends are due to a depression in the H_c^{PE} and H_c^{PP} values as a consequence of an increase in the surface free energy of the crystals (see eq. (3)) (28).

The use of the microhardness technique in blends of condensation polymers [PET/PEN and PET/polycarbonate (PC)] evidences the formation of copolymer sequences within the blends (30).

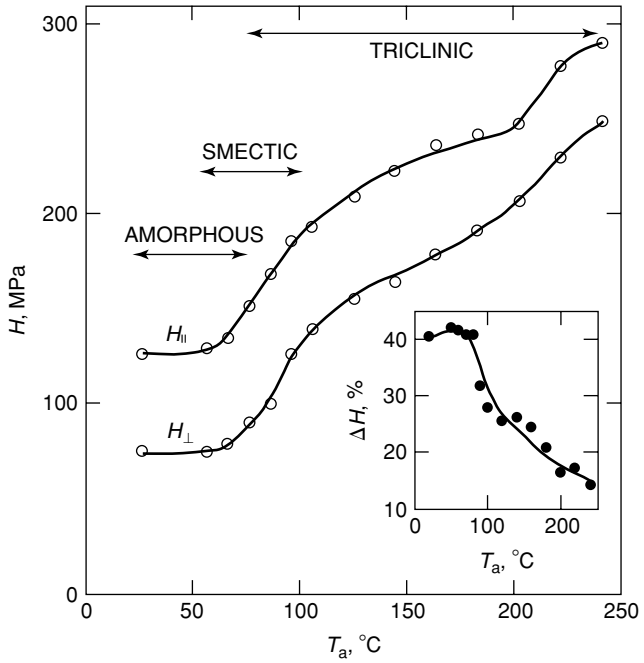

Fig. 7. Plots of $H_{\parallel}$ and $H_{\perp}$ as a function of annealing temperature for cold-drawn PET. The inlet illustrates the plot of indentation anisotropy ΔH vs T_a for the same material.

Indentation Anisotropy of Oriented Polymers

Uniaxial mechanical deformation produces a conspicuous anisotropic shape of the residual indentation (4). The anisotropy depends on the orientation of the diagonals of indentation relative to the axial direction. Two well-defined hardness values emerge. One value (maximum for a Vickers indenter) can be derived from the indentation diagonal parallel to the fiber axis, $d_{\parallel}$. The second one (minimum) is deduced from the diagonal perpendicular to it, $d_{\perp}$. The former value responds to an instant elastic recovery of the fibrous network in the draw direction. The latter value defines the plastic component of the oriented material. It is useful to define the indentation anisotropy as $\Delta H = 1 - (d_{\parallel}/d_{\perp})$.

A ΔH increase with increasing draw ratio λ has been found for solid-state extruded and highly drawn polymers, and a correlation between indentation anisotropy and Young's modulus has been found (4,31). Indentation anisotropy values of several carbon-fiber composites have been reported (32). Recently, the indentation anisotropy of cold-drawn PET, annealed at different temperatures, has also been examined (33).

Figure 7 illustrates the $H_{\parallel}$ and $H_{\perp}$ values as a function of annealing temperature T_a for cold-drawn PET. The $H_{\perp}$ increase with rising T_a reveals firstly, the gradual appearance of smectic domains (apparent at $T_a = 50^{\circ}C$) and secondly, the developing of a triclinic structure for $T_a \geq 80^{\circ}C$. The insert of Figure 7 shows the rapid decrease of ΔH with increasing T_a above 70°C. This result suggests that a molecular relaxation mechanism in the amorphous layers takes place above T_g

($T_g \approx 70^\circ$C), leading to a decrease in the elastic response of the fibrils to indentation along the chain direction.

Test Methods

Scratch Hardness Tests. The method is based on the ability of one solid to scratch another. A corner of a diamond cube is drawn across the sample surface under a force of 29.4 mN applied to the body diagonal of the cube; this creates a V-shaped groove of width λ, which is measured microscopically (34). The hardness is given by

$$\mathrm{HS} = \frac{10{,}000}{\lambda^2} \tag{6}$$

The constant 10,000 is arbitrary and λ is in μm.

Dynamic Rebound Test: Scleroscope. In this test, the rebound of a diamond-tipped weight dropped from a fixed height is measured (34). There are two models of the instrument: Model C (HSc) uses a hammer of small mass ($\approx$2.3 g) and a large height of fall ($\approx$251 mm); Model D (HSd) uses a hammer of about 36 g and a short fall ($\approx$18 mm).

Indentation Depth Reading: Rockwell Test. In this test, the depth of the indentation is read from a dial indicator; no microscope is required (34). In the Rockwell hardness tests, a load of 98 N is first applied to the surface and the depth of penetration is thereafter reckoned as the zero of measurement. A further load of 588, 980, or 1470 N is applied and removed leaving the additional depth of indentation recorded on a dial. The hardness is then expressed in terms of the dial reading on an arbitrarily numbered scale. The indenter used may be a steel spherical penetrator or a diamond cone with a hemispherical tip. The scales, indenter, and loads employed are chosen to adapt to the material properties. Results given by different testers are not readily interconverted.

Tests Based on the Optical Imaging of Indentation. Hardened steel, tungsten carbide, or diamond indenters are usually employed. Hardness values are determined from the load and the measurement of the residual indentation after load removal (1). The spacing between indents must be large enough (typically twice the width of the indentation) to be unaffected by deformation resulting from nearby indents. The sample thickness must be 10 or 1.5 times thicker than the width of the residual impression for spherical or pyramidal indenters, respectively. A microscope equipped with a micrometer eyepiece is used to measure the diameter of the impression up to 0.5 μm at most. The surface of the specimen must be flat, smooth, free of dirt, and unlubricated.

Brinell. In the Brinell test, a hardened steel ball is forced into the specimen. The standard test uses a 10-mm ball and a force of 29.42 kN (34). The Brinell hardness HB is equal to the applied force divided by the area of the indentation:

$$\mathrm{HB} = \frac{2P}{\pi D\left[1 - \sqrt{(1 - d/D)^2}\right]} \tag{7}$$

in which P is the force in N, D is the diameter of the ball in mm, and d is the diameter of the impression in mm. The minimum radius of a curved specimen surface is $2.5D$. Published tables simplify the conversion from the hardness values obtained with one standard load to the other (34).

Pyramid Indenters. The most common pyramid indenters are the *Vickers, Knoop*, and *Berkovich* indenters. The Vickers indenter consists of a square-based diamond pyramid with included angles (α) of 136° between nonadjacent faces. The Knoop test uses a rhombic-based diamond with included angles of 172° and 130° between opposite edges. The Berkovich indenter is a diamond trigonal pyramid whose facets form an angle of 65.3° with respect to the normal to the base.

Hardness value is calculated by dividing the load P by the facet or projected area of indentation, A:

$$H = \frac{P}{A} = C\frac{P}{d^2} \tag{8}$$

Here d is the average of both diagonal lengths, the length of the long diagonal or the height of the triangular impression for the Vickers, Knoop, and Berkovich indenters respectively. Hardness values in equation (8) are given in MPa if the force is in N and d in mm. C is a geometric constant whose value depends on the indenter shape and whether the projected area or the facet contact area of indentation is being used to calculate the hardness number. For a Vickers indenter, the facet area is most commonly used ($C = 1.854$). Knoop and Berkovich microhardness values are traditionally derived using the projected area of indentation ($C =$ 14.23 and 1.766 respectively).

The Vickers indenter penetrates the surface about twice as far as the Knoop indenter for a given load. The latter is very sensitive to material anisotropy because of the twofold symmetry of the indentation. The Berkovich indenter is preferred to the four-side pyramids when extremely small indentations are produced.

The indenter geometry is known to influence hardness values in polymers as well as in metals, ceramics, and glassy materials. For conical, spherical, and triangle-based pyramid indenters, hardness values are known to increase with decreasing included angle at the indenter tip (decreasing radius of the spheres) (1,35,36). This seems to be due to the detailed processes involved in the plastic flow around the indenter, together with a higher interface friction effect as the indenter included angle decreases (1,35). For the standard Brinell, Vickers, and Berkovich tests, a number of papers report on the correlation between the different hardness scales (1,37–39). Brinell and Vickers hardness values are almost identical up to a Brinell hardness of about 3 GPa (1). A few papers also show a good agreement between Vickers and Berkovich hardness numbers (37,38). Finally, a fairly good correspondence is also found for Knoop and Vickers hardness values (1,38,39) although significant deviations have also been reported (40).

Continuous Load–Depth Recording. In ultramicroindentation and nanoindentation devices the displacement and load are monitored continuously. It should be possible to vary the applied load, or imposed displacement, either in ramp mode or with a discontinuous increment (step mode) (41). Figure 8 illustrates a loading–hold–unloading cycle obtained for PET using an

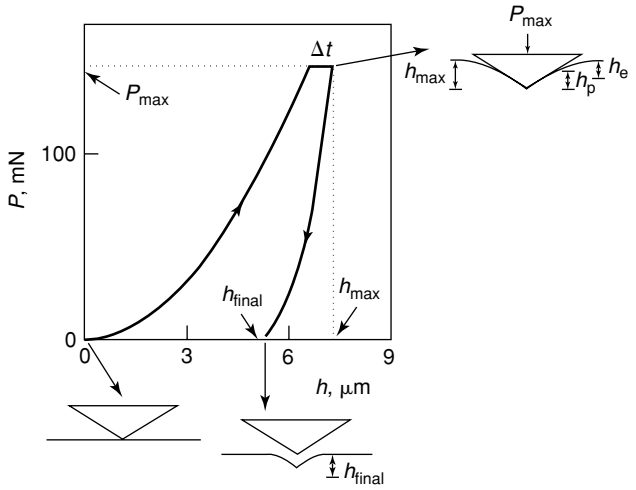

Fig. 8. Typical compliance curve for glassy PET obtained from continuous depth-sensing recording.

ultramicrohardness tester operating in ramp mode. The load is incremented at constant speed up to the maximum load P_{max} held thereafter for a period of time Δt and subsequently released at the same rate as in the loading cycle. Continuous depth-sensing recording does not give values of absolute hardness directly. This is because the area of indentation is not explicitly measured. However, the loading/unloading data can be processed on the basis of well-established assumptions to yield hardness and Young's modulus values (6,42). These approaches consider that the on-load maximum indentation depth h_{max} is the sum of the plastic and the elastic components of indentation, h_p and h_e respectively (see Fig. 8). It is further assumed that the area of contact between the indenter and specimen is determined by the plastic deformation only. The h_p value is then calculated from the analysis of the unloading curve (6,42). For a Vickers indenter, $A = 26.4h_p^2$, where A is the facet area of contact between the indenter and the specimen. Similar geometrical relationships between A and h_p can be derived for other indenters. Hardness is then calculated according to equation (8). The elastic modulus values may be derived from the analysis of the unloading curves.

Indentation studies on different polymeric materials suggest that the hardness values derived from continuous depth-sensing recording compare fairly well with the hardness numbers derived from the direct measurement of the size of indentation (35,43,44). This result suggests that hardness numbers determined from the contact area under load are comparable to post-indentation hardness values.

The actual trend in hardness testing is to use the nanoindentation instruments in conjunction with atomic force microscopes (45). Load–displacement measurements are used to derive hardness and elastic modulus data while the atomic force microscope yields additional topographic information of the indentation area. Measurements at depths of 1 nm can be performed.

BIBLIOGRAPHY

"Hardness" in *EPST* 1st ed., Vol. 7 pp. 470–478, by P. I. Donnelly, Hercules Inc.; "Hardness" in *EPSE* 2nd ed., Vol. 7, pp. 614–626, by F. J. Baltá-Calleja, J. Martinez-Salazar, and D. R. Rueda, Institute for Structure of Matter CSICC, Madrid, Spain.

1. D. Tabor, *The Hardness of Metals*, Oxford University Press, New York, 1951.
2. B. R. Lawn and V. R. Howes, *J. Mater. Sci.* **16**, 2745 (1981).
3. E. Amitay-Sadovsky and H. D. Wagner, *Polymer* **39**, 2387 (1998).
4. F. J. Baltá Calleja, *Adv. Polym. Sci.* **66**, 117 (1985).
5. J. B. Pethica, R. Hutchings, and W. C. Oliver, *Philos. Mag. A* **48**, 593 (1983).
6. W. C. Oliver and G. M. Pharr, *J. Mater. Res.* **7**, 1564 (1992).
7. F. J. Baltá Calleja, *Trends Polym. Sci.* **2**, 419 (1994).
8. F. J. Baltá Calleja and S. Fakirov, *Adv. Polym. Sci.* **5**, 246 (1997).
9. F. Ania, J. Martínez-Salazar, and F. J. Baltá Calleja, *J. Mater. Sci.* **24**, 2934 (1989).
10. S. Fakirov, F. J. Baltá Calleja, and M. Krumova, *J. Polym. Sci., Polym. Phys.* **37**, 1413 (1999).
11. J. M. Pastor, A. González, and J. A. De Saja, *J. Appl. Polym. Sci.* **38**, 2283 (1989).
12. C. Santa Cruz and co-workers, *J. Polym. Sci., Polym. Phys.* **29**, 819 (1991).
13. F. J. Baltá Calleja, C. Santa Cruz, and T. Asano, *J. Polym. Sci., Polym. Phys.* **31**, 557 (1993).
14. J. Kajaks and co-workers, *Polymer* **41**, 7769 (2000).
15. F. J. Baltá Calleja and H. G. Kilian, *Colloid Polym. Sci.* **263**, 697 (1985).
16. F. J. Baltá Calleja, O. Öhm, and R. K. Bayer, *Polymer* **35**, 4775 (1994).
17. F. J. Baltá Calleja and co-workers, *Polymer* **32**, 2252 (1991).
18. L. Giri and co-workers, *J. Macromol. Sci., B: Phys.* **36**, 335 (1997).
19. A. Flores and co-workers, *Colloid Polym. Sci.* **276**, 786 (1998).
20. F. J. Baltá Calleja, J. Martínez-Salazar, and T. Asano, *J. Mater. Sci. Lett.* **7**, 165 (1988).
21. S. Fakirov and co-workers, *J. Mater. Sci. Lett.* **17**, 453 (1998).
22. B. Wunderlich, *Macromolecular Physics*, Vol. **3**: *Crystal Melting*, Academic Press, New York, 1980, Chapt. "8".
23. F. J. Baltá Calleja and co-workers, *J. Mater. Sci.* **35**, 1315 (2000).
24. A. Flores and co-workers, *Polymer* **41**, 5431 (2000).
25. F. J. Baltá Calleja and co-workers, *J. Mater. Sci.* **30**, 1139 (1995).
26. V. Lorenzo, J. M. Pereña, and J. M. G. Fatou, *Die Angew. Makromol. Chem.* **172**, 25 (1989).
27. D. R. Rueda and co-workers, *J. Mater. Sci.* **29**, 1109 (1994).
28. F. J. Baltá Calleja and co-workers, *Macromolecules* **23**, 5352 (1990).
29. H. G. Fritz and co-workers, *J. Mater. Sci.* **30**, 3300 (1995).
30. F. J. Baltá Calleja and co-workers, *J. Macrom. Sci., B: Phys.* **36**, 655 (1997).
31. V. Lorenzo and J. M. Pereña, *J. Appl. Polym. Sci.* **39**, 1467 (1990).
32. W. P. Paplham and co-workers, *Polym. Composites* **16**, 424 (1995).
33. T. Asano and co-workers, *Polymer* **40**, 6475 (1999).
34. *Annual Book of ASTM Standard Part 10*, American Society for Testing and Materials, Philadelphia, 1978.
35. B. J. Briscoe and K. S. Sebastian, *Proc. R. Soc. Lond. A* **452**, 439 (1996).
36. M. V. Swain and J. S. Field, *Philos. Mag. A* **74**, 1085 (1996).
37. B. Rother and co-workers, *J. Mater. Res.* **13**, 2071 (1998).
38. M. Sakai, S. Shimizu, and T. Ishikawa, *J. Mater. Res.* **14**, 1471 (1999).
39. P. J. Blau, J. R. Keiser, and R. L. Jackson, *Mater. Charac.* **30**, 287 (1993).
40. P. J. Blau, *Metallography* **16**, 1 (1983).
41. H. M. Pollock, *ASTM Handbo.* **18**, 419 (1992).
42. M. F. Doerner and W. D. Nix, *J. Mater. Res.* **1**, 601 (1986).

43. B. J. Briscoe, K. S. Sebastian, and S. K. Sinha, *Philos. Mag. A* **74**, 1159 (1996).
44. A. Flores and F. J. Baltá Calleja, *Philos. Mag. A* **78**, 1283 (1998).
45. A. V. Kulkarni and B. Bhushan, *Thin Solid Films* **290/291**, 206 (1996).

F. J. BALTÁ CALLEJA
A. FLORES
Instituto de Estructura de la Materia, CSIC

HDPE. See ETHYLENE POLYMERS, HDPE.

HIGH DENSITY POLYETHYLENE. See ETHYLENE POLYMERS, HDPE.

HYDROGELS

Introduction

Hydrogels are hydrophilic polymers that absorb water and are insoluble in water at physiologic temperature, pH, and ionic strength because of the presence of a three-dimensional network. The cross-links can be formed by covalent bonds, or electrostatic, hydrophobic, or dipole–dipole interactions. The hydrophilicity is due to the presence of hydrophilic groups, such as hydroxyl, carboxyl, amide, and sulfonic groups along the polymer chain.

The area of hydrogel research has expanded dramatically in the last 10 years, primarily because hydrogels perform well for biomedical applications. This is true for both the synthetic and natural hydrogels. Hydrogels work well in the body because they mimic the natural structure of the body's cellular makeup. Recent advances in the use of hydrogels for tissue engineering, drug delivery, and contact lens application, to name but a few of the many biomedical applications of hydrogels, have led to (for the first time) the potential to design artificial organs in a controlled fashion, to deliver drugs to specific sites in the body, and to fabricate the first true extended wear contact lenses.

This article focuses on the biomedical applications of hydrogels. Several areas of nonbiomedical applications are also discussed. Hydrogels can be classified as synthetic, natural, "smart," and biodegradable hydrogels. There may be many more classes of hydrogels, but this class division is based on the current focus of hydrogel research. Hydrogels which are interpenetrating polymer networks (IPNs) and block copolymers, for example, are discussed throughout the article. The preparation of hydrogels focuses on the details of free-radical cross-linking polymerization, chemical cross-linking, irradiation cross-linking, and physical interaction cross-linking techniques.

Encyclopedia of Polymer Science and Technology. Copyright John Wiley & Sons, Inc. All rights reserved.

Properties

A hydrogel is a cross-linked polymer that swells in water to an equilibrium value. The dry hydrogel is called a *xerogel* or dry gel. When the hydrogel is dried, water evaporates from the gel and causes collapse of the gel structure. If water is removed without disturbing the network, either by freeze-drying or by organic solvent extraction techniques, the resultant hydrogel is extremely porous. These materials are referred to as *aerogels* (1). The amount of water a material needs to absorb to be classified as a hydrogel remains undefined, but most researchers generally agree that if a material absorbs at least 10% water and is insoluble in water, it can be classified as a hydrogel. The swollen equilibrated state of a hydrogel results from a balance between the osmotic driving forces that cause the water to enter the hydrophilic polymer and the cohesive forces exerted by the polymer chains in resisting expansion (2,3). They attain an equilibrium swelling state that depends on the osmotic driving forces and the cross-link density. An equilibrated state is reached quickly following immersion of the dry (xero) gel in water. Most hydrogels, in fact, reach an equilibrium concentration of water within 15 min of hydration time. The degree of hydration (water content) can be expressed using the following equation:

$$\%\text{Water(weight)} = [(\text{hydrated weight} - \text{dry weight})\text{hydrated weight}] \times 100$$

The degree of water absorption related to the dry state of the polymer is called *percent hydration*. This is calculated using the following equation:

$$\%\text{Hydration} = [(\text{hydrated weight} - \text{dry weight})\text{dry weight}] \times 100$$

The more hydrophilic the polymer and/or monomers used to prepare the hydrogel, the higher the degree of hydration. This hydration can also, to some extent, be controlled through cross-link density. The higher the degree of cross-linking for a given polymer system will result in a corresponding decrease in water content. An expression for polymer swelling is found in the Flory–Huggins equation where the volume fraction of the polymer in the swollen gel is expressed as

$$V_2 = \left(m_\mathrm{p} d_\mathrm{p}^{-1}\right) / \left(m_\mathrm{p} d_\mathrm{p}^{-1} + m_\mathrm{w} d_\mathrm{w}^{-1}\right)$$

where m_p and m_w are the weights of dry polymer and solvent, respectively, and d_p and d_w are the densities of dry polymer and solvent at 25°C (4,5).

The hydrophilicity of the hydrogel system can also be expressed by means of an interaction parameter (χ). This parameter defines the interaction energy during the process of hydration. The parameter is determined experimentally from stress–strain curves and the swelling characteristics of the hydrogel using the Flory–Huggins equation,

$$\chi = -\left[\nu_\mathrm{e} v_1 \left(\langle\alpha\rangle_0^2 (v_2)^{1/3} - v_2/2\right) + \ln(1 - v_2) + v_2\right] v_2^{-2}$$

where ν_e is the concentration of elastically effective chains in a volume unit of

unswollen polymer, v_1 is the molar volume of solvent, and $\langle\alpha\rangle$ the isotropic dilation factor. One can approximate $\langle\alpha\rangle^2_0$ to equal $(v_0)^{2/3}$ if the polymerization is performed in a solvent (v_0 in this case is the volume fraction of the monomer in the original mixture or the volume fraction of the polymer at network formation), and ν_e can be approximated from stress–strain curve.

The water that is contained in hydrogels is believed to consist of a "bound" water and "free" water (6). When the dry hydrogel polymer is placed in water, the hydrophilic groups along the polymer chain are hydrated first. Water will form a hydration sphere around these hydrophilic groups. This type of water is called *bound water*. The bound water molecules are believed to be tightly held in the hydrogel matrix through a series of chemical interactions, such as hydrogen bonding. As the hydrogel continues to hydrate, additional water that is absorbed by the hydrogel is referred to as *unbound or free water*. This water fills the voids and pores of the hydrogel. The water in this hydration sphere has less structure and higher mobility than does bound water. Higher water content hydrogels contain more free water. It is the free water that is believed to be responsible for the "end of day" dehydration characteristics of high water content hydrogel contact lenses. These types of water are determined experimentally using dsc (differential scanning calorimetry) and nmr (nuclear magnetic resonance) techniques. It is important to note, however, that not all researchers believe that free and bound water exists. From heat-capacity measurements in the hydrogel poly(HEMA) [poly(2-hydroxyethyl methacrylate)] and a study of the thermodynamics from mixing water with poly(HEMA), researchers have indicated that strong interactions of water with the polar groups along the polymer chain does not occur. Evidence as determined by pulsed gradient nmr indicates that all of the water in poly(HEMA) hydrogels diffuses as a homogeneous water phase (7).

The amount and type of water that is contained in the hydrogels determines the diffusion and transport characteristics of the hydrogel. This is important for drug delivery and contact lens application. It has been shown that the low water transport characteristics of some contact lens hydrogel system is the major factor responsible for contact lens adhesion. The oxygen permeability and water transport characteristics of conventional hydrogels increase with increasing levels of hydration. Details of the diffusion and dynamic transport behavior or hydrogels can be found in excellent reviews (8). The design of a high water content hydrogels for biomedical application where mechanical integrity is required can be a serious problem because of the fact that high water content hydrogels typically possess very poor tear strengths.

Classes of Hydrogels

Hydrogels can be classified as either synthetic or natural according to their origin, degradable or stable depending on their stability characteristics, and "intelligent" or conventional depending on their ability to exhibit significant dimensional changes with variations in pH, temperature, or electric field.

Conventional Synthetic Hydrogels. The class of conventional synthetic hydrogels is prepared by free-radical polymerization of vinyl-activated monomers. These monomers can be classified according to type and charge. The water content

of the resultant hydrogel can vary widely, depending on the hydrophilicity of the monomer and degree of cross-linking. A difunctional monomer is added to cross-link the polymer chains.

One of the most important classes of monomers used to prepare synthetic hydrophilic polymers and hydrogels are the methacrylates and acrylates. The principal monomer is shown in (**1**) where R=H (acrylate) and R=CH_3 (methacrylate). A wide variety of commercially available hydrophilic acrylates and methacrylates exist. A huge advantage of this class of monomers is their relative ease of polymerization and low cost. The monomer 2-hydroxyethyl methacrylate (HEMA) (**2**) has been used extensively in the contact lens industry. Poly(HEMA) possesses a water content of 38% and has excellent mechanical strength. The monomer glyceryl methacrylate (**3**) when polymerized and cross-linked results in a hydrogel of approximately 70% water, depending on its purity and degree of cross-linking.

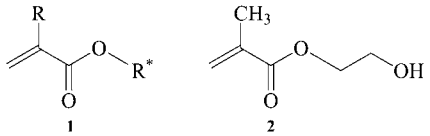

1

2

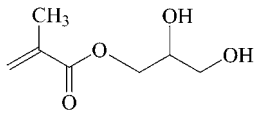

3

Another very important class of monomers used to prepare synthetic hydrogels is the acrylamide/methacrylamide (**4**) (R=CH_3 or H) based monomers. These include the monomers acrylamide (AA), *N*-methacrylamide (MAA), *N*,*N*-dimethylacrylamide (DMA), and diacetone acrylamide (DAA). The polymers prepared from AA, MAA, and DMA are all "super water absorbent" polymers, each capable of absorbing several times their weight in water. DMA is a particularly useful monomer for biomedical application in that it possesses excellent hydrolytic and thermal stability characteristics and moderately low levels of toxicity, unlike AA, which is extremely toxic. The polymerization of the monomer 2-hydroxyethylmethacrylamide (**5**) also results in a "super water absorbent" polymer. Despite its similar structure to the methacrylate analogue HEMA, this polymer is capable of water contents as high as 85%, simply because of substitution of the ester for an amide linkage.

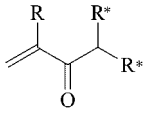

4

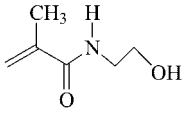

5

The class of hydrophilic monomers based on the cyclic lactams is also an important class of monomers. The most widely used lactam monomer is *N*-vinyl pyrrolidinone (NVP) (**6**). This is also a "super absorber." Hydrogels prepared from

this monomer absorb several times their weight in water, despite the hydrophobic aliphatic ring structure. Cross-linking agents for NVP and NVP-based copolymerizations include *N*,*N*-methylenebisacrylamide and allyl methacrylate. The monomer NVP is widely used for contact lens application, and in fact, most commercial contact lens materials contain NVP.

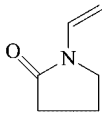

6

Monomers that contain ionic functionality are also widely used for the preparation of hydrogels. These include methacrylate, methacrylamide, and styrene-based monomers that contain acidic or basic functionality. In this class of monomers is included methacrylic acid, acrylamidomethylpropylsulfonic acid (**7**), and *p*-styrene sulfonate. These are typically used as comonomers at low concentration. The ionic functionality in a buffered saline environment dramatically increases the water content of the resultant hydrogel. For example, copolymerization of 2 wt% methacrylic acid with HEMA results in a hydrogel having a water content of 60% (compared with a 38% water content for HEMA alone). In a similar fashion, the cationic monomer methacryloyloxyethyltrimethylammonium chloride (MAC) is extremely hydrophilic. A hydrogel containing 60% NVP, 10% MAC, and 30% HEMA results in a material having an equilibrium water content of 87% (9).

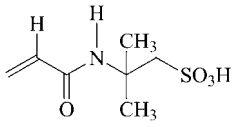

7

The copolymerization of MAC with methacrylic acid results in ampholytic hydrogels. These are hydrogels that contain both anionic and cationic characteristics (10). These materials exhibit interesting pH-dependent behavior. Zwitterionic hydrogels, based on 2-(methacryloyloxy)ethyl-2′-(trimethylammonium)ethyl phosphate inner salt (**8**), have also been designed for improved biocompatibility. These hydrogels mimic the zwitterionic structure of phospholipids such as phosphatidylcholine, which is a major component of the outer membrane of all living cells (11). Zwitterionic monomers contain both a cationic and anionic charge on the same molecule.

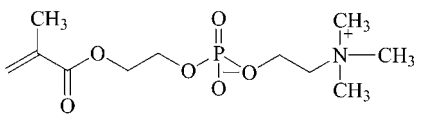

8

It is important to note that almost all high water content hydrogels possess poor mechanical properties. This is a huge disadvantage of hydrogels, especially when one needs to design a material for an application that requires some mechanical integrity. A homopolymer of poly(NVP), for example, resembles a hydrated gelatin. In order to overcome the poor strength of these materials, it is necessary to copolymerize these "super absorbent" monomers with monomers that are capable of improving the overall tear strength of the material. Several monomers have been successfully used. One such monomer is methyl methacrylate (MMA). Low concentrations of MMA in a copolymer formulation typically result in a reduction in water content, but a dramatic improvement in mechanical integrity is also observed. Monomers such as cyclohexyl methacrylate and *t*-butylcyclohexyl methacrylate also work well (12). These monomers improve the mechanical properties of hydrogel formulations by imparting rigidity to the polymer network. This approach, however, is seriously limited in that phase separation often occurs before acceptable properties are achieved. One approach to overcome this phase separation issue, while improving the overall hydrogel strength, is through the use of "hydrophilic-bulky" strengthening agents, such as 4-*t*-butyl-2-hydroxycyclohexyl methacrylate (TBE) (**9**) (13). Excellent mechanical characteristics and optical clarity have been achieved through the use of TBE. A 80/20 (w/w) copolymer of NVP and TBE results in an 85% water-containing hydrogel that possesses a tear strength equivalent to the 38% water-containing hydrogel poly(HEMA).

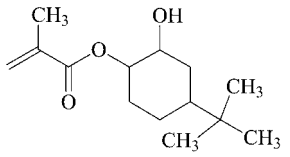

9

Silicone Hydrogels. A new class of hydrogels based on silicone has been developed (14). These materials were developed in an attempt to combine the high oxygen permeability of polydimethylsiloxane and the excellent water absorption characteristics of conventional non-silicone hydrogels. This new class of hydrogels was developed primarily for contact lens application. These silicone hydrogels are also prepared by free-radical polymerization techniques.

The biggest limitation in the design of silicone hydrogels is that silicone-based monomers are hydrophobic and insoluble in hydrophilic monomers. The copolymerization of methacrylate-functionalized silicones with hydrophilic monomers generally results in opaque, phase-separated materials. There have been essentially three approaches in the design of transparent silicone hydrogels, ie, in minimizing the phase separation that occurs during polymerization of methacrylate-functionalized silicones with hydrophilic monomers. One approach has involved a protection–deprotection procedure (**15**). This involves the protection of a hydrophilic monomer with a hydrophobic protecting group. Copolymerization of the protected monomer with a methacrylate-functionalized silicone, followed by removal of the protecting group, results in a transparent silicone hydrogel. For example, trimethylsilyl-protected 2-hydroxyethyl methacrylate is

readily soluble in silicone-based monomers. Copolymerization of the protected HEMA with the monomer methacryloyloxyethyl tris(trimethylsilyloxy)silane forms a transparent, hydrophobic material that, following immersion in a mild basic or acidic deprotecting solution and extraction to remove hexamethyldisiloxane, gives a transparent silicone-based hydrogel (**10**). This is a good approach in principle; however, it is extremely expensive because of the large number of processing steps and length of time required for complete deprotection.

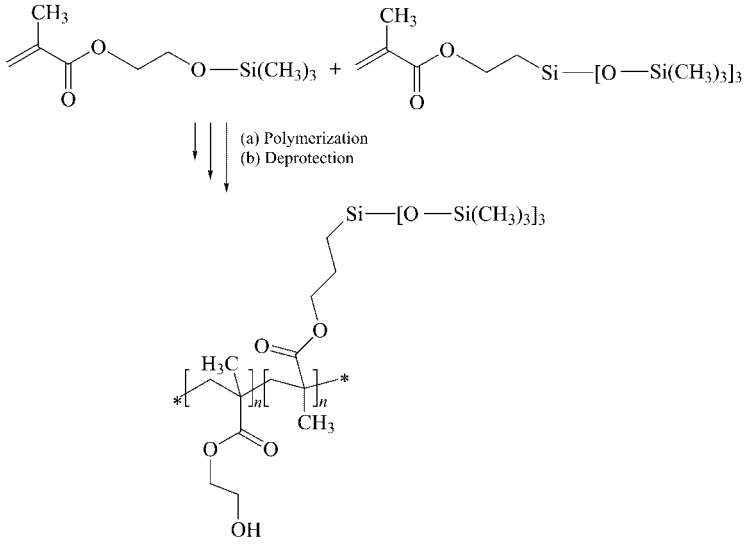

10

Another approach has been the use of a solubilizing co-solvent. For example, the addition of a co-solvent that is capable of solubilizing an incompatible mixture of silicone and a hydrophilic monomer, in many cases, results in transparent materials following cure. Examples of co-solvents include isopropyl alcohol, hexanol, and methyl dodecanoate. This approach has the additional advantage of controlling the glass-transition temperature of the material. The addition of higher concentrations of co-solvent results in a lower glass-transition temperature as a result of a higher polymer chain flexibility (higher free volume). It is imperative that the glass transition of the material is below the cure temperature in order to effect a complete cure.

The third and most successful approach has been the preparation of siloxanes containing hydrophilic groups to improve the solubility of silicone-based materials with hydrophilic monomers. In this approach several synthetic avenues have been pursued including the synthesis of hydrophilic-TRIS [tris(trimethylsiloxysilyl)propyl methacrylate] derivatives, siloxanes containing hydrophilic blocks, and siloxanes containing hydrophilic grafts, such as polyethyleneglycol-grafted silicones (**11**) (16–19).

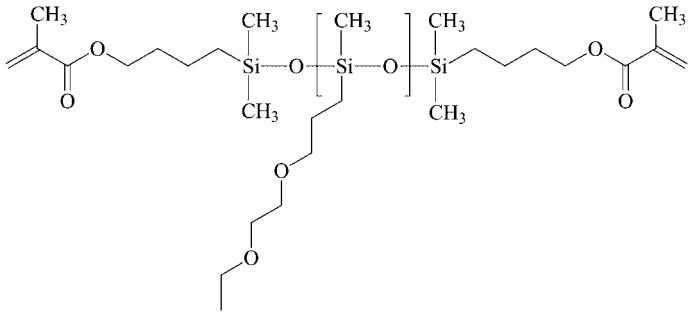

11

Natural Hydrogels. Naturally occurring water-soluble polymers include polynucleotides, polypeptides, and polysaccharides. These polymers are derived from a variety of naturally occurring sources such as plants, animals, and humans, or are synthesized. The polymer collagen, for example, is obtained from cows, pigs, and humans, depending on the type of collagen required. Polypeptides can be synthesized by a protection/solid support scheme or through recombinant DNA techniques. Hydrogels of naturally occurring polymers are prepared by the chemical or physical cross-linking of these polymers. The chemical cross-linking reaction of polysaccharides (alginate, chitin, chitosan, cellulose, oligopeptides, and hyaluronic acid (**12**)) and proteins (albumin, gelatin) leads to a variety of well-defined hydrogels (20–22). Hydrogels prepared from these polymers exhibit excellent biocompatibility, primarily because they mimic the structural components of the body. In humans, glycoaminoglycans are hydrogels that exist in the connective tissue, such as skin, tendon, and bone (23,24). Additional information on the naturally occurring polymers can be found in excellent reviews (25,26).

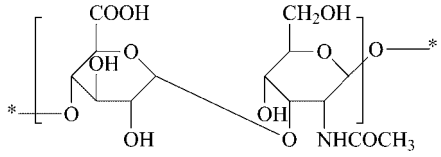

12

"Smart" Hydrogels. A truly amazing class of hydrogels that has found potential use for a wide variety of applications is the class of "smart" or "intelligent" hydrogels. Smart hydrogels are, in most respects, very much similar to conventional hydrogels. They are synthesized using similar methods and absorb water. Smart hydrogels, however, deserve to be in their own class. The uniqueness of this class is due to the unusual volume changes that these polymers exhibit under the application of very specific stimuli. Smart hydrogels exhibit significant volume changes in response to stimuli such as changes in pH, temperature, electric field, and light (27–29). The major reason for the interest in these polymer systems

is that the smart polymers, in most respects, behave like biopolymers in nature; small changes of some specific stimuli dictate most of the biochemical response in the body. The desire to form hydrogel systems that can mimic biological systems drives a huge area of research. This volume change is abrupt and occurs with only a small change in stimuli. In solution these changes are referred to as the lower critical solution temperature (LCST), where at a specified temperature the polymer precipitates from solution. For a hydrogel system, these changes are marked by an order of magnitude change in the size, shape, and water content of the hydrogel. The hydrogel returns to its original state when the stimuli is removed. These shifts are triggered by changes in the physical state of the hydrogel as a result of changes in the hydrophilic/hydrophobic microstructure of the hydrogel. In designing such systems, the goal is to control the balance of the hydrophobic/hydrophilic nature of the hydrogel system. The driving force behind these transitions varies, with common stimuli including (*1*) the neutralization of charged groups by either pH shift, (*2*) the addition of an oppositely charged polymer, and (*3*) change in the efficiency of hydrogen bonding with an increase in temperature or ionic strength (30).

Biodegradable Hydrogels. Biodegradable hydrogels, much similar to that of the smart hydrogels category, has expanded at such a fast pace that it now deserves to be in its own class. The uses of biodegradable hydrogels now encompass a wide variety of applications, for both biomedical and nonbiomedical uses. In the design of biomedical products, the basic objective is to fabricate materials that resorb or degrade in a physiological environment so that the device ultimately disappears with no adverse reaction (31,32). Degradable polymers undergo chain scission to form low molecular weight oligomers or monomers. Ultimately, the oligomers and monomers are either fully degraded to biosubstances or are eliminated by the body. Degradation is characterized by loss of molecular weight, loss of mass and mechanical strength. The definition of biodegradation is broad and includes a variety of degradative mechanisms, depending on whether the degradation follows (33). Degradation hydrolytic, thermal, or enzymatic degradation pathways (see BIODEGRADABLE POLYMERS, MEDICAL APPLICATIONS).

Methods of Preparation

Free-Radical Polymerization. Free-radical polymerization cross-linking is the preferred route used to prepare hydrogels from the class of acrylates, amides, and vinyl lactams. It can also be used to prepare hydrogels from the naturally occurring polymers if the polymer backbone or chain end of the natural polymer has been functionalized with a radically polymerizable group. It is also the preferred route to prepare interpenetrating network hydrogels (IPNs) using either synthetic monomers or natural polymers (again funtionalized with a radically polymerizable group). The IPNs hydrogels are networks that contain two polymer systems, each in its own cross-link network.

To form a hydrogel by free-radical polymerization, a difunctional cross-linking agent must be added to the polymerization. The classical gelation

theory can be applied to most of these polymerizations, especially for methacrylate–dimethacrylate monomer combinations that have similar reactivity (34). This theory allows for a fairly precise determination of the overall kinetics of the system, which includes estimates of the gelation and vitrification point. There are a variety of cross-linkers one can choose from. For methacrylate polymerizations, a common cross-linker is ethylene glycol dimethacrylate (**13**) that is added at a concentration of 0.1–1.0%. For acrylamide systems, methylene bisacrylamide is very common. For lactam-based systems, ethylene divinylurea works extremely well.

Problems arise when one attempts to copolymerize monomers of unlike reactivity, such as the copolymerization of HEMA with the vinyl lactam NVP. For this type of polymerization, a block-type copolymer possessing high levels of unreacted NVP results. This is due to the slow kinetics of NVP polymerization and unsuitable reactivity ratio of this comonomer system. The reactivity ratios (r_1 and r_2 values) result in a "blocky" backbone. This high level of unreacted NVP can be overcome by designing cross-linkers that are capable of polymerizing with both lactam and methacrylate functionality. For example, the cross-linker methacryloxyethyl vinyl carbonate (**14**) (MEVC) is an excellent example of a cross-linker that possesses reactivity for both a methacrylate and vinyl lactam functionality. The vinyl carbonate group has the same reactivity as the vinyl bond in NVP (35). The copolymerization of NVP and HEMA with MEVC results in a significant increase in water content (when compared with conventional methacrylate cross-linkers) because of the higher incorporation of NVP in the copolymer.

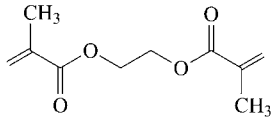

13

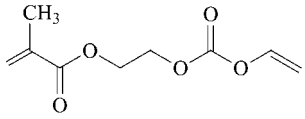

14

The chemistry of typical free-radical polymerizations involves an initiation, propagation, chain transfer, and termination step leading to the formation of a cross-linked polymer system (36). The initiation step (radical formation step) utilizes chemistries that when subjected to thermal or ultraviolet radiation form radicals that react with activated monomers, such as a methacrylate. A wide variety of thermal, ultraviolet, visible, and redox initiators are commercially available. Typical thermal initiators include the class of azo compounds, such as azobisisobutylonitrile (AIBN), and peroxide initiators, such as the peroxydicarbonates and the hindered peroctoates. Polymerization conditions vary

widely depending on the type of initiator and its half-life. For example, the respective 10-h half-life data of AIBN is 64°C, and for cumylperoxydecanoate the 10-h half-life is 38°C. This is extremely helpful in controlling polymerization exotherms, reactivity ratios, and monomer solubility. Typical commercially available ultraviolet and visible light initiators include the benzoin methyl ethers, acetophenones, and benzoyl phenyl phosphine oxides, to name but only a few.

The polymerizations can be performed either in solution or neat. There are advantages to both methods depending on the product end use. Solution polymerizations can be helpful when the preparation of large quantities of hydrogel are required. The solvent for most reactions is water; however, a wide variety of polar solvents can be used with the only requirement that they can be exchanged for water in the hydration step. The polymerization exotherm can be controlled by choice of solvent. For many copolymerizations, the addition of a suitable "solubilizing" solvent is necessary to solubilize monomers of widely varying hydrophilicity. Also, a solvent can aid in the molecular weight control. By use of a chain-transfer solvent such as an alkyl mercaptan, molecular weight and end-group functionality can be controlled (37).

Neat polymerizations, also sometimes referred to as bulk polymerizations, are typically performed between metal or glass plates utilizing a flexible spacer to accommodate shrinkage. Clamps are used to assure a complete seal. The metal plates are many times treated with a fluoro polymer, and the glass plates are treated with a chloromethylsilane to facilitate plate separation and to eliminate adhesion of the polymer film. The filled plates are cured in an oven or under ultraviolet or visible lights, depending on the desired initiation mode. Following the cure, the films are removed and extracted with an appropriate solvent. Neat polymerizations are very fast, usually requiring only minutes for total monomer conversion. This, however, limits the reaction size in that exotherms are difficult to control. A big advantage of neat polymerizations is that there is no need for solvent removal. Solvent removal can be very time-consuming, requiring either extensive thermal devolatilization or solution extraction steps.

Emulsion and suspension polymerizations are also an important route to obtain hydrogels by free-radical polymerization (38). For some applications, this is the preferred route, particularly when droplets or spheres of the hydrogel are desired. This is an important route to prepare hydrogels for drug delivery application. For these polymerizations, the initiator, solvent, and monomer are added together with a suspending agent and/or emulsifier. The cross-linker can be added but is not necessary, depending on whether one desires a soluble polymer. A major disadvantage of this route is that the emulsifier and/or suspending agent is sometimes difficult to remove.

Chemical Cross-Linking of Polymers. Another important method used to prepare hydrogels is by the cross-linking of hydrophilic polymers (39). This route can be employed for both the synthetic and naturally occurring polymers. In this reaction, a bifunctional cross-linking agent is added to a dilute solution of the hydrophilic polymer. The hydrophilic polymer contains functionality that is capable of reacting with the cross-linking agent. The reaction is typically in solution,

but may also be performed through a suspension reaction where microparticles or spheres are desired.

Most of the naturally occurring polymers can be cross-linked in this fashion. For example, the polymers albumin and gelatin can be cross-linked with formaldehyde or a difunctional dialdehyde (40,41). The aldehyde reacts with the amino group along the albumin polymer backbone (**15**). Also, using a similar approach, chrondroitin sulfate can be cross-linked with diaminododecane catalyzed by dicyclohexycarbodiimide (42). In this example, increasing the concentration of diaminododecane increased the degree of cross-linking. Cystein-bearing polypeptides can be cross-linked through cystein bonds (43,44). Another example is the cross-linking of poly(vinyl alcohol) using a diisocyanate-terminated poly(ethylene oxide). Hydrogels have also been prepared from functionalized poly(ethylene glycol) (PEG) through enzymatic cross-linking. PEG functionalized with a glutaminamide and a lysine-containing polypeptide were cross-linked by the reaction of a natural tissue enzyme, transglutaminase (**16**). Transparent gels of water contents as high as 90% have been prepared by this route (45).

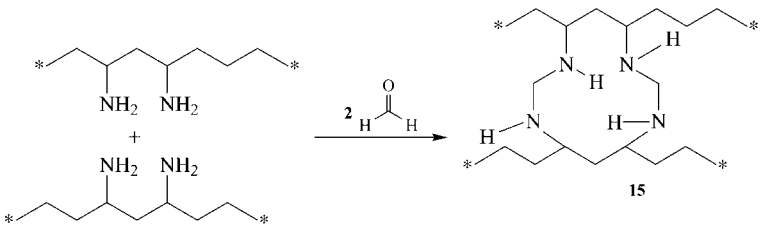

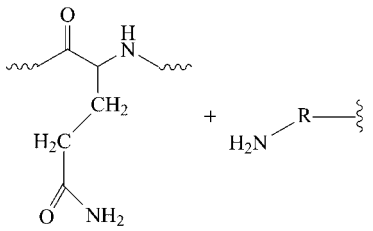

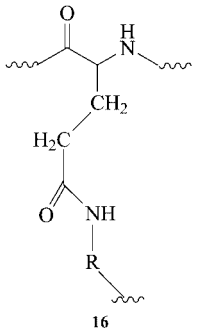

16

Irradiation Cross-Linking of Polymers. Hydrogels can also be obtained by ionizing-radiation techniques. This route can be employed for both the synthetic and naturally occurring polymers. *Ionizing radiation* is a radiation that possesses enough energy to ionize simple molecules either in air or water (46). The radiation can be in the form of an electron beam irradiation or γ–radiation. This cross-linking reaction can be accomplished by irradiation of a hydrophilic polymer in bulk or in solution. These reactions are usually performed in water. The preferred method, however, is irradiation of a polymer solution. The solution method is preferred because it requires less energy for formation of a macroradical, and radical efficiency is increased because of the reduced viscosity of the reaction mixture. When a polymer solution is irradiated, reactive sites along the polymer backbone are formed. The main reactive species (when water is used as the reactive solvent) are hydrated electrons, hydroxyl radicals, and hydrogen atoms. It is the hydroxy radicals, however, that lead to abstraction of hydrogen atoms along the polymer chain with formation of a "multisite" radical functionalized macromolecule. When these radicals combine, a cross-link is formed. This is not true for all polymer systems; some polymers, in fact, will degrade under ionizing radiation (47). Many polymers in solution will undergo simultaneous cross-linking and degradation reactions. Each polymer system is unique and the optimum irradiation conditions need to be determined experimentally to minimize chain degradation and maximize cross-linking reactions.

Gels through Physical Interactions. Hydrogels can also be formed through a series of physical interactions. It is this type of reaction that, in fact, provides most of the cellular network in the body. These physical interactions include polyelectrolyte complexation, hydrogen bonding, hydrophobic association, and crystalline entanglements. Typical methods to prepare films utilizing physical interactions involves solvent casting or precipitation techniques.

Polyelectrolyte Complexation. Hydrogels can be easily formed through the formation of polyelectrolyte complexes (48). The bonds formed through polyelectrolytic complexation occur between pairs of charged sites along the polymer backbone. The hydrogels formed through electrolytic complexation are insoluble in water, and the electrolytic bonds can be very stable depending on the pH of the system (7–10 kcal).

Polyelectrolyte complexes are divided into four subclasses depending on the basicity and acidity of the polyelectrolytes. These include strong acid–strong base, strong acid–weak base, weak acid–strong base, and weak acid–weak base subclasses. The composition of these complexes is dictated by the degree of dissociation of the electrolytic components.

The complexation of poly(sodium styrene sulfonate) and poly(4-vinylbenzyltrimethylammonium chloride) is easy to form (**17**) (49). By combining two water-based solutions of each polymer at equimolar concentration, the complex forms immediately as evident by the formation of white precipitate. Another example is the polyelectrolyte complexation of an amino group containing chitosan with the polymer sodium alginate (50). Sodium alginate also forms a strong complex through the association of calcium ions (51).

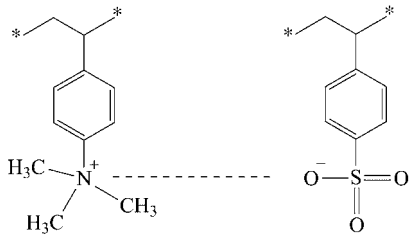

17

Hydrogen Bonding. Hydrogels can also be formed through the hydrogen bonding of macromolecular chains. A hydrogen bond is formed through the association of electron-deficient hydrogen and a functional group of high electron density. Similar to the polyelectrolytic complexes described above, hydrogen-bonded complexes occur in many biological systems. The hydrogen-bonded complex (**18**) of poly(acrylic acid) and poly(NVP) is one of the more common (52,53). This complex is affected by a variety of factors, such as the molar ratio of each polymer, the solution temperature, polymer concentration, type of solvent, and polymer structure (degree of association between complexing functionalities). This complex will not form a gel at neutral pH.

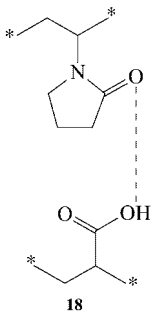

18

Hydrophobic Association. Hydrogels can also be formed through hydrophobic associations (54–58). Polymer systems such as block copolymers, graft copolymers, and polymer blends form microphase/microdomain separated structures. The hydrophobic domains in these structures behave as associated crosslink sites. These polymers combine hydrophobic segments that form unique hydrophobic phases dispersed (or surrounded) by hydrophilic water absorbing regions. These hydrophobic-associated polymer blends typically possess poor mechanical properties because of poor interfacial adhesion, and films are usually opaque because of macrophase polymer separation. Control of the size of the hydrophobic phase tends to improve the optical transparency and mechanical integrity. A precise balance needs to be established.

One of the major advantages of this approach is the resultant low cost economics of the system. Commercially available polymers can be used to generate a wide variety of high strength, low cost hydrogels. This is particularly true of polymer blends. The hydrophobic phases of blend hydrogels form multicross-link sites along the polymer backbone and, so loss of the water-soluble polymer is

minimized. This is extremely important for biomaterials where polymer leaching cannot be tolerated. Another advantage of this approach is that these polymer blends are soluble in organic solvents and flow at elevated temperatures. This allows for the processing of these hydrophobic blends by injection molding. Covalently cross-linked systems are insoluble in organic solvents and do not flow even at elevated temperatures. An excellent example of a hydrophobically associated hydrogel is the copolymer of poly(butyl methacrylate-*co*-methacrylamide-*co*-acrylic acid) with a blend of poly(*N*,*N*-dimethylacrylamide-*co*-*N*-vinylpyrrolidone) (59,60). Hydrophobic association is the predominant associated force holding this polymer blend together. It is reported that this polymer is stable in water at a pH range of 1–11.

Biomedical Applications of Hydrogels

One of the first areas of commercial application for hydrogels was contact lenses (61). In the 1950s and 1960s Otto Wichterle in Prague discovered the hydrogel poly(HEMA), and a very simple process to prepare contact lenses (62). The process consisted of spinning a monomer solution in a preformed optical quality mold. This ingenious work was completed on an old-fashioned "erector set" in the early morning hours of Christmas. Since that time the area of hydrogel research has expanded rapidly. Hydrogels have been used for a wide variety of nonbiomedical applications, but the primary area of hydrogel research has focused on biomedical applications. This is the result of the generally excellent biocompatibility exhibited by hydrogels. Hydrogels have been successfully used for a wide variety of biomedical applications including contact lenses, intraocular lenses, drug delivery devices, implants, and scaffolds for living cell encapsulations.

Contact Lenses.

Conventional Hydrogels. With the discovery of poly(HEMA), the contact lens industry began to flourish. This is because HEMA is a transparent, soft material that, when hydrated, absorbs 38% water, and as a result is very comfortable to wear. The HEMA lens also has excellent wetting characteristics and biocompatibility. Within a few years following this discovery, a number of companies began to market their own version of the HEMA lens. A multitude of new hydrogel contact lenses emerged (63–66). Most were based on copolymers of HEMA, NVP, and glyceryl methacrylate, together with cross-linkers and initiators. These materials were marketed as daily wear lenses, ie, wear the lens for one day, remove it at night for cleaning, and again wear the lens the next day.

With the huge success of the daily wear contact lens market, researchers began to look for ways to increase the contact lens wearing time. This started a huge research effort to design contact lens materials for extended wear application, with the primary goal to simplify the patients cleaning and wearing schedule. Such design was not a trivial task. The design of a new contact lens material for extended wear application requires a material to satisfy a number of very strict design requirements. The material must be optically transparent, possess chemical and thermal stability, biocompatibility, and be wettable to tears. It must also have suitable mechanical properties. This requires a material to have a low modulus for patient comfort and high tear strength for lens handling

durability. In addition, it is important that the material can be processed through free-radical polymerization techniques. Finally, the material must be permeable to oxygen. There is a lack of blood vessels in the corneal network, and so the cornea obtains almost all of its oxygen requirements from the atmosphere. Placing a contact lens over the eye that does not "breathe" may result in a number of physiological problems (microcysts, inflammation, infections, and corneal ulcers) (67).

There have been several approaches in the design of high oxygen permeable hydrogels for extended wear contact lens application. The first and simplest approach reduces the lens thickness to increase the oxygen transmissibility. The key intrinsic material properties that are a measure of oxygen diffusion are oxygen permeability (Dk), where D is the diffusion coefficient and k is a proportionality coefficient called the *Henry's law coefficient*, and oxygen transmissibility (DkL^{-1}), where the actual amount of oxygen reaching the cornea is inversely proportional to the lens thickness L. Several thin-lens designed contact lenses were introduced to the market with, however, limited success. These lenses were extremely difficult to handle, and most thin-lens designs did not provide enough oxygen permeability for extended lens wear application.

The second approach consists of designing hydrogels with a high water content. A direct correlation exists between water content and oxygen permeability, and so the higher the water content, the higher the hydrogel's oxygen permeability (Fig. 1, ■). There are two methods of designing high water hydrogels. The first involves the polymerization of highly hydrophilic monomers, such as NVP. The second utilizes the use of ionic monomers. The polymerization of HEMA with small concentrations of methacrylic acid, in a buffered saline environment results in a significant increase in water content. For example, with the addition of 2 wt% of methacrylic acid to HEMA, a 60% water content is realized (as compared with 38% for pure HEMA). Both methods require the use of cross-linkers and initiators and may need strengthening agents.

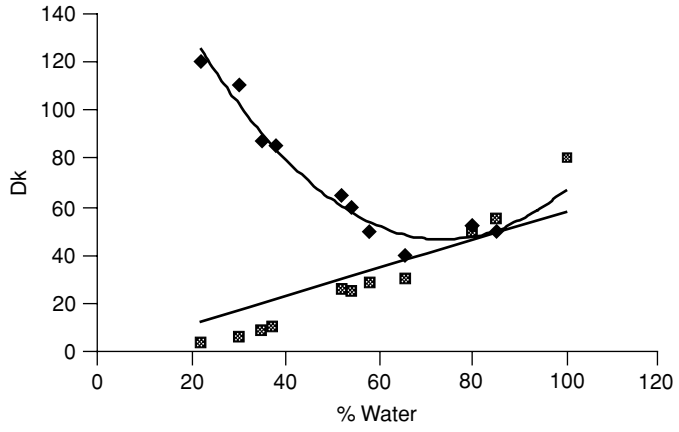

Fig. 1. Relationship between Dk and percent water for conventional hydrogels (■) and TPVC-based silicone hydrogels (◇) (Dk in units of Barrers).

At the time of the discovery of high water content hydrogels, these materials were considered a huge breakthrough with the potential, many practitioners believed, to be the "ultimate contact lens material." This promise, however, was short-lived. There are several limitations of high water content hydrogels. The first is that high water content hydrogels typically possess poor tear strengths and often exhibit a high affinity for protein, particularly for hydrogels possessing an ionic functionality (68). Deposits can affect material wetting, patient comfort, visual acuity, and may even cause inflammatory responses. In addition, in dry environments, high water content hydrogels can induce a clinical response known as *epithelial dehydration* (a dehydration of the corneal epithelial cells) (69). This results in damage to the corneal epithelial cells. This phenomenon is a result of the high rate of water evaporation that occurs with the high water content hydrogels.

Silicone Hydrogels. Another approach in the design of an extended wear contact lens consisted of the development of materials based on polydimethylsiloxane elastomers (PDMS). PDMS appeared to be an ideal polymer for use in an extended wear lens because it possessed a low modulus of elasticity, excellent transparency, and high oxygen permeability (70). The major drawback is that PDMS is completely nonwettable to tears, thus requiring surface treatment to impart wettability. These surface treatments were typically ineffective, resulting in surfaces that possessed marginal wetting characteristics and a high affinity for lipids. Another significant drawback was that silicone lenses under normal wear conditions adhered to the cornea. This was attributed to the low water transport and high recovery characteristics of silicone (See SILICONES).

In an attempt to combine the high oxygen permeability of PDMS and the excellent comfort, wetting, and deposit resistance of conventional hydrogels, the design of silicone-based hydrogels for contact lens application has been studied. This approach was also an attempt to design materials that did not adhere to the cornea. But most of all, it would provide lenses possessing levels of oxygen permeability high enough for extended wear application with minimal physiological impact.

One simple, yet elegant approach in the design of a transparent silicone hydrogel has been reported (71,72). This material has been introduced commercially under the trade name Balafilcon. This new silicone hydrogel system is based on a vinyl carbamate substituted TRIS derivative: (Tris(trimethylsiloxy)silylpropylvinylcarbamate) (TPVC, (**19**)). The TPVC molecule contains the hydrophobic silicone portion, and attached to this silicone is a hydrophilic vinyl carbamate group. This "direct hydrophilic" attachment now gives the silicone significant hydrophilic character. The TPVC molecule is soluble in all proportions with hydrophilic monomers, such as HEMA and NVP. In addition, the vinyl carbamate group provides a "polymerization link" for copolymerization with hydrophilic monomers. The polymerization reaction of TPVC with NVP (and a suitable cross-linker) cast using uv initiation methods, results in transparent, high Dk, low modulus gels that are insoluble in water. Figure 1 (◇) shows the relationship between oxygen permeability (Dk) versus percent water for the TPVC-based silicone hydrogels. This is an important relationship in that it clearly shows the Dk advantage in designing hydrogels based on silicone. In contrast to conventional non-silicone-based hydrogels, the Dk decreases with increasing

water content because of the lower concentration of TPVC in the higher water content copolymers.

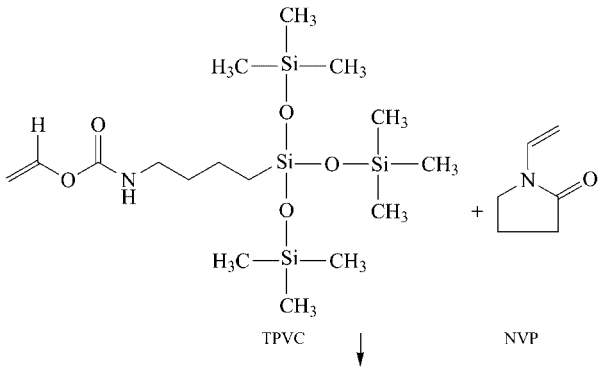

19

Intraocular Lenses. An intraocular lens (IOL) is an implant that is used to replace the diseased or damaged natural lens of the eye (73–77). The lens is supported in the eye through the use of haptics or loops that are attached directly to the IOL optics. There have been a wide variety of materials that have been successfully used as IOLs, ranging from the rigid poly(methyl methacrylate) to the soft elastomer silicone. The current trend in IOL research is to design materials that can be folded and inserted through a small corneal incision. The natural lens is removed using emulsification techniques, and the IOL lens is placed in the original capsule bag that held the lens. Once the IOL is inserted, the lens recovers to its original shape. The small incision is desirable to reduce the degree of induced astigmatism (loss of sphericity) in the operated eye and to minimize corneal trauma.

Hydrogels have also been successfully used for small incision IOLs. There are a number of commercially available hydrogel IOLs based predominately on HEMA, that range in water content from 17 to 28%. Aromatic-based methacrylates, such as phenylethyl methacrylate, are added to increase the refractive index of the lens. A higher refractive index will allow for a thinner IOL design (for power considerations) and result in an IOL that can be inserted through a smaller opening and recover its shape faster. A recent research effort has focused on an expandable IOL hydrogel where the lens is inserted in a dehydrated state and allowed to hydrate in the eye. This allows for the insertion of IOLs with reduced dimensions that make insertion through a small opening possible (78). Once the lens is implanted in the eye, it quickly hydrates, expands, and reaches its final dimensions within minutes.

Drug Delivery. The goal of drug delivery is to maintain the drug concentration in the body (plasma) within therapeutic limits for long periods of time. A constant drug release rate (zero-order) is desired. Conventional drug administration (oral delivery, injection) usually results in poor control of the plasma drug concentration. The controlled release of drugs from polymeric matrices has, however, been very successful. Many polymeric devices that deliver drugs at a

sustained release rate are now commercially available. Controlled release devices offer the desired therapeutic range of drug dose. Controlled drug delivery applications include sustained delivery (time) and target delivery systems (insertion at the diseased site). The delivery of drugs such as protein-based drugs, eg, insulin and growth factor, and also conventional drugs, eg, steroids and antibiotics, can be achieved.

Controlled release systems can generally be divided into three sections depending on their mode of release: diffusion controlled, chemical erosion, and solvent activated (79). In a diffusion-controlled device, the drug is surrounded by an inert barrier and diffuses from a reservoir, or the drug is dispersed throughout a polymer and diffuses from the polymer matrix. In a chemical erosion device, the drug is dispersed in a bioerodible polymer system or is covalently linked to a polymer backbone via a hydrolyzable linkage. As the polymer or hydrolyzable link degrades, the drug is released. In a solvent-activated device, the drug is dispersed within polymeric matrix and the device is swelled with a suitable solvent (usually water). As the device swells, the drug is released.

Conventional Hydrogels. Hydrogels have been used extensively in the field of controlled drug delivery (80–85). The advantages of using hydrogels in drug delivery systems are that they can be used at a local level, ie, insertion at the diseased site. This has become important because many of the new protein-based drugs require delivery in this fashion. The release of a growth factor, for example, to a specific site is highly desirable. This is because many biologically active polypeptides have very short half-lives and can not be administered orally (86). The hydrogel can be cross-linked at the diseased site by photopolymerization techniques, complexation, and enzymatic cross-linking. The hydrogel will also conform to the local anatomy (organs, vessels).

A wide variety of conventional cross-linked homo- and copolymeric hydrogels have been used for drug delivery application. In most hydrogels, the rate of diffusion through the bulk depends on two primary factors: the extent of cross-linking and water content. The extent of cross-linking determines the extent of swelling and the distance between chains within the hydrogel network. When entrapped drugs are diffusing within the network, the rate of diffusion can depend on the interchain separation and the size of the diffusing drug. The rate of diffusion is also controlled by water content. The general approach is to design hydrogels with very specific levels of hydrophilicity/hydrophobicity. This hydrophilic/hydrophobic balance controls water content and drug diffusion, where each drug will diffuse according to its dissolution profile (87). For water-soluble drugs dispersed in a high water content hydrogel, drug release will be rapid.

Hydrogel drug delivery systems can be used in the hydrated or dry states. The drug is incorporated during the polymerization process or through diffusion techniques using preformed films, tablets, etc (equilibrium absorption from concentrated drug solutions). A major limitation of incorporating the drug during the polymerizing process is that the drug will release during the extraction process (the process used to remove unreacted monomers) and, as a result, this technique is rarely used for biomedical applications. The diffusion method is a viable alternate to disperse and deliver drugs. In this method, the hydrogel is soaked in a drug solution until an equilibrium dispersion is reached. The hydrogel is then dried, packaged, and sterilized before use. Dried hydrogels release the drug as the

material hydrates (the drug will diffuse very slowly in an unhydrated hydrogel). The release of water-soluble drugs from a dry hydrogel involves the simultaneous absorption of water and desorption of drug through a swelling-controlled diffusion mechanism (88). As water penetrates a glassy hydrogel matrix that contains a dissolved or dispersed drug, the polymer swells and its glass-transition temperature is lowered. As the water enters the material, a water front forms that separates the glassy polymer from the swelled hydrated polymer. In regard to drug distribution and release, the solvent front separates the drug in the unhydrated core from the swollen water phase. As the water phase continues to grow and expand, the drug diffuses and is released. The drug release kinetics during this process can range from a square root of time dependence (Fickian) to a linear time (Case II transport) dependence. The Case II transport is governed by the rate of polymer relaxation. For most cases, the intermediate situation, which is termed non-Fickian (rate of Fickian diffusion and polymer relaxation are comparable), is observed (89). For example, thiamine HCl release from an initial dry poly(HEMA) hydrogel bead, as plotted versus the square root of time, shows an initial non-Fickian behavior with linearity established only after long periods of time.

Many conventional hydrogel designs that achieve zero-order drug-release are available. The manufacture of reservoir-based hydrogels (reservoir of drug encapsulated and surrounded by a polymer membrane) and matrix diffusion systems (drug is homogeneously dispersed in the hydrogel matrix) using common hydrogels, such as HEMA and glyceryl methacrylate, are relatively easy. The zero-order release rate can be achieved in many cases using either approach; however, the release rate of drugs from a matrix-type system typically declines continuously proportional to the square root of time. Soaking a poly(HEMA)/progesterone matrix, followed by uv irradiation in the presence of a cross-linker, can result in a rate-controlled membrane that exhibits a fairly steady release rate (90). Another use of a controlled release device makes use of a semicrystalline hydrogel (91). The hydrogels in these examples are based on poly(vinyl alcohol) and poly(ethylene oxide). In these systems, films are prepared through solution casting techniques. The films are subjected to an annealing process that creates varying degrees of crystallinity depending on the annealing time and temperature. The degree of crystallinity can be controlled and the degree of crystallinity is the controlling factor of drug release. The rate of crystal dissolution in water controls the rate of drug release. A commercial drug delivery application utilizing hydrogels has been introduced by Geltex pharmaceuticals (92). In this work a nonabsorbed hydrogel based on poly(allylamine) substituted with quaternary amine was designed for hypercholesterolemia (high cholesterol). The quaternary amine binds selectively with cholesterol. This polymer acts in the intestine as a bile acid scavenger to lower serum cholesterol levels in patients with increased risk of vascular disease. Bile acid sequestrants act by binding bile salts in the intestine and prevent them from passing through the intestinal wall and back into the blood stream. A U.S. NDA (new drug application) was filed in July 1999 with approval received in May 2000.

Degradable Hydrogels. Many research groups have studied the use of degradable hydrogels for drug delivery (93). The encapsulated drug will release at a controlled rate depending on such factors as pH, temperature, and cross-link density. Many examples of degradable drug delivery hydrogels can be found in the literature (39).

One of the first successful degradable release systems was based on the polyester hydrogels. These hydrogels are prepared by the copolymerization of malonate-type polyesters (polyesters that contain pendent backbone unsaturation) with monomers, such as NVP and acrylamide. Release of serum albumin occurs from these systems by a bulk erosion process. Other drugs can also be used. As the ester linkage of the polyester backbone hydrolyzes, the entrapped drug is gradually released to the surrounding environment. The release rate depends on the cross-link density. The degradation components of these erodible cross-linked polyesters result in nontoxic, water-soluble by-products. In a similar system, polyester macromers of a poly(ethylene glycol)-*co*-(lactic acid or glycolic acid) were prepared and evaluated for use as bioerodible hydrogels (94). These gels degrade upon hydrolysis of the oligo(α-hydroxy acid) regions and release the by-products poly(ethylene glycol), the hydroxy acid, and oligo(α-acrylic acid) (**20**). The degradation rate can be controlled by tailoring the concentration of α-hydroxy acid. If polymerized in contact with tissue, the gels adhere, and if polymerized prior to tissue placement, the gels are nonadhesive. The protein albumin was entrapped within these hydrogels and shown to release at a consistent rate. The release rate was dependent on the cross-link density and the molecular weight of the protein.

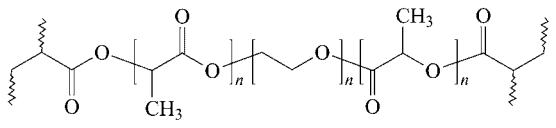

20

Drug-delivery devices combining cross-linked conventional hydrogels, where the drug is covalently linked via a degradable oligopeptide side chain, have been designed for targeted anticancer drugs. In this example, hydrogels of *N*-(2-hydroxypropyl)methacrylamide were prepared. The drug was attached synthetically by a degradable oligopeptide linkage. *In vitro* experiments have shown that these devices target ovarian carcinoma cells with promising results (95). Another interesting example of hydrogels for drug delivery utilizes the concept of degradable natural polymers (96). In this work, the natural oligosaccharide hyaluronic acid (HA) is chemically modified through the use of a pendent hydrazido functional group that is covalently linked to a wide variety of drugs, such as steroids. The covalent link is hydrolytically unstable and under mild conditions it releases the drug.

"Smart" Hydrogels. Research efforts on the design of smart hydrogels for drug delivery application has increased significantly over the past few years (30,31,97). Such systems show promise as drug-delivery devices because of the rapid release of conventional and protein-based drugs during the expansion/contraction of these hydrogel systems. Efforts have focused primarily on designing systems that make use of change in pH and temperature. The idea behind this approach is that smart hydrogels will both expand and contract, forming a hydrogel "switch" that releases drug or protein in a controlled fashion. When a drug is incorporated into a smart hydrogel, the diffusion of the polymer is dependent on the gel-state. Smart hydrogels can be designed to release drugs either above or below the lower critical solution temperature (LCST). Smart hydrogels

have been designed to release drugs at low pH (gastric release application) and at basic pH (intestinal release application).

Some brilliant work in this area has been described. Most of this has been based on the polymer poly(isopropyl acrylamide) (IPA) (97–99). IPA has a critical solution temperature close to that of body temperature (32°C). A large variety of IPA-based polymers (grafts, block) containing varying concentration of hydrophobic monomers have been synthesized. The concentration of hydrophobic monomer controls the critical solution temperature. Recent examples include the design of thermosensitive hydrogels as heparin-releasing polymers for the prevention of thrombosis. In this system, copolymers such as of *N*-isopropylacrylamide, butyl methacrylate, and acrylic acid were cross-linked together with heparin. At temperatures below the LCST, the polymer swelled significantly and solution loading of the drug was performed. Above the LCST, the gel de-swelled and released heparin. Another example makes use of a hydrogel based on an ether–urethane–isopropylacrylamide IPN for use as a heparin-release system. In this example, the "smart" polymer was applied as a coating on polyurethane catheters. This heparin-release coating system resulted in a significant reduction in thrombus formation on test surfaces in contact with venous blood (100).

The design of smart polymers as glucose-sensitive systems that release insulin has recently been described (101,102). The ultimate goal in this work is to design an artificial pancreas. This is accomplished by incorporating glucose oxidase into a pH- or temperature-sensitive smart polymer. An insulin-releasing drug-delivery system was produced by the incorporation of glucose oxidase, bovine serum albumin, and insulin into a gel of poly(*N*,*N*-dimethylamino)ethyl methacrylate-*co*-ethylacrylamide)(103,104). Exposure of this system to glucose in the desired physiological concentration range resulted in a reduction in the system pH and swelling of the polymer (as brought about by protonation of the polymer). This swelling causes a release of insulin. Another system based on a polymer complex of poly(*N*-vinyl-2-pyrrolidinone-*co*-phenylboronic acid acrylamide-*co*-dimethylaminopropylacrylamide) and poly(vinyl alcohol) also shows glucose sensitivity. In this system, a stable gel forms at pH 7.4 because of the "covalent" linkage of the boronate–hydroxy groups. The gel contains insulin. Through the addition of glucose, the complex dissociates and transforms the gel to a sol-state (the gel begins to solubilize) resulting in swelling and subsequent insulin release (105).

Tissue Engineering. The use of biomedical materials over the last 20 years has, in most respects, been extremely successful. A wide variety of materials have been developed that have been successfully used to replace hips, heart valves, and the natural lens of the eye, to name but a few successful applications. The major drawback in this area of research, however, is that these materials, for almost all cases, can only perform for short periods of time. No long-term replacements have to date been developed. The clinical needs are even greater in the case of organs, where replacement by organ transplantation is the only option. The area of tissue engineering, however, offers some intriguing possibilities.

The goal of tissue engineering is to create living, three-dimensional tissue/organs using cells obtained from readily available sources, such as cells obtained directly from the patient (31). The ultimate goal in this work is to grow cells specific to a particular organ and then to direct the cell growth to form the

actual organ. This theoretically can be accomplished through the attachment of specific cells to a scaffolding matrix that directs cell attachment, differentiation, and growth. In order to do this amazing feat, a physical scaffold is required to allow for the organization of cells to form the specific organ (to simulate cell growth, migration, and differentiation). These scaffolds need to interact with the cells through highly specific bioreactions that control cell adhesion and growth factor responses. The scaffolds are ideally biodegradable. Some fabulous work in this area has recently been reported.

The use of biodegradable hydrogels as a temporary-support template for cartilage has been reported (106). Cartilage is a biphasic material made up of collagen as the solid support suspended in a gel of proteoglycans. Within this gel are the chondrocytes that are responsible for maintaining the extracellular matrix of cartilage (glycosaminoglycans and type II collagen). For this work the hydrogel calcium alginate was used as the scaffold. The alginate polymer was prepared by dissolving in water and adding calcium ions to form a "complexed" cross-link polymer network. The immobilization of chondrocytes in alginate was accomplished simply by soaking the alginate in a solution of chondrocytes. Researchers have demonstrated that the chondrocytes maintained their structure, were capable of proliferating at rates significantly higher than that of monolayer cultures, maintained their production of glycosaminoglycans and collagen, and formed a mechanically functional matrix in a hydrogel network. This has all led to the first successful experiments that have shown that new cartilage can be created *in vivo* using hydrogel scaffolding.

In a similar concept, the design of biodegradable hydrogels for bone regeneration through growth factor release has been reported (107). In this research effort, gelatin was cross-linked with either glutaraldehyde or carbodiimide. The growth factor was added by solution adsorption into the preformed gelatin hydrogels. The cationic growth factor was held in the gelatin matrix through complexation with the anionic sites along the gelatin backbone. The gelatin enzymatically degrades in the body to release the growth factor. When implanted into a bone defect, the growth factor resulted in accelerated bone regeneration and closed the bone defect.

Wound Dressings. Hydrogels have also been used as wound dressings because most hydrogels are soft, flexible, conform to the wound, are biocompatible, and are permeable to water vapor and metabolites. As wound dressings, they absorb the exudate, do not stick to the wound, allow for access of oxygen to the wound site, and accelerate healing. This is actually a very large market with total sales of synthetic wound dressings, as reported in 1999, of $350 million (108). The dressing is usually applied as a thin preformed/prehydrated film. The hydrogel wound dressings are based on hydrocolloid/hydrogels and alginate dressings. Hydrophilic monomers and polymers used to prepare the hydrogel bandages are based on NVP, poly(ethylene oxide), and poly(vinyl alcohol).

Biosensors. A *biosensor* is a compact device or probe that detects, records, and transmits information regarding a physiological change or the presence of various chemical or biological materials in the environment. A biosensor is a probe that integrates a biological component, such as a biological product (enzyme or antibody), with an electronic component to yield a measurable response. Biosensors are used to monitor changes in the physiological environment (109). The usual

aim of a biosensor is to produce either discrete or continuous electronic signals that are proportional to a single analyte or a related group of analyte (110). The biosensors typically comprise a biological sensing element, a transducer, a signal conditioner, a data processor, a signal generator, and one or more organic or inorganic membranes. Hydrogels have been used as reactive matrix membranes in biosensors. Hydrogels possess several advantages over other materials in that they exhibit rapid and selective diffusion characteristics of the analyte, as well as provide support. For example, there has been a significant amount of success in the area of lipid bilayer based biosensor membranes. One of the early disadvantages of these bilayer probes was their poor ion diffusion characteristic. Hydrogels were successfully used to provide both the required ion diffusion and also the support for the thin lipid bilayer membrane (111). Among the various types of biosensors, those that measure glucose have received the most attention, due primarily to the fact that nearly 6% of the population suffers from diabetes (112). In these biosensors, the consumption of oxygen or the formation of hydrogen peroxide is monitored (enzyme glucose oxidase catalyzes the reaction of glucose and oxygen to form gluconic acid and hydrogen peroxide). Hydrogels are used as enzyme immobilization matrices in these type of biosensors. Enzyme entrapped in a hydrogel of poly(HEMA), polyacrylamide, and poly(vinyl alcohol) have been reported (113).

Surface Coatings Applications of Hydrogels. The surface treatment of polymeric materials is one of the most active research areas in the field of biomedical materials. It is generally agreed that the surface of any material is what dictates its cellular response in the body. Attempts to design biocompatible surfaces have been explored with significant success for many years. This approach, ie, minimization of chemical and physical interactions between the substrate polymer and blood, is the most promising avenue for short-term clinical success. It has been shown that materials functionalized with surfaces consisting of groups such as carboxylate, sulfate, or sulfonate groups act as antithrombogenic agents in that they repel plasma proteins and platelets. The grafting of poly(ethylene oxide) functionalized surfaces onto a variety of material substrate results in an increase in hydrophilicity and provides a reduction of complement activation and platelet adhesion (114). In a similar example, the grafting of poly(HEMA) onto a variety of surfaces has also provided an improvement in antithrombogenic properties. Novel techniques of surface modification, based on molecular imprinting, have led to hydrogel systems with the ability to recognize biological and pharmaceutical compounds. Gel surfaces can be molecularly designed for specific applications (115,116). For example, polyacrylamide gels modified with an adhesion receptor, asioaloglycoprotein, were prepared to study cell adhesion. This work, as well as other similar research efforts, has helped gain an understanding of the required surface functionality for improved receptor response (117,118). Also, in the area of contact lens research, the formation of a hydrogel surface on nonwetting substrates, such as silicone, provides an avenue for a wettable, biocompatible material possessing excellent comfort characteristics. These have all been made possible utilizing techniques such as plasma oxidation, the surface-initiated polymerization of hydrophilic monomers, and the graft functionalization of high molecular hydrophilic polymers through covalent coupling.

Plasma Surface Modification. One of the earliest approaches to design wettable, hydrogel-like surfaces was by glow discharge plasma and/or corona discharge techniques. Corona treatment of polymer surfaces consists of the reaction of oxygen with the polymer surface under an electric discharge to create polar functionality such as carboxyl, ether, carbonyl, or hydroxyl groups. The formation of polar groups raises the surface free energy and allows for surface wetting. Low pressure glow discharge oxygen plasma has also been used successfully on silicone-based materials. This results in a wettable surface that consists primarily of hydrated cross-linked silicate/silanol functionality. In fact, the Silsight™ silicone elastomer lens, commercialized primarily for pediatric aphakic (loss of natural crystalline lens) patients, is made wettable through oxygen plasma techniques.

Since these early efforts to generate wettable surfaces through oxidative treatments, a variety of novel plasma processes have been developed (119). These efforts have focused primarily on plasma polymerization (deposition). This effort is in an attempt to deposit a continuous thin hydrophilic polymer film layer. In this process, polymerizable gases (monomers) are introduced to the plasma reactor during or after the glow discharge treatment. The plasma conditions initiate polymerization that results in deposition of a thin polymer surface, where the surface chemistry can be manipulated by choice of monomer. This technique results in primarily a covalent polymer attachment.

Direct Covalent Coupling. Similar approaches to covalently attached polymers via glow discharge plasma have also been pursued. In these efforts, the polymers were solution-adsorbed and surface-grafted under inert gas plasma. A free-radical mechanism for the grafting has been proposed. This approach has been used to coat a variety of substrates with hydrogels. Upon plasma treatment radicals are formed on the surface that react with oxygen to form hydroperoxy compounds. The homolytic decomposition of the hydroperoxides form radicals that initiate the polymerization (thermal or ultraviolet) of hydrophilic monomers, such as HEMA (120). The adsorption can best be accomplished by using surface-active compounds that preferentially immobilize on the surface before introduction of the plasma.

In addition to the conventional plasma polymerization approaches, a significant number of research programs have focused on the design of wettable surfaces utilizing a combination of glow discharge plasma and polymer grafting through classical chemical reaction techniques (121). One approach demonstrates the successful covalent attachment of a polysaccharide (**21**). In this process, a silicone surface is aminated using glow discharge ammonia plasma. The aminated surface is then reacted with an oxidized dextran to form a covalently attached (via a Schiff-based linkage) dextran. Following reduction to a stable secondary amine linkage, a highly wettable surface is formed (122). Another approach makes use of covalent grafting utilizing solution techniques only. In this example, the vinyl acetate groups of a medical grade poly(ethylene-*co*-vinyl acetate-*co*-vinyl chloride) was saponified using a solution of methanol and sodium hydroxide and then reacted with hexamethylene diisocyanate to form a highly reactive isocyanate-modified surface. The resultant surface is then reacted, again via solution techniques, with an amine functionalized hydrophilic polymer (123).

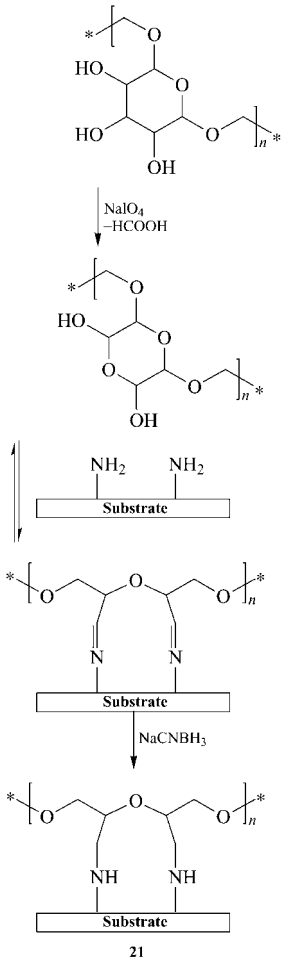

21

Hydrogel Surfaces through In Situ Polymerization Techniques. Several research groups have reported on efforts to design wettable silicone-based materials through *in situ* polymerization techniques. These are attempts to design wettable, biocompatible surfaces without the need for surface treatment. The primary driver for this research is cost. Without the need for a secondary surface treatment, a large reduction in lens cost would be achieved.

Significant progress in this area has been made. It has been shown recently that the polarity of the casting substrate may provide an avenue for surface wetting without surface treatment. The casting of silicone-based formulations from polar mold materials results in a surface rich character. For example, a copolymer based on a fluorinated silicone and the hydrophilic monomer, DMA was cast against the hydrophilic mold resin Barex (copolymer of acrylonitrile and styrene). X-ray photoelectron spectroscopy analysis of the surface showed a threefold increase in surface nitrogen concentration as compared with the same formulation cast from a hydrophobic polypropylene resin. The Barex cast material resulted in

a hydrogel-like surface as a result of the preferential polymerization–migration of DMA at the Barex surface.

The use of polymerizable surfactants (surface-active macromer, SAM) in silicone formulations has been explored to form hydrogel-like surfaces without a surface treatment (124). Several surface-active water-soluble macromers were evaluated. The SAMs were prepared using a two-step synthetic procedure. In this procedure, hydrophobic alkylmethacrylates or fluoromethacrylates monomers are polymerized with polyoxyethylene methacrylates using a functional mercaptan as a chain-transfer agent. The resultant hydroxyl or carboxylate capped macromer (**22**) is further functionalized with a polymerizable methacrylate.

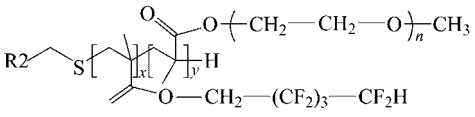

(22)

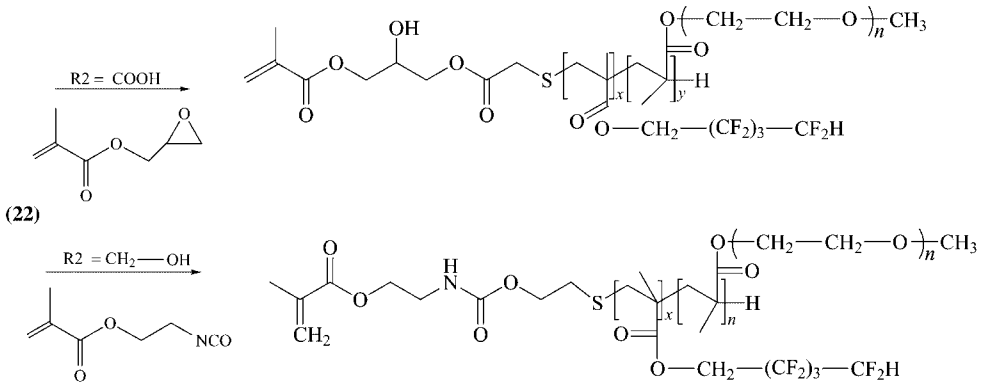

(22)

The SAMs are surface-active, yet possess significant hydrophilic character. They are simply added to a silicone formulation, at concentrations of 0.1–0.5%, and polymerized. It has been shown that the polymerization of SAMs in silicone-based formulations results in a significant increase in surface polarity. This is due to migration of the SAM to the mold–lens interface before polymerization. Clinical performance has also been improved. The incorporation of SAMs has had a positive effect on surface wetting and deposition characteristics.

Nonbiomedical Applications

This article has detailed a variety of biomedical applications of hydrogels. It is important to note, however, that many applications of hydrogels for

nonbiomedical use have been successfully designed. These include the use of hydrogels for chemical valves, bioseparation devices, biomimetic actuators, thermoresponsive surfaces, affinity precipitation, anodes for bridge-building application, water retention for soil application, and disposable diapers the details of which can be found in other articles (10,31,125–128).

BIBLIOGRAPHY

"Contact Lenses" in *EPST* 1st ed., Suppl. Vol. 1, pp. 158–219, by M. F. Refojo, Eye Research Institute of Retina Foundation; "Contact Lenses" in *EPSE* 2nd ed., Vol. 4, pp. 164–173, by H. K. Singer and E. C. Bellantoni, American Optical Corp., and A. R. Leboeuf, Barnes-Hind Pharmaceuticals, Inc.

1. K. Park, W. S. W. Shalaby, and H. Park, *Biodegradable Hydrogels For Drug Delivery*, Technomic Publishing Co, Inc., Lancaster, Pa., 1993, pp. 2–3.
2. J. M. Guenet, *Thermoreversible Gelation of Polymers and Biopolymers*, Academic Press, New York, 1992.
3. N. Peppas and Y. Yang, *Contact Lens* **7**, 300 (1981).
4. P. J. Flory, *J. Am. Chem. Soc.* **78**, 5222 (1956).
5. P. J. Flory, *Principles of Polymer Chemistry*, Cornell University Press, Ithaca, N.Y., 1953, Chapt. "XII", pp. 495–540.
6. J. M. Rosiak and F. Yoshii, *Nucl. Instrum. Methods Phys. Res.* **151**, 56–64 (1999).
7. L. J. C. Peschier and co-workers, *Biomaterials* **14**, 945–952 (1993).
8. N. A. Peppas and S. R. Lustig, in N. Peppas, ed., *Hydrogels in Medicine and Pharmacy*, Vol. **1**, CRC Press, Boca Raton, Fla., 1987, pp. 57–83.
9. V. Kudella, in H. Mark, N. Bikales, C. Overberger and G. Menges, eds., Encyclopedia of Polymer Science and Engineering, Vol. **7**, Wiley-Interscience, New York, 1987, p. 787.
10. S. D. Bruck, *J. Biomed. Mater. Res.* **7**, 387 (1973).
11. U.S. Pat. 5,739,236 (1998), R. J. Bowers, S. Jones, and P. Stratford (to Biocompatibles Ltd.).
12. U.S. Pat. 4,436,887 (1984), R. C. Chromecek and co-workers (to Bausch and Lomb).
13. U.S. Pat. 5,270,418 (1993), G. D. Friends and J. F. Künzler (to Bausch and Lomb).
14. J. Künzler, *Trends Polym. Sci.* **4**, 52 (1995).
15. U.S. Pat. 4,649,184 (1987), T. Yoshikawa (to Toyo Contact Lens Co., Ltd.).
16. U.S. Pat. 5,321,108 (1994), J. Künzler and R. Ozark (to Bausch and Lomb).
17. J. Künzler and R. Ozark, J. Appl. *Polym. Sci.* **65**, 1081 (1997).
18. U.S. Pat. 4,139,513 (1979), K. Tanaka and co-workers.
19. U.S. Pat. 4,260,725 (1981), P. L. Keogh, J. Künzler, and C. C. Niu.
20. L. Junqueira, J. Carneiro, and R. Kelley, *Basic Histology*, Appleton and Lange, Norwalk, conn., 1992.
21. W. S. W. Shalaby and K. Park, in J. C. Salamone, ed., *Polymeric Materials Encyclopedia*, CRC Press, Boca Raton, Fla., 1996, p. 2125.
22. A. Hoffman, in R. Kronenthal, Z. Oser and E. Martin, eds., *Polymer in Medicine and Surgery*, Plenum, New York, 1975.
23. S. D. Brook, *Properties of Biomaterials in Physiological Environments*, CRC Press, Boca Raton, Fla., 1980.

24. J. Andrade, ed., *Hydrogels for Medical and Related Applications*, American Chemical Society, Washington, D.C., 1976.
25. C. L. McCormick and J. Bock, in H. Mark, N. Bikales, C. Overberger, and G. Menges, eds., *Encyclopedia of Polymer Science and Engineering*, Vol. **17**, Wiley-Interscience, New York, 1989, pp. 737–784.
26. A. L. Lehninger, *Principles of Biochemistry*, Worth Publishers, New York, 1982, pp. 127–137.
27. T. Takagi, K. Takahashi, M. Aizawa, and S. Miyata, in *Proceedings of the First International Conference on Intelligent Materials*, Technomic Publishing Co., Inc., Lancaster, Pa., 1993.
28. H. G. Schield, *Prog. Polym. Sci.* **17**, 163–249 (1992).
29. A. S. Hoffman, *Artificial Organs* **19**, 458–467 (1995).
30. I. Y. Galaev and B. Mattiasson *TIBTECH* **17**, 335–340 (1999).
31. L. G. Griffith, *Acta Mater.* **48**, 263–277 (2000).
32. R. K. Kulkarni and co-workers, *J. Biomed. Mater. Res.* **5**, 169 (1971).
33. H. Park and K. Park, in R. Ottenbrite, S. Huang, and K. Park, eds., *Hydrogels and Biodegradable Polymers for Bioapplications*, ACS Symposium Series, Vol. **627**, American Chemical Society, Washington, D.C., 1996, pp. 1–10.
34. Ref. 8, pp. 11–12.
35. U.S. Pat. 5,310,779 (1994), Y. C. Lai (to Bausch and Lomb).
36. D. E. Gregonis, C. Chen, and J. Andrade, in Ref. 24, ACS Symposium Series, Vol. **31**, p. 88.
37. Y. Tsukahara and co-workers, *J. Polym. Sci. Part A: Polym. Chem.* **27**, 1099–1114 (1989).
38. G. Odian, *Principles of Polymerization*, 3rd ed., John Wiley and Sons, Inc., New York, 1991.
39. Ref. 1, pp. 35–66.
40. H. Akin and N. Hasirci, *Proc. Am. Chem. Soc. Polym. Div. Polym. Prepr.* **36**, 384–385 (1995).
41. K. Yamada and co-workers, *J. Neurosurg* **86**, 871, (1997).
42. A. Rubinstein, D. Nakar, and A. Sintov, *Pharm. Res.* **9**, 276–278 (1992).
43. Y. M. Lizuka and co-workers, *J. Appl. Polym. Sci.* **56**, 73–77 (1995).
44. N. Peppas, ed., *Hydrogels in Medicine and Pharmacy*, Vol. **2**, CRC Press, Boca Raton, Fla., 1987, pp. 1–48.
45. J. J. Sperinde and L. G. Griffith, *Macromolecules* **30**, 5255–5264 (1997).
46. A. S. Hoffman, *Radiat. Phys. Chem.* **9**, 207 (1977).
47. J. M. Rosiak and F. Yoshii, *Nucl. Instrum. Methods Phys. Res.* **151**, 56–64 (1999).
48. E. Tsuchida and K. Abe, in H. J. Cantow, ed., *Advances in Polymer Science*, Vol. **45**, Springer-Verlag, New York, 1982.
49. A. Rembaum, *Appl. Polym. Symp.* **22**, 299 (1973).
50. Y. Hagino and S. J. Huang, *Proc. ACS Div. Polym. Mater. Sci. Eng.* **72**, 249–250 (1995).
51. T. L. Bowersock and co-workers, *Proc. Am. Chem. Soc., Div. Polym. Mater.* **35**, 405–406 (1994).
52. H. Ohno, K. Abe, and E. Tsuchida, *Makromol. Chem.* **179**, 755 (1978).
53. F. E. Bailey and H. G. France, *J. Polym. Sci.* **49**, 397 (1961).
54. U.S. Pat. 4,085,168 (1978), R. Milkovich and M. T. Chiang (to CPC International Inc.).
55. U.S. Pat. 4,095,877 (1978), O. Wichterle, V. Stoy, and A. Stoy (to Ceskoslovenska akademic ved, (University in Prague).).
56. T. Nakashima and K. Takakura, J. Biomed. *Mater. Res.* **11**, 787 (1977).
57. T. Okano, M. Kitayama, and I. Shinohara, *J. Appl. Polym. Sci.* **22**, 369 (1978).

58. T. Okano and co-workers, *J. Biomed. Mater. Res.* **15**, 393 (1981).
59. K. R. Shah, in B. M. Culbertson, ed., *Contemporary Topics in Polymer Science*, Vol. **6**, Plenum, New York, 1989, p. 486.
60. K. R. Shah, in Ref. 21, pp. 3092–3097.
61. J. Künzler and J. McGee, *Chem. Ind.* **16**, 651, 1995.
62. U.S. Pat. 3,220,960 (1965), O. Wichterle and D. Lim (to Ceskoslovenska akademic ved, (University in Prague)).
63. S. Hosaka, J. Biomed. *Mater. Res.* **14**, 557 (1980).
64. O. Wichterle and R. Chromecek, *J. Polym. Sci.* **16**, 4677 (1969).
65. U.S. Pat. 3,957,362 (1976), W. Mancini, D. Korb, and M. Refojo (to Corneal Sciences, Inc.).
66. U.S. Pat. 4,625,009 (1986), T. Izumitani and co-workers.
67. B. Holden, G. Mertz, and J. McNally, *Invest. Ophthalmol. Vis. Sci.* **24**, 218 (1983).
68. E. J. Castillo and co-workers, *Biomaterials* **7**, 9–16 (1986).
69. L. Minarik and *J. Rapp, Contact Lenses (CLOA Journal)* **15**, 185–188 (1989); G. Orsborn and S. Zantos, *Contact Lenses (CLOA Journal)* **14**, 81–85 (1988).
70. J. Brandrup and J. Immergut, eds., *Polymer Handbook*, 3rd ed., Vol. **VI**, Wiley-Interscience, New York, 1989, p. 435.
71. Eur. Pat. 396,364 (1990), R. Bambury and D. Seelye (to Bausch and Lomb).
72. G. L. Grobe and co-workers, *Polym. Prepr. (Am. Chem. Soc., Div. Mater. Sci.)* **80**, 108 (1999).
73. U.S. Pat. 6,030,416 (2000), P. Huo, S. Zhou, and C. Liau (to Pharmacia & Upjohn AB).
74. U.S. Pat. 5,331,073 (1994), J. Weinschank and R. Christ.
75. R. Larsson and co-workers, *Biomaterials* **10**, 511–516 (1989).
76. M. F. Refojo, in P. Christel, A. Meunier, and A. J. C. Lee, eds., *Biological and Biomechanical Performance of Biomaterials*, Elsevier Science, Amsterdam, 1986.
77. T. Kohnen, R. J. Lambert, and D. D. Koch, *Ophthalmology* **104**, 1277–1286 (1997).
78. D. Schonfeld, *Ocular Surgery News*, 10–11 (2001).
79. S. J. Holland, B. J. Tighe, and P. L. Gould, *J. Controlled Release* **4**, 155–180 (1986).
80. N. Peppas, in Ref. 8, pp. 102–113.
81. D. Shino and co-workers, in *Proceedings of the First International Conference on Intelligent Materials*, Technomic Publishing Co., Inc., Lancaster, Pa., 1993, pp. 301–304.
82. S. Kitano and co-workers, *J. Controlled Release* **19**, 162–170 (1992).
83. R. W. Baker, M. E. Tuttle, and R. Helwing, *Pharm. Technol.* **8**(2), 26–30 (1984).
84. P. Hocking, *J.M.S.-Rev. Macromol. Chem. Phys., Part C* **32**, 35–54 (1992).
85. J. A. Hubbell, *MRS Bull.* **21**, 33 (1996).
86. J. Heller and co-workers, *Biomaterials* **4**, 262 (1983).
87. W. Mark Saltzman, *Drug Delivery*, Oxford University Press, Oxford 2001, pp. 259–261.
88. D. S. T. Hsieh, ed., *Controlled Release Systems: Fabrication Technology*, Vol. **2**, CRC Press, Boca Raton, Fla., 1988, pp. 61–73.
89. Ref. 88, pp. 74–75.
90. H. A. J. Struyker-Boudier, ed., *Rate-Controlled Drug Administration and Action*, CRC Press, Boca Raton, Fla., 1985, pp. 24–27.
91. S. K. Mallapragada and N. A. Peppas, *J. Controlled Release* **45**, 87–94 (1997).
92. R. Jones, *Curr. Opin. Cardiovasc., Pulm. Renal Invest. Drugs* **2**, 284–291 (2000).

93. S. J. Holland, B. J. Tighe, and P. L. Gould, *J. Controlled Release* **4**, 155–180 (1986).
94. A. S. Sawhney, C. P. Pathak, and J. A. Hubbell, *Macromolecules* **26**, 581–587 (1993).
95. J. Kopecek and P. Kopeckova, *Chem. Listy* **91**, 600–603 (1997).
96. T. Pouyani and G. D. Prestwich, *Bioconjugate Chem.* **5**, 339–347 (1994).
97. N. A. Peppas, *Curr. Opinm. Colloid Interface Sci.* **2**, 531–537 (1997).
98. N. A. Peppas, in R. Gurny, H. E. Junginger, and N. A. Peppas, eds., *Pulsatile Drug Delivery*, Wissenschaftlishe Verlagsgesellschaft, Stuttgart, 1993, pp. 41–56.
99. S. W. Kim, in N. Ogata, S. W. Kim, J. Feijen, and T. Okano, eds., *Advanced Biomaterials in Biomedical Engineering and Drug Delivery Systems*, Springer, Tokyo, 1996, pp. 125–133.
100. A. Gutowska and S. W. Kim, *Proc. Am. Chem. Soc. Div. Polym. Chem.* **212**, 115 (1996).
101. S. Kitano and co-workers, in *Proceedings of the First International Conference on Intelligent Materials*, Technomic Publishing Co., Inc., Lancaster, Pa., 1993, pp. 383–388.
102. T. Aoki and co-workers, *Polym. J.* **28**, 371–374 (1996).
103. J. Kost, *Pulsed and Self-Regulated Drug Delivery*, CRC Press, Boca Raton, Fla., 1990.
104. M. Goldraich and J. Kost, *Clin. Mater.* **13**, 135–142 (1993).
105. T. Aoki and co-workers, *Polym. J.* **28**, 371–374 (1996).
106. S. K. Ashiku, M. A. Randolph, and C. A. Vacanti, *Mater. Sci. Forum* **250**, 129–150 (1997).
107. Y. Tabata, M. Yamamoto, and Y. Ikada, *Pure Appl. Chem.* **70**, 1277–1282 (1998).
108. Synthetic Wound Dressings Market, Theta Report No. 610, New York, 1996.
109. K. Bruce Jacobson *Oak Ridge Natl. Lab Rev.* **29**(3), 1–18, 1996.
110. A. P. F. Turner, I. Karube and G. S. Wilson, *Biosensors: Fundamentals and Applications*, Oxford University Press, Oxford, 1987.
111. H. T. Tien and co-workers, *Anal. Sci.* **14**, 3–18, 1998.
112. W. J. Wizeman and P. Kofinas, *Biomaterials* **22**, 1485–1491, 2001.
113. M. Koudelke-Hep, P. van der Wal, D. J. Strike, and N. F. de Rooij, in Ref. 21, pp. 3368–3371.
114. D. Klee and H. Hoecker, in *Advances in Polymer Science*, Vol. **149**, Springer, Verlag, Berlin, 2000, pp. 1–57.
115. W. J. Wizeman and P. Kofinas, *Biomaterials* **22**, 1485–1491 (2001).
116. P. Bures and co-workers, *J. Controlled Release* **72**, 25–33 (2001).
117. P. H. Weigel and co-workers, *J. Biol. Chem.* **253**, 330 (1978).
118. L. G. Griffith and S. T. Lopina, *Biomaterials* **19**, 979 (1998).
119. E. M. Liston, L. Martinu, and M. R. Wertheimer, in M. Strobel, C. S. Lyons, and K. L. Mittal, eds., *Plasma Surface Modification of Polymers*, VSP, Utrecht, the Netherlands, 1994, pp. 3–39.
120. P. W. Rose and E. M. Liston, *Plast. Eng.* **41**, 41 (1985).
121. M. S. Sheu, A. S. Hoffman, B. D. Ratner, J. Feijen, and J. M. Harris, in Ref. 119, pp. 197–208.
122. L. Dai and co-workers, in B. D. Ratner and D. G. Castner, eds., *Surface Modification of Polymeric Materials*, Plenum Press, New York, 1996, pp. 147–156.
123. J. Wirshing, D. Klee, H. Hoecker, A. Dekker, and C. Mittermayer, in *Proc. 12th European Conference on Biomaterials*, Porto, 1995, p. 104.
124. P. V. Valint, D. Ammon, G. L. Grobe, and J. McGee, in Ref. 122, pp. 21–26.

125. M. Gupta and B. Mattiasson, in G. Street, ed., *Highly Selective Separations in Biotechnology*, Blackie Academic & Professional, London, 1994, pp. 7–33.
126. A. Hoffman, *J. Controlled Release* **6**, 297–305 (1987).
127. W. Heitz and co-workers, *Angew. Makromol. Chem.* **123/124**, 147 (1984).
128. G. Burillo and T. Ogawa, *Radiat. Phys. Chem.* **18**, 1143 (1981).

JAY FRIEDRICH KÜNZLER
Bausch and Lomb Inc.

β-HYDROXYALKANOATES.

See POLY3-(HYDROXYALKANOATES).

HYPERBRANCHED POLYMERS

Introduction

Material engineers have been trying to improve polymer properties with a variety of technologies and ingenuity. Polymers have been modified in numerous different ways in order to alter their properties. The most utilized ways to alter properties have either been to simply develop a new monomer and synthesize a new polymer or to modify an existing polymer by some chemical route. Modification normally consists of changing a catalyst or using different comonomers.

In nature, condensation of polyfunctional monomers, having two different functional groups, occurs under the enzymatic control, resulting in tree-shaped, highly branched, but still soluble, macromolecules. In 1952, Paul Flory (1) theoretically described hyperbranched polymers obtained by condensation of AB_x-monomers in a statistical growth process. Flory pointed out that such a molecule would have one A-group, DP+1 B-groups, and poor mechanical properties because of high branching and absence of chain entanglements. The synthesis of hyperbranched polymers remained an unsolved challenge for synthetic chemists and it was not until the late 1980s that the concept was reawakened by Kim and Webster who also coined the term hyperbranched (2,3).

Since then, synthetic chemists have explored numerous ways to achieve statistically branched macromolecular structures. In theory, all polymer-forming reactions can be utilized for the synthesis of hyperbranched polymers. In practice, some reactions are far more suitable than others.

The synthesis of dendrimers has been carried out in parallel to the exploration of hyperbranched polymers. The number of papers describing dendrimers by far exceeds the number of papers concerning hyperbranched polymers.

Encyclopedia of Polymer Science and Technology. Copyright John Wiley & Sons, Inc. All rights reserved.

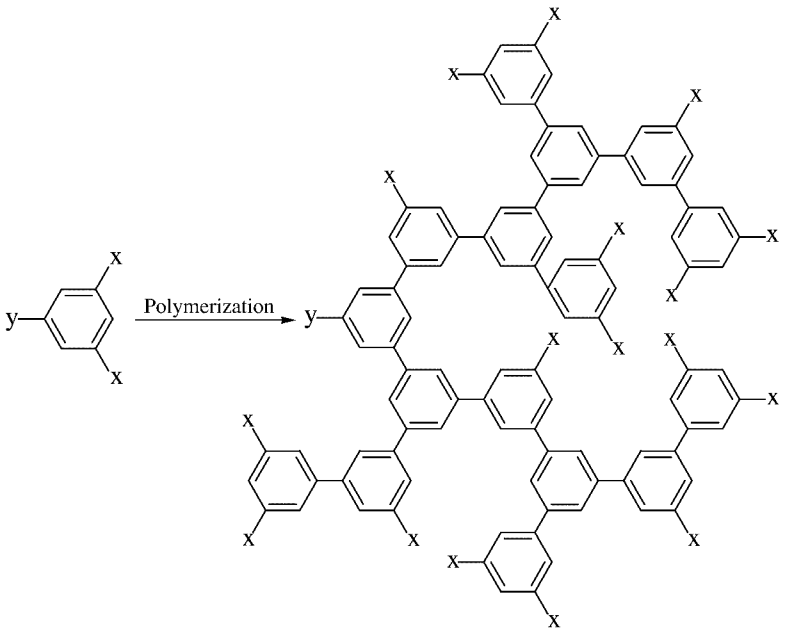

Fig. 1. Polyphenylenes were prepared via Pd(0) [such as $Pd(PPh_3)_4$] or Ni(II) catalyzed coupling reactions of various dihalophenyl derivatives such as dibromophenylboronic acid (3–5).

Monomers

Polyphenylenes. One of the first hyperbranched polymers described in the literature was the class of polyphenylenes (3–5). The polyphenylenes were prepared via Pd(0)- or Ni(II)- catalyzed coupling reactions of various dihalophenyl derivatives such as dibromophenylboronic acid. The polymers were highly branched polyphenylenes with terminal bromine groups which could be further transformed into a variety of structures, eg, methylol, litiate, or carboxylate (Fig. 1). The halofunctional hyperbranched polymers obtained have M_n between 2 and 32 kg/mol depending on the polymerization conditions.

Aliphatic Polyesters. Polyesters are an important class of condensation polymers, and the availability of a few commercial dihydroxy carboxylic acids has triggered several research groups to look into hyperbranched polyesters in great detail. Several old patents concerning highly branched and hyperbranched polyesters exist. One of the oldest patents, of 1972, concerns the polymers obtained by condensation of polyhydroxy monocarboxylic acids and their use in coatings (6). Essentially, one monomer, 2,2-bis(methylol)propionic acid (bis-MPA), has been used for the preparation of hyperbranched aliphatic polyesters. The cocondensation of bis-MPA and a four-functional polyol [di-(trimethylol)propane] resulting in hydroxy-functional hyperbranched polyesters has been described (7). The degree of branching has been found to be 0.45. The molecular weight and number of terminal hydroxyl groups can be varied by altering the stoichiometric ratio between the polyol core and bis-MPA.

Similar materials, hyperbranched polyesters based on bis-MPA and a polyol, are now commercially available from Perstorp AB (http://www.perstorp.com). under the trade name Boltorn (Fig. 2). The average number of hydroxyl groups per molecule can be tailored between 8 and 64 and the molecular weight can be varied between ca 2,000 and 11,000. The copolymerization of bis-MPA and a polyol core keeps the molecular weight distribution fairly low, typically below 2.

Aromatic Polyesters. Considerable attention has been paid to aromatic hyperbranched polyesters synthesized from monomers derived from 3,5-dihydroxy benzoic acid (DBA). The thermal stability of DBA is not good enough to allow direct esterification of DBA, and therefore chemical modifications are necessary. Some aromatic monomers used for the synthesis of hyperbranched polymers are presented in Figure 3.

In a systematic investigation of hyperbranched polyesters derived from 3,5-bis(trimethylsiloxy) benzoyl chloride (8–11), the monomers were condensed at 150–200°C and also by using low temperature esterification procedures. The polymers were found to have a degree of branching close to 0.55 and apparent molar masses (M_n) in the range of 16–60 kDa, as determined by gpc relative to linear polystyrene standards. Several functionalizations were made on the phenolic end groups in order to investigate how the nature of the end groups affected the glass-transition temperature (T_g).

Another investigation (12,13) describes hyperbranched polyesters derived from 3,5-bis(trimethylsiloxy) benzoyl chloride and from 3,5-diacetoxybenzoic acid, both of which yield phenolic polyesters after hydrolysis. Hyperbranched polyesters obtained from melt condensation of 5-acetoxyisophthalic acid and 5-(2-hydroxy)-ethoxyisophthalic acid respectively were also studied. The latter yields a soluble product while the former results in an insoluble polymer because of formation of anhydride bridges.

In a comparison (14) of the polyesterification of silylated 5-acetoxyisophthalic acid and of free 5-acetoxyisophthalic acid, the nonsilylated monomer yielded insoluble products, indicating that a cross-linked material was obtained. The degree of branching for these materials was found to be close to 0.6 and independent of reaction conditions. Star-shaped and hyperbranched polyesters have also been synthesized by polycondensation of trimethylsilyl 3,5-diacetoxybenzoate (15) and a number of hyperbranched polymers based on the trimethylsilylester of β-(4-hydroxyphenyl)propionic acid have been reported (16).

Aromatic hyperbranched polyesters have been synthesized from 5-(2-hydroxyethoxy)isophthalate copolymerized with 1,3,5-benzenetricarboxylate (core molecule) as a moderator of the molar mass (17). The degree of branching was found to be 0.60–0.67, as determined by ^{13}C nmr. Apparent molar masses (M_w) were found to be 5–36 kDa according to sec characterization using linear polystyrene standards.

Polyester-amides. DSM is marketing the poly(ester-amide) Hybrane™ which is the second commercially available hyperbranched polymer (Fig. 4) (http://www.hybrane.com). It is also a hydroxy-functional product, but instead of ester linkages it comprises amide and ester connectivities. The synthesis is accomplished in two steps: cyclic anhydrides are reacted with diisopropanolamine to give an amide-intermediate, carrying two hydroxyl groups and one carboxylic acid. The subsequent polymerization takes places via an oxazolinium-intermediate, which

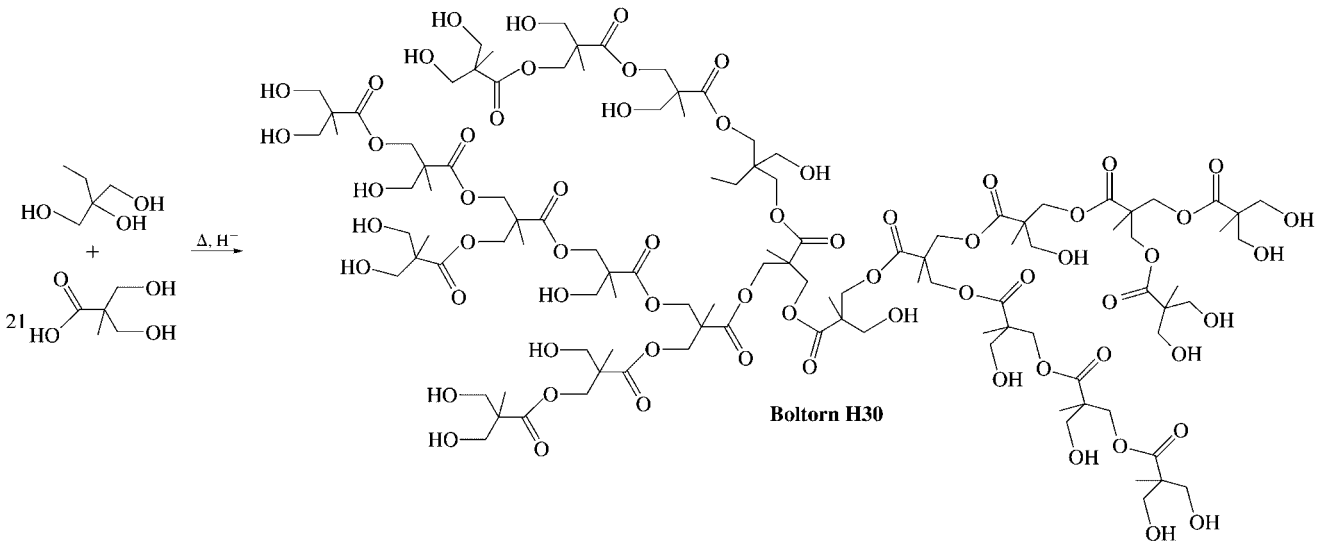

Fig. 2. Hyperbranched polyester based on bis-MPA and a polyol, commercially available from Perstorp AB (http://www.perstorp.com) under the trade name Boltorn.

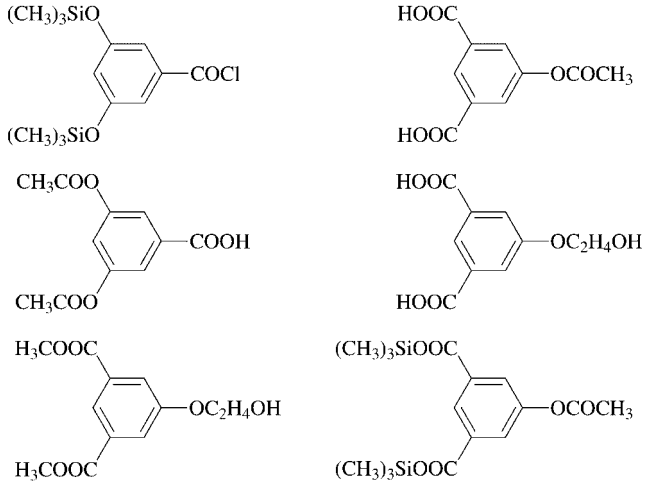

Fig. 3. Aromatic monomers used for the synthesis of hyperbranched polyesters (3–5).

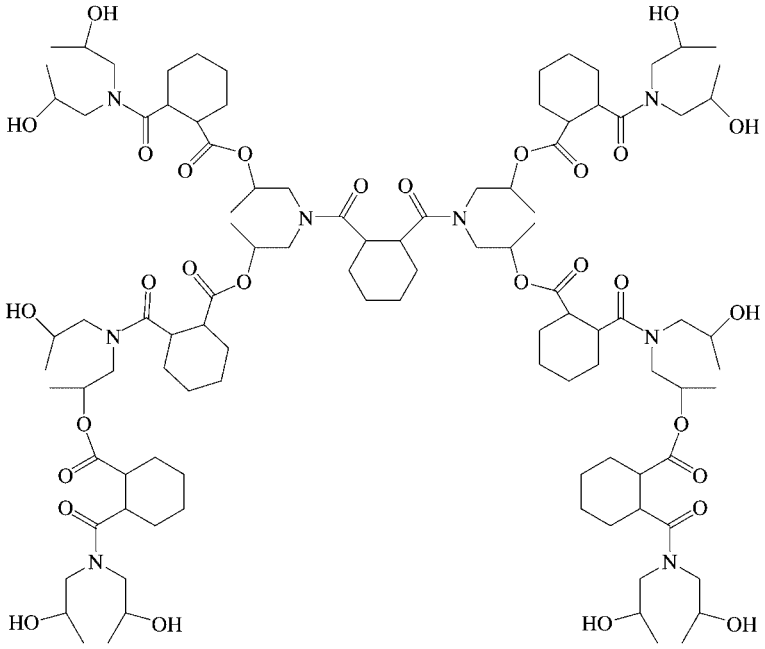

Fig. 4. Poly(ester-amide) Hybrane (http://www.hybrane.com).

results in the formation of a hydroxy-functional hyperbranched polymer. The properties of Hybrane can be altered by the choice of anhydride compounds.

Polyethers. A one-pot synthesis of hyperbranched benzylic polyethers based on self-condensation of 5-(bromomethyl)-1,3-dihydroxybenzene in solution has been developed (18). The effect of variation of reaction conditions such as monomer concentration, time, and type of solvent was explored and it was

concluded that an increased reaction time and polar solvents increased the molar mass while a change in monomer concentration had less effect. Polymers with molar masses up to 120 kg/mol, as determined with low angle laser light scattering, were obtained under optimum conditions. The desired O-alkylation was accompanied by approximately 30% C-alkylation. Therefore the degree of branching was difficult to determine. It was also shown that the phenolic end groups could easily be transformed into other moieties such as benzyl, silyl, or acetate end groups with a subsequent change in T_g and solubility of the polymers. However, one main problem which appeared was that the monomer showed to be extremely allergenic, which limits the use of this structure.

Aromatic Poly(ether-ketone)s. The synthesis of hyperbranched aromatic poly(ether-ketone)s based on monomers containing one phenolic group and two fluorides which were activated toward nucleophilic substitution by neighboring groups has been described (19,20). The molar mass and polydispersity of the formed poly(ether-ketone)s could be controlled by reaction conditions such as monomer concentration and temperature. The formed polymers had high solubility in common solvents such as THF.

Also, the synthesis of hyperbranched poly(ether-ketone)s based on AB_2-monomers having either one phenolic and two fluoride groups or two phenolic and one fluoride groups has been described (21).

Properties of Hyperbranched Polymers

One reason for the emerging interest in hyperbranched polymers and other macromolecular architectures is the possibility to obtain improved material properties compared to conventional, linear polymers. Already, Flory predicted that highly branched polymers would exhibit different properties compared to linear polymers (1). He stipulated that the amount of entanglements would be lower for polymers based on AB_x-monomers with subsequent reduction in mechanical strength, and this was one of the reasons why these polymers at that point were abandoned. Changes in properties related to architectural changes in hyperbranched polymers rather than chemical changes have to some extent been evaluated but a full understanding is still lacking. Two questions in this area of late have been focused on the extent to which these changes in properties occur and also why they occur.

Solution Properties. One of the first properties that was reported to differ for hyperbranched polymers as compared to linear analogues was the high solubility induced by the branched backbone. Hyperbranched polyphenylenes have very good solubility in various solvents as compared to linear polyphenylenes which have very poor solubility and the solubility depends to a large extent on the structure of the end groups, eg, highly polar end groups such as carboxylates would make the polyphenylenes even water-soluble (2).

Not only good solubility but also solution behavior differs for hyperbranched polymers compared with linear polymers. Hyperbranched polymers such as hyperbranched aromatic polyesters (12,13) exhibit a very low α-value in the Mark–Houwink–Sakurada equation and low intrinsic viscosities. This is consistent with highly branched and compact structures. A comparison has been made between linear polymers, hyperbranched polymers, and dendrimers with respect to

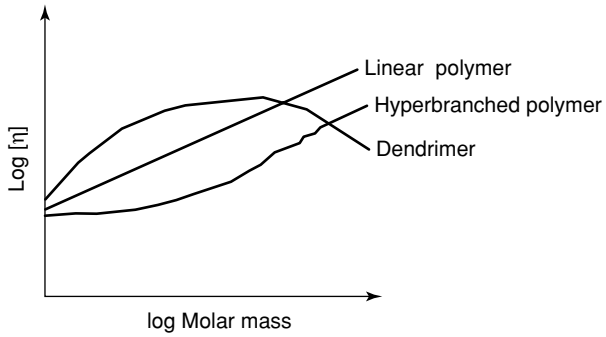

Fig. 5. Comparison between linear polymers, hyperbranched polymers, and dendrimers with respect to intrinsic viscosities as a function of molar mass (22).

intrinsic viscosities as a function of molar mass, which clearly shows the differences induced by variations in the backbone architecture (Fig. 5) (22).

Another special feature for dendritic polymers is the possibility to combine an interior structure with a certain polarity with a shell (end groups) having another polarity, eg, a hydrophobic inner structure and hydrophilic end groups. For example, hyperbranched polyphenylenes with carboxylate end groups have been described as unimolecular micelles where the carboxylate end groups make the polymer water-soluble and the hydrophobic interior can host a guest molecule (4). This has also been described by other authors (21), who solubilized hydrophobic molecules in water by using hyperbranched aromatic poly(ether-ketone)s having acid end groups. They did not see any critical micelle concentration (CMC) but observed a steady increase in solubility of the hydrophobic compound with polymer concentration. From these observations they concluded that a unimolecular micelle behavior applied. In a recent review (23), the guest-host possibility is described for various dendritic polymers with the aim toward medical applications such as drug delivery.

The size of dendritic polymers in solution has been shown to be greatly affected by solution parameters such as polarity and pH. For example, it has been shown that the size of dendrimers with carboxylic acid end groups in water can be increased by as much as 50% on changing the pH (24).

Thermal Properties. One of the first questions that arises when looking at a new group of polymers such as hyperbranched polymers is what determines the glass-transition temperature. The normal interpretation of T_g is related to relatively large segmental motions in the polymer chain segments, and the role of the end groups diminishes above a certain molecular weight. This is different in hyperbranched polymers since segmental motions are affected by the branching points and the presence of numerous end groups. The glass transition has instead been proposed (4,5) to be a translational movement of the entire molecule instead of segmental movement, hence increasing the importance of the end group structure. The backbone part of hyperbranched polymers was also suggested to affect the T_g but to a much lesser extent. The glass-transition temperature is one of the properties that has been reported for most of the hyperbranched polymers

described in the literature. The results have been either based on calorimetric or rheological measurements. Values of T_g for a series of hyperbranched aromatic polyesters with different end groups have been presented in a review paper (25). It was shown that the chemical structure of the end groups had a large impact on the T_g. The glass-transition temperature shifted as much as 100°C (from 255 to 150°C), going from carboxylic acid to acetate end groups. This and other reports (26) show the large impact of end group structure on the T_g, hence indicating the importance of this structural part. The backbone of course also affects the T_g, eg, an aliphatic polyester has a much lower T_g than an aromatic one (25). The T_g for polyether dendrimers has been found to follow a modified Flory equation where the amount and structure of end groups are accounted for indicating a similarity with T_g for linear polymers (27). However, no full model to predict the T_g for hyperbranched polymers exists since several other factors such as degree of branching, steric interactions due to crowding, backbone rigidity, and polarity in combination also play an important role for the glass-transition temperature. The glass-transition temperature of dendritic polymers is also discussed in another paper (28).

The thermal stability of hyperbranched polymers is related to the chemical structure in the same manner as that for linear polymers, eg, aromatic esters are more stable than aliphatic ones. The use of hyperbranched polymers have, however, in some cases been shown to improve the thermal stability when used as additives. An increased thermal stability of polystyrenes has been shown when a small amount of a hyperbranched polyphenylene was used as a rheology modifying additive to polystyrene.

A study of the PVT properties of hyperbranched aliphatic polyesters (29) showed that these polyesters were dense structures with smaller thermal expansion coefficients and lower compressibility compared to some linear polymers.

Mechanical and Rheological Properties. The rheological properties for hyperbranched polymers are characterized by a Newtonian behavior in the molten state, ie, no shear thinning or thickening is observed (29), indicating a lack of entanglements for these polymers. The nonentangled state imposes rather poor mechanical properties, resulting in brittle polymers. This has limited the use of these polymers as thermoplastics to applications where the mechanical strength is of minor importance. The large amount of branching also makes most of these polymers amorphous, although exceptions exist. Hence, these polymers are mainly suitable as additives or as thermosets when high mechanical strength is required for a certain application.

The melt behavior has been shown to be greatly affected by the structure of the end groups where an increase in polarity of the end groups can raise the viscosity several orders of magnitude (30) (Fig. 6). This is of great importance when looking at applications where a low viscosity is essential for the processing of the material (31).

Another difference is the relationship between molar mass and melt viscosity. The increase in melt viscosity with molar mass for linear polymers is linear with a transition when the molecular weight reaches the critical mass for entanglements M_c, where the slope increases. This is different for hyperbranched polymers. The viscosity increase is less pronounced and levels out at higher molar masses (29).

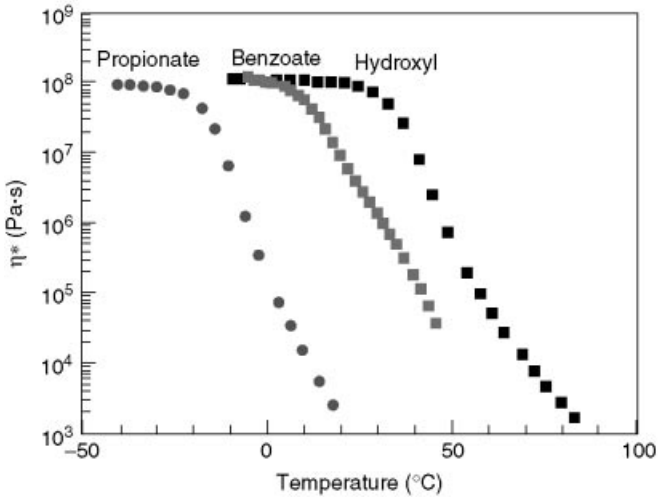

Fig. 6. Hyperbranched polyester based on bis-MPA and a polyol with end groups of different polarities (30).

Hyperbranched polymers are often referred to as Amorphous Polymers since the branching of the backbone reduces the ability to crystallize in the same manner as for linear polymers. Some exceptions have, however, been presented where the polymers have been modified to induce crystallization. Hyperbranched aliphatic polyesters were made semicrystalline by attaching alkyl chains with 14 carbons or longer as end groups (32). The crystallization was affected by several factors such as length of the end groups and the size of the hyperbranched polyester. Different combinations of these actors yielded different transition temperatures as well as different crystalline structures.

Polymerization

Polycondensation. The step-growth polymerization of AB_x-monomers is by far the most utilized synthetic pathway to hyperbranched polymers. A number of AB_2-monomers, suitable for step-growth polymerizations, are commercially available. This has, of course, sparked off the interest for hyperbranched condensation polymers, and a wide variety has been presented in the literature (11,25,33,34).

A typical condensation procedure involves the one-step reaction where the monomer and suitable catalyst/initiator are mixed and heated to the required reaction temperature. To accomplish a satisfactorily conversion, the low molar mass condensation product formed through the reaction has to be removed. This is most often pursued by a flow of inert gas and/or by reducing the pressure in the reaction vessel. The resulting polymer is usually used without any purification or, in some cases, after precipitation of the dissolved reaction mixture into a nonsolvent.

When polymerizing highly functional monomers one must always consider the occurrence of unwanted side reactions leading to the onset of gelation. In

the reacting AB_x-system the preferential reaction has to be A reacting with B. Unwanted side reactions have to be suppressed. Even a very low amount of A–A or B–B reactions would inevitably lead to gelation.

The one-pot polymerization of AB_2-monomers offers no control over molecular weight, and subsequently, gives rise to highly polydisperse polymers (1). The copolymerization of AB_2-monomers with B_y-molecules introduces a tool not only to control the molecular weight but also to reduce the molecular weight distribution.

In a classical step-growth polymerization of AB-monomers, backbiting occurs, resulting in formation of intramolecular cyclics. This of course puts the molecular growth to an end, since the functional groups are lost. When polymerizing AB_2-monomers, there is a possibility of losing the unique focal point because of intramolecular cyclics. This leads to the loss of the reactive A-group in the focal point but the cyclized molecule still holds a number of reactive B-groups, which can lead to further increase in molecular weight.

However, the maximum molecular weight and the rate of polycondensation are reduced by the occurrence of cyclization reactions. Although, one might speculate that a moderate degree of cycle formation is desired since this will reduce the molecular weight distribution.

One way to reduce the cycle formation is to add the AB_2-monomer successively throughout the reaction in a so called slow-addition. Several authors have shown that slow addition of monomer leads to a reduction in side reactions and an increase in molecular weight (35,36). Several authors have studied the occurrence of cyclization in hyperbranched systems (37,38).

Assuming that all B-groups have the same reactivity, the chemical reaction giving rise to a branched molecule is identical to the reaction resulting in a linear polymer. Statistically, this will eventually result in a hyperbranched polymer. However, dependent on the chemical structure of the monomer, steric effects might favor the growth of linear polymers. Computer simulations of condensation of AB_x-monomers and co-condensation of AB_x-monomers with B_y-functional cores have been published. Only a few papers deal with the experimentally studied structure buildup in hyperbranched polymers (39).

One discrepancy with condensation polymers is that they are sensitive toward hydrolysis, which might restrict the use of such polymers. Some hyperbranched polymers are synthesized by substitution reactions that provide more hydrolytically stable polymers.

Ring-Opening Procedures to Hyperbranched Polymers. The use of ring-opening polymerization for the synthesis of hyperbranched polymers has, so far, been rather limited. Conceptually, ring-opening polymerization holds an advantage over ordinary step-growth polymerizations in that no low molecular weight compound has to be removed. This facilitates the formation of high molecular weight compounds.

The Pd-catalyzed ring-opening polymerization of a cyclic carbamate in the presence of an initiator, which also acts as a core molecule, to afford a hyperbranched polyamine has been reported (40,41). The polymerization was denoted to be multibranching. Multibranching implies that the number of propagating chain ends increase with the progress of the polymerization.

Ring-opening polymerization of hydroxy-functional cyclic ethers could, in accordance with hydroxy-functional lactones, give rise to hyperbranched polyethers.

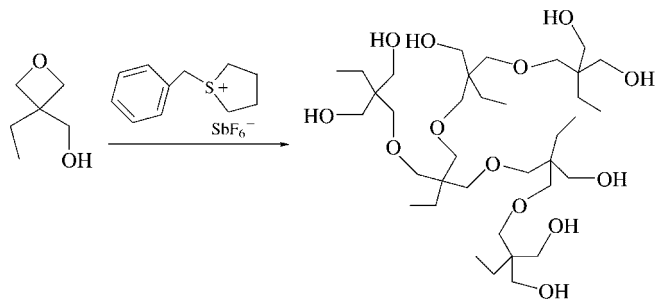

Fig. 7. Cationic ring-opening polymerization of 3-ethyl-3-(hydroxymethyl)oxetane to a hydroxy-functional hyperbranched polyether (45,46).

One example of such a compound is glycidol, an oxirane-ring substituted with a hydroxymethyl group. Already in the mid-1980s, both the anionic and cationic polymerizations of glycidol had been extensively investigated and it was concluded that branched polymers were formed (42,43). More recently, the anionic ring-opening polymerization of glycidol has been reported (44).

Anionic polymerization of 2-hydroxymethyloxetane is unsuccessful (34). The failure of such a reaction is most likely due to the fact that oxetanes are not known to ring-open under basic conditions. The successful cationic ring-opening polymerization of 3-ethyl-3-(hydroxymethyl)oxetane gave hydroxy-functional hyperbranched polyethers (45,46) (Fig. 7). The cationic polymerization can proceed according to two different mechanisms, activated chain end (ACE) or activated monomer mechanism (AMM) (45) (Fig. 8).

The ring-opening polymerization of an AB-monomer, 4-(2-hydroxyethyl)-ε-caprolactone, has been reported (47). ε-Caprolactone is easily polymerized using ring-opening polymerization under facile conditions, and the primary hydroxyl group can be used to initiate the polymerization. The polymers are reported to

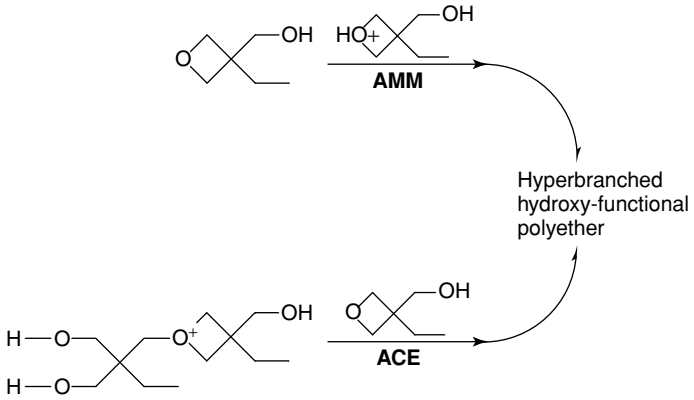

Fig. 8. Cationic ring-opening polymerization can proceed in accordance to two different mechanisms, activated chain end (ACE) or activated monomer mechanism (AMM).

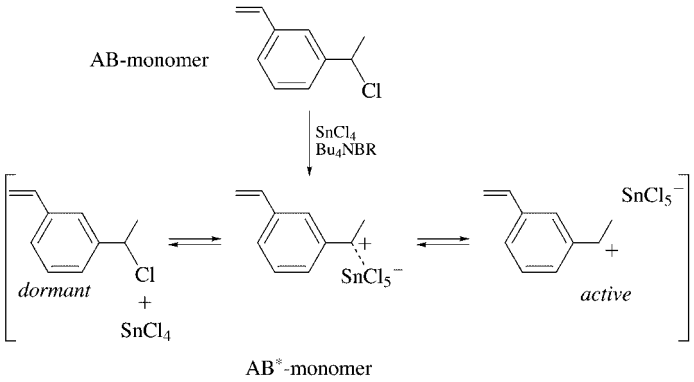

Fig. 9. Self-condensing vinyl polymerization (SCVP) (48).

have molecular weights in the range of 65,000–85,000 (PDI ca 3.2) as determined by sec.

Self-Condensing Vinyl Polymerization. The first hyperbranched vinyl polymer was presented in 1995 (48) and this marked the birth of the "second generation" of hyperbranched polymers. Hitherto, exclusively step-growth polymerization had been utilized to accomplish hyperbranched polymers. This had, of course, also limited the potential applications to areas where condensation-type polymers are acceptable.

3-(1-Chloroethyl)-ethenylbenzene was cationically polymerized in the presence of $SnCl_4$. The polymerization was termed "self-condensing" vinyl polymerization (SCVP) (Fig. 9) because the polymerization was found to proceed by repeated step-wise couplings of otherwise chain-growing species.

3-(1-Chloroethyl)-ethenylbenzene is an AB-monomer where the A-group is the readily polymerizable vinyl group and the B-group the latent initiator moiety, a benzyl halide. External activation of the labile B-group was afforded by the addition of $SnCl_4$ (Fig. 10).

The presentation of SCVP marked the onset of extensive research focussing on the use of vinyl monomers for the synthesis of hyperbranched polymers. Lately,

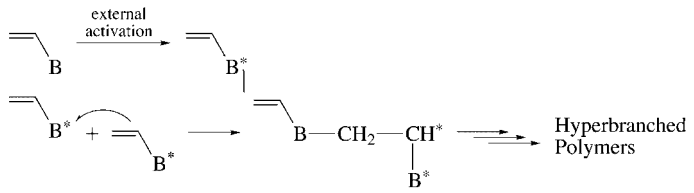

Fig. 10. AB∗ represents the activated monomer. The polymerization is initiated by the addition of B∗ to an A-group, which leaves a dimer carrying one double bond and two active sites, B∗. Given the chemical structure of the monomer, it can be assumed that the reactivities of A∗ and B∗ are similar and that is why both the initiating B∗-group and the newly created propagating cation can react with the vinyl group of another molecule (monomer or polymer) in the same way.

there has been a great interest in "living" free-radical procedures that possess accurate control over molecular weight, molecular weight distribution, and chain ends. The SCVP concept was further developed into TEMPO-initiated "living" free-radical polymerization synthesis of hyperbranched polystyrenes (49). The extensive development of metal-catalyzed "living" free-radical polymerization brought about new possibilities to use radical polymerization as a tool to obtain advanced macromolecular architectures. Atom-transfer radical polymerization (ATRP) techniques were developed to obtain hyperbranched polystyrenes (50), and the first use of group-transfer polymerization to obtain hyperbranched methacrylates was reported (51).

Since then, a number of different approaches, based on vinyl monomers and various initiating systems, have been explored to yield hyperbranched polymers such as poly(4-acetylstyrene) (52), poly(vinyl ether) (53), and polyacrylates (54).

The polymerization of AB$*$-functional vinyl monomers is fundamentally different from the step-growth polymerization of AB_2-monomers. Condensation of AB_2-monomers immediately results in hyperbranched polymers since the reactivity of the end groups are the same, regardless of what type of repeat unit (linear or dendritic) that is formed.

In the case of AB$*$-monomers it is not obvious how the chain growth takes place. Depending on the chemical structure of the monomer there will be a competition between conventional, linear, chain-growth polymerization, via the double bond, and the branching reaction, ie, where the group capable of initiation (B$*$), reacts with a vinyl group. If the reactivities of the two different propagating species are exactly the same, one envisions that a randomly branched system will be the result. However, all monomers attempted in SCVP so far possess unequal reactivity of the propagating sites. A systematic investigation on how the branching could be maximized by altering the reaction conditions when polymerizing 4-chloromethylstyrene using metal-catalyzed "living" free-radical polymerization was done (55).

Since free-radical polymerization is the most important industrial polymerization process, the development of polymerization procedures for vinyl monomers greatly opened up the application for hyperbranched polymers.

Proton-Transfer Polymerization. Proton-transfer polymerization (PTP) (Fig. 11) has been reported as a versatile route to hyperbranched polymers (56). Conceptually, PTP is an acid–base controlled reaction where the nucleophilicity and basicity of monomer and intermediates play important roles.

A base serves as an initiator and abstracts the labile proton from the monomer, forming a reactive nucleophilic species, $^{-}AB_2$, (**2**). This species rapidly adds to the B-group on a monomer, leaving an anionic site in the dimer, (**3**). This species is less nucleophilic than (**2**) and undergoes a rapid, thermodynamically driven, proton exchange with monomer, instead of nucleophilic addition. This produces a new nucleophile, (**2**), and an inactive dimer, (**4**). The multiplicity of reactive B-groups in each growing molecule that contains a single H–A group ensures the formation of a hyperbranched molecule.

The usefulness of the PTP concept was further demonstrated in a study (57) where hyperbranched aliphatic polyethers were synthesized from a diepoxide and a three-functional alcohol utilizing the concept of A_2–B_3 monomers.

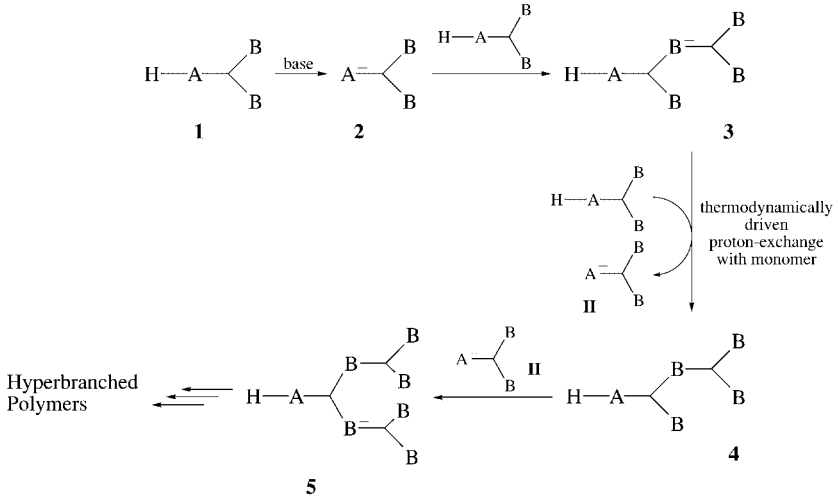

Fig. 11. Proton-transfer polymerization (PTP) (56).

Analytical and Test Methods

Degree of Branching. In a perfectly branched dendrimer only one type of repeat unit can be distinguished, apart from the terminal units carrying the chain ends. A more thorough investigation of a hyperbranched polymer (assuming high conversion of B-groups) reveals three different types of repeat units as illustrated in Figure 12. The constituents are *dendritic units* (*D*), fully incorporated A_xB-monomers; *terminal units* (*T*) having the two A-groups unreacted; and *linear units* (*L*) having one A-group unreacted. The linear segments are generally spoken of as defects. The term *degree of branching* (DB) was coined in 1991 (8) as (eq. (1))

$$\mathrm{DB} = (\Sigma D + \Sigma T)/(\Sigma D + \Sigma L + \Sigma T) \tag{1}$$

To date, two different techniques have been used to determine the degree of branching. The first technique (8) involves the synthesis of low molar mass

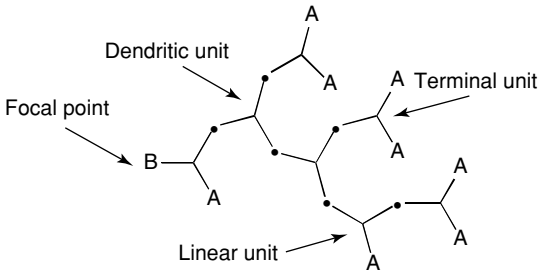

Fig. 12. The constituents in a hyperbranched polymer are *dendritic units* (*D*), fully incorporated A_xB-monomers; *terminal units* (*T*) having the two A-groups unreacted; and *linear units* (*L*) having one A-group unreacted.

model compounds resembling the repeat units to be found in the hyperbranched skeleton. The model compounds are characterized with ^{13}C nmr. From the spectra of the model compounds the different peaks in the spectra of the polymers can be assigned. The degree of branching is calculated from the integrals of the corresponding peaks in the spectrum of the polymer.

In a second method (38), based on the degradation of the hyperbranched backbone, the chain ends are chemically modified and the hyperbranched skeleton is fully degraded by hydrolysis. The degradation products are identified using capillary chromatography. Two chemical requirements have to be fulfilled to use this technique successfully. Firstly, degradation must not affect chain ends, and secondly, the conversion into elementary subunits must be complete.

The expression in equation (1) has been frequently used to characterize hyperbranched polymers. The definition leads to high DB values at low degrees of polymerization. Another expression for the degree of branching where also the degree of polymerization is taken into consideration has been introduced (58). The same group also published findings from computer simulations of ideal experiments where all the monomers are added to the core molecules, keeping the total number of molecules constant throughout the reaction (35). Increasing the functionality of the core resulted in decreased polydispersity for the final polymer. The degree of branching was found to have a limiting value of 0.66 with slow monomer addition at high degree of conversion.

It is of vital importance to understand how the degree of branching affects the properties of a hyperbranched polymer. One way to obtain polymers with higher degrees of branching is to use preformed dendron-monomers. Using this concept (21) it was found that the resulting polymers with the highest degree of branching also exhibited the highest solubility in organic solvents. This topic has also been studied by investigating the hyperbranched poly(siloxysilanes) obtained from AB_2-, AB_4-, and AB_6-monomers (59).

Uses

Numerous applications have been suggested for hyperbranched polymers but few have reached commercial exploitation. Only a few papers have been published where a certain application of a hyperbranched polymer has been addressed.

Thermosets. One area where hyperbranched polymers may find use is for thermoset applications. The low melt viscosity can improve the processing properties while extensive cross-linking can result in sufficient material strength.

Among the first studies presenting the use of hyperbranched polymers for thermoset applications was the synthesis of unsaturated polyester resins based on aliphatic hyperbranched polyesters (7). A number of resins with various amounts of maleate/allyl ether moieties were attached as end groups were synthesized. The resins could be cross-linked by a free-radical mechanism giving films with final film hardnesses depending on the amount of functional groups. Based on the same base polyester, several resins with different viscosities (before cure) and different curing rates could be obtained. The same group has also conducted studies of acrylated hyperbranched polyesters for electron beam curing (60).

Also, methacrylated polyesters and their use in photopolymerizations of films and fiber-reinforced polymer composites have been studied. The resins were found to have a low viscosity and a higher curing rate than those of corresponding linear unsaturated polyesters (61,62).

Coatings. The use of hyperbranched polymers as base for various coating resins has been described in the literature. Different resin types are obtained depending on the reactive end group structure which is attached to the hyperbranched polymer.

A number of different thermoset resin structures based on hyperbranched aliphatic polyesters have been described (63). The results can best be exemplified by their results on hyperbranched alkyd coating resins. A comparative study between an alkyd resin based on a hyperbranched aliphatic polyester and a conventional high solid alkyd, which is a less branched structure, yielded the following results. The hyperbranched resin had a substantially lower viscosity than the conventional resin with comparable molar mass, ie, less solvent is needed in order to obtain a suitable application viscosity. The hyperbranched resin also exhibited much shorter drying times than the conventional resin although the oil content was similar. These achievements would not be possible without a change in architecture of the backbone structure of the resins (Figs. 13 and 14).

Studies on acrylate resins (64,65) based on hyperbranched aliphatic polyesters have shown the possibility to vary both the polarity (wetting behavior) and T_g of the thermoset by changing either the polarity of the end groups or the cross-link density. This study shows that it is possible to vary the T_g within a large range (50–150°C) by changing the amount of reactive end groups (cross-linkable groups) utilizing the same hyperbranched polyester as a base structure. FT-Raman measurements of the residual unsaturation on these systems also showed that the acrylate functional end groups are all accessible to polymerization, ie, they are not trapped inside the hyperbranched polyester structure. The

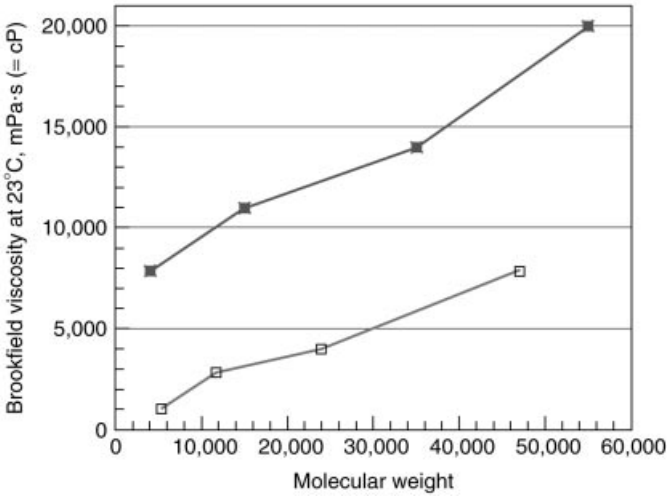

Fig. 13. Hyperbranched resins have a substantially lower viscosity than conventional resins with comparable molar mass (alkyd resin made from Boltorn). —■— Reference alkyds and —⊟— dendritic alkyds.

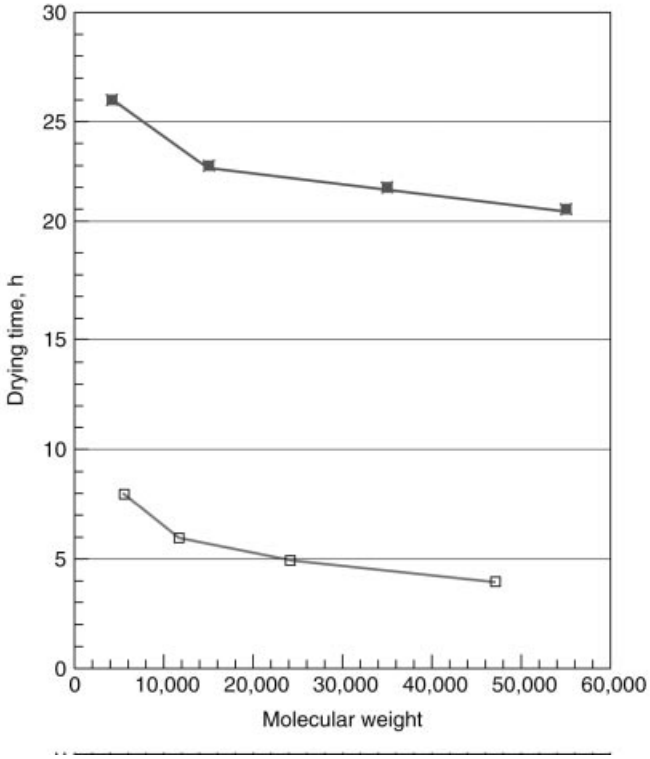

Fig. 14. Hyperbranched resins have much shorter drying times than conventional resins (alkyd resin made from Boltorn). ⊣■⊢ Reference alkyds and ⊣□⊢ dendritic alkyds.

uv polymerization of the resins also proceeded at a high rate compared to conventional acrylate resins. The structure of the nonreactive end groups affected the T_g to some extent although the cross-link density had a much larger impact on the T_g. The structure of the nonreactive end groups had a much larger effect on other properties such as the wetting behavior. Changing these groups from carboxylic acid groups to propionate groups increased the contact angle of water from 10° to 75°. Overall, it can be concluded that the thermoset properties can be greatly varied within a wide range by changes in functionality of the end groups while retaining the same backbone structure.

Solid thermoset resins have increasing importance in several fields; one of the dominating groups is powder coatings. Powder coatings are based on resins that are solid at ambient temperature and flow at elevated temperature to form a uniform coating layer. Most systems are based on amorphous reactive polymers that cross-link in the molten state forming a thermoset coating. It has been demonstrated that semicrystalline powder coatings based on hyperbranched polyesters can be synthesized (66).

ε-Caprolactone was grafted on hydroxy-functional hyperbranched aliphatic polyesters forming semicrystalline copolymers (Fig. 15). The crystallinity and rheological properties were found to be tailorable by means of the appropriate choice of hyperbranched polyester and the degree of polymerization of the crystalline

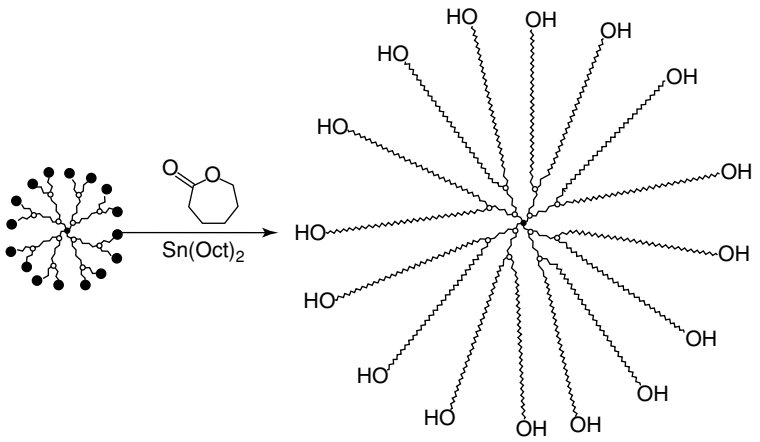

Fig. 15. Ring-opening polymerization of ε-caprolactone using Boltorn and stannous octanoate as a macroinitiator (66).

grafts (ε-PCL). Cross-linkable resins were obtained by methacrylation of the terminal hydroxyl groups. The resins were found to have suitable melt rheology for low temperature powder coatings. All resins were uv-cured in the molten state to yield flexible films with low levels of residual unsaturation. The properties of the final cross-linked films were shown to be dependent on the structure of the resins, ie, long side chains could crystallize in the network producing a semicrystalline network. Crystallization of short chains was hindered by the cross-linking.

Additives.

Toughening for Epoxy-Based Composites. One application that has been suggested for hyperbranched polymers is as additives where the hyperbranched polymers improve a property such as toughening (67). One reason for this is the possibility to adjust the polarity of the polymer to make it either compatible or incompatible with another polymer. Reaction-induced phase separation by adjusting the polarity of an hyperbranched aliphatic polyester relative to an epoxy/amine thermoset system has been demonstrated (67) (Fig. 6). An epoxy-modified hyperbranched polyester was used as toughener and the critical energy release rate G_{1c} of carbon fiber-reinforced epoxy was improved from 1.4/kJ/m^2 to 2.5/kJ/m^2 (1.19 ft·lbf/in^2). This result is obtained by a reaction driven phase separation. An advantage compared to the more conventional ones is that no filtering of toughener during fiber-impregnation can take place. The phase separation is accomplished by a careful design of reactivities of the different components as well as designing the surface polarity of the hyperbranched resin (67).

Processing Aids. The use of hyperbranched polyphenylenes as processing aid for polystyrenes has been reported (4). The melt viscosity of polystyrene was reduced while not affecting the final properties to any larger extent. The addition of the polyphenylenes also improved the thermal stability of the system.

The use of hyperbranched polymers as a processing aid for linear low density polyethylene (LLDPE) has been investigated (68). Various generations of Boltorn were used which had either 16 carbon atom alkanes or a mixture of 20/22 carbon atom alkanes on the end groups. Blends of up to 10% hyperbranched polymer

content were mixed via extrusion at 170°C to produce 1-mm diameter fibers. Processability, surface appearance, and the rheological properties of the blends were evaluated. It was found that the power requirement for extrusion was significantly decreased as a result of reduced blend viscosity, and also, the mass flow rate for a given extruder speed was greater than virgin LLDPE for all hyperbranched polymer blends. Melt fracture and sharkskin of the blends was successfully eliminated, and minimal preprocessing time was required for the effect to take place. Surface analysis using x-ray photoelectron spectroscopy and transmission electron microscope techniques were performed with both showing that the hyperbranched polymer had a preference to accumulate at the fiber surface. Rheological experiments were similarly affected, therefore, the blend viscosity is really a composite of a hyperbranched polymer rich phase and a neat LLDPE phase. It was suggested that the hyperbranched polymer rich phase acted as a lubricating layer at the polymer/die wall interface. The hyperbranched polymer with a greater degree of end group substitution acted better as a processing/rheological property aid. The results suggest that hyperbranched polymers, at trace levels of ~500 ppm, may offer a number of advantages when used as a processing aid for LLDPE.

Surface Modification. Corrosion of metal surfaces is a serious problem worldwide. It has been demonstrated that even rather thin organic layers can passivate and block electrochemical reactions on metal surfaces. Hydrophobic, fluorinated, hyperbranched poly(acrylic acid) films can block these unwanted electrochemical reactions (69–72). Hyperbranched films containing acrylic acid were synthesized on mercaptoundecanoic acid self-assembling monolayers on gold via sequential grafting reactions. This technique was shown to be useful to obtain thick and homogeneous films. The acid groups were accessible for modifications. Fluorination of these films gave surfaces that were analyzed with cyclic voltametry and ac-impedance measurements. These studies showed that the barrier toward redox reactions was greatly improved.

Conclusion

The area of hyperbranched polymers is a young and rapidly growing area within the field of macromolecules. A number of applications where the special properties of these polymers have already been described and some hyperbranched polymers are already in the marketplace. Numerous polymers with highly branched backbone structures have been synthesized and characterized. Dendritic polymers, comprising dendrimers and hyperbranched polymers, are polymers based on A_xB-monomers, ie, monomers having one B-functionality and two or more A-groups resulting in polymers with a potential branching point in each repeat unit. The difference between dendrimers and hyperbranched polymers is that the former are well-defined, layerwise constructed polymers with a branching point in each repeat unit, while the latter contain not fully reacted monomers in the polymer backbone. One main advantage of hyperbranched polymers over dendrimers is that the synthesis is less tedious, making more material available at a reasonable cost.

The synthesis of hyperbranched polymers can be made in several different ways. Classical condensation reactions are the most commonly used. The condensation reactions are either made in bulk or in solution where the A_xB-monomers

are condensated by themselves or in combination with a B_y-core monomer. The use of a B_y-core monomer improves the control over molecular weight and dispersity of the hyperbranched polymer. Another approach to the synthesis of hyperbranched polymers is the use of self-condensing vinyl polymerization, which is a way of using vinyl-functional monomers to obtain hyperbranched polymers. The introduction of this approach has greatly increased the number of possible monomers that can be used for this group of polymers.

A wide variety of hyperbranched polymers has been described in the literature. The properties of hyperbranched polymers have been shown to depend on several parameters, the most important ones are the backbone and the end-group structure in combination. The properties of hyperbranched polymers differ from linear polymers, for example, the solubility, which is much higher for hyperbranched polymers. Hyperbranched polymers normally exhibit an amorphous, nonentangled behavior, ie, a Newtonian behavior in the melt. Attachment of reactive end groups in various amounts leads to thermoset structures where the T_g and cross-link density can be greatly varied for the same hyperbranched polymer. A number of applications have already been suggested, related to the special properties of hyperbranched polymers.

BIBLIOGRAPHY

1. P. J. Flory, *J. Am. Chem. Soc.* **74**, 2718 (1952).
2. Y. H. Kim and O. W. Webster, *Abstracts of Papers of the Am. Chem. Soc.* **196**, 104–POLY (1988).
3. Y. H. Kim and O. W. Webster, *J. Am. Chem. Soc.* **112**, 4592–4593 (1990).
4. Y. H. Kim and O. W. Webster, *Macromolecules* **25**, 5561–5572 (1992).
5. Y. H. Kim and R. Beckerbauer, *Macromolecules* **27**, 1968–1971 (1994).
6. U.S. Pat. 3,669,939 (1972), S. A. Baker and D. J. Walbridge.
7. M. Johansson, E. Malmström, and A. Hult, *J. Polym. Sci., Part A: Polym. Chem.* **31**, 619–624 (1993).
8. C. J. Hawker, R. Lee, and J. M. J. Fréchet, *J. Am. Chem. Soc.* **113**, 4583–4588 (1991).
9. K. L. Wooley and co-workers, *Polym. J.* **26**, 187–197 (1994).
10. K. L. Wooley, J. M. J. Fréchet, and C. J. Hawker, *Polymer* **35**, 4489–4495 (1994).
11. J. M. J. Fréchet and C. J. Hawker, *Reactive and Functional Polymers* **26**, 127–136 (1995).
12. S. R. Turner, B. I. Voit, and T. H. Mourey, *Macromolecules* **26**, 4617–4623 (1993).
13. S. R. Turner and co-workers, *Macromolecules* **27**, 1611–1616 (1994).
14. H. R. Kricheldorf and O. Stober, *Macromol. Rapid Commun.* **15**, 87–93 (1994).
15. H. R. Kricheldorf, O. Stober, and D. Lubbers, *Macromolecules* **28**, 2118–2123 (1995).
16. H. R. Kricheldorf and T. Stukenbrock, *Polymer* **38**, 3373–3383 (1997).
17. W. J. Feast and N. M. Stainton, *J. Mater. Chem.* **5**, 405–411 (1995).
18. K. E. Uhrich and co-workers, *Macromolecules* **25**, 4583–4587 (1992).
19. T. X. Neena and co-workers, *J. Am. Chem. Soc.* **115**, 356 (1993).
20. T. X. Neena and co-workers, *Makromol. Symp.* **77**, 35 (1994).
21. C. J. Hawker and F. K. Chu, *Macromolecules* **29**, 4370–4380 (1996).
22. J. M. J. Fréchet, *Science* **263**, 1710 (1994).
23. K. Uhrich, *Trends Polym. Sci.* **5**, 388–393 (1997).
24. G. R. Newkome and co-workers, *Angew. Chem., Int. Ed. Engl.* **30**, 1178 (1991).
25. B. I. Voit, *Acta Polym.* **46**, 87–99 (1995).

26. B. I. Voit and S. R. P. Turner, *Angew. Makromol. Chem.* **223**, 13–27 (1994).
27. K. L. Wooley and co-workers, *Macromolecules* **26**, 1514–1519 (1993).
28. H. Stutz, *J. Polym. Sci., Part B: Polym. Phys.* **33**, 333 (1995).
29. A. Hult, E. Malmström, and M. Johansson, in J. Salamone, ed., *The Polymeric Materials Encyclopedia: Synthesis, Properties and Applications*, CRC Press, Boca Raton, Fla., 1996.
30. H. Ihre, M. Johansson, E. Malmström, and A. Hult, in G. R. Newkome, ed., *Advances in Dendritic Macromolecules*, Vol. **3**, JAI Press, London, 1996.
31. Y. D. Zhang and co-workers, *Macromol. Chem. Phys.* **197**, 667–676 (1996).
32. E. Malmström, M. Johansson, and A. Hult, *Macromol. Chem. Phys.* **197**, 3199–3207 (1996).
33. A. Hult, M. Johansson, and E. Malmström, *Hyperbranched Polymers*, Vol. **143**, Springer-Verlag, Berlin, 1999, pp. 1–34.
34. Y. H. Kim, *J. Polym. Sci., Part A: Polym. Chem.* **36**, 1685–1698 (1998).
35. R. Hanselmann, D. Holter, and H. Frey, *Macromolecules* **31**, 3790–3801 (1998).
36. G. M. Gong and J. M. J. Fréchet, *J. Polym. Sci., Part A: Polym. Chem.* **37**, 3193 (1999).
37. K. Dusek and co-workers, *Polym. Bull.* **42**, 489–496 (1999).
38. P. Kambouris and C. J. Hawker, *J. Chem. Soc., Perkin Trans. 1* 2717–2721 (1993).
39. D. Schmaljohann, H. Komber, and B. I. Voit, *Acta Polym.* **50**, 196–204 (1999).
40. M. Suzuki, A. Ii, and T. Saegusa, *Macromolecules* **25**, 7071–7072 (1992).
41. M. Suzuki and co-workers, *Macromolecules* **31**, 1716–1719 (1998).
42. E. J. Vandenberg, *J. Polym. Sci., Part A: Polym. Chem.* **23**, 915 (1985).
43. E. J. Vandeberg, *J. Polym. Sci., Part A: Polym. Chem.* **27**, 3113 (1989).
44. A. Sunder and co-workers, *Macromolecules* **32**, 4240–4246 (1999).
45. M. B. Bednarek and co-workers, *Macromol Rapid. Commun.* **20**, 369 (1999).
46. H. M. Magnusson, E. Malmström, and A. Hult, *Macromol. Rapid. Commun.* **20**, 453 (1999).
47. M. J. Liu, N. Vladimirov, and J. M. J. Fréchet, *Macromolecules* **32**, 6881–6884 (1999).
48. J. M. J. Fréchet and co-workers, *Science* **269**, 1080 (1995).
49. C. J. Hawker and co-workers, *J. Am. Chem. Soc.* **117**, 10763–10764 (1995).
50. S. G. Gaynor, S. Edelman, and K. Matyjaszewski, *Macromolecules* **29**, 1079–1081 (1996).
51. P. F. W. R. Simon and A. H. E. Müller, *Macromol. Rapid Commun.* **18**, 865 (1997).
52. P. Lu, J. K. Paulasaari, and W. P. Weber, *Macromolecules* **29**, 8583–8586 (1996).
53. H. M. Zhang and E. Ruckenstein, *Polym. Bull.* **39**, 399–406 (1997).
54. K. Matyjaszewski and co-workers, *Macromolecules* **30**, 5192–5194 (1997).
55. M. W. Weimer, J. M. J. Fréchet, and I. Gitsov, *J. Polym. Sci. Part A: Polym. Chem.* **36**, 955–970 (1998).
56. H. T. Chang and J. M. J. Fréchet, *J. Am. Chem. Soc.* **121**, 2313–2314 (1999).
57. T. Emrick, H. T. Chang, and J. M. J. Fréchet, *Macromolecules* **32**, 6380–6382 (1999).
58. H. Frey and D. Holter, *Acta Polym.* **50**, 67–76 (1999).
59. J. F. Miravet and J. M. J. Fréchet, *Abstracts of Papers of the Am. Chem. Soc.* **214**, 130-PMSE (1997).
60. M. Johansson and co-workers, *J. Appl. Polym. Sci.* **75**, 612–618 (2000).
61. B. Rånby and W. F. Shi, *J. Appl. Polym. Sci.* **12**, 1937 (1996).
62. B. Rånby and W. F. Shi, *J. Appl. Polym. Sci.* **12**, 1945 (1996).
63. K. Sörensen and B. Pettersson, *New Orleans, Louisiana*, 1994, p. 753.
64. M. Johansson and A. Hult, *J. Coat. Technol.* **67**, 35–39 (1995).
65. M. Johansson, G. Rospo, and A. Hult, *Abstracts of Papers of the Am. Chem. Soc.* **214**, 105-PMSE (1997).
66. E. M. M. Johansson, A. Jansson, and A. Hult, *J. Coat. Technol.* **72**, 49–54 (2000).

67. L. B. Pettersson and J. A. E. Manson, *Abstracts of Papers of the Am. Chem. Soc.* **214**, 104-PMSE (1997).
68. Y. Hong and co-workers, *J. Rheol.* **43**, 781 (1999).
69. Y. F. Zhou and co-workers, *Langmuir* **12**, 5519–5521 (1996).
70. M. Q. Zhao and co-workers, *Langmuir* **13**, 1388–1391 (1997).
71. Y. F. Zhou and co-workers, *J. Am. Chem. Soc.* **118**, 3773–3774 (1996).
72. M. L. Bruening and co-workers, *Langmuir* **13**, 770–778 (1997).

ANDERS HULT
Royal Institute of Technology

INJECTION MOLDING

Introduction

Injection molding is an extensive global manufacturing process for making simple to intricate plastic, ceramic, and metal parts. Injection molding converts wax, thermoplastics, thermosets as well as powdered metals, and magnesium into thousands of products (1,2). Commercial processes and equipment have been developed for a wide variety of materials, though the bulk of what is injection molded are thermoplastics. Applications appear limitless, from compact discs to jet plane canopies, to medical implants. Nearly all consumer products have some injection-molded components. In the year 2000 injection molding consumed approximately 32 wt% of all plastics sold worldwide, roughly 4.95×10^7 metric tons (3). This is second to extrusion which consumed 36 wt% of all plastics sold worldwide. The United States consumes about 33% of the plastic sold worldwide. In the United States, the plastics industry ranks as the fourth largest after motor vehicles, petroleum refining, and automotive parts. Plastic processing and products continue to grow at a faster pace than the national average. This is in spite of the trend of the United States going toward an information and service industry and away from manufacturing. In the United States there are about 6000 molding shops, down from a high of about 8000 in the early 1990s. Consolidation continues as monitored by the trade journals, for which web sites are listed (4–8). There are an estimated 80,000 injection presses in operation within the United States.

The injection-molding process provides low cost fabrication of large and small parts to precision tolerances. Many of these parts are nearly impossible to make in production volumes by other techniques. Injection molding can form parts as small as a cubic millimeter (micromolding), and parts as large as garbage dumpsters and 1.2×2.4 m (4×8 ft) filter panels are in production. A wide range of

Encyclopedia of Polymer Science and Technology. Copyright John Wiley & Sons, Inc. All rights reserved.

injection-molding processing capability characterizes the industry. Quality and tolerances can be high if scientific principles are followed. Tolerances near 0.025 mm (0.001 in.) are difficult to achieve but are possible if concurrent engineering is applied to certain parts. One of the strengths of injection molding over other plastic forming processes is that parts can have fine three-dimensional (3-D) details in their shape and surface finish. Typical nominal-wall thickness ranges from 0.5 to 6.4 mm (0.020–0.250 in.); however, thickness of 0.08–50 mm (0.003–2.0 in.) are also possible. Injection molding is the plastic processing method of choice for large quantities of identical parts. Quantities in the millions are possible with one or more molds that can form several parts at one time. The efficiency of this process has changed the quality of life for most Americans, especially low income households.

Properties of injection-molded parts can be unique. Given a metal or plastic's typical properties, injection molding imparts some of its own. Because of flow patterns, molecular orientation, and other factors, molded part properties are often different than those of the base material. An example of the benefits of orientation is the "living hinge", the flexible plastic hinge found on spice, shampoo, and dental floss containers. Properties of injection-molded parts can be flexible or stiff, soft or hard, tough or brittle, clear or opaque, specific chemically resistant and flame retardant. Parts can be tinted, colored, plated with various metals, and recycled.

Economic Aspects

Profit margins for the industry are generally low and have averaged around 6% as shown in Figure 1.

Another perspective to Figure 1 is to exclude resin cost and calculate the cost to run an injection-molding machine on an hourly basis. Usually this is expressed as a charge per hour for a given size machine. The range for hourly rates is US \$10–\$175/h, depending on machine size ranked in tons of clamp pressure. Machine clamp pressures range from 69 to 1.4×10^5 MPa (5–10,000 tons), most being below 1.4×10^4 MPa (1000 tons).

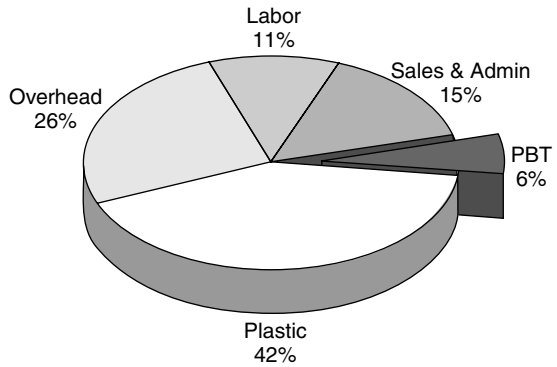

Fig. 1. Costs and profit margins for molders. *Source*: Facts & Figures of the US Plastics Industry, published yearly by The Society of the Plastics Industry, Inc. Includes custom and proprietary molders; PBT = profits before taxes.

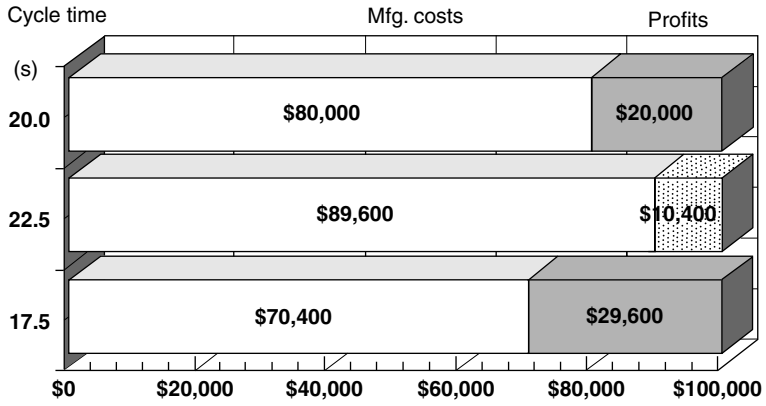

Fig. 2. Quoted profit per $100,000 of sales. Courtesy of D. Paulson.

Most businesses operating injection-molding shops (molders) will bid a job to make 20%, or greater, profit before taxes, yet they realize far less as Figure 1 shows. Resin cost is often included in part quotes, which means that if the price of the plastic increases the molder must absorb the cost, and profits decrease. Molders rarely have much of an influence on resin pricing. Quoting, therefore, should provide a mechanism that allows resin price fluctuations to be passed on to the customer, yet this is not common practice in the industry. Another reason for low profit margins is that when quoting, the exact cycle time (the time required to make a part) is not known or cannot easily calculated; that is, the quote is based on an estimated cycle time. Often after the mold is built and trialed, production cycles are longer than estimated or quoted and the molder cannot renegotiate the contract. This effect of cycle time on profit is known, yet poorly understood (9). The top bar of Figure 2 shows a typical bidding situation with a 20% return added to costs for a 20-s cycle.

The middle bar shows how a 10–15% cycle time increase, averaged to 22.5 s, can cut profits by nearly 50%. Using the same concept, a 10–15% decrease in cycle time improves profits by ~50%, for a 2.5-s decrease in cycle time. Few molders know their actual costs and most are not willing to spend money to shorten cycles.

This low profit margin is the cause for many consolidations and hurts a molder's ability to attract capital for machine replacement as new technology emerges. Figure 1 also points out that molders only sell time that is used to make acceptable parts. Any time not used to make acceptable parts such as mold changes, downtime, repairs, and time to make rejects is lost profit opportunity and must be kept to a minimum to be internationally competitive.

The Injection Molding Process and Machine

Injection molding is a forming process. Material (plastic, metal, ceramic, wax, etc) is fed into a hopper which delivers it to the feed section of the barrel and screw. The material is melted usually via a screw that melts or blends the material and then pushes liquefied material (eg, plastic) into the mold, which forms the part.

The injection-molding industry is relatively young when compared to other manufacturing processes, such as metals, wood, or cement. Although patented in 1870 by Smith and Locke and 1872 by Hyatt, the first commercial plunger machines were developed in the late 1920s and 1930s. Egan patented the reciprocating screw in 1956. Since then the elements of the machine have stayed the same but advances continue with the evolution of advanced computer controls, hydraulic circuits, and computer numerically controlled (CNC) all electric presses. There are several variations and extensions of injection molding within the industry that provide unique capabilities to the process and in turn special properties to parts. Virtually all share the common elements of the following:

(1) Material preparation: The plastic/metal/mixture may be cleaned, dried, colored, blended, heated, cooled, or in some way readied for use in the machine. This can be one resin, thermoplastic or thermoset, or combination of base resin and additives. Additives include colors, metal particles, foaming agents, antistatic agents, fillers, fibers, flow aids, stabilizers, antioxidants, mold-release agents, binders, flame retardants, etc.

(2) Material, usually dried plastic granules, is fed (usually by gravity) into a feed port or throat of a heating cylinder or barrel.

(3) Material melting and/or mixing, [usually thermoplastics via heat (heater bands) and mechanical shear (flights of a screw shearing the plastic at inside surface of a barrel wall)], preparing it to be pushed into the cavity: As the screw rotates, it pumps plastic forward to prepare enough material for injection. The injection unit, barrel, and screw are now something like a syringe ready to inject fluid.

(4) Filling the cavity by pushing the material under pressure [7 to ∼414 MPa (1000–60,000 psi)] into a mold cavity. The cavity sees less pressure, between 1.4 and 140 MPa (200–20,000 psi), because of large pressure losses as the plastic travels the path to the part. This path includes the nozzle of the injection-molding machine, the sprue (a tapered cone) that connects the nozzle to the runner, the runner (usually a round channel), and the gate or entryway to the part.

(5) The mold or tool that contains the cavity that forms the part and provides heat to cure thermoset parts or cooling to set up or freeze thermoplastic parts. Typically, the mold cools the molten plastic to a rigid or semirigid form so that it can withstand the force of ejection (part removal) and retain its shape. Not all of the energy to melt the plastic is removed by the mold. Cooling continues after ejection and the part continues to shrink. Parts made with certain plastics, ie, semicrystalline, may take 3 days to 6 weeks to stabilize. Post-molding conditioning can be critical to achieve desired performance, dimensional criteria, or flatness.

(6) The clamp which holds the mold halves together during filling and packing the part with plastic.

(7) Part removal or an ejection mechanism. This occurs after the clamp opens, separating the mold at the parting line into halves. The part is pushed (ejected) out of the mold and drops to a box, conveyor belt, or is taken out by a robot.

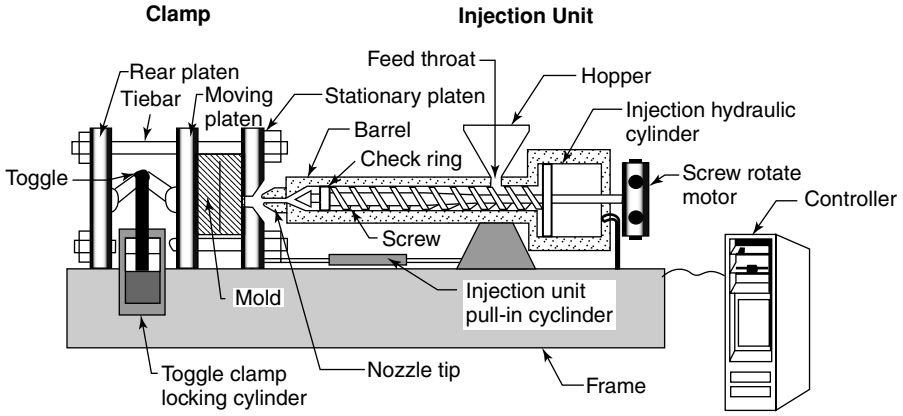

Fig. 3. Basic hydraulic (toggle clamp) injection-molding machine components. Illustration by John W. Bozzelli & Rick J. Bujanowski.

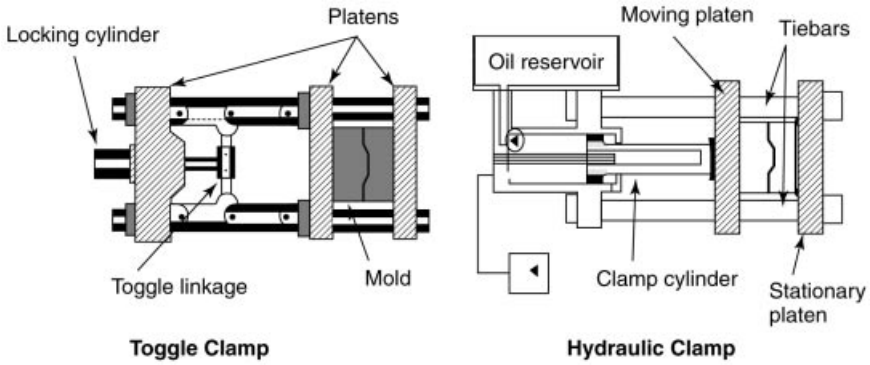

Fig. 4. Toggle and hydraulic clamps. Illustrations by Rick J. Bujanowski & John W. Bozzelli.

(8) A controller, usually a computer, that coordinates and controls the various steps of the process and components of the machine.

Figure 3 depicts many of these components in a typical hydraulic injection-molding machine with a toggle clamp.

There are a number of variations in machine construction and processing techniques (10). There are hydraulic (Fig. 4), hydromechanical, and toggle clamping machines (Fig. 4). There are also tiebar-less clamps as shown in Figure 5, and two-platen machines that were developed to save floor space over the normal three-platen machine.

Two-platen machines do away with the rear platen by locking the moving platen to the four tiebars. Here the moving platen closes on the mold as usual, then a tiebar locking mechanism locks onto the four tiebars, allowing a hydraulic pancake cylinder to build clamp pressure by pushing the moving platen toward the stationary platen. Clamps shown in Figures 3–5 are horizontal clamps; vertical

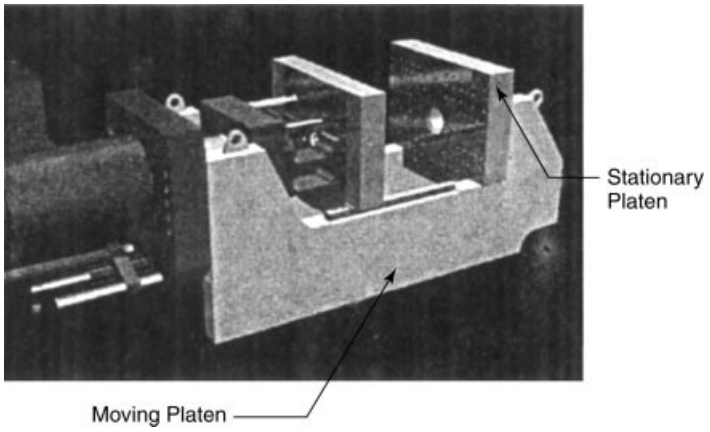

Fig. 5. Tiebar-less clamp. Courtesy of Engel Machinery Inc.

clamps are also available, where a platen moves up and down. Vertical clamps are useful in insert molding to use gravity to hold the insert in place as the mold closes. In all cases except in tiebar-less machines, the tiebars are stretched to build clamp pressure (tonnage) that holds the mold halves together during injection and packing of the plastic into the mold.

A significant shift in the industry, which started in the 1990s, is to use electric motor servo-drives rather than hydraulics to power machines. Greater accuracy, less noise, 20–60% less power requirements, and no hydraulic fluids are claimed advantages.

The process for making a part is called the molding cycle. This cycle is depicted in Figure 6 with the average time for that function stated as a percentage of the total cycle time.

A cycle or cycle time is the elapsed time required for the injection-molding machine to complete the process of forming a part. It can be timed starting at any point of the cycle to the same point on the next cycle. Cycle times range from below 4 s for compact discs to hours for jet canopies, both made from polycarbonate. Machines have been made that can cycle in less than one second.

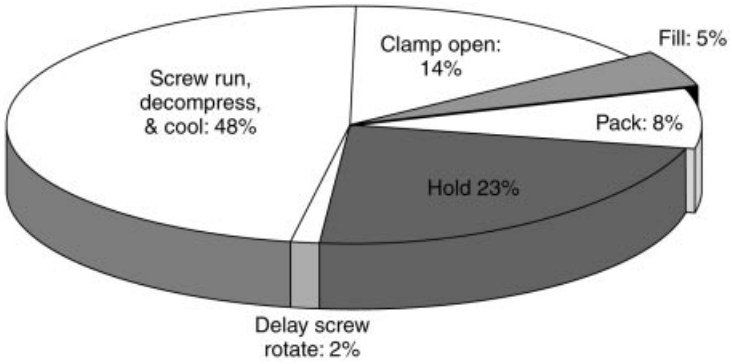

Fig. 6. The injection molding cycle.

Variations and Extension to the Injection-Molding Process

Injection Blow Molding. A preform (this looks like a test tube with bottle cap threads) is injection molded in one cavity, removed and then placed into another where it is pressurized with gas to stretch the hot preform into a thinner-walled seamless bottle or container such as a milk bottle or gas tank. This is depicted in Figure 7. This is an extension of injection molding more than a variation.

Injection Compression/Coining. With this technique the mold is only partially closed during injection. At the appropriate time and with the right amount of plastic in the mold, the clamp is then completely closed, forcing (compressing) the plastic to the shape of the mold cavity. A variation on this is coining. The clamp is closed but the mold has components that compress the plastic in the cavity as the plastic cools. Coining is where the cavity volume is changing during the solidification of the plastic. Plastic is injected into the cavity and then the movable platen closes completely, or a mold component moves to compress the plastic to compensate for shrinkage or densification.

Gas-Assist Injection Molding. Here, plastic is injected into the cavity until it is 50–85% full, then high pressure gas, usually nitrogen, is injected to finish filling the cavity by pushing the plastic flow front to the end of the cavity. This leaves a gas bubble or channel inside the part. This saves plastic, reduces cost, and often improves part strength especially in thick sections. Gas can be injected at the nozzle of the machine or directly into the mold as depicted in Figure 8. Gas-assist molding can be considered as a variation of co-injection molding where the outer layer or skin of the part is plastic and the core is a gas channel rather than another type of plastic.

Gas Pack or External Gas-Assist Injection Molding. This is a variation of coining but uses a gas, usually nitrogen, to pack out a certain section of a part to meet dimensional requirements. The gas is injected on the rear (ejector) side of the part to push the molten plastic against the cosmetic side of the mold surface.

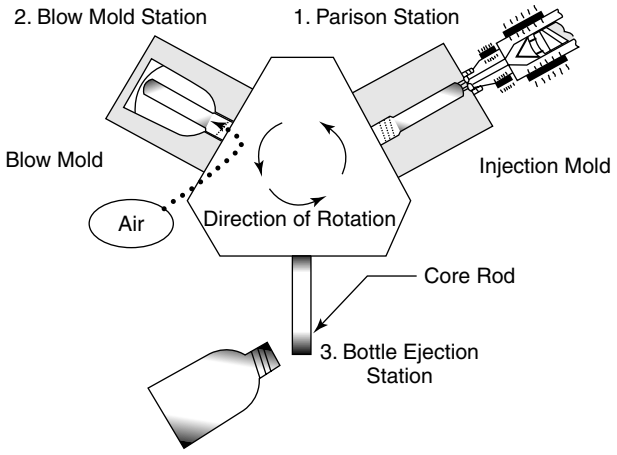

Fig. 7. Injection blow molding.

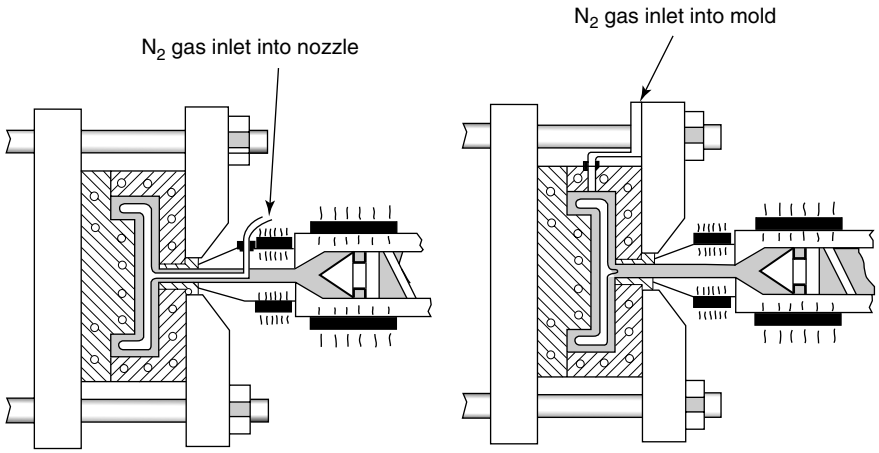

Fig. 8. Gas-assist injection molding (nozzle & mold gas entry with bubble in part). Illustration by Rick J. Bujanowski & John W. Bozzelli.

Gas-Counter Pressure Injection Molding. Normally, as plastic enters a mold it displaces the air within the cavity. The air is vented to the atmosphere via specially designed vents specific to the type of plastic being molded. In gas-counter pressure molding an O-ring is installed around the perimeter of the cavity and a gas pressurizes the cavity. During injection this counter pressure gas, usually between 345 and 2760 kPa (50–400 psi), prevents gases, water, nitrogen, etc from emerging to the surface. Gas-counter pressure molding will provide a smooth skin and nice appearance when processing plastic with a foaming agent. The counter pressure prevents the gas bubbles from developing at the surface.

Structural Foam Molding. Plastic pellets are blended with a chemical blowing (foaming) agent, usually in pellet form, and injected into the mold under normal molding conditions. The foaming agent can also be a gas or liquid. The cavity is filled only to 70–95% full and then the foaming agent releases a gas, usually nitrogen, to finish fill. The parts surface is usually splayed or rough. The resulting part has a significant density reduction, saving material costs. Density reduction ranges from 5 to 35% with an average in the 8–20% range, yet the parts are stiffer than solid wall parts. In combination with gas-counter pressure the rough surface caused by the gas bubbles coming to the surface can be eliminated. The counter pressure gas prevents the foam bubbles from developing at the surface; cosmetics are as good as regular injection molding. Injection and cavity pressures are lower than that with conventional injection molding and sometimes the term low pressure molding is applied. Machine and mold costs are lower due to the lower pressure requirements. Trexel Inc. has recently brought out a new variation to foam molding, the Mucel® Process. It injects high pressure gas (N_2 or CO_2) into the barrel achieving supercritical fluid conditions to dissolve the gas into the polymer. A special screw aids in dispersing the gas into the molten plastic before injection. Once in the cavity, small bubbles evolve as pressure is lowered as the part cools.

Thin-Wall Molding. This is identical in concept to normal injection molding but the parts produced have much thinner nominal walls; notebook computer

shells and cellular phone housings are examples. While an exact definition of "thin-wall" has not yet been defined, the range is often in the 0.08–0.80 mm (0.003–0.030 in.) range. Sometimes thin-wall is defined as a wall thickness to flow length ratio in the range of 150–300 to 1. Modified injection-molding machines that provide fast injection rates and higher injection pressures are usually required.

Insert Injection Molding. Plastic can be injected around another material or another plastic to form a part with plastic partially or completely encapsulating the other material or "insert." A metal grid, screw, or electronic circuit can be encapsulated by placing the item into a cavity, the mold closing around it forming the cavity and holding the insert in place and then injecting plastic. The plastic connectors on the end of a wire harness, automotive battery tops with terminals, and car windows with molded weather-stripping gasket are insert molded.

In-Mold Decorating. This is a variation of insert injection molding where the insert is a label, fabric, or some type of appliqué that is mounted flush to one side of a mold and held in place, sometimes by vacuum, and plastic is injected behind it. Wood-grain car dashboard pieces, labels on food containers, and fabric on seats are examples of in-mold decorating.

Multishot Injection Molding. This is similar to insert molding where the insert is usually another plastic component. A soft grip over a rigid plastic handle, many toothbrush handles with soft and hard sections, and an automotive tail-light with clear, red, and orange lenses are typical examples. State-of-the-art multishot molding uses an injection press fitted with two to six injection barrels. They can inject different colors or different materials simultaneously or through a timed sequence. Normally, the mold pivots or rotates between shots. The first part or inner section is made and then the second plastic is shot around or through the first.

Co-injection Molding. This type is similar to multishot molding. Using a timed or position sequenced injection, two or more plastics in different barrels can provide a skin or outside wall made of an expensive plastic with the core or inside filled with a foam, gas, or recycled or cheaper plastic. Fence rails or railroad ties can be made with a post-consumer or recycled plastic as the core on the inside and virgin prime material as the skin on the outside for acceptable appearance and performance.

Metal/Ceramic/Carbide Injection Molding or Powder Injection Molding (PIM). This is similar to plastic injection molding but the plastic resin is replaced with metal, a plastic–metal blend, or ceramic powder. For example, a plastic binder, often polypropylene or acetal, encapsulates or is used as a carrier for fine metal particles. Loading can be near 80% metal. This plastic–metal combination is forced under high pressure into the mold cavity. The "green" fragile part is ejected and then the plastic or binder is removed with acid, solvents, water, catalytic vapor, or heat. The resulting part is placed in a sintering oven and a precisely controlled heating regimen sinters the metal particles together yielding a metal part. Metal molding is an excellent technique to form complex metal shapes that would be difficult or impossible to machine. Ceramic molding is similar. Pure metal molding is also practiced. Magnesium in granular or powder form can be fed to a screw, melted, and injected into a mold.

Reaction Injection Molding. Two or more components are fed into the barrel feed throat, often preblended; the screw continues the mixing and then

injects the mixture into a mold. The mold can be heated or cooled. Once mixing is started a chemical reaction begins. Careful control of barrel and mold temperatures as well as residence time in the barrel are critical to prevent premature curing. It is possible to have the compound cure and seize the screw within the barrel.

Liquid Injection Molding. Molding machines with special barrels, screws, and feed systems mix and then inject liquids into a mold cavity. Similar to reaction injection molding the two liquids, often silicone or urethane based, react to form a thermoset part. Baby bottle nipples and keycap return springs are two current silicone type applications.

Micromolding. This is an extension of injection molding to extremely small part molding. Part weights in micromolding are already below 1.0 g. Technology is evolving to injection-mold parts in the milligram (or 10^{-3} g) range.

Components of a Successful Injection-Molding Product

A successful plastic product depends on the optimization of each of the following four principal components: part design, material selection and handling, tool design and construction, and processing/machine capabilities.

These interact with each other and they are equally important. One or more is often neglected by most in the molding industry, which causes delays in production and significant profit loss throughout the entire life cycle of the product. To employ all four from the beginning of a project is "concurrent" engineering and their implementation is scientific injection molding (SIM). SIM is a detailed strategy of optimizing each one of these components and not allowing errors to be compensated through processing. The synergy of working with all four from the beginning of a project has shown profit increases of 100% and faster development times to market and significantly fewer manufacturing problems.

Part Design. A successful plastic product must begin with a good part design. Because injection molding is a comparatively new and a rapidly expanding industry, it is often the case that an engineer with little plastics training is forced into plastic part design. This combination of no plastics experience and a tendency to apply rules for metals to complex shapes is ill-advised and often leads to project delays, failures, cost overruns, and production problems. Issues such as draft angles, weldlines, and polish in the direction of draw are singular to plastics. Plastics are unique, different than the materials most designers are familiar with and do not have a uniform set of precise design rules. A common mistake for the uninitiated designer is to increase nominal wall thickness to gain strength. With plastics, generally thicker means weaker due to more internal stresses. Thicker walls add weight and higher production cost because of longer cycle times. To gain stiffness or strength in a plastic wall, properly designed reinforcing ribs can be added.

Different plastics have different amount of shrink upon cooling, higher for semicrystalline resins (eg, polypropylene can shrink 0.030 in./in.) and lower for amorphous plastics (eg, polystyrene can shrink 0.006 in./in.). Further, shrinkage, especially for semicrystalline materials, varies due to thickness, cooling rate, and often color. Whatever stays hotter for a longer time will shrink more. Therefore, changes in nominal wall thickness cause differential cooling, which causes

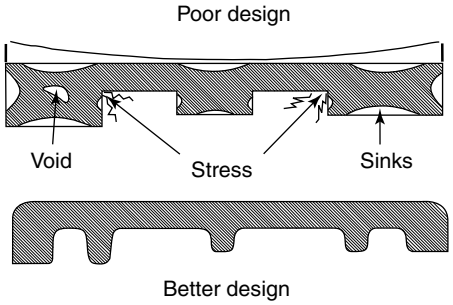

Fig. 9. Cooling and nominal wall thickness. Courtesy of Glenn Beall.

differential shrinkage that causes warp. Warp distorts the part out of dimensional tolerance. This distortion may be immediate after ejection from the mold, or after assembly in the application environment. For example, the fit and shape of an interior trim piece of a car's dashboard are fine in production and assembly, but once on the road and after a few thermal cycles (cool nights and hot days) the trim piece warps out of shape. With plastics, nominal wall-thickness changes and sharp corners should be avoided. If nominal wall-thickness changes are necessary the variation must be minimized. How fast the wall changes thickness will also influence properties and performance. Blending different thickness wall sections will minimize internal stresses. The first rule in plastic part design is uniform nominal wall thickness, yet few parts are designed on this basic premise. Figure 9 shows an application of uniform nominal wall thickness.

During part design one must take into consideration material, tool, and processing issues. When designing a part the mold is also being designed. For example, to have a dimensionally stable, high performance part it must be cooled as uniformly as possible. Is it possible to get water channels to all sections of the part so that it will cool evenly? Can the part be removed from the mold? Part design forces these and other tool construction details. Often the gate or entry point for the resin is determined by the cosmetic or performance requirements; however, it may not be possible because of mold building requirements. A good plastic part designer knows and comprehends the other three components and makes the difficult compromises to meet material, tooling, and processing requirements.

Schools and training programs have not kept up with demand for plastic part designers because of industry growth. Lack of proper training and drive for short product development times are two of the many causes for "engineering changes" as the mold is being built. That is, the design is changed after work has started on making the mold. Often a design change is made and there is no steel to accommodate the change. The mold builder cuts it to the previous design. Figures 10 and 11 depict the cost of engineering changes at different stages of a project and the impact design has on the profit margin of a project. Engineering changes must be completed in the design phase before production tooling is made. Unfortunately, the industry norm is to start cutting the tool (mold) before the design is finalized.

Industry trends will continue to challenge design. Trends to consolidate multiple functions into few parts for easier and faster assembly results in more

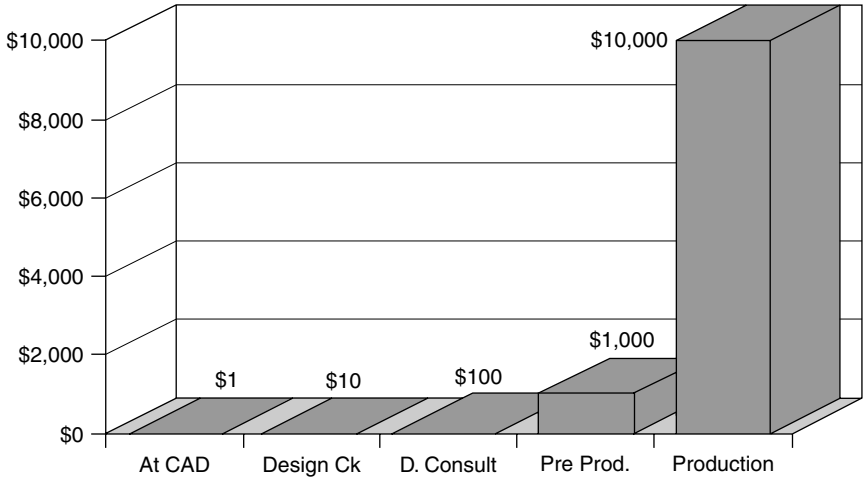

Fig. 10. Costs for design changes. Courtesy of Glenn Beall, data from Martin Marietta Co.

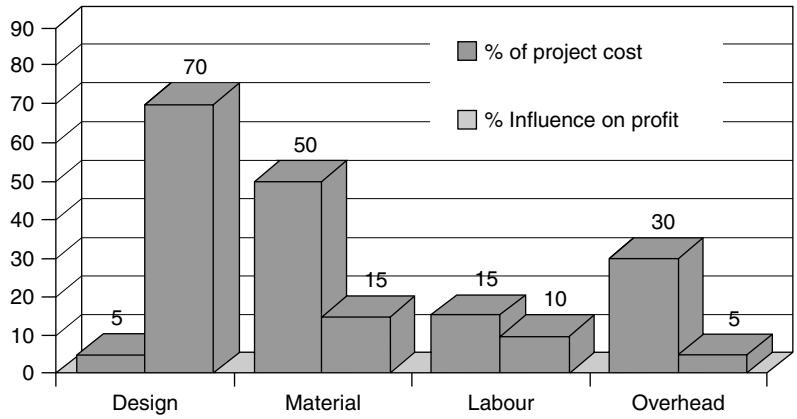

Fig. 11. Costs vs influence. Courtesy of Glenn Beall, data from Hewlett Packard/Ford Motor Co.

complex plastic part geometries. Thinner walls to save plastic and longer flow paths in larger parts are other trends that test design limits. It is imperative that part design heed fundamental design principles as outlined in References (11) and (12). Better performance is often tied to tighter tolerances. This forces more attention to the details in each of the four components for making a successful plastic part.

Material Selection and Handling. Material selection is usually done during early stages of part design. Involvement of processing and material specialists are valuable in optimizing this tough decision-making process. With data bases covering over 32,000 resins the task is daunting (13), especially when most of the data provided does a poor job of predicting the time and temperature behavior of plastic materials in end applications. Sepe's handbook provides practical time temperature data for 120 families of thermoplastic materials based on dynamic

mechanical analysis (14). Although most of the 32,000 resins are not used in large quantities many have specific properties and applications. During material selection the rush to production often takes precedence over the necessary thorough determination of the applications' physical requirements and exposure to environmental factors.

Thorough review of the performance criteria for the application is critical. Before a plastic is selected a list of criteria should be built on answers to questions such as transparency, use temperature, thermal cycle, dimensional tolerances, cosmetic aesthetics, agency approval UL, FDA, NSF etc, and wear and abrasion needs. Environmental conditions are crucial and must be evaluated under time, temperature, concentration of the chemical or radiation, and stress within and applied to the part. Strength, fatigue, rate of loading, elongation, cleaning aids or solvents, body oils or fluids, shipping and storage conditions, expected misuse, and liability concerns must also be considered. For all plastic product failures, 32% is due to environmental stress-crack resistance issues (15). Environmental concerns for waste disposal and recycling must also be evaluated.

The process of injection molding influences the material's properties. Parts made by injection molding retain stress developed during injection, packing, or cooling. Properties in the flow direction are often different than that in the cross flow direction for anisotropic behavior. Shrinkage can be greater in the cross flow direction, while tensile strength is stronger in the flow direction. Addition of additives often provides one benefit, such as color, mold release, radiation stabilization, or wear resistance, but compromise another property such as impact or elongation. Part performance is further complicated by use of temperature range, complex design features, nominal wall thickness, sharp internal corners, process variations, etc. The end result is that nearly all the typical property data sheets of a material supplier dictate that an injection-molded part must be tested in its end application to verify performance.

Material handling is part of the molding process. Plastic must be properly prepared before entry into the feed throat of an injection-molding machine. Plastic granules can get contaminated with foreign material during shipping, and handling especially in regrind operations. Fines, metal, dirt, moisture, or another plastic must be removed before processing. Typically, the only precaution taken is to pass the plastic over a magnet to trap ferrous metal fragments before use. For resins that are hygroscopic it is necessary to dry them to remove the moisture before processing. Polycarbonates, nylons, urethanes, and polyesters are examples of plastics that are sensitive to hydrolysis. Hydrolysis occurs as the polymer is melted in the barrel of the injection-molding machine in the presence of moisture and results in parts with poor physical properties. The parts may look acceptable but the molecular chains are shorter due to hydrolysis, and parts will not perform to expectations. Once dry, the resin must be conveyed and stored dry until processed. It is common for the industry to dry the plastic but convey and/or store it exposed to plant air. Normally, the plastic must be processed within 30 min before it readsorbs enough moisture to mandate redrying. Some resins especially sensitive to moisture adsorption and hydrolysis present a drying challenge because of poor dryer design, maintenance, and operation. Figure 12 shows a common layout of a two-bed desiccant dryer. Two-, three-, and four-bed desiccants are common in the industry.

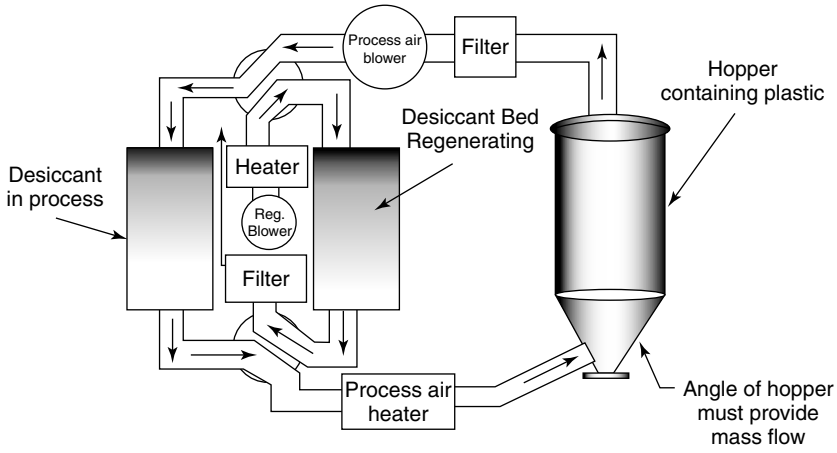

Fig. 12. Two-bed desiccant dryer.

Poor dryer maintenance leads to inactive desiccants, air leaks in hoses, clogged filters, defective heaters, and the inability to maintain a low dew point of the drying air. Parts made from improperly dried or wet resins should not be reground for reuse if the plastic is subject to hydrolysis. Degradation by hydrolysis destroys properties and is not reversible.

Blending in additives is another common resin preparation step before feeding plastic to the injection-molding machine. For most additives this is best done and usually performed at the plastic resin producer's facility after polymerization and before extrusion into pellets. However, at-the-press additives are popular. The additive can be granules, powders, or liquids, which can modify the base resins in appearance and performance. Coloring is an example of an additive used to change appearance. Typically, the natural resin is blended with a coloring agent. If the resin producer adds the color the resin is "precolored" as delivered to the molder. If the coloring is done at the molding shop it is called in-house coloring with natural resin and color concentrate or master batch coloring. The concentrated colorant, usually in granular form but can be powder or liquid, is blended with the natural resin (usually in a ratio of 20:1, ie, 20 kg of resin to 1 kg of colorant) and then fed into the feed throat of the molding machine. Colored plastic parts do not peel or show scratches like painted parts, the color is throughout the part. Colorants change not only the base resin's appearance but also its physical and processing properties. Different colors of the same resin will have different properties and may require different processing conditions. This is especially true for semicrystalline resins as colors often change the degree of crystallinity.

Tool Design and Construction. Mold design and construction is critical to all molding processes. Injection molding can not be accomplished without a mold or "tool." Building a mold is capital and time intensive (16). Tooling cost breaks down into 10% for engineering, 15% for material, and 75% labor. Current trends show that material and labor costs are increasing so much that low pressure forming processes that can function with less expensive tooling are gaining favor, such as rotomolding, blow molding, and thermoforming.

A mold performs many different functions. It can be highly complex leading to high initial cost and a maintenance burden. However, for the plastics industry simpler equates to elegance, lower cost, and higher production. The main functions of a mold are to form the shape and surface finish of the part from the molten plastic and then cool or heat the plastic to solidify or cure it so that the part can be removed from the mold. The demand for 3-D complex parts has evolved mold making into an art form second to none. Novel mold designs and construction techniques allow ever more complex shapes to be made to exacting tolerances. The mold must be ruggedly built to withstand repeated cycles, sometimes in the millions, and enormous pressures. The typical injection mold will be pressurized to 1.4–140 MPa (200–20,000 psi) to shape and pack a cavity full of plastic.

The simplest mold is the two-plate mold as depicted in Figure 13.

This two-plate mold forms one part with a cavity and core. The molten plastic enters the mold through the sprue bushing which mates perfectly with the nozzle of the molding machine. In Figure 13 the sprue bushing delivers molten plastic directly into the part. The part is "sprue gated." A "gate" is a restricted entry point for the plastic to fill the part. There are several gate designs, each with its unique advantages and disadvantages. In a multicavity tool the flow of plastic is channeled at right angles from the sprue bushing to the different cavities by means of a runner system as shown in Figure 14 (cold runner).

If multicavity molds must be built to meet product demand and the part must be center-gated (eg, round gears) there are two tooling options: a three-plate mold or a hot runner mold. A three-plate mold provides a runner path as shown in Figure 15, which allows for center-gating multiple parts.

Since this runner system comes out of the mold as the part is ejected, it is known as a cold runner. Ideally, the runner system provides the shortest path possible to each part with equal flow distance and equal pressure-drop to each

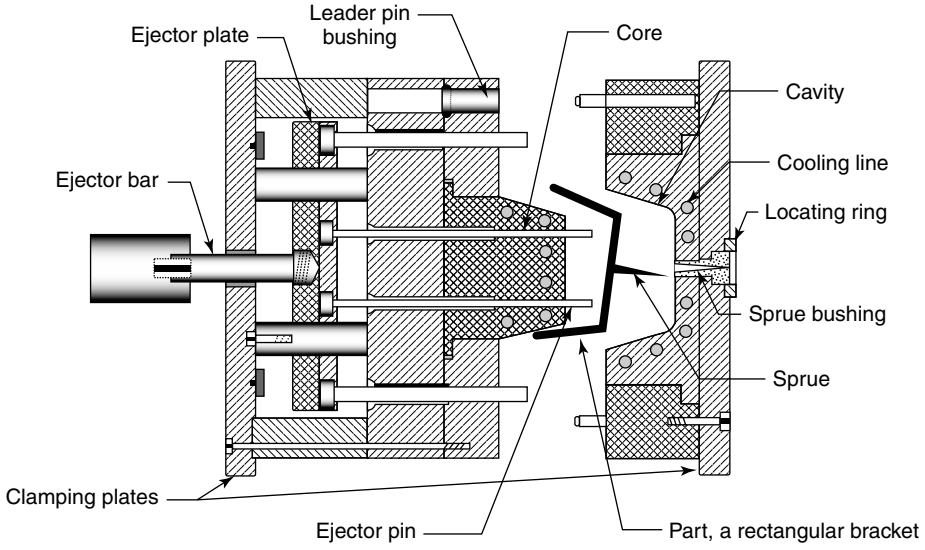

Fig. 13. Basic components of a two-plate mold. Illustration by John W. Bozzelli.

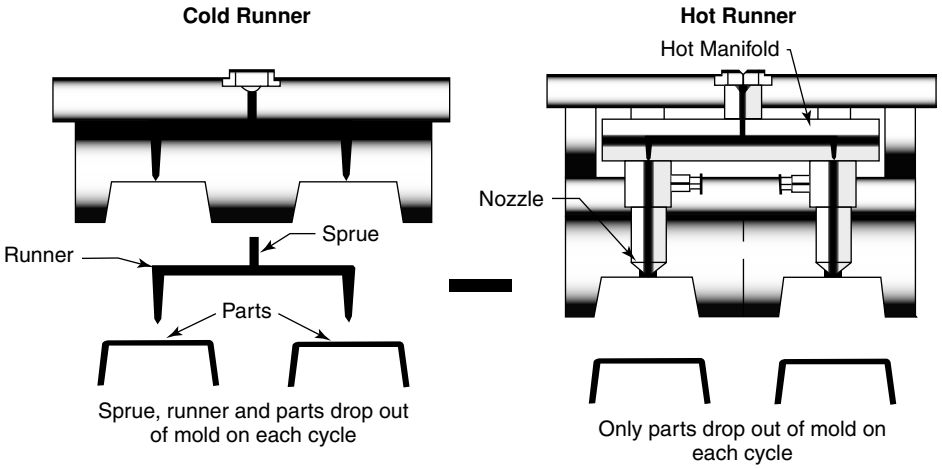

Fig. 14. Multicavity (two cavities) Cold and hot runners. Drawing courtesy of John Klees.

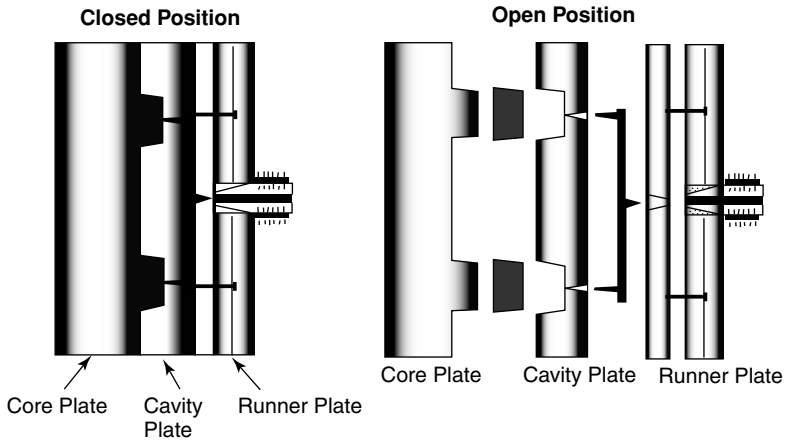

Fig. 15. Three-plate two-cavity mold.

part. Multicavity tools can make identical (Fig. 15) or nonidentical or dissimilar parts. Tools that make nonidentical parts are called family molds. Parts for a model airplane are made in one shot from a family tool and are usually packaged attached to the runner. Making quality parts in a family tool is more difficult than making parts in a multicavity tool with identical cavities because of flow imbalances. Usually, plastic will not fill a small part the same way as it will fill a large part within the same mold.

Multicavity tools can be built to make over 100 parts per cycle. These are complex molds that can cost hundreds of thousands of dollars. The cold runner systems in multicavity tools can be extensive, wasting plastic. The runner has to be separated from the part, handled, discarded, or reground for reuse if possible. An alternative to cold runners and a trend in the molding industry are hot runners or runnerless molds. Hot runners serve the same purpose as cold runners, ie,

to provide a flow channel to each cavity, but unlike cold runners, they are heated channels that keep the plastic molten during the entire cycle. The molten runner stays in the tool between shots, always ready to deliver plastic to the cavity. These hot runners are heated externally by surrounding the channel with an appropriate electric heating element or internally where the electric element is inside the channel. While this concept of hot runners may seem fairly easy to accomplish, a hot runner tool is more expensive, incurs higher maintenance costs, and often more difficult to start and run than cold runner counterparts. Runnerless mold design and construction adds several more degrees of complexity to an already intricate task. Mold making, especially hot runner tools, must be done by specialized mold makers in combination with mold filling simulation analysis. Figure 14 shows a balanced hot runner layout for two cavities. Figure 16 shows details of an internally vs externally heated hot tips used to deliver plastic to parts in hot runner tools.

With mold costs increasing due to complexity and required fast mold build times, the need to reliably predict plastic flow behavior has intensified. Mold filling simulation has evolved with the industry to become a significant factor in aiding the design and construction of molds (17). There are several software programs available. They range from those that make simple two-dimensional 2-D calculations quickly and inexpensively to the sophisticated 3-D software suites that can calculate pressure drops, shrinkage, warp, and cooling characteristics costing thousands of dollars. Highly trained, experienced engineers or technologists are needed to obtain reasonable predictions with this software.

Mold making is a complex and intricate undertaking. Skills required include the knowledge of machining various metals, computers, CNC programming, electronics, hydraulics, metallurgy, polymer flow, polymer shrinkage, etc. Mold makers have to make knowledgeable compromises on types of metal used to withstand corrosion, pressure, temperature, heat conduction, thermal expansion, etc. How the metal is cut, heat-treated, coated, or polished influences the quality and cost of the mold. The mere direction of polishing strokes can influence the ability for the plastic part to be ejected. Polish on a mold can be from a lens quality high polish

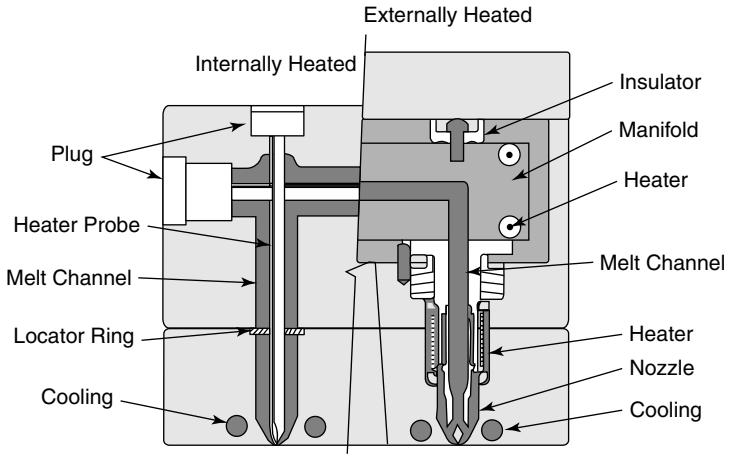

Fig. 16. Hot runner tips. Courtesy of Husky Injection Molding Systems Ltd.

or gloss to a texture that imitates wood or leather grain. Polishing can be 50% of the tooling cost.

The foremost challenge in tool building is fast response. How fast can the mold be made and at the least cost? With unrelenting demand for shorter lead times between concept to production, speed of part design and tool construction becomes strategic. Prototype tools are sometimes made before production tooling to test design or performance of both the part and the tool. An entire industry has developed to service "rapid prototype tooling," building some tools in days rather than weeks. The technologies that are currently in use include metal casting, laser sintering, metal spray-up, and Kirksite. As important as mold makers are to injection molding, the United States has yet to develop an organized apprentice program that can be compared to those of Europe and the Pacific rim. More mold makers are needed because of industry growth, demand for faster build times, and more complex tools, yet there is a decreasing supply of talented mold makers within the United States. With plastic a growth industry ranked fourth in the U.S. manufacturing community, this situation may inhibit growth and our ability to be internationally competitive.

Processing. For all plastic processings the goal is to optimize the process in order to provide volumes of parts with optimum performance in the least amount of time. This requires molding within the constraints of the plastic, tool, machine, and part. To accomplish this goal, molding must be scientific from the plastic's point of view and focus on four key processing variables: plastic flow rate or fill time, plastic pressure, plastic temperature, and plastic cooling rate and time.

These are plastic conditions, but the first consideration is that the injection molding machine does what is required and expected. Reliability and repeatability are one set of issues, while proper control of injection rate, molten plastic uniformity, and other variables are another. Because of the number of machine makers and variations in design and construction it is crucial to evaluate and monitor actual machine performance. Hydraulic vs toggle clamping, electric vs hydraulic drives, and different hydraulic architectures are some of the variations possible. Process or machine monitoring, while not commonly used in the industry, does provide scientific data to objectively evaluate machine performance (18,19). Hydraulic pressures, stroke position, temperatures, cavity, and nozzle plastic pressures are common variables monitored. Figure 17 shows a typical plot of hydraulic and cavity pressure curves vs time for a two-stage process. First stage fills the cavity to 99% full and the second stage finishes filling and packs the cavity to the required pressure and then holds the plastic in the cavity until the gate cools and freezes. After the second stage the screw rotates to plasticize or melt the plastic and charge the front of the screw with the next shot.

Plastic Flow Rate. Plastic viscosity changes with shear or injection rate. Thus, injection rate (or the time to fill a cavity 99% full) determines a resin's viscosity while filling the cavity. Normally viscosity vs shear rate data is gathered from a capillary rheometer and plotted on log scales to provide a straight line. Figure 18 is a viscosity vs shear rate curve for a typical plastic developed by using an injection-molding machine as a rheometer (20,21). This involves using the Hagan–Poiseuille equation to derive the relationship that viscosity is proportional to the pressure drop and time (fill time) as the plastic flows from the nozzle to the end of fill making a 95–99% full shot (short shot).

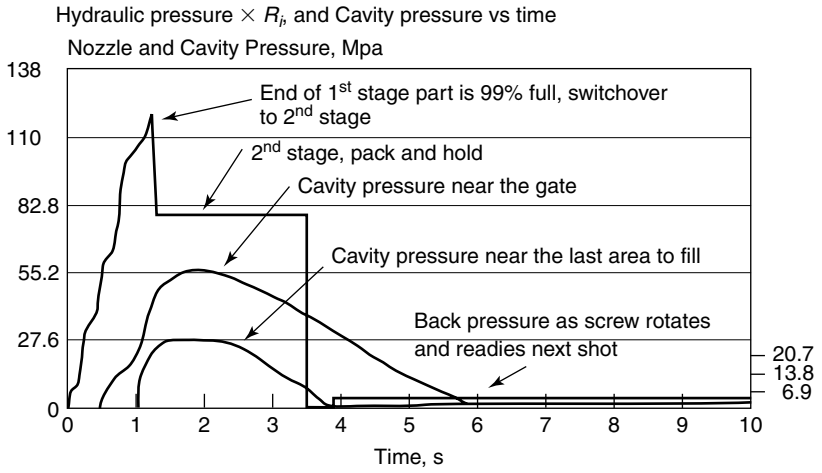

Fig. 17. Nozzle and cavity pressures vs time, good shot. Illustration by Rick J. Bujanowski & John W. Bozzelli. To convert MPa to psi, multiply by 145.

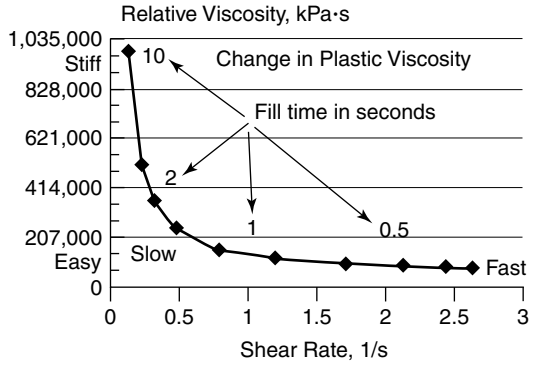

Fig. 18. Typical plastic flow. The change in plastic viscosity is at constant temperature. Shear rate correlates to flow rate or fill time. To convert kPa·s to psi·s, multiply by 0.145. To convert kPa·s to P, multiply by 10,000.

These data are then plotted on linear scales to dramatize (for the molder) the viscosity change in plastics relative to shear rate. For injection-molding processors (people who run the injection-molding machine) shear rate correlates to injection speed or fill time. The viscosity of plastics is high at slow injection rates and low at fast injection rates. The viscosity dependence on shear rate for plastics mandates that the molding machine accurately controls injection rate or "fill time" for process control. Injection speed or fill time must be controlled and constant to within ±0.04 s shot-to-shot and run-to-run. If fill time varies, viscosity will vary; if viscosity varies parts will vary. The flow-front shear rate is highly transient during filling, either accelerating or decelerating as it flows into a complex 3-D cavity during this fill time. Constant fill time is one way to keep these transient velocities consistent shot to shot. Machines must be set up and run to maintain a constant injection rate or fill time. Machines often have the ability to store

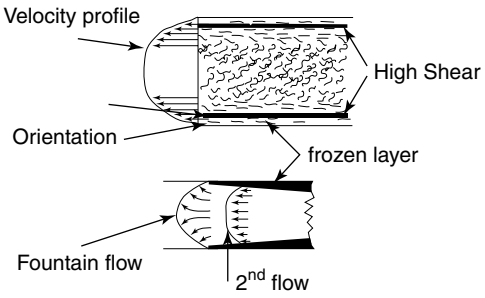

Fig. 19. Fountain flow.

process set points such as injection speed or velocity in millimeters per second. However, because of calibration errors and normal wear on a press, duplicating a millimeters per second (mm/s) set point called up from computer memory is no guarantee that fill time will be repeated. Unfortunately, the industry trend is to duplicate machine set points, not the actual velocities. It is best to monitor and control fill time.

Polymer flow through the nozzle, sprue, runner, gate, and part is best described with the concept of fountain flow. This describes the movement of the long-chain molecules. Figure 19 depicts this fountain flow concept where the long chains freeze at the side walls (there is zero velocity at the side walls of the flow path), orientate, and provide a velocity gradient and a high shear region just inside the frozen outer layer.

This explains why in-mold decorating can be done with delicate fabrics or paper labels without tearing the decoration while plastic flows over it to fill the cavity. Powdered-metal and metal molding do not exhibit this type of flow behavior.

Historically, most discussions on polymer flow focus only on viscosity. However, with many of the newer resins that are highly impact modified or have high elasticity, viscosity tells only part of the story for flow behavior. Two plastics can have identical viscosity characteristics and yet mold differently. Elastic response and the polymer's ability to transmit pressure become increasingly important as part designs increase in complexity. Both viscous and elastic response are required to properly characterize flow through complex cavities (22).

Controlling fill time is so important for plastic molding that a specific molding strategy has evolved. This strategy is based on separating fill (first stage or boost) from pack and hold (second stage). During fill, abundant hydraulic pressure (power) must be available to the hydraulic cylinder so that the flow-control valve on the injection-molding machine controls flow. First-stage hydraulic pressure set-point or limit must not control injection speed. There must be a pressure differential, ΔP, across the flow control valve so that the screw maintains injection velocity during fill. This concept of filling on first stage under velocity control is analogous to cruise-control on a car. If the plastic has to go through a gate or thin section, there has to be plenty of energy (hydraulic pressure) available to do it, just like a car going up a hill on cruise control. As with cruise control, if you run out of power (hydraulic pressure in the case of molding) you slow down. If you slow down, as the curve in Figure 18 shows, you move to the left and the plastic's viscosity gets stiffer. If the hydraulic injection cylinder does not have abundant hydraulic

pressure and the material gets stiffer due to a temperature change or different lot, you have a compounding effect. The injection speed slows, which in turn drives the viscosity stiffer and again the injection speed slows. This actually can end up as an unfilled part or short shot. Many molders run with little or no pressure differential across the flow-control device, preventing state-of-the-art closed loop machines from correctly controlling the first stage or filling the part. This is called "pressure-limited molding." Processing with an appropriate ΔP, not too high to flash the mold, allows the machine to attenuate viscosity changes on first stage. If the machine is set up correctly, it will adapt on any given shot to compensate for viscosity changes during filling the part. This removes the need for processors to tweak first-stage settings during production. Also, there is no lost production while waiting for someone to realize the machine is making unacceptable parts because of a change in viscosity such as a lot or temperature change.

Predicting the flow through the runner system (hot or cold), the gate and part is known as mold-filling simulation or mold-flow analysis as referenced in the tooling discussion. All deal with the viscosity vs shear rate relationship and continue to evolve. For example, why inside cavities on a multicavity (over four) mold fill differently than outside cavities has recently been explained ((23)). That is, some cavities fill first and others fill later during injection or the first stage. This happens even though the flow distance and pressure drop to each cavity is identical. This is known as unbalanced filling, which can make nonidentical parts even though the mold cavities are identical. It also sets up these cavities for nonuniform packing during the second stage. Once filling the mold is accomplished, the cavity must be packed with molten plastic to a pressure that provides appropriate dimensions and surface finish.

Plastic Pressure. The pressure gradient across a part establishes most of the part's attributes. The plastic pressure during pack and hold (second stage) influences dimensions, warp, gate area strength, gate vestige, and some visual characteristics such as sink marks and gloss. There is a pressure drop along the flow path from the plastic within the nozzle to the part's last area to fill. This pressure drop provides a measure of the difficulty of molding. The larger the pressure drop, the larger the amplification of the process variables. Determining this pressure drop is not straightforward, as different machines develop different plastic pressures at the same hydraulic pressures. By knowing a machine's intensification ratio (hydraulic ram area vs the area of the nonreturn valve acting like a piston pushing the plastic) we can calculate the plastic pressure in the nozzle. Often this plastic pressure is noted as injection pressure or specific pressure on a machine's specification sheet. Figure 20 depicts the hydraulic advantage or intensification ratio of hydraulic pressure intensified to plastic pressure in the nozzle.

During the early stages of the industry the machine producers made nearly all machines with a 10:1 intensification ratio with maximum injection pressures ~140 MPa (20,000 psi). If the maximum hydraulic pressure allowed to the hydraulic injection cylinder was 14 MPa (2000 psi), with an intensification ratio of 10:1, the maximum molten plastic pressure available in the nozzle was 140 MPa (20,000 psi). Today, machines are available with intensification ratios from 6:1 to 43:1 and corresponding plastic pressures up to ~415 MPa (60,000 psi). Figure 20 depicts a hydraulic cylinder and screw with a 16:1 intensification ratio.

This intensification ratio and resulting maximum available injection pressure were a factor in U.S. machine producers losing a significant portion of the

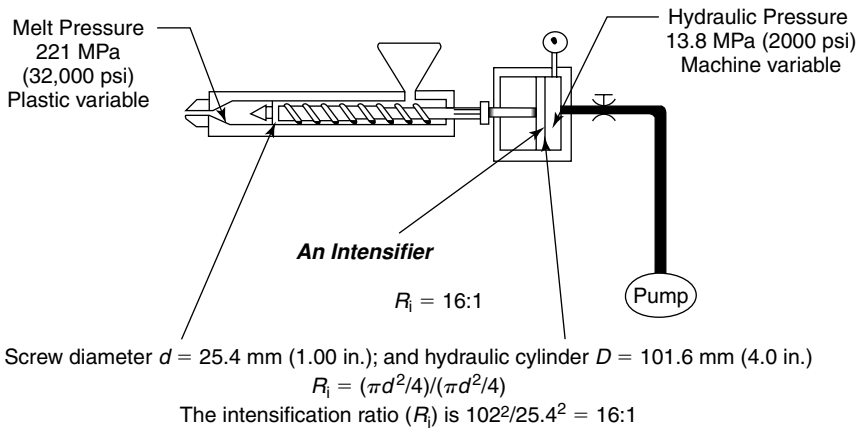

Fig. 20. Hydraulic vs plastic pressure. Illustration by John W. Bozzelli & Rick J. Bujanowski.

market to foreign competitors. The United States was slow to respond to the need for higher injection pressures required for long flow paths and complex thin-wall parts. It is suggested that machines purchased have at least 207 MPa (30,000 psi) of injection pressure, higher if the intention is for thin-wall molding. This will provide machines with greater flexibility in precision molding at no extra cost. They will also have better injection velocity control.

Over 90% of the hydraulic machine producers currently *do not* report plastic pressure on the controller or gauges. Hydraulic pressure is the standard. Production scheduling often forces a mold to be run in several different presses, each with a potentially different intensification ratio. Processors need to control this plastic pressure variable for consistent parts. Many molders reproduce hydraulic pressures (a machine variable) and not the critically important molten plastic pressures (the key plastic variable). With the advent of all electric machines this issue may resolve itself. Electric injection-molding machines use plastic pressure values for set points and reported pressures on their controllers. Injection pressure is sensed through a transducer mounted on the thrust bearing pushing on the screw, and it must read in plastic or injection pressure.

Knowing and controlling both injection and cavity pressures during filling (first stage) and packing (second stage) provides for excellent process control and part consistency. In the first stage (filling) the goal is to make a 99% full part before switching or transferring to the second stage (pack and hold). The part is slightly short or unfilled if the process was stopped at the end of the first stage. Since the part is short, the pressure near the last area to fill or the end of the flow front is zero. The pressure at the beginning of flow inside the nozzle can be calculated from the hydraulic pressure at the end of the first stage and using the intensification ratio. Thus, the plastic-pressure drop can be calculated for any short shot. By a series of short shots the pressure loss during the first stage (or filling the part) can be detailed without the use of cavity transducers. This data can be compared to mold-filling simulation calculations to check accuracy. A typical short shot study might show pressure losses as follows.

Nozzle	20.6 MPa	3,000 psi
Hot runner and gate	38.0 MPa	5,500 psi
Filling the part	82.7 MPa	12,000 psi
Total	*141.3* MPa	*20,500* psi

This information allows the processor to find high pressure-loss areas, which can be modified to provide easier flow and therefore a more robust molding process that makes acceptable parts. Lower pressure drop leads to better process control and consistency.

Switching from the first stage or velocity (V) control to the second stage or pressure (P) control is known as first to second stage transfer, or VP transfer. This switchover occurs as the screw moves forward and reaches a set point or position that provides the right amount of material to fill the mold 95–99.9% full. Other possible switchover conditions can be based on time, hydraulic pressure, or cavity pressure. Switchover by cavity pressure is more repeatable than by position, which is more repeatable than time. Switchover by hydraulic pressure is not recommended, as it limits the machine's ability to control velocity. To properly control the development of cavity pressure in the mold requires sharp machine response from the first to the second stage and accurate pressure control (see Figure 17, nozzle pressure curve).

The purpose of the second stage is to finish filling the mold and build cavity pressure to sufficient levels to replicate the shape and finish of the mold cavity. This is a different pressure loss than seen in filling or the first stage. Too much packing pressure will result in parts that are overpacked or flashed, causing wasted plastic and dimensional variances. Too little pressure or lack of control will produce nonfilled parts (shorts), dimensional variances, and unacceptable parts. Cavity pressure measurements (transducers are required) provide a methodology to verify part consistency. While cavity pressure measurement capability has been available for ~25 years, it is rarely used in the molding industry. Costs, incorrect placement, lack of large data gathering and storage capability, lack of training, delicate transducers (pressure sensors), and difficulty in interfacing with the molding machine have all been negative factors. Focus had only been on peak cavity pressures. More complete data can be found with cavity pressure curve integrals or area under the cavity pressure curves. For example, gate seal or plastic backflow out of the cavity is not seen if only peak pressures are monitored. Process monitoring instrumentation and appropriately located transducers can be used to inspect parts for 100% acceptance or rejection for dimensional tolerances. Cavity pressure measurements will not inspect for cosmetic or aesthetic criteria, which can be done via computer vision systems. Newer easier-to-use sensors that measure both cavity pressure and temperature are under development based on ultrasonics (24,25).

Before the amount of pressure to pack the part to the specified tolerances can be found, second stage (pack and hold) time must be determined. Second stage pressure is a timed event and must be on either (a) long enough to make sure the gate is frozen so plastic does not backflow out of the part or (b) for just long enough to pack the part out but not overpack the gate. Backflow of plastic out of the part into the runner can occur if second stage pressure timer ends before

the gate freezes. This allows the higher pressure that has been developed in the cavity to push plastic back out the gate so that the gate area of the part does not have molecules too closely packed or overpacked. Once the mold is filled, plastic cools and shrinkage requires more plastic to compensate. The amount of plastic that can be packed into the cavity during the second stage time depends on how long it takes for the gate to seal or freeze off. Gate freeze or gate seal time can be determined with a cavity pressure sensor near the gate or by plotting part weight vs increasing second stage (pack and hold) time. Cavity pressure curves from measurements near the gate will show changes in slope on the cooling portion (decreasing pressure vs time) of the curve between gate seal and gate unseal. However, cavity pressure data is rarely available. Part weight experiments are more common and require weighing parts, excluding the runners, as the processor changes the amount of second stage time. Part weight vs second stage time are recorded and graphed. The resulting graph shows stable part weights when the gate is sealed and a drop in weight at second stage times where the gate is not frozen. Part weight will vary as second stage time is changed until gate freeze occurs. Cycle time must be kept constant during this experiment to keep the energy load on the mold consistent.

Once gate seal time is established, the processor can optimize the amount of second stage pressure. It is this pack and hold pressure that establishes the parts dimensions and density. If running with second stage time long enough achieves gate seal, raising second stage pressure will increase part weight and size. Lower pressures produce lighter and smaller parts. A well-made mold that correctly accommodates for shrinkage (difficult to do) and the correct packing pressure will provide a part centered on the dimensional specifications. This provides an optimized process to meet dimensional criteria. The gate area will normally be packed to a higher pressure than the last area to fill. There is a pressure gradient from the gate area to the last area to fill. Within the part there is some pressure loss which can vary considerably on a shot-to-shot basis. The pressure gradient must be duplicated for consistent parts. This pressure gradient can be minimized if the processor runs with second stage times shorter than those needed for gate seal. Plastic can be allowed to backflow out of the cavity to reduce pressure near the gate after filling. These cavity pressures can be measured with cavity pressure transducers (see Fig. 17, the cavity pressure curves).

Correctly adjusting screw rotation speed, backpressure, clamp opening, ejection, and clamp closing will optimize the rest of the cycle. During screw rotation, there is pressure held against the hydraulic cylinder in the injection unit. This resistance pressure is called backpressure and must be overcome by the metering section of the screw acting like a pump pushing plastic in front of it, preparing for the next shot. Something like filling a syringe for a shot. With a properly designed screw, minimum screw rotation speeds to keep the cycle constant, and backpressures ~7.0 MPa (1000 psi) plastic pressure, uniform molten plastic consistency can be achieved. Clamp movement should be smooth and set appropriately to protect damaging the expensive mold. Ejection should not distort the part with too much speed or pressure.

The clamp keeps the mold halves together as cavity pressure develops during filling and second stage packing. Clamp force is generated by the stationary and rear platen stretching the four tiebars after the moving platen pushes the mold closed. It is important that the tool takes up most of platen area between the

tiebars and that the clamping force is uniform. Uniform clamp force around the parting line prevents excessive tool and clamp wear. Clamping a mold correctly requires a level machine, parallel platens, and uniform stretch of each of the four tiebars. Occasionally, high injection pressures will overcome the clamping force, separate the mold halves, then produce flashed parts. These must be trimmed or discarded. Clamping forces required are usually estimated and rarely scientifically calculated or measured. Industry guidelines vary from 20.7 to 68.9 MPa (1.5 to ~5 tons/in.^{2}) of the projected area of the part and runner. Thin-wall applications can require as much as 110 MPa (8 tons/in.^{2}).

Different types of molding machine clamps (toggles, hydraulic, and hydromechanical) have different advantages. Toggles are fast and energy efficient, yet it is difficult to set clamp tonnage accurately. Better toggle machines use strain gages to measure stretch of the tiebars which relates clamp tonnage. With toggles, clamp force changes as mold temperature changes due to the thermal expansion of the mold and machine components. Hydraulic clamps are easy to set, less energy efficient but are sometimes slower due to the large volume of oil necessary to fill the hydraulic cylinder. Hydraulic clamps automatically compensate for thermal mold expansion. Molding machines are ranked by clamp tonnage within the molding industry. Machines range from 69 to 1.4×10^5 MPa (5–10,000 ton/in.^{2}).

Plastic Temperature. Correct temperature and uniformity are crucial for a consistent process. Monitoring of plastic temperature is difficult and rarely utilized in the industry. Control of temperature is done via thermocouples partially embedded into the barrel wall, usually three to four along the length of the barrel. The actual molten plastic is not monitored for temperature and >90% of the temperature values provided as data are barrel wall temperatures that can be off by ±25°C (45°F). Temperature control is done via proportional-integral-derivative (PID) controllers or PID algorithms on computer controlled presses. Calibration of thermocouples is seldom done. PID temperature control of the nozzle tips is also important, yet ~40% of the industry uses variacs.

Heat necessary to melt the plastic granules comes from two sources. The heater bands start the melting process by getting the plastic to stick to the barrel wall. Between 10 and 40% of the heat necessary to melt the plastic comes from the heater bands. Most of the heat comes from the frictional or shear heat developed as the flights of the screw rotate within close proximity of the barrel wall. The flights shave plastic from the barrel wall into a spiral pool between the flights. Between 60 and 90% of the energy necessary to melt the plastic comes from screw rotation or shear at the barrel wall—flight interface. Temperature override can occur, and the open space between the heater bands is necessary for barrel cooling. Some machines have cooling fans placed between the heater bands to aid control.

Screw design and construction are important aspects to any plastic processing, yet design gets little attention in the injection-molding industry. Figure 21 shows a general–purpose screw which is what is specified or accepted for ~85% of machines delivered. The screw is divided into three zones: feed, normally 50% of the flights; transition, 25%; and metering, 25%.

The feed zone conveys plastic forward to the transition zone and has a constant root diameter. The root diameter tapers through the transition zone, which compresses the granules forcing air back toward and out of the feed throat and hopper. The main purpose of the transition zone is to compress the plastic and provide the shear heating to drive the melting process. Ideally, by the end of the

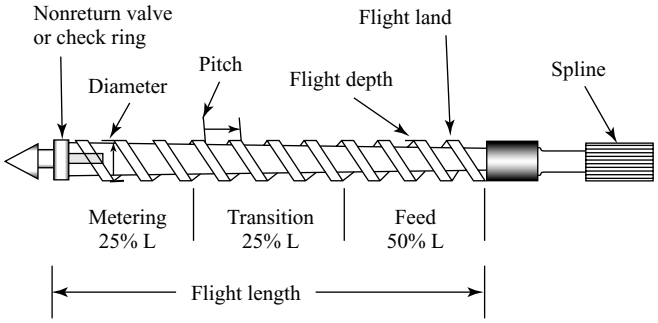

Fig. 21. Screw components. Illustration by Rick J. Bujanowski & John W. Bozzelli.

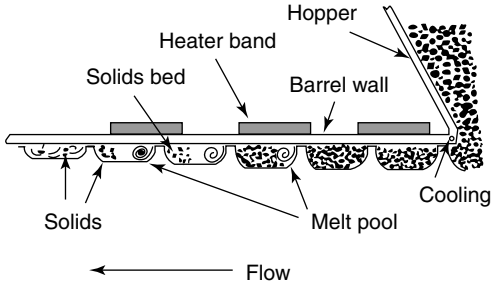

Fig. 22. Melt Model, solids pass. Illustration by John W. Bozzelli & Rick J. Bujanowski.

transition zone the plastic is melted, but usually the solid bed breaks up. Unmelted solids along with molten plastic get delivered to the metering section, which acts like a pump to push the plastic forward, charging plastic for the next shot (see Fig. 22).

As plastic is pushed forward (overcoming backpressure) the screw is forced to retract. There is now a cylinder of plastic in front of the screw tip and nonreturn valve. Upon injection, the screw moves forward seating the nonreturn valve or check ring, which acts like a plunger, piston, or ram to push the plastic out the nozzle tip into the sprue bushing of the mold.

Molten plastic uniformity is required for optimum processing performance; hence, screw specification is another strategic issue. The standard general-purpose screw is known to produce unmelted solids (26,27). These unmelted solids clog gates and produce inferior parts. Molten plastic uniformity can be achieved with state-of-art screws and metering sections as represented in Figure 23.

Screw and barrel specifications deal with type of material to be processed, shot volume, and plastic uniformity. Shot volume (the part, runner, and sprue)

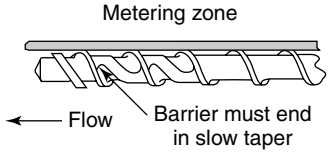

Fig. 23. Modified metering section. Illustration by Rick J. Bujanowski & John W. Bozzelli.

should be 25–65% of the barrel capacity. Barrel and screw hardness and corrosion resistance depend on the type of material to be processed. Glass fiber or other abrasive fillers require hard barrels to prevent excessive wear. Materials that may produce acid gases, HCl from PVC, or other volatiles that may chemically attack the barrel and screw call for more chemically resistant steels such as stainless or plating the screw with a chemically resistant metal such as nickel. Screw design specifications also involve compression ratio, how much is the plastic compressed within the flights of the screw from feed to metering zone, length-to-diameter ratio or L/D, and shape of the screw flights. The screw should be highly polished to allow plastic to slip on the screw and stick to the barrel, have sharp flights with a large trailing radius so as to prevent dead spots from causing degradation of the polymer.

Plastic Cooling Rate and Time. Cooling is over 90% of the molding cycle, so optimization is critical to provide the minimum cycle time and optimum profits. Analyzing the cycle in Figure 6 shows that cooling for the part actually occurs in each segment except for filling. Molding is a thermal process and so consistent steady-state conditions cycle to cycle are crucial. Within the cycle there are large swings in temperature, yet cycle-to-cycle consistency is paramount. This is the reason automatic cycles provide better quality and production over manual cycles. Automatic cycles allow the machine to cycle unattended. Manual cycle depend on an operator to take parts out of the mold, then re-cycling the process. Manual cycles do not run at a constant cycle time, allowing heat loads to vary on the mold and machine. Molds take several cycles to reach equilibrium because of the cooling process being a combination of radiation, air convection, and conduction cooling as coolant flows through the channels of the mold. Time to reach this steady-state mode can be minutes or hours depending on the part, tool size, and mold-cooling capacity. Often the machine's platens that hold the mold must come to temperature equilibrium with the environment before the cycles are in steady state. Thus, the machine's environment can and does influence the process. Air conditioning a molding plant is expensive but it aids in steady-state processing, leveling season heat and cooling loads on the mold.

Not all of the heat energy put into the resin must be removed by mold cooling. The part can be ejected warm as long as it is rigid enough to withstand the force of ejection and hold its shape during post-molding handling by humans, robots, conveyors, or as they accumulate in a box or bin. Part cooling will continue after ejection and must be kept consistent to maintain part uniformity and prevent warping. Whatever the cause, nonuniform cooling will add retained stress to a part. Nonuniform nominal wall thickness, improper packaging, even inconsistent part placement on a table after ejection can cause dimensional variations and warp. This is particularly important for semicrystalline, high shrink resins, which can take weeks to stabilize because of continued crystallization.

Mold cooling or temperature control is typically done with a thermolator that pumps water, water and ethylene glycol mixture, or oil through channels in the mold to heat or cool the plastic. Heat transfer (usually cooling) problems develop if corrosion or deposits accumulate in the channels (water lines) in the mold. Other issues are that water lines are not drilled uniformly around the part, coolant lines are not routed correctly, or coolant flow is not turbulent. Flow turbulence is defined by a Reynolds number of 3500 or greater and is difficult to achieve in some plants because of inadequate feed and return line size or restrictions in the tools cooling

channels. Molds often have different size cooling lines yet fed by the one multifrost manifold. Larger lines get more coolant flow at the expense of smaller lines, leading to nonuniform cooling. Chiller (refrigerated or chilled water) operation, cooling tower condition, water treatment, and filtration are important areas that demand constant monitoring to maintain optimum and consistent cooling. Certain cooling checks should be made on a routine basis. For instance, each cavity must receive the same coolant flow rate. Additionally, the pressure drop from inlet to outlet for each mold circuit should be ∼210 to 240 kPa (30–35 psi) pressure drop or greater. Temperature differential between inlet vs outlet should be below 2°C (4°F).

Handling of the parts after production must also be controlled for consistency. For high tolerance parts in semicrystalline resins (polyethylenes, nylons, acetal, and polypropylene), each part must be treated to the same post-mold conditions of handling, storage, etc. Cooling influences post-molding shrinkage. Parts in the center of a box do not cool like those on the sides, and the different cooling rate may be the cause of rejects. The concept is to treat every part the same. All parts must be ejected, cooled, and packaged identically, or differences in dimensions and warp develop even though parts were good out of the press.

BIBLIOGRAPHY

"Injection Molding" in *EPSE* 2nd ed., Vol. 8, pp. 102–138, by I. I. Rubin, Robinson Plastic Corp.

1. D. V. Rosato and D. V. Rosato, *Concise Encyclopedia of Plastics: Fabrication & Industry*, Kluwer Academic Publishers, Boston, Mass., 2000.
2. D. V. Rosato and D. V. Rosato, *Injection Molding Handbook*, 3rd ed., Kluwer Academic Publishers, Boston, Mass., 2000.
3. D. V. Rosato, *Injection Molding Newsletter* (53), 1–24 (Spring 2000).
4. *Injection Molding Magazine*, www.immnet.com.
5. *Modern Plastics*, www.modplas.com.
6. *Plastics News*, www.PlasticsNews.com.
7. *Plastics Engineering*, Society of Plastics Engineers, www.4spe.org.
8. *Modern Mold and Tooling*, 110 William St., New York, NY 10038.
9. D. C. Paulson, *Injection Molding Magazine*, Dec. 1994, p. 7.
10. F. Johannaber, *Injection Molding Machines, A User's Guide*, 3rd ed., Hanser Gardner Publications, Cincinnati, Ohio, 1994, 328 pp.
11. G. Beall, Plastic Part Design for Economical Injection Molding, Seminar Manual, 1982–2000.
12. R. A. Malloy, *Plastic Part Design for Injection Molding—An Introduction*, Hanser Gardner Publications, Cincinnati, Ohio, 1994, 460 pp.
13. *IDES Prospector*, www.idesinc.com, also available through the Society of Plastic Engineers, www.4SPE.org.
14. M. Sepe, *Dynamic Mechanical Analysis for Plastics Engineering*, Plastics Design Library, Norwich, N.Y., 1998, 189 pp.
15. M.Sepe, private communication, Dec. 1999.
16. R. G. W. Pye, *Injection Mold Design*, Longman Scientific and Technical, Essex, England, 1989.
17. P. Kennedy, *Flow Analysis of Injection Molds*, Hanser Gardner Publications, Cincinnati, Ohio, 1995, 237 pp.
18. D. C. Paulson, *Plastics and Rubber Processing*, March 1978, pp. 32–36.
19. R. J. Groleau, 1989 ANTEC, pp. 260–263.

20. J. W. Bozzelli and R. J. Groleau, Presented at the *Las Vegas West SPE Conference*, Feb. 1991.
21. J. Bozzelli, A. Larsen, and J. McDonnell, 1998 SPE ANTEC, paper number 346 on compact disc.
22. L. R. Schmidt, 1998 ANTEC paper number 719 on compact disk #9840CD, Printed volume pp. 3592–3597.
23. J. P. Beaumount, *J. Injection Molding Technol.* **1**(3), 133–143 (Sept. 1997).
24. S. Y. Baek, R. Edwards, and C. L. Thomas, 2000 SPE ANTEC, paper number 1038 on compact disk #0050CD.
25. E. C. Brown, A. J. Dawson, P. D. Coates, 2000 SPE ANTEC, paper number 592 on compact disk # 0050CD.
26. *Cylinder & Screw Handbook*, 6th ed., Westland Corp., Wichita, Kans., 1997, 33 pp.
27. *Plasticating Components*, Spirex Corp., Youngstown, Ohio, 2000, 114 pp.

JOHN W. BOZZELLI
Midland, Michigan

INORGANIC POLYMERS

Introduction

Inorganic polymer science represents an area that has been held back by the synthetic problem of constructing macromolecular chains. However, advances in the last two decades or so of the twentieth century have led to the preparation of a variety of new polymers that contain main group elements, transition-metals, and even lanthanides. It is plausible that some of these new materials, with properties that are difficult or impossible to achieve with existing organic materials, may fulfill the requirements of specialized markets; such developments remain an interesting future challenge. Polysiloxanes (silicones) represent the most well-developed class of inorganic polymers and these materials are discussed in a separate article (see SILICONES). In addition, although surveyed briefly in this article, more detailed information on POLYPHOSPHAZENES and POLYSILANES and POLYCARBOSILANES can be found elsewhere in the Encyclopedia. Here we focus on other main classes of inorganic polymers.

Inorganic Polymers Based on Main Group Elements

Polyphosphazenes. Polyphosphazenes (**1**) have a polymeric backbone composed of alternating phosphorus and nitrogen atoms. The side groups, R, can be alkoxy, aryloxy, amino, alkyl, aryl, inorganic, or organometallic groups. This large range of accessible structural variations is accompanied by a wide range of polymer properties that are highly dependent upon the nature of the side groups (see Table 1).

Encyclopedia of Polymer Science and Technology. Copyright John Wiley & Sons, Inc. All rights reserved.

Table 1. Properties of Selected Polyphosphazenes[a]

Formula	T_g, °C	T_m, °C	Properties
$[NP(O^nC_4H_9)_2]_n$	−105		Elastomer
$[NP(O^nC_3H_7)_2]_n$	−100		Elastomer
$(NPF_2)_n$	−96	−68, −40	Hydrolytically unstable elastomer
$[NP(OC_2H_5)_2]_n$	−84		Elastomer
$[NP(OCH_2CH_2OCH_2CH_2OCH_3)_2]_n$	−84		Water-soluble elastomer
$[NP(OCH_3)_2]_n$	−76		Elastomer
$(NPCl_2)_n$	−66	−7.2 (39)[b]	Hydrolytically unstable elastomer
$[NP(OCH_2CF_3)_2]_n$	−66	242	Microcrystalline thermoplastic (films)
$[N_3P_3(OCH_2CF_3)_5(CH_3)]_n$	−63		Elastomer
$[N_3P_3(OCH_2CF_3)_x(CH_2Si(CH_3)_3)]_n$	−61		Elastomer
$[NP(OCH_2CF_3)(OCH_2(CF_2)_xCF_2H)]_n$	−60[c]		Elastomer
$[NP(OC_9H_{19})_2]_n$	−56		Elastomer
$[NP(CH_3)(alkyl)]_n$	−50[d]		Amorphous gums or waxes
$[NP(CH_3)_2]_n$	−46	143	Microcrystalline powder
$[NP(^nC_6H_{13})_2]_n$	−29	129	Wax-like solid
$(NPBr_2)_n$	−15		Hydrolytically unstable, leathery material
$[NP(OC_6H_5)(OC_6H_4C_2H_5)]_n$	−10[e]	[f]	Elastomer
$[NP(OC_6H_5)_2]_n$	−8	390	Microcrystalline thermoplastic (films, fibers)
$[NP(OC_6H_4COOH)_2]_n$	−5		Glass, soluble in aqueous base
$[NP(OC_6H_4COOC_2H_5)_2]_n$	8	127	Microcrystalline thermoplastic (films)
$[NP(OC_6H_4CH_3)(OC_6H_4CHO)]_n$	11		Thermoplastic
$[NP(NHCH_3)_2]_n$	14		Water-soluble glass and film former
$[NP(OC_6H_5)(OC_6H_4C_6H_5\text{-}o)]_n$	24		Glass
$[NP(NHC_2H_5)_2]_n$	30		Glass, soluble in aqueous acid
$[NP(CH_3)(C_6H_5)]_n$	37		
$[NP(OC_6H_5)(OC_6H_4C_6H_5\text{-}p)]_n$	43		Glass
$[NP(CH_3)(alkyl)]_n$	∼50[g]		Amorphous gums or waxes
$[N_3P_3(OCH_2CF_3)_4(C_5H_4FeC_5H_4)]_n$[g]	61		Amber-colored glass
$[NP(NHC_6H_5)_2]_n$	91		Glassy thermoplastic
$[NP(OC_6H_4C_6H_5\text{-}p)_2]_n$	93	>350	Microcrystalline thermoplastic (high η)

[a] Refs. 1,2–3.
[b] For the stretched polymer.
[c] Varies with values x and ratio of side groups.
[d] Broad, poorly defined transitions.
[e] Varies with ratio of side groups.
[f] Complex melting phenomena.
[g] Ferrocenyl polymer.

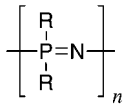

1

In addition, the phosphorus–nitrogen backbone inherently possesses a unique range of unusual properties. For example, it is extremely flexible which in turn can give rise to low glass-transition temperatures, particularly in the case of poly(alkoxyphosphazenes) such as the *n*-butoxy derivative ($T_g = -105^\circ$C) (1,4). Furthermore, the backbone is thermally and oxidatively stable, as well as optically transparent from 220 nm to the near infrared region, which makes it resistant to breakdown in many harsh environments, as evidenced by the flame-retardant properties of many polyphosphazenes.

Ring-Opening Polymerization (ROP). The first polyphosphazene synthesized, poly(dichlorophosphazene) (**2**), was prepared in cross-linked form by Stokes at the end of the nineteenth century by the thermal ROP of the cyclic trimer $[Cl_2PN]_3$ (**3**) (1). This material, referred to as "inorganic rubber," remained a chemical curiosity because of its intractability and hydrolytic instability until the mid-1960s when it was shown that if the ROP of pure $[Cl_2PN]_3$ is carried out carefully, uncross-linked poly(dichlorophosphazene) (**2**), which is soluble in organic solvents, is formed (5). Subsequent reaction of this highly reactive polymeric species with nucleophiles has been shown to yield a wide range of hydrolytically stable poly(organophosphazenes) (eq. 1) (1,6–8).

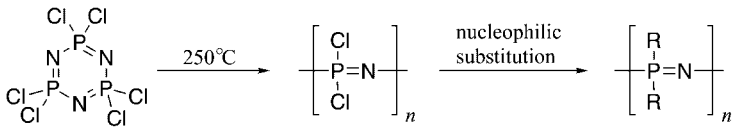

3 **2** **1** (1)

This macromolecular substitution route, used primarily with alkoxides, aryloxides, or primary amines, is largely responsible for the immense structural diversity of poly(organophosphazenes) and allows the tuning of certain properties and the introduction of others through the choice of nucleophile. Highlights concerning the use of the macromolecular substitution route with **2** and related materials involve the introduction of side groups, which lead to liquid crystallinity (see polymer **4**) (9), photochromism (10), photocross-linkability (11–13), and the preparation of novel polymers such as (**5**) with short-chain branching (14,15).

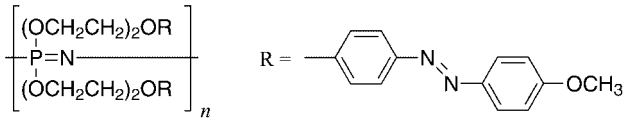

4

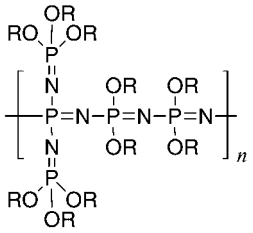

5

The thermal ROP route requires the synthesis and careful purification of the cyclic trimer $[Cl_2PN]_3$ and the use of elevated temperatures where control of molecular weight is very difficult and cross-linking can take place at high conversion, which can limit the yield.

Condensation Polymerization. Although several polyphosphazenes have been commercialized, much work has focused on the development of cheaper and more convenient methods for making these materials. Also, the reaction of poly(dichlorophosphazene) with organometallic reagents such as Grignard or organolithium reagents generally leads to chain cleavage as well as substitution, and thus macromolecular substitution does not provide a satisfactory route to polymers with only alkyl and aryl side groups bound by direct P—C bonds. To these ends several promising condensation routes have been developed.

In the early 1980s, a condensation route to polyphosphazenes from phosphoranimines was discovered (eq. 2) (16).

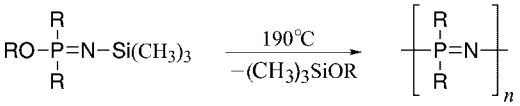

(2)

The polymerization is in fact a chain-growth reaction and allows access to high molecular weight polyphosphazenes such as poly(dimethylphosphazene) and poly(methylphenylphosphazene) (2). Methyl deprotonation/substitution of these polymers as well as electrophilic aromatic substitution of the phenyl substituents in poly(methylphenylphosphazene) have been developed as versatile strategies for the derivatization of both of these polymers (eq. 3) (3).

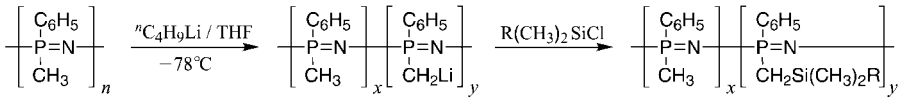

(3)

An alternative, direct route to fluoroalkoxy phosphazene polymers and aryl derivatives which also permits access to block copolymers has been developed (eqs. 4 and 5) (17,18).

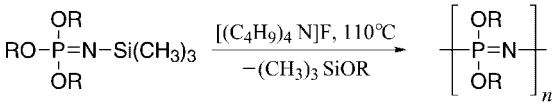

(4)

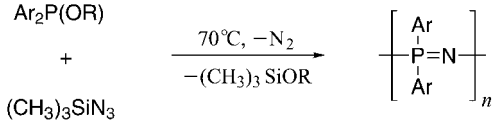

(5)

The development of condensation routes to poly(dichlorophosphazene) have also been reported. One promising route operates at 200°C (eq. 6) (19).

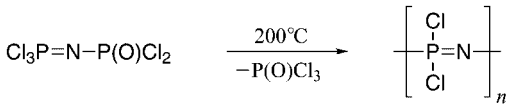

(6)

In 1995, details of a synthesis of poly(dichlorophosphazene) which operates at room temperature and allows for good molecular weight control were reported (eq. 7) (20). It involves the condensation of phosphoranimines in the presence of cationic initiators such as a PCl_5. The polymerization has been shown to proceed via a cationic chain-growth mechanism that shows "living" characteristics (21). Two equivalents of the initiator react with one equivalent of a chlorinated phosphoranimine to form a reactive ion pair (eg, $[Cl_3P{=}N{=}PCl_3]^+PCl_6^-$), which further reacts with monomer to propagate chain growth.

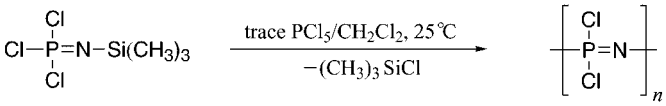

(7)

This synthetic method has been extended to the direct synthesis of poly(organophosphazenes) as well as the development of star and block copolymers. For example, triarmed star-branched polyphosphazenes (eg, **6**) can be synthesized through the initiation of trifunctional phosphoranimines (22). It has also been shown that the presence of "living" active sites at the termini of the polymer chains allows for addition of a second monomer and the formation of block copolymers (23), such as (**7**) which is formed through the initiation of a difunctional linear phosphoranimine and the subsequent introduction of two different monomers (24). These developments offer the prospect of improved routes

to phosphazene polymers, which may well facilitate more rapid and extensive commercialization.

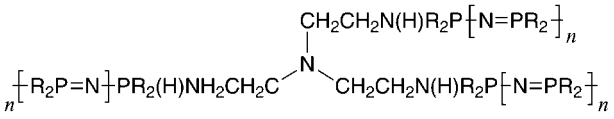

6

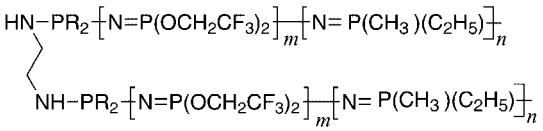

7

Monomer Synthesis. Both the ROP and condensation routes to poly(dichlorophosphazene) require high purity monomers. For the traditional ROP process, ultrahigh purity $[NPCl_2]_3$ is required. The most common method for its preparation is through the reaction of PCl_5 with NH_4Cl in a high boiling halogenated solvent, such as chlorobenzene or tetrachloroethane, at 150°C. The yields can approach 70–80% under specialized conditions, but 50% is more typical (25).

The phosphoranimine most commonly used in the aforementioned condensation route to poly(dichlorophosphazene) is $Cl_3P{=}NSi(CH_3)_3$. The synthesis of this compound has been described (21) and is based on a modification of an earlier procedure (26) involving the reaction of PCl_5 with $LiN(Si(CH_3)_3)_2$ at −78°C in hexane. However, the purification required by this method is a challenge and leads to an overall yield of <40%.

It has also been reported that the reaction of $N(Si(CH_3)_3)_3$ with PCl_5 can be manipulated to maximize yields of either the cyclic trimer (76%) or the pure phosphoranimine monomer (40%) through variations in reaction conditions (25). These reactions use milder conditions than previously reported methods, with higher yields. In addition, the major side product, $(CH_3)_3SiCl$, can be recycled to form one of the starting materials, $N(Si(CH_3)_3)_3$.

N-Silylphosphoranimines with alkyl and aryl substituents can be synthesized by reaction of commercial starting materials such as PCl_3, $((CH_3)_3Si)_2NH$, and Grignard reagents by way of a three-step process, with typical yields of 60–70%. These precursors are also accessible via a "one-pot" synthesis, which requires only isolation of the final product with yields of about 75% (3).

Uses. Some of the most useful polyphosphazene derivatives are fluoroalkoxy derivatives, and amorphous copolymers are very useful as flame-retardant, hydrocarbon-solvent, and oil-resistant elastomers and have found aerospace and automotive applications. Polymers such as the amorphous comb polymer poly[bis(methoxyethoxyethoxy)phosphazene] (**8**) are of considerable interest as components of polymeric electrolytes in battery technology (1).

Polyphosphazenes are also of interest as biomedical materials and bioinert, bioactive, membrane-forming, and bioerodable materials (1).

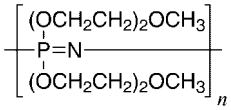

8

Polysilanes

Properties. Since the first reports of soluble and processible polysilanes (**9**) in the late 1970s, these macromolecules have attracted widespread interest from both a fundamental and an applied perspective (1,27–29). The use of Wurtz coupling has allowed the preparation of a range of polymers with alkyl or aryl substituents at silicon that are high in molecular weight with $M_n > 10^5$. Since 1980, there has been a remarkable growth in interest concerning these polymers and they have been found to possess a variety of fascinating properties. The backbone of silicon atoms gives rise to unique electronic and optical properties.

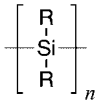

9

One of the most remarkable features of the all-silicon backbone is that it leads to the delocalization of σ electrons, a phenomenon which is virtually unknown in carbon chemistry (30). This can be understood in terms of the nature of the molecular orbitals associated with the Si—Si σ bonds. These are more diffuse than those associated with C—C σ bonds as they are constructed from higher energy 3*s* and 3*p* atomic orbitals. This leads to significant interactions between the adjacent Si—Si σ bonds along a polysilane chain, a situation analogous to that for the π bonds in π-delocalized polymers such as polyacetylene. Thus, a band model is more appropriate than a localized model (1,28). As a consequence of the delocalization of σ electrons, the σ—$\sigma*$ transition, which occurs at 220 nm in $(CH_3)_3Si—Si(CH_3)_3$, moves to lower energy as the number of silicon atoms in the chain increases. In the high polymers, the σ—$\sigma*$ band-gap transitions occur in the near uv region at ca 300–400 nm (Table 2). The lowest absorption bands of polysilanes have also recently been assigned to excitonic rather than interband transitions (32). The electron delocalization also leads to appreciable electrical conductivity following doping. For example, conductivities of up to 0.5 S/cm have been reported for polysilastyrene (**10**), after doping with AsF_5 (1). In addition, many of the polymers are thermochromic as the conformations adopted by the polymer change with temperature, which alters the degree of σ-delocalization along the main chain. Because of their low energy σ—$\sigma*$ transitions, polysilanes

Table 2. Ultraviolet–visible Absorption Data for Typical Polysilanes[a,b]

R_1	R_2	λ_{max}, nm	ε/SiSi
CH_3	$^nC_3H_7$	306	5600
CH_3	$^nC_4H_9$	304	
CH_3	$^nC_6H_{13}$	306	5100
CH_3	$^nC_{12}H_{25}$	309	5000
CH_3	C_2H_4-C_6H_5	303	9950
CH_3	$^cC_6H_{13}$	326/320	7390
$^nC_3H_7$	$^nC_3H_7$	310	
$^nC_4H_9$	$^nC_4H_9$	314	8400
$^nC_6H_{13}$	$^nC_6H_{13}$	316/317	9700
$^nC_{14}H_{29}$	$^nC_{14}H_{29}$	318	8400
$^nC_3H_7$	$^nC_6H_{13}$	322	10600
$^nC_6H_{13}$	$^nC_8H_{17}$	318	8785
CH_3	C_6H_5	341	9300
CH_3	p-$C_6H_4CH_3$	337/338	8600
CH_3	p-$C_6H_4OCH_3$	344	8180
CH_3	p-$C_6H_4O^nC_6H_{13}$	354	5400
CH_3	p-$C_6H_4C_6H_5$	352	4000
CH_3	β-naphthyl	350	2800
p-$C_6H_4C_2H_5$	p-$C_6H_4C_2H_5$	390	10200
p-$C_6H_4{}^nC_4H_9$	p-$C_6H_4{}^nC_4H_9$	395	26600
p-$C_6H_4{}^sC_5H_{11}$	p-$C_6H_4{}^sC_5H_{11}$	390	16200
p-$C_6H_4{}^tC_4H_9$	p-$C_6H_4{}^tC_4H_9$	376	3400
p-$C_6H_4{}^nC_6H_{13}$	p-$C_6H_4{}^nC_6H_{13}$	397	23300
m-$C_6H_4{}^nC_6H_{13}$	m-$C_6H_4{}^nC_6H_{13}$	400	21300
p-$C_6H_4{}^nC_6H_{13}$	p-$C_6H_4{}^nC_6H_{13}$	394	18600

[a] In solution.
[b] Refs. 28 and 31.

are photosensitive and have attracted considerable attention as photoresist materials in microlithography (1,27,28).

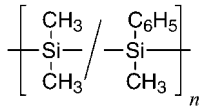

10

Synthesis. The first report of a soluble polysilane appeared in 1978 and the material was prepared by the treatment of a mixture of organodichlorosilanes with sodium metal (33). Instead of only the expected cyclic oligomers, a polymeric product, termed polysilastyrene (**10**), was formed. Poly(dimethylsilane) had been previously prepared as a highly crystalline insoluble material (1,27,28). The introduction of phenyl groups in the random copolymer reduces the crystallinity and allows the material to be soluble and processible.

The main method used to synthesize polysilanes involves the thermally-induced Wurtz coupling reaction of organodichlorosilanes with alkali metals (eq. 8). Although improvements in this process have been reported (eg, the use of ultrasound), the harsh conditions for this reaction tend to limit the side groups that can be successfully introduced to nonfunctionalized alkyl and aryl units and makes scale-up unattractive (1).

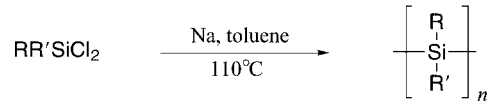

(8)

Because of these limitations, considerable effort has been focused on the development of new synthetic routes to polysilanes. Transition-metal-catalyzed dehydrogenative coupling, discovered in 1985 (eq. 9) (34), is potentially very attractive; however, the molecular weights of the polysilanes formed to date are generally quite low (M_n < 8,000). The catalysts used for these coupling reactions are usually titanocene or zirconocene derivatives (34,35).

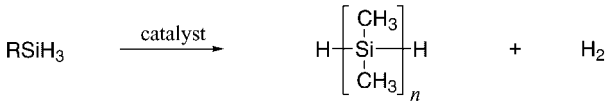

(9)

The catalytic dehydrogenation route yields novel polysilanes with Si—H functionalities, which are of interest as ceramic precursors (36). In addition, it has been shown that a variety of new side groups can be introduced using a derivatization approach (eq. 10) (37).

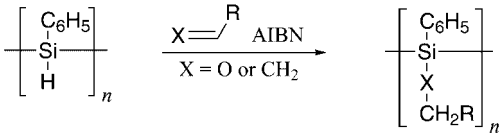

(10)

In 1991, a novel ROP route to polysilanes was reported (eq. (11)) (38). The key to this approach is to take readily accessible octaphenylcyclotetrasilane, which is too sterically crowded to undergo ROP, and to replace some of the phenyl groups by smaller methyl substituents (via a two-step process) to make the ring polymerizable.

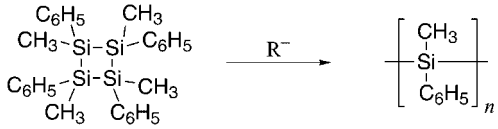

(11)

Another route to polysilanes that involves the anionic polymerization of disilabicyclooctadienes, which function as sources of masked disilenes (eq. 12), has been described (39,40). Amphiphilic block copolymers formed by this anionic route, such as poly(1,1-dimethyl-2,2-dihexyldisilene)-*b*-(2-hydroxyethyl methacrylate), undergo self-assembly to form micelles (41).

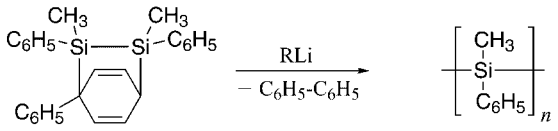

(12)

Uses. The delocalization of σ electrons in polysilanes gives rise to unique electronic and optical properties. Also, several polysilanes have been found to function as useful thermal precursors to silicon carbide fibers and these materials have attracted attention with respect to microlithographic applications and as polymerization initiators (1,27,28). The use of these materials as hole transport layers in electroluminescent devices has also been explored (42). Indeed, the photoconductivity of poly(methylphenylsilane) doped with C_{60} has been studied and has been found to be comparable with the best materials available (43).

Polygermanes and Polystannanes

Properties. The remarkable properties of polysilanes has led to significant interest in the development of polymer chains based on the heavier Group 14 elements, germanium and tin.

Studies of polygermanes indicate that the σ delocalization is even more extensive than for polysilanes and that the σ—$\sigma*$ band-gap transition for the high polymers is significantly red-shifted by ca 20 nm in comparison to the silicon analogues (44,45) (Table 3). Other studies have shown that these materials possess semiconductive behavior upon oxidative doping (49) as well as significant nonlinear optical behavior (50) and thermochromicity (45).

High molecular weight polystannanes possess σ electrons that are extensively delocalized as illustrated by the band-gap transition, which occurs at 384–388 nm for poly(dialkylstannanes) (in THF) and at even higher wavelengths for some poly(diarylstannanes) (Table 3) (48,51). In addition, exposure of thin films of the polymers to the oxidant AsF_5 leads to significant electronic conductivities of ca 0.01–0.3 S/cm (52). Polystannanes are highly photosensitive and exhibit photobleaching behavior, and on uv-irradiation depolymerize to yield cyclic oligomers. The materials are thermally stable to 200–270°C in air and, at more elevated temperatures, function as interesting precursors to SnO_2 (52).

Synthesis. Polygermanes (**11**) were prepared in the mid-1980s by Wurtz coupling techniques similar to those used to prepare the silicon analogues (eq. 13) (1). A variety of alkyl and aryl derivatives can be prepared by this method but the harsh reaction conditions are not tolerant of many functional groups (53).

Table 3. Ultraviolet–visible Absorption Data for Some Typical Polygermanes and Polystannanes $[ER_1R_2]_n$[a]

E	R_1	R_2	λ_{max}, nm
Ge	CH_3	C_6H_5	332[b]/327[c]
Ge	CH_3	p-C_6H_4F	336[b]
Ge	CH_3	p-$C_6H_4CF_3$	332[b]
Ge	CH_3	p-$C_6H_4CH_3$	326[b]
Ge	CH_3	m-$C_6H_4(CH_3)_2$	330[b]
Ge	CH_3	p-$C_6H_4OCH_3$	338[b]
Ge	C_2H_5	C_2H_5	293[c]
Ge	$^nC_3H_7$	$^nC_3H_7$	312[c]
Ge	$^nC_4H_9$	$^nC_4H_9$	325[c]
Ge	$^nC_5H_{11}$	$^nC_5H_{11}$	327[c]
Ge	$^nC_6H_{13}$	$^nC_6H_{13}$	325[c]
Ge	C_6H_5	$^nC_4H_9$	337[c]
Sn	p-$C_6H_4{}^tC_4H_9$	p-$C_6H_4{}^tC_4H_9$	432[d]
Sn	p-$C_6H_4{}^nC_6H_{13}$	p-$C_6H_4{}^nC_6H_{13}$	436[d]
Sn	o-$C_6H_4C_2H_5$	o-$C_6H_4C_2H_5$	468[d,e]
Sn	p-$C_6H_4O^nC_4H_9$	p-$C_6H_4O^nC_4H_9$	448[d]
Sn	o-C_2H_5-p-$O^nC_4H_9$—C_6H_4	o-C_2H_5-p-$^nC_4H_9$-C_6H_4	506[d]
Sn	p-C_6H_4—$N(Si(CH_3)_3)_2$	p-$C_6H_4N(Si(CH_3)_3)_2$	450[d]

[a] All values were measured in THF unless otherwise noted.
[b] Synthesized via demethanative coupling (46).
[c] Synthesized via electrochemical polymerization (47).
[d] Synthesized via catalytic polymerization (48).
[e] Value obtained on a thin film of the polymer.

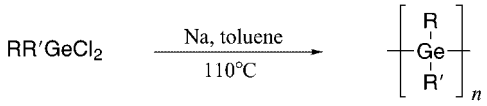

11 (13)

Dehydrocoupling has been investigated, but has proven relatively unsuccessful (54). Electrochemical reduction of halogermanes has proven somewhat successful and has provided a route to poly(germane–germane) and poly(germane–silane) copolymers (47,55). The ruthenium catalyst, $Ru(P(CH_3)_3)_4(CH_3)_2$, can be employed in the demethanative coupling of trimethylgermane, which gives relatively high molecular weight polygermanes under mild conditions (25°C) (eq. 14) (46,56).

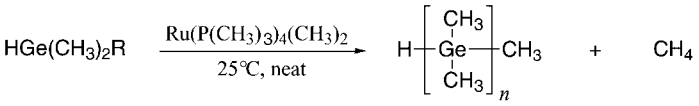

R = CH_3, Ar (14)

Early attempts to generate polystannanes by Wurtz coupling of organodichlorostannanes have yielded only low molecular weight oligomers and reduction products. The first high molecular weight materials were made using

transition-metal-catalyzed dehydrogenative coupling of secondary stannanes R_2SnH_2 (eq. 15) (51). Yellow polystannanes (**12**) (R = *n*-butyl, *n*-hexyl, or *n*-octyl) of substantial molecular weight (up to M_w = ca 96,000, M_n = ca 22,000) were prepared using various zirconium catalysts. This method is applicable to the preparation of poly(diarylstannanes) possessing solubilizing substituents (48,57). Interestingly, a change in catalyst from zirconocene-based systems to $HRh(CO)(P(C_6H_5)_3)_3$ has been shown to lead to highly branched polystannane structures (58).

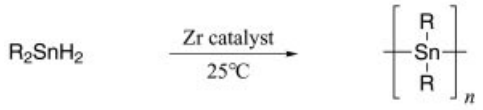

12 (15)

Uses. Both polygermanes and polystannanes may find applications because of their unique optical, electronic, and chemical properties. Some of these potential uses include photoresist layers (44,59,60), third-order nonlinear optical materials (50), charge transport polymers (61,62), photoconductors, microlithographic materials (63), and photoinitiators (59).

Boron-Containing Polymers

Boron-containing polymers are of considerable intrinsic interest, as possible reactive intermediates and as precursors to boron-based ceramics (64–69). The synthesis of polyborazines (**13**) (M_w up to ca 7600, M_n up to ca 3400) via thermally induced dehydropolymerization of borazines (eq. 16) has been reported (68). The polymers were isolated as white solids and characterization suggested the presence of a significantly branched structure. Pyrolysis at 1200°C yielded white turbostratic boron nitride in 85–93% yield.

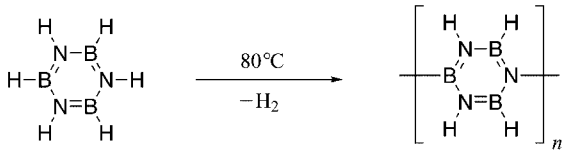

13 (16)

A wide range of novel polymers with boron in the backbone have been prepared by means of boration polymerizations (65,70–82). Diynes can be polymerized by hydroboration (70,71), phenylboration (65), and haloboration (72) to yield polymers (**14**),(**15**), and (**16**) (eq. 17). When an appropriate aromatic or heteroaromatic diyne is used, the resulting polymers have been shown to have extended π-conjugation through the vacant *p*-orbital of the boron atom (73,74). In fact, several have been shown to exhibit blue fluorescence emission.

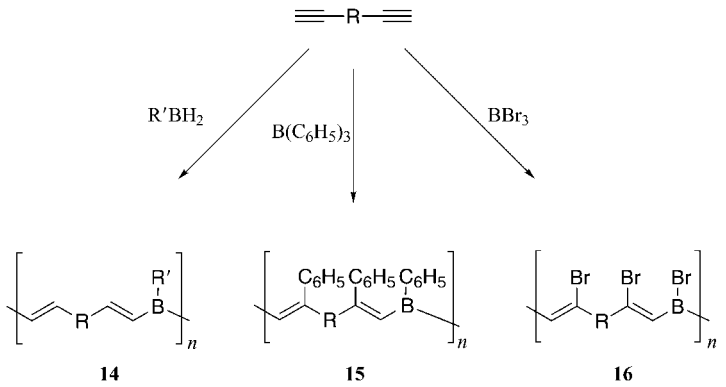

(17)

Diisocyanates have been shown to undergo haloboration–phenylboration polymerization to give halosubstituted polymers (**17**) (75). They also undergo alkoxyboration in the presence of mesityldimethoxyborane to produce poly(boronic carbamates) (**18**) (eq. 18) (76).

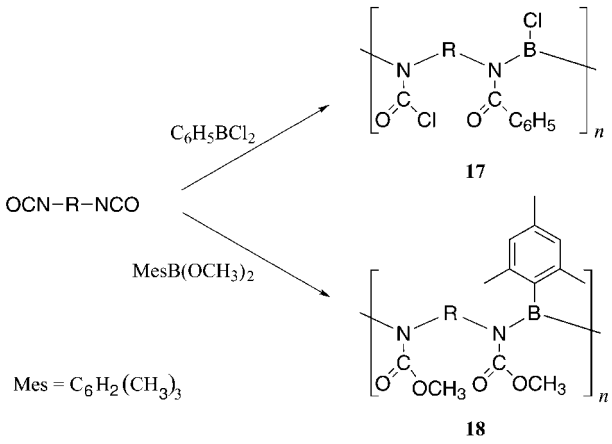

(18)

Dicyano compounds undergo hydroboration to produce poly(cyclodiborazanes) (**19**), which have proven relatively stable towards air and thermal oxidation (eq. 19) (77–79). Some examples have been prepared where the dicyano compound allows for incorporation of a charge transferred structure (80). These exhibit extended π-conjugation through the cycloborazane unit.

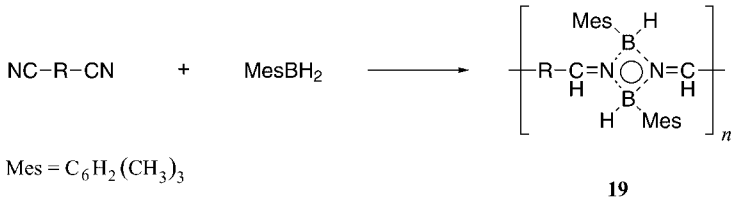

(19)

Finally, the polycondensation reaction between bifunctional Grignard reagents and aryldimethoxyboranes, carried out under a nitrogen atmosphere, in THF, gives rise to poly(phenylene-boranes) (**20**) (eq. 20) (83). The conjugated polymers may have potential applications in electronic devices such as LEDs.

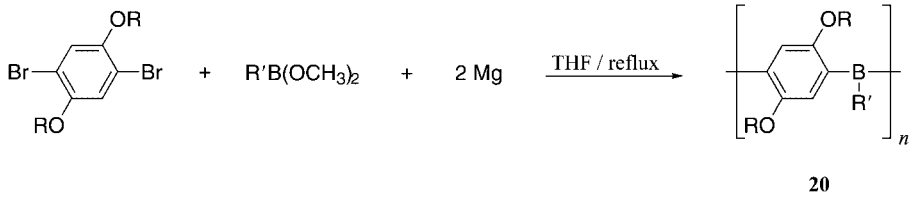

20

(20)

Transition-metal-catalyzed dehydrocoupling of phosphine–borane adducts (**21**) has been shown to give rise to high molecular weight polyphosphinoboranes (**22**) (84). In the 1950s and 1960s, several claims of the synthesis of polyphosphinoboranes (**22**) were made (eq. 21). The main route studied was the thermal dehydrocoupling of $R_2PH{\cdot}BH_3$ adducts at 200°C and above; however, structural characterization of the polymers was minimal and reported yields and molecular weights were very low (85,86).

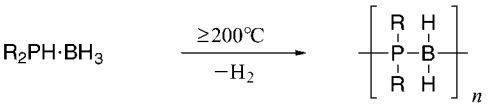

R = alkyl

21 **22**

(21)

The dehydrocoupling of various adducts (**21**) has now been studied in the presence of various catalysts, such as $RhCl_3$, $[Rh(\mu\text{—}Cl)(1,5\text{-cod})]_2$, and $[Rh(1,5\text{-cod})_2]^+$ (87). The bulky adduct (**21**) ($R_1 = R_2 = C_6H_5$) was shown to undergo dehydrogenative coupling to form only a linear dimer or a mixture of the cyclic trimer and tetramer, depending upon the temperature used. However, primary phosphine–borane adducts, such as $C_6H_5PH_2{\cdot}BH_3$ and $iC_4H_9PH_2{\cdot}BH_3$, were found to undergo catalytic dehydrogenative polymerization under similar conditions to yield soluble polyphosphinoboranes (**22**) (eq. 22). When the polymerization is carried out in solution, the resulting polymers are low in molecular weight (eg, $M_w \approx 5600$ for $R = C_6H_5$) whereas the neat polymerization affords high molecular weight phosphorus–boron polymers (eg, $M_w \approx 31{,}000$ for (**22**) $R = C_6H_5$). These polymers are air and moisture stable in the solid state, and detailed studies of the physical properties have yet to be conducted but the novel phosphorus–boron backbone allows for interesting possibilities such as low temperature flexibility, flame retardancy, and ceramic formation.

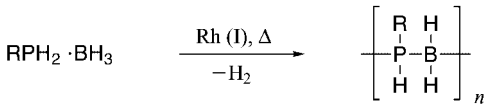

$R = C_6H_5, iC_4H_9$

22 (22)

Polycarbophosphazenes

Polycarbophosphazenes possess a backbone of phosphorus, nitrogen, and carbon atoms and can be regarded as derivatives of "classical polyphosphazenes" (**1**) in which every third phosphorus atom is replaced by carbon. The first examples of these materials were discovered in 1989 (88). Thermal ROP of a cyclic carbophosphazene was used to prepare the chlorinated polymeric species (**23**), which undergoes halogen replacement reactions with nucleophiles such as aryloxides and aniline to yield hydrolytically stable poly(aryloxycarbophosphazenes) (**24**) (M_w = ca 10^5, $M_n = 10^4$) (eq. 23) (88–91). The polymer backbone in these materials was found to be less flexible than in classical polyphosphazenes. For example, the halogenated polymer (**23**) possesses a T_g of −21°C compared to a value of −66°C for poly(dichlorophosphazene) (**2**).

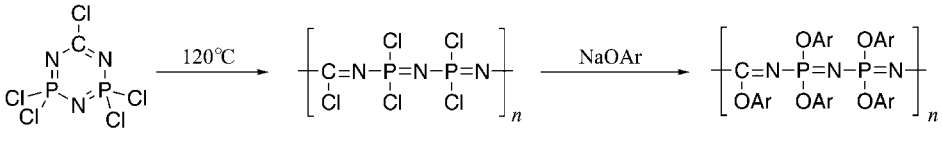

23 **24** (23)

The reaction of (**23**) with alkylamines has also been studied (91). The resulting poly(alkylaminocarbophosphazenes) are sensitive to hydrolysis. However, arylamino derivatives are moisture stable and, in addition, a novel, regioselectively substituted polymer (**25**) was successfully prepared via the sequential reaction with $NH(C_6H_5)_2$ and trifluoroethoxide anions (eq. 24).

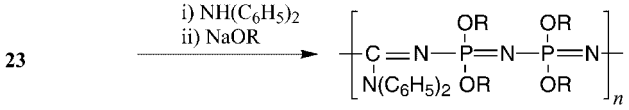

$OR = OCH_2CF_3$

25 (24)

Sulfur–Nitrogen–Phosphorus Polymers

Sulfur–nitrogen–phosphorus polymers possess backbones that can be regarded as compositional hybrids of those present in sulfur–nitrogen polymers, such as the solid-state polymer poly(sulfur nitride) $[SN]_x$ or polyoxothiazenes $[RS(O)=N]_n$ and classical polyphosphazenes, $[R_2P=N]_n$ (**1**) (92). Poly(sulfur nitride), $[SN]_x$, possesses remarkable properties such as electrical conductivity at room temperature and superconductivity below 0.3 K (93). $[SN]_x$ is insoluble and has a polymeric structure in the solid state with interchain S···S interactions. As these interactions are crucial to the properties of the material, $[SN]_x$ is best regarded as a solid-state polymer rather than a polymeric material with discrete macromolecular chains of the type discussed in this article.

The first well-characterized examples of sulfur–nitrogen–phosphorus materials, polythiophosphazenes, were reported in 1990 (94). These polymers were prepared via the thermal ROP of a cyclothiophosphazene (eq. 25). This yielded the hydrolytically sensitive polythiophosphazene (**26**) with a backbone of three-coordinate sulfur(IV), nitrogen, and phosphorus atoms. Although reaction of (**26**) with nucleophiles such as aryloxides yielded materials (**27**) with improved hydrolytic stability, degradation was still rapid except where very bulky substituents such as *o*-phenylphenoxy were present.

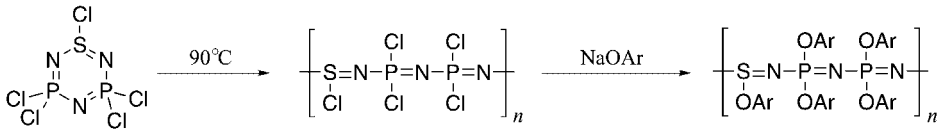

26 **27** (25)

Although the backbone of polythiophosphazenes appears to be quite fragile, a particularly interesting feature of the substitution reactions of (**26**) is that the S—Cl bond is much more reactive than the P—Cl bonds. Regioselective substitution at the sulfur center is possible and yields macromolecules (**29**) with different aryloxy substituents at sulfur and phosphorus (eq. 26) (94,95).

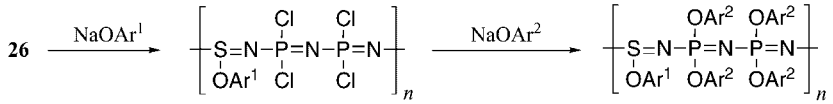

28 **29** (26)

In 1991, another class of sulfur–nitrogen–phosphorus polymers, polythionylphosphazenes, were reported (96,97). These materials, which possess four-coordinate sulfur(VI) atoms in the backbone, possess improved stability and were prepared by a thermal ROP of cyclic thionylphosphazenes (**30**), with either chlorine or fluorine at the sulfur(VI) center, at 165–180°C (eq. 27) (98). An

ambient temperature synthesis involving initiation by Lewis Acids such as $GaCl_3$ has been subsequently developed (99).

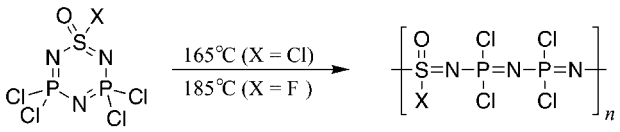

30 X = Cl or F **31** (27)

The halogenated polythionylphosphazenes (**31**) that are formed in these ROP reactions (together with small quantities of macrocyclic byproducts) are quite sensitive to hydrolysis but a variety of moisture-stable derivatives have been prepared by reaction of this species with aryloxides or amines (100–102). Mixed substituent aryloxy–alkoxy polymers have also been prepared (92). Interestingly, with aryloxides, regioselective substitution at phosphorus is observed and in the resulting polymers (**32**) the sulfur(VI)-halogen bond remains intact. Remarkably, this regioselectivity is the exact reverse of that detected for the polythiophosphazenes described earlier where the sulfur(IV)-halogen bond is more reactive. In contrast to the reactions with aryloxides, reaction with primary or secondary amine nucleophiles leads to substitution at both the phosphorus and the sulfur(VI) centers to give poly(aminothionylphosphazenes) (**33**) (102,103).

X = Cl or F R = alkyl or aryl

32 **33**

Ab initio calculations on isotactic polythionylphosphazene (**31**) (X = Cl or F) indicate a localized electronic structure for the polymer backbone and predict that a *cis–trans* helical conformation is the most energetically favorable for isolated macromolecules (104). This is in contrast to the analogous "classical" polyphosphazene (**1**) where a *trans*-planar conformation is preferred. Studies of the properties of the polythionylphosphazenes also reveal significant differences in thermal transition behavior and polymer morphology compared to classical polyphosphazenes. For example, the polymer $[NSOF\{NP(OC_6H_5)_2\}_2]_n$ is an amorphous elastomer ($T_g = -15^\circ C$), whereas the analogous classical polyphosphazene $[NP(OC_6H_5)_2]_n$ is a microcrystalline thermoplastic ($T_m = 390^\circ C$, $T_g = -6^\circ C$). The T_gs of the fluorinated polythionylphosphazenes are lower than those of the analogues with chlorine at sulfur. For example, for (**31**) (X = F) $T_g = -56^\circ C$ whereas for (**31**) (X = Cl) $T_g = -46^\circ C$ (101). Poly(aminothionylphosphazenes) possess high gas permeability and have found utility as matrices for phosphorescent dyes for oxygen sensing applications (105).

Also noteworthy is an interesting condensation route reported which leads to polymers with backbones of alternating S(O)—N and P—N units (106).

Preliminary reports of the first polythiazylphosphazenes (**34**), which possess three-coordinate sulfur(III) atoms, have appeared (eq. 28) (107). These materials would represent true hybrids of poly(sulfur nitride) and polyphosphazenes and further developments in this area should prove to be particularly interesting.

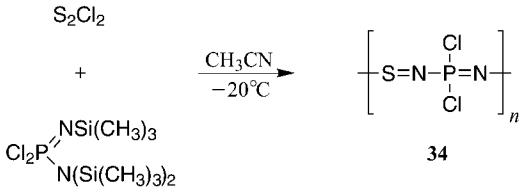

(28)

Polyoxothiazenes

Partially characterized polyoxothiazenes were briefly reported in the early 1960s (108). However, in 1992 the first well-characterized examples (**35**) with alkyl or aryl substituents at sulfur were described (109). These polymers, which possessed estimated molecular weights of M_w = ca 10^5 and M_n = ca 10^4, were synthesized via the condensation polymerization of *N*-silylsulfonimidates at 120–170°C over 2–8 days (eq. 29). These reactions are catalyzed by added Lewis acids (eg, $BF_3{\cdot}O(C_2H_5)_2$) and bases (eg, fluoride). By using a mixture of different sulfonimidates, random copolymers such as $[CH_3S(O){=}N]_m[C_6H_5S(O){=}N]_n$ were also successfully prepared. Free sulfonimidates were also found to thermally condense to yield poly(organooxothiazenes) at lower temperatures than their *N*-silyl analogues (eq. 29) (109,110).

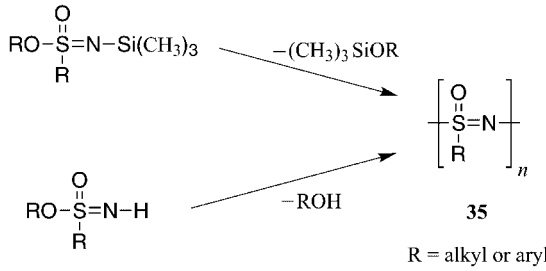

(29)

Polyoxothiazenes appear to be highly polar. For example, $[CH_3S(O){=}N]_n$ is soluble in DMF, DMSO, hot water, and concentrated H_2SO_4. Studies of the thermal transition behavior of these materials have indicated that they are amorphous, which is consistent with an atactic structure. Interestingly, the T_g of $[CH_3S(O){=}N]_n$ is ca. 60°C, which is dramatically higher than for $[(CH_3)_2P{=}N]_n$ (T_g = −46°C). This suggests a much less flexible backbone for polyoxothiazenes compared to polyphosphazenes, as might be expected from

studies on polythionylphosphazenes (vide supra). Thermogravimetric analysis (TGA) showed that the polymers are stable to weight loss up to ca 270°C (at a heating rate of 10°C/min). Theoretical studies on $[CH_3\ S(O){=}N]_n$ have indicated that a *cis–trans* helical conformation is the most stable for this polymer (110).

Inorganic Polymers Based on Transition Elements

Ferrocene-Based Polymers. The excellent thermal stability and interesting physical (eg, redox) properties associated with the ferrocene moiety have led to extensive efforts aimed at the incorporation of this unit into polymer structures. The inclusion of this moiety in the side-group structure of polymers has been very successful and requires only minor modifications of previously established synthetic methodologies. For example, poly(vinylferrocene) (**36**) can be prepared via the free radical addition polymerization of vinylferrocene (111). The incorporation of ferrocene moieties into the main chains of polymers where the metal atoms are separated by a considerable distance has also been achieved. The extensive organic chemistry of the metallocene nucleus has allowed for the preparation of well-defined difunctional ferrocenes that have been used in controlled polycondensation reactions to yield well-defined products of appreciable molecular weight. Examples of products derived from such reactions involve the poly(arylene–siloxane–ferrocenes) (eg, **37**) (112), ferrocene-containing polyesters (113), and novel "accordian" type polymers (114,115).

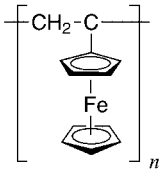

36

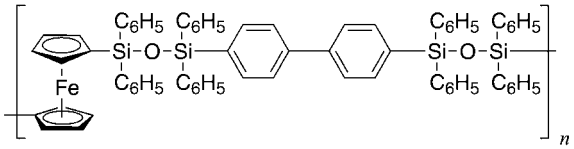

37

The versatile chemistry of the ferrocenyl moiety has also allowed for the preparation of a large number of dendrimeric structures with this group at the periphery (116–118). A series of dendrimers based upon polypropylenimine cores have been reported (119,120) and star-shaped macromolecules with ferrocene units at the periphery have been produced (121), as well as amido-ferrocene dendrimers (eg, **38**) (122). A convergent approach has allowed for the synthesis of dendrimers (**39**) for which the ferrocene units at the periphery display electronic interaction (123).

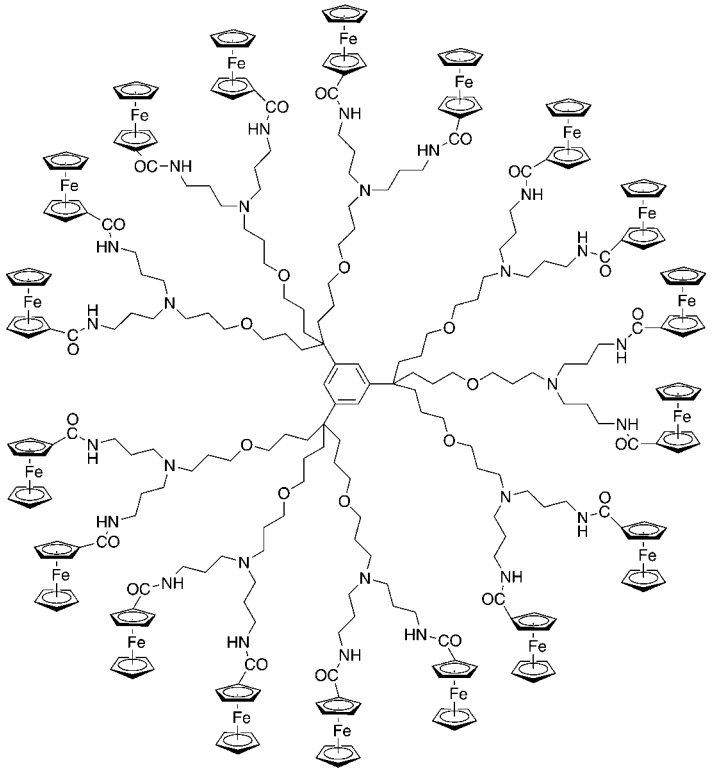

38

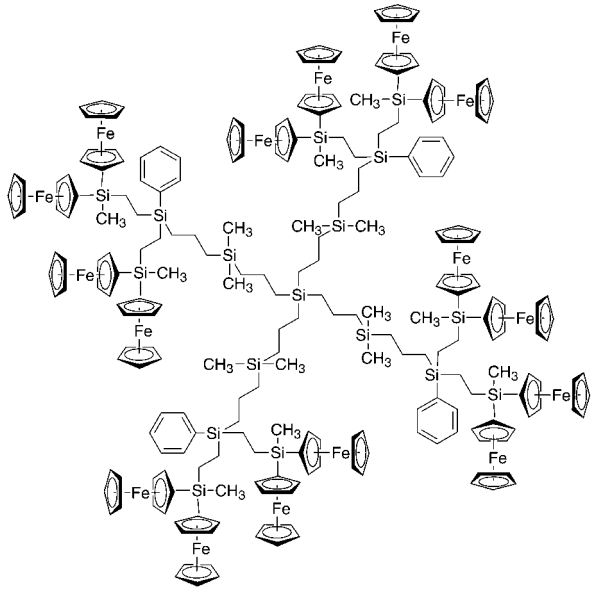

39

In contrast, very few examples of polymers with ferrocene units in close proximity, which could take advantage of interactions between the metal atoms, have been prepared. The development of materials with interesting physical (eg, electronic and/or magnetic) properties might be anticipated based on the properties of molecular species in which two ferrocene units are linked close together. Thus, in such systems the iron atoms can interact and in some cases yield delocalized, mixed valent species upon one-electron oxidation, even when the metal atoms are up to 0.7 nm apart (124,125). Work in this field has largely yielded low molecular weight ($M_n \ll 10{,}000$) and often poorly defined materials (126). For the synthesis of well-characterized polymers ($M_n <$ ca 11,000) with main chains of ferrocene groups and vinylene, divinylene, or oligovinylene units see Reference 127.

Polyferrocenylenes

A typical early route to polyferrocenylenes (**40**) with $M_n < 5000$ involved polycondensation processes such as the recombination of ferrocene radicals generated via the thermolysis of ferrocene in the presence of peroxides. However, these materials have been found to possess other fragments such as CH_2 and O in the main chain (128,129). More structurally well-defined polyferrocenylenes (**40**) ($M_n < 4000$) have been prepared (130) via the condensation reaction of 1,1-dilithioferrocene·TMEDA (tetramethylethylenediamine) with 1,1-diiodoferrocene and, significantly, the reaction of 1,1′-dihaloferrocenes with magnesium (eq. 30) has been shown to afford low molecular weight ($M_n = 4600$ for soluble fractions) materials with appreciable crystallinity (131). In the latter case, oxidation with 7,7,8,8-tetracyanoquinodimethane (TCNQ) afforded doped polymers that were delocalized on the Mössbauer time scale (ca 10^{-7} s) at room temperature and which possessed electrical conductivities of up to 10^{-2} S/cm.

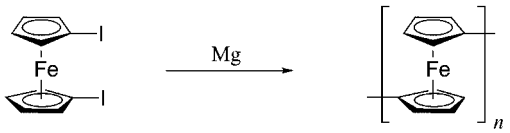

40 (30)

Polyferrocenylsilanes

Properties. Polyferrocenylsilanes possess a backbone of alternating ferrocene and organosilane units. Since the early 1990s when the first high molecular weight, well-characterized examples were prepared by a ROP approach, considerable effort has been directed towards understanding the properties of polyferrocenylsilane materials, the vast majority of which are soluble in common organic solvents (132,133). It was noted early on that electrochemistry of the high polymers such as (**41**) ($R = R' = CH_3$) possess two reversible oxidation waves in a 1:1 ratio (132,134). This provided clear evidence for the existence of interactions between the iron atoms, and led to the proposal that initial oxidation

occurred at alternating iron sites along the main chain. Work on model oligomers with between two and nine ferrocene units has provided clear evidence in support of this postulate (135). Similar electrochemical behavior has subsequently been detected for a range of other polyferrocenylsilanes (134). Oxidative doping of poly(ferrocenyldimethylsilane) with I_2 has been shown to yield semiconducting materials (σ = ca 10^{-4} S/cm) whereas the pristine materials are insulating (σ = ca 10^{-14} S/cm) (133). A report indicates that several tetracyanoethylene (TCNE)-oxidized low molecular weight polyferrocenylsilanes (M_w = ca 1500) show electron delocalization on the Mössbauer time scale (ca 10^{-7} s) and also ferromagnetic ordering at low temperatures (136). Studies of high molecular weight $M_w > 10^5$ analogues have not reproduced this behavior (137). Thin films of the homopolymers and block copolymers with organic or inorganic co-blocks are attracting attention for numerous applications, such as chemomechanical sensors, electrochromic materials, electrode mediators, variable refractive index materials, hole transport layers, charge dissipation coatings for dielectrics, lithographic resists, and photonic band-gap materials (133,138–144).

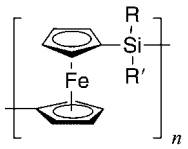

41

The polymers also exhibit interesting morphology and several of the symmetrically substituted derivatives will crystallize. For example, the dimethyl derivative (**41**) (R = R′ = CH_3) is an amber, film-forming thermoplastic and possesses a T_m at 120–145°C depending on crystallite size and a T_g at 33°C whereas, in contrast, the *n*-hexyl analogue (**41**) (R = R′ = *n*-hexyl) is an amber, gummy amorphous material with a T_g of −26°C (133). The packing in the crystalline regions of polymer (**41**) (R = R′ = CH_3) has been shown to be analogous to that of a linear pentamer (135,141,142). In addition, as the iron atom in ferrocene acts as a "molecular ball-bearing," this gives these polymers a large degree of conformational flexibility and consequently T_gs are lower than might be expected for polymers with such a bulky unit in the main chain (133) (Table 4).

Several polyferrocenylsilanes can be fabricated in the melt (eg, R = R′ = CH_3 above 150°C) (Fig. 1). Polyferrocenylsilanes have been found to exhibit excellent thermal stability to weight loss (up to 350–400°C) and have been shown to yield interesting composites containing Fe nanoparticles at 500–1000°C (145–147). Controlled cross-linking of the polyferrocenylsilanes can be used to make magnetic ceramic films and monoliths with the same shape as the polymer precursor as well as solvent-swellable, redox-active gels (148,149). The solution properties of polyferrocenylsilanes such as the dimethyl derivative (**41**) (R = R′ = CH_3) have been well-characterized by light-scattering experiments and viscometry and Mark–Houwink parameters have been established (150).

Table 4. Thermal Transition and gpc Molecular Weight Data for Selected Polyferrocenylsilanes[a]

R/OR	R′/OR′	T_g (T_m)[b], °C	M_n[c]	PDI[d]
H	H	16 (165)	–[e]	–[e]
CH_3	CH_3	33 (122–143)	3.4×10^5	1.5
C_2H_5	C_2H_5	22 (108)	4.8×10^5	1.6
$^nC_3H_7$	$^nC_3H_7$	24 (98)	8.5×10^4	2.7
$^nC_4H_9$	$^nC_4H_9$	3 (116,129)	3.4×10^5	2.6
$^nC_5H_{11}$	$^nC_5H_{11}$	−11 (80–105)	3.0×10^5	1.6
$^nC_6H_{13}$	$^nC_6H_{13}$	−26	7.6×10^4	1.5
CH_3	H	9 (87, 102)	4.2×10^5	2.0
CH_3	$CH_2CH_2CF_3$	59	8.1×10^5	3.3
CH_3	$CH{=}CH_2$	28	7.7×10^4	2.1
CH_3	$^nC_{18}H_{37}$	1 (16)	5.6×10^5	2.5
CH_3	C_6H_5	90	1.5×10^5	2.0
CH_3	Fc[f]	99	7.1×10^4	2.3
CH_3	$CH_2CH_2CH_2Cl$	27	2.7×10^5	1.5
OCH_3	OCH_3	19	1.5×10^5	1.9
OC_2H_5	OC_2H_5	0	3.8×10^5	2.1
OCH_2CF_3	OCH_2CF_3	16	2.2×10^5	1.2
$O^nC_4H_9$	$O^nC_4H_9$	−43	3.9×10^5	2.1
$O^nC_6H_{13}$	$O^nC_6H_{13}$	−51	0.9×10^5	2.4
$O^nC_{18}H_{37}$	$O^nC_{18}H_{37}$	(32)	2.3×10^5	2.2
OC_6H_5	OC_6H_5	54	2.3×10^5	2.0
$(OCH_2CH_2)OCH_3$	$(OCH_2CH_2)OCH_3$	−53	1.0×10^5	2.6
CH_3	$(OCH_2CH_2)_xOCH_3$[g]	−69, −72[h]	5.6×10^4, 1.9×10^5	2.3, 2.2

[a] Refs. 133 and 143.
[b] DSC data collected at a heating rate of $10^\circ C\ min^{-1}$.
[c] GPC data and molecular weight values are relative to polystyrene standards. Although in this case gpc provides only molecular weight estimates, absolute determinations of M_w by static light scattering for several polymers have indicated that gpc underestimates the real values by a factor of 2 (144).
[d] $PDI = M_w/M_n$.
[e] Insoluble polymer.
[f] $Fc = (\eta\text{-}C_5H_4)Fe(\eta\text{-}C_5H_5)$.
[g] $x \sim 8$.
[h] Two different molecular weight samples.

Water-soluble polyferrocenylsilanes have also been prepared and these possess, for example, oligoethoxy or ionic side chains (151,152). These materials can be used in layer-by-layer assembly processes to form superlattices with a range of potential applications (153). Novel random copolymers (**42**) with oligosilane spacers have also been prepared by using a thermal copolymerization process (154,155). These polymers possess interesting photophysical and charge transport properties. Indeed, the skeletons of the polysilane segments can be selectively cleaved using uv light because of the photosensitive nature of the Si-Si bond. Block copolymers containing polyferrocenylsilane blocks (*vide infra*) have demonstrated interesting self-assembly behavior and are of interest for nanostructure applications (156). For example, cylindrical worm-like micelles with a polyferrocenylsilane core

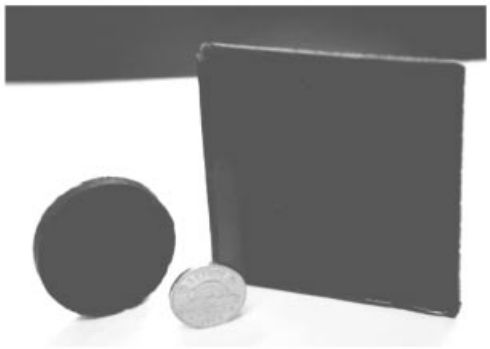

Fig. 1. Samples of melt processed polyferrocenylsilanes.

and a polysiloxane corona can be fabricated and are of potential use as semiconducting nanowires and as etching resists in nanolithography (157).

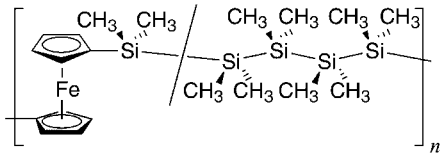

42

Synthesis.

Ring-Opening Polymerization. Early attempts to prepare macromolecules in which the ferrocene units are separated via an organosilane spacer group focused on the use of polycondensation reactions. Partially characterized, impure polyferrocenylsilanes were prepared via the reaction of dilithioferrocene with organodichlorosilanes. The molecular weights of 1400–7000 reported for these materials are characteristic of polycondensation processes where exact reaction stoichiometries are virtually impossible to achieve because one reactant, in this case dilithioferrocene, cannot be readily prepared in pure form (116).

In 1992, the first synthesis of high molecular weight polyferrocenylsilanes (**41**) ($M_w = 10^5$–10^6, $M_n > 10^5$) via a thermal ROP route was reported (132,158). This process involved heating silicon-bridged [1]ferrocenophanes (**43**) in the melt at 130–220°C (eq. 31). The presence of a single-atom bridging the ferrocene unit in the monomer leads to a strained structure in which the planes of the cyclopentadienyl rings are tilted with respect to one another by an angle of ca 21°. In contrast, in ferrocene the cyclopentadienyl rings are parallel. The presence of strain in the ferrocenophane, which has been measured to be ca 80 kJ/mol for (**43**) ($R = R' = CH_3$), is believed to provide the driving force for the ROP process (132,158).

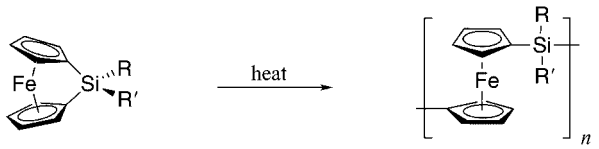

43 **41**

R = alkyl, aryl, ferrocenyl etc (31)

Since this initial discovery, a wide range of silicon-bridged [1]ferrocenophanes with either symmetrically or unsymmetrically substituted silicon atoms have been prepared and similarly polymerized (Table 4). Polymerization of a mixture of different silicon-bridged [1]ferrocenophanes has also been shown to yield random copolymers (159).

Silicon-bridged [1]ferrocenophanes undergo living anionic ROP using initiators such as n-C_4H_9Li in THF (160,161). This has permitted the synthesis of polyferrocenylsilanes with controlled molecular weights and narrow polydispersities and has also allowed the preparation of the first block copolymers containing skeletal transition-metal atoms (160,161). Block copolymers such as (**44**) have been prepared with other monomers that undergo anionic polymerization such as cyclic siloxanes (see eq. 32) or organic monomers such as polystyrene and isoprene (161,162). The resulting block copolymers undergo phase separation in the solid state and, in solution, micellar aggregates are formed (156,163).

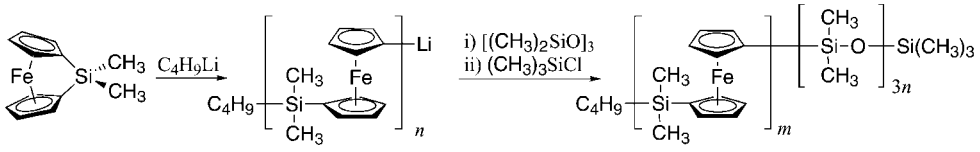

43 **41** **44**

(32)

Also, the transition-metal-catalyzed ROP of silicon-bridged [1]ferrocenophanes in the presence of various transition-metal complexes (eg, Pt^{II}, Pt^0, Rh^I, Pd^{II}) has been developed (164). This route, which takes place in solution at room temperature, is much milder than, and doesn't have the same stringent monomer purity requirements as, anionic ROP. Furthermore, molecular weight control is possible through the use of Si—H containing capping agents such as $(C_2H_5)_3SiH$, and access to block and graft copolymers and star polymers is possible (164,165).

Monomer Synthesis. Sila[1]ferrocenophane monomers such as (**43**) are readily available on a substantial laboratory scale (>100 g) from the reaction of dilithioferrocene tetramethylethylenediamine ($fcLi_2$·TMEDA) with the appropriate dichloroorganosilane (166). Spirocyclic sila[1]ferrocenophanes such as (**45**) and (**46**) are also easily synthesized (167). Sila[1]ferrocenophane monomers with alkoxy, aryloxy, and amino substituents at silicon are readily accessible through reaction of dichlorosila[1]ferrocenophane with the appropriate alcohol, phenol or amine in the presence of base (168).

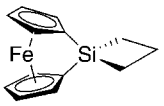

45

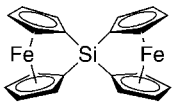

46

Other Polyferrocenes

The ROP route has been extended to the synthesis of other polymers from [1]ferrocenophane precursors. Polyferrocenylgermanes (**47**) were first reported in 1993 and have been well-characterized and possess quite similar thermal transition behavior, morphology, and electrochemical behavior to the analogous polyferrocenylsilanes (169). Poly(ferrocenylsilane-ferrocenylgermane) random copolymers (**48**) have also been prepared via the thermal polymerization of mixtures of the respective monomers (169).

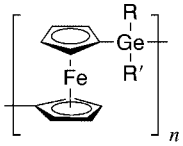

R = alkyl, aryl, etc

47

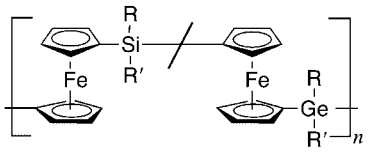

48

Polyferrocenylphosphines (**49**) (and the corresponding phosphine sulfides) are also accessible via the thermal ROP of phosphorus-bridged [1]ferrocenophanes (170). Polymers of this type have been previously prepared by condensation routes and the catalytic potential of some of their transition-metal derivatives has already been noted. In addition, the first sulfur-bridged [1]ferrocenophanes have been prepared and polymerized to give polyferrocenylsulfides, (eg, **50**) (171).

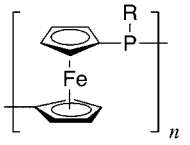

R = alkyl, aryl, etc

49

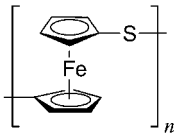

50

Hydrocarbon-bridged [2]-ferrocenophanes (**51**) possess strained ring-tilted structures (tilt-angles = ca 21°) and these species have been found to yield polyferrocenylethylenes (**52**) via ROP at 250–300°C (eq. 33) (172). As a consequence of the presence of a more insulating bridge, these polymers show much smaller interactions between the iron atoms compared to polyferrocenylsilanes.

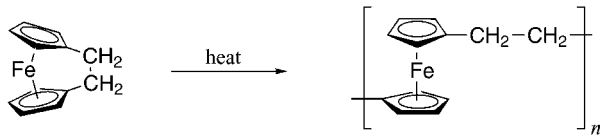

51 52 (33)

Analogous hydrocarbon-bridged [2]ruthenocenophanes (tilt angles = ca 29–30°) undergo thermal ROP to yield poly(ruthenocenylethylenes) (172). These materials exhibit significantly different electrochemistry from their iron analogues.

In early 1992, it was reported that [3]trithiaferrocenophanes, which are essentially unstrained, function as precursors to poly(ferrocenylene persulfides) via a novel atom abstraction polymerization route (eq. 34) (173). Thus, reaction of [3]-trithiaferrocenophanes (**53**) with $P(C_4H_9)_3$ led to the formation of the phosphine sulfide $S{=}P(C_4H_9)_3$ and the polymers (**54**).

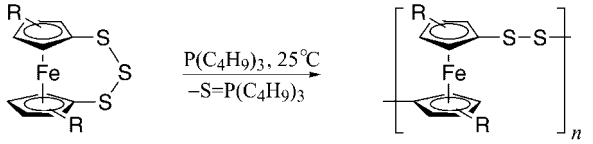

53 54 (34)

The presence of a butyl substituent on the cyclopentadienyl ring is necessary for the polymer to be soluble. The molecular weight (M_w) of (**54**) (R = n-C_4H_9) was determined to be 40,000 by gel permeation chromatography (gpc). The [3]ferrocenophanes (**53**) (R = H) and (**53**) (R = n-C_4H_9) can be copolymerized to give soluble copolymers with $M_w = 25{,}000$.

Poly(ferrocenylene persulfides) possess a range of novel properties (173–175). They are photosensitive and the S–S bonds can be reversibly reductively cleaved with $Li[B(C_2H_5)_3H]$ and then regenerated upon oxidation with I_2. Their electrochemical behavior is similar to that detected for polyferrocenylsilanes except that the interaction between the iron sites appears to be even greater. The atom abstraction route using $P(^tC_4H_9)_3$ as a desulfurization agent has also been extended to the preparation of other poly(ferrocenylene persulfides) with t-butyl substituents and also high molecular weight (M_w = 50,000–1,000,000) network polymers by the use of [3]ferrocenophanes with two trisulfido bridges as monomers (174).

Face-to-Face Metallocene Polymers

The development of rigid-rod metallocene polymers with a multistacked structure using condensation routes has been reported (176–180). This involved treatment of the ferrocene monomers (**55**) with $FeCl_2$ and $Na[N(Si(CH_3)_3)_2)]$ and this yielded purple polymers (**56**) with molecular weights up to $M_n = 18{,}000$, although higher

molecular components were also present (eq. 35). Mixed metal copolymers containing Ni and Fe whose soluble fractions were of low molecular weight ($M_n < 3000$) were also reported by using $Ni(acac)_2$ instead of $FeCl_2$ (176). The electrical and magnetic properties of these novel polymers and copolymers are clearly worthy of investigation. Interestingly, structural work on well-defined oligomers suggests that the stacked metallocene units in the polymer form a helical structure (180).

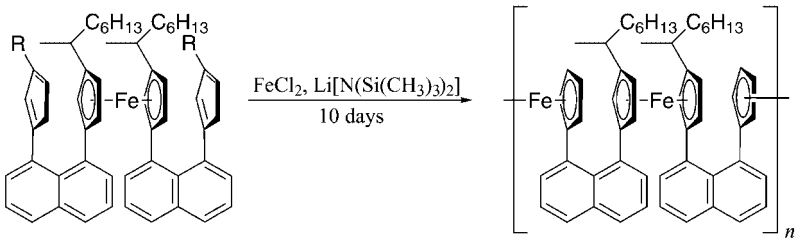

R = H or 2-octyl

55 **56** (35)

Coordination Polymers

In the past, attempts to prepare coordination polymers have been hindered by the insolubility and consequent intractability of the products. These problems arise from the inherent skeletal rigidity of these materials, and the introduction of solubilizing or flexibilizing groups either in the polymer backbone or side-group structure is necessary for useful products to be obtained. Such modification has yielded a range of interesting and well-characterized materials with intriguing properties. For example, novel liquid crystalline polymers (**57**) containing paramagnetic Cu^{II} centers have been prepared (181) and soluble, luminescent silver-containing polymers (**58**) have been reported (182).

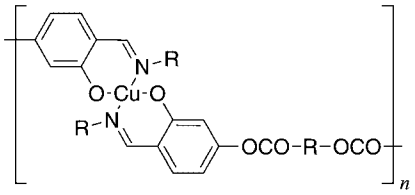

57

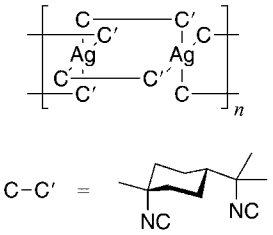

58

In addition, well-characterized lanthanide containing polymers (**59**), which possess polyelectrolyte behavior and exhibit interesting photophysical properties, have been reported (183). The tetradentate Schiff-Base ligands greatly stabilize the lanthanide ions in solution and allow for efficient energy transfer to the

lanthanide centers. Several of the polymers are soluble in polar organic solvents such as DMSO, and molecular weights (M_n) up to 1.8×10^4 have been established. The polymer (**59**) (Ln = Eu or Eu/Y) is an interesting candidate for luminescent and lasing applications (184). Similar polymers containing cerium and zirconium in the main chain have also been prepared and these possess M_n values up to 3×10^4 (185). Films of these polymers have conductivities of $\sim 10^{-7}$ S/cm which increase to $\sim 10^{-3}$ S/cm upon I_2 doping (186).

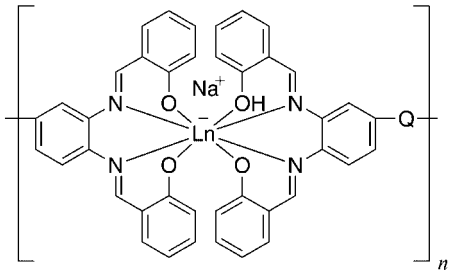

Ln = Eu, La, Gd, Y, Yb

Q = _, CH_2, SO_2

59

Phthalocyanine-based polymers, such as the "shish-kebab" polymers (**60**), are also of considerable interest and significant electrical conductivities of up to ca 0.1 S/cm have been detected for chemically or electrochemically doped materials (187,188). If flexible organic substituents are present on the periphery of the phthalocyanine ring, these materials can also be soluble (at least low molecular weight fractions).

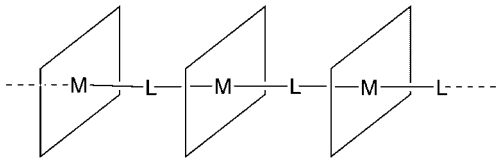

= phthalocyanine L = bipy, CN^-

M = Fe, Ru, Os, Co, Rh, Mn, Cr

60

Well-defined and readily soluble ruthenium coordination polymers (**61**) have been synthesized through the reaction of a bisbidentate ligand and a metal center that already possesses one bidentate ligand (189–191). In these complexes, the random stereospecificity at the ruthenium centers results in a ribbon-like conformation of the polymers with the extension of the chain dependent upon the substituent R. The Ru^{II} centers appear to behave independently and the polymers appear to be stable against heat and uv irradiation. They have molecular weights on the order of $M_w = 40{,}000$–$50{,}000$.

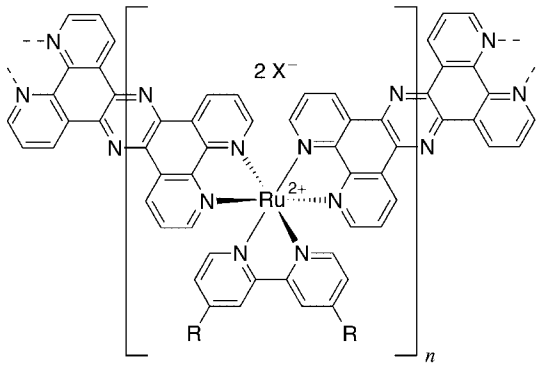

R = H, C_6H_5, CH_3, $CH_2—C_{10}H_{15}$

X^- = Cl^-, BF_4^-, PF_6^-, ...

61

A similar strategy applied to the reaction of a bistridentate monomer with an appropriate ruthenium compound gives rise to the rod-like polymers (**62**), which are soluble due to the *n*-hexyl substituents (192,193). These polymers display a pronounced polyelectrolytic effect in salt-free dimethylacetamide.

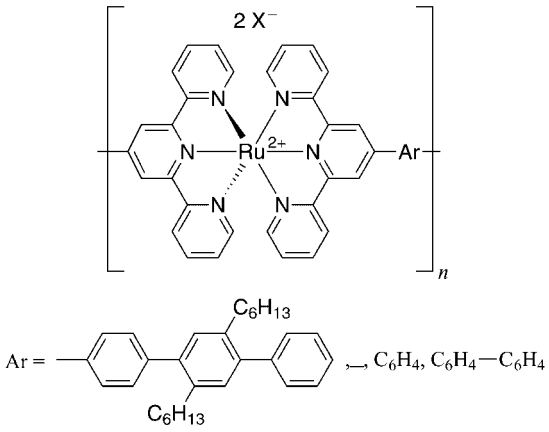

X^- = Cl^-, BF_4^-

62

Polythiophene-metal complex hybrid polymers such as (**63**) and (**64**) have been explored (194,195). The polythiophene-cobalt salen hybrid (**63**) participates in the electrocatalytic reduction of oxygen and is highly conducting in nature. Polymers such as (**64**) have also been shown to be conducting. A variety of related structures have been prepared and similar strategies have also resulted in the preparation of polymeric metallorotaxanes (196).

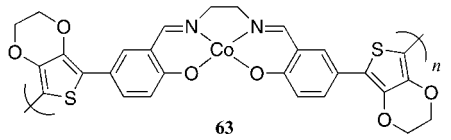

63

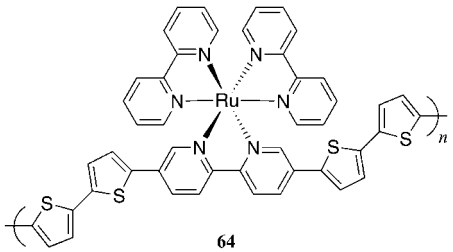

64

The generation of dendrimeric coordination polymers has also been an area of significant activity. Imaginative routes to novel Ru- or Pt-polypyridyl systems (eg, **65**) (197) have been reported and many other ligand systems have been exploited (117,118,198–201). These materials are of interest with respect to their photophysical and electrochemical properties and possibly their catalytic behavior.

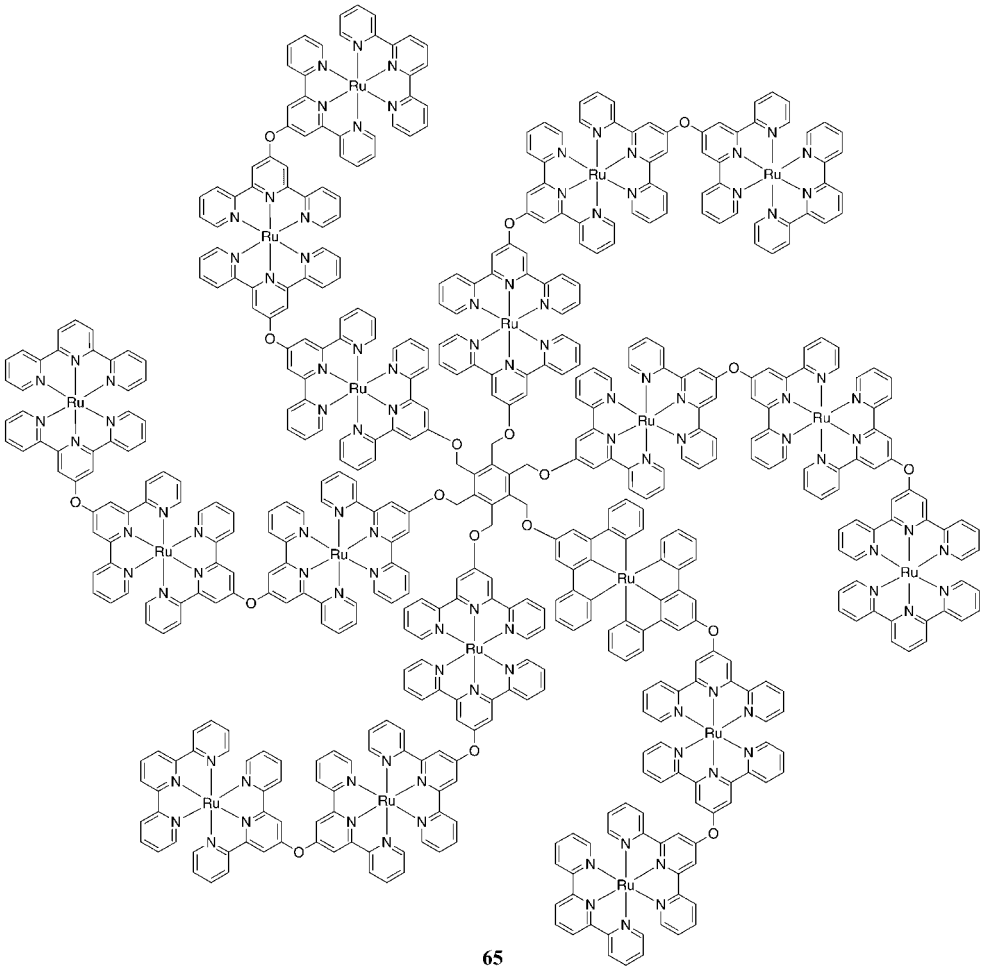

65

Rigid-Rod Organometallic Polymers

Macromolecules with backbones that possess conjugated C≡C units and transition-metal atoms, termed polymetallaynes, represent some of the best-characterized examples of transition-metal-based polymers prepared to date (202).

The first polymetallaynes contained nickel, palladium, or platinum atoms in the main chain and were isolated in 1977 as yellow, film forming materials (203–205). These were prepared by efficient copper halide-catalyzed coupling processes (eg, eq. 36) and possessed estimated molecular weights (M_w) from 13,000 to 120,000.

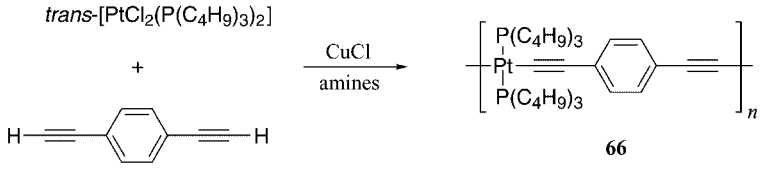

66

(36)

There has been an important expansion in this area which has yielded a range of new rigid-rod materials via the creative use of a variety of new and well-defined polycondensation strategies. For example, a new route to the polyplatinynes (**66**) that involved the reaction of *trans*-$PtCl_2(PR_3)_2$ complexes with bis(trimethylstannyl)diynes (eq. 37) has been reported (206). These rigid-rod polymers possessed estimated weight-average molecular weights up to ca 100,000 according to gpc measurements.

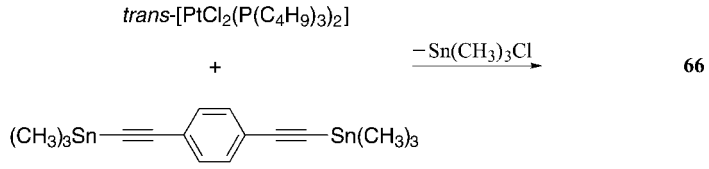

(37)

This synthetic procedure can be extended to allow the incorporation of other transition elements into the polymer main chain such as iron (to give **67**) by using $FeCl_2[(C_2H_5)_2\ PCH_2CH_2P(C_2H_5)_2]_2$ as the transition-metal-containing reactant (207). In addition, condensation routes to organonickel polymers (**68**), have been devised (208,209) and interesting organocobalt (210) and organozirconium (211) polymers containing metallacyclopentadiene moieties in the main chain have been reported.

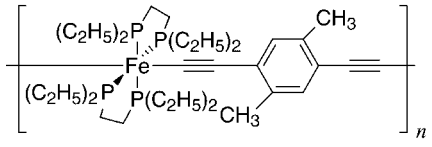

67

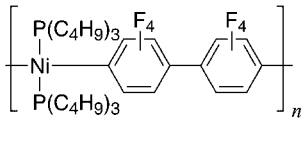

68

In another interesting synthetic development, it was shown that a range of rhodium-containing polymetallynes (**69**) are accessible via the reaction of the unsubstituted diynes with $Rh(PR_3)_4CH_3$ in a reaction that involves reductive elimination of methane and the loss of a phosphine ligand (eq. 38) (212). In the case where trimethylphosphine ligands are attached to rhodium, the polymers are insoluble but the tri(*n*-butyl)phosphine analogues are soluble and yield free-standing solvent-cast films from THF.

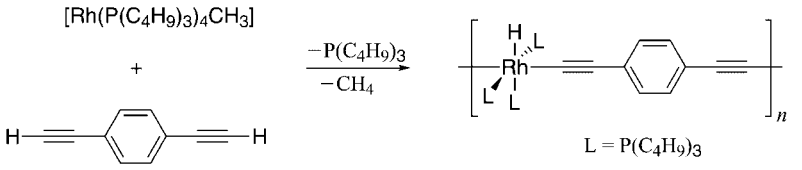

69 (38)

Over the past 15 years the physical properties of polymetallaynes have received continued attention because of their novel rigid-rod structures and their conjugated backbones (213–222). Thus, polyplatinynes form ordered, liquid crystalline mesophases in solvents in which they are soluble such as trichloroethylene (213), and these materials also possess novel, third-order nonlinear optical properties (214) that are of interest for electrooptic device applications. Optical absorption and photoluminescence spectroscopic studies and extended Hückel calculations have shown that polymetallaynes possess a delocalized polymer backbone whose electronic structure is modified by the nature of the transition metal, coligands, and the unsaturated hydrocarbon spacer (215–217). For example, optical band gaps for a series of polyplatinynes with platinum centers joined by σ-conjugated acetylide-arene linkages of varying length have been measured to be in the range of 2.5–3.1 eV, which is lower than for model complexes and is consistent with conjugation through the metal centers (216).

Other developments in the area of rigid-rod transition-metal-based polymers include the synthesis of a range of thermotropic liquid crystalline organocobalt polymers (eg, **70**) in which the metal is bound to skeletal cyclobutadiene units (eq. 39) (223).

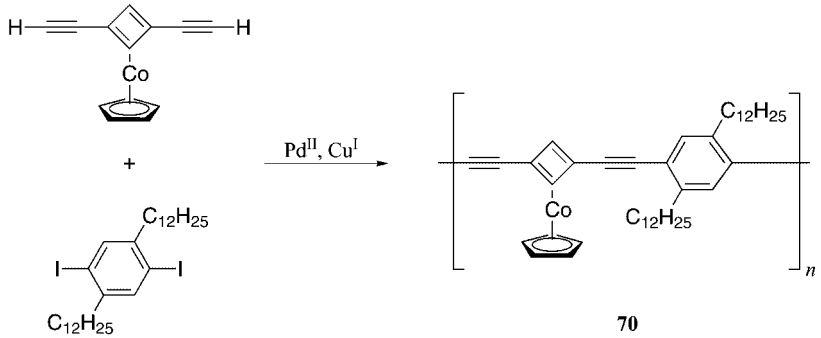

70 (39)

In addition, the preparation and characterization of novel lyotropic liquid crystalline aramides (**71**) with complexed chromium(tricarbonyl) units have been

reported (224). These materials are soluble in organic solvents, which leads to potential processing advantages for the uncomplexed organic polymer as the $Cr(CO)_3$ groups can be easily added and removed and poly(*p*-phenyleneterephthalamide) is only soluble in concentrated sulfuric acid (224,225). Work on the coordination of transition-metal fragments to π-hydrocarbon units can be found in Reference 226.

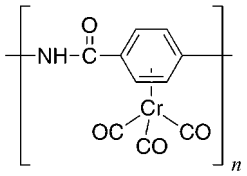

71

BIBLIOGRAPHY

"Inorganic Polymers" in *EPST* 1st ed., Vol. 8, pp. 664–691, by D. L. Venezky, U.S. Naval Research Laboratory; "Inorganic Polymers" in *EPSE* 2nd ed., Vol. 8, pp. 138–147, by A. Rheingold, University of Delaware.

1. J. E. Mark, H. R. Allcock, and R. West, *Inorganic Polymers*, Prentice Hall, Englewood Cliffs, N.J., 1992; I. Manners, *Angew. Chem. Int. Ed. Engl.* **35**, 1603 (1996); R. D. Archer, *Inorganic and Organometallic Polymers*, Wiley-VCH, New York, 2001.
2. R. H. Neilson and co-workers, *ACS Symp. Ser.* **572**, 232 (1994), and references therein.
3. P. Wisian-Neilson, *ACS Symp. Ser.* **572**, 246 (1994).
4. R. de Jaeger and M. Gleria, *Prog. Polym. Sci.* **23**, 179 (1998), and references therein.
5. H. R. Allcock and R. L. Kugel, *J. Am. Chem. Soc.* **87**, 4216 (1965).
6. H. R. Allcock, *J. Inorg. Organomet. Polym.* **2**, 197 (1992).
7. H. R. Allcock, *Chem. Mater.* **6**, 1476 (1994).
8. H. R. Allcock, *Adv. Mater.* **6**, 106 (1994).
9. H. R. Allcock and C. Kim, *Macromolecules* **22**, 2596 (1989).
10. H. R. Allcock and C. Kim, *Macromolecules* **24**, 2846 (1991).
11. H. R. Allcock, A. A. Dembek, and E. H. Klingenberg, *Macromolecules* **24**, 5208 (1991).
12. H. R. Allcock and C. G. Cameron, *Macromolecules* **27**, 3131 (1994).
13. G. Facchin and co-workers, *J. Inorg. Organomet. Polym.* **1**, 389 (1991).
14. D. C. Ngo, J. S. Rutt, and H. R. Allcock, *J. Am. Chem. Soc.* **113**, 5075 (1991).
15. H. R. Allcock and co-workers, *Macromolecules* **27**, 7556 (1994).
16. R. H. Neilson and P. Wisian-Neilson, *Chem. Rev.* **88**, 541 (1988); C. H. Walker, J. V. St. John, and P. Wisian-Neilson, *J. Am. Chem. Soc.* **123**, 3846 (2001).
17. R. A. Montague and K. Matyjaszewski, *J. Am. Chem. Soc.* **112**, 6721 (1990).
18. K. Matyjaszewski, *J. Inorg. Organomet. Polym.* **2**, 5 (1992); K. Matyjaszewski and co-workers, *J. Polym. Sci., Part A: Polym. Chem.* **30**, 813 (1992); K. Matyjaszewski and co-workers, *Polymer* **35**, 5005 (1994); U. Franz, O. Nuyken, and K. Matyjaszewski, *Macromolecules* **26**, 3723 (1993).
19. G. D'Halluin and co-workers, *Macromolecules* **25**, 1254 (1992).
20. C. H. Honeyman and co-workers, *J. Am. Chem. Soc.* **117**, 7035 (1995).
21. H. R. Allcock and co-workers, *Macromolecules* **29**, 7740 (1996).
22. J. M. Nelson and H. R. Allcock, *Macromolecules* **30**, 1854 (1997).
23. H. R. Allcock and co-workers, *Macromolecules* **30**, 2213 (1997).
24. H. R. Allcock and co-workers, *Macromolecules* **33**, 3999 (2000).

25. H. R. Allcock and co-workers, *Inorg. Chem.* **38**, 280 (1999).
26. E. Niecke and W. Bitter, *Inorg. Nucl. Chem. Lett.* **9**, 127 (1973).
27. R. West, *J. Organomet. Chem.* **300**, 327 (1986).
28. R. D. Miller and J. Michl, *Chem. Rev.* **89**, 1359 (1989).
29. K. Matyjaszewski, *J. Inorg. Organomet. Polym.* **1**, 463 (1991).
30. H. Teramae and K. Takeda, *J. Am. Chem. Soc.* **111**, 1281 (1989); J. T. Nelson and W. J. Pietro, *J. Phys. Chem.* **92**, 1365 (1988); A. Savin and co-workers, *Angew. Chem. Int. Ed. Engl.* **31**, 187 (1992).
31. P. Trefonas, *Encycl. Polym. Sci. Eng.* **13**, 162 (1987).
32. H. Tachibana and co-workers, *Phys, Rev. B* **47**, 4363 (1993).
33. K. S. Madiyasni, R. West, and L. D. David, *J. Am. Ceram. Soc.* **61**, 504 (1978).
34. C. Aitken, J. F. Harrod, and E. Samuel, *J. Organomet. Chem.* **279**, C11 (1985); C. T. Aitken, J. F. Harrod, and E. Samuel, *J. Am. Chem. Soc.* **108**, 4059 (1986).
35. T. D. Tilley, *Acc. Chem. Res.* **26**, 22 (1993), and references therein.
36. M. Scarlete and co-workers, *Chem. Mater.* **6**, 977 (1994).
37. Y.-L. Hsiao and R. M. Waymouth, *J. Am. Chem. Soc.* **116**, 9779 (1994).
38. M. Cypryk, Y. Gupta, and K. Matyjaszewski, *J. Am. Chem. Soc.* **113**, 1046 (1991); E. Fossum and K. Matyjaszewski, *Macromolecules* **28**, 1618 (1995).
39. K. Sakamoto and co-workers, *J. Am. Chem. Soc.* **111**, 7641 (1989).
40. H. Sakurai and co-workers, *ACS Symp. Ser.* **572**, 8 (1994).
41. T. Sanji, F. Kitayama, and H. Sakurai, *Macromolecules* **32**, 5718 (1999).
42. H. Suzuki and co-workers, *Adv. Mater.* **5**, 743 (1993).
43. Y. Wang, R. West, and C. H. Yuan, *J. Am. Chem. Soc.* **115**, 3844 (1993).
44. P. Trefonas and R. West, *J. Polym. Sci., Polym. Chem.* **23**, 2099 (1985).
45. R. D. Miller and R. Sooriyakumaran, *J. Polym. Sci., Part A: Polym. Chem.* **25**, 111 (1987).
46. S. M. Katz, J. A. Reichl, and D. H. Berry, *J. Am. Chem. Soc.* **120**, 9844 (1998).
47. M. Okano and co-workers, *Electrochim. Acta* **44**, 659 (1998).
48. V. Y. Lu and T. D. Tilley, *Macromolecules* **33**, 2403 (2000).
49. T. Hayashi and co-workers, *Chem. Lett.* 647 (1992).
50. T. Kodaira and co-workers, *Adv. Mater.* **7**, 917 (1995); J.-C. Baumert and co-workers, *Appl. Phys. Lett.* **53**, 1147 (1988).
51. T. Imori and T. D. Tilley, *Chem. Commun.* 1607 (1993).
52. T. Imori and co-workers, *J. Am. Chem. Soc.* **117**, 9931 (1995).
53. K. Mochida and H. Chiba, *J. Organomet. Chem.* **473**, 45 (1994).
54. C. Aitken and co-workers, *J. Organomet. Chem.* **349**, 285 (1988).
55. M. Okano, T. Toriumi, and H. Hamano, *Electrochim. Acta* **44**, 3475 (1999).
56. J. A. Reichl and co-workers, *J. Am. Chem. Soc.* **118**, 9430 (1996).
57. V. Lu and T. D. Tilley, *Macromolecules* **29**, 5763 (1996).
58. J. R. Babcock and L. R. Sita, *J. Am. Chem. Soc.* **118**, 12481 (1996).
59. K. Mochida and co-workers, *J. Organomet. Chem.* **542**, 75 (1997).
60. H. Ban, K. Deguchi, and A. Tanaka, *J. Appl. Polym. Sci.* **37**, 1589 (1989).
61. M. Abkowitz and M. Stolka, *Solid State Commun.* **78**, 269 (1991).
62. M. Abkowitz and M. Stolka, *J. Non-Cryst. Solids* **114**, 342 (1989).
63. K. Mochida and co-workers, *Appl. Organomet. Chem.* **11**, 949 (1997).
64. Y. Chujo, N. Takizawa, and T. Sakurai, *Chem. Commun.* 227 (1994).
65. Y. Chujo, *ACS Symp. Ser.* **572**, 398 (1994).
66. R. T. Paine and C. K. Narula, *Chem. Rev.* **90**, 73 (1990); R. T. Paine, *J. Inorg. Organomet. Polym.* **2**, 183 (1992).
67. R. T. Paine and L. G. Sneddon, *ACS Symp. Ser.* **572**, 358 (1994).
68. P. J. Fazen and co-workers, *Chem. Mater.* **2**, 96 (1990).
69. P. J. Fazen and co-workers, *Chem. Mater.* **7**, 1942 (1995).

70. Y. Chujo and co-workers, *Macromolecules* **24**, 345 (1991).
71. Y. Chujo and co-workers, *Macromolecules* **25**, 33 (1992).
72. Y. Chujo, I. Tomita, and T. Saegusa, *Macromolecules* **23**, 687 (1990).
73. N. Matsumi, K. Naka, and Y. Chujo, *J. Am. Chem. Soc.* **120**, 5112 (1998).
74. N. Matsumi, M. Miyata, and Y. Chujo, *Macromolecules* **32**, 4467 (1999).
75. Y. Sasaki and Y. Chujo, *Polym. Prepr. Jpn.* **45**, 214 (1996).
76. N. Matsumi and Y. Chujo, *Macromolecules* **31**, 3802 (1998).
77. Y. Chujo and co-workers, *Macromolecules* **25**, 27 (1992).
78. Y. Chujo, I. Tomita, and T. Saegusa, *Macromolecules* **27**, 6714 (1994).
79. N. Matsumi, K. Naka, and Y. Chujo, *Macromolecules* **31**, 8047 (1998).
80. N. Matsumi, T. Umeyama, and Y. Chujo, *Macromolecules* **33**, 3956 (2000).
81. N. Matsumi and co-workers, *Macromolecules* **31**, 3155 (1998).
82. N. Matsumi, K. Kotera, and Y. Chujo, *Macromolecules* **33**, 2801 (2000).
83. N. Matsumi, K. Naka, and Y. Chujo, *J. Am. Chem. Soc.* **120**, 10776 (1998).
84. H. Dorn and co-workers, *Angew. Chem. Int. Ed.* **38**, 3321 (1999).
85. R. I. Wagner and F. F. Caserio Jr., *J. Inorg. Nucl. Chem.* **11**, 259 (1959).
86. A. B. Burg, *J. Inorg. Nucl. Chem.* **11**, 258 (1959).
87. H. Dorn and co-workers, *J. Am. Chem. Soc.* **122**, 6669 (2000).
88. I. Manners and co-workers, *J. Am. Chem. Soc.* **111**, 5478 (1989).
89. H. R. Allcock and co-workers, *Macromolecules* **24**, 2024 (1991).
90. H. R. Allcock and co-workers, *Inorg. Chem.* **32**, 5088 (1993).
91. H. R. Allcock, S. M. Coley, and C. T. Morrissey, *Macromolecules* **27**, 2904 (1994).
92. I. Manners, *Coord. Chem. Rev.* **137**, 109 (1994).
93. M. M. Labes, P. Love, and L. F. Nichols, *Chem. Rev.* **79**, 1 (1979).
94. J. A. Dodge and co-workers, *J. Am. Chem. Soc.* **112**, 1268 (1990).
95. H. R. Allcock, J. A. Dodge, and I. Manners, *Macromolecules* **26**, 11 (1993).
96. M. Liang and I. Manners, *J. Am. Chem. Soc.* **113**, 4044 (1991).
97. M. Liang and I. Manners, *Makromol. Chem., Rapid Commun.* **12**, 613 (1991).
98. J. C. van de Grampel, *Rev. Inorg. Chem.* **3**, 1 (1981); J. C. van de Grampel, *Coord. Chem. Rev.* **112**, 247 (1992).
99. A. R. McWilliams and co-workers, *J. Am. Chem. Soc.* **122**, 8848 (2000).
100. Y. Ni and co-workers, *Angew. Chem. Int. Ed. Engl.* **34**, 998 (1995).
101. Y. Ni and co-workers, *Macromolecules* **25**, 7119 (1992).
102. Y. Ni and co-workers, *Macromolecules* **29**, 3401 (1996).
103. M. N. Nobis and co-workers, *Macromolecules* **33**, 7707 (2000).
104. R. Jaeger and co-workers, *Macromolecules* **28**, 539 (1995).
105. Z. Pang and co-workers, *Adv. Mater.* **8**, 768 (1996).
106. V. Chunechom and co-workers, *Angew. Chem. Int. Ed.* **37**, 1928 (1998).
107. T. Chivers and co-workers, in R. Steudel, ed., *Studies in Inorganic Chemistry, Vol. 14: The Chemistry of Inorganic Ring Systems*, Elsevier, Amsterdam, Netherlands, 1992, p. 271.
108. F. Seel and G. Simon, *Angew. Chem.* **72**, 709 (1960); G. W. Parshall, R. Cramer, and R. E. Foster, *Inorg. Chem.* **1**, 677 (1962).
109. A. K. Roy, *J. Am. Chem. Soc.* **114**, 1530 (1992).
110. A. K. Roy and co-workers, *J. Am. Chem. Soc.* **115**, 2604 (1993).
111. C. U. Pittman Jr. and co-workers, *Macromolecules* **3**, 746 (1970).
112. W. J. Patterson, S. P. McManus, and C. U. Pittman Jr., *J. Polym. Sci. Part A-1* **12**, 837 (1974).
113. K. Gonsalves, L. Zhan-ru, and M. D. Rausch, *J. Am. Chem. Soc.* **106**, 3862 (1984).
114. M. E. Wright, and M. S. Sigman, *Macromolecules* **25**, 6055 (1992).
115. M. E. Wright and co-workers, *Macromolecules* **27**, 3016 (1994).
116. P. Nguyen, P. Gómez-Elipe, and I. Manners, *Chem. Rev.* **99**, 1515 (1999).
117. M. A. Hearshaw and J. R. Moss, *Chem. Commun.* 1 (1999).

118. C. Gorman, *Adv. Mater.* **10**, 295 (1998).
119. B. Alonso and co-workers, *Chem. Commun.* 2575 (1994).
120. I. Cuadrado and co-workers, *Organometallics* **15**, 5278 (1996).
121. J.-L. Fillaut, J. Linares, and D. Astruc, *Angew. Chem. Int. Ed. Engl.* **33**, 2460 (1994).
122. C. Valério and co-workers, *J. Am. Chem. Soc.* **119**, 2588 (1997).
123. I. Cuadrado and co-workers, *J. Am. Chem. Soc.* **119**, 7613 (1997).
124. U. T. Mueller-Westerhoff, *Angew. Chem. Int. Ed. Engl.* **25**, 702 (1986).
125. W. H. Morrison Jr. and D. N. Hendrickson, *Inorg. Chem.* **14**, 2331 (1975); J. A. Kramer and D. N. Hendrickson, *Inorg. Chem.* **19**, 3330 (1980).
126. E. W. Neuse and H. Rosenberg, *J. Macromol. Sci., C: Rev. Macromol. Chem.* **4**, 1 (1970).
127. R. Bayer, T. Pöhlmann, and O. Nuyken, *Makromol. Chem., Rapid Commun.* **14**, 359 (1993); C. E. Stanton and co-workers, *Macromolecules* **28**, 8713 (1995).
128. C. U. Pittman Jr. and Y. Sasaki, *Chem. Lett.* 383 (1975).
129. N. Bilow, A. L. Landis, and H. Rosenberg, *J. Polym. Sci. Part A-1* **7**, 2719 (1969).
130. E. W. Neuse and L. Bednarik, *Macromolecules* **12**, 187 (1979).
131. T. Yamamoto and co-workers, *Inorg. Chim. Acta* **73**, 75 (1983).
132. D. A. Foucher, B.-Z. Tang, and I. Manners, *J. Am. Chem. Soc.* **114**, 6246 (1992).
133. I. Manners, *Chem. Commun.* 857 (1999).
134. D. A. Foucher and co-workers, *Angew. Chem. Int. Ed. Engl.* **32**, 1709 (1993).
135. R. Rulkens and co-workers, *J. Am. Chem. Soc.* **118**, 12683 (1996).
136. M. Hmyene and co-workers, *Adv. Mater.* **6**, 564 (1994).
137. J. K. Pudelski and co-workers, *Macromolecules* **29**, 1894 (1996).
138. L. I. Espada and co-workers, *J. Inorg. Organomet. Polym.* **10**, 169 (2000).
139. R. Resendes and co-workers, *Adv. Mater.* **12**, 327 (2000).
140. I. Manners, *Pure Appl. Chem.* **71**, 1471 (1999).
141. J. Rasburn and co-workers, *Chem. Mater.* **7**, 871 (1995); S. Barlow and co-workers, *J. Am. Chem. Soc.* **118**, 7578 (1996).
142. V. S. Papkov and co-workers, *Macromolecules* **33**, 7107 (2000).
143. K. Kulbaba and I. Manners, *Macromol. Rapid Commun.*, **22**, 711 (2001).
144. I. Manners, *Adv. Organomet. Chem.* **37**, 131 (1995).
145. R. Petersen and co-workers, *Chem. Mater.* **7**, 2045 (1995).
146. M. J. MacLachlan and co-workers, *Adv. Mater.* **10**, 144 (1998).
147. M. J. MacLachlan and co-workers, *J. Am. Chem. Soc.* **122**, 3878 (2000).
148. M. J. MacLachlan and co-workers, *Science* **287**, 1460 (2000).
149. M. J. MacLachlan, A. J. Lough, and I. Manners, *Macromolecules* **29**, 8562 (1996).
150. J. A. Massey and co-workers, *J. Polym. Sci. Part B: Polym. Phys.* **38**, 3032 (2000).
151. K. N. Power-Billard and I. Manners, *Macromolecules* **33**, 26 (2000).
152. F. Jäkle, Z. Wang, and I. Manners, *Macromol. Rapid Commun.* **21**, 1291 (2000).
153. M. Ginzburg and co-workers, *Langmuir* **16**, 9609 (2000).
154. E. Fossum and co-workers, *Macromolecules* **28**, 401 (1995).
155. R. Rulkens and co-workers, *Macromolecules* **30**, 8165 (1997).
156. J. A. Massey and co-workers, *Adv. Mater.* **10**, 1559 (1998).
157. J. A. Massey and co-workers, *J. Am. Chem. Soc.* **123**, 3147 (2001).
158. I. Manners, *Can. J. Chem.* **76**, 371 (1998).
159. J. K. Pudelski and co-workers, *Macromolecules* **28**, 7301 (1995).
160. R. Rulkens, Y. Ni, and I. Manners, *J. Am. Chem. Soc.* **116**, 12121 (1994).
161. Y. Ni, R. Rulkens, and I. Manners, *J. Am. Chem. Soc.* **118**, 4102 (1996).
162. J. A. Massey and co-workers, *J. Am. Chem. Soc.* **122**, 11577 (2000).
163. J. A. Massey and co-workers, *J. Am. Chem. Soc.* **120**, 9533 (1998).
164. P. Gómez-Elipe and co-workers, *J. Am. Chem. Soc.* **120**, 8348 (1998).
165. R. Resendes and co-workers, *Macromolecules* **33**, 8 (2000).
166. Y. Ni and co-workers, *J. Chem. Ed.* **75**, 766 (1998).
167. M. J. MacLachlan and co-workers, *Organometallics* **17**, 1873 (1998).

168. P. Nguyen and co-workers, *Macromolecules* **31**, 5977 (1998).
169. T. J. Peckham and co-workers, *Macromolecules* **29**, 2396 (1996).
170. T. J. Peckham and co-workers, *Macromolecules* **32**, 2830 (1999).
171. R. Rulkens and co-workers, *J. Am. Chem. Soc.* **119**, 10976 (1997).
172. J. M. Nelson and co-workers, *Chem. Eur. J.* **3**, 573 (1997).
173. P. F. Brandt and T. B. Rauchfuss, *J. Am. Chem. Soc.* **114**, 1926 (1992).
174. C. P. Galloway and T. B. Rauchfuss, *Angew. Chem. Int. Ed. Engl.* **32**, 1319 (1993).
175. D. L. Compton and T. B. Rauchfuss, *Organometallics* **13**, 4367 (1994); D. L. Compton and co-workers, *Chem. Mater.* **7**, 2342 (1995).
176. H. M. Nugent, M. Rosenblum, and P. Klemarczyk, *J. Am. Chem. Soc.* **115**, 3848 (1993).
177. M. Rosenblum, *Adv. Mater.* **6**, 159 (1994).
178. M. Rosenblum and co-workers, *Macromolecules* **28**, 6330 (1995).
179. R. Arnold, S. A. Matchett, and M. Rosenblum, *Organometallics* **7**, 2261 (1988); B. M. Foxman and co-workers, *Organometallics* **12**, 4805 (1993).
180. B. M. Foxman, D. A. Gronbeck, and M. Rosenblum, *J. Organomet. Chem.* **413**, 287 (1991).
181. M. Marcos, L. Oriol, and J. L. Serrano, *Macromolecules* **25**, 5362 (1992).
182. D. Perreault and co-workers, *Inorg. Chem.* **31**, 3688 (1992).
183. H. Chen and R. D. Archer, *Macromolecules* **28**, 1609 (1995).
184. H. Chen and R. D. Archer, *Macromolecules* **29**, 1957 (1996).
185. H. Chen, J. A. Cronin, and R. D. Archer, *Macromolecules* **27**, 2174 (1994).
186. J. A. Cronin, S. M. Palmer, and R. D. Archer, *Inorg. Chim. Acta* **251**, 81 (1996).
187. M. Hanack and M. Lang, *Adv. Mater.* **6**, 819 (1994).
188. T. J. Marks, *Angew. Chem. Int. Ed. Engl.* **29**, 857 (1990).
189. R. Knapp, A. Schott, and M. Rehahn, *Macromolecules* **29**, 478 (1996).
190. S. Kelch and M. Rehahn, *Macromolecules* **30**, 6185 (1997).
191. S. Kelch and M. Rehahn, *Macromolecules* **31**, 4102 (1998).
192. S. Kelch and M. Rehahn, *Chem. Commun.* 1123 (1999).
193. S. Kelch and M. Rehahn, *Macromolecules* **32**, 5818 (1999).
194. R. P. Kingsborough and T. M. Swager, *Chem. Mater.* **12**, 872 (2000).
195. S. S. Zhu, R. P. Kingsborough, and T. M. Swager, *J. Mater. Chem.* **9**, 2123 (1999).
196. J. Buey and T. M. Swager, *Angew. Chem. Int. Ed.* **39**, 608 (2000).
197. E. C. Constable and P. Harverson, *Inorg. Chim. Acta* **252**, 9 (1996).
198. S. Achar and R. J. Puddephatt, *Angew. Chem. Int. Ed. Engl.* **33**, 847 (1994).
199. S. Achar and R. J. Puddephatt, *Chem. Commun.* 1895 (1994).
200. S. Serroni and co-workers, *Angew. Chem. Int. Ed. Engl.* **31**, 1493 (1992).
201. G. R. Newkome and co-workers, *Chem. Commun.* 925 (1993).
202. M. H. Chisholm, *Angew. Chem. Int. Ed. Engl.* **30**, 673 (1991).
203. K. Sonogashira, S. Takahashi, and N. Hagihara, *Macromolecules* **10**, 879 (1977).
204. S. Takahashi and co-workers, *Macromolecules* **11**, 1063 (1978).
205. N. Hagihara, K. Sonogashira, and S. Takahashi, *Adv. Polym. Sci.* **41**, 149 (1981).
206. S. J. Davies and co-workers, *Chem. Commun.* 187 (1991).
207. B. F. G. Johnson and co-workers, *J. Organomet. Chem.* **409**, C12 (1991).
208. K. C. Sturge and co-workers, *Organometallics* **11**, 3056 (1992).
209. X. A. Guo and co-workers, *Macromolecules* **27**, 7825 (1994).
210. H. Nishihara and co-workers, *Adv. Mater.* **5**, 752 (1993); I. Tomita, A. Nishio, and T. Endo, *Macromolecules* **27**, 7009 (1994).
211. S. S. H. Mao and T. D. Tilley, *J. Am. Chem. Soc.* **117**, 5365 (1995).
212. H. B. Fyfe and co-workers, *Chem. Commun.* 188 (1991).
213. A. Abe, N. Kimura, and S. Tabata, *Macromolecules* **24**, 6238 (1991).
214. C. C. Frazier and co-workers, *Polymer* **28**, 553 (1987).
215. J. Lewis and co-workers, *J. Organomet. Chem.* **425**, 165 (1992).

216. M. S. Khan and co-workers, *J. Mater. Chem.* **4**, 1227 (1994).
217. G. Frapper and M. Kertesz, *Inorg. Chem.* **32**, 732 (1993).
218. W. J. Blau and co-workers, *J. Mater. Chem.* **1**, 245 (1991).
219. A. E. Dray and co-workers, *Synthetic Metals* **41–43**, 871 (1991).
220. C. W. Faulkner and co-workers, *J. Organomet. Chem.* **482**, 139 (1994).
221. K. A. Bunten and A. K. Kakkar, *J. Mater. Chem.* **5**, 2041 (1995).
222. G. Jia and co-workers, *Organometallics* **12**, 263 (1993).
223. M. Altmann and co-workers, *Adv. Mater.* **7**, 726 (1995).
224. A. A. Dembek, R. R. Burch, and A. E. Feiring, *J. Am. Chem. Soc.* **115**, 2087 (1993).
225. D. Tanner, J. A. Fitzgerald, and B. R. Phillips, *Angew. Chem. Int. Ed. Engl. Adv. Mater.* **28**, 649 (1989).
226. A. A. Dembek, P. J. Fagan, and M. Marsi, *Macromolecules* **26**, 2992 (1993); A. S. Abd-El-Aziz and C. R. de Denus, *Chem. Commun.* 663 (1994).

SARA C. BOURKE
IAN MANNERS
University of Toronto

INTERFACIAL PROPERTIES.

See SURFACE PROPERTIES.

LASER LIGHT SCATTERING

Introduction

In a broad definition, laser light scattering (LLS) could be grouped as inelastic (eg, Raman, fluorescence, and phosphorescence) and elastic (no absorption) light scattering. However, in polymer and colloid science, LLS is normally referred to in terms of static (elastic) or dynamic (quasi-elastic) measurements, or both (1). Static LLS as a classic and absolute analytical method measures the time-average intensity, and it has been long and widely used to characterize both synthetic and natural macromolecules (2). On the other hand, dynamic LLS measures the intensity fluctuation. This is where the word *dynamic* comes from. The visibility of the scattering objects (macromolecules or colloidal particles) in LLS depends on the refractive index difference (dn) between the scattering object and dispersion medium.

In the last two decades, thanks to the advance of stable laser, ultrafast electronics, and personal computer, LLS (especially dynamic LLS) has evolved from a very special instrument for physicists and physical chemists to a routine analytical tool in polymer laboratories or even to a daily quality-control device in production lines. Commercially available research-grade LLS instruments (eg, ALV, Germany, and Brookhaven, U.S.A.) are capable of making static and dynamic measurements simultaneously for studies of colloidal particles in suspensions or macromolecules in solutions as well as in gels and viscous media.

The interaction of laser light (an electromagnetic radiation) with matter can be described in terms of two fundamental quantities: the momentum transfer ($\boldsymbol{K}$) and the energy transfer ($\Delta\omega$), obeying the conservation equations:

Encyclopedia of Polymer Science and Technology. Copyright John Wiley & Sons, Inc. All rights reserved.

$$\hbar K = \hbar(k_I - k_S)$$
$$\text{and} \tag{1}$$
$$\hbar\Delta\omega = \hbar(\omega_I - \omega_S)$$

where $\hbar = h/2\pi$ with h being Planck's constant; $\boldsymbol{k}_{\mathrm{I}}$, $\boldsymbol{k}_{\mathrm{S}}$, and ω_{I}, ω_{S} are, respectively, the incident and scattered wave vectors with magnitudes $2\pi/\lambda_{\mathrm{I}}$, $2\pi/\lambda_{\mathrm{S}}$ and angular frequencies $2\pi\nu_{\mathrm{I}}$, $2\pi\nu_{\mathrm{S}}$. For structural and dynamic information, $\mathrm{R} \sim \boldsymbol{K}^{-1}$ can be used as a spatial resolution ruler in static LLS to probe the sizes of colloidal particles and macromolecules, and $\tau \sim 1/\Delta\nu = 1/(\nu_{\mathrm{I}} - \nu_{\mathrm{S}})$ can be used as a characteristic time range in dynamic LLS to measure the relaxation of colloids in suspension, or macromolecules in solution.

The amplitude of scattering vector $\boldsymbol{K}$, written as q [$=4\pi \sin(\theta/2)/\lambda$], is a pertinent parameter. In principle, one can change either the scattering angle θ or the wavelength λ of the beam in the scattering medium to alter q. However, in LLS, it is not practical to vary $\boldsymbol{K}$ by λ. Therefore, q is typically varied by θ in the range 15°–160°, implying that in static LLS we can only measure the size (R) down to about tens of nanometers, much larger than that in small-angle x-ray scattering (3). In dynamic LLS, translational motions of macromolecules or particles within the size range 1–1000 nm can be measured. The characteristic time of relaxation in dynamic LLS, which includes translational, rotational, and internal motions, could vary from seconds to tens of nanoseconds (4). There are different ways to measure the characteristic time (5), but we shall discuss only the commonly used self-beating intensity–intensity time correlation spectroscopy.

Many reviews, books, proceedings, and chapters have been published on the topic. Serious LLS users should consult References (1) and (2) and other books, rather than proceedings or articles, as reference materials. In particular, the first monograph on the theoretical aspects of dynamic LLS (6) is highly recommended because it remains as the best source reference. In this article there is concentration on experimental detail. Often, static and dynamic LLS are used separately; generally, polymer chemists are more familiar with static LLS and only use dynamic LLS to size particles, whereas polymer physicists are not custom to precise static LLS measurements and sample preparation. This seriously limits their application. This article specially deals with this problem by using several typical examples to show how static and dynamic LLS can be combined to extract more information, such as the characterization of molar mass distribution, estimation of composition distribution of a copolymer, the adsorption/grafting of polymer chains on colloidal particle surfaces, and the self-assembled nanostructure of block copolymers.

Static Laser Light Scattering

For the convenience of discussion, both macromolecules and colloidal particles are referred to as *particles* hereafter. When a light beam I_{INC} hits a solution, the excess Rayleigh ratio $R_{\mathrm{vv}}(q)$ of the solute particles for the vertically polarized incident and scattering lights has the form

$$\frac{HC}{R_{\mathrm{vv}}(q)} \approx \frac{1}{M_w P(q)} \tag{2}$$

where $H[=4\pi^2 n^{2T,P}_{0(\partial n/\partial C)}2/(N_A\lambda_0^4)]$ is an optical constant for a given polymer solution and a laser light source, $M_w(=\int_0^\infty f_w(M)\,M\mathrm{d}M\int_0^\infty f_w(M)\,\mathrm{d}M)$ is the weight-average molar mass and $f_w(M)$ is the weight distribution of molar mass. The scattering factor $P(q)$ for particles with different shapes have been previously derived (7, 8) and graphically displayed (9). It is related to q and the root-mean square z-average radius of gyration $\langle R_g{}^2\rangle_z{}^{1/2}$, or written as $\langle R_g\rangle$, where $\langle R_g{}^2\rangle_z$ is defined as $\int_0^\infty f_w(M)MR_g^2\mathrm{d}M/\int_0^\infty f_w(M)M\mathrm{d}M$. When $\langle R_g\rangle$ is smaller than $1/q$, ie, $q\langle R_g\rangle \ll 1$, we have

$$P(q)\approx 1-1/3q^2R_g^2+\cdots \tag{3}$$

It can be shown that equation (3) is not only valid for the Gaussian chain but also for particles with an arbitrary shape as long as $q\langle R_g\rangle \ll 1$. Considering the interparticle interference between the scattered lights, Debye (10) showed in 1947 that the concentration dependence can be virial expanded as a power series in the concentration, the combination of which with equations (2) and (3) leads to

$$\frac{HC}{R_{vv}(q)}\approx\frac{1}{M_w}\left(1+\frac{1}{3}\langle R_g^2\rangle_z q^2+\cdots\right)+2A_2C+\cdots \tag{4}$$

Where A_2 is the second virial coefficient. This is the most basic equation in static LLS. With $R_{vv}(q)$ measured over a series of C and q, one can obtain $<R_g>$ and A_2, respectively, from the slopes of $[HC/R_{vv}(q)]_{c\to 0}$ vs q^2 and $[HC/R_{vv}(q)]_{q\to 0}$ vs C; and M_w from $[HC/R_{vv}(q)]_{c\to 0,q\to 0}$. The Zimm plot, $HC/R_{vv}(q)$ vs (q^2+kC) with k an adjustable constant, allows the extrapolations of $q\to 0$ and $C\to 0$ to be made on a single grid (11). Figure 1 shows a typical Zimm plot for thermally sensitive and biocompatible poly(N-vinyl caprolactam) in water at 25°C (12).

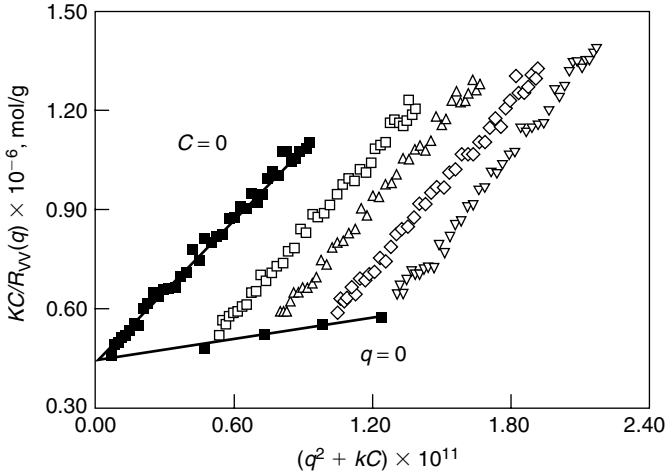

Fig. 1. Typical Zimm plot for thermally sensitive and biocompatible poly(N-vinyl caprolactam) ($M_w = 2.34\times 10^6$ g/mol, $<R_g> = 79$ nm, and $A_2 = 1.59\times 10^{-4}$ (mol·mL)/g^2) in water at 25°C.

It should be noted that equation (4) is valid under the restriction that the solution exhibits no absorption, no fluorescence, and no depolarized scattering. As for anisotropic rigid or rigid-like rods with a depolarized scattering, readers should refer to the excellent review article in Reference (13), and the references therein. As for the correction of absorption and fluorescence, readers are advised to refer to the characterization of Kevel in concentrated sulphuric acid (14–16). In practice, the Rayleigh ratio is determined by a relative method; namely, by measuring the scattering intensity of a standard, eg, benzene or toluene, we can calculate the Rayleigh ratio of a solution by

$$R_{vv}(q) = R^{o}_{vv}(q)\frac{\langle I\rangle_{\text{solution}} - \langle I\rangle_{\text{solvent}}}{\langle I^{o}\rangle}\left(\frac{n}{n^{o}}\right)^{\gamma} \tag{5}$$

where the superscript "o" denotes the standard and $<I>$ is the time-averaged scattering intensity. The term (n/n^{o}) is a refraction correction for the scattering volume and $1 \leq \gamma \leq 2$, depending on the detection optics. If a slit is used, we only need to correct the refraction in one direction ($\gamma = 1$). On the other hand, if a pinhole with a size much smaller than the beam diameter is used at the center of the scattering cell, we have to correct the refraction in two directions ($\gamma = 2$). When the pinhole size is comparable to the beam diameter, $1 < \gamma < 2$, which should be avoided. In practice, a slit ($\sim$200 μm) is preferred. Note that static LLS theory is not complicated, but the alignment of LLS spectrometer is much more difficult.

Dynamic Laser Light Scattering

When the incident light is scattered by a moving particle, the detected frequency of the scattered light will be slightly higher or lower owing to the Doppler effect, depending on whether the particle moves towards or away from the detector. The frequency distribution of the scattered light is slightly broader than that of the incident light. This is why dynamic LLS is also called quasi-elastic light scattering (QELS). In comparison with the incident light frequency ($\sim 10^{15}$ Hz), the frequency broadening Δf $\sim 10^{5}$–10^{7} Hz is so small, that it is difficult, if not impossible, to detect Δf in frequency domain. But, it can be recorded in the time domain via a time correlation function so that dynamic LLS is sometimes known as photon correlation spectroscopy (PCS).

Without a local oscillator (ie, a constant fraction of the incident light reaching the detector *intentionally* or *unintentionally* by various sources, such as surface scratching or reflection), the self-beating of the scattered electric field leads to the intensity–intensity time correlation function $G^{(2)}(q, t)$, which is related to the normalized scattered electric field–electric field time correlation function $|g^{(1)}(q, t)|$ $(=<\boldsymbol{E}(q, 0)\boldsymbol{E}*(q, t)>/<\boldsymbol{E}(q, 0)\boldsymbol{E}*(q, 0)>)$ by the Siegert relation:

$$G^{(2)}(q,t) = \langle I(q,0)I(q,t)\rangle = A(1 + \beta|g^{(1)}(q,t)|^{2}) \tag{6}$$

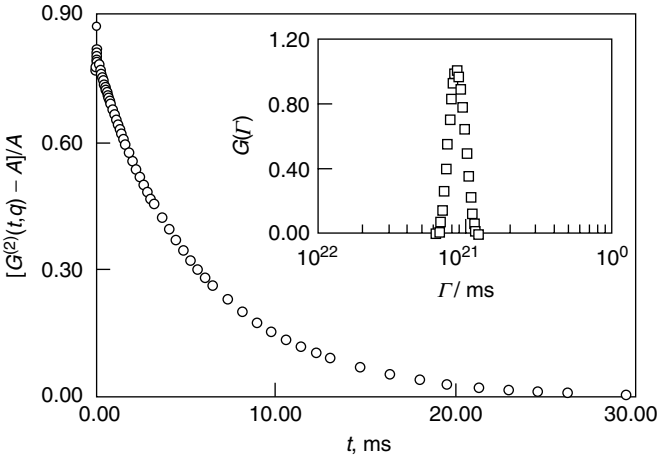

Fig. 2. Typical normalized intensity–intensity time correlation function for thermally sensitive and biocompatible poly(*N*-vinyl caprolactam) ($M_w = 2.34 \times 10^6$ g/mol, $<R_g> =$ 79 nm, and $A_2 = 1.59 \times 10^{-4}$ mol·mL/g^2) in water at 25°C.

where A ($\equiv <I(q, 0)I(q, 0)>$) is the baseline, t is the delay time, β is a parameter depending on the coherence of the detection optics, and $I(q, t)$ is the detected scattering intensity or photon counts at time t, including contributions from both solvent and solute. Therefore, $I_{\text{solution}}(q, t) = I_{\text{solvent}}(q, t) + I_{\text{solute}}(q, t)$. Figure 2 shows a typical normalized intensity–intensity time correlation function for thermally sensitive and biocompatible poly(*N*-vinyl caprolactam) in water at 25°C.

In a real experiment, β_{app} [$=\beta(I_{\text{solute}}/I_{\text{solution}})^2$] instead of β is measured by the extrapolation of $[G^{(2)}(q, t)]_{t\to 0}$ in equation (6) (17). The reader should be aware of this fact, especially for weakly scattered dilute low molar mass polymer solution. For example, if $I_{\text{solute}} = I_{\text{solvent}}$, $\beta_{\text{app}} = \beta/4$. Note that β is a constant for each given detection geometry so that it can be determined by using a strongly scattered object, such as narrowly distributed latex particles (~100 nm). Knowing β, one can calculate I_{solute} from β_{app}. A beginner in LLS should note that such a measurement is not a routine method and only reserved for some particular experiments in which a direct and accurate measurement of $I_{\text{solution}} - I_{\text{solvent}}$ is difficult. Generally, the relaxation of $|g^{(1)}(q, t)|$ includes both diffusion (translation and rotation) and internal motions. Let us first consider the translational diffusion relaxation. For a polydisperse sample with a continuous distribution of molar mass M or size R, we have

$$|g^{(1)}(q,t)| = \int_0^\infty G(\Gamma)e^{-\Gamma t}\mathrm{d}\Gamma \tag{7}$$

where $G(\Gamma)$ is the line width distribution. Note that by the definition of $|g^{(1)}(q, t)|$, $G(\Gamma)$ is an intensity distribution of Γ. For a dilute solution, the measured line width Γ is related to q, C, and the translational diffusion coefficient D by (18,19)

$$\Gamma = q^2 D(1 + k_d C)\left(1 + f\left\langle R_g^2\right\rangle_z q^2\right) \tag{8}$$

where k_d is the diffusion second virial coefficient and f is a dimensionless parameter depending on the structure, internal motions, and solvent. When $C \Rightarrow 0$ and $q \Rightarrow 0$, $\Gamma/q^2 \Rightarrow D$.

Equation (7) indicates that once $|g^{(1)}(q, t)|$ is determined from $G^{(2)}(q, t)$ through equation (6), $G(\Gamma)$ can be computed from the Laplace inversion of $|g^{(1)}(q, t)|$ (20–26). In the last three decades, many computation programs were developed. At the earlier stage, the caculation speed was a very important factor in the development. This constraint has gradually been removed in the last 10 years. Among many programs, the CONTIN program (27) is still the most used and accepted one. However, it should be noted that equation (7) is one of the first kind Fredholm integral equations. Its inversion is an ill-conditioned problem because of the bandwidth limitation of photon correlation instruments, unavoidable measurement noises, and a limited number of data points; namely, the inversion does not lead to a unique $G(\Gamma)$. Therefore, it is more important to *reduce the noises in the measured intensity time correlation function than to choose a program for data analysis* (26,27). It is crucial to thoroughly clean (ie, dust-free) the solution. A practical checkup is to measure the scattered intensity at 15° for 5–10 min. If there is no sharp intensity pulse, the sample is "clean." Unfortunately, many of the LLS users did not realize this problem or did not want to face it. It is dangerous to use a "dirty" solution and explain whatever comes from it.

It is worth noting that there is a temptation among LLS users to extract too much information from $G^{(2)}(q, t)$, actually from experimental noises. In the literature, three or four peaks in $G(\Gamma)$ were often reported. It has to be warned that even a bimodal distribution of $G(\Gamma)$ has to be justified by other physical evidences or preexperimental knowledge. This does not mean that many of the Laplace inversion programs developed in the past are useless. On the contrary, they have been quite successful in retrieving some desired information. Therefore, the Laplace inversion should be used with a clear understanding of its ill-conditioned nature and its limitation.

The contribution of the rotational relaxation to Γ has been discussed (6,13). At a very small scattering angle, the internal and rotational a relaxations are relatively so fast that its contribution to Γ can be neglected. The internal motions of a long flexible polymer chain, also known as the normal modes or "breathing modes," can only be observed at higher scattering angles. The spectral distribution of the light scattered from a flexible polymer chain has been derived (6,28). Figure 3 shows typical plots of $G(\Gamma/q^2)$ vs Γ/q^2 for a narrowly distributed high molar mass polystyrene standard in toluene at different x values (29). The change of $G(\Gamma/q^2)$ is due to the fact that the line width (Γ) associated to the translational diffusion increases with x, but those related to the internal motions are independent of the scattering angle.

The uninitiated reader may wish to consult books on polydispersity analysis (30,31). In practice, one can use a fast but limited cumulants analysis to obtain the average line width $<\Gamma>$ and relative width $\mu_2/<\Gamma>^2$ of $G(\Gamma)$ (20), wherein $[G^{(2)}(q, t) - A]/A$ is expanded as

$$\ln\left[\frac{G^{(2)}(q,t)-A}{A}\right] = \ln\beta - \langle\Gamma\rangle t + \frac{\mu_2 t^2}{2!} + \frac{\mu_3 t^3}{3!} + \cdots \tag{9}$$

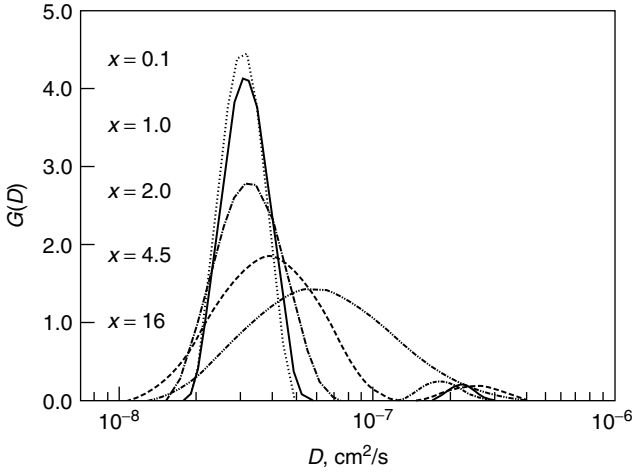

Fig. 3. x-dependence of $G(\Gamma/K^2)$ for a high molar mass polystyrene standard ($M_w = 1.02 \times 10^7$ g/mol and $M_w/M_n = 1.17$) in toluene at $T = 20^\circ$C, where $x = (R_gK)^2$ and $G(\Gamma/K^2)$ was calculated by using the CONTIN Laplace inversion program.

where $<\Gamma> = \int_0^\infty \Gamma G(\Gamma)\, d\Gamma$ and $\mu_m = \int_0^\infty (\Gamma - <\Gamma>)^m\, G(\Gamma)\, d\Gamma$. For $\mu_2/<\Gamma>^2 < 0.2$, the second-order cumulants fit is sufficient, while when $\mu_2/<\Gamma>^2 \sim 0.2$–$0.3$, the third-order cumulants fit is required. For an even higher value of $\mu_2/<\Gamma>^2$, we cannot simply use a higher order expansion to solve the problem because we do not know how many terms are sufficient to avoid an overfitting of experimental noises. For a broadly distributed sample, the Laplace inversion could yield more reliable $<\Gamma>$ and $\mu_2/<\Gamma>^2$ as long as the measured time correlation function is obtained within a proper bandwidth range and has a sufficient photon count, eg, the baseline has a total count over 10^6. The Laplace inversion method is particularly useful if $G(\Gamma)$ is a bimodal distribution where the two peaks are well separated by a factor of 2 or more.

Methods of Combining Static and Dynamic LLS

Dynamic LLS is famous for its application in particle sizing. $G(\Gamma)$ obtained from a dilute dispersion is converted to the hydrodynamic size distribution $f(R_h)$ by means of $D = \Gamma/q^2$ and the Stokes–Einstein relation $D = k_BT/6\pi\eta R_h$ with k_B, T, and η being the Boltzmann constant, the absolute temperature, and solvent viscosity, respectively. All the parameters in the conversion are either well-known constants or precisely measurable by other methods. Therefore, using dynamic LLS to size the particle size distribution is an absolute method without any calibration. Many commercial instruments have been successfully developed on this principle; details have been compiled in a book (32). However, a combination of static and dynamic LLS can provide much more than the characterization of the weight-average molar mass and the particle size distribution.

Characterization of Molar Mass Distribution. Among other methods, using a combination of static and dynamic LLS to characterize the molar mass

distribution of a polymer has yet to become popular because it requires a well-aligned spectrometer that is capable of doing both static and dynamic LLS, a better understanding of LLS theory, and a calibration between D and M. It is worth noting that LLS as a nonintrusive and nondestructive method has its own advantages, eg, it can use a strong corrosive solvent, such as concentrated sulphuric acid, and it can be operated at temperatures as high as 340°C. Though not involving fractionation as in gpc, $G(\Gamma)$ obtained in dynamic LLS could lead to the molar mass distribution if we have

$$D = k_D M^{-\alpha_D} \tag{10}$$

where k_D and α_D are two scaling constants (33). It has been confirmed that for a flexible polymer, $0.5 < \alpha_D < 0.6$ in a good solvent and $\alpha_D = 0.5$ in a Flory Θ-solvent; for a rigid rod-like chain, $\alpha_D = 1$; and for a semirigid worm-like chain, $0.6 < \alpha_D < 1$. Equations (2), (6) and (7) indicate that both $Mf_w(M)$ and $G(D)$ are proportional to the excess scattered intensity. Using equation (10), we have (19)

$$f_w(M) \propto D^{1+2/\alpha_D} G(D) \tag{11}$$

Therefore, one can transfer D to M and $f_w(M)$ to $G(D)$ if knowing k_D and α_D, very similar to gpc or the particle sizing where we know that $k_D = k_B T/6\pi\eta$ and $\alpha_D = -1$. Figure 4 shows such obtained differential weight distributions $f_w(M)$ of molar mass for four different poly(N-vinyl caprolactam) fractions in water at 25°C.

The most straightforward method for calibrating D vs M is to measure both D and M for a set of narrowly distributed samples with different molar masses (34,35). However, only a very few kinds of polymers, eg, polystyrene and

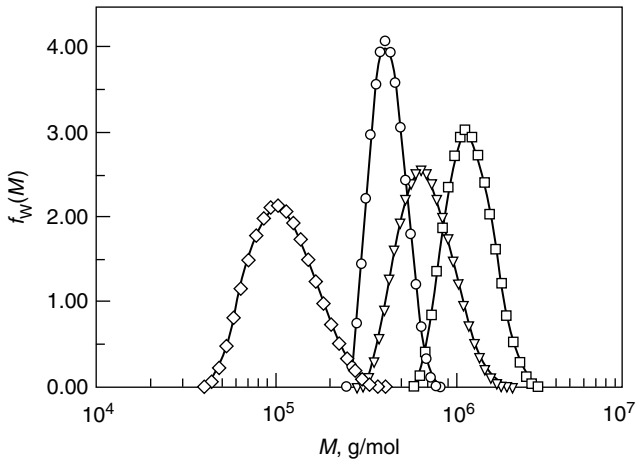

Fig. 4. Typical differential weight distributions $f_w(M)$ of molar mass for four different poly(N-vinyl caprolactam) fractions in water at 25°C, which were calculated by a combination of static and dynamic LLS results, ie, from the line-width distribution $G(\Gamma)$ and the weight-average molar mass (M_w).

poly(methyl methacrylate), can be prepared in such a manner. A traditional time-consuming fractionation method has to be used. Hence, we often have to satisfy ourselves with one or more broadly distributed samples. For two or more samples, one can determine both α_D and k_D from the measure values of M_w and $G(D)$ by a method described in Reference (19). In the case of only one sample, one can estimate α_D from the Mark-Houwink constant from the calibration between intrinsic viscosity and molar mass, ie, $[\eta] = k_\eta M_w{}^\alpha \eta$. It has been shown that $\alpha_D \approx (\alpha_\eta + 1)/3$ for a coil chain (33,36). With α_D estimated from α_η, M_w from static LLS, and $G(D)$ from dynamic LLS, one can determine k_D in the characterization of linear polyethylene in 1,2,4-trichlorobenzene at 135°C (37,38), where α_D was estimated from $\alpha_\eta = 0.72$ (39). Also, LLS can be combined with gpc to find α_D and k_D (40,41). Use of a combination of static and dynamic LLS to estimate the molar mass distribution of some special polymers has been reviewed (42).

Estimation of Copolymer Composition Distribution. A copolymer is normally polydisperse not only in molar mass but also in chain composition. A combination of static and dynamic LLS can be used to estimate its composition distribution. Consider a copolymer sample consisting of monomers A and B and suppose that the copolymer species "i" is characterized by the molar mass M_i and the weight fraction ($w_A(M_i)$). Assume that for a given M, there is no further composition heterogeneity. For a given copolymer in solvents 1 and 2, eq (12) applies (43,44)

$$\frac{f^{(1)}_{w,\mathrm{app}}(M)}{f^{(2)}_{w,\mathrm{app}}(M)} = \left\{ \frac{v^{(2)}}{v^{(1)}} \frac{w_A(M) v_A^{(1)} + \left[1 - w_A(M)\right] v_B^{(1)}}{w_A(M) v_A^{(2)} + \left[1 - w_A(M)\right] v_B^{(2)}} \right\}^2 \tag{12}$$

where $f_{w,\mathrm{app}}(M)$ is the apparent weight distribution, v is specific refractive index increment, and the superscripts denote two solvents. The values of v, v_A, and v_B in two solvents can be predetermined using differential refractometer. The ratio on the left-hand side can be determined as a function of M since $f_{w,\mathrm{app}}(M)$ and M_w is obtainable using Equations (10) and (11). Therefore, Equation (12) allows the determination of $w_A(M)$. Once $w_A(M)$ is known, $v(M)$ and $f_w(M)$ can be computed (43,44). Figure 5 shows such obtained weight composition for two PET–PCL samples with different weight-average molar masses but the same overall composition. It clearly shows that the PET content increases as the molar mass for $M < \sim 4 \times 10^4$ and approaches a constant value (~14%) in the high molar mass range.

Investigation of Interchain Aggregation. Using dynamic LLS to size polymer aggregates is only a simple application. A combination of static and dynamic LLS can lead to the weight fraction and molar mass of the aggregates. If a solution contains individual polymer chains and clusters (or aggregates), static LLS can lead to an apparent weight-average molar mass $M_{w,\mathrm{app}} = M_{w,L} w_L + M_{w,H} w_H$, where the subscripts "L" and "H" denote low molar mass polymer chains and high molar mass clusters, respectively, and w_L and w_H are their weight fractions with $w_L + w_H = 1$. If clusters are much larger than individual chains,

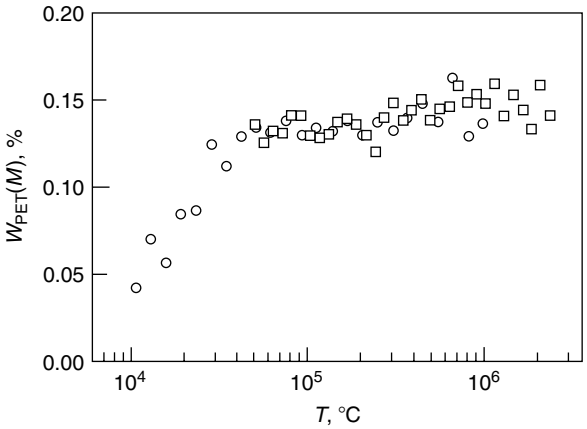

Fig. 5. Estimate of the chain composition distributions for low mass (○) and high mass □ 13% PET–PCL samples by a combination of static and dynamic LLS.

dynamic LLS can detect two distinct peaks $G_{\mathrm{L}}(D)$ and $G_{\mathrm{H}}(D)$, as shown in Figure 6 (45). The area ratio A_{r} of these two peaks equals the intensity ratio, ie,

$$A_r = \frac{A_L}{A_H} = \frac{\int_{\mathrm{o}}^{D_M} G_L(D)\mathrm{d}D}{\int_{\mathrm{D}_M}^{\infty} G_H(D)\mathrm{d}D} = \frac{M_{w,L}x_L}{M_{w,H}x_H} \tag{13}$$

with D_{M} being the cutoff translational diffusion coefficient between $G_{\mathrm{L}}(D)$ and $G_{\mathrm{H}}(D)$. Using Equations (12) and (13), one can calculate $M_{\mathrm{w,L}}x_{\mathrm{L}}$ and $M_{\mathrm{w,H}}x_{\mathrm{H}}$ from

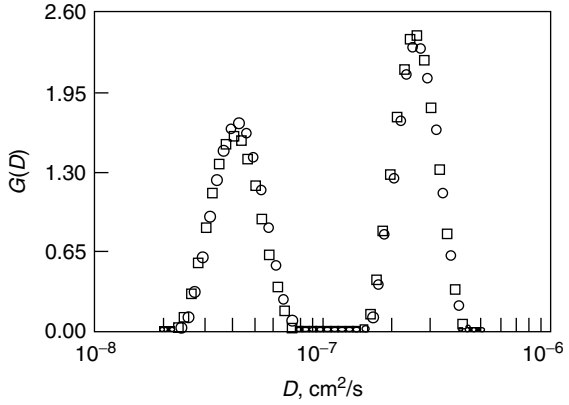

Fig. 6. Translational diffusion coefficient distributions $G(D)$ of a simulated polymer mixture at two scattering angles ("○", 14° and □, 17°). The mixture contains two polystyrene standards of distinctly different weight-average molar masses (3.0×10^5 and 5.9×10^6 g/mol) and a high mass polystyrene.

$M_{w,app}$ and A_r. Knowing any one of $M_{w,L}$, $M_{w,H}$, x_L, and x_H permits finding the rest of the three. This method has been thoroughly tested (45) and used to characterize thermoplastic polymers with phenolphthalein in their backbone chains (46).

Elucidation of Colloidal Particles. Besides sizing colloidal particles, one can use a combination of static and dynamic LLS to elucidate the structure and density of particles, the adsorbed surfactant or polymer layer, and the particle formation (47–52). The following is just one example of how to determine the particle density (ρ) by combining static and dynamic LLS. For a colloidal particle with a uniform density, its molar mass $M = (4/3)\pi R^3 \rho N_A$, where R is its radius and N_A is the Avogadro constant. D can be converted to R_h. In general, $R_h \geq R$, so that one can assume that $R_h = R + b$ with b being the thickness of the solvated layer. Thus,

$$D = \frac{1}{1 + b(4\pi\rho N_A/M)^{1/3}} \left(\frac{k_B T}{6\pi\eta}\right) (4\pi\rho N_A)^{1/3} M^{1/3} \tag{14}$$

Comparing equation (14) with equation (10) and considering $b \ll R$, one finds approximately $\alpha = 1/3$ and $k_D = (k_B T/6\phi\eta)(4\pi\rho N_A)^{1/3}/[1 + b(4\pi\rho N_A/M)^{1/3}]$. Replacing M in equation (14) with M_w given

$$M_w = \frac{1}{\left[1 + b\left(4\pi\rho N_A/M_w\right)^{1/3}\right]^3} \left(\frac{4\pi\rho N_A}{3}\right) \left(\frac{k_B T}{6\pi\eta}\right)^3 \Big/ \int_0^\infty G(D) D^3 \mathrm{d}D \tag{15}$$

Equation (15) contains two unknown parameters b and ρ. Knowing one of them, one can calculate the other from M_w and $G(D)$. In this way, it was found that the polystyrene nanoparticles made of only a few uncross-linked chains have a slightly lower density than bulk polystyrene or conventional polystyrene latex (53).

Study of Self-assembly of Diblock Copolymers. Diblock copolymer can self-assemble into a core–shell nanostructure in a selective solvent in which the core and shell are, respectively, made of the collapsed insoluble blocks and the swollen soluble blocks. For the first approximation, the core–shell nanostructure can be described by two concentric spheres with different, but uniform, densities (ρ_c and ρ_s). Instead of neutron scattering, a combination of static and dynamic LLS can also lead to the core radius (R_c) and shell thickness (ΔR) from $<R_g>/<R_h>$ by the following principle.

For a sphere with a uniform density, we can write the core and the shell masses (M_c and M_s) as $M_c = 4\pi\rho_c R_c^3/3$ and $M_s = 4\pi\rho_s(R^3 - R_c^3)/3$, where R_c is the core radius and R is the particle radius. According to the definition of R_g for a sphere, we have

$$R_g^2 = \frac{\int_v \rho(r) r^2 \mathrm{d}v}{\int_v \rho(r) \mathrm{d}v} = \frac{\int_0^{R_c} 4\pi\rho_c r^4 \mathrm{d}r + \int_{R_c}^{R} 4\pi\rho_s r^4 \mathrm{d}r}{M_c + M_s} = \frac{3\left[M_c R_c^2 R^3 - (M_c + M_s) R_c^5 + M_s R^5\right]}{5(M_c + M_s)(R^3 - R_c^3)} \tag{16}$$

Setting the mass ratio M_c/M_s as A and the radius ratio R_c/R as x, we can rewrite equation (16) as

$$\frac{R_g}{R_h} = \left\{ \frac{3\left[Ax^2 - (1+A)x^5 + 1\right]}{5(1+A)(1-x^3)} \right\}^{1/2} \tag{17}$$

where R has been replaced with R_h. Note that M_c/M_s equals to the molar mass ratio of the insoluble block to the soluble block, a constant for a given diblock copolymer. Therefore, for each measured $<R_g>/<R_h>$, we can find a corresponding x according to equation (17) and calculate R_c and ΔR since $R_c = <R_h>x$ and $\Delta R = <R_h> - R_c = <R_h>(1-x)$.

Figure 7 shows a typical average association chain number (n_{chain}) dependence of R_c and ΔR of self-assembled core–shell nanostructures of a rod-coil diblock copolymer, poly(styrene-*block*-(2,5-bis[4-methoxyphenyl]oxycarbonyl)styrene) (PS-b-PMPCS). The fact that R_c is nearly a constant and close to the contour length of the PMPCS block (~31 nm), but ΔR increases with n_{chain}, clearly reveals that when more copolymer chains are self-assembled into the core–shell nanostructure, the insoluble rod-like PMPCS blocks are simply inserted into the core, whereas the soluble coil-like polystyrene

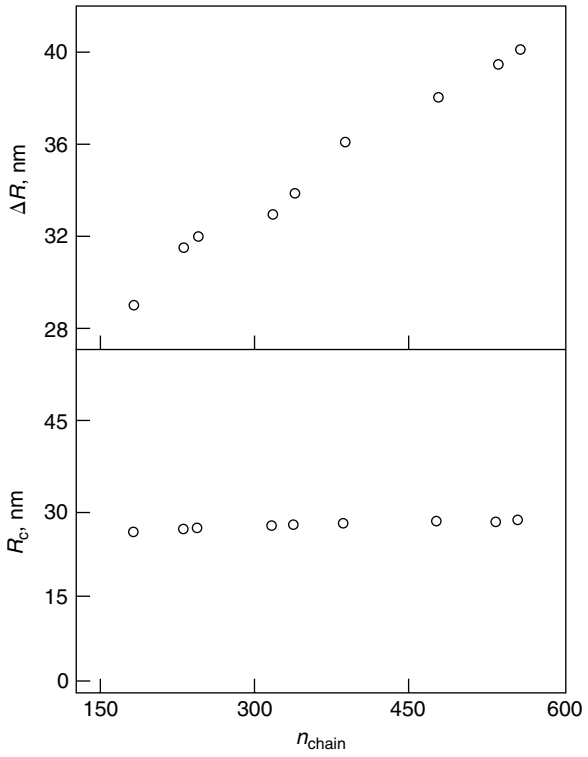

Fig. 7. Average association chain number dependence of the core radius (R_c) and shell thickness (ΔR_h) of self-assembled core–shell nanostructures of a rod-coil diblock copolymer, poly(styrene-*block*-(2,5-bis[4-methoxyphenyl]oxycarbonyl)styrene) PS-b-PMPCS in *p*-xylene at 25°C.

blocks are forced to stretch in the shell as a result of the repulsion in a good solvent.

Practice of Laser Light Scattering

A laser light scattering spectrometer contains a limited number of components; namely, the light source, the optics, the cell holder, and the detector. Nowadays, an LLS instrument should have a digital output (single-photon counting) from a fast photomultiplier, ie, the output current pulse should be treated by preamplifier/amplifier/discriminator before it is connected to a digital time correlator, a single plug-in board to a personal computer.

Light Source. Traditionally, the light source is a helium–neon (He–Ne) laser with a wavelength of 632.8 nm and an output power of 5–50 mW or an argon-ion (Ar^+) laser with a wavelength of 488 or 514.5 nm and an output power of 50–400 mW. Krypton lasers have also been used because their wavelength can be longer than 632.8 nm. The additional cost and somewhat short plasma tube life are drawbacks. The laser used in dynamic light scattering should have a TEM_{00} mode with a Gaussian intensity profile. The reader should choose a laser with a beam amplitude rms noise less than 0.5%. Noted that in dynamic LLS, long-term stability is not very important since the maximum delay time is usually no more than a few minutes, typically less than 1 s, but both the beam point and intensity stabilities are important from static LLS. More recently, there is a tendency to replace these gas lasers with solid-state CW lasers.

The frequency-doubled Nd-YAG laser (532 nm) is a much better choice nowadays if two wavelengths are not required. In comparison with gas lasers, the solid laser has the following advantages: (*1*) its beam diameter is smaller so that small scattering angles are easier to access; (*2*) it is ∼1000 times more coherent; (*3*) it is ∼10 times more stable; (*4*) it has a smaller overall size; (*5*) it is air-cooled and requires only plug-in electric power; and (*6*) its running cost is lower by a factor of ∼5 or more. It is expected that solid-state lasers will gradually replace gas lasers in most applications. The manufacturers have started to provide a new kind of solid-state CW diode lasers in visible (∼670 nm) and near visible (780–830 nm) range, which are particularly useful in the study of conjugated polymers.

Optics and Cell Design. It is well known that laser light follows Gaussian optics. If a laser beam is focused through an aperture by a lens, the diameter (d_s) of the focus spot will be $\sim 1.22 l\lambda\, f/r_0$ with f and r_0 being the focal length and beam radius, respectively. If $r_0 \sim 0.8$ mm, $\lambda \sim 532$ nm, and $f \sim 300$ mm, typically $d_s \sim 0.25$ mm so that the incident beam divergence (d_s/f) is less than 1 Mrad, which is sufficiently small. A polarizer may be placed in the light path before the incident beam strikes the sample cell to define the polarization (normally vertical) of the incident beam. Nowadays, the polarization ratio of lasers is better than 100:1 so that the polarizer is not necessary for a normal LLS measurement.

The conventional sample cell holder in LLS consists of a hollow cylindrical brass block with an outside diameter of 50–80 mm and an inside diameter of 10–20 mm, which matches the outside diameter of the scattering cell. The brass block is normally placed inside a cylindrical optical glass cup filled with a fluid

(eg, xylene, toluene, and silican oil), the refractive index of which matches that of glass ($\sim$1.5) to reduce the surface scattering and cell curvature. A proper alignment of the optical path requires the variation of the scattered intensity of a standard, benzene or toluene, after the scattering volume correction by sin θ is less than 1% (if the scattering volume is chosen by a slit) or 2% (if a small pinhole is used) over an angular range of $\sim 15^\circ$–150°. In principle, the scattering cell with an optical quality should be used. However, it is found in practice that a selected normal cylindrical sample vial is also satisfactory, which reduces the cost and makes it disposable.

On the other hand, if one is only interested in dynamic LLS, a rectangular cell can also be used or even preferred. It is noted that the scattering volume ($\sim 200 \times 300 \times 300\ \mu m^3$ or 0.02 μL) is so small that one can use a small scattering cell, eg, a melting-point capillary with a μL-solution volume for dynamic LLS (54), even though it is difficult to use it in static LLS. The scattering cell can also be a flow type (55) so that it can be used as an *in situ* LLS detector for gpc and electrophoresis. Another challenge in polymer analysis is to characterize polymers soluble only at high temperatures. An important advancement in this direction is the design of a novel light scattering cell holder that is capable of operating at temperatures as high as 340°C (56–61). It was first developed at State University of New York at Stony Brook and is now available in DuPont (Experimental Station), BASF (Ludwigshafen, Germany), and our laboratory.

It has to be stated that the optics together with the cell design in LLS are going through a drastic change because of the development of optical fiber technology (62–65). Figure 8 shows a fiber-optic detector probe comprising a single-mode optical fiber and a graded index microlens, which can form an integral part of the scattering cell. In this cell-detector probe design, the probes can eliminate the need for a goniometer, which is often one of the bulkier components of the spectrometer. Moreover, the probe can be in contact with the solution or dispersion so that the requirement of a transparent window in the sample chamber can be relaxed.

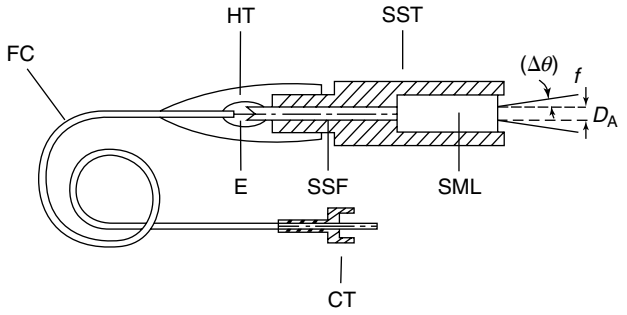

Fig. 8. Schematic of a typical fiber-optic probe. SST: a matching piece of cylindrical stainless steel; SML: SELFOC microlens; SSF: a stainless steel or ceramic ferrule used for mounting the bare optical fibre; E: epoxy used for holding fibre in ferrule; HT: heat shrink tubing; FC: fibre cable; CT: SMA type II male connector. D_A and $(\Delta\theta)$ are the effective detector aperture and divergence angle, respectively.

Detectors and Detection. Commercially available standard photomultiplier tubes (PMTs) with a low dark count (<30 Hz) and a short after-pulsing are normally used to count photons. When a He–Ne laser light source is used, an S-20 photocathode is preferable because of its higher sensitivity in the red range. PMTs, such as EMI 9863 and new Hamamatsu miniature PMTs, are more suitable. To reduce dark count, the PMT with a relatively smaller photocathode (typically 2.54 mm in diameter) should be used. If the laser light is in the blue and green range, PMTs with a bialkali photocathode is more adequate because it has a lower dark count at room temperature. The selected EMI 9893 PMT with a low dark count and a short after-pulsing has been popular for this purpose. The RCA C31034 PMT with a broad spectral response (300–800 nm) is good for the entire visible range, but it is more delicate and expensive. The silicon avalanche photodiode (SAP) is another new development and holds promise in making miniature light-scattering apparatuses. With a broad spectral response, SAPs are matched to diode lasers to simplify the LLS instrumentation, especially if it is combined with a fibre-optic probe, as recently demonstrated by ALV (Germany).

Figure 9 shows two commonly used configurations of the detection optics. In static LLS, the first pinhole (P1) can be replaced by a slit so that the alignment will be easier, but it has to be switched back to a pinhole for dynamic LLS, which makes simultaneous static and dynamic measurements impossible. In **A**-configuration, the scattering volume is mainly determined by the diameter (d_{P1}) of P1 (or the slit width). The first pinhole should be as close as possible to the cell, so that the scattering volume will be better defined. However, because of the existence of the cell holder and index matching cup, the first pinhole is normally 10–15 cm away from the scattering center. The second pinhole is located exactly on the focal plane of the lens and the opening angle of d_{P2}/f determines the uncertainty of the scattering angle ($\Delta\theta$). The coherent factor (β) in equation (6) is mainly determined by the opening angle of d_{P2}/L_0 but also influenced by d_{P1}. In this design, the alignment will be easier and the distance between the cell and the

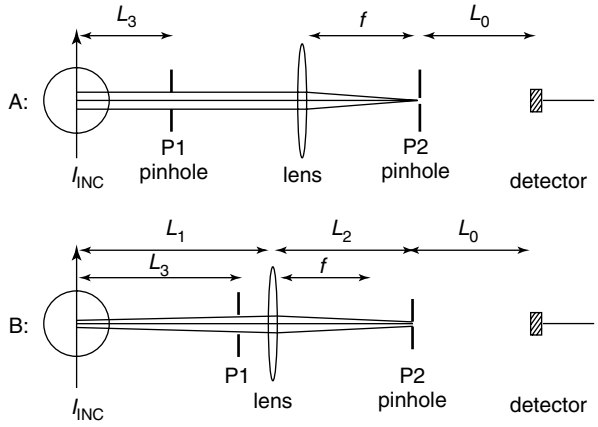

Fig. 9. Two commonly used configurations of the detection optics for both static and dynamic laser light scattering, where I_{INC} is the incident light and f the focal length.

detector could be smaller. In practice, $f \sim 10$ cm, $L_0 \sim 10$ cm, $d_{P1} \sim 200$–400 μm, and $d_{P2} \sim 100$–200 μm.

In **B**-configuration, L_1, L_2, and f are related by $1/L_1 + 1/L_2 = 1/f$, ie, the scattering center and the second pinhole are located exactly on the imagining planes of the lens. The scattering volume is precisely determined by d_{P2}. $\Delta\theta$ is determined by the opening angle of d_{P1}/L_3. Therefore, the first pinhole should be placed as close as possible to the lens, which has no difficulty in practice. If $L_1 = L_2 = 2f$, ie, the so-called $2f$–$2f$ configuration, the second pinhole is optically moved to the scattering center. β is still determined by the opening angle of d_{P2}/L_0. In this configuration, $f \sim 5$–10 cm, smaller than the previous one. For a given d_{P2}, the scattering volume can be enlarged by a factor of L_1/L_2 (normally, $L_1/L_2 \leq 3$) so that one can simultaneously have a stronger scattering intensity, a higher β, and a smaller $\Delta\theta$ for a given distance between the scattering center and the detector. However, the alignment is more difficult but manageable.

Sample Preparation. If a polymer can be dissolved in more than one solvent, the choice of solvent for LLS should be made generally according to the following guidelines: (*1*) colorless to avoid absorption; (*2*) a higher contrast, ie, a higher dn/dC; and (*3*) less polar and less viscous to make dust-free preparation easier. In practice, there may be no choice. For example, poly(1,4-phenyleneterephthalamide) (PPTA or Kevlar) is only soluble in very strong and viscous acids. In such a case, ultracentrifugation instead of filtration has to be used (16,66). As for a copolymer, the selection of proper solvents is even more difficult because at least two solvents that satisfy the three guidelines are needed. For this reason, only a few works related to copolymer characterization have been reported so far (67–70). As for polymers only soluble at high temperatures, the preparation of a polymer solution for LLS is a challenge. Finding a solvent with a high boiling point is often not easy, and dissolution and clarification at high temperatures are even more difficult. Two novel high temperature dissolution-and-filtration apparatuses have been developed (56,59).

Differential Refractometer. One of the most important parameters in static LLS is the specific refractive index increment (dn/dC), which is defined as $\lim_{C \Rightarrow 0}(dn/dC)_{T,P,\lambda}$. Equation (2) shows that an error of $E\%$ in dn/dC will lead to an error of $2E\%$ in M_w. The refractive index increment Δn of a polymer solution is usually measured using either a differential refractometer or an interferometer. In a differential refractometer, the light beam is refracted at the boundary between solution and solvent. Commonly, the beam displacement is directly measured and then converted to Δn after multiplying a calibration constant. The refractometer is normally calibrated by using a solution with an accurately known refractive index difference Δn (71,72). This is not an absolute method since the constant has to be calibrated at the same conditions as those used in LLS. In an interferometer, two light beams with identical geometrical paths passed two different optical paths. One passes through solution and the other passes through solvent. This method relies on the interference of the two beams. Its details can be found elsewhere (73,74). In a high temperature LLS measurement, the conventional divided differential refractometer cuvette has to be replaced by a deformed cylindrical light-scattering cell in which the laser beam is refracted by the solution/air interface (57).

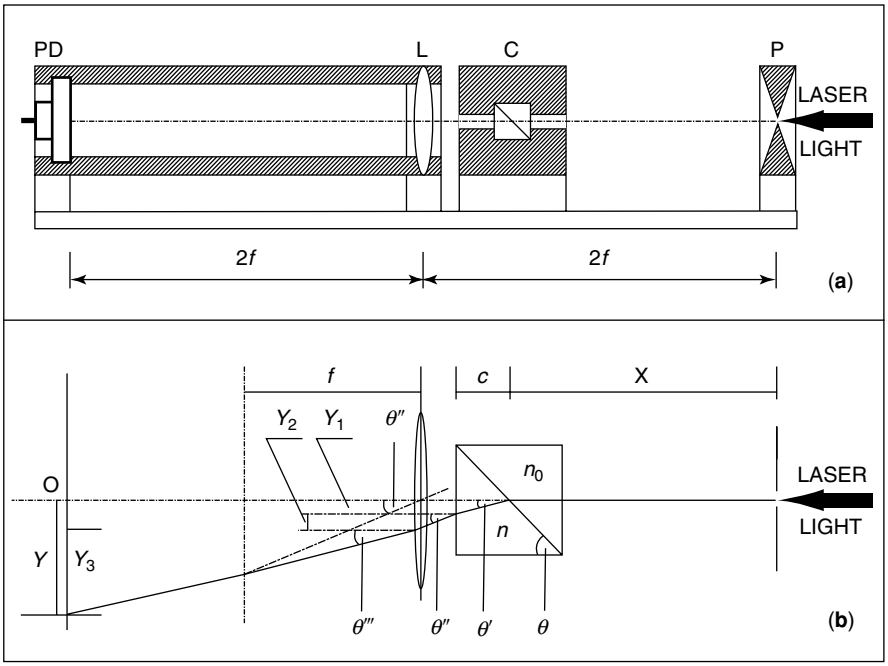

Fig. 10. **(a)** Schematic view of a novel differential refractometer (commercialized by ALV GmbH, Langen, Germany), which consists of a pinhole (P), a differential refractometer cuvette (C), a lens (L, $f = 10$ cm), and a position-sensitive detector (PD). All components are rigidly mounted on a 40-cm long optical rail. (**b**) Light path in which one compartment of the cuvette contains a solvent with refractive index n, and the other contains a solution with slightly different refractive index $n = n_0 + \Delta n$. The cuvette and angles θ', θ'' and θ''', (actually very small, $\sim$0.01 rad) are enlarged to make the light path distinct.

Figure 10 schematically shows a novel differential refractometer which was first designed by one of the authors (75) and later commercialized by ALV GmbH (Langen, Germany). A small pinhole (P) with a diameter of 200–400 μm is illuminated with a laser light. The illuminated pinhole is imaged to a position-sensitive detector (PD) (Hamamatsu S 3932) by a lens (L) located at an equal distance from the pinhole and the detector. The focal length (f) of the lens is 100 mm. This refractometer adopted a ($2f$–$2f$) design. Note that in a conventional ($1f$) design, a parallel incident light beam is used and the distance between the detector and the lens is only one focal length. The conventional design cannot solve the beam drift problem associated with a laser. A temperature-controlled refractometer cuvette (C) (Hellma 590.049-QS) is placed just in front of the lens. It is a flow cell divided into two compartments with a volume of $\sim$20 μL. All the components are rigidly mounted on a small optical rail. The refractometer has dimensions of only 40 cm in length, 15 cm in width and 10 cm in height. The length can be easily reduced to 20 cm with another lens if necessary. The output voltage (-10 to 10 V) from the position-sensitive detector is proportional to the displacement of the light spot from the center of the detector and can be measured by a digital voltmeter or an analogue-to-digital data acquisition system and a personal computer. Figure 10b

shows the basic principle and the light path of the refractometer, where θ', θ'', θ''', and the cuvette are drawn enlarged to make the details clear. It can be shown that $Y = K\Delta n$, where $K = [X + c''(1 - 1/n_0)] \tan(90^\circ - \theta)$. For a given optical setup and solvent, X, c, θ, n_0, and hence K are constants. Therefore, the signal is proportional to Δn. This ($2f$–$2f$) design is optically equivalent to placing the detector directly behind the pinhole, so that the beam drift problem is solved. The refractometer with its present dimensions can be easily installed into any existing laser light-scattering spectrometer (75).

BIBLIOGRAPHY

"Scattering" in *EPST* 1st ed., Vol. 12, pp. 355–397, by J. L. Lundberg, I. R. Hardin, and M. K. Tomioka, Clemson University; "Scattering" in *EPSE* 2nd ed., Vol. 15, pp. 1–68, by B. Gabrys and P. E. Tomlins, National Physical Laboratory; "Light Scattering" in *EPSE* 2nd ed., Vol. 8, pp. 721–794, by G. C. Berry, Carnegie-Mellon University.

1. B. Chu, *Laser Light Scattering*, 2nd ed., Academic Press, Inc., New York, 1991.
2. M. B. Huglin, *Light Scattering from Polymer Solution*, Academic Press, Inc., New York, 1972. Also, *Topics in Current Chemistry* **73**, 141 (1977).
3. O. Glatter and O. Kratky, *Small-angle X-ray Scattering*, Academic Press, Inc., New York, 1982.
4. S. B. Dubin, N. A. Clark, and G. B. Benedek, *J. Chem. Phys.* **54**, 5158 (1971).
5. G. D. Patterson, *Methods of Experimental Physics*, Vol. **16A**, Academic Press, Inc., New York, 1980, pp. 170–204.
6. B. J. Berne and R. Pecora, *Dynamic Light Scattering*, John Wiley & Sons, Inc., New York, 1976.
7. B. H. Zimm, *J. Chem. Phys.* **16**, 1093 (1948).
8. S. Chandrasekkar, *Rev. Mod. Phys.* **15**, 1 (1943).
9. P. Munk, *Introduction to Macromolecular Science*, John Wiley & Sons, Inc., New York, 1989, p. 255.
10. P. Debye, *J. Phys. Coll. Chem.* **51**, 18 (1947).
11. B. H. Zimm, *J. Chem. Phys.* **16**, 1100 (1948).
12. A. C. W. Lau and C. Wu, *Macromolecules* **32**, 581 (1999).
13. P. S. Russo, in W. Brown, ed., *Dynamic Light Scattering*, Chapter. "12", Oxford University Press, New York, 1993.
14. B. Chu, Q. Ying, C. Wu, and J. Ford, *Polym. Commun.* **25**, 211 (1984).
15. B. Chu, Q. Ying, and C. Wu, *Polymer* **26**, 1408 (1985).
16. Q. Ying and B. Chu, *Die Makromol. Chem., Rapid Commun.* **5**, 785 (1984).
17. S. T. Sun, I. Nishio, G. Swislow, and T. Tanaka, *J. Chem. Phys.* **73**, 5971 (1980).
18. W. H. Stockmayer and M. Schmidt, *Macromolecules* **17**, 509 (1984).
19. C. Wu, S. Q. Zhou, and W. Wang, *Biopolymer* **35**, 385 (1995).
20. D. E. Koppel, *J. Chem. Phys.* **57**, 4814 (1972).
21. A. K. Livesey, P. Licinio, and M. Delaye, *J. Chem. Phys.* **84**, 5102 (1986).
22. J. G. McWhirter and E. R. Pike, *J. Phys. A* **11**, 1729 (1978).
23. B. Chu, J. R. Ford, and H. S. Dhadwal, *Methods Enzymol.* **117**, 256 (1983).
24. B. Chu, C. Wu, and J. R. Ford, *J. Colloid Interface Sci.* **105**, 473 (1985).
25. J. Raczek, *Eur. Polym. J.* **19**, 607 (1983).
26. E. Nordmeier and M. D. Lechner, *Polym. J.* **21**, 623 (1989).
27. S. W. Provencher, *J. Chem. Phys.* **64**, 2772 (1976).
28. A. Perico, P. Piaggio, and C. Cuniberti, *J. Chem. Phys.* **62**, 2690 (1975).

29. C. Wu, K. K. Chan, and K. Q. Xia, *Macromolecules* **28**, 1032 (1995).
30. E. Q. Schulz-DuBois, ed., in *Proceedings of the 5th International Conference on Photon Correlation Techniques in Fluid Mechanics*, Springer-Verlag, New York, 1983.
31. B. E. Dahneke, ed., *Measurements of Suspended Particles by Quasi-elastic Light Scattering*, John Wiley & Sons, Inc., New York, 1983.
32. G. Gouesbet and G. Grehan, *Optical Particle Sizing*, Plenum Press, New York, 1988.
33. P. G. de Gennes, *Scaling Concepts in Polymer Physics*, Cornell University Press, Ithaca, N.Y., 1979.
34. B. Appelt and G. Meyerhoff, *Macromolecules* **13**, 657 (1980).
35. C. Wu and co-workers, *Acta Polymerica Sinica* **3**, 349 (1995).
36. P. J. Flory, *Principles of Polymer Chemistry*, Cornell University Press, Ithaca, N.Y., 1953.
37. B. Chu, M. Onclin, and J. R. Ford, *J. Phys. Chem.* **88**, 6566 (1984).
38. J. Pope and B. Chu, *Macromolecules* **17**, 2633 (1984).
39. A. Cervenka, *Makromol. Chem.* **170**, 239 (1973).
40. C. Wu, *Macromolecules* **26**, 5423 (1993).
41. C. Wu, *J. Polym. Sci., Polym. Phys. Ed.* **32**, 803 (1994).
42. C. Wu, *Adv. Polym. Sci.* **137**, 103 (1998).
43. C. Wu and co-workers, *J. Appl. Polym. Sci.* **53**, 1323 (1994).
44. C. Wu and co-workers, *Macromolecules* **27**, 6055 (1994).
45. C. Wu, M. Siddiq, and K. F. Woo, *Macromolecules* **28**, 4914 (1995).
46. C. Wu, M. Siddiq, and S. Q. Bo, *Macromolecules* **29**, 2989, 3157 (1996).
47. M. Li, M. Jiang, and C. Wu, *Macromolecules* **30**, 2201 (1997).
48. C. Wu, *Macromolecules* **27**, 7099 (1994).
49. C. Wu, M. Chen, and M. Akashi, *Macromolecules* **30**, 2187 (1997).
50. J. Gao, S. Q. Zhou, and C. Wu, *Polym. Eng. Sci.* **36**, 2968 (1996).
51. C. Wu and K. K. Chan, *J. Polym. Sci. Polym. Phys. Ed.* **33**, 919 (1994).
52. C. Wu, R. Y. Qian, D. H. Napper, *Macromolecules* **28**, 1592 (1994).
53. C. Wu, R. Y. Qian, and D. H. Napper, *Macromolecules* **28**, 1592 (1995).
54. R. Foord and co-workers, *Nature* **277**, 242 (1970).
55. B. Chu, R. Xu, T. Maeda, H. S. Dhadwal, *Rev. Sci. Instrum.* **59**, 716 (1988).
56. C. Wu, W. Buck, and B. Chu, *Macromolecules* **20**, 98 (1987).
57. B. Chu and C. Wu, *Macromolecules* **20**, 93 (1987).
58. B. Chu, C. Wu, and J. Zuo, *Macromolecules* **20**, 700 (1987).
59. B. Chu, C. Wu, and W. Buck, *Macromolecules* **21**, 397 (1988).
60. B. Chu, C. Wu, and W. Buck, *Macromolecules* **22**, 831 (1989).
61. C. Wu, *Makromol. Chem., Makromol. Symp.* **61**, 377 (1992).
62. R. G. Brown, *Appl. Opt.* **26**, 4846 (1987).
63. R. G. Brown and A. P. Jackson, *J. Phys. E* **20**, 1503.
64. H. S. Dhadwal and B. Chu, *Rev. Sci. Instrum.* **60**, 845 (1989).
65. H. S. Dhadwal, C. Wu, B. Chu, *Applied Optics* **28**, 4199 (1989).
66. B. Chu, C. Wu, J. Ford, *J. Colloid Interface Sci.* **105**, 473 (1985).
67. W. Bushuk and H. Benoit, *Can. J. Chem.* **36**, 1616 (1958).
68. B. Chu and co-workers, *Macromolecules* **18**, 1962 (1985).
69. W. H. Stockmayer and co-workers, *J. Polym. Sci.* **16**, 517 (1955).
70. C. Wu and co-workers, *Macromolecules* **27**, 6055 (1994).
71. M. Obasa and co-workers, *Polym. J.* **25**, 301 (1993).
72. *Application Notes LS7, Chromatix, Mountain View, Calif.*, 1985.
73. I. Baltog, C. Ghita, and L. Ghita, *Eur. Polym. J.* **6**, 1299 (1970).

74. *Application Notes Optilab 903, Wyatt Technology, Santa Barbara, Calif.*, 1992.
75. C. Wu and K. Q Xia, *Rev. Sci. Instrum.* **65**, 587 (1994).

CHI WU
University of Science and Technology of China
The Chinese University of Hong Kong
AIZHEN NIU
Nankai University

LDPE. See ETHYLENE POLYMERS, LDPE.

LIGHT-EMITTING DIODES

Introduction

The role of polymers in light-emitting diodes (LEDs) traditionally has been associated with the use as a structural material. Epoxy resins are routinely applied as the transparent "packaging material" in conventional LEDs in which light is generated at the junction of two *inorganic* semiconductors. The polymer provides the structural integrity of the device and serves as the optical medium that enables the extraction of light (1). During the last decade, however, LEDs have been developed in which the semiconducting, electroluminescent (EL) material itself is a polymer. These devices are usually referred to as polymer LEDs or PLEDs and have attracted significant attention in both academic and industrial environment. The principal interest in the use of EL polymers is based on their promise to combine the ease of processability and mechanical flexibility of macromolecular materials with the exceptional, readily-tailored properties of organic semiconductors. PLEDs offer the prospective of low production costs, light weight, large area, fast switching times, low power consumption, high brightness, large viewing angle, and crisp colors. Thus, the new technology may feature distinct advantages over existing flat-panel display devices such as conventional emissive displays, inorganic LEDs, and liquid crystal displays (LCDs). As a result, the list of potential applications of PLEDs ranges from small, low information-content displays for simple electronic devices such as pagers and portable phones to high resolution video-rate displays for use in desktop monitors and ultrathin television sets. In addition, PLEDs may be employed as flat lighting devices, for example in automotive rear lights or as backlights in LCDs.

Since the first demonstration of a PLED in 1990 (2), the field has progressed with an almost unbelievable pace, and the technology has matured to the edge

Encyclopedia of Polymer Science and Technology. Copyright John Wiley & Sons, Inc. All rights reserved.

of commercial exploitation (3). In view of the over 5000 publications on PLEDs published to date, it is clearly outside the scope of this article to review this exciting progess in detail. Rather, a comprehensive overview focusing on the general concepts, as well as the current state-of-the-art, is given. For a more detailed description regarding the chemical, physical, and engineering aspects of PLEDs, the reader is referred to a selection of excellent reviews which have appeared in the recent past (4–11). It should be noted that the discussion of LEDs based on low molecular weight organic emitters has been omitted here for apparent reasons. However, the latter share many of the features of PLEDs (12,13), and despite the more demanding device manufacturing processes of low molecular weight organic LEDs, their technological application is slightly more advanced than that of PLEDs (3–5,9).

Device Physics and Device Design Considerations

An LED is an electrooptical device that exploits the EL effect of a fluorescent, semiconducting material and emits electromagnetic radiation in the ultraviolet, visible, or infrared regime of the electromagnetic spectrum when an electric current is applied (1) (see LEDs (Light Emitting Diodes)). Conventional LEDs, commercially introduced in the 1960s, are based on inorganic semiconductors such as GaAs, GaP, AlGaAs, GaAsP, and InGaP. Electroluminescence in organic materials was originally discovered in the early 1960s (14), but useful devices were demonstrated only some 20 years later (12,13). Electric-field-induced light emission from a fluorescent, semiconducting polymer was first observed in 1990, when an electrical field was applied to a thin film of poly(*p*-phenylene vinylene) (PPV) (2).

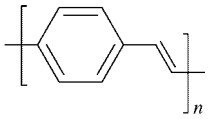

PPV

The LED reported then materialized the most simple device configuration of a PLED which, in accordance with the number of organic layers used, is usually referred to as a single-layer device (Fig. 1). The semiconducting polymer film (typical thickness 50–500 nm) is sandwiched between two electrodes, of which at least one has to be (semi)transparent in order to allow the generated light to escape from the device. Adopting a standard Schottky-configuration, a high work function anode such as semitransparent indium tin oxide (ITO) and a low work function cathode such as Al, Mg or Ca are employed, leading to nonlinear rectification and, thus, rendering the device into a diode. If an external voltage, or bias, is applied, oppositely charged carriers—holes and electrons—are injected above a threshold voltage from the electrodes into the conduction band (CB) and the valence band (VB), respectively, of the semiconducting polymer (Fig. 2). These electronic levels correspond to the electron affinity (EA) and ionization potential (IP) of the polymer. Because of the applied electric field (typically of the order

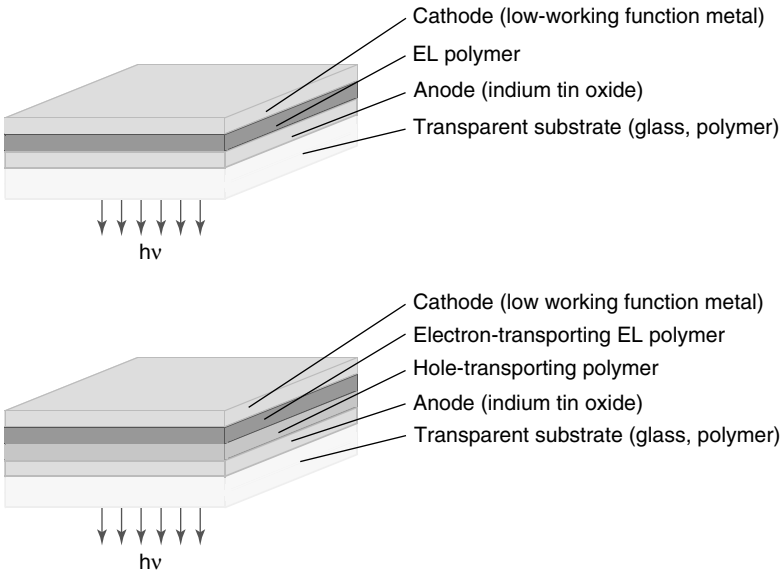

Fig. 1. Schematic drawings of the configurations of a single-layer PLED (top) and a two-layer PLED (bottom).

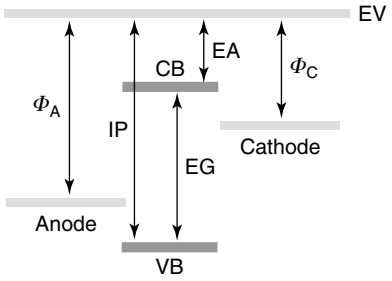

Fig. 2. Simplified schematic representation of the electronic energy levels in a single-layer PLED. CB and VB are the conduction band and valence band, respectively, of the semiconducting polymer, which equal to the ionization potential (IP) and electron affinity (EA) relative to vacuum level (EV). The work functions (or Fermi levels) for anode (Φ_A) and cathode (Φ_C) and the band gap (EG) are also indicated.

of 10^6 V/cm, corresponding to an operating voltage of a few volts), these carriers travel through the polymer toward the oppositely charged electrode. On their way, the charge carriers will either recombine within the emitting polymer layer with an opposite charge and form singlet and triplet excited states (excitons), or they reach the opposite electrode and discharge without having contributed to the EL effect. The singlet excited states created through charge-recombination are identical with those generated through photoexcitation, and, as in the case of fluorescence, they relax to the electronic ground state under the emission of light. The color of the latter is governed by the energy difference between the singlet excited state and the electronic ground state, also referred to as the band

gap (EG) of the EL polymer. The triplet excited states, by contrast, decay through nonradiative processes.

The theoretical internal quantum efficiency of a PLED, η_{int}, is defined as the number of photons generated per injected electron:

$$\eta_{\text{int}} = \eta_{\text{PL}} \eta_r \chi \tag{1}$$

η_{int} is primarily governed by the (solid-state) fluorescence quantum efficiency of the polymer, η_{PL}, which can exceed 65% (15), the fraction of injected charge carriers that form excited states, η_{r}, and the fraction of singlet excited states created (as opposed to triplets), χ. Unfortunately, spin statistics dictate a χ of only 1/4, although recent work suggests that this limitation can, in principle, be overcome (16). To make things worse, internal reflection effects, which are governed by the device's geometry and the refractive index of the light-emitting polymer (n), allow only a fraction of the generated light to be extracted from the device. Thus, in a typical device configuration, the external quantum efficiency of a PLED, η_{ext}, is lower than η_{int} by a factor of $2n^2$ (17):

$$\eta_{\text{ext}} = \eta_{\text{int}} / 2n^2 \tag{2}$$

Approximating the refractive index of the EL polymer with a value of 1.4 allows to put up an upper limit of about 5% for η_{ext}, which still compares favorably with the typical performance of conventional inorganic LEDs (0.2–8%) (1). It should be noted that special geometries may be used to improve the light extraction from the device (18). For engineering purposes, it is often desirable to express the performance of an LED through its power efficiency η_{pow}:

$$\eta_{\text{pow}} = \eta_{\text{ext}} E / U \tag{3}$$

η_{pow} is the optical power output divided by the electrical power input, and is calculated from η_{ext} using the applied voltage U and the average energy E of the emitted photons. Since the human eye is usually the detector for visible LEDs, the key performance parameter of an LED is the luminous efficiency η_{lum} (units: lm/W) which is a product of η_{ext} and the relative eye sensitivity curve S which has been defined by the Commission Internationale de L'Eclairage, CIE):

$$\eta_{\text{lum}} = \eta_{\text{ext}} S \tag{4}$$

Reference values that are frequently used to evaluate the performance of PLEDs are the luminous efficiencies of conventional inorganic LEDs (0.15–20 lm/W) or unfiltered incandescent lamps (17 lm/W) (1). Finally, the absolute brightness of an LED, or luminance (usually quoted in cd/m^2), and luminance per current density (cd/A) are also frequently used parameters to describe the performance of LEDs. Here, the brightness of a laptop computer (200 cd/m^2) or of a TV cathode ray tube (500 cd/m^2) are often employed as benchmarks (19).

As can be deduced from equation (1), the optimizations of charge-injection and charge-transport (both of which directly influence the fraction of injected charge carriers that form excited states, η_{r}) are important aspects for the design

of efficient PLEDs. In order to allow for efficient charge-injection and, concomitantly, low operating voltages, the work functions of cathode and anode should match the EA and IP (or in semiconductor terminology, conduction band and valence band) of the semiconducting emitter, respectively, as closely as possible. Unequal barrier heights at the two electrode–polymer junctions are undesirable because one carrier will be injected preferentially, leading to an increased driving voltage and a reduced luminous efficiency. At the other hand, most organic semiconductors are *p*-type conductors, allowing holes to be transported more efficiently than electrons. Consequently, substantial research efforts have been made regarding the identification of optimal electrode–polymer combinations. A general possibility, of course, is the chemical modification of the emitting polymer, with the intent to tailor—besides the color-determining band gap—its EA, IP, and/or charge-transport characteristics. Another strategy is the design of two-layer (or even three-layer) devices in which, for example, a hole-transporting polymer and an electron-transporting, light-emitting polymer are combined (7). The resulting heterojunction between the two semiconducting polymers allows to control the charge-injection rates and helps to confine the charge recombination to the emitting layer (Fig. 1). In addition, this architecture effectively reduces problems associated with the migration of oxygen and metal ions from the electrodes into the organic layer and the related creation of quenching sites in the emission zone. Consequently, the two-layer architecture has become the preferred PLED embodiment.

Materials

The design of PLEDs relies on a variety of different materials, including a transparent substrate, the (semi)transparent anode, a hole-transporting layer in case of the usual two-layer structure, the EL polymer itself, an additional electron-conducting/hole-blocking layer in case of a three-layer device, the cathode, and finally some additional packaging material(s).

Polymeric materials such as polyester-based films have initially been heralded as desirable substrates because of the unique potential to create mechanically flexible displays (20). However, moisture and oxygen have to be rigorously excluded from the device so as to prevent rapid degradation of the EL polymer and the cathode. Thus, in view of the notoriously poor barrier characteristics of polymeric substrates, glass is the current substrate and packaging material of choice because of its unmatched barrier characteristics. Nevertheless, recent studies have shown that the barrier characteristics of polymeric substrates can greatly be improved by applying a coating of silicon nitride or silicon oxynitride through a vapor deposition process (21).

Essentially all PLED devices described in the literature rely on ITO as the high work function anode material, although a number of alternative transparent conducting oxides have become available (22). ITO offers good electrical conductivity and a transmittance of $>85\%$ at a film thickness of <150 nm, and allows the generated light to escape from the device. ITO-coated glass is routinely used as the electrode material in LCDs and a variety of other applications and is readily available at comparably low cost. Most importantly, ITO offers a work function

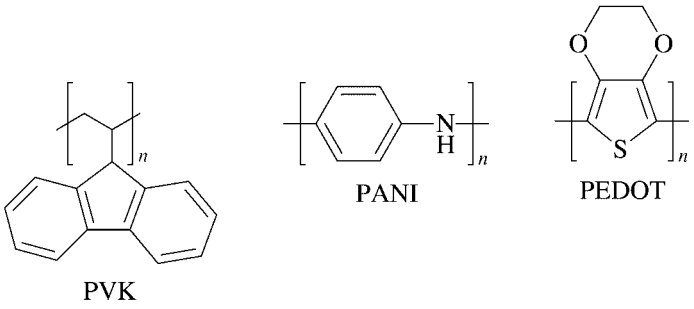

Fig. 3. Chemical structures of poly(vinylcarbazole) (PVK), poly(aniline) (PANI), and poly(3,4-ethylene dioxy thiophene) (PEDOT) which are frequently used as the hole-transport layer in two-layer devices.

of between 4.5 and 5.0 eV (relative to vacuum level), which matches the IP of frequently used conjugated organic polymers and allows for reasonably efficient hole-injection. Unfortunately, the electronic characteristics of ITO depend quite strongly on the manufacturing conditions and cleaning treatments. In addition, its surface structure can vary substantially, making the use of ITO often rather cumbersome.

As mentioned before, the two-layer architecture has become the preferred PLED embodiment (Fig. 1), thus requiring a first polymer layer with efficient hole-transport characteristics (6). Poly(vinylcarbazole) (PVK) is an extensively investigated, commercially available hole-conductor, which has been frequently used in this context (Fig. 3). Alternatively, polymeric triphenyldiamines have been employed (23). More recently, poly(aniline) (PANI) and poly(3,4-ethylene dioxy thiophene) (PEDOT) which are commercially available from Ormecon and Panipol Ltd. and Bayer AG, respectively, have found widespread application instead (4,10). Used in their electrically conducting form, these polymers not only allow efficient hole-injection and hole-transport, but also offer an effective electron transport. As a result, the electric field across this layer is dramatically reduced, limiting the undesired migration of charged species from the anode through the device (see LEDs (Light Emitting Diodes)).

Light generation is achieved in the actual light-emitting layer which, in a typical two-layer configuration, usually also acts as an electron-transport material; the design considerations for EL polymers are discussed in detail below, together with an overview of typical material systems.

Finally, a low work function cathode is required for electron-injection. A variety of different cathode materials have been employed, including Ca, Li, Mg, Al, Cr, or alloys of these metals, sometimes also combined with Ag. Since electron-injection is often a limiting factor for the device efficiency, the metal with the lowest work function of the above series (Ca, 2.9 eV) is a preferred option. However, while Ca-based devices may work well in the laboratory, the practical application of this metal is stifled by its sensitivity toward oxidation. Changing the cathode material to Mg (work function 3.7 eV) or Al (4.3 eV) leads to improved device stability, however, usually at the expense of an increase in driving voltage and a reduced device efficiency.

Development of EL Polymer Systems. The characteristics of the emissive layer are, of course, of predominant importance for optimum device performance. Thus, the design of light-emitting polymers has received particular attention during the last decade. In view of the abundance of EL polymers that have been synthesized and investigated to date (4–11), it is far beyond the scope of this review to provide a comprehensive overview. Consequently, a number of selected examples are presented which illustrate the various design concepts, are based on the most commonly employed building blocks, and are relevant from an application point of view. Important design considerations address the need for

(1) high intrinsic photoluminescence efficiency
(2) high purity (elimination of traps which provide nonemissive decay paths for excitons)
(3) adequate charge-transport characteristics (low barrier for charge-injection, reversible formation of charge carriers, balanced charge transport)
(4) appropriate color of emitted light
(5) high optical transparency (no re-absorption or scattering of the emitted light)
(6) good processability
(7) high film quality (homogeneous thickness of typically 50–500 nm, no pinholes or cracks, smooth surface, compatibility to adjacent layers)
(8) high thermomechanical stability (no softening under operating conditions)
(9) long lifetime (high thermal, light, oxidative, and environmental stability)
(10) low price

This list of fundamental requirements has indeed been a veritable challenge for materials design in terms of synthesis, understanding of structure–property relationships, and processing. The majority of the vast number of polymeric EL materials investigated to date origins from the family of conjugated polymers, ie, macromolecules featuring an extended π-conjugated backbone (Figs. 4a and b). Important examples of classes of conjugated polymers used as emitting layer in PLEDs (Fig. 5) include poly(arylene)s, poly(arylene vinylene)s, and, to some extent, also poly(arylene ethynylene)s (24). Unfortunately, the very same conjugation which renders these macromolecules semiconducting is also the origin of the difficulties that were initially encountered in attempts to process the early, more simple forms of these polymers into useful shapes, ie, high quality films. These difficulties are directly related to the fact that conjugated polymers are relatively rigid macromolecules which exhibit high melting enthalpies and low melting entropies, resulting in melting temperatures that are typically far beyond thermal decomposition. In addition, the nonpolar chemical nature of many conjugated polymers permits only modest enthalpic interactions with potential solvents, which prevents simple solution-processing. These problems have been overcome by a number of different design strategies which, naturally, follow those already successfully applied for nonconjugated rigid-rod polymers (25). The latter include (*1*) the use of so-called precursor routes; (*2*) the derivatization of π-conjugated polymers with flexible (or alternatively bulky) side chains which increase the entropy

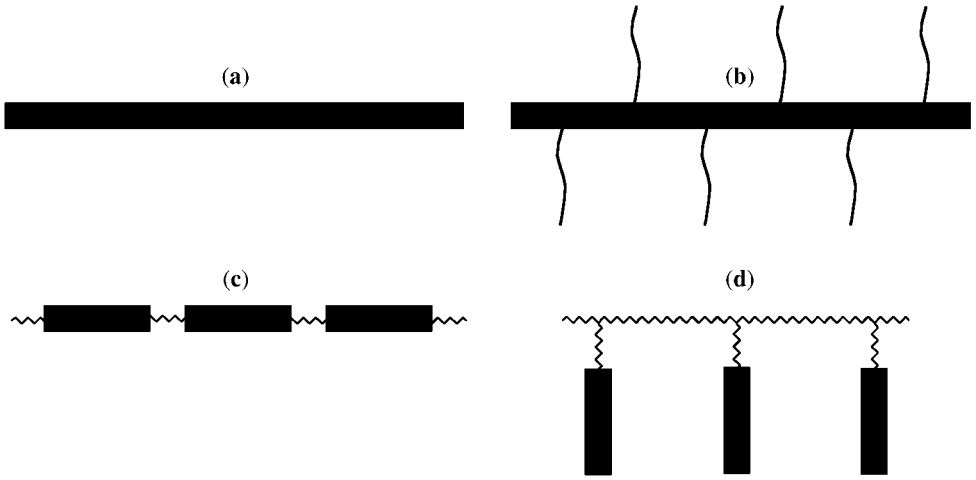

Fig. 4. Schematic representation of typical EL polymer architectures. (**a**) "Plain," conjugated main chain, (**b**) hairy-rod structure, (**c**) semiflexible, "segmented" structure, and (**d**) nonconjugated polymer with conjugated side chains. ▬, π-conjugated moiety; ∿∿, flexible segment; and —, solubilizing side chain.

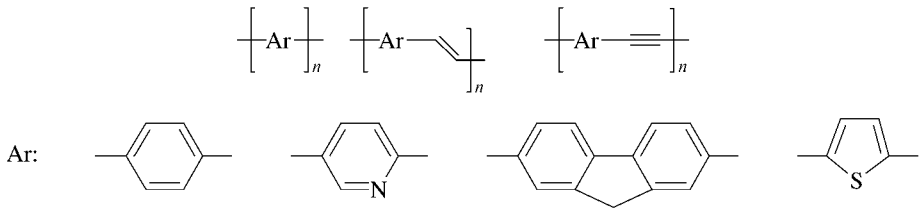

Fig. 5. Chemical structures (generalized) of different classes of conjugated polymers used as EL materials.

gain upon dissolution (and also reduce interchain interactions) and, thus, render the polymer soluble (Fig. 4b); (*3*) the introduction of flexible "spacer" units between the conjugated moieties which reduce the overall rigidity of the polymer backbone, again leading to improved solubility (Fig. 4c); and (*4*) the use of nonconjugated, processable polymers which feature the conjugated moieties in the form of side chains (Fig. 4d) *or* (*5*) as guest molecules which are not covalently connected to the matrix polymer but are rather dissolved or dispersed in the latter.

The so-called precursor route represents a particularly attractive way to synthesize and process underivatized π-conjugated polymers which were initially employed in many of the early studies on PLEDs, including PPVs and poly(*p*-phenylene)s (PPPs) (26,27). The concept relies on the three steps of synthesizing tractable, nonconjugated "precursor" macromolecules comprising appropriately selected leaving groups, processing of these precursor polymers according to standard (mostly solution-based) techniques, and converting the precursor

polymer into the final (intractable) conjugated species by (usually heat-induced) abstraction of the leaving group. A classical example is the synthesis of yellow-green-light-emitting PPV (see structure above) (28), which has been used and optimized by a variety of research groups (26,29). A special version of the precursor route that has received considerable attention in connection with the preparation of PPV-based LEDs makes use of a chemical vapor deposition (CVD) process (8,26). Here, the starting material is vaporized under high vacuum conditions and pyrolized to result in suitable monomers, which subsequently undergo CVD and polymerization on a substrate. This solvent-free process usually results in high quality films of a precursor-PPV, which can be subsequently converted to the conjugated form. However, all precursor methods suffer from major difficulties in that (*1*) the conversion from precursor to π-conjugated polymer is often not quantitative (leading to defects which may interrupt the conjugation in the polymer backbone), (*2*) the removal of low molecular weight conversion products (which may adversely affect some of the polymer's properties) is not trivial, (*3*) the precursor polymers often exhibit a limited oxidative stability, and (*4*) generally undesirable side reactions may occur. On the other hand, the process also allows to tune the material properties to a certain extent. For example, partial conversion of precursor/π-conjugated polymer results in segmented polymers (Fig. 4c) with improved performance and modified color of the emitted light, as described below.

A different approach is the design of inherently soluble, "hairy-rod" EL polymers according to the design strategy outlined in Fig. 4b. The latter allows film processing by standard solvent-based methods, eg, spin- and dip-coating, screen- and ink-jet printing, as well as Langmuir Blodgett (LB) techniques. The electronic properties of these macromolecules are primarily governed by the chemical structure of the conjugated polymer backbone itself, but a number of additional tools can be employed to further manipulate band gap (emission color), charge-injection/charge-transport characteristics, thermomechanical stability, thermal/oxidative stability, and other relevant properties (4,6,8,11). The incorporation of electron-deficient aromatic rings and the integration of electron-withdrawing or electron-donating substituents into the conjugated system are illustrative examples of how the electronic characteristics can be varied over a wide range. Another important general tool for property tailoring is the control of the effective conjugation length through the introduction of side chains which exhibit steric interactions and force the backbone to twist, or by using copolymers that comprise well-defined conjugated segments that are separated by aliphatic "spacer" moieties (Fig. 4c). Such segmented conjugated polymers (Fig. 4c), nonconjugated polymers with conjugated side chains (Fig. 4d), and also blends of nonconjugated matrix polymers and low molecular weight EL compounds (in which the crystallization-induced segregation of the EL guest molecules and the polymeric matrix poses a serious problem) were reviewed extensively in the literature (4,6,8,11,26). The nonconjugated spacer moieties disrupt the electronic conjugation, concomitant with a shift of the band gap toward higher energies, ie, into the blue regime of the visible spectrum, which with extended conjugated structures has proven to be difficult to access. Moreover, confinement of excitons is achieved by stifling the migration of the latter to quenching sites, which usually leads to

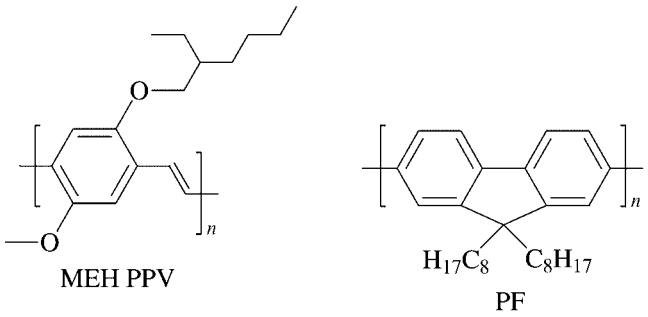

Fig. 6. Chemical structures of poly[2-methoxy-5-(2′-ethylhexyloxy)-*p*-phenylene vinylene] (MEH PPV) and poly(9,9-dioctyloxy fluorene).

an appreciable enhancement of luminescence efficiency. However, as mentioned heretofore, the nonconjugated moieties disrupt the electronic conjugation, suggesting intrinsic limitations with respect to charge transport (it should be noted in this context that also polymers with a fully conjugated backbone structure feature only a finite effective conjugation length which in case of PPV, for example, extends over less than 10 repeat units, cf Ref. 8).

From the multitude of organo-soluble conjugated EL materials investigated to date, two classes of materials seem to have shown the most promising overall matrix of properties, at least from an industrial point of view, namely derivatized PPVs and poly(fluorene)s. The most widely studied soluble PPV derivative is the orange-light-emitting poly[2-methoxy-5-(2′-ethylhexyloxy)-*p*-phenylene vinylene] (MEH PPV) which was introduced in 1991 (30). It was the first soluble light-emitting material to be used in a PLED (Fig. 6) (31). The alkyloxyy substituents not only render the polymer soluble but also shift the EL emission to higher wavelengths when compared to the parent PPV. A wide variety of poly(2,5-dialkoxy-*p*-phenylene vinylene)s and other 2,5-derivatized PPVs have since been investigated (4,6), and a few PPV derivatives, including a phenyl-substituted-PPV, have been developed for commercial exploitation for example by Covion and are used in the pilot production of Philips Electronics and Uniax Corp. (32). Besides the PPVs, poly(9,9-dialkyl fluorene)s (Fig. 6) have recently emerged as an extremely promising class of polymeric light-emitting materials (10), and a series of poly(fluorene) homo- and copolymers have been developed by the Dow Chemical Co. (32).

Towards Technological Exploitation

Only a decade after the first demonstration of electroluminescence in polymeric materials, the performance of PLEDs now appears to meet many of the requirements for applications at the low performance end of the display market, and the field has matured to the point of commercial exploitation; the most current overview of the state-of-the-art can be found in an outstanding review (4). A number of electronics and polymer companies, including Cambridge Display Technology Ltd., Covion, Dow Chemical Co., Philips Electronics, and Uniax Corp., have

disclosed prototypes or pilot products that offer a luminous efficiency η_{lum} between 10 and 22 lm/W at an (average) brightness between 100 and 1000 cd/m^2 (4,10,32). Thus, these devices clearly meet the brightness requirements for many display applications and also match the efficiency of conventional inorganic LEDs incandescent lamps. However, it should be noted that bright and efficient devices are primarily available in the green range of the emission spectrum, while presently available blue- and red-light-emitting materials result in devices which are substantially less bright and efficient (4,7). Thus, substantial progress regarding the availability of different colors is required before full-color devices based on red, green, and blue pixels can be made available.

Probably, one of the most critical aspects from an application point of view is that of device lifetime. Although the requirements for the latter strongly depend of the particular application, operating lifetimes of >10,000 h are usually targeted (4,5), often at elevated temperatures. Detailed studies conducted at a variety of laboratories (4,10) have indeed demonstrated that this requirement can, in principle, be met when adequately packaging the device. However, most of the "successful" lifetime studies were conducted under constant current conditions, and a gradual rise of the driving voltage was reported to maintain the initial current and brightness. This situation not only suggests an irreversible degradation of the device but also presents a challenge for the electronic device drivers.

The most basic device architecture of PLEDs has been described above; most technical applications rely on much more sophisticated designs. For example, almost every display application will demand arrays of many individually addressable pixels, similar to conventional LCDs (Fig. 7). Pixilated PLEDs rely on the creation of a "grid" of intersecting anode and cathode rows, which is usually generated by photolithographic patterning of the ITO anode into columns and vapor deposition of the cathode rows through a corresponding mask. As it is well known for LCDs (33), the devices can be operated in either passive- or active-matrix mode. Passive-matrix addressing relies on the consecutive addressing of the rows (typically within a period of 1/30 s or less) and on applying a simultaneous bias to the columns holding active pixels. Where an active row and column intersect, the electric field directly causes EL emission. This format, which is usually used for low resolution applications, requires high scanning rates in order to avoid flickering of the image. Moreover, because each pixel is active only for a short fraction of the cycle, it will require to generate very high intensity (ie, >10,000 cd/m^2) under a high current density during its "on" state in order to produce an acceptable average luminance. The active matrix architecture moderates the need to cycle at high rates by giving every pixel a "memory" in the form of a capacitor and a transistor. While this architecture seems mandatory for high resolution and large-area displays, it adds, of course, another layer of complexity to the device.

Another step toward high end application is, of course, the creation of multicolor devices, featuring red, green, and blue pixels. A variety of approaches have been suggested to achieve the latter, including (*1*) the use of uv or blue LEDs and external color conversion through green and red-light-emitting fluorescent dyes applied to the appropriate pixels, (*2*) the use of white LEDs in combination with conventional absorbing color filters, (*3*) the stacking of individual, independent device segments in vertical fashion, and (*4*) the use of advanced deposition

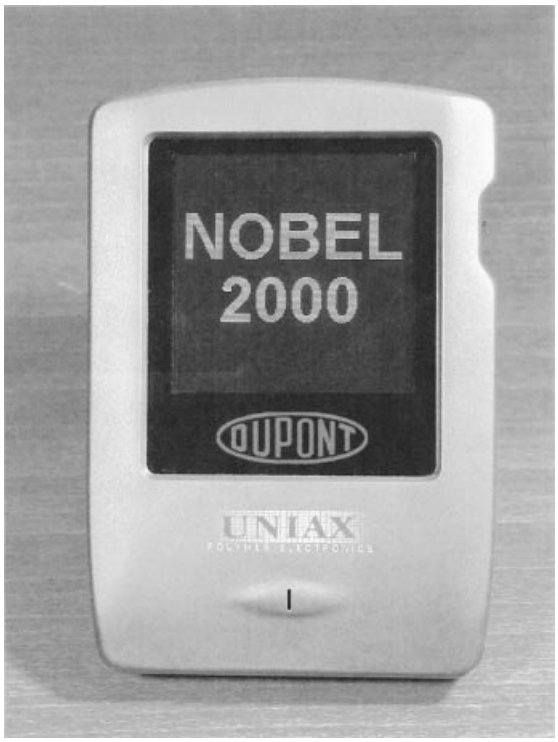

Fig. 7. Polymer LED passive matrix display; 160 × 160 pixels with pitch of 300 μm. Picture provided by Nobel Laureate Dr. Alan J. Heeger, courtesy of Uniax Corp., Santa Barbara, Calif.

processes that allow the deposition of different EL polymers in patterned fashion, for example, by ink-jet printing (4).

Another exciting development has been the design of PLEDs which emit linearly polarized light and, among other applications, might find use as backlights of conventional LCDs (8,34). The central feature in these devices is a high degree of uniaxial supramolecular orientation of the light-emitting polymer layer, which is most easily achieved by using thermotropic liquid-crystalline PLED materials such as poly(9,9-dialkyl fluorene)s or segmented poly(arylene vinylene)s. Monodomain alignment in thin films of these materials is usually accomplished by using an alignment layer such as a rubbed poly(imide) film, leading to highly polarized photo- and electroluminescence, with dichroic ratios (ratio of the intensity of emitted light polarized parallel and perpendicular to the orientation direction, respectively) that can exceed 20.

After only a decade of development, PLEDs indeed seem to have matured to the edge of commercial exploitation. The technology is expected to initially address the market for small- and medium-sized alphanumeric displays, as used in calculators, handheld telephones, pagers, car radios, personal digital assistants information readouts on household appliances, and in automobiles, which has a current annual volume of about US$2.5 billion, with high growth rates expected.

The display technologies traditionally employed in these applications are LCDs, vacuum fluorescence displays, and inorganic LEDs. Industrial sources estimate that by 2004–2005, organic LEDs (including PLEDs as well as LEDs based on small organic molecules) may capture between US$350 to US$700 million of that market (3,35). In the long run, PLEDs also have the potential to replace current high resolution video-rate displays in, eg, desktop monitors, ultrathin television sets, and the like.

BIBLIOGRAPHY

1. M. G. Craford and F. M. Steranka, in G. L. Trigg, ed., *Encyclopedia of Applied Physics*, Vol. **8**, VCH, Weinheim, 1994, pp. 485.
2. J. H. Burroughes and co-workers, *Nature* **347**, 539 (1990).
3. A. H. Tullo, *C&EN* 20 (June 26, 2000).
4. U. Mitschke and P. Bäuerle, *J. Mater. Chem.* **10**, 1471 (2000).
5. D. Kalinowski, *J. Phys. D: Appl. Phys.* **32**, R179 (1999).
6. A. Kraft, A. C. Grimsdale, and A. B. Holmes, *Angew. Chem. Int. Ed.* **37**, 403 (1998).
7. D. Bradley, *Curr. Opin. Solid State Mater. Sci.* **1**, 789 (1996).
8. A. Greiner, ed., *Polym. Adv. Technol.* (special topic issue) **9**, 369–490 (1998).
9. S. Miyata and H. S. Nalwa, eds., *Organic Electroluminescent Materials and Devices*, Gordon and Breach Science Publishers, Amsterdam, 1997.
10. M. T. Bernius, M. Inbasekaran, J. O'Brien, and W. Wu, *Adv. Mat.* **12**, 1737 (2000).
11. A. Greiner and co-workers, *Macromol. Chem. Phys.* **197**, 113 (1996).
12. C. W. Tang and S. A. VanSlyke, *Appl. Phys. Lett.* **51**, 913 (1987).
13. C. Adachi, T. Tsutsui, and S. Saito, *Appl. Phys. Lett.* **56**, 799 (1990).
14. M. Pope, H. Kallmann, and P. Magnante, *J. Chem. Phys.* **38**, 2042 (1963).
15. B. R. Hsieh and co-workers, *J. Am. Chem. Soc.* **129**, 231 (1998).
16. M. A. Baldo and co-workers, *Nature* **395**, 151 (1998).
17. N. C. Greenham, R. H. Friend, and D. D. C. Bradley, *Adv. Mater.* **6**, 491 (1994).
18. G. Gu and co-workers, *Opt. Lett.* **22**, 396 (1997).
19. C. Bastiaansen, T. Tervoort, and C. Weder, eds., *Macromolecular Symposia*, Vol. **154**, Wiley-VCH, Weinheim, 2000.
20. G. Gustafsson and co-workers, *Nature* **357**, 6378 (1992).
21. H. Kubota and co-workers, *J. Lumin.* **56**, 87 (2000).
22. *MRS Bulletin* **25**(8) (2000).
23. M. Thelakkat, R. Fink, F. Haubner, and H.-W. Schmidt, *Macromolecular Symposia*, Vol. **125**, Wiley-VCH, Weinheim, 2000, pp. 157.
24. C. Schmitz and co-workers, *Adv. Funct. Mater.* **11**, 41 (2001).
25. J. Moulton and P. Smith, in M. Lewin and J. Preston, eds., *Handbook of Fiber Science and Technology III, High-Technology Fibers, Part C*, Marcel Dekker, Inc., New York, 1993, pp. 275.
26. A. Greiner and co-workers, *Acta Polym.* **48**, 1 (1997).
27. D. Gin and V. Conticello, *Trends Polym. Sci.* **4**, 217 (1996).
28. U.S. Pat. 3,401,152 (1986), R. A. Wessling and R. G. Zimmerman. (to The Dow Chemical Company).
29. D. D. C. Bradley, *J. Phys. D: Appl. Phys.* **20**, 1389 (1987).

30. F. Wudl, P. M. Allemand, G. Srdanov, Z. Ni, and D. McBranch, *Materials for Nonlinear Optics: Chemical Perspectives*, American Chemical Society, Washington, D.C., 1991, pp. 683.
31. D. Braun and A. J. Heeger, *Appl. Phys. Lett.* **58**, 1982 (1991).
32. *URL: www.cdtltd.co.uk; www.covion.com; www.dow.com; www.dupont.com; www.philips.com; www.uniax.com.*
33. L. K. M. Chan, in R. J. Brook, M. C. Flemings, and S. Mahajan, eds., *The Encyclopedia of Advanced Materials*, Vol. **2**, Elsevier Science Ltd., Oxford, 1994, pp. 1294.
34. M. Grell and co-workers, *Adv. Mater.* **11**, 895 (1999).
35. D. E. Mentley, *Laser Focus World* **35**(5), 111 (1999).

ANDREAS GREINER
Universität Marburg Germany
CHRISTOPH WEDER
Case Western Reserve University

LIGNIN

Introduction

The word lignin is derived from the Latin word *lignum* meaning wood. It is a main component of vascular plants. Indeed, lignin is second only to polysaccharides in natural abundance, contributing 24–33% and 19–28%, respectively, to dry wood weights of normal softwoods and temperate-zone hardwoods.

According to a widely accepted concept, *lignin* [8068-00-6] may be defined as an amorphous, polyphenolic material arising from enzymatic dehydrogenative polymerization of three phenylpropanoid monomers, namely, coniferyl alcohol [485-35-5] (**2**), sinapyl alcohol [537-35-7] (**3**), and *p*-coumaryl alcohol (**1**).

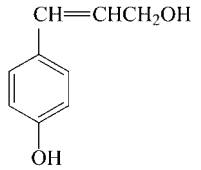

(**1**)

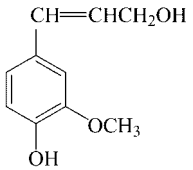

(**2**)

Encyclopedia of Polymer Science and Technology. Copyright John Wiley & Sons, Inc. All rights reserved.

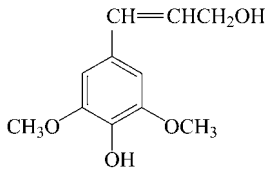

(**3**)

The traditionally held biosynthesis process, which consists essentially of random radical coupling reactions, sometimes followed by the addition of water, of primary, secondary, and phenolic hydroxyl groups to quinonemethide intermediates, leads to the formation of a three-dimensional polymer that lacks the regular and ordered repeating units found in other natural polymers such as cellulose and proteins. Traditionally no other enzymes or proteins are thought to be required (1).

The random biosynthesis process is under review. Dirigent proteins, acting as templates, are proposed to assist the orientation of lignin precursors to afford stereoselective phenoxy radical coupling (2,3).

Normal softwood lignins are usually referred to as guaiacyl lignins because the structural elements are derived principally from coniferyl alcohol (more than 90%), with the remainder consisting mainly of *p*-coumaryl alcohol-type units. Normal hardwood lignins, termed guaiacyl–syringyl lignins, are composed of coniferyl alcohol and sinapyl alcohol-type units in varying ratios. In hardwood lignins, the methoxyl content per phenylpropanoid unit is typically in the range of 1.2–1.5 (4). Grass lignins are also classified as guaiacyl–syringyl lignins. However, unlike hardwood lignins, grass lignins additionally contain small but significant amounts of structural elements derived from *p*-coumaryl alcohol. Grass lignins also contain *p*-coumaric, hydroxycinnamic, and ferulic acid residues attached to the lignin through ester and ether linkages (5).

The distribution of lignin in individual cells of lignified wood has been well examined. The lignin concentration is rather uniform across the secondary wall, but there is a significant increase in lignin concentration at the boundary of the middle lamella and primary wall region (6). This pattern of lignin distribution, with the highest concentration in the interfiber region and a lower, uniform concentration in the bulk of the cell walls, is typical for most wood cells. Thus lignin serves the dual purpose of binding and stiffening wood fibers through its distribution between and in the cell walls.

Lignin performs multiple functions that are essential to the life of the plant. By decreasing the permeation of water across the cell wall in the conducting xylem tissues, lignin plays an important role in the internal transport of water, nutrients, and metabolites. It imparts rigidity to the cell walls and acts as a binder between wood cells, creating a composite material that is outstandingly resistant to compression, impact, and bending. It also imparts resistance to biological degradation.

In commercial chemical pulping of wood, the reverse process in nature is performed to isolate fibers for papermaking. In the process, wood is delignified by chemically degrading and/or sulfonating the lignin to water-soluble fragments. The industrial lignins thus obtained are used in many applications.

Structure and Reactions

The structural building blocks of lignin are linked by carbon–carbon and ether bonds (7,8). Units that are trifunctionally linked to adjacent units represent branching sites which give rise to the network structure characteristic of lignin (see Figs. 1 and 2). Thus lignin consists of complex and diverse structures, including in softwood lignin an eight-member ring configuration (dibenzodioxocin) (11).

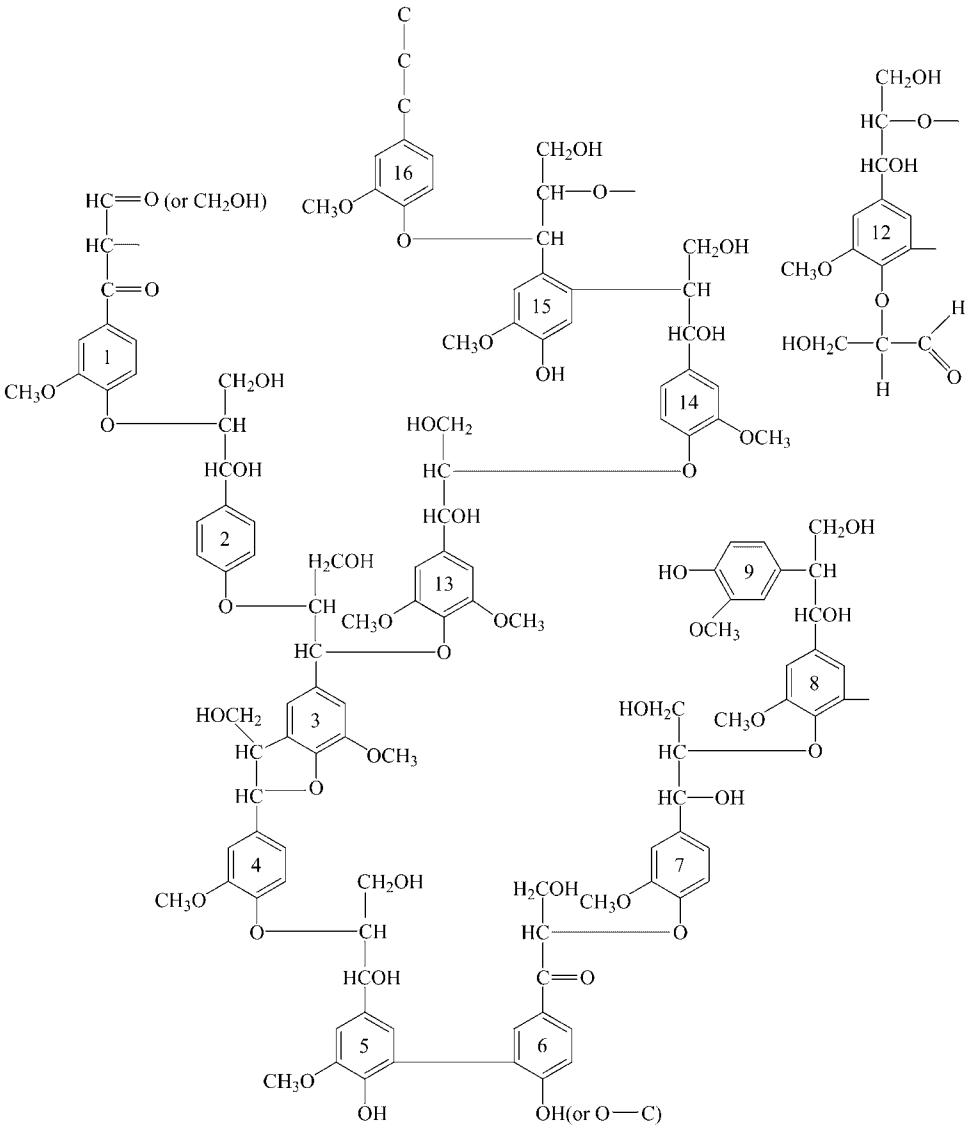

Fig. 1. Structural model of spruce lignin (9).

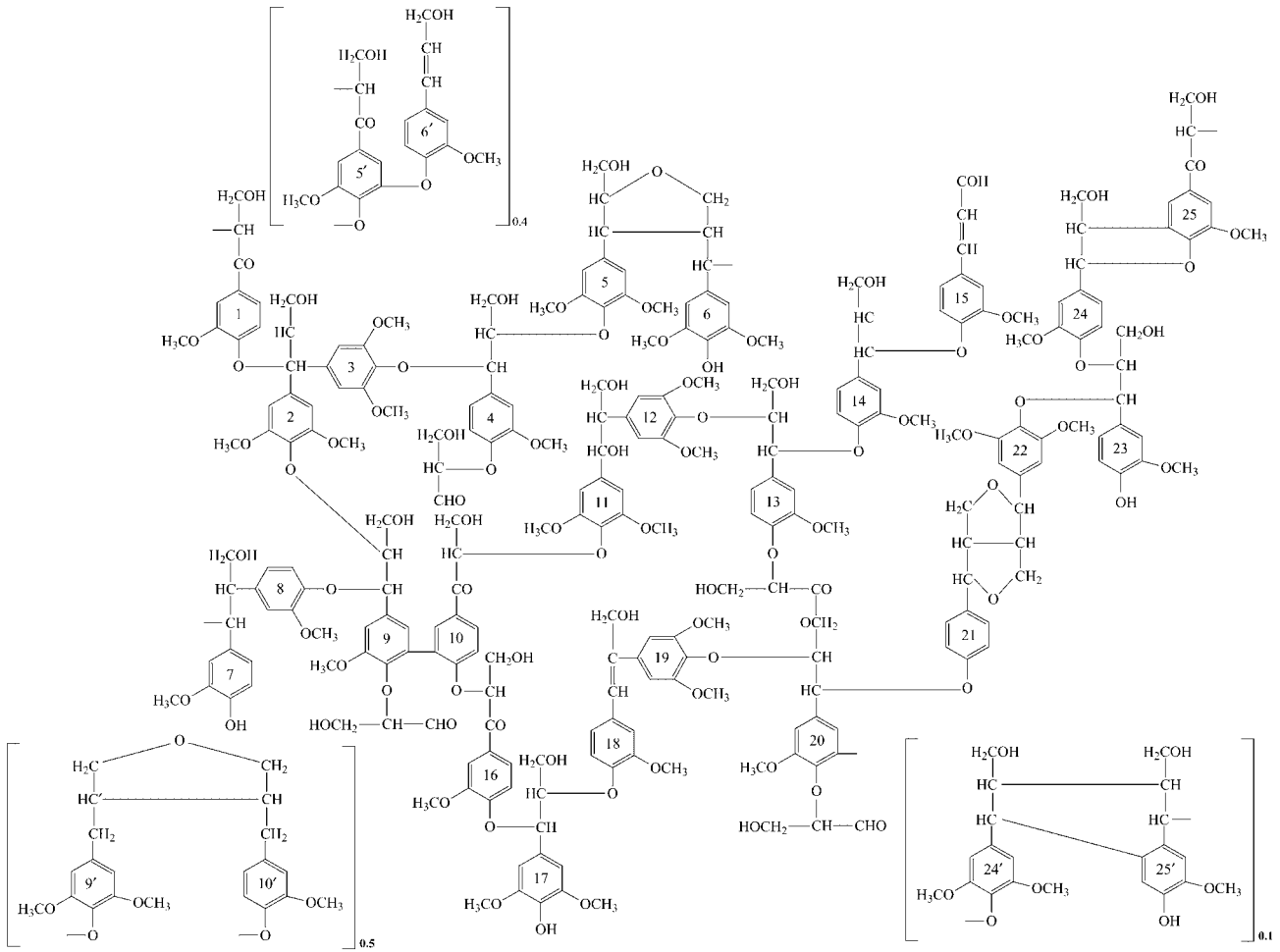

Fig. 2. Structural model of beech lignin (10).

Table 1. Types and Frequencies of Interunitary Linkages in Softwood and Hardwood Lignins (Number of Linkages per 100 C_9 Units)

Linkage	Softwood lignin[a]	Hardwood lignin[b]
β–*O*–4	49–51	65
α–*O*–4	6–8	
β–5	9–15	6
β–1	2	15
5–5	9.5	2.3
4–*O*–5	3.5	1.5
β–β	2	5.5

[a]Ref. 12.
[b]Ref. 7.

The types and frequencies of several prominent interunitary lignin linkages are summarized in Table 1.

Because the interunit carbon–carbon linkages are difficult to rupture without extensively fragmenting the carbon skeleton of the lignin, solvolysis of the ether linkages is often utilized as the best approach for degrading lignin. Of the functional groups attached to the basic phenylpropanoid skeleton, those having the greatest impact on reactivity of the lignin include phenolic hydroxyl, benzylic hydroxyl, and carbonyl groups. The frequency of these groups may vary according to the morphological location of lignin, wood species, and method of isolation.

Electrophilic Substitution. The processes by which the aromatic ring in lignin is modified by electrophilic substitution reactions are chlorination, nitration, and ozonation. Chlorination, widely used in multistage bleaching sequences for delignifying chemical pulps, proceeds by a rapid reaction of elemental chlorine with lignin in consequence of which the aromatic ring is nonuniformly substituted with chlorine. In nitration, nitro groups are introduced into the aromatic moiety of lignin with nitrogen dioxide (13). As one of several competing processes, electrophilic attack of ozone on lignin ultimately leads to ring hydroxylation (14).

Conversion of Aromatic Rings to Nonaromatic Cyclic Structures. On treatment with oxidants such as chlorine, hypochlorite anion, chlorine dioxide, oxygen, hydrogen peroxide, and peroxy acids, the aromatic nuclei in lignin typically are converted to *o*- and *p*-quinoid structures and oxirane derivatives of quinols. Because of their relatively high reactivity, these structures often appear as transient intermediates rather than as end products. Further reactions of the intermediates lead to the formation of catechol, hydroquinone, and mono- and dicarboxylic acids.

Aromatic rings in lignin may be converted to cyclohexanol derivatives by catalytic hydrogenation at high temperatures (250°C) and pressures [20–35 MPa (200–350 atm)] using copper–chromium oxide as the catalyst (15). Similar reduction of aromatic to saturated rings has been achieved using sodium in liquid ammonia as reductants (16).

Conversion of Cyclic to Acyclic Structures. Upon oxidation, the aromatic rings of lignin may be converted directly to acyclic structures, eg, muconic acid derivatives, or indirectly by oxidative splitting of *o*-quinoid rings. Further oxidation creates carboxylic acid fragments attached to the lignin network.

Ring Coupling and Condensation Reactions. Many oxidants, eg, ClO_2, O_2, generate free radicals in lignin. Coupling of such reactive radicals ultimately leads to diphenyl structures. In alkaline media, phenolic units may react with formaldehyde forming methylol derivatives that condense with themselves or with other phenols. This formaldehyde condensation reaction is the basis for using technical lignins in the preparation of adhesives.

Cleavage of Ether Bonds. Ether linkages at the α- and β-positions are the most abundant functional groups on the propanoid side chain of lignin. Under acidic conditions these linkages undergo solvolytic cleavage, initially forming secondary alcohols which are converted to carbonyl, ethylene, and carboxyl structures through a combination of dehydrations and allylic rearrangements, leading eventually to fragmentation of the side chain (17).

The alkali-promoted cleavage of α- and β-ether linkages, an important step in alkaline pulping processes, is mainly responsible for the fragmentation and dissolution of lignin in the pulping liquor. Addition of bisulfide ion to the aqueous alkaline media, as in the case of kraft pulping, enhances the rate and extent of β-aryl ether cleavage in phenolic units (18).

Cleavage of Carbon–Carbon Bonds. Under appropriate conditions, the propanoid side chain in lignin may be ruptured to form three-, two-, or one-carbon fragments. This carbon–carbon fragmentation occurs in a variety of laboratory treatments and technical processes such as in bleaching of chemical pulps with Cl_2, ClO_2, and O_2, in microbial degradation (19), and in photo-oxidation (20).

Substitution Reactions on Side Chains. Because the benzyl carbon is the most reactive site on the propanoid side chain, many substitution reactions occur at this position. Typically, substitution reactions occur by attack of a nucleophilic reagent on a benzyl carbon present in the form of a carbonium ion or a methine group in a quinonemethide structure. In a reversal of the ether cleavage reactions described, benzyl alcohols and ethers may be transformed to alkyl or aryl ethers by acid-catalyzed etherifications or transetherifications with alcohol or phenol. The conversion of a benzyl alcohol or ether to a sulfonic acid group is among the most important side-chain modification reactions because it is essential for the solubilization of lignin in the sulfite pulping process (21).

Formation and Elimination of Multiple Bond Functionalities. Reactions that involve the formation and elimination of multiple bond functional groups may significantly affect the color of residual lignin in bleached and unbleached pulps. The ethylenic and carbonyl groups conjugated with phenolic or quinoid structures are possible components of chromophore or leucochromophore systems that contribute to the color of lignin.

Reduction of ring-conjugated carbonyl groups to the corresponding primary and secondary alcohols is generally achieved by reaction with sodium borohydride. Ring-conjugated olefinic groups may be converted to their saturated components by hydrogenation.

Analytical Methods

Detection of Lignin. The characteristic color-forming response of lignified tissue and some lignin preparations on treatment with certain organic and inorganic reagents was recognized in the early nineteenth century. More than 150 color reactions have now been proposed for the detection of lignin (22). Reagents used in these reactions may be classified into aliphatic, phenolic, and heterocyclic compounds, aromatic amines, and inorganic chemicals. Among the important reactions are the Wiesner and Mäule color reactions.

The Wiesner Reaction. The reaction of lignified tissue and phloroglucinol–hydrochloric acid gives a visible absorption spectrum with a maximum at 550 nm. This has been attributed to coniferaldehyde units in lignin as the groups responsible for the color formation.

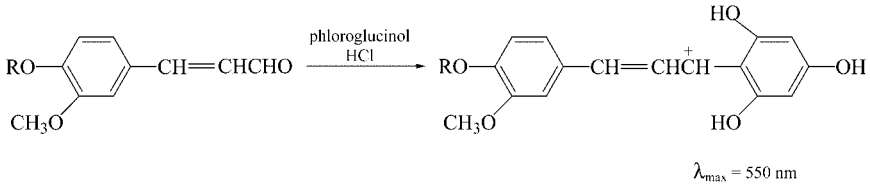

The Mäule Color Reaction. The procedure for this test consists basically of three sequential treatments of lignified material with 1% potassium permanganate, 3% hydrochloric acid, and concentrated ammonium hydroxide. A red-purple color develops for hardwoods and a brown color for softwoods. The steps comprising the Mäule reaction may be represented as follows (23,24):

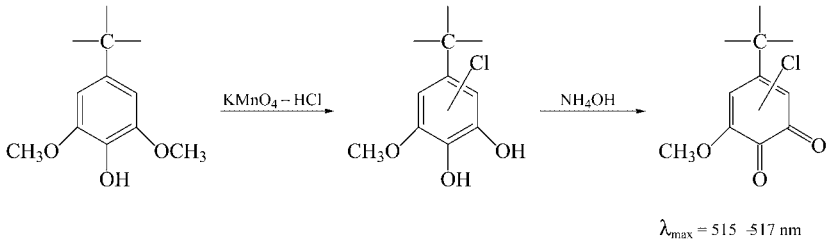

Determination of Lignin Content. Lignin content in plants (wood) is determined by direct or indirect methods (25). The direct method includes measurement of acid-insoluble (ie, Klason) lignin after digesting wood with 72% sulfuric acid to solubilize carbohydrates (26). The Klason lignin contents of representative lignified materials are shown in Table 2.

In contrast to the direct determination of lignin content, indirect methods do not involve the isolation of a lignin residue. These include spectrophotometric methods and procedures that are based on oxidant consumption. A uv microspectrophotometric method has been used to determine the distribution of lignin in the various cell wall regions of softwoods (27). Supplementing the uv-microscopic technique is a method in which lignin is brominated and the bromine uptake,

Table 2. Klason Lignin Contents of Lignified Materials[a]

Material	Klason lignin content, %
Softwoods	26–28.8
Hardwoods	22
Nonwood fibers	
Bagasse	19.6
Bamboo	22.2
Wheat straw	17.0
Kenaf	10.9
Sorghum	7.9
Pulp	
Pine kraft	4.8
Birch kraft	5.0
Spruce kraft	2.8
Birch acid sulfite	3.2
Birch bisulfite	4.0

[a]Ref. 25.

which is proportional to the lignin content, is determined by a combination of scanning or transmission electron microscopy (sem or tem) and energy dispersive x-ray analysis (edxa) (28). A number of spectral methods for determining lignin content are based on totally dissolving the sample in a suitable solvent and measuring the uv absorbance of the solution. Among the solvents used to dissolve lignocellulosic material are sulfuric acid, phosphoric acid, nitric acid, cadoxene, and acetyl bromide in acetic acid. The acetyl bromide method appears to have gained the most widespread acceptance (29).

The methods of oxidant consumption are used exclusively in the analysis of residual lignin in unbleached pulps. These procedures are all based on the common principle that lignin consumes the applied oxidants at a much faster rate than the carbohydrates, and oxidant consumption under carefully specified conditions can be regarded as a measure of lignin concentration in the pulp.

Two oxidants commonly used are chlorine and potassium permanganate. The *Roe chlorine number*, the uptake of gaseous chlorine by a known weight of unbleached pulp [ie, Technical Association of the Pulp and Paper Industry (TAPPI) Standard Method T202 ts-66] has been superseded by the simpler hypo number (ie, TAPPI Official Test Method T253 om-86), eg, chlorine consumption in treatment of the pulp with acidified sodium or calcium hypochlorite.

By far the most commonly used oxidation method is the corrected permanganate number test (30) in which the number of mL of 0.1 *N* $KMnO_4$ consumed by 1 g of oven-dried pulp under specified conditions (kappa number) is determined (TAPPI Historical Method T236 hm-85). Typical kappa numbers for representative pulps are shown in Table 3.

Characterization of Lignin. Lignin is characterized in the solid state by Fourier transform infrared (ftir) spectroscopy, uv microscopy, interference microscopy, cross polarization/magic angle spinning nuclear magnetic resonance (cp/mas nmr) spectroscopy, photoacoustic spectroscopy, Raman spectroscopy,

Table 3. Kappa Numbers for Typical Pulps[a]

Pulp	Kappa number range
Kraft (bleached grade)	
Softwood	25–35
Hardwood	14–18
Neutral sulfite semichemical (softwood)	80–100
Bisulfite (softwood)	30–50
Acid sulfite	
Softwood	16–22
Hardwood	14–20
Kraft (chlorinated and alkali extracted)	
Softwood	5–8
Hardwood	3–6

[a]Ref. 29.

pyrolysis-gas chromatography–mass spectroscopy, and thermal analysis. In solution, lignins are characterized by spectral methods such as uv spectroscopy, ftir spectroscopy, ^{1}H nmr spectroscopy, ^{13}C nmr spectroscopy, electron spin resonance spectroscopy (esr), and by several chemical degradation methods such as acidolysis, nitrobenzene and cupric oxidations, permanganate oxidation, thioacidolysis, hydrogenolysis, nuclear exchange reaction, ozonation and dfrc (derivitization followed by reductive cleavage). The details of these characterization methods have been discussed (31,32).

FTIR spectroscopy is a versatile, rapid, and reliable technique for lignin characterization. Using this technique, the *p*-hydroxyphenyl, guaiacyl, and syringyl units, methoxyl groups, carbonyl groups, and the ratio of phenolic hydroxyl to aliphatic hydroxyl groups can be determined. The uv microscopy method is best suited for investigating the topochemistry of lignin in wood, namely, for determining the concentration and chemical structure of lignin in different layers of the cell wall. CP/MAS NMR spectroscopy provides for another spectral technique whereby lignin can be characterized in the solid state. Results obtained by cp/mas nmr are in good agreement with Klason lignin contents for softwoods.

In solution, lignin is most conveniently analyzed qualitatively and quantitatively by uv spectroscopy. Typical absorptivity values D at 280 nm for milled wood lignins MWL(s) and other types of lignins are listed in Table 4. These values are used for quantitative determination of the lignins in suitable solvents.

^{1}H and ^{13}C nmr spectroscopies provide detailed information on all types of hydrogen and carbon atoms, thus enabling identification of functional groups and types of linkages in the lignin structure. Detailed assignments of signals in ^{1}H and ^{13}C nmr spectra have been published (34,35). A review of the use of ^{31}P nmr as an analytical tool for lignin is available (36). Through phosphitylation of the various hydroxyl groups present in lignin, unique quantitative and qualitative information has been obtained.

Electron spin resonance (esr) and electron paramagnetic resonance (epr) spectroscopy are essential tools for the study of structure and dynamics of molecular systems containing one or more unpaired electrons. These methods have found application as a highly sensitive tool for the detection and identification of

Table 4. Absorptivity Values *D* of Lignin at 280 nm[a]

Lignin	*D*, L/(g·cm)	Solvent
Spruce MW	16.7	2-Methoxyethanol
Spruce MW	20.7	Formamide
Spruce MW	19.5	Dioxane
Pine MW	18.8	2-Methoxyethanol/ethanol
Beach MW	13.3	Formamide
Maple MW	12.9	2-Methoxyethanol/ethanol
Poplar dioxane	12.6	Dioxane
Spruce lignosulfonate	11.9	Water
Beech lignosulfonate	10.4	Water
Pine kraft	24.6	Water
	26.4	2-Methoxyethanol/water

[a]Ref. 33.

free-radical species in lignin and lignin model compounds (37,38). Milled wood lignin generally exhibits a singlet esr signal with a *g*-value of 2.0023 and a line width of 1.6 mT (16 G), typical of a phenoxy radical.

Among the chemical degradation methods, acidolysis, nitrobenzene and cupric oxide oxidations, permanganate oxidation, thioacidolysis, and hydrogenolysis are all based on a common principle of chemically degrading lignin polymers to identifiable low molecular weight products through side-chain cleavages and maintaining the aromatic nature of the lignin units. By these methods, the make-up of monomeric units in the lignin (eg, guaiacyl–syringyl–*p* -hydroxyphenyl ratio) is determined. In addition, the identification of dimeric and trimeric degradation products reveals the types of linkages existing in the lignin. A new degradation method termed dfrc (derivatization followed by reductive cleavage) has been found to be simpler and is gaining acceptance (39). Combination of dfrc with ^{31}P nmr has revealed information about the structural nature of hydroxyl-bearing moieties of lignin (40).

A technique based on ozonation, in contrast, provides information on the structure of the lignin side chain by degrading the aromatic rings (41). Thus the side chain of the dominant structure in all native lignins, the arylglycerol–β-aryl ether moiety, can be obtained in the form of erythronic and threonic acids. Ozonation proves to be an elegant method for determination of the stereospecificity in lignin.

The quantities of noncondensed and condensed phenyl nuclei in various lignins and in the morphological regions of cell walls are determined by a nucleus exchange method (42). The data obtained from this method indicate that lignin in the middle lamella is more condensed than lignin in the secondary wall and that hardwood lignin is less condensed than softwood lignin. By combining nucleus exchange with nitrobenzene oxidation, the methylol groups formed in the condensation of lignin with formaldehyde can be directly measured without isolation of the lignin.

Functional Group Analysis. The move toward instrumental analysis and away from wet methods is illustrated in the methods of analysis of the various fuctional groups present in lignin. NMR has become a particularly useful tool.

Each section below contains information about both the classical wet method as well as references to the most current instrumental techniques.

The total hydroxyl content of lignin is determined by acetylation with an acetic anhydride–pyridine reagent, followed by saponification of the acetate, and followed by titration of the resulting acetic acid with a standard 0.05 *N* NaOH solution. Either the Kuhn–Roth (43) or the modified Bethge–Lindstrom (44) procedure may be used to determine the total hydroxyl content. The aliphatic hydroxyl content is determined by the difference between the total and phenolic hydroxyl contents. Total hydroxyl content has been determined, after derivitization, by ^{31}P, ^{13}C, ^{1}H, and ^{19}F nmr techniques. This was recently reviewed (45).

The phenolic hydroxyl group is one of the most important functionalities affecting the chemical and physical properties of lignin. It facilitates the base-catalyzed cleavage of interunitary ether linkages and oxidative degradation, and has a pronounced influence on the reactivity of lignin polymers in various modification reactions such as sulfomethylation with formaldehyde and bisulfite. Regarding classical analysis, the periodate method is based on the oxidation of a phenolic guaiacyl group with sodium periodate to orthoquinone structures, wherein nearly 1 mole of methanol per mole of phenolic hydroxyl group is released (46). Measurement of the methanol formed is approximately equivalent to the phenolic hydroxyl content. Another classic method is aminolysis (44) consisting of acetylation of lignin and aminolysis with pyrrolidine to remove acetyl groups such as 1-acetylpyrrolidine. The amount of removed acetyl is a measure of the phenolic hydroxyl content of lignin. These and other procedures for determining phenolic hydroxyl groups have been compared (47). The advantages and disadvantages of each of these methods compared with nmr spectroscopy has also been discussed (45). A simple and reliable ^{1}H nmr method that does not require derivitization has been reported. This method relies on D_2O exchange of the phenolic proton. An instrument capable of 500 MHz or greater is required (48). Table 5 lists the total phenolic and aliphatic hydroxyl contents of some representative milled wood, bamboo, and technical lignins.

As early as 1922, the presence of carbonyl groups in spruce lignin was postulated (50). Coniferaldehyde [458-36-6] has definitely been identified as a building block in lignin, and the α-carbonyl content has been found to increase in the milling of wood and during pulping processes. The total carbonyl content of lignin is determined by a borohydride or hydroxylamine hydrochloride method (51),

Table 5. Phenolic and Aliphatic Hydroxyl Contents of Milled Wood and Technical Lignins[a]

	Hydroxyl content, mol/C_9 unit		
Lignin	Total	Phenolic	Aliphatic
Spruce MWL	1.46	0.28	1.18
Bamboo MWL	1.49	0.36	1.13
Pine kraft lignin	1.35	0.58	0.77
Bamboo kraft lignin	1.00	0.44	0.56

[a] Ref. 49.

Table 6. Carboxyl Contents of Various Lignins[a]

Lignin	COOH, meq/g
Hardwood kraft	1.44
Hardwood native	0.92
Lignosulfonates	0.31–2.08
Wheat straw MWL	0.81
Spruce MWL	0.12
Decayed spruce	0.55
Softwood kraft	0.80

[a]Ref. 54.

and the α-carbonyl content from analysis of uv alkaline difference spectra. An ^{19}F nmr method employing quantitative trifluoromethylation of lignin was recently reported, which is claimed to be not only more precise than the previous methods, but can differentiate between the various types of carbonyl groups (52).

The method of choice for determining carboxyl groups in lignin is based on potentiometric titration in the presence of an internal standard, *p*-hydroxybenzoic acid, using tetra-*n*-butylammonium hydroxide as a titrant (53). The carboxyl contents of different lignins are shown in Table 6. In general, the carboxyl content of lignin increases upon oxidation.

Methoxyl groups are determined by the Viebock and Schwappach procedure (55). In treatment of lignin with hydroiodic acid, the methoxyl group is cleaved, forming methyl iodide which is quantitatively stripped from the reaction mixture and collected in a solution of sodium acetate and glacial acetic acid containing bromine. The bromine reacts with methyl iodide to form alkyl bromide and iodine bromide. The iodine thus produced is titrated with a dilute standard sodium thiosulfate solution by using 1% starch solution as an indicator. The methoxyl content can be quantitatively determined with high accuracy based on the quantity of iodine recovered. A technique that offers a simpler procedure using gas chromatography (gc) has been reported (56). This method relies on quantiative analysis of methyl iodide by gc after reaction with hydroiodic acid. This bypasses the complex apparatus, as well as the distillation, trapping, and titration steps.

Finally, the sulfonate content of lignin is determined by two main methods: one typified by conductometric titration in which sulfonate groups are measured directly, and the other which measures the sulfur content and assumes that all of the sulfur is present as sulfonate groups. The method of choice for determining the sulfonate content of lignin samples that contain inorganic or nonsulfonate sulfur, however, is conductometric titration (57).

Properties

Molecular Weight and Polydispersity. Because it is not possible to isolate lignin from wood without degradation, the true molecular weight of lignin

in wood is not known. Different methods for measuring the molecular weight of isolated lignins give various results, and aggregation of lignin molecules may prevent determination of real molecular weight. Light scattering and vapor-phase pressure osmometry are the traditional methods of analysis. Using these methods, the weight-average molecular weight M_w of softwood milled wood lignin is estimated to be 20,000; lower values have been reported for hardwoods (58).

Various methods based on sec (size exclusion chromatography) have been reported. An initial stumbling block for this method was an affinity between Lignin and early sec columns, and the use of linear polystyrene sulfonate standards (59). Since that time, various standardization techniques such as universal calibration, mals (multiple angle light scattering) and maldi-tof (matrix assisted laser desorption ionization-time of flight) mass spectrometry have been coupled with sec (60,61). With the maldi-tof method the M_w of softwood kraft lignin was found to be close to 3000. Purified softwood lignosulfonates have been estimated to have a M_w of 30,000 by mals (62). Kraft lignins invariably have lower molecular weights than lignosulfonates, indicative of a more extensive degradation of the lignin during the kraft pulping process. Hopefully, a method that gives the actual molecular weight of isolated lignins will be verified by one of the above listed techniques.

Solution Properties. Lignin in wood behaves as an insoluble, three-dimensional network. Isolated lignins (milled wood, kraft, or organosolv lignins) exhibit maximum solubility in solvents having a Hildebrand's solubility parameter, σ, of 20.5–22.5 $(J/cm^3)^{\frac{1}{2}}$ [10–11$(cal/cm^3)^{\frac{1}{2}}$], and $\Delta\mu$ in excess of 0.14 μm, where $\Delta\mu$ is the infrared shift in the O—D bond when the solvents are mixed with CH_3OD. Solvents meeting these requirements include dioxane, acetone, methyl cellosolve, pyridine, and dimethyl sulfoxide.

Thermal Properties. As an amorphous polymer, lignin behaves as a thermoplastic material undergoing a glass transition at temperatures that vary widely depending on the method of isolation, sorbed water, and heat treatment (62). Lignin stores more energy than cellulose in wood. For example, the glass-transition temperature T_g and heat capacity at 350 K for dioxane lignin are 440 K and 1.342 J/(g·K), respectively (63). Thermal softening of lignin at elevated temperatures accelerates the rate of delignification in chemical pulping and enhances the bond strength of fibers in paper- and boardmaking processes. In commercial thermomechanical pulping, a pretreatment of wood chips with sulfite lowers the T_g of lignin to 70–90°C (63), thus decreasing the power consumption in defibration. Other physical properties of lignin have been comprehensively reviewed (51).

Chemical Properties. Lignin is subject to oxidation, reduction, discoloration, hydrolysis, and other chemical and enzymatic reactions. Many are briefly described elsewhere (64). Key to these reactions is the ability of the phenolic hydroxyl groups of lignin to participate in the formation of reactive intermediates, eg, phenoxy radical (**4**), quinonemethide (**5**), and phenoxy anion (**6**):

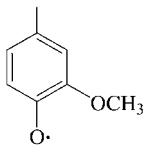

(**4**)

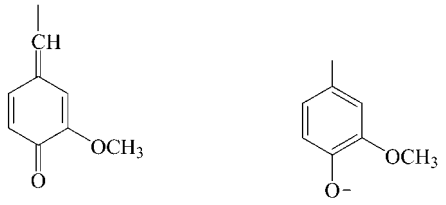

(**5**) (**6**)

The free-radical intermediate initiates light-induced discoloration (yellowing) and enzymatic degradation of lignin (38,65). Nucleophilic addition occurs at the quinonemethide center, of which the most important reactions are the addition of sulfonate groups to the α-carbon during sulfite pulping and the sulfide assisted depolymerization in kraft pulping (Fig. 3).

The significance of phenoxy anions is well-recognized in the isolation of kraft and other water-insoluble technical lignins by acid precipitation. The ionization of phenolic hydroxyl groups coupled with the reduction of molecular size renders native lignin soluble in the aqueous pulping solution, thus enabling its separation from the polysaccharide components of wood.

The aromatic ring of a phenoxy anion is the site of electrophilic addition, eg, in methylolation with formaldehyde. The phenoxy anion is highly reactive to

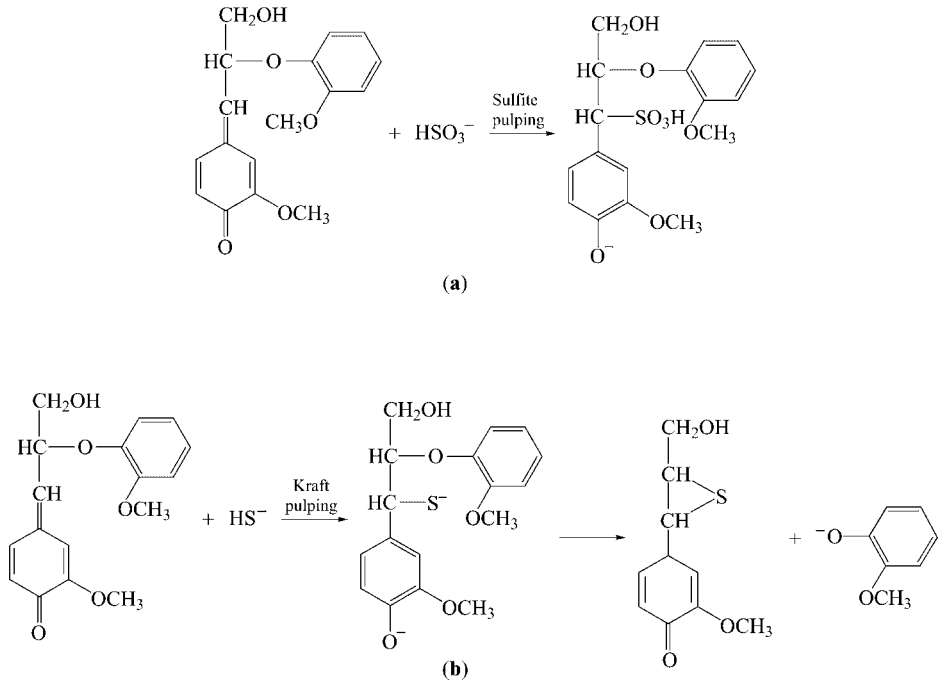

Fig. 3. Reactions at the quinonemethide center during pulping: (**a**) sulfite pulping and (**b**) kraft pulping.

many oxidants such as oxygen, hydrogen peroxide, ozone, and peroxyacetic acid. Many of the chemical modification reactions of lignin utilizing its aromatic and phenolic nature have been reviewed elsewhere (66).

During the last decade there has been increased interest in the use of lignolytic enzymes that degrade lignin, for the pulping of wood, bleaching of fiber, or for modification of lignin-based chemical feedstocks. The pretreatment of pulpwood with enzymes has seen limited commercial use. With a number of research groups dedicated to this technology, it should continue to gain commercial acceptance (67).

Industrial Lignins

Industrial lignins are by-products of the pulp and paper industry. Lignosulfonate [8062-15-5], derived from sulfite pulping of wood, and kraft lignin [8068-05-1], derived from kraft pulping, are the principal commercially available lignin types. Organosolv lignins [8068-03-9] derived from the alcohol pulping of wood are also reported to be available commercially, in the past, but is no longer available in any quantity (68).

The production capacity of lignin in the Western world is estimated to be ca 8×10^5 t/year (Table 7). Although the production of lignosulfonates has been declining, kraft lignin production has increased. Of the companies listed in Table 7, LignoTech Sweden and Westvaco produce kraft lignins. The rest produce lignosulfonates.

Advances in technology have increased the importance of lignin products in various industrial applications. They are derived from an abundant, renewable resource, and they are nontoxic and versatile in performance.

Lignosulfonates. Lignosulfonates, also called lignin sulfonates and sulfite lignins, are derived from the sulfite pulping of wood. In the sulfite pulping process, lignin within the wood is rendered soluble by sulfonation, primarily at benzyl alcohol, benzyl aryl ether, and benzyl alkyl ether linkages on the side chain of phenyl propane units (69). Some demethylation also occurs during neutral and alkaline sulfite pulping, and this leads to the formation of catechols and methane sulfonic acid (see Fig. 3).

Table 7. European and American Lignin Manufacturers

Producer	Country	Annual capacity, t/year
Borregaard LignoTech	Europe	400,000
	United States	70,000
Tembfibre	Europe	40,000
	Canada	40,000
Fraser Paper	United States	50,000
Tolmozzo	Italy	35,000
Westvaco	United States	30,000
Inland Paper	United States	20,00
Others		100,000
Total		*785.000*

Table 8. Compositions of Spent Sulfite Liquors[a]

Component	Percentage of total solids	
	Softwood	Hardwood
Lignosulfonate	55	42
Hexose sugars	14	5
Pentose sugars	6	20
Noncellulosic carbohydrates	8	11
Acetic and formic acids	4	9
Resin and extractives[b]	2	1
Ash	10	10

[a]Ref. 70.
[b]For example, polyphenolic oils and tall oils.

Depending on the type of pulping process, lignosulfonates of various bases, including calcium [8061-52-7], sodium [8061-51-6], magnesium [8061-54-9], and ammonium lignosulfonates [8061-53-8], can be obtained. Typical compositions for hardwood and softwood spent sulfite liquors are given in Table 8. In addition to whole liquor products, commercial forms of lignosulfonates include chemically modified whole liquors, purified lignosulfonates, and chemically modified forms thereof.

Isolation of Lignosulfonates. Various methods have been developed for isolating and purifying lignosulfonates from spent pulping liquors. One of the earliest and most widely used industrial processes is the Howard process, where calcium lignosulfonates are precipitated from spent pulping liquor by addition of excess lime. Lignin recoveries of 90–95% are obtainable through this process. Other methods used industrially include ultrafiltration and ion exclusion (69), which uses ion-exchange resins to separate lignin from sugars.

Laboratory methods for isolating lignosulfonates include dialysis (71,72), electrodialysis (73), ion exclusion (73,74), precipitation in alcohol (75,76), and extraction with amines (77–79). They can also be isolated by precipitation with long-chain substituted quarternary ammonium salts (80–82).

Physical and Chemical Properties of Lignosulfonates. Even unmodified lignosulfonates have complex chemical and physical properties. Their molecular polydispersities and structures are heterogeneous. They are soluble in water at any pH but insoluble in most common organic solvents.

Typical C_9 formulas reported for isolated softwood and hardwood lignosulfonates are $C_9H_{8.5}O_{2.5}(OCH_3)_{0.85}\ (SO_3H)_{0.64}$ and $C_9H_{7.5}\ O_{2.5}(OCH_3)_{1.39}(SO_3H)_{0.68}$, respectively. These correspond to monomer unit molecular weights of 235 for softwood lignosulfonates and 254 for hardwoods. Polymer molecular weights are polydisperse and difficult to determine precisely. However, a range of 1000–140,000 has been reported for softwood lignosulfonates (83), with lower values reported for hardwoods (84).

A number of different functional groups are present in lignosulfonates. ^{13}C nmr analysis of a purified sulfonated lignin from Western hemlock revealed 2.0% phenolic hydroxyl, 17.5% sulfonate, 12.5% methoxyl, and 0.6% carboxyl groups per unit weight of lignosulfonates (85). Additional studies indicate that

lignosulfonates also contain limited numbers of olefinic, carbonyl, and catechol groups (86).

Lignosulfonates exhibit surface activity but have only a slight tendency to reduce interfacial tension between liquids. When compared with true surface-active agents, they are not effective in reducing the surface tension of water or for forming micelles (87). Their surface activity can be improved, however, by introducing long-chain alkyl amines into the lignin structure (88), by ethoxylation of lignin phenolic structures (89), or by conversion to oil-soluble lignin phenols (90).

Lignosulfonate Uses. Worldwide, the single largest use of lignosulfonates is as water reducers for concrete. Both hardwood and softwood lignosulfonates are widely used as lower end water reducers. Recently, higher molecular weight products produced by fractionation of softwood lignosulfonates have been used as midrange water reducers, and efforts are underway to modify lignosulfonates for use as superplasticizers.

From a historical perspective, two other large-volume uses include production of vanillin and dimethyl sulfoxide (DMSO) (91). Commercially, softwood spent sulfite liquors or lignosulfonates can be oxidized in alkaline media by oxygen or air to produce vanillin [121-33-5].

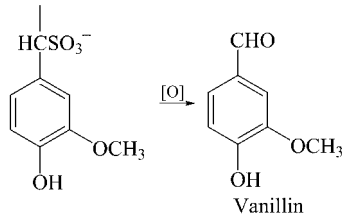

Vanillin

Through reaction with sulfide or elemental sulfur at 215°C, lignosulfonates can also be used in the commercial production of dimethyl sulfide and methyl mercaptan (92). Dimethyl sulfide produced in the reaction is further oxidized to DMSO, a useful industrial solvent.

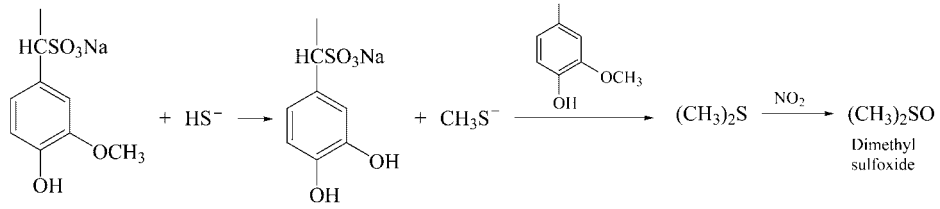

Dimethyl sulfoxide

Additional large-volume uses of lignosulfonates include animal feed pellet binders, dispersants for gypsum board manufacture, thinners/fluid loss control agents for drilling muds, dispersants/grinding aids for cement manufacture, and in dust control applications, particularly road dust abatement.

Lignin technology has advanced significantly, and increased research and development efforts have resulted in specialty uses in several key market areas.

Dye Dispersants. One such area is dye manufacture, where lignosulfonates act as primary dispersants, extenders, protective colloids, and grinding aids. Products produced by the reaction of lignosulfonates with benzyl alcohols have low azo dye reduction properties, low fiber-staining properties, high dispersion efficiency, good grinding aid qualities, and increased heat stability (66). Lignosulfonates prepared by sulfonation of kraft lignin are also widely used in this application. Such products are particularly useful in applications requiring superior heat stability.

Pesticide Dispersants. Modified lignosulfates and lignosulfonates derived from kraft lignins are used in the formulation of pesticides. In wettable powders, suspension concentrates, and water-dispersible granules, they act as dispersants and prevent sedimentation. They also act as binders in the production of granular pesticides. Typical usage levels in these types of products range from 2 to 10%.

Carbon Black Dispersant. Specially modified lignosulfonates are used in a wide range of pigment applications to inhibit settling and decrease solution viscosity. Applications include dispersants for dark pigment systems used to color textile fibers, coatings, inks , and carbon black. Lignosulfonates are also used as grinding aids and binders in the pelletizing of carbon black.

Water Treatment/Industrial Cleaning Applications. Boiler and cooling tower waters are treated with lignosulfonates to prevent scale deposition (93). In such systems, lignosulfonates sequester hard water salts and thus prevent their deposition on metal surfaces. They can also prevent the precipitation of certain insoluble heat-coagulable particles (94). Typical use-levels for such applications range from 1 to 1000 ppm.

In industrial cleaning formulations, lignosulfonates function as dirt dispersants and suspending agents (95). Rinsing properties are improved, corrosivity is reduced, and the amount of wetting agent needed is lowered when lignosulfonates are added to acid and alkaline industrial cleaning formulations. Typical use-levels in such formulations range from 0.05 to 2.0%.

Complexing Agent for Micronutrients. Complexes of lignosulfonates and iron, copper, zinc, manganese, magnesium, boron, or combinations of such are used to provide essential micronutrients to plants growing in metal-deficient soils. In most instances application of such complexes is by foliar spray. When applied in this manner the micronutrients can be readily absorbed by the plant without undesired leaf burn (96). Lignosulfonate complexes can also be used in soil treatment where they maintain availability of metals longer than if metals are applied alone (97).

Lignosulfonate–metal complexes are weaker complexes than those formed from amine-based complexing agents such as ethylenediaminetetracetic acid (EDTA). They are compatible with most pesticides/herbicides, but their use in phosphate fertilizers is not recommended

Oil-Well Cement Retarders. Sodium and calcium lignosulfonates are the most commonly used retarders for oil-well cements (98). They are effective with all Portland cements and are generally added in concentrations from 0.1 to 2%. Depending on their structure and purity and on the nature of the cement, they

are effective to about 250°F bottom hole circulating temperature. This range can be extended to 400°F by addition of sugar acids or sodium borate.

Expanders for Lead-Acid Batteries. Oxylignin, a sodium lignosulfonate derived from the vanillin process, is the premier expander for lead-acid batteries (99). When added to the negative plate at dosages of 0.1–0.5%, battery lifetimes are expanded from days to years.

Other Uses. Other uses of specially modified lignosulfonates include leather tanning (100), as flotation and wetting aids in ore processing, as sacrificial agents in enhanced oil recovery (101), as precipitating agents in protein recovery (102, 103), in deicing formulations (104), and as wood preservatives (105). Medicinally, lignosulfonates have been purported to have value as antithrombotic (106) and antiviral (107,108) agents.

Interest in acrylic-graft copolymers of lignosulfonates is also growing. Commercially such products have found use as dispersants/fluid loss control agents for oil-well drilling muds and cements (109,110), as scale control agents in water treatment (111), as water reducing agents in the manufacture of bricks and ceramic materials (112), and as low inclusion animal feed binders (113).

Kraft Lignins. Kraft lignins, also called sulfate or alkali lignins, are obtained from black liquor by precipitation with acid. Generally, acidification is conducted in two steps. In the first step, carbon dioxide from the waste gases of boiler fires or from lime kilns is used to reduce the pH of the liquor from 12 to 9–10. About three quarters of the lignin is precipitated in this step as a sodium salt. After isolation, the material thus obtained can be used as is or further refined by washing. By suspending the salt in water and lowering the pH to 3 or less with sulfuric acid, refined lignin is obtained.

Typical compositions for softwood and hardwood kraft black liquors are shown in Table 9. Most commercial kraft lignins are sulfonated kraft lignins or lignin amines. A few nonsulfonated products are, however, available.

Physical and Chemical Properties of Kraft Lignins. Kraft lignins are soluble in alkali (pH > 10.5), dioxane, acetone, dimethyl formamide, and methyl cellosolve. They are insoluble in water at neutral and acidic pH, have number-average molecular weights in the 2000–3000 range, and are less polydisperse

Table 9. Compositions of Kraft Black Liquors[a]

	Total solids, %	
Component	Softwood	Hardwood
Kraft lignin	45	38
Xyloisosaccharinic acid	1	5
Glucoisosaccharinic acid	14	4
Hydroxy acids	7	15
Acetic acid	4	14
Formic acid	6	6
Resin and fatty acids	7	6
Turpentine	1	
Others	15	12

[a]Ref. 48.

than lignosulfonates. A C_9 formula of $C_9H_{8.5}O_{2.1}S_{0.1}(OCH_3)_{0.8}(CO_2H)_{0.2}$ has been reported for softwood kraft lignin corresponding to a monomer molecular weight of about 180 (114). Because of the high degree of degradation during pulping, they also have a large number of free phenolic hydroxyl groups (4.0%).

The aromatic rings of kraft lignins can be sulfonated to varying degrees with sodium sulfite at high temperatures (150–200°C) or sulfomethylated with formaldehyde and sulfite at low temperatures (<100°C). Oxidative sulfonation with oxygen and sulfite is also possible.

Many of the chemical reactions used to modify lignosulfonates are also used to modify kraft lignins. These include ozonation, alkaline–air oxidation, condensation with formaldehyde and carboxylation with chloroacetic acid (115), and epoxysuccinate (116). In addition, cationic kraft lignins can be prepared by reaction with glycidylamine (117).

The physical and chemical properties of kraft lignin differ greatly from those of lignosulfonates. A summary of these differences is presented in Table 10.

Applications of Kraft Lignins. Because of the high fuel value of black liquor, kraft lignin products are generally used in high value applications. In many applications, the base lignin must be modified (ie, through sulfonation or oxidation) prior to use. Once modified, kraft lignins can be used in most of the same applications in which lignosulfonates are used. These include usage as emulsifying agents/emulsion stabilizers (118), as sequestering agents (119), as pesticide dispersants (120), as dye dispersants (66,121,122), as additives in alkaline cleaning formulations (123), as complexing agents in micronutrient formulations, as flocculants (124), and as extenders for phenolic adhesives (125). In addition, kraft lignins can also be used as an extender/modifier and as a reinforcement pigment in rubber compounding (126,127).

Sulfonated kraft lignins derivatized via ethoxylation have recently been used as dispersants in numerous applications including pesticides and dyestuffs (128). Propoxylated lignosulfonates have found use commercially as nonretarding dispersants for oil-well cements (129).

Table 10. Properties of Kraft Lignins and Lignosulfonates[a]

Property	Kraft lignins	Lignosulfonates
Molecular weight	2,000–3,000	20,000–50,000
Polydispersity	2–3	6–8
Sulfonate groups, meq/g	0	1.25–2.5
Organic sulfur, %	1–1.5	4–8
Solubility	Soluble in alkali (pH < 10.5), acetone, dimethylformamide, methyl cellosolve	Soluble in water at all pHs; insoluble in organic solvents
Color	Dark brown	Light brown
Functional Groups	Many phenolic hydroxyl, carboxyl, and catechol groups; some side-chain saturation	Fewer phenolic hydroxyl, carboxyl, and catechol groups; little side-chain saturation

[a]Ref. 70.

Toxicology of Lignosulfonates and Sulfonated Kraft Lignins. Rather extensive testing has shown that lignosulfonates are nontoxic. In most cases, LD_{50} values are greater than 5 g/kg. The safe use of lignosulfonates in the manufacturing and processing of a wide variety of food and food packaging applications is covered under the following U.S. Food and Drug Administration regulations: (*1*) as adjuvants in pesticide formulations exempt from the requirements of tolerance when applied pre- or postharvest (21 CFR 182.99, 40 CFR 180.1001); (*2*) as dispersant or stabilizers in pesticides applied pre- or postharvest to bananas (21 CFR 172.715); (*3*) as a boiler water additive used in the preparation of steam that will contact food (21 CFR 173.310); (*4*) as components of paperboard or paper in direct contact with moist, fatty, or dry food (21 CFR 176.170, 178.3120, 176.120, 176.180); (*5*) as component in food packaging adhesives (21 CFR 175.105); (*6*) as component of defoamers used in manufacturing food-packaging grade paper or paperboard (21 CFR 176.210); and (*7*) in animal feed as pelleting or binder aid (limit of 4%), surfactant in molasses (limit of 11%), and source of metabolizable energy (limit 4%) (21 CFR 573.600).

Organosolv Pulping Lignins. In organosolv pulping processes, hardwood chips are batch cooked for set times at appropriate temperatures and pH in an aqueous ethanol or methanol liquor. In the process, lignin, hemicelluloses, and other miscellaneous components of the wood are extracted into the alcoholic pulping liquor forming a black liquor. Organosolv lignin is recovered from the black liquor by precipitation, settled, centrifuged or filtered, and dried (127,130). The resulting lignin is a fine, brown, free-flowing powder.

Physical and Chemical Properties. Organosolv lignins are soluble in some organic solvents and in dilute alkali. They are insoluble in water at neutral or acidic pH. They have number-average molecular weights lower than 1000 and polydispersities between 2.4 and 6.3 (68). A C_9 formula of $C_9H_{8.53}O_{2.45}(OCH_3)_{1.04}$ has been reported for one organosolv lignin (68). This corresponds to a monomer molecular weight of 188.

Applications. These materials are still in developmental infancy, and are not currently available commercially. The lignins produced in these processes have potential application in wood adhesives, as flame retardants , as slow-release agents for agricultural and pharmaceutical products, as surfactants , as antioxidants, as asphalt extenders, and as a raw material source for lignin-derived chemicals.

Other Lignins. In addition to main commercial lignins, there are a number of other lignins of no or limited commercial value. One of these is produced almost exclusively in the Commonwealth of Independent States (CIS) where wood is used to produce glucose by acid hydrolysis. The lignin isolated as a by-product of this process is called acid hydrolysis lignin. It is claimed that in modified form such lignins can be used as rubber filling agents, as binders in wood adhesives, as additives in fabric treating compounds where they impart decay resistance, and as flotation aids in ore processing.

Numerous lignins have also been isolated in the laboratory including milled wood lignins, dioxane lignins, and enzymatically liberated lignins. These laboratory prepared lignins have different chemical and physical properties depending on the chemical modifications undergone during their isolation, and the quantities obtained are after limited.

BIBLIOGRAPHY

"Lignin" in *EPST* 1st ed., Vol. 8, pp. 233–272, by W. J. Schubert, Fordham University; "Lignin" in *EPSE* 2nd ed., Vol. 8, pp. 795–852, by W. G. Glasser and S. S. Kelley, Virginia Polytechnic Institute and State University.

1. J. L. McCarthy and A. Islam, in W. G. Glasser, R. A. Northey, and T. P. Schultz, eds., ACS Symposium Series 742: *Lignin: Historical, Biological, and Materials Perspectives*, ACS, Washington, D.C., 1999, p. 19, 20, 25, 26, 33.
2. N. G. Lewis, *Science* **275**, 362 (1997).
3. *Ref. 1*, pp. 38–39.
4. K. V. Sarkanen and H. L. Hergert, in K. Sarkanen and C. Ludwig, eds., *Lignins: Occurrence, Formation, Structure, and Reactions*, Wiley-Interscience, New York, p. 43.
5. P. Lewis and M. Paice, eds., ACS Symposium Series: *Plant Cell Wall Polymers: Biogenesis and Degradation*, ACS, Washington, D.C., 1989, p. 299.
6. B. J. Fergus, *The Distribution of Lignin in Wood as Determined by Ultraviolet Microscopy*, Ph.D. dissertations, McGill University, Montreal, Canada, 1968.
7. J. Gierer, *Wood Sci. Technol.* **19**, 289 (1985).
8. J. Gierer, *Wood Sci. Technol.* **20**, 1 (1986).
9. E. Adler, *Wood Sci. Technol.* **11**, 169 (1977).
10. H. H. Nimz, *Angew. Chem., Int. Ed.* **13**, 313 (1974).
11. P. Karhunen and co-workers, *Tetrahedron Lett.* **36**(1), 169–170 (1995).
12. M. Erickson, S. Larsson, and G. E. Miksche, *Acta Chem. Scand.* **27**, 903 (1973).
13. S. I. Andersson and O. Samuelson, *Sven. Papperstidn.* **88**, R102 (1985).
14. J. Gierer, *Holzforschung* **36**, 43 (1982).
15. E. E. Harris and H. Adkins, *Pap. Trade J.* **107**(20), 38 (1938).
16. N. N. Shorygina, T. Y. Kafeli, and A. F. Samechkina, *J. Gen. Chem.* **19**, 1558 (1949).
17. A. F. A. Wallis, in Ref. 4, p. 345.
18. J. Gierer, *Wood Sci. Technol.* **14**, 241 (1980).
19. T. K. Kirk and R. L. Farrell, *Ann. Rev. Microbiol.* **41**, 465 (1987).
20. G. Gellerstedt and E. L. Pettersson, *Acta Chem. Scand. B* **29**, 1005 (1975).
21. G. Gellerstedt, *Wood Sci. Technol.* **14**, 241 (1976).
22. J. Nakano and G. Meshitsuka, in Ref. 31, p. 23.
23. G. Meshitsuka and J. Nakano, *Mokuzai Gakkaishi* **24**, 563 (1988).
24. K. Iirama and R. Pant, *Wood Sci. Technol.* **22**, 167 (1988).
25. C. W. Dence, in Ref. 31, p. 37.
26. *TAPPI Test Method T222 om-83*, Atlanta, Ga., 1988.
27. B. J. Fergus and co-workers, *Wood Sci. Technol.* **3**, 117 (1969).
28. S. Saka, R. J. Thomas, and J. S. Gratzl, *Tappi* **61**(1), 73 (1978).
29. K. Iiyama and A. F. A. Wallis, *Wood Sci. Technol.* **22**, 271 (1988).
30. J. E. Tasman and V. Berzins, *Tappi* **40**, 691 (1957).
31. S. Y. Lin and C. W. Dence, eds., *Methods in Lignin Chemistry*, Springer-Verlag, Berlin, 1992.
32. Y. Z. Lai, H. Xu, and R. Yang, in Ref. 1, p. 239.
33. S. Y. Lin, in Ref. 31, p. 217.
34. K. Lundquist, in Ref. 31, p. 242.
35. D. Robert, in Ref. 31, p. 250.
36. D. S. Argyropoulos, *J. Res. Chem. Intermed.* **21**, 373–395 (1995).
37. C. Steelink, *Adv. Chem. Ser.* **59**, 51 (1966).
38. K. P. Kringstad and S. Y. Lin, *Tappi* **53**, 2296 (1970).
39. F. Lu and J. Ralph, *J. Agric. Food Chem.* **45**, 2590–2592 (1997).
40. S. Tohmura and D. S. Argyropoulos, *J. Agric. Food Chem.* **49**, 536–542 (2001).

41. K. V. Sarkanen, A. Islam, and C. D. Anderson, in Ref. 31, p. 387.
42. M. Fumaoka, I. Abe, and V. L. Chiang, in Ref. 31, p. 369.
43. R. Kuhn and H. Roth, *Ber. Dtsch. Chem. Ges.* **66**, 1274 (1933).
44. P. Mansson, *Holforschung* **37**, 143 (1983).
45. O. Faix, B. Andersons, D. S. Argyropoulos and D. Robert, in *8th International Symposium on Wood and Pulping Chemistry*, Helsinki, Finland, June 6–9, 1995, Vol. I, pp. 559–566.
46. E. Adler, S. Hernestam and I. Wallden, *Sven. Papperstidn.* **61**, 640 (1958).
47. O. Faix, C. Gruenwald, and O. Beinhoff, *Holforschung* **46**, 425 (1992).
48. E. Tiainen and co-workers, *Holzforschung* **53**, 529–533 (1999).
49. C.-L. Chen, in Ref. 31, p. 409.
50. P. Klason, *Ber. Dtsch. Chem. Ges.* **55**, 448 (1922).
51. C.-L. Chen, in Ref. 31, p. 446.
52. B. C. Ahvazi, C. Srestini and D. S. Argyropoulos, *J. Agric. Food Chem.* **47**, 190–201 (1999).
53. H. Pobiner, *Anal. Chim. Acta* **155**, 57 (1983).
54. C. W. Dence, in Ref. 31, p. 458.
55. F. Viebock and A. Schwappach, *Ber. Dtsch. Chem. Ges.* **63**, 2818 (1930).
56. S. M. Baker, *Holzforschung* **50**, 573–574 (1996).
57. S. Katz, R. P. Beatson, and A. M. Scallan, *Sven. Papperstidn.* **87**, R48 (1984).
58. W. Lange, O. Faix and O. Beinhoff, *Holzforschung* **37**, 63–67 (1983).
59. M. E. Himmel, J. Mylnár, and S. Sarkenen, in C. Wu, ed., *Handbook of Size Exclusion Chromatography*, Marcel Dekker, Inc., New York, 1995, 353–380.
60. A. Jacobs and O. Dahlman, *Nordic Pulp Paper Res. J.* **15**, 120–127 (2000).
61. *Wyatt Corporation Technical Brochure*.
62. H. Hatakeyama, K. Kubota, and J. Nakano, *Cellulose Chem. Technol.* **6** 521 (1972).
63. D. Atack, C. Heitner, and M. I. Stationwala, *Sven. Papperstidn.* **81**, 164 (1978).
64. D. A. I. Goring, in Ref. 31, p. 695.
65. T. K. Kirk, H. H. Yang, and K. Keyser, *Dev. Ind. Microbiol.* **19**, 51 (1978).
66. S. Y. Lin, *Progress in Biomass Conversion*, Vol. **4**, Academic Press, Inc., Orlando, Fla., 1983, p. 31.
67. T. Hattori and M. Shimada, in D. N.-S. Hon, N. Shiraishi, eds., *Wood and Cellulosic Chemistry*, Marcel Dekker, Inc., New York, 1998, 547–571.
68. J. H. Lora and co-workers, in W. G. Glasser and S. Sarkanen, eds., ACS Symposium Series 397: *Lignin—Properties and Materials*, ACS, Washington, D.C., 1989, p. 312.
69. H. Schneider and co-workers, *Int. Sugar J.* **77**, 259 (1975).
70. S. Y. Lin and I. S. Lin, in Ullmann's Encyclopedia of Industrial Chemistry, 5th ed., Vol. **15**, VCH, Weinheim, Germany, 1990, p. 305.
71. W. Q. Dean and D. A. I. Goring, *Tappi* **47**, 16 (1964).
72. A. E. Markham, Q. P. Peniston, and J. L. McCarthey, *J. Am. Chem. Soc.* **71**, 3599 (1949).
73. G. A. DuBey, T. R. McElhinney, and A. J. Wiley, *Tappi* **48**, 95 (1965).
74. V. F. Felicetta and J. L. McCarthey, *Tappi* **40**, 851 (1957).
75. J. Benko, *Tappi* **44**, 771 (1961).
76. J. L. Gardon and S. G. Mason, *Can. J. Chem.* **33**, 1477 (1955).
77. E. E. Harris and D. Hogan, *Ind. Eng. Chem.* **49**, 1393 (1957).
78. Y. Kojima and co-workers, *Jpn. Tappi* **15**, 607 (1961).
79. S. Y. Lin, in Ref. 31, p. 76.
80. L. Sato, *Science (Japan)* **13**, 403 (1943).
81. I. Croon and B. Swan, *Sven. Papperstidn.* **66**, 812 (1963).
82. G. R. Quimby and O. Goldschmid, *Tappi* **49**, 562 (1966).
83. W. Q. Yean and D. A. I. Goring, *Sven. Papperstidn.* **55**, 563 (1952).

84. E. Sjostrom and co-workers, *Sven. Papperstidn.* **65**, 855 (1962).
85. C. H. Ludwig and W. T. Zdybak, Paper presented at the *185th National Meeting of the American Chemical Society, Cellulose, Paper and Textile Division*, Seattle, Wash., Mar. 23, 1983.
86. D. W. Glennie, in Ref. 4, p. 614.
87. K. F. Keirstead, *Colloid Interface Sci.* **III**, 431 (1976).
88. U.S. Pat. 4,562,236 (1985), S. Y. Lin (to Reed Lignin, Inc.).
89. U.S. Pat. 5,094,296 (1990), M. G. DaGue (to Texaco, Inc.).
90. U.S. Pat. 5,095,986 (1990), D. G. Naae and C. A. Davis (to Texaco, Inc.).
91. R. A. Northey, ACS Symposium Series 476: *Emerging Technology of Materials and Chemicals from Biomass*, ACS, Washington, D.C., 1992.
92. U.S. Pat. 2,840,614 (1958), D. W. Gohen (to Crown Zellerbach Corp.).
93. U.S. Pat. 2,826,552 (1958), P. W. Bonewitz, E. H. Fults, and S. W. Hockett (to Bonewitz Chem., Inc.).
94. U.S. Pat. 3,317,431 (1967), S. Kaye (to Wright Chemicals).
95. U.S. Pat. 3,247,120 (1966), J. A. Von Pless (to Cowles Chem. Co.).
96. U.S. Pat. 3,244,505 (1966), C. Adolphson and R. W. Simmons (to Georgia Pacific).
97. A. Wallace and R. T. Ashcroft, *Soil Sci.* **82**, 233 (1956).
98. U.S. Pat. 4,069,217 (1989), W. J. Detroit and M. E. Sanford (to Reed Lignin, Inc.).
99. G. J. Szava, *J. Power Sources* **28**(1/2), 149 (1989).
100. U.S. Pat. 3,447,889 (1969), R. W. Simmons (to Georgia Pacific).
101. S. A. Hong and J. H. Bae, *SPE Reservoir Eng.* **11**, 467 (1990).
102. R. J. Sherman, *J. Food Tech.* **33**(6), 50 (1979).
103. E. I. Tonseth and H. B. Berridge, *Effluent Water Treat. J.* **3**, 124 (1968).
104. U.S. Pat. 4,824,588 (1989), S. Y. Lin (to Reed Lignin, Inc.).
105. U.S. Pat. 4,988,576 (1991), S. Y. Lin and L. L. Bushar (to Daishowa Chemicals, Inc.).
106. Eur. Pat. 0 303 236 A2 (1988), R. H. Samson and J. W. Hollis (to Reed Lignin, Inc.).
107. Jpn. Pat. 02,262,524 (1989), S. Toda and co-workers (to Noda Shokukin Kogyo).
108. Jpn. Pat. 03,206,043 (1991), H. Sakagami, Y. Kawazoe, and K. Konno (to Kawakami).
109. U.S. Pat. 4,676,317 (1987), S. E. Fry and co-workers (to Halliburton Co.).
110. Brit. Pat. 2,210,888 A (1988), C. D. Williamson (to Nalco, Inc.).
111. U.S. Pat. 4,891,415 (1990), S. Y. Lin and L. L. Bushar (to Daishowa Chemicals, Inc.).
112. U.S. Pat. 4,871,825 (1989), S. Y. Lin (to Reed Lignin, Inc.).
113. U.S. Pat. 4,952,415 (1989), T. S. Winowiski and S. Y. Lin (to Daishowa Chemicals, Inc.).
114. S. Y. Lin and W. J. Detroit, *Ekman-Days 1981 Int. Symp. Wood Pulp. Chem.* **4**, 44 (1981).
115. U.S. Pat. 3,841,887 (1974), S. I. Falkenhag and C. W. Bailey (to Westvaco).
116. U.S. Pat. 3,956,261 (1976), S. Y. Lin (to Westvaco).
117. U.S. Pat. 4,728,728 (1988), S. Y. Lin and L. H. Hoo (to Reed Lignin, Inc.).
118. U.S. Pat. 3,123,569 (1964), M. J. Borgfeldt (to Chevron Research and Technology).
119. H. T. Dellicolli, Westvaco Technology and Agricultural Micronutrients, Westvaco Company Brochure, 1992.
120. U.S. Pat. 3,986,979 (1976), H. H. Moorer and C. W. Sandefur (to Westvaco).
121. U.S. Pat. 4,670,482 (1987), P. Dilling (to Westvaco).
122. U.S. Pat. 4,740,590 (1988), P. Dilling (to Westvaco).
123. U.S. Pat. 3,803,041 (1974), M. S. Dimitri (to Westvaco).
124. U.S. Pat. 4,781,840 (1988), P. Schilling (to Westvaco).
125. K. Kratzl and co-workers, *Tappi* **45**, 113 (1962).
126. G. V. Rao and co-workers, *Ind. Pulp Paper 11* (June–July 1978).
127. S. I. Falkehag and co-workers, In *ACS Symposium on Renewable Resources for Plastics*, Philadelphia, Pa., 1975, p. 68.

128. *Surfactant Systems for Pesticides, Westvaco Company Brochure*, 1989.
129. U.S. Pat. 6,019,835 (2000), J. Chatterji and co-workers (to Halliburton Energy Services).
130. J. H. Lora and S. Aziz, *Tappi* **68**(8), 94 (1985).

STUART E. LEBO JR.
JERRY D. GARGULAK
TIMOTHY J. MCNALLY
LignoTech USA, Inc.

LINEAR LOW DENSITY POLYETHYLENE. See ETHYLENE POLYMERS, LLDPE.

LIQUID CRYSTALLINE POLYMERS, MAIN-CHAIN

Introduction

The liquid crystallinity of low molecular weight liquid crystals (LMWLCs) was found more than 100 years ago, when Reinitzer synthesized several esters of cholesterol. In the liquid crystalline (LC) state, the substance shows characteristics of a liquid in terms of its mobility, while it exhibits characteristics of a crystalline material in terms of its optical properties because of the anisotropy in the structure (1,2).

After more than two decades of research work on LMWLCs, Vorländer, in 1923, realized that liquid crystalline polymers (LCPs) must exist too (3,4). The first reference to a polymeric mesophase was in 1937 when Bawden and Pirie found that a solution of tobacco mosaic virus formed two phases, one of which was birefringent in certain concentrations (4). The first liquid crystalline phase for a synthetic polymer was a solution of poly(γ-benzyl-l-glutamate), reported by Elliot and Ambrose in 1950 (5). A few years later, Flory, based on the lattice model, proposed his well-known theory in treatment of liquid crystallinity in lyotropic systems (6). Flory proposed to divide the molecule into several submolecules, usually called segments, which consists of rigid rod-like moieties. Using this model, he concluded that molecular structure and geometry were the most important factors to induce liquid crystallinity. According to the Flory theory, a state with partial order can be formed above a critical concentration whereas the orientations of molecules are totally random below the critical concentration. The transition from a random to a partial order state is discontinuous. During the phase transition, isotropic phase and anisotropic phase coexist (7). The predicted critical axial ratio for the phase transition is 6.4 in a nonsolvent system (7). Flory later incorporated

Encyclopedia of Polymer Science and Technology. Copyright John Wiley & Sons, Inc. All rights reserved.

the temperature effect into the lattice model. For LMWLCs, the aspect ratio is defined as L/d, in which L is the length and d is the diameter of the molecule. For LCPs, the aspect ratio is replaced by the persistence ratio by substituting the molecule length L by the persistence length q.

The revelation of the theory to form the LC phase and the discovery of LC properties from rigid-chain polymers occurred coincidently, which led to an extensive search for new kinds of rigid-chain LCPs from academia and industry. DuPont scientists led the invention and successfully synthesized and identified lyotropic LCPs made of rigid wholly aromatic polyamides in the 1960s and later commercialized the high performance fiber under the name Kevlar (8,9). This became an important milestone in the development of LCPs. Since then, many LCPs with excellent mechanical properties have been synthesized and their applications in various areas have been explored. Workers at Carborundum in the early 1970s patented an aromatic copolyester based on a biphenol monomer and later used the trade name as Ekkcel I-2000 to test market (10,11). This material was diagnosed to possess LC characteristics several years after the invention. Eastman Kodak reported the first well-characterized thermotropic aromatic–aliphatic copolyesters by the reaction of *p*-acetoxybenzoic acid (ABA) and poly(ethylene terephthalate) (PET), later tested market under the trademark X7G (12–14). Both Ekkcel and X7G failed in commercialization because the former had to be processed at extremely high temperatures, whereas the later had too much PET which lowered the performance. Celanese developed various tractable wholly aromatic thermotropic polyesters and poly(ester-amide)s with the trademark Vectra in early 1980s, based on composition reported in patents and elsewhere (15,16). Early development of Vectra LCP aimed at fiber applications, and the unique applications in electrical and electronic interconnection devices were serendipitously discovered and developed in the 1980s. Today, Kelvar fibers have replaced steel, fiber glass, asbestos, and graphite for varieties of applications, including radial tires, brake linings, and composites. Vectra LCP series of resins have been molded for electronic, telecommunication, medical, and other applications. Extruded and blown films are used for strength members and print circuit board, respectively (5,17).

Thermotropic main-chain LCPs have unique combination of properties from both LC and conventional thermoplastic states; these include melt processibility, high mechanical properties, low moisture take-up, and excellent thermal and chemical resistance. With the successful development of these LCPs and recognition of their unique properties, comprehensive research and development have been carried out by both academia and industry (3,5,9,11,14,16–26). Among various R&D directions, the synthesis of new LCPs (3,14,16,17,19–22,24,26), their rheology behavior (27–31), morphology, compatibility and processing of LCPs and blends (32–34) have received most attention.

Synthesis of Main-Chain LCPs

Polyesters and poly(ester-amide)s are two important series of main-chain LCPs. In general, poly(ester-amide)s show increased thermal stability compared to polyesters (5,9,16). They both are synthesized by polycondensation reactions. In

order to increase the reactivity, monomers usually have to be acetylated *in situ* or before conducting the polycondensation reaction (5,9,16). Using the synthesis of LC polyester as an example, the synthesis procedure is described as follows. The transesterification reactions start with phenyl esters of diacids with acetylated aryl diols at relatively high temperatures. Normally, the reaction temperature is higher than the highest melting point of monomers. In order to reduce oxidation, the polymerization is commonly conducted in a nitrogen atmosphere. When low melt viscosity oligomers are obtained, the melt becomes turbid since the fluctuations of orientation of the mesogenic domains are in the range of the wavelength of visible light. A vacuum is then applied to the reaction system to further remove the by-products from the melt and to increase molecular weights. In order to facilitate the diffusion process, a stainless high-torque steel stirrer is desirable to improve the mixing and to accelerate the evolution of by-products, such as acetic acid. A multistep change in the temperature profile is the key to facilitate the molecular weight enhancement. The polymerization reaction can be carried out with or without a catalyst. Catalysts may affect the color and the thermal stability of the final product (18,35). In the reported kinetics study of bulk LCP polycondensation (36–38), for example, the ABA/2,6-acetoxynaphthoic acid (ANA) reaction system, the kinetics was investigated by titrimetry of evolved acetic acid trapped in a sodium hydroxide solution or monitoring the volume of acetic acid. It was found the polycondensation obeyed second-order kinetics irrespective of whether the reaction was catalyzed or uncatalyzed. A Similar conclusion was found for thin-film polymerizations (35).

Most monomers for LCP syntheses are highly crystalline, but do not have characteristics of liquid crystallinity (16,20–22,24–26). During the polymerization, an LC phase forms, and the LC texture evolves with the progress of polymerization and further annealing. To study the in situ morphological evolution of LCPs and annihilation of liquid crystal textures (or defects) during polymerization reactions, a powerful and convenient technique has been developed using the heat-stage polarizing microscope (39,40). This novel approach modernizes the previous film polymerization technique (41–44) and has been extended to investigate the reaction kinetics, effects of catalysts, and monomer structures on the formation of various main-chain LC polyesters and poly(ester-amide)s (35,45,46) as well as to study the evolution of surface energy of LCPs during the polymerization reactions (47). Figure 1 shows a typical evolution of polymerization for 73/27 ABA/ANA with a thickness of 10 μm at 230°C. After the monomer crystals melt and the reaction system reaches the proposed temperature, the reaction system becomes a homogenous phase as shown in Figure 1 (500 s). In the early stage of polycondensation reaction, oligomers form in the molten monomer phase. Their molecular weights and chain lengths increase with reaction time. When the chain lengths of oligomers reach a certain value, they form the LC phase and separate from the isotropic melt. Figure 1 (515 s) shows the reaction-induced phase-separation process during polymerization. The dark area in the micrographs is the isotropic phase; the bright area represents the LC phase. The first sign of forming the LC phase is that many bright LC domains instantaneously appear in the view range. Because of the polydispersity of the chain length, oligomers are partitioned within the isotropic and LC phases according to their chain lengths. A fraction with relatively longer chain lengths forms LC domains, while others remain in the isotropic

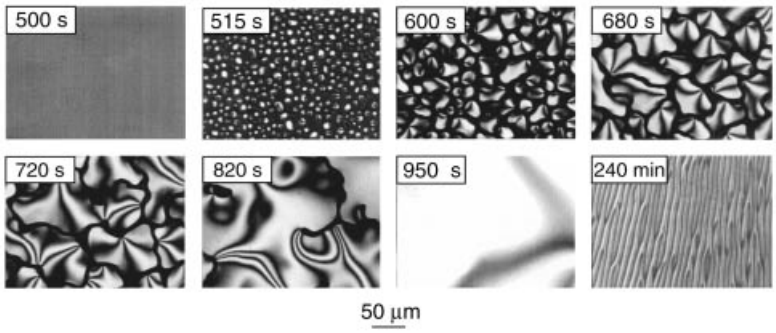

Fig. 1. Micrographs showing morphologies of 73/27 ABA/ANA polymerization reaction system at different reaction times. All the micrographs were obtained from the same area of the same sample. Reaction temperature: 230°C.

phase (39). After the appearance of LC phase, the sizes of LC domains quickly increase, and correspondingly the number of domains decreases because of domain growth and coalescence of adjacent LC domains. As a result, the total view area becomes an anisotropic LC phase (950 s).

LCPs exhibit a variety of textures of different length scales, originated from flow and deformation. A frequently observed texture called *banded texture or stripe texture* often emerges in the samples in which relaxation or shrinkage of molecular chains occurs. The conditions inducing this texture include the following: subjecting to shear and/or elongation flow (48), evaporating the solvent from a lyotropic LC (49,50), and quenching a thermotropic LC from a high temperature (51). As a consequence of stress relaxation after shear or volume deficiency induced by solvent evaporating or quenching, banded texture appears but the local order does not decrease significantly. In the 73/27 ABA/ANA reaction system, with the increase in molecular weight, the volume deficiency causes the appearance of banded texture since adhesion to the substrate prevents uniform shrinkage in three dimensions. Figure 1 (240 min) shows banded texture in the late reaction stage. However, the banded texture may not appear in some other compositions and reaction temperatures. For example, in some cases, the crystallization occurs and interrupts the formation of banded texture (39).

Modification of Main-Chain LCPs. Modifications of main-chain LCPs suitable for conventional processing equipment, without compromising the uniqueness of LC characteristics and the superior mechanical properties, have received most attention. Low cost LCPs are also in high demand. Most frequently used methods include synthesizing by random copolymerization, introducing kinks into the polymer chains by using meta or ortho linkages, introducing flexible linkages, and incorporating bulky side groups into the polymer chains (5,9,16–18,20–22).

Random Copolymerization. Random copolymerization is an effective way to disturb the regular structure of the polymer chain. The lack of periodicity along the chain inhibits crystallization, and thus reduces the crystallinity and depresses T_m (the transition temperature to form an LC phase), without necessarily leading to an additional loss of mesogenicity and T_i (the transition temperature

from an LC phase to an isotropic phase). This approach has been adapted when designing random copolymers such as Vectra A by Celanese (Ticona) with commercial success. Vectra A is a copolyester based on ABA and ANA with a mole ratio of 73/27. The melting point of this LCP is around 280°C, which is much lower than the melting points of either ABA or ANA homopolymers (5,16,18).

The morphologies of both ABA and ANA homopolymers and 73/27 ABA/ANA copolymer prepared by thin-film polymerization show that crystallization occurs in the homopolymerization systems and the liquid crystal state remains stable in the copolymerization system (39–44), clearly indicating that the random copolymerization is an effective way to retard the crystallization. Transmission electron microscopy revealed that the microstructures of homopolymers of ABA and ANA had more obvious lamellar texture (41–44).

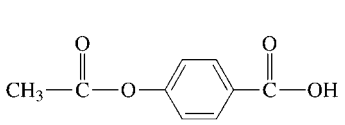

p-Acetoxybenzoic acid (ABA)

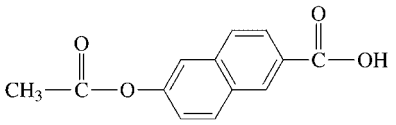

2,6-Acetoxynaphthoic acid (ANA)

Introduction of Kinks. Introduction of kinks into the polymer backbone effectively reduces the regularity of the molecules, and thus lowers the melting temperature. However, the incorporation of kinking units has an unfavorable influence on the liquid crystallinity since the kinks disrupt the straightness of the molecules. Also, the inducing of kinks into molecular chains is unfavorable for the thermal stability of the LCPs (16–26). The exact role of kinks has attracted remarkable attention because the formation of liquid crystallinity is not directly related to the kink content and many interesting phenomena have been found. For example, *m*-acetoxybenzoic acid (mABA) has a kink created by the meta linkage. However, the thin-film polymerization results of mABA/ANA indicate that the LC phase may still be observed even when the mABA content is as high as 66 mol% at 183°C (44).

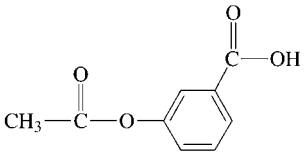

m-Acetoxybenzoic acid (mABA)

Isophthalic acid (IA) is a monomer extensively employed to modify LCPs because its cost is low and the meta linkage can induce a kink into the molecular chain. The resultant polymer has a lower T_m. However, the meta linkage also has a detrimental effect on the stability of the LC phase because it will disturb the LC character if its percentage is too high. In the thin-film polymerization of ABA/acetoxy acetanilide (AAA)/IA system, the critical meta-linked IA content is 26 mol% at 280°C, which means the liquid crystal phase can only be formed when IA content is lower than 26% and crystallization occurs once the IA content is higher than this critical point (45).

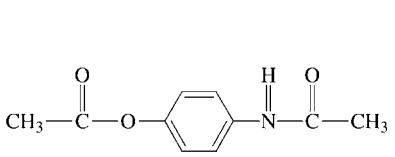

Acetoxy acetanilide (AAA)

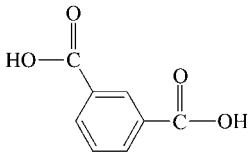

Isophthalic acid (IA)

Phthalic acid (PA) has an ortho linkage which can also introduce a kink into the molecular chain. However, it is seldom utilized to modify the LCPs because the liquid crystal phases are not stable for the systems containing PA units (46). Recently, it was found that, in the early stage of thin-film polymerization, both ANA/AAA/PA and ANA/AAA/IA systems form liquid crystal phase when the PA or IA content is 20%. However, with the further reaction going on, the ANA/AAA/PA system crystallizes, whereas the ANA/AAA/IA system remains in the LC state (46).

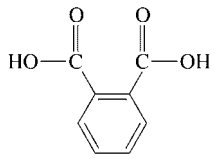

Phthalic acid (PA)

Since kinks shorten the persistence length of the polymer chain, the LC characteristics may be destabilized if the kink content is high. Figure 2 shows the critical ANA content for the two reaction systems, ANA/AAA/IA and ANA/AAA/PA, to form liquid crystallinity at different reaction temperatures. For the ANA/AAA/PA system, the window of reaction temperature is wide because of the low melting point (205°C) of PA, and the critical ANA content range is very

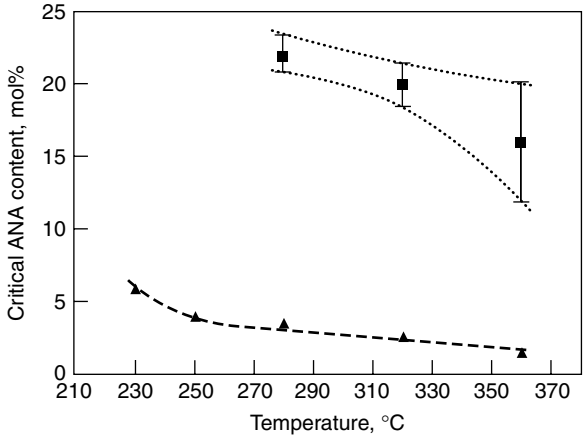

Fig. 2. The dependence of the critical ANA content for ANA/AAA/PA and ANA/AAA/IA systems on reaction temperature. ■ ANA/AAA/IA system; ▲ ANA/AAA/PA system.

narrow for all the temperatures we investigated. For the ANA/AAA/IA system, the reaction temperature window is restricted by the high melting point (342°C) of IA. When conducting the polymerizations at low temperatures, such as 250°C, the reactions are incomplete and IA crystals remain after reaction. So the reaction temperatures used have to be relatively high, from 280 to 360°C. The most striking and interesting phenomenon in Figure 2 is that PA has a much higher tendency to form liquid crystallinity than IA. One of the causes may be due to the *cis* conformation of the bridging groups, especially for the amide group, which can compensate for the 60° angular conformation induced by an ortho linkage. As a result, the reaction system containing PA may have more opportunities to form a relatively straight conformation than the system containing IA. The other possibility is that the resultant polymer in the ANA/AAA/PA system may form a spiral chain conformation because of the rotation of the bridging groups, thus inducing liquid crystallinity (46).

The final morphology of LCPs depends on kinks content because the elastic constants of LC during the reaction are strongly affected by the kink structure. During polymerization, the defects in the LC phase involve very high distortion energy in the case of rigid or semirigid polymers. Disclinations with opposite signs tend to attract each other in order to release the energy and lead to the annihilation and the decrease in the number of defects (52–55). Because the elastic constant values decrease with increasing kink content, the defect density increases with increasing kink content since LCPs with kinks cannot annihilate fast and completely in the reaction system (45,46).

Modification with Flexible Segments. Modification with flexible segments is another important way to improve the melt processibility. By inserting flexible segments to separate the mesogenic units along the polymer chain, the chemical periodicity of the molecule is preserved. These polymer systems are referred to as semirigid polymers. The influence of flexible linkages on the melting temperature can be considered in several ways. In addition to facilitate the motion of the polymer chain, the random distribution of monomeric units also decreases the melting temperature further if the flexible segments are introduced by a copolymerization. The disadvantages of introducing a flexible spacer to a polymer chain are that it disturbs the liquid crystallinity and affects the thermal stability of the resultant polymer.

The most typical spacer segments used consist of flexible polymethylene $-(CH_2)_n-$ of varying length n. T_i decreases in a zigzag fashion in homologous series in which the spacer length regularly increases. This zigzag characteristic is referred to the odd–even effect. T_i tends to be higher when there is an even number n of methylene groups in the spacer, but this oscillation is attenuated on ascending the series. This effect is best understood by assuming the conformation of the methylene spacer to be all trans, which has the lowest energy. An even-numbered polymethylene spacer possesses a set of low energy *trans* conformers that force the rigid units to adopt a collinear disposition. In contrast, an odd-numbered spacer places the two mesogenic groups in the angled orientation disfavoring the ordering of a nematic phase (19).

Introduction of Lateral Groups. Lateral groups have been introduced to lower the melting points of LCPs. Grafting bulky side groups onto the polymer main chain influences the melting temperature in several ways. It effectively

increases the interchain distance and reduces the interchain forces so that the efficiency of the chain packing is reduced. Moreover, this effect is much enhanced by the copolymerization because the randomness of the polymer chain further decreases the crystallinity and melting point (19,23). Unfortunately, the lateral group has a strongly unfavorable effect on the formation of liquid crystallinity, especially for the bulky lateral groups, which will immediately cause the loss of liquid crystallinity if they are randomly distributed in the molecular chain. Two reaction systems ANA/AAA/3-fluorophthalic acid (FPA) and ABA/AAA/PA were compared to identify the effect of lateral group on liquid crystallinity. Because of the kink structure of the PA unit and the different sizes of hydrogen and fluorine atoms affect the formation of crystallinity, the critical ABA content to form the LC phase for the ABA/AAA/FPA and ABA/AAA/PA systems at 280°C are 9 and 5%, respectively, indicating that fluorine atoms modify chain distance and conformation and lower the stability of the LC phase (56).

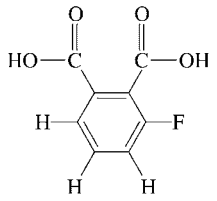

3-Fluorophthalic acid (FPA)

Rigid-chain polymers containing different concentration of laterally attached side rods have been demonstrated in bulk reactions using a Vectra LCP as the base material, as illustrated in Figure 3 (57). These polymers exhibit liquid crystallinity even up to a maximum side-rod concentration of 20 mol%. The crystallinity of the

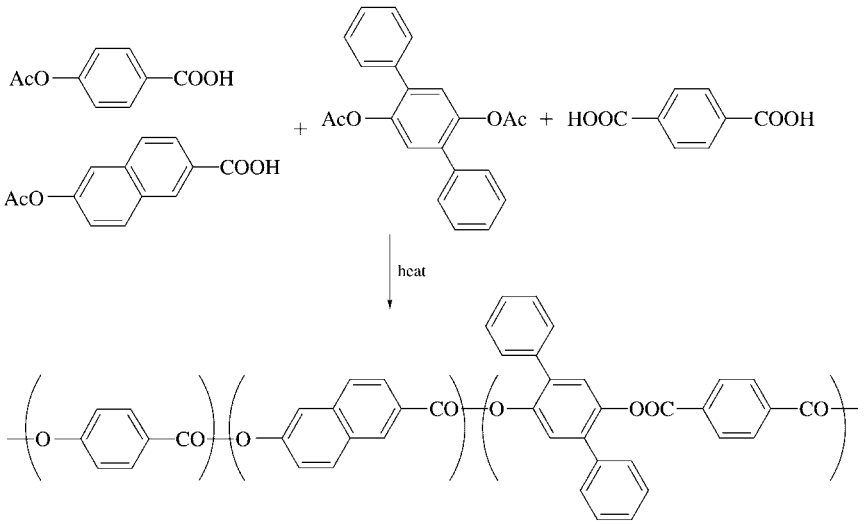

Fig. 3. Incorporation of laterally attached side rods.

polymers, however, decreases with the increase in the side-rod concentration. The advantage of these polymers is their lower dielectric constants compared with their parent polymers, ie, similar polymers but without laterally attached side rods. A dielectric constant of 2.6 can be achieved by incorporating 10 mol% of laterally attached side rods, which is 0.5 lower than that of its parent polymer. The reduction in dielectric constant may be attributed to low crystallinity and less dense packing structure of the polymers induced by incorporating of laterally attached side rods. This series of polymers also has good thermal stability (see also LIQUID CRYSTALLINE POLYMERS, SIDE-CHAIN).

Thermal Stability and Degradation

Thermal stability, degradation behavior, and kinetics of commercially available main-chain LC polyesters such as Ticona's Vectra, BP-Amoco's Xydar, DuPont's Zenite, Eastman's X7G, and Mitsui's LC polyimide have been reported (58–62). There are two degradation processes for most of these LCPs in air, but only one in N_2. By observing the ftir bands, it can be concluded that CO_2 is the dominant product in both N_2 and air, and it exists all through the degradation process. In air, the by-products may consist of H_2O, CO, CO_2, phenols, aryl esters, ketones, and others through dehydration, decarboxylation, and decarbonylation. The stability at the beginning of the decomposition process follows the order Xydar SRT-900 > Vectra A950 > Vectra B950 (60). The activation energy E_a of thermal degradation for Vectra A950 and Vectra B950 are about 232 and 197 kJ/mol in N_2, and 222 and 159 kJ/mol in air, respectively (60).

Crystallization

Crystallization of main-chain LCPs is considerably different from that of conventional polymers, such as polyethylene or PET. LCPs have reduced flexibility compared to the latter, which implies that large translations of their molecules are required for recrystallization. Thus the crystallization process in an LC phase may present its own peculiarities. The orientational order associated with mesophase may act as a precursor for further crystal growth, especially in monotropic LCPs where the metastability of mesophase generally leads to the formation of a more stable crystal phase.

The overall crystallization process includes two steps, primary nucleation followed by crystal growth. The process can be well described by the Avrami equation (63,64) as shown:

$$1 - \theta = \exp(-Kt^n)$$

where θ is the relative crystallinity at time t, n is the dimensionality of crystal growth, and K is a temperature-dependent constant that depends on the growth geometry, the number of nuclei present, and the linear growth rate of polymer crystals. For most LCPs, n is found to be less than 1 for the growth of liquid crystallinity.

The crystallization process for most commercially available LCPs can be found elsewhere (65–72). For most LCPs, there are two transition processes: one is a fast transition process, ascribed to the aggregation of rigid chains, and the other is a slow transition process developing gradually during the later heat-treatment stage. These two processes also manifest in different crystal structures. For LCPs synthesized from ABA/ANA compositions, the fast process leads to hexagonal packing with cylindrical symmetry along the chain direction, while the slow process gives rise to orthorhombic packing (66). The Avrami parameter n values for Vectra A are in the low range 0.2–0.5, which is due to the fact that each crystal does not grow with a constant radial growth rate (70). The crystallization and phase transition behavior in LC polyimides have been investigated (73–78). Smectic-layered structures have been found for some polyimides.

Surface Energy

The surface energies of Vectra A, Vectra B, and Xydar have been reported using contact angle techniques at room temperature (79,80). Experimental data suggest that surface energy values match between the two-liquid geometric method (81,82) and the three-liquid acid–base (83,84) method if a correct combination of testing liquids is used. However, three-liquid Lifshitz–van der Waals acid–base method is more suitable for the surface energy calculation of these three LCPs, and provides much more information, eg, acidity and basicity of LCP surfaces. The average surface energies of Vectra A-950, Vectra B-950, and Xydar are 41.0, 41.9, and 42.3 mJ/cm^2, respectively. In addition, all these three LCPs should be classed as monopolar Lewis bases because their Lewis acid components, γ^+, are negligible. The incorporation of a small amount of $-C(CF_3)_2-$ in the main chain can lower LCP's surface energy and the fluorocarbons are preferentially enriched at the air–polymer interface (85).

Morphology and Microstructure

In the LC phase and within a volume element, the molecules are aligned along one common direction in average, labeled by a unit vector $\boldsymbol{n}$. A region within the sample volume where the directon does not change very much is defined as a *domain*. The distribution of domain orientations within the sample forms texture (86,87). The various rheological behaviors, which strongly affect the processing conditions and final properties of these materials, are the results due to the interaction between the texture and the flow field. To sum up, the final properties are determined to a large extent by the microstructure, which, in turn, is due to a combination of the inherent properties of the LCPs and the flow conditions during processing.

It has been reported that three kinds of distinct fibrils could be observed in oriented LCP fibers, extrudates, and mold parts; they are 50-nm microfibrils, 500-nm fibrils and 5 μm macrofibrils (88). For highly oriented fine fibers, the LC domains are elongated along the fiber direction with a size of about 500 nm

in the transverse direction. A periodic and inherent defect layer of about 50 nm has also been noticed in the fiber structure. For large diameter extruded rods, the degree of orientation decreases from the outer skin to the core because the shear rate is higher at the outer skin than at the core (89). Increasing the draw ratio cannot eliminate the skin–core structure. However, by changing the temperature profile within the extrusion die, one may be able to induce a higher shear rate at the core and thus enhance the overall degree of orientation and fiber modulus (90). The mechanical properties of extruded LCP films in various directions follow typical macromolecular composites theory and can be predicted using the Tsai–Hill equation (91). Because of the complexity of flow patterns during the injection molding, a layered structure can be found in the cross-section of molded parts (5,16,88). Each layer corresponds to each flow pattern. However, the degree of orientation decreases as one proceeds from the skin to the core (88). Later studies revealed much detailed morphology of the nature of the microfibrillar hierarchy and the shape of the microfibrils was found to be tape-like (92,93).

LCP Rheology and Blends

Since the main characteristic of thermotropic LCP melts is the persistence of order in the material even when the stresses causing deformation are removed, the rheological behavior of LCP is different from normal polymers. The viscosity vs shear rate behavior for LCPs can be represented by three distinct regions: (*1*) a shear thinning region at low shear rates, (*2*) a Newtonian region in an intermediate shear rate region, (*3*) a power-law shear thinning region at high shear rates (27). Although very few sets of data show all the three regions in a single polymer, analysis of the published data of a number of authors for LCPs identified the three flow regions (28). An important characteristic of LCPs is that they have longer relaxation times compared with flexible coil polymers. Two relaxation times for LCP melts one for the stresses and the other for orientation have been reported (29). Although these phenomena were related through the stress-optical law for conventional flexible coil polymers, they were independent for LCPs. The relaxation time of orientation was longer than the relaxation time of stress; thus, the orientation LCPs achieved during processing was retained in the solid state more easily than for flexible chain polymers.

Using the unique and superior properties of LCPs to enhance the thermal and mechanical performance of various engineering resins, studies have been conducted since late 1980s (94–104). The LCP phase is preferentially oriented in the direction of flow. LCPs can also be viewed as a processing aid (lubricant), which effectively reduces the viscosity of the blends if the LCP content is low (32,94,96–99). It is found that the LCP domains do not always deform into fibrils as reinforced elements for some LCP/thermoplastic blends. One must provide adequate shear stress and torque history to deform LCPs into elongated fibrils. The rule of thumb is to have process conditions which yield the viscosity ratio of the dispersed LCP phase to the thermoplastic matrix to be lower than 1 (99,103). LCPs blends also suffer from poor adhesion strength between the LCP phase and the thermoplastic matrix. Forming cross-linkable LCP blends is one of the ways to overcome it

(105–107). LCP/LCP blends have also been developed (33,108) to yield LCPs with a better performance.

Applications of Main-Chain LCPs

Thermotropic LCPs have a great potential as structural materials. They have high strength and stiffness in the direction of the molecular alignment and their low melt viscosity and low shrinkage facilitate processing. Most applications of main-chain LCPs are based on the excellent mechanical properties of these materials (3,5,9,16,17,26,30). As we know, high modulus and high tensile strength occur when polymer molecules are aligned and extended. In ordinary isotropic polymers, the molecules tend to align and to uncoil in tensile and shear fields, but recoil and partially lose their orientation when removing the stress. To obtain high modulus, there are the following requisites: the individual molecule should be stiff, the alignment of the molecules has to be nearly prefect, and ratio of the aromatic to aliphatic linkages must be high. These conditions are satisfied by wholly aromatic LCPs because of their high tendency to align and to remain in that orientation. The chemical structures of wholly aromatic LCPs provide a good answer for these attainments.

Because thermotropic wholly aromatic LCPs have characteristics such as high strength, low melt viscosity, low shrinkage, ease of processibility, excellent thermal resistance, low water, and gas absorption, they have wide applications in following areas: fibers, rods, sheets, composites used in mechanical and chemical industries; chip carriers, connectors, switches used in electronics; connectors, couplers, buffers used in fiber optics; interior components, brackets in aerospace; and so on (3,5,9,16,17,26,30).

LCP fibers have high strength and stiffness and are lightweight. Fabrics of LCP fibers (such as Vectran fibers) have been used as ballistic garments, helmets, and military flak jackets. Excellent cut/tear resistance and thermal insulation also make LCP fibers desirable for protective gloves and clothing. Sheet products made from mineral-filled LCP variants or multilayer copper and LCP laminates have been used for thermoforming and electroplating for printed circuit board. Large-diameter melt-extruded LCP rods have been used to replace steel wire and even used as strength members in optical cable applications. This is because LCP rods have the following characteristics: lightweight and flexible, excellent tensile properties, which prevent optical fibers from breaking during the lay down process, very small negative coefficient of thermal expansion, which minimize the external stress, good chemical resistance, and almost zero water regain. LCP rivets offer an attractive alternative to metal for fasteners without the high cost and heavy weight of titanium or the corrosion problem associated with aluminum. Because Kevlar and Vectran fibers are strong, nonabrasive, dimensionally and thermally stable, they also have been used to reinforce brake linings. For injection-molding resins, the addition of fillers or fiber-reinforced elements into neat LCP resins may be the best approach to obtain high quality. Most commercial LCP products contain 30–70% fillers or fiber-reinforced elements in order to lower the LCP cost and have balanced mechanical and electrical properties. LCPs offer at least a few advantages over other engineering resins in electric applications, for example, low

mold shrinkage, fast cycling time, capability of molding thin parts, low moisture regain, and better chemical and mechanical properties. In addition, LCPs are little affected by radiation.

LCPs have been in commercial use for over 20 years, and new applications are still emerging. It is expected that commercial LCPs are still in the growth phase and that significant increases in usage will occur in the twenty-first century.

BIBLIOGRAPHY

"Liquid Crystalline Polymers" in *EPSE* 2nd ed., Vol. 9, pp. 1–61, by S. L. Kwolek, E. I. du Pont de Nemours & Co., Inc., P. W. Morgan and J. R. Schaefgen, Consultants.

1. H. Baumgärtel, E. U. Franck, W. Grünbein, and H. Stegemeyer, eds., *Topics in Physical Chemistry*, Vol. **3**: Liquid Crystals, Springer, New York, 1994.
2. G. W. Gray and P. A. Winsor, eds., *Liquid Crystals & Plastics Crystals*, Vol. **1**, John Wiley & Sons, Inc. New York, 1974.
3. A. A. Collyer, *Liquid Crystal Polymers: From Structures to Applications*, Elsevier Applied Science, London, 1992.
4. E. Chiellini, M. Giordano, and D. Leporini, eds., *Structure and Transport Properties in Organized Polymeric Materials*, World Scientific, Singapore, 1997.
5. T. S. Chung, G. W. Calundann, and A. J. East, *Encyclopedia of Engineering Materials*, Marcel Dekker, Inc., Vol. **2**, (1989), p. 625.
6. P. J. Flory, *Proc. R. Soc. London, ser. A* **243**, 73 (1956).
7. P. J. Flory, in *Recent Advances in LCPs*, Elsevier Applied Science, London, 1985.
8. U.S. Pat. 3575933 (1971), E. F. Hoegger, J. R. Schaefgen, and C. W. Stephens; U.S. Pats. 3600350 (1971) and 3671542 (1972), S. L. Lwolek; U.S. Pat. 3943110 (1976), P. W. Morgan (to E. I. du Pont de Nemours & Co., Inc.).
9. M. Jaffe, *Encyclopedia of Polymer Science and Engineering*, John Wiley & Sons, Inc., New York, Vol. **7**, (1987), p. 699.
10. U.S. Pat. 3637595 (1972), G. Cottis, J. Economy, and B. E. Nowak; U.S. Pat. 3759870 (1973), J. Economy and B. E. Nowak (to Carborundum).
11. J. Economy and co-workers, *J. Polym. Sci. Polym. Chem.* **14**, 2207 (1976).
12. U.S. Pats. 3778410 (1973) and 3804805 (1974), H. F. Kuhfuss and W. J. Jackson Jr.; U.S. Pats. 4153779 (1979), W. J. Jackson, G. G. Gebeau, and H. F. Kuhfuss, (to Eastman Kodak).
13. W. J. Jackson, *Brit. Polym. J.* **12**, 153 (1980).
14. W. J. Jackson, *Mole. Cryst. Liq. Cryst.* **169**, 23 (1989).
15. U.S. Pat. 4067852 (1978), 4161470 (1979), 4184996 (1980), G. W. Calundann; U.S. Pat. 4330457 (1982), A. J. East, L. F. Charbonneau, and G. W. Calundann (to Ticona).
16. G. W. Calundann, and M. Jaffe, in *Proceedings of the Robert A. Welch Conferences on Chemical Research*, Vol. XXVI, Synthetic Polymers, (1982), p. 247.
17. T. S. Chung, *Advances in Thermotropic LCPs*, Technomic, Lancaster, 2001.
18. T. S. Chung, *Polym. Eng. Sci.* **26**, 901 (1986).
19. A. A. Collyer, *Mater. Sci. Tech.* **5**, 309 (1989).
20. J. Economy and K. Goranov, *Adv. Polym. Sci.* **117**, 221 (1994).
21. J. I. Jin JI and C. S. Kang, *Prog. Polym. Sci.* **22**, 937 (1997).
22. H. Han and P. K. Bhowmik, *Prog. Polym. Sci.* **22**, 1431 (1997).
23. A. M. Donald and A. H. Windle, *LCPs*, Cambridge University Press, Cambridge, 1992.

24. V. P. Shibaev and L. Lam, eds., *LC and Mesomorphic Polymers*, Springer-Verlag, New York, 1994.
25. A. Ciferri, ed., *Liquid Crystallinity in Polymers: Princles and Fundamental Properties*, VCH Publishers, New York, 1991.
26. R. A. Weiss, and C. K. Ober, *LCPs*, American Chemical Society, Washington, D.C., 1990.
27. S. Onogi and T. Asada, in G. Astarita, G. Marrucci, and L. Nicolais, eds., *Rheology*, Plenum Press, New York, 1980.
28. K. F. Wissbrun, *J. Rheol.* **25**, 619 (1981).
29. R. E. Jerman and D. G. Baird, *J. Rheol.* **25**, 272 (1981).
30. F. N. Cogswell and K. F. Wissbrun, in D. Acierno, and A. A. Collyer, eds., *Rheology and Processing of LCPs*, Chapman & Hall, New York, 1996, Chapt. "4".
31. D. E. Turek and G. P. Simon, *Polymer* **34**, 2750 (1993).
32. A. Datta, and D. G. Baird, *Polymer* **36**, 505 (1995).
33. M. T. De Meuse and M. Jaffe, *Mol. Cryst. Liq. Cryst.* **157**, 535 (1988).
34. M. Jaffe, P. Chen, E. W. Choe, T. S. Chung, and S. Makhija, in P. Hergenroth eds., *Advances in Polymer Science*, Vol. **117**, Springer Verlag, New York, 1994, p. 297.
35. T. S. Chung and S. X. Cheng, *J. Polym. Sci, Part A: Polym. Chem.* **38**, 1257 (2000).
36. P. A. Williams, and co-workers, *Macromolecules* **29**, 1874 (1996).
37. X. Han and co-workers, *Macromolecules* **29**, 8313 (1996)
38. J. Mathew, and co-workers, *Macromolecules* **25**, 7338 (1992).
39. S. X. Cheng, T. S. Chung, and S. Mullick, *Chem. Eng. Sci.* **54**, 663 (1999).
40. S. X. Cheng, and T. S. Chung, *J. Phys. Chem., Part B* **103**, 4923 (1999).
41. J. Liu, F. Rybnikar, and P. H. Geil, *J. Polym. Sci., Part B: Polym. Phys.* **30**, 1469 (1992).
42. J. Liu, F. Rybnikar, and P. H. Geil, *J. Macromol. Sci., Part B: Phys.* **35**, 375 (1996).
43. A. Lucero and co-workers, *Polymer* **38**, 4387 (1997).
44. F. Rybnikar, B. L. Yuan, and P. H. Geil, *Polymer* **35**, 1831 (1994).
45. S. X. Cheng, T. S. Chung, and S. Mullick, *J. Polym. Sci., Part B: Polym. Phys.* **37**, 3084 (1999).
46. S. X. Cheng, and T. S. Chung, *J. Polym. Sci., Part B: Polym. Phys.* **38**, 2221 (2000).
47. T. S. Chung and K. X. Ma, *J. Phys. Chem., Part B* **103**, 108 (1999).
48. C. Viney and W. S. Putnam, *Polymer* **36**, 1731 (1995).
49. W. Wang, G. Lieser, and G. Wegner, *Makromol. Chem.* **194**, 1289 (1993).
50. J. Wang, S. Bhattacharya, and M. M. Labes, *Macromolecules* **24**, 4942 (1991).
51. S. Chen and co-workers, *Liq. Crys.* **13**, 365 (1993).
52. W. Wang, *Liq. Crys.* **19**, 251 (1995).
53. C. Liu, and M. Muthukumar, *J. Chem. Phys.* **106**, 7822 (1997).
54. D. K. Ding and E. L. Thomas, *Mol. Cryst. Liq. Cryst.* **241**, 103 (1994).
55. J. Gunther and co-workers, *Polymer* **39**, 4497 (1998).
56. S. X. Cheng and T. S. Chung, *Investigation of the Effect of Lateral Group on Liquid Crystallinity, in preparation.*
57. C. He and co-workers, *J. Polym. Sci., Part A: Polym. Chem.* **39**, 1242 (2001).
58. H. Sato and co-workers, *J. Anal. Appl. Pyrolysis* **37**, 173 (1996).
59. D. O. Hummel and co-workers, *Makromol. Chem.* **194**, 1545 (1993).
60. X. Jin and T. S. Chung, *J. App. Polym. Sci.* **73**, 2195 (1999).
61. T. S. Chung and X. Jin, *Polym. Eng. Sci.* **40**, 841 (2000).
62. K. P. Pramoda and A. Yamaguchi, *Polym. Deg. Stab.* **67**, 365 (2000).
63. M. Avrami, *J. Chem. Phys.* **7**, 1103 (1939).

64. M. Avrami, *J. Chem. Phys.* 212 (1940).
65. M. Jaffe, J. D. Menczel, and W. E. Bessey, in E. A. Turi, ed., *Thermal Characterization of Polymeric Materials*, Academic Press, San Diego, Calif., 1997. Chapt. "2".
66. S. Z. D. Cheng, and co-workers, *Macromolecules* **22**, 4240 (1989).
67. S. Z. D. Cheng and co-workers, *Macromolecules* **23**, 1196 (1990).
68. J. Blackwell, H. M. Cheng, and A. Biswas, *Macromolecules* **21**, 39 (1988).
69. N. D. Field and co-workers, *Macromolecules* **21**, 2155 (1988).
70. T. S. Chung and co-workers, *J. Appl. Polym. Sci.* **72**, 1139 (1999).
71. T. S. Chung and co-workers, *Polym. Eng. Sci.* **39**, 953 (1999).
72. K. P. Pramoda and T. S. Chung, *Polym. Prepr.* **41**, 1391, (2000).
73. H. R. Kricheldorf and N. Probst, *High Perform. Polym.* **7**, 471 (1995).
74. H. R. Kricheldorf, and M. Gurau, *J. Polym. Sci., Part A: Polym. Chem.* **33**, 2241 (1995).
75. H. R. Kricheldorf, *Advances in Polymer Science*, Vol. **141**, Springer-Verlag, Berlin, 1999, p. 83.
76. S. L. Liu and co-workers, *J. Polym. Sci., Part B: Polym. Phys.* **36**, 1679 (1998).
77. S. L. Liu and co-workers, *Polym. Eng. Sci.* **38**, 1845 (1998).
78. S. L. Liu and co-workers, *J. Polym. Sci., Part B: Polym. Phys.* **38**, 3018 (2000).
79. K. X. Ma, T. S. Chung, and R. J. Good, *J. Polym. Sci., Part B: Polym. Phys.* **36**, 2327 (1998).
80. T. S. Chung, K. X. Ma, and M. Jaffe, *Macrom. Chem. Phys.* **199**, 1013 (1998).
81. D. K. Owens and R. C. Wendt, *J. Appl. Polym. Sci.* **13**, 1741 (1969).
82. D. H. Kaelble, *J. Adhesn.* **2**, 50 (1970).
83. C. J. van Oss, M. K. Chaudhury, and R. J. Good, *Chem. Rev.* **88**, 927 (1988).
84. C. J. van Oss and co-workers, *J. Colloid Interface Sci.* **128**, 313 (1989).
85. K. X. Ma and T. S. Chung, *J. Phys. Chem. B* **105**, 4145 (2001).
86. P. G. de Gennes and J. Prost. *The Physics of Liquid Crystals*, Clarendon Press, New York, 1993.
87. S. Chandrasekhar, *Liquid Crystals*. Cambridge University Press, Cambridge, 1977.
88. L. C. Sawyer and M. Jaffe, *J. Mater. Sci.* **21**, 1897 (1986)
89. T. S. Chung, *J. Polym. Sci., Polym. Lett. Ed.* **24**, 299 (1986).
90. T. S. Chung, *J. Polym. Sci., Part B: Phys.* **26**, 1549 (1988).
91. Y. Ide and T. S. Chung, *J. Macromol. Sci., Part B: Phys.* **23**, 497 (1985).
92. L. C. Sawyer and co-workers, *J. Mater. Sci. Lett.* **11**, 69 (1992)
93. L. C. Sawyer and co-workers, *J. Mater. Sci.* **28**, 225 (1993)
94. A. Siegmann, A. Dagan, and S. Kenig, *Polymer* **26**, 1325 (1985).
95. T. S. Chung, *Plast. Engi.* **43**, 39 (Oct. 1987).
96. G. Kiss, *Polym. Eng. Sci.* **27**, 410 (1987).
97. S. G. James, A. M. Donald, and W. A. Macdonald, *Mol. Crys. Liq. Crys.* **153**, 491 (1987).
98. T. M. Malik, P. J. Carreau, and N. Chaplea, *Polym. Eng. Sci.* **29**, 600 (1990).
99. D. Dutta and R. A. Weiss, in D. N. Schulz and J. E. Glass, eds. *Polymers as Rheology Modifiers*, American Chemical Society, Washington, D.C., 1991, p. 145.
100. D. Beery, S. Kenig, and A. Siegmann, *Polym. Eng. Sci.* **31**, 451 (1991)
101. A. Mehta and A. I. Isayev, *Polym. Eng. Sci.* **31**, 971 (1991).
102. W. C. Lee and A. T. Dibenedetto, *Polym. Eng. Sci.* **32**, 400 (1992).
103. J. P. D. Souza and D. G. Baird, *Polymer* **37**, 1985 (1996).
104. H. Wang and co-workers, *Polymer Composites* **21**, 114–123 (2000).
105. X. Y. Zhao and co-workers, *J. Appl. Polym. Sci.* **69**, 349 (1998).
106. X. Y. Zhao and co-workers, *J. Appl. Polym. Sci.* **76**, 1141 (2000).

107. H. R. Kricheldorf and A. Gerken, *High Performance Polym.* **9**, 75 (1997).
108. B. Gupta and co-workers, *J. Appl. Polym. Sci.* **53**, 575 (1994).

TAI-SHUNG CHUNG
SI-XUE CHENG
Institute of Materials Research and Engineering
National University of Singapore
MICHAEL JAFFE
The State University of New Jersey

LIQUID CRYSTALLINE THERMOSETS

Introduction

Liquid crystalline thermosets (LCTs) may generally be defined as low molar mass, multifunctional monomers, which can be cured thermally, chemically, or photochemically in the melt state, leading to a highly cross-linked, high glass-transition temperature material which exhibits liquid crystalline order. These materials are expected to exhibit properties that combine the useful benefits of both cross-linked thermosets and liquid crystals, such as low viscosity for ease of processing, good dimensional stability, high glass-transition temperatures, good thermal stability, high mechanical properties, the ability to be oriented, and good barrier properties. Among the applications envisioned for these materials are high performance resins for composites, optical thin films, and packaging material for microelectronics. The eventual use of LCTs for these types of applications will depend on the continued investigation and development of their properties.

The first mention of LCTs is in a paper by de Gennes in 1969 (1). The first experimental investigations occurred in the 1970s (2,3). However, significant numbers of publications did not appear in the literature until the 1990s. Early efforts focussed primarily on the liquid crystalline structure of the monomers or the cured networks, whereas more recently there have been efforts to examine the evolution of structure during cure, the nature of the cure process, and a variety of properties.

Molecular Structure of Monomers

Quite a large number of different monomer structures have been synthesized (4). Reactive end groups utilized include epoxy (5–10), acrylate and methacrylate

Encyclopedia of Polymer Science and Technology. Copyright John Wiley & Sons, Inc. All rights reserved.

(11–14), maleimide and nadimide (15–21), vinyl (22,23), isocyanate and cyanate ester (24–27), and ethynyl (28–30). In one case, a dual-curing monomer containing both acrylate and ethynyl groups has been made (31). The mesogen is generally aromatic, and may include ester (6–8,10,16,19–21,25–30,32–34), amide (15,18), or azomethine (35,36) linkages. There may also be a flexible spacer, typically between the mesogen and the reactive group (10,13,37). Two fairly unusual structures involve twin mesogen LCTs, in which there are two mesogenic units separated by a flexible spacer (34,36,38,39), and LCTs in which the reactive group is placed between the flexible unit and the mesogen (40). It is also possible to create branched monomers that exhibit a liquid crystalline phase (41). While most monomers exhibit either achiral nematic or smectic phases, by appropriate choice of the monomer structure it is possible to create chiral smectic (42) and discotic phases (43). Tables 1 and 2 provide a representative list of monomers that have been synthesized. Two epoxies that have been extensively compared are shown below.

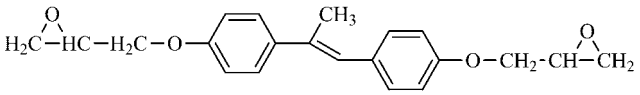

1

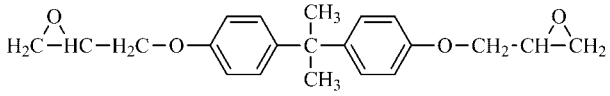

2

Diglycidyloxy-α-methylstilbene (**1**) is a liquid crystalline epoxy, while the diglycidyl ether of bisphenol A (**2**) is a typical non-liquid-crystalline epoxy.

LCT monomers follow the general rules for liquid crystalline behavior that have been found for nonreactive low molar mass liquid crystals (44–48). Thus, bulky substituents tend to destabilize the liquid crystalline phase (16,27–30,33,35), longer flexible units favor the formation of smectic phases (40,49), and odd–even effects are seen in the transition temperatures as a function of flexible spacer length (36,40,49). Rigid mesogens that form liquid crystalline order upon cure may not be liquid crystalline themselves. For example, **1** is itself a monotropic nematic, with a melting temperature of 128°C and an isotropic to nematic transition upon cooling of 95°C (50). Extension of **1** with a flexible unit such as glutaric acid creates an oligomer which is enantiotropic (8). In this case the structure may be likened to that of a main chain liquid crystalline polymer containing rigid and flexible segments. The phase diagram for binary mixtures of LCT monomers may be calculated using the same techniques as are employed for low molar mass liquid crystals, although slight discrepancies are found between theoretical and experimental phase diagrams (51). These discrepancies may be accounted for by the reactive nature of LCTs, whereby a complex mixture of partially reacted species is formed during the experiment that is not accounted for in the theory. It has also been found that the type of linkage can have an effect on the phases shown. For example, Lee and co-workers have examined the effect of an ester group versus an ether group between the mesogen and the flexible spacer of an epoxy LCT

Table 1. Representative Epoxy LCTs

Mesogen	End group	References
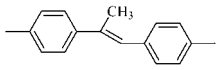	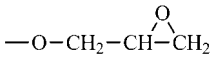	9
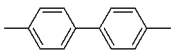	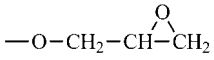	8
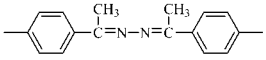	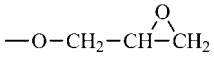	8
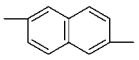	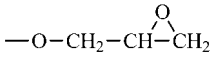	8
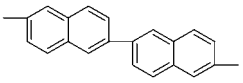	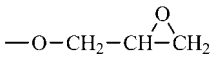	8
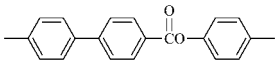	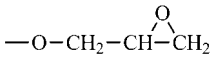	8
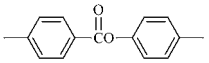	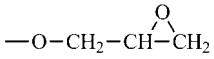	8
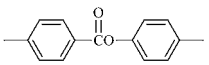	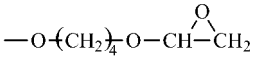	10
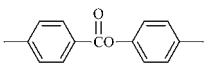	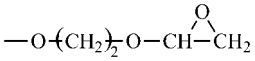	10
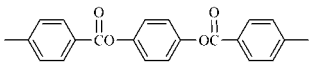	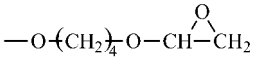	10
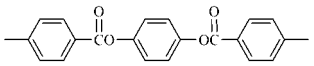	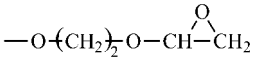	10
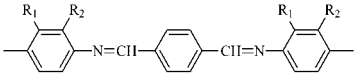	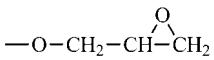	35
(R_1 and R_2 may be hydrogen or methyl)		
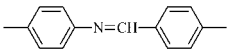	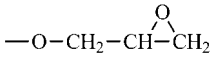	35
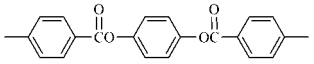	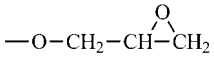	52
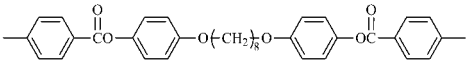	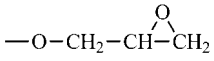	38
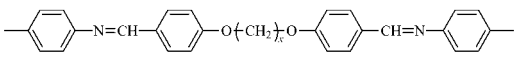	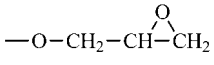	36
(*x* ranges from 6 to 9)		

(52). They found that the ester group leads to a monomer with a smaller nematic temperature range. As in low molar mass liquid crystals, this can be attributed to reduced intermolecular interactions due to the electron-withdrawing character of the ester group, and lower geometrical anisotropy due to the larger size of the ester group.

Table 2. Representative Miscellaneous LCTs

Mesogen	End group	References
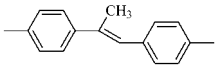	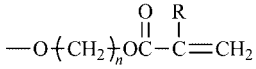 (R is hydrogen or methyl; $n = 3, 6, 11$)	11
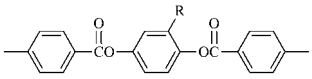 (R is hydrogen or methyl)	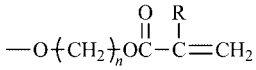 (R is hydrogen or methyl; $n = 6$)	12,14
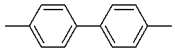	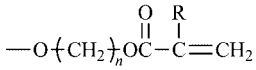	11,13
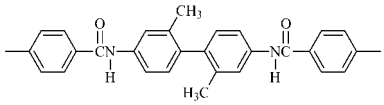	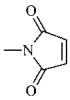	15
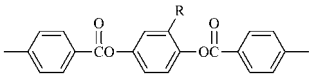 (R is hydrogen, methyl, or chlorine)		16
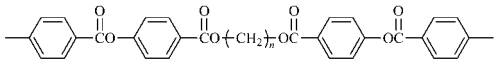 ($n = 5, 6, 8, 9$)	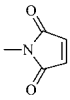	20
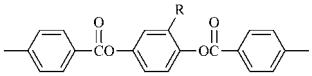 (R is hydrogen or methyl)	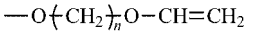	22
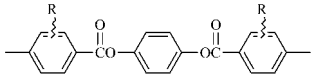 (R is methyl or chlorine)	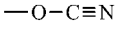	24
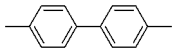	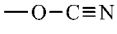	25,26
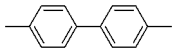	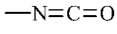	25,26
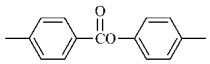	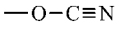	25,26
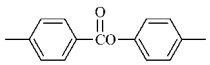	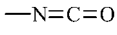	25,26
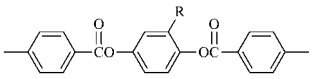 (R is hydrogen)	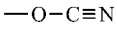	26
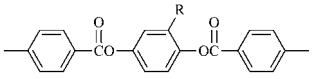 (R is hydrogen)	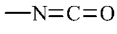	26

Table 2. (Continued)

Mesogen	End group	References
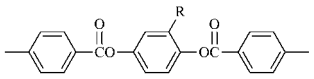 (R is hydrogen, methyl, methoxy, or chlorine)	—C≡CH	28
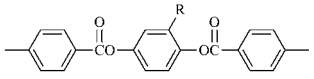 (R is hydrogen, methyl, methoxy, or chlorine)	—O—CH_2—C≡CH	29,30
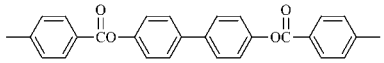	—C≡C— 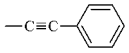	90

Cure Behavior

Reaction Kinetics. The presence of a liquid crystalline phase can have a dramatic effect on polymerization rates. The activation energy can be lower in the liquid crystalline phase, implying a higher rate constant (53). For those monomers which are initially isotropic, isothermal differential scanning calorimetry measurements show an initial exotherm due to the polymerization in the isotropic phase, followed by a second exotherm due to a rate acceleration when the reacting system undergoes a phase transition to a liquid crystalline phase. This phenomenon appears to be general, as it appears in both chain-growth (54–56) and step-growth (57–59) systems. Mormann and Bröcher found a similar second exotherm for an epoxy system that was undergoing a smectic to nematic transition during cure (60). This may be due to the lower viscosity of the nematic phase.

Several studies have compared the kinetic parameters that result from polymerization in different phases for chain-growth systems. Douglas and co-workers used Raman spectroscopy to compare liquid crystalline and non-liquid crystalline bisacetylene monomers (28). They found that the initial polymerization rate was higher in the liquid crystalline phase. Other studies have examined the photopolymerization of methacrylates and acrylates using differential scanning calorimetry. Hoyle and co-workers found there was no change in the initial polymerization rate as a function of phase, but the maximum rate was reached at lower conversions as the order of the phase increased (56). Guymon and Bowman performed a detailed kinetic study for liquid crystalline and non-liquid-crystalline diacrylates polymerized in a liquid crystalline solvent (61). Remarkably, they found that the polymerization rate is higher at lower temperatures, again due to the greater order present in the lower temperature liquid crystalline phases. A detailed analysis showed that this rate increase is caused by a decrease in the termination rate constant rather than by an increase in the propagation rate constant.

Kinetic studies have also been conducted on epoxy systems. For amine cure, it is generally assumed that the primary amine has a greater reactivity than the secondary amine. However, two studies found that for liquid crystalline epoxies the secondary amine is more reactive than the primary amine (62,63). There is no

complete explanation for this behavior, but it has been suggested that it is caused by the lower viscosity of the nematic phase. More detailed kinetic analysis has been done to model the kinetics during the complete reaction. Non-liquid crystalline epoxies are typically found to follow an autocatalytic model, in which one considers the reaction between an epoxide and an amine or anhydride hardener, with the reaction catalyzed by a species formed during the reaction (eg hydroxyl group). This model fits the isothermal differential scanning calorimetry data for both isotropic epoxies, and for liquid crystalline epoxies that show only a single exothermic peak during cure (57,64). For systems that do show a second peak due to a phase change during cure, modifications to the autocatalytic model are needed. The basic concepts inherent in these modifications are that the reaction proceeds at a different rate in the liquid crystalline phase than in the isotropic phase, and the isotropic and liquid crystalline phases contribute to the rate according to the relative proportion of each phase present. Liu and co-workers developed a model by modifying the autocatalytic model with a rate-enhancement term (57,59) and also introduced an error function so that the contribution of the rate-enhancement term increases as the conversion increases. Micco and co-workers also developed a model by assuming that the reaction rate is autocatalytic in the isotropic phase but linear with conversion to the liquid crystalline phase (58). They also assumed a form for the rate of growth of the liquid crystalline phase, and that the isotropic and liquid crystalline phases contributed to the overall rate in proportion to their volume fractions. Given the similarities of the two models, it is not surprising that both are able to model the double exotherm. Unfortunately, these models do not give much insight into the mechanism behind the rate enhancement, although Liu and co-workers do propose that their rate-enhancement term is associated with an increased concentration of reactive groups at the layer boundaries in the smectic phase.

Network Formation. Only very little work has been conducted on examining the effect that the liquid crystalline phase may have on the network formation. The two studies conducted indicate that in fact the liquid crystalline phase has no effect on gelation. Jahromi and co-workers examined the viscoelastic behavior of a liquid crystalline epoxy during cure at a single temperature (65). They found that the critical gelation exponent was equal to 0.5, which is also found for isotropic epoxies. Cho and Douglas performed measurements on a different epoxy at multiple temperatures, and found that the conversion at gelation was independent of cure temperature, as would be expected for a purely statistical step-growth process (66). Both studies found that the conversion at gelation was in good agreement with that calculated from standard theories of gelation via step growth. Thus it appears that, at least in epoxy systems, gelation is independent of the phase in which the cure reaction occurs.

Phase Evolution during Cure. Although the liquid crystalline properties of LCT monomers are easily understood on the basis of low molar mass liquid crystals, the structures of the resulting networks are much more complicated, resulting from an interplay among the monomer structure, the effect of cross-linking, and the cross-linking agent, if one is present. In some cases, there is no change in the liquid crystalline texture during cure, and the network exhibits the same liquid crystallinity as does the monomer (28,30,67). Even in such cases, however, there may be a slight loss of order at the molecular level due to the cross-linking reaction. Such an effect has been predicted theoretically (68),

and there is at least some experimental evidence that this may actually occur (69).

In many cases, however, the liquid crystalline order of the network is not the same as that of the monomer. Most common is the case in which the order of the network is actually greater than that of the monomer, in seeming contradiction with the theoretical calculations mentioned above. The most common example is **1**, which is a monotropic nematic liquid crystal as a monomer, and can be cured from the isotropic phase to give a liquid crystalline network (50,67,70). There are also other examples of this behavior (38,39,71–74), including systems which are initially nematic and then cure to give a smectic network (3,67,71). In general this behavior is explained on the basis of a minimum aspect ratio for the molecule that is required for liquid crystallinity to occur (28,39). It is assumed that the cure reaction increases the aspect ratio such that the molecules organize into a liquid crystalline phase. However, this explanation does not account for transitions from a monomer that is nematic to a network that is smectic, nor why some monomers that are initially isotropic form a network that is smectic. Therefore, it has also been suggested that specific molecular interactions between either the mesogens or the cross-linking molecules may be operative in the formation of smectic phases (38,69).

There are also several cases in which the molecular order decreases during cure, with the formation of a nematic network from a smectic monomer (75,76) or isotropic networks from both nematic and smectic monomers (28,40,76). This phenomenon is explained as being due to the disruption of the order due to the formation of cross-links. For example, Gavrin and Douglas synthesized a series of bisethynyl LCTs in which the cross-linking group is attached directly to the mesogen (40). In this particular case the cross-linking group is not decoupled from the mesogen through a flexible spacer, and thus if the distance between the molecules in the liquid crystalline phase is inconsistent with the bonding distance, the liquid crystallinity will be disrupted. This behavior is therefore similar to the general requirements for a flexible spacer to decouple the mesogen from the backbone in side-chain liquid crystalline polymers. However, other bisethynyl LCTs do not lose liquid crystallinity during cure (28), and thus there are clearly some details of this behavior that are not yet understood.

Another important factor affecting the network structure, at least in epoxies, is the cross-linking agent that is used. A study on this factor was conducted by Mihara and co-workers (77). They examined several combinations of mesogenic and nonmesogenic epoxies and amines. The most significant result from their study was that it is possible to create a liquid crystalline network if a mesogenic amine is used, even if the epoxy used is nonmesogenic. This clearly indicates the strong role that the hardener may play in determining the liquid crystalline structure of the network. Another example of this phenomenon occurs with **1** (50,70). When cured with a difunctional amine the resulting network forms a nematic structure. However, when cured with the unsymmetric tetrafunctional amine sulfanilamide, the resulting network forms a smectic structure. The authors propose that this difference is caused by the unequal reactivities of the two amine groups in sulfanilamide. The aromatic amine tends to react more easily, causing chain extension with little cross-linking, which is assumed to favor formation of the smectic phase. Only at the later stages of cure does the sulfonamide group react, resulting in cross-linking. However, Barclay and co-workers have found

that **1** and its oligomers cross-linked with the symmetric tetrafunctional amine methylenedianiline can form either a nematic or smectic phase, depending on the molecular weight distribution; oligomers with a narrower distribution tend to form the smectic phase (67). This result suggests that the most important factor may be the presence of molecular interactions that drive the formation of the smectic phase, and that a broader molecular weight distribution disrupts the regularity of that structure, leading to a nematic phase. Similarly, use of an aliphatic acid to cure 2,6-diglycidyloxynaphthalene results in a nematic network, despite the low aspect ratio of the epoxy monomer (72). In this case, hydrogen bonding may play an important role in the formation of the liquid crystalline structure.

It is apparent, then, that the formation of liquid crystalline structure in cured LCT networks is a complicated process and is currently difficult to predict. Nevertheless, for practical applications it is desirable to at least have knowledge of the liquid crystallinity that may form as a function of the cure conditions. To achieve this, a number of workers have created transformation diagrams that show the liquid crystalline phases that form as a function of cure temperature and cure time (28,30,36,38–40,70,71,73,78). Figure 1 is one example of these types of diagrams. One of the interesting questions that arises from these types of diagrams is the conversion dependence of the phase transformation. Several studies have addressed this issue by performing independent measurements of conversion versus time at various cure temperatures, and then converting the time axis to conversion (63, 66,78). They find that the conversion at which the transformation occurs increases with increasing cure temperature. This is because at higher cure temperatures the critical molecular length for liquid crystallinity to occur is higher, and thus a greater conversion is needed. This explanation is supported by experimental results on other systems, for which an increase in isotropization temperature as a function of cure time at a single cure temperature has been reported (50).

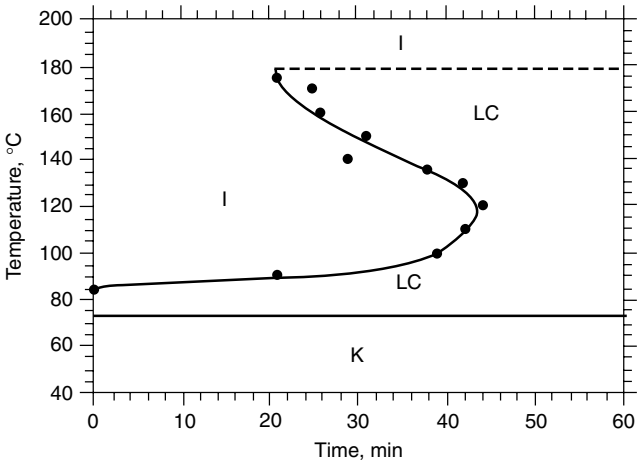

Fig. 1. Transformation diagram for **1** cured with sulfanilamide showing changes in morphology as a function of the cure time. This particular diagram shows the time at which phase transformations occur when the sample is cured isothermally at a given temperature. I, isotropic; LC, liquid crystalline; K, crystalline. Reprinted from Ref. 70, Copyright (1994), with permission from Elsevier Science.

Properties

Mechanical Properties. Liquid crystalline polymers are known to have outstanding mechanical properties due to their microdomain morphology and their ability to be oriented. It is expected, therefore, that LCTs may have the same advantages. The effects of orientation are considered in a later section; here we consider only macroscopically unoriented systems.

As part of their study on orientation effects, Benicewicz and co-workers measured the tensile modulus of **1**(69). They obtained a value of 3 GPa, which is typical for non-liquid-crystalline epoxies. Earls and co-workers also found flexural modulus values of approximately 3–4 GPa for both **1** and **2**(9). Tan and co-workers found even lower values of modulus for different liquid crystalline epoxies, although they did not make a direct comparison to isotropic systems (79). Ortiz and co-workers also found no enhancement in modulus for **1**, with the storage modulus in the glassy state actually lower than for an isotropic epoxy and the compressive modulus the same (80). From this limited data it appears that the liquid crystalline phase has no advantage for tensile modulus. This may not be surprising since modulus in the glassy state is governed by bond deformations and rotations, which will be relatively unaffected by the liquid crystalline state. Ortiz and co-workers did find, however, an increase in the dynamic modulus in the rubbery state above what is predicted from rubber elasticity theory (80). This increase is greater for the smectic phase than for the nematic phase. They explain this behavior by proposing that deformation due to motion of the cross-links in an ordered phase will disrupt that ordered phase, resulting in an additional free energy penalty due to the deformation. They also examined additional compressive properties, and found that the liquid crystalline phase results in a lower yield stress, no strain-softening region, and a lower strain at failure. They propose that this behavior occurs because the rigid and extended nature of the network segments prevents plastic deformation. Similarly, Earls and co-workers found a slightly lower flexural strength for **1** compared to that for **2**(9).

Enhancements in fracture toughness for LCTs are greater than for other properties. Several studies have examined the fracture behavior of LCT epoxies. Both Sue and co-workers and Ortiz and co-workers found that **1** cured in the liquid crystalline phase had a higher fracture toughness than **1** cured in the isotropic phase (80,81). Robinson and co-workers conducted a detailed investigation, comparing **1** and **2** cured with the same curing agent with the same cure cycle (82). By varying the epoxy-to-hardener ratio, they found that the morphology of **1** changed, with the domain size decreasing with increasing deviation from balanced stoiochiometry. As a result, the fracture toughness for **1** was higher than that for the isotropic epoxy only at and near the stoichiometric formulation. Carfagna and co-workers found that this increased fracture toughness extends to fiber-reinforced composites, although the increase in impact resistance for LCTs was not as great in the composites as for the neat resin (83). The mechanism for this enhanced fracture toughness has been investigated by TEM. Sue and co-workers found that the crack appears to grow preferentially at the boundaries of the liquid crystalline domain, resulting in crack deflection and segmenting, with this mechanism becoming less effective as the domain size decreases (81). Ortiz and co-workers found that failure occurs by formation of individual microcracks, which grow and

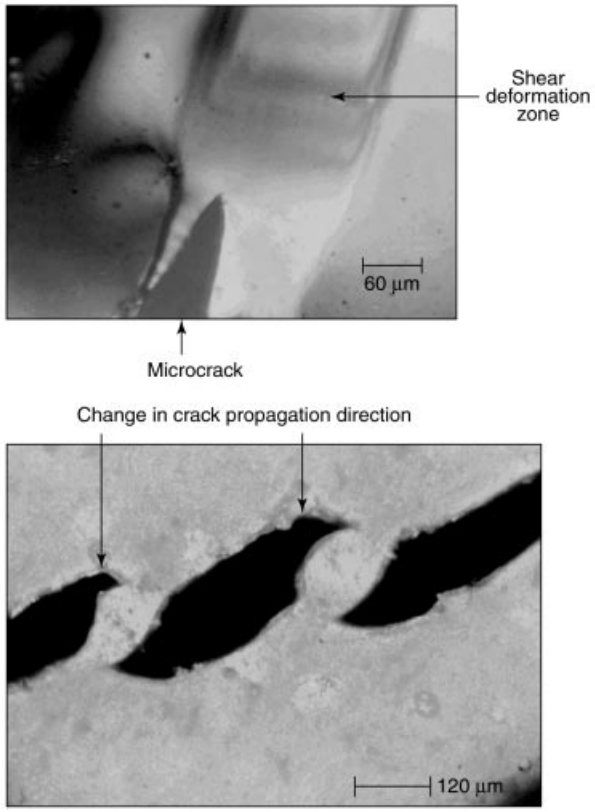

Fig. 2. Thin films of (**a**) **2** and (**b**) **1**, both cured with methylene dianiline, strained in tension, and observed between crossed polars in an optical microscope. In (**a**) can be seen the typical behavior of an isotropic epoxy: a single crack with birefringence caused by a shear deformation zone ahead of the crack tip. In (**b**) there are multiple cracks; these cracks undergo slow, stable propagation due to failure of individual liquid crystalline domains in front of and at the crack tip. Reprinted with permission from Ref. 84, Copyright (2000), Kluwer Academic Publishers.

coalesce, eventually resulting in failure (84). This is in contrast to the isotropic epoxy, which fails by formation and growth of a single crack. Figure 2 shows a comparison between the two systems. Ortiz and co-workers proposed that the individual microcracks undergo stable propagation due to failure of individual liquid crystalline domains (84). These mechanisms are consistent with the results of Robinson and co-workers (82), in that it would be expected for these toughening mechanisms to become less effective as the domain size decreases.

Several studies have examined the adhesive properties of LCTs. Ochi and Takashima, and Carfagna and co-workers both found an increase in the lap shear strength for an LCT epoxy compared to an isotropic LCT (85,86). However, Frich and Economy (87) found that the lap shear strength with a titanium substrate for an LCT that cures by transesterification was lower than that for an isotropic resin. Given the limited data available, it is not clear whether these differences are due to the substrates, surface pretreatment, the type of cure reaction, the liquid crystalline phase, or some other factor. However, most of these studies did find

that the failure mode for the LCT was cohesive or mixed cohesive and adhesive, as opposed to only adhesive for the isotropic thermosets. Thus, it appears that regardless of the lap shear strength, the LCT has a greater bonding strength to the substrates. In one case both materials failed in a cohesive manner, and thus the increased lap shear strength appears to be related to the higher fracture toughness of the liquid crystalline material (86).

Thermal Stability. Only a few studies have examined the thermal stability of LCTs. When the monomers are specifically designed to contain no aliphatic carbons, the thermal stabilities can be very high. For example, Melissaris and co-workers synthesized rigid rod monomers with ethynyl end groups (88,89), while Gavrin and co-workers synthesized monomers with phenylethynyl end groups (90). In both cases degradation temperatures were reported to be at least 400°C in both air and nitrogen atmospheres. Thermal stability has also been examined for epoxy LCTs. The thermal stability is affected by the type and concentration of hardener used; as the aliphatic content of the resin mixture increases, the thermal stability decreases (91,92). One study showed that an anhydride hardener resulted in lower thermal stability than an amine hardener, perhaps due to the difference in cross-link structure (93). In one study liquid crystalline epoxies were compared directly to **2**(94). When the epoxies were cured with an anhydride hardener the liquid crystalline epoxies showed a higher onset temperature for degradation, but when an amine hardener was used **2** had a higher onset temperature. In general, the results suggest that the high thermal stability is a consequence of the types of bonds present and is not significantly affected by the liquid crystalline phase.

Permeability. Liquid crystalline polymers are known to exhibit very low permeability to various permeants due to the packing of molecules in the liquid crystalline and crystalline states. The low permeability of LCPs can be understood on the basis of a two-phase model, in which it is assumed that the permeant does not penetrate into the domains, but can only diffuse through the domain boundaries (95–97). On the basis of these results, it might be expected that LCTs would also show low permeability. Carfagana and co-workers measured the sorption isotherm for **1** and found no difference in water sorption between the nematic and isotropic states (98). In contrast, Earls and co-workers found that **1** cured in the smectic state absorbed considerably less methylene chloride, methylethyl ketone, dimethyl formamide, and bleach after 30 days compared to that adsorbed by **2**; weight gains for **1** were all less than 1%, while weight gains for **2** ranged from 1.0% (bleach) to 26.6% (methylene chloride)(9). Feng also found considerable differences between **1** and **2** in the smectic phase (99). Using a permeation technique to measure the transport of water vapor through thin films, he found that the permeability, diffusion coefficient, and sorption coefficient were all substantially lower for **1**. From the limited data available, it appears that the liquid crystalline state present in the cured resin has an important effect on the diffusion properties, with the smectic phase being considerably less permeable than the nematic or isotropic phases.

Optical Properties. All of the optical applications of LCTs have considered the cholesteric phase. The cholesteric phase is interesting because thin films of a cholesteric liquid crystal oriented such that the helical axis is perpendicular to the plane of the film will selectively reflect circularly polarized light with a wavelength determined by the pitch of the helix. For low molar mass liquid crystals,

films are typically created by mixing a nematic liquid crystal with small amounts of a chiral molecule. The pitch of the helix is determined by both the concentration and the temperature, and thus they are utilized as simple temperature sensors. The goal of creating a cholesteric LCT is driven by the desire to permanently fix the helical pitch, and thus the reflected wavelength, for use in optical devices.

There are several approaches that have been used to create cholesteric LCTs. These include polymerizing nematic LCTs in the presence of a nonpolymerizable chiral molecule (100–104), polymerizing a non-liquid-crystalline monomer in the presence of a nonpolymerizable chiral molecule (105), and copolymerizing nematic and chiral LCTs (100,106). As with low molar mass liquid crystals, in general the pure cholesteric compounds do not reflect light in the visible range, although there is at least one example of a diacrylate which reflects red light when it is not polymerized (106).

Several studies have examined the properties of the cross-linked cholesteric LCTs and proposed some interesting applications. Hikmet and Zwerver showed that removal of the nonpolymerizable molecule leads to an irreversible change in the helical pitch, and thus the wavelength of reflected light (101). This change could be induced locally by writing with a laser beam, suggesting that these materials could be used for optical storage. Ishihara and co-workers used cholesteric LCTs as optical notch filters that filter light of specific wavelengths for displays, allowing better color purity for those displays (105). Heynderickx and Broer also considered cholesteric LCTs for display applications (104). In their case they used a cholesteric LCT film as a compensation foil to eliminate the wavelength dependence of transmission for a supertwisted nematic display.

Orientation of LCTs in External Fields

The liquid crystalline order of LCTs allows them to be oriented by external fields. Orientation may be induced at a surface, or by electric or magnetic fields. Curing the material subsequent to, or during, orientation leads to a cured thermoset which has some degree of macroscopic order. Unlike liquid crystalline polymers, shear fields and mechanical deformation in the uncured state are not considered to be as effective, because of the rapid relaxation of the monomers and the difficulty in maintaining such fields during the cure process. Nevertheless, mechanical deformation has been shown to be effective at orienting lightly cross-linked materials by heating above their T_g and subsequently cooling to lock in the orientation, although the ability to orient decreases dramatically with increasing cross-link density and the orientation is lost upon heating above T_g (107,108). The orientation process tends to enhance certain properties of the cured LCT, although the potential benefits have not yet been fully explored.

Surface Induced Orientation. Liquid crystals are well known to orient at surfaces (109). This effect is utilized in liquid crystal displays, in which orientation of the liquid crystal at a surface is transmitted throughout a thin film. Often this orientation can be achieved simply by rubbing a polymer such as polyimide repeatedly along a given direction. This rubbing process results in orientation of the liquid crystal along the rubbing direction. Given that this technique works well for low molar mass liquid crystals, it is not surprising that it has been utilized

to align thin films of LCTs (12,22,23,56,110). The technique appears to be very general, and has been applied to epoxies, vinyl ethers, and methacrylates, using both thermal and photoinitiated polymerization. The orientation in these systems can be measured using either infrared spectroscopy or X-ray scattering. The resulting orientation is expressed in terms of the second moment of the orientation function, or the orientation parameter, which is given by

$$\langle P_2 \rangle = \frac{1}{2}(3\langle \cos^2 \alpha \rangle - 1) \quad (1)$$

where α is the angle a molecule makes with respect to the alignment direction and the angular brackets denote an average over all molecules. The limiting values for $<P_2>$ are -0.5 for perfect orientation perpendicular to the alignment direction, 0 for no orientation, and 1.0 for perfect orientation parallel to the alignment direction. Values for $<P_2>$ resulting from surface-induced orientation typically range from 0.6 to 0.94, indicating a high degree of alignment.

An interesting application of surface-induced alignment of LCTs is orientation at the surface of fibers in fiber-reinforced composites. Adams and Mallon have shown that a low molar mass liquid crystal is oriented at the surface of a carbon fiber parallel to the fiber direction (111), while Sue and co-workers found that **1** can be oriented along the fiber direction, depending on the cure schedule and the epoxy/hardener formulation (112). These findings raise the possibility of creating fiber-reinforced composites with controlled matrix orientation and/or tailored interfaces, which may improve the fiber/matrix interface and result in improved properties (see REINFORCEMENT).

Electric-Field-Induced Orientation. Despite the fact that electric field orientation of liquid crystals is an important technology used, for example, in liquid crystal displays, there has been almost no work on the electric field alignment of LCTs. This may be because electric fields are effective only for thin films; the high field strengths required, on the order of 10^4 V/cm or greater, can lead to dielectric breakdown in thick samples. Nevertheless, although bulk orientation cannot be obtained via electric fields, use of electric fields does provide a complement to the surface-induced techniques described above.

The only description of electric field orientation comes out of work by Ober and co-workers (37,113). They used ac electric fields, which allowed them to control orientation either parallel or perpendicular to the field direction. This is caused by an electrohydrodynamic effect, by which there exists a critical field frequency, below which the molecule orients parallel to the electric field and above which the molecule orients perpendicular to the electric field. Ober and co-workers were able to show control over the direction of orientation in a cyanate ester LCT by changing the frequency of the applied field during the cure (113). In contrast, an epoxy LCT flipped from a parallel to a perpendicular orientation during isothermal cure at a given applied frequency (37). This was attributed to a change in the critical frequency due to the increase in viscosity during cure.

Magnetic-Field-Induced Orientation. Liquid crystals may be oriented in magnetic fields, even though they are diamagnetic, due to the anisotropy in their diamagnetic susceptibility. The advantage of magnetic fields over surface-induced orientation or electric fields is that samples are not confined to thin films.

In fact, orientation in magnetic fields is more efficient in thicker samples, due to anchoring effects at walls. The result is that magnetic fields are the only way to obtain samples of highly cross-linked materials on which bulk properties can be measured.

de Gennes has described the fundamental physics behind the orientation of liquid crystals in magnetic fields (109). Essentially, we can consider an isolated rod placed in a magnetic field. This rod experiences a torque due to the presence of the field, given by (109,114)

$$L_{\mathrm{M}} = -\frac{1}{2}\Delta\chi B^2 \sin 2\theta \tag{2}$$

where $\Delta\chi$ is the anisotropy in the diamagnetic susceptibility parallel and perpendicular to the molecular axis (χ_{par} - χ_{perp}), B is the magnetic field strength, and θ is the angle of the molecular axis with respect to the magnetic field direction. Most liquid crystals have a positive $\Delta\chi$, meaning that the molecular axis aligns parallel to the applied field. Opposing this magnetic torque is a viscous torque, given by

$$L_{\mathrm{V}} = -\gamma_1 \frac{\mathrm{d}\theta}{\mathrm{d}t} \tag{3}$$

where γ_1 is the rotational viscosity coefficient. Essentially, this viscous torque is caused by the drag exerted on the molecule by the surrounding medium. The time dependence of the orientation process can be obtained by assuming that steady state has been reached, i.e. the sum of these torques is zero. Solving the resulting differential equation leads to

$$\tan\theta = \tan\theta_0 \exp\left(\frac{-t}{\tau}\right) \tag{4}$$

where θ_0 is the initial angle of the molecule when the field is first applied, and τ is a relaxation time given by

$$\tau = \frac{\gamma_1}{\Delta\chi B^2} \tag{5}$$

There are two important assumptions in this approach. The first is that the viscosity is a constant. Clearly for LCTs this cannot be true, as the viscosity increases during cure. It is straightforward to include a time-dependent viscosity in the model, although it makes the solution of the differential equation more complicated. The implications of this time-dependent viscosity will be discussed below. The other assumption is that this is a monodomain sample, with all molecules at the same angle with respect to the magnetic field. To account for polydomain samples, it is possible to integrate equation 4 over all possible domain orientations. When this is done, the distribution function for domain orientations is given by (114)

$$\rho(\theta,t) = \frac{\sin\theta_0}{\sin\theta}\frac{\mathrm{d}\theta_0}{\mathrm{d}\theta} \tag{6}$$

where the relationship between θ_0 and θ is defined by equation 4. Finally, the model prediction for average orientation angle of the domains, $< \cos^2\theta >$, is

$$\langle \cos^2\theta \rangle = \frac{\int_0^{\pi/2} \rho(\theta,t) \sin\theta \cos^2\theta \, d\theta}{\int_0^{\pi/2} \rho(\theta,t) \sin\theta \, d\theta} \quad (7)$$

which can then be used to calculate $<P_2>$ using equation 1.

Experimentally, it has proven quite feasible to orient LCTs in magnetic fields. Two classes of materials have been studied: epoxies, which are thermally polymerized in the presence of a magnetic field (69,79,107,115–118). and acrylates or methacrylates, which are oriented in a magnetic field and then photopolymerized (12,56,119,120). Most of the work understanding the factors affecting the degree of orientation have been conducted on epoxies. From the model described above, we see that the factors that could improve orientation are higher field strength; lower initial viscosity and slower viscosity increase; longer time in the magnetic field; and a more anisotropic diamagnetic susceptibility. However, very few studies have examined these factors in detail. Benicewicz and co-workers have shown that orientation increases for **1** cured with sulfanilamide system up to a field strength of approximately 10 T (69). Lincoln and Douglas examined the combined effects of field strength, time in the field, and B-staging (prereaction) (118). They found that orientation increases with higher field strength, longer time in the field, and less B-staging (due to the lower viscosity).

The liquid crystalline phase present during the orientation process is also an important factor. Theoretically, the decrease in energy upon orientation of a single molecule in the gas phase is orders of magnitude less than the thermal energy, and thus a single molecule is randomized by thermal fluctuations. In a liquid crystalline phase, however, motions of the molecules are coupled, and thus the total energy decrease of the system is much greater than the thermal energy. In addition, it has been shown theoretically that packing constraints in a smectic liquid crystal cause orientation to be considerably more difficult than in a nematic (121). Thus, we would expect that under identical conditions nematic LCTs would show the greatest degree of orientation, smectic LCTs would show a lower degree of orientation, and isotropic thermosets would show no orientation. These expectations are confirmed by experimental results. Hoyle and co-workers photopolymerized a methacrylate LCT at various temperatures in a 0.53-T field (56). Substantial orientation was observed when polymerization was conducted at low temperatures in the nematic phase. However, no orientation was observed at high temperatures, when the monomer existed in the isotropic phase. Barclay and co-workers examined **1** and oligoethers of **1**, cured with methylene dianiline (67,107). Compound **1** showed much lower orientation compared to the oligoethers, because **1** itself is initially isotropic, while the oligoethers are initially nematic. Thus, the oligoethers have more time for orientation to occur, and presumably also have lower viscosity since orientation can occur before any chain branching or cross-linking can occur due to the cure reaction. Jahromi used deuterium NMR to show that the rate of orientation is lower in the smectic phase than in the nematic phase (115).

Very little work has been done to understand the kinetics of the orientation process. The model described above has been used to examine the factors affecting the degree of orientation (122). The rate of orientation is determined

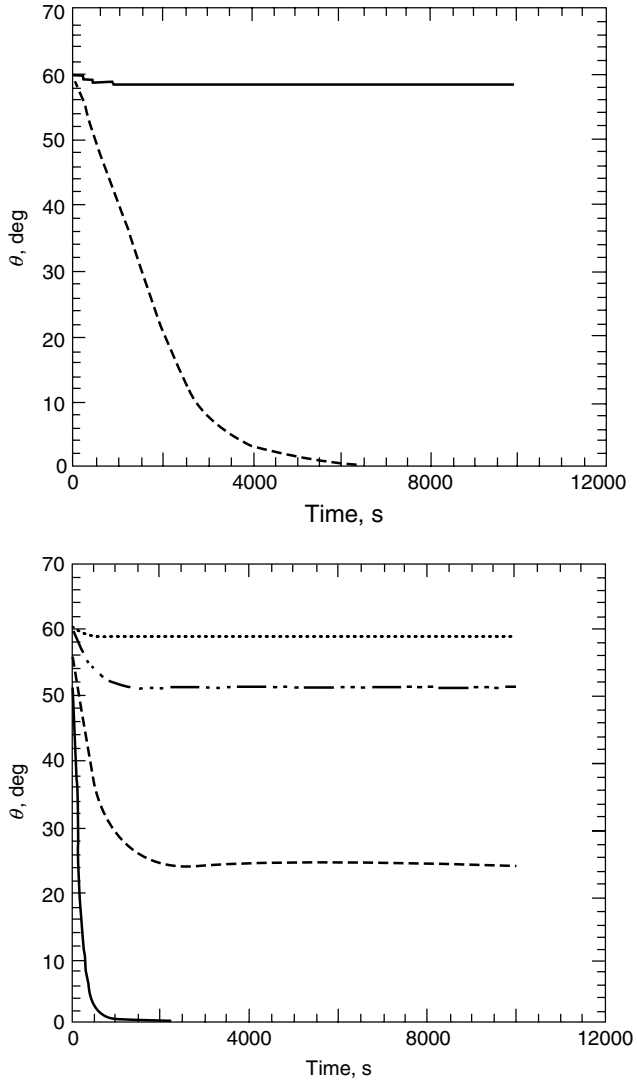

Fig. 3. Model calculations of the magnetic field orientation of liquid crystals. Calculations were conducted using equations 2 and 3. In (**a**) comparison is made between a nonreactive liquid crystal with a constant viscosity and a reactive liquid crystal with an exponentially increasing viscosity due to the cure reaction —— reactive; - - - - unreactive. In (**b**) is seen the effects of magnetic field strength for the reactive liquid crystal . . . . . 0.01 T; —— . . . 0.025 T; – – - 0.05 T; - - - - 0.1 T. From Ref. 122. To convert T to gauss, multiply by 10^4.

by a competition between the magnetic field and the viscosity. Figure 3a show the effect of the time-dependent viscosity as predicted by the above model. For a liquid crystal with a constant viscosity, the viscosity only serves to retard the orientation process; thus at long times the monodomain sample becomes completely oriented in the direction of the magnetic field. However, when the viscosity increases exponentially with time, there comes a point where the magnetic field strength is not sufficient to overcome the viscosity, and orientation ceases. In real systems, this point may correspond to the gel point. Figure 3b shows that if

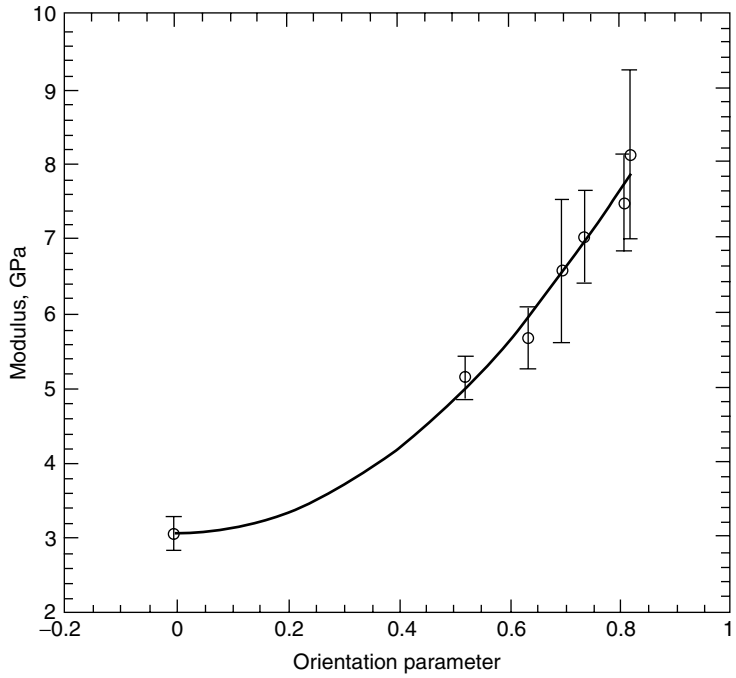

Fig. 4. Effect of magnetic field strength on the tensile modulus of compound **1** cured with sulfanilamide. The line is a quadratic fit to the data, which indicates that the modulus is determined by the average orientation of the molecules. Reprinted with permission from Ref. 69, Copyright (1998), American Chemical Society. To convert GPa to psi, multiply by 145,000.

the field strength is high enough complete orientation can be achieved before the viscosity increase overcomes the magnetic field. Unfortunately, there have been no detailed comparisons to date between this model and experimental results, and so the quantitative accuracy of this model cannot be evaluated. However, predicted trends do correspond to the experimental results described above.

A few studies have examined the effect of orientation on bulk properties. Figure 4 shows the change in tensile modulus with orientation for **1** cured with sulfanilamide. Overall, the tensile modulus can be increased three times by orientation. The authors interpret the quadratic dependence of the modulus on orientation parameter as indicating that the modulus depends on the average orientation of the smectic layers (69). Tan and co-workers also found an increase in tensile modulus upon orientation (79). It has also been shown that orientation leads to an anisotropic coefficient of thermal expansion (low thermal expansion in the direction of orientation) (69,107), as well as a higher tensile strength and elongation at break (79). In contrast, experiments using a non-liquid-crystalline epoxy show no enhancements in properties after curing in a magnetic field (123), further confirming that the liquid crystalline phase is needed for orientation to occur.

Future Directions for Research

The synthesis of LCT monomers and understanding of their cure behavior appears to be fairly well established. Although further effort may be needed to

identify LCT monomers appropriate for specific situations, the general principles of how molecular structure affects the phases present, and the development of different phase structures during cure, is well understood. Future work is likely to be focussed on properties and applications of LCTs. For example, only relatively little work has been conducted on bulk mechanical properties or permeability of solvents or gases in LCTs. Important fundamental questions remain regarding the mechanism of enhancement in these properties over conventional isotropic thermosets, as well as the origin of differences in properties between different liquid crystalline phases (eg nematic vs smectic). Considerable work is also needed to fully understand and control the orientation of LCTs using external fields. Finally, applications for LCTs are not yet developed. A few optical devices have been constructed using LCTs, but general application of LCTs to optical applications has not been demonstrated. Similarly, the use of LCTs in composite structures remains limited in scope. Substantial effort is needed to show whether LCTs can exhibit performance benefits that will justify their use in future applications.

BIBLIOGRAPHY

1. P. G. de Gennes, *Phys. Lett. A* **28**, 725 (1969).
2. L. Liebert and L. Strzelecki, *C. R. Acad. Sci. Paris* **276**, 647 (1973).
3. S. B. Clough, A. Blumstein, and E. C. Hsu, *Macromolecules* **9**, 123 (1976).
4. A. Shiota and C. K. Ober, *Prog. Polym. Sci.* **22**, 975 (1997).
5. C. Carfagna, E. Amendola, and M. Giamberini, *Prog. Polym. Sci.* **22**, 1607 (1997).
6. M. Giamberini, E. Amendola, and C. Carfagna, *Macromol. Chem. Phys.* **198**, 3185 (1997).
7. B. A. Rozenberg and L. L. Gureva, in S. M. Aharoni, ed., *Synthesis, Characterization, and Theory of Polymeric Networks and Gels*, Plenum Press, New York, 1992, p. 147.
8. M. Giamberini, E. Amendola, and C. Carfagna, *Recent Res. Dev. Polym. Sci.* **2**, 363 (1998).
9. U.S. Pat. 5,270,405 (1993), J. D. Earls, R. E. Hefner, and P. M. Puckett (to The Dow Chemical Company).
10. S. Jahromi, J. Lub, and G. N. Mol, *Polymer* **35**, 622 (1994).
11. U.S. Pat. 5,078,910 (1992), M. H. Litt (to Edison Polymer Innovation Corp.).
12. C. E. Hoyle, T. Watanabe, E. Brister, and J. W. Whitehead, *Polym. Prep.* **34**, 703 (1993).
13. M. H. Litt, W. T. Whang, K. T. Yen, and X. J. Qian, *J. Polym. Sci., Part A: Polym. Chem.* **31**, 183 (1993).
14. R. A. M. Hikmet, J. Lub, and P. M. Vanderbrink, *Macromolecules* **25**, 4194 (1992).
15. A. E. Hoyt and B. C. Benicewicz, *J. Polym. Sci., Part A: Polym. Chem.* **28**, 3403 (1990).
16. A. E. Hoyt and B. C. Benicewicz, *J. Polym. Sci., Part A: Polym. Chem.* **28**, 3417 (1990).
17. A. E. Hoyt, B. C. Benicewicz, and S. J. Huang, *ACS Symp. Ser.* **435**, 198 (1990).
18. U.S. Pat. 5,198,551 (1993), B. C. Benicewicz and A. E. Hoyt (to The United States of America as represented by the United States Department of Energy).
19. U.S. Pat. 5,114,612 (1992), B. C. Benicewicz and A. E. Hoyt (to The United States of America as represented by the United States Department of Energy).
20. K. Kallal-Bartolomeo, J. C. Milano, J. L. Vernet, and B. Gallot, *Macromol. Chem. Phys.* **201**, 2276 (2000).
21. H. R. Kricheldorf and T. Krawinkel, *Macromol. Chem. Phys.* **199**, 783 (1998).
22. R. A. M. Hikmet, J. Lub, and J. A. Higgins, *Polymer* **34**, 1736 (1993).
23. H. Andersson, U. W. Gedde, and A. Hult, *Polymer* **33**, 4014 (1992).

24. G. G. Barclay, C. K. Ober, K. I. Papathomas, and D. W. Wang, *Macromolecules* **25**, 2947 (1992).
25. W. Mormann and J. Zimmermann, *Polym. Mater. Sci. Eng.* **66**, 498 (1992).
26. W. Mormann, *Trends Polym. Sci.* **3**, 255 (1995).
27. W. Mormann and C. Kuckertz, *Macromol. Chem. Phys.* **199**, 845 (1998).
28. E. P. Douglas, D. A. Langlois, and B. C. Benicewicz, *Chem. Mater.* **6**, 1925 (1994).
29. H. R. Kricheldorf and A. Gerken, *High Perform. Polym.* **9**, 75 (1997).
30. D. A. Langlois, B. C. Benicewicz, and E. P. Douglas, *Chem. Mater.* **10**, 3393 (1998).
31. J. W. Schultz, J. Bhatt, R. P. Chartoff, R. T. Pogue, and J. S. Ullett, *J. Polym. Sci., Part B: Polym. Phys.* **37**, 1183 (1999).
32. R. A. M. Hikmet, J. Lub, and A. J. W. Tol, *Macromolecules* **28**, 3313 (1995).
33. W. Mormann and C. Irle, *Macromol. Symp.* **122**, 159 (1997).
34. K. Kurschner and P. Strohriegl, *Liq. Cryst.* **27**, 1595 (2000).
35. W. Mormann, M. Broche, and P. Schwarz, *Macromol. Chem. Phys.* **198**, 3615 (1997).
36. E. J. Choi, H. K. Ahn, J. K. Lee, and J. I. Jin, *Polymer* **41**, 7617 (2000).
37. A. Shiota and C. K. Ober, *Macromolecules* **30**, 4278 (1997).
38. A. Shiota and C. K. Ober, *Polymer* **38**, 5857 (1997).
39. A. Shiota and C. K. Ober, *J. Polym. Sci., Part A: Polym. Chem.* **34**, 1291 (1996).
40. A. J. Gavrin and E. P. Douglas, *Macromolecules* **34**, 5876 (2001).
41. W. Mormann and J. G. Zimmermann, *Liq. Cryst.* **19**, 481 (1995).
42. B. C. Baxter and D. L. Gin, *Macromolecules* **31**, 4419 (1998).
43. C. D. FavreNicolin and J. Lub, *Macromolecules* **29**, 6143 (1996).
44. M. J. S. Dewar and R. M. Riddle, *J. Am. Chem. Soc.* **97**, 6658 (1975).
45. M. J. S. Dewar and A. C. Griffin, *J. Am. Chem. Soc.* **97**, 6662 (1975).
46. S. A. Haut, J. P. Schroede, and D. C. Schroede, *J. Org. Chem.* **37**, 1425 (1972).
47. S. L. Arora, J. L. Fergason, and T. R. Taylor, *J. Org. Chem.* **35**, 4055 (1970).
48. M. J. S. Dewar and R. S. Goldberg, *J. Org. Chem.* **35**, 2711 (1970).
49. A. J. Gavrin, *PhD dissertation*, University of Florida, Gainesville, Fla., 2000.
50. Q. H. Lin, A. F. Yee, H. J. Sue, J. D. Earls, and R. E. Hefner, *J. Polym. Sci., Part B: Polym. Phys.* **35**, 2363 (1997).
51. A. E. Hoyt and S. J. Huang, *J. Macromol. Sci.—Pure Appl. Chem. A* **32**, 1931 (1995).
52. J. Y. Lee, J. S. Jang, S. M. Hong, S. S. Hwang, and K. U. Kim, *Polymer* **40**, 3197 (1999).
53. G. Schnurpfeil, A. Harder, H. Schroder, D. Wohrle, A. Hartwig, and O. D. Hennemann, *Macromol. Chem. Phys.* **202**, 180 (2001).
54. C. E. Hoyle, C. P. Chawla, D. Kang, and A. C. Griffin, *Macromolecules* **26**, 758 (1993).
55. C. E. Hoyle and T. Watanabe, *Macromolecules* **27**, 3790 (1994).
56. C. E. Hoyle, T. Watanabe, and J. B. Whitehead, *Macromolecules* **27**, 6581 (1994).
57. J. P. Liu, C. C. Wang, G. A. Campbell, J. D. Earls, and R. D. Priester, *J. Polym. Sci., Part A: Polym. Chem.* **35**, 1105 (1997).
58. G. Micco, M. Giamberini, E. Amendola, C. Carfagna, and G. Astarita, *Ind. Eng. Chem. Res.* **36**, 2976 (1997).
59. J. P. Liu, C. C. Wang, G. A. Campbell, J. D. Earls, and R. D. Priester, *J. Polym. Sci., Part A: Polym. Chem.* **36**, 1457 (1998).
60. W. Mormann and M. Brocher, *Polymer* **40**, 193 (1999).
61. C. A. Guymon and C. N. Bowman, *Macromolecules* **30**, 1594 (1997).
62. A. Mititelu, T. Hamaide, C. Novat, J. Dupuy, C. N. Cascaval, B. C. Simionescu, and P. Navard, *Macromol. Chem. Phys.* **201**, 1209 (2000).
63. E. Amendola, C. Carfagna, M. Giamberini, and G. Pisaniello, *Macromol. Chem. Phys.* **196**, 1577 (1995).
64. P. Punchaipetch, V. Ambrogi, M. Giamberini, W. Brostow, C. Carfagna, and N. A. D'Souza, *Polymer* **42**, 2067 (2001).

65. S. Jahromi, W. A. G. Kuipers, B. Norder, and W. J. Mijs, *Macromolecules* **28**, 2201 (1995).
66. S. Cho and E. P. Douglas, *Macromolecules* **35**, 4550 (2002).
67. G. G. Barclay, C. K. Ober, K. I. Papathomas, and D. W. Wang, *J. Polym. Sci., Part A: Polym. Chem.* **30**, 1831 (1992).
68. D. L. Kurdikar, H. M. J. Boots, and N. A. Peppas, *Macromolecules* **28**, 5632 (1995).
69. B. C. Benicewicz, M. E. Smith, J. D. Earls, R. D. Priester, S. M. Setz, R. S. Duran, and E. P. Douglas, *Macromolecules* **31**, 4730 (1998).
70. Q. H. Lin, A. F. Yee, J. D. Earls, R. E. Hefner, and H. J. Sue, *Polymer* **35**, 2679 (1994).
71. J. J. Mallon and P. M. Adams, *J. Polym. Sci., Part A: Polym. Chem.* **31**, 2249 (1993).
72. M. Giamberini, E. Amendola, and C. Carfagna, *Polym. Eng. Sci.* **39**, 534 (1999).
73. J. S. Grebowicz, *Macromol. Symp.* **104**, 191 (1996).
74. W. Mormann and M. Brocher, *Macromol. Chem. Phys.* **197**, 1841 (1996).
75. S. Osada, K. Tsunashima, T. Inoue, and S. Yano, *Polym. Bull.* **35**, 505 (1995).
76. S. Osada, S. Yano, K. Tsunashima, and T. Inoue, *Polymer* **37**, 1925 (1996).
77. T. Mihara, Y. Nishimiya, and N. Koide, *J. Appl. Polym. Sci.* **68**, 1979 (1998).
78. S. M. Hong, S. S. Hwang, and J. Y. Lee, *J. Polym. Sci., Part B: Polym. Phys.* **39**, 374 (2001).
79. C. B. Tan, H. Sun, B. M. Fung, and B. P. Grady, *Macromolecules* **33**, 6249 (2000).
80. C. Ortiz, R. Kim, E. Rodighiero, C. K. Ober, and E. J. Kramer, *Macromolecules* **31**, 4074 (1998).
81. H. J. Sue, J. D. Earls, and R. E. Hefner, *J. Mater. Sci.* **32**, 4031 (1997).
82. E. J. Robinson, E. P. Douglas, and J. J. Mecholsky Jr., *Polym. Eng. Sci.*, **42**, 269 (2002).
83. C. Carfagna, G. Meo, L. Nicolais, M. Giamberini, A. Priola, and G. Malucelli, *Macromol. Chem. Phys.* **201**, 2639 (2000).
84. C. Ortiz, L. Belenky, C. K. Ober, and E. J. Kramer, *J. Mater. Sci.* **35**, 2079 (2000).
85. M. Ochi and H. Takashima, *Polymer* **42**, 2379 (2001).
86. V. Ambrogi, C. Carfagna, M. Giamberini, E. Amendola, and E. P. Douglas, *J. Adhes. Sci. Technol.* **16**, 15 (2002).
87. D. Frich and J. Economy, *J. Polym. Sci., Part A: Polym. Chem.* **35**, 1061 (1997).
88. A. P. Melissaris, J. K. Sutter, M. H. Litt, D. A. Scheiman, and M. A. Schuerman, *Macromolecules* **28**, 860 (1995).
89. A. P. Melissaris and M. H. Litt, *Macromolecules* **27**, 2675 (1994).
90. A. J. Gavrin, C. L. Curts, and E. P. Douglas, *J. Polym. Sci., Part A: Polym. Chem.* **37**, 4184 (1999).
91. C. Farren, M. Akatsuka, Y. Takezawa, and Y. Itoh, *Polymer* **42**, 1507 (2001).
92. M. G. Lu, M. J. Shim, and S. W. Kim, *J. Appl. Polym. Sci.* **75**, 1514 (2000).
93. C. Carfagna, E. Amendola, and M. Giamberini, *Macromol. Chem. Phys.* **195**, 2307 (1994).
94. W. F. A. Su, K. C. Chen, and S. Y. Tseng, *J. Appl. Polym. Sci.* **78**, 446 (2000).
95. V. Vittoria, R. Russo, F. Decandia, P. L. Magagnini, and B. Bresci, *J. Polym. Sci., Part B: Polym. Phys.* **29**, 1163 (1991).
96. D. H. Weinkauf and D. R. Paul, *J. Polym. Sci., Part B: Polym. Phys.* **30**, 817 (1992).
97. D. H. Weinkauf and D. R. Paul, *J. Polym. Sci., Part B: Polym. Phys.* **30**, 837 (1992).
98. C. Carfagna, E. Amendola, M. Giamberini, G. Mensitieri, M. A. Delnobile, and A. G. Filippov, *Polym. Eng. Sci.* **35**, 137 (1995).
99. J. Feng, *PhD dissertation*, University of Florida, Gainesville, Fla., 2001.
100. A. Stohr and P. Strohriegl, *J. Macromol. Sci.—Pure Appl. Chem. A* **34**, 1125 (1997).
101. R. A. M. Hikmet and B. H. Zwerver, *Liq. Cryst.* **13**, 561 (1993).
102. R. A. M. Hikmet and B. H. Zwerver, *Liq. Cryst.* **12**, 319 (1992).
103. R. A. M. Hikmet and B. H. Zwerver, *Mol. Cryst. Liq. Cryst.* **200**, 197 (1991).
104. I. Heynderickx and D. J. Broer, *Mol. Cryst. Liq. Cryst.* **202**, 113 (1991).

105. S. Ishihara, F. Yokotani, Y. Matsuo, and K. Morimoto, *Polymer* **29**, 2141 (1988).
106. J. Lub, D. J. Broer, R. A. M. Hikmet, and K. G. J. Nierop, *Liq. Cryst.* **18**, 319 (1995).
107. G. G. Barclay, S. G. McNamee, C. K. Ober, K. I. Papathomas, and D. W. Wang, *J. Polym. Sci., Part A: Polym. Chem.* **30**, 1845 (1992).
108. A. Shiota and C. K. Ober, *J. Polym. Sci., Part B: Polym. Phys.* **36**, 31 (1998).
109. P. G. de Gennes and J. Prost, *The Physics of Liquid Crystals*, 2nd ed., Clarendon Press, Oxford, 1993.
110. D. J. Broer, J. Lub, and G. N. Mol, *Macromolecules* **26**, 1244 (1993).
111. P. M. Adams and J. J. Mallon, *Mol. Cryst. Liq. Cryst.* **208**, 65 (1991).
112. H. J. Sue, J. D. Earls, R. E. Hefner, M. I. Villarreal, E. I. Garcia-Meitin, P. C. Yang, C. M. Cheatham, and C. J. G. Plummer, *Polymer* **39**, 4707 (1998).
113. H. Korner, A. Shiota, T. J. Bunning, and C. K. Ober, *Science* **272**, 252 (1996).
114. J. S. Moore and S. I. Stupp, *Macromolecules* **20**, 282 (1987).
115. S. Jahromi, *Macromolecules* **27**, 2804 (1994).
116. C. K. Ober and G. G. Barclay, *Mater. Res. Soc. Symp. Proc.* **227**, 281 (1991).
117. C. B. Tan and B. M. Fung, *J. Polym. Sci., Part B: Polym. Phys.* **39**, 915 (2001).
118. D. M. Lincoln and E. P. Douglas, *Polym. Eng. Sci.* **39**, 1903 (1999).
119. J. W. Schultz, R. P. Chartoff, and J. S. Ullett, *J. Polym. Sci., Part B: Polym. Phys.* **36**, 1081 (1998).
120. J. W. Schultz and R. P. Chartoff, *Polymer* **39**, 319 (1998).
121. O. Parodi, *Solid State Commun.* **11**, 1503 (1972).
122. E. P. Douglas, *Polym. Prep.* **40**, 498 (1999).
123. R. Gerzeski, *Polym. Eng. Sci.* **39**, 2150 (1999).

ELLIOT P. DOUGLAS
University of Florida

LITERATURE OF POLYMERS. See INFORMATION RETRIEVAL.

LIVING POLYMERIZATION, ANIONIC. See ANIONIC POLYMERIZATION.

LLDPE. See ETHYLENE POLYMERS, LLDPE.

LOW DENSITY POLYETHYLENE. See ETHYLENE POLYMERS, LDPE.

MASS SPECTROMETRY

Introduction

For many years, mass spectroscopists have searched for ways to place charged polymeric molecules in the gas phase without degrading the polymer molecule. With charged polymer molecules in the gas phase, the many methods of mass spectrometry (ms) used for small molecules can be applied to large molecules. In the same way, placing unfragmented polymer molecules into the gas phase offers polymer science one of the most powerful absolute techniques that can be applied to single-chain characterization. The ms techniques offer the possibility to obtain polymer single-chain structural information as a function of its molecular mass, eg, repeat units, end groups, copolymer composition distributions, and polymer architecture, as well as the overall molecular mass distribution (MMD). One can also envision studying gas-phase chemical reactions involving polymer chains to further study chain structure, ie, copolymer sequencing, or chain branching. This hope has been realized in the last 10 years with the advent of soft ionization methods in mass spectrometry, matrix-assisted laser desorption/ionization (MALDI), and electrospray ionization (esi) methods. These methods place unfragmented high molecular weight polymer molecules in the gas phase. Using MALDI methods, one can examine polymers with molecular mass from about 500 to about 1,500,000 (1). Using esi methods, polymers with molecular masses up to 5,000,000 have been measured in the gas phase (2).

In this article, focus is on the soft ionization technique MALDI, which is mainly in use for synthetic polymers. ESI is briefly discussed, although the electrospray method has been generally confined to polar polymers, which are water-soluble. Other ionization methods that have been used on synthetic polymers, mainly laser desorption (LD) and field desorption (FD), are confined to low

Encyclopedia of Polymer Science and Technology. Copyright John Wiley & Sons, Inc. All rights reserved.

molecular mass polymers. LD and FD methods are discussed in some detail in other references on ms (3,4).

Readers should note: A search of the current literature will reveal that esi and MALDI methods are most commonly used on biopolymers. Any simple search using the names of these methods will give many more articles on biopolymer uses of these methods than articles on synthetic polymers.

In the last edition of this encyclopedia, a detailed discussion of traditional small molecule ms was given in connection with studies on the degradation of polymers and studies on additives in polymers. These topics will not be considered in this article. The reader is referred to the 1987 Encyclopedia article or other more current reviews (5,6).

This review begins with an abbreviated history of the work done to successfully place a high molecular mass polymer into the gas phase. Then there is a description of the two most common methods used to place charged high mass molecules into the gas phase, esi, and MALDI. Because of its dominant use with synthetic polymers, the MALDI method is described in detail, including sample preparation, data analysis, and the problems this method poses. The time-of-flight mass spectrometry (tof-ms) system is also described in detail since it is the most common in use today for synthetic polymers. References to other ms and detection systems are also provided for the interested reader. Additionally, issues of quantification will be reviewed because to determine MMD or molecular composition distribution (MCD) for copolymers one must be able to quantify the ms data. A variety of applications of MALDI to synthetic polymers are described.

History of MALDI and Electrospray

Electrospray ionization of polymers was introduced in 1968 (7) in an effort to study polystyrene by ms. In 1984, the technique was further developed for biopolymers (8). Spectra of poly(ethylene glycols) (PEG) up to molecular masses of 17,500 were also obtained using esi (9). In 1992, esi techniques were used to obtain ms on a poly(ethylene oxide) (PEO) of about 5,000,000 (2). Since esi techniques multiply charge macromolecules, both these studies were able to get spectra on a quadrupole ms with an m/z of less than 2000, where z is the number of charges. However, with many different n-mers in a normal narrow MMD of a synthetic polymer, the effect of z often as high as 40 means that one needs to obtain resolution in m/z of a small fraction of a mass unit to see the entire MMD.

In 1988, a laser-based desorption method was developed (10) which produced ions of both high molecular mass synthetic polymers and biopolymers. In that same year, the laser desorption technique using an organic molecule matrix now commonly called MALDI was developed (11). The technique was originally described for biopolymers. In 1992, it was shown that the MALDI technique could be applied to synthetic polymers (12–15).

The Analysis Process

Mass spectrometry may be viewed as comprised of three distinct processes: (1) The production of charged gas-phase species from the original analyte. This step

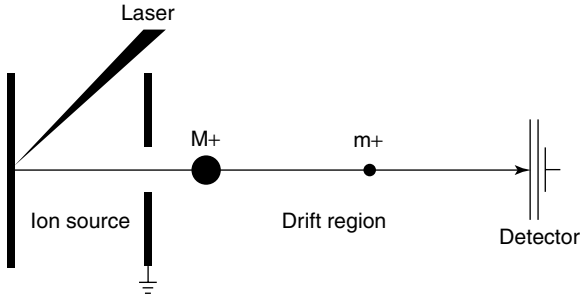

Fig. 1. Schematic of linear tof-MALDI instrument.

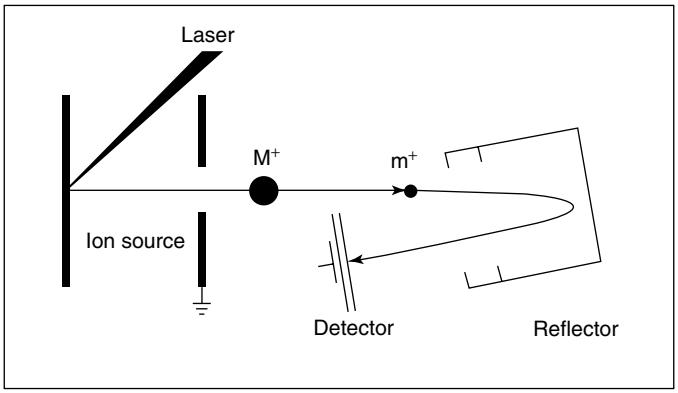

Fig. 2. Schematic of reflectron tof-MALDI instrument.

involves a way to get the analyte into the gas phase and a way to ionize it. For both MALDI and esi, these events occur in the same process; for other ms techniques used on lower mass molecules, this is not necessarily the same process; (2) The separation of the analytes by mass or, more correctly, by m/z; and (3) The detection of the ions.

Herein will be considered the MALDI-tof-ms with a microchannel plate (MCP) detector (see Fig. 1 for the schematic of a linear MALDI-tof-ms and Fig. 2 for the schematic of a reflectron MALDI-tof-ms). This is currently the instrument most commonly used to analyze synthetic polymers.

Introduction of the Polymer Molecule into the Gas Phase and Ion Formation. Since the advent of lasers, it has been hoped that with very short laser pulses of an appropriately chosen wavelength, energy could be transferred into the translational modes of the polymer molecule in such a rapid way that the molecule would go into the gas phase before it broke apart (fragmented). Although there had been numerous tries (7), only small polymers with masses less than 2000 or so could be gotten into the gas phase without significant fragmentation (16,17). These methods of laser desorption or field desorption are described in more detail in the previous encyclopedia article and recent books (3,4,18). Since these methods are limited to low molecular mass polymers they will not be considered here.

The MALDI Process. The MALDI process is the ablation of the analyte cocrystallized with an organic small molecule matrix, most commonly an organic acid. The process (11) initially used and also in common use today is as follows: A polymer (biological or synthetic) is cocrystallized or co-mixed with the matrix molecule in the solid phase. A short uv or ir laser pulse is used to ablate the matrix and the analyte mixture creating a plume of matrix and analyte species. The ablation process involves the uv or ir absorption by the matrix molecule. The laser energy excites the matrix molecule, causing it to vaporize and decompose into what is now considered a supersonic phase transformation (19). This process excites many modes of the matrix and transfers the energy from electronic or vibrational modes into translational modes in the matrix. For MALDI-tof-ms, the most commonly used laser is the 337-nm wavelength uv nitrogen laser. This laser has a pulse width of about 3 ns and generally performs well in the ablation of the matrices commonly used.

The laser energy per unit area is a variable that one can adjust with a variable absorbing neutral density filter. The ablation energy per unit area is usually adjusted to the lowest level that will produce polymer ions. This keeps the initial energy of the plume lower. Lower initial plume energy results in lower initial velocity distributions of the molecular ions, minimizing broadening and reducing the fragmentation of the polymer.

The matrix is selected to absorb most of the energy; few (if any) electronic states of the analyte (the polymer) are excited directly. However, since the analyte is intimately mixed with the matrix, the analyte is carried into the gas phase as a consequence of the phase transformation in the matrix. The analyte, the matrix molecules, clusters of matrix molecules, cations and cation clusters, as well as various combinations of each of these species have been detected in the plume from this laser ablation process (21–23).

For biopolymers, it is thought that the biopolymer is protonated by the many protons released in the plume and thus charged as a positive ion (4). For synthetic polymers, only those which have labile protons are easily charged in the same way (like polyacrylic acid and polystyrene sulfonate). Most synthetic polymers are charged by the addition of a metal ion. In some cases, adventitious metal ions are present in the matrix at concentrations sufficient to allow for their addition to the polymer in the gas phase. (Careful analysis of polymers of known end groups allows unambiguous identification of the attached metal cation.) In other cases, the ions have to be added to the matrix–polymer mixture to give enough of the proper ion to attach to the polymer. Generally, polar polymers are charged by alkali metal ions. These are either added to the solutions used to create the solid matrix analyte mix or often exist as impurities, either from the glassware or solvent used in the sample preparation or in the matrix material. For nonpolar polymers containing double bonds, transition-metal salts with Ag or Cu cations are added to the solution containing the matrix analyte mixture, and these ions charge the polymer in the gas phase. For reasons not completely understood at this time, regardless of the normal stable charged state of the metal ion ie, $+1$,$+2$, or $+3$, the MALDI process generally favors only singly charged n-mers in the gas phase (24). This generalization does not hold for very large molecular mass where multiply charged synthetic polymers can often be seen (1). Once charged, the metal polymer species is then accelerated into the separation region of the ms.

Other Soft Ionization Processes for Large Molecules. Electrospray ionization creates ions by a potential difference between a metal capillary tube and the inlet to the mass spectrometer. The electric field generates charged droplets in the form of a fine mist (see Ref. 25). Application of a drying gas or heat evaporates the solvent, reducing the droplet size and eventually resulting in the formation of molecular ions.

Truly monodispersed polymers like large biomolecules may be examined by esi-ms. These samples typically show a distribution of multiply charged molecules and no evidence of fragmentation. The multiple charging process has the effect of lowering the m/z values to a range easily measured by quadrupole ms, molecular mass typically in the range 500–2500. The molecular mass of biopolymers can be calculated since more than one charged state is observed. However, the multiple charging of esi is a drawback for synthetic polymers. Here, there are many n-mers even with a synthetic polymer having a narrow MMD. Each n-mer in the MMD forms many multiply charged species. These multiply charged species for each n-mer together with the distribution of n-mers results in an m/z spectrum that requires a resolution often not available in many mass spectrometers to separate all the species present. Because esi-ms uses solutions of the polymer as the sample, esi-ms is easily connected to liquid chromatography systems, such as hplc or sec. The coupling of esi with chromatographic process is often used to deconvolute the complex spectra described above (26).

The Separation Process. Once the analyte is in the gas phase as an ion, analytes must be separated on the basis of mass to charge (m/z). A variety of separation techniques are available. The most common form of ms separation is the quadrupole mass filter (3,4). Because this method is limited to m/z less than 3000 or so, it is not generally used with MALDI. However, a quadrupole is commonly used with esi where multiply charged analytes allow one to examine high masses for m/z less than 3000.

Fourier transform mass spectrometry (ftms) is an ion cyclotron resonance method (3,4). This method is currently limited to masses less than 20,000. Thus, it works well for lower molecular mass polymers. Often it is used with MALDI. However, the MALDI process is so energetic that the initial velocity of the analytes can cause some intensity difficulties that make the method difficult to quantify. Because of the expense of the magnet required to obtain quality data with this method, only a few laboratories use this method.

For MALDI, the most common mass separation technique is tof-ms. In its simplest form, the ions in the MALDI plume are accelerated by a high voltage (often as high as 25 kV) for a distance of a few millimeters during which the ions obtain a velocity v. The accelerated ions drift in an evacuated tube, typically about a meter long, at this velocity. (Some instruments have flight tubes as long as 6 m). The equation describing this simple process is

$$zeV = 1/2mv^2 \tag{1}$$

where V is the electric potential applied to accelerate an ion of charge ze. Once in the drift tube the translational energy of the ion is given by the r.h.s. of the equation. There is a correction for the initial velocity of the particle in equation (1) but if the field is large enough, this is a small correction (18,27). If the drift

tube is long compared to the acceleration region, then $v = L/(t - t_0)$ where L is the length of the drift tube and $t - t_0$ is the time from some arbitrary zero time t_0 set by the arrival of the ablating laser pulse. Thus, we have

$$m/z = 2eV(t - t_0)^2/L^2 \tag{2}$$

or

$$m/z = a(t - t_0)^2 \tag{3}$$

Equation (3) is the equation relating mass and charge to time, which is used as the general calibration for a tof-ms instrument. Often some small corrections are added to equation (3) (18,28) for the final tof calibration equation.

In current instruments, two modifications from a simple tof instrument are included. One is the reflectron, a set of ion mirrors which slow the ions down, reverses their direction, and by increasing the actual length of the flight path, increases the resolution. See Figure 2 for a schematic of an instrument with a reflectron. By appropriate choice of reflectron voltages and shape of the voltage fields, one can improve resolution even more. This is described in detail in other references (18). The overall effect of the reflectron is to make little change in equation (2) for use as a calibration equation.

Although the reflectron improves the resolution of the instrument, there can be loss of signal because of ion optics as well as late fragmentation. Fragmentation that occurs while the molecule is in the linear flight tube is considered late fragmentation. (Early fragmentation is fragmentation in the initial plume.) Molecules that fragment in the late fragmentation process will have the proper kinetic energy and arrive at the correct time at the detector in the linear region. Once in the reflectron, these ions are reacclerated with the mass of the charged fragment. Thus, they arrive at the reflectron detector at the "wrong" time.

The second modification is called delayed extraction. In earlier instruments, a single high voltage accelerating electric field was continuously applied while the plume was formed by laser ablation. Instruments with delayed extraction have a second field plate located a few millimeters away from the original field plate. The second field plate is energized for a brief time, keeping the plume trapped for a short time (hundreds of nanoseconds), between the two field plates. The second field is then suddenly dropped to zero potential, accelerating the ions from the contained plume. This brief containment of the analyte plume allows it to come to some modest equilibration, decreasing the range of initial translational velocities and thus improving the resolution of the final spectra (27,28).

Detectors. Several detectors are available for tof-ms instruments. An optimum detector should show no ion velocity dependence. The detector should not saturate or should have a sufficiently rapid recovery rate on the time scale of the smallest collection time interval. No current detector satisfies these requirements. Many of the most common detectors have been discussed (3).

The MCP detector is the most commonly used on instruments employed for the analysis of synthetic polymers. The MCP detector is made up of an assembly of lead glass capillaries coated on the inside with electron-emissive materials and fused together. The capillaries are biased by a high voltage. Ions strike the inside

wall, creating secondary electrons which amplify each ion impact signal with a gain of 10^3 or 10^4. Higher gains are obtained with two MCP detectors in series.

In a study (29) of differences in signals from two detectors, using the same tof instrument, equimass blends of narrow PMMA standards were used to simulate a wide polydispersity polymer and it was shown that different detection systems produced different MMD for the polymer blend using the same sample preparation method and the same analyzer conditions. The differences arose from detection mechanisms, saturation effects in the detector, and signal to noise problems.

Matrices for the MALDI Process. The matrix is crucial to the MALDI process. It is generally believed that how the polymer is situated in the matrix has a significant influence on the success of the MALDI process. Liquid matrices have been used in a number of applications for biopolymers but only a few applications for synthetic polymers. Solid matrices are most common for both biopolymers and synthetic polymer work. The earliest experiments (11) that described the MALDI technique employed solid matrices.

Liquid Matrices. Liquid matrices have the advantage that they present a homogeneous material for the polymer to reside in (in contrast to the crystal of a solid matrix which is discussed in a later section) and thus show less variation in signal as the laser probe is moved across the sample compared to use of a solid matrix with hand spotting (30). Furthermore, with a liquid matrix it is more likely that one can detect precipitation of the polymer sample in the sample preparation. Such an observation cannot be made during the solvent evaporation step of the solid matrix polymer preparation.

The major disadvantage of the liquid matrix is high vapor pressure of the liquid, often too high for the vacuum systems of many current tof instruments. The use of atmospheric pressure ms in MALDI analyses (31) may lead to the increased use of liquid matrices. Furthermore, the liquid matrices seem to have poorer mass resolution than the same polymer in solid matrices. Finally, many instruments are designed with vertical sample holders, which are not impossible to work with but certainly this sample alignment does not favor the use of these matrices. Little work has been done on this promising method of sample introduction.

m-Nitrobenzyl alcohol (*m*-NBA) and 2-nitrophenyl octyl ether (*o*-NPOE) are commonly used MALDI liquid matrices. These substances were originally used as fast ion bombardment (FAB) ms (3,4) liquid matrices. Liquid systems with liquid mediators and uv absorbers, some of which were normal solid matrices, have been developed (30). These gave excellent sodium cationized PEO spectra. A glycerol mediator with sodium and potassium ferrocyanide as the matrix absorber has been used (32,33).

Solid Matrices. Most work on synthetic polymers use the solid matrices developed for the biopolymer analysis. To use these matrices, solutions of polymer, matrix, and cationizing salt are mixed. The solvent is then allowed to evaporate from these solutions deposited onto a sample surface. The mass proportion ratios of the matrix:polymer:salt in the final solid mixture cover the range of 5:1:2 to 2000:1:1. These proportions are often dependent on molecular mass of the polymer (1). The choice of matrix compounds for synthetic polymers with respect to the polarity of the polymer have been discussed (34). As a general rule, matrix polarity should be matched with the polarity of the polymer so that both are soluble in a common solvent. Since the MALDI sample preparation requires intimate

mixing of matrix, analyte, and salt, this choice will assure the best co-mixing of the final solid mixture of the analyte and the matrix. The following table for the appropriate choice of matrix and polymer in terms of solvent strength may be helpful. The arrangement in the table is more hydrophilic at the top proceeding to more hydrophilic.

Matrix	Polymer
Thiourea	Poly(ethylene glycol)
Dihydrobenzoic acid	Poly(propylene oxide)
Cyanohydrobenzoic acid	Poly(vinyl acetate)
Ferulic acid	Poly(tetramethylene glycol)
Indol acrylic acid	Poly(methyl methacrylate)
Dithranol	Polystyrene
Retinoic acid	Polybutadiene
Diphenyl butadiene	Polydimethylsiloxane

Although this table provides a good first rule for the choice of various matrices for each polymers, its usefulness is often overridden by the sample preparation methods described later in this review.

A recent review (20) of MALDI of synthetic polymers offers an extensive reference list of polymers and the appropriate matrix to use with them.

Sample Preparation Methods for Solid Matrices. Sample preparation is critical to MALDI using solid matrices. The presumption is that the polymer and the salt must be well dispersed in the final matrix mixture to achieve a one-to-one representation of the polymer MMD in the solution to the polymer MMD in the gas phase. Yet, the matrix is commonly crystalline and the polymer may be either semicrystalline, like PEO, or glassy, like atactic polystyrene. Kinetic processes occurring during the loss of solvent from the solution of the mixture of matrix, salt, and polymer must occur either to co-crystallize the polymer with the matrix and salt or to embed the polymer in the defect structure of the organic matrix. To obtain the correct representation of the MMD in the ms, each n-mer in the MMD must occur in the ms in proportion to its appearance in the original MMD.

The intimate dispersion of the salt in the matrix is also important (35,36); if the salt is not well dispersed, there may be a loss of signal. The matrix is often an organic acid. By making the salt of the matrix acid and mixing this with the parent matrix acid, increased polymer signal is obtained. Too much salt, however, leads to no polymer signal since matrix salt alone is often not a good matrix for the polymer.

Generally, there are two common approaches to sample deposition onto the target surface, hand-spotting and electrospraying. In one approach, the solutions described above are hand-spotted from a microliter pipette onto a target plate; 0.5–2 μL of solution are used to deposit micrograms of polymer, matrix, and salt mixtures onto the plate. The solvent is allowed to evaporate rapidly (often with help from a fan or heating or by drawing the pipette tip across the plate, spreading the solvent out). One usually obtains crystals of the matrix. This is called "hand-spotting" or the "air-dried droplet technique." The advantage to this method is that it requires little additional equipment. However, the samples have large

signal variations across the target plate; one finds areas of large polymer signal, "a sweet spot," and other regions where no polymer signal is found. This inconsistency across the sample is reduced somewhat by a variety of modifications of the hand-spotting method. In a procedure used by various workers (37,38), the matrix crystals are crushed with a spatula. This leads to additional sample homogeneity. Others have examined the different modifications of the hand-spotting technique (39).

However, in general, hand-spotting leads to a relative standard deviation of 40% in the total signal intensity variation across the target surface. The electrospraying method of sample preparation, described below, can produce targets that exhibit less than 5% relative standard deviation of total signal intensity across the target surface (40).

The same solutions that are used for hand-spotting are used in the electrospray technique. These solutions, after mixing, are then drawn into a microliter syringe that is placed into a syringe pump. The needle of the syringe is held at a potential between 3 kV and 7 kV against the sample target as ground. When the solution is delivered at 2–20 μL/min, a fine spray of charged droplets is delivered out of the needle. The sprayed solvent evaporates from the droplets, and the polymer:salt:matrix mixture is deposited on the sample plate nearly dry (40,41). This procedure keeps the crystals of the matrix small (ca 2–5 μm diameter) (35,40) and the polymer matrix and salt in an intimate mixture.

The signal from electrospray sample deposition shows little shot-to-shot variability as long as the sample depth is thicker than the amount of sample that can be ablated by a few laser shots at the same location of the target (42). This methodology also shows good shot-to-shot repeatability for biopolymers (41).

Choice of Salts. Synthetic polymers generally obtain a charge by a different mechanism than biopolymers. Most biopolymers obtain a charge by addition or loss of a proton from the parent molecule. This is because biopolymers have acid groups available to them. For synthetic polymers like polystyrene sulfonic acid, this mode is also available. However, most synthetic polymers do not contain labile protons. Those synthetic polymers that are polar or contain double bonds can be cationized, however. The polar polymer molecules require a metal ion, often an alkali like Na^+ or K^+, to attach to the polymer *n*-mers to obtain a charge. The Na and K metal ions are usually found in the matrix itself or introduced through the glassware used in sample preparation. For example, with PEO or PMMA, the common matrices used for these polymers have enough Na and K so that one commonly sees ions with both Na and K attachment without the addition of any Na or K salt. One can also add salts to the sample preparation solutions causing these salts to attach to the polymer *n*-mers. For polymers with double bonds, polybutadiene or polystyrene for example, one normally has to add Ag or Cu salts. These metal salts are found to work best, although other salts also give spectra (43). In fact, some matrices give spectra for these polymers with Na or K salts but the quality of the spectra is poor compared to spectra obtained with transition-metal salts. Polymers without polarity or double bond, for example polyethylene or polypropylene, have difficulty being cationized. Only a few papers report MALDI spectra on these saturated hydrocarbon polymers (44,45).

Commonly, salts that are soluble in the same solvent as the polymer and the matrix are added to the polymer matrix solvent mix. Nitrate, chlorides, etc

are commonly tried, but these do not easily dissolve in the organic solvents commonly used (tetrahydrofuran, acetone, chloroform). One often uses trifluoroacetic acid (TFA) salts; for example, Ag TFA or CuTFA are commonly used to cationize polystyrene. Only one paper has reported any effect of the anion on the cationization process (46).

Other materials have been used to cationize the polymers. Metallocenes (ferrocene, nickelocene, and cobaltocene) have been used as cationizing agents for polystyrene and PEO (47). These cations have the advantage that they are soluble in many organic solvents and also do not have the isotopic splitting seen with Ag, which often complicates the interpretation of the MALDI spectra.

Quantification of MALDI for MMD and Moments of MMD

Mass Axis Quantification. Mass axis quantification is most easily done. Calibration of most tof instruments is usually done with biopolymers of known molecular masses. These biolpolymer are selected because they typically provide a single major peak whose mass is known accurately; thus, mass axis quantification is quite straightforward. Calibration usually can be done using three of these biopolymers. Collecting data with 2-ns time intervals, one can get better than single-unit resolution on an instrument with a 1.5-m flight tube in reflectron mode at about 7000. Good mass resolution and calibration is required for end group determination, copolymer composition determination, and for polymer architecture studies.

Signal Axis Quantification. For synthetic polymers, signal axis quantification is of utmost importance to obtain a good representation of the MMD or MCD or to compute the moments of the MMD to compare with classical polymer characterization methods like light scattering or membrane osmometry.

The signal axis may be in error due to a variety of reasons. Many of these issues have been discussed (48). Most of the issues related to uncertainties arising from sample preparation have been discussed in some detail in the earlier sections on matrices and sample preparation.

Uncertainties Arising from Ablation, Ionization, and Drift Regions. Little is known about the desorption/ionization process in MALDI. Work on the same type of polymer of different molecular masses suggests that higher ablation energies are required for polymers of higher molecular masses. Thus, since the normal procedure is to adjust the laser ablation energy to just above the threshold needed to obtain the polymer spectra in MALDI, the desorption process of MALDI could also cause the moments determined by mass spectrometry to be lower than the true moment. It is not known whether low mass molecules desorb better than higher mass molecules, but, if preferential desorption of low mass molecules occurs, it could account for the low MALDI values often reported when the moments from MALDI are compared to those obtained by classical methods (49–53).

For homopolymers, the dominant polymer repeat units commonly show high signal intensity. Also, less intense intermediate peaks may be seen adjacent to the major high intensity repeat units. These intermediate peaks more often than not have the same repeat unit as the major peaks. These intermediate peaks may arise from a variety of sources. It is most obvious that end groups or cations may

differ. One can have two different sets of end groups on linear chains or many different types of end groups on branched chains. This gives rise to a main group series of peaks arising from the major pair of end groups and a second series of peaks from the second set of end groups.

One may see additional peaks from different metal cations attaching to the polymer. As noted before for polar polymers like PEO and PMMA, one does not need to add salts to the matrix. Impurities in the matrix in the form of Na or K seem to be in sufficient concentration to cause the addition of Na or K to the polymers. For example, with PMMA it is not uncommon to see peaks separated by 16 u, the difference between the molecular mass of Na and K. This peak intensity will change by the addition of one or the other metal ion. All the above peaks will appear in both the linear and reflectron mode.

Some intermediate peaks will often appear differently in linear and reflectron modes for reasons other than sensitivity differences between the two modes. If the reflectron spectra is different from the linear spectra, this may be due to fragmentation during the flight down the linear flight tube. Of course, fragmentation occurring in the ablation region (the source region) cannot be detected this way. Ablation region fragmentation may be detected by the appearance of more n-mers in the low mass regions of the MMD as the laser energy is increased.

Finally, the intermediate peaks may arise from matrix adducts to the polymer. Matrix adducts of polystyrene polymers of molecular mass 3900 and 7000 of the form MatrixAgPolymer and MatrixAgAgPolymer have been found (21). Figure 3 shows the entire spectrum, and Figure 4 shows these adduct peaks in a polystyrene of molecular mass of about 7000 used in the NIST Interlaboratory Comparison (49,54).

Uncertainties Arising from the Detector. The detector is another influence on the MMD that may impact the moments calculated by MALDI-tof-ms. The

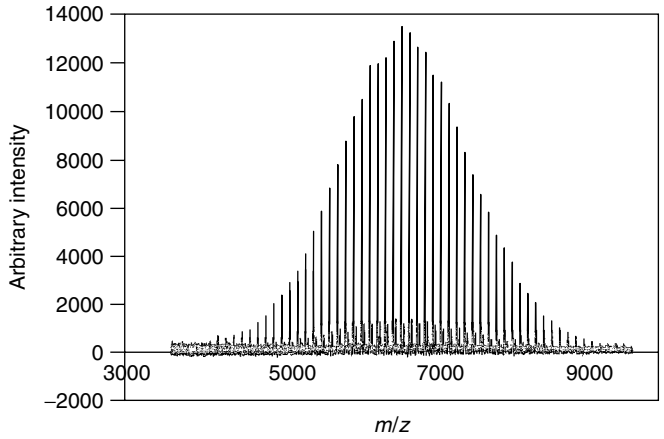

Fig. 3. MALDI-tof-ms of polystyrene around 7000 molecular mass. This MALDI spectrum was generated using dithranol as the matrix and AgTFA as the salt. The polystyrene, dithranol, and salt were dissolved in tetrahydrofuran. The solution was then electrosprayed onto the sample plate. The polymer analyzed in reflectron mode with an extraction voltage of about 25 keV.

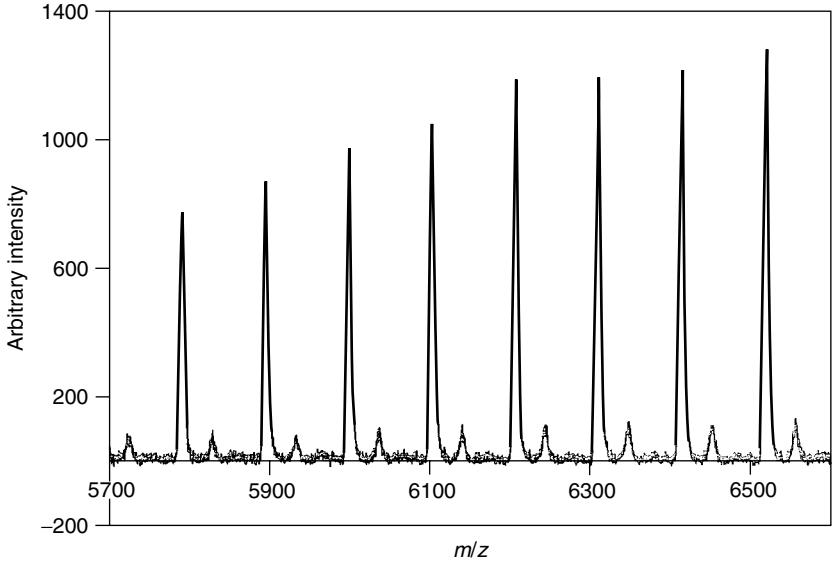

Fig. 4. Detail of MALDI-tof-ms of polystyrene polymer shown in Figure 3. The smaller peaks between the main peaks have been shown (21) to be the result of matrix adducts. This is an example where these intermediate peaks are not from polymer molecules terminated with other end groups or from *n*-mers charged with different salts.

detector in most of the instruments is an MCP detector. The smaller molecular mass molecules hit the detector first, and the larger molecules follow later. If there is saturation occurring in the detector, then there would be a discrimination against the high mass molecules. The issue of detector saturation has been discussed by many authors (51,55,56). Since the matrix molecules or low molecular mass polystyrene molecules could saturate the detector before the higher molecular mass molecules arrive at the detector, this would cause the computation of a lower M_n and M_w than the true values.

The detector may also be less sensitive to larger mass polymer molecules because of the way the ions are detected. MCP detectors count the number of ions by an ion-to-electron conversion when the ionized polymer collides with the detector plate. A bias occurs against the high mass species when the ion-to-electron conversion is diminished due to a decrease in the impact velocity of the larger ionic species (51,57). If a discrimination against the high mass polymer molecules exists, this would cause the estimated moments of the distribution to be less than the true value of the moment.

Uncertainties from Data Analysis. Baselines drawn in MALDI-tof-ms are similar to that of a spectroscopic or chromatographic system where a many-point baseline must be drawn. Baseline corrections may be a cause of the disagreement between the moments determined by classical methods and those determined by MALDI. There is much more noise in the low mass end of the spectra obtained by MALDI-ms. Some of this noise may arise from fragments of the polymer, clusters of matrix and salt, or metal clusters. If the baseline correction does not account for this difference in baseline noise, then these data may overweight the lower part

of the MMD and thus the calculated M_n and M_w would be expected to be lower than the true moments.

Assuming a correct baseline is drawn, the question arises as to how to compare the MMD estimated from a tof mass spectrometer to that obtained from size exclusion chromatography (sec) using a UV or differential refractive index (DRI) detector. A sec is the instrument most commonly used to obtain the MMD for synthetic polymers. The most obvious difference between the two techniques is that the tof detector counts numbers of ions of n-mers while the DRI or UV detectors on sec instruments measures mass concentration of the polymer. The mass concentration of the polymer is proportional to the product of the molecular mass of the n-mer and the number of molecules of that n-mer per unit volume. Thus, in the ms we obtain the number MMD while in the sec we normally obtain the mass MMD. Furthermore, the raw signal of each must be corrected for the transformation from time to mass, which is different for each instrument. This transformation has been discussed in detail (58).

Finally, there is a problem of the detection for higher n-mer masses in MALDI. Since the detector is an ion detector, a counter of the number of n-mers, peaks disappear into the noise before peaks would disappear into the noise on a normal sec detector, which detects the total mass associated with each n-mer. The consequences of this signal-to-noise problem on the polydispersity (M_w/M_n) studied by MALDI-tof-ms has been discussed (59).

The above discussion assumes that the polymer is a linear homopolymer. For branched polymer there is not a simple direct relationship of elution volume in sec to molecular mass. For a copolymer, the signal differs in both the DRI or the uv detector for different groups in the copolymer. Further, it is usually assumed that there is no effect of molecular mass on the DRI or uv response. Although this is the case for high molecular mass species, as we go to very short chains the DRI and uv are affected by the presence of end groups. This is discussed in more detail in the section on narrow MMD.

The effect of instrumental broadening on the sec data has not been discussed. For a polymer with little polydispersity the chromatographic broadening is important in sec and may lead to prediction of larger polydispersities than those found by MALDI. Some measurement condition differences which cause effects greater than those between the mass and number MMDs have been studied (60).

Applications of MALDI-tof-ms

Narrow MMD Homopolymers. Generally, most laboratories obtained reasonable agreement for narrow MMD polymers between moments of MMD obtained from MALDI and those obtained by classical methods, eg light scattering to obtain M_w and end group analysis or osmometry to obtain M_n or sec. Good agreement between classical methods and MALDI for polymers with $M_w/M_n < 1.2$ has been observed (61,62). A study (63) of PMMAs by sec and MALDI support this view. A careful study of polystyrene of molecular mass 5050, 7000, and 11,600 and blends of the three has been done (48). Using the polystyrene 5050 and 11,700 and studying changes in the MMD of the polymer of 7000 by blends, showed no systematic uncertainties within 0.5% in the MMD or the moments of the MMD.

A MALDI-tof-ms interlaboratory comparison was conducted by NIST among 23 laboratories using MALDI-tof-ms on a well-characterized polystyrene to assess the robustness of the method to determine the MMD (49). An example of a MALDI-tof-ms spectrum from this polymer is given in Figure 3. The polystyrene was synthesized to have a tertiary butyl end group at one end and a proton at the other. An nmr characterization of M_n was found to give 7050 ± 400. The M_w was found to be 7300 ± 600 by light scattering. The expanded uncertainty values following the "±" represent both type A uncertainties (statistical uncertainty) and type B uncertainties (systematic uncertainties) (64). An ftir spectroscopy confirmed the presence of a single pair of end groups and no other end groups in measurable amounts.

Each participating laboratory was asked to perform MALDI-ms using two distinct protocols. Each laboratory was asked to do three repeats of each protocol to check for intralaboratory variability.

By compiling all the returned data using all protocols into one preliminary analysis, it was found that MALDI-ms returned an M_n of 6600 ± 100 and an M_w of 6700 ± 90. The uncertainty values following the "±" represent only type A standard uncertainties (statistical uncertainty). These M_w and M_n obtained from MALDI were below the M_w and M_n of the classical methods but still within the overlapping uncertainty ranges. The statistical uncertainty in the ms measurements was very small, indicating that from laboratory to laboratory, reproducibility was extremely good.

In a few reported cases, the agreement for narrow distribution polymers has not been good (52). This can generally be attributed to the failure of the classical method at low molecular mass. For example, calibration of sec at low molecular mass is at best difficult. Furthermore, the effect of end groups on the detector response is often not taken into account nor is the effect of broadening on the computed moments properly taken into account at the lower molecular masses. For example, the DRI detector requires the dn/dc be constant, independent of molecular mass for the calculation performed by most current software programs. But dn/dc is known to be affected by end groups (65).

$$\mathrm{d}n/\mathrm{d}c = a + b/M \tag{4}$$

For most polymers, the second term on the r.h.s. has a contribution below 100 repeat units or molecular mass less than 10,000 for polystyrene.

Generally, the effect of not correcting for broadening is to increase the apparent values of sec values of M_n and M_w. This effect may be seen by comparing the moments calculated from sec and from MALDI in the data (63) on narrow MMD polymers.

Broad MMD Homopolymers. Early in the studies on MALDI of synthetic polymers, it was hoped that MALDI could be used successfully for both narrow and broad MMD. Soon it was discovered that for a variety of reasons the correct MMD of broad MMD polymers could not be obtained in one step by MALDI-tof-ms. Good agreement between MALDI and gpc for MMD moments for polymers with polydispersities less than $M_w/M_n = 1.1–1.2$ was found (50). Polymers with higher polydispersities regularly showed incorrect moments of the MMD (50,66).

A number of authors used the procedure of simulating a broad MMD by preparing a multicomponent blend of a number of narrow fractions to mimic a

broad MMD. This way of controlling the amount of each part of the MMD allowed them to show that they do not get the correct representation of the expected MMD from the mixed systems. This procedure also provides a method to examine the various causes of this problem, including instrumental effects (55), sample preparation (67), desorption/ionization issues (51), and laser power (68).

None of these studies have lead to significant improvements in doing the MALDI-ms of polymers with high polydispersities. Generally, this problem has been overcome by coupling MALDI-tof-ms to various chromatographic methods to separate polymers.

MALDI as a Chromatography Detector. The sec is the most commonly used chromatography technique for analysis of polymers. Two common approaches have been used to obtain a MMD from the combination of MALDI and sec. In one case, one fractionates the polymer using sec, collecting each fraction and obtaining the MALDI on each fraction. One then must combine the data from each MALDI spectra to create the MMD on the polymer. This is done by summing each MALDI chromatogram used in obtaining the moments to obtain M_n and M_w and the polydispersity (69). This technique is thought to suffer some of the discrimination issues brought out in the discussion in the broad MMD section (20).

In another method, fractions are taken from the sec at well-defined elution volumes. A MALDI analysis of these fractions is made and the peak of the mass MMD M_p is computed from the MALDI data on the fraction. The M_p so obtained is then used to calibrate the sec. The calibrated sec is then run to get the exact MMD of the polymer (70). A number of authors have used this technique. Two limitations of this technique should be mentioned. The first problem arises because one must have relatively narrow mass fractions in each sec fraction used for this to work. Thus, linear or lightly branched homopolymers or random or alternating copolymers meet this criterion. Branched polymers or polymers with rings or closed loops may show broad MMD fractions for narrow sec fractions. This is because branched polymers or polymers with rings and loops can have the same hydrodyamic volumes for molecules with widely varying masses (71–74). Block copolymers in a solvent such that one block is extended and the other is collapsed (with very different hydrodynamic volumes) may result in mass broadening too. This effect will make it difficult to assign a mass to the broadened fraction by MALDI and thus to get a good calibration for the sec columns. The second problem comes from the assignment of the total mass of the material in each sec fraction. For a copolymer, for example, a single detector may not be enough to assign the total mass of different groups at a given molecular mass. Two detectors at least may be required for copolymers.

In one case (71) a different phenomenon is observed: Poly(bisphenol A carbonate) terminated with hydroxyl groups undergoes self-association by hydrogen bonding in solution and these molecular aggregates remain in the sec column. In the application of the sec MALDI method, self-aggregation is suppressed in the sample preparation for the MALDI analysis and thus a very broad molecular mass for each MALDI appears. This is an extreme case where sec alone cannot provide a narrow MMD for MALDI.

A number of papers discuss placing a MALDI-ms instrument in line with a continuous chromatographic process (75,76). For example, a method called Aerosol MALDI has been developed. In this method, elutant from an sec is mixed with

matrix prior to pneumatic nebulization, which sprays directly into a mass spectrometer. MALDI is performed on aerosol particles using a 355-nm laser. The solvent is evaporated from the aerosol particles by passing the aerosol through a heated tube. This technique has been used successfully with PEG of mass 1000 u and polypropylene glycol also of mass 1000 u. Mass resolution with this method is less than with normal MALDI. In addition, the problem with data analysis is overwhelming. Baseline determinations, identification of peaks, and quantification are all problems.

The sec method separates polymers on the basis of the polymer size alone. In sec, only the interaction of a polymer which excludes it from the wall is operative. An attractive interaction between the polymer in solution and the solid portion of the porous separation medium can substantially affect molecular separation. The attractive interaction counterbalances the exclusion effect until a compensation point, "the adsorption theta point," is obtained (77,78). Selective molecular separation is lost at this compensation point. For an even greater attractive polymer porous media interaction, the polymer becomes adsorbed onto the surface of the porous media so that the higher molecular weight polymers exhibit an inhibited flow through the porous media. The change from an excluding interaction to an attractive interaction with the porous media can be affected by changing the solvent strength by use of mixed solvents.

For block copolymers, one can choose a solvent system that will have one block at the polymer compensation point and another block in the exclusion regime.

This chromatographic method has been used to examine the polyethylene oxide-*co*-polymethylene (PM) block system (79). The solvent is chosen so that the PEO is at its critical condition, ie, there is no separation with respect to the molecular mass of the PEO, but there is separation with respect to PM. MALDI-tof-ms was used as a detector on this system. Each separate PM peak was continuously transferred onto a MALDI target. The fractionation was made into separate PM peaks. Within each PM peak there is a MMD of PEO. This allowed the authors to estimate both the MMD and MCD for the whole polymer.

End Groups. Polymer end groups play an important role in determining polymer properties. This is increasingly important as the molecular mass of the polymer decreases. Low molecular mass polymers with well-defined end group functionality are used as prepolymers for many important final polymer products, ie, polyurethanes, epoxies, uv cure adhesives, and various other thermosets (qv). For example, polyurethanes are commonly made by a three-step processing in which the activity of the end groups is important in determining the final product (see POLYURETHANES).

Bulk functionality of prepolymers can be determined by nmr, uv–vis spectroscopy, or titration methods. The sec data from multiple detectors can sometimes be used to obtain estimates of functionality, but this is often not available due to the lack of difference of detector signal between the end group compared to the central groups. Even if this is possible, sec does not allow one to separate monofrom multifunctional end groups. Further, the calibration of sec at low molecular masses is, at best, difficult. MALDI-tof-ms offers a unique probe of the end group functionality as a function of the molecular mass of the polymer itself. For polymers of molecular masses below 10,000 or so, current commercially available MALDI-tof-ms instruments can differentiate end groups differing by a few mass

units. With the sensitivity of ftms, one can achieve single mass unit end group identification up to 20,000 (3).

PMMA with a variety of end groups was analyzed and it was shown that the various end groups can be identified (80). A variety of PMMAs of industrial relevance have also been examined and it was possible to distinguish many end groups using "time-lag-focusing" (delayed extraction) for polymers with molecular masses of 16,000 (81,82).

MALDI has been applied to the analysis of poly(alkylthiophenes) (PAT), a rigid rod-type polymer (83), and it was possible to determine the end-group compositions of the PAT samples; H/H, H/Br, and Br/Br end groups were found. The samples showed large variations in the presence of each end-group pair as a function of preparation conditions. Such end-group monitoring is necessary for the development of new materials from these polymers. Further, for the polymers with Br end groups, some end-group loss as a function of laser power was found, with more fragmentation at higher laser powers.

Finally, the end groups in poly(bisphenol A carbonate) have been examined (84). It was possible to distinguish among a variety of end groups for polymers with masses up to 16,000. This work was done with the MALDI acting as an sec detector.

Copolymers. MALDI-tof-ms of copolymers offers the opportunity to obtain an MMD and MCD. However, to obtain an MCD the ms can only be done on low mass copolymers. This is generally difficult because the number of *n*-mers separated by only a few mass units quickly becomes very high for copolymer composition near 50-50. If the mole faction of one of the copolymers is small, it is possible to obtain single or nearly single n-mer resolution for the MCD of the copolymer.

As simple example, MALDI-tof-ms has been used to study the number of α-methyl styrene (α-MeSty) repeat units in SRM 1487, a narrow MMD PMMA NIST standard reference material of about 6300 g/mol (62). Here, the major copolymer component is MMA and α-MeSty is the minor component. The α-MeSty is, in fact, part of the initiator for this polymer and the material is either a "MMA styrene MMA" triblock copolymer or a "styrene MMA" diblock copolymer, with the α-MeSty block length containing 0–6 α-MeSty.

In a more comprehensive study, the copolymer systems polystyrene-*block*-poly(α-MeSty) and poly(α-MeSty)-*block*-poly(4-vinyl pyridine) were examined (85–87). These copolymers have a much more complex MCD as a function of molecular mass than the one just discussed (62), and the resulting MALDI-tof-ms spectra reflect this complexity. In the work (87) on poly(α-MeSty)-*block*-poly(4-vinyl pyridine), polymers with different mole ratios of α-MeSty and 4-vinyl pyridine were studied. The composition of the maximum peak was used to start the analysis. The compositional assignment of this maximum peak was made from nmr data and/or the initial chemical composition of the polymer reaction mixture. The rest of the peaks were assigned by a procedure that references the composition of the main peak. From this analysis the two dimensional distribution of the di-block copolymer was obtained as shown in Figure 5. Such use of collateral data shows that ms alone may not be enough to obtain such a complex copolymer distribution. However, with the copolymer composition distribution, a richer understanding of the copolymer chemistry can be obtained.

In a study (85) on the copolymer system polystyrene-*block*-poly(α-MeSty), it was possible to confirm that the copolymer composition agrees with the predicted

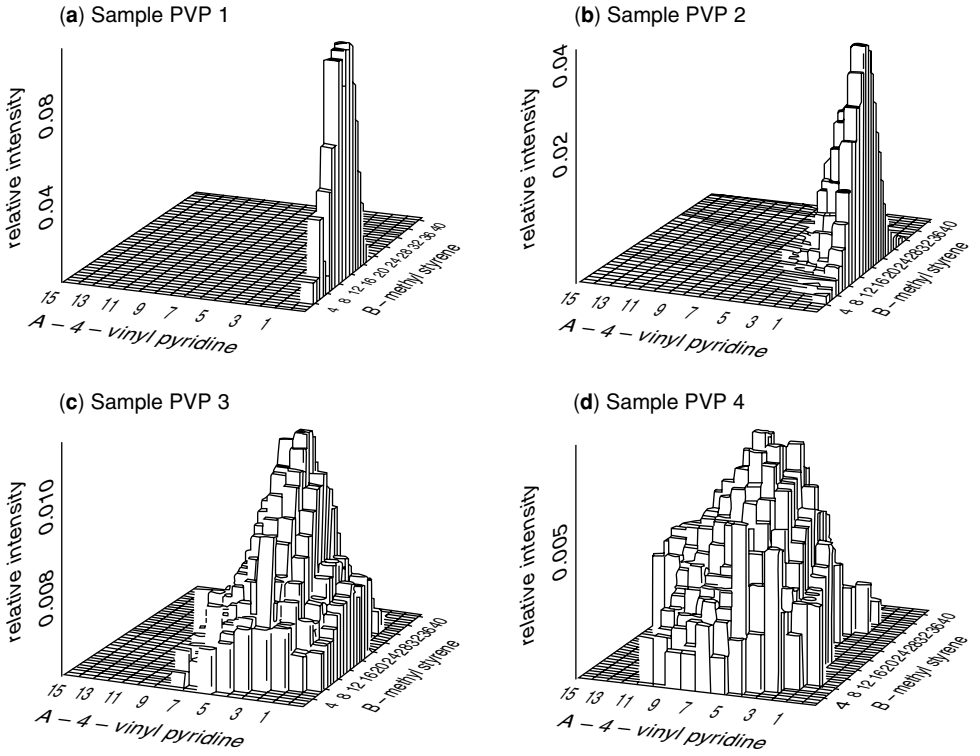

Fig. 5. MMD for one homopolymer and three copolymers of block copolymer of poly(α-MeSty)-*block*-poly(4-vinyl pyridine) as a function of mole fraction of poly(α-MeSty). (**a**) PVP1 is the MMD for poly(α-MeSty) homopolymer; (**b**) PVP2 is the MMD and MCD of the diblock copolymer poly(α-MeSty)-*block*-poly(4-vinyl pyridine) with 0.9 ± 0.1 mole fraction poly(α-MeSty); (**c**) PVP3 is the MMD and MCD of the diblock copolymer poly(α-MeSty)-*block*-poly(4-vinyl pyridine) with 0.63 ± 0.1 mole fraction poly(α-MeSty); (**d**) PVP2 is the MMD and MCD of the diblock copolymer poly(α-MeSty)-*block*-poly(4-vinyl pyridine) with 0.45 ± 1 mole fraction poly(α-MeSty). Reproduced from Ref. 87.

Zimm–Schulz distribution (88,89). Using an analysis method similar to that used previously on the poly(α-MeSty)-*block*-poly(4-vinyl pyridine) system, the MMD of both parts of the copolymer were determined. The data analysis method was claimed to verify the random coupling hypotheses. The hypothesis (90) that the polydispersity of individual blocks is higher than the polydispersity of the whole polymer was confirmed (85). That is, block copolymers with narrow MMD have broad complex chemical composition distribution.

The composition and sequence distribution of poly(butyleneadipate-*co*-butyleneterephthalate) have been studied (91). The intensity of the ms peaks was compared with theoretical intensities obtained using a Bernoulli distribution of the sequences. This result is in excellent agreement with nmr analysis of the bulk polymer.

Many other authors have shown MALDI-tof-ms of copolymers, but have not offered analysis to obtain a composition distribution as have the previous

authors. For example, the alternating copolymers of polycarbonate and two random copolyethers used as nonlinear optical materials were examined (92). Poly(*p*-phenylene ethynylene)-*block*-poly(ethylene oxide) has been studied (93). Also, styrene-*block*-isoprene copolymers have been examined (94). Much of the current work on copolymers has been reviewed (95).

MALDI to Elucidate Polymer Chemistry. Perhaps one of the most profitable future uses of MALDI will be for elucidation of polymer chemistry. Examining a reaction not yet complete or looking for polymer side products differing only by an end group will yield important reaction kinetics information. Unlike nmr, uv, or ftir, where one can perhaps find the presence of differing end groups or internal species for the overall MMD, MALDI can identify these species and how they can appear as a function of molecular mass. A caveat to all this work is the matrix attachment studies (21). Without careful studies of the linear and reflectron modes for each reaction examined and the effect of matrix and attached ion on the resultant spectra, one has to consider many of the conclusions from these studies tentative.

Some of the early examples of this use of MALDI to elucidate polymer chemistry are presented here. One can often elucidate polymer chemistry by examining the polymer products during or at the end of a reaction. Much of what has been discussed in the copolymer section relates to this. The work in References 85–87 describes the distribution from which the chemistry can be elucidated.

In the work on SRM 1487, a low molecular mass PMMA, the authors related their findings to the polymer chemistry of the initiator (62). Based on the synthesis information, SRM 1487 would have the following structure:

$$\text{H-PMMA-}\{\alpha\text{-MeSty}\}_m\text{-PMMA-H} \tag{5}$$

where m is the number of α-MeSty repeat units. The course of the anionic reaction of PMMA initiated by α-MeSty with a Na gegen-ion had been extensively studied (96,97) and the conclusion was that dimer and tetramer α-MeSty difunctional anion initiators are the dominant species in the initiation reaction ($m = 2$ or 4). MALDI studies suggested that all values of m from $m = 0$ to $m = 7$ were possible. However, no chains with $m = 6$ were found.

MALDI-tof-ms was used to examine the products from some anionic polymerizations with styrene initiated by *sec*-butyl-Li or t-$C_4H_9O(CH_2)_3$ Li and extended by isoprene (98). Several electrophilic reagents affected termination. The results showed unusual end group rearrangements to yield some end groups not normally expected. From this observation it was possible to suggest new mechanisms for the termination reaction of the polymer.

MALDI-tof-ms has been used to study the preparation of linear polysiloxanes with hydride end-capped and cyclic polysiloxanes from the ring-opening anionic polymerization reaction with hexamethylcyclotrisiloxane and octamethylcyclotrisiloxane (99). The PDMS reaction was followed by MALDI and the incorporation of the hydride end cap and the creation of the cyclics was studied as a function of time. Further studies (100) employed MALDI and sims; it was found that MALDI provides more reproducible relative intensities of the n-mers than does SIMS.

Polymer Architecture Elucidated by MALDI. Although ms is a mass determining device, ms studies in combination with an understanding of polymer chemistry allows one to make deduction on the architecture of polymer molecules. In this section, a study of trifunctional polymerizations similar to those studied by Flory in the early 1940s (see, for example, Ref. 101 is described). Here, however, instead of a carbon-based backbone a silicon-based backbone was studied.

The prepolymers of the polysilsesquioxanes were studied by MALDI-tof-ms (102,103). Polysilsesquioxanes are three-dimensional polymers with a repeat unit of the form $[RSiO_{3/2}]$ where each silicon is coordinated with three oxygen atoms. After a low temperature sol–gel synthesis and processing, silsesquioxanes are then fully cross-linked to from a fourfold coordinate structure. One important unknown in the processing of silsesquioxanes is the "degree-of-condensation" of the prepolymer silsesquioxanes before it is converted into the final product. That is, how many of the silicon atoms are threefold coordinated with bridging oxygen atoms and how many have terminal silanol (SiOH) groups?

In the polymerization process to create the prepolymer, a condensation reaction of two silanol groups to create one Si—O—Si bridge with the elimination of water occurs. In the prepolymer, these terminal silanol groups control the reactivity of the polymer in subsequent processing steps that result in a cross-linked product. Before the use of MALDI-ms only the average number of terminal silanol groups in the whole sample could be measured by ir spectroscopy. Condensation of SiOH groups out of the growing prepolymer silsesquioxane molecule can lead to the formation of intramolecular Si—O—Si bridges with the loss of water. This elimination reaction is easily identified via high resolution tof-ms. Figure 6 shows the overall spectrum while Figure 7 shows the detail of a single low mass oligomer

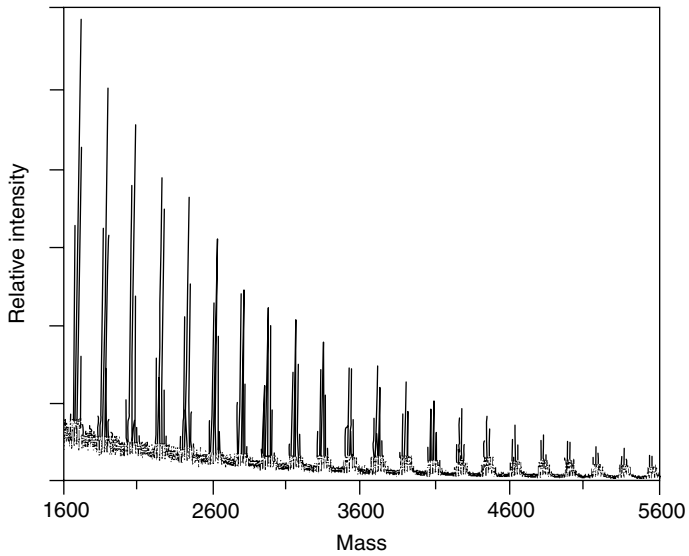

Fig. 6. The central portion of the full mass spectrum of a polysilsesquioxane prepolymer showing the characteristic shape of a condensation polymer. The major repeats show the changing number of $RSiO_{3/2}$ with a repeat of 188, 12 u.

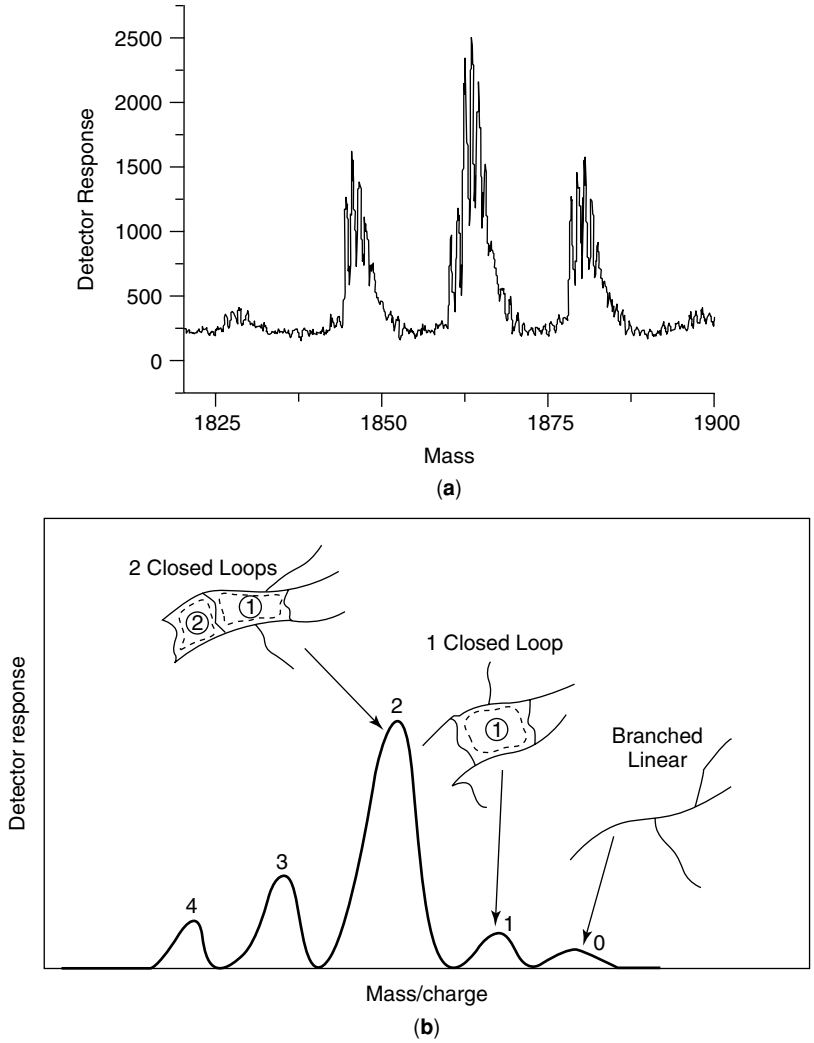

Fig. 7. (**a**) A single-repeat unit detail of the full mass spectrum shown in Figure 6. The distance between peaks in a single major cluster is 18 u, indicative of the intermolecular loss of water; (**b**) The schematic of the polymer ms shows the relation of each peak of the ms to the degree of intermolecular polymer condensation, the important polymer architecture change in this system.

from the overall spectrum. The maximum possible mass of an oligomer with n repeat units occurs when every silicon atom has one silanol group in addition to one R-group and two bridging oxygen atoms. However, the highest intensity peak generally does not occur at the maximum possible mass. Instead, lower mass peaks are more intense. These peaks correspond to the loss of water as a pair of —SiOH groups react. This indicates that intramolecular reactions are occurring.

Each loss of 18 u closes a loop in the molecule moving it away from a highly branched linear structure toward a closed polyhedron. In the limit of the loss of

all silanol groups, a fully condensed polyhedral structure results. For example, for n=8 the fully condensed structure is a cube with Si atoms at each corner and Si—O—Si linkages for the cube edges. Thus, the structure and chemical architecture of each n-mer can be deduced from MALDI-tof-ms.

In another determination of architecture by MALDI (84), the appearance of cyclics and linears in the poly(bisphenol A carbonate) has been investigated. It was possible to distinguish between the linear and cyclic species. From MALDI studies, a separate sec calibration line was obtained for the cyclic and the linear species. This work was done with the MALDI acting as an sec detector.

BIBLIOGRAPHY

"Mass Spectrometry" in *EPST* 1st ed., Vol. 8, pp. 412–419, by G. P. Shulman, Jet Propulsion Laboratory; "Mass Spectromety" in *EPSE* 2nd ed., Vol. 9, pp. 319–356, by K. D. Cook, University of Tennessee.

1. D. C. Schriemer and L. Li, *Anal. Chem.* **68**, 2721–2725 (1996).
2. T. Nohmi and J. B. Fenn, *J. Am. Chem. Soc.* **114**, 3241–3246 (1992).
3. J. L. Watson, *Introduction to Mass Spectrometry*, 3rd ed., Lippencott-Raven, New York, 1997.
4. G. Siuzdak, *Mass Spectrometry for Biotechnology*, Acedemic Press, San Diego, 1996.
5. P. B. Smith and co-workers, *Anal. Chem.* **69**, 95R–121R (1997).
6. P. B. Smith and co-workers, *Anal. Chem.* **71**, 61R–80R (1999).
7. M. Dole and co-workers, *J. Chem. Phys.* **49**, 2240–2249 (1968).
8. M. Ymashita and J. B. Fenn, *J. Phys. Chem.* **88**, 4451–4459 (1984).
9. S. F. Wong, C. K. Meng, and J. B. Fenn, *J. Phys. Chem.* **92**, 546–550 (1988).
10. K. Tanaka and co-workers, *Rapid Commun. Mass Spectrom.* **2**, 151 (1988).
11. M. Karas and F. Hillenkamp, *Anal. Chem.* **60**, 2299 (1988).
12. U. Bahr and co-workers, *Anal. Chem.* **64**, 2866 (1992).
13. P. O. Danis and co-workers, *Org. Mass Spec.* **27**, 843 (1992).
14. P. O. Danis and D. E. Karr, *Org. Mass Spectrom.* **28**, 923–925 (1993).
15. R. Abate and co-workers, *Rapid Commun. Mass Spectrom.* **7**, 1033–1036 (1993).
16. R. J. Cotter and co-workers, *Macromolecules* **19**, 2996–3001 (1986).
17. S. J. Pastor and C. L. Wilkins, *J. Amer. Soc. Mass Spectrom.* **8**, 225–233 (1997).
18. R. J. Cotter, *Time-of-Flight Mass Spectrometry*, American Chemical Society, Washington, D.C., 1997. ACS Professional Reference Books.
19. A. Vertes, G. Irinyi, and R. Gijbels, *Anal. Chem.* **65**, 2389–2393 (1993).
20. M. W. F. Nielen, *Mass Spectrom. Rev.* **18**, 309–344 (1999).
21. R. J. Goldschmidt and C. M. Guttman, *J. Amer. Soc. Mass Spectrom.* **11**, 1095–1106 (2000).
22. H. Rashidezadeh and B. C. Guo, *J. Amer. Soc. Mass Spectrom.* **9**, 724–730 (1998).
23. R. Knochenmuss, E. Lehmann, and R. Zenobi, *Eur. Mass Spectrom.* **4**, 421–426 (1998).
24. M. Karas, M. Gluckmann, and J. Schaefer, *J. Mass Spectrom.* **35**, 1–12 (2000).
25. A. G. Bailey, *Electrostatic Spraying of Liquids*, John Wiley & Sons, Inc., New York, 1988.
26. W. J. Simonsick and L. Prokai, *Adv. Chem. Ser.* **247**, 41–56 (1995).
27. M. L. Vestal, P. Juhasz, and S. A. Martin, *Rapid Commun. Mass Spectrom.* **9**, 1044–1050 (1995).

28. P. Juhasz, M. L. Vestal, and S. A. Martin, *J. Amer. Soc. Mass Spectrom.* **8**, 209–217 (1997).
29. H. C. M. Byrd and C. N. Mcewen, *Anal. Chem.* **72**, 4568–4576 (2000).
30. J. B. Williams, A. I. Gusev, and D. M. Hercules, *Macromolecules* **29**, 8144–8150 (1996).
31. V. V. Laiko, M. A. Baldwin, and A. L. Burlingame, *Anal. Chem.* **72**, 652–657 (2000).
32. P. Zollner, E. R. Schmid, and G. Allmaier, *Rapid Commun. Mass Spectrom.* **10**, 1278–1282 (1996).
33. P. Zollner and co-workers, *Int. J. Mass Spectrom. Ion Processes* **169**, 99–109 (1997).
34. S. D. Hanton and K. G. Owens, in *Proceedings of the 46th ASMS Conference on Mass Spectrometry and Allied Topics*, Orlando, Fla., 1998, Vol. 46, p. 1185.
35. S. D. Hanton, P. A. C. Clark, and K. G. Owens, *J. Amer. Soc. Mass Spectrom.* **10**, 104–111 (1999).
36. R. C. King and K. G. Owens, in *Proceedings of the 42nd ASMS Conference on Mass Spectrometry*, Chicago, Ill., 1994, Vol. 42, p. 977.
37. F. M. L. Amado and co-workers, *Rapid Commun. Mass Spectrom.* **11**, 1347–1352 (1997).
38. D. A. Allwood and co-workers, *Appl. Surf. Sci.* **103**, 231–244 (1996).
39. O. Vorm, P. Roepstorff, and M. Mann, *Anal. Chem.* **66**, 3281–3287 (1994).
40. W. R. Blair, C. M. Guttman, and W. E. Wallace, in *Proceedings of the 46th ASMS Conference on Mass Spectrometry and Allied Topics*, Orlando, Fla., 1998, Vol. 46, p. 1059.
41. R. R. Hensel, R. C. King, and K. G. Owens, *Rapid Commun. Mass Spectrom.* **11**, 1785–1793 (1997).
42. J. Axelsson and co-workers, *Rapid Commun. Mass Spectrom.* **11**, 209–213 (1997).
43. A. M. Belu and co-workers, *J. Amer. Soc. Mass Spectrom.* **7**, 11–24 (1996).
44. R. Chen and L. Li, in *Proceedings of the 48th ASMS Conference on Mass Spectrometry*, Long Beach, Calif., 2000, Vol. 48, p. 1211.
45. S. Weidner, A. Hollander, and G. Kuhn, *Rapid Commun. Mass Spectrom.* **11**, 447–450 (1997).
46. A. M. Hoberg and co-workers, *Eur. Mass Spectrom.* **4**, 435–440 (1998).
47. S. K. Poehlein and co-workers, *Rapid Commun. Mass Spectrom.* **13**, 1349–1353 (1999).
48. H. H. Zhu, T. Yalcin, and L. Li, *J. Amer. Soc. Mass Spectrom.* **9**, 275–281 (1998).
49. C. M. Guttman and co-workers, *Polym. Prepr.* **41**, 678–679 (1999).
50. G. Montaudo and co-workers, *Rapid Commun. Mass Spectrom.* **9**, 453–460 (1995).
51. D. C. Schriemer and L. A. Li, *Anal. Chem.* **69**, 4169–4175 (1997).
52. R. S. Lehrle and D. S. Sarson, *Rapid Commun. Mass Spectrom.* **9**, 91–92 (1995).
53. B. S. Larsen, W. J. Simonsick, and C. N. Mcewen, *J. Amer. Soc. Mass Spectrom.* **7**, 287–292 (1996).
54. C. M. Guttman and co-workers, *Anal. Chem.* **73**, 1252–1262 (2001).
55. C. N. McEwen, C. Jackson, and B. S. Larsen, *Int. J. Mass Spectrom. Ion Processes* **160**, 387–394 (1997).
56. A. Westman, G. Brinkmalm, and D. F. Barofsky, *Int. J. Mass Spectrom. Ion Processes* **169/170**, 79–87 (1997).
57. P. W. Geno and R. D. Macfarlane, *Int. J. Mass Spectrom. Ion Processes* **92**, 195–210 (1989).
58. C. M. Guttman, *Polym. Prepr.* **37**, 837–838 (1996).

59. D. A. Saucy and L. Zhu, in *Proceedings of the 47th ASMS Conference on Mass Spectrometry*, Dallas, Tex., 1999, Vol. 47, p. 3021.
60. C. Jackson, B. Larsen, and C. Mcewen, *Anal. Chem.* **68**, 1303–1308 (1996).
61. G. Montaudo and co-workers, *Macromolecules* **28**, 7983–7989 (1995).
62. C. M. Guttman, W. R. Blair, and P. O. Danis, *J. Polym. Sci., Part B: Polym. Phys.* **35**, 2409–2419 (1997).
63. P. M. Lloyd and co-workers, *Eur. Mass Spectrom.* **1**, 293–300 (1995).
64. S. F. Wong, C. K. Meng, and J. B. Fenn, *J. Phys. Chem.* **92**, 546–550 (1988).
65. U. Bahr and co-workers, *Anal. Chem.* **64**, 2866–2869. (1992).
66. G. Montaudo and co-workers, *Macromolecules* **28**, 4562–4569 (1995).
67. B. C. Guo and co-workers, *Rapid Commun. Mass Spectrom.* **11**, 781–785 (1997).
68. K. Martin and co-workers, *Rapid Commun. Mass Spectrom.* **10**, 1471–1474 (1996).
69. C. E. Kassis and co-workers, *Rapid Commun. Mass Spectrom.* **11**, 1134–1138 (1997).
70. M. W. F. Nielen, *Anal. Chem.* **70**, 1563–1568 (1998).
71. C. Puglisi and co-workers, *Rapid Commun. Mass Spectrom.* **13**, 2260–2267 (1999).
72. P. C. Hiemetz, *Polymer Chemistry*, Marcel Dekker, Inc., New York, 1984.
73. C. Wu, *Handbook of Size Exclusion Chromatography*, Marcel Dekker, Inc., New York, 1995.
74. W. W. Yau, J. J. Kirkland, and D. D. Bly, *Modern Size Exclusion Liquid Chromatography*, John Wiley & Sons, Inc., New York, 1979.
75. K. K. Murray and D. H. Russell, *J. Amer. Soc. Mass Spectrom.* **5**, 1–9 (1994).
76. A. I. Gusev, *Fresenius, J. Anal. Chem.* **366**, 691–700 (2000).
77. C. M. Guttman, E. A. Dimarzio, and J. F. Douglas, *Macromolecules* **29**, 5723–5733 (1996).
78. S. G. Entelis, V. V. Evreinov, and A. V. Gorshkov, *Adv. Polym. Sci.* **76**, 129 (1986).
79. J. Falkenhagen and co-workers, *Int. J. Polym. Anal. Char.* **5**, 549–562 (2000).
80. D. R. Maloney and co-workers, *J. Chem. Soc. Chem. Commun.* 561–562 (1995).
81. A. T. Jackson and co-workers, *J. Amer. Soc. Mass Spectrom.* **8**, 132–139 (1997).
82. A. T. Jackson and co-workers, *Rapid Commun. Mass Spectrom.* **11**, 520–526 (1997).
83. J. S. Liu, R. S. Loewe, and R. D. McCullough, *Macromolecules* **32**, 5777–5785 (1999).
84. C. Puglisi and co-workers, *Rapid Commun. Mass Spectrom.* **13**, 2260–2267 (1999).
85. G. Wilczek-Vera, P. O. Danis, and A. Eisenberg, *Macromolecules* **29**, 4036–4044 (1996).
86. Wilczek-Vera and co-workers, *Macromolecules* **32**, 2180–2187 (1999).
87. G. Wilczek-Vera and co-workers, *Rapid Commun. Mass Spectrom.* **13**, 764–777 (1999).
88. G. V. Schulz, *Z. Phys. Chem. B* **43**, 25 (1939).
89. B. H. Zimm, *J. Chem. Phys.* **16**, 1093, 1099 (1948).
90. D. Freyss, P. Rempp, and H. Beniot, *J. Polym. Sci (Phys.)* **B2**, 217 (1969).
91. M. S. Montaudo and F. Samperi, *Eur. Mass Spectrom.* **4**, 459–465 (1998).
92. D. Vitalini and co-workers, *Macromolecules* **29**, 4478–4485 (1996).
93. V. Francke and co-workers, *Macromol. Rapid Commun.* **19**, 275–281 (1998).
94. V. Schadler and co-workers, *Macromolecules* **29**, 4865–4870 (1996).
95. M. S. Montaudo, *Macromol. Symp.* **141**, 95–101 (1999).
96. V. Warzelhan, H. Hocker, and G. V. Schulz, *Makromol. Chem.* **181**, 149 (1978).
97. V. Warzelhan and G. V. Schulz, *Makromol. Chem.* **177**, 2185 (1976).
98. C. Wesdemiotis and co-workers, *Polym. Prepr.* **41**, 629–630 (2000).
99. S. K. Pollack and A. M. Morgan, *Polym. Prepr.* **41**, 631 (2000).

100. A. M. G. J. A. Hackridge, *Polym. Prepr.* **41**, 635 (2000).
101. P. C. Painter and M. M. Coleman, *Fundamentals of Polymer Science*, Technomic Publishing Corp., Lancaster, Pa., 1994.
102. W. E. Wallace, C. M. Guttman, and J. M. Antonucci, *J. Amer. Soc. Mass Spectrom.* **10**, 224–230 (1999).
103. W. E. Wallace, C. M. Guttman, and J. M. Antonucci, *Polymer* **41**, 2219–2226 (2000).

CHARLES M. GUTTMAN
NIST Polymers Division

MECHANICAL TESTING. See MECHANICAL PERFORMANCE.

MELAMINE RESINS. See AMINO RESINS AND PLASTICS.

MEMBRANE TECHNOLOGY

Membranes have gained an important place in chemical technology and are being used increasingly in a broad range of applications. The key property that is exploited is the ability of a membrane to control the permeation of a chemical species in contact with it. In packaging applications, the goal is usually to prevent permeation completely. In controlled drug delivery applications, the goal is to moderate the permeation rate of a drug from a reservoir to the body. In separation applications, the goal is to allow one component of a mixture to permeate the membrane freely, while hindering permeation of other components. Since the 1960s, membrane science has grown from a laboratory curiosity to a widely practiced technology in industry and medicine. This growth is likely to continue for some time, particularly in the membrane gas separation and pervaporation separation areas. Membranes will play a critical role in the next generation of biomedical devices, such as the artificial pancreas and liver. The total membrane market grew from $10 million to $2–3 billion in the 40 years prior to 2000. Spectacular growth of this magnitude is unlikely to continue, but a doubling in the size of the total industry to $5 billion during the decade following is likely.

Historical Development

Systematic studies of membrane phenomena can be traced to the eighteenth century philosopher scientists. For example, Abbé Nolet coined the word *osmosis* to describe permeation of water through a diaphragm in 1748. Through the nineteenth and early twentieth centuries, membranes had no industrial or commercial uses but were used as laboratory tools to develop physical/chemical theories.

For example, the measurements of solution's osmotic pressure made with membranes by Traube and Pfeffer were used by van't Hoff in 1887 to develop his

Encyclopedia of Polymer Science and Technology. Copyright John Wiley & Sons, Inc. All rights reserved.

limit law, which explains the behavior of ideal dilute solutions. This work directly led to the van't Hoff equation. At about the same time, the concept of a perfectly selective semipermeable membrane was used by Maxwell and others in developing the kinetic theory of gases.

Early investigators experimented with any type of diaphragm available to them, such as bladders of pigs, cattle, or fish and sausage casings made of animal gut. Later, collodion (nitrocellulose) membranes were preferred, because they could be made reproducibly. In 1907, Bechhold devised a technique to prepare nitrocellulose membranes of graded pore size, which he determined by a bubble test (1). Other workers (2–4) improved on this technique, and by the early 1930s microporous collodion membranes were commercially available. During the next 20 years, this early microfiltration membrane technology was expanded to other polymers, notably cellulose acetate. Membranes found their first significant application in the filtration of drinking water samples at the end of World War II. Drinking water supplies serving large communities in Germany and elsewhere in Europe had broken down, and filters to test for water safety were needed urgently. The research effort to develop these filters, sponsored by the U.S. Army, was later exploited by the Millipore Corp., the first and still the largest microfiltration membrane producer.

By 1960, the elements of modern membrane science had been developed, but membranes were used in only a few laboratory and small, specialized industrial applications. No significant membrane industry existed, and total annual sales of membranes for all applications probably did not exceed $10 million in 2000 dollars. Membranes suffered from four problems that prohibited their widespread use as a separation process: they were too unreliable, too slow, too unselective, and too expensive. Partial solutions to each of these problems have been developed since the 1960s, and now membrane-based separation processes are commonplace.

The seminal discovery that transformed membrane separation from a laboratory to an industrial process was the development, in the early 1960s, of the Loeb–Sourirajan process for making defect-free, high-flux, asymmetric reverse osmosis membranes (5). These membranes consist of an ultrathin, selective surface film on a microporous support, which provides the mechanical strength. The flux of the first Loeb–Sourirajan reverse osmosis membrane was 10 times higher than that of any membrane then available and made reverse osmosis practical. The work of Loeb and Sourirajan, and the timely infusion of large sums of research dollars from the U.S. Department of Interior, Office of Saline Water (OSW), resulted in the commercialization of reverse osmosis and was a principal factor in the development of ultrafiltration and microfiltration. The development of electrodialysis was also aided by OSW funding.

The 20-year period from 1960 to 1980 produced a significant change in the status of membrane technology. Building on the original Loeb–Sourirajan membrane technology, other processes, including interfacial polymerization and multilayer composite casting and coating, were developed for making high performance membranes. Using these processes, membranes with selective layers as thin as 0.1 μm or less can be made. Methods of packaging membranes into spiral-wound, hollow-fine-fiber, capillary and plate-and-frame modules were also developed, and advances were made in improving membrane stability. By 1980, microfiltration,

ultrafiltration, reverse osmosis, and electrodialysis were all established processes with large plants installed around the world.

The principal development in the 1980s was the emergence of industrial membrane gas separation processes. The first significant development was the Monsanto Prism® membrane for hydrogen separation, in the late 1970s (6). Within a few years, Dow was producing systems to separate nitrogen from air, and Cynara and Separex were producing systems to separate carbon dioxide from methane. These applications of membrane gas separation are now well established, and several thousand membrane plants have been installed. Gas separation technology is evolving and expanding rapidly, and further substantial growth will be seen, particularly in the separation of vapor/gas mixtures such as propylene from nitrogen and propane and butane from methane. The final development of the 1980s was the introduction of the first commercial pervaporation systems for dehydration of alcohol by GFT, a small German engineering company. By 1990, GFT had sold more than 100 plants. Many of these plants are small, but the technology has been demonstrated and a number of other important pervaporation applications are now at the pilot-plant stage.

Types of Membrane

Although this article is limited to synthetic membranes, excluding all biological structures, the topic is still large enough to include a wide variety of membranes that differ in chemical and physical composition and in the way they operate. In essence, a membrane is nothing more than a discrete, thin interface that moderates the permeation of chemical species in contact with it. This interface may be molecularly homogeneous, that is, completely uniform in composition and structure, or it may be chemically or physically heterogeneous, for example, containing holes or pores of finite dimensions. A normal filter meets this definition of a membrane, but, by convention, the term *membrane* is usually limited to structures that permeate dissolved or colloidal species, whereas the term *filter* is used to designate structures that separate particulate suspensions. The principal types of membrane are shown schematically in Figure 1 and are described briefly in the following subsections.

Isotropic Microporous Membranes. A *microporous membrane* is very similar in its structure and function to a conventional filter. It has a rigid, highly voided structure with randomly distributed, interconnected pores. However, these pores differ from those in a conventional filter by being extremely small, of the order of 0.01–10 μm in diameter. All particles larger than the largest pores are completely rejected by the membrane. Particles smaller than the largest pores, but larger than the smallest pores are partially rejected, according to the pore size distribution of the membrane. Particles much smaller than the smallest pores will pass through the membrane. Thus, separation of solutes by microporous membranes is mainly a function of molecular size and pore size distribution. In general, only molecules that differ considerably in size can be separated effectively by microporous membranes, for example, in ultrafiltration and microfiltration.

Nonporous, Dense Membranes. *Nonporous, dense membranes* consist of a dense film through which permeants are transported by diffusion under the

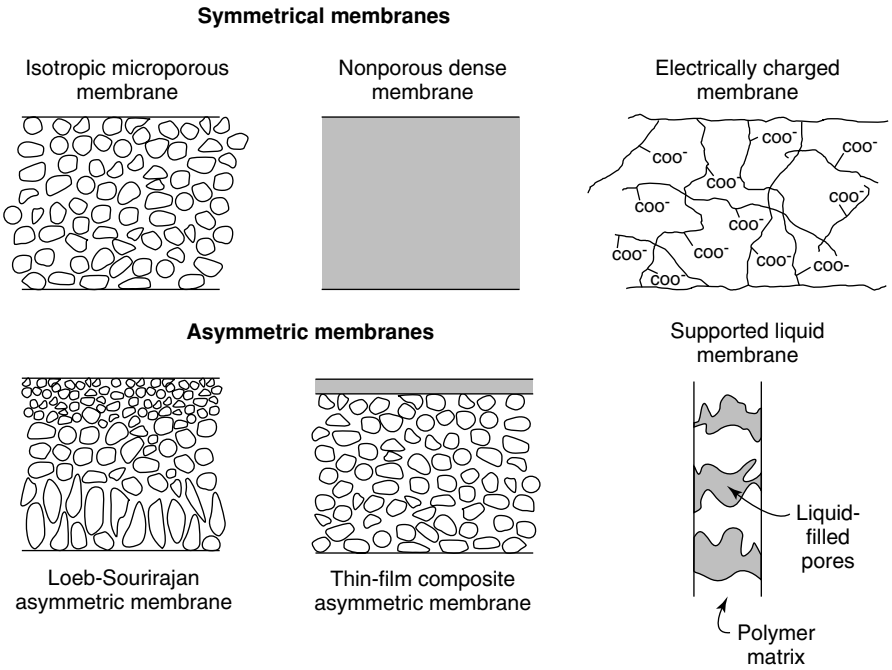

Fig. 1. Schematic diagrams of the principal types of membrane.

driving force of a pressure, concentration, or electrical potential gradient. The separation of various components of a solution is related directly to their relative transport rate within the membrane, which is determined by their diffusivity and solubility in the membrane material. An important property of nonporous, dense membranes is that even permeants of similar size may be separated when their concentration in the membrane material (ie, their solubility) differs significantly. Most gas separation, pervaporation, and reverse osmosis membranes use dense membranes to perform the separation. However, these membranes usually have an asymmetric structure to improve the flux.

Electrically Charged Membranes. *Electrically charged membranes* can be dense or microporous, but are most commonly microporous, with the pore walls carrying fixed positively or negatively charged ions. A membrane with positively charged ions is referred to as an *anion-exchange membrane* because it binds anions in the surrounding fluid. Similarly, a membrane containing negatively charged ions is called a *cation-exchange membrane*. Separation with charged membranes is achieved mainly by exclusion of ions of the same charge as the fixed ions of the membrane structure, and to a much lesser extent by the pore size. The separation is affected by the charge and concentration of the ions in solution. For example, monovalent ions are excluded less effectively than divalent ions and, in solutions of high ionic strength, selectivity decreases. Electrically charged membranes are used for processing electrolyte solutions in electrodialysis.

Asymmetric Membranes. The transport rate of a species through a membrane is inversely proportional to the membrane thickness. High transport rates

are desirable in membrane separation processes for economic reasons; therefore, the membrane should be as thin as possible. Conventional film fabrication technology limits manufacture of mechanically strong, defect-free films to about 20-μm thickness. The development of novel membrane fabrication techniques to produce asymmetric membrane structures was one of the major breakthroughs of membrane technology. *Asymmetric membranes* consist of an extremely thin surface layer supported on a much thicker porous, dense substructure. The surface layer and its substructure may be formed in a single operation or formed separately. The separation properties and permeation rates of the membrane are determined exclusively by the surface layer; the substructure functions as a mechanical support. The advantages of the higher fluxes provided by asymmetric membranes are so great that almost all commercial processes use such membranes.

Ceramic, Metal, and Liquid Membranes. The discussion so far implies that membrane materials are organic polymers and, in fact, the vast majority of membranes used commercially are polymer-based. However, in recent years, interest in membranes formed from less conventional materials has increased. Ceramic membranes, a special class of microporous membranes, are being used in ultrafiltration and microfiltration applications, for which solvent resistance and thermal stability are required. Dense metal membranes, particularly palladium membranes, are being considered for the separation of hydrogen from gas mixtures, and supported or emulsified liquid films are being developed for coupled and facilitated transport processes.

Preparation of Membranes and Membrane Modules

Because membranes applicable to diverse separation problems are often made by the same general techniques, classification by end-use application or preparation method is difficult. The first part of this section is, therefore, organized by membrane structure; preparation methods are described for symmetrical membranes, asymmetric membranes, ceramic and metal membranes, and liquid membranes. The final two subsections cover the production of hollow-fine-fiber membranes and membrane modules.

Symmetrical Membranes. Symmetrical membranes have a uniform structure throughout; such membranes can be either dense films or microporous.

Dense Symmetrical Membranes. These membranes are used on a large scale in packaging applications, and they are also used widely in the laboratory to characterize membrane separation properties. However, it is difficult to make mechanically strong and defect-free symmetrical membranes thinner than 20 μm, so the flux is low, and these membranes are rarely used in separation processes. For laboratory work, the membranes are prepared by solution casting or by melt pressing.

In solution casting, a casting knife or draw-down bar is used to spread an even film of an appropriate polymer solution across a glass plate. The casting knife consists of a steel blade, resting on two runners, arranged to form a precise gap between the blade and the plate on which the film is cast. A typical hand-casting knife is shown in Figure 2. After the casting has been made, it is left to stand, and the solvent evaporates to leave a uniform polymer film.

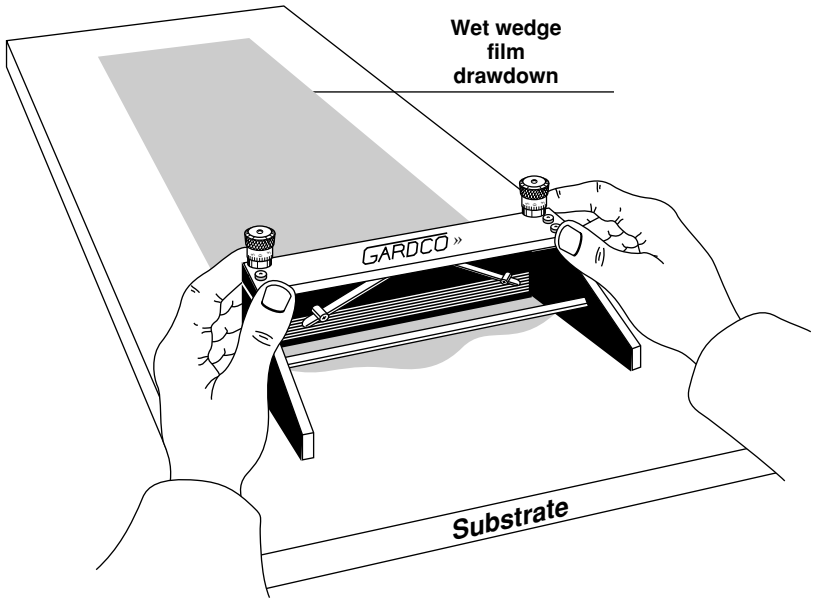

Fig. 2. A typical hand-casting knife. Courtesy of Paul N. Gardner Co., Inc.

Many polymers, including polyethylene, polypropylene, and nylons, do not dissolve in suitable casting solvents. In the laboratory, membranes can be made from such polymers by melt pressing, in which the polymer is sandwiched at high pressure between two heated plates. A pressure of 8–15 MPa (1000–2000 psi) is applied for 0.5–5 min, at a plate temperature just above the melting point of the polymer. Melt forming is commonly used to make dense films for packaging applications, either by extrusion as a sheet from a die or as blown film.

Microporous Symmetrical Membranes. These membranes, used widely in microfiltration, typically contain pores in the range of 0.1- to 10-μm diameter. As shown in Figure 3, microporous membranes are generally characterized by the average pore diameter d, the *membrane porosity* ε (the fraction of the total membrane volume that is porous), and the *tortuosity of the membrane*, τ, (a term reflecting the length of the average pore through the membrane compared to the membrane thickness). The most important types of microporous membrane are those formed by one of the solution-precipitation techniques discussed in the next section under Asymmetric Membranes; about half of microporous membranes are made in this way. The remainder is made by various proprietary techniques, the more important of which are outlined in the following subsections.

Irradiation. Nucleation track membranes were first developed by the Nuclepore Corp. (now a division of Whatman, Inc.) (7). The two-step preparation process is illustrated in Figure 4. A polymer film is first irradiated with charged particles from a nuclear reactor or other radiation source; particles passing through the film break polymer chains and leave behind sensitized/damaged tracks. The film is then passed through an etch solution, which etches the polymer preferentially along the sensitized nucleation tracks, thereby forming pores. The length of time the film is exposed to radiation in the reactor determines the number

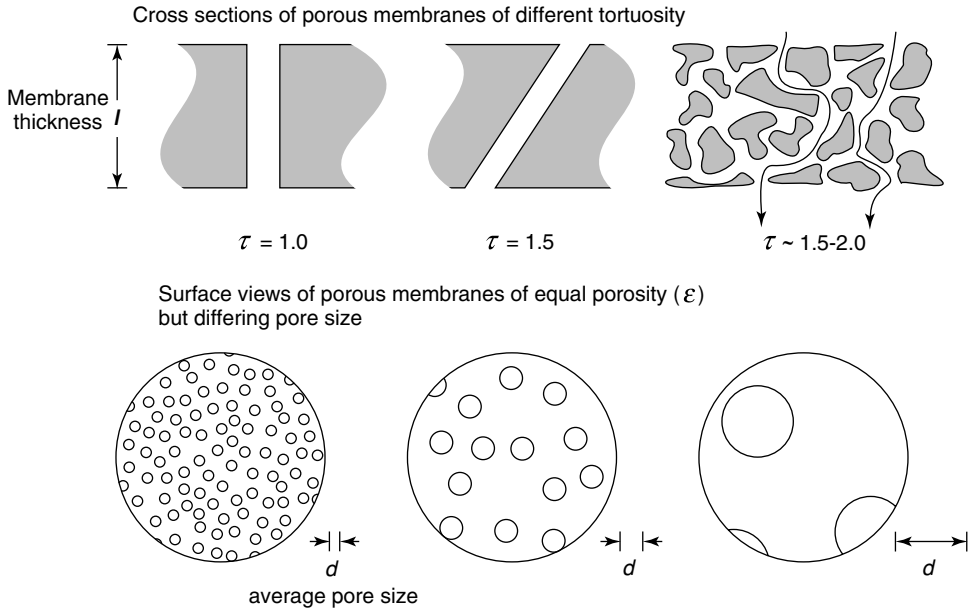

Fig. 3. Microporous membranes are characterized by tortuosity τ, porosity ϵ, and their average pore diameter d. (**a**) Cross sections of porous membranes containing cylindrical pores. (b) Surface views of porous membranes of equal ϵ, but differing pore size.

of pores in the film; the etch time determines the pore diameter. Because of the unique preparation techniques used to make nucleation track membranes, the pores are uniform cylinders traversing the membrane almost at right angles. The membrane tortuosity is, therefore, close to 1.0. The membrane porosity is usually relatively low, about 5%, so fluxes are low. However, because these membranes are very close to a perfect screen filter, they are used in analytical techniques that require filtration of all particles above a certain size from a fluid so that the particles can be visualized under a microscope.

Expanded Film. Expanded-film membranes are made from crystalline polymers by an orientation and stretching process. In the first step of the process, a highly oriented film is produced by extruding the polymer at close to its melting point coupled with a very rapid drawdown (8,9). After cooling, the film is stretched a second time, up to 300%, at right angles to the original orientation of the polymer crystallites. This second elongation deforms the crystalline structure of the film and produces slit-like voids 20–250 nm wide between crystallites. The process is illustrated in Figure 5. This type of membrane was first developed by the Celanese Corp. and is sold under the trade name Celgard; a number of companies now make similar products. The membranes made by W. L. Gore, sold under the trade name Gore-Tex, are made by this type of process (10).

The original expanded-film membranes were sold in rolls as flat sheets. These membranes had relatively poor tear strength along the original direction of orientation and were not widely used as microfiltration membranes. They did, however, find a principal use as porous, inert separating barriers in batteries and some medical devices. More recently, the technology has been developed to produce

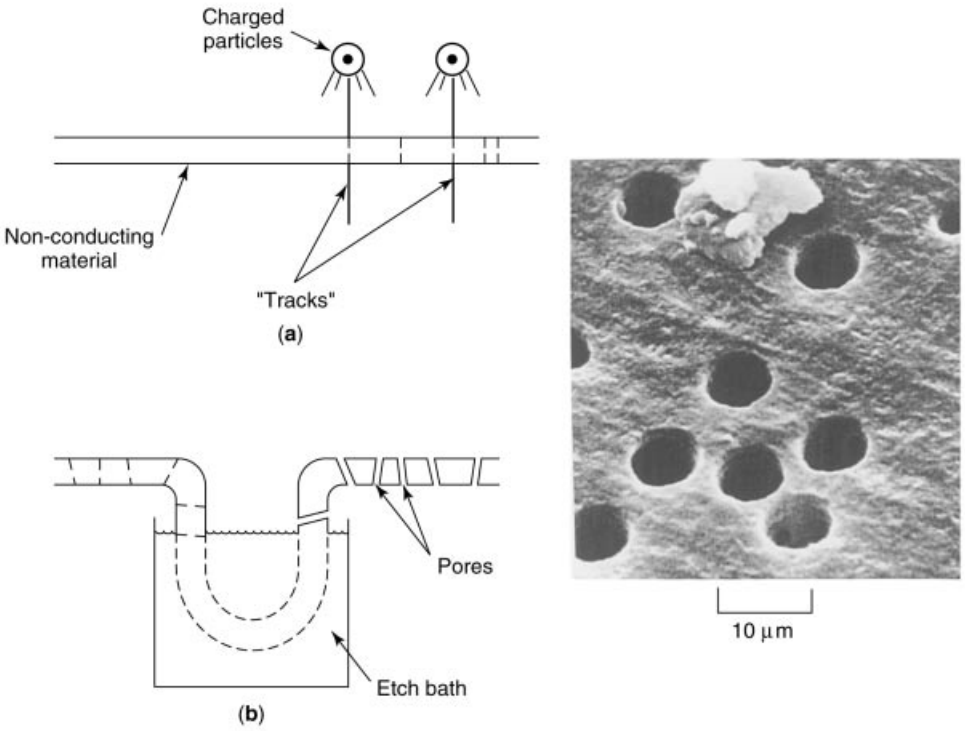

Fig. 4. Diagram and photograph of the two-step process to manufacture nucleation track membranes. (**a**) Polycarbonate film is exposed to charged particles in a nuclear reactor. (**b**) Tracks left by particles are preferentially etched into uniform cylindrical pores.

these membranes as hollow fibers, which are being used as membrane contactors (11,12).

Template Leaching. Template leaching offers an alternative manufacturing technique for insoluble polymers. A homogeneous film is prepared from a mixture of the membrane matrix material and a leachable component. After the film has been formed, the leachable component is removed with a suitable solvent and a microporous membrane is formed (13,14). The leachable component could be a soluble, low molecular weight solid or liquid, or even a polymeric material such as poly(vinyl alcohol) [PVA] or poly(ethylene glycol). The same general method is used to prepare microporous glass (15). In this case, a two-component glass melt is formed into sheets or small tubes, after which one of the components is leached out by extraction with an alkaline solution.

Asymmetric Membranes. In industrial applications other than microfiltration, symmetrical membranes have been displaced almost completely by asymmetric membranes, which have much higher fluxes. Asymmetric membranes have a thin, selective layer supported on a more open porous substrate. Hindsight makes it clear that many of the membranes produced in the 1930s and 1940s were asymmetric, although this was not realized at the time. The importance of the asymmetric structure was not recognized until Loeb and Sourirajan prepared the first high-flux, asymmetric, reverse osmosis membranes by what is

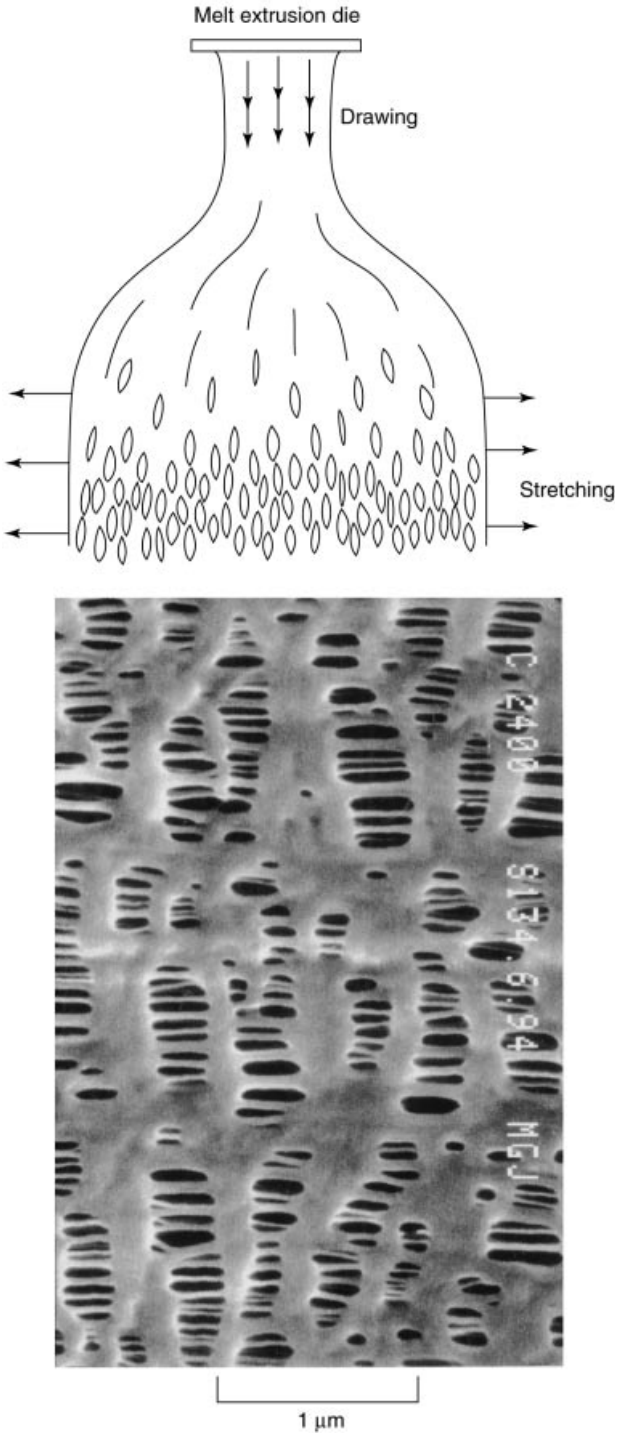

Fig. 5. Preparation method and scanning electron micrograph of a typical expanded polypropylene film membrane, in this case Celgard.

now known as the Loeb–Sourirajan technique (5). Loeb and Sourirajan's discovery was a critical breakthrough in membrane technology. The reverse osmosis membranes they produced were an order of magnitude more permeable than any symmetrical membrane produced previously. More importantly, demonstration of the benefits of the asymmetric structure paved the way for the development of other types of asymmetric membranes.

Phase Inversion (Solution Precipitation). *Phase inversion*, also known as *solution precipitation* or *polymer precipitation*, is the most important asymmetric membrane preparation method. In this process, a clear polymer solution is precipitated into two phases: a solid, polymer-rich phase that forms the matrix of the membrane, and a liquid, polymer-poor phase that forms the membrane pores. If precipitation is rapid, the pore-forming liquid droplets tend to be small and the membranes formed are markedly asymmetric. If precipitation is slow, the pore-forming liquid droplets tend to agglomerate while the casting solution is still fluid, so that the final pores are relatively large and the membrane structure is more symmetrical. Polymer precipitation from a solution can be achieved in several ways, such as cooling, solvent evaporation, precipitation by immersion in water, or imbibition of water from the vapor phase. Each technique was developed independently; only since the 1980s has it become clear that these processes can all be described by the same general approach based on polymer/solvent/nonsolvent phase diagrams. Thus, the Loeb–Sourirajan process, in which precipitation is produced by immersion in water, is a subcategory of the general class of phase-inversion membranes. The theory behind the preparation of membranes by all of these techniques has been discussed in a number of monographs and review articles (16–19).

Polymer Precipitation by Cooling. The simplest solution-precipitation technique is thermal gelation, in which a film is cast from a hot, one-phase polymer solution. When the cast film cools, the polymer precipitates, and the solution separates into a polymer matrix phase containing dispersed pores filled with solvent. The precipitation process that forms the membrane can be represented by the phase diagram shown in Figure 6. The pore volume in the final membrane is determined mainly by the initial composition of the cast film, because this determines the ratio of the polymer to liquid phase in the cooled film. However, the spatial distribution and size of the pores is determined largely by the rate of cooling and, hence, precipitation of the film. In general, rapid cooling produces membranes with small pores (20,21).

Polymer precipitation by cooling to produce microporous membranes was first commercialized on a large scale by Akzo (22). Akzo markets microporous polypropylene and poly(vinylidine fluoride) membranes produced by this technique under the trade name Accurel. Polypropylene membranes are prepared from a solution of polypropylene in *N*,*N*-bis(2-hydroxyethyl)tallowamine. The amine and polypropylene form a clear solution at temperatures above 100–150°C. Upon cooling, the solvent and polymer phases separate to form a microporous structure. If the solution is cooled slowly, an open cell structure results. The interconnecting passageways between cells are generally in the micron range. If the solution is cooled and precipitated rapidly, a much finer structure is formed. The rate of cooling is, therefore, a key parameter determining the final structure of the membrane (20).

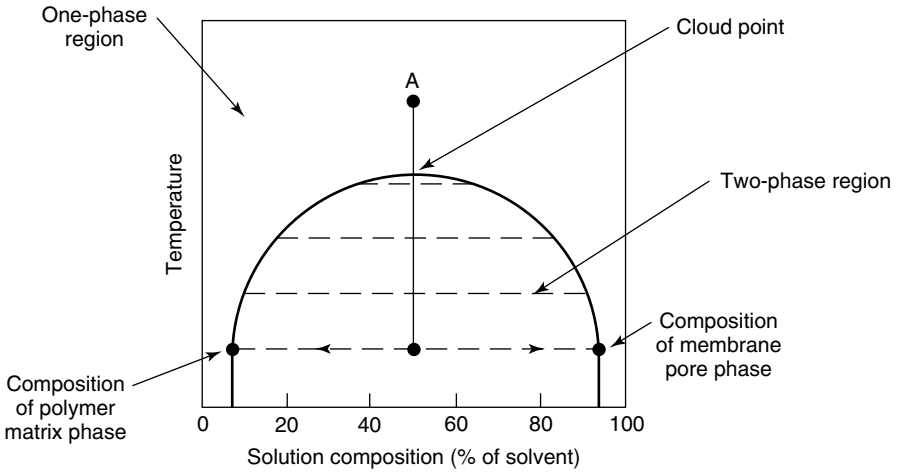

Fig. 6. Phase diagram showing the composition pathway traveled by the casting solution during precipitation by cooling. Point A represents the initial temperature and composition of the casting solution. The cloud point is the point of fast precipitation. In the two-phase region tie lines linking the precipitated polymer phase and the suspended liquid phase are shown.

A schematic diagram of the polymer precipitation process is shown in Figure 7. The hot polymer solution is cast onto a water-cooled chill roll, which cools the solution, causing the polymer to precipitate. The precipitated film is passed through an extraction tank containing methanol, ethanol, or isopropanol to remove the solvent. Finally, the membrane is dried, sent to a laser inspection station, trimmed and rolled up. The process shown in Figure 7 is used to make flat-sheet membranes. The preparation of hollow-fiber membranes by the same general technique has also been described.

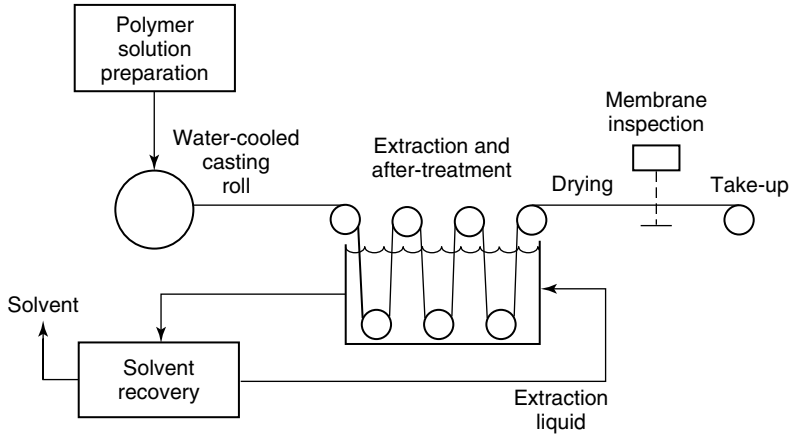

Fig. 7. Equipment to prepare microporous membranes by the polymer precipitation by cooling technique. Reprinted from Ref. 20, Copyright 1985, with permission American Chemical Society.

Polymer Precipitation by Solvent Evaporation. This technique was one of the earliest methods of making microporous membranes (1–4). In the simplest form of the method, a polymer is dissolved in a two-component solvent mixture consisting of a volatile solvent, such as acetone, in which the polymer is readily soluble, and a less volatile nonsolvent, typically water or an alcohol. The polymer solution is cast onto a glass plate. As the volatile solvent evaporates, the casting solution is enriched in the nonvolatile nonsolvent. The polymer precipitates, forming the membrane structure. The process can be continued until the membrane has completely formed, or it can be stopped, and the membrane structure fixed, by immersing the cast film into a precipitation bath of water or other nonsolvent. Scanning electron micrographs of some membranes made by this process are shown in Figure 8 (23).

Many factors determine the porosity and pore size of membranes formed by the solvent evaporation method. The average size of the nonsolvent droplets held in the polymer casting solution increases during the evaporation process. As Figure 8 shows, if the membrane is immersed in a nonsolvent after a short

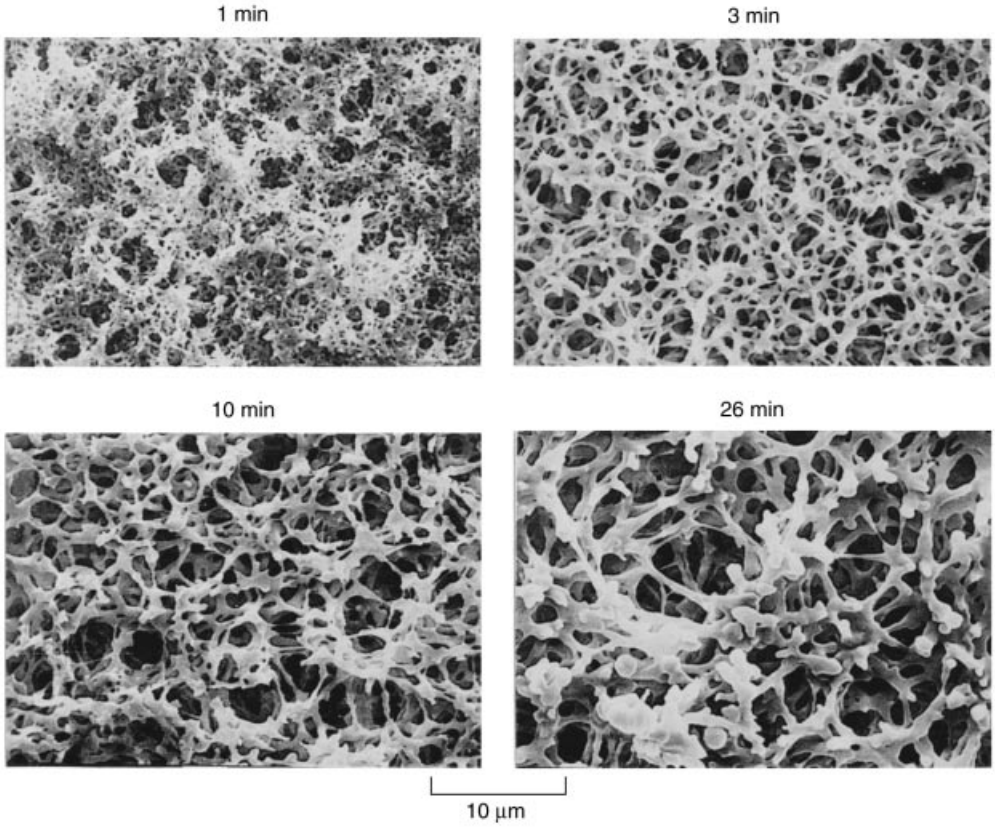

Fig. 8. Scanning electron micrographs of the bottom surface of cellulose acetate membranes cast from a solution of acetone (volatile solvent) and 2-methyl-2,4-pentanediol (nonvolatile solvent). The evaporation time before the structure is fixed by immersion in water is shown. Reprinted from Ref. 23, Copyright 1974, with permission from Elsevier Science.

evaporation time, the resulting membrane will be finely microporous. If the evaporation step is prolonged before fixing the structure by immersion in water, the average nonsolvent droplet diameter will be larger and consequently the average pore size will be larger. In general, increasing the nonsolvent content of the casting solution, or decreasing the polymer concentration, increases porosity. It is important that the nonsolvent be completely incompatible with the polymer. If partly compatible nonsolvents are used, the precipitating polymer phase contains sufficient residual solvent to allow it to flow and collapse as the solvent evaporates. The result is a dense rather than microporous film.

Polymer Precipitation by Imbibition of Water Vapor. Preparation of microporous membranes by simple solvent evaporation alone is not practiced widely. However, combinations of solvent evaporation with precipitation by imbibition of water vapor from a humid atmosphere are the basis of many commercial phase-inversion processes. The processes often involve proprietary casting formulations that are not normally disclosed by membrane developers. However, during the development of composite membranes at Gulf General Atomic, this type of membrane was prepared and the technology described in some detail in a series of Office of Saline Water Reports (24). These reports remain the best published description of the technique. The type of equipment used is shown in Figure 9. The casting solution typically consists of a blend of cellulose acetate and cellulose nitrate dissolved in a mixture of volatile solvents, such as acetone, and nonvolatile nonsolvents, such as water, ethanol, or ethylene glycol. The polymer solution is cast onto a continuous stainless steel belt. The cast film then passes through a series of environmental chambers; hot, humid air is usually circulated through the first chamber. The film loses the volatile solvent by evaporation and simultaneously absorbs water from the atmosphere. The total precipitation process is slow, taking about 10 min to complete. The resulting membrane structure is fairly symmetrical. After precipitation, the membrane passes to a second oven, through which hot, dry air is circulated to evaporate the remaining solvent and dry the film. The formed membrane is then wound on a take-up roll. Typical casting speeds are of the order of 0.3–0.6 m/min. This type of membrane is widely used in microfiltration applications (25).

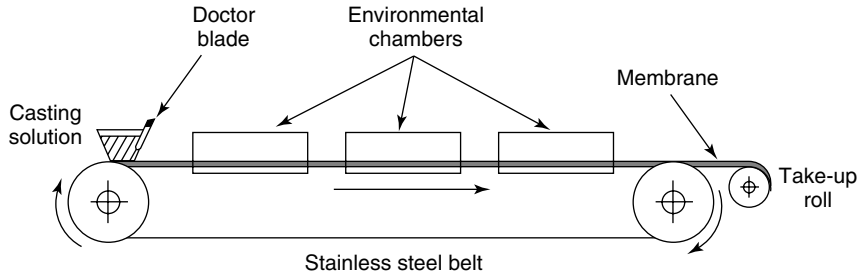

Fig. 9. Schematic of casting machine used to make microporous membranes by water-vapor imbibition. A casting solution is deposited as a thin film on a moving stainless steel belt. The film passes through a series of humid and dry chambers, where the solvent evaporates from the solution, and water vapor is absorbed from the air. This precipitates the polymer, forming a microporous membrane that is taken up on a collection roll.

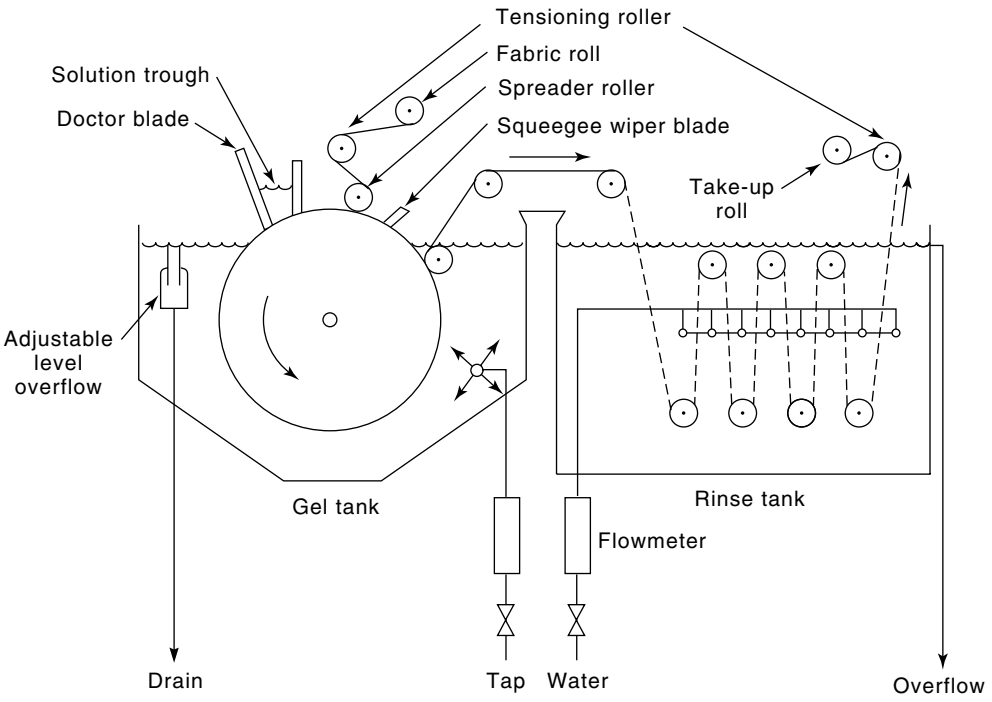

Fig. 10. Schematic of Loeb–Sourirajan membrane casting machine used to prepare reverse osmosis or ultrafiltration membranes. A knife and trough is used to coat the casting solution onto a moving fabric or polyester web which enters the water-filled gel tank. After the membrane has formed, it is washed thoroughly to remove residual solvent before being wound up.

Polymer Precipitation by Immersion in a NonSolvent Bath. This is the Loeb–Sourirajan process, the single most important membrane-preparation technique; almost all reverse osmosis, ultrafiltration, and many gas separation membranes are produced by this procedure or a derivative of it. A schematic of a casting machine used in the process is shown in Figure 10. A typical membrane casting solution contains approximately 20 wt% of dissolved polymer. This solution is cast onto a moving drum or paper web, and the cast film is precipitated by immersion in a water bath. The water precipitates the top surface of the cast film rapidly, forming an extremely dense, selective skin. This skin slows down the entry of water into the underlying polymer solution, which precipitates much more slowly, forming a more porous substructure. Depending on the polymer, the casting solution, and other parameters, the dense skin varies from 0.1 to 1.0 μm in thickness. Loeb and Sourirajan, the original developers of this process, were working in the field of reverse osmosis (5). Later, others adapted the technique to make membranes for other applications, including ultrafiltration and gas separation (6,19,26).

A great deal of work has been devoted to rationalizing the factors affecting the properties of asymmetric membrane made by this technique and, in particular, understanding those factors that determine the thickness of the membrane skin that performs the separation. The goal is to make this skin as thin as possible, but still defect free. The skin layer can be dense, as in reverse osmosis or gas

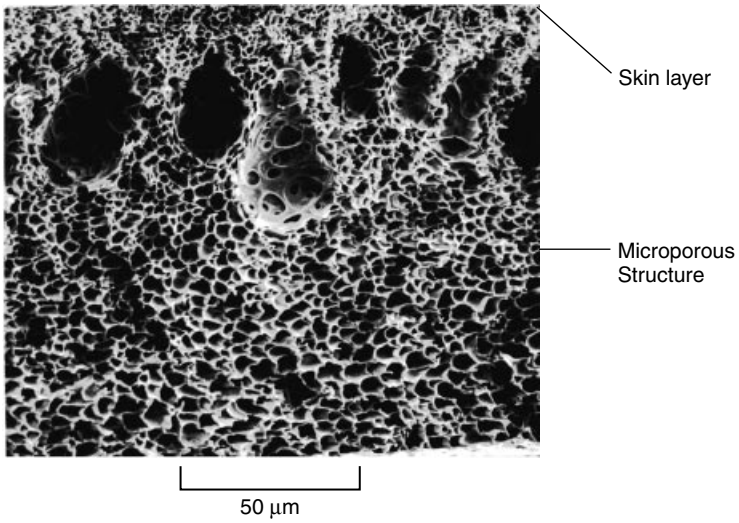

Fig. 11. Cross-sectional scanning electron micrograph of an asymmetric Loeb–Sourirajan ultrafiltration membrane. The large macrovoids under the membrane skin (top surface) are common in this type of ultrafiltration membrane.

separation, or finely microporous with pores in the 10- to 50-nm-diameter range, as in ultrafiltration. In good quality membranes made by this technique, a skin thickness as low as 50–100 μm can be achieved. A scanning electron micrograph of a Loeb–Sourirajan membrane is shown in Figure 11.

The phase-diagram approach has been widely used to rationalize the preparation of these membrane (16–19,26). The ternary phase diagram of the three-component system used in preparing Loeb–Sourirajan membranes is shown in Figure 12. The corners of the triangle represent the three components, polymer, solvent, and precipitant, while any point within the triangle represents a mixture of three components. The system consists of two regions: a one-phase region, where all components are miscible, and a two-phase region, where the system separates into a solid (polymer-rich) phase and a liquid (polymer-poor) phase. Although the one-phase region in the phase diagram is thermodynamically continuous, for practical purposes it can conveniently be divided into a liquid and solid gel region. Thus, at low polymer concentrations, the system is a low viscosity liquid, but, as the concentration of polymer is increased, the viscosity of the system also increases rapidly, reaching such high values that the system can be regarded as a solid. The transition between liquid and solid regions is, therefore, arbitrary, but can be placed at a polymer concentration of 30–40 wt%. In the two-phase region of the diagram, tie lines link the polymer-rich and polymer-poor phases. Unlike low molecular weight components, polymer systems in the two-phase region are often slow to separate into different phases and metastable states are common, especially when a polymer solution is rapidly precipitated.

The phase diagram in Figure 12 shows the precipitation pathway of the casting solution during membrane formation. During membrane formation, the system changes from a composition A, which represents the initial casting solution

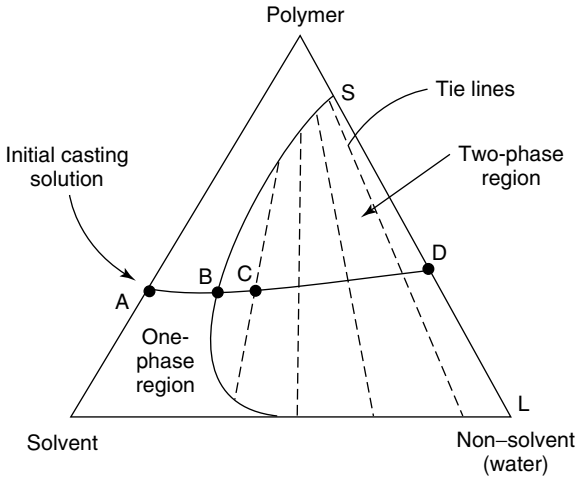

Fig. 12. Phase diagram showing the composition pathway traveled by a casting solution during the preparation of porous membranes by solvent evaporation: A, initial casting solution; B, point of precipitation; and C, point of solidification.

composition, to a composition D, which represents the final membrane composition. At composition D, the two phases are in equilibrium: a solid (polymer-rich) phase, which forms the final membrane structure, represented by point S, and a liquid (polymer-poor) phase, which constitutes the membrane pores filled with precipitant, represented by point L. The position D on the line S–L determines the overall porosity of the membrane. The entire precipitation process is represented by the path A–D, during which the solvent is exchanged by the precipitant. The point B along the path is the concentration at which the first polymer precipitates. As precipitation proceeds, more solvent is lost and precipitant is imbibed by the polymer-rich phase, so the viscosity rises. At some point, the viscosity is high enough for the precipitated polymer to be regarded as a solid. This composition is at C in Figure 12. Once the precipitated polymer solidifies, further bulk movement of the polymer is hindered. The rate and the pathway A–D taken by the polymer solution vary from the surface of the polymer film to the sublayer, affecting the pore size and porosity of the final membrane at that point. The nature of the casting solution and the precipitation conditions are very important in determining the kinetics of this precipitation process, and detailed theoretical treatments based on the ternary-phase-diagram approach have been worked out.

In the Loeb–Sourirajan process formation of minute membrane defects may occur. These defects, caused by gas bubbles, dust particles, and support fabric imperfections, are often very difficult to eliminate. These defects may not significantly affect the performance of asymmetric membranes used in liquid separation operations, such as ultrafiltration and reverse osmosis, but can be disastrous in gas separation applications. Henis and Tripodi (6), following earlier work (27) at General Electric, showed that this problem can be overcome by coating the membrane with a thin layer of relatively permeable material. If the coating is sufficiently thin, it does not change the properties of the underlying selective layer, but it does plug membrane defects, preventing simple convective gas flow through

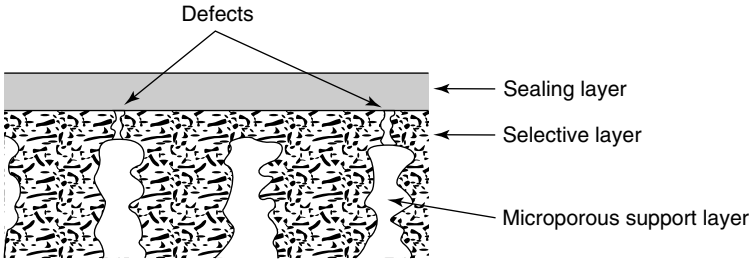

Fig. 13. Schematic of coated gas separation membrane.

defects. They applied this concept to sealing defects in polysulfone Loeb–Sourirajan membranes with silicone rubber (6). The form of these membranes is shown in Figure 13. The silicone rubber layer does not function as a selective barrier but rather plugs up defects, thereby reducing nondiffusive gas flow. The flow of gas through the portion of the silicone rubber layer over the pore is very high compared to the flow through the defect-free portion of the membrane. However, because the total area of the membrane subject to defects is very small, the total gas flow through these plugged defects is negligible. When this coating technique is used, the polysulfone skin layer of the Loeb–Sourirajan membrane no longer has to be completely free of defects; the Henis–Tripodi membrane can be made with a thinner skin than is possible with an uncoated Loeb–Sourirajan membrane. The increase in flux brought about by decreasing the thickness of the selective skin layer more than compensates for the slight reduction in flux caused by the silicone rubber sealing layer.

Cellulose acetate Loeb–Sourirajan reverse osmosis membranes were introduced commercially in the 1960s. Since then, many other polymers have been made into asymmetric membranes in attempts to improve membrane properties. In the reverse osmosis area, these attempts have had limited success, the only significant example being DuPont's polyamide membrane. For gas separation and ultrafiltration, a number of membranes with useful properties have been made. However, the early work on asymmetric membranes has spawned numerous other techniques in which a microporous membrane is used as a support to carry another thin, dense separating layer.

Interfacial Composite Membranes. A method of making asymmetric membranes, involving interfacial polymerization, was developed in the late 1960s. This technique was used to produce reverse osmosis membranes with dramatically improved salt rejections and water fluxes compared to those prepared by the Loeb–Sourirajan process (28). In the interfacial polymerization method, an aqueous solution of a reactive prepolymer, such as polyamine, is first deposited in the pores of a microporous support membrane, typically a polysulfone ultrafiltration membrane. The amine-loaded support is then immersed in a water-immiscible solvent solution containing a reactant, for example, a diacid chloride in hexane. The amine and acid chloride then react at the interface of the two solutions to form a densely cross-linked, extremely thin membrane layer. This preparation method is shown schematically in Figure 14. The first membrane was based on polyethyleneimine cross-linked with toluene-2,4-diisocyanate, to form the structure shown in

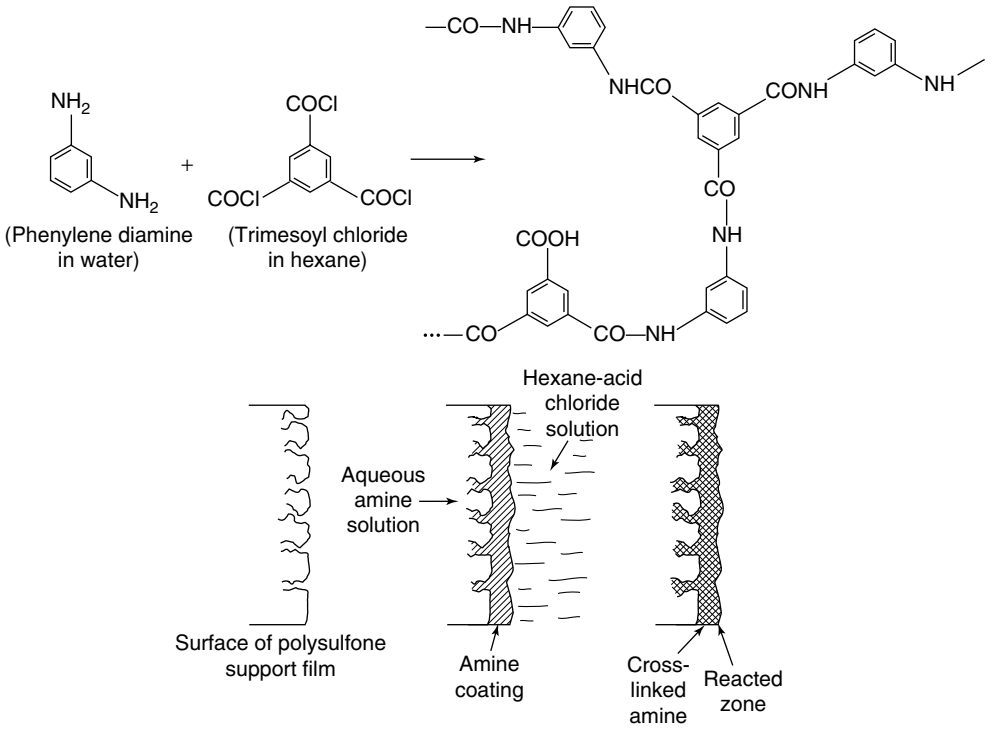

Fig. 14. Schematic of the interfacial polymerization process. The microporous film is first impregnated with an aqueous amine solution. The film is then treated with a multivalent cross-linking agent dissolved in a water-immiscible organic fluid, such as hexane or Freon-113. An extremely thin polymer film forms at the interface of the two solutions. The chemistry illustrated in this example is for the FT-30 membrane using the interfacial reaction of phenylene diamine with trimesoyl chloride. This membrane is widely used for desalination.

Figure 14. The process was later refined at FilmTec (28,29) and UOP (30) in the United States, and at Nitto (31) in Japan. The chemistry of these membranes has been reviewed (32).

Membranes made by interfacial polymerization have a dense, highly cross-linked interfacial polymer layer formed on the surface of the support membrane at the interface of the two solutions. A less cross-linked, more permeable hydrogel layer forms under this surface layer and fills the pores of the support membrane. Because the dense, cross-linked polymer layer can only form at the interface, it is extremely thin, of the order of 0.1 μm or less, and the permeation flux is high. Because the polymer is highly cross-linked, its selectivity is also high. The first reverse osmosis membranes made this way were 5–10 times less salt-permeable than the best membranes with comparable water fluxes made by other techniques.

Interfacial polymerization membranes are less applicable to gas separation because of the water-swollen hydrogel that fills the pores of the support membrane. In reverse osmosis, this layer is highly water swollen and offers little resistance to water flow, but when the membrane is dried and used in gas separations the gel becomes a rigid glass with very low gas permeability. This glassy polymer fills

the membrane pores and, as a result, defect-free interfacial composite membranes usually have low gas fluxes, although their selectivities can be good.

Solution-Cast Composite Membranes. Another very important type of composite membrane is formed by solution-casting a thin (0.5–2.0 μm) film on a suitable microporous film. Most solution-cast composite membranes are prepared by a technique pioneered at UOP (33). In this technique, a polymer solution is cast directly onto the microporous support film. The support film must be clean, defect-free, and very finely microporous, to prevent penetration of the coating solution into the pores. If these conditions are met, the support can be coated with a liquid layer 50–100 μm thick, which after evaporation leaves a thin selective film, 0.5–2 μm thick. This technique was used to form the Monsanto Prism® gas separation membranes (6) and at Membrane Technology and Research to form pervaporation and organic vapor/air separation membranes (34,35). A schematic drawing and scanning electron micrograph of this type of membrane are shown in Figure 15.

Composite membranes may consist of three or more layers. A highly permeable gutter layer is coated onto the support to provide a smooth, continuous

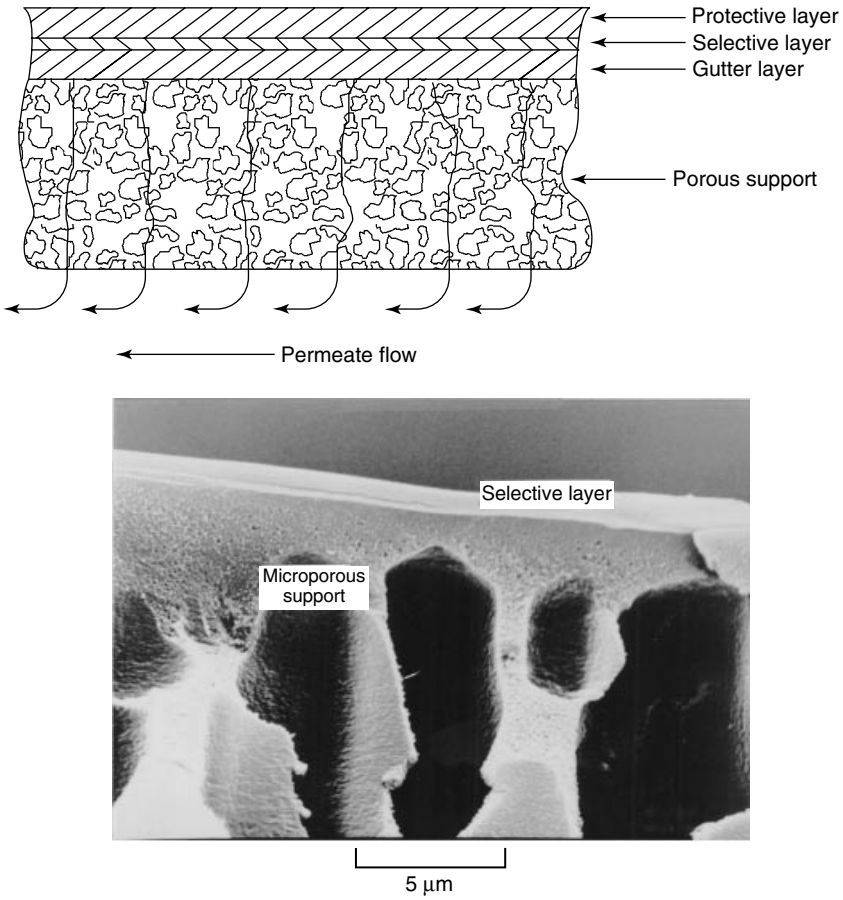

Fig. 15. Schematic drawing and scanning electron micrograph of a multilayer composite membrane.

Table 1. Summary of Less Widely Used Membrane Preparation Techniques

Preparation technique	Membrane characteristics	References
Plasma polymerization	Monomer is plasma polymerized onto the surface of a support film. Resulting chemistry is complex	36–39
Reactive surface treatment	An existing membrane is treated with a reactive gas of monomer to form an ultrathin surface layer	40–42
Dynamically formed membranes	A colloidal material is added to the feed solution of an ultrafiltration membrane. A gel forms on the membrane surface and enhances the membrane selectivity	43,44
Molecular sieve membranes	An ultrafine microporous membrane is formed from a dense, hollow-fiber polymeric membrane by carbonizing or from a glass hollow fiber by chemical leaching. Pores in the range 0.5–2 nm are claimed	45–48
Microporous metal membranes by electrochemical etching	Aluminum metal, for example, is electrochemically etched to form a porous aluminum oxide film. Membranes are brittle but uniform, with small pore size 0.02–2.0 μm	49,50

surface and to conduct the permeate to the pores of the microporous support. The thin, selective layer is coated onto the gutter layer, and finally a highly permeable top layer may be added to protect the membrane from damage during module preparation.

Other Asymmetric Membrane Preparation Techniques. A number of other methods of preparing membranes have been reported in the literature and are used on a small scale. Table 1 provides a brief summary of these techniques.

Metal Membranes. Palladium and palladium alloy membranes can be used to separate hydrogen from other gases. Palladium membranes were studied extensively during the 1950s and 1960s, and a commercial plant to separate hydrogen from refinery off-gas was installed by Union Carbide (51). The plant used palladium/silver alloy membranes in the form of 25-μm-thick films. The plant was operated for some time, but a number of problems, including long-term membrane stability under the high-temperature operating conditions, were encountered; later the plant was replaced by pressure-swing adsorption systems. Small-scale palladium membrane systems are still used to produce ultrapure hydrogen for specialized applications (52,53). These systems use palladium/silver alloy membranes, based on those developed in 1960 (54). Membranes with much thinner effective palladium layers than those that were used in the Union Carbide installation can now be made. One technique is to form a composite membrane

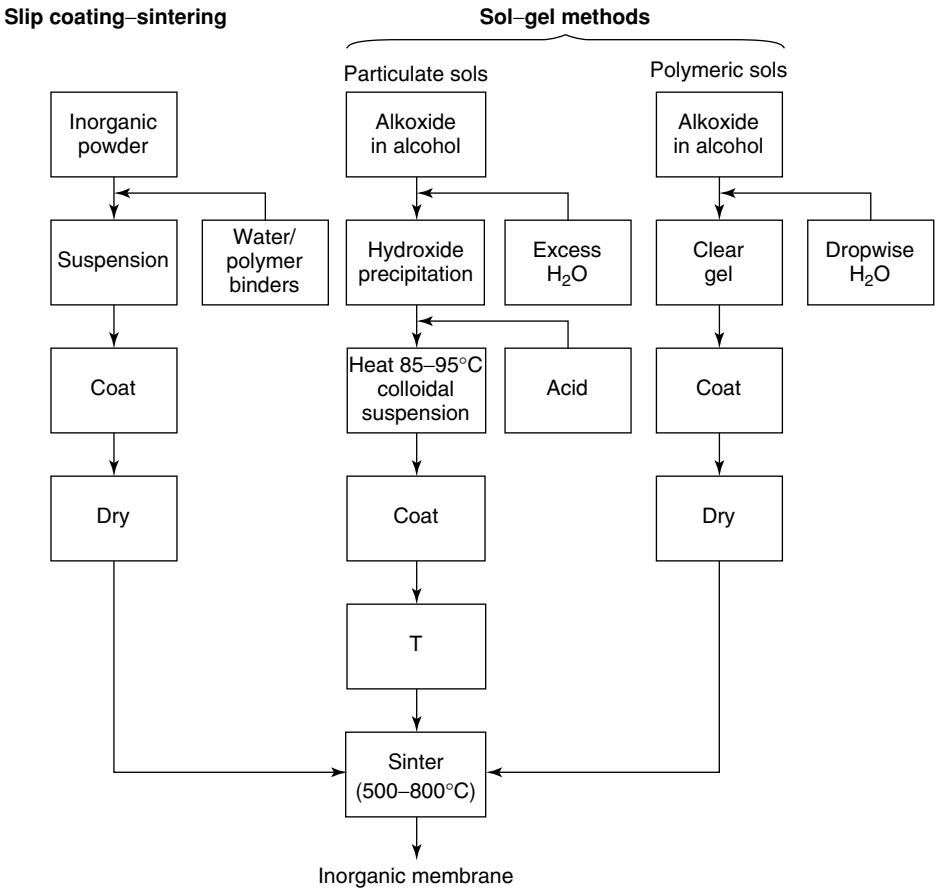

Fig. 16. Sol–gel and simple slip-coating–sintering process used to make ceramic membranes.

comprising a polymer substrate onto which is coated a thin layer of palladium or palladium alloy (55). The palladium layer can be applied by vacuum methods, such as evaporation or sputtering. Coating thicknesses of the order of 100 nm or less can be achieved.

Ceramic Membranes. A number of companies have developed ceramic membranes for ultrafiltration and microfiltration applications. Ceramic membranes have the advantages of being extremely chemically inert and stable at high temperatures, conditions under which polymer films fail. Most ceramic membranes are made by the slip-coating–sintering or sol–gel techniques outlined in Figure 16 (56–58).

The slip-coating–sintering process is the most widely used. In this process, a porous ceramic support tube is made by pouring a dispersion of a fine-grain ceramic material and a binder into a mold and sintering at high temperature. The pores between the particles that make up this support tube are large. One surface of the tube is then coated with a suspension of finer particles in a solution of a cellulosic polymer or PVA which acts as a binder and viscosity enhancer to hold

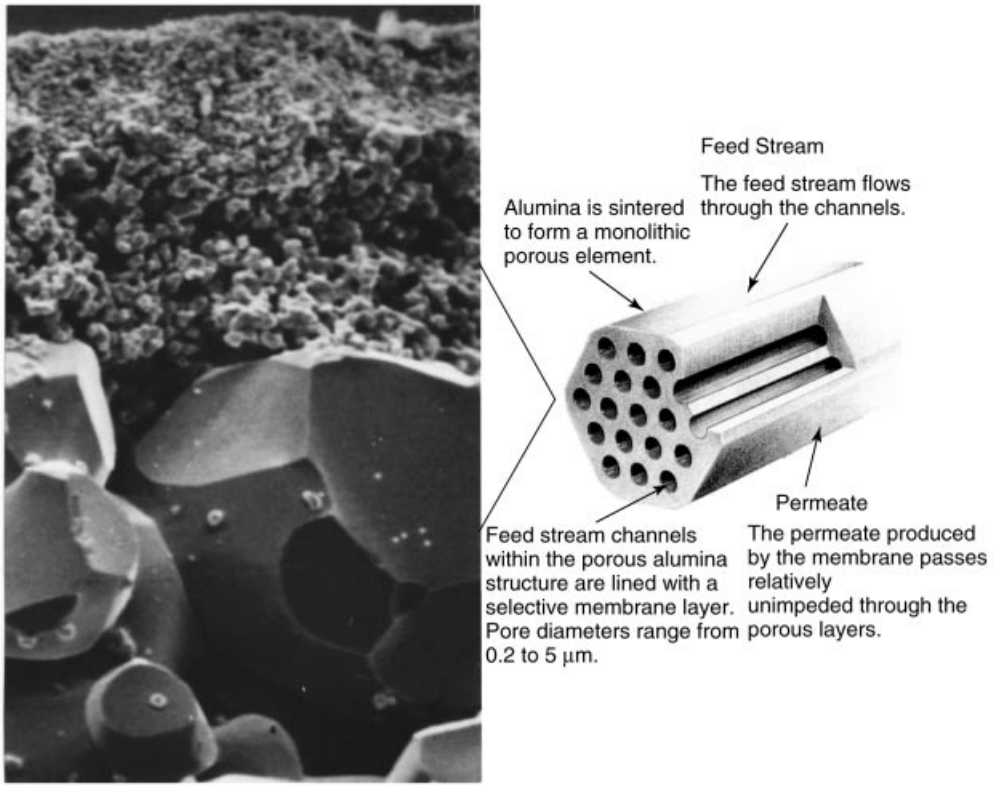

Fig. 17. Cross-sectional scanning electron micrograph of a three-layered alumina membrane/support (pore sizes 0.2, 0.8, and 12 μm, respectively).

the particles in suspension. This mixture is called a slip suspension; when dried and sintered at high temperatures, a finely microporous surface layer remains. Usually several slip-coated layers are applied in series, each layer being formed from a suspension of progressively finer particles and resulting in an anisotropic structure. Most commercial ceramic ultrafiltration membranes are made this way, generally in the form of tubes or perforated blocks. A scanning electron micrograph of the surface of this type of multilayer membrane is shown in Figure 17.

The slip-coating–sintering method can produce membranes with pore diameters down to about 10–20 nm. More finely porous membranes are made by sol–gel techniques. In the sol–gel process slip-coating is taken to the colloidal level. Generally the substrate to be coated with the sol–gel is a microporous ceramic tube formed by the slip-coating–sintering technique. The solution coated onto this support is a colloidal or polymeric gel of an inorganic hydroxide. These solutions are prepared by controlled hydrolysis of metal salts or metal alkoxides to hydroxides.

Sol–gel methods fall into two categories, depending on how the colloidal coating solution is formed. In the particulate–sol method a metal alkoxide is hydrolyzed by addition of excess water or acid. The resulting precipitate is maintained as a hot solution for some time before it is cooled and coated onto the microporous support membrane. After careful drying and sintering at 500–800°C,

a very finely microporous layer is formed. In the polymeric sol–gel process, partial hydrolysis of the metal alkoxide in alcohol is accomplished by adding the minimum of water to the solution. The alkoxide groups then react to form an inorganic polymer molecule that can be coated onto the microporous support. On drying and sintering, the inorganic polymer converts to a metal oxide ceramic film.

Liquid Membranes. A number of reviews summarize the considerable research effort in the 1970s and 1980s on liquid membranes containing carriers to facilitate selective transport of gases or ions (59,60). Although still being studied in a number of laboratories, the more recent development of much more selective conventional polymer membranes has diminished interest in processes using liquid membranes.

Hollow-Fiber Membranes. Most of the techniques described previously were developed originally to produce flat-sheet membranes, but the majority can be adapted to produce membranes in the form of thin tubes or fibers. Formation of membranes into hollow fibers has a number of advantages, one of the most important of which is the ability to form compact modules with very high surface areas. This advantage is offset, however, by the generally lower fluxes of hollow-fiber membranes compared to flat-sheet membranes made from the same materials. Nonetheless, the development of hollow-fiber membranes in the 1960s (61) and their later commercialization by Dow, Monsanto, DuPont, and others represents one of the most significant events in membrane technology.

Hollow fibers are usually of the order of 25 μm to 2 mm in diameter. They can be made with a homogeneous dense structure, or preferably with a microporous structure having a dense selective layer on the outside or inside surface. The dense surface layer can be integral, or separately coated onto a support fiber. The fibers are packed into bundles and potted into tubes to form a membrane module. More than a kilometer of fibers may be required to form a membrane module with a surface area of 1 m^2. A module can have no breaks or defects, requiring very high reproducibility and stringent quality control standards. Fibers with diameters 25–200 μm are usually called hollow-fine fibers. The fibers are too fine to allow the feed fluid to be pumped down the fiber bore so the feed fluid is generally applied to the outside of the fibers and the smaller volume of permeate removed down the bore. Fibers with diameters in the 200 μm to 2 mm range are called capillary fibers. The feed fluid is commonly applied to the inside bore of the fiber, and the permeate is removed from the outer shell.

Hollow-fiber fabrication methods can be divided into two classes (62,63). The most common is *solution spinning*, in which a 20–30% polymer solution is extruded and precipitated into a bath of a nonsolvent, generally water. Solution spinning allows fibers with the asymmetric Loeb–Sourirajan structure to be made. An alternative technique is *melt spinning*, in which a hot polymer melt is extruded from an appropriate die and is then cooled and solidified in air or a quench tank. Melt-spun fibers are usually relatively dense and have lower fluxes than solution-spun fibers, but, because the fiber can be stretched after it leaves the die, very fine fibers can be made. Melt spinning can also be used with polymers such as poly(trimethylpentene), which are not soluble in convenient solvents and are difficult to form by wet spinning.

Solution (Wet) Spinning. The most widely used solution spinneret system was first devised by Mahon (61). The spinneret consists of two concentric capillaries: the outer capillary having a diameter of approximately 400 μm and

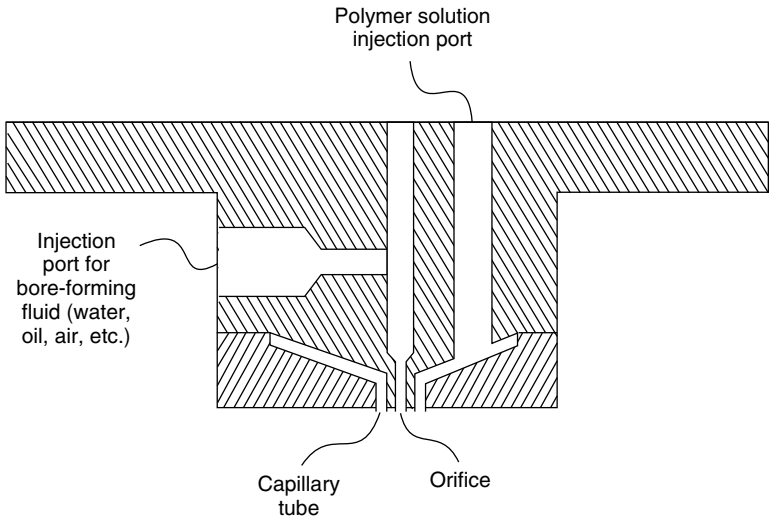

Fig. 18. Twin-orifice spinneret design used in solution-spinning of hollow-fiber membranes. Polymer solution is forced through the outer orifice, while bore-forming fluid is forced through the inner capillary.

the central capillary having an outer diameter of approximately 200 μm and an inner diameter of 100 μm. Polymer solution is forced through the outer capillary while air or liquid is forced through the inner one. The rate at which the core fluid is injected into the fibers relative to the flow of polymer solution governs the ultimate wall thickness of the fiber. Figure 18 shows a cross section of this type of spinneret.

A complete hollow-fiber spinning system is shown in Figure 19. Fibers are formed almost instantaneously as the polymer solution leaves the spinneret. The amount of evaporation time between the solution exiting the spinneret and entering the coagulation bath is a critical variable. If water is forced through the

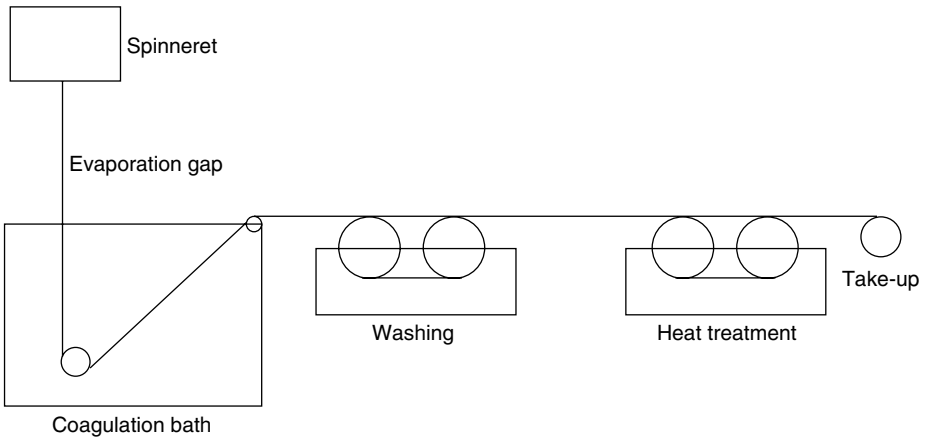

Fig. 19. A hollow-fiber solution-spinning system. The fiber is spun into a coagulation bath, where the polymer spinning solution precipitates to form the fiber. The fiber is then washed, dried, and taken up on a roll.

inner capillary, an asymmetric hollow fiber is formed with the skin on the inside. If air under a few pounds of pressure, or an inert liquid, is forced through the inner capillary to maintain the hollow core, the skin is formed on the outside of the fiber by immersion in a suitable coagulation bath (64).

Wet spinning of this type of hollow fiber is a well-developed technology, especially in the preparation of dialysis membranes for use in artificial kidneys. Systems that spin more than 100 fibers simultaneously on an around-the-clock basis are in operation. Wet-spun fibers are also used widely in ultrafiltration applications, in which the feed solution is forced down the bore of the fiber. Nitto, Asahi, Microgon, and Abcor all produce this type of fiber, generally with diameters of 1–3 mm.

Melt Spinning. In melt spinning, the polymer is extruded through the outer capillary of the spinneret as a hot melt, the spinneret assembly being maintained at a temperature between 100 and 300°C. The polymer can be extruded either as a pure melt or as a blended dope containing small amounts of plasticizers and other additives. Melt-spun fibers are usually stretched as they leave the spinneret, to form very thin fibers. Formation of such small-diameter fibers is a main advantage of melt spinning over solution spinning. The dense nature of melt-spun fibers leads to lower fluxes than can be obtained with solution-spun fibers, but, because of the enormous membrane surface area of these fine hollow fibers, this may not be a problem.

Membrane Modules. A useful membrane process requires the development of a membrane module containing large surface areas of membrane. The development of the technology to produce low cost membrane modules was one of the breakthroughs that led to the commercialization of membrane processes in the 1960s and 1970s. The earliest designs were based on simple filtration technology and consisted of flat sheets of membrane held in a type of filter press: these are called plate-and-frame modules. Systems containing a number of membrane tubes were developed at about the same time. Both of these systems are still used, but because of their relatively high cost they have been largely displaced by two other designs—the spiral-wound module and the hollow-fiber module.

Spiral-Wound Modules. Spiral-wound modules were used originally for artificial kidneys, but were fully developed for reverse osmosis systems. This work, carried out by UOP under sponsorship of the Office of Saline Water (later the Office of Water Research and Technology), resulted in a number of spiral-wound designs (65–67). The design shown in Figure 20 is the simplest and most common, and consists of a membrane envelope wound around a perforated central collection tube. The wound module is placed inside a tubular pressure vessel, and feed gas is circulated axially down the module across the membrane envelope. A portion of the feed permeates into the membrane envelope, where it spirals toward the center and exits through the collection tube.

Small laboratory spiral-wound modules consist of a single membrane envelope wrapped around the collection tube. The membrane area of these modules is typically 0.6–1.0 m^2. Commercial spiral-wound modules are typically 100–150 cm long and have diameters of 10, 15, 20, and 30 cm. These modules consist of a number of membrane envelopes, each with an area of approximately 2 m^2, wrapped around the central collection pipe. This type of multileaf design is illustrated in Figure 21 (66). Such designs are used to minimize the pressure drop encountered

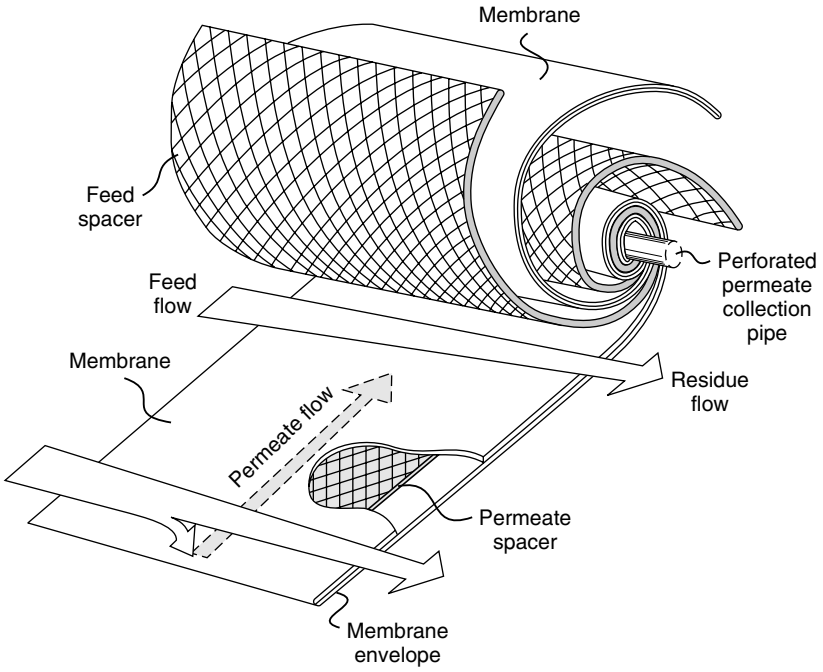

Fig. 20. Schematic of a spiral-wound membrane module.

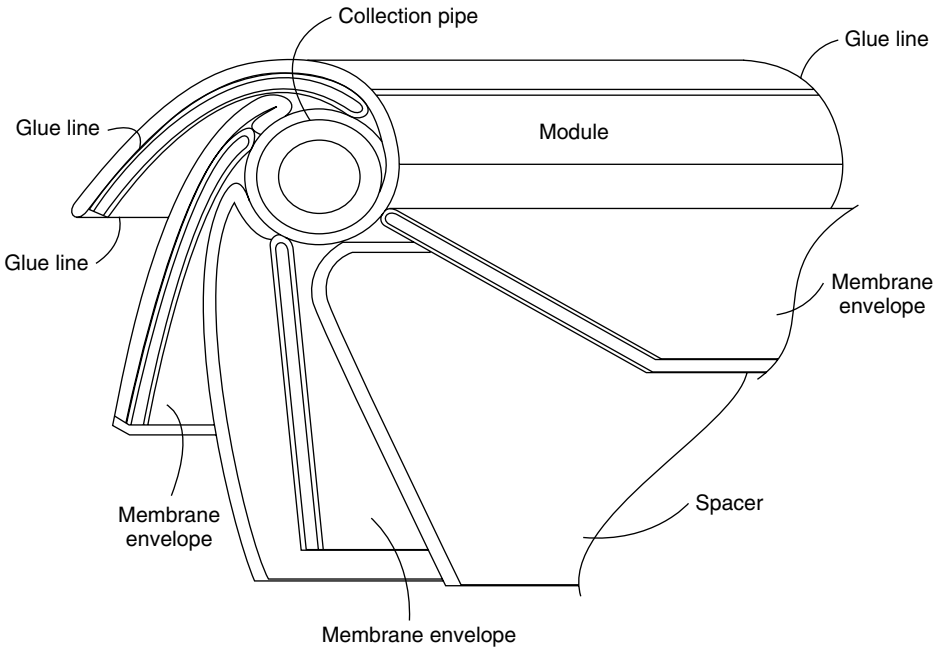

Fig. 21. Multileaf spiral-wound module, used to avoid excessive pressure drops on the permeate side of the membrane. Large, 30-cm-diameter modules may have as many as 30 membrane envelopes, each with a membrane area of about 2 m^2.

by the permeate fluid traveling toward the central pipe. If a single membrane envelope were used in these large diameter modules, the path taken by the permeate to the central collection pipe would be 5–25 m, depending on the module diameter. This long permeate path would produce a very large pressure drop, especially with high flux membranes. If multiple, smaller envelopes are used in a single module, the pressure drop in any one envelope is reduced to a manageable level.

Hollow-Fiber Modules. Hollow-fiber membrane modules are formed in two basic geometries. The first is the shell-side feed design illustrated in Figure 22a and used, for example, by Monsanto in their hydrogen separation systems or by DuPont in their reverse osmosis fiber systems. In such a module, a loop or a closed bundle of fiber is contained in a pressure vessel. The system is pressurized from the shell side; permeate passes through the fiber wall and exits through the open fiber ends. This design is easy to make and allows very large membrane areas to be contained in an economical system. Because the fiber wall must support a considerable hydrostatic pressure, these fibers are usually made by melt spinning and usually have a small diameter, of the order of 100-μm ID and 150- to 200-μm OD.

The second type of hollow-fiber module is the bore-side feed design illustrated in Figure 22b. The fibers in this type of unit are open at both ends, and the feed fluid is usually circulated through the bore of the fibers. To minimize pressure drops inside the fibers, the fibers often have larger diameters than the very fine fibers used in the shell-side feed system and are generally made by solution spinning. These so-called capillary fibers are used in ultrafiltration, in pervaporation, and in some low to medium pressure gas applications. Feed pressures are usually limited to less than 1 MPa (150 psig) in this type of module. A number of variants on the basic design have been developed and reviewed (68).

Plate-and-Frame Modules. Plate-and-frame modules were among the earliest types of membrane system; the design originates from the conventional filter-press. Membrane, feed spacers, and product spacers are layered together between two end plates, as illustrated in Figure 23 (69). A number of plate-and-frame units have been developed for small-scale applications, but these units are expensive compared to the alternatives, and leaks caused by the many gasket seals are a serious problem. Plate-and-frame modules are now generally limited to electrodialysis and pervaporation systems and a limited number of highly fouling reverse osmosis and ultrafiltration applications.

Tubular Modules. Tubular modules are now generally limited to ultrafiltration applications, for which the benefit of resistance to membrane fouling because of good fluid hydrodynamics overcomes the problem of their high capital cost. Typically, the tubes consist of a porous paper or fiberglass support with the membrane formed on the inside of the tubes, as shown in Figure 24. The first tubular membranes were between 2 and 3 cm in diameter, but more recently, as many as five to seven smaller tubes, each 0.5–1.0 cm in diameter, are nested inside a single, larger tube.

Module Selection. The choice of the appropriate membrane module for a particular membrane separation balances a number of factors. The principal factors that enter into this decision are listed in Table 2.

Cost, although always important, is difficult to quantify because the actual selling price of membrane modules varies widely, depending on the application.

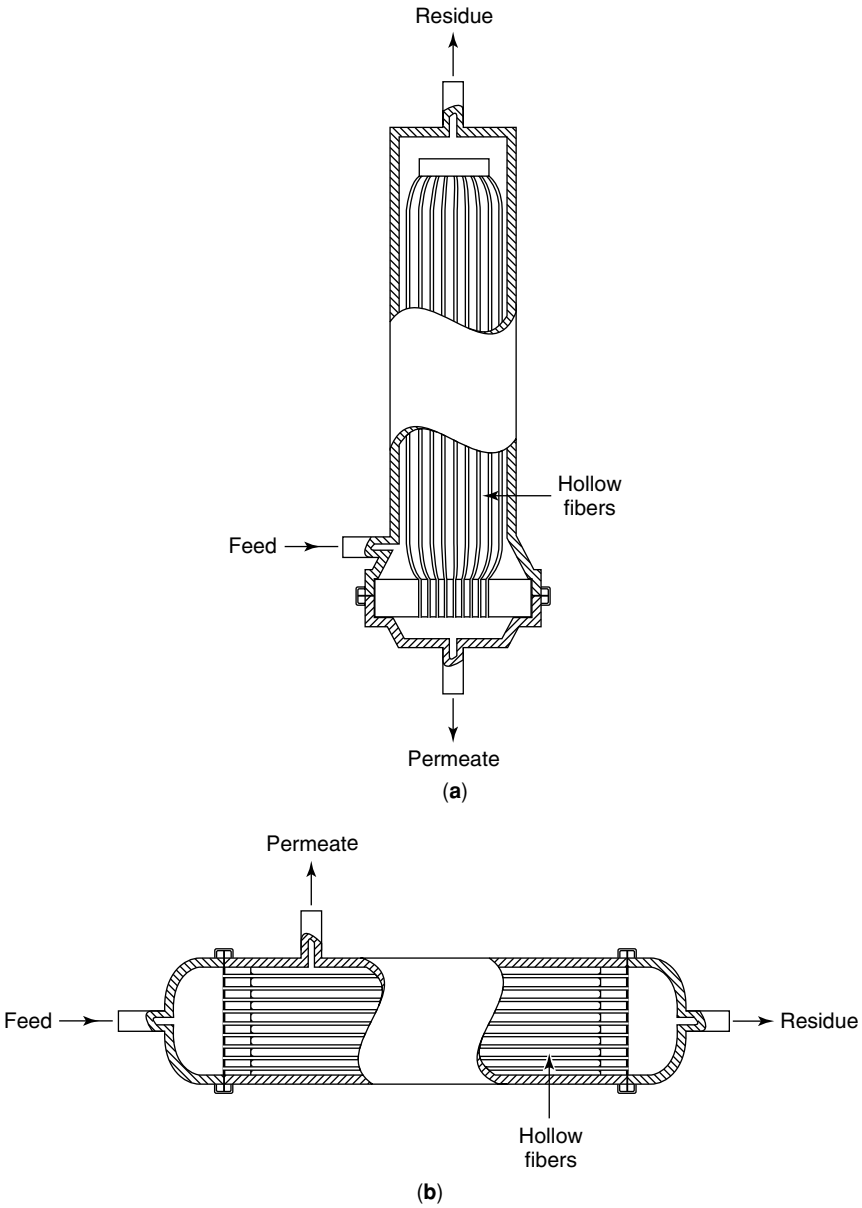

Fig. 22. Two types of hollow-fiber modules used for gas separation, reverse osmosis, and ultrafiltration applications. (**a**) Shell-side feed modules are generally used for high pressure applications up to ˜7 MPa (1000 psig). Fouling on the feed side of the membrane can be a problem with this design, and pretreatment of the feed stream to remove particulates is required. (**b**) Bore-side feed modules are generally used for medium pressure feed streams up to ˜1 MPa (150 psig), where good flow control to minimize fouling and concentration polarization on the feed side of the membrane is desired.

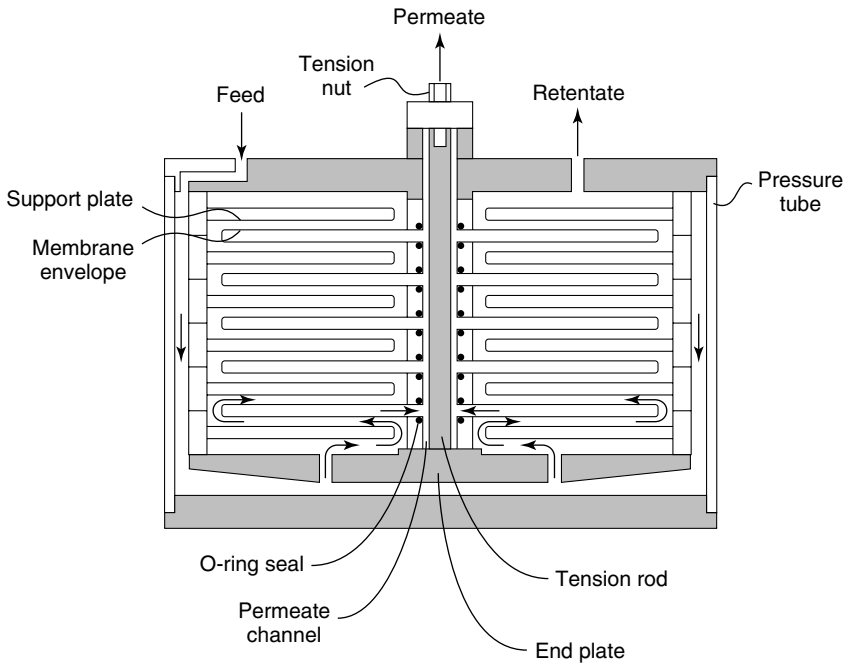

Fig. 23. Schematic of plate-and-frame module system. This design has good flow control, but the large number of spacer plates and seals leads to high costs.

Generally, high-pressure modules are more expensive than low-pressure or vacuum systems. The selling price also depends on the volume of the application and the pricing structure adopted by the industry. For example, spiral-wound modules for reverse osmosis of brackish water are produced by many manufacturers, resulting in severe competition and low prices, whereas similar modules for use in gas separation are much more expensive. Estimates of module manufacturing costs are given in Table 2; the selling price is typically two to five times higher.

A second factor determining module selection is resistance to fouling. Membrane fouling is a particularly important problem in liquid separations such as

Table 2. Characteristics of the Principal Module Designs

	Hollow-fine fibers	Capillary fibers	Spiral-wound	Plate-and-frame	Tubular
Manufacturing cost, $/m^2	2–10	5–50	5–50	50–200	50–200
Resistance to fouling	Very poor	Good	Moderate	Good	Very good
Parasitic pressure drop	High	Moderate	Moderate	Low	Low
Suitability for high pressure operation	Yes	No	Yes	Difficult	Difficult
Limitation to specific types of membrane	Yes	Yes	No	No	No

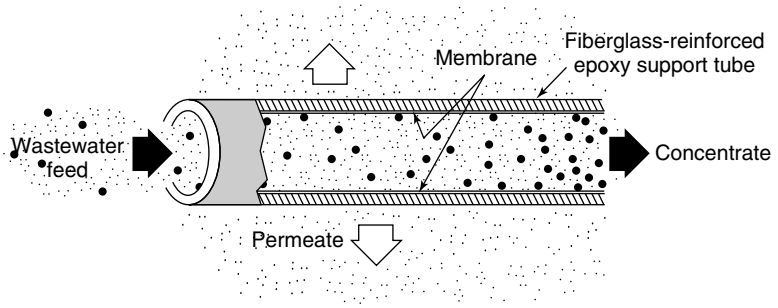

(**a**)

(**b**)

Fig. 24. (**a**) Typical tubular ultrafiltration module design. In the past, modules in the form of 2- to 3-cm-diameter tubes were common; more recently, 0.5- to 1.0-cm-diameter tubes, nested inside a simple pipe (**b**), have been introduced.

reverse osmosis and ultrafiltration. In gas separation applications, fouling is more easily controlled. Hollow-fine fibers are notoriously prone to fouling and can only be used in reverse osmosis applications if extensive, costly feed-solution pretreatment is used to remove all particulates. These fibers cannot be used in ultrafiltration applications at all.

A third factor is the ease with which various membrane materials can be fabricated into a particular module design. Almost all membranes can be formed into plate-and-frame, spiral, and tubular modules, but many membrane materials cannot be fabricated into hollow-fine fibers or capillary fibers. Finally, the suitability of the module design for high pressure operation and the relative magnitude of pressure drops on the feed and permeate sides of the membrane can sometimes be important considerations.

In reverse osmosis, most modules are of the hollow-fine-fiber or spiral-wound design; plate-and-frame and tubular modules are limited to a few applications in

which membrane fouling is particularly severe, for example, food applications or processing of heavily contaminated industrial wastewater. Currently, hollow-fiber designs are being displaced by spiral-wound modules, which are inherently more fouling resistant, and require less feed pretreatment. Also, thin-film interfacial composite membranes, the best reverse osmosis membranes now available, have not been fabricated in the form of hollow-fine fibers.

For ultrafiltration applications, hollow-fine fibers have never been seriously considered because of their susceptibility to fouling. If the feed solution is extremely fouling, tubular or plate-and-frame systems are still used. Recently, however, spiral-wound modules with improved resistance to fouling have been developed, and these modules are increasingly displacing the more expensive plate-and-frame and tubular systems. Capillary systems are also used in some ultrafiltration applications.

For high-pressure gas separation applications, hollow-fine fibers appear to have a major segment of the market. Hollow-fiber modules are clearly the lowest cost design per unit membrane area, and their poor resistance to fouling is not a problem in many gas separation applications. Also, gas separation membrane materials are often rigid glassy polymers such as polysulfones, polycarbonates, and polyimides, which can be easily formed into hollow-fine fibers. Of the principal companies servicing this area only Separex and GMS use spiral-wound modules. Both companies use these modules to process natural gas streams, which are relatively dirty, often containing oil mist and condensable components that would foul hollow-fine-fiber modules rapidly.

Spiral-wound modules are much more commonly used in low-pressure or vacuum gas separation applications, such as the production of oxygen-enriched air, or the separation of organic vapors from air. In these applications, the feed gas is at close to ambient pressure, and a vacuum is drawn on the permeate side of the membrane. Parasitic pressure drops on the permeate side of the membrane and the difficulty in making high-performance hollow-fine-fiber membranes from the rubbery polymers used to make these membranes both work against hollow-fine-fiber modules for this application.

Pervaporation operates under constraints similar to low-pressure gas separation. Pressure drops on the permeate side of the membrane must be small, and many pervaporation membrane materials are rubbery. For this reason, spiral-wound modules and plate-and-frame systems are both in use. Plate-and-frame systems are competitive in this application despite their high cost, primarily because they can be operated at high temperatures with relatively aggressive feed solutions, conditions under which spiral-wound modules might fail.

Membrane Applications

The principal use of membranes in the chemical processing industry is in various separation processes. Seven major membrane separation processes are discussed in this section. These can be classified into technologies that are developed, developing, or to-be-developed, as shown in Table 3. Membranes, or rather films, are also used widely as packaging materials. The use of membranes in various biomedical applications, for example, in controlled release technology and in

Table 3. Various Membrane Separation Technologies

	Process	Status
Developed technologies	Microfiltration	Well-established unit processes. No major breakthroughs seem imminent
Ultrafiltration		
Reverse osmosis		
Electrodialysis		
Developing technologies	Gas separation	A number of plants have been installed. Market size and number of applications served are expanding rapidly
Pervaporation		
To-be-developed technologies	Facilitated transport	Major problems remain to be solved before industrial systems will be installed

artificial organs such as the artificial kidney, lung, and pancreas are only covered briefly here.

The four developed processes are microfiltration, ultrafiltration, reverse osmosis, and electrodialysis. All are well established, and the market is served by a number of experienced companies. The first three processes are related to filtration techniques, in which a solution containing dissolved or suspended solids is forced through a membrane filter. The solvent passes through the membrane; the solutes are retained. The three processes differ principally in the size of the particles separated by the membrane. Microfiltration is considered to refer to membranes with pore diameters from 0.1 μm (100 nm) to 10 μm. Microfiltration membranes are used to filter suspended particulates, bacteria, or large colloids from solutions. Ultrafiltration refers to membranes having pore diameters in the range 2–100 nm. Ultrafiltration membranes can be used to filter dissolved macromolecules, such as proteins, from solution. Typical applications of ultrafiltration membranes are concentrating proteins from milk whey, or recovering colloidal paint particles from electrocoating paint rinse waters.

In reverse osmosis membranes, the pores are so small, in the range 0.5–2 nm in diameter, that they are within the range of the thermal motion of the polymer chains. The most widely accepted theory of reverse osmosis transport considers the membrane to have no permanent pores at all. Reverse osmosis membranes are used to separate dissolved microsolutes, such as salt, from water. The principal application of reverse osmosis is the production of drinking water from brackish groundwater or seawater. Figure 25 shows the range of applicability of reverse osmosis, ultrafiltration, microfiltration, and conventional filtration. In some recent work, membranes that fall into the overlapping area between very retentive ultrafiltration membranes and very open ultrafiltration membranes are sometimes called nanofiltration membranes. The membranes have apparent pore diameters between 0.5 and 5 nm.

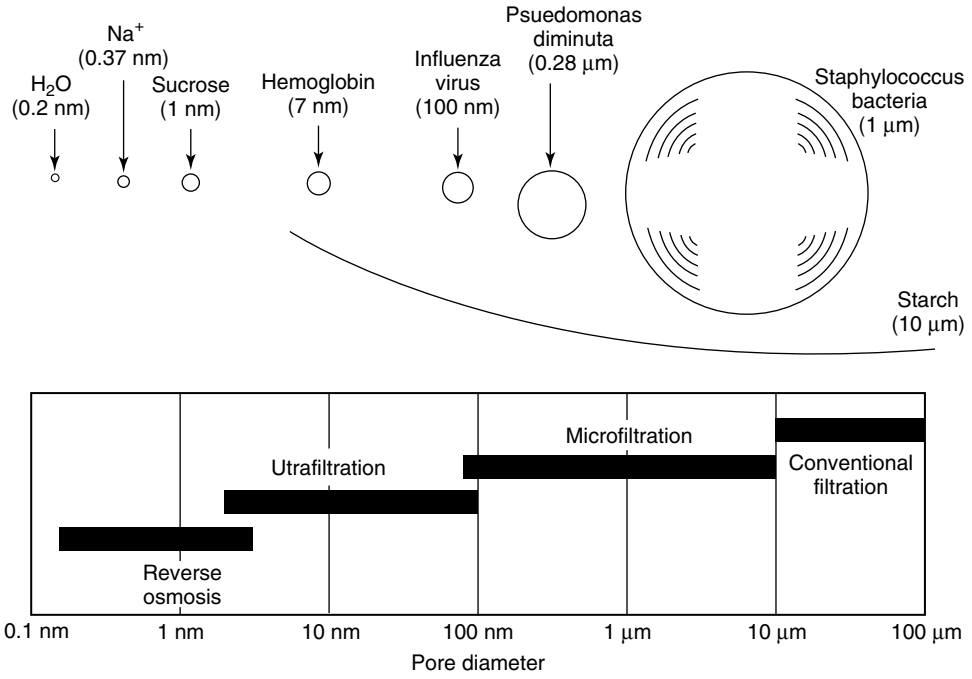

Fig. 25. Reverse osmosis, ultrafiltration, microfiltration, and conventional filtration are related processes differing principally in the average pore diameter of the membrane filter. Reverse osmosis membranes are so dense that discrete pores do not exist; transport occurs via statistically distributed free volume areas. The relative size of different solutes removed by each class of membrane is illustrated in this schematic.

The fourth fully developed membrane process is electrodialysis, in which charged membranes are used to separate ions from aqueous solutions under the driving force of an electrical potential difference. The process utilizes an electrodialysis stack, built on the plate-and-frame principle, containing several hundred individual cells formed by a pair of anion- and cation-exchange membranes. The principal current application of electrodialysis is the desalting of brackish groundwater. However, industrial use of the process in the food industry, for example to deionize cheese whey, is growing, as is its use in pollution-control applications.

Of the two developing membrane processes listed in Table 3, gas separation and pervaporation, gas separation is the more developed. At least 20 companies worldwide offer industrial membrane-based gas separation systems for a variety of applications. In gas separation, a mixed gas feed at an elevated pressure is passed across the surface of a membrane that is selectively permeable to one component of the feed. The membrane separation process produces a permeate enriched in the more permeable species and a residue enriched in the less permeable species. Important, well-developed applications are the separation of hydrogen from nitrogen, argon, and methane in ammonia plants; the production of nitrogen from air; the separation of carbon dioxide from methane in natural gas operations; and the separation and recovery of organic vapors from air streams. Gas separation is an area of considerable current research interest; the number of applications is expected to increase rapidly over the next few years.

Pervaporation is a relatively new process with elements in common with reverse osmosis and gas separation. In pervaporation, a liquid mixture contacts one side of a membrane and the permeate is removed as a vapor from the other. Currently, the only industrial application of pervaporation is the dehydration of organic solvents, in particular, the dehydration of 90–95% ethanol solutions, a difficult separation problem because an ethanol–water azeotrope forms at 95% ethanol. However, pervaporation processes are also being developed for the removal of dissolved organics from water and for the separation of organic solvent mixtures. These applications are likely to become commercial in the next decade.

The final membrane process listed in Table 3 is *facilitated transport*. No commercial plants are installed or are likely to be installed in the near future. Facilitated transport usually employs liquid membranes containing a complexing or carrier agent. The carrier agent reacts with one permeating component on the feed side of the membrane and then diffuses across the membrane to release the permeant on the product side of the membrane. The carrier agent is then reformed and diffuses back to the feed side of the membrane. The carrier agent thus acts as a shuttle to selectively transport one component from the feed to the product side of the membrane.

Facilitated transport membranes can be used to separate gases; membrane transport is then driven by a difference in the gas partial pressure across the membrane. Metal ions can also be selectively transported across a membrane driven by a flow of hydrogen or hydroxyl ions in the other direction. This process is sometimes called *coupled transport*.

Because the facilitated transport process employs a specific, reactive carrier species, very high membrane selectivities can be achieved. These selectivities are often far higher than those achieved by other membrane processes. This one fact has maintained interest in facilitated transport since the 1970s, but the problems of the physical instability of the liquid membrane and the chemical instability of the carrier agent are yet to be overcome.

Microfiltration. *Microfiltration* is generally defined as the separation of particulates between 0.1 and 10 μm by a membrane. Two principal types of membrane filter are used: depth filters and screen filters. Figure 26 compares typical pore sizes of depth and screen filters. Screen filters have small pores in the top surface that collect particles larger than the pore diameter on the surface of the membrane. Depth filters have relatively large pores on the top surface and so particles pass to the interior of the membrane. The particles are then captured at constrictions in the membrane pores or by adsorption onto the pore walls. Screen filter membranes rapidly become plugged by the accumulation of retained particles at the top surface. Depth filters, which have a much larger surface area available to collect the particles, provide a greater holding capacity before fouling.

Depth filters are usually preferred for the most common type of microfiltration system, illustrated schematically in Figure 27a. In this process design, called *dead-end or in-line filtration*, the entire fluid flow is forced through the membrane under pressure. As particulates accumulate on the membrane surface or in its interior, the pressure required to maintain the required flow increases until, at some point, the membrane must be replaced. The useful life of the membrane is proportional to the particulate loading of the feed solution. In-line microfiltration of solutions as a final polishing step prior to use is a typical application.

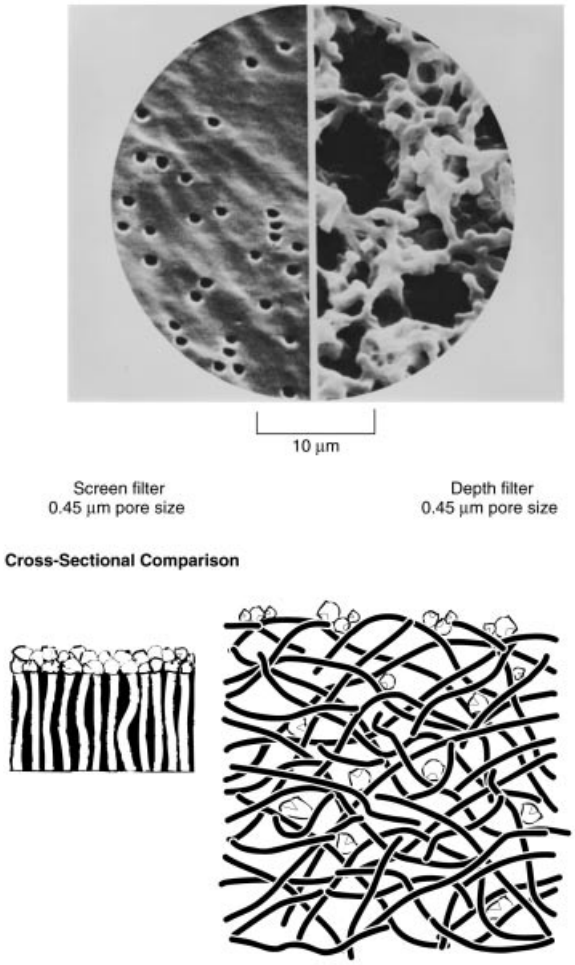

Fig. 26. Surface scanning electron micrograph and schematic comparison of nominal 0.45-mm screen and depth filters. The screen filter pores are uniform and small and capture the retained particles on the membrane surface. The depth filter pores are almost 5–10 times larger than the screen filter equivalent. A few large particles are captured on the surface of the membrane, but most are captured by adsorption in the membrane interior.

Increasingly, screen membranes are preferred for the type of cross-flow microfiltration system shown in Figure 27b. Cross-flow systems are more complex than the in-line (dead-end) filter systems because they require a recirculation pump, valves, controls, etc. However, a screen membrane has a much longer lifetime than a depth membrane and, in principle, can be regenerated by back flushing. Cross-flow filtration is being adopted increasingly for microfiltration of high-volume industrial streams containing significant particulate levels (70).

Ultrafiltration. The term ultrafiltration was coined in the 1920s to describe the collodion membranes available at that time. The process was first widely used in the 1960s when Michaels and others at Amicon Corp. adopted the then recently discovered Loeb–Sourirajan asymmetric membrane preparation

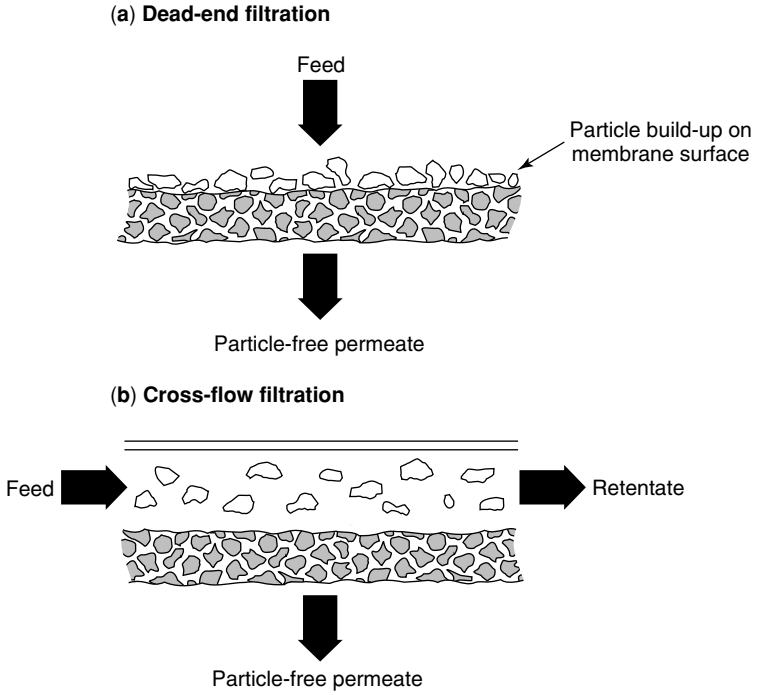

Fig. 27. Schematic representation of dead-end and cross-flow filtration with microfiltration membranes. The equipment used in dead-end filtration is simple, but retained particles plug the membranes rapidly. The equipment required for cross-flow filtration is more complex, but the membrane lifetime is longer.

technique to the production of ultrafiltration membranes (26). These membranes had pore sizes in the range 2–20 nm and found an immediate application in concentrating and desalting protein solutions in the laboratory. Later, Romicon, Abcor, and other companies developed the technology for a wide range of industrial applications. Early and still important applications were the recovery of electrocoat paint from industrial coating operations and the clarification of emulsified oily wastewaters in the metalworking industry. More recent applications are in the food industry for concentration of proteins in cheese production and for juice clarification (71). The current ultrafiltration market is in the range $150–250 million/year.

An example is the application of ultrafiltration to an automobile electrocoat paint operation shown schematically in Figure 28. Electrocoat paint is an emulsion of charged paint particles. The metal piece to be coated is made into an electrode of opposite charge to the paint particles and is immersed in a large tank of the paint. When a voltage is applied between the metal part and the paint tank, the charged paint particles migrate under the influence of the voltage and are deposited on the metal surface to form a coating over the entire wetted surface of the metal part. After electrodeposition, the piece is removed from the tank and rinsed to remove excess paint, after which the paint is cured in an oven.

The rinse water from the washing step rapidly becomes contaminated with excess paint, while the stability of the paint emulsion is gradually degraded

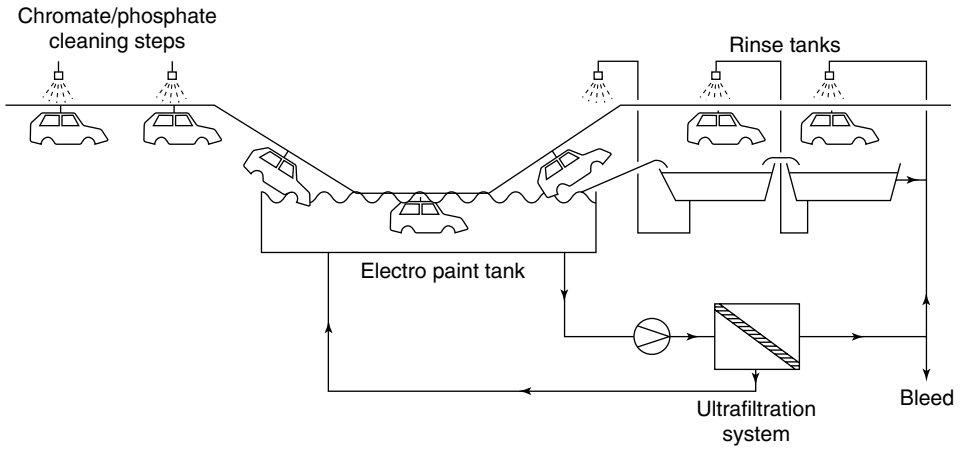

Fig. 28. Flow schematic of an electrocoat paint ultrafiltration system. The ultrafiltration system removes ionic impurities from the paint tank carried over from the chromate/phosphate cleaning steps and provides clean rinse water for the countercurrent rinsing operation.

by ionic impurities carried over from the cleaning operation before the paint tank. Both of these problems are solved by the ultrafiltration system shown in Figure 28. The ultrafiltration plant takes paint solution containing 15–20% solids and produces a clean permeate, containing the ionic impurities but no paint particles, which is sent to the countercurrent rinsing operation, and a slightly concentrated paint to be returned to the paint tank. A portion of the ultrafiltration permeate is bled from the tank and replaced with water to maintain the ionic balance of the process. A good review of other ultrafiltration applications is given in Reference (71).

Ultrafiltration membranes are usually asymmetric membranes made by the Loeb–Sourirajan process. They have a finely porous surface or skin supported on a microporous substrate. The membranes are characterized by their *molecular weight cutoff*, a loosely defined term generally taken to mean the molecular weight of the globular protein molecule that is 95% rejected by the membrane. A series of typical molecular weight cutoff curves are shown in Figure 29. Globular proteins are usually specified for this test because the rejection of linear polymer molecules of equivalent molecular weight is usually much less. Apparently, linear, flexible molecules are able to snake through the membrane pores, whereas rigid globular molecules are retained.

A key factor determining the performance of ultrafiltration membranes is concentration polarization, which causes membrane fouling due to deposition of retained colloidal and macromolecular material on the membrane surface. The pure water flux of ultrafiltration membranes is often very high—more than 1 $cm^3/(cm^2 \cdot min)$ [350 $gal/(ft^2 \cdot day)$]. However, when membranes are used to separate macromolecular or colloidal solutions, the flux falls within seconds, typically to the 0.1 $cm^3/(cm^2 \cdot min)$ level. This immediate drop in flux is caused by the formation of a gel layer of retained solutes on the membrane surface because of the concentration polarization. The gel layer forms a secondary barrier

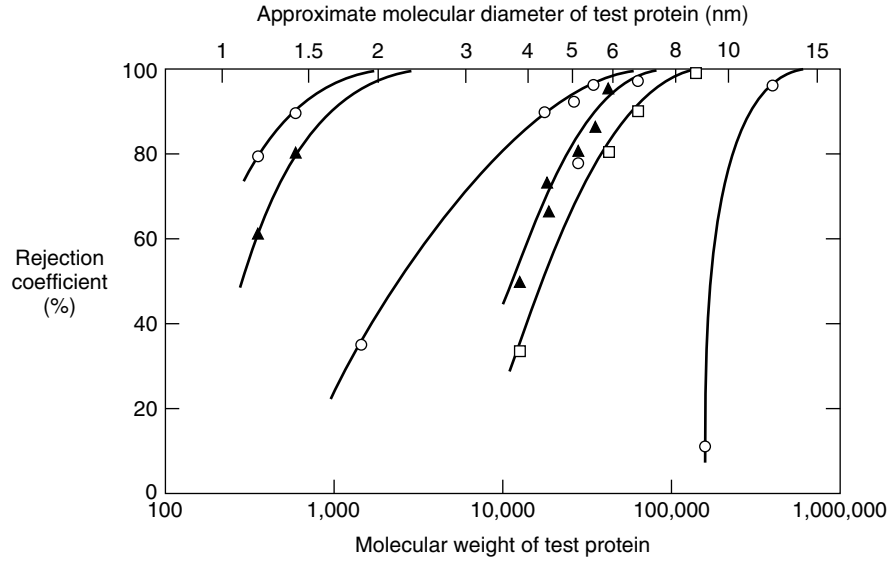

Fig. 29. Rejection of test proteins as a function of molecular weight, in a series of ultrafiltration membranes with different molecular weight cutoffs. As these data show, membranes with complete sharp molecular weight are not found outside of manufacturers' catalogs.

to flow through the membrane, as illustrated in Figure 30. This first decline in flux is determined by the composition of the feed solution and its fluid hydrodynamics. Sometimes the resulting flux is constant for a prolonged period, and when the membrane is retested with pure water, its flux returns to the original value. More commonly, however, a further slow decline in flux occurs over a period of hours to weeks, depending on the feed solution. Most of this second decrease in flux is caused by slow consolidation of the secondary layer formed by concentration polarization on the membrane surface. Formation of this consolidated gel layer, called *membrane fouling*, is difficult to control. Control techniques include regular membrane cleaning, back flushing, or using membranes with surface characteristics that minimize adhesion. Operation of the membrane at the lowest practical operating pressure also delays consolidation of the gel layer.

A typical plot illustrating the slow decrease in flux that can result from consolidation of the secondary layer is shown in Figure 31. The pure water flux of these membranes is approximately 200 L/min, but on contact with an electrocoat paint solution containing 10–20% latex, the flux immediately falls to about 40–50 L/min. This first drop in flux is due to the formation of the gel layer of latex particles on the membrane surface, as shown in Figure 30. Thereafter, the flux declines steadily over a 2-week period. This second drop in flux is caused by slow densification of the gel layer under the pressure of the system. In this particular example the densified gel layer could be removed by periodic cleaning of the membrane. When the cleaned membrane is exposed to the latex solution again, the flux is restored to that of a fresh membrane.

If the regular cleaning cycle shown in Figure 31 is repeated many times, the membrane flux eventually does not return to the original value on cleaning. Part of this slow, permanent loss of flux is believed to be due to precipitates on the

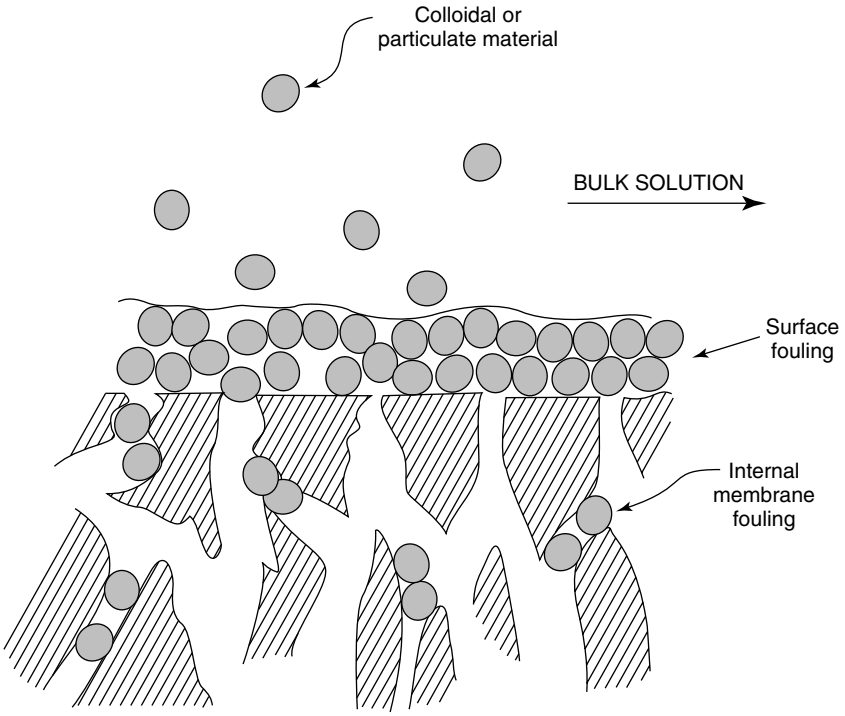

Fig. 30. Schematic representation of fouling on an ultrafiltration membrane. *Surface fouling* is the deposition of solid material on the membrane that consolidates over time. This fouling layer can be controlled by high turbulence, regular cleaning, and using hydrophilic or charged membranes to minimize adhesion to the membrane surface. Surface fouling is generally reversible. *Internal fouling* is caused by penetration of solid material into the membrane, which results in plugging of the pores. Internal membrane fouling is generally irreversible.

membrane surface that are not removed by the cleaning procedure. A further cause of the permanent flux loss is believed to be internal fouling of the membrane by material that penetrates the membrane pores and becomes lodged in the interior of the membrane, as illustrated in Figure 30.

As described previously, the initial cause of membrane fouling is concentration polarization, which results in deposition of a layer of material on the membrane surface. In ultrafiltration, solvent and macromolecular or colloidal solutes are carried toward the membrane surface by the solution permeating the membrane. Solvent molecules permeate the membrane, but the larger solutes accumulate at the membrane surface. Because of their size, the rate at which the rejected solute molecules can diffuse from the membrane surface back to the bulk solution is relatively low. Thus their concentration at the membrane surface increases far above the feed solution concentration. In ultrafiltration the concentration of retained macromolecular or colloidal solutes at the membrane surface is typically 20–50 times higher than the feed solution concentration. These solutes become so concentrated at the membrane surface that a gel layer is formed and becomes a secondary barrier to flow through the membrane. The formation of the gel layer

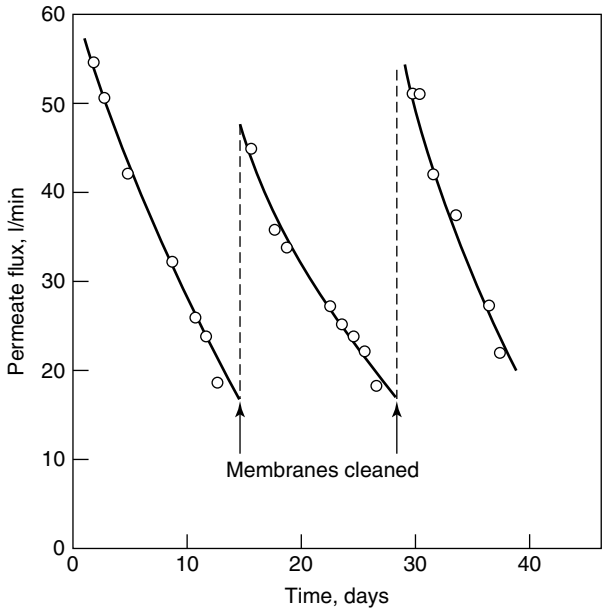

Fig. 31. Ultrafiltration flux as a function of time of an electrocoat paint latex solution. Because of fouling, the flux declines over a period of days. Periodic cleaning is required to maintain high fluxes.

is easily modeled mathematically and is reviewed in detail elsewhere (71–74). One consequence of the formation of the gel layer on the membrane surface is that ultrafiltration membrane fluxes reach a limiting plateau value that cannot be exceeded at any particular operating condition.

The effect of the gel layer on the flux through an ultrafiltration membrane at different feed pressures is illustrated by the experimental data in Figure 31. At a very low pressure p_1, the flux J_v is low, so the effect of concentration polarization is small, and a gel layer does not form on the membrane surface. The flux is close to the pure water flux of the membrane at the same pressure. As the applied pressure is increased to pressure p_2, the higher flux causes increased concentration polarization, and the concentration of retained material at the membrane surface increases. If the pressure is increased further to p_3, concentration polarization becomes enough for the retained solutes at the membrane surface to reach the gel concentration c_{gel}, and form the secondary barrier layer. This is the limiting flux for the membrane. Further increases in pressure only increase the thickness of the gel layer, not the flux.

Experience has shown that the best long-term performance of an ultrafiltration membrane is obtained when the applied pressure is maintained at or just below the plateau pressure p_3 shown in Figure 32. Operating at higher pressures does not increase the membrane flux but does increase the thickness and density of retained material at the membrane surface layer. Over time, material on the membrane surface can become compacted or precipitate, forming a layer of deposited material that has a lower permeability; the flux then falls from the initial value.

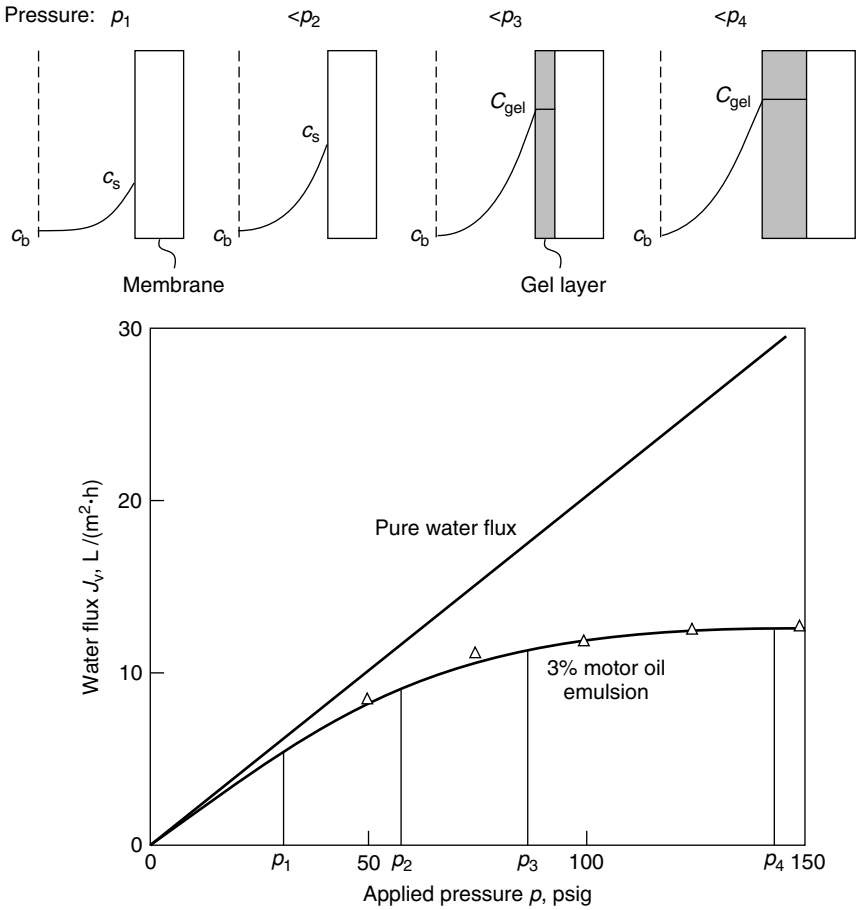

Fig. 32. The effect of pressure on ultrafiltration membrane flux and the formation of a secondary gel layer. Ultrafiltration membranes are best operated at pressures between p_2 and p_3 at which the gel layer is thin. Operation at high pressures such as p_4 leads to formation of thick gel layers, which can consolidate over time, resulting in permanent fouling of the membrane.

Reverse Osmosis. This was the first membrane-based separation process to be commercialized on a significant scale. As described previously, the breakthrough discovery that made reverse osmosis possible was the development of the Loeb–Sourirajan asymmetric cellulose acetate membrane. This membrane made desalination by reverse osmosis practical; within a few years commercial plants were installed. Currently, the total worldwide market for reverse osmosis membrane modules is about $300 million/year, split approximately between 15% hollow-fiber and 85% spiral-wound modules. The general trend of the industry is toward spiral-wound modules for this application, and the market share of the hollow-fiber products is falling (75).

The first reverse osmosis modules made from cellulose diacetate had a salt rejection of approximately 97–98%. This was enough to produce potable water (ie water containing less than 500-ppm salt) from brackish water sources, but was

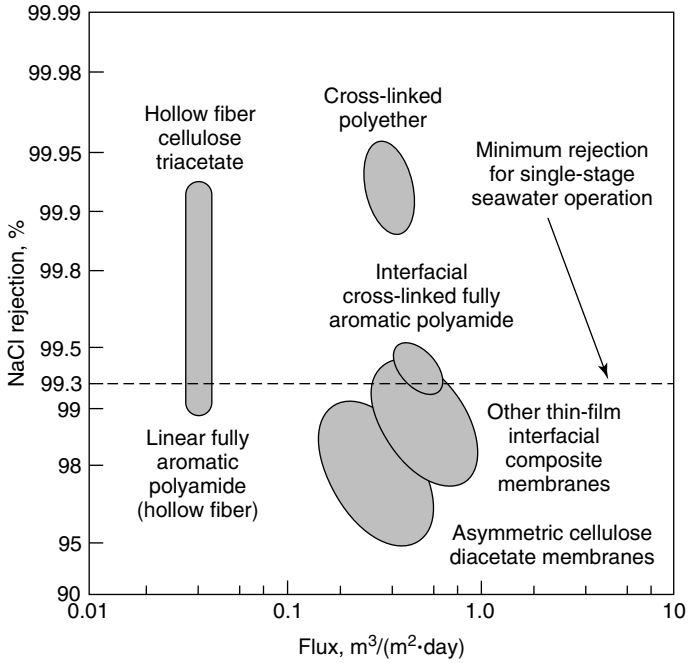

Fig. 33. Performance characteristics of membranes operating on seawater at 5.5 MPa (56 kg/cm^2) and 25°C (75).

not enough to desalinate sea water efficiently. In the 1970s, interfacial composite membranes with salt rejections greater than 99.5% were developed, making seawater desalination possible (28,29); a number of large plants are operating worldwide.

The performance characteristics of the membranes available in 1990 are shown in Figure 33. Hollow-fine-fiber membranes made by Toyobo and DuPont have relatively low fluxes, but because large membrane areas can be made so economically in hollow-fiber form, these membranes can still compete. The highest flux, highest performance membrane is the cross-linked polyether membrane formerly made by Toray. However, this membrane is unstable to oxidation, and all free oxygen and chlorine must be removed from the feed water to the membrane, a process that is expensive and subject to failure. As a result, most of the reverse osmosis membrane market is divided between various types of thin-film interfacial composite membranes and cellulose diacetate Loeb–Sourirajan membranes. Cellulose diacetate membranes still retain a fraction of the market because of their greater chemical and mechanical stability compared to interfacial composites. This advantage is gradually disappearing as improved interfacial composite membranes are developed (76).

The performance of reverse osmosis membranes is generally described by the water and salt fluxes (77,78). The water flux J_w is linked to the pressure and concentration gradients across the membrane by the term

$$J_w = A(\Delta p - \Delta \pi) \quad (1)$$

where A is a constant, Δp is the pressure difference across the membrane, and $\Delta\pi$ is the osmotic pressure differential across the membrane. As this equation shows, at low applied pressure when $\Delta p < \Delta\pi$, water flows from the dilute to the concentrated salt-solution side of the membrane by normal osmosis. When $p = \Delta\pi$, there is no flow. When the applied pressure is higher than the osmotic pressure ie, $\Delta p > \Delta\pi$, water flows from the concentrated to the dilute salt-solution side of the membrane.

The salt flux J_s across a reverse osmosis membrane can be described by the equation

$$J_s = B(c_1 - c_2) \tag{2}$$

where B is a constant and c_1 and c_2 are the salt concentration differences across the membrane.

It follows from these two equations that the water flux is proportional to the applied pressure, but the salt flux is independent of pressure. This means the membrane becomes more selective as the pressure increases. Selectivity can be measured in a number of ways, but conventionally, it is measured as the salt rejection coefficient R defined as

$$R = \left(1 - \frac{c_2}{c_1}\right) \times 100\% \tag{3}$$

Some data illustrating the effect of pressure on the water and salt fluxes and the salt rejection of a good quality reverse osmosis membrane are shown in Figure 34.

Although the principal application of reverse osmosis membranes is still desalination of brackish water or seawater to provide drinking water, a recent, significant market is production of ultrapure water by filtration of municipal drinking water. Such water is used in the electronics industry, where huge amounts of extremely pure water with a total salt concentration significantly below 1 ppb are required to wash silicon wafers.

A simplified flow scheme for a brackish water reverse osmosis plant is shown in Figure 35. In this example, it is assumed that the brackish water is heavily contaminated with suspended solids, so flocculation followed by a sand filter and a cartridge filter are used to remove particulates. The pH of the feed solution might be adjusted, followed by chlorination to sterilize the water to prevent bacterial growth on the membranes and addition of an antiscalant to inhibit precipitation of multivalent salts on the membrane. Finally, if chlorine-sensitive interfacial composite membranes are used, sodium sulfite is added to remove excess chlorine before the water contacts the membrane. Generally, more pretreatment is required in plants using hollow-fiber modules than in plants using spiral-wound modules. This is one reason why hollow-fiber modules have been displaced by spiral-wound systems in most brackish water installations.

A feature of the system design shown in Figure 35 is the staggered arrangement of the module pressure vessels. As the volume of the feed water is reduced as water is removed in the permeate, the number of modules arranged in parallel is also reduced. In the example shown, the feed water passes initially through four modules in parallel, then through two, and finally through a single module

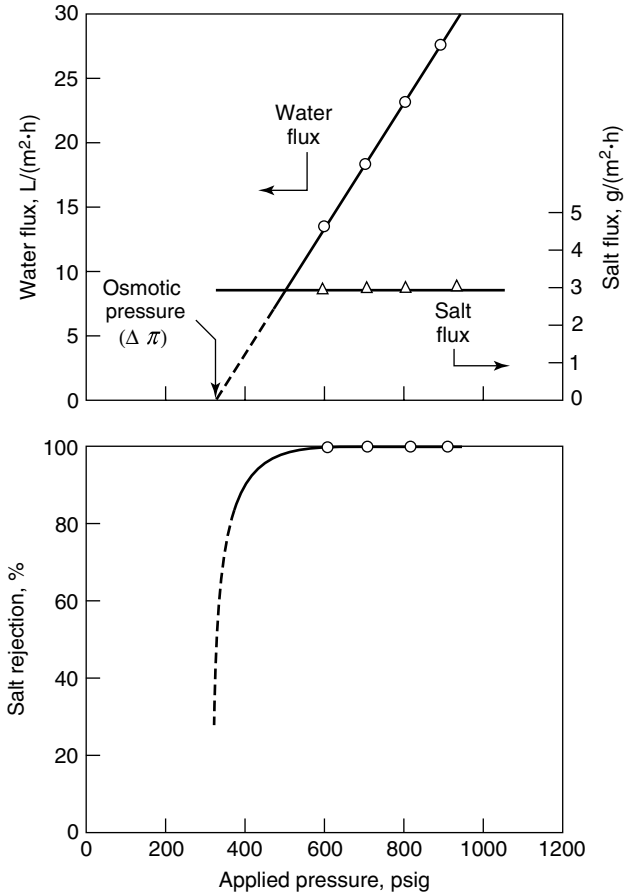

Fig. 34. Water and salt fluxes through a high performance reverse osmosis membrane, when tested with a 3.5% NaCl feed solution. The water flux increases, whereas the salt flux is essentially independent of applied pressure. To convert MPa to psig, multiply by 145 (78).

in series. This is called a *Christmas tree or tapered module design* and provides a high average feed solution velocity through the modules.

The operating pressure of reverse osmosis systems has gradually fallen over the past 20 years as the permeability and rejections of membranes have steadily improved. The first plants operated at pressures up to 60 atm, but typical brackish water plants now operate at pressures in the 10- to 20-atm range. Capital costs of brackish water plants have stayed remarkably constant for almost 20 years; the rule of thumb of $1.00/(gal·day) capacity is still true. Accounting for inflation, this, of course, reflects a very large reduction in real costs resulting from the better performance of today's membranes.

Electrodialysis. *Electrodialysis* is an electrochemical separation process in which a gradient in electrical potential is used to separate ions with charged, ionically selective membranes. A schematic of the simplest type of electrodialysis system is shown in Figure 36 (79–81). The process uses an electrodialysis stack,

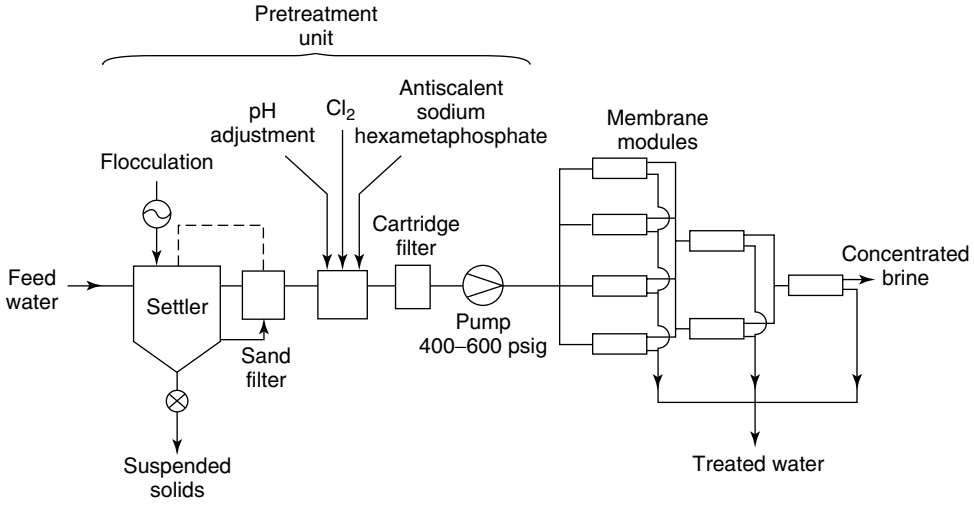

Fig. 35. Flow schematic of a typical brackish water reverse osmosis plant. The plant contains seven pressure vessels, each containing six membrane modules. The pressure vessels are in a "Christmas tree" array to maintain a high feed velocity through the modules.

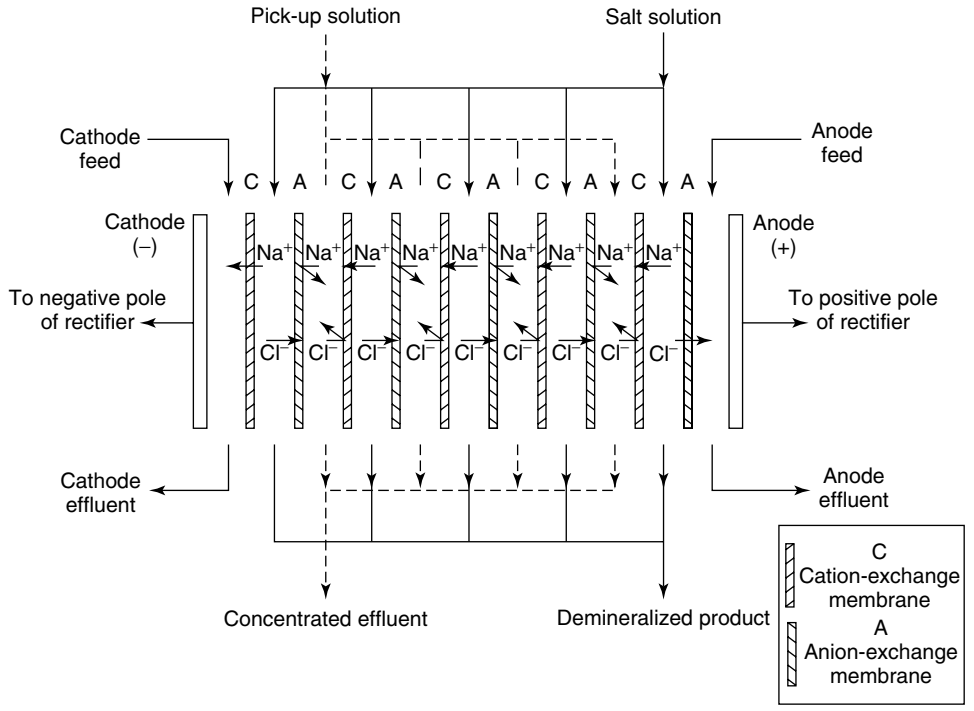

Fig. 36. Schematic diagram of a plate-and-frame electrodialysis stack. Alternating cation and anion permeable membranes are arranged in a stack of up to 100 cell pairs: C, cation-exchange membrane; A, anion-exchange membrane.

built on the plate-and-frame principle and containing several hundred cells each formed by a pair of anion- and cation-exchange membranes. Anion-exchange membranes contain fixed, positively charged entities, such as quaternary ammonium groups, fixed to the polymer backbone. These membranes are permeable to negatively charged ions, but positive ions are excluded from permeation by the fixed charges. Similarly, cation-exchange membranes contain fixed, negatively charged groups, such as sulfonic acid groups. Cationic membranes are permeable to positively charged ions, but not to negatively charged ions. The arrangement of the membranes in an electrodialysis stack is such that every second cell becomes depleted of salt, while the adjacent cells become concentrated in salt. The degree of concentration is determined by the rate of flow of solution through the stack.

Electrodialysis is used widely to desalinate brackish water, but this is by no means its only significant application. In Japan, which has no readily available natural salt brines, electrodialysis is used to concentrate salt from seawater. The process is also used in the food industry to deionize cheese whey, and in a number of pollution-control applications.

In the past, the principal problem inhibiting the use of electrodialysis was slow deterioration of the membranes by chemical degradation and scaling. In the 1970s the introduction of a process called *polarity reversal* reduced the scaling problem significantly. In this process, the flow of current through the electrodialysis stack is reversed periodically by reversing the polarity of the electrodes. When the polarity of the electrodes is reversed, the concentrated stream becomes the demineralized product stream and the demineralized stream becomes the concentrated stream; automatic valves are used to switch the streams. When the current is reversed, scale deposited on the membranes in the previous cycle is dissolved. Typically, the current of an electrodialysis stack is reversed every 15–20 min. One or two minutes production of the system is lost after each reversal, but the reduced scaling and fouling of the membranes more than compensates for this loss in productivity.

One of the most attractive features of electrodialysis is its energy efficiency. The electric current A needed to desalinate a solution is directly proportional to the quantity of ions transported through the membranes and is given by the equation

$$A = zFQ\Delta c/\xi \tag{4}$$

Here z is the electrochemical valence, F is the Faraday constant, Q is the feed solution flow rate, Δc is the difference in concentration between the feed and product solution, and ξ is the current utilization factor. The current utilization factor is always less than 100% because of losses in the stack. Because the membranes are not perfectly semipermeable, some co-ions diffuse across the membrane. Some water is also transferred across the membrane by osmotic flow. Finally, some current flows through the stack manifold and is dissipated as electrical heating. Nonetheless, electrodialysis uses significantly less energy than competitive processes such as evaporation or reverse osmosis, especially for low concentration feed solutions.

Gas Separation. During the 1980s, gas separation using membranes became a commercially important process; the size of this application is still increasing rapidly. In gas separation, one of the components of the feed permeates a selective membrane at a much higher rate than the others. The driving force is

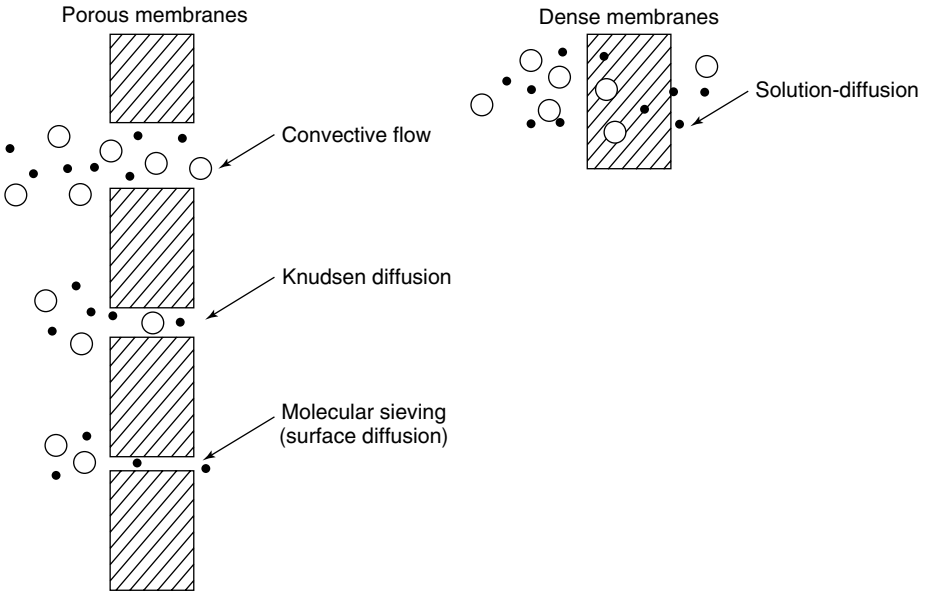

Fig. 37. Mechanisms for permeation of gases through porous and dense gas separation membranes.

the pressure difference between the pressurized feed gas and the lower pressure permeate.

Both porous and dense membranes can be used as selective barriers; Figure 37 illustrates the mechanism of gas permeation through both classes. Three types of porous membranes, differing in pore size, are shown. If the pores are relatively large, in the range 0.1–10 μm, gases permeate the membrane by convective flow, and no separation occurs. If the pores are smaller than 0.1 μm, then the pore diameter is the same size or smaller than the mean free path of the gas molecules. Diffusion through such pores is governed by Knudsen diffusion, and the transport rate of different gases is inversely proportional to the square root of the molecular weight. The latter relationship, sometimes called *Graham's law of diffusion*, was exploited on a massive scale in the separation of $U^{235}F_6$ and $U^{238}F_6$ during the Manhattan Project. Finally, if the membrane pores are very small indeed, of the order 0.5–2 nm, then molecules are separated by molecular sieving. Actual transport mechanisms through this type of membrane are complex and include both diffusion in the gas phase and diffusion of adsorbed species on the surface of the pores (surface diffusion). Nonetheless, ceramic and ultramicroporous carbon membranes have been prepared with extraordinarily high separations for very similar molecules (45–47).

Although microporous membranes are a topic of research interest, all current commercial gas separations are based on the fourth type of mechanism shown in Figure 37, namely diffusion through dense polymer films. Gas transport through dense polymer membranes is governed by the equation

$$J_i = \frac{P_i[p_{i(o)} - p_{i(l)}]}{l} \tag{5}$$

where J_i is the flux of component i, $p_{i(o)}$ and $p_{i(l)}$ are the partial pressure of the component i on either side of the membrane, l is the membrane thickness, and P_i is a constant called the membrane permeability, which is a measure of the membrane's ability to permeate gas (78). The ability of a membrane to separate two gases, i and j, is the ratio of their permeabilities, $\alpha_{i,j}$, called the membrane selectivity:

$$\alpha_{ij} = \frac{P_i}{P_j} \tag{6}$$

In this equation the permeabilities of gases are measured with the gas mixture. The selectivity calculated from the ratio of pure gas permeabilities is sometimes called the ideal gas selectivity and is often higher than the actual selectivity value. Permeability P_i can be expressed as the product of two terms. One, the diffusion coefficient D_i, reflects the mobility of the individual molecules in the membrane material; the other, the Henry's law sorption coefficient k_i, reflects the number of molecules dissolved in the membrane material. Thus, equation (6) can also be written as

$$\alpha_{ij} = \left(\frac{D_i}{D_j}\right)\left(\frac{k_i}{k_j}\right) \tag{7}$$

The ratio D_i/D_j is the ratio of the diffusion coefficients of the two gases and can be viewed as the mobility selectivity, reflecting the different sizes of the two molecules. The ratio k_i/k_j is the ratio of the Henry's law sorption coefficients of the two gases and can be viewed as the sorption or solubility selectivity, reflecting the relative condensabilities of the two gases. If molecule i is larger than j, then the mobility selectivity will always be less than 1. The sorption selectivity, however, is normally greater than 1, reflecting the higher condensability of large molecules compared to small ones. The balance between the sorption selectivity and the mobility selectivity determines whether a membrane material is selective for large or small molecules in a gas mixture.

In all polymer materials, the diffusion coefficient decreases with increasing molecular size, because large molecules interact with more segments of the polymer chain than small molecules do. Hence, the mobility selectivity always favors the passage of small molecules over large ones. However, the magnitude of the mobility selectivity term is different for glassy and rubbery materials (82), as the data in Figure 38 show. With increasing permeant size, diffusion coefficients in glassy materials decrease much more rapidly than diffusion coefficients in rubbers, in which the polymer chains can rotate freely. For example, the mobility selectivity of natural rubber for nitrogen over pentane is approximately 10. The mobility selectivity of polyvinyl chloride, a rigid, glassy polymer, for nitrogen over pentane is more than 100,000 (83).

The second factor affecting the overall membrane selectivity is the sorption or solubility selectivity. The sorption coefficient of gases and vapors, which is a measure of the energy required for the permeant to be sorbed by the polymer, increases with increasing condensability of the permeant. This dependence on condensability means that the sorption coefficient also increases with molecular

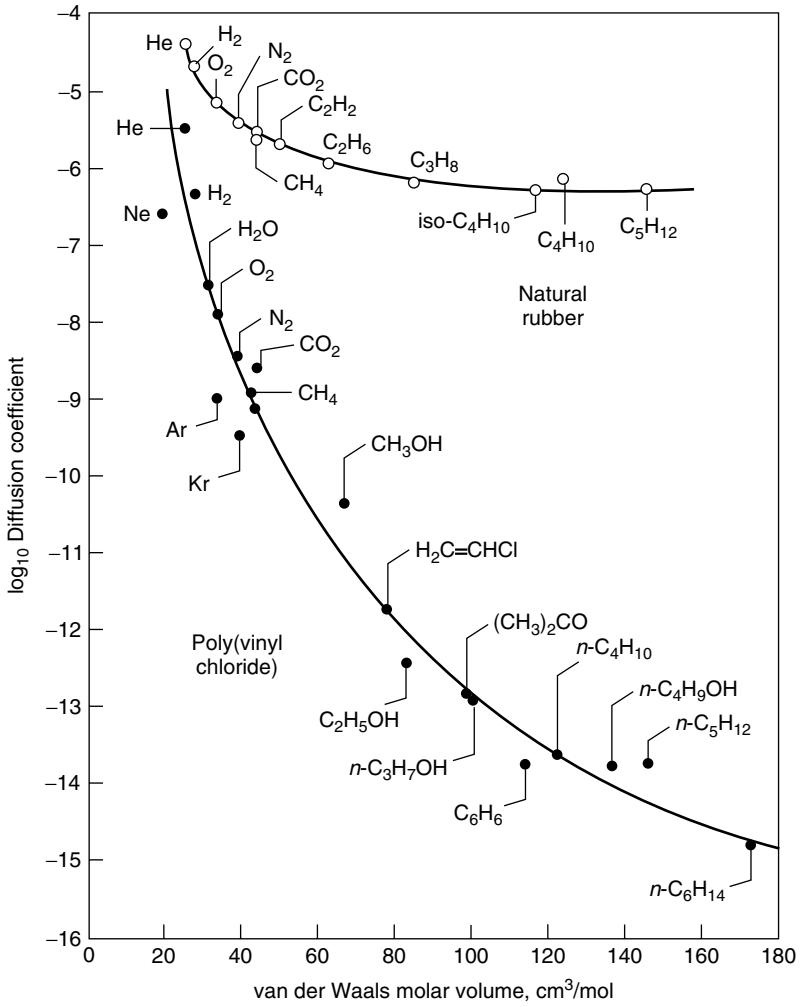

Fig. 38. Diffusion coefficient as a function of molar volume for a variety of permeants in natural rubber and in poly(vinyl chloride). Reprinted from Ref. 83, Copyright 1982, with permission from Elsevier Science.

diameter, because large molecules are normally more condensable than small ones. The Henry's law sorption coefficient can, therefore, be plotted against boiling point or molar volume as shown in Figure 39 (84). As the figure shows, sorption selectivity favors the larger, more condensable molecules, such as hydrocarbon vapors, over the permanent gases, such as oxygen and nitrogen. The difference between the sorption coefficients of permeants in rubbery and glassy polymers is far less marked than the differences in the diffusion coefficients.

It follows from the preceding discussion that the balance between the mobility selectivity term and the sorption selectivity term in equation (7) is different for glassy and rubbery polymers. This difference is illustrated by the data in Figure 40 (85). In glassy polymers such as polyetherimide, the mobility term is usually

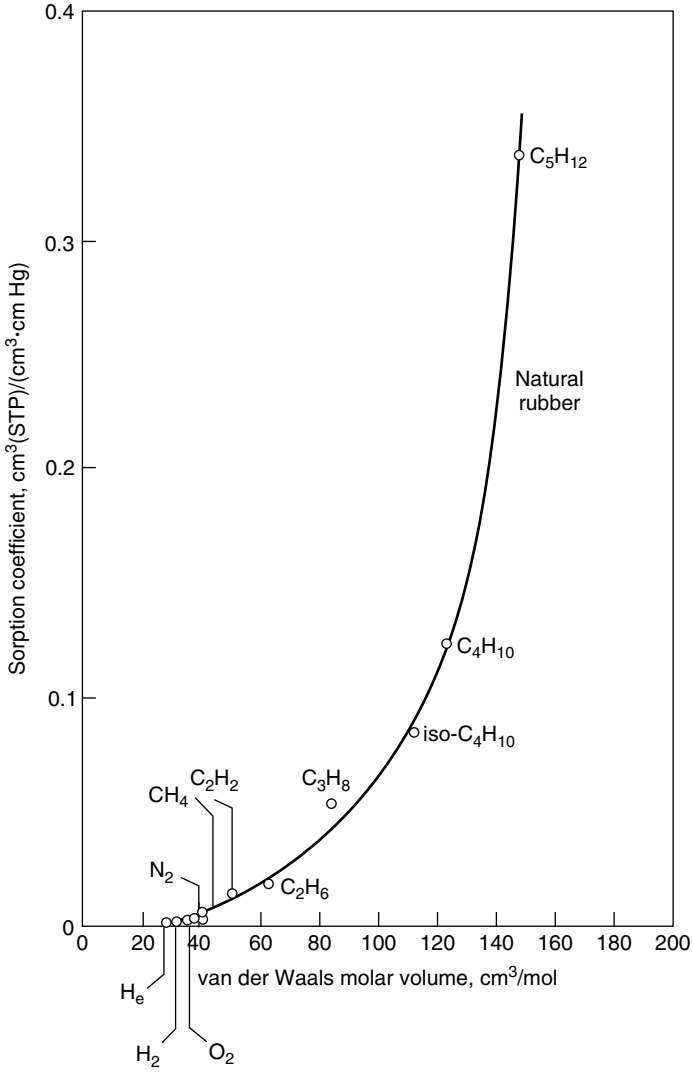

Fig. 39. Gas sorption coefficient as a function of molar volume for natural rubber membranes. Larger permeants are more condensable and have higher sorption coefficients.

dominant, permeability decreases with increasing permeant size, and small molecules permeate preferentially. When used to separate organic vapors from air, therefore, glassy membranes are air selective. In rubbery polymers, the sorption selectivity term is usually dominant, permeability increases with increasing permeant size, and large molecules permeate preferentially. The separation properties of polymer membranes for a number of the most important gas separation applications have been summarized in Reference 86.

Both hollow-fiber and spiral-wound modules are used in gas separation applications. Spiral-wound modules are favored if the gas stream contains oil mist or condensable vapors as in the separation of hydrocarbon vapors from

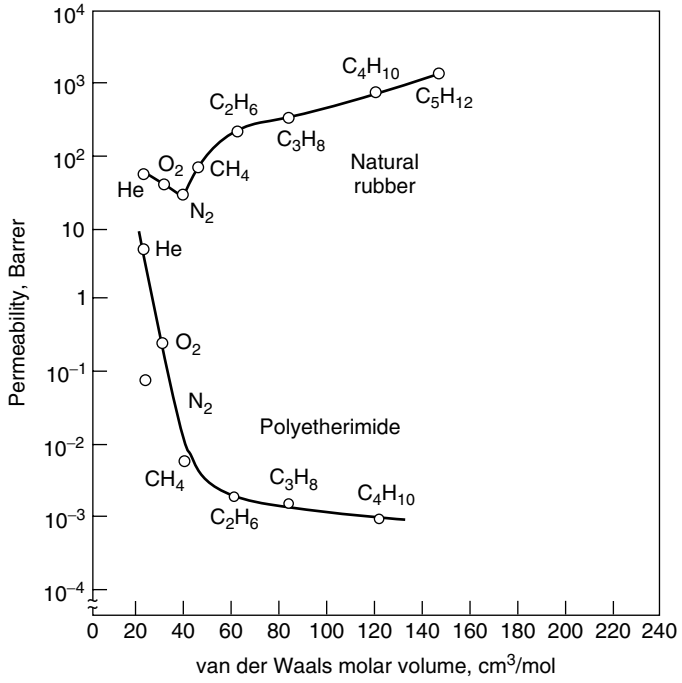

Fig. 40. Permeability as a function of molar volume for a rubbery and glassy polymer, illustrating the different balance between sorption and diffusion in these polymer types. The rubbery membrane is highly permeable; the permeability increases rapidly with increasing permeant size because sorption dominates. The glassy membrane is much less permeable; the permeability decreases with increasing permeant size because diffusion dominates (85).

$$1\ \text{Barrer} = \frac{0.335 \times 10^{-15}\text{m} \cdot \text{mol}}{\text{m}^2 \cdot \text{s} \cdot \text{Pa}} \left(\frac{10^{-18}\text{cm}^3(\text{STP}) \cdot \text{cm}}{\text{cm}^2 \cdot \text{s} \cdot \text{cm Hg}} \right)$$

nitrogen or hydrogen or in natural gas separations. Table 4 summarizes the current commercial gas separation applications (87,88). The first large-scale commercial application of gas separation was the separation of hydrogen from nitrogen in ammonia purge gas streams, launched in 1980 by Permea (now a division of Air Products). This process was followed by a number of similar applications, such as hydrogen/methane separation in refinery off-gases and hydrogen/carbon monoxide adjustment in oxo-chemical synthetic plants. Several hundred of these plants have now been installed.

Following Permea's success, several companies produced membrane systems to treat natural gas streams, particularly to separate carbon dioxide from methane. The goal is to produce a stream containing less than 2% carbon dioxide to be sent to the national pipeline and a permeate enriched in carbon dioxide to be flared or reinjected into the ground. Cellulose acetate is the most widely used membrane material for this separation, but because its carbon dioxide/methane selectivity is only about 15, two-stage systems are often required to achieve a sufficient separation. The membrane process is generally best suited to relatively small streams, but the economics have slowly improved over the years and more

Table 4. Gas Separation Application Areas for Membranes

Gas separation	Applications
O_2/N_2	Nitrogen from air, oxygen enrichment of air
H_2/hydrocarbons	Refinery hydrogen recovery
H_2/CO	Syngas ratio adjustment
H_2/N_2, Ar, CH_4	Ammonia purge gas
CO_2/CH_4	Acid gas treatment of natural gas
Hydrocarbons/air	Hydrocarbon recovery, pollution control
H_2O/air	Air dehumidification
H_2O/CH_4	Natural gas dehydration
H_2S/CH_4	Sour gas treatment of natural gas
He/CH_4	Helium separation from natural gas
He/N_2	Helium recovery

than 100 natural gas treatment plants have now been installed—some quite large. Figure 41 shows flow schematics for one-stage and two-stage carbon dioxide membrane separation plants.

By far the largest gas separation process in current use is the production of nitrogen from air. The first membranes used for this process were based on

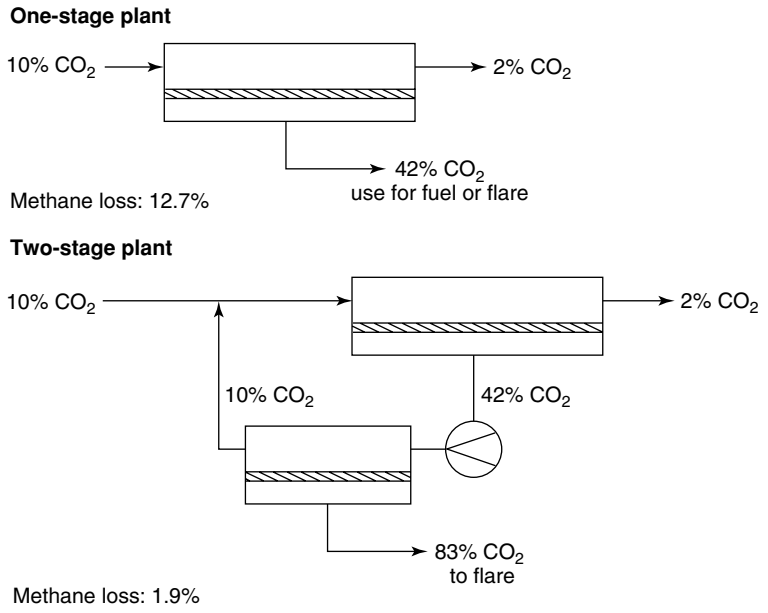

Fig. 41. Flow scheme of one-stage and two-stage membrane separation plants to remove carbon dioxide from natural gas (α_{CO2}/CH_4 of 15 is typical for cellulose acetate membranes). Because the one-stage design has no moving parts, it is very competitive with other technologies especially if there is a use for the low pressure permeate gas. Two-stage processes are more expensive because a large compressor is required to compress the permeate gas. However, the loss of methane with the fuel gas is much reduced.

polysulfone, poly(methyl pentane), and ethyl cellulose. These materials had oxygen/nitrogen selectivities of 4–5, and the economics of the process were marginal. The second-generation materials now used have selectivities in the range 7–8 and significantly higher fluxes. With these membranes, the economics of nitrogen production from air are very favorable, especially for small plants producing 0.14–14 standard m^3/min (5–500 scfm) of nitrogen. In this range, membranes are the low–cost process, and most new nitrogen plants use membrane systems. More than 5000 such systems have been installed.

A growing application of membrane systems is the removal of condensable organic vapors from air and other streams. Unlike the processes described earlier, organic vapor separation uses rubbery membranes, which are more permeable to the organic vapor. More than 100 organic vapor recovery plants have been installed. In Europe, most of the plants recover gasoline vapors from air vented during transfer operations; in the United States, most plants recover olefins and light hydrocarbons from chemical processing streams.

Pervaporation. In this separation process, illustrated schematically in Figure 42, a multicomponent liquid stream is passed across a membrane that preferentially permeates one or more of the components. As the feed liquid flows across

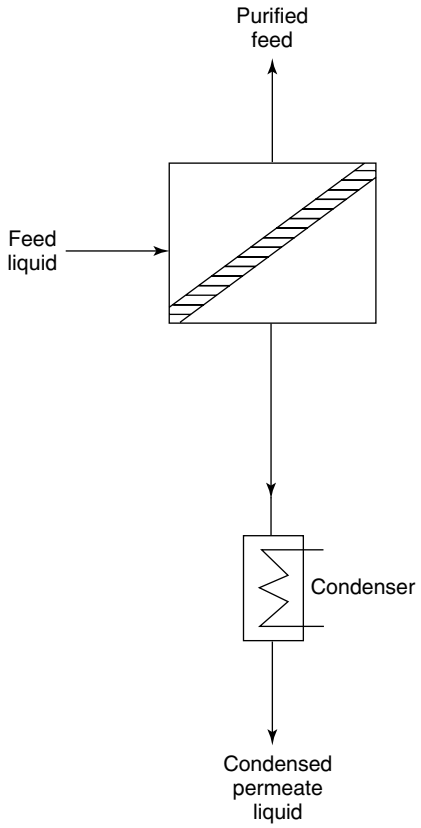

Fig. 42. Schematic of the basic pervaporation process.

the membrane surface, the preferentially permeated component passes through the membrane as a vapor. Transport through the membrane is induced by maintaining a vapor pressure on the permeate side of the membrane that is lower than the vapor pressure of the feed liquid. The pressure difference is achieved by cooling the permeate vapor to below the temperature of the feed stream, causing it to condense. This spontaneously generates a partial vacuum on the permeate side of the membrane. The condensate is then removed as a concentrated permeate fraction; the residue, depleted of the permeating component, exits on the feed side of the membrane. The process can be applied to the removal of dissolved water from organic solvents, to the extraction of organic solvents from water, and to the separation of mixed organic solvents.

The separation β_{pervap} achieved by a pervaporation process can be defined in the conventional way as

$$\beta_{\text{pervap}} = \frac{c_i''/c_j''}{c_i'/c_j'} \tag{8}$$

where c_i' and c_j' are the concentrations of components i and j on the feed liquid side and c_i'' and c_j'' are the concentrations of components i and j on the permeate side of the membrane. Because the permeate is a vapor, c_i'' and c_j'' can be replaced by p_i'' and p_j'', the vapor pressures of components i and j on the permeate side of the membrane. The separation achieved by the membrane can then be expressed by the equation

$$\beta_{\text{pervap}} = \frac{p_i''/p_j''}{c_i'/c_j'} \tag{9}$$

The most convenient mathematical method of describing pervaporation is to divide the overall separation processes into two steps, as shown in Figure 43 (89). The first is evaporation of the feed liquid to form a (hypothetical) saturated vapor phase on the feed side of the membrane. The second is permeation of this vapor through the membrane to the low pressure permeate side of the membrane. Although no evaporation actually takes place on the feed side of the membrane during pervaporation, this approach is mathematically simple and is thermodynamically completely equivalent to the physical process. The evaporation step from the feed liquid to the saturated vapor phase produces a separation β_{evap}, which can be defined as the ratio of the concentrations of the components in the feed vapor to their concentrations in the feed liquid,

$$\beta_{\text{evap}} = \frac{p_i'/p_j'}{c_i'/c_j'} \tag{10}$$

where p_i' and p_j' are the partial vapor pressures of the components i and j in equilibrium with the feed solution.

The second step, permeation of components i and j through the membrane, is related directly to conventional gas permeation. The separation achieved in this

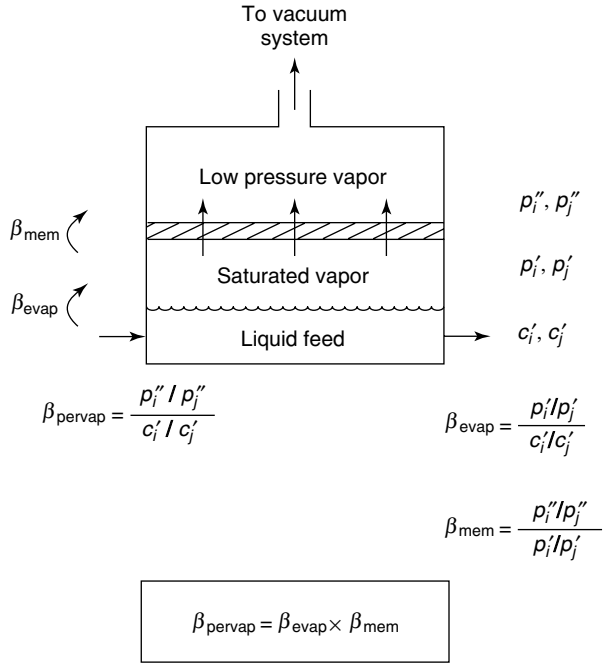

Fig. 43. The separation performed by a pervaporation membrane, β_{pervap}, is the product of the independent processes of evaporative separation β_{evap} and membrane permeation separation β_{mem}.

step, β_{mem}, can be defined as the ratio of components in the permeate vapor to the ratio of components in the feed vapor:

$$\beta_{mem} = \frac{p_i'' / p_j''}{p_i' / p_j'} \tag{11}$$

From the definitions given in equations (8–11), we can write the equality

$$\beta_{pervap} = \beta_{evap} \times \beta_{mem} \tag{12}$$

This equation shows that the separation achieved in pervaporation is proportional to the product of the separation achieved by evaporation of the liquid and the separation achieved by permeation of the components through a membrane. To achieve good separations both terms should be large. It follows that, in general, pervaporation is most suited to the removal of volatile components from relatively involatile components, because β_{evap} will then be large. However, if the membrane is sufficiently selective and β_{mem} is large, nonvolatile components can be made to permeate the membrane preferentially (89).

The selectivity of pervaporation membranes varies considerably and has a critical effect on the overall separation obtained. The range of results that can

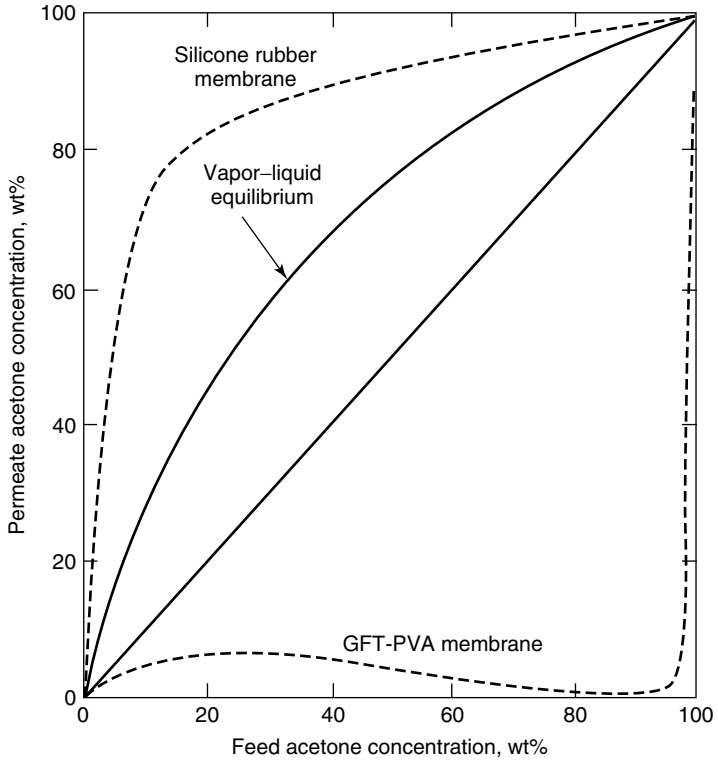

Fig. 44. The pervaporation separation of acetone–water mixtures achieved with a water-selective PVA membrane and with an acetone-selective silicone rubber membrane. The PVA membrane is best suited to removing small amounts of water from a concentrated acetone solution, whereas the silicone rubber membrane is best suited to removing small amounts of acetone from a dilute acetone stream. Reprinted from Ref. 91 by courtesy of Marcel Dekker, Inc.

be obtained for the same solutions and different membranes is illustrated in Figure 44 for the separation of acetone from water using two types of membrane (90,91). The figure shows the concentration of acetone in the permeate as a function of the concentration in the feed. The two membranes shown have dramatically different properties. The silicone rubber membrane removes acetone selectively, whereas the cross-linked PVA membrane removes water selectively. This difference occurs because silicone rubber is hydrophobic and rubbery, thus permeates the acetone preferentially. On the other hand, PVA is hydrophilic and glassy, thus permeates the small hydrophilic water molecules preferentially.

The acetone-selective, silicone rubber membrane is best used to treat dilute acetone feed streams and concentrate most of the acetone in a small volume of permeate. The water-selective PVA membrane is best used to treat concentrated acetone feed streams containing only a few percent water. Most of the water is then removed and concentrated in the permeate. Both membranes are more selective than distillation, which relies on the vapor–liquid equilibrium to achieve a separation.

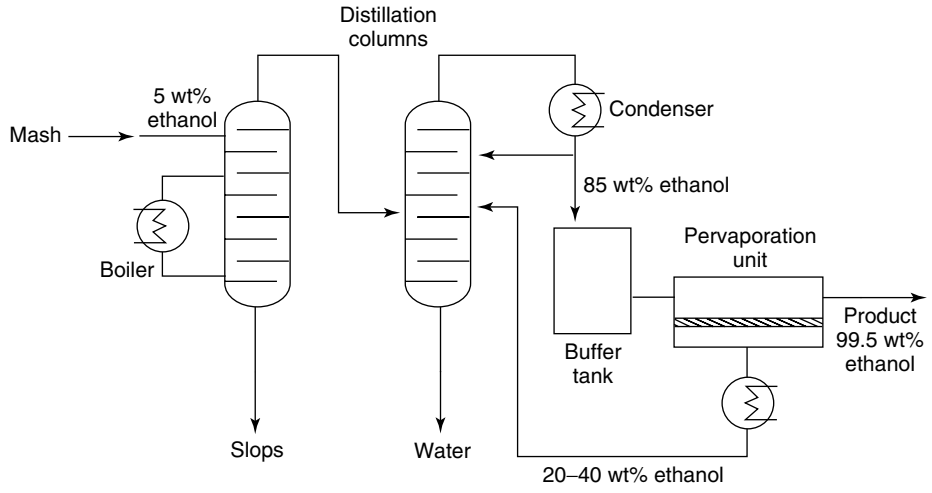

Fig. 45. Integrated distillation/pervaporation plant for ethanol recovery from fermentors. The distillation columns concentrate the ethanol/water mixture from 5 to 80%. The pervaporation membrane produces a 99.5% ethanol product stream and a 40–50% ethanol stream that is sent back to the distillation column.

Pervaporation now has two commercial applications. The first and most developed is the separation of water from concentrated alcohol solutions. The leader in this field, GFT of Neunkirchen, Germany, installed their first major plant in 1982. Currently, more than 100 plants have been installed by GFT for this application (92). The second application is the separation of small amounts of organic solvents from contaminated water (93). In both applications, organics are separated from water. This separation is relatively easy because organic compounds and water exhibit distinct membrane permeation properties as a result of their difference in polarity. The separation is also amenable to membrane pervaporation, because the feed solutions are relatively nonaggressive and do not chemically degrade the membrane.

A flow scheme for an integrated distillation–pervaporation plant operating on a 5 wt% ethanol feed from a fermentation mash is shown in Figure 45. The distillation column produces an ethanol stream containing 85–90 wt% ethanol, which is fed to the pervaporation system. To maximize the vapor pressure difference across the membrane, the pervaporation module usually operates at a temperature of 80°C with a corresponding feed stream vapor pressure of 400–600 kPa (4–6 atm). Despite these harsh conditions, the membrane lifetime is good and qualified guarantees for up to 4 years are given.

Figure 45 shows a single-stage pervaporation unit. In practice, at least three pervaporation stages are used in series, with additional heat being supplied to the ethanol feed between each stage. This compensates for pervaporative cooling of the feed and maintains the feed at 80°C. The heat required is obtained by thermally integrating the pervaporation system with the condenser of the final distillation column. Most of the energy used in the process is, therefore, low grade heat. Generally, about 0.5 kg of steam is required for each kilogram of ethanol

produced. The energy consumption of the pervaporation process is, therefore, about 559 kJ/L (2000 Btu/gal) of product, less than 20% of the energy used in azeotropic distillation, which is typically in the range 3–3.4 MJ/L (11,000–12,000 Btu/gal). Moreover, pervaporation uses very low grade steam, which is available in most industrial plants at very low cost.

Although most of the installed solvent dehydration systems have been for ethanol dehydration, dehydration of other solvents, including isopropanol, glycol, acetone, and methylene chloride, has been considered.

No commercial systems have yet been developed for the separation of the more industrially significant organic–organic mixtures. However, current technology now makes development of pervaporation for these applications possible, and a number of laboratories are actively developing the process. It can only be a matter of time before commercially significant organic–organic separations are attempted using pervaporation. The first pilot-plant results for an organic–organic application, the separation of methanol from methyl *tert*-butyl ether–isobutene mixtures, was reported by Air Products (94). This is a particularly favorable application, and currently available cellulose acetate membranes give good separation. Exxon and Texaco have worked on organic–organic separation by pervaporation, particularly the separation of aromatics from aliphatic hydrocarbons in refinery process streams.

Other Membrane Separation Techniques. The six membrane separation processes described earlier represent the bulk of the industrial membrane separation industry. A seventh process, dialysis, is used on a large scale to remove toxic metabolites from blood in patients suffering from kidney failure (95). The first successful artificial kidney was based on cellophane (regenerated cellulose) membranes and was developed by W.J. Kolf in 1945. Over the past 50 years, many changes have been made. Currently, most artificial kidneys are based on hollow-fiber modules having a membrane area of about 1 m^2. Cellulose fibers are still widely used, but are gradually being displaced by fibers made from polycarbonate, polysulfone, and other polymers, which have higher fluxes or are less damaging to the blood. As shown in Figure 46, blood is circulated through the center of the fiber, while isotonic saline, the dialysate, is pumped countercurrently around the outside of the fibers. Urea, creatinine, and other low molecular weight metabolites in the blood diffuse across the fiber wall and are removed with the saline solution. The process is quite slow, usually requiring several hours to remove the required amount of the metabolite from the patient, and must be repeated one to two times per week. Nonetheless, 100,000 patients use these devices on a regular basis.

In terms of membrane area used and dollar value of the membrane produced, artificial kidneys are the single largest application of membranes. Similar hollow-fiber devices are being explored for other medical uses, including an artificial pancreas, in which islets of Langerhans supply insulin to diabetic patients, or an artificial liver, in which adsorbent materials remove bilirubin and other toxins.

One other membrane separation technique, yet to be used on a commercial scale, is carrier facilitated transport. In this process, the membrane used to perform the separation contains a carrier which preferentially reacts with one of the components to be transported across the membrane. Most of the work on

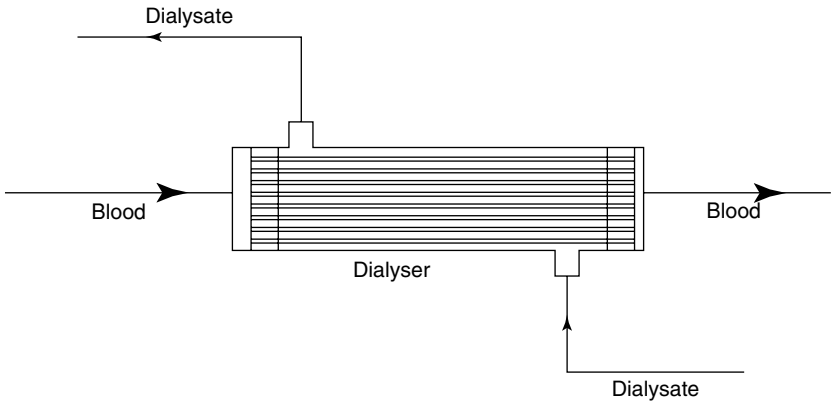

Fig. 46. Schematic of a hollow fiber artificial kidney dialyser used to remove urea and other toxic metabolites from blood. Several million of these devices are used every year.

carrier facilitated transport has employed liquids containing a dissolved complexing agent (59,60). Membranes are formed by holding the liquids by capillary action in the pores of a microporous film. The carrier agent reacts with one permeating component on the feed side of the membrane and then diffuses across the membrane to release the permeant on the product side of the membrane. The carrier agent is then reformed and diffuses back to the feed side of the membrane. Thus, the carrier agent acts as a selective shuttle to transport one component from the feed to the product side of the membrane. Facilitated transport membranes can be used to separate gases; membrane transport is then driven by a difference in the gas partial pressure across the membrane. Metal ions can also be transported selectively across a membrane, driven by a flow of hydrogen or hydroxyl ions in the opposite direction; this process is sometimes called coupled transport. Examples of facilitated transport processes for gas and metal ion transport are shown in Figure 47.

Because the facilitated transport process employs a reactive carrier species, very high membrane selectivities can be achieved. These selectivities are often far larger than those achieved by other membrane processes, a factor that has maintained interest in facilitated transport. However, no significant commercial applications exist or are likely to exist in the next decade. The principal problems are the physical instability of the membrane and the chemical instability of the carrier agent.

Membrane Contactors. In the membrane processes described earlier, the membrane acts as a selective barrier, allowing relatively free passage of one component while retaining another. In membrane contactors the membrane functions as an interface between two phases but does not control the passage of permeants across the membrane (12,13). Delivery or removal of gases from liquids is the largest application of contactors.

One example is the blood oxygenator used during surgery when the patient's lungs cannot function normally. A flow schematic of one of these hollow-fiber devices is shown in Figure 48. More than 1 million procedures per year use blood

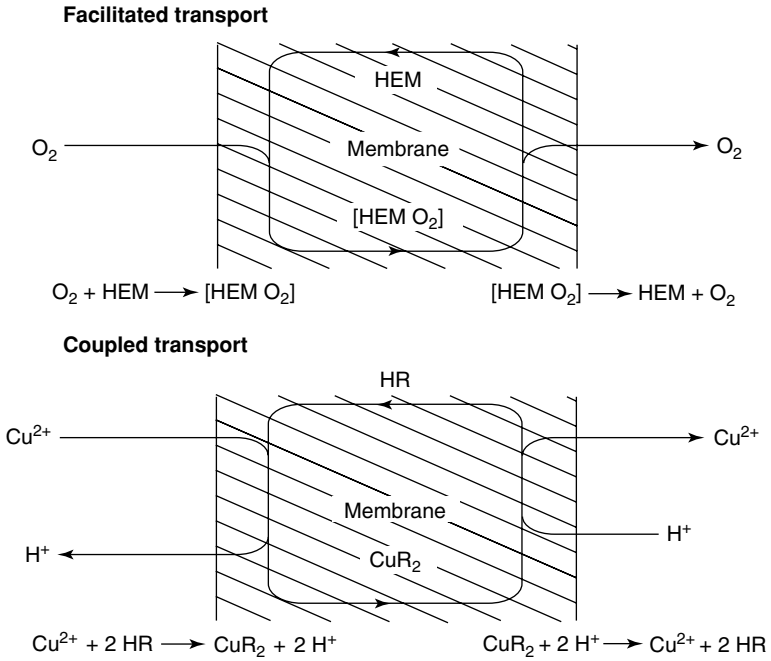

Fig. 47. Schematic examples of facilitated transport of gases and metal ions. The gas-transport example shows the transport of oxygen across a membrane using hemoglobin (HEM) as the carrier agent. The ion-transport example shows the transport of copper ions across the membrane using a liquid ion-exchange reagent as the carrier agent.

oxygenators. Each device costs about $500–600, so the total annual market is about $500 million.

Membrane contactors have also found some industrial applications, most commonly to deoxygenate ultrapure water for the electronics industry (96) or for boiler feed water and to adjust carbonation levels in beverages (97). Microporous hollow-fiber membrane modules are most commonly used. The aqueous phase is circulated on the shell side of the fiber and a gas sweep or vacuum flows down the inside of the fibers.

Controlled Drug Delivery. A significant application of membranes is to moderate the release of biologically active agents, such as insecticides, fertilizers, and most importantly, drugs. Although the concept of controlled drug release using a rate-controlling membrane to moderate drug delivery can be traced to the 1950s, the founding of the Alza Corp. in the late 1960s gave the entire technology a decisive thrust. The products developed by Alza during the subsequent 25 years stimulated the entire pharmaceutical industry (98,99).

Controlled release can be achieved by a wide range of techniques; a simple example, a transdermal patch, is illustrated in Figure 49. In this device, a drug is held in a reservoir surrounded by a membrane. With such a system, the release rate of drug is constant as long as a constant concentration of drug is maintained within the device. Such a constant concentration is maintained if the reservoir contains a saturated solution and sufficient excess of solid drug. Systems that

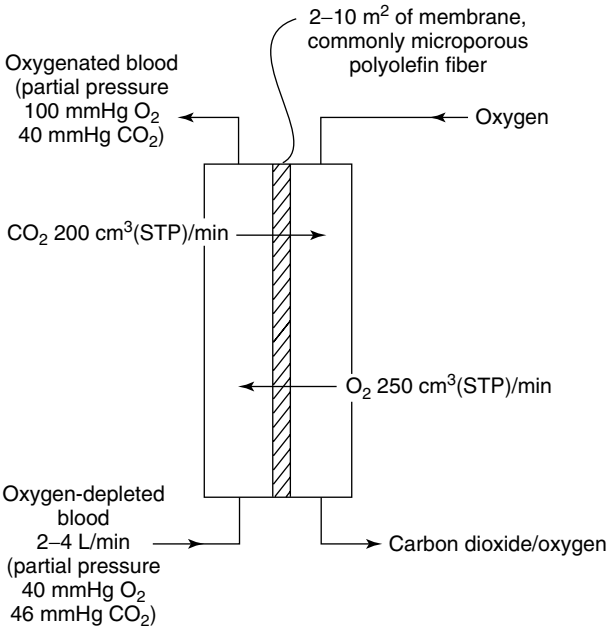

Fig. 48. Flow schematic of a membrane blood oxygenator. The device is designed to deliver about 250 cm^3(STP)/min of oxygen to the blood and remove about 200 cm^3(STP)/min of carbon dioxide from the blood.

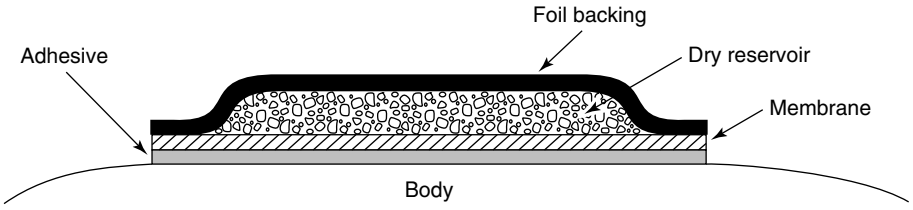

Fig. 49. Schematic of transdermal patch in which the rate of delivery of drug to the body is controlled by a polymer membrane. Such patches are used to deliver many drugs including nitroglycerine, estradiol, nicotine, and scopalamines.

operate by this principle are commonly used in transdermal patches to moderate delivery of drugs such as nitroglycerine (for angina), nicotine (for smoking cessation), and estradiol (for hormone replacement therapy) through the skin. Other devices using osmosis or biodegredation as the rate-controlling mechanism are also produced as implants and tablets.

The Future

Since the 1960s, membrane science has grown from a laboratory curiosity to a widely practiced technology in industry and medicine. This growth is expected

to continue for some time, particularly in the membrane gas separation and pervaporation separation areas. It is also clear that membranes will pay a critical role in the next generation of biomedical devices, such as the artificial pancreas and liver. The total membrane market has grown from $10 million to $2 billion in the 40 years prior to 2000. Spectacular growth of this magnitude is unlikely to continue, but a doubling in the size of the total industry to $5 billion during the decade following is likely.

BIBLIOGRAPHY

"Membranes" in *EPST* 1st ed., Vol. 8 pp. 620–638, by H. C. Friedlander, Union Carbide Research Institute; "Membranes" in *EPSE* 2nd ed., Vol. 9, pp. 509–579, by I. Cabasso, State University of New York-ESF at Syracuse.

1. H. Bechhold, *Z. Phys. Chem.* **60**, 257 (1907).
2. W. J. Elford, *Trans. Far. Soc.* **33**, 1094 (1937).
3. R. Zsigmondy and W. Bachmann, *Z. Anorg. Chem.* **103**, 119 (1918).
4. J. D. Ferry, *Chem. Rev.* **18**, 373 (1936).
5. S. Loeb and S. Sourirajan, *Saline Water Conversion-II*, American Chemical Society, Washington, D.C., 1963. Advances in Chemistry Series Number **28**.
6. J. M. S. Henis and M. K. Tripodi, *Sep. Sci. Techol.* **15**, 1059 (1980).
7. R. L. Fleischer, P. B. Price, and R. M. Walker, *Sci. Am.* **220**, 30 (June 30, 1969).
8. H. S. Bierenbaum and co-workers, *Ind. Eng. Chem. Prod. Res. Dev.* **13**(1), 2 (1974).
9. U.S. Pat. 4585604 (Apr. 29, 1986), K. Okuyama and H. Mizutani (to Mitsubishi Petrochemical Co.).
10. U.S. Pat. 4187390 (Feb. 28, 1980), R. W. Gore (to W. L. Gore and Associates, Inc.).
11. K. K. Sirkar, in W. S. W. Ho and K. K. Sirkar, eds., *Membrane Handbook*, Chapman and Hall, New York, 1992, pp. 885–912.
12. M. C. Yang and E. L. Cussler, *AIChE J.* **32**, 1910 (1986).
13. U.S. Pat. 4708799 (Nov. 24, 1987), K. Gerlach, E. Kessler, and W. Henne.
14. U.S. Pat. 4708800 (Nov. 24, 1987), T. Ichikawa and co-workers (to Terumo Kahushiki Kaisha).
15. U.S. Pat. 4778499 (Oct. 18, 1988), R. P. Beaver (to PPG Industries, Inc.).
16. H. Strathmann and co-workers, *Desalination* **16**, 179 (1975).
17. H. Strathmann and K. Kock, *Desalination* **21**, 241 (1977).
18. J. G. Wijmans and C. A. Smolders, in P. M. Bungay, H. K. Lonsdale, and M. N. de Pinho, eds., *Synthetic Membranes: Science, Engineering and Applications*, Reidel, Dordrecht, The Netherlands, 1986.
19. I. Pinnau and W. J. Koros, *J. Polym. Sci., Polym. Phys. Ed.* **31**, 419 (1993).
20. W. C. Hiatt, G. H. Vitzthum, K. B. Wagener, K. Gerlach, and C. Josefiak, in D. R. Lloyd, ed., *Materials Science of Synthetic Membranes*, American Chemical Society, Washington, D.C., 1985, pp. 229–244. ACS Symposium Series, Vol. **269**.
21. D. R. Lloyd, S. S. Kim, and K. E. Kinzer, *J. Membr. Sci.* **64**, 1 (1991).
22. U.S. Pat. 4247498 (Jan. 27, 1981), A. J. Castro (to Akzona, Inc.).
23. L. Zeman and T. Fraser, *J. Membr. Sci.* **87**, 267 (1994).
24. R. L. Riley, H. K. Lonsdale, L. D. LaGrange, and C. R. Lyons, Office of Saline Water Report No. 386, PB# 207036, Jan. 1969.

25. L. J. Zeman and A. L. Zydney, *Microfiltration and Ultrafiltration: Principles and Applications*, Marcel Dekker, Inc., New York, 1995.
26. U.S. Pat. 3615024 (Oct. 26, 1971), A. S. Michaels (to Amicon Corp.).
27. U.S. Pat. 3980456 (Sept. 14, 1976), W. R. Browall (to General Electric Co.).
28. L. T. Rozelle, J. E. Cadotte, K. E. Cobian, and C. V. Kopp Jr., in S. Sourirajan, ed., *Reverse Osmosis and Synthetic Membranes*, National Research Council of Canada, Canada, 1977, pp. 249–262. *Pub. NRCC* **15627**.
29. J. E. Cadotte, in *Ref. 20*, pp. 273–294.
30. R. L. Riley and co-workers, *Desalination* **19**, 113 (1976).
31. Y. Kamiyama and co-workers, *Desalination* **51**, 79 (1984).
32. R. J. Petersen, *J. Membr. Sci.* **83**, 81 (1993).
33. U.S. Pat. 4234701 (Jan. 1984), R. L. Riley and R. L. Grabowsky (to UOP, Inc.).
34. U.S. Pat. 4871378 (Oct. 3, 1989), I. Pinnau (to Membrane Technology and Research, Inc.).
35. U.S. Pat. 4553983 (Nov. 19, 1985), R. W. Baker (to Membrane Technology and Research, Inc.).
36. H. Yasuda, *J. Membr. Sci.* **18**, 273 (1984).
37. H. Yasuda, in Ref. 28, pp. 263–294.
38. A. R. Stancell and A. T. Spencer, *J. Appl. Polym. Sci.* **16**, 1505 (1972).
39. M. Kawakami and co-workers, *J. Membr. Sci.* **19**, 249 (1984).
40. U.S. Pats. 4657564 (Apr. 14, 1987), M. Langsam; 4759776 (July 26, 1988), M. Langsam and A. C. Savoca (both to Air Products and Chemicals, Inc.).
41. M. Langsam, M. Anand, and E. J. Karwacki, *Gas Sep. Purif.* **2**, 162–170 (1988).
42. J. M. Mohr and co-workers, *J. Membr. Sci.* **56**, 77–98 (1991).
43. K. A. Kraus, A. J. Shor, and J. S. Johnson, *Desalination* **2**, 243 (1967).
44. J. S. Johnson and co-workers, *Desalination* **5**, 359 (1968).
45. M. B. Rao and S. Sircar, *J. Membr. Sci.* **85**, 253 (1994).
46. K. Keizer and co-workers, *J. Membr. Sci.* **39**, 285 (1988).
47. J. E. Koresh and A. Soffer, *Sep. Sci. Technol.* **18**, 723 (1983).
48. U.S. Pat. 5288304 (Feb. 22, 1994), W. J. Koros and C. W. Jones (to The University of Texas System).
49. U.S. Pats. 4717455 (Jan. 5, 1988); 4722771 (Feb. 2, 1988), M. Textor, M. Werner, and W. Franschitz (to Swiss Aluminum, Ltd.).
50. R. C. Furneaux and co-workers, *Nature* **337**(6203), 147–149 (1989).
51. R. B. McBride and D. L. McKinley, *Chem. Eng. Prog.* **61**, 81 (1965).
52. R. E. Buxbaum and A. B. Kinney, *Ind. Eng. Chem. Res.* **35**, 530 (1996).
53. D. J. Edlund and J. McCarthy, *J. Membr. Sci.* **107**, 147 (1995).
54. J. B. Hunter, *Platinum Met. Rev.* **4**, 130 (1960).
55. A. L. Athayde, R. W. Baker, and P. Nguyen, *J. Membr. Sci.* **94**, 299 (1994).
56. H. P. Hsieh, in K. K. Sirkar and D. R. Lloyd, eds., *New Membrane Materials and Processes for Separation*, 1988, p. 1. AIChE Symposium Series, Vol. **84**.
57. T. J. Burggraaf and K. Keizer, in R. R. Bhave, ed., *Inorganic Membranes Synthesis, Characteristics, and Applications*, Chapman and Hall, New York, 1991.
58. A. Larbot and co-workers, *J. Membr. Sci.* **39**, 203 (1988).
59. R. W. Baker and I. Blume, in M. C. Porter, ed., *Handbook of Industrial Membrane Technology*, Noyes Publication, Park Ridge, N.J., 1990, pp. 511–588.
60. E. L. Cussler, in Ref. 87, pp. 273–300.
61. U.S. Pats. 3228876 (1966) and 3228877 (1966), H. I. Mahon (to The Dow Chemical Company).
62. I. Moch Jr., *Kirk Othmer Encyclopedia of Chemical Technology*, 4th ed., Vol. **13**, John Wiley & Sons, Inc., New York, 1995.

63. B. Baum, W. Holley Jr., and R. A. White, in P. Meares, ed., *Membrane Separation Processes*, Elsevier, Amsterdam, The Netherlands, 1976, pp. 187–228.
64. O. M. Ekiner and G. Vassilatos, *J. Membr. Sci.* **53**, 259 (1990).
65. U.S. Pat. 3367504 (Feb. 6, 1968), J. C. Westmoreland (to Gulf General Atomic, Inc.).
66. U.S. Pat. 3417870 (Dec. 24, 1968), D. T. Bray (to Gulf General Atomic, Inc.).
67. S. S. Kremen, in Ref. 28, pp. 371–386.
68. W. J. Koros and G. K. Fleming, *J. Membr. Sci.* **83**, 1 (1993).
69. R. Günther and co-workers, *J. Membr. Sci.* **121**, 95 (1996).
70. R. H. Davis, in W. S. W. Ho and K. K. Sirkar, eds., *Membrane Handbook*, Chapman and Hall, New York, 1992, pp. 480–505.
71. M. Cheryan, *Ultrafiltration and Microfiltration Handbook*, Technomic Publishing Co., Inc., Lancaster, Pa., 1998.
72. J. G. Wijmans and co-workers, *J. Membr. Sci.* **109**, 135 (1996).
73. R. W. Baker and H. Strathmann, *J. Appl. Polym. Sci.* **14**, 1197 (1970).
74. G. Belfort, R. H. Davis, and A. L. Zydney, *J. Membr. Sci.* **1**, 96 (1994).
75. R. L. Riley, in R. W. Baker and co-workers, eds., *Membrane Separation Systems—Recent Developments and Future Directions*, Noyes Data Corp., Park Ridge, N.J., 1991, pp. 276–328.
76. B. S. Parekh, ed., *Reverse Osmosis Technology*, Marcel Dekker, Inc., New York, 1988.
77. U. Merten, in U. Merten, ed., *Desalination by Reverse Osmosis*, MIT Press, Cambridge, Mass., 1966, pp. 15–54.
78. J. G. Wijmans and R. W. Baker, *J. Membr. Sci.* **107**, 1 (1995).
79. H. Strathmann, *Sep. Purif.* **14**, 41 (1985).
80. M. S. Mintz, *Ind. Eng. Chem.* **55**, 18 (1963).
81. E. Korngold, in G. Belfort, ed., *Synthetic Membrane Processes*, Academic Press, Inc., New York, 1984, pp. 192–220.
82. S. A. Stern, *J. Membr. Sci.* **94**, 1 (1994).
83. A. R. Berens and H. B. Hopfenberg, *J. Membr. Sci.* **10**, 283 (1982).
84. G. J. Van Amerongen, *J. Appl. Phys.* **17**, 972 (1946).
85. R. D. Behling, K. Ohlrogge, K.-V. Peinemann, and E. Kyburz, in A. E. Fouda, J. D. Hazlett, T. Matsuura, and J. Johnson, eds., *Membrane Separations in Chemical Engineering*, Vol. **85**, American Chemical Society, Washington, D.C., 1989, p. 68. AIChE Symposium Series No. **272**.
86. L. M. Robeson, *J. Membr. Sci.* **62**, 165 (1991).
87. D. R. Paul and Y. P. Yampol'skii, eds., *Polymeric Gas Separation Membranes*, CRC Press, Boca Raton, Fla., 1994.
88. R. Spilmann, *Chem. Eng. Prog.* **85**, 41 (1989).
89. J. G. Wijmans and R. W. Baker, *J. Membr. Sci.* **79**, 101 (1993).
90. A. H. Ballweg, H. E. A. Brüschke, W. H. Schneider, and G. F. Tusel, in *Proceedings of the Fifth International Alcohol Fuels Symposium*, Auckland, New Zealand, May 13–18, 1992, John McIndoe, Dunedin, New Zealand, 1982.
91. M. E. Hollein, M. Hammond, and C. S. Slater, *Sep. Sci. Technol.* **28**, 1043 (1993).
92. H. E. A. Brüschke, in R. Bakish, ed., *Proceedings of the Third International Conference on Pervaporation*, Nancy, France, Bakish Materials Corp., Englewood, N.J., 1988.
93. I. Blume, J. G. Wijmans, and R. W. Baker, *J. Membr. Sci.* **49**, 253 (1990).
94. M. S. K. Chen, G. S. Markiewicz, and K. G. Venugopal, *AIChE Symp. Ser.* **85**(272), 82–88 (1989).
95. T. Daugirdas and T. S. Ing., eds., *Handbook of Dialysis*, Little Brown and Co., Boston, 1988.

96. F. Wiesler and R. Sodaro, *Ultrapure Water* **35**, 53 (Sep. 1996).
97. U.S. Pats. 5565149 (Oct. 1996), J. K. R. Page and D. G. Kalhod (to Permea, Inc.); 5522917 (June 1996), K. Honda and M. Yamashita (to Miura, Inc.).
98. R. W. Baker, *Controlled Release of Biologically Active Agents*, John Wiley & Sons, Inc., New York, 1987.
99. L. F. Prescott and W. S. Nimmo, eds., *Novel Drug Delivery and Its Application*, John Wiley & Sons, Inc., Chichester, England, 1989.

RECENT MONOGRAPHS ON MEMBRANE TECHNOLOGY

GENERAL TEXTS

E. L. Cussler, *Diffusion*, Cambridge, London, 1984.
G. Belfort, ed., *Synthetic Membrane Processes*, Academic Press, Orlando, Fla., 1984.
R. E. Kesting, *Synthetic Polymeric Membranes*, 2nd ed., John Wiley & Sons, Inc., New York, 1985.
P. M. Bungay, H. K. Lonsdale, and M. N. de Pinho, eds., *Synthetic Membranes: Science and Engineering Applications*, Reidel, Dordrecht, The Netherlands, 1986.
M. C. Porter, ed., *Handbook of Industrial Membrane Technology*, Noyes Data Corp., Park Ridge, N.J., 1988.
R. Rautenbach and R. Albrecht, *Membrane Processes*, John Wiley & Sons, Inc., Chichester, England, 1989.
R. W. Baker and co-workers, *Membrane Separation Systems*, Noyes Data Corp., Park Ridge, N.J., 1991.
M. Mulder, *Basic Principles of Membrane Technology*, Kluwer Academic Publishers, Dordrecht, The Netherlands, 1991.
W. S. W. Ho and K. K. Sirkar, eds., *Membrane Handbook*, Chapman and Hall, New York, 1992.
R. W. Baker, *Membrane Technology and Applications*, McGraw-Hill, New York, 2000.

SPECIALIZED MONOGRAPHS

K. S. Spiegler and A. D. K. Laird, eds., *Principles of Desalination*, Academic Press, Inc., New York, 1980.
T. D. Brock, *Membrane Filtration*, Sci. Tech. Inc. Publishing, Madison, Wis., 1983.
M. Cheryan, *Ultrafiltration and Microfiltration Handbook*, Technomic Publishing Co. Inc., Lancaster, Pa., 1998.
R. W. Baker, *Controlled Release of Biologically Active Agents*, John Wiley & Sons, Inc., New York, 1987.
B. S. Parekh, ed., *Reverse Osmosis Technology*, Marcel Dekker, Inc., New York, 1988.
R. Bhave, ed., *Inorganic Membrane Synthesis Characteristics and Applications*, Van Nostrand Reinhold Co., Inc., New York, 1991.
R. Bakish, ed., *Proceedings of the International Conference of Pervaporation Processes*, Heidelberg, Germany, 1991, and Ottawa, Canada, 1992.
D. R. Paul and Y. P. Yampol'skii, eds., *Polymeric Gas Separation Membranes*, CRC Press, Inc., Boca Raton, Fla., 1994.

F. H. Weller, ed., *Electrodialysis (ED) and Electrodialysis Reversal (EDR) Technology*, Ionics, Inc., Watertown, Mass.

RICHARD W. BAKER
Membrane Technology & Research, Inc.

METALLOCENE CATALYSTS.

See SINGLE-SITE CATALYSTS.

METHACRYLIC ESTER POLYMERS

Introduction

Historically speaking, methacrylic ester polymers and acrylic ester polymers developed concomitantly. In 1933, acrylates were copolymerized with ethyl methacrylate; this work led to the commercialization of ethyl methacrylate monomer. The homopolymerization of methyl methacrylate [80-62-6] to form poly(methyl methacrylate) [9011-14-7] (PMMA) found a special market in safety glass which consisted of two glass plates separated by a thin layer of poly(methyl methacrylate). Cast sheets of PMMA were brought to market in the 1930s by the Rohm and Haas Co. and E. I. du Pont de Nemours & Co., Inc., in the United States as well as by Rohm and Haas AG and Imperial Chemicals Industries, Ltd., in Europe. These cast sheets were used as structural materials; the shatter resistance, light weight, high transparency, and moldability recommended the use of PMMA for windows and military aircraft canopies. Methacrylates entered the injection and compression molding arenas in 1938. Finally, during the 1930s, methyl methacrylate found a great deal of use as a comonomer in the production of acrylic polymers by emulsion and solution polymerization (1,2). These copolymers have primarily been employed as high quality paints and coatings.

Properties

Methacrylic ester monomers are a versatile group of monomers whose chemical properties are primarily determined by the nature of the R side-chain group in the structure

$$CH_2{=}C(CH_3)OOR$$

Encyclopedia of Polymer Science and Technology. Copyright John Wiley & Sons, Inc. All rights reserved.

Polymer physical and chemical properties also depend upon the R group, the molecular weight, and the tacticity of the polymer.

Methacrylic monomers differ from acrylics (see ACRYLIC ESTER POLYMERS) in that they have a methyl group in the α position of the vinyl group; this methyl group lends stability, hardness, and stiffness to the polymers formed from methacrylic ester monomers. Methacrylics will readily polymerize with other methacrylic and acrylic monomers. This ability to form copolymers among these two already diverse groups allows the industrial chemist to create polymers with an incredible breadth of properties ranging from tacky adhesives to hard powders and rigid sheets. Although more costly than many other commonly employed industrial monomers, methacrylics have found a great deal of industrial usage because of their unique balance of performance properties as well as their ease of use. Methacrylic ester monomers can be copolymerized readily with either methacrylic or acrylic ester monomers to form an even greater variety of acrylic copolymers. These polymers find applications that range from extremely tacky adhesives to hard powders and sheets.

Glass-Transition Temperature (T_g). Although often cited as a single value, the glass transition often takes place over a broad range of temperatures. The glass transition is manifested in a polymeric material as an embrittlement when moving across the range from high to low temperatures. Other properties, such as chemical reactivity, mechanical and dielectric relaxation, viscous flow, load-bearing capacity, hardness, tack, heat capacity, refractive index, thermal expansivity, creep and diffusion, register large changes after traversing the glass-transition range.

Methacrylic ester polymers display the same change from hard, brittle, glass-like materials below the T_g value to relatively soft, flexible, rubbery materials above the T_g. Movement to even higher temperatures can result in a change to a flowable, tacky material. Table 1 contains basic physical data (density, solubility parameters, and refractive index values) for the most common methacrylic ester polymers.

The glass transition can be measured by a variety of techniques. The most commonly accepted methods currently are differential scanning calorimetry (dsc) (3,13) and dynamic mechanical analysis (dma) (5,6). Other methods employed in the past have included the approximation methods of Vicat softening temperature and brittle point measurement. More accurate numbers were also determined by methods which rely on the changes manifested in the physical properties of the polymer, such as dilatometry (volume) and refractive index measurements. The T_g values for a large variety of polymers are found in References 6, 7, 14, and 15.

The tacticity of the polymer backbone can significantly influence the glass-transition temperature of a given type of polymer. In general, T_g values decrease in the order syndiotactic > atactic > isotactic (16). Free-radical polymerization (which constitutes the vast majority of industrial acrylic polymer production) generates mainly atactic polymers because of the symmetric nature of the radical species. Table 2 contains the T_g values for a variety of methacrylic ester polymers with different tacticity types.

A wide range of glass-transition temperatures can be accessed by copolymerizing methacrylic and acrylic ester monomers (Fig. 1). Values for the

Table 1. Physical Properties of Methacrylic Ester Polymers

Polymer	CAS registry number	T_g, °C[a]	Density[b] at 20°C, g/cm^3	Solubility parameter,[b,c] (J/cm^3)$^{1/2}$	Refractive index n_D^{20}[d]
Poly(methyl methacrylate)	[9011-14-7]	105	1.190	18.6	1.490
Poly(ethyl methacrylate)	[9003-42-3]	65	1.119	18.3	1.485
Poly(*n*-propyl methacrylate)	[25609-74-9]	35	1.085	18.0	1.484
Poly(isopropyl methacrylate)	[26655-94-7]	81	1.033		1.552
Poly(*n*-butyl methacrylate)	[9003-63-8]	20	1.055	17.8	1.483
Poly(*sec*-butyl methacrylate)	[29356-88-5]	60	1.052		1.480
Poly(isobutyl methacrylate)	[9011-15-8]	53	1.045	16.8	1.477
Poly(text-butyl methacrylate)	[25213-39-2]	107	1.022	17.0	1.4638
Poly(*n*-hexyl methacrylate)	[25087-17-6]	−5	1.007^{25}	17.6	1.4813
Poly(2-ethylbutyl methacrylate)	[25087-19-8]	11	1.040		
Poly(n-octyl methacrylate)	[25087-18-7]	−20	0.971^{25}	17.2	
Poly(2-ethylhexyl methacrylate)	[25719-51-1]	−10			
Poly(*n*-decyl methacrylate)	[29320-53-4]	−60			
Poly(lauryl methacrylate)	[25719-52-2]	−65	0.929	16.8	1.474
Poly(tetradecyl methacrylate)	[30525-99-6]	−72			1.47463
Poly(hexadecyl methacrylate)	[25986-80-5]				1.47503
Poly(octadecyl methacrylate)	[25639-21-8]	−100		16.0	
Poly(stearyl methacrylate)	[9086-85-5]			16.0	
Poly(cyclohexyl methacrylate)	[25768-50-7]	104	1.100		1.50645
Poly(isobornyl methacrylate)	[28854-39-9]	170(110)	1.06	16.6	1.5000
Poly(phenyl methacrylate)	[25189-01-9]	110	1.21		1.571
Poly(benzyl methacrylate)	[25085-83-1]	54	1.179	20.3	1.5680
Poly(ethylthioethyl methacrylate)	[27273-87-0]	−20			1.5300
Poly(3,3,5-trimethylcyclohexyl methacrylate)	[75673-26-6]	79			1.485

[a] Refs. 3–11.
[b] Refs. 4, 11, and 12.
[c] To convert (J/cm^3)$^{1/2}$ to (cal/cm^3)$^{1/2}$, divide by 2.05.
[d] Refs. 4, 9, 11, and 12.

Table 2. Glass-Transition Temperatures (°C) of Atactic, Syndiotactic, and Isotactic Methacrylic Ester Polymers[a]

Methacrylate	Atactic	Syndiotactic	Isotactic
Methyl	105	105	38
Ethyl	65	66	12
n-Propyl	35		
Isopropyl	84	85	27
n-Butyl	20		−24
Isobutyl	53		8
sec-Butyl	60		
text-Butyl	118	114	7
Cyclohexyl	104		110

[a]Refs. 12 and 14.

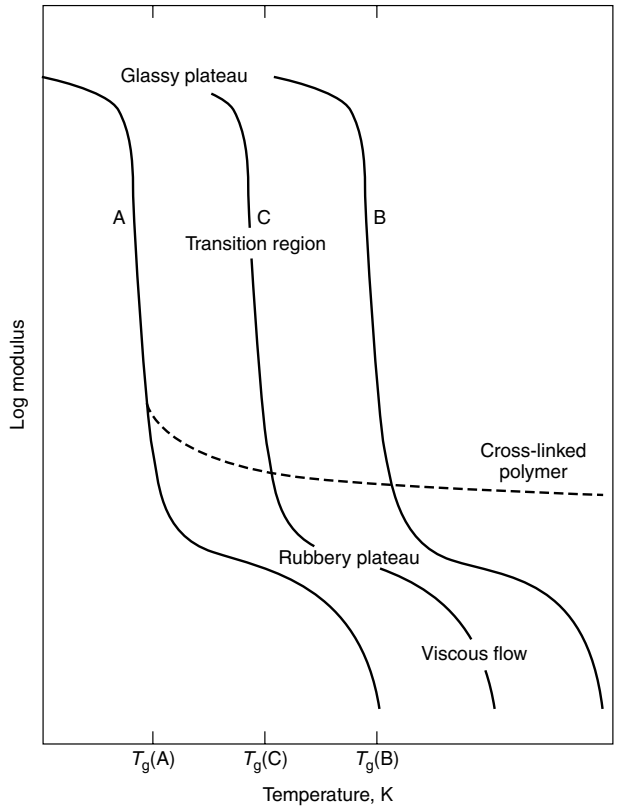

Fig. 1. Modulus–temperature curve of amorphous and cross-linked methacrylic polymers: A, a softer polymer; B, a harder polymer; and C, a 1:1 copolymer of A and B.

glass-transition temperature can be calculated from the overall composition of the polymer as well as the individual T_g values for the homopolymers of the constituent monomers (17). Soft (low T_g) components can be used as internal plasticizers or softeners which are permanently bound to the polymer backbone.

Modulus–temperature curves of the type shown in Figure 1 are useful for analyzing the degree of rigidity within a polymer. Not only can one observe the differences in hardness of a polymer, but cross-linking can also be measured through the proper use of the modulus–temperature curves (18). Cross-linking is generally used to increase the physical toughness and decrease the solubility of a polymer.

Molecular Weight. The properties of methacrylic ester polymers (and most other types of polymers for that matter) improve as molecular weight increases. Beyond a certain level (100,000–200,000 for methacrylic ester polymers) this improvement in polymer properties reaches a plateau. One example of a property that follows this trend is the glass-transition temperature which can be described by the equation

$$T_g = T_{gi} - k/M_n$$

where T_{gi} is the glass-transition temperature for a polymer of infinite molecular weight and M_n is the number-average molecular weight. Typical values of k fall in the range of 2×10^5 (10) for methacrylic polymers. Reference 19 summarizes the effect of molecular weight on polymer properties.

Mechanical Properties Related to Polymer Structure. Although the contributions of the side chains influence polymer properties in similar fashion for both methacrylic and acrylic compositions, methacrylates exhibit higher T_g values than their acrylic counterparts (same side chain) because the α hydrogen on the polymer backbone restricts the rotational motion of the backbone. This stiffening of the backbone is manifested as higher tensile strength and lower elongation for the methacrylic analogues to the acrylic polymers given the same side chain (see Table 3).

The smallest side-chain monomer in the alkyl methacrylate series, methyl methacrylate, polymerizes to form a hard material ($T_g = 105°C$) which can be cut into shapes. If the material is heated above its glass-transition temperature, the PMMA can be bent or molded to fit any form desired. Upon cooling, the material retains the molded shape upon cooling; in this manner, fighter plane canopies, among other objects, were made out of PMMA during World War II. This highly useful "flexible plastic glass" was sold by the Rohm and Haas Co. under the trade name Plexiglas for several decades.

As the side-chain length is increased for the methacrylate monomers, the T_g decreases rapidly for the series of C1–C12. *n*-Butyl methacrylate [97-88-1]

Table 3. Comparison of Mechanical Properties of Polyacrylate and Methyl Methacrylate[a]

	Tensile strength, MPa[b]		Elongation at break, %	
Ester	Polymethacrylate	Polyacrylate	Polymethacrylate	Polyacrylate
Methyl	62	6.9	4	750
Ethyl	34	0.2	7	1800
Butyl	6.9	0.02	230	2000

[a] Refs. 20 and 21.
[b] To convert MPa to psi, multiply by 145.

homopolymer, for example, has a T_g value of 20°C and is far softer than PMMA; lauryl methacrylate [142-90-5] continues the progression to softer, more rubbery materials ($T_g = -65$°C). After a certain length of chain is passed, the van der Waals attractive forces among the chains reach a level high enough that crystallization of the side chains takes place and the T_g moves to higher values. Octadecyl methacrylate [32360-05-7] polymerizes to form a hard polymer with a T_g of 36°C.

Another factor in the determination of how rigid a polymer backbone will be is the steric bulk of the side chain. Branching within the side chain will restrict the freedom of movement for the backbone in similar fashion as the α hydrogen of the methacrylate monomers. As cited above, *n*-butyl methacrylate homopolymer has a T_g value of 20°C; poly(*tert*-butyl methacrylate), on the other hand, has a T_g of 107°C. The effect is proportional to the overall size of the side chain as well; the longer and more branched the chain, the more movement will be restricted and T_g will be elevated.

Optical Properties. Poly(methyl methacrylate) is essentially transparent in the 400- to 700-nm visible light range (22); this clarity along with the ease of machining described above contributes to this material's popularity as a substitute for glass. The polymer gradually becomes less transparent as the wavelength range is increased until the material is opaque beyond 2800 nm. Additives are commonly incorporated in PMMA cast sheets to block the transmission of uv rays in the wavelength range 290–350 nm. Poly(methyl methacrylate) allows radio and television broadcast waves to transfer through the material while blocking α and β radiations (23).

Poly(methyl methacrylate) is capable of serving as a waveguide for visible light. When light is shone through the edge of PMMA, the light emerges through the opposite edge of the material, with virtually no loss of intensity; the primary reason for this property is that when visible light reaches the air/polymer interface at an angle of 42.2° or greater, it reflects back into the polymer intact. This useful optical property in combination with the mechanical properties described above has resulted in the PMMA's use in fiberoptics, automotive tailights, camera lenses, remote lighting, reducers, magnifiers, and prisms (24).

Electrical Properties. Poly(methyl methacrylate) has an extremely high surface resistivity which, combined with the weather resistance of the material, leads to the use of PMMA in high voltage applications. Some of these basic electrical properties (23) are listed in Table 4.

Chemical Properties. The chemical-resistance properties of methacrylic ester polymers are even higher than those of the acrylic esters. Methacrylic esters undergo a lower degree of hydrolysis in either acidic or alkaline media than acrylics. Both acrylics and methacrylics easily outperform vinyl acetate-containing polymers which are well known to be susceptible to hydrolysis of the side-chain ester. There are marked differences in the chemical-resistance properties of different forms of PMMA. The syndiotactic (alternating) form of PMMA is the most chemically inert. The rate of hydrolysis for syndiotactic PMMA is lower than that for isotactic (26); radical polymerizations generate large portions of syndiotactic PMMA and benefit in terms of stability.

In terms of solubility resistance (25), PMMA is generally not harmed by inorganic solutions, mineral oils, animal oils, low concentrations of alcohols, paraffins,

Table 4. Electrical Properties of 6.35-mm-thick Poly(methyl methacrylate) Sheet[a]

Property	Typical values	ASTM method
Dielectric strength	>16.9–20.9	D149
Short-term test, V/μm[b]		
Dielectric constant, V/mm[c]		D150
At 60 Hz	142–154	
At 1000 Hz	130–134	
Power factor, V/cm[d]		D150
At 60 Hz	20–24	
At 1000 Hz	16–20	
At 1,000,000 Hz	8–12	
Loss factor, V/cm[d]		D150
At 60 Hz	75–87	
At 1000 Hz	51–59	
At 1,000,000 Hz	24–31	
Arc resistance	No tracking	D495
Volume resistivity, Ω·cm	$1 \times 10^{14} - 6 \times 10^{17}$	D257
Surface resistivity, Ω/sq	$1 \times 10^{17} - 2 \times 10^{18}$	D257

[a]Ref. 25.
[b]To convert V/μm to V/mil, multiply by 25.4.
[c]To convert V/mm to V/mil, divide by 39.4.
[d]To convert V/cm to V/mil, divide by 394.

olefins, amines, alkyl monohalides, and aliphatic hydrocarbons and higher esters (>10 carbon atoms). Chemical species which will degrade PMMA include lower esters (ethyl acetate, isopropyl acetate), aromatic hydrocarbons (benzene, toluene, xylene, phenols), cresol, carbolic acid, aryl halides (chlorobenzene, bromobenzene), aliphatic acids (butyric acid, acetic acid), alkyl polyhalides (ethylene dichloride, methylene chloride), high concentrations of alcohols (methanol, ethanol, 2-propanol), and high concentrations of alkalies and oxidizing agents. In Table 5, the chemical- and photochemical-resistance properties of PMMA are compared to those of two other transparent plastic materials: polycarbonate and cellulos acetate butyrate (27). In terms of thermal stability, methacrylates will depolymerize (28) at a greater than 95% level when exposed to temperatures above 300°C.

Table 5. Relative Outdoor Stability of Poly(methyl methacrylate)[a]

	Light transmittance		Haze	
Material	Initial, %	After exposure,[b] %	Initial, %	After exposure,[b] %
Poly(methyl methacrylate	92	92	1	2
Polycarbonate	85	82	3	19
Cellulose acetate butyrate	89	68	3	70

[a]Ref. 27
[b]Three-year outdoor.

Methacrylate Monomers

Properties. Table 1 of methacrylic acid and derivatives (qv) lists many of the basic properties of methacrylic acid monomers. Tables 6 and 7 contain many of the additional physical and thermodynamic properties for commercially important monomers (29–32).

Manufacture of Monomers. The commercial processes for manufacturing these monomers are contained in Methacrylic acid and derivatives (33).

Handling, Health and Safety Factors. Mild steel is the material of choice for transporting and storing methacrylic ester monomers which are shipped by way of rail cars or tanker trucks. Stainless steel (Types 304 and 316) are used for transport and storage of acidic monomers.

Methacrylic monomers are relatively nontoxic, based upon oral, dermal, and inhalation exposure test data for rats and rabbits (30,34,35). However, these monomers can be skin sensitizers and are mildly to severely irritating after eye or skin contact. Liver and kidney damage can result from repeated near-lethal exposures. Overall toxicity is generally inversely proportional to the length of the side-chain ester group (see ACRYLIC AND METHACRYLIC ACID POLYMERS).

Radical Polymerization

The majority of commercial methacrylic ester polymers are produced by free-radical initiators. Peroxides and azo compounds function as typical initiators for this type of polymerization. Other possible routes for producing methacrylic polymers with radicals include photoinitiation and radiation-induced polymerization. Both γ ray and electron-beam radiation have been employed in the production of methacrylic ester polymers (36–38). At constant temperature, there is a first-order dependence of the polymerization rate on monomer concentration and a one-half-order dependence on initiator concentration. Rate data for the polymerization of various methacrylic monomers using the azo compound 2,2′-azobisisobutyronitrile [78-67-1] (AIBN) are shown in Table 8.

The polymerization of methacrylic monomers is highly exothermic and involves an increase in the density of the forming polymeric material. Both effects must be accounted for in industrial processes. The degree of shrinkage upon conversion from monomer to polymer decreases as the side-chain length increases, but on a molar basis, the shrinkage level is relatively constant (40).

The propagation mechanism for the free-radical polymerization of methacrylic monomers involves the head-to-tail chain addition of monomer units to grow the polymer chain. Chain termination can occur by either radical combination or disproportionation (41).

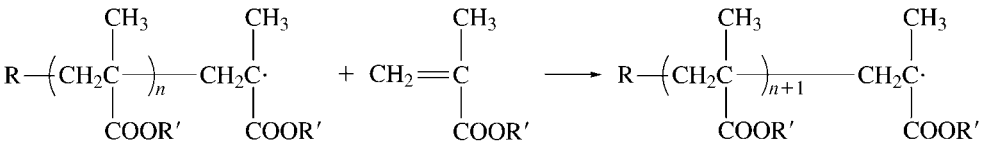

Table 6. Physical Properties of Commercially Available Methacrylate Monomers $CH_2{=}C(CH_3)COOR$[a]

Compound	Mol wt	Mp, °C	Bp, °C	Refractive index n_D^{25}	Density d_5^{25}, g/cm^3	Flash point, °C[b]		Typical inhibitor, ppm[c]
						COC	TOC	
Methacrylic acid	86.09	14	159–163[d]	1.4288	1.015	77		100 MEHQ
Methyl methacrylate	100.11	−48	100–101[d]	1.4120	0.939		13	10 MEHQ
Ethyl methacrylate	114.14		118–119[d]	1.4116	0.909	35	21	15 MEHQ
n-Butyl methacrylate	142.19		163.5–170.5[d]	1.4220	0.889	66		10 MEHQ
Isobutyl methacrylate	142.19		155[d]	1.4172	0.882		49	10 MEHQ
Isodecyl methacrylate	226		120[e]	1.4410	0.878	121		10 HQ + MEHQ
Lauryl methacrylate	262	−22	272–343[d]	1.444	0.868	132		100 HQ
Stearyl methacrylate	332	15	310–370[d]	1.4502	0.864	>149		100 HQ
2-Hydroxyethyl methacrylate	130.14	−12	95[g]	1.4505	1.064	108		1200 MEHQ
2-Hydroxypropyl methacrylate	144.17	< −70	96[g]	1.4456	1.027	121		1200 MEHQ
2-Dimethylaminoethyl	157.20	ca −30	68.5[g]	1.4376	0.933		74	200 MEHQ
2-tert-Butylaminoethyl methacrylate	185.25	> −70	93[g]	1.4400	0.914	11		1000 MEHQ
Glycidyl methacrylate	142.1		75[g]	1.4482	0.073		84	25 MEHQ
Ethylene glycol dimethacrylate	198.2		96–98[h]	1.4520	1.048	113		60 MEHQ
1,3-Butylene dimethacrylate	226		110[e]	1.4502	1.011	124		200 MEHQ
Trimethylolpropane trimethacrylate	338	−14	155[i]	1.471	1.06	>149		90 HQ

[a] Refs. 29–32.
[b] COC = Cleveland open cup; TOC = Tagliabue open cup.
[c] MEHQ = monomethylether of hydroquinone; HQ = hydroquinone.
[d] At 101 kPa (1 atm).
[e] At 0.4 kPa[f].
[f] To convert kPa to mm Hg, multiply by 7.5.
[g] At 1.3 kPa[f].
[h] At 0.53 kPa[f].
[i] At 0.13 kPa[f].

Table 7. Thermodynamic Properties of Methacrylates[a]

Methacrylate	Heat of vaporization, kJ/g[b]	Heat capacity, J/(g·K)[b]	Heat of polymerization, kJ/mol[b]
Methacrylic acid		2.1–2.3	56.5
Methyl methacrylate	0.36	1.9	57.7
Ethyl methacrylate	0.35	1.9	57.7
n-Butyl methacrylate		1.9	56.5
2-Hydroxyethyl methacrylate			49.8
2-Hydroxypropyl methacrylate			50.6
2-Dimethylaminoethyl methacrylate	0.31		

[a]Ref. 31.
[b]To convert J to cal, divide by 4.184.

Table 8. Polymerization Data for Methacrylic Ester Monomers[a]

Methacrylates	^{k}sp,[b] 44.1°C	Heat of polymerization, kJ/mol[c]	Shrinkage, vol%
Methyl	27[d]	57.7	21.0
Ethyl	25[e]	57.7	18.2
Butyl	41[d]	59.4	14.9

[a]Ref. 39.
[b]The units of ^{k}sp are $L^{1/2}/(mol^{1/2}\cdot h^{-1})$. Initial rate of polymerization is calculated from ^{k}sp and the concentration of AIBN using the following equation: initial rate of polymerization in %/h = ^{k}sp/AIBN.
[c]To convert kJ to kcal, divide by 4.184.
[d]In bulk.
[e]2.5 *M* solution in benzene.

In the case of free-radical polymerizations initiated by oxygen-based radicals (eg *t*-butoxy radical), hydrogen abstraction from both the polymer backbone and the α-methyl side chain also occurs (42–45).

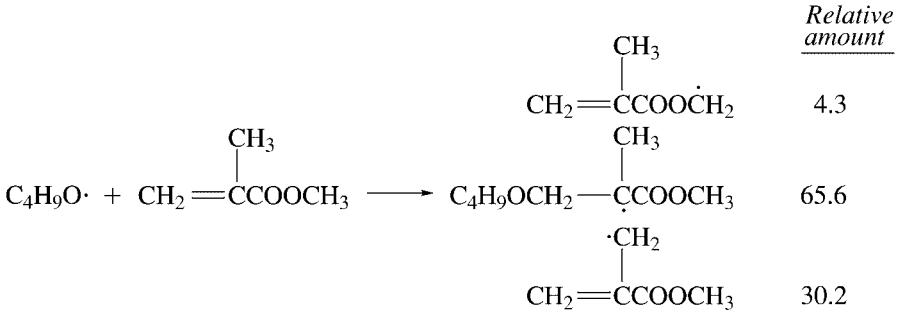

As in many free-radical processes, oxygen will form an adduct with the active radical end of a polymer and slow the rate of polymerization. An alternating polymer consisting of methyl methacrylate and dioxygen units can be formed through this inhibition mechanism. For this reason, a positive flow of nitrogen is typically used in industrial processes. Extra care must be taken to exclude oxygen when running polymerizations at lower temperatures where oxygen solubility in water is higher.

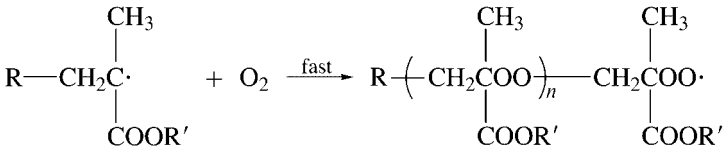

The addition of the O_2 unit is very rapid, but because of this relative stability of this adduct, the overall rate of polymerization slows down markedly. Termination levels increase as more O_2 adducts are formed.

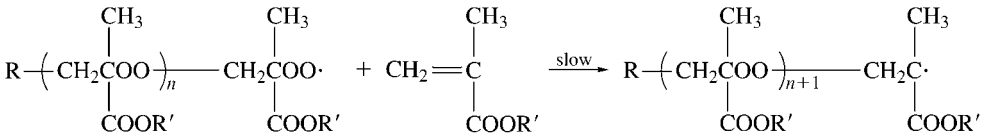

In addition to the decrease in overall polymerization rate, there are decreases in kinetic chain length and molecular weight distribution observed when these polymerizations are run in the presence of oxygen (46).

Copolymerization affords a great deal of leverage in tuning the final properties of methacrylic polymers. Methacrylic ester monomers copolymerize smoothly with acrylic monomers; this ease of copolymerization allows one to create copolymer materials with widely varying properties by using the soft, flexible acrylics with hard, brittle methacrylics. One can control properties further by controlling molecular architecture such that alternating polymer chains with methacrylate-rich and acrylate-rich segments are formed. Finally, specialty monomers can be used in small amounts to specifically target certain properties (eg film adhesion to certain substrates) or to allow for further reactions such as cross-linking. Some of the more common specialty functional monomers are displayed in Table 9.

Bulk Polymerization

Bulk polymerization is used primarily for the production of cast sheets of PMMA. During the course of these polymerizations, an autoacceleration known as the *Trommsdorf or gel effect* is observed at approximately 20–50% conversion. This phenomenon is attributable to an increase in viscosity as monomer is converted to polymer within the reactor. Once the viscosity reaches the critical point, termination begins to slow down below the rate of propagation. Therefore, the overall rate of polymerization increases and an increase in the rate of heat generated from the reactor is observed. Because termination is slowing, the molecular weight of material generated after the gel-effect point has been reached is higher than material generated earlier in the process; molecular weight in this case is limited only by the diffusion of monomer to the growing radical chain end (47).

Three main types of bulk polymerization are practiced commercially: batch cell casting, continuous casting, and continuous bulk. Batch cell casting is used to produce roughly half of the PMMA generated globally with the continuous casting and continuous bulk methods splitting the remainder of production equally. Sheets

Table 9. Common Functional Monomers for Copolymerization with Acrylic and Methacrylic Esters

Functionality	Monomer	Structure
Carboxyl	Methacrylic acid	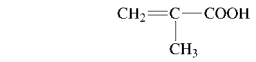
	Acrylic acid	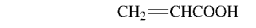
	Itaconic acid	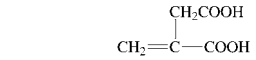
Amino	2′-text-Butylaminoethyl methacrylate	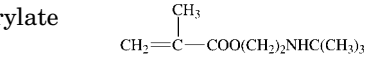
	2-Dimethylaminoethyl methacrylate	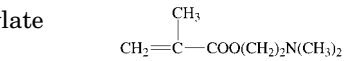
Hydroxyl	2′-Hydroxyethyl methacrylate	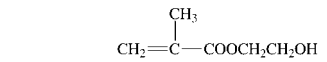
	2-Hydroxyethyl acrylate	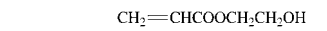
N-Hydroxymethyl	N-Hydroxymethyl acrylamide	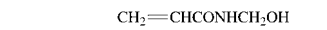
	N-Hydroxymethyl methacrylamide	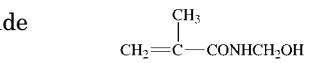
Oxirane	Glycidyl methacrylate	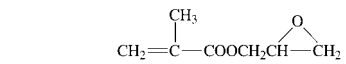
Multifunctional	1,4-Butylene dimethacrylate	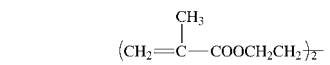

are produced with widths of approximately 1 m and lengths of several meters; thicknesses range from 0.16 to 15 cm.

Sheet Production. Poly(methyl methacrylate) sheets are produced with all three methods of bulk polymerization. Because of its inherent ease of operation, batch cell dominates this area (48–52). In this method, each sheet is formed in a mold composed of two plate glass sheets separated by a flexible spacer; a flexible spacer with springs attached is needed so that the plates can be brought closer together during the course of the polymerization to account for the increase in density as monomer is being converted to polymer. The mold is filled from one open corner with monomer (or monomer/polymer syrup), initiator, and other additives; the mold is then closed to begin the curing process. Curing itself is accomplished through the use of a carefully controlled temperature ramp to ensure complete cure and to minimize any possibility of losing control of the polymerization exotherm. The curing process takes anywhere from 10 h for thin sheets to several days for the thickest materials. Once formed, the polymer sheets are cooled separated from their reusable glass holders. The finished sheet is then annealed at 140–150°C over the course of several hours to reduce stress within the sheets and guarantee completeness of cure.

Monomer–polymer syrups are used to (*1*) aid in the shrinkage issues encountered in the formation of PMMA sheets, (*2*) shorten the polymerization induction period, and (*3*) lower the temperature necessary for initiation. These syrups contain roughly 20% polymeric material along with the monomer and can be made either by dissolving 20% finished PMMA in monomer or partially polymerizing

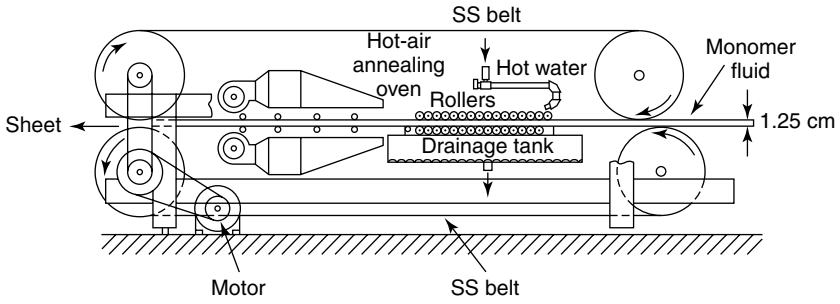

Fig. 2. Continuous process for manufacturing PMMA plastic sheet.

a batch of PMMA to the 20% level. Batch cell casting can also be used for the production of PMMA rods and tubes.

Continuous production of PMMA is accomplished using a method developed in 1968 (53). This method (Fig. 2) utilizes a polymer–monomer syrup which is delivered to a curing and annealing apparatus between two parallel stainless steel belts that are held at an angle to maintain the desired spacing between the belts. A gasket seals the reacting zone of the setup while it moves down the line at approximately 1 m/min. The reaction conditions for this type of reactor are ∼70°C for ∼45 and ∼10 min annealing time at ∼110°C. Masking tape is used to protect the sheets when they have cooled.

Poly(methyl methacrylate) is thermoplastic and can be formed into practically any shape when heated (54,55). Continuous production is employed when thin sheets are desired or highly filled materials (eg synthetic marble) are being formed.

Molding Powder. Poly(methyl methacrylate) is used extensively in injection and extrusion molding of plastics (56). The PMMA can take many forms from 0.3-cm pellets to fine beads and granulated powders. The molding powders are formed by extrusion of either bulk polymerized methyl methacrylate or from a polymer–monomer syrup which is heat-treated to remove the unreacted methyl methacrylate monomer. The PMMA emerges as a narrow rod which is chopped into the appropriately sized powder.

Synthetic Marble. Highly filled monomer or monomer–polymer syrup mixtures are used to form synthetic marble materials. A single belt approach can be employed in the formation of synthetic marble with only one smooth side (57,58). Aluminum oxide, calcium carbonate, titanium dioxide, etc, are used at loading levels of ∼60%; the specific materials of choice are determined according to the translucence, chemical-resistance, and water-resistance properties desired (59,60).

Solution Polymerization

Solution polymerization is a commercially significant means of manufacturing methacrylic polymers for the coatings, adhesives, and laminates markets. Soluble

Table 10. Chain-Transfer Constants for Methyl Methacrylate

Type	$C_s \times 10^5$ at 80°C	C_s at 60°C
Solvents[a]		
Benzene	0.8	
Toluene	5.3	
Chlorobenzene	2.1	
2-Propanol	19.1	
Isobutyl alcohol	2.3	
3-Pentanone	17.3	
Chloroform	11.3	
Carbon tetrachloride	24.2	
Chain-transfer agent[b]		
Carbon tetrabromide		0.27
Butanethiol		0.66
text-Butyl mercaptan		0.18
Thiophenol		2.7
Ethyl mercaptoacetate		0.63

[a]Refs. 58 and 59.
[b]Ref. 60.

peroxides, peroxypivalates, and azo initiators are used to initiate the polymerization in an organic solvent. Polymers with molecular weights in the range of 2000–200,000 are made by this process. Higher molecular weights generate viscosities which are very difficult to process and are typically made by other processes (61,62).

The solubility properties of solution polymers depend upon the length of the ester side chain. Polymers with less than four carbons are soluble in aromatic hydrocarbons and only sparingly soluble in aliphatic hydrocarbons. Those polymers which are made from higher alcohols are soluble in aliphatic hydrocarbons. Solvent plays a role not only in solubilizing the polymer but also as a chain transfer agent which helps control the viscosity of the solution polymer by keeping the molecular weight low. Chain transfer constants (C_s) for methyl methacrylate in common solvents are given in Table 10.

Initiator choice is another important consideration for solution polymerizations; the rate of thermolysis, cost, and initiator solubility in the diluent solvent are considerations in the choice of reaction solvent. Use levels range from a few hundredths of a percent to several percent by weight on the monomer used in the synthesis. The molecular weight of the polymer produced is inversely proportional to the level of initiator employed in the synthesis. Another consideration in the choice of initiator is the tendency of hydroperoxides to abstract hydrogens from the polymer backbone and side chains. *tert*-Amylhydroperoxide and di-*tert*-amylperoxide generate *tert*-amyloxy radicals which undergo β scission to generate ethyl radicals and one equivalent of acetone. The carbon-based ethyl radicals have lower energy than their oxygen-based sources (63). In addition to solvent and initiator selection, molecular weight can be controlled through the use of chain transfer agents and manipulation of the monomer concentration and reaction temperature (64).

Stainless steel is the material of choice for reactors used in solution polymerization. Nickel and glass can also be employed, provided that the reactor is constructed to withstand pressures of 446 kPa (65 psi). Because of the wide range of viscosities encountered in solution polymerization, a variety of stirring impellers are employed. For lower viscosities (<1000 cP) an anchor-type agitator is used; higher viscosities necessitate the use of a ribbon-type impeller, which sweeps virtually the entire volume of the reactor and, therefore, prevents polymer from remaining near the edges of the reactor.

Temperature control is of utmost importance in solution polymerizations because of the large quantity of heat liberated during the course of the polymerization. All industrial-scale reactors include cooling jackets and rupture disks in order to control the temperature and conditions within the reactor. In order to maintain efficient cooling of a solution polymer batch, it is imperative to maintain control over the viscosity of the batch. Another method for controlling reactor temperature is through the gradual addition of monomers to the batch; total cycle times for these batches generally fall in the range of 8–24 h (65). As a final precaution a chemical inhibitor is stored in the reactor area in order to quickly shut down the polymerization in the event that temperature control is compromised.

A typical reactor charge sheet for the solution polymerization of a terpolymer containing 27.5% 2-ethylhexyl acrylate, 41.3% methyl methacrylate, and 31.2% hydroxyethyl methacrylate is shown below:

Ingredient	Parts, wt%
Reactor charge	
Xylene	28.4
Ethoxyethanol	14.1
Monomer charge	
2-Ethylhexyl methacrylate	15.5
Methyl methacrylate	23.3
Hydroxyethyl methacrylate	17.6
Initiator charge	
tert-Butyl perbenzoate	1.1

For this polymerization, a reactor temperature of ~140°C is maintained for roughly 3 h while the monomer mixture is fed into the reactor. Following the completion of the monomer addition, the batch is held at 140°C to finish the batch. The final product consists of a 58% solids clear, viscous polymer which is cooled and packaged for delivery to the customer (66).

Stainless steel is used for the shipping and ground transport of methacrylic resins. Depending on the size of a particular order, these resins can be delivered in drums, tank trucks, or rail cars; water is rigorously excluded to prevent rusting and discoloration of the solution polymer. Because of the temperature dependence of the viscosity of these polymers, all transport containers are maintained at a specific temperature in order to permit effective transfer of the material once it has been delivered (67). Again, steel is the material of choice for the construction of transfer valves and pipes.

Emulsion Polymerization

Methacrylic ester latex polymers and copolymers are employed in the architectural coatings, paper, textile, floor polish, and leather industries. Methacrylic esters are most typically copolymerized with acrylates such as ethyl acrylate and butyl acrylate. These products are opaque, milky-white dispersions which can be formed at 30–60 wt% solids levels. One of the principal advantages to the use of emulsion polymerization versus solution polymerization is that the viscosity of the material is independent of molecular weight (68,69). Extremely high molecular weights (>1,000,000) can be obtained without any viscosity penalty being incurred. Particle sizes for these polymer latexes typically fall in the range of 0.1–1 μm. The polymerizations themselves take place very rapidly, with the latex water continuous phase providing a tremendous amount of heat capacity to the batch so that temperature control becomes more facile than in solution polymerization. The use of water also allows the polymer producer to eliminate the expensive and hazardous solvents often employed in solution polymerization.

Surfactants are employed to stabilize the emulsion polymer particles; anionic, cationic, and steric stabilizers are all used for the production of latexes, depending on whether one wants a negative, positive, or neutral potential surface on the formed polymer particle. The specific anionic options available for use are alkyl sulfates, alkyl sulfosuccinates, and alkylarene sulfonates and phosphates. Standard nonionic surfactants include alkyl or aryl polyoxyethylenes. In recent years, alkyl phenol ethoxylates have fallen into disfavor because of their reported problems with bioaccumulation in aquatic life. This still somewhat controversial, environmentally-driven issue has necessitated the use of alternative surfactants which have a lower impact on the environment. Typically, the aryl ring is eliminated to solve this problem.

Initiation for emulsion polymerizations occurs in the aqueous continuum; therefore, water soluble initiators such as ammonium or sodium persulfate are used. This oxidizing initiator can be cleaved either thermally or via redox reaction to generate sulfate radicals which function as the initiating species for these polymerizations. One of the advantages in using the redox approach for initiation is the temperature-independence of the rate for this reaction. Emulsion polymerizations can be run in the 25–60°C range versus 75–90°C for thermally initiated runs. In order to run a redox-initiated polymerization, a reductant is needed to directly or indirectly (through the use of a multivalent metal promoter) reduce the oxidant. Although there are many choices, common reductants include isoascorbic acid [89-65-6], sodium sulfoxylate formaldehyde [6035-47-8], and sodium hydrogensulfite [7631-90-5].

Reactors for the emulsion polymerization of methacrylic esters are made of stainless steel and are jacketed for temperature control; these reactors are built to withstand pressures of 446 kPa (65 psi) and contain emergency stacks with rupture disks in case of excess pressure buildup within the reactor. Agitation is a critical issue for emulsion polymerization. Variable-speed drive shafts are used along with stainless steel agitators to mix the batch. Baffles on the reactor walls are also common features of industrial emulsion polymerization reactors. Temperature control is maintained through the use of steam and cold water circulation with the jacket of the reactor. Feed lines for the monomer emulsion, initiators, and

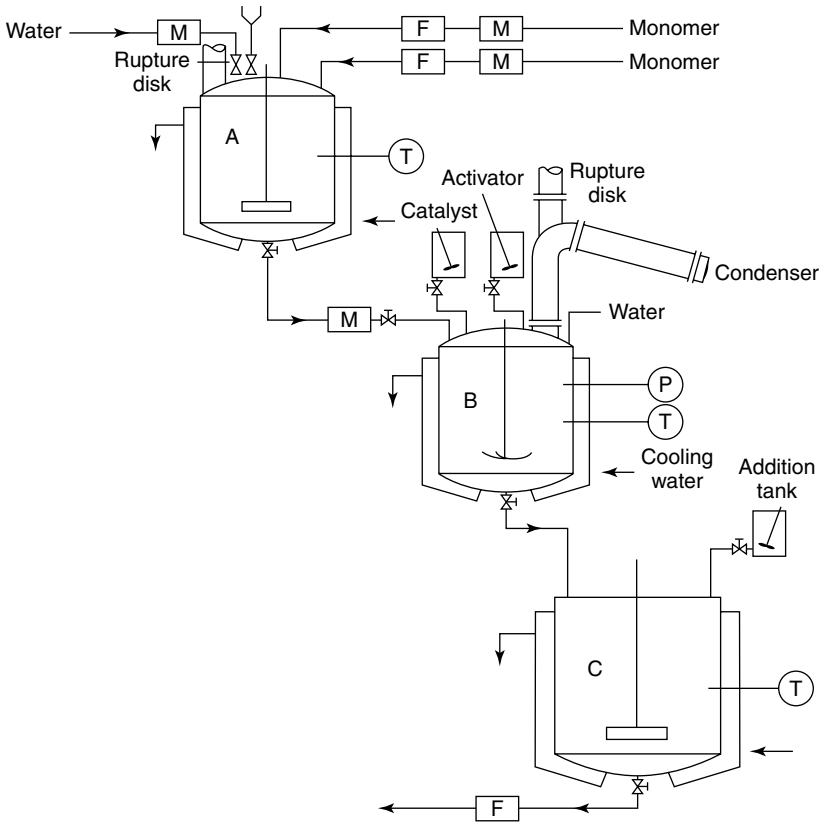

Fig. 3. Emulsion polymerization plant: A, emulsion feed tank; B, polymerization reactor; C, drumming tank; F, filter; M, meter; P, pressure gage; and T, temperature indication.

reductants are placed at the top of the kettle. Figure 3 contains a schematic for a typical industrial emulsion polymerization reactor.

Monomer emulsion preparation takes place in stainless steel tanks which are equipped with their own pressure gages, temperature indicators, and rupture disks. Because of the high (>70%) monomer content in a typical emulsion, close attention must be paid to the emulsion to ensure that it does not autoinitiate and produce an uncontrolled exotherm. Once safely formed, monomer emulsions can be added to the main reactor chamber either all at once or via gradual addition. Gradual addition is more commonly employed so that a high degree of temperature control is maintained.

Following the polymerization, the polymer latex is transferred to a drumming tank which serves as a temporary storage vessel from which the polymer is packaged for delivery to the customer. Drumming tanks are additionally used to adjust the pH, solids content, and other final properties of the latex. For this purpose, drumming tanks are equipped with their own agitation systems. Following filtration, the latex is transferred from the drumming tank into a storage vessel either for immediate delivery or for temporary storage on-site.

A typical recipe for an emulsion polymerization process is contained in the table below (70,71):

Ingredient	Parts
Monomer emulsion charge	
Deionized water	13.65
Sodium lauryl sulfate	0.11
Methyl methacrylate	22.50
Butyl acrylate	22.05
Methacrylic acid	0.45

This process generates a 50% methyl methacrylate, 49% butyl acrylate, and 1% methacrylic acid terpolymer at 45% solids. The monomer emulsion is first formed by adding the ingredients in the order listed while agitating the monomer emulsion container. The reactor charge (30.90 parts deionized water and 0.11 parts sodium lauryl sulfate) are added and heated to 85°C. The initiator (0.23 parts ammonium persulfate) is then charged prior to the beginning of the monomer emulsion feed. The emulsion is fed over 2.5 h, and a reactor temperature of 85°C is maintained during the monomer emulsion feed and subsequent polymerization. Upon completion of the emulsion feed, the reactor temperature is raised to 95°C for 0.5 h to complete the polymerization in terms of both monomer conversion and persulfate decomposition. The polymer latex is then cooled to room temperature, filtered, and packaged.

Latex polymers and copolymers of methacrylic esters are shipped in drums, tank trucks, and rail cars constructed of stainless steel or resin-coated steel and are insulated to prevent freezing of the latex. Storage tanks are, likewise, insulated and in some cases heated to prevent freezing of the latex material. Sedimentation, skinning (surface film), gritting (solids formation within latex), gumming (deposition on walls), and sponging (aerogel formation) are all concerns in the stabilization of methacrylic polymer dispersions. Other issues in the storage and handling of latexes include pH drift, evaporation, temperature fluctuation, shear and turbulence, and foaming (see FOAMS). Bactericides are commonly used to preserve polymer latexes from microbial attack (65).

Suspension Polymerization

In order to form polymer dispersions with particle sizes > 1 mm, suspension polymerization is used. The beads generated via this method of polymerization find their main usage in ion-exchange resins and molding powders. Molding powder compositions range from 100% methyl methacrylate to 20% acrylate copolymer for increased flexibility and improved processing properties. Amino or acid functional monomers are additional options in copolymer suspension polymerizations for ion-exchange; di- or tri-functional monomers are included in order to controllably cross-link the polymer beads.

The initial step in a suspension polymerization involves the suspension of 0.1- to 5-mm monomer droplets in water. The droplets are stabilized against

ripening by the inclusion of a protective colloid or suspension agent. Unlike emulsion polymerization, an oil-soluble initiator is used for suspension polymerizations. The initiator enters the monomer droplet and is thermally dissociated to produce radicals and initiate polymer chain growth. Water again served as a dispersion medium and a heat sink within these polymerizations. Particle sizes generated using this method are in the 0.1- to 5-mm range and are controlled through the suspension agent as well as the agitation rate. The polymer beads are isolated and washed via filtration or centrifugation.

Suspension agents commonly used include cellulose derivatives, polyacrylate salts, starch, poly(vinyl alcohol), gelatin, talc, clay, and clay derivatives (65,72). The primary role of these agents is to preserve a specific monomer droplet size and prevent the ripening (enlargement through coalescence) of the monomer droplets. Glycerols, glycols, polyglycols, and inorganic salts are also used to enhance suspension polymer properties (65). Finally, lubricants such as lauryl or cetyl alcohol and stearic acid and cross-linkers such as di- and trivinylbenzene, diallylesters of dibasic acids, and glycol dimethacrylates are common components of suspension processes.

Polymerization takes place within the monomer droplets and, therefore, follows a course consistent with the behavior of a bulk polymerization (65,73). Ideally, there are no transfer processes taking place between the aqueous continuum and the monomer droplets during these polymerizations. Initiators such as azo and peroxy compounds are chosen such that they are highly soluble in the monomer phase and highly insoluble in the aqueous phase; molecular weight distributions are determined in large part by the amount of initiator charged to a particular polymerization (65).

Reactor equipment is very similar to that used in emulsion polymerizations as depicted in Figure 3. The agitation and safety hardware are virtually identical as are the materials of construction. In a typical polymerization, water, suspension agents, monomer mixture, initiator, and other additives are charged to the reactor kettle in this order. The reaction mixture is then heated under careful agitation to the desired initiation temperature. Large rises in temperature and/or pressure are often encountered in suspension polymerizations; reaction times are quite rapid for this type of polymerization. Once finished, the slurry is cooled and filtered or centrifuged to isolate the polymer beads. The beads are then washed with copious amounts of water and dried either on aluminum trays in an oven maintained at 80–120°C or in a stainless steel rotary vacuum drier (65) (see DRYING).

A standard suspension polymerization process for the production of PMMA beads begins with the charging of 24.64 parts of methyl methacrylate and 0.25 parts of benzoyl peroxide to a 30°C solution containing 0.42 parts disodium phosphate, 0.02 parts monosodium phosphate, and 0.74 parts of Cyanomer A-370 (polyacrylamide resin) in 79.93 parts of deionized water. The reaction mixture is brought to 75°C and held there for 3 h. After cooling, the beads are isolated by filtration, washed with water, and dried (74).

Nonaqueous Dispersion Polymerization. A nonaqueous dispersion (NAD) polymer can be formed by first dissolving a methacrylic monomer in organic solvent and polymerizing to form an insoluble polymer in the presence of an amphipathic graft or block copolymer. The block or graft copolymer serves as a stabilizing agent and allows the insoluble methacrylic polymer to form a stable

Table 11. Examples of Methacrylic Nonaqueous Dispersion Polymers

Polymer	Diluent	Dispersant	Reference
Poly(methyl methacrylate)	Aliphatic hydrocarbon	Hydroxystearic acid–acrylic graft copolymer	70
Poly(methyl methacrylate)	Aliphatic hydrocarbon	Drying oil-modified polyester	72
Poly(methyl methacrylate)	Hexane	Isobutylene-*co*-isoprene graft copolymer	73
Poly(methyl methacrylate)	Methanol	Ethylene glycol–methyl methacrylate graft copolymer	74
Poly(ocytyl methacrylate)	methanol	Ethylene glycol–octyl methacrylate graft copolymer	70
Poly(methacrylic acid)	Chloroform–ethanol	Methacrylate functional polyester	70

colloidal particle. Particle sizes for these samples range from 0.1 to 1.0 μm with outliers in the range of 15 μm possible (75–77). These polymers are often used in the coatings industry as substitutes for aqueous emulsion polymers. The advantages of NAD polymers over emulsion polymers include low heat of evaporation and drying which is independent of the prevailing humidity level; disadvantages include toxicity of organic solvents, odor, cost, and flammability. Table 11 displays some examples of commercially significant NAD polymers.

Graft Polymerization

The construction of graft polymers involves the attachment of side branches of one composition to a main chain of a separate composition. One method of preparation depends upon the creation of radical sites along the main chain so that branches of the second composition can be grown out from monomer to create the grafted portions (78–80). Graft polymers may take the form of solution polymers, bulk polymers, or dispersions. methacrylate butadiene styrene (MBS) and methacrylate acrylonitrile butadiene styrene (MABS) are the most commercially significant graft polymers. Grafting methods used have included chemical (81,82), photochemical (83), radiation (83,84), and mastication (85). Methyl methacrylate has been grafted onto such diverse polymer backbones as cellulose (86), poly(vinyl alcohol) (87), polyester (88), polyethylene (89), poly(styrene) (90), poly(vinyl chloride) (91), and other alkyl methacrylates (92).

The preparation of MABS first involves the dissolution or dispersion of polybutadiene in a methyl methacrylate/acrylonitrile mixture which can either serve as the continuous phase in bulk polymerization or take the form of monomer droplets in suspension polymerization. The refractive indices of the two phases formed are matched such that the final material is tough, transparent, highly impact-resistant, and able to be melted and formed into diverse shapes.

MBS polymers are prepared via an emulsion polymerization process which consists of the formation of methyl methacrylate and styrene grafts on an already-formed styrene–butadiene backbone. The final product is used as an impact modifier in poly(vinyl chloride) materials.

Ionic Polymerization

Cationic polymerization is not an option in the formation of methacrylic ester polymers. Methacrylic monomers can, in fact, be used as solvents or colsolvents in the formation of polymer by a cationic mechanism (93,94).

Anionic polymerization, on the other hand, is frequently used to form methacrylic ester polymers. Initiation is accomplished in organic solvents via organometallic initiating species. Polymers of exceptionally narrow molecular weight distributions are possible by using anionic polymerization; molecular architecture can be finely (95) controlled as well. Polymers with high degrees of crystallinity are also obtainable through the careful control of reaction conditions. The method has not yet achieved large-scale commercial success because of the high costs involved in the formation of these polymers. Stereoregular poly(methyl methacrylate) (96,97) and poly(*n*-butyl methacrylate) have been prepared through the use of anionic polymerization. Polar solvents are used to form syndiotactic polymers and nonpolar solvents are employed in the formation of isotactic anionic polymers; solvent choice can, therefore, be used to form polymers with entirely different physical properties. The anionic polymerization of methacrylic esters has been covered extensively in the literature (98–101).

Michael additions are thought to be responsible for initiation in anionic polymerization:

Chain growth occurs through the head-to-tail addition of monomer units:

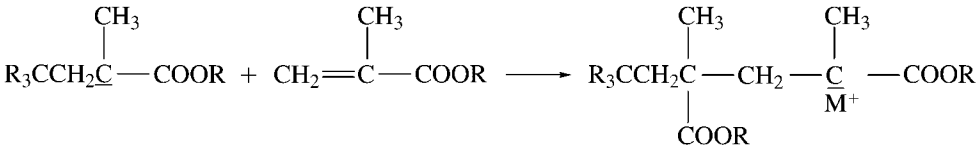

Although it is possible to polymerize both methacrylic and acrylic esters by anionic polymerization (102), copolymers of these two classes are not observed.

Group transfer polymerization, first reported by DuPont in 1983 (103), allows the production of methacrylic esters with controlled architectures. This technique uses a silyl ketene acetal initiator to produce block polymers, comb-graft polymers, star polymers, and functional polymers (103,104).

Living Polymerization

One of the most exciting areas currently in the radical polymerization of methacrylic ester monomers is the field of living polymerization. *Living polymers* are defined in Reference 105 as polymers that retain their ability to propagate for a long time and grow to a desired maximum size while their degree of termination or chain transfer is still negligible. Because of these properties, exceptional control can be exercised over the topology (ie linear, comb), composition (ie block, graft), and functional form (ie telechelic, macromonomer) of these polymers (106).

Atom transfer radical polymerization (ATRP) and nitroxide-mediated (107–109) polymerization both show promise in terms of the ability to fine-tune polymer architecture using living radical methods. ATRP has been successfully used in the polymerization of methyl methylacrylate using copper (110), ruthenium/aluminum alkoxide (111), iron (112), and nickel (113) catalyst systems.

Analytical Test Methods and Specifications

Plastic Sheet. Clear and colored transparent, clear and colored translucent, and colored semiopaque PMMA sheets are manufactured commercially. Properties such as uv resistance, mar resistance, crazing resistance, impact resistance, and flame resistance can be improved through the use of additives. Some of the physical properties of PMMAs are displayed in Table 12.

Solution Polymers. The main properties of interest for solution polymers are their composition, solids content, solvent type, viscosity, molecular weight, and glass-transition temperature. Composition information can be obtained through refractive index measurements, spectroscopic techniques, and pyrolytic gas–liquid chromatography. Solids content is measured by volatilizing the diluent solvent and measuring the percentage decrease in sample mass. Solution viscosities can be measured via Brookfield viscometer; intrinsic viscosity can be used to obtain estimates of solution polymer molecular weights (115).

Emulsion Polymers. Methacrylic ester latex properties for characterization include composition, solids content, particle-size distribution, viscosity, pH, glass-transition temperature, and minimum film-forming temperature. Composition information is obtained through nmr spectroscopy, pyrolytic gas chromatography, and refractive index measurement. Gravimetric methods are used to measure solids content; particle size distribution information is obtained through light scattering methods, microscopy, or capillary hydrodynamic flow techniques. Photon correlation spectroscopy is also used to measure particle size distributions (116). Viscosity measurements are made using Brookfield or similar

Table 12. Typical Properties of Commercial Poly(methyl methacrylate) Sheet[a]

Property	Value	ASTM test method
Specific gravity	1.19	D792-66
Refractive index	1.49	D542-50 (1965)
Tensile strength		D638-64T
Maximum, MPa[b]	72.4	
Rupture, MPa[b]	72.4	
Elongation, max, %	4.9	
Elongation, rupture, %	4.9	
Modulus of elasticity, MPa[b]	3103	
Flexural strength		D790-66
Maximum, MPa[b]	110.3	
Rupture, MPa[b]	110.3	
Deflection, max, cm	1.52	
Deflection, rupture, cm	1.52	
Modulus of elasticity, MPa[b]	3103	
Compressive strength		D695-68T
Maximum, MPa[b]	124.1	
Modulus of elasticity, MPa[b]	3103	
Compressive deformation under load[c]		D621-64
14 MPa[b] at 50°C, 24 h, %	0.2	
28 MPa[b] at 50°C, 24 h, %	0.5[d]	
Shear strength, MPa[b]	62.1	D732-46 (1961)
Impact strength		
Charpy unnotched, J/cm^2[e]	2.94	D255-56 (1961)
Rockwell hardness	M-93[d]	
Hot forming temperature, °C	144–182	
Heat distortion temperature		D648-56 (1961)
2°C/min, 1.8 MPa,[b] °C	96[d]	
2°C/min, 0.46 MPa,[b] °c	107[d]	
Maximum recommended continuous service temperature, °C	82–94	
Coefficient of thermal expansion, cm/cm/°C		
−40°C	5.0×10^{-5}	
−18°C	5.6×10^{-5}	
5°C	6.5×10^{-5}	
27°C	7.6×10^{-5}	
38°C	8.3×10^{-5}	
Coefficient of thermal conductivity, kW/(m·K)	0.00344	
Specific heat, 25°C, kJ/(kg·°C)[f]	0.452	

[a] Ref. 114.
[b] To convert MPa to psi, multiply by 145.
[c] Conditioned 48 h at 50°C.
[d] Values change with thickness; the reported value is for 0.635 cm.
[e] To convert J/cm^2 to lbf/in., divide by 0.0175.
[f] To convert kJ to kcal, divide by 4.184.

viscometers. Finally, glass-transition measurements can be made either by dma or dsc.

Emulsion polymers typically have a series of stability tests run on them before they are approved for sale commercially (117). These tests include freeze–thaw, mechanical shear, and thermal stability. The settling tendencies of a latex are assessed as is the formulation stability with regard to other dispersions, salts, surfactants, and pigments.

Suspension Polymers. Suspension polymers of methacrylic esters are characterized by their composition and particle size distribution. Because of their large particle sizes, these materials are typically passed through sizing screens which separate the various fractions according to polymer bead diameter. Materials destined for the molding powders market are subjected to melt-flow studies under the conditions of use that they will encounter for their specific application. Ion-exchange beads are, likewise, studied with regard to their ion-exchange capacity, density (wet and apparent), solvent swelling, moisture holding capacity, porosity, and salt-splitting characteristics (118).

Health and Safety Factors

Provided that there are no toxic additives or high levels of residual monomers, methacrylic ester polymers are classified as nontoxic. These materials find use in dental fillings, dentures, contact lenses, medicine dispensers, and food packaging. However, some acrylic and methacrylic dispersions can be skin or eye irritants due to the surfactants used in stabilization.

Because of the toxicity of the monomers involved in forming methacrylic ester polymers, extra precautions are taken to avoid any release of monomer into the surrounding area. Most industrial polymerization reactors are run with closed kettles to prevent monomer vapor from escaping into the surrounding air.

One of the hazards uniquely associated with the production of methacrylic powders and sheets is explosion of polymer dust. These materials are flammable and must be treated with care to avoid static discharges which can serve as ignition sources. Poly(methyl methacrylate) is widely used in buildings under codes which limit the fire hazards associated with this material. Solution polymers of methacrylic esters are considered flammable while latex emulsion polymers are nonflammable because of the aqueous continuous phase.

Uses

The primary market for methacrylate resins in the United States is in the glazing and skylights area. These resins also find significant usage in consumer products, transportation signs, lighting fixtures, plumbing (spas, tubs, showers, sinks, etc), panels, and siding (119,120).

Glazing. Methacrylic ester polymers are well-suited for use as glazing, lighting, or decorative materials because of their unique balance of light transmittance, light weight, dimensional stability, and formability as well as their

weather, impact, and bullet resistance. Some of the specific applications for these materials include windows for aircraft fuselages (121), banks, police cars, hockey rinks, storm doors, bath and shower doors, and showcases. The ability to manufacture either colored or clear versions of methacrylate sheets recommends their use in decorative window mosaics, side glazing, color coordinated structures, and sunscreens (122,123). Both sheets and molding pellets have been used for lighting, solar control, and in signs (124–128).

Medicine. For years, dentures, dental fillings, and denture bases have been made using methacrylic ester polymers (129,130) (see DENTAL MATERIALS). These polymers can also be used to prevent tooth decay in natural teeth by serving as a barrier which can be coated over the surface of the tooth. The dimensional behavior of these bone-cement composites has been reported (131) as has the structure of the cold-cured acrylic resin (132). Both hard and soft contact lenses have been made using polymethacrylates (133,134). hHYDROGELS (qv) comprising poly(2-hydroxyethyl methacrylate) are used in soft contact lenses (135,136).

Optics. Polymethacrylates are naturally good choices for the fiberoptics market because of their optical clarity and low thermal resistance (137). Fresnel and eyeglass lenses have been made using polymethacrylates (138–140).

Oil Additives. Long-chain polymethacrylates increase the viscosity of oil as temperature increases and are therefore used as additives to improve the performance of lubricating oils and hydraulic fluids in internal combustion engines (141). Through the careful control of polymer molecular weight and composition, oils of constant performance over broad temperature ranges are made possible (142). Polymethacrylates can be used to improve the viscosity index, sludge dispersancy, and antioxidant properties of an oil (143) (see ANTIOXIDANTS). Through the grafting of polyethylene and polypropylene onto long-chain polymethacrylates, multipurpose lubricants having viscosity index, pour point depression properties, and detergent dispersing capabilities are possible (144).

Other. Synthetic marble fixtures and bathtubs are made using methacrylic ester polymers (145,146). Opaque and clear methacrylate sheets have been used as structural components in the manufacture of recreational vehicles (147). These materials are additionally used for electrical insulation. Thermoplastic methacrylate resins are used in lacquer coatings for plastics, in printing inks, as heat seal lacquers for packaging, as screen printing media for decorative porcelain, in traffic paints, and for the protection of buildings from acid rain and weathering (148). Other copolymer used are discussed in the article ESTER POLYMERS.

BIBLIOGRAPHY

"Acrylic Ester Polymers" in *EPST* 1st ed., Vol. 1, pp. 246–328, by L. S. Luskin and R. J. Myers, Rohm and Haas Co.; "Acrylic and Methacrylic Polymers" in *EPST* 2nd ed., Vol. 1, pp. 211–299, by B. B. Kine and R. W. Novak, Rohm and Haas Co.

1. E. H. Riddle, *Monomeric Acrylic Esters*, Reinhold Publishing Corp., New York, 1954.
2. M. Salkind, E. H. Riddle, and R. W. Keefer, *Ind. Eng. Chem.* **51**, 1232, 132B (1959).
3. H. E. Bair, ASTM Spec. Tech. Publ. STP 1249, 1994, p. 50.

4. R. P. Chartoff, P. T. Weissman, and A. Sircar, ASTM Spec. Tech. Publ. STP 1249, 1994, p 88.
5. G. Xue, J. Dong, and J. Ding, *Mater. Eng.* **9**, 791 (1995).
6. D. W. VanKrevelen, *Properties of Polymers*, Elsevier Publishing Co., Amsterdam, the Netherlands, 1976.
7. H. B. Burrell, *Off. Dig. Fed. Soc. Paint Technol.* **34**, 131 (Feb. 1962).
8. S. Krause and co-workers, *J. Polym. Sci., Part A* **3**, 3573 (1965).
9. W. A. Lee and G. J. Knight, *Br. Polym. J.* **2**, 73 (1970).
10. R. H. Wiley and G. M. Braver, *J. Polym. Sci.* **3**, 647 (1948).
11. S. Krause and co-workers, *J. Polym. Sci., Part A* **3**, 455 (1965).
12. D. H. Klein, *J. Paint Technol.* **42**, 335 (1970).
13. F. Garbassi, *Polym. News* **22**, 355 (1997).
14. O. G. Lewis, *Physical Constants of Linear Homopolymers*, Springer-Verlag, New York, 1968.
15. J. Brandrup and E. H. Immergut, *Polymer Handbook*, 3rd ed., Wiley-Interscience, New York, 1989.
16. J. A. Shetter, *Polym. Lett.* **1**, 209 (1963).
17. T. G. Fox Jr., *Bull. Am. Phys. Soc.* **1**, 123 (1956).
18. L. E. Nielsen, *Mechanical Properties of Polymers and Composites*, Vol. **1**, Marcel Dekker, Inc., New York, 1974.
19. J. R. Martin, J. F. Johnson, and A. R. Cooper, *J. Macromol. Sci., c:Rev. Macromol. Chem.* **8**, 57 (1972).
20. W. H. Brendley Jr., *Paint Varn. Prod.* **63**, 23 (July 1973).
21. A. S. Craemer, *Kunststoffe* **30**, 337 (1940).
22. *Plexiglas Design and Fabrication Data, Plexiglas Cast Sheet for Lighting, PL-927a*, Rohm and Haas Co., Philadelphia, Pa.
23. *Plexiglas Design and Fabrication Data, PL-53i*, Rohm and Haas Co., Philadelphia, Pa.
24. *Optics, PL-897B*, Rohm and Haas Co., Philadelphia, Pa.
25. *Plexiglas Molding Pellets, PL-926a*, Rohm and Haas Co., Philadelphia, Pa.
26. F. J. Glavis, *J. Polym. Sci.* **36**, 547 (1959).
27. *Plexiglas Acrylic Plastic Molding Powder, PL-866*, Rohm and Haas Co., Philadelphia, Pa.
28. R. Simha, *Advances in Chemistry Series No. 34: Polymerization and Polycondensation Processes*, American Chemical Society, Washington, D.C., 1962, p. 157.
29. *Acrylic and Methacrylic Monomers—Typical Properties and Specifications, CM-16*, Rohm and Haas Co., Philadelphia, Pa.
30. *Storage and Handling of Acrylic and Methacrylic Esters and Acids, Bulletin 84C*, Rohm and Haas Co., Philadelphia, Pa.
31. L. S. Luskin, in E. C. Leonard, ed., *High Polymers, Vinyl and Diene Monomers*, Vol. **24**, Part 1, Wiley-Interscience, New York, 1970.
32. L. S. Luskin, in F. D. Snell and C. L. Hilton, eds., *Encyclopedia of Industrial Chemical Analysis*, Vol. **4**, Wiley-Interscience, New York, 1967, p. 181.
33. R. V. Porcelli and B. Juran, *Hydrocarbon Proc. Int. Ed.* **65**(3), 37–43 (1986).
34. F. E. Clayton and G. D. Clayton, eds., *Patty's Industrial Hygiene and Toxicology*, 4th ed., Wiley-Interscience, New York, 1991.
35. *Technical data, The Methacrylate Producers Association, Washington, D.C., 1843 and 1873.*
36. S. Egusa and K. Maguchi, *J. Polym. Sci.* **20**, 863 (1982).
37. R. R. Challa and co-workers, *J. Appl. Polym. Sci.* **31**, 27 (1985).
38. V. I. Lukhovitskii and co-workers, *Polym. Sci., Ser. A.* **38**, 1263 (1996).

39. *Preparation, Properties and Uses of Acrylic Polymers, CM-19*, Rohm and Haas Co., Philadelphia, Pa.
40. T. G. Fox Jr. and R. Loshock, *J. Am. Chem. Soc.* **75**, 3544 (1953).
41. D. Pramanick, R. Bhattacharyya, and B. Chakraborty, *Hungarian J. Ind. Chem.* **12**, 1 (1984).
42. P. G. Griffiths, E. Rizzardo, and D. H. Solomon, *J. Macromol. Sci., Chem.* **17**, 45 (1982).
43. P. G. Griffiths, E. Rizzardo, and D. H. Solomon, *Tetrahedron Lett.* **23**, 1309 (1982).
44. T. Nakamura and co-workers, *Macromolecules* **30**, 2843 (1997).
45. T. Nakamura and co-workers, *Polymer* **40**, 1395 (1999).
46. M. M. Mogilevich, *Russ. Chem. Rev.* **48**, 199 (1979).
47. J. Shen and co-workers, *Makromol. Chem.* **192**, 2669 (1991).
48. L. S. Luskin, J. A. Sawyer, and E. H. Riddle, in W. M. Smith, ed., *Polymer and Manufacturing and Processing*, Reinhold Publishing Corp., New York, 1964.
49. E. H. Riddle and P. A. Horrigan, in P. H. Groggins, ed., *Unit Processes in Organic Synthesis*, 5th ed., McGraw-Hill, Inc., New York, 1958.
50. J. O. Beattie, *Mod. Plast.* **33**, 109 (1956).
51. U.S. Pat. 3,113,114 (Dec. 3, 1963), R. A. Maginn (to E. I. du Pont de Nemours Co., Inc.).
52. U.S. Pat. 3,382,209 (May 7, 1968), W. G. Deschert (to American Cyanamid Co.).
53. U.S. Pat. 3,376,371 (Apr. 2, 1968), C. J. Opel (to Swedlow, Inc.).
54. *Forming Plexiglas Sheet, PL-4k*, Rohm and Haas Co., Philadelphia, Pa.
55. *Plexiglas Acrylic Sheet, PL-80M*, Rohm and Haas Co., Philadelphia, Pa.
56. *Plexiglas Molding Manual, PL-710*, Rohm and Haas Co., Philadelphia, Pa.
57. *Mod. Plast.* **47**, 6 (June 1970).
58. U.S. Pat. 3,706,825 (Dec. 19, 1972), N. L. Hall (to E. I. du Pont de Nemours & Co., Inc.).
59. *Plast. Ind. News* **32**, 11 (Nov. 1986).
60. U.S. Pat. 3,847,865 (Nov. 1984), R. B. Duggins (to E. I. du Pont de Nemours & Co., Inc.).
61. E. L. Madruga, J. San Roman, and P. Benedi, *J. Appl. Polym. Sci.* **41**, 1133 (1990).
62. I. Czajlik and T. Foldes-Berezanich, *Eur. Polym. J.* **17**, 131 (1981).
63. V. R. Kamath and J. D. Sargent, *J. Coat. Technol.* **59**, 51 (1987).
64. J. I. Kroschwitz, ed., *Encyclopedia of Polymer Science and Engineering*, 2nd ed., Vol. **3**, John Wiley & Sons, Inc., New York, 1985, pp. 288–290.
65. *The Manufacture of Acrylic Polymers, CM-107*, Rohm and Haas Co., Philadelphia, Pa.
66. Brit. Pat. 2,097,409A (Apr. 6, 1982), P. Bitler (to ICI Co.).
67. *Bulk Storage and Handling of Acryloid Coating Resins, C-186*, Rohm and Haas Co., Philadelphia, Pa.
68. P. A. Lovell and M. S. El-Aasser, *Emulsion Polymerization and Emulsion Polymers*, John Wiley & Sons, Inc., New York, 1997.
69. R. G. Gilbert *Emulsion Polymerization: A Mechanistic Approach*, Academic Press, New York, 1995.
70. U.S. Pat. 3,458,466 (July 29, 1969), W. J. Lee (to The Dow Chemical Company).
71. U.S. Pat. 3,344,100 (Sept. 26, 1967), F. J. Donat and E. H. Baker (to B. F. Goodrich Co.).
72. E. Giannetti and co-workers, *J. Polym. Sci., Polym. Chem.* **24**, 2517 (1986).
73. G. S. Whitby and co-workers, *J. Polym. Sci.* **16**, 549 (1955).
74. W. Cooper and co-workers, *J. Polym. Sci.* **34**, 651 (1959).

75. K. E. J. Barrett, ed., *Dispersion Polymerizations in Organic Media*, John Wiley & Sons, Inc., New York, 1975.
76. M. A. Winnik and co-workers, *Makromol. Chem., Macromol. Symp.* **10/11**, 483 (1987).
77. Brit. Pat. 1,002,493 (1965), C. J. Schmidle (to Rohm and Haas Co.).
78. T. O. Purcell Jr., in N. M. Bikales, ed., *Encyclopedia of Polymer Science and Technology*, Suppl. 1, Wiley-Interscience, New York, 1976, pp. 319–325.
79. R. J. Ceresa, *Block and Graft Copolymers*, Vol. **1**, Butterworth, Inc., Washington, D.C., 1962.
80. H. A. J. Battaerd and G. W. Tregear, *Polymer Reviews, Graft Copolymers*, Vol. **16**, Wiley-Interscience, New York, 1967.
81. W. Kobryner, *J. Polym. Sci.* **34**, 381 (1959).
82. P. W. Allen, *J. Polym. Sci.* **36**, 55 (1959).
83. W. Cooper, G. Vaughan, and R. W. Madden, *J. Appl. Polym. Sci.* **1**, 329 (1959).
84. W. Cooper and co-workers, *J. Polym. Sci.* **34**, 651 (1959).
85. D. J. Angier and W. F. Watson, *J. Polym. Sci.* **20**, 235 (1956).
86. T. Toda, *J. Polym. Sci.* **58**, 411 (1962).
87. U.S. Pat. 3,030,319 (Apr. 17, 1962), K. Kaizirman and G. Mino (to American Cyanamid Co.).
88. S. Lenka, *J. Polym. Sci., Polym. Lett. Ed.* **21**, 281 (1983).
89. A. Chapiro, *J. Polym. Sci.* **29**, 321 (1958).
90. Brit. Pat. 788,175 (Dec. 3, 1957), R. G. Norrish (to Distillers Co., Ltd.).
91. S. P. Rao and M. Santappa, *J. Polym. Sci., Part A-1* **5**, 2681 (1967).
92. R. K. Graham, M. S. Gluekman, and M. J. Kampf, *J. Polym. Sci.* **38**, 417 (1959).
93. T. Nishikubo, T. Ichijyo, and T. Takoha, *J. Appl. Polym. Sci.* **20**, 1133 (1976).
94. N. G. Gaylord and co-workers, *J. Polym. Sci. Polym., Chem. Ed.* **13**, 467 (1975).
95. T. Tsuruta, T. Makimoto, and H. Kanai, *J. Macromol. Chem.* **1**, 31 (1966).
96. J. Trekoval and D. Lim, *J. Polym. Sci., Part C* **4**, 333 (1964).
97. D. Braun and co-workers, *Makromol. Chem.* **51**, 15 (1962).
98. T. E. Long and co-workers, *J. Poly. Sci., Polym. Chem.* **27**, 4001 (1989).
99. K. Hatada, T. Kitayama, and K. Ute, *Prog. Polym. Sci.* **13**, 189 (1988).
100. A. H. E. Mueller, *American Chemical Society Symposium Series No. 166*, American Chemical Society, Washington, D.C., 1981, p. 441.
101. M. Van Beylen and co-workers, *Adv. Polym. Sci.* **86**, 87 (1988).
102. H. Yuki and co-workers, in O. Vogl and J. Furukawan, eds., *Ionic Polymerization*, Marcel Dekker, Inc., New York, 1976.
103. O. W. Webster, *Makromol. Chem., Macromol. Symp.* **70/71**, 75 (1993).
104. W. J. Brittain, *Rubb. Chem. Technol.* **65**, 580 (1992).
105. M. Szwarc, *J. Polym. Sci., Part A: Polym. Chem.* **36**, ix (1998).
106. T. E. Patten and K. Matyjaszewski, *Adv. Mater.* **10**, 901 (1998).
107. M. K. Georges and co-workers, *Macromolecules* **26**, 2987 (1993).
108. S. A. F. Bon and co-workers, *Macromolecules* **30**, 324 (1997).
109. C. J. Hawker and co-workers, *Macromolecules* **31**, 213 (1998).
110. J. S. Wang and K. Matyjaszewski, *Macromolecules* **28**, 7901 (1995).
111. M. Kato and co-workers, *Macromolecules* **28**, 1721 (1995).
112. T. Ando, M. Kamigaito, and M. Sawamoto, *Macromolecules* **30**, 4507 (1997).
113. C. Granel and co-workers, *Macromolecules* **29**, 8576 (1996).
114. *Plexiglas Acrylic Sheet, PL-783a*, Rohm and Haas Co., Philadelphia, Pa.

115. P. W. Allen, *Technique of Polymer Characterization*, Butterworths Scientific Publications, London, 1959.
116. H. G. Barth and S.-T. Sun, *Anal. Chem.* **65**, 55R (1993).
117. *Emulsion Polymerization of Acrylic Monomers, CM-104*, Rohm and Haas Co., Philadelphia, Pa.
118. R. Kunin, *Elements of Ion Exchange*, R. E. Krieger Publishing Co., Huntington, N.Y., 1971.
119. A. M. Dave, *Pop. Plast.* **31**(4), 27–30 (1986).
120. R. R. Jobanputra and R. C. Mathur, *Pop. Plast.* **33**(6), 31–32 (1988).
121. R. Hermann, *Mater. Des.* **9**, 339 (1988).
122. H. J. Gambino Jr., *Security You Can See Through, PL-1228*, Rohm and Haas Co., Philadelphia, Pa.
123. *Mod. Plast.* (5), 52 (May 1975).
124. *Plexiglas Molding Pellets, PL-926a*, Rohm and Haas Co., Philadelphia, Pa.
125. P. W. Allen and co-workers, *J. Polym. Sci.* **36**, 55 (1959).
126. *Sun Screen Innovations with Plexiglas, PL-935*, Rohm and Haas Co., Philadelphia, Pa.
127. *Transparent Plexiglas Solar Control Series*, Rohm and Haas Co., Philadelphia, Pa.
128. *Plexiglas DR Sign Manual, PL-1097e*, Rohm and Haas Co., Philadelphia, Pa.
129. W. D. Cook, D. R. Beech, and M. J. Tyas, *Biomaterials* **6**, 362 (1985).
130. J. M. Antonucci, *ACS Polymer Science and Technology Series* **34**, American Chemical Society, Washington, D.C. 1986, p. 277.
131. J. R. DeWijn, F. C. M. Driessenj, and T. J. J. H. Sloff, *J. Biomed. Mater. Res.* **9**(4), 99 (1975).
132. R. P. Kusy and D. T. Turner, *J. Dent. Res.* **53**, 948 (1974).
133. W. Timmer, *Chem. Tech.* **9**, 1975 (Mar. 1979).
134. B. J. Tighe, *Br. Polym. J.* **18**(1), 8–13 (1986).
135. J. P. Montheard, M. Chatzopoulos, and D. Chappard, *J. Macromol. Sci., c:Rev. Macromol. Chem. Phys.* **32**(1), 1 (1992).
136. E. J. Mack and co-workers, in N. A. Peppas, ed., *Hydrogels in Medicine & Pharmacy*, Vol. **2**, CRC Press, Inc., Boca Raton, Fla., 1987, p. 65.
137. C. Emslie, *J. Mater. Sci.* **23**, 2281 (1988).
138. I. Kaetsu, K. Yoshida, and O. Okubo, *J. Appl. Polym. Sci.* **24**, 1515 (1979).
139. H. Okubo, K. Yoshida, and I. Kaetsu, *Int. J. Appl. Radiat. Isot.* **30**, 209 (1979).
140. U.S. Pat. 4,146,696 (Mar. 17, 1979), H. M. Bond, D. L. Torgersen, and C. E. Ring (to Buckee-Mears Co.).
141. R. J. Kopko and R. L. Stambaugh, in *Fuels and Lubricants Meetings*, Houston, Tex., June 3–5, 1975, Society of Automotive Engineers, Inc., Warrendale, Pa. SAE Paper 750693.
142. U.S. Pat. 2,091,627 (Aug. 31, 1937), H. A. Bruson (to Rohm and Haas Co.).
143. U.S. Pat. 3,147,222 (Sept. 1, 1964), L. N. Bauer (to Rohm and Haas Co.).
144. U.S. Pat. 3,879,304 (Apr. 22, 1975), J. O. Waldbilling (to Texaco, Inc.).
145. A. S. Wood, *Mod. Plast.* **52**, 40 (Aug. 1975).
146. *Mod. Plast.* **49**, 44 (Aug. 1972).
147. R. Martino, *Mod. Plast.* **51**, 62 (Nov. 1974).
148. G. Kuhl and H.-D. Christian, *Pigment Resin Technol.* **16**(7), 4 (1987).

ROBERT V. SLONE
Rohm and Haas Company

MICROMECHANICAL PROPERTIES

Introduction

Mechanical properties of polymeric materials are important for nearly all applications in industry, technology, and the household. Particularly, stiffness, strength, and toughness are decisive properties in many uses. Mechanical properties depend strongly on chemical as well as on supermolecular structure of the polymeric material. While the chemical, molecular structure defines some basic properties such as rigidity, thermal softening, and melting behavior, the ultimate mechanical properties are fixed by the supermolecular structures or morphology. The same molecular structure can yield to many varied morphologies dependent on factors such as orientation due to fabrication, different cooling rates, changes in thermal history, and secondary crystallization.

However, not all of the manifold structural or morphological details influence the ultimate mechanical properties to the same degree. There are details which determine properties more than other ones, ie, there are so called "property determining structures." Besides, it is not sufficient to study the average structure and morphology of a material, but the variation of morphological details or extreme sizes of the details have to be known. Smaller structural details have become increasingly important for a defined improvement of mechanical properties with a shift from details on the micrometer scale to details on the nanometer scale, eg, in block copolymer or nanocomposites, Polymer-Clay.

The influence of all of the different structural details on the mechanical properties is determined by micromechanical processes, which appear under the applied loading conditions. Depending on the very different structural details and loading conditions, there is a very large variety of micromechanical processes of deformation and fracture. These processes define the *micromechanical properties* of a polymeric material or the *micromechanics*. Therefore, micromechanical properties form the bridge between structure or morphology and ultimate mechanical properties. Improved knowledge of the micromechanical properties allows a deeper insight into the influence of morphology on the mechanical properties, ie, it allows a better understanding of structure–property correlations (see Fig. 1).

A detailed knowledge of structure–property correlations is not only of academic interest but also important for the polymer industry. It enables a defined modification of the morphology for realizing special desired properties for practical applications. This way was called "microstructural construction of polymers" (1). In addition, study of micromechanics in polymeric model materials may reveal new micromechanical processes, yielding improved, new and up-to-now impossible combinations of different mechanical properties, eg, combinations of contradictory properties, such as stiffness, strength, and toughness. Transforming such new micromechanical mechanisms from model samples to technically usable materials by defined scaling-up may yield new classes of polymers, eg, in the field of nanostructured materials.

The term "*micromechanics*" covers all processes on mesoscopic, microscopic, and nanometer scales that occur inside a material in response to an external loading (2). These processes include reactions of macromolecules, such as stretching or

Encyclopedia of Polymer Science and Technology. Copyright John Wiley & Sons, Inc. All rights reserved.

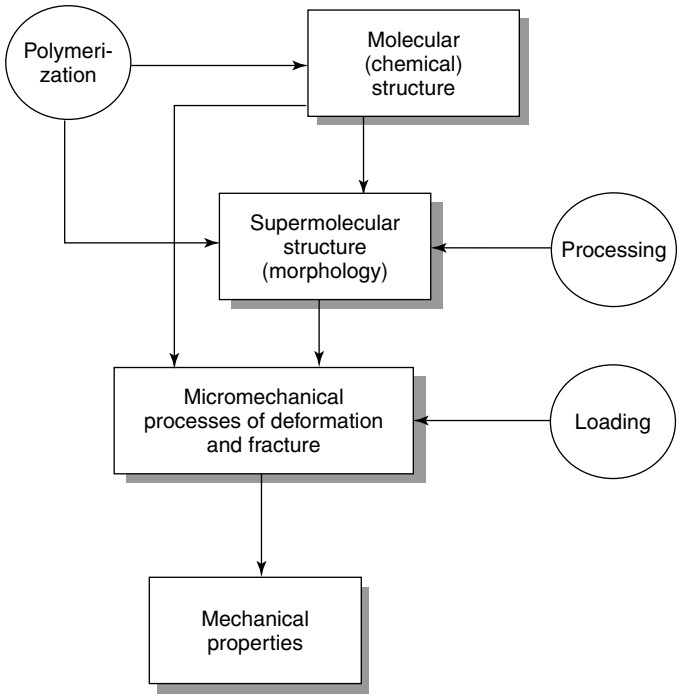

Fig. 1. Correlations between structure, morphology, micromechanical processes, and mechanical properties of polymers.

scission of molecular segments, reptation (snake-like) movement, microyielding, microcavitation, forming of crazes, shear bands or deformation zones up to crack initiation, propagation, and fracture.

Recently, several different techniques to study micromechanical properties have been applied. Besides spectroscopic and scattering techniques, the microscopic techniques of electron microscopy and atomic force microscopy are particularly useful for direct determination of micromechanical properties in polymers (2–7). A brief overview about successfully applicable techniques is given in this article. Using these techniques, micromechanical properties of different polymers that have been studied are also reviewed.

Every study of micromechanical processes must be coupled with a detailed investigation of the morphology and, in particular, of those structural parameters of most importance for the property of interest (see "representative volume" - below). Often, structural defects exist that are responsible for premature failure of materials. In the following, direct imaging techniques of electron microscopy and atomic force microscopy are discussed in more detail, since they allow a very direct determination of the micromechanical processes in dependence on the local morphology, and yield often a very clear picture of the micromechanical behavior of the material. Additional information about special micromechanical properties can be revealed by using several other techniques. However, unlike the direct microscopic methods, these techniques yield mainly integral results from a larger sample volume, but complete the picture.

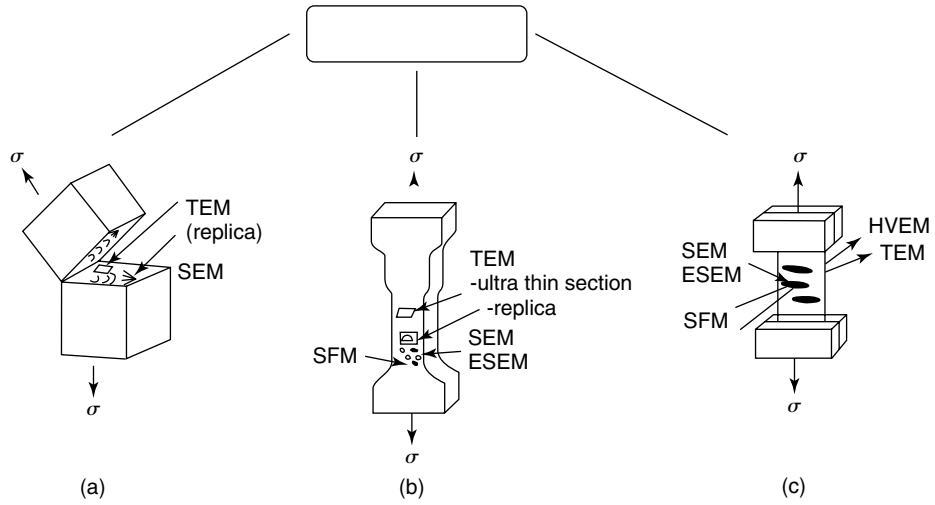

Fig. 2. Survey of (electron and scanning force) microscopic methods for investigating micromechanical processes in polymers. σ indicates the applied tension stress and the arrows indicate area and direction of investigation in the microscope (see text for full details). (**a**) fracture surfaces—tension test, impact test, broken pieces; (**b**) surfaces of deformed (loaded) bulk samples; (**c**) *in situ* deformation of thin samples.

Microscopic Techniques

A survey of successful methods is given in Figure 2, demonstrating three main techniques (2–4):

(1) Fracture surfaces can be directly investigated in the scanning electron microscope (sem, microfractography, Fig. 2a), demonstrating most significantly the final processes of deformation, crack initiation, and crack propagation up to fracture. In particular, structural heterogeneities (defects), which initiate fracture and influence crack path, can be detected (see FRACTOGRAPHY). Using sem, the surface topography of bulk specimen can be very easily inspected with the only precondition of coating with a thin conducting layer. Using thin replicas from the fracture surface, transmission electron microscopy (tem) can also be applied (however, preparation of thin replicas from a polymer surface is a relatively difficult procedure) (see MICROSCOPY).

(2) Deformation of bulk material is followed by investigation of the changes at the surfaces by sem, environmental scanning electron microscopy (esem, with the advantage of avoiding any conducting layer), and atomic or scanning force microscopy (sfm) or, after replication, by tem. Changes inside the bulk material are studied by preparation of ultrathin sections from deformed regions using a cryo-ultramicrotome (occasionally after selective chemical staining to improve the contrast) and by tem investigations (Fig. 2b). In semicrystalline polymers, changes of the crystalline orientation can be studied by electron diffraction.

(3) Samples of different thicknesses (usually semithin or ultrathin sections prepared by ultramicrotomy) can be deformed in tensile devices and the deformed samples investigated directly by sem, esem, sfm, tem, or high voltage electron microscopy (hvem) (Fig. 2c).

The advantage of techniques 1 and 2 is the possibility of studying bulk material, deformed under defined stress conditions and loading temperatures. Disadvantages of technique 1 lie in the difficulty of detecting the initial stages of deformation and in the impossibility of carrying out experiments *in situ*. In technique 2, problems may arise from a possible modification of the deformation structures at the sample surfaces in sem or sfm studies and from the danger of damaging the deformation structures by the preparation of ultrathin films (usually by ultramicrotomy) in tem studies.

Tests *in situ* can be performed by technique 2 only using an esem (because of avoiding a conducting surface layer) and by technique 3 using different microscopes in combination with tensile devices. Additional advantages of technique 3 lie in the investigation of processes by using special tensile devices to perform deformation tests at lower or higher temperatures (usually from -150°C to 200°C). Using these tensile stages, samples of different thicknesses can be studied: thicker samples (thick sections) can be investigated in an sem, esem, and sfm, revealing deformation processes near the surface. A method particularly advantageous is the investigation of semithin sections, up to several micrometers thick, in a 1000-kV hvem. Such samples, on one hand, show a relatively high mechanical stability and often they represent the micromechanical behavior typical for these polymers and, on the other hand, the investigation in an hvem enables high magnifications and resolutions. Ultrathin sections or films are necessary for using conventional 100- to 200- kV tem. These ultrathin samples are often mounted for supporting on a Cu grid (8) or on a film with a hole.

Using sfm, a direct study of surface structures is possible in air without the need for coating with a conducting layer and without any radiation damage, but with a resolution in the nanometer range. Therefore, this method is of particular interest for micromechanical investigations and real *in situ* tests.

Choice of the appropriate size and thickness of the sample depends on several factors, including the morphology of the polymeric material, sample shape or geometry, and stress state (eg, plane strain or plane stress state). Therefore, the various techniques mentioned above allow the study of very different polymers.

An often-discussed problem is the "transformation" of results from microscopic investigations on thin samples to the bulk material. The typical dimensions or features of the morphology (the "property determining structures") must be smaller than the sample thickness, that is, the samples have to contain a representative part of the morphology (a "representative volume"). If the thin sections contain a representative part of the morphology, the character of the deformation (the deformation mode) is often unchanged; however, the absolute values of deformation (degree of elongation) are usually higher in thin samples than in the bulk (2–4). Therefore, across the scale of structures, certain scales can correspond to specific properties. For example, modulus as measured by standard ISO tensile test with specimen cross-section 4 mm by 10 mm scales to volume fraction crystallinity in semicrystalline polymers, but yield stress, deformation, and crack

initiation and propagation may well relate to processes in amorphous, interlamellar regions or near molecular scale events five to six orders of magnitude in scale lower than that of the specimen geometry.

A general problem of all electron microscopic tests of polymers *in situ* is radiation damage. Polymers, as organic materials, are particularly sensitive to electron-beam irradiation with several primary effects (eg, ionization, rupture of chemical bonds) and secondary effects (eg, mass loss, cross-linking, reduction in crystallinity, charging up). The sensitivity to irradiation decreases with increasing carbon content in the polymeric material, for example in the sequence polytetrafluoroethylene (PTFE), poly (vinyl chloride) (PVC), poly(methyl methacrylate) (PMMA), polycarbonate (PC), polyethylene (PE), and polystyrene (PS) (9). Irradiation damage occurs very quickly during irradiation in the electron microscope. Such damaged specimens are frequently well suited for investigating morphology (10) (except by means of electron diffraction), but are not appropriate for tests *in situ*. The damage of the specimen can be somewhat reduced by taking precautions in the instrumentation and manner of operation (eg, use of "low dose" technique, highly sensitive photographic material, or of electronic image intensifiers with coupled image recording, application of higher acceleration voltage in an hvem) (2,11).

An additional problem associated with the direct investigation of polymeric materials by electron microscopy is in the usually low contrast between structural details. In connection with deformation, the effect of "straining-induced contrast enhancement" is of particular importance. Structural elements, such as particles, which possess a smaller Young's modulus than the surrounding material, show a preferred extensibility or deformation during stretching of the sample. In the direction of the electron beam, the thickness of the sample decreases at these places, thus causing a difference in the intensity of the transmitted electron beam and an enhanced contrast (2,10).

Scattering (Diffraction) Techniques

Different methods of measuring the scatter function of corpuscular as well as wave radiations are used for indirect measurements of microscopic heterogeneities or changes in morphology, which develop under the action of load, especially development, distribution and size of crazes and craze fibrils in amorphous and rubber-toughened polymers, and change of lamellae in semicrystalline polymers (see SCATTERING).

As it is well known from the principles of light and x-ray optical instruments, irradiation of a material having periodic structures results in interference phenomena when wavelength of the incident radiation and structural periodicity are in the same order of magnitude. X-ray diffraction was the first direct evidence for the presence of periodicity in inorganic crystalline solids. Correlation between wavelength of the incident ray, structural periodicity in the material under examination, and diffraction angle is expressed by Bragg's Law (1913). Although Bragg's Law was primarily used to explore the atomic structure of these solids, different diffraction techniques have been developed to study the structure of all states of matter with different beams, such as ions, electrons, neutrons, and

protons, whose wavelength is an integral multiple of the distance between two- or three-dimensional periodic structures.

Different types of radiation interact elastically with different structural units of the material to be investigated. So x-rays are scattered on electronic cloud, while electrons are deflected in the electric field of atomic nuclei. An exception includes neutron scattering where wavelength of incident radiation is larger than the diameter of atomic nuclei, so that scattering is independent on diffraction angle but depends on differences of scattering cross sections of atomic nuclei.

Wide-angle x-ray scattering (waxs) enables us to study changes in crystallinity and orientation (texture analysis) and, for instance, processes of lamellae twisting in semicrystalline polymers (12).

Small-angle x-ray scattering (saxs) is used to study fibrillar and lamellar structures and detects appearance of microcavities (13), eg, microvoids between craze fibrils and interfibrillar spacing (14). Using intense x-ray radiation from a synchrotron source, real-time measurements can be performed in a low speed and frequency range (15–19). Thus, some insight into stretching and buckling of craze fibrils during fatigue (17) and in development of crazes in PC during loading is gained (18).

Small-angle light scattering (sals) can be used if polymers are able to scatter light because of density or birefringence fluctuations in the order of wavelength of the light, eg, in the case of spherulites.

Small-angle scattering of electrons (saes) (15) can be performed in a tem using ultrathin specimens, yielding long periods of regular deformation structures (eg, craze fibrils). However, electron diffraction is seldom used for research of polymeric materials, since it needs a very long camera length and, therefore, a high apparative expenditure. A recent, and very convenient alternative method is the Fourier transform analysis of electron micrographs (2).

Small-angle neutron scattering (sans) enlightens the fluctuation of density, concentration, and magnetic properties in the material and, therefore, it enables investigation of changes of conformation of macromolecules and makes it possible, in combination with the other scattering techniques, to compare structures of crazes grown in samples of different thicknesses (19).

Interference Optics

In transparent materials, the classical methods of light-optical interference are widely used in the determination of small dimensions that are of the order of the wavelength of light. Successful applications are investigations of the micromechanics of crazes at crack tips in transparent glassy thermoplastics (20). Usually, fracture-mechanics specimen are used with an artificial crack and a craze ahead of the crack tip. The specimen, with a polished surface adjacent to the optical arrangement, is illuminated in reflection with monochromatic light under normal incidence and normal to the crack plane. Typical fringe systems appear because of the interference between reflections from the two crack faces and at the two boundaries between crazed and uncrazed material. From the accurately determined positions of the individual fringes and with the knowledge of the refractive index of the craze, the crack openings and craze thicknesses can be calculated.

The interference-optical method can easily be applied to static or very slow-moving cracks. Special experimental arrangements are necessary to investigate short-time problems of fast-moving cracks or high frequency fatigue.

Other optical methods include the shadow-optical method of caustics based on the deflection of light by the elastic-stress field around the crack tip. It gives direct information on the stress-intensity factor or the strain–energy release rate (21).

Spectroscopic Techniques (Rheooptical Methods)

A rheooptical method includes a mechanical test under static conditions (tensile test, stress relaxation, cyclic test) carried out simultaneously with an optical measurement. Among other optical methods such as x-ray scattering, nmr spectroscopy, polarized fluorescence or birefringence, the Fourier transform infrared (ftir) spectroscopy has become one of the most frequently applied tools in rheooptics (22). Advantage of infrared spectroscopy is its sensitivity, rapidity, and the ability to investigate changes of molecular orientations not only in separate structural units but also in various phases of multiphase systems. From the ratio of intensities of beams polarized parallel and perpendicular to the deformation direction, orientation functions can be calculated.

The ftir measurements can be performed both in transmission and in reflection mode. The transmission mode requires thin samples with thicknesses up to 500 μm depending on the nature of the material and the intensity of the interesting bands. No limit is in the reflection mode, but an extremely flat sample is required. The difficulty of rheooptical ftir spectroscopy is to find suitable bands for quantitative orientation measurements.

Microindentation Hardness

The indentation test is one of the simplest ways to measure mechanical properties of a material. The micromechanical behavior of polymers and the correlation with microstructure and morphology have been widely investigated over the past two decades (23). Conventional microindentation instruments are based on the optical measurement of the residual impression produced by a sharp indenter penetrating the specimen surface under a given load at a known rate. Microhardness is obtained by dividing the peak load by the contact area of impression. From a macroscopic point of view, hardness is directly correlated to the yield stress of the material, ie, the minimum stress at which permanent strain is produced when the stress is subsequently removed.

Although hardness derived from residual impression measurements is an indicator of the reversible plastic deformation processes, information about elastic release of the indentation depth is mostly lost. Continuous load-displacement monitoring (as the indenter is driven into and withdrawn from the film) substitutes the imaging method used in conventional microindenters. The need to characterize the surface of very thin films and near surfaces has led to the development of ultra- and nanoindentation testers with indentation depths within the submicrometer scale

Other Techniques

Additional details of micromechanical properties can be studied using several other techniques. These additional techniques include the following:

(1) **Dynamic mechanical relaxation tests:**

measurement of molecular mobility in different polymer phases as a function of temperature (24).

(2) **Nuclear magnetic resonance (nmr):**

determination of molecular mobility (25).

(3) **Electron spin resonance (esr):**

measurement of chain scission and radical formation (13).

(4) **Acoustic emission (AE):**

study of fracture processes, eg, rupture of fibers in fiber-reinforced thermoplastics (26).

(5) **Acoustic microscopy (ultrasound acoustic microscopy):**

determination of cracks near a surface (27).

Classification of Micromechanical Properties

The mechanical behavior of materials under stress can be graphically illustrated by macroscopically determined stress–elongation curves and characterized by typical values of moduli, strength, yield stress, strain, toughness, and others. Different types of stress–strain curves are schematically shown in Figure 3, which are connected with different groups of micromechanical processes.

Type a: Linear increase of load with very high modulus and strength with a low elongation at break; behavior is typical of high strength fibers (eg, highly oriented fibers of PE with ultrahigh molecular weight) and is mainly determined by the structure of microfibrils, appearance of molecular defects, and entanglements.

Types b and c: Nearly linear increase of load with high modulus up to a relatively high strength with quasibrittle fracture (type b) or semiductile behavior (type c) with a relatively small elongation at break. Examples are the amorphous

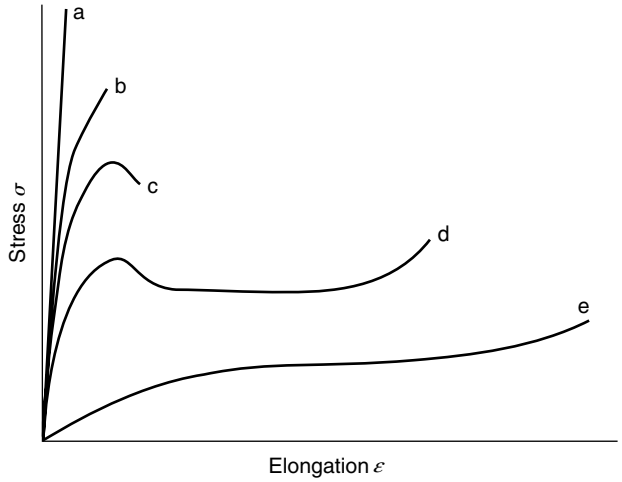

Fig. 3. Characteristic types of stress–elongation curves of polymers. See text for a description of types a–e indicated in the figure.

glassy polymers PS, SAN (styrene–acrylonitrile), and PMMA and the amorphous ductile polymers PVC and PC. Micromechanical properties are connected with local yield processes (see "Plastic Deformation Processes" below).

Type d: After a more or less pronounced yield point at a medium stress, a large elongation appears at nearly the same load (cold drawing). The ductile fracture can be preceded by an additional increase of load (strain hardening). Typical examples are the rubber-toughened or high impact polymers (HIPS, ABS, ACS) and the semicrystalline polymers PE or PP. Micromechanical mechanisms are discussed below in "Toughening Mechanisms," "Yielding in Semicrystalline Polymers," and "Yielding in Block Copolymers."

Type e: Slow and continuous increase of load, homogeneous deformation, and fracture at large elongations. This behavior is typical to rubber and rubber-like materials.

The curves in Figure 3 illustrate the deformation behavior of different polymers at room temperature. However, nearly all polymers can be made to show tensile engineering stress-engineering strain curves a–e dependent on temperature, strain rate, geometry, and stress state.

Plastic Deformation Processes in Amorphous Homopolymers

Local plastic deformation processes in amorphous glassy or semiductile polymers (corresponding to curves b and c in Fig. 3) may appear at different scales, and are sketched in Figure 4. Also in macroscopic brittle materials, macromolecular segments are deformed (eg, by stretching or disentanglement) until chain scission and microvoid formation occur at highly localized places of stress concentration on a microscopic scale (nanometer scale). A relatively sharp crack propagates without large energy absorption and produces a brittle fracture (on the top in

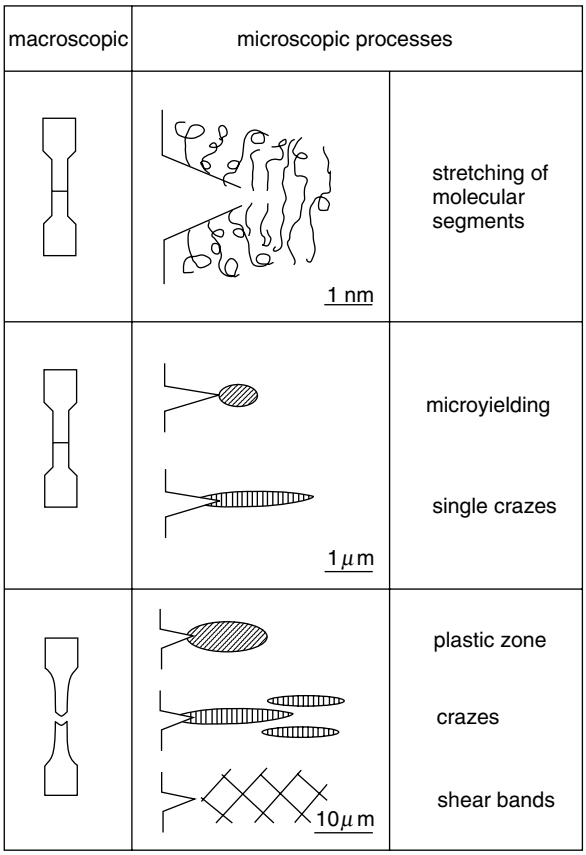

Fig. 4. Schematic representation of basic mechanisms of local, plastic deformation on different scales in amorphous polymers (group I mechanisms). The left shows what is visible on the macroscopic scale, while the center illustrates the microscopic processes, as described on the right (hatched areas are plastically deformed).

Fig. 4). Semibrittle materials show a small volume of plastically stretched polymeric material ahead of a crack tip on a micrometer scale, eg, in the form of crazes or shear bands. Macroscopic fracture is quasibrittle or semiductile, occasionally with necking. Larger plastic deformation involves large volumes on a mesoscopic scale (10-μm scale), including formation of larger or multiple crazes or shear bands. In this sequence (from top to bottom in Fig. 4), the plastic deformation involves larger volumes, yielding an increase in the amount of energy absorption (an increase of toughness).

Crazing in Amorphous, Glassy Polymers. Deformation structures typical of amorphous, glassy polymers are the so-called crazes. Crazes are long, narrow plastic deformation zones, sharply delimited from the surroundings (28). Polymeric material is to a high degree plastically deformed in crazes (in PS usually up to about 150–250%). Figure 5a shows a craze in PS having well-ordered thin fibrils of 5–20 nm in diameter, running in the direction of tension, whereas the longitudinal directions of the crazes are perpendicular to the tension. An

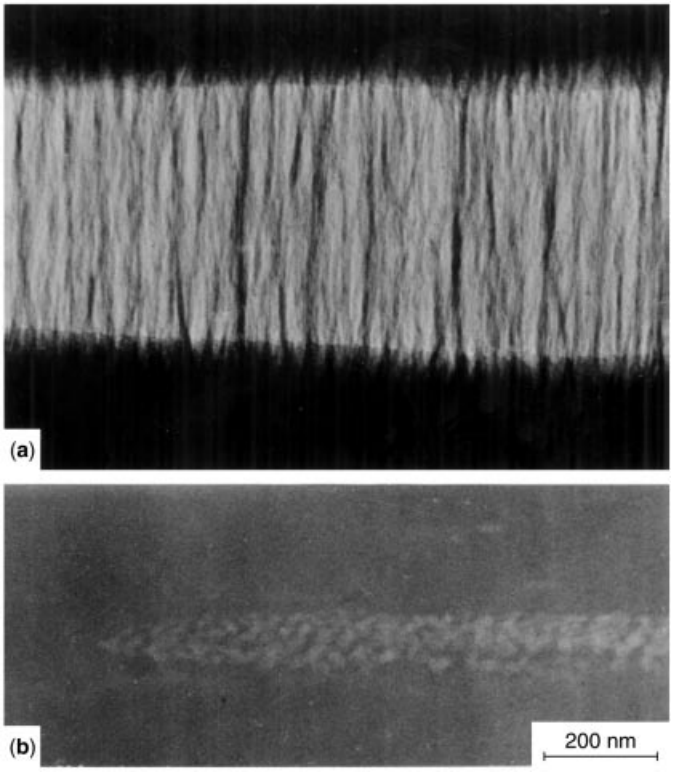

Fig. 5. Structure of a craze in PS (deformed semithin section in HVEM). (a) Fully developed craze with a clearly pronounced fibrillation; (b) domain-like structure of a pre-craze ahead of the true craze.

advantageous method of determining the center-to-center distance of fibrils is optical diffraction of electron micrographs, proving center-to center distances of 10–50 nm (2). The structure first visible ahead of the craze tip, ie, in the transformation or processing zone of the craze, is shown in the micrograph of Figure 5b, revealing bright "domain"-like spots of 20–50 nm in diameter. There is a critical minimum diameter $d_{\min}$ of less than 20 nm of the domains. These domains appear brighter than the surrounding material as they are slightly plastically deformed. All domains are arranged in a narrow band with a thickness of a few tens of nanometers and a length of usually some micrometers. These zones ahead of the fully developed crazes are called "pre-crazes" (2,29). They considerably contributed to better understanding of the formation mechanism of crazes.

The initiation and formation of crazes can be discussed in connection with the entanglement model (30,31). In amorphous polymers, the macromolecules are assumed to form topological links, ie, the so-called entanglements, responsible for strength and deformability of the polymeric material. Entanglements are formed only if the length or molecular mass of macromolecules are high enough (existence of a critical entanglement molecular mass, about 17,500 for PS). Adjacent entanglements can be considered to form a network. The average diameter of the

meshes of this network in PS is about 15 nm (with an entanglement distance of ~10 nm). The material between the entanglements (ie, in the meshes of the network) is assumed to be mechanically weaker. During stretching, the meshes are preferentially deformed, yielding the domain-like structure of the pre-crazes (Fig. 5b). After stronger deformation the domains rupture, forming microvoids. The entangled material between these microvoids is plastically stretched and transformed into the fibrils of a developed craze (Fig. 5a). During this process the microvoids coalesce partially and are transformed from a closed cell structure into an open cell structure. This crazing mechanism based on such an "entanglement network model" or "domain model" (31) probably describes details of formation of fibrillated crazes better than other models.

The fibrillar structure of the crazes is typical of PS. Another glassy polymer is styrene–acrylonitrile (SAN) copolymer with a PS content of usually about 74%. In this material the dominant deformation structures are homogeneously deformed zones, but in many cases they coexist with the fibrillated crazes (2,29). Depending on the loading conditions (stress state, loading velocity, temperature), the deformation character can be shifted from one to another. Another typical glassy polymer is PMMA with a typical appearance of homogeneously deformed crazes at room temperature (29).

Measurement of microindentation experiments on crazes in the micron range revealed additional information about micromechanical properties of the craze fibrils (32). The craze zones' microhardness was determined and the elastic moduli of the crazed material were calculated from the elastic recovery curves of indentations. The crazes were created in miniaturized tensile samples of some amorphous polymers (PS, SAN, PMMA, PVC) during slow crack propagation under fatigue loading at room temperature. The calculated elastic moduli of the stretched material inside the crazes are higher than those of the bulk material. This is consistent with the concept of the oriented entanglement network and the highly oriented polymer chains within the craze.

The transition from the undeformed glassy polymer to the highly plastically deformed crazes at temperatures below the glass-transition temperature can also be discussed in connection with the universal appearance of multiple glass-transition of macromolecules (33). The basic idea is that a localized stress concentration increases the local free volume and reduces locally the glass-transition temperature to the level of test temperature. Therefore, the increase in external stress results in a step-by-step transition from the glassy behavior of the undeformed polymer material to more flexible modes and a mobile state of macromolecules. The rapid changes of macromolecular mobility in dependence on stress state were demonstrated by electron microscopy of the pre-craze structures and the corresponding real crazes (34).

Although crazes are typical of amorphous glassy polymers, crazes or craze-like features have also been observed in many other amorphous polymers (see below), semicrystalline polymers (eg, in PE, PP, PA), and in rubber-modified high impact polymers (eg, HIPS, ABS). In the literature they were often designated as microcracks, deformation zones, or yield zones (28).

Yielding in Amorphous Ductile Polymers. Typical amorphous ductile polymers are PVC and PC. Deformation at room temperature results in the

formation of shear bands or homogeneous deformation bands (2,29). It is generally accepted that crazes with a fibrillated internal structure appear if the entanglement density is low, ie, if the distance between entanglements is large (as in PS) (28,30). With decreasing entanglement distance (or molecular weight), there is a transition to a finely fibrillated form of crazes and to homogeneous deformation bands.

The influence of entanglement density on internal structure of crazes and deformation bands can be demonstrated by a special effect in PC (as an example of a high-temperature-resistant polymer). Usual bisphenol A polycarbonate (BPA-PC) shows a glass-transition temperature T_g of 148°C and chemically modified versions on the base of trimethylcyclohexane (TMC-PC from Bayer AG) reach a T_g of 238°C because of a reduced chain mobility. Because of the good compatibility with usual PC, blends with T_gs between 148°C and 238°C are available (35). Here, blends with T_g of 180°C and 200°C are used (called PC-2 and PC-3, respectively). The usual PC as well as the types with higher glass-transition temperatures show a characteristic transition in the deformation behavior. At room temperature and somewhat higher temperatures, typical shear bands and homogeneous deformation zones appear. At temperatures between 60 and 80°C below the particular glass-transition temperature, there is a transition into the formation of fibrillated crazes. With increasing deformation temperature, the fibrillation of the crazes becomes coarser (increase of the long period of fibrillation). This effect is summarized in Figures 6 and 7.

These transitions in the deformation character can be understood by processes on the macromolecular level. With increasing temperature, the stress necessary for thermally induced disentanglement drops more rapidly than the stress necessary for molecular mobility (yield stress). There are three regions depending on temperature of deformation:

(1) $T \approx$ RT (well below T_g): High entanglement density and high macromolecular mobility (yield stress lower than disentanglement stress) result in homogeneous yielding (shear bands and deformation zones).
(2) $T \approx T_g - \Delta T$ (ΔT = 60–80°C): Thermally induced disentanglement (reduced disentanglement stress up to the range of yield stress or reduction of entanglement density) results in the transition from homogeneous yielding to crazing.
(3) $T < T_g$ ($T \approx T_g$): Intense thermally induced disentanglement (lower disentanglement stress than yield stress) results in coarsening of craze structure with increasing fibril thickness and fibril spacing.

The effect of coarsening of the fibrillar structure of crazes with increasing temperature below the glass-transition temperature has been also found in SAN and PC by electron microscopy and saxs (34).

Fibrillated crazes are usually thinner than the homogeneous deformation bands. Therefore, the whole content of polymeric material, which is plastically deformed, is smaller in the crazes and larger in the shear bands or deformation zones. The result is shown macroscopically in the unusual effect of a decrease of toughness and an embrittlement with increasing temperature.

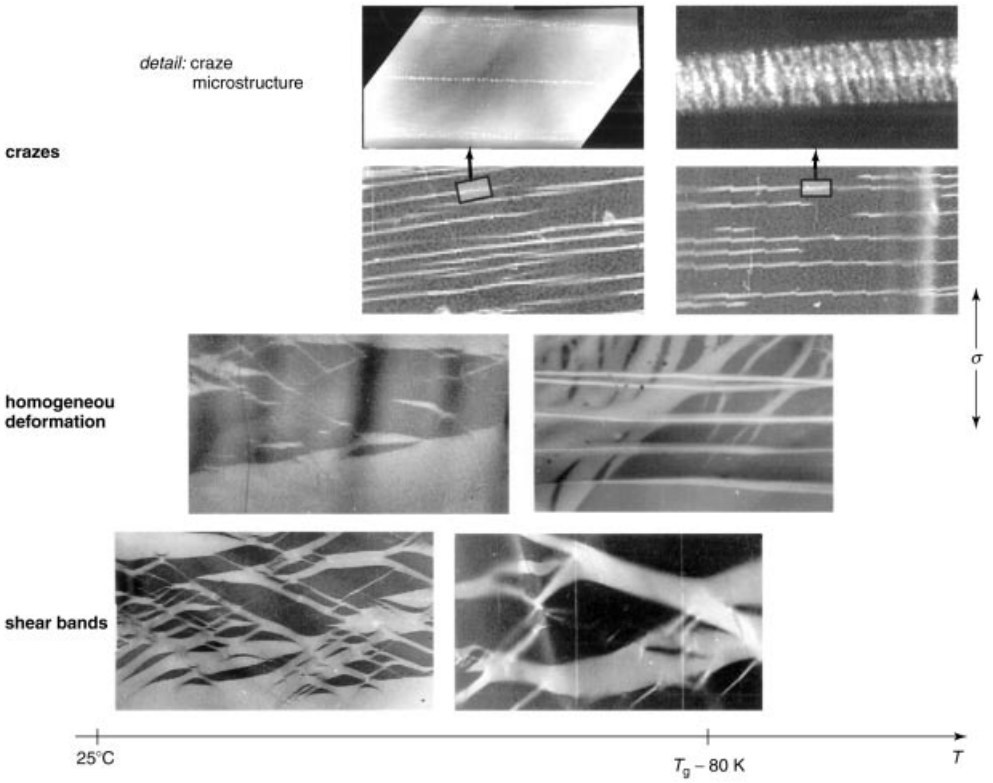

Fig. 6. Influence of the deformation temperature T on type and internal structure of deformation zones in PC (RT = room temperature, T_g = glass-transition temperature; deformed thin specimens, 200-kV tem).

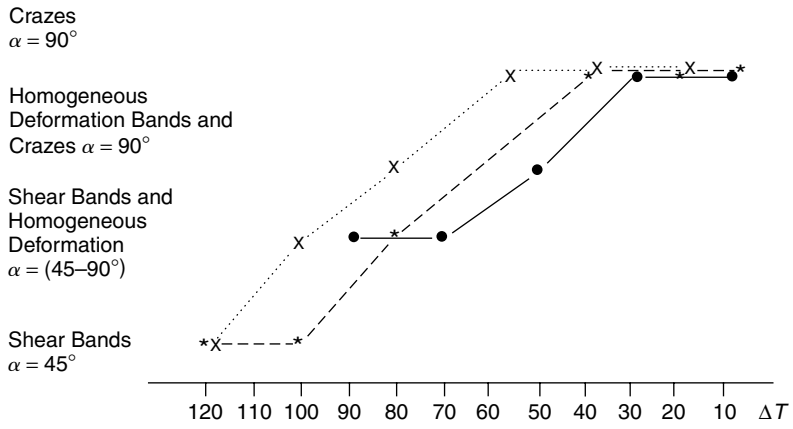

Fig. 7. Schematic drawing of the transition in the deformation behavior in dependence on the difference between test temperature T and glass-transition temperature T_g of usual and high temperature PC ($\Delta T = T_g - T$; α = angle between length orientation of the deformation bands or crazes and direction of loading; T_g of materials used: usual BPA-PC, 148°C; PC-2, 180°C; PC-3, 200°C). x ..... PC-3; ∗—— PC-2; ·—PBA-PC.

Mechanisms of Enhancing the Toughness in Heterogeneous Polymers

The toughness of a material can be enhanced by increasing the ability of the material to deform plastically. This is achieved in toughening mechanisms (see IMPACT RESISTANCE). The idea common to all of these mechanisms is the initiation of a very large number of very small local yield events. Mechanisms that have been discussed and that have been carried out in practice are sketched in Figure 8. Type A involves the initiation of a large number of microcracks by (usually) inorganic particles, short fibers, or something similar; because the increased energy absorption occurs only through the creation of new internal surfaces, a noticeable effect is to be expected only in very brittle material or at low temperatures. In type B, ductile particles, distributed in a brittle matrix, are plastically stretched in the area of the crack tip, bridging the two crack surfaces. This "bridging mechanism"

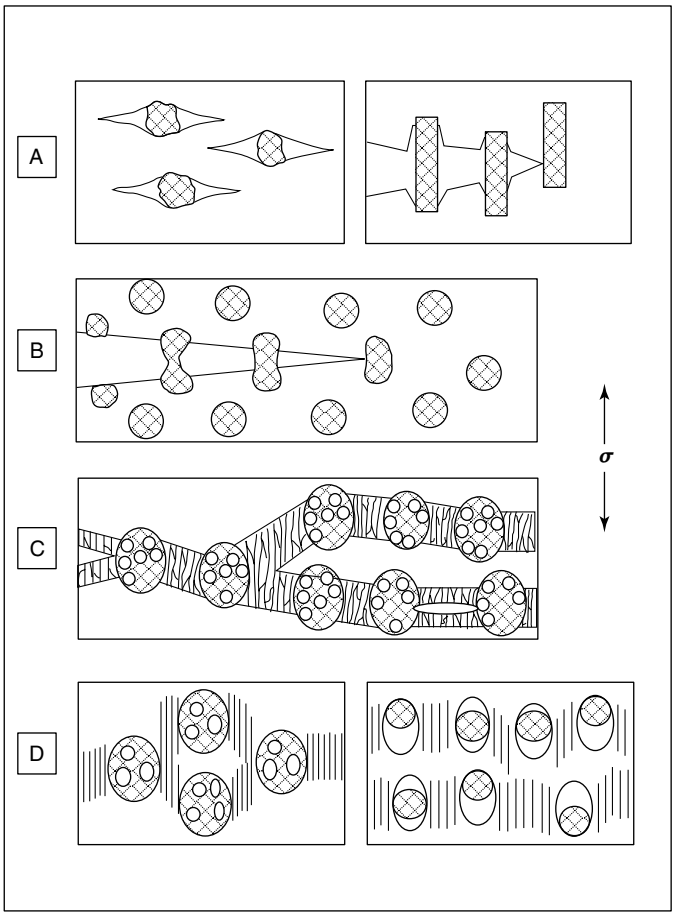

Fig. 8. General mechanisms of enhancing the toughness of structurally modified polymers-group II mechanisms (in the boxes the crosshatched areas are inorganic particles, fibers or weak (rubber-like) particles distributed in a bulk matrix polymer; σ indicates the applied tension stress).

is also effective only in brittle materials, such as in epoxies (of course, it appears also in rubber-toughened polymers, but not as a main energy-absorbing factor). Types C and D behavior involves the initiation of a large number of small plastic zones (crazes or shear bands), induced by stress concentration at soft structural heterogeneities, eg, rubber particles. While in type C stress concentration at the soft rubber particles is sufficient for craze initiation [this mechanism is the typical mechanism of high impact polystyrene (HIPS)], in type D cavitation inside or at the particles is necessary for intense plastic yielding between the particles (typical of toughened semicrystalline polymers such as toughened PP or PA).

A precondition of toughness enhancement is prevention of premature crack propagation; there are some "crack stop mechanisms" including effects of crack tip blunting, reduction of critical stress concentrations, or reduction of crack length and crack propagation velocity (2).

Toughening of a brittle matrix polymer by rubber particles with a volume content of about 5–25% is of major importance to the plastic industry. It has proved so effective that the technology has been extended to almost all of the commercial glassy thermoplastics (including PS, SAN, PMMA, PVC), many semicrystalline polymers (such as PP and PA), and several thermosetting resins. Rubber toughening of polymers involves three important steps of deformation, which can be summarized in a so-called "three-stage mechanism of toughening" (2,36) (see Fig. 9).

(1) The first step at individual rubber particles is stress concentration σ_K and often cavitation inside the rubber particles.
(2) If the particle volume content is in average above 10%, a remarkable superposition of the individual particle stress fields appears. The result is a higher stress concentration σ_K' and the more intense initiation of local matrix yielding in the form of fibrillated crazes, homogeneous crazes, or shear yielding.
(3) The third step is stabilizing the deformation structure by preventing a premature crack propagation (by crack stop mechanisms such as limitation of crack length or crack tip blunting at or in the rubber particles) and by stabilizing the rubber particle cavities due to the plastically deformed adjacent rubber and matrix strands.

The dominant matrix deformation mechanism depends mainly on the type of matrix material, but strongly also on test temperature, strain rate of testing, and on type, shape, and size of rubber particles (2,36–38). Fibrillated crazes are typical of toughened PS (HIPS), a coexistence or a transition from fibrillated crazes to homogeneous ones is typical of toughened SAN (ABS), homogeneous deformation appears in many grades of ABS, toughened PVC, and toughened PMMA. Shear yielding is the dominant mechanism of the toughened semicrystalline polymers PA and PP.

Rubber toughening is often assumed to be identical to the modification by rubber particles. However, there is an alternative and also very effective possibility of rubber toughening of amorphous polymers—the *rubber network toughening* (2). Here, small thermoplastic particles, eg, PVC particles (about 1 μm in diameter),

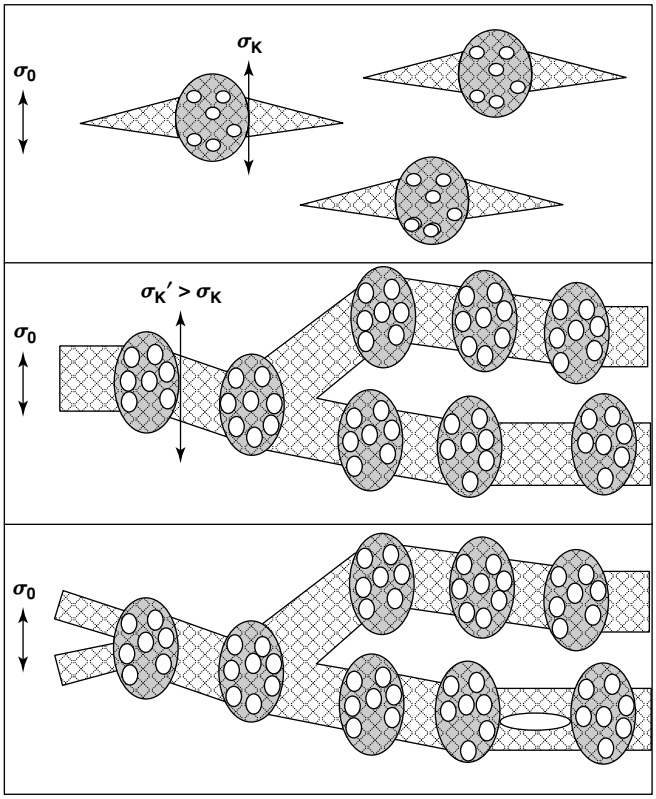

Fig. 9. Schematic presentation of the three-stage mechanism of toughening with multiple initiation of local yield events (eg, crazes as in case C in Fig. 8).

are embedded by a network or honeycomb structure of rubber (for instance EVAc). Since there are very tiny network layers in the range of a few tens of nanometers, the rubber content is usually below 10%, ie, the PVC content reaches more than 90%. During loading, the rubber network is stretched, which initiate the PVC particles to yield and to absorb deformation energy. A deformation mechanism similar to the network toughening is the so called *inclusion yielding*, where stiffer thermoplastic particles are distributed in a somewhat softer matrix (eg, SAN particles distributed in a PC matrix) (39). Under load, the particles are forced to deform plastically. Both mechanisms demonstrate the possibility to transform stresses via a softer matrix, which are high enough to reach the yield stress of the stiffer particles.

Most of these micromechanical processes are highly localized and depend strongly on the local morphology. Therefore, direct imaging by electron microscopy techniques with a high local resolution are of particular importance, and most of our knowledge of rubber toughening arises from the application of such techniques (2,36–38).

Toughened Polymers with Amorphous Matrix. The fundamental deformation step is the formation of crazes in the stress field around the rubber

particles (ie, in the zones of highest stress concentration, the equatorial zones around the particles). It can clearly be shown that crazes start in the matrix directly at the interface to the rubber particles. If the distance between rubber particles is small enough, crazes are intensively formed between the particles (cf Fig. 9).

HIPS deforms generally by formation of fibrillated crazes, whereas many ABS grades show the formation of fibrillated crazes and homogeneous crazes (homogeneous deformation bands, shear deformation). A transition between these deformation modes appear in dependence on loading velocity and particularly on test temperature. Such transitions can be advantageously studied by electron microscopy and using a special tensile holder with cooling and heating facilities (40).

Very fine and well-dispersed morphologies can be obtained by blending the glassy polymer with core-shell particles. Successful materials possess three-stage core-shell particles (40). In the example used here, the particles consist of a single core of PMMA, surrounded by a 20-nm thick inner shell of grafted and lightly cross-linked poly(butyl acrylate-*co*-styrene) (PBA) and an outer grafted shell of PMMA. This PMMA layer is about 10 nm thick, and is sufficiently miscible with SAN or PMMA as matrix materials to provide good adhesion between the modifier particles and the matrix.

The typical micromechanical behavior of this material at room temperature is shown in Figure 10. The lower magnification in Figure 10a shows a dense pattern of cavitated and elongated rubber particles and plastically deformed matrix material between the particles. The matrix deformation occurs mainly in the form of homogeneous shear deformation zones and a small number of short and relatively thin fibrillated crazes (40).

The cavitation mechanism within the modifier particles begins with microvoid formation and fibrillation in the butyl acrylate shell, as shown in higher magnification in Figure 10b. The fibrillated shells with the internal PMMA cores resemble spiders. The fibrils are connected by the PMMA cores, and the cavities in

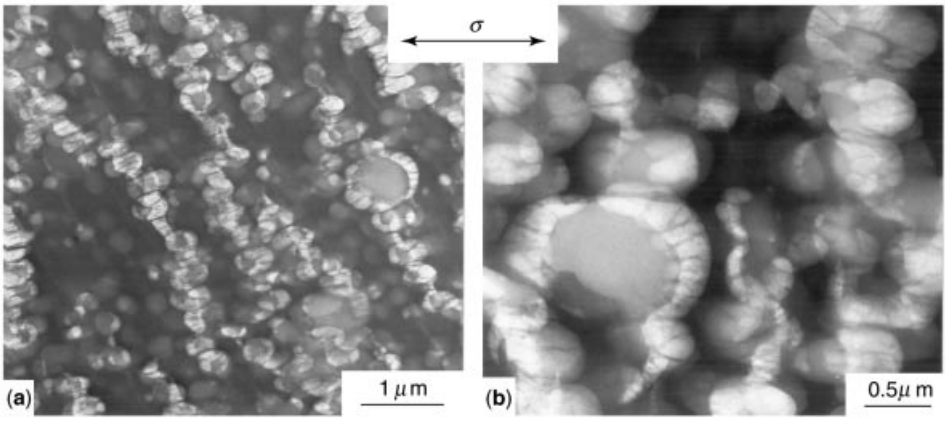

Fig. 10. Deformation structures of an SAN/PBA blend. (**a**) lower magnification; (**b**) higher magnification (tem micrographs, deformation direction, see arrow).

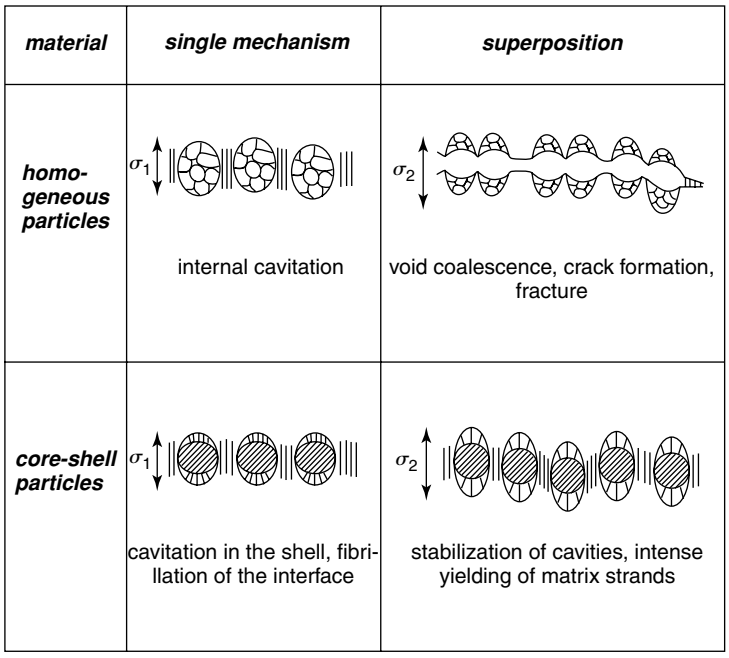

Fig. 11. Comparison of the action of homogeneous and core-shell particles in toughened polymers concerning the single mechanism at particles and the superposition effect between particles.

the PBA shells are limited in their size by the fibrils between the core and the outer shell. This stabilization of cavities by the core-shell structure is an advantage of this type of particles over homogeneous rubber particles. This remarkable difference between homogeneous rubber particles and core-shell particles is sketched in Figure 11. In both cases, the starting mechanisms of cavitation inside the particles, stress concentration at the surface of the particles, and initiation of plastic yielding of adjacent matrix parts are very similar. However, if we consider later stages of deformation, superposition of stresses between the particles occur and differences become visible. In the often possible case of closely connected homogeneous rubber particles, the voids inside the particles can coalesce, leading to larger voids, crack initiation and, consequently, a premature fracture. Using core-shell particles, the individual microvoids are stabilized in their size, and void coalescence is prevented, with the result of an intense plastic yielding of the matrix.

Usually, the hard polymer cores of the modifier particles are not deformed, as is visible in the micrographs of Figure 10. This is usually accepted since it hardly seems possible to deform a glassy polymer core inside a rubbery shell. However, there are results that show that a plastic yielding of the hard cores should be possible: fibrils are drawn out from the PMMA cores, leading to a flattening of the cores. The stretching of the cores into fibrils is very similar to the mechanism of fibril drawing in craze formation. This mechanism of yielding of glassy cores inside modifier particles is a new toughening mechanism, contributing to energy absorption during deformation (1,40). A precondition to this effect is that the rubbery shell of the modifier particles forms fibrils showing a remarkable strain

hardening effect, leading to stresses in the fibrillated shell, which are high enough to draw fibrils from the hard core.

The advantage of core-shell particles to toughen PMMA has been demonstrated by investigation of deformed samples by HVEM (41). Besides core-shell and homogeneous rubber particles, many other types of rubber particles have been studied (eg, cells, drops, coils). A qualitative and quantitative estimation of the size and structure of differently shaped rubber particles on the toughness of modified PS on the basis of detailed electron microscopic studies can be found in Reference 42.

Usually, ABS polymers show a good toughness by an intense formation of stress-induced crazes or homogeneous deformation zones at and between rubber particles. Recently, a surprising effect has been found in some ABS grades: When creep tests were performed with loads well below the yield stress and if the specimens were tested afterwards in the tensile mode, samples broke atypically brittle at a low strain level (43). Such a drastic embrittlement was observed after preloading with stresses between 25 and 55% of the short-term yield stress. Lower and higher preloading stresses yield only a smaller reduction of toughness.

The microscopic investigation revealed the reason of this effect. The materials showing the embrittlement possess a pronounced bimodal distribution of the rubber particles with smaller particles of 50–250 nm and a smaller fraction of bigger ones between 350 nm and 1 μm. During preloading of this material, a few extremely long crazes with lengths up to a few millimeters are formed (Fig. 12). They start at the biggest rubber particles often near the sample surfaces and propagate in a straight line across the material without being influenced by the other smaller particles. It seems that, for the long crazes, the material behaves like a homogeneous material. During subsequent tensile test, cracks can propagate very quickly in these long crazes and initiate the brittle fracture.

This special type of craze, for which ABS had not been known up to now, is called "macrocraze." The formation of macrocrazes correspond to the large distance between the very big rubber particles and can be understood in connection with changes of Young's modulus both of the matrix and the rubber particles during loading. It is known that the moduli of thermoplastics and rubber decrease with decreasing load velocity $\dot{\varepsilon}$ (in tensile test or with decreasing frequency in torsion pendulum test). This is schematically drawn in Figure 12c for SAN matrix and small and big rubber particles, as used in the ABS of Figures 12a and b. The big rubber particles show another constitution than the smaller ones and possess a higher deformability or lower modulus. This is detectable from *in situ* deformation tests of the material in the HVEM (using a technique described in more detail in Ref. 2. Starting with deformation tests with a very high speed (impact test or test at low temperatures below glass-transition temperatures of rubber particles), the modulus of rubber particles is very high, comparable with the modulus of the glassy SAN matrix (the modulus ratio G_R/G_M is nearly 1). Therefore, there is nearly no stress concentration at the rubber particles ($\sigma_c \approx \sigma_0$), and no crazes are initiated. With decreasing test speed (with a load rate in the usual application range or with increasing temperature to room temperature) the modulus of the glassy matrix is unchanged, but the modulus of rubber particles decreases drastically. In this range, the ratios of moduli G_R/G_M are much lower than 1, and the

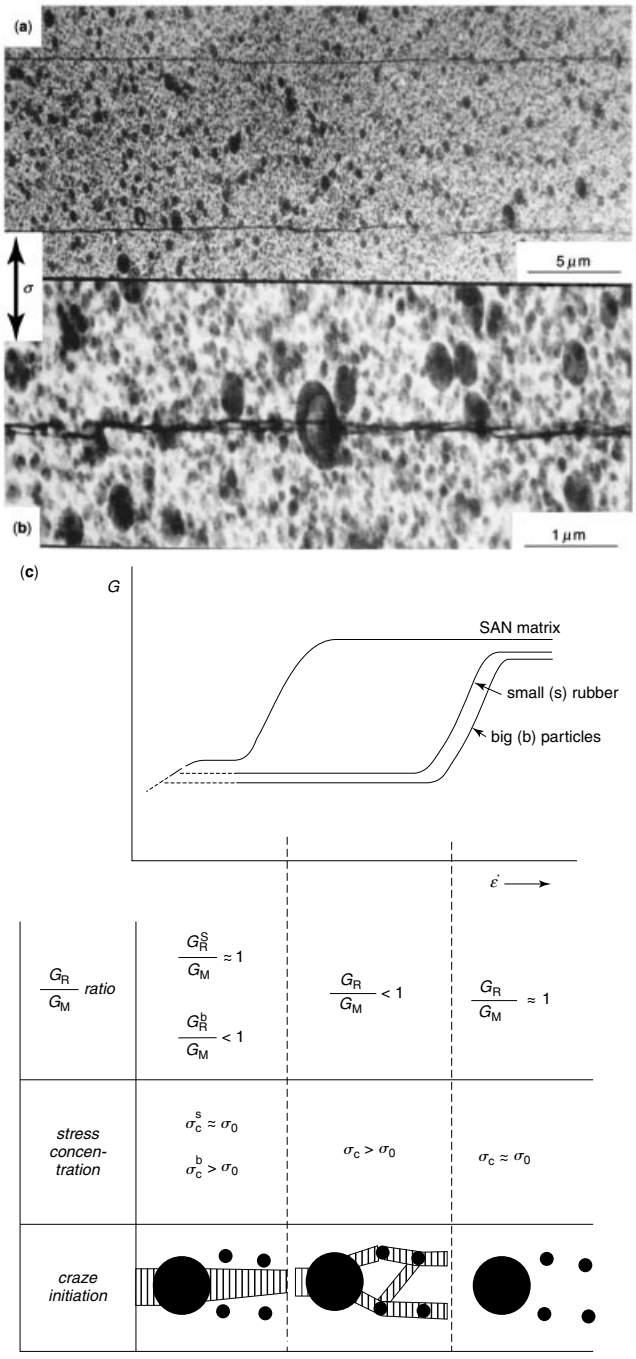

Fig. 12. (**a**, **b**) Formation of very long, tiny crazes (so-called macrocrazes) after preloading in an ABS with only a few large rubber particles (sample preloaded for 166 h with 40% of yield stress, stained with OsO_4, 1-μm thick ultramicrotome section, HVEM). (**a**) general view of two macrocrazes; (**b**) higher magnification of part of a macrocraze; (**c**) schematic of the decrease of the shear modulus G of thermoplastic SAN matrix material and cross-linked rubber with decreasing load rate $\dot{\varepsilon}$ (corresponding to an increased temperature). Below: ratio of moduli G_R and G_M of rubber and matrix, corresponding stress concentration and initiation and propagation of crazes. From Reference 16.

stress concentration at rubber particles reaches a maximum ($\sigma_c/\sigma_0 > 1$). This results in an intense initiation of crazes at larger as well as smaller rubber particles (range of intense plastic energy absorption, range of toughness).

A further decrease of test speed $\dot{\varepsilon}$ down to very low values corresponds to the situation during creep and static preloading. Here, the modulus of the glassy SAN matrix decreases to the level of the rubber. Under the action of a tensile stress this situation can be considered similar to the glass-transition range of matrix material, discussed in detail in References 33 and 34. While the smaller (harder) rubber particles show a modulus similar to the matrix modulus (moduli ratio $G_R^s/G_M \approx 1$) the bigger (weaker) rubber particles are somewhat weaker than the matrix (moduli ratio $G_R^b/G_M < 1$).

Therefore, only the largest rubber particles are able to stress concentrate and to initiate crazes. ABS regions with the smaller rubber particles do not show any differentiation in modulus (they behave like a homogeneous material). Here, the crazes that are initiated at the largest rubber particles propagate without modification and can grow to macrocrazes.

Toughened Polymers with Semicrystalline Matrix. It is well known that toughness of semicrystalline polymers such as PA (polyamide) and PP can be increased similar to the amorphous polymers by the addition of relatively small amounts of rubber particles such as EPR or EPDM. As in HIPS and ABS, the modifier particles act as stress concentrators, initiating a plastic deformation of matrix strands between the particles as the main energy absorption step. In impact-modified PA and PP at room temperature, plastic deformation takes place through shear deformation (mechanism of multiple shear deformation).

In contrast to crazing, shear deformation does not involve dilatation of material, but relief of local plastic constraint by formation of voids and subsequent strain field interactions between voids often enhance localized shear yielding and is an important precondition of effective toughening. Figure 13 shows scanning force micrographs of highly deformed parts of PP toughened by an addition of 20% EPDM rubber particles. The particles are cavitated and fibrillated and, together with the adjacent matrix strands, they are strongly plastically deformed, elongating up to 900%. Details of the influence of particle type, internal structure, and size of particles, as well as of interparticle distance, are discussed in References 36, 44, and 45.

Toughened PP shows a decrease of toughness with decreasing temperature. In stress–strain tests, Young's modulus and strength increase but elongation at break and the area below stress–strain curve (corresponding to toughness) decrease. This change is connected with changes in micromechanical processes. Transmission electron micrographs of PP/EPDM deformed at RT and -40°C are shown in Figure 14. Figure 14b reveals a coexistence of shear yielding and crazing, and Figure 14c shows only formation of fibrillated crazes at and between elongated particles.

The use of core-shell particles has an advantage over homogeneous rubber particles that is very similar to that discussed above (cf Fig. 11). An additional advantage is that they enable a low temperature toughness. Deformation tests of PP with core-shell EPR (ethylene–propylene–rubber) particles at very low temperatures of up to -100°C revealed that the EP shell is cavitated and elongated

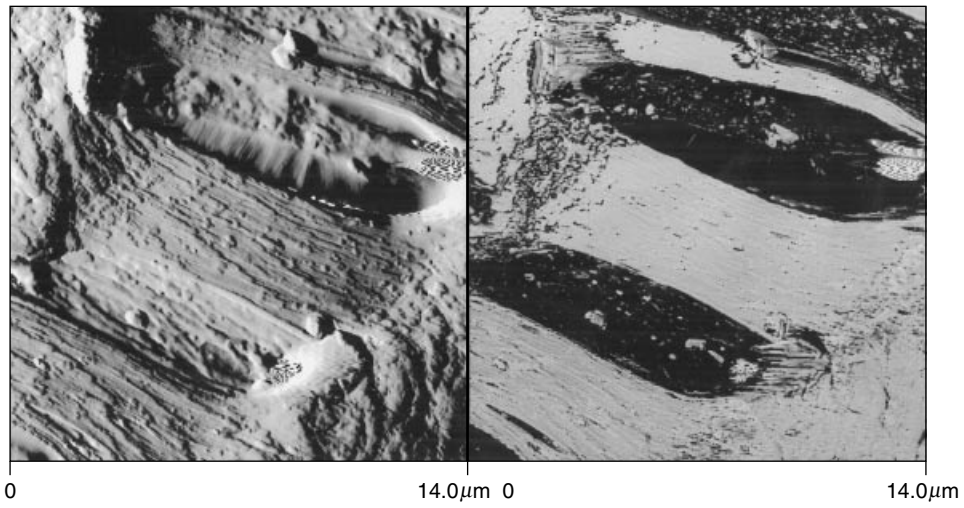

Fig. 13. Scanning force micrographs of a deformed PP/EPDM blend revealing the elongated particles with the highly plastically stretched matrix strands in between (deformation direction from top left to bottom right; sfm tapping mode: left, amplitude signal; right, phase signal).

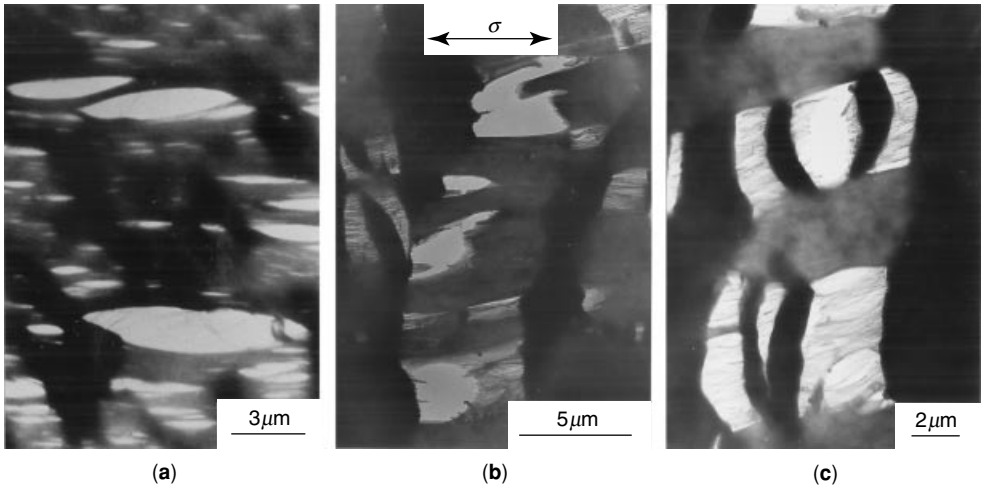

Fig. 14. Deformation structures of PP impact-modified with EPDM at different test temperatures: (**a**) RT – cavitated particles as well as adjacent matrix strands are strongly plastically deformed by shear yielding; (**b**) −40°C—coexistence of shear yielding and crazing; (**c**) −40°C – fibrillated crazes between elongated particles (thin sections, deformed and investigated by hvem (**a**) and tem (**b** and **c**)). From Reference 1.

with fibrillation inside, and the adjacent matrix parts show fibrillated crazes (1). It is an effect far below the glass-transition temperature of the rubber phase, and it demonstrates that toughening processes are not limited by the glass-transition temperature of modifier particles. The important step is local stress concentration at the voided particles, which initiate the formation of crazes. These micromechanical results reveal that it should be possible to increase low temperature toughness

of PP and other semicrystalline polymers. Essential structural preconditions are the use of modifier particles that are able to cavitate and to stabilize cavities so as to avoid growth of voids into cracks.

Polymer Blends. The aim of producing polymer blends is to improve different properties and to reduce costs. There are many publications and books, which review preparation and structure of multiphase polymer blends (38). A central problem is to realize an optimum morphology, eg, an optimum size of particles of the polymer, which is in the minority in a matrix of a polymer in majority. One attractive route to multiphase polymeric materials, which promotes high interfacial adhesion and excellent morphology control, together with related mechanical properties, is *in situ* formation of compatibilizing during reactive blending. Using compatibilizers, the size of dispersed particles in a matrix can be decreased. As shown in Reference 46, the size of PA 6 particles in a PP matrix can be drastically reduced using increasing amounts of an SEBS-*g*-MA compatibilizer, however, not the smallest, but an optimum size and constitution of particles yielding the best properties.

Often, blending a polymer with particles of a second polymer is connected with an increase of toughness. As an example, blends of a metallocene-based high density ethene/1-hexene copolymer (HDPE, density 0.93 g/cm^3) with 20 vol% of an elastomeric ethene/1-hexene copolymer (VLDPE, hexene content 17.2 mol%, density 0.867 g/cm^3) were used as model blends to study the morphology development and the micromechanical behavior (47,48). Use of the sfm tapping mode and a special force modulation technique enabled local deformations of the sample and changes in the morphological structures in a defined specimen area to be recorded directly while the external elongation was successively increased. In order to carry out *in situ* deformation experiments, the sfm was equipped with a deformation unit and a periodic pattern was evaporated on the back side of the sample. Figure 15 illustrates the positioning of the sample. The optical micrographs show an overview (Fig. 15a) of the sample with the evaporated pattern and two artificial notches (diffuse black areas) on the left and on the right, and in Figure 15b the marked area in the sample center. The sfm phase signal image in Figure 15c shows the blend morphology with elastomeric particles (appearing bright) in the HDPE matrix with crystalline lamellae (occurring dark owing to their higher stiffness in comparison to the adjacent interlamellar amorphous areas).

The micrographs of Figure 16 illustrate typical results of the sfm *in situ* tensile test. The images show a sample area of 2 μm $\times$ 2 μm marked in Figure 15c before deformation (at the top) and after a deformation of about 35% (at the bottom). On the left, the height signal images show the surface topography, and on the right-hand side, the sample is visible in phase signal images. A comparison of the micrographs shows that the area between the dotted lines is nearly homogeneously strained. However, deformations on the submicron range are strongly inhomogeneous. Especially, the strong deformation of the elastomeric particles is accompanied by a very heterogeneous deformation of the surrounding semicrystalline matrix. Adjacent segments between particles (perpendicular to the load direction) reveal a considerably increased elongation, whereas segments between particles in the direction of loading are nearly not deformed. This correlates with the distribution of stress concentration around soft particles. Additionally, the behavior of crystalline lamellae under stress can

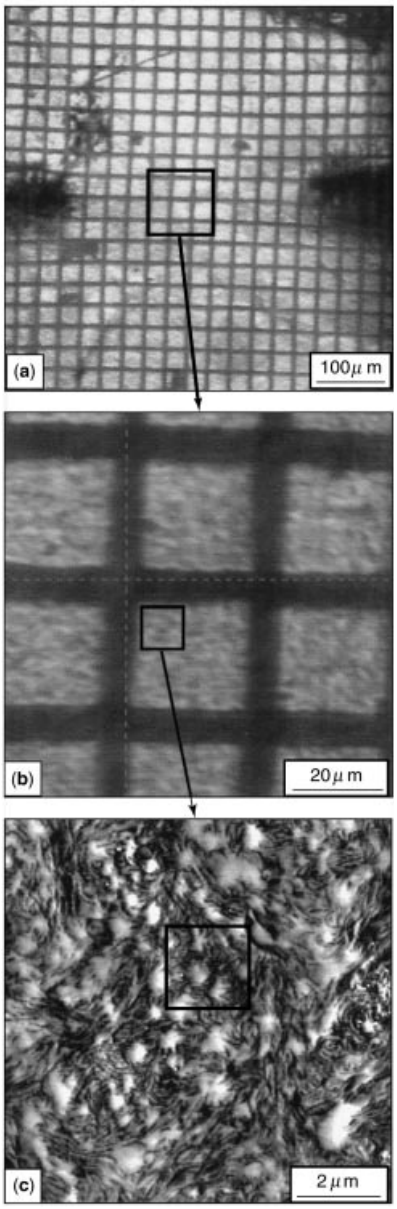

Fig. 15. Specimen from an HDPE/VLDPE blend for *in situ* sfm deformation test with an evaporated pattern to observe an area of interest; (**a**, **b**) optical micrographs; (**c**) sfm phase signal image in tapping mode. From Reference 48.

be directly observed. The appearance of the crystalline lamellae is improved in Figure 17 after an imaging processing by a high pass filter (48). These micrographs very clearly reveal that the lamellae are composed of single crystal blocks (in an appearance as beaded strings). Some types of deformation behavior of lamellae are visible:

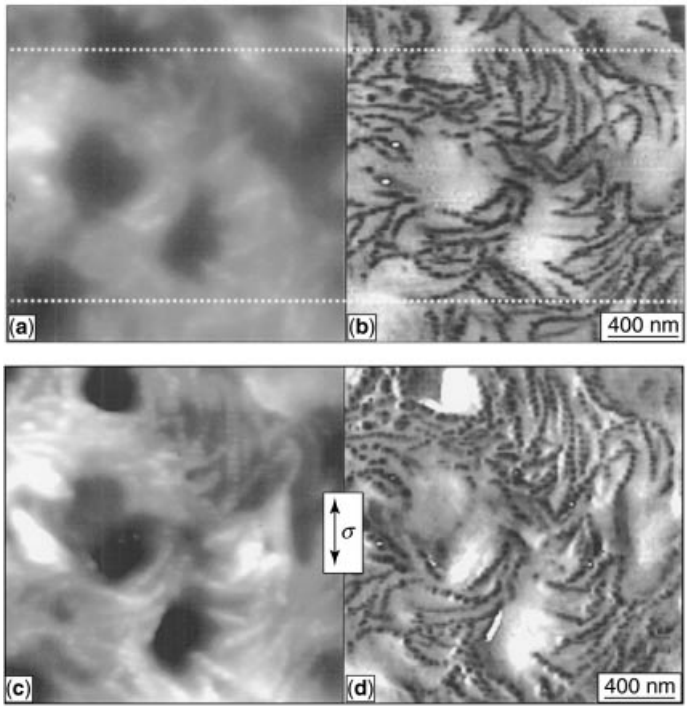

Fig. 16. Marked specimen area from Figure 15 before deformation (**a**, **b**) and after deformation (**c**, **d**) in sfm tapping mode height images (**a**, **c**) and phase signal images (**b**, **d**). From Reference 48.

(1) Lamellar segments perpendicular to the loading direction (segment between the points A and B in Fig. 17) rotate in stress direction without changing the segment length.
(2) Lamellae aligned in loading direction (segment between points C and D) are stretched with an increasing separation of the crystalline blocks.
(3) Lamellae in other orientations show a combination of both effects; for example, segment between the points E and F reveals a rotation and an elongation.

Yielding in Semicrystalline Polymers. In the literature, it is often assumed that the large plastic deformation of the semicrystalline polymers such as PE or PP is a continuous orientation of the chain segments in the deformation direction (ie, a continuous change in the *c*-texture). This assumption is mainly based on x-ray scattering measurements. The result of steadily increasing *c*-axis orientation is based on averages from a relatively large volume of a sample. Direct electron microscopic investigations revealed that the improvement of the *c*-axis orientation results from a superposition of several local deformation processes. In detail, the orientation of PE has been divided into three stages (2,4,49). In the first stage, mainly the amorphous, interlamellar parts contribute to the deformation.

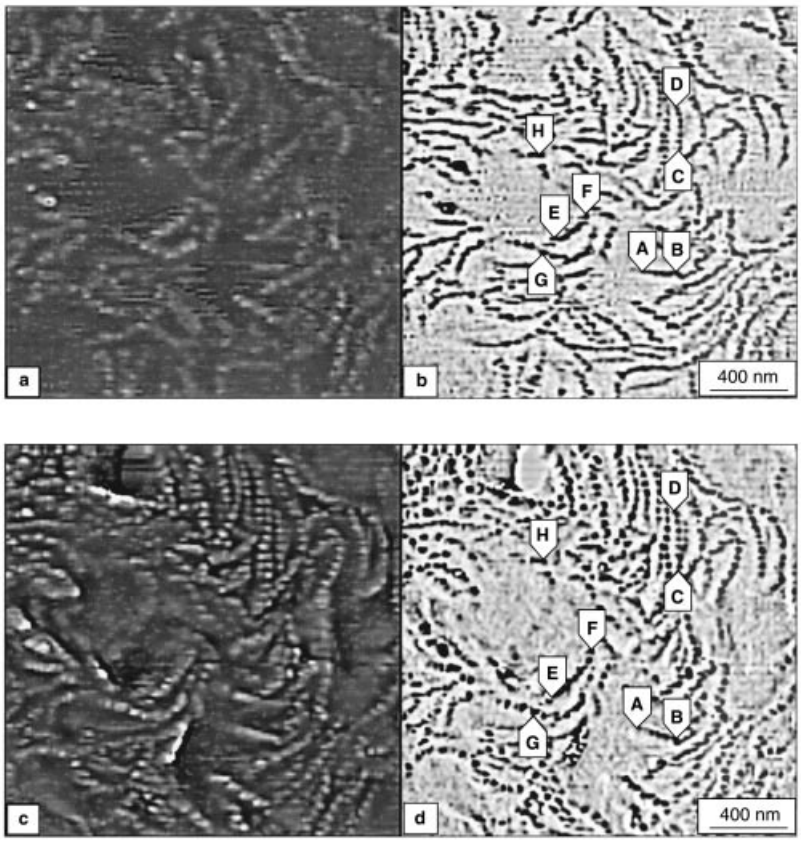

Fig. 17. Micrographs of Figure 16 after additional image processing; the capitals mark lamellar segments under different degree of deformation (eg, twisting, stretching, block separation). From Reference 48.

Larger lamellae can break into shorter pieces, and the lamellae tend to twist with their length direction toward the deformation direction. The processes of twisting and orientation of the lamellae do not appear homogeneously in the whole sample. There are smaller regions with a pronounced or stronger orientation and others with a weaker one. This makes clear that the deformation at the beginning strongly depends on the yield properties of the amorphous material between the lamellae. In the second stage a transition from the lamellar appearance into a microfibrillar arrangement occurs, with the improvement of the *c*-axis orientation in the third stage.

Some aspects of the first stage of deformation are visible in the *in situ* deformation test of a PE blend by sfm in Figures 16 and 17 and are also revealed by tem studies of crack-tip crazes in PE (48).

Yielding in Block Copolymers. While polymer blends show macrophase-separated morphologies, which often lead to a deterioration of mechanical properties because of the immiscibility of the components, in block copolymers microphase-separated structures at the typical size scale 10–100 nm

are observed. A wide spectra of mechanical properties and micromechanical deformation mechanisms are observed in such block copolymers attributable to the existence of a large variety of highly ordered microphase separated morphologies with a periodicity in the range of radius of gyration of the copolymer molecules (50,51). While a great deal of work has been carried out on morphology and phase behavior of these fascinating materials, only a little has been done regarding the correlation between morphology, mechanical properties, and underlying micromechanical processes of deformation and fracture.

Pioneering works on the micromechanical deformation mechanisms in block copolymers date back to the mid-eighties when cavitation mechanism in styrene–butadiene (SB) diblock copolymers containing PB cylinders in a PS matrix was proposed (52,53). Based mainly on tem investigations, a two-step craze growth mechanism was proposed:

(1) In the first stage the PB cylinders are strongly deformed till the cavitation stress of PB is reached. As a consequence, the PB cylinders cavitate resulting in the formation of voids.
(2) In the second step PS is plastically deformed by local stress concentration resulting in a cellular deformation structure.

Mechanical behavior of block copolymers are governed by the molecular architecture (AB diblock, ABA or ABC triblock, $(AB)_n$ star block, etc), symmetry of the blocks, and microphase-separated morphology (50). Most extensively studied and more interesting from the technical point of view are SBS triblock copolymers based on polystyrene and polydienes (PB or PI), where the outer glassy styrene blocks physically cross-link the elastomeric B phase at both the ends. In SBS triblock copolymers of sufficient molecular weight, the mechanical properties can be tailored simply by adjusting its composition. Thermoplastic elastomers having dispersed glassy phase (spheres or hexagonally arranged cylinders) in a rubbery matrix like Kraton (Shell Chemical Co.) or Styroflex (BASF AG) have elongations at break that are severalfold and tensile strengths above 30 MPa. These high values are contributed with stretching the elastomeric network and rotation and orientation of the dispersed phase. The tem, ftir spectroscopy, and saxs studies of SBS triblock copolymers with styrene cylinders revealed that the initial stage of tensile deformation is governed by preferential orientation of elastomeric chains and later stages by a breakdown of the glassy domains (54).

Another class of copolymers having interesting mechanical properties are weakly segregated block copolymers. One of the most striking effect observed in these block copolymers is a synergism in tensile properties (51,55,56). In a certain composition range, the tensile strength was found to exceed that of pure PS, as illustrated in Figure 18. Irrespective of the block copolymer architecture (diblock, triblock, or star block), this effect was observed and shows that it is attributed to the widened interface resulting from enhanced phase mixing. Therefore, in triblock copolymers this synergistic effect occurs over a broader composition range than in diblock copolymers because of enhanced miscibility of triblock copolymers. The deformation structures observed in these block copolymers depend in detail on type and orientation of the microphase-separated morphology. Particularly interesting are the mechanisms of “craze termination,” “craze tip blunting,” and

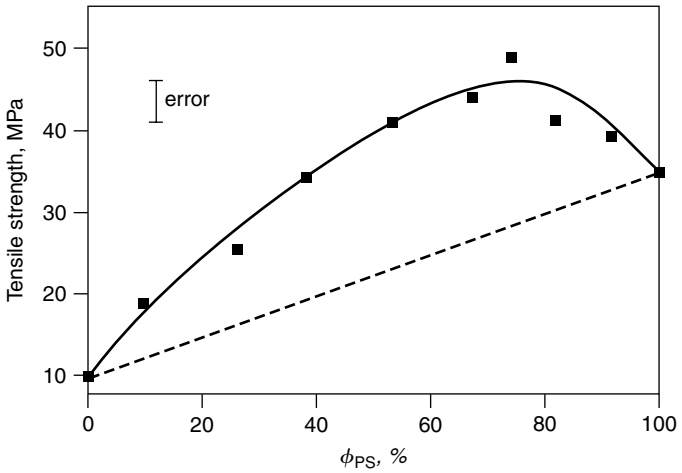

Fig. 18. Dependence of tensile strength on volume fraction of PS for PBMA-*b*-PS-*b*-PBMA triblock copolymers and pure PS and PBMA (strain rate 1.6×10^{-4} s^{-1}). From Reference 51.

"craze deviation" during propagation of crazes through an arrangement of stacks of lamellae (51,55).

A craze in a block copolymer with lamellar morphology is shown in Figure 19a with an internal structure of highly extended craze fibrils of PS and PBMA. The PBMA lamellae are cavitated and, therefore, appear brighter than the dark, thicker PS lamellae. Because of the microvoids in the PBMA lamellae, a stress concentration is built up in the adjacent PS lamellae that initiate a large plastic deformation of these PS lamellae. This is similar to the mechanism as described by Argon for PS-*b*-PB diblock copolymers (53). The diameter of the PS fibrils is 15–25 nm with long periods of about 100–130 nm. In the undeformed material the PS lamellae are about 80–90 nm thick. This is much larger than

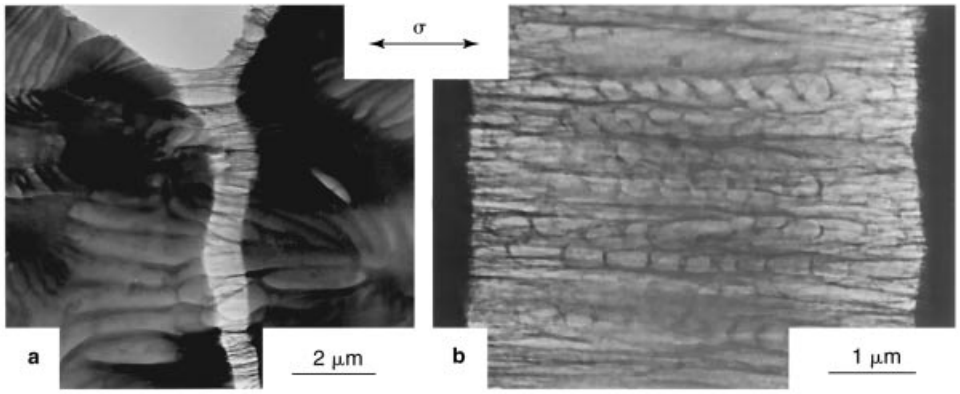

Fig. 19. hvem micrographs of crazes in PS-*b*-PBMA diblock copolymers with different morphology. (**a**) Lamellar morphology, PS volume content 67%; (**b**) Hexagonally packed PBMA cylinders, PS volume content 76%.

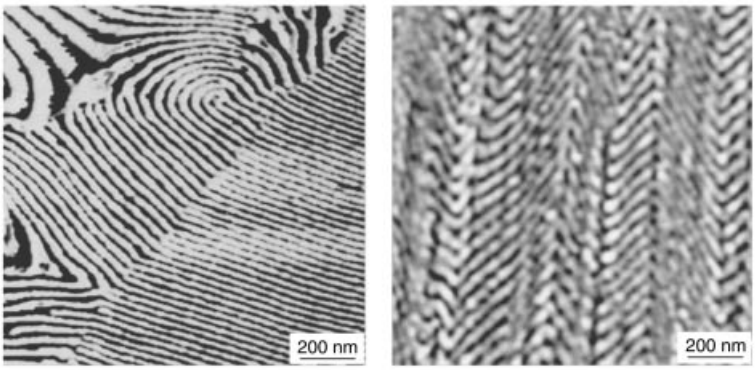

Fig. 20. Tapping mode sfm images of a lamellar SBS triblock copolymer before (left) and after deformation (right); deformation direction vertical, PS phase appears light.

the thicknesses of the deformed PS lamellae, clearly indicating their large plastic deformation.

A craze in a block copolymer with PBMA cylinders is shown in Figure 19b with an internal cellular structure of the craze. The PBMA cylinders are cavitated in the craze and, therefore, appear bright. This is followed by a large plastic deformation of the PS parts (appearing dark) up to fibrils.

In block copolymers with lamellar morphology, mechanical properties and deformation structures vary with the orientation of the lamellae with respect to the direction of applied load. When the material is loaded in a perpendicular direction to the lamellar orientation, lamellae are folded in a fish-bone-like arrangement (57). Such a lamellar folding in a solution cast film of an SBS triblock copolymer is shown in Figure 20 (58).

Nowadays, star-block copolymers are earning growing interest because of their improved mechanical and rheological properties. Introducing a "tapered chain" and giving the stars a highly asymmetric block structure lead to the evolution of a nonclassical lamellae-like morphology in spite of a very high styrene content (about 75%) and correspondingly high ductility (59). Investigating such asymmetric SB star-block copolymers with alternating PS and PB lamellae confirmed the result of a high plastic deformation of the PS lamellae (60) which is also shown in the crazes of Figure 19. tem micrographs of stained samples of a star-block copolymer with a PS content of 74% show alternating PS and PB lamellae (see Fig. 21a). Thicknesses and long periods of the PS lamellae range between 10–25 nm and 30–50 nm, respectively. Tension of the sample in a parallel direction to the length direction of the lamellae shows a stretching of the whole morphology (Fig. 21b). The PS as well as the PB lamellae are highly plastically deformed in parallel direction to the applied stress. This is clearly indicated by a reduced thickness and long period of PS lamellae up to 7–15 nm and 20–35 nm, respectively (see Figs. 21c and 21d). Here, the lamellae are deformed without any cavitation or microvoid formation and without the formation of local craze-like deformation bands. The deformation of the lamellae reaches elongations up to 300%; this corresponds to the typical elongations of the fibrils inside the crazes in PS.

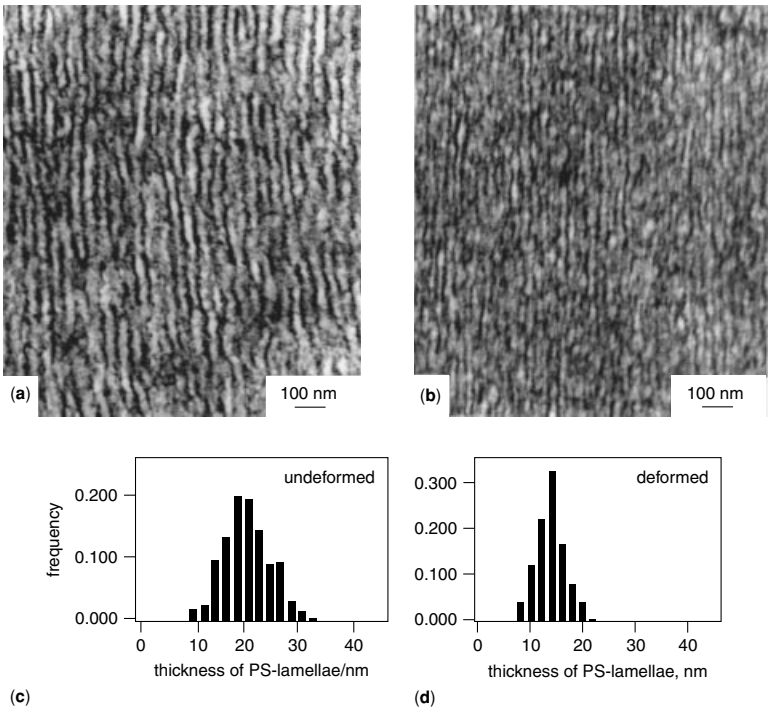

Fig. 21. Morphology of an injection-molded specimen of a star-block copolymer with a PS content of 74% with lamellar arrangement of PS and PB lamellae before and after deformation. (**a**) PS and PB lamellae before deformation; (**b**) Plastically stretched PS and PB lamellae deformed in parallel direction to lamellar orientation (**a**, **b** tem micrographs of chemically stained thin sections, PB lamellae appear dark; arrow shows direction of tension) Frequency distributions of thicknesses of PS lamellae (**c**) before and (**d**) after deformation. From Ref. 60.

This homogeneous yielding of PS lamellae together with adjacent PB ones can be considered as a new deformation and toughening mechanism, called *thin layer yielding mechanism*. This effect appears only in thin PS layers with a thickness smaller than a critical thickness (see Fig. 22). This critical thickness D_{crit} is comparable with the maximum thicknesses of the craze fibrils in PS, ie, in the range of 20 nm. The difference between fibril stretching in PS crazes and thin layer yielding of PS lamellae is to be seen in the fact that craze fibrils are stretched between microvoids, whereas the PS lamellae are deformed together with the adjacent PB lamellae.

These results show that the tensile properties of block copolymers, such as stiffness, tensile strength, elongation at break, and toughness, can be improved as compared to those of pure homopolymers, polymer blends, and rubber-toughened polymers. Moreover, this demonstrates the possibility of creating a new class of polymers with improved properties based on materials with structures at the nanometer scale.

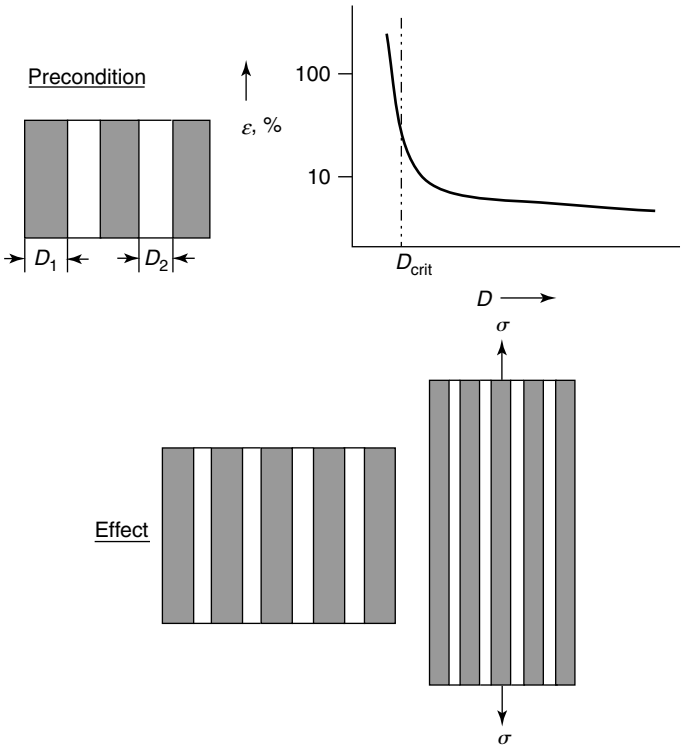

Fig. 22. Schematic drawing of the principle of the thin layer mechanism (D, D_{crit}, ε, and σ stand for PS layer thickness, critical layer thickness, elongation at break, and load direction).

ACKNOWLEDGMENTS

The author thanks Prof. Dr. U. Gösele, Max Planck Institute of Microstructure Physics in Halle/S., for providing the opportunity to carry out deformation tests in the 1000-kV hvem and Dr. R. Godehardt, Dr. J.U. Starke, W. Lebek, S. Henning, M. Ensslen, and R. Adhikari for performing deformation tests on several polymers in hvem, tem, and sfm. He gratefully thanks the Deutsche Forschungsgemeinschaft (DFG) for financial support in several projects.

BIBLIOGRAPHY

"Micromechanical Measurements" in *EPSE* 2nd ed., Vol. 9, pp. 745–760, by W. Döll and L. Könczöl, Fraunhofer-Institut für Werkstoffmechanik, and L. Bevan, North East London Polytechnic.

1. G. H. Michler, *Polym. Adv. Technol.* **9**, 812 (1998).
2. G. H. Michler, *Kunststoff-Mikromechanik: Morphologie, Deformations- und Bruchmechanismen*, Carl Hanser-Verlag, München, 1992.
3. G. H. Michler, *Trends Polym. Sci.* **3**, 124 (1995).
4. G. H. Michler, *J. Macromol. Sci., Phys. B* **38**(5/6), 787 (1999).

5. I. Narisawa, *Festigkeit polymerer Materialien (Russian translation from Japanese)*, Chimia, Moscow, 1987.
6. A. C. Roulin-Moloney, ed., *Fractography and Failure Mechanisms of Polymers and Composites*, Elsevier Applied Science Publishers Ltd., London, 1989.
7. R. C. Cieslinski, H. C. Silvis, and D. J. Murray, *Polymer* **36**(9), 1827 (1995).
8. E. J. Kramer, in H. H. Kausch, ed., *Crazing in Polymers, Adv. Polym. Sci.* **52/53**, 1 (1983).
9. D. Vesely, A. Low, and M. Bevis, in *Proc. EMAG on Developments in Electron Microscopy and Analysis* , Bristol, 1975, Academic Press, Inc., Orlanda, Fla., 1976, p. 333.
10. G. H. Michler, *Ultramicroscopy* **15**, 81 (1984).
11. L. C. Sawyer and D. T. Grubb, *Polymer Microscopy*, Chapman & Hall, London, 1987.
12. D. Hofmann and co-workers, *J. Appl. Polym. Sci.* **39**, 1595 (1990).
13. E. E. Tomashevskii and co-workers, *Int. J. Fract.* **11**, 803 (1975).
14. E. Paredes and E. W. Fischer, *Makromol. Chem.* **180**, 2707 (1979).
15. H. R. Brown, *Polym. Sci.: Polym. Phys. Ed.* **21**, 483 (1983).
16. S. Suehiro and co-workers, *Macromolecules* **19**, 745 (1988).
17. P. J. Mills, H. R. Brown, and E. J. Kramer, *J. Mater. Sci.* **20**, 4413 (1985).
18. T. Pomper and co-workers, *J. Macromol. Sci., Phys. B* **38**(5/6) 869 (1999).
19. H. R. Brown and co-workers, *Polym. Eng. Sci.* **24**, 825 (1984).
20. W. Döll, in H. H. Kausch, ed., *Crazing in Polymers, Adv. Polym. Sci.* **52/53**, 105 (1983).
21. J. F. Kalthoff, in A. S. Kobayashi, ed., *Handbook on Experimental Mechanics*, Prentice-Hall, Inc., Englewood Cliffs, N.J., 1986, p. 430.
22. H. W. Siesler, in S. Fakirov, ed., *Oriented Polymer Materials*, Hüthing & Wepf Verlag, Heidelberg, 1996, p. 138.
23. F. J. Baltá Calleja and S. Fakirov, *Trends Polym. Sci.* **5**, 246 (1997).
24. E. J. Donth, *Glasübergang*, Akademie-Verlag, Berlin, 1981.
25. W. Klöpffer, *Introduction to Polymer Spectroscopy*, Springer-Verlag, New York, 1984.
26. L. Könczöl, A. Hiltner, and E. Baer, *J. Appl. Phys.* **60**, 2651 (1986).
27. J. Baumann and G. Fritsch, *Phys. Unserer Zeit* **19**, 16 (1988).
28. H. H. Kausch, ed., *Crazing in Polymers*, Vol. **2**, Springer-Verlag, New York, 1990.
29. G. H. Michler, *J. Mater. Sci.* **25**, 2321 (1990).
30. E. J. Kramer and L. L. Berger, in Ref. 28, Chapt. "1", p. 1.
31. G. H. Michler, *Plaste u. Kautschuk* **38**, 268 (1991).
32. G. H. Michler and co-workers, *Philos. Mag. A* **79**, 167 (1999).
33. E. Donth and G. H. Michler, *Colloid Polym. Sci.* **267**, 557 (1989).
34. J.-U. Starke, G. Schulze, and G. H. Michler, *Acta Polym.* **48**, 92 (1997).
35. G. Kämpf, D. Freitag, and G. Fengler, *Kunststoffe* **82**, 385 (1992).
36. G. H. Michler and J. U. Starke, in C. K. Riew and A. J. Kinloch, eds., *Toughened Plastics II*, 1996, Chapt. "17", p. 251. ACS No. 252.
37. C. B. Bucknall, *Toughened Plastics*, Applied Science Publishers, London, 1977.
38. D. R. Paul and C. B. Bucknall, eds., *Polymer Blends*, Vols. **1** and **2**, John Wiley & Sons, Inc., New York, 2000; see in particular Vol. **2**, Chapt. "22", p. 83.
39. J. Kolarik and co-workers, *Polym. Eng. Sci.* **37**, 128 (1997).
40. J.-U. Starke and co-workers, *J. Mater. Sci.* **32**, 1855 (1997).
41. J. Laatsch and co-workers, *Polym. Adv. Technol.* **9**, 716 (1998).
42. G. H. Michler, B. Hamann, and J. Runge, *Angew. Makromol. Chem.* **180**, 169 (1990).
43. H. Gust, R. Hengl, and P. Eyerer, *Adv. Polym. Technol.* **10**, 1 (1990).
44. G.-M. Kim and co-workers, *J. Appl. Polym. Sci.* **60**, 1391 (1996).
45. G.-M. Kim and G. H. Michler, *Polymer* **39**, 5689 (Part 1), 5699 (Part 2) (1998).
46. G.-M. Kim and co-workers, *Acta Polym.* **49**, 88 (1998).
47. R. Godehardt and co-workers, *J. Macromol. Sci., Phys. B* **38**, 817 (1999).
48. G. H. Michler and R. Godehardt, *Cryst. Res. Technol.* **35**(6/7), 863 (2000).
49. G. H. Michler, *Colloid Polym. Sci.* **270**, 627 (1992).

50. A. Keller and J. A. Odell, in M. J. Folkes, ed., *Processing, Structure and Properties of Block Copolymers*, Elsevier Applied Science Publishers, London, 1985, Chapt. "2", p. 29.
51. R. Weidisch and G. H. Michler, in F. J. Baltá Calleja and Z. Roslaniec, eds., *Block Copolymers*, Marcel Dekker, Inc., New York, 2000, Chapt. "8", p. 215.
52. C. E. A. Schwier, A. S. Argon, and R. E. Cohen, *Polymer* **26**, 1985, 1985.
53. A. S. Argon and R. E. Cohen, in Ref. 28, p. 301.
54. J. Sakamuto and co-workers, *Polymer* **34**, 4837 (1993).
55. R. Weidisch and co-workers, *Polym. Adv. Technol.* **9**, 727 (1998).
56. R. Weidisch and co-workers, *J. Mater. Sci.* **35**, 1257 (2000).
57. E. L. Thomas, R. Albalak, and Y. Cohen, in *Proc. 11th. Int. Conf. on Deformation, Yield and Fracture of Polymers*, Cambridge, U.K., 10–13 Apr. 2000, p. 191.
58. R. Adhikari and co-workers, *J. Macromol. Sci., Phys. B* in press.
59. K. Knoll and N. Nießner, *Macromol. Symp.* **132**, 231 (1998).
60. G. H. Michler and co-workers, *J. Appl. Polym. Sci.* in press.

GOERG H. MICHLER
Martin-Luther-Universität Halle-Wittenberg

MODELING OF POLYMER PROCESSING AND PROPERTIES

Introduction

The properties of polymeric systems are strongly dependent on their structure which is itself fully controlled by the processing conditions. Thus, it is now well accepted that the mechanical strength of polymer fibers steadily increases with an improvement of the orientation of the macromolecular chains (1). This is the reason why fiber spinning is typically followed by a drawing step with the purpose of aligning and extending the chains along the fiber axis. In some applications, the polymer must be processed from solution, and fiber formation itself requires a coagulation step in order to consolidate the polymer into a solid filament suitable for drawing. In that case, the solvent-coagulant exchange at the polymer interface strongly controls the internal structure of the fiber (2), and hence its ultimate tensile strength and elongation at break. In other techniques, fiber formation from solution occurs upon rapid quenching to a lower external pressure and/or temperature (3). In this case, the size and the porosity of the fiber is strongly dependent on the polymer concentration and quenching conditions.

A theoretical description of all the factors controlling the effect of processing conditions on polymer structure and properties is extremely complex because of the need to consider a wide variety of different factors such as polymer concentration, molecular weight, as well as external variables (time, temperature, pressure). In view of this complexity, this work has focused on the development of kinetic Monte-Carlo lattice models. These models are mesoscopic in the sense that the unit lattice length is of the order of the statistical segment length for the polymer chain and atomic level details are omitted. The objective of this review is to describe these models in some detail and show their value in getting a better

Encyclopedia of Polymer Science and Technology. Copyright John Wiley & Sons, Inc. All rights reserved.

understanding of the interplay between processing conditions, polymer structure, and product properties.

Polymer Drawing

This section focusses on polymer deformation in the *solid state*. Models for flow-induced structure and orientation in the *molten state* have been presented in References 4 and 5. Most previous approaches (1,6,7) for describing the deformation of solid polymer systems are essentially phenomenological and static representations which are incapable of providing a unified description of the various morphological changes that may occur depending on the dynamics and on the structure at the molecular level. All these models are incapable of simultaneously providing quantitative information on (*1*) stress–strain behavior, molecular extension, and fracture; (*2*) morphological changes that occur during deformation; and (*3*) the effect of testing variables, such as temperature and strain rate.

One model for the deformation of polymer solids has been described at length in References 8 and 9. It is briefly reviewed here. Figure 1 gives this model representation of the entangled solid polymer network prior to deformation. The entanglements, ie, knots formed between chains, are denoted by the heavy black circles. For polyethylene in the melt, the molecular weight between entanglements, $M_e^{melt} = 1900$, which corresponds to $n = 14$ statistical segments. For solution cast polyethylene samples, M_e is easily obtained from

$$M_e = M_e^{melt}/\phi \tag{1}$$

in which ϕ denotes the polymer concentration. The dotted lines in Figure 1 represent the attractive (van der Waals or hydrogen) intermolecular bonds connecting sections either of the same chain or of different chains. Tensile drawing is assumed to occur along the y-axis.

The network is deformed at a constant temperature T and a rate of elongation ε. During deformation, the bonds between chains are allowed to break according to the Eyring kinetic theory of fracture (7), ie, at a rate

$$v = \tau \exp[-(U - \beta\sigma)/kT] \tag{2}$$

Here, τ is the thermal vibration frequency, U and β are the activation energy and volume, and

$$\sigma = M_\varepsilon \tag{3}$$

is the local stress. In equation (3), ε is the local strain and K is the elastic constant for the bond. The breaking of these attractive bonds leads to a release of the chain strands, which are now available to support the external load. Once broken, these bonds are assumed not to reform.

As the stress of the "freed" chain strands increases, slippage through entanglements sets in at a rate that has the same functional form as that for the attractive bonds (eq. (2)) but with different values for the activation energy U and

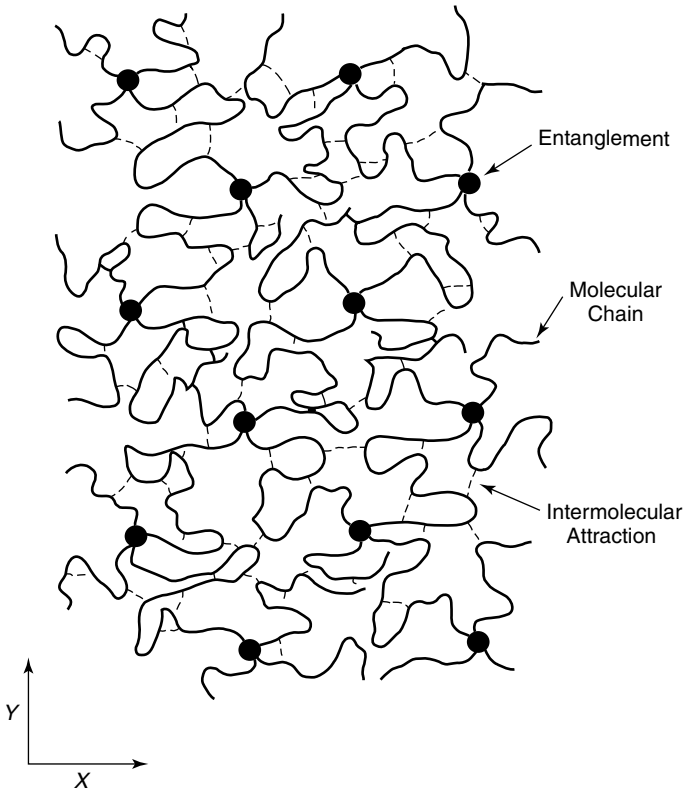

Fig. 1. Schematic representation of a model for an unoriented polymer network. The heavy black circles represent the entanglement loci and the dotted lines denote the attractive bonds between chains. Reprinted with permission from Ref. 8. Copyright (1987) American Chemical Society.

volume β. In eq. (2), σ now represents the difference in stress in two consecutive chain strands that are separated by an entanglement. This stress difference is calculated using the rubber elasticity theory (10). Thus, the stress on a stretched chain strand having a vector length $\boldsymbol{r}$ is given by

$$\sigma = \alpha kTL^{-1}(r/nl) \tag{4}$$

In equation (4), n denotes the number of statistical chain segments of length l in the strand whereas L^{-1} is the inverse Langevin function and α is a proportionality constant.

Equations (2) and (3) for the attractive bond breaking process are executed on the computer with the help of a Monte-Carlo lottery in which bond i breaks according to a probability

$$p_i = v_i/v_{\max} \tag{5}$$

Here, v_i is obtained from equation (2), whereas $v_{\max}$ is the rate of breakage of the most strained bond in the array. After each visit of a bond, the time t is

incremented by $1/[v_{max}n(t)]$ where $n(t)$ is the total number of intact bonds at time t. The simulation of chain slippage through entanglements is executed using a similar technique in which $n(t)$ now denotes the total number of entanglements left at time t. The present model also allows for chain breaking when the local draw ratio on a particular chain strand exceeds its maximum value given by the square root of its number of statistical segments.

After a very small time interval δt has elapsed, the attractive bond breaking, chain slippage, and fracture processes are halted and the network is elongated along the tensile y-axis by a small constant amount determined by the rate of elongation ε. The network is then relaxed to its minimum energy configuration, using a series of fast computer algorithms, described in Reference 11, which steadily reduce the net residual force acting on each entanglement point. Upon completion of network relaxation, the Monte-Carlo process of bond breakings and chain slippage is restarted for another time interval δt, and so on and so forth, until the network fails.

Morphologies of Deformation. Figure 2 shows a series of calculated stress–strain curves for melt-crystallized polyethylene at three different molecular weight values ($M = 1900$, 9500, and 250,000). The lowest molecular weight sample exhibits a low elongation at break and brittle failure. As the molecular weight is increased ($M = 9500$), the stress–strain curve exhibits a so-called yield

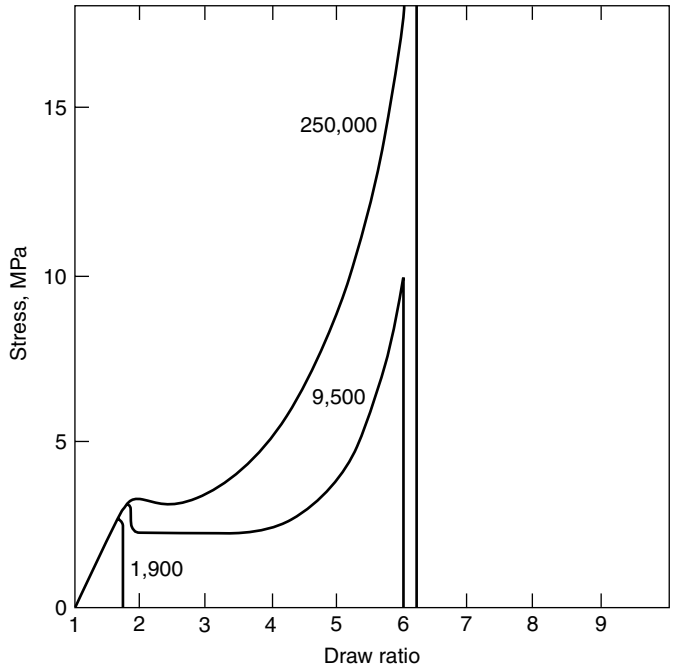

Fig. 2. Calculated stress–strain curves for three poylethylene samples of different molecular weights. To convert MPa to psi, multiply by 145. Reprinted with permission from Ref. 8. Copyright (1987) American Chemical Society.

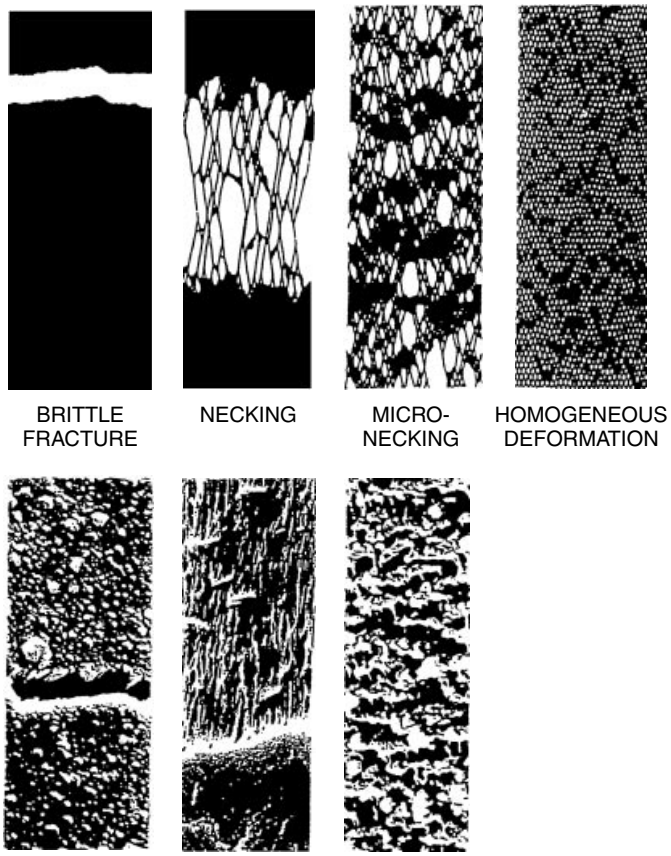

Fig. 3. Dependence of morphology on molecular weight. *Top*: Deformation morphologies obtained from the model for melt-crystallized polyethylene at increasing values of the molecular weight. From left to right: $M = 1900$, $M = 8500$, $M = 20{,}000$, and $M = 250{,}000$. *Bottom*: Experimental morphologies obtained at comparable molecular weights. Reprinted with permission from Ref. 8. Copyright (1987) American Chemical Society.

point (the first maximum in the stress–strain curve), followed by a flat region characteristic of neck formation. At draw ratio values $\lambda < 4$, strain hardening is observed. For the highest $M = 250{,}000$, strain hardening occurs almost immediately past the yield point.

A set of computer-generated morphologies is presented in Figure 3 (top) for different melt-crystallized polyethylene samples with increasing values (from left to right) of the molecular weight. As was clearly exemplified in the stress–strain curve (Fig. 2), the low molecular weight sample exhibits brittle failure with a sharp breaking surface. As the molecular weight is increased, a necking mode of deformation is observed, ie, a region of highly deformed molecular chains bridging two sections in which the macromolecules are still in a random coil configuration. This necking region propagates along the sample by continuously drawing more and more chains from the undeformed sections into the deformed region. At $M = 20{,}000$ a micro-necking morphology is observed in which numerous necks are obtained. For still higher $M = 250{,}000$, the number of micro-necks becomes

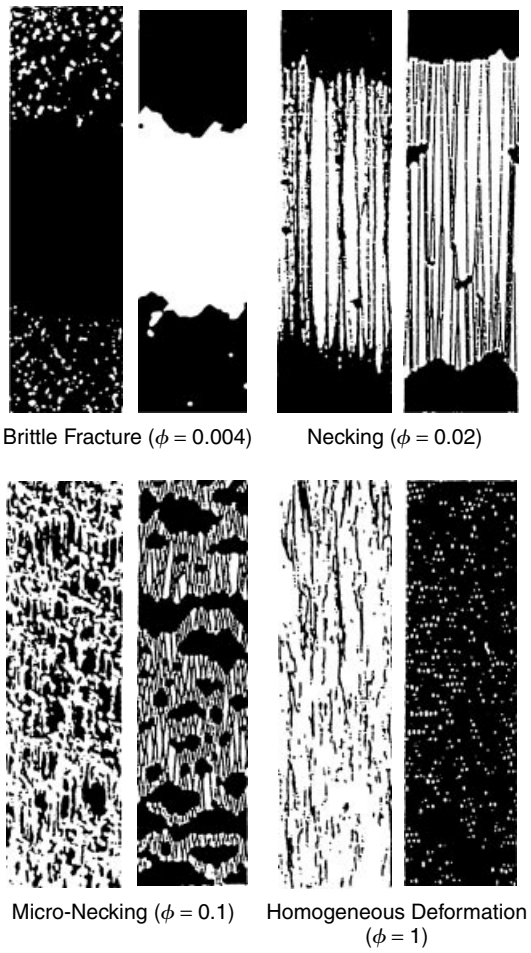

Fig. 4. Dependence of morphology on degree of dilution ϕ ($M = 500{,}000$). Deformation morphologies obtained from experiment (left) and from the model (right) for solution cast polyethylene at increasing values of the entanglement spacing factor ϕ. From left to right: $\phi = 0.004$, $\phi = 0.02$, $\phi = 0.1$, and $\phi = 1$. In all cases, $M = 475{,}000$. Reprinted with permission from Ref. 9. Copyright (1988) American Chemical Society.

so large that the deformation becomes essentially homogeneous. The bottom of the figure shows experimental morphologies obtained at comparable molecular weight values. An excellent agreement between theory and experiment is found.

A similar set of transitions can be obtained by keeping the molecular weight constant and varying the entanglement spacing, as is obtained in solution cast samples (see eq. (1)). Figure 4 shows a sequence of experimental (left) and calculated (right) morphologies for $M = 475{,}000$ at increasing values of ϕ (9). As with the results of Figure 3, model morphologies are in good qualitative agreement with experimental observation. This illustrates that the present approach is capable of handling the very complex issue of connecting events on the molecular level to macroscopic properties and features.

Importance of Drawing Conditions. As noted in the introduction, the mechanical properties of polymeric fibers are strongly dependent on the length of the macromolecular chains and also on their orientation with respect to the fiber axis. Since orientation increases with draw ratio (1), it is of uttermost importance to identify the factors controlling polymer drawability. A detailed study of the importance of temperature and elongation rate on the maximum draw ratio of melt-crystallized polyethylene, using the model described above, has been presented in Reference 12. This work was motivated by early experimental investigations which seemed to indicate that, for each molecular weight, there may exist an optimum draw temperature and/or rate of deformation (13,14). Figure 5a shows the

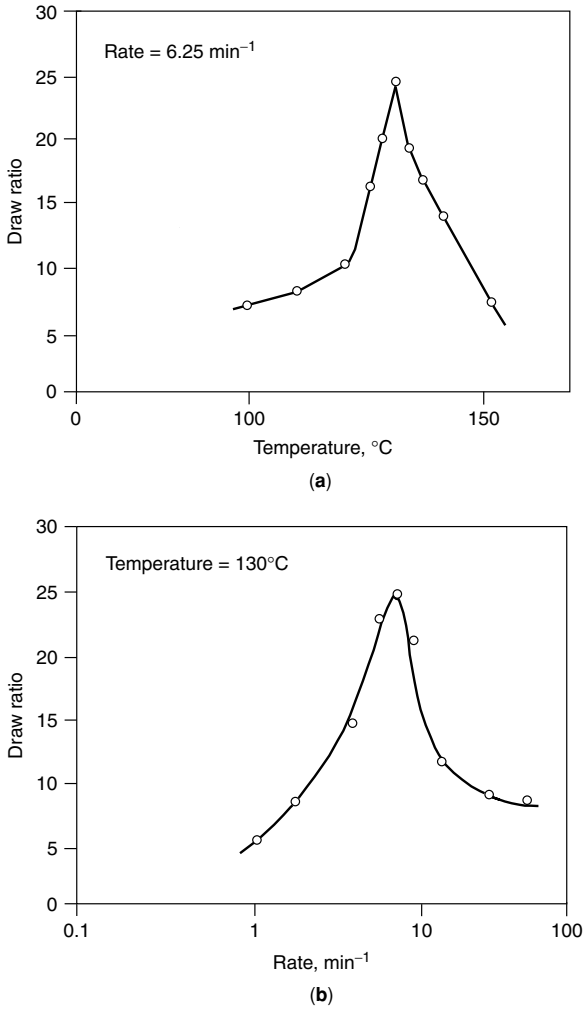

Fig. 5. Calculated dependence of the maximum draw ratio on testing conditions for melt-crystallized polyethylene with $M = 143{,}000$. (a) Dependence on temperature at constant elongation rate (6.25 min^{-1}); (b) Dependence on elongation rate at constant temperature (130°C). Reprinted with permission from Ref. 12. Copyright (1988) American Chemical Society.

calculated dependence of the draw ratio on temperature for *monodisperse* melt-crystallized polyethylene with $M = 143{,}000$. The figure reveals a sharp maximum in the draw ratio at $T = 130^{\circ}$C. A careful examination of the present model results gives the following insight. At low temperature $T < 100^{\circ}$C, all the samples break at their "natural" draw ratio $\lambda = 5$, as determined from the number of statistical segments between entanglements in the melt. As the temperature is increased, the model results reveal an onset of slippage of chains through entanglements, which leads to a steady increase in drawability. There is, however, an upper limit to that increase. Thus, at $T = 130^{\circ}$C, the rate of chain slippage becomes comparable to the rate of straining the overall sample and any further increase in temperature leads to a progressive decrease in drawability. Results (not reproduced) for other *monodisperse* molecular weights show a similar behavior with different values for the optimum drawing temperature. These observations are of importance since they predict that the sharp optimum of Figure 5a cannot be observed for a polydisperse sample as every single molecular weight in the distribution has an optimum temperature window which will be different from the others. Also, since our model is based on a thermally activated rate theory, we expect that results similar to those of Figure 5a will be obtained when keeping the temperature constant and varying the elongation rate. A confirmation of that model prediction is given in Figure 5b.

A further test of our model results is presented in Figure 6, which displays actual experimental samples drawn to their breaking point at different values of the deformation temperature and at a constant elongation rate of 23 min^{-1}. The samples are for NBS SRM 1484 linear polyethylene which has a close-to monodisperse molecular weight distribution with $M_{\text{n}} = 111{,}000$ and $M_{\text{w}} = 125{,}000$. It is evident that, for this particular rate, the optimum drawing temperature is around 75°C. Note that the location of the optimum temperature window is different from that predicted from our model simulations (see Fig. 5a). A better fit could have been obtained by adjusting the activation energy for chain slippage, which has not been attempted in the present calculations.

The results discussed above for monodisperse polyethylenes clearly demonstrate that each molecular weight exhibits a different temperature or elongation window within which optimum drawing occurs. The model reveals that, within those windows, the rate of slippage of chains through entanglements reaches its optimum value. These observations strongly point to the need for very accurate control of the temperature and rate of deformation for optimum drawing, particularly for high molecular weight polymers.

Polymer Coagulation

Polymer coagulation defines the process by which a solution of a polymer in a good solvent is quenched in a nonsolvent, leading to solvent–nonsolvent exchange and polymer precipitation. This process is at the basis of a wide range of industrial processes including wet spinning (3), fibridation (15), and membrane formation (16). A major drawback of the solution/coagulation process is that the coagulant moves into the polymer gel by forming large tear-dropped macrovoids (fingers), which are usually very difficult to eliminate. Several theories have been

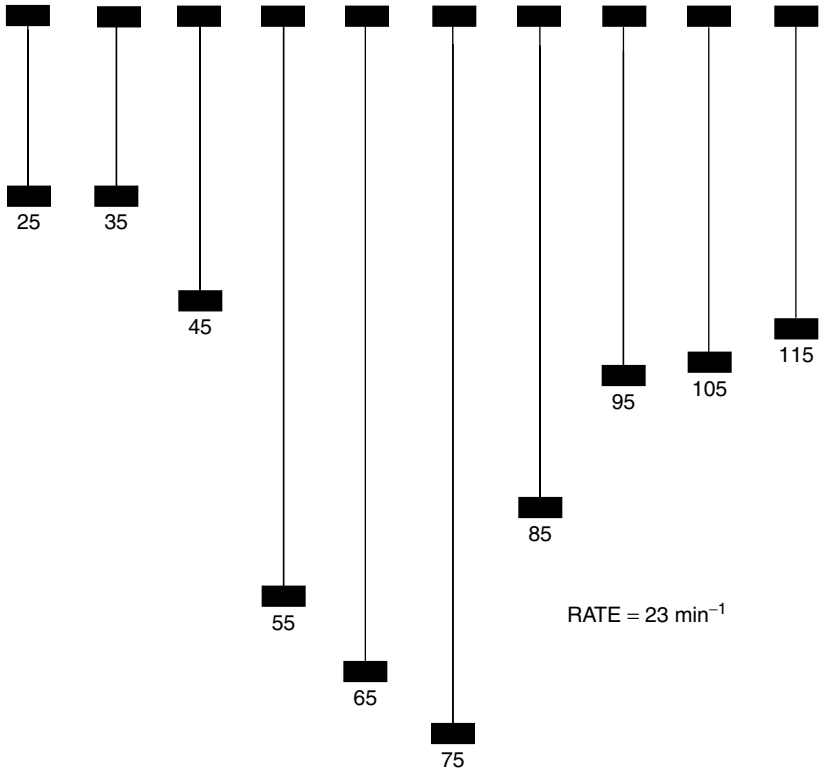

Fig. 6. Dependence of maximum draw ratio on temperature (°C) (Polyethylene $M = 10^5$). Actual melt-crystallized NBS SRM 1484 polyethylene samples drawn to break at different temperatures. The elongation rate was 23 min^{-1}. Reprinted with permission from Ref. 12. Copyright (1988) American Chemical Society.

proposed for describing finger formation. These include linear stability analyses of the solvent–nonsolvent exchange at the polymer interface (17,18) and studies of the mass transfer paths before the onset of phase separation (19–21). All these studies are based on the derivation of analytical equations for diffusion of the polymer, solvent, and coagulant. In view of the great complexity of the problem, all previous models had to resort to several simplifying assumptions: (*1*) the diffusion process is purely one-dimensional, (*2*) thermodynamic equilibrium is always preserved at the bath–polymer interface, (*3*) phase separation is not considered and is assumed to occur through nucleation and growth. In fact, it is now well accepted that polymer coagulation is a *nonequilibrium* process, entirely controlled by the rate of solvent–coagulant exchange through the interface.

In view of the great difficulties associated with analytical studies of the development of polymer structure during coagulation, a computer simulation of the ternary diffusion process is employed. One approach has been described at length in Reference 22. In brief, the coagulation process is simulated on a lattice, whose sites represent either a nonsolvent, a solvent, or a polymer aggregate. For simplicity, all three components are assumed to have equal molar volume and the

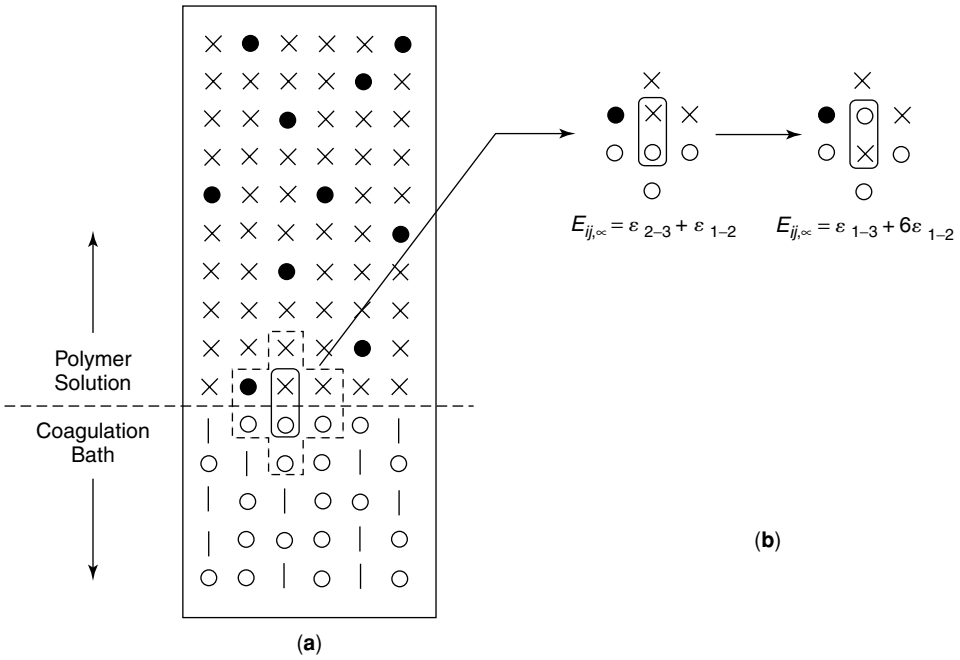

Fig. 7. Schematic representation of a lattice model for diffusion of a coagulant into a polymer solution. The polymer, the solvent, and the coagulant particles, are denoted by symbols ●, ×, and ○, respectively. The diffusion process is simulated through a series of two-particle exchanges on nearest-neighbor lattice sites. The rates of exchange are obtained from equation (6) in which $E_{ij,\alpha}$ and $E_{ji,\alpha}$ are the interaction energies of the pair with nearest-neighbor particles, before and after the exchange (see Fig. 7b). As diffusion proceeds, the coagulant–polymer interface (dashed line) moves upwards and, since the coagulation bath is assumed to be infinite, the lattice sites below that interface are being continuously replenished with coagulant particles (see text). Courtesy of *Journal of Polymer Science*.

simulation is limited to a two-dimensional geometry similar to that encountered in typical experimental studies. In these setups, a drop of polymer solution is placed between two microscope slides whereas the coagulant is introduced near the edge (2,23). A schematic representation of the two-dimensional model of polymer coagulation is given in Figure 7a. The polymer solution is represented by a lattice of sites which are filled-in, according to the polymer weight fraction, by either a solvent or a polymer particle. A detailed study of the importance of the polymer particle "size" can be found in Reference 24. The bottom five rows of the lattice represent the infinite bath filled-in with coagulant particles. Coagulant, solvent, and polymer sites are referred to by indexes 1, 2, and 3 respectively. The ternary polymer–solvent–coagulant diffusion process is simulated as follows. A pair of nearest-neighbor—i and j—lattice sites are picked at random. Denoting by α the local environment for that pair, the rate for an exchange $ij \rightarrow ji$ within α is calculated from (25)

$$v_{ij\rightarrow ji,\alpha} = \tau_{i,j} - 1\exp[\beta(E_{ij,\alpha} - E_{ji,\alpha})/2] \tag{6}$$

In equation (6), $\tau_{i,j}^{-1}$ is related to the mutual diffusion coefficient $D_{i,j}^{\infty}$ of i and j particles *at infinite dilution* through (26)

$$D_{i,j}^{\infty} = \tau_{i,j}^{-1(\delta x)} 2 \tag{7}$$

where δx denotes the unit lattice length. Note that, in equation (6), all the effects of particle interactions are relegated to the Boltzmann exponent of (half) the energy difference between initial and final states for the exchanging pair. That functional form is guided by a requirement of commutativity of the individual two-particle exchanges (25). Using equation (6), a probability for exchange is then calculated through

$$p_{ij \to ji,\alpha} = v_{ij \to ji,\alpha} / v_{\max} \tag{8}$$

in which $v_{\max}$ denotes the highest rate of exchange among all the pairs on the lattice (see also eq. (5)). Having determined the probability p for an exchange $ij \to ji$ (eqs. 6–8), a random number between 0 and 1 is generated and the move is allowed if that number falls below p. After each visit of a pair and whether the pair is allowed to exchange or not, the overall "time" t is incremented by $1/[v_{\max} n]$ in which n denotes the total number of pairs of sites on the lattice (note the similarity with our Monte-Carlo process for polymer drawing, as described earlier). In addition to two-particle exchanges, the model also allows for small clusters to move through a series of one-lattice-step displacements of entire rows or columns of polymer particles. Also, since the coagulant bath is assumed to be infinitely large, solvent particles diffusing into the bath to a depth of more than 5 lattice units with respect to the polymer–bath interface are systematically removed from the lattice and replaced by coagulant particles.

Skin and Finger Formation. First attention is turned to the application of the model to the coagulation of a solution of 20% Nomex®, an aromatic polyamide commercialized by DuPont, dissolved in *N*-methylpyrrolidinone (NMP). An estimation of the range of values of the model parameters can be found in Reference 22. Figure 8 shows the calculated morphology obtained after precipitation in water for a time $t = 0.02$ s. Only the polymer particles have been represented. The figure clearly reveals that the coagulant diffuses inside the polymer gel through a series of finger-like structures. The latter have a strikingly similar shape and originate through regularly spaced pores in a thin skin, in perfect agreement with experimental observation (2). Note the important shrinkage of the polymer gel whose initial position was located at the bottom of the figure. A careful analysis of our model results leads to the following insight into the origin of the skin/finger formation. Immediately upon immersion of the polymer gel in the coagulation bath, the fast solvent-coagulant exchange across the interface combined with the large repulsive forces between polymer and coagulant cause an immediate precipitation at the interface. This process is too fast for any segregation of the Nomex particles into polymer-rich and polymer-poor domains and, as a result, a thin skin starts to form. Since the polymer concentration is low, the skin, in its early stages, is not homogeneous and it presents defects along its contour. The latter form the initiation pores for fingers, which then quickly grow inside the polymer solution as it is faster for a solvent particle to exit through a pore

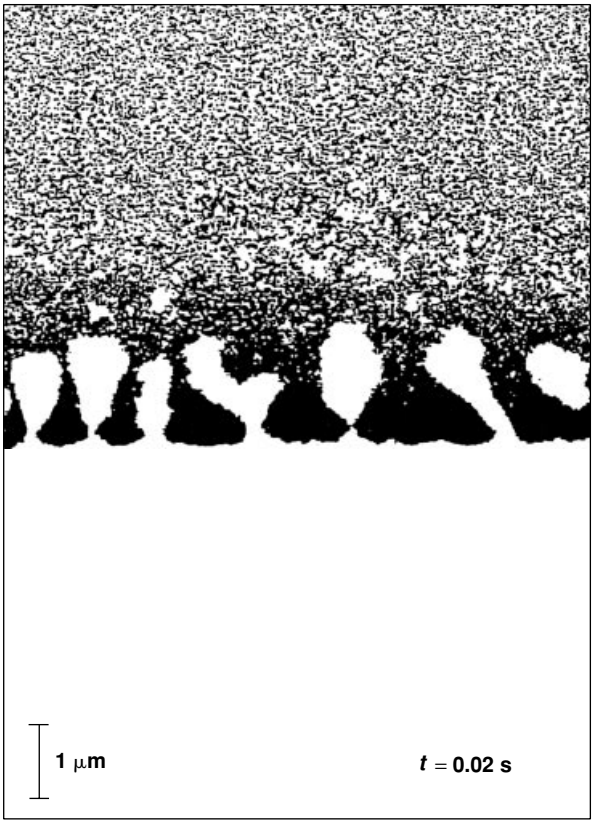

Fig. 8. Calculated coagulant–polymer interface for a 20% solution of Nomex in NMP precipitated in water at $t = 0.02$ s. The figure is for a square lattice of 450 × 600 sites; only polymer particles (symbol •) have been represented. The figure is for $\varepsilon_{1-2} = 0.77$, $\varepsilon_{2-3} = 0$, and $\varepsilon_{1-3} = 2.8$. Courtesy of *Journal of Polymer Science*.

than through a defect-free skin. In support of the proposed mechanism for finger formation, experiments clearly reveal that fingers do not develop when a skin is absent or when the polymer volume fraction is too high, ie, when skin defects are less probable.

Importance of the Solvent–Coagulant Miscibility. To recall, the miscibility between solvent and coagulant is, in this model, controlled by the interaction energy parameter ε_{1-2}. A study of the effect of that parameter on the morphology of the precipitated polymer is presented in Figures 9a–d, for approximately the same coagulation time $t = 0.02$–0.03 s. For perfect mixing ($\varepsilon_{1-2} = 0$, Fig. 9a), the polymer is seen to coagulate into large agglomerates of ca 0.3 mm in diameter (dust-like structure). As the miscibility of solvent and coagulant decreases ($\varepsilon_{1-2} = 0.5$ and $\varepsilon_{1-2} = 0.77$, Figs. 9b and 9c), the present model results clearly reveal the development of finger-like structures which also become more regular as ε_{1-2} increases. Finally, for very immiscible solvent and coagulant ($\varepsilon_{1-2} = 1.5$, Fig. 9d), the formation of a sponge-like structure with spherical pores filled-in with

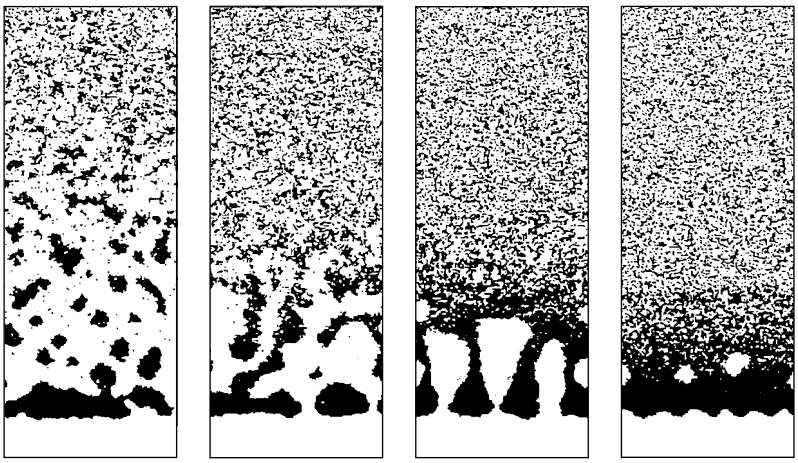

Fig. 9. Effect of the solvent–coagulant miscibility on polymer structure. (a) $\varepsilon_{1-2} = 0$, (b) $\varepsilon_{1-2} = 0.5$, (c) $\varepsilon_{1-2} = 0.77$, and (d) $\varepsilon_{1-2} = 1.5$. The structures are for a coagulation time $t = 0.02$ s, except (d) which is for $t = 0.03$ s. All the other parameters are the same as in Figure 8. The extent of shrinking of the polymer–coagulant interfaces with respect to their initial positions have not been represented. Courtesy of *Journal of Polymer Science*.

coagulant is observed. It is interesting to note that the sequence of precipitated morphologies obtained in Figure. 9 through a decrease in solvent–coagulant miscibility is also very similar to that observed experimentally (27) when increasing the initial polymer concentration. Based on our understanding from the model, this is not surprising since a decrease in solvent–coagulant miscibility effectively makes solvent and polymer particles more alike as far as the coagulant is concerned. A further investigation of the model results also reveals that the transition from sponge to finger to dust-like structures is also accompanied by a dramatic increase of the rate of coagulation, in perfect agreement with experimental observation. Thus, for the dust-like structure studied in Figure 9a, it is found that the diffusion coefficient for the penetration depth of the coagulation front is around 10^{-5} cm^2/s. For the sponge-like structure of Figure. 9d, a diffusion coefficient of ca 2×10^{-7} cm^2/s is found.

Effect of Additives in the Coagulant. In industrial applications, the coagulant power and coagulant–solvent miscibility are often varied through the incorporation of additives into the coagulant. These additives may consist of pure polymer solvent or of large amounts of inorganic salts. The presence of an additive in the coagulant can be easily accounted for in the lattice model (28). Figures 10a–c show the effect of adding $CaCl_2$ to water during coagulation of a 20% solution of Nomex in NMP. The figures clearly reveal a transition from a finger-like to a dense polymer structure at ~50% $CaCl_2$ concentration. Further investigation of the model results reveals that the transition is not associated with any decrease in the rate of coagulation, which stays at high values around 10^{-5} cm^2/s. The approach, therefore, clearly confirms the advantages of using high salt concentrations in the coagulant. Further study of the model results also reveals that

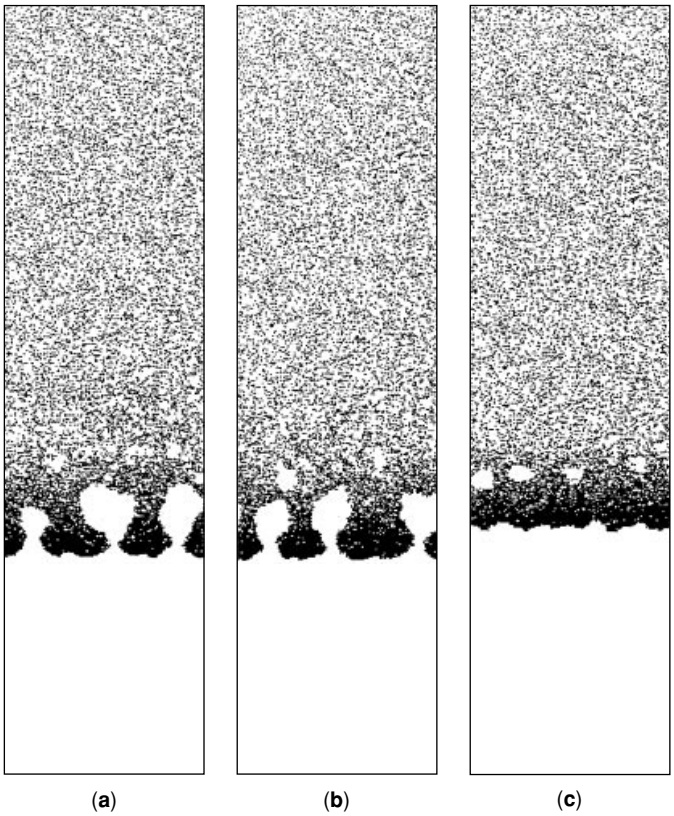

Fig. 10. Effect of adding increasing amounts of $CaCl_2$ to the aqueous coagulant. The amounts of $CaCl_2$ are as follows: (a) 35%, (b) 40%, and (c) 50%. All three figures are for a coagulation time $t = 0.015$ s. Reprinted from Ref. 28. Copyright (1995), with permission from Excerpta Medica Inc.

the success of that technique rests upon the use of a salt that is poorly miscible with the polymer solvent. This observation is in line with the previous finding (see Fig. 9) that a decrease in solvent–coagulant miscibility leads to more dense polymer structures. The effect of adding high concentrations of the solvent to the aqueous bath has also been studied. At 35–49% solvent, the model results clearly reveal a transition from a finger-like morphology into a more uniform structure, as observed experimentally (29,30). However, in contrast to the case of a salt addition, that transition is also associated with a dramatic decrease in the rate of coagulation. Thus, with 49% solvent in the coagulant, no polymer has yet precipitated after $t = 0.02$ s and coagulation becomes an extremely slow process entirely controlled by particle nucleation and growth.

Admittedly, these results are for short coagulation times ($t < 0.03$ s) which has allowed the study of structures no larger than a few microns in depth. Therefore, it could be argued that, being for small coagulation times $t < 0.03$ s, the results of the present paper are not representative of the fully coagulated structures that sometimes require up to a few minutes to obtain. In support of these results, it

should be noted, however, that actual micrographs of coagulated morphologies obtained at different times, ranging from a few seconds to several minutes, do not reveal any evidence for a change in polymer structure with time. Thus, a change in these calculated morphologies at later times remains improbable and the gross morphology of the final polymer structure should be adequately described by the present model results.

Polymer Quenching

The previous section presented a model study of the coagulation of a polymer solution brought upon by *diffusion* of a nonsolvent. The present section focuses on the faster process of phase separation inside a binary polymer–solvent system induced by an abrupt change in external temperature and/or pressure. This problem is of obvious importance in polymer processing techniques based on thermally induced phase separation (31) or on rapid expansion of supercritical solutions (32). A typical example of the latter is the flash spinning process. Here, a polymer solution is first heated under high pressure and then rapidly released through a spinnerette, leading to the formation of a fibrillar polymeric network.

Equilibrium properties of polymers in dilute solutions are reasonably well understood (33) and polymer–solvent phase equilibria can be easily obtained through the use of the classical Flory-Huggins mean-field lattice model (34) or, alternatively, from more recent computer simulations of Gibbs ensembles (35,36). On the other hand, the development of polymer morphology inside the coexistence curve is only poorly understood and previous work has been restricted essentially to kinetic studies of the collapse of a *single* polymer chain (37–39). For that reason, attention is turned to multichain systems and focus is on the very early stages ($t \ll 1$ s) of spinodal decomposition, during which equilibrium concentrations and morphologies are being established. The purpose of developing such a multichain model is to get a better understanding of the dependence of polymer structure on molecular weight, polymer concentration, and quenching conditions.

In this model (40), first an array of polymer chains at infinite temperature is constructed for a given value of the chain volume fraction V_f and chain length N (henceforth in statistical segment units). This is obtained by randomizing an ordered array of chains by a series of Monte-Carlo moves of two kinds. The first is a *nonlocal* reptation which randomly moves a bond from one end of a chain to the other (36). The second incorporates *local* random moves such as end-flip, 2-bond kink jump, and 3-bond crankshaft motion (41). Upon completion of that process, an interaction energy $\varepsilon < 0$ is imposed between pairs of nonbonded nearest-neighbor chain segments and the system is quenched to a finite temperature T. The new state of the polymer chains is then obtained, as a function of time, by using the *local* Monte-Carlo moves described above (ie, nonlocal reptation is excluded) which are made to occur at a rate (see also eq. (6))

$$v = \tau^{-1} \exp[-\beta(U_f - U_i)/2] \tag{9}$$

in which U_f and U_i denote the local energy in the final and initial states, respectively, whereas τ corresponds to the reorientation time of a statistical segment,

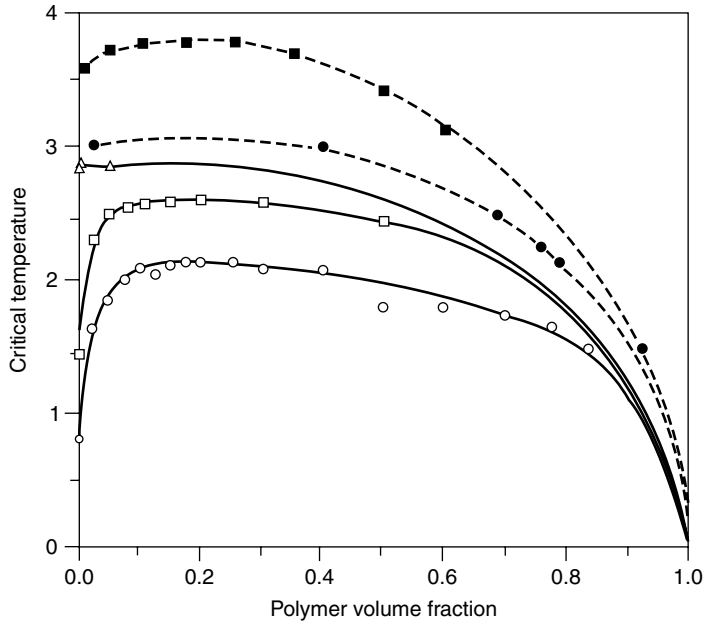

Fig. 11. Dependence of the critical temperature $-k_B T_c/\varepsilon$ on polymer volume fraction. Results obtained by the present approach are denoted by open symbols ○, $N = 20$; □,: $N = 60$; and △: $N = 1000$. Both local and nonlocal (ie, reptation) moves have been used in our Monte-Carlo simulations. Filled-in symbols are reproduced from Reference 35 (●, $N = 100$) and Reference 36 (⬒, $N = 64$). The curves are drawn to guide the eye. Reprinted with permission from Ref. 40. Copyright (1997) American Chemical Society.

which is of the order of 10^{-8} s. As in all previous models, after each attempted move, the overall "time" t is incremented by $1/[v_{max}n]$ in which v_{max} represents the highest rate among all n possible moves on the lattice.

The polymer–solvent phase equilibria are obtained from a study of the behavior of the specific heat

$$C = [\langle \nu^2 \rangle - \langle \nu \rangle^2]\varepsilon^2/[(N+1)k_B T^2] \tag{10}$$

in which ν denotes the number of nearest neighbor nonbonded polymer segments. The critical temperature $-k_B T_c/\varepsilon$ for phase separation is obtained from the location of the maximum in a plot of C vs T. Model results for the dependence of that critical value on the polymer volume fraction V_f are presented in Figure 11 for chains of length $N = 20$ (symbol ◯), 60 (□), and 1000 (△). The figure reveals a pronounced asymmetry of the curves and a shift of their maxima toward higher T_c and lower V_f with an increase in N, in perfect agreement with experimental observation. Also represented are theoretical predictions obtained from two previous approaches: (*1*) the slab geometry model (Ref. 35; symbol ●) and (*2*) the Gibbs ensemble simulations (Ref. 36; symbol ⬒). Both sets of results are in good qualitative agreement with model predictions.

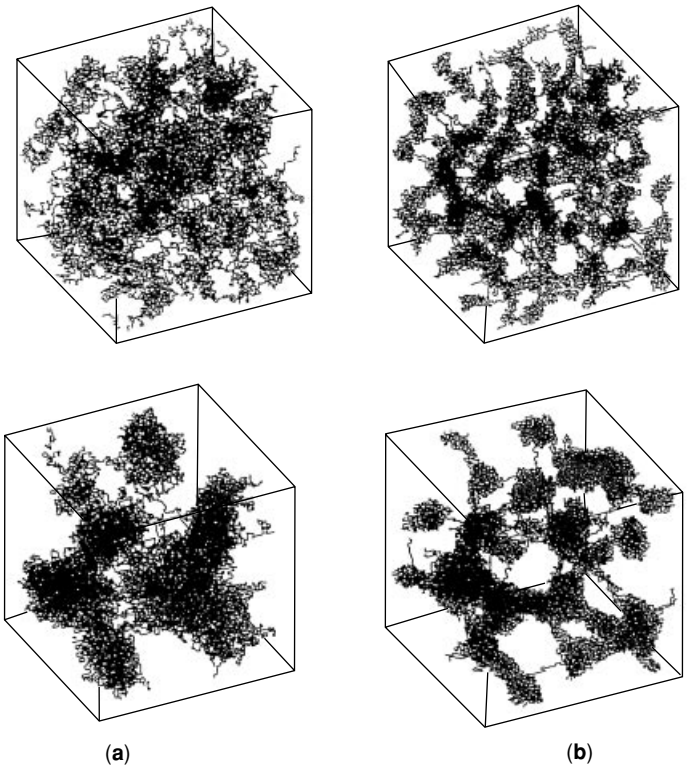

Fig. 12. Polymer morphologies obtained at $-k_B T/\varepsilon = 2.5$ and 1.0 for two different simulation times: $t = 5 \times 10^3 \tau$ (top) and $t = 15 \times 10^4 t$ (bottom). The representations are for cubic lattices of 70 unit lengths (~70 nm) in each direction. Reprinted with permission from Ref. 40. Copyright (1997) American Chemical Society.

Effect of Quench Depth. Now attention is turned to an analysis of the structure development upon quenching inside the binodal curves of Figure 11. The results are presented in Figure 12 for two (reduced) temperatures $-k_B T/\varepsilon = 2.5$ (Fig. 12a) and $-k_B T/\varepsilon = 1.0$ (Fig. 12b). The top set of morphologies is for a short time $t = 5 \times 10^3 \tau$. A bicontinuous sponge-like morphology is observed, in agreement with experimental observation (31,42) and with a recent viscoelastic model study (43). High temperatures (left) are seen to lead to a coarser morphology, whereas lower ones (right) form a lacy structure with fine and dense fibrils. Further study of the model results indicates that, within that early stage, spinodal decomposition occurs to quickly establish equilibrium concentrations and the polymer forms a continuous percolated structure whose fine features are exacerbated at very deep quenches. For large simulation times $t = 10^5 \tau$ (bottom set of morphologies in Fig. 12), the figures reveal a substantial coarsening of the structures and a progressive breaking up of the continuous polymer gel into isolated spherical aggregates. This is the so-called percolation-to-cluster transition. Within that regime, it was also found that the rate of coarsening increases with a decrease in quenching temperature.

The Case of Mixed Solvent Systems. There has been a recent interest in the use of mixed solvent systems for polymer processing and isolation. It is now common in industrial processes for polymer coagulation to employ solvent mixtures which are designed to bring the polymer solution close to its solubility limit. The formulation of these systems is often empirical and the behavior of polymer chains in mixed solvents is still poorly understood. The present study focuses on a 70/30 blend of chains of two different lengths $N_1 = 4000$ and $N_2 = 50$ (in statistical segment units). The blend is dissolved at 3.3% concentration in two different solvents: (*1*) a mixture of 80% good solvent (repulsive interaction energy with the polymer $\varepsilon = 1$) and 20% bad solvent ($\varepsilon = 41$) and (*2*) a single solvent system with average solvent power. The study proceeds as follows (44). First the two polymer solutions are equilibrated at high temperatures. These solutions are then quenched inside the two-phase region at the same temperature T until thermodynamic equilibrium is achieved. The polymer structures obtained in the two solvents for a quenching temperature $T = 40$ are depicted in Figures 13a and 13b. In the average solvent case (Fig. 13a), the polymer blend is seen to precipitate in a dense spherical globule. For the solvent mix (Fig. 13b), on the other hand, the precipitated structure is more diffuse and a fraction of the chains remains soluble in the solvent phase. Further investigation of the model results reveals that those chains, which represent about 5% of the total polymer mass, are made exclusively of the short length component. The presence of that soluble fraction is due to preferential adsorption of the good solvent by the low molecular weight chains (44–46). These results are of great importance as they indicate that quenching a polydisperse system below the cloud point may induce molecular weight segregation between the two phases: the longer chains, which precipitate out first, tend to populate the polymer-rich phase whereas the shorter

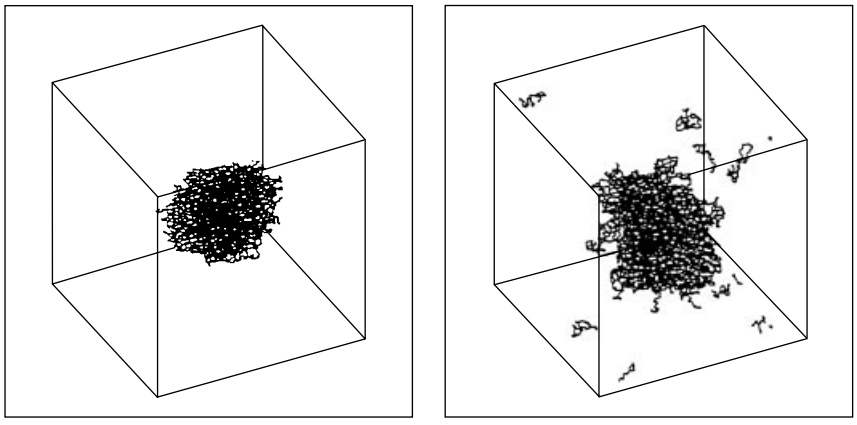

Fig. 13. Effect of solvent characteristics on precipitated polymer morphologies. The figure is for a blend precipitated in (a) the average solvent and (b) a mixture of 80% good solvent ($\varepsilon = 1$) with 20% bad solvent ($\varepsilon = 41$). Total polymer concentration is 3.3% and quenching temperature is set at $T = 40$ (in k_B units). The representation is for a simple cubic lattice of $70 \times 70 \times 70$ sites. Courtesy of *Journal of Polymer Science.*

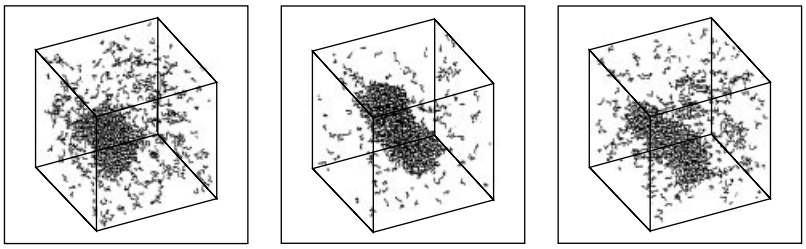

Fig. 14. Effect of quench depth, T, on precipitated polymer morphologies. (a) $T = 20$, (b) $T = 10$, and (c) $T = 2$ (in k_B units). The figure is for a 32/68 blend of chains of lengths $N_1 = 4000$ and $N_2 = 10$, dissolved in a mixture of 80% good solvent ($\varepsilon_{2-3} = -0.25$) with 20% bad solvent ($\varepsilon_{1-3} = 45$). Total polymer concentration is 3.3%. Courtesy of *Journal of Polymer Science*.

chains, having greater solubility, remain in the solvent phase. The effect of quench depth on the soluble polymer fraction has also been studied. The model results are shown in Figure 14 for a 32/68 blend of chains of lengths $N_1 = 4000$ and $N_2 = 10$, precipitated at increasing quench depths: (*1*) $T = 20$; (*2*) $T = 10$, and (*3*) $T = 2$ (in k_B units). The model reveals that the soluble fraction first decreases and then increases with quench depth. This increase is due to a higher preferential adsorption at low temperatures. It should be noted also that this effect seems to be indicative of a solvent mixture in which the good solvent has a tendency to form a complex with the polymer ($\varepsilon_{2-3} = -0.25$).

Thermally Bonded Nonwovens

Mechanical Properties. The processing of fibers into planar fibrous materials such as papers, nonwovens, and wood fiber boards has received a lot of attention over the years because of their great versatility and their ease of manufacturing into complex shapes for a wide range of applications. In spite of its importance, little attention has been paid to the fracture behavior of fibrous sheets. Previous theories are based on random lattice models with various types of disorder (47,48). The fibrous nature of the networks has been included in more recent approaches (49,50). These models, however, are confined to two-dimensional representations and, as such, they are incapable of describing actual sheet structures in which bonding between layers plays a major role. They are also based on simplified fracture criteria and provide only static calculations of stress–strain curves. Again, analytical approaches that attempt to tackle all the aspects of paper deformation are clearly impossible and, for that reason, one needs to turn to computer modeling. Here the focus is on nonwoven sheets, such as Tyvek®, which are formed by pressing spunbonded fibrous webs (layers) between two smooth heated rolls. These webs are created through flash spinning of a solution of high density polyethylene through a spinneret containing a single hole.

In the model (51), a spunbonded web (henceforth referred to as "layer") is represented by an array of fiber strands connected on a two–dimensional x-y lattice.

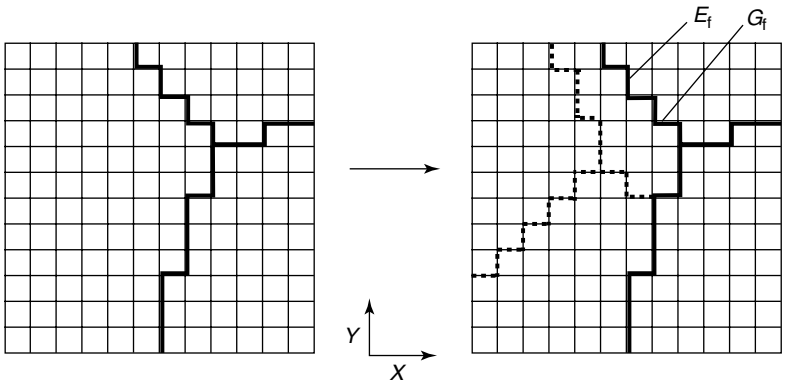

Fig. 15. Model construction of a fibrous layer. E_f and G_f denote the elastic tensile and shear modulus for the fiber. Reprinted from Ref. 51. Copyright (1997), with permission from Excerpta Medica Inc.

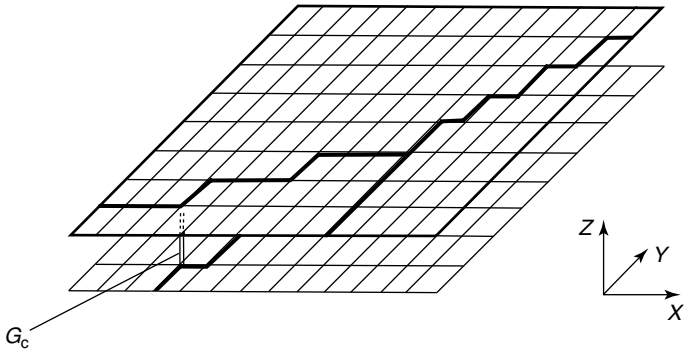

Fig. 16. Consolidation into a sheet structure. G_c denotes the shear modulus of the bonds introduced during consolidation. Reprinted from Ref. 51. Copyright (1997), with permission from Excerpta Medica Inc.

This array is built in a sequence of steps. At each step, a lattice site is chosen at random and three fiber strands are constructed from that site until they reach either the edge of the lattice or a previously constructed strand (see Fig. 15). Each of the strands within a layer is modeled as a ribbon, made itself of a series of lattice bonds. The sheet structure is then obtained by piling up a series of layers on top of each other along the z-axis and consolidation is realized through bonding nearest-neighbor fiber sites between layers (see Fig. 16). Upon tensile deformation, the individual fiber bonds are stretched and their local stresses combined with thermal activation rate theory (see eq. (2)) define probabilities for bond rupture. As in previous models, at regular time intervals, the individual lattice sites are relaxed toward mechanical equilibrium with their neighbors by a systematic sequence of operations which steadily reduce the net residual force acting on each site.

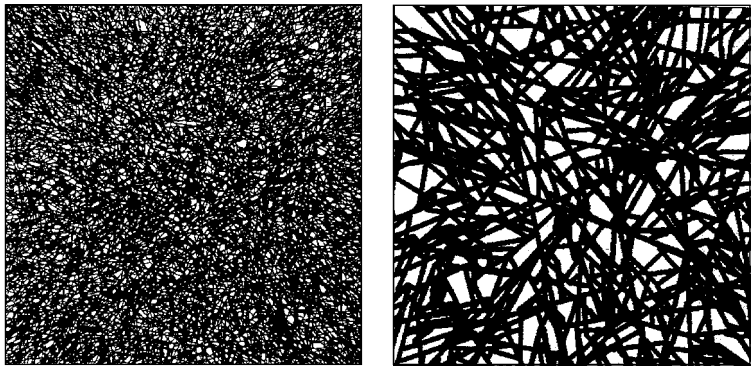

Fig. 17. Actual computer representations of two 3-layer sheets having different fiber cross sections. The top structure is for a square cross section (aspect ratio $\alpha = 1$), whereas the bottom is for ribbon-like fibers (cross-section aspect ratio $\alpha = 7$). Both structures are for a 37% fiber volume fraction. Reprinted from Ref. 57. Copyright (1998), with permission from Excerpta Medica Inc.

The results, to be presented below, will be for application to Tyvek sheets. Figure 17 shows actual computer representations of two 3-layer sheets having different fiber cross sections. The *lhs* structure is for a square cross section (aspect ratio $\alpha = 1$), whereas the *rhs* is for ribbon-like fibers with cross-section aspect ratio $\alpha = 7$. Both structures are for a 37% fiber volume fraction. Note that the sheet of Figure 17b has a fewer number of pores but, more larger voids. Figure 18 shows calculated stress–strain curves for polyethylene sheets for two different values of the shear modulus G_f of the fiber. The two curves show the presence of two distinct regions characterized by different moduli. Within the first region, which extends to ~9% elongation, computer results reveal an extensive deformation of the consolidating bonds. These bonds start to break at 2–4% elongation, which results in a continuous bending down of the stress–strain curve. At higher elongations, one enters the second region which is characterized by a gradual increase in the load supported by the fibers. As a result, the slope of the curve within that region is seen to be strongly dependent on the fiber shear modulus G_f. The latter observation is in line with the previous model finding (52) in that the *tensile* deformation of structures reinforced with randomly oriented fibers is fully controlled by the *shear* modulus of the fibers.

Permeability. Nonwoven fibrous media are also being extensively used in filtration and barrier applications. Several analytical approaches have been proposed for describing the dependence of their permeability on the shape and volume fraction of fibers (53–56). For simplicity, all these studies assumed that the fibrous media is made of a regular array of equidimensional cells, each consisting of a fiber segment surrounded by air. This is certainly not the case experimentally as fibrous media are made from a deposition process in which fibers are laid into a dense and compact mat. In one approach (57), the permeability of the sheet to diffusional flow is studied by a Monte-Carlo process. Here, the sheet is put in contact with a large external bath of small particles which diffuse through the

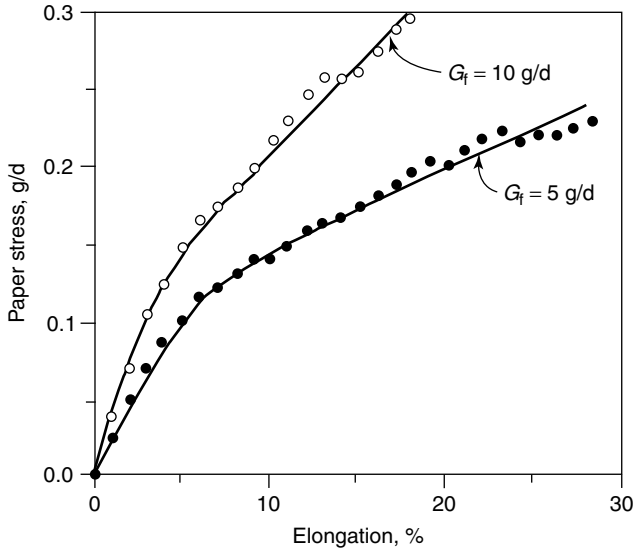

Fig. 18. Calculated stress–strain curves for two polyethylene sheets with $G_f = 10$ g/d and $G_f = 5$g/d (10 g/$d \cong$1 GPa). In reference to the units commonly used in the paper industry, a stress of 0.1 g/d is equivalent to a load of 10 lbs/in. on a 7 mil sheet. The curve is drawn to guide the eye. Reprinted from Ref. 51. Copyright (1997), with permission from Excerpta Medica Inc.

structure by hopping between nearest-neighbor lattice sites. This model allows one to study in detail the importance of the sheet density, fiber shape, and the role of interstitial voids between layers.

Model results for the dependence of diffusivity D (see Ref. 57) on fiber volume fraction V_f are presented in Figure 19. For simplicity, the data have been normalized by the diffusivity D_0 at $V_f = 0$. First, square fibers are examined ($\alpha = 1$, Fig. 9a). Calculated data have been represented by symbols ○ and ● for sheets of 5 and 10 layers, respectively. For both sheets, the diffusivity shows a monotonic decrease with fiber volume fraction up to $V_f = 0.4$. Also represented in the figure (symbol +) are calculated data from Reference 53 The predictions are higher than the present study because, as stated earlier, previous approaches assume each fiber to be surrounded by air so that the pores always belong to the continuous phase, except at $V_f = 1$. Ribbon-like fibers with $\alpha = 7$, are shown in Figure 19b. Comparison with the previous figure shows a strong decrease in diffusivity with an increase in cross-section aspect ratio α. These observations may seem surprising in view of the large pore areas previously observed in Figure 17b at large $\alpha = 7$. At constant V_f, diffusivity is, however, mainly controlled by the *tortuosity* of the diffusion path across the sheet. The length of that path obviously increases with α, as wide fibers act as large obstacles which force a diffusing particle to wander within a plane perpendicular to flow. Also represented in Figure 19b are predictions from previous theories (54,56) for $\alpha = 6$. As in Figure 19a, these approaches lead to an overestimation of the diffusivity at high V_f because they neglect contacts between fiber elements.

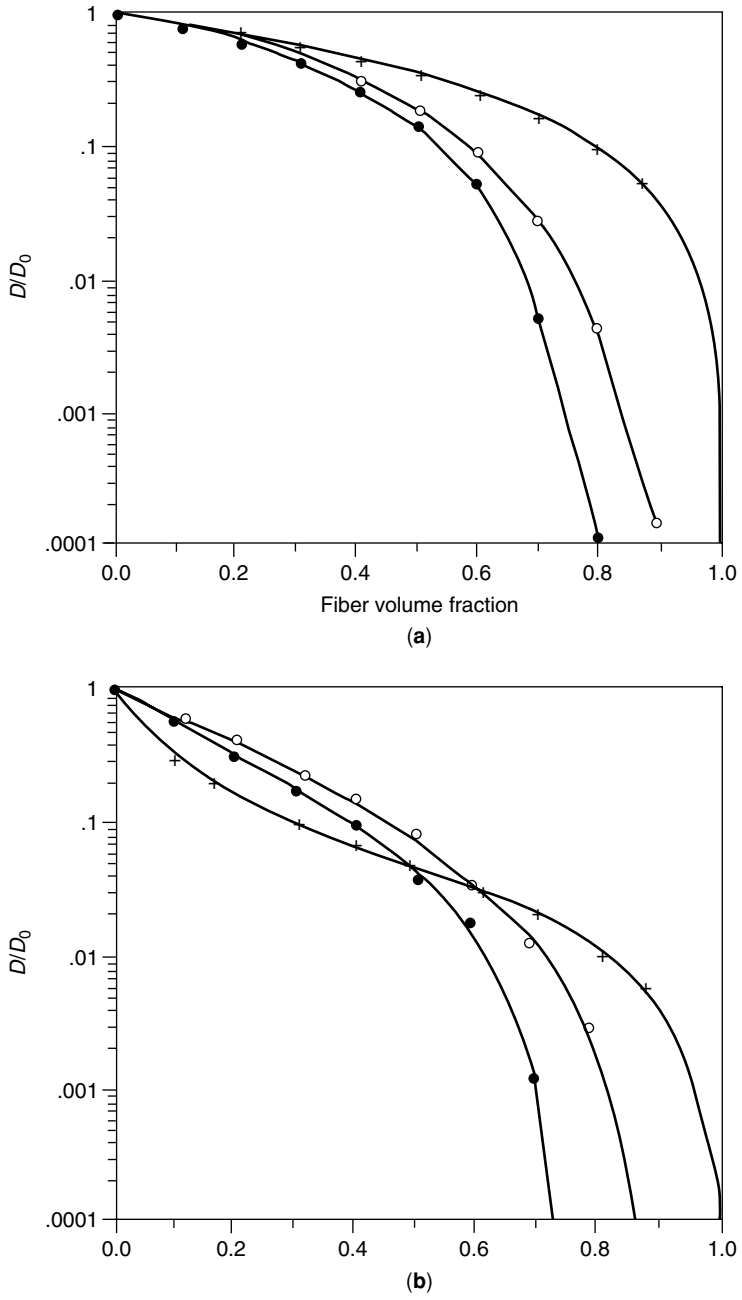

Fig. 19. (a) Normalized diffusivity D/D_0 for sheets of fibers with $\alpha = 1$. Symbols are as follows: ◯ and •, data calculated with our model for 5- and 10-layer sheets; +, model data taken from Reference 53. (b) Same as Figure 19a but, for sheets of fibers with $\alpha = 7$. Model data taken from Reference 56 for $\alpha = 6$ are denoted by the symbol +. Other model data obtained in Reference 54 fall along the same line. Reprinted from Ref. 57. Copyright (1998), with permission from Excerpta Medica Inc.

Conclusions

In summary, a series of kinetic Monte-Carlo models for the study of the effect of processing conditions on polymer structure and properties have been presented. These models are mesoscopic in the sense that the unit lattice length is of the order of the statistical segment length for the polymer chains and atomic level details are omitted. There studies have clearly revealed the importance of molecular weight, molecular weight distribution, and density of entanglements in controlling the drawability of flexible polymers in the solid state. The approach has also allowed description in detail of the processes of coagulation and quenching of a polymer solution and reproduction the wide variety of different polymer structures that can be obtained. Finally, turning to the processing of fibers into planar fibrous materials such as papers and nonwovens, it has been shown that kinetic Monte-Carlo models can be equally successful at predicting their mechanical and permeability properties.

BIBLIOGRAPHY

1. I. M. Ward, *Mechanical Properties of Solid Polymers*, 2nd ed., John Wiley and Sons, Inc., New York, 1990.
2. H. Strathmann, *ACS Symposium Series 269: Materials Science of Synthetic Membranes*, American Chemical Society, Washington, DC, 1985, p. 165.
3. W. E. Dorogy and A. K. St Clair, *J. Appl. Polym. Sci.* **43**, 501 (1991).
4. L. J. Mendes and co-workers, *J. Polym. Sci., Polym. Phys.* **37**, 2571 (1999).
5. A. K. Doufas and A. J. McHugh, *J. Rheol.* **45**, 403 (2001).
6. A. J. Kinloch and R. J. Young, *Fracture Behavior of Polymers*, Applied Science, London, 1983.
7. H. H. Kausch, *Polymer Fracture*, Springer-Verlag, Berlin, 1978.
8. Y. Termonia and P. Smith, *Macromolecules* **20**, 835 (1987).
9. Y. Termonia and P. Smith, *Macromolecules* **21**, 2184 (1988).
10. L. R. G. Treloar, *The Physics of Rubber Elasticity*, 2nd ed., Clarendon, Oxford, 1958.
11. Y. Termonia, P. Meakin, and P. Smith, *Macromolecules* **18**, 2246 (1985).
12. Y. Termonia, S. R. Allen, and P. Smith, *Macromolecules* **21**, 3485 (1988); Y. Termonia and P. Smith, *Colloid Polym. Sci.* **270**, 1085 (1992); Y. Termonia and P. Smith, *Macromolecules* **26**, 3738 (1993).
13. G. Capaccio, T. A. Crompton, and I. M. Ward, *J. Polym. Sci., Polym. Phys. Ed.* **14**, 1641 (1976); G. Capaccio, T. A. Crompton, and I. M. Ward, *J. Polym. Sci., Polym. Phys. Ed.* **18**, 310 (1980).
14. T. Kanamoto and co-workers, *Macromolecules* **21**, 470 (1988).
15. J. E. Van Trump, DuPont Progress Report, PR-90-24, 1990; PR 92-11 (1992).
16. R. E. Kesting, *Synthetic Polymeric Membranes*, 2nd ed., John Wiley & Sons, Inc., New York, 1985.
17. R. J. Ray, W. B. Krantz, and R. L. Sani, *J. Membr. Sci.* **23**, 155 (1985).
18. P. Neogi, *AIChE J.* **29**, 402 (1983).
19. C. Cohen, G. B. Tanny, and S. Prager, *J. Polym. Sci., Polym. Phys. Ed.* **17**, 477 (1979).
20. A. J. Reuvens, F. W. Altena, and C. A. Smolders, *J. Polym. Sci., Polym. Phys. Ed.* **24**, 793 (1986); A. J. Reuvens, J. W. A. van den Berg, and C. A. Smolders, *J. Membr. Sci.* **34**, 45 (1987); A. J. Reuvens and C. A. Smolders, *J. Membr. Sci.*,, **34**, 45 (1987).
21. L. Yilmaz and A. J. McHugh, *J. Membr. Sci.* **28**, 287 (1986); A. J. McHugh and L. Yilmaz, *J. Membr. Sci.* **43**, 319 (1989).

22. Y. Termonia, *Phys. Rev. Lett.* **72**, 3678 (1994); Y. Termonia, *J. Polym. Sci., Polym. Phys. Ed.* **33**, 279 (1995).
23. M. A. Frommer and D. Lancet, in H. K. Lonsdale and H. E. Podall, eds., *Reverse Osmosis Membrane Research*, Plenum Press, New York, 1972, p. 85.
24. Y. Termonia, *J. Polym. Sci., Polym. Phys. Ed.* **36**, 2493 (1998).
25. Z. Alexandrowicz and Y. Termonia, *Mol. Phys.* **38**, 47 (1979).
26. Y. Termonia, *Mol. Phys.* **38**, 65 (1979).
27. H. Strahmann and co-workers, *Desalination* **16**, 179 (1975).
28. Y. Termonia, *J. Membr. Sci.* **104**, 173 (1995).
29. H. Strathmann, K. Kock, and P. Amar, *Desalination* **16**, 179 (1975).
30. C. A. Smolders and co-workers, *J. Membr. Sci.* **73**, 259 (1992).
31. D. R. Lloyd, S. S. Kim, and K. E. Kinzer, *J. Membr. Sci.* **64**, 1 (1991); S.-W. Song and J. M. Torkelson, *Macromolecules* **27**, 6389 (1994).
32. C. A. Eckert, B. L. Knutson, and P. G. Debenedetti, *Nature* **383**, 313 (1996).
33. P. G. de Gennes, *Scaling Concepts in Polymer Physics*, Cornell University Press, Ithaca, New York, 1988; M. Doi and S. F. Edwards, *The Theory of Polymer Dynamics*, Oxford Science, New York, 1989; J. des Cloiseaux and G. Jannink, *Polymers in Solution*, Clarendon, Oxford, 1990.
34. P. J. Flory, *J. Chem. Phys.* **9**, 660 (1941); M. L. Huggins, *J. Chem. Phys.* **9**, 440 (1941).
35. W. G. Madden, A. I. Pesci, and K. F. Freed, *Macromolecules* **23**, 1181 (1990).
36. A. D. Mackie, A. Z. Panagiotopoulos, and S. K. Kumar, *J. Chem. Phys.* **102**, 1014 (1995).
37. A. Byrne and co-workers, *J. Chem. Phys.* **102**, 573 (1995).
38. B. Ostrovsky and Y. Bar-Yam, *Comput. Polym. Sci.* **3**, 9 (1993).
39. Y. A. Kuznetsov, E. G. Timoshenko, and K. A. Dawson, *J. Chem. Phys.* **103**, 4807 (1995); J. Ma, J. E. Straub, and E. I. Shakhnovich, *J. Chem. Phys.* **107**, 2615 (1995).
40. Y. Termonia, *Macromolecules* **30**, 5367 (1997).
41. A. Sariban and K. Binder, *Macromolecules* **24**, 578 (1991).
42. J. H. Aubert and R. L. Clough, *Polymer* **26**, 2047 (1985); J. H. Aubert, *Macromolecules* **23**, 1446 (1990).
43. T. Taniguchi and A. Onuki, *Phys. Rev. Lett.* **77**, 4910 (1996).
44. Y. Termonia, *J. Polym. Sci., Polym. Phys. Ed.* **37**, 2782 (1999).
45. B. E. Read, *Trans. Faraday Soc.* **56**, 382 (1960).
46. A. Dondos and H. Benoit, *Makromol. Chem.* **133**, 119 (1970); A. Dondos and H. Benoit, *Makromol. Chem.* **179**, 1051 (1978).
47. P. M. Duxbury, P. D. Leath, and P. L. Beale, *Phys. Rev., B* **36**, 367 (1987).
48. P. D. Beale and D. J. Srolovitz, *Phys. Rev., B* **37**, 5500 (1989).
49. M. J. Alava and R. K. Ritala, *Physica Scripta, T* **33**, 155 (1990); *J. Phys.: Condens. Matter* **2**, 6093 (1990).
50. J. Astrom and co-workers, *J. Appl. Phys.* **75**, 2383 (1994).
51. Y. Termonia, *Chem. Eng. Sci.* **52**, 3003 (1997).
52. Y. Termonia, *J. Polym. Sci., B* **32**, 969 (1994).
53. L. Rayleigh, *Philosoph. Mag.* **34**, 481 (1892).
54. W. T. Brydges, S. T. Gulati, and G. Baum, *J. Mater. Sci.* **10**, 2044 (1975).
55. E. L. Cussler and co-workers, *J. Membr. Sci.* **38**, 161 (1988).
56. L. Nilsson and S. Stenstrom, *Chem. Eng. Sci.* **50**, 361 (1995).
57. Y. Termonia, *Chem. Eng. Sci.* **53**, 1203 (1998).

YVES TERMONIA
E. I. du Pont de Nemours, Inc.

NANOCOMPOSITES, POLYMER–CLAY

Introduction

Polymer matrix nanocomposites are a fairly new class of engineered materials which offer for a broad range of properties, an interesting and even radical alternative to more conventional filled polymers, yet at much lower filler loadings. They can be defined as polymer matrix systems in which the dispersed inorganic reinforcing phase has at least one of its dimensions in the nanometer range, which is quite close to the scale of elementary phenomena at the molecular level. The resulting unique combination of large interfacial area and small interparticle distance strongly influences nanocomposite behavior.

Current status of research and industrial development of polymer nanocomposites clearly outlines the prominent position of clay nanocomposites and the present review is mainly devoted to the latter materials.

From a general point of view, filler aspect ratio is a pertinent parameter to distinguish between various types of nanocomposites. Table 1 summarizes typical dimensions of particles under concern. Spherical silica particles are an example of isotropic nanoparticles which either provide increased composite stiffness while retaining matrix transparency, or exhibit novel optical properties by forming colloidal crystals. Although it is obviously critical to the optical behavior, it is generally observed that optimum mechanical properties are not achieved in conjunction with the best state of dispersion (1). When only two dimensions are in the nanometer range, fiber-like structures, such as whiskers or carbon nanotubes, with aspect ratios ranging between 50 and 1000 are dealt with. For instance, cellulose whiskers extracted from tunicate shells have been shown to dramatically improve composite stiffness in the case of poly(vinyl chloride) or

Encyclopedia of Polymer Science and Technology. Copyright John Wiley & Sons, Inc. All rights reserved.

Table 1. Typical Nanofiller Dimensions

Material	Shape	Typical dimensions
Silica particles	Spheres	Diameter: 30–150 nm
Cellulose whiskers	Rigid rods	Diameter: 15 nm; length: 1 μm
Carbon nanotubes	Flexible tubes (multiwall)	Diameter: 30 nm; length: 10–50 μm
Layered silicates	Flexible discs	Diameter: 50–500 nm; thickness: 1 nm

poly(styrene-*co*-butyl acrylate) matrix in the rubbery state. In the latter material a 3 order of magnitude modulus improvement is achieved at only 6 mass% whisker content. Percolation of a rigid whisker network is evoked to account for such a property increase (2). Reaching a conductivity percolation threshold at very low loadings, owing to the nanoscale dispersion of carbon nanotubes with large aspect ratio, has also been of prime importance for designing conductive polymer blends with electrostatic paintability, while limiting resin embrittlement (3). Preliminary experiments with carbon nanotube–polymer composites also underline the potential of this nanofiller for entering the field of composite materials for structural applications as well (4). Opportunities for functional and/or structural applications of carbon nanotubes will mainly depend on the capacity to reach large-scale production at moderate cost and to monitor composite elaboration while retaining nanotube integrity.

Among the variety of composites that display unique structure and behavior at the nanometer level, as compared to classical micrometer scale particulate filled materials, the use of layered silicates as a reinforcing phase is by far the most successful way of designing polymer nanocomposites with a broad range of markedly modified properties. A report from Toyota Central Research Laboratories of the development of a polyamide-6 (PA6)-based clay nanocomposite with remarkable thermomechanical behavior, at low clay loadings relative to conventional filler additives (below 5 mass% instead of 20–30 mass%), triggered extensive research efforts worldwide (5). In fact the benefits were shown not only for strength and stiffness, but also for thermal stability and barrier properties (6). Accordingly, the following presentation focuses on these materials, starting with a brief description of the layered silicates commonly used, followed by nanocomposite structural characterization and elaboration routes. Various properties of interest are reviewed together with the currently emerging structure–property relationship schemes.

Polymer-Layered Silicate Nanocomposites

Layered silicates, the more widely used in polymer nanocomposites, belong to the same structural group, the 2:1 phyllosilicates, and more specifically to the smectite group. They comprise natural clay minerals such as montmorillonite, hectorite, and saponite and also synthetic layered minerals, fluorohectorite, laponite, or magadiite. An idealized structure for montmorillonite is presented in Figure 1. Elementary clay platelets consist of a 1-nm-thick layer made of two tetrahedral sheets of silica fused to an edge-shared octahedral sheet of alumina or magnesia. Isomorphic cation substitution results in an excess of negative charges within

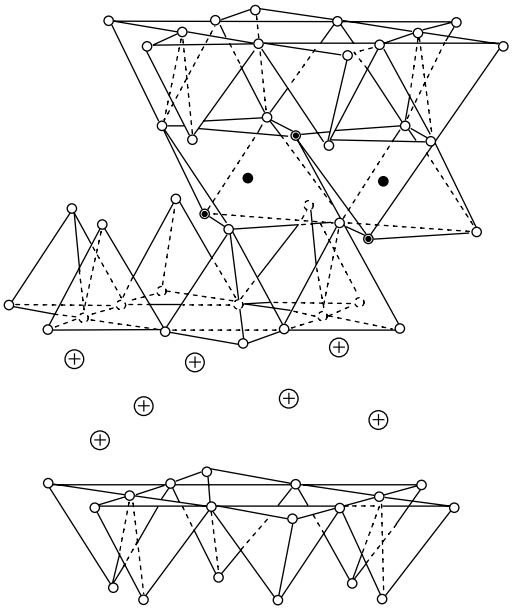

Fig. 1. Structure of montmorillonite. ● Al or Mg; ◉ OH; ◯ O; ⊕ exchangeable cations.

the layer. Stacking of the layers leads to a regular van der Waals gap called *gallery* or *interlayer*. Cations located in the galleries (eg Ca^{2+}, Na^{+}) counterbalance the excess layer charges. They are usually hydrated. This negative surface charge is quantified as the cation-exchange capacity (CEC), usually in the range from 80 to 150 meq/100 g for smectites. The interlayer space can be penetrated by organic cations or polar organic liquids as well. Exchange reactions with organic cations (aminoacids, alkylammonium ions, etc) enable to render the silicate surface organophilic. A key parameter of the stacking is the basal spacing or *d*-spacing, which ranges from 0.96 nm (ie, the layer thickness) in the fully collapsed state to about 2 nm, depending on the nature of the interlayer cation and the amount of adsorbed water (7). Individual lamellae have a high aspect ratio, with a diameter typically in the range 50–500 nm. Primary crystals (also called *tactoids*) consist of 8–10 lamellae, with usually disordered stacking. Their aggregation leads to a turbostratic structure. This organization is reflected in the x-ray diffraction (xrd) pattern where diffuse *hk* bands rather than sharp *hkl* reflections are observed. The basal reflection (001) is of more interest since it is used to derive the *d*-spacing. It will be dependent on the amount and nature of intercalated molecules in the galleries.

Characterization of Nanocomposite Microstructure. Mixing clay with a polymer does not necessarily lead to a nanocomposite. Elaboration strategies are aimed at monitoring dispersion of the inorganic compound at the nanometer level, that is down to the elementary clay platelet. Figure 2 provides a schematic illustration of the various microstructures readily achievable, namely a conventional filled polymer with clay particles in the micrometer range, an

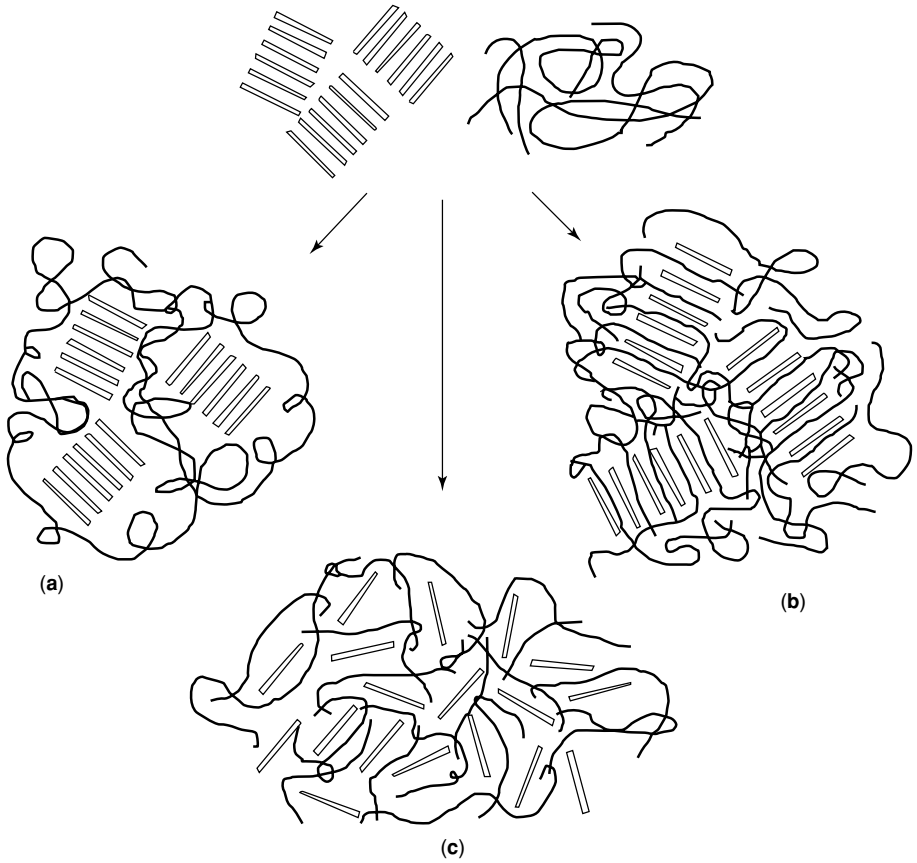

Fig. 2. Schematic representation of clay platelet dispersion as (**a**) primary crystals, (**b**) intercalated, or (**c**) exfoliated structures.

intercalated nanocomposite in which extended polymer chains are intercalated in the gap between silicate layers while the stacking order is retained (note that in this case the host gallery height is much smaller than the radius of gyration of the polymer chain), and a delaminated (or exfoliated) nanocomposite where clay layers are individually dispersed in the host polymer matrix.

The two basic tools used to elucidate nanocomposite morphology are x-ray diffraction (xrd) and transmission electron microscopy (tem). They provide complementary information on clay dispersion in the host matrix.

The basal plane reflection (00l) diffraction peak yields a direct evaluation of the d-spacing between the clay lamellae, as long as layer registry is preserved to some extent. It allows therefore to follow the structural evolution from the pristine clay stacking to any intercalated state. With changes in d values in the range 1–4 nm, such data are accessible at low diffraction angle, ie, for $1 < 2 < 9^{\circ}$. Follow up of the increase in peak width at half maximum also reflects the increase in the degree of disorder in layer stacking during the intercalation process [see eg, (8)].

Figure 3 illustrates the change in d-spacing of a stearylammonium-modified montmorillonite (C_{18}Mt) blended with a maleic anhydride-modified polypropylene

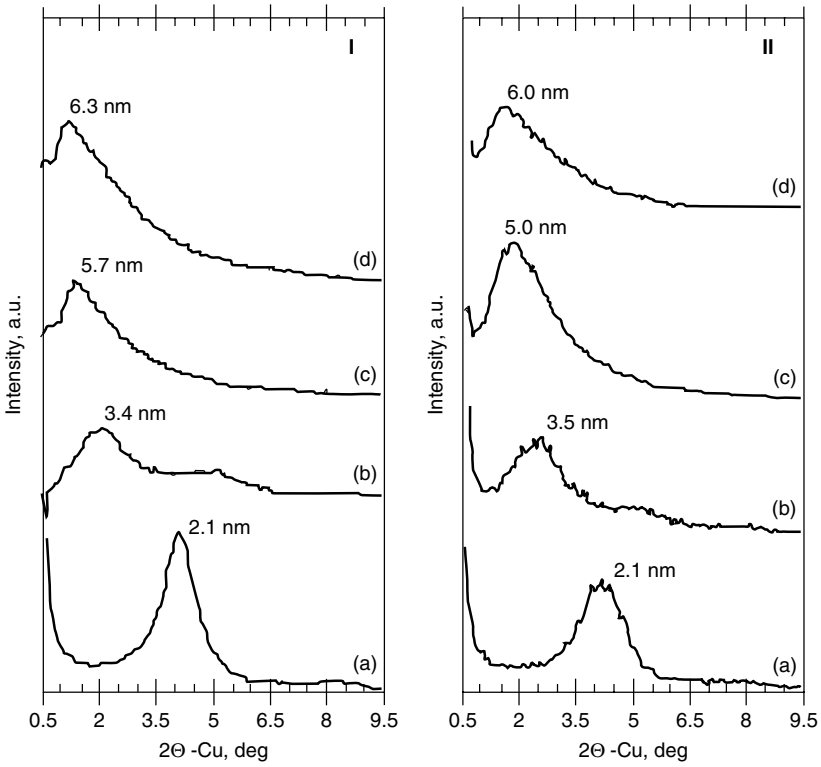

Fig. 3. Evolution of the *d*-spacing showing montmorillonite intercalation in PP-MA oligomer (**I**), and no subsequent change upon further blending with PP (**II**). Reproduced from Ref. 9.

oligomer (PP-MA). As the amount of the latter component is increased, the interlayer distance increases drastically (spectra Ia–d), indicating the efficiency of the intercalation process. Spectrum IIa reveals the lack of intercalation of C_{18}Mt by pure PP. Spectra IIb–d do not show any change in the state of intercalation assessed in Spectra I when the PP-MA intercalated organoclay is further dipersed in a PP matrix. It is concluded that PP penetration in the galleries is not favored in this particular case (9).

Whenever the xrd pattern becomes silent, meaning that the interlayer spacing is no longer accessible by conventional wide-angle x-ray diffraction, the need still remains to have access to a mesoscale description of the spatial distribution of the clay platelets. Small-angle x-ray scattering may provide some answers regarding average interparticle distance, and also about platelet orientation with respect to process geometry (10).

Transmission electron microscopy has the great advantage to give a direct view of the microstructure. Typical micrographs reveal alternating dark and bright bands refering to the silicate layers and polymer matrix respectively. The illustrations of Figure 4 show exfoliated and intercalated-exfoliated structures in the case of 1 and 5 mass% dimethylditallow ammonium-modified montmorillonite

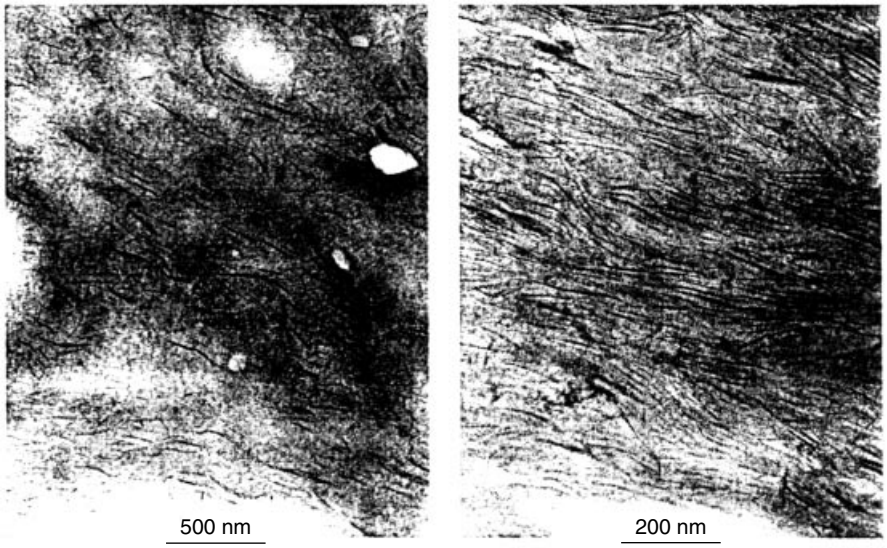

Fig. 4. Transmission electron microscopy of water-aided melt-dispersed organoclay in PA6. Courtesy of Dr M. van Es, DSM Reseach, Geleen.

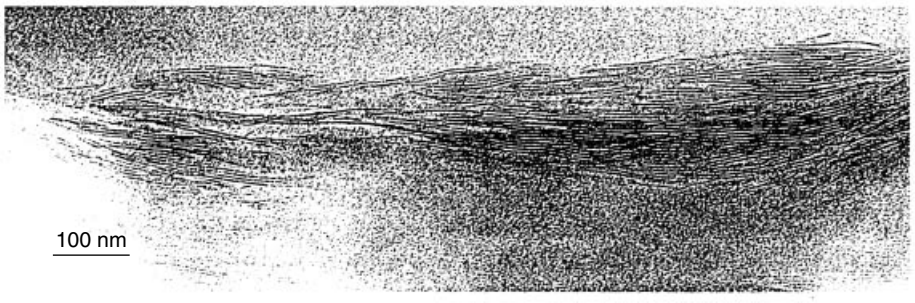

Fig. 5. Transmission electron microscopy of a melt-intercalated organoclay tactoid in a PP matrix. Courtesy of Dr M. Bacia, UST Lille.

dispersed by melt extrusion in a PA6 matrix. Additionally tem enables imaging of any mesoscale long-range ordering of the clay. It also reveals platelet flexibility promoted by the high aspect ratio and nanometer thickness as illustrated in Figure 5 for an intercalated organoclay tactoid in a PP matrix. An accurate description of polymer clay nanocomposites is therefore available from a combination of electron microscopy and xrd techniques.

Elaboration of Polymer–Organoclay Nanocomposites

Various methods have been developed in order to prepare polymer-layered silicate nanocomposites. These include *in situ* polymerization, polymer intercalation in

solution, emulsion polymerization in the presence of layered silicates, and melt intercalation. A few examples are given below to illustrate the different strategies. Review articles are available for more detailed information [see eg (11–13), and references therein].

***In situ* Polymerization.** Early works in the 1960s (14) demonstrated the feasability of intercalation polymerization of methyl methacrylate (MMA) after insertion–adsorption of the polar monomer between the lamellae of a sodium montmorillonite. Polymerization was initiated by free-radical catalysts or with γ irradiation. Renewed interest for the method in the last decade came from the work on PA6–clay hybrids at Toyota Central Research Laboratories (5), following a scheme adopted earlier by Unitika Co. (15). Sodium montmorillonite was first cation exchanged with ω-amino acids [$H_3N^+(CH_2)_{n-1}COOH$]. X-ray diffraction data show that the basal spacing is highly sensitive to the length of the alkyl chain. For $n > 11$, the ω-amino acid chain lies slanted to the layer and provides optimum swelling behavior by ε-caprolactam. 12-Amino-l-lauric acid ($n = 12$) modified montmorillonite (12-Mt) was used for performing the *in situ* ring-opening polymerization of ε-caprolactam. The carbonyl end groups of 12-Mt initiate polymerization and an increasing amount of polyamide-6 is bonded to the clay as the 12-Mt clay content is increased as clearly established by nmr studies (16). The resulting hybrid is either exfoliated at low 12-Mt content or increasingly intercalated beyond 10 wt% clay. In an alternative approach, the same team successfully developed a so-called one-pot synthesis of PA6–clay hybrid without preliminary cation exchange of the montmorillonite. Ring-opening polymerization of ε-caprolactam with 6-amino-l-caproic acid as an accelerator was performed in a water dispersion of montmorillonite in the presence of an acid. Phosphoric acid seems to be the best candidate to achieve true exfoliation in this particular process (17). 12-Amino-l-lauric acid was also successfully used both as a fluorinated silicate modifier and as a monomer in order to prepare a polyamide-12-based nanocomposite with exfoliated–intercalated structure (18). Some attempts to produce polystyrene (PS)-based nanocomposites through the *in situ* polymerization route have been reported (19). Intercalated structures are obtained. Intercalative polymerization of ε-caprolactone has also been achieved in the presence of α-protonated amino acid-exchanged montmorillonite. Upon heating, the organic acid groups initiate ring-opening polymerization of the monomer and the resulting polymer is ionically bound to the silicate platelets with a good level of delamination as revealed by xrd (20). *In situ* polymerization has also been extended to polyolefins, polyesters, or polycarbonate in recent years.

The production of thermoset-based nanocomposites by the same method has been investigated by many authors (21–23). In the case of epoxy–clay nanocomposites, the organophilic clay is first swollen in the mixture of epoxy prepolymer and curing agent. The gel state and final structure are strongly dependent on the nature of the onium ion, cross-linking amine, and curing conditions. In particular, larger chain length of the alkylammonium and ion-exchange with protonated primary amines should be preferred. Polyurethane networks are equally good candidates for clay nanolayer reinforcement (22). The approach consists in solvating polyol precursors in montmorillonite exchanged with long-chain onium ions and further adding the diisocyanate curing agent. Intercalated tactoids are obtained in the final cured nanocomposite.

Intercalation in Solution. In the case of water-soluble polymers, it is possible to prepare solvent-cast nanocomposites by using water as a cosolvent. Pristine montmorillonite can be easily dispersed in water, owing to its hydrophilic character, and blending for instance with polymers such as poly(ethylene oxide) (PEO) or poly(vinyl alcohol) (PVOH) is thus achievable (see eg (24–26)). Intercalated–exfoliated structures are observed for PVOH-based nanocomposites. On the contrary, in the presence of PEO, intercalated silicate layers are organized as large clay tactoids; this indicates that reaggregation of the initial silicate water suspension occurred during the film casting process. A similar elaboration strategy has also been developed, starting from an organoclay. In the examples of poly(ε-caprolactone) and poly(*l*-lactide), chloroform was used as a cosolvent. In both situations no evidence of intercalation could be found but the clay tactoids displayed a remarkable geometric arrangement, with their surfaces lying parallel to the cast film surface (27). These few illustrations are indicative of the high sensitivity of the final materials structure to the nature of the host matrix and to the interplay of polymer–polymer and polymer–clay interactions.

The above technique can be advantageously adapted to a situation where the polymer of interest is not soluble in any solvent, as is the case for polyimides. The polyimide precursor, ie, a poly(amic acid) solution in dimethylacetamide, is prepared and blended to a dispersion of an organomodified montmorillonite in the same solvent. Dimethylacetamide is then gradually removed, and upon heating the poly(amic acid) film at 300°C under nitrogen atmosphere the polyimide–clay hybrid is obtained. When an ammonium salt of dodecylamine is used in the ion-exchange process, true exfoliation is achieved and furthermore the clay platelets align parallel to the film surface (28).

Emulsion Polymerization. Considering the high hydrophilic character of sodium montmorillonite, it was anticipated that polymerization in an aqueous medium might provide an alternative route for polymer–clay nanocomposite preparation. The first report dealing with such an approach concerned the emulsion polymerization of MMA dispersed in a water phase in the presence of Na^+-montmorillonite. The structural analysis confirms intercalation of the PMMA in the clay galleries. A PS–clay nanocomposite has been elaborated according to the same procedure, with the same resulting intercalated morphology. Intercalation by the emulsion technique was also achieved for an epoxy system, again without requiring any ion-exchange treatment (29).

Melt Intercalation. Although emulsion polymerization or *in situ* polymerization may be considered as viable routes for industrial-scale production, as exemplified for PA6 with the latter process, melt compounding remains the most obvious route for cost-effective development of nanoreinforced polymers. The first industrial applications refer to the PA6–clay hybrid *in situ* polymerization process patented by Toyota (30), but growing interest in achieving clay nanodispersion by melt compounding is observed worldwide (31). Patent literature is clearly indicative of the current trend with many references to polyamides and other polar polymers such as polyesters or polyimides [see eg (32)]. Emphasis is put on the nature of the surfactant and processing conditions. Nonpolar polymers such as polyolefins are also highly attractive candidates with research efforts primarily driven by the automotive market. Polypropylene–clay hybrids have been prepared by melt mixing an organoclay, maleic anhydride-modified PP oligomers (PP-MA),

and PP. The polar PP-MA intercalates in the clay galleries and the quality of clay dispersion in the hybrids are clearly affected by the degree of miscibility of the polar oligomers in PP (9,33).

Direct melt intercalation of PEO in pristine montmorillonite by static annealing of cold-pressed powder mixture slightly above the melting temperature of PEO has been reported (34). The resulting *d*-spacing of the order of 1.8 nm indicates that the PEO chains are constrained in a 0.8-nm interlayer space. Differential scanning calorimetry studies reveal that the polymer is deprived of any thermodynamic transition. Neither the heat capacity jump characteristic of the glass transition nor the melting endotherm is observed. Chain dynamics appear quite peculiar in these systems. Thermally stimulated current results point at the essentially noncooperative nature of the motions of the confined chains. Intercalation kinetics have also been followed by xrd monitoring of the basal spacing reflection in model systems consisting of monodisperse PS and organically modified fluorohectorite. The most striking result is that the mobility of the polymer chains in this confined environment seems larger than that in the bulk melt (34,35). Spin-echo nmr experiments using deuterated PS suggest the coexistence of multiple environments, from solid-like to liquid-like, for intercalated chains. Molecular dynamics simulations relate this complex dynamic behavior to strong density inhomogeneity normal to the surface [(36), and Refs. 45 to 49 therein].

An extensive investigation of nanocomposite preparation with the aid of a swelling agent that is known to intercalate the clay provides some additional interesting experimental ground on the phase behavior. The results underline the influence of the polymer/swelling agent miscibility (as assessed by a solubility parameter approach) on nanocomposite formation. The example of an epoxy monomer as the swelling agent shows that either complete miscibility or strong immiscibility are preferable (37).

Structure Development in Polymer–Clay Nanocomposites

Whatever the elaboration route is, understanding phase behavior of the resulting nanocomposites is of prime importance to achieve reliable material development.

A lattice-based mean field model has been developed in order to address the problem of nanocomposite formation (38). By deriving the evolution of the free energy of the system with interlayer spacing, the model provides some basic predictions regarding the equilibrium states (ie, exfoliated, intercalated, or immiscible), in relation to the enthalpic and entropic factors of the interacting constituents, namely the silicate, the tethered surfactant chains, and the polymer. Polymer confinement results in entropy loss but the latter may be compensated in part by the entropy gain induced through the increase in conformational freedom of the tethered surfactant chain upon layer separation. As a consequence, melt intercalation is predicted to depend primarily on energetic (enthalpic) factors. Polar polymers or polymers containing groups interacting with the silicate surface will favor polymer–clay hybrid formation (35,38).

A theoretical investigation of the phase behavior of model analogues of polymer–clay nanocomposites has been conducted (39). Combining a self-consistent field model with density functional theory, the investigation underlines

some trends regarding phase morphology and stability for these systems. In particular, the calculations point at the key influence of the surfactant chain length. Polymer-like values lead to enhanced miscibility of the clay platelets and polymer matrix (exfoliated structure), even at moderate level of interactions between the grafted chains and polymer melt (39). The equilibrium behavior of a mixture of functionalized and nonfunctionalized chains (taken chemically identical) in the presence of two infinite planar surfaces has alternatively been considered using scaling theory. Functionalized chains have a telechelic architecture; ie, the active groups are located at each end of the chain. Qualitative phase diagrams are derived with prime consideration of the respective influences of interaction energy between the surface and the end group, and volume fraction ϕ of functionalized chains. Provided the interaction energy ε is high enough, exfoliation occurs more easily as ϕ is increased, whereas low ε values result in an immiscible mixture (40).

Nanocomposites Behavior

Thermal Stability. Thermal stability improvement was already recognized in the pioneering work by Blumstein on PMMA intercalated in montmorillonite. Intercalated PMMA degraded at a temperature 50°C higher than that of conventional unfilled PMMA. In recent years, thermogravimetric analysis of various polymer–clay systems have confirmed this observation even for low nanofiller loadings [see eg (13,41), and references therein]. A particularly striking example is that of cross-linked poly(dimethylsiloxane) incorporating 10 mass% exfoliated organomontmorillonite (42) for which thermal stability under nitrogen flow is enhanced by 140°C. Overall, restricted thermal motion in silicate interlayers and hindering of the diffusion of decomposition products are certainly key factors, but polymer structure and nature of the degradation mechanisms and degradation conditions are equally important to account for the disparities observed in literature.

Owing to what has been said previously on the role of the organic modifier of the layered silicate in elaboration and phase behavior of the polymer–clay nanocomposites, understanding of the key structural factors that influence its thermal degradation is of prime importance. Major concern is of course toward processing conditions and fire-retardant behavior as well. Recent work (43) on alkyl quaternary ammonium montmorillonite by a combination of thermogravimetric analysis, Fourier transform infrared spectroscopy, and mass spectrometry points at the complex degradation behavior of the organic surfactant. The initial degradation temperature is insensitive to chain architecture and length, or exchange ratio. Compared to the parent alkyl ammonium, the thermal stability of a fraction of the surfactant is substantially lowered because of catalytic sites on the layered silicates. Polymer processing generally implying temperatures higher than 180°C, chemical degradation of the surfactant is expected to occur. Many questions remain regarding the role of the decomposition products on the melt intercalation mechanism and subsequent nanocomposite phase stability. In this respect the potential of nmr techniques to follow the fate of the organic modifier seems quite promising (44).

Crystal Organization. Semicrystalline polymer nanocomposites present a unique interplay between nanoscale morphology of crystal lamellae on one hand and clay platelet organization on the other. Considering the importance of interfacial interactions and the confined chain environment, one may expect drastic changes in crystal organization. The case of PA6–clay hybrids is rather well documented. The preferred orientation of the silicate layers under melt-flow conditions, together with polymer confinement, will affect crystallization behavior. For instance, in injection-molded bars, close to the surface both the silicate layers and polymer chain axes (and hence lamella thickness) are parallel to the surface, whereas the chain axes rotate by 90° inside the bar and remain perpendicular to the silicate layers (45). Clay also favors nucleation of the γ phase (16,44), contrary to bulk PA6 which predominantly crystallizes in the more stable α form. The elevated temperature (205°C) crystal morphology of PA6–clay hybrids has been examined by performing simultaneous small- and wide-angle x-ray scattering (46). These results clearly establish that the nanoscale correlations of the silicate layer organization (40–60 nm) affect polymer crystallization, resulting in a less-ordered crystal γ phase. Evidence is also provided of the impact of polymer-layer interactions (tethered vs nontethered chains), the more defective lamellae pertaining to the *in situ* polymerized (tethered) nanocomposites. Spherulitic structure is unable to develop as in bulk polymers, which ought to influence the nonelastic mechanical response. Similar crystallization behavior is also observed in other semicrystalline polymers such as poly(ε-caprolactone) or poly(ethylene terephtalate) nanocomposites (27,47). The observation of high melting temperature phases, though defective, might come from a reduced entropy of fusion ΔS_f due to the confined crystallization environment.

Fire-Retardant Behavior. Controlling polymer flammability remains a key issue in numerous applications of engineering plastics and commodity polymers as well. The fire-retardant additive approach provides cost-effective solutions, but generally at the expenses of some physical and mechanical properties. There is also growing pressure for environmentally safe products and processes, including recyclability and use of halogen-free compounds. For these reasons, recognition of improved flammability properties in the case of polymer–clay nanocomposites has triggered the development of extensive research programs on a large variety of materials (41,48,49).

Cone calorimetry is used to evaluate the flammability under fire-like conditions. Relevant parameters such as the rate of heat release (HRR) and its peak value, heat of combustion (Hc), smoke yield (specific extension area, SEA), and carbon monoxide yield are obtained. Table 2 shows some typical data for layered silicate nanocomposites based on organically treated montmorillonite, with polyamide 6, poly(propylene-*graft*-maleic anhydride), and polystyrene as the host matrix. Nanocomposites under investigation have either delaminated (PA6) or intercalated–delaminated structures. In all cases there is a substantial reduction in peak HRR value (50–75%), whereas Hc and CO formation show little variation.

Table 2 also compares the PS–clay nanocomposite with a PS–clay mix for which intercalation does not occur. The kinetics of heat release are displayed in Figure 6. In the case of the mix, particle dispersion is only achieved at the primary particle micrometer level. The peak HRR value remains identical to

Table 2. Cone Calorimeter Data[a]

	Residue yield, %	Peak HRR, kW/m^2	Mean HRR, kW/m^2	Mean Hc, MJ/kg	Total heat released, MJ/m^2	Mean SEA, m^2/kg	Mean CO yield, kg/kg
Nylon-6	1.0	1011	603	27	413	197	0.01
Nylon-6–clay 2% delaminated	3.0	686	390	27	406	271	0.01
Nylon-6–clay 5% delaminated	5.7	378	304	27	397	296	0.02
PS	0	1118	703	29	102	1464	0.09
PS–clay mix 3% immiscible	3.2	1080	715	29	96	1836	0.09
PS–clay 3% intercalated	3.7	567	444	27	89	1727	0.08
PP-*g*-MA	0	2028	861	38	219	756	0.04
PP-*g*-MA–clay 5% intercalated	8.0	922	651	37	179	994	0.05

[a]After Ref. 48.

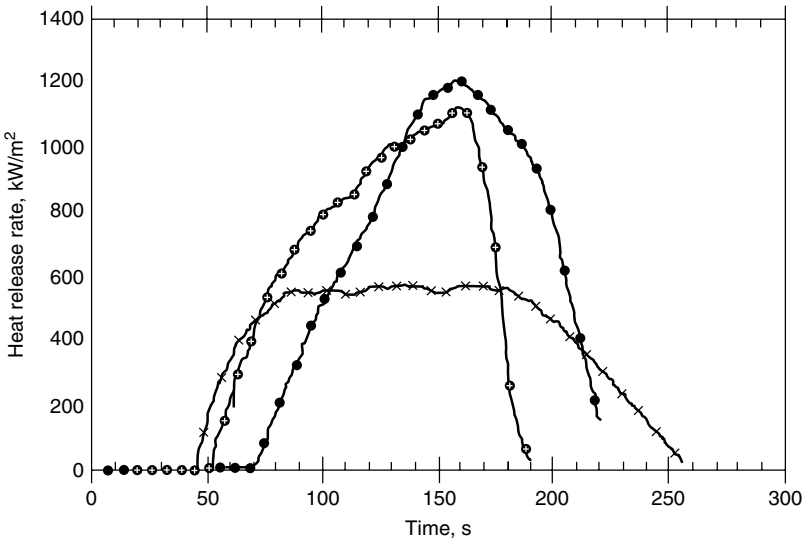

Fig. 6. Kinetics of heat release rate for PS-based compounds. Reproduced from Ref. 48. -●- PS pure; -⊖- PS immiscible (3% silicate); ⋆ PS intercalated (3% silicate).

that of pure PS while the intercalated PS–clay nanocomposite shows a 50% reduction.

The observed reduced flammability in the nanocomposites may not be attributed to an additional retention of carbon alone since the residue yields are not markedly increased. Some key insights are provided by radiative gasification experiments which enable to follow pyrolysis either in a nitrogen or in a nitrogen–oxygen atmosphere. The example of PA6 nanocomposites is revealing

enough of enhanced char formation and reduced mass loss rate in comparison to pure PA6. The current interpretation of these results is that the nanocomposite flame-retardant mechanism occurs through the build up of a reinforced char layer, which acts as an insulator, and a mass transport barrier so as to slow down the escape of the decomposition products. Developments according to this concept include the use of a PA6–clay nanocomposite in intumescent formulations as in the case of ethylene–vinyl acetate copolymers with ammonium polyphosphate (50). Enhanced flame-retardant performance is related to the formation of a thermally stable phosphocarbonaceous structure in the char, and the blend even shows a slight improvement in mechanical behavior.

Processing conditions also strongly influence the flame-retardant behavior. For example, in the case of PS-based nanocomposites, extrusion above 180°C under partially oxidative conditions yields an intercalated nanocomposite but with no flammability improvement, whereas the melt-extruded system at 170°C under nitrogen or vacuum exhibits flame-retardant efficiency (41). The way thermal degradation of the organic modifier alters the flammability reduction mechanism has yet to be understood.

Barrier Properties. Early work in the Toyota Research group acknowledged the great potential of polymer–clay nanocomposites to reduce moisture absorption and decrease water and gas permeability, even at low clay loadings (6). A further advantage for packaging applications lies in the fact that lowering of permeability is achieved while preserving transparency, owing to the suitable dispersion of platelets smaller than the wavelength of visible light.

The example of polyimide clay films illustrates the dramatic decrease of permeability coefficients. Only 2 mass% montmorillonite loading reduces the permeability by more than 50% of the pure polymer value for water vapor, oxygen, or helium. Notwithstanding possible changes in diffusion and/or solubility, it has been postulated that the major role of the clay platelets consists in substantially increasing the path length of the permeant, that is by creating a highly tortuous path, due to the high aspect ratio of the clay. A simple theory derived by Nielsen expresses the relative permeability as follows:

$$P_c/P_o = 1/[1+(L/2W)V_f]$$

in which V_f is the volume fraction of plates, L is the plate length, and W is the thickness. P_c and P_o stand for the nanocomposite and polymer permeability respectively.

Using equivalent loadings of clay but varying the aspect ratio yields results in fairly good agreement with the theoretical prediction (28). In the same way, a significant reduction in water vapor permeability was observed in the case of a poly(ε-caprolactone)–organomontmorillonite nanocomposite, showing a fivefold reduction at only 4.8 vol% clay whereas it is only halved at best with a 20 vol% conventionally filled silicate composite (20). The tortuosity model shows discrepancies between actual aspect ratios measured by tem and values deduced from curve fitting. Among the reasons for that are the deviations from the ideal dispersion of platelets parallel to the film surface, and possible aggregation of individual platelets.

Although tortuosity plays a role in barrier enhancement, some other factors ought to be taken into account (see BARRIER POLYMERS). Recent work on MXD6

Table 3. Comparison of PA6 and PA6–Clay Hybrids Mechanical Properties[a]

Property	PA6 clay hybrid	PA6
Tensile strength, MPa[b]		
At 23°C	97	69
At 120°C	32	27
Tensile modulus, GPa[c]		
At 23°C	1.9	1.1
At 120°C	0.6	0.2
Flexural strength, MPa[b]		
At 23°C	143	89
At 120°C	33	12
Flexural modulus, GPa[c]		
At 23°C	4.3	2.0
At 120°C	1.2	0.3
Izod impact, J/m[d]	18	21
Charpy impact, KJ/m^2[e]	6.1	6.2
HDT (1.82 MPa), °C	152	65

[a]After Ref. 5.
[b]To convert MPa to psi, multiply by 145.
[c]To convert GPa to psi, multiply by 145,000.
[d]To convert J/m to ft·lbf/in., divide by 53.38.
[e]To convert kJ/m^2 to ft·lbf/in.^{2}, divide by 2.4.

nanocomposites is indicative of an oxygen permeation reduction in humid environment far beyond what is expected from the increase in path length alone (51). In the light of the findings regarding chain packing and dynamics in such confined environments (36), models for the prediction of barrier properties ought to take into account the changes induced in terms of solubility and diffusion. A conceptual model has been proposed (52). So far no general predictive approach is available.

Mechanical Behavior. Being able to improve strength and stiffness with limited alteration of toughness is a goal readily achievable with polymer–clay nanocomposites (see MECHANICAL PROPERTIES; REINFORCEMENT).

Table 3 gathers some key data of the original work by the Toyota group (5), which show the dramatic influence of organomontmorillonite on mechanical properties of PA6–clay hybrids at low mineral loading (4.7 mass%). The improvement in strength is claimed to have little or no influence on impact properties as evaluated from Izod or Charpy tests. Increase in modulus is paralleled by a substantial rise in heat distortion temperature. A concept of constrained polymer region related to the ion-bonding strength of clay and PA6 is introduced to account for the observed behavior.

Linear Elastic and Rubber Elastic Behavior. Although stiffening is quite noticeable in the glassy regime of the amorphous phase, the most spectacular effect is seen in the rubber elastic regime phase, as already evoked in the case of reinforcement by cellulose whiskers (2). The PA6–clay hybrids example presented in Table 3 is quite representative of the situation encountered with semicrystalline thermoplastics, but elastomeric networks benefit as well of clay layer dispersion with a two- to threefold increase in modulus for polyurethane or epoxy networks

(22). In the meantime, improved elongation at break is observed, contrary to what is seen in classical filled systems, presumably due in part to dangling chain formation in the network (see ELASTICITY, RUBBER-LIKE). The dynamic mechanical loss peak related to the glass-transition mechanism is equally informative on the extent of polymer–clay interaction. This shows mainly in the reduction of the loss peak area and/or in the evolution of the peak temperature with clay content and elaboration conditions (5,53). Predictive modeling of both storage and loss modulus faces a complex challenge in order to account for the mechanical coupling between the phases, the potential existence of an interphase, and/or a certain degree of connectivity between the fillers. In the latter situation, a percolation approach should be useful (2,54). Otherwise models derived from Halpin–Tsai equations seem quite promising for modulus prediction in relation to clay platelet arrangement (55,56).

Plasticity and Rupture. The main drawback identified regarding the solid-state drawing behavior is certainly the limited elongation at break encountered for most thermoplastic–clay nanocomposites (9,33) in the vicinity or below the glass-transition temperature. Nanovoiding and subsequent extensive fibrillation of the polymer matrix is clearly evidenced from volume strain measurements during drawing (53) and from *in situ* tem observations (57). Such enhancement of nanoscale plasticity offers an opportunity for optimizing the stiffness/toughness balance. However critical microvoids may develop from areas where load transfer is no more achievable because of splitting of clay platelet aggregates. This points at the most critical issue in nanocomposite development, ie, monitoring of elaboration and processing conditions.

Key Role of Processing. Scarce work has been devoted to the influence of processing on microstructure and properties of polymer–clay nanocomposites (58, 59). It is shown that twin-screw extrusion enables achieving a significant degree of dispersion of the clay platelets, provided residence time and degree of shearing are optimized in conjunction with the nature of the organoclay. Thermal stability of the organic modifier is again at the heart of the problem.

In the same way as demonstration was made in the last decade of the importance of processing to design polymer blends, taking the full benefits of the interesting combination of properties displayed by polymer nanocomposites will mainly rely on key developments in the field of processing. Automotive and packaging markets are undoubtedly the driving force for it.

BIBLIOGRAPHY

1. J. M. Jethmalani and W. T. Ford, *Chem. Mater.* **8**, 2138 (1996); Z. Pu and co-workers, *Chem. Mater.* **9**, 2442 (1997).
2. L. Chazeau and co-workers, *J. Appl. Polym. Sci.* **71**, 1797 (1999); V. Favier and co-workers, *Polym. Eng. Sci.* **37**, 1732 (1997).
3. J. J. Scobbo, in SPE Antec 98 Proceedings, 1998, p. 2468.
4. D. Quian and co-workers, *Appl. Phys. Lett.* **76**, 2868 (2000); L. Jin, C. Bower, and O. Zhou, *Appl. Phys. Lett.* **73**, 1197 (2000).
5. A. Usuki and co-workers, *J. Mater. Res.* **8**, 1174 (1993); Y. Kojima and co-workers, *J. Mater. Res.* **8**, 1185 (1993).
6. A. Okada and co-workers, *Polym. Prep.* **28**, 447 (1987).

7. W. A. Deer, R. A. Howie, and J. Zussman, *An Introduction to Rock-Forming Minerals*, 2nd ed., Longman Scientific, Essex, U.K., 1992.
8. R. A. Vaia and co-workers, *Chem. Mater.* **8**, 2628 (1996).
9. N. Hasegawa and co-workers, *J. Appl. Polym. Sci.* **67**, 87 (1998).
10. K. Varlot and co-workers, *J. Polym. Sci., Part B* **39**, 1360 (2001).
11. E. P. Giannelis, *Adv. Mater.* **8**, 29 (1996).
12. P. C. Lebaron, Z. Wang, and T. J. Pinnavaia, *Appl. Clay Sci.* **15**, 11 (1999).
13. M. Alexandre and P. Dubois, *Mater. Sci. Eng.* **28**, 1 (2000).
14. A. Blumstein, *J. Polym. Sci., Part A* **3**, 2653 (1965).
15. Jpn. Pat. JP-A- 51-109998 (1976), S. Fujiwara and T. Sakamoto (to Unitika).
16. R. D. Davis, W. L. Jarrett, and L. J. Mathias, *Polym. Mater. Sci. Eng.* **82**, 272 (2000).
17. Y. Kojima and co-workers, *J. Polym. Sci., Part A* **31**, 1755 (1993).
18. P. Reichert and co-workers, *Acta Polym.* **49**, 116 (1998).
19. A. Akelah and A. Moet, *J. Mater. Sci.* **31**, 3589 (1996); J. G. Doh and I. Cho, *Polym. Bull.* **41**, 511 (1998).
20. P. B. Messersmith and E. P. Giannelis, *J. Polym. Sci., Part A* **33**, 1047 (1995).
21. P. B. Messersmith and E. P. Giannelis, *Chem. Mater.* **6**, 1719 (1994).
22. T. Lan, P. D. Kaviratna, and T. J. Pinnavaia, *J. Phys. Chem. Solids* **57**, 1005 (1996); Z. Wang, T. Lan, and T. J. Pinnavaia, *Chem. Mater.* **8**, 2200 (1996); Z. Wang and T. J. Pinnavaia, *Chem. Mater.* **10**, 1820 (1998); Z. Wang and T. J. Pinnavaia, *Chem. Mater.* **10**, 3769 (1998).
23. C. Zilg, R. Mülhaupt, and J. Finter, *Macromol. Chem. Phys.* **200**, 661 (1999).
24. P. Aranda and E. Ruiz-Hitzky, *Chem. Mater.* **4**, 1395 (1992); J. Wu and M. M. Lerner, *Chem. Mater.* **5**, 835 (1993).
25. R. A. Vaia and co-workers, *J. Polym. Sci., Part B* **35**, 59 (1997).
26. N. Ogata, S. Kawakage, and T. Ogihara, *J. Appl. Polym. Sci.* **66**, 573 (1997); K. E. Strawhecker and E. Manias, *Chem. Mater.* **12**, 2943 (2000).
27. N. Ogata and co-workers, *J. Polym. Sci., Part B* **35**, 389 (1997); G. Jimenez and co-workers, *J. Appl. Polym. Sci.* **64**, 2211 (1997).
28. K. Yano and co-workers, *J. Polym. Sci., Part A* **31**, 2493 (1993); K. Yano, A. Usuki, and A. Okada, *J. Polym. Sci., Part A* **35**, 2289 (1997).
29. D. C. Lee and L. W. Jang, *J. Appl. Polym. Sci.* **61**, 1117 (1996); M. W. Noh and D. C. Lee, *Polym. Bull.* **42**, 619 (1999); D. C. Lee and L. W. Jang, *J. Appl. Polym. Sci.* **68**, 1997 (1998).
30. U.S. Pat. 4,739,007 (Apr. 19, 1988), A. Okada and co-workers (to Toyota Co.).
31. L. Liu, Z. Qi, and X. Zhu, *J. Appl. Polym. Sci.* **71**, 1133 (1999).
32. WO Pat. 93-04117 (Mar. 4, 1993), M. R. Maxfield and co-workers (to Allied-Signal Inc.); WO Pat. 99-29767 (June 17, 1999), R. A. Korbee and co-workers (to DSM NV); WO Pat. 99-32403 (July 1, 1999), R. B. Barbee and co-workers (to Eastman Chemical Co.); WO Pat. 99-50340 (Oct. 7, 1999), H. Okamoto and co-workers (to Toyota Co.); WO Pat. 2000034180 (June 15, 2000), J. N. Gilmer and co-workers (to Eastman Chemical Co.).
33. M. Kawasumi and co-workers, *Macromolecules* **30**, 6333 (1997).
34. R. A. Vaia and co-workers, *J. Polym. Sci., Part B* **35**, 59 (1997); R. A. Vaia and co-workers, *Macromolecules* **28**, 8080 (1995).
35. E. P. Giannelis, R. Krishnamoorti, and E. Manias, *Adv. Polym. Sci.* **138**, 107 (1999).
36. R. A. Vaia and E. P. Giannelis, *MRS Bull.* **26**, 394 (2001).
37. H. Ishida, S. Campbell, and J. Blackwell, *Chem. Mater.* **12**, 1260 (2000).
38. R. A. Vaia and E. P. Giannelis, *Macromolecules* **30**, 7990 (1997); 8000 (1997).
39. V. V. Ginzburg, C. Singh, and A. C. Balazs, *Macromolecules* **33**, 1089 (2000).
40. D. V. Kuznetsov and A. C. Balazs, *J. Chem. Phys.* **112**, 4365 (2000).
41. J. W. Gilman and co-workers, *Chem. Mater.* **12**, 1866 (2000).
42. S. D. Burnside and E. P. Giannelis, *Chem. Mater.* **7**, 1597 (1995).

43. W. Xie and co-workers, *Chem. Mater.* **13**, 2979 (2001).
44. D. L. Vanderhart, A. Asano, and J. W. Gilman, *Macromolecules* **34**, 3819 (2001).
45. Y. Kojima and co-workers, *J. Polym. Sci., Part B* **33**, 1039 (1995).
46. D. M. Lincoln and co-workers, *Polymer* **42**, 1621 (2001).
47. Y. Ke, C. Long, and Z. Qi, *J. Appl. Polym. Sci.* **71**, 1139 (1999).
48. J. W. Gilman, T. Kashiwagi, and J. Lichtenham, *SAMPE J.* **33**, 40 (1997); J. W. Gilman, *Appl. Clay Sci.* **15**, 31 (1999).
49. D. Porter, E. Metcalfe, and M.-J. K. Thomas, *Fire Mater.* **24**, 45 (2000).
50. S. Bourbigot and co-workers, *Fire Mater.* **24**, 45 (2000).
51. T. Lan, Y. Liang, G. W. Beall, and K. Kamena, in "Additives 1999" Conference Proceedings, San Francisco, Calif., 1999.
52. G. W. Beall, in T. J. Pinnavaia and G. W. Beall, eds., *Polymer-Clay Nanocomposites*, (Wiley Series in Polymer Science), John Wiley & Sons, Inc., New York, 2001, p. 267.
53. J. M. Gloaguen and J. M. Lefebvre, *Polymer* **42**, 5841 (2001).
54. E. Reynaud, C. Gauthier, and J. Perez, *Rev. Metall.-CIT* 169 (Feb. 1999).
55. M. van Es, F. Xiqiao, J. van Turnhout, and E. van der Giessen, in "Additives 2000" Conference Proceedings, San Francisco, Calif., 2000.
56. D. A. Brune and J. Bicerano, *Polymer* **43**, 369 (2002).
57. G. M. Kim and co-workers, *Polymer* **42**, 1095 (2001).
58. H. R. Dennis and co-workers, *Plast. Eng.* **57**, 1, 56, (2001).
59. J. W. Cho and D. R. Paul, *Polymer* **42**, 1083 (2001); T. D. Fornes and co-workers, *Polymer* **42**, 9929 (2001).

JEAN-MARC LEFEBVRE
Université des Sciences et Technologies de Lille

NOVOLAKS. See PHENOLIC RESINS.

NUCLEIC ACIDS. See POLYNUCLEOTIDES.

NYLON. See POLYAMIDES.

OLEFIN-SULFUR DIOXIDE POLYMERS. See POLYSULFONES.

ORGANOMETALLIC POLYMERS. See METAL CONTAINING POLYMERS.

ORIENTED FILMS. See FILMS, ORIENTATION.

PACKAGING, FLEXIBLE

Introduction

Flexible packaging is used to deliver a product from the manufacturer or distributor to the retailer or ultimate consumer and protect that product during shipping, display, and storage. The total North American market for flexible packaging was estimated to be worth approximately $17 billion in the year 2000 (1). Flexible packaging provides a lightweight, cost-effective means for the transportation, storage, and display of many products. Flexible packaging offers many advantages over competitive rigid packaging including reduced weight and volume of packaging material used, and subsequently discarded, as well as increased consumer convenience. Whatever the application or use, polymer materials are selected, and the entire packaging structure is designed, to meet the performance requirements specific to that particular application.

Performance requirements may include the requirements of all users in the value chain. For consumers this may mean the packaging protects the product, identifies the product, and is easy to open. For retailers the packaging may provide eye-catching graphics that help sell the product and is of the proper physical form for display purposes. For the packager, flexible packaging may need to provide high packaging speeds and low scrap rates, as well as meeting the functional requirements for protecting the product inside the package. Specific performance requirements will vary greatly from one type of package to another. But in every case meeting the performance requirements will help assure proper protection of the goods being packaged.

Encyclopedia of Polymer Science and Technology. Copyright John Wiley & Sons, Inc. All rights reserved.

Forms of Flexible Packaging

Flexible packaging films may be in the forms of wraps, bags, and pouches of many shapes and sizes. Packages may be as small as a single-serving sugar pouch or as large as a palletized load of mulch bags. Packaging may be supplied to the packaging end-user in the form of premade bags or pouches, or rolls of film. The film may be applied directly to the packaged goods, as in the case of stretch film, or may be formed into a package in-line with the filling machinery, as in the case of a bag formed on a vertical form/fill/seal machine used to package candy. Some packages are formed in a step that occurs well before the product is packaged. Then the product is placed inside the package and the package is secured.

Key Performance Requirements. Some of the key performance requirements for high performance flexible packaging include the following. Barrier properties: to keep oxygen, water, light, or grease from entering the package or from leaving the package. Barrier properties may be characterized by measuring the permeation of oxygen and water vapor through the packaging material. Selective permeability: to allow oxygen and carbon dioxide to permeate through the package at a calculated rate, in order to extend the life of fresh-cut produce, for example. Oxygen, carbon dioxide, and water vapor permeability are frequently measured and specified (see BARRIER POLYMERS). Abuse resistance: to prevent damage to the packaging material and its contents during shipping and storage. Abuse resistance may include puncture resistance, tear strength, impact strength, and modulus. Some packages require good toughness at refrigerated or freezer temperatures. Sealability: to allow packages to be made at high packaging speeds and keep the product secure by preventing the package seams from failing. Sealability may be characterized by heat seal and hot tack strength, heat seal and hot tack initiation temperatures, seal-through-contamination performance, caulkability, and seal integrity. *Hot tack* refers to the strength of the seal while still in the molten state. It is critically important for packages where the product drops into the package while the seal is still partly molten. *Caulkability* refers to the ability of the sealant material to flow, filling in gaps around folds, wrinkles, or product contaminants. Machineability: to allow the packaging films to be easily run on high speed automatic packaging equipment. Machineability is governed largely by film modulus, film thickness, seal properties, and coefficient of friction. Consumer appeal: package appearance is an important factor driving product preference by consumers. Appeal is largely related to print quality and package gloss. Film thickness and modulus may also impact consumer appeal.

Polymer Materials Frequently Used in Flexible Packaging. Polymer materials commonly used in flexible packaging include linear low density polyethylene (LLDPE) (ETHYLENE POLYMERS, LLDPE, PROPYLENE POLYMERS (PP)), low density polyethylene (LDPE) (ETHYLENE POLYMERS, LDPE), high density polyethylene (HDPE) (ETHYLENE POLYMERS, HDPE), high molecular weight high density polyethylene (HMW-HDPE), and polypropylene (PP). Higher value, more specialty polymers used include polyolefin plastomers (POP), ultralow density polyethylene (ULDPE) (Ethylene Polymers, VLDPE), metallocene-catalyzed linear low density polyethylene (mLLDPE), enhanced polyethylene (EPE), ethylene vinyl acetate (EVA) copolymers, acid copolymers, (IONOMERS), nylon or polyamide

(PA), poly(ethylene terephthalate) (PET), ethylene vinyl alcohol (EVOH), and poly(vinylidene chloride) (PVDC). See POLYAMIDES, PLASTICS; POLYESTERS, THERMOPLASTIC; VINYL ACETATE POLYMERS; VINYL ALCOHOL POLYMERS; VINYLIDENE CHLORIDE POLYMERS (PVDC). See also FILMS AND SHEETING.

These polymers are selected for the specific performance that they provide, and are combined in the final package design to meet all the requirements for the specific application in which they are being used. Often there are many different combinations of materials or film constructions that will meet the minimum performance requirements of an application. In these cases selection of the final packaging structure may be based on considerations such as availability from multiple suppliers and ability to provide differentiation over competitive packaging. For example a combination of a box and an inner liner may be used or a stand-up pouch may be used, each combination providing the minimum requirements for product protection and safety. One manufacturer may select to use a box and inner liner and other manufacturers may elect to package their product in a stand-up pouch for the same product. Or one manufacturer may choose to use a stand-up pouch and another manufacturer may choose to use a pillow pouch for the same product.

Polymers may also be combined with other materials, such as foil or paper, to create a flexible package with performance attributes not achievable by the polymers alone. This is done through the lamination or extrusion coating process, described below.

Manufacturing Techniques

Polymer films may be manufactured by blown film or cast film extrusion or by extrusion coating of a polymer onto another substrate such as paper or aluminum foil (see FILMS, MANUFACTURE; EXTRUSION). Blown films are made by melting and pumping polymer through an annular die. Cast films are made by melting and pumping polymer through a flat die. The extrusion coating process is similar to the cast film process except that the molten polymer is coated directly onto another material. The selection of manufacturing process is governed by factors such as the size of the job to be run, the type of packaging material to be made, performance requirements for the end-user packaging, and availability of equipment. Cast film extrusion equipment typically operates at much higher output rates than blown film equipment, so it may be advantaged for production of large volumes of film of a single type, such as in the manufacture of stretch film. Blown film extrusion typically runs at a lower rate and may result in film with improved physical properties. Blown film also allows for adjustment of the bubble size and resulting width of the film produced, a key advantage when films of many different widths must be produced on the same machine.

The coextrusion process is used to combine multiple materials into a single film (see COEXTRUSION). Both blown films and cast films may be coextruded in three, five, seven, or more layers. The combination of multiple materials in a single film allows a cost-effective means of combining the performance properties of several polymers in a single film. One example would be the coextrusion of a

barrier polymer such as EVOH or PVDC with a sealant resin such as LLDPE, EVA, or a POP. Coextrusion is widely used in producing high performance packaging films such as those used to package foods. It is also widely used to produce industrial films such as stretch film, and is increasingly used in producing other types of industrial films.

Polymer films may be stretched, or oriented, to impart improved properties useful for a variety of packaging applications. Oriented film is produced by a double bubble or tenter frame process. A thick film or sheet is manufactured at a thick gauge, typically 0.254–0.508 mm (10–20 mil) and is subsequently oriented (stretched) in a semisolid state to many times its original dimensions (see FILMS, ORIENTATION). The multiple-step production is normally done in a continuous operation. The stretching of the sheet to make the final film may occur simultaneously in the machine and transverse directions, or the stretching may occur sequentially. After orienting, the films are typically 12.7–25.4 μm (0.5–1.0 mil) thick. The film is typically supplied in roll form. Biaxially oriented polypropylene (BOPP) is most often manufactured using a tenter frame process. Oriented polyethylene films are usually manufactured using a double bubble process. PVC films may also be oriented. Some oriented films are crosslinked to further enhance their performance. Compared to other films, oriented films typically provide improved optical properties, higher stiffness, and increased film shrinkage during packaging, which leads to improved package appearance.

Lamination is used to combine two or more films into a single packaging structure. It allows for the combination of materials that cannot be coextruded. An example would be a lamination of aluminum foil and a polyethylene sealant film. More complicated laminations may include multiple types of polymer film, paper, and foil. Laminations can be categorized into main types: adhesive laminations and extrusion laminations. In adhesive laminations, the substrates are combined using an adhesive material. In extrusion laminations the substrates are adhered together using a molten polymer, often LDPE, as the adhesive layer. Lamination offers an additional benefit of allowing for the protection of the printing ink between layers of polymer, thus providing superior graphics to packages which are surface printed. Many packages with superior graphics, such as glossy stand-up pouches, have a reverse printed outer layer laminated to structural and sealant materials. Laminations are also used to provide a barrier to oxygen, moisture, or light. The barrier functionality may be provided by foil or a barrier polymer such as EVOH or PVDC. Most high value processed meat and cheese packages are laminations. This allows for both the combinations of various materials into the packaging structure and for the superior graphic properties possible by reverse printing the surface layer of the package and protecting the printing inks within the package itself. Since laminations are more costly than coextruded or monolayer films, laminations are generally reserved for use in higher value applications.

Metallization is used to apply a thin coating of metal, typically a form of aluminum, to a polymer film. This provides improved oxygen and water barrier properties as well as barrier to light. The best known use of metallized film is probably potato chip bags. Metallized films may also be used for nuts and salty snacks. Metallized films may be coated to provide sealability or may be laminated to

another polymer film to provide improved properties such as seal integrity. Other types of coatings, whether to provide barrier properties of other functionality, may also be applied to polymer films used in flexible packaging.

Methods of Producing Packages. Packages may be formed in-line by a variety of techniques or may be supplied to the packer as preformed pouches or bags. Packaging may be created by wrapping or shrinking a basic film around a bundle of goods. Examples of in-line packaging forming include vertical form/fill/seal (VFFS), horizontal form/fill/seal (HFFS), and thermoform/fill/seal. In VFFS operations, film from a roll is passed through a series of rollers and is shaped by a forming collar into a tube. The film moves in a vertical direction (down) over a filling tube. A vertical seal is made, forming the film into a continuous tube. As the film continues through the machine, a horizontal seal is made, perpendicular to the machine direction of the film, forming the bottom-end seal of the bag. The product is dropped into the partially formed bag and the top-end seal is made. The process may operate in a step-wise or continuous manner. One example of a product normally packaged on VFFS equipment is fresh-cut produce. In HFFS operations, the film moves in a horizontal direction during the packaging step, eliminating the need for high hot tack strength. One application that typically uses HFFS equipment is chunk cheese. In thermoform/fill/seal operations, a bottom web is formed, product is added, and the top web, which is normally flat, is sealed to the bottom web. Thermoform/fill/seal packaging is frequently used for bacon and processed meats. Stand-up pouches and other types of packaging may be formed in-line with the filling equipment, or may be fully or partially prefabricated prior to the filling step.

Uses and Types of Flexible Packaging

Flexible packaging is used for the packaging of all types of items including food products, medical devices, industrial goods, and consumer goods. The packaging types can be described in terms of the products being packaged, such as bakery goods, or by the type of packaging being used, such as shrink film. Major uses for flexible packaging are described below.

Food Packaging. One key use of high performance flexible packaging films is the packaging of food for distribution and retail sale. Food products are increasingly being packaged at the manufacturer end for sale to the ultimate consumer in the original package. This is a change from the traditional distribution system where the product was wrapped for the consumer at the butcher shop.

Fresh Red Meat. Fresh red meat is often transported in large pieces from the slaughtering house to local butcher shops in large barrier bags. These bags are designed to provide a barrier to oxygen. As well as oxygen barrier, package toughness and seal integrity are key requirements for these bags. These bags may contain PVDC or EVOH as a barrier material, along with layer of various PE resins for toughness and sealability.

Processed Meat. Processed and cook-in meat such as luncheon meat, ham, bologna, and salami are packaged in barrier films that are designed to

keep oxygen from entering the package. This extends the shelf-life of the meat product and allows the retailer to display the product for sale for an extended period of time. It also allows the consumer to keep the product in their refrigerator, unopened, for some period of time after purchase. These packages are often printed with eye-catching graphics to increase the likelihood of retail sale. These films may contain a barrier polymer, printing surface such as PET or nylon, toughness layers of LLDPE or ULDPE, and a sealant layer that could be LLDPE, a POP, or an ionomer. In addition to low permeability to oxygen, abuse resistance and seal integrity are critical to maintaining the proper atmosphere inside the package. Optical properties such as high gloss and high clarity are important to create consumer appeal. Barrier requirements for processed meats range from 0.2 to 1.0 $cm^3/(100\ in.^2 \cdot day \cdot atm)$ for oxygen transmission rate (OTR) and 0.2–0.5 $g/(100\ in.^2 \cdot day)$ for water vapor transmission rate (WVTR).

Case-Ready Meat. An emerging use for plastic packaging is in the packaging of case-ready meats. In this application, a smaller package of fresh meat is packaged immediately after the slaughtering operation and distributed through retail stores directly to consumers. This saves the step of having the local butcher cut and prepare the individual cuts of meat for retail sale. It allows for reduced labor at the retail level and better usage of various cuts of meat. It also provides an improved level of food safety because handling of the raw food is reduced. Pork products such as pork loins and ribs are commonly sold in case-ready flexible packaging. Beef and other meat products are increasingly being sold in case-ready packaging. Different types of case-ready systems operate using different systems for product protection and extension of shelf-life. Some products are packaged in barrier packages, totally excluding oxygen from the package. Some case-ready systems package the food in a high oxygen environment, and these systems also use barrier films. Other systems package the meat in a bag or tray/lid combination that allows oxygen to permeate the package at the proper time to allow reddening of the meat that is expected by consumers.

Retortable Pouches. A growing use of flexible packaging is in the replacement of metal cans with retortable pouches. These pouches are typically laminations containing biaxially oriented nylon for toughness, foil for oxygen barrier, and a PP sealant film. These pouches may contain items like tuna, pet food, and soup. The food items are held at elevated temperature after packaging, so the packages must remain intact at elevated temperatures. A minimum requirement might be the ability to withstand a temperature of 130°F for 20 min. In addition to temperature resistance, toughness, seal strength, and barrier properties are critically important.

Bakery Products. Bakery products such as bread, bagels, and tortillas are usually sold in plastic bags. These bags are typically surface printed LDPE or LLDPE and their main functional requirement is to protect the product from drying out or being damaged during distribution. Good machineability is required for high packaging speeds. These films are typically surface printed monolayer structures. A haze of 5% or less is typically required of these high clarity films. Films generally require COF of below 0.2 for fast packaging speeds.

Candy and Confectionery Packaging. Candy and other sweets are packaged in flexible packaging. At the smallest level, individual bite-size portions of a candy product may be packaged in a small pouch or a twist–wrap type package. Candy bars are typically wrapped with oriented PP film that has been surface printed. These items may then be packaged in a secondary bag, which may be a laminated structure containing polyethylene and sometimes reverse printed BOPP films. The outer bags must have sufficient toughness to protect the food inside. The films are generally very glossy for maximum consumer appeal. To provide fast packaging speeds the films need to have high hot tack strength combined with low hot tack and heat seal initiation temperatures.

Cheese. Most cheese sold in the United States is prepackaged in some type of flexible packaging. Types of cheese packaging include individually wrapped slices of processed cheese, chunk cheese, and shredded cheese. Both chunk cheese and shredded cheese require substantial barrier to oxygen to prevent mold growth and spoilage. Either EVOH or PVDC may provide the oxygen barrier. While EVOH is generally coextruded into the film structure, PVDC may be coated onto the surface of a film via a coating process. They also require excellent seal integrity and abuse resistance to prevent the controlled atmosphere inside the package from being lost. Cheese packages are often laminations made with reverse printed outer webs containing PET or nylon for superior graphical presentation. They may also be extrusion coated structures where the sealant layer has been extrusion coated onto the outer layer. Sealant layers may consist of EVA, an ionomer, or a POP. Low heat seal initiation temperature (90°C or below) and good seal through contamination performance are required of the sealant material used. Processed cheese typically require films with OTR of 0.6–1.0 $cm^3/(100\ in.^2 \cdot day \cdot atm)$ and WVTR of 1.0 $g/(100\ in.^2 \cdot day)$.

Fresh-Cut Produce. Key performance requirements for fresh-cut produce packaging include proper oxygen and carbon dioxide permeability, seal integrity, machineability, and consumer appeal. Consumer appeal includes both feel and appearance. Feel is generally determined by film thickness and modulus while appearance is governed by print quality and film optical properties such as clarity, haze, and gloss. In order to extend the shelf-life of the produce being packaged, films must provide a level of oxygen permeability that is properly matched to the respiration rate of the produce inside the package. Cut produce respires after harvesting consuming oxygen and giving off carbon dioxide. By controlling the permeation of gases through the package the environment inside the package is controlled, respiration is slowed, and shelf-life is extended. The bags must have complete seal integrity in order to prevent the unplanned transfer of gases between the bags and the environment. Bags may contain PP, LLDPE, ULDPE, EVA, or POP. Oxygen transmission rate requirements vary widely depending on the type of produce being packaged, but common items range from about 100 $cm^3/(100\ in.^2 \cdot day \cdot atm)$ for caesar salad mixes, 150–200 $cm^3/(100\ in.^2 \cdot day \cdot atm)$ for iceberg salad mixes, ad 200–350 $cm^3/(100\ in.^2 \cdot day \cdot atm)$ for specialty salad mixes such as baby greens and exotic lettuces.

Frozen Foods (Fruits, Vegetables, IQF Poultry). Frozen foods are packaged in a variety of packaging types. Examples of frozen foods packaged in flexible packaging include frozen fruits, vegetables, french fries, and individually quick frozen chicken breasts. Many frozen foods are packaged in surface printed

polyethylene films. Some higher value added items are packaged in laminations, which may be shaped into stand-up pouches. Most frozen food bags are made on standard VFFS machinery. Low temperature toughness, modulus, high hot tack strength, and high seal strength are key requirements for frozen food packaging. Some packages are clear and require good clarity, while others are pigmented and require good gloss. LLDPE, ULDPE, EVA, and POP resins are all commonly used in creating frozen food packaging. Stiffness must be adequate for high speed packaging, and packaging films must have tear and puncture strength high enough to prevent package damage during transportation and storage.

Crackers, Cookies, and Cake Mixes. Inner Liners are used for packaging products such as cereal, crackers, and cookies inside a box. The key performance requirement for packaging these products is most often moisture barrier. The packaging film selected must be capable of keeping the product dry and in excellent condition upon delivery to the consumer. The packaging must offer seal integrity and machineability as well. Certain products have additional requirements such as puncture resistance—to keep the product from poking through the packaging film—and flavor and aroma barrier for highly flavored cereals. Most inner liners contain HDPE for its moisture barrier properties and a sealant layer which may be EVA or POP. Heat seal initiation temperatures of 90°C and below are commonly required. MVTR of 0.2 g/(100 in.^{2}·day·atm) or below is often required.

Salty Snacks. Salty snacks are frequently high in fat content and may require a package that provides an oxygen barrier in order to prevent the fat in the food from going rancid. They may also require grease resistance to keep the package from leaving an oily spot. Salty snacks may be packaged in barrier films containing foil, a metallized polymer film, or a barrier polymer such as EVOH or PVDC.

Potato Chips. Potato chips are often packaged in metallized films. Metallization of a polymer film provides a combination of oxygen barrier, moisture barrier, and light barrier. The use of a clear polymer film would not provide equivalent light barrier. Seal strength must be optimized to provide a secure package that can be easily opened by the consumer. Seal integrity and consumer appeal are also critical for this type of snack food packaging.

Ice. Ice bags are a specific type of carry-out bag used to transport manufactured ice. These bags are typically surface printed monolayer films. EVA copolymer is frequently used for these bags for its combination of sealability, low temperature toughness, and ease of manufacture into a film. Ice bags require good low temperature toughness, especially puncture strength, and adequate seal strength to prevent the bags from bursting. The bags must not, however, be so strong that the consumers cannot easily get to the ice inside the package.

Medical Device Packaging. Flexible films are used to package many types of medical devices. These packages must protect the device from contamination. Some medical devices are sterilized after packaging, and for these devices the packaging must be compatible with the sterilization procedure and must then maintain the sterile environment until the package is opened. Seal integrity and abuse resistance are key requirements for medical packaging (see MEDICAL APPLICATIONS).

Industrial Packaging.

Heavy Duty Shipping Sacks. Heavy duty shipping sacks are used for the transportation of items such as resin, salt, pet food, fertilizer, chemicals, topsoil, bark mulch, and compressed bales of fiber glass insulation. They typically contain 40 pounds or more of product. Heavy duty shipping sacks may be supplied as preformed bags or as rollstock, which is formed into bags in a continuous VFFS operation. Special machinery is required to form heavy duty shipping sacks on VFFS machinery in a high-speed continuous operation. These bags need moderate COF because they must easily pass through the packaging equipment, but stacked bags must slide off each other. Bags filled with hot products, such as salt, must also be able to withstand the filling temperatures without excessive stretching or dimpling of the film. Film toughness and creep resistance are also of key importance in many heavy duty shipping sack applications.

Shrink Film. Shrink film is used to collate bundles of goods. Industrial shrink film is typically manufactured by the blown film process from a blend of LDPE and LLDPE. Specialty polymers may be used to impart specific properties required for specialty applications of industrial shrink film. The use of LDPE, with its long chain branching and high level of molecular entanglement results in a film with a significant amount of molecular orientation locked into the film after fabrication. When the film is subsequently heated the oriented molecules tend to relax and return to an unoriented state. This allows the film to be shrunk around the packaged goods by the application of heat. This is most typically done in a shrink tunnel or sometimes with a hot air gun. Common uses of shrink film include cases of bottled water and soft drinks. Industrial shrink films are typically several mils thick. Shrink films require good shrinkage properties and holding force as well as enough abuse resistance to protect the product being packaged.

High Clarity Shrink Film (Oriented). Oriented, high clarity shrink film is used for the protection and display of high value consumer goods. It is distinguished from regular shrink film by its superior clarity and appearance, as well as increased shrinkage properties and higher stiffness. Goods are packaged by wrapping the film loosely around the goods, sealing the film to make a completely enclosed bag, and then shrinking the film by passing the package through a shrink tunnel or oven. Small holes may be poked in the film before wrapping to allow air to escape from the surface of the package while the film is shrinking. As in industrial shrink film, heat causes the molecules in the film to relax, causing the film return to its original unoriented size, and it shrinks tightly around the packaged goods. Since the polymer molecules in oriented shrink film are much more highly oriented, a greater level of shrinkage may be obtained. Boxed software and stationery products are often wrapped with high clarity shrink film. Ice cream cartons and other food products are also wrapped in high clarity shrink film. Optical properties, seal properties, shrinkage, and holding force are key requirements for oriented shrink film (see FILMS, ORIENTATION).

Liners. Liners, called trash bags by most consumers, are used for waste disposal in homes and businesses. Liners range in size from small bags used to line a bathroom wastebasket to large lawn and leaf bags sized to hold 40 gallons or more of waste. Liners may be supplied on a continuous roll, which

has been perforated for easy separation of the individual bags, or as separate bags contained in a box or bag. Liners are made from blown film, and the bags may be aligned in either the machine or cross direction. Bags supplied on rolls are aligned with the machine direction of fabrication, and the width of the bag is equal to the layflat obtained during blown film extrusion. Some bags, such as drawstring bags, may be aligned in the cross direction, or transverse to the direction of fabrication. These bags have seals on their sides that run perpendicular to the direction of fabrication. Liners are made primarily from LLDPE. Key properties include tear strength, impact strength, and tensile strength and modulus.

Storage Bags. Storage bags are small polyethylene bags, normally containing a plastic zipper or other closure, used by consumers and businesses for storing small quantities of food or other products. They are typically made from LDPE or LLDPE or blends of these two materials. Bag thickness may range from less than 1 mil to more than 3 mils depending on total bag size and intended use. Most bags are unprinted, though some contain a special labeling area on the outside of the bag for use by the consumer in marking the bags with a brief description of the items placed inside the bags. Most bags are clear to allow consumers to see the product inside the bag. Since many bags have zipper closures, the bags must be made from materials that are compatible with the simultaneous extrusion or attachment of the zippers.

Carry-Out Bags. Carry-out bags are used by consumers to carry purchased merchandise to their homes or businesses. These bags are typically polyethylene structures. Many are surface printed monolayer films. Some are coextruded films for enhanced performance. Examples include the merchandise bags used by department stores and discount stores and grocery sacks used at supermarkets. Depending on the specific use the bags may be fabricated from high molecular weight HDPE, LDPE, or LLDPE. Tensile strength and toughness are key requirements, although some carry-out bags are highly oriented HMW-HDPE, and consequently have low MD tear strength.

Stretch Film. Stretch film, or stretch/cling film, is used in the unitization of goods for transportation. A thin film is stretched, either by machine or by hand, and wrapped around multiple smaller packages to hold the goods together. The film clings to itself and to the pallet, securing the load. In its most common form, stretch/cling film is applied to a pallet of goods using a power prestretch pallet wrapper in an automated operation. In this operation the film is stretched, typically between 100 and 300% of its original length, by a set of rollers turning at different speeds and is then applied to a pallet of goods, which sit atop a moving turntable. Machine wrap film is typically supplied on rolls that are 20 or 30 in. wide. Hand wrap film is supplied on smaller rolls. Stretch/cling films may be manufactured by either a cast film or blown film process. Most stretch/cling films are coextruded structures, and LLDPE is the primary component of most stretch films. For specialized applications, coextrusions containing minor layers of PP, EVA, POP, or ULDPE may be employed. For most stretch film structures, a resin with good inherent cling is used as one or both surface layers, or a tackifier such as polyisobutylene is added to the structure to provide the proper level of cling force. Stretch film is used to hold entire or partial pallets of goods, such as resin bags, fertilizer bags, cartons of consumer goods or food products, together

during shipment. Most stretch film is removed by the retailer prior to the display of the packaged items for sale. Consumers can frequently view pallets of lawn and garden products, such as bark mulch and topsoil, still wrapped with stretch film on display at home improvement warehouses. Stretch films must have good stretchability, load retention, and puncture resistance.

Stretch Hooder. Stretch hooder film is used to form a large bag capable of containing an entire pallet of goods. Film is supplied on rolls and formed into a gusseted bag during the packaging operation. The bag is then stretched to increase its circumference and, while under tension, placed over a pallet of goods. The tension on the film is released as the film covers the goods, and the film contracts and secures the load. The main advantage of stretch hooder packaging over regular stretch wrap is that the load is completely covered on the top and sides. The chief disadvantage is that considerably more polymer is required to make a stretch hooder bag than to make enough stretch/cling film to contain the same load. Stretch hooder film is made on blown film extrusion equipment. Stretch hooder films must have good elastic memory and good abuse resistance.

BIBLIOGRAPHY

"Packaging Materials" in *EPST* 1st ed., Vol. 9, pp. 709–714, by S. Sacharow, Reynolds Metals Co.; "Packaging Materials, Flexible Materials" in *EPSE* 2nd ed., Vol. 10, pp. 684–695, by A. L. Brody, Schotland Business Research, Inc.

1. L. L. Hoover, *Flexible Packag.* 22–27 (Oct. 2000).
2. W. A. Jenkins and J. P. Harrington, *Packaging Foods with Plastics*, Technomic Publishing Co., Lancaster, Pa., 1991.
3. L. K. Mergenhagen and N. F. Whiteman, in *Polymers, Laminations, and Coatings Conference*, 1993.
4. T. I. Butler, S. Lai, and R. Patel, In *SPI International Plastics Exposition and Conference*, Chicago, 1994.
5. J. J. Wooster, in *Film Pack Conference*, Philadelphia, 1999.
6. T. D. Stirling, in *Future-Pak Conference*, Chicago, 1997.
7. M. F. Simpson and J. L. Presa, in *Future-Pak Conference*, Chicago, 1996.
8. J. S. Brandenburg and M. Davis, in *Specialty Polyolefins Conference (SPO)*, Houston, 1996, pp. 213–229.
9. J. V. Krohn and D. W. Jordy, *Tappi J.* **80**(3), 151–155 (1996).
10. G. Ealer, in *Polymers, Laminations, and Coatings Conference*, 1990, pp. 327–333
11. N. F. Whiteman, J. A. deGroot, L. K. Mergenhagen, and K. B. Stewart, in *RETEC Conference*, Houston, 1995.
12. B. Lipsitt, *Plast. Eng.* 25–28 (Aug. 1997).
13. C. L. Dawson and J. Tunison, in *Specialty Polyolefins Conference (SPO)*, Houston, 1996, pp. 231–245.
14. K. T. Higgins, *Food Eng.* 46–54 (Nov. 2000).
15. T. Bezigian, *Converting Mag.* 54–57 (Sept. 1997).
16. P. T. DeLassus, *Tappi J.* **77**(1), 109–113 (Jan. 1994).

JEFFREY J. WOOSTER
The Dow Chemical Company

PAN. See ACRYLONITRILE POLYMERS.

PBT. See POLYESTERS, THERMOPLASTIC.

PERFLUORINATED POLYMERS, PERFLUORINATED ETHYLENE–PROPYLENE COPOLYMERS

Introduction

Perfluorinated ethylene–propylene (FEP) resin is a copolymer of tetrafluoroethylene (TFE) and hexafluoropropylene (HFP) [116-15-4]; thus, its branched structure contains units of $-CF_2-CF_2-$ and of $-CF_2-CF(CF_3)-$. It retains most of the desirable characteristics of polytetrafluoroethylene (PTFE) but with a melt viscosity (MV) low enough for conventional melt processing. The introduction of HFP lowers the melting point of PTFE from 325°C to about 260°C.

The desire for a resin with PTFE properties yet capable of being fabricated by conventional melt processing led to the discovery of this product (1). It allows melt extrusion of wire insulations of longer continuous lengths than the batchwise paste extrusion of PTFE as well as the injection molding of intricately shaped parts. The FEP polymer is melt-fabricable without severe sacrifice in mechanical properties because the perfluoromethyl side groups on the main polymer chain reduce crystallinity, which varies between 30 and 45%. This change in the crystallinity causes FEP and other copolymer particles to behave differently from PTFE particles; they do not fibrillate like PTFE particles and therefore do not agglomerate easily.

As a true thermoplastic, FEP copolymer can be melt-processed by extrusion and compression, injection, and blow molding. Films can be heat-bonded and sealed, vacuum-formed, and laminated to various substrates. Chemical inertness and corrosion resistance make FEP highly suitable for chemical services; its dielectric and insulating properties favor it for electrical and electronic services; and its low frictional properties, mechanical toughness, thermal stability, and nonstick quality make it highly suitable for bearings and seals, high temperature components, and nonstick surfaces.

Mechanical properties are retained up to 200°C, even in continuous service, which is better than with most plastics. At high temperatures, these copolymers react with fluorine, fluorinating agents, and molten alkali metals. They are commercially available under the DuPont trademark Teflon FEP fluorocarbon resin. A similar product is manufactured by Daikin Kogyo and Dyneon and sold under the trademarks Neoflon and Hostaflon, respectively. The People's Republic of China

Encyclopedia of Polymer Science and Technology. Copyright John Wiley & Sons, Inc. All rights reserved.

also manufactures some FEP products. Additional information on specific manufacturers' products can often be obtained by consulting their internet web sites (for example, www.dupont.com/teflon).

Monomers

Preparation. The preparation, properties, and uses of TFE have been described. Hexafluoropropylene was initially prepared by pyrolysis of PTFE (2,3) and by fluorination of 1,2,3-trichloropropane followed by dehalogenation (4). A number of other routes are described in the patent literature (5–10). Hexafluoropropylene can be prepared in high yield by thermally cracking TFE at reduced pressure at 700–800°C (11,12). Pyrolysis of PTFE at 860°C under vacuum gives a 58% yield of HFP (13). Fluorination of 3-chloropentafluoro-1-propene [79-47-0] at 200°C over activated carbon catalyst yields HFP (14). Decomposition of fluoroform [75-46-7] at 800–1000°C in a platinum-lined nickel tube is another route (15). The thermal decomposition of sodium heptafluorobutyrate [2218-84-4], $CF_3CF_2CF_2CO_2Na$ (16), and copyrolyses of fluoroform and chlorotrifluoroethylene [79-38-9] (17), and chlorodifluoromethane [75-45-6] and 1-chloro-1,2,2,2-tetrafluoroethane [2837-89-0] (18) give good yields of HFP.

Properties and Reactions. The properties of HFP are shown in Table 1. It does not homopolymerize easily and hence can be stored as a liquid. It undergoes many addition reactions typical of an olefin. Reactions include preparation of linear dimers and trimers and cyclic dimers (21,22); decomposition at 600°C with subsequent formation of octafluoro-2-butene and octafluoroisobutylene (23); oxidation with formation of an epoxide (24), an intermediate for a number of perfluoroalkyl perfluorovinyl ethers (25,26); and homopolymerization to low molecular weight liquids (27,28) and high molecular weight solids (29,30). Hexafluoropropylene reacts with hydrogen (31), alcohols (32), ammonia (33), and the halogens and their acids, except I_2 and HI (31,34–36). It is used as a comonomer to produce elastomers and other copolymers (37–41). The toxicological properties are discussed in Reference 42.

Copolymers

Hexafluoropropylene and tetrafluoroethylene are copolymerized, with trichloracetyl peroxide as the catalyst, at low temperature (43). Newer catalytic methods, including irradiation, achieve copolymerization at different temperatures (44,45). Aqueous and nonaqueous dispersion polymerizations appear to be the most convenient routes to commercial production (1,46–50). The polymerization conditions are similar to those of TFE homopolymer dispersion polymerization. The copolymer of HFP–TFE is a *random copolymer*; that is, HFP units add to the growing chains at random intervals. The optimal composition of the copolymer requires that the mechanical properties are retained in the usable range and that the MV is low enough for easy melt processing.

Table 1. Properties of Hexafluoropropylene[a]

Properties	Value
Molecular weight	150.021
Boiling point at 101 kPa[a], °C	−29.4
Freezing point, °C	−156.2
Critical temperature, °C	85
Critical pressure, kPa[b]	3254
Critical density, g/cm^3	0.60
Vapor pressure at K, kPa[b]	
$243.75 < T < 358.15$	$\log P$ (kPa) $= 6.6938 - 1139.156/T$
Liquid density, g/cm^3	
60°C	1.105
20°C	1.332
0°C	1.419
−20°C	1.498
Heat of formation for ideal gas at, 25°C, ΔH, kJ/mol[c],[d]	−1078.6
Flammability limits in air at 101 kPa[a]	Nonflammable for all mixtures of air and hexafluoropropylene
Heat of combustion, kJ/mol[c],[d]	879
Toxicity, LC_{50} (rat), 4 h, ppm[e]	3000

[a]Ref. 4.
[b]To convert kPa to mm Hg, multiply by 7.5.
[c]To convert kJ to kcal, divide by 4.184.
[d]Ref. 19.
[e]Ref. 20.

Hexafluoropropylene–tetrafluoroethylene copolymers are available in low MV, extrusion grade, intermediate viscosity, high MV, and as dispersions. The low MV resin can be injection molded by conventional thermoplastic molding techniques. It is more suitable for injection molding than other FEP resins (51).

The extrusion grade is suitable for tubing, wire coating, and cable jacketing. It is less suitable for injection molding than the low MV resin because of its relatively high MV. The intermediate MV (Teflon FEP-140) resin is used for insulation of wires larger than AWG 12 (American wire gauge) and applications involving smaller wire sizes, where high current loads or excessive thermal cycling may occur. It is also ideal for jacketing wire braid construction, such as coaxial cables, and for heater cable jackets.

The high MV resin is used as liners for process equipment. Its MV is significantly higher than that of other resins, and therefore it is unsuitable for conventional injection molding. Stress-crack resistance and mechanical properties are superior to those of the other three products (52) (Table 2).

Modified HFP–TFE polymers offer a combination of high stress-crack resistance and high extrusion rates. Use of perfluorovinyl ethers as modifiers make it possible to achieve the superior performance without losing excellent chemical inertness and thermal stability (53–55).

Both high and low color concentrates are available for pigmenting extruded coatings of FEP resins. The concentrates are prepared for melt dispersion in

Table 2. Properties of Teflon FEP Fluorocarbon Resin[a]

Mechanical property	ASTM method	Teflon 110	Teflon 100	Teflon 140	Teflon 160
Melt flow number, g/10 min	D2116		7.0	3.0	1.5
Specific gravity	D792	2.13–2.17	2.13–2.17	2.13–2.17	2.13–2.17
Tensile strength at 23°C, MPa	D1708	20	23	30	31
Elongation at 23°C, %	D1708	300	325	325	305
Compressive strength, MPa	D695		21	21	23
Flexural strength at 23°C, MPa	D790		18	18	18
Impact strength at 23°C, J/m	D256		No break	No break	No break
Flexural modulus at 23°C, MPa	D790	655	620	620	586
Hardness durometer, Shore D	D2240	55	56	56	57
Coefficient of friction, metal/film	D1894		0.27	0.27	0.235
Deformation under load at 23°C, 6.9 MPa, 23 h, %	D621	1.8	0.5	0.5	0.5
Water absorption, 24 h, %	D570	<0.01	0.004	0.004	0.004
Linear coefficient of expansion °C	E831				
0–100°C			13.5×10^{-5}	13.9×10^{-5}	7.6×10^{-5}
100–150°C			20.8×10^{-5}	21.2×10^{-5}	11.5×10^{-5}
150–200°C			26.6×10^{-5}	27.0×10^{-5}	14.2×10^{-5}

[a]Compression-molded specimens; property data on extruded wire specimens are similar.

extrusion applications. The pigments (thermally stable) are purified and carefully selected to meet electrical, mechanical, and thermal end use specifications. Color concentrate pellets are easily dispersed among clear pellets by conventional tumbling. The ratio of concentrate to natural resin varies, depending on the wire size, insulation thickness, and color intensity desired.

An FEP copolymer dispersion is available as a 55-wt% aqueous dispersion containing 6% nonionic surfactant (on a solids basis) and a small amount of anionic dispersing agent. Its average particle size is ca 0.2 μm.

Properties. The crystallinity of FEP polymer is significantly lower than that of PTFE (70 vs 98%). The structure resembles that of PTFE, except for a random replacement of a fluorine atom by a perfluoromethyl group (CF_3). The crystallinity after processing depends on the rate of cooling the molten polymer. The presence of HFP in the polymer chain tends to distort the highly crystallized structure of the PTFE chain and results in a higher amorphous fraction.

In the free-radical polymerization of FEP copolymers, chain termination occurs by binary coupling of chain ends, thus contributing to high molecular weights. Linear viscoelastic properties of these polymers in the amorphous melts were measured by dynamic rheometry. The FEP samples had high molecular weights and were found to verify the relation of zero shear viscosity vs $(\text{mol wt})^3$ predicted by the reptation theory. At lower molecular weights, the empirical relation of viscosity vs $(\text{mol wt})^{3.4}$ holds (56).

Transitions and Relaxations. Only one first-order transition is observed, the melting point. Increasing the pressure raises the melting point. At low pressures, the rate of increase in the melting point is ca 1.74°C/MPa (0.012°C/psi); at high pressures this rate decreases to ca 0.725°C/MPa (0.005°C/psi). Melting increases the volume by 8%. In the presence of the HFP comonomer, crystal distortion occurs with an increase in intramolecular distance that, in turn, reduces the melting point (57).

The relaxation temperature appears to increase with increasing HFP content. Relaxation involves 5–13 of the chain carbon atoms. Besides α and γ relaxations, one other dielectric relaxation was observed below −150°C, which did not vary in temperature or in magnitude with comonomer content or copolymer density (58). The α relaxation (also called Glass I) is a high temperature transition (157°C), and γ relaxation (Glass II) (internal friction maxima) occurs between −5 and 29°C. The chain conformation and crystal structure of a series of HFP–TFE copolymers containing up to 50 mol% of HFP were studied (59). Increasing HFP content leads to significant departures from the highly ordered crystalline structure of PTFE. The helical conformation of the chain relaxes and untwists to accommodate the $-CF_3$ pendant group in the HFP unit.

Thermal Stability. The polymer is thermally stable and can be processed at ca 270°C. Thermal degradation is a function of temperature and time, and the stability is therefore limited. The melt-flow rate (thermal degradation) increases significantly for short periods above 280°C, and degradation occurs at lower temperatures with longer hold times. The hourly weight loss is 0.0004% at 230°C, 0.001% at 260°C, 0.01% at 290°C, 0.02% at 320°C, 0.08% at 340°C, and 0.3% at 370°C. Degradation is not significant if the change in melt-flow rate during molding is <10%. Physical strength decreases after prolonged exposure above 205°C, which accounts for the lower temperature rating of FEP resins (60).

Radiation Effects. The primary effect of radiation is the degradation of large molecules to small molecules. Molecular weight reduction can be minimized by excluding oxygen. If FEP is lightly irradiated at elevated temperatures in the absence of oxygen, cross-linking offsets molecular breakdown (58,61).

The degree to which radiation exposure affects FEP resins is determined by the energy absorbed, regardless of the type of radiation. Changes in mechanical properties depend on total dosage, but are independent of dose rate. The radiation tolerance of FEP in the presence or absence of oxygen is higher than that of PTFE by a factor of 10:1. Vacuum uv irradiation seems to provide a high potential for surface modification as compared to plasma treatment (62).

Mechanical Properties. Extensive lists of the physical properties of FEP copolymers are given in References 63–67–68. Mechanical properties are shown in Table 3. Most of the important properties of FEP are similar to those of PTFE; the main difference is the lower continuous service temperature of 204°C of FEP compared to that of 260°C of PTFE. The flexibility at low temperatures and the low coefficients of friction and stability at high temperatures are relatively independent of fabrication conditions. Unlike PTFE, FEP resins do not exhibit a marked change in volume at room temperature because they do not have a first-order transition at 19°C. They are useful above −267°C and are highly flexible above −79°C (69).

Static friction decreases with an increase in load, and the static coefficient of friction is lower than the dynamic coefficient. The tendency to creep must be considered carefully in FEP products designed for service under continuous stress. Creep can be minimized by suitable fillers. Fillers are also used to improve wear resistance and stiffness. Compositions such as 30% bronze-filled FEP, 20% graphite-filled FEP, and 10% glass-fiber-filled FEP offer high PV values [∼400(kPa·cm)/s] and are suitable for bearings.

Articles fabricated from FEP resins can be made bondable by surface treatment with a solution of sodium in liquid ammonia, or naphthalenyl sodium in tetrahydrofuran (69) to facilitate subsequent wetting. Exposing the surface to corona discharge (70) or amines at elevated temperatures in an oxidizing atmosphere (71) also makes the resins bondable. Some of the more recent work is described in References 72,73–74.

Vibration-dampening properties at sonic and ultrasonic frequencies are excellent. However, the thickness of the resin must be sufficient to absorb the energy produced; this is usually determined experimentally.

Electrical Properties. Because of excellent electrical properties, FEP is a valuable and versatile electrical insulator. Within the recommended service temperature range, PTFE and FEP have identical properties as electrical insulators. Volume resistivity, which is $>10^{17}$ Ω·cm, remains unchanged even after prolonged soaking in water; surface resistivity is $>10^{15}$ Ω/sq.

At low frequencies, the dielectric constant of FEP remains the same (∼2). However, at >100 MHz the constant drops slightly with increasing frequency. As a true thermoplastic, FEP has a void content of zero and most of the fabricated material has a density of 2.14–2.17 g/cm^3. The National Bureau of Standards has selected Teflon FEP resins for dielectric reference specimens because of the stability of their dielectric constant. The dissipation factor has several peaks as

Table 3. Mechanical Properties of FEP[a]

Property	Value	ASTM method
Specific gravity	2.14–2.17	D792-50
Thermal conductivity, W/(m·K)		Cenco-Fitch
−129–182°C	2.4	
−253°C	1.4	
Water absorption in 24 h, 3.175-mm-thick sample,		D570-547
% wt increase	<0.1	
Dimensional change at 23°C	None	
Coefficient of thermal expansion per °C		D696-44
>23°C	9.3×10^{-5}	
<23°C	5.7×10^{-5}	
Specific heat, kJ/(kg·K)[b]		
20°C	1.09	
100°C	1.17	
260°C	1.30	
Heat distortion, °C		D648-56
455 kPa[c]	70	
1820 kPa[c]	51	
Tensile yield strength, av, MPa[d]		D638-527
−251°C	165	
−160°C	131	
−129°C	96	
−73°C	62	
−56°C	27	
0°C	14	
23°C	12	
70°C	7	
121°C	3.5	
Tensile modulus, Pa[e]		
−251°C	57	
−160°C	50	
−129°C	36	
−73°C	24	
23°C	4	
100°C	1	
Tensile elongation, %		D638-527
−251°C	4	
−160°C	10	
−129°C	110	
−73°C	200	
23°C	350	
Flexural modulus, Pa[e]		D747-50
−251°C	53	
−160°C	47	
−101°C	32	
−23°C	6.6	
55°C	3.4	

Table 3. (Continued)

Property	Value	ASTM method
Compressive strength, MPa[d]		D695
−251°C	251	
−160°C	207	
23°C	15	
55°C	11	
100°C	3.4	
Izod impact strength, notched, J/m[f]		D256-56
23°C	No break	
Hardness durometer, shore D		D2240-T
23°C	59	
Taber abrasion, g/MHz, 100-g load CS–17 wheel	7.5	

[a]Measured on Teflon FEP T–100.
[b]To convert kJ to kcal, divide by 4.184.
[c]To convert kPa to atm, multiply by 0.01.
[d]To convert MPa to psi, multiply by 145.
[e]To convert Pa to mm Hg, multiply by 7.5×10^{-3}.
[f]To convert J/m to ftċlbf/in., divide by 53.38 (see ASTM D256).

a function of temperature and frequency (3×10^{-4} at 100 kHz; 7×10^{-4} at 1 MHz). The magnitude of the dissipation factor peak is greater for FEP than for PTFE because the molecular structure of the former is less symmetrical. The dissipation factor is hardly affected by irradiation annealing (75) and unaffected by humidity. The dielectric strength is high (80 GV/mm for 0.25-mm film at 23°C) and unaffected by thermal aging at 200°C. At high frequencies, the dielectric properties deteriorate in the presence of corona. If the voltage stress is not high enough to cause corona ignition, an infinitely long dielectric life is expected at any frequency. Corona discharges on the surface or in a void initiate dielectric breakdown (76). The FEP resins are recommended for continuous service up to 205°C. Although they begin to melt flow at 270°C, they retain some structural integrity up to 250°C (75).

Chemical Properties. The FEP resin is inert to most chemicals and solvents, even at elevated temperatures and pressures. However, it reacts with fluorine, molten alkali metal, and molten sodium hydroxide. Acids or bases are not absorbed at 200°C and exposures of 1 year. The absorption of organic solvents is less than 1% at elevated temperatures and long exposure times. Absorption of chemicals or solvents has no effect on the chemical integrity of the FEP molecule and is a reversible physical process.

Gases and vapors permeate FEP resin at a rate that is considerably lower than that of most plastics. Because FEP resins are melt processed, they are void-free and permeation occurs only by molecular diffusion. Variation in crystallinity and density is limited, except in unusual melt-processing conditions.

Because of its low permeability, FEP polymer is used extensively in the chemical industry. Its permeation characteristics are similar to those of PTFE (Table 4). An inverse relationship between permeability and film thickness applies to FEP.

Table 4. Permeability of FEP Fluorocarbon Resins to Liquid Vapors and Gases

	Permeability constant,[a,b] 10^{15} mol/(m·s·Pa)		
Vapor	23°C	35°C	50°C
jAcetic acid		9.07	
Acetone	0.37		3.23
Benzene	0.75		
Carbon tetrachloride	0.24	0.41	
Decane	112.18		33.48
Depentene	23.50		10.67
Ethyl acetate	0.27	2.06	4.09
Ethanol	1.61	4.66	
H_2SO_4, 98%	21.70		
Toluene	5.38		
Water	8.14	20.32	18.26

[a] Ref. 65 Test method ASTM E96-35T (at vapor pressure; for 25.4-μm film thickness). Values are averages only and not for specification purposes.
[b] Original data converted to SI units using vapor pressure data from Ref. 77.

Weathering. Articles fabricated from FEP are unaffected by weather, and their resistance to extreme heat, cold, and uv irradiation suits them for applications in radar and other electronic components. For example, after 15 years of solar exposure in Florida, the tensile strength and light transmission (96%) of a 25-μm-thick film was unchanged and the film remained crystal clear (78). Elongation increased slightly for the first 5–7 years of outdoor exposure, probably as a result of stress relaxation. Beyond 10 years, a small decrease was observed.

Optical Properties. Teflon FEP fluorocarbon film transmits more ultraviolet, visible light, and infrared radiation than ordinary window glass. The refractive index of FEP film is 1.341–1.347 (79).

Fabrication

Standard thermoplastic processing techniques can be used to fabricate FEP. Thermal degradation must be avoided, and a homogeneous structure and good surface quality must be maintained.

Injection Molding. Compared to most thermoplastic products, even the low MV resin has a significantly higher MV and therefore requires higher processing temperatures, slower injection rates, special mold design, and corrosion-resistant material of construction. When the flow velocity in melt processing exceeds a critical value, melt fracture occurs. The critical shear rate of FEP is much lower than that of other thermoplastics. Recommendations for materials of construction and the screw design, valves, smear heads, nozzle, operating conditions, and mold design are given in References 52,80, and 81.

Pigments (thermally stable at processing temperature) are dry blended with the resin before molding. At loadings of 0.1–1%, pigments have no appreciable effect on the dielectric strength, dielectric constant, or mechanical properties. The

dissipation factor of pigmented resin varies with the pigment and its amount (82).

Extrusion. Conventional melt-extrusion equipment is used in processing FEP resins. Commercial pigments are mixed with the resin before extrusion into wire coating, tubing, rods, molding, beading channels, etc. Coating thicknesses of 0.076–2.54 mm have been extruded over such materials as silicone rubber, poly(vinyl chloride), glass braid, metal-shielded cables, twisted conductors, and parallel multiconductor cables.

For primary insulation or cable jackets, high production rates are achieved by extruding a tube of resin with a larger internal diameter than the base wire and a thicker wall than the final insulation. The tube is then drawn down to the desired size. An operating temperature of 315–400°C is preferred, depending on holdup time. The surface roughness caused by melt fracture determines the upper limit of production rates under specific extrusion conditions (83,84). Corrosion-resistant metals should be used for all parts of the extrusion equipment that come in contact with the molten polymer (85).

Tubing is made in a wide range of sizes and is used as slip-on electrical insulation, instrument tubing, and for hoses. Small tubing, called spaghetti tubing, can be produced by a free-extrusion technique, whereas hose-size tubing is produced by conventional forming-box techniques; FEP also is extruded into films.

Dispersion Processing. The commercial aqueous dispersion of FEP contains 55 wt% of hydrophobic, negatively charged FEP particles and ca 6 wt% (based on FEP) of a mixture of nonionic and anionic surface-active agents. The average particle size is ca 0.2 μm. The dispersion is processed by the same technique used for PTFE dispersion. For example, the fabric is coated with FEP dispersion, the water is evaporated from the coating, the wetting agent is removed, and the FEP layer is fused with the fabric.

Dispersion is used as a coating for glass fabric, chemical barriers, and wire-insulating tapes; as adhesive coatings for bonding seals and bearings of PTFE to metallic and nonmetallic components; and as antifriction or antistick coatings for metals. The fusion of FEP to provide a continuous film depends on a time–temperature relationship; 1 min at 400°C or 40 min at 290°C is sufficient to achieve good fusion (86).

Other Techniques. The FEP resin is bonded to metal surfaces by the application of heat and pressure; it can be heat sealed or hot-gas welded. Heating FEP at 260°C and allowing it to cool slowly results in stress relieving, or annealing. The FEP film is used to weld PTFE-coated surfaces.

Effects of Fabrication on Product Properties. Extrusion conditions have a significant effect on the quality of the product (85). Contamination can be the result of corrosion, traces of another resin, or improper handling. Corrosion-resistant Hastelloy C parts should be used in the extruder. Surface roughness is the result of melt fracture or mechanical deformation. Melt fracture can be eliminated by increasing the die opening, die temperature, and the melt temperature and by reducing the extrusion rate. Bubbles and discoloration are caused by resin degradation, air entrapment, or condensed moisture. Excessive drawdown, resin degradation, or contamination can result in pinholes, tears, and cone breaks. The blisters are caused by degassing of primary coatings, and loose coatings are caused by rapid cooling and long cones.

Testing and Standards. Requirements for extrusion and molding grades are cited in ASTM specifications (87) and in Federal specification LP-389A of May 1964 (88). For fabricated shapes, FEP film and sheet are covered by Aeronautical Material Specifications (AMS) 3647 and LP-523 (89). Besides the specifications covered by the Fluorocarbons Division of the Society of the Plastics Industry, Inc. (90), other specifications are listed in Reference 91.

Economic Aspects

Because of the high cost of HFP, FEP is more expensive than PTFE. In the United States, in 2000, FEP sold at prices up to $35.2/kg, depending on the type and quantity. Most grades are marketed in a colorless, translucent, extruded pellet form. The dispersion containing about 55% solids is priced at ca $44/kg. FEP sales have increased rapidly because of usage in plenum cable.

Health and Safety

The safety precautions required in handling HFP–TFE copolymers are the same as those applied to handling PTFE (92). Large quantities have been processed safely by many different fabricators in a variety of operations. With proper ventilation, the polymer can be processed and used at elevated temperatures without hazard. The fumes from heated FEP or its thermal decomposition products are toxic in high concentrations, like the fumes or decomposition products of other polymers. Ventilation should be provided in areas where the resin is at processing temperature (270–400°C). At ambient temperatures, FEP resin is essentially inert. Inhalation of fumes given off by heated FEP resin may result in influenza-like symptoms. They may occur several hours after exposure and disappear within 35–48 h, even in the absence of treatment; the effects are not cumulative (52). Such attacks usually follow exposure to vapors evolved from the polymer without adequate ventilation or from smoking tobacco or cigarettes contaminated with the polymer. Toxicology study of the particulates and fumes is reported in Reference 93.

Applications. The principal electrical applications include hookup wire, interconnecting wire, coaxial cable, computer wire, thermocouple wire, plenum cable, and molded electrical parts. Principal chemical applications are lined pipes and fittings, over-braided hose, heat exchangers, and laboratory ware. Mechanical uses include antistick applications, such as conveyor belts and roll covers. A recent development of FEP film for solar collector windows takes advantage of light weight, excellent weatherability, and high solar transmission. Solar collectors made of FEP film are efficient, and installation is easy and inexpensive.

BIBLIOGRAPHY

"Tetrafluoreoethylene Polymers, Copolymers with Hexafluoropropylene" in *EPST* 1st ed., Vol. 13, pp. 654–670, by D. I. McCane, E. I. du Pont de Nemours & Co., Inc.;

"Tetrafluoroethylene Polymers,Tetrafluoroethylene–Hexafluoropropylene Copolymers" in *EPSE* 2nd ed., Vol. 16, pp. 601–613, by S. V. Gangal, E. I. du Pont de Nemours & Co., Inc.

1. U.S. Pat. 2946763 (July 26, 1960), M. I. Bro and B. W. Sandt (to E. I. du Pont de Nemours & Co., Inc.).
2. U.S. Pat. 2394581 (Feb. 12, 1946), A. F. Benning, F. B. Dowing, and J. D. Park (to Kinetic Chemicals, Inc.).
3. E. G. Young and W. S. Murray, *J. Am. Chem. Soc.* **70**, 2814 (1949).
4. A. L. Henne and T. P. Waalkes, *J. Am. Chem. Soc.* **68**, 496 (1946).
5. U.S. Pat. 3446858 (May 27, 1969), H. Shinzu and co-workers (to Daikin Kyogo Co.).
6. U.S. Pat. 3459818 (Aug. 15, 1969), H. Ukihashi and M. Hisasue (to Asahi Glass Co.).
7. U.S. Pat. 3873630 (Mar. 25, 1975), N. E. West (to E. I. du Pont de Nemours & Co., Inc.).
8. U.S. Pat. 5043491 (Aug. 27, 1991), J. Webster and co-workers, (to E. I. du Pont de Nemours & Co., Inc.).
9. U.S. Pat. 5057634 (Oct. 15, 1991), J. Webster and co-workers (to E. I. du Pont de Nemours & Co., Inc.).
10. U.S. Pat. 5068472 (Nov. 26, 1991), J. Webster and co-workers (to E. I. du Pont de Nemours & Co., Inc.).
11. U.S. Pat. 3758138 (Aug. 7, 1956), D. A. Nelson (to E. I. du Pont de Nemours & Co., Inc.).
12. B. Atkinson and A. B. Trenwith, *J. Chem. Soc., Part II* 2082 (1953).
13. U.S. Pat. 2759983 (Aug. 21, 1956), J. S. Waddell (to E. I. du Pont de Nemours & Co., Inc.).
14. U.S. Pat. 3047640 (July 31, 1962), R. F. Sweeny and C. Woolf (to Allied Chemical Corp.).
15. U.S. Pat. 3009966 (Nov. 21, 1961), M. Hauptschein and A. Fainberg (to Pennsalt Chemicals Corp.).
16. L. T. Hals, T. S. Reid, and G. H. Smith, *J. Am. Chem. Soc.* **73**, 4054 (1951); U.S. Pat. 2668864 (Feb. 9, 1954), L. T. Hals, T. S. Reid, and G. H. Smith (to Minnesota Mining and Manufacturing Co.).
17. G. Pass, *J. Chem. Soc., Part I* **824** (Jan. 1965); U.S. Pat. 3318963 (May 9, 1967), G. Pass (to Imperial Chemical Industries, Ltd.).
18. Ger. Pat. 1236497 (Mar. 16, 1967), W. Oese, H. Dude, and F. Reinke (to VEB Fluorwerke Dohma).
19. H. C. Duus, *Ind. Eng. Chem.* **47**, 1445 (1955).
20. J. W. Clayton, *Occup. Med.* **4**, 262 (1962).
21. U.S. Pat. 2918501 (Dec. 22, 1959), W. J. Brehm and co-workers (to E. I. du Pont de Nemours & Co., Inc.).
22. U.S. Pat. 3316312 (Apr. 25, 1967), D. I. McCane and I. M. Robinson (to E. I. du Pont de Nemours & Co., Inc.).
23. R. A. Matula, *J. Phys. Chem.* **72**, 3054 (1968).
24. U.S. Pat. 3358003 (Dec. 12, 1967), H. S. Eleuterio and R. W. Meschke (to E. I. du Pont de Nemours & Co., Inc.).
25. U.S. Pat. 3180895 (Apr. 27, 1965), J. F. Harris Jr. and D. I. McCane (to E. I. du Pont de Nemours & Co., Inc.).
26. U.S. Pat. 3291843 (Dec. 13, 1966), C. G. Fritz and S. Selman (to E. I. du Pont de Nemours & Co., Inc.).
27. E. V. Volkova and A. E. Skobina, *Vysokomol. Soedin.* **6**, 964 (1964).
28. Fr. Pat. 1524571 (May 10, 1968), S. W. Osborn and E. Broderich (to Thiokol Chemical Corp.).
29. U.S. Pat. 2983764 (May 9, 1961), D. F. Knaack (to E. I. du Pont de Nemours & Co., Inc.).
30. U.S. Pat. 2958685 (Nov. 1, 1960), H. S. Eleuterio (to E. I. du Pont de Nemours & Co., Inc.).

31. I. L. Knunyants, E. I. Mysov, and M. P. Krasuskaya, *Izv. Akad. Nauk. SSSR Otd. Khim. Nauk.*, 906 (1958).
32. I. L. Knunyants, A. E. Shchekotikhin, and A. V. Fakin, *Izv. Akad. Nauk. SSSR Otd. Khim. Nauk.*, 282 (1953).
33. I. L. Knunyants, L. S. German, and B. L. Dyatkin, *Izu. Akad. Nauk. SSSR Otd. Khim. Nauk.*, 1353 (1956).
34. R. N. Haszeldine and B. R. Steele, *J. Chem. Soc.*, 1592 (1953).
35. W. T. Miller, Jr., E. Bergman, and A. H. Fainberg, *J. Am. Chem. Soc.* **79**, 4159 (1957).
36. I. L. Knunyants, V. V. Shokina, and N. D. Kuleshova, *Izv. Akad. Nauk SSSR Otd. Khim. Nauk* 1936 (1960).
37. U.S. Pat. 3467636 (Sept. 16, 1969), A. Nersasian (to E. I. du Pont de Nemours & Co., Inc.).
38. U.S. Pat. 3536683 (Oct. 27, 1970), F. V. Bailor and J. R. Cooper (to E. I. du Pont de Nemours & Co., Inc.).
39. U.S. Pat. 3790540 (Feb. 5, 1974), J. E. Dohany and A. C. Whiton (to Pennwalt Corp.).
40. U.S. Pat. 3817951 (June 18, 1974), D. N. Robinson (to Pennwalt Corp.).
41. U.S. Pat. 3868337 (Feb. 25, 1975), P. Gros (to Society Superflexit).
42. G. L. Kennedy Jr., *Crit. Revs. Toxicol.* **21**(2), 149–170 (1990).
43. U.S. Pat. 2598283 (May 27, 1952), W. T. Miller (to U.S. Atomic Energy Commission).
44. R. A. Naberezhnykh and co-workers, *Dokl. Akad. Nauk SSSR* **214**, 149 (1974).
45. A. S. Kabankin, S. A. Balabanova, and A. M. Markevich, *Vysokomol. Soedin. Ser. A* **12**, 267 (1970).
46. Br. Pat. 781532 (Aug. 21, 1957), C. G. Krespan (to E. I. du Pont de Nemours & Co., Inc.).
47. U.S. Pat. 3132124 (May 5, 1964), M. J. Couture, D. L. Schindler, and R. B. Weiser (to E. I. du Pont de Nemours & Co., Inc.).
48. U.S. Pat. 4380618 (1983), A. Khan and R. Morgan (to E. I. du Pont de Nemours & Co., Inc.).
49. U.S. Pat. 4384092 (1983), J. Herison (to Ugine Kuhlmann).
50. U.S. Pat. 4861845 (1989), E. Slocum, A. Sobrero, and R. Wheland (to E. I. du Pont de Nemours & Co., Inc.).
51. R. S. Atland, *Modern Plast.* **62**, 200 (1985).
52. Teflon-FEP Fluorocarbon Resin, Techniques for Injection Molding, Information Bulletin 95d, E. I. du Pont de Nemours & Co., Inc., Wilmington, Del., 1969.
53. U.S. Pat. 5677404 (Oct. 14, 1997), L. M. Blair (to E. I. du Pont de Nemours & Co., Inc.).
54. U.S. Pat. 5688885 (Nov. 18, 1997), L. M. Blair (to E. I. du Pont de Nemours & Co., Inc.).
55. U.S. Pat. 5700889 (Dec. 23, 1997), L. M. Blair (to E. I. du Pont de Nemours & Co., Inc.)
56. S. Wu, *Macromolecules* **18**, 2023–2030 (1985).
57. R. K. Eby, *J. Appl. Phys.* **34**, 2442 (1963).
58. R. K. Eby and F. C. Wilson, *J. Appl. Phys.* **33**, 2951 (1962).
59. M. L. White and co-workers, *J. Polym. Sci., Part B: Polym. Phys.* **36**, 2811–2819 (1998).
60. Safe Handling Guide, Teflon Fluorocarbon Resins, du Pont Materials for Wire and Cable, Bulletin E-85433, E. I. du Pont de Nemours & Co., Inc., Wilmington, Del., 1986.
61. R. Y. M. Huang and P. J. F. Kanitz, *Polym. Prepr. Am. Chem. Soc. Div. Polym. Chem.* **10**, 1087 (1969).

62. V. N. Vasilets and co-workers, *J. Polym Sci., Part I: Polym. Chem.* **36**, 2215–2222 (1998).
63. R. J. Diamond, *Plastics* **27**, 109 (1962).
64. J. Frados, ed., *Modern Plastics Encyclopedia*, Vol. **46**, No. 10A, McGraw-Hill Book Co., Inc., New York, 1969, p. 974.
65. *J. Teflon* **11**(1), 8 (1970).
66. J. A. Brydson, *Plastics Materials*, Iliffe Books, Ltd., London, 1966, Chapt. "10", pp. 203–218.
67. Teflon 100 FEP–Fluorocarbon Resin—Melt Processible Resin, Information Bulletin X-90a, E. I. du Pont de Nemours & Co., Inc., Wilmington, Del., 1960.
68. *Teflon Fluorocarbon Resins, Mechanical Design Data*, 2nd ed., E. I. du Pont de Nemours & Co., Inc., Wilmington, Del., 1965.
69. A. A. Benderly, *J. Appl. Polym. Sci.* **6**, 221 (1962).
70. Brit. Pat. 890466 (Feb. 28, 1962), D. L. Ryan (to E. I. du Pont de Nemours & Co., Inc.).
71. U.S. Pat. 3063882 (Nov. 13, 1962), J. R. Chesire (to E. I. du Pont de Nemours & Co., Inc.).
72. R. R. Rye and G. W. Arnold, *Langmuir* **5**, 1331 (1989).
73. D. T. Clark and D. R. Hutton, *J. Polym. Sci., Polym. Chem. Ed.* **25**, 2643 (1987).
74. R. C. Bening and J. J. McCarthy, *Polym. Prep.* **29**, 336 (1988).
75. Electrical/Electronic Design Data for Teflon, E. I. du Pont de Nemours & Co., Inc., Wilmington, Del.
76. J. C. Reed, E. J. McMahon, and J. R. Perkins, *Insulation (Libertyville, III.)* **10**, 35 (1964).
77. D. W. Green, ed., *Perry's Chemical Engineers' Handbook*, 6th ed., McGraw-Hill Book Co., Inc., New York, 1984.
78. Teflon Solar Film for Solar Collectors, Bul. No. E21605 E. I. du Pont de Nemours & Co., Inc., Wilmington, Del.
79. Teflon FEP–Fluorocarbon Film, Bulletin T-5A, Optical, E. I. du Pont de Nemours & Co., Inc., Wilmington, Del.
80. Injection Molding Guide for Teflon FEP, PFA and Tefzel, Bulletin No. E-96680, E. I. du Pont de Nemours & Co., Inc., July 1987.
81. "Teflon/Tefzel" Injection Moulding Trouble-Shooting Guide, Bulletin No. E-96164 (Rev.), E. I. du Pont de Nemours & Co., Sept. 1991.
82. L. H. Gillespe, D. O. Saxton, and F. M. Chapman, *New Design Data for Teflon*, E. I. du Pont de Nemours & Co., Inc., Wilmington, Del., 1960.
83. *J. Teflon* **18**(1), 8 (1977).
84. Technical Information, Melt Extrusion Guide, Bulletin No. H-45321, E. I. du Pont de Nemours & Co., Inc., Mar. 1993.
85. *Teflon FEP–Fluorocarbon Resin—Techniques for Processing by Melt Extrusion*, 2nd ed., Information Bulletin X-82, E. I. du Pont de Nemours & Co., Inc., Wilmington, Del., 1960.
86. Properties and Processing Techniques for Teflon 120 FEP–Fluorocarbon Resin Dispersion, Preliminary Information Bulletin No. 20, E. I. du Pont de Nemours & Co., Inc., Wilmington, Del., 1961.
87. Scos *Annual Book of ASTM Standards*, Vol. 08.01 American Society for Testing and Materials, Philadelphia, Pa., 1993.
88. *Federal Supply Service Bureau Specification L-P-389A*, Section SW, 470E L'Enfant Plaza, Washington, D.C.
89. Technical Data, SAE International, Inc., Warrendale, Pa., 1993.
90. Scos *Annual Book of ASTM Standards*. Vol. 08.03, American Society for Testing and Materials, Philadelphia, Pa., 1993.

91. Technical Data, Society of the Plastics Industry, Inc., Fluorocarbon Division, Washington, D.C., 1993; *J. Teflon* **15**(1), 10 (1974).
92. *Guide to Safe Handling of Fluoropolymer Resins*, 3rd ed., Fluoropolymers Division of the Society of the Plastics Industry, Inc., Washington, D.C., 1998.
93. K. P. Lees and W. C. Seidal, *Inhalation Toxicol.* **3**, 237 (1991).

GENERAL REFERENCES

"Fluorinated Ethylene–Propylene Copolymers," under "Fluorine Compounds, Organic," in *ECT* 4th ed., Vol. 11, pp. 644–656, by S. V. Gangal, E. I. du Pont de Nemours & Co., Inc.

SUBHASH V. GANGAL
E. I. du Pont de Nemours & Co., Inc.

PERFLUORINATED POLYMERS, POLYTETRAFLUOROETHYLENE

Introduction

Polytetrafluoroethylene (PTFE) [9002-84-0], more commonly known as Teflon (E.I. du Pont de Nemours & Co., Inc.), a perfluorinated straight-chain high polymer, has a most unique position in the plastics industry because of its chemical inertness, heat resistance, excellent electrical insulation properties, and low coefficient of friction over a wide temperature range. Polymerization of tetrafluoroethylene monomer gives this perfluorinated straight-chain high polymer with the formula $-(CF_2-CF_2)_n-$. The white to translucent solid polymer has an extremely high molecular weight, in the $10^6 - 10^7$ range, and consequently has a viscosity in the range of 1–10 GPa·s ($10^{10} - 10^{11}$ P) at 380°C. It is a highly crystalline polymer and has a crystalline melting point. Its high thermal stability results from the strong carbon–fluorine bond and characterizes PTFE as a useful high temperature polymer.

The discovery of PTFE (1) in 1938 opened the commercial field of perfluoropolymers. Initial production of PTFE was directed toward the World War II effort, and commercial production was delayed by DuPont until 1947. Commercial PTFE is manufactured by two different polymerization techniques that result in two different types of chemically identical polymer. Suspension polymerization produces a granular resin, and emulsion polymerization produces the coagulated dispersion that is often referred to as a fine powder or *PTFE dispersion*.

Because of its chemical inertness and high molecular weight, PTFE melt does not flow and cannot be fabricated by conventional techniques. The suspension-polymerized PTFE polymer (referred to as *granular PTFE*) is usually fabricated by modified powder metallurgy techniques. Emulsion-polymerized PTFE behaves

Encyclopedia of Polymer Science and Technology. Copyright John Wiley & Sons, Inc. All rights reserved.

entirely differently from granular PTFE. Coagulated dispersions are processed by a cold-extrusion process (like processing lead). Stabilized PTFE dispersions, made by emulsion polymerization, are usually processed according to latex processing techniques.

Manufacturers of PTFE include Daikin Kogyo (Polyflon), DuPont (Teflon), Dyneon, Asahi Glass, Ausimont (Algoflon and Halon), and the CIS (Fluoroplast). India and The People's Republic of China also manufacture some PTFE products. Additional information on specific manufacturers' products can often be obtained by consulting their internet web sites (for example, www.dupont.com/teflon).

Monomer

Preparation. The manufacture of tetrafluoroethylene (TFE) [116-14-3] involves the following steps (2–9). The pyrolysis is often conducted at a PTFE manufacturing site because of the difficulty of handling TFE. New discoveries have made it somewhat easier to use it at remote places (10).

$$CaF_2 + H_2SO_4 \longrightarrow CaSO_4 + 2\,HF$$

$$CH_4 + 3\,Cl_2 \longrightarrow CHCl_3 + 3\,HCl$$

$$CHCl_3 + 2\,HF \xrightarrow{SbF_3} CHClF_2 + 2\,HCl$$

$$2\,CHClF_2 \xrightarrow{\Delta} CF_2{=}CF_2 + 2\,HCl$$

Pyrolysis of chlorodifluoromethane is a noncatalytic gas-phase reaction carried out in a flow reactor at atmospheric of subatmospheric pressure; yields can be as high as 95% at 590–900°C. The economics of monomer production is highly dependent on the yields of this process. A significant amount of hydrogen chloride waste product is generated during the formation of the carbon–fluorine bonds.

A large number of by-products are formed in this process, mostly in trace amounts; more significant quantities are obtained of hexafluoropropylene, perfluorocyclobutane, 1-chloro-1,1,2,2-tetrafluoroethane, and 2-chloro-1,1,1,2,3,3-hexafluoropropane. Small amounts of highly toxic perfluoroisobutylene, $CF_2{=}C(CF_3)_2$, are formed by the pyrolysis of chlorodifluoromethane.

In this pyrolysis, subatmospheric partial pressures are achieved by employing a diluent such as steam. Because of the corrosive nature of the acids (HF and HCl) formed, the reactor design should include a platinum-lined tubular reactor made of nickel to allow atmospheric pressure reactions to be run in the presence of a diluent. Because the pyrolysate contains numerous by-products that adversely affect polymerization, the TFE must be purified. Refinement of TFE is an extremely complex process, which contributes to the high cost of the monomer. Inhibitors are added to the purified monomer to avoid polymerization during storage; terpenes such as *d*-limonene and terpene B are effective (11).

Tetrafluoroethylene was first synthesized in 1933 from tetrafluoromethane, CF_4, in an electric arc furnace (12). Since then, a number of routes have been

Table 1. Physical Properties of Tetrafluoroethylene[a]

Property	Value
Boiling point at 101.3 kPa,[b] °C	−76.3
Freezing point, °C	−142.5
Liquid density at t°C, g/mL	
$-100 < t < -40$	$=1.202-0.0041t$
$-40 < t < 8$	$=1.1507-0.0069t-0.000037t^2$
$8 < t < 30$	$=1.1325-0.0029t-0.00025t^2$
Vapor pressure at T K, kPa[c]	
$196.85 < T < 273.15$	$\log_{10} P_{\mathrm{kPa}} = 6.4593-875.14/T$
$273.15 < T < 306.45$	$\log_{10} P_{\mathrm{kPa}} = 6.4289-866.84/T$
Critical temperature, °C	33.3
Critical pressure, MPa[d]	39.2
Critical density, g/mL	0.58
Dielectric constant at 28°C	
at 101.3 kPa[b]	1.0017
at 858 kPa[b]	1.015
Thermal conductivity at 30°C, m W/(m·K)	15.5
Heat of formation for ideal gas at 25°C, ΔH, kJ/mol[e],[f]	−635.5
Heat of polymerizationof 25°C to solid polymer ΔH, kJ/mol[e],[f]	−172.0
Flammability limits in air at 101.3 kPa[c], vol%	14–43

[a] From Ref. 22, unless otherwise stated.
[b] To convert kPa to atm, multiply by 0.01.
[c] To convert kPa to psi, multiply by 0.145.
[d] To convert MPa to atm, divide by 0.101.
[e] To convert J to cal, divide by 4.184.
[f] Ref. 23.
[g] Ref. 24.

developed (13–19). Depolymerization of PTFE by heating at ca 600°C is probably the preferred method for obtaining small amounts of 97% pure monomer on a laboratory scale (20,21). Depolymerization products contain highly toxic perfluoroisobutylene and should be handled with care.

Properties. Tetrafluoroethylene (mol wt 100.02) is a colorless, tasteless, odorless, nontoxic gas (Table 1). It is stored as a liquid; vapor pressure at −20°C is 1 MPa (9.9 atm). It is usually polymerized above its critical temperature and below its critical pressure. The polymerization reaction is highly exothermic.

Tetrafluoroethylene undergoes addition reactions typical of an olefin. It burns in air to form carbon tetrafluoride, carbonyl fluoride, and carbon dioxide (25). Under controlled conditions, oxygenation produces an epoxide (26) or an explosive polymeric peroxide (25). Trifluorovinyl ethers, RO—CF=CF_2, are obtained by reaction with sodium salts of alcohols (27). An ozone–TFE reaction is accompanied by chemiluminescence (28). Dimerization at 600°C gives perfluorocyclobutane, C_4F_8; further heating gives hexafluoropropylene, CF_2=$CFCF_3$, and eventually perfluoroisobutylene, CF_2=$C(CF_3)_2$ (29). Purity is determined by both gas–liquid and gas–solid chromatography; the ir spectrum is complex and therefore of no value.

Uses. Besides polymerizing TFE to various types of high PTFE homopolymer, TFE is copolymerized with hexafluoropropylene (30), ethylene (31), perfluorinated ether (32,33), isobutylene (34), propylene (35), and in some cases it is used as a termonomer (36). It is used to prepare low molecular weight polyfluorocarbons (37) and carbonyl fluoride (38), as well as to form PTFE *in situ* on metal surfaces (39). Hexafluoropropylene [116-15-4] (40,41), perfluorinated ethers, and other oligomers are prepared from TFE.

In the absence of air, TFE disproportionates violently to give carbon and carbon tetrafluoride; the same amount of energy is generated as in black powder explosions. This type of decomposition is initiated thermally and equipment hot spots must be avoided. The flammability limits of TFE are 14–43%; it burns when mixed with air and forms explosive mixtures with air and oxygen. It can be stored in steel cylinders under controlled conditions inhibited with a suitable stabilizer. The oxygen content of the vapor phase should not exceed 10 ppm. Although TFE is nontoxic, it may be contaminated by highly toxic fluorocarbon compounds.

Manufacture of PTFE

Engineering problems involved in the production of TFE seem simple as compared with those associated with polymerization and processing of PTFE resins. The monomer must be polymerized to an extremely high molecular weight in order to achieve the desired properties. The low molecular weight polymer does not have the strength needed in end use applications.

Polytetrafluoroethylene is manufactured and sold in three forms: granular, fine powder, and aqueous dispersion; each requires a different fabrication technique. Granular resins are manufactured in a wide variety of grades to obtain a different balance between powder flows and end use properties (Fig. 1). Fine powders that are made by coagulating aqueous dispersions are also available in various grades. Differences in fine powder grades correspond to their usefulness in specific applications and to the ease of fabrication. Aqueous dispersions are sold in latex form and are available in different grades. A variety of formulation techniques are used to tailor these dispersions for specific applications.

Polymerization. In aqueous medium, TFE is polymerized by two different procedures. When little or no dispersing agent is used and vigorous agitation is maintained, a precipitated resin is produced, commonly referred to as granular resin. In another procedure, called *aqueous dispersion polymerization*, a sufficient dispersing agent is employed and mild agitation produces small colloidal particles dispersed in the aqueous reaction medium; precipitation of the resin particles is avoided. The two products are distinctly different, even though both are high molecular weight PTFE polymers. The granular product can be molded in various forms, whereas the resin produced by the aqueous dispersion cannot be molded, but is fabricated by dispersion coating or conversion to powder for paste extrusion with a lubricant medium. Granular resin cannot be paste extruded or dispersion coated.

Granular Resins. Granular PTFE is made by polymerizing TFE alone or in the presence of trace amounts of comonomers (42–44). An initiator, a small amount of dispersing agent, and other additives (45) may be present; an alkaline

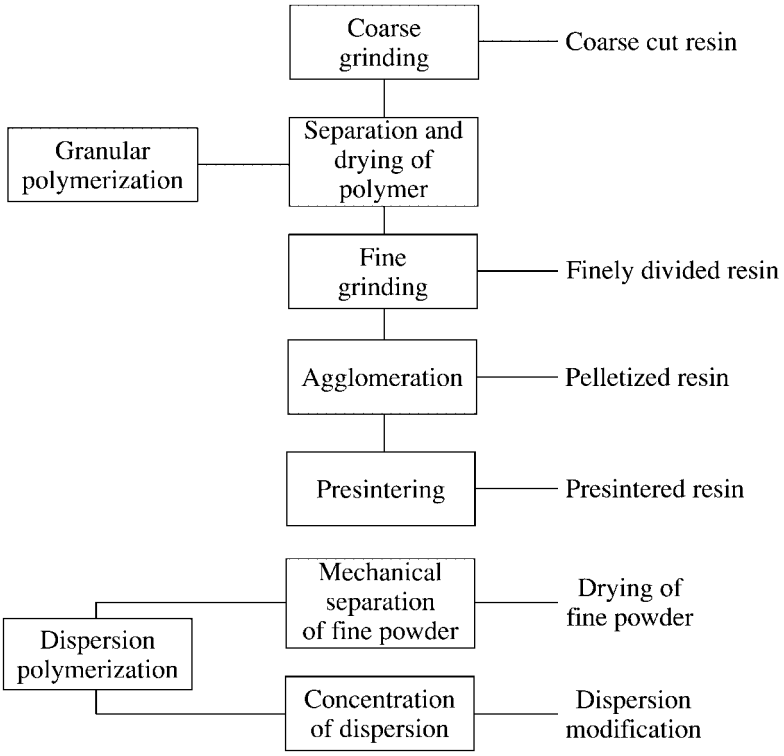

Fig. 1. Granular, fine powder, and dispersion PTFE products.

buffer is occasionally used (46). In the early stages of polymerization, an unstable dispersion is formed, but lack of dispersing agent and vigorous agitation cause the polymer to partially coagulate; the remainder of the process is fairly complex. The polymerized product is stringy, irregular, and variable in shape. The dried granular polymer is ground to different average particle sizes, depending on the product requirements, eg, the flow and other properties. Coarser fabrication of particles leaves a higher void in the sintered article. A better balance between handleability and moldability (ability to mold and sinter in the absence of voids) is achieved by agglomerating the finely divided resin to ca 400–800 μm (47–49). For ram extrusion of granular resin into long tubes and rods, a partially presintered resin is preferred. Granular PTFE resin is nonflammable.

Fine Powder Resins. Fine powder resins are made by polymerizing TFE in an aqueous medium with an initiator and emulsifying agents (50). The polymerization mechanism is not a typical emulsion type, but is subject to some of the principles of emulsion polymerization. The process and ingredients have a significant effect on the product. It is extremely important that the dispersion remains sufficiently stable throughout polymerization, avoiding premature coagulation (51), but unstable enough to allow subsequent coagulation into a fine powder. Gentle stirring ensures dispersion stability. The amount of emulsifying agent in the polymerization process is usually less than its critical micelle concentration.

The rate of polymerization and the particle shape are influenced by the amount of the emulsifying agent (52–55). The particle structure can be influenced by the polymerization process. Most of the particles are formed in the early stages of the polymerization process and the particles grow as the batch progresses; hence, the radial variation in molecular weight and polymer composition within the dispersion particle can be achieved by controlling the polymerization variables, including ingredients and operating conditions (56–62).

The thin dispersion rapidly thickens into a gelled matrix and coagulates into a water-repellent agglomeration that floats on the aqueous medium as the mechanical agitation is continued. The agglomeration is dried gently; shearing must be avoided.

Aqueous Dispersions. The dispersion is made by the polymerization process used to produce fine powders of different average particle sizes (63). The most common dispersion has an average particle size of about 0.2 μm, probably the optimum particle size for most applications. The raw dispersion is stabilized with a nonionic or anionic surfactant and concentrated to 60–65 wt% solids by electrodecantation, evaporation, or thermal concentration (64). The concentrated dispersion can be modified further with chemical additives. The fabrication characteristics of these dispersions depend on polymerization conditions and additives.

Filled Resins. Fillers such as glass fibers, graphite, asbestos, or powered metals are compounded into all three types of PTFE. Compounding is achieved by intimate mixing. Coagulation of the polymer with a filler produces a filled fine powder.

Properties

The properties described herein are related to the basic structure of PTFE and are exhibited by both granular and fine powder products. The carbon–carbon bonds, which form the backbone of the PTFE chain, and the carbon–fluorine bonds are extremely strong and are the key contributors in imparting an outstanding combination of properties. The fluorine atoms form a protective sheath over the chain of carbon atoms. If the atoms attached to the carbon-chain backbone were smaller or larger than fluorine, the sheath would not form a regular uniform cover. This sheath shields the carbon chain from attack and confers chemical inertness and stability. It also reduces the surface energy resulting in low coefficient of friction and nonstick properties.

Polytetrafluoroethylene does not dissolve in any common solvent; therefore, its molecular weight cannot be measured by the usual methods. A number-average molecular weight has been estimated by determining the concentration of end groups derived from the initiator. Earlier estimates, based on an iron bisulfite system containing radioactive sulfur, ^{35}S, ranged from 142×10^3 to 534×10^3 for low molecular weight polymer. The same technique applied to polymers of industrial interest gave molecular weights of $389\times10^3 - 8900\times10^3$ (65,66). In the absence of a normal molecular weight determination method, an estimated relative molecular weight is used for all practical purposes. It is obtained by measuring the specific gravity, following a standardized fabricating and sintering procedure (ASTM D1457-83). Because the rate of crystallization decreases with increasing

molecular weight, samples prepared from the high molecular weight polymer and cooled from the melt at a constant slow rate have lower standard specific gravities than those prepared from low molecular weight polymer cooled at the same rate (67). The correlation between number-average molecular weight (M_n) based on end group estimations, and standard specific gravity (SSG) is given by

$$SSG = 2.612 - 0.058 \log_{10} M_n$$

The SSG procedure assumes absence of voids (or constant void content). Voids depress the values of the measured specific gravity. The inaccuracies that result from voids can be corrected by applying ir techniques (68).

Melting and recrystallization behavior of virgin PTFE has been studied by dsc (69). A quantitative relationship was found between M_n and the heat of crystallization (ΔH_c) in the molecular weight range of $5.2\times10^5 - 4.5\times10^7$, where ΔH_c is heat of crystallization in J/g, which is independent of cooling rates of 4–32°C/min.

$$M_n = 2.1\times10^{10}\,\Delta H_c^{-5.16}$$

At ca 342°C, virgin PTFE changes from white crystalline material to almost transparent amorphous gel. Differential thermal analysis indicates that the first melting of virgin polymer is irreversible and that subsequent remeltings occur at 327°C, which is generally reported as the melting point. Most of the studies reported in the literature are based on previously sintered (ie, melted and recrystallized) polymer; very little work is reported on the virgin polymer. Melting is accompanied by a volume increase of ca 30%. Because the viscosity of the polymer at 380°C is 10 GPa·s (10^{11} P), the shape of the melt is stable. The melting point increases with increasing applied pressure at the rate of 1.52°C/MPa (0.154°C/atm) (70).

Virgin PTFE has a crystallinity in the range of 92–98%, which indicates an unbranched chain structure. The fluorine atoms are too large to allow a planar zigzag structure, which would permit chain flexibility; therefore the chains are rigid (71). Electron micrographs and diffraction patterns (72) of PTFE dispersion particles indicate that the rod-like particles present in virgin PTFE dispersions are fully extended chain crystals containing few defects. The spherical particles appear to be composed of similar rod-like entities that are wrapped around themselves in a more or less random fashion.

Between 50 and 300°C, PTFE obeys the relationship between stress τ and the apparent shear rate γ: $\tau = K\gamma^{1/4}$. Melting of PTFE begins near 300°C. Above this temperature, the shear stress at constant shear rate increases and the rheological exponent rises from 0.25 to 0.5 at the final melting point (73).

Transitions. Transitions observed by various investigators (74–80), their interpretation, and the modes of identification are shown in Table 2. Besides the transition at the melting point, the transition at 19°C is of great consequence because it occurs at ambient temperature and significantly affects the product behavior. Above 19°C, the triclinic pattern changes to a hexagonal unit cell. Around 19°C, a slight untwisting of the molecule from a 180° twist per 13 CF_2 groups to a 180° twist per 15 CF_2 groups occurs. At the first-order transition at 30°C, the

Table 2. Transitions in Polytetrafluoroethylene

Temperature, °C	Region affected	Technique	Reference
1st order			
19	Crystalline, angular, displacement causing, disorder	Thermal methods, x ray, nmr	75
30	Crystalline, crystal disordering	Thermal methods, x ray, nmr	75
90 (80 to 110)	Crystalline	Stress relaxation, Young's modulus, dynamic methods	78
2nd order			
−90 (−110 to −73)	Amorphous, onset of rotational motion around C—C bond	Thermal methods, dynamic methods	79
−30 (−40 to −15)	Amorphous	Stress relaxation, thermal expansion, dynamic methods	78
130 (120 to 140)	Amorphous	Stress relaxtion, Young's modulus, dynamic methods	78

hexagonal unit cell disappears and the rod-like hexagonal packing of the chains in the lateral direction is retained. Below 19°C there is almost perfect three-dimensional order; between 19 and 30°C, the chain segments are disordered; and above 30°C, the preferred crystallographic direction is lost and the molecular segments oscillate above their long axes with a random angular orientation in the lattice.

The dynamic mechanical properties of PTFE have been measured at frequencies from 0.033 to 90 Hz. Abrupt changes in the distribution of relaxation times are associated with the crystalline transitions at 19 and 30°C (81). The activation energies are 102.5 kJ/mol (24.5 kcal/mol) below 19°C, 510.4 kJ/mol (122 kcal/mol) between the transitions, and 31.4 kJ/mol (7.5 kcal/mol) above 30°C.

Polytetrafluorothylene transitions occur at specific combinations of temperature and mechanical or electrical vibrations. Transitions, sometimes called *dielectric relaxations*, can cause wide fluctuations in the dissipation factor.

Mechanical Properties. Mechanical properties of PTFE depend on processing variables, eg, preforming pressure, sintering temperature and time, cooling rate, void content, and crystallinity. Properties, such as the coefficient of friction, flexibility at low temperatures, and stability at high temperatures, are relatively independent of fabrication. Molding and sintering conditions affect flex life, permeability, stiffness, resiliency, and impact strength. The physical properties of PTFE have been reviewed and compiled (82–84) (Table 3).

A marked change in volume of 1.0–1.8% is observed for PTFE in the transition zone from 18 to 25°C. An article that has been machined on either side of this zone changes dimensions when passing through the transition zone; hence, the final operating temperature of a precision part must be accurately determined.

Table 3. Typical Mechanical Properties of Molded and Sintered PTFE Resins[a]

Property	Granular resin	Fine powder	ASTM method
Tensile strength at 23°C, MPa[b]	7–28	17.5–24.5	D638-61T
Elongation at 23°C, %	100–200	300–600	D628-61T
Flexural strength at 23°C, MPa[b]	Does not break		D790-61
Flexural modulus at 23°C, MPa[b]	350–630	280–630	D747-61T
Impact strength, J/m[c]			
at 21°C	106.7		D256–56
at 24°C	160		
at 77°C	>320		
Hardness durometer, D	50–65	50–65	D1706-59T
Compression stress, MPa[b]			
at 1% deformation at 23°C	4.2		D695-52T
at 1% offset at 23°C	7.0		D695-52T
Coefficient of linear thermal expansion 12×10^{-5} per °C, 23–60°C	12×10^{-5}		D696-44
Thermal conductivity, 4.6-mm thickness, W/(m·K)	0.24		Cenco-Fitch
Deformation under load, at 26°C, 24 h, %			D621-59
6.86 MPa[b]		2.4	
13.72 MPa[b]	15		
Water absorption, %	< 0.01	< 0.01	D570-54T
Flammability	Nonflammable		D635-56T
Static coefficient of friction with polished, steel	0.05–0.08		

[a] Ref. 83.
[b] To convert MPa to psi, multiply by 145.
[c] To convert J/m to ft·lbf/in., divide by 53.38.

Articles fabricated of PTFE resins exhibit high strength, toughness, and self-lubrication at low temperatures. They are useful from 5 K and are highly flexible from 194 K. They tend to return to their original dimensions after a deformation. At sintering temperature, they rapidly recover their original shapes. For most applications no special precautions are necessary because decomposition rates below the recommended maximum service temperature of 260°C are very low. Impact strength is excellent over a wide range of temperatures. Static friction decreases with an increase in load. Static coefficient of friction is lower than the dynamic coefficient and therefore reduces stick–slip problems.

The surface of PTFE articles is slippery and smooth. Liquids with surface tensions below 18 mN/m (=dyn/cm) are spread completely on the PTFE surface; hence, solutions of various perfluorocarbon acids in water wet the polymer (85). Treatment with alkali metals promotes the adhesion between PTFE and other substances (86) but increases the coefficient of friction (87).

Filled Resins. Filled compositions meet the requirements of an increased variety of mechanical, electrical, and chemical applications. Physical properties of filled granular compounds are shown in Table 4 (88,89).

Table 4. Properties of Filled PTFE Compounds[a]

Property	Unfilled	Glass fiber, wt%		Graphite, 15 wt%	Bronze, 60 wt%
		15	25		
Specific gravity	2.18	2.21	2.24	2.16	3.74
Tensile strength, MPa[b]	28	25	17.5	21	14
Elongation, %	350	300	250	250	150
Stress at 10% elongation, MPa[b]	11	8.5	8.5	11	14
Thermal conductivity, mW/(m·K)	0.244	0.37	0.45	0.45	0.46
Creep modulus, kN/m[c]	2	2.21	2.1	3.4	6.2
Hardness durometer, Shore D	51	54	57	61	70
Izod impact, J/m[d]	152	146	119		
PV[e] for 0.13-mm radial wear in 1000 h, unlubricated, (kPa·m)/s[f]	0.70	106	177	52	281
Wear factor, 1/Pa[g]	5×10^{-14}	28×10^{-17}	26×10^{-17}	100×10^{-17}	12×10^{-17}
Coefficient of friction					
static, 3.4 MPa[b] load	0.08	0.13	0.13	0.10	0.10
dynamic at PV[e] = 172 (kPa.m)/s[f]		0.15–0.24	0.17	0.15	0.15
V = 900 m/s	0.01		−0.24	−0.18	−0.22

[a] Ref. 88.
[b] To convert MPa to psi, multiply by 145.
[c] To convert kN/m to lbf/in., divide by 0.175.
[d] To convert J/m to ftlbf/in., divide by 53.38.
[e] PV = pressure × velocity.
[f] To convert kPa to psi, multiply by 0.145.
[g] To convert 1/Pa to (in.^{3}·min)/(ft·lbf·h), divide by 2×10^{-7}.

Chemical Properties. Vacuum thermal degradation of PTFE results in monomer formation. The degradation is a first-order reaction (90). Mass spectroscopic analysis shows that degradation begins at ca 440°C, peaks at 540°C, and continues until 590°C (91).

Radiation Effects. Polytetrafluoroethylene is attacked by radiation. In the absence of oxygen, stable secondary radicals are produced. An increase in stiffness in material irradicated in vacuum indicates cross-linking (92). Degradation is due to random scission of the chain; the relative stability of the radicals in vacuum protects the materials from rapid deterioration. Reactions take place in air of oxygen and accelerated scission and rapid degradation occur.

Crystallinity has been studied by x-ray irradiation (93). An initial increase caused by chain scission in the amorphous phase was followed (above 3 kGy or 3×10^5 rad) by a gradual decrease associated with a disordering of the crystallites. The amorphous component showed a maximum of radiation-induced broadening in the nmr at 7 kGy (7×10^5 rad).

In air, PTFE has a damage threshold of 200–700 Gy (2×10^4–7×10^4 rad) and retains 50% of initial tensile strength after a dose of 10^4 Gy (1 Mrad), 40% of initial tensile strength after a dose of 10^5 Gy (10^7 rad), and ultimate elongation of 100% or more for doses up to 2–5 KGy ($2\times10^5 - 5\times10^5$ rad). During irradiation, resistivity decreases, whereas the dielectric constant and the dissipation factor increase. After irradiation, these properties tend to return to their preexposure values. Dielectric properties at high frequency are less sensitive to radiation than are properties at low frequency. Radiation has very little effect on dielectric strength (94).

Absorption, Permeation, and Interactions. Polytetrafluoroethylene is chemically inert to industrial chemicals and solvents even at elevated temperatures and pressures (95). This compatibility is due to the strong interatomic bonds, the almost perfect shielding of the carbon backbone by fluorine atoms, and the high molecular weight of the polymer. Under some severe conditions PTFE is not compatible with certain materials. It reacts with molten alkali metals, fluorine, strong fluorinating agents, and sodium hydroxide above 300°C. Shapes of small cross section burn vertically upward after ignition in 100% oxygen. Because gases may be evolved, the weight loss during sintering of a blend of PTFE and white asbestos is many times greater than loss from pure PTFE. Finely divided aluminum and magnesium thoroughly mixed with finely divided PTFE react vigorously after ignition or at high temperatures.

Absorption of a liquid is usually a matter of the liquid dissolving in the polymer; however, in the case of PTFE, no interaction occurs between the polymer and other substances. Submicroscopic voids between the polymer molecules provide space for the material absorbed, which is indicated by a slight weight increase and sometimes by discoloration. Common acids or bases are not absorbed up to 200°C. Aqueous solutions are scarcely absorbed at atmospheric pressure. Even the absorption of organic solvents is slight, partially resulting from the low wettability of PTFE. Since absorption of chemicals or solvents has no substantial effect on the chemical bond within the fluorocarbon molecule, absorption should not be confused with degradation; it is a reversible physical process. The polymer does not suffer loss of mechanical or bulk electrical properties unless subjected to severely fluctuating conditions.

Dynamic mechanical measurements were made on PTFE samples saturated with various halocarbons (96). The peaks in loss modulus associated with the amorphous relaxation near −90°C and the crystalline relaxation near room temperature were not affected by these additives. An additional loss peak appeared near −30°C, and the modulus was reduced at all higher temperatures. The amorphous relaxation that appears as a peak in the loss compliance at 134°C is shifted to 45–70°C in the swollen samples.

The sorption behavior of perfluorocarbon polymers is typical of nonpolar partially crystalline polymers (97). The weight gain strongly depends on the solubility parameter. Little sorption of substances such as hydrocarbons and polar compounds occurs.

As an excellent barrier resin, PTFE is widely used in the chemical industry. However, it is a poor barrier for fluorocarbon oils because similarity in the chemical composition of a barrier and a permeant increases permeation. Most liquids and gases (other than fluorocarbons) do not permeate highly crystalline PTFE. Permeabilities at 30°C [in 10^{15} × mol/(m·s ·Pa)] are as follows: CO_2, 0.93; N_2, 0.18; He, 2.47; anhydrous HCl, <0.01.

Gases and vapors diffuse through PTFE more slowly than through most other polymers (Table 5). The higher the crystallinity, and the less space between polymer molecules, the slower the permeation. Voids greater than molecular size cause an increase in permeability. However, the permeability of the finished article can be controlled by molding the resin to low porosity and high density. The optimum specific gravity for low permeability and good flexural properties is 2.16–2.195. Permeability increases with temperature as a result of the increase in activity of the solvent molecules and because of the increase in vapor pressure of the liquids. Swelling of PTFE resins and film is very low.

Electrical Properties. Polytetrafluoroethylene is an excellent electrical insulator because of its mechanical strength and chemical and thermal stability, as well as excellent electrical properties (Table 6).

Table 5. Permeability of PTFE Resin to Vapors

	Permeability constant[a,b], × 10^{15} mol/(m·s·Pa)	
Permeant	23°C	30°C
Benzene	1.81	2.93
Carbon tetrachloride	0.13	
Ethanol	1.88	
HCL, 20%	<0.71	
Piperidine	0.96	
H_2SO_4, 98%	54.20	
Water		20.70

[a]Ref. 95. Test method ASTM E96-35T (at vapor pressure; for 25.4-μm film thickness). Values are averages only and not for specification purposes.

[b]Original data converted to SI units using vapor pressure data from Ref. 98.

Table 6. Electrical Properties of Polytetrafluoroethylene[a]

Property	Granular	Fine powder	ASTM method
Dielectric strength, short time, 2-mm thickness, V/mm	23,600	23,600	D149-55T
Surface arc-resistance, s	>300	>300	D495-55T
Volume resistivity, Ω·cm	$>10^{18}$	$>10^{18}$	D257-57T
Surface resistivity at 100% Rh, Ω/sq	$>10^{16}$		D257-57T
Dielectric constant, at 60 to 2×10^9 Hz	2.1	2.1	D150-59T
Dissipation factor, at 60 to 2×10^9 Hz	0.0003		D150-59T

[a]Ref. 83.

It does not absorb water and volume resistivity remains unchanged even after prolonged soaking. The dielectric constant remains constant at 2.1 for a temperature range of −40 to 250°C and a frequency range of 5–10 GHz.

Articles fabricated according to standard practice should have dielectric constants in the range of 2.05±0.5 when tested at room temperature (RT). The dielectric constant varies with density and factors that affect density. Machined components can be fabricated to a predetermined dielectric constant by controlling the rod density during processing by adjusting the preforming pressure on the resin and cooling after sintering. The dielectric constant and the density have a linear relationship. Predictable variations in the dielectric constant result from density changes that accompany thermal expansion occuring with increasing temperature. The dielectric constant did not change over two to three years of measurements.

The dissipation factor (the ratio of the energy dissipated to the energy stored per cycle) is affected by the frequency, temperature, crystallinity, and void content of the fabricated structure. At certain temperatures and frequencies, the crystalline and amorphous regions become resonant. Because of the molecular vibrations, applied electrical energy is lost by internal friction within the polymer, which results in an increase in the dissipation factor. The dissipation factor peaks for these resins correspond to well-defined transitions, but the magnitude of the variation is minor as compared to other polymers. The low temperature transition at −97°C causes the only meaningful dissipation factor peak. The dissipation factor has a maximum of 10^8–10^9 Hz at RT; at high crystallinity (93%) the peak at 10^8–10^9 Hz is absent.

As crystallinity increases, the internal molecular friction and the dissipation factor decrease. Voids reduce the dissipation factor in proportion to the percentage of microvoids present. Certain extruded shapes utilize air to reduce the effective dielectric constant and dissipation factor of a coaxial cable. The dielectric strength of these resins is high and is unaffected by thermal aging at 200°C. Frequency has a marked effect on the dielectric strength because corona discharge becomes more continuous as frequency increases. If the voltage stress is not high enough to cause corona ignition, a very long dielectric life is anticipated at any frequency. Corona discharges on the surface or in a void initiate dielectric breakdown (99). Surface arc resistance of these resins is high and not affected by heat aging. The resins do not track or form a carbonized conducting path when subjected to a surface arc in air. Polytetrafluoroethylene resins are capable of continuous service up to 260°C

and can withstand much higher temperatures for limited periods of time. They do not melt or flow and retain some strength even in the gel state which begins at 327°C.

Fabrication

Granular Resins. These resins are sold in different forms; an optimum balance between handleability and product properties is desired. A free-flowing resin is used in small and automatic moldings. A finely divided resin is more difficult to handle but it distributes evenly in large moldings and has superior properties in sintered articles; it is used for large billet- and sheet-molding operations. A presintered resin with low crystallinity and superior handleability is highly suitable for ram extrusion.

Virgin PTFE melts at about 342°C; viscosity, even at 380°C, is 10 GPa·s (10^{11} P). This eliminates processing by normal thermoplastic techniques, and other fabrication techniques had to be developed: the dry powder is compressed into handleable form by heating above the melting point. This coalesces the particles into a strong homogeneous structure; cooling at a controlled rate achieves the desired degree of crystallinity.

Molding. Many PTFE manufacturers give detailed descriptions of molding equipment, and procedures are presented in Reference 100. Round piston molds for the production of solid or hollow cylinders are the most widely used. Because preforming usually takes place below 100°C, carbon steel is a suitable material of construction. The compression ratio (ie, the bulk volume of the powder to the specific volume of the unsintered molding) for granular resins is 3:1 to 6:1. The powder should be evenly distributed and leveled in the mold, and to ensure adequate compression uniformly throughout the preform, maximum pressure should be maintained for a sufficient length of time, and then be released slowly.

Automatic molding permits high speed mass production and can be effective. Automatic presses can be operated mechanically, pneumatically, or hydraulically. The mold is filled by means of a special metering system from a storage hopper containing a free-flowing resin. Loading buckets that shuttle back and forth over the single-cavity mold are also used. Because automatic molding requires short cycles, the powder is usually compressed at high speed with a high preform pressure. Small articles such as rings, bushings, washers, gaskets, and ball-valve seats can be molded by this technique.

Isostatic molding allows uniform compression from all directions. A flexible mold is filled with a free-flowing granular powder and evacuated, tightly sealed, and placed in an autoclave containing a liquid that can be raised to the pressure required for performing. The moldings require subsequent finishing because close tolerance cannot be achieved.

Sintering. Electrical ovens with air circulation and service temperatures up to 400°C are satisfactory for sintering. In free sintering—the cheapest and most widely used process—a preformed mold is placed in an oven with a temperature variation of ±2°C. In pressure sintering, the preform is not removed from the mold; instead the mold containing the preform is heated in an oven until the sintering temperature is reached. During sintering and cooling, the mold

is again placed under pressure but lower than the preform pressure. Pressure-sintered products have internal stresses that can be relieved by subsequent annealing. In the pressure-cooling process, pressure is applied on the molded article after it has reached sintering temperature and is maintained throughout the cooling period. The final product has a lower void content than the free-sintered mold.

To improve homogenity, the preformed article is heated to 370–390°C. The time required for heating and sintering depends on the mold dimensions; cooling, which affects the crystallinity and product properties, should be slow.

Free-sintered articles do not have the same dimensions as the mold cavity because they shrink at right angles to the direction of the preform pressure and grow in the direction of the applied pressure.

For processing after sintering, in the least expensive method for sintered PTFE tape or sheet, a large billet is skived on a lathe after it has been sintered and cooled. High precision articles are machined from ram-extruded rods.

Articles that are too complicated to be made by machining are made by coining. A sintered molding is heated to its melting point, transferred to a mold, and quickly deformed at low pressure, where it is held until it has cooled sufficiently to retain the improved shape. However, the coined molding, if reheated to a high temperature, returns to its original shape, and hence there is a limit on the maximum temperature to which coined moldings can be heated.

Ram Extrusion. Compression molding is not suitable for the manufacture of continuous long moldings such as pipes or rods. In ram extrusion, a small charge of PTFE powder is preformed by a reciprocating ram and sintered. Subsequent charges are fused into the first charge, and this process continues to form homogeneous long rods (101). The die tube, which is made of a corrosion-resistant material, is heated by resistance heating. Good temperature control is essential, and the melted and compacted powder must not pass any constrictions in its path. Thermal expansion and friction produce great resistance to movement, and as a result, a considerable force is required to push the polymer through the tube. A high quality surface finish on the inside of the tube reduces the pressure. If adequate bond strength between successive charges is not developed, the extrudate may break at the interface (poker chipping). Free-flowing powders and presintered resins are preferred for ram extrusion. Ram-extruded rods are used for automatic screw machining. Tubing is used as pipe liners or stock from which seals, gaskets, and bellows are machined.

Fine Powder Resins. Fine powder PTFE resins are extremely sensitive to shear. They must be handled gently to avoid shear, which prevents processing. However, fine powder is suitable for the manufacture of tubing and wire insulation for which compression molding is not suitable. A paste-extrusion process may be applied to the fabrication of tubes with diameters from fractions of a millimeter to about a meter, walls from thicknesses of 100–400 μm, thin rods with up to 50-mm diameters, and cable sheathing. Calendering unsintered extruded solid rods produces thread-sealant tape and gaskets.

The paste-extrusion process includes the incorporation of ca 16–25 wt% of the lubricant (usually a petroleum fraction); the mixture is rolled to obtain uniform lubricant distribution. This wetted powder is shaped into a preform at low pressure (2.0–7.8 MPa or 19–77 atm), which is pushed through a die mounted

in the extruder at ambient temperature. The shear stress exerted on the powder during extrusion confers longitudinal strength to the polymer by fibrillation. The lubricant is evaporated and the extrudate is sintered at ca 380°C.

The exact amount of lubricant required for extrusion depends on the design of the extruder, the reduction ratio (ie, ratio of the cross-sectional preform area to the cross-sectional area in the die), and the quality of the lubricant. A low lubricant content results in a high extrusion pressure, whereas a high lubricant content causes a poor coalescence and generates defects in the extrudate.

Fine powder resins can be colored with pigments that can withstand the sintering temperature. The pigment should be thoroughly mixed with the powder by rolling the mixture before adding the lubricant. Detailed design parameters of the paste extruder are given in References 100, 102 and 103.

The extrudate is dried and sintered by passing it through a multistage oven located immediately after the extruder. Pipes and rods may be heated up to 380°C. The throughput rate depends on the length of the sintering oven. Residence time varies from a few seconds for thin-walled insulations on a wire to a few minutes for large diameter tubing. For short residence times temperatures may be as high as ca 480°C. The extrusion pressure depends on the reduction ratio, the, extrusion rate, the lubricant content, and the characteristics of the extruder.

To produce unsintered tape by paste extrusion, the fine powder is lubricated and preformed according to the procedure described earlier. The preform is extruded in the form of rods, which are calendered on hot rolls to the desired width and thickness. (104).

Different resins have been developed for use in different reduction–ratio application ranges (105,106). The powders suitable for high reduction–ratio applications, such as wire coatings, are not necessarily suitable for the medium reduction–ratio applications, such as tubings, or the low reduction–ratio applications, such as thread-sealant tapes or pipe liners. Applications and processing techniques are being used, which utilize the unique combination of properties offered by PTFE in fine powder form (107–109).

Dispersion Resins. Polytetrafluoroethylene dispersions in aqueous medium contain 30–60 wt% polymer particles and some surfactant. The type of surfactant and the particle characteristics depend on the application. These dispersions are applied to various substrates by spraying, flow coating, dipping, coagulating, or electrodepositing (110).

Aqueous dispersion is sprayed on metal substrates to provide chemical resistance, nonstick, and low friction properties. The coated surface is dried and sintered. Impregnation of fibrous or porous materials with these dispersions combines the properties of the materials with those of PTFE. Some materials require only a single dipping, eg, asbestos. The material is usually dried after dipping. For high pressure sealing applications, sintering at 380–400°C increases strength and dimensional stability. For film castings, the dispersion is poured on a smooth surface; the formed film is dried and sintered and peeled from the supporting surface.

Aqueous dispersions are used for spinning PTFE fibers. The dispersion is mixed with a matrix-forming medium (111,112) and forced through a spinneret

into a coagulating bath. The matrix material is removed by heating and the fibers are sintered and drawn molten to develop their full strength.

Effects of Fabrication on Physical Properties of Molded Parts. The physical properties are affected by molecular weight, void content, and crystallinity. Molecular weight can be reduced by degradation but not increased during processing. These factors can be controlled during molding by the choice of resin and fabricating conditions. Void distribution (or size and orientation) also affects properties; however, it is not easily measured.

Preforming primarily affects void content, sintering controls molecular weight, and cooling determines crystallinity. Voids caused by insufficient consolidation of particles during preforming may appear in the finished articles. Densities below 2.10 g/cm^3 indicate a high void content. Electrical and chemical applications require a minimum density of 2.12–2.14 g/cm^3. Particle size, shape, and porosity are also important in determining void content. Although void content is determined largely by particle characteristics and preforming conditions, sintering conditions can also have an effect. Temperatures too high or too low increase void content. Excessively high sintering temperature can decrease the molecular weight. The final crystallinity of a molding depends on the initial molecular weight of the polymer, the rate of cooling of the molding, and to a lesser extent on sintering conditions. The degree of crystallinity of moldings is affected by the cooling or annealing conditions.

Flexural modulus increases by a factor of 5 as crystallinity increases from 50 to 90% with a void content of 0.2%; however, recovery decreases with increasing crystallinity. Therefore, the balance between stiffness and recovery depends on the application requirements. Crystallinity is reduced by rapid cooling but increased by slow cooling. The stress-crack resistance of various PTFE insulations is correlated with the crystallinity and change in density due to thermal mechanical stress (113).

Applications

Consumption of PTFE increases continuously as new applications are being developed. Electrical applications consume half of the PTFE produced; mechanical and chemical applications share equally the other half. Various grades of PTFE and their applications are shown in Table 7.

Electrical Applications. The largest application of PTFE is for hookup and hookup-type wire used in electronic equipment in the military and aerospace industries. Coaxial cables, the second largest application, use tapes made from fine powder resins and some from granular resin. Interconnecting wire applications include airframes. Other electrical applications include computer wire, electrical tape, electrical components, and spaghetti tubing.

Mechanical Applications. Seals and piston rings, basic shapes, and antistick uses constitute two-thirds of the resin consumed in mechanical applications. Bearings, mechanical tapes, and coated glass fabrics also consume a large amount of PTFE resins. Seals and piston rings, bearings, and basic shapes are manufactured from granular resins, whereas the dispersion is used for glass–fabric coating

Table 7. Applications of Polytetrafluoroethylene Resins

Resin grade	Processing	Description	Main uses
Granular			
Agglomerates	Molding, preforming, sintering, ram extrusion	Free-flowing powder	Gaskets, packing, seals, electronic componenets, bearings, sheet, rod, heavy-wall tubing; tape and molded shapes for nonadhesive applications
Coarse	Molding, preforming, sintering	Granulated powder	Tape, molded shapes, nonadhesive applications
Finely divided	Molding, preforming, sintering	Powder for highest quality, void-free moldings	Molded sheets, tape wire wrapping, tubing, gaskets
Presintered	Ram extrusion	Granular, free-flowing powder	Rods and tubes
Fine powder			
High reduction ratio	Paste extrusion	Agglomerated powder	Wire coating, thin-walled tubing
Medium reduction ratio	Paste extrusion	Agglomerated powder	Tubing, pipe, overbraided hose, spaghetti tubing
Low reduction ratio	Paste extrusion	Agglomerated powder	Thread-sealant tape, pipe liners, tubing, porous structures
Dispersion			
General purpose	Dip coating	Aqueous dispersion	Impregnation, coating, packing
Coating	Dip coating	Aqueous dispersion	Film, coating
Stabilized	Coagulation	Aqueous dispersion	Bearings

and antistick applications. Most pressure-sensitive mechanical tapes are made from granular resins.

Chemical Applications. The chemical processing industry uses large amounts of granular and fine powder PTFE. Soft packing applications are manufactured from dispersions, and hard packings are molded or machined from stocks and shapes made from granular resin.

Overbraided hose liners are made from fine powder resins by paste extrusion, and thread-sealant tapes are produced from fine powder by calendering. Fabricated gaskets are made from granular resins and pipe liners are produced from fine powder resins. Fibers and filament forms are also available.

Highly porous fabric structures, eg, Gore-Tex, that can be used as membranes have been developed by exploiting the unique fibrillation capability of dispersion-polymerized PTFE (107).

Micropowders

The PTFE micropowders, also called waxes, are TFE homopolymers with molecular weights significantly lower than that of normal PTFE (114). The molecular weight for micropowders varies from 2.5×10^4 to 25×10^4, whereas that of normal PTFE is of the order of 10×10^6. Micropowders are generally white in color and are friable. The average agglomerate particle size is between 5 and 10 μm and is composed of smaller, "as polymerized" primary particles which are approximately 0.2 μm in diameter. The dsc curves of lower molecular weight micropowder show a higher heat of crystallization and melting (second heating) than normal PTFE. This is due to the higher crystallinity of the micropowder.

The production of micropowders involves the scission of the high molecular weight PTFE chain by gamma or electron beam irradiation at a variety of dosage levels. An increase in dosage reduces the molecular weight. The irradiated low molecular weight material is ground to a particle size ranging from 1 to 25 μm in the final product.

Economic Aspects

Polytetrafluoroethylene homopolymers are more expensive than most other thermoplastics because of high monomer refining costs. For extremely high molecular weights, ingredients and manufacturing process must be free of impurities, which increases costs. In the United States, the 2000 list prices from primary producers were between $15.2/kg and $20.4/kg, depending on the resin type. For example, granular PTFE resins cost $15.2–20.4/kg supplied in 45.45-kg containers. The coagulated fine powders cost $23.2–30.3/kg packaged in 45.45-kg containers. Formulated dispersions are $21.9–35.4/kg in 19- or 113-L containers. Although fine powder sales have increased in recent years, the sales of granular PTFE are the highest on a worldwide basis. Most of the resin is consumed in the United States (ca 9000 t in 1991), followed by Europe and Japan.

Testing and Standards

A description of PTFE resins and their classification are given in ASTM D1457-83. A comprehensive listing of industrial and military specifications covering mechanical, electrical, and chemical applications of PTFE can be found in Reference 115.

Health and Safety

Exposure to PTFE can arise from ingestion, skin contact, or inhalation. The polymer has no irritating effect to the skin, and test animals fed with the sintered polymer have not shown adverse reactions. Dust generated by grinding the resin also has no effect on test animals. Formation of toxic products is unlikely. Only the heated polymer is a source of a possible health hazard (116,117).

Because PTFE resins decompose slowly, they may be heated to a high temperature. The toxicity of the pyrolysis products warrants care where exposure of personnel is likely to occur. Above 230°C decomposition rates become measurable (0.0001% per hour). Small amounts of toxic perfluoroisobutylene have been isolated at 400°C and above; free fluorine has never been found. Above 690°C the decomposition products burn but do not support combustion if the heat is removed. Combustion products consist primarily of carbon dioxide, carbon tetrafluoride, and small quantities of toxic and corrosive hydrogen fluoride. The PTFE resins are nonflammable and do not propagate flame.

Prolonged exposure to thermal decomposition products causes so-called polymer fume fever, a temporary influenza-like condition. It may be contracted by smoking tobacco that has been contaminated with the polymer. It occurs several hours after exposure and passes within 36–48 h; the temporary effects are not cumulative.

Large quantities of PTFE resins have been manufactured and processed above 370°C. In various applications they are heated above the recommended use temperatures. No cases of serious injury, prolonged illness, or death have been reported resulting from the handling of these resins. However, when high molecular weight PTFE is converted to micropowder by thermal degradation, highly toxic products result.

Micropowders are added to a wide variety of material used in industry, where they provide nonstick and sliding properties (111). They are incorporated into the product by blending and grinding. To disperse well, the powder must have good flow properties. Conditions that make the powder sticky should be avoided.

The PTFE micropowders are commonly used in plastics, inks, lubricants, and finishes such as lacquer. Lubricants containing micropowders are used for bearings, valve components, and other moving parts where sliding friction must be minimized or eliminated. Nonstick finished that require good release properties, for example, in the food and packaging industry, commonly use PTFE micropowders.

In some applications the high heat stability of the micropowder can be utilized over a reasonably wide temperature range. A maximum service

temperature is normally 260°C, provided the crystalline melting point is between 320 and 335°C. Exposure above 300°C leads to degradation and possible evolution of toxic decomposition products.

The particulate morphology of PTFE micropowder in printing inks provides desirable gloss to the printed product. Its inherent lubricity results in good wear and slip properties and surface smoothness. The chemical resistance of the micropowder is as high as that of high molecular weight PTFE. It is therefore used in applications requiring service in strong or corrosive chemical environments such as concentrated mineral acids and alkalies.

BIBLIOGRAPHY

"Tetrafluoreoethylene Polymers" in *EPST* 1st ed., Vol. 13, pp. 623–654, by D. I. McCane, E. I. du Pont de Nemours & Co., Inc.; "Tetrafluoroethylene Polymers, Polytetrafluoroethylene (homopolymer)" in *EPSE* 2nd ed., Vol. 16, pp. 577–600, by S. V. Gangal, E. I. du Pont de Nemours & Co., Inc.

1. U.S. Pat. 2230654 (Feb. 4, 1941), R. J. Plunkett (to Kinetic Chemicals, Inc.).
2. J. D. Park and co-workers, *Ind. Eng. Chem.* **39**, 354 (1947).
3. J. M. Hamilton, in M. Stacey, J. C. Tatlow, and A. G. Sharpe, eds., *Advances in Fluorine Chemistry*, Vol. **3**, Butterworth & Co., Ltd., Kent, U.K., 1963, p. 117.
4. J. W. Edwards and P. A. Small, *Nature* **202**, 1329 (1964); *Ind. Eng. Chem. Fundam.* **4**, 396 (1965).
5. F. Gozzo and C. R. Patrick, *Nature* **202**, 80 (1964).
6. Jpn. Pat. 6015353 (Oct. 14, 1960), M. Hisazumi and H. Shingu.
7. U.S. Pat. 2994723 (Aug. 1, 1961), O. Scherer and co-workers (to Farbewerke Hoechst).
8. Brit. Pat. 960309 (June 10, 1964), J. W. Edwards, S. Sherratt, and P. A. Small (to ICI).
9. U.S. Pat. 3459818 (Aug. 5, 1969), H. Ukahashi and M. Hisasne (to Asahi Glass Co.).
10. U.S. Pat. 5345013 (Sept. 6, 1994), D. J. Van Bramer, M. B. Shiflett, and A. Yokozeki (to E. I. du Pont de Nemours & Co., Inc.).
11. U.S. Pat. 2407405 (Sept. 10, 1946), M. A. Dietrich and R. M. Joyce (to E. I. du Pont de Nemours & Co., Inc.).
12. O. Ruff and O. Bretschneider, *Z. Anorg. Allg. Chem.* **210**, 173 (1933).
13. E. G. Locke, W. R. Brode, and A. L. Henne, *J. Am. Chem. Soc.* **56**, 1726 (1934).
14. O. Ruff and W. Willenberg, *Chem. Ber.* **73**, 724 (1940).
15. L. T. Hals, T. S. Reid, and G. H. Smith, *J. Am. Chem. Soc.* **73**, 4054 (1951); U.S. Pat. 2668864 (Feb. 9, 1954), (to Minnesota Mining and Manufacturing Co.).
16. U.S. Pat. 3009966 (Nov. 21, 1961), M. Hauptschein and A. H. Fainberg (to Pennsalt Chemical Corp.).
17. U.S. Pat. 3471546 (Oct. 7, 1969), G. Bjornson (to Phillips Petroleum Co.).
18. U.S. Pat. 3662009 (May 9, 1972), W. M. Hutchinson (to Phillips Petroleum Co.).
19. U.S. Pat. 3799996 (Mar. 26, 1974), H. S. Bloch (to Universal Oil Products).
20. E. E. Lewis and M. A. Naylor, *J. Am. Chem. Soc.* **69**, 1968 (1947).
21. U.S. Pat. 3832411 (Aug. 27, 1974), B. C. Arkles and R. N. Bonnett (to Liquid Nitrogen Processing Co.).
22. M. M. Renfrew and E. E. Lewis, *Ind. Eng. Chem.* **38**, 870 (1946).
23. H. C. Duus, *Ind. Eng. Chem.* **47**, 1445 (1955).

24. W. M. D. Bryant, *J. Polym. Sci.* **56**, 277 (1962).
25. A. Pajaczkowski and J. W. Spoors, *Chem. Ind.* **16**, 659 (1964).
26. Brit. Pat. 931587 (July 17, 1963), H. H. Gibbs and J. L. Warnell (to E. I. du Pont de Nemours & Co., Inc.).
27. U.S. Pat. 3159609 (Dec. 1, 1964), J. F. Harris Jr. and D. I. McCane (E. I. du Pont de Nemours & Co., Inc.).
28. F. S. Toby and S. Toby, *J. Phys. Chem.* **80**, 2313 (1976).
29. B. Atkinson and V. A. Atkinson, *J. Chem. Soc. Part II*, 2086 (1957).
30. U.S. Pat. 2946763 (July 26, 1960), M. I. Bro and B. W. Sandt (to E. I. du Pont de Nemours & Co., Inc.).
31. U.S. Pat. 3847881 (Nov. 12, 1974), M. Mueller and S. Chandrasekaran (to Allied Chemicals Co.).
32. U.S. Pat. 3528954 (Sept. 15, 1970), D. P. Carlson (to E. I. du Pont de Nemours & Co., Inc.).
33. U.S. Pat. 5760151 (June 2, 1998) R. Aten, C. W. Jones, and A. H. Olson (to E. I. du Pont de Nemours & Co., Inc.).
34. U.S. Pat. 3475391 (Oct. 28, 1969), J. N. Coker (to E. I. du Pont de Nemours & Co., Inc.).
35. U.S. Pat. 3846267 (Nov. 5, 1974), Y. Tabata and G. Kojima (to Japan Atomic Energy Research Institute).
36. U.S. Pat. 3467636 (Sept. 16, 1969), A. Nersasian (to E. I. du Pont de Nemours & Co., Inc.).
37. U.S. Pat. 3403191 (Sept. 24, 1968), D. P. Graham (to E. I. du Pont de Nemours & Co., Inc.).
38. U.S. Pat. 3404180 (Oct. 1, 1969), K. L. Cordes (to E. I. du Pont de Nemours & Co., Inc.).
39. U.S. Pat. 3567521 (Mar. 2, 1971), M. S. Toy and N. A. Tiner (to McDonnell Douglas).
40. U.S. Pat. 3446858 (May 27, 1969), H. Shingu and co-workers (to Daikin Kogyo Co.).
41. U.S. Pat. 3873630 (Mar. 25, 1975), N. E. West (to E. I. du Pont de Nemours & Co., Inc.).
42. U.S. Pat. 3855191 (Dec. 17, 1974), T. R. Doughty, C. A. Sperati, and H. Un (to E. I. du Pont de Memours & Co., Inc.).
43. U.S. Pat. 3655611 (Apr. 11, 1972), M. B. Mueller, P. O. Salatiello, and H. S. Kaufman (to Allied Chemicals Co.).
44. K. Hintzer and G. Lohn, in Scheirs, ed., *Modern Fluoropolymers*, John Wiley & Sons, New York, 1997.
45. U.S. Pat. 4189551 (Feb. 19, 1980), S. V. Gangal (to E. I. du Pont de Nemours & Co., Inc.).
46. U.S. Pat. 3419522 (Dec. 31, 1968), P. N. Plimmer (to E. I. du Pont de Nemours & Co., Inc.).
47. U.S. Pat. 3766133 (Oct. 16, 1973) R. Roberts and R. F. Anderson (to E. I. du Pont de Nemours & Co., Inc.).
48. Jap. Pat. WO9905203 (Feb. 4, 1999), A. Funaki and T. Takakura (to Asahi Glass Co., Ltd.).
49. Jap. Pat. WO9906475 (Feb. 11, 1999), M. Asano, M. Sukegawa, and M. Tsuji (to Daikin Industries, Ltd.).
50. U.S. Pat. 2612484 (Sept. 30, 1952), S. G. Bankoff (to E. I. du Pont de Nemours & Co., Inc.).
51. U.S. Pat. 4186121 (Jan. 29, 1980), S. V. Gangal (to E. I. du Pont de Nemours & Co., Inc.).
52. U.S. Pat. 4725644 (1988), S. Malhotra (to E. I. du Pont de Nemours & Co., Inc.).

53. T. Folda and co-workers, *Nature* **333**, 55 (1988).
54. B. Luhmann and A. E. Feiring, *Polymer* **30**, 1723 (1989).
55. B. Chu, C. Wu, and W. Buck, *Macromolecules* **22**, 831 (1989).
56. U.S. Pat. 4576869 (Mar. 18, 1986), S. C. Malhotra (to E. I. du Pont de Nemours & Co., Inc.).
57. U.S. Pat. 4363900 (Dec. 14, 1982), T. Shimizu and S. Koizumi (to Daikin Kogyo Co.).
58. U.S. Pat. 4766188 (Aug. 23, 1988), T. E. Attwood and R. F. Bridges (to ICI).
59. U.S. Pat. 4036802 (July 19, 1977), R. V. Poirier (to E. I. du Pont de Nemours & Co., Inc.).
60. U.S. Pat. 4129618 (Dec. 12, 1978), J. M. Downer, W. G. Rodway, and L. S. J. Shipp, (to ICI).
61. U.S. Pat. 4840998 (June 6, 1989), T. Shimizu and K. Hosokawa, (to Daikin Kogyo Co.).
62. U.S. Pat. 4879362 (Nov. 7, 1979), R. A. Morgan (to E. I. du Pont de Nemours & Co., Inc.).
63. U.S. Pat. 4342675 (Aug. 3, 1982), S. V. Gangal (to E. I. du Pont de Nemours & Co., Inc.).
64. U.S. Pat. 2478229 (Aug. 9, 1949), K. L. Berry (to E. I. du Pont de Nemours & Co., Inc.).
65. K. L. Berry and J. H. Peterson, *J. Am. Chem. Soc.* **73**, 5195 (1951).
66. R. C. Doban and co-workers, Paper Presented at *130th Meeting of the American Chemical Society*, Atlantic City, N.J., Sept. 1956.
67. C. A. Sperati and H. W. Starkweather, *Fortschr. Hochpolym. Forsch.* **2**, 465 (1961).
68. R. E. Moynihan, *J. Am. Chem. Soc.* **81**, 1045 (1959).
69. T. Suwa, M. Takehisa, and S. Machi, *J. Appl. Polym. Sci.* **17**, 3253 (1973).
70. P. L. McGeer and H. C. Duus, *J. Chem. Phys.* **20**, 1813 (1952).
71. C. W. Bunn, *J. Polym. Sci.* **16**, 332 (1955).
72. H. D. Chanzy, P. Smith, and J. Revol, *J. Polym. Sci. Polym. Lett. Ed.* **24**, 557 (1986).
73. H. W. Starkweather Jr., *J. Polym. Sci. Polym. Phys. Ed.* **17**, 73–79 (1979).
74. U.S. Pat. 4840998 (June 6, 1989), R. H. H. Pierce and co-workers, (to Daikin Kogyo Co.).
75. E. S. Clark, and L. T. Muus, Paper Presented at *133rd Meeting of the American Chemical Society*, New York, Sept. 1957.
76. E. S. Clark, Paper Presented at *Symposium on Helices in Macromolecular Systems*, Polytechnic Institute of Brooklyn, Brooklyn, N. Y., May 16, 1959.
77. C. A. Sperati, in J. Brandrup and E. H. Immergut, eds., *Polymer Handbook*, 2nd ed., John Wiley & Sons, Inc., New York, 1975, pp. V-29–36.
78. Y. Araki, *J. Appl. Polym. Sci.* **9**, 3585 (1965).
79. N. G. McCrum, *J. Polym. Sci.* **34**, 355 (1959).
80. E. S. Clark, *Polymer* **40**(16), 4659–4665 (1999).
81. H. W. Starkweather Jr., *Macromolecules* **19**, 2541 (1986).
82. J. T. Milek, A Survey Materials Report on PTFE Plastics, AD 607798, U. S. Department of Commerce, Washington, D.C., Sept. 1964.
83. Teflon Fluorocarbon Resins Mechanical Design Data, Bulletin, E. I. du Pont de Nemours & Co., Inc. Wilmington, Del., Sept. 1964.
84. *Teflon® PTFE Fluoropolymers Resin*, Properties Handbook, 22313D, E. I. du Pont de Nemours & Co., Inc., Wilmington, Del., July 1996.
85. M. K. Bernett and W. A. Zisman, *J. Phys. Chem.* **63**, 1911 (1959).

86. U.S. Pat. 2871144 (Jan. 27, 1959), R. C. Doban (to E. I. du pont de Nemours & Co., Inc.).
87. A. J. G. Allan and R. Roberts, *J. Polym. Sci.* **39**, 1 (1959).
88. Filled Compounds of Teflon® PTFE, Bulletin E-96215, E. I. du Pont de Nemours & Co., Inc., Wilmington, Del., Mar. 1989.
89. Teflon® Fluoropolymer, Technical Information, A Tribological Characterization of Teflon® PTFE compounds, Bulletin H-38205, E. I. du Pont de Nemours & Co., Inc., June 1992.
90. J. C. Siegle and co-workers, *J. Polym. Sci. Part A* **2**, 391 (1964).
91. G. P. Shulman, *Polym. Lett.* **3**, 911 (1965).
92. L. A. Wall and R. E. Florin, *J. Appl. Polym. Sci.* **2**, 251 (1959).
93. W. M. Peffley, V. R. Honnold, and D. Binder, *J. Polym. Sci.* **4**, 977 (1966).
94. *J. Teflon (DuPont)* **10**(1) (Jan.–Feb. 1969).
95. *J. Teflon (DuPont)* **11**(1) (Jan.–Feb. 1970).
96. H. W. Starkweather Jr., *Macromolecules* **17**, 1178 (1984).
97. H. W. Starkweather Jr., *Macromolecules* **10**, 1161 (1977).
98. D. W. Green, ed., *Perry's Chemical Engineers' Handbook*, 6th ed., McGraw-Hill Book Co., Inc., New York, 1984.
99. J. C. Reed, E. J. McMahon, and J. R. Perkins, *Insulation (Libertyville, III.)* **10**, 35 (1964).
100. S. Ebnesajjad, *Non-melt Processible Fluoroplastics*, Vol. **1**, Plastics Design Library, Division of William Andrew, Inc., 2000. Handbook Series.
101. Teflon® PTFE Fluoropolymer Resin, Ram Extrusion Processing Guide, Bulletin 213428B, E. I. du Pont de Nemours & Co., Inc., Sept. 1995.
102. Teflon® Fluoropolymer Resin, Processing Guide for Fine Powder Resins, Bulletin 190617D, E. I. du Pont de Nemours & Co., Inc., Dec. 1994.
103. Teflon® 62, Hose and Tubing, Bulletin H-11959, E. I. du Pont de Nemours & Co., Inc. Feb. 1991.
104. Teflon® PTFE, Thread Sealant Tape Processing Guide, Bulletin 198112B, E. I. du Pont de Nemours & Co., Inc., Nov. 1992.
105. U.S. Pat. 3142665 (July 28, 1964), A. J. Cardinal, W. L. Edens, and J. W. Van Dyk (to E. I. du Pont de Nemours & Co., Inc.).
106. U.S. Pat. 4038231 (July 26, 1977), J. M. Douner, W. G. Rodway, and L. S. J. Shipp (to ICI).
107. U.S. Pat. 3962153 (June 8, 1976), R. W. Gore (to W. L. Gore and Assoc.).
108. U.S. Pat. 3993584 (Nov. 23, 1976), J. E. Owen and J. W. Vogt (to Kewanee Oil Co.).
109. U.S. Pat. 3704171 (Nov. 28, 1972), H. P. Landi (to American Cyanamid Co.).
110. Teflon® PTFE, Dispersions Properties and Processing Techniques, Bulletin No. X-50G, E-55514-2, April 1983.
111. U.S. Pat. 3051545 (Aug. 28, 1962), W. Steuber (to E. I. du Pont de Nemours & Co., Inc.).
112. P. E. Frankenburg, *Ullmann's Encyclopedia of Industrial Chemistry*, 5th ed., Vol. **A-10**, VCH Publishing, Inc., New York, 1987, pp. 649, 650.
113. R. L. Baillie, J. J. Bednarczyk, and P. M. Mehta, Paper Presented at *35th International Wire and Cable Symposium*, Chery Hill, N.J., Nov. 18–20, 1986.
114. Zonyl® Fluoroadditives, Bulletin H-81712, E. I. du Pont de Nemours & Co., Inc., Sept. 1995.
115. *J. Teflon (Du Pont)* **8**, 6 (Nov. 1967).
116. *Teflon Occupational Health Bull.* **17**(2) (1962) (Published by Information Service Division, Deptartment of National Health and Welfare, Ottawa, Canada).

117. *Guide to the Safe Handling of Fluoropolymer Resins*, 3rd ed., Fluoropolymers Division of the Society of the Plastics Industry, Inc., Washington, D.C., 1998.

GENERAL REFERENCE

"Tetrafluoroethylene Copolymers with Ethylene" under "Fluorine Compounds, Organic" in *ECT* 4th ed., Vol. 11, pp. 657–671, S. V. Gangal, E. I. du Pont de Nemours & Co., Inc.

SUBHASH V. GANGAL
E. I. du Pont de Nemours & Co., Inc.

PERFLUORINATED POLYMERS, TETRAFLUOROETHYLENE–ETHYLENE COPOLYMERS

Introduction

Copolymers of ethylene [74-85-1] and tetrafluoroethylene [116-14-3] (ETFE) have been a laboratory curiosity for more than half a century. These polymers were studied in connection with a search for a melt-fabricable polytetrafluroethylene (PTFE) resin (1–5); interest in them fell with the discovery of TFE–HFP (FEP) copolymers (6). In the 1960s, however, it became evident that a melt-fabricable fluorocarbon resin was needed with higher strength and stiffness than those of PTFE resins. Earlier studies indicated that ETFE [11939-51-6] might have the right combination of properties. Subsequent research efforts (7) led to the introduction of modified ETFE polymer [25038-71-5] (Tefzel) by E. I. du Pont de Nemours & Co., Inc., in 1970.

Modified ETFE are the products of real commercial value because they have good tensile strength, moderate stiffness, high flex life, and outstanding impact strength, abrasion resistance, and cut-through resistance. Electrical properties include low dielectric constant, high dielectric strength, excellent resistivity, and low dissipation factor. Thermal and cryogenic performance and chemical resistance are good. These properties, combined with elasticity, make this material an ideal candidate for heat-shrinkable film and tubing. This family of copolymers can be processed by conventional methods such as melt extrusion, injection molding, transfer molding, and rotational molding. The properties of the copolymers vary with composition; polymers containing 40–90% TFE (by weight) soften between 200 and 300°C, depending on composition (1). The TFE segments of the molecules account for >75% of the weight of an approximately 1:1 mole

Encyclopedia of Polymer Science and Technology. Copyright John Wiley & Sons, Inc. All rights reserved.

ratio copolymer. The two monomers combine readily into a nearly 1:1 alternating structure. Such polymers exhibit a unique combination of mechanical, chemical, and electrical properties as well as excellent weatherability. However, thermal stress-crack resistance is poor. The copolymer can be modified with a termonomer that undergoes free-radical polymerization and does not cause undesirable chain transfer or termination during polymerization. The modified copolymer exhibits almost the identical physical, chemical, and electrical properties characteristic of the 1:1 alternating copolymer, but retains high ultimate elongation up to 200°C.

Ethylene and TFE are copolymerized in aqueous, nonaqueous, or mixed medium with free-radical initiators. The polymer is isolated and converted into extruded cubes, powders, and beads, or a dispersion. This family of products is manufactured by DuPont, Dyneon, Daikin, Asahi Glass, and Ausimont and sold under the trade names of Tefzel, Hostaflon ET, Neoflon EP, Aflon COP, and Halon ET, respectively. Additional information on specific manufacturers' products can often be obtained by consulting their internet web sites (for example, www.dupont.com/teflon).

Monomers

Tetrafluoroethylene of purity suitable for granular or dispersion polymerizations is acceptable for copolymerization with ethylene. Polymerization-grade ethylene is suitable for copolymerization with TFE. Modifying termonomers, eg, perfluorobutylethylene and perfluoropropylene, are incorporated by free-radical polymerization.

Manufacture

Tetrafluoroethylene–ethylene copolymers have tensile strengths two to three times as high as the tensile strength of PTFE or of the ethylene homopolymer (1). Because these copolymers are highly crystalline and fragile at high temperature, they are modified with a third monomer, usually a vinyl monomer free of telegenic activity. The termonomer provides the copolymer with side chains of at least two carbon atoms, such as perfluoroalkylvinyl or vinylidene compounds, perfluoroalkyl ethylenes, and perfluoroalkoxy vinyl compounds. For high tensile properties and cut-through resistance, a molar ratio of ethylene and TFE between 60:40 and 40:60 is required (8,9).

Copolymerization is effected by suspension or emulsion techniques under such conditions that TFE, but not ethylene, may homopolymerize. Bulk polymerization is not commercially feasible because of heat-transfer limitations and explosion hazard of the comonomer mixture. Polymerizations typically take place below 100°C and 5 MPa (50 atm). Initiators include peroxides, redox systems (10), free-radical sources (11), and ionizing radiation (12). Mixtures of inert solvent and water can be used, where the polymerization occurs in the solvent medium, while the water serves to lower the viscosity of the mixture and to remove the heat of polymerization (13,14).

Purely aqueous polymerization systems give copolymers that are not wetted by the reaction medium. The products agglomerate and plug valves, nozzles, and tubing, and adhere to stirrer blades, thermocouples, or reactor walls. These problems do not occur in organic media or mixtures of these with water.

Aqueous emulsion polymerization is carried out using a fluorinated emulsifier, a chain-transfer agent to control molecular weight, and dispersion stabilizers such as manganic acid salts and ammonium oxalate (15,16).

To obtain a 50:50 molar ratio of monomers in the polymer, a mixture of about 75:25 TFE to ethylene must be initially charged to the reactor, depending on reactor pressure and temperature. Reactivity ratios for this system have been studied (17,18). The effects of temperature, addition of termonomer, and ethylene/TFE ratio on degree of alternation and on molecular structure have been studied (19). Melting point of ETFE are higher than would be predicted based upon a linear relationship between polyethylene and PTFE melting points. ETFE is unique in this respect. All other common copolymers of TFE exhibit either linear or depressed melting points when compared to a line between the respective homopolymer melting point and that of PTFE. This positive melting point deviation occurs from about 35:65 to 65:35 mole ratios and is at a maximum at the 50:50 alternating copolymer, which melts at about 285°C, compared to about 235°C for the 65:35 TFE/ethylene composition. Melting points are lowered by the incorporation of modifier, but the overall shape of a curve of the positive melting point deviation is unaltered. The ability of adjacent chains to interpenetrate is thought to be responsible for this behavior. For the same reason, stiffness follows a similar positive deviation, also reaching a maximum at the 50:50 composition. Reactivity ratios of ethylene and TFE are as follows:

Temperature, °C	$r(C_2F_4)$	$r(C_2H_4)$
−35	0.014 ± 0.008	0.010 ± 0.02
65	0.045 ± 0.010	0.14 ± 0.03

These values indicate strong alternation tendencies that decrease with increasing temperature. Computations show that 1:1 ETFE obtained at −30 and 65°C should have about 97 and 93%, respectively, of alternating sequences (20).

Properties

The equimolar copolymer of ethylene and TFE is isomeric with poly(vinylidene fluoride) but has a higher melting point (21,22) and a lower dielectric loss (23,24). A copolymer with the degree of alternation of about 0.88 was used to study the structure (25). The unit cell was determined by x-ray diffraction (26,27). Despite irregularities in the chain structure and low crystallinity, a unit cell and structure was derived that gave a calculated crystalline density of 1.9 g/cm^3. The unit cell is believed to be orthorhombic or monoclinic ($a = 0.96$ nm, $b = 0.925$ nm, $c = 0.50$ nm; $\gamma = 96°$).

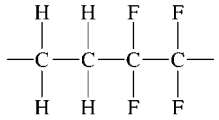

Ethylene–tetrafluoroethylene unit

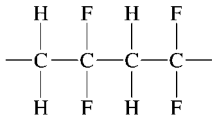

Poly(vinylidene fluoride) segment

The molecular conformation is that of extended zigzag. Molecular packing appears to be orthorhombic, each molecule having four nearest neighbors with the CH_2 groups of one chain adjacent to the CF_2 groups of the next. The x-ray spectrum of a 1:1 copolymer has two main peaks at $Z_0 = 19.63^\circ$ and $Z_0 = 21.00^\circ$, corresponding to Bragg distances of 0.45 and 0.42 nm, respectively. Compression-molded samples are 50–60% crystalline; however, crystallinity is greatly affected by composition, quench rate, and temperature.

Alternation is usually above 90%. Nearly perfect alternation of isomeric units in a ca 1:1 monomer ratio has been confirmed by infrared spectroscopy. Bands at 733 and 721 cm^{-1} have an intensity proportional to the concentration of $(CH_2)_n$ groups ($n = 4$ and <6, respectively) present in a copolymer containing 46 mol% TFE; intensity decreases with increasing concentration of fluorinated monomer.

The molecular weight and its distribution have been determined by laser light scattering, employing a new apparatus for ETFE dissolution and solution clarification at high temperature; diisobutyl adipate is the solvent at 240°C. The molecular weight of molten ETFE is determined by high temperature rheometry (28).

This polymer can be dissolved in certain high boiling esters at temperatures above 230°C (29–31), permitting a weight-average molecular weight determination by light scattering. Solution viscosity data suggest that the polymer exists as a slightly expanded coil under similar conditions (32).

Transitions. Samples containing 50 mol% TFE with ca 92% alternation were quenched in ice water or cooled slowly from the melt to minimize or maximize crystallinity, respectively (24). Internal motions were studied by dynamic mechanical and dielectric measurements, and by nuclear magnetic resonance. The dynamic mechanical behavior showed that the α relaxation occurs at 110°C in the quenched sample; in the slowly cooled sample it is shifted to 135°C. The β relaxation appears near −25°C. The γ relaxation at −120°C in the quenched sample is reduced in peak height in the slowly cooled sample and shifted to a slightly higher temperature. The α and γ relaxations reflect motions in the amorphous regions, whereas the β relaxation occurs in the crystalline regions. The γ relaxation at −120°C in dynamic mechanical measurements at 1 Hz appears at −35°C in dielectric measurements at 10^5 Hz. The temperature of the α relaxation varies from 145°C at 100 Hz to 170°C at 10^5 Hz. In the mechanical measurement it is 110°C. There is no evidence for relaxation in the dielectric data.

The activation energy is 318.1 kJ/mol (76 kcal/mol) for the α relaxation and 44.3 kJ/mol (10.6 kcal/mol) for the γ relaxation. These relaxations are attributed to the motion of long and short segments in the amorphous regions, respectively. As ETFE is isomeric with poly(vinylidene fluoride) (23), the γ relaxations occur at about the same temperature. Activation energies are similar and are attributed to the motion of short amorphous segments. The β relaxation in PVF_2 is considered to be the main-chain amorphous relaxation and is analogous to the α relaxation in the ETFE. However, the arrangement of dipoles in the all-trans conformation is more symmetrical.

Physical and Mechanical Properties. Modified ETFE has a good combination of mechanical properties, including excellent cut-through and abrasion resistance, high flex life, and exceptional impact strength. As wire insulation, it withstands physical abuse during and after installation. Lightweight wire constructions are designed with a minimum diameter and are useful as single, general-purpose insulation and for multiple or composite constructions.

Modified ETFE is less dense, tougher, and stiffer and exhibits a higher tensile strength and creep resistance than PTFE, PFA, or FEP resins. It is ductile, and displays in various compositions the characteristic of a nonlinear stress–strain relationship. Typical physical properties of Tefzel products are shown in Table 1 (33,34). Properties such as elongation and flex life depend on crystallinity, which is affected by the rate of crystallization; values depend on fabrication conditions and melt cooling rates.

Light transmittance of 25-μm films in the visible-to-ir range varies from 91 to 95% for Tefzel 200 and from 89 to 93% for Tefzel 280. In the uv range, transmittance increases from 50% at 200 nm to 90% at 400 nm.

Thermal Properties. Modified ETFE has a broad operating temperature range up to 150°C for continuous exposure (33). Cross-linking by radiation improves the high temperature capability further. However, prolonged exposure to higher temperatures gradually impairs the mechanical properties and results in discoloration. Thermal and oxidative degradation studies (35,36) suggest that main carbon chain sequences of two or more ethylene links are thought to be subject to thermal and oxidative degradation. To enhance the thermal stability of ETFE resins stabilizers may be added for high temperature applications (37). The copolymer will not support combustion in air. Limiting oxygen index (LOI) is about 30–31, depending on monomer ratio. LOI increases gradually as fluorocarbon content is increased up to the alternating composition. It then increases rapidly to the index of PTFE (38).

The thermodynamic properties of Tefzel 200 and 280 are shown in Table 2; the annual rate of loss of weight with thermal aging for Tefzel 200 ranges from 0.0006 g/g at 135°C to 0.006 g/g at 180°C after an initial loss of absorbed gases of 0.0013 g/g at elevated temperature. The excellent thermal stability of ETFE is demonstrated by aging at 180°C; at this temperature, the annual weight loss of six parts per 1000, or a 1% weight loss, takes almost 2 years.

Friction and Bearing Wear of the Glass-Reinforced Copolymer. Glass reinforcement improves the frictional and wear properties of modified ETFE resins (HT-2004). For example, the dynamic coefficient of friction [689.5 kPa (100 psi) at >3 m/min] for Tefzel 200 is 0.4, which drops to 0.3 for the 25% glass-reinforced product at these conditions (33). The wear factor also improves from

Table 1. Typical Properties of Tefzel[a]

	ASTM method	Tefzel 200, 280	Tefzel[b] HT-2004
Ultimate tensile strength, MPa[c]	D638	44.8	82.7
Ultimate elongation	D887-64T	200[d]	8
Compressive strength, MPa[c]	D695	48.9	68.9
Shear strength, MPa[c]		41.3	44.8
Heat deflection temp., °C	D648		
at 0.45 MPa		104	265
at 1.8 MPa		74	210
Max continuous use temp., no load, °C		150[e]	200
Low temp. embrittlement	D746	below −100°C	
Tensile modulus, MPa[c]	D638	827	8270
Flexural modulus, MPa[c]	D790	96.5	6550
Impact strength notched Izod	D256		
at −54°C, J/m[f]		>1067	373
at 23°C		no break	485
Deformation under load, 13.7 MPa at 50°C, %	D621	4.11	0.68
Coefficient of linear expansion per °C	D696-70		
20–30°C		9×10^{-5}	3×10^{-5}
50–90°C		9.3×10^{-5}	1.7×10^{-5}
140–180°C		14×10^{-5}	3.2×10^{-5}
Specific gravity	D792	1.70	1.86
Refractive index n_D		1.4028	
Flammability	UL 94	94V-O	94V-O
	D635	ATB[g] <5 s; ALB 10 mm	
Melting point, dta peak, °C		270	270
Water absorption at saturation, %	D570	0.029	0.022
Hardness			
Rockwell	D785	R50	R74
Durometer D		D75	
Coefficient of friction[h]			
Dynamic, 689 kPa (at >3 m/min)		0.4	0.3
Static, 689 kPa			0.3

[a] At 23°C and 50% Rh, unless otherwise specified.
[a] Reinforced with 25 wt% glass fiber.
[a] To convert MPa to psi, multiply by 145.
[a] Elongations between 100 and 300% are achieved with varying methods of sample fabrication.
[a] Long-term heat-aging tests on Tefzel 280 are in progress. Early data indicate that initial properties are retained after more than 2000 h at 200°C. It is expected that the continuous use temperature of Tefzel 280 will be above 150°C.
[a] To convert J/m to ft·lbf/in., divide by 53.38.
[a] ATB; average time of burning to nearest 5 s; ALB: average length of burn to nearest 5 mm. Test bar thickness = 2.9 mm.
[a] Mating material AISI 1018 Steel, Rc20, 16AA.

12×10^{-14} to 32×10^{-17} 1/Pa [6000×10^{-10}–16×10^{-10} (in.^{3}·min)/(ft·lbf·h)]. These frictional and wear characteristics, combined with outstanding creep resistance, indicate suitability for bearing applications. Glass-reinforced ETFE is less abrasive on mating surfaces than most glass-reinforced polymers. Its static

Table 2. Thermodynamic Properties of Modified ETFE

Property	Tefzel 200 and 280
Melting point, °C	270
Specific heat	0.46–0.47
Heat of sublimation, kJ/mol	50.2
Heat of fusion[a], J/g	46.0
Heat of combustion, kJ/g	13.72
Thermal conductivity, W/(m·K)	0.238
Critical surface tension of molten resin, mN/m (=dyn/cm)	22

[a] Little dependence on temperature.

Table 3. Bearing Wear Rate[a]

		Wear factor K, 10^{17} 1/Pa[c]	
Pressure, kPa[b]	Velocity, cm/s	Tefzel	Metal
On steel[d]			
6.8	2.5	32	8
6.8	5.1	28	12
6.8	7.6	38	26
6.8	8.9	60	32
6.8	10.2	fail	
On aluminum[e]			
2.0	5.1	2400	2400
0.68	25.4	960	780

[a] Thrust-bearing tester, no lubricant, ambient air temperature, metal finish 406 nm.
[b] To convert kPa to psi, multiply by 0.145.
[c] To convert 1/Pa to $(in.^3 \cdot min)/(ft \cdot lbf \cdot h)$, divide by 2×10^{-7}.
[d] AISI 1018.
[e] LM24M (English).

coefficient of friction depends on bearing pressure; for Tefzel HT-2004 the coefficient of friction changes from 0.51 at 68 Pa to 0.34 at 3.43 kPa (0.5 psi).

Dynamic friction depends on pressure and rubbing velocity (PV). The generation of frictional heat depends on the coefficient of friction and the PV factor. For the glass-reinforced product, temperature buildup begins at about PV 10,000 and thermal runaway occurs just below PV 20,000. High wear rates begin above PV 15,000. The wear rate depends on the type of metal rubbing surface and finish, lubrication, and clearances. Lubrication, hard shaft surfaces, and high finishes improve wear rates. Table 3 gives wear factors for steel and aluminum. Because the wear rate of both ETFE and the metal is much higher for aluminum than for steel, an anodized surface is preferred with aluminum.

Electrical Properties. Modified ETFE is an excellent dielectric (Table 4). Its low dielectric constant confers a high corona-ignition voltage. The dielectric constant does not vary with frequency or temperature. Both dielectric strength (ASTM D149) and resistivity are high. The loss characteristics are minimum; the dissipation factor, although low, increases at higher frequencies. Glass reinforcement increases losses and the dielectric constant rises from 2.6 to 3.4 (from 10^2

Table 4. Electrical Properties of ETFE Resins

	ASTM test	ETFE	Reinforced
Dissipation factor	D150		
10^2 Hz		0.0006	0.004
10^3 Hz		0.0008	0.002
10^4 Hz			0.002
10^5 Hz			0.003
10^6 Hz		0.005	0.005
10^9 Hz		0.005	
10^{10} Hz		0.010	0.012
Volume resistivity, Ω·cm	D257	$>10^{16}$	10^{16}
Surface resistivity, Ω/sq	D257	$>10^{16}$	10^{15}
Arc resistance, s	D495	75	110

to 10^{10} Hz); the dissipation factor is increased by 10-fold. Exposure to radiation also increases losses. Dielectric strength is not reduced by thermal aging, unless a physical break occurs in the material. The short-time test of ASTM D149 gives values of 16–20 kV/mm with 3-mm-thick specimens to 160–200 kV/mm with films 25–75 μm thick. Tracking resistance is about 70 s by ASTM D495. This is comparable to materials considered to be nontracking; under unusual conditions tracking occurs. When these resins are foamed they provide insulation with even lower dielectric constant (39).

Chemical Resistance and Hydrolytic Stability. Modified ETFE are resistant to chemicals and solvents (Table 5) that often cause rapid degradation in other plastic materials. Performance is similar to that of perfluorinated polymers (40), which are not attacked by strong mineral acids, inorganic bases, halogens, and metal salt solutions. Organic compounds and solvents have little effect. Strong oxidizing acids, organic bases, and sulfonic acids at high concentrations and near their boiling points affect ETFE to varying degrees.

Physical properties remain stable after long exposure to boiling water. Tensile strength and elongation of Tefzel 200 are unaffected after 3000 h in boiling water. The higher molecular weight ETFE behaves similarly, whereas the glass-reinforced product shows a reduction of 25–35% in tensile strength with loss of reinforcement.

Water absorption of Tefzel is low (0.029 wt%), which contributes to its outstanding dimensional stability as well as to the stability of mechanical and electrical properties regardless of humidity.

High temperature resistance of ETFE and other fluoropolymers in automotive fuels and their permeation resistance have been discussed (41,42).

The ETFE can be cross-linked by radiation (43), despite the high content of TFE units. The recommended upper continuous use temperature for commercial ETFE is 150°C. Physical strength can be maintained at higher temperatures when cross-linking agents are incorporated and cured by peroxide or ionizing radiation (44). The cut-through resistance of thin-wall wire insulation to a physical abuse during installation or use is increased at temperature up to 200°C. Short-term excursions to 240°C are possible for highly cross-linked resins. Cross-linking

Table 5. Tefzel Resistance to Chemicals after 7 Days of Exposure[a]

Chemical	Boiling point, °C	Test temp., °C	Retained properties, %		
			Tensile strength	Elongation	Weight, gain
Organic acids and anhydrides					
Acetic acid (glacial)	118	118	82	80	3.4
Acetic anhydride	139	139	100	100	0
Trichloroacetic acid	196	100	90	70	0
Hydrocarbons					
Mineral oil		180	90	60	0
Naphtha		100	100	100	0.5
Benzene	80	80	100	100	0
Toluene	110	110			
Amines					
Aniline	185	120	81	99	2.7
Aniline	185	180	95	90	
N-Methylaniline	195	120	85	95	
N,*N*-Dimethyl aniline	190	120	82	97	
n-Butylamine	78	78	71	73	4.4
Di-*n*-butylamine	159	120	81	96	
Di-*n*-butylamine	159	160	55	75	
Tri-*n* butylamine	216	120	81	80	
Pyridine	116	116	100	100	1.5
Solvents					
Carbon tetrachloride	78	78	90	80	4.5
Chloroform	62	61	85	100	4.0
Dichloroethylene	77	32	95	100	2.8
Methylene chloride	40	40	85	85	0
Freon 113	46	46	100	100	0.8
Dimethylformamide	154	90	100	100	1.5
Dimethyl sulfoxide	189	90	95	95	1.5
Skydrol		149	100	95	3.0
Aerosafe		149	92	93	3.9
A-20 stripper solution		140	90	90	
Ethers, ketones, esters					
Tetrahydrofuran	66	66	86	93	3.5
Acetone	56	56	80	83	4.1
Acetophenone	201	180	80	80	1.5
Cyclohexanone	156	156	90	85	0
Methyl ethyl ketone	80	80	100	100	0
n-Butyl acetate	127	127	80	60	0
Ethyl acetate	77	77	85	60	0
Other organic compounds					
Benzyl alcohol	205	120	97	90	
Benzoyl chloride	197	120	94	95	
o-Cresol	191	180	100	100	
decalin	190	120	89	95	
Pathaloyl chloride	276	120	100	100	
Inorganic acids					
Hydrochloric (conc)	106	23	100	90	0

Table 5. (Continued)

Chemical	Boiling point, °C	Test temp., °C	Retained properties, %		
			Tensile strength	Elongation	Weight, gain
Hydrobromic (conc)	125	125	100	100	
Hydrofluoric (conc)		23	97	95	0.1
Sulfuric (conc)		100	100	100	0
Nitric, 70% (conc)	120	120	0	0	
Chromic	125	125	66	25	
Phosphoric (conc)		100			
Halogens					
Bromine (anhy)	59	23	90	90	1.2
Chlorine (anhy)		120	85	84	7
Bases, peroxides					
Ammonium hydroxide		66	97	97	0
Potassium hydroxide, 20%		100	100	100	0
Sodium hydroxide, 50%		120	94	80	0.2
Hydrogen peroxide, 30%		23	99	98	0
Other inorganic compounds					
Ferric chloride, 25%	104	100	95	95	0
Zinc chloride, 25%	104	100	100	100	0
Sulfuryl chloride	68	68	86	100	8
Phosphoric trichloride	75	75	100	98	
Phosphoric oxychloride	104	104	100	100	
Silicon tetrachloride	60	60	100	100	

[a] Changes in properties <15% are considered insignificant; test performed on 250–1250 μm microtensile bars; tensile strength, elongation, and weight gain determined within 24 h after termination of exposure.

reduces plasticity but enhances high temperature properties and nondrip performance. The irradiated resin withstands a 400°C solder iron for 10 min without noticeable effect.

Modified ETFE has excellent weather resistance; tensile strength and elongation are not affected. On the other hand, tensile and elongation properties of the glass-reinforced compound show a significant reduction.

Modified ETFE films are used as windows in greenhouses and conservatories because of their high transparency to both uv and visible light and excellent resistance to weathering (45). Pigmented films are applied on white boards and in outdoor advertising laminates. Biaxially oriented films have tensile properties and toughness similar to polyester films (46).

Vacuum Outgassing and Permeability. Under vacuum, modified ETFE give off little gas at elevated temperatures. The loss rate is about one-tenth of the acceptable maximum rates for spacecraft uses. Exposing 750-μm specimens for 24 h at 149°C to a high vacuum results in a maximum weight loss of 0.12%; volatile condensible material is less than 0.02%.

The following permeability values were determined on Tefzel film (100μm, ASTM D1434) at 25°C [1 nmol (m· s·GPa) = 0.5 (cm^3·mil)/(100 $in.^2$dia·atm)]:

	nmol/(m·s·GPa)
Carbon dioxide	500
Nitrogen	60
Oxygen	200
Helium	1800
Water vapor (ASTM E96)	3.3

Fabrication

Modified ETFE are commercially available in a variety of physical forms (Table 6) and can be fabricated by conventional thermoplastic techniques. Commercial ETFE resins are marketed in melt-extruded cubes, that are sold in 20-kg bags or 150-kg drums. In the United States, the 1992 price was $27.9–44.2/kg, depending on volume and grade; color concentrates are also available.

Like other thermoplastics, they exhibit melt fracture (47) above certain critical shear rates. In extrusion, many variables control product quality and performance (48).

Melt Processing

Articles are made by injection molding, compression molding, blow molding, transfer molding, rotational molding, extrusion, and coating. Films can be thermoformed and heat sealed (33). Because of high melt viscosity, ETFE resins are usually processed at high temperatures (300–340°C).

Injection-molded articles shrink about 1.5–2.0% in the direction of resin flow and about 3.5–4.5% in the transverse direction under normal molding conditions. A 25% glass-reinforced composition shrinks only about 0.2–0.3% in the flow direction and about 3.0% in the transverse direction. Although shrinkage depends on shape and processing conditions, uniformity is excellent.

Table 6. Forms of Modified ETFE Resins

Tefzel grade	Form	Melt flow,[a] g/10 min	Application
210	Extruded cubes	45	Injection molding, thin coating
200	Extruded cubes	8	General purpose, insulation, tubing, fasteners
280	Extruded cubes	3	Chemical resistance, jacketing, havy-wall, logging cables
HT-2000	Compacted powder	8	Compounded products
HT-2010	Compacted powder	3	Compounded products, coating lining
HT-2010	Compacted powder	45	Coating

[a] At 297°C and 45 N (5 kgf) load.

Molten ETFE polymers corrode most metals, and special corrosion-resistant alloys are recommended for long-term processing equipment; short-term prototype runs are possible in standard equipment.

Forming and Machining. Articles can be formed below the melting point with conventional metal-forming techniques. Tetrafluoroethylene–ethylene copolymers are readily machined with the same tools and feed rates as are used for nylon and acetal. For best dimensional stability, the article should be annealed at the expected use temperature before the final machine cut.

Coloring and Decorating. Commercial pigments that are thermally stable at the resin processing temperature may be used. Pigments may be dry-blended with the resin, or ETFE pellets may be blended with color concentrates, which are available in pellet form.

Nontreated surfaces can be hot-printed with special foils in a manner similar to a typewriter ribbon. The type is heated to about 321°C, and a printing pressure of 172–206 kPa (25–30 psi) is applied for about 0.25 s; no further treatment is required.

Stripes may be applied to wire coated with ETFE fluoropolymer over DuLite 817-5002 fluoropolymer clear enamel or other bases. Thermally stable pigments are required. Stripes may be applied by gravure-wheel-type applicators and oven-cured in-line.

Assembly. The success of many applications depends on the ability of ETFE fluoropolymer to be economically assembled.

Screw Assembly. Self-tapping screws are used for joining ETFE parts. For maximum holding power, the boss diameter should be about double the screw diameter, and the engagement length about 2.5 times the screw diameter; lubricants should be avoided. Threaded inserts can be molded in place, pressed in, or driven in ultrasonically.

Snap-Fit and Press-Fit Joints. Snap-fit joints offer the advantage that the strength of the joint does not diminish with time because of creep. Press-fit joints are simple and inexpensive, but lose holding power. Creep and stress relaxation reduce the effective interference, as do temperature variations, particularly with materials with different thermal expansions.

Cold or Hot Heading. Rivets or studs can be used in forming permanent mechanical joints. The heading is made with special tools and preferably with the rivet at elevated temperatures. Formed heads tend to recover part of their original shape if exposed to elevated temperatures, resulting in loose joints. Forming at elevated temperature reduces recovery.

Spin Welding. Spin welding is an efficient technique for joining circular surfaces of similar materials. The matching surfaces are rotated at high speed relative to each other and then brought into contact. Frictional heat melts the interface and, when motion is stopped, the weld is allowed to solidify under pressure.

Ultrasonic Welding. Ultrasonic welding has been applied to Tefzel with weld strength up to 80% of the strength of the base resin. Typical conditions include a contact pressure of 172 kPa (25 psi) and 1–2 s cycle time. The two basic designs, the shear and butt joints, employ a small initial contact area to concentrate and direct the high frequency vibrational energy.

Potting. Potting of wire insulated with Tefzel has been accomplished with the aid of a coating of a colloidal silica dispersion. The pots produced with a polysulfide potting compound meeting MIL-S-8516C Class 2 standards exhibit pullout strengths of 111–155 N (25–35 lbf).

Bonding. Surface treatment, such as chemical etch, corona, or flame treatments, is required for adhesive bonding of Tefzel. Polyster and epoxy compounds are suitable adhesives.

ETFE respond well to melt bonding to untreated aluminum, steel, and copper with peel strengths above 3.5 kN/m (20 lbf/in.). For melt bonding to itself, hot-plate welding is used. The material is heated to 271–276°C, and the parts are pressed together during cooling.

The plasma surface treatment of ETFE to improve adhesion has been studied (49).

Testing and Standards

A description of modified ETFE and their classification is given by the American Society for Testing and Materials under the designation D3159-83 (50). A comprehensive listing of industrial and military specifications is available (51).

Applications. Tefzel 200 is a general-purpose, high temperature resin for insulating and jacketing low voltage power wiring for mass transport systems, wiring for chemical plants, and control and instrumentation wiring for utilities. In injection-molded form, it is used for sockets, connectors, and switch components (52). Because of excellent mechanical properties it provides good service in seal glands, pipe plugs, corrugated tubing, fasteners, and pump vanes. In chemical service, it is used for valve components, laboratory ware, packing, pump impellers, and battery and instrument components.

Tefzel 210, the high melt-flow resin, provides a high speed processing product for use in coating of fine wire and injection molding of thin-walled or intricate shapes. It is also used for other fine-wire applications requiring high line speeds and mechanical strength, but where harsh environmental conditions are not anticipated.

For high temperature wiring with mechanical strength and stress-crack and chemical resistance, Tefzel 280 is preferred. Rated by UL at 150°C, it is widely used for insulating and jacketing heater cables and automotive wiring and for other heavy-wall application where temperatures up to 200°C are experienced for short peirod of time or where repeated mechanical stress at 150°C is encountered. It is also suitable for oil-well logging cables and is used in transfer moldings and extrusions for lined chemical equipment. It is injection molded into articles with metal inserts, thick sections, and stock shapes.

Health and Safety

Large quantities of Tefzel have been processed and used in many demanding service applications. No cases of permanent injury have been attributed to these resins, and only limited instances of temporary irritation to the upper respiratory tract have been reported (53).

As with other melt-processible fluoropolymers, trace quantities of harmful gases, including hydrogen fluoride, diffuse from the resin even at room temperature. Therefore, the resins should be used in well-ventilated areas. Even though the resin is physiologically inert and nonirritating to the skin, it is recommended that spills on the skin be washed with soap and water. These resins are stable at 150°C and are recommended for continuous use at this temperature. Degradation, as measured by weight loss, is insignificant up to the melting point of 270°C. At processing temperatures sufficient quantities of irritating and toxic gases are generated to require removal of the gases by exhaust hoods over the die and at the hopper heater. For extrusion into water, a quench tank or partially filled container for purging is recommended. In extrusion operations proper procedures must be maintained to control temperature and pressure. The weight loss with increasing temperature is as follows:

Temperature, °C	Hourly weight loss, %
300	0.05
330	0.26
350	0.86
370	1.60

To remove all decomposition products, a "total-capture" exhaust hood is recommended.

Under normal processing conditions at 300–350°C, Tefzel resins are not subject to autocatalytic degradation. However, extended overheating can result in "blow-backs" through extruder feed hopper or barrel front.

Prolonged soldering in confined spaces with restricted air circulation requires ventilation. A small duct fan is recommended for hot-wire stripping. Tefzel articles should not be exposed to welding conditions.

The limiting oxygen index of Tefzel as measured by the candle test (ASTM D2863) is 30%. Tefzel is rated 94 V-0 by Underwriters, Laboratories, Inc., in their burning test classification for polymeric materials. As a fuel, it has a comparatively low rating. Its heat of combustion is 13.7 MJ/kg (32,500 kcal/kg) compared to 14.9 MJ/kg (35,000 kcal/kg) for poly(vinylidene fluoride) and 46.5 MJ/kg (110,000 kcal/kg) for polyethylene.

Bulk quantities of Tefzel fluoropolymer resins should be stored away from flammable materials. In the event of fire, personnel entering the area should have full protection, including acid-resistant clothing and self-contained breathing apparatus with a full facepiece operated in the pressure-demand or other positive-pressure mode. All types of chemical extinguishers may be used to fight fire involving Tefzel resins. Large quantities of water may be used to cool and extinguish the fire.

The DuPont Haskell Laboratory for Toxicology and Industrial Medicine has conducted a study to determine the acute inhalation toxicity of fumes evolved from Tefzel fluoropolymers when heated at elevated temperatures. Rats were exposed to decomposition products of Tefzel for 4 h at various temperatures. The approximate lethal temperature (ALT) for Tefzel resins was determined to be 335–350°C. All

rats survived exposure to pyrolysis products from Tefzel heated to 300°C for this time period. At the ALT level, death was from pulmonary edema; carbon monoxide poisoning was probably a contributing factor. Hydrolyzable fluoride was present in the pyrolysis products, with concentration dependent on temperature.

BIBLIOGRAPHY

"Fluorinated Plastics, Tetrafluoroethylene Copolymers with Ethylene" in *EPST* 1st ed., Suppl. Vol. 1, pp. 268–278, by R. L. Johnson, E. I. du Pont de Nemours & Co., Inc.; "Tetrafluoroethylene Polymers, Tetrafluoroethylene–Ethylene Copolymers" in *EPSE* 2nd ed., Vol. 16, pp. 626–642, by S. V. Gangal, E. I. du Pont de Nemours & Co., Inc.

1. U.S. Pat. 2468664 (Apr. 26, 1949), W. E. Hanford, and J. R. Roland, (to E. I. du Pont de Nemours & Co., Inc.).
2. U.S. Pat. 2479367 (Aug. 16, 1949), R. M. Joyce Jr. (to E. I. du Pont de Nemours & Co., Inc.).
3. Brit. Pat. 1166020 (Oct. 1, 1969), M. Modena and co-workers (to Montecatini Edison, SpA).
4. Jpn. Kokai 6422586 (Sept. 12, 1964), K. Hirose and co-workers (to Nitto Chemical Industry, Co., Ltd.).
5. Belg. Pat 725356 (Feb. 14, 1969), Z. Kenkyusho (to Asahi Glass, Ltd.).
6. U.S. Pat. 2946763 (July 26, 1960), M. I. Bro and B. W. Sandt (to E. I. du Pont de Nemours & Co., Inc.).
7. D. P. Carlson, *Development of Tefzel Fluoropolymer Resins*, unpublished paper, 1972.
8. U.S. Pat. 3624250 (Nov. 30, 1971), D. P. Carlson (to E. I. du Pont de Nemours & Co., Inc.).
9. U.S. Pat. 4123602 (Oct. 31, 1978), H. Ukihashi and M. Yamake (to Asahi Glass Co.).
10. Brit. Pat. 1353535 (May 22, 1974), R. Hartwimmer (to Farbwerke Hoechst, AG).
11. U.S. Pat. 3401155 (Sept. 10, 1986), G. Borsini and co-workers (to Montecatini Edison, SpA).
12. Y. Tabata, H. Shibano, and H. Sobue, *J. Polym. Sci. Part A* **2**, 1977 (1964).
13. U.S. Pat. 4521575 (June 4, 1985), S. Nakagawa and K. Ihara (to Daikin Kogyo Co. Ltd.).
14. U.S. Pat. 4614276 (Sept. 30, 1986), K. Ihara and T. Nakagawa (to Daikin Kogyo Co. Ltd.).
15. U.S. Pat. 3960825 (June 1, 1976), D. N. Robinson and co-workers (to Pennwalt Corp.).
16. U.S. Pat. 4338237 (July, 1982), R. A. Sulzbach and co-workers (to Hoechst Aktiengesellschaft).
17. M. Iuliano and co-workers, *Makromol. Chem.* **190**, 827–835 (1989).
18. F. Kostov and A. Nikolov, *J. Appl. Polym. Sci.* **57**, 1545–1555 (1995).
19. R. Naberezhnykh and co-workers, *Vysokomol. Soedin.* **19**(1), 33–37 (1977).
20. M. Modena, C. Garbuglio, and M. Ragazzini, *Polym. Lett.* **10**, 153 (1972).
21. M. Modena, C. Garbuglio, and M. Ragazzini, *J. Polym. Sci. Part B* **10**, 153 (1972).
22. F. S. Ingraham and D. F. Wooley Jr., *Ind. Eng. Chem.* **56**(9), 53 (1964).
23. S. Yano, *J. Polym. Sci. Part A2* **8**, 1057 (1970).

24. H. W. Starkweather, *J. Polym. Sci. Part A2* **11**, 587 (1973).
25. F. C. Wilson, and H. W. Starkweather, *J. Polym. Sci. Part A2* **11**, 919 (1973).
26. T. Tanigami and co-workers, *Polymer* **27**, 999–1006 (1986).
27. T. Pieper, B. Heise, and W. Welke, *Polymer* **30**, 1768–1775 (1989).
28. B. Chu and Chi Wu, *Macromolecules* **20**, 93–98 (1987).
29. B. Chu, C. Wu, and W. Buck, *Macromolecules* **22**, 371 (1989).
30. B. Chu and C. Wu, *Macromolecules* **19**, 1285 (1986).
31. B. Chu, and C. Wu, *Macromolecules* **20**, 98 (1987).
32. Z. Wang, A. Tontisakis, W. Tuminello, W. Buck, and B. Chu, *Macromolecules* **23**, 1444 (1990).
33. *Tefzel Fluoropolymer, Design Handbook*, E. I. du Pont de Nemours & Co., Inc., Wilmington, Del., 1973.
34. *Tefzel—Properties Handbook*, E-31301-6, E. I. du Pont de Nemours & Co., Inc., Wilmington, Del., Dec. 1999.
35. J. Morelli and co-workers, *J. Appl. Polym. Sci.* **43**, 601–611 (1991).
36. S. Malkevich, L. Tarutina, and L. Chereshkevich, *Plasticheskie massy* **6**, 5–7, (1960).
37. U.S. Pat. 4390655 (June 28, 1983), J. C. Anderson (E. I. du Pont de Nemours & Co., Inc.).
38. D. L. Kerbow, in J. Scheirs, ed., *Modern Fluoropolymers*, John Wiley & Sons, New York, 1997, p. 301.
39. S. K. Randa, C. R. Frywald, and D. P. Reifschneider, in *Proceedings of the 36th International Wire and Cable Symposium*, Arlington, Va., 1987, pp. 14–22.
40. Technical Information, Tefzel Fluoropolymer Resin, Chemical Use Temperature Guide, Bulletin 195062E, E. I. du Pont de Nemours & Co., Inc., Wilmington, Del., 1995.
41. M. Carpenter, S. Chillons, and R. Will, Paper presented at the *International Congress and Exposition*, Detroit Mich., Feb. 25–Mar. 1, 1991, Society of Automobile Engineers (SAE) International Technical Paper Series 910103.
42. D. Goldsberry, S. Chillons, and R. Will, Paper Presented at the *International Congress and Exposition*, Detroit, Mich., Feb. 25–Mar. 1, 1991. SAE Technical Paper Series 910104.
43. U.S. Pat. 3738923 (June 12, 1973), D. P. Carlson and N. E. West (E. I. du Pont de Nemours & Co., Inc.).
44. U.S. Pat. 4155823 (May 22, 1979), A. J. Gotcher and P. B. Gemeraad (Raychem Corp.).
45. J. Emsley, *New Scientist* **46** (Apr. 22, 1989).
46. U.S. Pat. 4510301 (Apr. 9, 1985), S. B. Levy (E. I. du Pont de Nemours & Co., Inc.).
47. Technical Information, Jacketing Rate Calculation, Bulletin No. 10, Fluoropolymers Division Technical Service Laboratory, E. I. du Pont de Nemours & Co., Inc., Wilmington, Del., Aug. 1982.
48. Extrusion Guide for Melt Processible Fluoropolymers, Bulletin E-41337, E. I. du Pont de Nemours & Co., Inc., Wilmington, Del.
49. S. Kaplan, O. Kolluri, G. Hansen, R. Rushing, and R. Warren, Technical Paper Presented at *Conference on Adhesives*, Society of Manufacturing Engineers, Atlanta, Ga., Sept. 12, 1989.
50. Modified ETFE-Fluorocarbon Molding and Extrusion Materials, ASTM D3159-95a, American Society for Testing and Materials, Philadelphia, Fa., 1998.
51. J. Teflon **15**(1), 1974.
52. Tefzel Fluoropolymers, Product Information (DuPont Materials for Wire and Cable), Bulletin E-81467, E. I. du Pont de Nemours & Co., Inc., Wilmington, Del., May 1986.

53. *Guide to the Safe Handling of Fluoropolymer Resins*, 3rd ed., Fluoropolymers Division of the Society of the Plastics Industry, Inc., Washington, D.C., 1998.

GENERAL REFERENCES

"Tetrafluoroethylene Copolymers with Ethylene" under "Fluorine Compounds, Organic" in *ECT* 4th ed., Vol. 11, pp. 657–671, S. V. Gangal, E. I. du Pont de Nemours & Co., Inc.

SUBHASH V. GANGAL
E. I. du Pont de Nemours & Co., Inc.

PERFLUORINATED POLYMERS, TETRAFLUOROETHYLENE–PERFLUORODIOXOLE COPOLYMERS

Copolymers of tetrafluoroethylene and 2,2-bistrifluoromethyl-4,5-difluoro-1,3-dioxole (PDD) are perfluorinated amorphous polymers and possess unusual combination of properties. They retain the outstanding chemical, thermal, and surface properties of perfluorinated polymers in addition to having excellent electrical and optical properties; and have solubility at ambient temperature in a normal fluorosolvent. This family of copolymers is manufactured by DuPont and sold under the trade name of Teflon AF, amorphous fluoropolymers.

All tetrafluoroethylene-based homo- and copolymers, described in earlier papers, are semicrystalline with distinct melting points. On the other hand, tetrafluoroethylene–PDD copolymers are totally amorphous and can be tailored for specific glass-transition temperatures by altering the polymer composition (1). So these perfluorinated amorphous polymers exhibit properties derived from their amorphous structure and perfluorinated chains.

Monomer

Preparation. 2,2-Bistrifluoromethyl difluoro-1,3-dioxole (PDD) monomer is synthesized in four steps (2). In the first step, hexafluoroacetone and ethylene oxide are reacted to form 2,2-bistrifluoromethyl-4,5-dichloro-4,5-difluoro-1,3-dioxolane. This product is then fully chlorinated and subsequently partially fluorinated to difluoro-1,3-dioxolane. In the last step, the fluorinated product is dechlorinated to obtain the final product, PDD.

Encyclopedia of Polymer Science and Technology. Copyright John Wiley & Sons, Inc. All rights reserved.

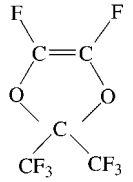

PDD Monomer

Properties. PDD is a colorless liquid with the boiling point of 33°C (3). It is very reactive and can homopolymerize, and therefore, needs to be stored at low temperature with a small amount of free-radical inhibitor. PDD can copolymerize with tetrafluoroethylene or other fluorinated monomers, such as vinylidene fluoride, vinyl fluoride, or chlorotrifluoroethylene.

Copolymerization. Copolymers of tetrafluoroethylene and PDD can be synthesized by free-radical initiators in either aqueous or nonaqueous medium (1). The homopolymer of PDD results in an amorphous polymer with the glass-transition temperature T_g of 335°C. This polymer is difficult to melt process because of the narrow processing window below its decomposition temperature. Copolymers can be prepared with any proportion of tetrafluoroethylene and PDD. Polymers containing less than 20 mol% PDD tend to be partially crystalline. At 20 mol% PDD, the T_g of the copolymer is about 80°C. The glass-transition temperature increases with an increase in PDD. The commercial Teflon AF products are copolymers of tetrafluoroethylene and PDD, and have glass-transition temperatures of 160 and 240°C for Teflon AF-1600 and Teflon AF-2400, respectively (4). During aqueous polymerization small amounts of acid fluoride or carboxylic acid end groups may be produced by ring-opening. For many applications these unstable ends are removed and converted to perfluorinated end groups by first treating the polymer with ammonia, followed by fluorination (5).

Properties. Teflon AF copolymers have many characteristics similar to those of other copolymers of tetrafluoroethylene, such as high-temperature stability, excellent chemical resistance, low surface energy, low water absorption, and high limiting oxygen index (LOI). On the other hand, many properties are different because of their amorphous structure. These polymers are soluble at ambient temperature in fluorinated solvents. They are transparent and have low refractive index. They are significantly stiffer and have high gas permeability. The glass-transition temperature of tetrafluoroethylene–PDD copolymers is sensitive to the structure of the dioxide monomer. It is likely that steric interactions involving the two trifluoromethyl groups lead to a highly congested chain structure with limited mobility (6). The structural study of these polymers indicate that there are microvoids in their structure and probably cause lower than expected polymer density, low dielectric constant, low refractive index, high gas permeability, and low thermal conductivity. Most likely the origin of these microvoids is loose chain packing caused by the high energy for rotation and reorientation of the dioxole ring containing polymer chain (7).

Table 1 summarizes mechanical, electrical, optical, and thermal properties of Teflon AF-1600 and AF-2400 (10). The dielectric constant for Teflon AF is lower than that for PTFE and is unaffected by humidity.

Table 1. Properties of Teflon AF-1600 and AF-2400

Property	AF-1600	AF-2400	ASTM method	Refs
Melt viscosity, Pa·s[a]			D3835	8
at 250°C	2650			
at 350°C		540		
Density, g/cm^3	1.78	1.67	D792	4
Water absorptivity; 1	<0.01	<0.01	D570	9
Contact angle, water, deg	104	105		8
Critical surface energy, mN/m(=dyn/cm)	15.6–15.7	15.6–15.7		8
Electrical properties				
Dielectric strength, kV(0.1 mm)$^{-1}$	2.1	1.9	D149	4
Dielectric constant				
1 MHz	1.934	1.904	D150	8
1 GHz	1.93	1.897		
13.6 GHz	1.927	1.89		
Dissipation factor				
1 MHz	0.00012	0.00012	D150	4
1GHz	0.00018	0.00024		
13.6 GHz	0.00020	0.00035		
Flammability, LOI %O_2	95	95		9
Hardness, Rockwell	103	97.5	D785	8
Refractive index	1.31	1.29	D542	9
Optical transmissions	>95	>95	D1003	9
Tensile strength @ break, MPa[a]			D638	8
23°C	27	26		
150°C	8			
220°C		4		
Elongation @ break, %				
23°C	17	8	D638	9
150°C	89			
220°C		8		

To convert MPa to psi, multiply by 145.
To convert Pa·s to P, multiply by 10.

The low temperature dielectric properties invetigation (11) revealed that the γ relaxation found at −186°C for PTFE is only one-third the intensity for AF-1600 and AF-2400. This relaxation is attributed to the cooperative motion of the four carbon atoms of a TFE dimer unit. The low concentration of such units in AF explains the difference in the intensity of γ relaxation.

The refractive index of Teflon AF is the lowest known for any solid organic polymer (12). One of the key properties of AF is its solubility in fluorinated solvents, such as "Fluorinert" FC-72, -75, and -40, perfluorobenzene, perfluoromethylcyclohexane, perfluorodimethylcyclohexane, perfluoroctane, or perfluorodecalin.

The thermal stability of Teflon AF approaches that of other perfluorinated polymers. At 260°C after 4 h of exposure no weight loss was observed. The weight losses after the exposure at 360, 380, 400, and 420°C were 0.3, 0.5, 1.9, and 8.8%, respectively.

Copolymers of PDD with other fluoromonomers are discussed in Reference 3.

Fabrication. Teflon AF is processed by a wide variety of techniques. AF solutions can be used for spin coating, dip coating, spraying, or casting. Melt-processing techniques such as extrusion and injection molding are used. Compression molding has also been used effectively. Spin coating is used to produce very thin and uniform coatings on flat substrates. The film thickness is influenced by the nature of the substrate, the spin speed, and the concentration of the solution. Dip coating is suitable for nonplanar surfaces (13). Compression molding is done about 100°C above T_g and may require longer heat-up time than other polymers because of its lower thermal conductivity. Laser ablation and vacuum pyrolysis techniques are also used (14,15).

Health and Safety. Safe practices employed for handling PTFE and PFA resins are adequate for Teflon AF (20). Adequate ventilation is required for processing above 330°C.

Applications and Economic Aspects. Teflon AF is used to provide antireflective coatings (16), low dielectric coatings, pellicles used in electronic chips (17), cladding in plastic optical fiber (18), as a low dielectric insulator, to coat gas separation membranes (19).

The PDD monomer used for AF is very expensive, which results in making AF products very costly. These polymers in solid form are sold in 25 and 500 g packages at prices $500 and $5000, respectively. The solutions are available in 100 mL and 1 L packages. They contain 1–18% solids, depending on the grade. The prices for solutions range from $70 for 1% solids of AF-2400 in 100 mL to $7810 for 18% solids of AF-16015-18 in 1 L package.

BIBLIOGRAPHY

1. U.S. Pat. 3978030 (Aug. 31, 1976), P. R. Resnick (to E. I. du Pont de Nemours & Co., Inc.).
2. U.S. Pat. 3865845 (Feb. 11, 1975), P. R. Resnick (to E. I. du Pont de Nemours & Co., Inc.).
3. P. R. Resnick and W. H. Buck in J. Scheirs, ed., *Modern Fluoropolymers*, John Wiley & Sons, Inc., New York, 1997, pp. 397–419.
4. W. H. Buck and P. R. Resnick, Teflon® AF Technical Bulletin H-52454-1, E. I. du Pont de Nemours & Co., Inc., Wilmington, Del., 1993.
5. U.S. Pat. 4946902 (Aug. 7, 1990), P. G. Bekiarian, M. D. Buckmaster, and R. A. Morgan (to E. I. du Pont de Nemours & Co., Inc.).
6. M. Hung, *Macromolecules* **26**, 2829 (1993).
7. W. J. Davies and R. A. Pethrik, *Eur. Poly. J.* **30**, 1289 (1994).
8. P. Gunther, H. Ding, and R. Gerhard-Multhaupt, in *Proceedings of the 1993 IEEE Conf. on Electrical Insulation and Dielectric Phenomena* 1993, pp. 197–202.
9. M. S. Jahan, D. R. Ermer, and D. W. Cooke, *Radiation Phys. Chem.* **41**(1/2), 77–83 (1993).
10. D. L. Kerbow and C. A. Sperati, in J. Brandrup, E. H. Immergut, and E. A. Grulke, eds., *Polymer Handbook*, 4th ed., Wiley-Interscience, New York, 1999, pp. V-31–58.

11. H. Starkweather and co-workers, *Macromolecules* **24**, 3853 (1991).
12. W. Groh and A. Zimmermann, *Micromolecules* **24**, 6660 (1991).
13. I. M. Thomas and J. H. Campbell, *SPIE* **1441**, 294 (1990).
14. G. B. Blanchet, *Appl. Phys. Lett.* **62**, 479 (1993).
15. J. Griesar and co-workers, *Proc. SPIE* **1330**, 111 (1990).
16. H. G. Floch and P. F. Belleville, *SPIE* **1758**, 135 (1992).
17. U.S. Pat. 5061024 (Oct. 29, 1991), D. E. Keys (to E. I. du Pont de Nemours & Co., Inc.).
18. U.S. Pat. 4530569 (July 23, 1985), E. N. Squire (to E. I. du Pont de Nemours & Co., Inc.).
19. C. C. Cho, R. M. Wallace, and L. A. Files-Sesler, *J. Electronic Mat.* **23**, 827 (1994).
20. *Guide to the Safe Handling of Fluoropolymer Resins*, 3rd ed., Fluoropolymers Division of the Society of the Plastics Industry, Inc., Washington, D.C., 1998.

SUBHASH V. GANGAL
E. I. du Pont de Nemours & Co., Inc.

PERFLUORINATED POLYMERS, TETRAFLUOROETHYLENE–PERFLUOROVINYL ETHER COPOLYMERS

Introduction

Perfluoroalkoxy (PFA) fluorocarbon resins are designed to meet industry's needs in chemical, electrical, and mechanical applications. These melt-processible copolymers contain a fluorocarbon backbone in the main chain and randomly distributed perfluorinated ether side chains:

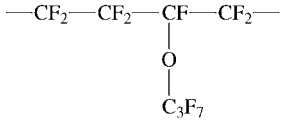

A combination of excellent chemical and mechanical properties at elevated temperatures results in reliable, high performance service to the chemical processing and related industries. Chemical inertness, heat resistance, toughness and flexibility, stress-crack resistance, excellent flex life, antistick characteristics, little moisture absorption, nonflammability, and exceptional dielectric properties are among the characteristics of these resins.

The introduction of a perfluoromethyl side chain (Teflon FEP) greatly reduces the crystallinity of polytetrafluoroethylene (PTFE). Crystallinity is reduced

Encyclopedia of Polymer Science and Technology. Copyright John Wiley & Sons, Inc. All rights reserved.

even further by replacing the short side chain with a long side chain, such as perfluoropropyl ether. In contrast to Teflon FEP, only a small amount of vinyl ether is required to reduce crystallinity and develop adequate toughness.

Tetrafluoroethylene (TFE) [116-14-3] and perfluorovinyl ether are copolymerized in aqueous (1,2) or nonaqueous (3) media. The polymer is separated and converted into various forms, such as extruded cubes, powders, beads, or dispersions. This family of products is manufactured by DuPont, Daikin, Dyneon, and Asahi Glass and sold under the trade names of Teflon PFA, Neoflon AP, Hostaflon TFA, and Aflon PFA, respectively. Additional information on specific manufacturers' products can often be obtained by consulting their internet web sites (for example, www.dupont.com/teflon).

Monomers

Preparation. The preparation of TFE has been described previously. Perfluorovinyl ethers (4–7) are prepared by the following steps. Hexafluoropropylene (HFP) [116-15-4] is oxidized to an epoxide HFPO [428-59-1] (5) which, on reaction with perfluorinated acyl fluorides, gives an alkoxyacyl fluoride.

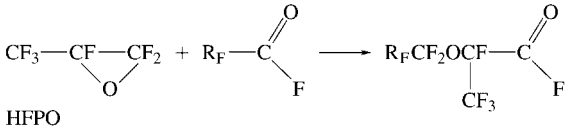

The alkoxyacyl fluoride is converted to vinyl ethers by treatment with base at ca 300°C (8).

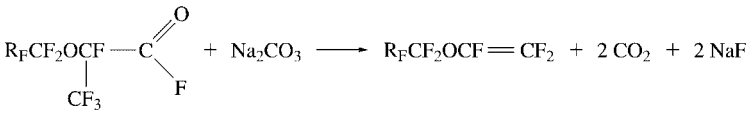

where $R_F = F(CF_2)_n$.

Alkoxyacyl fluorides are also produced by an electrochemical process (9).

The preparation of perfluoromethyl and perfluoroethyl vinyl ethers is described in References 10 and 11.

Properties. Properties of perfluoropropyl vinyl ether (PPVE) [1623-05-8], a colorless, odorless liquid (mol. wt. 266), are shown in Table 1. Perfluoropropyl vinyl ether is an extremely flammable liquid and burns with a colorless flame. It is significantly less toxic than HFP; the average lethal concentration (ALC) is 50,000 ppm (12).

Table 1. Properties of Perfluoropropyl Vinyl Ether, $F_3C—CF_2—CF_2—O—CF=CF_2$

Property	Value
Critical temperature, K	423.58
Critical pressure, MPa[a]	1.9
Critical volume, $cm^3/(g·mol)$	435
Surface tension, mN/m(=dyn/cm)	9.9
Boiling point, °C	36
Specific gravity at 23°C,	1.53
Vapour density at 75°C, g/cm^3	0.2
Vapour pressure at 25°C, kPa[b]	70.3
Solubility in water	0
Odor	None
Color	Colorless
Flash point, °C	−20
Flammable limits in air,[c] vol.%	1

[a]To convert MPa to atm, divide by 0.1013.
[b]To convert kPa to psi (psia), multiply by 0.145.
[c]Extremely flammable.

Copolymerization

Tetrafluoroethylene–perfluoropropyl vinyl ether copolymers [26655-00-5] are made in aqueous (1,2) or nonaqueous media (3). In aqueous copolymerizations water-soluble initiators and a perfluorinated emulsifying agent are used. Molecular weight and molecular weight distribution are controlled by a chain-transfer agent. Sometimes a second phase is added to the reaction medium to improve the distribution of the vinyl ether in the polymer (13); a buffer is also added. In nonaqueous copolymerization, fluorinated acyl peroxides are used as initiators that are soluble in the medium (14); a chain-transfer agent may be added for molecular weight control.

Temperatures range from 15 to 95°C, and the pressures from 0.45 to 3.55 MPa (65–515 psi). The temperatures used for the aqueous process are higher than those for the nonaqueous process.

Alkyl vinyl ethers tend to rearrange when exposed to free radicals (15). Temperatures must be kept low enough to prevent termination by free-radical coupling. In the aqueous process, temperatures below 80°C minimize the number of acid end groups derived from vinyl ether transfer. In the nonaqueous process, temperature must also be limited to avoid excessive vinyl ether transfer as well as reaction with the solvent. End groups are stabilized by treating the polymer (16) with methanol, ammonia, or amines (17–19). Treatment of PFA with elemental fluorine generates CF_3 end groups and a very low level of contamination (20), which is important for the semiconductor industry (21).

The polymer is separated from the medium and converted to useful forms such as melt-extruded cubes for melt-processible applications. Teflon PFA is also available as a dispersion, a fine powder, or in unmelted bead form.

Description and classification of PFA resins are given in Reference 22. Various specifications are given in Reference 23.

A family of copolymers containing TFE and perfluoromethyl vinyl ether modified with PPVE referred to as MFA is produced by Ausimont (24). The relatively small pendant group —O—CF3 seems to have a similar effect on the crystallinity reduction as is exhibited by —CF3 in FEP (perfluoropropylene–tetrafluoroethylene copolymer); however, the higher reactivity of perfluoromethyl vinyl ether than that of HFP makes the polymerization process more efficient. The performance characteristics are described in References 11 and 25.

A new family of copolymers called Teflon HP Plus has been introduced by DuPont using perfluoroethyl vinyl ether analogous to PPVE used to produce the standard PFA (26). A significantly higher reactivity of perfluoroethyl vinyl ether has made it possible to produce copolymers with widely different comonomer concentrations on a commercial scale while reducing the tendency to rearrange and form acid end groups from vinyl ether transfer. Even though perfluoroethyl group provides a somewhat shorter pendant group, its effect on the reduction of crystallinity is very similar to that of perfluoropropyl group. This makes the perfluoroethyl vinyl ether an optimum commonomer to produce a versatile family of products.

Properties

The melting point of commercial Teflon PFA is 305°C, ie, between those of PTFE and FEP. Second-order transitions are at −100, −30, and 90°C, as determined by a torsion pendulum (27). The crystallinity of the virgin resin is 65–75%. Specific gravity and crystallinity increase as the cooling rate is reduced. An ice-quenched sample with 48% crystallinity has a specific gravity of 2.123, whereas the press-cooled sample has a crystallinity of 58% and a specific gravity of 2.157.

Mechanical Properties. Table 2 shows the physical properties of Teflon PFA (28,29). At 20–25°C the mechanical properties of PFA, FEP, and PTFE are similar; differences between PFA and FEP become significant as the temperature is increased. The latter should not be used above 200°C, whereas PFA can be used up to 260°C. Tests at liquid nitrogen temperature indicate that PFA performs well in cryogenic applications (Table 3).

Unfilled Teflon PFA has been tested in mechanical applications, using Teflon FEP 100 as a control (30). Tests were run on molded thrust bearings at 689.5 kPa (100 psi) against AISI 1080, Rc 20, 16AA steel, and at ambient conditions in air without lubrication. A limiting PV value of 5000 was found. Wear factors and dynamic coefficients of friction are shown in Table 4.

Hardness is determined according to ASTM D2240 on 7.6 × 12.7 × 0.48 cm injection-molded panels (31). Results on the D scale are 63–65 for Teflon PFA and 63–66 for Teflon FEP.

Chemical Properties. A combination of excellent chemical and mechanical properties at elevated temperatures results in high performance service in the chemical processing industry. Teflon PFA resins have been exposed to a variety of organic and inorganic compounds commonly encountered in chemical service (32). They are not attacked by inorganic acids, bases, halogens, metal salt solutions,

Table 2. Properties of Teflon PFA

Property	ASTM method	Teflon 340	Teflon 350
Nominal melting point, °C		302–306	302–306
Specific gravity	D3307	10.6	1.8
Continuous use temp., °C		260	260
Tensile strength, MPa[a]			
at 23°C	D1708	28	31
at 250°C		12	14
Tensile yield, MPa[a]			
at 23°C	D1708	14	15
at 250°C		3.5	4.1
Ultimate elongation, %			
at 23°C		300	300
at 250°C	D1708	480	500
Flexural modulus, MPa[a]			
at 23°C	D790	655	690
at 250°C		55	69
Creep resistance[b] tensile, modulus, MPa[a]			
at 20°C	D695	270	270
at 250°C	D695	41	41
Hardness durometer	D2240	D60	D60
MIT folding endurance, 775–200 μm film thickness, cycles		50,000	500,000
Water absorption, %	D570	0.03	0.03
Coefficient of linear thermal expansion per °C	D696		
20–100°C		12×10^{-5}	12×10^{-5}
100–150°C		17×10^{-5}	17×10^{-5}
150–210°C		20×10^{-5}	20×10^{-5}

[a]To convert MPa to psi, multiply by 145.
[b]Apparent modulus after 10 h: stress = 6.89 MPa at 20°C, 6.89 kPa at 250°C.

Table 3. Cryogenic Properties of Teflon PFA Resins

Property	ASTM method	At 23°C	At −196°C
Yield strength, MPa[a]	D1708[b]	15	
Ultimate tensile strength, MPa[a]	D1708[b]	18	129
Elongation, %	D1708[b]	260	8
Flexural modulus, MPa[a]	D790-71[c]	558	5790
Impact strength, notched Izod, J/m[d]	D256-72a[e]	No break	64
Compressive strength, MPa[a]	D695		414
Compressive strain, %	D695		35
Modulus of elasticity, MPa[a]	D695		4690

[a]To convert MPa to psi, multiply by 145.
[b]Crosshead speed B, 1.3 mm/min; used at both temperatures for more direct comparision.
[c]Method 1, Procedure B.
[d]To convert J/m to ft·lbf/in., divide by 53.38.
[e]Method A, head weight is 4.5 kg at 23°C and 0.9 kg at 160°C.

Table 4. Teflon PFA Fluorocarbon Resin Thrust-Bearing Wear-Test Results[a]

Velocity, m/min	Wear factor K, 10^{17}, 1/Pa[b]	Dynamic coefficient of friction	Test duration, h
Teflon PFA			
TE-9704			
0.91	3.12	0.210	103
3.05	3.67	0.214	103
9.1	1.96	0.229	103
15.24	1.38	0.289	103
Teflon FEP 100			
0.91	3.71	0.341	104
3.05	2.19	0.330	104
9.1	3.16	0.364	104
15.24	1.60	0.296	103

[a]Mating surface: AISA 1018 steel, R*c* 20, 16AA; contact pressure: 689 kPa; at20°C in air; no lurbricant.
[b]To convert 1/Pa to (in.^{3}·min)/(ft·lbf·h), divide by 2×10^{-7}.

organic acids, and anhydrides. Aromatic and aliphatic hydrocarbons, alcohols, aldehydes, ketones, ethers, amines, esters, chlorinated compounds, and other polymer solvents have little effect. However, like other perfluorinated polymers, they react with alkali metals and elemental fluorine.

Thermal Stability. Teflon PFA resins are very stable and can be processed up to 425°C. Thermal degradation is a function of temperature and time. A significant increase in melt flow rate indicates degradation after a short time above 425°C; at lower temperatures degradation takes longer. Degradation is not significant if the change in melt flow rate of the resin during molding is below 20%. Degradation is also indicated by the formation of small bubbles or discoloration; however, high stock temperatures may cause slight discoloration without adversely affecting properties.

Heat aging at 285°C, a temperature slightly below but near the melting point, increases the strength of Teflon PFA. Samples aged in a circulating air oven for 7500 h at 285°C show a decrease in melt flow number as defined by ASTM D2116. A decline in melt flow number indicates an increase in average molecular weight, which is also indicated by a 25% increase in tensile strength and enhanced ultimate elongation. Toughness is also measured by MIT flex life, which improves severalfold on heat aging at 285°C.

When exposed to fire, Teflon PFA contributes little in fuel value and is self-extinguishing when the flame is removed. The fuel value is approximately 5.4 MJ/kg (2324 Btu/lb). It passes the UL-83 vertical-flame test and is classified as 94VE-O according to UL-94. The limiting oxygen index (LOI) by ASTM D2863 is above 95%.

Electrical Properties. The electrical properties of Teflon PFA are given in Table 5. The dielectric constant of PFA resins is about 2.06 over a wide range of frequencies (10^2–2.4×10^{10} Hz), temperatures, and densities (ASTM D150). The values for PFA density vary only slightly, 2.13–2.17, and the dielectric

Table 5. Electrical Properties of Teflon PFA

Property	ASTM method	Value
Dielectric strength,[a] kV/m		79
Volume resistivity, Ω·cm	D257	10^{18}
Surface resistivity, Ω/sq	D257	10^{18}
Dissipation factor	D150	
at 10^2 Hz		0.000027
at 10^6 Hz		0.000080
at 10^7 Hz		0.000145
at 10^9 Hz		0.00115
at 3×10^9 Hz		0.00144
at 1.4×10^{10} Hz		0.00131
at 2.4×10^{10} Hz		0.00124

[a] Short term, 250-μm-thick sample.

constant varies only about 0.03 units over this range, among the lowest of all solid materials. Humidity has no measurable effect on the dielectric constant of PFA. The dielectric strength (short-term) of PFA resins is 80 kV/mm (0.25-mm films, ASTM D149); FEP films give similar results, whereas PTFE films are typically measured at 47 kV/mm. Like other fluoropolymer resins, PFA loses dielectric strength in the presence of corona discharge. The dissipation factor at low frequency (10^2–10^4 Hz) decreases with increasing frequency and decreasing temperature. Temperature and frequency have little influence on the dissipation factor over the frequency range 10^4–10^7 Hz. As frequencies increase to 10^{10} Hz, there is a steady increase in dissipation factor. Above 10^7 Hz, increases measured at room temperature are highest; a maximum at about 3×10^9 Hz is indicated. The higher dissipation factor with increasing frequency should be considered in electrical insulation applications at high frequencies. The volume and surface resistivities of fluorocarbon resins are high and are not affected by time or temperature. When tested with stainless steel electrodes (ASTM D495), no tracking was observed for the duration of the test (180 s), indicating that PFA resin does not form a carbonized conducting path (33,34).

Optical Properties and Radiation Effects. Within the range of wavelengths measured (uv, visible, and nir radiation), Teflon PFA fluorocarbon film transmits slightly less energy than FEP film (35) (Table 6). In thin sections, the resin is colorless and transparent; in thicker sections, it becomes translucent. It is highly transparent to ir radiation; uv aborption is low in thin sections. Weather-O-Meter tests indicate unlimited outdoor life.

Like other perfluoropolymers, Teflon PFA is not highly resistant to radiation (36). Radiation resistance is improved in vacuum, and strength and elongation are increased more after low dosages (up to 30 kGy or 3 Mrad) than with FEP or PTFE. Teflon PFA approaches the performance of PTFE between 30 and 100 kGy (3–10 Mrad) and embrittles above 100 kGy (10 Mrad). At 500 kGy (50 Mrad) PTFE, FEP, and PFA are degraded. The effect of radiation on tensile strength and elongation is shown in Table 7.

Table 6. Optical Properties of Teflon PFA Film

Property	ASTM method	Value
Refractive index[a]	D542-50	1.350 ± 0.002
Haze, %	D10003-52	4
Light transmission, %		
Ultraviolet[b] 0.25–0.40 μm		55–80
Visible, 0.40–0.70 μm		80–87
Infrared, 0.70–2.1 μm		87–93

[a]Measured at 546 nm and 20°C.
[b]Cary Model Spectrophotometer.

Table 7. Effects of Radiation on Tensile Strength of PFA[a]

	ASTM D1708	
Exposure, kGy	Tensile strength, MPa[b]	Elongation, %
0	30.27	358
5	28.20	366
10	24.96	333
20	21.24	302
50	14.55	35
200		<5
500		<5

[a]*Sample:* 250-μm compression-molded films of Teflon PFA 340. *Source:* G.E. resonance transformer, 2 MeV capacity, at a current of 1 mA.
[b]To convert MPa to psi, multiply by 145.

Fabrication

Teflon PFA resins are fabricated by the conventional melt-processing techniques used for thermoplastics (37). Processing equipment is constructed of corrosion-resistant materials and can be operated at 315–425°C. A general-purpose grade, PFA 340, is designed for a variety of molding and extrusion applications, including tubing, shapes, and molded components, in addition to insulation for electrical wire and cables. Because of the excellent thermal stability of PFA 350, a wide range of melt temperatures can be used for fabrication. Extrusion temperatures are 20–26°C above the melting point.

Teflon PFA 440 HP is a chemically modified form of PFA 340 that provides additional benefits such as enhanced purity and improved thermal stability. This product is suitable for producing tubing, pipe linings for production of ultrapure chemicals, semiconductor components, and fluid handling systems for high performance filters (38).

Extrusion. Like other thermoplastics, Teflon PFA resin exhibits melt fracture above certain critical shear rates. For example, samples at 372°C and 5-kg load show the following behavior:

Teflon PFA	Melt flow, g/10 min	Critical shear rate, s^{-1}
340	14	50
310	6	16
350	2	6

Because Teflon PFA melt is corrosive to most metals, special corrosion-resistant alloys must be used for the extrusion equipment, such as Hastelloy C, Monel 400, and Xaloy 306. Barrels, liners, screws, adapters, breaker plates, and dies are made of corrosion-resistant metals (39). Corrosion is promoted by resin degradation and high processing temperatures, long residence times, or dead spots. Extruders used with Teflon FEP are also suitable for PFA resins. Heaters and controllers capable of accurate operation in the range of 330–425°C are required. Extruder barrels should have three or four independently controlled heating zones, each equipped with its own thermocouple and temperature-indicating control.

The screw consists of a feed section, a rapid transition section, and a metering section; a rounded forward end prevents stagnation. The breaker plate that converts the rotary motion of the melt into smooth, straight flow should have as many holes as possible; both ends of each hole should be countersunk for streamlined flow.

The temperature of the melt downstream from the breaker plate may exceed the front barrel temperature because of the mechanical work transmitted to the resin by the screw; it varies with screw speed and flow rate. The melt temperature is measured by a thermocouple inserted into the melt downstream from the breaker plate. A hooded exhaust placed over the extruder die and feed hopper removes decomposition products when the extrudate is heated.

High melt strength of Teflon PFA 350 permits large reductions in the cross section of the extrudate by drawing the melt in air after it leaves the die orifice (40). At a given temperature, the allowable flow rates are limited at the low end by resin degradation and at the high end by the onset of melt fracture. A broader range of specific gravities (2.13–2.17) may be obtained in articles fabricated from PFA 350 than from FEP 160. Unlike with PTFE, higher crystallinity in PFA seems to have little effect on flex life.

Injection Molding. Any standard design plunger or reciprocating screw injection machine can be used for PFA 340, although a reciprocating screw machine is preferred (41). Slow injection into mold cavities avoids surface or internal melt fracture, and control of ram speed is important at low speed. Corrosion-resistant metals are used for parts in continuous contact with molten resin; Hastelloy C and Xaloy 306 or 800 are recommended.

Because the mold is usually maintained at temperatures below the melting point of the resin, corrosion on the mold surface is less than in the molding machine. Nonreturn ball check valves and ring check valves are used; the latter is preferred for PFA. A streamlined flow must pass through the valve, preventing areas of stagnant flow or holdup and localized degradation.

A smear head causes less stagnation and overpacking than a nonreturn valve. A conventional-type reverse-tapered nozzle with the bore as large as possible without sudden changes in diameter is preferred. Independently controlled, zone-type heaters for heating the nozzle and at least two zones on the cylinder are used.

At a holdup time longer than 10–15 min at a high temperature, resin degradation is avoided by keeping the rear of the cylinder at a lower temperature than the front. At short holdup times (4–5 min), cylinder temperatures are the same in rear and front. If melt fracture occurs, the injection rate is reduced; pressures are in the range of 20.6–55.1 MPa (3000–8000 psi). Low back pressure and screw rotation rates should be used.

The cycle can usually be estimated on the basis of about 30 s/3 mm of thickness; most of it is devoted to ram-in-motion time (except for very thin sections). The mold temperature used with PFA 340 is often the highest temperature that allows the part to be ejected undamaged from the mold and retain its shape while cooling.

The resin must be of highest purity for optimum processing characteristics and properties. Degradation results in discoloration, bubbling, and change in melt flow rate.

Transfer Molding. Valve and fitting liners are made by a transfer-molding process (42), with the valve or fitting serving as the mold. Melted resin is forced into the fitting at a temperature above the melting point of the resin. The melt may be produced by an extruder or an injection molding machine or melted cubes contained in a melt pot and transferred by applying pressure to a piston in the pot. After the resin transfer is completed, the fitting is cooled under pressure. Stock temperatures of 350–380°C and fitting temperatures of 350–370°C are used to process PFA 350. A slight adjustment in the cooling cycles may be required for transfer molding PFA 350 because it has higher melting and freezing points than FEP.

Rotocasting Teflon PFA Beads. The resin has sufficient thermal stability for a commercial rotocasting operation; that is, TE-9738 has a melting point of about 303°C. In rotocasting trials, incoming flue gas temperatures of 355–365°C (43,44) and heat cycles of 90–180 min have been used. Conventional rotations for major and minor axes can be applied without modifications; Freecote 33 performs adequately as a mold release agent. Mold release instructions can be followed without modification. Heating cylces, including a preheat and a fusion stage, give consistent rotocasting. Preheating at 15–30°C below the fusion temperature takes 10–25 min. Heat-cycled Teflon PFA rotocastings are translucent white, often with bluish tinge. Rotocastings that have been heated too long may darken to a translucent brown. Uniform cooling is essential for undistorted, stress-free products; combinations of air and water are employed. The rotocasting is cooled below the resin melting temperature with air at ambient temperature and then with a water spray, and finally with a stream of air.

Dispersion Processing. A commercial aqueous dispersion of Teflon PFA 335 contains more than 50 wt% PFA particles, about 5 wt% surfactants and fillers. This dispersion is processed by the same technique as for PTFE dispersion. It is used for coating various surfaces, including metal, glass, and glass fabrics. A

thin layer of Teflon PFA coating can also serve as an adhesive layer for PTFE topcoat.

Powder Coating. Teflon PFA is also available in a finely divided powder form. It can be used to produce thin layers on various surfaces by heating these surfaces above the melting point of PFA and then bringing the powder in contact with them. This allows a thin layer of the powder to melt on the surface of the substrate.

For some applications the powder is suspended in an aqueous medium or a solvent with the help of emulsifying agents and then sprayed onto the substrate. The powder is also used as a filler to prepare sprayable compositions of PTFE dispersions, which then can be used to coat various substrates (45).

Pigmentation. Commercial color concentrates of Teflon PFA containing approximately 2% pigment can be easily dispersed in clear extruded cubes. The resin can also be dry-blended with stable inorganic pigments. At 0.1–1% of concentration, the pigment has no appreciable effect on the dielectric strength and constant or mechanical properties. The dissipation factor of pigmented resin varies with the type and concentration of the pigment.

Pigment used for dry blending is dried overnight at 150°C in a vacuum oven to remove absorbed gases and moisture. It is screened through a 149-μm (100-mesh) screen directly onto the cubes, which are rolled or tumbled for at least 15 min. The pigmented resin is stored in an airtight container to prevent absorption of moisture.

Applications and Economic Aspects

The perfluorovinyl ether comonomer used for PFA is expensive, as is PFA. Most PFA grades are sold as extruded, translucent cubes in various colors at $50.00–65.00/kg. Some PFA types are also marketed in nonextruded forms.

Teflon PFA can be fabricated into high temperature electrical insulation and components and materials for mechanical parts requiring long flex life. Teflon PFA 350 is used as liner for chemical process equipment, specialty tubing, and molded articles for a variety of applications. Teflon PFA 340 is a general-purpose resin for tubing, shapes, primary insulation, wire and cable jacketing, injection- and blow-molded components, and compression-molded articles. Teflon PFA 440 HP is a chemically modified form of PFA 340 with enhanced purity and improved thermal stability while processing. This resin is suitable in semiconductor manufacturing, fluid handling systems for industry or life sciences, and instrumentation for precise measurements of fluid systems.

Health and Safety

Safe practices employed for handling PTFE and FEP resins are adequate for Teflon PFA (46); adequate ventilation is required for processing above 330–355°C. In rotoprocessing, a vacuum (250–750 Pa or 1.8–5.6 mm Hg) in the oven ensures exhaust to the outside (45). Removal of end caps or opening of sealed parts in a

well-ventilated area ensures ventilation of decomposition fumes. During rotoprocessing, molds should be vented.

BIBLIOGRAPHY

"Fluorinated Plastics, Tetrafluoroethylene Copolymers with Perfluoroalkoxy Pendant Groups" in *EPST* 1st ed., Suppl. Vol. 1, pp. 260–267, by R. L. Johnson, E. I. du Pont de Nemours & Co., Inc.; "Tetrafluoroethylene Polymers, Tetrafluoroethylene–Perfluorovinyl Ether Copolymers" in *EPSE* 2nd ed., Vol. 16, pp. 614–626, by S. V. Gangal, E. I. du Pont de Nemours & Co., Inc.

1. U.S. Pat. 3132123 (May 5, 1964), J. F. Harris and D. I. McCane (to E. I. du Pont de Nemours & Co., Inc.).
2. U.S. Pat. 3635926 (Jan. 18, 1972), W. F. Fresham and A. F. Vogelpohl (to E. I. du Pont de Nemours & Co., Inc.).
3. U.S. Pat. 3536733 (Oct. 27, 1970), D. P. Carlson (to E. I. du Pont de Nemours & Co.).
4. U.S. Pat. 3358003 (Dec. 12, 1967), H. S. Eleuterio and R. W. Meschke (to E. I. du Pont de Nemours & Co., Inc.).
5. U.S. Pat. 3180895 (Apr. 27, 1965), J. F. Harris and D. I. McCane (to E. I. du Pont de Nemours & Co., Inc.).
6. U.S. Pat. 3250808 (Oct. 10, 1966), E. P. Moore, A. S. Milian Jr., and H. S. Eleuterio (to E. I. du Pont de Nemours & Co., Inc.).
7. U.S. Pat. 4118421 (Oct. 3, 1978), T. Martini (to Hoechst Aktiengesellschaft).
8. U.S. Pat. 3291843 (Dec. 13, 1966), C. G. Fritz and S. Selman (to E. I. du Pont de Nemours & Co., Inc.).
9. U.S. Pat. 2713593 (July 1955), T. J. Brice and W. H. Pearlson (to Minnesota Mining and Manufacturing Co.).
10. U.S. Pat. 5777179 (July 7, 1998), P. Resnick, B. Liang, and M. Hung (to E. I. du Pont de Nemours & Co., Inc.).
11. P. Pozzoli, G. Vita, and V. Arcella, in J. Scheirs, ed., *Modern Fluoropolymers*, John Wiley & Sons, Inc., New York, p. 373.
12. A. H. Olson, E. I. du Pont de Nemours & Co., Inc., private communication, 1992.
13. U.S. Pat. 4499249 (Feb. 12, 1985), S. Nakagawa and co-workers (to Daikin Kogyo Co., Ltd.).
14. U.S. Pat. 2792423 (May 14, 1957), D. M. Young and W. N. Stoops (to Union Carbide and Carbon Corp.).
15. R. E. Putnam, in R. B. Seymour and G. S. Kirshenbaum, eds., *High Performance Polymers: Their Origin and Development*, Elsevier Scientific Publishing, Inc., New York, 1986, p. 279.
16. M. Pianca and co-workers, *J. Fluorine Chem.* **95**, 71–84 (1999).
17. U.S. Pat. 3674758 (July 4, 1972), D. P. Carlson (to E. I. du Pont de Nemours & Co., Inc.).
18. U.S. Pat. 4599386 (July 8, 1986), D. P. Carlson and co-workers (to E. I. du Pont de Nemours & Co., Inc.).
19. PCT Int. Appl. WO 8911495 (1989), M. D. Buckmaster (to E. I. du Pont de Nemours & Co., Inc.).
20. U.S. Pat. 4943658 (1988), J. Imbalzano and D. Kerbow (to E. I. du Pont de Nemours & Co., Inc.).

21. C. J. Goodman and S. Andrews, *Solid State Technol.* **65** (July 1990).
22. PFA-Fluorocarbon Molding and Extrusion Materials, ASTM 3307-86, American Society for Testing and Materials, Philadelphia, Pa., 1987.
23. J. Teflon **15**(1) (1974).
24. U.S. Pat. 5463006 (Oct. 31, 1995), J. A. Abusleme and P. Colaianna (to Ausimont, S. p. A.).
25. *Hyflon® MFA, Fluoropolymers 620 and 640, Properties and Applications Selection Guide*.
26. U.S. Pat. 5760151 (June 2, 1998), R. M. Aten, C. W. Jones, and A. H. Olson (to E. I. du Pont de Nemours & Co., Inc.).
27. R. A. Darby, E. I. du Pont de Nemours & Co., Inc., private communication, 1992.
28. PFA Fluorocarbon Resins, Sales Brochure, E08572, E. I. du Pont de Nemours & Co., Inc., Wilmington, Del.
29. M. I. Bro and co-workers, in *29th International Wire and Cable Symposium*, Cherry Hill, N.J., Nov. 1980.
30. Teflon PFA Fluorocarbon Resins: Wear and Frictional Data, APD #2 Bulletin, E. I. du Pont de Nemours & Co., Inc., Wilmington, Del., 1973.
31. Teflon PFA Fluorocarbon Resins: Hardness, APD #4 Bulletin, E. I. du Pont de Nemours & Co., Inc., Wilmington, Del., 1973.
32. Teflon PFA Fluorocarbon Resins: Chemical Resistance, PIB #2 Bulletin, E. I. du Pont de Nemours & Co., Inc., Wilmington, Del., 1972.
33. E. W. Fasig, D. I. McCane, and J. R. Perkins, Paper presented at the *22nd International Wire and Cable Symposium*, Atlantic City, N.J., Dec. 1973.
34. Handbook of Properties for Teflon PFA, Sales Brochure, E46679, E. I. du Pont de Nemours & Co., Inc., Wilmington, Del., Oct. 1987.
35. Teflon PFA Fluorocarbon Resins: Optical Properties, APD #6 Bulletin, E. I. du Pont de Nemours & Co., Inc., Wilmington, Del., 1973.
36. Teflon PFA Fluorocarbon Resins: Response to Radiation, APD #3 Bulletin, E. I. du Pont de Nemours & Co., Inc., Wilmington, Del., 1973.
37. K. Hintzer and G. Lohr, in J. Scheirs, ed., *Modern Fluoropolymers*, John Wiley & Sons, Inc., New York, p. 223.
38. Teflon PFA 440 HP, Product information, H-27760, E. I. du Pont de Nemours & Co., Inc., Wilmington, Del., 1990.
39. Teflon PFA Fluorocarbon Resin: Injection Molding of Teflon PFA TE-9704, PIB #4 Bulletin, E. I. du Pont de Nemours & Co., Inc., Wilmington, Del., 1973.
40. Technical Information, Melt Extrusion Guide, Bulletin No. H-45321, E. I. du Pont de Nemours & Co., Inc., Wilmington, Del., Mar. 1993.
41. Injection Molding Guide for Teflon® FEP, PFA and Tefzel®, Bulletin No. E-96680, E. I. du Pont de Nemours & Co., Inc., Wilmington, Del., July 1987.
42. Technical Information, Transfer Moulding Guide, Bulletin No. H-34556, E. I. du Pont de Nemours & Co., Inc., Wilmington, Del., Jan. 1972.
43. Technical Information, No. 11, Processing Guidelines for Du Pont Fluoropolymer Rotocasting Powders of Tefzel and Teflon PFA, E. I. du Pont de Nemours & Co., Inc., Wilmington, Del., 1982.
44. Teflon PFA TE-9783 Rotation Molding Powder, Technical Information, H-26600, E. I. du Pont de Nemours & Co., Inc., Wilmington, Del., June 1990.
45. Brit. Pat. 2051091B (Feb. 9, 1983), J. E. Bucino (to Fluorocoat Ltd.).
46. *Guide to the Safe Handling of Fluoropolymers Resume*, 3rd ed., Fluoropolymers Division of the Society of the Plastics Industry, Inc., Washington, D.C., 1998.

GENERAL REFERENCE

"Tetrafluoroethylene Copolymers with Perfluorovinyl Ethers" under "Fluorine Compounds, Organic," in *ECT* 4th ed., Vol. 11, pp. 671–683, by S. V. Gangal, E. I. du Pont de Nemours & Co., Inc.

SUBHASH V. GANGAL
E. I. du Pont de Nemours & Co., Inc.

PET. See POLYESTERS, THERMOPLASTIC.

PHA. See POLY3-(HYDROXYALKANOATES).

PHOSGENE

Introduction

Phosgene [75-44-5] (carbonyl chloride, carbon oxychloride, chloroformyl chloride), Cl_2CO, is a colorless liquid with a low boiling point. The compound was first prepared in 1812 by J. Davy from the photochemical reaction of carbon monoxide and chlorine. Phosgene may be formed at elevated temperatures by oxidation of chlorinated solvents (1–5). Phosgene has been used in the preparation of a great variety of chemical intermediates. In addition, it is now widely used in the preparation of isocyanates, which are then used in the preparation of Polyurethanes (PUR), in the manufacture of Polycarbonates, and in the synthesis of chloroformates and carbonates, which are used as intermediates in the synthesis of pharmaceuticals and pesticides. Because of phosgene's toxicity, a high level of safety technology has been developed to ensure its safe handling.

Properties

Some physical properties of phosgene are listed in Table 1. At room temperature and pressure, phosgene is a colorless gas. Impurities may discolor phosgene, tranforming it from clear to pale yellow to green. Phosgene has a characteristic odor. At the time of intital exposure, the odor of phosgene gas can be detected only briefly. At ca 0.5 ppm in air, the odor has been described as pleasant and similar to that of newly mowed hay or cut green corn. However, at high concentrations, the odor may be strong, stifling, and unpleasant.

Encyclopedia of Polymer Science and Technology. Copyright John Wiley & Sons, Inc. All rights reserved.

Table 1. Some Physical Properties of Phosgene[a]

Properties and characteristics	Value
Molecular weight	98.92
Melting point, °C	−127.84
Boiling point, °C[b]	7.48
Density at 20°C, g/cm^3	1.387
Vapor pressure at 20°C, kPa[c]	161.68
Vapor density (air = 1.0)	3.4
Critical temperature, °C	182
Density at critical point, g/cm^3	0.52
Critical pressure, MPa[d]	5.68
Latent heat of vaporization, at 7.5°C, J/g[e]	243
Molar heat capacity of liquid, at 7.5°C, J/K[e]	100.8
Molar heat of formation, kJ[e]	
From elements	218
From CO and Cl_2	108
Molar entropy, J/K[e]	
At 7°C	280
At 25°C	284
Surface tension, mN/m (=dyn/cm)	
At 0.0°C	34.6
At 16.7°C	20.1
At 34.5°C	17.6
At 46.1°C	15.9

[a] Ref. 6.
[b] At 101.3 kPa[c] = 1 atm.
[c] To convert kPa to psi, multiply by 0.145.
[d] To convert MPa to psi, multiply by 145.
[e] To convert J to cal, divide by 4.184.

In general, phosgene is soluble in aromatic and aliphatic hydrocarbons, chlorinated hydrocarbons, and organic acids and esters. It is removed easily from solvents by heating or sparging with air or nitrogen, but because of its toxicity, great care must be taken to control its presence in the atmosphere.

Phosgene is a planar molecule. The interatomic distances are 0.128 nm for C—O and 0.168 nm for C—Cl (1). The Cl—C—Cl angle is 117°. Infrared, ultraviolet, and Raman spectral properties are described in References 7,8–9.

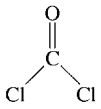

Reactions. Phosgene interacts with many classes of inorganic and organic reagents. The reactions are described extensively in the literature, eg, see References 10,11–12. Reaction with sodium takes place at room temperature, but reaction with zinc requires warming.

Oxides and sulfides of metals react with phosgene at elevated temperatures, usually yielding very pure chlorides. The reaction of phosgene with cadmium

sulfide is a good method for preparing carbonyl sulfide (carbon oxysulfide), COS. The reactions of phosgene with calcium, magnesium, tin, and zinc oxide have been described (13–18). The reactions of titanium oxide with phosgene, tungsten trioxide with phosgene, and the chlorination of oxides of interest in the nuclear field, especially uranium oxide, plutonium oxide, and thorium oxide, have also been characterized (19–24).

Phosphates and silicates of metals often react with phosgene at elevated temperatures and yield the metal chloride and phosphorus oxychloride or silicon dioxide. The reaction with ferric phosphate at 300–350°C has been proposed as a synthetic method for phosphorus oxychloride, $POCl_3$.

Anhydrous aluminum chloride forms a variety of complexes with phosgene, eg, $Al_2Cl_6 \cdot 5COCl_2$ at low temperatures, $Al_2Cl_6 \cdot 3COCl_2$ at 30°C, and $Al_2Cl_6 \cdot COCl_2$ at above 55°C. Reaction with aluminum bromide yields carbonyl bromide, $COBr_2$, and aluminum chlorobromide, $AlCl_2Br$. Reaction of antimony trifluoride with phosgene and chlorine yields carbonyl fluoride (25). Phosgene reacts with sodium fluoride and HCN, yielding phosgene fluorocyanide and carbonyl fluoride (26).

$$AlBr_3 + COCl_2 \longrightarrow COBr_2 + AlCl_2Br$$

$$SbF_3 + COCl_2 + Cl_2 \longrightarrow COF_2$$

$$NaF + HCN + COCl_2 \longrightarrow COFCN + COF_2$$

Phosgene reacts slowly with cold water to produce CO_2 and HCl, and more quickly at higher temperatures (27). In the reaction of gaseous phosgene with water, it is difficult to get the necessary intimate mixing of the gas and the water.

$$COCl_2 + H_2O \longrightarrow 2\,HCl + CO_2$$

Ammonia reacts vigorously with phosgene. The products are urea, biuret, ammelide (which is a polymer of urea), cyanuric acid, and sometimes cyamelide (which is a polymer of cyanic acid). The secondary products probably arise through the very reactive intermediate carbamyl chloride, NH_2COCl.

Phosgene reacts with a multitude of nitrogen, oxygen, sulfur, and carbon centers. Reaction with primary alkyl and aryl amines yields carbamoyl chlorides which are readily dehydrohalogenated to isocyanates:

$$RNH_2 + COCl_2 \longrightarrow RNHCOCl + HCl$$

$$RNHCOCl \longrightarrow RN{=}C{=}O + HCl$$

Secondary amines form carbamoyl chlorides:

$$R_2NH + COCl_2 \longrightarrow R_2NCOCl + HCl$$

α-Amino acids react readily with phosgene to form oxazolidine-2,5-diones:

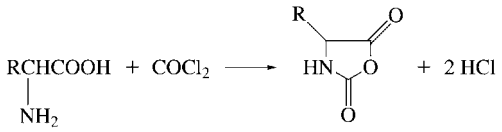

Hydrazine reacts with phosgene, yielding carbohydrazide:

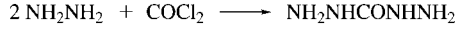

The reaction of phosgene with alcohols yields chloroformates, and with a basic catalyst present, carbonates are formed.

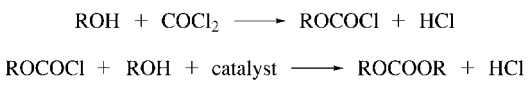

This reaction is commercially important since it serves as a basis for the manufacture of Polycarbonates.

Carboxylic acids react with phosgene to produce give acid chlorides (28).

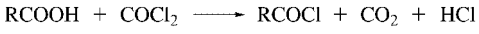

Ketones also react with phosgene:

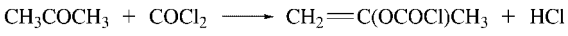

Amides react with phosgene to yield nitriles (qv).

Phosgene can also initiate ring opening.

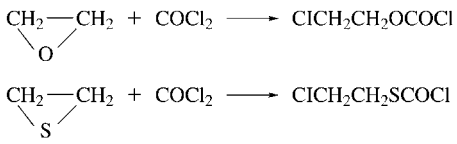

Although $POCl_3$ is the traditional reagent in the Vilsmeier aldehyde synthesis, phosgene may be employed and its role, as well as that of the intermediates, has been studied extensively (29–31).

Manufacture

Phosgene is manufactured by the reaction of carbon monoxide with chlorine over activated carbon. However, depending on the quantity of phosgene needed and the availability of the raw materials, numerous variations of this basic synthetic process are being practiced. Continuous processing and a high degree of automation are required for phosgene purification, condensation, and storage. Because of its toxicity, careful and extensive safety procedures and safety equipment are incorporated in plant design and operation. The entire phosgene manufacturing process consists of preparing and purifying carbon monoxide, preparing and purifying chlorine, metering and mixing of the reactants, reacting the mixed gases over activated carbon, purifying and condensing the resulting phosgene, and recovering trace phosgene to assure worker and environmental safety.

Carbon monoxide may be manufactured according to standard processes from coke, ie, from coal, or by controlled oxidation of hydrocarbon fuels. A carbon monoxide process that yields a gas of the highest possible purity must be chosen. Noncondensable impurities are particularly objectionable since their presence makes the recovery of all the phosgene difficult. Water must be removed from the starting gas to preclude hydrochloric acid formation in the converter. The hydrocarbon and hydrogen content should be minimized because reaction of chlorine with methane or hydrogen could ignite a reaction between chlorine and steel, thereby destroying the equipment. Other impurities might poison the catalyst. Sulfides must be excluded since they produce sulfur chlorides which usually are very undesirable impurities. The chlorine must be as dry and pure as the carbon monoxide so as to avoid corrosion of the equipment and decomposition of phosgene by water and other impurities.

Activated carbon of high adsorptive capacity is suitable for use as a catalyst; it need not be treated with metallic salts or other substances. If starting materials of high purity are employed, excellent and economic catalyst efficiency is obtained. A special carbon catalyst has been shown to give lifetimes that are 5–10 times longer than that of conventional activated carbon and also significantly lower levels of the by-product, carbon tetrachloride (32).

The phosgene generators employed are relatively simple tubular heat exchangers that are filled with granulated activated carbon. Because the reaction is rapid and exothermic, efficient heat removal is important since decomposition of phosgene into its starting materials begins to take place at 200°C. The temperature of the carbon bed in the initial reaction zone of the tubes can reach 400°C, but it rapidly falls to product temperatures of 40–150°C. The reaction is normally run at normal pressure or at a slight excess pressure. A phosgene generation system which monitors the phosgene requirements of a plant and responds by producing only the needed amounts has been developed (33,34).

A flow diagram of the production of phosgene appears in Figure 1. Carbon monoxide and chlorine gas are mixed in equimolecular proportions. A small amount of excess carbon monoxide is used to ensure complete reaction of the chlorine. The product gases can be condensed to liquid phosgene and uncondensed gases, which are then scrubbed for removal of remaining phosgene. Uncondensed gaseous phosgene can be employed for in-line operations. The solvent used for absorption is typically the solvent used in a later process step. The remaining

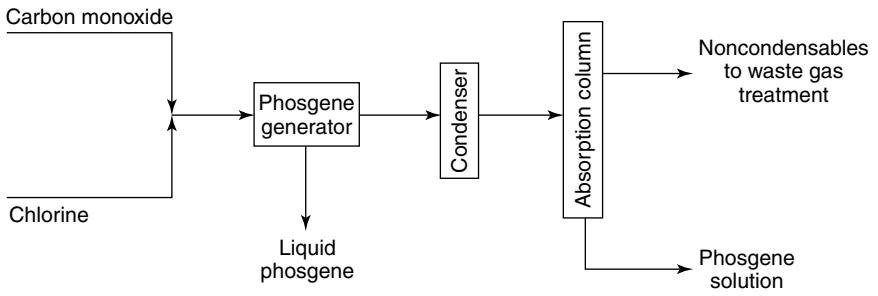

Fig. 1. Manufacture of phosgene from carbon monoxide and chlorine.

nonabsorbable gas stream is fed to the waste gas treatment system to be freed from phosgene.

Several methods of decomposing phosgene in waste gas streams are used. These are as follows:

Decomposition by caustic scrubbing. The waste gas stream is led through packed towers where a sodium hydroxide solution is introduced at the top of the towers. Venturi scrubbers could also be used. Make-up sodium hydroxide is added under pH control. The efficiency of scrubbing concentrated phosgene gas with caustic decreases significantly at caustic concentration below 4 wt% NaOH (35).

Decomposition with moist activated carbon. The waste gas stream is passed through packed activated carbon towers where water is fed at the top of the towers. The water is normally recycled. If the hydrochloric acid concentration in the recycled water exceeds 10%, the decomposition efficiency is greatly reduced. Thus a sufficient supply of fresh water must be assured (36).

Combustion. The waste gas stream is burned to convert phosgene to carbon dioxide and hydrochloric acid. An advantage of this method is that all components of the waste gas, such as carbon monoxide and solvent, are burned (37).

The outlet gas from the phosgene decomposition equipment is continuously monitored for residual phosgene content to ensure complete decomposition.

Analytical and Test Methods

Phosgene in air and in mixture with other gases can be detected by a variety of methods (38). Trace quantities to a lower limit of 0.05 μg/L air can be detected by uv spectroscopy (39). Both ir and gas chromatographies have been used extensively to measure phosgene in air at 1 ppb–1 ppm (7,40,41). Special and multiple-column gas-chromatographic methods have been used for more complex mixtures of gases containing phosgene (42–44). High performance liquid chromatography methods can also be used and offer detection limits of 5- to 10-ppb phosgene (45,46). Absolute determination of phosgene at levels below 100 ppb has been reported using pulsed flow coulometry (47). Laser photoacoustic spectroscopy has been used to detect phosgene at ppb levels (48).

Methods and instruments that are used to monitor phosgene content in air are well developed and have been reviewed (49–51). One detection instrument is

a porous tape that measures the concentration of phosgene in air in quantities as small as 6 ppb (52). Fourier transform infrared spectrometry techniques have been used to permit line and area monitoring in the area around phosgene plants (53).

Phosgene dose-indicator badges for personnel exposure monitoring are commercially available and validated (54,55). This is a simple, visually readable, passive sampler based on phosgene indicator paper which is impregnated with a solution of 4-*p*-nitrobenzylpyridine and *N*-benzylaniline. These indicator badges are used at a number of plant sites using phosgene.

Liquid phosgene is assayed by an iodometric method which involves the following reaction (56):

$$COCl_2 + 2\,NaI \longrightarrow CO + I_2 + 2\,NaCl$$

The released iodine is titrated with sodium thiosulfate.

The following specifications and standards have been reported (6):

Assay	Percent
$COCl_2$, min	99.0
Cl_2 (free), max	0.1
HCl, max	0.2

Storage and Handling

All phosgene containers require a Class A, poison-gas label as well as a corrosive label. Phosgene is transported in steel cylinders which conform to rigid safety-design specifications. The cylinders undergo special hydrostatic testing at 5.5 MPa (800 psi), and extension rings are incorporated in the cylinders to protect the valves. Phosgene is shipped in cylinders ranging in size from 43 to 909 kg. Careful testing for leaks is required after filling, and a vapor space must be accommodated in the storage vessel; excessive filling with liquid phosgene must be avoided.

Transportation requirements and classifications for phosgene are as follows:

DOT shipping name	Phosgene
DOT hazard class	2.3
RQ	Yes – 10 pounds
DOT labels	Poison, Corrosive
DOT placards	Poison
Bill of lading description	Phosgene, 2.3, UN1076, RQ (phosgene), inhalation hazard, poison gas and corrosive labels affixed
UN/NA number	UN1076
Additional DOT requirements	Return of empty containers: residue last contained: phosgene, 2.3, UN1076, RQ (phosgene), inhalation hazard, poison gas and corrosive labels affixed

Because phosgene reacts with water, great care must be taken to prevent contamination with traces of water since this could lead to a build up of pressure through the formation of hydrogen chloride and carbon dioxide. Wet phosgene is very corrosive; therefore, phosgene should never be stored with any quantity of water (4).

Health and Safety Factors

The odor threshold for phosgene is ca 0.5–1 ppm, but varies with individuals. Olfactory fatigue occurs after prolonged exposure (57). Phosgene may irritate the eyes, nose, and throat. The permissible exposure TLV by volume in air is 0.1 ppm (58). The TLV refers to the average airborne concentration at which it is believed nearly all workers may be repeatedly exposed on a daily basis without adverse effect. It is a time-weighted average for an 8-h day or a 40-h week and should be used as a guide for control only. The NIOSH REL (ceiling value) is 0.2 ppm for a 15-min excursion (59). Long-term exposure to phosgene has been reviewed, and potential hazards may exist at <0.2 ppm (60). Medical problems associated with phosgene exposure have been reviewed (61–63), and therapy for phosgene poisoning has also been reviewed (64–67).

When phosgene is inhaled, it reacts very little with the aqueous film on the mucous membranes of the upper respiratory tract. Most of it reaches the pulmonary alveoli, where gas exchange occurs. Here phosgene reacts with NH_2, OH, and SH groups of the blood–air barrier. This causes the blood–air barrier to lose its function as a membrane between the blood vessels and the pulmonary alveoli. As a result, blood plasma is able to pass from the blood vessels into the pulmonary alveoli, thereby increasingly disturbing the gas exchange.

Breathing phosgene causes pulmonary edema, which may be characterized by a delayed onset. The onset of pulmonary edema is a function of both concentration and length of exposure. Typically exposure above 50 ppm-minutes can lead to pulmonary edema (67). Exposed persons must be removed immediately from the contaminated area and decontaminated. Rescue workers should wear self-contained breathing apparatus. Injured persons should not be allowed any physical activity, and a physician should be consulted immediately. It is advisable to keep an exposed individual under the observation of a physician for 6–24 h, depending on the circumstances of exposure. In some instances this can be accomplished at the plant medical facility, or the exposed individual may require hospitalization.

In handling phosgene, extensive safety precautions and procedures are required to prevent exposure to phosgene. The first point is to design the phosgene system to prevent phosgene emissions from the closed equipment. Chemically resistant, high quality materials are used for plant equipment and lines which are inspected regularly. Pumps that are hermetically sealed to the outside or utilize multiple mechanical seals with buffer fluids are used for phosgene-containing streams. Stringent requirements are set for the quality and design of phosgene process control equipment, and critical areas have redundant control systems. The second point is to quickly detect leaks and contain or decompose escaped phosgene. This includes such measures as continuous alarm systems to monitor the working

atmosphere, systems for decomposing escaped phosgene (eg steam-ammonia curtains for gaseous emissions), jacketed pipes, and complete containments for phosgene plants (68,69). Vacuum systems are also used to mitigate phosgene releases. These systems consist of a series of vacuum hoses that can be put near a small leak to draw in escaping phosgene, which is then sent to a decomposition unit. More detailed information on current industrial practices for safely manufacturing or handling phosgene are available through the Chemical Manufacturers Association Phosgene Panel, Washington, D.C.

In case of extensive leaks or spills, immediate evacuation upwind of the phosgene source is necessary. Phosgene is 3.4 times as heavy as air and may collect in low-lying areas (6). Water should not be used on the source of a phosgene leak as the resulting corrosion enlarges the leak. Suitable personal protective equipment includes eye protection and respiratory equipment. In case of fire, it is essential to cool all phosgene-containing vessels. Leaks of liquid phosgene or phosgene solutions can be effectively combated by covering the phosgene-containing liquid with an absorbent and decomposition agents.

Waste Disposal. Because of its low boiling point and high toxicity, measures must be taken to prevent the entrance of phosgene into drains or sewers. If recycle of phosgene is not feasible, phosgene waste can be handled by one of the decomposition methods mentioned in the Manufacture section, ie, caustic scrubbing, moist activated carbon towers, or combustion.

Uses

Phosgene is an important and widely used intermediate. Practically all phosgene manufacture is captive, ie, it is used in the manufacture of other chemicals within the plant boundary. Only VandeMark (owned by Groupe SNPE) sells phosgene on the merchant market. Phosgene manufacturers with captive consumption in the United States are Aventis, BASF, Bayer, Dow, DuPont, GE Plastics, Huntsman/ICI, Lyondell, PPG, Twin Lake Chemicals, VandeMark, and Zeneca. The U.S. production of phosgene for 1999 was 1.55×10^6 t, and for 2000, it was approximately 1.61×10^6 t (70). The primary use of phosgene is the manufacture of isocyanates for the polyurethane industry, in which ca 80% of the phosgene output in the United States is consumed. The manufacture of toluene diisocyanate [1321-38-6] accounts for ca 40% of the phosgene consumption, while methylene diphenyl diisocyanate (MDI) [101-68-8] and polymeric MDI [9016-87-9] account for ca 40%. The polycarbonate industry accounts for ca 13% of the phosgene consumption, and the remaining 7% is used to produce aliphatic diisocyanates, monoisocyanates, chloroformates, agrochemicals, and intermediates for pharmaceuticals and dyestuffs. Although several commercial phosgene-free processes for producing polyisocyanates and polycarbonates have been announced, they are not expected to make large inroads into phosgene demand in the near future (71–75).

Phosgene can be employed in a variety of metal-recovery operations, eg, in the recovery of platinum, uranium, plutonium, and niobium (76–80). Phosgene has been proposed for the manufacture of aluminum chloride, beryllium chloride, and boron trichloride (81–83). Phosgene has been patented as a stabilizer, either by itself or in combination with thionyl chloride, for liquid SO_2 (84).

Phosgene is also used in the production of chloroformates, ie, chlorocarbonates, which are intermediates in the production of ore-flotation agents, perfumes, herbicides, and insecticides, and especially in the preparation of pharmaceuticals (85). Chloroalkyl chlorocarbonates have been manufactured as intermediates for pharmaceuticals and pesticides (86,87). Phosgene is also employed in the manufacture of carbonic esters. Phosgene has been suggested as a starting material for the manufacture of carbon tetrachloride and other chlorinated hydrocarbons (88–92). A number of pesticides have been patented based on the reaction of a thiol or dithiol with phosgene to form thiol chloroformates (93,94). The preparation of aromatic acids using phosgene and detailed process for the manufacture of terephthalic acid from toluene and phosgene have been described (95,96).

An important direct use of phosgene is in the preparation of polymers. Polycarbonates are the most significant and commercially valuable group. However, the use of phosgene has been described for other polymer systems, eg, fiber-forming polymeric polyketones and polyureas (97,98).

BIBLIOGRAPHY

1. L. C. Riusema and L. G. Silverstein, *Am. Ind. Hyg. Assoc. J.* **33**(1), 35 (1972).
2. M. H. Noweir, E. A. Pfitzer, and T. F. Hatch, *Am Ind. Hyg. Assoc. J.* **34**(1), 25 (1973).
3. H. F. Anderson, J. A. Dahlberg, and R. Wettstrom, *Ann. Occup. Hyg.* **18**, 129 (1975).
4. H. B. Singh, *Nature* **264**, 428 (1976).
5. M. J. Thomson and co-workers, *Combust. Flame* **98**, 350 (1994).
6. *Chemical Safety, Data Sheet SD-95*, Manufacturing Chemists Association, Washington, D.C., Revised (1978).
7. G. G. Esposito, *Anal. Chem.* **49**, 1774 (Oct. 1977).
8. V. Henri and O. R. Howell, *Proc. R. Soc. London, Ser. A* **128**, 190 (1930).
9. R. Anathakrishnan, *Proc. Indian Acad. Sci. Sect. A* **5**, 285 (1937).
10. H. Babad and A. G. Zieler, *Chem. Rev.* **73**(1), 75 (1973).
11. J.-P. Senet, *The Recent Advance in Phosgene Chemistry*, Group SNPE, Paris, Vol. **1**, 1997; Vol. **2**, 1999.
12. T. A. Ryan, C. Ryan, E. A. Seddon, and K. R. Seddon, *Phosgene and Related Carbonyl Halides*, Elsevier Science B.V., Amsterdam, 1996.
13. A. N. Ketov, V. V. Pechkovskri, and L. P. Kostin, *Issled. Obl. Khim. Tekhnol. Mineral's Solei Okislov, Akad. Nauk SSR Sb. Statei* 202 (1965); *Chem. Abstr.* **65**, 1753a (1966).
14. A. N. Ketov, V. V. Pechkovskri, and L. P. Kostin, *Izv. Vyssh. Uchebn. Zaved., Tsvetn. Met.* **7**(2), 94 (1964); *Chem. Abstr.* **61**, 3894h (1964).
15. A. N. Ketov, V. V. Pechkovskri, and L. P. Kostin, *Zh. Neorg. Khim.* **9**, 467 (1964).
16. Yu. P. Kuznetsov, E. S. Petrov, and A. I. Vakhrusheva, *Izv. Sib. Otd. Akad. Nauk SSSR, Ser. Khim. Nauk* **1**(2), 63 (1969); *Chem. Abstr.* **71**, 1841p (1969).
17. Yu. P. Kuznetsov, E. S. Petrov, and A. I. Vakhrusheva, *Izv. Sib. Otd. Akad. Nauk SSSR, Ser. Khim. Nauk* **1**(3), 60 (1969); *Chem. Abstr.* **71** 116862c (1969).
18. A. N. Ketov, V. V. Pechkovskii, and L. P. Kostin, *Sb. Nauchn. Tr. Permsk. Politekhn. Inst.* **14**, 3 (1963); *Chem. Abstr.* **62**, 3642e (1965).
19. A. N. Ketov, V. V. Pechkovskii, and I. M. Kolesov, *Izv. Vyssh. Uchebn. Zaved., Khim. Khim. Tekhnol.* **9**, 570 (1967); *Chem. Abstr.* **66**, 592761k (1967).

20. A. N. Ketov and I. M. Kolesov, *Sb. Nauchn. Tr. Permsk. Politekhn. Inst.* **18**, 42 (1965); *Chem. Abstr.* **66**, 7991 (1967).
21. D. Naumann, *Kernenegie* **5**(2), 188 (1962).
22. R. J. Sorenson, U.S. Atomic Energy Commission, HW-79141, 1963, p. 22.
23. D. T. Peterson and D. J. Sundquist, *U.S. Atomic Energy Commission* (IS-917), p. 30 (1964).
24. I. S. Pap and co-workers, *J. Therm. Anal.* **36**, 1765 (1990).
25. R. Hazeldine and H. Iserson, *J. Am. Chem. Soc.* **79**, 5801 (1957).
26. C. W. Tullock and D. D. Coffman, *J. Org. Chem.* **25**, 2016 (1960).
27. R. Mertens and co-workers, *Angew. Chem.* **106**, 1320 (1994).
28. Ger. Pat. 4,028,774 (Dec. 3, 1992), P. Ksoll and co-workers (to BASF A.G.).
29. G. Martin and M. Martin, *Bull. Soc. Chim. Fr.* (8), 637 (1963).
30. H. H. Bosshard and H. Zollinger, *Helv. Chim. Acta* **42**, 1659 (1959).
31. *Chemistry & Industry* 682 (Sept. 21, 1992).
32. L. Abrams, W. V. Cicha, L. E. Manzer, and S. Subramoney, *Studies in Surface Science and Catalysis*, Elsevier Science B.V., Amsterdam, 2000, p. **130**.
33. U. Osterwalder, *Ber. Int. Kolloq. Verhuetung Arbeitsunfaellen Berufskrankrankh. Chem. Ind.* **10**, 785; *Chem. Abstr.* **104**, 111756 (1985).
34. *Chem. Eng.* 27 (Nov. 10, 1986).
35. *Unpublished papers on the Caustic Scrubbing of Phosgene, Department of Army, Office of the Program for Chemical Demilitarization*, 1975–1978.
36. Ger. Pat. 961681 (1953), H. Wollthan, and W. Groves (to Bayer A.G.).
37. K. Hess and R. Kotkamp, *Chem. Ing. Tech.* **45**, 873 (1973).
38. P. C. Nigam and S. Prasad, *Indian J. Environ. Health* **28**, 218 (1986); *Chem. Abstr.* **105**, 196347 (1986).
39. W. B. Crummett and J. D. Melean, *Anal. Chem.* **37**, 424 (1965).
40. B. B. Baker, *Am. Ind. Hyg. Assoc. J.* **35**, 735 (1974).
41. D. Reichert, U. Splengler, and D. J. Henschler, *Chromatograph* **179**(1), 181 (1979).
42. R. J. Graham and F. D. Stevenson, *J. Chromatogr.* **47**, 555 (1970).
43. P. K. Basu, C. J. King, and S. Lynn, *J. Chromatogr. Sci.* **10**, 419 (1972).
44. H. Geisser and W. Richarz, *J. Chromatogr.* **147**, 453 (1978).
45. W. S. Wu and S. Virindar, *Analyst* **118**, 1285 (1993).
46. R. J. Rando, H. G. Poovey, and S. N. Chang, *J. Liq. Chromatogr.* **16**, 3291 (1993).
47. H. B. Singh, D. Lillian, and A. Appleby, *Anal. Chem.* **47**, 860 (1975).
48. X. Luo, F. Y. Shi, and J. X. Lin, *Int. J. Infrared Millimeter Waves* **12**(2), 141 (1991); *Chem. Abstr.* **115**, 34533 (1991).
49. M. H. Noweir and E. A. Pfitzer, *Am. Ind. Hyg. Assoc. J.* **32**(3), 163 (1971).
50. B. W. Thomas, *Oil Gas J.* **63**(24), 119, 121 (1965).
51. R. M. Tuggle and co-workers, *Ind. Hyg. Assoc. J.* **40**, 387 (1979).
52. N. Nakano, A. Yamamoto, and Y. Kobayashi, *Talanta* **42**, 641 (1995).
53. R. H. Hunt, in *Optical Remote Sensing and Applications to Environmental and Industrial Safety Problems*, Apr. 6–8, 1992, Air and Waste Management Association, Pittsburgh, Pa., 1992, p. 446.
54. *K&M Environmental Safe Air System Validation Report for Phosgene, Virginia Beach, Va.*
55. *Bacharach Inc. Environmental Testing of Colorimetric Phosgene Dosimeter Badges, Pittsburgh, Pa.*
56. C. A. Rush and C. E. Danner, *Anal. Chem.* **20**, 644 (1948).
57. G. Leonardos, D. Kendall, and N. Barnard, *J. Air Pollut. Control Assoc.* **19**, 91 (1969).

58. *Threshold Limit Values for Chemical Substances and Physical Agents*, American Conference of Governmental Industrial Hygienists, Washington, D.C., 1994.
59. *Phosgene Criteria Document*, NIOSH 76-137, Washington, D.C.
60. S. A. Cucinell, *Arch. Environ. Health* **28**, 272 (May 1974).
61. W. F. Diller, *J. Occup. Health* **20**, 189 (Mar. 1978).
62. W. F. Diller, *Toxicol. Ind. Health* **1**(2), 7 (1985).
63. Y. L. Yue and co-workers, *J. Appl. Physiol.* **69**, 1615 (1990).
64. W. F. Diller and R. Zante, *Toxicol. Ind. Health* **1**(2), 117 (1985).
65. *Critical Review of the Medical Management of Acute Phosgene Poisoning*, International Isocyanate Institute; Ref. 11358.
66. *Options for Medical Management of Phosgene Poisoning*, International Isocyanate Institute; Ref. 11359.
67. *Phosgene Pulmonary Exposure Information*, 2nd ed., Chemical Manufacturers Association Phosgene Panel, Sept. 1996
68. *Chem. Week* 34 (May 28, 1986).
69. *Chem. Eng.* **99**(5), 5 (May 1992).
70. *Chemical Economics Handbook Data Summary – Phosgene*, 687.1000E, SRI International, July 2000.
71. S. Fukuoka, M. Chono, and M. Kohno, *J. Org. Chem.* **49**, 1458 (1984).
72. U.S. Pat. 4,146,727 (1979), E. T. Shaw and J. G. Zajanek (to Arco).
73. K. A. Henderson Jr. and V. A. Alexanian, *Org. Prep. Proced. Int.* **18**, 149 (1986).
74. U.S. Pat. 5,189,205 (Feb. 23, 1993), W. D. McGhee and T. E. Waldman (to Monsanto Co.).
75. W. McGhee and co-workers, *J. Org. Chem.* **60**, 2820 (1995).
76. Ger. Pat. 1,077,642 (Mar. 17, 1960), G. R. Bond Jr. (to Houdry Process Corp.).
77. U.S. Pat. 2,890,099 (June 6, 1959), H. B. Rhodes, W. F. Pesold, and J. M. Hirshon (to U.S. Atomic Energy Commission).
78. Fr. Pat. 1,472,438 (Mar. 18, 1965) (to Atomic Energy Research Institute).
79. H. L. Brandt, AEC Accession No. 42455, Rept. No. HW-83235, CFSTI, 20, Washington, D.C., 1964.
80. U.S. Pat. 3,212,847 (Oct. 19, 1965), B. J. Lerner (to Dominium Gulf Co.).
81. J. Hille and W. Dürrwächter, *Angew. Chem.* **72**, 850 (1960).
82. U.S. Pat. 3,146,065 (Aug. 25, 1964), R. O. Bach (to Beryllium Metals and Chemical Corp.).
83. R. K. Pearson and co-workers, U.S. Atomic Energy Commission, CCC-1024-TR-234, 1957.
84. U.S. Pat. 3,042,490 (July 3, 1960), T. W. Saults and J. J. Wimberly (to Tennessee Corp.); Brit. Pat. 975,318 (Nov. 18, 1964), R. V. Riley, T. F. Eden, and W. D. Hopkinson (to Stavely Iron & Chemicals Co., Ltd.).
85. U.S. Pat. 3,152,167 (Oct. 6, 1964), M. Sletzinger (to Merck & Co., Inc.).
86. J. V. Swintosky and co-workers, *J. Pharm. Sci.* **55**, 992 (1966).
87. Ger. Pat. 1,179,922 (Oct. 22, 1964), H. Grassner and F. Stolp (to Badische Anilin & Soda Fabrik A.G.).
88. R. N. Haszeldine and H. Iserson, *J. Am. Chem. Soc.* **79**, 5801 (1957).
89. O. Glemser and co-workers, *Angew. Chem.* **75**, 823 (1963).
90. Ger. Pat. 1,188,570 (Mar. 11, 1965), W. Ziegenbein and K. H. Hornung (to Chemische Werke Huels A.G.).
91. U.S. Pat. 3,406,212 (Oct. 15, 1968), K. O. Christie and A. E. Pavlath (to Stauffer Chemical Co.).
92. Ger. Pat 1,133,716 (July 26, 1962), D. Ludsteck and co-workers (to Badische Anilin & Soda Fabrik A.G.).

93. U.S. Pat. 3,277,143 (Oct. 4, 1966), H. Tilles (to Stauffer Chemical Co.).
94. U.S. Pat. 3,093,537 (June 11, 1963), H. Tilles.
95. U.S. Pat. 2,552,591 (May 15, 1951), W. H. C. Rueggeberg, R. K. Frantz, and A. Ginsburg (to United States Army).
96. F. Runge, H. Reinhard, and G. Kühnhanss, *Chem. Tech. Berlin* **8**, 644 (1956).
97. Ger. Pat. 1,148,073 (May 2, 1963), R. Moroni and E. Dumont (to Collo-Rheincollodium Koeln G.M.b.H.).
98. U.S. Pat. 3,412,072 (Nov. 19, 1968), C. J. Bouboulis and I. Kirschenbaum (to Esso Research & Engineering Co.).

KENNETH L. DUNLAP
Bayer Corporation

PHOSPHORUS-CONTAINING POLYMERS AND OLIGOMERS

Introduction

The only valid generalization about phosphorus polymers is that they tend to be flame retardant (1,2). The flame-retardant effect depends heavily on the phosphorus content. Red (polymeric) phosphorus, despite its combustibility, is a commercial flame-retardant additive. Other features of many phosphorus polymers are adhesion to metals, metal ion-binding characteristics, and increased polarity (2). The flexible P—O—C linkages tend to impart lower glass-transition temperatures. Phosphorus polymers with acid groups are used industrially for ion exchange, adhesion, and scale inhibition. Some form water-soluble coatings used as primers in metal protection and for photolithographic plates. The binding properties have led to dental applications. Cellulose phosphates have found some drug and ion-exchange uses. Academic interest has been stimulated by the relationship of certain phosphate polymers to natural products, such as the nucleic acids (see POLYNUCLEOTIDES).

This review gives most attention to those phosphorus polymers which have attained commercial use or which have been (or currently are) the subject of serious development efforts. Other reviews encompass phosphorus polymers of mainly academic interest (3,4). The commercial examples tend to be specialty polymers and none have attained large volume usage. One reason is cost. In addition, those polymers having P—O links are usually more hydrolyzable than corresponding C—O bonded polymers, and moreover the phosphorus acids which are liberated tend to catalyze further hydrolysis. Hydrolytically stable phosphine oxide

Encyclopedia of Polymer Science and Technology. Copyright John Wiley & Sons, Inc. All rights reserved.

types are known but are costly. Another hydrolytically stable class, the polyphosphazenes, is discussed in a separate article.

Phosphorus-containing oligomers (low polymers) have been included in this article because they have become more important commercially than high polymers, since they can be used as additives or coreactants to introduce sufficient phosphorus for flame retardancy or some other desired property provided by phosphorus, such as metal binding (5,6).

The modification of conventional polymers with small amounts of phosphorus, reactives, or comonomers to impart flame retardancy (1,4,6) or improve other properties has become commercially significant, and is discussed separately below in connection with the polymer class being modified.

Polymeric Form of Elemental Phosphorus

Phosphorus occurs in several allotropic forms. The principal commercial form is white (or yellow) phosphorus; the molecule consists of four phosphorus atoms arranged in a tetrahedron. Heating white phosphorus at 270–400°C, preferably with a catalyst, produces red phosphorus, a stable, nontoxic, high melting, insoluble polymeric solid. Red phosphorus (often stabilized by additives) has been used for many decades as the igniting agent for the striking surface of safety matches. It is insoluble, thermally quite stable, and nontoxic; while it can be ignited, it is surprisingly effective as a flame retardant for plastics, and it is now finding commercial use, especially in Europe to flame-retard nylon. Other applications and its mode of action have been reviewed (7).

To prevent decomposition of red phosphorus to the toxic and highly flammable white form, it is stabilized with additives (8) and/or encapsulated with a thermoset resin.

The structure of red phosphorus is not fully established. It is believed (9) to be a cross-linked polymer with chains having the structure shown in Figure 1.

Inorganic Phosphorus Polymers

Inorganic polyphosphates are covalently linked polymers (10,11). Chains of repeating phosphate units are formed by eliminating the elements of water from adjacent orthophosphate units. Such polycondensations take place, for instance, when orthophosphoric acid is heated, producing a broad distribution of linear molecules of various chain lengths corresponding to the general formula $HO[P(O)(OH)O]_nH$. A table of compositions for various weight percentages of P_2O_5 is given in Reference 10.

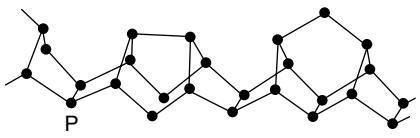

Fig. 1. Probable structure of red phosphorus.

Polyphosphoric acid itself has found utility mainly as a supported catalyst in the petroleum industry for alkylation, olefin hydration, polymerization, and isomerization, and for syntheses of fine chemicals and dyes. It is used to phosphorylate alcohol groups, for example in the production of anionic phosphate surfactants.

Heating alkali metal or alkaline earth metal dihydrogen phosphates produces polymeric salts (cyclic metaphosphates and linear polyphosphates) and cross-linked polyphosphates (ultraphosphates), depending on temperature and the presence of other ingredients (11,12). This complex group of polymers includes materials with crystalline, glass-like, fibrous, or ceramic properties as well as some with thermoplastic and thermoset characteristics; some are useful as binders for metals, ceramics, and dental restorations. Reviews are available on glasses (12,13), crystalline compounds (14), and polyphosphate fibers (15).

The water-soluble poly- and metaphosphates exhibit chelating properties. Glassy sodium metaphosphate (DP ca 15–20) is used in water treatment for scale inhibition (16). Long-chain sodium polyphosphates (metaphosphates) are used as preservatives in red meat, poultry, and fish (16). Long-chain sodium and potassium phosphates are added to sausage meat to improve color and texture (16).

Polyphosphates are produced naturally in some yeasts, comprising up to 30% of their total phosphate and up to a 600 degree of polymerization (17). These probably provide energy storage for the yeasts.

Some of the inorganic phosphate polymers possess properties resembling those of glassy organic plastics. Corning has attempted to commercialize low-melting phosphate-containing glasses as reinforcing fibers with excellent dimensional stability (18,19). The fibers can be made *in situ* by stirring in a high temperature thermoplastic melt. Phosphate glasses can also be molded at 360–400°C to make high refractive index lenses (20).

Heating of ammonium phosphates under an atmosphere of ammonia or in the presence of urea produces ammonium polyphosphate (21,22). At a high degree of polymerization, the product is a water-insoluble solid. This form of ammonium polyphosphate is used commercially as a flame-retardant additive for plastics and as the latent acid component in intumescent paints, mastics, and caulks (23,24). The water resistance can be further enhanced by encapsulation with a resin.

Polymeric Phosphorus Oxynitrides and Phosphorus Iminoimides

Condensed phosphoramides with linear, cyclic, or cross-linked structures are produced by the reaction of $POCl_3$ with ammonia. The higher molecular weight products are insoluble in water and on further heating are converted to a cross-linked insoluble polymer, phosphorus oxynitride $(PON)_x$ (25). Phosphorus oxynitride can be made by prolonged heating of melamine phosphates (26), urea phosphate (26), or ammonium phosphate under conditions where ammonia is retained (27). Phosphorus oxynitride is an effective flame retardant in those polymers, such as nylon 6, which can be flame retarded by exclusively char-forming condensed-phase means. However, phosphorus oxynitride is ineffective (at least by itself) in those

polymers, such as polybutylene terephthalate, which pyrolyze easily to volatile fuel (28–30).

An imido analog of phosphorus oxynitride, phospham, $(PN_2H)_x$, is made as the exhaustive self-condensation product of aminophosphazenes, but also may be made directly from elemental phosphorus and ammonia or from phosphorus pentasulfide and ammonia. Phospham is probably a thermoset phosphazene imide. It can be amorphous or crystalline. It is also an effective and thermally stable flame retardant, especially for high-temperature-processed polyamides (31). It was available for a short time as a development product from Japan.

Amorphous polymeric dielectric films of phosphorus nitrides and oxynitrides ("Phoslon") can be prepared on electronic substrates by chemical vapor deposition (32).

Organic Phosphorus Polymers

Phosphines. Polymeric phosphines exhibit strong metal-binding properties. Nonpolymeric phosphines, in particular triphenylphosphine, are employed as ligands for cobalt and rhodium in hydroformylation catalysts used in plasticizer manufacture. Extensive efforts have been made to attach phosphine–metal complexes to polymers in order to facilitate catalyst recovery and enhance selectivity (33). Problems of cost, catalyst life and activity, heat transfer, and mass transfer seem to have prevented commercialization.

Polymers from diarylphosphinylstyrenes have been prepared as ligands (34). Styryldiphenylphosphine monomer, commercially available in laboratory quantities, is easily polymerized or copolymerized (34,35). Copolymers of styryldiphenylphosphine with styrene cross-linked with divinylbenzene are commercially available in laboratory quantities.

Some polymeric phosphonium salts have been reported to have advantages in reaction rate or ease of separation relative to monomeric phosphonium salts as catalysts for nucleophilic reactions where the large cation favors nucleophilic reactivity of the anion (36).

Phosphine Oxides. The outstanding property of polymeric phosphine oxides is their stability. Since the electron pair of the phosphine structure has been donated to an oxygen atom, the phosphine oxide group is unreactive, although it is very polar and subject to strong hydrogen bonding.

Polymeric phosphine oxides are made by a variety of condensation- and addition-polymerization methods. Radical-initiated copolymerization of compounds with $RPCl_2$ structures with olefins produces polydichlorophosphanes, which on hydrolysis yield polyphosphine oxides (37). Where *p*-xylylene (produced by pyrolysis) is the olefin, this copolymerization affords quite tenacious high-temperature thermoplastic phosphine oxides (38).

Polystyrenes with attached phospholene oxide rings are recoverable catalysts for converting isocyanates to carbodiimides (39).

A series of polyesters and polyethers made from aromatic phosphine oxides exhibit stability as well as flame resistance (40,41). Aromatic polyethers containing phosphine oxide structures are made according to the following reaction (41–43):

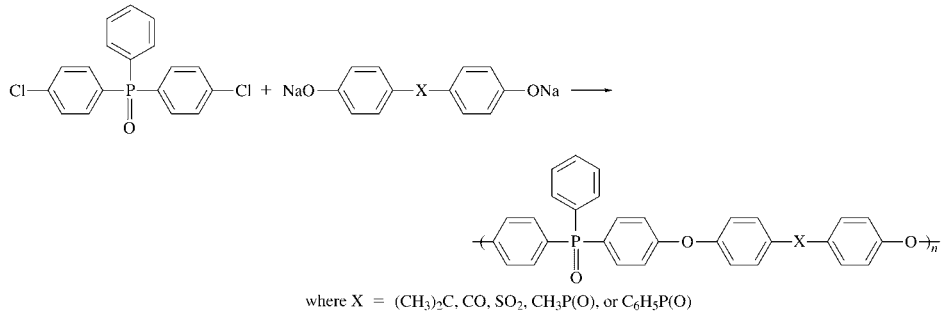

where X = $(CH_3)_2C$, CO, SO_2, $CH_3P(O)$, or $C_6H_5P(O)$

These polymers show good flame resistance and low smoke, and some have been introduced on a development scale for potential use in graphite composites and as electrical insulation for aircraft. Some polyphosphine oxides have been shown to be suitable for optical applications (44).

Aliphatic polyamides with a phosphine oxide unit in the dicarboxylic acid portion or the diamine portion of the polymer chain have been described (45–47). These were intended to have flame resistance while retaining adequate thermal and hydrolytic stability. The effect of the phosphine oxide on softening and heat distortion temperatures of these structures has been studied (48); some show elevated glass-transition temperatures (T_g) and softening temperatures compared to the phosphorus-free analogs, others show depressed melting behavior and loss of crystallinity. Increasing the content of phosphine oxide depresses the melting point and in most cases the crystallinity. In some cases incorporation of phenylphosphine oxide structures improves thermal properties.

One comparative study showed that the flame retardancy of an aromatic phosphine oxide copolymer was no better than that achieved by a similar amount of phosphine oxide structure as an additive (49).

Aromatic polycarbonates containing diphenylphosphine oxide units attached laterally to the chain (using the diol made by adding diphenylphosphine oxide to benzoquinone) have been shown in a General Electric patent to achieve flame retardancy without loss of T_g or impact strength (50). The required intermediate, diphenylphosphinous chloride, is commercially available, but this application has not been commercialized.

Polyimides containing phosphine oxide structures have been explored in the quest for highly stable thermoplastics. In the search for flame-retardant, heat-stable composites for aerospace applications, structures such as the following were prepared:

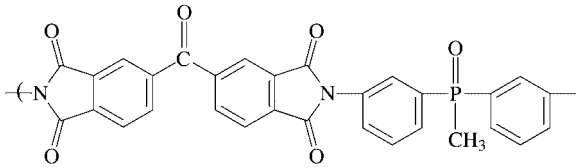

This polymer is stable to 400°C and shows excellent adhesion to glass-fiber reinforcement (51–53).

Phosphine oxide-containing polyimides were produced at NASA by polymerization of phosphine oxide-containing maleimides illustrated by the following structure (54):

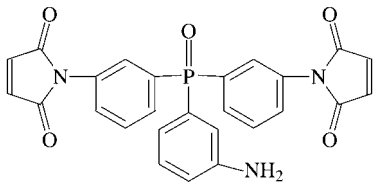

Ammonia-cross-linked textile finishes from tetrakis(hydroxymethyl) phosphonium salts have a primarily phosphine oxide structure and are discussed under the topic of cellulosic textile finishes.

Phosphinites and Phosphonites. In common with phosphines these classes of phosphorus structures have unshared electron pairs on the phosphorus. They tend to be unstable to oxidation and are good metal binders. Consequently, they have been prepared as antioxidant scavengers, catalyst ligands, and ion-extraction reagents, but no commercial applications of polymeric phosphinites or phosphonites are known.

Phosphites. Phosphites, mostly nonpolymeric, are employed as the peroxide-decomposing components of antioxidant systems for polyolefins and diene rubbers.

Polyphosphites, actually poly(hydrogen phosphonate)s, have been described as being made by transesterification of dialkyl phosphites with diols, but some examples have been shown to proceed concurrently with dealkylation and formation of acid end groups (55). If the acid end groups are realkylated such as by diazomethane, high molecular weight poly(hydrogen phosphonates) can be made (56). The use of diphenyl hydrogen phosphonate instead of dialkyl hydrogen phosphonate also permits achieving high molecular weight. These phosphite polymers can be oxidized to synthetic analogs of the nucleic acid backbone.

An oligomeric phenyl dipropylene glycol phosphite, averaging eight phosphite groups per mole, is a commercial color stabilizer (Doverphos 12, Dover Chemical Corp.) for rigid and plasticized PVC.

$$(C_6H_5O)[P(OC_6H_5)OC_3H_6OC_3H_6O]_7P(OC_6H_5)_2$$

Typical use levels are 0.25–1% in vinyls and polyurethanes.

A lower oligomeric dipropylene glycol phosphite, averaging three phosphite groups and five hydroxyl groups (GE's Weston PTP Phosphite) is used in foamed polyurethanes to control color development and prevent bun scorching.

Phosphinates. Phosphinate structures confer flame retardancy to polyester fibers (discussed separately below).

Esters of P-phenyl-P-vinylphosphinic acid can be polymerized to high molecular weight by free-radical initiators. The monomers are prepared from phenylphosphonous dichloride (57).

Oligomeric phosphinic/carboxylic acid copolymers are made by radical-catalyzed polymerization of acrylic and/or maleic acid in the presence of

hypophosphorous acid or sodium hypophosphite. The phosphinic unit is incorporated by a chain-transfer reaction (58,59). Products of this type are effective scale inhibitors for water treatment, and are commercially used.

(Hydroxymethyl)phenylphosphinic acid (an adduct of formaldehyde and phenylphosphinic acid) can be thermally dehydrated to form oligomers which are useful in flame retarding polyethylene terephthalate (60). These may have reached commercial usage in Europe.

A large and varied family of polymers have been made from a cyclic phosphinate made commercially from *o*-phenylphenol by the following reaction sequence:

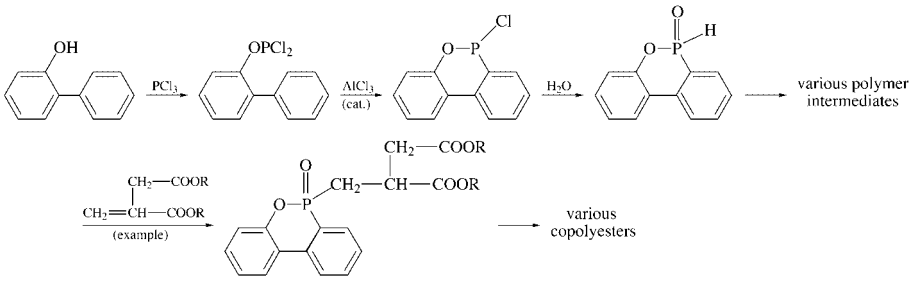

The key intermediate, a cyclic hydrogenphosphinate, 9,10-dihydro-9-oxa-10-phosphaphenanthrene-10-oxide, has been converted, originally by Japanese manufacturers, to a variety of difunctional polymer intermediates. Addition to itaconic ester produces a dicarboxylic ester commercially used to make thermoplastic polyesters. This technology is discussed below in connection with modified polyester fibers and epoxy resins. Addition of the hydrogen phosphonate to itaconic acid and copolyesterification can be done in a single operation (61).

The cyclic hydrogen phosphinate can also be added to benzoquinone to make a substituted hydroquinone and a diglycidyl ether therefrom, discussed below in connection with epoxy resins.

Phosphinates made from acrylic acid and methyl- or phenylphosphonous dichloride are used commercially to provide inherent flame retardancy to polyester fibers.

Phosphonates. The principal synthetic routes include addition and condensation methods. Although a large number of vinyl and diene phosphonate monomers have been described in the literature (2,5,7,62), only bis(2-chloroethyl) vinylphosphonate (Akzo-Nobel's Fyrol Bis-Beta monomer), vinylphosphonic acid (Clariant), and dimethyl vinylphosphonate (Clariant) have been offered commercially. The diethyl vinylphosphonate is available in laboratory quantities.

Vinylphosphonates are slow to homopolymerize. They copolymerize with most common monomers but particularly well with vinyl acetate (63), vinyl chloride, and acrylonitrile (64). The copolymerization Q and e values for bis(2-chloroethyl) vinylphosphonate are 0.23 and 1.73, respectively (65), reflecting an electron-poor double bond and low resonance stabilization of the free radical. They are also prone to chain transfer. Representative copolymers have been studied and evaluated for their expected flame-retardant action (66) but cost considerations have generally not encouraged commercial use of vinylphosphonate esters for this purpose.

Plasticized vinyl polymers are made by terpolymerization of bis(2-chloroethyl) vinylphosphonate with vinyl chloride and alkyl acrylates (67–69). These terpolymers can be calendered to films and were for a time in commercial development by Stauffer Chemical Co., for use as truck and container decals with permanent plasticity.

Vinylphosphonic acid is produced in Germany and used, initially by Hoechst, later by others to manufacture a hydrophilic poly(vinylphosphonic acid) prepared by free-radical polymerization in a solvent (70,71). Poly(vinylphosphonic acid) is mainly used for the treatment of aluminum photolithography plates before application of the photosensitive layer (72,73). The coating improves the developing and printing characteristics of the plate. Dental cement applications of cross-linked poly(vinylphosphonic acid) have also been studied (74). Vinylphosphonic acid copolymers with vinylsulfonic acid have been patented as scale inhibitors for water treatment (75).

Isopropenylphosphonic acid polymers are water-soluble and are believed to have found commercial utility as scale inhibitors (76). A flame-retardant copolymer of α-phenylvinylphosphonic acid with styrene has been patented (77).

The tetraethyl ester of 1,1-vinylidenediphosphonic acid has been used to make cross-linked copolymers which are ion-exchange resins with selective chelation properties for toxic metal cations (78). An alternative method for introducing the diphosphonic acid structure is by reaction of a methylenediphosphonic ester with chloromethylated styrene copolymer beads (79). At least one such resin class, Diphonix, also containing sulfonic acid and other functional groups, has shown promise for treatment of radioactive waste and for iron control in copper electrowinning (80,81).

An oligomeric vinylphosphonate was commercialized in the 1970s as a flame-retardant finish on cotton, principally for children's sleepwear (82).

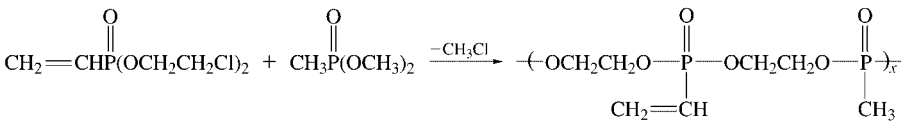

Upon free-radical-initiated curing, usually with a comonomer such as *N*-methylolacrylamide or with an amino resin, this monomer produces a cross-linked finish for cotton, resistant to laundering (83–85). This product was discontinued in the United States for marketing and cost reasons, but was later used in Japan for some nonapparel applications.

Vinylbenzylphosphonate diethyl ester was prepared by the Arbuzov reaction of vinylbenzyl chloride with triethyl phosphite, and this monomer was used as a precursor for experimental resins with metal-binding properties (86).

Copolymers of diethyl (methacryloyloxymethyl)phosphonate have recently been reinvestigated for possible flame-retardant use (87). Various acrylate and methacrylate monomers with phosphonic acid groups, which aid bonding to dentine, have shown promise for dental restoration purposes (88). Various allyl phosphonates (89) have been proposed for these uses but none appear to have found application.

Condensation Polymerization Routes to Polymeric Phosphonates. Reaction of a phosphonyl dichloride with an aliphatic diol produces polyphosphonates which are low melting and hydrophilic. Industrial interest has been concentrated on the polyphosphonates made from aromatic diols or aromatic phosphonyl dichlorides.

Because of the commercial availability of phenylphosphonyl dichloride (benzene phosphorus oxydichloride, BPOD), much work has been done on this intermediate to make polymeric phosphonates as flame-retardant thermoplastics or as additives for thermoplastics. In an early study, Toy (90) carried out the polycondensation of BPOD and dihydric phenols in a melt. Coover and McConnell added the use of an alkaline earth halide catalyst (91). For enhancement of the flame-retardant effectiveness as fiber additives, tetrabromobisphenols were used to make polyphosphonates (92). Various cocondensed polyesters with both phosphonate ester units and dicarboxylic ester units have been described and patented.

Toyobo in Japan introduced commercially the polymer or oligomer from phenylphosphonic dichloride and 4,4′-sulfonylbisphenol as an additive for polyester fibers, initially to meet the Japanese flame-retardant regulations for home furnishings (93,94).

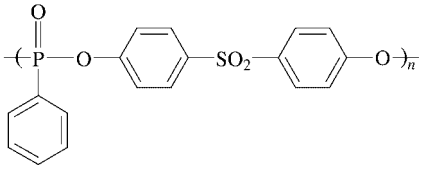

This oligomer, which seems to have a higher flame-retardant effect than the sulfur-free analogs, has been further studied and piloted in the United States (95–97). Its manufacture and use has also been developed in China and it is made there on a commercial scale (98).

Interfacial polycondensations for the synthesis of polyphosphonates by reaction of phosphonyl dichlorides with diols can be very rapid and, under favorable conditions, give high molecular weights (99,100).

Transesterification of a Phosphonate with a Diol. This method proceeds well in the case of *O,O*-dialkyl hydrogen phosphonates (101) but less selectively with *O,O*-dialkyl alkyl- or arylphosphonates. With *O,O*-diaryl alkylphosphonates, ester exchange is an effective route to polymeric phosphonates (102–104):

Higher molecular weights can be attained by adding tri- or tetrahydric phenols or triaryl phosphates to the reaction mixture (105). A transparent flame-retardant poly(methylphosphonate) thermoplastic made by this technology was for a time in development by Bayer (103). Mechanical properties were excellent, although resistance to hot water was somewhat deficient.

Transalkylation of a Phosphonate with a Dihalide. This route is especially useful with *O,O*-dimethyl phosphonates and bis-primary dihalides, eg, in the production of a poly(ethylene methylphosphonate) (106):

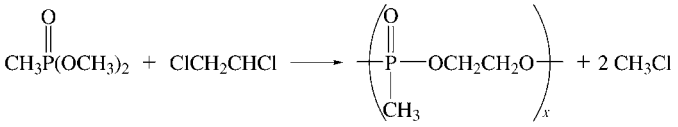

The reaction proceeds most readily in the presence of a basic catalyst (7,106). This chemistry was used for the commercial manufacture of a flame-retardant hydroxyl-terminated oligomer (7,107) suitable for flame-retarding thermoset resins and resin-impregnated paper.

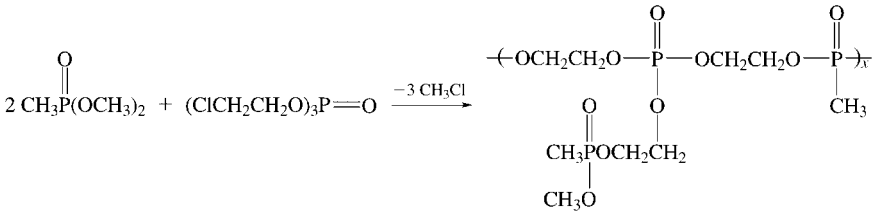

This route was superseded by an alternative halogen-free process using phosphorus pentoxide, as described below.

Arbuzov Polycondensation. To date industrial applications have been limited to production of oligomeric flame retardants, such as the conversion of tris(2-chloroethyl) phosphite to a mixture of its intramolecular Arbuzov rearrangement product, bis(2-chloroethyl) 2-chloroethylphosphonate and its oligomeric intermolecular Arbuzov products (108,109), where $x = 2$–6:

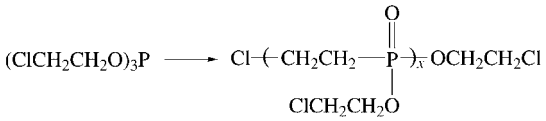

The detailed structure of the oligomers is open to some question; isomers and branched structures are likely. A product of this reaction, a mixture of monomeric and lower oligomeric compounds, is sold as Antiblaze 78 (A&W, now Rhodia) for flame retardance in urethane foam.

Arbuzov Cyclopolycondensation. This versatile reaction and related cyclopolymerizations have been extensively studied (101,110,111). A typical example is the cyclopolycondensation of methyl ethylene phosphite (112):

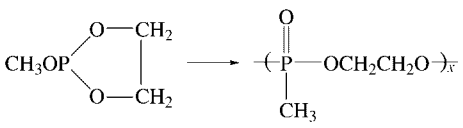

Insertion of an Alkylene Oxide into a Phosphonic Anhydride. A useful route to oligomeric flame retardants is based on the following two-step synthesis (113):

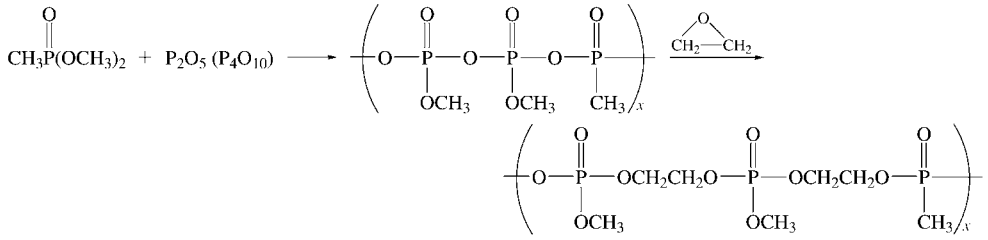

By inclusion of a limited amount of water or alcohol in the synthesis, oligomers of this type can be made with controlled hydroxyl content. Such products are exemplified by Akzo Nobel's Fyrol 51 or Fyrol 58 flame retardants which are useful as reactive oligomers in thermosets. In resin-treated automotive air filters this type of product is chemically linked into the resin and resists leaching by water when the filters are cleaned. Fyrol 51 has also found utility in making flame-retarded polyurethanes and textile finishes.

Insertion of a Diepoxide into a Phosphonate Ester. The insertion reaction of bisphenol A diglycidyl ether with diaryl aryl- or alkylphosphonates was shown to give polyphosphonates of moderate molecular weight (114).

Condensation of Phosphites with Aldehydes or Ketones. A phosphonate oligomer, Phosgard C22R (formerly made by Monsanto) flame retardant, has been used commercially as an additive in acrylics and thermoset plastics (115).

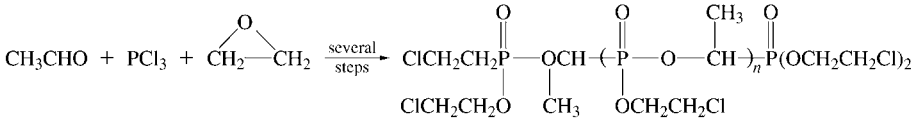

A related product was developed at Rohm and Haas Co., from acetone, ethylene glycol, and PCl_3, and probably has been used in flame-retarded acrylic sheets. (116,117).

Friedel-Crafts Reaction of PCl_3 on Styrenic Polymers, Followed by Oxidation. Ion-exchange resins with selective affinity for lanthanides and other "hard" cations have been made by the aluminum chloride-catalyzed reaction of PCl_3 with macroporous cross-linked styrenic resin beads. The initially formed phosphonous dichloride was hydrolyzed and oxidized to a resin with phosphonic acid groups (118).

Phosphonylation of a Carboxylic Acid Polymer. The reaction of a water-soluble polycarboxylic acid with phosphorous acid is said to yield a polymer with hydroxybis(phosphonic acid) structures. These are effective scale-inhibiting agents for aqueous systems (119) but not known to have been commercialized. A similar reaction in a Chinese study is said to result in the replacement of carboxyl groups by phosphonic acid groups (120) to produce polymers with similar utility.

Phosphates. Polymeric phosphates are used for the preparation of flame-retardant polymers, ion-exchange resins, and models for natural biopolymers such as nucleic acids, teichoic acids (components of bacterial cell walls) (121), and polynucleotides, which are discussed in a separate article. Synthetic poly(1,3-alkylene phosphates) as mimics of the natural teichoic acids have been studied, particularly in respect to Mg^{2+} binding and ion transport (122).

Addition polymerization of unsaturated phosphate monomers has been extensively investigated, but to date only a few industrial applications have been found. Dental anticaries applications of phosphoenol pyruvate polymers and copolymers with acrylic acid have been demonstrated *in vitro* (123).

Monoallyl phosphates undergo chain transfer at the allylic methylene group and polymerize poorly (89). Triallyl phosphate polymerizes with free-radical initiation to a hard, clear cross-linked polymer. This monomer was briefly piloted by the former Marbon Co. but not successfully commercialized.

Acid phosphate monomers made from hydroxyethyl acrylate or methacrylate and P_2O_5 are useful acrylic or epoxy coating components and dental adhesives (124), and promote adhesion to metal substrates (125–128). The mono(methacryloxyethyl) phosphate and di(methacryloxyethyl) phosphate are available as Kayamer PM-1 and PM-2 from Nippon Kayaku, or the mixture as Ebecryl 170 from UCB Radcure:

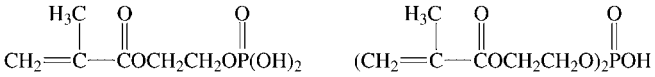

Polycondensation of Phosphoryl Dihalides with Diols. Poly(arylene aryl phosphate)s can be made stepwise by first preparing a phenyl phosphorodichloridate which reacts with a dihydric phenol, or in one step by the reaction of phosphorus oxychloride with a mixture of monohydric and dihydric phenols. Depending on the reactant ratio, the products can be oligomers or high molecular weight thermoplastic or thermoset polymers (129).

Aromatic phosphate polymers were found to have good transparency, hardness, and adhesion, but too brittle and hydrolytically unstable.

Oligomeric aromatic phosphates have been patented and commercially used as flame-retardant additives mainly for impact-resistant polystyrene blends with polyphenylene oxide and polycarbonate blends with acrylonitrile–butadiene–styrene (ABS) copolymers (130,131). They have also been shown useful in thermoplastic polyesters (92). The principal commercial examples are based on phenol and resorcinol (Akzo-Nobel's Fyrolflex RDP) or phenol and bisphenol A (Akzo-Nobel's Fyrolflex BDP or Albemarle's Ncendx P-30). Although these have the diphosphate as their principal ingredient, they also contain higher oligomers.

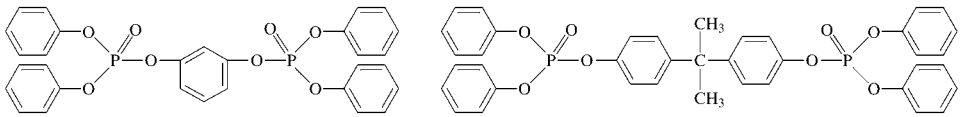

Some patents and publications suggest flame retardancy advantages for the higher oligomers (132,133). A systematic study of the oligomers and polymers made from alkyl and aryl dichlorophosphates and dihydric phenols showed that their flame retardancy (as expressed by oxygen index) is a function of phosphorus content and of thermal stability (134).

Insertion of Phosphorus Pentoxide into a Phosphate, Followed by Epoxide Insertion. The insertion of phosphorus pentoxide into a trialkyl phosphate or a tris(haloalkyl) phosphate produces oligomeric metaphosphoric anhydrides, which upon further insertion of an epoxide into the P—O—P linkages affords oligomeric phosphates. An older route for the chloroethyl phosphate oligomers used a transalkylation reaction for polycondensation, producing dichloroethane as by-product.

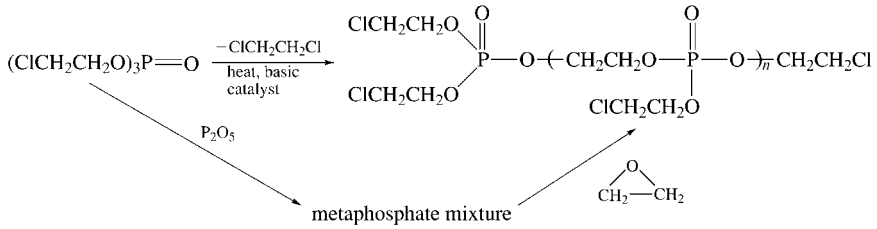

By inclusion of a proton source, such as H_3PO_4, water, or an alcohol, these oligomers can be made with hydroxyl functionality. Thus, a hydroxyl-terminated ethyl ethylene phosphate, Exolit OP 550, is made from triethyl phosphate, P_2O_5, phosphoric acid, water, and ethylene oxide. It has been introduced by Clariant as a reactive flame retardant for polyurethane foams (135).

The reaction of a trialkyl phosphate, P_2O_5, and ethylene oxide, omitting the addition of a proton source unlike the preceding synthesis, can produce a substantially nonfunctional oligomer (136). A product of this type, Akzo Nobel's Fyrol PNX, has been introduced as a high efficiency flame retardant for flexible or rigid polyurethane and polyisocyanurate foams. Because of its oligomeric character, it has low vapor emission (thus freedom from window fogging) in applications such as automobile seating (137).

Diepoxide Reaction with Phosphoric Acid. The reaction of phosphoric acid with diepoxides can produce linear polymers or gels which can be hydrolyzed to water-soluble poly(alkylene phosphates) (138,139).

Polycondensation of Compounds Containing a Phosphate Linkage. Polycondensation of tris(2-chloroethyl) phosphate, preferably in the presence of a nucleophilic catalyst, affords an oligomeric phosphate which was for a time produced by this process as a flame retardant for polyurethane foams, thermoset resins, and air-filter products (140–142). A preferred method, avoiding a chlorinated coproduct, is based on addition of phosphorus pentoxide and ethylene oxide to the tris(2-chloroethyl) phosphate, as discussed above.

Cyclopolymerization of Five- or Six-Membered Ring Phosphates. Poly(ethylene methyl phosphate) is formed from cyclic methyl ethylene phosphate (110).

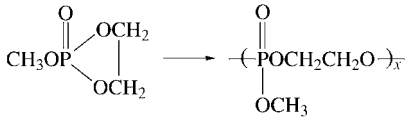

The reaction is thermally reversible and, consequently, polymers and oligomers with P(=O)OCCOP(=O)O linkages cannot be used in high temperature applications.

Production of poly(alkylene hydrogen phosphates) can be accomplished by ring-opening polymerization of cyclic hydrogen phosphonates, followed by oxidation (for example by chlorination and hydrolysis). The intermediate chloride can also be converted to esters or amides (111).

Phosphorus–Nitrogen Polymers. The most extensively investigated class of such polymers is the polyphosphazenes, which have been reviewed in regard to flame retardancy (143) and which are discussed in a separate article in this Encyclopedia. Research on polymeric phosphonamides, phosphoramides, and phosphorimides has not as yet led to commercial results.

Condensation Polymerization of Phosphonyl Dihalides or Phosphoryl Dihalides with Diamines. Polyphosphonamides have been prepared by interfacial reaction of phenylphosphonic dichloride with diamines (99,144); these products have apparently not been commercialized. Polyphosphonic amides have been shown to have useful flame-retardant efficacy in polyolefin formulations with other phosphorus additives (145).

Film-forming polyphosphoramides (146) form reverse-osmosis membranes impervious to urea and appear to have promise for artificial kidney applications.

Condensation Polymerization of Phosphonate Esters or Diamides with Diamines and Related Reactions. Treatment of diphenyl methylphosphonate with diamines produces thermoplastic materials with elemental compositions corresponding to polymeric phosphonamides or imides (102,147,148).

Phosphorus-Modified Plastics, Resins, and Textiles

In many cases, only small quantities of phosphorus are introduced by various means into a polymer to achieve desired properties such as flame retardancy or improved adhesion.

Polyolefins. Polyethylene can be phosphorylated with phosphorus trichloride and oxygen by a free-radical chain reaction (118,149–151). Side reactions include separate oxidation of the phosphorus trichloride and of the polymer. Hydrolysis gives phosphonic acid structures, which can impart flame retardancy and improved adhesion to surfaces. These materials have been explored for dental and bone therapy applications but no commercial use is known.

Styrene Resins. The introduction of phosphorus acid groups into polystyrene gives ion-exchange resins with different selectivities than the usual sulfonated types. In one method $-PCl_2$ groups are attached to the aromatic ring by reaction of polystyrene (or cross-linked styrene–divinylbenzene copolymer) with phosphorus trichloride with an aluminum chloride catalyst (152). After hydrolysis and oxidation, the aromatic rings contain $P(O)(OH)_2$ groups. Hydrolysis alone gives polystyrenes with phosphinic acid groups (153). Polystyrenes with phosphonic or phosphinic acid groups show selective ion-exchange properties toward metals (154) (see ION-EXCHANGE RESINS; STYRENE POLYMERS).

A macroporous polystyrene–divinylbenzene with sodium phosphonomethylaminomethyl groups has been marketed as Duolite ES-467 ion-exchange resin

(Rohm and Haas Co.) which is highly effective in chelating divalent metal cations. It removes traces of calcium from saturated sodium chloride brine, such as the feed streams to chlorine-caustic electrolytic cells (155). This resin also has high affinity for lead and zinc, and has been used for treating industrial-waste streams and cooling-tower waters.

Vinyl and Acrylic Polymers. Vinyl and acrylic polymers containing phosphorus are prepared from a phosphorylated monomer or by treating the polymer with a phosphorus compound.

Phosphonate groups are introduced into PVC via the Arbuzov reaction with a trialkyl phosphite (149); this reaction is slow and is accompanied by dehydrochlorination of the PVC and by intramolecular Arbuzov rearrangement of the phosphite (156,157). However, this reaction of phosphites may play a role in stabilizing PVC.

Acrylic dental adhesives have been modified with a phosphate ester linkage by reaction of a glycidyl methacrylate or hydroxyethyl methacrylate with phosphorus oxychloride (158). One such product, a 3M Scotchbond, adheres to dentine as well as to tooth enamel. Adhesion to enamel can be improved in dental bonding cements by including an acryloxyalkyl- or acryloxyaryl acid phosphate component (159). Japanese products utilize an unsaturated phosphinic acid monomer to improve adhesion (160).

Phosphorus acid groups can be introduced into acrylic acid polymers by use of chain transfer during polymerization in the presence of phosphorous acid (which provides a phosphonic acid end group) or hypophosphorous acid (which can provide a phosphinic acid middle or end group) (61,161). Certain water-soluble polymers of the Belclene 700 series (originally Ciba Geigy, later FMC) contain phosphinic or phosphonic acid groups, believed to have been made in this manner. These polymers are effective scale inhibitors and can be used in industrial and institutional washing formulations to aid soil removal and dispersion with control of water-hardness deposits.

Thermoplastic Polyesters. Cocondensation with a phosphorus acid, diol, or diester introduces a small amount of phosphorus into polyesters for flame retardancy, color stability, electrical properties, or antistatic properties. Hoechst and Toyo Spinning (Toyobo) have increased the flame retardancy of poly(ethylene terephthalate) fibers by incorporating small amounts of phosphinates.

The Hoechst technology is shown by the following sequence (162,163):

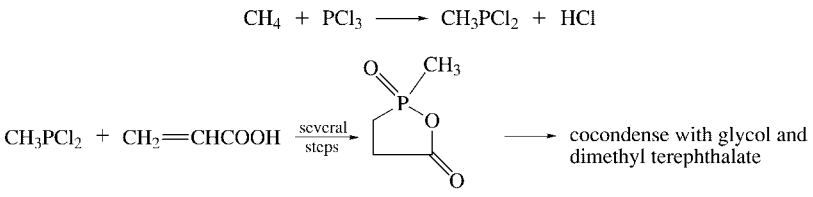

The flame-retardant polyester fiber was marketed originally by Hoechst, later by Ticona as Trevira CS, and now by Kosa in the United States as Avora FR, and is used for decorative fabrics and curtains, upholstery fabrics, hospital bedding, and sleeping bags. These fibers also exhibit low smoke evolution, good appearance, and light stability.

Technology originally developed at Toyobo for polyester fiber places the phosphinate group on a side chain in a modified poly(ethylene terephthalate) by cocondensation with a phosphinate of the following structure (164–166):

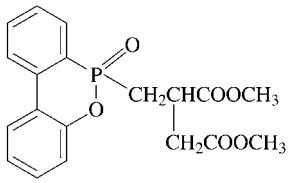

This is an addition product of a hydrogen phosphinate with dimethyl itaconate. A diol with the same ring system can also be used to make other phosphorus-containing thermoplastic polyesters (167).

Numerous patents disclose alternatives for flame-retardant polyester fibers by introducing small amounts, such as less than 1%, of phosphorus. The cocondensation of less than 1% of phenylphosphonic acid into the polyester has been claimed sufficient to flame retard it to a Japanese standard (168). Perhaps of commercial utility is a polyester fiber made by transesterifying the oligomer of phenyl(hydroxymethyl)phosphinic acid into molten poly(ethylene terephthalate) (169).

Polyester Resins (Thermoset). Many patents describe polyesters containing an alkylene oxide reaction product with a phosphonic or phosphoric acid to promote flame retardance; some patents describe transesterifying a neutral or acid phosphate directly into the reaction mixture (170).

Small amounts of phosphorus sufficient to induce flame retardancy are incorporated by transesterification of dimethyl methylphosphonate or other phosphonates with unsaturated polyester resins (171,172).

The phosphorus can also be introduced in the form of a vinylphosphonate for copolymerization with styrene in the curing step. Polyesters of this type, with bis(2-chloroethyl) vinylphosphonate as part of the cross-linking system, were marketed for a time (173). The only use of phosphorus compounds in any significant volume in polyester resins has been that of triethyl phosphate or dimethyl methylphosphonate for viscosity reduction and flame retardancy in filled-polyester, sheet-molding compositions.

Polyamides. Bis(carboxyethyl)alkylphosphine oxide units can be introduced into the backbone of nylon-6,6 to impart flame retardancy with minimal sacrifice of physical properties. (174). Despite much effort on this approach, these products failed to reach commercialization probably for cost reasons. Small amounts of bis(carboxyethyl)phosphinic acid salts can be introduced into the chain of polyamide-6,6 to impart inherent flame retardancy and stain resistance to carpet fiber (175).

Epoxy Resins. In the combustion of epoxy resins, phosphorus inhibits the evolution of fuel gases and increases char (176). Much attention has been given to phosphorus additives or reactives in epoxy resins used as coatings for the purpose of increased adhesion to surfaces (177,178) and for fire resistance. More recently, a great deal of attention has been given to phosphorus-containing, flame-retarded electrical/electronic laminates and encapsulated electronic parts.

Some of this effort has been directed to replacement of tetrabromobisphenol A, a major reactive component of circuit boards (wiring boards). Extensive development of flame-retarded halogen-free circuit boards has taken place especially in Europe and the Far East to find alternatives to tetrabromobisphenol A-based epoxy circuit boards. The use of phosphate ester additives usually depresses the thermomechanical properties excessively, and so the use of reactive phosphorus compounds has been the preferred approach.

Phosphorus can be introduced into epoxy resins in diverse ways using reactive means. Diglycidyl phenylphosphonate (179) has been found useful for electronic epoxy products but cost has retarded its commercial development.

Phosphorus can be introduced into epoxy resins by introducing phosphorus halides pre-cure or as part of curing step (in either case, a β-chloroalkoxy phosphorus ester structure is produced), but these reagents are generally too corrosive and labile, and this approach has not been commercialized. Incorporation of phosphoric acid (180) or polyphosphoric acid (181) has shown somewhat more promise. Epoxy resins modified by reaction with alkyl acid phosphates, such as butoxyethyl acid phosphate, had development efforts by Dow Chemical Co. (182). Extensive study was done at Ford Co. on epoxy coatings, with alkyl acid phosphates reacted into the epoxy structure (126) for purposes of improved adhesion and corrosion protection. Reaction of dialkyl or diphenyl phosphates with epoxy resins and subsequent curing gave products with intumescent flame-retardant properties but diminished thermal stability. The use of diphenyl phosphate raised the glass-transition temperature (183) in some epoxy resins. The reaction of epoxy groups with phosphorus acids generates β-hydroxyalkyl phosphate or phosphonate linkages, along with hydroxy(polyoxyalkylene) phosphates or phosphonates, and also some self-condensation of the epoxy groups. In some cases, gelation occurs.

Oligomeric phosphoric/phosphonic anhydrides can be incorporated into epoxy resins to make prepolymers or used as curing agents (184–186).

The chain extension of epoxy resins can be conducted with dihydric phenolic resins containing phosphate linkages. Bis(3-hydroxyphenyl) phenyl phosphate can be used as a chain extender for epoxy resins, and can afford a UL-94 V-0 level of flame retardancy with phosphorus content as low as 1.5% after cure (187); however, the glass-transition temperature (T_g) is lowered by the flexible phosphate group.

The problem of achieving a high T_g in a circuit-board laminate (to avoid distortion during soldering) is alleviated by the use of a pendant rigid phosphorus-containing ring structure, namely the 9,10-dihydro-9-oxa-10-phosphaphenanthrene group, the synthesis of which was shown above.

This ring system has been used in epoxy resins as well as in thermoplastic polyesters. It has been the subject of many patents and publications, and is commercially produced in Europe and the Far East. Its original use was in Toyobo's flame-retardant polyester fiber, in the form of the itaconic ester adduct.

The hydrogen phosphinate itself can be reacted directly into epoxy resins to produce presumably a β-hydroxyphosphinate structure (188); however, this consumes epoxy functionality and creates chain ends which tend to reduce the T_g.

A more selective means for incorporation of this ring system is to react the hydrogen phosphinate with benzoquinone by reductive addition to produce the phosphinyl-substituted hydroquinone (189,190). This can be used as a chain

extension reagent with an epoxy resin to obtain flame retardancy with an improvement of T_g. A still further elaboration of this cyclic structure is the reaction of the hydroquinone with epichlorohydrin and base to make a diglycidyl ether (191) which can be used as part of the epoxy resin.

The same ring system can also be introduced into a novolac hardener by phosphinylation of one or more of the hydroxyl groups of the novolac, leaving the remaining groups to serve for the cross-linking (192).

A cyclic neopentyl hydrogen phosphonate can be added to the epoxy group to impart flame retardancy although the creation of an end group does tend to lower T_g (193).

Phosphonated aromatic diamines (195) can serve as flame-retardant curing agents for epoxy resins. Phosphoramides and bis(aminophenyl)methylphosphine oxide have been evaluated in the quest for stable, fire-resistant epoxy composites for aerospace applications (196–198). Economical means for producing the phosphine oxide structure have been lacking.

Phosphine oxide diols and triols were shown at FMC to be excellent reactive flame retardants or synergists with good thermal and hydrolytic stability in epoxy resins (199).

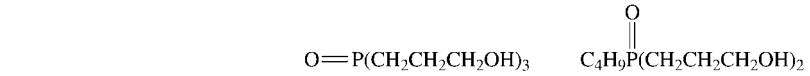

Their cost has retarded commercialization.

Polyurethanes and Isocyanurate-Modified Polyurethanes. Phosphorus flame retardants, both additive and reactive, are used in large quantities in Polyurethanes. Rigid urethane foams employed in thermal insulation must adhere to stringent fire regulations. Flexible foams used in automotive seating must pass the MVSS-302 fire standard; in furniture foam, they must pass the California state standard and other local fire codes.

Additive flame retardants continue to dominate the flexible foam market despite extensive work on reactive phosphorus compounds (200,201). A phosphonate–phosphate diol (6) has been used as a component of a blended flame retardant for flexible polyurethanes. A reactive phosphate diol (135) has recently been introduced by Clariant for use in flexible polyurethanes.

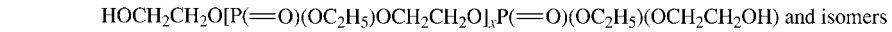

Reactive flame retardants have long been used in rigid foams. A successful early example, the diol Vircol 82 (Rhodia), is a diol made by reaction of dibutyl acid pyrophosphate with propylene oxide (202).

A phosphonate diol (Akzo-Nobel's Fyrol 6) is used in rigid foams, especially spray, froth, pour-in-place, and quasi-prepolymer foam formulations. It is a condensation product of diethanolamine with formaldehyde and diethyl phosphonate (203):

The diol structure permits permanent incorporation of the phosphonate group into the urethane foam. The phosphonate linkage is on a side chain rather

than in the backbone of the polyurethane, which increases the hydrolytic stability, and the amino group aids catalysis of the foaming.

A diol containing a phosphine oxide structure was shown to be useful in urethane coatings, adhesives, and rigid foams (204). Advantages included shelf stability of the amine catalyst–polyol mixture, low smoke, and good resistance to humidity (205).

A phosphorus-containing isocyanate can also be employed, although P(=O)N=C=O types, in general, are expensive to synthesize and, moreover, give hydrolytically unstable urethanes. The only phosphorus-containing isocyanate currently on the market is Bayer's Desmodur RFE, a solution in ethyl acetate of tris(*p*-isocyanatophenyl) thionophosphate (206).

This compound is not employed in urethanes. It is a cross-linking agent for adhesives and is used to increase bonding to rubber and plastic substrates and resistance to heat and solvents.

Phenolic and Amino Resins. Numerous patents describe incorporation of phosphorus to increase flame retardancy. Paper impregnated with phenolic resins or amino resins, such as that used in automotive air filters, is treated with oligomeric phosphates or phosphonates (6). Being low in volatility, they are retained during use. Large air filters must retain the flame retardant during washing and reuse; reactive (hydroxyl-terminated) phosphonate–phosphate oligomers are used for this application (207). Such structures presumably become chemically bound to the resin by formation of ether linkages.

Electronic circuit boards based on phenolic resin can be flame retarded by aryl phosphates including oligomeric types made by transesterification of aryl phosphates with novolacs (208). These partially phosphorylated novolacs are then incorporated into the thermoset structure.

Cellulosic Resins. In general, phosphorylation of cellulose or treatment of cellulose with phosphorus-containing resins produces a flame-retardant effect by increasing char yield although lowering the decomposition temperature somewhat. The mechanism has been extensively studied (209–211).

The direct phosphorylation of cellulose has been studied extensively, particularly to prepare flame-retardant cotton fabric or paper and ion-exchange materials (212). Heating cellulose with phosphoric acid results in little phosphorylation and much degradation. However, in the presence of urea or dicyandiamide, a sufficient degree of phosphorylation is achieved to impart self-extinguishing properties while allowing retention of useful strength. Such processes have been employed for semidurable, flame-retardant finishing of draperies. Resistance to a few washes is improved by using an amino resin such as methylolurea or methylolated dicyandiamide. Wood has been commercially treated for flame retardancy by aminoplast–phosphoric acid compositions (213).

Cellulose can also be phosphorylated by heating it with polyphosphoric salts, such as sodium hexametaphosphate (214). A water-insoluble sodium cellulose phosphate, Selectacel phosphate cation exchanger (Polysciences), is used in chromatography. A more highly substituted version, Selectacel SCP or Calcibind exchanger, is approved by the FDA for binding calcium in the gastrointestinal tract as a treatment for absorptive hypercalciurea (a disease causing recurrent calcium kidney stones) (215) (see CELLULOSE ESTERS, INORGANIC). Starches are phosphorylated by treatment with sodium orthophosphate, pyrophosphate,

metaphosphate, or tripolyphosphate (216). By varying the reagents and conditions, a wide range of properties can be achieved. A phosphate-treated starch swellable in cold water is used in instant puddings. Water-resistant phosphorylated starch is useful in paper sizing. A hydroxypropyl starch phosphate (Midwest Grain Products' Cosmogel 46) is heat and pH tolerant, and hydrates to a thick smooth paste useful in skin and hair care products.

Flame-Retardant Finishes on Cellulosic Substrates. The flame retarding of cotton and viscose-rayon fabrics has been the object of a large worldwide effort on phosphorus-containing finishes (217–219). The commercial cotton finishes are based on tetrakis(hydroxymethyl)phosphonium salts, usually the chloride or sulfate (220). These salts are prepared by reaction of formaldehyde with phosphine in the presence of an acid.

$$PH_3 + 4\,HCHO + HCl \rightarrow (HOCH_2)_4P^+Cl^-$$

The tetrakis(hydroxymethyl)phosphonium salts are applied to cellulosic fabric, most commonly as a urea precondensate (Albright & Wilson's, now Rhodia's Proban), and cured with ammonia vapor (221–223). The finish, after oxidation by air or hydrogen peroxide, has phosphine oxide structures in a cross-linked amino resin network, probably also lightly linked to the cellulose. This finish is durable to multiple launderings and is used for industrial cotton garments (224).

Other commercial finishes for cotton are less resistant to harsh laundering conditions, but can be applied by conventional pad-dry-cure methods. For example, the Ciba Pyrovatex CP flame retardant is based on the methylolated reaction product of dimethyl phosphite with acrylamide, which is condensed on the cotton fabric with an amino resin (225,226) to make a cross-linked amino resin containing a dimethyl phosphonate structure. Pyrovatex CP is principally $(CH_3O)_2P(O)CH_2CH_2C(O)NHCH_2OH$ with related side-reaction products (227,228). The chemistry of the Pyrovatex finish involves linkages both to cellulose directly and to aminoplast resins which then link to cellulose.

Phosphorylated Proteins. Naturally occurring phosphorus-containing proteins include such important examples as casein, discussed elsewhere in this Encyclopedia. In living organisms, proteins are often phosphorylated enzymatically on the serine or tyrosine hydroxyl group as an activation or regulation step, and over-phosphorylation may play a role in disease; this biochemistry is outside the scope of the present article.

Efforts to manufacture phosphorylated proteins by modification of nonphosphorus proteins have been reviewed (229). Phosphorylation of proteins with phosphorus oxychloride causes cross-linking and insolubilization, but improves gel-forming and water-binding properties. Phosphorylation with sodium trimetaphosphate improves functional properties of soybean protein, including water solubility. Nutritional and toxicological investigations are needed before such modified natural proteins can be used in foods (230).

BIBLIOGRAPHY

"Phosphorus-containing Polymers" in *EPST* 1st ed., Vol. 10, pp. 123–139, by Manfred Sander, Batelle Institute, and in *EPST* 2nd ed., Vol. 11, pp. 96–126 by Edward D. Weil, Stauffer Chemical Co.

1. E. D. Weil, in M. Grayson, ed., *Kirk-Othmer Encyclopedia of Chemical Technology*, 3rd ed., Vol. **10**, Wiley-Interscience, New York, 1980; in Ref. 2, Vol. **2**, Chapt. "4", pp. 103–128.
2. S. R. Sandler and W. Karo, *Polymer Synthesis*, 2nd ed., Academic Press, Inc., New York, 1992, pp. 460–546.
3. S. Maiti, S. Banerjee, and S. K. Palit, *Prog. Polym. Sci.* **18**, 227–261 (1993).
4. E. D. Weil, *J. Fire Flammability/Fire Retardant Chem.* **1**, 125 (1974).
5. S. V. Shulyndin, Ya. A. Levin, and B. E. Ivanov, *Russ. Chem. Rev. (Engl. Trans.)* **50**, 865 (1981).
6. E. D. Weil, R. B. Fearing, and F. Jaffe, *J. Fire Retardant Chem.* **9**, 39 (1982).
7. E. D. Weil, Paper at *11th Annual BCC Conference on Flame Retardancy*, Stamford, Conn., May 22–24, 2000.
8. J. J. McCallum and J. F. Alder, *J. Chem. Tech. Biotechnol.* **44**, 121–133 (1989).
9. H. Hartl, *Angew. Chem., Int. Ed. Engl.* **34**, 2637–2638 (1998).
10. A. D. F. Toy, in J. C. Bailar, H. J. Emeleus, R. Nyholm, and A. F. Trotman-Dickenson, eds., *Comprehensive Inorganic Chemistry*, Vol. **2**, Pergamon Press, Oxford, U.K., 1973, Chapt. "20".
11. N. H. Ray, *Inorganic Polymers*, Academic Press, Inc., London, 1978.
12. A. E. R. Westman, in E. J. Griffith and M. Grayson, eds., *Topics in Phosphorus Chemistry*, Vol. **9**, John Wiley & Sons, Inc., New York, 1977, pp. 231–405.
13. R. Brow, ed., *Structure, Properties and Applications of Phosphate and Phosphate-Containing Glasses: Proceedings of the 15th University Conference on Glass Science*, Rolla, Missouri, June 20–23, 1999, Elsevier, Amsterdam, 2000. *J. Non-Cryst. Solids* **263/264** (2000).
14. M. T. Averbuch-Pouchot and A. Durif, *Topics in Phosphorus Chemistry*, World Science Publishers, Singapore, 1996.
15. E. Griffith, ed., *Phosphate Fibers*, Plenum, New York, 1995.
16. A. D. P. Toy and E. N. Walsh, *Phosphorus in Everyday Living*, American Chemical Society, Washington, D.C., 1987.
17. P. Langen, in H. C. Schröder and W. E. G. Müller, eds., *Progress in Molecular and Subcellular Biology*, Vol. **23**, Springer Verlag, Berlin, 1999, pp. 19–26.
18. U.S. Pat. 4,940,677 (July 10, 1990), G. H. Beall and C. J. Quinn (to Corning, Inc.).
19. C. J. Quinn and G. H. Beall, in L. L. Hench and J. K. West, eds., *Chemical Processes and Advanced Materials*, John Wiley & Sons, Inc., New York, 1992, pp. 799–805.
20. U.S. Pat. 5,153,151 (Oct. 6, 1992), B. G. Aitken (to Corning, Inc.).
21. U.S. Pat. 3,723,074 (Mar. 27, 1973), P. G. Sears and H. L. Vandersall (to Monsanto Co.).
22. C. Y. Shen, N. E. Stahlheber, and D. R. Dyroff, *J. Am. Chem. Soc.* **91**, 62–67 (1969).
23. H. L. Vandersall, *J. Fire Flammability* **2**, 97 (1971).
24. H. Staendeke, in *Flame Retardant Coatings: Problems and Opportunities*, Proceedings of the Meeting of the Fire Retardant Chemicals Association, Pinehurst, N.C., Oct. 27–30, 1985, FRCA, Lancaster, Pa., *Flame Retardant Coatings: Problems and Opportunities*, Proceedings of the Meeting of the Fire Retardant Chemicals Association, Pinehurst, N.C., 1985, pp. 29–50.
25. E. Stegor and G. Mildner, *Z. anorg. allgem. Chemie* **332**, 314–321 (1964).
26. Brit. Pat. 1,461,615 (1977), K. Sommer (to Benckiser-Knapsack).
27. Fr. Pat. Appl. 2,617,152 (publ. Dec. 30, 1988), R. Marchand, Y. Laurent, and P.-N. Fevennec (to Centre National de la Research Scientifique).
28. E. D. Weil, in *Conference on Recent Advances in Flame Retardancy of Polymeric Materials*, Stamford, Conn., May 18–20, 1993.

29. E. D. Weil, in *Proceedings of the 2nd Beijing International Symposium/Exhibition on Flame Retardants*, Geological Publishing House, Beijing, China, 1993, pp. 285–290.
30. S. V. Levchik and co-workers, *Angew. Makromol. Chem.* **264**, 48–55 (1999).
31. E. D. Weil and N. Patel, *Fire and Materials* **18**, 1–7 (1994).
32. P. C. Li and L. C. Hua, *J. Electrochem. Soc.: Solid State Sci. Technol.* 366–372, (Feb. 1986).
33. N. L. Holy, in L. H. Pignolet, ed., *Homogeneous Catalysis with Metal Phosphine Complexes*, Plenum Publishing Corp., New York, 1983, Chapt. "14".
34. R. Rabinowitz, R. Marcus, and J. Pellon, *J. Polym. Sci., Part A* **2**, 1241 (1962).
35. W. M. McKenzie and D. C. Sherrington, *J. Polym. Sci., Polym. Chem. Ed.* **21**, 431 (1983).
36. H. J. Cristau and F. Plénat, in F. R. Hartley, ed., *Chemistry of Organophosphorus Compounds*, Vol. **3**, John Wiley & Sons, Inc., Chichester, U.K., 1994, pp. 159–160.
37. A. Boryniec and B. Lasziewicz, *J. Polym. Sci., Part A* **1**, 1963 (1963).
38. L. A. Errede and N. Knoll, *J. Polym. Sci.* **60**, 33 (1962).
39. U.S. Pat. 4,068,055 (Jan. 10, 1978), C. S. Smith (to Upjohn Co.).
40. U.S. Pats. 4,463,159 (July 31, 1984) and 4,472,570 (Sept. 18, 1984), S. Besecke and co-workers (both to Rohm GmbH).
41. U.S. Pat. 4,492,805 (Jan. 8, 1985), S. Besecke and co-workers (to Rohm GmbH).
42. S. Hashimoto, I. Furukawa, and K. Ueyama, *J. Macromol. Sci. Chem., Part A* **11**, 2167 (1977).
43. D. J. Riley and co-workers, *Polym. Eng. Sci.* **37**, 1501–1511 (1997).
44. U.S. Pat. 6,040,416 (Mar. 21, 2000), V. N. Sekharipuram and co-workers (to Johnson & Johnson Vision Products, Inc. and Virginia Tech Intellectual Properties, Inc.).
45. S. W. Shalaby and co-workers, *J. Polym. Sci., Polym. Chem. Ed.* **13**, 669 (1975).
46. J. Pellon and W. G. Carpenter, *J. Polym. Sci., Part A* **1**, 863 (1963).
47. U.S. Pat. 4,032,517 (June 28, 1977), O. A. Pickett Jr. and J. W. Stoddart (to Monsanto Co.).
48. J. Pellon, *J. Polym. Sci., Part A* **1**, 3561 (1963).
49. T. Kashiwagi, J. W. Gilman, J. E. McGrath, and I.-Y. Wan, in *New Dev. Future Trends Fire Saf. Global Basis, Int. Conf.*, Fire Retardant Chemicals Association, Lancaster, Pa., 1997, pp. 197–219.
50. U.S. Pat. 5,194,564 (Mar. 16, 1993), G. C. Davis, C. A. A. Claesen, and E. M. A. Gijzen (to General Electric Co.).
51. I. K. Varma and B. S. Rao, *J. Appl. Polym. Sci.* **28**, 2805 (1983).
52. U.S. Pat. 4,433,115 (Feb. 21, 1984), I. K. Varma, G. M. Fohlen, and J. A. Parker (to United States of America is represented by the Administrator of the National Aeronautics and Space Administration).
53. I. K. Varma, G. M. Fohlen, and J. A. Parker, *J. Polym. Sci., Polym. Chem. Ed.* **21**, 2017 (1983); *Contemp. Top. Polym. Sci.* **4**, 115 (1984).
54. I. K. Varma, G. M. Fohlen, and J. A. Parker, *J. Macromol. Sci. Chem., Part A* **19**, 209 (1983).
55. W. Vogt and S. Balasubramanian, *Makromol. Chem.* **163**, 111 (1973).
56. K. E. Branham, J. W. Mays, and G. M. Gray, *Polym. Prepr.* **40**(1), 78–79 (Mar. 1999).
57. Ger. Pat. 2,344,332 (Jan. 15, 1981), H.-J. Kleiner (to Hoechst AG).
58. U.S. Pat. 5,085,794 (Feb. 4, 1992), J. F. Kneller and co-workers (to Nalco Chemical Co.).

59. U.S. Pats. 4,046,707 (Sept. 6, 1977); 4,105,551 (Aug. 8, 1978); 4,127,483 (Nov. 28, 1978); and 4,159,946 (July 3, 1979), M. J. Smith and co-workers (all to Ciba Geigy Ltd.).
60. U.S. Pat. 4,812,501 (Mar. 14, 1989), G. Cipriani and A. Mariano (to Enichem Sintesi S.p.A.).
61. S.-J. Chang and F.-C. Chang, *J. Appl. Polym. Sci.* **72**, 109–122 (1999).
62. E. L. Gefter, *Organophosphorus Monomers and Polymers* (English translation by G. Kosolapoff), Assoc. Technical Services, Inc., Glen Ridge, N.J., 1962.
63. Ya. A. Levin, G. B. Fridman, and B. Ye. Ivanov, *Polym. Sci. U.S.S.R. (Engl. Transl.)* **17**, 971 (1975).
64. U.S. Pats. 3,725,359 (Apr. 3, 1973) and 3,792,113 (Feb. 12, 1974), P. Kraft and S. Altscher (both to Stauffer Chemical Co.).
65. R. Gallagher and J. C. H. Hwa, *J. Polym. Sci., Polym. Symp.* **64**, 329 (1978).
66. M. Banks, J. R. Ebdon, and M. Johnson, *Polymer* **35**, 3470–3473 (1994).
67. U.S. Pats. 3,725,509 (Apr. 3, 1973); 3,819,770 (June 25, 1974); 3,857,906 (Dec. 31, 1974); 3,943,085 (Mar. 9, 1976); 3,948,842 (Apr. 6, 1976); 3,991,134 (Nov. 9, 1976); 3,992,337 (Nov. 16, 1976); and 3,992,481-2 (Nov. 16, 1976), P. Kraft and S. Altscher (all to Stauffer Chemical Co.).
68. U.S. Pat. 4,210,739 (July 1, 1980), R. E. Gallagher and co-workers (to Stauffer Chemical Co.).
69. U.S. Pat. 4,147,853 (Apr. 3, 1979), J. C. Goswami and R. Querido (to Stauffer Chemical Co.).
70. F. Rochlitz and H. Vilcsek, *Angew. Chem.* **74**, 970 (1962).
71. Ger. Pat. 1,106,963 (May 18, 1961), W. Herbst, F. Rochlitz, and H. Vilcsek (to Farbwerke Hoechst AG).
72. U.S. Pat. 4,153,461 (May 8, 1979), G. Berghauser and F. Uhlig (to Hoechst AG).
73. U.S. Pat. 4,448,647 (May 15, 1984), T. N. Gillich and co-workers (to American Hoechst Corp.).
74. J. Baybrook and J. W. Nicholson, *J. Mater. Chem.* **3**, 361–365 (1993).
75. Eur. Pat. 0,643,081 (1994) (to Hoechst AG).
76. U.S. Pats. 4,446,028 and 4,446,046 (May 1, 1984), L. W. Becker (both to Betz Laboratories, Inc.).
77. Brit. Pat. Appl. 2,276,388 A (Sept. 29, 1994), A. Archer and M. Zakikhani (to Albright & Wilson).
78. S. D. Alexandratos and co-workers, *Macromolecules* **29**, 1021–1026 (1996).
79. S. D. Alexandratos and co-workers, *J. Appl. Polym. Sci.* **61**, 273–278 (1996).
80. E. P. Horwitz, R. Chiarizia, S. D. Alexandratos, and M. Gula, in A. H. Bond, M. L. Dietz, and R. D. Rogers, eds., *ACS Symposium Series, Vol. 716: Metal Ion Separation*, American Chemical Society, Washington, D.C., 1999, pp. 206–215.
81. R. Chiarizia and co-workers *Separation Science and Technology* **32**(1–4), 1–35 (1997).
82. U.S. Pats. 3,822,327 (July 2, 1974); 3,855,359 (Dec. 17, 1974); 4,017,257 (Apr. 12, 1977); and 4,067,927 (Jan. 10, 1978); E. D. Weil (all to Stauffer Chemical Co.).
83. B. J. Eisenberg and E. D. Weil, *Text. Chem. Color.* **6**(8), 180 (1974).
84. W. A. Reeves and Y. B. Marquette, *J. Fire Retardant Chem.* **5**, 65 (1978).
85. K. Masuda and M. Tomita, *J. Fire Retardant Chem.* **3**, 53, 164 (1976).
86. Z. Yu, W.-X. Zhu, and I. Cabasso, *J. Polym. Sci, Polym Chem. Ed.* **28**, 227–230 (1990).
87. J. B. Ebdon and co-workers, *Polym. Degrad. Stab.* **70**, 425–436 (2000).
88. F. Zeuner and co-workers, *Phosphorus, Sulfur and Silicon* **144–146**, 133–136 (1999).

89. C. E. Schildknecht, *Allyl Compounds and Their Polymers*, John Wiley & Sons, Inc., New York, 1973, pp. 674–678.
90. U.S. Pat. 2,435,252 (1948), A. D. F. Toy (to Victor Chemical Works).
91. H. W. Coover, R. L. McConnell, and M. A. McCall, *Ind. Eng. Chem.* **52**, 409 (1960).
92. U.S. Pat. 3,932,351 (Jan. 13, 1976), H. L. King (to Monsanto Co.).
93. Jpn. Kokai 72 39,154 (Dec. 6, 1972), K. Murayama and R. Yamatera (to Toyobo Co., Ltd.).
94. U.S. Pat. 3,719,727 (Mar. 6, 1973), Y. Masai, Y. Kato, and N. Fukui (to Toyo Spinning Co.).
95. K. S. Kim, *J. Appl. Polym. Sci.* **28**, 1119 (1983).
96. K. S. Kim, *J. Appl. Polym. Sci.* **28**, 2439 (1983).
97. U.S. Pat. 4,206,296 (June 3, 1980), A. J. Yu, S. Altscher, and K. S. Kim (to Stauffer Chemical Co.).
98. Chin. Pat. CN 1167167 A (Dec. 10, 1997), Y. Xia and co-workers (Qingdao University).
99. C. E. Carraher Jr., *Inorg. Macromol. Rev.* **1**, 287 (1972).
100. M. Richards and co-workers, *J. Polym. Sci., Part A: Polym. Chem.* **29**, 1157–1165 (1991).
101. G. M. Gray, K. E. Branham, L.-H. Ho, and J. W. Mays, in J. F. Harrod and R. M. Laine, eds., *Inorganic and Organometallic Oligomers and Polymers*, Kluwer Academic Publishers, Dordrecht, the Netherlands, 1991, pp. 249–263.
102. U.S. Pat. 4,152,373 (May 1, 1979), M. L. Honig and E. D. Weil (to Stauffer Chemical Co.).
103. M. Schmidt and co-workers, *Angew. Makromol. Chem.* **132**, 1 (1985).
104. U.S. Pat. 4,332,921 (June 1, 1982), M. Schmidt, J. Wank, and E. Reese (to Bayer AG).
105. U.S. Pats. 4,331,614 (May 25, 1982) and 4,415,719 (Nov. 15, 1983), M. Schmidt and co-workers (both to Bayer AG).
106. U.S. Pat. 3,956,431 (May 11, 1976), M. L. Honig and E. D. Weil (to Stauffer Chemical Co.).
107. U.S. Pats. 4,086,303 (Apr. 25, 1978); 4,152,371 (May 1, 1979); and 4,202,842 (May 13, 1980), E. D. Weil (all to Stauffer Chemical Co.).
108. J. Gloede and H. Gross, *J. Gen. Chem. U.S.S.R. (Engl. Transl.)* **54**, 1285 (1984).
109. U.S. Pat. 4,144,387 (Mar. 13, 1979), J. J. Anderson and co-workers (to Mobil Oil Co.).
110. G. Lapienis and S. Penczek, in K. J. Ivin, ed., *Ring-Opening Polymerization*, Elsevier Science Publishing Co., New York, 1983, Chapt. "13".
111. Ref. 2, pp. 486–493.
112. U.S. Pat. 3,890,411 (June 17, 1975), K. S. Shim (to Stauffer Chemical Co.).
113. U.S. Pat. 4,199,534 (Apr. 22, 1980), R. B. Fearing (to Stauffer Chemical Co.).
114. S. Minegishi and co-workers, *J. Appl. Polym. Sci., Part A: Polym. Chem.* **37**, 959–965 (1999).
115. U.S. Pats. 3,014,956 (Dec. 26, 1961) and 3,042,701 (July 3, 1962), G. Birum (both to Monsanto Co.).
116. U.S. Pat. 3,371,131 (Feb. 27, 1968), A. Carson, W. E. Feely, and M. J. Hurwitz (to Rohm & Haas Co.).
117. U.S. Pat. 3,468,980 (Sept. 23, 1969), G. E. Forsyth (to Rohm & Haas Co.).
118. J. Baddiley, *Acc. Chem. Res.* **3**, 98 (1970).
119. H. Egawa, K. Yamase, and A. Jyo, *J. Appl. Polym. Sci.* **52**, 1153–1164 (1994).
120. U.S. Pat. 4,207,405 (June 10, 1980), W. F. Masler III and D. C. Spaulding (to B. F. Goodrich Co.).
121. Z.-M. Wang and S.-C. Zu, in *Proc. 4th Asian-Pacific Corrosion Control Conference*, East China Institute of Chemical Technology, Shanghai, 1985, pp. 1020–1028.

122. S. Penczek and P. Klosinski, in C. G. Gebelein, ed., *Biomimetic Polymers*, Plenum Press, New York, 1990, pp. 223–252.
123. A. R. Elmes and co-workers, *Eur. Polym. J.* **33**, 1659–1664 (1997).
124. U.S. Pat. 4,499,251 (Feb. 12, 1985), I. Omura and co-workers (to Kuraray Co., Ltd.).
125. U.S. Pat. 3,754,972 (Aug. 28, 1973), R. deMajistre, G. M. Parker, and R. Sirkoch (to PPG Industries, Inc.).
126. R. O. Carter III, J. L. Parsons, and J. W. Holubka, *Ind. Eng. Chem. Res.* **26**, 1518–1523 (1987).
127. U.S. Pats. 3,524,903 (Aug. 18, 1970) and 3,574,794 (Apr. 13, 1971), S. R. Hargis Jr. (both to The Dow Chemical Company).
128. M. J. Chen, J. Kiplinger, N. Johnson, E. M. Walsh, and H. Adam, Paper at *International Corrosion Exhibition (ICE)*, Oct. 2000.
129. K. S. Annakutty and K. Kishore, *Polymer* **29**, 756–764 (1988).
130. U.S. Pat. 4,481,338 (Nov. 6, 1984), V. Serini and co-workers (to Bayer AG).
131. Jpn. Kokai Tokkyu Koho 59 24,736 [84 24,736] (Feb. 8, 1984) and 59 45,351 [84 45,351] (Mar. 14, 1984) (both to Adeka Argus Chemical Co., Ltd.).
132. R. Deanin and M. Ali, in G. Nelson, ed., *ACS Symposium Series, Vol. 599: Fire and Polymers II*, American Chemical Society, Washington, D.C., 1995, pp. 56–64.
133. X. Wang and co-workers, *Chem. Abstr.* **131**, 352076 (2000).
134. K. S. Annakutty and K. Kishore, *Polymer* **29**, 1273–1276 (1988).
135. U.S. Pat. 5,608,100 (Mar. 4, 1997), M. Sicken (to Hoechst AG.); U.S. Pat. 5,985,965 (Nov. 16, 1999), M. Sicken and H. Staendeke (to Clariant GmbH).
136. U.S. Pats. 4,382,042 (May 3, 1983) and 4,458,035 (July 3, 1984), T. Hardy and F. Jaffe (both to Stauffer Chemical Co.).
137. R. Crowell, Paper at *Fire Retardant Chemicals Association Spring Conference*, Washington, D.C., Mar. 2000.
138. S. Penczek, P. Kubisa, P. Klosinski, T. Biela and A. Nyk, *ACS Symposium Series, Vol. 496: Catalysis in Polymer Synthesis*, 1992, pp. 248–257.
139. A. Nyk, P. Klosinski, and S. Penczek, *Makromol. Chem.* **192**, 833–846 (1991).
140. U.S. Pat. 3,513,644 (May 26, 1970), E. D. Weil (to Stauffer Chemical Co.).
141. U.S. Pat. 3,896,187 (July 22, 1975), E. D. Weil (to Stauffer Chemical Co.).
142. U.S. Pat. 4,013,814 (Mar. 22, 1977), E. D. Weil (to Stauffer Chemical Co.).
143. C. W. Allen, *J. Fire Sci.* **11**, 320–328 (1993).
144. D. M. Harris, R. L. Jenkins, and M. L. Nielsen, *J. Polym. Sci.* **35**, 540 (1959).
145. PCT Appl. WO 93/22373 (Nov. 11, 1993), A. J. Lindsay (to Minnesota Mining and Manufacturing Co.).
146. M. A. Kraus and M. Nemas, *J. Polym. Sci., Polym. Lett. Ed.* **19**, 617 (1981).
147. U.S. Pat. 4,701,554 (Oct. 20, 1987), H. Kauth and co-workers (to Bayer AG).
148. U.S. Pat. 4,587,362 (May 6, 1986), M. Honig and E. D. Weil (to Stauffer Chemical Co.).
149. A. P. Khardin, O. I. Tuzhikov, and S. N. Bondarenko, *Russ. Chem. Rev. (Engl. Transl.)* **52**, 662 (1983).
150. J. P. Schroeder and W. P. Sopchak, *J. Polym. Sci., Part A-1* **47**, 417 (1970).
151. R. A. Weiss, R. W. Lenz, and W. J. MacKnight, *J. Polym. Sci., Polym. Phys. Ed.* **15**, 1409ff (1977); *J. Polym. Sci., Polym. Phys. Ed.* **16**, 1101 (1978).
152. R. Bogoczek and J. Surowiec, *J. Appl. Polym. Sci.* **26**, 4161 (1981).
153. S. D. Alexandratos and co-workers, *Macromolecules* **18**, 829 (1985).
154. S. D. Alexandratos and co-workers, *Macromolecules* **18**, 836 (1985).
155. J. J. Wolff and R. E. Anderson, in *Adsorption and Ion Exchange* (AIChE Symposium Series 219), Vol. **78**, American Institute of Chemical Engineers, New York, 1982, pp. 46–53.

156. N. A. Mukmeneva and co-workers, *Proc. Acad. Sci. U.S.S.R (Engl. Transl.)* **233**(3), 174 (1977).
157. P. A. Kirpichnikov, N. A. Mukneneva, and D. G. Pobedimski, *Russ. Chem. Rev. (Engl. Transl.)* **52**, 1051 (1983).
158. Eur. Pats. 84407 A2 (July 27, 1983); 61240 A2 (Sept. 29, 1982); and 58483 A2 (Aug. 25, 1982), J. E. Bunker (all to Minnesota Mining and Manufacturing Co.).
159. U.S. Pat. 4,514,342 (Apr. 30, 1985), R. W. Billington, G. B. Blackwell, and T. E. Prodger, (to Dentsply, Ltd.).
160. U.S. Pat. 4,222,780 (Sept. 16, 1980), K. Shibatani, I. Omura, and J. Yamauchi, (to Kuraray Co., Ltd.).
161. U.S. Pat. 5,866,664 (Feb. 2, 1999), T. F. McCallum III and B. Weinstein (to Rohm and Haas Co.).
162. U.S. Pat. 4,033,936 (July 5, 1977), U. Bollert, E. Lohmar, and A. Ohorodnik (to Hoechst AG).
163. S. Black, *J. Soc. Dyers Colorists* **108**, 372–373 (1992).
164. V. Freudenberger and F. Jacob, *Angew. Makromol. Chem.* **105**, 203 (1982).
165. U.S. Pat. 4,127,590 (Nov. 28, 1978), S. Endo and co-workers (to Toyo Boseki KK).
166. C. S. Wang, J. Y. Shieh, and Y. M. Sun, *Eur. Polym. J.* **35**, 1465–1472 (1999).
167. C. S. Wang, and C. H. Lin, *Polymer* **40**, 747–757 (1999).
168. Jpn. Kokai Tokkyo Koho 5 991,122 (May 24, 1984) (to Japan Exlan Co., Ltd.).
169. U.S. Pat. 4,981,945 (Jan. 1, 1991), G. Landoni and C. Neri (to Enichem Synthesis, S.p.A.).
170. R. C. Nametz, *Ind. Eng. Chem.* **59**(5), 99 (1967).
171. U.S. Pat. 4,360,647 (Nov. 23, 1982), R. E. Hefner Jr. (to The Dow Chemical Company).
172. U.S. Pat. 5,571,888 (Nov. 5, 1996), Y.-N. Cheng and co-workers (to Industrial Technology Institute).
173. Fr. Pat. 1,584,020 (Dec. 12, 1969), O. Zaske, C. H. Fintelmann, and H. B. Igdaroff (to Vistron Co.).
174. U.S. Pats. 4,032,517 (June 28, 1977) and 4,092,302 (May 30, 1978), O. A. Pickett Jr. and J. W. Stoddard (both to Monsanto Co.).
175. U.S. Pat. 5,545,833 (Aug. 13, 1996), J. W. Stoddard (to Monsanto Co.).
176. F. J. Martin and K. R. Price, *J. Appl. Polym. Sci.* **12**, 143 (1968).
177. J. L. Massingill, *J. Coatings Technol.* **63**(797), 47–54 (1991).
178. R. O. Carter III, J. L. Parsons, and J. W. Holubka, *Ind. Eng. Chem. Res.* **26**, 1518–1523 (1987).
179. Ger. Appl. DE 19747553 A1 (publ. Apr. 29, 1999), W. von Gentzkow and co-workers (to Siemens A.-G).
180. U.S. Pat. 5,389,704 (Feb. 14, 1995), Y. Yabu (to The Dow Chemical Company).
181. J. A. Mikroyannidis and Z. Nir, *J. Appl. Polym. Sci.* **30**, 83 (1985).
182. U.S. Pat. 4,613,661 (Sept. 23, 1986), H. G. Langer and co-workers (to The Dow Chemical Company).
183. D. Derouet, F. Morvan, and J. C. Brosse, *J. Appl. Polym. Sci.* **62**, 1855–1868 (1996).
184. Eur. Pat. 794236 (Sept. 10, 1997), G. Scholz, S. Hoerold, and W. Pirig (to Hoechst AG).
185. Eur. Pat. 794205 (Sept. 10, 1997), H. Kleiner, S. Hoerold, and G. Scholz (to Hoechst AG).
186. U.S. Pat. 4,952,646 (Aug. 28, 1990), E. D. Weil, J. Tomko, and F. Jaffe (to Akzo America).
187. C.-S. Wang, and J.-Y. Shieh, *Eur. Polym. J.* **36**, 443–452 (2000).
188. C.-S. Wang and C. H. Lin, *J. Polym. Sci., Part A: Polym. Chem.* **37**, 3903–3909 (1999).

189. C.-S. Wang and M.-C. Lee, *Polymer* **41**, 3631–3638 (2000).
190. C.-S. Wang and J.-Y. Shieh, *J. Appl. Polym. Sci.* **73**, 353–361 (1999).
191. J.-Y. Shieh and C.-S. Wang, *J. Appl. Polym. Sci.* **78**, 1636–1644 (2000).
192. Japan. Kokai Tokkyu Koho JP 2000 265,040 (Sept. 26, 2000), H. Moriyama, Y. Takahashi, and M. Yoshisawa (to Dainippon Ink and Chemicals, Inc.).
193. PCT Appl. WO 98/07731 (Feb. 26, 1998), A. J. Buser and J. A. J. Schutyser (to Akzo Nobel).
194. J. A. Mikroyannidis and D. A. Kourtides, in C. K. Riew and J. K. Gillham, eds., *Advances in Chemistry Series, Vol. 208: Rubber-Modified Thermoset Resins*, American Chemical Society, Washington, D.C., 1984, pp. 351–356.
195. U.S. Pat. 3,645,971 (Feb. 29, 1972), R. R. Hindersinn (to Hooker Chemical Co.).
196. R. W. Hunter, and R. M. Washburn, in H. Lee, ed., *Advances in Chemistry Series, Vol. 92: Epoxy Resins*, American Chemical Society, Washington, D.C., 1970, pp. 208–223.
197. U.S. Pat. 3,516,965 (June 23, 1970), R. M. Washburn (to McDonnell Douglas Corp.).
198. S. V. Levchik and co-workers, *Polym. Adv. Technol.* **7**, 823–830 (1996).
199. E. R. Fretz and J. Green, *Print. Circuit Fabr.* **6**(5), 55 (1983).
200. A. J. Papa, *Ind. Eng. Chem. Prod. Res. Dev.* **9**, 478 (1970).
201. A. J. Papa, in W. C. Kuryla and A. J. Papa, eds., *Fire Retardancy of Polymeric Materials*, Vol. **3**, Marcel Dekker, Inc., New York, 1975, pp. 1–133.
202. Brit. Pat. 954,792 (Apr. 8, 1964), C. L. Harowitz (to Virginia-Carolina Chemical Corp.).
203. U.S. Pat. 3,235,517 (Feb. 15, 1966), T. M. Beck and E. N. Walsh (to Stauffer Chemical Co.).
204. U.S. Pat. 4,456,742-3 (June 24, 1984), F. T. H. Lee and J. Green (to FMC Corp.).
205. J. Green, *Plast. Compound.* 30 (Nov.–Dec. 1984).
206. U.S. Pat. 3,136,806 (June 9, 1964), H. Holtschmidt (to Farbenfabriken Bayer AG).
207. E. D. Weil, J. Kearnan, and G. Leitner, in *TAPPI Paper Synthetics Conference Papers*, TAPPI, Atlanta, Ga., pp. 301–305.
208. Jpn. Kokai Tokkyo Koho 60/124630 A2 (July 3, 1985) (to Hitachi Chemical Co.).
209. A. A. Faroq and co-workers, *Polym. Degrad. Stab.* **44**, 323–333 (1994).
210. B. K. Kandola and co-workers, *J. Macromol. Sci., C: Rev. Macromol. Chem. Phys.* **36**, 721–794 (1996).
211. S. LeVan, in R. Rowell, ed., *The Chemistry of Solid Wood* (Adv. Chem. Ser.), American Chemical Society, Washington, D.C., 1984, 531–574.
212. E. E. Nifant'ev, *Russ. Chem. Rev. (Engl. Transl.)* **34**, 942 (1965).
213. U.S. Pat. 4,461,720 (July 24, 1984), A. G. Lovyet and D. J. Morgan (to Hoover Treated Wood Products, Inc.).
214. M. E. Hall and A. R. Horrocks, *Trends Polym. Sci.* **1**, 55 (1993).
215. C. Y. C. Pak and co-workers, *Am. J. Med.* **71**, 615 (1981); *FDA Drug Bull.* **13**(1), 1 (1983).
216. C.-T. Kim and co-workers, *Starch/Stärke* **51**, 280–286 (1999).
217. A. R. Horrocks, *Rev. Prog. Coloration* **16**, 62 (1986).
218. M. Lewin and S. Sello, eds., *Chemical Finishing of Fibers and Fabrics, Functional Finishes*, Vol. **2**, Marcel Dekker, Inc., New York, 1984.
219. A. R. Horrocks, in D. Heywood, ed., *Textile Finishing*, Vol. **2**, Society of Dyers and Colorists, Bradford, U.K., in press.
220. S. L. Vail, D. J. Daigle, and A. W. Frank, *Text. Res. J.* **52**, 671, 678, 738 (1982); D. J. Daigle and A. W. Frank, *Text. Res. J.* **52**, 751 (1982).
221. U.S. Pat. 4,311,855 (Jan. 19, 1982), R. Cole and J. E. Stephenson (to Albright & Wilson).
222. W. F. Herbes, K. H. Remley, and J. B. Tracek, *Am. Dyest. Rep.* 72 (Sept. 1976).
223. U.S. Pats. 4,078,101 (Mar. 7, 1978) and 4,145,463 (Mar. 20, 1979), R. Cole (both to Albright & Wilson, Ltd.).

224. E. D. Weil, *Am. Dyest. Rep.* **76**(1), 41 (1987); *Am. Dyest. Rep.* **76**(2), 40 (1987).
225. R. Aenishanslin and co-workers, *Text. Res. J.* **39**, 375 (1969).
226. R. Aenishanslin and N. Bigler, *Textilveredlung* **3**, 467 (1968).
227. F. Lohse, in *Proceedings of the International Symposium on Flame Retardants*, Beijing, China, Nov. 1–5, 1989, International Academic Publishers, Beijing, 1989, pp. 489–494.
228. A. I. Kapura, *J. Fire Sci.* **12**, 3–13 (1994).
229. A. W. Frank, *CRC Crit. Rev. Biochem.* **16**(1), 51 (1984).
230. F. F. Shih, in S. Magdassi, ed., *Surface Activity of Proteins*, Marcel Dekker, Inc., New York, 1996, pp. 91–113.

EDWARD D. WEIL
Polytechnic University

PHOTORESISTS. See LITHOGRAPHC RESISTS.

PIEZOELECTRIC POLYMERS

Introduction

Piezoelectric polymers have been known for more than 40 years, but in recent years they have gained repute as a valuable class of "smart materials." There is no standard definition for smart materials, and terms such as intelligent materials, smart materials, adaptive materials, active devices, and smart systems are often used interchangeably. The term "*smart material*" generally designates a material that changes one or more of its properties in response to an external stimulus.

The most popular smart materials are piezoelectric materials, magnetostrictive materials, shape-memory alloys, electrorheological fluids, electrostrictive materials, and optical fibers. Magnetostrictives, electrostrictives, shape-memory alloys, and electrorheological fluids are used as actuators; optical fibers are used primarily as sensors (see SHAPE MEMORY POLYMERS)

Among these active materials, piezoelectric materials are most widely used because of their wide bandwidth, fast electromechanical response, relatively low power requirements, and high generative forces. A classical definition of piezoelectricity, a Greek term for "pressure electricity," is the generation of electrical polarization in a material in response to mechanical stress. This phenomenon is known as the direct effect. Piezoelectric materials also display the converse effect: mechanical deformation upon application of an electrical charge or signal. Piezoelectricity is a property of many noncentrosymmetric ceramics, polymers, and biological systems. Pyroelectricity is a subset of piezoelectricity, whereby the polarization is a function of temperature. Some pyroelectric materials are ferroelectric, although not all ferroelectrics are pyroelectric. Ferroelectricity is a property of certain dielectrics that exhibit spontaneous electric polarization (separation of the center of positive and negative electric charge that

Encyclopedia of Polymer Science and Technology. Copyright John Wiley & Sons, Inc. All rights reserved.

Table 1. Comparison of Properties of Standard Piezoelectric Polymer and Ceramic Materials

	$d_{31}{}^a$, pm/V	$g_{31}{}^a$, (mV·m)/N	k_{31}	Salient features
Poly(vinylidene fluoride) (PVDF)	28	240	0.12	Flexible, lightweight, low acoustic and mechanical impedance
Lead zirconium titanate (PZT)	175	11	0.34	Brittle, heavy, toxic

Values shown are absolute values of constants.

makes one side of the crystal positive and the opposite side negative) that can be reversed in direction by applying an appropriate electric field. Ferroelectricity is named by analogy with ferromagnetism, which occurs in materials such as iron. Traditionally, ferroelectricity is defined for crystalline materials, or at least in the crystalline region of semicrystalline materials. More recently, however, a number of researchers have explored the possibility of ferroelectricity in amorphous polymers, that is, ferroelectricity without a crystal lattice structure (1).

Characteristics of Piezoelectric Polymers. The properties of polymers are very different from those of inorganics (Table 1), and they are uniquely qualified to fill niche areas where single crystals and ceramics cannot perform as effectively. As noted in Table 1, the piezoelectric strain constant (d_{31}) for the polymer is lower than that of the ceramic. However, piezoelectric polymers have much higher piezoelectric stress constants (g_{31}) which indicates that they are much better sensors than ceramics. Piezoelectric polymeric sensors and actuators offer the advantage of processing flexibility because they are lightweight, tough, readily manufactured in large areas, and can be cut and formed into complex shapes. Polymers also exhibit high strength and high impact resistance (2). Other notable features of polymers are low dielectric constant, low elastic stiffness, and low density, which result in high voltage sensitivity (excellent sensor characteristic) and low acoustic and mechanical impedance (crucial for medical and underwater applications). Polymers also typically possess high dielectric breakdown and high operating field strength, which means that they can withstand much higher driving fields than ceramics. Polymers offer the ability to pattern electrodes on the film surface and pole only selected regions. Based on these features, piezoelectric polymers possess their own established area for technical applications and useful device configurations.

Structural Requirements for Piezoelectric Polymers. The piezoelectric mechanisms for semicrystalline and amorphous polymers differ. Although the differences are distinct, particularly with respect to polarization stability, in the simplest terms, four critical elements exist for all piezoelectric polymers, regardless of morphology. These essential elements are (*1*) the presence of permanent molecular dipoles, (*2*) the ability to orient or align the molecular dipoles, (*3*) the ability to sustain this dipole alignment once it is achieved, and (*4*) the ability of the material to undergo large strains when mechanically stressed (3).

Semicrystalline Polymers

Mechanism of Piezoelectricity in Semicrystalline Polymers. Semicrystalline Polymers must have a polar crystalline phase to render them piezoelectric. The Morphology of such polymers consists of crystallites dispersed within amorphous regions, as shown in Figure 1a. The amorphous region has a glass-transition temperature that dictates the mechanical properties of the polymer, and the melting temperature of the crystallites dictates the upper limit of the use temperature. The degree of crystallinity in such polymers depends

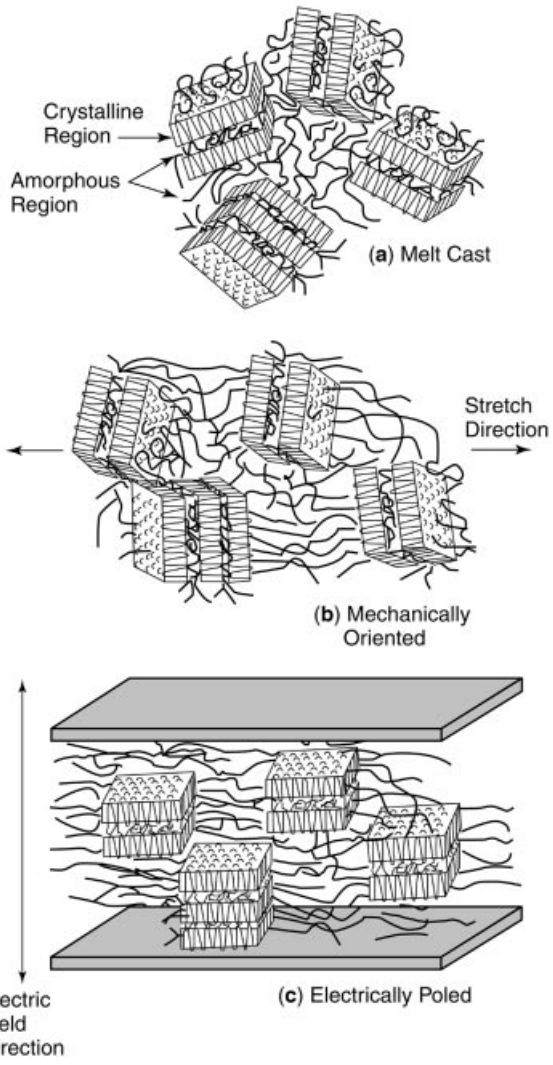

Fig. 1. Schematic illustration of random stacks of amorphous and crystal lamellae in the PVDF polymer: (**a**) the morphology after the film is melt cast; (**b**) after orientation of the film by mechanically stretching several times its original length; and (**c**) after depositing metal electrodes and poling through the film thickness.

on the method of preparation and thermal history. Most semicrystalline polymers have several polymorphic phases, some of which may be polar. Mechanical orientation, thermal annealing, and high voltage treatment are all, it has been shown, effective in inducing crystalline phase transformations. Stretching the polymer aligns the amorphous strands in the film plane, as shown in Figure 1b, and facilitates uniform rotation of the crystallites by an electric field. Depending on whether stretching is uniaxial or biaxial, the electrical and mechanical properties (and therefore the transduction response) are either highly anisotropic or isotropic in the plane of the polymer sheet. Electrical poling is accomplished by applying an electric field across the thickness of the polymer, as depicted in Figure 1c. An electric field of the order of 50 MV/m is typically sufficient to effect crystalline orientation. Polymers can be poled by using a direct contact method or corona discharge. The latter is advantageous because contacting electrodes is not required and samples of large area can be poled continuously. This method is used to manufacture commercial poly(vinylidene fluoride) (PVDF) film (see VINYLIDENE FLUORIDE POLYMERS(PVDF)). Some researchers have also successfully poled large areas of polymer films by sandwiching them between polished metal plates under a vacuum. This method eliminates electrical arcing of samples and the need for depositing metal electrodes on the film surface. The amorphous phase of semicrystalline polymers supports the crystal line orientation, and polarization is stable up to the Curie temperature. This polarization can remain constant for many years if it is not degraded by moisture uptake or elevated temperatures.

Piezoelectric Constitutive Relationships. The constitutive relationships that describe piezoelectric behavior in materials can be derived from thermodynamic principles (4). A tensor notation is adopted to identify the coupling between the various entities through mechanical and electrical coefficients. The common practice is to label directions as depicted in Figure 2. The stretch direction

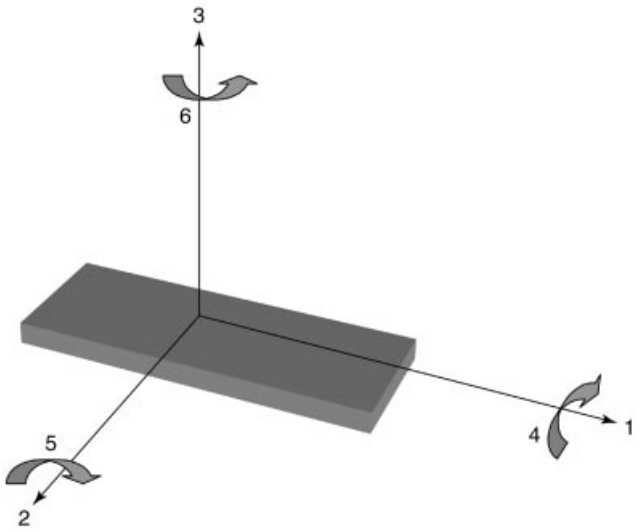

Fig. 2. Tensor directions for defining the constitutive relationships.

is denoted as "1." The "2" axis is orthogonal to the stretch direction in the plane of the film. The polarization axis (perpendicular to the surface of the film) is denoted "3." The shear planes, indicated by the subscripts "4," "5," and "6," are perpendicular to the directions "1," "2," and "3," respectively. By reducing the tensor elements and using standard notations (5), the resulting equations can be displayed in matrix form as follows:

$$\begin{vmatrix} S_1 \\ S_2 \\ S_3 \\ S_4 \\ S_5 \\ S_6 \end{vmatrix} = \begin{vmatrix} d_{11} & d_{12} & d_{13} \\ d_{21} & d_{22} & d_{23} \\ d_{31} & d_{32} & d_{33} \\ d_{41} & d_{42} & d_{43} \\ d_{51} & d_{52} & d_{53} \\ d_{61} & d_{62} & d_{63} \end{vmatrix} \begin{vmatrix} E_1 \\ E_2 \\ E_3 \end{vmatrix} + \begin{vmatrix} s_{11}^E & s_{12}^E & s_{13}^E & s_{14}^E & s_{15}^E & s_{16}^E \\ s_{21}^E & s_{22}^E & s_{23}^E & s_{24}^E & s_{25}^E & s_{26}^E \\ s_{31}^E & s_{32}^E & s_{33}^E & s_{34}^E & s_{35}^E & s_{36}^E \\ s_{41}^E & s_{42}^E & s_{43}^E & s_{44}^E & s_{45}^E & s_{46}^E \\ s_{51}^E & s_{52}^E & s_{53}^E & s_{54}^E & s_{55}^E & s_{56}^E \\ s_{61}^E & s_{62}^E & s_{63}^E & s_{64}^E & s_{65}^E & s_{66}^E \end{vmatrix} \begin{vmatrix} X_1 \\ X_2 \\ X_3 \\ X_4 \\ X_5 \\ X_6 \end{vmatrix} \tag{1}$$

$$\begin{vmatrix} D_1 \\ D_2 \\ D_3 \end{vmatrix} = \begin{vmatrix} \varepsilon_{11}^T & \varepsilon_{12}^T & \varepsilon_{13}^T \\ \varepsilon_{21}^T & \varepsilon_{22}^T & \varepsilon_{23}^T \\ \varepsilon_{31}^T & \varepsilon_{32}^T & \varepsilon_{33}^T \end{vmatrix} \begin{vmatrix} E_1 \\ E_2 \\ E_3 \end{vmatrix} + \begin{vmatrix} d_{11} & d_{12} & d_{13} & d_{14} & d_{15} & d_{16} \\ d_{21} & d_{22} & d_{23} & d_{24} & d_{25} & d_{26} \\ d_{31} & d_{32} & d_{33} & d_{34} & d_{35} & d_{36} \end{vmatrix} \begin{vmatrix} X_1 \\ X_2 \\ X_3 \\ X_4 \\ X_5 \\ X_6 \end{vmatrix} \tag{2}$$

Piezoelectricity is a cross coupling among the elastic variables, stress X and strain S, and the dielectric variables, electric charge density D and electric field E. Note that D is named in analogy to the B field in ferromagnetism, although some authors also refer to it as dielectric or electric displacement. There does not seem to be a standard nomenclature; however, it is the opinion of the authors of this article that electric charge density is a better description of this property. The combinations of these variables define the piezoelectric strain constant d, the material compliance s, and the permittivity ε. Other piezoelectric properties are the piezoelectric voltage constant g, stress constant e, and strain constant h given by the equations in Table 2. For a given constant, the first definition in the table refers to the direct effect, and the second refers to the converse effect. The piezoelectric constants are interrelated through the electrical and mechanical properties of the material. Electric field strength and displacement charge density are related through the dielectric constant, $\varepsilon\varepsilon_0$ (where ε_0 is the permittivity of free space), and stress and strain are related through the compliance according to

Table 2. Definitions of Piezoelectric Constants

Equations	Units
$d = (\mathrm{d}D/\mathrm{d}X)_\mathrm{E} = (\mathrm{d}S/\mathrm{d}E)_\mathrm{X}$	C/N or m/V
$e = (\mathrm{d}D/\mathrm{d}S)_\mathrm{E} = -(\mathrm{d}X/\mathrm{d}E)_\mathrm{S}$	C/m or N/Vm
$g = (\mathrm{d}E/\mathrm{d}X)_\mathrm{D} = (\mathrm{d}S/\mathrm{d}D)_\mathrm{X}$	Vm/N or m^2/C
$h = (\mathrm{d}E/\mathrm{d}S)_\mathrm{D} = -(\mathrm{d}X/\mathrm{d}D)_\mathrm{S}$	V/m or N/C

$$d_{ij} = \varepsilon_0 \varepsilon_i g_{ij} \tag{3}$$

$$e_{ij} = s_{ij} d_{ij} \tag{4}$$

The polarization P is a measure of the degree of piezoelectricity in a given material. In a piezoelectric material, a change in polarization ΔP results from an applied stress X or strain S under conditions of constant temperature and zero electric field. A linear relationship exists between ΔP and the piezoelectric constants. Because of material anisotropy, $\boldsymbol{P}$ is a vector that has three orthogonal components in the 1, 2, and 3 directions. Alternatively, the piezoelectric constants can be defined as

$$\Delta P_i = d_{ij} X_j \tag{5}$$

$$\Delta P_i = g_{ij} S_j \tag{6}$$

The electrical response of a piezoelectric material is a function of the electrode configuration relative to the direction of the applied mechanical stress. For a coefficient d_{ij}, the first subscript is the direction of the electric field or charge displacement, and the second subscript gives the direction of the mechanical deformation or stress. The C_{2v} crystallographic symmetry typical of synthetic oriented, poled polymer film leads to cancellation of all but five of the d_{ij} components (d_{31}, d_{32}, d_{33}, d_{15}, and d_{24}). If the film is poled and biaxially oriented or unoriented, $d_{31} = d_{32}$ and $d_{15} = d_{24}$. Most natural biopolymers possess D_∞ symmetry which yields a matrix that possesses only the shear piezoelectricity components d_{13} and d_{25}. Because the d_{33} constant is difficult to measure without constraining the lateral dimension of the sample, it is typically determined from equation 7 which relates the constants to the hydrostatic piezoelectric constant, d_{3h}.

$$d_{3h} = d_{31} + d_{32} + d_{33}. \tag{7}$$

The electromechanical coupling coefficient k_{ij} represents the conversion of electrical energy into mechanical energy and vice versa. The electromechanical coupling can be considered a measure of transduction efficiency and is always less than unity as shown here:

$$k^2 = \frac{\text{Electrical energy converted to mechanicalenergy}}{\text{Input electricalenergy}} \tag{8}$$

$$k^2 = \frac{\text{Mechanical energy converted to electricalenergy}}{\text{Input mechanicalenergy}} \tag{9}$$

Some k coefficients can be obtained from a measured d constant as follows:

$$k_{31} = \frac{d_{31}}{\sqrt{s_{11}^E \varepsilon_3^T}} \tag{10}$$

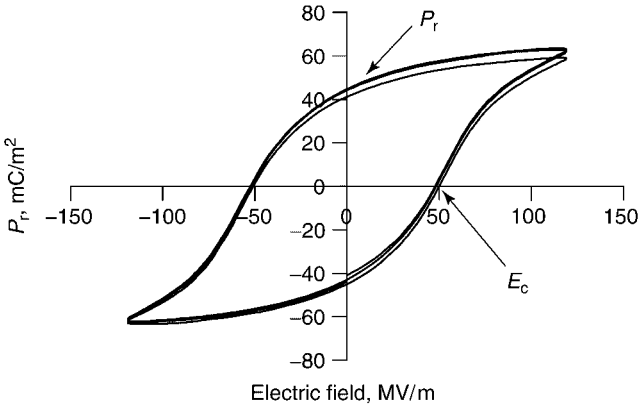

Fig. 3. Typical ferroelectric hysteretic behavior for PVDF.

Ferroelectricity in Semicrystalline Polymers. At high electric fields, the polarization in semicrystalline polymers such as PVDF is nonlinear with the applied electric field. This nonlinearity in polarization is defined as hysteresis. The existence of spontaneous polarization together with polarization reversal (as illustrated by a hysteresis loop) is generally accepted as proof of ferroelectricity. Figure 3 is an example of the typical hysteretic behavior of PVDF. Two other key properties typically reported for ferroelectric materials are the coercive field and the remanent polarization. The coercive field E_c, which marks the point where the hysteresis intersects the horizontal axis, is about 50 MV/m at room temperature for many ferroelectric polymers. The remanent polarization P_r corresponds to the point where the loop intersects the vertical axis. The values of E_c and P_r depend on temperature and frequency. The Curie temperature T_c is generally lower than but close to the melting temperature of the polymer. Below T_c, the polymer is ferroelectric and above T_c, the polymer loses its noncentrosymmetric nature.

Although ferroelectric phenomenon has been well documented in ceramic crystals, the question of whether polymer crystallites could exhibit dipole switching was debated for about a decade after the discovery of piezoelectricity in PVDF. Inhomogeneous polarization through the film thickness that yielded higher polarization on the positive electrode side of the polymer led to speculations that PVDF was simply a trapped charge electret. These speculations were dispelled when x-ray studies (6) demonstrated that polarization anisotropy vanishes because of high poling field strengths and that true ferroelectric dipole reorientation occurs in PVDF. One researcher used infrared to attribute the polarization reversal in PVDF to 180° dipole rotation (7). Others documented the same via x-ray pole analysis and infrared techniques for odd-numbered nylons (8).

State of the Art. Pioneering work in the area of piezoelectric polymers (9) led to the development of strong piezoelectric activity in poly(vinylidene fluoride) (PVDF) and its copolymers with trifluoroethylene (TrFE) and tetrafluoroethylene (TFE). These semicrystalline fluoropolymers represent the state of the art in piezoelectric polymers and are currently the only commercial piezoelectric polymers.

Table 3. Comparison of Piezoelectric Properties of Some Semicrystalline Polymeric Materials

Polymer	Structure	T_g, °C	T_m, °C	Max. use temp., °C	d_{31}, pC/N	Reference
PVDF	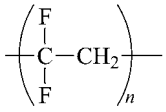	−35	175	80	20–28	2
PTrFE	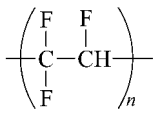	32	150	90–100	12	2
Nylon-11	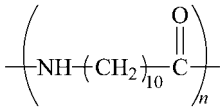	68	195	185	3 at 25°C, 14 at 107°.C	22
Polyurea-9	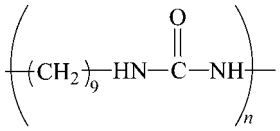	50	180	—	—	28

Odd-numbered nylons, the next most widely investigated semicrystalline piezoelectric polymers, have excellent piezoelectric properties at elevated temperatures but have not yet been embraced in practical application. Other semicrystalline polymers including polyureas, liquid crystalline polymers, biopolymers, and an array of blends have been studied for their piezoelectric potential and are summarized in the following section. The chemical repeat unit and piezoelectric constants of several semicrystalline polymers are listed in Table 3.

Poly(vinylidene fluoride) (PVDF). Interest in the electrical properties of PVDF began in 1969 when it was shown (9) that poled thin films exhibit a very large piezoelectric coefficient, 6–7 pC/N, a value about 10 times larger than had been observed in any other polymer. As seen in Table 3, PVDF is inherently polar. The spatially symmetrical disposition of the hydrogen and fluorine atoms along the polymer chain gives rise to unique polar effects that influence the electromechanical response, solubility, dielectric properties, and crystal morphology and yield an unusually high dielectric constant. The dielectric constant of PVDF is about 12, which is four times greater than that of most polymers, and makes PVDF attractive for integration into devices because the signal-to-noise ratio is smaller for higher dielectric materials (see DIELECTRIC RELAXATION). The amorphous phase in PVDF has a Glass Transition that is well below room temperature (−35°C); hence, the material is quite flexible and readily strained at room temperature. PVDF is typically 50–60% crystalline, depending on thermal and processing history, and has at least four crystal phases (α, β, γ, and δ); at least three are polar. The most stable, nonpolar α phase results upon casting PVDF from a melt and can be transformed into the polar β phase by mechanical stretching at elevated temperatures

or into the polar δ phase by rotating the molecular chain axis in a high electric field ($\sim$130 MV/m) (10). The β phase is most important for piezoelectricity and has a dipole moment perpendicular to the chain axis of 7×10^{-30} C·m (2.1 D). After poling PVDF, the room temperature polarization stability is excellent; however, polarization and piezoelectricity degrade as temperature increases and are erased at its Curie temperature. Previously, it was believed that polarization stability was defined only by the melting temperature of the PVDF crystals. Recently, however, some researchers suggest that the polarization stability of PVDF and its copolymers is associated with coulombic interactions between injected, trapped charges and oriented dipoles in the crystals (11). It has been hypothesized that the thermal decay of the polarization is caused by the thermally activated removal of the trapped charges from the traps at the surface of the crystals. The role of trapped charges in stabilizing orientation in both semicrystalline and amorphous polymers is still a subject that needs further study. The electromechanical properties of PVDF have been widely investigated. For more details, the reader is referred to the wealth of literature that exists on the subjects of piezoelectric, pyroelectric, and ferroelectric properties (2,6,12,13), and the morphology (14–16) of this polymer (see VINYLIDENE FLUORIDE POLYMERS).

Poly(vinylidene fluoride–trifluoroethylene and tetra fluoro ethylene) Copolymers. Copolymers of vinylidene fluoride with trifluoroethylene (TrFE) and tetrafluoroethylene (TFE) also exhibit strong piezoelectric, pyroelectric, and ferroelectric effects. These polymers are discussed together here because they behave similarly when copolymerized with PVDF. An attractive morphological feature of the comonomers is that they force the polymer into an all-trans conformation that has a polar crystalline phase, which eliminates the need for mechanical stretching to yield a polar phase. P(VDF–TrFE) crystallizes to a much greater extent than PVDF (up to 90% crystalline) and yields a higher remanent polarization, a lower coercive field, and much sharper hysteretic loops. TrFE also extends the use temperature by about 20°C to close to 100°C. Conversely, copolymers with TFE exhibit a lower degree of crystallinity and a suppressed melting temperature, compared to the PVDF homopolymer. Although the piezoelectric constants for the copolymers are not as large as those of the homopolymer, the advantages of P(VDF–TrFE) in processibility, enhanced crystallinity, and higher use temperature make it favorable for applications.

Researchers have recently reported that highly ordered, lamellar crystals of P(VDF–TrFE) can be made by annealing the material at temperatures between the Curie temperature and the melting point. This material is referred to as a "single crystalline film." A relatively large single crystal of P(VDF–TrFE) 75/25 mol% copolymer was grown that exhibits a room temperature $d_{33} = -38$ pm/V and a coupling factor $k_{33} = 0.33$ (17).

The result of introducing defects into the crystalline structure of P(VDF–TrFE) copolymer on electroactive actuation has been studied using high electron irradiation (18). Extensive structural investigations indicate that electron irradiation disrupts the coherence of polarization domains (all-trans chains) and forms localized polar regions (nanometer-sized, all-trans chains interrupted by trans and gauche bonds). After irradiation, the material exhibits behavior analogous to that of relaxor ferroelectric systems in inorganic materials. The resulting material is no longer piezoelectric, but rather exhibits a large electric field-induced strain

(5% strain) because of electrostriction. The basis for such large electrostriction is the large change in the lattice strain as the polymer traverses the ferroelectric to paraelectric phase transition and the expansion and contraction of the polar regions. Piezoelectricity can be measured in these and other electrostrictives when a dc bias field is applied. Irradiation is typically accomplished in a nitrogen atmosphere at elevated temperatures using irradiation dosages up to 1,200 kGy (120 Mrad).

Polyamides. A low level of piezoelectricity was first reported in polyamides (also known as nylons) in 1970 (19). A systematic study of odd-numbered nylons, however, initiated in 1980 (20) and served as the impetus for more than 20 years of subsequent investigations of piezoelectric and ferroelectric activity in these polymers. The monomer unit of odd nylons consists of even numbers of methylene groups and one amide group whose dipole moment is 12.3×10^{-30} C·m (3.7 D). Polyamides crystallize in all-trans conformations and are packed to maximize hydrogen bonding between adjacent amine and carbonyl groups, as seen in Figure 4 for an even-numbered and an odd-numbered polyamide. The amide dipoles align synergistically in the odd-numbered monomer, resulting in a net dipole moment. The amide dipole cancels in an even-numbered nylon, although remanent polarizations have been measured for some even-numbered nylons, as discussed later in this article. The unit dipole density depends on the number of methylene groups present, and polarization increases from 58 mC/m^2 for nylon-11 to 125 mC/m^2 for nylon-5 as the number of methylene groups decreases (8).

Polyamides are hydrophilic. Because water absorption is associated with hydrogen bonding to the polar amide groups, the hydrophilicity increases as the

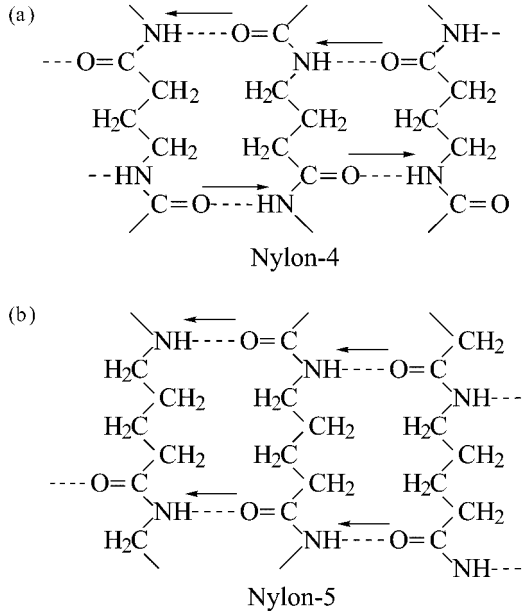

Fig. 4. Schematic depiction of hydrogen-bonded sheets showing dipole directions in the crystal lattices of (**a**) even (nylon-4) and (**b**) odd polyamides (nylon-5).

density of amide groups increases. Water absorption in nylon-11 and nylon-7 has been shown to be as high as 4.5% (by weight) and more than 12% for nylon-5 (21), whereas it is less than 0.02% for PVDF and its copolymers. Studies have shown that water absorption can have a dramatic effect on the dielectric and piezoelectric properties of nylons; however, water does not affect the crystallinity or orientation in thermally annealed films (21). Thus, films can be dried to restore their original properties.

At room temperature, odd-numbered nylons have lower piezoelectric constants than PVDF; however, when examined above their glass-transition temperatures, they exhibit comparable ferroelectric and piezoelectric properties and much higher thermal stability. The piezoelectric d and e constants increase rapidly as temperature increases. Maximum stable d_{31} values of 17 pC/N and 14 pC/N are reported for nylon-7 and nylon-11, respectively. Corresponding values of the electromechanical coupling constant k_{31} are 0.054 and 0.049. Studies have also shown that annealing nylon films enhances their polarization stability because it promotes denser packing of the hydrogen-bonded sheet structure in the crystalline regions and hinders dipole switching because of lowered free volume for rotation (22).

Though widely studied, piezoelectric polyamides have not been widely used in applications partly because of their low room temperature piezoelectric response and the problem of moisture uptake.

Liquid Crystalline Polymers. Liquid crystals consist of highly ordered rodlike or disk-like molecules. At their melting points they partially lose crystalline order and generate a fluid but ordered state. They can form layered structures called smectic phases or nematic phases that have an approximately parallel orientation of the molecular long axis. It was first predicted in 1975 that spontaneous polarization could be achieved in liquid crystals based on symmetry arguments (23). Subsequently, it has been shown that liquid crystalline molecules whose chiral carbon atoms link a mesogenic group and end alkyl chains may exhibit ferroelectric behavior in the smectic C phase (SmC$*$) (24). In this phase, the molecular axis tilts from the normal to the layer plane, and the molecular dipoles align in the same direction, yielding a net polarization. If such liquid crystalline molecules are introduced into the backbone or as a side group on a polymer, a ferroelectric liquid crystalline polymer can be obtained. There are three requirements for spontaneous polarization in a liquid crystal: a center of chirality, a dipole moment positioned at the chiral center that acts transverse to the molecular long axis, and a tilted smectic phase (25).

Polyureas. Polyureas are thermosets, long used as insulators in a number of applications. Until a few years ago, ureas were available mostly as insoluble powders or highly cross-linked resins. In 1987, a vapor deposition polymerization method was successfully developed that was later applied to synthesizing polyureas (26,27). Typically, a vapor deposition technique is used by evaporating OCN–R_1–NH_2 and H_2N–R_2–NH_2 monomers simultaneously on a substrate (where R_1 and R_2 are various aliphatic or aromatic groups). This prevents cross-linking and allows processing thicknesses in the hundreds of nanometers to tens of micrometers.

An exploration (27) of the dielectric and pyroelectric properties of polyurea films led to the discovery of their piezoelectricity. From the early 1990s to the

present, various aromatic and aliphatic polyureas were synthesized, and it was shown that they are piezoelectric (28,29). Aromatic polyureas were the first polyurea structures identified as piezoelectric. They exhibit a piezoelectric e constant of 15 mC/m^2 and have high temperature stability, which remains independent of temperature up to 200°C. Their pyroelectric coefficient is high because of their low dielectric loss compared to other polymers. The d constant is about 5 pC/N at room temperature and increases as temperature increases (28).

Owing to their structures, aliphatic polyureas possess higher flexibility in their molecular chains. Similarly to polyamides, hydrogen bonds play a large role in stabilizing the orientation polarization that is imparted. Polyureas that have an odd number of methyl groups exhibit overall nonzero polarization. Polyurea-9 was synthesized and processed first, and an e constant of 5 mC/m^2 was reported (29). Then, polyureas that have a smaller number of carbons were attempted because it was surmised that they should lead to a higher density of urea bond dipoles. Toward that end, polyurea-5 was synthesized, and it was found that the e and d constants are twice those of polyurea-9. Aliphatic polyureas exhibit ferroelectric hysteresis and in addition, are piezoelectric when they have odd numbers of methyl groups. Their thermal stability and piezoelectric coefficients depend highly on the poling temperature (typically 70–150°C) but are lower than those of aromatic polyureas.

Biopolymers. Piezoelectricity of biopolymers was first reported in keratin in 1941 (30). When a bundle of hair was immersed in liquid air, an electric voltage of a few volts was generated between the tip and the root. When pressure was applied on the cross section of the bundle, an electric voltage was generated. Subsequently, piezoelectricity has been observed in a wide range of other biopolymers including collagen (31,32), polypeptides like poly(γ-methylglutamate) and poly(γ-benzyl-L-glutamate) (33,34), oriented films of DNA (35), poly(lactic acid) (36), and chitin (37). Most natural biopolymers possess D_∞ symmetry and so they exhibit shear piezoelectricity. A shear stress in the plane of polarization produces an electric displacement perpendicular to the plane of the applied stress and results in a $-d_{14} = d_{25}$ piezoelectric constant. The piezoelectric constants of biopolymers are small relative to synthetic polymers; they range in value from 0.01 pC/N for DNA to 2.5 pC/N for collagen. The electromechanical effect in such polymers is attributed to the internal rotation of polar atomic groups linked to asymmetrical carbon atoms. Keratin and some polypeptide molecules assume an α-helical or a β-sheet crystalline structure in which the CONH dipoles align synergistically in the axial direction.

Currently, the physiological significance of piezoelectricity in many biopolymers is not well understood, but it is believed that such electromechanical phenomena may have a distinct role in biochemical processes. For example, it is known that electric polarization in bone influences bone growth (38). In one study, a piezoelectric PVDF film was wrapped around the femur of a monkey. Within weeks, a remarkable formation of new bone was observed. The motion of the animal caused deformation of the film, which produced a neutralizing ionic current in the surrounding tissue. This minute fluctuating current appears to stimulate the metabolic activity of bone cells and leads to the proliferation of bone.

Amorphous Polymers

The purpose of this section is to explain the mechanism and key components required for developing piezoelectricity in amorphous polymers and to present a summary of the polarization and electromechanical properties of the amorphous polymers currently under investigation.

Dielectric Theory. The piezoelectricity in amorphous polymers differs from that in semicrystalline polymers and inorganic crystals in that the polarization is not in a state of thermal equilibrium, but rather a quasi-stable state because of the freezing-in of molecular dipoles. The result is a piezoelectric-like effect. A theoretical model for polymers that have frozen-in dipolar orientation was presented to explain piezoelectricity and pyroelectricity in amorphous polymers such as poly(vinyl chloride) (39).

One of the most important properties of an amorphous piezoelectric polymer is its Glass Transition temperature because it dictates use temperature and defines the poling process conditions. T_g is (the temperature below which the material exhibits glass-like characteristics, and above which it has rubber-like properties). Orientation polarization of molecular dipoles is responsible for piezoelectricity in amorphous polymers. It is induced, as shown in Figure 5, by applying an electric field E_p at an elevated temperature ($T_p \geq T_g$) where the molecular chains are sufficiently mobile and allow dipole alignment with the electric field. Partial retention of this orientation is achieved by lowering the temperature below T_g in the presence of E_p, resulting in a piezoelectric-like

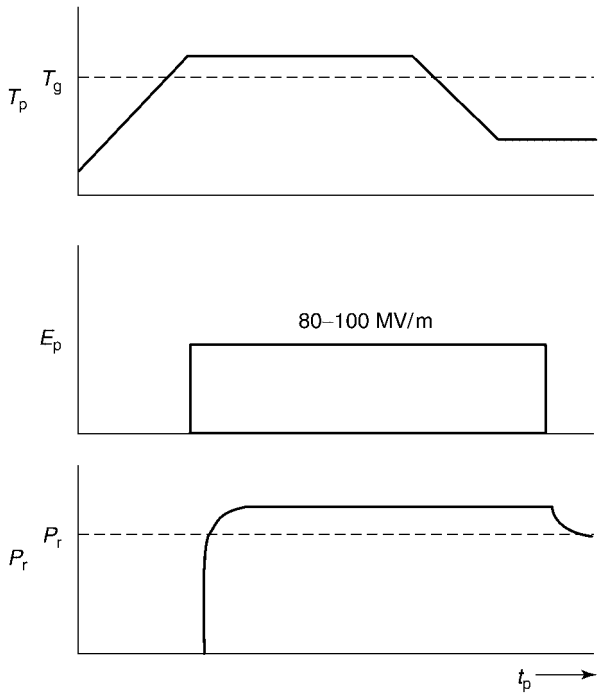

Fig. 5. Poling profile of an amorphous polymer.

effect. The remanent polarization P_r is directly proportional to E_p and the piezoelectric response. The procedure used to prepare a piezoelectric amorphous polymer clearly results in both oriented dipoles and space or real charge injection. The real charges are usually concentrated near the surface of the polymer, and they are introduced because of the presence of the electrodes. Interestingly, some researchers (40,41) have shown that the presence of space charges does not significantly affect piezoelectric behavior. The reason is twofold. The magnitude of space charges is usually not significant with respect to polarization charges. Secondly, space charges are essentially symmetrical with respect to the thickness of the polymer; therefore, when the material is strained uniformly, the contribution to the piezoelectric effect is negligible.

In what follows, the origins of the dielectric contribution to the piezoelectric response of amorphous polymers are addressed. The potential energy U of a dipole μ at an angle θ with the applied electric field is $U = \mu\ \mathbf{E} \cos\theta$. Using statistical mechanics and assuming Boltzman's distribution of dipole energies, the mean projection of the dipole moment $\langle\mu\rangle_E$ in the direction of the applied electric field is obtained:

$$\frac{\langle\mu_E\rangle}{\mu} = \coth\frac{\mu E_p}{kT} - \frac{kT}{\mu E} \tag{11}$$

This is the Langevin equation that describes the degree of polarization in a sample when an electric field E is applied at temperature T. Experimentally, a poling temperature in the vicinity of T_g is used to maximize dipole motion. The maximum electric field that may be applied, typically 100 MV/m, is determined by the dielectric breakdown strength of the polymer. For amorphous polymers, $\mu E/kT$ is much less than 1; this places these systems well within the linear region of the Langevin function. The remanent polarization P_r is simply the polarization during poling minus the electronic and atomic polarizations that relax at room temperature, once the field E_p is removed. The following linear equation for remanent polarization results when the Clausius–Mossotti equation is used to relate the dielectric constant to the dipole moment (42):

$$P_r = \Delta\varepsilon\ \varepsilon_0 E_p \tag{12}$$

It can be concluded that remanent polarization and hence the piezoelectric response of a material are determined by $\Delta\varepsilon$; this makes it a practical criterion to use when designing piezoelectric amorphous polymers. The Dielectric relaxation strength $\Delta\varepsilon$ may be the result of either free or cooperative dipole motion. Dielectric theory yields a mathematical approach for examining the dielectric relaxation $\Delta\varepsilon$ due to free rotation of the dipoles. The equation incorporates Debye's work based on statistical mechanics, the Clausius–Mossotti equation, and the Onsager local field and neglects short-range interactions (43):

$$\Delta\varepsilon_{\text{calculated}} = \frac{N\mu^2}{3kT\varepsilon_0}\left(\frac{n^2+2}{3}\right)^2\left[\frac{3\varepsilon(0)}{2\varepsilon(0)+n^2}\right]^2 \tag{13}$$

where N is the number of dipoles per unit volume, k is the Boltzmann constant, $\varepsilon(0)$ is the static dielectric constant, and n is the refractive index. One way to measure P_r in amorphous polymers is the thermally stimulated current (TSC) method (refer to section on characterization). P_r can be calculated from the liberated charge during TSC, and by reconciling that with the Onsager relationship, the dipole density can be calculated:

$$P_r = \frac{N\mu^2 E_p}{3kT_p}\left(\frac{\varepsilon_\infty + 2}{3}\right)^2\left[\frac{3\varepsilon(0)}{2\varepsilon(0)+\varepsilon_\infty}\right] \tag{14}$$

The piezoelectric constants are related to the polarization. From basic thermodynamics,

$$d_{3i} = \left(\frac{\partial P}{\partial \sigma_i}\right)_{\gamma,T} \tag{15}$$

A molecular theory of the direct piezoelectric effect in poled amorphous piezoelectric polymers has been developed. An expression for the hydrostatic coefficient appears in the original paper (41). Later, this theory was extended, and an equation for d_{31} was obtained (44,45). By differentiating equation 14 and modifying it to account for dimensional effects such as stretching (44,46),

$$d_{31} = P_r(1-\gamma)S_{11} + \frac{P_r(1-\gamma)}{3}(\varepsilon_\infty - 1)S_{11} \tag{16}$$

where γ is Poisson's ratio, ε_∞ is the permittivity at high frequencies, and S_{11} is the compliance of the polymer. The first term accounts for dimensional effects, and the second term gives the contribution of the local field effect.

Polarizability and Poling Conditions. Designing an amorphous polymer that has a large dielectric relaxation strength and hence piezoelectric response requires the ability to incorporate highly polar groups at high concentrations and cooperative dipole motion. A study of the relationship between relaxation times, poling temperatures, and poling fields is crucial to achieving optimal dipole alignment. Theoretically, the higher the electric field, the better the dipole alignment. The value of the electric field is limited, however, by the dielectric breakdown of the polymer. In practice, 100 MV/m is the maximum field that can be applied to these materials. Poling times need to be of the order of the relaxation time of the polymer at the poling temperature.

During poling, the temperature is lowered to room temperature, while the field is still on, to freeze-in the dipole alignment. In a semicrystalline material, however, locking-in the polarization is supported by the crystalline structure of the polymer, and it is therefore stable above the glass-transition temperature of the polymer. Because the remanent polarization in amorphous polymers is lost in the vicinity of T_g, their use is limited to temperatures well below T_g. This means that the polymers are used in their glassy state, where they are quite stiff and thus limit the ability of the polymer to strain as stress is applied. A piezoelectric amorphous polymer may be used at temperatures near its T_g to optimize its mechanical properties, but not too close so as to maintain the remanent polarization.

Although there are few data that address the stability of piezoelectric activity in amorphous polymers, it is clear that time, pressure, and temperature can contribute to dipole relaxation in these polymers. For a given application and use temperature, the effect of these parameters on the stability of the frozen-in dipole alignment should be determined.

Examples of Amorphous Piezoelectric Polymers. The literature on amorphous piezoelectric polymers is much more limited than that for semicrystalline systems. This is in part because no amorphous piezoelectric polymers have responses high enough to attract commercial interest. Much of the previous work on amorphous piezoelectric polymers was in nitrile-substituted polymers, including polyacrylonitrile (PAN) (47–49), poly(vinylidene cyanide–vinyl acetate) (PVDCN/VAc) (50–54), poly(phenyl ether nitrile) (PPEN) (55,56), and poly(1-bicyclobutanecarbonitrile) (57). Weak piezoelectric activity in poly(vinyl chloride) (PVC) and poly(vinyl acetate) (PVAc) has also been found (11,41,58,59). The most promising of these materials are vinylidene cyanide copolymers that exhibit large dielectric relaxation strengths and strong piezoelectricity. Table 4 shows the molecular structures of the most commonly encountered amorphous piezoelectric polymers.

Poly(vinylidene chloride). The carbon–chlorine dipole in poly(vinylidene chloride) (PVDC) has been oriented to produce a low level of piezoelectricity. The piezoelectric and pyroelectric activities generated in PVDC are stable and reproducible. PVDC has been used as a basis for understanding and studying piezoelectricity in amorphous polymers (39). The piezoelectric coefficients d_{31} of PVDC are reportedly in the range of 0.5–1.3 pC/N. This response was improved by simultaneous stretching and corona poling of film (44). The enhanced piezoelectric coefficient d_{31} ranged from 1.5–5.0 pC/N (see VINYLIDENE CHLORIDE POLYMERS (PVDC)).

PVDCN Copolymers. In 1980, exceptionally strong piezoelectric activity was found (50) in the amorphous copolymer of VDCN and VAc. The copolymer was poled at 150°C (20°C below its T_g) and cooled to room temperature in the electric field. A $P_r = 55$ mC/m^2 was obtained in a poling field of 50 MV/m. That is comparable to the P_r of PVDF. When local ordering, or paracrystallinity, is inherent in the polymer or is induced by mechanical stretching, an increase in the value of the remanent polarization is observed. For example, some researchers (51) assert that the large discrepancy between the measured and calculated $\Delta\varepsilon$ for PVDCN/VAc may be attributed to locally ordered regions in the polymer. $\Delta\varepsilon_{\text{calculated}} = 30$ for the copolymer PVDCN/VAc, and $\Delta\varepsilon_{\text{measured}} = 125$ (51). This large discrepancy in the values of $\Delta\varepsilon$ is indicative of cooperative motion of several nitrile dipoles within the locally ordered regions of the polymers. Cooperativity means that multiple nitrile dipoles respond to the applied electric field in a unified manner, instead of each dipole acting independently. Although the existence of cooperative dipole motion clearly increases the piezoelectric response of amorphous polymers, the mechanisms by which cooperativity can be systematically incorporated into the polymer structure remain unclear at this time (59).

The large relaxation strength exhibited by PVDCN/VAc gives it the largest value of P_r and hence d_{31} of all of the amorphous polymers. A number of authors have suggested that PVDCN/VAc also exhibits ferroelectric-like behavior (51–53) because of switching of the nitrile dipoles in an a.c. field. The switching time is long compared to that of a normal ferroelectric polymer.

Table 4. Structure, Polarization, and T_g of Piezoelectric Amorphous Polymers

Polymer	Structure	T_g, °C	d_{31}, pC/N	P_r, mCm^2	Reference
PVC	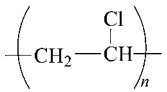	80	5	16	44
PAN	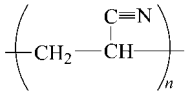	90	2	25	49
PVAc	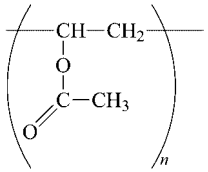	30	—	5	59
P(VDCN/VAc)	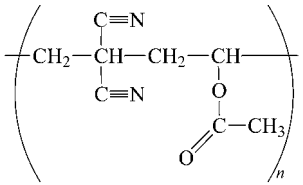	170	10	50	51
PPEN	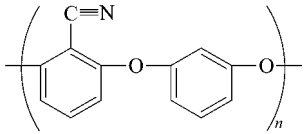	145	—	12	55
(β-CN) APB/ODPA	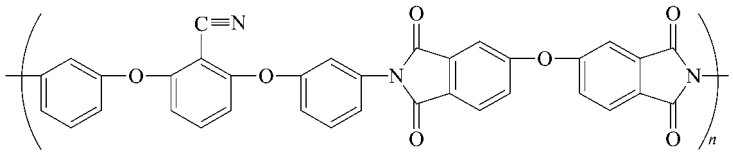	220	5 at 150°C	20	59

Other VDCN Polymers. The homopolymer of vinylidene cyanide is thermally unstable (60) and highly sensitive to moisture, but VDCN can be polymerized with a variety of monomers in addition to VAc, such as vinyl benzoate (VBz), methyl methacrylate (MMA), and others that form highly alternating chains. All of these copolymers show some degree of piezoelectricity although lower than PVDCN/VAc, which is explained by different activation energies for dipole orientation in the glassy state and different chain mobility that depends on the side group.

Polyacrylonitrile. Polyacrylonitrile (PAN) is one of the most widely used polymers (see ACRYLONITRILE POLYMERS). Shortly after it was shown that the PVDCN/VAc system is piezoelectric, researchers turned their attention to PAN because of its similarity to the aforementioned polymers. The presence of the large nitrile dipole in PAN indicated that it can be oriented by an applied electric field. PAN presented some challenges not encountered in other nitrile-substituted polymers, however. Although theoretical calculations predicted strong piezoelectric behavior, it was difficult to pole. Several investigators (47–49) proposed that the difficulty of poling PAN in the unstretched state is related to the strong dipole–dipole interaction of nitrile groups of the same molecule that repel each other, and thus prevent normal polarization. Upon stretching, the intermolecular dipole interactions facilitate packing of the individual chains and give rise to ordered zones. The remanent polarization of both unstretched and stretched PAN has been measured using the TSC method, and a twofold increase in remanent polarization (TSC peak at 90°C) was observed for PAN that was stretched to four times its original length (47). Another approach is the copolymerization of PAN with another monomer. Researchers have reported reduction of the hindering effect of the dipole–dipole interactions and enhancement of the internal mobility of the polymer segments when PAN is copolymerized with PA(polystyrene) or MMA. Ferroelectric behavior has been observed in P(AN–MMA), where, for given temperature and field conditions, a characteristic hysteretic loop is obtained (49). It was concluded that it may be one rare example where both ferroelectric and frozen-in dipole orientations are superimposed.

Nitrile-Substituted Polyimide. Amorphous Polymers that contain polar functional groups were synthesized (61–63) and investigated for use as high temperature piezoelectric sensors. (β-CN) APB/ODPA polyimide is one such system. The (β-CN) APB/ODPA polyimide possesses the three dipole functionalities shown in Table 5. Typically, the functional groups in amorphous polymers are pendent to the main chain. The dipoles, however, may also reside within the main chain of the polymer, such as the anhydride units in the (β-CN) APB/ODPA polyimide. The nitrile dipole is pendent to a phenyl ring ($\mu = 4.2$ D), and the two anhydride dipoles ($\mu = 2.34$ D) are within the chain, resulting in a total dipole moment of 29.4×10^{-30} C·m (8.8 D) per repeat unit.

The remanent polarization P_r of the (β-CN) APB/ODPA polymer found by the TSC method was approximately 20 mC/m^2 when poled at 80 MV/m above the T_g for 1 h (64). Excellent thermal stability was observed up to 100°C, and no loss of the piezoelectric response was seen after aging at 50°C and 100°C for as long as 500 h.

Partially cured films of the (β-CN) APB/ODPA system were simultaneously corona-poled and cured to enhance dipolar orientation and minimize localized

Table 5. Values of Dipole Moments Within Nitrile-Substituted Polyimide

Dipoles	Dipole identity	Dipole moment, C·m[a]
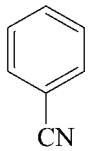	Pendent nitrile group	1.39×10^{-29}
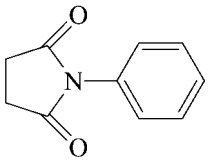	Main-chain dianhydride group	7.8×10^{-30}
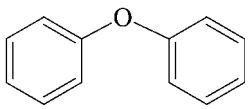	Main-chain diphenyl ether group	4.33×10^{-30}

[a]To convert C·m to Debye, multiply by 2.997×10^{29}.

arcing during poling. The aligned polar groups should be immobilized by additional imidization and subsequent cooling in an electric field. Both the T_g and the degree of imidization increase almost linearly as the final cure temperature is increased (64). The value of P_r was higher for films cured at lower temperatures. The mobility of the molecules in a partially imidized state should be higher than that in the fully cured state and therefore produce a higher degree of dipole orientation.

The importance of dipole concentration in ultimate polarization is evident from a comparison of PAN and the (β-CN) APB/ODPA polyimide. PAN has a single nitrile dipole per repeat unit ($\mu = 3.5$ D) resulting in a dipole concentration of $1.34 \times 10^{28}/m^3$. This translates into an ultimate polarization of 152 mC/m^2 (20). The (β-CN) APB/ODPA polyimide, on the other hand, has a total dipole moment of 8.8 D per monomer. The dipole concentration of (β-CN) APB/ODPA, however, is only $0.136 \times 10^{28}/m^3$, resulting in an ultimate polarization of 40 mC/m^2, which is less than a fourth of that of PAN. As a result, similar polyimides that have increased nitrile concentrations were synthesized and characterized. Studies of these polymers show that polarization is significantly increased by increasing dipole concentration. Structure–property investigations designed to assess the effects of these dipoles on T_g, thermal stability, and overall polarization behavior are currently being pursued.

Even-Numbered Nylons. Nylon 6I and 6I/6T exhibit a *D–E* hysteretic loop across a temperature range of 30–65°C at a fixed maximum field of 168 MV/m (65). The remanent polarization increases as the temperature increases. Note that nylon 6I and 6I/6T are completely amorphous. The P_r is about 30 mC/m^2 (see POLYAMIDES, AROMATIC).

Aliphatic Polyurethane. Some researchers (1) have suggested that aliphatic polyurethane systems exhibit ferroelectricity that stems from the amorphous part at temperatures above the glass-transition temperature. This "liquid state"

ferroelectricity is very peculiar, seems to exist, and is supported by the hydrogen bonds present.

Characterization and Modeling

Most piezoelectric characterization methods were developed for crystalline ceramics and had to be adapted for piezoelectric polymers. Methods based on resonance analysis and equivalent circuits that can be used to characterize semicrystalline PVDF and its copolymers are outlined in IEEE standards (66). Details for applying resonance analysis to piezoelectric polymers have recently been explored (67). Because of the lossy nature of some polymers, the IEEE standards are not adequate, and other techniques are needed to describe piezoelectric properties more accurately.

Quasi-static direct methods are both versatile and well suited to investigating fully the piezoelectric response of polymers. Direct methods of this type are especially appropriate for amorphous polymers. TSC measurements (68) are used to measure the remanent polarization imparted to a polymer, and direct strain or charge measurements are used to investigate the piezoelectric coefficients with respect to the electric field, frequency, and stress.

TSC is a valuable tool for characterizing piezoelectric polymers. After poling a polymer, a measure of the current dissipation and the remanent polarization as a function temperature can be obtained by TSC. As the sample is heated through its glass-transition temperature (or Curie temperature for a semicrystalline polymer) at a slow rate (typically 1–4°C/min), the depolarization current is measured by an electrometer. The remanent polarization is equal to the charge per unit area and is obtained from the data by integrating the current with respect to time and plotting it as a function of temperature:

$$P_{\mathrm{r}} = \frac{Q}{A} = \frac{1}{A}\int I(t) - \mathrm{d}t. \tag{17}$$

Figure 6 illustrates a typical TSC result. Because permanent dipoles are immobile at temperatures well below T_{g}, the current discharge remains low in this temperature range. As temperature increases to and beyond the T_{g}, however, the onset of dipole mobility contributes to a significant increase in the current peak. The peak in the current and the subsequent polarization maximum usually occurs in the vicinity of the T_{g}.

Direct methods for measuring the strain that results from applying a field or vice versa, applying a strain, and measuring the accumulated charge are abundant. Interferometers, dilatometers, fiber-optic sensors, optical levers, linear variable displacement transducers, and optical methods are employed to evaluate the piezoelectric strain (converse effect) (69–72). The "out-of-plane" or thickness piezoelectric coefficient d_{33} can be ascertained as a function of the driving field and frequency. The coefficient is measured based on the equation

$$S_{33} = d_{33}E_3, \tag{18}$$

where S_{33} is the strain and E_3 is the applied electric field.

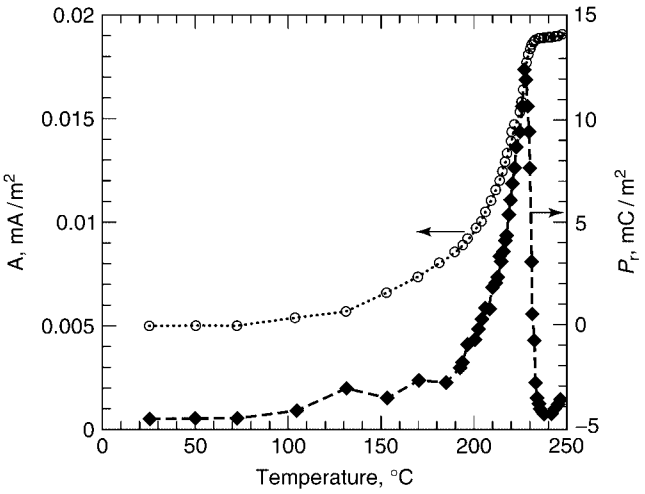

Fig. 6. Plot of thermally stimulated current for a typical amorphous poled polymer.

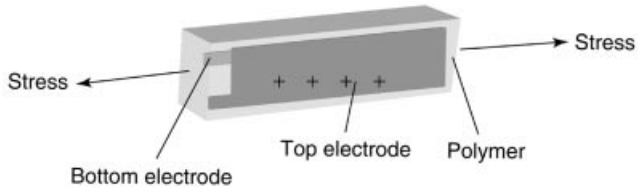

Fig. 7. Direct effect in polymers.

A modified Rheovibron, or similar techniques, have been used to measure the direct piezoelectric effect, where charges accumulated on the surfaces of the polymer are measured (59). The piezoelectric coefficient d_{31} can be obtained by straining the polymer in the direction of applied stress using a force F as depicted in Fig. 7. A charge Q is generated on the surface of the electrodes. A geometric factor is used to produce a geometrically independent parameter, surface charge density per unit applied stress:

$$d_{31} = \frac{Q/(WL)}{F/(Wt)}, \tag{19}$$

which has units of pC/N. W, L, and t are the width, length, and thickness of the sample, respectively.

Modeling. The methodology for modeling piezoelectric behavior in polymers varies, depending on the targeted properties. Approaches cover the range from macroscale to micro and atomistic scales. A detailed review of computational methods applied to electroactive polymers has been published (73).

In some cases, modeling can predict behavior where experiments cannot. Using molecular dynamics, the orientation polarization of the (β-CN) APB/ODPA polymer was assessed by monitoring the angle θ that the dipoles make with an

applied electric field (74). The bulk P_r was calculated, and the results agreed extremely well with experimental results (61). Computational modeling, however, gave insight into the contributions of the various dipoles present in a way experimental results could not. The model predicted that 40% of the orientation polarization was due to the dianhydride within the backbone of the ODPA monomer and demonstrated the importance of the flexible ether linkage (oxygen atom) in facilitating dipole alignment. Modeling insight of this kind is invaluable in guiding the synthesis of new materials.

Modeling of PVDCN/VAc can also play a role in understanding the cooperative motion responsible for the high dielectric relaxation strength of this class of polymers, not possible experimentally (75). Mesoscale simulation has been used to describe polarization reversal in PVDF films (76).

Applications and Future Considerations. The potential for applying piezoelectric and other electroactive polymers is immense. To date, ferroelectric polymers have been incorporated into numerous sensing and actuating devices for a wide array of applications. Typical applications include devices in medical instrumentation, robotics, optics, computers, and ultrasonic, underwater, and electroacoustic transducers. One important emerging application area for electroactive polymers is the biomedical field where polymers are being explored as artificial muscle actuators, as invasive medical robots for diagnostics and microsurgery, as actuator implants to stimulate tissue and bone growth, and as sensors to monitor vascular grafts and to prevent blockages (77,78). Such applications are ideal for polymers because they can be made biocompatible, and they have excellent conformability and impedance that match body fluids and human tissue. The intent of this article is not to detail specific applications; the interested reader may consult excellent sources on applications of piezoelectric and ferroelectric polymers (79–81).

In the future, we believe that fertile research areas for piezoelectric polymers will include work to enhance their properties, to improve their processibility for incorporation in devices, and to develop materials that have a broader use temperature range. Fundamental structure–property understanding has enabled the development of numerous semicrystalline and amorphous polymers. Based on this knowledge, future research that focuses on property enhancement via new chemistries that have higher dipole concentrations and incorporate dipole cooperativity may yield improved materials. Property enhancements may also be gained from processing studies to alter polymer morphology such as those used to make "single crystalline" fluoropolymers. Development of materials that can operate in extreme environments (high temperature and subambient temperature) is also important for expanding the use of piezoelectric polymers. Piezoelectric and pyroelectric constants of polymers are considerably lower than those of ferroelectric inorganic ceramics. Improvements in properties by incorporating polymers in composites with inorganics to obtain higher electromechanical properties and better mechanical properties are also valuable. To date, piezoelectric polymer–ceramic composites have been made wherein the polymer serves only as an inactive matrix for the active ceramic phase. This is due to the mismatch in permittivity between the polymer and ceramic which makes it difficult to pole both phases. Research that results in active polymer and ceramic phases could yield interesting electromechanical properties.

BIBLIOGRAPHY

1. T. Yuki, K. Shida, T. Koda, and S. Ikeda, 10th Int. Symp. Electrets, 1999, pp. 675–677.
2. G. T. Davis, in C. P. Wong, ed., *Polymers for Electronic and Photonic Applications*, Academic Press, Boston, Mass., 1993, p. 435.
3. M. G. Broadhurst and G. T. Davis, in G. M. Sessler, ed., *Electrets*, Vol. **33**, Springer-Verlag, New York, 1980, p. 283.
4. W. P. Mason, *Physical Acoustics and the Properties of Solids*, Van Nostrand, Princeton, N.J., 1958.
5. J. F. Nye, *Physical Properties of Crystals*, Clarendon Press, Oxford, 1957.
6. R. G. Kepler and R. A. Anderson, *J. Appl. Phys.* **49**, 1232–1235 (1978).
7. J. P. Luongo, *J. Polym. Sci. A-2* **10**, 1119–1123 (1972).
8. B. Z. Mei, J. I. Schienbeim, and B. A. Newman, *Ferroelectrics* **144**, 51–60 (1993).
9. H. Kawai, *Jpn. J. Appl. Phys.* **8**, 975 (1969).
10. K. Tashiro, H. Tadokoro, and M. Kobayashi, *Ferroelectrics* **32**, 167 (1981).
11. T. Furukawa, *IEEE Trans. Electr. Insul.* **24**, 375–393 (1989).
12. G. M. Sessler, *J. Acoust. Soc. Am.* **70**, 1596–1608 (1981).
13. A. J. Lovinger, *Science* **220**, 1115–1121 (1983).
14. J. B. Lando and W. W. Doll, *J. Macromol. Sci.-Phys. B2* 205 (1968).
15. A. J. Lovinger, in D. C. Basset, ed., *Developments in Crystalline Polymers*, Vol. **1**, Applied Science, London, 1982, p. 242.
16. G. T. Davis and co-workers, *J. Appl. Phys.* **49**, 4998 (1978).
17. K. Omote, H. Ohigashi, and K. Koga, *J. Appl. Phys.* **81**, 2760 (1997).
18. Q. M. Zhang, V. Bharti, and X. Zhao, *Science* **280**, 2101–2104 (1998).
19. H. Kawai and I. Henji, *Oyo Buturi* **39**, 413 (1970).
20. B. A. Newman and co-workers, *J. Appl. Phys.* **51**, 5161–5164 (1980).
21. B. A. Newman, K. G. Kim, and J. I. Scheinbeim, *J. Mater. Sci.* **25**, 1779–1783 (1990).
22. Y. Takase and co-workers, *Macromolecules* **24**, 6644–6652 (1991).
23. R. B. Meyer and co-workers, *J. Phys. Lett. (Paris)* **36**, 69 (1975).
24. P. Le Barny and J. C. Dubois, in C. B. McArdle, ed., *Side Chain Liquid Crystal Polymers*, Blackie, New York, 1989, p. 130.
25. G. Scherowsky, in H. S. Nalwa, ed., *Ferroelectric Polymers, Chemistry, Physics and Application*, Marcel Dekker, New York, 1995, p. 435.
26. Y. Takahashi and co-workers, *J. Vac. Sci. Technol. A* **5**, 2253 (1987).
27. Y. Takahashi, M. Iijima, and E. Fukada, *Jpn. J. Appl. Phys.* **28**, L408–L410 (1989).
28. T. Hattori and co-workers, *J. Appl. Phys.* **79**, 1713–1721 (1996).
29. E. Fukada, *IEEE Trans. Ultrasonics Ferroelectrics Frequency Control* **47**, 1277–1290 (2000).
30. A. J. P. Martin, *Proc. Phys. Soc.* **53**, 183 (1941).
31. E. Fukada, in Ref. 25, p. 393.
32. H. Maeda and E. Fukada, *Biopolymers* **21**, 2055 (1982).
33. M. Date, S. Takashita, and E. Fukada, *J. Polym. Sci. A-2* (8), 61 (1970).
34. T. Furukawa and E. Fukada, *J. Polym. Sci., Polym. Phys. Ed.* **14**, 1979 (1976).
35. Y. Ando and E. Fukada, *J. Polym. Sci., Polym. Phys. Ed.* **14**, 63 (1976).
36. E. Fukada, *Rep. Prog. Polym. Phys. Jpn.* **34**, 269 (1991).
37. Y. Ando, E. Fukada, and M. J. Glimcher, *Biorheology* **14**, 175 (1977).
38. E. Fukada, in R. O. Becker, ed., *Mechanisms of Growth Control*, Charles C. Thomas, Springfield, Ill., 1981, p. 192.
39. M. G. Broadhurst, C. G. Malmberg, F. I. Mopsik, and W. P. Harris, in M. M. Perlman, ed., *Electrets: Charge Storage and Transport in Dielectrics*, The Electrochemical Society, Princeton, N.J., 1973, pp. 492–504.
40. M. G. Broadhurst and co-workers, *Polym. Prepr.* **14**, 820 (1973).

41. F. I. Mopsik and M. G. Broadhurst, *J. Appl. Phys.* **46**, 4204–4208 (1975).
42. B. Hilczer and J. Malecki, in *Electrets* (Studies in Electrical and Electronic Engineering, Vol. **14**). Elsevier, New York, 1986, p. 19.
43. H. Frohlick, *Theory of Dielectrics (Monographs on the Physics and Chemistry of Materials, No. 42.*, Oxford, U.K., 1958, p. 15.
44. V. Bharti, T. Kaura, and R. Nath, *IEEE Trans. Dielectr. Electr. Insul.* **2**(6) (1995).
45. H. Stefanou, *J. Appl. Phys.* **50**, 1486–1490 (1979).
46. R. Meyrueix and O. Lemonnier, *Phys. D Appl. Phys.* **27**, 379–386 (1994).
47. R. J. Comstock, S. I. Stupp, and S. H. Carr, *J. Macromol. Sci. Phys. 3* **13**(1), 101–115 (1977).
48. H. Ueda and S. H. Carr, *Polym. J.* **16**, 661–667 (1984).
49. H. von Berlepsch and co-workers, *IEEE Trans. Electr. Insul.* **24**, 357–362 (1989).
50. S. Miyata and co-workers, *Polym. J.* **12**, 857–860 (1980).
51. T. Furukawa and co-workers, *Jpn. J. Appl. Phys.* **25**, 1178–1182 (1986).
52. I. Seo, *Ferroelectrics* **171**, 45–55 (1995).
53. P. A. Mirau and S. A. Heffner, *Polymer* **33**, 1156–1161 (1992).
54. M. Sakurai and co-workers, *Polym. Commun.* **32**, 397–399 (1991).
55. S. Tasaka, T. Toyama, and N. Inagaki, *Jpn. J. Appl. Phys.* **33**, 5838–5844 (1994).
56. T. Takahashi and co-workers, *Polymer* **36**, 3803–3808 (1995).
57. H. K. Hall and co-workers, *Polym. Bull.* **17**, 135–136 (1987).
58. V. Bharti and R. Nath, *J. Appl. Phys.* **82**, 3488–3492 (1997).
59. Z. Ounaies, J. A. Young, and J. S. Harrison, in I. M. Khan and J. S. Harrison, eds., *An Overview of the Piezoelectric Phenomenon in Amorphous Polymers*, American Chemical Society, Washington, D.C., 1999.
60. S. Tasaka and co-workers, *Polymer* **30**, 1639–1642 (1989).
61. Z. Ounaies, J. A. Young, J. O. Simpson, and B. L. Farmer, Mater. Res. Soc. Proc.: Mater. Smart Syst. II, Vol. 459, Materials Research Society, Pittsburgh, Pa., 1997, p. 59.
62. J. O. Simpson, Z. Ounaies, and C. Fay, Mater. Res. Soc. Proc.: Mater. Smart Syst. II, Vol. 459, Materials Research Society, Pittsburgh, Pa., 1997, p. 53.
63. Z. Ounaies, C. Park, J. S. Harrison, J. G. Smith, and J. Hinkley, SPIE Proc., Electroactive Polym. Actuators Devices, Vol. 3669, Newport Beach, Calif., 1999, p. 171.
64. C. Park, Z. Ounaies, J. Su, J. G. Smith Jr., and J. S. Harrison, Mater. Res. Soc. Proc.: Electroactive Polym., Vol. 600. 1999.
65. Y. Murata, K. Tsunashima, and N. Koizumi, 8th Int. Symp. Electrets (ISE 8), 1994, pp. 709–714.
66. IEEE Standard on Piezoelectricity (IEEE Standard 176-1987), Institute of Electrical and Electronic Engineers, New York, 1989.
67. S. Sherritt and Y. Bar-Cohen, in Y. Bar-Cohen, ed., *Electroactive Polymer (EAP) Actuators as Artificial Muscles: Reality, Potential and Challenges*, SPIE Press, Bellingham, Wash., 2001, p. 405.
68. J. van Turnhout, *Polym. J.* **2**, 173–191 (1971).
69. J. T. Dawley, G. Teowee, B. J. J. Zelinski, and D. R. Uhlmann, *Piezoelectric Characterization of Bulk and Thin Film Ferroelectric Materials Using Fiber Optics*, MTI Instruments Inc., Application Note.
70. W. Y. Pan, H. Wang, and L. E. Cross, *Jpn. J. Appl. Phys.* **29**, 1570 (1990).
71. Q. M. Zhang, W. Y. Pan, and L. E. Cross, *J. Appl. Phys.* **63**, 2429 (1988).
72. T. L. Jordan, Z. Ounaies, and T. L. Turner, *Mater. Res. Soc. Symp. Proc.* **459**, 231 (1997).
73. K. E. Wise, in Ref. 67, pp. 267–284.
74. J. A. Young, B. L. Farmer, and J. A. Hinkley, *Polymer* **40**, 2787 (1999).
75. K. E. Wise, 3rd SIAM Conf. Math. Aspects Mater. Sci., Philadelphia, Pa., May 21–24, 2000.
76. T. Koda, K. Shibasaki, and S. Ikeda, *Comp. Theor. Polym. Sci.* **10**, 335–343 (2000).

77. Y. Bar-Cohen, in Ref. 67, p. 615.
78. D. DeRossi and P. Dario, in P. M. Galletti, D. E. DeRossi, and A. S. DeReggi, eds., *Medical Applications of Piezoelectric Polymers*, Gordon & Breach, New York, 1988, p. 83.
79. G. M. Garner, in T. Wang, J. Herbert, and A. Glass, eds., *The Applications of Ferroelectric Polymers*, Blackie, London, 1988, p. 190.
80. T. R. Meeker, in Ref. 79, p. 305.
81. E. Yamaka, in Ref. 79, p. 329.

J. S. HARRISON
NASA Langley Research Center
Z. OUNAIES
Virginia Commonwealth University

PLASTICIZERS

Introduction

A plasticizer is a liquid that is added to a material (usually a resin or elastomer) making that material softer, more flexible (by decreasing the glass-transition temperature T_g of the polymer), and easier to process. This broad definition encompasses the use of water to plasticize clay for the production of pottery, and oils to plasticize pitch for caulking boats. The most widely plasticized polymer is poly(vinyl chloride) (PVC) because of its excellent plasticizer compatibility characteristics. The development of plasticizers closely follows the development of this commodity polymer; however, plasticizers are also used with other polymer types.

The amount of plasticizer added to a polymer varies depending on the effect required. A small addition of plasticizer may be made to improve the workability of the polymer melt. This contrasts with large additions made with the specific intention of completely transforming the properties of the product. PVC without a plasticizer, ie, unplasticized PVC (PVC-U), is used in applications such as pipes, siding, and window profiles. With plasticizer added, articles such as automotive interior trim, jacketing, cable insulations, and PVC floorings are formed.

There are presently ~300 plasticizers manufactured. Of these ~100 are of commercial importance. A list of some common commodity and specialty plasticizers can be found in Table 1.

Types of Plasticizers

Two principal methods exist for softening a polymer to bring about the dramatic effects of plasticization. A rigid polymer may be internally plasticized by chemically

Encyclopedia of Polymer Science and Technology. Copyright John Wiley & Sons, Inc. All rights reserved.

Table 1. Commonly Used Plasticizers

Plasticizers	Carbon chain	Molecular weight	Vapor pressure, Pa[a] (mm Hg @ 200°C)	Specific gravity 25° / 25°C	Viscosity, mPa·s(cP)@25°C
Dinormalhexyl phthalate (DnHP)	l6[b]	335	400	1.008	30
Diisoheptyl phthalate (DIHP)	7	362	280	0.983	30
Diheptyl phthalate (DnHP)	l7	362	253	0.983	30
Di(2-ethylhexyl) phthalate (DEHP)	8	391	173	0.982	58
Diheptylnonyl phthalate (DnHNP)	l7, l9	398	147	0.978	49
Dinormaloctyldecyl phthalate (DNODP)	l6, l8, l10	401	80	0.965	34
Diheptylnonylundecyl phthalate (DnHNUP)	l7, l9, l11	414	107	0.969	41
Diisononyl phthalate (DINP)	9	418	67	0.970	72
Dinonyl phthalate (DNP)	9	418	57	0.971	80
Dinormalnonyl phthalate (DnNP)	l9	418	43	0.967	39
Diisodecyl phthalate (DIDP)	10	447	47	0.964	88
Dinormalnonyldecylundecyl phthalate (DnNDUP)	l9, l10, l11	450	40	0.958	48
Dinonylundecyl phthalate (DnNUP)	l9, l11	458	40	0.954	50
Diundecyl phthalate (DUP)	l11	475	80	0.952	54
Diisoundecyldodecyl phthalate (DUDP)	11, 12	502	20	0.955	185
Ditridecyl phthalate (DTDP)	13	530	11	0.951	160
Di(2-ethylhexyl) teraphthalate (DOTP)	8	391	160	0.981	63
Butylbenzyl phthalate (BBP)	4, 7	312	253	1.119	42
Diheptylnonyl adipate (DnHNA)	l7, l9	370	440	0.920	12
Di(2-ethylhexyl) adipate (DEHA)	8	370	307	0.924	14
Diisononyl adipate (DINA)	9	398	227	0.924	2.0
Diisodecyl adipate (DIDA)	10	426	77	0.916	25
Triheptylnonyl trimellitate (TnHNTM)	l7, l9	530	16	0.984	105
Tri(2-ethylhexyl) trimellitate (TOTM)	8	530	21	0.987	220
Triisononyl trimellitate (TINTM)	9	589	13	0.975	315
Di(2-ethylhexyl) sebacate (DOS)	8	426	131	0.911	25
Di(2-ethylhexyl) azelate (DOZ)	8	412	147	0.914	15

[a]To convert Pa to mm Hg, divided by 133.3.
[b]l is linear.

modifying the polymer or monomer so that the flexibility of the polymer is increased. Alternatively, a rigid polymer can be externally plasticized by the addition of a suitable plasticizing agent. The external plasticizing route is more common because of lower overall costs, and the use of external plasticizers allows the processor a certain degree of freedom in developing formulations for a range of products.

Internal Plasticizers. There has been much dedicated work on the possibility of internally plasticized PVC (FPVC). However, in achieving this by copolymerization significant problems exist: (*1*) the affinity of the growing polymer chain for vinyl chloride rather than a comonomer implies that the incorporation of a comonomer into the chain requires significant pressure; (*2*) since the use of recovered monomer in PVC production is standard practice, contamination of vinyl chloride with comonomer creates additional problems, and (*3*) the complexity of the reaction can lead to longer reaction times and increased costs.

External Plasticizers. There are two groups of external plasticizers, primary and secondary. A primary plasticizer, when added to a polymer, causes elongation and softness to be increased. These changes are brought about by mechanisms described in the following section. A secondary plasticizer, when added to the polymer alone, does not bring about these changes and may have limited compatibility with the polymer. However, when added to the polymer in combination with a primary plasticizer, secondary plasticizers enhance the plasticizing performance of the primary plasticizer. Secondary plasticizers are also known as extenders.

Theory and Mechanism of Plasticizer Action

Four general theories have been proposed to explain external plasticizer action. Some theories involve detailed analysis of polarity, solubility, and interaction parameters and the thermodynamics of polymer behavior, whereas others treat plasticization as a simple lubrication of chains of polymer from each other. An understanding of the plasticization process can be gained by combining ideas from each theory, and an overall theory of plasticization must include all these aspects.

The steps involved in the incorporation of a plasticizer into a PVC product can be divided into five distinct stages:

(1) Plasticizer is mixed with PVC resin—adsorption step.
(2) Plasticizer penetrates and swells the resin particles—adhesion step.
(3) Polar groups in the PVC resin are freed from each other—absorption step.
(4) Plasticizer polar groups interact with the polar groups on the resin—intermolecular plasticizing step.
(5) The structure of the resin is re-established, with full retention of plasticizer—intramolecular plasticizing step.

Steps 1 and 2 can be described as physical plasticization, and the precise details of how this is carried out depends on the applications technology involved, ie, suspension or dispersion PVC. The rate at which step 2 occurs depends on the

plasticizer viscosity, degree of branching, resin pore size and free volume, and particle size.

Steps 3 and 4, however, can be described as chemical plasticization since the rate at which these processes occur depends on the chemical properties of molecular polarity, molecular volume, and molecular weight. An overall mechanism of plasticizer action must give adequate explanations for this as well as the physical plasticization steps.

The importance of step 5 cannot be stressed too strongly, since no matter how rapidly and easily steps 1–4 occur, if plasticizer is not retained in the final product the product will be rendered useless.

The Lubrication Theory. The lubrication theory is based on the assumption that the rigidity of the resin arises from intermolecular friction binding the chains together in a rigid network. On heating, these frictional forces are weakened to allow the plasticizer molecules to lubricate the chains. Once incorporated into the polymer, the plasticizer molecules shield the chains from each other, thus preventing the reformation of the rigid network (1).

The Gel Theory. This theory extends the lubrication theory by having the plasticizer break the resin–resin attachments of a three-dimensional honeycomb or gel structure and by masking these centers of attachment from each other, preventing their reformation. This gel is formed by loose attachments occurring at intervals along the polymer chain. This facilitates the movement of plasticizer molecules, thus imparting flexibility.

The Free Volume Theory. The Free Volume Theory is a further extension of the lubricity and gel theories and can be used to explain both external and internal plasticization. Free volume is a measure of the internal space available in a polymer for the movement of the polymer chain, which imparts flexibility to the resin. Plasticizers increase the free volume of the resin and ensure that free volume is maintained as the resin–plasticizer mixture is cooled from the melt, preventing interactions between neighboring polymer chains. For the plasticized resins, free volume can arise from motion of the chain ends, side chains, or the main chain. The fact that free volume increases with molecular motion is useful in explaining internal plasticization achieved by side-chain addition, where each side chain acts as a small molecule and free volume of the system is increased.

The introduction of a plasticizer, which is a molecule of lower molecular weight than that of the resin, has the ability to impart a greater free volume per volume of material because there is an increase in the proportion of end groups and the plasticizer has a glass-transition temperature (T_g) lower than that of the resin itself.

Thermodynamic or Mechanistic Theory. From the observation of migration of plasticized polymers it is clear that plasticizer molecules are not bound permanently to the polymer, but rather a dynamic equilibrium exists between solvation and desolvation of the polymer chains by plasticizer. Different families of plasticizers are attracted to the polymer by forces of different magnitude but the attraction is not permanent. There is a continuous exchange where a plasticizer molecule becomes attached to an active group on the polymer chain only to be dislodged and replaced by another plasticizer molecule.

Antiplasticization. Many resins tend to become more ordered and compact as existing crystallites grow or new crystallites form at the expense of the fluid

parts of the amorphous material. For small additions of plasticizer, the plasticizer molecules may be totally immobilized by attachment to the resin by various forces. These tend to restrict the freedom of small portions of the polymer molecule necessary for the absorption of mechanical energy. This results in a more rigid resin with a higher tensile strength and base modulus than the base polymer itself. This phenomenon is termed antiplasticization. Above these low concentrations the polymer becomes plasticized.

Interaction Parameters.

The Hildebrand Solubility Parameter. This parameter, defined by δ (eq. 1), can be estimated based on data for a set of additive constants F, for the more common groups in organic molecules to account for the observed magnitude of the solubility parameter:

$$\delta = \sum F/V \tag{1}$$

where V represents molar volume. Solubility parameters can be used to classify plasticizers of a given family in terms of their compatibility with PVC (2).

Polarity Parameter. This parameter, defined by ϕ (eq. 2), shows a good correlation with plasticizer activity for nonpolymeric plasticizers. The parameter is defined as

$$\phi = [M(A_p/P_0)]/1000 \tag{2}$$

where M is the molar mass of plasticizer, A_p the number of carbon atoms in the plasticizer excluding aromatic and carboxylic acid carbon atoms, and P_0 the number of polar (eg, carbonyl) groups present. The 1000 factor is used to produce values of convenient magnitude. Polarity parameters provide useful predictions of the activity of monomeric plasticizers but not activity of plasticizers from different families.

The Solid-Gel Transition Temperature. This temperature or clear point, T_m, is a measure of plasticizer activity and is the temperature at which a single grain of PVC dissolves in excess plasticizer. The more efficient plasticizers show lower values of T_m as a result of their higher solvating power. This can be correlated with the ease of processing of a given plasticizer, with a control PVC resin.

The Flory–Huggins Interaction Parameter. These ideas, based on a study of polymer miscibility, have been applied to plasticizers according to the following equation (eq. 3) in which V_1 is the molar volume of the plasticizer, obtained from molar mass figures and density values at T_m, and χ represents the interaction parameter.

$$1/T_m = 0.002226 + 0.1351(1 - \chi)/V_1 \tag{3}$$

Specific Interactions. Some mechanism of attraction and interaction between PVC and plasticizer must exist for the plasticizer to be retained in the polymer after processing.

The role of specific interactions in the plasticization of PVC between the carbonyl functionality of the plasticizer were proposed on the basis of results from Fourier transform infrared spectroscopy. Reported shifts in the absorption frequency of the carbonyl group of the plasticizer ester to lower wave number are indicative of a reduction in polarity. These ideas have been extended using newer analytical techniques, in particular molecular modeling and solid-state nuclear magnetic resonance spectroscopy (nmr).

Molecular Modeling. A range of plasticizer molecule models and a model for PVC have been generated and energy minimized to observe their most stable conformations. Such models highlight the free volume increase caused by the mobility of the plasticizer alkyl chains. More detailed models have also been produced to concentrate on the polar region of the plasticizer and its possible mode of interaction with the polymer (3).

Solid-State Nuclear Magnetic Resonance Spectroscopy. Advances in technology have made the study of solids by NMR techniques of considerably greater ease. For the accumulation of solid-state ^{13}C nmr spectra, cross-polarization magic angle spinning (cpmas) can be utilized to significantly reduce signal-broadening effects present in solid state but not in the liquid state. The technique has been used to study the molecular effects of plasticization by comparing spectral shifts of PVC and plasticizer under various degrees of processing.

Phthalate Esters

The family of phthalate esters are the most abundantly produced worldwide. The plasticizer esters are produced from orthophthalic and terephthalic acid reacted with an appropriate alcohol (eq. 4). Phthalate esters are manufactured from methanol (C_1) up to C_{17} (4) alcohols although phthalate use as PVC plasticizers is generally in the range C_6 to C_{13}. Low molecular weight phthalates find use in nitrocellulose; higher phthalates as synthetic lubricants for the automotive industries.

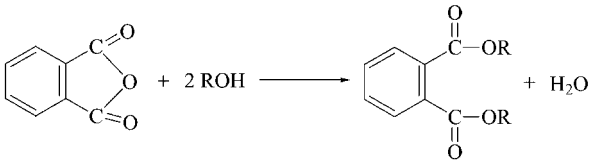

(4)

Di-2-ethylhexyl phthalate(DEHP) [117-81-7], also known as dioctyl phthalate (DOP), is generally considered as the industry standard. The reason for this is that it is in the mid-range of plasticizer properties. DEHP (or DOP) is the phthalate ester of 2-ethylhexanol, which is normally manufactured by the dimerization of butyraldehyde (eq. 5), the butyraldehyde itself being synthesized from propylene.

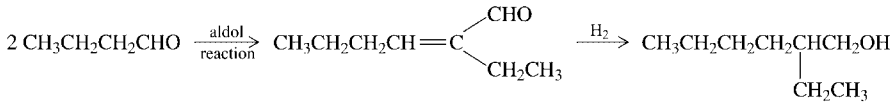

(5)

The widespread use of this plasticizer is a reflection of its all-around general-purpose plasticizing performance and its properties, suitable for a great many standard products. It possesses good plasticizing efficiency, fusion rate, and viscosity which, coupled with a competitive price, make it attractive to the PVC compounder and processor.

Diisononyl phthalate and diisodecyl phthalate are produced by esterification of oxo-alcohols of carbon chain length 9 and 10. The oxo-alcohols are produced through the carbonylation of alkenes (olefins). The hydroformylation or carbonylation process (eq. 6) adds a carbon unit to an alkene chain by reaction with carbon monoxide and hydrogen with heat, pressure, and catalyst. In this way a C_8 alkene is carbonylated to yield a C_9 alcohol. Because of the distribution of the C=C double bond in the alkene and the varying effectiveness of certain catalysts, the position of the added carbon atom can vary and an isomer distribution is generally created in such a reaction. The nature of this distribution depends on the reaction conditions. Consequently, these alcohols are termed *iso-alcohols* and the subsequent phthalates *iso-phthalates*.

Another method of producing a nonyl alcohol, which has gained predominance in the past few years, is by the dimerization process. In this process *n*-butylenes react to form an octene. Then through hydroformylation the 8-carbon olefin is converted to a nonyl alcohol (eq. 6). This alcohol has specific branching and some linearity that provides the corresponding ester with improved properties over esters made from isononyl alcohol.

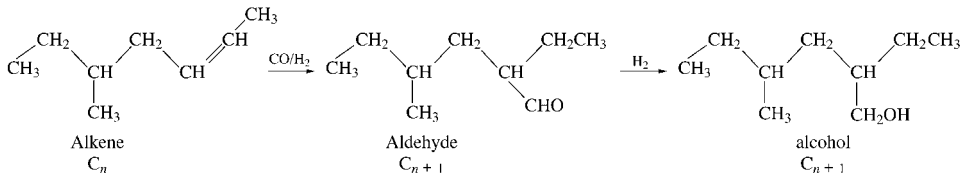

(6)

The C_9 and C_{10} phthalates (DINP, DNP, and DIDP) generally compete with DEHP as commodity general-purpose plasticizers. Other phthalates are available at opposite ends of the carbon number range [eg, diisohexyl phthalate (DHP, C_6) and diisotridecyl phthalate (DTDP, C_{13})], but these serve more specialty markets. The C_8 phthalate, diisooctyl phthalate (DIOP), is also a commodity plasticizer where it is used as an alternate to DEHP for environmental reasons.

The fourth process used to produce phthalate alcohols is the Ziegler process and the Ziegler displacement process. In the Ziegler process straight chain even-numbered carbon alcohols are produced from ethylene. Triethylaluminum is produced from aluminum, hydrogen, and ethylene. With the addition of more

ethylene the chain is lengthened in two-carbon increments. Oxidation and hydrolysis yield the primary even-numbered alcohols.

With the Ziegler displacement process the higher alkyl group is displaced from the chain growth product by ethylene. This yields a mixture of even-numbered linear alpha olefins with the trialkyl aluminum being recycled. The odd-numbered linear alcohols are produced through hydroformylation of the olefin and hydrogenation of the odd-numbered aldehydes.

The linear phthalates produced from these alcohols provide many advantages over their branched counterparts. Among these are processability, efficiency, volatility, viscosity, thermal stability, light stability, low temperature, and long-term permanence.

Citrate esters have gained some importance as an alternate to DEHP in medical, toy, and food applications. The citrate esters are more volatile, less compatible, more water sensitive, more difficult to fuse, and more costly than DEHP.

Adipate Esters

Alcohols of similar chain length to those used in phthalate manufacture can be esterified with adipic acid rather than phthalic anhydride to produce the family of adipate plasticizers. For example, esterification of 2-ethylhexanol with adipic acid yields di-2-ethylhexyl adipate (DEHA), also known as dioctyl adipate (DOA).

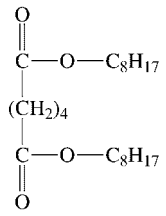

Di-2-ethylhexyl adipate

The family of adipic acid esters in PVC applications has improved low temperature performance relative to phthalates and lower plastisol viscosities, because of the lower inherent viscosities of the plasticizer. Adipates used are typically in the C_7–C_{10} range. Incompatibility problems can be encountered at higher carbon numbers, especially at high addition levels. Adipates are more volatile and have higher migration rates than phthalates. Because they are a specialty for the PVC industry, they are higher priced. As a result, it is not uncommon to encounter adipates used in blends with phthalates to produce a compromise of properties. Because of these limitations, linear phthalates are often used in place of adipates wherever possible.

Trimellitate Esters

These materials are produced by the esterification of a range of alcohols with trimellitic anhydride (TMA), which is similar in structure to phthalic anhydride with the exception of the third functionality (COOH) on the aromatic ring.

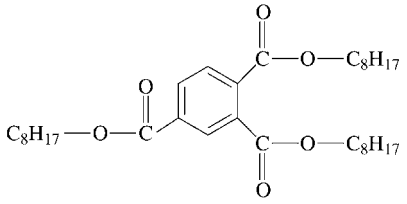

Tris-2-ethylhexyl trimellitate

Esters are produced in the ratio of 3 mol of alcohol to 1 mol of anhydride. Common esters in this family are tris-2-ethylhexyl trimellitate (trioctyl trimellitate, TOTM); L79TM, an ester of mixed linear C_7 and C_9 alcohols; L810TM, an ester of mixed linear C_8 and C_{10} alcohols; and trüsononyl trimellitate (TNTM), an ester based on isononyl alcohol.

In a flexible PVC compound the trimellitates are less volatile and have improved thermal stability over the phthalate and polymeric plasticizers. Their plasticizing effectiveness and compatibility are similar to phthalates. They offer better moisture and water resistance than the phthalates or polymeric plasticizers. Large volumes of trimellitate esters are used in 90°C and 105°C UL rated insulation compounds. Because of their extraction and migration resistance, thermal stability, and low volatility, the trimellitates are used in conjunction with 911P and DUP in automotive interior trim applications where windshield fogging is an issue.

Phosphate Esters

The principal advantage of phosphate esters is improved fire retardancy. The fire performance of PVC itself, relative to other polymeric materials, is very good because of its high halogen content, but the addition of plasticizers reduces this. Consequently, there is a need, in certain demanding applications, to improve the fire-retardant behavior of flexible PVC by reducing the limiting oxygen index (LOI) and smoke. Phosphate esters are combined with brominated phthalates for use in FPVC UL rated plenum cable applications. Tris-2-ethylhexyl phosphate shows good compatibility with PVC and also imparts good low temperature performance in addition to good fire retardancy.

2-Ethyhexyl diphenyl phosphate has widespread use in flexible PVC applications because of its combination of properties of plasticizing efficiency, low temperature performance, migration resistance, and fire retardancy.

Sebacate and Azelate Esters

Esters produced from 2-ethylhexanol and higher alcohols with linear aliphatic acids are used in some demanding flexible PVC applications where superior low temperature performance is required. Di-2-ethylhexyl sebacate (DOS) and di-2-ethylhexyl azelate (DOZ) are the commonly used members of this group. They offer superior low temperature performance but poorer compatibility, and command a significant premium. Their usage is generally limited to extremely demanding low temperature flexibility specifications, eg, underground jacketing cable in arctic environments.

Polymeric Plasticizers

Polymeric or polyester plasticizers are a class offering very good characteristics of low volatility, solvent, oil, stain, fat, and migration resistance to plasticized PVC. Polymerics usually are high molecular weight, linear, saturated, terminated polyesters of adipic, azelaic, or glutaric acids and propylene or butylene glycols. In most cases, termination is done by monohydric alcohols or monocarboxylic fatty acids. Polymerics have one of the following structures:

$$\underset{\mathbf{1}}{T_1\text{-}[G\text{-}A]_n\text{-}G\text{-}T_1} \qquad \underset{\mathbf{2}}{T_2\text{-}[A\text{-}G]_n\text{-}T_2}$$

where A is a dibasic acid, G a glycol, T_1, a fatty acid, T_2 a monohydric alcohol, and n the number of repeating units.

When polycondensation is carried out with a stoichiometric excess of acid (**1**), the carboxylic end groups are esterified with monoalcohols whereas with excess diol (**2**), the terminal hydroxy groups react with acetic acid or longer chain monocarboxylic acid. The polycondensation reaction yields a broad molecular weight distribution.

Choice of acid, glycol, and terminators is very important since the total architecture of the molecule is critical to achieve good compatibility with PVC because of the high molecular weight of the polyester. Because of their high molecular weight, polymeric plasticizers need to be heated up prior to dry blending and require a higher process temperature.

Because of lower efficiency than a monomeric plasticizer and higher costs, polymerics are used frequently in combination with phthalates to improve migration resistance and oil extraction characteristics over the phthalate system. Upholstery and aircraft seating subject to extraction by body or hair oil are examples of useful applications. Refrigerator gasketing, electrical tape, decals, and oil-resistant electrical wire use high levels of polymerics frequently as the sole plasticizer (5).

Polyester plasticizers range in viscosity from 900 to 300,000 m Pa·s (cP), as shown in Table 2. They can be classified as low, medium, and high viscosity products. As the viscosity increases the extraction resistance improves and the plasticizing efficiency decreases.

The chemical nature of the polymeric plasticizer can be used to classify them in relation to end-product performance. Table 2 shows that the acid component, diol component, and end groups as well as the molecular weight determine the performance properties.

Secondary Plasticizers

Also known as extenders, secondary plasticizers continue to play a significant role in flexible PVC formulations. They do not impart flexibility to the PVC resin alone, but when combined with a primary plasticizer act in such a way as to add flexibility and other properties to the final product (6). The majority of secondary plasticizers

Table 2. Polyester (Polymeric) Plasticizers: Composition, Properties, and Applications

Dicarboxylic acid	Diol	Viscosity	Properties and applications
Adipic acid	1,2-Propane diol, 1,3-propane diol, 1,3-butane diol, 1,4-butane diol, 1,6-hexane diol, neopentyl glycol	High, >10,000 mPa·s (cP); medium, 4000–8000 mPa·s (cP)	High resistance to gasoline, oils, fats, and bitumen; migration-resistant; tubing, films, cable insulation, and jacketing
		Low, <4000 mPa·s (cP)	Oil and fat resistance markedly less satisfactory; for spread coating alone or in combination with high viscosity esters; other uses as above
Azelaic acid	1,2-Propane diol, 1,3-propane diol, 1,3-butane diol, 1,4-butane diol, 1,5-pentane diol, 1,6-hexane diol	High, >10,000 mPa·s (cP)	High oil, gasoline, and fat resistance; adhesive tapes; other uses as for polysebacates
		Medium, 4000 to 8000 mPa·s (cP)	Easily processible; good compatibility; generally applicable polyester plasticizers
o-Phthalic acid	Ethylene glycol, 1,2-Propane diol, 1,3-Propane diol, 1,3-Butane diol, 1,4-Butane diol	Low, <4000 mPa·s (cP)	Easily processible; poor resistance to oils, fats, gasoline; reduced flexibility at low temperature
		<2000 mPa·s (cP)	Easy processing; for special applications
Sebacic acid	Ethylene glycol, 1,3-Propane diol, 1,3-Butane diol, 1,4-Butane diol, Neopentyl glycol	High, >10,000 mPa·s (cP)	Good resistance to gasoline, oil, fat, uv light; highly migration-resistant; good electrical properties; for high quality articles
		Medium, 4000–8000 mPa·s (cP)	Good compatibility with PVC, easily processible; for spread coating; protective clothing

in use are chlorinated paraffins, which are hydrocarbons chlorinated to a level of 30–70%. For a given hydrocarbon chain, viscosity increases with chlorine content, as does the fire retardancy imparted to the formulation. These materials aid fire retardancy because of their chlorine content. Chlorinated paraffins of the same chlorine content may have different volatilities and viscosities if they are based on different hydrocarbon chains.

Phthalate-chlorinated paraffin compatibility decreases as the molecular mass of the phthalate and the plasticizer content of the PVC formulation increase. Usually the chlorinated paraffin portion of the total plasticizer should not exceed 15%. Many compatibility graphs are available in the literature (7).

Other materials that are often referred to as secondary plasticizers include materials such as epoxidized soybean oil (ESO), epoxidized linseed oil (ELO), and epoxidized tallate oil (ETO). These act as secondary stabilizers because of their epoxy content by removing the HCI from the degrading polymer. The ETO provides the best low temperature properties of the epoxidized oils.

Plasticized Polymers: The Dominance of PVC

Over 90% of the plasticizer volume is used by the PVC industry. The reason for such high usage with PVC is that the benefits imparted by the plasticization of PVC are far greater than those imparted to other polymers. PVC is the only polymer able to accept and retain large concentrations of plasticizer. This is due in part to a morphological form comprising highly amorphous, semicrystalline, and highly crystalline regions. Without the wide range of additives available, eg, plasticizers, stabilizers, fillers, lubricants, and pigments, PVC would be of little use. The development of PVC as a commodity polymer is fundamentally linked to the development of its additives.

Different types of PVC exist on the market. The two principal types are suspension and paste PVC; the latter includes the majority of emulsions and dispersion PVC polymers. The plasticizer applications technologies associated with these two forms are distinctly different and are discussed separately. Details of the polymerization techniques giving rise to these two distinct polymer types can be found in many review articles (8) (see VINYL CHLORIDE POLYMERS).

Applications Technology

Suspension PVC. These polymers are produced by suspending vinyl chloride in water and polymerizing this monomer using a monomer-soluble initiator. PVC polymers produced via a suspension polymerization route have a relatively large particle size (typically 100–150 μm). Suspension polymers produced for the flexible sector have particles that are highly porous and are therefore able to absorb large amounts of liquid plasticizer during the mixing cycle. A typical flexible PVC formulation can be found in Table 3.

Using a ribbon blender, the resin, stabilizer, lubricant, and filler are heated to 70°C. The plasticizer is then distributed through piping running the length of the blender, and the heat remains on the jacketed blender until the dry point is

Table 3. Typical Flexible PVC Formulations

Ingredient	Parts by weight	Parts per hundred resin (phr)	wt%
PVC	75	100	50
Plasticizer	45	60	30
Filler	26.25	35	17.5
Stabilizer	3	4	2
Lubricant	0.75	1	0.5
Total	150	200	100

reached. If the plasticizer is preheated the dry point will be reached in less time. Polymeric plasticizers must be preheated to 70–80°C.

With a high speed mixer, set the jacket temperature at 90°C. Charge the resin and dry stabilizer, mix at high speed to 60°C. Add the plasticizer and other liquids and mix to the dry point at 70–85°C. Add the other solids and drop at 90–105°C with monomeric plasticizers. For polymerics, drop at 100–115°C. This dry blend can be either stored or processed immediately. Processing of suspension resin formulation is performed by a variety of techniques such as extrusion, injection molding, and calendering to fuse the PVC and produce the end product.

The dry blend can also be extruded and the extrudate pelletized to produce pellets of PVC compound, which can then be reprocessed to produce the final article. This has the benefit of ease of processing and storage of raw materials since all the formulation ingredients are contained in the gelled compound.

Plastisols. Plastisol-forming polymers are produced by microsuspension polymerization or dispersion polymerization (9). Microsuspension produces very fine particles of monomer to ensure that small particle sizes of polymer are produced. In emulsion or dispersion polymerization the vinyl chloride is dispersed in a water-soluble initiator; the vinyl chloride particles are small and stabilized using surfactants. There are also several variations of these two basic techniques.

Much lower particle size resins are produced when compared to suspension resins (1 μm vs 150 μm) with some residual surfactant from the polymerization process retained on the polymer. The small particle size imparts a lack of porosity to the resin and the demands on plasticizer behavior in a plastisol tend to be more complex. Choice of plasticizer is made with consideration given to the required viscosity of the plastisol and the required rheology of the plastisol. It is common to encounter formulations with two or three different plasticizers.

Plastisols differ from their suspension analogues in that after mixing with plasticizer they produce a paste or plastisol, similar in appearance to paint, rather than a dry blend. For plastisols charge 80% of the liquids into the mixer. Start the agitator and add the solids in the following sequence: filler, blending resin, dispersion resin. At no time should the mix temperature reach 35°C. This can be controlled through jacketing and the addition of some of the 20% of liquids originally held back. Take the mix through a high shear stage to break down the agglomerates. This will minimize viscosity buildup on aging due to plasticizer solvation. When there are no more lumps in the plastisol, add the remainder of the liquids and mix for homogeniety. The plastisol must be de-aerated before use, unless it is a foam plastisol. The plastisol can then be spread, coated, rotationally cast, or sprayed for processing.

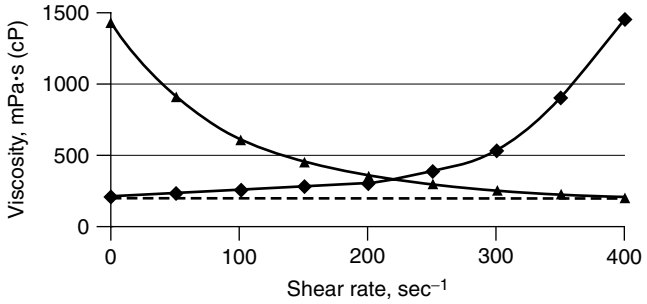

Fig. 1. Rheological behavior. - - - Newtonian; —•— dilatent; —▲— pseudoplastic.

Because the formulation ingredients in a plastisol are in liquid form, viscosity of the plastisol is of great importance and the intrinsic viscosity of the plasticizer contributes significantly to the plastisol viscosity, as does the precise polymerization conditions of the resin. The desired plastisol viscosity can be obtained by careful selection of polymer, plasticizer, and other formulation ingredients, but the shear rate applied to the plastisol also affects the viscosity. PVC plastisols are either (*1*) pseudoplastic, ie, viscosity decreases with shear; (*2*) near-Newtonian, ie, viscosity remains nearly constant with shear; or (*3*) dilatant, ie, viscosity increases with shear (see Fig. 1).

Effect of Plasticizer Choice on the Properties of Flexible PVC

A change in plasticizer affects the properties of a flexible PVC article. Certain properties are more important for some applications than others and some plasticizers find more extensive use in some application areas than others. The PVC technologist must ascertain the most important properties for an application and then make the correct choice of plasticizer. The two structural parameters that affect plasticizer performance are chain length or molecular weight and linearity.

In general, as the ester chain length increases, the following performance changes occur: solvation power decreases, efficiency decreases, volatility decreases, low temperature flex improves, low temperature brittleness improves, and compatibility decreases.

A comparison of linear vs branched chains show the following:

(1) Linear chains have a faster dry blend time.
(2) Branched chains have a faster fusion time.
(3) Branched chains are more compatible.
(4) Linear chains have better low temperature brittleness and flexibility.
(5) Linear chains are more efficient.
(6) Linear chains are less volatile.
(7) Branched chains have better electrical properties.
(8) Linear chains exhibit better uv stability and long-term permanence.
(9) Linear chains provide higher thermal stability.

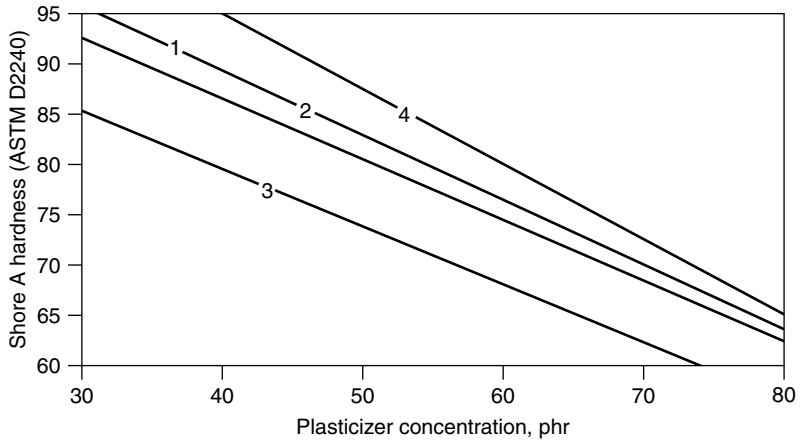

Fig. 2. Relative efficiency of plasticizers where (1) represents DEHP; (2) Palatinol® 9P; (3) DEHA; and (4) TOTM. (Palatinol is a registered trademark of BASF and 9P is a linear C_9 phthalate.)

Plasticizer Efficiency. This is a measure of the concentration of plasticizer required to impart a specified softness to PVC or shore hardness (Fig. 2). For a given acid constituent of plasticizer ester, ie, phthalate, adipate, etc, plasticizer efficiency decreases as the carbon number of the alcohol chain increases, eg, for phthalate esters efficiency decreases in the order BBP > DIHP > DOP > DINP > DIDP > DTDP (10). In addition to size of the carbon number of the alcohol chain, the amount of branching is also significant; the linear plasticizers are more efficient. Choice of the acid constituent can also be significant. For equivalent alcohol constituents, phthalate and adipate esters are both considerably more efficient than their trimellitate equivalent.

High Temperature Performance. High temperature performance in flexible PVC is related to plasticizer volatilization and plasticizer degradation (Fig. 3). Plasticizer volatilization, both from the finished article during use at elevated temperatures (eg, in electrical cable insulation) and also during processing [ie, release of plasticizer volatile organic compounds (VOCs)], is directly related to the vapor pressure and volatility of the plasticizer. The higher molecular weight phthalates give superior performance in this area. Higher molecular weight esters such as trimellitates are even less volatile and trimellitate esters find extensive use in the demanding wire and cable and automotive specifications, which have strict mass loss requirements. Branched esters have higher volatilities than their linear equivalents.

With regards to VOCs in the workplace, the same structure relationships apply. Not only does excessive plasticizer volatilization have environmental consequences, but since not all the plasticizer in use is entering the PVC resin this results in a harder material than anticipated. As a result of environmental protection legislation, more end users are looking at means of reducing or recovering and reusing plasticizer fumes and breakdown products.

Plasticizer molecules can undergo thermal degradation at high temperatures. Esters based on the branched alcohol isomers are more susceptible to such

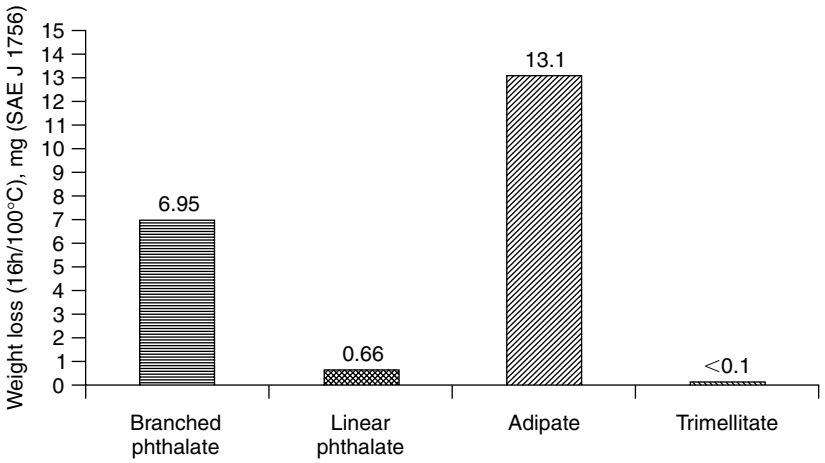

Fig. 3. Volatile loss of plasticizers from flexible PVC (Shore A80).

degradation because they have more tertiary carbon sites. With the addition of an antioxidant (topanol CA) to the plasticizer, its thermal properties can be improved.

Low Temperature Performance. The ability of plasticized PVC to remain flexible at low temperatures is of great importance in certain applications, eg, roofing, swimming pool liners, and tarpaulins. There is a significant contribution to low temperature performance from the alcohol portion of the ester, the greater the linearity of the plasticizer the greater the low temperature flexibility. The choice of the acid constituent of the plasticizer ester is also important. The linear aliphatic adipic, sebacic, and azeleic acids give excellent low temperature flexibility compared to the corresponding phthalates and trimellitates (Fig. 4).

Processing Properties. The dry blend and fusion characteristics of an FPVC are related to the molecular weight and degree of branching of the

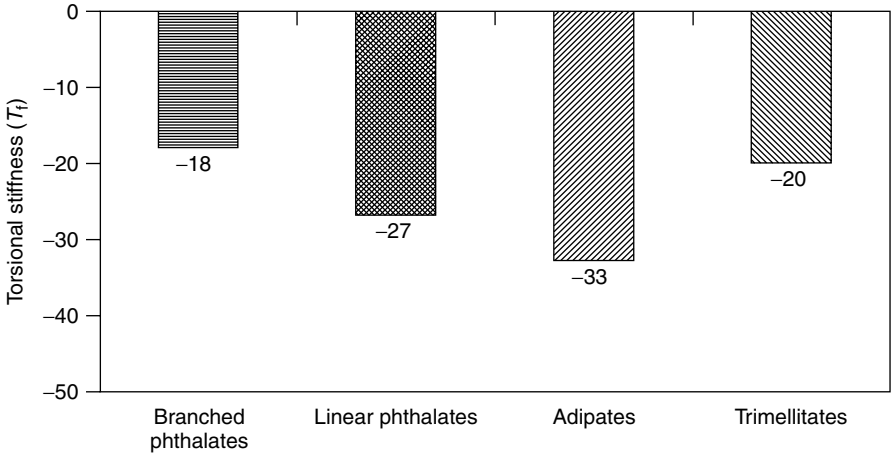

Fig. 4. Low temperature flexibility of plasticized PVC.

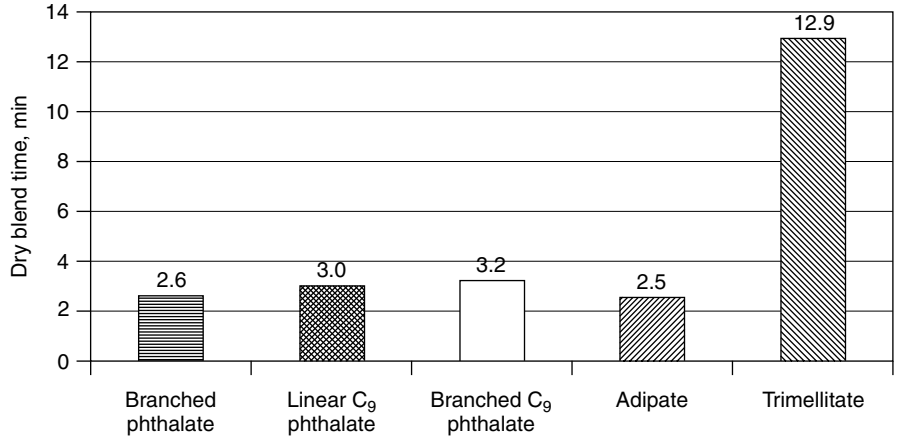

Fig. 5. Dry blend time of plasticized PVC.

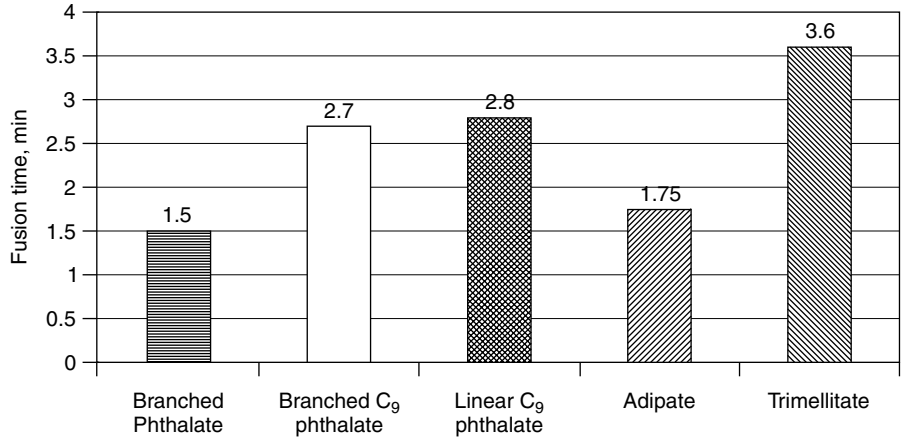

Fig. 6. Fusion time of plasticized PVC. Jacket temperature 96°C; rotor speed 63 rpm.

plasticizer (Fig. 5). In general, the shorter the chain length and the more linear the plasticizer, the shorter the dry blend time.

The fusion characteristics are a measure of the ability of a plasticizer to fuse with the polymer and develop maximum mechanical properties (Fig. 6). Fusion properties are often measured either as a processing temperature or time so as to obtain these properties. Ease of fusion is related to plasticizer branching and molecule size. The greater the branching of a plasticizer molecule, the greater attraction it has for the PVC polymer chain and the less additional energy, in the form of heat, is required. The smaller the plasticizer molecule the easier it is for it to enter the PVC matrix; larger molecules require more thermal energy to establish the desired interaction with the polymer. Thus, for the phthalate esters ease of fusion rate decreases in the order BBP > DIHP > DOP > DINP > DIDP.

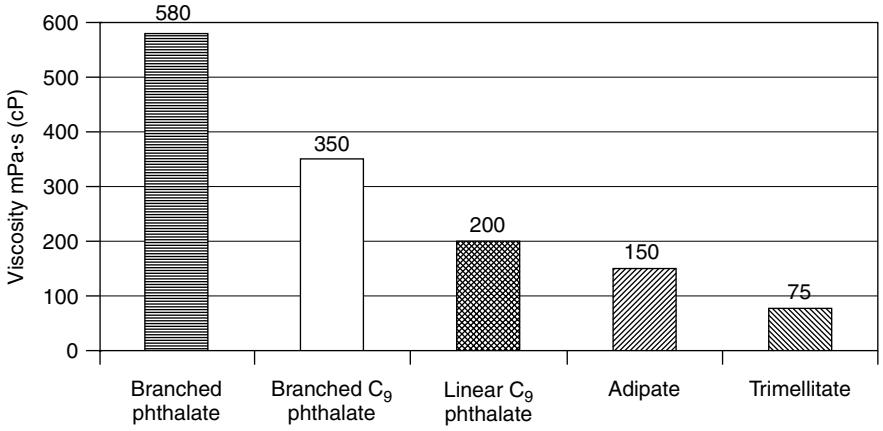

Fig. 7. Storage stability of plastisols (change in viscosity after 30 days).

Plastisol Viscosity and Viscosity Stability. After the primary contribution of the resin type in terms of its particle size and particle size distribution, plastisol viscosity has a secondary dependence on plasticizer viscosity (Fig. 7). The lower molecular weight and more linear esters have the lowest viscosity and hence show the lowest plastisol viscosity. Esters based on aliphatic acids, being of lower viscosity than the corresponding aromatic acids, show lower plastisol viscosities. Adipate esters have found widespread use in plastisol applications in blends with other esters. Plastisols are often mixed and then stored rather than processed immediately. It is of great importance in this case for the plasticizer to show viscosity stability at the storage temperature. It is not advisable to use a plasticizer of too great an activity, since grain swelling, leading to plastisol viscosity increase, can occur at room temperature for some active plasticizer systems.

Migration and Extraction. When plasticized PVC comes into contact with other materials, plasticizer may migrate from the plasticized PVC into the other material (Fig. 8). The rate of migration depends not only on the plasticizer but also on the nature of the contact material.

Plasticizer can also be extracted from PVC by a range of solvents, including water. The aggressiveness of a particular solvent depends on its molecular size and its compatibility with both the plasticizer and PVC. Water extracts plasticizer very slowly, oils are slightly more aggressive, and low molecular weight solvents are the most aggressive.

The key characteristic for migration and extraction resistance is molecular size. In general, the larger the plasticizer molecule the less it tends to migrate or be extracted.

Automotive Fogging. The term automotive fogging relates to the condensation of volatile material on a car windshield causing a decrease in visibility where light hits it. Although this volatile material may arise from a variety of sources, materials from inside the car may contribute to windshield fogging because of the high temperatures that can be encountered inside a car in a dry hot climate. In the case of flexible PVC such a contribution may arise from emulsifiers in the polymer, lubricants, stabilizers, plasticizers, and coating on the modifier.

Fig. 8. Plasticizer absorption by contact material in relation to chain length of the alcohol in the plasticizer. Solid lines indicate linear alcohol and dashed lines indicate branched alochol. —◇— Vinoflex® 507 rigid PVC; —■— Polystyrol® 475 K impact polystyrene; —▲— Terluran® 877 T (ABS); —●— Luran® 368 R (SAN); —⊠— Lupolen® 6011 L (HDPE); - -◇- - Vinoflex® 507 rigid PVC; - -■- - Polystyrol® 475 K impact polystyrene; - -▲- - Terluran® 877 T (ABS); - -●- - Luran® 368 R (SAN); ⊠ Lupolen® 6011 L (HDPE);

In each case manufacturers have studied their products in detail and recommend low fogging polymers, lubricants, stabilizers, and plasticizers. Tests have been designed (SAE J 1756) to assess the fogging performance of both the PVC sheet and the raw materials used in its production (Fig. 9). These tests involve heating of the sheet or raw material for a specified period at a set temperature in an enclosed apparatus with a cooled glass plate above the sheet or raw material. The reflectance of the glass plate is then compared before and after the test to ascertain the degree of fogging. In such a test, the fogging performance of a plasticizer is related to its volatility, vapor pressure, mass, and surface tension. The higher molecular weight and more linear plasticizers give superior performance. Trimellitate esters and 911 phthalates, with their high degree of linearity and low viscosity for plastisol applications, are used as low fogging plasticizers for these applications.

Long-term Permanence. Outdoor weatherability is dependent on branching and a properly stabilized formulation. Typically, to determine the permanence of FPVC accelerated uv weathering and thermal stability, studies are performed in the laboratory and outdoor weathering studies are carried out in Arizona, Florida, and northern industrial climate such as in New Jersey or Ohio. The percent elongation retained and discoloration are the measurable criteria.

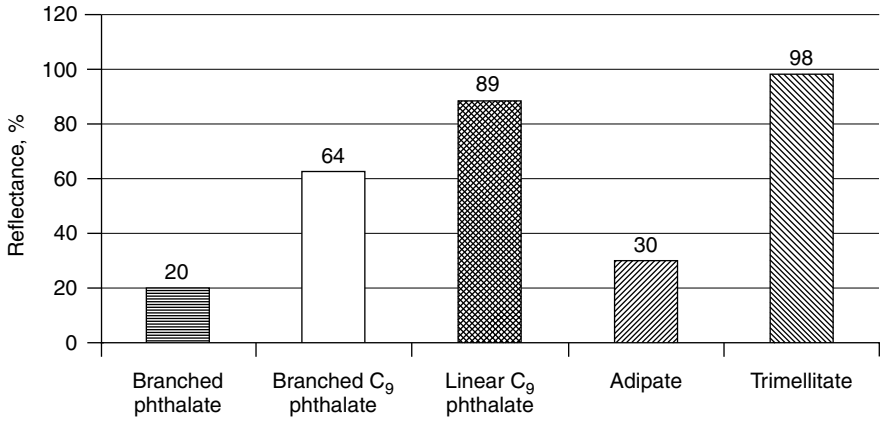

Fig. 9. Fogging of plasticized PVC for 3 h at 100°C (SAE J1756).

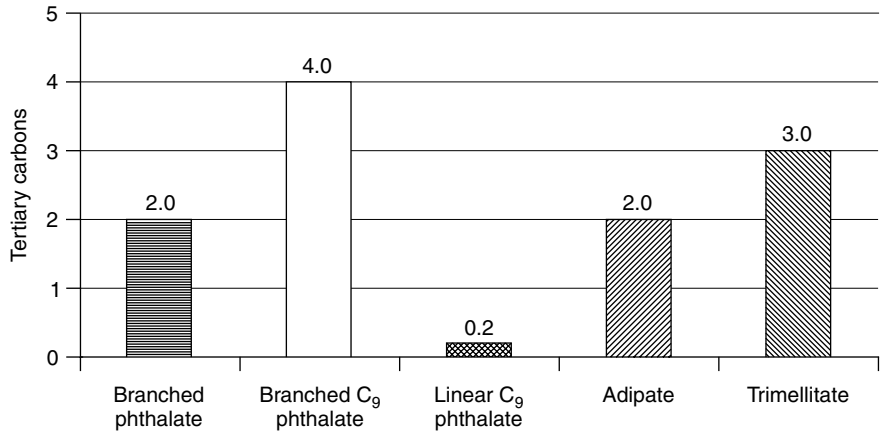

Fig. 10. Effect of branching on tertiary carbons.

Tertiary carbon sites on the plasticizer are weak spots where heat or light can initiate radical formation, which leads to degradation of the FPVC (Fig. 10). The higher the number of tertiary carbons the greater the probability for degradation and limited outdoor life.

Overall Assessment of Properties. Table 4 shows the effect for each criterion of increasing plasticizer concentration, increasing the size of the plasticizer molecule, increasing the linearity of the plasticizer molecule, and changing the acid constituent of the ester. There is no perfect plasticizer for every application. Choice depends on the performance requirements for the end use application and economics.

The Plasticization of Polymers Other Than PVC

The plasticization of PVC accounts for the majority of plasticizer use. However, a significant amount of plasticizers are used in non-PVC polymers. Although PVC

Table 4. Structure: Property Relationships of Plasticizers[a]

Property, at equal softness	Increased concentration	Increased size	Increased linearity	Acid[b] used / Acid[b] used
Higher efficiency	–	P	I	Ph = Ad > Tr
Thermal resistance	P	I	I	Tr > Ph > Ad
Low temperature	I	I	I	Ad > Ph = Tr
Fusion	(I)	P	(P)	Ph > Ad ≥ Tr
Plastisol				
Viscosity	I	(I)	I	Ad > Ph
Aging	–	I	(I)	Ad > Ph
Migration/extraction	P	I	I	Tr > Ph > Ad
Fogging	P	I	I	Tr > Ph > Ad
Long-term permanence	–	P	I	Ph > Tr > Ad

[a] I = improved performance; P = poorer performance; ( ), marginal performance.
[b] Ph = phthalate; Ad = adipate; Tr = trimellitate.

stands alone in its ability to accept and retain large quantities of commercial plasticizer, effective plasticization of other resins may be possible if certain conditions specific to the polymer of interest are met.

The first factor to be considered when looking at the plasticization of a polymer is the need. Even though some polymers may be compatible with large concentrations of plasticizer, the resultant softening benefits may be of little use. Other factors are short- and long-term compatibility.

For a plasticizer to enter a polymer structure the polymer should be highly amorphous. Once it has penetrated the polymer the plasticizer fills free volume and provides polymer chain lubrication, increasing rotation and movement.

The plasticizer content of a polymer may be increased by the suppression of crystallization in the polymer, but if crystallization subsequently occurs, the plasticizer exudes. For highly crystalline resins such as nylon, the small amounts of plasticizer allowable can change the nature of the small amorphous regions with a consequent overall change in properties.

Acrylic Polymers. Although considerable information on the plasticization of acrylic resins is scattered throughout journal and patent literature, the subject is complicated by the fact that the acrylic resins constitute a large family of polymers rather than a single polymeric species. A variation in physical properties may be obtained through copolymerization of two or more acrylic monomers selected from the available esters of acrylic and methacrylic acid (see ACRYLIC ESTER POLYMERS; METHACRYLIC ESTER POLYMERS).

Plasticizers are used with acrylics to produce tough flexible coatings. Compatabilities with common plasticizers are up to 10 wt% although with low molecular weight plasticizers, it can be higher. Plasticizers for acrylics include most of the common esters. There has been interest in the development of acrylic plastisols similar to PVC plastisols. Clearly, the same aspects of both plastisol viscosity and viscosity stability are important. Patents appear in the literature indicating that the number of available plasticizers that show both good compatibility with acrylic resins and satisfactory long-term plastisol stability may be fewer than those showing equivalent properties with dispersion PVC resins.

Patents have appeared which show the formulations containing PMMA emulsion polymer and PMMA suspension polymer combined with butyl benzyl phthalate and octyl benzyl phthalate. When replacing PVC applications the use of phosphate plasticizers may be required to give equivalent fire retardance.

Nylon. The high degree of crystallinity in nylon means that plasticization can occur only at very low levels. Plasticizers are used in nylon but are usually sulfonamide-based since these are generally more compatible than phthalates. These plasticizers help improve the processing of the nylon.

Poly(ethylene terephthalate). Poly(ethylene terephthalate) (PET) is a crystalline material and hence difficult to plasticize. Since PET is used as high strength film and textile fiber, plasticization is not usually required. Plasticizers may be used in small amounts as processing aids and external lubricants.

The main area of interest for plasticizers in PET is in the area of dyeing. Because of its lack of hydrogen bonds, PET is relatively difficult to dye. Plasticizers used in this process can increase the speed and intensity of the dyeing process. The compounds used, however, tend to be of low molecular weight since high volatility is required to enable rapid removal of plasticizer from the product (see POLYESTERS, THERMOPLASTIC).

Polyolefins. Interest has been shown in the plasticization of polyolefins but plasticizer use generally results in a reduction of physical properties, and compatibility can be achieved only up to 2 wt%. Most polyolefins give adequate physical properties without plasticization.

Polystyrene. Polystyrene shows compatibility with common plasticizers but is usually internally flexibilized with butadiene rubber. Small amounts of plasticizer are used to increase the flexibility further.

Fluoroplastics. Conventional plasticizers are used as processing aids for fluoroplastics up to a level of 25%. However, certain grades of Kel-F (chlorotrifluoroethylene) contain up to 25 wt% to improve elongation and increase softness. The plasticizers used are usually low molecular weight oily chloroethylene polymers.

Rubbers. Heavy petroleum oils, coal tars, and other predominantly hydrocarbon products have been used in rubber processing and formulations for many years. Esters such as DOA, DOP, and DOS, can be used with latex rubber, nitrile rubber, and chloroprene to reduce the T_g. The level of plasticizer is usually around 10–15 phr.

Economic Aspects

Worldwide consumption of plasticizers is estimated at 4.9×10^6 t (Fig. 11; Table 5) (11).

The distribution of plasticizers into various applications is shown in Figure 12.

Health and Safety Aspects

Numerous toxicological studies have been conducted on a variety of plasticizers. Because DEHP is the most widely used plasticizer and is a well-defined single

Table 5. North American Plasticizer Market[a]

Plasticizer	Market share, %
Overall market	
C_8 phthalates	20
C_9 and C_{10} phthalates	35
C_4 phthalates	1
Linear phthalates	28
Other specialties	16
Specialty market	
Epoxies[b]	19
Adipates	31
Phosphates	9
BBP	13
Polymerics	9
Trimellitates	14
Other	5

[a]Approximate split by grade types.
[b]ESO, etc.

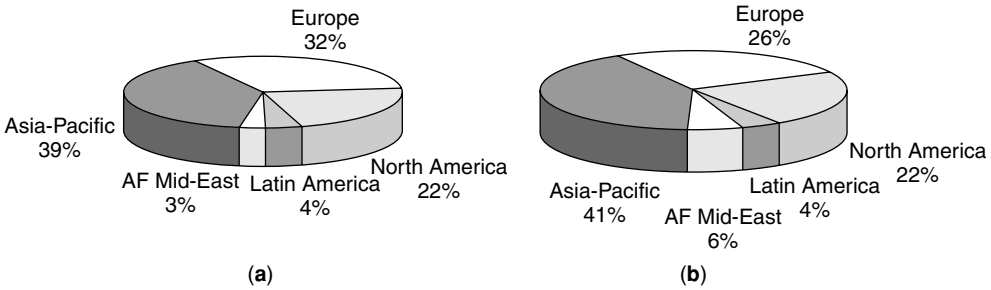

Fig. 11. Worldwide plasticizer production (**a**) and consumption (**b**). ■ is Africa and the Middle Eastern countries.

substance, it is the plasticizer that has been most thoroughly investigated in terms of its toxicology. There are more than 1000 scientific publications on the toxicology and environmental effects of DEHP (12).

Acute Toxicity. This studies the effect of the plasticizer on the species, usually a rodent, using a high dose where only a single or a few doses are given. Plasticizers posses a low acute toxicity with an LD_{50} greater than 2000 mg/kg body weight for oral route of exposure. Animal tests have indicated that plasticizers do not irritate the skin or eyes and are nonsensitizing.

Chronic Toxicity. Various animal species have undergone repeated oral exposure to phthalates for periods up to two years. Tumors were found in rodents at a dose level higher than what humans are exposed to. In mechanistic studies these tumors were found to be specific to rodents and therefore the effect is not relevant for humans. At lower dose levels, still many times higher than what humans are exposed to, no tumors are present. In these mechanistic studies phthalates were not genotoxic. Both *in vivo* and *in vitro* studies did not indicate

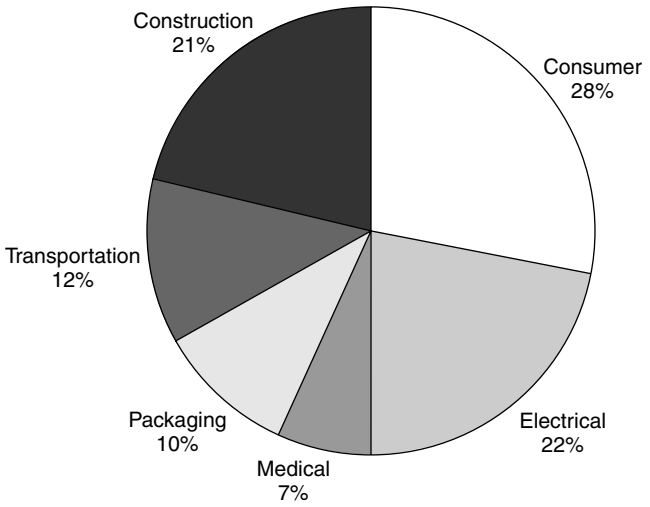

Fig. 12. Plasticizer market breakdown in North America.

any mutagenic potential. The DNA binding studies were also negative. These studies also showed that phthalates are weak peroxisome proliferators; however, peroxisome proliferation is species specific to rodents. Peroxisome proliferation was not evident in monkey and marmoset studies. Hypolipidemic drugs administered to rodents and humans cause peroxisome proliferation in the rodent but not in the human. The International Agency for Research on Cancer (IARC), a World Health Organization agency, has downgraded DEHP to category 3. DEHP is not classifiable as to its carcinogenicity to humans. The Canadian government has classified DEHP in Group IV—unlikely to be a carcinogen to humans.

Endocrine Modulation. Some scientists claim that chemicals in the environment may adversely affect the body's endocrine system and hormones. In studying phthalates, researchers looked at their ability to mimic the female hormone estrogen. The majority of the *in vitro* (test tube) and all the *in vivo* studies indicate that phthalates do not cause estrogenic effects. Although the mechanism is unknown, recent studies show that phthalates do not bind to the androgen receptor. Additional studies are under way to investigate whether phthalates produce other hormonal changes.

Developmental and Reprotoxicity. Some of the phthalates have shown reproductive effects in rodents at high dose levels. The relevance to humans is in question as primates appear resistant to the reproductive effects seen in rodents when tested with DEHP or DINP for 13 weeks at 2500 mg/kg/day (13).

Comparing estimates of the average human daily lifetime exposure to DEHP (0.3–6 μg/kg/day) to the level at which no effects are observed in rats indicates a margin of safety of 10,000 mg/kg/day for humans.

The Effect of Plasticizers on the Environment. Approximately 5 million tons of plasticizer is used annually in the world (14). Over 90% of the worldwide consumption is used to make FPVC, and 95% of these PVC plasticizers are

phthalate esters. Relatively few plasticizers are used in sufficient quantity to pose an environmental impact. For plasticizer grade esters phthalates are photodegradable, biodegradable, and are not bioaccumulative. They do not pose a hazard within their solubility parameter.

Phthalates can be emitted to the environment during their production, transportation, compounding and processing, life cycle, and disposal.

Because of the effect of uv degradation and microbial attack, a significant proportion of the emissions from the flexible PVC consists of plasticizer degradation products. In these instances, therefore, the level of plasticizers appearing in the environment will be significantly less than indicated by the plasticizer loss data.

Phthalate plasticizers are produced by esterification of phthalic anhydride in closed systems and so losses to the atmosphere are minimal. Inquiries of all the principal plasticizer producers indicate a maximum total emission of 0.02–0.1%, ninety percent of which is to the water compartment. This level is expected to decrease because of improvements in plant water treatment facilities.

The road, rail, and marine transport of phthalates is carried out by international companies with sophisticated tank cleaning facilities. Wash waters from these modern facilities are passed through a series of separators to remove any residual plasticizer, which is then incinerated. It is estimated that, as a result of cleaning and spillages, the maximum emission to the environment is 0.01%.

Process operations often do not involve direct use or contact with process water. Based on the manufacturing technology applied, aqueous emissions are expected to be minimal. During the production of FPVC products, plasticizers may be exposed for up to several minutes at temperatures of ~180°C. The loss of plasticizer by evaporation and degradation can be significant.

Air extracted from spread coating ovens contains typically 500 mg/m^3 plasticizer, which is present mostly as a condensate since the saturation concentration of common plasticizers in air is low. In those installations with filtration equipment, the average phthalate concentration in the air is reduced from 500 mg/m^3 to below 20 mg/m^3. The use of incineration equipment to clean the exhaust air reduces the residual phthalate concentration to practically zero. The use of filters and incinerators on calendering and spread coating plants is steadily increasing due primarily to the need to reduce emissions of solvents and other volatile organic compounds to the atmosphere.

Knowledge of the quantity of plasticizer used in each application together with the level of exhaust air treatment allows estimation of the level of plasticizer lost to atmosphere during these processes to be between 0.007 and 0.68%, with an average of 0.11%.

Emissions During Interior End Use. The majority of flexible PVC is used indoors in applications such as flooring, wall covering, upholstery, and wire and cable. Environ Corp. developed a model that attempts to quantify the plasticizer losses that occur in a typical room. Using theoretical and semiexperimental approaches they have arrived at an emission rate at 25°C of 2.3×10^{-4} $mg/s/m^2$. Using this emission rate with data on the annual production of PVC flooring, wall covering, etc, and estimates of their lifetimes, the plasticizer losses from all indoor flexible PVC articles can be calculated.

Emissions During Exterior End Use. When flexible PVC is used in exterior applications, plasticizer loss may occur due to a number of processes which include evaporation, microbial attack, hydrolysis, degradation, exudation, and extraction. The data from FPVC roofing has been used to estimate the plasticizer losses from all outdoor applications at 0.7–1%. This estimate may be too high. Much of this extracted plasticizer does not end up in the environment because considerable degradation takes place during the extraction process.

Emissions During Disposal and Incineration. The increasing use of modern incinerators to dispose of domestic waste results in complete combustion of plasticizers to carbon dioxide and water. The main route by which organic components are removed from a landfill is by ingress of water, extraction, and subsequent loss of water from the site to the environment. There are approximately 2000 active landfill sites with an annual combined water ingress of $40 \times 106\ m^3$. The solubility of the most common plasticizer, DEHP, in water is difficult to measure. The true solubility is considered to be around 50 μg/L, but various values are given in the literature. Assuming a worst case solubility of 1 ppm, then the maximum quantity of plasticizer extracted in the United Kingdom is 0.005%. A maximum of 0.02% plasticizer could be emitted to the environment from landfills in Western Europe. To obtain a more precise estimate of the situation, 25 effluent water samples from a variety of types of landfills have been analyzed. The highest concentration of DEHP detected was 30 parts per billion. If the highest figure is used instead of the assumed 1 ppm then the quantity from the whole of Europe becomes 0.0006%. In conclusion, the DEHP estimated emission factors for industrial point sources are as follows: air, 0.05–0.5 wt%; surface water, 0.001–0.01 wt%; soil, 0.001–0.01 wt%. Lower molecular weight phthalates would be greater and higher molecular weight phthalates would be less.

Storage and Handling

PVC plasticizers are viscous liquids with high boiling points and a very low vapor pressure. Their flash points are all well over 100°C so they are not classified as a flammable liquid. They are thermally stable and are practically insoluble in water. They have an indefinite shelf life in a sealed container. They can be stored safely in carbon steel storage tanks or drums for extended periods of time.

Tanks may be installed in a vertical or horizontal position. The vertical position is preferred to minimize air contact with the plasticizer and for drainage. The bottom of the tank should be inclined at 2–5% in the direction of the outlet valve. Underground storage tanks are not recommended. Besides carbon steel, storage tanks are made of stainless steel, aluminum alloy ($AlMg_3$), fiberglass reinforced plastic, and high density polyethylene.

The containment basin and walls should be constructed of concrete and be large enough to contain the tank's entire contents. If a basin serves more than one tank, its capacity must be sufficient to contain 110% of the largest tank plus the maximum rainfall in a 24-h period. Most plasticizers do not require heated

storage facilities although a heated plasticizer will flow more easily and have a faster dry blend time. Diundecyl phthalate and some polymeric plasticizers should be stored indoors or in a heated storage tank because of their higher pour point and crystallization.

All plasticizers should be filtered prior to compounding to prevent contamination of the FPVC and damage to the process equipment. For handling plasticizers personnel should wear neoprene gloves, chemical goggles, chemical splash suits, and boots. Spills should be contained, solidified, and placed in a suitable container for disposal as per federal, state, and local regulations. Waste disposal is by incineration or burial in a licensed facility. Plasticizers should not be discharged into waterways or sewer systems without proper authority as per federal, state, and local regulations.

BIBLIOGRAPHY

"Plasticizers" in *EPST* 1st ed., Vol. 10, pp. 228–306, by J. R. Darby and J. K. Sears, Monsanto Co.; "Plasticizers" in *EPSE* 2nd ed., Suppl. Vol., pp. 568–647, by J. K. Sears and N. W. Touchette, Consultants.

1. J. K. Sears, N. Touchette, and J. R. Darby, in R. W. Tess and G. W. Pohlein, eds., *Applied Polymer Science*, 2nd ed., American Chemical Society, Washington, D.C., 1985.
2. C. J. Howick, *Plasticizer Rubber Compos.: Proc. Appl.* **23**, 53–60 (1995).
3. *Chemistry in Britain, Computational Chemistry*, Nov. 1990.
4. L. I. Nass and C. A. Heiberger, *Encylopedia of PVC*, 2nd ed., **4** vols. Marcel Dekker, Inc., New York, 1986–1998.
5. L. Meier, in R. G. Achter and H. Müller, eds., *Plastics Additives*, 3rd ed., Hanser Publishers, New York, 1990.
6. L. Krauskopf and J. T. Lutz Jr., in E. J. Wickson, ed., *Handbook of PVC Formulating*, Wiley-Interscience, New York, 1993.
7. J. K. Sears and J. R. Darby, *The Technology of Plasticizers*, Wiley-Interscience, New York, 1982.
8. D. L. Buszard, in W. V. Titow, ed., *PVC Technology*, 4th ed., Elsevier, New York, 1984.
9. H. Sarvetnick, *Plastisols and Organosols*, Robert E. Krieger Publishing, Malabar Fla., 1983.
10. L. Krauskopf and W. Arndt, in J. Edenbaum, ed., *Plastics Additives and Modifiers Handbook*, Van Nostrand Reinhold Co., Inc., New York, 1992.
11. *Modern Plastics Encyclopedia*, Vol. **77**, No. 12, McGraw-Hill Co., Inc., New York, Nov. 2000.
12. L. B. Weisfeld, in J. T. Lutz Jr. and R. F. Grossman, eds., *Polymer Modifiers and Additives*, Marcel Dekker, Inc., New York, 2001.
13. Y. Kurata and co-workers, *Toxicol. Sci.* **42**, 49–56 (1998).
14. *Phthlate Esters Panel of American Chemical Council, Arlington, Va.*, www.phthalates.org.

BRIAN L. WADEY
BASF Corporation

PMMA. See METHACRYLIC ESTER POLYMERS.

POLY(3-HYDROXYALKANOATES)

Introduction

Poly(3-hydroxyalkanoates) (PHAs) are a family of polyesters accumulated as inclusion bodies (Fig. 1) by a wide variety of bacteria. They are water-insoluble, relatively resistant to aqueous hydrolysis but are readily biodegraded in any natural environment where microbial diversity exists. They can be produced from renewable resources and waste materials and, although temperature-sensitive, are potentially recyclable. Many PHAs have mechanical properties similar to those of common synthetic plastics.

Most PHAs contain exclusively 3-hydroxycarboxylate units (Fig. 2a) but many microorganisms can also accumulate a polymer containing 4-hydroxycarboxylate monomers [eg 4-hydroxybutyrate (4HB), where $p = 2$ and R = H] when fed the appropriate substrate. The most common PHA is poly(3-hydroxybutyrate) homopolymer (PHB, where R = CH_3). This was discovered and studied by Lemoigne during the 1920s (1). It was first suspected that these granules were lipid bodies as they were stained with hydrophobic dyes. Lemoigne proved that they were high molecular weight polyesters, years before the pioneering work of Carothers (2) on synthetic polyesters.

Although copolymers of 3-hydroxyalkanoates were identified as early as the 1960s (3), little importance was attributed to them. The term PHA only came into use during the 1980s to refer to PHB and the other 3-hydroxyalkanoate polymers. This definition had not been in use very long when copolymers containing 4-HB (4) or 5-hydroxyvalerate (5-HV) (5) were discovered. Their production involved the same enzymes as those for the synthesis of PHB but they contained units that had the hydroxyl group on the fourth or fifth carbon rather than the third. For this reason, the term PHA is now most commonly defined as polyhydroxyalkanoate. This also includes polymers containing units with double bonds and other reactive groups in their side chain. The term PHA is generally applied to the biologically synthesized polymers.

Two major classes of PHAs are known to exist. PHAs whose polymeric units are predominantly five carbons or less are classified as short-chain-length PHAs (SCL PHAs) while all others are referred to as medium-chain-length PHAs (MCL PHAs). The term MCL was coined because the number of carbons in the monomers roughly corresponds to those of medium-chain-length carboxylic acids. PHA nomenclature may still be in a state of flux as new structures continue to be discovered.

Encyclopedia of Polymer Science and Technology. Copyright John Wiley & Sons, Inc. All rights reserved.

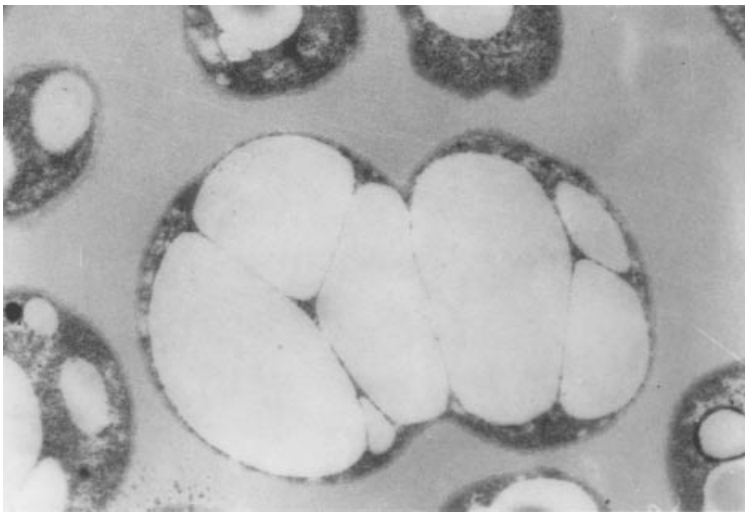

Fig. 1. PHB inclusion bodies in *Alcaligenes latus* (electron micrograph courtesy of Dr. G. Braunegg, Technical University of Graz, Graz, Austria).

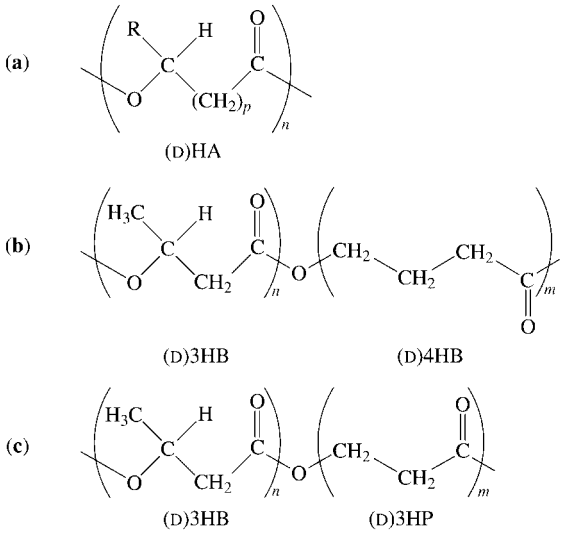

Fig. 2. Typical PHA structures including (**a**) General structure of polyhydroxyalkanoate subunits, P(HA), (**b**) P(3HB-*co*-4HB) copolymer, and (**c**) P(3HB-*co*-3HP) copolymer.

Properties

PHB exists in an amorphous state inside the bacterial cell. This seems to be necessary for its biosynthesis and there are several theories explaining how this state is maintained (6,7). Melting or solvent casting usually results in highly crystalline PHB because of its stereoregular nature. Crystallization may be avoided if the granules are isolated from the bacterial cells by a gentle enzymatic method,

which results in a stable latex suspension (6), but most PHB products are highly crystalline in nature. The rate of crystallization after melt processing can be increased by adding nucleating agents such as boron nitride, and by allowing the product to stabilize at the optimal crystallization temperature (about 60°C). The main drawbacks against the use of PHB are its brittle nature and its tendency to degrade near its melt temperature. Inclusion of a plasticizer (often a biodegradable one, such as triacetin) and annealing after initial crystallization aid in increasing flexibility. It has been demonstrated that impurities significantly increase the degradation rate (8). Thus a short processing time in the melt and a highly pure grade of polymer is recommended for PHB processing.

Effect of Side-Chain Length on PHA. The use of copolymers is another way to avoid degradation while increasing flexibility during melt processing of SCL PHA. Increasing the HV content of poly(3-hydroxybutyrate-*co*-3-hydroxyvalerate) [P(HB-*co*-HV)] from 0 to about 30% (expressed as mol% in this article) results in a concommitant decrease in melting point and Young's modulus (Table 1) but crystallinity remains high as a result of a phenomenon known as *cocrystallization* or *isodimorphism* (17). Above 30% HV the melting point begins to rise again. Increasing 4HB or 3-hydroxypropionate (3HP) monomers also lowers the melting point and gives a more flexible polymer. However, crystallinity decreases with increasing 4HB and 3HP since isodimorphism does not occur in these copolymers (18,19). Both 4HB and 3HP have much lower melting and glass-transition temperatures.

Conventional equipment used to process polyethylene can be used for pellets of PHA plasticized with a nucleating agent to form blow-molded, injection-molded, and film products. A key requirement is temperature control. It is recommended to operate at the lowest possible temperature and to keep the residence time at a minimum since the melting point of PHB is about 178°C and thermal degradation begins at about 180°C (depending on the purity). P(HB-*co*-HV) with a high HV content can have a melting point as low as 136°C. For most applications, it is suggested to process at a maximum temperature of 170°C, a maximum residence time of 3 min, and that molds and blow pin temperatures be kept at about 60°C (20). Mechanical properties deteriorate rapidly if the weight-average molecular weight falls below 400,000 g/mol.

Homopolymers of MCL PHA have not been biosynthesized to date. Although polymers designated as poly(3-hydroxyoctanoate) (PHO) have predominantly 3-hydroxyoctanoate repeating units (Fig. 2a where $P = 1$ and R = C_5H_{11}), they contain significant quantities (10% or greater) of other monomers, usually 3-hydroxydecanoate and 3-hydroxyhexanoate, depending on the bacterium and the carbon source. Melting temperature, Young's modulus, and tensile strength decrease as the length of the MCL PHA side chain increases (Table 1). MCL PHA can be toughened by annealing, which results in the formation of "crystalline cross-links."

Polymer Blends Incorporating PHA. The mechanical properties, morphology, biodegradability, and thermal and crystallization behavior of PHAs melt-blended or solvent-cast with nonbiodegradable polymers [such as poly(vinyl acetate)] and with biodegradable materials [such as wood cellulose fibers (21) and starch] have been reviewed (22). PHB blends with poly(ethylene oxide), poly(vinyl alcohol), poly (L-lactide), poly(D,L-lactide), poly(ε-caprolactone), poly(3-butyrolactone), P(HB-*co*-HV), and cellulose and starch derivatives have been

Table 1. Properties of Various PHAs[a] Compared to Polypropylene (PP)[b]

Physical properties	PP[c]	P(3HB)[c]	P(3HB-3HV)[d] (0–25%)	P(3HO)[e]	P(3HP)[f]	P(3HB-3HP)[f] (0–88%)	P(4HB)[g]	P(3HB-4HB) (0–49%)[h]
Crystalline melting point, °C	171 to 186	171 to 182	179 to 137	61	77	177 to 61	53	177 to 150
Glass-transition temp., °C	−10	−5 to 5[i]	10 to −6	−35	−19	4 to −15	−48	4 to 23
Crystallinity, %	65 to 70	60 to 80	80 to 30	30	37	60 to >13		60 to 15
Molecular weight M_w (10^5)	2.2 to 7	1 to 8	3	5	2	4 to 15		5 to 8
Molecular weight distribution	5 to 12	2.2 to 3			1.4	2.0 to 3.2		
Density, g/cm	0.905 to 0.94	1.23 to 1.25	1.20	1.0				
Tensile strength/MPa[j]	38	40	40 to 30	6 to 10			104	43 to 10
Young's modulus, GPa[k]	1.7	3.5 to 4.0	3.5 to 0.7				149	
Elongation to break, %	400	6 to 8	8 to 10	300 to 450			1000	5 to 511

[a]For additional properties, see Ref. 9.
[b]Structures are shown in Figures 2a–c.
[c]Ref. 10.
[d]Ref. 11.
[e]Ref. 12.
[f]Ref. 13.
[g]Ref. 14.
[h]Ref. 15.
[i]Ref. 16.
[j]To convert MPa to psi, multiply by 145.
[k]To convert GPa to psi, multiply by 145,000.

shown to be completely biodegradable (23). In a reactive blending process, the components have been mixed with a peroxide. This decomposes to form free radicals which cross-link the polymers (24).

Applications

The first commercial user of the P(HB-*co*-HV) resin was Wella AG, Darmstadt, Germany. They packaged hair and skin care products in injection blow-molded bottles. These products were introduced to the American and Japanese markets in 1991 and 1992 respectively.

Since PHAs are isotactic, they can serve as a feedstock for enantiomeric compounds, which can be used in the synthesis of chiral chemicals such as antibiotics, vitamins, fragrances, and pheromones. Optically pure monomers may be obtained from PHAs by chemical hydrolysis at 80–160°C using a titanate catalyst (25) or by enzymatic hydrolysis using extracellular bacterial depolymerases. It is possible to synthesize the optically active monomers by using bacteria, which can make the polymer but lack the 3-hydroxyalkanaote polymerase (Fig. 3a) or possess a high activity of intracellular PHA depolymerase. Monomers such as 4HB have therapeutic applications as an intravenous anaesthetic, for the treatment of narcolepsy, alcohol, heroin, and nicotine addiction (26).

PHB and P(3HB-*co*-4HB) have been evaluated for the controlled release of drugs (26,27). The drug may be microencapsulated in PHB and injected subcutaneously, or may be pressed into a pill and administered orally. Degradation is slow in the human body as it does not contain PHA depolymerases. Aqueous hydrolysis is probably responsible for *in vivo* degradation. PHB tablets of 60 mg (6.0 mm in diameter and 2.0 mm in thickness) degraded at a rate of 0.2 mg/week in the tissue of mice. In its present form, it might be considered for long-term applications in the body. PHB has been evaluated for use in surgical devices such as sutures, prosthetics, pins, dressings, and a three-dimensional heart valve scaffold (28). The monomers of PHB are natural metabolites found in the human body and are not toxic to humans. PHB and P(3HB-*co*-4HB) have been shown to be compatible with human tissue and mouse fibroblast cells. These materials elicit only a very mild immunological response in mice or rats (27).

Films of PHB and P(HB-*co*-HV) have piezoelectric properties. A charge is generated if a PHB crystal is deformed by hydrostatic force, thermal expansion, or other forces. Some synthetic piezoelectric polymers such as poly(vinylidene fluoride) are known to stimulate bone growth. It has been suggested that films of PHB and P(HB-*co*-HV) wrapped around bone fractures may accelerate the healing process (27).

PHAs are moisture-resistant and have gas barrier properties similar to the best coated films. They have potential use as plastic moisture barriers. Possible markets include mulch films, food and agricultural packaging, drink cartons, feminine hygiene products, disposable diapers, and disposable kitchen items, such as plastic films which are difficult to separate for recycling. Coatings may be applied with PHA as an amorphous latex which can be either reconstituted from the crystalline form of the polymer or obtained directly from a bacterial suspension by enzymatically dissolving the other cellular components. In the latter case, it

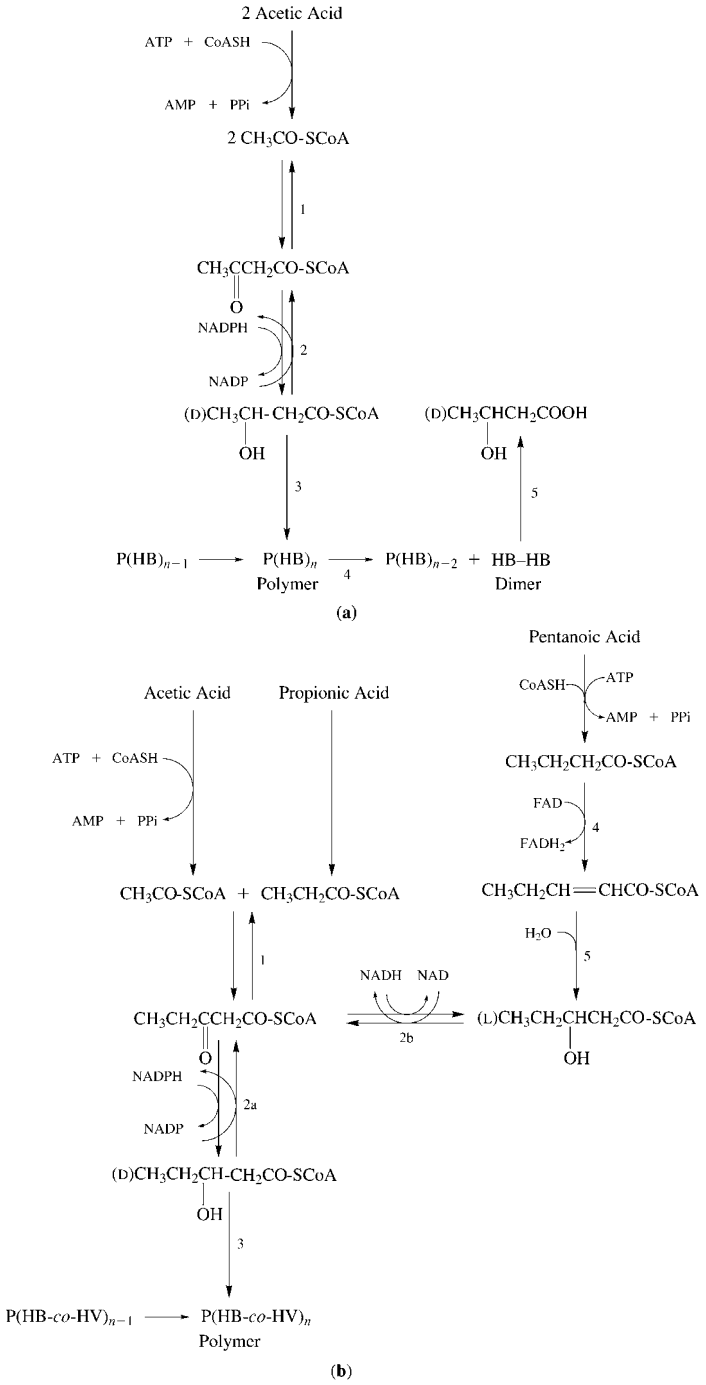

Fig. 3. (**a**) Biosynthesis of SCL PHA; 1, 3-ketothiolase; 2, NADPH-dependent acetoacetyl-CoA reductase; 3, SCL PHA polymerase; 4, SCL PHA depolymerase; 5, D(−)-3-hydroxybutyrate-dimer hydrolase. (**b**) Biosynthesis of P(HB-*co*-HV), 1, 3-ketothiolase; 2a, NADPH-dependent acetoacetyl-CoA reductase; 2b, NADH-dependent acetoacetyl-CoA reductase; 3, SCL PHA polymerase; 4, fatty acyl-CoA dehydrogenase; 5, enoyl-CoA hydratase.

is important that the granules are not dried prior to use as they would become crystalline. The latex may be applied as a spray to a material such as paper, dried and cross-linked using heat or uv light. The MCL PHAs are promising as coatings (29) since they are less crystalline than the SCL PHAs, and the microorganisms which synthesize them can introduce different functional groups (30).

Degradation of PHA

SCL PHA has been shown to degrade as rapidly as cellophane, much more rapidly than poly-L-lactic acid and aliphatic polyesters such as poly(butylene succinate) and poly(butylene succinate-*co*-ethylene succinate) under anaerobic conditions (31), faster than polycaprolactone under aerobic conditions, and faster than paper during composting (32). Although PHAs degrade rapidly in most nonsterile natural environments, they are much less susceptible to abiotic hydrolysis than most other "environmentally degradable" polymers. For example, although P(HB-*co*-HV) is less readily hydrolyzed under aseptic conditions (33), it generally degrades much more rapidly than polycaprolactone in septic environments.

PHA Biodegradability. One of the attractive features of PHAs products is that they can be biodegraded in a variety of environments including compost, soil, and sea water, under aerobic or anaerobic conditions. The rate of degradation in nature depends on environmental factors such as pH, temperature, moisture level, quantity of microorganisms capable of degrading PHAs, nutrients other than a carbon source, and on characteristics of the PHA material such as its thickness, surface area, molecular weight, crystallinity, and the presence of other components such as a filler. Standard methods for the determination of biodegradability have been developed for international standards organizations. For example, ISO/FDIS14855 is the compostability testing method. It is identical to ASTM D5338 and to the DIN (German) Standard.

Enzymatic Degradation of PHAs. The extracellular and intracellular depolymerases for the degradation of PHAs function differently. In both cases, the substrate is PHA but there is a difference in crystallinity. PHA granules inside the cell are amorphous (the native form). However in extracellular degradation, PHA has been removed from the cell and has been "processed," becoming a more crystalline material with both amorphous and crystalline regions. Intracellular depolymerases demonstrate low activity with semicrystalline PHA and extracellular depolymerases poorly attack amorphous PHA. Extracellular degradation is important in an environmental context as it would be the primary mechanism for the disappearance of a PHA product during composting or wastewater treatment.

Intracellular Degradation. Native PHB granules isolated from *Rhodospirillium rubrum* (34), *Azotobacter beijerinckii* (35), and *Zooglea ramigera* (36) were shown to be self-hydrolyzing while those of *Bacillus megaterium* (34) were not and those of *Alcaligenes eutrophus* (now called *Ralstonia eutropha*) did so at a very low rate (37). Depolymerization in *B. megaterium* requires a heat-labile factor associated with the granule and three soluble components: a heat-stable protein activator, PHB depolymerase, and a hydrolase. The concerted action of the first three components resulted in monomers and 15–20% dimers with the hydrolase converting the dimers to monomers.

Active intracellular depolymerases could lead to "turn over" of accumulated PHAs in the presence of excess carbon and/or PHA catabolism under carbon limitation. When *R. eutropha* containing PHB was placed in a nitrogen-free medium with valeric acid as the sole carbon source, many HB units were replaced by HV units or "turned over" (38). Similarly when cells containing P(HB-*co*-HV) were placed in the same medium with butyric acid as the sole carbon source, the HV content of the cells decreased.

The production of PHA depolymerase is repressed in most PHA-degrading bacteria when an easily degradable carbon source is present. When the carbon substrate is exhausted, the depolymerase synthesis is derepressed. Once the PHA monomers are released, they can be repolymerized, serve as a source of carbon and energy for growth or be excreted. If the microorganism is lacking the hydroxyalkanoic acid dehydrogenase or this enzyme has a low activity, the monomer will accumulate as hydroxycarboxylic acids. It has been demonstrated that this approach can be used to produce a high yield of pure enantiomers (39).

Extracellular Degradation. Although aqueous and enzymatic hydrolyses contribute to degradation in the environment, aqueous hydrolysis is very slow compared to enzymatic hydrolysis. It took about 16 weeks to produce a 30% weight loss of a P(HB-*co*-9%4HB) film (12 mm in diameter and 70 μm in thickness) in 0.01 *M* phosphate buffer at 70°C and pH 7.4 (16). Because of random hydrolytic chain scission, the number-average molecular weight (M_n) decreased from 226,000 to 13,000 in 55 days, with little change in actual weight (8%). At day 110, the extent of weight loss had increased to 30%. Degradation (usually monitored as weight loss) is typically much more rapid in the presence of active microorganisms. For example, a 75-μm-thick film completely degraded in anaerobic sewage in 1 week, in a well-watered soil at 25°C in 12 weeks, and in an estuarine sediment at 20°C in 8 weeks (40).

An initial sequence of events for a PHB film buried in a well-watered soil has been described (40). The first step is a wetting-out process, in which aqueous hydrolysis is probably responsible for the increase in the number of hydroxyl and carboxylic acid groups at the surface. After 1 week, the plastic surface becomes more hydrophilic. Bacterial and fungal colonization then occurs. Microbial attack (primarily due to extracellular enzymes) takes place at the surface (41,42) which becomes more pitted, increasing the surface area for degradation. Surface area is further increased by blending with a more rapidly biodegradable polymer such as starch. In a P(HB-*co*-19%HV)–starch composite, the degradation rate increased with the starch content (43). Starch was lost more rapidly than the P(HB-*co*-19%HV) starting at both surfaces, then toward the center. As the starch was removed, a larger internal surface area was available for PHA degradation. At least 31vol% starch granules is required to have continuity of all internal surfaces in a polyethylene–starch composite (44).

The mechanism of extracellular degradation of PHA is not yet well understood. A wide variety of microorganisms (fungi, aerobic and anaerobic bacteria) have been implicated but only *Pseudomonas lemoignei*, *Alcaligenes faecalis*, and *Comamonas* sp. have been studied in detail. Production of extracellular PHA depolymerases is induced by the presence of PHA as the sole carbon source. Generally, a PHB depolymerase acts from the hydroxyl terminus to form dimers (or trimers, depending on the depolymerase) and a trace amount of monomer. An

oligomer hydrolase further hydrolyzes the dimers (or trimers but not the polymeric material) to monomers which can then be used as a source of carbon and energy. Since the depolymerase acts at the hydroxyl end (sequentially removing monomers, dimers, or trimers), there should be a very slow change in the M_n. The rate of weight loss should not depend on the initial molecular weight and it has been shown that high and low molecular weight PHBs were indeed degraded at the same rate (41). There is no significant change in the molecular weight of the bulk of a film or blow-molded product as degradation takes place at the surface.

Although extracellular depolymerases act on semicrystalline PHA, the degradation rate has been shown to decrease with increasing crystallinity of PHB films (45). For a blow-molded, P(HB-*co*-16%HV) product (a 20-μm cross section was exposed to partially purified PHB hydrolase from *Penicillium funiculosum*), the degradation rate is faster at the less crystalline surface than at the more crystalline core (42). Furthermore, it has been shown that the amorphous regions on the surface of PHB films are degraded preferentially whereas microbial colonization takes place at spherical holes which tend to be at the crystal centers and at the boundary between spherulites (46).

The enzyme specificity depends to some extent on the composition of the PHA which induced the degradation. In general, enzymes induced by SCL PHAs will not act on MCL PHAs and those induced by MCL PHAs will not act on SCL PHAs. The specificity based on the composition of the PHA inducer is not as clear within each group of depolymerases. P(HB-*co*-HV) was degraded more slowly than PHB, and P(4HB) was degraded more quickly than PHB (41) by PHB-induced depolymerases. However, PHB, PHV, and P(HB-*co*-HV) were degraded at comparable rates by purified PHV depolymerase (PHV as sole carbon source) from *P. lemoignei* (47). It has been suggested that P(4HB) degraded faster because 4HB monomers were more sterically accessible to the enzyme than were 3HB monomers (41).

PHA Synthesis

Synthetically, PHB is produced from racemic 3-butyrolactone and P(HB-*co*-HV) is made from a mixture of 3-butyrolactone and 3-valerolactone, with triethylaluminum and water as catalyst (48). Although the stereospecificity of the resulting polymer can be controlled to a certain extent by adjusting the ratio of triethylaluminum and water, synthetic PHAs are usually optically inactive and hence only partially biodegradable.

SCL PHA Biosynthesis. During PHB synthesis, 3-ketothiolase catalyzes the condensation of two acetyl-CoAs to produce acetoacetyl-CoA which is stereospecifically reduced by an independent reductase to produce D(−)-3-hydroxybutyryl-CoA (35,49) (Fig. 3). First elucidated in *A. beijerinckii*, the presence of this synthetic route was confirmed in *R. eutropha*. These four-carbon monomers are then added to the growing PHB chain by a polymerase. If propionic acid is supplied during the fermentation, some of the acid is converted to proprionyl-CoA. A portion of this proprionyl-CoA is condensed with acetyl-CoA via 3-ketothiolase to produce five-carbon monomers (Fig. 3b). This is the most common pathway of P(HB-*co*-HV) production. Most PHB-accumulating bacteria will

produce P(HB-*co*-HV). Since acetate is needed for this synthetic route and some propionic acid is decarboxylated before monomer synthesis, usually less than 50% of the monomers will be HV even if a feed of pure propionic acid is added. This yield can be increased in *R. eutropha* by decreasing the dissolved oxygen concentration in the bioreactor during the accumulation phase (50).

High yields of HV are obtained when pentanoic acid is used because acetyl-CoA is no longer required since pentanoic acid is metabolized directly to L-(3)-hydroxyvaleryl-CoA which is subsequently racemized (at least in *R. eutropha*) to D-(3)-hydroxyvaleryl-CoA (51) (Fig. 3b). Although some acetate is produced, leading to HB monomer formation, PHAs with greater than 90% HV content can be obtained. SCL PHA producers have not been reported to accumulate monomers with side chains longer than C_2 or C_3 but can produce P(3HB-*co*-4HB) when fed 4-hydroxybutyric acid or 1,4-butanediol. *R. eutrophus* accumulates terpolyesters of 3HB, 3HV, and 5HV monomers when fed a mixture of pentanoic and 5-chloropentanoic acids. Even among SCL-accumulating microorganisms, there may be differences in the PHA synthetic pathway. For example, in *R. rubrum*, L-(+)-3-hydroxybutyryl-CoA is racemized to D-(−)-3-hydroxybutyrl-CoA using enoyl-CoA hydrases.

In most SCL PHA-accumulating bacteria, high intracellular levels of NADH and acetyl-CoA greatly stimulate the rate of PHA synthesis. Thus, if the growth rate is limited by a nutrient other than the source of carbon and energy, PHA is accumulated in the cell. By definition, the PHB content of the cells is stable under balanced growth conditions, while carbon and energy limitations increase depolymerase activity, leading to a decrease in cellular PHA content.

MCL PHA Biosynthesis. MCL PHA was first identified in mixed cultures in activated sludge (52) and marine sediments (53). The unusual manner in which these materials crystallized led to some debate as to whether they were copolymers or mixtures of homopolymers (54). The breakthrough in MCL PHA technology came when it was discovered that *Pseudomonas oleovorans* would accumulate MCL PHA when fed with the appropriate alkane, alkanoate, or alkanol (30,55,56). Shortly thereafter, several other ribosomal RNA homology group I pseudomonads were found that could also accumulate MCL PHA from the above substrates. Many pseudomonads can produce MCL PHA from simple carbohydrates such as glucose (57,58) although the yield is usually much lower. This led to the belief that MCL PHA could be derived from fatty acid synthesis as well as fatty acid degradation (59).

In fatty acid synthesis or degradation (Fig. 4), once the substrate is in the form of alkanoyl-CoA, a two-step process involving a 3-ketoacyl-CoA reductase and a PHA synthase occurs. The reduction step requires NADPH. A suitable supply of intracellular substrate appears to be the key factor controlling the rate of biosynthesis. If *P. oleovorans* is fed octanoate, it accumulates much more PHA than if hexanoate or dodecanoate are added. Nevertheless, the synthase is relatively nonspecific. *P. oelovorans* can accumulate polymers in which the side chain of the monomers contain double bonds, branches, cyclic structures, or even halogen atoms if the appropriate substrate is supplied.

Much less polymer is produced from carbohydrates (ie fatty acid synthesis) than from alkanes or related substrates (ie fatty acid degradation). This is possibly due to a shortage of acceptable substrate for the synthase. Pseudomonads

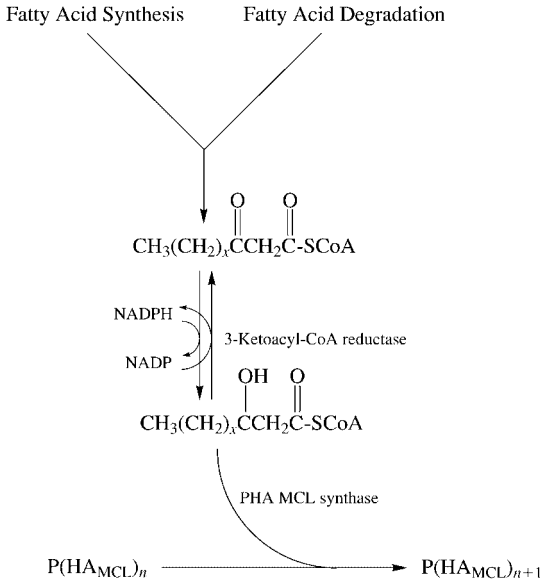

Fig. 4. Biosynthesis of MCL PHA. Substrate may result from fatty acid degradation, or from fatty acid synthesis. The substrate must be transferred from the acyl carrier protein (ACL) to Coenzyme A (CoA) if derived from fatty acid synthesis.

that produce PHA from glucose, accumulate a polymer where 3-hydroxydecanoate units dominate. They also frequently use 3-hydroxydecanoate as an intermediate metabolite for the synthesis of other materials such as biosurfactants (60). Blocking these pathways could result in increased polymer production.

The intracellular PHA depolymerase system can act very efficiently in MCL PHA producers. Carbon limitation often leads to extremely rapid depolymerization. The diversity of metabolic machinery among PHA-accumulating microorganisms indicates that unusual and potentially valuable PHA copolymers await discovery.

Synthesis in Transgenic Plants. PHB can be synthesized in plants in which the bacterial reductase and polymerase genes have been introduced. Although virtually all organisms possess the third gene in the SCL PHA pathway, coding for 3-ketothiolase, its activity and specificity vary, and it may not be present in all eucaryote organelles. Production is usually increased by cloning the 3-ketothiolase gene with the other two. Although transgenic plants are easily created, productivity remains problematic. The SCL PHA pathway was first cloned into *Arabidopsis thaliana*, the *Escherichia coli* of plant biotechnology (61). The yield was low, 0.1% dry weight, and the plants were stunted. However, granules similar to those found in bacteria were produced. The initial cloning strategy targeted the cytoplasm and granules were also found in the cell nucleus. Subsequent work has targeted the plastid which is also the site of starch and oil synthesis in plants. This has resulted in increased yields of up to 14% dry weight in the leaves of *A. thaliana*. These plants grew well but were chlorotic probably because of large amounts of PHB in the chloroplasts. Present research centers on oil and starch producing plants since these are already adapted to have large amounts of

storage material in the plastids (62), but other strategies are also being assessed. Although MCL PHA has been produced in transgenic plants (63), yield is low, partially because of a lack of understanding of the link between fatty acid synthesis and MCL PHA synthesis.

Separation of PHA from Biomass

All separation processes to date have been developed for microbial rather than plant biomass but many of these approaches could also be applied to recovery of PHA from plants. As a first step in the recovery from microbial biomass, the cells are separated from the fermentation broth usually by centrifugation or flocculation. In the latter case, the pH of fermentation broth is adjusted to 9 and the broth is heated; the pH is readjusted to 5 (64), and the biomass is recovered by centrifugation or filtration. The wet biomass may be freeze- or spray-dried to remove water. Processes to separate the intracellular PHA from the rest of the microbial biomass may be divided into two categories: (*1*) selective solubilization of PHA in an organic solvent, leaving the majority of the other biomass components in suspension and (*2*) destruction (eg enzymatic solubilization) of cellular components other than PHA, leaving the PHA granules in suspension. Physical treatments such as drying, heating, freezing and thawing, repeated centrifugation, and exposure to acids and organic solvents may result in crystallization of native PHA.

Solvent Extraction of PHAs. The majority of the patented separation processes describe the extraction of PHB from microbial biomass using organic solvents such as chlorinated hydrocarbons (eg chloroform or 1,2-dichloroethane), azeotropic mixtures [eg 1,1,2-trichloroethane with water (65)]; chloroform with methanol, ethanol, acetone, or hexane (66), and cyclic carbonates [eg hot (120–150°C) ethylene carbonate or 1,2-propylene carbonate (67)] in which the polymer is soluble. With the wider variety of PHAs which can be produced today, the choice of solvents should be carefully considered. In general, solvents which are suitable for PHB should be equally good for any SCL and MCL PHA. The reverse may not be true. For example, while semicrystalline PHB is insoluble in acetone, MCL PHA will dissolve in it.

Cells may be pretreated to make the polymer more accessible to the extraction solvent. This may involve washing in a hydrophilic solvent in which the polymer is insoluble (such as methanol or acetone for SCL PHA and methanol for MCL PHA), or physical disruption such as grinding, wet-milling, French press, or freezing and thawing cycles. Pretreatment with acetone has been shown to have the added advantage of removing certain polar lipid impurities and increasing the amount of PHB recovered (68).

After solvent extraction, the polymer solution is separated from the cellular residue by filtration or centrifugation. PHB is then precipitated from the chlorinated hydrocarbons or azeotropic mixtures with a cold nonsolvent, such as methanol. In the cases of ethylene carbonate and 1,2-propylene carbonate, the majority of the PHB precipitates on cooling (67).

PHA solutions become too highly viscous to process easily at concentrations of greater than 5 wt%. As a result, large amounts of solvent are required to obtain sufficiently dilute solutions to enable easy separation. A significant portion of

the PHB may remain unextracted in the biomass (68). Solvent extraction is not considered economical unless cheap solvent and energy for solvent recovery are available. However, solvent extraction is useful when the PHA content of the biomass is low or when high purity is required.

Although thermal degradation of PHB in air or a nitrogen atmosphere has been well studied (69), there are few examples which show that PHB degrades in organic solvents. The molecular weight is known to decrease in propylene carbonate and ethylene carbonate at 110–140°C (67), in chloroform–methanol mixtures at room temperature (70), and in methylene chloride, chloroform, and 1,2-dichloroethane at their boiling points (68).

Solvent extraction is a commonly used laboratory technique for PHA recovery, especially for molecular weight determination. Usually, methanol- (or ethanol-) pretreated, lyophilized biomass is heated in chloroform under reflux conditions for about 1 h. The polymer solution is recovered by filtration or centrifugation, and the polymer is precipitated in cold ethanol or methanol. The polymer may be further purified by redissolving in chloroform and reprecipitating in cold ethanol. It should be noted that about 25% of the "original" molecular weight (determined by chloroform extraction under ambient conditions) is lost when refluxed in chloroform for 1 h (68).

Removal of Cellular Components Other Than PHA.

Enzymatic Methods. Classical enzymatic treatment (involving lysozyme, proteinases, DNAses, etc) with or without a surfactant step can be used to remove the non-PHA biomass (71). Biologists have used these methods to prepare native PHB granules to study intracellular enzymatic degradation. On a commercial level, a process in which the fermentation broth may be first heated to 80°C to denature DNA and some proteins has been described (72). A series of enzymes [such as lysozyme, phospholipase, lecithinase, or alcalase (proteinase)] are then used to obtain a product which is 90–95% pure with 6–7% proteins and some peptidoglycan as major impurities. There may be a final wash with hydrogen peroxide to whiten the product. This was the method used for the production of P(HB-*co*-HV) (73), which was sold under the trade name Biopol by Zeneca, and later by Monsanto. When PHA granules recovered by enzymatic treatment are freeze-dried, they have a hard, crystalline shell and an amorphous core (6).

Chemical Methods. Strong oxidizing agents such as sodium hypochlorite at pH 10 have been used to dissolve the cellular biomass under conditions which result in significant loss of PHA molecular weight. However, by optimizing the operating conditions, PHB with a weight-average molecular weight of 600,000 g/mol and 95% purity has been obtained from *R. eutropha* biomass containing 50% PHB with an initial molecular weight of 1,200,000 g/mol. When the biomass is pretreated with a surfactant, less contact time with hypochlorite is needed to obtain PHB with the same purity. This allows an even higher molecular weight (800,000 g/mol) to be obtained (74). Never-dried granules obtained by surfactant-hypochlorite treatment also have an external crystalline shell and an amorphous core (75). Similar PHB recovery, molecular weights, and purity may be obtained when sodium hypochlorite is omitted and only an NaOH solution at pH 13 is used.

Physical Methods. Although there are many methods (eg reciprocating pump, ball mill) to physically disrupt microbial cells, there have been few processes which are based on these principles proposed for the large-scale recovery of PHAs. A process in which a biomass suspension was heated to 220°C

under nitrogen in an autoclave and then forced through a fire-jet into a tank of cold water has been patented (76). Cell breakage occurred, releasing PHB granules which were suspended in 50% aqueous acetone to remove lipids and to cause flocculation.

Commercial Production

PHB remained an academic curiosity until the fifties and sixties when W.R. Grace and Co. in the United States produced small quantities for commercial evaluation. They obtained patents for production processes and manufactured articles such as sutures and prosthetic devices (77) but eventually abandoned the project because of low PHB yields and difficulties in the separation process. About 10 years later, Imperial Chemical Industries (ICI) began a program in PHA production and product development. They patented (78) the first commercial process to produce SCL PHA copolymer (P(HB-*co*-HV)).

Choice of Production Strain and Process. The most important economic considerations are substrate costs, reactor productivity, and separations costs. SCL PHA can be produced from hydrolyzed starch (glucose), lactose (recombinant *E. coli* on cheese whey), cane or beet molasses (*Azotobacter vinelandii* or *Alcaligenes latus* on sucrose), waste wood (fermented hydrolyzed hemicellulose), methanol, and even mixtures of hydrogen and carbon dioxide (*R. eutropha*). Addition of an appropriate cosubstrate such as propionic acid results in P(HB-*co*-HV) synthesis in any of these processes although the percentage of HV can vary considerably depending on the bacterial strain. High productivity has been reported for several of these substrates. Using *R. eutropha* growing on glucose, 164 g/L of biomass containing 76% PHB has been produced in a fed-batch process in only 50 h (79). Densities well in excess of 100 g/L have been reported for fed-batch processes using *E. coli* strains with multicopy plasmids containing the key SCL PHA synthetic genes (80) as well as for methylotrophs growing on methanol (81). In recombinant *E. coli* strains, PHB content is frequently reported as being in excess of 90% of the biomass dry weight, making the separation process much simpler.

MCL PHA. The highest productivity results from using octanoic or nonanoic acids, but these are toxic at concentrations of several grams per liter and their low solubility may limit the growth rate because of poor mass transfer. Sodium salts of these acids are much more soluble but the final product concentration in fed-batch culture is limited by the accumulation of toxic concentrations of sodium ions in the medium. In any event, the present cost of both the salts and the acids prohibit their use in commercial production. Most microorganisms which make MCL PHA produce lipases and grow well on vegetable oils but the lipase concentration may limit the production rate. A *Pseudomonas putida* strain has been grown in fed-bath culture from oleic acid (a fatty acid commonly found in plant oils) to a biomass concentration of 92 g/L containing 45% PHA in 26 h (82). Because of their low density, these PHAs float to the surface after breakage of the bacterial cell and can thus be easily and cheaply separated from the rest of biomass.

Commercial Production Methods. Tredegar Industries has used recombinant *E. coli* to produce over 100 g/L of biomass containing at least 80% PHB by dry weight at the pilot-scale level. Mild detergent treatment and washing

steps followed by spray drying result in a white product which is 98% pure (83).

Fermentation and separation processes were developed for the pilot-scale production of PHB using an *A. latus* strain as well as its further processing into consumer products. Up to 1 ton/week of PHB was produced in Austria in a 15,000-L bioreactor (84). This technology is currently owned by the German company Biomer. The Biomer fermentation process is relatively simple with multistaging from the petri dish to a shake flask to a small fermentor which is then used to inoculate the production reactor (Fig. 5a). If sufficient carbon source (molasses) is added during the fed-batch process, up to 60 g/L of PHB may be obtained. The

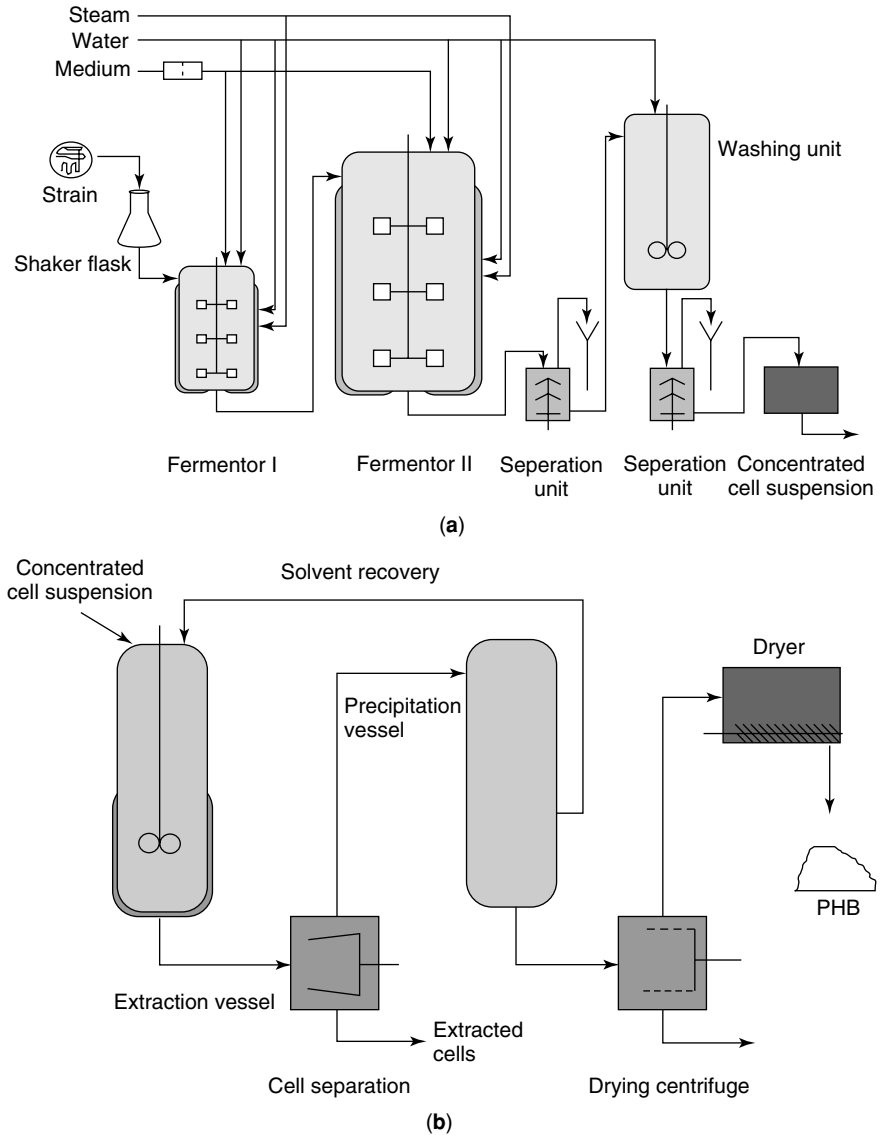

Fig. 5. (**a**) Biomer PHB fermentation process. (**b**) Biomer PHB separation process.

resulting biomass is washed in water. The concentrated cell suspension is then subjected to methylene chloride extraction (Fig. 5b). The resulting slurry is separated in a decanter. The solvent phase is then injected into hot water in a precipitation vessel where methylene chloride evaporates and PHB precipitates. After water removal (drying), PHB can then be processed into a marketable product.

Biopol [P(HB-*co*-HV)] has been produced from glucose and propionic acid in 35,000-L airlift reactors and in up to 200,000-L stirred tank reactors (85). Phosphate limitation (after about 60 h of growth) is used to trigger the accumulation phase in a strain of *R. eutropha*. Phosphate limitation was found to give better results than nitrogen limitation (86). Although solvents (chloroform or methylene chloride extraction after a hot methanol wash) may be used when high purity is required, the P(HB-*co*-HV) is usually obtained by treatment of the biomass with a series of surfactants, enzymes, and possibly oxidizing agents to dissolve the non-PHA biomass. The product is essentially a latex that may then be washed, spray-dried, compounded with nucleating agents and plasticizers, and extruded in the form of pellets. Until recently, several grades of Biopol were available at a cost of about 17.60/kg. Monsanto reported that Biopol production costs were 25–30% greater than those of polyolefins and has discontinued production.

Copersucar (Sao Paulo, Brazil) currently manufactures up to 5 tons of PHB per month in a fed-batch process using a 20,000-L fermentor equipped with a Frings aeration system. A *Burkholderia* sp. or *R. eutropha* mutant lacking PHA depolymerase is grown on inverted sugar and mineral salts. The PHB accumulation phase is triggered by phosphate limitation. The PHB is extracted in a mixture of boiling alcohols (a waste from ethanol distillation) under reflux. The cellular debris is removed and the polymer precipitates on cooling. Solvent is recovered by injecting the solvent/PHB paste on boiling water under vaccum. Copersucar may be able to sell PHB much more cheaply than its competitors as it has access to inexpensive carbon (sucrose) and energy (bagasse) sources.

Future Prospects

Cost of production is not a major consideration if PHA is to be used exclusively for specialty applications. However, if PHA is to be economically competitive with synthetic plastics, it must be produced on a far larger scale than any other aerobically produced microbial product. An additional problem arises from the fact that PHAs are intracellular products. Thus the amount that can be produced per cell has physical limitations.

In a typical PHA fermentation process, the cost is divided fairly evenly between substrate cost, capital, and operating expenditures in the fermentation process and the cost of separating the PHA from the microbial biomass. Typically the yield of dry biomass from a hexose sugar such as glucose is about 42% for *R. eutropha*. If the final biomass contains 75 wt% by weight of recoverable PHA, then the yield of PHA from the total amount of substrate supplied is about 32%. Thus, if carbon substrate was available at $500/t, the cost of the carbon source alone would be $1560/t, making the product twice as expensive as bulk synthetic plastics.

New methods such as the incorporation of temperature-sensitive plasmids for the production of autolytic enzymes should reduce separation costs. The direct

use of PHA-containing bacteria in melt processing (ie no separation process apart from water removal) has also been proposed. However, even assuming a negligible cost for the carbon source by using a waste material such as cheese whey permeate, and neglecting the separation costs, studies have shown that PHA produced in bioreactors could not be economically competetive with synthetic bulk plastics in the foreseeable future. The volumetric production rate cannot compete with chemical processes and this rate is limited by the oxygen transfer rate of present day bioreactors. New technologies must be developed for commercial PHA production.

In vitro synthesis of PHA granules from activated substrates may eventually become commercially feasible. In *R. eutropha*, the maximum rate of PHA synthesis occurs early in accumulation phase and deteriorates slowly thereafter. One would therefore expect that the maximum amount of PHA accumulation would depend on enzymatic activity or on NADPH or substrate supply. However the most detailed published study on this process points to a physical limitation (86) where polymer synthesis slows to a virtual stop simply because there is no more space available. If this is indeed the case, then the way around such a limitation is to produce the PHA granules outside the cells. This has been achieved (87,88). Commercial exploitation of this process requires a source of the biosynthetic enzymes (easily achievable through molecular biological techniques), substrates, NADP, and a method for NADP reduction already used in commercial steroid transformation processes. This would eliminate or greatly reduce separation costs. The present economic and technical barrier to this process is the lack of an inexpensive method to link coenzyme A to the appropriate carboxylic acid.

It is likely that in the near future, starch, oilseed, or leguminous plants will be used to produce PHAs. Other plant materials such as cellulose and starch are already used to make plastics or plastic-like materials. Hemicelluloses have been used directly and/or converted to organic acids for PHA production at a laboratory scale. Thus any waste from the separation of PHA from plants could be hydrolyzed, fermented to lactic, acetic, and propionic acids, and then fed into bioreactors for the production of specialty PHAs. Polylactides and other polymers of organic acids could be produced in the same plant as could polysaccharides. Plant materials may become a major source of plastic materials in the next century with PHAs leading the way.

BIBLIOGRAPHY

1. L. Lemoigne, *Bull. Soc. Chim. Biol. (Paris)* **8**, 770–782 (1926).
2. W. H. Carothers, in H. Mark and G. S. Whitby, eds., *Collected Papers of Wallace H. Carothers*, Interscience Publishers, New York, 1946.
3. J. Davis, *Appl. Microbiol.* **4**, 301–304 (1964).
4. Y. Doi and co-workers, *Macromolecules* **21**, 2722–2727 (1988).
5. Y. Doi and co-workers, *Makromol. Chem., Rapid Commun.* **8**, 631–635 (1987).
6. C. Lauzier, J.-F. Revol, and R. H. Marchessault, *FEMS Microbiol. Rev.* **103**, 299–310 (1992).
7. D. M. Horowitz and co-workers, *Nature* **363**, 23 (1993).
8. P. Kopinke, M. Remmler, and K. Mackenzie, *Polym. Degrad. Stab.* **52**, 25–38 (1996).
9. I. Noda, R. H. Marchessault, and M. Terada, in J. Mark, ed., *Polymer Data Handbook*, Oxford University Press, New York, 1999, pp. 586–599.

10. H. Brandl and co-workers, *Adv. Biochem. Eng. Biotechnol.* **41**, 77–93 (1990).
11. H. Mitomo, P. Barham, and A. Keller, *Polym. J.* **19**, 1241–1253 (1987).
12. K. D. Gagnon and co-workers, *Macromolecules* **25**, 3723–3728 (1992).
13. Y. Doi, H. Abe, E. Shimamura, M. Hiramitsu, and S. Nakamura, in J. C. Salamone, ed., *Polymeric Materials Encyclopedia*, CRC Press, Inc., Boca Raton, Fla., 1996, pp. 4304–4309.
14. S. Y. Lee, *Biotechnol. Bioeng.* **49**, 1–14 (1996).
15. Y. Doi, *Microbial Polyesters*, VCH Publishers, Inc., New York, 1990.
16. P. Barham and co-workers, *J. Mater. Sci.* **19**, 2781–2794 (1984).
17. T. Bluhm and co-workers, *Macromolecules* **19**, 871–2876 (1986).
18. M. Kunioka, A. Tamaki, and Y. Doi, *Macromolecules* **22**, 694–697 (1989).
19. A. Cao and co-workers, *Macromol. Chem. Phys.* **198**, 3539–3557 (1997).
20. *Biopol Nature's Plastic: Properties and Processing*, Monsanto, St. Louis, Mo., 1996, pp. 13–15.
21. H. Brandl and co-workers, *Can. J Microbiol.* **41**(1), 143–153 (1995).
22. H. Verhoogt, B. Ramsay, and B. Favis, *Polymer* **35**, 5155–5169 (1994).
23. L. Zhang and co-workers, *Polymer* **38**, 6001–6007 (1997).
24. M. Grimaldi and co-workers, *J. Mat. Sci.* **31**, 6155–6162 (1996).
25. D. Seebach and M. Zueger, *Hel. Chim. Acta* **65**, 495 (1982).
26. K. Sudesh, H. Abe, and Y. Doi, *Prog. Polym. Sci.* **25**, 1503–1555 (2000).
27. R. M. Lafferty, B. Korsatko, and W. Korsatko, in H.-J. Rehm and G. Reed, eds., *Biotechnology*, Vol. **6**, VCH Publishers, Inc., Weinheim, 1988, pp. 135–176.
28. R. Sodain and co-workers, *Tissue Eng.* **6**, 183–188 (2000).
29. U.S. Pat. 5451456 (Sept. 19, 1995), R. H. Marchessault, P. F. Lepoutre, and P. E. Wrist (to Pulp and Paper Research Institute of Canada).
30. R. G. Lageveen and co-workers, *Appl. Environ. Microbiol.* **54**, 2924–2932 (1988).
31. P. Shin, M. Kim, and J. Kim, *J. Environ. Polym. Degrad.* **5**, 33–39 (1997).
32. U. Pagga, D. Beimborn, and M. Yamamoto, *J. Environ. Polym. Degrad.* **4**, 173–178 (1996).
33. M. Yasin and B. J. Tighe, *Biomaterials* **13**, 9–16 (1992)
34. J. M. Merrick and M. Doudoroff, *Nature (London)* **189**, 890–892 (1961).
35. A. J. Anderson and E. A. Dawes, *Microbiol. Rev.* **54**, 450–472 (1990).
36. T. Saito and co-workers, *FEMS Microbiol. Rev.* **103**, 333–338 (1992).
37. H. Hippe and H. G. Schlegel, *Arch. Mikrobiol.* **56**, 278–299 (1967).
38. Y. Doi and co-workers, *FEMS Microbiol. Lett.* **65**, 165–170 (1990).
39. S. Y. Lee, Y. Lee, and F. Wang, *Biotechnol. Bioeng.* **65**, 363–368 (1999).
40. P. A. Holmes, in D. C. Basset, ed., *Developments in Crystalline Polymers*, Elsevier, New York, 1988, pp. 1–65.
41. Y. Doi and co-workers, *Macromolecules* **23**, 26–31 (1990).
42. M. Parikh, R. A. Gross, and S. P. McCarthy, *Polym. Mat. Sci. Eng.* **66**, 408–410 (1992).
43. B. A. Ramsay and co-workers, *Appl. Environ. Microbiol.* **59**, 1242–1246 (1993).
44. R. P. Wool, J. S. Peanasky, J. M. Long, and S. M. Goheen, in S. A. Barenberg, J. L. Brash, R. Narayan, and A. E. Redpath, eds., *Degradable Materials*, Proceedings of the First International Scientific Concensus Workshop, CRC Press, Inc., Boca Raton, Fla., 1990.
45. Y. Kumagai, Y. Kanesawa, and Y. Doi, *Makromol. Chem.* **193**, 53–57 (1992).
46. H. Nishida and Y. Tokiwa, *J. Environ. Polym. Degrad.* **1**, 65–80 (1993).
47. B. Müller and D. Jendrossek, *Appl. Microbiol. Biotechnol.* **38**, 487–492 (1993).
48. S. Bloembergen, D. A. Holden, and R. H. Marchessault, *Polym. Prepr.* **29**, 594–595 (1988).
49. A. Steinbüchel, in D. Byrom, ed., *Biomaterials*, Macmillan, New York, 1991, pp. 124–213.

50. G. Lefebvre, M. Rocher, and G. Braunegg, *Appl. Environ. Microbiol.* **63**, 827–833, (1997).
51. Y. Doi and co-workers, *J. Chem. Soc., Chem. Commun.* 1635–1636 (1987).
52. L. L. Wallen and W. K. Rohwedder, *Environ. Sci. Technol.* **8**, 576–579 (1974).
53. R. H. Findlay and D. C. White, *Appl. Environ. Microbiol.* **45**, 71–78 (1983).
54. R. H. Marchessault, H. Morikawa, and J.-F. Revol, *Macromolecules* **17**, 1882–1884 (1984).
55. M. J. de Smet and co-workers, *J. Bacteriol.* **154**, 870–878 (1983).
56. H. Brandl and co-workers, *Appl. Environ. Microbiol.* **54**, 1977–1982 (1988).
57. A. Timm and A. Steinbüchel, *Appl. Environ. Microbiol.* **56**, 3360–3367 (1990).
58. G. W. Haywood and co-workers, *Appl. Environ. Microbiol.* **56**, 3354–3359 (1990).
59. G. N. M. Huijberts and co-workers, *J. Bacteriol.* **176**, 1661–1666 (1994).
60. F. G. Jarvis and M. J. Johnson, *J. Am. Chem. Soc.* **71**, 4124–4127 (1949).
61. Y. Poirier and co-workers, *Science* **256**, 520–523 (1993).
62. C. Nawrath, Y. Poirier, and C. Somerville, *Mol. Breed.* **1**, 105–122 (1995).
63. V. Mittendorf and co-workers, *Proc. Natl. Acad. Sci. U.S.A.* **95**, 13397–13402 (1998).
64. U.S. Pat. 4358583 (Sept. 11, 1982), J. Walker and J. R. Whitton (to Imperial Chemical Industries, Plc).
65. U.S. Pat. 4705604 (Nov. 10, 1987), N. Vanlautem and J. Gilain (to Solvay and Co.).
66. U.S. Pat. 4562245 (Dec. 31, 1985), R. F. Stageman (to Imperial Chemical Industries, Plc).
67. U.S. Pat. 4101533 (July 18, 1978), R. M. Lafferty and E. Heinzle (to Agroferm AG).
68. J. A. Ramsay and co-workers, *Biotechnol. Tech.* **8**, 589–594 (1994).
69. N. Grassie, E. J. Murray, and P. A. Holmes, *Polym. Degrad. Stab.* **6**, 95–103, (1984).
70. A. H. de Mola, M. Marx-Figini, and R. V. Figini, *Makromol. Chem.* **176**, 2655–2667 (1975).
71. R. Greibel, Z. Smith, and J. M. Merrick, *Biochemistry* **7**, 3767–3681 (1968).
72. U.S. Pat. 4910145 (Mar. 20, 1990), P. A. Holmes and G. B. Lim (to Imperial Chemical Industries, Plc).
73. D. Byrom, in E. A. Dawes, ed., *Novel Biodegradable Microbial Polymers*, Kluwer Academic Publishers, Dordrecht, the Netherlands, 1990, pp. 113–117.
74. J. A Ramsay and co-workers, *Biotechnol. Tech.* **4**, 221–226 (1990).
75. C. A. Lauzier and co-workers, *Tappi J.* **76**, 71–77 (1993).
76. Eur. Par. Appl. 46335 (Feb. 24, 1980), P. A. Holmes and E. Jones (to Imperial Chemical Industries, Plc).
77. U.S. Pat. 3225766 (Dec. 28, 1965), J. N. Baptist and J. B. Ziegler (to W.R. Grace and Co.).
78. Eur. Pat. 69497 (Apr. 15, 1987), P. A. Holmes, L. F. Wright, and S. H. Collins (to Imperial Chemical Industries, Plc).
79. B. S. Kim and co-workers, *Biotechnol. Bioeng.* **43**, 892–898 (1994).
80. B. S. Kim, S. Y. Lee, and H. N. Chang, *Biotechnol. Lett.* **14**, 811–816 (1992).
81. D. Bourque, Y. Pomerleau, and D. Groleau, *J. Microbiol. Biotechnol.* **44**, 367–376 (1993).
82. G. N. M. Huijberts, H. van der Wal, R. A. Weusthuis, and G. Eggink, in *Abstract 5th International Symposium on Bacterial Polyhydroxyalkanoates*, Davos, Switzerland, Aug. 1996. (Abstract).
83. F. Merchant, D. E. Dennis, R. Merchant, and C. F. Batrell, in *4th International Symposium on Bacterial Polyhydroxyalkanoates*, Montreal, Canada, Aug. 1994. (Abstract).
84. U. J. Hänggi, in Ref. 72, pp. 65–70.
85. D. Byrom, *Int. Biodeter. Biodegrad.* **31**, 199–203 (1993).
86. D. G. H. Ballard, P. A. Holmes, and P. J. Senior, *Recent Advances in Mechanistic and Synthetic Aspects of Polymerization* **215**, 293–314 (1987).
87. R. J. Griebel and J. M. Merrick. *J. Bacteriol.* **108**, 782–789 (1971).

88. T. U. Grengross and D. P. Martin, *Proc. Natl. Acad. Sci. U.S.A.* **92**, 6279–6283 (1995).

BRUCE A. RAMSAY
Polyferm Canada,
JULIANA A. RAMSAY
Queen's University

POLY(ACRYLIC ACID). See ACRYLIC (AND METHACRYLIC) ACID POLYME.

POLY(CYCLOHEXYLENE TEREPHTHALATE).
See CYCLOHEXANEDIMETHANOL POLYESTERS.

POLY(ETHYLENE-NORBORNENE). See ETHYLENE-NORBORNENE COPOLYMERS.

POLY(METHACRYLIC ACID). See ACRYLIC (AND METHACRYLIC) ACID POLYME.

POLY(TRIMETHYLENE TEREPHTHALATE)

Introduction

Poly(trimethylene terephthalate) (PTT, also abbreviated as 3GT) is an aromatic polyester made by the melt polycondensation of 1,3-propanediol (PDO) with either terephthalic acid (TPA) or dimethyl terephthalate (DMT). Although available commercially only since 1998, it was one of the three polyesters first synthesized by Whinfield and Dickson (1) in 1941. Two of which, the so-called even-numbered poly(ethylene terephthalate) (PET) and poly(butylene terephthalate) (PBT) for the number of methylene units in their chemical structures, are well-established high volume polymers. However, the odd-numbered PTT remained an obscure polymer. It was never commercialized until recently because PDO was very expensive and was available only as a small volume fine chemical.

In the early 1970s, there were interests to commercialize PTT (2–4); however, they were short-lived. Despite making significant progress in lowering PDO manufacturing cost, the economics was still not good enough. Interest was revived in the late 1980s when Shell Chemical Co. (5) and Degussa (6) had breakthroughs in PDO manufacturing technologies. Shell began selling PTT in 1998 and completed building a new PDO plant (7). It was followed by DuPont announcing the building of a PTT plant by first using PDO acquired from Degussa, and later using PDO from bioengineering route (currently under development) when it becomes available (8). More than half a century after it was first synthesized, PTT finally joined PET and PBT and became a commercial reality. PTT from Shell is trademarked as Corterra polymer and DuPont's trademark is Sorona 3GT.

Encyclopedia of Polymer Science and Technology. Copyright John Wiley & Sons, Inc. All rights reserved.

1,3-Propanediol Monomer

1,3-Propanediol [504-63-2], also called trimethylene glycol, is a colorless, clear liquid with a boiling point of 214°C. The traditional synthesis route, practiced by Degussa, is to hydrate acrolein (9) under pressure with an acid catalyst such as acidic ion-exchange resin into 3-hydroxypropanal (3-HPA). This intermediate is not isolated. The aqueous solution is hydrogenated into PDO using Raney nickel catalyst. A new commercial route developed by Shell uses ethylene oxide (EO) as the starting raw material. Ethylene oxide is first hydroformylated into 3-HPA, using a combination of CO and H_2 synthesis gas with cobalt catalyst (5). 3-HPA is concentrated and hydrogenated into PDO. Commercial quantities of PDO are now available from both processes. A third route with the potential of further lowering PDO cost is by enzymatic fermentation (10,11) of glycerol and alcohol. This bio-route is under active development by DuPont and Genencore International. With advances in biogenetic engineering, new strains of engineered bacteria were reported to improve yield and selectivity that can be scaled up for commercial production.

Polymerization

PTT is melt-polymerized by either the transesterification of PDO with DMT or by the direct esterification of PDO with TPA. The process is similar to the polymerization of PET but with several important differences. Since the reactivity of PDO is much lower than that of ethylene glycol, "hot" catalysts such as titanium butoxide (12) and dibutyl tin oxide (13), normally too fast for PET, are used to polymerize PTT. Melt polymerization is carried out between 250 and 275°C, about 40°C lower than that used for PET. PTT has different polymerization side reaction products. Instead of cyclic trimers, PTT produces cyclic dimers. It also gives off acrolein and allyl alcohol instead of acetaldehyde gaseous by-products. Acrolein requires special handling and disposal.

Direct esterification of PDO with TPA is the preferred commercial route to polymerize PTT because it is more economical than using DMT. Figure 1 shows the reaction scheme. Because TPA has a melting point > 300°C and has poor solubility in PDO, esterification is carried out in the presence of a "heel" and under a pressure of 70–150 kPa at 250–270°C for 100–140 min. *Heel* is an oligomeric PTT melt with a degree of polymerization (DP) of 3–7 purposely left in the reaction vessel from a previous reaction to act as a reaction medium and to increase TPA solubility. The esterification step is self-catalyzed by TPA. After reaching a DP of about 3–7, 40–50% of the oligomers is transferred to the polymerization vessel. Titanium butoxide or dibutyl tin oxide catalyst (50–150 ppm) is added to initiate polymerization at 260–275°C. Vacuum (<0.15 kPa) is applied to remove the condensed water until the polymer reaches an intrinsic viscosity (IV) of 0.7–0.9 dL/g.

To obtain higher molecular weight PTT with IV > 1.0 dL/g, melt-polymerized chips are further solid-stated (14,15) at 180–210°C under nitrogen to prevent polymer yellowing from prolonged melt polymerization. Solid-stating also helps driving off residual gaseous by-products in the polymer chips; however, the molecular weight distribution is broadened from 2 to about 2.5.

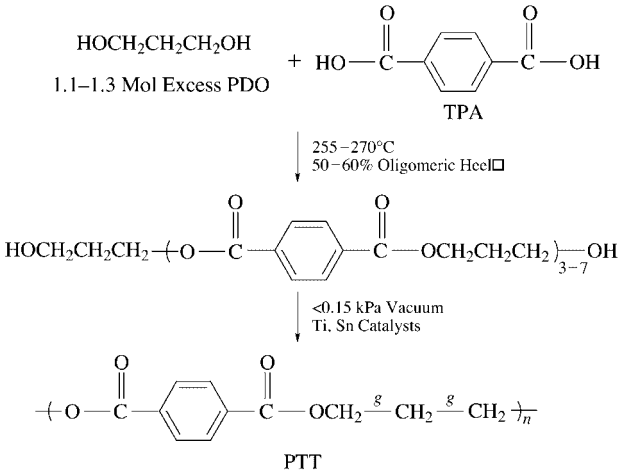

Fig. 1. PTT polymerization by direct esterification of TPA with PDO. *Gauche* conformation of PTT's methylene units is indicated by *g*.

Side Reactions and Thermal Degradation

PTT melt undergoes several side reactions during polymerization and melt processing. It has been proposed that PTT undergoes thermal degradation similar to PET via McClafferty rearrangement of the ester moiety (16,17). The carbonyl group abstracts a β-methylene hydrogen through a six-membered cyclic transition state, and this event is followed by chain scission giving terminal carboxyl and vinyl end groups in the fragmented chains. Further scission of the vinyl end gives allyl alcohol and its oxidative product acrolein. Under inert atmosphere, PTT has similar thermogravimetric weight loss profile as PET (18) with only one main decomposition step. Degradation in air was, however, different and involved two mechanisms. At about 300°C, degradation was decomposition-controlled. At a higher temperature, the rate increased and degradation changed to diffusion-controlled.

Cyclic oligomer is generated by chain backbiting similar to that in PET. Instead of cyclic trimer, PTT forms cyclic dimer with a melting point of 254°C. During polymerization, some PDO is dimerized into dipropylene ether glycol (DPG) and are incorporated in PTT as copolymer. Presence of DPG moiety lowers the polymer's melting point and affects the fiber's dye uptake. These side reactions could be suppressed to various extents by adding antioxidants and phosphites, using high purity PDO, and controlling the polymerization conditions (19).

Thermal Properties

PTT is a semicrystalline polymer with a glass-transition temperature T_g of 45°C and a melting point T_m of 228°C, both measured by a differential scanning calorimeter (dsc). The T_g of PTT is dependent on the polymer's crystallinity. It

Table 1. Thermal Properties of PTT

Property	Value	Reference
Melting point, °C	228	–
Equilibrium melting point, °C	244, 248	21,22
Heat of fusion ΔH_f, kJ/mol	30±2	23
Fully amorphous heat capacity, J/(K·mol)	94	23
Crystallization half-time @ 180°C, min	2.4	24
Cold crystallization temperature, °C	65	–
Glass-transition temperature, °C	45	–
Thermal diffusivity, m^2/s		
@ 25°C	1.36×10^{-7}	25
@ 140°C	0.99×10^{-7}	25

remains at 45°C up to about 30% crystallinity, and increases rapidly to about 70°C when crystallinity reaches 50% (20). The heat of fusion ΔH_f for a 100% crystalline PTT is 30 ± 2 kJ/mol. Other thermal properties are shown in Table 1. When PTT was rapidly quenched from the melt, the dsc heating scan showed a cold crystallization exotherm at about 65°C; however, a slowly cooled PTT does not cold crystallize. Therefore, the crystalline morphology is dependent on the melt quench history, and affects the drawing behavior of the polymer. The reversible and irreversible heat capacities were measured using adiabatic calorimetry, dsc, and temperature-modulated dsc (23,26). The measured heat capacities for both solid state and liquid state PTT agreed well with values calculated from the Tasarov equation based on polymer chain skeletal vibration contributions (Fig. 2).

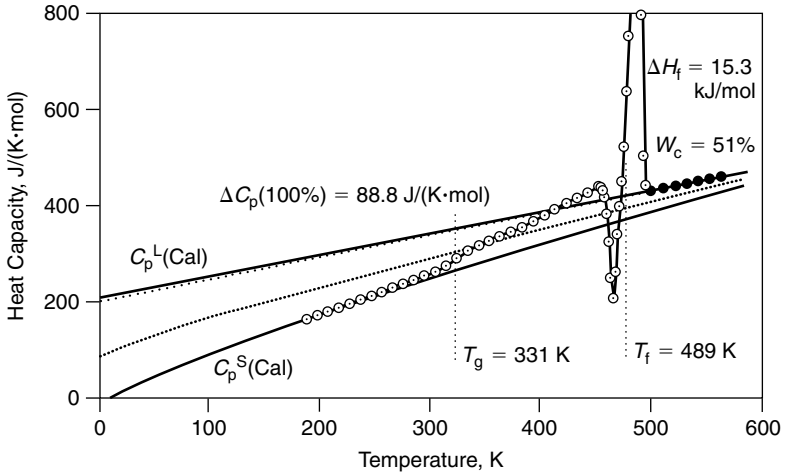

Fig. 2. Experimental and calculated heat capacities of solid and liquid PTT. –•– C_p (Exp); –•– Standard DSC;——C_p^L (Exp); . . .. . . C_p^L (Cal). From Ref. 23, Copyright © 1998 by John Wiley and Sons, Inc. Reprinted by permission of John Wiley & Sons, Inc.

Crystallization Kinetics

A comparison of the isothermal crystallization kinetics of PET, PTT, and PBT using a dsc showed that PTT has a crystallization rate in between those of PET and PBT (24). The Avrami rate constant K was of the order of 10^{-3}–10^{-2} min^{-n} when crystallized at 175–195°C. It is about an order of magnitude higher than PET but an order of magnitude lower than PBT when they were compared with the same degree of undercooling from the melt. PTT has a spherulitic growth rate of 117–4.7 μm/min, and it requires 4.8 kcal/mol of work for lamellae chain folding (22). On the basis of secondary nucleation analysis, a multiple nucleation crystallization mechanism transitioned from regime II to regime III at around 194°C was reported (22). Since the work of chain folding and the nucleation mechanism transition temperature were between literature values of PET and PBT, the three polyester crystallization rates rank in the same order.

A rapidly quenched PTT cold crystallizes when it is heated to above its T_g. It was found that PTT cold crystallized at a much faster rate than PET by following the increase in PTT crystalline band at 1220 cm^{-1} using rapid scanning Raman spectroscopy (27). At 71°C, PTT crystallized and reached 80% of its equilibrium crystallinity in <1 min whereas PET did not cold crystallize at all.

Molecular Weights

As a norm, molecular weight M of a polyester is given by its intrinsic viscosity (IV), also called limiting viscosity number $[\eta]$; M and $[\eta]$ are related to each other through the Mark–Houwink equation

$$[\eta] = KM^{\alpha} \tag{1}$$

where K and α are constants unique to the solvent and temperature used in measuring IV. Because of the fast crystallization rate, PTT chips have higher crystallinity than PET and are much more difficult to dissolve. A stronger solvent such as hexafluoroisopropyl alcohal (HFIPA) is used to dissolve PTT at room temperature. However, by heating to 110°C and taking care to ensure complete dissolution, mixtures of tetrachloroethane/phenol, typically used for PET, have been successfully used for PTT. Table 2 shows PTT's Mark–Houwink constants for various solvents (28,29), and the methods of molecular weight measurement.

In practice, IV is often measured using the simplified single-point method to save time. Simplified equations (30–33) gave good estimations of IV compared to the more rigorous Huggins or Kraemer plots to within ±3% when the solution concentration is kept at <0.005 g/dL (28).

Crystal Structure

Like PET and PBT, PTT crystallizes into the triclinic crystal structure (34–37). Unit cell dimensions obtained from wide-angle x-ray diffraction (waxd) are a=0.459, b=0.621, c=1.831 nm, $\alpha = 98°$, β=90°, γ=112° (34). The c-axis contains

Table 2. PTT Mark–Houwink Constants

Solvent	Temperature, °C	Molecular weight[a] determination[a] method[a]	K, 10^4 dL/g	α	Reference
HFIPA	35	sals	5.51	0.71	24
HFIPA	35	Hydroxyl group	10.0	0.70	–
60/40 Tetrachloroethane/ phenol	30	sals	5.36	0.69	24
50/50 Tetrachloroethane/ phenol	20	sals	8.2	0.63	25

[a]sals = small-angle light scattering.

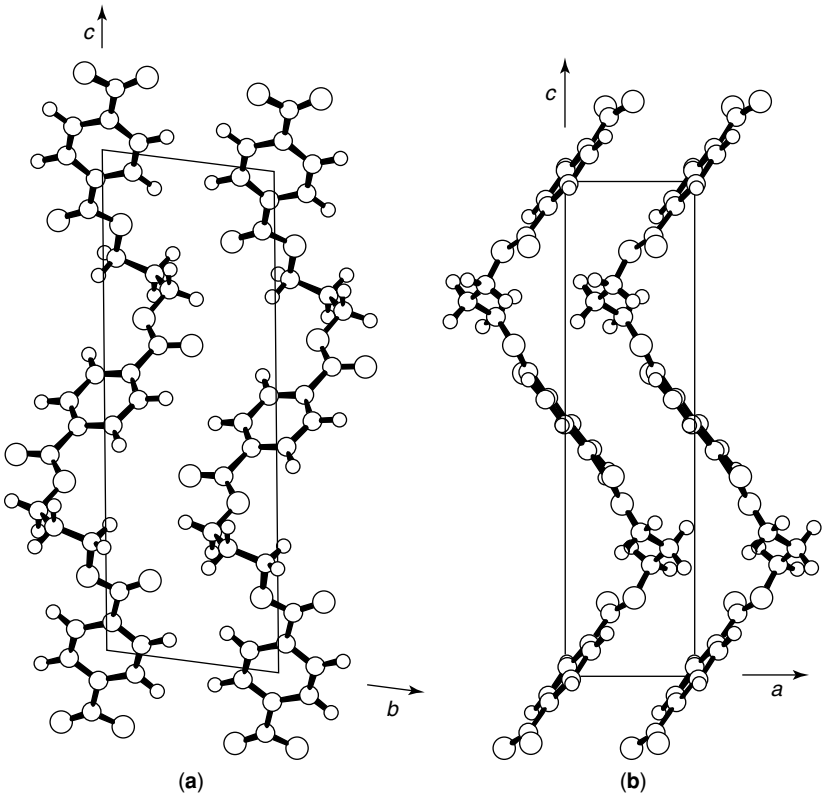

Fig. 3. Crystal structure of PTT viewed in the (**a**) *bc*-plane and (**b**) *ac*-plane showing the zizzag chain from the *gauche–gauche* conformation of the methylene units. Reprinted from Ref. 34, Copyright 1979, with permission from Elsevier Science.

two PTT repeating units with the methylene groups arranged in a *gauche–gauche* conformation. When viewed in the *ac*- and *bc*-plane, the chains are arranged in a highly contracted zizzag manner compared to that of PBT and PET (Fig. 3). There are disagreements in the reported crystal densities. Densities based on waxd crystal structures are much higher than those obtained by electron diffractions (38).

Measurements of the densities of a series of 19 PTT samples with dsc crystallinities from 14 to 35% gave an extrapolated crystal density of 1441 kg/m^3, in closer agreement to the waxd unit cell density (39). Until more work was done, the author's research group used 1432 kg/m^3 for crystallinity measurement, based on crystal structure parameters (34). Using a group contribution method, an amorphous density of 1295 kg/m^3 was calculated (25) in good agreement with the extrapolated value obtained by Ziabicki (39).

PTT waxd crystal orientation function f_c can be measured from the azimuthal scan of 010 reflection. The Herman orientation function equation using this reflection has been given by (38), and is based on Wilchinsky's treatment of uniaxial orientation:

$$f_c = 1 - 3\cos^2\phi_{010,Z} \tag{2}$$

where $\langle\cos^2\phi_{010,Z}\rangle$ is the average cosine angle of the normal of (010) plane made with the draw direction Z.

Mechanical Properties

Table 3 compares properties of PTT, PET, and PBT (40). They were measured on injection-molded samples using ASTM test methods. Tensile strength, flexural modulus, and notched Izod impact of PTT fall in between those of PET and PBT. All three polymers have similar electrical properties except for PET which has lower volume resistivity. The lower moisture absorptions of PTT and PBT are due to the high crystallinities from fast crystallization.

Dynamic Mechanical Properties. The PTT dynamic mechanical relaxation spectrum shows three viscoelastic relaxations (41). α-Relaxation occurs at -70°C and is the glass-transition temperature. T_g obtained by dynamic mechanical methods is usually higher than that from a dsc, and is frequency dependent.

Table 3. Comparison of PTT, PET, and PBT Properties

Property	PET	PTT	PBT
Tensile strength, MPa[a]	72.5	67.6	56.5
Flexural modulus, GPa[b]	3.11	2.76	2.34
Heat distortion temperature @ 1.8 MPa, $^\circ$C	65	59	54
Notched Izod impact, J/m[c]	37	48	53
Specific gravity, kg/m^3	1400	1350	1340
Mold shrinkage, m/m	0.03	0.02	0.02
Dielectric strength, V/μm	0.407	0.393	0.296
Dielectric constant at 1 MHz	3.0	3.0	3.1
Dissipation factor at 1 MHz	0.02	0.015	0.02
Volume resistivity, 10^{-16} Ω·cm	0.1	1.0	1.0
Moisture absorption, 14 days, %	0.49	0.15	0.2

[a] To convert MPa to psi, multiply by 145.
[b] To convert GPa to psi, multiply by 145,000.
[c] To convert J/m to ft·lbf/in., divide by 53.38.

α-Relaxation as high as 91°C has been reported (42). There are two subzero relaxations. β-Relaxation occurs at about −70°C. It originated from the amorphous phase (43), and has been attributed to the reorientation of the hydroxyl groups and local motions of the carboxyl groups. γ-Relaxation occurs at about −105°C and overlaps with the β-relaxation peak as a shoulder. This relaxation comes from the cooperative movement of the methylene segments containing at least three consecutive methylene units (44), and is therefore a low temperature motion of the trimethylene glycol portion of the polymer.

Elastic Recovery. The fiber industry has long been aware of PTT having the best tensile elastic recovery and resiliency among the three aromatic polyesters (45). This property is very desirable for fiber applications such as in carpets and textile apparels. The driving force for PTT's good elastic recovery comes from the response of its molecular chain to the applied strain.

It has been shown (46) that PTT has a very low theoretical crystal modulus, 2.59 GPa (375, 550 psi), compared to 107 GPa (1.55×10^7 psi) of PET (47) because of PTT's highly contracted helical-like conformation, whereas PET chain is fully extended with trans conformation. When a PTT fiber is stretched *in situ* in a waxd, the fiber period, measured from the Bragg d-spacing, increases immediately and is proportional to the applied strain up to 4% strain before deviating from affine deformation (48). Up to this critical strain the crystal deformation is reversible. The response of microscopic crystalline chains to macroscopic deformation explains why PTT has the best elastic recovery among the three aromatic polyesters. Further, PTT's elastic recovery and permanent set are nearly the same as nylon-6,6 up to 30% strain (25).

Melt Rheology. Figure 4 shows the melt viscosity as a function of shear rate for a 0.92 dL/g IV fiber grade PTT from 245 to 275°C (49). At 265°C, the melt viscosity profile is nearly the same as that of PET at a typical processing temperature of 290°C. At high shear rates of 10^3–10^4 s^{-1}, found in injection

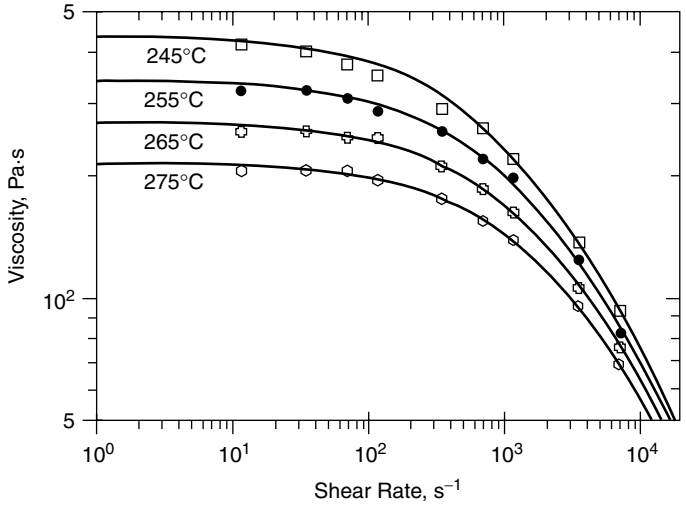

Fig. 4. Fiber grade 0.92 dL/g IV PTT capillary rheometer melt viscosity as a function of shear rate from 245 to 275°C. To convert Pa · s to P, multiply by 10.

molding and fiber spinning, the melt shear thins. It can be approximated as a power law fluid. However, PTT is more sensitive to shear thinning than PET with a non-Newtonian power law index n of 0.64 compared to 0.79 of PET (26).

Processing and Applications

Most of the developments to date have focused on textile and carpet fiber applications because PTT has a combination of several properties particularly suited for these applications. Table 4 compares PTT fiber properties with those of PET, nylon-6, and nylon-6,6 (20), (50), (51).

PTT fibers and yarns have bulk, resiliency, stretch-recovery, softness, hand, and drape similar to nylons and are much better than PET. As a polyester, it is inherently resistant to most stains that are acidic in nature because it does not have dye sites. It also has a lower static propensity. It is dyed with disperse dyes, but at a lower temperature than PET because of a lower T_g. The combinations of these properties are attractive to carpet and textile manufacturers for some applications where PTT could replace nylon or PET. It also offers the potential of creating new fiber products by using the unique combinations of these properties, which are not found in either nylon or PET.

Fiber end-use applications include (*1*) ready-to-wear, active-wear, intimate apparels, inner linings where stretch-recovery, softness, hand, and drape are the key attributes; (*2*) carpets where resiliency, newness retention, stain resistance, and low static generation provide values over currently used materials in some market segments; (*3*) automotive and home upholstery utilizing the easy dyeing, stain resistance, stretch-recovery properties. Within a short period of time since the polymer's commercialization, PTT ready-to-wear stretch apparels (52) and resilient floor coverings had already appeared in the market (since 1999).

Other applications are in monofilaments, nonwovens, films, engineering thermoplastics, and molded goods. Paper forming fabrics made with PTT monofilaments have been patented (53) for use in papermaking machines because PTT combines the chemical resistance of a polyester and the resiliency of the less chemical resistant nylon. PTT non-woven fabric shows better dimensional

Table 4. Comparison of PTT, PET, and Nylon Fiber Properties

Property	PTT	PET	Nylon
Yarn bulk and crimp	Excellent	Good	Excellent
Resiliency, stretch-recovery	Excellent	Fair	Excellent
Dyeing	Very good disperse-dyed at atmospheric boil without carrier	Good, disperse-dyed under pressure with carrier	Excellent, acid dyed
Stain resistance	Excellent	Excellent	Poor to very good
Electrostatic propensity	Excellent	Excellent	Poor to very good
Hand and softness	Excellent	Excellent	Very good
Drape	Excellent	Fair	Excellent

stability and is softer than polypropylene (54). Other applications include synthetic leathers (55) and flexible transparent film for packagings (56).

Fiber Processing. PTT used for fiber applications has IV of 0.80–0.92 dL/g ($M_n \approx$ 16,000–20,000). Prior to melt processing, the polymer chips must be dried to a moisture level of <30 ppm to avoid hydrolytic degradation. A close-loop hot air dryer is preferred. PTT is dried at 130°C and at a dew point of <−40°C for 6 h. Because of the faster crystallization rate, PTT chips are already semicrystalline after palletizing, and do not require a precrystallization step prior to drying as in PET.

The dried polymer is extruded at 250–265°C into fibers using conventional processing machines for bulk continuous filaments (BCF), partially oriented yarn (POY), spin-draw yarn (SDY), and staple fiber.

Carpets. The process of making PTT BCF carpets has been described in detail (57). The extruded yarn is drawn between sets of heated godets to a draw ratio 2.8–3.5 (58,59). It is then textured with hot air at 160–220°C and at a pressure of 0.6–1.0 MPa (87–145 psi) (60). Heat-setting with steam is at 135–145°C or at 175–195°C (61) when heat-set with the less effective heat conducting superheated steam. Tufted carpets are dyed with disperse dyes at atmospheric boil (62) in a continuous or a batch process. PTT carpets show excellent resiliency equivalent to a nylon in walk tests, have lower static charge of <3.5 kV, and are resistant to coffee, mustard, betadine, red acid dyes, and other stains (63).

Textile Fibers. PTT POY is spun using PET POY or SDY fiber spinning machines. Table 5 shows the tenacities and elongations of PTT fiber as a function of spinning speed (64). Tenacity increases while the elongation decreases with increasing speed. The PTT fiber stress–strain curve, unlike PET, has an inflexion point like a knee (45,65). A fully oriented PTT fiber has a modulus of 2.58 GPa (374,000 psi) compared to 9.15 GPa (1.33×10^6 psi) of PET (45).

PTT yarn has been textured by false-twist method at 140–160°C (64). Crimp development was almost twice as high as PET with crimp contraction reaching about 50%. When PTT yarns with a high level of crimp contraction are knitted into stretch fabrics, the amount of stretch achieved is equivalent to PET stretch fabrics incorporated with 6–8% of Spandex (66). In addition to stretch, PTT fabrics tend to have softer hand and better drape than PET. Since PTT does not absorb moisture like nylon, PTT fabrics also have a desirable dry touch and comfort.

Table 5. Tensile Properties of 150 dtex[a]/34-filament PTT Fiber as a Function of Spinning Speed

Spinning speed, m/min	Tenacity N/tex[b]	Elongation, %
600	0.090	252
1000	0.124	176
1500	0.148	146
2000	0.162	125
2500	0.195	97
3000	0.188	68

[a] 150 dtex = 135 den.

[b] To convert N/tex to g·f/den, multiply by 11.33.

Table 6. Properties of Glass-Filled Polyesters

Property	PET	PTT	PBT
Glass content, wt%	28	30	30
Tensile strength, MPa[a]	159	159	115
Flexural modulus, GPa[b]	8.97	10.4	7.60
Heat distortion temperature @ 1.8 MPa, °C	224	216	207
Notched Izod impact, J/m[c]	101	107	85
Specific gravity, kg/m^3	1560	1550	1530
Mold shrinkage, m/m	0.002	0.002	0.002

[a]To convert MPa to psi, multiply by 145.
[b]To convert GPa to psi, multiply by 145,000.
[c]To convert J/m to ft·lbf/in., divide by 53.38.

Dyeing. Because of its low T_g, PTT is disperse-dyed at atmospheric boil without using carriers for plasticization (62,67,68). Most countries have legislations prohibiting or regulating the use of the environmentally harmful biphenyl type carriers. PTT is thus a much more environmentally friendly polymer than PET in this respect, although PET is now dyed under pressure at 130°C without using carrier. The dye uptake of PTT and PET fibers has been compared by measuring their Kulbelka–Munk, K/S, values as a function of dyeing temperature (68). PTT reached and leveled off at K/S of about 16 at 100°C whereas PET did not absorb much dye at this temperature. Dye uptake only leveled off at >120°C dyeing temperature with a less dense color shade K/S value of 13.

Injection Molding. Several patents describe the injection molding of PTT for applications as transparent heat-resistant bottles (69), impact, heat, and bending resistant electrical connectors (70) and others. Neat PTT can be injection molded at 250–260°C into a mold maintained at 70–80°C under a holding pressure of 3.1–4.2 MPa (450–609 psi) and a cycle time of 40 s (40). Colder mold temperature tends to cause uneven crystallization with the formation of an amorphous transparent skin and a highly opaque crystalline core. The spherulites formed ranged from small and disordered at the outer edges to more perfect and larger in the core with high stress-concentration interfaces. In extreme cases, the molded article could become brittle. Glass-filled PTT crystallizes at a much faster rate and reduces the cycle time to 30 s. Table 6 compares the properties of a 30% glass-filled PTT with PET and PBT (40). The heat distortion temperature is greatly improved by the glass from 59 to 216°C. Notched Izod impact is similar to that in PET and slightly better than in PBT.

Health and Safety

Since PTT is a new commercial product, Shell took up the responsibility of product stewardship (71) and registered the polymer on the chemical inventory lists of several countries. As a high molecular weight polymer, PTT is biologically inactive and requires safe handling like other commercial polymers.

When PTT is exposed to high heat such as during drying and melt processing, it releases acrolein, allyl alcohol, and cyclic dimer by-products (71). Among them,

acrolein is of special concern because it is a very strong lacrymator. It also irritates lung and respiratory tracts and affects breathing. The effects are acute and do not have cumulative long-term effects. OSHA industrial hygiene guidelines for time-weighted exposure limit of acrolein over a period of 8 h is 0.1 ppm, and the short-term exposure limit for 15 min is 0.3 ppm. Therefore, adequate ventilation must be provided to avoid acrolein exposure.

BIBLIOGRAPHY

1. Br. Pat. 578079 (June 14, 1946), J. R. Whinfield and J. T. Dickson.
2. U.S. Pat. 3984600 (Oct. 5, 1976), S. Kawase and T. Kuratsuji (to Teijin Ltd.).
3. U.S. Pat. 3584103 (June 8, 1971), M. E. Harris (to E. I. du Pont de Nemours & Co., Inc.).
4. Br. Pat. 1254826 (Nov. 24, 1971) (to Fiber Industries, Inc.).
5. Eur. Pat. Appl. 478850A1 (Aug. 4, 1992), E. Drent; U.S. Pat. 5684214 (Nov. 4, 1997), P. R. Weider, J. B. Powell, and K. T. Lam (to Shell Oil Co.).
6. P. Nager, Paper presented at *CHEMSPEC Asia '91*, Tokyo, Japan, June 24–25, 1991.
7. H. H. Chuah, Paper presented at *Tifcon '96*, The Textile Institute, Blackpool, U.K., Nov. 6, 1996.
8. DuPont Sorona™ Selected As Brand Name for 3GT Polymer, Press Release, April 11, 2000, E. I. du Pont de Nemours & Co., Inc., Wilmington, Del.
9. Process Economics Program Report 227, 1,3-Propanediol and Polytrimethylene Terephthalate, SRI International, 1999.
10. DE 3734764 A1 (May 3, 1989), K. Tran-Dinh and F. F. Hill (to Hüls AG).
11. WO 9928480 (June 10, 1999), R. V. Nair and co-workers (to E. I. du Pont de Nemours & Co., Inc., and Genecor International, Inc.).
12. U.S. Pat. 4611049 (Sept. 9, 1986), T. Kuratsuji and T. Miki (to Teijin Ltd.).
13. U.S. Pat. 5340909 (Aug. 23, 1994), M. L. Doerr, J. J. Hammer, and J. R. Dees (to Hoechst Celanese Corp.).
14. H. H. Chuah, R. W. Vinson, and C. W. Ulzelmeier, Research Awareness Bulletin, Shell Chemical Co., July 1993, p. 101.
15. U.S. Pat. 5763104 (June 9, 1998), J. M. Stouffer, E. N. Blanchard, and K. W. Leffew (to E. I. du Pont de Nemours & Co., Inc.).
16. H. H. Chuah and S. L. Wallace, Research Awareness Bulletin, Shell Chemical Co., Aug. 1993, p. 97.
17. S. Schauhoff, *Chem. Fibers Int.* **46**, 263 (1996).
18. X.-S. Wang, X.-G Li, and D. Yan, *Polym. Degrad. Stab.* **69**, 361 (2000).
19. U.S. Pat. 6093786 (July 25, 2000), D. R. Kelsey (to Shell Oil Co.).
20. H. H. Chuah, H. S. Brown, and P. A. Dalton, *Int. Fiber J.* **10**(5), 50 (1995).
21. K. M. Lee, K. J. Kim, and Y. H. Kim, *Polymer (Korea)* **23**, 56 (1999).
22. J. M. Huang and F. C. Chang, *J. Polym. Sci., Part B: Polym. Phys. Ed.* **38**, 934 (2000).
23. M. Pyda and co-workers, *J. Polym. Sci., Part B: Polym. Phys. Ed.* **36**, 2499 (1998).
24. H. H. Chuah, *Polym. Eng. Sci.* **41**, 308 (2001).
25. H. H. Chuah, *Introduction to PTT Chemistry & Technology*, Short course at Shell Chemical Company, Westhollow Technology Center, Dec. 1995.
26. M. Pyda and B. Wunderlich, *J. Polym. Sci., Part. B: Polym. Phys. Ed.* **38**, 622 (2000).
27. B. J. Bulkin, M. Lewin, and J. Kim, *Macromolecules* **20**, 830 (1987).
28. H. H. Chuah, D. Lin-Vien, and U. Soni, *Polymer* **42**, 7137 (2001).

29. H. L. Traub, and co-workers, *Die Angew. Makromol. Chemie* **230**, 179 (1995).
30. O. F. Solomon and I. Z. Ciutã, *J. Appl. Polym. Sci.* **6**, 683 (1962).
31. N. Kuwahara, *J. Polym. Sci. A* **1**, 2395 (1963).
32. S. H. Maron, *J. Appl. Polym. Sci.* **5**, 282 (1961).
33. M. V. R. M. Rao, and M. Yaseen, *J. Appl. Polym. Sci.* **31**, 2501 (1986).
34. I. J. Desborough, I. H. Hall, and J. Z. Neisser, *Polymer* **20**, 545 (1979).
35. Y. Chatani and co-workers, *Ann. Meet. Soc. Polym. Sci. Kyoto*, Preprints, 1977, p. 427.
36. S. Poulin-Dandurand and co-workers, *Polymer* **20**, 419 (1979).
37. B. Moss and D. L. Dorset, *J. Polym. Sci., Part B: Polym. Phys. Ed.* **20**, 1789 (1982).
38. H. H. Chuah and B. T. A. Chang, *Polym. Bull.*, (in press).
39. A. Ziabicki, *Research on PolyTrimethylene Terephthalate and Corterra® Fibers*, Seminar presented at Shell Chemical Company, Westhollow Technology Center, Feb. 1999.
40. K. Dangayach, H. Chuah, W. Gergen, P. Dalton, and F. Smith, in *Proc. SPE 55th Ann. Tec. Conf. & Exhibits*, 1997, p. 2097.
41. C. C. González, J. M. Pereña, and A. Bello, *J. Polym. Sci., Part B: Polym. Phys. Ed.* **26**, 1397 (1988).
42. G. Farrow, J. McIntosh, and I. M. Ward, *Makromol. Chem.* **38**, 147 (1960).
43. J. G. Smith, C. J. Kibler, and B. J. Sublett, *J. Polym. Sci., Part. A-1* **4**, 1851 (1966).
44. N. G. McCrum, B. E. Read, and G. Williams, *Anelastic and Dielectric Effects in Polymeric Solids*, John Wiley & Sons, Inc., New York, 1967.
45. I. M. Ward, M. A. Wilding, and H. Brody, *J. Polym. Sci., Part B: Polym. Phys. Ed.* **14**, 263 (1976).
46. K. Nakamae and co-workers, *Zairyo* **35**, 1066 (1986).
47. I. Sakurada and K. Kaji, *J. Polym. Sci., Part C* **31**, 57 (1970).
48. R. Jakeways and co-workers, *J. Polym. Sci., Part B: Polym. Phys. Ed.* **13**, 799 (1975).
49. K. Dangayach, K. Ghosh, H. H. Chuah, B. Cristea, and W. P. Gergen, Paper presented at *ETP'99*, Zurich, June 7–9, 1999.
50. F. W. Werny, *Carpet & Rug Industry* **23**(6) 38 (1995).
51. Sorona™ 3GT's Attributes, Website product information, E. I. du Pont de Nemours & Co., Inc., 2000.
52. C. Heschmeyer, *Int. Fiber J.* **15**(4), 66 (2000).
53. U.S. Pat. 5104724 (Apr. 14, 1992), C. Y. Hsu (to Wangner System Corp.).
54. C. Hwo and co-workers, Poly(trimethylene phthalates or napthalate) and Copolymers: New Opportunities in Film, Engineering Thermoplastic and Other Applications, Technical Bulletin, SC:2731-98, Shell Chemical Co., 1998.
55. Jpn. Pat. 11222780 (Aug. 17, 1998) G. Bungo and M. Akiharu (to Asahi Chemical Industry Co., Ltd.).
56. Jpn. Pat. 08325391 (Dec. 10, 1996), T. Sato, T. Imamura, and T. Matsumoto (to Nippon Esters, Ltd.).
57. H. H. Chuah, Processing of Corterra® Polytrimethylene Terephthalate Polymer for Bulk Continuous Filament Carpets, Technical Bulletin SC:2528-98, Shell Chemical Co., 1998.
58. U.S. Pat. 5645782 (July 9, 1997), J. M. Howell, W.-H. Tung, and F. Werny (to E. I. du Pont de Nemours & Co., Inc.).
59. U.S. Pat. 6113825 (Sept. 5, 2000), H. H. Chuah (to Shell Oil Co.).
60. F. Werny and H. Chuah, *Int. Fiber J*. **11**(4), 62 (1996).
61. J. D. Polejes and co-workers, *Int. Fiber J*. **13**(6), 26 (1998).
62. H. H. Chuah, F. Werny, and T. Langley, *Book Pap.—Int. Conf. Exhib.*, The American Association of Textile Chemists and Colorists, 1995, pp. 98–106.

63. H. H. Chuah, *Chem. Fiber Int*. **46**, 424 (1996).
64. H. S. Brown and H. H. Chuah, *Chem. Fiber Int*. **47**, 72 (1997).
65. H. L. Traub, P. Hirt, and H. Herlinger, *Chem. Fiber Int.* **45**, 110 (1995).
66. M. Moerman, Corterra® PTT Polymers: Downstream Textile Development Generation 1 Information Package, Shell Chemical Co., 2000.
67. H. L. Traub, P. Hirt, and H. Herlinger, *Melliand Textilber* **76**, 702 (1995).
68. Y. Yang and co-workers, *Textile Chemist and Colorist & American Dyestuff Reporter* **1**(3), 50 (1999).
69. Jpn. Pat. Appl. 05031789 (Feb. 9, 1993), K. Kawaguchi, T. Nakane, and K. Hijikata (to Polyplastics Co.).
70. Jpn. Pat. 11054189 (Feb. 26, 1999), H. Matsumoto and co-workers (to Toray Industries, Inc.).
71. K. S. Kiibler and co-workers, Byproduct Emissions from Poly(trimethylene terephthalate): Studies on the Release of Acrolein and Allyl Alcohol During Processing, Storage, and Shipping of PTT, Technical Information Report, WTC-3659, Shell Chemical Co., 2000.

HOE H. CHUAH
Shell Chemical Company

POLY(VINYL ACETATE). See VINYL ACETATE POLYMERS.

POLY(VINYL ALCOHOL). See VINYL ALCOHOL POLYMERS.

POLY(VINYL CHLORIDE). See VINYL CHLORIDE POLYMERS.

POLY(VINYL ETHER). See VINYL ETHER POLYMERS.

POLY(VINYL FLUORIDE). See VINYL FLUORIDE POLYMERS.

POLY(VINYLIDENE CHLORIDE). See VINYLIDENE CHLORIDE POLYMERS.

POLY(VINYLIDENE FLUORIDE). See VINYLIDENE FLUORIDE POLYMERS.

POLYACETAL. See ACETAL RESINS.

POLYACRYLAMIDE. See ACRYLAMIDE POLYMERS.

POLYACRYLATES. See ACRYLIC ESTER POLYMERS.

POLYACRYLONITRILE. See ACRYLONITRILE POLYMERS.

POLYAMIDES, AROMATIC

Introduction

Aromatic polyamides first appeared in the patent literature in the late 1950s and early 1960s, when a number of compositions were disclosed by researchers at DuPont (1–3). These polymers were made by the reaction of aromatic diamines with aromatic diacid chlorides in an amide solvent. Over 100 examples of aromatic polymers and copolymers described in patents were listed in a 1989 book (4). Another extensive list of polymers was provided in the previous edition of this encyclopedia (5).

Forty years later, after the expenditure of much time and money, the number of commercially important aromatic polyamide polymers has been reduced to three—two homopolymers, poly(*m*-phenylene isophthalamide) (MPDI) and poly(*p*-phenylene terephthalamide) (PPTA), and one copolymer, copoly(*p*-phenylene/3,4′-diphenyl ether terephthalamide) (ODA/PPTA) (6):

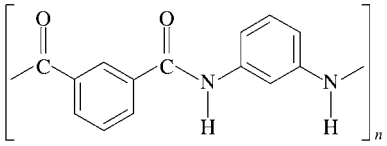

poly(*m*-phenylene isophthalamide) MPDI

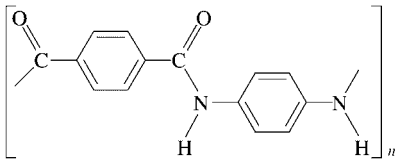

poly(*p*-phenylene terephthalamide) PPTA

Encyclopedia of Polymer Science and Technology. Copyright John Wiley & Sons, Inc. All rights reserved.

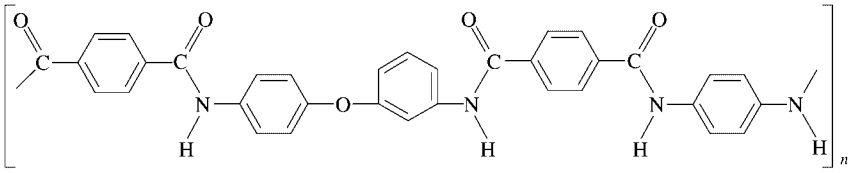

copoly(*p*-phenylene/3,4′-diphenyl ether terephthalamide ODA/PPTA

Because fibers from these aromatic polyamides have properties that differ significantly from the class of fibers known as polyamides (see Polyamides, fibers), the U.S. Federal Trade Commission adopted the term *aramid* as designating fibers of the aromatic polyamide type in which at least 85% of the amide linkages are attached directly to two aromatic rings.

The important properties of this class of polymers include thermal and chemical stability and the potential for high strength and modulus. Aliphatic polyamides melt at temperatures below 300°C, whereas most aromatic polyamides do not melt or melt above 350°C. Aramids also exhibit greater chemical resistance and low flammability. These properties derive from the aromatic character of the polymer backbone that can provide high chain rigidity. Aromatic polyamide fibers can have very high strength and modulus, and these properties persist at elevated temperatures. Because of their low density, aromatic polyamides have higher specific strength and modulus than steel or glass. In recent years, design engineers have been able to utilize these unique properties to create products which protect personnel from fire, bullets, and cuts, reduce the weight of aircraft and automobiles, and hold oil drilling platforms in place.

There are several other aromatic polymers, not polyamides, but which form fibers with high chain rigidity and similar properties. These would include poly(*p*-phenylene benzobisthiazole) (PBT) and poly(*p*-phenylene benzobisoxazole) (PBO) (Ref. 4, Chapt. VII):

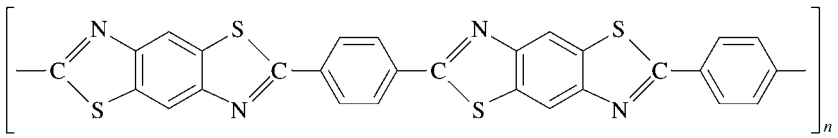

poly(*p*-phenylene benzobisthiazole) PBT

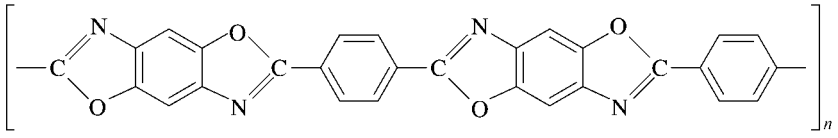

poly(*p*-phenylene benzobisoxazole) PBO

There is no systematic nomenclature for aromatic polyamides; however, several codes can be found in the literature. Poly(*m*-phenylene isophthalamide) is referred to as MPD-I or MPDI, poly(*p*-phenylene terephthalamide) is referred to as PPTA or PPD-T, and copoly(*p*-phenylene/3,4′-diphenyl ether terephthalamide) is referred to as ODA/PPTA or HM–50. Another important polymer, although not

available in commercial quantities, is poly(*p*-benzamide), PBA. Codes will be used throughout the article to refer to these materials.

Sources of Ingredients

The principal ingredients for the manufacture of aromatic polyamides on a commercial scale are the diamine and diacid chloride monomers, plus the solvents used for the polymerization reaction. The chemical processes reported to be used for preparation of each of these ingredients are described in this section.

Solvents. The key polymerization solvents are readily available from several sources. They are dimethylacetamide (DMA), dimethylformamide (DMF), *N*-methyl-2-pyrrolidinone (NMP), and hexamethylphosphoramide (HMPA).

Monomers. *m*-Phenylene diamine (MPD) can be prepared by the continuous liquid phase hydrogenation of *m*-dinitrobenzene at moderate temperatures (7). One process employs a dispersion of the *m*-dinitrobenzene in water (8); another uses a solvent, such as DMF, which dissolves both the reactant and the MPD product (9). Catalysts for the hydrogenation include platinum, palladium, and nickel that must be recovered by filtration. Purification steps include vacuum distillation.

p-Phenylene diamine (PPD) can be made in a two-stage process (10). In the first stage aniline and sodium nitrite undergo diazotization to form benzenediazonium chloride, which in turn reacts with excess aniline to form the intermediate, diphenyltriazine. At low pH, diphenyltriazine is rearranged into *p*-aminoazobenzene. Finally, *p*-aminoazobenzene is cleaved by catalytic hydrogenation into PPD and aniline. The aniline is recycled to the first-stage reaction. The PPD then undergoes a series of purification steps, including vacuum distillation.

3,4′-Diaminodiphenyl ether (3,4′-ODA) can be prepared from 3,4′-dichlorodiphenyl ether by treatment with aqueous ammonia in the presence of an amide solvent (eg, NMP), using copper as a catalyst (11). Dichlorodiphenyl ether is prepared by treating the sodium salt of *p*-chlorophenol with *m*-dichlorobenzene in the presence of aqueous NaOH, followed by removal of the water and subsequent treatment with dimethylene glycol diethyl ether and CuCl (12).

Phthaloyl chlorides [isophthaloyl chloride (ICL) and terephthaloyl chloride(TCL)] are made by at least two processes, both involving the chlorination of phthalic acid. In the first (13), xylene is chlorinated by a photochemical reaction to form hexachloroxylene. The hexachloroxylene then reacts with phthalic acid to give the corresponding phthaloyl chloride and by-product HCl. Phthaloyl chloride is purified by double distillation. To produce ICL by this reaction, *m*-xylene and isophthalic acid are the starting materials. To produce TCL, the process starts with *p*-xylene and terephthalic acid. Phthaloyl chlorides can also be produced by reacting intermolecular anhydrides of the corresponding acids with phosgene, in the presence of an amide catalyst such as DMF or DMA (14).

Polymer Properties

A wide variety of aromatic polyamide polymers and copolymers have been disclosed in the patent literature. Table 1 provides a partial list of structures, the

Table 1. Examples of Aromatic Polyamides

Polymer	η_{inh} dl/gm	Melting temperature from DTA, °C	10% Weight loss temperature, °C	Reference
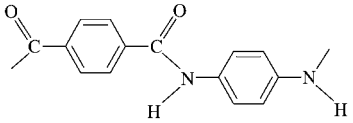	0.83	435	458	15
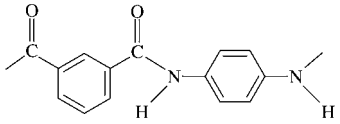	0.48	530	513	15,16
	5.0		568	
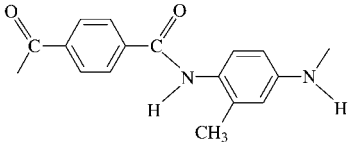	0.46	422	452	15,16
	1.10		512	
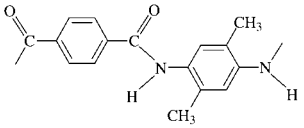	0.34	518	505	15,16
	0.32	545	487	
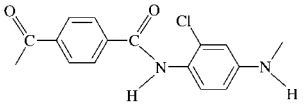	0.67	496	473	15
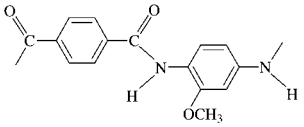	1.73	508	516	16
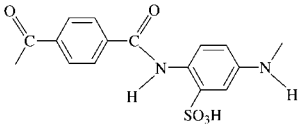	1.29	402	435	16
		528		
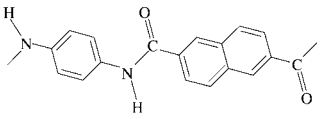	1.11	350	353	16
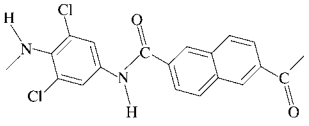	2.48			17
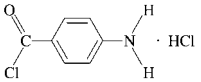	1.99			17

inherent viscosity of the polymer (a measure of molecular weight), and two thermal characteristics of the polymers. Many additional examples can be found in the literature (4,5).

With the exception of the A–B type polymer, poly(*p*-benzamide) (PBA), the polymerizations are of the A–A plus B–B type. A further distinction can be made between monomers with para orientation, eg, PPTA and those with meta orientation, eg, MPDI. The meta-oriented polymers are less easily crystallized, and therefore usually remain in solution throughout the polymerization. In some cases they can be spun into fibers directly from the polymerization medium. On the other hand, para-oriented polymers will tend to crystallize as they reach a certain chain length, so that they precipitate from the polymerization solution. This can limit the level of molecular weight that can be achieved, as will the nature of the solvent and the polymerization temperature.

Another important characteristic of the monomers is the presence of pendant groups attached to the aromatic ring. These pendant groups include alkyl, halogen, alkoxy, cyano, acetyl, and nitro. In addition to the simple phenylene compounds, diamines and diacid chlorides based on naphthalene and 4,4′-biphenyl have been used. A variety of monomers with bridging units of the following form have also been explored:

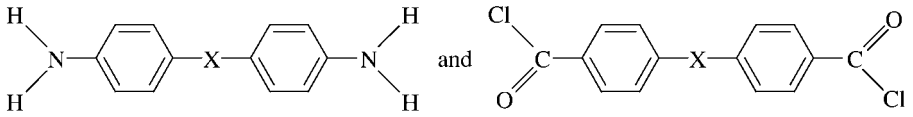

where X can be oxygen, sulfur, sulfone, keto, amine, or isopropylidene.

Thus, the number of chemical structures that could be (and has been) explored is quite large, especially when one considers the possible copolymer combinations.

Molecular Weight. The number-average molecular weight (M_n) of aromatic polyamides is generally in the range of 10,000–30,000, which is typical of condensation polymers. Because the measurement of M_n and M_w (weight-average molecular weight) is difficult and time consuming, the molecular weight of aromatic polyamides is commonly characterized by a dilute solution viscosity parameter termed *inherent viscosity* (η_{inh}). Inherent viscosity is an approximation of "intrinsic viscosity" ($[\eta]$), which, in turn, is classically related to molecular weight by the Mark–Houwink equation.

$$[\eta] = kM_w^a$$

Values of k and a in this equation have been measured for several aromatic polyamide solutions in 96% sulfuric acid (18,19).

PPTA	$k = 0.008$, $a = 1.09$
Poly(tetramethyl-*p*-phenylene terephthalamide)	$k = 0.0063$, $a = 0.96$
Poly(*p*-phenylene-2,5-dimethyl terephthalamide)	$k = 0.0021$, $a = 1.16$
MPDI	$k = 0.013$, $a = 0.84$

k has the units mL/g (divide by 100 to obtain the more commonly used units for η_{inh} of dL/g).

The viscosity/molecular weight relationship deviates from the Mark-Houwink equation at high levels of molecular weight (18). For PPTA this nonlinearity is pronounced above $M_w = 40{,}000$. Thus, at high levels of molecular weight, inherent viscosity will be somewhat misleading as an indicator of M_w.

Inherent viscosity is defined as

$$\eta_{inh} = \ln(t_{soln}/t_{solv})/c$$

where t_{soln} is the flow time for the polymer solution in the viscometer, t_{solv} is the flow time of the solvent, and c is the concentration of polymer in the solution specified as 0.5 g/dL (20). Thus, η_{inh} has the units of reciprocal concentration. Different solvents have been used. For the *para*-oriented polymers, the normal solvent is 96–98% sulfuric acid. For the meta-oriented polymers amide solvents are often used in place of sulfuric acid.

Molecular Weight Distribution. The polydispersity index (M_w/M_n) for PPTA has been estimated by gel permeation chromatography to be near 2 for low molecular weight polymers and nearer to 3 for polymers with $M_w > 35{,}000$ (18).

Thermal Properties. High melting point is one of the key distinguishing properties of aromatic polyamides. (In most cases the melting point exceeds the decomposition temperature, so that the material chars). A number of scientists have studied the thermal characteristics of aromatic polyamides by the differential thermal analysis (dta). Data for melting point are included in Table 1. The melting points of these polymers were empirically identified with the endothermic phase transitions from DTA measurements. One study did not detect a melting point for PPTA (15) while another (16) did (530°C). This has been attributed to molecular weight differences.

Thermogravametric analysis (tga) provides a measure of polymer thermal stability. In this test, polymer samples are heated at a programmed rate and sample weight is recorded as a function of temperature. Two studies (15,16) made tga measurements and reported the temperature for 10% weight loss (see Table 1). The thermal stability of these polymers is lower in air than in nitrogen.

Solubility. Solubility of selected aromatic polyamides in a variety of solvents has also been measured (15). In general, PPTA is soluble only in strong acids, such as sulfuric, hydrofluoric and methanesulfonic acids (all of the polymers cited are soluble in these acids). MPDI is also soluble in the amide solvents (DMF, DMA, and NMP) and in dimethyl sulfoxide, as are most of the substituted variations of these two polymers. Solubility in the amide solvents is increased by the addition of salts such as LiCl and $CaCl_2$. This class of polymers is generally not soluble in formic acid or *m*-cresol, which are common solvents for aliphatic polyamides.

Analytical and Test Methods. The properties described previously are all determined by well-known techniques in polymer chemistry. A description of each of the methods can be found in textbooks (20).

Laboratory Synthesis

Solution Polymerization. Most of the examples in the patent literature utilize solution polymerization. In this technique, an aromatic diamine is dissolved in an amide solvent and a stoichiometric quantity of an aromatic diacid chloride is added to the diamine solution while stirring vigorously. Important factors include monomer stoichiometry, ingredient and solvent purity, anhydrous conditions, diamine concentration (and therefore polymer concentration), and temperature of the starting diamine solution.

The primary polymer properties that are sought in these polymerizations are high polymer molecular weight and freedom from impurities that could impact the properties of products prepared from the polymer. All of the factors listed earlier can affect molecular weight. Stoichiometric imbalance will lead to excess ends that cannot react. Impurities, including water, can react with the active ends of one of the monomers. High temperature can lead to side reactions that produce unreactive ends. Since the reaction between an acid chloride and an amine is highly exothermic, the heat generated can significantly increase the temperature of the polymerizing solution. The extent of the temperature rise will depend on the diamine concentration and the degree of cooling.

For polymers that remain soluble in the polymerizing medium, such as MPDI in NMP, the reaction is rapid even at low temperature. For those that do not remain soluble, the choice of solvent becomes very important. More powerful solvents can produce polymers with higher molecular weights. Lower temperatures can also retard the precipitation of the polymer.

A 1965 book (21) discusses low temperature solution polycondensation at length, although it does not deal with the reaction of aromatic diamines with aromatic diacid chlorides by this method. The book also discusses interfacial polymerization.

A mechanism for these low temperature polymerizations has been proposed (Ref. 4, pp. 115–119). It involves an initial stage in which the amine reacts with an acid chloride liberating a molecule of HCl. The HCl, in turn, forms a complex with either an unreacted amine end or a molecule of solvent. An equilibrium is established between the amine hydrochloride and the solvent hydrochloride that depends on the basicity of the solvent. The first stage proceeds until half of the amine has reacted, at which point nearly all of the amine ends have formed an HCl complex. The second stage of the reaction is much slower and depends on the availability of free amine.

Poly(p-benzamide). PBA is an interesting case. One monomer from which a high molecular

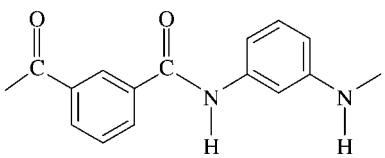

weight polymer can be made is *p*-aminobenzoyl chloride hydrochloride. This monomer can be synthesized from *p*-aminobenzoic acid and thionyl chloride,

forming the intermediate, sulfinyl aminobenzoyl chloride, followed by treatment with dry HCl in ether (22). When this monomer is dissolved in an amide solvent such as DMA, an equilibrium is set up between the amine hydrochloride of the monomer and the solvent hydrochloride. Some free amine is formed and the polymerization proceeds. As one would expect, this monomer is extremely sensitive to water and heat.

Poly(m-phenylene isophthalamide). The formation of MPDI is an example of a polymerization in which the polymer remains soluble in the polymerizing medium. Suitable solvents are NMP and DMA with the possible addition of LiCl or $CaCl_2$. MPD is dissolved in anhydrous solvent at a concentration of up to 1.0 mol/L and cooled to 0°C, stirring vigorously. Solid ICL is added and the stirring is continued for 30 minutes. The resulting polymer remains in solution and has an η_{inh} of 1.8 (3).

Poly(p-phenylene terephthalamide). PPTA provides an example of a polymer that has very limited solubility in suitable solvents. In the laboratory, PPD is dissolved in an amide solvent in concentrations up to 0.5 mol/L. The solution is cooled to near 0°C, stirring vigorously. Solid TCL in an equal stoichiometric quantity is added and within a few minutes the solution becomes opalescent. Vigorous stirring is continued as the polymerizing mixture solidifies and then breaks into particles with the consistency of wet sawdust. This crumb can then be neutralized with dilute caustic, washed with water, and dried. The resulting polymers exhibit η_{inh} as high as 6.0 (23).

Because polymerization will proceed much more slowly when the polymer becomes insoluble, the selection of the solvent has an important effect on the level of molecular weight that can be achieved. Solvents using mixtures of HMPA and NMP or HMPA and DMA produce polymers with higher molecular weight than any of the three solvents alone (24). Similarly, salts can be added to amide solvents to increase the solubility of PPTA and thereby increase the η_{inh} level that can be obtained (24). The combination of NMP and $CaCl_2$ is especially useful for providing high molecular weight PPTA (25). Another approach for increasing the level of molecular weight that can be attained is the use of an acid acceptor, such as tertiary amines (26) and tributyl amine (27).

Copolymers. A large number of copolymer compositions have been prepared, many by low temperature solution polymerization, including ODA/PPTA (Ref. 4 pp. 145–172; 28,29).

Interfacial Polymerization. Some of the earliest reports of the preparation of aromatic polyamides employed interfacial polymerization. In this technique the diacid chloride is dissolved in a solvent with limited water solubility and then added to an aqueous solution of the diamine with vigorous stirring. The aqueous solution contains a base that neutralizes the HCl that is generated. One example is the preparation of MPDI using tetrahydrofuran as the solvent for ICL (2).

This process is difficult to develop at a commercial scale. A modified process for producing MPDI allows the ICL and MPD to react slowly in a solution without an acid acceptor. This reactive solution is then added to an aqueous solution containing an acid acceptor and stirred vigorously to build molecular weight in an interfacial-type polymerization. This process gives higher molecular weight than

solution polymerization techniques and therefore, improved fiber properties. This is the process that Teijin uses to produce the polymer for their MPDI product, Teijinconex® (30).

Vapor Phase Polymerization. PPTA can be formed by vapor phase polymerization at temperatures above 250°C (31). The polymer produced appears to have a high degree of branching, which makes the spinning of fibers with high strength more difficult. Improved products may be formed by using an acid acceptor that would permit shorter reaction times (32).

Commercial Polymerization Processes

There are relatively few commercial products based on aromatic polyamides. These are listed in Table 2. Processes for producing the polymers, for those products where reliable information has been published, are described.

MPDI. The commercial process for MPDI has been proposed (5) based on the patent literature (35). A block diagram of the process is shown in Figure 1.

The diamine noted in the figure is actually a 9.3% solution of MPD in DMA in the patent example, and the diacid chloride is molten ICL. The MPD solution is cooled to −15°C, while the molten ICL is supplied at 60°C. The heat of reaction brings the temperature of the effluent from the mixer to 74°C. This effluent is then cooled before $Ca(OH)_2$ is added to neutralize the HCl formed in the polymerization reaction. Finally, the polymer solution is blended, deaerated, and filtered before being pumped to storage for use in spinning. The MPDI of the patent example has an η_{inh} of 1.65.

A second polymer process is the modified interfacial polymerization described earlier (30). In this process, the polymer is isolated and dried, then redissolved for spinning, as shown in Figure 2.

PPTA. The commercial process for PPTA has been proposed (5) based on the patent literature (36,37). A block diagram of the process is shown in Figure 3.

Table 2. Commercial Products Based on Aromatic Polyamide Polymers

Polymer	Type of product	Trade name	Capacity,[a] t/year	Manufacturer
MPDI	Fiber	Nomex	15,900	E. I. du Pont de Nemours & Co.
MPDI	Fiber	Teijinconex	2,300	Teijin Co., Ltd.
MPDI	Fiber	Fenylon	900	Russian State Complex
PPTA	Fiber	Kevlar	29,900	E. I. du Pont de Nemours & Co.
PPTA	Fiber	Twaron	11,000	Accordis (Twaron Products bv)
PPTA	Fiber	Fenylon ST	1,300	Russian State Complex
ODA/PPTA	Fiber	Technora	800	Teijin Co., Ltd.
Aramid copolymer	Film	Mictron	400	Toray Industries, Inc.
PPTA	Film	Aramica	200	Asahi Chemical Industry, Ltd.

[a]Data for fiber capacities from SRI International (33); data for film capacities from *Japan Chemical Week* (34).

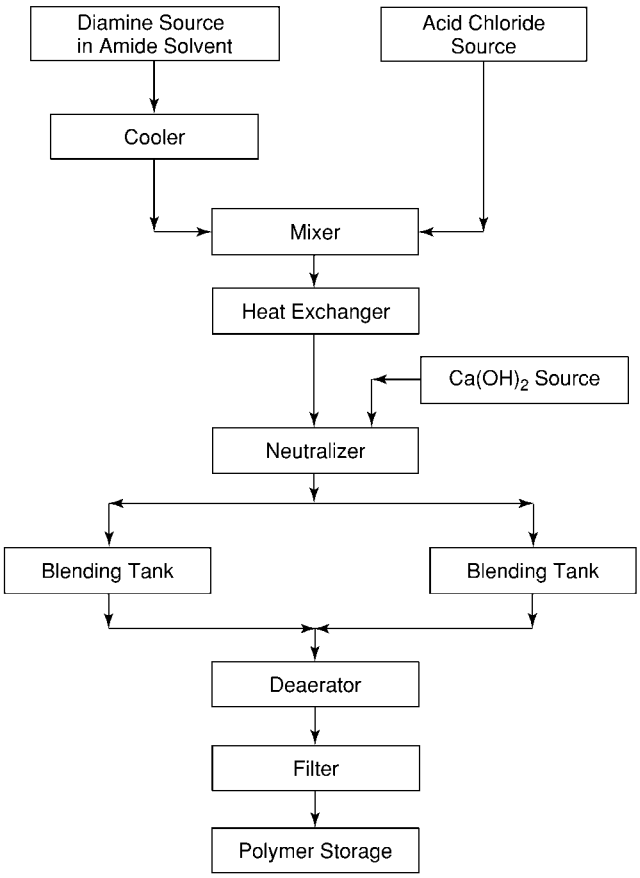

Fig. 1. Preparation of MPDI via low temperature solution polymerization (35).

In this process, PPD is dissolved in HMPA and then mixed with molten TCL in a series of mixers equipped to remove some of the heat of reaction. The polymer/solvent crumb is then washed with water, filtered, and dried. For health reasons, HMPA has been replaced by NMP/$CaCl_2$ as a solvent.

A similar process has been described for the production of PPTA for the Twaron process (10), although the polymerization reaction is done in batch reactors. The solvent is NMP containing $CaCl_2$. The polymer has a molecular weight (M_n) of 18,000–19,000.

ODA/PPTA. The polymerization process for producing ODA/PPTA has been described (6,28,29). PPD and 3,4′-ODA are dissolved in a solvent such as NMP and then reacted with TCL to form the copolyamide. The composition is likely 50% 3,4′-ODA and 50% PPD. When the reaction is complete the HCl formed is neutralized by the addition of $Ca(OH)_2$ to give a stable viscous solution that is suitable for spinning. The inherent viscosity is in the 2–3 dL/g range and the polymer concentration is around 6 wt%. The process is quite similar to that shown in Figure 1 after accounting for the use of two diamines.

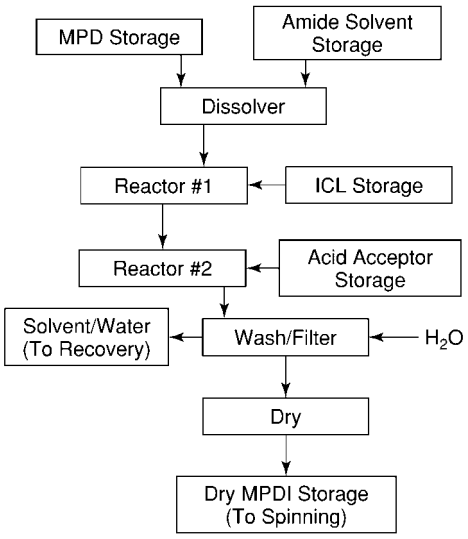

Fig. 2. Preparation of MPDI via interfacial polymerization (30).

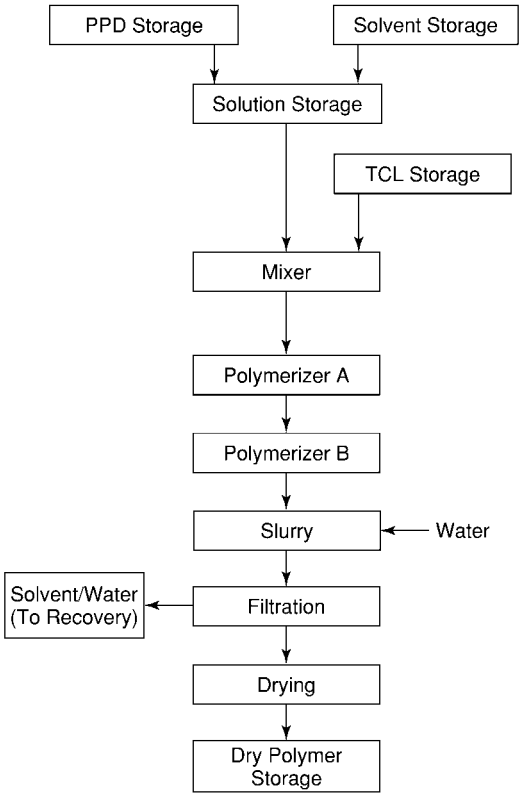

Fig. 3. Preparation of PPTA via low temperature solution polymerization (37).

Processing of Aromatic Polyamides

Most of the aromatic polyamides we have discussed so far have high melting points that prevent the type of melt processing common to aliphatic polyamides, polyolefins, and other polymers. Thus, most applications are based on forms of the polymer that can be prepared from solutions of the polymers. These would include fiber, films, and pulp.

Techniques for processing polymer solutions are well known (See Fibers) and include wet spinning and dry spinning of fibers and solution casting of films. In order to minimize the cost of commercial processes, large numbers of fibers must be handled together, at high speed, and with minimum interruptions to the operation. Commercial processes for forming aromatic polyamide products are described in this section, focusing on the types of solution that are employed and the methods used to coagulate the fibers and complete the development of the fiber structure.

Wet Spinning MPDI. A flow diagram for the wet spinning of MPDI to form Teijinconex is shown in Figure 4 (30).

The process involves dissolving the dry, salt-free polymer in an organic solvent at low temperature and then heating the dispersion to near 100°C to form a clear solution. This solution is wet spun into an aqueous solution containing a high concentration of an inorganic salt. The coagulated fiber is washed, and then drawn and post-treated. The fiber has excellent mechanical properties.

Figure 5 describes another wet spinning process for MPDI (38).

Dry Spinning MPDI. The dry spinning of MPDI from a DMF/$LiCl_2$ solution into an air column maintained at 225°C has also been described (3). After the

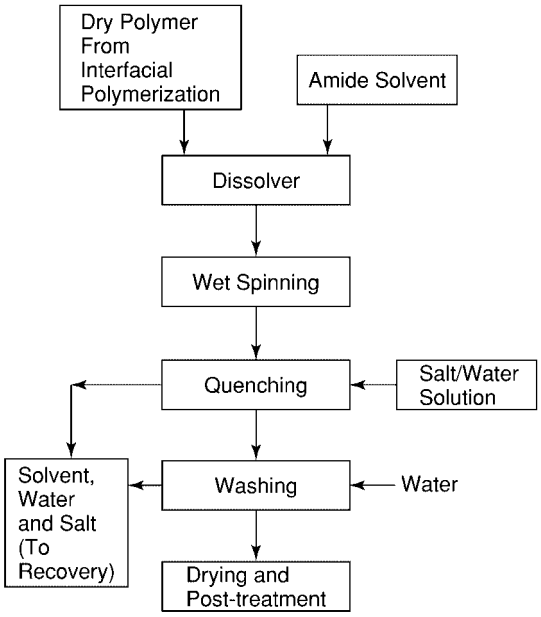

Fig. 4. Wet spinning of MPDI (30).

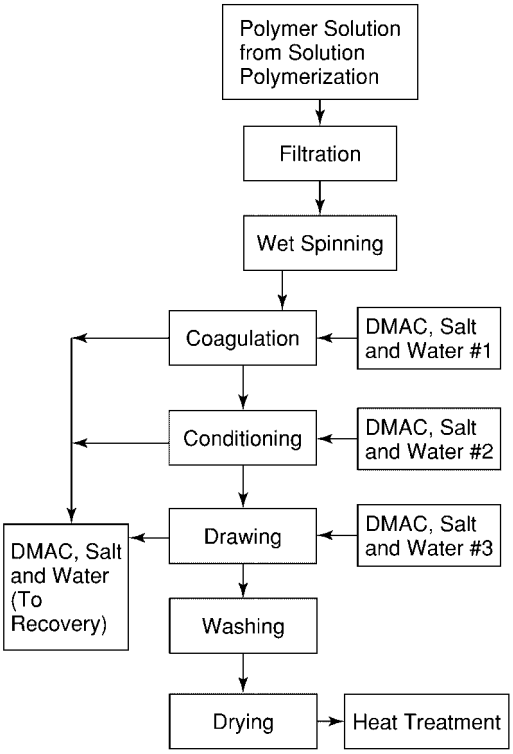

Fig. 5. Wet spinning of MPDI (38).

fibers thus formed are drawn 4.75× and the remaining solvent and salt removed by extraction in hot water, they exhibit a tenacity of 0.6 GPa and an elongation of 30%.

Spinning of PPTA. Unlike MPDI, high molecular weight PPTA is not soluble in amide solvents, with or without the addition of inorganic salts. Formation of fibers from PPTA became possible when it was discovered that concentrated solutions of the polymer in 100% sulfuric acid had relatively low viscosity, could be spun at moderate temperatures, and that the PPTA did not degrade rapidly at those conditions (36). This discovery was the result of the study of nematic solutions of PBA and PPTA (22,36) and substantiated the theoretical predictions of Flory (39). A schematic of such a process is shown in Figure 6.

The patent literature (36) describes a spinning process in which PPTA is dissolved in 98–100% sulfuric acid at a concentration of greater than 18%. The solution is pumped through a spinneret into an aqueous coagulating/quenching bath, with an air gap separating the spinnerets from the bath (40). The fiber is then washed thoroughly with water and dried.

Fibers formed by this spinning process are highly oriented even without the type of high temperature drawing common for other polyamide fibers, and have high stiffness (tensile moduli of 50–75 GPa). Even higher moduli (Kevlar 149 has a modulus of 180 GPa) can be obtained by subjecting the fibers to a stretching

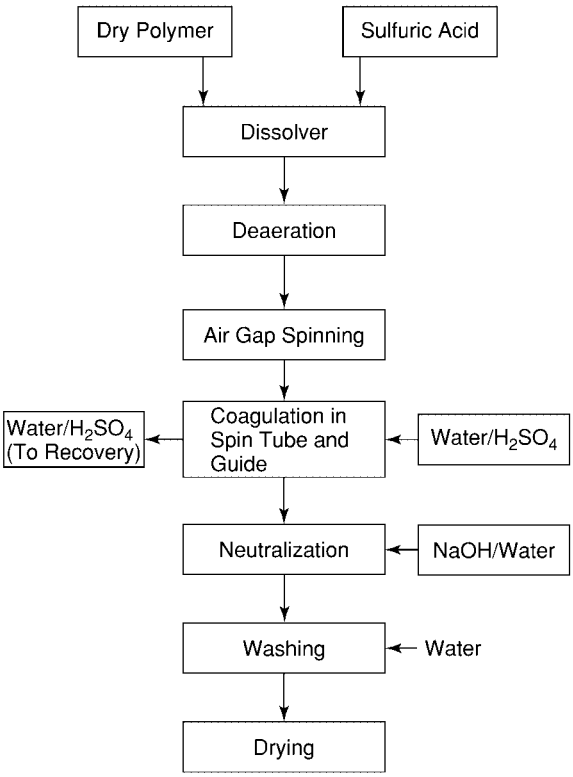

Fig. 6. Air gap spinning of PPTA (36).

process at high temperature (41–43). This would appear to be the basis for the high modulus versions of Kevlar and Twaron.

Wet Spinning of ODA/PPTA. The literature (28,29) describes the wet spinning of the copolyamide, ODA/PPTA, from a solution in NMP and $CaCl_2$ that had been filtered and deaerated. The solution is then pumped through a spinneret into a hot water/$CaCl_2$ bath. Next the filaments are washed with hot water and dried. The dried fibers are subjected to 8.5× stretch in a heated cell containing 510°C nitrogen. The fibers have tenacities in the 2.6–3.3 GPa range, depending on the ratio of DPE to PPD. The process is similar to that described in Figure 5.

Post-Spinning Processes. A significant portion of the aramid fiber sold in recent years has been in the form of staple, floc, or pulp products that are produced by the fiber manufacturer. Short fiber products are produced by cutting continuous filament yarn into lengths that range from about 1 mm to over 100 mm. Products in the 1- to 6-mm length range are referred to as *floc*, while the longer products are called *staple*. All of the continuous filament products described previously are also offered in cut-fiber forms.

Pulp is highly fibrillated, high surface area (7–15 m^2/g) short length product that is made by passing an aqueous slurry of cut PPTA fiber through a refiner

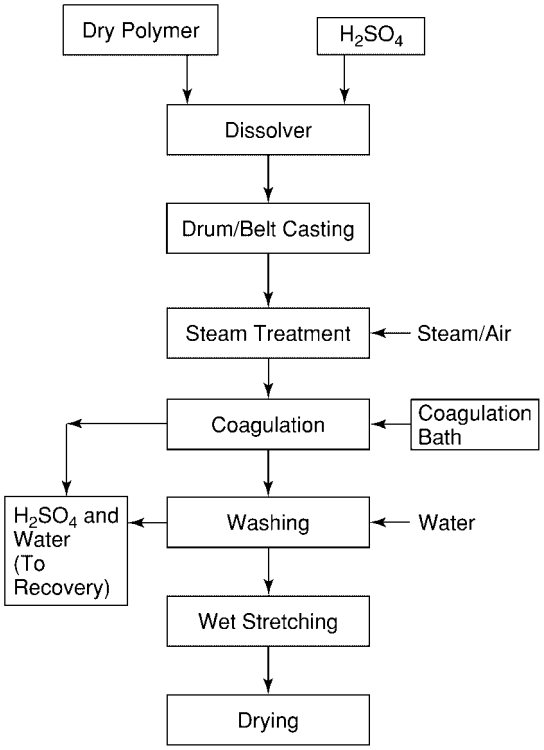

Fig. 7. Process for casting PPTA film (46).

(10). MPDI is not offered in pulp form, but methods for producing pulp have been disclosed (44,45).

Film Casting of PPTA. A technique has been developed for producing biaxially oriented PPTA film (46). A schematic of this process is shown in Figure 7.

This process involves dissolving PPTA in sulfuric acid at concentrations that produce a liquid crystal state. The viscous solution is extruded through a die onto a drum or belt where it is subjected first to high humidity warm air. This can convert the film from an anisotropic solution to an isotropic one. This is important for the production of a balanced film (machine direction or MD compared to transverse direction or TD), because anisotropic solutions of PPTA have a strong tendency to fibrillate. This solution is then dipped into a coagulating liquid, such as dilute sulfuric acid, which sets the film. Next the film is washed with water to remove the acid, after which it is biaxially stretched to provide orientation and then dried. Finally, the film is heat-treated while retaining the orientation.

Fiber and Film Properties

Physical, chemical, electrical, and mechanical properties of fibers are described in this section, with emphasis on commercially available fibers and the properties of importance in the markets they serve.

Table 3. Crystal Lattice Parameters of PPTA, PBA, and MPDI[a]

	PPTA	PBA	MPDI
Crystal system	Orthorhombic	Orthorhombic	Triclinic
Space group	$P2_1/n$-C_{2h}^5	$P2_12_12_1$-D_2	$P1$-C_1^1
Lattice constant			
a, nm	0.780	0.771	0.527
b, nm	0.519	0.814	0.525
c, nm	1.29	1.28	1.13
α, deg			111.5
β, deg			111.4
γ, deg	90		88.0
Number of chains in a unit cell	2	2	1
Density, g/cm^3			
Calculated	1.50	1.54	1.45
Observed	1.43–1.45	1.48	1.38

[a]Ref. 48.

Fiber Structure. An extensive description of the structure of PPTA (Kevlar) fibers has been provided in a 1993 book (47), including a description of the crystal lattice (48), estimates of apparent crystallite size and percent crystallinity, a description of fibrillar and pleat structure, and evidence of a skin-core structure. Crystal lattice structure and dimensions for PBA and MPDI (Nomex) fibers are also included, as shown in Table 3. The structure of Twaron is essentially the same (10), while the crystal structure of Teijinconex is nearly identical to the MPDI fiber in Table 3. PPTA fibers are highly crystalline, ranging from 68 to 95% crystalline depending on the heat treatment of the fiber and the crystallinity measurement technique. MPDI fibers are also highly crystalline, although the crystal lattice is quite different from that of PPTA (30).

It has been proposed that PPTA fibers have an unusual radial orientation of hydrogen-bonded sheets and a pleated structure (49). When this model is combined with proposals for a skin-core structure (50–52), one can visualize a comprehensive picture of PPTA structure.

Fiber Properties. Most commercially available fibers are now available in a variety of forms, including continuous filament yarns of different deniers, staple products of various lengths, pulp, paper products, and some nonwoven fabrics. Physical and chemical properties have most often been determined for the yarn products, with the understanding that these properties would usually apply to the other forms as well. While there is some variation in properties among the various deniers, it is usually not large. Representative properties of the major types of commercial yarn are shown in Tables 4 and 5. These properties are taken from the catalogs published by each manufacturer (53,54). Test methods are described in Table 6.

The products available commercially at this time fall into several categories. The MPDI products provide high temperature durability, low flammability, inherent dielectric strength, and excellent chemical resistance, combined with low modulus and high elongation. These products are well suited to fabrics for protective clothing, paper in electrical uses, and high temperature filtration applications.

Table 4. Properties of Aramid Fibers

		MPDI			PPTA				
		Nomex	Teijinconex		Kevlar		Twaron		ODA/PPTA
Property	Test Method[a]	430	Std	HT	K-29	K-49	Std	HM	Technora
Density, g/cm^3	a	1.38	1.38	1.38	1.44	1.44	1.44	1.45	1.39
Equilibrium moisture content, % at:									
65% RH	b	5.2	5.2	5.2	4.0	3.7	6.5	2.5	1.8
95% RH	b	7.0	9.0	9.0	6.5	6.3	–	–	–
Tensile properties at room temperature[b]									
Strength, GPa	c	0.59	0.61–0.68	0.73–0.86	2.9	3.0	2.9	2.9	3.4
Elongation, %	c	31	35–45	20–30	3.6	2.4	3.6	2.5	4.6
Modulus, GPa	c	11.5	7.9–9.8	11.6–12.1	71	112	70	110	72
Thermal Properties									
Specific heat, J/kg·K	d	72	60	60	81	81	81	81	96
Thermal conductivity, W/m·K	e	0.25	0.11	0.11	2.5	2.5	–	–	0.5
Coefficient of thermal expansion, cm/(cm·°C)	f	1.8×10^{-5}	1.5×10^{-5}	1.5×10^{-5}	-4.0×10^{-6}	-4.9×10^{-6}	-3.5×10^{-6}	-3.5×10^{-6}	-6×10^{-6}
Heat of combustion, J/kg	g	28×10^{6}	–	–	35×10^{6}	35×10^{6}	–	–	–
Flammability, LOI, %	h	28	29–32	29–32	29	29	29	29	–
Decomposition (in N_2) temperature, °C	j	400–420	400–430	400–430	520–540	520–540	520–540	520–540	500
Tensile properties measured at elevated temperatures[a]									
Tensile strength, GPa measured at T=									
150°C	k	0.46	0.48	0.69	2.5	2.7	–	–	–
200°C	k	0.39	0.41	0.64	2.2	2.6	–	–	–
250°C	k	0.32	0.35	0.57	2.0	2.4	–	–	>1.7
Tensile modulus, GPa measured at T=									
150°C	k	10.6	6.1	8.6	60	91	–	–	–
200°C	k	9.9	5.1	7.0	58	89	–	–	–
250°C	k	9.4	4.3	6.1	–	–	–	–	>37

Tensile property retention									
Hot air exposure—% strength retained after:									
100 h @ 180°C	l	100	99	99	95	–	86	–	98
1000 h @ 180°C	l	99	95	95	60	–	80	–	85
100 h @ 250°C	l	95	85	85	35	–	55	–	75
1000 h @ 250°C	l	73	75	75	<10	–	–	–	25
Saturated steam exposure—% strength retained after:									
400 h @ 120°C	l	–	70	–	25	–	–	–	100
100 h @ 140°C	l	–	86	–	–	–	–	–	–
1000 h @ 150°C	l	70	<50	–	–	–	–	–	–

[a] See Table 6.

[b] To convert strength and modulus values to cN/dTex, multiply GPa by 10.0 and divide by density (g/cm^3); to convert cN/dtex to gpd, multiply by 1.133.

Table 5. Chemical Resistance of Aramid Fibers

Chemical	Time, h/Temp., °C	Percent strength retention				
		MPDI		PPTA		ODA/PPTA
		Nomex	Teijinconex	Kevlar	Twaron	Technora
40% H_2SO_4	100/95		28			90
10% H_2SO_4	100/21	90–100	98	90–100		
10% H_2SO_4	1000/21		95	69	35[a]	
10% HCl	1000/21		20–60		35	10
10% HNO_3	100/21	60–80	90–100	20–60		
10% HNO_3	2200/21				15[a]	
10% NaOH	100/95		<10			75
10% NaOH	1000/21	90–100	90	46		
40% NaOH	1000/21	80–90	76			
28% NH_4OH	1000/21	90–100	90–100	90–100	65[a]	
0.01% NaClO	1000/21	90–100		16		
10% NaClO	100/95					55
0.4% H_2O_2	1000/21	90–100	56–75			
10% NaCl	1000/21	90–100			100[a]	
100% Acetic acid	1000/21		90–100		90[a]	
90% Formic acid	100/21	90–100	90–100	90–100		
90% Formic acid	100/99	60–80	90–100	0–20		
100% Acetone	1000/21	90–100	90–100			
100% Acetone	100/56	80–90		90–100		
100% Benzene	1000/21	90–100	90–100	100		
100% Ethyl alcohol	1000/21	90–100	90–100	100		
100% Ethyl alcohol	100/77	90–100		90–100		
50% Ethylene glycol	1000/99	80–90	90–100	60–80		
10% Formaldehyde	1000/21	90–100	90–100			
100% Gasoline	1000/21	90–100	90–100	90–100		
100% Methyl alcohol	1000/21	90–100	90–100	90–100		
100% Perchloroethylene	10/99	90–100		90–100		
100% Tetrahydrofuran	1000/21		90–100			

[a]Measurements made after 3 months (2200 h) of exposure at room temperature.

PPTA and ODA/PPTA provide high tensile strength and modulus, coupled with high use temperature and low flammability. The high modulus versions of PPTA provide value in protective apparel, ropes, and fiber optic applications, while the standard versions are used in asbestos replacement and rubber reinforcement markets. Figure 8 shows modulus vs tenacity for a wide variety of fiber products.

Film Properties. The two commercial aramid films are both based on PPTA. Aramica is a homopolymer, while Mictron is most likely a copolymer or a terpolymer. They provide excellent strength and stiffness, along with high temperature stability. Table 7 lists some of the key properties of these materials.

Uses

The properties of aromatic polyamide fibers and films are sufficiently different from those of the products that preceded them that many new uses and

Table 6. Test Methods

Note	Property	Test Description + ASTM Reference
a	Density	Density gradient tube at 21°C, ASTM D1505-96
b	Equilibrium moisture content	Fiber is bone dried and then exposed to the specified humidity at room temperature for >24 h.
c	Tensile properties	Instron Tester. Details depend on type of fiber. ASTM D885-85 (1.1 TM) for Kevlar; D885 M for Twaron; DuPont Test Method 12002 for Nomex
d	Specific heat	Differential scanning calorimeter, ASTM E1269
e	Thermal conductivity	Guarded-comparative longitudinal heat flow, ASTM E1225-87
f	Coefficient of thermal expansion	Untwisted fiber is held at constant tension, then length changes are measured as temperature is cycled between 25 and 150°C
g	Heat of combustion	Oxygen consumption calorimeter, ASTM E1354-97
h	Flammability—LOI	Oxygen index, ASTM D2863-97
j	Decomposition temperature	Differential thermal analysis, ASTM E1356-91
k	Tensile properties vs temperature	Sample and Instron acclimated for 5 min prior to testing as above (c)
l	Exposure tests	Samples exposed to specified conditions, then reconditioned to RT and 55% RH before testing as above (c)

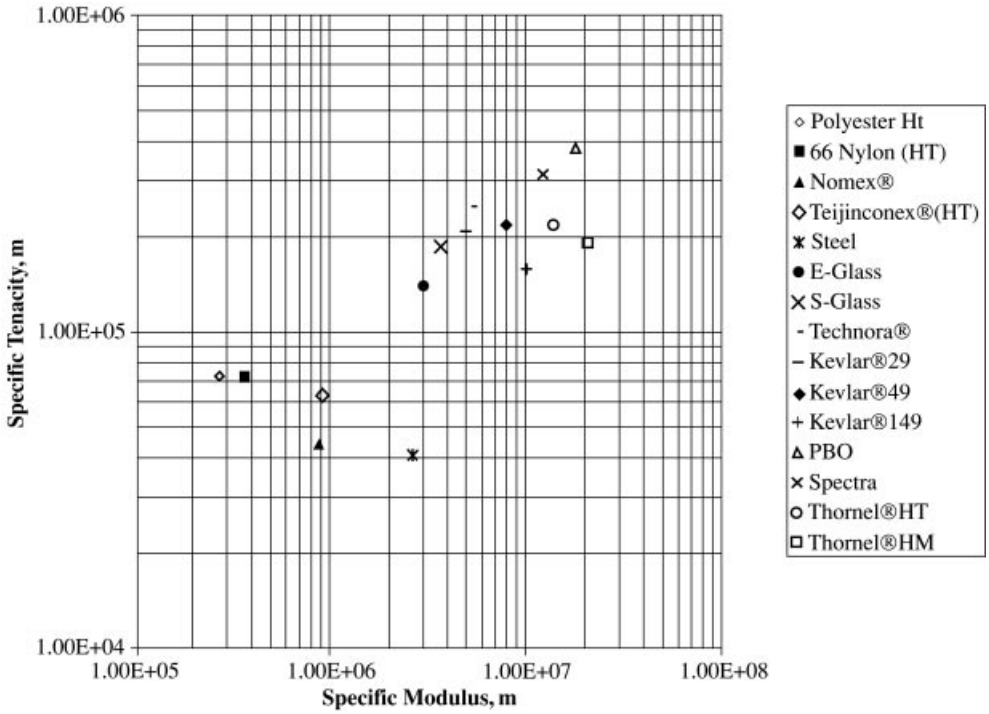

Fig. 8. Modulus tenacity map for industrial fibers.

Table 7. Properties of Aramid Films and Papers

	Mictron	Aramica	Nomex	Thermount
Reference	55	55,56	57	58
Polymer	PPTA	PPTA	MPDI	PPTA
Form	Film	Film	Paper	Paper
Source	Toray	Asahi	DuPont	DuPont
Type		M type	410	N710
Thickness, μm	25	25	127	97
Density, g/cm^3	1.50	1.40	0.87	0.64
Mechanical properties (MD/TD)				
Tensile strength, GPa	0.5	0.5/0.3	0.1/0.05	0.2
Elongation, %	60	15/25	16/13	1.5
Tensile modulus, GPa	13/9	19/10	–	5.4
Initial tear strength, kg	–	25	3.3/1.6	–
Melting point, °C	Does not melt	Does not melt	Does not melt	Does not melt
Long-term heat resistance, °C	180	ca 200	ca 200	ca 200
Thermal expansion, 10^{-5} °C^{-1}	0.1	0.2	–	−0.7
Moisture absorption, %	1.5	2.8	–	
@ 75% RH/Room temp.				
@ 55% RH				1.6
Electrical properties				
Dielectric constant @ 1 KHz	–	4.0	2.4	3.9[a]
Dissipation factor @ 1 KHz	–	0.02	0.006	0.02[a]
Volume resistivity, Ω·cm	5×10^{17}	10^{16}	5×10^{16}	–
Surface resistivity, Ω/sq	–	10^{16}	10^{16}	–
Dielectric strength, KV/mm	300	230	25	82[a]

[a]Epoxy impregnated laminate.

applications have been developed. Applications are summarized according to general market groupings, specifying the type of fiber or film used but not the specific product.

MPDI Fibers.

Textiles. MPDI fibers have found a substantial market as the fiber used to produce garments designed to protect workers from the hazard of fire. Obviously this includes firefighters and racecar drivers, but it is also becoming standard clothing for workers who operate in chemical factories and other places where the danger of flash fires is real. Key properties include its inherent flame resistance; abrasion, wear, and chemical resistance which allows clothing to be washed and worn many times; and high elongation and low modulus which allows the design of comfortable clothing. Antistatic properties and other characteristics can be incorporated by use of fiber blends.

MPDI fabrics have also been used as a fire blocking material in aircraft seat upholstery, where regulations require such functionality. They are finding increasing use as a fire block in hospitals and as upholstery where fire resistance is important.

Another major market for MPDI fabrics is as bag filters for a number of industries, such as power plants, cement factories, and steel factories, where the ability to withstand hot, corrosive gases is critical.

Paper. An equally important use of MPDI fiber are products in the form of paper. Paper can be made from a mixture of MPDI fibrids and floc (45). The mixture is slurried in water and processed on a conventional paper machine. The primary market for these papers is as electrical insulation in motors, generators, and transformers. The key properties are chemical resistance, good insulating characteristics, and high temperature stability.

Another significant market based on paper is that of honeycomb sandwich structures for aircraft interior floors and panels. The MPDI provides thermal stability during processing and, in the form of honeycombs, gives an exceptional stiffness to weight ratio.

PPTA and ODA/PPTA Fibers.

Protective Clothing. PPTA fibers have become the standard from which body armor for the protection of police and military personnel is made. The primary properties are high strength and light weight. These protective fabrics must be thicker than their fire protection cousins, but they still must be designed to be comfortable. PPTA is also used to make cut resistant fabrics for use in gloves and chain saw chaps.

Composites. High strength and low weight provides the basis for the use of PPTA reinforced composites for the strength members in aircraft, boats, the transportation industry, and sports equipment. Related applications would include providing the protective shielding in lightweight helmets for the military and as rigid armor in military vehicles, police cars, helicopters, and banks.

PPTA is also used in pulp form in a variety of automotive and industrial applications such as brake and clutch linings, gaskets, and nonwoven felts, where it has replaced asbestos. Key performance attributes are chemical resistance, thermal stability, and wear resistance.

Ropes and Cables. Here, again, high specific strength and stiffness are important. Cables based on PPTA fibers anchor oil rigs and provide ship to shore mooring lines. PPTA fibers also provide tension reinforcement for fiber optic cables, where high stiffness and dielectric properties are key advantages. ODA/PPTA fibers are used in a variety of applications where high strength and abrasion resistance are important.

Rubber Reinforcement. PPTA fibers were developed originally to replace polyester and steel as the reinforcing fiber in tires. That market continues to be important today, although it never reached the level envisioned in the 1960s. Key market segments today include high performance automobile tires, heavy-duty machinery and aircraft tires and, on the other end of the spectrum, puncture resistant, high performance bicycle tires. PPTA and ODA/PPTA are also used as reinforcement in rubber transmission belts and hoses.

Other Markets. PPTA fibers are used to form nonwoven sheet reinforcements that are used as substrate for printed wiring boards where low thermal expansion or the ability to use laser drilling technology are important. Other applications for aramid fibers include cement reinforcement, the engineered lumber

industry, boat sails, parachute fabrics, reinforcement in athletic shoes, pulp as a thixatropic agent, etc. Like most new materials, the development of new applications is a continuing process and is driven by the ingenuity of designers.

PPTA Films.

Recording Media. PPTA film provides a three- to fourfold advantage in tensile modulus over polyester film which is the preeminent material of the industry. High temperature stability is another important feature in this market. These property advantages offer the possibility of substantial miniaturization, and are the primary basis for the development of this film. At this time, the markets and products are still in the development stage.

Resin and Fibrid Forms. More recently commercialized product forms of PPTA and MPDI are respectively, resin and fibrid. The resin (polymer) form is finding utility as a reinforcing agent or as a wear additive in a variety of thermoplastic matrices. The high surface area fibrid form is used as a thixatrope and as a reinforcing agent in coating, sealant, plastic, elastomer, and composite applications.

Economic Aspects

Aramid products have now been commercially available for nearly 40 years. Table 2 provides a summary of current (as of 1999) capacities to produce these products, with total worldwide capacities of 19,000 t of *m*-aramid fiber, 43,000 t of *p*-aramid fiber, and 600 t of *p*-aramid film. Table 8 shows total world consumption of Aramid fibers between 1979 and 1998 (33), indicating sales near 90% of capacity for *m*-aramid and near 60% for *p*-aramid. Sales of both types have been increasing at a rate of over 4.5%/year for the past 10 years.

Prices of Aramid products vary widely depending on the denier of the product and the part of the world the product is sold. In general, *m*-aramids fall in the $20–60/kg range while *p*-aramids fall in the $10–30/kg range (33). Staple is less expensive than continuous filament yarn.

Table 8. Consumption of Aramid Fibers (thousands of metric tons)

	Year			
	1979	1986	1992	1998
m-Aramids				
United States	4	5	5	7
Europe and Russia	1	4	4	7
Japan and Asia	<1	1	3	3
Total	*6*	*10*	*12*	*17*
p-Aramids				
United States	5	9	8	10
Europe and Russia	<1	4	8	12
Japan and Asia	1	1	3	3
Total	*6*	*14*	*19*	*25*

Health and Safety

No matter the process, the safety requirements in the production of aramid fibers and films are substantial. The monomers used in these processes are highly toxic and are sometimes handled at high temperatures (7). They require protective clothing and great care to avoid any contact. At least one potential solvent for the polymerization (HMPA) was found to be carcinogenic in rats (59) and was discontinued as the solvent for the commercial process. Sulfuric acid is used in the fiber formation of PPTA, and protective clothing is a requirement for all personnel who enter the spinning area. The high strength of PPTA fibers makes handling the yarn at high speed a hazardous enterprise, and special training of production workers is especially important.

PPTA and MPDI are relatively safe products that present minimal risk to human health and the environment. MPDI fabrics have been worn for over 30 years without significant effect on the skin, and PPTA products have a similar history. The Food and Drug Administration now provides that many forms of PPTA fiber may be safely used as components of articles that come in repeated contact with food.

During the processing of these fibers some respirable fibrous particles are always produced, and inhalation of these particles should be minimized. Adherence to good industrial hygiene practices for ventilation and cleanup will protect against significant exposure (60).

BIBLIOGRAPHY

"Polyamides, Aromatic" in *EPSE* 2nd ed., Vol. 11, pp. 381–409, by J. Preston, Research Triangle Institute.

1. Belg. Pat. 569760 (1958) (to E. I. du Pont de Nemours & Co., Inc.).
2. U.S. Pat. 3006899 (Oct. 31, 1961) H. W. Hill, S. L. Kwolek and P. W. Morgan (to E. I. du Pont de Nemours & Co., Inc.).
3. U.S. Pat. 3063966 (Nov. 13, 1962), S. L. Kwolek, P. W. Morgan, and W. R. Sorenson (to E. I. du Pont de Nemours & Co., Inc.)
4. H. H. Yang, *Aromatic High-Strength Fibers*, John Wiley & Sons, New York, 1989, pp. 70–111
5. J. Preston, *Encyclopedia of Polymer Science and Technology*, 2nd ed., Wiley-Interscience, New York, 1988
6. S. Ozawa, *Polym. J. (Tokyo)* **19**, 119 (1987)
7. J. K. Stille and T. W. Campbell, *Condensation Monomers*, John Wiley & Sons, New York, 1972, p. 558
8. U.S. Pat. 2619503 (Nov. 25, 1952), R. G. Benner and A. C. Stevenson (to E. I. du Pont de Nemours & Co., Inc.)
9. U.S. Pat. 2894036 (July 7, 1959), D. E. Graham (to General Aniline and Film Corp.)
10. H. M. Caesar, *Chemical Fibers International*, 161–164 Apr., (2000)
11. Jpn. Pat. 01085951 (Mar. 30, 1989), H. Oshino, E. Mine, and K. Sumitani (to Teijin Chem. Ind.)
12. Jpn. Pat. 63041434 (Feb. 22, 1988), H. Oshino, A. Namatame, and K. Sumitani (to Teijin Chem. Ind.)

13. Brit. Pat. 946491 (Jan. 15, 1964) and 949574 (Feb. 12, 1964) (to Diamond Alkali Corp.)
14. U.S. Pat. 3318950 (May 9, 1967), F. J. Christoph Jr., S. H. Parker, and R. L. Seagraves (to E. I. du Pont de Nemours & Co., Inc.)
15. R. Takatsuka and co-workers, *J. Polym. Sci.* **15**, 1905 (1977)
16. A. K. Chaudhuri, B. Y. Min, and E. M. Pearce, *J. Polym. Sci., Polym. Chem. Ed.* **18**, 2949 (1980)
17. U.S. Pats. 3671542 (June 20, 1972) and 3819587 (June 25, 1974), S. L. Kwolek (to E. I. du Pont de Nemours & Co., Inc.)
18. M. Arpin and C. Strazielle, *Polymer*, **18**, 591 (1977)
19. V. N. Tsvetkov, *Rigid-Chain Polymers*, Consultants Bureau, New York, 1989
20. F. W. Billmeyer Jr., *Textbook of Polymer Science*, John Wiley & Sons, Inc., New York, 1984, Chapts. "7" and "8".
21. P. W. Morgan, *Condensation Polymers: By Interfacial and Solution Methods*, Wiley-Interscience, New York, 1965
22. S. L. Kwolek, and co-workers, *Macromolecules* **10**, 1390 (1977)
23. T. I. Bair, P. W. Morgan, and F. L. Killian, *Macromolecules* **10**(6), 1396 (1977)
24. A. A. Federov, V. M. Savinov, and L. B. Sokolov, *Polym. Sci. USSR* **12**, 2475 (1970)
25. U.S. Pat. 4308374 (Dec. 29, 1981), L. Vollbracht and T. J. Veerman (to AKZO NV); U.S. Pat. 4297478 (Oct. 27, 1981), V. Rocklus, J. Sacco (to Rhône-Poulenc-Textile)
26. U.S. Pat. 4169932 (Oct. 2, 1979), L. B. Sokolov, V. M. Savinov, and V. S. Petrukhin
27. U.S. Pat. 4684409 (Aug. 4, 1987), J. D. Hodge and K. S. Lee (to E. I. du Pont de Nemours & Co., Inc.)
28. S. Ozawa, and K. Matsuda, *Handbook of Fiber Science and Technology, Vol III: High Technology Fibers, Part B*, Marcel Dekker, Inc., New York, 1989
29. U.S. Pat. 4075172 (Feb. 21, 1978), S. Ozawa, and co-workers, (to Teijin Ltd.)
30. H. Fujie, *Nikkakyo Geppo* **40**, 8 (1987)
31. R. M. Ikeda, and co-workers, *J. Appl. Polym. Sci.* **25**, 1391 (1980)
32. Jpn. Pat. 54033591 (Mar. 12, 1979), F. Takashi, N. Hirosaku, and M. Toshiaki (to Asahi Chemical Industry Co., Ltd)
33. *Chemical Economics Handbook—Specialty Organic Fibers (Aramid Fibers)*, SRI International, Menlo Park, Calif., Nov. 1999.
34. *Japan Chemical Week*, and Feb./Apr. 1999
35. U.S. Pat. 3287324 (Nov. 22, 1966), W. Sweeny (to E. I. du Pont de Nemours & Co., Inc.)
36. U.S. Pat. 3767756 (Oct. 23, 1973), H. Blades (to E. I. du Pont de Nemours & Co., Inc.)
37. U.S. Pat. 3850888 (Nov. 26, 1974), J. A. Fitzgerald and K. K. Likhyani (to E. I. du Pont de Nemours & Co., Inc.)
38. U.S. Pat. 5667743 (Sept. 16, 1997), T. M. Tai and co-workers, (to E. I. du Pont de Nemours & Co., Inc.)
39. P. J. Flory, *Proc. R. Soc. London, Ser. A* **234**, 73 (1956)
40. U.S. Pat. 3414645 (Dec. 3, 1968), H. S. Morgan (to Monsanto Co.)
41. U.S. Pats. 3869429 and 3869430 (Mar. 4, 1975), H. Blades (to E. I. du Pont de Nemours & Co., Inc.)
42. U.S. Pat. 4500278 (Feb. 19, 1985), S. R. Cochran (to E. I. du Pont de Nemours & Co., Inc.)

43. U.S. Pat. 5009830 (Apr. 23, 1991), T. S. Chern (to E. I. du Pont de Nemours & Co., Inc.)
44. U.S. Pat. 3018091 (Jan. 23, 1962), R. B. Duggan (to E. I. du Pont de Nemours & Co., Inc.)
45. U.S. Pat. 3756908 (Sept. 4, 1973), G. C. Gross (to E. I. du Pont de Nemours & Co., Inc.)
46. U.S. Pat. 4752643 (June 21, 1988), T. Imanishi and S. Muraoka (to Asahi Chemical Industry Co, Ltd.)
47. H. H. Yang, *Kevlar® Aramid Fiber*, John Wiley & Sons, Inc., New York, 1993
48. K. Tashiro, M. Kobayashi, and H. Tadokoro, *Macromolecules* **10**, 413 (1977)
49. M. G. Dobb, D. J. Johnson, and B. P. Saville, *J. Polym. Sci., Polym. Phys. Ed.* **15**, 2201 (1977)
50. R. J. Morgan, C. O. Pruneda, and W. J. Steele, *J. Polym. Sci., Polym. Phys. Ed.* **21**, 1757 (1983)
51. R. E. Wilfong and J. Zimmerman, *J. Appl. Polym. Sci., Polym. Symp.* **31**, 1 (1977)
52. V. Gabara, in H. Brody, ed. *Synthetic Fibre Materials*, Longman Scientific and Technical, Essex, England, 1994, Chapt. "9".
53. Technical Guide for NOMEX® Brand Fiber, H-52703, E. I. du Pont de Nemours & Co., Inc, Wilmington, Del., Apr. 1999; Technical Guide for KEVLAR® Aramid Fiber, H-77848, E. I. du Pont de Nemours & Co., Inc., Wilmington, Del., Apr. 2000; Forgoing the Future with KEVLAR®, H-51009, E. I. du Pont de Nemours & Co., Inc., Wilmington, Del., Oct. 1997; Teijinconex®—Technical Information, CN02/91.2, Teijin Ltd., Japan; Teijinconex® Aromatic Polyamide Fiber, Tejin Ltd., Japan; High Tenacity Aramid Fiber: Technora®, Teijin Ltd., Japan; Twaron®—Product Information: Yarns, Fibers and Pulp, Akzo Fibers Division, the Netherlands; Twaron® in Brake Linings and Clutch Facings, Akzo Nobel, the Netherlands.
54. J. G. Hust, *Cryogenics* **15**, 126–128 (1975)
55. S. Yasufuku, *IEEE Electrical Insulation Magazine* **11**(6), 27–33 (1995)
56. Technical Brochure, Aramica Film, 1991 Asahi Chemical Industry America, Inc.
57. NOMEX® Aramid Paper Type 410—Typical Properties, H-22368, E. I. du Pont de Nemours & Co., Wilmington, Del., Aug. 1998.
58. G. L. Hendren, and co-workers, *Advanced Materials*, **10** 1233–1237 (1998)
59. J. A. Zapp Jr., *Science* **190**, 422 (1975)
60. E. I. du Pont de Nemours & Co., Inc., Properties and Processing of DuPont KEVLAR® Aramid Yarn for Mechanical Rubber Goods, A-88950, June 1993.

GENERAL REFERENCES

P. W. Morgan, *Condensation Polymers: By Interfacial and Solution Methods*, John Wiley & Sons, Inc., New York, 1965.
W. B. Black and J. Preston, eds., *High Modulus Wholly Aromatic Fibers*, Marcel Dekker, Inc., New York, 1973.
H. H. Yang, *Aromatic High-Strength Fibers*, John Wiley & Sons, Inc., New York, 1989.

H. H. Yang, *Kevlar Aramid Fiber*, John Wiley & Sons, Inc., New York, 1993.
V. Gabara, in H. Brody, ed., *Synthetic Fibre Materials*, Longman Scientific and Technical, Essex, England, 1994, Chapt. "9".

J. GALLINI
E. I. du Pont de Nemours, & Company, Inc.

POLYAMIDES, FIBERS

Polyamide fibers are spun from linear thermoplastic polymers having recurring amide groups made from diamines and dicarboxylic acids $(CONH{-}R{-}NHCO{-}R')_n$ or lactams $(RCONH)_n$. Polyamides are generally referred to as nylons when R and R′ are essentially aliphatic, alicyclic, and less than 85% of the amide linkages are attached directly to two aromatic rings. When these linkages are equal to or greater than 85% aromatic, the fibers are referred to as aramids. Polyamides from the condensation of diamines and dicarboxylic acids are termed AABB type, and those from lactams, AB type. Aliphatic polyamides are identified by numerals that indicate the number of carbon atoms in the monomer. One number is used for the AB type and two numbers, the first designating the diamine, for the AABB type. For example, the polyamide made from caprolactam (six carbons) is nylon-6 [25038-54-4], and those from hexamethylenediamine and adipic acid, nylon-6,6 [9011-56-6]. Monomers containing ring structures are coded by either a single letter such as T for terephthalic acid (nylon-6,T) or an abbreviated form such as PACM for bis(*p*-aminocyclohexyl)methane, eg, PACM-12. In designating a random copolyamide, the components are named in order of decreasing percentages, followed by their weight percentages in parentheses. For example, if hexamethylenediamine adipic acid, sebacic acid, and dodecanedioic acid are copolymerized to give 50% nylon-6,6, 40% nylon-6,10, and 10% nylon-6,12, the product can be designated as nylon-6,6/6,10/6,12 (50/40/10). A block copolyamide, which is made by melt-blending two polyamides or a yarn consisting of fibers spun from two different polymer melt streams such as nylon-6,6 and nylon-6,10, can be designated as nylon-6,6//6,10 (50//50).

Wallace H. Carothers and his research team at DuPont discovered nylon-6,6, which is covered in his patents issued in 1937 and 1938. Diamines from C_2 to C_{18} were synthesized and reacted with aliphatic and aromatic dicarboxylic acids to make polyamides, which were then melt spun and evaluated as fibers. Nylon-6,6 was ultimately selected for scale-up and development because of its favorable

Encyclopedia of Polymer Science and Technology. Copyright John Wiley & Sons, Inc. All rights reserved.

melting point (~260°C), best balance of properties, and lower manufacturing cost. DuPont announced nylon-6,6 as the first synthetic fiber on Oct. 27, 1938, completed the pilot plant in Wilmington, Delaware, in July 1938, and introduced nylon to the market as Exton bristles for Dr. West's toothbrushes (1). The first nylon filament plant was built in 1939 at Seaford, Delaware, and nylon stockings went on sale nationally on May 15, 1940.

In 1929, while employed at the Agfa Film Factory near Leipzig, Germany, Paul Schlack discovered caprolactam, the intermediate for nylon-6 (2). He polymerized caprolactam to nylon-6 and was granted a patent in 1941 assigned to I. G. Farbenindustrie (3). Nylon-6 was developed and commercially introduced as Perlon in 1940 (4,5). I. G. Farbenindustrie had evaluated many polyamide constituents without finding an improvement over nylon-6 and nylon-6,6 (6). In Italy, Societa Rhodiaceta started making nylon-6,6 in 1939. In the United Kingdom, ICI and Coutaulds formed British Nylon Spinners in 1940 and started to manufacture nylon-6,6 in 1941. In the United States, Chemstrand started spinning nylon-6,6 in 1952, and by 1955 Allied Chemical, American Enka, and Industriale Rayon started spinning nylon-6 fibers.

Approximately 4×10^6 t of nylon fiber is produced annually worldwide; nylon-6 and nylon-6,6 account for about 98% of the total production. Nylon fibers are used in the flooring, apparel, industrial and transportation industries. The advantages of nylon fibers over other synthetic fibers are high strength, durability, resilience, ease of dyeability, and low specific gravity.

In 1998, the worldwide nylon fibers market was shared by DuPont with 27%; BASF, 9%; Rhodia, 9%; Solutia, formerly Monsanto fibers, 7%; AlliedSignal, 7%; and the remaining 41% by many smaller manufacturers (7). The downturn in the fiber business, worldwide recession, overcapacity, and competition from polyester fibers in the late 1980s led to acquisitions and merges. Some mills started to melt spin their own fibers, notably nylon-6, during this period (8,9).

Properties of Nylon-6 and Nylon-6,6

Both the inherent properties and those that can be engineered into the fiber and ultimately into the fabricated article account for the diverse end uses of nylon. For every end use, the fiber must offer performance and/or a perceived market value, meet mill acceptance standards, and have favorable economics.

The properties of textile fibers can be divided into three categories—geometric, physical, and chemical—which can be measured with available methods (10–12). Perceived values such as tactile aesthetics, style appearance of apparel fabrics, comfort of hosiery, as well as color, luster, and plushness of carpets are difficult to quantify and are not always associated with the properties of the fiber, but rather with the method of fabric construction and finishing.

The most useful synthetic fibers for textile applications are linear, semicrystalline, oriented polymers, whose properties are defined by molecular structure and molecular organization. The first level of molecular organization is the chemical structure that defines the structure of the repeating unit in the base polymer

and the nature of the polymeric link. This relates directly to chemical reactivity, dyeability, moisture absorption, and swelling characteristics, and indirectly to all physical properties. Macromolecular structure, the second level, describes the family of polymer molecules in terms of chain length, chain-length distribution, chain stiffness, molecular size, and molecular shape. The third level, supermolecular organization, describes the arrangement of the polymer chains in three-dimensional space. Levels two and three are directly related to the physical properties of textile fibers and have a significant bearing on some of their chemical characteristics. The chemical and macromolecular structures of polyamide fibers can be determined by chemical and instrumental analysis (13). The supermolecular organization of nylon-6 and nylon-6,6 have been defined in terms of crystallinity, crystalline and amorphous orientation, and chain folds by xrd, fiber density, dsc, and nmr methods (10,14–18).

Molecular chains in a polyamide fiber are held in specific structural configurations by weak van der Waal and strong intermolecular hydrogen-bonding forces between amide groups. An increase in the number of amide bonds raises the melting point in a homologous series, with the AABB type having the higher melting points T_m in the series (Fig. 1). AABB polymers have a more symmetrical repeating unit than AB. Other things being equal, the more symmetrical the repeating unit, the higher the T_m.

Nylon-6 and nylon-6,6 are isomers that share the same empirical formula, $C_6H_{11}NO$; density, 1.14 gm/cm^3; refractive index n_D, 1.530 (unoriented fiber); and many other properties (19). However, they differ in melting point by 40°C because of differences in the alignment of molecular chains and crystallization behavior (18). These parameters are important in fiber formation in melt spinning, but are not as significant as the glass-transition temperature T_g in the downstream processing of the fiber into a specific end-use article (20). The T_g which signifies a transition from a glassy to a rubbery state, plays a role in the drawing, texturing, and dyeing of a fiber. By controlling melt spinning and downstream processing, the fiber properties of both nylon types can be adjusted to accommodate a variety of end-use performance requirements.

Tensile Properties. Tensile properties of nylon-6 and nylon-6,6 yarns, shown in Table 1, are a function of polymer molecular weight, fiber spinning speed, quenching rate, and draw ratio. The degree of crystallinity and crystal and amorphous orientation obtained by modifying elements of the melt-spinning process have been related to the tenacity of nylon fiber (18).

Tensile properties of synthetic and natural fibers (or yarn) are measured from stress–strain curves as shown in Figure 2. These measurements are not only important in determining the suitability of a nylon fiber for a specific end use, but also in comparing it to other fiber types. Nylon staple generally has higher elongation but similar tenacity to regular nylon filament because of differences in melt-spinning conditions, such as draw ratio and quench rate, and because it is usually a crimped product. Both nylon fiber forms have a lower modulus than polyester, cotton, silk, Nomex and Kevlar; the last two are aramids produced by DuPont. Increasing the tenacity increases the modulus of nylon, but it is still lower than polyester and Kevlar. The toughness of nylon is approximately 20% higher than polyester and much higher than silk, cotton, wool, Nomex and Kevlar.

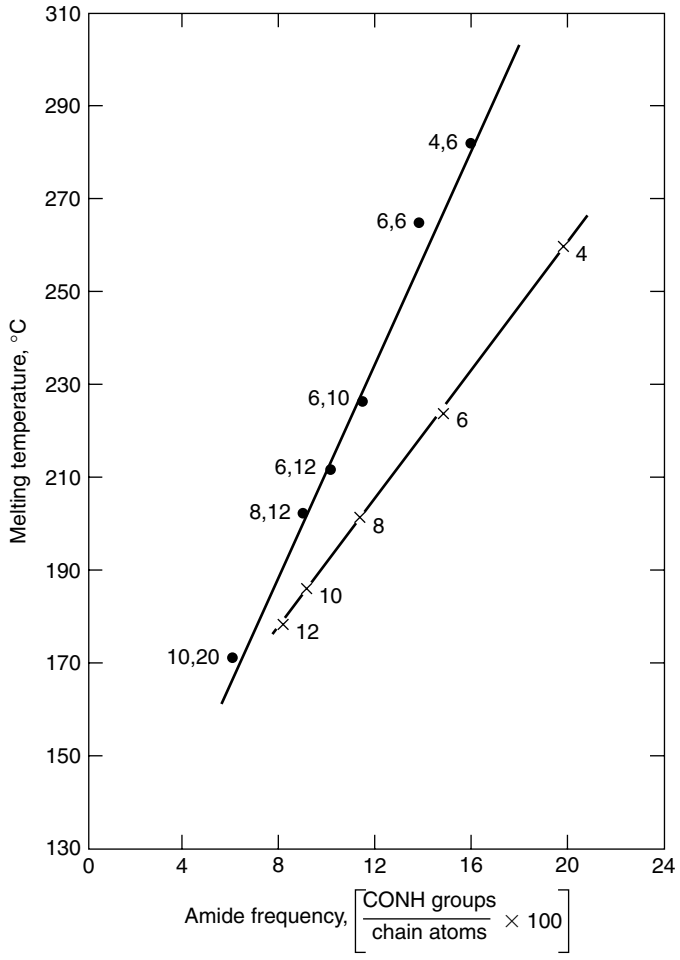

Fig. 1. Effect of amide frequency on the melting points of AB-type (×) and AABB-type (•) polyamides. The number on the curves indicate the specific nylon.

Definitions of the commonly measured tensile properties are as follows: *Linear density* (tex) is the weight in grams of 1000 m of yarn. *Tenacity* (N/tex). is the tensile stress at break and is expressed in force-per-unit linear density of unstrained specimen. *Knot tenacity* is the tensile stress required to rupture a single strand of yarn with an overhand knot tied in the segment of sample between the testing clamps. It is expressed as force-per-unit linear density and is an approximate measure of the brittleness of the yarn. *Loop tenacity* is the tensile stress required to rupture yarn when one strand of yarn is looped through another and broken. It is expressed as force-per-unit linear density. Loop tenacity is an indication of brittleness, but is not considered as sensitive as the knot test. Reported values are one-half the actual test values.

Breaking strength is the maximum load required to rupture a fiber. It is expressed in grams. *Tensile strength* is the maximum stress or load per unit area

Table 1. Tensile Properties of Nylon-6 and Nylon-6,6[a] Continuous-Filament Yarns[b]

	Nylon-6		Nylon-6,6	
Property	Regular tenacity	High tenacity	Regular tenacity	High tenacity
Breaking tenacity, N/tex[c]				
Standard	0.35–0.64	0.57–0.79	0.20–0.53	0.52–0.86
Wet	0.33–0.55	0.51–0.72	0.18–0.48	0.45–0.71
Loop	0.34–0.49	0.45–0.89	0.18–0.45	0.44–0.67
Knot	0.34–0.48	0.42–0.59	0.18–0.45	0.44–0.67
Tensile strength, MPa[d]	503–690	703–862	275–731	593–924
Breaking elongation, %				
Standard	17–45	16–20	25–65	15–28
Wet	20–47	19–33	30–70	18–32
Average modulus (stiffness), N/tex[c]	1.6–2.0	2.6–4.2	0.44–2.1	1.9–5.1
Average toughness, N/tex[c]	0.06–0.08	0.06–0.8	0.07–0.11	0.07–0.11
Elastic recovery, %	98–100 at 1–10%	99–100 at 2–8%	88 at 3%	89 at 3%
Moisture regain at 21°C, %				
65% RH	2.8–5.0	2.8–5.0	4.0–4.5	4.0–4.5
95% RH	3.5–8.5	3.5–8.5	6.1–8.0	6.1–8.0

[a]Conditioned at 65% RH and 21°C.
[b]Ref. 21.
[c]To convert N/tex to g/den, multiply by 11.33.
[d]To convert MPa to psi, multiply by 145.

in units of Pascal (1 MPa = 145 psi). Tensile strength (MPa) = tenacity (N/tex) × specific gravity × 1005. *Elongation at break* is the increase in sample length during a tensile test and is expressed as a percentage of original length. *Tensile modulus*, ie, Young's modulus, also called *initial modulus* or *elastic modulus*, is the load required to stretch a specimen of unit cross-sectional area by a unit amount. It is expressed as the ratio of the tensile stress divided by the tensile strain in the initial straight-line portion of the stress–strain curve, extrapolated to 100% sample elongation. *Work-to-break* is the actual work required to rupture the material. It is proportional to the total area under the stress–strain curve. *Yield point*, or *elastic limit*, is the point on the stress–strain curve where the load and elongation cease to be directly proportional. It is the point at which the stress–strain curve deviates from the tangent drawn to the initial straight-line portion of the curve, as in tensile modulus determinations.

Creep is the change in shape of a material while subject to a stress; it is time-dependent. *Elasticity*, the ability of a fiber to return to its original dimensions upon release of a deformation stress, is described by the tenacity of the yield point on the stress–strain curve. *Toughness*, the ability of a fiber to absorb work before it ruptures, is evaluated from the area under the total stress–strain curve. The toughness index is defined as one-half the product of the stress and strain at break

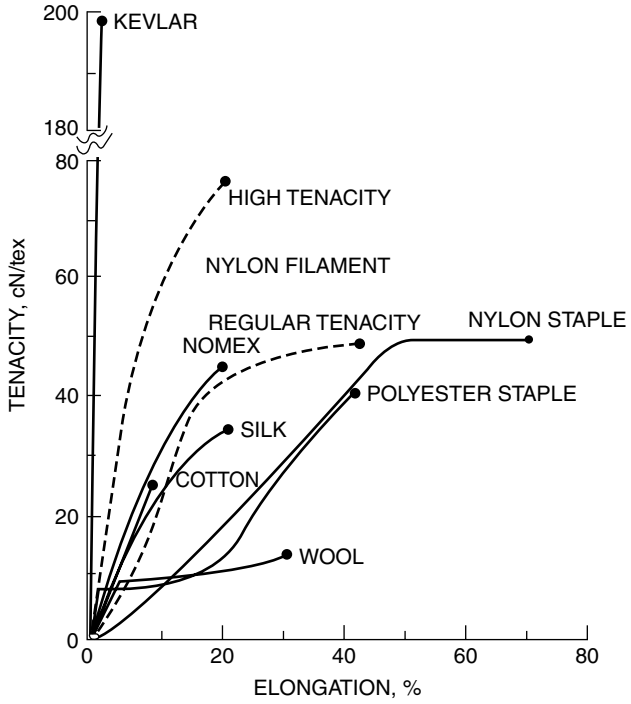

Fig. 2. Stress–strain curves of some textile fibers (22). To convert cN/tex to N-tex, divide by 100.

and is also in units of gram-per-unit linear density. *Creep and recovery* define the plasticity or plastic flow of a fiber in relation to load and time (21). At a critical applied load above the yield point, the fiber extends very rapidly and continues to extend at a much slower rate as time progresses, spanning from a few seconds to over a month. When the load is removed, the reverse process occurs. The fiber recovers part of its extension very rapidly and then begins to contract over a period of time (delayed recovery). The recovery is a relaxational phenomenon where the stress that generated the deformation is dissipated as a function of time, which in effect is complimentary to creep. The quantification of the plastic flow of a fiber resulting from molecular motions induced by the deformation and recovery processes is dependent on load, time, and temperature (22).

Elastic recovery is the ability of a fiber to regain its original form after being stretched at a specified percentage of its length. Shrinkage induced by hot–wet treatment of a fiber is also a form of stress relaxation. Compared to other fibers, nylon fibers have an outstanding degree of elasticity, recovering well from high loads and extension.

Temperature and Moisture Properties. Thermal treatment and moisture affinity significantly influence the physical properties of nylon fibers and fabrics. The absorption of water causes the fiber to swell, which alters its dimensions and in turn changes the size, shape, stiffness, and permeability of yarns and fabrics. It also alters the frictional and static behavior of yarns in mill processing as well as the performance of fabrics during use. Water, a powerful plasticizer for

nylon, preferentially penetrates the amorphous regions, readily hydrogen-bonds to the amide, and increases molecular chain mobility (23–28). As a result, the absorbed water lowers tensile modulus, the work to elongate and work recovery (29,30), and the glass-transition temperature (31). The crystallinity of nylon also increases as it absorbs water (32), which breaks up intermolecular hydrogen bonding and allows the hydrocarbon chain segments to pack better. Water also affects the heat setting properties of nylon yarns and fabrics (33,34). The moisture regain of nylon-6 and nylon-6,6 is shown in Table 1. For comparison, polyester has a moisture regain of approximately 0.4%, acrylic 1.5%, cotton 8%, and wool 16%.

Because of water's plasticizing effect, the water content of nylon fibers and fabrics must be known and controlled when measuring physical properties. Prior to the measurement, samples are conditioned at a specified temperature and relative humidity (rH) for at least 24 h.

Nylon-6 softens at 170°C and melts at 215–220°C. Nylon-6,6 softens at 234°C and melts at 255–260°C. Nylons also have thermal behavior properties between the melting and glass-transition temperatures that are important in fiber melt spinning and drawing and in fiber-to-fabric processing. These behavior properties are the result of relaxational phenomena due to the onset of mobility of the aliphatic chain segments in the amorphous and crystalline regions and occur between 70 and 180°C (28,35). Typical unrestrained nylon-6,6 fibers begin to shrink as the temperature increases from 25 to 70°C with the application of dry heat. At 70°C the fiber undergoes crystallization that tends to reduce chain mobility. From 70 to 115°C the fiber continues to shrink and at 115–125°C loses absorbed and bonded water. The crystal structure also changes from the triclinic to the hexagonal form. At 170–180°C, the hexagonal crystals begin to break up and the polymer chains take on a fluid-like mobility. Because of its higher temperature profile, nylon-6,6 requires higher fiber melt processing, texturing, heat setting (36), and end-use application temperatures (eg, thermal bonding) than nylon-6.

Electrical Properties. Nylon has low electrical conductivity (high electrical resistivity) and behaves like an insulator. Nylon-6 has a resistivity of 6×10^{14} Ω·cm when dry and a resistivity of 2×10^{8} Ω·cm when conditioned at 100% (RH) at 20°C (37); nylon-6,6 responds similarly.

Because of its insulating nature, nylon can accumulate positive or negative electrical charges on its surface when rubbed or in contact with other substances, followed by separation. These charges do not dissipate readily and can cause problems in fiber processing and certain end-use applications. Consequently, antistatic agents are added to spin finishes to facilitate fiber processing, conductive fibers are added to carpets to prevent static shock, and antistats are added to the fibers to prevent static cling of women's slips.

The dielectric constant of nylon-6,6 (at 1000 Hz) is 4.0 at 22°C and 18% (rH), and increases to 20.0 when wet (38).

Optical Properties. When light falls on a nylon fiber, it can be partially transmitted, absorbed, or reflected, depending on the cross-section shape and the nature of any second substance added during polymerization or melt spinning. Additive-free nylon with a standard round cross section has a translucent high sheen luster. The inherent luster of the fiber and the color introduced in dyeing are important optical properties that relate to a fabric's visual quality and its acceptance by the customer. Fibers that need to be opaque or to cover well in

certain applications such as apparel are melt spun from polymer containing TiO_2 delusterant.

Optical properties also provide useful structure information about chemically similar fibers. The orientation of the molecular chains of a fiber can be estimated from differences in the refractive indexes measured with the optical microscope, using light polarized in the parallel and perpendicular directions relative to the fiber axis (39,40). The difference of the principal refractive indexes is called the *birefringence*, which is generally used to monitor the orientation of nylon filament in melt spinning (43). Birefingence can also be used to distinguish nylon from other chemically dissimilar fiber types as illustrated:

	Refractive index		Birefringence
	$n_{\parallel}$	$n_{\perp}$	$(n_{\parallel}—n_{\perp})$
Nylon	1.578	1.522	0.056 (Strong)
Polyester	1.706	1.546	0.160 (Intense)
Acrylic	1.511	1.514	−0.003 (Weak)

Chemical Properties. The chemical reactivity of nylon is a function of the amide groups and the amine and carboxyl ends. The aliphatic segment of the chain is relatively stable.

Solvolysis and Reactivity. Generally, nylon is insoluble in organic solvents, but soluble in formic acid, some phenolic solvents, and fluorinated alcohols such as hexafluoro-2-propanol. Nylon is relatively inert to alkalies. Dilute solutions of strong mineral acids, such as sulfuric and hydrochloric, weaken nylon fibers and hydrolyze them at high concentration and elevated temperature. Strong oxidizing agents and mineral acids such as potassium permanganate solution and nitric acid degrade nylon. Nylon, however, can be bleached in most bleaching solutions common to household and commercial mill applications. Nylon can be hydrolyzed by water under pressure at 150°C and above. The amine end group of a nylon fiber can undergo the same reactions as primary amines, such as neutralization, acylation, and dehydrohalogenation of alkylbromides at elevated temperatures (41).

The amine ends also react with atmospheric contaminants, such as SO_2 and oxides of nitrogen and ozone, under ambient storage conditions (42). This phenomenon is referred to as aging and results in reduced acid-dye affinity.

Thermochemical Properties. Thermal oxidation of nylon-6 and nylon-6,6 starts to occur at 120–140°C, ultimately leading to product yellowing and strength loss. Prolonged exposure at 50–60°C above the melting point will cause crosslinking and the formation of gel, and in the case of nylon-6, depolymerization emitting caprolactam. Thermal degradation of polyamides involves complex chemical reaction paths that are a function of the chemical structure, temperature, length of time exposed, and levels of moisture and oxygen.

The preferred and also the most effective thermal stabilizers for nylon subjected to hot-stretching in tire cord manufacturing are salts and organic derivatives of copper (43–47). The copper salt is added before polymerization at concentrations that give 30- to 70-ppm Cu in the spun yarn. Alkali metal iodides or bromides are also added at 0.1–0.3% for synergism and stabilization of the

cuprous/cupric moieties during melt processing (48). Organic antioxidants such as hindered phenols alone and in combination with organic phosphites are moderately effective.

Photolytic Properties. The extent of photodegradation of nylon-6 and nylon-6,6 depends on the intensity and spectral distribution of the light source, the length of time exposed, humidity, air quality, and the presence of photosensitizers on and below the fiber surface. Photosensitizers include the degradation products created during melt spinning and high temperature fiber processing, TiO_2 (the standard fiber delusterant), iron salt contamination, as well as certain dyes and dye bath chemicals. The chemistry of the photodegradation of nylon is as complex as thermal degradation and has also been studied extensively (49,51–53).

Nylon-6 and nylon-6,6 fibers degrade when exposed directly to sunlight outdoors and under glass or to a source of uv radiation in the 300- to 400-nm wavelength range, resulting in the formation of hydroperoxides, chain scission, yellowing, and strength loss (53). In contrast, polyester, if shielded by glass, and acrylic fibers have outstanding resistance to direct sunlight. Polyester is therefore preferred for window curtain fabric and acrylic for outdoor furniture.

The prepolymer copper-based antioxidants described earlier are also effective photostabilizers for nylon and are used in yarns for parachutes. Soluble copper salts (eg, $CuSO_4$) can also be applied to fibers as part of the finish or to fabrics as post-treatments to protect against uv exposure.

The TiO_2 delusterant is photostabilized by adding manganese salts of pyrophosphorous acids, phosphites, and phosphates (54,56,57) in the prepolymer, or by using TiO_2 coated with a manganese compound (57,58).

Staple Properties. In contrast to continuous filament, spun nylon staple yarns have a softer, warmer tactile hand and a more natural appearance. Nylon staple is used as the pile material in plush carpets and woven velour automotive upholstery fabrics because of its high strength, abrasion resistance, and ease of recovery from pile crush and distortion. It is also used in blends with natural fibers and regenerated cellulosics and acrylics primarily to add strength in yarn spinning of both coarse and fine count yarns and for weaving apparel greige goods.

To accommodate the various uses in 100% form and in blends, the tenacities and elongations of the nylon staple offerings range from 0.3 to 0.6 N/tex (3–7 g/denier) and from 50 to 100% elongation. Most other fiber properties of nylon staple differ little from those of the continuous filament; property characteristics of nylon-6 and nylon-6,6 are similar.

The multiplicity of nylon blends, processing systems, and uses requires a large variety of staple types. Tex per filament may be 0.1–2 (1–20 denier), the cross section may be round or modified, the luster may be bright or dull, crimp may be present or absent, and the fiber may be heat-set or not, depending on its use. The staple length is about 4 cm for cotton system processing, 5–7 cm for the woolen system, 8–10 cm for the worsted system, and about 18–20 cm for carpet staple.

Preparation of Nylon-6 and Nylon-6,6 Polymer

Fiber quality polymer requires that ingredients have optimum purity; are protected from exposure to oxygen; the equipment be maintained, cleaned,

and purged; and new additives be pretested for melt stability and polymer reactivity.

Hexamethylenediamine [124-09-4] and adipic acid [124-04-9] are used in the commercial production of nylon-6,6, and ε-caprolactam [105-60-2] is used for nylon-6.

Nylon-6,6 is made by the polycondensation of hexamethylene diamonium adipate salt with removal of water.

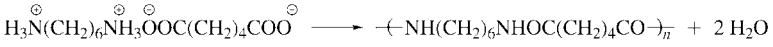

The diamine and diacid react in equimolar quantities to form a salt having a pH of 7–7.5 and stored as a 50–60% aqueous solution. Nylon-6,6 can be polymerized in either a batch or continuous process. In the batch process, the salt is transferred to an evaporator where it is heated at 150–160°C and concentrated to 80–85% by the removal of water. Additives such as chain terminators, dye modifiers, and antioxidants are introduced. The mixture is pumped into an autoclave purged with nitrogen and heated under pressure from 210 to 275°C until prepolymer having about 4000 molecular weight is formed. At this point, TiO_2 delusterant can be added. The pressure is gradually released and the temperature is maintained to remove more water in order to increase the degree of polymerization. After the molten polymer has equilibrated to the desired molecular weight, it is extruded under pressure in the form of a ribbon, which is quenched on a water-cooled casting wheel and cut into flakes of a specified size. The flake is dried in a flake conditioner and packaged.

The number-average molecular weight is adjusted in the 12,000–15,000 range for apparel fibers, >20,000 for high strength yarns for tires and industrial end uses.

Nylon-6 is the polyamide formed by the ring-opening polymerization of ε-caprolactam. The polymerization of ε-caprolactam can be initiated by acids, bases, or water. Hydrolytic polymerization initiated by water is often used in industry. The polymerization is carried out commercially in both batch and continuous processes by heating the monomer in the presence of 5–10% water to temperatures of 250–280°C for periods of 12 to more than 24 h. The chemistry of the polymerization is shown by the following reaction sequence.

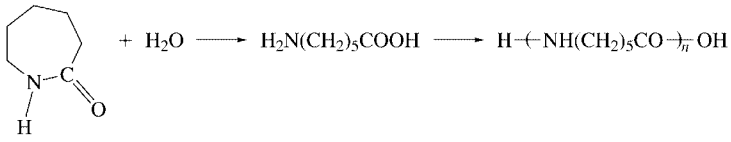

Depending on the final polymerization conditions, an equilibrium concentration of monomers (ca 8%) and short-chain oligomers (ca 2%) remains (59). Prior to fiber spinning, most of the residual monomer is removed. In the conventional process, the molten polymer is extruded as a strand, solidified, cut into chip, washed with water to remove residual monomer, and dried. In some newer continuous processes, the excess monomer is removed from the molten polymer by vacuum stripping.

The addition of small, but specific, amounts of a monofunctional acid to the polymerization is often used to control molecular weights and catalyze reactions. The polymerization is controlled to produce a number-average molecular weight of 18,000–30,000, depending on the end use.

Nylon-6 can be easily polymerized at atmospheric pressure. A continuous process was developed in 1940, called the VK process, which in German stands for *vereinfacht kontinuierlich*, or simplified continuous (60). The VK process is widely used in industry in the 1990s, whereas batch processes, being less economical, are gradually phased out of use. Procedures are also available for making gram quantities of nylon-6 and nylon-6,6 in the laboratory (61).

Manufacture of Nylon-6 and Nylon-6,6 Fibers and Yarns

All commercial linear polyamides that melt at or below 280°C are melt—rather than solution—spun into fiber because melt spinning is more economical.

Polyamide fibers are manufactured by melt spinning (or extrusion), followed by drawing (or stretching). In spinning, the molten polymer is delivered from an extruder or a metal-grid melter, or directly from continuous polymerization located upstream of the spinning machine. The molten polymer passes through a filter and a spinnerette. The emerging molten filaments are quenched by cross-flow air in a vertical chimney, attenuated partially in the molten state to achieve the desired spun tex and partially in the solid state to develop some degree of orientation. The filaments are converged and a finish preparation is applied to the yarn to provide lubrication and static protection prior to winding on a bobbin. In a two-step process, the spun yarn packages are first lagged in a conditioned area to facilitate drawing and to maintain package integrity. The yarns are then drawn to approximately 130% (draw ratio of 1.3) up to 600% (draw ratio of 6.0) of their original length, resulting in higher tensile strength, lower elongation, and oriented crystallization. The drawing process is controlled and modified to achieve the yarn properties for specific end use. Conventional drawing is used for moderate tenacity apparel straight (flat) yarns and heat is applied, followed by a heat-relaxation step for the high tenacity, low shrinkage tire yarns. For carpets and some apparel applications, flat yarns are textured (crimped) to impart softness and fabric cover (bulk).

Combinations of two or more of the above steps into consecutive processes, such as spin–draw or spin–draw–texture, reduce manufacturing costs. In addition to continuous-filament yarn, nylon is also offered in staple, tow, and flock forms. Staple is made by cutting crimped continuous-filament yarn into 3- to 20-cm lengths. In manufacturing, tow is made by combining many yarn ends, either flat or crimped, to give a total tow size of 6–111 ktex. Flock is made by precision-cutting tow into 0·5- to 3-mm fiber lengths.

Spinning Continuous-Filament Yarns

In the first commercial process for melt-spinning nylon, polymer chips were stored under nitrogen pressure in a sealed hopper from which they flowed by gravity to a pancake coil heated by a central Dowtherm system (62). The nitrogen pressure

moved the molten polymer to a gear pump that forced the metered polymer stream through a sand-filled filter pack and a spinneret, both maintained at the desired temperature by the single Dowtherm system for the entire machine. The molten filaments were quenched by a cross flow of air at ambient temperature in a chimney with side panels to prevent outside air disturbances. The quenched filaments were converged over a ceramic guide to form the single threadline per spinnerette. Finish was applied by a roll and the threadline wound on friction-driven bobbins at speeds of a few hundred meters per minute. The spun yarn was taken to another machine, the draw twister, where it was drawn, given twist for coherence, and wound on shipping packages containing about 0.5 kg of yarn.

Over the years, fiber producers have improved on the basic design and developed more efficient spinning machines that have lowered manufacturing costs and improved yarn quality. In the early 1950s, the continuous polymerization (CP) process for nylon was combined directly with the spinning machine to eliminate the use of polymer chips. The capacity of a CP direct-spinning machine can be as high as 70,000 t/year and the machine is used in the production of apparel, carpet, industrial yarn, and staple. Extruders are also used to melt polymer chips. They can be horizontal or vertical, vented or unvented, having capacities up to 5000–7000 t/year.

Molten polymer must be delivered to the spinnerette in precisely metered amounts or the filaments will vary in size and give unacceptable products. A metering pump is installed after the extruder to discharge exact volumes of molten polymer per unit time against pressures as high as 70 MPa (10,000 psi) at temperatures in the 300°C range. The molten polymer is also filtered under high shear to remove gel particles and particulate matter that can clog spinnerette holes. A filtration-shear device is attached directly to the distribution plate and spinneret. The typical pack for spinning low tex yarns is a cylindrical cavity about 3.7 cm in diameter and 3.7 cm in height, filled with layers of sand, the finest on the bottom and the coarsest on top. Fine-mesh screens in the bottom and top of the cavity keep the sand in place. Specially designed screens and sintered metal are replacing the sand. Pack designs must avoid stagnant spots where polymer can be trapped and thermally degrade, thus increasing the pressure drop through the pack and shortening its life.

Early spinnerettes were 316-stainless steel disks, ∼5 cm in diameter, 0.5 cm in thickness, and with 13 round holes. Over the years, the increased productivity demands have led to as many as 500 holes for larger disk spinnerettes and 4000 holes for rectangular shape spinnerettes.

The molten filaments are extruded through the spinnerette down a vertical chimney where they are air-quenched. The filaments are then converged to form the threadline in the V shape formed by crossed ceramic pins or other similar devices. The threadline passes to the floor below where finish is applied and is wound up on the spin bobbins.

In earlier years, the windup speed was 275–375 m/min with 0.5 kg of yarn per bobbin. In the 1990s, winders are designed for 10- to 25-kg bobbins, two or more bobbins per winder, operating at speeds up to 6000 mpm, and equipped with automatic bobbin changers.

A conventional spinning apparatus is shown in Figure 3 (63). Polymer chips are melted in a larger extruder, which, in turn, feeds a manifold spinning line.

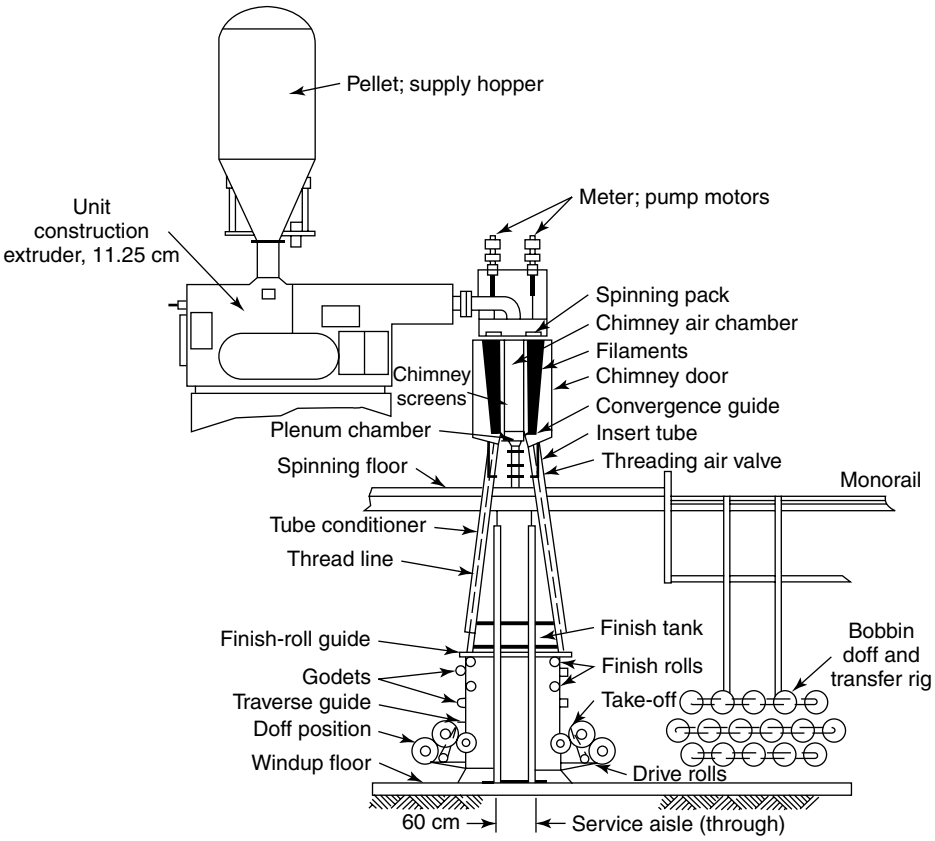

Fig. 3. Conventional melt spinning apparatus. Reproduced with permission from Ref. 66. Copyright © 1966 Noyes Publications.

The feed lines are made as short as possible and the polymer is distributed to a series of spin packs and chimneys where the yarn is quenched. The yarn passes to the tube conditioner, over finish rolls and take-up godet rolls, and then to winders. Spare winders switch over rapidly to a new roll during the doffing operation to avoid yarn loss. The yarns then pass on monorail conveyors to the drawing areas. In plant production, multiple yarns are spun simultaneously, each with many filaments. Efforts must be taken from polymer makeup through spinning to control the uniformity of each end of yarn and to minimize defects that can result in breaks and down time. A significant design trend in spinning has been toward modern short and ultrashort compact machines (64,65). The concept is to have one floor spinning where the maximum distance between spin die and winder is 1.3–2 m compared to conventional processes having up to 5 m between spinnerette plate and winder.

Draw–Twist Process. This is a two-step split process where yarn spun onto bobbins at 300–3000 m/min is lagged and then taken to a draw-twisting operation (Fig. 4a). The degree of drawing or stretching is accomplished by adjusting the speed of the draw rolls, which run faster than the feed rolls. The drawn yarn is

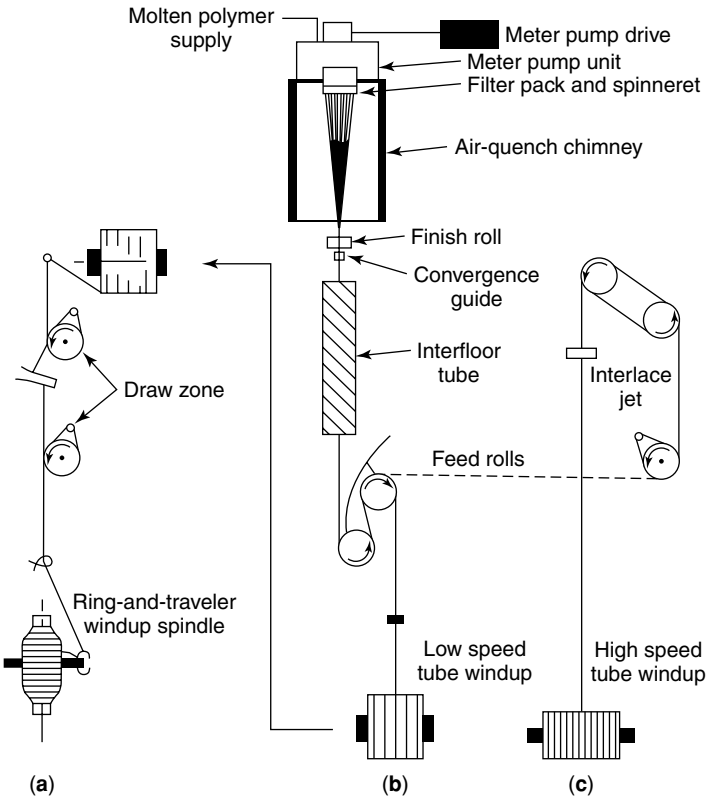

Fig. 4. Melt spin–draw processes for nylon yarn (**a**) draw–twist process, (**b**) conventional spinning process, and (**c**) coupled process.

then twisted for coherence and wound on a pirn with a standard ring-and-traveler mechanism. Yarns for apparel, hosiery, and industrial end uses have been made by this process.

Spin–Draw Process. In the early 1960s, a single-step process was commercialized in which the spinning and drawing steps were combined (Figs. 4b and 4c). This required the development of high speed drawing, winding technology, and air jet interlacing to tangle instead of twisting the yarn. For apparel and carpet yarn end uses, the process utilizes the conventional cold draw; for tire and high strength industrial yarn applications, heated-draw assists such as jets, rotating pins, shoes, roll chests, and yarn relaxation steps are added (66). The spin–draw process has also been combined with continuous polymerization. The double-sided unit in Figure 3 is commonly used where the stretch godets and draw assists are installed before the windup (67,68).

In the coupled process (Fig. 4c), the draw ratio, which affects the tenacity and elongation, lowers with increasing spinning speed. As draw ratio is increased, tenacity and initial modulus increase and elongation decreases.

New Developments in Spinning and Drawing. The continual effort by the fiber producers to increase production, lower manufacturing costs, and improve quality has led to a better understanding of the effects of the spinning and

drawing process on physical and molecular structure of fibers (69–77). The polymer factors that affect melt spinning are molecular weight and polydispersity index, which is the ratio of weight-average molecular weight M_w to number-average molecular weight M_n. M_w is determined by solution viscosity and M_n by end-group analysis. In spinning, the tensile stress of the extruded fiber is affected by the polymer melt viscosity, spinning speed, cooling rate, and its degree of structural orientation.

The earlier work cited was in the 100- to 2400-m/min spinning speed range, but the later effort is focused at 4000–6000 m/min (78,79). The effect of spinning speed on residual drawing was classified by the degree of fiber orientation (80). Low orientation yarns (LOY) have a high residual drawing, low crystallinity, and limited storage stability. These yarns are subsequently processed through the draw-twisting process. Medium oriented yarns (MOY) processed at 1800–2800 m/min are slightly more crystalline, but still have limited storage stability. Partially oriented yarns (POY) processed at 3000–4000 m/min are partially drawn (70–100% elongation) with some residual drawing, but still have low crystallinity. Partially or spin-oriented nylon feed yarns were developed in the early 1970s to meet the needs of increased false-twist texturing speeds (81). In processing, the drawing step is eliminated and the orientation required for draw texturing is controlled in spinning. POY yarns have also been used in the 1990s in the process of draw warping to make flat yarn warps for weaving and knitting (81–84). A process has been defined for making feed yarns that impart excellent uniformity with structure-sensitive large acid dye molecules in dyeing fabrics from warp-drawn yarns (85). Highly oriented yarns (HOY) spun at 4000–6000 m/min are not fully drawn (50–60% elongation). Fully oriented yarns (FOY) with elongations of 20–30% require spinning speeds of well over 6000 m/min.

Molecular weight has a strong effect on the properties of high speed melt-spun nylon. Generally, higher molecular weight leads to higher modulus and filament tenacity and lower elongation to break (86). In spinning POY nylon, the yarn bundle can be transferred directly to winders capable of 4500–6500 m/min, (which is referred to as godetless spinning), or through a set of driven godets (87). Improvements in the processing and properties of nylon-6,6 have been made by modifying quench and windup hardware (64,88), using higher than usual molecular weights (86,89), adding a trifunctional branching agent to increase melt viscosity (90), incorporating minor amounts of hydrogen-bonding agents in high molecular weight polymer (87), and adding pyrogenic silica to the polymer (91). The hydrogen-bonding agents include nylon-6 monomer or 2-methylpentamethylene diamine.

Texturing Processes. Texturing is the conversion of flat continuous-filament yarns to crimped ones so as to simulate properties inherent in natural and synthetic spun staple yarns, such as thermal insulation, fullness, cover (bulk), softness, and moisture transport. In texturing, the geometry and, to a degree, the surface of the filaments are mechanically deformed by bending, twisting, or compressing to introduce permanent wavy (crimp) loops and coils. Prior to the texturing step, heat is applied in the range of 100–190°C to soften the filaments. After texturing, the yarn is cooled to set the crimp and the mechanical deformation is removed by tensioning the yarn during package windup. Texturing affects the tensile properties, dyeability, and the macromolecular structure of the fibers in a

nonuniform way that can cause dye structure and barré problems in dyeing fabrics. Depending on how the filaments have been mechanically deformed and the temperature used, differential stresses and random disoriented molecular chains are set in specific configurations to give one of three classifications of textured yarns: stretch, modified stretch–bulk, or bulk. The textured stretch or bulk is developed when the yarn experiences a stress-relaxing environment under low or no tension, as in steaming hot air, or dyeing. Stretch yarns have high extensibility and good recovery, but only moderate bulk compared to modified stretch and high bulk-textured yarns.

Descriptions of the various texturing processes and latest machine modifications to increase quality, speed, and efficiency have been the subject of numerous reviews (92–96). In air jet or Taslan texturing, the yarn is introduced into a venturi tube in the air jet where the turbulence from a stream of compressed air cause the filaments to entangle and form surface loops. The product has bulk, but no stretch, and the process can be varied to give a range of bulk and novelty effects (97). In false-twist texturing, a specially made yarn is heated by a radiant or contact heater just below the melting point, twisted as high as 30–40 turns/cm, then untwisted and packaged at windup speeds as high as 1200 m/min. Draw-texturing is a continuous process where partially oriented yarns are drawn and false-twist-textured. A continuous high speed spin–draw–false-twist-texturing process for nylon has also been developed (98). False-twist-textured filaments are coiled, have good bulk, but are regarded primarily as stretch yarns.

In another form, bulked continuous-filament (BCF) yarns are spin-drawn and textured with a fluid jet in a continuous one-step process. After drawing, the yarn is heated over rolls in a hot chest and passed through a hot air or superheated steam jet under controlled conditions. In some designs, texturing is achieved by impinging the yarn onto a baffle plate, a screen, or the walls of a specially shaped chamber (99–102). BCF yarns have bulk with some stretch and each filament has a random, three-dimensional curvilinear crimp form. Edge crimping is accomplished by drawing a heated yarn over a knife edge that compresses (flattens) the edge side and stretches the outside of the filament. The metastable stresses so imposed are relaxed during heating, causing the yarn to crimp and coil to give a stretch yarn (103–105). Gear crimping is adaptable to draw-twisting or spin–draw–texture operation and generally used to texture high tex yarns. Stuffer-box crimping is used for both low and high tex yarns and for crimping tow for staple. Most of the crimped nylon made in the United States is stuffer-boxed, gear, false-twist, and air- or fluid-jet-crimped.

Commercial textured yarns cover a range of yarn sizes and end uses. The 1.7- to 3.3-tex (15- to 30-denier) yarns for hosiery are false-twist-textured, as is the 4.4- to 22.2-tex (40- to 200-denier) yarns for apparel. The 56- to 333-tex (500- to 3000-denier) yarns for carpets, upholstery, and soft-sided luggage are air- and fluid-jet-textured.

Most of the textured apparel and industrial yarns are woven or knitted directly into fabric. The carpet BCF yarns can be tufted directly off package into loop pile or velvet constructions. For the textured saxony constructions, the BCF and the spun staple yarns must be ply-twisted and heat-set. The heat-setting temperature for nylon-6 and nylon-6,6 is 180–220°C in hot–dry atmosphere, and 120–140°C in saturated steam. The yarns are twist-set in pressurized autoclaves

or continuously on the Superba and Suessen machines (106). Before setting the twist, the yarn is heated and relaxed for predevelopment of the bulk.

Staple Fiber. Staple manufacturing consists of spinning, drawing, crimping, cutting, and baling (107). The spun yarn from individual spinnerettes, ranging from several hundred to a few thousand filaments, are piddled into a can, lagged, the ends of which combined into a tow, and drawn. Finish is applied in spinning to help drawing, and is usually applied again after drawing to assist in the crimping and cutting operations. In crimping, multiple tow ends are forced continuously into a constricted stuffer box by preset feed rolls. The box is sealed by an adjustable hinged and weighted gate. The tow ends filling the chamber are arranged in uniform folds by compression. When the pressure in the stuffer box exceeds the pressure of the hinged gate, the gate rises to permit discharge of the crimped tow, and then falls, thereby repeating the process (108). Prior to cutting, water is applied to the crimped tow to reduce static and maintain wear life of the knives. The compact spinning systems, approximately 6 m high by 6 m wide and developed for nylon, polyester, and polypropylene, can be integrated into accommodating, designed downstream staple process operations (crimping, heat-setting, cutting, baling) to reduce space and cost as well as to expand product flexibility and improve quality (109). This process is a spin–draw type where tow is fed directly to drawing and then through the staple-making operations. The spinning and drawing speeds must be coordinated for proper performance. When utilizing the conventional low speed staple process, the spinning and drawing speeds must be reduced substantially. To compensate for the loss in throughput capacity per position, spinnerets having high number of holes (8000–75,000) are used. In another process where spinning and drawing are maintained close to conventional spinning, the stuffer-box crimper must be designed to process large tow titers, and to prevent the sticking of filaments on the roller and escaping of filaments that break loose from the bundle. Developed by Takehara, Japan, a high speed crimper capable of 6000 m/min avoids the problems encountered with the conventional roller (110). The Takehara Type T-K-K has a large-diameter ring roller that rotates in one direction, and an inner roller that lies on the inner surface of the ring roller and rotates with it in the same direction and with the same speed while holding the tow to be crimped (111).

Staple is used directly in the manufacturing of nonwoven fabrics and spun into yarn through the cotton, worsted, and woolen systems in 100% form or in blends with other synthetic or natural fibers.

Flock. *Flocking* is the mechanical and/or electrostatic application of finer fiber particles to adhesive-coated fabrics, paper, yarns, plastic, or metal objects (112). Flocking offers a soft, velvety surface for decorative and visual appeal and has a wide variety of functions: sound dampening, thermal insulation, friction reduction of sliding surfaces, increased surface exposure for evaporation and filtering, buffing and polishing, liquid retention or dispersal, cushioning of heavy objects, and even preventing the settling of barnacles on boat hulls (113).

Flock is made by precision-cutting drawn, uncrimped tow using a rotary or guillotine cutter into 0.3- to 6-mm lengths, depending on the denier per filament. The higher the denier per filament, the longer the tolerable length before curvature of the cut fiber becomes a problem in flock preparation. The tow presented to the cutter can be a combination of tow with lower total tow ktex creeled directly

out of shipping boxes or a tow that had been scoured, pad-dyed, rinsed, and treated with special finish on a continuous range. The tow size can be from 111 to 3889 ktex (1,000,000–35,000,000 denier) at the cutter.

Whether the process is continuous or batch, the flock must be similarly treated for electrostatic application. The spin finish is removed by scouring and then a finish mixture is applied to impart the following properties to the flock (114): (*1*) good siftability; (*2*) low interfiber adhesion needed for proper coverage, (*3*) good movement and orientation in the electrostatic field needed to get the flock to go straight into the adhesive coating, (*4*) correct level of conductivity appropriate to the strength of the field and compatible with an ac- or dc-applied voltage, and (*5*) good wetting-out properties in the adhesive. Fiber length has a great effect on flock properties; increasing the fiber length decreases the number of fibers sifted, the number of fibers flocked, and the percentage of maximum flock density (115).

Nylon is the preferred fiber for flocking because of its good chemical bonding to a wide range of adhesives, its toughness, and its ease of dyeability and printability. Nevertheless, the tow must be manufactured with the proper ktex, cohesion, and spin finish to be readily converted to flock.

Finishes. Fiber finishes are designed to provide fiber cohesion, lubricity, and static-free operability at low and high traverse speeds over a variety of metallic and ceramic surfaces encountered in fiber plant and mill operations (116–118). Fiber cohesion is important in that loose or protruding filaments can catch on processing equipment and cause snags and breaks, or become entrapped within a windup package, causing unevenness in texturing, knitting, and weaving. Finishes, consisting primarily of lubricants, emulsifiers, and antistatic agents, are generally applied as aqueous emulsions at concentrations giving a finish-on-yarn level of 0.3–1% after the evaporation of water.

In application, the aqueous-finish emulsion is pumped to a holding or storage tank from which it is circulated through a system that feeds the spinning machine. The finish is applied by passing the yarn either through the circulating finish across a constantly revolving "kiss" roll that is partially immersed in the emulsion, or through a slotted pin or guide in which the emulsion stream is metered through an orifice.

Modified Cross Sections. Nylon filaments are spun in a variety of cross-section shapes that include the conventional round to irregular solid and hollow shapes (Fig. 5). The cross-section shape is an important variant in designing the functionality and luster of fibers. The round cross section is used for strength in industrial applications and for subdued luster in apparel and upholstery. The multilobal cross sections are used to enhance bulk and for bright luster in both BCF and spun staple yarns for carpets and upholstery. The grooves in the multilobal shapes also enhance moisture transport by wicking water through capillary action. Flat-sided ribbon-like cross sections provide cover in apparel applications.

Bright (no delusterant) round and hollow fiber cross sections have a smooth sheen-like luster, whereas multilobal cross sections vary from bright sheen to bright glitter luster, depending on how they are designed to converge and transmit internally reflected light (119).

In spinning the different fiber cross sections, spinnerette orifice shape and dimensions must be made to exacting tolerances, and changes in polymer melt

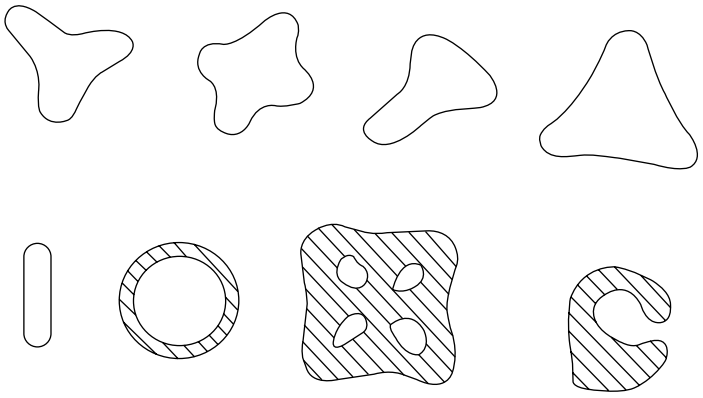

Fig. 5. Typical nylon fiber cross-section shapes.

viscosity, block temperature, and air quenching conditions must be anticipated to assure the desired shape, spinning continuity, and quality yarn. In spinnerette manufacture, the final orifice is produced after counterboring all but the thin sections of the spinnerette blank. Noncircular spinnerette orifice shapes are made by electron-beam milling and electrodischarge machining. For the solid, nonround shapes, a single orifice design is used. Various specific orifice shapes have been developed and fiber cross sections have been defined using mathematical relationships (120,121).

In making hollow fibers, both pre- and post-coalescent spinnerettes and spinning techniques can be used. The former requires injection of a gas through the capillary to create the void (122,123), whereas the latter involves entrapment of gas (air, nitrogen) by coalescence of the molten polymer spun exiting from a segmented orifice designed to give the desired number of cross-section holes, shape, and percent void (124,125).

The open hollow-fiber shape shown in Figure 5 is made by a unique process requiring bicomponent yarn technology (169). A yarn is spun with a water-soluble copolyester core and nylon sheath where the core is dissolved out with an alkali treatment in fabric dyeing.

Additives. Additives can be introduced in salt preparation, polymerization, or the molten polymer stream prior to extrusion of the filaments. Additives are used to alter the basic characteristics and performance of the fiber and can be classified by function.

Delusterants reduce the transparency, increase the whiteness, and alter the fiber's reflectance of light. TiO_2 is the delusterant of choice for all melt-spun fiber types because of its high cover, whiteness, and chemical and thermal stability. The anatase, not the rutile form of TiO_2, is preferred because it is softer and contributes less to abrasion wear of machine guides and rolls. Nylon is translucent and requires TiO_2 in most textile and home furnishing applications for the cover and to reduce objectionable sheen and gloss in fabrics. Semidull nylon yarns contain ca TiO_2, 0.3%; middull, ca 1.0%; and fulldull, ca 1.5–2.0%.

TiO_2 requires careful slurry preparation and introduction to the nylon to minimize the formation of agglomerates and to maintain an average particle size

of 0.1–0.5 μm in fiber. Otherwise, filter packs will clog and require frequent replacement. TiO_2 is added as an aqueous dispersion to the prepolymer in the manufacturing of nylon-6,6, and to the caprolactam in the manufacturing of nylon-6, frequently as a master batch containing up to 30% TiO_2 in low molecular weight polymer (127). Nonmelt-compatible polymeric materials such as poly(oxyethylenes), polystyrene (128), and poly(methyl pentene) (129) have also been used as delusterants.

Colorants can be introduced into the fiber by adding dyes and pigments in salt preparation, during polymerization, or into the molten polymer just before spinning (130). Pigmented fibers are referred to as mass-dyed, dope-dyed, solution-dyed, or producer-colored. Inorganic pigments are used more than the organics, especially where high color, light, and crock fastness are required, such as in upholstery and carpet for automotive interiors. The organic pigments have higher chroma, but are not as colorfast to heat and light. Nylon-6 can accommodate more pigments than nylon-6,6 because of its lower melt-processing temperatures. Like TiO_2, the pigments must be dispersible and heat stable in polymer and fiber manufacturing. A common and efficient approach to adding pigment to the base polymer in spinning is first to disperse the pigment as a concentrate in a carrier polymer, usually a lower melting copolymer. The concentrates range from 25 to 50% pigment content and are offered as a single color or a compounded color blend in pellet or flake form. The flake can be blended with the base polymer flake at a specified loading and charged to the feed hopper of the spinning process or remelted in a vessel that allows it to be metered directly into the molten polymer prior to spinning. Quality pigmented fibers are spun with processes equipped with mixing screws and volumetric or gravimetric automatic feeders. Typical pigments for nylon are carbon black, red iron oxide, aluminum cobalt blue, and phthalocyanine blue and green. Carbon black enhances nylon's resistance to photodegradation. A number of light-stable pigments that are also environmentally friendly are available (131).

Antioxidants are used to prevent thermal and oxidative degradation of nylon in manufacturing, post-fiber and fabric processing, and final use.

Antistats such as polyoxyethylenes (132,133) and *N*-alkyl polycarbonamide (134) are added to nylon to reduce static charge and improve moisture transport and soil release in fabrics. These additives also alter the luster of fiber spun from bright polymer. Static reduction in carpets is achieved primarily by the use of fibers modified with conductive carbon black.

Antimicrobial agents are used where there is a need to inhibit bacterial and fungal growth. The additives can consist of copper, germanium, zinc and zinc compounds, metal oxides or sulfides, metal zeolites, as well as silver and copper oxide coated inorganic core particles (135–140).

Flame retardants designated for nylon plastics, such as halogenated organic and phosphorous derivatives, are difficult to spin into fiber because of the high loading required for effectiveness and their adverse effects on melt viscosity and fiber physical properties.

Both fiber producers and fabric mills have realized that many of the performance variants that are difficult to incorporate into fiber melt spinning can be accomplished by post-treating yarns or fabrics. Mills can apply flame retardants, softeners, dye-fade inhibitors, and stain- and soil-resisting agents as part of the finishing of a fabric.

Dyeability

Nylon is atmospherically dyed using established trade procedures for staple (stock dyed), yarn (yarn dyed), fabric (piece dyed) for batch dyeing systems (becks, jets, kettles), for continuous dyeing systems [pad – dye, steam (fixation), rinse], and for printing systems (flatbed, rotary screen, roller and transfer) (141–143). Because of their physical and chemical structure, nylon-6 and nylon-6,6, unlike the principal synthetic and natural fibers, have an affinity for every dye class as summarized in Table 2 (144).

Commonly used dyes are the disperse, acid, and premetallized. Disperse dyes are easy to apply, but have marginal wash and lightfastness on nylon. Acid dyes, unlike the disperse dyes, are water soluble, interact with the amine ends, and, as expected, have better wash and lightfastness than the disperse dyes. There are two categories of acid dyes. Those containing one sulfonate group on the dye molecule are referred to as leveling acid dyes and those containing two or more sulfonates, nonleveling or critical acid dyes. Premetallized dyes are large metal complex molecules that respond like critical acid dyes. They have the best wash and lightfastness and are used for high uv-exposure end uses such as automotive upholstery. Leveling acid dyes are used in piece dyeing and wet roller and screen printing of carpets, upholstery, and apparel. Disperse dyes are used to dye carpets and for transfer printing primarily of flocked upholstery and carpets. In transfer printing, dyes printed on special papers are transferred to the fabric under heat and pressure.

Effect of Fiber Properties. Acid dyes are attracted to the accessible amine ends of the nylon chains located in the amorphous regions of the fiber. Acid dye affinity of nylon can be adjusted by adding excess diamine or diacid to the polymer salt or by changing the molecular weight in polymerization. A light acid-dyeable nylon-6,6 is spun with 15–20 amine ends, expressed in terms of gram equivalents per 10^6 grams of polymer. A medium or regular acid-dyeable nylon has 35–45 and a deep acid-dyeable nylon has 60–70 amine ends. Ultradeep acid-dyeable nylons have 80 amine ends or more and are made by adding basic compounds such as *N*-(2-aminoethyl)piperazine in polymerization to enhance the total available dye sites (145). Nylon-6,6 can also be made base-dyeable by

Table 2. Dye Affinity of Major Textile Fibers[a]

	Dye types[b]							
Fiber types	Direct	Vat	Reactive	Sulfur	Acid	Premet	Cationic	Disperse
Cellulose	D	D	D	D	S	S	–	–
Wool	S	SS	HS	S	D	D	–	D
Nylon	S	HS	HS/D	HS	D	D	D	D
Acetate	S	S	S	S	–	–	–	D
Acrylic	–	–	–	–	–	–	D	D
Polyester, 2GT	–	–	–	–	–	–	D	D
Polypropylene	–	–	–	–	–	–	–	–

From Ref. 147, reprinted with permission from AATCC.

D = dyes; S = stains; HS = heavy stain; SS = slight stain; D = requires special polymer; Requires carrier or high pressure and temperature.

increasing the level of carboxyl ends (146) or by introducing sulfonic acid groups through the addition of a copolymerizable dicarboxylic acid derivative to a polymer salt, such as the sodium salt of 3,5-dicarboxybenzene sulfonate (147). By using the proper dyes, dye-bath auxiliaries, and pH control, light, medium, and deep acid- and base-dyeable yarns can be dyed in combination in a single bath to give multitonal and two-color styling effects. This concept of differential-dyeing yarns is unique to nylon and is used extensively in the piece dyeing of carpet, apparel, and upholstery fabrics.

Macromolecular structure and supermolecular organization also affect dye affinity. Drawn (oriented) nylon-6 has more of a random open structure than nylon-6,6 (148). Nylon-6, therefore, dyes more rapidly than nylon-6,6, but is also more susceptible to color crocking, especially with disperse dyes. High dye rates can be achieved with nylon-6,6 by adding a minor random copolyamide component in polymerization. Also, any melt-spinning process adjustment or post-fiber and fabric treatment that decreases orientation in the amorphous domain increases dyeability. Examples are lowering the draw ratio, applying steam or swelling chemicals (eg, phenol), and texturing particularly with pre- or post-heat relaxation (149, 150). Nonuniform drawing or heat application can cause streaks with structure-sensitive nonleveling and premetallized dyes. Variations in fiber geometry and cross-section shape and yarn crimp level in texturing cause optically related color streaks. The streaks are caused by a single yarn or groups of yarns that appear to take up dye differently from neighboring groups of yarns. The yarns differing in heat history, amine-end sites, and/or processing tensions will cause streaks.

The appearance of streaks with leveling or nonleveling acid and premetallized dye can be subdued by increasing the dye-bath pH, at a sacrifice in dye exhaust, by adding chemical agents that retard the dye strike or, more effectively, by metering all or a portion of the dye in a concentrated solution at or near the dyeing temperature of the fiber (87.8–104.4°C) instead of at the usual 26.7–48.9°C practiced by the trade (151).

For end uses demanding high dye lightfastness such as automotive interior fabrics, select premetallized dyes and uv inhibitors are applied through the dye bath (152,153). Nylon can also be co-dyed with polyurethane elastomeric fibers, wool, acrylics, polyesters, and cellulosics (154).

Modified Nylon-6 and Nylon-6,6 Fibers

Bicomponent and Biconstituent Fibers. Bicomponent fibers consist of two polymers of the same generic class, eg, nylon-6 and nylon-6,10; biconstituent fibers consist of two dissimilar generic polymers, eg, nylon-6,6 and polyester. Both fiber types are made separately by melt-spinning the two different polymers through a common, specially designed spinneret such as the one in Figure 6 (155). The spinneret hole and block channels can be designed so that the two polymers emerge side by side, as sheath–core or conjugate fibers. The fibers are processed through conventional drawing or spin–draw operations. The original intent of the side-by-side bicomponent yarn was to impart stretch in tricot knit and hosiery applications. Nylon-6 and nylon-6,6 homopolymers were paired to a copolyamide on the basis of shrinkage difference as measured on the individually

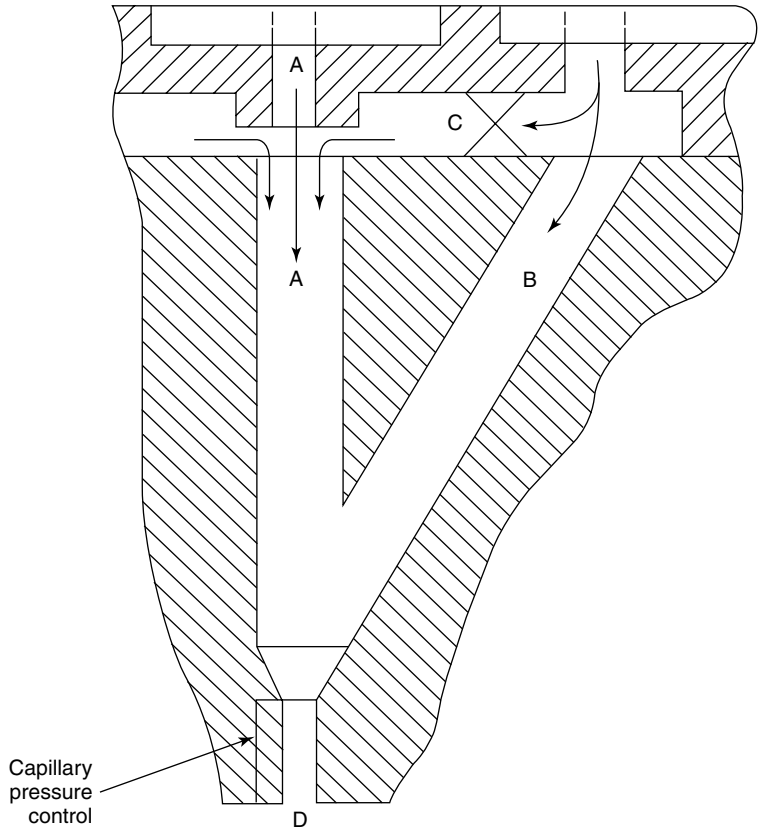

Fig. 6. Bicomponent spinneret for sheath-core fiber where A represents copolymer; B, homopolymer; and D, bicomponent fiber capillary exit. If side-by-side fiber is desired, the interconnecting channel C is sealed at X.

spun polymers. Depending on the differential shrinkage, the bicomponent yarn would assume a level of helical crimp in dyeing or steaming.

Examples of earlier bicomponent stretch yarns were spun with a nylon-6,6 sheath and core compositions of nylon-6,6/6,10 (50/50) and nylon-6,6/6 (80/20). Stretch was also achieved by spinning side-by-side two nylon-6,6 polymers having a relative viscosity difference of at least 15 units (156), and by spinning nylon-6 with a melt-spinnable polyurethane (157).

Most of the stretch hosiery today are made from textured POY and with elastomeric spandex fibers.

Bicomponent technology has been used to introduce functional and novelty effects other than stretch to nylon fibers. For instance, antistatic yarns are made by spinning a conductive carbon-black polymer dispersion as a core with a sheath of nylon (158) and as a side-by-side configuration (159). At 0.1–1.0% implants, these conductive filaments give durable static resistance to nylon carpets without interfering with dye coloration.

Dye selectivity can be altered by spinning a high amine-end nylon core with a sulfonate-containing nylon sheath (160). In standard dyeing conditions, the core

accepts leveling acid dyes, but not critical or basic dyes; the sheath accepts basic dyes. The effect creates a third color when dyed in combination with acid- and base-dyeable yarns.

Microdenier fibers, ie, very fine fibers, can be made by spinning biconstituent conjugate fibers such as those illustrated in Figure 7. The technology was developed by Kanebo and marketed under the fabric names Belseta and Glacem. The concept, referred to as alkalization, is to spin a readily alkali-soluble copolyester with nylon and then to dissolve away the polyester in the fabric stage. For example, the wedge-like nylon portion of the round 1.7-decitex (1.5 denier) filament in Figure 7 can split into eight components, each 0.20 decitex (0.18 denier) (161). The hexagonal cross-section fiber is of the "islands-in-the-sea" type where the orange wedge-shaped nylon "islands" in the copolyester "sea" connect slightly at the matrix center (162).

Microdenier nylon and polyester were a significant spinning breakthrough when demonstrated in 1985. The finer-than-silk fibers added a new dimension to fabric aesthetics, comfort, and performance. Microdenier nylons are used in weaving, warp knits, and weft knits for sports-, leisure-, and fashion-wear. Polyester can be melt spun at 0.55 decitex/filament, but the finest nylon is spun at 1.1 decitex/filament. The ultramicro staple nylons made by the polyester alkalization procedure are used to manufacture suede and water-resistant fabrics.

Copolymers. There are two forms of copolymers: block and random. A nylon block copolymer can be made by combining two or more homopolymers in the melt. The composition of the melt is a function of temperature and more so of time. Two homopolyamides in a moisture-equilibrated molten state undergo amide interchange where amine ends react with the amide groups. As time progresses, the two homopolyamides in the melt form a block and eventually a random copolymer as a result of amide interchange. Block copolymerization is a way of introducing a new variant into a base polymer without grossly affecting the spinning

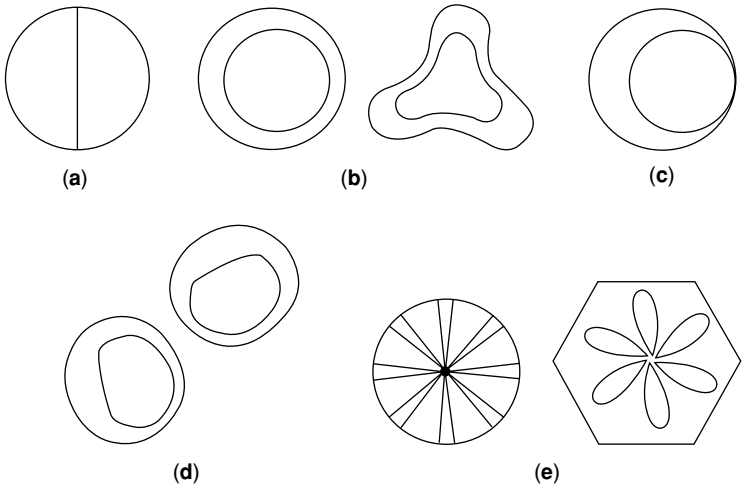

Fig. 7. Bicomponent cross-section forms: (**a**) side by side, (**b**) concentric sheath core, (**c**) eccentric sheath core, (**d**) kidney-shaped sheath core, and (**e**) conjugate.

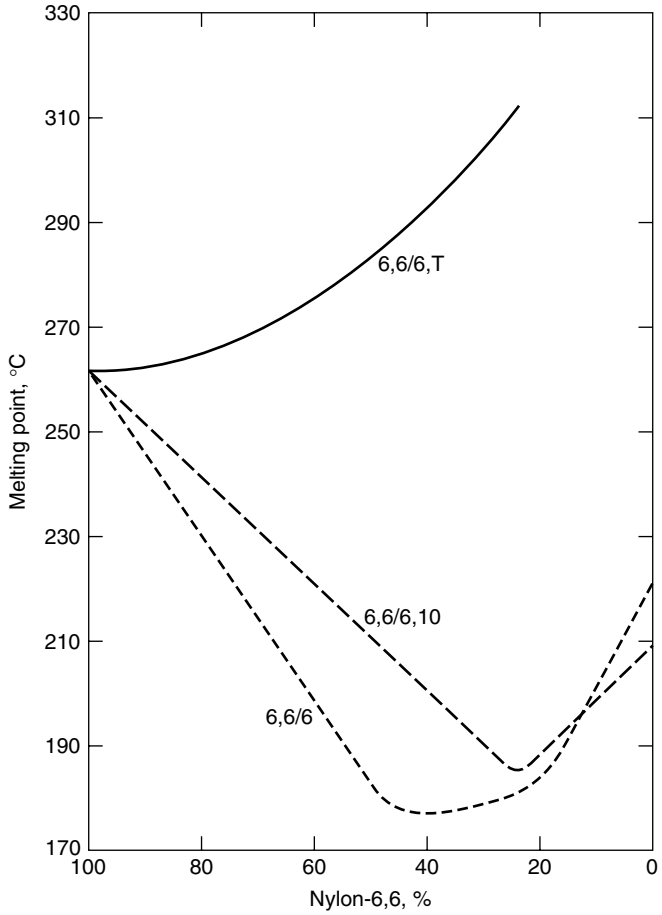

Fig. 8. Melting point–composition curves for random copolyamides of nylon-6,6.

performance and physical properties of the yarn. The process requires careful control, however, to maintain the desired composition in order to ensure uniform product and spinning continuity. Examples of this technology are the block copolymers of poly(4,7-dioxadecamethyleneadipamide) and poly(dioxaarylamide) with nylon-6 (163,164) for hydrophilic nylons.

Random copolymers are made by combining two or more monomers in the polymerization process. The melting temperature of random copolymers are lowered as the regularity with which the monomer groups are spaced along the backbone is reduced. Hydrogen bonding between the amides is also reduced. This is illustrated in the melting point–composition relationship for nylon-6,6/6 and nylon-6,6/6,10 in Figure 8. Crystallinity and orientation are also reduced with increasing randomization. However, in the case of nylon-6,6/6,T, the crystallinity is not reduced because the copolyamide segment is similar in size to that which is replaced. Such monomers which can be exchanged or replace each other in the crystal lattice are often termed *isomorphic monomers*.

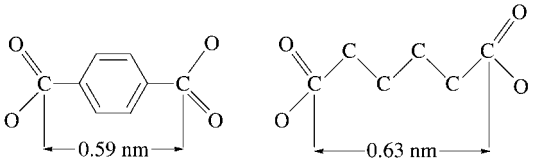

Random copolyamides that melt below 200°C are difficult to process through melt spinning because they are difficult to crystallize and consequently remain tacky through the windup. Copolyamides that melt above 300–310°C are also difficult to process because of their higher melt viscosities and greater susceptibility to thermal oxidation.

The general properties of random copolyamides are high dyeability (especially with nonleveling large dye molecules), lower melting and softening points, reduced dry and wet strength properties, high creep failure, and high shrinkage. The last property led to the use of the copolyamides in bicomponent self-crimping yarns. Copolyamides are also suitable for thermal bonding of fiber and fabrics because of their low softening temperature. Random copolyamides are also used to modify the dyeability of nylon-6,6. The addition of 0.5–2% comonomer increases the dyeing rate to almost that of nylon-6. Comonomers are also used as assists in the high speed godetless spinning of draw-texturing feed yarns. Nylon-6,6 copolyamides with ethyltetramethyleneadipamide, pentamethyleneadipamide, or 2-methylpentamethyleneadipamide units lower the gelation rate of nylon-6,6 at the spinning temperature of nylon-6,6 (165–167).

Graft Polymers. The grafting of polymers on nylon fiber surfaces as a means of altering chemical or physical properties has been explored and demonstrated over the years. However, a process has not yet been found that is safe, economical, and efficient for grafting yarns at conventional spinning speeds. Nevertheless, efforts continue because the property changes are dramatic and permanent, and because the process is more conducive to slower speed fabric-finishing processes. Vinyl monomers can be grafted to almost any nylon by ionizing radiation usually from a Co-60 source, high energy uv radiation, or chemical means. Radiation grafting of acrylonitrile on nylon-6 gives basic dyeability, and that of styrene, hydrophobicity (168). Nylon-6,6 can also be made basic-dyeable by chemically grafting acrylic or methacrylic acid with a water-soluble formaldehyde sulfoxylate salt (169). The friction of nylon fibers can be changed by grafting poly(dimethylsiloxane) macromolecules to the surface (170).

Nylon carpet fibers can be made to resist stain from certain acidic artificial and natural colorants found in soft drinks, juices, coffee, and red wines, by grafting a phenyl–vinyl and ether–maleic anhydride copolymer to the fiber surface using uv light and a photoactivator in the solution (171). However, there are other techniques for blocking the stain-sensitive amine ends that are more commercially applicable and efficient. They include (*1*) the post-treatment of nylon carpets with an alkali metal silicate in a phenol–formaldehyde product (172) or with a sulfonated naphthol or sulfonated phenol–formaldehyde product at a specific pH (173), (*2*) manufacturing of carpets with only cation-dyeable nylon yarn and dyeing or printing them to shade and acceptable lightfastness with premetallized or acid dyes

(177), and (*3*) melt-spinning of fibers–pigmented or producer-colored fibers–from nylon polymer containing a high level of a sulfonated derivative (174,175).

Other Nylons

Poly(tetramethylenediamine-*co*-adipic acid), nylon-4,6 [24936-71-8], polymer introduced as Stanyl by Dutch State Mines is spun into a high-temperature-resistant, high-tenacity filament yarn, Stanylenka 460 HRST, by Akzo Nobel Faser AG in Wuppertal, Germany. Stanylenka is intended for industrial applications including tire cord and automotive airbags because of its enhanced heat capacity, improved chemical resistance, better dimentional stability, and higher modulus than nylon-6,6 (176). The fiber melts at 285°C and has a density of 1.18 g/cm^3.

Poly(bis-[*p*-aminocyclohexyl]methane-*co*-dodecanedioic acid), PACM-12 [24936-74-1], introduced by DuPont as Qiana in 1968 was later withdrawn from the market. This diamine exists in several cis–trans and trans–trans isomeric forms that influence fiber properties, such as shrinkage and tenacity. The product offered silk-like hand and luster, dimensional stability, and wrinkle resistance similar to polyester. The yarn melted at 280°C, had a high wet glass-transition temperature of ∼85°C, and a density of 1.03 g/cm^3; the last was lower than that of nylon-6 and nylon-6,6. Qiana required a carrier for effective dyeing.

Poly(hexamethylenediamine-*co*-dodecanedioic acid), nylon-6,12 [24936-74-1], melts at 212°C, has a density of 1.06 g/cm^3, and has a lower moisture regain than that of nylon-6,6. Nylon-6,12 is used primarily for fishing lines and toothbrush bristles. It has a good apparel fiber properties, but is not as readily dyeable as nylon-6,6.

Poly(butyrolactam), nylon-4 [24938-566-27], melts at 268°C, has a density of 1.25 g/cm^3, and has a moisture regain of 6–9%, which is similar to cotton at 60% RH. It is easier to dye than nylon-6 and cotton, but is difficult to manufacture (177).

Applications

World production of nylon fibers is expected to reach 4×10^6 t in the year 2000 (178). Just under 50% of this volume will be produced in the United States and Western Europe, while future production growth will be predominantly in developing regions of China and southeast Asia (179). Production by polyamide type is about 70% nylon-6 and 30% nylon-6,6 (180).

Nylon and polyester make up almost 75% of world's synthetic fiber production (178). As the various market segments and end-use technologies have developed over the years for these maturing synthetic fibers, nylon has moved specifically into higher value applications where its unique properties justify the higher price. Nylon has grown more slowly than polyester, and now nylon filament production volume is one-third of polyester (179). Nylon filament prices are generally higher than those of polyester filament, for example, ranging from around 25% higher for tire reinforcement to over twice as much for some apparel yarns (181).

Principal market segments for nylon are carpet face yarns, which in the United States account for 70% share of nylon consumption; knit and woven apparel

at 18% share; industrial end uses such as tires and reinforced rubber products at 7%; and all other uses at 5% (182).

Nylon is the preferred fiber for carpets because of its excellent wear resistance, appearance retention, and ease of coloration. For a given appearance retention and wear life, particularly in plushes, less nylon (in terms of weight per unit area) is required than for polyester or polypropylene. Technical innovations such as soil and stain resistance and antistatic carpeting have contributed significantly to the growth of nylon in this industry. Branding or certification programs, including DuPont's Stainmaster∗, Solutia's Wear-Dated∗, Allied's Anso∗, and BASF's Zeftron∗, and others, have been used to grow volume and market share. In the 1990s, the industry also saw much push toward lower cost, nonbranded offerings, and significant industry integration, mergers, and reorganization. Nylon filament and staple have 60% share of carpet face fiber usage in the United States, exceeding 2 billion pounds per year; polypropylene filament has grown to almost 30% share, while staple fibers of polyester and other materials make up the rest (182).

Recycling of carpet components, especially the face fiber, has received much attention during the 1990s because over 4 billion pounds of post-consumer and manufacturing carpet-related waste is discarded annually, usually to landfills (183). The industry and major nylon fiber and carpet producers have demonstrated and are implementing collection methods, material management methods, and technologies to recycle waste carpet materials in a variety of bulk composites, reformed plastics via component separation and remelt, and recovered base polymer ingredients for both nylon-6 and nylon-6,6. Less than 1% of the discarded material is currently being recycled (183), but significant growth in recycled volume is expected during the next 5 years (184).

Two largest segments of industrial nylon applications are (1) reinforcing yarns in tires and (2) woven fabrics for airbags in automobiles. Because of its excellent strength, adhesion to rubber, and fatigue resistance, nylon is the preferred fiber in bias-ply industrial/commercial tires (eg, for short-distance trucks, construction/agricultural equipment, racing cars, and airplanes), in mini-spare passenger car tires, and in off-road vehicles tires. Polyester is the dominant fiber used in the carcass of radial passenger car tires because of its relative cost and higher modulus versus nylon. Nearly all high performance radial passenger car tires have nylon cap plies (above steel belts) to improve high speed durability.

In 1984 the U.S. Department of Transportation ruled that all new cars sold in the United States must be equipped with automatic crash-restraints for driver and front-seat passenger by 1990. This led to the adoption of the airbag concept, which created a new fabric opportunity for nylon industrial yarns. Airbag usage in light vehicles grew to over 110 million units by the year 2000, as frontal airbag installations for drivers and passengers reached 100% in the United States and approached 70% in Europe and Japan (185). Significant additional growth is expected as other regions adopt this concept, and adoptions of side-impact airbags increase. The air bag fabric is woven with high tenacity nylon industrial yarns, generally nylon-6,6, ranging from 47 to 94 tex (420–840 denier), in plain or rip-stop construction, and then scoured, heat-set, and coated with a neoprene formulation to protect the fabric from environmental pollutants and changes in temperature and humidity.

Other applications for the heavier denier, industrial grade nylon yarns include cordage, hose, webbing, sport goods, coated fabrics, belting, printer ribbon tapes, personal flotation devices, luggage, upholstery (automotive, contract), home furnishings, and papermaker felts (staple).

In apparel applications, nylon is preferred over polyester in warp knit fabrics for lingerie because of nylon's relatively fine denier, low weight, and softness; and in circular knit fabrics for sheer hosiery and pantyhose for these same reasons plus its superior textured yarn properties (especially stretch/recovery). Nylon is also the companion yarn of choice in stretch knit and woven constructions that incorporate elastane fibers, such as Dupont's Lycra∗ or Bayer's Dorlastan∗, because of textile processing compatibility (especially dyeing) versus polyester and elastane, in addition to nylon's preferred tactile aesthetics. Volume growth of nylon in apparel is expected to continue at relatively low rates, around 2.0% per year (186), but higher growth in value is expected as the recent consumer/retailer demands for high value, branded fabrics and garments continue (187). Examples of these specialty offerings are the stretch fabrics with elastane yarn, typically 5–20% of the composition; and branded offerings differentiated by aesthetics or functional performance, like Dupont's Tactel∗, Nylstar's Meryl∗, and BASF's Ultra Touch∗. Because of their softness, drape, and comfort, one denier per filament and microdenier yarns (less than 1 denier/filament) continue to gain popularity as compared to the workhorse 3 denier/filament yarns in previous years.

BIBLIOGRAPHY

"Polyamide Fibers" in *EPST* 1st ed., Vol. 10, pp. 347–460, by O. E. Snider and R. J. Richardson, Allied Chemical Corp.; "Polyamides, Fibers" in *EPSE* 2nd ed., Vol. 11, pp. 410–445, by J. H. Saunders, Consultant.

1. G. B. Kauffman, *Chem. Tech.* **17**, 725 (1988).
2. W. R. Potsch, *Chem. Fibers Int.* **47**, 432 (1997).
3. U.S. Pat. 2241321 (May 6, 1941), P. Schlack (to I. G. Farbenindustrie AG).
4. P. A. Schlack, *Chemiefasern/Textilindus*. **17**, 961 (1967).
5. H. Klare, *Technologie und Chemie der Synthetischem Fasern aus Polyamiden*, Verlag Technik, Berlin, 1954, p. 13.
6. H. Hupff, *Synthetic Fiber Development in Germany*, Part II, H. M. Stationery Office, London, 1945, p. 101.
7. I. McAllister III, *Textile World* **48**(11), 41 (1998).
8. M. S. Reisch, *C&EN* **31**(71), 12 (Aug. 2, 1993).
9. I. McAllister III, *Textile World* **149**(7), 154 (1999).
10. W. E. Morton and J. W. S. Hearle, *Physical Properties of Textile Fibers*, Textile Institute, Manchester, U.K., 1993.
11. H. D. W. Smith, *Rayon Tex. Mar.* **26**, 271 (1945).
12. R. Meredith, *Mechanical Properties of Textile Fibers*, Interscience Publishers, New York, 1956, Chapt. "16".
13. F. D. Snell and L. S. Ettre, eds., *Encyclopedia of Industrial Chemical Analysts*, Vol. **17**, John Wiley & Sons, Inc., New York, 1973, pp. 275–305.
14. C. W. Bunn and E. V. Garner, *Proc. Royal Soc. London Ser. A* **189**, 39 (1947).
15. P. F. Dismore and W. O. Statton, *Polym. Sci. Part C* **13**, 133 (1966).
16. H. F. Mark, S. M. Atlas, and E. Cermia, eds., *Man-Made Fibers: Science and Technology*, Vol. **1**, Wiley-Interscience, New York, 1967, pp. 24–374.

17. J. H. Dumbleton, D. R. Buchanan, and B. B. Bowles, *J. Appl. Polym. Sci.* **12**, 2067 (1968).
18. R. F. Stepaniak and co-workers, *J. Appl. Polym. Sci.* **23**, 1747 (1979).
19. J. Brandrup and E. H. Immergut, eds., *Polymer Handbook*, Wiley-Interscience, New York, 1989, pp. V-109, VI-258.
20. R. A. F. Moore, *Tex. Chem. Color.* **21**(2), 19 (1989).
21. Ref. 10, pp. 341–356.
22. D. G. Hunt and D. W. Darlington, *Polymer* **20**, 241 (1979).
23. H. H. Starkweather Jr. and co-workers, *J. Polym. Sci.* **21**, 189 (1956).
24. R. Puffr and J. Sebenda, *J. Polym. Sci., Part C* **16**, 79 (1967).
25. H. G. Olf and A. Peterlin, *J. Polym. Sci., Part A2* **11**, 2033 (1971).
26. E. G. Smith, *Polymer* **17**, 7751 (1976).
27. G. Weber, *Angew. Makromol. Chem.* **74**, 187 (1978).
28. A. Anton, *Text. Res. J.* **43**, 524 (1973).
29. W. T. Holfeld and M. S. Shepard, *Can. Tex. J.* **94**, 80 (1977).
30. J. Freitag, *Man-Made Fiber Yearbook*, Chemiefasern/Textilindus., Germany, 1989, p. 58.
31. G. J. Kettle, *Polymer* **18**, 742 (1977).
32. G. Hinrickson, *Colloid Polym. Sci.* **256**, 9 (1978).
33. J. L. Rush and J. C. Miller, *Am. Dyest. Rep.* **24**(2), 37 (1969).
34. M. E. Gibson Jr. and co-workers, *Tex. Chem. Color.* **18**(9), 55 (1980).
35. N. S. Murty and co-workers, *Macromolecules* **24**, 3215 (1991).
36. H. W. Schmidlin, *Preparation and Dyeing of Synthetic Fibers*, Reinhold Publishing Corp., New York, 1963, p. 45.
37. H. F. Mark, S. M. Atlas, and E. Cernia, *Man-Made Fibers*, Vol. **2**, John Wiley & Sons, Inc., New York, 1968, p. 280.
38. M. Dole and B. Wunderlich, *Macromol. Chem.* **34**, 29 (1969).
39. *AATCC Technical Manual*, American Association of Textile Chemists and Colorists, Research Triangle Park, N.C., 1993, p. 50.
40. Ref. 10, p. 564.
41. A. Anton, *Tex. Chem. Color.* **13**(2), 46 (1981).
42. M. Makansi, *Tex. Chem. Color.* **18**, 27 (1986).
43. N. B. Neiman, *Aging and Stabilization of Polymers*, Consultants Bureau, New York, 1965, p. 249.
44. U.S. Pat. 2705227 (Mar. 29, 1955), G. S. Stanatoff (to E. I. du Pont de Nemours & Co., Inc.).
45. U.S. Pat. 3113120 (Dec. 3, 1963), P. V. Papero and R. L. Morter (to Allied Chemical Corp.).
46. U.S. Pat. 3272773 (Aug. 13, 1966), D. H. Edison (to E. I. du Pont de Nemours & Co., Inc.).
47. U.S. Pat. 3457325 (July 22, 1969), A. Anton (to E. I. du Pont de Nemours & Co., Inc.).
48. K. Janssen, P. Gijaman, and D. Tummers, *Polym. Degrad. Stab.* **46**, 127 (1995).
49. R. F. Moore, *Polymer* **4**, 493 (1963).
50. W. H. Sharkey and W. E. Mochel, *J. Am. Chem. Soc.* **81**, 3000 (1959).
51. C. V. Stephenson, B. C. Moses, and W. S. Wilcox, *J. Polym. Sci.* **55**, 477 (1961).
52. G. Reinert and F. Thommen, *Tex. Chem. Color.* **23**, 31 (1991).
53. A. Anton, *J. Appl. Polym. Sci.* **9**, 1631 (1965).
54. U.S. Pat. 2887462 (May 19, 1955), J. G. Van Oot (to E. I. du Pont de Nemours & Co., Inc.).
55. U.S. Pat. 3002947 (Oct. 3, 1961), D. E. Maple (to E. I. du Pont de Nemours & Co., Inc.).

56. U.S. Pat. 3242134 (Mar. 22, 1966), P. V. Papero (to Allied Chemical Corp.).
57. U.S. Pat. 4710535 (Dec. 1, 1987), P. Perrot and G. Vuillemey (to Rhone-Poulenc Fibers).
58. M. Wedler and J. Kastner, *Man-Made Fiber Yearbook*, Chemical Fibers International, Germany, 1998, p. 60.
59. H. K. Reimschuessel, *J. Polym. Sci. Macromol. Rev.* **12**, 65 (1977).
60. H. Ludewig, *Faserforsh. Textiltech.* **2**, 341 (1951); obituary, *Acta Polym.* **35**, 113 (1984).
61. W. R. Sorenson and T. W. Campbell, *Preparative Methods of Polymer Chemistry*, Interscience Publishers, New York, 1961, pp. 60, 236.
62. F. S. Fiordan Jr. and J. H. Saunders, eds., *Forty Years of Melt Spinning*, American Chemical Society, Washington, D.C., 1981.
63. A. Alexander, *Man-Made Fiber Processing*, Noyes Data Corp., Parkridge, N.J., 1966, p. 82.
64. U.S. Pat. 4804508 (Feb. 14, 1989), J.-P. Double and C. Lecluse (to Rhone-Poulenc Fibers).
65. I. E. Lenk, *Man-Made Fiber Yearbook*, Chemiefasern/Textilindus., Germany, 1994, p. 62.
66. U.S. Pat. 3311691 (Mar. 29, 1967), A. N. Good (to E. I. du Pont de Nemours & Co., Inc.).
67. H. Klare, *Synthetic Fibers from Polyamides*, Akademie-Verlag GmbH, Berlin, 1963.
68. F. Fourne, *Synthetische Fasern*, Wissenschaftlicher Verlag, Stuttgart, Germany, 1964, p. 39.
69. A. Ziabicki, *Fundamentals of Fiber Formation*, John Wiley & Sons, Inc., New York, 1976.
70. A. Wasiak and A. Ziabicki, *Appl. Polym. Symp.* **27**, 111 (1975).
71. J. E. Spruiell and J. L. White, *Appl. Polym. Symp.* **27**, 121 (1975).
72. J. G. Bankar, J. E. Spruiell, and J. L. White, *J. Appl. Polym. Sci.* **21**, 2341 (1977).
73. M. D. Danford, J. E. Spruiell, and J. L. White, *J. Appl. Polym. Sci.* **22**, 3351 (1978).
74. J. Gianchandani, J. E. Spruiell, and E. S. Clark, *J. Appl. Polym. Sci.* **27**, 3527 (1982).
75. W. O. Statton, *J. Polym. Sci., Part A2* **10**, 1587 (1972).
76. J. P. Bell, *Tex. Res. J.* **42**, 292 (1972).
77. J. Elad and J. M. Schultz, *J. Polym. Sci., Polym. Phys. Ed.* **22**, 781 (1984).
78. G. Perez and E. Jung, in ISF-85, Hakone, Japan, 1985, p. 20.
79. H. Brever and co-workers, *Chemiefasern/Textilindus.* **42**, 87 (1992).
80. H. Treptow, *Man-Made Fiber Yearbook*, Chemiefasern/Textilindus., Germany, 1986, p. 6.
81. R. T. Maier, in Ref. 80, p. 106.
82. R. C. Mears, in Ref. 80, p. 108.
83. J. F. Hagewood, *Man-Made Fiber Yearbook*, Chemiefasern/Textilindus., Germany, 1988, p. 102.
84. I. F. Maag, *Man-Made Fiber Yearbook*, Chemiefasern/Textilindus., Germany, 1990, p. 79.
85. U.S. Pat. 5219503 (June 15, 1993), R. L. Boles Jr. and co-workers (to E. I. du Pont de Nemours & Co., Inc.).
86. K. Koyanna, J. Suryadevara, and J. E. Spruiell, *J. Appl. Polym. Sci.* **31**, 2203 (1986).
87. U.S. Pat. 5202182 (Apr. 13, 1993), B. H. Knox and co-workers (to E. I. du Pont de Nemours & Co., Inc.).

88. U.S. Pat. 5182068 (Jan. 26, 1993), J. Richardson (to Imperial Chemical Industries PLC).
89. U.S. Pat. Re 33059 (U.S. Pat. 4583357) (Sep. 19, 1989), J. M. Chamberlin and co-workers (to Monsanto Co.).
90. U.S. Pat. 4721650 (Jan. 26, 1988), W. J. Nunning and co-workers (to Monsanto Co.).
91. U.S. Pat. 5238637 (Aug. 24, 1993), O. Chaubet and co-workers (to Rhone-Poulenc Fibers).
92. K. Chan, *Textile Asia* **30**(8), 60 (1999).
93. H. M. El-Behery, in Draw Texturing Technical Conference, Clemson, S.C., Apr. 10–11, 1973.
94. R. W. Mason, *Textile Maintenance & Engineering* 83 (May 1999).
95. H. Schellenberg, in Ref. 80, p. 96.
96. T. Ishida, *JTN* **427**(6), 98 (1990).
97. U.S. Pats. 2783609 (Mar. 5, 1957), 2852906 (Sep. 23, 1958), and 2869967 (Jan. 20, 1959), A. L. Breen (to E. I. du Pont de Nemours & Co., Inc.).
98. U.S. Pat. 4648240 (Mar. 10, 1987), R. S. Hallsworth and S. Rodney (to E. I. du Pont de Nemours & Co., Inc.).
99. U.S. Pat. 3005251 (Oct. 24, 1961), C. E. Hallden Jr. and K. Murenbeeld (to E. I. du Pont de Nemours & Co., Inc.).
100. U.S. Pat. 2942402 (June 28, 1960), C. W. Palm (to Celanese Corp.).
101. U.S. Pat. 2884756 (May 5, 1959), W. I. Head (to Eastman Kodak Co.).
102. U.S. Pat. 2852906 (June 23, 1958), A. L. Breen (to E. I. du Pont de Nemours & Co., Inc.).
103. U.S. Pat. 2875502 (May 3, 1959), H. W. Matthews and W. K. Wyatt (to Turbo Machine Co.).
104. U.S. Pat. 2245874 (June 17, 1941), W. S. Robinson.
105. Brit. Pat. 801147 (Oct. 12, 1955), J. A. Place (to British Nylon Spinners Ltd.).
106. F. Werny and co-workers, *Ullmann's Encyclopedia of Industrial Chemistry*, VCH Verlagsgesellschaft, Weinheim, Germany, 1988, p. 263.
107. Ref. 63, pp 149, 150.
108. U.S. Pat. 2575781 (Nov. 20, 1951), J. L. Barach (to Alexander Smith).
109. S. D. Fredericks, *Int. Fiber J.* **5**(4) 49–62 (1990).
110. *Chemiefasern / Textilindus.* **43/95**, 487 (E77) (1993).
111. U.S. Pat. 4908920 (May 20, 1990), Katsuomi Takehara (to Kabushiki Kaisha Takehara Kikai Kenkyusho).
112. *Design with Flock in Mind*, American Flock Association, Boston, Mass., 1992.
113. U.S. Pat. 5618588 (April 8, 1997), Kjell K. Alm (to Sealflock Aktiebolzo).
114. W. Irganells and N. Ranadan, *J. Soc. Dyers Colour.* **108**, 270 (1992).
115. R. L. Coldwell and H. P. Solomon, *IEEE Trans. Ind. Appln.* **14**(2), 175 (Mar./Apr. 1978).
116. P. E. Slade, *Handbook of Fiber Finish Technology*, Marcel Dekker, Inc., New York, 1997.
117. H. R. Billica, *Fiber Prod.* **12**(2), 21 (1984).
118. H. R. Billica, *Fiber Prod.* **12**(3), 24 (1984).
119. A. Anton, K. A. Johnson, and P. A. Jansson, *Tex. Res. J.* **48**, 247 (1978).
120. U.S. Pats. 2939201 and 2939202 (June 7, 1960), M. C. Holland (to E. I. du Pont de Nemours & Co., Inc.).
121. U.S. Pat. 3109220 (Nov. 5, 1963), A. H. McKinney and H. E. Stanley (to E. I. du Pont de Nemours & Co., Inc.).
122. U.S. Pat. 3075242 (Jan. 29, 1963), E. Grafried (to W. C. Heraeus).
123. U.S. Pat. 3081490 (Mar. 19, 1963), W. Heymen and W. Martin (to Vereingte Glanzstoff-Fabriken AG).

124. U.S. Pat. 3745061 (July 10, 1973), A. J. Champaneria and M. R. Lindbeck (to E. I. du Pont de Nemours & Co., Inc.).
125. U.S. Pat. 5190821 (Mar. 2, 1993), M. T. Goodall, C. A. Jackson, and P. H. Lin (to E. I. du Pont de Nemours & Co., Inc.).
126. *JTN* **459**(2), 44 (1993).
127. U.S. Pat. 2689332 (Aug. 8, 1958), G. A. Nesty (to Allied Chemical Corp.).
128. U.S. Pat. 3903348 (Sep. 2, 1975), B. B. Esteridge and B. M. Lyon (to Akzona Inc.).
129. U.S. Pat. 5407745 (April 18, 1995), V. G. Bankar and W. H. Tung (to E.I. du Pont de Nemours & Co., Inc.).
130. P. Schaeffer, *Chem. Tech.* **12**, 242 (1960).
131. S. S. Parikh and co-workers, *Material Processes and Products in Interior Trim, Seating & Headliners*, Society of Automotive Engineers, Inc., Detroit, Mich., 1991, p. 47.
132. U.S. Pat. 3329557 (July 4, 1967), E. E. Magat and D. Tanner (to E. I. du Pont de Nemours & Co., Inc.).
133. U.S. Pat. 3388104 (June 11, 1968), L. W. Crojatt Jr. (to Monsanto Co.).
134. U.S. Pat. 3900676 (Aug. 19, 1975), T. Alderson (to E. I. du Pont de Nemours & Co., Inc.).
135. Jpn. Pat. 03275603-A (9204) (Dec. 6, 1991), T. Kawachi (to Teisan Seiyaku KK).
136. World Pat. 09207037-A (9220) (Mar. 30, 1992), A. K. Philpott (to Aboe Pty. Ltd.).
137. Jpn. Pat. 04240205-A (9241) (Aug. 27, 1991), Y. Takeda and I. Yuaja (to Kuraray Co., Ltd.).
138. Jpn. Pat. 04248943-A (9242) (Sept. 4, 1992), Y. Mizukami, H. Tamemasa, and Y. Kimuka (to Kanebo Ltd.).
139. Eur. Pat. 505638-A1 (9240) (Sept. 30, 1992), Z. Hagiwara and M. Okubo (to Hagiwara Giken KK).
140. U.S. Pat. 5180585 (Jan. 19, 1993), H. W. Jacobson, S. L. Samuels, and M. H. Scholla (to E. I. du Pont de Nemours & Co., Inc.).
141. J. R. Aspland, *Textile Dyeing and Coloration*, AATCC, Research Triangle Park, N.C., 1997, pp. 228, 243, 258, 273.
142. C. B. Smith, *Dyeing and Printing Guide*, ATI, Nov. 1990, p. 35.
143. *Dyeing Primer*, AATCC, Research Triangle Park, N.C., 1981
144. A. Anton, TCC&ADR **32**(3), 26 (Mar. 2000).
145. U.S. Pat. 3375651 (Apr. 2, 1968), L. B. Greeson, Jr. (Monsanto Co.).
146. U.S. Pat. 4017255 (Apr. 12, 1977), M. C. Cobb (Imperial Chemical Industries).
147. U.S. Pat. 3184436 (May 18, 1965), E. E. Magat (E. I. du Pont de Nemours & Co., Inc.).
148. G. A. Nesty, *Tex. Res. J.* **29**, 765 (1944).
149. J. L. Rush and J. C. Miller, *Am. Dyest. Rep.* **58**, 37 (1969).
150. R. A. F. Moore and H. D. Weigman, *Tex. Res. J.* **56**, 180 (1986).
151. U.S. Pat. 5230709 (July 27, 1993), W. T. Holfeld and D. E. Mancuso (E. I. du Pont de Nemours & Co., Inc.).
152. A. Anton, *Tex. Chem. Color.* **4**(10), 32 (1982).
153. U.S. Pat. 4902299 (Feb. 20, 1990), A. Anton (E. I. du Pont de Nemours & Co., Inc.).
154. J. R. Aspland, *Tex. Chem. Color.* **25**(9), 79 (1993).
155. U.S. Pat. 3399108 (Aug. 27, 1968), E. H. Olson (to E. I. du Pont de Nemours & Co., Inc.).
156. U.S. Pat. 4740339 (Apr. 26, 1988), H. C. Bach and W. B. Black (to Monsanto Co.).
157. J. H. Saunders and co-workers, *J. Appl. Polym. Sci.* **19**, 1387 (1975).
158. U.S. Pat. 4064075 (Aug. 27, 1968), D. R. Hull (to E. I. du Pont de Nemours & Co., Inc.).
159. U.S. Pat. 3969559 (May 27, 1975), N. W. Boe (to Monsanto Co.).
160. U.S. Pat. 4075378 (Feb. 21, 1978), A. Anton and J. A. B. Nolin (to E. I. du Pont de Nemours & Co., Inc.).

161. S. Shiomura, *Tex. Asia* **22**(9), 140 (1991).
162. U.S. Pat. 5047189 (Sept. 10, 1991), C.-L. Lin (to Nan Ya Plastics Corp.).
163. U.S. Pat. 4113794 (Sept. 12, 1978), R. M. Thompson and R. S. Stearns (to Sun Ventures, Inc.).
164. U.S. Pat. 4168602 (Sept. 25, 1979), R. M. Thompson, (Sun Ventures, Inc.).
165. U.S. Pat. 5110900 (May 5, 1992), J. A. Hammond Jr. and D. N. Marks (to E. I. du Pont de Nemours & Co., Inc.).
166. U.S. Pat. 5185428 (Feb. 9, 1993), J. A. Hammond Jr. and D. N. Marks (to E. I. du Pont de Nemours & Co., Inc.).
167. U.S. Pat. 5194578 (May 16, 1993), A. Anton (to E. I. du Pont de Nemours & Co., Inc.).
168. K. El-Salmawi and co-workers, *Am. Dyest. Rep.* **82**(5), 47 (1993).
169. U.S. Pat. 3394985 (July 30, 1968), H. H. Froehlich (to E. I. du Pont de Nemours & Co., Inc.).
170. S. Michielsen, in *Joint International Conference with the Fiber Society*, The Textile Institute of Materials, U.K. and Institut Textile de France, Apr. 21–24, 1997, p. 111.
171. U.S. Pat. 5236464 (Aug. 17, 1993), D. K. Barnes and co-workers (to AlliedSignal, Inc.).
172. U.S. Pat. 4501591 (Feb. 26, 1985), P. A. Ucci and R. C. Blythe (to Monsanto Co.).
173. U.S. Pat. 4780099 (Oct. 25, 1988), I. Greschler and co-workers (to E. I. du Pont de Nemours & Co., Inc.).
174. U.S. Pat. 5889138 (Nov. 3, 1998), A. Anton and co-workers (to E. I. du Pont de Nemours & Co., Inc.).
175. U.S. Pat. 5889138 (Mar. 30, 1999), A. W. Summers (to Solutia, Inc.).
176. V. Siejak, in Ref. 58, pp. 24, 34.
177. C. E. Barnes, *Lenzinger Berichte* **62**, 62 (Mar. 1987).
178. P. Short, C&EN, 25 (May 15, 2000).
179. *Fiber Organon*, 104, 105 (June 2000).
180. W. Bongard, *Chem. Fibers Int.* **50**, 254 (2000).
181. P. Short, *Women's Wear Daily* 12 (July 25, 2000).
182. J. E. Luke, *America's Textile Industries* 19, (Jan. 2001).
183. J. Hagewood, *Int. Fiber J.* **14**(3), 48 (1999).
184. H. Miller, *Int. Fiber J.* **14**(3), 54 (1999).
185. M. Whyte, *Industrial Fabric Products Review* **76**(6), 32 (1999).
186. R. Reichard, *Textile World* 20 (Jan. 2000).
187. J. E. Luke, *America's Textile Industries* 54 (Feb. 2000).
188. W. N. Rozelle, ed., *Textile World Manmade Fiber Chart*, Primedia Intertec Publication, Oakland Park, Kan., 1998.
189. Ref. 10, pp. 282–284; Ref. 21; *Multifiber Bulletin X-273, DuPont Fibers*, Apr. 1993.
190. Ref. 37, p. 259.
191. U.S. Pat. 6013111 (Jan. 11, 2000), W. G. Jenkins (to Burlington Industries, Inc.).

GENERAL REFERENCES

M. Lewin and E. M. Pearce, *Handbook of Fiber Chemistry*, 2nd ed., Marcel Dekker, Inc., New York, 1998, pp. 72–152.
F. Fourne', *Synthetic Fibers: Machines and Equipment*, Hanser/Gardner Publications, Inc., Cincinnati, Ohio, 1999, pp. 34–66.

R. B. Seymour and R. S. Porter, eds., *Manmade Fibers: Their Origin and Development*, Elsevier Applied Science, New York, 1993, pp. 227–277.
W. E. Morton and J. W. S. Hearle, *Physical Properties of Textile Fibres*, The Textile Institute, Manchester, U.K., 1993.
H. F. Mark, S. M. Atlas, and E. Cernia, eds., *Man-Made Fibers Science and Technology*, **3** vols., Wiley-Interscience, New York, 1967–1968.
F. D. Snell and L. S. Ettre, eds., *Encyclopedia of Industrial Chemical Analysis*, Vol. **17**, John Wiley & Sons, Inc., New York, 1973, pp. 275–305.

ANTHONY ANTON
BENNETT R. BAIRD
E. I. du Pont de Nemours & Company, Inc.

POLYAMIDES, PLASTICS

Introduction

The use of polyamides in plastic applications dates back to the original commercialization of this polymer. The first polyamide application was the introduction by DuPont in 1938 of nylon-6,6 for tooth brush filaments (1). Although fiber applications soon dominated, the use of polyamides as plastics grew steadily from the 1950s and is estimated to represent more than 25% of total polyamide use in the year 2000 or 1.65 million metric tons per year (2). Growth is about 8–9% per annum compared to less than 1.5% for fibers (3).

Polyamides were the first engineering plastics and still represent by far the biggest and most important class of these types of material. The combination of mechanical and thermal properties allows them to be employed for highly specified end uses and often for metal replacement applications (see Engineering Thermoplastics, Survey).

Polyamides comprise a range of materials, depending on the monomers employed. Nylon-6,6 [32131-17-2] and nylon-6 [25038-54-4] continue to be the most popular types, still accounting for more than 90% of nylon use. Table 1 gives a summary of the properties of the more common types which are currently commercially available. In recent years there has been increasing interest in polyamides with higher melting points to extend the boundaries of this polymer type to satisfy more stringent high temperature automotive and electronic applications. This has resulted in the development of nylon-4,6 and several semiaromatic nylons.

Encyclopedia of Polymer Science and Technology. Copyright John Wiley & Sons, Inc. All rights reserved.

Table 1. Properties of the More Common Nylons, Dry as Molded

Property	Nylon-6,6[a]	Nylon-6[b]	Nylon-11[c]	Nylon-12[d]	Nylon-6,9[e]	Nylon-6, 12[a]	ASTM test method
CAS Registry Number	[32131-17-2]	[25038-54-4]	[25035-04-5]	[24937-16-4]	[28757-63-3]	[24936-74-1]	
Specific gravity	1.14	1.13	1.04	1.02	1.09	1.07	D792
Water absorption, wt%							
24 h	1.2	1.6	0.3	0.25	0.5	0.25	
Equilibrium at 50% rh	2.5	2.7	0.8	0.7	1.8	1.4	
Saturation	8.5	9.5	1.9	1.5	4.5	3.0	
Melting point, °C	255	215	194	179	205	212	D2117
Tensile yield strength, MPa[f]	83	81	55	55	55	61	D638
Elongation at break, %	60–90	50–150	200	200	125	150	D638
Flexural modulus, MPa[f]	2800	2800	1200	1100	2000	2000	D790
Izod impact strength, J/m[g]	53–64	55–65	40–68	95	58	53	D256
Rockwell hardness, R scale	121	119	108	107	111	114	D785
Deflection temperature under load, °C							D648
At 0.5 MPa[f]	235	185	150	150	150	180	
At 1.8 MPa[f]	90	75	55	55	55	90	
Dielectric strength, kV/mm							D149
Short time	24	17	16.7	18	24	16	
Step by step	11	15		16	20		
Dielectric constant							D150
At 60 Hz	4.0	3.8	3.7	4.2	3.7	4.0	
At 10^3Hz	3.9	3.7	3.7	3.8	3.6	4.0	
At 10^6 Hz	3.6	3.4	3.1	3.1	3.3	3.5	
Starting acid[h] or lactam	Adipic acid[h]	Caprolactam	11-Aminoundecanoic acid	Dodecanolactam	Azaleic[h] acid[h]	Dodecanedioic[h] acid[h]	

[a]Ref. 4.
[b]Ref. 5.
[c]Ref. 6.
[d]Ref. 7.
[e]Ref. 8.
[f]To convert MPa to psi, multiply by 145.
[g]To convert J/m to ft·lbf/in., divide by 53.38.
[h]The starting amine is hexamethylenediamine for Nylon-6,6, Nylon-6,9, and Nylon-6,12.

Physical Properties

The original development of polyamides, initially nylon-6,6 then nylon-6, concentrated on their potential as fiber-forming materials where strength, elasticity, and high dye uptake were considered the most important properties, along with the ability to withstand ironing temperatures. It soon became apparent, however, that the properties of the material held many advantages for use as a plastic. In particular, the relatively high tensile strength and stiffness, together with good toughness, high melting point (and therefore temperature stability), and good chemical resistance, all combined to allow a wide range of applications. The material soon came to be seen as an engineering plastic that could be used for metal replacement in structural or semistructural end uses. These properties are present to a greater or lesser extent in the entire semicrystalline polyamide family and form the basis for the continuing success and growth of these materials.

Appropriate choice of monomer can provide a balance of properties to meet particular types of applications. In general, the effects of different monomers and therefore the property balance of different types of nylon can be summarized as follows: lengthening the aliphatic segments between the amide groups results in lower moisture absorption, reduced strength and stiffness, and lower melting point (eg, nylon-11 or nylon-12 compared to nylon-6,6). The introduction of aromatic groups increases stiffness and strength but reduces moisture uptake and, to a lesser extent, impact strength. Some semiaromatic polyamides also have an increased melting point.

In addition to the semicrystalline nylons, which comprise the vast majority of commercial resins, nylon is also available in an amorphous form that gives rise to transparency and improved toughness at the expense of high temperature properties and chemical stress-crack resistance. Table 2 shows the properties of some different polyamide types.

Crystallinity. The presence of the polar amide groups allows hydrogen bonding between the carbonyl and NH groups in adjacent sections of the polyamide chains. For common nylons such as nylon-6,6 and nylon-6, the regular spatial alignment of amide groups allows a high degree of hydrogen bonding to be developed when chains are aligned together, giving rise to a crystalline structure in that region. These nylons are semicrystalline materials that can be thought of as a combination of ordered crystalline regions and more random amorphous areas having a much lower concentration of hydrogen bonding. This semicrystalline structure gives rise to the good balance of properties. The crystalline regions contribute to the stiffness, strength, chemical resistance, creep resistance, temperature stability, and electrical properties; the amorphous areas contribute to the impact resistance and high elongation. The crystallinity can be disrupted by substituents on the chains that interfere with the alignment process. Amorphous nylons are produced by deliberately engineering this effect, eg, nylon-NDT/INDT (also known as PA-6-3-T or PA-TMDT), which uses trimethyl-substituted hexamethylenediamine isomers combined with terephthalic acid.

Thermal Properties. The high melting point of polyamides such as nylon-6,6 is a function of both the strong hydrogen bonding between the chains and the crystal structure. This also allows the materials to retain significant stiffness above the glass-transition temperature (T_g) and almost up to the melting point.

Table 2. Properties of Other Nylons, Dry as Molded

Property	Nylon-4,6	Nylon-MXD,6	Nylon-NDT/INDT	Polyphthalamide (PPA)
CAS registry number	[50327-22-5]	[25805-74-7]	[9071-17-4]	
Water absorption, %				
24 h	2.0	0.31		0.81
50% rh	3.4		3.0	
Saturation	13.0	5.5	7.0	
Melting point, °C	295	243	amorphous	310
Glass-transition temperature, T_g, °C	~85	102	149	123–135
Tensile strength, MPa[a]	95	103	85	104
Flexural modulus, MPa[a]	3100	4500	2900	3300
Elongation at break, %	50	2.3	70	6.4
Notched Izod impact strength, J/m[b]	110	20	~160	53
DTUL[c] at 1.8 MPa[a], °C	160	96	130	120
Starting materials				
Amine	diaminobutane	*m*-xylylenen-diamine	trimethylhexa-methylene-diamine	hexamethylene-diamine
Acid	adipic acid	adipic acid	terephthalic acid	adipic acid, iso/terephthalic acids
Reference	9	10	11	12

[a]To convert MPa to psi, multiply by 145.
[b]To convert J/m to ft·lbf/in., divide by 53.38.
[c]Deflection temperature under load.

The effect is further increased when reinforcements such as glass fiber are added, giving a high deflection temperature under load even at high loading. The effect also results in the sharp melting points of nylon as the majority of the hydrogen bonding rapidly breaks down at that temperature, giving a low viscosity, water-like melt. The melting point is mainly related to the degree of hydrogen bonding between the chains, which depends on the density of amide groups. The melting point therefore drops as the length of aliphatic groups between the amide links increases (eg, nylon-6,6 melting at 264°C, compared to nylon-6,12 at 212°C). The influence of structure on the melting point is further complicated by factors that affect the ease of crystallization. For even–even nylons such as nylon-6,6 and nylon-6,12, the monomers have a center of symmetry and the amide groups easily align to form hydrogen bonds in whichever direction the chains are facing when placed on top of one another. For even nylons, such as nylon-6, that have no center of symmetry, the amide groups are in the correct positions only if the chains are aligned in one particular direction (antiparallel). For this reason, nylon-6 has a melting point more than 40°C lower than nylon-6,6, despite having the same density of amide groups. It also has a slower crystallization rate and therefore wider processing window. Other types of nylon, such as even–odd and odd nylons, also differ from the above types for similar reasons of crystallization and crystal packing. In addition, crystallization is impeded and melting point reduced by copolymerization and substituents on the chains, although in certain cases isomorphism of comonomers avoids this effect, eg, terephthalic acid increases the melting point of nylon-6,6.

In recent years, polyamides have been increasingly used in higher temperature applications (mainly automotive) and in addition to the newer high melting point materials, glass-reinforced nylon-6,6, in specially modified formulations, has been shown to be suitable for use in replacing metals at temperatures which would not have been considered possible a few years ago (13).

Moisture Absorption. A characteristic property of nylon is the ability to absorb significant amounts of water (14) (Fig. 1). This again is related to the polar amide groups around which water molecules can become coordinated. Water absorption is generally concentrated in the amorphous regions of the polymer where it has the effect of plasticizing the material by interrupting the polymer hydrogen bonding, making it more flexible (with lower tensile strength) and increasing the impact strength. The T_g is also reduced. Moisture absorption, determined by both the degree of crystallinity and the density of amide groups, is, as with the melting point, reduced with increasing length of aliphatic groups in the chain. Aromatic monomers also reduce the moisture absorption. Nylon-6 has a higher moisture absorption than nylon-6,6 because of its lower crystallinity. The effect of moisture absorption on the mechanical properties of nylon-6,6 is included in Table 3.

Electrical Properties. Nylons are frequently used in electrical applications mainly for their combination of mechanical, thermal, chemical, and electrical properties. They are reasonably good insulators at low temperatures and humidities and are generally suitable for low frequency, moderate voltage applications. The relatively high dissipation factor of nylon causes problems under conditions of high electrical stress, particularly when moist, because of the likelihood of overheating. Dry nylon has volume resistivities in the 10^{14}–10^{15} Ω·cm region, but this decreases with increasing moisture and temperature. Dielectric

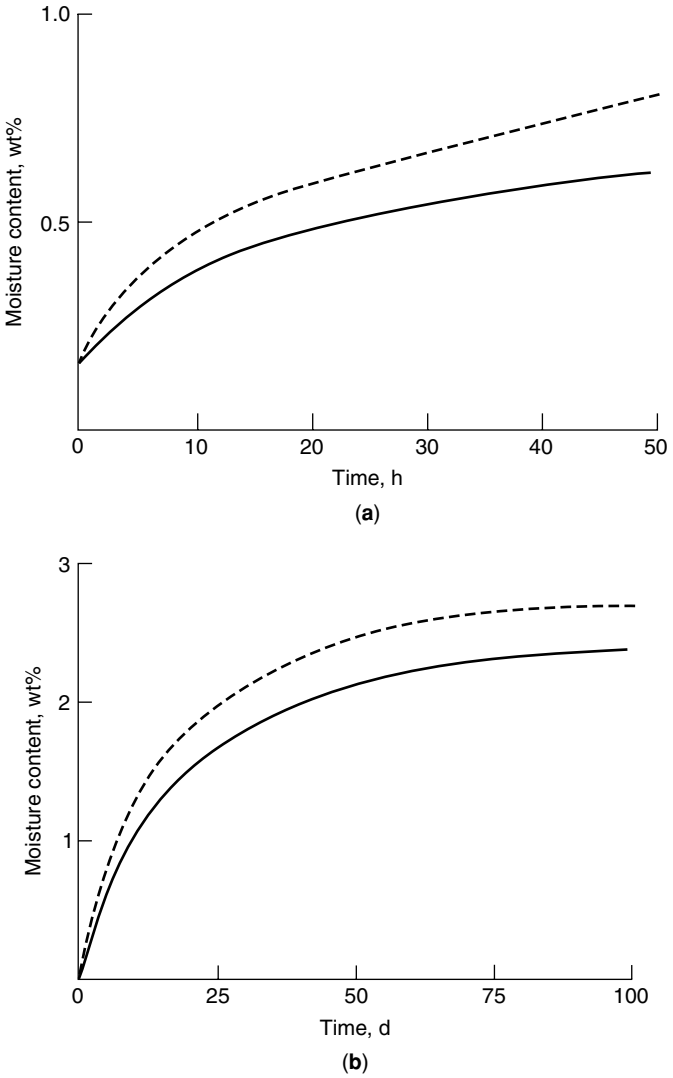

Fig. 1. Rate of moisture pickup for nylon-6,6 (——) and nylon-6 (—) granules at 50% rh and 23°C: (**a**) 0–48 h, (**b**) 0–100 days.

constant displays large increases with moisture and temperature. For moist nylon, however, the value decreases with increasing frequency, as the water molecules are less able to respond at higher frequencies.

Nylons have excellent arc and tracking resistance. Arc resistance is not affected by moisture or temperature up to about 100°C. Comparative tracking resistance of most unmodified nylons is greater than 600 V. Incorporation of additives such as flame retardants often reduces the electrical properties because of the introduction of ionic species.

Flammability. Most nylons are classified V-2 by the Underwriters' Laboratory UL-94 test, which means that these nylons are self-extinguishing within a

Table 3. Effect of Additives on Nylon-6,6 and Nylon-12

Property	Nylon-6,6[a]				
30 wt% Glass fiber[a]	Impact modifier[a]	Nylon-6,6 + Nylon-12[b]			Nylon-12 + plasticizer[b]
Tensile strength, MPa[c]					
Dry	83	193	52	50–55	27
50% rh[d]	77	130	41		
Flexural modulus, MPa[c]					
Dry	2800	9300	1800	1500	330
50% rh[d]	1200	6600	900		
Elongation at break, %					
Dry	60	3	60	200	300
50% rh[d]	>300	5	210		
Notched Izod impact strength, J/m[e]					
Dry	53	110	910	60	No break
50% hr[d]	112	133	1070		
Deflection temperature under load at 1.8 MPa[c], °C	90	254	83	50	55

[a]Ref. 4.
[b]Ref. 7.
[c]To convert MPa to psi, multiply by 145.
[d]50% rh = conditioned to 50% relative humidity at 23°C.
[e]To convert J/m to ft·lbf/in., divide by 53.38.

certain time scale under the conditions of the test. They achieve this performance by means of giving off burning drips. Inclusion of reinforcement such as glass fiber converts this behavior to HB, where the sample continues to burn as a result of the reinforcement holding it together. The flammability performance can be improved by adding flame-retardant additives that can eliminate burning drips and produce nylon that meets the most stringent UL-94 test (V-0), even with materials containing glass fibers.

Mechanical Properties

The semicrystalline structure of most commercial nylons imparts a high strength (tensile, flexural, compressive, and shear) as a result of the crystallinity and good toughness (impact strength) due mainly to the amorphous region. The properties of nylon are affected by the type of nylon (including copolymerization), molecular weight, moisture content, temperature, and the presence of additives. Strength and modulus (stiffness) are increased by increasing density of amide groups and crystallinity in aliphatic nylons; impact strength and elongation, however, are decreased. Nylon-6 having a lower crystallinity than nylon-6,6 has a

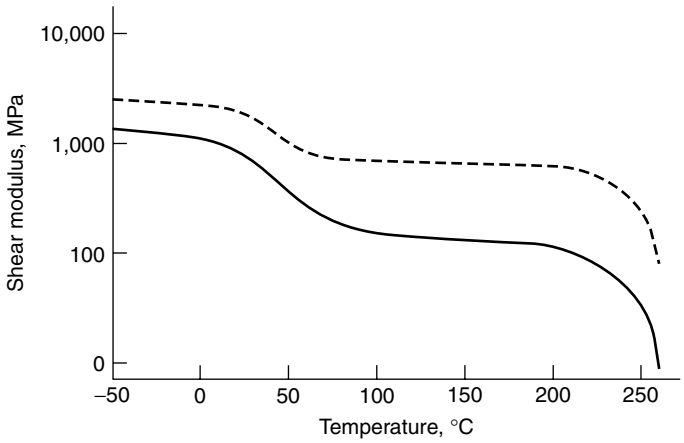

Fig. 2. Effect of temperature on the shear modulus of dry nylon-6,6 (——) and nylon-6,6 plus 30% glass fiber (—). To convert MPa to psi, multiply by 145.

higherimpact strength and slightly lower tensile strength. Nylons containing aromatic monomers tend to have increased stiffness and strength by virtue of the greater rigidity of the chains. Increasing molecular weight gives increased impact strength without having a significant effect on tensile strength. Moisture content affects the properties of nylon-6 and nylon-6,6; the effect is similar to that of temperature. Increasing moisture content reduces the T_g above which the modulus and tensile strength drop significantly; however, some polyamides with a high T_g, such as those containing aromatic monomers, have little change in properties with changing moisture as the T_g remains above room temperature. Increasing moisture for nylon-6 and nylon-6,6 also gives a steady increase in impact strength as a result of increasing plasticization, although at very low temperatures moisture can embrittle nylon. For nylons that absorb lower amounts of water, the effects on properties are less.

The effect of temperature on properties can be seen in Figure 2, which shows the effect on modulus of increasing temperature of unmodified and glass-reinforced nylon-6,6. Impact strength, however, shows a steady increase with temperature as it does with moisture.

Generally, nylon is notch-sensitive and the unnotched impact strength is dramatically reduced when a notch or flaw is introduced into the material. This needs to be considered when designing parts so that sharp angles are avoided where possible. This notch sensitivity can be considerably reduced by incorporating impact modifiers. For the most effective of these materials, the notched impact strength approaches the unnotched impact performance of the unmodified resin. The increased ductility of the material that accompanies impact modification does, however, reduce stiffness and strength. Moisture conditioning of moldings is often used to increase impact strength and flexibility before such operations as snap fitting or assembling cable ties, which can be avoided in some cases by using impact-modified resins. The effect of impact modifier on the properties of nylon-6,6 is shown in Table 3.

Properties such as stiffness and strength can be considerably increased by adding a reinforcing agent to the polymer, particularly glass or carbon fiber. Inclusion of a filler or reinforcement forces the material to fail in a brittle rather than ductile fashion. As a result, the unnotched impact strength and elongation are reduced, although the notched impact strength may be increased. These materials maintain their mechanical integrity under a high load almost up to the melting point of the nylon, eg, deflection temperature under load (see Table 3). Mechanical properties can also be modified by the inclusion of Plasticizers, which have a similar effect to that of water in breaking down hydrogen bonding in the amorphous region and increasing ductility, flexibility, and impact strength. Table 3 also shows the effect of glass and plasticizers on nylon-6,6 and nylon-12 properties, respectively.

As with most plastics the properties of nylons are time-dependent. The strain in a molding constantly under load increases with time (creep); equally, the load or stress required to maintain a constant deformation decays with time (stress relaxation). Some creep curves are given in Figure 3. Glass-fiber reinforcement considerably improves the creep performance. Nylons have good resistance to dynamic fatigue, ie, the application of cyclic loads. This is influenced both by the frequency and wave form imposed as well as by moisture, temperature, and the presence of notches. Again, glass-fiber reinforcement considerably improves the number of cycles that can be withstood. Nylon-6,6 has much better fatigue resistance than nylon-6, and it is claimed that nylon-4,6 is much better still (9). Nylon is also particularly resistant to damage from repeated impacts; much better, for example, than some metals that have a high impact resistance to a single blow.

Two more properties for which nylon shows particular advantages are abrasion resistance and coefficient of friction. These properties make the material suitable for use in, for example, unlubricated bearings and intermeshing gears;

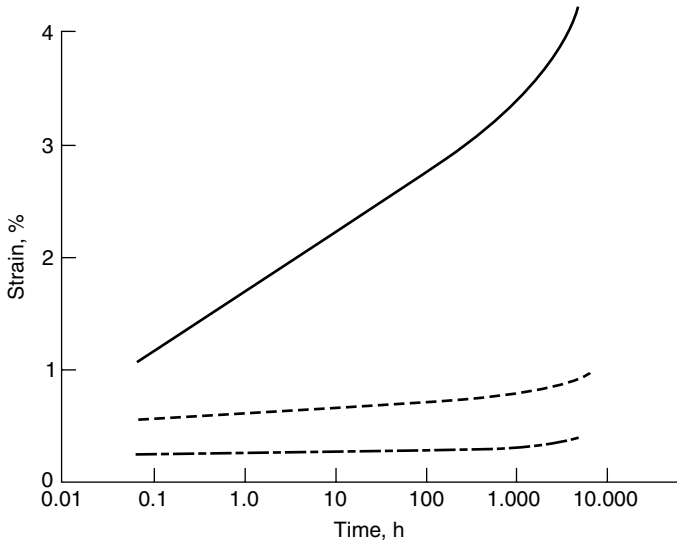

Fig. 3. Tensile creep of nylon-6,6 at 50% rh, 23°C, and 15 MPa (2175 psi) (——), reinforced by 15 wt% glass (—), and 33 wt% glass (– -).

nylon has been used in such applications from an early stage in its development. Wear and friction properties can be further improved by use of appropriate additives; for example, abrasion resistance can be increased considerably by the use of aramid-fiber reinforcement and PTFE, graphite or molybdenum disulphide have been used to significantly reduce friction (and often also wear) in moving parts.

Chemical Properties

Hydrolysis and Polycondensation. One of the key properties of polyamides relates to the chemical equilibrium set up when the material is polymerized. The polymerization of nylon is a reversible process and the material can either hydrolyze or polymerize further, depending on the conditions.

In the melt the material is in a dynamic situation and only at a certain (equilibrium) moisture content does the rate of hydrolysis equal the rate of polymerization. This equilibrium moisture content (in a sealed system) depends on the polymer, the temperature, the molecular weight, and the end group balance of the polymer. Below this moisture content, the melt increases in viscosity (polymerizes) and above it hydrolysis occurs with reduction in viscosity and molecular weight. For nylon-6,6, the equilibrium moisture content is close to 0.15% for most standard injection-molding resins; however, the figure is less for reinforced materials as less nylon is present per unit weight. For high molecular weight nylons used for extrusion applications, the equilibrium moisture content is less as the concentration of end groups is less; therefore, these materials need to be processed at lower moisture contents to avoid lowering the molecular weight. Nylons also polymerize in the solid form (solid-phase or solid-state polymerization) if heated significantly above 100°C in the absence of water. The equilibrium also means that nylons can hydrolyze when parts are exposed to aqueous environments for long periods at high temperatures, leading to loss of properties. However, this depends on the conditions of exposure. Nylon-6,6 has long been used successfully for automobile radiator end tanks and washing machine valves and has recently been used for pump housings for the boilers of domestic central heating systems (15). Nylons that absorb lower amounts of moisture have improved hydrolysis resistance, and semiaromatic nylons have been used for some higher temperature applications (16).

Thermal Degradation. Although nylons have good thermal stability, they tend to degrade in the melt when held for long periods of time or at high temperatures. This is particularly the case for nylons containing adipic acid such as nylon-6,6. The adipic acid segment can cyclize, leading to chain scission and the production of cyclopentanone and derivatives and evolution of carbon dioxide and ammonia. Alongwith reduction of molecular weight, cross-linking also occurs, and the material eventually sets into an intractable gel. This is normally not a problem with plastics processing operations where the residence time is relatively short, but loss of molecular weight during injection molding can occur as a result of this, particularly at high temperatures (over 300°C) or where the shot size is a small proportion of the machine capacity. Significant evolution of carbon dioxide also occurs. Processing machines should not be left containing molten nylon for any length of time but should be either emptied or purged out with, for example, a polyolefin.

Oxidation. All polyamides are susceptible to oxidation. This involves the initial formation of a free radical on the carbon alpha to the NH group, which reacts to form a peroxy radical with subsequent chain reactions leading to chain scission and yellowing. As soon as molten nylon is exposed to air it starts to discolor and continues to oxidize until it is cooled to below 60°C. It is important, therefore, to minimize the exposure of hot nylon to air to avoid discoloration or loss of molecular weight. Similarly, nylon parts exposed to high temperature in air lose their properties with time as a result of oxidation. This process can be minimized by using material containing stabilizer additives. Improvements in recent years have allowed nylons to be used at higher temperatures without problems, and formulations to minimize yellowing with aging have been developed.

Ultraviolet Aging. Nylon parts exposed to sunlight and uv rays undergo a similar free-radical aging process. Again, this can be reduced with appropriately stabilized materials.

Effect of Chemicals and Solvents. Nylons have excellent resistance to many chemicals, although the effect varies depending on the nature of the nylon. Generally, polyamides tend to be particularly resistant to nonpolar materials such as hydrocarbons. Resistance is least to strong acids and phenols which are most effective at disrupting the hydrogen bonding and which can sometimes dissolve the nylon. Highly polar materials such as alcohols are absorbed and sometimes dissolve the nylons containing lower concentrations of amide groups. Ethylene glycol, which is used in engine coolants, is absorbed by polyamide and dissolves nylon-6,6 (and nylon-6) above 160°C. Certain metal salts can attack nylon causing stress cracking, eg, zinc or calcium chloride, or even dissolve the material in alcoholic solution, eg, lithium chloride.

Manufacture

Solid-State Polymerization. There is a limit to the molecular weight that can be obtained in a melt-polymerization process as a result of degradation with long melt residence times and limits to the diffusion rate of moisture out of high viscosity melts. In order to produce high molecular weight resins to be used in, for example, extrusion operations, it is necessary to polymerize further by heating in the solid state. This is carried out under vacuum, steam, or inert gas. Nylon-6,6, for example, can be solid-state-polymerized in the temperature range of 150–240°C. Below the melting point, the hydrolysis rate is negligible compared to the reaction time, and degradation reactions are also much reduced. This process can be carried out by a batch or continuous process. The batch process involves tumbling granules in a heated rotating vessel under vacuum or a stream of inert gas. The continuous process uses a column with heating and cooling sections, granules enter at the top and exit at the bottom against a counter current of inert gas, and the residence time is set to give the molecular weight increase required.

Compounding. Although low levels of additives such as lubricants can often be incorporated during the polymerization process (internally or surface coated onto granules), in order to add the required higher levels of, eg, glass-fiber reinforcement, impact modifiers, or flame retardants, it is necessary for the nylon

to undergo a second manufacturing step to melt-incorporate the additives. This is carried out by extrusion compounding, which usually consists of a gravimetric feed of additives and nylon granules to a single- or twin-screw extruder. The screw conveys the mixture along a heated barrel and, by the action of shear on the polymer, melts the material and mixes in the ingredients. Twin-screw extruders usually have intermeshing co-rotating screws that are more effective at mixing the material than single-screws, and can be built up from modular components, allowing flexibility in selecting the average and localized shear/mixing regime along the screw. Additives such as glass fiber can be added along the barrel and into the melt in such designs; screw-side feeders can be used to do this. A vacuum line attached to a vent in the barrel allows the removal of moisture and volatiles. Material is extruded through a die into laces, which are water-cooled and pelletized. An alternative compounder is the co-kneader design which is a modification of a single-screw extruder but has axial motion as well as rotation and mixing pins engaging with the (modified) screw. This system allows a higher level of mixing to be achieved without generating excessive temperatures (particularly useful for temperature-sensitive additives) but requires a secondary crosshead or gear pump to develop pressure for lace extrusion (17).

Additives and Modifications. For plastics uses, nylon is only rarely employed as the pure polymer, and is almost always modified to some extent even if only with the addition of a small amount of lubricant. There has been a dramatic increase in the range and number of combinations of additives used to modify nylons, resulting in a huge expansion in the number of commercial grades available and the uses to which they can be put. It is not unusual to find formulations that contain less than 50% nylon and half a dozen or more additives.

Lubricants. Lubricants are used to improve the melt flow, screw feeding, and mold release of nylons. Long-chain acids, esters, and amides are used together with metal salts, eg, metal stearates. Improved melt flow is mainly a function of molecular weight reduction during molding. Mold release is improved by waxes of limited compatibility with nylon, which migrate to and lubricate the mold surface. High molecular weight silicones have also been used to improve flow and mold release of polyamide.

Nucleants. Although nylons crystallize quickly, it is often an advantage, particularly for small parts, to accelerate this process to reduce cycle time and increase productivity. Nylon-6, which crystallizes more slowly than nylon-6,6, particularly benefits from nucleation in unreinforced formulations. Nucleants are generally fine-particle-size solids or materials that crystallize as fine particles before the nylon. The materials, eg, finely dispersed silicas or talc, seed the molten nylon and result in a higher density of small uniformly sized spherulites; in nylon-6, the crystalline form is also changed. Nucleation increases tensile strength and stiffness but makes the material more brittle. Mold shrinkage is lower for nucleated resins.

Stabilizers. Stabilizers are often added to slow down the rate of oxidation and uv aging. Heat stabilizers can be organic antioxidants (such as hindered phenols or aromatic amines), hydroperoxide decomposers, or metal salts. The latter are most commonly used in the form of copper halide mixtures. This system, which has the side effect of discoloring the nylon, acts as a regenerative free-radical suppressor. Above about 120°C, the copper halide system is by far the most effective

and allows the use of glass-reinforced nylon-6,6 in high temperature automotive underhood applications. Ultraviolet stabilizers can be free-radical acceptors, uv absorbers, or hindered amine light stabilizers. Commonly, mixtures are used to give optimal performance, eg, a uv absorber such as a benzotriazole (or recently triazine) compound, to harmlessly absorb much of the uv energy, combined with a hindered amine light stabilizer (plus optionally a hindered phenol) to suppress reactive free radicals (18). The most common uv stabilizer, however, continues to be finely dispersed carbon-black pigment.

Impact Modifiers. Notched impact strength and ductility can be improved with the incorporation of impact modifiers, which can also lower the brittle–ductile transition temperature and give much improved low temperature toughness. Impact modifiers are rubbers (often olefin copolymers) that are either modified or contain functional groups to make them more compatible with the nylon matrix. Dispersion of the rubber into small (micrometer size) particles is important in order to obtain effective toughening (19). Impact modifiers can be combined with other additives, such as glass fiber and minerals, in order to obtain a particular balance of stiffness and toughness. Modified acrylics, silicones, and polyurethanes have also been proposed as impact modifiers.

Flame Retardants. Flame retardants are added to nylon to eliminate burning drips and to obtain short self-extinguishing times. Halogenated organics, together with catalysts such as antimony trioxide, are commonly used to give free-radical suppression in the vapor phase, thus inhibiting the combustion process. Additives that have been used are brorninated polystyrene, decabromodiphenyl oxide, and chlorinated dodecahydrodimethanodibenzocyclooctene (Dechlorane plus). In Europe, red phosphorus is widely used. It is effective at much lower levels and promotes char formation as well as inhibiting combustion, but is a more hazardous raw material to handle and the compounds are not available in light colors. Concern about the possibility of dioxin formation from resins containing halogenated organics, particularly those containing phenoxy groups, has led to increasing interest in nonhalogen, nonphosphorus flame retardants. Melamine derivatives have been widely used in unreinforced compositions and products have been developed based on magnesium hydroxide, although the high levels needed result in very poor mechanical properties. Recently nonhalogen, nonred phosphorus glass-reinforced flame retardant materials have been reported (20).

Plasticizers. Plasticizers are used to increase the flexibility of nylon and improve impact strength. They are most commonly used in nylon-11 and nylon-12 for such applications as flexible fuel hoses for automobiles. Plasticizers for polyamide are often sulphonamides, although others such as long-chain diols have been used as well as the caprolactam monomer in unextracted nylon-6. The latter material has been used for applications such as fishing lines.

Reinforcement. Nylon is particularly suitable for reinforcement and the melt incorporation of short glass fibers has long been practiced, being developed around 1960 by ICI in England (21) and Fiberfil Inc. in the United States (22). The tensile strength of nylon-6,6 is increased by more than 2.5 times and stiffness by almost 4 times by adding 30% glass fiber. Glass fiber also improves dimensional stability, notched impact strength, temperature performance and long-term creep, and is normally used in the 15–60 wt% range. The glass fibers used need to be treated with a specific sizing to enable bonding with the nylon and dispersion in

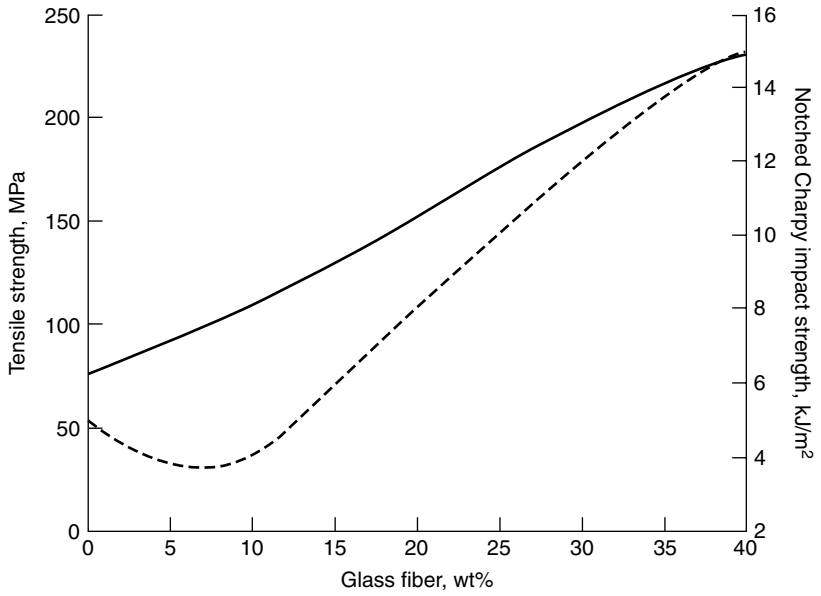

Fig. 4. Variation of tensile strength (——) and notched impact strength (—) with glass fiber level in nylon-6,6. To convert kj/m^2 to ft·lbf/in^2, divide by 2.10.

the melt; the size formulations are proprietary but often contain an aminosilane coupling agent and a polyurethane or acrylic binder. Special sizing compositions have been developed to improve the retention of properties of nylon-6,6 when exposed to hot engine coolant, and glass fibers further improved in this respect continue to be developed. The fibers are normally added as 3- or 4.5-mm chopped strands (bunches of filaments), but the fiber length in the final product drops to a fraction of a millimeter after dispersion in the extruder. Figure 4 shows the relationship between glass fiber content and typical properties in nylon-6,6.

A disadvantage of glass fibers is the warpage of flat moldings. This is the result of differential shrinkage caused by anisotropy from the glass fibers, which tend to align with the direction of melt flow. Mineral reinforcements are used to obviate this by stiffening the material with a more isotropic mixture. Properties are lower than for glass fiber. Minerals having a higher aspect ratio, such as talc and mica, tend to have higher stiffness and strength; surface-treated kaolin and wollastonite have better impact properties. Combinations with glass are also used. Other reinforcements include mineral fibers, carbon fiber, and para-aramid fibers (Kevlar). Carbon fibers give very high stiffness but are much more expensive than glass; aramid fibers increase abrasion resistance.

Nanocomposites. These are materials in which nanometer size silicate layers are uniformly dispersed into polyamides to give high levels of reinforcement at very low levels (eg, 5%). The layer-type clay minerals are treated to make the layers separate allowing them to be incorporated into the polymer structure (intercalation). Initial developments involved incorporation during nylon polymerization but extrusion compounding routes have now been developed. Some advantages of this technology are low density and isotropic shrinkage (23).

Polymer Blends. Commercial blends of nylon with other polymers have also been produced in order to obtain a balance of the properties of the two materials or to reduce moisture uptake. Blends of nylon-6,6 with poly(phenylene oxide) have been most successful, but blends of nylon-6,6 and nylon-6 with polyethylene or polypropylene have also been introduced (24).

Pultrusion. A special variant of compounding is pultrusion, which is used in the manufacture of long fiber reinforced polyamide materials. In this technique, fibers (eg, glass fibers) are pulled through polymer melt usually with some mechanism to spread the fibers to allow complete wetting. On cutting the resulting lace, the glass fiber length becomes equal to the length of the granule. These materials can give high stiffness and impact strength combined with lower warpage (25) but need to be processed carefully (large gate size, low back pressure) to avoid reducing the glass fiber length to that of a standard short glass fiber product.

Processing

Nylons need to be processed dry to avoid molecular weight loss and processing problems. Figure 5 indicates both the usable moisture range for nylon-6,6 and nylon-6 in injection molding and the relationship with temperature (26). Extrusion applications require lower moisture contents (max 0.1–0.15% for nylon-6,6 and nylon-6) as do some other nylon types (eg, max 0.1% for nylon-11 and nylon-12; 0.05% for nylon-4,6). The materials are normally supplied dry by the manufacturer

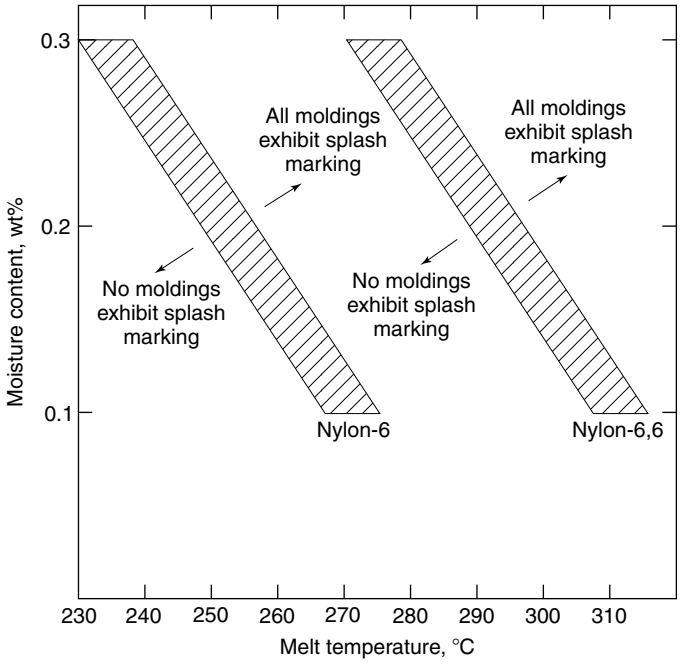

Fig. 5. Relationship between moisture content and temperature for an unvented cylinder during injection molding.

in moistureproof packaging such as foil-lined 25-kg bags or lined 1-ton boxes. Once opened, the material should be used within a few hours or resealed. Material that has absorbed some moisture can be redried using a vacuum oven at 80°C or a dehumidifier hopper drier.

Material should not be processed at too high a temperature, eg, preferably not above 310°C for nylon-6,6 or 290°C for nylon-6, in order to avoid degradation. Residence times at the higher temperatures should be kept to a minimum. Molten nylon should not be left in an idle machine for more than 30 min maximum. Exposure of molten and hot nylon to air should also be minimized to avoid discoloration.

Generally, nylon scrap or regrind can be reused satisfactorily, provided that it is dry. The level allowed depends on the amount of degradation and the specification of the final products.

Injection Molding. This is the largest single processing route for nylon, taking more than 60% of the material produced. This technique is generally carried out using a screw preplasticizing injection-molding machine (27–29) (see INJECTION MOLDING). Nylons can often be processed on general-purpose screws having a constant decreasing flight depth along the screw, but better performance can be achieved by a nylon-type screw having a sharp reduction in flight depth within a few flights in the compression or transition zone. This allows for the sharp melting point of semicrystalline nylons, which results in a rapid reduction in bulk density.

The sharp melting point and the low melt viscosity also mean that nylon can give problems with nozzle drool and/or premature freeze-off. For this reason, it is normally necessary to use either a reverse-taper nozzle (fitted with a heater to avoid freeze-off), a mechanical shut-off nozzle, or melt decompression. The design of molds should also take into account this low viscosity and sharp melting point. Mold surfaces should be well-mated to avoid flash.

Table 4 gives injection-molding temperatures for various nylons. Typical molding conditions for polyamides are as follows: average injection velocity, 100–300 mm/s; hold pressure, 70–90 MPa; hold pressure time, 20–30 s; maximum injection pressure, 70–90 MPa; cooling time, $\leq$10 s; and total cycle time, $\leq$50 s. Nylons generally require a fast injection speed and are particularly good for achieving fast cycle times because of the low viscosity and rapid setting-up.

Significant mold shrinkage occurs with nylon, mainly on account of the increase in density with crystallization. This can give rise to voiding and sink marks in moldings. The dimensional stability can be much improved by using reinforcing agents or nucleated materials.

Developments in injection molding that have become increasingly important include gas injection and fusible-core molding. Gas injection enables a saving in part weight and avoidance of sink marks in thick sections. This technique has recently been upgraded for use in tubing applications where the hollow core formed by the gas pushing out molten nylon from the center becomes the bore of the tube. Special materials are required to give a smooth internal surface. Fusible-core technology involves overmolding a low melting metal alloy core that is subsequently melted out in an oil bath. This technique allows much more complex moldings containing internal passageways to be produced. The method had become important for making automobile air inlet manifolds but is now being mainly overtaken in

Table 4. Injection-Molding Temperatures for Different Polyamides[a]

Polyamide	Melt temperature, °C[b]	Mold temperature, °C
Nylon-6	250–290	80
Nylon-6,6	290–300	80–100[b]
Nylon-4,6	315	120
Nylon-6,9 and nylon-6,10	270	80
Nylon-6,12	240–270	80
Nylon-11	210–260	80
Nylon-12	200–250	70–80[c]
Nylon-MXD,6	250–280	130
Nylon-NDT/INDT	280–300	80
Polyphthalamide[d]	327–332	135–150

[a]Ref. 30.
[b]The higher temperatures are used for glass-filled or high viscosity materials and the lower temperatures for low viscosity or plasticised resins.
[c]The lower mold temperature is used if >5% plasticizer.
[d]Ref. 31.

this application by vibration welded parts. Another very recent technique, which is really a development of gas injection, is water injection. In this process, water under high pressure replaces gas in ejecting molten nylon from the center of a part; the advantage is more efficient cooling, shorter cycle times, and the potential to produce larger diameter tubes (32).

Extrusion. Extrusion accounts for about 30% of nylon produced and is used in various processes (33). Nylons can be extruded on conventional equipment having the following characteristics. The extruder drive should be capable of continuous variation over a range of screw speeds. Nylon often requires a high torque at low screw speeds; typical power requirements would be a 7.5-kW motor for a 30-mm machine or 25-kW for a 60-mm one. A nylon screw is necessary and should not be cooled. Recommended compression ratios are between 3.5:1 and 4:1 for nylon-6,6 and nylon-6; between 3:1 and 3.5:1 for nylon-11 and nylon-12. The length-to-diameter ratio L/D should be greater than 15:1; at least 20:1 is recommended for nylon-6,6, and 25:1 for nylon-12.

Typical operating temperatures are shown in Table 5. Most extrusion operations require high viscosity (high molecular weight) nylon in order to give a high melt strength to maintain the shape of the extrudate. In the following sections,

Table 5. Typical Temperatures (°C) for Nylon Extrusion

Location	Nylon-6,6[a]	Nylon-6[a]	Nylon-12[b]
Screw			
Feed zone	265–275	220–230	185–205
Compression zone	275–285	235–250	190–215
Metering zone	285–295	245–265	190–220
Head	285–295	250–270	200–230
Die	285–295	250–270	195–230

[a]Ref. 33.
[b]Ref. 34.

reference is made to three broad viscosity ranges that correspond to these approximate number-average molecular weights when nylon-6,6 is used: high viscosity nylon ($M_n = 30{,}000$–$40{,}000$), medium viscosity (20,000–30,000), and standard viscosity (15,000–18,000, as used for injection molding).

Film. Nylon film can be produced as either tubular or cast film. In tubular film, melt is extruded through a screen pack and a tubular die, and a bubble is formed with air pressure. Total drawdown (extension of the melt) of the order of 10:1 to 20:1 is achieved. High viscosity nylon is required for this operation. A relatively stiff, hazy film is produced; nylon-6 has a lower haze level than nylon-6,6. Cast film is produced from medium viscosity nylon by extruding through a straight slot die and then rapidly quenching on highly polished rolls at a controlled temperature; speed of the rolls affects drawdown as above. Nylon film is also produced as coextruded multilayer structures mainly with olefin-type polymers. Nylon film has a low permeability to oxygen, nitrogen, and carbon dioxide, but a high permeability to water vapor (see BARRIER POLYMERS).

Tubing and Pipe. Medium to high molecular weight polymers are used for tube extrusion. Small bore tube (up to 10 mm) can be extruded through a conventional die and cooled in an open water bath. Air is injected into the center of the tube, using a torpedo to prevent the extrudate from collapsing and to adjust the wall thickness. For tubing larger than 10 mm, a pressure sizing die is used and tube is drawn into the water bath through a series of sizing plates in the end of the bath, 25–50 mm away from the die. A drawdown of about 2:1 is usually used, but this depends on the molecular weight and line speed. High molecular weight nylons require less drawdown than the less stiff lower molecular weight materials. Similar methods are used for large diameter pipe, for which high viscosity material is normally used, particularly with high wall thicknesses. As this is a slow operation, melt temperatures are kept up to 30°C above the normal melt temperature.

Monofilament. Standard and medium viscosity nylons are used. Close control of diameter is important and a gear pump is used before the die (after filtering through a fine filter pack) to minimize pressure variations. The die hole diameter is normally 1.5–2 times the diameter of the undrawn filament. The filaments are drawn through a quench tank at approximately 40°C, separated and then drawn by passing through two sets of rolls (running at different speeds) separated by a heated chamber. The drawn filament is set by passing through a final heated conditioning chamber.

Rod and Profiles. Medium to high viscosity grades are used. Accurate temperature control is important. For rods of diameters greater than 3 mm, slow solidification is essential to avoid voids and cracks caused by nonuniform shrinkage. Two processes are used. For rods up to 150 mm, a forming box is used whereby nylon is extruded under pressure through a water-cooled cylindrical tube. The tube is isolated from the die by a nonmetallic gasket, the rod is pulled off at a constant rate by a haul-off. The second process, which can be used for more complex shapes, involves extruding the nylon into a series of interconnecting open-ended molds.

Wire and Cable Coating. Nylons are widely used for wire covering and sheathing cable. In the latter application, nylon is usually overcoated onto insulation of another material, such as PVC, in order to provide cut and abrasion resistance. In a specialized application, nylon-11 and nylon-12 are used to provide

termite resistance. Amorphous polyamides have been used for sheathing of optical fiber cables.

Blow Molding. Blow Molding of nylons has become more important as a means of making large hollow moldings. In addition to high molecular weight nylon, resins modified to increase melt strength and containing glass fiber have been introduced, and impact modifiers are often used to increase melt elasticity. Blow molding of nylons is usually carried out by extrusion blow molding, whereby melt is produced in an extruder and formed into a tube called a parison (35). The molten parison is captured in a mold that pinches and seals the ends, and the rigid hollow part is formed by inflation under air pressure. Intermittent extrusion blow molding is most common, which involves the storing of melt in an accumulator die head until required to form the next parison, melt storage with a reciprocating screw or accumulator pot with ram is often used. Continuous blow molding and injection blow molding (for small parts) can also be used. The parison can also be inflated using suction blow molding and this technique is now becoming increasingly important. Suction blow molding is especially suitable for 3-D parts where the parison can be effectively pulled through complex mold shapes using vacuum. The design of the manifold and accumulator head should be such as to avoid material hold-up locations (giving degradation and gel formation), and should also incorporate even, carefully controlled heating. Adequate venting of the head is necessary to avoid buildup of gas.

Rotomolding. Nylon-6, nylon-11, and nylon-12 can be used in rotomolding and are generally supplied for these applications as a powder or with a small pellet size. The process involves tumbling the resin in a heated mold to form large, thin-walled moldings. Nylon-11 and nylon-12 use mold temperatures of 230–280°C and nylon-6 is processed at over 300°C. An inert gas atmosphere is preferred to avoid oxidation.

Reaction Injection Molding. RIM uses the Anionic polymerization of nylon-6 to carry out polymerization in the mold. A commercial process involves the production of block copolymers of nylon-6 and a polyether by mixing molten caprolactam, catalyst, and polyether prepolymer, and reacting in a mold (36,37).

Powder Coating. Nylon-11 and nylon-12 are used in powder form for anticorrosion coating of metals. Dip coating and electrostatic and flame spraying are used. Dip coating, which involves immersing a preheated article into fluidized nylon powder, is most suitable for automation.

Assembly Techniques. After molding, parts produced in more than one component can be assembled by snap fit, bolting, rivetting, welding, or gluing. Welding has become much more widespread in the last 10 years, with vibration welding in particular finding use to produce complex parts such as automotive air intake manifolds in a more cost effective manner than the capital intensive lost core process. Ultrasonic welding is also used (requires the nylon parts to be dry) and recently both hot plate and laser welding (38) have attracted considerable interest. Special polyamide materials have been developed for both these latter techniques. Polyamide parts can also be glued together, aided by the high surface energies of these polymers. Joint strengths are however much lower than when welded. Certain epoxy and polyurethane glues can be used sucessfully with polyamides although epoxies may give better resistance to temperature. Nylon–nylon joints are stronger than, for example, nylon–aluminum.

Table 6. Worldwide Polyamide Consumption in 1998 (10^3 t)[a]

Region	Auto	Electrical/electronic	Film	Other	Total
North America	186	86	69	154	495
Europe	158	120	74	220	572
Asia Pacific	93	68	61	113	335
Rest of the world	7	9	16	31	63
Total	*444*	*283*	*220*	*518*	*1465*

[a]Ref. 3.

Applications

More than 60% of nylon is used in injection-molding applications. About 55% of this use is in the transportation industries, and most of this use is concerned with automobile production. Table 6 shows the split of applications for which nylon was used worldwide in 1998 (3). Descriptions of uses for polyamides, split into the principal application areas are given below.

Automotive. Not only is this the biggest single application area for polyamides but the rapid increase in the number of new applications is strongly influencing the overall growth rates for the polymer type. Metal replacement is being driven by both weight savings (and therefore fuel efficiency) and lower manufacturing costs.

Underhood. Polyamides have been used under the hood for a long time and applications such as radiator end tanks, filter housings, connectors and cable ties, together with nylon-11 and nylon-12 for fuel hoses have been long established. Certain applications such as filter housings may have mainly switched to lower cost polymers such as polypropylene but this has been far more than balanced by a huge growth in new uses. During the 1990s nylon air intake manifolds had essentially replaced aluminum and use of polyamides had extended to fuel rails, fans, fan shrouds, thermostat housings, and valve and engine covers. Some of the latest developments are front end modules (often nylon/metal hybrid structures) (39) and water tubes or water rails to replace rubber hoses in the coolant circuit. These tubing parts can potentially be made by either gas injection molding or blow molding, depending on the complexity and functionality required.

Interior. Again, polyamides have been used for some time for switches, handles, seat belt components, etc. Big new applications include air bag containers (very tough stiff resins are required to withstand the explosive inflation forces), pedals, and pedal boxes. Polyamides have also been used to replace metals in seat systems (39).

Exterior. Probably the biggest exterior application for polyamides is for wheel covers where mineral reinforced compositions are used to get the required degree of dimensional stability and flatness. Moves to use lower cost polymers have had limited success so far because of the better resistance of nylon to temperatures developed during braking. Other exterior applications include sun roof surrounds, door handles, fuel filler flaps, etc. One special application is the use of a nylon product (DuPont Selar®) as a fuel barrier material in polyethylene fuel tanks.

Electrical/Electronic. The electrical insulating properties of polyamides together with temperature performance, toughness, and inherent low flammability have long driven use in electrical and electronic applications. Uses include cable ties, connectors, light housings, plugs, and switches. Flame-retardant materials are also used for switchgear, housings, relays, circuit breaker components, and terminal strips. The advent of higher melting, higher heat-distortion temperature polyamides has allowed more temperature sensitive applications to convert to plastics. A new area for these types of products is for printed circuit boards using surface mount technology for which resistance to soldering temperatures is necessary. One additional application area is for housings for electronic equipment using products modified to provide an electromagnetic barrier and static dissipation.

Consumer. Polyamides are used in a number of consumer applications. A long-standing use is for power tool housings made from glass-reinforced nylon-6 or nylon-6,6 often containing impact modifier. A variation of this is a chain saw handle made using gas injection to reduce the weight; nylon monofilament is also used for strimmer cord. Sports equipment is one area in which polyamide use has expanded significantly and nylon has been used in ski boots and ski bindings, ice or roller skates, sports shoe soles, and tennis rackets (using carbon fiber reinforcement). Other miscellaneous applications include lighters, kitchen utensils, toothbrush filaments (nylon-6,12), chair bases and arms, spectacle frames, sewing thread, and packaging film (including cook-in-the-bag envelopes).

Industrial. This covers a huge range of unrelated areas of use. Nylon has been used from the early days in various gears and pulleys as well as in bearings and bearing cages, fasteners, and valves. Low melting nylon terpolymers are used as hot melt adhesives, nylon-12 for wire coating (including dish washer baskets), and amorphous nylons are used for transparent filter bowls and flow meters and for protecting optical fiber cables. Other uses have been stadium seats, sliding rails for conveyors, washing machine valves, castors, rail insulator pads, fishing lines, window thermal insulation, and film for medical applications. Some recent applications are pump housings for central heating systems (15) and an all-nylon shopping trolley (40).

Recycling

The issue of the recycling of polyamide parts has become a hotly debated issue since the second half of the 1990s. In the light of expected future legislation, a number of pilot schemes have been started to investigate collecting and recycling parts such as automotive components. The most advanced schemes however concentrate on reusing nylon carpets in plastic end uses. These processes are complex and expensive as considerable pretreatment of the post-consumer article is required before it can be reused in a plastics compounding process. The product can be recompounded directly (mechanical recycling) which invariably leads to a lower quality resin as contamination and/or unwanted ingredients cannot be entirely removed. The route to highest quality resin is achieved by chemical recycling in which the polyamide is taken back to monomer, purified, and repolymerized. A plant to chemically recycle nylon-6 had been started in the United States in 1999

(41) and a demonstration plant to recycle nylon-6,6 (as well as mixtures with nylon-6) was due to be commissioned in 2001 (42). The final development of recycling will probably involve a balance of part reuse, energy recovery, mechanical recycling, and chemical recycling.

Economic Aspects

The principal worldwide manufacturers of nylon resins are given in Table 7. Total sales of nylon plastics in the United States and Canada in 1998 were 495,000 t (3). West European sales were 572,000 t and sales in Asia Pacific (including Japan) were 335,000 t (3). Table 8 shows the variation of price across different polyamide types. Current estimates of growth for polyamide plastics are 9% p.a. for nylon-6 and 8.2% for nylon-6,6 (3). With fiber growth at 1.3% and 1.4% respectively, this represents a greater than 6 times higher growth rate for plastics. Published literature values for polyamide prices had remained stable through the second half of the 1990s (44) but in Europe at least, real prices had been dropping to the point at which major suppliers had needed to announce price increases in late 1999 and 2000 in order to get back to reinvestment economics (particularly in view of major oil and raw material cost increases).

Specifications, Standards, and Quality Control

Raw material specifications may be agreed between the supplier and the molder or end user, or they may be defined as requirements by an external body. The standards ASTM D4066 (45) and ISO 1874-1/2 identify how to classify and specify nylon materials and give details of tests and test methods that may be used, as well as required values. ASTM D5336 for polyphthalamides is also used. The tests include mechanical, thermal, electrical, and flammability properties as appropriate. In addition to these, it is normally necessary to specify the viscosity of the material, maximum moisture content, and ash content (if reinforced). Viscosity is generally measured as solution viscosity that corresponds directly to molecular weight, rather than melt viscosity, which is moisture-dependent. In the United States, solution viscosity is generally measured as relative viscosity (ASTM D789) or inherent viscosity (ASTM D2857), normally in 90% formic acid or *m*-cresol solvent. Elsewhere, viscosity measurements mainly use the internationally agreed viscosity number (ISO 307) in formic acid, sulfuric acid, or *m*-cresol. Moisture content is determined according to ASTM D789. The test employs a coulometric Karl Fischer titration technique using a nitrogen-flushed heated chamber to drive moisture into the solution. Commercial equipment is available to carry out this test. Manufacturer's quality control tests normally include tests for contamination, color, moisture, ash, viscosity, packaging (qv), and other properties as appropriate.

In recent years most polyamide suppliers have made data available using a common computer database software known as CAMPUS (Computer Aided Material Preselection by Uniform Standards). All data in this database is measured in common ISO format (ISO 10350 for single point and ISO 11403-1/2 for

Table 7. Manufacturers of Polyamide Plastics

Manufacturer	Nylon type	Trade name
United States		
E. I. du Pont de Nemours & Co., Inc.	6,6, 6,12, and others	Zytel and Minlon[a]
Ticona U.S.	6,6	Celanese
Solutia	6,6, 6,9	Vydyne
Honeywell	6	Capron
BASF Corp.	6	Ultramid
EMS-American Grilon, Inc.	6	Grilon
Nylon Corp. of America	6	Nycoa
Atofina Chemicals, Inc.	11	Rilsan
BP Amoco	PPA	Amodel
France		
Atofina	11, 12	Rilsan
	Polyamide blends	Orgalloy
Rhodia	6,6, 6,10	Technyl
Germany		
BASF AG	6, 6,6, 6,10	Ultramid
Bayer AG	6	Durethan
DuPont de Nemours	6,6	Zytel and Minlona[a]
Degussa-Hüls AG	12	Vestamid
	NDT/INDT	Trogamid
Italy		
Rhodia	6, 6,6	Technyl
Radici Novacips SpA	6, 6,6	Radilon
Netherlands		
DSM	6, 6,6	Akulon
	4,6	Stanyl
Japan		
Asahi Chemical Industry Co., Ltd.	6,6	Leona
Mitsubishi Engineering-Plastics Corp.	6, 6,6	Novamid
	MXD,6	Reny
Mitsui Chemicals	66,6T, 6T,6I	Arlen
Toray Industries, Inc.	6, 6,6, 12	Amilan
Ube Industries, Ltd.	6, 6,6, 12	Ube Nylon
Unitika, Ltd.	6, 6,6	Unitika
Switzerland		
EMS Chemie AG	6, 6,6, copolymers	Grilon
	12, transparent amorphous	Grilamid
	Amorphous copolymers	Grivory
United Kingdom		
BIP Plastex Ltd.	6	Beetle
Israel		
Nilit	66	Polynil

[a]Mineral filled.

multipoint data) and allows easy data retrieval and comparison between grades and suppliers. The CAMPUS internet site (http://www.campusplastics.com/) contains a listing of the participating companies and in many cases gives links to where their data can be downloaded.

Table 8. Prices of Polyamides 2000[a]

Type	Price, $/kg
Nylon-6	2.84–2.93
Mineral filled	2.69–2.87
30% Glass fiber	3.70–3.92
Nylon-6,6	3.00–3.15
Mineral filled	2.82–3.00
30% Glass fiber	3.64–3.86
Nylon-6,9	5.51–6.09
Nylon-6,10	6.31–6.90
Nylon-6,12	6.31–7.21
Nylon-4,6	6.50
Nylon-11	7.25–7.52
Nylon-12	7.01–7.52
Transparent amorphous	5.45–7.94

[a]Ref. 44.

BIBLIOGRAPHY

"Polyamides, Plastics" in *EPST* 1st ed., Vol. 10, pp. 460–482, by E. C. Schule, Allied Chemical Corp. "Polyamides, Plastics" in *EPSE* 2nd ed., Vol. 11, pp. 445–476, by R. J. Welgos, Allied Chemical Corp.

1. M. I. Kohan, *Nylon Plastics Handbook*, Carl Hanser Verlag, Munich, Germany, 1995.
2. B. De Bièvre, in *Polyamide 2000 World Congress (Conf.)*, Mar. 2000, Session I/2, Maack Business Services, Zürich.
3. F. Charaf, in *Polyamide 2000 World Congress (Conf.)*, Mar. 2000, Maack Business Services, Zürich.
4. Zytel Nylon Resins, Product Guide and Properties, E. I. du Pont de Nemours & Co., Inc., Wilmington, Del., 1998.
5. Capron Nylon Homopolymers for Molding and Extrusion, Honeywell, Morristown, N.J., 1998.
6. Design Guide to a Versatile Engineering Plastic, Atofina, France, 1984.
7. Vestamid, Range of Grades, Degussa-Hüls AG, Germany, 1988.
8. Vydyne Engineering Plastic Composite Data Sheet, Solutia, St. Louis, Mo., 1992.
9. Stanyl, General Information, DSM, Heerlen, the Netherlands, 1995.
10. New Engineering Plastics, Reny, Mitsubishi Engineering-Plastics Corp., Tokyo, Japan, 1994.
11. Technical Information, Trogamid-T, Degussa-Hüls AG, Germany, 1987.
12. *Plast. Technol.* **37**, 45 (Apr. 1991).
13. F. Spitznagel, M. Schuchard, and M. Welch, *Kunststoffe* **88**(3), 308–314 (1998).
14. Design Information on Zytel®/Minlon® Resins, Module II, E. I. du Pont de Nemours & Co., Inc., Wilmington, Del., 1998.
15. P.-A. Bardh, *Engineering Design* **99**(2), 6–7 (1999).
16. T. D. Boyer, G. L. Glass, and J. Solenberger, in *Proc. Electr./Electron. Insul. Conf. 23rd*, 1997, pp. 367–370.
17. W. Henschel, in *Adv. Plast. Technol. APT '96, Int. Conf.*, Paper 21, Institute of Plastics and Paint Industry, Gliwice, Poland, 1996, pp. 1–35.
18. P. Schrijver-Rzymelka, *Kunststoffe* **89**(7), 87–90 (1999).
19. U.S. Pat. 4174358 (Nov. 13, 1979), B. N. Epstein (to E. I. du Pont de Nemours & Co., Inc.).

20. R. V. Kasowski, S. L. Tang, M. M. Martens, T. Court, and K. Cosstick, in *New Adv. Flame Retard. Technol., Fire Retard. Chem. Assoc., Fall Conf.*, Fire Retardant Chemicals Association, Lancaster, Pa., 1999.
21. Brit. Pat. 950656 (Feb. 26, 1964), J. Maxwell and A. Rutherford (to ICI).
22. *Chem. Week* 109 (Jan. 25, 1964).
23. P. C. LeBaron, Z. Wang, and T. J. Pinnavaia, *J. Appl. Clay Sci.* **15**(1/2), 11–29 (1999).
24. O. Poyet, J.-C. Causse, and H.-J. Caupin, in *Polyamide 2000 World Congress (Conf.)*, Mar. 2000, Session X/3, Maack Business Services, Zürich.
25. J. Hollin, D. Miller, and D. Vantour, *J. Reinf. Plast. Compos.* **17**(18), 1617–1624 (1998).
26. Maranyl Nylon Compounds, Injection Moulding, N102, 11th ed., Du Pont de Nemours Int. SA, Geneva, Switzerland, 1987.
27. Moulding Manual for DuPont Minlon® and Zytel® Resins, TRZ 30, H-53792, Du Pont de Nemours Int. SA, Geneva, Switzerland, 1996.
28. J. B. Dym, *Injection Molds and Molding*, Van Nostrand Reinhold Co., Inc., New York, 1979.
29. I. I. Rubin, *Injection Molding Theory and Practice*, John Wiley & Sons, Inc., New York, 1972.
30. ISO 1874-2, *Plastics Polyamide (PA) Moulding and Extrusion Materials, Part 2: Preparation of Test Specimens and Determination of Properties*, International Standards Organization, Geneva, Switzerland, 1995.
31. ASTM D5336-93, *Standard Specification for Polyphthalamide (PPA) Injection-Molding Materials*, ASTM, Philadelphia, Pa., 1993.
32. W. Michaeli, A. Brunswick, and C. Kujat, *Kunststoffe Plast. Europe* **90**(8), 25 (2000).
33. Maranyl Nylon Compounds, Extrusion, N103, Du Pont De Nemours Int. SA, Geneva, Switzerland, 1987.
34. Rilsan Technical Bulletin, Atofina, France, 1984.
35. Blow Molding Processing Manual, L-11866, Du Pont de Nemours Int. SA, Geneva, Switzerland, 1999.
36. Nyrim Nylon Block Copolymers, Solutia, St. Louis, Mo., 1992.
37. U.S. Pat. 4031164 (June 21, 1977), R. M. Hedrick and J. D. Gabbert (to Monsanto Co.).
38. C. Bonten, E. Schmachtenberg, and C. Tüchert, *Kunststoffe Plast. Europe* **90**(10), 59 (2000).
39. H. Meier, in *Polyamide 2000 World Congress (Conf.)*, Mar. 2000, Session X/1, Maack Business Services, Zürich.
40. R. Bauer, *Kunststoffe Plast. Europe* **90**(6), 17 (2000).
41. M. Booij, in *Polyamide 2000 World Congress (Conf.)*, Mar. 2000, Session III/4, Maack Business Services, Zürich.
42. P. Penone, in *ETP2000 Conf. Plastic Technology, Gaudner Publications, Inc.* June 2000, Maack Business Services, Zürich.
43. *Plast. Technol.* **46** 158 (Oct. 2000).
44. *Plast. Technol.* Monthly. **46** (Oct. 2000).
45. ASTM D4066-93, *Standard Specification for Nylon Injection and Extrusion Materials (PA)*, ASTM, Philadelphia, Pa., 1993.

GENERAL REFERENCES

Reference 1 above is an excellent reference book covering all aspects of nylon technology. R. S. Williams and T. Daniels, *Rapra Rev. Rep.* **3**(3), 33/1–33/116 (1990). Useful review of polyamide plastics with 473 references.

ROBERT J. PALMER
Du Pont de Nemours International S.A.

POLYBENZIMIDAZOLE POLYMERS (PBI). See RIGID ROD POLYMERS.

POLYBENZOTHIAZOLES (PBT). See RIGID ROD POLYMERS.

POLYBENZOXAZOLES (PBO). See RIGID ROD POLYMERS.

POLYBUTADIENE. See BUTADIENE POLYMERS.

POLYBUTENES. See BUTENE POLYMERS.

POLYCHLOROPRENE. See CHLOROPRENE POLYMERS.

POLYCYANOACRYLATES

Introduction

Cyanoacrylate polymers are commercially important materials as structural adhesives. They combine rapid curing and high strength and are widely used to bond a diverse range of substrate surfaces, including metals, ceramics, plastics, rubbers, and biologically derived materials. The corresponding monomers were first isolated in 1947 by Ardis at B. F. Goodrich (1). Subsequently, Eastman Kodak patented them as adhesive compositions in 1957 (2) and the first commercial adhesive formulation, based on methyl 2-cyanoacrylate, was introduced in 1958 (3). Today, cyanoacrylates represent a billion dollar industry serving medical, electronic, engineering, and consumer markets worldwide. Although adhesive compositions still constitute the major segment of the business, there is growing interest and activity in the use of these polymers in other areas. These include binding agents for the controlled delivery of drugs, coatings for lithographic printing plates, waveguides for optical sensors, photoresists, and holographic recording media.

Physical Properties of Monomers

Cyanoacrylate monomers are generally low viscosity, colorless liquids that are unstable in the absence of acidic stabilizers. The commercially important materials are lower alkyl esters of 2-cyanoacrylic acid including methyl, ethyl, *n*-propyl, allyl, *n*-butyl, isobutyl, 2-methoxyethyl, 2-methoxypropyl, and *n*-octyl derivatives. The structures of some of these monomers are shown in Figure 1. The physical properties of these and related monomers are reported in detail in several previous

Encyclopedia of Polymer Science and Technology. Copyright John Wiley & Sons, Inc. All rights reserved.

Table 1. Properties of Some Common Cyanoacrylate Monomers[a]

	Methyl	Ethyl	Isopropyl	Allyl	*n*-Butyl	2-Methoxyethyl
Boiling point, °C	85–86	92–93	109–112	120–122	118–120	136–138
at kPa[b,c]	1.5	1.3	1.6	1.6	1.1	0.1
Viscosity at 25°C, mPa·s(=cP)	2	2	2	2	2	3
Density, g/cm^3	1.10	1.05	1.01	1.05	0.98	1.06
Refractive index n_{20}^{D}	1.44	1.43	1.43	1.46	1.43	1.43[d]
Flash point, °C	83	83	–	82	85	–
Surface tension[b] at 30°C, mN/m (=dyn/cm)	44.5	38.8	34.5	39.5	34.2	41.5
Lap-shear adhesive strength, MPa[e,f]	22.0	17.2	20.9g	21.5	15.7	18.6

[a] Data from Ref. 3 unless otherwise indicated.
[b] Data from Ref. 5.
[c] To convert kPa to mm Hg, multiply by 7.5.
[d] n_{D30} from Ref. 5.
[e] ASTM D1002, steel substrates.
[f] To convert MPa to psi, multiply by 145.

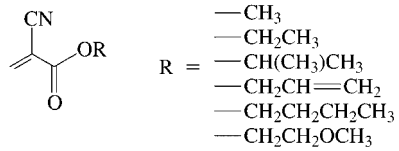

Fig. 1. Some commercially important cyanoacrylate monomers.

publications (3–5). A summary of the bulk physical properties of some common monomers is presented in Table 1.

The lower esters of alkyl 2-cyanoacrylates (eg, methyl, ethyl esters) provide adhesives with excellent lap-shear strengths to a variety of different substrates (3). They are, however, brittle materials and generally require the addition of a rubber-toughening agent to improve peel strength and impact resistance (4). The low esters have pungent odors whereas the higher esters, in particular the alkoxyalkyl esters, are virtually odorless (3).

Chemical Properties of Monomers

The chemical properties of cyanoacrylate monomers are primarily determined by the highly electron-deficient nature of the alkene double bond. In the presence of catalytic amounts of basic or nucleophilic species they undergo rapid anionic bulk polymerization reaction and this chemistry is discussed in more detail later. Under neutral or acidic conditions, cyanoacrylates are good dienophiles and readily undergo [4+2] cycloaddition reactions with conjugated dienes such as butadiene or anthracene (6,7). However, in the presence of stiochiometric quantities of electron-rich monomers, such as vinyl ethers, they undergo heterodiene cycloadditions to give substituted dihydropyrans (8) (Fig. 2). The diene adducts

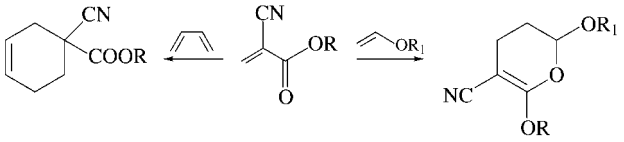

Fig. 2. Cycloaddition reactions of cyanoacrylates.

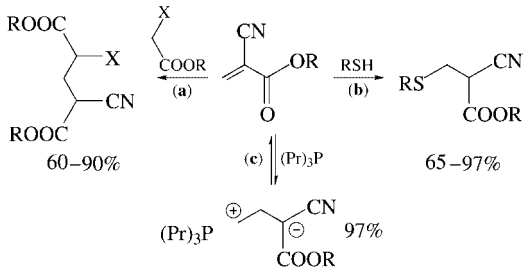

Fig. 3. Michael-type addition reactions to cyanoacrylates: (a) 5% piperidine, acetonitrile, 20°C, X = NO_2, CN, COR; (b) acetone, 3.5 h, 20°C, R = CH_2COOH, C_2H_4SH; (c) dry benzene, 3 h, 20°C.

are stable and are frequently used to characterize the more reactive monomers. In contrast, the dihydropyrans are unstable and are readily isomerized or polymerized (8,9).

Cyanoacrylates may also add to a variety of organic acids in piperidine-catalyzed Michael-type reactions (10–12). Thus nitro-, cyano-, and acetoacetates give the corresponding glutarate derivatives in moderate to high yields (Fig. 3a). However, as the acidity of the organic acid decreases, the yield of Michael adduct decreases and polymerization predominates. From a synthetic viewpoint the reaction is useful only for acids having $pK_a < 13$. Similarly, thiols and thiocarboxylic acids add to cyanoacrylate monomers to give the corresponding β-thioethers in high yields (11,12). This reaction proceeds at room temperature and does not require a catalyst (Fig. 3b). However, slow addition of monomer to thiol is required to ensure that polymerization does not occur. Similar techniques are used to prepare internal zwitterionic salts of cyanoacrylates and trialkylphosphines (Fig. 3c) (10,11,13). The salts are stable over several months, provided they are stored under anhydrous conditions.

Manufacture of Monomer

Cyanoacrylate monomers are usually prepared by a base-catalyzed Knoevenagel condensation of alkyl cyanoacetate and formaldehyde to give an intermediate low molar mass polymer which is then depolymerized under acidic conditions at elevated temperatures (14–17). Figure 4 depicts the process for the production of methyl 2-cyanoacrylate.

The condensation step is preferably carried out with paraformaldehyde in the presence of a nonaqueous solvent to facilitate the removal of water by azeotropic distillation (15). The reagents are generally employed in stiochiometric amounts,

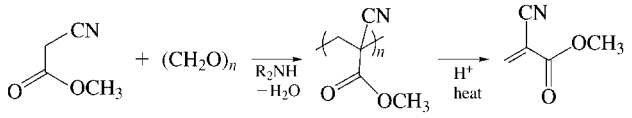

Fig. 4. Synthetic route for production of methyl 2-cyanoacrylate.

although a small excess of cyanoacetate may be employed to reduce the viscosity of the intermediate polymer solution, thus improving its processing characteristics (16). On completion of the condensation step, the solvent is removed and the oligomer treated with anhydrous acid, such as P_2O_5, to neutralize the catalyst and remove traces of residual water. The depolymerization reaction is carried out under reduced pressure at temperatures in the range 150–250°C and is facilitated by the addition of a nonreactive heat transfer medium, such as tricresyl phosphate (15). Acidic vapor-phase stabilizers, such as SO_2, and free-radical inhibitors, such as 1,4-hydroquinone, are also added to ensure stability of the monomer as soon as it is formed (15,16). On heating, the polymer decomposes to produce monomer vapor, which is passed through a distillation condenser and collected as a liquid. The crude monomer obtained in this way is then purified by redistillation and carefully stabilized with low levels of acidic inhibitors (18).

Other methods for the synthesis of cyanoacrylate monomers include pyrolysis of 3-alkoxy-2-cyanopropionates (1), transesterification of cyanoacrylates with alcohols (19,20), displacement of monomer from the corresponding anthracene Diels–Alder adduct by treatment with maleic anhydride (7,21), esterification of cyanoacrylic acid or cyanoacryloyl chloride with alcohols (22), and the oxidation of alkyl 2-cyanopropionate phenyl selenides with hydrogen peroxide (23). These alternative methods are particularly useful for the preparation of monomers not readily prepared by thermal decomposition of cyanoacrylate polymer.

Polymerization

Cyanoacrylate monomers undergo extremely rapid polymerization in the presence of catalytic amounts of anionic initiators or certain covalent bases such as tertiary amines and phosphines. The reaction is completely inhibited by strong acids and is thus anionic in nature. The kinetics of base-catalyzed solution polymerization has been studied in detail utilizing adiabatic calorimetry (24–35). These studies show that in the absence of strong acid the polymerization has no intrinsic termination reaction. The overall kinetics depends on the rate of initiation and may be distinguished between those reactions in which initiators exhibit very rapid rates of initiation (eg, hydroxyl ions or phosphines) and those where the initiation sequences are relatively slow (eg, acyclic amines or pyridine). With rapid initiators, nearly ideal living polymerization conditions exist and molecular weights are in close approximation to the theoretical values from the monomer/initiator ratios employed (25). For such cases a classical anionic polymerization mechanism is postulated (Fig. 5). With covalent bases such as tertiary amines, the initiation step involves one or more reversible monomer addition reactions before the propagation sequence becomes established and the polymerization proceeds via a zwitterionic mechanism (29,30).

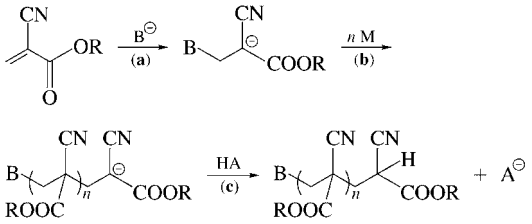

Fig. 5. Base (B)-catalyzed anionic polymerization mechanism of cyanoacrylate monomer (M): (a) initiation, (b) propagation, and (c) transfer/termination by acid (HA).

Although cyanoacrylate polymers are most commonly prepared by anionic polymerization, they may also be prepared by free-radical polymerization using conventional radical initiators (36–38), provided adequate amounts of anionic polymerization inhibitors are employed. Bulk photoanionic polymerization of cyanoacrylates has also been described by a number of workers (39–43). These systems rely on the *in situ* generation of an anionic initiator from a neutral species, following absorption of light of an appropriate wavelength. The zwitterionic and radical copolymerization of cyanoacrylates has also been reported for a number of comonomers including vinyl ethers (44), ketene acetals (45), furan (46), vinyl ketones (47), and ethylene (48).

Properties of Polymers

The physical properties of poly(alkyl 2-cyanoacrylates) are discussed in a recent review (49). The polymers are colorless and amorphous solids that readily undergo retropolymerization reactions at temperatures in the region 140–180°C (50). Glass-transition temperatures T_g vary depending on the method of measurement, conditions of synthesis, etc, with values typically in the range of −78 to +165°C (*n*-decyl and methyl cyanoacrylate polymers respectively). The solubility of methyl, ethyl, and *n*-butyl cyanoacrylate polymers were systematically determined in a wide range of common solvents (51). The polymers are generally soluble in polar aprotic solvents (eg, DMSO, DMF) and insoluble in both nonpolar solvents (eg, hexane, ether) and polar solvents (eg, methanol, water). Solubility improves as the size of the alkyl group increases. Intrinsic viscosities $[\eta]$ of ethyl and *n*-butyl cyanoacrylate polymers have been measured in a number of different solvents and found to give linear log–log relationships with number-average molecular weight M_n over approximately 2 orders of molecular weight range. The Mark–Houwink constants were determined and found to be internally self-consistent for a range of different solvents (51).

The thermodynamic properties of several cyanoacrylate polymers have been determined using precision adiabatic and isothermal calorimetry (52–55). The Gibbs free energy ΔG_0 estimated from the enthalpy ΔH_0 and entropy ΔS_0 of the bulk polymerization of various monomers showed that polymerization is thermodynamically feasible over the temperature range −270 to +160°C at standard pressure. Ceiling temperatures T_c for polymerization were derived from the thermodynamic data and represent the upper temperature limit of polymerization.

Table 2. Thermodynamic Parameters for Some Cyanoacrylate Polymerizations at 25°C and Atmosphere Pressure (101.3 kPa)

Parameter[a]	Ethyl	Allyl	*N*-Decyl
$-\Delta H_0$, kJ/mol	48	64	69
$-\Delta S_0$, J/mol·K	88	85	141
$-\Delta G_0$, kJ/mol	21	39	39
T_c, °C	267	307	217
T_g, °C	149	122	−78
Ref.	55	52	53

[a]To convert J to cal, divide by 4.184.

Glass transitions (T_g) were obtained from plots of heat capacity with temperature and clearly show a decrease in value as the size of the alkyl side chain increases. Typical data are presented in Table 2..

Cyanoacrylate polymers are also rapidly degraded in solution at temperatures substantially below T_c in the presence of basic species (56,57). Size exclusion chromatography showed that an initial high molecular solution of unimodal polycyanoacrylate degrades over 60s at ambient temperature to produce a lower molecular weight distribution following the addition of a catalytic amount of hydroxide ion. This degradation was attributed to a chain-end unzipping of monomer followed by its immediate repolymerization to produce an intermediate bimodal distribution of molecular weights.

Dynamical mechanical analyses are reported for a range of solvent cast films of cyanoacrylate polymers ranging in molecular weight from 75,000 to 330,000 (58). The storage moduli decrease with increasing size of the alkyl side chain and generally fall off sharply at temperatures above T_g. An exception to this trend is poly(allyl 2-cyanoacrylate), which exhibits an increase in modulus that is attributed to cross-linking through the unsaturated side group. Refractive indices of cyanoacrylate polymers are in the range 1.45–1.48 and dielectric constants vary from 3.3 to 5.4 at 1 MHz (3).

Economic Aspects

The principal manufacturers and suppliers of cyanoacrylate monomers include Henkel (Loctite Div.), National Starch, Toagosei, Sumitomo, and Three-bond. The largest market for these materials is in the formulation of so-called *instant adhesives* for which the U.S. production is now estimated in the region 2000 t annually. Although this represents a relatively small fraction of the total volume of adhesives business, it corresponds to a disproportionately high value due to the high costs of cyanoacrylate monomers.

Specifications and Standards

Cyanoacrylates are generally specified in relation to their intended end use (see section on Uses). For adhesives this will usually include details of the physical properties of uncured formulations (eg, viscosity, density, flash point), curing

performance and conditions in a standard joint configuration (cure time, effect of humidity, etc) and a variety of physical, chemical, and materials performance properties (T_g, adhesive strength, durability, chemical resistance etc). These data are generally available in technical product bulletins provided by the manufacturers and suppliers of the various monomers.

Analytical and Test Methods

Cyanoacrylate monomers and polymers are routinely characterized by all common chromatographic and spectroscopic techniques including ir, nmr, ms, gc, sec, and uv analytical techniques. The levels of acid stabilizers in monomers are usually determined by potentiometric titration. Microstructural assignments of anionically and zwitterionically polymerized poly(ethyl 2-cyanoacrylate) have been unambiguously determined using DEPT and ^{1}H–^{13}C HETCOR nmr analysis (59).

Health and Safety Factors

Volatile cyanoacrylate monomers, in particular methyl and ethyl cyanoacrylates, have characteristic acrid odors. Exposure to these materials at levels in the range of 1–5 ppm results in irritation to the eyes, nose, and throat (3). It is recommended that these monomers be used in a well-ventilated area, that skin and eye contact be avoided, and that the user be familiar with the relevant safety data supplied by product manufacturers. A recent epidemiological study in workers with occupational exposure to monomer vapors concluded that there was no increased risk of pulmonary obstruction (eg, asthma) on exposure to average short-time concentrations of less than 0.5 ppm (60). Polymerization of cyanoacrylates is rapid and exothermic and particular care should be taken to avoid burns, which can result from the unexpected bulk polymerization of inadequately stabilized or contaminated monomer samples.

Uses

Adhesives represent by far the most important use of cyanoacrylates. They are marketed throughout the world for both industrial and consumer use. They polymerize rapidly on contact with many surfaces and exhibit excellent adhesive strength to a wide variety of different materials. The beneficial adhesive properties are attributed to a combination of good wetting of surfaces by the monomers, the high polarity of the polymer, and the high molecular weight of the bulk polymer, which is frequently in excess of 10^6. The typical adhesive product comprises a mixture of monomers, stabilizers, and additives (such as thickeners, rubbers, fillers) to control the rheology of the uncured composition and properties of the cured adhesive. Several comprehensive reviews on cyanoacrylate adhesives have been published (3,4).

Traditionally cyanoacrylates have been used to facilitate the automated assembly of various devices and components including computers, calculators, electric motors, medical equipment, optical components, jewelry, and sporting

goods. More recently, cyanoacrylate adhesives are being used in surgical areas such as tissue adhesives for wound closure (61), sealing corneal perforations (62), and for the control of gastrointestinal bleeding (63). Cyanoacrylate adhesives are associated with a comparatively low incidence of post-operative infection and the cured polymers are generally considered to be biodegradable, biocompatible, nontoxic, and nonallergenic (61,63). Cyanoacrylate esters with higher alkyl group side chains (eg, *n*-butyl, *n*-octyl) are preferred for surgical applications, as they have been shown to be less toxic to surrounding tissues (62).

Cyanoacrylate polymers are also extensively used in the production of encapsulated colloidal nanoparticles for targeted drug delivery systems and are particularly useful in the treatment of certain cancers (64). Their good encapsulation properties, low toxicity, and satisfactory biocompatibility make them attractive for this application. By forming amphiphilic copolymers of cyanoacrylate and ethylene oxide, the therapeutic activity of entrapped compounds can be enhanced. The copolymer functions to prolong the circulation lifetime of the nanoparticles after they have been introduced into the bloodstream (65).

Other potential uses of cyanoacrylate polymers include the development and characterization of latent fingerprints by vapor-phase deposition of polymer (66) and the deposition and growth of plasma-resistant photoresist films by interfacial polymerization from the vapor phase (67). Potential applications in the optical area include the formation of high tilt angle alignment layers in liquid crystal devices (68), the production of holographic media for optical data storage (69), and the production of waveguide sensors for the detection of organic vapors (70). Polycyanoacrylate films containing infrared dyes are readily ablated on exposure to laser light and may be used to produce lithographic printing plates with good ink receptivity, adhesion, and wear resistance (71).

BIBLIOGRAPHY

"2-Cyanoacrylic Ester Polymers" in *EPST* 1st ed., Vol. 1, pp. 337–342, by H. W. Coover Jr. and T. H. Wicker Jr., Tennessee Eastman Co., a division of Eastman Kodak Co., "Acrylic and Methyacrylic Ester Polymers, 2-Cyanoacrylic Ester Polymers" in *EPSE* 2nd ed., Vol. 1, pp 299–305, by H. W. Coover Jr. and J. M. McIntire, Eastman Kodak Co.

1. U.S. Pat. 2467926 1947, A. E. Ardis (to The B.F. Goodrich Co.).
2. U.S. Pat. 2794788 (1957), H. W. Coover and N. H. Shearer (to Eastman Kodak Co.).
3. H. W. Coover, D. W. Dreifus, and J. T. O'Connor, in I. Skeist, ed., *Handbook of Adhesives*, 3rd ed., Van Nostrand Reinhold, Co., Inc., New York, 1990, pp. 463–477.
4. G. H. Millet, in S. R. Hartshorn, ed., *Structural Adhesives, Chemistry and Technology*, Plenum Press, New York, 1986, pp. 249–307.
5. V. Vijayalakshmi, J. N. Vani, and N. Krishnamurti, *J. Adhes. Sci. Techol.* **4**, 733 (1990).
6. U.S. Pat. 2467927 (1947), A. E. Ardis (to The B. F. Goodrich Co.).
7. U.S. Pat. 4012402 (1977), C. J. Buck (to Johnson & Johnson).
8. H. A. Rasoul and H. K. Hall, *J. Org. Chem.* **47**, 2080 (1982).
9. I. Cho and J.-Y. Lee, *Macromolecules* **16** 1245 (1983)
10. Y. G. Gololobov, G. D. Kolomnikova, and T. O. Krylova, *Russ. J. General Chem.* **64**, 373 (1994).
11. Y. G. Gololobov and T. O. Krylova, *Heteroat. Chem.* **6** 271 (1995).
12. I. I. Kandror and co-workers, *Izv. Akad. Nauk. SSSR, Ser. Khim.* (12), 2816 (1991).

13. T. O. Krylova and co-workers, *Russ. J. General Chem.* **64**, 371 (1994).
14. U.S. Pat. 2467927 (1947), A. E. Ardis (to B. F. Goodrich Co.).
15. U.S. Pat. 2721858 (1955), F. B. Joyner and G. F. Hawkins (to Eastman Kodak Co.).
16. U.S. Pat. 3254111 (1966), G. F. Hawkins and H. F. McCurry (to Eastman Kodak Co.).
17. J. M. Rooney, *Polym. J.* **13**, 975 (1981).
18. U.S. Pat. 2794788 (1957), H. W. Coover and N. H. Shearer (to Eastman Kodak Co.).
19. Russ. Pat. SU 726086 (1980), J. Voitekunas and co-workers (to USSR Academy of Sciences).
20. U.S. Patent 6096848 (2000), Y. Gololobov, W. Gruber, and C. Nicolaisen (to Henkel).
21. L. Giral and co-workers, *Ann Pharm. Fr.* **43**, 439 (1960).
22. PCT Pat. Application WO 9415907 (1994), V. A. Dyatlov and G. A. Katz (to Eurotax Ltd.).
23. P. Klemarczyk, *Polymer* **39** (1), 173 (1998).
24. E. F. Donnelly and co-workers, *J. Polym. Sci. Polym. Lett.* **15**, 399 (1977)
25. D. C. Pepper, *J. Polym. Sci., Polym. Symp.* **62**, 65 (1978).
26. D. C. Pepper, *Polym. J. (Tokyo)* **12**, 629 (1980).
27. D. S. Johnston and D. C. Pepper, *Makromol. Chem.* **182**, 393 (1981).
28. D. S. Johnston and D. C. Pepper, *Makromol. Chem.* **182**, 407 (1981).
29. D. S. Johnston and D. C. Pepper, *Makromol. Chem.* **182**, 421 (1981).
30. D. C. Pepper and B. Ryan, *Makromol. Chem.* **184**, 383 (1983).
31. D. C. Pepper and B. Ryan, *Makromol. Chem.* **184**, 395 (1983).
32. D. C. Pepper, *Makromol. Chem.* **188**, 527 (1987).
33. J. P. Cronin and D. C. Pepper, *Makromol. Chem.* **189**, 85 (1988).
34. I. C. Eromosele and D. C. Pepper, *Makromol. Chem.* **190**, 3085 (1989).
35. I. C. Eromosele and D. C. Pepper, *Makromol. Chem.* **190**, 3095 (1989).
36. A. J. Canale and co-workers, *J. Appl. Polym. Sci.* **4**, 231 (1960).
37. J. C. Bevington and J. A. Jemmett, *J. Chem. Soc., Faraday Trans.* **69**, 1866 (1977).
38. B. Bunichiro, M. Yoshioka, and T. Otsu, *Makromol. Chem.* **184**, 1025 (1983).
39. C. Kutal, P. A. Grutsch, and D. B. Yang, *Macromolecules* **24**, 6872 (1991).
40. B. J. Palmer and co-workers, *Macromolecules* **28**, 1328 (1995).
41. N. Arsu, A. Onen, and Y. Yagci, *Macromolecules*, **29**, 8973 (1996).
42. R. B. Paul and co-workers, *Polymer* **38**, 2011, (1997).
43. Y. Yamaguchi and co-workers, *Macromolucles* **31**, 5155 (1998).
44. H. A. Rasoul and H. K. Hall Jr., *J. Org. Chem.* **47**, 2080, (1982).
45. T. Yokozawa, K. D. Ando, and T. Endo, *Macromolecules* **27**, 1978 (1994).
46. E. Oikawa, F. Aoki, and K. Katano, *Polym. J.* **11**, 257 (1997).
47. K. Maruyama and co-workers, *Int. J. Adhesn. Adhesv.* **9** (3), 143 (1989).
48. C. D. Eisenbach, W. Liebert, and B. Sperlich, *Angew. Makromol. Chem.* **223**, 81 (1994).
49. J. Woods, in J. C. Salamone, ed., *Polymeric Materials Encyclopedia*, Vol. **2**, CRC Press, Inc., Boca Raton, 1996, p. 1632.
50. J. M. Rooney, *Br. Polym. J.* **13**, 160, (1981).
51. E. F. Donnelly and D. C. Pepper, *Makromol. Chem., Rapid Commun.* **2**, 439 (1981).
52. E. G. Kiparisova and co-workers, *Polym. Sci.* **35**, 743 (1993).
53. T. A. Bykova and co-workers, *Polym. Sci.* **35**(1), 8 (1993).
54. T. A. Bykova and co-workers, *Polym. Sci.* **33**, 2453 (1991).
55. T. A. Bykova and co-workers, *Polym. Sci.* **33**, 537 (1991).
56. B. Ryan and G. McCann, *Makromol. Rapid Commun.* **17**, 217 (1996).
57. D. R. Robello, T. D. Eldridge, and M. T. Swanson, *J. Polym. Sci. Part A* **37**, 4570 (1999).
58. K. H. Cheung and co-workers, *Makromol. Chem.* **188**, 3041 (1987).
59. D. R. Robello, T. D. Eldridge, and F. M. Michaels, *J. Polym. Sci. Part A* **37**, 2219 (1999).
60. M. Goodman and co-workers, *J. Toxicol. Environ. Health, Part A* **59**, 135 (2000).
61. R. Vanholder and co-workers, *Biomaterials*, **14**, 737 (1993).

62. G. R. John in T. J. Zimmerman, ed., *Textbook of Ocular Pharmacology*, Lippincott-Raven, Pa, 1977, p. 671.
63. D. Katti and N. Krishnamurti, *J. Appl. Polym. Sci.* **74**, 336 (1999).
64. F. Lescure and co-workers, *J. Colloid Interface Sci.* **154** (1), 77 (1992).
65. M. T. Peracchia and co-workers, *Pharm. Res.* **15**, 550 (1998).
66. D. T. Burns and co-workers, *Anal. Chim. Acta* **362**, 171 (1998).
67. J. Woods and co-workers, *Polymer* **30**, 1091 (1989).
68. C. B. McArdle and J. Woods, in K. L. Mittal and K.-W. Lee, eds., *Polymer Surfaces and Interfaces*, VSP Publishers, Utrecht, the Netherlands, 1997, p. 225.
69. R. A. Rupp and co-workers, *Polymer* **38**, 2299 (1997).
70. R. P. Podgorsek and co-workers, *Sensors and Actuators B* **51**, 146, (1998).
71. U.S. Pat. 5605780 (1996), M. S. Burberry, C. D. DeBoer and S. W. Weber (to Eastman Kodak Co.).

JOHN WOODS
Loctite Corporation

POLYDIACETYLENE. See DIACETYLENE AND TRIACETYLENE POLYME.

POLYESTERS, FIBERS

Introduction

Over 17,000 kt (>35 billion pounds) of polyester fiber are produced each year, making it the most widely used fiber in the world (1) (Fig. 1). Its commercial domination of textile and industrial markets is due to a unique blend of high performance, low cost, and benign impact on the environment. The polyester fiber industry shares raw material supplies with the large global markets for poly(ethylene terephthalate) (PET) beverage containers (recycleable into fibers) and automobile antifreeze and so it is based on a large and stable infrastructure. The public image of polyester fiber is less than glamorous, but it is unlikely that a more versatile and economical fiber will replace it anytime soon.

W. H. Carothers at DuPont invented the polymer family known as polyester over 70 years ago (2–5). The polyester fiber industry developed in the post-World War II period, along with other "miracle" synthetic fibers of the time. Synthetic fibers revolutionized the textile industry, providing a number of advantages over traditional plant and animal fibers:

(1) Increased fiber strength and uniformity allowed finer yarns, higher processing speeds, less waste, and a wider range of fabric possibilities.
(2) Better thermal stability enabled "permanent press" fabrics that were easier to care for.

Encyclopedia of Polymer Science and Technology. Copyright John Wiley & Sons, Inc. All rights reserved.

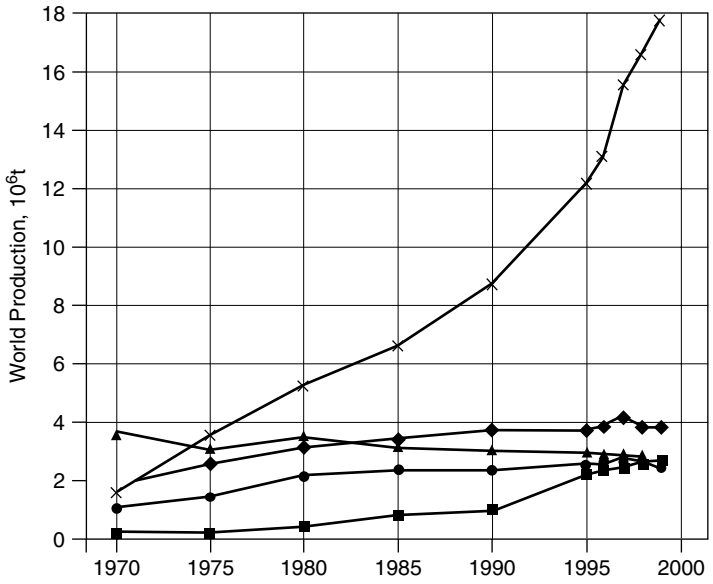

Fig. 1. Historical growth of polyester fibers (PES = PET). Synthetic fibers—World production by fiber class. PES, PA, Cellulose, PAC, and Misc. Reprinted with permission from Ref. 2.

Many of those synthetic fibers remain in special applications, but polyester has captured the largest share of the markets for cotton blending, apparel, and rubber reinforcement. With the economic advantage of large production scale, its dominance has continued to grow at the expense of natural and other synthetic fibers.

A polyester fiber is defined by the U.S. Federal Trade Commission as "A manufactured fiber in which the fiber forming substance is any long-chain synthetic polymer composed of at least 85% by weight of an ester of a substituted aromatic carboxylic acid, including but not restricted to substituted terephthalic units, $p(-R-O-CO-C_6H_4-CO-O-)_x$ and parasubstituted hydroxybenzoate units, $p(-R-O-CO-C_6H_4-O-)_x$."

Carothers' original polyesters used aliphatic dicarboxylic acids and had low melting points. Fibers made from these polymers were not commercially interesting. Nearly a decade later, J. R. Whinfield and J. T. Dickson working for Calico Printers Assoc., Ltd. produced a high melting point polyester from aromatic terephthalic acid and ethylene glycol. They assigned patent rights to ICI in 1947, and the PET industry was born. Today, the term "polyester" is nearly synonymous with PET, although other members of the family continue to be used in special applications.

Historical Development

A patent-sharing arrangement gave DuPont initial control over PET in the United States while ICI Chemicals dominated patents in the rest of the world (6–9).

The success of PET fibers encouraged opposition from wool and cotton producers, and competition from other chemical and textile firms. ICI sublicensed the PET technology to companies in Japan and Western Europe, and installed fiber plants with a number of affiliates around the world. DuPont built fiber plants in the Americas and Europe.

PET fibers rapidly became a worldwide venture, with each producer developing their own designs of fiber-making equipment and their own market segments. The large chemical firms, who could afford the R&D to develop the best products with the most efficient and reliable manufacturing processes, established industry leadership.

As the technology developed, PET fibers penetrated into a number of end-use areas, broadly classified as *staple fibers, textile filament*, and *industrial filament*. These end uses have different requirements in terms of fiber properties and physical geometry, and so different fiber manufacturing processes have evolved according to the special needs of each market segment.

Staple PET fibers are typically packaged in bales and blended with natural staples such as cotton or wool. They are designed with cut lengths and diameters similar to their blend partners, ∼30 to 100 mm in length and ∼10 to 20 μm in diameter. Fiber diameter is an important parameter affecting both bending stiffness and light reflection, which affect fabric feel and appearance. Staple fibers are formed into yarns by the ancient practice of fiber spinning, where the fibers are twisted together to form a continuous strand and the number of fibers in the cross section controls the fineness of the yarn. These yarns are formed into fabrics by the traditional methods of weaving or knitting. The protruding free ends of twisted staple yarns contribute to fuzzy fabric surfaces, which greatly impact the perceived comfort of apparel fabrics. PET staple fibers must possess three-dimensional structure (or "crimp") and surface lubricity to allow the fibers to be processed in textile machinery and to mingle evenly with other fibers in the blend.

Initially developed for textiles and apparel, staple fibers are finding increasing applications in nonwovens markets. In these applications, fibers are formed directly into fabrics through carding, dry-lay, or wet-lay forming processes and held together by entanglement, resin bonding, or thermal bonding. Such nonwoven products are used for filters, interliners, cushioning material, etc.

Textile filament yarns are continuous yarns, with fabric aesthetics akin to natural silk. Fiber diameter plays a strong role in fabric suppleness, and *texturing* of the yarn is also used to impart three-dimensional structure and pleasing fabric feel. In contrast to the high-volume, low-speed processes for staple fibers, continuous yarns are produced at relatively high speeds (∼100 m/s) and sold on bobbins; high speed winder technology has been a crucial factor in the growth of these markets. The world's current production of polyester fibers for textiles is split roughly evenly between staple and filament yarns (1).

Industrial (nontextile) end uses constitute the third major market for PET fibers. *Industrial filament yarns* are used for reinforcement of rubber or high strength industrial fabrics. Most passenger car tires produced in the United States are reinforced with yarns made from high molecular weight PET polymers, processed to yield high strength and low shrinkage. Neither dyeability or appearance is important, but the physical and chemical properties of the fibers are critical.

The manufacturing processes for textile filament, staple, and industrial filament yarns have become so specialized that it is not possible to make one such

class of fibers on the others' equipment. Within these classes, there are production machines specialized for certain types of fibers for certain types of consumer products. Large machines designed to produce high volumes of commodity products (eg, staple for cotton blending) at high efficiency and low cost are not well suited to the efficient production of specialty staple variants (eg, fibers with special dyeing properties) and vice versa.

Additives and copolymers have extended the use of PET fibers into areas where the original commodity products had deficiencies in eg, soil-resistance, static protection, or poor dyeability. Newer members of the polyester family have found applications in markets where more stretchiness or resiliency were desired (using longer aliphatic chains) or to gain higher modulus, temperature resistance, and strength (with fully aromatic polymers).

Chemical and Physical Structure

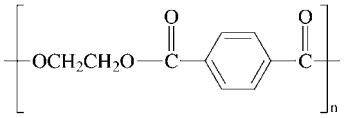

Poly(ethylene terephthalate) (PET)

PET polymer is composed of repeating units of the above monomer, each unit having a physical length of about 1.09 nm and a molecular weight of about 200. Ideally, it is capped on the left by H—, and on the right by —OH when produced from ethylene glycol and terepthalic acid. Polymerization is thus accompanied by the production of water, which is removed under elevated temperature and vacuum. Accordingly, the presence of water in the molten state will rapidly depolymerize the structure, so that thorough drying of the polymer prior to melt spinning of fibers is a prerequisite.

The PET polymer structure can also be generated from the reaction of ethylene glycol and dimethyl terephthalate, with methyl alcohol as the by-product; a few producers still use this route. The aromatic ring coupled with the short aliphatic chain is responsible for a relatively stiff polymer molecule, as compared with more aliphatic structures such as polyolefin or polyamide. The lack of segment mobility in the polymer chains results in relatively high thermal stability, as discussed later.

Melt Behavior. The degree of polymerization is adjusted to yield the desired balance of molten viscosity (for fiber extrusion) and filament strength. A textile grade polymer will have an average number of ~100 repeat units per molecule so that the extended length of a typical polymer chain is about 100 nm with a molecular weight about 20,000. Higher levels of polymerization produce higher strength fibers, but the melt viscosity and stability of the melt to even tiny amounts of moisture become extreme. Measurement of the average degree of polymerization is typically accomplished by measurement of either the molten viscosity (eg, by measuring pressure drop through a calibrated orifice) or the viscosity of a dilute solution of the polymer in an appropriate solvent (10). The latter is a measure of polymer chain length known as "intrinsic viscosity" or IV. A typical IV level, in *o*-chlorophenol (OCP) solvent, for the aforementioned textile

grade polymer is 0.62. [Different solvents will generate different IV numbers (11)]. The IV in OCP is connected to the number-average molecular weight (M_n) of the polymer by the Mark–Houwink formula for PET (11):

$$IV_{OCP} = 1.7 \times 10^{-4} (M_n)^{0.83} \quad (1)$$

A useful formula to predict the (low shear) melt viscosity of PET from its IV is as follows:

$$\eta_0 = 0.0129 (IV_{OCP})^{5.35} \exp\left(\frac{6800}{T}\right) \quad (2)$$

where η_0 is the Newtonian melt viscosity (Paċs) and T the absolute temperature (K).

If moisture is present before the polymer is melted, hydrolytic degradation will occur. Each water molecule will break a chain, increasing the total number of polymer chains by one. The effect on the average molecular weight is as follows:

$$M_n' = \frac{M_n}{1 + \frac{xM_n}{1800}} \quad (3)$$

where M_n is the starting average molecular weight, M_n' the average molecular weight after reaction with water, and x the weight percent of water.

Equation (3) can be used with equations (1) and (2) to determine the effect of moisture on IV and melt viscosity.

It can be seen from these relationships that higher IVs produce rapid increases in melt viscosity, and increased sensitivity of the polymer to hydrolytic degradation. The technology required to process high IV (ca 0.9–1.0) materials used for industrial fibers is more demanding than that for textile materials. Pressure requirements for polymer flow, for example, are ~10 times higher.

In addition to hydrolytic degradation, random chain scissions will occur at elevated temperatures and these scissions lead to a gradual loss of average molecular weight in the polymer melt. The chemistry of thermal degradation is different from hydrolytic degradation; it results in different types of end groups on the polymer chains. The chemical species that are generated during thermal degradation reactions are deleterious to fiber properties, leading to loss of thermal stability and, in the presence of oxygen, to cross-linked gel particles.

Polymer Structure. In the absence of any mechanism to induce preferential orientation in the polymer molecules, PET will freeze as a clear, glassy solid with a specific gravity of 1.33 (11). The molecular structure is similar to that of a bowl of spaghetti, with the polymer chains randomly coiling about one another. The chains are attracted to each other through van der Waal forces. This attraction can be overcome with the addition of thermal energy, which induces molecular vibration and bond rotations. Some chain segments pack together more closely than others, particularly if they are run parallel to each other for a section of their lengths. Stronger bonds form in these regions. If sufficient molecular alignment is present, regions of the microstructure pack into an ordered, repetitive structure and become crystalline (Fig. 2).

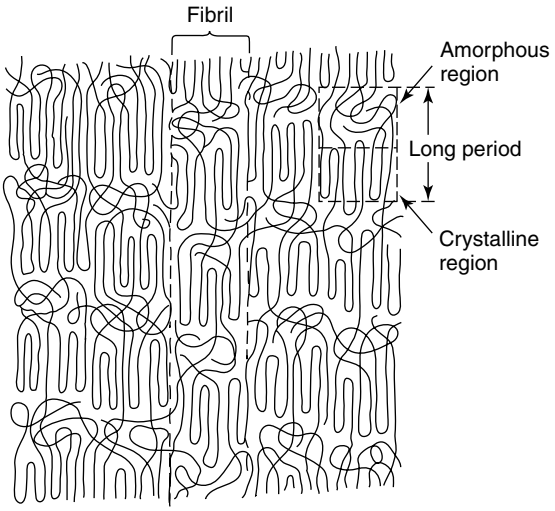

Fig. 2. Microstructure of an oriented, partially crystalline PET fiber (8).

An amorphous polymer in a state of molecular alignment is not a stable structure; it is metastable. It can change either to a more perfectly ordered, crystalline structure or to a more disordered, nonoriented structure. In either case, the free energy of the system is reduced. Given enough time and/or thermal energy, an oriented amorphous polymer will change in either or both of these directions.

The van der Waals attraction forces in the amorphous regions can be overcome at relatively low temperatures. The glass-transition temperature (T_g) is the characteristic temperature at which this occurs. At temperatures above T_g, spontaneous molecular rearrangement becomes easier, allowing plastic deformation and the generation of crystalline order with the release of heat. The stronger bonding forces in the crystalline phase require higher temperatures in order to be re-broken, and this phase transition represents a true melting point T_m. However, even this transition is not sharply defined in a real polymer because the melting temperatures depend on the size of the crystallites. Smaller crystallites melt more easily.

As determined from x-ray diffraction, the unit cell of crystalline PET is triclinic with a repeat distance of 1.075 nm along the major axis (11,12). This corresponds to >98% of the theoretical extended length of the monomer repeat unit (12). There is very little extensibility remaining in a PET crystal, resulting not only in high modulus but also a relatively short extension range over which the crystal can be extended and still recover elastically. The density of the crystalline structure is 9% higher than the amorphous structure, with SG = 1.45 (11).

A considerable amount of molecular orientation along the fiber axis is induced in the fiber manufacturing process, and crystallization will occur in regions where adjacent polymer chains are sufficiently extended and aligned so that bonds can form between adjacent chains. The rate of crystallization for oriented fibers under tension is thousands of times faster than for unoriented, quiescent melts. The length of the polymer chain which will be continuously entrapped within a

crystalline region is typically ~20 repeat units, before entanglement with another chain terminates the process. But crystalline regions do come in different sizes, and the size and distribution of these crystallites contribute to fiber properties such as dyeability and shrinkage. It is the crystalline regions that tie together the spaghetti-like polymer structure to give fibers with high strength and temperature stability (see Table 1).

Table 1. Properties of PET Fibers

Diameter, μm	10–50
Tenacity, MPa[a]	
Textile fiber	450–750
Industrial fiber	850–1050
Elongation, %	10–50
Initial modulus, MPa[a]	
Textile fiber	$\leq$6,000
Industrial fiber	$\leq$14,500
Shrinkage @160°C, %	
Textile fiber	5–15
Industrial fiber	2–5
Specific gravity	
Molten	1.21
Amorphous	1.33
Crystalline	1.44
Glass transition, °C	
Amorphous	67
Oriented, crystalline	125
Crystalline melt point, °C	265–275
Heat capacity, J/(kg·K)[b]	
@25°C	63
@200°C	105
Heat of fusion, kJ/kg[b]	120–140
Thermal conductivity W/(m·K)	0.14
Thermal volumetric expansion, 1/°C	
30–60°C	1.6×10^{-4}
90–190°C	3.7×10^{-4}
Moisture regain, %	
65% rh	0.6
Total immersion	0.8
Refractive index	1.58–1.64
Dielectric constant	
60 Hz	3.3
1 GHz	2.8
Electric resistivity, ohm·cm	
Dry	10^{18}
0.5% moisture	10^{12}
Solvents	*o*-Chlorophenol, hexafluoroisopropyl alcohol, hot alkali
Nonsolvents	alcohol, gasoline, most acids

[a]To convert from MPa to psi, multiply by 145.
[b]To convert from J to cal, divide by 4.184.

The T_g of amorphous PET is in the range of 65–75°C, and this can increase to ~125°C after being drawn and partially crystallized, reflecting the reduced rotational mobility of the chain segments. The crystallite melting points range from ~265 to 285°C. Usually, however, a single melt temperature is quoted for PET, eg, the temperature of maximum heat absorption in a differential scanning calorimeter (dsc).

Among the spectrum of melt-spinnable fibers such as polyolefins and nylons, PET stands at the upper end in terms of crystalline melt temperature and glass-transition temperature. This provides superior dimensional stability for applications where moderately elevated temperatures are encountered, eg, in automobile tires or in home laundering and drying of garments. It is generally agreed that the high thermal stability results from the aromatic rings that hinder the mobility of the polymer chain.

More elastic, less stiff polyesters can be prepared from diols with longer aliphatic chain lengths, eg, from propylene (3G) or butylene (4G) glycols in combination with terephthalic acid [see POLY(TRIMETHYLENE TEREPHTHALATE)]. These polymers crystallize in a form with significantly less extension of the molecule; approximately 75 and 87% of the fully extended form for the 3GT and the 4GT polymers, respectively (12).

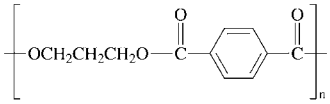
Poly(trimethylene terephthalate) (PTT)

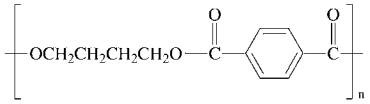
Poly(tetramethylene terephthalate) (PBT)

Along with the increased softness and springiness of the polymers comes a reduction in melting points and glass-transition temperatures, not always welcome. These polyester variants command a higher price simply because they are more rare; their raw materials are more expensive because they are not produced on the massive scale of the PET raw materials.

One alternative to PET fiber which did compete historically was poly(1,4-cyclohexylene dimethylene terephthalete), commercialized under the name Kodel II by Eastman. This polyester gained an early footing because it was not covered by the existing patents, and was able to establish a raw material base from which it could compete both technically and economically [see POLY(CYCLOHEXYLENE TEREPHTHALATE)].

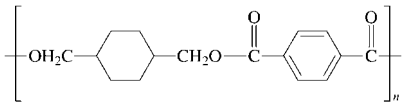
Poly(cyclohexylene dimethylene terephthalate)

This PCT fiber has better resiliency than PET, without compromising high temperature resistance. It successfully competes in the high-end carpet yarn market against nylon, where PET was limited by its relatively lower wear resistance. Recycling of PET bottles has provided a source of low cost resins that are used for carpets in less critical markets.

Fiber Geometry. Solid PET polymer is relatively hard and brittle. It must be formed into very fine fibers in order to exhibit bending stiffness that is low enough for textile materials. Most commercial PET fibers are produced in a diameter range of about 10–50 μm, considerably smaller than a human hair. Within this range lies a vast difference in the softness, drape, and feel of fabrics formed from the fibers, since bending stiffness of a cylindrical fiber depends on the 4th power of its diameter.

One key requirement in the commercial production of fibers is controlling fiber diameters within narrow ranges of the target. Another is controlling the internal structure of the fiber, particularly the orientation of the polymer molecules. It is orientation of the polymer molecules along the fiber axis that controls the morphology and hence the fiber properties such as dye uptake, shrinkage, and tensile strength.

The production process for fibers starts with the extrusion of molten PET through small holes at slow speeds, but the fibers will be stretched by hundreds of times their initial lengths before the production process is completed. The stretching process is responsible for diameter reduction and for alignment of the polymer molecules in the direction of the stretching. As this alignment proceeds, the polymer chains pack increasingly closer to each other, and the density of the material rises progressively, becoming crystalline in some regions. The fiber density is a guide to the amount of orientation present in the fiber; a finished PET fiber is typically ~50% crystalline.

Chemical and Physical Modifications

In many applications, modification of PET fiber properties is desirable in order to enhance certain features of the product or to enhance the process of converting fibers into finished goods. In these cases, most of the basic PET fiber properties are acceptable but certain enhancements are desired, even at the expense of other properties or costs that will be affected by the modification. These side effects are always present; it is the goal of fiber development personnel to engineer the best compromise.

What follows are some of the most common variations that have been applied to PET fibers; more complete information is available in the literature (13).

Low Pill Fibers. In staple yarns that do not contain high twist levels, it is relatively easy for individual fibers to work their way to the yarn surface under the influence of friction. This will cause long filaments to appear at the surface of the fabric, which then become entangled to form unsightly fuzz balls or "pills." With natural fibers, these pills readily break off after the attaching filament is repeatedly flexed. With PET, the attaching filaments are too tough to break, and the pills accumulate. It is difficult to prevent pills from forming and far easier to modify the PET fiber so that it will more readily break under repeated flexing. The simplest way to do this is to reduce the molecular weight of the polymer, thereby reducing fiber strength. This also reduces the melt viscosity, which can create some problems with the stability of the melt-spinning process.

Some anti-pill fibers are made by including a small amount of a cross-linking agent in the polymer (eg, pentaerythritol) (Fig 3). This increases melt viscosity

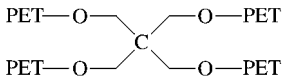

Fig. 3. Cross-linking of PET chains by reaction with pentaerythritol.

while embrittling the fiber and reducing its flex life. The penalty is a fiber that is somewhat weaker during processing and more subject to breakage during yarn and fabric formation. An alternative is to treat fabrics with an alkaline bath that partially dissolves the PET fibers to make them weaker; this also changes the hand of the fabric. The most elegant approach is to include a chemical cross-linker that is not activated until the fabric is formed and put into an activating bath.

Deep Dye Fibers. The PET polymer molecule contains no chemically active species for attachment of dye molecules. Instead, "disperse" dyes are used which diffuse into the fiber and become physically entrapped in the tangle of polymer chains in the amorphous regions. (The dye molecules are too large to fit within the more closely-packed crystalline regions.) In order to encourage rapid diffusion into the structure, it is common to use pressurized dye baths and/or "structure-opening" chemicals that encourage swelling of the amorphous regions. The presence of large amounts of crystallinity and/or high orientation (hence closer packing of polymer chains) in the amorphous regions will inhibit the dye diffusion process. Differences in fiber orientation cause differences in dye depth.

A common method to increase the dyeing rate is to inhibit the formation of crystalline regions during fiber manufacture. To this end, it is sufficient to break up the regularity of the repeating ET units of PET. Small amounts of *other* types of monomers which are incorporated into the chain will do this, as they form copolymers.

Monomer units for this purpose include adipic acid or isophthalic acid to substitute for some of the terephthalic acid (Fig. 4a). Similarly, propane or butane diol, or poly(ethylene glycol) can be substituted for some of the ethylene glycol.

The result is a fiber that is less crystalline and dyes more readily. The downside is an unavoidable reduction in transition temperatures, a less stable structure more prone to shrinkage, and the easier escape of dye molecules and oligomers which can deposit onto the surfaces of textile processing equipment. Depending

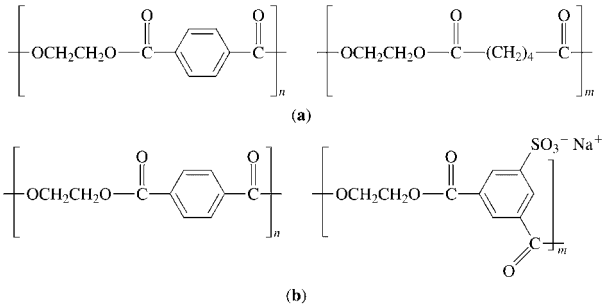

Fig. 4. (**a**) Deep-dye PET, modified by copolymerization with adipic acid and (**b**) Cat-dye PET, enabled by addition of sulphoisophthalic acid.

on level and type of comonomer used, increased problems with lightfastness or polymer degradation can also occur.

Ionic Dyeability. As noted earlier, PET has no dye attachment sites for chemically active dyes. It is possible to add ionic dyeability by forming copolymers of PET with monomer species that possess such sites, for example, on a pendent side chain. The most common of these has been the incorporation of a sodium salt of a dicarboxylic acid, eg, of 5-sulphoisophthalic acid. The acidic sulpho-group allows the attachment of cationic dye molecules, in addition to disperse dyes (Fig. 4b).

If both the modified and the unmodified fibers are put into a dye bath containing a mixture of disperse and cat dyes, they will emerge with two different colors. This is not only a good parlor trick, but is useful in the creation of specialty fabrics when the two different yarns are woven into fabrics with a predetermined pattern. The multicolored pattern emerges upon dyeing.

Since the basic structure of the modified fiber is a copolymer, rapidity of dyeing is also gained with these cat-dye fibers. Losses in fiber strength, temperature stability, and increased hydrolytic degradation are prices paid for the dyeability enhancement.

Some efforts have been made to incorporate sites into PET that accept *acid* dyes, but most of these alkaline-containing additives cause degradation and discoloration of the polymer. No acid-dye PET polymer has been commercially successful.

Antistatic/Antisoil Fibers. The nonionic character of the PET molecule makes the polymer hydrophobic and oleophilic. Without polar species, the ability to transport electrical charge along the fiber is poor. If excess static charges build up on PET fibers, as will happen unavoidably upon contact with other materials, these charges will not quickly leak away. The result can be clinging of fabrics to the skin or discharges of static electricity. (This problem is reduced at higher humidity levels because the small amount of water absorbed by the PET provides polar, charge-carrying molecules for quicker draining of the static charge.) PET's attraction for nonpolar, oily materials means that oils, which are difficult to remove, can easily stain fibers.

During the manufacture and processing of fibers, it is common to employ surface lubricants, wetting agents, and antistatic treatments to assist in processing. These are temporary, however, and a longer-term solution typically requires polymer additives or copolymers. (Copolymerization typically results in greater permanence than additives which can migrate to the fiber surface and be lost.)

Poly(ethylene glycol) (PEG) is frequently added to PET to confer antistatic and/or antisoil behavior. The ether groups running along the backbone of the PEG are sufficiently polar to attract moisture and to provide charge-transfer sites. This benefits both the electrical conductivity and the ability of water or detergent molecules to lift the oily stains. By using long-chain PEG additives, a block copolymer is formed. This avoids some of the thermal stability losses that occur with random copolymers.

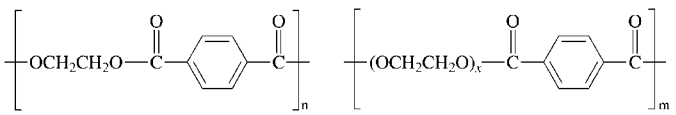

PET copolymerized with poly(ethylene glycol)

It is also possible to add PEG at the last stages of polymerization, so that much of the additive remains agglomerated in a separate phase. In this case, subsequent scouring of the fibers removes much of the soluble PEG, leaving microscopic voids in the fibers. These voids can act as reservoirs for moisture, and will also decrease light transmission and increase the reflectance properties of the fibers.

High Shrink Fibers. Although high fiber shrinkage is not usually desirable, an exception is when high and low shrink fibers are intimately combined. As the yarn or fabric shrinks because of the high shrink component, the excess length in the low shrink component forms loops at the yarn and fabric surfaces, providing texture. In filament yarn fabrics, these projecting loops can mimic the feel and appearance of staple yarn fabrics. Lack of crystallization in oriented fibers allows high shrinkage so that copolymers or non-heatset (noncrystallized) PET fibers can be used for these purposes.

Low Melt Fibers. Noncrystalline polymers or copolymers can also be used to generate fibers with relatively low softening temperatures. Such fibers can be blended with regular fibers, eg, staples, and bonded together by applying sufficient heat to melt the low temperature component. Such fibers need not be exotic. The use of undrawn, amorphous fibers suffices for many such purposes, for example, bonded nonwoven webs formed from a mix of drawn and undrawn PET staple fibers. Without crystalline structure, the undrawn fibers will soften and become tacky at relatively low temperatures.

Bicomponent (Bico) Fibers. Bico fibers are a new class of fibers, rather than a subset of PET fibers. Bico fibers are formed from two different polymers, which are melted separately and then combined into a single fiber at the last moment before extrusion. In some cases the fibers are actually extruded separately, and then combined while they are still molten so that they fuse together after spinning.

The most common cross-sectional fiber shapes are core-sheath and side-side configurations (Fig. 5). By encasing a PET core in a modified sheath, it is possible

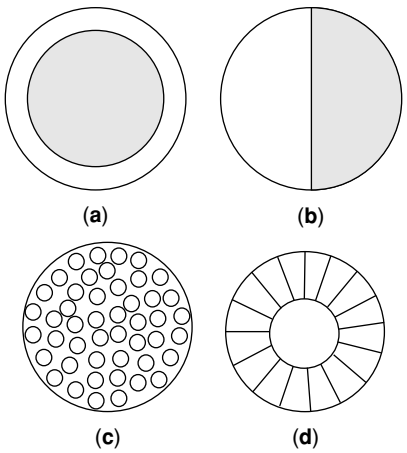

Fig. 5. (**a**) Cross-section of core/sheath bico fiber, (**b**) cross-section of side/side bico fiber, (**c**) "Islands-in-the-sea" bico fiber, and (**d**) segmented bico fiber.

to provide desirable surface characteristics (eg, antistatic/antisoil) with minimal effect on fiber strength. A popular application is to use sheath material with a lower melt point than the core. A nonwoven fabric can be formed from such fibers and then heated to a temperature sufficient to melt the sheath to bond the fibers together. Since the core component is not melted, the binder fiber retains its integrity and strength.

The side-side configuration is usually used to impart crimp to the fiber. If formed from fiber materials with differing shrinkage characteristics, and treated after fiber formation to develop the shrinkage, the differential lengths will cause the fibers to contract into a helical shape and develop three-dimensional crimp. Such self-crimping fibers provide a different type of bulk and hand than do conventionally crimped fibers.

Bico fibers have been available for at least 30 years, but only recently have they developed widespread applications. Bico production equipment is relatively more complex and expensive and so the fibers require higher selling prices. As these fibers become more common in specialty markets, production cost is decreasing and they are now beginning to find uses in commodity applications.

Hollow Fibers. In some applications it is desirable to generate increased bulk without adding weight, eg, for insulation or padding. A solution is to make fibers that are larger in diameter and stiffer, but with internal voids to reduce weight. (Think of a core-sheath heterofil with an air core.) By extruding hollow fibers, weight reductions of 20% or greater can be achieved, a not inconsiderable advantage. Foaming agents in the polymer (eg, dissolved CO_2) have also been used to generate microporous, lightweight fibers.

Microfibers. A PET microfiber is loosely defined as one with a decitex per filament below about 1. (Decitex is a measure of fiber size. If 10,000 m of fiber weighs x grams, the decitex of the fiber $= x$.) This translates to a fiber diameter of $\sim$10 μm or less. In fabric form, such fibers provide a very soft hand and a low luster appearance. They can also make moisture-repellant fabrics without sacrificing comfort or air porosity, ideal for sportswear. The larger fiber surface area also can be useful for filtration applications.

Traditional melt spinning is not the best way to make microfibers. Technical problems occur with very low mass throughputs, and economics suffer. By employing bico technology, it is possible to extrude larger shapes that can be separated into smaller components after extrusion.

The "islands-in-the-sea" approach uses bico technology to extrude filaments that contain a multiplicity of small fibrils encased in a soluble matrix (Fig. 5c). After fiber processing and fabric formation, the matrix is dissolved away to leave behind the microfibers. Fibers with submicron diameters can be produced. The process is expensive, but luxurious fabrics and nonwoven materials such as Ultrasuede® are made this way.

Bico technology can also be used to form composite fibers that can be broken apart, by using polymers with poor mutual adhesion (eg, polyolefin and PET). A fiber made with a dozen or more segments, alternating between two polymer types, can be post-processed to form separated fibrils of the two different materials. The shapes of the fibrils can affect the aesthetics of the fabrics, for example, sharp edges on the fibrils confer crispness and the sound of silk to fabrics.

Light Reflectance. The light reflectance of yarns and fabrics can be quite sensitive to the size and shape of the fibers. Two types of light interactions occur:

(1) Light is reflected from the surface of the fiber because of the change in refractive index from air into polymer (for PET, $n = 1.6$). This is specular reflection, similar to reflection from a mirror, and causes no coloration of the reflected light.
(2) Light that is transmitted through the fiber surface can interact with the molecular structure, eg, dye molecules, and thereby change its spectral character before being emitted back through the surface.

The mixture of these two types of light is what meets the eye, and the ratio of these two components affects the perceived depth of color. The more the specular reflection, the less the apparent color depth. Fine fibers of PET usually appear white, even though the polymer chips that they are made from may appear grey in color. This is a consequence of the high amount of specular reflection of ambient light, emanating from the large surface area of the fibers. Additionally, any relatively large surface areas of specular reflection can generate visible points of light when they are oriented to reflect from point sources; these cause the fibers or fabrics to glitter.

Larger diameter fibers have proportionally less surface to volume ratio and so proportionally less specular reflection; thus they appear darker than small fibers containing the same amount of dye. But larger fibers also have relatively flatter surfaces and are more prone to glitter. It has long been practiced to include microscopic fragments of highly reflective material in the polymer so as to opacify the fibers and diffuse surface reflections and glitter. Powdered titanium dioxide is the common additive used for this. It gains its reflective properties by means of exceedingly high refractive index. The quantity of TiO_2 in the polymer is controlled to produce "clear" or "dull," or "semi-dull" fibers for various types of fabrics.

It is possible to microscopically roughen the fiber surface to diffuse the surface reflections by other methods, eg, by chemically etching the surfaces with corrosive solvents. Many of these solvents will preferentially dissolve the amorphous regions, leaving the undissolved crystalline formations standing proud at the surface. Powdered materials with refractive indices similar to PET can be incorporated in the polymer to create rougher fiber surfaces with much less light reflectance from the additive/polymer interfaces. Cab-O-Sil®, a powdered silica, is one such material.

In addition to the aforementioned methods, fiber shape is exploited to produce differences in appearance. Surface lobes can break up smoothness and reduce glitter, and triangular or T shapes can generate subtle sheen effects to fabrics and yarns. Patent literature is filled with various cross-sectional shapes that have been used to provide visual and tactile effects that are not possible with natural fibers.

Surface Friction and Adhesion. Control of fiber friction is essential to the processing of fibers, and it is sometimes desirable to modify fiber surfaces for particular end uses. Most fiber friction modifications are accomplished by coating the fibers with lubricants or finishes. In most cases, these are temporary treatments that are removed in final processing steps before sale of the finished good.

In some cases a more permanent treatment is desired and chemical reactions are performed to attach different species to the fiber surface, eg, siliconized slick finishes or rubber adhesion promoters. Polyester's lack of chemical bonding sites can be altered by surface treatments that generate free radicals, such as with corrosive chemicals (eg, acrylic acid) or by ionic bombardment with plasma treatments. The broken molecular bonds produce more polar sites, providing increased surface wettability and reactivity.

The physical topology of the fiber surface also has a strong effect on friction. A microscopically smooth surface will generate more intermolecular attraction sites than will a roughened surface. It has been long known that including particulate additives (eg, TiO_2 or Cab-O-Sil) in the polymer reduces fiber friction, and that polished rolls generate more friction against PET fibers than do rougher rolls.

Antiflammability and Other Applications. Problems can occur with garments made from thermoplastic polymer fibers when they are exposed to flames; the molten polymer can stick to skin and cause burns. If the molten polymer itself supports continued combustion, the problem is worse. Additives that contain bromine or phosphorus have been used to reduce combustibility of PET, but these additives are typically expensive and/or deleterious to fiber properties. Here, bico technology is applicable so that antiflammable additives can be incorporated into the sheath without sacrificing the strength of the core of the fiber.

Other applications that have been developed for PET fibers include the incorporation of fragrances, antibacterial or absorbent additives, and also pigmented fibers for permanent coloration. Here again, the bico technology offers a route to such specialty fibers with lower raw material costs and fewer processing faults.

Melt Spinning of PET Fibers

A large part of the attractiveness of PET is that it is melt-spinnable into fibers, providing a clean, pollution-free manufacturing process. The goals of melt spinning include not only the stable formation of fine fibers but also the control of the microstructure of those fibers. Ideally, this is done at as high a throughput rate as possible for economic reasons.

Typical equipment used to make PET fibers is shown in Figure 6. Prior to melting, the polymer chips must be thoroughly dried, typically under vacuum at elevated temperature for several hours. The equilibrium moisture content of PET under ambient conditions is about 0.5% (11) and this much moisture would cause unacceptable levels of depolymerization. The dried polymer chips are fed to an extruder which melts the chips and forwards them to a metering pump, which delivers a volumetrically controlled flow of polymer into a heated spinning pack.

Modern large-scale PET fiber facilities have evolved to a continuous process of PET polymer production, and have integrated the processes of polymerization and fiber extrusion. This avoids the equipment, energy, and manpower needed to solidify and pelletize the polymer, dry it, and remelt it. In large plants that operate continuously for months at a time, huge quantities (more than 200 tons per day) of fiber are produced from a single line. Such fibers may be used, for example, in commodity markets such as woven or knitted apparel, or for tire reinforcement. For more specialized markets, which require modified polymers in

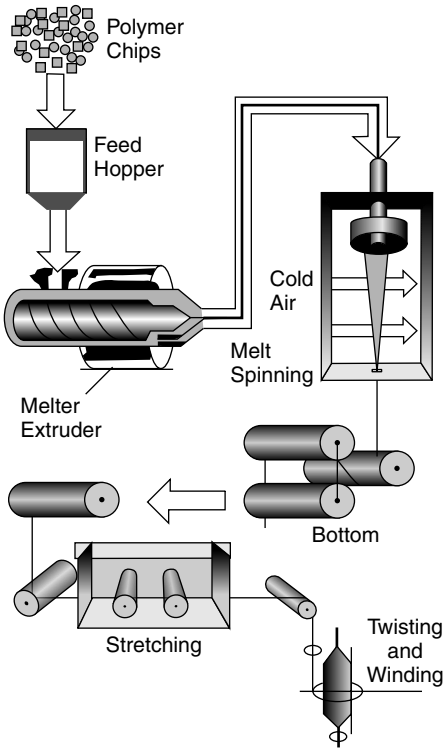

Fig. 6. Melt spinning process. From www.fibersource.com.

smaller quantities, the downtime and waste associated with changeovers of such large lines is prohibitive; smaller batch lines based on PET chips are preferred. Whether fed by a continuous polymerization (CP) process or by remelted chips, however, the spinning processes are basically the same.

Under typical conditions of 290°C spinning temperature, the molten viscosity is ca 200–2000 Paċs (2000–20,000 P) depending on average molecular weight. This is extremely viscous—similar to hot asphalt. The pump must provide a pressure of 10–20 MPa (∼100–200 bar) to force the flow through the pack, which contains filtration media (eg, a sand bed) to remove any particles larger than a few micrometers.

At the bottom of the pack, the polymer exits into the air through a multiplicity of small holes through a thick plate of metal (the spinneret). The number of holes can range up to several thousands per spinneret. Each spinneret hole is ca 0.2–0.4 mm in diameter with a typical flow rate in the range of about 1–5 g/min (less for fine fibers, more for heavy fibers). Although a round hole is most common, it is not unusual for the hole to have a complex shape intended to provide fiber cross sections of unusual shape, as noted earlier. The mass flow rate through the spinneret is controlled by metering pumps feeding the pack. A take-up device, typically a rotating roll system with a controlled surface speed, controls the final speed of the extruded filaments. Assuming the same flow rate to every spinneret

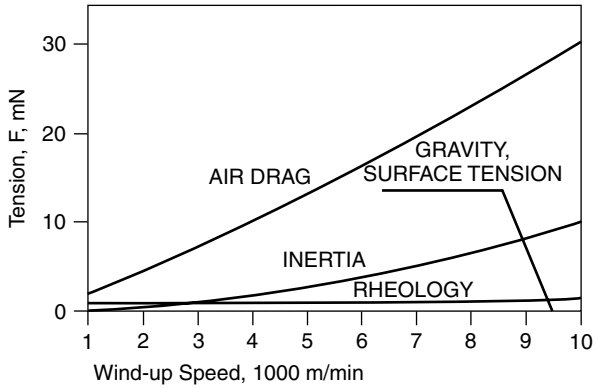

Fig. 7. Typical forces acting upon spinning threadline (14). To convert from mN to dyne, multiply by 100.

hole, the final diameter of the filaments is fixed by the flow rate and the take-up speed; the spinneret hole size does not affect fiber diameter.

The structure and properties of the filaments are controlled by the threadline dynamics, especially in the molten region between the exit from the spinneret and the freezing point of the fibers. After freezing, the fibers will be traveling at the take-up speed, which is typically 100–200 times faster than their exit speed from the spinneret hole. Thus, considerable acceleration (and stretching) of the threadline occurs after extrusion. The forces acting on the fibers in this transition region include gravity, surface tension, rheological drag, air drag, and inertia (Fig. 7). Because both temperature and threadline speed are rapidly changing, these force balances also change rapidly along the threadline. The dynamics of threadline formation are reasonably well understood and have been successfully modeled. Numerous references on the subject are available (15,16).

While traversing the spinneret hole (typically 1.5–5.0 times longer than it is wide), the molten fibers are in a state of viscous shear that induces molecular orientation along the fiber axis. Upon exit from the hole, the filaments slow down and bulge slightly, as the molecules relax and disorient. This is "die swell." From the die swell region onward, the filaments accelerate, and it becomes an ongoing competition between orientation (induced by extensional flow) vs thermal disorientation (due to molecular relaxation). Near the spinneret, the filament is still hot, the polymer is relatively fluid, and little net orientation is present in the threadline. Further down, the filament is cooler, the polymer more viscous, and thermal disorientation less; net orientation is higher. Orientation increases progressively and reaches a maximum as the threadline "freezes," ie, stops extending, usually within ∼1 m from the spinneret. The amount of orientation that is frozen into the spun fiber is directly related to the stress level in the fiber at the freeze point (15).

A key parameter which controls the rate at which orientation is being generated is the rate of extension

$$v' = \frac{dv}{dx} \tag{4}$$

where v is the local threadline velocity and x the distance along threadline.

For a Newtonian polymer, the stress required to deform the polymer at this extension rate is simply $\eta v'$, where η is the extensional viscosity of the polymer (which changes rapidly as the polymer cools) PET is not strictly Newtonian, else it could not be fiber-forming. Fiber forming polymers develop increasing tension because of retraction forces as they become oriented, so that localized necks do not grow and become discontinuities. An exception to this behavior occurs at high shear rates, and is discussed later.

The fiber extension also corresponds to acceleration of the material at a rate equal to vv', and the inertial resistance to this acceleration is responsible for a tension gradient along the filament. Finally, the air resistance of the fiber generates surface drag forces that increase with velocity so that a further tension gradient appears because of air drag. These are the three dominating forces—rheological, inertial, and air drag—that control spinning threadline dynamics and velocity profiles over the range of typical spinning speeds. Gravity and surface tension forces are relatively much smaller.

Starting with a more viscous polymer (whether due to higher molecular weight or lower extrusion temperature) will produce higher final orientation. And so will increasing the total amount of stretch, the "draw-down" ratio. The primary tool for controlling the net orientation, though, is the speed of the process, ie, the take-up speed. By increasing the velocity and extension rate of the filaments, the orientating mechanism becomes more dominant over the thermal relaxation mechanisms, and more net orientation is frozen into the fibers. Since molecular orientation is such a critical parameter, several methods have been developed to measure it. One of the most common is filament birefringence, taking advantage of the fact that oriented PET is a birefringent material. The refractive index for light polarized along the fiber axis is different than the index for polarization across the axis. The difference in these indices increases as the orientation increases. This difference can be measured by viewing fibers under a microscope with polarized light (17). This method requires only a very small sample of fibers, as compared with other methods that may depend on measurement of, for example, fiber shrinkage, shrinkage forces, or residual extensibility. Obviously, a higher level of v' corresponds to larger rheological and inertial forces, and higher v creates more air drag. Thus, high speed spinning is also high stress spinning.

The melt-spinning process for PET fibers can conveniently be divided into three regions of take-up speed:

(1) In low speed spinning (<1000 m/min), the spinning threadline forces are dominated by rheological deformation. Air drag may also play a role for fine filaments (with high surface–volume ratios), but drag is generally small in the fiber formation region near the spinneret where velocities are lower and diameters larger. The acceleration rate is too small for inertia to play a role. Only a small amount of residual orientation is frozen into the threadline, since thermal disorientation predominates over the orientating effects of fiber extension.

(2) In medium-speed spinning (ca 1000–4000 m/min), the air speed generates higher drag and faster cooling. The inertial effects are also greater, being proportional to velocity and extensional shear rate. The resulting higher

stress at the freeze point increases the orientation frozen into the spun fibers.

(3) At speeds beyond ~4000 m/min, inertial and air-drag effects become the dominant contributors to fiber stress. Sufficient orientation can be induced so that significant crystallization occurs in the as-spun fiber. The structure begins to partition into either highly oriented crystalline regions or amorphous regions of relatively low orientation. There is relatively less of the "oriented-amorphous" structure.

The structure-partitioning effect at high speeds is believed to arise from the scaffold of oriented regions that develop within the structure and support the fiber stress. This leaves the less-ordered regions free to relax and disorient so that a two-phase structure begins to appear where there was before a broad continuum of orientations. In this region, the highly ordered sections behave as a solid, with tensile stresses proportional to deformation, while the less-ordered regions behave more like a fluid with stresses proportional to *rate* of deformation. This is a mixture of solid and liquid phases.

It has been observed that, at speeds sufficient to induce crystallization, fiber deformation will become concentrated into a "neck" region where the final amount of stretching will occur over a very short distance. The origins of this neck have been a source of speculation and research (15,16) and efforts have been made to link necking and crystallization in a cause–effect relationship. Current evidence favors the explanation that this phenomenon is similar to necking behavior seen when cold-drawing plastic materials (14). This means that the molten filament passes through a stage where resistance to deformation decreases along the threadline. The decrease in resistance is initiated by "shear-thinning," where the apparent viscosity of the polymer decreases at increased shear rates. High shear rates promote a high level of molecular orientation within the melt, which then allows the molecules to slip by each other more easily. As the thinning process accelerates, the decrease in cross-sectional area concentrates the stress, while the overall tension remains constant. This produces a rapidly thinning neck. The necking stops when sufficient orientation has been induced so that further elongation requires additional force, and the resistance has become elongation-dependent rather than elongation rate-dependent. Classically, the liquid has become a solid. Coincidentally, the high levels of orientation allow crystallization to occur very rapidly after stretching has stopped.

Another feature of high speed spinning is that the fiber macrostructure becomes nonuniform, with more orientation and crystallinity near the fiber surface than in the interior. This is a result of nonuniform solidification, where rapid cooling generates lower temperature and higher viscosity at the surface. This leads to an oriented surface "skin" which supports the spinning stress, whereas higher temperatures in the interior allow more relaxation and disorientation.

The skin-core structure is a macroscopic analogue of the partitioned structure within the fiber. Since fiber stresses become concentrated in the oriented regions, there is a loss of participation of some of the interior molecules to resist subsequent strains. Under fiber extension, the taut molecules will break first, triggering rupture of the fiber before the unoriented molecules contribute much resistance. A loss of overall fiber strength and tenacity results.

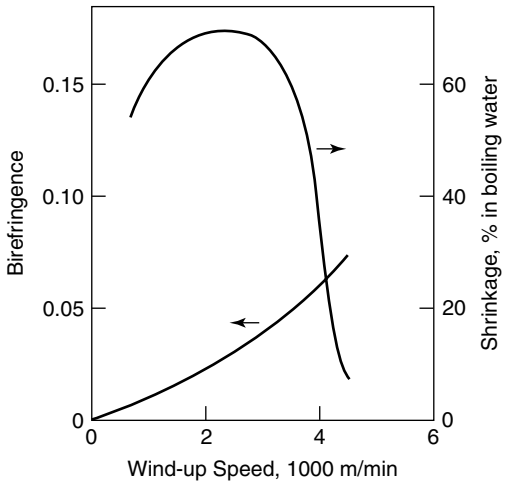

Fig. 8. Orientation and shrinkage of spun yarn vs spinning speed (18).

Insight into the spun yarn structure can be gained by observing its behavior in boiling water. The combination of elevated temperature and the plasticizing effect of the water molecules allows relaxation of the oriented regions, resulting in yarn shrinkage (Fig. 8). As spun orientation becomes greater, the spun yarn shrinkage will increase up to a point. At sufficiently high levels of orientation, the plasticizing effect of the heat and moisture will allow crystallization to proceed within the hot water, and this will inhibit shrinkage in the amorphous regions. This rate differential will increase at higher spinning speeds. Additionally, the reduction of amorphous orientation accompanying crystallization in high speed spun yarns will depress their shrinkage even further.

In summary, the strongest PET fibers are formed by slow-speed spinning processes. A benefit of high speed spinning is that it generates less of the intermediate "oriented-amorphous" structure that is prone to thermal shrinkage. The most thermally stable fibers are therefore formed by high speed spinning processes. It is possible to increase spinning speeds to the point that very little extensibility remains in the fibers, but the microstructure becomes so highly paritioned that little strength remains. Nearly all commercial spinning processes leave at least ~100% extensibility remaining in the spun fibers, and do further downstream processing at lower temperatures in order to develop the most useful fiber properties.

Spinning Process Control. There are a number of factors available for controlling the spinning process, to control thereby the properties of the fibers. These include melt viscosity (via temperature and/or polymerization level), hole diameter and throughput, spinning speed, and the cooling rate of the filaments after extrusion. In the ideal world, each fiber would have an identical history and microstructure. In reality, each filament is subjected to different thermal histories according to its position within the threadline relative to the flow of cooling air. Uneven heat losses from the spinneret face also lead to different extrusion temperatures among the filaments. Consequently, different filaments have different

average orientation levels. Additionally, any particular filament will have varying levels of orientation along its length because of microscale fluctuations in cooling rate, eg, air turbulence.

The fiber orientation uniformity is also affected by small-scale or timewise variations in polymer viscosity related to breakage of polymer chains during the extrusion process. The degradation occurs as a result of residual moisture that immediately reacts to break chains, and by thermal degradation that occurs more gradually over time (2). Different residence times and temperature histories within the laminar flow streamlines lead to different viscosities, and hence different orientation levels in the final fibers.

A primary goal of extrusion equipment and process design is to minimize the orientation variability among filaments, since variability can have undesirable effects on product uniformity (eg, dye uptake level) and on yarn strength and processing performance. As a rule, higher throughput rates and/or more filaments per spinneret create greater difficulties in achieving uniform cooling and fiber properties. There is a compromise between fiber uniformity and production economics, since larger scale processes are more economical.

This tradeoff between product uniformity and production economics has affected the process design for various types of PET fibers. Products such as textile filament yarn have a strong requirement for uniform dye uptake, within and between bobbins of yarn used for weaving or knitting. No opportunity is available for "blending out" dye differences with continuous filament (CF) yarns. Continuous filament yarns are made on spinning machines with a relatively small number and low density of holes per spinneret, and the supply of cooling air is controlled very carefully to minimize variability. These are relatively low throughput processes.

In contrast, staple fibers are always blended during the textile process, either among themselves or with other fibers. Small fiber orientation differences that might occur between various spinning machines, or over small periods of time, will be blended out so that dye uptake differences occur over such a fine scale as to be invisible to the eye in the final fabric. For this reason, tolerance for fiber nonuniformity is greater for staple than for filament products. Consequently, the spinning processes used for staple allow much higher throughput rates, with much higher numbers of holes per spinneret. This allows staple fiber to be produced at less cost than filament yarn, and the selling prices of the fibers reflect this; filament PET yarns command significantly higher prices than do commodity staples. Continuous filament products, however, do not require post-processing in order to be converted into yarns suitable for knitting and weaving.

Relative scales of the spinning processes for staple and filament products are depicted in Table 2. The industrial filament process is intermediate to the staple and textile filament processes, in terms of both spinning throughput and fiber

Table 2. Scales of Spinning for Various Products

	Staple filament	Industrial filament	Textile filament
Filaments per spinneret	6000	750	140
Pack throughput (kg/h)	240	100	12
CV of orientation	~15%	~10%	~5%

orientation uniformity (here measured by spun birefringence level). Industrial yarns must be uniform enough to be drawn to much higher tenacity levels than staple yarns, but are not dyed and therefore not subject to the more demanding uniformity requirements of textile yarns.

Although it is evident that fiber orientation level affects dye uptake, and that orientation uniformity translates to dye uniformity, it is less obvious that orientation uniformity will affect yarn strength. The breakage of fiber bundles is controlled by the "weak link" principle, where the early breakage of a few high orientation fibers will initiate a catastrophic failure sequence among surviving fibers within the bundle (19,20). This comes about as a result of load transfer from the broken fibers to the unbroken survivors via fiber–fiber friction, and hence stress concentration. Variable extensibility of the fibers within a yarn can thereby result in yarn strength that is much lower than the average strength of the component fibers.

Drawing of Spun Filaments

The purpose of drawing is to further align and stabilize the structure of the fibers. Additional diameter reduction occurs in this step. Drawing occurs at a much lower temperature than spinning, typically just above T_g, so that there is minimal thermal disorientation to compete with orientation induced during stretching. Fibers may have been extended by a factor of 100–200 during spinning, but a draw ratio in the range of about 2–5 is typically enough to induce the maximum amount of fiber orientation short of breakage. Drawing is more efficient at orienting the structure.

The amount of drawing used depends on (*1*) the amount of orientation already present from spinning and (*2*) the desired level of fiber properties. High levels of final orientation are desired for technical fibers where high tenacity and high initial modulus are needed. Less orientation may be needed for textile fibers, so that dye penetration is faster and the fibers are less stiff.

Figure 9 displays the stress–strain behavior of PET fibers that were prepared from the same spun yarn but drawn to different ratios. The curves represent the elongation and stress in terms of initial fiber area (decitex). The open circles represent true stress values, where stress values at break are corrected for the decreased area of the fiber after extension on the testing device.

As expected, the residual extensibility of the fiber decreases at higher draw ratios. What is not so predictable is that the true stress at failure increases as the draw ratio increases; fiber failure strength is improved by drawing the yarn. If a curve is drawn to connect the endpoints of the stress–strain curves, it is seen that there is an inverse relation between tenacity and elongation to break (e_b). The form of this relationship is

$$t = \frac{K}{e_b^{\alpha}} \tag{5}$$

where t is engineering tenacity, K and α are constants.

Experimentally, $\alpha \sim 0.3$. The value of K is a measure of inherent fiber strength and will depend on the molecular weight of the polymer. K will also increase if post-draw heatsetting is used to crystallize the structure.

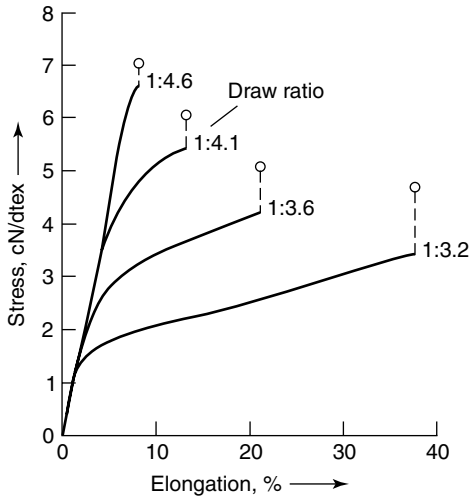

Fig. 9. Stress–strain curves of PET filaments drawn at different draw ratios (21). To convert cN/dtex to g·f/den, multiply by 113.

The presence of significant crystallinity in the fibers prior to drawing is detrimental to a smooth and continuous drawing process. Free extension of the polymer chains is inhibited by crystalline tie points, which must be disrupted for molecular extension to occur while drawing. If very high final fiber orientations are desired, then high drawing stresses may be generated, which can cause frequent breakouts of the drawing process at the sites of small fiber defects. Increasing the drawing temperature to compensate for the high tension will only hasten the crystallization process, compounding the problem. For most PET fiber production, inhibiting spun orientation is an advantage since it will allow a higher final draw ratio, which will allow higher spinning speed and throughput. An exception is when the final fiber properties require very high levels of thermal stability which can be provided by a network of small, very numerous crystallites that are "seeded" during the spinning process.

The use of a post-draw heatsetting (or annealing) step usually accompanies the drawing process. It is the purpose of this step to stabilize the structure and make it stronger. The level of yarn tension and the annealing temperature both can have significant effects on the final properties. Basically, there are two separate processes occurring during annealing: (*1*) crystallization in the most highly oriented regions and (*2*) chain disorientation via bond rotation in amorphous regions. The relative rates of these two processes are affected differently by tension and temperature and so a significant range of different fiber properties can be achieved according to the balance of these two variables.

High temperature (~200°C), high tension heatsetting promotes a high level of orientation in the amorphous regions and hence high fiber modulus and relatively lower dyeing rate. Dyeing rate can be improved by reducing the heatsetting temperature so that less crystallization occurs. If temperature is raised even higher, however, the structure can generate fewer larger crystals as the smaller ones melt and the larger ones become more perfect. This will also enhance

dyeability, since there are fewer crystallites to inhibit diffusion of the large dye molecules.

If the fibers are heated with low tension, then disorientation of the amorphous regions occurs and the fibers are left with low shrinkage forces (and modulus), but high dyeability. It may be desired to complete stress-relaxation while the filaments are held in some particular shape so that the memory of this shape is frozen into the microstructure. This might be done by twisting the yarn to form helical fibers, or by compressing them into random or regular modes of buckling. Such fibers retain crimp or texture, further enhancing their fabric aesthetics or their processability on textile machinery.

Commercial Drawing Processes. The drawing process can be continuous with spinning or it can be done as a separate step. The former simplifies handling, but can require very high final roll speeds since the drawing rolls must operate at several times the spinning speed. Such spin-draw processes are commonly used for high strength industrial yarns, at final speeds up to ca 8000 m/min (300 mph). This speed imposes severe demands on rolls and winders that can operate at high centrifugal forces (~10,000 g) and can control the yarn temperatures in the few milliseconds of contact time that are available.

At the other extreme are discontinuous staple fiber processes that operate at relatively slow speeds (<500 m/min). In order to obtain high throughput rates, the spun yarns from many spinnerets are collected and drawn in parallel. A modern staple line might process up to $\sim 5 \times 10^6$ filaments at a time, producing fiber at the rate of 200–300 tons/day. After crimping, such fibers are usually cut into short (<50 mm) lengths and baled. Depicted below is a modern drawing line for PET staple fibers. Such lines can be purchased as a package installation from equipment vendors, as can lines to produce the PET polymer and spin it into fibers (Fig. 10).

The third major PET fiber type is continuous filament textile yarn and this also uses a discontinuous production process. In this case the spun yarns are produced at speeds up to ~5000 m/min, precluding further in-line processing because of exceedingly high speed requirements. The spun yarns are highly oriented (known as POY, for Partially Oriented Yarn) and are wound onto packages then subsequently processed on another machine which provides the final orientation, texturing, and setting in an integrated process. Most commonly, POY yarns are heatset in a highly twisted configuration and then untwisted. The memory of twist produces a fiber bundle with helical filaments, providing bulk and stretchiness. Textured CF yarns may be knitted or woven directly into fabrics, eliminating the steps of blending and yarn formation used for staple fibers such as cotton or wool.

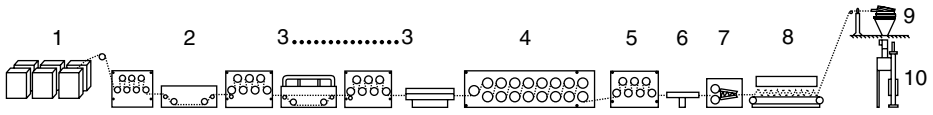

Fig. 10. Staple fiber line: (1) spun yarn supply cans, (2) lubricating bath, (3) two-stage drawing, (4) heatsetting, (5) cooling, (6) reheating, (7) crimping, (8) drying, (9) cutting, and (10) baling.

More akin to silk yarns, continuous filament POY produces lighter fabrics of 100% PET. Such yarns have provided a fertile field for imaginative engineering of cross-sectional shapes, fiber sizes, and combinations of color and texture. An entire field of specialty filament yarns called Shingosen has been developed in Japan (2), providing novel and luxurious fabrics that cannot be duplicated with natural fibers.

The Future of Polyester Fibers

From the proprietary developments by chemical industries in the mid-twentieth century, the technology for making PET fiber has become readily available. Entire plants can be purchased from machinery suppliers for textile or industrial fibers, continuous filaments, or staple. This has led to rapid expansion of PET fiber plants into developing countries by governments and/or large investment firms that supply fiber for labor-intensive fabric and apparel industries based in those countries. To an increasing degree, such apparel is imported back to the countries where the technology originated, displacing fiber and textile businesses there. This trend will continue as the world economy becomes more global.

Standardization of the world fiber business on PET guarantees that future fiber technology efforts will remain focused on this polymer. Costs and efficiencies will get better, and other fiber types will become even less competitive. Domination of the PET commodity fiber business by Asian countries will encourage more efforts by Western and Japanese producers to further expand into niche markets with special fiber types, and to further displace natural and other synthetic fibers from their markets.

The types of products that contain PET fibers will expand, especially in areas such as nonwoven fabrics used for disposable items, eg, industrial fabrics for diapers, disposable wipes, filters, etc. These are products that do not require much hand labor and are relatively protected from the low labor costs in developing countries. It is certain that bicomponent fibers based on PET will become more prevalent as the production technology becomes more widespread, where the bico approach can enhance properties or economics.

The domination of PET is likely to continue so long as the raw material costs remain low, and these are currently driven by the cost of oil. Although synthetic fibers use only ∼1% of the petroleum stream, they are in competition for that resource with fuels which use up to 50 times as much. Efforts are already in place for chemical producers to supply raw materials from renewable biological sources, and so it is possible that even the increasing cost of oil will not diminish the dominance of polyester. When contrasted with increasing costs of land and resources for natural fiber production, as food for an increasing population competes for the same land, the use of PET fibers will likely become even more prevalent than today.

BIBLIOGRAPHY

"Polyesters, Fibers" in *EPSE* 1st ed., Vol. 11, pp. 1–41, by G. Farrow and E. S. Hill, Fiber Industries, Inc. and P. L. Weinle, Celanese Fibers Marketing Co.; "Polyesters, Fibers"

in *EPSE* 2nd ed., Vol. 12, pp. 118–193, by G. W. Davis and J. R. Talbot, Celanese Corp.

1. Paraxylene and Derivatives—World Supply and Demand Report, PCI, 1999.
2. *Int. Fiber J.* **15**(3), 8 (2000).
3. W. H. Carothers and J. A. Arvin, *J. Amer. Chem. Soc.* **51**, 2560 (1929).
4. W. H. Carothers, *Chem. Rev.* **8**, 353 (1931).
5. U.S. Pat. 2,071,250 (1937), W. H. Carothers (to E. I. du Pont de Nemours & Co., Inc.).
6. Brit. Pat. 578,079 (1946), J. R. Whinfield and J. T. Dickson (to ICI).
7. U.S. Pat. 2,465,319 (1949), J. R. Whinfield and J. T. Dickson (to ICI).
8. U.S. Pat. 2,518,283 (1950), E. F. Casassa (to E. I. du Pont de Nemours & Co., Inc.).
9. U.S. Pat. 2,534,028 (1950), E. F. Izard (to E. I. du Pont de Nemours & Co., Inc.).
10. A. Ziabicki and H. Kawai, *High Speed Fiber Spinning—Science and Engineering Aspects*, Krieger, Malabar, Fla., 1991.
11. H. F. Mark, S. M. Atlas, and E. Cernia, eds., *Man-Made Fibers, Science and Technology*, Vol. **3**, John Wiley and Sons, Inc., New York, 1968.
12. U.S. Pat. 3,671,379 (1972), E. F. Evans and N. C. Pierce (to E. I. du Pont de Nemours & Co., Inc.).
13. J. Militky and co-workers, *Modified Polyester Fibres*, Elsevier, New York, 1991.
14. L. R. G. Treloar and G. Riding, *J. Text. Inst.* **54**, T156–T170 (1963).
15. T. Nakajima, *Advanced Fiber Spinning Technology*, Woodhead, Cambridge, 1994.
16. J. Kim and S. Kim, *J. Appl. Polym. Sci.* **76**, 446–456 (2000).
17. C. R. Desper, *CRC Crit. Rev. Macromol. Sci.* 501–543 (Aug. 1973).
18. *Polyester—50 Years of Achievement*, The Textile Institute, Manchester, U.K., 1993.
19. D. Zimliki, Modeling the Strength of Flat Yarns, Twisted Yarns, and Two-Ply Cords from Single Filament Data, M. S. Thesis, Department of Chemical Engineering, Clemson University, 1998.
20. I. M. Ward, *J. Macromol. Sci. Phys. B* **1**, 4 (1967).
21. H. Luckart, W. Kagi, U. Kemp, and W. Stibal, *Ullmann's Encyclopedia of Industrial Chemistry*, 5th ed., A10, VCH Publishers, New York, 1987.

GENERAL REFERENCES

A partial listing of organizations with affiliations to the fiber and textile industries, including reference libraries and personnel:
The Textile Institute, University of Manchester (Manchester, U.K.).
IRC in Polymer Science and Technology, Leeds U. (Leeds, U.K.).
Nonwovens Cooperative Research Center, North Carolina State University (Raleigh, N.C.).
Center for Advanced Engineering of Fibers and Films, Clemson University (Clemson, S.C.).
Textiles and Nonwovens Development Center, University of Tennessee (Knoxville, Tenn.).
Textile Research Institute, Princeton University (Princeton, N.J.).
Institute of Textile Technology, University of Virginia (Charlottesville, Va.).
Web sites with links to reference materials or fiber materials:
http://www.fibersource.com/
http://www.geocities.com:0080/~spanoudi/tradname.html
http://www.tx.ncsu.edu/research/tipub/books.htm

http://www.textileinstitutebooks. com/Merchant2/merchant.mv
http://www.fabriclink.com

GLEN REESE
Kosa

POLYETHERETHERKETONES (PEEK). See ENGINEERING THERMOPLASTICS.

POLYETHYLENE. See ETHYLENE POLYMERS.

POLYISOBUTYLENE. See BUTYL RUBBER.

POLYISOPRENE. See ISOPRENEPOLYMERS.

POLYKETONES

Introduction

Nearly 40 years have evolved between the first discovery by Reppe of transition-metal-catalyzed CO/ethene copolymerization and the discovery in 1983, at Shell, of a class of highly active, high yield palladium catalysts for the synthesis of high molecular weight, perfectly alternating CO/ethene copolymers [PK-E, Fig. 1]. This class of catalysts is also active for the co- and terpolymerization of CO with alkenes other than ethene, both simple aliphatic and heteroatom functionalized, thus providing access to a family of completely new polyketone polymers.

The high activity catalysts have made it possible to produce perfectly alternating copolymers in an ultrapure state, with very low levels of catalyst residues. Extensive research efforts have subsequently provided further advances in the manufacture and stabilization of polyketones and led to the development of easily melt-processable polyketone grades. For the first time, the intrinsic physicochemical and mechanical properties of these polymers could thus be assessed.

Aliphatic polyketones described here are a family of semicrystalline thermoplastics obtained by co- or terpolymerization of CO and ethene and/or higher α-olefins. Main emphasis will be on CO/ethene/propene-based terpolymers [PK-EP]. These polymers can be produced with a wide range of compositions and molecular weights. Various aspects of polyketone catalysis, the polymerization process, the types and properties of polyketones, and their applications are reviewed. A number of reviews on polyketones have appeared in recent years (1–5).

In 1996, Shell started commercial production of a number of PK-EP engineering thermoplastic grades, marketed under the trade name of Carilon Polymer.

Encyclopedia of Polymer Science and Technology. Copyright John Wiley & Sons, Inc. All rights reserved.

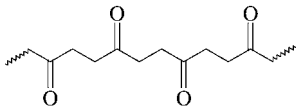

Fig. 1. CO/ethene-based PK-E. *Note:* Applied notation for perfectly alternating CO/α-olefin polyketones: PK-M_1M_2-n, in which M_1 and M_2 are abbreviations for the types of α-olefins incorporated in the co- or terpolymer chain [eg M = ethene (E), propene (P), butene (B), pentene (P), hexene (H), octene (O), decene (D), dodecene (Do), tetradecene (Td), hexadecene (Hd), octadecene (Od), icosene (Ic), and styrene (S)] and n, the molar monomer index $\{n = [100 \times [M_2]/([M_1] + [M_2])]\}$, is the percentage of M_2 (in mol%) on the total amount of α-olefin incorporated in the polymer backbone. For example, PK-E represents a copolymer build up of CO and ethene, while PK-EP-6 represents a terpolymer build up of CO, ethene, and propene in a molar ratio of 100:94:6.

Because of a strategic change in product portfolio initiated in 2000, Shell International Chemicals has announced its withdrawal from the engineering plastics market.

Physical Properties and Manufacture of Monomers

Ethene, propene, and CO are gases under ambient conditions. Their most important properties are given in Table 1. Ethene and propene are primarily obtained from cracking of higher hydrocarbons, or from dehydrogenation of ethane and propane, respectively. Carbon monoxide may be obtained by steam reforming of hydrocarbons (petroleum gas, natural gas, mineral oil, biomass) or gasification of coal into synthesis gas, followed by separation.

Copolymerization

Perfectly Alternating Copolymers. Nickel was the first transition metal found to catalyze the copolymerization of ethene and CO. In the late 1940s, Reppe and Magin (BASF) showed that $K_2Ni(CN)_4$ in water catalyzed the production of low melting polyketone oligomers in addition to diethyl ketone and propionic acid, albeit with a poor activity of ~0.8 g PK-E/(g Ni·h) (6). Also, rhodium-based catalysts showed some activity (7,8). Palladium(II) systems were first disclosed by Gough (ICI). Although these palladium(II) dichloride complexes bearing monodentate phosphine ligands showed a moderate activity,

Table 1. Physical Properties of the Monomers

Physical property	Ethene	Propene	CO
Molecular weight	28.054	42.080	28.010
Boiling point, °C	−103.7	−47.7	−191.5
Melting point, °C	−169.2	−185.3	−204.0
Critical pressure, MPa[a]	5.12	4.65	3.50
Critical temperature, °C	9.9	92.0	−140.2

[a]To convert MPa to psi, multiply by 145.

~300 g PK-E/(g Pd·h), severe conditions were required (250°C, 200 MPa) (9). In the early 1980s, Sen reported that certain monodentate phosphine modified palladium(II) complexes containing the virtually noncoordinating tetrafluoroborate anion produced PK-E under very mild conditions. However, the reaction rates were very low, ~4 g PK-E/(g Pd·h), as were the molecular weights (10,11). The real breakthrough came in 1983, when Drent (Shell) discovered that palladium(II)-based catalysts modified with the combination of a diphosphine ligand (L_2) and weakly or noncoordinating anions (X, eg sulfonates), produce high molecular weight PK-E at high rates [up to 6000 g PK-E/(g Pd·h) for $Pd(dppp)X_2$ (**1**)], at relatively mild reaction conditions (90°C, 4–6 MPa) (12,13).

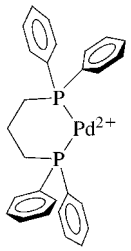

$Pd(dppp)^{2+}$ (**1**)

Copolymerization is carried out in methanol, which also constitutes an initiation and chain transfer reagent (eq. 1).

$$n\,CH_2{=}CH_2 + n\,CO + CH_3OH \longrightarrow H{-}[CH_2CH_2C(O)]_n{-}OCH_3 \qquad (1)$$

Although the catalysts L_2PdX_2 were initially prepared *in situ* (eq. 2), preformed complexes exhibit a similar performance (14–16).

$$Pd(OOCCH_3)_2 + L_2 + 2\,HX \longrightarrow L_2PdX_2 + 2\,CH_3COOH \qquad (2)$$

Since this finding, a large variety of transition-metal-based catalysts have been reported for the production of perfectly alternating aliphatic polyketones (17–27). Particularly suitable systems include palladium(II)- or nickel(II)-based complexes modified with a neutral or anionic bidentate chelating ligand and weakly coordinating anions X (such as OTs^-, OTf^-, TFA^-, BF_4^- and tetra-arylborates) (2,3,13).

Besides ethene, a variety of α-olefins can be effectively copolymerized with CO. These include

(1) propene and higher aliphatic α-olefins (2,14,15,28–35)
(2) functionalized α-olefins in which the functionality (eg $-CH_2OH$, $-CH_2CN$, $-CH_2Cl$, $-COOH$, $-COOR$, epoxide) is separated by at least one methylene group from the olefinic group (2,5,36–38).
(3) styrene and its (functionalized) derivatives (4,39–47)
(4) α,ω- and 1,2-dienes (48–53)

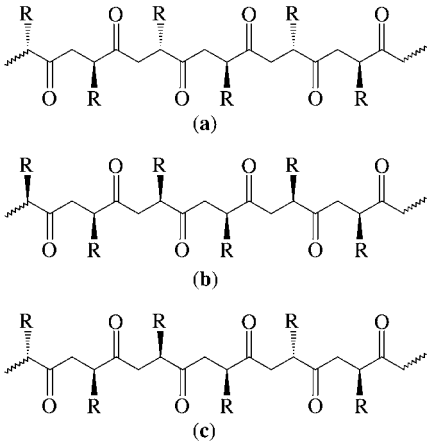

Fig. 2. Polyketone stereoisomers: (**a**) isotactic; (**b**) syndiotactic; (**c**) atactic.

Additionally, certain *internal* olefins can be copolymerized with CO, albeit at much reduced rates. For example, by employing 2-butene, low molecular weight oligomers of poly(1,5-ketone) are obtained by a sequence of insertion and isomerization steps (54). Copolymers with *strained* internal olefins such as (functionalized) norbornene or norbornadiene can also be made (55).

Besides copolymers, a variety of perfectly alternating CO/olefin terpolymers have been produced (31,56–64). The two olefins are usually randomly incorporated in the polymer chain, to a degree which is equally proportional to their concentration and relative rate of incorporation.

Copolymerization of CO and α-olefins can be achieved with almost perfect control of the chemo-, regio- (via either 1,2- or 2,1-insertion), and stereoselectivity in nearly all cases (2–4,33). Syndio-, iso-, and atactic copolymers can be produced on purpose (Fig. 2). For propene, highly isotactic materials can be prepared using chiral ligands (33,65,66). For styrene, chain-end control results in syndiotactic structures for a suitable choice of ligands (39,41). This chain-end control can, however, be overruled by application of certain chiral ligands to give isotactic structures (67). Epimerization of syndio- or isotactic polyketones into atactic materials occurs by heating, or by treatment with a strong base or a strong acid (68).

Interestingly, the palladium-catalyzed copolymerization of propene and CO may yield a polyspiroketal product, which can be converted into a polyketone (PK-P) by heating or dissolution (69,70). This conversion is reversible (eq. 3). In the presence of an acid the polyspiroketal structure can be (partly) restored (4,54). Also copolymers of higher α-olefins tend to adopt the polyspiroketal form (4).

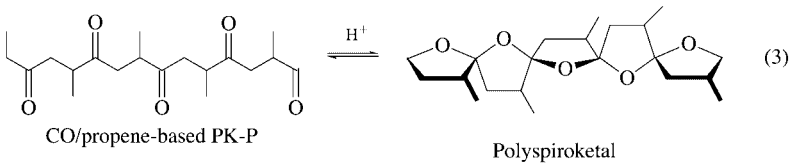

(3)

The choice of the most effective catalyst system is highly dependent on the type of olefin under consideration. Polymerization of CO and aliphatic α-olefines is most suitably carried out employing a catalytic system modified with a symmetrical, C_3-bridged aryldiphosphine ligand (2,71). However, these systems are not suitable for copolymerization of CO and styrene (41). For this reaction palladium(II)-based catalysts modified with a conjugated diimine (39,41), a bisoxazoline (43,44), a phosphine–phosphite (43), or a phosphine–imine ligand (43) have been employed, in, under chain-transfer conditions, combination with an oxidant promotor, such as 1,4-benzoquinone or 1,4-naphthoquinone (39–47,72), or a polar, acidic type of solvent (73,74).

Polyketone catalysis can be carried out in a wide variety of solvents, including water [using sulfonated ligands (75–79)], aprotic solvents [in which alumoxanes can be used as cocatalysts (80,81)], and even in solvent-free systems (62,82). However, methanol remains the solvent of choice for industrial polyketone production. Aliphatic polyketones can also be manufactured in a gas-phase process (83,84).

Nonperfectly Alternating Copolymers. Nonperfectly alternating polyketones, having a CO content of less than 50%, may be obtained either by a free-radical polymerization (3,85–87) or by application of certain *neutral* palladium(II)-based catalysts (88). However, the products are not identical. The nonperfectly alternating copolymers produced with a palladium(II)-based catalyst consist of a random combination of $-CH_2CH_2C(O)-$ and $-CH_2CH_2-$ units, while those produced by a free-radical polymerization also contain branched structure elements.

Catalyst Evaluation and Development. After the discovery of $(dppp)PdX_2$ [(**1**), dppp = 1,3-(diphenylphosphino)propane] as an efficient catalyst for CO/α-olefin copolymerization and Shell's decision to start process and product development work on this new engineering thermoplastic, an intensive search began toward the identification of more efficient catalyst systems for the production of PK-EP-6 [Shell's commercial polyketone grade, which contains 6 mol% of propene]. The target was not just to simply increase the activity, but also to find catalysts exhibiting an optimal balance on criteria including activity and stability of the catalyst, relative rate of propene/ethene incorporation, the molecular weight and molecular weight distribution of the terpolymer, product bulk density, particle size distribution, reactor fouling, the influence of residual catalyst on the melt-stability of the terpolymer, and the synthetic accessibility and manufacturing costs of the diphosphine ligand.

It had already been found that catalysts based on C_3-bridged aryldiphosphines (dppp) were more active than their C_2- or C_4-bridged counterparts (12,13). Substitution of the aryldiphosphines by alkyldiphosphines gives moderately active catalysts, but the molecular weight of the products is rather low (89). In 1986, it was discovered that replacement of the phenyl substituents on phosphorus by *o*-anisyl groups [$Pd(bdompp)X_2$ (**2**), bdompp 1,3-bis-(di-(2-methoxyphenyl)phosphino)propane], not only gave more active catalysts, but also produced co- and particularly terpolymers with a considerably higher molecular weight (Table 2) (90).

Table 2. Performance of Selected Catalysts in CO/Ethene Copolymerization[a]

Catalyst	Diphosphine ligand (L_2)	Rate, kg/(g Pd·h)	LVN,[b] dL/g
1	dppp	7.1	1.05
2	bdompp	12.7	1.58
3	diEt-XPhos	42.7	1.20

[a]Reaction conditions: Catalyst–$Pd(OAc)_2/L_2$/trifluoroacetic acid = 1/1.02/6, solvent = methanol, $T = 90°C$, $P_{tot} = 5$ MPA (50 bar), $CO/C_2^{=} = 1/1$ (gas cap), 6 wt% seed/methanol (C_2^2 = ethene).
[b]LVN = limiting viscosity number (see also Table 3).

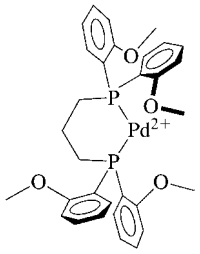

$Pd(bdompp)^{2+}$(**2**)

This finding offered the advantage of producing PK-EP-6 (LVN 1.7) at a much higher rate of 8–10 kg/(g Pd·h) (at 80°C) than with (**1**), which produces this material at a rate of only 1 kg/(g Pd·h) (at 45°C). At 80°C, the rate of (**2**) is first-order in ethene up to the highest partial pressures investigated (6 MPa), first-order in CO up to 0.5 MPa, and becomes zero-order in CO between 1 and 4 MPa. Taking the relative molar solubilities (inverse Henry constants) of CO, ethene, and propene in methanol at 80°C (1:5.4:11) into account, the ratio of rate constants for the incorporation of the three monomers by (**2**) was found to be

$$k_{co}:k_{c_2}:k_{c_3} = 1300:19:1$$

On a molecular scale this means that CO-insertion is much faster than ethene-insertion, while, in turn, propene-insertion is considerably slower than that of ethene. The rate constants for incorporation of other α-olefins are similar to that found for propene. The rate-dependency on the monomer concentration is highly dependent on the catalyst employed. For example, the rate of a Pd(dppp)-based catalyst (**1**) is first-order in CO over a much larger pressure span than that of (**2**) (91).

The structures of all further improved catalysts are based on modifications of this basic ligand concept: combination of a C_3-bridged disphosphine and *o*-anisyl groups on phosphorus. In 1987, it was found that substitution of the central carbon atom of the C_3-bridge by a $Si(CH_3)_2$ unit (diMe-Si-XPhos) gave the most active type of catalyst systems discovered thus far (92). In the 1990s, it was found that substitution of one or both protons at the central carbon atom of the C_3-bridge by aliphatic groups (eg diEt-XPhos, (**3**)) provided similar high activity catalysts

(93–95). Moreover, this type of catalysts exhibits a higher olefin/CO reactivity ratio, offering the advantage of using a lower olefin/CO ratio in the batch slurry polymerization process for PK-EP-6, thus lowering the olefin recycling costs.

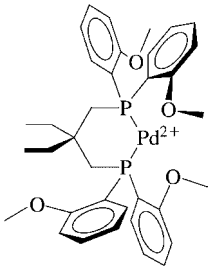

$Pd(diEt\text{-}XPhos)^{2+}$ (**3**)

Recently, certain nickel(II)-based catalysts have been found to exhibit activities similar to that of the most active palladium(II)-based catalysts (96,97). However, thus far the industrial applicability of these low cost nickel catalysts is limited because of the poor rate of propene incorporation during CO/ethene/propene terpolymerization.

Reaction Mechanism of Polyketone Catalysis

Propagation. The catalytically active species in polyketone formation is a square-planar cationic palladium(II) complex, L_2PdR^+, where L_2 represents the bidentate ligand and R is the growing polymer chain. The fourth coordination site at palladium may be occupied by an anion, a solvent molecule, a carbonyl group of the chain (*vide infra*), or a monomer molecule. Model studies indicate that having a strongly coordinating group at this position strongly reduces the rates of the insertion steps (98–100). Thus, competition for the vacant site appears to be an important factor affecting the performance of the catalyst, and provides an explanation for the sensitivity to the choice of solvent and counterion.

The palladium–diphosphine-catalyzed copolymerization of CO with aliphatic olefins occurs in a perfectly alternating way, and propagation "errors" (double CO or olefin sequences) are not observed. The origin of the perfectly alternating nature of the copolymers has received ample attention, both in experimental (101–106) and in theoretical studies (107–110). The mechanism for copolymer chain growth involves two sequential propagation steps: the reversible migratory insertion of CO into the Pd–alkyl bond of the growing polymer chain, followed by the irreversible migratory insertion of ethene into the resulting Pd–acyl bond (Fig. 3). Various intermediates in the catalytic cycle have been isolated or were characterized spectroscopically (82,98–105,111,112). Double CO-insertion does not occur because it is thermodynamically uphill, while double ethene-insertion is kinetically hampered owing to the much higher affinity of cationic palladium(II)-centers for CO over ethene, combined with the much higher rate of CO-insertion in the Pd–alkyl bond over ethene-insertion.

Bidentate ligands give copolymerization catalysts which are far superior to those bearing monodentate ligands (1,2). The most obvious difference between

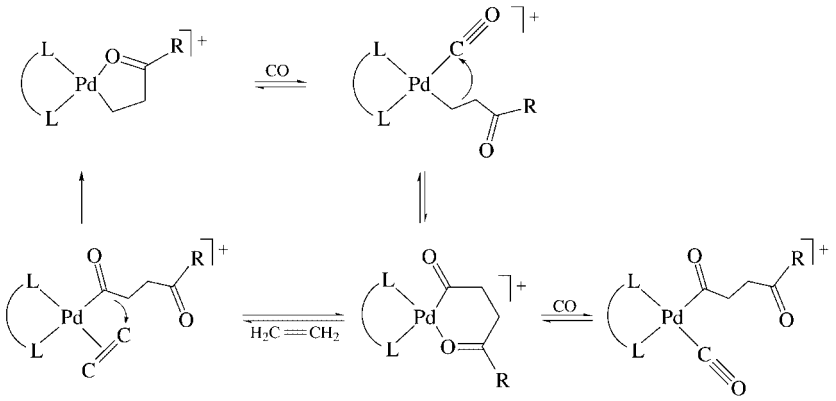

Fig. 3. Proposed propagation mechanism; R represents the growing copolymer chain.

mono- and bidentate ligands is that the latter are always cis-chelate coordinated at the d^8-square-planar palladium center, whereas the former can also coordinate in a trans fashion. If a bidentate ligand is used, the starting or growing copolymer chain and the "empty" fourth coordination site are always cis to each other, which is the ideal position for migratory insertion reactions. If a monodentate phosphine is used, both palladium(II)-alkyl and palladium(II)-acyl species prefer a trans position of the two phosphine ligands, which hampers migratory insertion reactions and facilitates termination.

Initiation and Termination (Chain Transfer). End-group analysis (^{13}C nmr) of CO/ethene copolymer produced in *methanol* showed the presence of 50% ester [-C(O)OCH_3, **E**] and 50% ketone [-C(O)CH_2CH_3, **K**] groups, in accordance with the average overall structure of the polymer molecule as given in equation 1. It is not a priori clear which group is the "head" and which is the "tail" of the polymer. Moreover, gc and ms analyses of oligomer fractions show, in addition to the expected keto-ester (**KE**) chains, the presence of diester (**EE**) and diketone (**KK**) compounds (13).

$CH_3CH_2[C(O)CH_2CH_2]_nC(O)OCH_3$ $\quad n \geq 0$
Keto-ester (**KE**)

$CH_3O[C(O)CH_2CH_2]_nC(O)OCH_3$ $\quad n \geq 1$
Diester (**EE**)

$CH_3CH_2[C(O)CH_2CH_2]_nH$ $\quad n \geq 1$
Diketone (**KK**)

At low temperatures ($\leq 85^\circ$C) employing $Pd(dppb)^{2+}$ as the catalyst, the majority of the polyketone chains are **KE**, with only small but balancing quantities of **EE** and **KK** chains (13). At higher temperatures, the same products are produced in a ratio (**KE**:**EE**:**KK**) close to 2:1:1. These observations have been rationalized by assuming two competing termination mechanisms (13); *protonolysis* (*H*), leading to the formation of a ketone end group (**K**) and *methanolysis* (*M*), giving an ester end group (**E**). After termination via protonolysis a Pd-*methoxy* species is

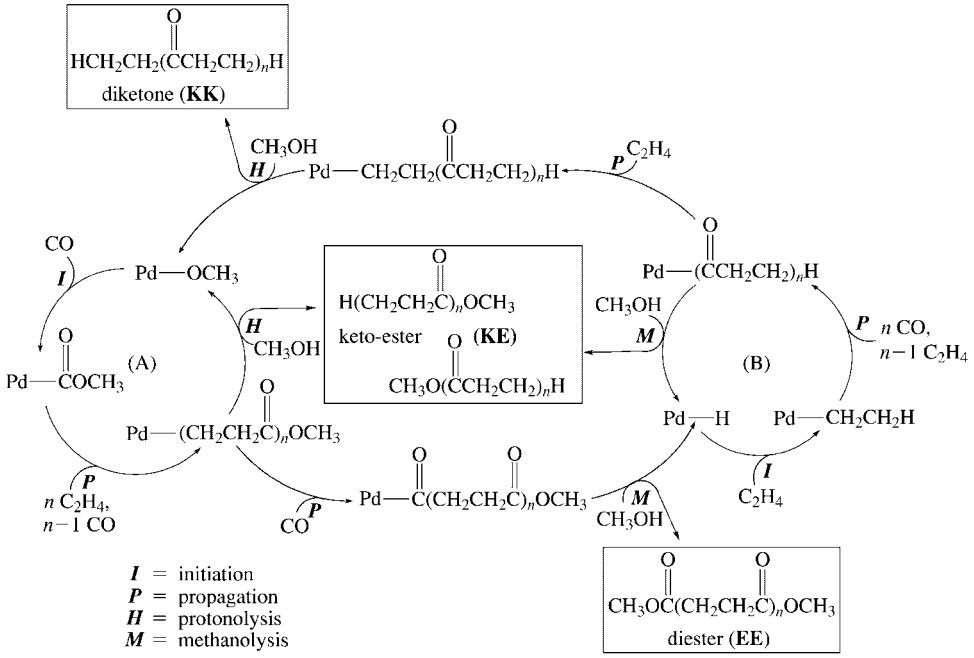

Fig. 4. Proposed chain transfer mechanisms, the *methoxy* cycle (A) and the *hydride* cycle (B) (reprinted in slightly adjusted form from Ref. 2).

obtained, which gives rise to the formation of an **E** end group at the start of the next copolymer chain it produces (cycle A), whereas after alcoholysis a Pd-*hydride* species is obtained, giving a **K** end group in the next chain (cycle B).

In Figure 4 the formation is summarized of the three possible polymeric chains, **KE**, **EE** and **KK**, formed by the two initiation–propagation–termination cycles A and B. Individually both cycles produce **KE** molecules, but the cycles are connected by the two "cross" termination steps which give **EE** and **KK** chains.

The formation of appreciable amounts of **EE** and **KK** at higher temperatures demonstrates that both chain transfer cycles contribute with comparable rates. The almost complete absence of the "crossover" products **EE** and **KK** at *lower* temperatures indicates that *one* cycle dominates. Rapid protonolysis and slow methanolysis would produce **KE** product via $PdC(O)OCH_3^+$ initiation (cycle A). Rapid methanolysis and slow protonolysis would produce the same product, but now via PdH^+ initiation (cycle B). Hence, product distribution alone is not sufficient to decide which cycle is responsible for the production of **KE** under these conditions. Crossover from A and B must have the same rate as termination within B, since the termination rate does not depend on how the chain started. Similarly, crossover from B to A has the same rate as termination within A. If the ratio of alcoholysis to protonolysis is k, the ratio of the products will be **EK**:**EE**:**KK** $= 1 + k^2$:k:k. A ratio of 2:1:1 implies that both termination steps contribute equally (k . Based on this finding, the ratio to which the chain transfer cycles A and B occur can be determined. The actual mechanism of alcoholysis has not been elucidated as yet.

In aprotic solvents and for CO/α-olefin- and CO/styrene-based copolymers, formation of vinyl-ketone [$R^1R^2C{=}C(R^3)C(O){-}$] and butenyl-ketone end groups has been reported (2,72,114).

Nature of the Catalyst in Polyketone Catalysis

Under actual slurry process conditions, 70–90°C; 5MPa (50 bar) CO/ethene, the nature of the initially homogeneous palladium(II)-based polyketone catalyst is rather complex. It may be present in at least three different states (I–III), each exhibiting its own kinetics. State I represents the running catalyst species, $[L_2Pd(CH_2CH_2C(O))_nCH_2CH_3]^+$ or $[L_2Pd(CH_2CH_2C(O))_nOCH_3]^+$, in the *homogeneous phase*, so being completely dissolved in methanol. Because of growth of the copolymer chain, the solubility of these species gradually decreases and at a certain chain length n, the running catalyst precipitates and becomes heterogeneous. Copolymer chain end-group analysis revealed that this phase transition occurs when n is about 13–20 and is accompanied by a change in the extent to which the two termination reactions, *alcoholysis* and *protonolysis* (*vide supra*), occur while the ratio of chain transfer vs propagation (k_t/k_p) increases (115).

The states II and III represent two types of heterogeneous catalyst species. Size exclusion chromatography showed the molecular weight distributions of CO/ethene-derived polyketone to be bimodal (116), indicating the presence of two different types of propagating catalyst sites that are not in fast equilibrium (117). The molecular weight distribution could be fitted with a combination of a Flory–Schulz distribution (type II; $M_w/M_n = 2$), typical of a homogeneous polymerization catalyst (118), and a Wesslau distribution (type III; $M_w/M_n \gg 2$), typical of a heterogeneous polymerization catalyst (119). It is conceivable that the catalytic sites producing a Wesslau distribution are sterically or physically congested, for example, because they are caught in the matrix or micropores of the polymer particles. The sites producing a Flory–Schulz distribution may be located on the external surface of the polyketone particles and therefore all face a similar environment. The ratio of polymer chains produced by the type II and III sites was found to be dependent on the copolymer particle size. Larger particles contain more of the longer chains produced by type III sites. Because of particle growth and agglomeration during a batch slurry run, the Wesslau contribution increases with time, and, as a consequence, the average molecular weight of the product gradually increases.

Manufacturing Process

The production of aliphatic polyketones at larger scale started in the market development unit (MDU; production capacity: 500 t/a) in Moerdijk, the Netherlands, in 1986 at Shell. The first commercial plant (capacity 7 kt/a) for the production of aliphatic polyketones came on stream in Carrington, U.K., in 1996. Production is carried out in a batch slurry process, by terpolymerization of CO, ethene, and propene in methanol at 70–90°C and 40–60 bar. The catalyst Pd(bdompp)$(TFA)_2$ (**2**) is suitably prepared in acetone by mixing palladium acetate,

1,3-bis-(di-(*o*-methoxyphenyl)phosphino)propane, and trifluoroacetic acid in a 1:1.02:4–10 ratio (see eq. 2).

The catalyst Pd concentration in the reaction solvent is usually about 5 ppm. The activity of the catalyst is about 8–10 kg terpolymer/(g Pd·h), throughout a batch run, typically lasting 8 h. The main commercial polyketone grades, PK-EP-6, contain about 6 mol% of propene and have a melting point of about 220°C and M_n = 37,000–52,000. After work-up and drying, the product is obtained as a snow white powder with a bulk density of 300–500 kg/m^3, and an average polymer particle size typically in the range of 200–600 μm, depending on the grade produced. The amount of Pd residue in the product is generally well below 10 ppmw.

The molecular weight of the various product grades is controlled mainly by the reaction temperature, the overall pressure, and the partial pressure ratio of the monomers. A small amount of water (2 vol%) is added to the reaction mixture to reduce the amount of methanol chemically bound to the terpolymer in the form of ketal groups. The initially encountered problems of extensive reactor fouling and low bulk density of the product were overcome simultaneously by introduction of a seed powder (typically 4–10 wt% PK-EP-6) in the reactor prior to the start of the polymerization and the use of an excess of acid in the catalyst solution. Both the seed powder and the excess of acid assist agglomeration of the newly formed terpolymer particles. The required excess of acid depends on the desired molecular weight.

A similar aliphatic polyketone product, Ketonex™, has been produced at pilot-plant scale by BP in Grangemouth, Scotland (120,121). Production was presumably carried out in a continuous slurry process.

Properties

Physical and Mechanical Properties. Perfectly alternating aliphatic polyketones based on ethene and CO, $-[CH_2CH_2C(O)]_n-$ (PK-E), have a relatively high melting point (T_m) of 257°C (122,123). This is about 125°C higher than the T_m of polyethylene, and reflects the strong polar group contribution, resulting from the regularly repeating ketone units. The alternating ketone groups in the polymer backbone confer polarity and high cohesive energy density to the polymer. The strong polar intermolecular forces, combined with a flexible polymer backbone, yield a semicrystalline material with a typical density of 1.24 g/cm^3 and a glass-transition temperature (T_g) near 15°C.

X-ray diffraction studies showed that the crystalline phase of PK-E may exist in two different forms, α and β (124,125). In both forms the copolymer chains are in an all-trans configuration, but the modes of chain packing differ. At room temperature, the crystalline phase exists primarily in the α-form. Depending on the way the material is prepared and pressure-treated, a phase transition takes place at about 120°C to the β-form. Above 120°C, the crystalline phase is exclusively in the β-form until it melts. This crystalline phase transition (CPT) is reversible, ie, upon cooling, the β-form (partly) transforms into the α-form again. The transition is accompanied by a volume change of about 5–7% (calculated densities for the α- and β-form are 1.383 and 1.297 g/cm^3, respectively) (124). In the differential scanning calorimetry thermogram, the CPT is observed as a small endotherm at 120°C

(126,127). The processes of spinning and drawing lead to the transformation of the β-crystalline part of PK-E into oriented α-crystalline material (128).

The crystallinity, T_m, and T_g of PK-E can be influenced by introduction of a third monomer such as propene (PK-EP) or a higher α-olefin such as decene (PK-ED) or dodecene (PK-EDo) (56–58). For example, random incorporation of 6 mol% propene in the polymer backbone (PK-EP-6) results in reduction of T_m from 257 to 220°C, while incorporation of 4 mol% dodecene (PK-EDo-4) reduces T_m to about 230°C. In PK-EP, propene is predominantly incorporated in the polymer chain in the 1,2- or 2,1-mode and, according to ^{13}C nmr in solution, only a small fraction is incorporated in the 1,3-mode.

Semicrystalline polyketones are insoluble in common organic solvents, and dissolve only in highly polar and acidic solvents such as hexafluoroisopropanol and *m*-cresol (>60°C). Related to this, polyketones demonstrate a high resistance to a broad range of chemicals and constitute good barriers both to small gases (such as oxygen) and to automotive fuels (129,130). Semicrystalline polyketones exhibit typical engineering thermoplastic characteristics, such as high impact strength, high heat distortion temperature, modulus (131), high resilience, and good wear and abrasion behavior. In a falling-weight impact test, PK-EP containing 3–6 mol% propene shows ductile failures down to −50°C. Replacement of the propene by 4 mol% dodecene (PK-EDo-4) lowers this temperature to −70°C. Also other mechanical properties of PK-EDo-4, such as stiffness, stability, and notched Izod impact strength, are significantly better than those of PK-EP-6.

Characteristics of typical low molecular weight (LMW) and high molecular weight (HMW) commercial grade materials of PK-EP-6 are given in Table 3.

The HMW grade is the standard grade for injection molding. The LMW grade is a high melt-flow injection molding grade and also the base material for compounding. Typical properties of the HMW grade are summarized in Table 4.

Relationships exist between T_g, T_m, and the type of termonomer introduced in the polymer and between T_g and the ductile to brittle temperature transition of polyketones in notched Izod or falling-weight impact strength test. For decene- or dodecene- containing grades T_m and T_g decrease simultaneously, while for propene-containing grades the opposite is observed (5).

Next to semicrystalline materials, perfectly alternating polyketones have also been manufactured, which exhibit amorphous, elastomeric, viscous, or side-chain liquid crystalline characteristics. An overview of some different types of polyketones is given in Table 5.

Oligomers of PK-P and PK-EP with a C_3/C_2 ratio of >0.4 are highly viscous liquids which can be cross-linked with a range of multifunctional reagents, such

Table 3. Characteristics of Two PK-EP-6 Grades[a]

Designation	MF,[b] g/10 min	η_0,[a] Pa·s	M_n[d]	M_w[d]	M_z[d]	LVN,[e] dL/g
LMW	64	190	37,000	100,000	230,000	1.1
HMW	6.9	2000	52,000	175,000	465,000	1.8

[a]Composed of CO, ethene, and 6 mol% propene; $T_m = 220$°C.
[b]Melt flow (MF) index at 240°C and 2.16-kg load (according to ASTM D1238).
[c]Zero shear viscosity at 230°C.
[d]Molecular weight from gpc in HFIPA relative to PMMA standards.
[e]Limiting viscosity number (LVN) in *m*-cresol at 60°C.

Table 4. Typical Properties of HMW PK-EP-6[a]

Property	Value, units	Test method
General properties		
Melting temperature	220°C	
Specific gravity	1.24 g/cm^3	ISO 1183
Mold shrinkage, flow direction	~2%	ISO 294-4
Mold shrinkage, perpendicular	~2%	ISO 294-4
Water absorption equilibrium @ 50%	0.5% m/m	ASTM D570
Volume flow rate	5–6 mL/10 min	ISO 1133 (240°C and 2.16 kg)
Thermal properties		
Heat distortion temperature	100°C	ISO 75/A (1.8 MPa)
Vicat softening point	205°C	ISO 306/B50 (50 N)
Relative temperature index	90°C	UL-746B (mechanical without impact)
Mechanical properties		
Tensile strength at yield	60 MPa[b]	ISO 527-1 (50 mm/min)
Elongation at yield	25%	ISO 527-1 (50 mm/min)
Tensile strength at break	55 MPa[b]	ISO 527-1 (100 mm/min)
Elongation at break	>300%	ISO 527-1 (100 mm/min)
Tensile modulus	1.4 GPa[c]	ISO 527-1 (1 mm/min)
Flexural modulus	1.4 GPa[c]	ISO 178
Notched Charpy impact strength @ 23°C	18 kJ/m^2[d]	ISO 179/1A
UL-94 flammability		
Flame resistance	HB	UL-94
Limiting oxygen index	21%	ISO 4589
Glow wire flammability index (2 mm)	750°C	IEC 695-2-1
Electrical properties		
Dielectric constant		
@ 50 Hz	6.6	IEC 250
@ 1 kHz	6.3	
@ 1 MHz	5.7	
Dissipation factor		
@ 50 Hz	0.026	IEC 250
@ 1 kHz	0.02	
@ 1 MHz	0.07	
Volume resistivity	10^{13} ω ·cm	IEC 93
Surface resistivity	10^{14} ω	IEC 93
Electrical strength	18 kV/mm	IEC 243-1 (1.6 mm; silicone oil)
Comparative tracking index	600 V	IEC 112

[a]Composed of CO, ethene, and 6 mol% propene; at 23°C and 50% relative humidity, unless otherwise stated.
[b]To convert MPa to psi, multiply by 145.
[c]To convert GPa to psi, multiply by 145,000.
[d]To convert kJ/m^2 to ft·lbf/in.^{2} divide by 2.10.

Table 5. Overview of Various Types of Aliphatic Polyketones

Type	Monomers	Appearance	Potential uses	Source
PK-E	CO/C_2^{2-}	Semicrystalline; $T_m = 257°C$	Engineering thermoplast	10–13, 122
PK-EP	$CO/C_2^{=}/C_3^{2-}$ ($C_3 < 10$ mol%)[a]	Semicrystalline; $T_m = 180–250°C$	*Vide infra* (section D)	56
PK-EP	$CO/C_2^{=}/C_3^{=}$ ($C_3 > 20$ mol%)[a]	LMW: highly viscous	Thermosetting resins	132, 133
		$M_w > 10^5$ g/mol[b]: elastomeric	Films, adhesives	5, 58
PK-EDo	$CO/C_2^{=}/C_n^{2-}$ ($C_3 < 10$ mol%)[a]	Semicrystalline; $T_m = 180–250°C$	Engineering thermoplast	57
PK-P	$CO/C_3^{=}$	Atactic LMW: highly viscous	Thermosetting resins	132–134
		$M_w > 10^5$ g/mol: elastomeric[c]	Films, adhesives	5, 35
		Isotactic: semicrystalline	–	33, 64, 66
PK-S	CO/styrene	Syndiotactic: semicrystalline; $T_m = 280°C$	–	4, 39, 47
		Atactic: amorphous; $T_g \approx 100°C$	–	135
		Isotactic: semicrystalline; T_m = n.d.	–	
PK-ES	$CO/styrene/C_2^{=}$	Semicrystalline or amorphous	–	62, 64, 136
PK-Hd	CO/C_{16}^{2-}	$M_n \approx (5–8) \times 10^3$ g/mol,[d] highly viscous; $T_m = 13°C$	Wax crystal growth modifiers that lower the pour point of gas oils and crude oils	5, 137–139
PK-POd	$CO/C_3^{=}/C_n^{=}$ ($n = 18, 20$)	Elastomeric	Elastomers	5, 59

[a] On total amount of olefins. Olefins are represented C_n = where the superscript indicates a double bond and subscript n denotes the number of carbons in the olefin.
[b] Measured by gpc (rel. to polystyrene).
[c] Stereoirregular; regioregularity: 50–55% head-to-tail units.
[d] Measured by gpc (rel. to PMMA).

as diamines, to obtain new, both thermoset and thermoreversible, performance resin systems (79,132,133). These systems, marketed by Shell under the trade name Carilite, (can) find application in coatings, composites, and adhesives.

Product Stability. During melt-processing, polyketones undergo intermolecular and intramolecular aldol condensation reactions (140–144). The intermolecular degradation reactions (*cross-linking*) lead to an increase in the melt viscosity and limit the melt-processing window (145). These reactions are catalyzed by impurities, such as salts (ions) and catalyst residues (146). Because of the lower melting point, the PK-EP grades (with $T_m \approx 220^\circ C$) have a substantially improved melt-processing window compared to PK-E ($T_m \approx 257^\circ C$). This, in combination with the application of high turnover palladium catalysts, improved manufacturing techniques (147), and the discovery of efficient melt-stabilizers such as calcium hydroxy apatite (148,149) led to a significant reduction in cross-linking during melt-processing. As a result, polyketone thermoplastics have become readily processable using conventional techniques, such as injection molding, extrusion, blow molding, hot-plate molding, and fiber spinning.

During aerobic heat aging, aliphatic polyketones can undergo complex oxidation reactions, manifested in part by molecular weight loss. Specific hindered phenolic type antioxidants have been identified, which significantly reduce molecular weight loss, allowing maintenance of mechanical properties for a long period (150). The typical continuous use temperature or UL index of stabilized neat PK-EP is currently 90–95°C. [*Note*: *UL index* (Underwriters' Laboratory) is defined as the (service) temperature at which the polymer loses 50% of a certain property within an agreed period of time. The property selected is the most critical property in the application envisaged. UL indices are found by extrapolation in an Arrhenius plot of failure vs aging temperatures. Usually they are based on extrapolation to 11000 h.]

Because of the presence of carbonyl groups, aliphatic polyketones are prone to degradation upon exposure to uv light. The mechanisms are based on chain-scission reactions, described in the literature as Norrish type I and Norrish type II reactions (151). Addition of uv absorbers is required to improve the photostability of unpigmented polyketone polymers, but is less effective for maintenance of surface-related properties (152,153). Ultravioletabsorbing pigments such as carbon black can also be used to significantly retard photodegradation in aliphatic polyketones.

Filled and Reinforced Aliphatic Polyketone Compounds. Aliphatic polyketones can be compounded with inorganic fillers, reinforcing agents, and lubricants (154). Compounds are produced using a co-rotating twin-screw extruder, with a typical melt temperature of 260°C.

Within Shell Chemicals, a number of fillers have been evaluated. These include chopped glass fibers, mica, wollastonite (a calcium silicate mineral), and calcium carbonate (nonreinforcing mineral filler). In all cases improvements in flexural modulus, flexural strength, and heat distortion temperature were found, the levels corresponding to the reinforcing ability of the filler. Fiber glass gave the best improvement, followed in decreasing order by mica, wollastonite, and calcium carbonate. The notched Izod values followed this same order of ranking, with the exception that mica-filled PK-EP-6 exhibits the lowest impact values. The results demonstrate that aliphatic polyketones can be readily compounded

with traditional fillers at relatively high loading levels and that filled polyketones exhibit property relationships similar to those of other engineering thermoplastics.

Flame-Retardant Aliphatic Polyketone Compounds. In the electrical and electronic industries, there is an increasing demand for materials with good flame retardancy (UL-94 VO rating and limiting oxygen index $\geq$ 28%). This often necessitates the addition of flame-retardant additives into plastics. Various halogenated compounds are very effective flame retardants. In recent years, however, governmental, regulatory, and public pressures have supported the use of halogen- and red phosphorus-free flame retardants because of environmental, toxicity, corrosivity, and smoke generation concerns. In this context, much attention has been given to hydrated fillers, such as aluminum and magnesium hydroxide, which function by releasing water upon endothermic decomposition. Polyketones have been found to be excellent base materials for halogen- and red phosphorus-free flame retardants at loading levels much lower than generally required in other thermoplastics (20–30% vs typically 50–60% for polyolefins and polyamides). This low loading level helps to preserve mechanical properties and the ductility and toughness of the aliphatic polyketone. On account of its low viscosity, which facilitates filler incorporation, a relatively high melt-flow aliphatic polyketone is used as a base material for flame-retardant compositions. Since aliphatic polyketones are generally melt-processed at temperatures above the decomposition temperature of aluminum hydroxide, but below that of magnesium hydroxide, the latter was selected as flame retardant for polyketones (155). In addition, a unique mineral, partially hydrated magnesium calcium carbonate ($MgCaCO_3$) was found to exhibit good flame retardancy for polyketones, even at low loading levels.

Of the hydrated fillers evaluated, magnesium hydroxide is more efficient than $MgCaCO_3$. Surface modification of magnesium hydroxide preserves impact properties. Addition of glass fibers increases the strength, rigidity, and dimensional stability of halogen- and red phosphorus-free flame-retardant aliphatic polyketone compositions.

Uses

The processing advantages offered by aliphatic polyketones have proven to be particularly attractive. The polymer is suitable for many conventional melt-processing methods, without any need for predrying. Injection molding of aliphatic polyketones is characterized by fast setting, ensuring that molding times are short. Comparative tests with other engineering thermoplastics have shown that reductions in cycle time of up to 50% can be achieved by using aliphatic polyketones, without any compromise in the functionality of the molded parts or the overall balance of performance properties. The shrinkage of nonfilled grades is isotropic. Moldings exhibit an excellent mold definition and are marr-resistant. If molded correctly, even large, flat moldings are warp-free. Parts can be assembled "dry as molded" without any need for conditioning or annealing.

Automotive Applications. Aliphatic polyketones (PK-EP-6) are characterized by the following performance attributes: good thermal dimensional stability, good low temperature impact behavior, and excellent resistance to fuels

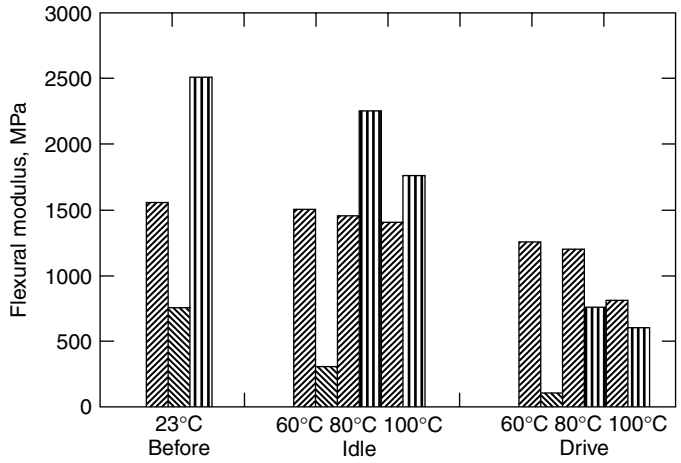

Fig. 5. Aging performance in diesel fuel (3000 h). ▨ PK; ▧ HDPE; ▥ POM. To convert Mpa to psi, multiply by 145.

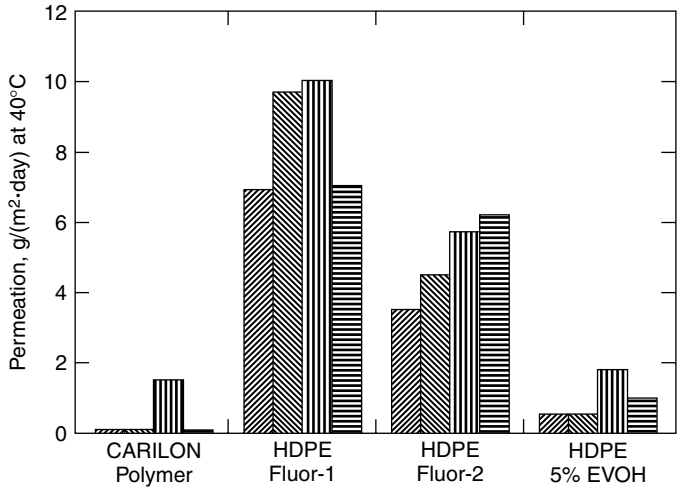

Fig. 6. Fuel permeation. ▨ Petrol; ▧ TF1; ▥ TF2; ▤ TF3. *Note:* Based on European standard fuel Halterman (CEC-RF-08-A-85). TF-1 = 90% + 10% EtOH, TF-2 = 92.5% + 7.5% EtOH, TF-3 = 95% + 5% EtOH. HDPE Fluor-1 and HDPE Fluor-2 refer to fluorinated HDPE fuel tanks from different suppliers. HDPE 5% EVOH is an HDPE, ethylene vinyl alcohol multilayer system.

(Fig. 5), coolants, transmission fluids, oils, and greases, with virtually no fuel permeation (Fig. 6). These attributes make these materials well suitable for a variety of automotive applications, such as fuel tanks, fuel system components, fuel pumps, fuel filters, injection rails, sensors, transmission seal rings, bearing cages, and rubber reinforcements (156). Only relatively small molecules capable of hydrogen bonding, such as water and methanol, give rise to a minor degree of

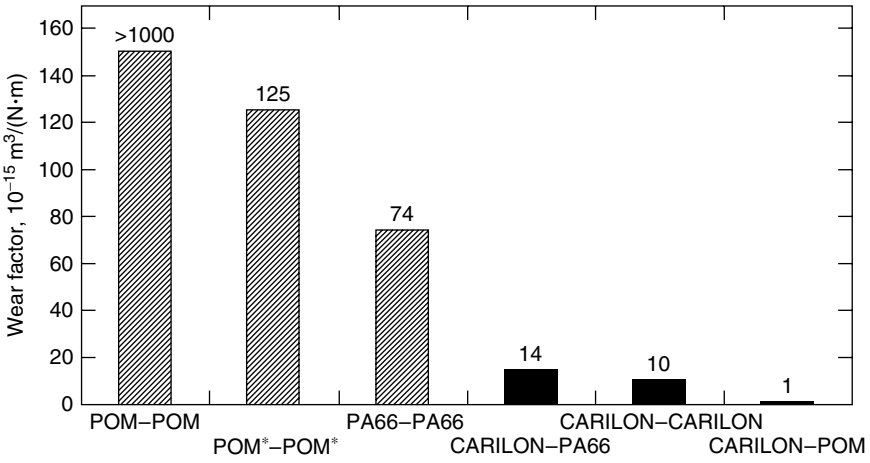

Fig. 7. Wear resistance of like and unlike polymer pairings. POM∗: POM, PTFE-modified.

swelling, exhibiting a plasticizing mechanism. PK-EP-6 is particularly resistant to aqueous media, including weak acids, bases, and salt solutions such as zinc chloride (up to 50%).

Polyketones can be considered for both monolayer and multilayer constructions. The combination of good barrier properties, dimensional stability in the presence of fuel, and high burst pressures affords the possibility of a simple monolayer construction. Should multiple layers be required, an inexpensive two-layer construction based on polyethylene and polyketones has been demonstrated to exhibit good structural strength, barrier performance, and interlayer adhesion, both with and without a tie layer.

Consumer Applications. The excellent wear resistance of aliphatic polyketones is a particularly interesting feature. Field experience has shown that tribological arrangements such as gear trains can become more attractive if at least one of the components is made from aliphatic polyketones (157) (Fig. 7). In plastic arrangements where lubrication is not desired, arrangements with aliphatic polyketones generate low wear and low noise. The wear characteristics of aliphatic polyketones in like polymer pairings is much lower than which would be achieved with polyamide–polyamide or polyacetal–polyacetal arrangements, and this even applies when comparisons are made with specially lubricated PTFE-modified materials.

Aliphatic polyketones are used in power lawn and garden industry because of the good wear resistance, insensitivity to water, chemical resistance, and ease of molding. Other application areas related to the good wear performance are in sports and recreational equipments. Outlets are also found in the medical sector because of the autoclavability, sterilizability, and chemical resistance of aliphatic polyketones. Polyketones are FDA-approved, which is important for food contact applications.

Electrical and Electronic Applications. Flame-retardant aliphatic polyketone compounds are formulated to meet UL-94 V-0 and V-1 classifications,

and offer a good balance between flame resistance, electrical properties, stiffness, toughness, and elongation at break. High tracking resistance is complemented by resistance to electrolytic corrosion, high glow wire temperature, and low smoke density. No corrosive flue gases are produced, and flame retardancy is achieved with mineral flame retardants. Aliphatic polyketone compounds have found outlets in connectors, cable ties, and electromechanical devices.

Industrial Applications. Aliphatic polyketones possess a combination of properties such as chemical resistance, resilience, snapability, tribological properties, and impact performance, that are important for industrial applications. Aliphatic polyketones are able to withstand cleaning processes such as spraying with hot and cold water, blowing with hot air, exposure to hot steam, and exposure to detergents or weak bleaches. Typical areas of application are bottling, cleaning, conveyor belting, pumps or offshore applications, pipe-liner applications, and industrial filters and brushes.

Fiber Applications. Aliphatic polyketones also offer high potential as an anisotropic material (158). The maximum stretch ratio which has been obtained for aliphatic polyketones is 26:1. This has been determined for fibers produced via solution-spinning (159,160), the spin technique allowing the largest degree of disentanglements. The maximum stretch ratio of aliphatic polyketones is higher than that of polyamides and polyesters (respectively 6:1 and 10:1), but lower than that of polypropylene and polyethylene (respectively 48:1 and 300:1) (161). This indicates the ease of stretching and the intrinsic ability of polyketones to obtain a more oriented molecular structure than polyamides and polyesters. Because of the presence of carbonyl groups, the level of secondary molecular interactions on the other hand is stronger than for polyolefins, allowing an oriented molecular structure to be maintained in use, a weakness for polyolefins, as is indicated by the poor creep resistance of polyolefins.

Although PK-EP-6 can be solution-spun with excellent results (162), the most feasible/economic way to produce fibers is via melt-spinning. Melt-spun aliphatic polyketone fibers can be stretched to high ratios, yielding high levels of molecular orientation, and so strong and stiff fibers, as is demonstrated in Figure 8.

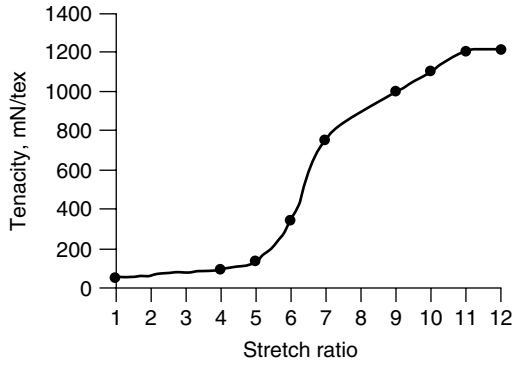

Fig. 8. Tenacity as a function of the stretch ratio of melt-spun aliphatic polyketones (PK-EP-6). To convert mN/tex to g·f/den, multiply by 11.33×10^{-3}.

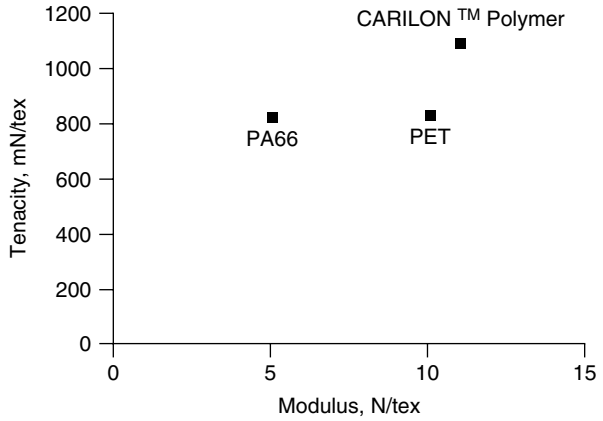

Fig. 9. Balance between tenacity and modulus for different fiber meterials. To convert mN/tex to g·f/den, multiply by 11.33×10^{-3}.

As Figure 9 shows, aliphatic polyketone fibers position well as compared to melt-spun polyamide-66 and poly(ethylene terephthalate) fibers.

The good tensile properties achievable with fibers made from PK-EP-6 make it an obviously attractive material for reinforcement in rubber applications, such as tires, hoses, and belts. In view of the inherent structure of aliphatic polyketones, which is vulnerable to photolytic attack if not adequately protected, direct exposure to sunlight should be limited, which is avoided in the case of rubber reinforcements.

The good chemical and hydrolytic resistance of aliphatic polyketone fibers, which has to be balanced with its thermal oxidative stability, provides them new opportunities as filter material, eg papermaking cloth or fuel filters.

Outlook

The development of aliphatic polyketones adds a new chapter to the history of polymers. These perfectly alternating co- or terpolymers are accessible by the transition-metal-catalyzed polymerization of readily available, cheap feedstocks, CO and olefins. The origin of the remarkable, perfectly alternating nature of the polymers can be found in a subtle interplay between thermodynamic and kinetic factors during catalysis, along with the interaction of the polar polymer chain-end with the electrophilic catalytic metal center. A parallel is noticed between polyketone catalysis and modern olefin polymerization catalyzed by early transition-metal or iron complexes. However, while in the latter, electrophilic activation of just one type of monomer, ie olefins, is involved, polyketone catalysis requires the simultaneous activation of two totally different types of monomers, ie CO and olefins, with different coordination capabilities and reactivity characteristics. It is therefore not surprising that the present, first generation of commercial palladium(II)-based polyketone catalysts show as yet a considerably lower activity than homogeneous polyolefin catalysts. Although the current catalyst activity is sufficiently high to make production of polyketones economically viable,

future catalyst research has to be directed toward the development of more active, more efficient, and (better) recyclable catalytic systems. Most recent research (*vide supra*) has already shown that subtle changes in catalyst structure can afford a huge boost in activity and monomer reactivity ratio, while a first high activity catalyst based on nickel(II) has just been discovered.

As shown, aliphatic polyketones present a broad new class of polymers with a wide range of properties and applications. An important additional asset of these polymers is their ecological friendliness. In production, their direct synthesis from readily available base-chemicals, principally accessible from renewable feedstocks such as ethanol or biomass, overcomes the synthesis of complex monomers, which is often unavoidably accompanied by the generation of significant waste streams, as in the case of other engineering plastics such as polyamides. In use, because of their unique balance of properties and associated wide range of applications, polyketones can play a vital role in the sustainable development of mobility by significant weight reduction of automotive vehicles, as well as by reduction of hydrocarbon emissions from these vehicles by the use of integrated nonhydrocarbon permeable polyketone fuel systems. In addition, polyketones can be recycled and, since they contain only C, H, and O-atoms, are perfectly suited for clean energy production or for recycling back to feedstock, eg by gasification, at the end of their service life.

Aliphatic polyketones are still in an early phase of product development and at present, only terpolymers based on CO, ethene, and propene are in a well-enough advanced state of development for use as engineering thermoplastics. Future research into the structure–performance relationships of co- and terpolymers based on these and other olefinic monomers will lead to a controlled molecular tailoring and designing of polymers with desired properties.

ACKNOWLEDGMENTS

The authors acknowledge the valuable contributions of all those within Shell who have contributed to the development of Carilon Polymer and Carilite. We thank Shell International Chemicals for their permission to publish this paper.

BIBLIOGRAPHY

"Olefin-Carbon Monoxide Polymers" in *EPST* 1st ed., Vol. 9, pp. 397–402, by G. Pieper, Farbenfabriken, AG; "Olefin-Carbon Monoxide Polymers in *EPSE* 2nd ed., Vol. 10, pp. 369–373, by H. Starkweather, E. I. du Pont de Nemours & Co., Inc.

1. A. Sen, *Acc. Chem. Res.* **26**, 303 (1993).
2. E. Drent and P. H. M. Budzelaar, *Chem. Rev.* **96**, 663 (1996).
3. A. Sommazzi and F. Garbassi, *Prog. Polym. Sci.* **22**, 1547 (1997).
4. K. Nozaki and T. Hiyama *J. Organomet. Chem.* **576**, 248 (1998).
5. A. S. Abu-Surrah and B. Rieger, *Top. Catal.* **7**(1–4), 165 (1999).
6. U.S. Pat. 2,577,208 (1951), W. Reppe and A. Magin (to Badische Aniline & Soda-Fabrik Akt. Ges.).
7. Y. Iwashita and M. Sakuraba, *Tetrahedron Lett.* **26**, 2409 (1971).
8. A. Sen and J. S. Brumbaugh, *J. Organometal. Chem.* **279**, C5 (1985).

9. Brit. Pat. Appl. 1,081,304 (1967), A. Gough (to Imperial College Industries).
10. A. Sen and T.-W. Lai, *J. Am. Chem. Soc.* **104**, 3520 (1982).
11. T. W. Lai and A. Sen, *Organometallics* **3**, 866 (1984).
12. Eur. Pat. Appl. 121,965 (Oct. 17, 1984), E. Drent (to Shell Int. Res. Maatsch. B.V.).
13. E. Drent, J. A. M. van Broekhoven, and M. J. Doyle, *J. Organomet. Chem.* **417**, 235 (1991).
14. Z. Jiang and co-workers, *Macromolecules* **25**, 2999 (1992).
15. J. W. Chien, A. X. Zhao, and F. Xu, *Polym. Bull.* **28**, 315 (1992).
16. U. Daum, *Poly-(1-Oxo-Trimethylene) Synthese, Charakterisierung und polymer-analoge Umsetzungen, Ph.D. Thesis, ETH, Zurich*, 1988.
17. U. Klabunde and co-workers, *J. Organomet. Chem.* **334**, 141 (1987).
18. W. Keim, H. Maas, and S. Mecking, *Z. Naturforsch.* **50b**, 430 (1995).
19. M. G. Gardener and co-workers, *J. Organomet. Chem.* **572**, 239 (1999).
20. F. J. Parlevliet and co-workers, *Organometallics* **18**, 3394 (1999).
21. S. Y. Desjardins and co-workers, *J. Organomet. Chem.* **554**, 163 (1997).
22. G. K. Barlow and co-workers, *Organometallics* **19**, 1470 (2000).
23. B. Dömhover and co-workers, *Angew. Chem., Int. Ed. Engl.* **37**, 3050 (1998).
24. S. Doherty and co-workers, *Organometallics* **18**, 3558 (1999).
25. W. Keim and H. Maas, *J. Organomet. Chem.* **514**, 271 (1996).
26. E. Lindner and co-workers, *Inorg. Chim. Acta* **103**, 296 (1999).
27. C. Bianchini and co-workers, *New. J. Chem.* **23**, 929 (1999).
28. Eur. Pat. Appl. 181,014 (May 14, 1986), E. Drent (to Shell Int. Res. Maatsch. B.V.).
29. Eur. Pat. Appl. 322,018 (June 28, 1989), E. Drent and R. L. Wife (to Shell Int. Res. Maatsch. B.V.).
30. Eur. Pat. Appl. 376,364 (July 4, 1990), J. A. Van Doorn, P. K. Wong, and O. Sudmeijer (to Shell Int. Res. Maatsch. B.V.).
31. Eur. Pat. Appl. 384,517 (Aug. 29, 1990), P. K. Wong (to Shell Int. Res. Maatsch. B.V.).
32. Eur. Pat. Appl. 393,790 (Oct. 24, 1990), P. W. N. M Van Leeuwen, C. F. Roobeek, and P. K. Wong (to Shell Int. Res. Maatsch. B.V.).
33. A. Batistini, G. Consiglio, and U. W. Suter, *Angew. Chem., Int. Ed. Engl.* **31**, 303 (1992).
34. M. Barsacchi and co-workers, *Macromolecules* **25**, 3604 (1992).
35. A. S. Abu-Surrah and co-workers, *Macromolecules* **29**, 4806 (1996).
36. Eur. Pat. Appl. 272,727 (June 29, 1988), E. Drent (to Shell Int. Res. Maatsch. B.V.).
37. Eur. Pat. Appl. 463,689 (Jan. 2, 1992), E. Drent (to Shell Int. Res. Maatsch. B.V.).
38. J. T. Lee and H. Alper, *Chem. Commun.* 2189 (2000).
39. Eur. Pat. Appl. 229,408 (July 22, 1987), E. Drent (to Shell Int. Res. Maatsch. B.V.).
40. Eur. Pat. Appl. 235,865 (Sept. 9, 1987), J. A. M. van Broekhoven and E. Drent (to Shell Int. Res. Maatsch. B.V.).
41. M. Barsacchi and co-workers, *Angew. Chem., Int. Ed. Engl.* **30**, 989 (1991).
42. Eur. Pat. Appl. 486,103 (May 20, 1992), A. W. de Jong and J. J. Keijsper (to Shell Int. Res. Maatsch. B.V.).
43. M. Brookhart and co-workers, *J. Am. Chem. Soc.* **116**, 3641 (1994).
44. S. Bartolini, C. Carfagna, and A. Musco, *Macromol. Rapid Commun.* **16**, 9 (1995).
45. K. Nozaki and co-workers, *J. Am. Chem. Soc.* **119**, 12779 (1997).
46. A. Aeby, A. Gsponer, and G. Consiglio, *J. Am. Chem. Soc.* **120**, 11000 (1998).
47. R. Koster and R. H. Birk, *Polym. Prepr.* **37**, 525 (1996).

48. Neth. Pat. Appl. 88 01168 (Dec. 1, 1989), E. Drent (to Shell Int. Res. Maatsch. B.V.).
49. Eur. Pat. Appl. 504,985 (Sept. 23, 1992), E. Drent (to Shell Int. Res. Maatsch. B.V.).
50. S. L. Borkowsky and R. W. Waymouth, *Macromolecules* **29**, 6377 (1996).
51. K. Nozaki and co-workers, *Bull. Chem. Soc. Jpn.* **69**, 2043 (1997).
52. S. Kacker and A. Sen, *J. Am. Chem. Soc.* **119**, 10028 (1997).
53. K. Osahada, J.-C. Choi, and T. Yamamoto, *J. Am. Chem. Soc.* **119**, 12390 (1997).
54. Z. Jiang and A. Sen, *J. Am. Chem. Soc.* **117**, 4455 (1995).
55. M. D. E. Forbes and co-workers, *J. Am. Chem. Soc.* **117**, 3946 (1995).
56. Eur. Pat. Appl. 213,671 (Mar. 11, 1987), J. A. M. van Broekhoven, E. Drent, and E. Klei (to Shell Int. Res. Maatsch. B.V.).
57. A. A. Smaardyh and co-workers, *Internal Shell reports*, 1998, 1999.
58. A. S. Abu-Surrah and co-workers, *Macromol. Rapid Commun.* **17**, 559 (1996).
59. A. S. Abu-Surrah, R. Wursche, and B. Rieger, *Macromol. Chem. Phys.* **198**, 1197 (1997).
60. U.S. Pat. 4,970,294 (1990), E. Drent and R. L. Wife (to Shell Oil Co.).
61. Eur. Pat. Appl. 404,228 (Dec. 27, 1990), P. K. Wong (to Shell Int. Res. Maatsch. B.V.).
62. A. Sen and Z. Jiang, *Macromolecules* **26**, 911 (1993).
63. D.-J. Liaw, J.-S. Tsai, and B.-F. Lay, *Polym. J.* **28**, 806 (1996).
64. A. Aeby and G. Consiglio, *Helv. Chim. Acta* **81**, 35 (1998).
65. Z. Jiang and A. Sen, *Macromolecules* **27**, 2694 (1994).
66. K. Nozaki, N. Sato, and H. Takaya, *J. Am. Chem. Soc.* **117**, 9911 (1995).
67. M. Brookhart and co-workers, *J. Am. Chem. Soc.* **118**, 3641 (1994).
68. M. Brookhart and co-workers, *J. Am. Chem. Soc.* **114**, 5894 (1992).
69. A. Batistini and G. Consiglio, *Organometallics* **11**, 1766 (1992).
70. P. K. Wong and co-workers, *Ind. Eng. Chem. Res.* **32**, 986 (1993).
71. P. W. N. M. van Leeuwen, C. F. Roobeek, and H. van der Heijden, *J. Am. Chem. Soc.* **116**, 12117 (1994).
72. V. Busico and co-workers, *Makromol. Chem., Rapid Commun.* **14**, 261 (1993).
73. B. Milani and co-workers, *Organometallics* **16**, 5064 (1997).
74. B. Milani and co-workers, *Organometallics* **19**, 3435 (2000).
75. Z. Jiang and A. Sen, *Macromolecules* **27**, 7215 (1994).
76. G. Verspui, F. Schanssema, and R. A. Sheldon, *Chem. Commun.* 401 (1998).
77. G. Verspui, G. Papadogianakis, and R. A. Sheldon, *Angew. Chem., Int. Ed. Engl.* **39**, 804 (2000).
78. C. Bianchini and co-workers, *Macromolecules* **32**, 3859 (1999).
79. PCT Int. Appl. WO 0068296 (published: Nov. 16, 2000), A. A. Broekhuis and co-workers (to Shell Int. Res. Maatsch. B.V.).
80. Eur. Pat. Appl. 590,942 (Apr. 6, 1994), J. H. Brophy, N. A. Cooley, and M. J. Green (to BP Chem. Ltd.).
81. Y. Koide, S. G. Bott, and A. R. Barron, *Organometallics* **15**, 2213 (1996).
82. W. P. Mul and co-workers, *Angew. Chem., Int. Ed. Engl.* **39**, 1848 (2000).
83. Eur. Pat. Appl. 248,483 (Dec. 9, 1987), M. J. Doyle and co-workers (to Shell Int. Res. Maatsch. B.V.).
84. Eur. Pat. Appl. 501,576 (Sept. 2, 1992), E. Drent and J. J. Keijsper (to Shell Int. Res. Maatsch. B.V.).
85. Ger. Pat. 863,711 (Aug. 27, 1941), F. Ballauf, O. Bayer, and L. Leichman (to Farbenfabriken Bayer AG).
86. U.S. Pat. 2,495,286 (Jan. 24, 1950), M. M. Brubaker (to E. I. du Pont de Nemours & Co., Inc.).
87. M. M. Brubaker, D. D. Coffman, and H. H. Hoehn, *J. Am. Chem. Soc.* **74**, 1509 (1952).

88. Eur. Pat. Appl. 632,084 (Jan. 4, 1995), E. Drent and D. Pello (to Shell Int. Res. Maatsch. B.V.).
89. Eur. Pat. Appl. 522635 (Jan. 13, 1993), E. Drent and J. J. Keijsper (to Shell Int. Res. Maatsch. B.V.).
90. Eur. Pat. Appl. 257663 (Mar. 2, 1988), J. A. M. van Broekhoven, and R. L. Wife (to Shell Int. Res. Maatsch. B.V.).
91. D. Fatutto, L. Tonolio, and R. V. Chaudhari, *Catal. Today* **48**, 49 (1999).
92. Eur. Pat. Appl. 300,583 (Jan. 25, 1989), J. A. van Doorn and co-workers (to Shell Int. Res. Maatsch. B.V.).
93. Eur. Pat. Appl. 454,270 (Oct. 30, 1991), J. J. Keijsper and A. W. van der Made (to Shell Int. Res. Maatsch. B.V.).
94. Eur. Pat. Appl. 743,336 (Nov. 20, 1996), F. Baardman and co-workers (to Shell Int. Res. Maatsch. B.V.).
95. Int. PCT Pat. Appl. WO 00/08030 (Feb. 17, 2000), W. Eilenberg and co-workers (to Shell Int. Res. Maatsch. B.V.).
96. Int. PCT Pat. Appl. WO 00/09583 (Feb. 24, 2000), J.-K. Buijink, E. Drent, and J. C. Suykerbuyk (to Shell Int. Res. Maatsch. B.V.).
97. Int. PCT Pat. Appl. WO 00/09584 (Feb. 24, 2000), J.-K. Buijink, E. Drent, and J. C. Suykerbuyk (to Shell Int. Res. Maatsch. B.V.).
98. G. P. C. M. Dekker and co-workers, *J. Organomet. Chem.* **430**, 357 (1992).
99. R. van Asselt and co-workers, *J. Am. Chem. Soc.* **116**, 977 (1994).
100. B. A. Markies and co-workers, *J. Am. Chem. Soc.* **117**, 5263 (1995).
101. J.-T. Chen and A. Sen, *J. Am. Chem. Soc.* **106**, 1506 (1984).
102. A. Sen, and co-workers, *J. Am. Chem. Soc.* **109**, 148 (1987).
103. G. P. C. M. Dekker and co-workers, *Organometallics* **11**, 1598 (1992).
104. F. C. Rix, M. Brookhart, and P. S. White, *J. Am. Chem. Soc.* **118**, 4746 (1996).
105. C. S. Shultz and co-workers, *J. Am. Chem. Soc.* **122**, 6351 (2000).
106. K. Vrieze and co-workers, *New. J. Chem.* **21**, 807 (1997).
107. P. Margl and T. Ziegler, *J. Am. Chem. Soc.* **118**, 7337 (1996).
108. P. Margl and T. Ziegler, *Organometallics* **15**, 5519 (1996).
109. M. Svensson, T. Matsubara, and K. Morakuma, *Organometallics* **15**, 5568 (1996).
110. K. E. Frankcombe and co-workers, *Organometallics* **16**, 3199 (1997).
111. F. Ozawa and co-workers, *J. C. S. Chem. Commun.* 1469 (1991).
112. C. Carfagna and co-workers, *Chem. Commun.* 1113 (1998).
113. M. A. Zuideveld and co-workers, *J. Am. Chem. Soc.* **120**, 7977 (1998).
114. G. J. P. Britovsek and co-workers, *J. C. S. Chem. Commun.* 1632 (1993).
115. W. P. Mul, E. Drent, P. J. Jansens, A. H. Kramer, and M. H. W. Sonnemans, *J. Am. Chem. Soc.* **123**, 5350–5351 (2001).
116. P. J. Jansens, and F. H. Geuzebroek, *internal Shell report*, 1996.
117. G. Odian, *Principles of Polymerization*, 3rd ed., John Wiley & Sons, Inc., New York, 1991, p. 385.
118. P. J. Flory, *Principles of Polymer Chemistry*, Cornell University Press, Ithaca, N.Y., 1953, Chapts. "3, 8, and 9".
119. T. Keii and co-workers, *Makromol. Chem.* **185**, 1537 (1984).
120. J. G. Bonner and A. K. Powell, *Polym. Mater. Sci. Eng.* **76**, 108 (1997).
121. *European Chemicals News* 25–31 (Oct. 1999).
122. C. E. Ash, *J. Mater. Educ.* **16**, 1 (1994).
123. R. L. Danforth, J. M. Machado, and J. C. M. Jordaan, in *Proc. of the 1995 ANTEC Conf.*, Boston, May 7–11, 1995, Vol. II, p. 2316.
124. B. J. Lommerts, E. A. Klop, and J. Aerts, *J. Polym. Sci., Part B: Polym. Phys.* **31**, 1319 (1993).

125. E. A. Klop and co-workers, *J. Polym. Sci., Part B: Polym. Phys.* **33**, 315 (1995).
126. B. J. Lommerts, *Structure development in polyketone and polyalcohol fibers, Ph.D. Dissertation*, University of Groningen, 1994.
127. J. M. Lagaron and co-workers, *Polymer* **41**, 3011 (2000).
128. J. M. Lagaron, A. K. Powell, and N. S. Davidson, *Macromolecules* **33**, 1030 (2000).
129. M. A. del Nobile and co-workers, *J. Appl. Polym. Sci.* **50**, 1261 (1993).
130. D. H. Weinkauf, P. A. Kinneberg, and C. A. Ash, in *Proc. of the 1995 ANTEC Conf.*, Boston.
131. A. Wakker, H. G. Kormelink, P. Verbeke, and J. C. M. Jordaan, *Plast. Eur. Kunststoffe*, Sept. 1995, p. 110.
132. U.S. Pat. 5,952,459 (Sept. 14, 1999), A. A. Broekhuis and J. Freriks (to Shell Oil Co.)
133. B. T. A. Chang and co-workers, in *49th Proc. of the Electron. Compon. Technol. Conf.*, 1999, pp. 49–55.
134. Eur. Pat. Appl. 181,014 (May 14, 1986), E. Drent (to Shell Int. Res. Maatsch. B.V.).
135. Eur. Pat. Appl. 345,847 (Dec. 13, 1989), J. A. van Doorn and E. Drent (to Shell Int. Res. Maatsch. B.V.).
136. S. Kacker, J. A. Sissano, and D. N. Schultz, *J. Polym. Sci., Part A: Polym. Chem.* **38**, 752 (2000).
137. Eur. Pat. Appl. 468,594 (Jan. 29, 1991), E. Drent, H. P. M. Tomassen, and M. J. Reynhout (to Shell Int. Res. Maatsch. B.V.).
138. Eur. Pat. Appl. 479,353 (Apr. 8, 1991), M. J. Reynhout, H. P. M. Tomassen, and D. Bodt (to Shell Int. Res. Maatsch. B.V.).
139. Eur. Pat. Appl. 482,686 (Apr. 29, 1992). (1991), J. F. H. Braams and M. J. Reynhout (to Shell Int. Res. Maatsch. B.V.).
140. S. Shkolnik and E. D. Weil, *J. Appl. Pol. Sci.* **69**, 1691 (1998).
141. O. Chiantore and co-workers, *Macromolecules* **30**, 2589 (1997).
142. G. Conti and A. Sommazzi, *J. Mol. Struct.* **294**, 275 (1993).
143. J. C. W. Chien and A. X. Zhao, *Polym. Degrad. Stab.* **40**, 257 (1993).
144. S. De Vito and co-workers, *Polym. Int.* **353**, 45 (1998).
145. J. M. Machado, M. Londa, P. Verbeke, and W. P. Gergen, in *Proc. of the 1995 ANTEC Conf.*, Boston, May 7–11, 1995, Vol. II, p. 2335.
146. C. A. Ash, D. G. Waters, and A. A. Smaardijk, in *Proc. of the 1995 ANTEC Conf.*, Boston, May 7–11, 1995, Vol. II, p. 2319.
147. Eur. Pat. Appl. 600,554 (June 8, 1993), J. C. M. Jordaan and co-workers (to Shell Int. Res. Maatsch. B.V.).
148. U.S. Pat. 5,122,564 (June 16, 1992), E. R. George (to Shell Oil Co.).
149. Eur. Pat. Appl. 478088 (Apr. 1, 1992), E. R. George and co-workers (to Shell Int. Res. Maatsch. B.V.).
150. U.S. Pat. 5,082,885 (Jan. 21, 1992), R. Q. Kluttz and J. L. M. Syrier (to Shell Oil Co.).
151. F. Y. Xu and J. C. W. Chien, *Macromolecules* **26**, 3485 (1993).
152. Int. PCT Pat. Appl. WO 9633237 (Oct. 24, 1996), C. E. Ash and D. G. Waters (to Shell Int. Res. Maatsch. B.V.).
153. Int. PCT Pat. Appl. WO 9633236 (Oct. 24, 1996), C. E. Ash, D. G. Waters, and D. H. Weinkauf (to Shell Int. Res. Maatsch. B.V.).
154. R. P. Gingrich, J. M. Machado, M. Londa, and M. G. Proctor, in *Proc. of the 1995 ANTEC Conf.*, Boston, May 7–11, 1995, Vol. II, p. 2345.
155. M. Londa, R. P. Gingrich, H. G. Kormelink and M. G. Proctor, in *Proc. of the 1995 ANTEC Conf.*, Boston, May 7–11, 1995, Vol. II, p. 2351.
156. J. A. Grande, in *Modern Plastics*, Jan. 1998, p. 40.
157. J. W. Kelly, D. R. Roane, and D. M. Le, in *Proc. of the 1995 ANTEC Conf.*, Boston, May 7–11, 1995, Vol. III, p. 3819.
158. H. G. Kormelink, M. Vlug, and J. E. Flood, *Chem. Fibers Int.* **49**, 208 (1999).

159. Eur. Pat. Appl. 360,358 (Mar. 28, 1990), A. W. van Breen, J. H. van Deursen, and F. I. M. Wetser (to Shell Int. Res. Maatsch. B.V.).
160. Eur. Pat. Appl. 456,306 (Nov. 13, 1991), B. J. Lommerts and co-workers (to Akzo N.V.).
161. J. Smook, G. J. H. Vos, and H. L. Doppert, *J. Appl. Polym. Sci.* **41**, 105 (1990).
162. Eur. Pat. Appl. 310,171 (Apr. 5, 1989), J. M. Beyen and co-workers (to Shell Int. Res. Maatsch. B.V.).

E. DRENT
W. P. MUL
A. A. SMAARDIJK
Shell International Chemicals B.V.

POLYMETHACRYLATES. See METHACRYLIC ESTER POLYMERS.

POLYNUCLEOTIDES

Introduction

Hereditary information is stored within the nucleic acids DNA and RNA. Natural nucleic acids are polymeric, consisting of monomers known as nucleotides, and hence the term "polynucleotide" can be used to refer to DNA and RNA. Information is encoded within the sequence of nucleotides in these polymers as specific tracts defined as genes. The information is passed on to progeny by replication and converted into protein products by *transcription*/*translation* (a process known as gene expression). While considerable progress in understanding the biological role of nucleic acids was made in the first half of the twentieth century, it was the proposal of the double-helical structure for DNA in 1953 (1) that allowed researchers to begin probing, mimicking, and manipulating the nucleic acids at the molecular level (2). The importance of this cannot be overstated: virtually all advances in molecular biology and biotechnology rest on the foundations of nucleic acid chemistry and biology.

This article describes the structural and functional properties of the polynucleotides, DNA and RNA., beginning with a description of how these polymers are synthesized through enzymatic catalysis or by stepwise, solid-supported chemical methods. Next, the structural features of DNA and RNA are described, followed by the most commonly used methods for studying the properties of polynucleotides.

A variety of synthetic polynucleotide analogues are presented next. Once the DNA structure and base-pairing rules were identified, synthetic chemists could begin preparing unnatural analogues. These compounds are important for testing various theories regarding the relationship between the primary structures of DNA/RNA and their tendency to fold into specific three-dimensional structures.

Encyclopedia of Polymer Science and Technology. Copyright John Wiley & Sons, Inc. All rights reserved.

In addition, synthetic analogues are finding increasing utility as diagnostic probes and therapeutic agents.

Next strategies for sequence-specific recognition of polynucleotides are described. Preservation and processing of the genetic information *in vivo* requires sequence-specific recognition of DNA and RNA by proteins and other nucleic acids. Unraveling biological mechanisms for recognition has led to several classes of compounds that can be designed to bind to most, if not all, sequences of DNA and RNA. The most successful of these compounds are themselves oligomeric or polymeric, reflecting the need for relatively large molecular structures to interact sequence specifically with polynucleotides.

The penultimate section of this article presents one of the truly paradigm-shifting discoveries of the late twentieth century: the demonstration that RNA could act as an enzyme, catalyzing a variety of chemical reactions. The extension of this work to the *in vitro* evolution of sequences with unique catalytic and binding properties represents the introduction of the nucleic acids into what was once thought to be the exclusive realm of proteins.

Finally, the article concludes with a description of how polynucleotides are finding applications in materials sciences. In particular, the sequence-specific molecular recognition mechanisms that define precise, relatively rigid three-dimensional structures have led materials scientists to adopt polynucleotides as construction materials for the noncovalent synthesis of intricate, ordered structures. Thus, the very molecules that fueled the biotechnological revolution are now being incorporated into the foundation of the next revolution, namely nanoscience and nanotechnology.

The following sections describe in fairly general terms the chemistry, biology, and physics of DNA, RNA, and their synthetic analogues. Key references to books, review articles, and the primary literature are provided to permit the interested reader to find more detailed descriptions of the various topics.

Polynucleotide Structure

The most widely recognized secondary structure for a biopolymer is the DNA double helix. However, DNA is capable of forming a variety of nonduplex secondary structures either transiently or at equilibrium. Moreover, the structural landscape available to RNA is vast, because RNA normally exists in the absence of a complementary strand. This allows RNA to fold into complex three-dimensional shapes, analogous to proteins, and exhibit many diverse functions. This section reviews the primary, secondary, and tertiary structures adopted by polynucleotides.

Primary Structure. The primary structure of DNA differs from RNA only in the absence of the 2′-OH group and the replacement of the uracil nucleobase with thymidine (Fig. 1). The monomer itself comprises a phosphate group, a ribose or deoxyribose sugar ring, and a nucleobase. Each of these components is important for the formation of the most common of DNA and RNA structures, the right-handed double helix. DNA and RNA polymers are polyelectrolytes by virtue of the anionic phosphate groups positioned at regular intervals along the phosphodiester backbone. These charges introduce to the polynucleotides intra- and interstrand electrostatic repulsive forces that affect the thermodynamic stabilities of various secondary and tertiary structures. Meanwhile, the backbone sugar rings

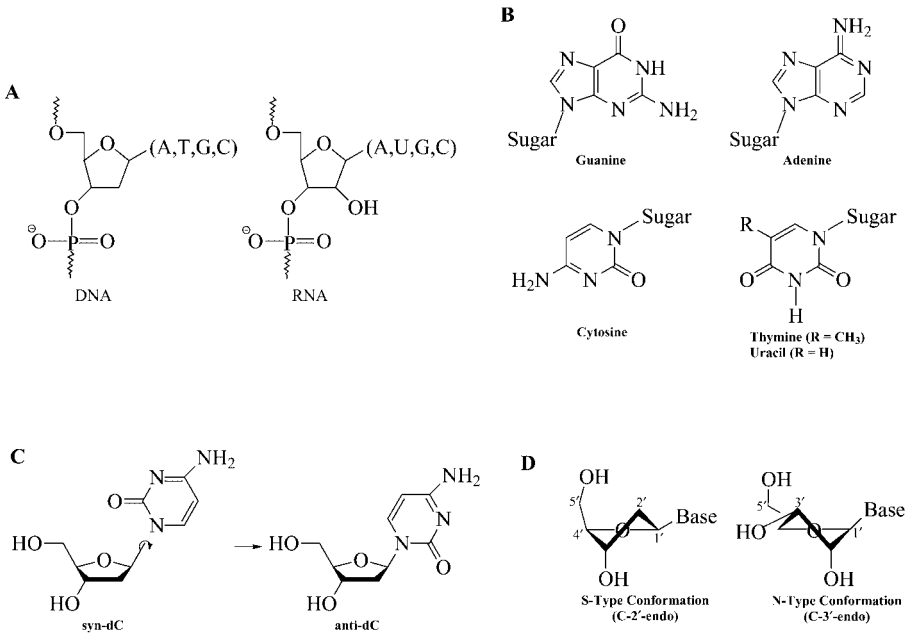

Fig. 1. Elements of DNA/RNA primary structure. (**A**) backbone units, (**B**) nucleobase structures, (**C**) glycosidic bond rotation interconverts syn and anti conformations, and (**D**) preferred sugar puckers for deoxyribose (left) and ribose (right).

can adopt two limiting conformations, the C3′-endo and the C2′-endo, that influence the orientation of the backbone and the base (Fig. 1). Also, the orientation of the nucleobase relative to the sugar ring (ie syn or anti) is variable but crucial to secondary structure formation (Fig. 1) (3,4).

The primary structure of oligonucleotides can be written using the notation 5′-dpApGpTpC-3′. The 5′ refers to the position of the exocyclic methylene carbon of the DNA backbone (Fig. 1). The "d" denotes that the sugar rings are deoxyribose; in the case of RNA the "d" will not be present. The "p" refers to the locations of the phosphate groups that create phosphodiester linkages to the 5′ and/or the 3′ sugar carbons of the adjacent monomers, and A, G, T, and C are abbreviations for adenosine, guanosine, thymidine, and cytidine respectively (U = uridine in RNA). In addition to the standard nucleobases, a variety of modified nucleobases are found in RNA, particularly transfer RNA. These modifications are introduced post-transcriptionally by enzymes.

Secondary Structure.

The Double Helix. The most common secondary structure formed by DNA and RNA is the double-stranded helix (1). The double helix places the negatively charged phosphate groups on the periphery where they are exposed to water, while the bases are π stacked in the interior with the nucleobases forming interstrand pairs through hydrogen-bonding interactions (Fig. 2) (5). Wrapping of the two strands around one another creates two concave surfaces, referred to as the *minor and major grooves*. The edges of the base pairs form the floors of the grooves, while the sugar rings and phosphate groups comprise the walls of the grooves.

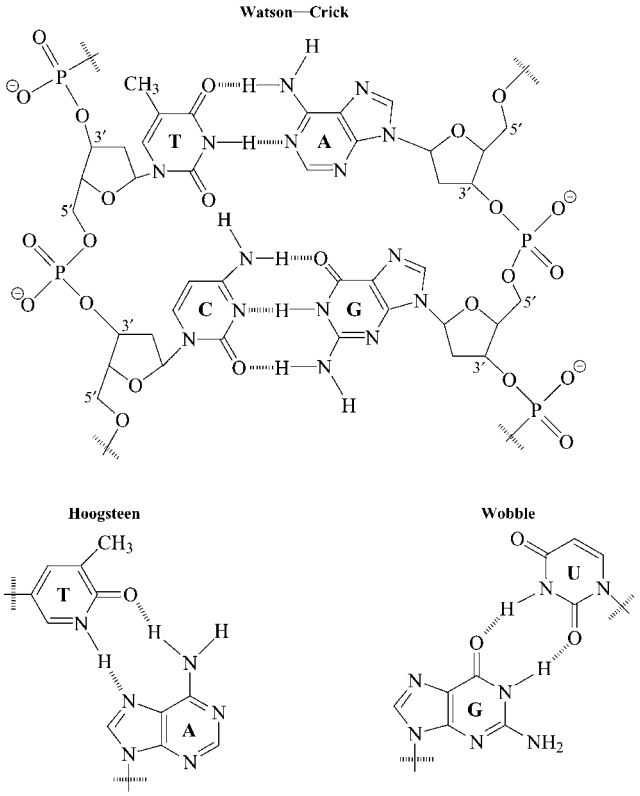

Fig. 2. Hydrogen-bonding patterns in polynucleotides, including Watson–Crick pairing characteristic of duplex DNA and RNA (top); Hoogsteen pairing formed in triplex structures (bottom left); and wobble pairing often found in RNA (bottom right).

The canonical Watson–Crick base pairs utilize NH and NH_2 groups of the nucleobases as hydrogen bond donors, while the electron pairs of carbonyl carbons and ring nitrogens serve as hydrogen bond acceptors (Fig. 2). The recognition of the purine bases (A and G) by the pyrimidine bases (T and C) establishes the fidelity of DNA transcription. Non-Watson–Crick base pairs have been observed, the most important of which are the Hoogsteen pairs and the "wobble" pairs (Fig. 2). These noncanonical base pairs give rise to triplex structures, and also allow for the considerable variations from the standard duplex form observed in many DNA and RNA sequences.

Given the conformational flexibility of the monomer units, it is no surprise that the double helical secondary structure can actually be subdivided into families of structurally distinct polymorphs (see Table 1 for helix parameters) (6). DNA double helices most commonly adopt the B-form, while A-form helices are the most common RNA secondary structures. These helices have a right-handed helix sense and utilize the Watson–Crick base pairing mentioned above (Fig. 3). In addition, both the A- and B-form orient the glycosidic bond in the anti conformation. A major difference between the A- and B-form structures is the positioning of the base pairs relative to the helix axis. In B-DNA the base pairs are centered

Table 1. Helix Parameters

Parameter	A-Form DNA	B-Form DNA	Z-Form DNA	A-Form RNA
Helix twist	Right	Right	Left	Right
Residues per turn	11	10.5	11.6	11
Helix diameter, nm	2.3	2.0	1.8	–
Sugar pucker	C3′-endo	C2′-endo	C2′-endo	C3′-endo
Glycosidic bond orientation	anti	anti	anti (A, T, C), syn (G)	anti
Displacement of bp from axis, nm	0.45	−0.002 to −0.18	−0.2 to −0.3	0.44
Major groove	Narrow, deep	Wide, deep	Flat, very shallow	1
Minor groove	Wide, shallow	Narrow, deep	Narrow, very deep	1

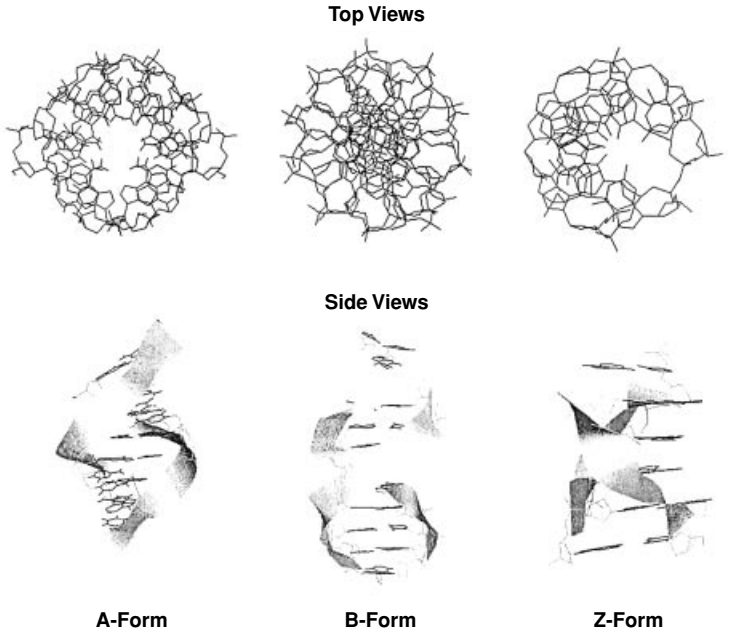

Fig. 3. Top and side views of three DNA double-helical conformations. In the side views, the base pairs are shown in black and ribbons are traced along the DNA backbones to illustrate the helicity.

on the helix axis and lie roughly perpendicular to the axis. In A-DNA the base pairs are shifted toward the minor groove by 0.45 nm and are tilted, leading to a deep and narrow major groove, but a shallow and wide minor groove relative to B-DNA (3,4). When viewed from the above, this leads to a "filled" cylinder for B-DNA, but an open channel running through A-DNA (Fig. 3).

Z-DNA is a left-handed double-stranded helix (Fig. 3) favored by high concentrations of NaCl or $MgCl_2$ and alternating G–C sequences. Z-DNA is less tightly wound (11.6 vs 10.5 base pairs per helical turn) and therefore forms a narrower helix than B-DNA. Z-DNA has a characteristic zigzag appearance to its backbone,

which arises from alternation between the syn and anti conformations of the guanine and cytosine bases respectively. This leads to a major groove that is extremely shallow (almost flat) and a minor groove that is very deep (7). Although B-form DNA is most common *in vivo*, the existence of Z-form DNA *in vivo* has led to intensive studies of its potential biological role (8).

The A-, B-, and Z-form helices are model helices that do not fully represent the range of helical structures observed by nmr and x-ray analysis of DNA and RNA. Each base sequence can have its own structure that will influence the curvature, rigidity, and even the groove widths and depths. While the degree to which the local structure of double-helical DNA varies with sequence has been recently questioned (9), extreme cases such as the highly curved structures of oligo(dA)–oligo(T) sequences are well-established (3,4). Moreover, biologically relevant properties such as hydration, flexibility, and the positioning of hydrogen-bond donor and acceptor groups in the two grooves are clearly sequence-dependent.

Triplexes and Beyond. Watson–Crick base pairing leaves hydrogen-bond donor and acceptor groups exposed in the major groove of B-form DNA. Oligonucleotides can bind within the major groove of B-form DNA to form triple-helical complexes stabilized by Hoogsteen hydrogen bonding (Fig. 2). These structures form most readily at homopurine–homopyrimidine sequences, using either homopurine or homopyrimidine third strands (10–12). Although most studies have utilized a separate third strand to form the triplex, certain sequences of duplex DNA can form triplexes by folding back of one strand into the major groove of the duplex at a remote site, leaving its partner strand unpaired. This structure, referred to as "H-DNA," (13) has not yet been identified *in vivo*, although speculation has focused on its possible involvement during genome replication.

Tetrahelical structures of DNA can also form from guanine-rich sequences (14). These structures are stabilized by G-tetrads formed via Hoogsteen hydrogen bonding of four guanines in a roughly square orientation (Fig. 4). Adjacent tetrads stack on top of one another, but with a potassium or magnesium cation sandwiched in between. Quadruplexes can form from four separate strands, two separate strands, or from the intramolecular folding of a single strand. It is postulated that G-quadruplexes are formed in the single-stranded extensions of chromosomes

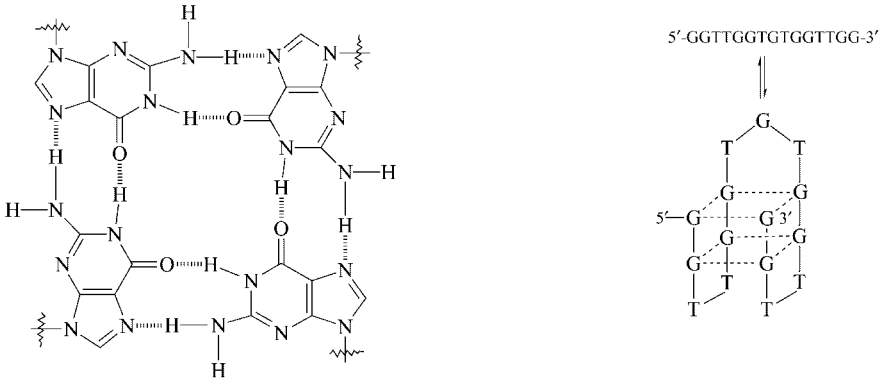

Fig. 4. Hydrogen bonding pattern in guanine (G)-tetrads (left) and intramolecular folding of a 15-base DNA sequence into a G-quadruplex motif (right).

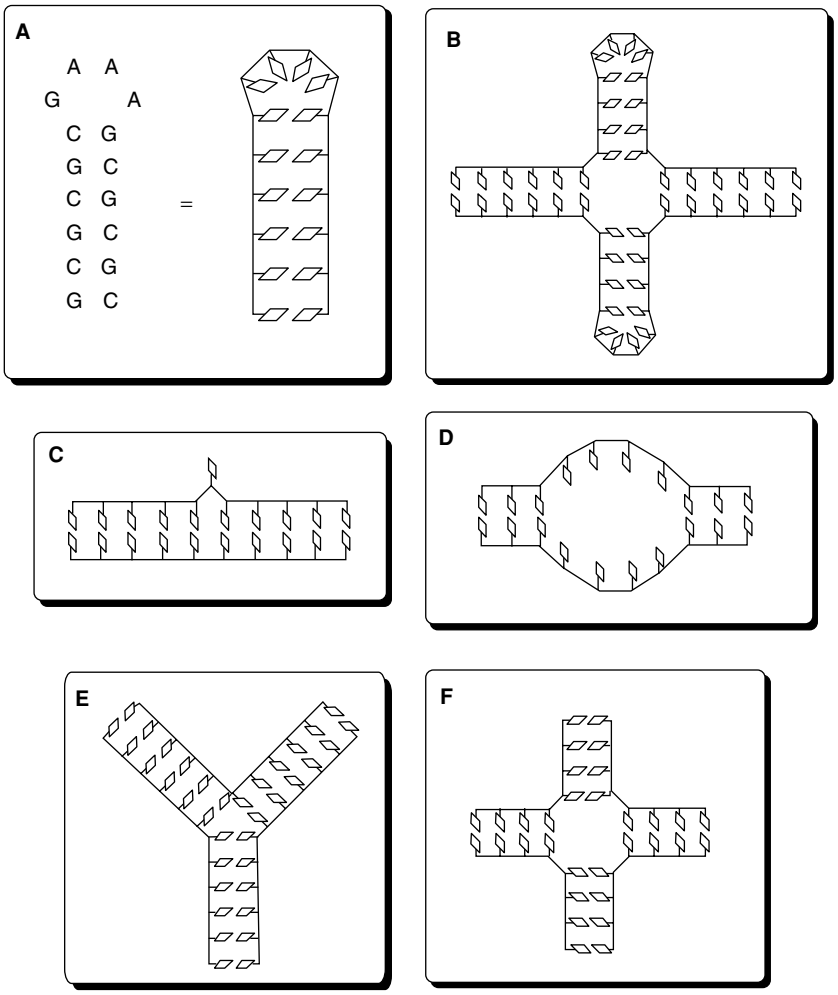

Fig. 5. Nonduplex polynucleotide secondary structures: hairpin (**A**), cruciform (**B**), bulge (**C**), bubble (**D**), three-way junction (**E**), and four-way junction (**F**).

known as telomeres. Telomeric DNA consists of thousands of repeats of a G-rich sequence that can form G-quadruplexes. Telomeric repeats are lost over the life cycle of somatic cells, and when the telomere becomes suitably short, cell death is triggered. This loss of repeats is compensated for by the enzyme telomerase, which extends the telomeres and therefore cell life. Telomerase activity has been observed in over 80% of all tumor types, suggesting a link with cell immortalization and tumorigenesis and spurring intense study of the G-quadruplex as a specific target for antitumor drugs (10).

Other Oligonucleotide Structures. DNA and RNA sequences can form many nonduplex secondary structures (Fig. 5). For example, bulges are formed when one or more unpaired bases are present within one strand of an otherwise base-paired structure. Unpaired bases present on both strands at a given

position are referred to as *bubbles*. Whether these non-hydrogen-bonded bases are stacked within the helix or flipped out toward the aqueous solvent is highly sequence-dependent. Bulges have been implicated in protein/RNA recognition and are sometimes necessary for the tertiary folding of catalytic RNAs (15,16).

Hairpins can form when there are complementary sequences within the same strand but separated by a noncomplementary region, such as the sequence 5′-CGCGCGCGAAAGCGCGCG-3′ where the central GAAA forms the loop and the underlined bases at the termini form the stem (Fig. 5). If a hairpin is formed within the context of double-stranded DNA, the complementary strand can also fold into a hairpin, yielding a cruciform structure, or remain unpaired. Such structures likely serve as binding sites for proteins. Furthermore, the hairpin motif is one of the most common secondary structure elements observed in RNA (17).

With appropriately designed sequences, three-way and four-way junctions can form (Fig. 5) (15). The four-way junction is particularly noteworthy, as it constitutes the key intermediate in homologous recombination, where the two chromosomes within a given pair mix with one another (18,19). Four-way junctions formed from synthetic oligonucleotides have provided useful models for these intermediates and have been used as design elements in nanoconstruction (*vide infra*).

Tertiary Structure. Unlike DNA, an RNA molecule normally exists *in vivo* in the absence of its complementary strand. This allows RNA to fold into a plethora of sequence-dependent three-dimensional structures. The secondary structures are based on loops, bulges, and helices, but many of these elements can bend, turn, and fold upon themselves, allowing for tertiary interactions to occur between unpaired hydrogen-bonding sites. For example, two complementary loop sequences can hybridize with one another to form a short Watson–Crick duplex that stabilizes an entropically unfavorable conformational restriction (Fig. 6). However, two secondary structure elements need not recognize one another through Watson–Crick base pairing. Certain loop sequences will bind tightly to helical regions in a sequence-specific manner. In many cases, these tertiary interactions are stabilized by hydrogen bonding involving the 2′-OH group from the ribose ring, a feature that is missing from a corresponding DNA polynucleotide (20). These long-distance (relative to the primary structure) interactions allow for many three-dimensional shapes to be formed (21,22). This leads to an almost endless variety of structure in DNAs and RNAs that allows for the specific recognition of biological macromolecules, and even reaction catalysis.

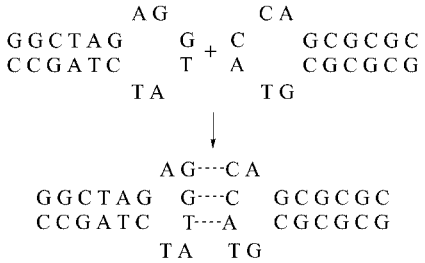

Fig. 6. Tertiary interaction between two complementary loops forms a "kissing complex" through Watson–Crick base pairing.

Methods for Characterizing Polynucleotides

A wide variety of techniques are commonly used to characterize DNA and RNA. Perhaps the most useful is gel electrophoresis, which takes advantage of the fact that these compounds are polyelectrolytes (23). In electrophoresis, nucleic acid molecules are separated on the basis of length by migration through a polymer gel under the influence of an electric field, with longer molecules migrating more slowly through the gel. The gel is most commonly composed of agarose, a natural polysaccharide, or cross-linked polyacrylamide. By increasing the percentage of acrylamide monomer and the number of cross-links in the gel, greater resolution of polymer lengths can be achieved. In fact, two DNA or RNA molecules that are tens to hundreds of nucleotides long but differ in length by a single nucleotide can be resolved. Most often, the polynucleotides are covalently labeled with radioactive P-32, allowing the positions of different DNA or RNA to be revealed by autoradiography or phosphorimagery. Nonradioactive detection systems employing fluorescent stains or chemoluminescent reporters are also commonly used. Detection of damaged nucleotides, identification of protein or drug binding sites, and quantitation of the thermodynamics and kinetics of molecular recognition by/of nucleic acids are just a few of the many applications of gel electrophoresis. In addition, gel electrophoresis performed on a preparative scale allows for the purification of a particular nucleic acid from a complex mixture since the desired DNA or RNA can be extracted from the gel after electrophoresis.

Additionally, capillary gel electrophoresis (CGE) has become an increasingly important method for DNA sequencing because of its high resolution (single nucleotide), fast run times, and high sensitivity (24). Capillary electrophoresis is actually a family of related separation techniques that use narrow-bore fused silica capillaries to separate a complex array of large and small molecules. High voltages are used to separate the molecules on the basis of differences in size, charge, and hydrophobicity. CGE uses a gel to perform the sieving of the DNAs or RNAs and an in-line uv or laser-induced fluorescence detector (in conjuction with staining dyes) for product analysis (25). These methods do not require the time normally spent to stain and photograph gels, and ultimately allow for high throughput analysis because of automated sample processing (26,27).

Specific polynucleotides are usually identified in gels by comparison of their mobilities with those of standards of appropriate length. However, mass spectrometry is being increasingly applied to the analysis of nucleic acids, particularly with respect to their complexes with proteins and small molecules (9,28–30). Soft ionization methods such as matrix-assisted laser desorption and electrospray are used to introduce the complexes into the gas phase but with insufficient energy so as to promote dissociation of the molecular components. The mass of the complex provides information on the identities of the components and their stoichiometries.

The thermodynamics of molecular recognition events involving polynucleotides are of great interest and can be studied by a variety of optical and calorimetric techniques. The most commonly used method involves recording the uv absorbance of a sample at 260 nm as a function of temperature (31). For example, when a DNA duplex is formed, the absorbance is lower because of stacking of the nucleobases than when the two strands are separated from one another.

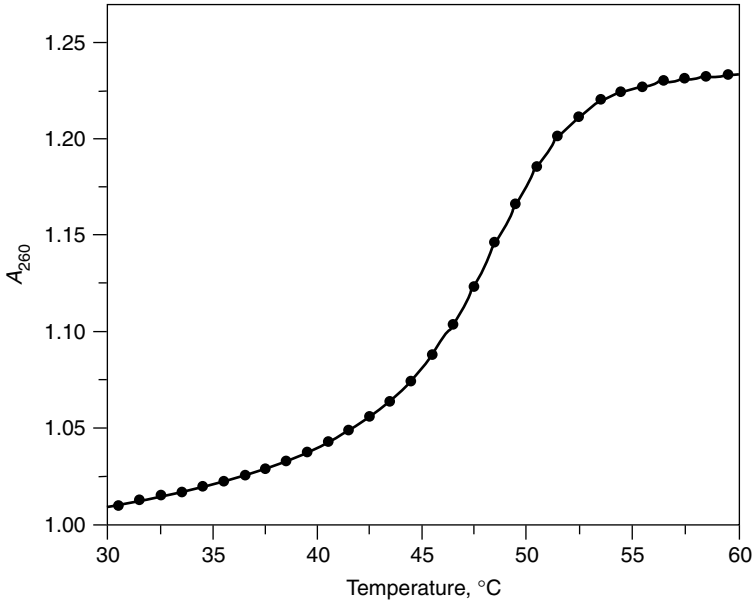

Fig. 7. Typical thermal denaturation curve plotting the uv absorbance at 260 nm (A_{260}) of a polynucleotide sample versus temperature. The "melting temperature" (T_m) of this sample is ca 48°C.

Thus, heating of a DNA duplex leads to an increase in absorbance, because the temperature is raised through the point at which there is sufficient thermal energy to disrupt the hydrogen-bonding and base-stacking interactions that are primarily responsible for the stability of the double-helix (Fig. 7). The midpoint of this transition is referred to the "melting temperature" (T_m) for the duplex. Curve-fitting of the temperature-dependent absorbance data or measurement of the concentration dependence of the T_m permits extraction of the free-energy, enthalpy, and entropy changes involved in forming a hybrid from isolated strands.

Alternatively, two different types of calorimetry can be used to analyze polynucleotides. In isothermal titration calorimetry, a solution containing one component (eg, single strand of DNA or RNA) is titrated into a solution containing the other component (eg, the complementary strand) at constant temperature (32). The amount of heat released upon binding of the two components is measured directly, and the concentration dependence permits extraction of the equilibrium binding constant and free-energy change for the reaction. Differential scanning calorimetry uses a constant concentration of the components used to form the complex of interest, and measures the heat taken up by the system as the temperature increases (33). (Or, conversely, the heat released as the system is cooled.) At the T_m, a discontinuity in the heat absorbed/released is detected and can be used to determine the enthalpy change for the transition.

Polynucleotide structures can be studied by a number of methods having varying levels of resolution. Offering the highest resolution are multidimensional nmr spectroscopy (34) and x-ray crystallography (9), both of which provide precise interatomic distances and angles. However, these are both very time-intensive

methods requiring expensive instrumentation and large amounts of material. Moreover, crystallization of nucleic acids, especially RNA, is still unpredictable. Lower resolution methods include circular dichroism (CD) spectropolarimetry (35,36) and structure probing experiments using chemical (37,38) or enzymatic (39,40) nucleases. CD relies on the differential absorption of left- and right-handed circularly polarized light by chiral chromophores or achiral chromophores bound in a chiral environment. Polynucleotides with different secondary or tertiary structures will exhibit different CD spectra, allowing, for example, distinction among the different families of DNA structures described above. In addition, molecular modeling and other computational methods are becoming increasingly sophisticated in their approaches to predicting three-dimensional structure based on primary sequence (41).

Structure probing experiments involve the use of chemical or enzymatic cleavage agents ("nucleases") to degrade the DNA or RNA backbone with predictable degrees of sequence or structure selectivity. Formation of intermolecular complexes or folding into stable tertiary structures alters the reactivity of the polynucleotide to these cleavage agents, resulting in either more or less cleavage at key positions. This can be detected using radiolabeled polynucleotide and gel electrophoresis, since cleaved substrates migrate faster than uncleaved substrates and the site of cleavage can be pinpointed. The high resolution of gel electrophoresis allows precise mapping of inter- and intramolecular interactions by this method. Figure 8 illustrates one application of this method, in which binding

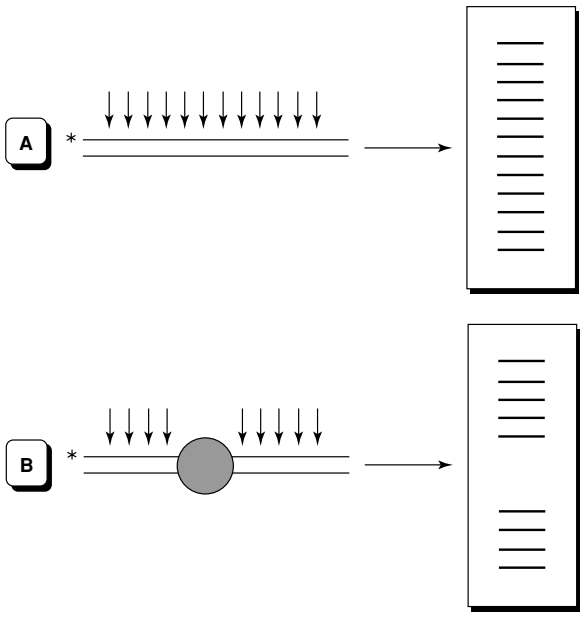

Fig. 8. Schematic of a footprinting experiment. In Part A radiolabelled DNA is cleaved by a chemical or enzymatic nuclease with no sequence selectivity (arrows). This leads to an autoradiogram exhibiting a ladder pattern corresponding to cleavage of the DNA at all positions. In Part B a ligand blocks cleavage at its binding site, leading to missing bands on the autoradiogram: the "footprint".

of a protein to a specific sequence of DNA prevents enzymatic cleavage at the binding site. The resulting "footprint" in the autoradiogram not only demonstrates that the protein is bound to the DNA, but also identifies the precise position of the binding site.

Enzymatic and Chemical Synthesis of Polynucleotides

At first glance, DNA and RNA appear to be random copolymers comprising four different monomers. However, the importance of the information encoded within nucleic acids requires that the monomers be arranged in a specific sequence. (Imagine how inefficient it would be to try to find a specific book within a library in which the books were shelved randomly.) Moreover, the replication of DNA through enzymatic means must repeatedly generate the required sequence with high fidelity. Hence, the process by which the polymer is synthesized must be under direct control at each step in the propagation. Otherwise, not only would a random sequence result, but also each molecule in the population would likely have a different sequence from all others. (While this is clearly undesirable in a biological context, the ability to synthesize randomized pools of polynucleotide sequences has been exploited in the generation of functional polynucleotides, as described henceforth.) This section will describe both enzymatic and chemical strategies for the synthesis of polynucleotides of well-defined sequences and lengths.

Enzymatic Synthesis. DNA and RNA are biosynthesized by polymerase enzymes. RNA is synthesized from a DNA strand with the assistance of an RNA polymerase enzyme. Inversely, DNA can be synthesized from an RNA strand with a reverse transcriptase (RT) enzyme. This mechanism is important because of "retroviruses" (such as HIV) in which RT makes up part of the viral replication cycle. (HIV-RT is an important target for anti-HIV therapy.) In any enzymatic synthesis of DNA or RNA, it is critical to the life of the organism that these enzymes synthesize their respective polynucleotides in a specific sequence of monomer units. The enzymes are able to accomplish this by utilizing a "template" strand to direct the synthesis. By reading the sequence of nucleobases on the template, the enzymes select the complementary monomer for incorporation into the propagating strand (Fig. 9). It was widely accepted that the polymerase enzymes accomplish this by matching the nucleotide to the template on the basis of complementary

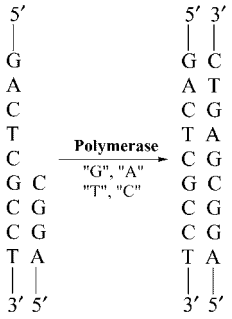

Fig. 9. Templated synthesis of DNA and RNA by polymerase enzymes.

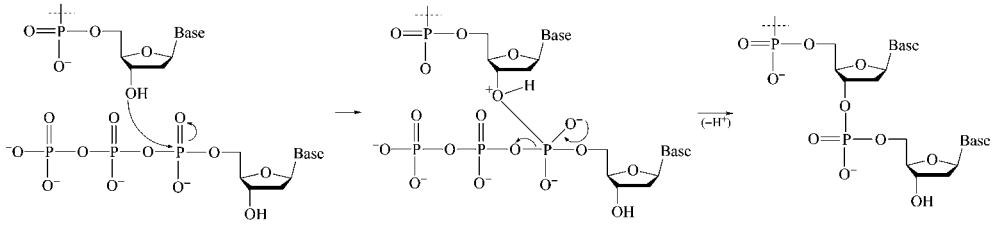

Fig. 10. Chemical reaction catalyzed by DNA polymerase. The 3′-OH of the growing DNA strand attacks the α-phosphorus of the dNTP, releasing pyrophosphate and forming a phosphodiester linkage.

hydrogen bonding. However, recent research indicates that for DNA polymerase, at least, the enzyme matches the shape of the incoming nucleotide to the template rather than reading the specific arrangement of hydrogen-bond donor and acceptor groups (42,43). The enzyme will continue to read the template strand and extend the newly synthesized strand until it reaches a particular sequence on the template, which acts as a pause or stop position indicating where the propagation should be terminated. The monomers used during DNA and RNA synthesis are nucleoside triphosphates. The reason for the triphosphate "tail" on the monomer becomes apparent when one considers the bond-forming reaction catalyzed by the polymerase enzyme: nucleophilic attack by the 3′-OH group of the propagating strand on the α-phosphate leads to release of inorganic pyrophosphate as a leaving group (Fig. 10).

Polymerase enzymes are used extensively in the laboratory for the synthesis and manipulation of DNA and RNA (44). One of the most important applications of enzymatic DNA synthesis is in the polymerase chain reaction (PCR), which is used to amplify minute quantities of DNA from a variety of sources, including crime scene evidence, archaeological specimens, or medical samples (45). In PCR, two short oligonucleotide primers are first synthesized by chemical methods. These primers are complementary to the 5′-ends of the two strands which form the DNA duplex of interest (Fig. 11). A large excess of the primers is mixed with the target DNA along with a DNA polymerase enzyme and the nucleoside triphosphate monomers. The sample is heated to disrupt the target duplex. Then, as the

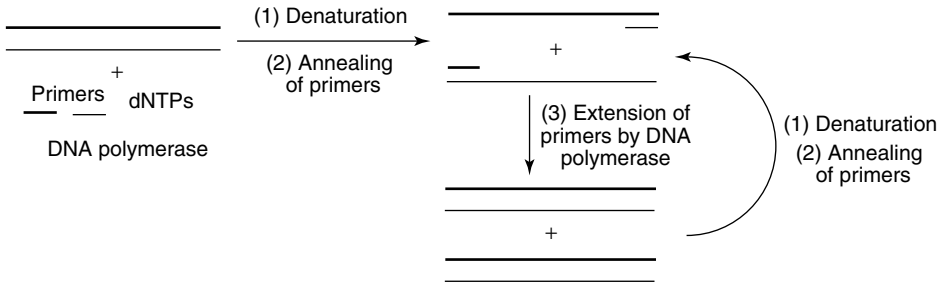

Fig. 11. The polymerase chain reaction, used to amplify small quantities of DNA through repetitive denaturation/annealing/extension cycles.

sample cools, the excess of primers competes kinetically with the complementary strands to form short primer-target duplexes. DNA polymerase then extends the primers to form full-length duplexes with both of the original strands. Subsequent heating, hybridization, and extension cycles lead to amplification of the DNA target concentration. Thus, PCR increases the amount of DNA that can be used for applications such as (*1*) diagnostic tests and assays; (*2*) *in vitro* transcription/translation to make mRNA and, ultimately, protein; and (*3*) insertion into recombinant DNA vectors for the expression of proteins of interest by organisms such as *E. coli* (bacteria) or *S. cerevisae* (yeast).

Chemical Synthesis. In the 1960s, the chemical synthesis of polypeptides was revolutionized through use of an insoluble solid support (46). A similar approach to the synthesis of polynucleotides was developed in the 1980s (47,48). Solid-phase synthesis benefits from short reaction times (because of high concentrations of reagents) and easy purification involving simple filtration, since the desired product remains covalently bound to the support.

The solid support used for DNA synthesis is usually controlled pore glass, functionalized with surface groups that permit attachment of the first monomer by an ester group. Monomers are added to the solid support in a predetermined sequence to form the desired oligo- or polynucleotide. A single round of extension, involving the addition of one monomer, actually consists of four chemical reactions (Fig. 12). In the first step, a dimethoxytrityl-protecting group is removed from the terminal 5′-OH. The next monomer is then added as the β-cyanoethyl-protected phosphoramidite. This coupling reaction forms a phosphite and is catalyzed by

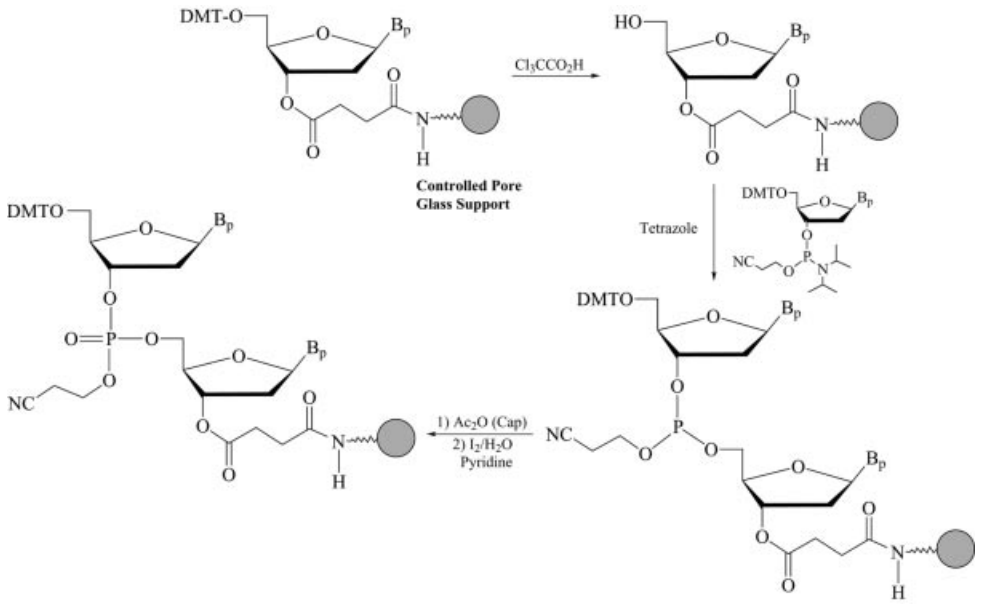

Fig. 12. The key steps in solid-phase chemical synthesis of DNA oligonucleotides. Each cycle consists of deprotection, coupling, capping, and oxidation steps and results in addition of one monomer onto the chain.

tetrazole. Any unreacted 5′-OH groups are "capped" through reaction with acetic anhydride. Finally, the phosphite is oxidized to a phosphotriester.

After the desired sequence is completed, the polynucleotide is released from the solid support, and protecting groups are removed via hydrolysis with ammonium hydroxide. The DNA is purified by gel electrophoresis or hplc and characterized by mass spectrometry. Similar methods are used to synthesize RNA oligomers, although the 2′-OH group on the ribose ring must be protected.

Solid-phase DNA and RNA synthesis are now fully automated and DNA oligomers can be purchased from many different vendors for less than $1/base. The ready availability of custom-synthesized DNA has contributed to the rapid growth in molecular biology, especially through providing primers for PCR amplification of desired DNA sequences. Other applications include synthesis of DNA oligomers for "gene-chip" analyses and libraries of DNA agents to be used in drug discovery. Furthermore, the chemical synthesis method permits the preparation of oligomers based on completely unnatural backbones, as described in the following section.

Synthetic Polynucleotide Analogues

Synthetic oligonucleotides are finding applications as antigene and antisense reagents, where sequence-specific binding to genomic DNA by triplex formation or to messenger RNA by duplex formation perturbs gene expression. The ability to selectively block expression of targeted genes is of great value both in the laboratory as well as in the clinic. However, oligonucleotides based on natural backbones are not optimized for these applications since single-stranded nucleic acids are readily degraded by nuclease enzymes and are not readily taken up by cells. Much effort has been directed toward the improvement of oligonucleotides for these applications. Modifications of the bases, sugar rings, and phosphodiester backbone (including replacement of the entire backbone) have been reported. A short list of analogues that have shown improved properties include phosphorothioates (49), PNA (peptide nucleic acid) (50,51), LNA (locked nucleic acid) (52,53), 2′-O-alkylated RNA and RNA/DNA chimeras (54), HNA (hexitol nucleic acid)(55,56), and phosphoramidates (49,57) (Fig. 13).

Antisense molecules should exhibit several properties: (*1*) high affinity and specificity for the target sequence (in order to overcome local secondary and tertiary structure); (*2*) nuclease resistance (stability to enzymes that destroy DNA and RNA); (*3*) RNase H activation (the ability to use enzymes *in vivo* to catalytically degrade a target mRNA); (*4*) spontaneous uptake by animal and human tissues; (*5*) low toxicity; and (*6*) high solubility. In addition, the ability to serve as a PCR primer is extremely useful for diagnostic applications. Finally, the ability to be incorporated into standard chemical and/or enzymatic syntheses and a low cost for synthesis of the monomer units are obviously important for commercial applications (58). The performance of various analogues are collected in Table 2. Four of the most promising synthetic analogues are described in greater detail below.

Phosphorothioates. Phosphorothioates are one of the earliest groups of DNA analogues. Phosphorothioate oligonucleotides involve a modification of the phosphodiester linkage of DNA wherein one of the nonbridging oxygen atoms is

Table 2. Properties of Oligonucleotide Analogues

Analogue	Improved affinity	Nuclease stability	RNase H activity	PCR primer	Clinical trials
DNA	−	−	+	+	−
RNA	−	−	−	+	−
Phosphorothioate	−	+	+	+	+
Phosphoramidate	+	+	−	+	−
2′-*O*-CH_3-RNA	+	+	−	+	−
2′-*O*-CH_3-RNA/DNA	+	+	+	+	+
PNA	+	+	−	−	−
LNA	+	+	Poor	+	−
LNA/DNA	+	+	+	+	−

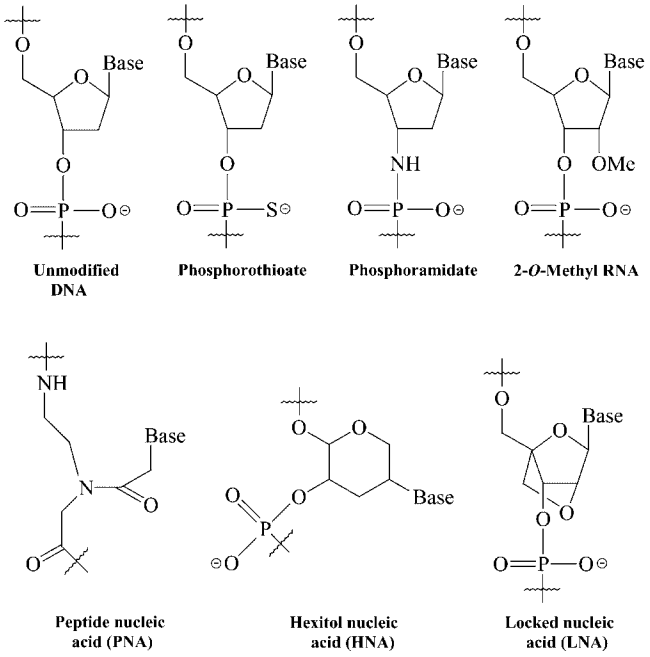

Fig. 13. Synthetic analogues of DNA and RNA, with unmodified DNA shown for comparison.

replaced by a sulfur atom (49). Phosphorothioates are one of the most commonly used analogues for antisense studies, and a great deal of clinical data has been acquired for these compounds. The first antisense oligonucleotide drug that has been approved for use is a phosphorothioate (Fomivirsen^{TM}), which is used to treat a viral infection of the eye (59).

Phosphorothioates can be incorporated into DNA sequences by solid-phase synthesis techniques. The chemical synthesis of the monomer units creates a chiral center at the modified phosphorous atom. These diastereomers can be separated for chemical synthesis, while any enzymatic incorporation results in only the

formation of the (R)-internucleotide linkage. (If the diastereomers are not separated prior to chemical synthesis, the final product will actually contain 2^n distinct compounds, where n is the number of phosphorothioate monomers incorporated into the sequence.) The use of a mixture of compounds can lead to ambiguous pharmacological results as well as regulatory issues (49).

The beneficial aspects of phosphorothioates include their ability to be spontaneously taken up by certain animal and human tissues, low toxicity, the ability to recruit RNase H, a moderate stability to nucleases and to base-catalyzed hydrolysis, and ease of synthesis. However, incorporation of phosphorothioate linkages into oligonucleotides reduces their affinity relative to unmodified DNA, enhances the tendency to form secondary structure, and increases nonspecific binding to proteins. These effects can lead directly to poor target binding. However, both laboratory and clinical data indicate that phosphorothioates can overcome these deficiencies so as to be effective antisense drugs and reagents.

PNA (Peptide Nucleic Acid). PNA is a DNA analogue where the entire phosphodiester backbone is replaced with *N*-2-aminoethylglycine backbone, and the linkage to the nucleobase is replaced with acetyl linker (50). This arrangement of atoms fits the bonding arrangement of DNA by containing six single bonds in the backbone repeat unit, and three single bonds from the backbone to the nucleobase (Fig. 13). This variation on DNA is interesting because the chemical character has been altered significantly: PNA has the attributes of both proteins and nucleic acids (60–62).

As a hybridization agent, PNA binds to RNA and DNA with significantly higher affinity (ΔT_m per monomer $\sim +3.5^\circ$C) and specificity than does unmodified DNA (63,64). The stability order for PNA, RNA, and DNA hybrids is as follows: PNA/PNA > PNA/RNA > PNA/DNA > RNA/DNA > DNA/DNA (65). This ordering is at least partially because of the uncharged character of the PNA backbone. PNA is capable of forming both antiparallel (N-terminus of the PNA aligned with the 3′-terminus of the DNA/RNA target) and parallel duplexes. The parallel duplex exhibits a T_m that is $\sim$1–2°C (per base pair) lower than the corresponding antiparallel duplex (50). In addition, homopyrimidine PNAs cooperatively form 2:1 triplexes with complementary homopurine DNAs. The first PNA strand forms a Watson–Crick duplex with the DNA strand, while the second PNA binds in the major groove by Hoogsteen hydrogen bonding (66). The x-ray structure of a PNA_2/DNA triplex shows hydrogen bonding between the backbone NH of the Hoogsteen PNA strand and phosphate oxygen of the DNA backbone (67), contributing to exceptionally high stability for these complexes. This strong binding property allows homopyrimidine PNAs to form strand displacement complexes when targeted toward duplex DNA and has led to study of PNA as an antigene agent (68).

PNAs are resistant to nuclease and protease enzymes, exhibit improved affinity and specificity relative to DNA oligonucleotides, and are efficiently prepared through solid-phase peptide synthesis. The uncharged character of PNA causes low aqueous solubility, although this is readily alleviated by the addition of lysine units at either terminus. One disadvantage of PNA as an antisense agent is that PNA/RNA duplexes do not induce RNase H activation. Thus, standard PNA cannot cause the catalytic degradation of RNA targets, although equipping the PNA with its own catalytic group is being pursued. Nevertheless, the improved

hybridization properties of PNA have allowed its use in many biotechnological applications such as hybridization arrays (69), oligonucleotide capture (70), and PCR clamping (71). PNA has also been shown to be capable of inhibiting human telomerase (72,73) and the expression of genes *in vivo* (74,75). It is also important to note that even though PNA is a DNA analogue, its self-recognizing properties and distinct chemical structure may allow its use in other applications not currently associated with nucleic acids technology.

LNA (Locked Nucleic Acid). LNA nucleotides incorporate a methylene bridge between the 2′-oxygen and 4′-carbon of ribose (Fig. 13) (52). This bridge conformationally locks the ribose into the 3′-endo conformation, thereby reducing the flexibility of the monomer and preorganizing the sugar ring into the conformation required for A-form duplexes (76). This modification results in dramatic increases in duplex stability, with ΔT_m values approaching 10°C per LNA monomer. However, as more LNA bases are incorporated, the increase per LNA base is reduced. In addition, incorporation of LNA monomers into longer oligomers (over ten bases long) leads to less duplex stabilization than in shorter sequences. These effects can reduce the overall stabilization per monomer to ∼2°C, which implies that LNA monomers will be used most effectively in short oligonucleotides (77).

The high affinity of LNAs coupled with nuclease resistance, RNase H activation, and commercial availability define LNA as the best of the RNase H activating oligonucleotide analogues to date (Table 2). It is important to note that an oligonucleotide comprised of all LNA monomers does not strongly activate RNase H, unlike LNA–DNA chimeras (ie, oligomers which contain both LNA and DNA monomers) (77). LNA–DNA chimeras have been used to produce an antisense effect on the G-protein-coupled receptor in living rat brain (78). This successful result implies both low toxicity and good potential for antisense applications. It also exemplifies another significant advantage of LNA relative to PNA: its ability to be incorporated into any phosphoramidite-based synthetic scheme. Thus, chimeric structures in which LNA residues are interspersed among DNA monomers allow the affinity enhancement due to LNA to be realized while maintaining the RNase H-activating properties of unmodified DNA. This can be extended further by also incorporating phosphorothioate residues to take advantage of their pharmacokinetic properties.

Phosphoramidates. Phosphoramidates are another commercially available DNA analogue where the 3′-oxygen of the phosphodiester center is replaced with an amino or aminoalkyl group (Fig. 13) (49). Phosphoramidates exhibit complete resistance to nuclease P1 and snake venom phosphodiesterase and a moderate improvement in affinity for DNA and RNA targets (ΔT_m per monomer = ∼4°C for 2′-fluoro N3′–P5′ phosphoramidates) (57). However, they exhibit no RNase H activity (49).

Sequence-Specific Recognition of Polynucleotides. Genetic information is stored permanently in DNA and transiently in RNA. Molecular recognition events are critical to accessing, reading, replicating, and utilizing the genome. In addition, the use of synthetic ligands to bind to specific sequences of DNA and RNA lies at the heart of numerous applications, ranging from gene therapy to molecular diagnostics. The highly divergent three-dimensional structures of natural DNA and RNA require distinct strategies for recognition of biologically relevant targets. A number of low molecular weight compounds have demonstrated

impressive recognition capabilities for polynucleotides. (79,80) However, given the polymeric nature of both DNA and RNA, it stands to reason that the most effective reagents should themselves be oligomeric or polymeric. Natural and synthetic ligands of this type that recognize DNA and RNA sequence specifically will be described in this section.

DNA. By far, the most common secondary structure for DNA is the double helix. Sequence-specific recognition of double-helical DNA relies on several factors. First, the array of functional groups exposed in the major and minor grooves can be read by DNA-binding ligands. This is referred to as "direct readout." However, more subtle factors may also be involved, such as sequence-dependent variation in the shape, flexibility, and hydration of the DNA. Ligands which discriminate among sequences based on these parameters utilize "indirect readout" of the sequence information.

DNA-binding ligands range in size from multidomain proteins (with molecular weights in excess of 10^5 kDa) to small molecules (with molecular weights as low as 300 Da). Larger ligands have greater potential for sequence-specific recognition because they can generate a more extended binding interface, where hydrogen bonding, electrostatic attractions, van der Waals contacts, and desolvation contribute to a favorable ΔG for association. Proteins recognize DNA sequences through a myriad of contacts involving all of these forces. Of the vast array of DNA-binding proteins that have been discovered and characterized, the most promising class with respect to predetermining the sequence that will be targeted is the zinc finger proteins (81). This group of proteins folds into a three-dimensional structure that is stabilized by a zinc ion which chelates four separate protein side chains. Each zinc finger domain recognizes three base pairs of DNA sequence specifically through contacts made in the major groove, and covalent linkage of separate domains through peptide chains allows for modular recognition of extended sequences. These proteins are able to function as artificial transcription factors, leading to enhanced or reduced gene expression, depending on the targeted gene (82).

The major groove of DNA is also the recognition site for triplex-forming oligonucleotides (TFOs) (12). As discussed above, Hoogsteen hydrogen bonding interactions allow sequence-specific recognition of DNA. TFOs have successfully inhibited gene expression through binding to target sequences in duplex DNA both *in vitro* (83,84) and *in vivo* (85). However, Hoogsteen recognition of DNA has not been generalized, meaning that only a relatively small subset of all possible sequences can be effectively bound by this strategy.

Numerous modifications of the natural DNA backbone have been utilized to try to improve the binding affinity and, therefore, biological utility of TFOs. PNA forms triplex structures with duplex DNA targets, although the triplex incorporates two PNA strands and one of the two DNA strands. This "strand invasion complex" leaves the second DNA strand locally displaced. Since triplex formation by this mechanism still relies on Hoogsteen hydrogen bonding, it suffers from the same sequence limitations as unmodified DNA. Strand invasion by mixed sequence PNA is generally unfavorable. However, adding a second PNA strand complementary to the displaced DNA strand leads to formation of a double-invasion complex, an approach that might be generalizable to any sequence (86).

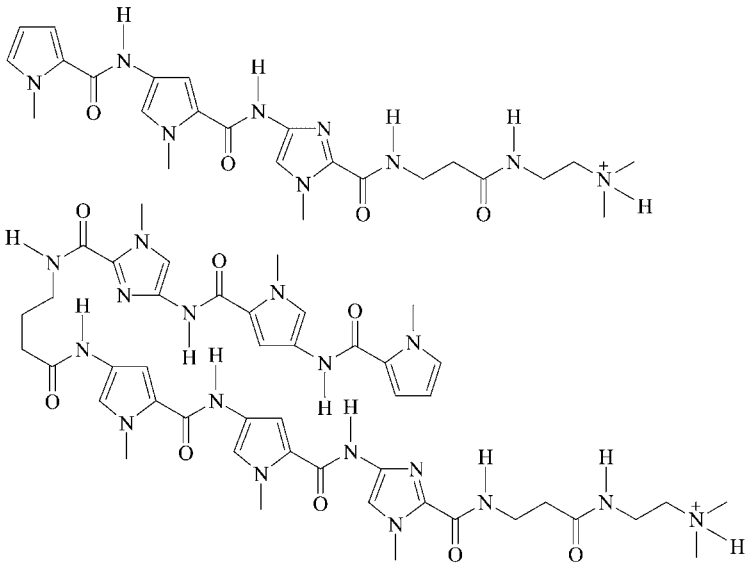

Fig. 14. Polyamide molecules that bind in the minor groove of DNA sequence-specifically. The three-ring compound binds as a cofacial dimer to give a 2:1 stoichiometry. The six-ring compound folds into a hairpin structure and binds as a 1:1 complex.

Strand invasion by LNA has not been reported. However, given the high stability offered by the LNA modifications, it is possible that these oligomers will bind sequence specifically to duplex DNA, although the stoichiometry and sequence restrictions cannot be predicted at this time.

The zinc finger proteins and TFOs access sequence information through the major groove. However, sequence discrimination can also be achieved using the information available in the minor groove of duplex DNA. In this context, a series of oligomeric ligands comprising heterocyclic groups (*N*-methylimidazole, *N*-methylpyrrole, 3-hydroxy-*N*-methylpyrrole) linked via amide connections (Fig. 14) are noteworthy. Two such molecules can bind simultaneously in a face-to-face orientation within the minor groove of DNA (87,89). Alternatively, intramolecular dimerization in the minor groove arises when two polyamides are covalently linked (90). Moreover, the precise sequence of heterocycles within the oligomer can be designed to recognize virtually any sequence of DNA. Control of gene expression using this class of ligands has been reported (91–93).

RNA. High resolution nmr, x-ray crystallography, and computational structure prediction methods are just beginning to illuminate the structural diversity embodied in RNA. Understanding the structure a particular RNA sequence folds into is of great interest, for, as with all biomolecules, the three-dimensional structure is intimately related to the function. However, with such a diverse structure-space covered by RNA, it is highly unlikely that a general protein-based approach to sequence-specific recognition can be achieved in the near future. Instead, the most successful RNA-binding strategies are based on the antisense approach, wherein an oligonucleotide or mimic is targeted to a complementary sequence within the RNA (84).

Natural systems often use antisense agents to control levels of gene expression. For example, if the protein derived from a given messenger RNA is not needed at a particular time, the expression can be downregulated by synthesizing a complementary RNA that binds to the mRNA and prevents its translation by the ribosome. This natural strategy led to the development of antisense therapeutics based on DNA oligonucleotides. In this strategy, binding of the DNA oligonucleotide is envisioned to inhibit gene expression in two ways. First, binding of the DNA to the mRNA target could prevent translation by a steric blockage of the ribosome. Of greater potential though, is the ability of DNA/RNA hybrids to activate the enzyme RNase H, which hydrolyzes the RNA component of the hybrid, leading to dissociation of the DNA antisense agent. This allows the antisense agent to potentially block translation of multiple mRNA molecules.

There are three potential pitfalls to the antisense strategy. First, unmodified DNA oligonucleotides are rapidly degraded by nuclease enzymes in the body, effectively eliminating the therapeutic activity before the DNA can ever reach the mRNA target. This deficiency has been overcome by synthesizing analogues of DNA that are stable to nuclease degradation, although these analogues also reduce the ability of RNase H to recognize the resulting hybrid with RNA (78,94,95). The second deficiency involves the possibility that the antisense agent will bind nonspecifically to other biomolecules *in vivo*. There is considerable evidence that antisense agents can affect a wide variety of biochemical pathways in addition to the expression of the specific gene being targeted. Finally, if an antisense agent successfully avoids degradation and nonspecific binding, it must still overcome the folded structure of the RNA, which can impose significant thermodynamic and kinetic obstacles to hybridization (96).

These factors point back to the need for increased understanding of RNA secondary and tertiary structure. In particular, sites that are near the surface of the folded structure and are not involved in base pairing with other portions of the RNA are likely to be the most viable targets for antisense agents. Currently, large libraries of potential antisense agents covering most of the target RNA sequence are synthesized and then screened individually for inhibition of gene expression. This can be a time-consuming and expensive procedure, especially as more costly modifications such as PNA or LNA are introduced. Rational design of antisense agents, based primarily on knowledge of the RNA structure, should significantly improve the initial phase of the drug discovery process.

Functional Polynucleotides

As mentioned above, once freed from the constraints of a complementary strand, polynucleotides can fold into a wide range of three-dimensional structures, leading to a diverse array of functions. Two specific types of functional polynucleotides are (*1*) aptamers, which bind noncovalently but selectively to ligands and (*2*) enzymes, which catalyze chemical reactions similar to protein enzymes. While a few examples of both natural aptamers and enzymes have been discovered, far more have been identified from synthetic combinatorial libraries through *in vitro* selection methods. The general approach to selection of functional polynucleotides is described below, followed by specific examples of nucleic acid–based aptamers and enzymes.

***In Vitro* Selection.** The concept of generating combinatorial libraries of molecules and then screening them for either structural or functional characteristics has reached many areas of chemistry and biology (97). Nucleic acid-based technology has followed this trend with the development of the *in vitro* selection or SELEX (Systematic Evolution of Ligands by EXponential amplification) method (98), in which a large population of randomized DNA or RNA sequences is generated and then screened for efficient binding to small molecules, proteins, metals, other nucleic acids, or even for catalytic ability (99). DNA and RNA molecules selected for binding to specific ligands are called *aptamers* (derived from aptus, "to fit"), while those *molecules that catalyze chemical reactions and fulfill criteria for enzyme activity* are referred to as *ribozymes* or *deoxyribozymes*. The generation of functional polynucleotides from randomized pools has provided considerable insight into the process of evolution at the molecular level and substantiated the idea that nucleic acids catalyzed important biological reactions before proteins were evolved for that purpose (100,101).

In the SELEX process (Fig. 15), a pool of DNA is chemically synthesized with a constant region (containing an RNA polymerase promoter and any other necessary sites for protein recognition) at the 5′-end, a run of randomized positions, and then another constant region at the 3′-end. The randomized positions are introduced by adding a mixture of all four phosphoramidites during the tetrazole-mediated coupling step in solid-phase synthesis. This yields a pool of 4^n total sequences, where n is the number of randomized positions. The pool is amplified via PCR, using primers that are specific to the two constant regions. If DNA aptamers or deoxyribozymes are desired, the pool is then subjected to its first round of selection. However, if RNA aptamers or ribozymes are to be selected, the DNA pool is first transcribed into RNA using RNA polymerase.

After the selection step, the enriched pool is then amplified. For DNA pools, PCR can be performed directly, while RNA pools require (*1*) RT to make the corresponding DNA, (*2*) PCR, and (*3*) and transcription to generate the amplified, enriched RNA pool. To allow molecular evolution to occur, rather than simple selection, mutagenic PCR can be performed. In this case, the DNA polymerase that is used to amplify the pool is prone to make errors during synthesis leading to incorporation of an incorrect nucleotide. This allows for single "mutations" to be introduced into selected sequences in an essentially random fashion. Subsequent rounds of selection and amplification ultimately lead to high affinity aptamers or high activity catalysts. Examples of these functional polynucleotides are described below.

Aptamers. A selection process, most often affinity chromatography, is used to select the sequences that bind the desired target. In this approach, the ligand of interest is covalently attached to the matrix used for chromatography. Those sequences that are retained on the column are either nonspecifically adsorbed to the matrix or specifically bound to the ligand. The adsorbed sequences can usually be rinsed away with a number of washes while the higher affinity, specifically bound sequences are retained. These sequences can then be eluted from the column with either a buffer that weakens the aptamer/small molecule interaction (such as a high salt buffer) or a buffer containing the free small molecule. The resulting enriched pool is then amplified and then subjected to further rounds of selection. The selection pressure can be increased by using higher temperature,

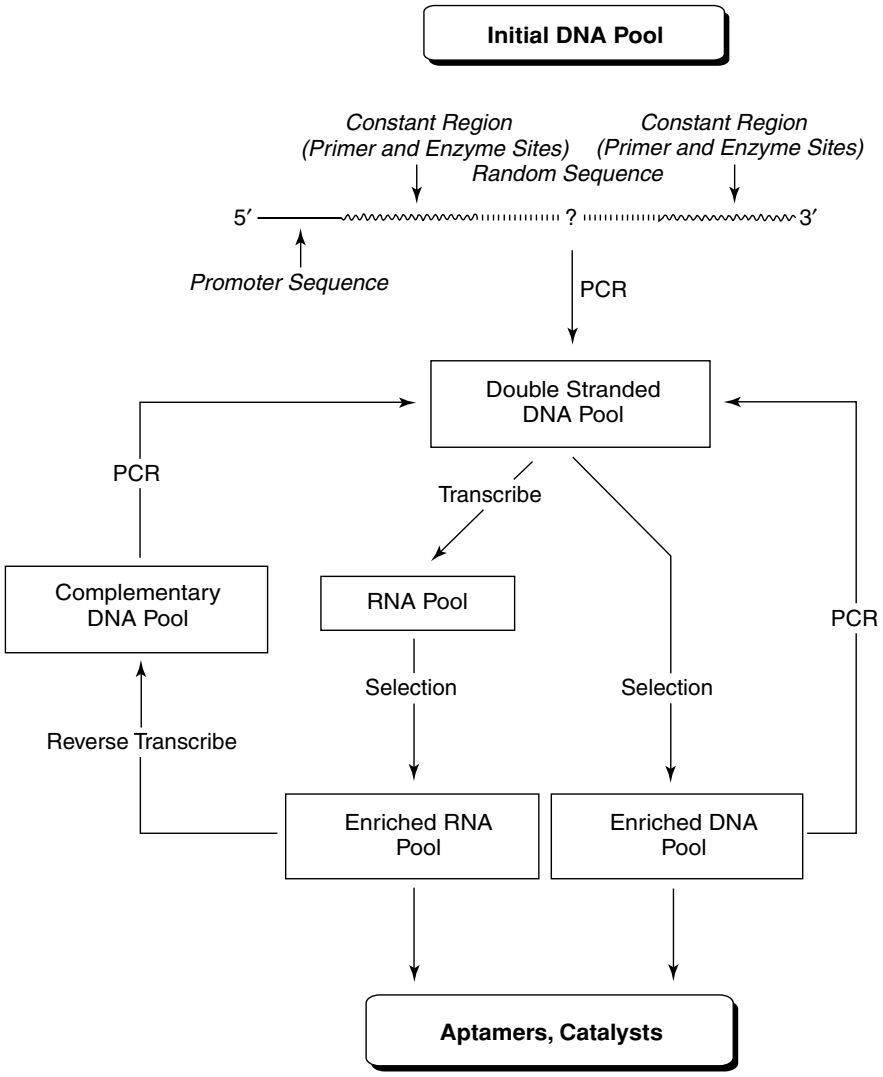

Fig. 15. Flow chart for *in vitro* selection of aptamers and catalysts from randomized DNA and RNA pools.

variations in ionic strength, and competitive binding, favoring retention of only the highest affinity aptamers on the column.

Table 3 collects examples of ligands used to select aptamers from either DNA or RNA pools. A variety of structural motifs have been effectively targeted with this procedure, including amino acids, organic dyes, and nucleotides. In addition, SELEX has been used to identify aptamers for protein targets, such as thrombin (101). It is well-known that many biological events occur because of the interaction of proteins with nucleic acids. However, the vast majority of proteins do not normally interact with DNA or RNA. Aptamers selected for binding to such

Table 3. Small Molecule Targets for Aptamer Selection

Small molecule	K_D, μm	Reference
ATP/adenosine	1	102
Guanosine	31	103
7-Methyl-GTP	0.5	104
Flavin	0.5	105
NAD	2.5	106
Arginine	0.33	107
Tryptophan	18	108
Streptomycin	1	109
Chloroamphenicol	2.1	110

proteins could disrupt the activity of these proteins, sparking great interest in the discovery of aptamers for protein recognition. The inhibition of protein activity is a primary strategy for pharmaceutical agents so that aptamers could conceivably be applied as drugs, although some modification of the DNA/RNA structure will likely be required in order to avoid enzymatic degradation *in vivo*.

Catalysts. SELEX has been used to create nucleic acids that are capable of catalyzing reactions. This idea was strongly influenced by the discovery of RNAs that catalyze RNA cleavage and ligation reactions (ribozymes) (112,113). Selection strategies have been used to screen combinatorial libraries of sequences for catalytic activity. Methods for selecting nucleic acid enzymes are somewhat different from aptamer selection strategies, since simple binding to an affinity column does not necessarily correlate with efficient catalysis. Thus, while binding to a column is a useful approach for isolation of desired sequences from the pool, the binding should be coupled to some chemical reaction. For example, selection of an RNA-cleaving DNA enzyme has been accomplished using a pool of DNA sequences with a single RNA linkage (incorporated through enzymatic extension) and capped with a biotin group (114). The randomized region is separated from the biotin cap by the RNA linkage. It is then passed through a streptavidin column, allowing all sequences to be retained on the column via the high affinity biotin/streptavidin interaction. Changing the buffer to one that promotes folding (eg, high ionic strength or addition of metal ions) allows those sequences that are able to cleave themselves to be released from the column in the selection step. These sequences are then amplified by PCR using a primer that has a biotin group attached to it. The pool is then ready for the next round of selection. Methods have also been used to create ribozymes and DNA enzymes that are capable of cleaving RNAs in a sequence-specific manner. Table 4 provides examples of reactions catalyzed by nucleic acid enzymes. These range from cleavage and ligation reactions, which have natural analogues, to glycosidic bond formation and insertion of metals into porphyrins. While the functional diversity of nucleic acid enzymes is likely to be limited in comparison with protein enzymes (because of the smaller number of functional groups present in the former), these polynucleotides are capable of performing an impressive array of functions.

Table 4. Reactions Catalyzed by Oligonucleotide Enzymes

Polynucleotide	Reaction catalyzed	Reference
RNA and DNA	Phosphodiester transfer of DNA and RNA	115–117
RNA and DNA	Phosphodiester hydrolysis of DNA and RNA	118–121
RNA and DNA	Acyl transfer	122–125
RNA	Glycosidic bond formation	126
RNA and DNA	Metal insertion into porphyrins	127,128

Use of Polynucleotides as Building Materials for Nanoconstruction

Biological structures are assembled on the nanometer or micron length scale and consist primarily of noncovalently associated subunits. The molecular recognition mechanisms that have evolved to permit assembly of such large structures provide stunning examples of "programmed synthesis," in which the final three-dimensional structure is encoded within the structures of the individual subunits. While it is the function of these assemblies that most often attracts our attention, it is the structure that permits the function. Moreover, the specific intermolecular forces that allow these assemblies to form are highly directional, allowing objects to be positioned spatially with great precision.

The sequence-specific hydrogen-bonding pattern that defines the DNA double helix protects the integrity of the genetic information and provides a molecular level mechanism for replication of the genome. However, the double helix is also beginning to serve as an inspiration for nanomaterials scientists, who see the relatively rigid, regular structure as an ideal construction scaffold (129). For example, when two objects are attached at the 5′-ends of complementary DNA strands, hybridization to form a duplex will position the two objects at a predetermined distance. Alternatively, DNA "three-way" and "four-way" junctions can be used to arrange objects in more complex patterns (Fig. 16). The "objects" positioned on the DNA scaffolding can range from small molecules that function as electron (130) or energy (131,132) donor and acceptor groups to inorganic nanoparticles (133–138). This nanoconstruction strategy is largely generalizable since a range of chemistries is available to permit attachment of the molecule of interest to a DNA oligomer.

Further elaboration into network structures can be realized if a cross-linking group is included. Two-dimensional networks formed from cross-linked four-way junctions have been imaged by atomic force microscopy (139). In addition, gold nanoparticles having dozens of copies of an attached DNA oligonucleotide can be cross-linked by another DNA oligomer to yield elegant superstructures, as revealed by electron microscopy (140). This self-assembly process also has immediate practical utility: when the nanoparticles cluster together, they undergo a color change from red to blue, providing a sensitive colorimetric indicator for the specific sequence of DNA required to form the cross-linked network (141).

Polynucleotides have other molecular recognition mechanisms that permit formation of stable three-dimensional structures. For example, folded RNAs are often stabilized by a tertiary interaction known as a GNRA tetraloop–receptor

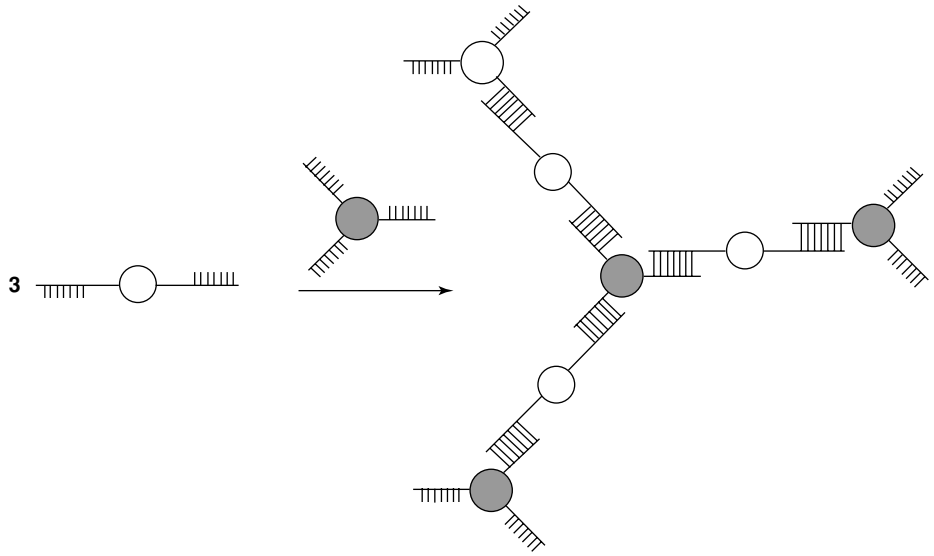

Fig. 16. Use of Watson–Crick base pairing to assemble organized, network structures.

motif. In these cases, a four-base single-stranded loop region of the RNA consisting of the sequence 5′-GNRA-3′ (where N = any base and R = G or A) binds within the major groove of a specific RNA sequence. This association does not involve Watson–Crick base pairing, yet it is sequence-specific. Short RNA sequences have been synthesized containing both a GNRA tetraloop and a receptor within a hairpin structure (142). The rigidity of the intervening duplex prevents an intramolecular association of the loop and receptor, leading to the formation of self-assembled structures through intermolecular interactions. RNA is unlikely to be a practical construction material because of its relatively high cost and low chemical stability. However, the rich variety of nonduplex secondary and tertiary structures exhibited by RNA polynucleotides can be exploited to form novel architectures.

Outlook

The biological polynucleotides DNA and RNA provide essential information for the maintenance and propagation of life. The structure and function of these polymers continue to be studied using the techniques of biology, chemistry, and physics. The growing application of polynucleotides in biotechnology and medicine, as laboratory reagents, and as nanomaterials can be attributed not only to their central importance in nature, but also to their ease of synthesis, manipulation, and characterization. The continued study and application of polynucleotides and their synthetic analogues in both biological and materials science contexts will undoubtedly lead to truly breathtaking discoveries in the future.

BIBLIOGRAPHY

"Polynucleotides" *EPST* 1st ed., Vol. 11, pp. 364–379, by H. Kossel, Universität Freiburg; Suppl. Vol. 2, pp. 510–610, by R. D. Blake, University of Maine; "Polynucleotides" *EPSE* 2nd ed., Vol. 12, pp. 699–785, by Wilhelm Guschlbauer, Centre d'Etudes Nucléaires de Saclay, France.

1. J. D. Watson and F. H. C. Crick, *Nature* **171**, 737–738 (1953).
2. S. M. Hecht, ed., *Bioorganic Chemistry: Nucleic Acids*, Oxford University Press, New York, 1996.
3. G. M. Blackburn and M. J. Gait, eds., *Nucleic Acids in Chemistry and Biology*, 2nd ed., Oxford University Press, New York, 1996.
4. P. Belmont, J.-F. Constant, and M. Demeunynck, *Chem. Soc. Rev.* **30**, 70–81 (2001).
5. R. E. Dickerson, *Adv. Enzymol.* **211**, 67–111 (1992).
6. W. Saenger, *Principles of Nucleic Acid Structure*, Springer-Verlag, New York, 1984.
7. A. Rich, A. Nordheim, and A. H.-J. Wang, *Annu. Rev. Biochem.* **53**, 791–846 (1984).
8. B. H. Johnston, *Methods., Enzymol.* **211**, 127–158 (1992).
9. X. Shui and co-workers, *Biochemistry* **37**, 8341–8355 (1998).
10. D. E. Gilbert and J. Feigon, *Curr. Opin. Struct. Biol.* **9**, 305–314 (1999).
11. J. C. Francois, J. Lacoste, and L. Lacroix, *Methods Enzymol.* **313**, 74–95 (2000).
12. M. D. Frank-Kamenetskii and S. M. Mirkin, *Annu. Rev. Biochem.* **64**, 65–95 (1995).
13. S. M. Mirkin, M. D. Frank-Kamenetskii, *Annu. Rev. Biophys. Biomol. Struct.* **23**, 541–576 (1994).
14. J. R. Williamson, *Annu. Rev. Biophys. Biomol. Struct.* **23**, 703–730 (1994).
15. D. M. J. Lilley, *Biopolymers* **48**, 101–112 (1998).
16. C. E. Pearson and co-workers, *Cell Biochem.* **63**, 1–22 (1996).
17. G. Varani, *Annu. Rev. Biophys. Biomol. Struct.* **24**, 379–404 (1995).
18. M. Kvaratskhelia, *J. Mol. Biol.* **297**, 923–932 (2000).
19. M. F. White and co-workers, *J. Mol. Biol.* **269**, 647–664 (1997).
20. R. T. Batey, R. P. Rambo, and J. A. Doudna, *Angew. Chem. Int. Ed.* **38**, 2326–2343 (1999).
21. G. L. Conn and D. E. Draper, *Curr. Opin. Struct. Biol.* **8**, 278–285 (1998).
22. M. Chastain and I. Tinonco, *Prog. Nucleic Acid Res.* **41**, 131–177 (1991).
23. D. Rickwood and B. D. Hames, *Gel Electrophoresis of Nucleic Acids: A Practical Approach*, Oxford University Press, New York, 1990.
24. L. Kotler and co-workers, *Proc. Nat. Acad. Sci. USA* **90**, 4241–4245 (1993).
25. H. E. Schwartz and K. J. Ulfelder, *Anal. Chem.* **64**, 1737 (1992).
26. V. Dolnik, *J. Biochem. Biophys. Methods* **41**, 103–119 (1999).
27. H. Watzig, M. Degenhardt, and A. Kunkel, *Electrophoresis* **19**, 2695–2752 (1998).
28. K. X. Wan, T. Shibue, and M. L. Gross, *J. Am. Chem. Soc.* **122**, 300–307 (2000).
29. V. Tereshko, G. Minasov, and M. Egli, *J. Am. Chem. Soc.* **121**, 3590–3595 (1999).
30. S. A. Hofstadler and R. H. Griffey, *Chem. Rev.* **101**, 377–390 (2001).
31. L. A. Marky and K. J. Breslauer, *Biopolymers* **26**, 1601–1620 (1987).
32. J. E. Ladbury and B. Z. Chowdhry, *Chem. Biol.* **3**, 791–801 (1996).
33. T. V. Chalikian and co-workers, *Proc. Nat. Acad. Sci. USA* **96**, 7853–7858 (1999).
34. K. Wüthrich *NMR of Proteins and Nucleic Acids*, John Wiley & Sons, Inc., New York, 1986.
35. A. Rodger and B. Nordén, *Circular Dichroism and Linear Dichroism*, Vol. **1** Oxford University Press, Oxford, 1997.
36. K. Nakanishi, N. Berova, and R. W. Woody, *Circular Dichroism: Principles and Applications*, VCH Publishers, New York, 1994.
37. T. D. Tullius, In Ref. 2, pp. 144–162.
38. D. S. Sigman, A. Mazumder, and D. M. Perrin, *Chem. Rev.* **93**, 2295–2316 (1993).

39. G. Knapp, *Methods Enzymol.* **180**, 192–212 (1989).
40. J. A. Jaeger, J. SantaLucia Jr., and I. Tinoco, *Annu. Rev. Biochem.* **62**, 255–287 (1993).
41. V. Lehnert and co-workers, *Chem. Biol.* **3**, 993–1009 (1996).
42. T. J. Matray and E. T. Kool, *J. Am. Chem. Soc.* **120**, 6191–6192 (1998).
43. E. T. Kool, *Annu. Rev. Biophys. Biomol. Struct.* **30**, 1–22 (2001).
44. M. Van Cleve, in Ref. 2, pp. 75–104.
45. J. F. Burke, *PCR: Essential Techniques*, John Wiley & Sons, Inc., New York, 1996.
46. R. B. Merrifield, *J. Am. Chem. Soc.* **85**, 2149 (1963).
47. S. L. Beaucage and M. H. Caruthers, *Tetrahedron Lett.* **22**, 1859–1862 (1981).
48. S. L. Beaucage and M. H. Caruthers, in Ref. 2, pp. 36–74.
49. S. Verma and F. Eckstein, *Annu. Rev. Biochem.* **67**, 99–134 (1998).
50. M. Egholm and co-workers, *Nature* **365**, 566–568 (1993).
51. P. E. Nielsen and M. Egholm, *Peptide Nucleic Acids. Protocols and Applictions*, Horizon Scientific, Norfolk, Conn. 1999.
52. S. K. Singh and co-workers, *Chem. Commun.* 455–456 (1998).
53. A. A. Koshkin and co-workers, *J. Am. Chem. Soc.* **120**, 13252–13253 (1998).
54. R. I. Hogrefe, *Antisense Nucleic Acid Drug Dev.* **9**, 351–357 (1999).
55. C. Hendrix and co-workers, *Chem. Eur. J.* **3**, 1513–20 (1997).
56. C. Hendrix and co-workers, *Chem. Eur. J.* **3**, 110–20 (1997).
57. R. G. Schultz and S. M. Gryaznov, *Nucleic Acids Res.* **24**, 2966–2973 (1996).
58. E. Uhlmann and A. Peyman, *Chem. Rev.* **90**, 543–584 (1990).
59. C. Marwick, *J. Am. Med. Assoc.* **280**, 871 (1998).
60. D. R. Corey, *Trends Biotechnol.* **15**, 224–229 (1997).
61. P. E. Nielsen, *Acc. Chem. Res.* **32**, 624–630 (1999).
62. P. E. Nielsen and G. Haaima, *Chem. Soc. Rev.* **26**, 73–78 (1997).
63. T. Ratilainen and co-workers, *Biochemistry* **37**, 12331–12342 (1998).
64. T. Ratilainen and co-workers, *Biochemistry* **39**, 7781–7791 (2000).
65. S. Tomac and co-workers, *J. Am. Chem. Soc.* **118**, 5544–5552 (1996).
66. S. K. Kim and co-workers, *J. Am. Chem. Soc.* **115**, 6477 (1993).
67. L. Betts and co-workers, *Science* **270**, 1838–1841 (1995).
68. D. Y. Cherny and co-workers, *Proc. Natl. Acad. Sci. USA* **90**, 1667–1674 (1993).
69. C. Carlsson and co-workers, *Nature* **380**, 207 (1996).
70. H. Ørum and co-workers, *BioTechniques* **19**, 472–480 (1995).
71. H. Ørum and co-workers, *Nucleic Acids Res.* **21**, 5332–5336 (1993).
72. J. C. Norton and co-workers, *Nat. Biotech.* **14**, 615–620 (1996).
73. B.-S. Herbert and co-workers, *Proc. Natl. Acad. Sci. USA* **96**, 14276–14281 (1999).
74. D. F. Doyle and co-workers, *Biochemistry* **40**, 53–64 (2001).
75. T. Mayhood and co-workers, *Biochemistry* **39**, 11532–1139 (2000).
76. K. Bondensgaard and co-workers, *Chem. Eur. J.* **6**, 2687–2695 (2000).
77. D. A. Braasch and D. R. Corey, *Chem. Biol.* **8**, 1–7 (2001).
78. C. Wahlestedt and co-workers, *J. Proc. Natl. Acad. Sci. USA* **97**, 5633–5638 (2000).
79. W. D. Wilson, in Ref. 3, pp. 329–374.
80. J. A. Mountzouris and L. H. Hurley, in Ref. 2, pp. 288–323.
81. J. S. Berg, *Acc. Chem. Res.* **28**, 14–19 (1995).
82. R. R. Beerli, B. Dreier, and C. F. Barbas, *Proc. Natl. Acad. Sci. USA* **97**, 1495–1500 (2000).
83. M. Grigoriev and co-workers, *J. Biol. Chem.* **267**, 3389–3395 (1992).
84. P. S. Miller, in Ref. 2, pp. 347–374.
85. S. Cogoi and co-workers, *Biochemistry* **40**, 1135–1143 (2001).
86. J. Lohse, O. Dahl, and P. E. Nielsen, *Proc. Natl. Acad. Sci. USA* **96**, 11804–11808 (1999).
87. M. Mrksich and co-workers, *Proc. Natl. Acad. Sci. USA* **89**, 7586–7590 (1992).
88. W. S. Wade, M. Mrksich, and P. B. Dervan, *J. Am. Chem. Soc.* **114**, 8783–8794 (1992).

89. B. H. Geierstanger and co-workers, *Science* **266**, 646–650 (1994).
90. M. Mrksich, M. E. Parks, and P. B. Dervan, *J. Am. Chem. Soc.* **116**, 7983–7988 (1994).
91. A. K. Mapp and co-workers, *Proc. Natl. Acad. Sci. USA* **97**, 3930–3935 (2000).
92. L. A. Dickinson and co-workers, *Biochemistry* **38**, 10801–10807 (1999).
93. J. M. Gottesfeld and co-workers, *Nature* **387**, 202–205 (1997).
94. M. A. Bonham and co-workers, *Nucleic Acids Res.* **23**, 1197–1203 (1995).
95. H. Knudsen and P. E. Nielsen, *Nucleic Acids Res.* **24**, 494–500 (1996).
96. P. P. Zarrinkar and J. R. Williamson, *Science* **265**, 918–924 (1994).
97. S. E. Osborne and A. D. Ellington, *Chem. Rev.* **97**, 349–370 (1997).
98. J. Abelson, *Science* **249**, 488–9 (1990).
99. D. S. Wilson and J. W. Szostak, *Annu. Rev. Biochem.* **68**, 611–647 (1999).
100. L. Gold and co-workers, *Proc. Natl. Acad. Sci. USA* **94**, 59–64 (1997).
101. D. P. Bartel and P. J. Unrau, *Trends Cell Biol.* **9**, M9–M13 (1999).
102. M. Sassanfar and J. W. Szostak, *Nature* **364**, 550–553 (1993).
103. G. J. Connell and M. Yarus, *Science* **264**, 1137–1141 (1994).
104. A. A. Haller and P. Sarnow, *Proc. Natl. Acad. Sci. USA* **94**, 8521–8526 (1997).
105. P. Burgstaller and M. Famulok, *Angew. Chem., Int. Ed. Engl.* **33**, 1084–1087 (1994).
106. C. T. Lauhon and J. W. Szostak, *J. Am. Chem. Soc.* **117**, 1246–1257 (1995).
107. A. Geiger and co-workers, *Nucleic Acids Res.* **24**, 1029–1036 (1996).
108. M. Famulok and J. W. Szostak, *J. Am. Chem. Soc.* **114**, 3990–3991 (1992).
109. S. T. Wallace and R. Schroeder, *RNA* **4**, 112–123 (1998).
110. D. H. Burke and co-workers, *Chem. Biol.* **4**, 833–843 (1997).
111. L. C. Bock and co-workers, *Nature* **355**, 564–6 (1992).
112. A. J. Zaug and T. R. Cech, *Nucleic Acids Res.* **10**, 2823–2838 (1982).
113. A. J. Zaug and T. R. Cech, *Science* **231**, 470–475 (1986).
114. R. R. Breaker and G. F. Joyce, *Chem. Biol.* **1**, 223–229 (1994).
115. D. P. Bartel and J. W. Szostak, *Science* **261**, 1411–1418 (1993).
116. E. H. Ekland, J. W. Szostak, and D. P. Bartel, *Science* **269**, 364–370 (1995).
117. B. Cuenoud and J. W. Szostak, *Nature* **375**, 611–614 (1995).
118. T. Tuschl, P. A. Sharp, and D. P. Bartel, *EMBO J.* **17**, 2637–2650 (1998).
119. V. K. Jayasena and L. Gold, *Proc. Natl. Acad. Sci. USA* **94**, 10612–10617 (1997).
120. R. R. Breaker and G. F. Joyce, *Chem. Biol.* **2**, 655–660 (1995).
121. R. R. Breaker, *Nat. Biotechnol.* **15**, 427–431 (1997).
122. M. Illangasekare and co-workers, *Science* **267**, 643–647 (1995).
123. A. Jenne and M. Famulok, *Chem. Biol.* **5**(1), 23–34 (1998).
124. B. Zhang and T. R. Cech, *Nature* **390**, 96–100 (1997).
125. T. M. Tarasow, S. L. Tarasow, and B. E. Eaton, *Nature* **389**, 54–57 (1997).
126. P. J. Unrau and D. P. Bartel, *Nature* **395**, 260–263 (1998).
127. M. M. Conn, J. R. Prudent, and P. G. Schultz, *J. Am. Chem. Soc.* **118**, 7012–7013 (1996).
128. Y. Li and D. Sen, *Nat. Struct. Biol.* **3**, 743–747 (1996).
129. N. C. Seeman, *Annu. Rev. Biophys. Biomol. Struct.* **27**, 225–248 (1998).
130. C. J. Murphy and co-workers, *Science* **262**, 1025–1029 (1993).
131. S.-I. Kawahara, T. Uchimaru, and S. Murata, *Chem. Commun.* 563–564 (1999).
132. D. J. Hurley and Y. Tor, *J. Am. Chem. Soc.* **120**, 2194–2195 (1998).
133. A. P. Alivisatos and co-workers, *Nature* **382**, 609–611 (1996).
134. C. A. Mirkin and co-workers, *Nature* **382**, 607–609 (1996).
135. C. J. Loweth and co-workers, *Angew. Chem. Int. Ed.* **38**, 1808–1812 (1999).
136. G. P. Mitchell, C. A. Mirkin, and R. L. Letsinger, *J. Am. Chem. Soc.* **121**, 8122–8123 (1999).
137. J. J. Storhoff and C. A. Mirkin, *Chem. Rev.* **99**, 1849–1862 (1999).
138. S. M. Waybright and co-workers, *J. Am. Chem. Soc.* **123**, 1828–1833 (2001).
139. C. Mao, W. Sun, and N. C. Seeman, *J. Am. Chem. Soc.* **121**, 5437–5443 (1999).

140. R. C. Mucic and co-workers, *J. Am. Chem. Soc.* **120**, 12674–12675 (1998).
141. J. J. Storhoff and co-workers, *J. Am. Chem. Soc.* **120**, 1959–1964 (1998).
142. L. Jaeger and N. Leontis, *Angew. Chem. Int. Ed.* **39**, 2521–2524 (2000).

STUART A. KUSHON
BRUCE A. ARMITAGE
Carnegie Mellon University

POLYOXYMETHYLENE. See ACETAL RESINS.

POLYPHENYLENE ETHER. See POLYETHERS, AROMATIC.

POLYPROPYLENE. See PROPYLENE POLYMERS.

POLYSULFIDES

Introduction

Polysulfide polymers have the following general structure:

$$HS\text{—}(\text{—}R\text{—}S_x\text{—})\text{—}SH$$

1

where x is referred to as the rank and represents the average number of sulfur atoms in the polysulfide unit. This article is limited to polymers where R is an aliphatic group and $x > 1$. The rank x usually ranges from slightly less than 2 to about 4. A recent monograph (1) provides extensive information on the history, properties, and uses of aliphatic polysulfides. Other sulfur-containing polymers have been reviewed elswhere (2).

The history of polysulfides began over 150 years ago. In 1838, chemists in Switzerland reported that the reaction of chloraetherin (1,2-dichloroethane) with potassium polysulfide gave a rubbery, intractable, high sulfur semisolid. Subsequently there were reports of similar products obtained by various methods, but the first useful products were developed from studies in the late 1920s. This work led to the formation of the Thiokol Corp., which began production of the ethylene tetrasulfide polymer Thiokol® A in 1928. This was the first synthetic elastomer manufactured commercially in the United States. One of the first successful applications of Thiokol A [14807-96-6] was for seals where its resistance to solvents justified its relatively high price.

These new synthetic rubbers were accessible from potentially low cost raw materials and generated considerable worldwide interest. For a time, it was hoped that the polysulfide rubbers could substitute for natural rubber in automobile

Encyclopedia of Polymer Science and Technology. Copyright John Wiley & Sons, Inc. All rights reserved.

tires. Unfortunately, these original polymers were difficult to process, evolved irritating fumes during compounding, and properties such as compression set, extension, and abrasion resistance were not suitable for this application.

During the 1930s, gradual improvements in the product and in how it was processed overcame some of the drawbacks of this material. Nonetheless, the applications were limited and Thiokol Corp. struggled to remain solvent. The first year Thiokol Corp. reported a profit was in 1941, 13 years after its foundation. The profitability was achieved when the U.S. Air Force discovered that the aliphatic polysulfides were useful as a fuel-resistant sealant for aircraft tanks and hoses. Polysulfides also began to be used as sealants for boat hulls and decks.

The most significant improvement came in the early 1940s when a method for preparing thiol-terminated liquid polysulfides was developed. Cure of the liquid polysulfides could be accomplished by oxidative coupling. So a rubber product could be compounded without the need of heavy mixing equipment. One of the first large-scale applications of the liquid polysulfides was as a binder for solid rocket fuel. From about 1946 until 1958, these binders were used in various rocket systems and the aliphatic polysulfides achieved commercial success. The switch to predominately liquid-fueled rockets in 1958 ended this phase of the polysulfide business.

Since then, uses have shifted toward civilian applications. Polysulfides have unusually good resistance to solvents and to the environment and they have good low temperature properties. They are particularly useful in a variety of sealant applications. For example, the outstanding resistance of polysulfides to petroleum products has made them the standard sealant for virtually all aircraft integral fuel tanks and bodies. Another important application is in insulating glass window sealants. Sealants based on liquid polysulfides have had an excellent record since the 1950s and are the worldwide market leader in these applications.

Polysulfides also have a long record as construction sealants. In 1953, the Lever House in New York was one of the first high rise buildings to abandon the traditional structural masonry for the attractive curtain wall construction. Originally, the joints were sealed with a typical oil-based caulk. Within 6 months, there were serious leakage problems through virtually every joint. The original sealant was removed and replaced with a polysulfide-based elastomeric sealant that could expand and compress with the movements of the panels. Much of this original sealant was still performing in the 1990s. Polysulfides became the first high performance elastomeric sealants to be used in building construction and have been applied successfully to many large-scale projects around the world.

Some of the early Thiokol solid rubbers are still made and used in printing rolls, solvent-resistant spray hoses, gaskets, and gas-meter diaphragms. Many of the polysulfide products have been in use since the 1940s with an excellent track record. Continuing improvements keep these products competitive.

Physical Properties

The commercial polysulfides are made from bis-chloroethylformal (formal) as shown later in equation (12). In some products 1,2,3-trichloropropane is added as a branching agent. Table 1 shows typical properties of polysulfides available from the Rohm and Haas Co.

Table 1. Properties of LP Liquid Polysulfide Polymers[a]

Property specification requirements	LP-31	LP-2	LP-32	LP-12	LP-3	LP-33	LP-977	LP-980
Viscosity at 25°C, Pa·s[a]	95–155	41–52.5	41–52.5	41–52.5	0.94–1.44	1.5–2	10–15	10–15
Moisture content, %	0.12–0.22	0.3 max	0.27 max	0.27 max	0.1 max	0.1 max	0.26 max	0.26 max
Mercaptan content, %	1.0–1.5	1.50–2.00	1.50–2.00	1.50–2.00	5.9–7.7	5.0–6.5	2.5–3.5	2.5–3.5
General properties								
Average molecular weight	8,000	4,000	4,000	4,000	1,000	1,000	2,500	2,500
Pour point, °C	10	7	7	7	−26	−23	4	4
Branching agent, %	0.5	2.0	0.5	0.2	2.0	0.5	2.0	0.5
Average viscosity								
at 4°C, Pa·s[b]	740	380	380	380	9	16.5	77	77
at 65°C, mPa·s (=cP),	14,000	6,500	6,500	6,500	150	210	1,100	1,100
Low temperature flexibility[c] at 9 MPa[d], 69°C	−54	−54	−54	−54	−54	−54	−54	−54

[a] All products listed have flash point (PMCC) > 177°C. The specific gravity at 25°C ranges from 1.27 to 1.31. CAS Registry Number for all the LPs listed is [68611-50-7], ie, they are copolymers made from (**3**) and 1,2,3-trichloropropane, and sodium polysulfide.

[b] To convert Pa·s to P, multiply by 10.

[c] Cured compound.

[d] To convert MPa to psi, multiply by 145.

The solid polysulfide products are light brown millable rubbers. Thiokol ST [9065-29-6] (**2**) is made as in equation (12). Its Mooney viscosity (ML 1 + 3 at 100°C) ranges from 20 to 60. Thiokol FA [68611-48-3] is a copolymer made from formal (**3**) and ethylene chloride with sodium polysulfide; its Mooney viscosity (ML 1 + 4 at 121°C) ranges from 60 to 112. Both rubbers have excellent resistance to a wide range of chemicals. They also have low permeability to gases, water, and organic liquids. They have excellent low temperature flexibility, and they show superior resistance to the effects of sunlight, ozone, aging, and weathering.

$$HS(C_2H_4OCH_2OC_2H_4SS)_nC_2H_4OCH_2OC_2H_4SH$$

2

$$ClCH_2CH_2—O—CH_2—O—CH_2CH_2Cl$$

3

Chemical Properties

Curing Agents. The rich chemistry of the thiol end group provides versatility in modifying and curing polysulfide polymers. A recent review article describes reactions and mechanisms for curing agents commonly used with polysulfide polymers (3).

Two-Part Oxidative Curing. The most common means of curing polysulfides is by chain extension with oxidizing agents, eg, equation (1), where R—SH represents liquid polysulfide, O the oxidizing agent, and the product is a disulfide.

$$2\,R—SH + O \longrightarrow R—S—S—R + H_2O \quad (1)$$

Because thiols are easily oxidized, a host of organic and inorganic oxidants may be used. Mild oxidants such as oximes, nitro compounds, or air can be effective. Various oxidants have been used in special applications, but only a few are used in large-scale applications.

For a long time, lead(IV) oxide (PbO_2) was the most widely used oxidizing agent for the high molecular weight liquid polysulfides (mol wt > 2500). It was not suitable for lower molecular weight polymers because of the difficulty in controlling the strongly exothermic reaction. Since the early 1970s, manganese dioxide (MnO_2) has become the predominate oxidizing agent. Manganese dioxide [11129-60-5] has several advantages over lead, such as reduced toxicity, better pot life stability, and better light resistance, elasticity, and recovery for the cured rubber.

A newer curing system is sodium perborate monohydrate [10332-33-9] ($NaBO_2H_2O_2H_2O$). Since this is a well-known bleaching agent used in certain laundry cleaning formulations, it is produced on a large scale at a reasonable price. Sodium perborate offers several advantages as a curing agent for building sealants. One is that it has a light color rather than the dark color of manganese or lead oxides. Thus, it is nonstaining and sealants can be manufactured in a variety of colors. Sealants cured with sodium perborate have low modulus, excellent

elasticity, and outstanding resistance to water, weather, uv light, and mold, even without additives. They have good adhesion to most surfaces and are environmentally friendly.

One-Part Curing Systems. The inorganic peroxide curing agents for liquid polysulfides are activated by water. By formulating and packaging polysulfides under anhydrous conditions, one-part sealants are prepared. These cure when exposed to atmospheric moisture and are used in construction sealant applications. The curing agents most commonly used have been calcium peroxide, zinc peroxide/amine, zinc/lithium peroxide, or manganese dioxide. Sodium perborate is also effective in preparing light-colored, faster curing, one-part sealants.

Polysulfide polymers' resistance to moisture vapor transmission is a positive characteristic for applications like insulating glass sealants, but it is a drawback for one-part moisture curing sealants because it leads to relatively slow cure rates. Toray Thiokol has developed new faster curing one-part compositions based on polysulfides with silylthio end groups (4).

Epoxy Resins. Polysulfides may also be cured by reaction with epoxy resins according to the reaction in equation (2). Amines or other catalysts are used and often primary or secondary amine resins are cured together with the polysulfide.

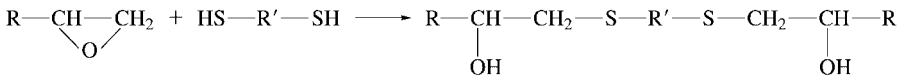

(2)

LP-3, the lowest molecular weight liquid polysulfide, is used as a reactive diluent to lower the viscosity of the formulation and to facilitate mixing and application of the resin. The liquid polysulfide also acts as a flexibilizer. The addition of LP-3 to epoxy formulations gives products with good flexibility, high impact strength, excellent chemical resistance, and good adhesion. ELP-3 [117527-71-6] (**4**) is an epoxy-terminated polysulfide derived from LP-3. An advantage of this product is its low odor, especially in comparison with the thiol-terminated LP-3.

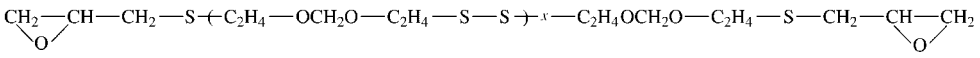

4

Diisocyanates or Polyisocyanates. The thiol end groups of the liquid polysulfides are quite reactive with isocyanates (eq. 3). Typical diisocyanates, such as 1,3-toluene diisocyanate (*m*-TDI) and diphenylmethane-4,4′-diisocyanate (MDI), are effective in curing liquid polysulfides. Using liquid polysulfides instead of the common hydroxy-terminated polymers brings the advantages of the polysulfide to the cured product. Thus, good chemical and solvent resistance, weatherability, adhesion, etc, can be attained. The isocyanate-cured systems have some advantages over oxidative-cured systems, such as improved adhesion to plastic substrates. There are also drawbacks to this method of curing. For example, water must be eliminated from the formulation to prevent foaming. This requires additional steps to dry all of the formulation ingredients (fillers, plasticizers, liquid polysulfide, etc) and to protect them from atmospheric moisture. Also, the mix ratio must be tightly controlled to give close to stoichiometric amounts of

polysulfide and isocyanate. Actually, a slight excess of isocyanate is usually used. For the oxidative-cured formulations, a significant excess of oxidant is used and the ratio is more forgiving. Furthermore, the isocyanates are more hazardous to work with than the commonly used oxidizing curing agents.

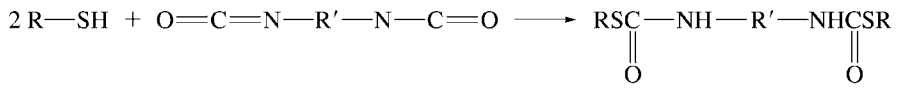

(3)

Phenolic Resins. At elevated temperatures, phenolic resins are cured with polysulfide resins through a condensation reaction. The product may be considered a block copolymer of the rigid phenolic resin and the flexible polysulfide. Thus, the polysulfide acts to flexibilize the resulting polymer.

Miscellaneous Curing Reactions. Other functional groups can react with the thiol terminal groups of the polysulfides to cross-link the polymer chains and build molecular weight. For example, aldehydes can form thioacetals and water. Organic and inorganic acids or esters can form thioesters. Active dienes such as diacrylates can add to the thiols (5). Examples of these have been mentioned in the literature, but none have achieved commercial significance.

Reactions of the Disulfide Group. Besides the thiol end groups, the disulfide bonds also have a marked influence on both the chemical and physical properties of the polysulfide polymers. One of the key reactions of disulfides is nucleophilic attack on sulfur (eq. 4). The order of reactivity for various thiophiles has been reported as $(C_2H_5O)_3P > R^-, HS^-, C_2H_5S^- > C_6H_5S^- > C_6H_5P, CN^- > SO_3^{2-} > OH^- > 2,4\text{-}(NO_2)_2C_6H_3S^- > N_3^- > SCN^-, I^-, C_6H_5NH_2$ (6). These thiophiles are capable of splitting the disulfide bond and thus reducing the molecular weight of the polymers.

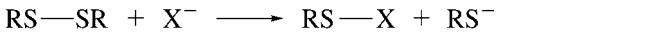

(4)

An important aspect of this is the splitting of the polymer chain with thiol (eq. 5) or mercaptide ion (thiol + base catalyst). In fact, sodium sulfide or organic monothiols, eg, mercaptoethanol or decylmercaptan, are utilized to lower the molecular weight of polysulfides or to limit the extent of curing reactions.

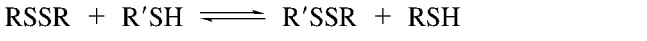

(5)

This reaction also plays a role in the degradation of polysulfides. A backbiting mechanism as shown in equation (6) results in formation of the cyclic disulfide (**5**). Steam distillation of polysulfides results in continuous gradual collection of (**5**). There is an equilibrium between the linear polysulfide polymer and the cyclic disulfide. Although the linear polymer is favored and only small amounts of the cyclic compound are normally present, conditions such as steam distillation, which removes (**5**), drives the equilibrium process toward depolymerization.

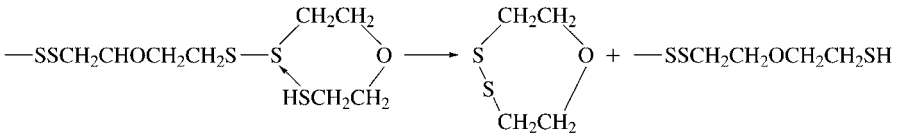

5 (6)

Another aspect of the splitting reaction (eq. 5) is that it allows for the potential recycle of cured polysulfide. Oxidatively cured polysulfides can be broken down by adding low molecular weight liquid polysulfide with mixing and heating. The resulting liquid material can be reworked and cured again (7). A related reaction is disulfide interchange (eq. 7). This process leads to redistribution of the polymers. For example, if thiol-terminated polymers made from different monomers are combined, they redistribute to form a random polymer. Thus, block copolymers of polysulfides are difficult to obtain. One way to make use of this phenomenon is shown in equation (8). Here a high molecular weight thiol-terminated polysulfide polymer is reduced to a lower molecular weight polymer with hydroxyl terminals. In this way a different functionality can be introduced into the end group.

$$\mathrm{RSSR} + \mathrm{R'SSR'} \longrightarrow 2\,\mathrm{RSSR'} \tag{7}$$

$$\mathrm{RSSR} + \mathrm{HOCH_2CH_2SSCH_2CH_2OH} \longrightarrow 2\,\mathrm{RSSCH_2CH_2OH} \tag{8}$$

Disulfide interchange also affects the physical properties of the cured polysulfide polymers. Polysulfide polymers undergo stress relaxation in a manner markedly different from conventional rubbers. Stress applied to stretch a sample of polysulfide rubber rapidly falls to zero. There is no change in the chemical and physical properties of the polymer recovered after the tests. The polysulfide polymer can be repeatedly recycled through the relaxation process. With vulcanized hydrocarbon rubbers, the stress decay takes place much more slowly and the activation energy for the relaxation is higher. Studies have attributed the behavior of the polysulfides to interchange between the polysulfide linkages of adjacent polymer chains (8). Addition of free sulfur or free thiol groups dramatically increases the rate of relaxation. Small amounts of free thiol can increase the rate several hundredfold (8).

Disulfides are susceptible to attack by strong oxidizing agents and this can result in decomposition of polysulfides. For example, nitric acid causes violent decomposition of polysulfide polymers.

Manufacture and Processing

Polysulfide polymers are made commercially according to the reactions shown in equations (9), (10), (11), (12). Details of the process and alternative approaches have been described (1,9). Although other dihalides can be used, its favorable

economics, minimal competition with ring formation, and the desirable physical properties of the resulting polymer have made bis-chloroethylformal the monomer of choice. Only occasionally are other dihalides used in special applications. 1,2,3-Trichloropropane [96-18-4] is sometimes added as a branching agent.

Many of the reagents used are hazardous and require special equipment and handling. There is an ongoing effort to minimize waste from the processes. Excess 2-chloroethanol (eq. 10) is removed from the product by distillation and recycled. Little waste is generated in equations (9) and (10). In the polymerization reaction (eq. 11), excess sodium polysulfide is required to drive the reaction to completion. Specialized equipment is used for washing and collecting the high molecular weight solid polymer in order to optimize its recovery. The wash water contains NaCl, the excess sodium polysulfide, and only small amounts of organics. The amount of excess Na_2S_x is minimized. High molecular weight solid (**2**) is converted to liquid polysulfide (**2**) by reaction with NaSH and Na_2SO_3.

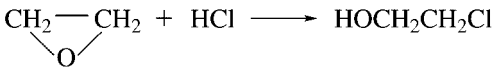

(9)

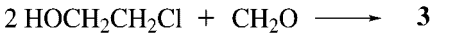

(10)

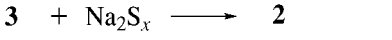

(11)

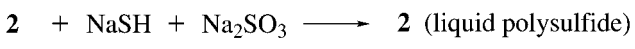

(12)

Formulation. Polysulfide-based sealants are formulated with appropriate ingredients to obtain the desired properties for a particular application. A typical formulation contains liquid polysulfide polymer, curing agent, cure accelerators (bases) or retarders (acids), fillers, plasticizers, thixotropes, and adhesion promoters.

For a two-part (A and B) sealant, Part A consists of liquid polysulfide, filler, plasticizer, thixotrope, and adhesion promoter. Part B contains the curing agent, plasticizer, a small amount of filler, and the accelerator or retarder. Part A can be mixed on any type of mixer that will ensure thorough dispersion. Generally, the equipment should utilize a double-arm kneading action mixer or a combination kneading action and high speed dispersing blade. Representative types are Change Can, Ross Planetary or Power Mixer, Meyers Mixer, Kneader Extruder, and Hockmeyer Mixer. Optimum dispersion of the fillers is obtained on a paint mill where the fillers are subjected to a grinding action that breaks down the agglomerates. If the mixer itself provides sufficient grinding of the pigments, then milling can be eliminated. The curing paste (Part B) can be prepared either by ball milling or three-roll paint milling. Paint milling is generally preferred; however, solvent-based pastes are best prepared in a ball mill to minimize solvent

loss. In order to obtain the most uniform results, pastes containing the accelerators or retarders should be aged for at least two weeks at room temperature prior to use.

The one-part sealant bases require drying the ingredients. Predrying the ingredients before manufacturing is cumbersome and expensive. Other alternatives include vacuum drying during manufacture, azeotropic distillation to remove water before moisture-sensitive components are added, and use of desiccants. The most common method is through the use of the desiccant barium oxide (10). The mixing is done on equipment as described, except the processes are carried out under an atmosphere of dry nitrogen and the final step is to combine the pastes into a single mix.

Specifications and Testing

Typical specifications for the polysulfide polymers are summarized in Table 1. Specifications for the sealants vary widely depending on the specific application and the needs of the applicators. Standards for sealant testing vary in different countries. Ultimately, the tests should simulate the environment the sealants will be exposed to and measure their performance under these conditions.

Examples of typical tests for sealants include those for stability, curing rate, and physical properties of cured sealants. Stability varies with formulation and storage temperature, and may range from 3 months to over 1 year. Curing characteristics include tack-free time (which varies with relative humidity and can range from hours to days), work life, and cure time. Cured sealant tests include adhesion to appropriate substrates, measurement of physical and mechanical properties (eg, tensile strength, elongation, modulus, hardness, compression and recovery, and low temperature flexibility), and assessing the effects of exposure to conditions in the environment where they will be used (uv light, water or special fluids, and a range of temperatures).

Health and Safety

As might be expected for sulfur-containing polymers, the polysulfides have a characteristic odor. Although the odor is somewhat objectionable, it probably arises from small amounts of low molecular weight dimercaptans or from cyclic sulfides or disulfides. The lower molecular weight polymers exhibit the strongest odor. Toxicity tests conducted on a representative LP brand liquid polysulfide used in a typical sealant application indicate that the polymers are not eye irritants and have a low order of oral toxicity ($LD_{50} > 5$ g/kg). Tests on the lower molecular weight liquid polysulfide products show similar findings. These materials are not eye or skin irritants, do not cause allergic skin reactions, and are not toxic when administered orally ($LD_{50} > 3.4$ g/kg). Rats exposed to a low molecular weight LP at a level of 230 mg/L for 4 h developed apparent eye and respiratory tract irritation. But this level far exceeds that which would be encountered in an industrial setting. Under the criteria set forth under OSHA's Hazard Communication Standard (29 CFR 1910.1200), liquid polysulfide products are classed as nonhazardous.

When considering sealants or other formulated products, the health and safety considerations relating to the other ingredients should be taken into account.

Economic Aspects

Worldwide production capacity of liquid polysulfides is about 36,000 t, with manufacturing sites in the United States, Japan, and Germany. Total consumption is about 27,000 t. Approximately 50% is for insulating glass sealants, 30% for construction applications, and ~10% for aircraft sealants. In addition, about 900 t of the solid polysulfide rubbers are sold each year.

Most of the polysulfide sales are in Europe, the United States, and Japan. Polysulfide sealants have ~83% of the market share of insulating glass sealants in Europe, 35% in the United States, and a total of ~60% worldwide. Polysulfides have only a modest share of the building sealant market. Polysulfides are virtually the only sealant specified for aircraft integral fuel tanks worldwide. In addition, they comprise about 90% of other aircraft sealant applications. The total volume used in the aircraft sealant market fluctuates with aircraft construction and repair.

Overall, demand for polysulfides in the United States is expected to remain flat for the next 5 years, but a 2–3% average annual increase in demand is expected in other countries (11) (see SEALANTS).

Uses

Insulating Glass Sealants. One of the largest scale applications of polysulfide polymers is as a sealant for insulating glass windows. The window consists of two panes of glass separated by a hollow spacer that is filled with desiccant to remove moisture or volatiles from the air space. This prevents condensation and fogging of the window at low temperature. Dual seal windows contain a primary seal along the edge of the spacer that is usually made from polyisobutylene (PIB). PIB has good resistance to moisture vapor transmission and extends the life of the unit. The outer edge of the unit is closed off with the secondary seal of polysulfide or other sealant material. The intermediate air space is sometimes filled with an inert gas such as argon to improve insulation and reduce noise. Polysulfide sealants have low permeability for water vapor or inert gas and can be used either in dual- or single-seal units. In the dual-seal units, if there are small leaks in the primary seal, the polysulfide provides a good backup. Other sealants such as silicones have high permeability, and can only be used in dual-seal units that rely on the integrity of the primary seal.

Besides water vapor and gas diffusion, other requirements for good edge sealants are water resistance, uv resistance, heat/cold resistance (−40 to 80°C), adhesion to glass and metal, and good characteristics for application. Polysulfide sealants have maintained an excellent record in use since the 1950s. Development of new polysulfides and sealant formulations continues in order to meet market needs of the 1990s.

Aircraft Sealants. Polysulfides have been used for sealing fuel tanks and aircraft structural components since the 1940s. There are stringent requirements for these sealants. They must have outstanding resistance to fuels and excellent adhesion to many different materials such as various metal alloys and protective coatings used in aircraft construction. The sealants must also perform in extremely variable weather conditions (12). The polysulfides have an excellent performance record.

Construction Sealants. In the 1950s, curtain wall construction became dominant in high rise buildings. This technique requires sealing of the joints against wind and weather. Sealants used up until that time were not suitable to withstand the temperature changes, sun, wind, rain, vibration, etc. Polysulfide-based sealants were developed for this application and have served in many large-scale projects since that time. Polysulfide construction sealants are used to seal glass in aluminum frames, concrete moving joints, steel/stone joints, and in other applications. For earlier sealants, in order to obtain good adhesion to the variety of substrates, primers were usually used. Besides the disadvantage of requiring application of the primer, there was the risk that the primer would not be properly or uniformly applied. More recently, polysulfide sealants have been developed that incorporate adhesion promoters in the formulation and eliminate the need for primers (13).

Below-Ground Sealants. Immersion in water for long periods or continuous exposure to high humidity are especially difficult conditions for organic-based materials to withstand. Sealants for use in water purification plants or wastewater treatment plants have special demands for physical, chemical, and microbiological properties. Polysulfide-based sealants have proved themselves useful in this area. Special consideration must also be given to the other ingredients, eg, fillers, plasticizers, adhesion promoters, or curing agents, in formulating for these applications (14).

The chemical and fuel resistance of polysulfides makes them useful as sealants and coatings for secondary containment areas, where they prevent chemicals, solvents, fuels, etc from seeping into the ground in the event of spillage or a storage tank leak (15). Polysulfide-based coatings and sealants are also used for bridges, air fields, and road construction.

Epoxy Flexibilizers. Polysulfides are useful as flexibilizers in epoxy resin formulations. Compounders can target the properties desired for a particular application through the selection and balance of the epoxy, the liquid polysulfide–epoxy ratio, curing agent, and filler. Most of the compounds are two-component: one containing the epoxy resin, the second containing polymer and curing agent. Probably, the most important factor is the ratio of polysulfide to epoxy resin. The most effective ratio ranges from 2 to 1 liquid polysulfide to epoxy. Liquid polysulfide–epoxy formulations are used for a variety of applications including adhesives, protective coatings, barrier coatings, electrical potting compounds, resilient plastic tooling materials, aggregate liquid polysulfide–epoxy mortars, and surface sealers.

Water Dispersions. Polysulfide products are offered as aqueous dispersions (Thiokol WD-6). These are useful for applying protective coatings to line fuel tanks and for concrete, wood, and in some cases fabrics, felt, leather, and paper.

It has been found that a stable emulsion can be made that contains both LP and manganese oxide curing agent. The emulsion can be thinned and applied as a spray coating. After it is applied, water evaporates and the LP cures to form a solid rubber (16).

Rubber Articles. The solid polysulfide rubber products Thiokol FA and Thiokol ST are used in the manufacture of printing rollers, printing blankets, gas-meter diaphragms, O-rings, and specialty molded items.

BIBLIOGRAPHY

"Polysulfide Polymers" in *EPST* 1st ed., Vol. 11, pp. 425–447, by M. B. Berenbaum, Thiokol Chemical Corp.; "Polysulfide" in *EPSE* 2nd ed., Vol. 13, pp. 186–196, by S. Ellerstein, Thiokol Chemical Corp.

1. H. Lucke, *ALIPS Aliphatic Polysulfides*, Hüthig & Wepf, Basel, Switzerland, 1994.
2. A. Duda and S. Penczec, in J. I. Kroschwitz, ed., *Encyclopedia of Polymer Science and Engineering*, Wiley and Sons, Inc., New York, 1989, pp. 246–368.
3. G. B. Lowe, *Int. J. Adhes. Adhesiv.* **17**, 345–348 (1997).
4. Jpn. Pat. 09255750 (1997), S. Yoshidie and Y. Minoru (to Toray Thiokol).
5. S. J. Hobbs, *Polym. Mater. Sci.* **67**, 415 (1992).
6. W. A. Pryor, *Mechanisms of Sulfur Reactions*, McGraw-Hill Book Co., Inc., New York, 1962, pp. 59–64.
7. Ger. Pat. Appl. DE 4142500 (1991), R. J. Hecktor and co-workers (to Metallgesellschaft AG).
8. A. V. Tobolsky and W. J. MacKnight, *Polymeric Sulfur and Related Polymers*, Wiley-Interscience, New York, 1965.
9. D. E. Vietti, *Comprehensive Polymer Science*, Vol. **5**, Pergamon Press, Oxford, U.K., 1989, pp. 533–542.
10. U.S. Pat. 3912696 (1975), J. I. Doughty (to Minnesota Mining and Manufacturing Co.).
11. J. G. Lacson, A. De Boo, and Y. Yoshida, *Chemical Economics Handbook*, SRI International, Menlo Park, Calif., 1999.
12. D. B. Paul, P. J. Hanhela, and R. H. E. Huang, *Polymer Science and Technology*, Plenum Press, New York, 1988, pp. 269–280.
13. A. R. Fiorillo and J. R. Harding, in D. H. Nicastro, ed., *Science and Technology of Building Seals, Sealants, Glazing and Waterproofing*, Vol. **4**, ASTM STP 1243, ASTM, Philadelphia, Pa., 1994.
14. T. Lee, *Science and Technology of Building Sealants, Glazing and Waterproofing*, Vol. **4**, ASTM STP 1243, ASTM, Philadelphia, Pa., 1995.
15. T. Lee, T. Rees, and A. Wilford, in C. J. Parise, ed., *Science and Technology of Building Seals, Sealants, Glazing and Waterproofing*, STP 1168, ASTM, Philadelphia, Pa., 1992, pp. 47–56.
16. U.S. Pat. 5073577 (1991), P. H. Anderson (to Morton International, Inc.).

GENERAL REFERENCES

M. B. Berenbaum, in N. G. Gaylord, ed., *Polyethers*, Part III, Vol. **13**, Wiley-Interscience, New York, 1962, p. 43.

E. R. Bertozzi, *Rubber Chem. Technol.* **41**, 114 (1968).
D. Vietti, in J. I. Kroschwitz, ed., *Encyclopedia of Chemical Technology*, Vol. **19**, John Wiley & Sons, Inc., New York, 1996, p. 933.
E. M. Fettes, in N. Kharasch, ed., *Organic Sulfur Compounds*, Vol. **1**, Pergamon, London, 1961, p. 266.
H. Lucke, *ALIPS Aliphatic Polysulfides*, Hüthig & Wepf, Basel, Switzerland, 1994.
J. R. Panek, in N. G. Gaylord, ed., *Polyethers*, Part III, Vol. **13**, Wiley-Interscience, New York, 1962, p. 115.
A. V. Tobolsky and W. J. MacKnight, *Polymeric Sulfur and Related Polymers*, John Wiley & Sons, Inc., New York, 1965.
A. V. Tobolsky, *The Chemistry of Sulfides*, Wiley-Interscience, New York, 1968.
D. E. Vietti, *Comprehensive Polymer Science*, Vol. **5**, Pergamon, London, 1989, p. 533.

DAVID VIETTI
Rohm and Haas Company

POLYSULFONES

A polysulfone is characterized by the presence of the sulfone group as part of its repeating unit. Polysulfones may be aliphatic or aromatic. Aliphatic polysulfones were synthesized by radical-induced copolymerization of olefins and sulfur dioxide and characterized many years ago. However, they never demonstrated significant practical utility because of their relatively unattractive physical properties, notwithstanding the low cost of their raw materials (1,2). The polysulfones discussed in this article are those based on an aromatic backbone structure. The term polysulfones is used almost exclusively today to denote aromatic polysulfones.

Polysulfones comprise a class of amorphous thermoplastic polymers characterized by high glass-transition temperatures, good mechanical strength and stiffness, and outstanding thermal and oxidative resistance. These polymers are characterized by the presence of the para-linked diphenylenesulfone group

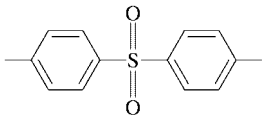

as part of their backbone repeat units. By virtue of their mechanical, thermal, and other desirable characteristics, these polymers enjoy an increasingly wide and diversified range of commercial applications. The basic repeat unit of any polysulfone contains sulfone, aryl, and ether units as part of the main backbone structure. These polymers are thus often referred to in the polymer literature as poly(arylethersulfone)s. Other names include polysulfones, polyethersulfones, and polyarylsulfones, and the lack of standardized nomenclature has often resulted

Encyclopedia of Polymer Science and Technology. Copyright John Wiley & Sons, Inc. All rights reserved.

Table 1. Chemical Structures and Glass-Transition Temperatures (T_g) of Polysulfone, Polyethersulfone, and Polyphenylsulfone

Polymer	CAS nos.	Repeat unit structure	T_g, °C
Polysulfone (PSF)	[25135-51-7]	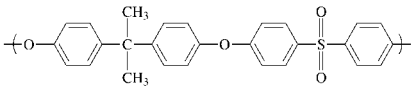	185
Polyethersulfone[a] (PES)	[25667-42-9]	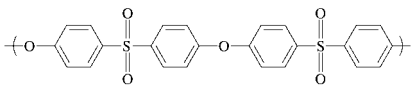	220
Polyphenylsulfone (PPSF)	[25608-64-4]	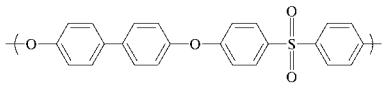	220

[a]PES repeat unit structure can alternately be drawn as

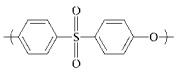

in confusion over the meaning of a designation. The different designations are somewhat arbitrary and all refer to the same class of polymers.

In addition to sulfone, phenyl, and ether moieties, the main backbone of polysulfones can contain a number of other connecting units. The most notable such connecting group is the isopropylidene linkage, which is part of the repeat unit of the well-known bisphenol A based polysulfone. It is difficult to clearly describe the chemical makeup of polysulfones without reference to the chemistry used to synthesize them. There are several routes for the synthesis of polysulfones, but the one which has proved to be most practical and versatile over the years involves aromatic nucleophilic substitution. In this polycondensation, equimolar quantities of 4,4′-dihalodiphenylsulfone [usually dichlorodiphenylsulfone (DCDPS)] and a bisphenol are allowed to react in the presence of base to form the aromatic ether bonds and eliminate an alkali salt as a by-product. Today, this route is employed almost exclusively for the manufacture of polysulfones on a commercial scale.

The diphenylsulfone group is supplied to the repeat unit of all polysulfones by DCDPS. Differentiation among various polysulfones comes from the choice of bisphenol. Three different and commonly used bisphenols lead to three commercially important polysulfones referred to generically by the common names polysulfone (PSF), polyethersulfone (PES), and polyphenylsulfone (PPSF). Other common shorthand designations for polysulfone and polyphenylsulfone are PSU and PPSU, respectively. The repeat units of these polymers are shown in Table 1.

Polymerization

Nucleophilic Substitution Route. Commercial synthesis of poly(arylethersulfone)s is accomplished via the nucleophilic substitution polycondensation route. This synthesis route, discovered at Union Carbide in

the early 1960s (3,4), involves reaction of the bisphenol of choice with 4,4′-dichlorodiphenylsulfone in a dipolar aprotic solvent in the presence of an alkali base. Examples of dipolar aprotic solvents include *N*-methyl-2-pyrrolidinone (NMP), dimethyl acetamide (DMAc), sulfolane, and dimethyl sulfoxide (DMSO). Examples of suitable bases are sodium hydroxide, potassium hydroxide, and potassium carbonate. In the case of polysulfone (PSF) synthesis, the reaction is a two-step process in which bisphenol A [80-05-7] is first converted *in situ* to the dialkali metal salt (1) by reaction with base (eg, two molar equivalents of NaOH), followed by the nucleophilic substitution reaction of (**3**) with 4,4′-dichlorodiphenylsulfone [80-07-9] (2). Polysulfone is typically prepared as described in Reference 5 according to equation (1), where $n = 40–60$. The minimum degree of polymerization is dictated by the minimum molecular weight required to achieve useful mechanical properties from the polymer. For polysulfone, this corresponds to a reduced viscosity of about 0.35 dL/g (in chloroform at 25°C and 0.2 g/dL concentration).

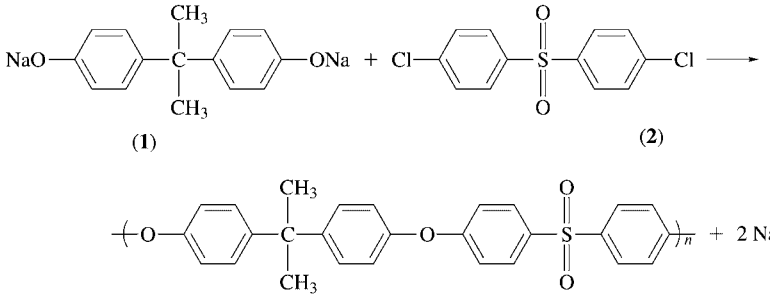

(1)

The rate of polymerization in this type of reaction depends on both the basicity of the bisphenol salt and the electron-withdrawing capacity of the activating group (in this case sulfone) in the dihalide monomer. Also affecting reactivity is the electronegativity of the halogen in the dihalide monomer. The difluoride-based sulfone monomer is more reactive than the dichloride and thus gives higher polymerization rates, but the dichloride is by far the more economical raw material. Another important consideration in reactivity and the attainment of high molecular weight is the purity of the 4,4′-isomer in the dichlorodiphenyl sulfone monomer. Chlorines in the meta position on the phenyl ring are not activated and do not undergo nucleophilic displacement. Hence, a significant presence of the 3,4′-isomer of the sulfone monomer can act as a monofunctional terminating species for the polycondensation and prevent the attainment of target molecular weights. Factors governing rates of reaction have been discussed (6).

DMSO is an effective solvent for the polymerization as it affords good solubility for both the polymer and the disodium salt of bisphenol A [2444-90-8]. Typical polymerization temperatures for polysulfone are in the range 130–160°C. At temperatures below 130°C, the polymerization slows down considerably because of poor solubility of the disodium salt of bisphenol A.

The reaction of NaOH with bisphenol A generates water. This water must be thoroughly removed from the system to allow the reaction to be driven to

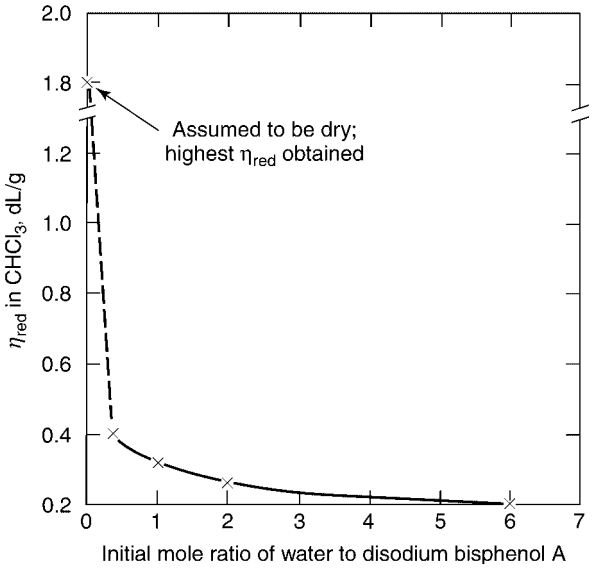

Fig. 1. Effect of water presence in polysulfone polymerization on maximum attainable polymer reduced viscosity.

completion, and more importantly, to prevent hydrolysis of the DCDPS monomer (**4**). Failure to remove all of the water prior to the introduction of DCDPS results in regeneration of NaOH, which rapidly reacts with DCDPS to form the monosodium salt of 4-chloro-4′-hydroxydiphenylsulfone [18995-09-0] (**6**) (6).

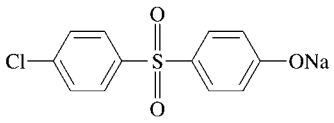

(**3**)

With as little as 0.5% hydrolysis of the sulfone monomer, the polymerization stoichiometric balance is sufficiently upset to prevent high molecular weight polymer from being achieved. The dependence of maximum attainable PSF molecular weight on water content during polymerization can be inferred from Figure 1.

Molecular weight control for this type of condensation polymerization, eg, by nucleophilic substitution, is typically achieved by one of several methods: (*1*) the addition of a monohalogen compound such as chloromethane once target molecular weight has been achieved in the reaction vessel (such compounds terminate chain growth by reacting with available sodium phenate end groups to form nonreactive methoxyl end groups on the chains); (*2*) the use of excess DCDPS monomer to limit the maximum attainable molecular weight by means of stoichiometric imbalance; and (*3*) the use of monohydric phenols or monohalo-activated aromatic compounds as chain terminators. Generally, the first or the second method (or a combination of them) is used. In the case of termination methods (*2*) or (*3*), the terminator

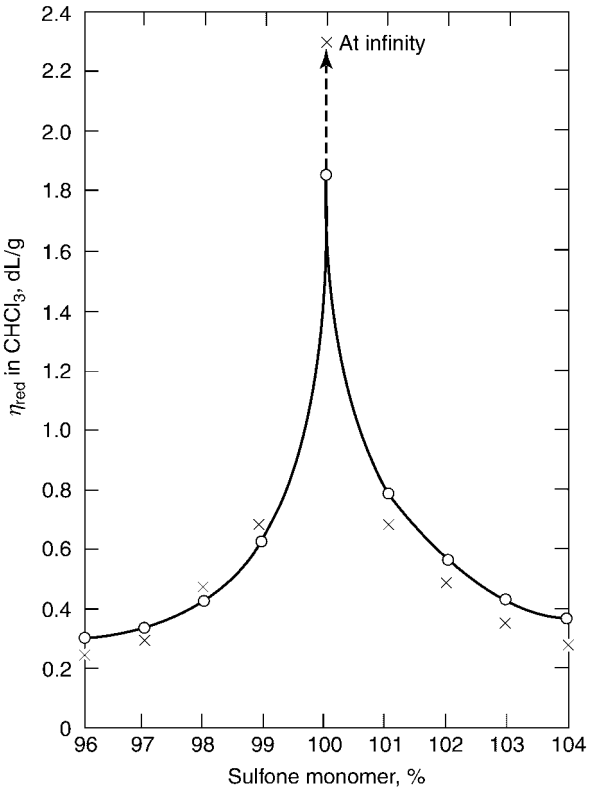

Fig. 2. Effect of stoichiometric imbalance in polysulfone polymerization on maximum attainable polymer reduced viscosity where × is theoretical and ○, experimental.

is typically added at the beginning of the reaction along with the monomer. The actual effect of any such terminator depends on its relative reactivity as well as the amount added. The terminator unbalances the stoichiometry of the two monomers, thereby placing a ceiling on the maximum attainable degree of polymerization according to Carothers' principle of functionality. A mole ratio of unity for the two parent monomers results in the highest attainable molecular weight as illustrated in Figure 2. The most favorable reaction rates are also achieved by maintaining the monomer ratio at or very near unity.

The polymerization of polyethersulfone (PES) and polyphenylsulfone (PPSF) are analogous to that of PSF, except that in the case of these two polymers, solvents that are higher boiling than DMSO are needed because of the higher reaction temperatures required. Diphenyl sulfone, sulfolane, and NMP are examples of suitable solvents for PES and PPSF polymerizations. Chlorobenzene or toluene are used as cosolvents at low concentrations. These cosolvents form an azeotrope with water as they distill out of the reaction mixture, thereby keeping the polymerization medium dehydrated. Potassium carbonate is a suitable choice for base. The syntheses of PES and PPSF also differ from that of PSF in that the reaction is carried out in a single-step process. In other words, the formation of the dipotassium salt of the bisphenol is not completed in a separate first step. Equations (2)

and (3) represent polymerizations based on the dipotassium salts of bisphenol S and biphenol to make PES and PPSF, respectively.

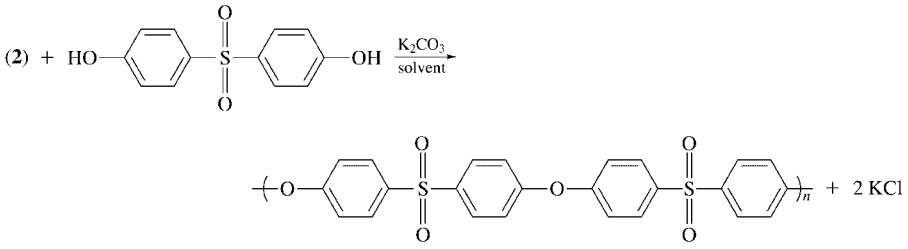

(2)

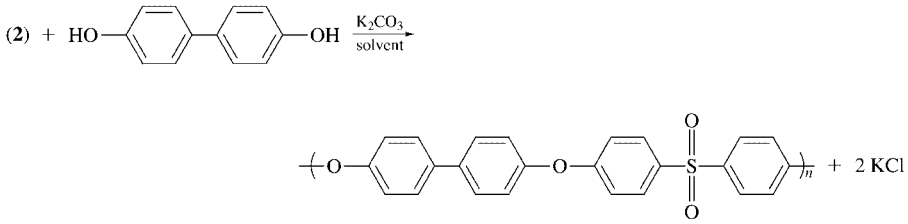

(3)

An alternative synthesis route for PES involves the partial hydrolysis of dichlorodiphenyl sulfone (**4**) with base to produce 4-chloro-4′-hydroxydiphenylsulfone [7402-67-7] followed by the polycondensation of this difunctional monomer in the presence of potassium hydroxide or potassium carbonate (7).

As a variation on the base-catalyzed nucleophilic displacement chemistry described, polysulfones and other polyarylethers have been prepared by cuprous chloride-catalyzed polycondensation of aromatic dihydroxy compounds with aromatic dibromo compounds. The advantage of this route is that it does not require that the aromatic dibromo compound be activated by an electron-withdrawing group such as the sulfone group. Details of this polymerization method, known as the Ullman synthesis, have been described (8).

A method for the polymerization in nondipolar aprotic solvents has been developed and reported (9,10). The method relies on phase-transfer catalysis. Polysulfone is made in chlorobenzene as solvent, with (2.2.2)cryptand as catalyst (9). Less reactive crown ethers require dichlorobenzene as solvent (10). High molecular weight polyphenylsulfone can also be made by this route in dichlorobenzene; however, only low molecular weight PES is achievable by this method. Crosslinked polystyrene-bound (2.2.2)cryptand is found to be effective in these polymerizations which allow simple recovery and reuse of the catalyst.

Other Synthesis Routes. Several alternative routes to the nucleophilic substitution synthesis of polysulfones are possible. Polyethersulfone can be synthesized by the electrophilic Friedel–Crafts reaction of bis(4-chlorosulfonylphenyl)ether [121-63-1] with diphenyl ether [101-84-8] (11–13).

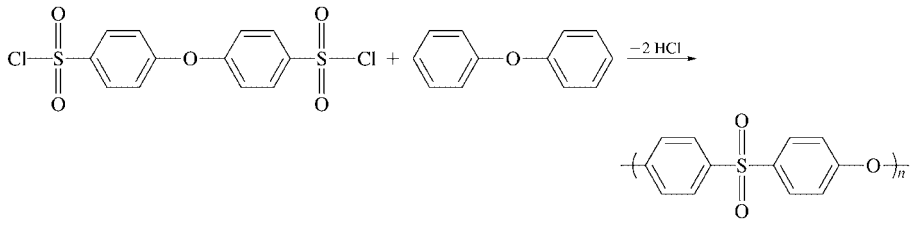

(4)

The same reaction can be carried out with 4-chlorosulfonyldiphenyl ether [1623-92-3] as a single monomer.

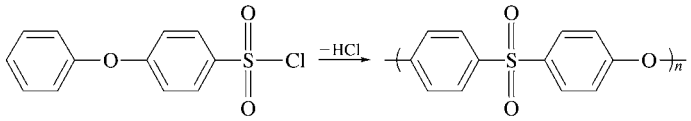

(5)

The single-monomer route (eq. (5)) is preferred, as it gives more para-linked repeat units and therefore a straighter backbone than the two-monomer route. Other sulfone-based polymers can be similarly produced from sulfonyl halides with aromatic hydrocarbons. The key step in these polymerizations is the formation of the carbon–sulfur bond. High polymers are achievable via this synthesis route although the resulting polymers are not always completely linear.

An elegant synthesis method which is specific to sulfone polymers containing phenyl–phenyl linkages (such as PPSF) is the nickel-catalyzed coupling of aryl dihalides. The scheme for this synthesis is composed of two steps. First, an aromatic dihalide intermediate is formed which carries the backbone features of the desired polymer. This aromatic dihalide intermediate is then self-coupled in the presence of zero-valent nickel, triphenylphosphine, and excess zinc to form the biphenyl- or terphenyl-containing polymer. Application of this two-step scheme to PPSF can be depicted as follows.

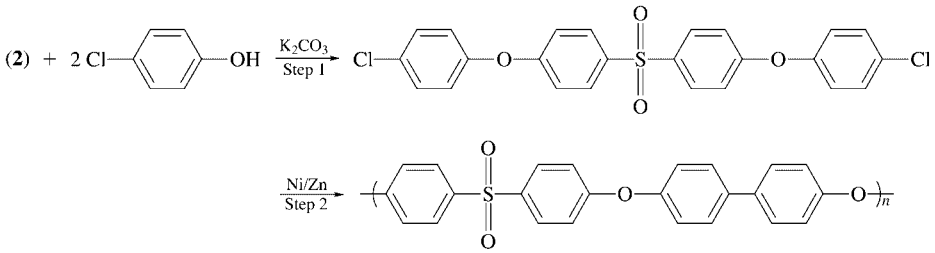

The first step in this scheme is a classical aromatic nucleophilic substitution. Details of the method have been expounded upon (14–17). References 14 and 15 are concerned with the synthesis of the diaryl halide intermediate, whereas References 16 and 17 discuss the synthesis of the polymers, with emphasis on the polymerization of PPSF by this route.

Oxidative coupling of aromatic compounds has been applied successfully to synthesize a polyarylethersulfone via the Scholl reaction (18). High molecular weight polymer was obtained by treatment of 4,4′-di(1-napthoxy)diphenylsulfone and 4,4′-di(napthoxy)benzophenone with ferric chloride. Equimolar amounts of the Lewis acid are required and the method is limited to napthoxy-based monomers and other systems that can undergo the Scholl reaction.

Properties

Structure–Property Relationships. The characteristic feature of each of the polymers in Table 1 is the highly resonant diaryl sulfone grouping. As a consequence of the high oxidation state of the sulfur atom being in its highest state of oxidation and the enhanced resonance of the sulfone group in the para position, these resins offer outstanding thermal stability and resistance to thermal oxidation. The thermal stability is further augmented by the high bond dissociation energies inherent in the aromatic backbone structure. As a result, these polymers can be melt-fabricated at temperatures of up to 400°C with no adverse consequences. The high degree of oxidative stability also allows for prolonged or continuous exposure to temperatures of anywhere between 150 and 190°C, depending on polymer, formulation, and use conditions. The ether linkages in these polymers contribute to chain flexibility, leading to mechanical toughness and favorable melt rheological properties for conventional thermoplastic fabrication. The relatively inert ether and sulfone backbone functionalities contribute to resistance against hydrolysis and chemical attack by acids and bases. Medical and food contact applications for polysulfones are possible in part because of this characteristic.

The high glass-transition temperatures (T_g) of polysulfones are attributed to the rigid phenyl rings in the backbone and also the sulfone group, which increases T_g by providing strong dipole–dipole interactions between chains and by restricting rotation of the aromatic units relative to other connecting groups. The ether groups in these polymers are the main flexibilizing units, and the T_gs of polysulfones are inversely related to the ether content in the backbone on a repeat unit weight basis. Other connecting groups either increase or decrease chain rigidity and T_g according to an increase or decrease in the conformal freedom and polarity of those units. The most convenient way to tailor properties of a polysulfone to specific needs is through the appropriate selection of the bisphenol. The T_gs of polysulfones based on the polycondensation of DCDPS with different bisphenols are listed in Table 2.

The three polysulfones in Table 1 exhibit several important common attributes, but there are distinguishing features for each member of this group. Examination of the structures of the repeat units shows that a primary distinguishing feature of PES is that it contains almost double the sulfone group content on a weight basis compared to PSF. Another differentiation is that the flexibilizing isopropylidene unit is absent in PES. As a consequence of these structural changes, the T_g of PES is 35°C higher than that of PSF. On the other hand, because the sulfone group is the most hygroscopic moiety in the backbone of these polymers and the isopropylidene group is hydrophobic, the moisture uptake at

Table 2. Glass-Transition Temperatures of Polysulfones Produced from the Polycondensation of 4,4′-dichlorodiphenylsulfone with Various Bisphenols[a]

Bisphenol	Structure	T_g[b], °C
4,4′-dihydroxydiphenyl oxide	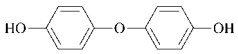	170
4,4′-dihydroxydiphenyl sulfide	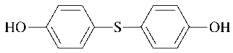	175
4,4′-dihydroxydiphenyl methane	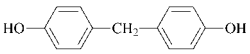	180
2,2′-bis(hydroxyphenyl)-propane	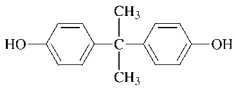	185
Hydroquinone	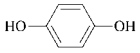	200
2,2′-bis(hydroxyphenyl)-perfluoropropane	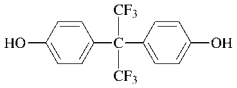	205
4,4′-dihydroxydiphenyl phenone	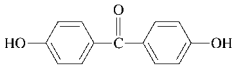	205
4,4′-dihydroxydiphenyl sulfone	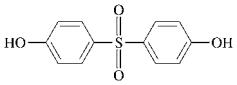	220
4,4′-dihydroxydiphenyl	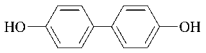	220
1,4-bis(4-hydroxyphenyl) benzene		250
4,4′-bis(4″-hydroxybenzenesulfonyl) diphenyl	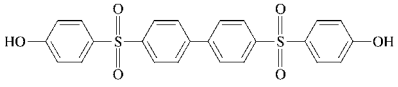	265

[a]Ref. 17.
[b]Glass-transition temperatures reported to nearest 5°C.

equilibrium is significantly lower for PSF than it is for PES (Table 3). The ability to minimize water absorption of a polymer is desirable for most engineering applications. Thus, backbone structure of a polysulfone is tied to physical properties and ultimately to performance and suitability for various applications.

Mechanical properties of aromatic polysulfones are also intimately tied to backbone structure. For the achievement of good strength and toughness together with favorable melt processing characteristics, the first and foremost requirement is a linear (unbranched) and para-linked chemical structure for the aryl groups in the backbone. The mechanism of permanent deformation is not the same in all polysulfones. Rather, it is dependent on subtle backbone structural features, the best illustration of which is the significant improvement in impact and toughness properties of PPSF over those of PES and PSF. The dependence of polysulfone mechanical toughness on backbone structural features has been discussed in detail (19).

Table 3. Physical and Thermal Properties of PSF, PES, and PPSF

Property	ASTM test method	PSF	PES	PPSF
Color		Light yellow	Light amber	Light amber
Clarity		Transparent	Transparent	Transparent
Haze[a], %	D1004	<7	<7	<7
Light transmittance[b], %		80	70	70
Refractive index	D1505	1.63	1.65	1.67
Density, g/cm^3	D1505	1.24	1.37	1.29
Glass-transition temperature[c], °C		185	220	220
Heat deflection temperature[d], °C	D648	174	204	207
Continuous service temperature[e], °C		160	180	180
Coefficient of linear Thermal expansion	D696	5.1×10^{-5}	5.5×10^{-5}	5.5×10^{-5}
Specific heat at 23°C, J/g·K		1.00	1.12	1.17
Thermal conductivity, W/m·K	C177	0.26	0.18	0.35
Water absorption, %				
In 24 h	D570	0.22	0.61	0.37
At equilibrium	D570	0.62	2.1	1.1
Mold shrinkage, cm/cm	D955	0.005	0.006	0.006
Temperature @ 10% TGA[f] wt. loss				
In nitrogen		512	547	550
In air		507	515	541

[a] As measured on 3.1-mm thick specimens.
[b] Typical values—varies with color.
[c] Onset value as measured by differential scanning calorimetry.
[d] As measured on 3.1-mm thick ASTM specimens under a load of 1.82 MPa.
[e] Practical maximum long-term use temperatures for PSF and PES based on UL-746 thermal rating data; value for PPSF is an estimate.
[f] Thermogravimetric analysis run at heating rate of 10°C/min and 20 mL/min gas (nitrogen or air) flow rate.

Physical, Chemical, and Optical Properties. Aromatic polysulfones possess several common key attributes including high T_gs (generally >170°C) and a high degree of thermal oxidative stability (Table 3). Thermal oxidative stability of PSF, PES, and PPSF can be inferred from the thermogravimetric data shown in Figure 3. Because of their fully amorphous nature, these resins exhibit optical transparency. The T_g of polysulfones reduced via nucleophilic polycondensation can be tailored by the choice of the bisphenol as illustrated in Table 2. By virtue of the chemically nonlabile aromatic ether backbone, these polymers exhibit superb resistance to hydrolysis in hot water and steam environments. Furthermore, they can withstand acidic and alkali media over a wide range of concentrations and temperatures.

In addition to conferring transparency on these polymers, the amorphous noncrystallizable nature of polysulfones assures minimal shrinkage during

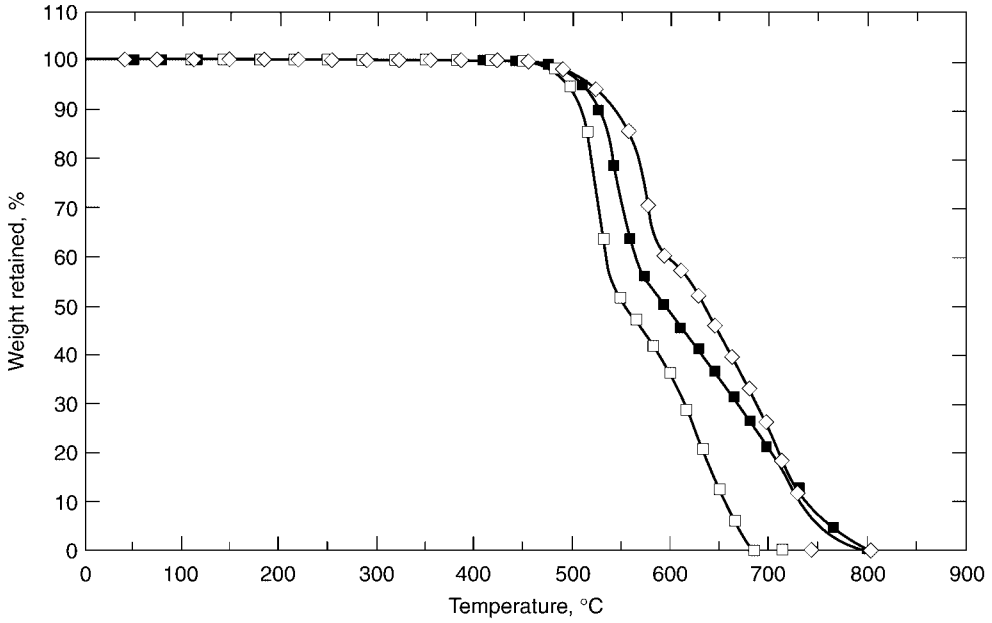

Fig. 3. Thermogravimetric analysis (TGA) curves in air for PSF (□), PES (■), and PPSF (◇). TGA in nitrogen at a heating rate of 10°C/min. From Ref. 17.

fabrication of the resins into finished parts. The absence of crystallinity also assures dimensional stability during the service life of the parts where high use temperatures are encountered. Good dimensional stability is important to many structural, engineering, and electronic applications.

Although commercially available polysulfones are transparent in their natural form, they show a slight yellow-amber tinge. This color is related to the high melt processing temperatures required during resin manufacture and finishing steps. Great progress has been made over the years in controlling and minimizing color (yellowness) in polysulfones. Among the three commercially available polysulfones, the bisphenol A based polymer (PSF) exhibits the lowest color and highest transmittance of visible light. The light transmittance value ranges given in Table 3 are based on the color ranges that are typical for commercially available grades. Because of their highly aromatic character, sulfone polymers exhibit high refractive indices relative to amorphous polymers based on olefinic or other aliphatic backbones.

Because of the presence of the sulfone moiety, polysulfones are slightly hygroscopic. Absorbed water expands linear dimensions of a polysulfone of the order of 0.010–0.012% for every 0.1 wt% of moisture absorbed. This dimensional change is relatively small, but it can be important in applications where very close dimensional tolerances are a requirement. In addition to effecting small dimensional changes, absorbed moisture causes a slight plasticization of the plastic, contributing to some lowering of stiffness and strength in hot, wet environments. This effect is again small and can easily be compensated for by judicious part design and engineering.

Mechanical Properties. Polysulfones are rigid and tough with practical engineering and strength and stiffness properties even without reinforcement. Their strength and stiffness at room temperature are high compared to traditional aliphatic backbone amorphous plastics. The polymers exhibit ductile yielding over a wide range of temperatures and deformation rates. High unnotched impact resistance has been tied to a second-order (β) transition which is observed in these polymers under dynamic mechanical thermal analysis. The β-transition occurs at around -100°C and is believed to be due to two mechanisms. The first involves 180° flips of aromatic units around the ether bond (20). The second has been proposed to be a concerted motion of the sulfone group with complexed, absorbed water (21). The presence of moisture increases the magnitude of the β-transition peak, although moisture is not necessary for the existence of the transition. The effect of polysulfone backbone structure on the sub-T_g relaxations has been the subject of detailed study (22).

The room temperature mechanical properties of bisphenol A, bisphenol S, and biphenol-based polysulfones are given in Table 4. The elongation at yield of these polymers is highest for PPSF, while PES offers slightly higher tensile strength than the other two polymers. Otherwise, the tensile and flexural properties for these three polymers are quite comparable. The main distinguishing

Table 4. Typical Room-Temperature Mechanical Properties of PSF, PES, and PPSF

Property	ASTM test method	PSF	PES	PPSF
Tensile[a] (yield) strength, MPa[b]	D638	70.3	83.0	70.0
Tensile modulus, GPa[c]	D638	2.48	2.60	2.30
Elongation at yield, %	D638	5.7	6.5	7.2
Elongation at break, %	D638	75	40	90
Flexural strength, MPa[b]	D790	106	111	105
Flexural modulus, GPa[c]	D790	2.69	2.90	2.40
Compressive strength, MPa[b]	D695	96	100	99
Compressive modulus, GPa[c]	D695	2.58	2.68	1.73
Shear (yield) strength, MPa[b]	D732	41.4	50	62
Notched Izod impact, J/m[d]	D256	69	85	694
Unnotched Izod impact	D256	NB[e]	NB	NB
Tensile impact, kJ/m^2[f]	D1822	420	340	400
Poisson ratio, at 0.5% strain	–	0.37	0.39	0.42
Rockwell hardness	D785	M69	M88	M86
Abrasion resistance[g], mg/1000 cycles	D1044	20	19	20

Note: These and other properties reported throughout, as well as the summary of possible applications for these resins are based on the best available information. Including the information is not intended to be taken as a recommendation for a particular use, or as an endorsement of any particular material.

[a]Tensile, flexural, and impact properties based on 3.1-mm thick ASTM specimens.

[b]To convert MPa to psi, multiply by 145.

[c]To convert GPa to psi, multiply by 145,000.

[d]To convert J/m to ft·lbf/in., divide by 53.38.

[e]No break.

[f]To convert kJ/m^2 to ft·lbf/in.^{2}, divide by 2.10.

[g]Taber abrasion test using CS-17 wheel and 1000-g load for 1000 cycles.

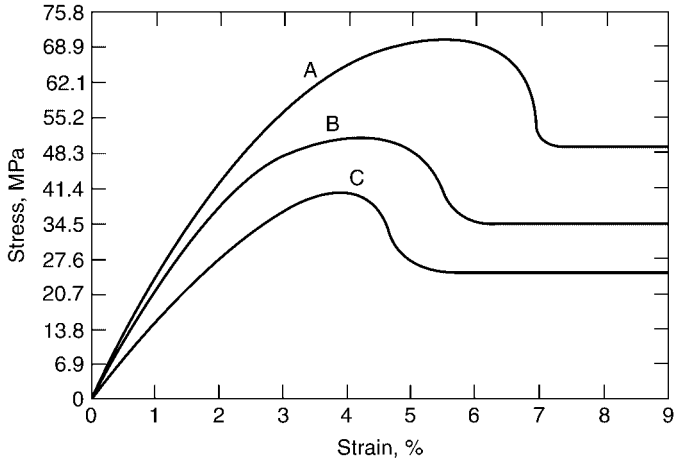

Fig. 4. Tensile stress–strain curves for polysulfone showing yield behavior at A, 20°C; B, 99°C; and C, 149°C. To convert MPa to psi, multiply by 145.

feature in the mechanical properties of PPSF is its "supertough" behavior exemplified by a very high value for notched impact strength. In addition, PPSF has the ability to retain a high degree of ductility after prolonged heat exposure. The data in Table 4 represent short-term mechanical properties under simple loading conditions. These values should be regarded as typical values for generic polysulfone, polyethersulfone, and polyphenylsulfone of practical molecular weights. Assessment of the mechanical performance of an engineering polymer for a specific end use should include consideration of the long-term aspects such as creep and fatigue properties where applicable. Temperature and environmental factors should also be taken into consideration.

The effect of temperature on tensile stress–strain behavior of PSF is depicted in Figure 4. The resin continues to exhibit useful mechanical properties at temperatures up to 160°C under prolonged or repeated thermal exposure. This temperature limit is extended to about 180°C in PES and PPSF. The tensile and flexural properties as well as resistance to cracking in chemical environments can be substantially enhanced by the addition of fibrous reinforcements such as chopped glass fiber. Mechanical properties at room temperature for glass fiber-reinforced polysulfone, polyethersulfone, and polyphenylsulfone are shown in Table 5.

Flammability. An important consideration in the selection of thermoplastic resins involves the need for good flame retardancy characteristics (see FLAMMABILITY). Polysulfones exhibit excellent inherent burning resistance characteristics compared with those of many engineering thermoplastics. The wholly aromatic polysulfones such as PES and PPSF possess particularly outstanding flame retardancy and very low smoke release characteristics. The flammability of PSF is also good but can be enhanced further by the addition of small proportion of a nonhalogen-based flame retardant. This forms the basis of the Udel P-1720 commercial polysulfone grade from British Petroleum. Flammability properties of various polysulfones are given in Table 6.

Table 5. Typical Physical and Mechanical Properties of Glass Fiber-Reinforced (GR) Polysulfone, Polyethersulfone, and Polyphenylsulfone

		Polysulfone			Polyethersulfone			Polyphenylsulfone
Property	ASTM test method	10% GR	20% GR	30% GR	10% GR	20% GR	30% GR	30% GR
Tensile strength, MPa[a]	D638	77.9	96.5	108	86	105	126	120
Tensile modulus, GPa[b]	D638	3.65	5.17	7.38	3.8	5.7	8.6	9.2
Tensile elongation, %	D638	4.1	3.2	2.0	5.8	3.2	1.9	2.4
Flexural strength, MPa[a]	D790	128	148	154	145	162	179	173
Flexural modulus, GPa[b]	D790	3.79	5.52	7.58	4.1	5.2	8.1	8.0
Izod impact, J/m[c]	D256	64	69	74	48	59	75	75
Tensile impact, kJ/m^2[d]	D1822	101	114	109	59	65	71	83
Heat deflection temperature, °C	D648	179	180	181	211	214	216	210
CLTE, mm/mm·°C	D696	3.6	2.5	2.0	3.6	3.1	3.1	–
Specific gravity	D1505	1.33	1.40	1.49	1.43	1.51	1.58	1.53
Mold shrinkage, mm/mm	D955	0.004	0.003	0.002	0.005	0.004	0.003	0.003

[a]To convert MPa to psi, multiply by 145.
[b]To convert GPa to psi, multiply by 145,000.
[c]To convert J/m to ft·lbf/in., divide by 53.38.
[d]To convert kJ/m^2 to ft·lbf/in.^{2}, divide by 2.10.

Table 6. Flammability and Burning Behavior of PSF, PES, and PPSF

Property	Test method	PSF	PES	PPSF
Flammability rating	UL-94	V-0 at 6.1 mm[a]	V-0 at 0.8 mm[a]	V-0 at 0.8 mm[a]
Limiting oxygen index	ASTM D286	30.0	38.0	38.0
Smoke density[b]	ASTM E662	90 at 1.5 mm[a]	35 at 6.2 mm[a]	30 at 6.2 mm[a]
Self-ignition temperature, °C	ASTM D1929	621	502	–

[a]Thickness.
[b]Specific optical density, D_m - flaming condition.

Table 7. Electrical Properties of PSF, PES, and PPSF

Property	ASTM test method	PSF	PES	PPSF
Dielectric strength (3.2 mm[a]), kV/mm	D149	16.6	15.5	14.6
Volume resistivity, ohm·cm	D257	7×10^{16}	9×10^{16}	9×10^{15}
Dielectric constant	D150			
At 60 Hz		3.18	3.65	3.44
At 10^3 Hz		3.17	3.65	3.45
At 10^6 Hz		3.19	3.52	3.45
Dissipation factor	D150			
At 60 Hz		0.0008	0.0019	0.0006
At 10^3 Hz		0.0008	0.0023	–
At 10^6 Hz		0.0051	0.0048	0.0076

[a]Thickness.

Electrical Properties. Polysulfones offer excellent electrical insulative capabilities and other electrical properties as can be seen from the data in Table 7. The resins exhibit low dielectric constants and dissipation factors even in the GHz (microwave) frequency range. This performance is retained over a wide temperature range and has permitted applications such as printed wiring board substrates, electronic connectors, lighting sockets, business machine components, and automotive fuse housings, to name a few. The desirable electrical properties along with the inherent flame retardancy of polysulfone make these polymers prime candidates in many high temperature electrical and electronic applications.

Resistance to Chemical Environments and Solubility. As a rule, amorphous plastics are susceptible, to various degrees, to cracking by certain chemical environments when the plastic material is placed under stress. The phenomenon is referred to as environmental stress-cracking (ESC), and the resistance of the polymer to failure by this mode is known as environmental stress-cracking resistance (ESCR). The tendency of a polymer to undergo ESC depends on several factors, the most important of which are applied stress, temperature, and the concentration of the aggressive species. Polysulfones, being completely amorphous, exhibit susceptibility to stress cracking by some organic environments. The potency of the stress-cracking agent is generally related to the match between the solubility parameter of the solvent and that of the polymer. For example, PSF, which has a solubility parameter $\delta = 21.8\ (J/cm^3)^{1/2}$, resists aliphatic hydrocarbons

Table 8. Resistance[a,b] of Natural (Unreinforced) PSF, PES, and PPSF Resins to Various Chemical Environments[c]

	Ranking		
Environment	PSF	PES	PPSF
Aliphatic hydrocarbons	1	1	1
Aromatic hydrocarbons	10	9	7
Alcohols/Glycols	2	2	2
Esters	9	8	6
Ketones	10	8	7
Chlorinated hydrocarbons	10	8	8
Aliphatic amines	2	1	1
Aromatic amines	8	7	6
Electrolyte solutions	1	1	1
Acids[b]	3	2	1
Bases	3	2	1
Ionic surfactants	1	1	1
Nonionic surfactants	5	4	3

[a]Ranking codes: 1 = excellent; 5 = good; 10 = very poor.
[b]Data are for comparative purposes only; actual resistance depends on many factors including stress, temperature, concentration, and exposure duration.
[c]Stress-cracking resistance is substantially enhanced in the presence of reinforcement such as glass fibers.
[d]Nonoxidizing.

(lower δ) and most alcohols (higher δ), but readily undergoes stress cracking by ketones, which have δ-values sufficiently close to that of the polymer.

The exact mechanism of ESC of a polymer is still not completely understood, but in essence it involves a weakening of the secondary (intermolecular) bonds between neighboring polymer chains because of the solubility of the chemical in the polymer. As a result, a number of crazes are generated at the stressed surface of the polymer; if the number of crazes is large the stress level is moderated and cracking is prevented, or at least delayed. If only a few crazes form, on the other hand, they tend to grow and propagate as cracks, resulting in rupture.

The ESCR performance of PSF, PES, and PPSF is summarized in Table 8. These polymers are highly resistant to hydrolysis by hot aqueous media, including boiling water, high pressure steam, mineral acids and alkalis, and salt solutions. This resistance is usually a key reason behind the selection of polysulfones over the other engineering plastics like polycarbonates, polyesters, polyamides, and polyetherimides (23). The resistance to stress cracking by organic solvents varies according to the one-dimensional solubility parameter concept described above. The most problematic solvents are aromatics, chlorinated hydrocarbons, ketones, and esters. The resistance of the three polysulfones to these and other environments in general follows the ascending order PSF < PES < PPSF, as illustrated in Table 8. When the aggressive environment does not actually dissolve or swell the polymer, the ESCR problem can usually be overcome by the use of a glass

fiber-reinforced grade of the polysulfone resin of interest. Glass fiber or any other effective reinforcing agent usually provides enough added load-bearing capability to compensate for the ESCR deficiency of the polymer.

Solubility of the three commercial polysulfones follows the order PSF > PES > PPSF. At room temperature, all three of these polysulfones as well as the vast majority of other aromatic sulfone-based polymers can be readily dissolved in a handful of highly polar solvents to form stable solutions. These powerful solvents include NMP, DMAc, pyridine, and aniline. 1,1,2-Trichloroethane and 1,1,2,2-tetrachloroethane are also suitable solvents but are less desirable because of their potentially harmful health effects. In addition to being soluble in the aforementioned list, PSF is also readily soluble in a host of less polar solvents by virtue of its lower solubility parameter. These solvents include tetrahydrofuran (THF), 1,4 dioxane, chloroform, dichloromethane, and chlorobenzene. The relatively broad solubility characteristics of PSF have been key in the development of solution-based hollow-fiber spinning processes in the manufacture of polysulfone asymmetric membranes (see MEMBRANE TECHNOLOGY). The solvent list for PES and PPSF is short because of the propensity of these polymers to undergo solvent-induced crystallization in many solvents. When the PES structure contains a small proportion of a second bisphenol comonomer, as in the case of RADEL A (British Petroleum) polyethersulfone, solution stability is much improved over that of PES homopolymer.

Radiation Resistance. Polysulfones exhibit resistance to many electromagnetic frequencies of practical significance, including microwave, visible, and infrared. Especially notable is the excellent resistance to microwave radiation, which has contributed to the excellent fit of polysulfones in cookware applications. Polysulfone also shows good resistance to x-rays, electron beam (24), and gamma (25,26) radiation under many practical application conditions.

Like the majority of aromatic polymers, polysulfones exhibit poor resistance to uv light. Polysulfones absorb in the uv region, with attendant discoloration and losses in mechanical properties due to polymer degradation at, and directly beneath, the exposed surface. Prolonged exposure to sunlight is therefore not recommended for these polymers in neat form. Retention of mechanical integrity is improved with pigmentation and/or reinforcement of the resin, and almost full resistance to uv is achieved when the resins are pigmented with high loadings of carbon black. Painting of the part is another option that can be used to avoid the effects of uv light. The retention of mechanical integrity of PPSF upon exposure to uv light is somewhat better than it is for either PSF or PES, especially when the resin is in an opaque form by virtue of pigmentation. This greater apparent resistance to uv is a consequence of the more inherently ductile nature of PPSF compared to both PSF and PES.

Fabrication

As with most linear amorphous polymers, polysulfones are fully thermoplastic materials and readily flow at temperatures $\geq 150^{\circ}C$ above their respective T_gs. The backbone structure is extremely thermally stable during melt processing, remaining unchanged even when subjected to several melt fabrication cycles.

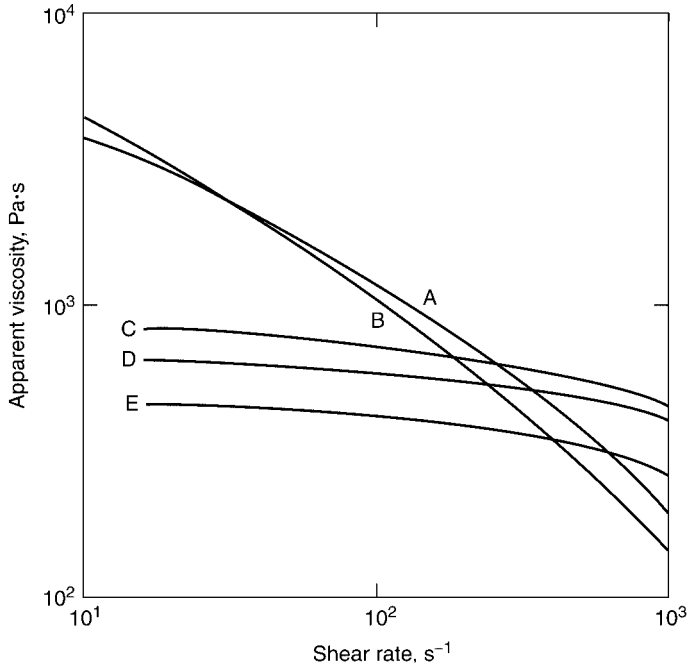

Fig. 5. Melt viscosity dependence on shear rate for various polymers: A, low density polyethylene at 210°C; B, polystyrene at 200°C; C, UDEL P-1700 (PSF) at 360°C and RADEL R-5000 (PPSF) at 380°C; D, LEXAN 104 polycarbonate at 315°C; and E, RADEL A-300 (PES) at 380°C. To convert Pa·s to P, multiply by 10.

Polysulfones can be melt-processed on conventional equipment used for thermoplastics fabrication. Typical melt viscosity behavior as a function of shear rate is shown in Figure 5 for polysulfones and some other polymers. As illustrated in these plots, the shear thinning characteristics of polysulfones are much more muted than they are for aliphatic backbone polymers such as the polyethylene and polystyrene shown to illustrate this point. The rheological behavior of polysulfones is fundamentally more similar to that of bisphenol A polycarbonate.

Injection molding is the most common fabrication technique. Polymer melt temperature for PSF injection molding can be in the range 325–400°C depending on part thickness, length, complexity, and other factors. PES and PPSF are generally molded using temperatures in the range 360–400°C. Mold temperatures suitable for PSF injection molding are in the range 100–170°C; for PES and PPSF this range is 120–190°C. Lower mold temperatures can be used but are not recommended as they can result in unacceptably high levels of molded-in residual stresses in the parts. Because of the relatively high viscosities of polysulfones and the limited shear-thinning they exhibit over the practical range of shear rates, generous sizing of runners and gates in mold design is recommended. The insensitivity to shear has the beneficial effect of resulting in parts that are low in molecular orientation, and hence are much more nearly isotropic than those molded from many other thermoplastics.

Polysulfones are easily processed by other fabrication techniques commonly used for thermoplastics, including extrusion, thermoforming, and blow molding. Extrusion into film, sheet, tubing, or profile can be accomplished on conventional extrusion equipment with a metering screw of moderate depth having a 2.5:1 compression ratio. Stock temperatures during extrusion of PSF, PES, and PPSF are in the range 315–375°C depending on grade of resin viscosity and type of product being produced. A common fabrication technique is sheet extrusion followed by thermoforming. Prior to thermoforming, the sheet must be dry to prevent foaming. The surface temperatures required to produce the necessary sag are in the range 230–260°C for PSF and 275–305°C for PES and PPSF. Blow molding of polysulfones is possible on most commercial blow molding equipment, provided the equipment is capable of maintaining melt temperatures in the range 300–360°C.

Once formed, parts made of polysulfones (particularly those produced by injection molding) can be annealed to reduce molded-in stress. Increased stiffness, dimensional stability, and resistance to creep during service life of the part are generally enhanced if molded-in stresses are reduced. More importantly, the resistance of the part to ESC or crazing is usually improved if molded-in stresses are minimized. Annealing can be easily accomplished either in an air oven or a glycerol bath. Typical time–temperature conditions for the proper annealing of polysulfones in an air oven are 1 h/170°C for PSF and 1 h/200°C for PES and PPSF. Annealing at similar temperatures by immersion in hot glycerol can be accomplished in 1–5 min. Because overannealing may result in a reduction of impact toughness, the use of conservative molding practices, most notably a hot mold and appropriate part and gating designs, to produce low stress parts is preferred whenever contact with aggressive chemical environments is anticipated for the component during its service life.

Prior to melt processing, the resin must be dried to reduce the level of absorbed atmospheric moisture, which can be as high as 0.8 wt%. For injection-molding operations, a moisture content below 0.05 wt% is appropriate, but for extrusion applications such as film or sheet the moisture level should not exceed 0.01 wt%. The presence of significant amounts of moisture during melt processing causes bubbling and foaming of the trapped moisture, which leads to structural and appearance defects in the fabricated parts. Drying to the targeted 0.05 wt%, moisture can be easily achieved in a circulating hot air oven or a dehumidifying hopper dryer in 3–4 h at 135–165°C. Drying temperatures can be increased to 180°C for PES and PPSF, if it is desired to cut down on drying time.

Post-Fabrication Operations. Sulfone polymers are amenable to most post-fabrication operations. Because of their high T_gs and inherent toughness characteristics, the resins can be machined with conventional metal working techniques such as drilling, tapping, sawing, turning, milling, and routing. They can also be polished to a high gloss. Cutting or machining oil is generally not required or recommended, but water can be used to reduce heat. Sulfone polymers can be joined by a variety of techniques. Joining sulfone polymers to themselves or to similar materials often employs ultrasonic welding, heat staking, and spin welding. Solvent bonding can also be used for self-bonding, but it is generally not recommended and should only be used as a last resort. Traditional adhesive bonding can be used, especially when polysulfone must be joined to a dissimilar material. Products manufactured from sulfone resins can also be easily finished and

decorated by printing, painting, laser etching, or by the application of hot stamping patterns. Metallic patterns and finishes can be applied by vacuum metalizing, cathode sputtering, as well as flame/arc spraying.

Blends and Alloys

The blending of two or more polymers to achieve unique property combinations of the parent polymers continues to be an attractive way to tailor existing commercial polymers to specific end use requirements. The blending of polysulfones with other polymers presents opportunities, but at the same time poses some significant technical challenges. Miscibility of PSF or PES with any nonsulfone-based polymer is extremely rare. Some examples of limited miscibility have been uncovered and discussed (27–31). Only one of these cases involves stable one-phase behavior in the melt state (31). The inert nature of the phenyl, sulfone, and ether moieties precludes interchain reactions, such as ester–ester interchange, which can facilitate the achievement of miscibility in otherwise immiscible systems. As a result, blends of PSF or PES with other nonsulfone-based polymers generally rely on interfacial adhesion and good shear mixing during compounding to produce an intimately mixed blend with good mechanical compatibility. None of the binary blends comprising PSF, PES, and PPSF are miscible, although their blends form mechanically compatible mixtures with relatively stable phase morphologies. Properties of these blends are available (32–34). Blends comprising two or more polysulfones can provide a convenient way to achieve specific properties or simply to reduce cost (35).

One of the factors precluding blending of polysulfones and commodity polymers such as styrenics and polyolefins is the fact that these polymers do not possess the requisite thermal stability to endure melt processing in the temperature range that is required for polysulfones. As a result, there are few commercially available polymer types that make good candidates for blending with polysulfones. These are, in general, other engineering thermoplastics, such as polycarbonates, some polyesters, polyimides , polyaryletherketones, and poly(phenylene sulfide) (PPS). Polymer blends involving polysulfones are discussed in numerous patents and journal articles, eg, a study (36) dealing with the interaction energies of polysulfones with several polymers as they relate to miscibility. Properties of PSF–PPS blends are well documented (37,38). Another study (39) describes the mechanical and rheological properties of PSF when blended with a thermotropic liquid crystalline polyester.

For reasons that are not fully understood, PPSF exhibits generally improved compatibility characteristics over either PSF or PES in a number of systems. An example of this is blends of PPSF with polyaryletherketones (40,41). These blends form extremely finely dispersed systems with synergistic strength, impact, and ESCR properties. Blends of PPSF with either PSF or PES are synergistic in the sense that they exhibit the supertoughness characteristic of PPSF at PSF or PES contents of up to 35 wt% (33,34). The miscibility of PPSF with a special class of polyimides has been discovered and documented (42). The miscibility profile of PPSF with a group of high temperature ($T_g > 230^\circ C$) polysulfones has been reported (43).

Proprietary blend formulations based on polysulfone, polyethersulfone, and polyphenylsulfone are sold commercially by British Petroleum to meet various end use requirements. The blends based on polysulfone are sold under the Mindel trademark. A glass fiber-reinforced blend based on PES is offered under the trade name Radel AG-360. This offers most of the performance characteristics of 30% glass fiber-reinforced polyethersulfone, but at a lower cost. Two blend product lines are offered based on PPSF. These are designated as the Radel R-4000 and R-7000 series products. The former is a lower cost alternative to Radel R PPSF homopolymer offering most of the performance attributes unique to PPSF. The R-7000 series of resins have been formulated for use in aircraft interiors for civil air transport. They exhibit a very high degree of resistance to flammability and smoke release.

Health and Safety

Polysulfones are chemically inert polymers for the most part and to date (ca 2000) have known negative health effects. These polymers have been used for many years in applications where safety is of utmost importance. Numerous grades comply with U.S. and international governmental regulations for direct contact with food. Polysulfone has been in use for food processing (qv), plumbing, and medical and prosthetic device applications since the 1960s. Various grades of polysulfone, polyethersulfone, and polyphenylsulfone meet U.S. Food and Drug Administration (FDA) requirements for direct food contact. Similar approvals are given by the U.S. National Sanitation Foundation under Standard 51 permitting use of certain polysulfone, polyethersulfone, and polyphenylsulfone resins in food processing equipment. Radel R polyphenylsulfone complies with *U.S. Pharmacopeia* Class VI requirements for use in medical device components. Many regulatory bodies around the world have sanctioned the use of various sulfone polymer grades in potable water delivery applications. Various commercial grades of polysulfone, polyethersulfone, and polyphenylsulfone are also listed in Underwriters Laboratories' Recognized Component Directory.

The thermally and oxidatively stable backbones of polysulfones preclude development of any significant amount of toxic, volatile by-products from thermal degradation when the resins are heated during melt processing. The polymers remain essentially odorless when injection-molded at temperatures of up to 380°C. At temperatures above 380°C, trace amounts of sulfur dioxide, methane, and other organic compounds and residual solvents begin to evolve. As for other plastic materials, adequate ventilation of the molding area is recommended when injection molding polysulfones.

Uses

Sulfone polymers are used in a wide variety of applications that take advantage of their hydrolytic and acid/caustic stability, clarity, high heat-deflection temperatures, as well as a number of other features. These application areas include cookware and appliances, electrical and electronic packaging and substrates,

Table 9. Examples of Uses for PSF, PES, and PPSF

Area/Use	PSF	PES	PPSF
Food service/food processing			
Microwave cookware	×	×	
Coffee carafes	×		
Milking equipment components	×		
Nonstick cookware coatings		×	
Functional plumbing			
Valve components	×		×
Faucets	×		
Fittings	×		×
Water heater dip tubes	×		
Electrical/electronic			
Circuit breaker housings		×	
Electronic connectors	×	×	×
Fiber optic connectors		×	×
Lighting sockets		×	
Transformer magnet wire coating			×
Business machine components	×	×	
Transportation			
Automotive fuses	×	×	
Automotive lamp reflectors	×	×	
Locomotive battery cases		×	
Aircraft interior parts			×
Medical			
Dental instruments	×	×	×
Surgical instrument trays	×		×
Hemodialysis membranes	×		
Laboratory animal cages	×		×
Industrial			
Pump components		×	
Flow meters	×		
Sight glasses	×		
Tower packing		×	
Gas separation membranes	×		
Water purification membranes	×		

automotive and aerospace parts and components, and a host of industrial and plumbing uses. Table 9 shows some of the more typical applications for each of PSF, PES, and PPSF. Because they share common fundamental features, PSF, PES, and PPSF could, in principle, be used interchangeably for many applications. In those instances, PSF is selected whenever possible because of its lower cost. PES is selected over PSF in applications requiring additional heat resistance or chemical resistance. PPSF offers a substantial improvement over PES in hydrolytic stability, impact, chemical resistance, and flammability resistance, while it maintains the same thermal resistance capabilities as those of PES. It is generally selected for most demanding end uses, when both PSF and PES fall short of meeting requirements.

The polysulfones resin family offers many desirable properties for cookware products in both commercial and consumer markets. In addition to those mentioned above, other noteworthy features are resistance to hot greases and detergent solutions and microwave transparency. Coffee carafes, steam-heated food service trays, and a variety of plastic parts used in household appliances are a few examples of these uses. Sulfone polymers are also used in automated dairy processing components as an alternative to stainless steel because of their clarity, hydrolytic stability, and resistance to sterilization.

Household plumbing components have been successfully produced from polysulfone and polyphenylsulfone, and this is a growing applications area for these polymers. Such fabricated parts offer excellent hydrolytic stability as well as resistance to dissolved chlorine, which is commonly used by many municipalities as part of water purification regimes. In some cases, polysulfones are used in chemical processing equipment because of their very good resistance to some chemical environments. Examples of such uses include corrosion-resistant pipe, pumps, filter modules, support plates, and tower packing. In the case of severe chemical environments glass-reinforced grades can be used to enhance resistance and prolong service life.

In the electrical and electronic industry, sulfone polymers are used in many applications including lighting sockets, circuit breaker components, fuses, and a wide variety of connectors. High dielectric strength, low dissipation across wide temperature and frequency ranges, and flame retardancy characteristics make PSF, PES, and PPSF suitable for these and other applications. The high dimensional stability of these polymers makes them suitable for a variety of precision business machine parts. PPSF is also used as a magnet wire coating because of its high temperature capability, high dielectric strength, and toughness (44).

Medical applications such as instrument trays, devices, and handles are also commonly fabricated from PSF and PPSF. Products made from PSF and PPSF offer resistance to sterilization by using boiling water, steam, gamma radiation, ethylene oxide, and a wide range of disinfectants. PPSF is especially preferred when the sterilization environments are more severe.

One unique application area for PSF is in membrane separation uses. Asymmetric PSF membranes are used in ultrafiltration, reverse osmosis, and ambulatory hemodialysis (artificial kidney) units. Gas-separation membrane technology was developed in the 1970s based on polysulfone hollow-fiber membranes. The PRISM (Monsanto) gas-separation system based on this concept has been a significant breakthrough in gas-separation technology (see MEMBRANE TECHNOLOGY). Additional details are available on the use of polysulfone in membrane separations (45), as well as gas transport properties of polysulfone and polyethersulfone (46–50).

There are four commercial suppliers that manufacture polysulfones: BP Amoco Corp. in the United States, BASF Corp. in Germany, Sumitomo Chemical Co. in Japan, and Gharda Chemicals in India. A listing of the resins supplied by each of these companies along with the trade names particular to each of these suppliers is shown in Table 10. All four companies supply a polyethersulfone-type product. Polysulfone is supplied by three of the four (see Table 10) and, as of this writing, BP Amoco is the sole supplier of polyphenylsulfone.

Table 10. Manufacturers and Trade Names of Commercially Available Polysulfones[a]

Supplier	Polysulfone types offered	Trade name
BP Amoco	PSF	Udel
	PES	Radel A
	PPSF	Radel R
BASF	PSF	Ultrason S
	PES	Ultrason E
Gharda Chemicals	PSF	Gafone S
	PES	Gafone
Sumitomo	PES	Sumikaexcel

[a]As of Nov. 1, 2000.

BIBLIOGRAPHY

"Polysulfones" in *EPST* 1st ed., Vol. 11, pp. 447–463, by R. N. Johnson, Union Carbide Corp.; "Polysulfones" in *EPSE* 2nd ed., Vol. 13, pp. 196–211, by J. E. Harris and R. N. Johnson, Union Carbide Corp.

1. E. J. Goethals, in N. M. Bikales, ed., *Encyclopedia of Polymer Science and Technology*, Vol. **13**, Interscience Publishers, a Division of John Wiley & Sons, Inc., New York, 1969, pp. 448–477.
2. A. H. Fawcett, in J. I. Kroschwitz, ed., *Encyclopedia of Polymer Science and Engineering*, 2nd ed., Vol. **10**, John Wiley & Sons, Inc., New York, 1987, pp. 408–432.
3. U.S. Pat. 4108837 (Aug. 22, 1978), R. N. Johnson and A. G. Farnham (to Union Carbide Corp.).
4. R. N. Johnson and co-workers, *J. Polym. Sci., Part A-1* **5**, 2375 (1967).
5. M. J. El-Hibri, in J. I. Kroschwitz, ed., *Encyclopedia of Chemical Technology*, 4th ed., Vol. **19**, John Wiley & Sons, Inc., New York, 1996, p. 947.
6. S. R. Shulze, in *155th Natl. Am. Chem. Soc. Meet.*, San Francisco, Calif., Mar.–Apr. 1968, p. L-090. Abstract of Paper.
7. Brit. Pat. 1153035 (Sept. 24, 1965), D. A. Barr and J. B. Rose (to Imperial Chemical Industries).
8. U.S. Pat. 3332909 (July 25, 1967), A. G. Farnham and R. N. Johnson (to Union Carbide Corp.).
9. U.S. Pat. 5239043 (Aug. 24, 1993), S. Savariar (to Amoco Corp.).
10. U.S. Pat. 5235019 (Aug. 10, 1993), S. Savariar (to Amoco Corp.).
11. U.S. Pat. 4008203 (Feb. 15, 1977), M. E. B. Jones (to Imperial Chemical Industries).
12. B. E. Jennings, M. E. B. Jones, and J. B. Rose, *J. Polym. Sci., Part C: Polym. Lett.* **16**, 715 (1967).
13. J. B. Rose, *Polymer* **15**, 456 (1974).
14. I. Colon and D. R. Kelsey, *J. Org. Chem.* **51**, 2627 (1986).
15. U.S. Pat. 4263466 (Apr. 21, 1981), I. Colon, L. M. Maresca, and G. T. Kwiatkowski (to Union Carbide Corp.).
16. U.S. Pat. 4400499 (Aug. 23, 1983), I. Colon (to Union Carbide Corp.).
17. G. T. Kwiatkowski and co-workers, *Makromol. Chem., Macromol. Symp.* **54/55**, 199–224 (1992).
18. V. Percec and H. Nava, *J. Polym. Sci., Part A: Polym. Chem.* **26**, 783 (1988).
19. T. E. Attwood, M. B. Cinderey, and J. B. Rose, *Polymer* **34**, 1322 (1993).

20. J. J. Dumias and co-workers, *Macromolecules* **19**, 1884 (1986).
21. L. M. Robeson, A. G. Farnham, and J. E. McGrath, *Appl. Polym. Symp.* **26**, 373 (1975).
22. C. L. Aitken, W. J. Koros, and D. R. Paul, *Macromolecules* **25**, 3424 (1992).
23. L. M. Robeson and S. T. Crisafulli, *J. Appl. Polym. Sci.* **28**, 2925 (1983).
24. A. Davis and co-workers, *Makromol. Chem.* **129**, 63 (1969).
25. J. R. Brown and J. H. O'Donnell, *Polym. Lett.* **8**, 121 (1970).
26. A. R. Lyons, M. C. R. Symons, and J. K. Yandel, *Makromol. Chem.* **157**, 103 (1972).
27. D. J. Walsh and V. B. Singh, *Makromol. Chem.* **185**, 1979 (1984).
28. D. J. Walsh, S. Rostami, and V. B. Singh, *Makromol. Chem.* **186**, 145 (1985).
29. H. Nakamura and co-workers, *Polymer* **31**, 303 (1990).
30. K. Jeremic, F. E. Karasz, and W. J. Macknight, *New Polym. Mater.* **3**, 163 (1992).
31. U.S. Pat. 5191035 (Mar. 2, 1993), M. J. El-Hibri, J. E. Harris, and J. L. Melquist (to Amoco Corp.).
32. U.S. Pat. 4743645 (May 10, 1988), J. E. Harris and L. M. Robeson (to Amoco Corp.).
33. U.S. Pat. 5086130 (Feb. 4, 1992), B. L. Dickinson, M. J. El-Hibri, and M. E. Sauers (to Amoco Corp.).
34. U.S. Pat. 5164466 (Nov. 17, 1992), M. J. El-Hibri, B. L. Dickinson, and M. E. Sauers (to Amoco Corp.).
35. U.S. Pat. 6075100 (June 13, 2000), M. J. El-Hibri (to BP Amoco Corp.).
36. T. A. Callaghan and D. R. Paul, *J. Polym. Sci., Part B: Polym. Phys.* **32**, 1847 (1994).
37. M.-F. Cheung and co-workers, *Polymer* **31**, 2299 (1990).
38. M.-F. Cheung, A. Golovoy, and H. van Oene, *Polymer* **31**, 2307 (1990).
39. S. M. Hong and co-workers, *Polym. J.* **23**, 1347 (1991).
40. U.S. Pat. 4804724 (Feb. 14, 1989), J. E. Harris and L. M. Robeson (to Amoco Corp.).
41. U.S. Pat. 4713426 (Dec. 15, 1987), J. E. Harris and L. M. Robeson (to Amoco Corp.).
42. U.S. Pat. 5037902 (Aug. 6, 1991), J. E. Harris and G. T. Brooks (to Amoco Corp.).
43. U.S. Pat. 4804723 (Feb. 14, 1989), J. E. Harris and L. M. Robeson (to Amoco Corp.).
44. S. A. Weinberg, M. J. El-Hibri, and J. A. Rock, in *Electrical Manufacturing & Coil Winding 1998 Preceedings*, Cincinatti, Ohio, Electrical Manufacturing & Coil Winding Association, Inc., Imperial Beach, Calif., 1998, p. 159.
45. W. J. Koros and R. T. Chern, in R. W. Rousseau, ed., *Handbook of Separation Process Technology*, John Wiley & Sons, Inc., New York, 1987.
46. A. J. Erb and D. R. Paul, *J. Membr. Sci.* **8**, 11 (1981).
47. K. Ghosal and R. T. Chern, *J. Membr. Sci.* **72**, 91 (1992).
48. J. S. McHattie, W. J. Koros, and D. R. Paul, *Polymer* **32**, 840 (1991).
49. J. S. McHattie, W. J. Koros, and D. R. Paul, *Polymer* **32**, 2618 (1991).
50. K. Ghosal, R. T. Chern, and B. D. Freeman, *J. Polym. Sci., Part B: Polym. Phys.* **31**, 891 (1993).

M. JAMAL EL-HIBRI
SHARI A. WEINBERG
BP Amoco Polymers, Inc.

POLYTETRAFLUORETHYLENE. See PERFLUORINATED POLYMERS.

POLYTRIACETYLENE. See DIACETYLENE AND TRIACETYLENE POLYMERS.

POLYURETHANES

The polymers known as polyurethanes include materials that incorporate the carbamate group, —NHCOO—, as well as other functional groups, such as ester, ether, amide, and urea. The name polyurethane is derived from ethyl carbamate, known as urethane. Polyurethanes are usually produced by the reaction of a polyfunctional isocyanate with a macroglycol, a so-called polyol, or other reactants containing two or more groups reactive with isocyanates. Often a combination of a macroglycol and a short-chain glycol extender is used to produce segmented block copolymers. The macroglycols are based on polyethers, polyesters, or a combination of both. In recent years diamines have also been used as comonomers in order to achieve higher reaction rates in molding and spray applications. In addition to the linear thermoplastic polyurethanes, obtained from difunctional monomers, branched or cross-linked thermoset polymers are made with higher functional monomers. Linear polymers have good impact strength, good physical properties, and excellent processibility, but limited thermal stability (owing to their thermoplasticity). Thermoset polymers, on the other hand, have higher thermal stability but sometimes lower impact strength (rigid foams). The higher functionality is obtained with higher functional isocyanates (polymeric isocyanates), or with higher functional polyols. Cross-linking is also achieved by secondary reactions. For example, urea groups are generated in the formation of water-blown flexible foams. An isocyanato group reacts with water to form a carbamic acid, which dissociates into an amine and carbon dioxide, with the latter acting as a blowing agent. The amine reacts with another isocyanate to form a urea linkage. Further reaction of the urea group with the isocyanate leads to cross-linking via a biuret group. Water-blown flexible foams contain urethane, urea, and some biuret groups in their network structure. Urea-modified segmented polyurethanes are manufactured from diisocyanates, macroglycols, and diamine extenders. Polyurethane network polymers are also formed by trimerization of part of the isocyanate groups. This approach is used in the formation of rigid polyurethane-modified isocyanurate (PUIR) foams.

The addition polymerization of diisocyanates with macroglycols to produce urethane polymers was pioneered in 1937 by O. Bayer (1). The rapid formation of high molecular weight urethane polymers from liquid monomers, which occurs

Encyclopedia of Polymer Science and Technology. Copyright John Wiley & Sons, Inc. All rights reserved.

even at ambient temperature, is a unique feature of the polyaddition process, yielding products that range from cross-linked networks to linear fibers and elastomers. The enormous versatility of the polyaddition process allowed the manufacture of a myriad of products for a wide variety of applications.

The early German polyurethane products were based on tolyene diisocyanate (TDI) and polyester polyols. In addition, a linear fiber, Perlon U, was produced from the aliphatic 1,6-hexamethylene diisocyanate (HDI) and 1,4-butanediol. Commercial production of flexible polyurethane foam in the United States began in 1953. In Germany a toluene diisocyanate consisting of an isomeric mixture of 65% 2,4-isomer and 35% 2,6-isomer was used in the manufacture of flexible foam, whereas in the United States the less expensive 80:20 isomer mixture was used. In 1956, DuPont introduced poly(tetramethylene glycol) (PTMG), the first commercial polyether polyol; the less expensive polyalkylene glycols appeared by 1957. The availability of the lower cost polyether polyols based on both ethylene and propylene oxides provided the foam manufacturers with a broad choice of suitable raw materials, which in turn afforded flexible foams with a wide range of physical properties. Polyether polyols provide foams with better hydrolytic stability whereas polyester polyols give superior tensile and tear strength. The development of new and superior catalysts, such as Dabco (triethylenediamine) and organotin compounds, has led to the so-called one-shot process in 1958, which eliminated the need for an intermediate prepolymer step. Prior to this development, part of the polyol was treated with excess isocyanate to give an isocyanate-terminated prepolymer. Further reaction with water produced a flexible foam.

The late 1950s saw the emergence of cast elastomers, which led to the development of reaction injection molding (RIM) at Bayer AG in Leverkusen, Germany, in 1964. Also, thermoplastic polyurethane (TPU) elastomers and Spandex fibers were introduced during this time. In addition, urethane-based synthetic leather was introduced by DuPont under the trade name Corfam in 1963.

The late 1950s also witnessed the emergence of a new polymeric isocyanate (PMDI) based on the condensation of aniline with formaldehyde. This product was introduced by the Carwin Co. (later Upjohn and Dow) in 1960 under the trade name PAPI. Similar products were introduced by Bayer and ICI in Europe in the early 1960s. The superior heat resistance of rigid foams derived from PMDI prompted its exclusive use in rigid polyurethane foams. The large-scale production of PMDI made the coproduct 4,4′,-methylenebis(phenyl isocyanate) (MDI) readily available, which has since been used almost exclusively in polyurethane elastomer applications. Liquid derivatives of MDI are used in RIM applications, and work has been done since the 1990s to reinforce polyurethane elastomers with glass, graphite, boron, and aramid fibers, or mica flakes, to increase stiffness and reduce thermal expansion. The higher modulus thermoset elastomers produced by reinforced reaction injection molding (RRIM) are also used in the automotive industry. In 1969 Bayer pioneered an all-plastic car having RIM-molded bumpers and fascia; in 1983 the first plastic-body commercial automobile (Pontiac Fiero) was produced in the United States.

The polymerization step can be conducted in a mold, in an extruder (TPU production), or continuously on a conveyor (block foam production). Also, spraying

of the monomers onto the surface of a substrate produces polyurethane coatings. The resulting polymers can be thermoplastic, which allows reprocessing by injection molding, extrusion, blow molding, and other remelting processes, or they are thermoset polymers as used in the RIM process in the molding of automotive bumpers, or in the manufacture of cellular polyurethanes.

Polyurethanes are a primary component of the global polymer market. They amount to about 6% of the total world plastic use. The world consumption of polyurethanes in 2000 was about 8 million tons, with a global growth averaging around 3–4% a year. The Western Hemisphere uses about 3 million metric tons per annum, Western Europe approximately 2.6 million metric tons per annum, the remainder being used in Asia and Africa.

Today's global polyurethane industry has been reshaped by several mergers of the 1980s and 1990s. Some of the familiar players, such as ICI, Upjohn, Olin, Rhone Poulenc, Union Carbide, and Arco, sold their polyurethane businesses; Bayer, the principal global isocyanate producer, strengthened its position in polyether polyols by acquiring the Arco polyol business in 1999. Also Dow, the other leading producer of polyether polyols, acquired Union Carbide in 1999, which further strengthened its position in polyols. The primary polyurethane players of the new millennium are Bayer, BASF, Dow, and Huntsman, the latter through the purchase of the global ICI business. Lyondell, which acquired the TDI businesses from Olin and Rhone Poulenc, sold the Arco polyol business to Bayer in 1999, thereby indicating their intent to eventually exit polyurethanes. Over the years the primary polyurethane chemical producers underwent forward integration by buying primary polyurethane system houses, ie their principal customers. Recent examples include the acquisition of Essex, a leading producer of automotive windshield adhesives and sealants, and of Flexible Products and General Latex, which are polyurethane foam system houses, by Dow; and BASF acquired IPI International, a producer of insulation foam systems.

In Asia and South America, the primary global chemical producers formed joint ventures with primary local companies, some of which established small volume manufacturing sites. In contrast, Dow/Mitsubishi built an isocyanate distillation plant in Yokaichi, Japan, to separate PMDI/MDI feedstock. Dow has another distillation plant in Delfzjiel, Holland, which has been increased by 60% in 2000. In this plant feedstock from Dows Estarreja, Portugal, plant is separated into PMDI and MDI. Although distillation plants are less costly, the other primary producers seem to be involved in building global-size facilities in Asia. For example, BASF plans to build a new 140-kt/a TDI plant in Yosu, South Korea by 2003. A present MDI plant at this site will be simultaneously expanded to 160 kt/a. Also, several major facilities are planned for mainland China. A recent project by Bayer, the building of a major TDI plant in Taiwan, was cancelled because of local opposition to the plant. Enichem in Italy, which acquired its isocyanate technology from ICI, is a regional producer of isocyanates and polyols.

The major producers of polyurethane chemicals also manufacture TPU elastomers. DuPont was also at one time involved in polyurethanes, but it sold its TDI technology to Dow and excited the synthetic leather business. However, DuPont is still the principal force in the production of polyurethane fibers (Lycra). Through the acquisition of Uniroyal and Witco, the Crompton & Knowles Corp. became a

principal force in polyurethane elastomers, which are now sold under the trade name CK Witco. Manufacturing and marketing arrangements include a rigid foam system marketing deal between Huntsman and Shell, and a manufacturing joint venture of BASF and Shell. The latter is named Basell CV, which opened a new styrene monomer/propylene oxide plant at Moerdijk in the Netherlands with a capacity of 250 kt/a of propylene oxide. Another plant in Singapore is scheduled to open in 2002. Some of the new polyols are used to supply Huntsman, which is the only primary polyurethane company without a polyol manufacturing capability.

One of the current trends in polyurethanes is the gradual replacement of TDI by the less volatile PMDI or MDI in many applications. The production of PMDI/MDI is a coproduct process, which is economically viable because the market requires amounts of both isocyanates in the amounts presently produced. All primary producers remove some of the higher priced MDI (up to 50%) by vacuum distillation. A process for the manufacture of only MDI does not exist.

Elimination of chlorinated fluorocarbon (CFC) blowing agents and the reduction of emission of volatile organic compounds (VOCs) have been ongoing. The latter leads to a rapid increase in the use of water-based polyurethane dispersions in coating applications. Flexible foam producers have eliminated auxiliary blowing agents, and the rigid foam producers use water-blown formulations in combination with hydrochlorofluorocarbons (HCFCs), hydrofluorocarbons (HFCs), or hydrocarbons. Adhesives and sealants are reformulated from solvent-based products to 100% solid-and water-based systems.

Isocyanates

The synthesis, reactions, and manufacture of isocyanates were reviewed in 1997 (2), and the chemistry and technology of isocyanates is the subject of a recent book (3).

The standard method of synthesis of isocyanates is the phosgenation of amines or amine salts. The phosgenation of amines to isocyanates was pioneered by Hentschel in 1884 (4). Using this method, a solution of the diamines in chlorobenzene is added to excess phosgene in the same solvent below 20°C. The resultant slurry consisting of the dicarbamoyl chloride (**1**) and the diamine dihydrochloride (**2**) is treated with excess phosgene at temperatures up to 130°C. Upon heating above 65°C the dicarbamoyl chloride dissociates to generate diisocyanate (**3**). The conversion of **2** is very slow, and the use of polar solvents or higher pressures increases the rate of reaction.

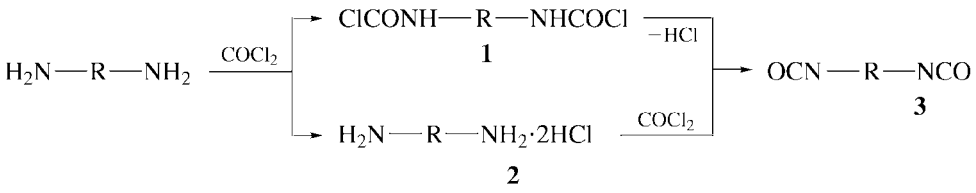

In the laboratory a slurry of the diamine salts, obtained by treating a solution of the diamines with hydrogen chloride or carbon dioxide, is treated above 100°C until a clear solution is obtained. Instead of the toxic phosgene gas, the liquid trichloromethyl chloroformate (diphosgene) (5) or the solid bistrichloromethyl carbonate (triphosgene) (6) can be used in the laboratory. The phosgene oligomers have to be used with caution because the toxic monomer can be generated readily and all reactions have to be performed under a fume hood.

In the continuous manufacture of diisocyanates, the by-products (hydrogen chloride and excess phosgene) are vented and separated. The recovered phosgene is recycled and part of the hydrogen chloride is used in the aniline/formaldehyde condensation. The solvents used in the phosgenation of the diamines are aromatic hydrocarbons, especially chlorobenzene and *o*-dichlorobenzene. Occasionally, more polar solvents, such as ethyl acetate, dioxane, nitrobenzene, or dimethylsulfone, are used. Excess phosgene can also be used as solvent if the reaction is conducted under high pressure. Dimethylformamide (DMF) and phenyltetramethylguanidine catalyze the phosgenation reaction (7).

Aliphatic diamines are also phosgenated in a two-phase reaction using methylene chloride and aqueous sodium hydroxide. The diamine and phosgene are dissolved in methylene chloride and the form **2** is instantaneously neutralized with sodium hydroxide. The generated diisocyanate remains in the solvent phase, and excess phosgene is also neutralized with sodium hydroxide, which enhances the safety of phosgene handling. The highly exothermic reaction requires efficient cooling. A disadvantage of this process is the use of a slight excess of phosgene, which cannot be recovered.

Instead of phosgene and its oligomers, oligomeric *t*-butylcarbonates are also used to convert diamines into diisocyanates. For example, sterically hindered aromatic diamines react with di-*t*-butyldicarbonate in the presence of dimethylaminopyridine in acetonitrile at room temperature to give sterically hindered aromatic diisocyanates. In this manner 3,6-3′,6′-tetramethyl MDI is obtained in 93% yield (8). Also, aliphatic diamines react with di-*t*-butyltricarbonate at room temperature to give a high yield of the corresponding diisocyanates (9).

Since the early 1970s, attempts have been made by the principal global producers of isocyanates to avoid the use of the toxic phosgene in the manufacture of isocyanates. Attempts to produce TDI and PMDI by nonphosgene processes have failed. However, two aliphatic diisocyanates, CHDI and TMXDI, are manufactured using nonphosgene processes. Hüls and BASF have also announced plans to use nonphosgene processes for the manufacture of IPDI in their new plants which are under construction. In the new, nonphosgene chemistry, isocyanic acid, generated by thermolysis of urea, reacts with diamines to give a bis-urea derivative. Subsequent reaction with diethylamine affords tri-substituted urea derivatives, which are thermolyzed in an inert solvent in the presence of an acidic catalyst to give the diisocyanate (10). Gaseous ammonia is the only by-product in this process. Also, reaction of aliphatic diamines with carbon dioxide, in the presence of triethylamine, affords biscarbamate salts, which can be dehydrated with phosphoryl chloride to give the diisocyanate (11).

Another laboratory method of synthesis of diisocyanates is the thermolysis of bisacylazides (**4**) (Curtius reaction). For example, dicarboxylic acid chlorides react

with trimethylsilyl azide to give (**4**), which is thermolyzed in an inert solvent to give the diisocyanates (**5**), $n = 3$–10 (12).

$$\mathrm{ClCO{-}(CH_2)_n{-}COCl} + 2\ \mathrm{(CH_3)_3SiN_3} \rightarrow \underset{\mathbf{4}}{\mathrm{N_3CO(CH_2)_nCON_3}} \rightarrow \underset{\mathbf{5}}{\mathrm{OCN(CH_2)_nNCO}} + 2\ \mathrm{N_2}$$

The preparation of aliphatic diisocyanates, using bisacylazides, has to be conducted with caution because an explosion occurred in the preparation of ethylene diisocyanate by using this method (13). Ethylene diisocyanate is readily obtained by dehydrochlorination of a heterocyclic allophanoyl chloride derivative obtained in the phosgenation of ethyleneurea (14).

The commodity aromatic isocyanates TDI and PMDI/MDI are most widely used in the manufacture of urethane polymers. Tolylene diisocyanate, TDI, is a distilled 80:20 mixture of 2,4- and 2,6-isomers. However, pure 2,4-TDI and a 65:35 mixture of the 2,4- and 2,6-isomers are also commercially available. Pure 2,4-TDI, mp 19.5–21°C, is obtained on cooling of 80:20 TDI. The manufacture of TDI involves nitration of toluene, hydrogenation to the diamines, and phosgenation. Separation of the undesired ortho derivatives, such as 2,3- and 3,4-dinitrotoluene, is necessary because their presence interferes with the polymerization of TDI (15).

The other commodity isocyanate, PMDI/MDI, is based on benzene. Mononitration of benzene, catalytic reduction to aniline, followed by condensation of aniline with formaldehyde produces oligomeric amines, which are phosgenated to give mixtures of PMDI and MDI. MDI is separated from PMDI by continuous thin-film vacuum distillation.

PMDIs are crude products that vary in exact composition. The main constituents are 40–60% MDI; the remainder is the other isomers of MDI, triisocyanates, and higher molecular weight oligomers. Important product variables are functionality and acidity. Rigid polyurethane foams are mainly manufactured from PMDI. The so-called pure MDI is a low melting solid that is used for high performance polyurethane elastomers and spandex fibers.

Liquid MDI (Isonate 143-L) is produced by converting some of the isocyanate groups in MDI to carbodiimide groups, which react with the excess isocyanate present to form a small amount of the trifunctional four-membered ring cycloadduct (16). The presence of the cycloadduct lowers the melting point of MDI to give a liquid product. In most applications the trifunctional cycloadduct will dissociate into difunctional monomers; therefore, this type of liquid MDI can be used in the manufacture of linear polyurethanes. Liquid MDI products are also made by reaction of the diisocyanate with small amounts of glycols. These products are called prepolymers. MDI products enriched in 2,4-MDI are also available. The latter are used in the manufacture of flexible MDI foams.

The manufacture of the oligomeric amine precursors for PMDI/MDI is conducted by continuously adding formaldehyde to aniline in the presence of less than the stoichiometric amount of hydrochloric acid at room temperature in agitated reactors. The reaction mixture is gradually heated to 100°C over a period of several hours. The reaction can also be conducted under pressure at higher temperatures in order to increase the rate of reaction. However, the oligomeric amines produced in this manner contain higher amounts of 2,2′- and 2,4′-methylenedianiline

(MDA). The acid-catalyzed aniline/formaldehyde reaction proceeds in two steps. At room temperature aniline reacts with formaldehyde to form N-substituted carbonium ions which attack aniline in the para- and ortho-position to give a mixture of *p*-aminobenzylamine (PABA), (**6**), *o*-aminobenzylamine (OABA), (**7**), and oligomeric benzylamines. Subsequent heating affects dissociation of the benzylamines to give C-bonded carbonium ions, which form another C—C bond in their reaction with aniline.

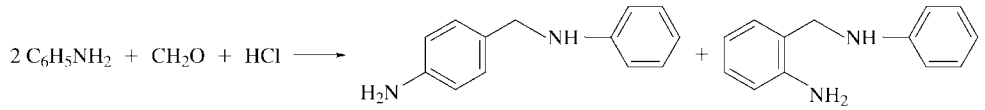

6 **7**

$$\mathbf{6} + C_6H_5NH_2 + HCl \rightarrow 4,4'\text{-MDA} + 2,4'\text{-MDA} + \text{oligomers}$$

$$\mathbf{7} + C_6H_5NH_2 + HCl \rightarrow 2,4'\text{-MDA} + 2,2'\text{-MDA} + \text{oligomers}$$

The variables affecting the product distribution are aniline concentration, hydrochloric acid concentration, and temperature. The higher the excess of aniline, the higher is the diamine concentration. Higher hydrochloric acid concentration and lower initial temperature favor the formation of 4,4′-MDA. Attempts were made over the years to replace the aqueous hydrochloric acid catalyst with slower reacting solid acidic clay catalysts, but the obtained product distribution was different, and therefore this approach was never used.

The commercial manufacture of TDI and PMDI/MDI is the continuous phosgenation under pressure of the amine precursors in an inert solvent at elevated temperatures. The by-products, hydrogen chloride and excess phosgene, are continuously vented and separated. The recovered phosgene is recycled and the hydrogen chloride is used in the aniline/formaldehyde condensation, or it is sold or reoxidized to chlorine to be reused in the manufacture of phosgene. In case of the manufacture of PMDI, some of the diisocyanate (MDI) is separated by continuous vacuum distillation using a wiped film evaporator. In this operation the residual PMDI, which still contains MDI, is only subjected to a short heat treatment. The advantage of the simultaneous manufacture of both isocyanates is a quantitative yield because the by-products of the phosgenation reaction are contained in the residual PMDI.

The current prices of the commodity aromatic isocyanates (DM/kg) are TDI: 3.6; PMDI: 2.8; MDI: 4.3. The light-stable aliphatic isocyanates are somewhat more expensive.

Several higher-priced aromatic diisocyanates, such as *p*-phenylene diisocyanate (PPDI), 1,5-naphthalene diisocyanate (NDI), and bitolylene diisocyanate (TODI), are also available. These symmetrical high melting diisocyanates give high melting hard segments in polyurethane elastomers.

Aromatic diisocyanates are also obtained in the coupling of suitable monoisocyanates. For example, reaction of 4-isocyanatobenzoyl chloride (**8**) with a trimethylsiloxy-substituted isocyanate (**9**) affords diisocyanato benzoates (**10**) (17).

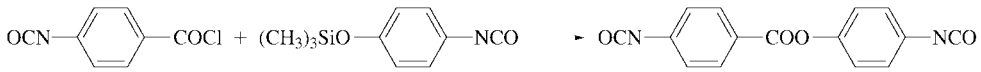

8 **9** **10**

Triad diisocyanates (**12**) are obtained in the reaction of two equivalents of 4-isocyanatobenzoyl chloride with the silylated hydroquinone derivative (**11**) (18).

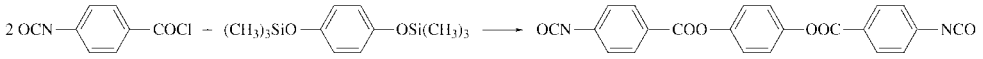

11 **12**

The aromatic triisocyanate (**13**) is obtained in the reaction of 4-nitrophenol and thiophosphoryl chloride, followed by reduction and phosgenation. (19). This triisocyanate is sold under the trade name Desmodur RF (Bayer) as a glue for rubber adhesive solutions.

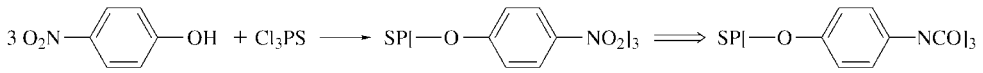

13

Aromatic triisocyanates as cross-linkers are more readily obtained by trimerizing 2,4-TDI. In this reaction the more reactive isocyanate group in the 4-position undergoes trimerization to produce a triisocyanate (20).

Also, aromatic polyisocyanates are obtained in the copolymerization of styrene with cinnamoyl azide (21). Blocked polyisocyanates (**14**) are obtained from *p*-nitrostyrene and carbon monoxide in methanol, using a ruthenium catalyst (22).

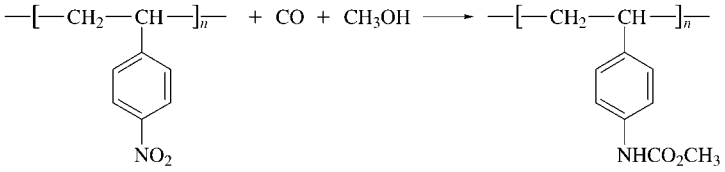

14

Polyurethanes obtained from aromatic diisocyanates undergo slow oxidation in the presence of air and light causing discoloration, which is unacceptable in some applications. In contrast, polyurethanes obtained from aliphatic diisocyanates are color stable, although it is necessary to add antioxidants and uv-stabilizers to the formulations to maintain the physical properties of the polymers with time.

The elusive parent diisocyanate, O=C=N–N=C=O, is only stable at $-75^{\circ}C$, and therefore it is not suitable as a monomer for polyurethanes (23). The least costly aliphatic diisocyanate is hexamethylene diisocyanate (HDI), which is obtained by phosgenating the nylon intermediate hexamethylenediamine (HDA). Because of its low boiling point, HDI is mostly used in the form of its derivatives, such as biurets, allophanates, dimers, or trimers (24). Isophorone diisocyanate (IPDI) and its derivatives are also used in the formulation of rigid coatings, while hydrogenated MDI (HMDI) and cyclohexane diisocyanate (CHDI) are used in the formulation of flexible coatings and polyurethane elastomers.

HDA is commercially produced from adipic acid or butadiene. The catalytic hydrogenation of adiponitrile to HDA is common in both routes. The phosgena-

Table 1. Phosgenation Processes for Aliphatic Diisocyanates

Method	Rate of reaction	Diamine concentrations	Yields
Diamine salts[a,b]	Very slow	Lowest	Highest
Diamines	Faster	Higher	High
Two-phase[c]	Very fast	High	Lower

[a] Hydrochlorides or carbamates from diamines and carbon dioxide.
[b] This reaction can also be conducted using excess phosgene as solvent.
[c] Using water, sodium hydroxide, and methylene chloride.

tion of the diamine is conducted continuously in chlorobenzene. In Table 1 the advantages and disadvantages of several phosgenation processes for aliphatic diisocyanates are shown.

In a recent patent a nonphosgene synthesis of HDI is described (25). Reaction of HDA with urea and ethanol, in the presence of $Co(OAc)_2$ at 170–175°C, affords the biscarbamate, which is thermolyzed in a thin-film evaporator at 260–270°C.

The other significant aliphatic diisocyanate, IPDI, is based on isophorone chemistry. Trimerization of acetone gives isophorone (**15**), which on reaction with HCN affords the β-cyanoketone (**16**). Reductive amination of (**16**) to the diamine (**17**), followed by phosgenation, gives IPDI (**18**).

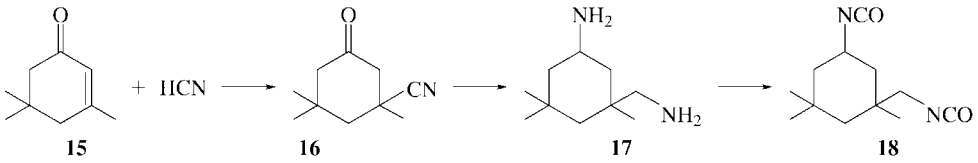

15 **16** **17** **18**

An example of a nonphosgene route to IPDI is the reaction of **17** with urea and *n*-butanol in the presence of dibutyl carbonate at 210–220°C. Thermolysis of the biscarbamate at 270–280°C at 30 mbar affords **18** (26). IPDI is a mixture of 72% cis isomers and 28% trans isomers (27).

HMDI was originally produced by DuPont as a coproduct in the manufacture of Quiana fiber. After terminating Quiana production DuPont sold the product to Bayer. Today, a crude mixture of the diamines obtained in the acid-catalyzed aniline/formaldehyde reaction is supplied by Bayer to Air Products, which is performing the ring hydrogenation. The phosgenation of the ring hydrogenated diamines is performed by Bayer. Commercial HMDI is a mixture of three stereo isomers (trans–trans, mp 65°C; cis–trans, mp 36°C; and cis–cis, mp 61°C). The direct formation of a blocked HMDI is conducted by ring hydrogenation of caprolactam blocked MDI (28).

Semicommercial aliphatic diisocyanates include *trans*-cyclohexane-1,4-diisocyanate (CHDI) and *m*-tetramethylxylylene diisocyanate (TMXDI). A coproduct in the production of TMXDI is *m*-isopropenyl-α,α-dimethylbenzyl isocyanate (TMI), which can be copolymerized with other olefins to give aliphatic polyisocyanates. These aliphatic diisocyanates are manufactured using nonphosgene routes. Akzo has developed the CHDI process based on scrap polyester fiber. Ring hydrogenation of dimethyl terephthalate (DMT), transesterification with diethylene glycol, followed by reaction with ammonia provides a diamide, which

is N-chlorinated. Hofmann rearrangement in the presence of diethylamine produces the blocked diisocyanate, which is subsequently deblocked on heating in the presence of hydrogen chloride (29). Cyclohexyl diisocyanate (CHDA) can also be obtained by catalytic hydrogenation of *p*-phenylenediamine. Most likely, this approach has economic advantages over the multistep process based on fiber scrap.

The manufacture of TMXDI, developed by American Cyanamid, is based on the reaction of *m*-isopropylidenebenzene (**19**) with ethyl carbamate to give the blocked diisocyanate (**20**). Thermolysis affords a mixture of TMXDI (**21**) and the monoisocyanate (TMI) (**22**) (30).

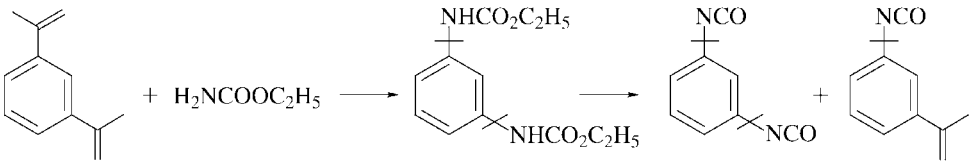

19 **20** **21** **22**

The coupling of ω-isocyanatocarboxylic acid chlorides (**23**) with silylated aliphatic hydroxy-isocyanates (**24**) is another method of synthesis of aliphatic diisocyanates (**25**), containing ester groups in their structure (31).

$$OCN(CH_2)_nCOCl + OCN(CH_2)_4OSi(CH_3)_3 \longrightarrow OCN(CH_2)_nCOO(CH_2)_4NCO$$

23 **24** **25**

In Table 2 the physical properties and the manufacturers of the commercial isocyanates are listed.

Blocked and Modified Isocyanates

Masked or blocked diisocyanates are used in coating applications. The blocked diisocyanates are storage-stable, nonvolatile, and easy to use in powder coatings. Blocked isocyanates are produced by reaction of the diisocyanate with blocking agents such as caprolactam, 3,5-dimethylpyrazole, phenols, oximes, acetoacetates, or malonates. Upon heating at 120–160°C, the blocked isocyanates dissociate and the generated free isocyanate reacts with hydroxyl groups available in the formulation to give high molecular weight polyurethanes. In the case of acetoacetates and malonates, the free isocyanates are not regenerated, but the adducts undergo transesterification reactions with the present polyol upon heating (32). A phenol-blocked methylene diisocyanate (**27**) is obtained in the reaction of phenyl carbamate (**26**) with formaldehyde (33).

$$2\ C_6H_5OCONH_2 + CH_2O \rightarrow C_6H_5OCONHCH_2NHCOOC_6H_5$$

26 **27**

The blocking of isocyanato groups with phenol is used in the formation of hyperbranched polyurethanesfrom a benzylalcohol derivative, having two

Table 2. Properties of Commercial Isocyanates

Name	Structure	CAS Reg. No.	Boiling point °C$_{kPa}$[a]	Melting point °C	Producer
PPDI	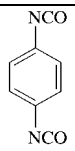	[104-49-4]	$110–112_{1.6}$	94–96	Akzo
TDI	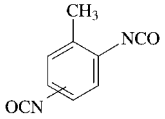	[1321-38-6]	$121_{1.33}$	14[b]	BASF, Bayer, Dow, Lyondell, Enichem, Mitsui
MDI	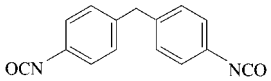	[101-68-8]	$171_{0.13}$	39.5	BASF, Bayer, Dow, Enichem
PMDI	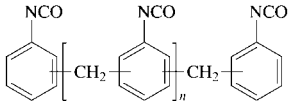	[9016-87-9]			
NDI	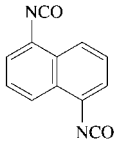	[3173-72-6]	$244_{0.017}$	130–132	Bayer, Mitsui
TODI	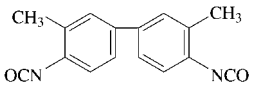	[91-97-4]	$160–170_{0.066}$	71–72	Nippon-Soda
XDI	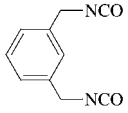	[3634-83-1]	$159–162_{1.6}$		Takeda
TMXDI	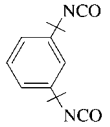	[58067-42-8]	$150_{0.4}$		American Cyanamid
HDI	$OCN(CH_2)_6\ NCO$	[822-06-0]	$130_{1.73}$		Bayer, Lyondell, Mitsui, Hüls
TMDI	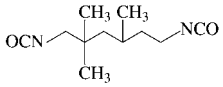	[83748-30-5]	$149_{1.33}$		Hüls
	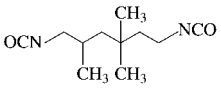	[15646-96-5]			
CHDI	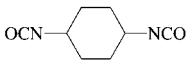	[2556-36-7]	$122–124_{1.6}$		Akzo
HXDI	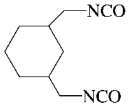	[38661-72-2]	$98_{0.053}$		Takeda

Table 2. (Continued)

Name	Structure	CAS Reg. No.	Boiling point °C$_{kPa}$[a]	Melting point °C	Producer
IPDI	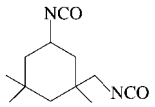	[4098-71-9]	$153_{1.33}$		BASF, Bayer, Hüls, Lyondell
HMDI[c]	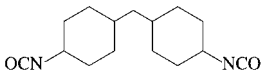	[5124-30-1]	$179_{0.12}$	trans–trans 65 cis-trans 36 cis–cis 61	Bayer

[a]To convert kPa to mm Hg, multiply by 7.5.
[b]Mixture of 80% 2,4-isomer [584-84-9] and 20% 2,6-isomer [91-08-7].
[c]Mixture of stereoisomers.

$NHCOOC_6H_5$ groups in the 3,5-position (34). Intramolecular dimers derived from long-chain aliphatic diisocyanates (35) and macrocyclic ureas (36) are also used as masked aliphatic diisocyanates.

Blocked aliphatic isocyanates or their derivatives are used for one-component coating systems. Masked polyols are also used for this application. For example, polyols capped with vinyl or isopropenyl ethers produce polyacetals, which do not react with isocyanates. Hydrolysis of the acetals with moist air regenerates the hydroxyl groups, which undergo polyurethane reaction with isocyanate-terminated prepolymers (37). In addition, substituted oxazolines are used as masked cross-linkers (38). Ketimine cross-linkers are also utilized in the formulation of one-component coating systems (39). Hydrolysis of ketimines produces diamines, which undergo a very fast reaction with isocyanate-terminated prepolymers. Blocked isocyanates are also used in the cross-linking of acrylic resins for automotive coatings. Incorporation of masked diisocyanates into epoxy resins lowers the moisture absorption in the derived coatings (40).

Other modified commercial diisocyanates include diisocyanate prepolymers, biurets, and isocyanurates (trimers). Asymmetric trimers (iminooxadiazine diones) are also obtained from aliphatic diisocyanates, using fluoride-based catalysts. The modifications of the commercial isocyanates are necessary to lower their melting points, or to lower their vapor pressure. The prepolymers used in the manufacture of polyurethanes are mainly urethane modified diisocyanates, formed in the reaction of the diisocyanate with a small amount of a macrodiol. Hydroxy-terminated prepolymers can also be prepared, but they are of no commercial significance. To raise the vapor pressure of aliphatic diisocyanates they are converted into allophanates, biurets, or triisocyanurates (trimers). HDI is mainly used as the biuret, (**28**), which is formed in the reaction of 3 mol of HDI with 1 mol of water, or other active hydrogen containing compounds, such as hydrated inorganic salts, tertiary alcohols, formic acid, pivalic acid, hydrogen sulfide, monoamines, or diamines.

$$3\ OCN{-}R{-}NCO + H_2O \rightarrow OCN{-}R{-}NHCON(RNCO)CONH{-}R{-}NCO$$

28

High temperature (>270°C) reaction of HDA with excess HDI is a commercial process to produce the HDI biuret (41). The excess HDI is removed by thin-film vacuum distillation. For the conversion of HDI into a triisocyanurate

derivative (trimer), using benzyltrimethyl ammonium hydroxide as the catalyst, it is advantageous to remove carbon dioxide from the diisocyanate by sparging with nitrogen (42). When tributylphosphine is used as the catalyst a mixture of dimers and trimers (3:2) is obtained (43). Sometimes prepolymers are used as coreactants in the trimerization of HDI (44). Also, mixtures of HDI and IPDI are used to generate the mixed trimers (45). On standing, HDI biurets slowly generate monomeric HDI; therefore, it is advantageous to use allophanates as the diisocyanate derivatives because allophanates do not dissociate on standing. Glycols, polyols, or monoalcohols are used to initiate allophanate formation.

The derivatization of IPDI is easier to accomplish because of the different reactivities of the two isocyanate groups in the molecule. For example, preferential dimerization of the primary isocyanate group is observed in the trialkylphosphine-catalyzed reaction (46). Trimerization of IPDI in the presence of quaternary ammonium salts affords mainly the isocyanurate trimer (47). Attempted biuret formation from IPDI and $Na_2SO_4 \cdot 10H_2O$ gives a mixture of ureas and biurets (48). A biuret derivative is also obtained from IPDI and HDA (49).

The use of catalysts plays a role in determining which isocyanate group in IPDI is more reactive. For example, in the reaction of IPDI with *n*-butanol at 50°C the secondary isocyanate group is 1.6 times more reactive than the primary isocyanate group in both stereoisomers. Using dibutyltin dilaurate as the catalyst, the reactivity of the secondary NCO group is about 12 times higher than the primary NCO group. However, using a tertiary amine catalyst (DABCO) the primary NCO group is 1.2 times more reactive than the secondary NCO group (50). The selective reactivities of the isocyanate groups in IPDI can be utilized to generate a diol containing an acrylic double bond for cross-linking (51). Reaction of the initially formed carbamate (**29**) with diethanolamine affords the diol (**30**).

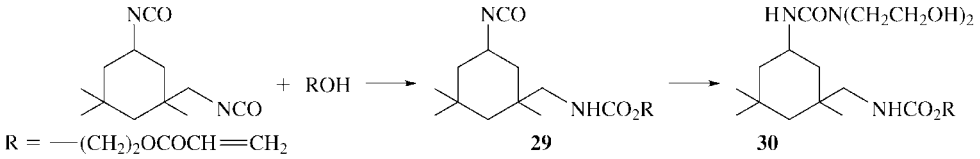

The selective reaction of the *p*-isocyanato group in 2,4-TDI is used to produce the TDI dimer, which is a higher melting solid diisocyanate. In Table 3 some modified commercial diisocyanates are listed.

Polyols

Polyether Polyols. The polyether polyols used in the manufacture of polyurethanes are hydroxy-terminated macromolecules, with molecular weights ranging from 250 to 8000. Lyondell/Bayer has provided pilot plant diols/triols having molecular weights of 10,000 to 15,000 for lubricant and surfactant applications. The hydroxy functionality can range from 2 to 8. The economically attractive polyether polyols based on alkylene oxides are listed in Table 4.

Other speciality initiators derived from natural products are also manufactured. Examples include formose, lactose,α-methyl glucoside, and

Table 3. Modified Commercial Diisocyanates

Modification	Description	Unreacted isocyanate, %[a]	Viscosity at 25°C, MPa[b]	NCO[c]	Application and trade names
Urethane	MDI and low mol. weight weight polyether diol	60	800	22	PU RIM elastomers Lupranate MP 102 (BASF) Mondur PF (Bayer) Isonate 181 (Dow)
	TDI and low mol. weight triol[d]	<0.5	2,000	12.5	Coatings Mondur CB (Bayer)
	MDI and polyester Polyol	13	2,000[d]	6.5	Elastomers Baytec (Bayer)
Allophanate	TDI and low mol. weight diol	70	20	4.0	Flexible PU foam Mondur HR (Bayer)
Biuret	HDI[e]	<0.7	10,000	22	Coatings Desmodur N (Bayer)
Dimer	TDI	<0.7	Solid	13 (48)[f]	Desmodur TT (Bayer)
Trimer	IPDI[g]	<0.7	2,000	12	Coatings (Huels)
Carbodiimide	MDI, partial reaction	70	40	29	Elastomers Lupranate MM 103 (BASF) Mondur CD (Bayer) Isonate 143-L (Dow)

[a] Based on total mixture.
[b] To convert MPa to psi, multiply by 145.
[c] Wt% NCO (equivalent weight = 42).
[d] Removal of excess isocyanate under vacuum.
[e] Partial reaction followed by removal of excess isocyanate.
[f] In parentheses: amount of isocyanate available after thermolysis of the dimer.
[g] 30% solvent modification.

Table 4. Commercial Polyether Polyols

Product	Nominal functionality	Initiator	Cyclic ether[a]
Poly(ethylene glycol) (PEG)	2	Water or EG[b]	EO
Poly(propylene glycol) (PPG)	2	Water or PG	PO
PPG/PEG[c]	2	Water or PG	PO/EO
Poly(tetramethylene glycol) (PTMG)	2	Water	THF
Glycerol adduct	3	Glycerol	PO
Trimethylolpropane adduct	3	TMP	PO
Pentaerythritol adduct	4	Pentaerythritol	PO
Ethylenediamine adduct	4	Ethylenediamine	PO
Phenolic resin adduct	4	Phenolic resin	PO
Diethylenetriamine adduct	5	DETA	PO
Sorbitol adduct	6	Sorbitol	PO
Sucrose adduct	6	Sucrose	PO

[a]EO: ethylene oxide, PO: propylene oxide, THF: tetrahydrofuran.
[b]EG: ethylene glycol, PG: propylene glycol.
[c]Random or block copolymers.

soybean-derived polyols. Propoxylation of dairy waste also affords polyether polyols. DuPont has developed a fermentation process to convert glucose into 1,3-propanediol, a useful polyurethane extender.

The alkylene oxide polymerization is usually initiated by alkaline hydroxides, especially potassium hydroxide. In the base-catalyzed polymerization of propylene oxide (PO), some rearrangement occurs to give allyl alcohol. Further reaction of allyl alcohol with PO produces a monofunctional alcohol. Therefore, polyether polyols derived from PO are not truly difunctional. By using zinc hexacyano cobaltate as catalyst, a more difunctional polyol is obtained (52). Olin has introduced the difunctional polyether polyol under the trade name Poly-L. This product is now available from Arch Chemicals. Similar polyols free of monol contamination are available from Arco/Lyondell/Bayer and Asahi.

Ethylene oxide is manufactured by direct oxidation of ethylene, in contrast PO is only obtained in coproduct processes. The classical process, chlorination of propylene, is still used by Dow, one of the world's largest producer of polyether polyols. In contrast, all other producers use the Halcon process, based on the simultaneous production of PO and styrene monomer or *t*-butyl alcohol. In view of the demise of MTBE (methyl-*t*-butyl ether based on *t*-butyl alcohol) as a fuel additive, the styrene coproduct process (POSM) will remain as the economically viable route to PO. A recent example is the new (SMPO) plant of Basell at Moerdijk in the Netherlands. The largest producer of PO, the former Arco (now Lyondell), has sold its global polyol business to Bayer in 1999. Lyondell will also provide Bayer a long-term, low cost supply of PO. Recently, Dow announced that it also will use the POSM route to PO in a new facility.

The backbone of the polyether polyols are either PO homopolymers or random or block copolymers with ethylene oxide. Important characteristics of the polyol are their hydroxy functionality, hydroxy equivalent weight, and their

reactivity and compatibility with the other components used in the polyurethane formulation. Blending of polyols of different functionality, molecular weight, and reactivity can be used to tailor a polyol for a specific application. Since primary hydroxy groups are more reactive than secondary hydroxy groups, it is advantageous to produce block copolymers with terminal primary hydroxyl groups by using ethylene oxide last in a block copolymer. Capping with ε-caprolactone also produces primary hydroxyl groups. Trichlorobutylene oxide-derived polyols are used as fire retardants. The hydrophobicity of polyether polyols can be modified by homo- or copolymerization with 1,2-butylene oxide or styrene oxide. The higher molecular weight polyether polyols are soluble in organic solvents. Poly(PO) is soluble in water up to a molecular weight of 760, and copolymerization with ethylene oxide expands the range of water solubility. Random copolymers are obtained by polymerizing mixtures of PO and ethylene oxide. The viscosity of polyether polyols increases with hydroxyl equivalent weight.

With amine initiators the so-called self-catalyzed polyols are obtained, which are used in the formulation of rigid spray foam systems. The rigidity or stiffness of a foam is increased by aromatic initiators, such as Mannich bases derived from phenol, phenolic resins, toluenediamine, or methylenedianiline (MDA). BASF/Dow have formed a venture into Mannich polyols for spray foam applications.

In the manufacture of highly resilient flexible foams and some thermoset RIM elastomers, graft or polymer polyols are used. Graft polyols are dispersions of free-radical-polymerized mixtures of acrylonitrile and styrene partially grafted to a polyol. Polymer polyols are available from BASF, Dow, and Union Carbide. *In situ* polyaddition reaction of isocyanates with amines in a polyol substrate produces polyharnstoff dispersion (PHD) polyols, which are marketed by Bayer (53). In addition, blending of polyether polyols with diethanolamine, followed by reaction with TDI, also affords a urethane/urea dispersion (54). The polymer or PHD-type polyols increase the load bearing properties and stiffness of flexible foams. Interreactive dispersion polyols are also used in RIM applications where elastomers of high modulus, low thermal coefficient of expansion, and improved paintability are needed.

Polyester Polyols. Initially polyester polyols were the preferred raw materials for polyurethanes, but today the less expensive polyether polyols dominate the polyurethane market. An exception are the inexpensive aromatic polyester polyols, which have been introduced for rigid foam applications. These are obtained from residues of terephthalic acid production or by transesterification of DMT or poly(ethylene terephthalate) (PET) scrap with glycols. TBI of France is the first European company to manufacture aromatic polyester polyols directly from PET scrap bottles at lssoire with a capacity of 10 kt/a. Phthalates and terephthalates are also used.

Polyester polyols are based on saturated aliphatic or aromatic carboxylic acids and diols or mixtures of diols. The carboxylic acid of choice is adipic acid because of its favorable cost/performance ratio. For elastomers, linear polyester polyols of molecular weight of ca 2000 are preferred. Branched polyester polyols, formulated from higher functional glycols, are used for foam and coating applications. Polyester polyol-derived polyurethanes have a lower hydrolytic stability

compared to polyurethanes made from polyether polyols, but they have better oxidative and thermal stabilities.

In addition, polyester polyols are made by the reaction of caprolactone with diols. Poly(caprolactone diols) are used in the manufacture of TPU elastomers with improved hydrolytic stability (55). The hydrolytic stability of the poly(caprolactone diol)-derived TPUs is comparable to TPUs based on the more expensive long-chain diol adipates (56). Polyether/polyester polyol hybrids are synthesized from low molecular weight polyester diols, which are extended with PO.

The most important chain extenders are ethylene glycol, diethylene glycol, propylene glycol, 1,4-butanediol, cyclohexanedimethanol, and hyroquinone dihydroxyethyl ether. Recently, 1,3-propanediol (57) and 1,2,4-butanetriol (58) have become available as new polyurethane raw materials. Since ethylene glycol-extended polyurethanes are prone to thermal degradation, ethylene glycol is only used as a RIM extender in thermoset polyurethanes.

Linear Polyurethanes and Poly(urethane ureas)

The chemistry and technology of polyurethanes is described in Reference 59. Numerous co-workers at Bayer have contributed to this book. Another important compilation of polyurethane technology can be found in Reference 60. This book is comprised of articles from Dow scientists. Also, a summary of polyurethane chemistry and technology is found in the somewhat older book compiled by ICI researchers (61).

Polyurethanes are generally obtained by reacting a difunctional hydroxy compound with a diisocyanate to yield A_2B_2 polymers. AB-type polyurethanes are obtained by cationic ring-opening polymerization of cyclic carbamates (62). Polymerization of monomers containing a hydroxyl and an isocyanate group in the monomer also affords AB polymers. The latter are usually generated *in situ* because of the incompatibility of both groups. An exception are substituted isocyanatophenols obtained in the phosgenation of aminophenols. While 4-isocyanatophenol undergoes homopolymerization after removal of the solvent, alkyl substituents adjacent to the functional groups increase the stability of isocyanatophenols (63). The reactive functional groups can also be generated from suitable precursors. For example, 4-hydroxybenzoyl azide, upon thermolysis, produces the AB homopolymer (64). From 4-(2-hydroxyethoxy)benzoyl azide the corresponding aliphatic/aromatic AB polyurethanes are obtained, the coproduct being gaseous nitrogen (65). An aliphatic AB monomer can be generated from aminoalcohols and di-*t*-butyltricarbonate. In the presence of $Zr(acac)_4$ the monomer undergoes homopolymerization. In this manner aliphatic polyurethanes $-[-(CH_2)_x-NHCO-]-_n, X = 4–12$ are obtained (66). These reactions are summarized in Table 5. Desilylation of silylated hydroxyester isocyanates with HF in pyridine also affords the corresponding AB homopolymer (67).

The generation of isocyanates from azide precursors is also utilized in the formation of hyperbranched polyurethanes **33** by thermolysis of 3,5-dihydroxybenzoyl azide (**31**) (68). The ABB-type monomer (**32**), generated *in situ*, undergoes polymerization to form a network polymer.

Table 5. AB Polyurethanes Generated from Hydroxyl Group Containing Monomers

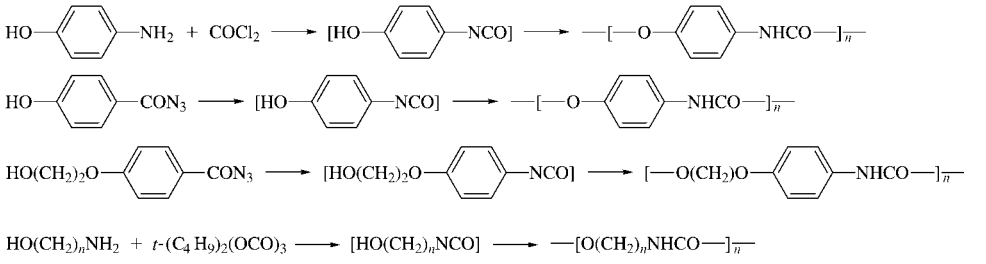

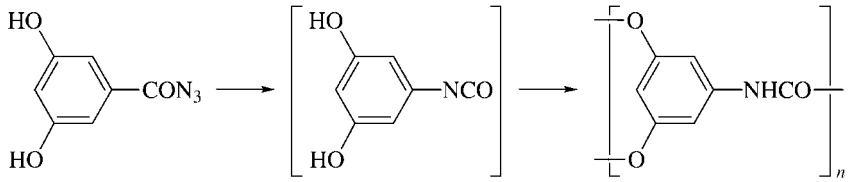

31 **32** **33**

The majority of commercial polyurethanes are A_2B_2 polymers. The useful physical properties of polyurethanes are derived from their molecular structure and determined by the choice of building blocks as well as the supramolecular structures caused by atomic interaction between chains. The ability to crystallize, the flexibility of the chains, and spacing of polar groups are of considerable importance, especially in linear thermoplastic materials. In rigid cross-linked systems, such as polyurethane foams, other factors such as density determine the final properties.

The unique properties of linear TPUs are attributed to their long-chain structure. TPU elastomers are segmented block copolymers, comprising of hard- and soft-segment blocks. The soft-segment blocks are formed from long-chain polyester or polyether polyols and MDI; the hard segments are formed from short-chain diols, mainly 1,4-butanediol, and MDI. Under ambient conditions the higher-melting hard segments are incompatible with the soft segments, and microphase separation occurs. The hard segments aggregate into crystalline domains, in which hydrogen bonding of the —NH— groups of the urethane chain bond to neighboring carbonyl groups occurs. Upon melting, the crystalline domains are disrupted and the polymer can be processed. In Table 6 the melt temperature of hard segments formed from MDI and glycols are shown. The 1,4-butanediol extended MDI-based polyurethane has the highest melting hard segment (69).

The symmetrical MDI is more suitable for the preparation of segmented polyurethane elastomers having excellent physical properties. Segmented polyurethanes are also obtained from 2,6-TDI, but an economically attractive separation process for the TDI isomers has yet to be developed.

The melt viscosity of a TPU depends on the weight-average molecular weight and is influenced by chain length and branching. TPUs are viscoelastic

Table 6. T_m of Model Hard Segments Derived from MDI and Glycols

Linear glycol	Hard segment T_m, °C
1,2-	199.7
1,3-	203.8
1,4-	208
1,5-	172.2
1,6	168
1,7-	164
1,8-	176
1,10-	174

Table 7. Macrodiols for TPU (mol wt 2000)

Polyol	T_g, °C	T_m, °C
Poly(propylene glycol)	−73	–
Poly(tetramethylene glycol)	−100	32
Poly(1,4-butanediol adipate)	−71	56
Poly(ethanediol 1,4-butanediol adipate)	−60	17 (37)
Poly(caprolacton) diol	−72	59
Poly(1,6-hexanediol carbonate)	−62	49

materials which behave like a glassy, brittle solid, an elastic rubber, or a viscous liquid, depending on temperature and time scale of measurement. With increasing temperature, the material becomes rubbery because of the onset of molecular motion. At higher temperatures a free-flowing liquid forms. The melt temperature of a polyurethane is important for processibility. Melting should occur well below the decomposition temperature. Below the glass-transition temperature (T_g), the molecular motion is frozen, and the material is only able to undergo small-scale elastic deformations. For amorphous polyurethane elastomers, the T_g of the soft segment is ca −50 to −60°C, whereas for the amorphous hard segment, T_g is in the 20–100°C range. The T_g and T_m of the more common macrodiols used in the manufacture of TPU are listed in Table 7.

Polyester and polyether diols are used together with MDI to manufacture TPU elastomers. The polyester diols are obtained from adipic acid and diols such as ethylene glycol, 1,4-butanediol, or 1,6-hexanediol. The preferred molecular weights are 1000–2000, and low acid numbers are essential to ensure optimal hydrolytic stability. Also, caprolactone-derived diols and polycarbonate diols are used. Polyether diols are mainly poly(tetramethylene glycol) (PTMG), but polyalkylene oxide-derived diols are also used. TPUs contain wax to aid in mold release and diatomaceous silica for added slip and as antiblocking agents in films. Antioxidants (hindered phenols or hindered amines) and uv-stabilizers (benzotriazoles) are also added to improve the environmental resistance.

The bulk polymerization of the polyurethane monomers is conducted by mixing the liquid monomers and catalysts at room temperature (one-step method),

or by prereacting the diisocyanates with part of the polyol to form a prepolymer, which is subsequently reacted with the remaining polyol to form the final polymer (two-step method). Part of the heat of reaction of the polymerization process is not generated if prepolymers are used. Prepolymers are often made at a ratio of NCO/OH of 2:1 in order to minimize free diisocyanate; prepolymers with a ratio of NCO/OH larger than 2:1 are called quasi prepolymers and these contain free diisocyanate. HDI or TDI prepolymers free of the diisocyanate are often made by removing the volatile diisocyanate by continuous vacuum distillation. Preformulated systems containing an isocyanate A side and a polyol B side, the latter also containing catalysts, surfactants, and blowing agents, are available from system houses. Carbodiimide-modified MDI offers advantages in polyester-based systems because of improved hydrolytic stability (70).

Solution polymerization of the monomers is also conducted in some applications. The solvents used have to be inert to isocyanates. Highly polar solvents (DMF, etc), which are excellent solvents for polyurethanes, have to be used with caution (71). Polyurethanes are also obtained by interfacial polymerization of isocyanatocarboxylic chlorides and glycols to give polyester urethanes (72).

In view of the morphological differences of MDI- and TDI-derived polyurethanes, the former are more suitable for the preparation of segmented polyurethane elastomers, while the latter are mainly used in the construction of flexible polyurethane foams. Segmented TPUs with excellent physical properties are also obtained from 2,6-TDI (73).

For economic reasons the bulk one-step polyaddition method is predominantly used to produce polyurethanes. For example, TPUs are produced by reaction extrusion. In this process the liquid monomers are mixed in a twin screw extruder, and the finished polymer is continuously extruded and pelletized. In the formulation of extrusion-grade TPUs a slight excess of the macrodiol is used. Reaction extrusion is also used in the manufacture of polyurethane engineering thermoplastics produced from MDI and higher boiling glycols, such as 1,6-hexanediol and cyclohexanedimethanol (74). These polymers were introduced by Upjohn/Dow under the trade name Isoplast. Blends of engineering plastics (ABS, acetal, nylon, polyesters, and polycarbonates) with TPUs are also finding uses in some polymer applications (75). The blends or alloys are readily produced by dry-blending and reextrusion.

Segmented elastomeric polyurethane fibers (Spandex fibers) based on MDI have also been developed. DuPont introduced Lycra in 1962. The generic name Spandex fibers designates elastomeric fibers, in which the fiber-forming substance is a long-chain polymer consisting of >85% of polyurethane. Extenders used in Spandex fibers include hydrazine and ethylenediamine. DuPont uses a dry-spinning process in which the polymer solution in DMF is extruded through a spinerette into a column of circulating hot air. Other producers that use the dry-spinning process include Bayer (Dorlastan) and Asahi Chemical Industry (Asahi Kasei Spandex). Wet-spinning processes are also used, in which isocyanate-terminated prepolymers are extruded into a nonaqueous diamine bath. Globe manufacturing is producing Glospan, using this process. Nishin Spinning Co. uses a melt extrusion process to produce Mobilon.

Poly(urethane ureas) are obtained in many aromatic isocyanate applications. For example, water-blown flexible polyurethane foam incorporates urea

linkages in its network structure. The reaction of the isocyanate with water provides an amine function, which reacts with more isocyanate to afford the urea segments. Poly(urethane ureas) are also used in elastomer applications, where diamines are used as chain extenders. Examples include cast elastomers made from TDI prepolymers and MOCA (3,3′-dichloro-4,4′-diaminodiphenylmethane) and RIM elastomers, using diethyltoluenediamine (DETDA) as a chain extender. This chemistry is also used in the formulation of spray elastomers. Aromatic amine-terminated polyols, obtained by hydrolysis of prepolymers based on 2,4-TDI and PPG or polyester polyols, are used with solid high melting aromatic diisocyanates to give one-component systems that cure without moisture. Amine-terminated polyols are also used in RIM and spray applications.

Because of the versatility of the polyurethane system it is possible to introduce comonomers which can affect the physical properties of the derived polymers. For example, photo cross-linkable polyurethanes are formulated using 2,5-dimethoxy-2,4′-diisocyanato stilbene as a monomer (76). Comonomers, having an azoaromatic chromophore, are used in optical bleaching applications (77), or in the formation of photorefractive polymers (78). The latter random polymers have second-order nonlinear optical (NLO) properties. Linear polymers are also obtained from HDI/PTMG and diacetylenic diols. These polymers can be cross-linked through the acetylenic linkages producing a network polymer with properties similar to poly(diacetylenes) (79).

Thermodegradable polyurethanes are produced from MDI, polycaprolactone diol, and 2,2-azobis(2-cyanopropanol). The polymers degrade at about 120°C, and the initial weight loss corresponds to the amount of azo groups in the polymer (80). When the polymerization of MDI and 1,4-butanediol is conducted in 60-crown-20 (60C20) or 36-crown-12 (36C12), respectively, polyrotaxenes are obtained consisting of polyurethane chains enclosed in the crown ethers (81).

Polyurethane Ionomers

The versatility of the polyurethane system is further exemplified by the formulation of ionic polymers (see IONOMERS). Polyurethane ionomers are segmented polymers in which ionic groups are separated by long-chain apolar segments (82). In the presence of water the ionic centers are hydrated. This effect enables ionomers to form stable dispersions in water, and solventless polyurethane coatings are formulated in this manner. The use of *N*-alkyldiethanolamines or dimethylol propionic acid as extenders allows incorporation of ionic groups into the polymer backbone. Also, reaction of—NH—group containing polyurethane chains with sodium hydride, followed by reaction with 1,3-propane sultone, affords ionomers. When the ionic centers are located in the hard segment, they align to form a domain morphology. Anionic dispersions have greater stability than cationic dispersions, but cationic polymers show better adhesion to glass.

Examples of the grafting of ionic groups to the urethane or urea backbone in linear polymers are shown in Table 8.

Ionic polymers are also formulated from TDI and MDI (86). Poly(urethane urea) and polyurea ionomers are obtained from divalent metal salts of *p*-aminobenzoic acid, MDA, dialkylene glycol, and 2,4-TDI (87). In the case of

Table 8. Grafting of Ionic Groups to Linear Polymers

Functional group	Acid precursor	Base	Pendant group	Reference
—NH—	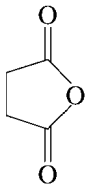	KOH	$\rangle NCOCH_2CH_2COOK$	83
—NH—	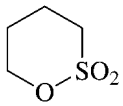	KOH	$\rangle N(CH_2)_3SO_3K$	84
—NHCONH—		Et_3N	—NHCON$(CH_2)_3SO_3^-(C_2H_5)_3NH^+$	83
—NHCONH—	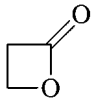		—NHCONCH$_2$CH$_2$COOH	83
—NHCONH—	CH_2O, $NaHSO_3$		—NHCONCH$_2$SO$_3$Na	85

polyureas, the glycol extender is omitted. If TDI is used in coating applications, it is usually converted to a derivative to lower the vapor pressure. A typical TDI prepolymer is the adduct of TDI with trimethylolpropane (Desmodur L).

Liquid Crystalline Polyurethanes

Liquid crystalline polyurethanes are formulated from mesogenic diols, such as 4,4′-bis(ω-hydroxyalkoxy)biphenyls and 2,4-TDI. Examples of the mesogenic diols include 4,4′-bis(6-hydroxyhexoxy)biphenyl (88) and 4,4′-bis(2-hydroxyethoxy)biphenyl (89). More rigid diisocyanates, such as 2,5-TDI and PPDI, are also used with mesogenic diols to form liquid crystal polyurethanes (90). Partial replacement of the mesogenic diols by PTMG with different molecular weights shows that the lower molecular weight flexible spacers form a more stable mesophase and exhibit higher crystallinity (91) (see LIQUID CRYSTALLINE POLYMERS, MAIN-CHAIN; LIQUID CRYSTALLINE POLYMERS, SIDE-CHAIN).

Another approach to liquid crystal polyurethanes involves the attachment of cholesterol to the polyurethane chain utilizing the dual reactivity in 2,4-TDI. In the initial reaction of the diisocyanate with cholesterol the 4-carbamate is produced, which on reaction with diethanolamine affords a diol, which is subsequently polymerized with 2,4-TDI (92).

Liquid crystal polyurethanes are also obtained from mesogenic ester diisocyanates (17). Also, a triad diol, bis(*p*-oxymethylphenyl)terephthalate, is used with HDI, HMDI, or TDI to give liquid crystal polyurethanes (93).

Thermoset Polyurethanes

Flexible Polyurethane Foams. The largest market segment in polyurethanes consists of flexible foams. A flexible polyurethane foam results from the reaction of an aromatic diisocyanate with a mixture of a polyol, water, a surfactant, and a catalyst. Sometimes a coblowing agent is added, but this practice is no longer viable because of environmental considerations. The reaction of the diisocyanate with water generates carbon dioxide gas, which is used as the blowing agent. The simultaneously generated urea acts as a chain extender. The number of moles of water in a polyurethane flexible foam formulation is typically 1–5 times the number of equivalent moles of polyol. Most commercial flexible foam is produced from TDI. In the 2,4-isomer the initial reaction occurs at the nonhindered isocyanate group in the 4-position. The unsymmetrically substituted ureas formed in the subsequent reaction with water are more soluble in the developing polymer matrix. Low density flexible foams are not readily produced from MDI or PMDI; enrichment of PMDI with the 2,4′-isomer of MDI affords a steric environment similar to the one in TDI, which allows the production of low density flexible foams that have good physical properties (94). The use of high performance polyols based on a copolymer polyol allows production of high resiliency (HR) slabstock foam from either TDI or MDI (95).

Flexible foams are three-dimensional agglomerations of gas bubbles separated from each other by thin sections of polyurethanes and polyureas. The microstructures observed in TDI- and MDI-based flexible foams are different. In TDI foams monodentate urea segments form after 40% conversion, followed by a bidentate urea phase, which is insoluble in the soft segment. As the foam cures, annealing of the precipitated discontinuous urea phase occurs to optimize alignment through hydrogen bonding (96).

The formation of cellular products also requires surfactants to facilitate the formation of small bubbles necessary for a fine-cell structure. The most effective surfactants are polyoxyalkylene–polysiloxane copolymers. The length and ethylene oxide/PO (EO/PO) ratio of the pendant polyether chains determine the emulsification and stabilizing properties. In view of the complexity of the interaction of surfactant molecules with the growing polymer chains in foam production, it is essential to design optimal surfactants for each application. Flexible polyurethane foams require surfactants that promote improved cell-wall drainage. This allows the cell walls to become more open during the foaming reaction. Also, the shift away from TDI to MDI in molded HR foams adds new demands on foam surfactants (97).

Flexible slab or bun foam is poured by multicomponent machines at rates of >45 kg/min. One-shot pouring from traversing mixing heads is generally used. A typical formulation for furniture-grade foam having a density of 0.024 g/cm^3 includes a polyether triol (mol wt 3000); TDI; water; catalysts, ie, stannous octoate in combination with a tertiary amine; and surfactant. Coblowing agents are often used to lower the density of the foam and to achieve a softer hand. Coblowing agents are methylene chloride, methyl chloroform, acetone, and CFC 11, but the last has been eliminated because of its ozone-depletion potential. Additive systems (98) and new polyols (99) are being developed to achieve softer low density foams. Higher density (0.045 g/cm^3) slab or bun foam, also called HR foam, is

similarly produced, using polyether triols having molecular weight of 6000. The use of polymer polyols improves the load-bearing properties.

The uncatalyzed reaction of diisocyanates with macroglycols is of no significance in the formation of polyurethanes. Tailoring of performance characteristics to improve processing and properties of polyurethane products requires the selection of efficient catalysts. In flexible foam manufacturing a combination of tin and tertiary amine catalysts are used in order to balance the gelation reaction (urethane formation) and the blowing reaction (urea formation). The tin catalysts used include dibutyltin dilaurate, dibutylbis(laurylthio)stannate, dibutyltinbis-(isooctylmercapto acetate), and dibutyltinbis(isooctylmaleate). The principal tertiary amines used are Dabco (1,4-diazabicyclo[2.2.2]octane) and higher boiling linear tertiary amines, such as pentamethyldipropylenetriamine and bis(dimethylaminoethyl) ether. Hydroxy groups containing tertiary amines are also used because they become incorporated into the polymer structure, which eliminates odor formation in the foam. Delayed-action or heat-activated catalysts are of particular interest in molded foam applications. These catalysts show low activity at room temperature but become active when the exotherm builds up. In addition to the phenol salt of 1,8-diazabicyclo[5.3.0]undec-7-ene (DBU) the benzoic acid salt of Dabco is also used.

Catalysts for urethane applications are sold by Air Products (Dabco), Abbott (Polycat), Kao Corp. (Kaolizer), Tosoh Corp. (Toyocat), and Union Carbide (Niax). Organic mercury compounds were used in cast elastomers and in RIM systems to extend cream time, ie, the time between mixing of all ingredients and the onset of creamy appearance, but are no longer used today because of toxicity concerns.

For the reaction of TDI with a polyether triol, bismuth or lead compounds can also be used. However, tin catalysts are preferred mainly because of their slight odor and the low amounts required to achieve high reaction rates. Carboxylic acid salts of calcium, cobalt, lead, manganese, zinc, and zirconium are employed as cocatalysts with tertiary amines, tin compounds, and tin–amine combinations.

Flame retardants are incorporated into the formulations in amounts necessary to satisfy existing requirements. Reactive-type diols, such as *N,N*-bis(2-hydroxyethyl)aminomethyl phosphonate (Fyrol 6), are preferred, but nonreactive phosphates (Fyrol CEF, Fyrol PCF) are also used. Often, the necessary results are achieved using mineral fillers such as alumina trihydrate or melamine. Melamine melts away from the flame and forms both a nonflammable gaseous environment and a molten barrier that helps to isolate the combustible polyurethane foam from the flame. Alumina trihydrate releases water of hydration to cool the flame, forming a noncombustible inorganic protective char at the flame front. Flame-resistant upholstery fabric or liners are also used.

There are four main types of flexible slabstock foam: conventional, HR, filled, and high load-bearing foam. Filled slabstock foams contain inorganic fillers to increase the foam density and improve the load-bearing characteristics. High load-bearing formulations incorporate a polymer polyol. Slabstock flexible foam is produced on continuous bun lines. The bun forms while the material moves down a long conveyor. In flat-top bun lines, the liquid chemicals are dispensed from a stationary mixing head to a manifold at the bottom of a trough. More rectangular foams are produced by several newer processes such as Draka, Petzetakis, Hennecke, Planiblock, and Econo Foam. However, the most popular rectangular block

foam process is the Maxfoam process. The high outputs require faster and longer conveyors. An exception is the Vertifoam process in which the reaction mixture is introduced at the bottom of an enclosed expansion chamber. The chamber is lined with paper or polyethylene film, which is drawn upward at a controlled rate. Because the Vertifoam machine is much smaller than the horizontal machines, operational savings can be achieved (100). Two newer slabstock foam manufacturing processes have been developed. The Cannon CarDio process injects liquid carbon dioxide into the foam mix to reduce the density whereas the Bayer/Hennecke NovaFlex process is conducted under reduced pressure to lower the density.

The properties of thermoset flexible polyurethane foams are related to density; load-bearing properties are likewise important. Under normal service temperatures, flexible foams exhibit rubber-like elasticity to deformations of short duration but creep under long-term stress. Maximum tensile strength is obtained at densities of ca 0.024–0.030 g/cm^3. The densities are controlled by the amount of water in the formulation and may range from 0.045 to 0.020 g/cm^3 by raising the amount of water from 2 to 5%. Auxiliary blowing agents are also used to reduce density and control hardness. The size and uniformity of the cells are controlled by the efficiency of mixing and the nucleation of the foam mix. Flexible foams are anisotropic and the load-bearing properties are best when measured in the direction of foam rise.

A high rate of block foam production (150–220 kg/min) is required in order to obtain large slabs to minimize cutting waste. Bun widths range from ca 1.43 to 2.2 m, and typical bun heights are 0.77–1.25 m. In a flexible foam plant, scrap can amount to as much as 20%. Most of it is used as carpet underlay and in pillows and packaging. The finished foam blocks are stored in a cooling area for at least 12 h before being passed to a storage area or to slitters where the blocks are cut into sheets. In the production plant the fire risk must be minimized. Temperatures of up to 150°C can be reached in the interior of the foam blocks. Blowing of ambient air through the porous foam allows dissipation of the heat generated in the exothermic reaction.

Most flexible foams produced are based on polyether polyols; ca 8–10% (15–20% in Europe) of the total production is based on polyester polyols. Flexible polyether foams have excellent cushioning properties, are flexible over a wide range of temperatures, and can resist fatigue, aging, chemicals, and mold growth. Polyester-based foams are superior in resistance to dry-cleaning and can be flame-bonded to textiles.

In recent years, molded flexible foam products are becoming more popular. The bulk of the molded flexible urethane foam is employed in the transportation industry, where it is highly suitable for the manufacture of seat cushions, back cushions, and bucket-seat padding. TDI prepolymers were used in flexible foam molding in conjunction with polyether polyols. The introduction of organotin catalysts and efficient silicone surfactants facilitates one-shot foam molding, which is the most economical production method.

The need for heat curing has been eliminated by the development of cold-molded or HR foams. These molded HR foams are produced from highly reactive polyols and are cured under ambient conditions. The polyether triols used are of molecular weight 4500–6500 and are high in ethylene oxide (usually >50% primary hydroxyl content). Reactivity is further enhanced by triethanolamine, liquid

aromatic diamines, and aromatic diols. Generally, PMDI, TDI, or blends of PMDI–TDI are used. Load-bearing characteristics are improved by using polymer polyol. HR foams exhibit relatively high SAC (support) factors, ie, load ratio, excellent resiliency (ball rebound > 60%), and improved flammability properties.

Semiflexible molded polyurethane foams are used in other automotive applications such as instrument panels, dashboards, arm rests, head rests, door liners, and vibrational control devices. An important property of semiflexible foam is low resiliency and low elasticity, which results in a slow rate of recovery after deflection. The isocyanate used in the manufacture of semiflexible foams is PMDI, sometimes used in combination with TDI or TDI prepolymers. Both polyester as well as polyether polyols are used in the production of these water-blown foams. Sometimes integral skin molded foams are also produced.

Rigid Polyurethane Foams. Almost all rigid cellular polyurethanes are produced from PMDI. Some formulations, particularly those for refrigerator and freezer insulation, are based on modified TDI (golden TDI) or TDI prepolymers, but these are being replaced by PMDI formulations. The polyaddition reaction is influenced by the structure and functionality of the monomers, including the location of substituents in proximity to the reactive isocyanate group (steric hindrance) and the nature of the hydroxyl group (primary or secondary). Impurities also influence the reactivity of the system; for example, acid impurities in PMDI require partial neutralization or larger amounts of the basic catalysts. The acidity in PMDI can be reduced by heat or epoxy treatment, which is best conducted in the plant. Addition of small amounts of carboxylic acid chlorides lowers the reactivity of PMDI or stabilizes isocyanate-terminated prepolymers.

The polyols used include PO adducts of polyfunctional hydroxy compounds or amines (see Table 4). The amine-derived polyols are used in spray foam formulations where high reaction rates are required. Crude aromatic polyester diols are often used in combination with the multifunctional polyether polyols. Blending of polyols of different functionality, molecular weight, and reactivity is used to tailor a polyol for a specific application. The high functionality of the polyether polyols combined with the higher functionality of PMDI contributes to the rapid network formation required for rigid polyurethane foams.

From the onset of creaming to the end of the rise during the expansion process, the gas must be retained completely in the form of bubbles, which ultimately results in the closed-cell structure. Addition of surfactants facilitates the production of very small uniform bubbles necessary for a fine-cell structure.

Reactive or nonreactive fire retardants, containing halogen and phosphorus, are often added to meet the existing building code requirements. The most commonly used reactive fire retardants are Fyrol 6, chlorendic anhydride-derived diols, and tetrabromophthalate ester diols (PHT 4-Diol). There is a synergistic effect of nitrogen and phosphorus observed in P–N compounds. Phosphonates, such as Fryol 6, are effective in char formation, whereas phosphine oxide-derived fire retardants are reactive in the gas phase. Because the reactive fire retardants are combined with the polyol component, storage stability is important. Nonreactive fire retardants include halogenated phosphate esters, such as tris(chloroisopropyl) phosphate (TMCP) and tris(chloroethyl) phosphate (TCEP), and phosphonates, such as dimethyl methylphosphonate (DMMP). Highly halogenated aromatic compounds, borax, and melamine are also used as fire retardants in rigid foams.

Insulation foams are halocarbon-blown. Chlorofluorocarbons, eg, CFC-11 (bp 23.8°C) and CFC-12 (bp −30°C), were used extensively as blowing agents in the manufacture of rigid insulation foam. Because of the mandatory phaseout of CFCs by Jan. 1, 1996, it had become necessary to develop blowing agents that have a minimal effect on the ozone layer. As a short-term solution, two classes of blowing agents are considered: HCFCs and HFCs. For example, HCFC 141b, CH_3CCI_2F (bp 32°C), is a drop-in replacement for CFC-11, and HFC 134a, CF_3CH_2F (bp −26.5°C), was developed to replace CFC-12. HCFC 142b, CH_3CCIF_2 (bp −9.2°C), is the blowing agent used in the 1990s. Addition of water or carbodiimide catalysts to the formulation generates carbon dioxide as a coblowing agent. Longer-range environmental considerations have prompted the use of hydrocarbons such as pentanes and cyclopentane as blowing agents. Pentane-blown foams have already been used in the appliance industry in Europe. Pentane-based formulations are typically used in conjunction with water. Because rigid foams blown with alternative blowing agents have lower values [(m·W)/(m·K)] of about 19.5, as compared to 18.0 for CFC-11-blown foams, they are thus less efficient in their insulation performance. In addition, because rigid polyurethane foams at a density of 0.032 g/cm^3 are ca 97% gas, the blowing agents determine the *k*-factor (insulation value).

The catalysts used in the manufacture of rigid polyurethane foams include tin and tertiary amine catalysts. Combinations of catalysts are often used to achieve the necessary balance of reaction rates. This is especially necessary if part of the blowing agent is carbon dioxide, generated in the reaction of the isocyanate with added water. New surfactants are required for the emerging water-coblown formulations, using pentanes as the main blowing agent (101). A typical water-coblown rigid polyurethane formulation is shown in Table 9 (102).

Rigid polyurethane foam is mainly used for insulation. The configuration of the product determines the method of production. Rigid polyurethane foam is produced in slab or bun form on continuous lines, or it is continuosly laminated between either asphalt or tar paper, or aluminum, steel, and fiberboard, or gypsum facings. Rigid polyurethane products, for the most part, are self-supporting, which makes them useful as construction insulation panels and as structural elements in construction applications. Polyurethane can also be poured or frothed into suitable cavities, ie, pour-in-place applications, or be sprayed on suitable surfaces. Spray-applied polyurethane foams are produced in densities ranging from 0.021 to 0.048 g/cm^3. The lower density foams are used primarily in nonload-bearing applications, eg, cavity walls and residential stud-wall insulation, whereas the

Table 9. Typical Rigid Polyurethane Panel Formulation

Ingredients	Parts
PMDI	135
Polyol	98
Water	1.9
Catalyst	2.0
Surfactant	2.0
HFC 134a	17.0

higher density foams are used in roofing applications. Applicators can buy formulated systems consisting of the isocyanate component, as well as the polyol side containing the catalysts, surfactants, and blowing agent.

During the molding of high density rigid foam parts, the dispensed chemicals have to flow a considerable distance to fill the cavities of the mold. In the filling period, the viscosity of the reacting mixture increases markedly from the initial low value of the liquid mixture to the high value of the polymerized foam. If the viscosity increases rapidly, incomplete filling results. Chemical factors that influence flow properties are differential reactivity in the polyol components and the addition of water to the formulation. Because venting holes allow the escape of air displaced by the rising foam, a moderate degree of overpacking is often advantageous. Newer high pressure RIM machines have simplified the mold-filling procedure, so filling of intricate molds is no longer a problem.

Rigid polyurethane foam is often poured into cavities, providing both thermal insulation and physical strength. Aircraft carrier hulls and refrigerators and freezers are insulated by in-place applied rigid polyurethane foam.

Many of the rigid insulation foams produced in the 1990s are PUIR foams. In the formulation of poly(urethane isocyanurate) foams an excess of PMDI is used. The isocyanate index can range from 105 to 300 and higher. PUIR foams have a better thermal stability than polyurethane foams (103). The cyclotrimerization of the excess isocyanate groups produces heterocyclic triisocyanurate groups, which do not revert to the starting materials but rather decompose at much higher temperatures. In the decomposition of the PUIR foams a char is formed, which protects the foam underneath the char.

The formation of isocyanurates in the presence of polyols occurs via intermediate allophanate formation, ie, the urethane group acts as a cocatalyst in the trimerization reaction. By combining cyclotrimerization with polyurethane formation, processibility is improved, and the friability of the derived foams is reduced. The trimerization reaction proceeds best at 90–100°C. These temperatures can be achieved using a heated conveyor or a RIM machine. The key to the formation of PUIR foams is catalysis. Strong bases, such as potassium acetate, potassium 2-ethylhexoate, and tertiary amine combinations, are the most useful trimerization catalyst. A review on the trimerization of isocyanates is available (104).

Modification of cellular polymers by incorporating amide, imide, oxazolidinone, or carbodiimide groups has been attempted but only the PUIR foams were produced in the 1990s. PUIR foams often do not require added fire retardants to meet most regulatory requirements (105). A typical PUIR foam formulation is shown in Table 10 (106).

The physical properties of rigid urethane foams are usually a function of foam density. A change in strength properties requires a change in density. Rigid polyurethane foams that have densities of <0.064 g/cm^3, used primarily for thermal insulation, are expanded with HCFCs, HFCs, or hydrocarbons. Often water or a carbodiimide catalyst is added to the formulation to generate carbon dioxide as a coblowing agent. High density foams are often water-coblown. In addition to density, the strength of a rigid foam is influenced by the catalyst, surfactant, polyol, isocyanate, and the type of mixing. By changing the ingredients, foams can be made that have high modulus, low elongation, and some brittleness (friability), or relative flexibility and low modulus.

Table 10. Typical PUIR Foam Formulation

Ingredients	Parts
PMDI (250 Index)	208.7
Terate 203[a]	100
Dabco K-15	5.2
Dabco TMR 30	1.2
Surfactant	2.0
HCFC 141b	35.0

[a]Crude aromatic polyester.

Rigid polyurethane foams generally have an elastic region in which stress is nearly proportional to strain. If a foam is compressed beyond the yield point, the cell structure is crushed. Compressive strength values of 10–280 kPa (1–14 psi) can be obtained using rigid polyurethane foams of 0.032-g/cm^3 density. In addition, the elastic modulus, shear strength, flexural strength, and tensile strength all increase with density.

Most low density rigid polyurethane foams have a closed-cell content of $>$90%. Above 0.032 g/cm^3, closed-cell content increases rapidly and is generally $>$99% above 0.192 g/cm^3. Bun foam, produced under controlled conditions, has a very fine-cell structure with cell sizes of 150–200 μm.

The availability of PMDI also led to the development of PUIR foams by 1967. The PUIR foams have superior thermal stability and combustibility characteristics, which extend the use temperature of insulation foams well above 150°C. The PUIR foams are used in pipe, vessel, and solar panel insulation; glass-fiber-reinforced PUIR roofing panels having superior dimensional stability have also been developed.

Strong bases, such as potassium acetate, potassium 2-ethylhexoate, or amine–epoxide combinations are the most useful trimerization catalysts. Also, some special tertiary amines, such as 2,4,6-tris(*N,N*-dimethylaminomethyl) phenol (DMT-30), 1,3,5-tris(3-dimethyl-aminopropyl)hexahydro-*s*-triazine, and ammonium salts (Dabco TMR) are good trimerization catalysts.

Semirigid foams are also manufactured. These foams do not fully recover after deformation; they are used in the construction of energy-absorbing automobile bumpers. Integral skin molded foams have an attached densified water skin, which is produced during manufacture. The preferred isocyanate for integral skin foams is carbodiimide-modified liquid MDI, which is used with ethylene oxide-capped polyols or polymer polyols. Thicker skins are obtained by lowering mold temperatures and increasing the percentage of overpack.

Interpenetrating Polymer Networks (IPNs)

Polyurethanes are used extensively in the formation of IPNs because of their inertness and reaction latitudes. They are formed from isocyanate-terminated prepolymers, and chain extension and cross-linking are accomplished using mixtures of diols and triols. The other polymer component involved in the formation of the polyurethane-derived IPNs include *p*-styrene, poly(methyl

methacrylate), polyacrylate, polyacrylamide, poly(vinyl chloride)(PVC), nylon 6, unsaturated polyesters, and epoxy polymers. The urethane prepolymers, chain extenders, and cross-linkers as well as the second monomer and its respective cross-linker can be reacted sequentially or simultaneously in solution or better in bulk. The polyurethane chains in the IPNs have reduced hydrogen bonding because of the presence of the polymer chains formed from the second monomer, which interfere with hydrogen bonding.

Sometimes the formation of polyurethane IPNs is conducted under pressure. For example, a 50:50 polyurethane–polystyrene (PU–PS)IPN is obtained from MDI and PTMG, using 1,4-butanediol and trimethylolpropane as extender and cross-linker. The styrene is cross-linked with divinyl benzene. Increased pressure (up to 20,000 kg/cm^2) increases the mixing of the components as well as the degree of cross-linking (107). In a similar manner IPNs derived from HDI and polystyrene are obtained (108). A simultaneous poly(isocyanurate)–nylon 6 IPN is obtained by mixing a HDI biuret/caprolactam initiator with caprolactam monomer and a prepolymer made from HMDI and a diol at 95°C, followed by polymerization at 140°C, to afford the poly(isocyanurate) star-shaped nylon-6 IPN (109). PU–PVC IPNs are obtained from MDI and poly(caprolactone) (PCL) and PVC. It was found by nitroxide spin labeling studies that the polyurethane consists of a crystalline PCL and an amorphous PCL phase, and that PVC acts as a plasticizer between the phases (110). A polyurethane–polyester IPN with a ratio typical for sheet molding compound (SMC) is obtained from Isonate 143-L (liquid MDI) poly(caprolactone triol), an unsaturated polyester resin and styrene monomer (111). The polymerization is conducted at 60°C, using different initiators (*t*-butylperoxy-2-ethylhexanoate and cobalt naphthenate) to control the reaction rates. The polyester has a solvent effect on the polyurethane reaction. Prior to gelation, the reaction resembles a solution polymerization, and after gelation a bulk polymerization. A recent book reviews PU-derived IPNs (112).

Thermoset Polyurethane Elastomers

Thermoset polyurethanes are cross-linked polymers, which are produced by casting or RIM. For cast elastomers, TDI in combination with 3,3′-dichloro-4,4′-diphenylmethanediamine (MOCA) are often used.

RIM is another important polymerization method used in the manufacture of thermoplastic or thermoset polyurethanes. This high pressure reactive casting process is conducted in RIM machines. Differences between the low pressure casting process and the high pressure RIM process are in the speed and efficiency of mixing. The isocyanates used in the formulation of RIM systems are liquid MDI products (carbodiimide-modified MDI or MDI prepolymers) and PMDI for structural (SRIM) applications. Also, glass reinforced versions are known as RRIM. The RIM process used in the automotive industry consists of high pressure impingement mixing of reactive liquid monomers resulting in short molding cycles. The principal advantage of this process results from the fact that molds are filled with liquids, which requires only 50 lb/in.^{2} clamping pressure as compared to the 2–5 tons/in.^{2} needed for injection molding of TPUs. In order to improve the green strength of the resultant polymers diamine extenders, such as diethyl

Table 11. Properties of RIM Systems

	Flexural modulus, MPa[a]		
Properties	0.137–0.517	0.517–1.03	1.37–2.75
Tensile elongation, % break	100–300	50–200	<50
Izod impact, J/m[b]	534–801	267–801	<267
Impact strength	High	Medium high	Low
Material description	Elastomer	Pseudo plastic	Plastic
Automotive application	Fascia	Fender	Hood or deck lid

[a]To convert MPa to psi, multiply by 145.
[b]To convert J/m to ft·lb/in., divide by 53.38.

toluenediamine (DETDA), are incorporated in the newer automotive systems. Also, internal mold release (IMR) agents based on zinc stearate compatibilized with primary amines were introduced in 1985. The IMR systems are used to reduce the need to apply external mold release agents. An IMR system offers reduced cycle times, improved productivities, less frequent mold cleaning, and lower scrap rate. In the RIM technology, aromatic diamine chain extenders, such as DETDA, are used to produce poly(urethane ureas) (113), and replacement of the polyether polyols with amine-terminated polyols produces polyureas (114). Some physical properties of RIM systems are listed in Table 11.

Polyurethane Coatings

Polyurethane coatings are used wherever applications require abrasion resistance, skin flexibility, fast curing, good adhesion, and chemical resistance. The polyaddition process allows formulation of solvent based or solventless liquid two-component systems, water-based dispersions, or powder coatings. Two-component polyurethane coatings are prepared by mixing the A and B components prior to application to the substrate. The TDI-trimethylolpropane adduct, the HDI biuret, and the isocyanurate of HDI or IPDI are often used as the polyisocyanate component. These systems cure at ambient temperature to give coatings with excellent properties. In order to increase the pot life of the coating systems, one-component moisture coatings are developed. These systems are based on PMDI, MDI, TDI, or HDI and a polyfunctional polyether polyol. These prepolymers (NCO content 3–16%) are stable when stored under dry conditions at ambient temperature. Blocked isocyanates are also used in the formulation of one-component systems. Thus, storage stable one-component coatings that are heat curable can be formulated by mixing blocked polyisocyanates with macrodiols. Also, solvent-free polyurethane powder coatings are known. Both thermoplastic and thermoset binder systems can be used in powder coatings. Thermoplastic powders are mainly used in thick coating applications (125–1000 μm). Polyester polyurethane powders use caprolactam-blocked IPDI or TDI adducts as cross-linking agents. Caprolactam does not cause yellowing and diffuses with a minimum of degassing. Powdered polyesters and blocked isocyanate adducts must be solids with melting points above 50°C to prevent agglomeration during storage. Powder coating systems also

contain pigments, fillers, catalysts (stannous octoate, etc), and small amounts of flow-control additives, and they are cured by baking at 180–200°C for 15–30 min.

Solutions (5–25% solids) of fully reacted polyurethanes based on MDI or IPDI are also used in coating applications. These coatings are used mostly as finish coats on flexible substrates. Because of concern over airborne solvents aqueous polyurethane dispersions are used today. These polymers are prepared by incorporating ionic groups into their backbone, and both cationic and anionic groups are utilized in the preparation of the ionomers. The solvent and water resistance of films formed from aqueous dispersions can be improved by cross-linking. Ionomers are also used in the formulation of speciality adhesives.

Polyurethane coatings are mainly based on aliphatic isocyanates and acrylic or polyester polyols because of their outstanding weatherability. For flexible elastomeric coatings, HMDI and IPDI are used with polyester polyols, whereas higher functional derivatives of HDI and IPDI with acrylic polyols are mainly used in the formulation of rigid coatings. Plastic coatings, textile coatings, and artificial leather are based on either aliphatic or aromatic isocyanates. For light-stable textile coatings, combinations of IPDI and IPDA (as chain extender) are used. The poly(urethane urea) coatings are applied either directly to the fabric or using transfer coating techniques. The direct-coating method is applied for rainwear because the microporous coating is permeable to air and water vapor, but not to liquid water. Microporous polyurethane sheets (poromerics) are used for shoe and textile applications. Alcantara is an artificial velour leather used in the fabrication of fashion wear. Polyurethane binder resins are also used to upgrade natural leather.

Waterborne polyurethane coatings are formulated by incorporating ionic groups into the polymer backbone. These ionomers are dispersed in water through neutralization. The experimental 1,12-dodecane diisocyanate is especially well suited for the formation of waterborne polyurethanes because of its hydrophobicity (115). Cationomers are formed from IPDI, *N*-methyldiethanolamine, and poly(tetramethylene adipate diol) (116); anionic dispersions are obtained from IPDI, PTMG, PPG, and dimethylol propionic acid (117). The ionic groups can also be introduced in the polyol segment. For example, reaction of diesterdiol, obtained from maleic anhydride and 1,4-butanediol, with sodium bisulfite produces the ionic building block, which on reaction with HDI gives a polyurethane ionomer (118). The weatherability of aliphatic polyurethane coatings is related to their structures. Polyester polyol-based polyurethanes are more uv-resistant than polyether polyol-based polyurethanes, but the latter offer better hydrolytic stability (see URETHANE COATINGS).

For baking enamels and wire and powder coatings, blocked isocyanates are used. Blocked polyurethane coatings do not cure below a certain threshold baking temperature. Catalysts, such as tertiary amines or organometallic tin compounds, are used to lower the curing temperature.

Uses

Furniture and Bedding. In most geographic regions flexible foam applications represent the largest volume uses of polyurethanes. The bulk of the use

is for furniture, automotive seating, bedding, and packaging applications. With a broad range of available load-bearing capacity and resiliency, these materials offer degrees of comfort and protection not approached by any other single cushioning material. Flexible slabstock foam is used approximately 60% in furnishings, 35% in automotive application (seating, crash pads, head-armrests, trim, sound insulation, vibration dampening, carpet backing, sun visors, instrument panels, and energy management), and 5% in packaging and other applications. Bedding applications are centered on flexible foam mattresses of a variety of sizes and densities. However, polyurethane mattresses are still encountering significant competition from traditional coil-spring mattresses. Polyurethane foam mattresses are commonly found in hospitals, hotels, universities, and other high volume institutional-type applications. Foaming in-place is often used for packaging of delicate instruments and military parts.

Carpet cushioning is another application for both prime foam and rebounded scrap foam. The prime foam is virgin foam used as a separate carpet underlay or attached directly to the back of the carpet. The latter allows rapid continuous application of liquid chemicals using reaction polymerization technologies. Systems based on prepolymers of TDI or MDI are used in combination with conventional polyols and inorganic fillers. The rebounded scrap foam is made by adhesive binding ground flexible foam scrap, and it is used as a separate carpet underlay.

A significant volume of flexible foam is used in speciality applications, some of which continue to use the earliest type flexible polyester polyurethane foam used mainly for textile lamination. Reticulatd foams are used in air filters.

Construction. Building and construction markets use rigid polyurethane foam produced as boardstock (either produced continuously, discontinuously, or cut from rigid foam buns). The boardstock is then used as roof or wall insulation for commercial and residential buildings, as well as in refrigerated buildings and metal door cores. Residential sheathing uses an aluminum foil-faced boardstock often produced using continuous lamination technologies. Rigid polyurethane foam can also be spray-applied, a technique that is well suited for retrofitting commercial roofs and industrial tank and pipe insulation.

Other significant applications for rigid polyurethane foam include domestic refrigerators and coolers, insulated trailer trucks, shipping containers, and railway cars. Marine applications utilize the flotation/buoyancy characteristics of rigid foams for recreational boats and aircraft carriers. Semirigid polyurethane foam is also used as foam-in-place packaging foam. Polyurethane products are also used in the construction of masks and other life-like surfaces, puppetry, animatronics, and props and sets, both life-size and miniature, for the movie industry.

Spraying of the foam formulation by special two-stream spray guns onto suitable surfaces is often conducted. On-site applications for spray foam include roofs, tanks, vessels, cavity walls, and pipes. Spray-applied polyurethane foams are produced in densities ranging from 1.3 to 3.0 lb/ft^2 (21–48 kg/m^3). The lower-density foams are used primarily in nonload-bearing applications (cavity walls and residential stud-wall insulation). The higher-density foams are used in roofing applications. The 1:1 volume ratio of the A and B components required for spray foams excludes the poly(isocyanurate) chemistry from this application. In spray foam formulations, PMDI in combination with the more reactive amine polyols

are used, and sometimes diamine extenders are added to increase the reaction rate.

Ships transporting liquid natural gas (LNG) are usually insulated with rigid PUIR foam laminates, which provide temperature stabilities from −180 to 150°C. The main fuel tank of the National Aeronautics and Space Administration (NASA) space shuttles is also insulated with PUIR foam. Rigid polyurethane foam is used in engineered foam-in-place packaging of industrial or scientific equipment and in the molding of furniture, simulated-wood ceiling beams, and a variety of decorative and structural furniture components. Rigid foam is also used for the repair of river barges.

Automotive Applications. The global automotive industry utilizes every variation of polyurethane technology. Examples include automotive seating, RIM bumber and fascia, RRIM for light weight rocker panels, rigid polyurethane insulation foam for the walls of refrigerated trucks and underfloor sound insulation, interior panels, and high performance paints and coatings. In 1999 a total of 1.161 million tons of polyurethanes were used in automotive applications (United States: 596 kt/a, Europe: 365 kt/a, and Asia: 200 kt/a).

Recent trends are the increased use of MDI-based flexible foams because higher density foams with good comfort are obtained. Also, dual hardness foam cushioning can be produced more easily with MDI systems. Hot cure TDI foams are being phased out. In Table 12 the distribution of the systems used in the global automotive seating production are shown.

The growth rate of polyurethane RIM/RRIM parts is slowed to only about 1% because of the need to develop products with easier recycling routes, but RRIM-based composite pickup-truck boxes weighing up to 115 kg are currently produced using two separate RRIM molding processes. This trend may positively influence the future growth rate of polyurethane parts. In 1998 RIM/RRIM consumption in Europe was 8935 kt/a, while in the United States, 39,900 kt/a was consumed. The Asian market amounted to 8205 kt/a.

Automotive shock absorbers based on 1,5-NDI and ethylene glycol adipates (Vulkollan) are used in the global automotive markets (total consumption in 1998 was 10.2 kt/a). Systems based on MDI are also used.

For door panels structural RIM molding is used, and fiber reinforced polyurethane interior materials use long fiber injection technologies or compression molding processes. A trend to eliminate PVC in interior panels

Table 12. Global Automotive Seating Systems

System	%
TDI HR cold cure	20
TDI hot cure	22
MDI HR cold cure	33
TM-20 HR[a]	16
Others[b]	3

[a] 80:20 Blend of TDI 80 with PMDI.
[b] Foams produced with cross-linkers or modified grades of TDI.

presents an opportunity for polyurethanes in skins for door and instrument panels. Also, colored polyurethane skins based on aliphatic isocyanates are backfoamed with conventional MDI-based polyurethane spray foam (Recticel process).

Aqueous two-component polyurethane systems for automotive topcoats are under development. Currently the automotive topcoats are made from solvent-based two-component or blocked one-component systems based on HDI trimer (Desmodur N) or IPDI trimer (Desmodur Z) or both in conjunction with an acrylic polyol. The polyurethane topcoats provide the vehicles with a tough and durable finish with excellent long-lasting glossy appearance ("wet look") One-component aqueous dispersions are already used in electrodeposition primers and pigmented base coats. Soft-feel polyurethane coatings are increasingly used for instrument panels and seat covers.

Polyurethane foams are increasingly used for insulation, sound proofing, and carpet backing in automotive applications. Examples include instrument panels, dashboards, armrests, door liners, sound/vibration dampening mats, bumper cores, and sun visors. These semirigid foams are mainly based on PMDI. Semirigid integral skin foams characterized by a tough elastomeric polyurethane skin formed during manufacture of the low density foam core are also used in interior trim parts. Recently Volkswagon insisted on the elimination of amine emission from polyurethane foams installed in their vehicles. The use of reactive tertiary amine catalysts which become bound to the polyurethane foam would solve this problem.

Automotive windshield and backlight sealants were introduced by Essex (now Dow Chemical) in the 1970s. Excellent tensile strength and toughness combined with good adhesion to primed glass allow automobiles to pass 40 mh rollover tests without the windshield popping out. One component windshield sealants utilize diethylmalonate blocked MDI prepolymers to ensure package stability. In the presence of both tin and mercury or bismuth salts, moisture will cure the sealant under ambient conditions. The U.S. market for automotive sealants in 1997 was 68.5 kt/a.

Antilacerent windshields were also considered by bonding single or multiple layers of polyurethanes to the interior windshield. However, the emergence of the use of air bags in cars has eliminated the need for antilacerent windshields. However, modular window gaskets are produced using the RIM process. The MDI systems based on polyether polyols, glycol, or DETDA extenders require painting in order to achieve good weatherability.

Footwear. Polyurethanes are among the most useful materials for footwear applications. The low weight and high level of comfort of microcellular polyurethane soles and their ease of production, using a reaction molding process led to rapid global adaptation of this technology. Apart from the dominant use of microcellular polyurethane elastomers in the production of shoe soles (street shoes, sport shoes, leisure shoes, and safety shoes), polyurethane flexible or semiflexible foams with or without an integral skin are commonly used to produce in-soles and ski-boot liners. Polyurethanes also offer processing advantages, such as direct molding of the shoe soles to the shoe uppers.

Two basic types of polyurethanes are available as shoe-soling products: polyester- and polyether-based systems. The polyester systems were first

introduced because of their high quality in applications such as safety shoes, boots, and sport shoes. They are also very suitable for direct soling. Lower-cost polyether systems were introduced in the 1970s. Polyether-based systems are the choice for street shoes because of their excellent hydrolytic stability. Polyether polyurethanes also provide better flex resistance at low temperature because of the lower glass transition temperature of the polyether chain. Usually a highly reactive 4000 molecular weight polyether diol is used in combination with a MDI prepolymer and 1,4-butanediol, and small amounts of triols are added to improve the green strength and demolding time. A controlled amount of water and fluorocarbon blowing agents are used in combination with tertiary amine and tin catalysts.

Millable Polyurethane Gums and Elastomers. Polyurethanes with the rheology of natural rubber, so-called *millable gums*, are made by mixing hydroxy-terminated prepolymers and isocyanate cross-linking agents, such as the 2,4-TDI dimer, and other additives on a rubber mill. The milled compound is shaped, compression molded, and heat cured. Millable polyurethane gums are used in synthetic rubber applications such as shock-damping mounts, roll covers, and parts for military vehicles.

Polyurethane elastomers containing ultra high molecular weight polyethylene (UHMWPE) as fillers show improved abrasion resistance. The UHMWPE is dispersed in the polyol in the formation of the filled polyurethanes. Commercial uses include gears, rollers, bushings, and mining screens.

Polyurethanes are also used in the construction of sport surfaces such as all-weather athletic areas, outdoor game areas, children's playgrounds, tennis courts, and multisport halls. The polyether polyurethane systems, mainly based on PMDI, are applied by a pour-in-place method. Often additional rubber granules are added to the system.

Solid polyurethane industrial tires are produced for off-road machines (fork and lift trucks, wheelchairs), pneumatic tires for tractors, backhoe loaders, soft-cast elastomer tires for heavy vehicles and skateboard and roller skate wheels. Polyurethane tires for passenger cars have not as yet been commercialized. Pneumatic tires for tractors are produced using the RIM process. Soft-cast polyurethane elastomers are also used for puncture-free tires, especially for heavy vehicles, replacing the air in pneumatic tires.

Another important application for solid polyurethane elastomers are sealing gaskets in sewage clay pipes. These gaskets are made by casting liquid elastomer systems directly onto the extremities of the pipe. The solidified elastomer will adhere well to the ceramic surface.

Elastomeric spandex fibers are used in hosiery and sock tops, girdles, brassieres, support hose, and swim wear. The use of spandex fibers in sport clothing is increasing.

Polyurethane Adhesives and Sealants. Polyurethane adhesives are known for excellent adhesion, flexibility, toughness, high cohesive strength, and fast cure rates. Polyurethane adhesives rely on the curing of multifunctional isocyanate-terminated prepolymers with moisture or on the reaction with the substrate, eg, wood and cellulosic fibers. Two-component adhesives consist of an isocyanate prepolymer, which is cured with low equivalent weight diols, polyols, diamines, or polyamines. Such systems can be used neat or as solution. The two

components are kept separately before application. Two-component polyurethane systems are also used as hot-melt adhesives.

Waterborne adhesives are preferred because of restrictions on the use of solvents. Low viscosity prepolymers are emulsified in water, followed by chain extension with water-soluble glycols or diamines. PMDI, which has a shelf life of 5–6 h in water, can be used as a cross-linker. Waterborne polyurethane coatings are used for vacuum forming of PVC sheeting to ABS shells in automotive interior door panels, for the lamination of ABS/PVC film to treated polypropylene foam for use in automotive instrument panels, as metal primers for steering wheels, in flexible packaging lamination, as shoe-sole adhesive, and as tie coats for polyurethane-coated fabrics. PMDI is also used as a binder for reconstituted wood products and as a foundry core binder.

Typical one-component elastomeric adhesive formulations are based on a linear poly(butylene adipate) of molecular weight 2000, MDI and 1,4-butanediol as chain extender. Crystallization of the soft polyol segment below 40°C, which occurs after evaporation of the solvent, causes a gain in bond strength. Upon heating of the film with an infrared lamp, the adhesive can be reactivated for bonding. The adhesive systems are manufactured by dissolving the elastomeric polyurethane in the desired solvent or solvent mixture and adding other polymers, fillers, and stabilizers. The polyurethane adhesive technology is also utilized in the formulation of architectural sealants, which are also supplied as both one- and two-component systems. These systems are often modified with epoxy, acrylic, or other polymers and with stabilizers and fillers. One-component automotive windshield sealants utilize diethyl malonate-blocked MDI prepolymers. In the presence of tin, mercury, or bismuth salts moisture will cure the sealant under ambient conditions.

Polyurethane sealant formulations use TDI or MDI prepolymers made from polyether polyols. The sealants contain 30–50% of the prepolymer; the remainder consists of pigments, fillers, plasticizers, adhesion promoters, and other additives. The curing of the sealant is conducted with atmospheric moisture.

Biomedical Polyurethane Applications. Numerous different type of aromatic and aliphatic polyether urethanes and poly(urethane ureas) as well as siloxane–urethane copolymers have been developed for many biomedical applications. The principal products are segmented TPUs based on PTMEG as the soft segment. Biomer, developed by DuPont in the 1960s, uses a diamine as extender, and solutions of the polymer in dimethyl acetamide (DMAc) became available. Biomer was later sold to Ethicon, who withdrew the product from the market in 1991. Pellethane, a TPU based on PTMEG, MDI, and 1,4-butanediol was introduced by Upjohn in the 1970s. Pellethane was used extensively in pacemaker leads, but Dow Chemical, who purchased the chemical division of Upjohn in 1985, decided not to sell Pellethane for biomedical applications, because of potential liabilities. A TPU based on a polycarbonate macroglycol and MDI was introduced recently by Cardiotech (Chromoflex). Improved biodurability was claimed for these polymers (119). Also, Bayer developed improved series of TPUs (Texin 5590), for biomedical applications based on IPDI, using a diamine extender. These poly(urethane ureas) have a higher modulus to allow easy insertion of catheters.

Male polyurethane condoms in the United States had 5% of the market in 1999. The excellent physical properties of TPU films allow the manufacture of very thin condoms by cutting and welding or by solvent dipping.

Polyurethane gels were also developed by Bayer (Levagel) for biomedical applications. These gels are based on quadrafunctional polyether polyols and aliphatic isocyanate prepolymers. The new gels are used in very soft padding for artificial limbs and in the development of wound dressing products. The gels can be foamed to enhance breathability to oxygen and water vapors to promote healing.

Binder Applications. Reconstituted wood products, such as particle boards, wafer boards, medium density fiberboards, and oriented standboards, increasingly use PMDI as a liquid adhesive to bind the wood products. Wood has many hydroxyl groups containing compounds such as cellulose, hemicellulose, and lignin. Polymeric isocyanate binder resins will react with these hydroxyl groups to form chemical bonds between the wood chips. PMDI is a 100% active liquid binder that is easily atomized and provides excellent bonding efficiencies. Dow has developed Isobind, a special PMDI for this application as well as process technology called Optimax, which is available under a licensing agreement with Carbocol Systems, Inc. The use of isocyanate binders achieves faster cure rates and lower temperature cure as compared to other binder resins. Isocyanate binders cure at about 100°C, while phenol/formaldehyde resins cure at 150°C or higher. The demands of public regulatory agencies for control of formaldehyde products, used extensively as wood binding resins, have intensified interest in formaldehyde-free isocyanate binders.

The PMDI-derived reconstituted wood products have found applications as siding materials, shelves, cabinets, furniture, and pallets. Extra large panels are finding uses in the mobile home industry, where entire walls are fabricated from a single continuous panel with greater rigidity and strength. Shipping containers of lighter weight and uniform properties can also be made. PMDI can also be used as a binder for agro waste products. For example, three-layer laminates consisting of top and bottom layers of coconut husks and a core layer consisting of wood chips provide attractive building panels. Waste straw and bagasse is also used in the manufacture of solid wood-like boards.

The use of PMDI as a binder for foundry cores, rubber waste products, and solid rocket fuel are also known. Isocyanate-terminated prepolymers, often prepared from TDI or MDI with polyether polyols are also used as binders for composite products that require elastomeric properties. Athletic surfaces are sometimes prepared from ground rubber tire scrap bonded with isocyanate-based prepolymers. Similarly, flexible polyurethane foam scrap is bonded with isocyanate prepolymers to form rebonded foam useful as carpet underlay. Solidification of incineration ashes with PMDI-based binder systems is another waste disposal application. In this manner hazardous waste materials undergo chemical fixation and detoxification.

The thickening of SMC can be accelerated using hydroxy-terminated unsaturated polyesters in conjunction with isocyanate-terminated prepolymers. Polyurethane ionomer-based sizings for glass fibers used in RRIM applications are also known.

Synthetic leather products are also produced using a urethane binder. These poromeric materials are produced from textile-length fiber mats impregnated with DMF solutions of polyurethanes. Permeability to moisture vapor is the key property needed in synthetic leather. In addition to shoe applications, poromerics are

Table 13. Major Polyurethane Applications in the United States/ Canada and Europe

Market	United States/Canada (%)	Europe (%)
Construction	26	23
Furniture and Bedding	23	24
Elastomers	9.6	7
Coatings	9	10
Appliances	6	7
Footwear	1.0[a]	8

[a] Footwear is no longer manufactured in the United States and Canada.

used for handbags, luggage, and apparel. Polyurethane films having oxygen and water permeability are applied in bandages and wound dressings and as artificial skin for burn victims.

Economic Aspects

In 1998 a total of 2642 kt/a of polyurethanes were consumed in the United States (91%) and Canada (9%). The European consumption in 1998 was 2169 kt/a, and the Asian Pacific Region consumed 1807 kt/a of polyurethane chemicals. Therefore, the total global polyurethane consumption was of the order of 8000 kt/a in 2000. In Table 13 a comparison of significant American and European applications as percentages of the previously mentioned total amounts are shown. With the exception of footwear, the use by application in both regions is almost identical.

The flexible foam market is the largest global polyurethane consumption. In the United States and Canada a total of 1114 kt/a was used in flexible foam applications in 1998. Flexible slab foam is used predominantly in furniture, carpet underlay, and bedding; molded foam is used extensively in transportation. Carpet underlay is manufactured from either virgin or scrap polyurethane foam, which is combined with a binder adhesive.

Of the 687 kt/a of rigid foam produced in the United States and Canada in 1998, more than 50% was used in the construction industry. About 60% of this total was used in laminated boards and insulation panels; about 30% was poured at construction site. Insulated appliances (132 kt/a) and tank and pipe insulation (79 kt/a) are other important uses of rigid insulation foam. Rigid polyurethane foam is produced from PMDI. Another important application of PMDI is particle board binder resins. A total of 160 kt/a of PMDI was used in this application in the United States and Canada in 1998.

The total elastomer consumption in the United States and Canada in 1998 accounted for 245 kt/a. Automotive RIM applications accounted for 65.3 kt/a, TPU for 53.5 kt/a, and Spandex for 26.5 kt/a. Cast elastomers had the highest consumption (100 kt/a). Coatings consumption in the United States and Canada in 1998 was 237 kt/a, and powder coatings accounted for about 20% of the total. Adhesives (105 kt/a) and sealants (80 kt/a) were other important polyurethane applications.

The polyurethane industry is dominated by the multinational isocyanate producers. The principal isocyanate producers (BASF, Bayer, Dow) also manufacture polyols. Dow is one of the largest global producers of polyether polyols, and

Bayer acquired the other primary polyether polyol producer, when it purchased the polyol business of Arco (now Lyondell) in 1999. Also, in 1999 Dow further strengthened its position in polyols when it acquired Union Carbide. Polyether polyols, mainly used for flexible foam production, account for 65 wt% in a flexible foam formulation, 35% in rigid polyurethane foams, and even less in PUIR foams.

The former Olin and Rhone Poulenc TDI production facilities are still operated by Lyondell, but it is unlikely that Lyondell will continue the isocyanate business without the polyether polyol business it sold to Bayer.

Health and Safety Factors; Environmental Aspects

The primary route of exposure to most isocyanates is through inhalation. Isocyanate vapors and aerosol can irritate the mucous membranes in the respiratory tract (nose, throat, lungs) causing nasal irritation, sore throat, coughing, chest discomfort, shortness of breath, and reduced lung function. Persons with a nonspecific bronchial hyperreactivity can respond to extremely low concentrations with similar symptoms as well as asthma attack. Exposure to higher concentrations may lead to bronchitis, bronchial spasm, and pulmonary edema. These effects are usually reversible. As a result of repeated overexposure or a single large dose, certain individuals may develop isocyanate sensitization (chemical asthma), which may cause a reaction to a later exposure at very low concentrations. These symptoms, which can include chest tightness, wheezing, cough, shortness of breath, or asthmatic attack, could be immediate or delayed up to several hours after exposure. Chronic overexposure to isocyanates has been reported to cause lung damage (including decrease in lung function), which may be permanent. Sensitization can either be temporary or permanent.

Both chlorofluorocarbons and methylene chloride are used as blowing agents. Inhalation of high concentrations of chlorofluorocarbons can be dangerous and may cause anesthesia and unconsciousness. Severe acute exposures have caused cardiac arrhythmias, including ventricular fibrillation. Since chloroflurocarbon vapors are heavier than air, high concentrations can accumulate in confined or low-lying areas, displacing air or oxygen supply. Although these materials are considered nonflammable, they can heated to decomposition, generate highly toxic phosgene and carbonyl fluoride. In addition, when confined and subject to high temperatures, chlorofluorocarbons may present an explosion hazard.

Like chlorofluorocarbons, methylene chloride is difficult to ignite, but when heated to decomposition, can produce toxic materials such as hydrogen chloride, carbon dioxide, and carbon monoxide. Upon skin contact methylene chloride can cause irritation, drying, and weakening of the skin. Inhalation can cause central nervous system depression, resulting in impaired judgment and reduced motor ability. Inhalation of high concentrations causes cancer in laboratory animals. It is therefore extremely important to follow the manufacturer's recommendation for the safe use and handling of methylene chloride.

Although the products of combustion vary, virtually all polyurethane foams and materials burn, often generating a variety of toxic, potentially lethal gases

and dense smoke. The type and amount of combustion products vary with product composition, fire conditions, oxygen concentration, and other factors. As in all organic fires, the main toxicant is carbon monoxide. Like other nitrogen-containing polymers oxides of nitrogen and hydrogen cyanide can also be released. Fully cured polyurethanes present no health hazards; they are chemically inert and insoluble in water and are the most organic solvents. However, dust can be generated in fabrication, and inhalation of the dust should be avoided. Polyether-based polyurethanes are not degraded in the human body, and are therefore used in biomedical applications.

Some of the chemicals used in the production of polyurethanes, such as the highly reactive isocyanates and tertiary amine catalysts, must be handled with caution. The other polyurethane ingredients, polyols and surfactants, are relatively inert materials having low toxicity.

Isocyanate Toxicity. Isocyanates in general are toxic chemicals and require great care in handling. Oral ingestion of substantial quantities of isocyanates can be tolerated by the human body, but acute symptoms may develop from the inhalation of much smaller amounts. The inhalation of isocyanates presents a hazard for the people who work with them as well as the people who live in the proximity of an isocyanate plant. Adequate control of exposure is necessary to achieve a safe working environment. The suppliers Material Safety Data Sheets (MSDS) have to be consulted for the most current information on the safe handling of isocyanates.

Respiratory effects are the primary toxicological manifestations of repeated overexposure to diisocyanates (120). Once a person is sensitized to isocyanates, lower concentrations can trigger a response (121). Most of the industrial diisocyanates are also eye and skin irritants. Controlling dermal exposure is good industrial hygiene practice. The 1997 American Conference of Governmental Industrial Hygienists (ACGIH) exposure guideline for TDI is 0.005 ppm as a TWA-TLV (an 8-h time-weighted average concentration); the 1997 TLV for TDI in Japan is 20 ppb.

Overexposure to TDI can cause chemical bronchitis (isocyanate asthma) in sensitized individuals. Transient acute asymptomatic changes in respiratory function and deterioration of lung function following long-term repeated exposure have also been encountered. Allergic sensitization may occur within months or after years of exposure to isocyanates. Animal studies using TDI showed no teratologic response at exposure concentrations up to 0.5 ppm. A chronic gavage study indicated tumor formation in the animals, but the study was found to be of doubtful toxicological relevance because of the method used and the excessively high dose levels. Vapor exposure to MDI is limited by the low vapor pressure, corresponding to a saturated atmosphere of 0.1 mg/m^3 at 25°C. An acute aerosol inhalation study on PMDI using rats indicated that the 4-h LC_{50} is 490 mg/m^3. The current ACGIH TLV for MDI is 0.051 mg/m^3 (0.005 ppm) as a TWA. The OSHA PEL is 0.02 ppm as a ceiling limit.

The toxicity of aliphatic diisocyanates also warrants monitoring exposure to its vapors. HDI has a moderate potential for acute systemic dermal toxicity; rabbit dermal LD_{50} is 570 mL/kg. However, HDI is severely irritating to the skin and eyes. Irritation, lacrimation, rhinitis, burning sensation to throat and chest, and coughing have all been reported in humans following acute inhalation

Table 14. Acute Toxicity of Diisocyanates in Rats[a]

Isocyanate	LC_{50}, mg/kg	1 h LC_{50}, mg/m^3	Std. vapor pressure conc., ppm
HDI	710	310[b]	6.8
IPDI	>2,500	260	0.34
TDI	5,800	58–66	19.6
MDI	>31,600		0.1
NDI	>10,000		0.02[c]

[a]Ref. 122.
[b]4 h.
[c]Vapor pressure at 50°C.

exposure to HDI. HMDI has a low eye and dermal irritation potential, as well as a low potential for acute toxicity. Exposure to HMDI aerosol can cause dermal sensitization of laboratory animals. IPDI can cause skin sensitization reactions as well as eye irritation. The acute toxicity of diisocyanates in rats is shown in Table 14.

There are a multitude of governmental requirements for the manufacture and handling of isocyanates. The U.S. Environmental Protection Agency (EPA) mandates testing and risk management for TDI and MDI under Toxic Substance Control Administration (TSCA). Annual reports on emissions of both isocyanates are required by the EPA under SARA 313.

Thermal degradation of isocyanates occurs on heating above 100–120°C. This reaction is exothermic, and a runaway reaction can occur at temperatures > 175°C. In view of the heat sensitivity of isocyanates, it is necessary to melt MDI with caution and to follow suppliers' recommendation. Disposal of empty containers, isocyanate waste materials, and decontamination of spilled isocyanates are best conducted using water or alcohols containing small amounts of ammonia or detergent. For example, a mixture of 50% ethanol, 2-propanol, or butanol; 45% water; and 5% ammonia can be used to neutralize isocyanate waste and spills. Spills and leaks of isocyanates should be contained immediately, ie, by dyking with an absorbent material, such as saw dust.

The total U.S. airborne emission of volatile TDI is estimated by the International Isocyanate Institute (III) to be <25 t, or less than 0.005% of the annual U.S. production. Published data show that TDI has a 1/3 life of 8 s in air at 25°C and 50% RH, and a 0.5-s to 3-day half-life in water, depending on pH and agitation. Without agitation, isocyanates sink to the bottom of the water and react slowly at the interface. Because of this reactivity, there is no chance of bioaccumulation.

Toxicity of Tertiary Amine Catalysts. The liquid tertiary aliphatic amines used as catalysts in the manufacture of polyurethanes can cause contact dermatitis and severe damage to the eye. Inhalation can produce moderate to severe irritation of the upper respiratory tracts and the lungs. Ventilation, protective clothing, and safety glasses are mandatory when handling these chemicals.

Toxicity of Polyurethanes. These polymers can be considered safe for human use. However, exposure to dust, generated in finishing operations, should be avoided. Ventilation, dust masks, and eye protection are recommended in foam

fabrication operations. Polyurethane or polyisocyanurate dust may present an explosion risk under certain conditions. Airborne concentrations of 25–30 g/m^3 are required before an explosion occurs. Inhalation of thermal decomposition products of polyurethanes should be avoided because carbon monoxide and hydrogen cyanide are among the many products present.

Because polyurethanes are combustible, they have to be applied in a safe and responsible manner. At no time should exposed foam be used in building construction. An approved fire-resistive thermal barrier must be applied over foam insulation on interior walls and ceilings. Model U.S. building codes specify that foam plastic used on interior walls and ceilings must have a flame-spread rating, determined by ASTM E84, of <75 and smoke generation of <450. The foam plastic must be covered with a fire-resistive thermal barrier either having a finish rating of not less than 15 min or equivalent to 12.7-mm gypsum board, or having a flame-spread rating of <25, smoke generation of <450 (if covered with approved metal facing), and protection by automatic sprinklers. Under no circumstances should direct flame or excessive heat be allowed to contact polyurethane or polyisocyanurate foam. The ASTM numerical flame-spread rating is not intended to reflect hazards presented under actual fire conditions.

Recycling of Polyurethanes. For polyurethanes a wide variety of recycling procedures are considered. Examples include mechanical recycling (rebounded foam, adhesive pressing, particle bonding, regrind, injection molding, compression molding), chemical recycling (glycolysis, hydrolysis), feedstock recovery (pyrolysis, hydrogenation, gasification), and energy recovery (incineration). Especially, the large amounts of polyurethanes generated by ELV (end-of-life disposal of motor vehicles) is of present concern. An average of 20 kg of polyurethane per car is globally used.

The glycolysis procedure, pioneered by Upjohn in the 1970s (123), produces reusable polyols. In this process cut-up or pulverized polyurethane products are fed continuously or in batches into a heated reactor containing single glycol or mixtures of glycol at 185–210°C. A clear solution of a urethane polyol in the used glycol is obtained. This polyol, in admixture with virgin polyol, can be used for the manufacture of rigid polyurethane foams. Several pilot plants operate in Europe to produce polyols for rigid foam manufacture using variations of this process. In one process mixtures of polyurethane and PET scrap are used. Even rigid foam from insulated underground pipelines are recycled using the glycolysis process. The chemistry of the glycolysis process involves transesterification of the carbamate groups in the polyurethanes with the reactive solvent. In this manner three-dimensional network polymers are converted into soluble linear polyurethane group containing polyols.

In order to reuse such a polyol in flexible foam manufacture a subsequent propoxylation step becomes necessary, and Dow Chemical has developed a "tandem chemolysis" process for flexible polyurethane polyols.

Flexible polyurethane foam generated in production or recovered after use as seating foam or packaging foam can be recycled by shredding and mixing with a polyurethane binder to produce carpet underlay. Annually, ca 70 kt/a of carpet underlay produced in the United States is made from recycled flexible foam. Powdered flexible foam is also used as filler (up to 30%) in the manufacture of flexible foam products.

BIBLIOGRAPHY

"Polyurethanes" in *EPST* 1st ed., Vol. 11, pp. 506–563, by K. A. Pigott, Mobay Chemical Co.; "Polyurethanes" in *EPSE* 2nd ed., Vol. 13, pp. 243–303, by J. K. Backus et al., Mobay Corp., a Bayer USA Co.

1. O. Bayer, *Angew. Chem. A* **59**, 257 (1947).
2. H. Ulrich, *Kirk-Othmer Encyclopedia of Chemical Technology*, 4th ed., Vol. **24**, John Wiley & Sons, Inc., New York, 1997, pp. 695–726.
3. H. Ulrich, *The Chemistry and Technology of Isocyanates*, John Wiley & Sons, Inc., Chichester, 1996.
4. W. Hentschel, *Ber. Dtsch. Chem. Ges*.**17**, 1284 (1884).
5. K. Kurita, T. Matsumura, and Y. Iwakura, *J. Org. Chem*. **41**, 2070 (1976).
6. H. Eckert and B. Forster, *Angew. Chem*.**99**, 922 (1987).
7. U.S. Pat. 3492331 (1970), A. A. R. Sayigh and H. Ulrich (to The Upjohn Co.).
8. H. J. Knölker, T. Braxmeier, and G. Schlechtingen, *Angew. Chem. Int. Ed.* **34**, 2497 (1995).
9. H. W. Peerlings and A. W. Meijer, *Tetrahedron Lett*. **40**, 1021 (1999).
10. Eur. Pat. Appl. EP 408277 (1991), E. T. Shawl, J. G. Zajazek, and H. S. Kessling, Jr.
11. T. E. Waldmann and W. D. McGhee, *J. Chem. Soc., Chem. Comm.* 957 (1994).
12. T. Ohkubo and R. Okada, in *Proceedings Polyurethane World Congress*, Vancouver, Canada, 1993, p. 527.
13. J. A. Maclaren, *Chem. Ind. (London)* 395, (1971).
14. H. Ulrich, J. N. Tilley, and A. A. R. Sayigh, *J. Org. Chem*. **29**, 2401, 3334 (1964).
15. W. J. Schnabel and E. Kober, *J. Org. Chem*. **34**, 1162 (1969).
16. U.S. Pat. 3384653 (1968), W. E. Erner and A. Odinak (to The Upjohn Co.).
17. W. Mormann and M. Brahm, *Macromolecules* **24**, 1096 (1991).
18. W. Mormann and M. Brahm, *Polymer* **34**, 187 (1993).
19. H. Holtschmidt and G. Oertel, *Angew. Chem. Int. Ed.* **1**, 617 (1962).
20. P. I. Kordomenos, A. H. Dervan, and J. Kresta, *J. Coat. Technol.* **54**, 43 (1982).
21. A. Liebersohn and D. H. Kohn, *J. Appl. Polym. Sci.* **23**, 3445 (1979).
22. S. R. Gaonkar and co-workers, *Macromolecules* **23**, 3533 (1990).
23. G. Maier and co-workers, *Angew. Chem. Int. Ed.* **35**, 1696 (1996).
24. H. J. Laas, R. Halpaap, and J. Pedain, *J. Prakt. Chem.* **336**, 185 (1994).
25. Eur. Pat. 566925 (1992) (to BASF).
26. DE 3314790 (1983) (to BASF).
27. M. Rochery, I. Vroman, and T. M. Lam, *Liebigs Ann. Chem.* **37**, 259 (2000).
28. Eur. Pat. 23649 (1981) R. Yamamoto and co-workers (to Mitsui Toatsu).
29. Brit. Pat. 2031907 (1980), H. Zengel and co-workers (to BASF).
30. U.S. Pat. 4439616 (1984), B. Singh, L. W. Chang, and P. S. Forgioni (to American Cyanamid).
31. W. Mormann and G. Leukel, *J. Polym. Sci. A* **27**, 4341 (1989).
32. Z. W. Wicks Jr., *Progr. Org. Coat.* **9**, 3 (1981).
33. Z. Wirpsza, in *Proceedings of UTECH*, The Hague, the Netherlands, 1994.
34. R. Spindler and J. M. J. Frechnet, *Macromolecules* **26**, 4809 (1993).
35. R. Richter, B. Tucker, and H. Ulrich, *J. Org. Chem*. **46**, 5226 (1981).
36. H. Ulrich, B. Tucker, and R. Richter, *J. Org. Chem.* **43**, 1544 (1978).
37. U.S. Pat. 3923744 (1975), M. V. Sorensen, R. C. Whiteside, and R. A. Hickner (to The Dow Chemical Company).
38. D. C. Scholl, in *Proceedings of Water Borne and Higher Solids Conference*, New Orleans, La., 1985, p. 120.
39. M. Bock and R. Halpaap, *J. Coat. Tech.* **59**, 755 (1987).
40. S. V. Lonikar and co-workers, *J. Appl. Polym. Sci.* **28**, 759 (1990).

41. Eur. Pat. 277353 (1987), H. Woynar, K. König, and J. Pedain (to Bayer A.G.); *Chem. Abstr.* **109**, 191, 119 (1981).
42. Ger. Offen. 3806276 (1989), J. Pedain, M. Bock, and C. G. Dieris (to Bayer A.G.); *Chem. Abstr.* **112**, 99, 527 (1990).
43. Ger. Offen. 3809261 (1989), J. Pedain, K. König, and W. Dell (to Bayer A.G.); *Chem. Abstr.* **112**, 100, 822 (1990).
44. Eur. Pat. 336205 (1988), J. Pedain and co-workers (to Bayer A.G.); *Chem. Abstr.* **112**, 141, 369 (1990).
45. Eur. Pat. 478990 (1990), H. J. Lass and co-workers (to Bayer A.G.); *Chem. Abstr.* **116**, 237, 531 (1992).
46. Ger. Pat. 1934763 (1971), K. Schmitt, J. Disteldorf, and F. Schmitt (to Huels); *Chem. Abstr.* **75**, 7537 (1971).
47. U.S. Pat. 4469867 (1984), J. Disteldorf and W. Hübel (to Huels).
48. T. Lesiak, A. Balewski, and W. Czerwinski, *Angew. Makrom. Chem.* **93**, 61 (1981).
49. A. Balewski and T. Lesiak, *Angew. Makrom. Chem.* **142**, 79 (1986).
50. K. Hatada and co-workers, *J. Appl. Polym. Sci., Part A-1* **28**, 3019 (1990).
51. Eur. Pat. 414102 (1991), U. Keppeler and M. Bobrich (to BASF); *Chem. Abstr.* **116**, 61, 329 (1992).
52. C. P. Smith, J. W. Reisch, and J. M. O'Connor, *J. Elast. Plast.* **24**, 306 (1992).
53. K. G. Spitler and J. J. Lindsey, *J. Cell. Plast.* **17**, 43 (1981).
54. U.S. Pat. 4761434 (1985), M. Dietrich (to Bayer A.G.).
55. H. W. Bonk and co-workers, *J. Elastom. Plast.* **3**, 157 (1971).
56. C. S. Schollenberger and F. D. Stewart, *Advances in Urethane Science and Technology*, Vol.**1**, Technomics, Stamford, Conn., 1971, p. 65.
57. *Chem. Eng. News* 10 (July 17, 1995).
58. Eur. Pat. 297444 (1989), M. Eggersdorfer and co-workers; *Chem. Abstr.* **111**, 77, 493 (1989).
59. G. Oertel, *Polyurethane Handbook*, 2nd ed., Carl Hanser Publishers, Munich, Germany, 1993.
60. W. F. Gum, W. Riese, and H. Ulrich, *Reaction Polymers*, Hanser Gardner Publications, Munich, Germany, 1992.
61. G. Woods, *The ICI Polyurethanes Book*, John Wiley & Sons, Inc., New York, 1987.
62. S. Neffgen, H. Keul, and H. Höcker, *Macromolecules* **30**, 1289 (1997).
63. H. Ulrich, R. Richter, and B. Tucker, *Synthesis* 277 (1979).
64. J. F. Kinstle and L. E. Sepulveda, *J. Polym. Sci., Polym. Lett.* **15**, 467 (1977).
65. N. D. Ghatke and J. Y. Jadhar, *J. Polym. Sci. A* **21**, 1941 (1983).
66. R. M. Versteegen, R. P. Sijbesma, and E. W. Meijer, *Angew. Chem. Int. Ed.* **38**, 2917 (1999).
67. W. Mormann, N. Tiemann, and E. Turuskan, *Polymer* **30**, 1127 (1989).
68. A. Kumar and S. Ramakrishnan, *J. Chem. Soc., Chem. Commun.* 1953 (1993).
69. Y. Chamberlin and co-workers, *J. Polym. Sci. A* **20**, 1445 (1982).
70. H. W. Bonk, H. Ulrich, and A. A. R. Sayigh, *J. Elast. Plast.* **4**, 259 (1979).
71. H. Ulrich, *J. Polym. Sci.: Macromol. Rev.* **11**, 93 (1976).
72. Y. Iwakura and co-workers, *Makromol. Chem.* **95**, 205 (1966).
73. D. W. House, W. M. Baumann, and R. V. Scott, in *Proceedings Polyurethane World Congress*, Aachen, Germany 1987, p. 340.
74. U.S. Pat. 4567236 (1986), D. J. Goldwasser and R. Oertel (to The Upjohn Co.).
75. H. W. Bonk, R. S. Drzal, G. N. Georgacopoulos, and T. M. Shah, in *Proceedings of the SPE 43rd Annual Technical Conference*, New York, 1985, p. 1300.
76. U.S. Pat. 3555071 (1971), D. V. Rao, A. A. R. Sayigh, and H. Ulrich (to The Upjohn Co.).
77. T. Burniana and co-workers, *J. Macromol. Sci., Pure Appl. Chem. A* **32**, 1397 (1995).

78. M. Chen and co-workers, *Macromolecules* **25**, 4032 (1992).
79. M. F. Rubner, *Macromolecules* **17**, 2114 (1986).
80. Y. Shimura and D. Chen, *Macromolecules* **26**, 5004 (1993).
81. Y. X. Shen and H. W. Gibson, *Macromolecules* **25**, 2058 (1992).
82. D. Dietrich, W. Keberle, and H. Witt, *Angew. Chem.* **82**, 53 (1970).
83. Ger. Pat. 1237306 (1964), W. Keberle, D. Dietrich, and O. Bayer.
84. Ger. Pat. 922736 (1952), G. Pieper and co-workers; *Chem. Abstr.* **55**, 10, 912 (1961).
85. Brit. Pat. 1076909 (1965), W. Keberle and D. Dietrich.
86. H. A. Al-Salah and co-workers, *J. Polym. Sci. B* **24**, 2681 (1986).
87. H. Matsuda and S. Takechi, *J. Polym. Sci. A* **29**, 83 (1991).
88. S. K. Pollack and co-workers, *Macromolecules* **25**, 2381 (1992).
89. G. Smith and co-workers, *Macromolecules* **23**, 3389 (1990).
90. J. Back Lee and co-workers, *Macromolecules* **26**, 4989 (1993).
91. B. Szczepaniak and co-workers, *J. Polym. Sci. A* **31**, 3223 (1993).
92. M. Tanaka and T. Nakaya, *J. Macromol. Sci., A: Chem.* **26**, 1655 (1989).
93. M. Tanaka and T. Nakaya, *J. Macromol. Sci., A: Chem.* **24**, 777 (1987).
94. K. Diblitz and C. Diblitz, in *Proceedings of the Polyurethane World Congress*, Vancouver, Canada, 1993, p. 619.
95. H. Mispreuve and P. Knaub, in *Proceedings of the Polyurethane World Congress*, Vancouver, Canada, 1993, p. 297.
96. J. V. McClusky and co-workers, in *Proceedings of the Polyurethane World Congress*, Vancouver, Canada, 1993, p. 507.
97. D. R. Battice and W. J. Lopez, *J. Cell. Plast.* **23**, 158 (1987).
98. R. M. Hennington, V. Zellmer, and M. Klincke, in *Proceedings of SPI 33rd Annual Conference*, 1990, p. 492.
99. J. S. Hicks and A. K. Schrock, in *Proceedings of SPI 33rd Annual Conference*, 1990, p. 348.
100. A. C. M. Griffiths and P. Shreeve, *Cell. Polym.* 195 (1984).
101. J. Grimminger and K. Muha, in *Proceedings Polyurethane World Congress*, Vancouver, Canada, 1993, p. 279.
102. C. Cecchini, V. Cancellier, and B. Cellarusi, in *Proceedings Polyurethane World Congress*, Vancouver, Canada, 1993, p. 354.
103. H. Ulrich, *J. Cell. Plast.* **17**, 31 (1981).
104. A. K. Zhitinkina, N. A. Shibanova, and O. G. Tarakanov, *Russ. Chem. Rev.* **54**, 1104 (1985).
105. H. E. Reymore, R. J. Lockwood, and H. Ulrich, *J. Cell. Plast.* **14**, 95 (1978).
106. T. W. Bodnar, J. J. Koch, and J. D. Thornsberry, in *Proceedings Polyurethane World Congress*, Nice, France, 1991, p. 191.
107. T. P. Russell and co-workers, *Macromolecules* **26**, 1922 (1993).
108. H. Lee and S. C. Kim, *Macromolecules* **19**, 644 (1986).
109. W. L. Chang, K. C. Frisch, and K. Ashida, *J. Polym. Sci. A* **27**, 3619 (1989).
110. S. Schlick and co-workers, *Macromolecules* **22**, 822 (1989).
111. Y. S. Yang and L. J. Lee, *Macromolecules* **20**, 1490 (1987).
112. L. H. Sperling, D. Klempner, and L. A. Utracki, *Interpenetrating Polymer Networks*, American Chemical Society, Washington, D.C., 1994. Advances in Chemistry Series No. 239.
113. U.S. Pat. 4219502 (1980), K. G. Ihrman and M. Brandt.
114. H. G. Schmelzer and co-workers, *J. Prakt. Chem.* **336**, 483 (1994).
115. R. A. Smiley, S. Yang, H. X. Xiao, K. C. Frisch, and J. Kresta, in *Proceedings UTECH'90*, 1990, p. 205.
116. J. C. Lee and B. Kim, *J. Polym. Sci. A* **32**, 1983 (1994).
117. B. K. Kim, J. C. Lee, and K. H. Lee, *J. Macromol. Sci., Part A: Chem.* **31**, 1241 (1994).

118. D. Dietrich, *Proc. Org. Coat.*, **9**, 281 (1981).
119. R. J. Carson and A. Edwards, *Urethane Technology* 24 (Dec. 1999/Jan. 2000).
120. A. W. Musk, J. M. Peters, and D. H. Wegman, *Am. J. Ind. Med.* **13**, 331 (1988).
121. M. H. Karol, *CRC Crit. Rev. Toxicol*. **16**, 349 (1986).
122. I. F. Carney, *Toxicology of Isocyanates*, International Isocyanate Institute, Inc., New Canaan, Conn., 1980.
123. H. Ulrich and co-workers, *Polym. Eng. Sci.* **18**, 844 (1978).

HENRI ULRICH

POLYVINYLCARBAZOLE. See VINYLCARBAZOLE POLYMERS.

POLYVINYLPYRROLIDINONE. See VINYL AMIDE POLYMERS.

POM. See ACETAL RESINS.

PRESSURE-SENSITIVE ADHESIVES

Introduction

A *pressure-sensitive adhesive* (PSA) is a viscoelastic material that adheres without the need of more than light pressure and requires no activation by water, solvent, or heat. The bond that is formed should be a permanent bond in the sense that the PSA remains bonded unless removal is desired and activated by the user. The Pressure Sensitive Tape Council suggests a number of other desirable features of many PSAs, including aggressive tack, the ability to adhere to a variety of surfaces, and to be removed cleanly without leaving residue. A common element to all PSAs is a polymeric network. This network may be uncross-linked or cross-linked, and it may also contain nonpolymeric additives that affect adhesive properties.

PSAs were first used commercially in medical applications in the late 1800s and entered commercial industrial use in the 1920s with the advent of masking tape and shortly thereafter, cellophane tape (1). The earliest PSAs used natural rubber and this elastomer remains one of the three main classes of polymers used in PSAs today. The other two are acrylics, which were introduced in the 1950s, and synthetic block copolymers, which were introduced in the 1960s. PSAs are used in a wide variety of industries today with the majority of PSAs delivered in the form of tapes or labels.

PSA Tape Construction

Because of their sticky nature, PSAs are not available as a bulk material for direct use. By far the most common method of using PSAs is as a tape, which is a thin

Encyclopedia of Polymer Science and Technology. Copyright John Wiley & Sons, Inc. All rights reserved.

coating of PSA coated on a flexible backing material. Tapes are available as rolls (eg, box-sealing tape, transparent office tape), pads or sheets (eg, labels, stamps), and individual pieces (eg, medical bandages, decals). The simplest tape form is a single-sided tape in which one side of the backing is completely coated with a PSA. More complex variations are also available: double-sided tapes, strip coated single-sided tapes (eg, repositionable notes), pattern coated single-sided tapes (eg, some wound dressings), and transfer tapes (ie, where the adhesive layer can be applied to a surface without a backing). There are an extremely large number of variations of PSA tapes available, depending on the types of PSA used, backing materials used, and the overall construction.

A general tape construction includes a thin adhesive layer (10–750 μm) attached to a film or paper backing. It is important for the adhesive to remain attached to the backing, and in some cases it is necessary to provide a chemical primer coating or a surface treatment to the backing to ensure this. Flame and corona treatments are common methods to increase the surface energy of the film. In the case of a roll of tape, the side of the tape opposite from the adhesive is usually treated with a release coating to allow for unwinding of the tape (see Fig. 1a for schematic of laminate construction). Stacks or pads of tape may also be made using the same laminate structure with the exception that a release liner is placed under the bottom piece of tape in the pad. Individual pieces of tape (eg, adhesive bandages) can also be prepared by attaching a release liner to each piece of tape (see Fig. 1b). A transfer tape can be made by replacement of the backing with a second release liner. This allows for the user to apply a free film of PSA to a surface by removing one liner, applying the tape, and then removing the second liner. Alternatively, a single liner that is coated on both sides can be used to prepare a roll form of transfer tape.

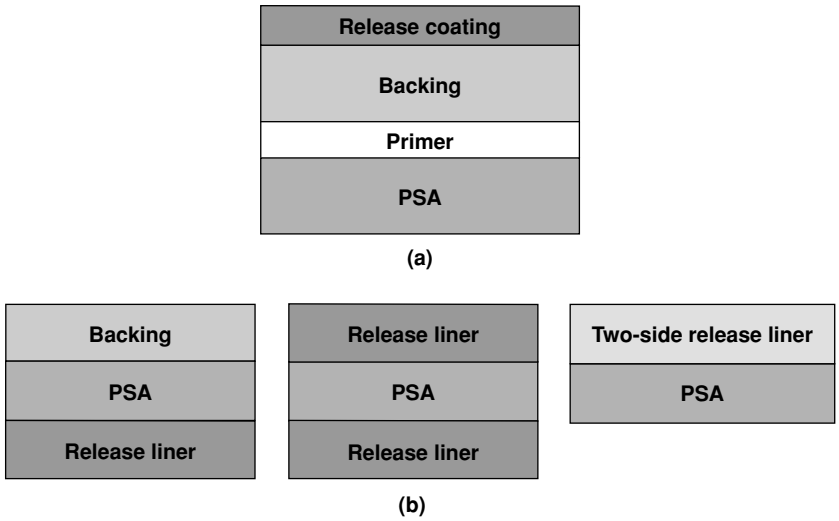

Fig. 1. (**a**) Linerless construction. (**b**) Liner constructions.

Release Surfaces. Since PSAs will adhere to many surfaces with only light to moderate pressure, it is necessary to protect the surface of the PSA until just prior to use. This is done by keeping the PSA in contact with a release surface, that is, a surface that the PSA can be easily peeled from without damaging the PSA. The force needed to remove a PSA from the release surface can vary greatly, ranging from 5 g/25 mm width (premium release) to 2000 g/25 mm width (tight release). The primary requirements are that the force is low enough to avoid splitting the adhesive layer, avoid removing the adhesive from the backing, and avoid deforming the backing during removal. The force of removal should be high enough to avoid having the PSA accidentally come free from the release surface before the user intends to apply it.

Typical release surfaces are made using a release coating, a microscopically thin layer of a low surface energy material that is applied to a supporting substrate. In a roll of tape the release coating is applied to the side of the backing opposite the PSA, so that when rolled upon itself the PSA will be in contact with the release surface (often called a low adhesion backsize in this application). Alternatively, the release coating may be provided on a separate liner that is discarded after being removed from the PSA. The most common release coatings use silicones, long alkyl chain branched polymers, and fluorinated polymers. In addition to providing a low energy surface, many release coatings also contain low molecular weight material that can provide a weak boundary layer between the adhesive and the polymerized portion of the release coating. Although effective for release purposes, the transfer of low molecular weight compounds (particularly silicones) to the surface of the adhesive can sometimes have a negative effect on its subsequent adhesion properties.

Some smooth surfaces have a low enough surface energy that they can serve as a release surface without the addition of a special coating. Many plastics, such as polyethylene, polypropylene, and poly(vinyl chloride), can be release surfaces for some adhesives. Another approach for release without a special coating employs a rough surface, such as a fabric or specially microreplicated surface, that minimizes contact of the PSA with the surface. One should be careful about the tendency of a PSA to flow and fill in crevices when roughness is used to provide release, since this can lead to variations in release force with aging.

Additives. Many PSAs contain additives that, unlike tackifiers or plasticizers, are not intended to affect the inherent PSA properties. Pigments, such as titanium dioxide, are added to change a PSA's appearance. Metal particles or carbon black can be added to provide electrical conductivity. Drugs such as nitroglycerin, nicotine, or estradiol are added for use in transdermal drug delivery.

The most commonly used additives, however, are stabilizers. These are usually added to protect the PSA from thermal-oxidative degradation or from photodegradation, and are generally present at low levels in a formulation (eg, about 0.5–2 wt%). Hindered phenols (eg, Irganox available from Ciba Specialty Chemicals) are most commonly used to prevent thermally induced oxidation, although phosphites and thioethers are also used, sometimes in combination with each other. Ultraviolet absorbers, hindered amines, or simple pigments are most commonly added for protection from photodegradation.

Types of Tape

Industrial Tape. Packaging tapes represent the largest volume of PSA tapes and typically use stiff, oriented polypropylene or polyester film backings to provide low extensibility and high shear strength. Addition of glass or plastic fibers in the lengthwise direction is used in filament tape to provide extremely high tensile strength. Masking tape, the earliest example of industrial tape, typically has a crepe paper backing saturated with rubber. The creping allows for conformability when uneven surfaces are masked, paper allows for easy hand tearability, and the rubber saturation provides resistance to paints and solvents. A number of electrical tapes use plasticized PVC or other similar soft backings to provide conformability for wire wrapping applications.

Consumer and Office Tape. Clear, cellulose acetate tape is widely used as a general-purpose office tape. Paper tapes of all types provide hand tearability and ease of printing, but are generally not used for applications where high strength is required. Strip coated labels are used as repositionable notes.

Medical. Medical tapes often have cloth or cloth-like backings for comfort and breathability. Numerous synthetic breathable, conformable nonwovens (eg, spunlaced polyester such as Sontara, a trademark of DuPont; creped polypropylene) have been developed for such purposes. In some instances, film tapes are preferred to provide a barrier for wound coverage or to increase hydration to speed transdermal drug delivery. Electrically conductive adhesives are used for electrode applications.

Labels. Labels typically have a paper backing, but film backed labels are becoming more common. Labels can be both permanent or repositionable, and water dispersible PSAs are used for compatibility with recycling operations.

Other. Specialized PSA tapes with virtually any possible backing are also available: hook-and-loop (eg, Velcro, a trademark of Velcro USA, Inc.) backing, reflective tapes, magnetic backing, furniture pads, wall hooks, carpet tiles, etc.

Specialty Constructions. Although not solely pressure-sensitive, there are a number of materials which are responsive to other stimuli to either activate, deactivate, or modify PSA-type behavior. Medical adhesives that are not tacky at room temperature, but which undergo a phase transition leading to PSA properties at body temperature, can be used for ease of handling and positioning (2). In a reverse mode, PSAs for medical use that lose their adhesive properties on demand have been developed to make tapes that can be removed with little or no trauma. This transition can be achieved by exposure to light which causes cross-linking and a subsequent stiffening of the PSA (3) or alternatively by swelling with water to effect a phase separation of a water soluble tackifier that disrupts the skin/PSA interface (4,5). Other removal approaches have included application of heating or cooling (2) to effect a phase change of part of the adhesive or application of various solvents or oils to disrupt the interface between PSA and adherend (6). Stretch release tapes allow for a clean and easy removal by using a large stretching deformation in the backing to cause a low removal force at the interface between substrate and PSA (7).

Test Methods

Three main types of test methods are used to determine the physical properties of PSAs: peel, tack, and shear (8) (see also ADHESION). Standard test methods are available for all three properties, and numerous additional variations of tests measuring these properties have also been used (9). Environmental conditions are an extremely important factor in all PSA testing. PSAs are almost always very sensitive to temperature. Many PSAs are also sensitive to humidity, particularly if stored in environments where they can either absorb or lose moisture.

Peel Adhesion. In a peel adhesion test a length of tape is adhered to a surface and then the tape is removed by lifting away from the surface in a specified manner. The results are reported as the force required for a given width of tape. It is important to note whether the mode of failure is adhesive (ie, between adhesive and substrate), transfer (ie, between adhesive and film backing), or cohesive (ie, splitting of the adhesive layer). The standard ASTM method (10) involves adhering the tape to a carefully controlled stainless steel test plate and then peeling the tape from the plate at a controlled rate of 15 cm/min and 180° angle (see Fig. 2). Substrates other than steel (eg, polyethylene, phenolic resin, skin) may be used to try to better model actual use conditions. Similarly, the rate and angle of peel may be modified where appropriate to better match actual usage conditions. Other important factors to control in a peel test include the type of rolldown with which the tape is applied (eg, hardness and diameter of roller, load applied, rate of rolldown, number of passes of roller) and the amount of time the tape is allowed to dwell prior to removal.

It should be understood that, strictly speaking, peel is a tape property rather than a PSA property. That is, the backing or other construction of the tape can often have a strong influence on the peel adhesion. The primary backing effects are the influence on actual peel angle, which can differ from the nominal angle if the backing is sufficiently stiff, and backing deformation, which can occur if the adhesive force is sufficiently large to exceed the strength of the backing.

The peel tests described above are applied rate tests, but peel tests may also be performed as applied load tests. The easiest applied load test to perform is to adhere a tape to a substrate and attach a weight to one end of the tape such that the weight hangs freely below the substrate. The rate at which the load peels the tape from the substrate is then recorded. A low load, low rate variation on this test is a so-called flagging test, in which a tape is wound around a cylinder and

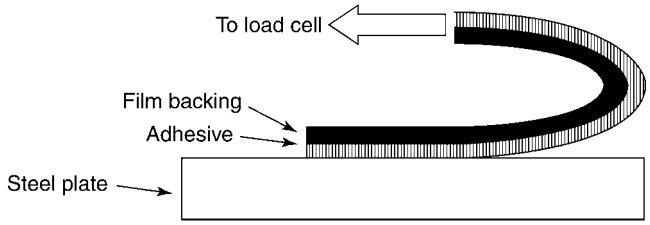

Fig. 2. 180° peel adhesion.

then the rate at which the tape unwinds is measured. In this case, the only load present is due to the weight of the tape and any stress put into the tape during application.

Tack. Tack is in many ways similar to peel adhesion in that a bond is formed and then broken in a lifting manner. When dealing with theoretical descriptions of tack, all of the same considerations that are involved with peel adhesion mechanics are employed. In a practical sense, however, the bond formed in a tack test typically exists for only a short time and is formed with a relatively light amount of force when compared to a peel test. In addition, the test is typically performed with the tape held fixed and a probe or ball being used to contact the tape.

The most common ASTM standard method is a probe tack method (11), in which a cylindrical probe is raised into contact with the adhesive surface of the tape and then pulled back (see Fig. 3). The maximum force attained during removal is reported as the tack value. Typical conditions involve an application pressure of 100 g/cm^2, a contact time of 1 s, and a removal rate of 1 cm/s, but all of these parameters may be varied with most test equipment.

Another ASTM standard method, rolling ball tack (12), involves placing a piece of tape, adhesive side up, at the base of an inclined surface. A steel ball is allowed to roll down the incline from a fixed height, and the distance that the ball travels across the adhesive surface of the tape is taken as a tack value. Longer distances of travel indicate that the tape is less tacky. Other tests involving drums, rollers, or loops of tape have also been used, but are not as common.

Although it can be influenced by backing properties, rolling ball tack is generally considered to be fairly independent of the backing. Probe tack can be more dependent on backing properties, but very flexible backings may be reinforced with more rigid backings in order to reduce the influence of backing on the tack value. More sophisticated tack tests have been developed that measure force throughout the entire debonding process in conjunction with video observation of the bond (13) or using atomic force microscopy as a probe (14).

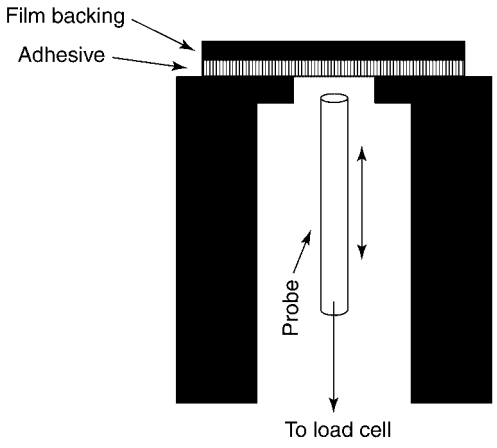

Fig. 3. Probe tack test.

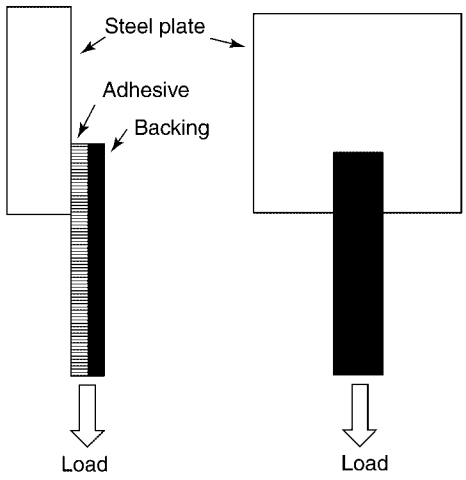

Fig. 4. Shear holding power test. Side view and front view.

Shear Holding Power. Shear represents an entirely different property from peel and tack, and is more related to bulk material properties rather than interfacial properties. The most common ASTM standard method is a holding-power test (15), in which a fixed area of a piece of tape is applied to a vertical test panel and a weight is hung from the free end of the tape (see Fig. 4). The length of time until the load of the weight pulls the tape from the test panel is recorded as the shear holding time. Of particular importance in this test is the mass of the weight used and the area of tape applied to the test panel. Typical contact areas are 0.5 × 0.5 in. (1.27 × 1.27 cm) and 1.0 × 1.0 in. (2.54 × 2.54 cm). Typical weights are 500–1000 g.

As with other pressure-sensitive adhesive tests, the temperature is an important variable and tests are typically carried out at room temperature. A variation on this method is the SAFT test (shear-adhesion-failure temperature) in which the test apparatus is placed in an oven where the temperature is set to rise at 4.5°C/min. The temperature at which the tape fails is recorded as the SAFT value.

In theory, shear is strictly a bulk property of the adhesive that is not affected by surface interactions or the backing in a tape construction. In practice, however, the shear holding power can be affected both by backing and by surface interactions. The force in the shear holding test appears to be entirely in the direction of the hanging tape, but since it is a single-overlap shear joint there are forces generated normal to the plate that can lift the tape from the plate in a peel mode (16). This can be significant for very firm adhesives that have very little tendency to slip in a shear mode, but may be easier to peel from the steel surface. A clear indication that this is occurring is when the mode of failure is described as "pop-off" (ie, the tape falls cleanly from the plate instead of slipping down the face of the plate). Another potentially interfering factor is backing deformation. This is particularly true for tapes with easily deformable backings, but can also be seen for tapes with relatively stiff backings that have adhesives that are extremely resistant to shear

deformation. The backing deformation can cause curling or buckling of the tape that can also lead to the introduction of additional peel forces.

Rheological Tests. Other rheological tests that measure viscoelastic properties are available. Dynamic mechanical rheometry (DMA or DMTA when temperature is included) involves a parallel plate rheometer that can deform a disk of material in a shearing motion. This is done as a function of frequency of shearing and often with varying temperature. The shear storage and loss moduli, G' and G'', or the dynamic viscosity can be obtained with this test. These rheological properties can be related to tack, peel, and shear, and have found much use in development and analysis of PSAs (17). Another way to obtain shear modulus is to use a double-overlap shear apparatus in which the load is applied to a slip plate instead of directly to the tape. This configuration removes both the peel forces associated with single-overlap shear and the potential deformation that may occur in the standard shear holding test.

Materials

There are three major classes of polymers used in PSAs today: block copolymer, natural rubber, and acrylic. A number of other polymers used in smaller, specialty applications include silicones, polyisobutylenes, polyolefins, styrene-butadiene, poly(vinyl alkyl ether)s, and polyurethanes.

Block-Copolymer Rubbers. Block copolymer rubbers are thermoplastic elastomers that are the most widely used class of PSAs (see ELASTOMERS, THERMOPLASTIC). The most commonly used are ABA block copolymers, where A is polystyrene and B is a polydiene. Polyisoprene (R = CH_3) and polybutadiene (R = H) are the most common B polymers, giving SIS and SBS copolymers, respectively (see BUTADIENE POLYMERS; ISOPRENE POLYMERS).

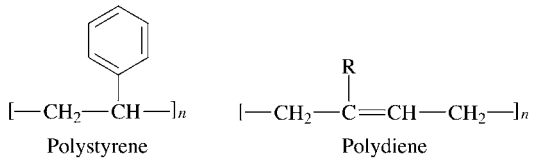

Polystyrene Polydiene

The mechanism by which these perform is based on phase separation of the polystyrene and the polydiene. The polystyrene is generally present in an amount from 10 to 20% of the rubber, and as the minor component it phase separates into microscopic spherical domains that act as cross-links at each end of a polydiene polymer chain. Molecular weights of the entire block copolymer are typically of the order of 100,000–200,000 g/mol. At room temperature the polystyrene is glassy ($T_g \sim 100°C$) and the polydiene is rubbery ($T_g \sim -70°C$). Each SIS (or SBS) polymer chain will have each chain end anchored in a glassy polystyrene domain, with a rubbery polyisoprene link connecting them. Thus the material acts as a cross-linked rubber. When the temperature is increased to above the polystyrene T_g, the microscopic polystyrene domains can be melted, allowing the individual polymer chains to flow and this allows the material to be hot-melt processed. Upon cooling

the domain, structure is reformed. A tackifier is always needed, and plasticizers are often added as well to increase tack and reduce cost.

Block copolymers are synthesized by an organic solution anionic polymerization that can lead to high purity, fairly monodisperse, and relatively low cost polymers. The solvent is then removed from the polymer which is available commercially in the form of rubber pellets or crumb. Adhesives can be prepared by dissolving the rubber in solvent, formulating with tackifier and/or plasticizer, and subsequently coating from the same solvent. This is typically used for small volume products or for small-scale laboratory experiments.

More typical, though, is hot-melt processing of these adhesives. The rubber is blended with tackifier and/or plasticizer in a bulk mixer or extruder at elevated temperature (eg, 150–200°C), coated as a molten liquid, and cooled. The lack of need for post-curing is a significant advantage over natural rubber PSAs. The high purity and consistency of the input rubber is also an advantage when compared to natural rubber.

The high degree of cross-linking gives adhesives with high cohesive strength, but can be a disadvantage in situations where stress relaxation of the adhesive is beneficial. A number of variations on the basic SIS or SBS copolymers are available. Differing amounts of di-block, SI or SB, polymer may be included which causes incomplete cross-linking, and will typically lead to higher adhesion, better stress relaxation, and lower shear strength.

Typical formulations are shown in Table 1 (18). The rolling ball tack is clearly dependent on the amount of tackifier with lower levels of tackifier giving superior rolling ball tack. The probe tack also shows a decrease in force with increasing tackifier. Shear holding strength shows an increase with increasing coupling efficiency because of the formation of a stronger cross-link network. Interesting differences between shear holding power to steel and to kraft paper illustrate the importance of the substrate selection when testing a PSA. The peel adhesion behavior is somewhat more complicated, since it is strongly influenced both by

Table 1. PSA Performance Tests[a]

Formulation[a]	1	2	3	4	5	6	7	8	9
Tackifier[b]	75	75	75	100	100	100	150	150	150
% S–I–S[c]	25	50	80	25	50	80	25	50	80
Rolling ball, cm	.94	.56	3.4	1.2	1.4	3.6	30+	30+	30+
Probe tack, kg	1	1.2	.9	1.5	1.5	1.3	1.7	1.6	1.2
180° Peel, N/cm[d]	15.1[e]	10.5	7.4	17.5[e]	22.4[e]	10.5	18.2[e]	24.9[e]	9.8[f]
Shear, min									
Steel[g]	84	206	1180	168	229	1112	202	590	424
Kraft[g]	55	661	>1500	42	458	>1500	41	153	847

[a] All formulations contain 100 parts block copolymer (S–I + S–I–S) and 2 parts Butazate stabilizer. Except where indicated the test methods are ASTM standards noted above.
[b] Wingtack 95 (trademark to Goodyear Chemical).
[c] % S–I–S is the number of S–I–S molecules divided by the number of S–I–S + S–I molecules.
[d] To convert N/cm to ppi, divide by 1.75.
[e] Cohesive failure.
[f] Shocky peel.
[g] Holding power to steel and kraft paper, PSTC-7 (see Ref. 9).

initial adhesion and by the ability of the adhesive to deform and absorb energy upon removal. Increasing tackifier levels will generally increase adhesion because of the dilution of the polymer network, which increases molecular mobility and reduces the PSA storage modulus. However, increasing tackifier will also increase the T_g of the PSA, and if the T_g reaches or exceeds the use temperature then the material will entirely lose PSA properties.

Antioxidants are usually employed to prevent oxidation of the double bond in either of the polydienes. Specialty grades are available where the polydiene has been hydrogenated, which gives much better chemical stability and uv resistance. Multiarm and star-block copolymers are some examples of specialty copolymers that can be used to modify the performance of block copolymer adhesives (19).

These PSAs are still commonly referred to in much of industry as Kraton (a trademark of Shell Chemical) adhesives, although block-copolymer rubbers are also available worldwide from several other major sources: Dexco, Enichem, and Nippon-Zeon. The most common uses of block-copolymer PSAs are in packaging tapes, although they find use in nearly all types of PSA applications.

Natural Rubber. Natural rubber is obtained from the *Hevea brasiliensis* tree as a latex. It is primarily *cis*-1,4-polyisoprene with small amounts of bound proteins and other contaminants (see RUBBER, NATURAL).

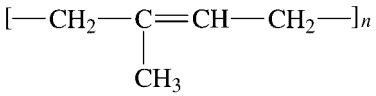

The latex is ammoniated, coagulated, and air dried or smoked to obtain gum rubber. As with most other rubbers, a tackifier must be blended with natural rubber in order to produce a PSA, since the rubber itself has a very low glass-transition temperature ($T_g \sim -70^\circ C$) and a high shear storage plateau modulus. The molecular weight of the input rubber is quite high, greater than 1,000,000 g/mol, and so the rubber is usually milled between steel rolls to break the rubber chains and reduce the molecular weight to make subsequent processing easier (20).

When coated from solvent, natural rubber can be used to make a PSA with a combination of good cohesive shear strength and the ability to dissipate stress within a bond. This is due to the ability of the high molecular weight of the polyisoprene to establish good shear strength without the need for cross-linking. The lack of cross-linking aids in stress relaxation. Because of the double bond in polyisoprene, natural rubber is subject to oxidation, and antioxidants are typically added to the adhesive formulations.

Natural rubber can also be formulated and coated directly from latex, although the costs are typically higher than compounding of gum rubber and coating from solvent. Hot-melt processing of natural rubber is a newer technology that offers the possibility of efficient, solvent-free production (21). Because the high molecular weights of the natural rubber will not survive a hot-melt extrusion or mixing process, it is necessary to post-cure hot-melt natural rubber adhesives with, for example, electron beam radiation curing if high cohesive strength is necessary.

The most common uses of natural rubber PSAs are in masking tapes, packaging tapes, duct tapes, and other cloth tapes.

Acrylics. Acrylic adhesives are copolymers produced from esters of acrylic acid (see ACRYLIC ESTER POLYMERS). An acrylic copolymer suitable for use in a PSA must contain a significant fraction of a monomer that gives a homopolymer with a low glass-transition temperature (T_g). This monomer will typically give a homopolymer with a T_g less than −20°C and usually in the range of −40 to −80°C. It is this low T_g monomer that gives the PSA its soft, tacky properties. The most common monomers used to give low T_g polymers are 2-ethylhexyl acrylate, isooctyl acrylate (3M Company manufactures isooctyl acrylate for internal consumption), and butyl acrylate.

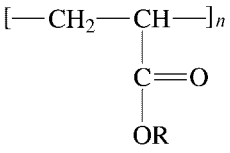

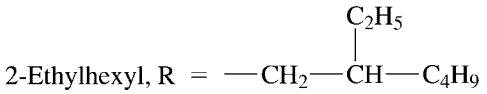

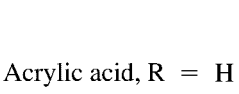

The tacky characteristic of an acrylic copolymer was described as early as 1933 (22). On their own, these low T_g homopolymers are tacky, but they lack the cohesive strength needed to make suitable PSAs, and therefore need reinforcement to prevent the PSA from splitting and oozing during use. There are a number of methods for providing this reinforcement, including the addition of high T_g monomers to the copolymer; addition of monomers that cause intermolecular interactions between individual copolymers; covalent cross-linking of the copolymer; and physical cross-linking of the copolymer via graft or block copolymers.

The first useful acrylic PSAs were introduced in the 1950s with the incorporation of high T_g functional monomers (23), such as acrylic acid and acrylamide, used for reinforcement. This continues to be a widely used approach for acrylic PSA reinforcement. Typical acrylic PSAs contain up to 10% of these reinforcing monomers. Additional high T_g, but nonfunctional, monomers may also be added to the copolymer, with some typical examples being vinyl acetate, ethyl acrylate, methyl acrylate, and methyl methacrylate.

Graft copolymers that provide reinforcement may be prepared in a manner somewhat similar to that of the rubber block copolymers. The graft copolymers are prepared by adding macromonomers (ie, polymers with a reactive functional group on one end) during copolymerization. Typical macromonomer examples are polystyrene or poly(methyl methacrylate)s, with molecular weights between 2000 and 50,000 g/mol, that are terminated with a reactive acrylate group. The block structure that forms differs from the A–B–A rubber copolymers, since the macromonomers are incorporated into the polymer at random. The combination of polydispersity in the length of the acrylic backbone, polydispersity in the number of grafts per backbone, and polydispersity in the length of each graft generally leads to adhesives that do not possess as much elastic strength as the A–B–A rubber copolymers.

Acrylic adhesives tend to be more stable than rubber-based adhesives since they have a saturated backbone. They are also generally designed so that they function as PSAs without the need for any tackification or plasticization, although tackifiers can be added to modify adhesion or reduce cost. Both of these features help to differentiate them from rubber-based PSAs. The ability to avoid use of tackifiers and antioxidants makes acrylics a good choice for medical applications where minimal skin irritation is desired.

Acrylic PSAs can be prepared by a number of synthetic routes and the subsequent processing into a PSA tape naturally varies. The earliest synthetic method was free-radical polymerization in an organic solvent. The resulting solution is usually directly coated to make a tape or mixed with other components (eg, additional solvent, tackifier) prior to coating, but it may also be dried of solvent to provide bulk adhesive for later compounding steps.

Acrylics can also be prepared in water by either emulsion or suspension polymerization. Both of these water-based polymerizations rely on the insolubility of the acrylate monomers in a continuous aqueous phase which leads to the creation of small polymeric particles dispersed in water. Although superficially similar, there are important differences between the two types of polymerization, with the most significant being that suspension particles are typically 50–500 μm in diameter, whereas emulsion particles are typically 50–200 nm in diameter (24). Emulsions are widely used since the small particle size can lead to well-stabilized dispersions and also help to effect good film forming properties. Emulsions have an advantage over solution polymers, since the molecular weight of the polymer can be controlled independently of the rate of reaction, allowing for very high molecular weights to be obtained. Suspensions are less common, but in some cases the large particle size can be used to control tape properties. One prominent example is in repositionable notes (eg, Post-It, a trademark of 3M) which take advantage of the low surface contact area of the large particles to keep adhesion at a controlled, low level.

Acrylics can also be bulk polymerized. One method for bulk polymerization involves coating a mixture of acrylic monomers along with a photoinitiator onto a film and uv curing to form the adhesive in place. Also being solventless, this can be an attractive method for making thick coatings. In addition, novel phase structure can be imparted by in place curing in some instances [eg, bicontinuous microemulsions (25)].

Acrylic PSAs find wide use in office tapes, medical tapes, packaging tapes, automotive tapes, and specialty applications where good stability is desired.

Specialty Materials.

Silicones. Most silicone PSAs are based on a poly(dimethylsiloxane) network that is chemically cross-linked during a curing process.

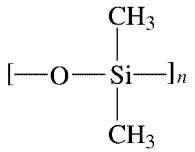

This cross-linked network is generally prepared by addition of a multifunctional, reactive silicate resin to a long chain poly(dimethylsiloxane). They can be prepared to have very high temperature performance, good solvent resistance, and low irritation in medical applications (see SILICONES). Among their disadvantages, however, is that they tend to be expensive, are usually applied from solvent, and usually need a specialty release liner, since they will not release well from most silicone-based release liners (26).

Polyisobutylene. Polyisobutylene (PIB) is an all hydrocarbon elastomer prepared by cationic polymerization of isobutylene.

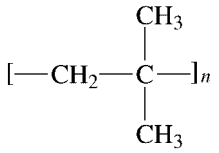

The lack of double bonds gives it good chemical stability. PIB varies from a liquid to a rubber as the molecular weight is shifted from low (<5000 g/mol) to high (>100,000 g/mol). PIB PSAs are usually prepared as a mixture of PIB rubber with a tackifier or oil in a manner similar to other rubber-based PSAs. Low molecular weight PIB can also be used as a tackifier in blends with high molecular weight PIB or in blends with other rubbers as well. One advantage of a high and low molecular weight blend of PIBs is that this takes full advantage of the inherent chemical stability. These adhesives are typically used in applications where good aging or chemical resistance is needed (eg, pipe wrap, electrical tapes) or in medical applications where low skin irritation potential is beneficial. Among their disadvantages is that they are difficult to cross-link, so that they usually have low cohesive strength, and very high molecular weight PIBs need to be solvent processed since they become difficult to hot-melt process (27).

Polyolefins. A variety of amorphous poly(α-olefins) have been used as the base elastomer in PSAs.

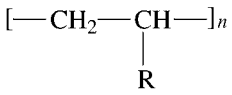

Polypropylene, R = CH_3 Polyhexene, R = C_6H_{13},

Typical polypropylene and polyethylene materials are highly crystalline and thus have little applicability in PSAs. The key to using a polyolefin in a PSA is to select one with a high degree of amorphous character. These range from amorphous polypropylene or propylene–ethylene copolymers to poly(α-olefins) with longer side chains that disrupt crystallinity (28,29). Polyolefins are usually either tackified or cross-linked to produce suitable PSA properties. The lack of double bonds provides stability benefits similar to those in PIB. The raw materials are generally low cost and can be hot-melt processed. Among their disadvantages is that they

do not yet have the wide range of formulation flexibility that can be achieved with block-copolymer or acrylic PSAs.

Tackifiers/Plasticizers

As mentioned above, tackifiers and/or plasticizers are often used as part of many PSA formulations, most particularly in synthetic and natural rubber PSAs. Tackifiers and plasticizers are low molecular weight compounds that are compatible with the base polymer of the PSA. They act as a diluent in the base polymer of the PSA because they are not part of the polymeric network made up by the base polymer (30). They must be compatible with the base polymer to avoid problems of phase separation. In particular, if the tackifier/plasticizer has a lower surface energy than the base polymer, then phase separation can create a layer of pure tackifier/plasticizer on the surface of the PSA and destroy the tack of the formulation. The most common tackifiers are based on rosin acids, small-chain hydrocarbons, and terpenes.

A typical rosin acid is abietic acid, although the acids used for most rosin-based tackifiers are chemically modified, often by hydrogenation and/or esterification to form more stable products.

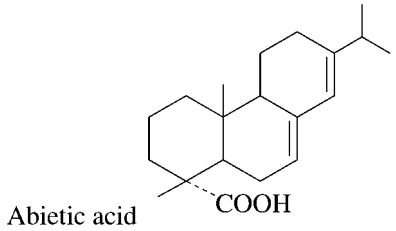

Abietic acid

The small chain hydrocarbon tackifiers are oligomers with molecular weights in the range of several hundred to 2000 g/mol. They are typically obtained from petroleum feed streams and fall into three general classes. The most common C-5 aliphatic hydrocarbons are *cis*- and *trans*-piperylene and isoprene.

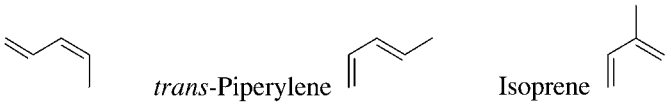

cis-Piperylene *trans*-Piperylene Isoprene

The similarity in chemical structure to isoprene explains why these are quite compatible with natural rubber and synthetic isoprene-based polymers (or block copolymers). The C-9 aromatic hydrocarbon resins include indene- and styrene-based oligomers. Because of the difference in chemical structure these will associate with the end-blocks in S–I–S copolymers, and thus have a reinforcing effect and improve high temperature performance. Finally, mixtures of aliphatic and aromatic hydrocarbon resins are commonly used as a way to tailor compatibility and physical properties of the resultant PSAs.

Terpenes are similar to the aliphatic hydrocarbon resins in that the most common, α- and β-pinene, can be considered to be dimers of isoprene.

α-Pinene β-Pinene

Like rosins, terpenes are derived from pine trees (via turpentine) or other natural sources, such as citrus peels.

The difference between plasticizers and tackifiers is somewhat arbitrary and the effect of this difference is described below in the section on Physical Properties. Plasticizers are typically lower in molecular weight and melting or softening point than are tackifiers. Hydrocarbon oils including aromatic, naphthenic, and paraffinic are commonly used with rubber-based adhesives. Phthalates, such as dioctyl phthalate or dibutyl phthalate, are more typically used in small amounts with acrylics. Since plasticizers are usually low molecular weight compounds, there is often more latitude in the chemical types that will be compatible with the base polymer because of the contribution from entropy of mixing.

Physical Properties

By definition a PSA must have physical properties that differ from most ordinarily encountered materials. It should behave like a liquid when it is forming a bond with a substrate, but after application it should behave like a solid in order to retain the bond. This dual liquid–solid behavior should be present without the need to make any chemical or physical modifications to the PSA, but should rather be an intrinsic material property.

When acting as a liquid it must have an appropriate surface energy that will allow it to wet a substrate. Liquids with appropriate surface energy have the capability to easily wet a substrate because of the high degree of molecular mobility that they possess. Except in very limited circumstances though, (eg, two smooth glass plates "bonded" together by a thin layer of liquid), they do not have enough strength to keep two surfaces bonded together. So in order to have the needed strength to be a PSA, a material must be a solid, but it must be capable of behaving like a liquid during the time it takes to form a bond (of the order of 1 s).

Polymers are the only class of materials that possess this combination of properties. Because of their extended, chain-like molecular structure they form networks (which may or may not be cross-linked) that resist large-scale molecular motion, and therefore provide solid-like behavior. The portions of the polymer molecule in between network junctions, however, can undergo small-scale motion that is similar to that of a liquid when viewed on a short time scale. An important feature of all PSAs is the glass transition temperature T_g of its polymeric components. If the PSA is cooled below its T_g, then it will behave like a glassy solid, since even the small-scale, between-network motions will be frozen. Above its T_g, though, the

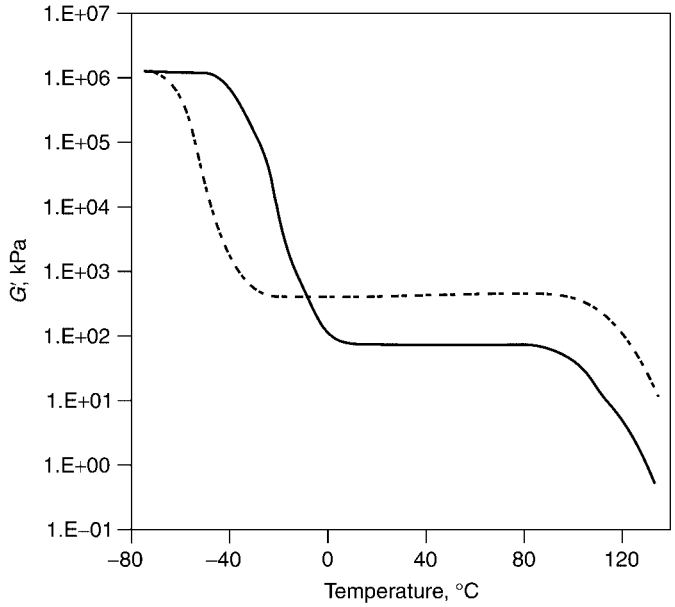

Fig. 5. Storage modulus of rubber (dotted line) and rubber+resin PSA (solid line) as a function of temperature. To convert kPa to psi, multiply by 0.145.

small-scale, between-network motion provides the liquid-like behavior needed for bonding.

The ability to form an initial bond is most generally referred to as the "tack" of a PSA. It is necessary for the glass transition of the PSA to be below the application temperature. It is also necessary, however, for the plateau storage modulus G' of the PSA to be low enough to allow the PSA to deform sufficiently to make good intermolecular contact with the adherend. The Dahlquist criterion for bonding states that G' needs to be less than 100 kPa on a 1-s time scale. This is a good general rule of thumb, although the amount of intermolecular contact will also be influenced by PSA thickness, surface roughness, and application pressure.

In Figure 5, the storage modulus of a typical cross-linked rubber is compared to that of a PSA made from a mixture of the rubber and tackifier. The rubber has a low T_g, which is why it is soft and rubbery at room (or use) temperature, but its modulus is too high for it to be a PSA. Addition of tackifier decreases the modulus below the Dahlquist criterion and allows for the mixture to be a PSA. The effect of dilution of the rubber network with a tackifier can be predicted by rubber elasticity theory using the equation below (31,32). The effect of fillers can also be predicted.

$$G_e \cong v^2(\rho/M_e)RT(1 + 2.5c + 14.1c^2)$$

where G_e is the plateau modulus, v the volume fraction of network molecules

in the continuous phase, ρ the density, M_e the entanglement spacing molecular weight, R the gas constant, T the temperature, and c the filler volume fraction. In the common case of an S–I–S block copolymer, the continuous phase comprises the polyisoprene and mid-block tackifiers and the filler volume comprises the polystyrene and end-block tackifiers.

Although the T_g of the mixture increases with additional tackifier, it is still below room temperature. Addition of more tackifier will continue to reduce the plateau storage modulus, but will eventually raise the T_g above the use temperature and the subsequent mixture would have no tack.

As described above, the distinction between plasticizers and tackifiers is somewhat arbitrary, but the important difference between the two is that addition of a plasticizer will not affect or will lower the T_g of the PSA formulation. The effect of lowering the modulus is the same as for a tackifier.

The glass-transition temperature of the mixture can be approximately calculated using the Fox equation (33):

$$\frac{1}{CT_g} = \frac{x_1}{Tg_1} + \frac{x_2}{Tg_2} + \cdots + \frac{x_n}{Tg_n} \quad (1)$$

where CT_g is the calculated glass-transition temperature; $x_1, x_2, \ldots, x_n$ are the weight fractions of the adhesive components; and $T_{g1}, T_{g2}, \ldots, T_{gn}$ are the T_g's for the individual components. More complex approximations for the glass-transition temperatures are also available (33,34).

Once a bond is created, the PSA should resist removal (unless controlled or easy removal is a desired feature for a particular product). Adhesion can be looked at as being controlled by two primary components. The *intrinsic adhesion* (also called *the work of adhesion*) between the adhesive and substrate is caused by intermolecular interactions. These can be van der Waals interactions for nonfunctional adhesives (eg, rubbers, polyolefins) or can also include hydrogen bonding, acid–base interactions, or actual covalent chemical bonding (35). The intrinsic adhesion, however, is generally small when compared to the practical strength of the adhesive bond, which is the force of adhesion that is actually measured (36). This is due to the second contribution to the force of adhesive removal, which is the ability of the adhesive to viscoelastically deform and absorb energy prior to debonding. The adhesive force for PSA bonds has been extensively analyzed using the theory of fracture mechanics (37–44). In a general sense, one can say that debonding occurs when the adhesive has been deformed sufficiently to store enough elastic stress to overcome the intrinsic work of adhesion.

In Figure 6, a generalized peel force vs peel rate curve is shown. At very low peel rate the dotted line indicates that the adhesive is undergoing cohesive failure. As the tape is slowly lifted away from the substrate the adhesive is able to undergo viscous deformation and absorb all of the energy being imparted by the peel before it can be transferred to the surface. Put another way, the viscous dissipation is rapid enough at slow peel rates to prevent the adhesive from building up enough stored elastic energy to overcome the intrinsic adhesion at the surface. The modulus of the adhesive increases with increasing rate leading to

increasing peel adhesion force. A transition will occur at a sufficiently high peel rate where the adhesive can now build up enough stored elastic energy to cleanly and smoothly remove from the substrate. Beyond this transition rate the peel force again increases with increasing peel rate (shown by the solid line) until another transition occurs to "shocky" peel. This "shocky" peel is related to the increased stiffening and glass-like behavior of the adhesive at increasing peel rate. In a roll unwind case, the unwinding tape will accelerate as it passes this shocky peel transition since the peel force will now begin to decrease with increasing rate. Since most peel is performed by pulling the tab end of a tape at a constant rate, the tape unwinding from the roll will move faster than the tab being pulled until slack accumulates in the tape, causing the effective peel rate at the roll to drop to near zero. As the tab end continues to be pulled the slack is taken up and this process is repeated to give a jerky or shocky peel. The peel force shown in Figure 3 for the shocky region (dashed line) is an average peel force, since the instantaneous peel forces measured will vary greatly.

A specific type of adhesive failure is "lift" which is a very slow low-angle peel of a tape at its edges. The optimal physical properties to resist lift often differ from those necessary to provide high short-term peel adhesion. Longer time (low frequency) material properties become important, and the ability of the adhesive or backing to relax stress over time also becomes important, since stresses imparted to the tape during application can lead to long-term failure if they cannot be dissipated.

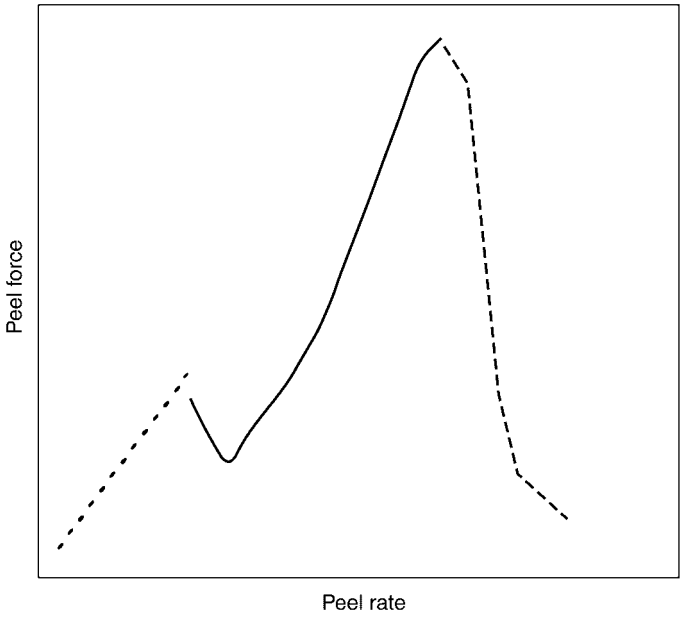

Fig. 6. Peel force vs peel rate schematic showing cohesive failure (dotted line), adhesive failure (solid line), and shocky peel (dashed line).

Another undesirable feature of a PSA tape is creep or oozing. This is most often seen with uncross-linked adhesives that undergo viscous flow over long times. This is governed by properties similar to those that govern lift, except that the ability of the adhesive to relax stress through flow (which helps reduce lift) can lead to increased creep. It is usually necessary to strike a balance between lift, creep, and the short-term tack and adhesion properties needed in a PSA tape.

General Manufacture

A wide variety of methods have been used to make PSAs and PSA tapes, ranging from multistep processes to completely integrated manufacturing methods. Synthesis of the PSA (or PSA-component-like rubber) can be a solvent-based process (eg, organic solution, emulsion, or suspension polymerization) or a solventless process (eg, reactive extrusion, bulk polymerization).

A common thread through nearly all PSA tape manufacture is a processing step where the PSA is present as part or all of a liquid phase (distinguished from the "liquid-like" behavior it shows during use) that may be applied to a surface in a thin coating. This liquid phase is obtained in three primary ways. The PSA is dissolved as a solution in organic solvent or water and the solvent or water is removed by drying after the coating step. The PSA is heated to a temperature at which it becomes molten (ie, hot-melt processing) and the PSA is cooled after the coating step. The PSA is formed by coating low molecular weight liquid compounds that may be polymerized in place after coating. General industry trends are toward solventless processes since these eliminate the use of hazardous organic solvents and the high energy usage due to drying.

The PSA is usually coated directly onto the backing film, although it may also be coated onto the release liner and subsequently laminated to the backing film. Coating on liner is usually done with soft or stretchy backings that can deform during oven drying or with cure-in-place systems where the backing may absorb the liquid prepolymer mixture before polymerization can occur.

Economic Aspects

Of the three major classes of polymers in use today, acrylics make up the largest volume of material at 33% of the total PSA market. Synthetic block-copolymer elastomer represents 25% of the total PSA market. Since these are almost universally compounded with tackifying resins, the amount of PSA produced using block copolymers could be twice as large as the amount of elastomer used. Natural rubber represents 22% of the total PSA market, but is also compounded with resin to produce a PSA, and so the total amount of PSA produced is also larger (45). This represents a shift toward acrylics from 10 years ago when the relative

amounts of acrylic, block copolymer, and natural rubber elastomer was 23, 29, and 28%, respectively (46).

Estimated production (47) volumes (by area coated) of tapes and labels in 1997 were 7.5×10^9 m^2 in the United States, 7.7×10^9 m^2 in Europe, and $(6–8) \times 10^9$ m^2 in Asia. Estimated use of PSAs (by mass) in 1998 was 250,000 t in the United States and 295,000 t in Europe. Estimated sales volumes of pressure-sensitive products in 1999 were $\$11 \times 10^9$ m^2 in the United States, $\$8.4 \times 10^9$ m^2 in Europe, and $\$1.9 \times 10^9$ m^2 in Japan, with global growth rates for these markets estimated at between 4 and 6% annually for tapes and between 7 and 11% annually for labels (47,48).

BIBLIOGRAPHY

"Pressure-Sensitive Adhesives and Products" in *EPSE* 2nd ed., Vol. 13, pp. 345–368, by S. C. Temin, Consultant.

1. D. Satas, in D. Satas, ed., *Handbook of Pressure Sensitive Adhesive Technology*, 3rd ed., Satas & Associates, Warwick, R.I., 1999, p. 1.
2. U.S. Pat. 5412035 (May 2, 1995), E. E. Schmitt and co-workers (to Landec Co.).
3. WO 0061692 (Oct. 19, 2000), C. Ansell (to Smith & Nephew, Plc.).
4. U.S. Pat. 5032637 (July 16, 1991), D. J. Therriault and J. E. Workinger (to Adhesives Research, Inc.).
5. U.S. Pat. 5352516 (Oct. 4, 1994), D. J. Therriault and M. J. Zajaczkowski (to Adhesives Research, Inc.).
6. U.S. Pat. 5336207 (Aug. 9, 1994), M. A. Norcia (to Smith & Nephew United, Inc.).
7. U.S. Pat. 6106937 (Aug. 22, 2000), M. D. Hamerski (to Minnesota Mining and Manufacturing Co.).
8. R. P. Muny, *Adhesives & Sealants Industry* 42 (Feb. 2000).
9. *Test Methods for Pressure Sensitive Adhesive Tapes*, Pressure Sensitive Tape Council, Chicago, 1996.
10. ASTM D3330, *Annual Book of ASTM Standards*, Vol. 15.09, 1999.
11. ASTM D2979, *Annual Book of ASTM Standards*, Vol. 15.06, 1999.
12. ASTM D3121, *Annual Book of ASTM Standards*, Vol. 15.06, 1999.
13. A. Zosel, in *Proceedings of the Pressure Sensitive Tape Council: 23nd Annual Technical Seminar*, New Orleans, La., Pressure Sensitive Tape Council, Chicago, 2000, p. 193.
14. A. Paiva and co-workers, *Macromolecules* **33**, 1878 (2000).
15. ASTM D3654, *Annual Book of ASTM Standards*, Vol. 15.09, 1999.
16. A. V. Pocius, *Adhesion and Adhesives Technology: An Introduction*, Carl Hanser Verlag, Munich, 1997, pp. 42–45.
17. S. G. Chu, in D. Satas, ed., *Handbook of Pressure Sensitive Adhesive Technology*, 2nd ed., Van Nostrand Reinhold Co., Inc., New York, 1989, p. 158.
18. U.S. Pat. 4096203 (June 20, 1978), D. J. St. Clair (to Shell Oil Co.).
19. U.S. Pat. 5412031 (May 2, 1995), J. Ma and M. K. Nestegard (to Minnesota Mining and Manufacturing Co.).
20. R. E. Bennett, in A. K. Bhowmick, M. M. Hall, and H. A. Benarey, eds., *Rubber Products Manufacturing Technology*, Marcel Dekker, Inc., New York, 1994, p. 855.
21. U.S. Pat. 5549033 (July 23, 1996), T. D. Bredahl and co-workers (to Minnesota Mining and Manufacturing Co.).

22. Ger. Pat. 575327 (1933), W. Bauer (to Roehm and Haas AG).
23. U.S. Pat. 2884126 (Apr. 28, 1959), E. W. Ulrich (to Minnesota Mining and Manufacturing Co.). Reissued as U.S. Pat. RE24906 (Dec. 13, 1960).
24. G. Odian, *Principles of Polymerization*, 3rd ed., John Wiley & Sons, Inc., New York, 1991, pp. 302, 341.
25. U.S. Pat. 5670557 (Sept. 23, 1997), T. M. Dietz and co-workers (to Minnesota Mining and Manufacturing Co.).
26. L. A. (Sobieski) Jones, in Ref. 1, p. 550.
27. J. J. Higgins, F. C. Jagisch, and K. O. McElrath, in Ref. 1, p. 321.
28. Pressure-Sensitive Adhesives Based on Amorphous Polyolefin from Eastman Chemical Company, Publication WA-23A, Feb. 1999.
29. U.S. Pat. 5112882 (May 12, 1992), G. N. Babu and co-workers (to Minnesota Mining and Manufacturing Co.).
30. J. A. Schlademan, in *Proceedings of the Pressure Sensitive Tape Council: 22nd Annual Technical Seminar*, Washington, D.C., Pressure Sensitive Tape Council, Chicago, 1999, p. 87.
31. G. Kraus and K. W. Rollmann, *J. Appl. Polym. Sci.* **21**, 3311 (1977).
32. G. Kraus, K. W. Rollmann, and R. A. Gray, *J. Adhesn.* **10**, 221 (1979).
33. P. R. Couchman, *Macromolecules* **11**, 1156 (1978).
34. A. S. Cantor, *J. Appl. Polym. Sci.* **77**, 826 (2000).
35. J. Comyn, *Adhesion Science*, Royal Society of Chemistry, Cambridge, U.K., 1997, pp. 3–10.
36. Ref. 16, p. 140.
37. B. Z. Newby and M. K. Chaudhury, *Langmuir* **13**, 1805 (1997).
38. A. N. Gent and C. W. Lin, *J. Adhesn.* **30**, 1 (1989).
39. W. F. Parsons, M. A. Faust, and L. E. Brady, *J. Polym. Sci.* **16**, 775 (1978).
40. A. N. Gent and G. R. Hamed, *Polym. Eng. Sci.* **17**, 462 (1977).
41. K. R. Shull and A. J. Crosby, in *Proceedings of the 23rd Annual Meeting of the Adhesion Society*, Myrtle Beach, S.C., Adhesion Society, Blacksburg, Va., 2000, p. 113.
42. A. J. Crosby and K. R. Shull, *J. Polym. Sci., Part B: Polym. Phys.* **37**, 3455 (1999).
43. E. H. Andrews and A. J. Kinloch, *Proc. R. Soc. London, Ser. A* **332**, 385 (1973).
44. C. Creton, in H. E. H. Meijer, ed., *Materials Science and Technology: A Comprehensive Treatment*, Vol. **18**, Wiley-VCH, New York, 1997, p. 708.
45. D. Satas, in Ref. 1, p. 6.
46. D. Satas, in Ref. 17, p. 4.
47. R. A. Higham, in R. A. Higham, ed., *Pressure Sensitive Industry: Markets and Technology Yearbook: 1999*, Data Transcripts, Surrey, U.K., 1999.
48. J. Talmage, *Adhesive Technol.* 10 (Sept. 2000).

GENERAL REFERENCES

D. Satas, ed., *Handbook of Pressure Sensitive Adhesive Technology*, 3rd ed., Satas & Associates, Warwick, R.I., 1999.
I. Benedek, *Development and Manufacture of Pressure-Sensitive Products*, Marcel Dekker, Inc., New York, 1999.
I. Skeist, *Handbook of Adhesives*, 3rd ed., Van Nostrand Reinhold Co., Inc., New York, 1990.
A. V. Pocius, *Adhesion and Adhesives Technology: An Introduction*, Carl Hanser Verlag, Munich, 1997.

J. Johnston, *Pressure Sensitive Adhesive Tapes*, Pressure Sensitive Tape Council, Northbrook, Ill., 2000.

ADAM S. CANTOR
3M Healthcare Markets

PSA. See PRESSURE SENSITIVE ADHESIVES.

PULTRUSION. See COMPOSITES, FABRICATION.

PVC. See VINYL CHLORIDE POLYMERS.

PVDC. See VINYLIDENE CHLORIDE POLYMERS.

PVDF. See VINYLIDENE FLUORIDE POLYMERS.

PVF. See VINYL FLUORIDE POLYMERS.

PVK. See VINYLCARBAZOLE POLYMERS.

PVP. See VINYL AMIDE POLYMERS.

REINFORCEMENT

Introduction

In antiquity, mechanical properties were often the decisive factor in materials selection. Today, they still limit the size of our bridges and skyscrapers, and the performance of our airplanes. The second part of the twentieth century has seen significant developments in our understanding of fundamental material science, and thus also of the mechanical performance of materials. This understanding has generated profound changes in the field, leading to new families of materials, new concepts, and wide-ranging improvements in the mechanical behavior and in all other properties of materials. In our energy-conscious society, materials and structures are required to be more performant, lightweight, and cheap. The best answer to these requirements is often provided through the powerful concept of reinforcement of a "matrix" material with a second-phase dispersion (particles, fibers). This concept was already known to our ancestors. Indeed, the book of Exodus provides an often quoted reference to straw-reinforced clay bricks prepared by the Hebrews, and plant fibers in pottery artefacts were used early on in Central and South America. In these early examples however, the aim was to prevent cracking of the brittle material rather than reinforcement. The concept of reinforcement of materials by a second-phase solid is omnipresent in nature as well, from human bones (hydroxyapatite platelets within a collagen fibrillar matrix) to fingernails and rhinoceros horn (both consist of keratin fibers dispersed in a protein matrix), to the various types of wood (cellulosic fibers in a lignin matrix). A more subtle concept related to reinforcement in nature concerns the hierarchical microstructures (including the various degrees of symmetry) which so far have only partially been applied to synthetic composites, and a promising future seems to lie ahead for the observation of (and lessons to be learned from) the reinforced

Encyclopedia of Polymer Science and Technology. Copyright John Wiley & Sons, Inc. All rights reserved.

structures that appear in nature, a field commonly termed biomimetics. It is an interesting fact that many natural forms of reinforcement possess a nanometric dimension whereas most current synthetic composites include fibers in the micrometer range. Expected benefits of such "miniaturization" would range from a higher intrinsic strength of the reinforcing phase (and thus of the composite) to more efficient stress transfer, to possible new and more flexible ways of designing the mechanical properties of yet even more advanced composites. First these arguments are reviewed, then the concept of stress transfer leading to the principle of reinforcement is discussed. This is followed by specific materials aspects and by a short account of possible future forms of reinforcement.

Strength of Reinforcement

Strength as a Function of Dimension. The strength of materials increases as the scale decreases. In reinforcing fibers, for example, this is true whether the scale is taken as the diameter of the fiber or as its length. It is true too for the characteristic (or average) dimension of a reinforcing particle or a platelet. This phenomenon is usually called the size effect and has two types of explanation, based on probabilistic arguments and fracture mechanics. From a probabilistic viewpoint, Weibull (1) and Freudenthal (2) proposed a formal link between the probability of occurrence of a critical defect in a solid of (dimensionless) volume V, the concentration of defects, and the size (length, area, volume) of the solid specimen:

$$F(V) = 1 - \exp[-(V/V_0)] \tag{1}$$

where V_0 is the (dimensionless) mean volume per defect (thus, $1/V_0$ is the mean concentration of defects). As seen in equation 1, the probability of occurrence of a critical defect (and thus of failure) increases rapidly with increasing size for a given defect concentration. Equation 1 does not explicitly include any assumption regarding the physical nature of the process. Stress may then be drawn in by assuming that the original density of flaws in the material, $1/V_0$, increases as the applied stress σ increases according to some physical law. For example, if a simple power law

$$V_0^{-1} = (\sigma/a)^b \tag{2}$$

is assumed, where a and b are constants termed the scale and shape parameters, the widely used two-parameter Weibull distribution is obtained. Specifically for a fiber viewed as a chain of elementary links or elements, the weakest-link argument is involved as follows. If each element in the chain-like structure has a failure probability $F(\sigma)$ under a stress σ, then its probability of survival is $1-F(\sigma)$. The probability of survival of a chain of n elements is then $[1-F(\sigma)]^n$, from which it results immediately that the probability of failure, $F_n(\sigma)$, of the chain (or the fiber) is given by

$$F_n(\sigma) = 1 - [1 - F(\sigma)]^n \tag{3}$$

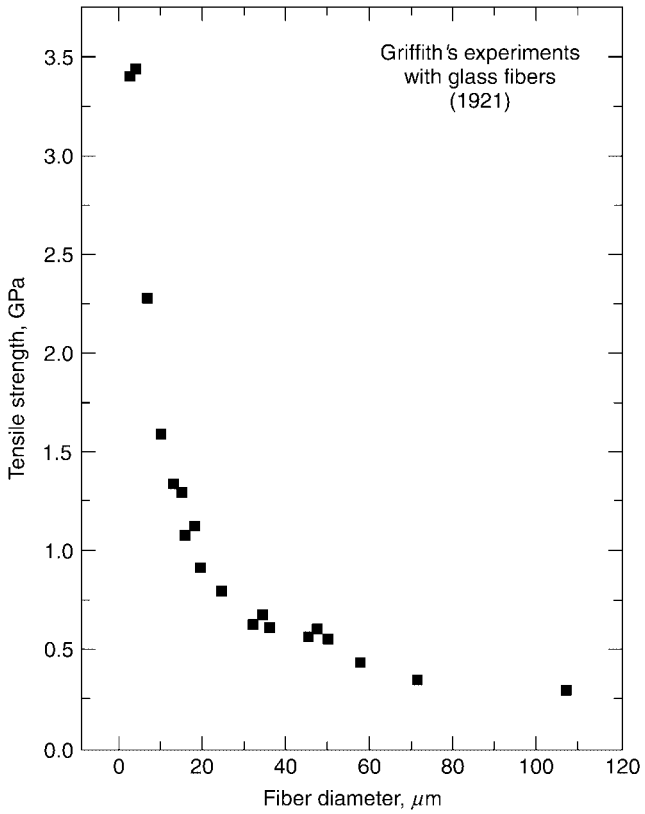

Fig. 1. Plot adapted from the 1920 experiment of Griffith with glass fibers, illustrating the effect of fiber diameter on strength (3). To convert GPa to psi, multiply by 145,000.

If the probability of failure, $F(\sigma)$, of a single element is a Weibull distribution, it is immediately apparent that the probability of failure of the chain is again a Weibull distribution with the same shape parameter b but with a lower value of the scale parameter a. The latter may easily be shown to be equivalent to a lower mean strength. Thus, the larger the specimen, the higher its probability of failure. The same conclusion is reached when fracture mechanics arguments are used, based on the original observation of Griffith (Fig. 1) with freshly drawn glass fibers of varying diameters. A dependence between strength (σ_f) and size (D) of the form

$$1/\sigma_f = p + qD^{1/2} \tag{4}$$

(p and q are constants) is obtained for reinforcing materials such as ultrahigh molecular weight polyethylene (UHMWPE) fibers and polydiacetylene fibers (4). An extensive discussion of size effects in fibers and composites may be found elsewhere (4,5).

Strength as a Function of Interfacial Area and Interaction. The mechanical effectiveness of reinforced materials is a function of the efficiency with

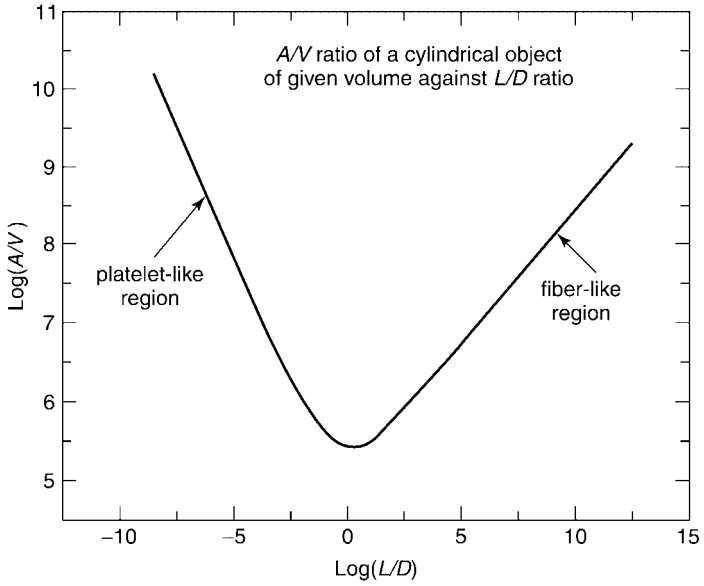

Fig. 2. Surface area-to-volume ratio (A/V) of a cylindrical object of given volume against aspect ratio (L/D). The shape of the object fluctuates between a fiber and a platelet, and maxima of the area-to-volume ratio are obtained either for a very long and thin fiber or a very wide and thin platelet. Adapted from Ref. 9.

which loads are being transferred from the external source to the reinforcing phase, via the matrix or binder. This efficiency is, in turn, a function of the available interfacial area between the reinforcing agent and the matrix, and of the quality of the interface. Generally speaking, the stress transfer efficiency increases with the area-to-volume ratio of the reinforcing agent, and with the interfacial adhesion. The first point may be illustrated by taking a small cylindrical particle of length 1 mm and diameter 5 μm, and varying its length and diameter so as to keep the volume constant. As seen in Figure 2, the shape of the particle fluctuates between a fiber and a platelet, and maxima of the area-to-volume ratio are obtained either for a very long and thin fiber or a very wide and thin platelet. Interestingly, these two cases are frequently encountered in nature's composite materials when high strength or stiffness is the determining factor. The second point, namely, the effect of interfacial adhesion on strength and stiffness of composites, has been extensively studied and the major developments are summarized in a subsequent section.

Strength as a Function of the Type of Reinforcing Material. It is possible to use simple models to select materials that a priori should be suitable as reinforcements. The theoretical tensile strength $\sigma_{\max}$ of a solid is given by (6)

$$\sigma_{\max} = (E \cdot \gamma / a_0)^{1/2} \tag{5}$$

where E and γ are the Young's modulus and the surface energy of the solid, respectively, and a_0 is the atomic spacing. When looking for strong solids, we therefore

look for substances of high elastic modulus, high surface energy, and small atomic spacing. This suggests that atoms with small atomic radii should be considered: beryllium, boron, carbon, nitrogen, oxygen, aluminum, and silicon are good choices, and the strongest materials always contain one of these elements (7). Based on the above, it would seem that polymers are not appropriate, because of their "softness" and low modulus, but this is not so. Theoretical calculations show that well-oriented high molecular weight polymers have very high moduli and strength, with the added advantage of low density. All the above considerations explain the appearance, from the early 1960s, of high performance fibers such as carbon and boron, followed by silicon carbide, Kevlar, UHMWPE, and more.

Strength and Fiber Flexibility. Flexibility of fibers used in high performance composites is necessary because of the intense bending strains and stresses applied to the fibers during operations such as weaving, knitting, and filament winding. The flexibility of a fiber will be higher when its curvature is as large as possible and when the bending moment necessary to reach a given curvature is as small as possible. Flexibility is thus defined as (for a circular fiber) $\varphi = 64/E\pi d^4$, where E and d are the fiber bending modulus and diameter, respectively (8). As seen, the effect of size (diameter) is by far the strongest, and thus nanoscale reinforcement promotes high flexibility.

The Principles of Reinforcement

When combining highly performant fibers with polymers, a composite with improved mechanical properties is formed. The stress applied from an external source to the composite is transferred to the fibers (which are the load-bearing element) through the fiber–matrix interface, and the mechanism of this stress transfer and the ensuing reinforcement effect may be described as follows. The situation is different when fibers are long or short.

Long Fibers. The composites used in the most advanced applications (in aerospace, for example) normally include long (or continuous) fibers from which laminated structures are formed. When the fibers are more rigid than the matrix (which is the case in practically important composites), assuming a perfectly bonded interface between fiber and matrix, and loading parallel to the fiber array, the transfer of stress from the applied load to the fibers is achieved from the ends of the specimen through the loading mechanism, resulting in a fairly uniform stress field in the composite. Thus, a simple rule of mixtures

$$E_{\mathrm{L}} = E_{\mathrm{f}}V_{\mathrm{f}} + E_{\mathrm{m}}V_{\mathrm{m}} \tag{6}$$

emerges for the longitudinal Young's modulus of the composite, where the subscripts f and m designate the fiber and the matrix, and E and V are the Young's modulus and fiber volume fraction respectively. Equation 6 usually provides a good fit to experiment. For the transverse Young's modulus of the composites, the often quoted inverted rule of mixtures

$$1/E_{\mathrm{T}} = (V_{\mathrm{f}}/E_{\mathrm{f}}) + (V_{\mathrm{m}}/E_{\mathrm{m}}) \tag{7}$$

does not usually provide a good fit. The semiempirical Halpin–Tsai equation

$$E_T = E_m\left[\frac{1+\varsigma\eta V_f}{1-\eta V_f}\right] \tag{8}$$

provides a better estimate, with

$$\eta = \frac{(E_f/E_m)-1}{(E_f/E_m)+\varsigma} \tag{9}$$

and where ζ is an empirical parameter which is equal to 2 for circular or square fibers. Similar equations exist for the other elastic constants (9). The strength of composites with continuous fibers is given by

(1) *Low fiber volume fraction*

$$\sigma_L = \sigma_{mu}(1-V_f) \tag{10}$$

(2) *High fiber volume fraction*

$$\sigma_L = \sigma_{fu}V_f + \sigma_m^*(1-V_f) \tag{11}$$

where σ_{mu}, σ_{fu}, and σ_m* are the strength of the matrix, the strength of the fiber, and the stress in the matrix at the strain at which the fiber breaks. In the above models, the following assumptions were made: (*1*) the fibers are more brittle and have a much higher tensile modulus than the matrix; (*2*) the fibers and the matrix behave in a linear elastic fashion until failure; (*3*) the strain in the fiber and the matrix are equal (perfect interfacial bonding); and (*4*) all fibers have the same tensile strength. For very high fiber content, a good approximation of the longitudinal properties of continuous, unidirectional composites is as follows (from eqs. 6 and 11):

$$\begin{aligned} E_L &= E_f V_f \\ \sigma_L &= \sigma_{fu} V_f \end{aligned} \tag{12}$$

In reality, none of the four assumptions above are obeyed exactly in many industrial composites: Glass fibers are often as brittle as epoxy resins; most polymer matrices behave in a nonlinear elastic or plastic fashion beyond a certain strain; the quality of interfacial bonding varies according to the composite system, and is statistical along the fiber length; and the tensile strength of fibers is statistical rather than uniform because of the presence of various defect populations (as briefly discussed earlier).

The statistical strength of fibers is usually described as follows. If the probability of failure, $F(\sigma)$, of a single fiber unit element is a Weibull distribution

$$F(\sigma) = 1 - \exp[-(\sigma/a)^b] \tag{13}$$

it is immediately apparent that the probability of a long fiber (viewed as a chain of n unit elements) is again a Weibull distribution

$$F_n(\sigma) = 1 - \exp[-n(\sigma/a)^b] \tag{14}$$

with the same shape parameter, b, but with a smaller scale parameter:

$$a_n = an^{-1/b} \tag{15}$$

Thus the strength is "self-similar." The mean strength is defined as

$$\bar{\sigma} = \int_{-\infty}^{+\infty} \sigma f(\sigma) \mathrm{d}\sigma \tag{16}$$

where $f(\sigma)$ is the density function ($=\mathrm{d}F(\sigma)/\mathrm{d}\sigma$). Using $a_n = aL^{-1/b}$, one has

$$F_{\mathrm{n}}(\sigma) = 1 - \exp\left[-(\sigma/a_{\mathrm{n}})^b\right] \tag{17}$$

where L is the (nondimensional) fiber length rather than the number of fiber elements. It is easy to show that the mean of the distribution is given by

$$\bar{\sigma} = a_n \Gamma[1 + (1/b)] \tag{18}$$

where $\Gamma(\cdot)$ is the Gamma function, the values of which can be found in tables. The coefficient of variation is

$$cv \cong 1.2/b \tag{19}$$

A higher strength variability is found in ceramic fibers (such as alumina), which have a relatively low Weibull shape parameter. Typical Weibull parameters for commercial fibers are shown in Table 1. The statistical variability of bundles and composites is a function of the fiber variability but is generally lower than

Table 1. Typical Value Ranges for the Weibull Scale and Shape Parameters of Fibers[a]

Fiber	Scale parameter, MPa[b]	Shape parameter
E-glass	3000–3500	4–6
HM carbon	1300–3000	1.7–2.6
HS carbon	1700–2100	2.8–5.3
Kevlar 49	3000–3500	7–10
UHMWPE	2200–4000	6–8
SiC	2500–4000	–
Boron	2700–3700	8–10

[a] Gauge length ~10 cm.
[b] To convert MPa to psi, multiply by 145.

that of the single fibers. Calculations of the composite statistical strength grow rapidly complex (10) and this topic is beyond the scope of the present article.

Short Fibers. Stress transfer in discontinuous fiber composites, which include the cases of either short or broken fibers, is more complex than in continuous fiber composites. The shear and tensile stress and strain fields will not, in this case, be uniform. If both the matrix and the fiber are elastic, the tensile stress profile in the fiber is given by (7)

$$\sigma_f = E_f \varepsilon \left[1 - \frac{\cosh\beta(l/2 - x)}{\cosh\beta l/2} \right] \tag{20}$$

where ε is the imposed strain (thus, the strain in the matrix away from the fiber), l is the fiber length, and the origin of the x-axis is in the middle of the fiber. The parameter β, the so-called shear-lag parameter, has units of reciprocal length and is equal to

$$\beta = \left[\left(\frac{G_m}{E_f} \right) \left(\frac{2\pi}{A_f \ln(R/r_f)} \right) \right]^{1/2} \tag{21}$$

where G_m is the matrix shear modulus, A_f and r_f are the fiber cross section and radius, respectively, and R is the distance from the fiber axis at which the matrix displacement is unaffected by the fiber presence (thus, $2R$ may be viewed as the average interfiber spacing, and R/r_f is a function of fiber packing). A simple force balance model gives the shear stress profile at the fiber–matrix interface:

$$\tau = \varepsilon (G_m E_f)^{1/2} \left(\frac{\pi r_f^2}{2A_f \ln(R/r_f)} \right)^{l/2} \left(\frac{\sinh\beta(l/2 - x)}{\cosh\beta l/2} \right) \tag{22}$$

The measured shear stresses in the matrix at the ends of fibers are in fact much larger than those given by equation 22 because of stress concentration effects. Therefore, the maximum shear stress will be the smaller of the following two stresses: the shear yield stress of the matrix, or the shear strength of the fiber–matrix interface. Whichever of these two stresses is attained first will control the load transfer phenomenon.

Based on this simple model, the composite modulus is

$$E_c = E_f V_f \left(1 - \frac{\tanh\beta l/2}{\beta l/2} \right) + E_m (1 - V_f) \tag{23}$$

From equations 20, 22, and 23, it is seen that

(1) If the fiber is long enough, the stress in the fiber will increase from zero at the two ends to a maximum value $\sigma_{fu} = E_f \varepsilon$.
(2) The shear stress has a maximum value at the fiber ends and a minimum at the center.
(3) The larger the value of the load transfer parameter β (or the smaller the length β^{-1}), the more rapid is the stress increase in the fiber from its ends.

For polymer composites, the fiber is usually elastic but the matrix is plastic beyond a certain strain level. Frictional slip and plastic flow of the matrix have been observed to occur in these systems, with some prevalence of the first mechanism. A simple equilibrium of force gives

$$\frac{l}{d} = \frac{\sigma_f}{2\tau} \tag{24}$$

where d is the fiber diameter and τ is either the matrix shear yield strength (τ_y) or more likely in polymers, the interface shear strength (τ_i). If the fiber is long enough, beyond a certain critical length l_c, there is enough stress transferred in the fiber to break it, at a stress σ_{fu}:

$$\frac{l_c}{d} = \frac{\sigma_{fu}}{2\tau_i} \tag{25}$$

Even for $l > l_c$, the average stress $\bar{\sigma}_f$ in the fiber is still less than its maximum in the center:

$$\bar{\sigma}_f = \sigma_f\left(1 - \frac{1-\beta}{l/l_c}\right) \tag{26}$$

Interfacial Adhesion. Various tests have been developed to measure the strength of the fiber–matrix adhesive bond. Two schools of thought have emerged, the first one focusing on a relatively approximate but rapid testing of comparatively large, real-life specimens, and the second on the more elaborate testing of much smaller model specimens. Both approaches have advantages and drawbacks. Examples of the first type include the well-known interlaminar shear strength (or ILSS) test and the transverse strength test. Examples of the second type include the single-fiber composite test (also called the fragmentation test), the single-fiber pull-out test, and the microbond test. Reviews of these tests exist in the literature (11). A more recent technique, microRaman spectroscopy, provides an accurate measurement of the tensile stress profile in a single fiber, and a measure of the interfacial shear strength, provided that the fiber has a Raman spectrum that includes a strain-sensitive band. There is currently no universally agreed upon method that provides a single measure of interfacial adhesion in composites. This is an area that has been the subject of intense research over the last decade and a thorough description of this field is beyond the scope of the present article.

Types of Reinforcement

The structural characteristics of a host polymer material—the matrix—may be improved by including a dispersed material—the reinforcing phase—in various ways. The dispersed phase may be continuous (fiber, tape) or discontinuous (particulate, flake, whisker). We restrict the discussion to reinforcing phases used in fiber (or whisker) form since this article deals with mechanical reinforcement effects rather than with considerations of cost reduction, electrical properties, or

other nonmechanical aspects. In polymer matrix composites, reinforcing fibers are used mainly to improve stiffness and strength. Taking stiffness as an example, the low modulus value (1–5 GPa typically) of most polymer matrices is readily and dramatically increased by the presence of glass or carbon fibers (typical modulus: 72 GPa and 250–750 GPa, respectively). Advanced fiber composite materials take advantage of the highly directional properties of fibers to generate superior structural properties. The main fibers in use for composites applications include the various types of glass and carbon/graphite, boron, silicon carbide, alumina, the aramids, and polyethylene. Fibers at the experimental stage include polybenzoxazole (PBO) and polybenzothiazole (PBT). The diameter of most of these fibers varies from a few to about one hundred microns, whereas their length ranges between a few millimeters up to fully continuous. Whiskers have diameters in the nanometer range, and lengths down to the submicron range (so do carbon nanotubes, which are briefly considered at the end of the article). Whiskers are thin, elongated single crystals with properties much superior to those of the bulk material from which they are made. Typical whiskers include aluminum oxide (Al_2O_3), silicon carbide (SiC), carbon, silicon nitride (Si_3N_4), nickel aluminide ($NiAl_3$), iron, nickel, and copper. Single fibers, which are difficult to handle individually, are usually gathered into bundles such as yarns, tows, or strands of a few hundreds up to 100,000 or more single fibers. Such spools are the starting elements in the fabrication of a structure. They are combined with polymers using various techniques, to form intermediate flat sheets ("prepregs," random mats, woven and knitted fabrics, braids, and more recent noncrimp fabrics) or direct final shapes (using filament winding, for example). The overall fiber architecture is controlled by the selection of appropriate reinforcement formats and processing routes. Table 2 shows the maximum achievable fiber volume fraction using different reinforcement formats, and compares the orientation factor which is 1 for a uniaxial array, 0.3 for a quasi-isotropic lay-up, and 0.12 for a random three-dimensional (3-D) lay-up (11). No less important is the type of fiber surface treatment applied

Table 2. Connection Between the Reinforcement Format, the Manufacturing Process, the Fiber Orientation Factor, and the Maximum Fiber Volume Fraction[a]

Reinforcement format	Applicable process	Orientation factor	Maximum fiber volume fraction
UD tow	Filament winding; pultrusion	1.00	0.80
UD prepreg	Autoclave; resin film infusion	1.00	0.65
Multiaxial prepreg	Autoclave; resin film infusion	0.31	0.60
2-D noncrimp fabric	Resin film infusion; resin transfer molding	0.30	0.55
Woven 2-D fabric	Resin transfer molding; wet lay-up	0.27	0.50
Orthogonal 3-D fabric	Resin transfer molding	0.30	0.40
Random planar	Sheet molding compound; resin transfer molding; wet lay-up	0.30	0.30
Random 3-D short fiber	Bulk molding compound; injection molding	0.12	0.20

[a]Adapted from Ref. 12.

Table 3. Properties of Representative Fiber and Whisker Materials

Material	Fiber diameter, μm	Tensile modulus, GPa[a]	Tensile strength, GPa[a]	Density, g/cm^3	Thermal expansion coefficient, 10^{-6} K^{-1}
E-glass	10–20	72	3.5[b]	2.54	5.0
S-glass	12	86	4.6[b]	2.50	5.6
High modulus PAN-based carbon	6–8	290–590	2.5–3.9	1.70–1.94	−1.0 to −1.2
High strength PAN-based carbon	5–8	230–295	3.5–7.1	1.76–1.82	−0.4 to −1.0
High modulus Pitch-based carbon	10	520–830	2.1–2.2	2.03–2.18	−1.4
Boron	140	385–400	2.8	2.63	4.9
Silicon carbide	142	400	3.3	3.08	4.86
Silicon carbide (Nicalon)	15	200	2.8	2.60	3.1
Alumina (Al_2O_3) FP	20	379	1.9	3.95	8.3
Nextel (Al_2O_3) 610	10–12	380	3.1	3.9	8.0
Saffil (Al_2O_3–SiO_2)	3	100–300	1.0	3.3–3.5	—
PBT (heat-treated)	—	331	4.2	1.58	—
Kevlar 149	12	180	3.6	1.47	−2.0
Kevlar 49	12	130	3.6	1.45	−2.0
Kevlar 29	12	60	3.8	1.44	−2.0
UHMWPE (Dyneema SK60)	15	87	2.7	0.97	−12.0
UHMWPE (Spectra 1000)	30	172	3.0	0.97	—
Aluminium oxide whiskers	2.8–9.8	427	20.7	3.97	—
Beryllium oxide whiskers	9.8–29	344	13.1	2.86	—
Silicon carbide whiskers	0.75–2.8	482	20.7	3.22	—

[a]To convert GPa to psi, multiply by 145,000.
[b]Virgin strength values. Actual strength values prior to incorporation into composite are about 2.1 GPa (Ca 300,000 psi).

to enhance handling, processing, fiber–matrix adhesion, and to reduce fiber breakage or fiber-to-fiber adhesion. Many properties of the composite structures, including impact resistance and damage tolerance, are strongly dependent on the quality of the fiber–matrix interfaces.

The properties of the major fibers used in composites are given in Table 3. The specific strength against Young's modulus is plotted in Figure 3.

Glass Fibers. Glass is the most widely used reinforcing material. Its advantages include low cost, high tensile and impact strengths, and high chemical resistance. The estimated annual production of glass fibers for the year 2000 was 1800 kton, compared to 18, 12, and 5 kton for carbon, aramid, and other fiber types respectively (12). The advantages of glass fibers include low cost, high tensile and impact strengths, and high chemical resistance. Their drawbacks include a relatively low modulus, self-abrasiveness, low fatigue resistance, and poor adhesion to matrix resins. Typical compositions and properties of three glasses used for fiber manufacture, E (electrical), C (chemical), and S (high tensile strength), are given in Table 4.

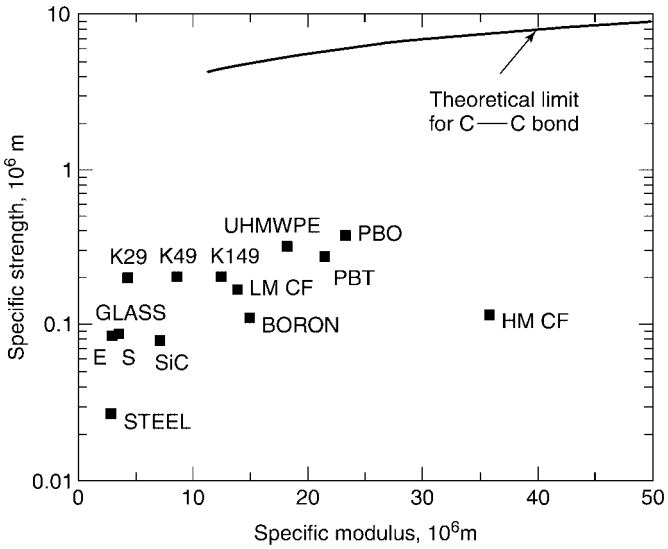

Fig. 3. Specific strength against specific Young's modulus for the major fibers used in polymer composites. The theoretical line for the C—C bond was calculated using the Orowan–Polanyi formula (eq. 5) normalized by the density ρ, namely,; $\sigma/\rho = (\gamma/\rho a_0)^{1/2}(E/\rho)^{1/2}$, with the surface energy $\gamma \approx 4.2$ J/m^2, the length of the C—C bond $a_0 \approx 0.15$ nm, $\rho = 1.8$ g/cm^3 (=17652 N/m^3).

Glass fibers are produced in either continuous filament or staple form. The glass is melted, and fibers are made by rapid mechanical drawing of the forming filaments through orifices. Silica-based glass fibers possess a tetrahedron network structure of oxygen atoms around a silicon atom, all bonded together by covalent

Table 4. Composition (in wt%) and Basic Properties of Glass Types Used in Fiber Form

	E-glass	C-glass	S-glass
Composition			
SiO_2	55.2	65	65
Al_2O_3	14.8	4	25
B_2O_3	7.3	5	—
MgO	3.3	3	10
CaO	18.7	14	—
Na_2O	0.3	8.5	—
K_2O, Fe_2O_3, F_2	0.8	0.5	—
0.5			
Property			
Density, g/cm^3	2.54	2.46	2.45
Tensile strength of single fiber at 25°C, GPa[a]	3.6	3.0	4.2
Tensile strength of strand, GPa	1.7–2.7	1.6–2.3	2.1–3.1
Elastic modulus at 25°C, GPa	75	73	86
Coefficient of linear thermal expansion, 10^{-6} °C	5	8	5

[a]To convert GPa to psi, multiply by 145,000.

bonds. The oxygen atoms are shared between tetrahedra, and the resulting 3-D rigid network structure leads to isotropic properties, in contrast to those of carbon and aramid fibers, which are anisotropic. Elements such as calcium, sodium, and potassium are also present within the network (but are not linked directly to it) and form ionic bonds with the oxygen atoms. Their presence improves the fiber formability but tends to lower its stiffness and strength. The virgin glass fiber strength falls rapidly in the presence of humidity or of mineral acids, and during processing operations in which the fibers may rub against each other. A water-based thin coating called a sizing is therefore applied to the fiber during manufacture. The size usually contains a film-former polymer, a lubricant, and (usually) an organosilane coupling agent with the structure X_3SiR. The R group may react with the polymer matrix, while the X groups can hydrolyze in the presence of water to form silanol groups, which then condense with the silanol groups at the surface of the glass fibers to form siloxanes. The sizing has several roles: protection of the fiber surface from damage, binding the fibers together for easier processing, lubricating the fibers for abrasion resistance during processing, imparting antistatic properties, and increasing the fiber–matrix interfacial bonding.

Carbon or Graphite Fibers. Carbon fibers consist of small crystallites of turbostratic graphite. These resemble graphite single crystals except that the layer planes are not packed in a regular fashion along the *c*-axis direction. In a graphite single crystal, the carbon atoms in a basal plane are arranged in hexagonal arrays and held together by strong covalent bonds. Between the basal planes, only weaker van der Waals forces exist. Therefore, the single crystals are highly anisotropic with in-plane moduli of the order of 1000 GPa whereas the modulus perpendicular to the basal planes is only about 35 GPa. It is thus apparent that to produce high modulus and high strength fibers, the basal planes of graphite must be parallel to the fiber axis. There are several routes for the production of carbon fibers: from rayon-based fibers, from polyacrylonitrile (PAN), from pitch, and from pyrolitic deposition. These processes are now briefly summarized (13).

From Rayon-Based Fibers. Rayon filaments are stretched in a series of steps in an inert atmosphere at temperatures of around 2700°C (4900°F). The tension, along with the high temperatures, converts the polymer to graphite and causes the graphite layer planes to align with the fiber axis, imparting high strength and high modulus to the fibers.

From PAN. Polyacrylonitrile (PAN) is a long-chain linear polymer composed of a carbon backbone with attached carbonitrile groups. The conversion of PAN fibers into carbon fibers involves

(1) heating in an inert atmosphere or vacuum to cyclize the PAN;

(2) treating the fibers in an oxidizing atmosphere at temperatures typically in the range of 200–300°C (392–572°F) while under tension to avoid shrinkage. This treatment converts thermoplastic PAN into a nonplastic cyclic or ladder structure which is capable of withstanding the high temperatures present in the subsequent carbonization treatment. During the oxidizing treatment, considerable reorganization of the polymer chains occurs, involving 3-D linking of the parallel molecular chains by oxygen bonds

(however, some uncertainty still exists regarding the reaction mechanisms during the oxidation treatment of PAN in air). This imparts rigidity along the chain;

(3) further graphitization under stress of the stabilized PAN fibers at higher temperatures in an inert atmosphere.

From Mesophase Pitch. Coal tar pitch (a mixture of many species of hydrocarbons and heterocyclic molecules) is heated for up to 40 h at approximately 450°C (800°F), forming a viscous liquid with a high degree of molecular order known as mesophase (a form of liquid crystal). The mesophase is then rapidly spun through small orifices (spinnerets), aligning the mesophase molecules along the fiber axis. The fibers are thermoset at relatively low temperatures and then heated at 1700–3000°C (3100–5400°F).

From Pyrolitic Deposition. Pyrolitic deposition of hydrocarbons from the gas phase may lead to the formation of carbon fibers. Gases such as methane, benzene, and naphthalene can be used, with deposition temperatures of about 1100°C. A thin tube of carbon is formed on a substrate and then grows by a surface diffusion mechanism. The turbostratic carbon is formed in concentric layers parallel to the fiber axis, and fiber lengths of up to 5 cm may be obtained. Although there is little commercial use of fibers with such short length (and with poor control of the diameter), except as fillers to make polymers conductive for static charge dissipation, a highly graphitic structure results, which may be appropriate for specific applications.

The preferred orientation of a carbon fiber, and thus its modulus, can be enhanced by stretching the fiber during one of the processing stages. For carbon fibers derived from PAN, this stretch orientation is usually carried out during the low temperature heat treatment. Additional factors that might influence the elastic modulus of carbon fiber include the heat treatment temperature (HTT), boron doping, and neutron irradiation. The strength of a carbon fiber depends on the type of the precursor fiber, processing conditions (such as HTT), preoxidation conditions, and the presence of flaws and defects. The strength of PAN-based carbon fibers was observed to increase with increasing HTT and to reach a maximum value at about 1500°C (2732°F) before starting to decrease at higher HTTs. Various mechanisms have been proposed to explain this behavior. Like the modulus, the strength of a carbon fiber is significantly influenced by the preoxidation conditions of PAN fibers. Defects in carbon fibers appear, however, to be the most significant strength-limiting factor.

The surface of carbon fibers is usually oxidized to increase the adhesion with the resin matrix. Oxidizing treatments include wet chemical treatments with sodium hypochlorite or nitric acid. Such treatments generally produce two effects with epoxy resins: first, an outer, defect-laden fiber surface layer is removed; second, surface oxygen groups are added, which can interact with the resin matrix. In addition to oxidative surface treatments, there may be surface treatment with finishes or sizings to enhance compatibility of the fibers with the polymer matrix.

Carbon fibers are available with a wide range of modulus and strength. The theoretical modulus of graphite is in the vicinity of 1035 GPa, and the theoretical values of strength range from 100 to 200 GPa (7). Tensile strengths of 20 and

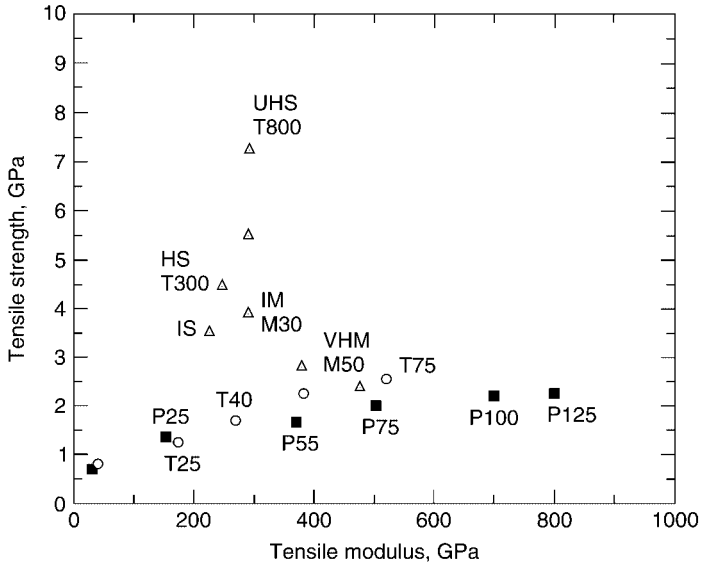

Fig. 4. Mechanical properties of major carbon fibers: ■, pitch; ○, Rayon; and △ PAN. To convert GPa to psi, multiply by 145,000.

7 GPa have been reported with carbon whiskers and continuous carbon fibers, respectively. Carbon fibers can be approximately classified into five groups in terms of their tensile modulus (E) and strength (σ_u): Ultrahigh modulus ($E >$ 400 GPa), high modulus (300 $< E <$ 400 GPa), intermediate modulus (250 $< E$ 300 GPa), high strength ($\sigma_u > 3.8$ GPa), and high strain carbon fibers ($\varepsilon_f > 1.8\%$). The properties of carbon fibers are listed in Table 3 and Figure 4. Note the negative thermal expansion coefficient in the longitudinal direction of carbon fibers, which makes them especially useful in applications requiring thermal management such as instrumentation housings with dense electronics. Finally, the more recent Conoco's carbon fiber technology is a mesophase-pitch-based product offering unique, high performance properties for a broad range of target applications. As a randomly oriented, continuous filament, nonwoven mat (CFM), it is a significant departure from traditional carbon fiber products, which are largely manufactured in tow form—and it is compatible with many high speed manufacturing operations.

Aramid Fibers. Aramid (aromatic polyamide) fibers such as Kevlar (DuPont) and Twaron (Akzo Nobel) are made of poly(paraphenylene terephthalamide). The polymer can be prepared by solution polycondensation of *p*-phenylene diamine and terephthaloyl chloride at low temperatures. The fiber is spun by extrusion of a solution of the polymer in a suitable solvent (for example, sulphuric acid), followed by stretching and thermal annealing treatment. Technora (Teijin) fibers are slightly different from Kevlar and Twaron as they consist of a copolymer: poly(paraphenylene terephthalamide-*co*-3,4-oxydiphenylene terephthalamide). Various grades of Kevlar fibers are produced (Kevlar-29, 49, and 149), Kevlar-49 being the one more commonly used in composite structures.

X-ray diffraction studies show that the structure of Kevlar-49 consists of rigid linear molecular chains that are highly oriented in the fiber axis direction, with the chains held together in the transverse direction by hydrogen bonds. Thus, the polymer molecules form rigid planar sheets. The strong covalent bonds in the fiber axis direction provide high longitudinal strength, whereas the weak hydrogen bonds in the transverse direction result in low transverse strength. Aramid fibers exhibit skin and core structures. The core consists of layers stacked perpendicular to the fiber axis that are composed of rod-shaped crystallites with an average diameter of 50 nm. These crystallites are closely packed and held together with hydrogen bonds nearly in the radial direction of the fiber.

The theoretical modulus of the poly(paraphenylene terephthalamide) molecule has been calculated to be about 250 GPa. However, the modulus of commercially available *p*-aramid fibers ranges from 60 to 186 GPa. The elastic modulus of the fiber is closely related to the crystalline orientation angle. The theoretical strength per unit weight (tenacity) of aramid fiber has been estimated to be 20.7 N/tex (235 g/den) in textile units, assuming that the fiber is composed of a perfectly oriented single crystal consisting of infinitely long polymer molecules. The current commercially available *p*-aramid yarns possess a strength of up to 2.2 N/tex (25 g/den). The aramid fibers have an elastic modulus over 20 times greater than that of nylon fibers. The more rigid and complex molecules impart higher mechanical properties and improved thermal resistance to aramid fibers. These fibers with high specific strength have great cohesiveness and a tendency to form fibrils; they absorb much more energy than brittle fibers. However, they have a highly anisotropic structure that leads to low longitudinal shear moduli, poor transverse properties, and low axial compressive strengths. This directional trade-off arises because of the much weaker lateral bonding mechanisms. While glass and carbon fiber composites show similar tensile and compressive strengths, the compressive strength of unidirectional composites containing Kevlar-49 fibers could be as low as 25% of their tensile strength. The interfacial bond strength between aramid fibers and epoxy resins is normally lower than what is experienced with carbon fiber composites. Work has been carried out on various surface coating, sizing, or plasma treatments to improve interfacial properties of aramid composites.

Further improvement in mechanical properties of aramids appears possible since calculations based on perfect alignment and crystalline order predict a theoretical modulus of about 220–245 GPa. The properties of aramid fibers are compared in Table 5. Like carbon, aramid fibers have a negative thermal expansion coefficient in the longitudinal direction. Aramids have high impact resistance, and they have found their way into the markets of soft and rigid (composite) armors.

Polyethylene Fibers. Solid-state drawing can be used to produce high modulus polyethylene fibers from high density polyethylene. The linearity and crystallinity of this polymer impart a significant degree of order in the polymer structure prior to drawing, thus permitting a highly extended chain configuration to be attained through post-fiber-formation drawing. The modulus of the fiber is proportional to the draw ratio (ratio of final fiber diameter to initial fiber diameter) of the fiber. High draw ratios are essential for producing high strength fibers. For an UHMWPE (MW$\sim 10^6$ g/mol), the natural draw ratio is around 5:1,

Table 5. Aramid Fiber Properties

	Twaron (Akzo)	Twaron HM	Kevlar 29	Kevlar 49	Kevlar 149	HM-50 (Teijin)
Density, g/cm^3	1.44	1.45	1.44	1.44	1.47	1.39
Tensile strength, GPa[a]	2.8	2.8	2.8	2.8	2.8	3.0
Tensile modulus, GPa	80	125	62	124	186	74
Tensile strain, %	3.3	2.0	3.5	2.5	1.9	4.2
Coefficient of thermal expansion,C 10^{-6} °C						
Longitudinal						
0–100°C	—	—	−2.0	—	—	—
100–200°C	—	—	−4.1	—	—	—
200–260°C	—	—	−5.3	—	—	—
Radial						
0–100°C	—	—	59	—	—	—

[a]To convert GPa to psi, multiply by 145,000.

where further orientation can no longer be imposed. However, draw ratios of 50:1 to 70:1 are necessary to obtain high strength fibers. These draw ratios can be achieved by dissolving UHMWPE in a solvent (decalin, paraffin oil, or paraffin wax) to reduce intermolecular entanglements, making it possible to achieve greater fiber orientation. Typically, a 5–10% solution of polymer in solvent is prepared at 150°C. The dilute solution is then cooled to ∼135°C and forms a "gel," a porous, crystallized solid with minimal entanglement density. This gel is spun into fibers and then ultradrawn at 120°C to reach the final fiber diameter and strength.

Similar to other polymer-based high performance fibers, the transverse and longitudinal compressive strengths of polyethylene fibers are relatively low. Epoxy composites containing PE fibers show poor compressive response. Their interlaminar shear strength is lower than that achievable with carbon fiber composites, mainly because of the usually poor bonding between PE fibers and the epoxy matrix. This poor bonding results from their fibrillar structure and low surface energy. Cold plasma treatments of PE fiber surface are a possible way for better interfacial bonding in these composites.

The physical and chemical properties of the gel-spun PE fibers are similar to other PE fibers (eg, solid-state drawn) except that they are of extremely high strength and modulus. These fibers, similar to the aramid fibers, produce high strength and high modulus materials at a significant weight savings over conventional fibers. In fact, UHMWPE fibers, with a density of 0.97 g/cm^3, are even lighter than aramid fibers. This low density feature, coupled with high strength and modulus values, has made UHMWPE fibers the most outstanding among the currently commercial reinforcing fibers in terms of specific strength and specific modulus (Tables 3 and 6).

Because of their low softening point, PE fibers do not retain their strength at temperatures above 145°C. Therefore, these fibers should not be used as reinforcements in many injection molding or sheet molding processes. The creep resistance of these fibers under high load is rather poor. However, their good

Table 6. Comparison Between the Theoretical Strength of Polymers and the Strength of Commercial Fibers

Polymer	Density, g/cm^3	Theoretical strength, N/tex[a]	Strength of commercial fibers, N/tex[a]
PE	0.97	32.8	0.79 (not gel spun)
Nylon 6	1.14	27.9	0.84
POM	1.41	23.3	—
PVA	1.28	20.8	0.84
Kevlar	1.44	20.7	2.2
PET	1.37	20.5	0.84
PP	0.91	19.3	0.79
PVC	1.39	14.9	0.35
Rayon	1.50	11.7	0.46
PMMA	1.19	7.7	—

[a]To convert N/tex to gf/den, multiply by 11.33.

resistance to aqueous and low temperature organic environments have made them attractive materials for marine tow ropes, mooring cables, fishing nets, and sail cloth. Similar to aramids, the ballistic resistance of UHMWPE is outstanding and these fibers are used in soft and rigid (composite) armors. The low dielectric and low loss tangent properties, and hence good microwave transparency, of PE fibers have made them viable candidate reinforcements for radome systems. The fibers produced include Spectra (Honeywell), Dyneema (DSM), and Toyobo (Toyobo). Future applications should include sporting goods, low temperature pressure tanks, and medical devices.

Rigid Rod Polymer Fibers. Poly(*p*-phenylene benzobisthiazole), or PBT, is a stiff chain polymer which can be synthesized and spun into the fiber form by a dry jet-wet spinning technique using a large air gap. A high draw ratio is imposed on the fiber, following spinning to create a high level of orientation. Fibers of high strength and high modulus are obtained with a further heat treatment of drawn fibers in a nitrogen environment. In addition to possessing extremely high specific modulus and strength (Table 3), PBT also has very good chemical resistance to all solvents but strong acids. Good thermal stability is another advantage associated with this fiber over all the currently available commercial polymer fibers. Physical properties are said to be retained at up to 700°C for short-term exposure and at 350°C for an extended period of time. Rigid rod polymers such as polybenzobisoxazoles (PBO) and self-reinforcing liquid crystalline polyesters can also be fabricated into a fiber form. Thermotropic liquid crystalline polymers can orient themselves into highly ordered states and can be thermally processed, as opposed to the lyotropic aramids which must be solution-processed into reinforcing fibers.

Polymer fibers have a high potential as future reinforcements, as may be seen from the comparison of theoretical and experimental strengths presented in Table 6.

Boron Fibers. Boron filaments have been used for many years as a reinforcement for both polymers and metal matrices. Boron-fiber-reinforced

composites offer a unique combination of mechanical and physical properties. The elastic modulus of boron fiber is high (Table 3), providing good stiffness to the reinforced composites. Boron fiber was first used in military aircraft, and boron-fiber-reinforced aluminum was employed for tube-shaped truss members to reinforce the space shuttle structure. However, the rapid reaction of boron fiber with molten aluminum and long-term degradation of diffusion-bonded boron/aluminum at temperatures greater than 480°C may preclude its use for high temperature applications. These drawbacks will also be a real concern in using potentially more economical fabrication methods, such as squeeze casting or low pressure high temperature pressing for metal matrix composites. Boron-fiber-reinforced metal matrix composites typically contain approximately 50% filament by volume. Major applications for boron/aluminum include tubular struts used in the mid-fuselage section of the space shuttle electronic modules. This is because boron/aluminum possesses high strength and stiffness, lightweight, high thermal conductivity, and low thermal expansion. Boron-reinforced metal composites are also being considered for uses in jet-engine fan blades, aircraft wing skins, structural support members, and landing-gear components.

Boron filament is manufactured by chemical vapor deposition (CVD), which involves the formation of solid by decomposition or reduction of gaseous molecules upon a heated substrate (tungsten or carbon filaments). The filaments are heated to approximately 1260°C and then pulled through a boron trichloride/hydrogen environment. The linear deposition rate is slow (about 50 mm/h), and many reactors must be run in parallel to achieve an appreciable production rate. The majority of the boron filaments are used in continuous fiber–epoxy composites. Boron–epoxy composites offer high strengths and stiffness in tension, compression, and bending. The high mechanical properties of boron-reinforced composites have led boron fibers to be applied for many high stress applications. Boron composites have been utilized in numerous aircraft and helicopter designs, eg, stabilizer and rudder in the F-15 fighter plane. In sports goods, a small quantity of boron–epoxy composites have been used to improve strength, stiffness, and sensitivity of rackets, fishing rods, and golf-club shafts.

Silicon Carbide Fibers. Silicon carbide (SiC) filaments are produced by a CVD technique. The β-SiC is obtained by the reaction of silane and hydrogen gases with the carbon filament being the substrate for deposition. The SiC fibers have mechanical and physical properties equal to those of boron, and can be used at higher temperatures than the present boron fiber when available in production quantities. CVD SiC fibers are primarily used for reinforcing metal and ceramic matrices. Alternatively, SiC fibers can be made from a polycarbosilane precursor which is meltspun at 350°C. The final form is obtained by pyrolyzing the fiber at 1200°C in an inert environment.

The use of advanced ceramics in applications such as gas-turbine engines has been limited partially because of their brittle nature, which often leads to catastrophic failure. However, the fracture toughness of a ceramic can be significantly improved by the addition of SiC fiber. The high mechanical properties of SiC fibers (Table 3) result in higher composite strength, stiffness, and toughness. The fibers have been evaluated in various glass, ceramic, and glass–ceramic matrices. The use of these high density fibers in polymer matrix composites has yet

to be explored. Two of the most thoroughly studied SiC fibers are Nicalon (Nippon Carbon Co) and SCS (AVCO).

The SiC fiber is qualified for use in aluminum, magnesium, and titanium. An extensive design database for hot-molded SiC reinforced 6061 aluminum is available. Property data on investment-cast SiC/Al are more limited. SiC-fiber-reinforced titanium parts typically are fabricated by press bonding or hot isostatic pressing. Composites of SiC/Ti have been shown to successfully withstand extended exposure at high temperature. SiC fibers retain usable strengths at up to 1000°C, and have the unique characteristic of retaining basic fiber strength in molten aluminum for up to half an hour. This characteristic should greatly reduce the cost and difficulty of producing SiC/Al composites.

Other Ceramic Fibers. Alumina polycrystalline filaments (Al_2O_3) are of interest mainly for metal matrix composites. They have a high resistance to oxidation, tensile strength and modulus of up to 2 and 380 GPa, respectively, and an excellent strength retention up to 1370°C. Their density is 3.95 g/cm^3. DuPont's FP polycrystalline alumina yarn has a 100% α-alumina composition, and a remarkably high compressive strength of about 6.9 GPa.

Saffil alumina–silica fibers have excellent thermal insulation behavior and resilience up to 1600°C. Their diameter is small, about 3 μm.

Additional ceramic fibers include 3M Nextel metal oxides fibers, and Quartz fibers (from Quartzel and Saint-Gobain) with excellent dielectric properties and near-zero thermal expansion coefficient.

Prospects for Alternative and/or Future Reinforcement

Self-Reinforcing Composites—Molecular Reinforcement. The idea of molecular reinforcement rests on the transfer of the fiber reinforcement concept to the molecular level. It was predicted that increasing the aspect ratio by decreasing the diameter would lead to a single molecule "fiber" as the ultimate reinforcing material (14). Liquid crystals may be formed *in situ* in a polymer by taking advantage of the self-orienting characteristics of anisotropic melts and solutions of polymers. In this way, the liquid crystals, because of their high level of orientation, take the place of fibers in a composite, and the self-reinforced resin is its own composite. Although most of the work in this area involves aromatic polyesters and copolyesters, recently published work gives a promising application of blending liquid crystal polymers with more conventional polymers in which the reinforcing component is dispersed microscopically or molecularly. The concept of developing polymers that can form liquid crystals during fabrication into structures (for example, by injection molding) is receiving considerable attention, for in this way it may be possible to produce composites with high performance economically. For a review, see Reference 15.

Natural Fiber Composites. Replacing synthetic fibers with natural fibers such as hemp and flax has both environmental and economic advantages. Unlike carbon and glass fibers, natural fibers are abundantly available from renewable resources. In terms of cost, natural fibers are cheaper than the synthetic alternatives. Natural fibers and plant-based resins have been shown to combine to produce low cost composites with good mechanical properties (a tensile strength

in the 30 MPa range has been obtained for a composite containing about 30 wt% flax, while a tensile modulus of 4.7 GPa was obtained for a 40 wt% flax composite. Similar numbers were obtained for hemp composites. Composites from renewable resources offer significant potential for new high volume, low cost applications (16).

Carbon Nanotubes. Carbon nanotubes are giant linear fullerenes (closed, convex cage molecules containing only hexagonal and pentagonal faces) having a tubular geometry, which were discovered in 1991 (17). Nanotubes may arise as concentric cylinders and form multiwalled carbon nanotubes, or as single-shell cylinders or single-wall nanotubes, which are closed at their ends. The preparation and physical properties of nanotubes are currently the subject of intense research (18,19). Estimates for the Young's modulus of a carbon nanotube are consistent with the exceptionally high values already measured for a graphene sheet, about 1.2 TPa. Single-wall carbon nanotubes are also expected to be very strong and to resist fracture under extension and compression. Unlike carbon fibers, single-wall nanotubes are remarkably flexible (by many orders of magnitudes compared to conventional high performance fibers, because of their small diameter; see the definition of flexibility above), but should regain their original shape when the stresses distorting it are removed. The excellent mechanical properties of carbon nanotubes would make them ideal for composites applications, which would have significant consequences in structural applications.

BIBLIOGRAPHY

"Reinforcement" in *EPST* 1st ed., Vol. 12, pp. 42–57, by G. Kraus, Phillips Petroleum Co.; "Reinforcement" in *EPSE* 2nd ed., Vol. 14, pp. 391–410, by J. M. Patterson and S. Tsai, USAF Materials Laboratory.

1. W. Weibull, *J. Appl. Mech.* **18**, 293 (1951).
2. A. M. Freudenthal, in H. Liebowitz, ed., *Fracture*, Vol. **2**, Academic Press, New York, 1968, p. 592.
3. A. A. Griffith *Philos. Trans. R. Soc. London, Ser. A* **221**, 163 (1920).
4. H. D. Wagner, in K. Friedrich and R. B. Pipes, eds., *Application of Fracture Mechanics to Composite Materials*, Vol. **6**, Elsevier Science Publishers B.V., Amsterdam, 1989, Chapt. "2", pp. 39–77.
5. H. D. Wagner, *J. Polym. Sci., Polym. Phys.* **27**(1), 115 (1989).
6. A. H. Cottrell, *The Mechanical Properties of Matter*, John Wiley & Sons, Inc., New York, 1964, p. 234.
7. A. Kelly and N. H. Macmillan, *Strong Solids*, Oxford Science Publications, Oxford, 1986.
8. D. Hull and T. W. Clyne, *An Introduction to Composite Materials Cambridge Solid State Science Series*, Cambridge University Press, Cambridge, 1996.
9. R. F. Gibson, *Principles of Composite Material Mechanics*, McGraw-Hill, Inc., New York, 1994.
10. T.-W. Chou, *Microstructural Design of Fiber Composites*, Cambridge University Press, Cambridge, 1992, Chapt. "3".
11. R. E. Swain and co-workers, *J. Thermoplastic Compos. Mater.* **3**(1), 12 (1990).
12. M. G. Bader, *J. Microsc.* **201**(Part 2), 110 (2001).
13. J.-B. Donnet and R. C. Bansal, *Carbon Fibers* International Fiber Science & Technology Series, Marcel Dekker, Inc., New York, 1984.

14. P. Lindenmayer, *Polym. Eng. Sci.* **15**, 236 (1975).
15. B. Schartel and J. H. Wendorff, *Polym. Eng. Sci.* **39**(1), 128 (1999).
16. G. I. Williams and R. P. Wool, *Appl. Comp. Mater.* **7**(5/6), 421 (2000).
17. S. Iijima, *Nature* **354**, 56 (1991).
18. J. P. Salvetat and co-workers, *Appl. Phys. A, Mater. Sci. Proc.* **69**(3), 255 (1999).
19. D. Tomanek and R. J. Enbody, eds., *Science and Application of Nanotubes*, Kluwer Academic Publishers, Boston, Mass., 1999.

H. D. WAGNER
Weizmann Institute of Science

RELEASE AGENTS

Introduction

Release agents are substances that control or eliminate the adhesion between two surfaces. They find considerable use in the adhesive, food, furniture, glass, metal, plastics, rubber, printing, and packaging industries. They expedite many industrial handling and processing operations, particularly of polymers, such as calendering, casting, embossing, extrusion, forming, labeling, laminating, machining, molding, packaging, protecting, and transferring. They are known by a variety of terms descriptive of their effect, including abherents, abhesives, antiblocking agents, antistick agents, external lubricants, surface lubricants, mold-release agents, parting agents, and slip agents. Expectedly, release agents are usually applied directly to surfaces. However, it is sometimes possible to incorporate them into the bulk of the material being treated. Such processing aids are known as internal release agents. They act by migration to the surface and consequently also have an inevitable, internal lubricant effect. Likewise, materials intended as internal lubricants may also exhibit release characteristics, particularly when used at high concentration, if some of the material finds its way to the exterior.

Release agents function by either lessening intermolecular interactions between the two surfaces in contact or preventing such close contact. Thus, they can be low surface-tension materials based on aliphatic hydrocarbon or fluorocarbon groups, or they can be particulate solids. These two categories are by no means mutually exclusive; certain waxes, for instance, can exhibit characteristics of both types. The principal classes of materials used are waxes, fatty acid metal soaps, other long-chain alkyl derivatives, polymers, and fluorinated compounds.

Encyclopedia of Polymer Science and Technology. Copyright John Wiley & Sons, Inc. All rights reserved.

Product Types and Requirements

Release agents are available in a wide variety of forms and are formulated for numerous modes of application. Product types include neat liquids, solutions, powders, flakes, pastes, emulsions, dispersions, sprays, and films. Some are general-purpose inert products intended for a broad range of applications, including home consumer uses, whereas others are highly specific, designed to cross-link or react *in situ* with particular substrates. As with most other formulated processing aids, there is a trend away from products containing volatile organic compounds and ozone-depleting substances, and toward water-based and high solids formulations. Users are also switching from the heavier metal soaps such as lead stearate [7428-48-0]. Another trend that helps reduce solvent and carrier use is toward semipermanent release treatments for multiple releases that have to be applied less frequently. Many products serve more than one processing function and contain other additives, such as antioxidants and wetting agents. The composition of these multifunctional and reactive products is usually proprietary information.

Suppliers of release agents vary from large, basic polymer producers to small, regional formulators and distributors. Examples from among the hundreds of such suppliers include the following: Axel Plastics Research Laboratories, Inc.; Barlocher GmbH; Chem-Pak, Inc.; Dexter Adhesive and Coating Systems; Dicronite Dry Lube; Dow Corning Corp.; DuPont Coating and Release Systems; Endura Coatings, Inc.; Ferro Corp.; Th. Goldschmidt AG; Kluber Chemie KG; Mann Formulated Products, Inc.; Price-Driscoll Corp.; Releasomers, Inc.; Rhodia, Inc.; and Witco Corp.

Many more suppliers and information about their product line can be obtained from compilations such as the *Modern Plastics World Encyclopedia* (1) and the *Thomas Register of American Manufacturers* (2). Obviously, the choice will depend on the processing conditions involved and the nature of the contacting substrates (3). In addition to ease of release, other important requirements are minimal buildup of residues on mold substrate, minimal effect on the molded article, adequate film-forming ability, compatibility with other operational conditions and procedures, health and safety requirements, and cost.

The prevention of residue buildup in polymer processing from either the mold release agent or the molding compound is a common product shortcoming (4). Should it occur, ease of cleanability of the mold surface becomes important. Undesirable effects on molded article surfaces include blistering, streaking, discoloration, stress cracking, and swelling. Film-forming ability is critical in casting and molding operations where melt flow might displace the release agent. Cohesive strength and substantivity to the mold can be enhanced by incorporation of polar groups but this may have a detrimental effect on release performance. Time is often a key operational condition. For example, water or solvent carriers must fully evaporate before a mold is filled. This can be critical in automated processes and limits release agent choice. Similarly, elevated temperature applications require good thermal and oxidative stability to prevent formation of polar, adhesive-like groups. Health and safety concerns are use specific; processing and packaging of foodstuffs and drugs requiring the most stringent consideration. Cost effectiveness, the number of acceptable releases per unit cost, is the key cost-related requirement.

These criteria guide product selection, but trials under production conditions are prudent. Some standard test methods are available that closely simulate actual end-use conditions. For example, ASTM D3354-89 (5) quantifies the degree of blocking, ie unwanted adhesion, between plastic layers. There are also standard test methods for determining coefficients of friction (D1894-95 and D3028-95) and surface gloss and haze (D2475-90 and D1003-95) that can reflect release agent effects on substrate surfaces. The impact of release additives on bulk properties must also be considered, particularly with integral additives to plastics. For example, partial solubility usually confers some plasticizing effect that may improve impact strength but could reduce heat distortion temperature. Some release additives such as metallic soaps have antioxidant and heat-stabilizer benefits that are exploited in multipurpose formulations.

Classification of Release Agents

A classification by chemical type is given in Table 1. It is neither rigorous nor complete and some materials could appear in more than one of these classifications. Polyethylene waxes [9002-88-4], for example, could be considered both as synthetic waxes and as polyolefins. The broad classes of release materials are listed in the chemical class column, and the principal types in the chemical subdivision column, with a single example in the specific examples column. No attempt has been made to incorporate actual commercial products as many are mixtures and some are of proprietary composition. For example, metallic soaps are often used in combination with hydrocarbon waxes to produce finely dispersed suspensions.

Table 1. Chemical Classification of Release Agents

Chemical class	Chemical subdivision	Specific example
Waxes	Petroleum waxes	Paraffin wax [8002-74-2]
	Vegetable waxes	Carnauba wax [8015-86-9]
	Animal waxes	Lanolin [8006-54-0]
	Synthetic waxes	Polyethylene wax [802-88-4]
Fatty acid metal soaps	Metal stearates	Magnesium stearate [557-04-0]
	Other	Calcium ricinoleate [6865-33-4]
Other long-chain alkyl derivatives	Esters	Diethylene glycol monostearate [106-11-6]
	Amides and amines	Ethylene bis(stearamide) [110-30-5]
	Acids and alcohols	Oleic acid [112-80-1]
Polymers	Polyolefins	Polypropylene [9003-07-0]
	Silicones	Polydimethylsiloxane [9016-00-6]
	Fluoropolymers	Polytetrafluoroethylene [9002-84-0]
	Natural polymers	Cellophane [9005-81-6]
	Other	Poly(vinyl alcohol) [9002-89-5]
Fluorinated compounds	Fluorinated fatty acids	Perfluorolauric acid [307-55-1]
Inorganic materials	Silicates	Talc [14807-96-6]
	Clays	Kaolin [1332-58-7]
	Other	Graphite [7782-42-5]

Many products also contain formulating aids such as solvents, emulsifiers, and biocides.

Mechanism of Release

Because release agents are used to reduce the adhesion between materials, it is self-evident that the mechanisms of adhesion and the properties that affect it are the key to understanding release phenomena. These main mechanisms are chemical reaction across the interface, interdiffusion, electrostatic attraction, surface energetics and wettability, and mechanical interlocking. Important surface and interfacial properties include surface topography, surface composition, surface energy and its effect on substrate and adhesive wettability, and the thermodynamic work of adhesion. Key bulk properties of the thin-film interfacial phase include its ability to set to a cohesive solid after wetting the substrate and its viscoelastic response to deformation controlled by factors such as degree of crystallinity, molecular weight and distribution, number of cross-links, and presence of fillers. The absence of weak boundary layers can also be crucial to developing good adhesion between phases.

Inversion of these arguments indicates that release agents should exhibit several of the following features: (*1*) act as a barrier to mechanical interlocking; (*2*) prevent interdiffusion; (*3*) exhibit poor adsorption and be unreactive with at least one of the contact phases; (*4*) have low surface tension, resulting in poor wettability, ie negative spreading coefficient, of the release substrate by the adhesive; (*5*) low thermodynamic work of adhesion; (*6*) low intermolecular forces across the interface, eg an absence of electrostatic or polar attractions; (*7*) display nonsetting or low cohesive interactions within the release phase; and (*8*) provide a weak boundary layer.

Many of these features are interrelated. Finely divided solids such as talc [14807-96-6] are excellent barriers to mechanical interlocking and interdiffusion. They also reduce the area of contact over which short-range intermolecular forces can interact. Because compatibility of different polymers is the exception rather than the rule, preformed sheets of a different polymer usually prevent interdiffusion and are an effective way of controlling adhesion, provided no additional strong interfacial interactions are thereby introduced. Surface tension and thermodynamic work of adhesion are interrelated, as shown in equations (1), (2), (3) (6), and are a direct consequence of the intermolecular forces that also control adsorption and chemical reactivity.

The work of adhesion, W_A, is the change in energy per unit surface area when two phases come into contact, as shown in equation (1) where σ_1 and σ_2 are the surface energy of each phase and σ_{12} the interfacial energy between them.

$$W_A = \sigma_1 + \sigma_2 - \sigma_{12} \quad (1)$$

If the adhesive is phase 1 and the release coating is phase 2, then the spreading coefficient S of 1 on 2 is as given in equation (2).

$$S = \sigma_2 - \sigma_1 - \sigma_{12} \quad (2)$$

Because the work of cohesion, W_C, of the adhesive is $2\sigma_1$, equation (3) follows.

$$W_A - W_C = S \tag{3}$$

Thus when the forces of adhesion are less than those of cohesion, ie when W_A is less than W_C, the spreading coefficient is negative and failure will be at the interface between the adhesive and release coating, the desired situation in a release coating application. Conversely, when the spreading coefficient is positive, undesirable cohesive failure in the adhesive or release coating will be the case. These simple, fundamental equations demonstrate the clear requirement that the release-coating surface energy be lower than that of the adhesive. Table 2 lists the surface energy of some common release substrates.

There are three broad types of intermolecular forces of adhesion and cohesion (7): quantum mechanical forces, pure electrostatic forces, and polarization forces. Quantum mechanical forces account for covalent bonding. Pure electrostatic interactions include Coulomb forces between charged ions, permanent dipoles, and quadrupoles. Polarization forces arise from dipole moments induced by the electric fields of nearby charges and other permanent and induced dipoles. Ideally, the forces involved in the interaction at a release interface must be the weakest possible. These are the polarization forces known as *London or dispersion forces* that arise from interactions of temporary dipoles caused by fluctuations in electron density. They are common to all matter and their energies range from 0.1 to 40 kJ/mol. Solid surfaces with the lowest dispersion-force interactions are those that comprise aliphatic hydrocarbons, and fluorocarbons, and that is why such materials dominate the classification table (Table 1) and the surface energy table (Table 2).

Table 2. Surface Tensions of Various Release Substrates

Substrate	Surface tension,[a] mN/m	Reference
Carnauba wax [8015-86-9]	38[b]	9
Paraffin wax [8002-74-2]	23	10
Octadecylamine monolayer [124-30-1]	22	11
Stearic acid monolayer [57-11-4]	21	11
Polyethylene [9002-88-4]	33	12
Polypropylene [9003-07-0]	29	12
Poly(dimethylsiloxane) [9016-00-6]	24	12
Poly(methylnonafluorohexylsiloxane) [115287-18-8]	16.3	12
Poly(vinyl fluoride) [24981-14-4]	28	12
Poly(vinylidene fluoride) [24937-79-9]	25	12
Polytetrafluoroethylene [9002-84-0]	18.3	12
10-Monohydroperfluoroundecanoic acid monolayer [1765-48-6]	15	13
Poly(pentadecafluorooctyl methacrylate) [29014-57-1]	10.6	12
n-Perfluoroeicosane [37589-57-4]	6.7[c]	14
Perfluorolauric acid monolayer [307-55-1]	6	13

[a] Critical surface tension of wetting, unless otherwise indicated.
[b] Extrapolated value from higher temperature measurements on liquid material.
[c] Solid surface energy, geometric mean approach.

Aliphatic fluorocarbons are the lowest surface-energy solids known. Among the hydrocarbons, the lowest surface energy values are found for surfaces comprising closely packed methyl groups. It has been shown from the studies of critical surface tension of wetting that the order of increasing surface energy of fluorocarbon and hydrocarbon constituent groups is CF_3- < -CF_2- < CH_3- < -CH_2- (8). Organic waxes and other long-chain alkyl derivatives achieve a methyl-rich surface by alignment of the alkyl chains. A related surface can be obtained with plentiful methyl groups along a polymer chain, as in the case of poly(dimethylsiloxane) [9016-00-6]. Such is the extreme localization of these atomic force fields, that there is little direct effect on surface energy from the underlying partially-polar siloxane backbone. Because of this very short, nanoscale, range of operation of dispersion forces, release can also be effected by minimizing the degree of contact between surfaces using finely divided solids. Some, such as microcrystalline wax [64742-42-3] and hydrophobic silica [7631-86-9], combine the two effects in what is sometimes referred to as a microscopic ball-bearing mechanism. Recent studies on the fundamentals of release have also pointed to the importance of a low glass-transition temperature as well as low surface energy. See, for example, the studies of Newby and Chaudhury (15) on fundamentals of release from viscoelastic adhesives. More detailed publications on specific mechanistic aspects of release agents are available, for example, metallic stearates (16), fatty amides (17), application of fluorochemicals to textiles (18), release of polyurethanes (19), and silicone-coated release papers (20).

Industrial Applications

Metal and Glass. Although one might expect that high thermal stability would be a prerequisite for release agent use with molten metals and glasses, it is not necessarily the case. Mineral oils are widely used in molding and shaping glass, despite the smoke and residue buildup entailed. Heat-resistant, graphite-containing resins are also used. Phenolic resins are used in this application and also in mold fabrication for metal castings.

In this process, sand and resin are mulled together and applied to a pattern and hardened to give a mold. Release agents prevent adhesion of the resin binder to the pattern, enabling the mold to be cleanly separated. They also improve the mold release properties after the casting of the metal. Internal mold release agents such as calcium stearate [1592-23-0] have other beneficial effects, such as reduced agglomeration of the resin-coated particles and lower muller power requirements. External release agents such as aqueous silicone emulsions or wax dispersions are used both in the mold making and casting steps. Similar release agents are used in a variety of other metal-forming operations, including the injection molding of low melting aluminum alloys, drawing of ferrous metals, and hobbing and stamping with application to both the tool and product surfaces.

Rubber, Plastics, and Textiles. Release agents are widely used to achieve release of polymers and release from polymers. They are useful in many polymer-processing applications, such as extrusion, calendering, molding, and embossing. By preventing the polymer from sticking and building up on process equipment, rejects are reduced or eliminated. In subsequent machining,

packaging, and labeling operations, abherents allow faster, more continuous handling. Release from polymer applications varies from the familiar example of fluorocarbon-treated cookware to the use of shrink films of polytetrafluoroethylene [9002-84-0] or polyethylene [9002-88-4] over rollers in the ink, printing, polymer processing, and coating industries. A significant aspect of such applications is anti-deposition coatings to reduce accumulation of pollutants and other undesirable matter. Examples include non-thrombogenic surfaces in biomedical uses, low soiling materials for solar-energy collectors, and soil-release agents in powdered detergents. Anti-redeposition agents and soil-release polymers have become important additives to today's laundry products (21).

In the extrusion of thermoplastic polymer powder or granules, release agents aid in the flow and keep the finished product from sticking when stacked. They can also reduce possibility of thermal breakdown by reducing energy requirements and cycle times. Production of granules of particularly adhesive polymers such as polystyrene [9003-53-6] would be impossible without such aids. In the mixing, sheeting, and calendering of natural rubber [9006-04-6], release agents prevent sticking to rollers, thereby maintaining continuous operation. Waxes, metal stearates, and silicones are widely used; solid abherents are popular for dusting finished, unfilled products.

Molding operations such as the manufacture of automobile seat foams and reaction injection molding and blow molding techniques consume considerable quantities of release agents. Many polymers are molded, but polyurethanes present a particular challenge, owing to the likelihood of adhesive bonding of isocyanates to the mold. Polymer films are often used to allow castings to separate from the mold. A specific example is the use of regenerated cellulose (cellophane [9005-81-6]) films in the manufacture of corrugated, glass-reinforced polyester building panels. The molds can also be made from inherently releasing polymers such as silicones.

Adhesive Transfer Processes. There are several important material-transfer applications involving polymer products that are so critically dependent on controlled adhesion that they merit separate mention from general polymer release problems. They include hot stamping foils, release coatings for pressure-sensitive adhesive (PSA) products, photocopier materials, transfer coatings, and transfer printing of textiles.

Hot stamping foils are a type of composite, decorative laminate that uses a polymer carrier film, either polyester or cellophane, together with an external release agent, usually a wax, to transfer coatings to surfaces to be decorated. The transferred coating is rapidly bonded using heat and pressure. Particular attention must be paid to foil detail and surface area, nature of the transferred coating, and avoidance of premature release during slitting and winding of the foils. Some foils are metallized by vacuum deposition; hence there must be no volatiles or migration to interfere with subsequent adhesion on hot stamping.

Silicone products dominate the PSA release liner market, but Werner-type chromium complexes such as stearato chromic chloride [12768-56-8] are also used. Various substrates are used, including coated Kraft papers and polyethylene or polyester films. Silicone coatings that cross-link to form a film are used in various forms such as solvent and solventless dispersions, and emulsions. Technical requirements include good release, no contamination of the adhesive,

adequate anchorage to the substrate, no blocking in rolls, good solvent holdout with solvent-based adhesives, and good thermal and dimensional stability. Poly(dimethylsiloxane)-based products are used for organic PSA release; fluorosilicones such as poly(methylnonafluorohexylsiloxane) [115287-18-8] are needed for silicone PSAs.

Transfer of toner material between rollers and eventually onto the paper is a demanding process. Because speed is of the essence, a combination of temperature and pressure is used to ensure adequate flow of the thermoplastic toner when fusing the image. Temperatures close to 200°C are used, requiring good thermal stability of both the rollers and the release agents. To prevent adhesion of melted toner to the heated roller, its outer layer, at least, is usually a silicone or fluorocarbon material. Often a release agent or fuser oil is also applied to the fuser roll to ensure adequate release. Silicones are widely used on account of their excellent thermal and chemical stability. Another approach is to incorporate the release agent in the toner. Polyethylene and polypropylene [9003-07-0] waxes are dispersed in the toner and migrate to the surface during the fusing step.

Transfer coating is a combination of casting and coating used to create composite materials such as simulated suede leather. A polyurethane film is cast on a release sheet and dried; a second solution is cast on the dried film and then laminated to a suitable fabric when still wet. The release paper is then stripped away when the material has dried. Flexographic printing directly onto fabrics is beset by shrinkage and register problems that are considerably eased by transfer printing from a release sheet of abherent-treated paper. This is printed on the release side by the direct gravure method, dried, and rewound. Direct gravure offers precision and color possibilities not otherwise obtainable. The roll of preprinted release is then forwarded to the fabric converters for unwinding and pressure-heat lamination of the preprint to the fabric.

Furniture. The furniture industry uses a lot of auxiliary release agents in the general gluing and veneering of wood and wood-based materials, as well as in a variety of coating processes. For example, when applying paper impregnated with phenolic and melamine resins for wood surface finishes, the reverse side of the sheet must be coated with a release agent to prevent sticking to the press surface. Mineral oils, paraffin waxes, fatty esters, and specialized paintable silicones are all used for this purpose. Silicone rubber molds are also utilized in the furniture industry; they generally have adequate release properties and require no additional release agents.

Food. Household food uses of release materials such as polyolefin refrigerator ice trays, other foodstuff molds, wax paper, release-coated pans and bake ware, and nonstick cooking sprays are very familiar. One of the oldest methods is the use of flour to release dough from preparation surfaces. Other natural abherents include confectioners' sugar, rice flour, and rice paper. The use of abherent surfaces in the food industry not only decreases product loss, but also eases equipment cleaning. semipermanent release coatings based on silicone resins and polytetrafluoroethylene can last for months whereas wax coatings are removed after each batch of cooking during cleaning and reapplied prior to the next use. Vegetable and animal fats applied pure or as emulsions are used in this way in the bakery industry. Bakery liners are also employed, and can often be reused several times. Glassine and parchment papers treated with chromium complexes

are examples. Note that the trivalent chromium complexes used do not share the hexavalent chromium health hazard.

Economic Aspects

The low surface energy and inertness of the materials used as release agents are exploited in numerous other coating applications and processing aid operations, such as water repellents, polishes, defoamers, and pigment and filler treatments. Consequently, it is difficult to obtain unambiguous economic information regarding release agent consumption. The 1997 Encyclopedia estimate quoted an earlier 1992 figure for worldwide consumption of lubricant and mold-release plastics additives of $(130–140) \times 10^3$ t. The United States, Western Europe, and the rest of the world accounted for one-third each of this activity. This is still a good estimate as the small growth in new markets is balanced by the trend toward semipermanent mold-release compounds.

Estimates can also be made for certain product types in applications that are critically dependent on release agents. For example, silicone release coatings for PSAs account for ca $\$100 \times 10^6$ in the United States, with the rest of the world consuming a similar amount. Growth is limited in many of these release applications with price increases largely offset by production and use efficiencies. Release agent product prices cover a very broad range from a few dollars per kilogram for simple solvent dispersions of stearates and paraffin waxes up to $100/kg for some complex, reactive, proprietary compositions. They may sometimes be the only alternative, but they are often cost effective even when less expensive materials can be used, because of the lower use level or less frequent application rate required. A release agent should be selected not on the basis of unit cost, but for its impact on overall processing and finishing costs.

Health and Safety Factors

Most general-purpose release agents have been developed for this market, in part because of their low toxicity and chemical inertness and do not usually present health and safety problems. Some of the solvent dispersions require appropriate care in handling volatile solvents, with some suppliers offering water-based alternatives. Some of the solids, particularly finely-divided, hydrophobic solids, can also present inhalation problems. Some of the metallic soaps are toxic, although there is a trend away from the heavier, more toxic metals such as lead. The reactive type of release coating with monomers, prepolymers, and catalysts can require specialized handling procedures. The potential user with health and safety questions is advised to consult the manufacturer directly.

Principal health and safety concerns involve contact with foodstuffs and drugs. U.S. Government regulations governing the use of additives such as release agents are listed in the *Code of Federal Regulations*. Title 21 contains the rules established by the U.S. Food and Drug Administration. Part 175 deals with indirect food additives, ie adhesives and components of coatings; part 175.300 specifically covers resinous and polymeric materials for use as components of coatings. This regulation contains a section on release agents that are the basic polymer of the coating, including polyethylene wax, polytetrafluoroethylene,

and silicones, as well as a section on surface lubricants, including glyceryl monostearate [31566-31-1]. Regulations are subject to change, and the *Code of Federal Regulations* is revised at least annually and also updated in the daily issues of the *Federal Register*. Details of regulatory practice differ between countries and a multitude of regulations exist worldwide. Local health and safety information on a particular product is best obtained directly from the formulator or manufacturer. Their skill and experience is the best defense against hazards associated with the use of release agents.

BIBLIOGRAPHY

"Release Agents" in *ECT* 4th ed., Vol. 21, pp. 207–218, by M. J. Owen, Dow Corning Corp.

1. *Modern Plastics World Encyclopedia 2000* **76**(12) (1999).
2. *Thomas Register of American Manufacturers*, 80th ed., Thomas Publishing Co., New York, 1990 [Also available on http://tr.thomasregister.com].
3. C. Kirkland, *Plast. Technol.* **26**, 65 (1980).
4. *Plast. World* **41**, 100 (1983).
5. *Annual Book of ASTM Standards*, Vols. **08.01** and **08.02**, American Society of Testing and Materials, West Conshohocken, Pa., 1996.
6. M. J. Owen, in W. J. Van Ooij and H. R. Anderson, eds., *Mittal Festchrift on Adhesion Science and Technology*, VSP, Utrecht, the Netherlands, 1998, p. 255.
7. J. N. Israelachvili, *Intermolecular and Surface Forces*, Academic Press, Inc., San Diego, Califo., 1989, p. 21.
8. W. A. Zisman, *Adv. Chem. Ser.* **43**, 1 (1964).
9. F. E. Bartell and H. H. Zuidema, *J. Am. Chem. Soc.* **58**, 1453 (1936).
10. D. K. Owens and R. C. Wendt, *J. Appl. Polym. Sci.* **13**, 1741 (1969).
11. E. G. Shafrin and W. A. Zisman, *J. Phys. Chem.* **61**, 1046 (1957).
12. M. J. Owen, in J. E. Mark, ed., *Physical Properties of Polymers Handbook*, AIP Press, Woodbury, N.Y., 1996, p. 673.
13. W. A. Zisman, in P. Weiss, ed., *Symposium on Adhesion and Cohesion*, Elsevier Science, New York, 1962, p. 176.
14. T. Nishino and co-workers, *Langmuir* **15**, 4321 (1999).
15. B.-M. Z. Newby and M. K. Chaudhury, *Langmuir* **13**, 1805 (1997).
16. S. H. Collins, *Plast. Compounding* **6**, 38 (1983).
17. K. Coupland, A. J. Maltby, and D. A. Parker, in *AddCon Asia '97, Int. Plast. Addit. Modif. Conf.*, Rapra Technology, Shrewsbury, U.K., 1997. Paper 15/1-paper15/5.
18. L. G. Cote, *Text. Wet. Process, [Conf.]*, Clemson University, Clemson, S.C., 1998, pp. xv/1–xv/16.
19. B. J. Briscoe and S. S. Panesar, *J. Adhesn. Sci. Technol.* **2**, 287 (1988).
20. J. D. Jones and M. J. Owen, in J. C. Salamone, ed., *The Polymeric Materials Encyclopedia*, Vol. **10**, CRC Press, Inc., Boca Raton, Fla., 1996, p. 7688.
21. A. J. O'Lenick Jr., *J. Surfactants Deterg.* **2**, 553 (1999).

MICHAEL J. OWEN
Dow Corning Corporation

RHEOLOGICAL TESTING. See VISCOMETRY.

RNA. See POLYNUCLEOTIDES.

SHAPE-MEMORY POLYMERS

Introduction

Besides finding high performance materials, material scientists concentrate on designing "intelligent" and "self-repairing materials." In this context, materials showing a thermally induced shape-memory effect, such as metallic alloys or gels, have been studied intensively, and a class of polymers showing shape-memory behavior has found growing interest (1–5). The relatively easy manufacturing and programming of shape-memory polymers makes these materials a cheap and efficient alternative to well-established metallic alloys. These polymers usually surpass by far the recovery properties of shape-memory alloys, which can recover deformations of 8% at maximum. Taking into consideration the importance of polymeric materials in daily life, a very broad spectrum of possible applications for intelligent polymers opens up, covering an area from minimally invasive surgery to high performance textiles, and to self-repairing plastic components in all kinds of technical devices.

Stimuli-sensitive implant materials have a high potential for applications in minimally invasive surgery. Degradable implants could be inserted into the human body in a compressed (temporary) shape through a small incision where they obtain their shape relevant for the specific application after warming up to body temperature. After a defined time period the implant is degraded. In this case subsequent surgery to remove the implant is not necessary. For applications in biomedicine, it is necessary to have tailor-made shape-memory polymers whose thermal, mechanical, or degradation properties can be varied over a wide range. A substantially new development in this context is polymer systems. These are families of polymers in which macroscopic properties can be controlled by a

Encyclopedia of Polymer Science and Technology. Copyright John Wiley & Sons, Inc. All rights reserved.

specific variation of molecular parameters. In this way shape-memory polymers having a specific combination of properties required for specific applications can be obtained by slight variation of the molecular structure and chemical composition.

Definitions of Shape-Memory Polymer and Related Technical Terms

Shape-memory polymers are stimuli-responsive materials. Upon application of an external stimulus they have the ability to change their shape. A change in shape initiated by a change in temperature is called *thermally induced shape-memory effect*. The shape-memory effect results from the polymer's structure, that is, its morphology in combination with a certain processing and programming technology. Therefore, shape-memory behavior can be observed for several polymers that may differ significantly in their chemical composition.

The process of programming and recovering the shape of a polymer is shown schematically in Figure 1. The polymer is processed into its permanent shape by conventional methods. Afterwards, it is deformed and the desired temporary shape is fixed. The latter process is called programming. The programming process consists of heating the sample, deforming and cooling the sample, or drawing the sample at a low temperature ("cold drawing"). The permanent shape is now stored while the sample is in the temporary shape. Heating the programmed polymer above a temperature higher than the transition temperature T_{trans} results in activating the shape-memory effect. As a consequence, the recovery of the memorized, permanent shape can be observed. Cooling of the polymer below the transition temperature leads to solidification of the material. However, the polymer sample does not return to its temporary shape. The described effect is called a *"one-way" shape-memory effect*. The programming process including a mechanical deformation can be repeated. The new temporary shape is not necessarily

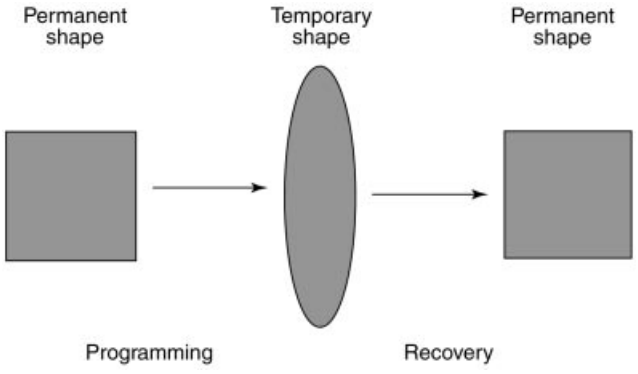

Fig. 1. Schematic demonstration of the thermally induced one-way shape-memory effect. By the programming process the permanent shape is transferred to the temporary shape. Heating up of the sample to a temperature above the switching transition T_{trans} initiates the recovery of the permanent shape. From Ref. 2.

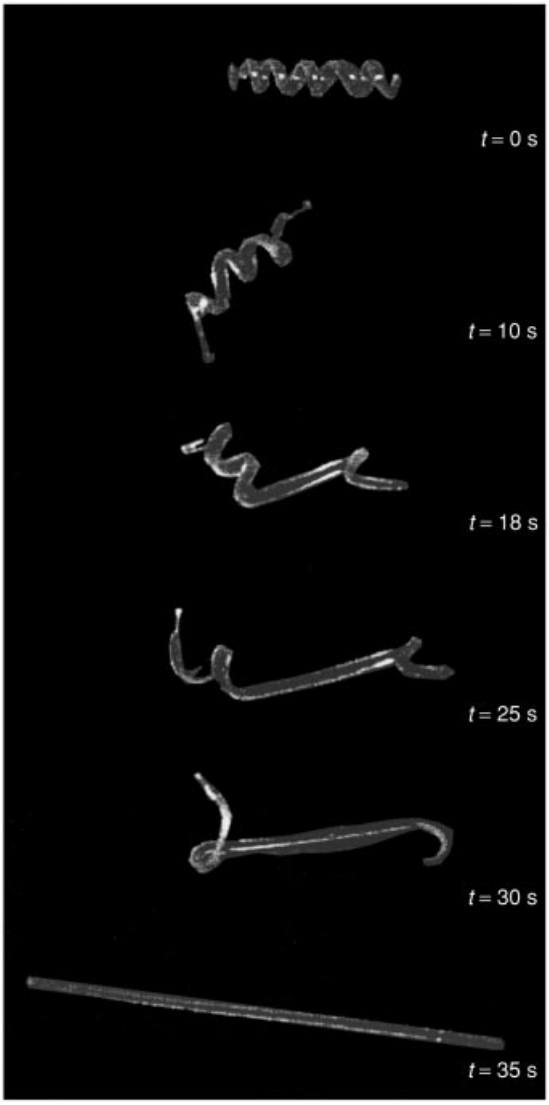

Fig. 2. The series of photos demonstrates (top–down) the transition from the temporary shape (spiral) to the permanent shape (rod) for a shape-memory network that has been synthesized of poly(ε-caprolactone)dimethacrylate and butylacrylate (comonomer content: 50 wt%). The switching temperature of this polymer is 46°C. The recovery process takes 35 s when heated up to 70°C.

supposed to match the temporary shape resulting from the former programming process.

In Figure 2, a photo sequence demonstrates impressively the performance of shape-memory polymers. The permanent shape of the polymer sample is that of a rod. This rod has been deformed to a spiral (temporary shape) during the programming process. Under the influence of hot air having a temperature of 70°C the permanent shape is recovered as soon as

the switching temperature T_{trans} is reached. With optimized programming conditions the permanent shape can be recovered with an accuracy of more than 99% (1).

Molecular Mechanism of the Shape-Memory Effect

All shape-memory polymers discussed henceforth are *elastomers*. On the molecular level they represent polymer networks consisting of segment chains that are connected by netpoints. The netpoints can be formed by entanglements of the polymer chains or intermolecular interaction of certain polymer blocks. These cross-links are called *physical netpoints*. Cross-links in the form of covalent bonds form *chemical netpoints*. An elastomer exhibits a shape-memory functionality if the material can be stabilized in the deformed state in a temperature range that is relevant for the particular application. This can be achieved by using the network chains as a kind of molecular switch. For this purpose, it should be possible to limit the flexibility of the segments as a function of the temperature. This process is supposed to be reversible. The ability to incorporate a control function into the material provides a thermal transition T_{trans} of the network chains in the temperature range of interest for the particular application. At temperatures above T_{trans} the chain segments are flexible, whereas the flexibility of the chains below this thermal transition is at least partly limited. In the case of a transition from the rubber-elastic, ie viscous, to the glassy state the flexibility of the entire segment is limited. The molecular mechanism of programming the temporary and recovering the permanent shape is demonstrated schematically in Figure 3 for a linear multiblock copolymer as an example of a thermoplastic shape-memory polymer with a crystalline hard segment.

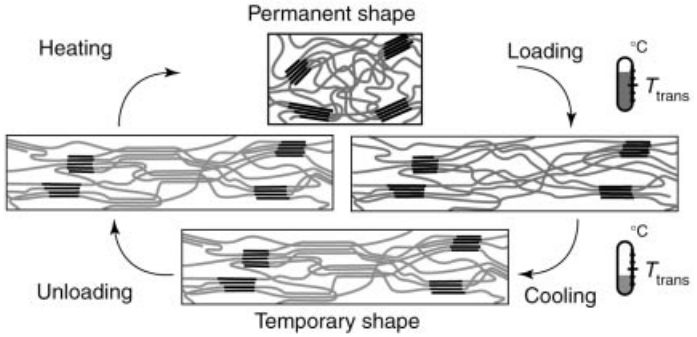

Fig. 3. Schematic demonstration of the molecular mechanism of the thermally induced shape-memory effect for a multiblock copolymer, $T_{trans} = T_m$. If the rise in temperature is higher than T_{trans} of the switching segments, these segments are flexible (marked red, here) and the polymer can be deformed elastically. The temporary shape is fixed by cooling down below T_{trans} (marked blue, here). If the polymer is heated up again the permanent shape is recovered.

Table 1. Possible Combinations of Hard-Segment- and Switching-Segment-Determining Blocks in Linear, Thermoplastic Block Copolymers with Thermally Induced Shape-Memory Effect[a]

Thermal transition determining the permanent shape at T_{perm}	Hard-segment-determining block (Block A)		Switching-segment-determining block (Block B)		Phase-separated block copolymers	
	Highest thermal transition	Second thermal transition	Highest thermal transition	Second thermal transition	T_{perm}	Possible switching transitions T_{trans}
Melting point	$T_{m,A}$	$T_{g,A}$	$T_{m,B}$	$T_{g,B}$	$T_{m,A}$	$T_{m,B}$, $T_{g,A}$, $T_{g,B}$
$T_{perm} = T_{m,A}$	$T_{m,A}$	$T_{g,A}$	$T_{m,B}$	$T_{g,B}$	$T_{m,A}$	$T_{m,B}$, $T_{g,mix}$
	$T_{m,A}$	$T_{g,A}$	$T_{g,B}$		$T_{m,A}$	$T_{g,A}$, $T_{g,B}$
	$T_{m,A}$	$T_{g,A}$	$T_{g,B}$		$T_{m,A}$	$T_{g,mix}$
Glass transition	$T_{g,A}$		$T_{m,B}$	$T_{g,B}$	$T_{g,A}$	$T_{m,B}$, $T_{g,B}$
($T_{perm} = T_{g,A}$)	$T_{g,A}$		$T_{m,B}$	$T_{g,B}$	$T_{g,A}$	$T_{m,B}$, $T_{g,mix}$
	$T_{g,A}$		$T_{g,B}$		$T_{g,A}$	$T_{g,B}$

[a]Ref. 2.

The mechanism of the thermally induced shape-memory effect of linear block copolymers is based on the formation of a phase-separated morphology with one phase acting as molecular switch. The phase showing the highest thermal transition T_{perm} is by the formation of physical netpoints, on the one hand providing the mechanical strength of the material, especially at $T < T_{perm}$, and on the other hand the fixation determining the permanent shape. The materials are divided into two categories according to the thermal transition of the particular switching segment the shape-memory effect is based on. Either the transition temperature T_{trans} is a melting temperature T_m or a glass-transition temperature T_g. In case of a melting temperature one observes a relatively sharp transition in most cases, whereas glass transitions always extend over a broad temperature interval. In case there is no sufficient phase separation between the "hard-segment-determining" block (Block A) and the "switching-segment-determining" block (Block B), mixed glass-transition temperatures $T_{g,mix}$ between the glass transiton of the "hard-segment- and the switching-segment-determining" blocks may occur. Mixed glass-transition temperatures are also qualified to act as switching transitions for the thermally induced shape-memory effect. Table 1 gives an overview about possible combinations of "hard-segment- and switching-segment-determining" blocks in linear, thermoplastic shape-memory polymers (2).

In chemically cross-linked shape-memory networks the permanent shape is stabilized by the covalent netpoints. In analogy to linear block copolymers with shape-memory, the temporary shape of covalently cross-linked shape-memory networks can be fixed either by crystallizable segment chains or by a glass transition of the segment chains that is in the temperature range of interest.

Cyclic Thermomechanical Characterization

The shape-memory effect can be quantified by cyclic thermomechanical investigations. Typically, measurements are performed by means of a tensile tester equipped with a thermochamber. During this experiment, different test programs are applied that differ, for example, in the programming procedure (cold drawing at $T < T_{trans}$ or temporary heating up of the polymer sample to a temperature $T > T_{trans}$) or in the control parameter of the tensile tester (stress- or strain-controlled). A single cycle includes the programming of the sample and the recovery of its permanent shape.

A typical test program is described in the following: the test piece is heated up to a temperature T_{high} that is above the switching temperature T_{trans} and is elongated to the maximum strain ε_m. In case of thermoplastics, it is important not to exceed the highest thermal transition T_{perm}; otherwise, the polymer sample would melt. The sample is cooled down below the transition temperature T_{trans} to a temperature T_{low} under constant strain ε_m. In this way, the temporary shape is fixed. Retracting the clamps of the tensile tester to the original distance of 0% strain causes the sample piece to bend. After increasing the temperature to T_{high} ($>T_{trans}$) the sample contracts and the permanent shape is recovered. The cycle can begin again.

The result of such a measurement is usually presented in a tensile stress (σ)–strain (ε) curve (see Fig. 4a). This is why this test protocol is often called a two-dimensional measurement. Figure 4 schematically represents curves obtained as results from mechanical measurements. If the stretched sample is cooled down (Position ② in Fig. 4a) different effects can result in changes of the curves' course. Here, differences in the expansion coefficient of the stretched sample at temperatures above and below T_{trans}, as a consequence of the entropy elasticity and volume changes due to crystallization, are inducing changes in mechanical stress σ. The latter is the case if T_{trans} is a melting point.

The elastic modulus $E(T_{high})$ at a temperature T_{high} can be determined from the initial slope in the program step ① (Fig. 4a) also the elastic modulus of the stretched sample at a temperature T_{low} can be determined from the slope of the curve in the program step ③ (Fig. 4a). Important quantities to be determined describing the shape-memory properties of the material for a certain maximum strain ε_m are the *strain recovery rate* R_r and the *strain fixity rate* R_f. Both can be determined according to equations 1 and 3. The strain recovery rate R_r quantifies the ability of the material to memorize its permanent shape and is a measure of how far a strain that was applied in the course of the programming, $\varepsilon_m - \varepsilon_p(N-1)$, is recovered in the following shape-memory transition. For this purpose the change in strain that is applied during programming in the Nth cycle, $\varepsilon_m - \varepsilon_p(N-1)$, is compared with the change in strain that occurs with the shape-memory effect, $\varepsilon_m - \varepsilon_p(N)$:

$$R_r(N) = \frac{\varepsilon_m - \varepsilon_p(N)}{\varepsilon_m - \varepsilon_p(N-1)} \tag{1}$$

where $\varepsilon_p(N-1)$ and $\varepsilon_p(N)$ represent the strain of the sample in two successively passed cycles in the stress-free state before yield stress is applied. The *total strain*

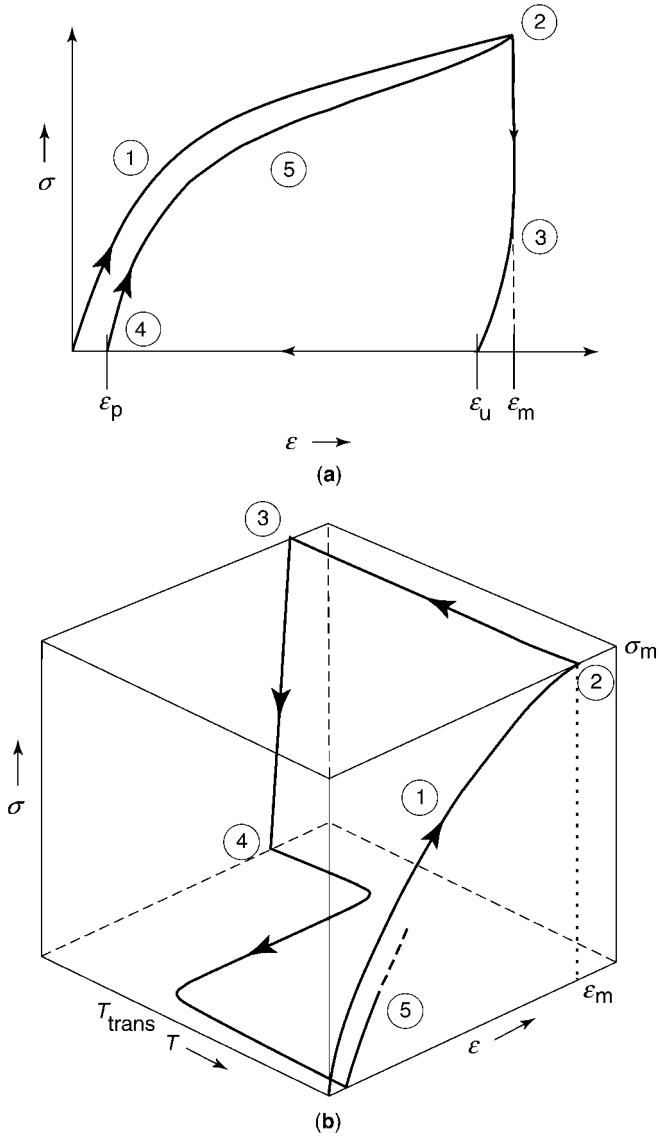

Fig. 4. Schematic demonstration of the results of the cyclic thermomechanical investigations for two different test programs: (**a**) ε–σ diagram: ① stretching to ε_m at T_{high}; ② cooling to T_{low}, while ε_m is kept constant; ③ clamp distance is driven back; ④ at $\varepsilon = 0\%$ heating up to T_{high}; ⑤ beginning of the second cycle. (**b**) ε–T–σ diagram: ① stretching to ε_m at T_{high}; ② cooling down to T_{low} with cooling rate $k_{cool} = dT/dt$ while σ_m is kept constant; ③ clamp distance is reduced unless stress-free state $\sigma = 0$ MPa is reached; ④ heating up to T_{high} with a heating rate $k_{heat} = dT/dt$ at $\sigma = 0$ MPa; ⑤ beginning of the second cycle. From Ref. 2.

recovery rate $R_{r,tot}$ is defined as the strain recovery after N passed cycles referred to the original shape of the sample piece:

$$R_{r,tot}(N) = \frac{\varepsilon_m - \varepsilon_p(N)}{\varepsilon_m} \tag{2}$$

The strain fixity rate R_f describes the ability of the switching segment to fix the mechanical deformation which has been applied during the programming process. It describes how exactly the sample can be fixed in the stretched shape after a deformation to ε_m. The resulting temporary shape $\varepsilon_u(N)$ always differs from the shape achieved by deformation.

$$R_f(N) = \frac{\varepsilon_u(N)}{\varepsilon_m} \tag{3}$$

The strain fixity rate R_f is given by the ratio of the strain in the stress-free state after the programming step in the Nth cycle, $\varepsilon_u(N)$, and the maximum strain ε_m (1).

As indicated in Figure 4 the first cycles can differ from each other. With an increasing number of cycles the curves become more similar. The process of deformation and recovery of the permanent shape becomes highly reproducible. The changes in the first cycles are attributed to the history of the sample piece. In this respect, processing and storage play an important role. During the first cycles, a reorganization of the polymer on the molecular scale takes place as a reaction on the deformation in a certain direction. Singlepolymer chains arrange in a more favorable way with regard to the deformation direction. Covalent bonds may be broken during this process. An important variable that cannot be determined by a two-dimensional measurement is T_{trans}. In this respect, the "three-dimensional" test record that is given schematically in Figure 4b is interesting. In contrast to the two-dimensional measurement, here, the sample piece is cooled down in a controlled way (constant cooling rate) at a constant tensile stress σ_m. The change in strain in this program step is influenced by the temperature dependence of the thermal expansion coefficient of the stretched polymer and volume effects, which is based on the thermal transition T_{trans}, eg, a crystallization process. Having reached T_{low} the strain is reduced until a stress-free state is reached. The sample is now heated up to T_{high} at a constant heat rate. During this experiment the tensile stress is kept constant at 0 MPa; this means that the clamps are following the shape change of the test piece. In this way, the shape change caused by the shape-memory effect is recorded as a function of the temperature. From the interpretation of the ε–T plane in the ε–T–σ diagram not only T_{trans} but also the temperature interval can be determined in which the shape-memory effect takes place (Fig. 4b).

Examples for Shape-Memory Polymers

The following examples show thermally induced shape-memory. The first three examples are exclusively physically cross-linked. These examples are two polyurethanes representing thermoplastic shape-memory polymers with $T_{trans} = T_m$ or T_g, and a high molecular weight, amorphous polynorbornene. Examples of covalently cross-linked shape-memory networks are so-called heat-shrinkable materials and a shape-memory network with a crystallizable switching segment ($T_{trans} = T_m$) that has been developed for biomedical application.

Polyurethanes with Poly(ε-caprolactone) Switching Segment. Polyesterurethanes with a "hard-segment-determining" block of 4,4′-methylenebis(phenylisocyanate) (MDI) and 1,4-butanediol can be synthesized by the prepolymer method (6–11). The highest thermal transition T_{perm} corresponding to the melting temperature of the "hard-segment-determining" blocks is found between 200 and 240°C. Poly(ε-caprolactone)diols with a number-average molecular weight (M_n) between 1600 and 8000 form the switching segments. The switching temperature for the shape-memory effect can be varied between 44 and 55°C depending on the weight fraction of the switching segments (variation between 50 and 90 wt%) and the molecular weight of the used poly(ε-caprolactone)diols. In polyurethanes with a high molecular weight of the used poly(ε-caprolactone) the "switching-segment-determining" blocks can crystallize optimally and so the temporary shape is set ideally. Moreover, a high weight fraction of "hard-segment-determining" blocks guarantees an optimum stabilization of the permanent shape. As a consequence, polyurethanes that combine a high molecular weight of the used poly(ε-caprolactone) and a high weight fraction of "hard-segment-determining" blocks show the best shape-memory properties. The strain recovery rate comes up to 98% at maximum strains ε_m of 80%. Nonetheless, the shape-memory properties are strongly influenced by the degree of the applied strain. The strain recovery rates decrease if the applied strains ε_m are increased from 80 to 250%. Decisive factors influencing the recovery properties are, besides the crystallinity of the switching segments, the formation and stability of the hard-segment-forming domains, especially, in the temperature range above the melting temperature of the switching-segment crystallites. For a content of hard-segment-forming domains below 10 wt% the hard-segment domains are not able to form stable physical cross-links. During the initial three cycles a slight increase in the switching temperature can be observed. This behavior is interpreted in terms of the destruction of weak netpoints, followed by an increasing formation of an ideal elastic network.

Polyurethanes with Poly(tetrahydrofuran) Switching Segment. Materials with a mixed glass-transition temperature $T_{g,mix}$ are systems with poly(tetrahydrofuran)- (poly(THF)-) switching-segment blocks having number-average molecular weights of 250 and 650 and a hard-segment-forming phase based on MDI and 1,4-butanediol. The hard segment is made using the prepolymer method (12,13). The highest thermal transition T_{perm} corresponds with the melting temperature of the "hard-segment-determining" blocks. The block copolymers exhibit a $T_{g,mix}$ between 16 and 54°C in case of the switching segment with M_n = 250 depending on the hard-segment content (hardsegment content between 57 and 95 wt%), a $T_{g,mix}$ between −13 and 38°C for the switching segment with M_n = 650 (hard-segment content between 32 and 87 wt%), and a $T_{g,mix}$ of −36–22°C for the switching segment with M_n = 1000 (hard-segment-content between 23 and 81 wt%). If poly(THF)diols with M_n = 2000 or 2900 are used one cannot observe a mixed T_g because of the good separation of the different blocks. Here, the occurring glass-transition temperatures are also dependent on the hard-segment content because of the hard segments' property to hinder the mobility of the switching-segment chains. The shape recovery rate increases with increasing hard-segment content, reaching values up to 99% for the material with a switching segment with

$M_n = 250$ and a hard-segment content of 75 wt%. For materials with a switching segment with $M_n = 650$ complete recovery is not reached until the hard-segment content is 87%. After approximately 100 repetitions a constant shape recovery rate of 95% is reached.

Polynorbornene. Norsorex is a linear, amorphous polynorbornene having shape-memory properties. It was developed by the companies CdF Chemie and Nippon Zeon in the late 1970s. The molecular weight of this polynorbornene is about 3×10^6 (3,14). It is produced by a ring-opening metathesis polymerization of norbornene using a tungsten–alkylidene catalyst. This polynorbornene has a content of 70–80 mol% of trans-linked norbornene units and a glass-transition temperature between 35 and 45°C (14,15). The shape-memory effect of this strictly amorphous material is based on the formation of a physically cross-linked network due to entanglements of the high molecular weight, linear polymer chains. The thermal transition from the glassy state to the rubber-elastic state can be used as switching transition (16). Consequently, upon reaching the glass-transition temperature T_g the material softens abruptly. If the chains are stretched quickly in this state and the material is rapidly cooled down again below T_g, as an answer to this, the polynorbornene chains can neither slip off each other rapidly enough nor can entanglements disentangle. By rapid cooling the induced elastic stress can be frozen within the material. After heating up again above T_g, because of the thermally induced shape-memory effect a recovery of the material's shape can be observed. The described Norsorex is not inevitably purely amorphous. There are reports of a high molecular weight polynorbornene with a high content of trans-linked norbornene units showing a tendency toward strain-induced crystallization (14,15). Because of this observation the possibility must not be excluded that crystallites acting as physical netpoints contribute to the shape-memory effect.

"Heat-Shrinkable" Polymers. Since the 1960s, polyethylene covalently cross-linked by means of ionizing radiation has found broad application as heat shrink foil or tubing especially for the insulation of electric wires or as protection against corrosion of pipe lines (17–22). These materials are marketed under the term *heat-shrinkable materials*. The mechanism of the heat-shrinking process corresponds to the thermally induced shape-memory effect. The permanent shape is fixed by covalent cross-links. The switching process is controlled by the melting temperature of the polyethylene crystallites.

Biodegradable Polymer Networks with Shape-Memory. Based on oligo(ε-caprolactone)diol representing the component to form a crystallizable switching segment, a polymer system with an AB-polymer network structure has been developed (1). For this purpose oligo(ε-caprolactone)diols have been functionalized with methacrylate end groups that can undergo a polymerization reaction. The comonomer of choice is *n*-butyl acrylate because of the low T_g (−55°C) of pure poly(*n*-butyl acrylate); this supposedly determines the amorphous network chains of the expected network. The molecular weight of the used oligo(ε-caprolactone)dimethacrylate cross-linking agent and the content of the comonomer butyl acrylate represent the molecular parameters controlling crystallinity, eg T_{trans}, and mechanical properties. The number-average molecular weights of the oligo(ε-caprolactone)dimethacrylates used were 2000 and 10,000. The cross-link density in the case of the oligo(ε-caprolactone)dimethacrylate

(M_n = 2000) was varied by addition of 11–90 wt% butyl acrylate and for the oligo(ε-caprolactone)dimethacrylate (M_n = 10,000) by addition of 20–71 wt% butyl acrylate. The cross-link density increases with decreasing content of butyl acrylate. The butyl acrylate content influences the thermal properties of the formed AB network, especially for the oligo(ε-caprolactone)dimethacrylate with M_n 2000. Here, only in the case of a very low content of butyl acrylate of 11 wt%, a melting point at a $T_m = 25^\circ$C can be observed. The corresponding homonetwork of oligo(ε-caprolactone) dimethacrylate has a melting point at $T_m = 32^\circ$C. All other networks of this series were found to be completely amorphous. For the networks of butyl acrylate and oligo(ε-caprolactone)dimethacrylate with M_n 10,000 the melting point decreases from 51 to 44°C with increasing butyl acrylate content. With increasing butyl acrylate content the mechanical properties of both materials with oligo(ε-caprolactone) segments with M_n = 2000 and 10,000 change in such a way that the values of the elastic modulus (E), the tensile strength (σ_{max}), and the tensile stress at break (σ_R) decrease for about an order of magnitude. The absolute values are an order of magnitude higher for the series with oligo(ε-caprolactone) segments with M_n = 10,000. In cyclic thermomechanical tensile tests for the network with oligo(ε-caprolactone) segments (M_n = 10,000), strain fixity rates between 95 and 85% and strain recovery rates from 98 to 93% could be obtained. After three thermocycles all materials reached a constant strain recovery rate of 99%. In *in vitro* tests these shape-memory networks appear to be promising in their biocompatibility.

BIBLIOGRAPHY

1. A. Lendlein, A. M. Schmidt, and R. Langer, *Proc. Natl. Acad. Sci. U.S.A.* **98**, 842 (2001).
2. A. Lendlein and S. Kelch, *Angew. Chem., Int. Ed.*, in press.
3. K. Nakayama, *Int. Polym. Sci. Technol.* **18**, T43–T48 (1991).
4. U.S. Pat. 5,128,197 (1992), K. Kobayashi and S. Shunichi (to Mitsubishi Heavy Industries Ltd.).
5. U.S. Pat. 6,160,084 (2000), R. S. Langer and co-workers (to MIT).
6. B. K. Kim, S. Y. Lee, and M. Xu, *Polymer* **37**, 5781–5793 (1996).
7. F. Li and co-workers, *J. Appl. Polym. Sci.* **62**, 631–638 (1996).
8. F. Li and co-workers, *J. Appl. Polym. Sci.* **64**, 1511–1516 (1997).
9. B. K. Kim and co-workers, *Polymer* **39**, 2803–2808 (1998).
10. H. M. Jeong, B. K. Kim, and Y. J. Choi, *Polymer* **41**, 1849–1855 (2000).
11. H. M. Jeong and co-workers, *J. Mater. Sci.* **35**, 279–283 (2000).
12. J. R. Lin and L. W. Chen, *J. Appl. Polym. Sci.* **69**, 1563–1574 (1998).
13. J. R. Lin and L. W. Chen, *J. Appl. Polym. Sci.* **69**, 1575–1586 (1998).
14. K. Sakurai and T. Takahashi, *J. Appl. Polym. Sci.* **38**, 1191–1194 (1989).
15. K. Sakurai, T. Kashiwagi, and T. Takahashi, *J. Appl. Polym. Sci.* **47**, 937–940 (1993).
16. P. T. Mather, H. G. Jeon, and T. S. Haddad, *Polym. Prepr. (Am. Chem. Soc., Div. Polym. Chem.)* **41**, 528–529 (2000).
17. A. Charlesby, *Atomic Radiation and Polymers*, Pergamon Press, Oxford, 1960, pp. 198, 257.
18. S. Ota, *Radiat. Phys. Chem.* **18**(1/2), 81–87 (1981).
19. W. Chen, K. Xing, and L. Sun, *Radiat. Phys. Chem.* **22**, 593–601 (1983).
20. G. Kleinhans, W. Starkl, and K. Nuffer, *Kunststoffe* **74**, 445–449 (1984).

21. G. Kleinhans and F. Heidenhain, *Kunststoffe* **76**, 1069–1073 (1986).
22. S. Machi, *Radiat. Phys. Chem.* **47**, 333–336 (1996).

ANDREAS LENDLEIN
STEFFEN KELCH
Deutsches Wollforschungsinstitut

SINGLE-SITE CATALYSTS

Introduction

In 1953, Karl Ziegler discovered that the activation of certain early transition metal halides with aluminum alkyls resulted in the formation of new organometallic catalysts capable of polymerizing ethylene at room temperature and ambient pressure (1–3). In 1954, Giulio Natta and co-workers from the Politecnico di Milano and Montecatini for the first time prepared crystalline isotactic polypropylene (iPP) by using the heterogeneous $TiCl_4/(C_2H_5)_3Al$ Ziegler catalyst system (4–8). Three years later, in 1957, the first PP plant went on line at the Montecatini site in Italy. Only six years later, in 1963, Karl Ziegler and Giulio Natta shared the Nobel Prize in chemistry for their landmark discoveries that laid the foundation for today's multibillion-dollar-a-year polyolefin industry (see ZIEGLER–NATTA CATALYSTS).

The industrial and academic impact of Ziegler–Natta catalysis has been tremendous (9–11). Several generations of catalysts and processes have been introduced on a commercial scale to produce a variety of polymeric materials ranging from fibers to commodity thermoplastics, engineering plastics, and elastomers. At the turn of the millennium, over 40 million tons of polyolefins per year worldwide are produced using the Ziegler–Natta technology. Modern $MgCl_2$-supported Lewis-base-modified catalyst systems produce spherical pellet-sized polyolefin replicas with catalytic activities exceeding 1 ton of polymer per gram of transition metal, thus eliminating the need for pelletizing extrusion and additional polymer purification steps. Annual demand for polyethylene (PE), the number one commodity plastic, is approaching 50 million metric tons. Polypropylene (PP) is ranked third, after poly(vinyl chloride) (PVC), and has the fastest growing market (see ETHYLENE POLYMERS; PROPYLENE POLYMERS (PP)).

Encyclopedia of Polymer Science and Technology. Copyright John Wiley & Sons, Inc. All rights reserved.

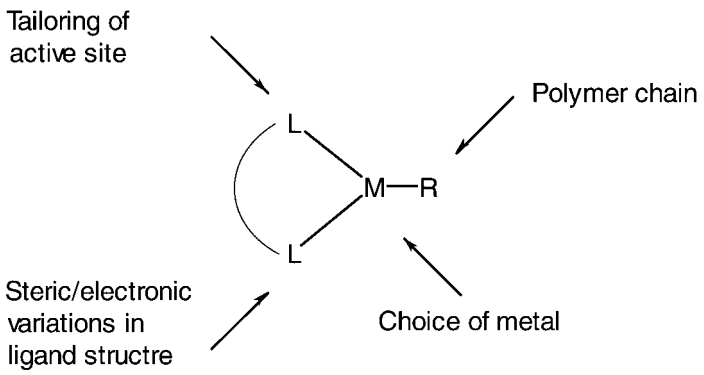

Fig. 1. General structure of single-site catalysts.

Fifty years after the initial discoveries, Ziegler–Natta catalysis remains as an outstandingly vital field. The recent rapid scientific and technological outburst of single-site transition metal catalysts is undoubtedly one of the most remarkable developments in the application of molecular organometallic chemistry to catalysis and polymer science (for reviews and general references, see Refs. 12–38). These predominantly homogeneous catalyst systems consist of well-defined active sites with the general formula [L_nMR], where L_n represents an organic ligand set bound to the transition metal M, and R is the growing polymer chain or initiating group (Fig. 1).

By variation of the organic ligand and thus the steric and electronic environment of the metal center, these catalysts can be tailored to control the olefin polymerization reaction in an unprecedented fashion. Almost any vinyl monomer, irrespective of its molecular weight or steric hindrance, can be polymerized by choosing the proper catalyst and polymerization conditions. Virtually all feasible polymer microstructures ranging from atactic to isotactic, hemiisotactic, syndiotactic, and stereoblock poly-α-olefins can be produced by rational modification of the catalyst structure. In addition, molecular weight, molecular weight distribution, comonomer content, and end-group composition of the produced polymer can be varied independently. Entirely new polyolefin materials, not accessible with traditional Ziegler–Natta catalysts, have also emerged through single-site catalyst (SSC) technologies. Notable examples include syndiotactic polystyrene, thermoplastic PP-based elastomers, as well as cycloaliphatic polymers obtained by cyclopolymerization of nonconjugated dienes or direct polymerization of cycloolefins, such as norbornene and cyclopentene (see ELASTOMERS THERMOPLASTIC; ETHYLENE-NORBORNENE COPOLYMERS).

The first generations of SSCs were based on Group 4 metallocene complexes as pioneered by Ewen, Kaminsky, and Brintzinger. More recent examples include alternative ligand systems complexed with Group 4 metals, as well as several late transition-metal-based catalyst systems developed by Brookhart, Gibson, Grubbs, and others. The less oxophilic late transition metals are even capable of incorporating a variety of polar comonomers into polyolefin chains.

This article provides a broad overview of the current status and the enormous amount of literature on single-site olefin polymerization catalysts. For the

sake of consistency, *single-site catalyst* is used in this article for describing a catalyst system or precursor consisting of essentially uniform active centers producing narrow molecular weight distribution polymers ($M_w/M_n \approx 2$), in accordance with Schulz–Flory statistics. Since several of these catalysts have two coordination sites located at the same metal center, the term *single-center catalyst* is also in common use. The references have, with a few exceptions, been selected from the open literature with the main emphasis on the well-established Group 4 metallocenes and the recently developed late transition metal catalysts. For detailed descriptions of the various catalysts and processes as well as references to the extensive patent literature, the reader is referred to the original publications cited in the bibliography and the available reviews and text books (12–38).

Evolution and Classification of SSC Systems

Classical Ziegler–Natta catalysts are multisited and heterogeneous with the polymerization taking place on edges and dislocations of transition metal halide crystals. Development of homogeneous single-site olefin polymerization catalysts was initiated by efforts to model the reaction mechanisms of the heterogeneous catalysts. In 1955, Breslow and Newburg (39,40) and Natta and co-workers (41) discovered that titanocene dichloride (Cp_2TiCl_2) could be activated for ethylene polymerization by addition of aluminum alkyls $(C_2H_5)_2AlCl$ or $(C_2H_5)_3Al$. The first soluble catalysts were inactive for polymerization of propylene and exhibited much lower activities in ethylene polymerization than their heterogeneous counterparts. Nevertheless, these and other subsequent early studies (42–49) contributed significantly to the understanding of both heterogeneous and homogeneous Ziegler–Natta catalysis.

In the mid-1970s, a series of serendipitious discoveries initiated the rapid development in single-site olefin polymerization catalysis, which in less than 25 years has revolutionized modern polymer synthesis. In 1973, Reichert and Meyer observed a remarkable increase in polymerization activity by adding small amounts of water to the $Cp_2TiCl_2/C_2H_5AlCl_2$ metallocene catalyst system (50). Similar observations were reported by Long and Breslow for $Cp_2TiCl_2/(CH_3)_2AlCl$ (51). In 1975, Sinn and Kaminsky discovered an enormous and unexpected increase in polymerization activity after addition of considerable amounts of water to the otherwise inactive $Cp_2Ti(CH_3)_2/(CH_3)_3Al$ mixture (52). The suspected formation of methylaluminoxane (MAO) by partial hydrolysis of $(CH_3)_3Al$ was subsequently supported by its controlled synthesis. The direct activation of titanocenes and zirconocenes with preformed MAO gave exceedingly active catalysts for polymerization of ethylene (53). For the first time, homogeneous metallocene-based SSCs became more active than the commercially used heterogeneous Ziegler–Natta catalyst systems. In addition, the MAO-activated Group 4 metallocenes were capable of polymerizing propylene and higher α-olefins (54,55), although only atactic polymers of prochiral monomers were obtained (because of the achiral nature of the catalytic site).

Group 4 Metallocene-Based Catalysts. Revolutionary breakthroughs occurred in the early 1980s when Ewen (56) and Kaminsky (57) reported that MAO-activated C_2 symmetric chiral *ethylene*-bridged bis(tetrahydroindenyl)

Group 4 *ansa*-metallocenes *rac*-$C_2H_4(IndH_4)_2MCl_2$ (M = Ti, Zr), developed by Brintzinger and co-workers (58–60), polymerized propylene to iPP. The prefix *ansa* from Latin (for bent, handle) was first used for compounds with an alkane bridge across an arene ring, and later adopted by Brintzinger as a short notation for metallocene derivatives with an interannular bridge.

Since the mid-1980s billions of dollars have been invested worldwide in research focusing on modifying and improving the metallocene-based olefin polymerization catalysts. Key structures are summarized in Figure 2.

In 1988, Ewen reported the first preparation of a C_s symmetric *ansa*-metallocene catalyst precursor $[(CH_3)_2C(Cp)(Flu)]ZrCl_2$ producing syndiotactic polypropylene (sPP) (61), and a few years later its C_1 symmetric modification

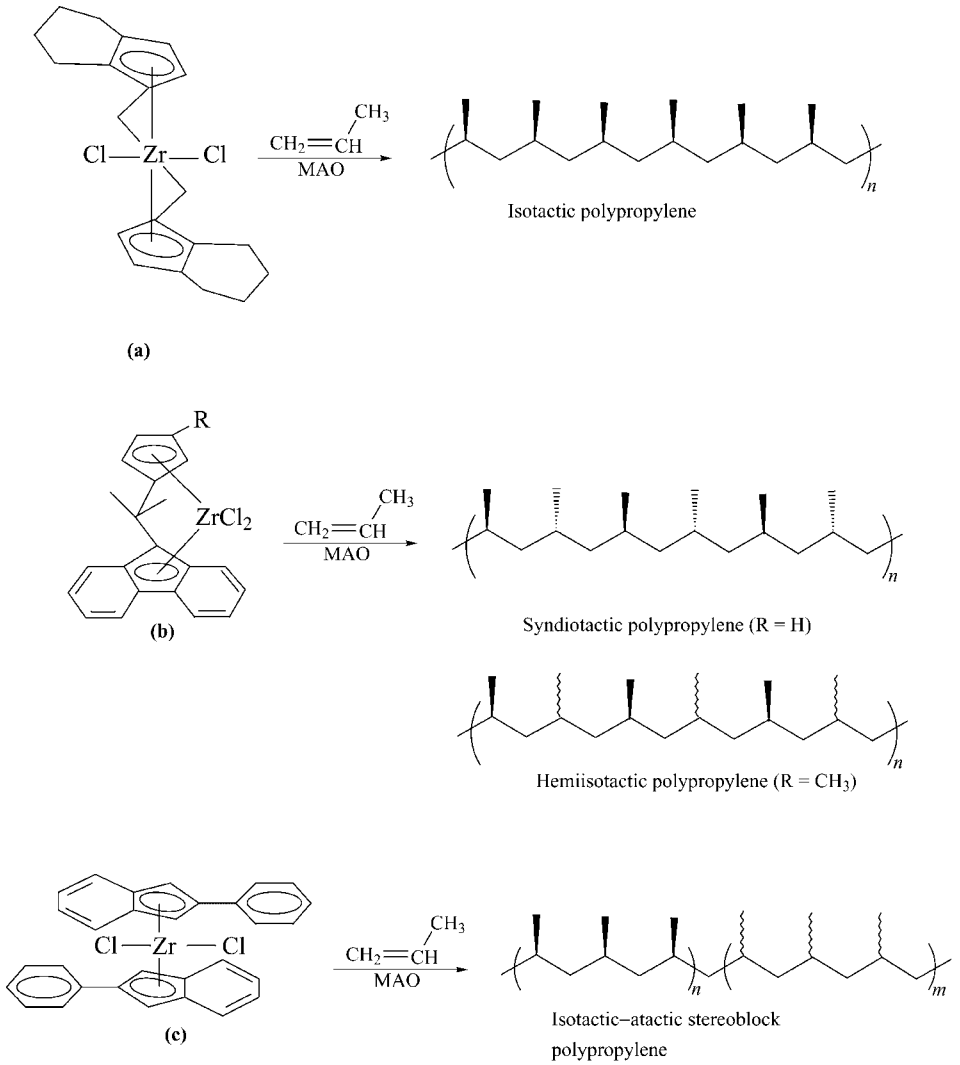

Fig. 2. Key metallocene catalysts for olefin polymerization: (**a**) *rac*-$C_2H_4(IndH_4)_2ZrCl_2$ (56–60); (**b**) $(CH_3)_2C(3\text{-R-Cp})(Flu)ZrCl_2$ (R = H, CH_3) (61,62); (**c**) $(2\text{-}C_6H_5\text{-Ind})_2ZrCl_2$ (63).

$[(CH_3)_2C(3\text{-}CH_3Cp)(Flu)]ZrCl_2$ for hemiisospecific propylene polymerization (62). In 1995, Coates and Waymouth described an unbridged bis(2-phenylindenyl) zirconocene producing elastomeric isotactic–atactic stereoblock PP (63), presumably by oscillating stereocontrol in which the catalyst switches between isospecific and aspecific conformations during the growth of a single polymer chain.

In these pseudotetrahedral bis(cyclopentadienyl) metallocenes the d^0 central transition metal (Ti, Zr, or Hf) is bound to two η^5-cyclopentadienyl-type ring ligands and two σ-ligands (usually Cl or CH_3), one or both of which are removed upon formation of the active catalyst. The most commonly employed cyclopentadienyl ligands are based on plain or substituted cyclopentadienyl (Cp), indenyl (Ind), tetrahydroindenyl ($IndH_4$), and fluorenyl (Flu) anions. Because of the high structural diversity of the available ligand structures, the steric and electronic environment of the active site can be modified by variation of the ligand size, shape, and substitution pattern (for representative examples of structural variations, see Refs. 13, 33, and 58–93). The function of the interannular *ansa*-bridging group is to lock the ancillary ligand in the desired conformation or symmetry, thus allowing steric control over the enantiodifferentiating steps in stereoselective olefin polymerization or differentiation of olefins of different sizes in copolymerization reactions.

The most notable examples of monocyclopentadienyl-based catalyst precursors are the "constrained geometry" *ansa*-monoCp-amido Group 4 complexes (25,94–105) (Fig. 3) developed by Dow Chemical Co. (106) and Exxon Chemical Co. (107) (for further references to the patent literature, see Ref. 25). The original ligand design was introduced for organoscandium complexes (108). A remarkable feature of these catalysts is the open nature of the active site which allows the incorporation of higher α-olefins, including styrene, in copolymerization with ethylene. Incorporation of vinyl-terminated macromonomers results in the formation of long-chain branched ultralow-density polyethylenes possessing unique rheological properties. The titanium-based constrained geometry catalysts (CGCs) are generally preferred over their zirconium and hafnium analogues showing higher activities and producing polymers with higher molecular weights. Several structural modifications of the CGCs including monoCp-alkoxide analogues have been described (109–111).

Monocyclopentadienyl and (monoindenyl)titanium trichlorides are generating interest as catalyst precursors for syndiospecific polymerization of styrene (112–127). A class of highly active olefin polymerization catalysts based on a (monocyclopentadienyl)titanium dimethyl cation $[CpTi(CH_3)_2]^+$, generated by

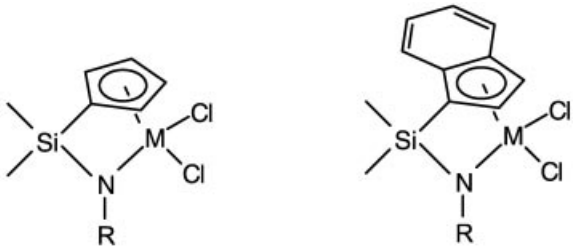

Fig. 3. Prototypical Group 4 constrained geometry catalysts (CGC). M = Ti, Zr; R = alkyl, aryl; Cp = cyclopentadienyl, tetramethylcyclopentadienyl.

methyl abstraction from $CpTi(CH_3)_3$ or $Cp*Ti(CH_3)_3$ (Cp* = pentamethylcyclopentadienyl), has been described (127–132).

Alternative Early Transition Metal Catalysts. Bis(cyclopentadienyl) Group 3 and lanthanide complexes of the type L_2MR (L = bridged or unbridged Cp or related ligands; M = Sc, Y, La, Nd, Sm, Lu; R = H, alkyl) have received interest, mainly in mechanistic studies, as single-component olefin polymerization catalysts (133–141). Other examples of potential early transition metal nonmetallocene SSC precursors (26) include the aminoborole (142), boratabenzene (143–147), diamido (148–164), and chelating alkoxide complexes (165–168) of the Group 4 metals (Fig. 4).

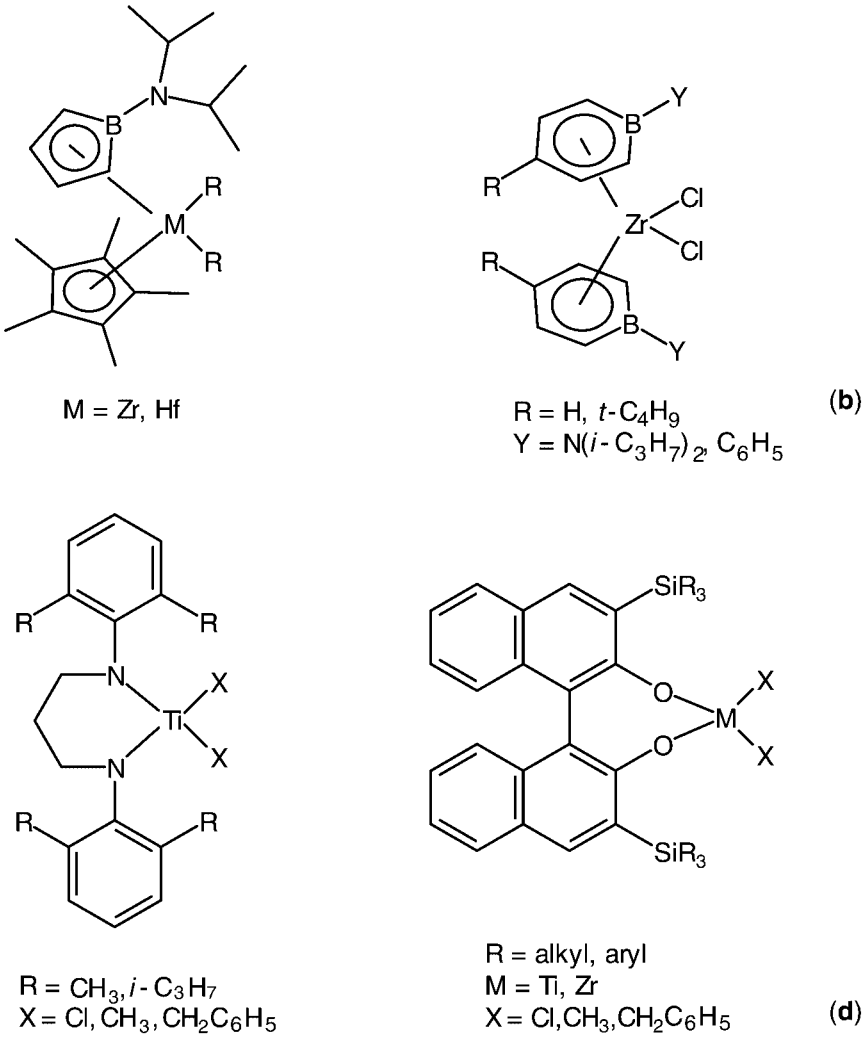

Fig. 4. Examples of potential nonmetallocene early transition metal SSC precursors: (**a**) aminoborole; (**b**) boratabenzene; (**c**) diamido; and (**d**) chelating alkoxide Group 4 metal complexes.

Group 5 metal catalysts based on various cyclopentadienyl and dianionic mixed ligand and related complexes of tantalum (169,170), niobium (171,172), and vanadium (173,174) have also been described.

Late Transition Metal Catalysts. In contrast to early transition metal catalysts, late metal systems most often dimerize or oligomerize olefins due to competing β-hydride elimination (175,176). For example, soluble Ni(II)-based ethylene oligomerization catalysts form the basis for the Shell Higher Olefin Process (SHOP) (177,178). In 1995, a series of highly electrophilic nickel(II) and palladium(II) complexes were reported (179–182). These complexes incorporate bulky diimine ligands (Fig. 5), which upon activation with MAO polymerize ethylene and α-olefins with high activities comparable to those of metallocene catalysts. In these complexes, the presence of equatorial sterically demanding aryl substituents effectively blocks the associative olefin exchange, retarding the chain transfer and resulting in high molecular weight polymers. Copolymerization of ethylene and propylene with functionalized vinyl monomers was reported shortly after the initial findings (193,194). The first reports stimulated an extensive search for other late transition metal olefin polymerization catalysts. Subsequent studies on these and related nickel and palladium systems using neutral or anionic chelating N—N, N—O, and N—P ligands have been described by several academic and industrial groups (for reviews and references to the patent literature, see Refs. 26, 195, and 196).

During 1997 and 1998, highly active iron(II)- and cobalt(II)-based ethylene polymerization catalysts bearing 2,6-bis(imino)pyridyl ligands (Fig. 5) were described independently by Brookhart (183,184), and Gibson (187,188), as well as by DuPont (185,186). Oligomerization of ethylene to linear α-olefins (189) as well

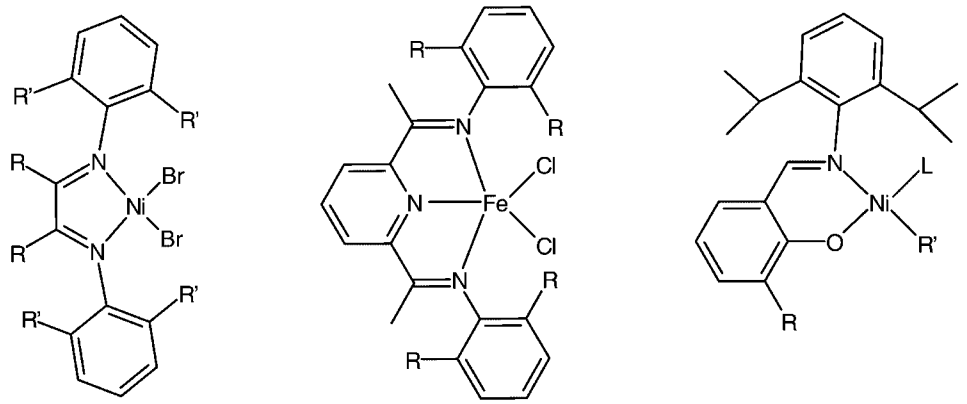

Fig. 5. Late transition metal SSC precursors based on (**a**) diimine (179–182), (**b**) 2,6-bis(imino)pyridyl (183–190), and (**c**) salicylaldimine (191,192) ligands.

as polymerization of propylene (190), using the iron-based catalysts, was reported in subsequent papers.

A family of neutral single-component salicylaldimine nickel(II) catalysts (Fig. 5) that produce high molecular weight PE, polymerize functionalized olefins, and require no cocatalyst have been reported (191,192). These catalysts can be regarded as an extension of the original SHOP oligomerization systems where the P—O chelate of the neutral SHOP catalyst has been replaced with a sterically demanding N—O ligand leading to high molecular weight products.

Catalyst Generation

Active Species and Function of the Cocatalyst. The active species in olefin polymerization is, in most cases, a coordinatively unsaturated cationic metal alkyl $[L_nMR]^+$ (197). Activity and stereoregularity of the produced polymer are determined by the steric and electronic properties of the ancillary ligand set L_n and the ion–ion interactions between the highly electrophilic metal cation and its counterion. Several methods exist for generating the active catalyst (for a review on cocatalysts for metal-catalyzed olefin polymerization, see Ref. 198). MAO is by far the most common cocatalyst (28), including large-scale industrial production. The exact composition, structure, and function of the aluminoxane cocatalysts are still a matter of controversy (199–202); controlled hydrolysis of $Al(CH_3)_3$ produces a complex mixture of cyclic and linear oligomeric MAOs, possibly containing cluster-like or supramolecular aggregates with the general formula $(CH_3AlO)_n$ (Fig. 6). The degree of oligomerization varies from 5 to 20.

In the case of Group 4 metallocene dihalide catalyst precursors L_2MX_2 (eq. 1), addition of MAO generates first a monomethyl complex L_2MXCH_3 (203,204). Excess MAO gives the dialkylated species $L_2M(CH_3)_2$. Presumably, some of the Al centers in MAO have a high propensity to abstract a methyl anion from $L_2M(CH_3)_2$ forming a weakly coordinating anion $[CH_3—MAO]^-$. The metallocene cation $[L_2MCH_3]^+$ is stabilized coordinatively by the $[CH_3—MAO]^-$ counterion, which in the presence of olefins gives way to olefin-separated ion pairs $[L_2M(olefin)CH_3]^+[CH_3—MAO]^-$. Repeated olefin insertion to the metal–alkyl bond forms the polyolefin.

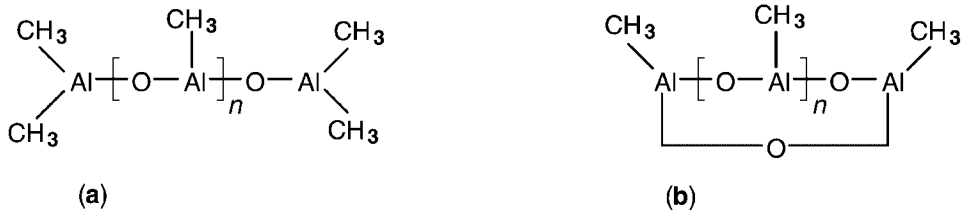

Fig. 6. Generalized structures of MAO: linear (**a**), and cyclic (**b**).

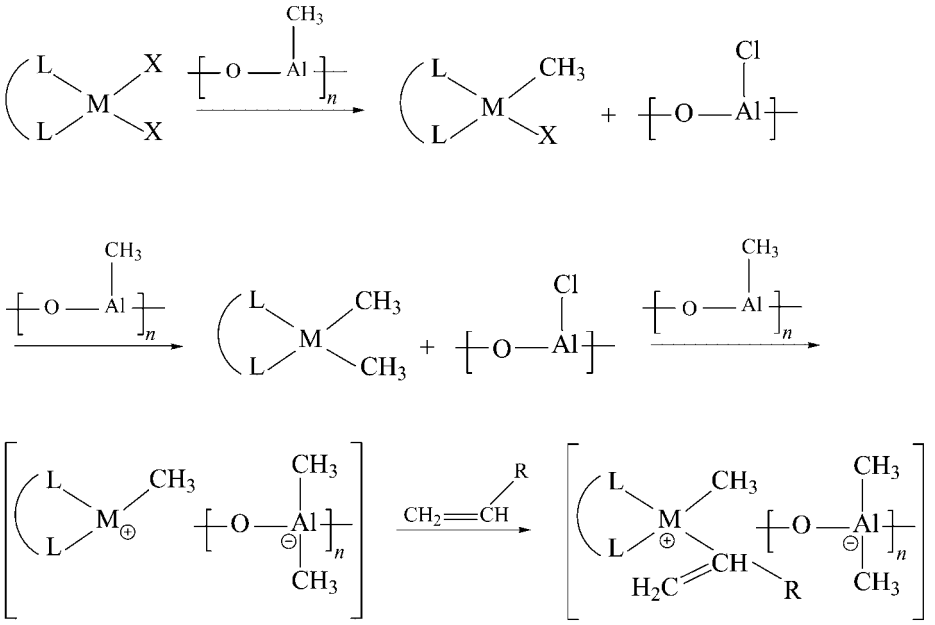

(1)

A large excess of MAO is usually required to achieve high polymerization activities. For Group 4 metallocene/MAO catalyst systems, activity maxima are generally found at [Al]:[M] ratios ranging from 1000:1 to 10,000:1. The excess MAO is possibly required to shift the equilibrium involving the metal monoalkyl and MAO to the cationic active species. In addition, MAO has been found to reactivate inactive complexes formed by hydrogen tranfer reactions and to prevent the deactivation of the catalyst by bimolecular processes. Aluminoxanes also scavenge impurities such as water and oxygen from the reaction medium.

Intensive work has been carried out to develop stoichiometric activators for metallocene and other SSCs (17,198). Early systems based on tetraphenylborate or other carborane anions exhibited only low polymerization activities as a result of the strong interaction of the cationic metal center with the counterion (197,205–213). The introduction of perfluorinated tetraphenylborate $[(C_6F_5)_4B]^-$ (214,215) produced exceedingly active cationic metallocene catalysts for polymerization of α-olefins. The application of $[(C_6F_5)_4B]^-$, $[(C_6F_5)_3BCH_3]^-$, and related fluoroarylborate counterions in various homo- and copolymerization reactions has been studied in detail (62,216–237). Methods for generating the cationic metal complex include mixing of metal dialkyl with dimethylanilinium tetrakis(perfluorophenyl)borate $[NH(CH_3)_2C_6H_5]^+[(C_6F_5)_4B]^-$, alkyl anion transfer with trityl tetrakis(perfluorophenyl)borate $[(C_6H_5)_3C]^+[(C_6F_5)_4B]^-$, and methyl abstraction from the metal dialkyl complex with $(C_6F_5)_3B$. Other base-free or weakly stabilized metal alkyl cations, including metallocene–borate–betaine complexes (238–242), other zwitterionic catalyst systems (230,243–247), and Al-, Nb-, and Ta-based perfluoroaryloxide anions (248) have been developed.

Polymerization Mechanism. The basic mechanistic steps of olefin coordination to the metal center and the subsequent insertion into the metal–carbon bond are not entirely understood. Several plausible hypotheses have been

suggested (249–257), most notably the Cossee-Arlman model based on *cis*-insertion of an α-olefin into the metal–carbon bond (eq. 2) (249–252). Both kinetic isotope studies and molecular modeling suggest that the transition state of the insertion step is stabilized by agostic interactions between the metal center and an α-hydrogen atom of the growing chain (for a review, see Ref. 20). The agostic interaction apparently increases the rigidity of the transition state resulting in an increase in the rate of olefin insertion and, in the case of chiral catalysts, an increase in stereospecificity.

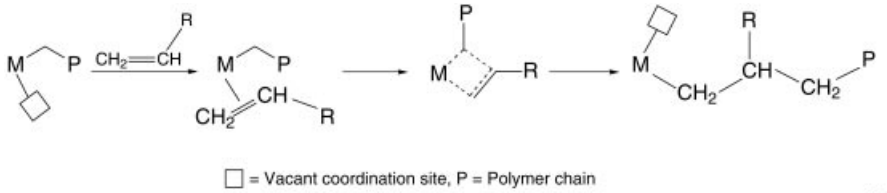

(2)

The molecular weight of the produced polymer is determined by the relative rates of monomer insertion and chain termination (Fig. 7) (for a review on chain transfer processes in propylene polymerization, see Ref. 258). The dominant chain termination process in olefin polymerization involves an intramolecular β-H elimination (259,260) producing a vinylidene-terminated polymer chain and a metal hydride. Termination by β-elimination may occur either by direct hydrogen transfer from the polymer chain to the metal center, or by transfer of a β-H from the polymer chain to a carbon atom of a coordinated olefin (261). The rate of the latter process increases with olefin concentration in parallel with increased rate of propagation, whereas the rate of the former is olefin-independent. Intramolecular β-alkyl elimination (261–263) produces a metal–alkyl and an allyl-terminated chain end. Reinsertion of terminally unsaturated polymer chains results in long-chain branching. Saturated chain ends are obtained in the presence of chain-transfer agents, such as H_2 or aluminum alkyls (eg, complexed MAO). Hydrogen functions as an effective means to control the molecular weight of polyolefins (264,265),

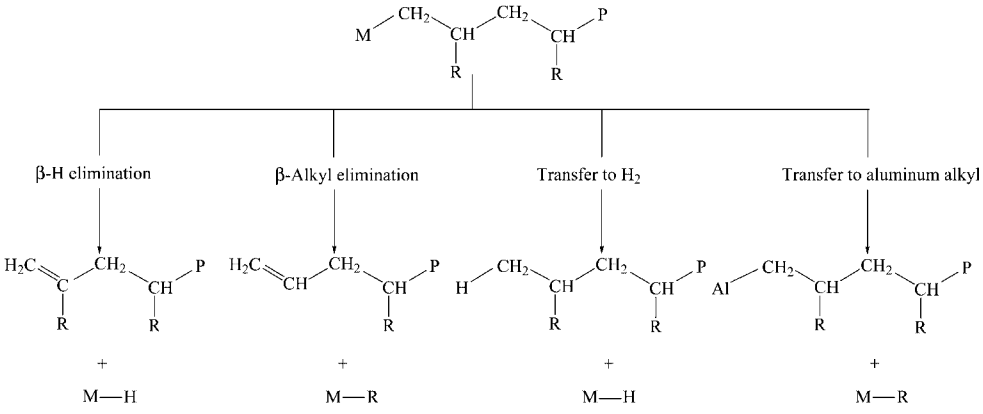

Fig. 7. Chain termination processes in olefin polymerization.

producing an alkyl-terminated chain end and a metal hydride. Transalkylation to the aluminum cocatalyst results in a metal–alkyl and an aluminum-terminated polymer chain, which for PP generates isopropyl end groups after hydrolysis of the carbon–aluminum bond (266–271). The barrier to exchange of alkyl groups between the transition metal and aluminum compounds decreases with increasing electron density at the metal center (267,271).

Mechanisms of Stereocontrol. Stereochemistry of the olefin insertion step can be controlled by both the steric environment of the active site (enantiomorphic-site control) as well as the growing polymer chain (chain end control). In chain end stereocontrol, stereospecificity arises from the chiral β-carbon atom of the last enchained monomer unit, which in turn influences the stereochemistry of monomer addition. Chain-end control is usually less effective than site control and has been observed for some achiral metallocenes at low polymerization temperatures. Partially iPP resulting from chain end stereocontrol has been obtained with Cp_2TiPh_2/MAO (56,272). The syndiospecific polymerization of 1-butene using the $Cp*_2MCl_2$/MAO (M = Zr, Hf) catalyst systems has been described (273). Predominantly sPP has been obtained under chain end control, using Brookhart's diimine nickel catalysts (274–277).

Stereoselectivity of C_2 symmetric Group 4 *ansa*-metallocenes in isospecific propylene polymerization results from an enantiomorphic-site control mechanism. Chain propagation proceeds prevailingly via 1,2 (primary) monomer insertion. Both coordination sites of the C_2 symmetric catalyst are homotopic and thus selective for the same olefin enantioface. Repulsive interactions force the coordinated propylene monomer into that enantiofacial approach to the metal–alkyl unit which has the methyl substituent of the monomer *trans* to the β-C atom of the growing polymer chain (Fig. 8). To avoid repulsive interaction with the ligand, the growing chain preferably obtains a conformation where the first C—C bond is directed toward the most open sector of the ligand framework. Repeated chain migratory insertion with the same olefin enantioface generates an isotactic polymer chain.

Experimental proof for the presented mechanism has been obtained by propylene oligomerization studies with enantiomerically pure *ansa*-metallocene catalysts (259,264,278,279). The participation of α-agostic interactions in the insertion process by polymerization of α-deuterated olefins has been demonstrated (280,281). Agostic interactions control the stabilities of the alternative transition states for propylene insertion. Of the two possible orientations of the polymer chain involving a three-membered Zr—H(α)—C(α) ring, one is sterically hindered by collision of the growing chain with a β-substituent of the chiral ligand. The other one is essentially unencumbered placing the β-C in the open position of the ligand framework. The stereochemistry of the propylene insertion step has been studied using a *s-cis*-η^4-butadiene complex derived from a C_2 symmetric bis(indenyl) *ansa*-zirconocene *rac*-$(CH_3)_2Si(Ind)_2ZrCl_2$ (242).

Syndiospecific propylene polymerization with C_s symmetric *ansa*-metallocene catalysts proceeds in an analogous fashion (Fig. 8). The growing polymer chain is directed away from the bulkier cyclopentadienyl ligand, and the favored propylene enantioface places the methyl substituent *trans* to the growing chain. Migratory insertions result in regular alternation of the monomer approach from the left and right side of the metallocene wedge, consequently producing the syndiotactic polymer (61,76).

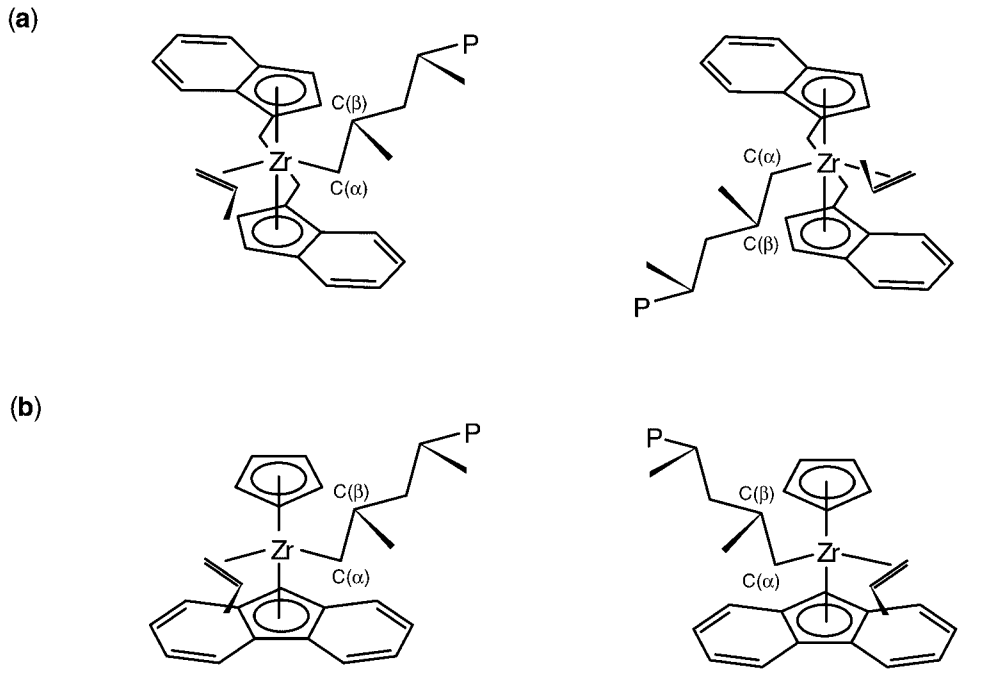

Fig. 8. Enantioselective coordination of propylene to the coordination sites of a C_2 symmetric isospecific metallocene catalyst (**a**) (only one enantiomer of the racemic pair is shown), and a C_s symmetric syndiospecific metallocene catalyst (**b**) [$(CH_3)_2C$ bridge omitted for clarity].

Theoretical Studies

Numerous theoretical studies on both early and late transition metal SSCs have appeared in recent years covering nearly all aspects of the olefin polymerization process (for reviews, see Refs. 282 and 283). The employed methodologies include molecular mechanics (284–291), ab initio electronic structure methods (292–297), density functional studies (298–303), as well as various hybrid techniques (304–308), such as the combination of quantum and molecular mechanics (QM/MM). A detailed description of these studies is outside the scope of this article; nevertheless, these theoretical investigations have played a major role in elucidating the elementary steps of olefin complexation, chain propagation, and chain termination as well as the mechanisms of stereocontrol in catalytic olefin polymerization.

Polymerization of Ethylene

The properties of polyethylene are strongly influenced by its molecular weight, molecular weight distribution, and branching content. Three major classes of polyethylene are commercially available. Conventional low density polyethylene (LDPE) is produced at high polymerization temperatures and pressures. As a

consequence of the radical polymerization mechanism, LDPE contains both short- and long-chain branching. Heterogeneous Ziegler–Natta catalysts polymerize ethylene to highly linear high density polyethylene (HDPE) characterized by excellent strength but poor melt processability. Linear low density polyethylene (LLDPE) is traditionally obtained by controlled incorporation of higher α-olefins such as 1-hexene or 1-octene into polyethylene, using Ziegler–Natta or chromium catalysts (see ETHYLENE POLYMERS, LLDPE).

In contrast to multisite heterogeneous Ziegler–Natta systems, metallocenes and other SSCs allow a precise control of the polymerization reaction resulting in narrow distribution of all molecular characteristics, including molecular weight distribution, comonomer distribution and architecture, and content of branches.

Homopolymers. Both unbridged and stereorigid (bridged) metallocenes have been employed in polymerization of ethylene. Cp_2ZrCl_2/MAO homopolymerizes ethylene with 10–100 times higher activity compared to conventional Ziegler–Natta catalysts. The insertion rate is comparable to reaction rates observed in enzymatic systems, and polymerization activities reaching 40,000 kg PE/g Zr/h have been reported for this catalyst system alone (18,22,55). Essentially linear homopolyethylenes (HDPE) are obtained in most cases using bis(cyclopentadienyl), bis(indenyl), and related metallocene catalysts. The choice of metal and ligand substitution pattern highly influences the polymerization performance. Activity generally decreases in the order of Zr > Ti > Hf. Increasing electron-donating ability of the ligand substituents appears to increase the activity in the cyclopentadienyl series whereas steric crowding has a detrimental effect. Consequently $(CpCH_3)_2ZrCl_2$ is more active than $(CpC_2H_5)_2ZrCl_2$ or $Cp*_2ZrCl_2$ (266). Substituted bis(indenyl) (71) and bis(fluorenyl) (90,309) *ansa*-metallocenes display, in some cases, very high activities exceeding those of Cp_2ZrCl_2. Molecular weight can be controlled by addition of hydrogen or by increasing the polymerization temperature. Hafnium complexes produce higher molecular weight polymers than their zirconium analogues. The stronger Hf–carbon σ-bond slows down both bond-making and bond-breaking processes resulting in a lower activity and higher molecular weight.

The nickel and palladium diimine catalysts developed by Brookhart (Fig. 5a) display some unique properties; for example, they can produce highly branched polymers from a single ethylene feedstock. Polymers derived from the nickel catalysts are generally less branched than those obtained with their palladium analogues, and products ranging from conventional LLDPE to amorphous, elastomeric, or hyperbranched materials can be obtained by variation of the metal, monomer concentration, polymerization temperature, and pressure. The branch formation is explained by a *chain walking mechanism* (179,185,186,310), where the growing polymer chain undergoes a series of β-hydride eliminations and reinsertions resulting in migration of the metal species along the polymer backbone.

Activities of the MAO-activated nickel catalysts are comparable to those of metallocenes, and turnover frequencies of 3.9×10^5 h^{-1} corresponding to 11,000 kg PE/mol Ni/h were reported in the initial publications (179). Molecular weights can be varied from oligomers to high polymers (M_w = 30,000 to > 1,000,000) depending on the catalyst structure and polymerization conditions (185). The palladium analogues display more moderate activities, but due to the extensive "chain walking" the range of accessible materials is broadened

considerably. DuPont is currently developing its Versipol™ (E.I. du Pont de Nemours & Co., Inc.) catalyst technology based on the Brookhart-type late transition metal catalyst systems (186).

The 2,6-bis(imino)pyridyl iron catalysts (Fig. 5b) show likewise extremely high activities in homopolymerization of ethylene. Upon activation with modified MAO, turnover frequencies of greater than 10^7 h^{-1} corresponding to 330,000 kg PE/mol Fe/h have been reported (187). The highest molecular weights (M_w) exceed 500,000 (192). The recently discovered single-component nickel catalysts (Fig. 5c) can produce homopolyethylenes with $M_w > 250{,}000$ and turnover frequencies ranging from 0.5×10^6 to 3.0×10^6 g PE/mol Ni/h at low temperatures and pressures (196). The total content of methyl, ethyl, propyl, and butyl branches remains under 10 branches per 1000 carbon units under optimal polymerization conditions. At slightly elevated polymerization temperatures, activities comparable to those of the first metallocenes and Brookhart's diimino nickel catalysts were observed.

Copolymers with Propylene and Higher α-Olefins. Group 4 metallocene catalyzed copolymerization of ethylene with higher α-olefins such as 1-butene, 1-pentene, 1-hexene, or 1-octene produces well-defined copolymers with random distribution of the comonomer (311–322). The copolymerization rates are often higher than those of the corresponding homopolymerizations. Chiral C_2 symmetric *ansa*-metallocenes incorporate higher α-olefins more readily than the unbridged complexes. Syndiospecific C_s symmetric metallocene catalysts show even better copolymerization characteristics. Alternating copolymers of ethylene and 1-octene have been obtained with some *meso*-diastereomers of bridged bis(indenyl) catalysts (323). Among the various polyolefins produced using SSC technology the LLDPE-grades show perhaps the greatest industrial potential.

Copolymers of ethylene and propylene show, in some cases, elastic properties (324,325). Further incorporation of dienes, such as ethylidenenorbornene or 1,4-hexadiene, produces ethylene–propylene–diene monomer (EPDM) elastomers. Kaminsky (326) and Waymouth (327) have reported the predominantly alternating copolymerization of ethylene and propylene, using C_1 and C_s symmetric (cyclopentadienyl)(fluorenyl) *ansa*-zirconocene-based catalysts (eq. 3), demonstrating yet another example of preparation of new materials through rational exploitation of SSC systems.

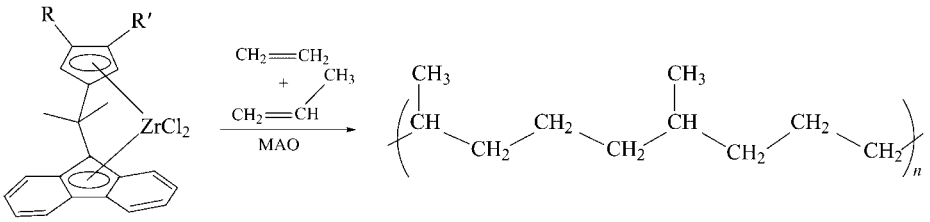

R = H; R′ = CH_3;
R = H; R′ = i-C_3H_7;
R = H; R′ = t-C_4H_9;
R = R′ = CH_3.

(3)

Long-Chain Branching. The constrained geometry Group 4 catalysts of the Dow and Exxon chemical companies allow the incorporation of, besides C_4–C_{20} α-olefins, even styrene (99,328), isobutylene (329), and vinyl-terminated macromonomers into HDPE or LLDPE polyethylene chains (see Ref. 25 and references to the patent literature therein). At high polymerization temperatures (typically $T_p = 130$–$160^\circ C$) these catalysts produce controlled amounts of vinyl-terminated polymers or oligomers that are reinserted to the growing polymer chain. Typical levels of long-chain branching (LCB) range from 1 to 3 branches per 1000 carbon atoms. The resulting materials exhibit some unique properties since the presence of LCB significantly affects the melt viscosity, elasticity, shear thinning, and extension thickening of the produced polymer, thus improving its processability. Typically, the LCB-PEs exhibit the strength and toughness of LLDPE while having the melt processability of LDPE (25). Formation of very low levels of long-chain branched material has been reported also for ethylene bridged bis(indenyl) *ansa*-zirconocene/MAO catalyst systems (330–332).

Polymerization of Propylene

Stereoselective polymerization of α-olefins, especially propylene, has received an enormous amount of attention in recent years (see PROPYLENE POLYMERS (PP)). Group 4 metallocene-based SSCs allow the production of PP in a considerably wider range of composition and microstructures than any other catalytic system (Fig. 9) (for reviews, see Refs. 14, 333, and 334). The physical properties of polyolefins are strongly influenced by their microstructures. Highly stereoregular iPPs and sPPs are crystalline thermoplastics whereas stereorandom atactic polypropylene (aPP) is an amorphous elastomer. The most efficient tool for determining the microstructure and stereoregularity of poly-α-olefins is ^{13}C nmr spectroscopy. Tacticity of the polymer is commonly expressed in terms of its pentad content, which is the fraction of stereosequences containing five adjacent stereocenters. An isotactic [*mmmm*] pentad consists of a sequence of five identical stereocenters, whereas in the syndiotactic [*rrrr*] pentad the configuration of the stereocenters is regularly alternating. The [*mmmm*] pentad content of highly iPP approaches 100% whereas perfectly atactic polymers consist of a statistical mixture of all 10 possible pentads.

Because of the steric constraints of the metallocene catalysts, propylene insertion mainly proceeds in a regioregular fashion (1,2-insertion), although occasional 2,1-regioinversions are observed. The amount of regioerrors depends on the structure of the catalyst and affects the crystallinity and melting point of the produced polymer (14,84,85,334). Insertion of propylene into a growing chain with a 2,1 last-inserted unit is usually exceedingly slow because of the highly unfavorable nonbonded interactions, and the chain end may isomerize to a more reactive 3,1-unit, which would then be followed by a regioregular primary insertion.

Isolated stereoerrors result from regioregular 1,2-insertions of the wrong olefin enantioface. Alternatively, a regioregular last-inserted monomer unit may undergo an epimerization reaction producing an inversion of configuration. Recent studies (280,281,335–342) suggest that the major part of stereoerrors in iPPs in fact results from the chain end epimerization reaction, rather than from regioirregular 2,1-insertions or regioregular insertions with the incorrect enantioface.

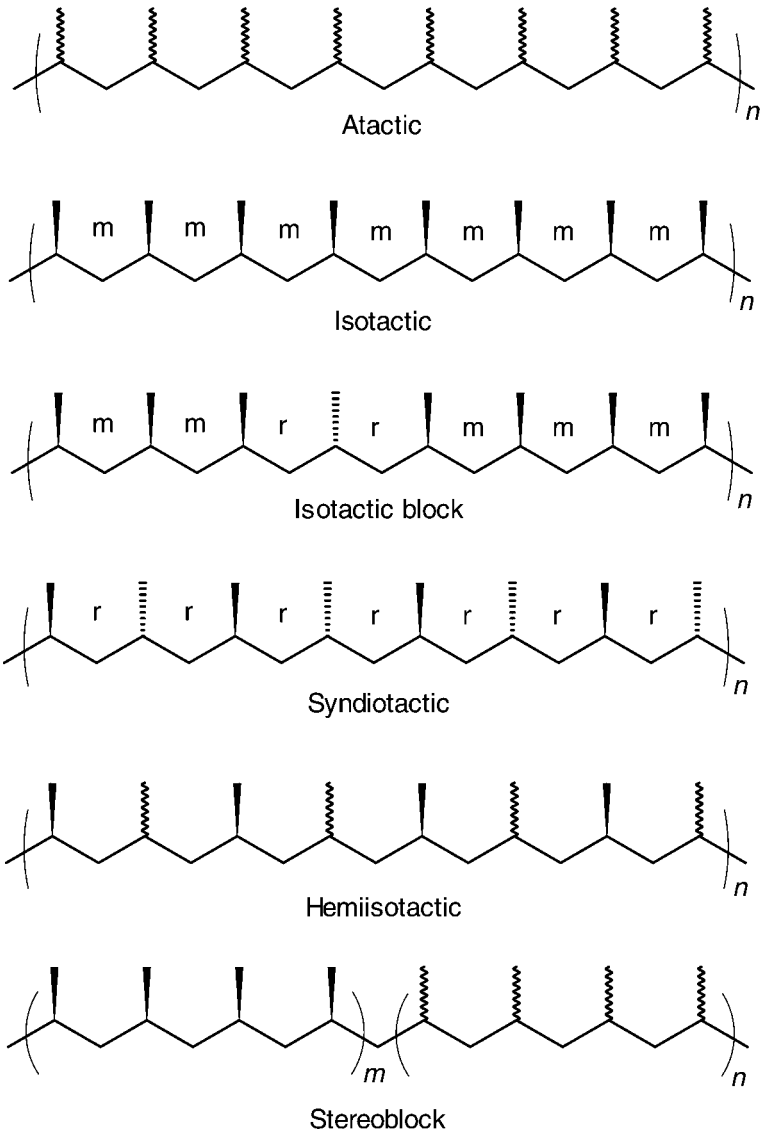

Fig. 9. PP microstructures.

Homopolymers.

Atactic Polypropylene. Low molecular weight aPP waxes can be obtained from solvent extraction of iPP prepared with heterogeneous Ziegler–Natta catalysts. The product is neither completely atactic nor fully amorphous, and finds limited use as an additive in bitumen and adhesives (22). Achiral and unbridged metallocene catalysts such as Cp_2ZrCl_2 also produce mainly low molecular weight aPP, although at low temperatures partially isotactic material has been obtained by chain end control mechanism (56). High molecular weight, fully atactic

elastomeric aPP has been obtained using a C_{2v} symmetric bis(fluorenyl) *ansa*-zirconocene catalyst $(CH_3)_2Si(Flu)_2ZrX_2$/MAO (X = Cl, CH_3) under technical production conditions (83,343). Molecular weights (M_w) ranging from 100,000 to 400,000 and polymerization activities corresponding to 1300–11,200 kg PP/mol Zr/h were obtained at $T_p = 50°C$ at variable monomer concentrations. The low densities, high transparency, softness, low modulus, and high elongation of these polymers result from the totally amorphous state of the polymer chains (22).

Isotactic Polypropylene. IPP is generally obtained with C_2 symmetric *ansa*-metallocene catalysts. In most cases, bridged bis(indenyl)- or bis(tetrahydroindenyl)-derived Group 4 complexes are used (56,57,62,65–71, 84,85,87,344,345), with a few exceptions based on C_2 symmetric substituted bis(cyclopentadienyl) analogues (346,347) and some sterically congested C_1 symmetric catalysts (72,73,78,348–354). A series of unbridged asymmetrically substituted bis(indenyl) and bis(tetrahydroindenyl) zirconocenes that produce partially iPP under enantiomorphic site control at low polymerization temperatures has been described (355–357). In these catalysts, the isospecific conformational isomer is stabilized by partially hindered ligand rotation. An unbridged bis(1-methylfluorenyl)zirconium dichloride/MAO catalyst system reportedly produces iPP even at elevated polymerization temperatures (78,358). Chiral disposal of the substituted fluorenyl ligands results from a strongly hindered rotation around the Zr—C_5 axis. Several other bridged or unbridged metallocene catalysts lacking C_2 symmetry have been employed in propylene polymerization producing PPs with variable microstructures ranging from nearly atactic to partially isotactic materials (63,64,88,89,93,359–379). Remarkable examples are the elastomeric PPs (*vide infra*) obtained with C_1 symmetric *ansa*-metallocenes (89,366–373) and the isotactic–atactic stereoblock elastomeric PPs (63,64,374–379).

The original Brintzinger-type catalyst systems based on *rac*-$C_2H_4(IndH_4)_2TiCl_2$ and its zirconocene analogue exhibit reasonably high activities in propylene polymerization; however, the molecular weights, melting points, and isotacticities of the produced iPPs are by far inferior to those of heterogeneous Ziegler–Natta catalysts when employed under technical conditions. For example, bulk polymerization of propylene at 70°C using *rac*-$C_2H_4(IndH_4)_2ZrCl_2$/MAO produces iPP with M_w = 15,000 and $T_m = 125°C$ (344), whereas commercial Ziegler–Natta grades of iPP have molecular weights between 100,000 and 500,000 and melting points ranging from 160 to 165°C. Rational structural modifications (68–71,344) of the original catalysts culminated in the 1994 publications of the Hoechst group (71) and Brintzinger (65) describing true high performance metallocene catalysts for isospecific propylene polymerization (Fig. 10). The 2,2′-dialkyl-4,4′-diaryl-substituted dimethylsilylene bridged bis(indenyl) *ansa*-zirconocene catalysts polymerize propylene to highly iPP with stereoselectivities, polymer melting points, and molecular weights comparable to those obtained with heterogeneous Ziegler–Natta catalysts (Table 1) (65,67,71,344,380–382). These metallocene-based catalysts are over 40 times more active than the conventional systems. Hydrogen gas has to be applied as a molecular weight regulator, even under technical polymerization conditions, in order to produce commercial iPP grades.

The 2,2′-alkyl substitution at the C_5 rings of the bis(indenyl) *ansa*-zirconocene catalysts dramatically improves the molecular weight of the produced

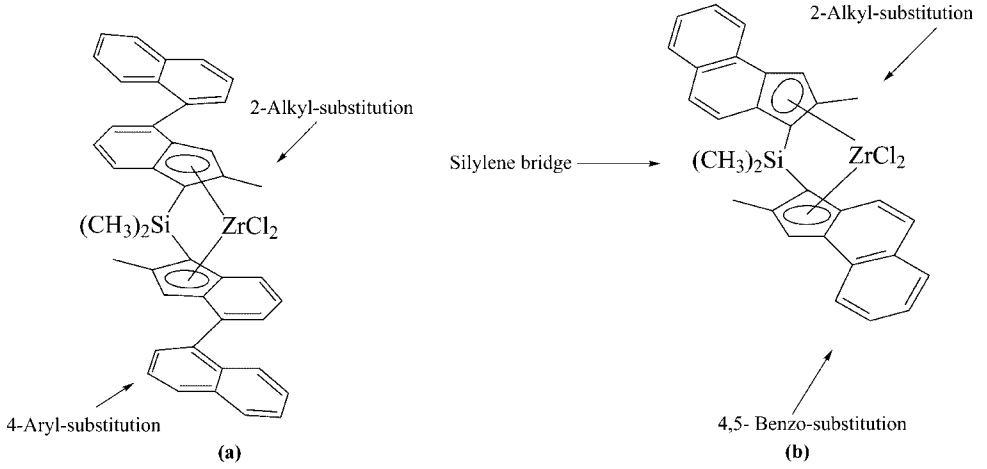

Fig. 10. High performance metallocene catalysts for isospecific polymerization of propylene. (**a**) Hoechst group (71); (**b**) Brintzinge (65).

PP (65,67,70,71,344). The observed enhancement has been explained by a combination of steric and electronic influence on the chain-termination reaction. Enhanced rigidity of the ligand framework combined with a direct steric interaction of the alkyl group with the growing polymer chain decreases the rate of β-elimination. Electron donation from the alkyl substituent may further decrease the local Lewis acidity of the central metal atom, thus reducing its tendency for β-H abstraction.

The role of the substituents in β-position to the interannular bridge, ie, 4,4′-positions of the six-membered rings of the indenyls, appears to be twofold. The gain in stereospecificity by enlarging the 4,4′-substituents from isopropyl to naphthyl, as shown in Table 1, results from indirect steric control (71). The high rotational barrier of the naphthyl substituent places it in an optimal position for interaction with the growing chain. The synergistic effect of 2-alkyl-4-aryl substitution further

Table 1. Propylene Polymerization Performances of Various Bis(indenyl) *ansa*-zirconocene/MAO Catalyst Systems[a,b]

Metallocene/catalyst	*A*, kg PP/mmol M/h	M_w	[*mmmm*] Pentad, %	T_m, °C
rac-$C_2H_4(Ind)_2ZrCl_2$	188	24,000	78.5	132
rac-$(CH_3)_2Si(Ind)_2ZrCl_2$	190	36,000	81.7	137
rac-$(CH_3)_2Si(2\text{-}CH_3\text{-}Ind)_2ZrCl_2$	99	195,000	88.5	145
rac-$(CH_3)_2Si(2\text{-}CH_3\text{-}4\text{-}i\text{-}C_3H_7\text{-}Ind)_2ZrCl_2$	250	210,000	88.6	150
rac-$(CH_3)_2Si(2\text{-}CH_3\text{-Benz}[e]Ind)_2ZrCl_2$	400	330,000	88.7	146
rac-$(CH_3)_2Si(2\text{-}CH_3\text{-}4\text{-}C_6H_5\text{-}Ind)_2ZrCl_2$	550	730,000	95.1	157
rac-$(CH_3)_2Si(2\text{-}CH_3\text{-}4\text{-Naph-}Ind)_2ZrCl_2$	880	920,000	99.1	161
$Ti/MgCl_2$/ED	20	900,000	99	162

[a] A Conventional heterogeneous Ziegler–Natta catalyst ($Ti/MgCl_2$/electron donor) is included for comparison.

[b] Technical reaction conditions (T_p = 70°C; liquid propylene; [Al]:[Zr] = 15,000:1) (Refs. 68–71 and 344).

improves the catalyst rigidity and enhances the stereospecificity. Secondly, electron donation from the aryl or alkyl substituents may stabilize the cationic active species or facilitate its formation (65,67,71). The resulting increase in polymerization activity also influences the polymer molecular weight by increasing the ratio of the rates of chain propagation vs. chain termination. Even higher polymerization activities have been reported by using the 2,2-di-*n*-propyl-4,4-di-9-phenanthryl substitution pattern (382).

The structure of the interannular bridge mainly influences the stereospecificity and polymerization activity of the bis(indenyl) catalysts. Replacement of the ethylene bridge of *rac*-$C_2H_4(Ind)_2ZrCl_2$ by a one-membered silylene (65–71) or germylene (69) bridge improves the stereoselectivity whereas a one-membered carbon bridge decreases both the stereoselectivity and molecular weight of the produced polymer (69,87,344). Longer than two-atom bridges decrease the activity and stereoselectivity because of the distortion of the molecular C_2 symmetry and narrowing of the coordination gap aperture (68,383,384). Aromatic substitution on the bridge enhances the molecular weight, although the size of the effect appears to be unpredictable (69,71,344). Electron withdrawing substituents in the six-membered rings of the indenyl ligands decrease the polymerization activity and molecular weight (75,82). Dimethylamino-substituents in the 2,2′-positions result in modest activities and stereospecificities; *rac*-$(CH_3)_2Si(2\text{-}(CH_3)_2NInd)_2ZrCl_2$/MAO polymerizes propylene to iPP with $[mmmm] = 85\%$, $T_m = 132^\circ C$, and $M_n = 30{,}000$ ($T_p = 50^\circ C$; $P = 2$ bar), albeit suffering from long induction periods apparently resulting from interaction of the amino groups with the cocatalyst (66). *tert*-Butyldimethylsiloxy-substituted analogues exhibit likewise modest activities and stereospecificities but polymerize propylene and ethylene without the induction delay (91,271).

Alkyl or silyl substitution in the 3,3′-positions of the five-membered rings of ethylene and dimethylsilylene bridged bis(indenyl) catalysts markedly decreases the polymerization activity and results in a complete loss of stereoselectivity (62,69,344,385). Bilateral coverage of the coordination sites by the 3,3′-substituents and the hydrogen atoms of the 4,4′-positions equalizes the energetic differences between the two enantiofacial orientations of the incoming propylene monomer (386). An exception to this are the single carbon bridged 3,3′-substituted catalysts *rac*-$R_2C(3\text{-}(CH_3)_3C\text{-}Ind)_2ZrCl_2$ (R = H, CH_3) (Fig. 11) (85,345) that

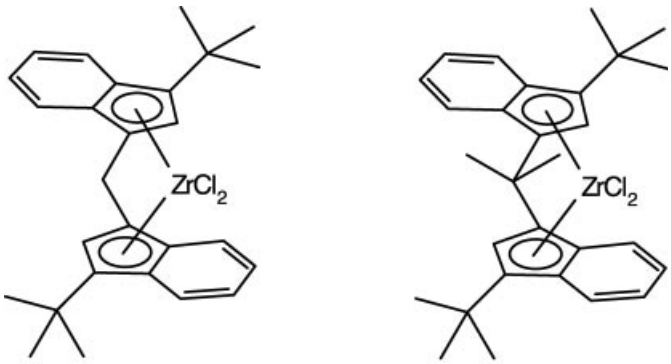

Fig. 11. Single carbon bridged isospecific metallocene catalysts.

produce highly isotactic polymers. For example, the methylene bridged complex *rac*-$H_2C(3\text{-}(CH_3)_3C\text{-}Ind)_2ZrCl_2$ and its dimethyl analogue produce, in combination with MAO, fully regioregular iPP ([*mmmm*] = 95–98%) with medium–high molecular weights (M_w = 70,000–780,000) and high melting points (T_m = 154–163°C) in the T_p range of 30–70°C (345). The polymer properties and polymerization activities are inferior to those obtained with the high-performance 2,2′-dialkyl-4,4′-diaryl-substituted Hoechst catalysts. An advantage with the Montell systems is, however, their simple and inexpensive ligand and catalyst synthesis.

Syndiotactic Polypropylene. Before the report on the first syndiospecific *ansa*-metallocene catalyst (61), only partially sPP had been obtained with vanadium-based Ziegler–Natta catalysts at low polymerization temperatures (387). The C_s symmetric metallocene-based systems are the first examples of catalysts that are capable of producing highly sPP in high yield and are practical for industrial scale-up. The properties of metallocene sPP differ substantially from those of iPP, especially in their considerably higher room temperature impact strength, higher optical clarity, and resistance against uv radiation.

The polymerization behavior of the original Ewen catalyst has been studied in detail (61,62,388). For example, bulk polymerization of propylene at 50°C using $(CH_3)_2C(Cp)(Flu)ZrCl_2$/MAO produces sPP having syndiotactic pentad content [*rrrr*] = 82%, M_w = 133,000, and T_m = 140°C (62). Higher syndiotacticities are obtained at lower polymerization temperatures. Several structural variations of the original catalyst are reported in the literature (62,74,76–78,385,389–400) (Fig. 12). Hafnocene-based catalysts exhibit a lower activity and slightly lower syndiospecificity but produce polymers with higher molecular weights. The titanium analogues suffer from both poor activities and poor stereoselectivities (389). Replacement of the isopropylidene bridge of $(CH_3)_2C(Cp)(Flu)ZrCl_2$ with an aromatic Ph_2C bridge improves both the syndiotacticity and molecular weight of the polymer (77), whereas considerably lower stereoselectivities are observed for the ethylene (78,390,396) and $(CH_3)_2Si$ (391) bridged analogues. Exceedingly active regio- and syndiospecific metallocene catalysts have been obtained by replacing the fluorenyl ligand of $(C_6H_5)_2C(Cp)(Flu)ZrCl_2$ with the sterically demanding octamethyloctahydrodibenzofluorenyl (Oct) moiety. The produced sPPs have syndiotactic pentad contents [*rrrr*] approaching 99% and melting temperatures as high as 153°C have been reported (399,400), demonstrating for the first time the dramatic effect of distal ligand perturbations on the polymer stereochemistry.

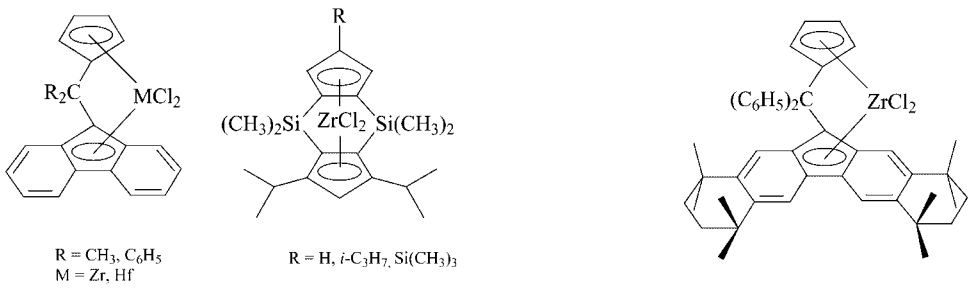

Fig. 12. Metallocene catalysts for syndiospecific polymerization of propylene.

The doubly bridged C_s symmetric bis(cyclopentadienyl)zirconocene catalysts developed by Bercaw and co-workers are likewise highly regio- and syndiospecific (397,398). Bulk polymerization of propylene at 20–70°C gave sPPs with pentad contents [*rrrr*] = 45.4–97.5% and molecular weights M_w of 130,000–1,250,000 depending on the catalyst substitution pattern and the employed polymerization temperature (76). The highest reported polymerization activity corresponding to 16,900 kg PP/g Zr/h was obtained at 70°C using the (1,2-$(CH_3)_2Si)_2$(Cp)(3,5-*i*-$(C_3H_7)_2$-Cp)$ZrCl_2$/MAO catalyst system.

Hemiisotactic PP. As first demonstrated by Ewen (62), the C_1 symmetric metallocene $(CH_3)_2$C(3-CH_3Cp)(Flu)$ZrCl_2$ produces hemiisotactic polypropylene (hitPP) consisting of alternating isotactic and stereorandom monomer placements. The two coordination sites of this catalyst are different; the isospecific site is blocked by both the Cp-methyl substituent and the fluorenyl C_6 ring whereas the aspecific site is unilaterally framed by the second fluorenyl moiety. As the growing chain occupies the more hindered site, the two conformations in which the first C—C bond is directed toward the substituted side of the Cp ring or toward the fluorenyl ring have equal probabilities. Consequently monomer insertion from the less hindered site is aspecific. At the less hindered site the polymer chain is oriented toward the open sector of the ligand framework resulting in stereospecific monomer insertion from the more hindered site, thus forming the hemiisotactic microstructure.

Copolymers with Higher α-Olefins. Several researchers (381,401–404) have copolymerized propylene with 1-hexene (402–404) and 1-octene (381,401), using various MAO-activated metallocene catalysts. Random distribution of the comonomer was observed in all cases. Comonomer incorporation is dependent on the catalyst structure; combination of benzannelation and 2-methyl substitution of silylene bridged bis(indenyl) ligands in *rac*-$(CH_3)_2Si$(2-CH_3-benz[*e*]Ind$)_2ZrCl_2$ was found to enhance both the molecular weight and comonomer content of the propylene–octene copolymers (401). Poly(propylene)-*graft*-poly(styrene) copolymers have been prepared using the *rac*-$(CH_3)_2Si$(2-CH_3-benz[*e*]Ind$)_2ZrCl_2$/MAO catalyst in copolymerization of propylene with allyl-terminated polystyrene macromonomers (405). Graft copolymers with a polystyrene content ranging from 7 to 72% were obtained. The same catalyst system was used for copolymerization of propylene with an aPP macromonomer (406).

Elastomeric Polypropylene (elPP). PPs consisting of blocks of atactic and isotactic stereosequences behave as thermoplastic elastomers. This material was identified for the first time by Natta in 1959 during fractionation studies of first generation Ziegler–Natta iPP (407). The elastomeric properties of these polymers are believed to result from cocrystallization of isotactic stereoblocks in neighboring PP chains to form a physically cross-linked elastomer. More recently, elPP has been prepared using supported tetraalkyl Group 4 catalysts (408,409).

A number of Group 4 metallocene catalysts have been shown to produce PP elastomers (Fig. 13). The production of elPP has been reported using asymmetrically substituted *ansa*-titanocene catalysts $CH_3CH((CH_3)_4Cp)$(Ind)$TiCl_2$/MAO under a variety of polymerization conditions (366–370). The formation of short isotactic sequences in predominantly atactic polymer chains was proposed to originate from sequential monomer insertion at the aspecific and isospecific coordination sites of the catalyst, although this mechanism has been challenged. elPPs

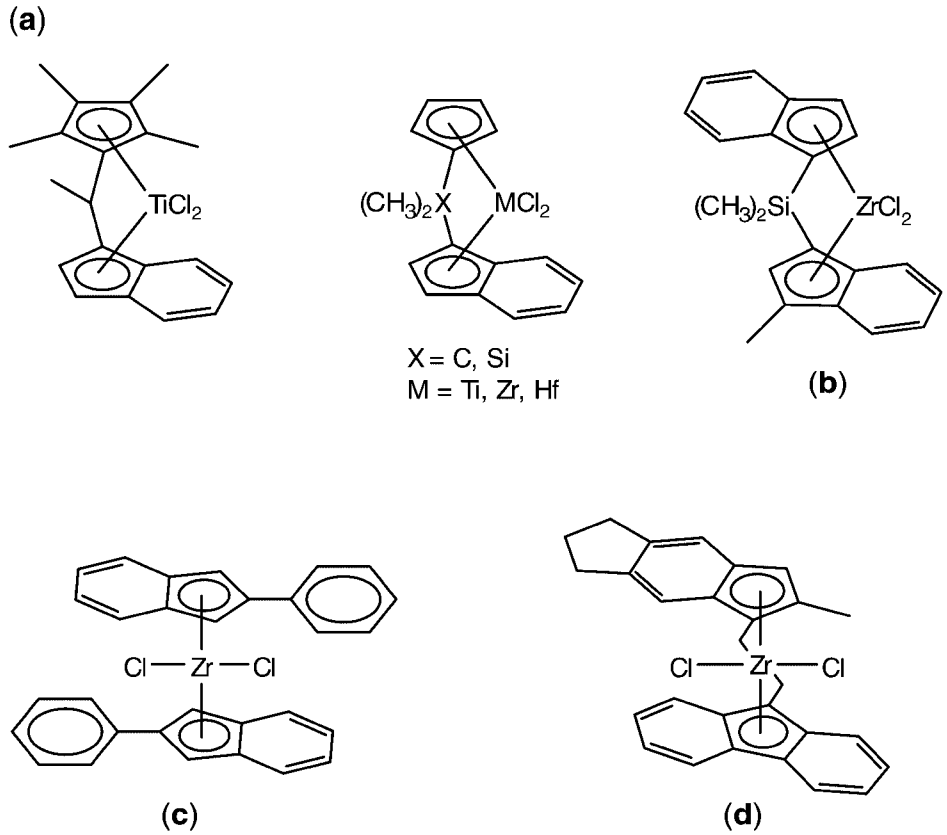

Fig. 13. Metallocene catalysts for preparation of elastomeric PP. (**a**) Titanocene Catalysts (366–370); (**b**) (371–373); (**c**) See also Figure 14 (63,64,374–379); (**d**) Zirconocene Catalysts (89).

have also been prepared using a related class of MAO-activated metallocenes $(CH_3)_2X(Cp)(Ind)MCl_2$ (X = C, Si; M = Ti, Zr, Hf) (371,372). Microstructures of the PPs produced were found to be sensitive to both catalyst structure and polymerization conditions with the hafnium-based systems yielding the best elastomeric properties. The mechanism suggested (371,372) involves random monomer insertion at the isospecific and aspecific coordination sites, respectively. In a more recent report, the preparation of high molecular weight semicrystalline elPP using the asymmetrically substituted *rac*-like diastereomer of $(CH_3)_2Si(Ind)(3\text{-}CH_3Ind)ZrCl_2$ in combination with MAO has been described (373). The obtained polymers exhibited isotactic pentad contents [*mmmm*] = 30.4–41.9% and molecular weights (M_w) of 37,000–115,000 depending on the monomer concentration and polymerization temperature.

A series of C_1 symmetric *ansa*-zirconocene catalysts based on an ethylene bridged mixed ligand (indenyl)(fluorenyl) framework has been described (89). These complexes, upon activation with MAO, retain their high activities even at elevated polymerization temperatures producing PPs of variable isotacticities [*mmmm*] = 19.9–72.1% and molecular weights (M_w) up to 230,000 depending on

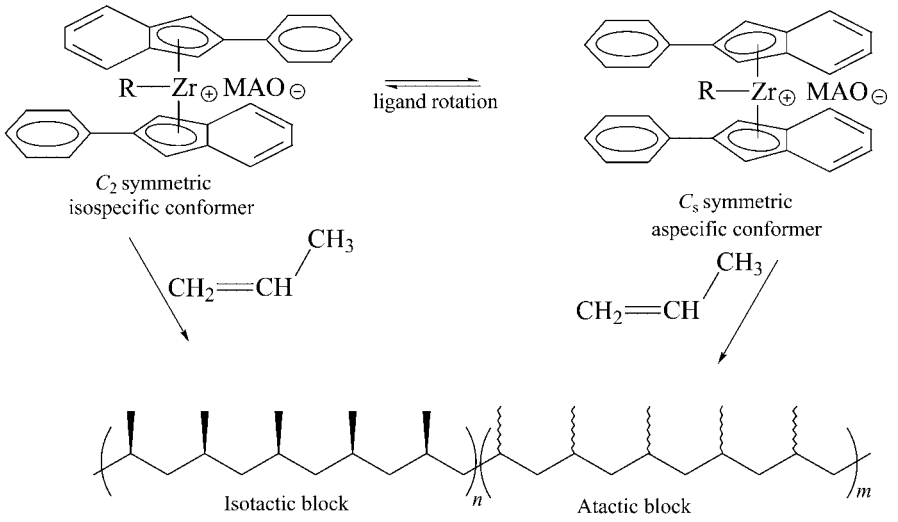

Fig. 14. Oscillating stereocontrol for production of isotactic–atactic stereoblock PP.

the employed catalyst, polymerization temperature and monomer concentration. The presence of two different coordination sites allows precise control of stereoerror formation resulting in bulk properties ranging from flexible semicrystalline thermoplastics to excellent thermoplastic elastomers.

The oscillating catalysts that have been developed are based on unbridged bis(2-arylindenyl) Group 4 metallocenes that presumably interconvert between an isospecific and aspecific conformer on the time scale of the polymerization reaction producing isotactic–atactic stereoblock polymers (Fig. 14) (63,64,374–379). The size of the stereoblocks is controlled by the relative rates of chain propagation and ligand isomerization. The nature of the substituent in 2-position of the indenyl ligand is crucial for obtaining elastomeric material. The prototypical bis(2-phenylindenyl)zirconium dichloride/MAO system produces elPP having pentad contents $[mmmm] = 6.3–28.1\%$ as a function of the monomer concentration and polymerization temperature (63). The 3,5-trifluoromethyl-substituted analogue $[2\text{-}(3,5\text{-}(CF_3)_2\text{-}C_6H_5)Ind]_2ZrCl_2$ produces PP of considerably higher isotacticity and crystallinity; values up to $[mmmm] = 73\%$ were reported for the MAO-activated catalyst system (64). Several other modifications generating mainly aPP have been reported in subsequent papers (374–379).

A related strategy based on reversibly bridged donor–acceptor substituted metallocenes, potentially providing access to elastomeric polyolefins, has been described (93). In these complexes one of the cyclopentadienyl or indenyl ligands contains a donor group (eg, diethylphosphanyl or dimethylamino) whereas the other one is substituted with an acceptor (eg, dichloroboranyl). Ligand rotation can be controlled by temperature-dependent donor–acceptor interaction. For example, *rac*-$[(C_2H_5)_2P(2\text{-}CH_3Ind)][Cl_2B(2\text{-}CH_3\text{-}Ind)]ZrCl_2$ activated with triisobutylaluminum and $[NH(CH_3)_2C_6H_5]^+[(C_6F_5)_4B]^-$ produces at room temperature (bulk polymerization of propylene) highly iPP with $[mmmm] = 94\%$, $T_m = 158°C$, and $M_v = 2{,}000{,}000$. At 50°C the pentad content drops to $[mmmm] = 82\%$ and

molecular weight to $M_v = 434{,}000$, whereas the melting temperature remains high, $T_m = 154^\circ C$, indicating the formation of aPP sequences together with long isotactic blocks.

Other Monomers

Cycloolefins. A distinct feature of the Group 4 metallocene/MAO catalyst systems is their ability to polymerize cyclic olefins without ring-opening metathesis, a reaction characteristic of heterogeneous Ziegler–Natta catalysts. Cyclobutene, cyclopentene, norbornene, and dimethanooctahydronaphthalene are readily homopolymerized to isotactic polycycloalkenes, using chiral *ansa*-zirconocene catalysts (18,22,24,203,410–412) (eq. 4). Homopolymers of the cyclic olefins are not processable because of their high melting points (400–500°C) and insolubility in common organic solvents. Cycloolefin copolymers (COCs), produced by copolymerization of cyclic monomers with ethylene or propylene, are however amorphous thermoplastics exhibiting heat resistance up to 200°C combined with high rigidity, toughness, and environmental stability (18,22,24,410,413–418). The excellent stiffness and low density of COCs combined with their stability against hydrolysis and chemical degradation renders them as potential materials for compact discs, lenses, and optical fibers.

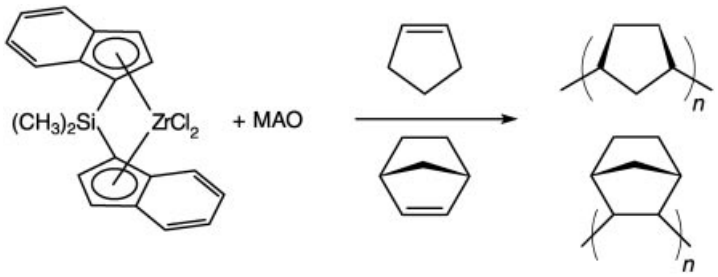

(4)

Dienes. Group 4 metallocene catalysts are capable of polymerizing both conjugated and nonconjugated dienes. Polymerization of α,ω-dienes affords cyclopolymers with remarkably high cyclo- and regioselectivities (269,270,419–425). Insertion of the terminal double bond of the nonconjugated diene into the metal–carbon bond is followed by intramolecular cyclization that produces the polymeric ring structure interspaced by methylene groups. Tacticity of the cyclopolymer is determined by the enantiofacial selectivity of the insertion step and is influenced by the symmetry and structure of the catalyst precursor. Diastereoselectivity of the cyclization step (ie, whether cis or trans rings are formed) is likewise influenced by catalyst structure and sterical environment of the active site. For example, in the polymerization of 1,5-hexadiene, Cp_2ZrX_2/MAO (X = Cl, CH_3) produces (at ambient temperature) predominantly atactic *trans*-poly(methylene-1,3-cyclopentane) (PMCP) whereas the sterically congested $Cp*_2ZrCl_2$/MAO catalyst produces mainly the atactic *cis* product (419–422). Interestingly, the *cis*-connected atactic PMCPs have melting points reaching $T_m = 171^\circ C$, whereas the

trans-PMCP showed a considerably lower melting point of $T_m = 86^\circ C$ (421). The synthesis of optically active cyclopolymers from 1,5-hexadiene using enantiomerically pure *ansa*-metallocene catalysts (423,424), the cyclopolymerization of functionalized α,ω-dienes (425), and the post-functionalization of hydroxy-terminated PMCP (269,270) are discussed separately (*vide infra*).

Styrene. Syndiotactic polystyrene (sPS) is a high melting stereoregular polymer first prepared in the mid-1980s using an undisclosed titanium-based catalyst in combination with aluminum activators (112). In contrast to isotactic polystyrene (iPS), which shows a very low crystallization rate and is thus useless for most commercial applications, sPS has a fast crystallization rate, higher melting point compared with iPS (270°C vs 230°C), superior heat and chemical resistance, as well as low specific gravity, low dielectric constant, and high modulus of elasticity. These unique properties have resulted in remarkable interest in sPS as an attractive low cost replacement for expensive engineering plastics (see SYNDIOTACTIC POLYSTYRENE).

A variety of Group 4 metal complexes, in combination with common olefin polymerization activators, have been evaluated as potential catalysts for syndiospecific polymerization of styrene (for reviews, see Refs. 114, 115, 123, and 426). Monocyclopentadienyl and monoindenyl titanocenes generally exhibit the highest activities (eq. 5) (112–127). Curiously, half-sandwich titanium-trifluoride-based catalysts are more active than their trichloride analogues (124,427,428). The polymerization mechanism for sPS formation is under debate. Kinetic studies and spectroscopic investigations of the catalytic systems suggest a cationic Ti(III) complex as the active species (123).

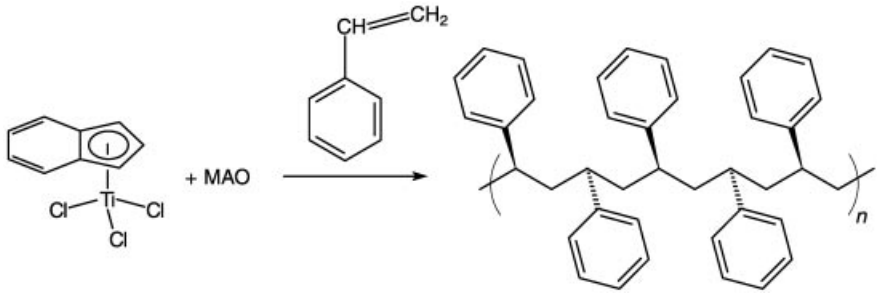

(5)

Functional Polymers

Controlled *in situ* incorporation of polar or reactive functional groups into polyolefins is a long-standing challenge (429–431). End uses of polyolefins are restricted by their chemical inertness and lack of adhesive properties. The absence of polar groups results in a poor affinity for functional additives such as dyes, paints, and antioxidants, and limits the compatibility of polyolefins with functional polymers, biomaterials, metal, and glass. Traditional Ziegler–Natta catalysts are highly oxophilic and readily poisoned by Lewis-basic comonomers (alcohols, ethers, carboxylic acids, esters, and amines). Recently, considerable advances toward functionalized polyolefins have been made by direct polymerization and

copolymerization of functional monomers over SSCs as well as by various associated indirect post-polymerization methods.

Homo- and Copolymerization of Polar Monomers.

Metallocene Catalysts. Group 4 metallocene-based catalysts are, under proper polymerization conditions, tolerant to selected polar comonomers. Various functionalized dienes and α-olefins have been polymerized using cationic metallocene catalysts (425,432,433). Polymerization activities were lower than those observed for the analogous nonpolar monomers. Silyl-protected 1,6-heptadien-4-ols are readily cyclopolymerized by the sterically hindered $[Cp*_2ZrCH_3]^+X^-$ catalyst [$X = B(C_6F_5)_4$ or $CH_3B(C_6F_5)_3$] with turnovers reaching 280 (59% conversion) (eq. 6) (425). Deprotection of the silyl group generates the corresponding polyalcohol. Tertiary amines were homo- and copolymerized using both aspecific and isospecific metallocene catalysts (425,432,433). Borate cocatalysts gave higher activities than MAO-based catalyst systems. Optimum activities were achieved using diisopropyl-substituted amine with an olefin tether of three carbon atoms. Catalyst stereospecificities were essentially insensitive to monomer functionality.

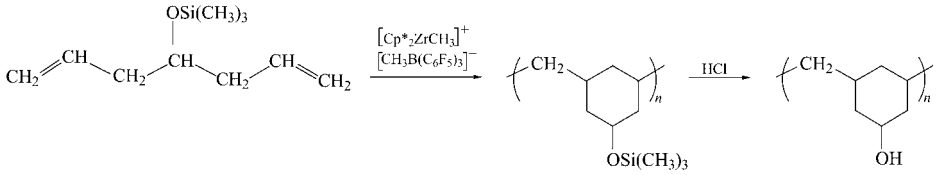

(6)

Other examples of polar comonomers incorporated by Group 4 metallocenes include silylamines (434), protected alcohols (435,436) and carboxylic acids (436), ω-chloroolefins (437), and primary long-chain hydroxyalkenes (438,439). The copolymerization of propylene with a hindered phenolic stabilizer 6-*tert*-butyl-2-(1,1-dimethylhept-6-enyl)-4-methylphenol over an isospecific metallocene/MAO catalyst system has been described (440). A novel strategy for preparation of polyolefin graft copolymers has been developed by combination of metallocene and "living" free radical polymerization techniques (441–443). Copolymerization of an alkene-substituted hindered alkoxyamine with ethylene or propylene affords well-defined macroinitiators with 2,2,6,6-tetramethylpiperidine-*N*-oxyl (TEMPO) chain ends to which polystyrene, acrylate, and butadiene side chains can be grafted in a "living" fashion.

In addition, Group 4 metallocene-type catalyst systems have been employed in living ring-opening polymerization of lactones (444–446) and carbonates (447). Various metallocene or lanthanocene complexes have been used as initiators for homo- and copolymerization of methacrylates, acrylates, and the synthesis of block copolymers (224,448–457). Single-site-type zinc alkoxide complexes have been described for ring-opening polymerization of lactides (458).

Late Transition Metal Catalysts. In contrast to early transition metals, late transition metal catalysts (26,185) are considerably less oxophilic and are tolerant to a wide range of functional groups. The α-diimine palladium complexes developed by Brookhart (179,180,183,184) copolymerize ethylene and propylene with alkyl acrylates (180,183) and protected alcohols (459) to high molecular weight

random copolymers, albeit at reduced activities. The ethylene acrylate copolymers are amorphous, highly branched materials with ~100 branches/1000 carbon atoms. Typical T_g values range from −67 to −77°C.

The neutral salicylaldimine nickel complexes described by Grubbs and coworkers (195,196) show unprecedented functional group tolerance and are capable of incorporating substituted norbornenes, carbon monoxide, and α–ω functional olefins into polyolefins with well-defined compositional distributions (eq. 7) (196). Furthermore, ethylene can be homopolymerized with these catalysts in the presence of various functional additives including acetone, water, ethyl alcohol, and triethyl amine. In the presence of 1500 equivalents of H_2O, polyethylene was produced at a rate of 5.4×10^4 g PE/mol Ni/h.

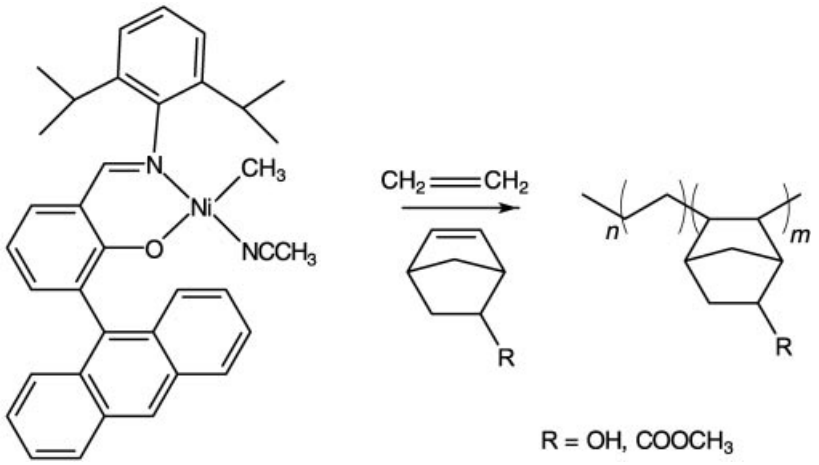

(7)

Modification of Preformed Polymers. Alkene end groups of polyolefins can be functionalized in a post-polymerization process. PPs with olefinic end groups have been prepared using the isospecific $(CH_3)_2Si(3\text{-}(CH_3)_3C\text{-}5\text{-}CH_2Cp)_2ZrCl_2$/MAO catalyst system (460). The vinylidene chain ends react further to give a range of monofunctional PPs with anhydride, silane, thiol, epoxy, borane, and carboxylic acid end groups. Thiol functionalized polymers were used as chain-transfer agents in free radical polymerizations of styrene and acrylics to form PP block copolymers. A similar approach has been applied using aluminum (461) and borane (462) reagents. Ethylene or propylene have been copolymerized with unsymmetrical dienes, using MAO-activated metallocene catalysts (463–465). Selective incorporation of the α-olefinic double bonds of the comonomers provides access to polymers containing internal unsaturations that can be converted to various functional groups.

Yet another methodology involves the metallocene-catalyzed copolymerization of olefins with borane containing monomers (466,467). The incorporated borane group can be quantitatively converted to a hydroxy group or transformed into a stable polymeric radical suitable for free radical grafting of acrylates.

Chain Transfer to Organometallic Compounds. Hydroxy-terminated poly(methylene-1,3-cyclopentane) has been prepared by selective chain transfer to aluminum in the cyclopolymerization of 1,5-hexadiene with the sterically

congested $Cp_2{*}ZrCl_2$/MAO catalyst (269,270). Aluminum alkoxide of the produced polymer was used as a macroinitiator for ring-opening polymerization of ε-caprolactone to produce diblock copolymers (270).

A similar strategy was used to prepare borane-terminated polyethylenes with $[Cp{*}_2ZrCH_3]^+X^-$ [X = $B(C_6F_5)_4$ or $CH_3B(C_6F_5)_3$] in the presence of 9-borabicyclo[3.3.1]nonane chain-transfer agent (468). The borane end group was selectively oxidized and transformed to a polymeric radical for grafting of methyl methacrylate.

Silyl-capped polyolefins have been prepared by employing organotitanium-mediated silanolytic chain-transfer processes (469,470). Various monomers including ethylene, propylene, 1-hexene, and styrene were homo- and copolymerized using the cationic $[((CH_3)_2Si((CH_3)_4Cp)(CH_3)_3CN)TiCH_3]^+X^-$, [*rac*-$C_2H_4(Ind)_2TiCH_3]^+X^-$, and $[Cp{*}_2TiCH_3]^+X^-$ [X = $B(C_6F_5)_4$] metallocene catalyst systems in the presence of organosilanes ($C_6H_5SiH_3$, $C_6H_5CH_3SiH_2$), $(CH_3)_2SiH_2$, $(C_2H_5)_2SiH_2$) (470). Silyl-linked linear A–A and star block copolymers as well as A–B block copolymers were obtained in catalytic cycles using polyfunctional silabenzenes.

Enantioselective Polymerization

The characteristic functionalities of naturally occurring polymers are, in most cases, related to their specific chiral structure. In nature, proteins, nucleic acids, and polysaccharides are constructed of readily available chiral monomers such as sugars and amino acids. Both natural and synthetic chiral polymers are finding application as chromatographic supports, polymeric reagents and catalysts, chiral membranes, and materials for preparation of cholesteric liquid crystal polymers (471,472).

High molecular weight stereoregular vinyl polymers contain mirror planes of symmetry perpendicular to the molecular axis (Fig. 15) and thus do not have inherent chirality associated with the main chain. Synthesis of chiral polymers from vinyl monomers, with the exception of low molecular weight oligomers,

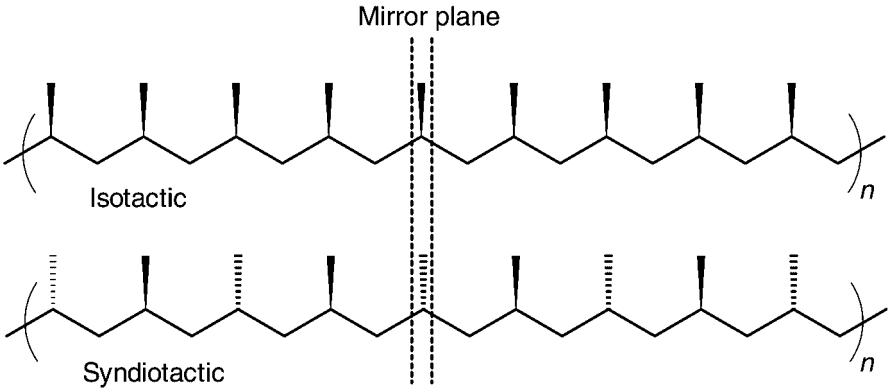

Fig. 15. Mirror planes of symmetry in stereoregular vinyl polymers.

requires more complex polymer architectures to circumvent the symmetry constraints.

Enantiomerically pure SSCs (79), readily available through resolution of the racemic C_2-symmetric Brintzinger-type *ansa*-metallocenes (59,473–475), have attracted considerable interest in catalytic and enantioselective C—C bond formation reactions (476). Despite the aforementioned symmetry concerns, these catalysts have opened new possibilities in synthesis and design of chiral macromolecules.

Polymerization and Oligomerization of Prochiral Olefins. The synthesis of optically active iPP and polybutene with the enantiomerically pure catalyst derived from (*S*,*S*)-$C_2H_4t(IndH_4)_2ZrCl_2$ has been reported (311,477). The obtained polymers showed fairly large optical activities in soaked suspensions ($[\alpha]_D = -123^\circ$, -250° for PP, $+130^\circ$ for polybutene) attributed to a helical conformation or predominant screw sense. As expected, racemization occurred when the polymer was heated or completely dissolved.

Oligomerization of α-olefins can be promoted by two methods: (*1*) reducing the monomer concentration in the polymerization medium thus favoring β-H elimination over chain propagation and (*2*) conducting the polymerization in the presence of H_2 gas. Optically active low molecular weight oligomers of propylene and butene have been prepared using the (*S*,*S*)-$C_2H_4(IndH_4)_2ZrCl_2$ catalyst at high temperature and low alkene concentration (478). The binaphtholate (*R*,*R*)-$C_2H_4(IndH_4)_2Zr$(BINOL) has been used for asymmetric oligomerization of propylene (479,480), 1-pentene (480), and 4-methyl-1-pentene (480) in the presence of hydrogen and deuterium chain-transfer agents. A detailed microstructural analysis of the oligomeric fractions showed for the first time that the stereoregulation of the polymerization reaction with these catalyst systems results from preferential addition of one enantioface of the prochiral monomer to the growing polymer chain.

Cyclopolymerization. As discussed earlier, nonconjugated dienes can be polymerized with metallocene-based catalysts to afford cyclopolymers. In contrast to linear polyolefins which have only two microstructures of maximum order (isotactic and syndiotactic), cyclic polymers have four microstructures due to the possibility of configurational isomerism (cis vs trans) in the main chain (Fig. 16). Of these the *trans*-diisotactic structure contains no mirror planes of symmetry and is chiral by virtue of its main-chain stereochemistry (481). Two criteria for chirality of this microstructure are the presence of trans rings and isotacticity (the same

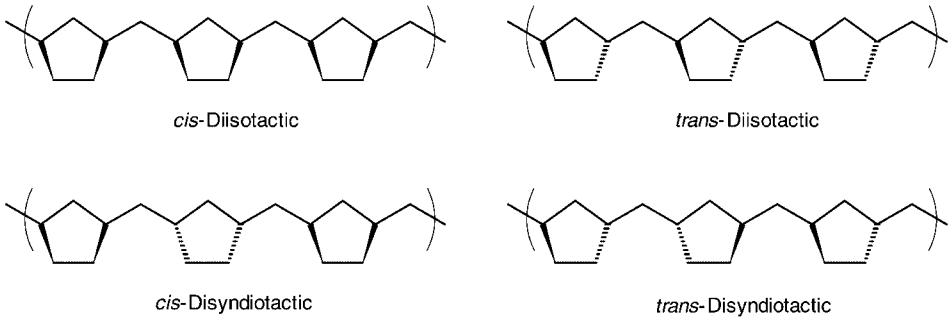

Fig. 16. Poly(methylene-1,3-cyclopentane) structures of maximum order.

relative configuration of every other stereocenter). All other structures contain mirror planes within the repeating subunits.

Using both enantiomers of the resolved $C_2H_4(IndH_4)_2Zr$(BINOL)/MAO catalyst 1,5-hexadiene has been polymerized to obtain optically active poly(methylene-1,3-cyclopentane) (eq. 8) (423,424). The polymer obtained with the (*R*,*R*) catalyst displayed a molar optical rotation of $[\Phi]_{405}^{28} = +51.0^\circ$ ($c = 0.8$ in $CHCl_3$). Microstructural analysis by ^{13}C nmr indicated an enantiofacial selectivity of 91% for the olefin insertion step and 72% content of trans rings. Cyclopolymerization with the (*S*,*S*) catalyst gave the enantiomeric polymer with $[\Phi]_{405}^{28} = -51.2^\circ$. Interestingly, the measured optical rotations are considerably higher than that obtained for diasteromerically pure model compound *trans*-(1*R*,3*R*)-1,3-dimethylcyclopentane, possibly resulting from a preferential helical conformation in solution.

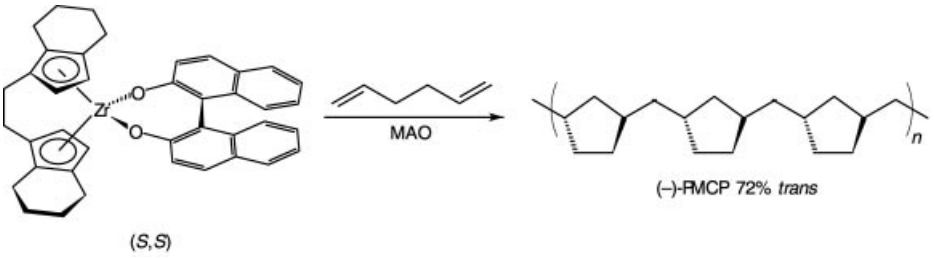

(8)

Styrenic Copolymers. Alternating copolymerization of vinyl monomers with carbon monoxide produces polyketones with stereogenic centers along the polymer backbone (482). Brookhart and co-workers have reported the copolymerization of *p-tert*-butylstyrene and CO under the enantiomorphic site control mechanism, using an enantiomerically pure cationic palladium catalyst based on a C_2-symmetric bisoxazoline ligand (eq. 9) (483). The obtained copolymer showed a high molar optical rotation of $[\Phi]_{589}^{25} = -536^\circ$ ($c = 0.5$ in CH_2Cl_2) resulting from main-chain chirality. ^1H and ^{13}C NMR analysis revealed a high degree of stereoregularity (>98%) confirming the isotactic microstructure. The narrow molecular weight distribution ($M_w/M_n = 1.4$) of this polymer is consistent with the Schulz–Flory statistics for a SSC.

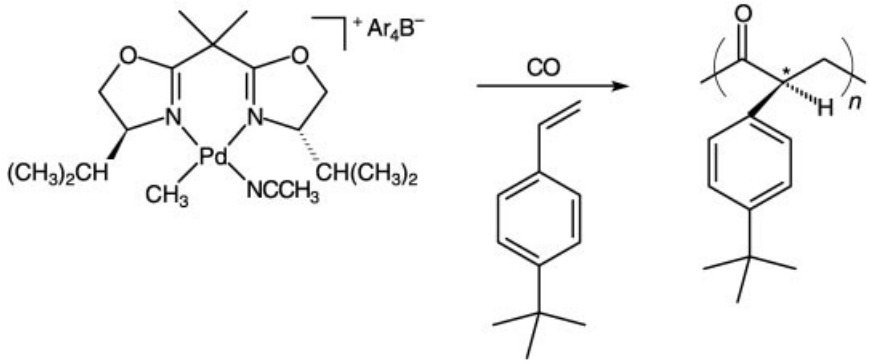

(9)

Heterogenization of SSCs

Essentially homogeneous SSCs have to be supported for use in industrial gas-phase, slurry, and bulk-monomer polymerization processes (for reviews, see Refs. 484–491). Not surprisingly, most of the information on the supported catalyst systems has been published only in the patent literature (for extensive coverage, see Ref. 490). The main problems are associated with catalyst feeding, reactor fouling, and controlled particle morphology of the produced polymer. Continuous operation of gas-phase polymerization processes requires the use of free-flowing catalyst particles that can be easily fed into the reactor. Controlled growth of the polymer particles during the polymerization reaction (Fig. 17) is likewise essential, since overheating and subsequent melting of the forming polymer grains may result in sheets and lumps that disturb the agitation, fluidization, and product removal processes.

The most common inorganic supports used for heterogenization of metallocenes are various types of silica, alumina, and magnesium compounds (381,484–502), although other less conventional carrier materials based on zeolites (503–505), mesoporous (MCM-41) silica (506–510), cyclodextrin (511,512), polystyrene (513–515), polysiloxanes (516,517), and sulfated zirconia (518) have been reported. Self-supporting catalyst systems based on olefin or alkyne functionalized metallocenes have also been described (519). In this case, the initially homogeneous metallocene is incorporated into the growing polymer chain, which upon precipitation from the reaction mixture functions as a heterogeneous catalyst system.

Immobilization of metallocenes on the carrier materials can be accomplished by various methods, including (*1*) direct impregnation of the activated metal complex/aluminoxane mixture; (*2*) premodification of the support with MAO or aluminum alkyls followed by reaction with the metallocene; (*3*) anchoring of the metallocene to the support through covalent bonds followed by activation with the cocatalyst. Similar approaches can be applied to the boron-activated catalyst systems (489,490).

In most cases, properties of the polymers obtained with the supported catalysts are similar to those obtained with their homogeneous analogues. The

Fig. 17. Replication of catalyst morphology in isospecific propylene polymerization with heterogeneous metallocene catalyst: SEM image of the heterogeneous catalyst SiO_2/MAO/$(CH_3)_2$Si(2-CH_3-benz[*e*]Ind)$_2ZrCl_2$ (left), and SEM image of PP powder (ρ = 0.22 g/mL) produced in hexane with triisobutylaluminum as external activator at 40°C (right). [From Ref. 492. Copyright © John Wiley & Sons, Inc. Reprinted by permission of John Wiley & Sons, Inc.]

single-site nature of the metallocene is generally preserved, although activites are often remarkably reduced. The surrounding carrier material may increase the steric hindrance around the active sites, thus contributing to decreased overall productivities. On the other hand, enhanced site-isolation may suppress binuclear chain transfer and deactivation pathways resulting in improved molecular weights and, most notably, satisfactory activities at considerably reduced cocatalyst concentrations. Supported metallocene catalysts are commonly activated with [Al]:[M] ratios in the range of 50–400:1, far below those required for their homogeneous counterparts.

Despite the technological difficulties associated with catalyst preparation, leaching and process parameters, the number of announcements on commercial production of polyolefins with heterogeneous SSCs is, at the time of writing, rapidly increasing. The advanced supported SSCs are highly active and suitable for use as drop-in catalysts in existing commercial plants. These catalysts produce coherent polymer grains that are enlarged replicas of the catalyst particles exhibiting the desired bulk densities and other material properties. Dow and Exxon have been the key players in commercialization of SSC technologies. Both companies launched their homogeneous high pressure and solution ethylene polymerization processes in 1991. BASF commercialized its heterogeneous metallocene-based polyethylene in 1995. Several other companies, including Exxon, Mitsui Petrochemical, Borealis Polymers and Elenac (BASF/Shell joint venture), are now producing commercial grades of metallocene polyethylenes in gas-phase or slurry processes (489). Isotactic metallocene PPs are limited to speciality polymers produced by Targor (BASF/Hoechst) and Exxon. sPP, EPDM-polymers, ethylene–styrene copolymers, sPS, and cyclic olefin copolymers are, at the time of writing, in earlier development cycles.

BIBLIOGRAPHY

1. Ger. Pat. 973 626 (filed Nov. 17, 1953) K. Ziegler and co-workers, *Chem. Abstr.* **54**, 14794b (1960).
2. K. Ziegler and co-workers, *Angew. Chem.* **67**, 426 (1955).
3. K. Ziegler, *Angew. Chem.* **76**, 545–553 (1964).
4. Ital. Pat. 526 101 (filed June 8, 1954), G. Natta, P. Pino, and G. Mazzanti.
5. G. Natta and co-workers, *J. Am. Chem. Soc.* **77**, 1708–1710 (1955).
6. G. Natta, *J. Polym. Sci.* **16**, 143–154 (1955).
7. G. Natta, *Angew. Chem.* **68**, 393–403 (1956).
8. G. Natta, *Angew. Chem.* **76**, 553–566 (1964).
9. H. Sinn and W. Kaminsky, *Adv. Organomet. Chem.* **18**, 99–149 (1980).
10. T. Simonazzi and U. Giannini, *Gazz. Chim. Ital.* **124**, 533–541 (1994).
11. P. Galli, *Macromol. Symp.* **89**, 13–16 (1995).
12. K. B. Sinclair and R. B. Wilson, *Chem. Ind. (London)* 857–862 (1994).
13. P. C. Möhring and N. J. Coville, *J. Organomet. Chem.* **479**, 1–29 (1994).
14. H. H. Brintzinger and co-workers, *Angew. Chem., Int. Ed. Engl.* **34**, 1143–1170 (1995).
15. G. W. Coates and R. M. Waymouth, in E. W. Abel, F. G. A. Stone, and G. Wilkinson, eds., *Comprehensive Organometallic Chemistry II*, Pergamon, Oxford, 1995, pp. 1193–1208.
16. S. S. Reddy and S. Sivaram, *Prog. Polym. Sci.* **20**, 309–367 (1995).
17. M. Bochmann, *J. Chem. Soc., Dalton Trans.* 255–270 (1996).

18. W. Kaminsky, *Macromol. Chem. Phys.* **197**, 3907–3945 (1996).
19. A. E. Hamielec and J. B. P. Soares, *Prog. Polym. Sci.* **21**, 651–706 (1996).
20. R. H. Grubbs and G. W. Coates, *Acc. Chem. Res.* **29**, 85–93 (1996).
21. M. Bochmann, *Curr. Opin. Solid State Mater. Sci.* **2**, 639–646 (1997).
22. W. Kaminsky and M. Arndt, *Adv. Polym. Sci.* **127**, 143–187 (1997).
23. A. A. Montagna, A. H. Dekmezian, and R. M. Burkhart, *CHEMTECH* **27**(12), 26–31 (1997).
24. W. Kaminsky, *J. Chem. Soc., Dalton Trans.* 1413–1418 (1998).
25. A. L. McKnight and R. M. Waymouth, *Chem. Rev.* **98**, 2587–2598 (1998).
26. G. J. P. Britovsek, V. C. Gibson, and D. F. Wass, *Angew. Chem., Int. Ed. Engl.* **38**, 428–447 (1999).
27. I. Tritto and U. Giannini, eds., *Macromol. Symp.* **89**, 1–586 (1995).
28. H. Sinn and W. Kaminsky, eds., *Macromol. Symp.* **97**, 1–246 (1995).
29. R. F. Jordan, ed., *J. Mol. Catal. A: Chem.* **128**, 1–337 (1998).
30. T. J. Marks and J. C. Stevens, eds., *Topics Catal.* **7**, 1–210 (1999). (Special Issue on Advances in Polymerization Catalysis, Catalysts and Processes.)
31. J. A. Gladysz, ed., *Chem. Rev.* **100**, 1167–1682 (2000) (Special Issue on Frontiers in Metal-Catalyzed Polymerization.)
32. G. Fink, R. Mülhaupt, and H. H. Brintzinger, eds., *Ziegler Catalysts: Recent Scientific and Technological Improvements*, Springer-Verlag, Berlin, 1995.
33. A. Togni and R. L. Halterman, eds., *Metallocenes*, Wiley-VCH, Weinheim, 1998.
34. G. M. Benedikt and B. L. Goodall, eds., *Metallocene Catalyzed Polymers. Materials, Properties, Processing & Markets*, Plastics Design Library, New York, 1998.
35. G. M. Benedikt, ed., *Metallocene Technology in Commercial Applications*, Plastics Design Library, New York, 1999.
36. W. Kaminsky, ed., *Metalorganic Catalysts for Synthesis and Polymerization: Recent Results by Ziegler–Natta and Metallocene Investigations*, Springer-Verlag, Berlin, 1999.
37. J. Scheirs and W. Kaminsky, eds., *Metallocene-Based Polyolefins. Preparation, Properties and Technology*, Wiley, New York, 1999.
38. P. Arjunan, J. E. McGrath, and T. L. Hanlon, eds., *Olefin Polymerization: Emerging Frontiers*, American Chemical Society, Washington, DC, 2000. ACS Symposium Series, Vol. 749.
39. D. S. Breslow and N. R. Newburg, *J. Am. Chem. Soc.* **79**, 5072–5073 (1957).
40. D. S. Breslow and N. R. Newburg, *J. Am. Chem. Soc.* **81**, 81–86 (1959).
41. G. Natta and co-workers, *J. Am. Chem. Soc.* **79**, 2975–2976 (1957).
42. H. Sinn and F. Patat, *Angew. Chem.* **70**, 496–500 (1958).
43. G. Natta, P. Corradini, and I. W. Bassi, *J. Am. Chem. Soc.* **80**, 755–756 (1958).
44. J. C. W. Chien, *J. Am. Chem. Soc.* **81**, 86–92 (1959).
45. W. P. Long and D. S. Breslow, *J. Am. Chem. Soc.* **82**, 1953–1957 (1960).
46. G. Mazzanti and G. Natta, *Tetrahedron* **8**, 86–100 (1960).
47. H. Sinn and F. Patat, *Angew. Chem.* **75**, 805–813 (1963).
48. G. Henrici-Olivé and S. Olivé, *Angew. Chem.* **79**, 764–773 (1967).
49. G. Henrici-Olivé and S. Olivé, *J. Organomet. Chem.* **16**, 339–341 (1969).
50. K. H. Reichert and K. R. Meyer, *Makromol. Chem.* **169**, 163–176 (1973).
51. W. P. Long and D. S. Breslow, *Liebigs Ann. Chem.* 463–469 (1975).
52. A. Andersen and co-workers, *Angew. Chem., Int. Ed. Engl.* **15**, 630–632 (1976).
53. H. Sinn and co-workers, *Angew. Chem., Int. Ed. Engl.* **19**, 390–392 (1980).
54. J. Herwig and W. Kaminsky, *Polym. Bull.* **9**, 464–469 (1983).
55. W. Kaminsky and co-workers, *Makromol. Chem., Rapid Commun.* **4**, 417–421 (1983).
56. J. A. Ewen, *J. Am. Chem. Soc.* **106**, 6355–6364 (1984).
57. W. Kaminsky and co-workers, *Angew. Chem., Int. Ed. Engl.* **24**, 507–508 (1985).

58. H. Schnutenhaus and H. H. Brintzinger, *Angew. Chem., Int. Ed. Engl.* **18**, 777–778 (1979).
59. F. R. W. P. Wild and co-workers, *J. Organomet. Chem.* **232**, 233–247 (1982).
60. F. R. W. P. Wild and co-workers, *J. Organomet. Chem.* **288**, 63–67 (1985).
61. J. A. Ewen and co-workers, *J. Am. Chem. Soc.* **110**, 6255–6256 (1988).
62. J. A. Ewen and co-workers, *Makromol. Chem., Macromol. Symp.* **48/49**, 253–295 (1991).
63. G. W. Coates and R. M. Waymouth, *Science* **267**, 217–219 (1995).
64. E. Hauptman, R. M. Waymouth, and J. W. Ziller, *J. Am. Chem. Soc.* **117**, 11586–11587 (1995).
65. U. Stehling and co-workers, *Organometallics* **13**, 964–970 (1994).
66. E. Barsties and co-workers, *J. Organomet. Chem.* **520**, 63–68 (1996).
67. N. Schneider and co-workers, *Organometallics* **16**, 3413–3420 (1997).
68. W. A. Herrmann and co-workers, *Angew. Chem., Int. Ed. Engl.* **28**, 1511–1512 (1989).
69. W. Spaleck and co-workers, *New. J. Chem.* **14**, 499–503 (1990).
70. W. Spaleck and co-workers, *Angew. Chem., Int. Ed. Engl.* **31**, 1347–1350 (1992).
71. W. Spaleck and co-workers, *Organometallics* **13**, 954–963 (1994).
72. J. A. Ewen and M. J. Elder, in Ref. 32, pp. 99–109.
73. J. A. Ewen, *Macromol. Symp.* **89**, 181–196 (1995).
74. J. A. Ewen and co-workers, *J. Am. Chem. Soc.* **120**, 10786–10787 (1998).
75. I.-K. Lee and co-workers, *Organometallics* **11**, 2115–2122 (1992).
76. D. Veghini and co-workers, *J. Am. Chem. Soc.* **121**, 564–573 (1999).
77. A. Razavi and J. L. Atwood, *J. Organomet. Chem.* **459**, 117–123 (1995).
78. A. Razavi and co-workers, in Ref. 32, pp. 111–147.
79. R. L. Halterman, *Chem. Rev.* **92**, 965–994 (1992).
80. Z. Chen and R. L. Halterman, *Organometallics* **13**, 3932–3942 (1994).
81. R. L. Halterman, D. Combs, and M. A. Khan, *Organometallics* **17**, 3900–3907 (1998).
82. N. Piccolrovazzi and co-workers, *Organometallics* **9**, 3098–3105 (1990).
83. L. Resconi and co-workers, *Organometallics* **15**, 998–1005 (1996).
84. L. Resconi and co-workers, *Organometalllics* **15**, 5046–5059 (1996).
85. L. Resconi and co-workers, *J. Am. Chem. Soc.* **120**, 2308–2321 (1998).
86. C. J. Schaverien and co-workers, *J. Am. Chem. Soc.* **120**, 9945–9946 (1998).
87. V. A. Dang and co-workers, *Organometallics* **18**, 3781–3791 (1999).
88. B. Rieger and co-workers, *Organometallics* **13**, 647–653 (1994).
89. U. Dietrich and co-workers, *J. Am. Chem. Soc.* **121**, 4348–4355 (1999).
90. H. G. Alt, W. Milius, and S. J. Palackal, *J. Organomet. Chem.* **472**, 113–118 (1994).
91. R. Leino and co-workers, *Organometallics* **15**, 2450–2453 (1996).
92. H. J. G. Luttikhedde and co-workers, *Organometallics* **15**, 3092–3094 (1996).
93. K. A. Ostoja Starzewski and co-workers, *Angew. Chem., Int. Ed. Engl.* **38**, 2439–2443 (1999).
94. J. Okuda, *Chem. Ber.* **123**, 1649–1651 (1990).
95. J. Okuda and co-workers, *Organometallics* **14**, 789–795 (1995).
96. F. Amor and J. Okuda, *J. Organomet. Chem.* **520**, 245–248 (1996).
97. D. W. Carpenetti and co-workers, *Organometallics* **15**, 1572–1581 (1996).
98. S. Ciruelos and co-workers, *Organometallics* **15**, 5577–5585 (1996).
99. F. G. Sernetz, R. Mülhaupt, and R. M. Waymouth, *Macromol. Chem. Phys.* **197**, 1071–1083 (1996).
100. F. G. Sernetz and co-workers, *J. Polym. Sci., Part A: Polym. Chem.* **35**, 1571–1578 (1997).
101. A. L. McKnight and co-workers, *Organometallics* **16**, 2879–2885 (1997).
102. Y.-X. Chen and T. J. Marks, *Organometallics* **16**, 3649–3657 (1997).
103. P.-J. Sinnema and co-workers, *Organometallics* **16**, 4245–4247 (1997).

104. L. Duda and co-workers, *Eur. J. Inorg. Chem.* 1153–1162 (1998).
105. A. Bertuleit and co-workers, *Top. Catal.* **7**, 37–44 (1999).
106. Eur. Pat. Appl. EP 416815 (1991); U.S. Pat. Appl. 401345 (1989), J. C. Stevens and co-workers (to The Dow Chemical Company); *Chem. Abstr.* **115**, 93163m (1991).
107. Eur. Pat. Appl. EP 420436 (1991); U.S. Pat. Appl. 406945 (1989), J. A. M. Canich (to Exxon Chemical Co.); *Chem. Abstr.* **115**, 184145y (1991).
108. P. J. Shapiro and co-workers, *Organometallics* **9**, 867–869 (1990).
109. B. Rieger, *J. Organomet. Chem.* **420**, C17–C20 (1991).
110. Y.-X. Chen and co-workers, *Organometallics* **16**, 5958–5963 (1997).
111. E. E. C. G. Gielens and co-workers, *Organometallics* **17**, 1652–1654 (1998).
112. N. Ishihara and co-workers, *Macromolecules* **19**, 2464–2465 (1986).
113. N. Ishihara, M. Kuramoto, and M. Uoi, *Macromolecules* **21**, 3356–3360 (1988).
114. N. Ishihara, *Macromol. Symp.* **89**, 553–562 (1995).
115. K. Yokota and co-workers, in Ref. 36, pp. 435–445.
116. T. E. Ready and co-workers, *Macromolecules* **26**, 5822–5823 (1993).
117. A. Kucht and co-workers, *Organometallics* **12**, 3075–3078 (1993).
118. T. E. Ready, J. C. W. Chien, and M. D. Rausch, *J. Organomet. Chem.* **519**, 21–28 (1996).
119. P. Foster, J. C. W. Chien, and M. D. Rausch, *Organometallics* **15**, 2404–2409 (1996).
120. A. Zambelli, L. Oliva, and C. Pellechia, *Macromolecules* **22**, 2129–2130 (1989).
121. C. Pellechia and co-workers, *J. Am. Chem. Soc.* **117**, 6593–6594 (1995).
122. A. Grassi and co-workers, *Macromolecules* **31**, 5588–5591 (1998).
123. C. Pellechia and A. Grassi, *Top. Catal.* **7**, 125–132 (1999).
124. W. Kaminsky and co-workers, *Macromolecules* **25**, 7647–7650 (1997).
125. N. Schneider, M.-H. Prosenc, and H.-H. Brintzinger, *J. Organomet. Chem.* **545/546**, 291–295 (1997).
126. G. Xu, *Macromolecules* **31**, 586–591 (1998).
127. E. F. Williams, M. C. Murray, and M. C. Baird, *Macromolecules* **33**, 261–268 (2000).
128. R. Quyoum and co-workers, *J. Am. Chem. Soc.* **116**, 6435–6436 (1994).
129. Q. Wang and co-workers, *Organometallics* **15**, 693–703 (1996).
130. T. L. Tremblay and co-workers, *Chem. Commun.* 831–832 (1997).
131. S. W. Ewart and M. C. Baird, *Top. Catal.* **7**, 1–8 (1999).
132. M. C. Baird, *Chem. Rev.* **100**, 1471–1478 (2000).
133. P. L. Watson, *J. Am. Chem. Soc.* **104**, 337–339 (1982).
134. P. L. Watson, *J. Am. Chem. Soc.* **104**, 6471–6473 (1982).
135. D. Stern, M. Sabat, and T. J. Marks, *J. Am. Chem. Soc.* **112**, 9558–9575 (1990).
136. P. J. Shapiro and co-workers, *Organometallics* **9**, 867–869 (1990).
137. P. J. Shapiro and co-workers, *J. Am. Chem. Soc.* **116**, 4623–4640 (1994).
138. J. P. Mitchell and co-workers, *J. Am. Chem. Soc.* **118**, 1045–1053 (1996).
139. J. H. Gilchrist and J. E. Bercaw, *J. Am. Chem. Soc.* **118**, 12021–12028 (1996).
140. M. B. Abrams and co-workers, *Organometallics* **18**, 1389–1401 (1999).
141. E. Ihara and co-workers, *Macromol. Chem. Phys.* **197**, 1909–1917 (1996).
142. A. Pastor and co-workers, *J. Organomet. Chem.* **528**, 65–75 (1997).
143. G. C. Bazan and co-workers, *J. Am. Chem. Soc.* **118**, 2291–2292 (1996).
144. G. C. Bazan and co-workers, *Organometallics* **16**, 2492–2494 (1997).
145. A. J. Ashe III and co-workers, *Organometallics* **17**, 3883–3888 (1998).
146. A. J. Ashe III, S. Al-Ahmad, and X. G. Fang, *J. Organomet. Chem.* **581**, 92–97 (1999).
147. A. J. Ashe III, X. G. Fang, and J. W. Kampf, *Organometallics* **18**, 1363–1365 (1999).
148. S. A. A. Shah and co-workers, *Organometallics* **15**, 3176–3181 (1996).
149. J. D. Scollard, D. H. McConville, and J. J. Vittal, *Organometallics* **14**, 5478–5480 (1995).
150. J. D. Scollard and co-workers, *Macromolecules* **29**, 5241–5243 (1996).
151. J. D. Scollard and D. H. McConville, *J. Am. Chem. Soc.* **118**, 10008–10009 (1996).

152. J. D. Scollard, D. H. McConville, and S. J. Rettig, *Organometallics* **16**, 1810–1812 (1997).
153. J. D. Scollard and co-workers, *J. Mol. Catal. A: Chem.* **128**, 201–214 (1998).
154. L.-C. Liang and co-workers, *J. Am. Chem. Soc.* **121**, 5797–5798 (1999).
155. S. Tinkler and co-workers, *Chem. Commun.* 2623–2624 (1996).
156. H. Mack and M. Eisen, *J. Organomet. Chem.* **525**, 81–87 (1996).
157. A. D. Horton and J. de With, *Chem. Commun.* 1375–1376 (1996).
158. A. D. Horton and co-workers, *Organometallics* **15**, 2672–2674 (1996).
159. N. A. H. Male, M. Thornton-Pett, and M. Bochmann, *J. Chem. Soc., Dalton Trans.* 2487–2494 (1997).
160. R. Baumann, W. M. Davis, and R. R. Schrock, *J. Am. Chem. Soc.* **119**, 3830–3831 (1997).
161. R. R. Schrock and co-workers, *Organometallics* **18**, 3649–3670 (1999).
162. B. Tsuie and co-workers, *Organometallics* **16**, 1392–1400 (1997).
163. Y. M. Jeon and co-workers, *Organometallics* **17**, 3161–3163 (1998).
164. C. H. Lee, Y.-H. La, and J. W. Park, *Organometallics* **19**, 344–351 (2000).
165. A. van der Linden and co-workers, *J. Am. Chem. Soc.* **117**, 3008–3021 (1995).
166. S. Fokken and co-workers, *Organometallics* **15**, 5069–5072 (1996).
167. S. Fokken and co-workers, *Organometallics* **16**, 4240–4242 (1997).
168. F. G. Sernetz and co-workers, *Macromolecules* **30**, 1562–1569 (1997).
169. K. Mashima, S. Fujikawa, and A. Nakamura, *J. Am. Chem. Soc.* **115**, 10990–10991 (1993).
170. K. Hakala and co-workers, *Macromol. Rapid Commun.* **18**, 635–638 (1997).
171. J. Jaffart and co-workers, *Eur. J. Inorg. Chem.* 425–428 (1998).
172. A. Spannenberg and co-workers, *Angew. Chem., Int. Ed. Engl.* **37**, 3363–3365 (1998).
173. P. T. Witte, A. Meetsma, and B. Hessen, *Organometallics* **18**, 2944–2946 (1999).
174. M. P. Coles and co-workers, *J. Organomet. Chem.* **591**, 78–87 (1999).
175. M. Peuckert and W. Keim, *Organometallics* **2**, 594–597 (1983).
176. G. Wilke, *Angew. Chem., Int. Ed. Engl.* **27**, 185–206 (1988).
177. W. Keim and co-workers, *Angew. Chem., Int. Ed. Engl.* **17**, 466–467 (1978).
178. W. Keim, *Angew. Chem., Int. Ed. Engl.* **29**, 235–244 (1990).
179. L. K. Johnson, C. M. Killian, and M. Brookhart, *J. Am. Chem. Soc.* **117**, 6414–6415 (1995).
180. C. M. Killian and co-workers, *J. Am. Chem. Soc.* **118**, 11664–11665 (1996).
181. S. A. Svejda, L. K. Johnson, and M. Brookhart, *J. Am. Chem. Soc.* **121**, 10634–10635 (1999).
182. D. P. Gates and co-workers, *Macromolecules* **33**, 2320–2334 (2000).
183. M. Brookhart and B. L. Small, in *9th IUPAC Symposium on Organometallic Chemistry Directed Towards Organic Synthesis*, Göttingen, Germany, July 20–25, 1997. Book of Abstracts, p. 447.
184. B. L. Small, M. Brookhart, and A. M. A. Bennett, *J. Am. Chem. Soc.* **120**, 4049–4050 (1998).
185. WO 98/27124 (1998), A. M. A. Bennett (to E.I. du Pont de Nermours & Co., Inc.); *Chem. Abstr.* **129**, 122973x (1998).
186. A. M. A. Bennett, *CHEMTECH* **29**(7), 24–28 (1999).
187. G. J. P. Britovsek and co-workers, *Chem. Commun.* 849–850 (1998).
188. G. J. P. Britovsek and co-workers, *J. Am. Chem. Soc.* **121**, 8728–8740 (1999).
189. B. L. Small and M. Brookhart, *J. Am. Chem. Soc.* **120**, 7143–7144 (1998).
190. B. L. Small and M. Brookhart, *Macromolecules* **32**, 2120–2130 (1999).
191. C. Wang and co-workers, *Organometallics* **17**, 3149–3151 (1998).
192. T. R. Younkin and co-workers, *Science* **287**, 460–462 (2000).
193. L. K. Johnson, S. Mecking, and M. Brookhart, *J. Am. Chem. Soc.* **118**, 267–268 (1996).

194. S. Mecking and co-workers, *J. Am. Chem. Soc.* **120**, 888–899 (1998).
195. S. D. Ittel, L. K. Johnson, and M. Brookhart, *Chem. Rev.* **100**, 1169–1204 (2000).
196. S. D. Ittel, in Ref. 36, pp. 616–628.
197. R. F. Jordan, *Adv. Organomet. Chem.* **32**, 325–387 (1991).
198. E. Y.-X. Chen and T. J. Marks, *Chem. Rev.* **100**, 1391–1434 (2000).
199. J. Bliemeister and co-workers, in Ref. 32, pp. 57–82.
200. H. Sinn and co-workers, in Ref. 36, pp. 105–122.
201. D. W. Imhoff and co-workers, *Organometallics* **17**, 1941–1945 (1998).
202. D. W. Imhoff and co-workers, *Organometallics*, **1**, 177–191 (1998).
203. W. Kaminsky and R. Steiger, *Polyhedron* **7**, 2375–2381 (1988).
204. D. Cam and U. Giannini, *Makromol. Chem.* **193**, 1049–1055 (1992).
205. M. Bochmann and L. M. Wilson, *J. Chem. Soc., Chem. Commun.* 1610–1611 (1986).
206. M. Bochmann and co-workers, *Organometallics* **7**, 1148–1154 (1988).
207. M. Bochmann, A. J. Jaggar, and J. C. Nicholls, *Angew. Chem., Int. Ed. Engl.* **29**, 780–782 (1990).
208. R. F. Jordan and co-workers, *J. Am. Chem. Soc.* **108**, 7410–7411 (1986).
209. R. F. Jordan and co-workers, *J. Am. Chem. Soc.* **109**, 4111–4113 (1987).
210. R. F. Jordan and co-workers, *Organometallics* **8**, 2892–2903 (1989).
211. G. G. Hlatky, H. W. Turner, and R. E. Eckman, *J. Am. Chem. Soc.* **111**, 2728–2729 (1989).
212. A. D. Horton and J. H. G. Frijns, *Angew. Chem., Int. Ed. Engl.* **30**, 1152–1154 (1991).
213. J. J. W. Eshuis and co-workers, *Organometallics* **11**, 362–369 (1992).
214. Eur. Pat. Appl. EP 277,004 (1988), H. W. Turner (to Exxon Chemical Co.); *Chem. Abstr.* 110, 58290a (1989).
215. U.S. Pat. Appl. 459,921 (1990), G. G. Hlatky, D. J. Upton, and H. W. Turner (to Exxon Chemical Co.); *Chem. Abstr.* 115, 256897v (1991).
216. X. Yang, C. L. Stern, and T. J. Marks, *J. Am. Chem. Soc.* **113**, 3623–3625 (1991).
217. X. Yang, C. L. Stern, and T. J. Marks, *J. Am. Chem. Soc.* **116**, 10015–10031 (1994).
218. P. A. Deck and T. J. Marks, *J. Am. Chem. Soc.* **117**, 6128–6129 (1995).
219. M. A. Giardello and co-workers, *J. Am. Chem. Soc.* **117**, 12114–12129 (1995).
220. L. Jia and co-workers, *Organometallics* **14**, 3135–3137 (1995).
221. Y.-X. Chen and co-workers, *J. Am. Chem. Soc.* **118**, 12451–12452 (1996).
222. Y.-X. Chen, C. L. Stern, and T. J. Marks, *J. Am. Chem. Soc.* **119**, 2582–2583 (1997).
223. L. Jia and co-workers, *Organometallics* **16**, 842–857 (1997).
224. Y.-X. Chen and co-workers, *J. Am. Chem. Soc.* **120**, 6287–6305 (1998).
225. L. Luo and T. J. Marks, *Top. Catal.* **7**, 97–106 (1999).
226. M. V. Metz and co-workers, *Angew. Chem., Int. Ed. Engl.* **39**, 1312–1316 (2000).
227. M. Bochmann and S. J. Lancaster, *Organometallics* **12**, 633–640 (1993).
228. M. Bochmann and co-workers, *Organometallics* **13**, 2235–2243 (1994).
229. M. Bochmann and S. J. Lancaster, *J. Organomet. Chem.* **497**, 55–59 (1995).
230. M. Bochmann, *Top. Catal.* **7**, 9–22 (1999).
231. V. C. Williams and co-workers, *J. Am. Chem. Soc.* **121**, 3244–3245 (1999).
232. V. C. Williams and co-workers, *Angew. Chem., Int. Ed. Engl.* **38**, 3695–3698 (1999).
233. V. C. Williams and co-workers, *Organometallics* **19**, 1619–1621 (2000).
234. J. C. W. Chien, W.-M. Tsai, and M. D. Rausch, *J. Am. Chem. Soc.* **113**, 8570–8571 (1991).
235. J. C. W. Chien, W. Song, and M. D. Rausch, *Macromolecules* **26**, 3239–3240 (1993).
236. A. R. Siedle and R. A. Newmark, *J. Organomet. Chem.* **497**, 119–125 (1995).
237. G. Kehr and co-workers, *Chem. Eur. J.* **6**, 258–266 (2000).
238. B. Temme and co-workers, *Angew. Chem., Int. Ed. Engl.* **34**, 1755–1757 (1995).
239. B. Temme, J. Karl, and G. Erker, *Chem. Eur. J.* **2**, 919–924 (1996).
240. J. Karl, G. Erker, and R. Fröhlich, *J. Am. Chem. Soc.* **119**, 11165–11173 (1997).

241. J. Karl and G. Erker, *Chem. Ber.* **130**, 1261–1267 (1997).
242. M. Dahlmann and co-workers, *J. Am. Chem. Soc.* **121**, 2820–2828 (1999).
243. M. Bochmann, S. J. Lancaster, and O. B. Robinson, *J. Chem. Soc., Chem. Commun.* 2081–2082 (1995).
244. X. Song and M. Bochmann, *J. Organomet. Chem.* **545/546**, 597–600 (1997).
245. Y. Sun and co-workers, *J. Am. Chem. Soc.* **119**, 5132–5143 (1997).
246. W. E. Piers, *Chem. Eur. J.* **4**, 13–18 (1998).
247. W. E. Piers, Y. Sun, and L. M. Lee, *Top. Catal.* **7**, 133–143 (1999).
248. Y. Sun and co-workers, *Organometallics* **19**, 1625–1627 (2000).
249. P. Cossee, *Tetrahedron Lett.* **17**, 12–16 (1960).
250. P. Cossee, *Tetrahedron Lett.* **17**, 17–21 (1960).
251. P. Cossee, *J. Catal.* **3**, 80–88 (1964).
252. E. J. Arlman and P. Cossee, *J. Catal.* **3**, 99–104 (1964).
253. M. L. H. Green, *Pure Appl. Chem.* **50**, 27–35 (1978).
254. K. J. Ivin and co-workers, *J. Chem. Soc., Chem. Commun.* 604–606 (1978).
255. Z. Dawoodi and co-workers, *J. Chem. Soc., Chem. Commun.* 1410–1411 (1982).
256. D. T. Laverty and J. J. Rooney, *J. Chem. Soc., Faraday Trans. 1* **79**, 869–878 (1983).
257. M. Brookhart and M. L. H. Green, *J. Organomet. Chem.* **250**, 395–408 (1983).
258. L. Resconi, I. Camurati, and O. Sudmeijer, *Top. Catal.* **7**, 145–163 (1999).
259. W. Kaminsky, A. Ahlers, and N. Möller-Lindenhof, *Angew. Chem., Int. Ed. Engl.* **28**, 1216–1218 (1989).
260. B. J. Burger and co-workers, *J. Am. Chem. Soc.* **112**, 1566–1577 (1990).
261. T. Tsutsui, A. Mizuno, and N. Kashiwa, *Polymer* **30**, 428–431 (1989).
262. J. J. W. Eshuis and co-workers, *J. Mol. Catal.* **62**, 277–287 (1990).
263. L. Resconi and co-workers, *J. Am. Chem. Soc.* **114**, 1025–1032 (1992).
264. W. Kaminsky and H. Lüker, *Macromol. Chem., Rapid Commun.* **5**, 225–228 (1989).
265. T. Tsutsui, N. Kashiwa, and A. Mizuno, *Macromol. Chem., Rapid Commun.* **11**, 565–570 (1990).
266. J. C. W. Chien and B.-P. Wang, *J. Polym. Sci., Part A: Polym. Chem.* **28**, 15–38 (1990).
267. A. R. Siedle and co-workers, *Polyhedron* **9**, 301–308 (1990).
268. L. Resconi, S. Bossi, and L. Abis, *Macromolecules* **23**, 4489–4491 (1990).
269. A.-L. Mogstad and R. M. Waymouth, *Macromolecules* **25**, 2282–2284 (1992).
270. A.-L. Mogstad and R. M. Waymouth, *Macromolecules* **27**, 2313–2315 (1994).
271. R. Leino and co-workers, *Macromolecules* **30**, 3477–3483 (1997).
272. G. Erker and C. Fritze, *Angew. Chem., Int. Ed. Engl.* **31**, 199–202 (1992).
273. L. Resconi, L. Abis, and G. Franciscono, *Macromolecules* **25**, 6814–6817 (1992).
274. C. Pellechia and A. Zambelli, *Macromol. Rapid Commun.* **17**, 333–338 (1996).
275. C. Pellechia and co-workers, *Macromolecules* **29**, 6990–6993 (1996).
276. C. Pellechia and co-workers, *J. Mol. Catal. A: Chem.* **128**, 229–237 (1998).
277. G. Milano and co-workers, *Organometallics* **19**, 1343–1349 (2000).
278. P. Pino, P. Cioni, and J. Wei, *J. Am. Chem. Soc.* **109**, 6189–6191 (1987).
279. R. Waymouth and P. Pino, *J. Am. Chem. Soc.* **112**, 4911–4914 (1990).
280. M. K. Leclerc and H. H. Brintzinger, *J. Am. Chem. Soc.* **117**, 1651–1652 (1995).
281. M. K. Leclerc and H. H. Brintzinger, *J. Am. Chem. Soc.* **118**, 9024–9032 (1996).
282. A. K. Rappé, W. M. Skiff, and C. J. Casewit, *Chem. Rev.* **100**, 1435–1456 (2000).
283. K. Angermund and co-workers, *Chem. Rev.* **100**, 1457–1470 (2000).
284. L. Cavallo, G. Guerra, and P. Corradini, *Gazz. Chim. Ital.* **126**, 463–467 (1988).
285. P. Corradini and co-workers, *Gazz. Chim. Ital.* **118**, 173–177 (1988).
286. L. Cavallo and co-workers, *Macromolecules* **24**, 1784–1790 (1991).
287. G. Guerra and co-workers, *J. Am. Chem. Soc.* **116**, 2988–2995 (1994).
288. L. Cavallo and G. Guerra, *Macromolecules* **29**, 2729–2737 (1996).
289. G. Guerra and co-workers, *J. Am. Chem. Soc.* **119**, 4394–4403 (1997).

290. Z. Yu and J. C. W. Chien, *J. Polym. Sci., Part A: Polym. Chem.* **33**, 125–135 (1995).
291. Y. van der Leek and co-workers, *Chem. Eur. J.* **3**, 585–591 (1997).
292. L. A. Castonguay and A. K. Rappé, *J. Am. Chem. Soc.* **114**, 5832–5842 (1992).
293. E. P. Bierwagen, J. E. Bercaw, and W. A. Goddard III, *J. Am. Chem. Soc.* **116**, 1481–1489 (1994).
294. R. J. Meier and co-workers, *J. Am. Chem. Soc.* **116**, 7274–7281 (1994).
295. T. Yoshida, N. Koga, and K. Morokuma, *Organometallics* **14**, 746–758 (1995).
296. R. D. J. Froese and co-workers, *J. Am. Chem. Soc.* **119**, 7190–7196 (1997).
297. E. A. H. Griffiths and co-workers, *Chem. Commun.* 1333–1334 (1999).
298. D. G. Musaev and co-workers, *J. Am. Chem. Soc.* **119**, 367–374 (1997).
299. J. C. W. Lohrenz, T. K. Woo, and T. Ziegler, *J. Am. Chem. Soc.* **117**, 12793–12800 (1995).
300. T. K. Woo and co-workers, *J. Am. Chem. Soc.* **118**, 13021–13030 (1996).
301. M. S. W. Chan and co-workers, *Organometallics* **18**, 4624–4636 (1999).
302. M.-H. Prosenc and H.-H. Brintzinger, *Organometallics* **16**, 3889–3894 (1997).
303. S. Lieber, M.-H. Prosenc, and H.-H. Brintzinger, *Organometallics* **19**, 377–387 (2000).
304. T. Yoshida, N. Koga, and K. Morokuma, *Organometallics* **15**, 766–777 (1996).
305. R. D. J. Froese, D. G. Musaev, and K. Morokuma, *J. Am. Chem. Soc.* **120**, 1581–1587 (1998).
306. L. Deng and co-workers, *J. Am. Chem. Soc.* **119**, 6177–6186 (1997).
307. L. Dengl, P. Margl, and T. Ziegler, *J. Am. Chem. Soc.* **121**, 6479–6487 (1999).
308. P. Margl, L. Dengl, and T. Ziegler, *Organometallics* **18**, 5701–5708 (1999).
309. H. G. Alt and A. Köppl, *Chem. Rev.* **100**, 1205–1222 (2000).
310. Z. Guan and co-workers, *Science* **283**, 2059–2062 (1999).
311. W. Kaminsky, K. Külper, and S. Niedoba, *Makromol. Chem., Macromol. Symp.* **3**, 377–387 (1986).
312. H. Drögemüller, K. Heiland, and W. Kaminsky, in W. Kaminsky and H. Sinn, eds., *Transition Metals and Organometallics as Catalysts for Olefin Polymerization*, Springer-Verlag, Berlin, 1988, pp. 303–308.
313. K. Heiland and W. Kaminsky, *Makromol. Chem.* **193**, 601–610 (1992).
314. J. C. W. Chien and D. He, *J. Polym. Sci., Part A: Polym. Chem.* **29**, 1585–1593 (1991).
315. J. C. W. Chien and D. He, *J. Polym. Sci., Part A: Polym. Chem.* **29**, 1595–1601 (1991).
316. J. C. W. Chien and T. Nozaki, *J. Polym. Sci., Part A: Polym. Chem.* **31**, 227–237 (1993).
317. T. Uozumi and K. Soga, *Makromol. Chem.* **193**, 823–831 (1992).
318. N. Herfert, P. Montag, and G. Fink, *Makromol. Chem.* **194**, 3167–3182 (1993).
319. J. Koivumäki, G. Fink, and J. V. Seppälä, *Macromolecules* **27**, 6254–6258 (1994).
320. J. Suhm, M. J. Schneider, and R. Mülhaupt, *J. Polym. Sci., Part A: Polym. Chem.* **35**, 735–740 (1997).
321. M. J. Schneider and co-workers, *Macromolecules* **30**, 3164–3168 (1997).
322. M. Miri, D. Hetzer, A. Miles, M. Pecak, and B. Riscili, in Ref. 36, pp. 509–515.
323. T. Uozumi and co-workers, *Macromol. Rapid Commun.* **18**, 883–889 (1997).
324. M. Galimberti and co-workers, *Macromol. Symp.* **89**, 259–275 (1995).
325. R. Kravchenko and R. M. Waymouth, *Macromolecules* **31**, 1–6 (1998).
326. M. Arndt and co-workers, *Macromol. Chem. Phys.* **199**, 1135–1152 (1998).
327. M. K. Leclerc and R. M. Waymouth, *Angew. Chem., Int. Ed. Engl.* **37**, 922–925 (1998).
328. G. Xu, *Macromolecules* **31**, 2395–2402 (1998).
329. T. D. Shaffer, J. A. M. Canich, and K. R. Squire, *Macromolecules* **31**, 5145–5147 (1998).
330. J. F. Vega and co-workers, *Macromolecules* **29**, 960–965 (1996).
331. A. Malmberg and co-workers, *Macromolecules* **31**, 8448–8454 (1998).
332. E. Kokko and co-workers, *J. Polym. Sci., Part A: Polym. Chem.* **38**, 376–388 (2000).
333. G. W. Coates, *Chem. Rev.* **100**, 1223–1252 (2000).

334. L. Resconi and co-workers, *Chem. Rev.* **100**, 1253–1346 (2000).
335. L. Resconi and co-workers, *Macromolecules* **28**, 6667–6676 (1995).
336. L. Resconi, *J. Mol. Catal. A: Chem.* **146**, 167–178 (1999).
337. V. Busico and R. Cipullo, *J. Am. Chem. Soc.* **116**, 9329–9330 (1994).
338. V. Busico and co-workers, *Macromolecules* **27**, 7538–7543 (1994).
339. V. Busico and R. Cipullo, *J. Organomet. Chem.* **497**, 113–118 (1995).
340. V. Busico and co-workers, *J. Am. Chem. Soc.* **118**, 2105–2106 (1996).
341. V. Busico and co-workers, *Macromolecules* **30**, 3971–3977 (1997).
342. V. Busico and co-workers, *J. Mol. Catal. A: Chem.* **128**, 53–64 (1998).
343. L. Resconi, F. Piemontesi, and R. L. Jones, in G. M. Benedikt and B. L. Goodall, eds., *Metallocene Catalyzed Polymers. Materials, Properties, Processing & Markets*, Plastics Design Library, New York, 1998, pp. 43–55.
344. W. Spaleck and co-workers, in Ref. 32, pp. 83–97.
345. L. Resconi and co-workers, *Organometallics* **19**, 420–429 (2000).
346. T. Mise, S. Miya, and H. Yamazaki, *Chem. Lett.* 1853–1856 (1989).
347. S. Collins and co-workers, *Organometallics* **10**, 2061–2068 (1991).
348. M. A. Giardello and co-workers, *J. Am. Chem. Soc.* **115**, 3326–3327 (1993).
349. M. A. Giardello and co-workers, *J. Am. Chem. Soc.* **117**, 12114–12129 (1995).
350. Y. Obora and co-workers, *Organometallics* **16**, 2503–2505 (1997).
351. S. Miyake, Y. Okumura, and S. Inazawa, *Macromolecules* **28**, 3074–3079 (1995).
352. H. Deng and co-workers, *Macromolecules* **29**, 6371–6376 (1996).
353. W. Spaleck and co-workers, *Macromol. Symp.* **89**, 237–247 (1995).
354. A. Razavi and co-workers, *Macromol. Symp.* **89**, 345–367 (1995).
355. G. Erker and co-workers, *J. Am. Chem. Soc.* **115**, 4590–4601 (1993).
356. G. Erker and co-workers, *J. Organomet. Chem.* **450**, 1–7 (1993).
357. M. Knickmeier, G. Erker, and T. Fox, *J. Am. Chem. Soc.* **118**, 9623–9630 (1996).
358. A. Razavi and J. L. Atwood, *J. Am. Chem. Soc.* **115**, 7529–7530 (1993).
359. G. Erker and co-workers, *J. Am. Chem. Soc.* **114**, 10983–10984 (1992).
360. G. Erker and co-workers, *Chem. Ber.* **127**, 1551–1553 (1994).
361. B. Rieger and co-workers, *Macromolecules* **23**, 3559–3568 (1990).
362. R. Fierro, J. C. W. Chien, and M. D. Rausch, *J. Polym. Sci., Part A: Polym. Chem.* **32**, 2817–2824 (1994).
363. M. L. H. Green and N. Ishihara, *J. Chem. Soc., Dalton Trans.* 657–665 (1994).
364. B. Rieger, *Polym. Bull.* **32**, 41–46 (1994).
365. W. Spaleck and co-workers, *J. Mol. Catal. A: Chem.* **128**, 279–287 (1998).
366. D. T. Mallin and co-workers, *J. Am. Chem. Soc.* **112**, 2030–2031 (1990).
367. J. C. W. Chien and co-workers, *J. Am. Chem. Soc.* **113**, 8569–8570 (1991).
368. G. H. Llinas and co-workers, *Macromolecules* **25**, 1242–1253 (1992).
369. J. C. W. Chien and co-workers, *J. Polym. Sci., Part A: Polym. Chem.* **30**, 2601–2617 (1992).
370. G. H. Llinas and co-workers, *Organometallics* **12**, 1283–1288 (1993).
371. W. J. Gauthier and co-workers, *Macromolecules* **28**, 3771–3778 (1995).
372. W. J. Gauthiuer and S. Collins, *Macromolecules* **28**, 3779–3786 (1995).
373. A. M. Bravakis and co-workers, *Macromolecules* **31**, 1000–1009 (1998).
374. R. Kravchenko, A. Masood, and R. M. Waymouth, *Organometallics* **16**, 3635–3639 (1997).
375. J. L. Maciejewski Petoff and co-workers, *Organometallics* **16**, 5909–5916 (1997).
376. M. D. Bruce and co-workers, *J. Am. Chem. Soc.* **119**, 11174–11182 (1997).
377. S. Lin and co-workers, *J. Mol. Catal. A: Chem.* **136**, 23–33 (1998).
378. R. Kravchenko and co-workers, *J. Am. Chem. Soc.* **120**, 2039–2046 (1998).
379. P. Witte, T. K. Lal, and R. M. Waymouth, *Organometallics* **18**, 4147–4155 (1999).
380. S. Jüngling and co-workers, *J. Polym. Sci., Part A: Polym. Chem.* **33**, 1305–1317 (1995).

381. S. Jüngling, S. Koltzenburg, and R. Mülhaupt, *J. Polym. Sci., Part A: Polym. Chem.* **35**, 1–8 (1997).
382. N. Kashiwa, S. Kojoh, J. Imuta, and T. Tsutsui, in Ref. 36, pp. 30–37.
383. J. A. Bandy and co-workers, *J. Chem. Soc., Dalton Trans.* 2207–2216 (1991).
384. T. K. Han and co-workers, *Macromolecules* **28**, 4801–4805 (1995).
385. J. A. Ewen, *Macromol. Symp.* **89**, 181–196 (1995).
386. L. Cavallo and co-workers, *Polymer* **32**, 1329–1335 (1991).
387. G. Natta, I. Pasquon, and A. Zambelli, *J. Am. Chem. Soc.* **84**, 1488–1490 (1962).
388. J. A. Ewen and co-workers, *Stud. Surf. Sci. Catal.* **56**, 439–482 (1990).
389. F. Grisi and co-workers, *J. Mol. Catal. A: Chem.* **140**, 225–233 (1999).
390. B. Rieger, T. Repo, and G. Jany, *Polym. Bull.* **35**, 87–94 (1995).
391. K. Patsidis and co-workers, *J. Organomet. Chem.* **509**, 63–71 (1996).
392. H. G. Alt, R. Zenk, and W. Milius, *J. Organomet. Chem.* **514**, 257–270 (1996).
393. H. G. Alt and R. Zenk, *J. Organomet. Chem.* **518**, 7–15 (1996).
394. H. G. Alt and R. Zenk, *J. Organomet. Chem.* **522**, 39–54 (1996).
395. H. G. Alt and E. Samuel, *Chem. Soc. Rev.* **27**, 323–329 (1998).
396. H. Lee and co-workers, *J. Organomet. Chem.* **561**, 37–47 (1998).
397. T. A. Herzog, D. L. Zubris, and J. E. Bercaw, *J. Am. Chem. Soc.* **118**, 11988–11989 (1996).
398. S. Miyake and J. E. Bercaw, *J. Mol. Catal. A: Chem.* **128**, 29–39 (1998).
399. S. A. Miller and J. E. Bercaw, *Abstr. Papers Am. Chem. Soc.* **217**, 151–INOR (1999).
400. S. A. Miller, *Metallocene-Mediated Olefin Polymerization: The Effects of Distal Ligand Perturbations on Polymer Stereochemistry, Ph.D. Thesis, California Institute of Technology, Pasadena, Calif.*, 2000.
401. M. J. Schneider and R. Mülhaupt, *Macromol. Chem. Phys.* **198**, 1121–1129 (1997).
402. F. Forlini and co-workers, *Macromol. Chem. Phys.* **198**, 2397–2408 (1997).
403. F. Forlini and co-workers, *Macromol. Chem. Phys.* **201**, 401–408 (2000).
404. I. Kim and Y. J. Kim, *Polym. Bull.* **40**, 415–421 (1998).
405. O. Henschke, A. Neubauer, and M. Arnold, *Macromolecules* **30**, 8097–8100 (1997).
406. T. Shiono, S. M. Azad, and T. Ikeda, *Macromolecules* **32**, 5723–5727 (1999).
407. G. Natta, *J. Polym. Sci.* **34**, 531–549 (1959).
408. J. W. Collette and co-workers, *Macromolecules* **22**, 3851–3858 (1989).
409. J. W. Collette and co-workers, *Macromolecules* **22**, 3858–3866 (1989).
410. W. Kaminsky and R. Spiehl, *Makromol. Chem.* **190**, 515–526 (1989).
411. W. Kaminsky, A. Bark, and M. Arndt, *Makromol. Chem., Macromol. Symp.* **47**, 83–93 (1991).
412. M. Arndt and W. Kaminsky, *Macromol. Symp.* **97**, 225–246 (1995).
413. W. Kaminsky, R. Engehausen, and J. Kopf, *Angew. Chem., Int. Ed. Engl.* **34**, 2273–2275 (1995).
414. W. Kaminsky and A. Noll, in Ref. 32, pp. 149–158.
415. B. A. Harrington and D. J. Crowther, *J. Mol. Catal. A: Chem.* **128**, 79–84 (1998).
416. M. Arndt and I. Beulich, *Macromol. Chem. Phys.* **199**, 1221–1232 (1998).
417. I. Tritto and co-workers, in Ref. 36, pp. 493–501.
418. A. L. McKnight and R. M. Waymouth, *Macromolecules* **32**, 2816–2825 (1999).
419. L. Resconi and R. M. Waymouth, *J. Am. Chem. Soc.* **112**, 4953–4954 (1990).
420. L. Cavallo and co-workers, *Macromolecules* **26**, 260–267 (1993).
421. O. R. de Ballesteros and co-workers, *Macromolecules* **28**, 2383–2388 (1995).
422. S. A. Miller and R. M. Waymouth, in Ref. 32, pp. 441–454.
423. G. W. Coates and R. M. Waymouth, *J. Am. Chem. Soc.* **113**, 6270–6271 (1991).
424. G. W. Coates and R. M. Waymouth, *J. Am. Chem. Soc.* **115**, 91–98 (1993).
425. M. R. Kesti, G. W. Coates, and R. M. Waymouth, *J. Am. Chem. Soc.* **114**, 9679–9680 (1992).

426. N. Tomotsu and co-workers, *J. Mol. Catal. A: Chem.* **128**, 167–190 (1998).
427. G. Xu and E. Ruckenstein, *J. Polym. Chem., Part A: Polym. Chem.* **37**, 2481–2488 (1999).
428. W. Kaminsky, D. Arrowsmith, and C. Strübel, *J. Polym. Chem., Part A: Polym. Chem.* **37**, 2959–2968 (1999).
429. U. Giannini and co-workers, *J. Polym. Sci.: Part C* **22**, 157–175 (1968).
430. J. Boor Jr., *Ziegler–Natta Catalysts and Polymerizations*, Academic Press, New York, 1979.
431. T. Simonazzi, A. De Nicola, M. Aglietto, and G. Ruggeri, in G. Allan, S. L. Aggarwal, and S. Russo, eds., *Comprehensive Polymer Science*, First Supplement, Pergamon Press, Oxford, 1992, pp. 133–158.
432. U. M. Stehling and co-workers, *Macromolecules* **31**, 2019–2027 (1998).
433. U. M. Stehling and co-workers, *Macromolecules* **32**, 14–20 (1999).
434. M. J. Schneider, R. Schäfer, and R. Mülhaupt, *Polymer* **38**, 2455–2459 (1997).
435. R. Goretzki and G. Fink, *Macromol. Rapid Commun.* **19**, 511–515 (1998).
436. M. M. Marques and co-workers, *J. Polym. Sci., Part A: Polym. Chem.* **37**, 2457–2469 (1999).
437. S. Bruzard and co-workers, *Macromol. Chem. Phys.* **198**, 291–303 (1997).
438. P. Aaltonen and B. Löfgren, *Macromolecules* **28**, 5353–5357 (1995).
439. P. Aaltonen and co-workers, *Macromolecules* **29**, 5255–5260 (1996).
440. C.-E. Wilén and J. H. Näsman, *Macromolecules* **27**, 4051–4057 (1994).
441. U. M. Stehling and co-workers, *Macromolecules* **31**, 4396–4398 (1998).
442. P. A. Fox, R. M. Waymouth, and C. Hawker, *Polym. Prepr. (Am. Chem. Soc., Div. Polym. Chem.)* **40**, 872–873 (1999).
443. W. Wiyatno and co-workers, *Polym. Prepr. (Am. Chem. Soc., Div. Polym. Chem.)* **41**(1), 85–86 (2000).
444. J. Okuda and I. L. Rushkin, *Macromolecules* **26**, 5530–5532 (1993).
445. J. Okuda and co-workers, *J. Organomet. Chem.* **501**, 37–39 (1995).
446. M. Hayakawa and co-workers, *Macromol. Chem. Phys.* **198**, 1305–1317 (1997).
447. M. Hayakawa and co-workers, *Macromol. Rapid Commun.* **17**, 865–870 (1996).
448. H. Yasuda and co-workers, *J. Am. Chem. Soc.* **114**, 4908–4910 (1992).
449. D. G. Ward and S. Collins, *J. Am. Chem. Soc.* **114**, 5460–5462 (1992).
450. Y. Li and co-workers, *Macromolecules* **30**, 1875–1883 (1997).
451. H. Nguyen and co-workers, *Macromolecules* **33**, 1508–1510 (2000).
452. M. A. Giardello and co-workers, *J. Am. Chem. Soc.* **117**, 3276–3277 (1995).
453. K. Soga and co-workers, *Macromolecules* **27**, 7938–7940 (1994).
454. H. Deng, T. Shiono, and K. Soga, *Macromolecules* **28**, 3067–3073 (1995).
455. H. Deng and K. Soga, *Macromolecules* **29**, 1847–1848 (1996).
456. L. S. Boffa and B. M. Novak, *Macromolecules* **27**, 6993–6995 (1994).
457. L. S. Boffa and B. M. Novak, *Macromolecules* **30**, 3494–3506 (1997).
458. M. Cheng and co-workers, *J. Am. Chem. Soc.* **121**, 11583–11584 (1999).
459. S. G. Correia and co-workers, *J. Polym. Sci., Part A: Polym. Chem.* **37**, 2471–2480 (1999).
460. R. Mülhaupt, T. Duschek, and B. Rieger, *Makromol. Chem., Macromol. Symp.* **48/49**, 317–332 (1991).
461. T. Shiono and K. Soga, *Macromolecules* **25**, 3356–3361 (1992).
462. T. Shiono and co-workers, *Macromolecules* **26**, 2085–2089 (1993).
463. T. C. Chung, H. L. Lu, and C. L. Li, *Macromolecules* **27**, 7533–7537 (1994).
464. W. Kaminsky, D. Arrowsmith, and H. R. Winkelbach, *Polym. Bull.* **36**, 577–584 (1996).
465. M. Hackmann and co-workers, *Macromol. Chem. Phys.* **199**, 1511–1517 (1998).
466. T. C. Chung and H. L. Lu, *J. Mol. Catal. A: Chem.* **115**, 115–127 (1997).
467. T. C. Chung and W. Janvikul, *J. Organomet. Chem.* **581**, 176–187 (1999).

468. G. Xu and T. C. Chung, *J. Am. Chem. Soc.* **121**, 6763–6764 (1999).
469. K. Koo and T. J. Marks, *J. Am. Chem. Soc.* **120**, 4019–4020 (1998).
470. K. Koo and T. J. Marks, *J. Am. Chem. Soc.* **121**, 8791–8802 (1999).
471. Y. Okamoto and T. Nakano, *Chem. Rev.* **94**, 349–372 (1994).
472. F. Ciardelli, in J. I. Kroschwitz, ed., *Encyclopedia of Polymer Science and Engineering*, Vol. **10**, Wiley, New York, 1987, pp. 463–493.
473. A. Schäfer and co-workers, *J. Organomet. Chem.* **328**, 87–99 (1987).
474. S. Collins, B. A. Kuntz, and Y. Hong, *J. Org. Chem.* **54**, 4154–4158 (1989).
475. B. Chin and S. L. Buchwald, *J. Org. Chem.* **62**, 2267–2268 (1997).
476. A. H. Hoveyda and J. P. Morken, *Angew. Chem., Int. Ed. Engl.* **35**, 1262–1284 (1996).
477. W. Kaminsky, *Angew. Makromol. Chem.* **145/146**, 149–160 (1986).
478. W. Kaminsky, A. Ahlers, and N. Möller-Lindenhof, *Angew. Chem., Int. Ed. Engl.* **28**, 1216–1218 (1989).
479. P. Pino, P. Cioni, and J. Wei, *J. Am. Chem. Soc.* **109**, 6189–6191 (1987).
480. P. Pino and co-workers, *Makromol. Chem.* **191**, 1677–1688 (1990).
481. M. Farina, *Top. Stereochem.* **17**, 1–111 (1987).
482. A. Sen, *Acc. Chem. Res.* **26**, 303–310 (1993).
483. M. Brookhart and co-workers, *J. Am. Chem. Soc.* **116**, 3641–3642 (1994).
484. M. R. Ribeiro, A. Deffieux, and M. F. Portela, *Ind. Eng. Chem. Res.* **36**, 1224–1237 (1997).
485. C. Jenny and P. Maddox, *Curr. Opin. Solid State Mater. Sci.* **3**, 94–103 (1998).
486. H. C. L. Abbenhuis, *Angew. Chem., Int. Ed. Engl.* **38**, 1058–1060 (1999).
487. J. C. W. Chien, *Top. Catal.* **7**, 23–26 (1999).
488. W. Kaminsky and H. Winkelbach, *Top. Catal.* **7**, 61–67 (1999).
489. M. O. Kristen, *Top. Catal.* **7**, 89–95 (1999).
490. G. G. Hlatky, *Chem. Rev.* **100**, 1347–1376 (2000).
491. G. Fink and co-workers, *Chem. Rev.* **100**, 1377–1390 (2000).
492. S. Jüngling, S. Koltzenburg, and R. Mülhaupt, *J. Polym. Sci., Part A: Polym. Chem.* **35**, 1–8 (1997).
493. U.S. Pat. 4,808,561 (1989), H. Welborn (to Exxon Chemical Co.); *Chem. Abstr.* **106**, 157033 (1987).
494. J. C. W. Chien and D. He, *J. Polym. Sci., Part A: Polym. Chem.* **29**, 1603–1607 (1991).
495. S. Collins, W. M. Kelly, and D. A. Holden, *Macromolecules* **25**, 1780–1785 (1992).
496. W. Kaminsky and F. Renner, *Makromol. Chem., Rapid Commun.* **14**, 239–243 (1993).
497. K. Soga and M. Kaminaka, *Macromol. Chem. Phys.* **195**, 1369–1379 (1994).
498. K. Soga, H. J. Kim, and T. Shiono, *Macromol. Chem. Phys.* **195**, 3347–3360 (1994).
499. K. Soga and co-workers, *Macromol. Symp.* **97**, 53–62 (1995).
500. M. C. Sacchi and co-workers, *Macromol. Rapid Commun.* **16**, 581–590 (1995).
501. G. G. Hlatky and D. J. Upton, *Macromolecules* **29**, 8019–8020 (1996).
502. D. Harrison and co-workers, *J. Mol. Catal. A: Chem.* **128**, 65–77 (1998).
503. S. I. Woo, Y. S. Ko, and T. K. Han, *Macromol. Rapid Commun.* **16**, 489–494 (1995).
504. M. Michelotti and co-workers, *J. Mol. Catal. A: Chem.* **129**, 241–248 (1998).
505. M. Michelotti and co-workers, *J. Mol. Catal. A: Chem.* **152**, 167–177 (2000).
506. T. Maschmeyer and co-workers, *Nature* **378**, 159–162.
507. Y. S. Ko and co-workers, *Macromol. Rapid Commun.* **17**, 749–758 (1996).
508. J. Tudor and D. O'Hare, *Chem. Commun.* 603–604 (1997).
509. L. K. Van Looveren and co-workers, *Angew. Chem., Int. Ed. Engl.* **37**, 517–520 (1998).
510. K. Kageyama, J. Tamazava, and T. Aida, *Science* **285**, 2113–2115 (1999).
511. D. Lee and K. Yoon, *Macromol. Rapid Commun.* **15**, 841–843 (1994).
512. D. Lee and K. Yoon, *Macromol. Symp.* **97**, 185–193 (1995).
513. H. Nishida and co-workers, *Macromol. Rapid Commun.* **16**, 821–830 (1995).
514. T. Kitagawa and co-workers, *Polymer* **38**, 615–620 (1997).

515. S. B. Roscoe and co-workers, *Science* **280**, 270–273 (1998).
516. T. Arai and co-workers, *Macromol. Chem. Phys.* **198**, 229–237 (1997).
517. K. Soga and co-workers, *Macromol. Chem. Phys.* **198**, 2779–2787 (1997).
518. H. Ahn and T. J. Marks, *J. Am. Chem. Soc.* **120**, 13533–13534 (1998).
519. H. G. Alt, *J. Chem. Soc., Dalton Trans.* 1703–1709 (1999).

REKO LEINO
Åbo Akademi University

SOLUTION POLYMERIZATION. See BULK AND SOLUTION POLYMERIZATION.

s-POLYSTYRENE. See SYNDIOTACTIC POLYSTYRENE.

STABILIZATION

Introduction

The performance of most polymer artifacts is adversely affected during the various stages of their lifecycle: manufacture, storage, processing/fabrication, and the service environment. Molecular oxygen is the main cause of irreversible polymer deterioration leading to loss of useful properties and ultimate mechanical failure. Its deleterious effect is accelerated by several other factors: temperature, sunlight, ozone, atmospheric pollutants, water, mechanical stress, adventitious metal, and metal ion contaminants. Most organic polymers, therefore, require protection against degradation, which can be achieved by the use of oxidation inhibitors referred to hereafter as *antioxidants* or *stabilizers*. Indeed the commercialization of some of the high tonnage polymers such as polypropylene (PP), and their use for outdoor applications, would not have been possible without the successful development of antioxidants. The use of very efficient stabilizers is also in great demand for applications involving second-life polymers, with reprocessing and recycling of thermoplastics as means of conservation of materials. Apart from cost and customer specifications, the amount of protection offered by antioxidants and stabilizers can vary enormously depending on the chemical structure of polymers, their physical and morphological characteristics, the manufacturing process, and service conditions of end-use articles (1–7).

The development of antioxidants and stabilizers started in the early part of the twentieth century as an empirical science (8–11). Progress in stabilization technology was made possible through a basic understanding of the underlying mechanisms of polymer oxidation. The terminologies used to describe antioxidants are wide ranging and reflect the polymer matrix. For example, in rubber technology, the terms antidegradants, antifatigue agents, and antiozonants are

Encyclopedia of Polymer Science and Technology. Copyright John Wiley & Sons, Inc. All rights reserved.

used, whereas in the plastics industry they are invariably referred to as melt (or processing) antioxidants, and heat and light stabilizers (or photoantioxidants). The terms primary and secondary antioxidants are also used, but the distinction is rather arbitrary and does not relate to their mechanisms of action. Although antioxidants and stabilizers are normally used at low concentrations (generally $<1\%$) they are key ingredients in the compounding of polymers. The continuous growth of polymer markets has ensured a parallel growth in demand for antioxidants and stabilizers, especially in the large tonnage polymers, with principal applications in packaging, building, automotive, electrical, and electronics systems.

This article aims to present a coherent treatment of the fundamental aspects of the science of polymer stabilization technology. The state of the art is discussed, with particular emphasis on recent developments and progress. A brief introduction to certain aspects of oxidation of polymers is given first before discussing the role of antioxidants, with examples to illustrate their basic mechanisms of action.

Oxidation of Polymers

Early works on free-radical chain theory for autoxidation of hydrocarbons (12–16) have shown that oxidation of hydrocarbons occurs autocatalytically, that is, the reaction starts slowly, possibly with a short induction period, followed by gradual increase in the rate (ascribed to the buildup of hydroperoxides) which will eventually subside giving rise to a sigmoidal curve as a function of time. The length of the short induction period is reduced or removed by the presence of initiators (eg, peroxides, azo compounds) and extended by antioxidants and stabilizers (Fig. 1). The basic autoxidation theory of hydrocarbons, involving a complex set of elementary reaction steps, was subsequently extended to oxidation of polymers (17–21). However, studies of oxidation in polymers, both in the solid phase (eg, under service conditions in presence of heat or light) and in the viscous melt during processing, are more complex than in liquid hydrocarbons because of the problems of oxygen diffusion, solubility, and effects of polymer crystallinity and morphology (4,22). The role of hydroperoxides in autoxidation of polymers cannot be overemphasized as they are associated with changes in molar mass of polymers and its properties leading ultimately to catastrophic failure (see Fig. 2).

Scheme 1 describes the free-radical process of polymer oxidation in terms of three basic steps: initiation, propagation, and termination (18). Although the origin of the first initiating macroalkyl radical is still controversial, many factors, eg, heat, mechanical stress, light, and transition metal impurities contribute to its formation (reaction (1a)). However, the direct reaction of polymers with oxygen (reaction (1b)) is generally not favored because of thermodynamic and kinetic considerations. It can only occur in polymers with very labile C—H bonds to give a relatively stable alkyl radicals that terminate, rather than propagate, the oxidation chain reaction. Oxygen can easily penetrate the amorphous regions of polymers; for example, in semicrystalline polymers these regions are highly oxidizable.

Propagation reactions involve the very fast reaction of oxygen with polymer alkyl radicals. Rate constants for reactions of most alkyl radicals with oxygen is of the order 10^7–10^9 $mol^{-1} \cdot s^{-1}$ (23). These reactions lead to the formation of macroalkylperoxyl radicals (Scheme 1, reaction 2), followed by abstraction of a

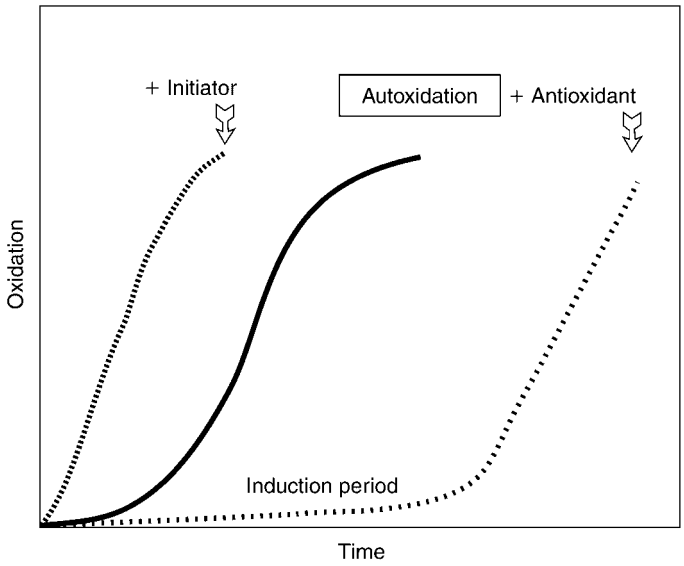

Fig. 1. Generalized scheme for changes in autoxidation curve, caused by presence of initiators and antioxidants.

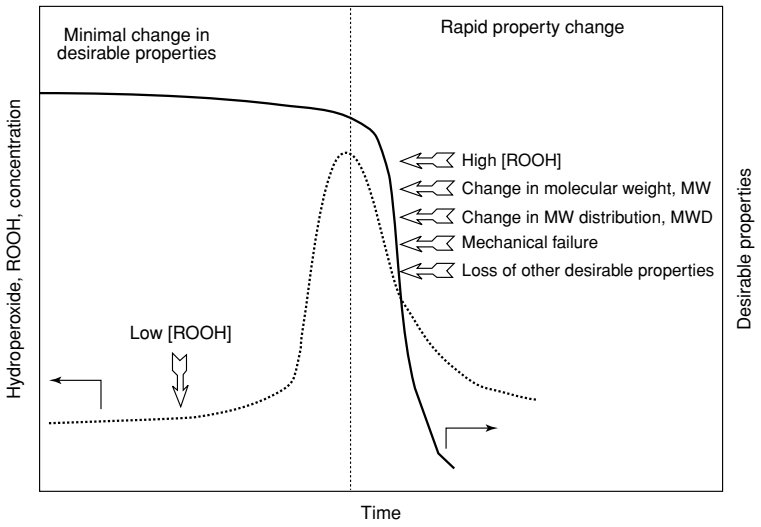

Fig. 2. Generalized scheme relating hydroperoxide concentration and loss of useful properties.

hydrogen from another polymer molecule (reaction 3). This latter reaction involves the breaking of a C—H bond and, therefore, a higher activation energy as compared to reaction 2. The rate of this reaction, which in most polymers determines the overall oxidation rate (rate determining step of autoxidation, RDS), is a function of both the C—H bond strength (allyl < benzyl and tertiary < secondary

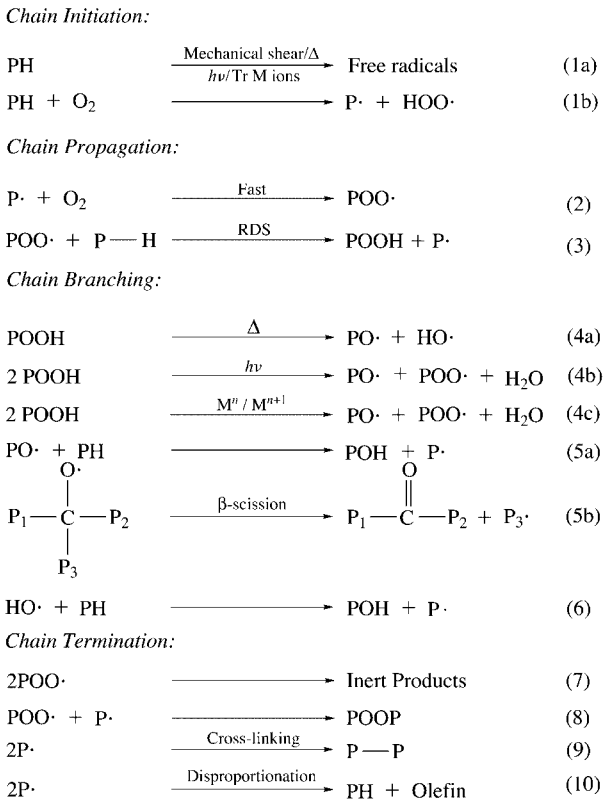

Scheme 1. Free-radical chain reaction involved in polymer oxidation.

< primary) and the stability of the macroalkyl radical formed (21,24–26). Reaction 3 gives macrohydroperoxides, the first molecular product of the chain oxidation process. These can undergo homolysis (bond dissociation energy of RO—OH is about 175 $kJ \cdot mol^{-1}$) under the effect of heat, light, or metal ions (from polymerization or pigments), giving rise to alkoxyl and hydroxyl macroradicals (reactions 4a–4c). Both these radicals can abstract a hydrogen from another polymer molecule, leading to new macroalkyl radicals (reactions 5a and 6), which continue the chain reaction. Alkoxyl radicals can undergo further reactions, eg, β-scission (see reaction 5b), which lead to cleavage of the polymer backbone and generation of further radicals.

The oxidative process terminates eventually through combination or disproportionation reactions involving the various propagating radicals. The exact nature of the terminating step, however, depends on the structure of the substrate as well as on oxygen concentration. Since reaction 3 is rate determining, alkylperoxyl radicals are the predominant reactive species under normal oxygen pressure (ie, $[POO\cdot] > [P\cdot]$) and termination occurs primarily through reaction 7, leading to diperoxides, carbonyl compounds, and alcohols (27–31). In the presence of limited amount of oxygen, eg, during polymer extrusion, alkyl radicals predominate (ie, $[P\cdot] > [POO\cdot]$) and termination reactions 8–10 assume greater significance.

These bimolecular termination reactions can lead to cross-linking with an increase in molar mass and/or disproportionation which takes place without changes in molar mass of the polymer (reactions 9 and 10). Other polymer radical reactions, including fragmentation and addition to double bonds to give rise to further free radicals, can also take place depending on the reaction conditions. These molecular changes lead ultimately to loss of mechanical properties (eg, impact strength, tensile strength, elongation) and premature failure, modification of surface appearance (eg, crack formation, loss of gloss, "chalking"), and, in many cases, to discoloration and yellowing.

Effect of Temperature and Water. Thermal oxidation of plastics and rubbers can occur at all stages of their lifecycle but is most pronounced during melt processing. The combined effects of temperature (180–330°C) and shear lead to mechanical rupture of polymer chains and formation of reactive mechano-alkyl radical ($R\cdot$). The thermal history of a polymer, therefore, has major consequences on its subsequent in-service performance. Table 1 summarizes the factors affecting polymer degradation at different stages of its lifecycle.

The nature of the polymer matrix exerts a profound effect on the mechanochemistry of the system. For example, thermal processing of poly(vinyl chloride) (PVC) results primarily in elimination/dehydrochlorination and discoloration rather than a change in molar mass. The formation of PVC macroradicals is

Table 1. Factors Affecting Degradation of Polymers at Different Stages of Their Lifecycle

Factors governing polymer degradation	Processing[a]	Service lifetime[b]
Physical state	Melt	Solid
Temperatures	180–320°C	−30 to 150°C
Oxygen concentration	Oxygen deficient conditions	Normal oxygen level
Exposure time	Minutes	Hours to Years
Radical concentrations	$[R\cdot] \gg [ROO\cdot]$	$[ROO\cdot] \gg [R\cdot]$
Hydroperoxide, ROOH, concentration	Low	Higher
Rate of ROOH decomposition	Fast	Moderate, depending on temperature
Factors accelerating the oxidation	Heat	Heat (lower temp.)
	Shear	Uv light
	Oxygen (Limited)	Oxygen, ozone
	Impurities and defects (from polymer manufacture, see Table 2)	Oxygenated moieties (from processing, see Table 2)
		Atmospheric pollutants (PNA,[c] S and N oxides)
		Water, solvents
		Metal ions, eg, copper

[a] For example, extrusion.
[b] For example, heat, uv radiation.
[c] PNA = polynuclear aromatic compounds.

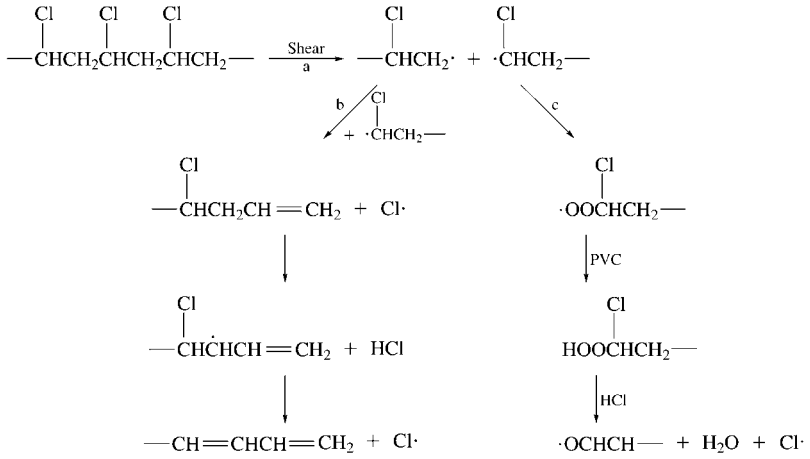

Scheme 2. Reactions of macroalkyl radical during high temperature processing of PVC.

followed by two competing reactions: elimination of HCl, leading to intense discoloration of the polymer (due to formation of conjugated double bonds) (Scheme 2, route b) and peroxidation (route c). The damage was found to be greatest during the first few minutes of processing when viscosity is highest (2,32–36).

Polyolefins, on the other hand, undergo changes in molar mass although the effect is not so visible as is the case for PVC. For example, PP undergoes mainly chain scission whereas polyethylene (PE) undergoes predominantly cross-linking (37–45) (Scheme 3). The presence of various unsaturated groups (eg, vinyl, vinylidene, *trans*-vinylene) as impurities in PE plays an important role in the overall oxidation and cross-linking of the polymer. Macroalkyl and macroalkoxyl radicals are intermediates and are ultimately responsible for the formation of various impurities including macrohydroperoxides, carbonyl groups, and double bonds (see Scheme 3). Polystyrene (PS) behaves similarly to PP under processing conditions where decomposition of tertiary hydroperoxides results in chain scission and reduction in molar mass (46) (Scheme 4).

All thermoplastic polymers, therefore, show a high rate of mechano-thermal degradation in the initial stages of the processing operation, giving rise to a buildup of irregularities into the macromolecule with profound effects on polymer performance during aging (1,2,37).

Although less systematic work has been carried out on mechano-thermal oxidation of other polymers during processing, generally they degrade in similar way to that of polyolefins, styrenics, and PVC. For example, aliphatic polyamides and polyesters, which are more stable under processing conditions than polyolefins, undergo free-radical attack, after initial formation of mechano radicals, by hydrogen abstraction at methylene groups in position α to the nitrogen (polyamides) or oxygen (polyesters) atoms, resulting in peroxidation and reduction in molar mass (2,47–49) (see Scheme 5).

It is important to point out that these polymers, along with other heteroatom-containing polymers such as polycarbonates (PC) and poly(ethylene terephthalate) (PET), are also highly susceptible to hydrolytic degradation (Scheme 6),

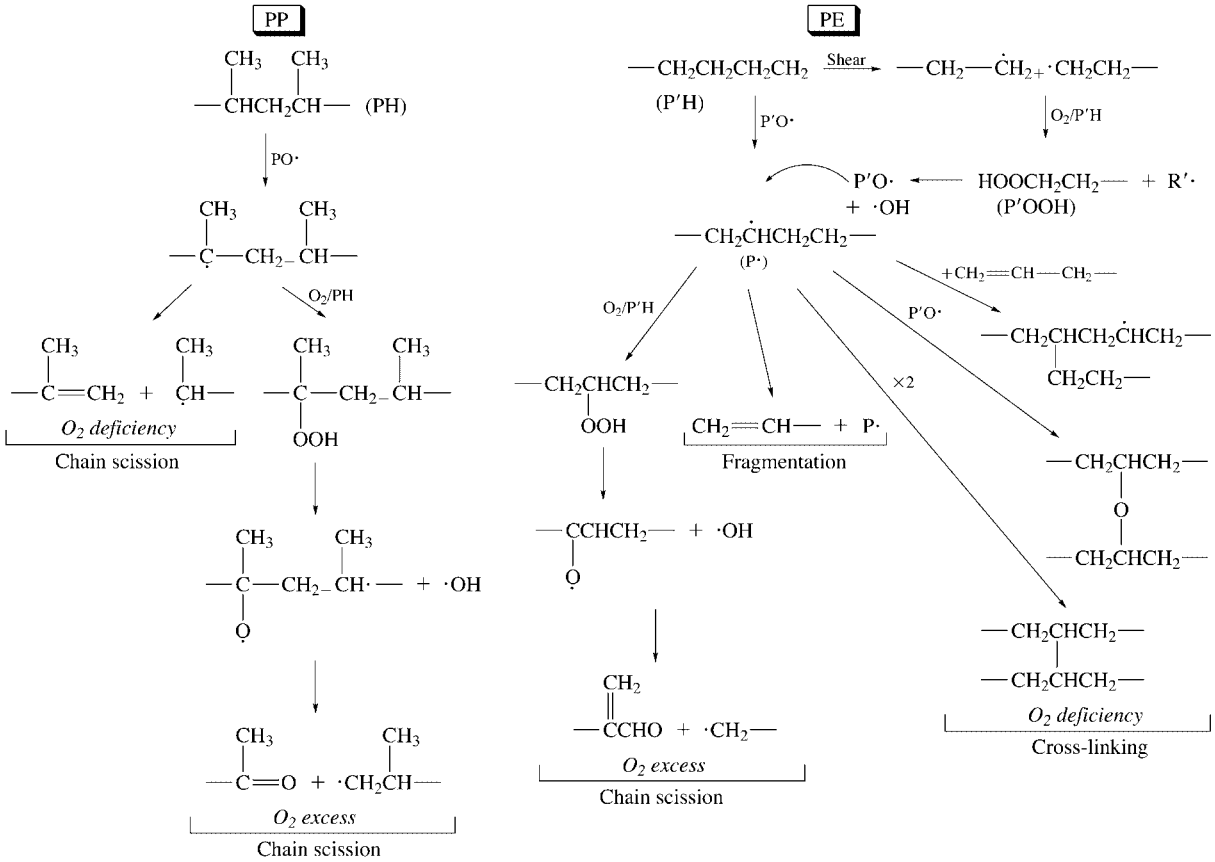

Scheme 3. Reactions of macroalkyl radicals during high temperature processing of polyolefins.

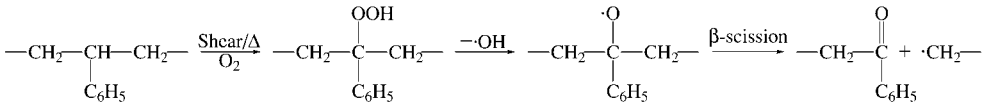

Scheme 4. Chain scission of PE hydroperoxides formed during melt processing.

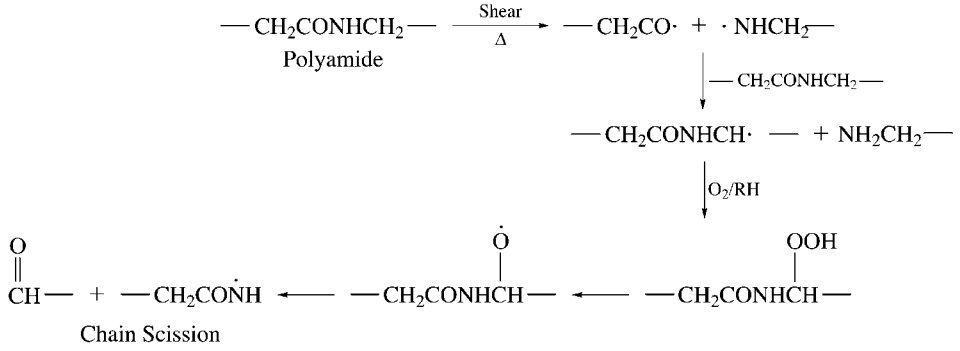

Scheme 5. Reactions of polyamides during high temperature processing.

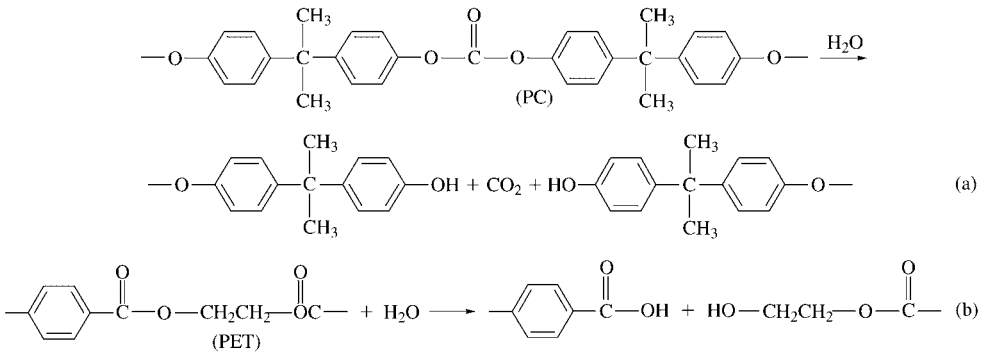

Scheme 6. Hydrolytic degradation of PC (**a**) and PET (**b**).

giving rise to chain scission, reduction in molar mass, and deterioration of mechanical properties. These polymers must be dried before melt processing, which is normally performed at temperatures of up to 300°C.

Polymers may be further subjected to the effect of temperature during their service performance, and their oxidation is referred to here as long-term thermal oxidation and is related to many applications including automotive (eg, under the bonnet), domestic appliances, and electronics systems. In addition to temperature, both polymer morphology and sample thickness influence significantly the long-term thermal oxidative behavior of polymers. As previously discussed alkylperoxyl radicals predominate under these oxidation conditions (see Table 1). For thin polymer samples ($<3 \times 10^{-3}$ cm) oxygen diffusion is not rate determining and the main termination process (in the absence of antioxidants) is a bimolecular reaction of alkylperoxyl radicals (Scheme 1, reaction 7). For thick polymer sections, and particularly at high temperatures, oxygen may become deficient

inside the sample during long-term thermal exposure, hence increasing the role of alkyl radicals in polymer oxidation which necessitates different strategies for its inhibition.

Effect of Ultraviolet Light and Outdoor Environment. The second stage of the polymer lifecycle, where oxidative degradation is a main cause for concern, occurs during outdoor exposure. The chemical impurities, eg, hydroperoxides, carbonyl compounds and unsaturation, which are generated during polymer manufacture and processing/fabrication, can further sensitize and accelerate polymer degradation under service conditions. Based purely on chemical structure, many of the polymers are intrinsically transparent to the shorter wavelengths of the sun spectrum (<290 nm). However, commercial hydrocarbon polymers, eg, PE and PP, are highly sensitive to outdoor weathering due to the presence of light absorbing impurities, especially oxygen-containing species. In view of the important role of oxygen-containing species as photoinitiators, the prior thermal history of polymers has a profound effect on their subsequent photo-oxidative behavior in service. Hydroperoxides formed during melt processing (and to a lesser extent during manufacturing and storage) are the most important photoinitiators during the early stages of polymer photo-oxidation (see Scheme 1, reaction 4b), while the derived carbonyl-containing products exert deleterious effects during the later stages by Norrish types I and II photocleavage processes, resulting in backbone scission (50–55) (Scheme 7).

It is important to point out that exposure of polymer articles to outdoor weathering results in photo-oxidation due to the direct effect of uv light (sunlight). This oxidation process is also affected by other environmental factors including heat, atmospheric pollutants, water (particularly in the case of polymers containing heteroatoms), and ozone (especially for unsaturated elastomers) (see Table 2). These factors may catalyze the formation of free radicals and light-sensitive chromophoric groups and initiate photo-oxidation (56–63). Under photo-oxidative conditions there is a high alkyl-to-alkylperoxyl radical ratio because of the higher rate of initiation, compared to oxidation under thermal conditions, and relatively low rate of oxygen diffusion in the solid polymer (22,64).

The photo-oxidative behavior of commercial polymers is widely different. The most photo-oxidizable polymers are the unsaturated rubbers with labile R—H bond and are generally heavily filled with carbon black (an effective sun-screen; see later) in outdoor applications. Similarly, rubber modified plastics, eg, high impact polystyrene (HIPS) and acrylonitrile–butadiene–styrene (ABS), are more

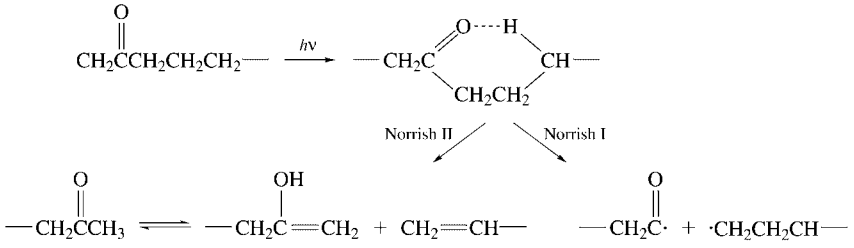

Scheme 7. Photolysis of PE (the Norrish reactions).

Table 2. Important Photoinitiators for Polyolefin Photo-oxidation

Stage	Photoinitiators
Polymer manufacture	Defects: unsaturation
	Impurities: transition metal ions present as catalyst residues
	Impurities: hydroperoxides and carbonyl compounds formed by adventitious oxidation
Processing and fabrication	Oxygenated moieties: hydroperoxides and carbonyl compounds formed by high temperature oxidation
	Transition metal ions from machinery or compounding ingredients
Environmental exposure	Atmospheric pollutants, eg, polynuclear aromatic compounds, nitrogen and sulfur oxides
	Carbonyl compounds by photolysis of hydroperoxides
	Unsaturation by photolysis of ketones
	Water
	Ozone

susceptible to photo-oxidation than polyolefins because of the rapid peroxidation of the rubber component that will sensitize the polymer to further photo-oxidation (65) (Scheme 8).

Light absorbing impurities and chromophoric groups present in commercial polyolefins (see Table 2) are responsible for their inherent photo-oxidative shortcomings (54). The photostability of the different members of the polyolefin family, however, vary significantly depending on their chemical and morphological structures; generally PP and high density polyethylene (HDPE) are more susceptible to photo-oxidation than low density polyethylene (LDPE) (37,66). PVC and PS should be relatively stable to photo-oxidation, but their thermal history exerts significant effects on their subsequent photo-oxidative behavior (67–70). The photo-oxidative stablility of engineering polymers such as aliphatic polyesters and polyamides is generally higher than that of polyolefins, albeit similar processes of peroxidation, photoinduced reactions, and chain scission are involved (71–76,76–81). Similarly, other engineering polymers such as PC, polysulphones, and poly(phenylene oxide) (PPO) are more stable to uv light than, for example, polyolefins and PVC. Prolonged outdoor exposure of these polymers lead to changes in their molar mass,

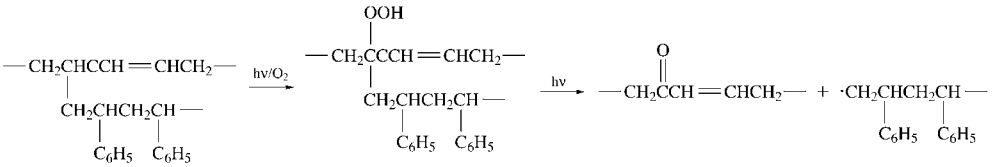

Scheme 8. Photoxidation of polybutadiene–polystyrene graft copolymer (HIPS).

reduction in mechanical properties, particularly impact strength and increasing yellowing, properties which can be particularly important in some applications, eg, the use of PC to replace glass for outdoor uses (55,81–84). The outdoor performance of all polymers can, however, be markedly improved by photo antioxidants and uv stabilizers.

Antioxidants in Polymer Stabilization—A Mechanistic Overview

Scheme 9 shows the two main oxidative cycles. Antioxidants and stabilizers can be classified according to their mode of action in interrupting the oxidative cycles: chain breaking and preventive (85,86). Examples of some commercial antioxidants from the different classes (87) are shown in Table 3 under their "primary" mode of action, albeit most antioxidants operate by more than one mechanism.

Chain-Breaking Antioxidants. Chain-breaking (CB) antioxidants (sometimes referred to as primary antioxidants) interrupt the primary oxidation cycle by removing the propagating radicals, ROO· and R· (85,88–92). Chain breaking donor (electron or hydrogen atom donors) (CB-D) antioxidants operate by reducing ROO· to ROOH (hydrogen atom donors) (see Scheme 10, reaction 10a). To be effective, CB-D antioxidants must compete with the chain propagating step (reaction 10b) and prevent hydrogen abstraction from the polymer. The antioxidant radical (A·) generated during this process must itself be stable (nonpropagating) and leads to stable molecular products (reaction 10c). Hindered phenols and aromatic amines (see Table 3, **AOs 1–12**) are some of the important examples of commercial CB-D antioxidants (see ANTIOXIDANTS).

Chain-breaking acceptor (CB-A) antioxidants, on the other hand, act by oxidizing alkyl radicals in a stoichiometric reaction and hence are only effective under oxygen-deficient conditions (reaction 10d). Antioxidants with structures based on benzofuranone derivatives (lactones) and hydroxylamines, as well as on quinones and stable free radicals, are good examples of CB-A antioxidants (91–96). Hindered amine derivatives [often referred to as hindered amine stabilizers (HAS); eg, **AOs 25–27**, Table 3 also function by a chain-breaking mechanism and, through their transformation products, are able to trap both R· and ROO· in a cyclical regenerative mechanism (50,55,62,94,97–100); for simplified reaction mechanism, see Scheme 11.

Preventive Antioxidants. Preventive antioxidants (sometimes referred to as secondary antioxidants) interrupt the second oxidative cycle by preventing or inhibiting the generation of free radicals (see Scheme 9). The most important preventive mechanism is the nonradical hydroperoxide decomposition (PD) (86,101). Phosphite esters and sulfur-containing compounds (eg, **AOs 15–24**, Table 3) are the most important classes of peroxide decomposers. Phosphites reduce hydroperoxides to alcohols and are themselves oxidized to the corresponding phosphates with a 1:1 stoichiometry and are referred to as stoichiometric peroxide decomposers (PD-S) (Scheme 12, reaction 12a). In addition to their peroxidolytic activity, some phosphite esters also behave as catalytic peroxidolytic agents (PD-C), and others (eg, hindered aryl phosphites; (see **AOs 15–18**, Table 3) are also capable of functioning by a chain-breaking mechanism (Scheme 12, reactions 12b and 12c). The contribution of each of these modes of action to the overall mechanism

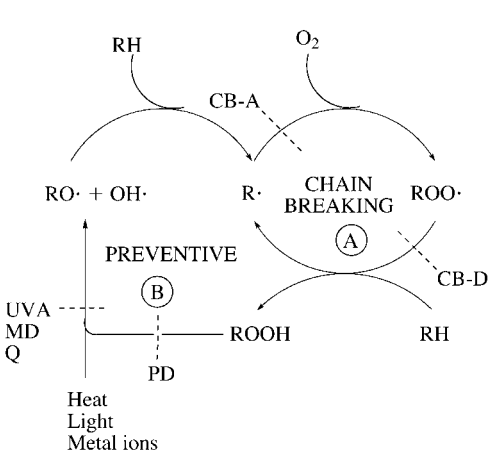

CB-A – Chain-Breaking Acceptors
Lactones
Hydroxylamines
Hindered Amine Photo-AOs through Derived Nitroxyl Radical

CB-D – Chain-Breaking Donors
Phenolic AOs—Synthetic & Biological
Aromatic Amines

PD – Peroxide Decomposers
Phosphites
Sulphur-Containing AOs
Nickel Complexes
Hydroxylamines

UVA – UV Absorbers
Hydroxy benzophenones
Hydroxy benzotriazoles

MD – Metal Deactivators

Q – Quenchers

Scheme 9. Oxidative degradation processes, antioxidant mechanisms, and some examples representing different antioxidant classes.

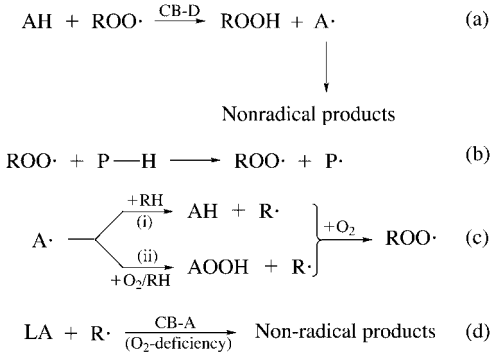

Scheme 10. Main reactions and competing pathways involved in chain-breaking antioxidant activity, where AH is a CB-D antioxidant, eg hindered phenol, A. is the antioxidant radical, and 1A is a CB-A antioxidant.

depends on the structure of the phosphite, oxidizability of the substrate, and the reaction conditions (102–104). Reaction 12d shows the hydrolysis of phosphite esters. Sulfur compounds, eg, thioethers and esters of thiodipropionic acid and metal dithiolates (see **AOs 19–24**, Table 3), decompose hydroperoxides catalytically (PD-C) whereby one antioxidant molecule destroys several hydroperoxides through the intermediacy of sulfur acids (Scheme 13) (86,101,105–107).

Metal ion deactivators (MD) act, primarily, by retarding metal-catalyzed oxidation of polymers (see Scheme 1, reaction 4c). They are used in polymers that are in contact with metals such as copper in wires and power cables. Metal deactivators are normally polyfunctional metal chelating compounds (eg, **AOs 33**,

Table 3. Some Examples of Commercial Antioxidants Representing the Principal Antioxidant Mechanisms

Antioxidant	Code	Trade name	Molecular mass
CHAIN-BREAKING ANTIOXIDANTS			
Hindered phenols			
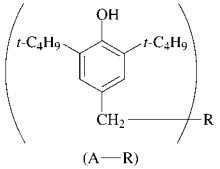 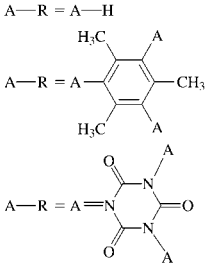 A—R = A—H; A—R = A—CH_3; A—R = A=N; A—R = A—$CH_2CO_2C_{18}H_{37}$; A—R = [A—$CH_2CO_2CH_2$—$\frac{1}{4}$ C; A—R = [A—$CH_2CONH(CH_2)_3$—$\frac{1}{2}$; A—R = [A—$CH_2COO(CH_2)_3$—$\frac{1}{2}$	**AO 1**	BHT	220
	AO 1	BHT	220
	AO 2	Irganox 1330	775
	AO 3	Irganox 3114	784
	AO 4	Irganox 1076	531
	AO 5	Irganox 1010	1178
	AO 6	Irganox 1098	637
	AO 7	Irganox 259	639
	AO 8	Irganox 3052	385
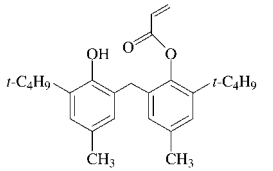	**AO 9**	Irganox 1081	359
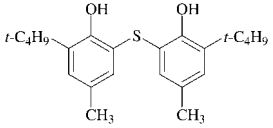			

Table 3. (Continued)

Antioxidant	Code	Trade name	Molecular mass	
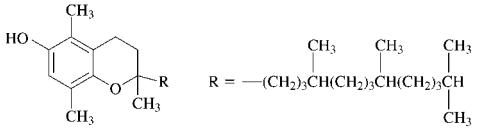	**AO 10**	Irganox E 201	431	
Aromatic amines				
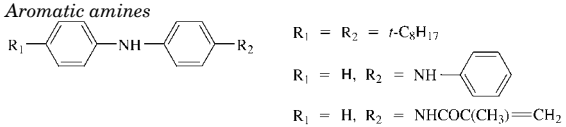	**AO 11**	Nonex OD	393	
	AO 12a	Nonex DPPD	260	
	AO 12b	–	252	
Lactones				
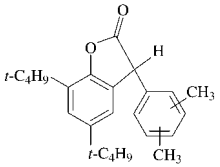	**AO 13**	HP 136	351	
Hydroxylamines				
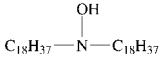	**AO 14**	Irgastab FS 042	537	
PREVENTIVE & PHOTO-ANTIOXIDANTS				
Peroxide decomppsers				
$(C_{12}H_{25}O)_3P$	**AO 15**	Ultranox TLP	586	Phosphiteesters
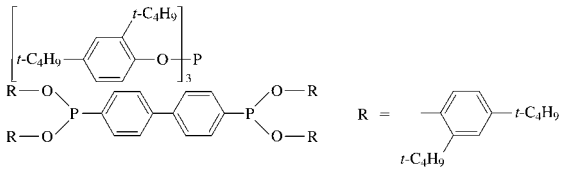	**AO 16**	Irgafos 168	647	
	AO 17	Irgafos P-EPQ	991	

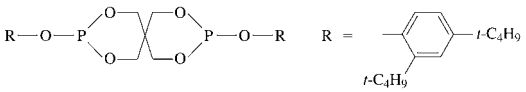

	AO 18	Ulrtanox U-626	
$R = C_{18}H_{37}$	**AO 19**	lrganox PS 802	683
$R = C_{12}H_{25}$	**AO 20**	Irganox PS 800	515
X = C, Y = NR_2, R = C_4H_9, M = Zn, $n = 2$			
X = C, Y = NR, M = Fe, $n = 3$	**AO 22**	Iron dithiocarbamate	
X = P, Y = OR_2, M = Ni, $n = 2$	**AO 23**	Nickel dithiophosphate	
X = C, Y = OR, M = Ni, $n = 2$	**AO 24**	Nickel xanthate	

Photoantioxidants, Hindered amine stabilizers

R = H	**AO 25**	Tinuvin 770	481
$R = CH_3$	**AO 26a**	Tinuvin 765	509
	AO 26b	Tinuvin 626	3100–4000

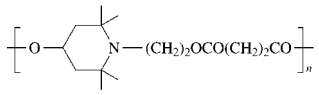

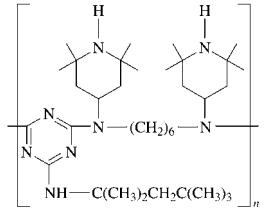

AO 27	Chimassorb944	2000–3100

Table 3. (Continued)

Antioxidant		Code	Trade name	Molecular mass	
UV absorbers					
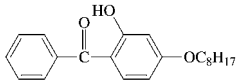		**AO 28**	Chimassorb 81	326	UVA
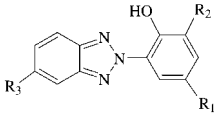	$R_1 = R_2 = t\text{-}C_4H_9$, $R_3 = H$	**AO 29**	Tinuvin 320	323	
	$R_1 = C_{12}H_{25}$, $R_2 = CH_3$, R_3=H	**AO 30**	Tinuvin 571	394	
	$R_1 = R_3 = H$, $R_2 = CH_3$	**AO 31**	Tinuvin P	225	
	$R_1 = t\text{-}C_4H_9$, $R_2 = CH_3$, $R_3 = Cl$	**AO 32**	Tinuvin 326	316	
Metal deactivators					
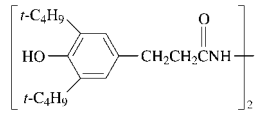		**AO 33**	Irganox MD 1024	553	MD
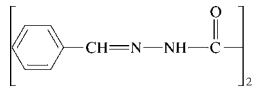		**AO 34**	Eastman OABH	294	
Hydrogen chloride scavengers					
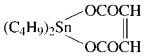		**AO 35**	Dibutyl tin maleate	347	HCI scavengers
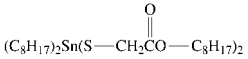		**AO 36**	Dioctyltin thioglycolate	750	

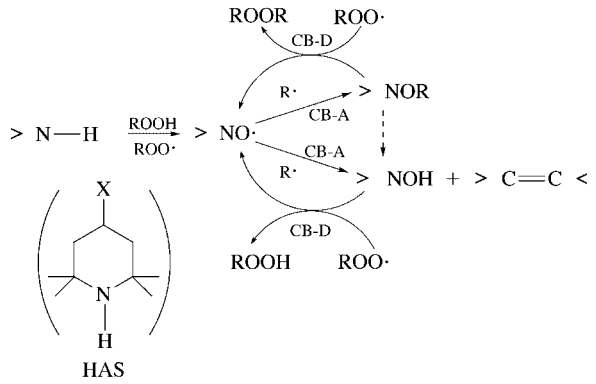

Scheme 11. Regenerative chain-breaking mechanism of hindered amine stabilizers.

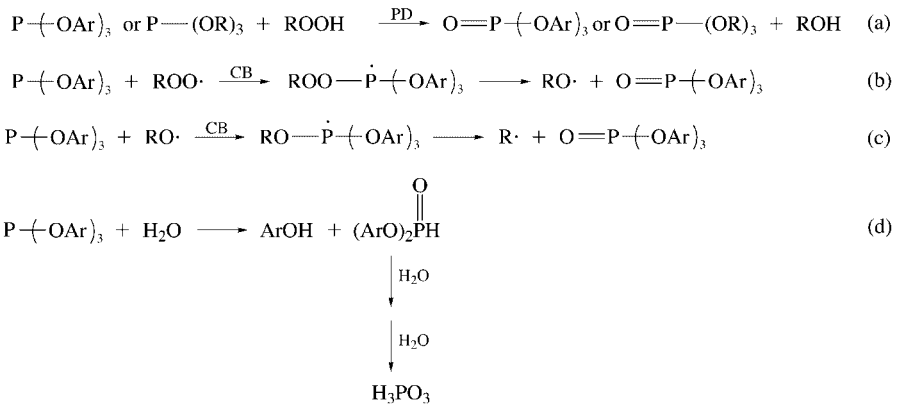

Scheme 12. Peroxidolytic and chain-breaking activity of phosphorous antioxidants.

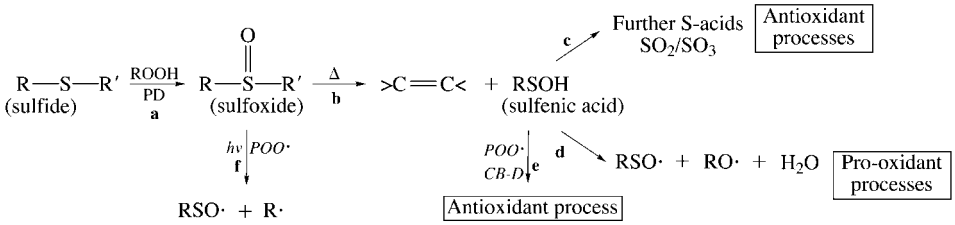

Scheme 13. Peroxidolytic activity of simple alkyl sulfides.

34, Table 3) that form stable metal complexes with reduced catalytic activity of the metal (108–110). Ultraviolet absorbers (UVA) act by absorbing uv light, hence retarding the formation and photolysis of hydroperoxides. Typical examples that are based on 2-hydroxybenzophenone and 2-hydroxybenzotriazole structures are given in Table 3 (**AOs 28–32**). These compounds are photostable and have high molar extinction coefficient in the spectral region 300–360 nm. Their activity is

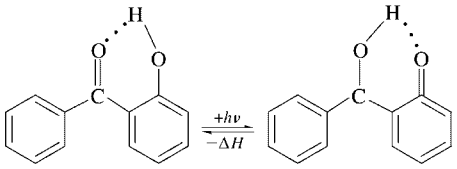

Scheme 14. Simplified view of the energy dissipation involving *o*-hydroxybe nzophenones.

based essentially on absorption of the harmful uv radiation and its harmless dissipation as heat. For example, uv light induces intramolecular hydrogen transfer in 2-hydroxybenzophenones to give an enol which is converted, in a radiationless process, back to the original ketone (111–114) (Scheme 14).

Performance of Stabilizers and Antioxidants

The commercial success of stabilizers and antioxidants depends not only on their inherent chemical effectiveness but also on their physical characteristics, toxicological considerations, and cost. Under aggressive service conditions their performance can be dominated by their physical characteristics. They can be lost from polymers through volatilization during processing and fabrication, or by exudation and solvent extraction during end use. This problem is particularly severe in the case of semicrystalline polymers and with polymer artifacts, eg, coatings, fibers, films, with high surface-to-volume ratio (4,5). In practice, therefore, their efficiency is a product of a complex relationship between all the chemical and physical factors. Chemical factors include structure, hydrolytic-, thermal-, and photo-chemical stability of both the parent molecule and its transformation products. Physical factors include solubility, diffusivity, volatility, leachability, as well as their interactions with the polymer substrate, including chemical and morphological features.

Physical loss of antioxidants into the contact media can have severe toxicological consequences in addition to risks associated with premature failure of the polymer product. Most countries have stringent regulations regarding the use of these additives in applications involving the human environment, eg, food packaging and medical applications. Although all stabilizers and antioxidants which are licensed for use in polymers for food contact and medical applications have to undergo strict toxicity testing regimes, their approval, however, does not necessarily mean that their oxidation products (derived from the parent molecule during processing, or as a result of their protective action in the substrate) are also nontoxic.

Chemical Effects. The intrinsic chemical activity of stabilizers and antioxidants is a function of their molecular structure. This can be determined accurately in a model substrate where they are fully soluble under test conditions that eliminate physical loss. However, using the chemical activity alone as an indicator can lead to unreliable predictions on the efficiency of antioxidants in polymers under practical conditions because of the dominating influence of physical factors under certain environments.

Some stabilizers, notably aromatic amines and some hindered phenols, impart discoloration or yellowing to the polymer substrate during processing and fabrication or during long-term use. This is highly undesirable in plastics and is largely due to the formation of quinonoid-type transformation products of the parent molecule (88,89). Aromatic amines cause extensive discoloration and are therefore employed almost exclusively in the stabilization of rubbers. Some stabilizers are also sensitive toward hydrolysis, especially phosphites, and to a lesser extent, phosphonites (Scheme 12, reaction 12d). This results not only in the loss of their antioxidant activity but also in the formation of species that may lead to corrosion of machinery during processing (104). Special care must be taken, therefore, during storage and handling of hydrolytically sensitive stabilizers.

Physical Effects. High chemical efficiency of antioxidants does not itself guarantee successful long-term protection of polymers under aggressive environment where their physical loss would drastically reduce their performance. For example, although the hindered phenol BHT (**AO 1**, Table 3) has very high intrinsic chemical activity, it is ineffective in protecting thermoplastic polymers because of its rapid physical loss and depletion through volatilization from the polymer (51). Indeed the physical behavior of stabilizers is a significant factor affecting their permanency, efficiency, and acceptability, especially in polymer applications destined for aggressive service environments such as organic solvents, including dry cleaning solvents, hot water and detergents, hot oils, acids, fatty food, hot air, and intense solar radiation. Physical factors which control the effectiveness and permanence of antioxidants include distribution, solubility, diffusivity, volatility, and leachability. To tackle the problem of physical loss, further commercial developments have led to the synthesis of higher molecular mass antioxidants based on the same hindered phenol function, eg, Irganox 1010 and Irganox1 330 (**AOs 5**, **2**, Table 3), which have outperformed BHT under these conditions (1,90).

Distribution and Polymer Morphology. In order to inhibit polymer oxidation, sufficient concentration of antioxidants must be present at the various oxidation sites. Examination of the distribution of photoantioxidants in typical commercial semicrystalline polymers, such as polyolefins, has shown (5,22,115) that they are rejected into the amorphous region on the boundaries of spherulites. Such nonuniform distribution of antioxidants leads to an increase in their concentration in the amorphous region, which is most susceptible to oxidation since the crystalline phase is normally impermeable to oxygen (5). However, in the case of polymer blends, a nonuniform distribution of antioxidants can undermine the overall stability of the blend, especially if it does not occur in favor of the more oxidizable component in the formulation.

Compatibility with Polymers. Stabilizers and antioxidants are generally less soluble in polymers than in lower molar mass liquid models. Although these compounds are usually highly soluble at the elevated processing temperatures, they may, on cooling to room temperature, precipitate out as a separate phase and exude to the polymer surface, leading to a buildup of a concentration gradient near the surface, forcing further migration of antioxidant from the bulk (5,22). Thus, compounds with low solubility and high diffusion rate are prone to blooming and loss to the surrounding medium by evaporation (air stream as contact media) or through leaching (extraction by a liquid contact media), leaving behind an unprotected polymer surface. Generally, the compatibility of stabilizers in host

polymers is improved when both have similar characteristics. Thus, for example, in nonpolar hydrocarbon polymers, compatibility decreases with increasing polarity of the stabilizers and increases with the number, length, and branching of the inert alkyl substituents attached to the stabilizer function (116,117) (eg, **AOs 2–5**, **20**, **30**, Table 3).

Diffusion, Volatility, and Leachability. The permanency of stabilizers and antioxidants is affected by diffusion characteristics of the parent molecule, the nature (gas, liquid, solid) of the surrounding medium, and temperature (5,7,116). For example, the diffusion coefficient of antioxidants decreases with increasing polar interactions with the polymer, increasing molecular mass of antioxidants, and branching in their alkyl side chain.

In the presence of a stream of hot air or high temperature and low pressure (eg, during polymer melt processing) volatility becomes very important; it is governed by the rate of diffusion of antioxidants, which, in turn, determines the rate at which the surface is replenished (5). The influence of polymer sample shape and the structure and molecular mass of antioxidants on volatility has received much attention. The rate of evaporation of antioxidants from rubber and PE, for example, was found (116) to be inversely proportional to the thickness of the sample and directly proportional to its surface area. Volatility, and the other physical characteristics of antioxidants, are critically dependent on the test conditions. This is illustrated in Table 4 for a series of antioxidants containing the same hindered phenolic functional group (see A—R with R= $-CH_2COOR'$ in Table 3) but differing only in the length of the chemically inert alkyl chain, R′ (51). In a model hydrocarbon, eg, dodecane, all the antioxidants in the series show similar antioxidant activities in a closed system (measured by oxygen absorption) at the same molar concentration. In PP under the same conditions, however, the antioxidant activity of the same series of antioxidants varies by a factor of 4, the optimum occuring at $R' = C_{12}H_{25}$. In an air oven, on the other hand, only the antioxidant with $R' = C_{18}H_{37}$ (ie, Irganox 1076, **AO 4** in Table 3) has any significant activity. At 100°C, but under otherwise identical conditions, somewhat better discrimination is observed between the lower members of the series, and only the C_{12} and C_{18} analogues show significant antioxidant activities (116). Further, the antioxidant activity of this series in an air-oven test is inversely related to volatility in a nitrogen stream (see Table 4).

In liquid contact media (eg, foodstuffs, oils, solvents), the rate of loss of antioxidants from the polymer surface depends both on their diffusion coefficient and on their partition coefficient between the liquid and the polymer. This is complicated by the ability of different solvents (liquid media) to swell polymers to different extents, giving rise to an increase in the diffusion coefficient of the antioxidant, which lead to higher loss rates (7). As in the case of volatilization, the rate of leachability of antioxidants from the surface of polymers into liquid contact media increases with temperature and surface area-to-volume ratio, eg, in thin polymer samples.

Thermal Stabilization

Stabilization of polymers against the effect of temperature is required both to prevent mechano-thermal oxidation at the processing stage (melt-processing

Table 4. Effectiveness of a Series of Hindered Phenol Antioxidants[a]

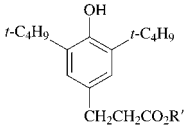

	Molecular weight	$T^{1/2,b}$ h	S,[c] g/100 g	D_c[d]	Induction period, h	
					PP_c[e]	PP_o[f]
CH_3[g]	292	0.28	32	25	95	2
C_6H_{13}	362	3.60	∞	23	312	2
$C_{12}H_{25}$	446	83.0	∞	20	420	2
$C_{18}H_{37}$	530	660.0	64	20	200	165
BHT,[h]	220	0.10	100	150	140	2

[a] They are compared at the same molar concentration (2×10^{-3} mol/100 g) in dodecane and in PP at 140°C (51).
[b] $T^{1/2}$ = antioxidant half-life in PP in N_2 stream at 140°C.
[c] S = solubility in hexane at 25°C.
[d] D_c = induction period in decalin by oxygen absorption at 140°C.
[e] PP_c = induction period in PP film by oxygen absorption at 140°C.
[f] PP_o = induction period in PP film in a moving air stream at 140°C by carbonyl measurement.
[g] Molecular formulas in this column represent R′.
[h] **AO 1**, in Table 3.

stabilizers) and to afford protection during in-service (long-term thermal stabilizers). In addition, the thermal stability of reprocessed polymers (recycled) must be preserved and reinforced by additional stabilization for further reprocessing and end use (recycling stabilizers).

Melt-Processing Stabilizers. Melt processing of polymers in screw extruder or a shearing mixer is accompanied by degradative processes including mechanical scission of the polymer backbone and formation of macroradicals. In an extruder, where the amount of oxygen is small, the alkyl radicals play an important role and become involved in the termination of the autoxidation process (as seen earlier $[R\cdot] \gg [ROO\cdot]$; see Table 1). However, both alkyl and alkylperoxyl radicals are formed in polymer melts, and hence, antioxidants that can remove macroradicals (in a chain-breaking mechanism, CB-D and/or CB-A) and destroy hydroperoxides (in a preventive mechanism, PD) should provide effective stabilization during processing.

The choice of antioxidants for melt stabilization vary, depending on

(1) structure and oxidizability of the base polymer
(2) extrusion/processing temperature
(3) rate of application of mechanical stress
(4) type and amount of structural defects and impurities
(5) performance targets of the end-use applications.

Thus, structural differences in polyolefins result in very different levels of their oxidizability. PP, for example, is very sensitive to oxidation and cannot be processed without adequate stabilization. HDPE is less sensitive to oxidation than PP and lower antioxidant concentrations are normally needed, whereas LDPE (processed around 200°C) is more stable and may even be used (for certain

applications) without the addition of an antioxidant. Unlike PS, rubber modified styrene blends and copolymers (eg, HIPS, ABS, SAN) are very sensitive to oxidation during processing and require substantial levels of stabilizers during melt processing. PVC, on the other hand, is very highly sensitive to the presence of structural defects and impurities that contribute effectively to initiating oxidation and generating color and corrosive HCl; thus, appropriate stabilization is essential.

Chain-Breaking Antioxidants. Sterically hindered phenols (efficient CB-D antioxidants) have been used extensively as melt-processing stabilizers in plastics. The primary step in their stabilizing action involves the scavenging of alkylperoxyl radicals ($ROO^{\cdot}$), which gives rise to harmful hydroperoxides (Scheme 10, reaction a). In practice, therefore, hindered phenols are generally used in combination with a peroxide decomposer, typically a hydrolysis-resistant phosphite (1–3,37,88,90,118,119). The structure of synthetic hindered phenols used to stabilize different polymers affects their efficiency depending on the degree of steric hindrance and the nature of the para-substituents. Generally, decreasing steric hindrance in the 2- and 6-positions results in increasing the rate of hydrogen abstraction from the phenol. Similarly, the nature of para-substituents affects the extent of discoloration as it determines the nature of transformation products obtained from the parent phenol (120–124).

Discoloration is typically caused by the formation of colored conjugated quinonoid-type transformation products with visible absorption wavelengths, typically >400 nm (125). Schemes 15 and 16 show some key reactions of hindered phenols used for polymer stabilization to illustrate the effects of different para-substituents:

(1) Unsubstituted, mono- or di-substituted methyl group (methyl-type); typical examples include **AOs 1–3** in Table 3; and

(2) Propionic acid derivative group of the general type $-CH_2CH_2COX$ (where X=OR or NR); examples include **AOs 4–7**, in Table 3 (propionate type). Propionate esters **AOs 4** and **5** are good stabilizers for polyolefins and styrenics, the propionamide **AO 6** is used in aliphatic polyamides, and the ester **AO 7** is suitable for polyesters.

The major transformations of phenolic antioxidants during melt processing, with both types of para-substitents (methyl and propionate types), consist of quinone-type products, C–C and C–O coupling product. Transformation products of antioxidants can greatly influence the extent of stabilization imparted to the polymer. Transformation products can exert anti- or pro-oxidant effects, hence synergizing or antagonizing the action of the parent antioxidant. For example, the formation of peroxydienones (PxD) (see Scheme 15, reaction b) from BHT (**AO 1**, Table 3) leads to pro-oxidant effects, whereas the C–C coupling products (DB) (eg Scheme 15, reaction c) and quinonoid products (SQ) (eg, Scheme 15, reactions d and f) exert antioxidant effects.

The mechanism of action of hindered phenols is centered on the nature of the initially formed phenoxyl radicals which undergo complex reactions, including bimolecular disproportionation, giving rise to a quinonemethide (QM) as well as

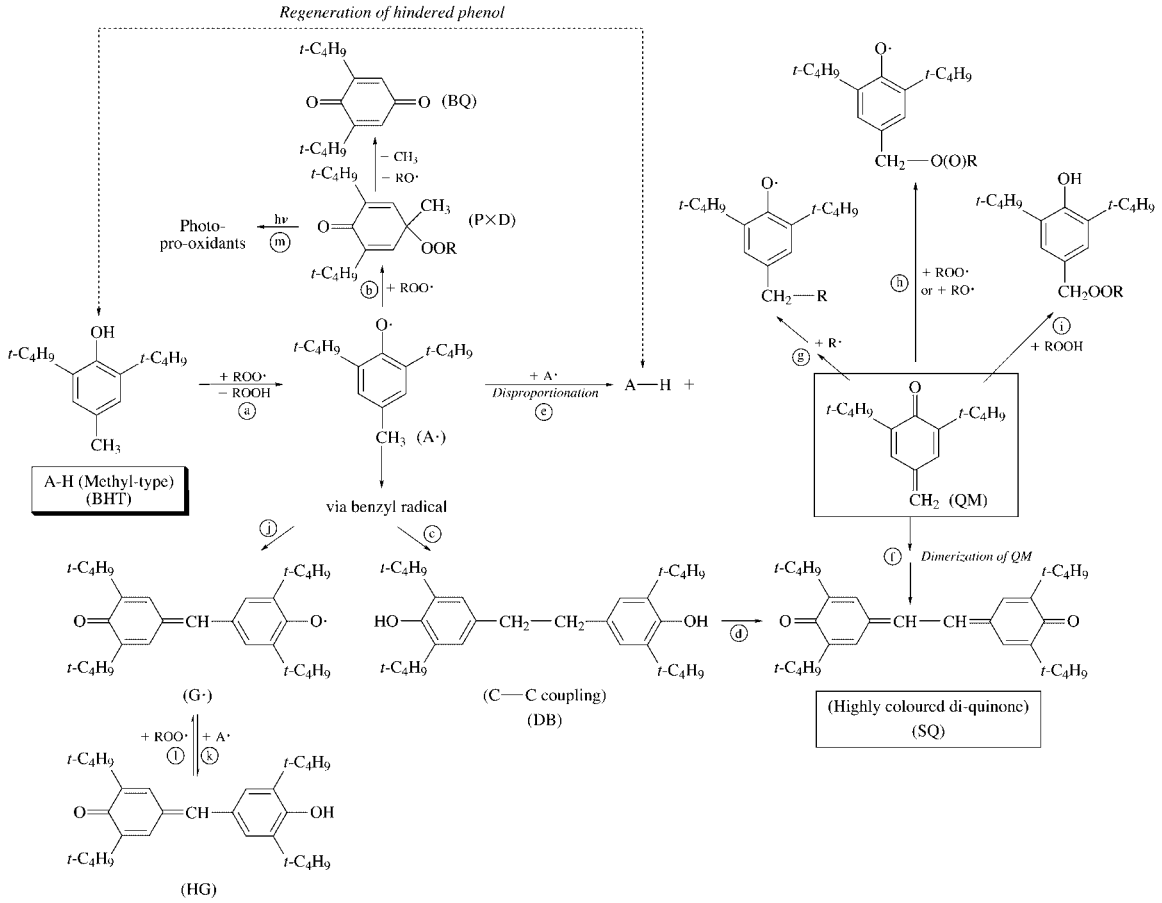

Scheme 15. Key reactions that take place during the antioxidant action of 4-methyl-containing hindered phenols.

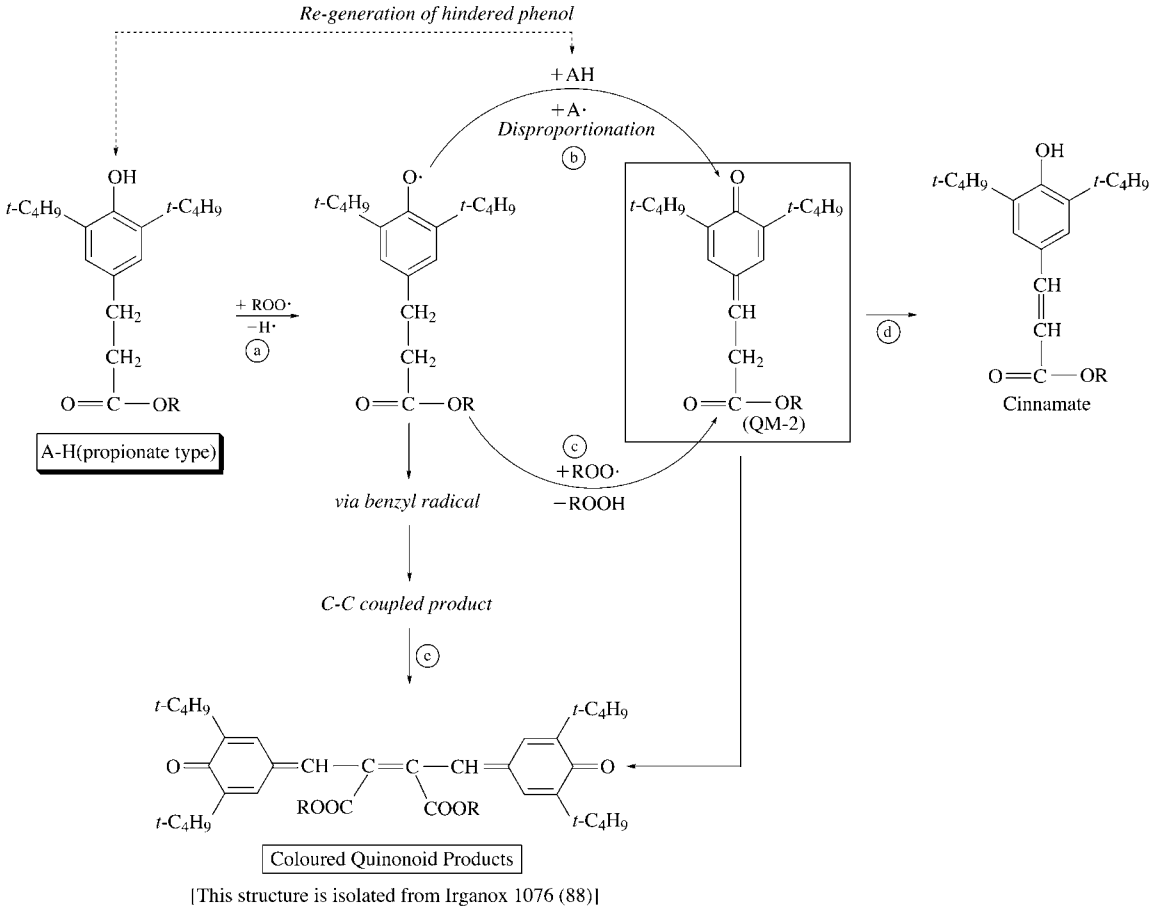

Scheme 16. Key reactions that take place during the antioxidant action of 4-methyl-containing hindered phenols.

on the regeneration of the parent phenol for further scavenging of another ROO· radical (Scheme 15, reactions e and f; Scheme 16, reaction b) and hence increasing the stability of the polymer (90,120,121). In the case of the propionate type, the QMs can also be formed by reaction of the corresponding phenoxyl radical with a second ROO· radical (Scheme 16, reaction c); these QMs have been shown (120) to isomerize further to the corresponding cinnamate (Scheme 16, reaction d). Although the starting hindered phenols themselves are not capable of acting by CB-A mechanism (because of their inability to deactivate R·), the derived QMs and other quinonoid products are effective CB-A antioxidants. The QMs are capable of deactivating not only the alkyl radicals but also other propagating species (alkoxyl, alkyperoxyl) as well as hydroperoxides (95,126,127) (see Scheme 15, reactions g–i). Furthermore, quinones which are stable in their oxidized and reduced forms, eg, galvinoxyl (G·) and hydrogalvinoxyl (HG) may deactivate both alkyl and alkylperoxyl radicals (via CB-A and CB-D mechanisms, respectively) in a redox reaction (see Scheme 15, reactions k and l) and are thus highly efficient antioxidants. Table 5 shows a comparison of the melt-stabilizing effect of the different oxidation products of BHT in PP with the parent stabilizer molecule (95). In addition to synthetic hindered phenols, the biological hindered phenol antioxidant vitamin E (see **AO 10**, Table 3) has also been shown to be an extremely highly effective melt stabilizer (see later under Biological Antioxidant).

Hindered phenols-derived quinones are CB-A antioxidants and are also effective melt stabilizers. The bifunctional hindered phenol semiacrylate antioxidant (**AO 8**, Table 3), which acts primarily by deactivating alkyl radicals, is an effective processing stabilizer for styrene–butadiene–styrene copolymers (93,128). More recent developments have resulted in the commercialization of new CB-A antioxidants including lactone-based stabilizers and hydroxylamines. The lactone stabilizers (see **AO 13**, Table 3), which are used commercially in blends with hindered phenols and phosphites, have been shown (92,93) to be efficient in oxygen-deficient environment particularly during melt processing, by trapping the macroalkyl radicals (Scheme 17). Similarly, the hydroxylamines (see **AO 14**, Table 3), which can also scavenge the macroalkyl radicals via the intermediacy of nitrones, have been shown (91,94) to be highly efficient (Scheme 18).

Table 5. Melt Stabilizing Activity of BHT and Its Oxidation Products[a]

	ΔMFI[c]	
Code[b]	4.5[d]	0.5[d]
BHT	100	270
BQ	55	65
SQ	50	60
G·	45	45
QM	40	55

[a] Ref. 95
[b] For structures see Fig. 6.
[c] ΔMFI is the percent increase in melt flow index of the polymer compared with an unprocessed control after a single pass extrusion at 270°C and 100 rpm.
[d] Concentration of antioxidant in 10^{-4} mol/100 g.

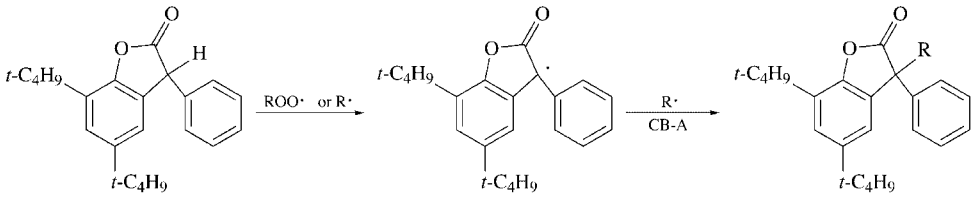

Scheme 17. Chain-breaking reactions involved in the antioxidant action of benzofuranes (lactone stabilizers).

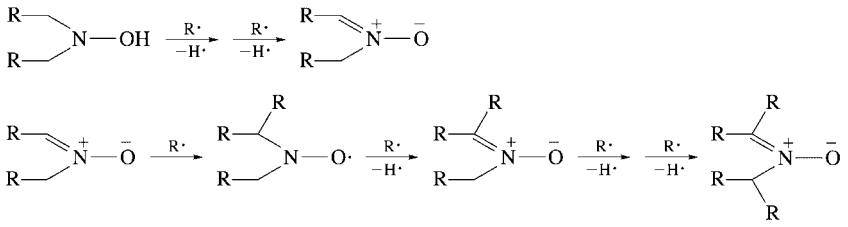

Scheme 18. Chain-breaking reactions involving hydroxylamine antioxidants and nitrones.

Hydrogen Chloride Scavengers. The aim of melt stabilization of PVC is to reduce the formation of HCl and hydroperoxides in the polymer, and to combat the development of unsaturation, which is both the source of color and further instability (2,129–132). In general, plasticized PVC is processed at lower temperatures than rigid PVC, and lesser damage is therefore expected during its melt processing. The elimination of labile chlorine atoms from the polymer backbone is the most important stabilization mechanism for PVC. Metal carboxylates (eg, lead carbonate, calcium, barium and zinc soaps) and tetravalent derivatives of tin (eg, dibutyl tin maleate; AO 35, Table 3) are frequently used for PVC stabilization, and the dialkyl tin carboxylates are in general more effective as chlorine-trapping reagents than the metal group II carboxylates (130–132). Both dialkyl tin maleates and thioglycollates (eg, AO 36, Table 3) function by eliminating HCl. In addition, the maleates function also by removing the unsaturation and limiting color development, whereas the thioglycollates have an additional peroxidolytic function.

Peroxide Decomposers as Processing Stabilizers. Alkyl and aryl phosphite esters (see Scheme 12) are effective melt stabilizers. They are often used in combination with hindered phenols (see Table 6). Phosphites generally function by a stoichiometric peroxidolytic mechanism (PD-S); Table 7 illustrates the benefits of using the commercial phosphites TNPP (**AO 15**) and Irgafos P-EPQ (**AO 17**, Table 3) for melt stabilization (95). The unique phosphite **AO 37** and its phosphate transformation products **AOs** 38 and 39, (Table 7), which were shown (104,133–135) to operate by a catalytic mechanism (PD-C), are particularly effective at low concentration of the parent stabilizer molecule (see AO 37, Table 7) (95). Phosphites are, however, generally susceptible to hydrolysis. For example, hydrolysis of aryl phosphites leads to the formation of low molecular mass phenol and a

Table 6. Melt Stabilizing Efficiency of Phosphites in PP[a]

Antioxidant	Wt%	MFI,[b] g/10 min
Control (no antioxidant)	0	11.7
Irganox 1010 (**AO 5**)	0.05	5.9
Irganofos 168 (**AO 14**)	0.05	7.7
Irganox PS 800 (**AO 18**)	0.1	8.4
Irganox 1010 + Irgafos 168	0.05 + 0.05	4.3
Irganox 1010 + Irganox PS 800	0.05 + 0.10	4.9

[a]Processed in internal mixer at 190°C.
[b]Melt flow index (MFI) measured at 230°C and 2.16 kg.

Table 7. Effect of Some Peroxidolytic Antioxidants as Melt Stabilizers for PP at 270°C[a]

		ΔMFI[b]	
Phosphorous antioxidant	Code	4.5[c]	0.5[c]
TNPP	**AO 15**	40	150
Irgafos P-EPQ	**AO 17**	40	120
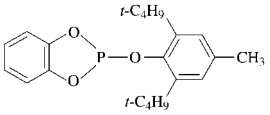	**AO 37**	60	85
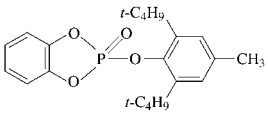	**AO 38**	75	150
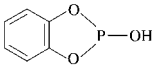	**AO 39**	80	100
Irganox PS 800 (Sulfide)	**AO 20**	170	190
[$ROCOCH_2CH_2$+SO_2 (Irg PS800-sulfoxide)	**AO 40**	50	50

[a]Ref. 95
[b]ΔMFI is the percent increase in the melt flow index of the polymer compared with an unprocessed control after a single pass extrusion at 270°C and 100 rpm.
[c]Concentration of antioxidant in 10^{-4} mol/100 g.

hydrogen phosphite which is further hydrolyzed to phosphorous acid (Scheme 12, reaction d) (102,104). The consequence of the hydrolysis of phosphites is the reduction of flow properties of the additive system (ie, undesirable change in handling characteristics), increase in corrosion of metal surfaces, formation of dark-colored spots and gel formation. In practice, therefore, only hydrolysis-resistant phosphites (and phosphonites) are used and these are generally based on sterically hindered phenols.

Sulfur-containing compounds are highly effective **PD** antioxidants but they are more complex in their behavior than the phosphites. They react with hydroperoxides in a catalytic process, which leads to the formation of various sulfur acids that are responsible for the catalytic nonradical destruction of hydroperoxides. The "simple" dialkyl sulfides, eg, thiodipropionate esters such as Irganox PS800 and PS 802 (**AOs 19** and **20**, Table 3), function as weak melt stabilizers. They give

rise to a pro-oxidant effect in the polymer because of the generation of free radicals (see Scheme 13, reaction d) by an initial redox reaction with hydroperoxides (95). The sulfoxide transformation product (AO 40, Table 7) formed from thiodipropionate esters is more effective melt stabilizers (see Table 7) because they give rise to sulfenic acid, which is an efficient chain-breaking antioxidant (2) (see Scheme 13, reaction e). In view of the prodegradant effects of thiodipropionate esters, in practice, these sulfide antioxidants are always used in combination with CB-D antioxidants, such as Irganox 1010 (**AO 5** in Table 6), to deactivate the free radicals formed.

Long-Term Thermal Stabilizers. Under normal conditions of long-term thermal oxidation, alkylperoxyl radicals are normally present in large excess over alkyl radicals (see Table 1). In thin samples ($<3 \times 10^{-3}$ cm), oxygen diffusion is not rate determining, and the main termination process is the bimolecular reaction of alkylperoxyl radicals (Scheme 1, reaction 7). Hindered phenols and aromatic amines (CB-D) are highly effective inhibitors of these radicals and are therefore used as long-term stabilizers. In practice, they are used in combination with peroxide decomposers such as phosphite esters (see Table 8) (1).

Many sulfur-containing PD antioxidants, especially the metal dithiolates, are very effective long-term thermal stabilizers (also melt and photo antioxidants; see later). This versatility in antioxidant action is the direct consequence of their highly effective PD activity (54,105,107,136–140). Moreover, the effectiveness of dithiolate antioxidants, within any one series depends strongly on their solubility in the polymer. For example, in the case of nickel dialkyldithiophosphate (NiDRP, **AO 23**, Table 3) series, the lower molecular weight members of the series are less soluble, and less effective than the higher members (see Fig. 3) (141). The zinc dialkyl dithiocarbamate (ZnDRC, **AO 21**) series too show similar behavior (142).

In the case of PVC, long-term thermal stabilization is normally achieved by the same antioxidants used for melt stabilization. Thiotin stabilizers, eg, **AO 36**, are more effective as thermal antioxidants than the more traditional dialkyl tin

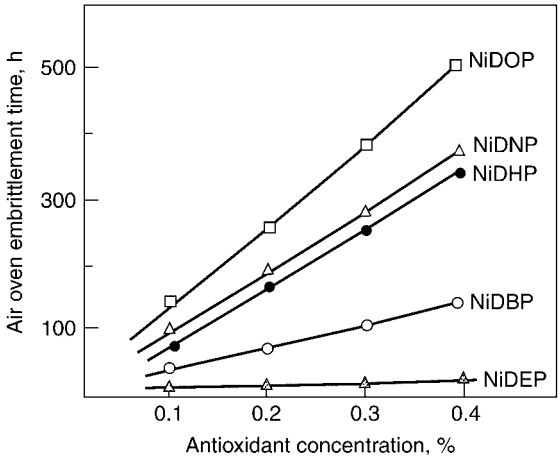

Fig. 3. Effect of length of R group in NiDRP [0.4%] on thermoxidative stability of PP at 140°C.

Table 8. Long-Term Thermal Stabilization of Different Polymers in Draft Air Oven[a]

PP[b]		LLDPE[c]		PA 6.6[d]			PBT[e]	
Formulation	EMT,[f] days	Formulation	EB_{t50},[g] days	Formulation	TS_{t50},[h] days	EB_{t50},[i] days	Formulation	EB_{t50},[j] days
Control	1	Control	21	Control	13	4	Control	3
AO 5 (0.05%)	22	**AO 4** (0.03%)	225	**AO 6** (0.5%)	$\gg$80	15	**AO 5** (0.25)	12
AO 5 (0.1%)	30	**AO 5** (0.03%)	400	**AO 6** + **AO 16** (0.25% + 0.25%)	89	16	**AO 6** + **AO 16** (0.13% + 0.13%)	14
							AO 2 (0.25%)	15
							AO 7 (0.25%)	11
							AO 7 + **AO 16** (0.13% + 0.13%)	20

[a] Ref. 1.
[b] PP: 30 μm-thick tape.
[c] LLDPE: 100-μm-thick octene comonomer film.
[d] PA 6.6: 1-mm-thick injection molded at 285°C.
[e] PBT: 1-mm-thick injection molded at 225°C.
[f] EMT = time to embrittlement at 120°C.
[g] EB_{t50} = time to 50% retained elongation at 100°C.
[h] TS_{t50} = time to 50% retained tensile strength at 120°C.
[i] EB_{t50} = time to 50% retained elongation at 120°C.
[j] EB_{t50} = time to 50% retained elongation at 160°C.

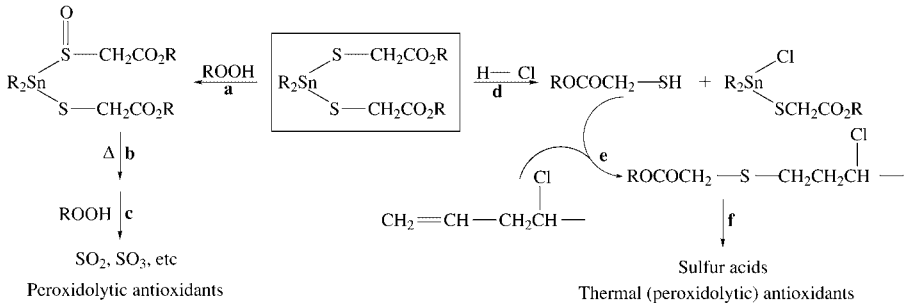

Scheme 19. Stabilization mechanism of thiotin stabilizers in PVC for long-term thermal stability.

maleates, eg, **AO 35** (32) and result in drastic reduction, even disappearance, of both the unsaturation and peroxides from the polymer. This is almost certainly due to the presence of sulfur in the thiotin molecule which offers highly effective PD activity. The acidic species are formed by reaction with hydroperoxide (see Scheme 19, reactions a–c>) in a manner which is analogous to the formation of sulfur acids from thiodipropionate ester. Moreover, reaction with HCl results in the formation of thioglycollate (Scheme 19, reaction d), which adds to the developing monomeric unsaturation (formed by HCl elimination), thus removing the sensitizing allylic methylene groups (see Scheme 19, reaction e). The monosulfides formed are themselves effective macromolecular antioxidants.

Photostabilization

As with thermal stabilizers, photostabilizers must satisfy basic chemical and physical requirements. In addition, they must be photostable, ie, stable to uv light, able to withstand continuous periods of uv exposure without being prematurely destroyed, or effectively transformed into sensitizing products. There are essentially three classes of compounds that are categorized as photostabilizers: uv absorbers and pigments, peroxide decomposers including nickel complexes, and sterically hindered amine light stabilizers (see UV STABILIZERS).

Ultraviolet Absorbers and Pigments. Most of the UVA used commercially fall into two main classes of compounds: the 2-hydroxybenzophenones (eg, **AO 28**, Table 3) and the 2-hydroxybenzotriazoles (eg, **AOs 29–32**, Table 3) with the 2-hydroxy group being essential for their activity (143). These UVA operate by additional mechanisms too, for example, by removing initiating radicals (eg, alkoxyl radicals) in a weak CB-D mechanism (see Scheme 20). (144–146). Further, UVA, such as **AO 28**, synergize effectively with peroxide decomposers, eg, metal dithiolates (see Table 15 later).

Ultraviolet-screening pigments have been used extensively to protect polymers against the harmful effect of uv radiation. For example, carbon black imparts an extraordinary stabilizing power, mainly on account of its high uv-absorbing capacity. However, like other UVA, carbon black has additional photoantioxidant

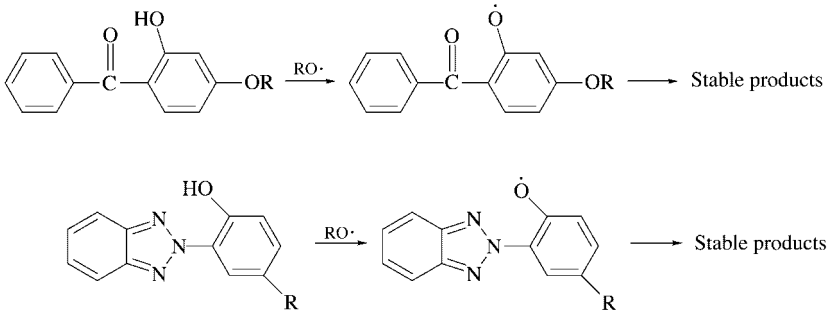

Scheme 20. Chain-breaking stabilizing activity of UVA.

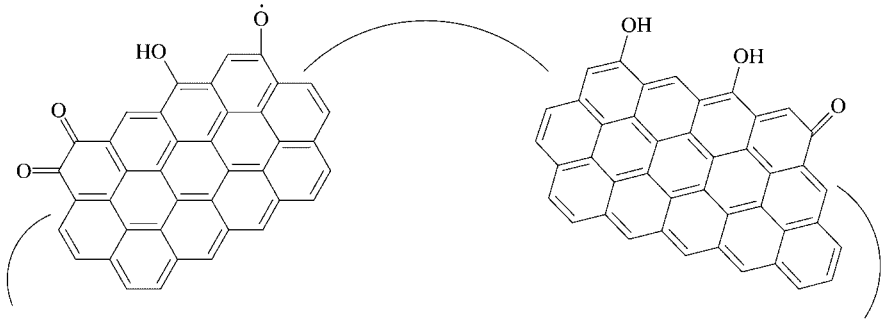

Fig. 4. Carbon black, simplified structure.

activities associated with its chemical structure (147,148). Carbon black has a highly condensed aromatic ring structure with small amounts of phenolic, ketonic, carboxyl functions, and a relatively high concentration of 'oxyl' radicals which are stabilized in the conjugated system (see Fig. 4). These structural features give carbon black its radical scavenging ability and CB function (147). Carbon black has (PD) activity too because of its acidic nature (148).

Peroxide Decomposers and Nickel Complexes. The photostability of these stabilizers vary according to the stability of their transformation products to uv light. Simple sulfides such as the thiodipropionate esters (eg, **AO 19** or **AO 20**, Table 3), which are good melt stabilizers, are unstable to light because of dissociation of their primary oxidation products to photoinitiating radicals (see Scheme 13, reaction f), and are not useful as photostabilizers. Similarly, conventional chain-breaking antioxidants, such as hindered phenols which are excellent melt and long-term stabilizers, have only very limited photostabilizing activity due to photo–pro-oxidant effects of some of their transformation products (see Scheme 15, reaction m).

Metal complexes of dithioic acids, eg, dithiocarbamates, dithiophosphates, xanthates (MDRC, MDRP, MRX, respectively) (see **AOs 21–24**, Table 3), which are highly effective catalytic peroxide decomposers (PD-C) and excellent melt stabilizers, are generally effective photostabilizers (101,105,136,137,139,149). Their

Table 9. Effect of Different Metal Dithiolates on the Photostability (Embrittlement Time, EMT) of PP Processed at 190°C[a]

Antioxidant	Concentration, 10^{-4} mol/100 g	UV-EMT, h
Unstabilized PP	0	90
ZnDEC	2.5	175
NiDEC	0.25	140
NiDEC	2.5	740
NiDEC	3	790
NiDEC	10	840
FeDMC	0.25	85
FeDMC	2.5	150
FeDMC	5	336
NiOctX	3	700
CoOct X	3	1600
Chimassorb 81	3	245
NiDBP + Chimassorb 81	6	2650

[a]For structures, see Table 3.

effectiveness is attributed mainly to the much higher uv stability of dithiolates as compared to simple sulfides. However, both the nature of the metal ion in the dithiolate complexes and their concentration play a crucial part in their overall effectiveness as uv stabilizers. Transition metal complexes containing Ni, Co, and Cu are more photostable than Zn- and Fe-containing complexes, and hence are more effective (see Table 9). Furthermore, the photoantioxidant activity of nickel dithiolates is greatly affected by their solubility in the polymer (117) as was shown previously in their use as thermal stabilizers (see Fig. 3). These peroxide decomposers also synergize effectively when used in combination with UVA (see Table 9). Like most other metal dithiolates, the primary oxidation product formed during the antioxidant function of NiDRP (**AO 23**, Table 3) is the corresponding disulfide, DRDS, which undergoes further oxidation to give different sulfur acids (the real catalysts for peroxide decomposition) (Scheme 21).

Processing history can have a profound effect on the photoantioxidant activity of sulfur compounds. For example, the effective melt stabilizer thiophosphoryl disulphide, DRDS, formed as the primary oxidation product of NiDRP (see Scheme 21) is further converted to a more effective photoantioxidant by oxidative processing (150) (see Table 10). Similar oxidative processing (in presence of excess oxygen or added hydroperoxide and with increasing time) results in enhanced photoantioxidant activity of other sulfur-peroxidolytic antioxidants such as the mercaptothiazolines, RMTZ (151) (see Table 10). The oxidative transformation products of RMTZ have been identified (152) as more complex thiazolines

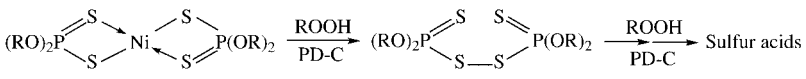

Scheme 21. Simplified mechanism of stabilization of nickel dithiophosphate and thiophosphoryl disulfide.

Table 10. Effect of Oxidative Processing on Photoantioxidant Activity of Dibutyl Thiophosphoryl Disulfide (DBDS) in PP[a]

Processing conditions in internal mixer, 190°C	UV-Embrittlement time, h			
	DBDS	DBDS+TBH*	RMTZ (R = Eth)	Unstabilized PP
Closed mixer, 5 min	–	700	–	–
Closed mixer, 10 min	250	–	670	90
Open mixer, 10 min	280	–	750	55
Open mixer, 15 min	–	–	850	–

[a]Refs. 150 and 151.

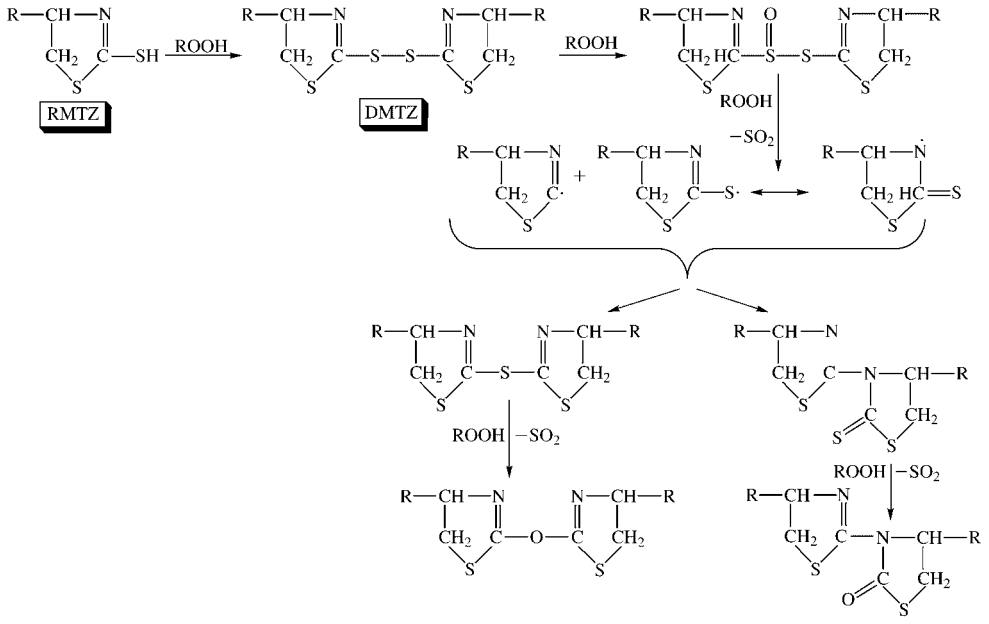

Scheme 22. Oxidative transformation of mercaptothiazolines during processing (152).

formed through the intermediacy of the disulfide, DMTZ. Further oxidation progressively depletes DMTZ of its sulfur content through the loss of low molecular mass sulfur acids (see Scheme 22). The final photoproducts absorb uv light above 290 nm, which, together with the slow libration of sulfur acids, is the reason for their improved photostabilizing activity with increasing processing severity.

Hindered Amine. Significant commercial development has been based on hindered piperidines (known as HALS, Hindered Amine Light Stabilizers) (see **AOs 25** and **26**, Table 3), which have been used extensively as photostabilizers in commercial polymers. HALS is a unique class of photostabilizers which do not subscribe to the general mechanisms of photostabilization: they are not uv screens, do not quench singlet oxygen or triplet carbonyls, and do not catalyze hydroperoxide decomposition. Their effectiveness, however, has been shown to be due to their primary transformation product, the corresponding nitroxyl radicals (>NO·), which is capable of scavenging alkyl radicals in competition with oxygen,

Table 11. Ultraviolet Stabilizing Effect of HALS-Based Antioxidants in PP[a]

Antioxidant	UV-EMT, h
AO 28, > N—H	750
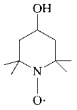	920
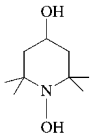	1040
Control, no HAS	90

[a] Concentration of each is 6×10^{-4} mol/100 g.

ie, an effective CB-A antioxidant. Its photostabilizing mechanism also involves the regeneration of the nitroxyl radical from both the corresponding hydroxylamine (>NOH an effective CB-D) and alkylhydroxylamine (37,50,96,98,100,153,154) (see Scheme 11). The overall photoantioxidant efficiency is due to the complementary nature of the acceptor- and donor-antioxidant, (CB-A/CB-D) mechanisms of the >NO·/>NOH, both of which were shown (96) to be significantly more effective than the parent amine stabilizer (see Table 11 for **AO 28** and its derivatives).

Time-Controlled Stabilization

Environmental considerations and specialty applications continue to generate new markets for polymers. The need for polymers with limited lifetime, eg, for food (especially fast-food) packaging, in agricultural products, eg, mulching films and certain medical and pharmaceutical products, has encouraged the development of degradable plastics. These products are designed for a limited lifetime use after which they degrade rapidly. Degradable plastics should ideally fulfil the following requirements (155):

(1) The degradation process should occur at a controllable and predetermined rate to allow for safe-use. During its useful service life, the polymer is stabilized and retains its mechanical strength.
(2) At the end of service life, degradation is triggered off, with rapid catastrophic failure in mechanical strength, concomitant with the formation of low molar mass polymer degradation products.
(3) Complete degradation should follow, whereby the degradation products formed above would be assimilated by microorganisms to give biomass and, ultimately, carbon dioxide and water.

One approach that meets the above requirements involves the use of transition metal dithiolates for time-controlled stabilization. These can fulfil their

stabilizing function during processing, manufacture, and throughout the short service life, but subsequently photodegrade and catalyze photo-oxidative degradation of the polymer, thus referred to as "antioxidant-photoactivators" (37,138,155–157).

Ultraviolet exposure of polyolefins containing metal dithiolate stabilizers reveals the presence of an initial induction period, which is directly proportional to the stabilizer concentration and which ends very sharply upon its consumption. The end of the induction period marks the start of photo-oxidation, which proceeds at a rate which is primarily a function of the concentration and the nature of the free metal ion produced (37,101,105,158). Although all dithiolates are powerful peroxidolytic antioxidants and excellent melt stabilizers of polymers, they exhibit different uv stability depending on the metal center. The iron complexes, eg, FeDRC, exhibit very unique concentration-dependent behavior on uv-exposure compared to their nickel analogues, eg, NiDRC. In the case of NiDRC, increasing its concentration results in an increase in the induction period to photo-oxidation and a decrease in the post-induction rate of photo-oxidation, whereas the FeDRC shows a contrasting behavior whereby both the induction period and post-induction rate increase with increase in concentration (156). Thus, at low concentrations (below 0.05%) in polyolefins the FeDRC complexes photolyze rapidly, giving a minimal induction period to photo-oxidatoin; at higher concentrations, however, a longer induction period becomes evident, followed by inversion of activity, which results in rapid photo-oxidation (see Fig. 5) (156).

Photoactivation of FeDRC complexes produces iron carboxylates which are very powerful sensitizers of photo-oxidation due to their participation in redox reactions with hydroperoxides (37) (see Scheme 23) (in contrast, NiDRC complexes are not photoactivators since the librated free metal ion has no photo–prooxidant activity). On the other hand, the observed photoinduction period at higher concentrations of FeDRC (see Fig. 5) is a direct consequence of its photoantioxidant behavior due to oxidation of the sulfur ligand to low molar mass sulfur acids

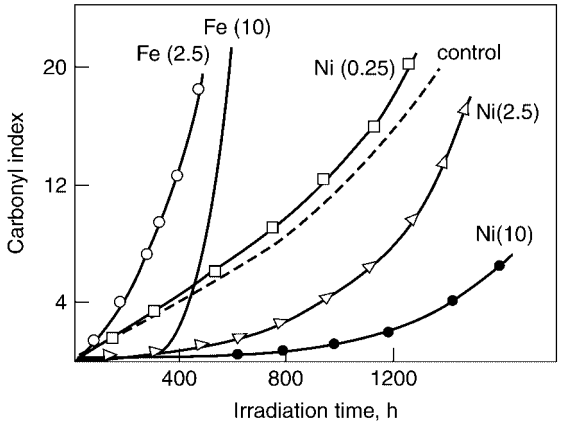

Fig. 5. Time-controlled photodegradation of LDPE stabilized with different concentrations of the photosensitize iron dithiocarbamate (FeDRC) and the photostabilizer nickel dithiocarbamate (NiDRC). Numbers on curves are antioxidant concentration in 10^{-4} mol/100 g (156).

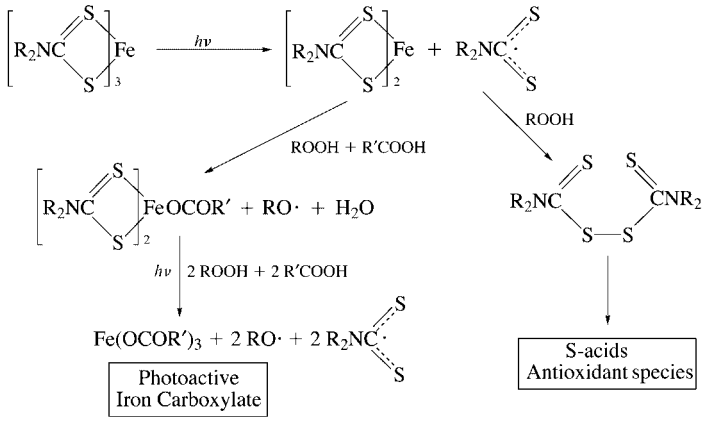

Scheme 23. Mechanism of action of the antioxidant-photoactivator FeDRC.

which are powerful antioxidants (158) by a mechanism similar to that described for the dithiophosphate.

It is this inversion in activity of FeDRC complexes from being photoantioxidants to becoming photoactivators (at the end of the induction period) which has made these antioxidant-photoactivators most suitable for the precise time-controlled stabilization. This has led to their commercial use in photobiodegradable plastics which are widely used in agricultural applications, eg, mulching films (155). In severe climates under intense uv radiation and high temperatures, two-component systems, which are based on combinations of iron and nickel dithiocarbamates, are generally used. This is mainly due to the fact that to achieve a reasonable length of the photoinduction period, a relatively high concentration of FeDRC is required, whereas a similar effect can be achieved with much lower concentrations of the more photostable nickel complexes (156). Overall, the choice of the final precise antioxidant-photoactivator system will depend on the required length of induction period and the rate of the activation process dictated by the end-use application.

Other Developments for More Efficient and Safer Stabilization

The problems of antioxidant loss from polymers in contact media, especially in human-contact applications, have generally been associated with the use of traditional low molecular mass antioxidants. Alternative types of antioxidants have been developed to address both questions of safety and efficiency. Three different approaches are highlighted here.

Higher Molar Mass Antioxidants. To address the problem of physical loss of antioxidants, oligomeric and macromolecular antioxidants were developed. A broad range of such antioxidants (both thermal- and photoantioxidants) have been synthesized (159) using a variety of methods (eg, free-radical

Table 12. Effect of Thermal Treatment and Latex Application on Polypropylene Multifilaments[a]

	Exposure time to 50% loss of tenacity, h		
		Treated	
Antioxidant	Untreated	20 min at 120°C	Acrylic latex and 20 min at 120°C
Control	490	550	460
Tinuvin 770 **(AO 25)**			
0.15	3600	1800	570
0.30	4600	2300	650
0.6	7400	5200	750
Tinuvin 622 **(AO 26b)**			
0.15	2950	2200	2450
0.30	4250	4200	3711
0.60	5500	5500	5600

[a]Ref. 160.

Table 13. Effect of HAF Carbon Black and Antioxidant on Heat Stability[a]

Vulcanizate	UTS	M_{100}	EB
No antioxidant	69	86	81
2% poly(BQ/PPD)[b]	108	123	99
2% poly(Nonox/DME)[c]	92	117	92

[a]In peroxide-cured ethylene–propylene rubber in air at 80°C. Percentage retention of properties after 230 days aging. UTS = ultimate tensile strength; M_{100} = Mooney viscosity; EB = elongation to break (161).

[b]Polymeric aromatic amine antioxidant produced by a reaction between *p*-phenylenediamine and benzoquinone at room temperature.

[c]Polymeric aromatic amine antioxidant produced by a reaction between diphenyl-*p*-phenylenediamine and xylene glycol dimethyl ether in presence of stearic chloride as catalyst.

polymerization, ring-opening polymerization, and polycondensation processes). These antioxidants show superior retention, and hence superior performance under demanding service conditions, eg, at elevated temperatures in the presence of oils and other solvents (see Tables 12 and 13) (160,161). The synthetic routes to these macromolecular antioxidants are, however, generally more expensive and their characteristics are not always fully defined. Furthermore, their high molar masses could lead to a lowering of compatibility with the host polymer with serious consequences, especially in crystalline polymers, to adversely affect their performance. Indeed, only a relatively few cost-effective macromolecular antioxidants are in commercial use (159).

Reactive Antioxidants. Reactive antioxidants are compounds containing one or more antioxidant functions (the antioxidant component) and one or more chemical functions capable of reacting either with monomers (same or different) or with polymers (the reactive component). The antioxidant

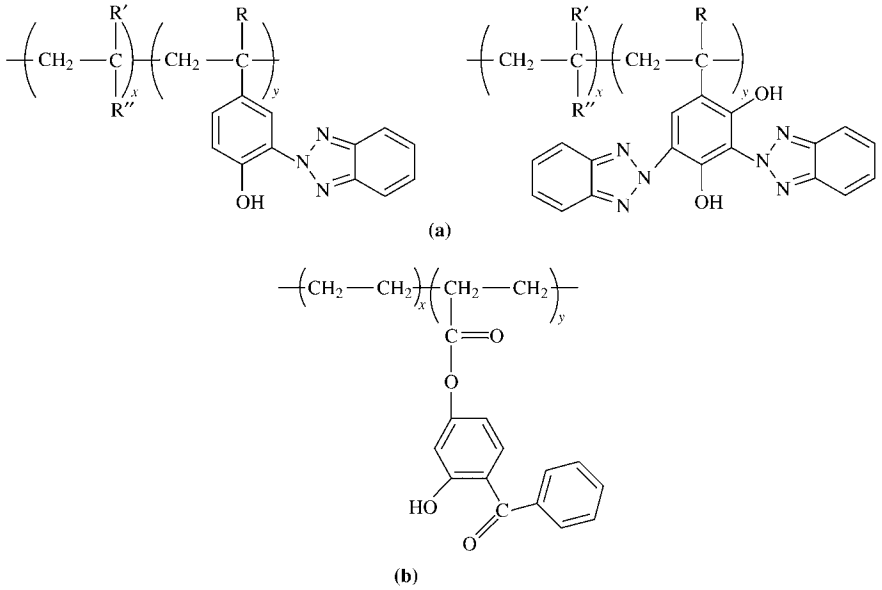

Scheme 24. Examples of antioxidant modified polymers prepared by copolymerization of various monomers with reactive UVAs. (**a**) **Hydroxy benzotriazole-based antioxidants**: R=H, CH_3 (antioxidants with vinyl or isopropenyl reactive groups); R′=C_6H_5, R″=H (styrene), R′=$COCH_3$, R″=CH_3 (methyl methacrylate); R′=$COOCH_3$, R″=H (*n*-butyl acrylate). (**b**) **Hydroxy benzophenone-based antioxidant** copolymerized with ethylene.

moiety can be based on any of the conventional antioxidant functions discussed earlier, whereas the reactive group can be chosen from a variety of polymerizable or nonpolymerizable functions, eg, vinyl, allyl, α–β unsaturated acyl or amide groups (eg, acryloyl, acrylamide, methacryloyl, or methacrylamide), styrene, isopropenyl, epoxy, and mercaptan (162). There are basically two main approaches to adopt:

Copolymerization during Polymer Manufacture. Extensive work has been documented on the synthesis and successful copolymerization of a large number of polymerizable UVA containing one or two UVA functions (see Scheme 24 for selected examples) (163,164). However, the use of such antioxidants has been beset by high synthetic costs.

The use of phenolic and amino-based antioxidants (ie, thermal stabilizers) by this approach has been limited because they inhibit the free-radical polymerization process (polymerization inhibitor) leading to lower efficiency. One of the few commercial products produced is based on the polymerizable chain breaking antioxidant (**AO 12b**, Table 3), designed for NBR rubbers (Chemigum HR 665) that has been shown to offer superior antioxidant performance, especially under aggressive (hot oil/high temperature) conditions, compared to low molecular mass conventional aromatic amine antioxidants (165). In spite of the successful synthesis and copolymerization of a large number of reactive antioxidants, there is a lack of major commercial development and production of antioxidant systems

based on this approach. This is almost certainly due to both low efficiency of polymerization in the presence of certain antioxidant functions and, more importantly, to the high costs generally involved in the synthesis and production of tailor-made "speciality" materials for each specific application. However, this approach may be utilized in certain target applications where performance and reliability, especially under a demanding environment, is the ultimate design prerequisite, eg, in space and military applications.

Chemical Grafting Post Polymer Manufacture. Various chemical routes have been exploited to achieve grafting of reactive antioxidants onto preformed commercial polymers. Different routes are available, depending on the method used to achieve grafting reactions during vulcanization, by decomposition of free-radical initiators (peroxides, hydroperoxides, AIBN), by uv or γ irradiation of polymer surfaces, by mechanical scission, and during melt processing in the presence of added initiators. The main prerequisite here is that the reaction leading to chemical attachment of the antioxidant should be achieved without detriment to the overall polymer properties or the basic processes involved, eg, vulcanization in case of rubbers or melt processing/fabrication in plastics (162,166).

Reactive antioxidants containing some of the basic photoantioxidant functions (eg, HAS, UVA) and one or more polymer reactive functions can be made to react with polymers during melt processing. These reactions are normally achieved in the presence of a very small concentration of a free-radical initiator, and in some cases also in the presence of a coreactive monomer (162,166–176). Both chemical factors and processing parameters can be manipulated to achieve high levels of grafting of the functional antioxidants on the polymer. Table 14 illustrates the advantages, especially under extractive conditions, of using reactive photo-antioxidants which are highly grafted on PP, compared to traditional nonreactive (nongraftable) analogues (170–175). The grafted HAS photoantioxidant AOTP, for example, shows superior performance under extractive conditions compared to the commercial HAS, Tinuvin 770 (**AO 25**, Table 3) because it is less readily lost from the polymer during processing and service. Furthermore, both grafted HAS antioxidants, eg, AOTP (monofunctional) and AATP (bifunctional), structures in Table 14, synergize effectively when used in combination with other classes of photostabilizers, eg, UVA such as Chimassorb 81 (**AO 28**, Table 3). A graftable UVA based on a hydroxybenzophenone structure, HAEB, is also shown to give effective synergism in combination with a highly grafted hindered phenol, DBBA, when the grafting of the latter was conducted in the presence of a reactive nonantioxidant comonomer, Tris (see Table 14 for structure). The co-grafting of this polyfunctional comonomer (Tris) with mono-vinyl antioxidants (and other monofunctional additives) in extruders or internal mixers has been shown (174) to lead to the production of highly grafted antioxidants in noncross-linked polymer products without detriment to the physical and morphological characteristics (eg, crystallinity) of the polymer. Highly grafted and "permanently fixed" antioxidant concentrates (masterbatches) can be produced for blending with, and dilution in, polymers in the same way as conventional antioxidants.

It is important to point out here that there are different approaches to the grafting of antioxidants on polymers, each with its set of advantages and disadvantages. However, the behavior of grafted reactive antioxidants is similar to that

Table 14. Ultraviolet Embrittlement Times (EMT) of PP Films[a]

Antioxidant structure	Composition without and with grafted (g) antioxidants	Conc. in PP film, %	EMT, h	
			Before extraction	After extraction
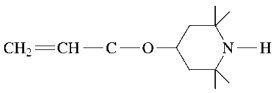 (AOTP)	AOTP-g	0.4	–	1200
AOTP-g + Chimassorb 81 (**AO 28**)	0.4 + 0.2	3000	–	
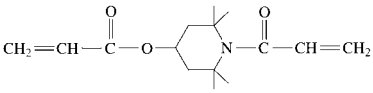 (AATP)	AATP-g	0.4	1850	
AATP-g + Chimassorb 81 (**AO 28**)	0.4 + 0.1	2050		
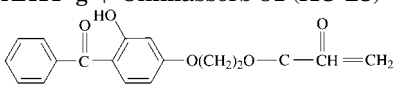 (HAEB)	HAEB	0.3	330	70
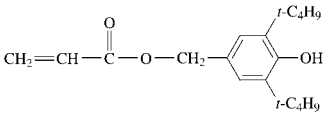 (DBBA)	DBBA	0.2	205	80
$(HAEB\text{-}g + DBBA\text{-}g)_{Tris}$	0.2 + 0.2	1160	1130	
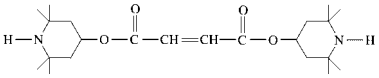 (BPM)	BPM-g	0.1	2850	1400
Irganox 1010 + Chimassorb 81	**AO 5** + **AO 28**	0.2 + 0.2	1750	70
Chimassorb 81	**AO 28**	0.4	330	110
Tinuvin 770	**AO 25**	0.4	1500	130
$(CH_2{=}CHCOOCH_2)_3CCH_2CH_3$	Tris			

[a]Films contain different grafted (g) reactive antioxidants when used alone and in combination with other stabilizers. Extraction in dichloromethane.

of their "traditional" low molecular mass analogues but offer greater permanency and stabilization of polymer compositions under more demanding conditions.

Biological Antioxidant. Safety issues and costly toxicity tests have focused attention on a new stabilization strategy that exploit the use of a fat-soluble biological antioxidant (vitamin E). α-Tocopherol (**AO 10**, Table 3), the most bioactive form of vitamin E, is a highly efficient biological chain-breaking antioxidant which is known to be involved in the natural defense mechanisms of living organisms (177,178).

Studies on vitamin E in polymers have demonstrated its high antioxidancy in different polymers, especially as a melt-processing stabilizer in polyolefins (119,179–186). Figure 6 shows the superior performance of vitamin E when compared to Irganox 1010 during melt extrusion of PE and PP at all concentrations and, in particular, at very low concentrations. Vitamin E can, therefore, be

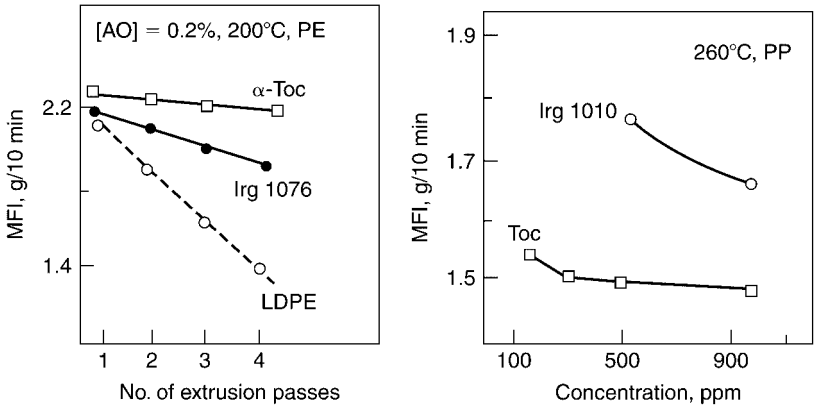

Fig. 6. The melt stabilizing activity of tocopherol and synthetic hindered phenols in PE and PP (119).

employed cost-effectively to stabilize polyolefins using only a small fraction of the concentration needed of typical synthetic hindered phenols. Its effectiveness is attributed to its efficient deactivation of macroradicals and to its oxidative transformation products which are themselves highly effective melt stabilizers (119).

In general, sterically hindered phenols contribute to some discoloration (yellowing) of polyolefins mainly through the formation of colored oxidation products, eg, quinonoid structures, and interactions with catalyst residues (187,188). The extent of discoloration depends on the chemical structure of the parent

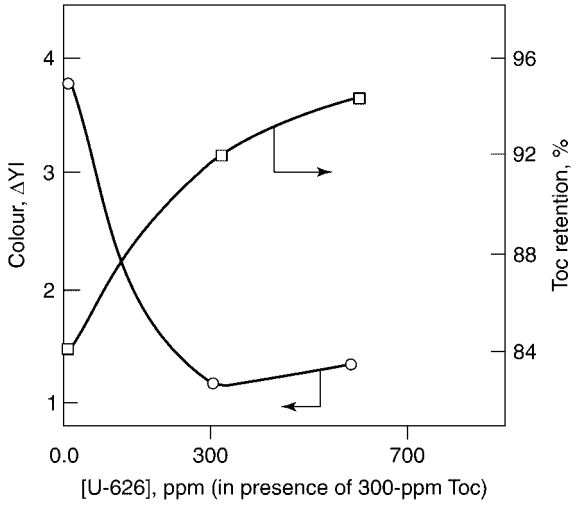

Fig. 7. Effect of the phosphite U-626 concentration in combinations containing 300-ppm Toc on color stability of PP and on the extent of tocopherol retention; PP extrusion at 260°C (119).

antioxidant, the oxidation products, and the type and amount of catalyst residues in the polymer. The use of a small concentration of certain co-stabilizers, such as phosphite esters, with hindered phenols result in reduced discoloration. In the case of vitamin E, the use of a small concentration of the phosphite U-626 (**AO 18**, Table 3) results in drastic reduction in discoloration, as well as an increase in the level of retention of the parent vitamin (see Fig. 7) (119). The reduction in consumption of other synthetic hindered phenol antioxidants by phosphite co-stabilizers has been reported, although the mechanism is not fully understood (189,190). In the case of the hindered aryl phosphite Ultranox U626 used in

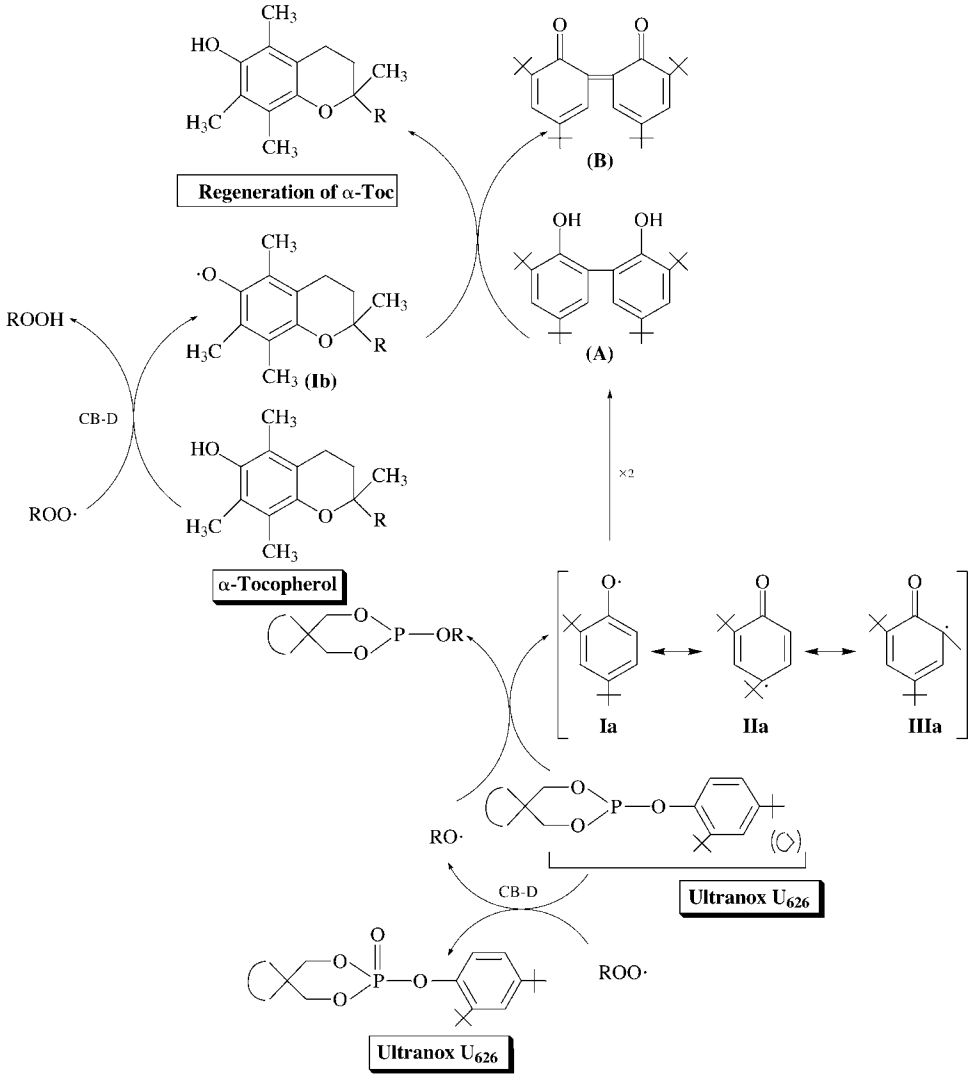

Scheme 25. Cooperative interactions between aromatic phosphite and tocopherol, resulting in the regeneration of tocopherol.

combination with tocopherol, the evidence (191) points out to the regeneration of the parent tocopherol through a redox reaction between products of the two stabilizers. Scheme 25 illustrates this and shows that the phenoxyl radical produced through the CB activity of Ultranox U-626 undergoes a C—C coupling reaction to produce a hindered phenol dimer (**A**) which can react further with the tocopheroxyl radical in a redox process that regenerates the parent hindered phenol (119).

Synergism and Antagonism

The cooperative interaction between two or more antioxidants (or antioxidant functions) that enhances the stabilization of a polymer by more than the sum of the individual effects of the antioxidants is referred to as *synergism*. Often, the overall effectiveness of the synergistic system is much greater than can be achieved by either of the antioxidants, even at higher concentration, and hence the practical importance of synergism. Synergism can result from the combined action of two

Table 15. Synertistic and Antagonistic Effects on Photostability of LDPE processed at 150°C

Stabilizer system	Concentration, 10^{-4} mol/100 g	Photo-embrittlement time, h		Reference
		Observed	Calculated effect[a,b]	
Control PP (no antioxidant)	–	l000	–	105
ZnDEC	3	l400	–	105
NiDEC	3	l800	–	105
Tinuvin 77O	3	2400	–	105
Irganox lO76	3	l750	–	105
NiDBP	2.5	2800	–	3
NiBX	2.5	2500	–	3
CuDIP	2.5	2300	–	3
Chimassorb 81	3	l650	–	
Synergistic systems				
NiDEC + Chimassorb 81	3 + 3	–	–	105
ZnDEC + Chimassorb 81	3 +	4000	3000	105
NiDBP + Chimassorb 81	2.5 + 2.5	5500	4500	3
NiBX + Chimassorb 81	2.5 + 2.5	4900	4200	3
CuDIP + Chimassorb 81	2.5 + 2.5	5350	4000	3
Antagonistic systems				
NiDEC + Irganox lO76	3 + 3	l580	3550	105
ZnDEC + Irganox lO76	3 + 3	l250	3l50	105
NiDEC + Tinuvin 77O	3 + 3	l850	4200	105
NiDBP + Irganox lO76	2.5 + 5	–	–	3

[a] Concentration of HOBP in this case was $5 \times l0^{-4}$ mol/l00 g.

[b] $\%\text{Synergism} = \frac{(E_s - E_c) - (E_1 - E_c) + (E_2 - E_c)}{E_1 - E_c + E_2 - E_c} \times 100$, where E_s is the embrittlement time of synergist; E_c is the embrittlement time of control; E_1 is the embrittlement time of antioxidant 1; and E_2 is the embrittlement time of antioxidant 2.

chemically similar antioxidants, eg, two hindered phenols (*homosynergism*), or from two different antioxidant functions present in the same stabilizer molecule, eg, Irganox 1081 (**AO 9**, Table 3) (*autosynergism*), or when separate stabilizer molecules that carry different antioxidant functions are physically blended in a stabilizer formulation (*heterosynergism*). Conversely, though infrequently, two antioxidants may interact antagonistically to cause a decrease in the sum of their individual contributions (2,51,192).

Highly effective UV-stabilizing systems can be achieved by the use of synergistic mixtures of compounds acting by different mechanisms. Table 15 illustrates the synergism obtained from combinations of different metal dithiolates with the UVA Chimassorb 81 (**AO 28**, Table 3) in LDPE (see Section on Antioxidants in Polymer Stabilization). In contrast to the synergistic effect obtained during thermal stabilization when hindered phenol antioxidants are mixed with sulfur-containing compounds, combinations of a phenolic antioxidant (eg, Irganox 1076; **AO 4**, Table 3) with metal dithiolates lead to antagonism during

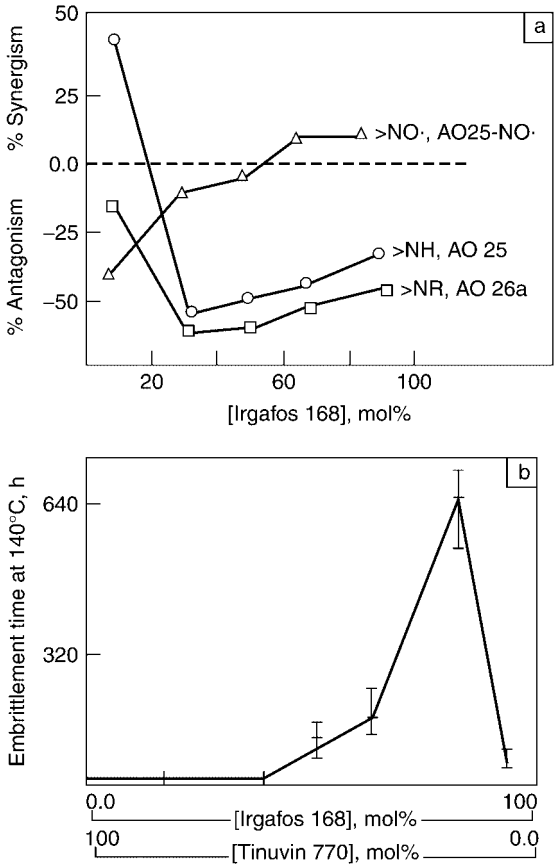

Fig. 8. Effect of molar composition of mixture of HALS and Irgafos 168 (total [AO] = 7×10^{-3} mol/kg in each case) on (**a**) extent of synergism and antagonism during photooxidation of PP (193), and (**b**) thermoxidative stability of PP in air oven (195).

photostabilization (see Table 15) (3,105). This antagonistic behavior has been attributed to sensitisation leading to photolytic destruction of the dithiolates by oxidation products of phenols, particularly stilbenequinones. Stabilizers that contain two different antioxidant functions (eg, PD and CB activities) in the same molecule, such as phenolic sulfides, show much higher molar intrinsic activity as thermal antioxidants (due to autosynergism) than conventional hindered phenols with only CB activity (51).

Hindered piperidines (HAS) exhibit a complex behavior when present in combination with other antioxidants and stabilizers. As discussed earlier (see section on Hindered Amine) these have to be oxidized first to the corresponding nitroxyl radical before becoming effective. Consequently, both CB-D and PD-C antioxidants that remove alkyl peroxyl radicals and hydroperoxides, respectively, antagonize the uv-stabilizing action of this class of compounds (see Fig. 8a) (193,194). However, since the hindered piperidines themselves are neither melt- nor thermal-stabilizers for polymers, they have to be used with conventional antioxidants and stabilizers. Effective synergism in both melt and thermal stabilization has been achieved when secondary and tertiary HALS were used in combination with both aromatic and aliphatic phosphites, the synergistic optimum depending on the structure of the phosphite (see Fig. 8b) (195). Hindered piperidines have also been reported to synergize with UVA, eg, benzotriazoles, in different polymers such as PP, PS, and ABS (53,196).

Conclusion

The combined effects of oxygen, water, heat, and light are generally extremely detrimental to the lifetime performance of polymers during processing, fabrication, and throughout the useful lifetime of its artifacts, recycling, and subsequent lifecycles. Stabilizers and antioxidants are, therefore, essential ingredients in almost all plastics formulations. Hydroperoxides are key initiators of oxidative degradation resulting in free-radical formation in polymers. Antioxidants are used to prevent the formation of hydroperoxides and/or to convert them into harmless chemicals (peroxidolytic antioxidants), or to deactivate the free radicals, eg, alkyl and alkylperoxyl, formed (chain-breaking antioxidants).

Apart from economic factors, the choice of stabilizers for end-use application is dictated by chemical, physical, and toxicological considerations. Stabilization of polymers during melt processing, heat aging, and outdoor exposure is normally achieved through the use of synergistic combinations of well-known commercial stabilizers with complementary antioxidant mechanisms. For example, the use of chain-breaking hindered phenols in combination with peroxidolytic phosphite antioxidants is a common practice to affect melt stabilization of polymers, whereas the use of different HAS in the presence or absence of uv absorbers is a general approach to photostabilisation. Ultimately, however, the selection of an antioxidant package needs to be specifically tailored for the end-use application with due attention to other critical considerations, for example, color and toxicity. Issues of efficiency and safety (including migration) of stabilizers have been at the forefront of recent progress made in the areas of macromolecular, reactive, and biological antioxidants. Further progress will almost certainly involve optimization and fine

tuning of the physical and chemical performance of the wide range of commercially available antioxidants and stabilizers.

BIBLIOGRAPHY

"Stabilization" in *EPST* 1st ed., Vol. 12, pp. 725–768, by L. I. Nass, Consultant; "Stabilization" in *EPSE* 2nd ed., Vol. 15, pp. 539–583, by W. L. Hawkins, Consultant.

1. F. Gugumus, in J. Pospisil and P. Klemchuk, eds., *Oxidation Inhibition of Organic Materials*, Vol. **1**, CRC Press, Boca Raton, Fla., 1990, p. 61.
2. G. Scott, in G. Scott, ed., *Atmospheric Oxidation and Antioxidants*, Vol. **2**, Elsevier Applied Science Publishers, London, 1993, p. 141.
3. S. Al-Malaika, in G. C. Eastmond, A. Ledwith, S. Russo, and P. Sigwalt, eds., *Comprehensive Polymer Science*, Vol. **6**, Pergamon Press, N.Y., 1989, p. 539.
4. N. C. Billingham, in P. Klemchuk and J. Pospisil, eds., *Oxidation Inhibition of Organic Materials*, Vol. **2**, CRC Press, Boca Raton, Fla., 1990, p. 249.
5. N. C. Billingham and P. D. Calvert, *Dev. Polym. Deg.* **3**, 139 (1980).
6. S. Al-Malaika, in G. Pritchard, ed., *Plastics Additives*, Chapman and Hall, London, 1998, p. 55.
7. S. Al-Malaika, M. D. R. J. Goonetileka, and G. Scott, *Polym. Deg. Stab.* **32**, 231 (1991).
8. C. Moureu and C. Dufraisse, *Bull. Soc. Chim.* **31**, 1152 (1922).
9. C. Dufraisse, *Rubb. Chem. Tech.* **6**, 157 (1933).
10. C. Moureu and C. Dufraisse, *Chem. Rev.* **3**, 113 (1926–27).
11. S. Al-Malaika, in R. Seymour and R. D. Deanin, eds., *History of Polymer Composites*, VNU Science Press BV, the Netherlands, 1987, p. 223.
12. H. L. J. Backstrom, *J. Am. Chem. Soc.* **49**, 1460 (1929); *Z. Phys. Chem. B* **25**, 99 (1934).
13. J. L. Bolland, *Quart. Rev.* **3**, 1 (1949).
14. J. L. Bolland and G. Gee, *Trans. Faraday Soc.* **42**, 236 (1946).
15. L. Bateman, *Quart. Rev.* **8**, 147 (1954).
16. L. Bateman and A. L. Morris, *Trans. Farad. Soc.* **49**, 1026 (1953).
17. G. Scott, *Atmospheric Oxidation and Antioxidants*, Elsevier, New York, 1965, p. 66.
18. S. Al-Malaika, in G. Scott, ed., *Atmospheric Oxidation and Antioxidants*, Vol. **1**, Elsevier, New York, 1993, p. 45.
19. W. L. Hawkins, *Polymer Stabilization*, John Wiley & Sons, Inc., New York, 1972.
20. D. Barnard, L. Bateman, and J. F. Smith, in L. Bateman, ed., *Chemistry and Physics of Rubber-Like Substances*, Applied Science Publishers, London, 1963, p. 593.
21. L. Reich and R. S. Stivala, *Autoxidation of Hydrocarbons and Polyolefins*, Marcel Dekker, Inc., New York, 1969, p. 1.
22. N. C. Billingham, in Ref. 2, p. 219.
23. E. T. Denisov, *Handbook of Antioxidants, Bond Dissociation Energies, Rate Constants, Activation Energies and Enthalpies of Reactions*, CRC Press, Boca Raton, Fla., 1995.
24. J. A. Howard, in J. K. Kochi, ed., *Free Radicals*, John Wiley & Sons, Inc., New York, 1973, p. 2.
25. J. A. Howard, K. U. Ingold, and M. S. Symonds, *Can. J. Chem.* **46**, 1017 (1968).
26. S. Korcek, and co-workers, *Can. J. Chem.* **50**, 2285 (1972).
27. G. A. Russel, *J. Am. Chem. Soc.* **79**, 3871 (1957).
28. J. A. Howard, *Adv. Free Radical Chem.* **4**, 49 (1972).
29. J. A. Howard and K. U. Ingold, *Can. J. Chem.* **43**, 2729 (1965).
30. J. A. Howard and K. U. Ingold, *Can. J. Chem.* **45**, 783, 789 (1967).
31. J. A. Howard, K. Adamic, and K. U. Ingold, *Can. J. Chem.* **47**, 3793, 3803 (1969).

32. B. B. Cooray and G. Scott, in G. Scott, ed., *Developments in Polymer Stabilization*, Vol. **2**, Applied Science Publishers, London, 1980, p. 53.
33. G. Scott, M. Tahan, and J. Vyvoda, *Chem. Ind.* 903 (1976).
34. G. Scott, M. Tahan, and J. Vyvoda, *Eur. Polym. J.* **14**, 377 (1978).
35. A. Guyot, *J. Vinyl Technol.* **7**, 92 (1985).
36. A. Michel, *J. Vinyl Technol.* **7**, 77 (1985).
37. S. Al-Malaika and G. Scott, in N. S. Allen, ed., *Degradation and Stabilization of Polyolefins*, Applied Science Publishers, London, 1983, p. 283.
38. K. B. Chakraborty and G. Scott, *Polym. Deg. Stab.* **1**, 37 (1979).
39. K. B. Chakraborty and G. Scott, *Eur. Polym. J.* **13**, 73 (1977).
40. M. Iring and F. Tudos, *Prog. Polym. Sci.* **15**, 217 (1990).
41. H. Hinsken, and co-workers, *Polym. Deg. Stab.* **34**, 279 (1991).
42. S. S. Stivala, J. Kimura, and S. M. Gabbay, in Ref. 37, p. 63.
43. R. T. Johnston and E. J. Morrison, in R. L. Clough, N. C. Billingham, and K. T. Gillens, eds., *Advances in Chemistry Series No. 249: Polymer Durability*, American Chemical Society, Washington, D. C., 1996, p. 651.
44. S. Moss and H. Zweifel, *Polym. Deg. Stab.* **25**, 217 (1989).
45. W. O. Drake, and co-workers, *Angew. Makromol. Chem.* **176/177**, 215 (1990).
46. G. Geuskens, and co-workers, *Polym. Deg. Stab.* **3**, 295 (1980–1981).
47. B. F. Sagar, *J. Chem. Soc. B* **428**, 1047 (1967).
48. A. Casale and R. S. Porter, *Polymer Stress Reactions*, Vol. **1**, Academic Press, New York, 1979, p. 69.
49. A. Casale and R. S. Porter, *Polymer Stress Reactions*, Vol. **2**, Academic Press, New York, 1979, p. 370.
50. D. J. Carlsson, A. Graton, and D. M. Wiles, in G. Scott, ed., *Developments in Polymer Stabilization*, Vol. **1**, Applied Science Publishers, London, 1979, p. 219.
51. Ref. 37, p. 247.
52. S. Al-Malaika and G. Scott, *Polym. Deg. Stab.* **5**, 415 (1983).
53. F. Gugumus, in Ref. 50, p. 261.
54. D. J. Carlsson and D. M. Wiles, *J. Macromol. Sci., Part C: Rev. Macromol. Chem.* **14**(1), 65 (1976).
55. F. Gugumus, in Ref. 4, p. 29.
56. A. Davis and D. Sims, *Weathering of Polymers*, Applied Science Publishers, London, 1983, p. 137.
57. F. H. Winslow, W. Matreyek, and A. M. Trozzolo, *S.P.E. Trans.* **18**, 776 (1972).
58. H. H. G. Jellinek, ed., *Photochemistry of Air Pollution*, Academic Press, New York, 1961.
59. J. A. Kuczkowski, in Ref. 1, p. 274.
60. E. M. Fettes, ed., *Chemical Reactions of Polymers*, Wiley-Interscience, New York, 1964.
61. H. H. G. Jellinek, ed., *Aspects of Degradation and Stabilization of Polymers*, Elsevier, Amsterdam, 1978.
62. G. Scott, in Ref. 2, p. 385.
63. D. J. Carlsson and D. M. Wiles, *Macromolecules* **9**, 695 (1976).
64. G. Scott, *Pure Appl. Chem.* **52**, 365 (1980).
65. G. Scott, in Ref. 50, p. 314.
66. W. L. Hawkins, in W. L. Hawkins, ed., *Polymer Stabilization*, Wiley, New York, 1972, p. 9.
67. G. Ayrey, B. C. Head, and R. C. Poller, *J. Polym. Sci., Macromol Rev.* **8**, 1 (1974).
68. H. O. Wirth and H. Andreas, *Pure Appl. Chem.* **49**, 627 (1977).
69. G. Scott, M. Tahan, and J. Vyvoda, *Eur. Polym. J.* **14**, 1021 (1978).
70. B. B. Cooray and G. Scott, in Ref. 50, p. 53.
71. L. Tang, and co-workers, *Makromol Chem.* **182**, 3477 (1981).

72. L. Tang, D. Sallet, and J. Lemair, *Macromolecules* **15**, 1432 (1982).
73. L. Tang, D. Sallet, and J. Lemair, *Macromolecules* **15**, 1437 (1982).
74. L. Tang, D. Sallet, and J. Lemair, *Macromolecules* **18**, 1771 (1985).
75. L. Tang, D. Sallet, and J. Lemair, *Macromolecules* **19**, 579 (1986).
76. J. Lemair and co-workers, *Polym. Deg. Stab.* **15**, 1 (1986).
77. A. Rivaton, *Polym. Deg. Stab.* **41**, 283 (1993).
78. A. Rivaton, *Polym. Deg. Stab.* **41**, 297 (1993).
79. M. Day and D. M. Wiles, *J. App. Polym. Sci.* **16**, 175 (1972).
80. M. Day and D. M. Wiles, *J. App. Polym. Sci.* **16**, 175 (1972).
81. A. Factor, W. V. Ligon, and R. J. May, *Macromolecules* **20**, 2462 (1987).
82. A. Davis and J. H. Golden, *J. Macromol. Sci., Part C: Rev. Macromol. Chem.* **3**, 49 (1969).
83. D. Bellus, P. Hrdlovic, and Z. Manasek, *J. Polym. Sci., Part B* **4**, 1 (1966).
84. H. S. Munro and D. T. Clark, *Polym. Deg. Stab.* **17**, 319 (1987).
85. G. Scott, in Ref. 18, p. 121.
86. Ref. 18, p. 161.
87. R. Gachter and H. Muller, eds., *Plastics Additives Handbook*, 2nd ed., Hanser Publishers, Munich, 1987.
88. J. Pospisil, in Ref. 50, p. 1.
89. J. Pospisil, in G. Scott, ed., *Developments in Polymer Stabilization*, Vol. **7**, Applied Science Publishers, London, 1984, p. 1.
90. H. Zweifel, in R. L. Clough, K. T. Gillen, and N. C. Billingham, eds., *Advances in Chemistry Series No. 249*, American Chemical Society, Washington, D.C., 1996, p. 375.
91. D. Horsey, in *Proceedings of the International Conference Additives-96*, Houston, Tex., 1996.
92. P. Nesvadba, in *Proceedings of the International Conference Additives-97*, Florida, 1997.
93. H. Zweifel, *Stabilization of Polymeric Materials*, Springer, Verlag, 1998, p. 53.
94. K. B. Chakraborty and G. Scott, *J. Polym. Sci., Polym Lett.* **22**, 553 (1984).
95. T. J. Henman, in Ref. 50, p. 39.
96. G. Scott, in Ref. 89, p. 65.
97. E. T. Denisov, in G. Scott, ed., *Developments in Polymer Stabilization*, Vol. **3**, Applied Science Publishers, London, 1980, p. 1.
98. V. Ya Shlyapintokh and V. B. Ivanov, in G. Scott, ed., *Developments in Polymer Stabilization*, Vol. **5**, Applied Science Publishers, London, 1982, p. 41.
99. H. Berger, T. A. B. M. Bolsman, and D. M. Brouwer, in G. Scott, ed., *Developments in Polymer Stabilization*, Vol. **6**, Applied Science Publishers, London, 1983, p. 1.
100. S. Al-Malaika, E. O. Omikorede, and G. Scott, *J. App. Polym. Sci.* **33**, 703 (1987).
101. S. Al-Malaika, in G. Scott, ed., *Mechanisms of Polymer Degradation and Stabilization*, Elsevier Science Publishers, New York, 1990, p. 61.
102. K. Schwetlick, in Ref. 101, p. 23.
103. D. G. Pobedimskii, N. A. Mukmeneva, and P. A. Kirpichnikov, in Ref. 32, p. 125.
104. K. Schwetlick and W. D. Habicher, in Ref. 90, p. 349.
105. S. Al-Malaika, K. B. Chakraborty, and G. Scott, in Ref. 99, p. 73.
106. G. Scott, in Ref. 99, p. 29.
107. J. R. Shelton, in G. Scott, ed., *Developments in Polymer Stabilization*, Vol. **4**, Applied Science Publishers, London, 1981, p. 23.
108. Z. Osawa, in Ref. 89, p. 193.
109. M. G. Chan, in Ref. 1, p. 225.
110. H. Muller, in Ref. 87, p. 75.

111. J. G. Calvert, J. N. Pitts Jr., *Photochemistry*, John Wiley & Sons, Inc., New York, 1967, p. 534.
112. H. J. Heller and H. R. Blattmann, *Pure Appl. Chem.* **30**, 145 (1972).
113. H. J. Heller and H. R. Blattmann, *Pure and Appl. Chem.* **36**, 141 (1973).
114. F. Gugumus, in Ref. 87, p. 128.
115. N. C. Billingham, P. Prentice, and T. J. Walker, *J. Polym. Sci., Polym. Symp.* **57**, 287 (1976).
116. J. Luston, in Ref. 32, p. 185.
117. S. Al-Malaika, P. Desai, and G. Scott, *Plast. Rubber Process. Appln.* **5**, 15 (1985).
118. K. Schwarzenbach, in Ref. 87, p. 1.
119. S. Al-Malaika and co-workers, *Polym. Deg. Stab.* **64**, 145 (1999).
120. J. Pospisil, in Ref. 4, p. 33.
121. J. Pospisil, in Ref. 6, p. 73.
122. J. Pospisil, *Polym. Deg. Stab.* **39**, 103 (1993).
123. J. Pospisil, *Polym. Deg. Stab.* **40**, 217 (1993).
124. A. F. Bickel and E. C. Kooyman, *J. Chem. Soc.* 2218 (1956).
125. P. P. Klemchuk and P. L. Horng, *Polym. Deg. Stab.* **34**, 333 (1991).
126. J. A. Kuczkowski, in Ref. 1, p. 247.
127. R. H. Bauer and G. M. Coopinger, *Tetrahedron* **19**, 1201 (1963).
128. S. Yachigo and co-workers, *Polym. Deg. Stab.* **39**, 317 (1993).
129. H. Andreas, in Ref. 87, p. 193.
130. G. Ayrey and R. C. Poller, in Ref. 32, p. 1.
131. B. B. Cooray and G. Scott, in Ref. 32, p. 53.
132. A. Guyot and A. Michel, in Ref. 32, p. 89.
133. K. Humphries and G. Scott, *J. Chem. Soc., Perkin Trans. 1* 831 (1973).
134. K. Humphries and G. Scott, *Pure Appl. Chem.* **324**, 697 (1982).
135. D. G. Pobedimskii, N. A. Mukmeneva, and P. A. Kirpichnikov, in Ref. 32, p. 125.
136. S. K. Ivanov, in Ref. 97, p. 55.
137. H. S. Laver, in Ref. 50, p. 167.
138. S. Al-Malaika, A. Marogi, and G. Scott, *J. App. Polym. Sci.* **30**, 789 (1985).
139. S. Al-Malaika and G. Scott, *Eur. Polym. J.* **16**, 503 (1980).
140. J. A. Howard and co-workers, *Can. J. Chem.* **51**, 1543 (1973).
141. S. Al-Malaika, M. Coker, and G. Scott, *Unpublished work*.
142. K. B. Chakraborty, W. R. Poyner, and G. Scott, *Plast. Rubber Process. Appl.* **3**, 59 (1983).
143. J. F. Rabek, *Mechanisms of Photophysical Processes and Photochemical Reactions*, John Wiley & Sons, Inc., New York, 1987, p. 594.
144. D. J. Carlsson, T. Suprunchuk, and D. M. Wiles, *J. App. Polym. Sci.* **16**, 615 (1972).
145. P. Vink, in Ref. 97, p. 117.
146. K. B. Chakraborty and F. Scott, *Eur. Polym. J.* **15**, 35 (1979).
147. W. L. Hawkins, in H. F. Mark and J. I. Kroschwitz, eds., *Encyclopedia of Polymer Science and Technology*, 2nd ed., Vol. **15**, John Wiley & Sons, Inc., New York, 1989, p. 539.
148. G. Scott, *Atmospheric Oxidation and Antioxidants*, 1st ed., Elsevier, Amsterdam, 1965, p. 287.
149. T. Colclough and J. I. Cunneen, *J. Chem. Soc.* 4790 (1964).
150. S. Al-Malaika, M. Coker, and G. Scott, *Polym. Deg. Stab.* **10**, 173 (1985).
151. S. Al-Malaika and co-workers, *Polym. Deg. Stab.* **10**, 55 (1985).
152. S. Al-Malaika and co-workers, *Polym. Deg. Stab.* **13**, 261 (1985).
153. P. P. Klemchuk and M. E. Gande, *Polym. Deg. Stab.* **22**, 241 (1988).
154. P. P. Klemchuk and M. E. Gande, *Polym. Deg. Stab.* **27**, 75 (1990).

155. D. Gilead and G. Scott, in Ref. 98, p. 71.
156. S. Al-Malaika, A. Marogi, and G. Scott, *J. App. Polym. Sci.* **31**, 685 (1986).
157. S. Al-Malaika, A. Marogi, and G. Scott, *Polym. Deg. Stab.* **18**, 89 (1987).
158. S. Al-Malaika, A. Marogi, and G. Scott, *J. App. Polym. Sci.* **33**, 1455 (1987).
159. J. Pospisil, in Ref. 1, p. 193.
160. J. Sedlar, in Ref. 4, p. 1.
161. D. K. Thomas, in Ref. 50, p. 137.
162. S. Al-Malaika, in S. Al-Malaika, ed., *Reactive Modifiers in Polymers*, Blackie Academic Professional, London, 1997, p. 266.
163. O. Vogl, A. C. Albertsson, and Z. Janovic, in P. Klemchuck, eds., *Polymer Degradation and Stabilization*, American Chemical Society, Washington, D.C., 1985, p. 197. ACS Symposium Series, Vol. **280**.
164. S. Fu, A. Gupta, A. C. Albertsson, and O. Vogl, in N. S. Allen and J. F. Rabek, eds., *New Trends in the Photochemistry of Polymers*, Elsevier Applied Science, London, 1985, p. 247.
165. J. W. Horvath, D. C. Grimm, and J. A. Stevick, *Rubber Chem. Technol.* **48**, 337 (1975).
166. G. Scott, in G. Scott, ed., *Developments in Polymer Stabilization*, Vol. **8**, Applied Science Publishers, London, 1987, p. 209.
167. D Munteanu, in Ref. 166, p. 179.
168. S. Al-Malaika, in S. Al-Malaika, A. Golovoy, and C. A. Wilkie, eds., *Chemistry and Technology of Polymer Additives*, Blackwell Science, Oxford, 1999, p. 1.
169. S. Al-Malaika, in J. L. Benham and J. F. Kinstle, eds., *ACS Symposium Series. No. 364: Chemical Reactions on Polymers*, American Chemical Society, Washington, D.C., 1988, p. 409.
170. S. Al-Malaika, G. Scott, and B Wirjosentono, *Polym. Deg. Stab.* **40**, 233–238 (1993).
171. S. Al-Malaika and N. Suharty, *Polym. Deg. Stab.* **49**, 77–89 (1995).
172. S. Al-Malaika and co-workers, *J. App. Polym. Sci.* **44**, 1287–1296 (1992).
173. S. Al-Malaika, A. Q. Ibrahim, and G. Scott, *Polym. Deg. Stab.* **22**, 233 (1988).
174. U.S. Pat. 5,382,633 (1995), G. Scott and S. Al-Malaika.
175. U.S. Pat. 4,959,410 (1990), G. Scott, S. Al-Malaika, and A. Ibrahim.
176. Y. N. Sharma and co-workers, *J. App. Polym. Sci.* **27**, 2605 (1982).
177. G. W. Burton and co-workers, *J. Am. Chem. Soc.* **102**, 7791 (1980).
178. G. W. Burton and K. U. Ingold, *Acc. Chem. Res.* **194**, (1986).
179. S. Al-Malaika, H. Ashley, and S. Issenhuth, *J. Polym. Sci., Part A: Polym. Chem.* **32**, 3099–3113 (1994).
180. S. Al-Malaika and S. Issenhuth, in Ref. 90, p. 425.
181. S. Al-Malaika and S. Issenhuth, *Polym. Deg. Stab.* **65**, 143 (1999).
182. S. Al-Malaika and co-workers, *Polym. Deg. Stab.* in press.
183. S. Al-Malaika and S. Issenhuth, *Polymer* **42**, 2915 (2001).
184. S. Al-Malaika, in *Proceedings of Addcon World 2000*, Basel, Switzerland, Oct. 2000, RAPRA Technology, Shrewsbury. Paper 15.
185. J. Ghosh, in *Proceedings of Additives '99*, San Francisco, 1999, Executive Conference Management, Michigan. Paper 2.
186. S. F. Laermer and F. Nabhulz, *Plast. Rubber Process. Appln.* **14**, 235 (1990).
187. J. Pospisil, *Adv. Polym. Sci.* **36**, 69 (1980).
188. J. E. Kresta and J. Majer, *J. Appl. Polym. Sci.* **13**, 1859 (1969).
189. W. O. Drake and co-workers, *Angew. Makromol. Chem.* **176**, 215 (1990).
190. J. Schiers, J. Pospisil, M. J. O'Connor, and S. W. Bigger, in Ref. 90, Chapt. "24".
191. S. Al-Malaika, M. Khayat, I. Pullright, and P. Hurley, *Unpublished work*.
192. S. Al-Malaika and G. Scott, *Eur. Polym. J.* **19**, 241 (1983).
193. I. Bauer and co-workers, *Polym. Deg. Stab.* **55**, 217 (1997).

194. F. Tudos, G. Balint, and T. Kelen, in Ref. 99, p. 121.
195. I. Bauer and co-workers, *Polym. Deg. Stab.* **48**, 427 (1995).
196. H. K. Muller, in Ref. 162, p. 55.

S. AL-MALAIKA
Aston University

STRESS RELAXATION. See VISCOELASTICITY.

STYRENE POLYMERS

Introduction

Polystyrene (PS), the parent of the styrene plastics family, is a high molecular weight, linear polymer. Its chemical formula $[-CH(C_6H_5)CH_2-]n$, where n (which for commercial uses) is between 800 and 1400, tells little of its properties. The main commercial form of PS (atactic PS) is amorphous and hence possesses high transparency. The polymer chain stiffening effect of the pendant phenyl groups raises the glass-transition temperature (T_g) to slightly over 100°C. Therefore, under ambient conditions, the polymer is a clear glass, whereas above the T_g it becomes a viscous liquid which can be easily fabricated, with only slight degradation, by extrusion or injection-molding techniques. It is this ease with which PS can be converted into useful articles that accounts for the very high volume (>20 billion pounds per year) used in world commerce. Even though crude oil is the source of the polymer, the energy savings and environmental impact accrued during fabrication and use, compared to alternative materials, more than offsets the short life of many PS articles (1).

Commercial manufacture of PS in North America began in 1938 by The Dow Chemical Co. The polymerization process involved loading 10-gal cans with neat styrene monomer and immersing the can in a liquid bath heated at progressively higher temperatures over several days until the monomer conversion reached 99%. The solid polymer was removed from the cans and any rust spots chipped off the cylinders of polymer with a hatchet (Fig. 1). The cylinders of polymer were finally ground into a powder and packaged for shipment to customers.

Within a few years, Dow replaced the "can process" with the more economical continuous bulk polymerization process still used today. Generally, the key problems associated with manufacture of the polymer are removal of the heat

Encyclopedia of Polymer Science and Technology. Copyright John Wiley & Sons, Inc. All rights reserved.

Fig. 1. Dow Chemical worker chipping rust from cylinders of PS made using the "can process" (ca 1940).

of polymerization and pumping of highly viscous solutions. Conversion of the monomer to the polymer is energetically very favorable and occurs spontaneously on heating without the addition of initiators or catalysts. Because it is a continuous polymerization process, material-handling problems are minimized during manufacture. By almost any standard, the polymer produced is highly pure and is usually greater than 99 wt% PS; however, for particular applications processing aids are often deliberately added to the polymer. Methods for improving the toughness, solvent resistance, and upper use temperature have been developed. Addition of butadiene-based rubbers increases impact resistance, and copolymerization of styrene with comonomers such as acrylonitrile or maleic anhydride produces heat- and solvent-resistant plastics. Uses for these plastics are extensive. Packaging applications, eg, disposable cups, meat and food trays, and egg cartons, are among the largest area of use for styrene plastics. Rigid foam insulation in various forms is being used increasingly in the construction industry, and modified styrene plastics are replacing steel or aluminum parts in automobiles. These applications result in energy savings beyond the initial investment in crude oil. The cost of achieving a given property, eg, impact strength, is among the lowest for styrene plastics as compared to other competitive materials.

Properties

The general mechanical properties of styrene polymers are given in Table 1. Considerable differences in performance can be achieved by using the various styrene plastics. Within each group, additional variation is expected. In choosing an appropriate resin for a given application, other properties and polymer behavior during fabrication must be considered. These factors depend on the combination of inherent polymer properties, the fabrication technique, and the devices, eg, a mold used for obtaining the final object. Accordingly, consideration must be given to such factors as the surface appearance of the part and the development of anisotropy, and its effect on mechanical strength, ie, long-term resistance of the molding to external strain.

Table 1. Mechanical Properties of Injection-Molded Specimens of Main Classes of Styrene-Based Plastics[a]

Property	Polystyrene (PS)	Poly (styrene-*co*-acrylonitrile) (SAN)[b]	Glass-filled PS[c]	High impact PS (HIPS)[d]	HIPS	Acrylonitrile–butadiene–styrene terpolymer (ABS)[d]		Standard ABS	Super ABS
						Type 1	Type 2		
CAS registry number	[9003-53-6]	[9003-54-7]			[9003-53-6]			[9003-56-9]	
Specific gravity	1.05	1.08	1.20	1.05	1.05	1.05	1.05	1.04	1.04
Vicat softening point, °C	96	107	103	103	95	99	108	103	108
Tensile yield, MPa[e]	42.0	68.9	131	39.6	29.6	31.0	53.8	41.4	34.5
Elongation at rupture, %	1.8	3.5	1.5	15	58	55	10	20	60
Modulus, MPa[e]	3170	3790	7580	2690	2140	2620	2620	2070	1790
Impact strength (notched Izold), J/m[f]	21	21	80	96	134	193	187	267	428
Dart-drop impact strength	Very low	Very low	Medium high	Low	Medium high	Medium high	High	Very high	Very high
Relative ease of fabrication	Excellent	Excellent	Poor	Excellent	Excellent	Excellent	Good	Good	Medium good

[a] Ref. 2
[b] 24 wt% acrylonitrile.
[c] 20% glass fibers.
[d] Medium molecular weight.
[e] To convert MPa to psi, multiply by 145.
[f] To convert J/m to ft·lbf/in., divide by 53.38.

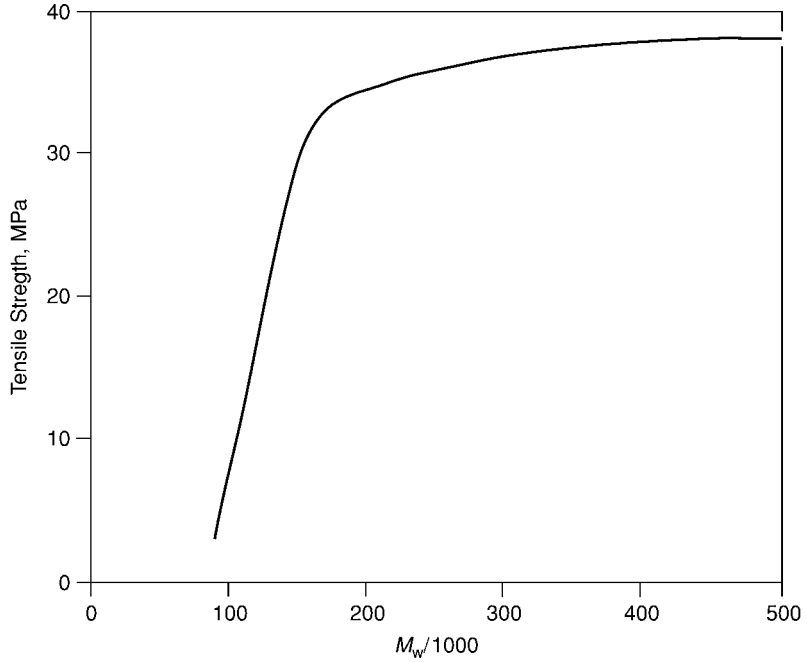

Fig. 2. PS tensile strength vs M_w (5). To convert Mpa to psi, multiply by 145.

Physical. An extensive compilation of physical properties of PS is given in References 2 and 3. In general, a polymer must have a weight-average molecular weight (M_w) about 10 times higher than its chain entanglement molecular weight (M_e) to have optimal strength. Below M_e, the strength of a polymer changes rapidly with M_w. However, at about 10 times M_e, the strength reaches a plateau region (Fig. 2). For PS, the M_e is 18,100 (4). Thus, PS having a $M_w < 150{,}000$ is generally too brittle to be useful. This indicates why no general-purpose molding and extrusion grades of PS having $M_w < 180{,}000$ are sold commercially.

Stress–Strain. The strain energy, derived from the area under the stress–strain curve, is considered to indicate the level of strength of a polymer. High impact PS (HIPS) has a higher strain energy than an acrylonitrile–butadiene–styrene (ABS) plastic, as shown in Figure 3. However, based on different impact-testing techniques, ABS materials are generally more ductile than HIPS materials (6,7). The failure of the stress–strain curve to reflect this ductility can be related to the fact that ABS polymers tend to show only localized flow or necking tendency at low rates of extension and, therefore, fail at low elongation. HIPS extends uniformly during such tests, and the test specimen whitens over all of its length and extends well beyond the yield elongation. However, at higher testing speeds, ABS polymers deform more uniformly and give high elongations.

Tensile strengths of styrene polymers vary with temperature. Increased temperature lowers the strength. However, tensile modulus in the temperature region of most tests (−40–50°C) is affected only slightly. The elongations of PS and styrene copolymers do not vary much with temperature (−40–50°C), but the elongation

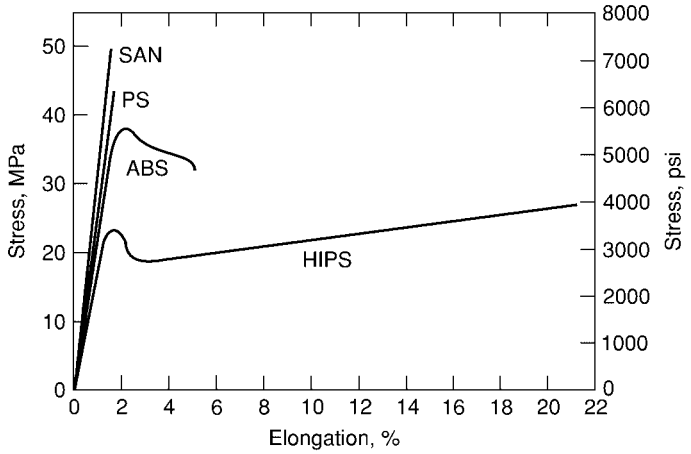

Fig. 3. Stress–strain curves for styrene-based plastics. To convert Mpa to psi, multiply by 145.

of rubber-modified polymers first increases with increasing temperature but ultimately decreases at high temperatures.

The molecular orientation of the polymer in a fabricated specimen can significantly alter the stress–strain data as compared with the data obtained for an isotropic specimen, eg, one obtained by compression molding. For example, tensile strengths as high as 120 MPa (18,000 psi) have been reported for PS films and fibers (8). Polystyrene tensile strengths below 14 MPa (2000 psi) have been obtained in the direction perpendicular to the flow.

Creep, Stress Relaxation, and Fatigue. The long-term engineering tests on plastics in extended use environments and temperatures are required for predicting the overall performance of a polymer in a given application. Creep tests involve the measurement of deformation as a function of time at a constant stress or load. For styrene-based plastics, many such studies have been carried out (9,10). Creep curves for styrene and its copolymers at room temperature show low elongation with only small variation with stress, whereas the rubber-modified polymers exhibit a low elongation region, followed by crazing and increasing elongation, usually to ca 20%, before failure (Fig. 4).

Creep tests are ideally suited for the measurement of long-term polymer properties in aggressive environments. Both the time to failure and the ultimate elongation in such creep tests tend to be reduced. Another test to determine plastic behavior in a corrosive atmosphere is a prestressed creep test in which the specimens are prestressed at different loads, which are lower than the creep load, before the final creep test (11).

Stress-relaxation measurements, where stress decay is measured as a function of time at a constant strain, have also been used extensively to predict the long-term behavior of styrene-based plastics (9,12). These tests have also been adapted to measurements in aggressive environments (13). Stress-relaxation measurements are further used to obtain modulus data over a wide temperature range (14).

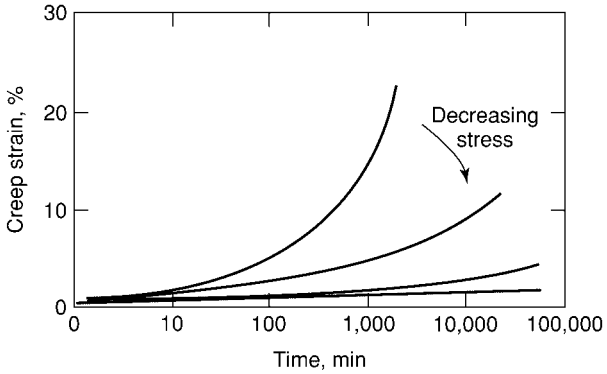

Fig. 4. Typical creep behavior for rubber-modified styrene polymers.

Fatigue is another property which is of considerable interest to the design engineer. Cyclic deflections of a predetermined amplitude, short of giving immediate failure, are applied to the specimen, and the number of cycles to failure is recorded. In addition to mechanically induced periodic stresses, fatigue failure can be studied when developing cyclic stresses by fluctuating the temperature.

Fatigue in polymers has been reviewed (15). Detailed theory and practice of fatigue testing are covered. Fatigue tests are carried out for two main reasons: to learn the inherent fatigue resistance of the material and to study the relationship between specimen design and fatigue failure. Fatigue tests are carried out both in air and in aggressive environments (16).

Melt Properties. The melt properties of PS at temperatures between 120 and 260°C are very important because it is in this temperature range that it is extruded to make sheets, foams, and films, or is molded into parts. Generally, it is desired to make parts having high strength from materials having low melt viscosity for easy melt processing. However, increased polymer molecular weight increases both strength and melt viscosity. The melt viscosity of PS can be decreased to improve its melt processability by the addition of a plasticizer such as mineral oil. However, the addition of a plasticizer has a penalty, ie, the heat-distortion temperature is lowered. In applications where heat resistance is very important, melt processability can be influenced, without a significant effect on heat resistance, by control of the polydispersity (17), by branching (18), or by the introduction of pendant ionic groups, eg, sodium sulfonate (19,20).

Impact Strength. When they fail, thermoplastic polymers typically dissipate energy either through microscopic shearing and/or crazing. Because of its inherently high entanglement molecular weight (19,000 g/mol), PS under plain strain conditions (thick parts) does not form shear bands. Thus, pure PS fails under tensile stress because of the formation of crazes (regions of microfibrils that bridge the top and bottom of a precursor crack) that rapidly develop into cracks and propagate catastrophically. Essentially, PS under plane strain conditions has a high yield stress and a low break stress. There can be very high local strains in the region of a craze, but very little material is deformed and little energy is dissipated. The crazes usually initiate at imperfections, such as surface scratches

or impurities in the bulk, and so as soon as one craze starts to form, the stress is concentrated at that site, the craze grows into a crack, and failure soon follows at very small macroscopic strain. Toughening PS involves finding ways to force it to form more crazes, thus dissipating more energy, or forcing it to deform by microscopic shear banding (21–24).

There are basically two different approaches used, and two different types of materials employed to obtain toughened PS. The first involves the use of dispersed rubber particles, which could have a variety of compositions including polybutadiene (PB) or various elastic block copolymers, in a continuous PS matrix. The second involves the use of styrenic block copolymers, or blends of block copolymers with PS homopolymer, where the block copolymer forms the continuous phase.

Dispersed rubber particles are the basis of toughening in HIPS. The toughening mechanism is quite complex, and the various ways in which dispersed rubber particles toughen PS have been discussed in detail (21–26). There are several ways in which the dispersed particles result in increased energy absorption during failure, but just two dominate. First, rubber particles result in the formation of multiple crazes, and thus the absorption of more energy. A rubber particle (assumed to be approximately spherical in shape) has a much lower modulus than PS. When a macroscopic tensile stress is applied to a medium containing soft, dispersed spheres, there is a stress concentration at the equator of the spheres, where the poles are in the direction of the applied stress. The stress at a distance from the particle is proportional to the particle size. It has been pointed out that for crazes to develop, a stress greater than that at the tip of a craze must extend at least three craze fibril dimensions into the matrix (22). Thus, while all particles result in stress concentration, small particles will not induce crazing because the critical stress does not extend far enough into the matrix. For HIPS, in which the rubber particles are composed of PB with PS occlusions, the minimum particle size to induce crazing is about 0.8 μm (22). Optimum toughening occurs with rubber particles from 1.0 to 2.0 μm.

The second major way in which rubber particles toughen PS is by allowing the formation of shear bands. Depending on the rubber particle size and volume fraction, the ligaments of PS between the rubber particles can become small enough (about 3.0 μm) so that if the rubber particles cavitate (due to triaxial stresses imposed by tensile deformation) the PS ligaments are under stress rather than strain (26). Under these conditions, the PS can shear band, thus absorbing considerable amounts of energy. Recent experimental work has emphasized the importance of shearing in addition to crazing in contributing to toughness in rubber-modified PS (24). Unfortunately, there are minimum rubber volume fractions and particle sizes for this mechanism to be effective, and those restrictions can result in significant light scattering and opacity as well.

The particle size restrictions for toughening PS depend on the mechanical properties of the rubber particle. For a HIPS rubber particle, with a Young's modulus of 333 MPa, the minimum size is 0.8 mm, while for a pure PB particle, with a Young's modulus of 47 MPa, the critical size is 0.44 mm (27). The stiffer the particle, the larger it must be. HIPS systems with bimodal particle size distributions can also be effective in toughening (28), but the bimodal particle size distribution is generally detrimental to optical clarity.

Dispersed rubber particles make other, less significant, contributions to the toughening of PS. Provided they are reasonably well adhered to the matrix and are somewhat tough, they can effectively terminate crazes and retard crazes from developing into cracks. The act of cavitation, either internal to the particle or at the particle–matrix interface, can absorb some energy, but an insignificant amount. Some adhesion of the rubber particle to the PS matrix is needed, but the exact role is not clear (23,25). In HIPS, the needed adhesion is provided by the PS that is grafted to the rubber particles during the polymerization process.

In summary, in order for dispersed rubber particles to toughen PS, they must be above a critical size, which is of the order of 0.8 μm, depending on the nature of the rubber. Higher concentrations of rubber particles will increase toughness by enabling more shear banding. Some adhesion between the rubber and matrix is also required.

HIPS materials can have a glossy or a dull surface appearance. This surface appearance is a function of surface roughness, which is caused by how much the rubber particles disrupt the surface regularity. The rubber particles near the surface can disrupt the surface by causing either depressions or elevations. These irregularities are caused not only by the nature of the rubber particles (eg, size and shape) but also by processing conditions. For example, during injection molding, the surface of the polymer is pressed against a very smooth polished mold surface and quenched locking in the smooth surface. However, when HIPS is extruded into sheets and thermoformed into parts, it is allowed to cool slowly giving the rubber particles near the surface time to relax. Polybutadiene rubber particles shrink upon cooling more than the PS matrix, thus causing depressions (29).

Material Types

General-Purpose (not rubber-toughened) PS (GPPS). GPPS is a high molecular weight ($M_w = 2–3 \times 10^5$), crystal-clear thermoplastic that is hard, rigid, and free of odor and taste. Its ease of heat fabrication, thermal stability, low specific gravity, and low cost results in moldings, extrusions, and films of very low unit cost. In addition, PS materials have excellent thermal and electrical properties, which make them useful as low cost insulating materials.

Commercial PSs are normally rather pure polymers. The amount of styrene, ethylbenzene, styrene dimers and trimers, and other hydrocarbons is minimized by effective devolatilization or by the use of chemical initiators (30). Polystyrenes with low overall volatile content have relatively high heat-deformation temperatures. The very low content of monomer and other solvents, eg, ethylbenzene, in PS is desirable in the packaging of food. The negligible level of extraction of organic materials from PS is of crucial importance in this application because of taste and odor issues.

When additional lubricants, eg, mineral oil and butyl stearate, are added to PS, easy-flow materials are produced. Improved flow is usually achieved at the cost of lowering the heat-deformation temperature. Stiff-flow PS has a high molecular weight and a low volatile level and is useful for extrusion applications. Typical levels of residuals in PS grades are listed in Table 2. Differences in molecular weight distribution are illustrated in Figure 5.

Table 2. Residuals in Typical Polystyrene, wt%

	Grade	
Polystyrene	Extrusion	Injection molding
Styrene	0.04	0.1
Ethylbenzene	0.02	0.1
Styrene dimer	0.04	0.1
Styrene trimer	0.25	0.8

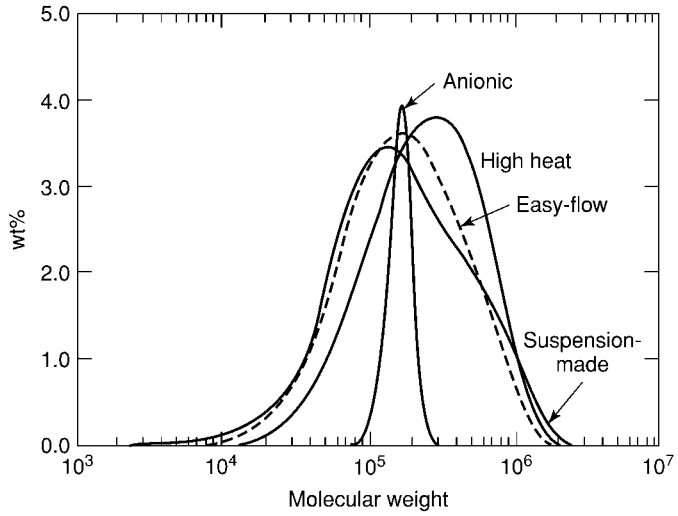

Fig. 5. Molecular weight distribution curves for representative PSs.

Specialty PS.

Ionomers. Polystyrene ionomers are typically prepared by copolymerizing styrene with an acid functional monomer (eg, acrylic acid) or by sulfonation of PS followed by neutralization of the pendant acid groups with monovalent or divalent alkali metals. The introduction of ionic groups into PS leads to significant modification of both solid state and melt properties. The introduction of ionic interactions in PS leads to increasing T_g, rubbery modulus, and melt viscosity (20). For the sodium salt of sulfonated PS, it has been shown that the mode of deformation changes from crazing to shear deformation as the ion content increases (31,32).

Tactic PS. Isotactic (iPS) and syndiotactic (sPS) PSs can be obtained by the polymerization of styrene with stereospecific catalysts of the Ziegler–Natta-type. Aluminum-activated $TiCl_3$ yields iPS while soluble Ti complexes [eg, $(\eta^5\text{-}C_5H_5)TiCl_3$] in combination with a partially hydrolyzed alkylaluminum [eg, methylalumoxane] yield sPS. The discovery of the sPS catalyst system was first reported in 1986 (33). As a result of the regular tactic structure, both iPS (phenyl groups cis) and sPS (phenyl groups alternating trans) are highly crystalline. Samples of iPS quenched from the melt are amorphous, but become

crystalline if annealed for some time at a temperature slightly below the crystalline melting point. The rate of crystallization is relatively slow compared to sPS and with other crystallizable polymers, eg, polyethylene or polypropylene. This slow rate of crystallization is what has kept iPS from becoming a commercially important polymer even though it has been known for over 40 years. sPS, on the other hand, crystallizes rapidly from the melt and is currently in the process of being developed for commercial use in Japan by Idemitsu Petrochemical Co. and in the United States and Europe by The Dow Chemical Co. In the amorphous state, the properties of iPS and sPS are very similar to those of conventional atactic PS. Crystalline iPS has a melting temperature of around 240°C, while sPS melts at about 270°C (34). In the crystalline state, both iPS and sPS are opaque and are insoluble in most common organic solvents.

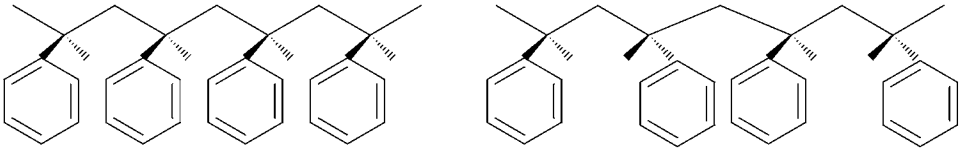

Isotactic Syndiotactic

Stabilized PS. Stabilized PSs are materials with added stabilizers, eg, uv screening agents and antioxidants. Early stabilization systems for PS included alkanolamines and methyl salicylate (35). In recent years, improved stabilizing systems have been developed; these involve a uv-radiation absorber, eg, Tinuvin P (Ciba Specialty Chemicals) with a phenolic antioxidant. Iron as a contaminant, even at a very low concentration, can cause color formation during fabrication; however, this color formation can be appreciably retarded by using tridecyl phosphite as a costabilizer with the uv-radiation absorber and the antioxidant (36). Rubber-modified styrene polymers are heat-stabilized with nonstaining rubber antioxidants, eg, Irganox 1076 (Ciba). Typically, stabilizer formulations for PS are designed by trial and error. However, recently a predictive model was developed for PS photodegradation allowing the prediction of weatherability of PS containing a certain concentration of a uv absorber (37).

Ignition-Resistant PS. Polymers containing flame retardants have been developed. The addition of flame retardants does not make a polymer noncombustible, but rather increases its resistance to ignition and reduces the rate of burning with minor fire sources. The primary commercial developments are in the areas of PS foams (see FOAMED PLASTICS) and television and computer housings. Both inorganic (hydrated aluminum oxide, antimony oxide) and organic (alkyl and aryl phosphates) additives have been used (38). Synergistic effects between halogen compounds and free-radical initiators have been reported (39). Several new halogenated compounds and corrosion inhibitors are effective additives (40) (see CORROSION AND CORROSION INHIBITORS). The polymer manufacturer's recommendations with regard to maximum fabrication temperature should be carefully observed to avoid discoloration of the molded part or corrosion of the mold or the machine.

Antistatic PS. Additives or coatings are utilized to minimize primarily dust-collecting problems in storage (see ANTISTATIC AGENTS). Large lists of commercial antistatic additives have been published (38). For styrene-based polymers, alkyl and/or aryl amines, amides, quaternary ammonium compounds, anionics, etc are used (see ADDITIVES).

Branched PS. Random-chain branching is found, to some extent, in all commercial free-radically produced polymers. Branching takes place during manufacture by chain transfer to polymer and can also take place in the polymer after manufacture by exposure to uv or other forms of radiation. Chain branching in some polymers is known to improve certain properties and is practiced commercially (eg, polyethylene and polycarbonate). In PS, many types of branch structures have been synthesized and the effect of branch structure on properties studied. Some of the branch structures possible in PS are shown in Figure 6.

Most of the recent studies of branched PS have focused on new synthetic methodologies (41–52) and on rheological properties (53–56).

Anionic polymerization has been the polymerization mechanism most widely used to make and study branched PSs. This is likely due to the ability to control the termination step, which is required for making many of the branch architectures shown in Figure 6. However, all large-scale PS production plants utilize free-radical polymerization chemistry. This is likely due to the cost associated with monomer purification needed for the anionic chemistry (57).

The PS business is extremely cost competitive. Oftentimes, an improvement in properties which is possible with a modification that would add a few percentage to the manufacturing cost is not practical because the customer will not pay the increased cost. Any property advantage must be very significant before the customer will pay more. It is likely that branching in PS may lead to improved performance of PS in certain applications. However, it is uncertain whether the

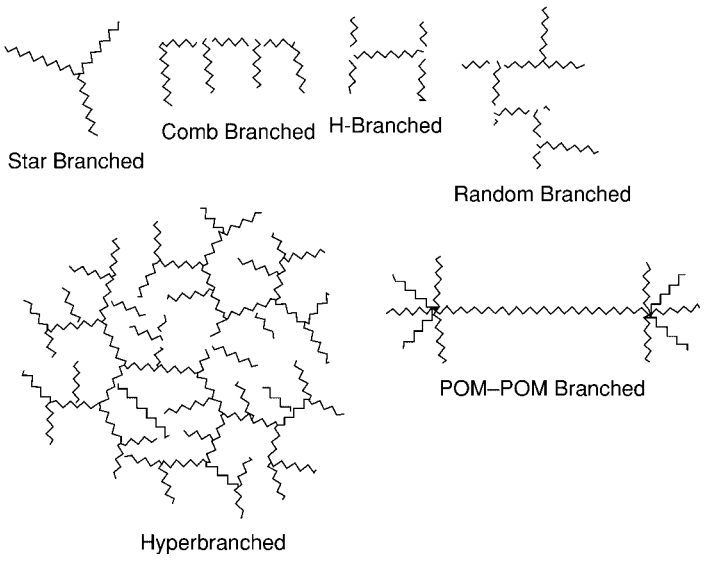

Fig. 6. Several possible PS branch architectures.

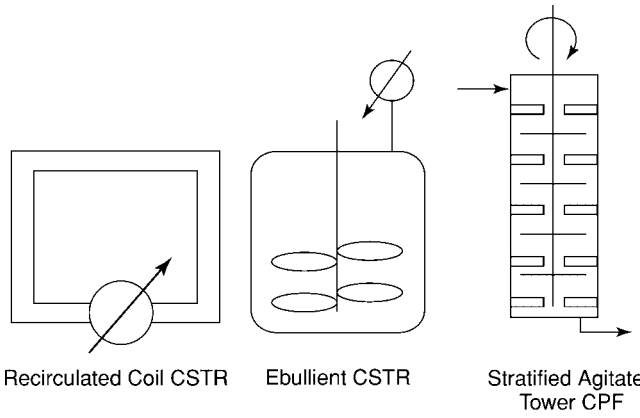

Fig. 7. Two Continuous stirred tank reactors (CSTR) and a continuous plug flow reactor (CPFR) configuration utilized for continuous mass polymerization of styrene.

increased performance will be significant enough to allow an increase in the selling price of the resin.

Since all commercial PS is currently manufactured using continuous free-radical bulk polymerization, most industrial research aimed at producing branched PS have been limited to free-radical chemistry. In general, the type of branch architecture that is possible using free-radical chemistry is limited to random-branched structures. Three reactor types are used commercially for continuous free-radical bulk polymerization of styrene (Fig. 7). These three reactor types are characterized as being either plug-flow or backmixed. Continuous plug-flow reactors (CPFR) typically have excellent radial mixing but virtually no backmixing, unless they are recirculated. These reactors are usually described as stratified agitated tower reactors. Continuous stirred tank reactors (CSTR), on the other hand, have high degrees of backmixing. They are usually single-staged and operated isothermally and at constant monomer conversion. CPFR-type reactors, on the other hand, are multistaged, having a temperature profile of typically 100–170°C. Two general configurations of CSTR reactors are utilized commercially, ie, recirculated coil and ebullient.

Typically, a few percentage by weight of a chain-transfer solvent (eg, ethylbenzene) is utilized during continuous free-radical bulk polymerization. The addition of a chain-transfer solvent to the polymerization decreases polymer molecular weight and therefore overall plant capacity when making high molecular weight products. However, the presence of some chain-transfer solvent is essential in keeping the polymerization reactor from becoming eventually fouled with gel and insoluble cross-linked polymer. The mechanism of buildup during continuous free-radical bulk polymerization without a chain-transfer solvent is likely chain transfer to polymer.

Peroxide initiators typically utilized for the manufacture of PS form *t*-butoxy (58) and/or acyloxy radical intermediates (59). These radicals have a strong propensity to abstract H-atoms. This propensity has found utility when making HIPS. For example, the use of initiators which generate *t*-butoxy radicals increases

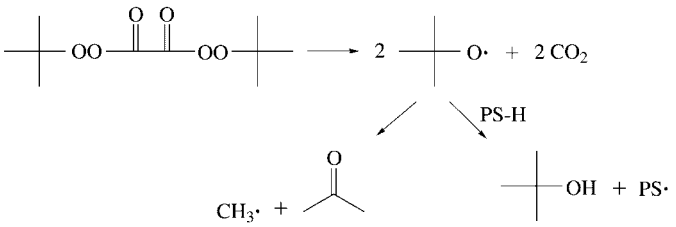

Fig. 8. Formation of *t*-butoxy radicals and their use to measure H-abstraction.

the level of grafting of PS onto PB rubber. The increase in grafting is generally thought to be due to H-abstraction from the rubber backbone by *t*-butoxy radicals (60). This raises questions regarding the extent of H-abstraction from the PS backbone during polymerization; that is, the use of initiators that generate potent H-abstracting radicals may increase the extent of long-chain branching during PS manufacture. This question has been investigated by decomposing bis(*t*-butylperoxy)oxalate in benzene solutions of PS (61,62). Bis(*t*-butylperoxy)oxalate decomposes upon heating to form two *t*-butoxy radicals and carbon dioxide. Once the *t*-butoxy radicals are formed they either abstract an H-atom or decompose to form acetone and a methyl radical (Fig. 8).

The extent of H-abstraction was determined by measuring the ratio of *t*-butyl alcohol (TBA)/acetone produced. Using cumene as a model for PS, a high level of H-abstraction was observed. However, PS showed a very low level of H-abstraction, which decreased further as the degree of polymerization (DP) of the PS was increased (Fig. 9). This was explained by the coil configuration of the PS chains restricting access of the *t*-butoxy radicals to the labile tertiary benzylic H-atoms on the PS backbone.

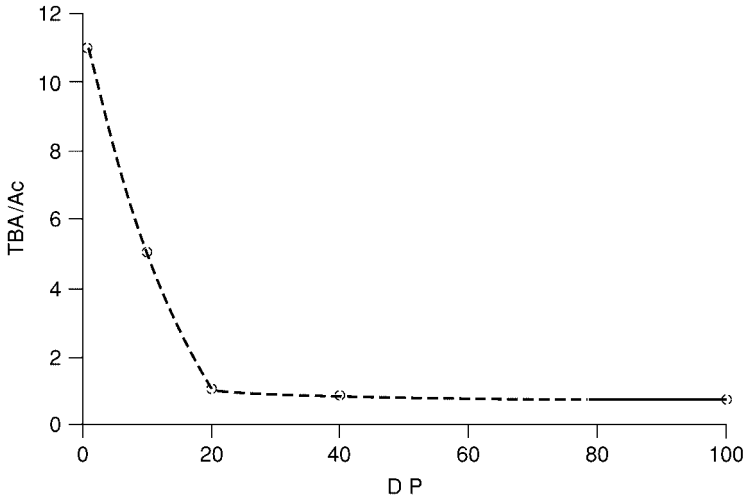

Fig. 9. H-abstraction as the ratio of *t*-butyl alcohol (TBA) to acetone (Ac) vs DP of PS (61,62).

The long-chain branching that takes place during PS manufacture in using continuous free-radical bulk polymerization reactors is extremely small. However, manufacturers of PS for film applications, where gel particles are a big problem, constantly monitor their product for gel. If the level of gel gets too high, the polymerization reactor must be cleaned to remove the coating of gel on the reactor walls. The mechanism of gel formation is not certain, but it is generally believed that a polymer layer forms on metal surfaces inside the polymerization reactor (63). The layer is dynamic, but the polymer chains that are in the layer are exposed to a free-radical environment for a longer period of time than are polymer chains in solution. The longer PS is exposed to free radicals, the more backbone H-abstraction can take place. Furthermore, the concentration of PS in the absorbed layer is very high. Thus, the "gel" effect (Trommsdorff effect) (64) may contribute to increased molecular weight growth in the layer. In any event, the layer of polymer ends up becoming higher in molecular weight than other chains. Eventually, cross-links form between the chains leading to infinite molecular weight. This effect not only can lead to the formation of gel, but can eventually result in reactor fouling if not controlled. Suspension polymerization does not have this problem. Addition of low levels (ie, 100–500 ppm) of a divinyl monomer to suspension styrene polymerization leads to the formation of branched PS without problems with reactor fouling. However, even though suspension polymerization can be used to produce branched PS, it is no longer practiced commercially for economic reasons.

The approaches to branching during continuous bulk free-radical polymerization that have been reported include the addition of a small amount of divinyl monomer (65), vinyl functional initiator (66), polyfunctional initiator (67), and vinyl functional chain-transfer agent (68) to the polymerization mixture. Researchers at Dow have investigated all of these approaches in using continuous free-radical bulk polymerization and found that they all lead to gel and eventual reactor fouling after a few days of continuous operation, even in the presence of a chain-transfer solvent. They found that only if a chain-transfer agent is added to the continuous free-radical bulk polymerization to maintain a high level of termination, could branched PS be produced without reactor fouling (69).

More recently, Dow researchers developed a new approach to making branched PS using continuous free-radical bulk polymerization, which eliminates the potential of reactor fouling by carrying out the branching after the polymer exits the polymerization reactor (70). The concept is to incorporate latent functional groups into the polymer backbone during the polymerization, which subsequently react to form a cross-link after the polymer exits the polymerization reactor (Fig. 10). The requirement is that the functional groups be inert at polymerization temperatures (100–160°C) and then during the devolatilization step while

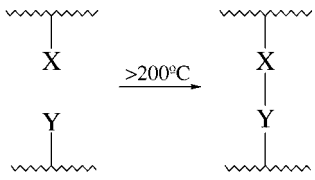

Fig. 10. General approach to post-polymerization reactor branching (cross-linking).

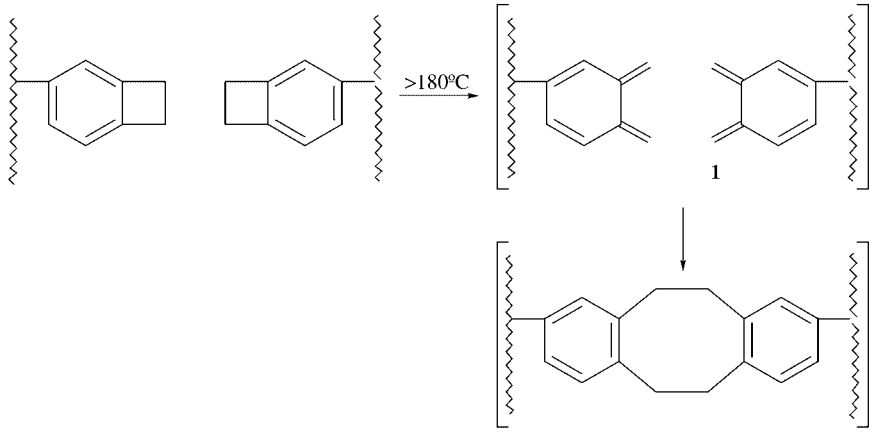

Fig. 11. Branching (cross-linking) chemistry of pendant BCB-functionalized PS.

the polymer is heated to 240°C, the groups must efficiently couple in the viscous polymer melt.

The functional group that worked best was benzocyclobutene (BCB) (48,71). BCB functional initiators were used to place BCB functional groups on the PS chain ends and BCB functional comonomers were used to place BCB groups pendant along the PS backbone. BCB is a very unique molecule in that it is totally inert at temperatures <180°C. However, at temperatures >200°C the strained four-membered ring opens resulting in the formation of a highly reactive orthoquinonemethide intermediate (**1**), which couples with another orthoquinonemethide on another PS chain resulting in the formation of a cross-link (Fig. 11).

One of the key reasons that it is difficult to long-chain branch PS without formation of cross-linked gel is due to the fact that the main mechanism of termination taking place in normal free-radical polymerization processes is radical coupling. Thus, dynamic (growing) high molecular weight branched polystyryl radicals couple together. This problem can be virtually eliminated using new controlled radical polymerization techniques. Soluble hyperbranched PS, previously only prepared using anionic polymerization chemistry, has been prepared using this technique. The controlled radical polymerization process was carried out using styrene having an alkoxyamine substituent (**2**) making it an A_2B monomer, which is well known to yield soluble hyperbranched polymers (72).

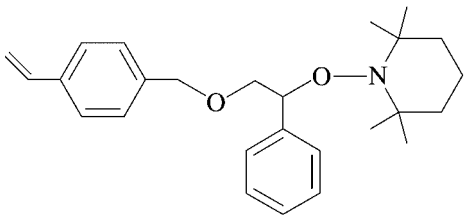

2

Styrene Copolymers. Acrylonitrile, butadiene, α-methylstyrene, acrylic acid, and maleic anhydride have been copolymerized with styrene to yield commercially significant copolymers. Acrylonitrile copolymer with styrene (SAN) is the largest volume styrenic copolymer and is used in applications requiring increased strength and chemical resistance over PS. Most of these polymers have been prepared at the crossover or azeotrope composition, which is ca 24 wt% acrylonitrile (see COPOLYMERIZATION).

Copolymers are typically manufactured using well-mixed CSTR processes to eliminate composition drift that causes a loss in transparency. SAN copolymers prepared in batch or continuous plug-flow processes, on the other hand, are typically hazy because of composition drift. SAN copolymers with as little as 4 wt% difference in acrylonitrile composition are immiscible (73). SAN is extremely incompatible with PS. As little as 50 ppm of PS contamination in SAN causes haze. Copolymers with over 30 wt% acrylonitrile are available and have good barrier properties. If the acrylonitrile content of the copolymer is increased to >40 wt%, the copolymer becomes ductile. SAN copolymers constitute the rigid matrix phase of the ABS engineering plastics.

Unlike PS homopolymers, SAN copolymers turn yellow upon heating. The extent of discoloration is proportional to the percentage of acrylonitrile in the copolymer (74). Generally, the mechanism of discoloration is thought to involve cyclization of acrylonitrile polyads in the polymer backbone, as depicted in Figure 12. However, recent studies have revealed that oligomers also contribute to discoloration. Specifically, one of the SAN trimer structures containing one styrene and two acrylonitrile units was found to thermally decompose resulting in the formation of a naphthalene derivative (Fig. 13), which readily oxidizes to form a highly colored species. The relative contribution of oligomers and polymer backbone polyad cyclization to overall discoloration is about equal.

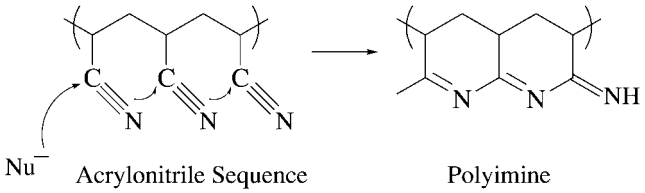

Fig. 12. Formation of red/yellow upon heating SAN triad in polymer backbone.

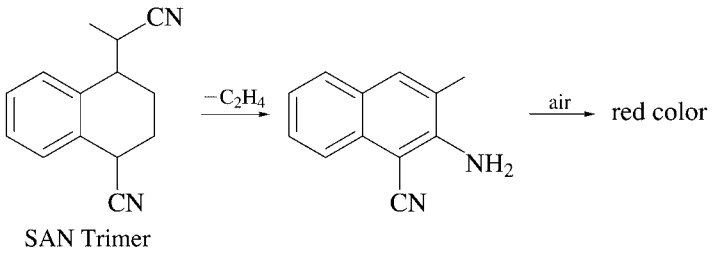

Fig. 13. Formation of red/yellow upon heating SAN trimer.

Styrene–butadiene copolymers are mainly prepared to yield rubbers (see ELASTOMERS; STYRENEUTADIENE COPOLYMERS). Many commercially significant latex paints are based on styrene–butadiene (weight ratio usually 60:40 with high conversion) copolymers (see COATINGS; PAINT). Most of the block copolymers prepared by anionic catalysts, eg, *sec*-butyl lithium, are also elastomers. However, some of these block copolymers are thermoplastic rubbers, which behave like cross-linked rubbers at room temperature but show regular thermoplastic flow at elevated temperatures (75,76). Diblock (styrene–butadiene) and triblock (styrene–butadiene–styrene) copolymers are commercially available. Typically, they are blended with PS to achieve a desirable property, eg, improved clarity/flexibility (76) (see POLYBLENDS). These block copolymers represent a class of new and interesting polymeric materials (77,78). Of particular interest are their morphologies (79–82), solution properties (83,84), and mechanical behavior (85,86).

Maleic anhydride readily copolymerizes with styrene to form an alternating structure. Accordingly, equimolar copolymers are normally produced, corresponding to 48 wt% maleic anhydride. However, by means of CSTR processes, copolymers with random low maleic anhydride contents can be produced (87). Depending on their molecular weights, these can be used as chemically reactive resins, eg, epoxy systems and coating resins, for PS-foam nucleation, or as high heat-deformation molding materials (88).

Recently, it has been discovered that styrene forms a linear alternating copolymer with carbon monoxide using palladium(II)–phenanthroline complexes. The polymers are syndiotactic and have a crystalline melting point $\sim 280^{\circ}$C (89). Currently, Shell Oil Co. is commercializing carbon monoxide α-olefin plastics based upon this technology (90).

Currently, Dow is commercializing ethylene–styrene interpolymers (ESI). Dow uses what they call a constrained-geometry metallocene catalyst (91). The classical heterogeneous Ziegler–Natta catalysts are generally ineffective for copolymerizing ethylene with styrene. ESI made by Dow have a "pseudorandom" structure meaning they do not contain any regioregularly arranged SS sequences, even at styrene contents approaching 50 mol%. Dow claims that the constrained-geometry of the catalyst (caused by the chelate ligand) plays a critical role in favoring the incorporation of the styrene. The technical significance of Dow's new catalyst is that the ESI resins are not contaminated with polyethylene or PS homopolymers, which generally results using alternate catalyst systems. A wide range of ESI resins have been prepared depending upon the ethylene/styrene ratio in the polymerization feed. Incorporation of high amounts of styrene into the copolymer requires the use of very high ratios of styrene. This presents a challenge at the end of the process because the unreacted styrene is removed by high temperature vacuum devolatilization, which can lead to some contamination by atactic PS (by spontaneous free-radical polymerization) if not done properly. ESI copolymers containing low levels of styrene are crystalline thermoplastics (92) while increasing the styrene content leads to a rapid decrease in crystallinity affording materials displaying excellent elastomeric properties (93). ESI containing about 20 mol% styrene are excellent compatibilizers for PE–PS blends (94).

Hydrogenated PSs. Dow researchers have successfully developed a new hydrogenation catalyst that allows complete hydrogenation of the phenyl rings on PS without degrading the molecular weight of the polymer (95). Complete

Table 3. Glass-Transition Temperatures of Substituted Polystyrene

Polymer	CAS registry number	T_g °C
Polystyrene	[9003-53-6]	100
Poly(*o*-methylstyrene)	[25087-21-2]	136
Poly(*m*-methylstyrene)	[25037-62-1]	97
Poly(*p*-methylstyrene)	[24936-41-2]	106
Poly(2,4-dimethylstyrene)	[25990-16-3]	112
Poly(2,5-dimethylstyrene)	[34031-72-6]	143
Poly(*p*-*tert*-butylstyrene)	[26009-55-2]	130
Poly(*p*-chlorostyrene)	[24991-47-7]	110
Poly(α-methylstyrene)	[25014-31-7]	170

hydrogenation of the phenyl rings of PS increases the glass-transition temperature (T_g) to ~140°C (96). Because of the hydrophobicity and low birefringence of the saturated polymer, it is well suited for use in optical media applications. Dow is currently planning to commercialize hydrogenated PS for use as a substrate for DVD discs.

Polymers of Styrene Derivatives. Many styrene derivatives have been synthesized and the corresponding polymers and copolymers prepared (97). The glass-transition temperatures for a series of substituted styrene polymers are shown in Table 3. The highest T_g is that of poly(α-methylstyrene), which can be prepared by anionic polymerization. Because it has a low ceiling temperature (61°C), depolymerization can occur during fabrication with the produced monomer acting as a plasticizer and lowering the heat distortion to 110–125°C (98). The polymer is difficult to fabricate because of its high melt viscosity and is more brittle than PS, but can be toughened with rubber.

Some polymers from styrene derivatives seem to meet specific market demands and to have the potential to become commercially significant materials. For example, monomeric chlorostyrene is useful in glass-reinforced polyester recipes since it polymerizes several times as fast as styrene (98). Poly(sodium styrenesulfonate) [9003-59-2] is a versatile water-soluble polymer and is used in water-pollution control and as a general flocculant (99,100). Poly(vinylbenzyl ammonium chloride) [70504-37-9] has been useful as an electroconductive resin (101). (see ELECTRICALLY-CONDUCTING POLYMERS).

Transparent Impact PS (TIPS). Rubber is incorporated into PS primarily to impart toughness. The resulting materials are commonly called high impact PS (HIPS) and are available in many different varieties. In standard HIPS resins, the rubber is dispersed in the PS matrix in the form of discrete particles. The mechanism of rubber-particle formation and rubber reinforcement and several general reviews of HIPS and other heterogeneous polymers have been published (102–108). The photomicrographs in Figure 14 show the different morphologies possible in HIPS materials prepared using various types of rubbers (109,110). If the particles are much larger than 5–10 μm, poor surface appearance of moldings, extrusions, and vacuum-formed parts are usually noted. Although most commercial HIPS contains ca 3–10 wt% PB or styrene–butadiene copolymer rubber, the presence of PS occlusions within the rubber particles gives rise to a 10–40% volume

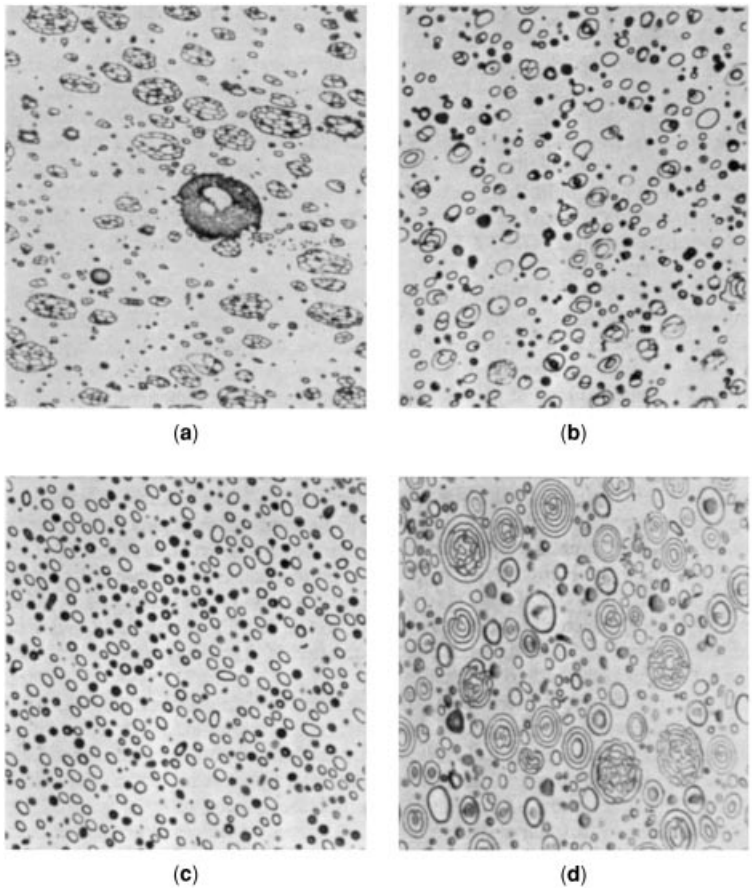

Fig. 14. Electron photomicrographs of several HIPS resins prepared using different types of rubbers.

fraction of the reinforcing rubber phase (108,111). Accordingly, a significant portion of the PS matrix is filled with rubber particles. Techniques have been published for evaluating the morphology of HIPS (110,112,113).

Polystyrene, by itself, is low in cost, relatively clear (90% transparency), has a moderate tensile modulus (3.3 GPa), and is relatively brittle (G_{1c} about 150 J/m^2). For many commercial applications, the optical clarity is a significant advantage, but the pure polymer is far too brittle for many applications and so some means must be taken to toughen it. Approaches to toughening include modifying the backbone structure by introducing comonomers (for example making SAN), adding plasticizers, and blending with various rubbers and elastomers. All of these options for toughening can have a deleterious effect on the desirable properties; comonomers raise the cost, plasticizers lower the modulus, and rubber fillers can destroy transparency. HIPS resins are opaque. The opacity is due to the scattering of light as it passes through the sample. This scattering is caused because the PB rubber particles and PS phase have different refractive indices. There are two ways to solve this problem and stop the light scattering: (*1*) adjust the relative

refractive indices of the two phases so they are nearly the same or (2) shrink the sizes of the PS and rubber phases to <20 nm. Most companies that want to market products for TIPS applications utilize the latter technique and have designed high styrene content microphase separated block copolymer rubbers that when blended with PS result in very small phase domain sizes. The refractive indices of PS and PB are 1.59 and 1.51, respectively. The technique of refractive index matching can be accomplished by either raising the refractive index of PB by copolymerizing refractive index enhancing comonomers with butadiene (eg, styrene, vinylbiphenyl, vinylnaphthalene) or by reducing the refractive index of PS by copolymerizing methyl methacrylate into the PS backbone (114).

TIPS resins made by blending high styrene content (~75 wt%) styrene–butadiene block copolymers with GPPS have good slow speed toughness (ie, 30% elongation), but poor high speed toughness. Phillips Petroleum became the first company (1972) to market these resins (115). Phillips calls their styrene–butadiene block copolymer resins for TIPS blending K-resins. They have a radial or star block structure with polybutadiene at the core and PS at the tips of the arms. The PS segments have a bimodal molecular weight distribution. These materials are produced by polymerizing styrene first with *sec*-butyl lithium (sBL). Once the desired molecular weight is reached, more sBL is added followed by more styrene. The added sBL initiates new chains while styrene also adds to the existing living PS chains. The result is a bimodal mixture of polystyryl lithium. Once the styrene is all converted, butadiene is added to form a mixture of styrene–butadiene block copolymers having the same butadiene block length and two different PS block lengths. At this point, the butadiene segment is still living. Silicone tetrachloride is added as a coupling agent resulting in the formation of the star block copolymer (**3**).

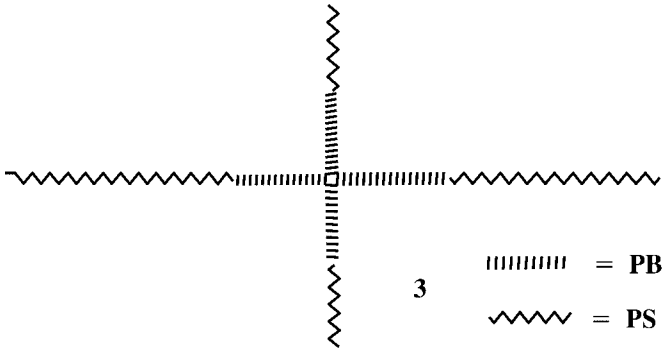

3

Several other companies also market transparent styrene–butadiene block copolymers for TIPS applications. BASF markets styrene–butadiene block copolymers having a similar structure (Styrolux); however, rather than pure PB segments, they make a gradient or taper styrene–butadiene block having a T_g of −30 °C (116). Their process to make this special architecture is similar to Phillips in that they prepare a bimodal mixture of polybutadienyl lithiums. However, then a mixture of butadiene and styrene are added to make the taper block. After the taper block is made, more styrene is added to add a short PS block. A tetrafunctional coupling agent is then added to form the star structure. BASF teaches

that the purpose of the long PS block is to enhance compatibility in blends with PS (116). Fina markets linear styrene–butadiene triblock materials under the trade name Finclear. These linear triblock resins are not just simple high styrene content styrene–butadiene–styrene triblock materials. Rather, they use the taper block concept; that is, rather than having pure PS and PB segments in the block copolymer, there is a gradient change over or tapering of the styrene to butadiene segments.

Unlike for PS, very little work has been published on the fracture of block copolymers. There is a substantial amount of literature on PS toughened by blending with block copolymers. In those systems, the block copolymer is dispersed, and provided the proper particle size and modulus are obtained, substantial improvements in toughness are obtained, as described above for HIPS. For the neat block copolymers, however, fracture mechanisms are fundamentally different than for PS.

Results on the fracture of KR01 and KR03, both Phillips K-resins, have been reported (117). KR01 has an overall molecular weight of 180,000 (M_w), while for KR03 the molecular weight is 220,000 (M_w). KR03 is asymmetrical, with one long PS block, while KR01 is fairly symmetrical. The different block structures result in quite different morphologies, which in turn impart quite different fracture properties. KR01 has basically a cylindrical morphology consisting of wavy rods of polybutadiene, about 20 nm in diameter, in a PS matrix. The cylindrical morphology is expected based on the volume fraction of PB. In KR03, the PB is in a disrupted lamellar morphology. The rubber phase is in sheets about 20 nm thick, but the sheets are neither flat nor continuous, although annealing sharpens the morphology somewhat. KR01 fractures in a manner similar to PS. There are well-defined crazes, and no deformation outside of the craze region. In KR03, there is significant microcracking (better termed nanocracking), voiding in the PB phase, and significant deformation. Argon refers to the failure of KR03 as a form of crazing and he reports strains to failure of 9% and 110% for KR01 and KR03, respectively, while Phillips product literature gives corresponding values of 20% and 160%. Notched Izod impact strengths have been reported as 0.4 ft·lb/in. and 0.75 ft·lb/in. for KR01 and KR03, respectively. The change in morphology has an appreciable effect on toughness (117).

The individual components (PS and styrene–butadiene block rubber) that make up TIPS are optically transparent. Ignoring the effects of surface imperfections (scratches, roughness), blends and block copolymers become hazy and the transparency is reduced due to light scattering from regions of differing refractive index. In very qualitative terms, significant light scattering will occur when regions of differing refractive index have dimensions of the order of the wavelength of visible light. For systems with dispersed rubber particles, like HIPS, that condition means that the rubber particles must be less than about 100 nm in diameter for the material to be transparent. Unfortunately, this requirement for clarity is inconsistent with the requirement for toughness of a minimum rubber particle size of 0.8 μm. The domain sizes in block copolymers are much smaller, of the order of 20 nm, and so block copolymers tend to be highly transparent. When homopolymers are blended with blocks, however, inhomogeneities in composition and refractive index can develop, and if the dimensions are large enough, light scattering can be significant.

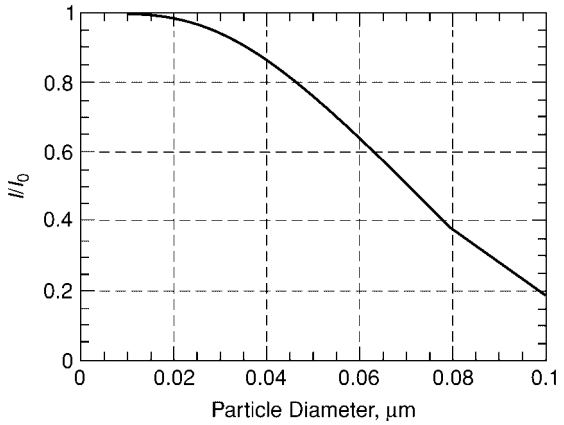

Fig. 15. Transmittance vs particle size for PB particles in a PS matrix with a path length of 1.0 mm. The calculation assumes 10 vol% of spherical particles and is for light with 0.55 μm wavelength.

Block copolymers of styrene and butadiene are highly transparent, despite the large refractive index difference between PS and PB and the fact that the blocks are phase separated. Styrolux and KR03 resins have transparencies around 90%. The transparency is due to the very small domain size, which is typically of the order of 20 nm. Spheres of equivalent size would scatter very little light, as shown from the data in Figure 15. In block copolymers the domain sizes are determined primarily by block molecular weights, and for commercial polymers the domains will always be small enough that they will not be a significant source of scattering. As long as block copolymer composition is uniform, degradation is avoided, smooth surfaces are maintained and fabricated articles are generally clear.

As a means of reducing cost and increasing modulus, GPPS is often blended with block copolymers, despite the fact that the blends tend to have inferior optical clarity than the pure block copolymers. There is some evidence that the addition of GPPS can raise the T_g of the block copolymer system (118). Several examples of how adding GPPS to block copolymers effects clarity have been provided (116,119). The solubility of the GPPS in the PS blocks depends on the relative molecular weights. With identical molecular weights the solubility is expected to be unlimited, and depending on block copolymer geometry (star vs linear) solubility may be maintained with a GPPS/block ratio of up to 1.5 (118). The reason that Styrolux and KR03 are asymmetrical, with on average one long PS block per molecule, is probably to enhance solubility of GPPS.

When GPPS of the proper molecular weight is added to a lamellar block copolymer, like KR03 or Styrolux, it is absorbed by the PS phase and hence swells it. With no added homopolymer, the block copolymer does not scatter light because all of the domains are much smaller than the wavelength of light, even though the PS domains will be larger than the butadiene domains, and to visible light the material has a uniform refractive index. If the GPPS is uniformly absorbed by the PS blocks the material remains transparent, even if the PS domains become comparable in size to the wavelength of light. In this case, the system is

transparent because the PB domains are still very small and evenly dispersed. Optically, the system is very similar to HIPS, except that it is easier to maintain the dispersion due to the block structure. As GPPS is added, the average refractive index of the material increases, but to visible light there is not a refractive index gradient that would result in scattering. The blend may begin to scatter light for one of two reasons. First, if large volumes of GPPS are added, even if miscibility with the blocks is maintained, variations in PS domain sizes can occur due to random fluctuations in morphology. When these domains become large, they will begin to scatter. If the GPPS begins to phase separate, then it will very quickly grow into domains that will cause significant scattering. The key to maintaining clarity is solubility of the added GPPS in the PS blocks. It has been shown how in a lamellar Styrolux system, added GPPS swells the PS blocks but leaves the butadiene block domains essentially unchanged (116). A blend with 60 vol% Styrolux and 40% GPPS has about 78% transmittance, compared to 90% for the pure block copolymer. Transmission electron micrographs show that the butadiene domains are essentially the same size in the blend and pure block copolymer (Fig. 16), but that the PS domains grow. Eventually, regions that are relatively high in PS develop that are large enough to scatter light. Individual PS domains are not that large by themselves. In contrast, it has also been shown that in a styrene–butadiene–styrene triblock system, added GPPS readily phase separates, forms relatively large domains of pure PS, and results in much higher light scattering.

In summary, optical clarity in TIPS systems depends on minimizing light scattering, which arises from having regions of differing refractive index. The dimensions of these scattering centers is dictated by the size of dispersed rubber particles (as in HIPS), by the morphological features in block copolymers, or by compositional fluctuations in blends of block and homopolymers. The conundrum for HIPS-type materials is that rubber particles large enough to toughen PS are also large enough to cause significant light scattering. In block copolymers, the morphological features are too small to scatter significantly and so these systems are highly transparent. Blends of high styrene content (>70 wt% styrene)

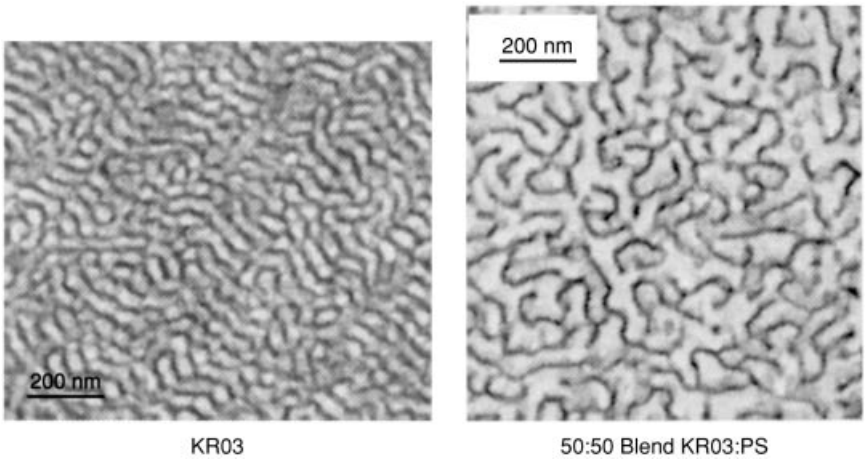

Fig. 16. TEM of KR03 and 50:50 blend of KR03 and PS.

block and GPPS remain transparent as long as gross phase separation can be prevented.

Besides transparency and toughness, modulus is also a key property for TIPS. The two approaches to toughening PS involve the addition of a relatively low modulus rubber phase. Adding rubber unavoidably lowers the modulus of the resulting composite; exactly how much depends on the resulting morphology. For systems with dispersed rubber particles, in which the PS remains the continuous phase, simple mechanical models do a good job of predicting modulus as a function of rubber phase volume fraction. In fact, measuring the dynamic modulus at small strains can be used to quantitatively evaluate the volume fraction of elastomer. The modulus of rubber-modified PS is given approximately by (120)

$$1/G = 1/G_1[1 + 1.86(\phi_1/\phi_2)]$$

where the assumption is made that the elastomer is in dispersed spherical domains, and Poisson's ratio for PS is 0.35. G is the shear modulus of the composite, G_1 the modulus of the PS matrix, and ϕ_1 and ϕ_2 the volume fractions of the PS and elastomer phases, respectively. In the case of HIPS with occluded PS in the rubber phase, the volume fraction of elastomer phase ϕ_2 is the total volume fraction of particles, not the volume of PB. A plot of modulus ratio vs effective volume fraction of rubber is given in Figure 17. At effective elastomer volume fractions up to 0.30 (including occluded and grafted PS), an upper limit on what is typically used for HIPS, the reduction in modulus is only 45%.

For lamellar morphologies, the situation is quite different. There are no good mechanical models for predicting the modulus of these systems, mostly because there is not an adequate way to describe the morphology. The modulus of a lamellar system depends on the relative volume fractions of the two phases, their individual moduli, and the orientation and aspect ratio of the lamellae. The last two parameters are almost impossible to determine in real systems; so, predicting moduli based on volume fractions and individual phase moduli is virtually impossible. If the rubber phase is co-continuous, as it is in lamellar systems like the K-resins, the modulus is significantly reduced relative to PS or HIPS. For KR03, the ratio G/G1 is typically 0.42 (121).

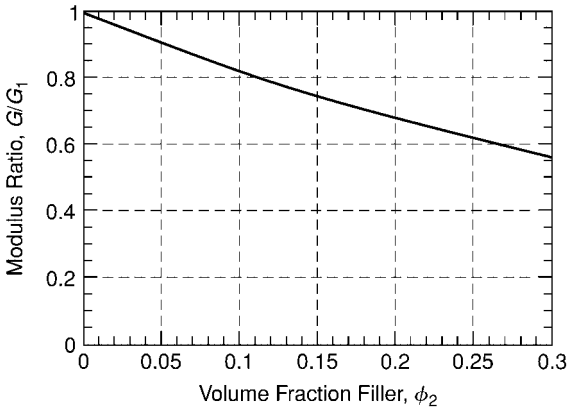

Fig. 17. Modulus ratio vs soft phase volume fraction for systems like HIPS.

Acrylonitrile–Butadiene–Styrene (ABS) Polymers. ABS polymers have become important commercial products since the mid-1950s. The development and properties of ABS polymers has been discussed in detail in Reference 122. ABS polymers, like HIPS, are two-phase systems in which the elastomer component is dispersed in the rigid SAN copolymer matrix. The electron photomicrographs in Figure 18 show the difference in morphology of mass versus emulsion ABS polymers. The differences in structure of the dispersed phases are primarily a result of differences in production processes, types of rubber used, and variation in rubber concentrations.

Because of the possible changes in the nature and concentration of the rubber phase, a wide range of ABS polymers are available. Generally, they are rigid [modulus at room temperature, 1.8–2.6 GPa, ie, (2.6–3.8) $\times$ 10^5 psi] and have excellent notched impact strength at room temperature (ca 135–400 J/m, ie,

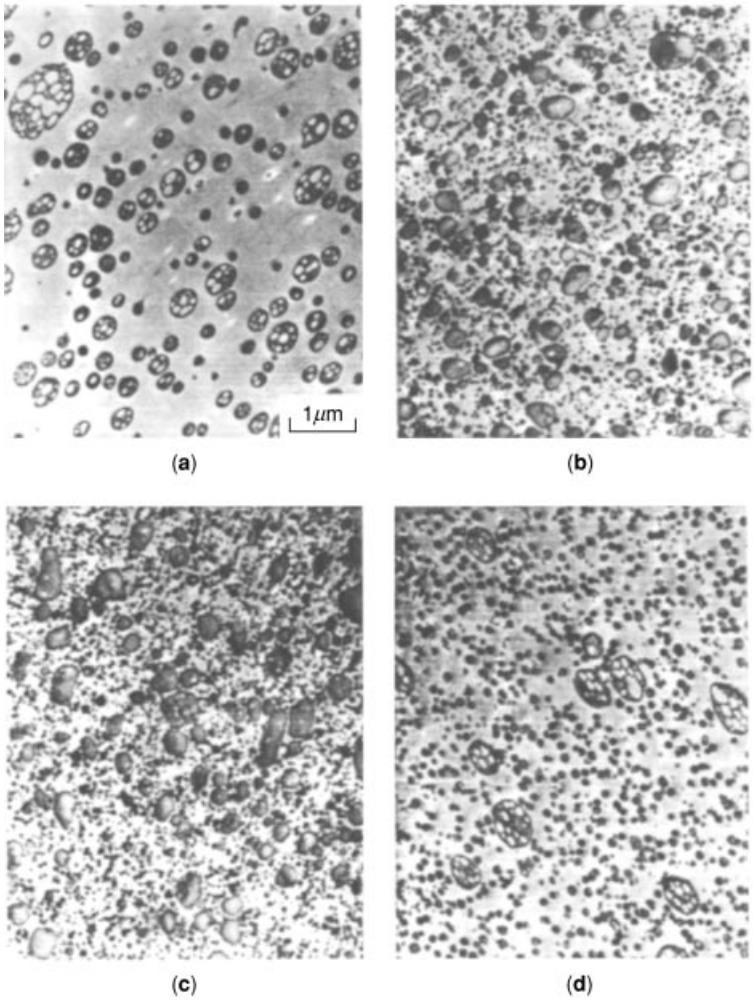

Fig. 18. Electron photomicrographs of some commercial ABS resins produced by bulk, emulsion, or a mixture of the two processes.

2.5–7.5 ft·lb/in.) and at lower temperatures, eg, at −40°C (50–140 J/m, ie, 0.94–2.6 ft·lb/in.). This combination of stiffness, impact strength, and solvent resistance makes ABS polymers particularly suitable for demanding applications. Another important attribute of several ABS polymers is their minimum tendency to orient or develop mechanical anisotropy during molding (123,124). Accordingly, uniform tough moldings are obtained. In addition, ABS polymers exhibit good ease of fabrication and produce moldings and extrusions with excellent gloss, which can be decorated by many techniques, eg, lacquer painting, vacuum metallizing, and electroplating (125–128). In the case of electroplating, the strength of the molded piece is significantly improved (123). When an appropriate decorative coating or a laminated film is applied, ABS polymers can be used outdoors (129).

ABS can be blended with bisphenol A polycarbonate resins to make a material having excellent low temperature toughness. The most important application of this blend is for automotive body panels.

When inherent outdoor weatherability is important, acrylonitrile–ethylene–styrene (AES) or acrylonitrile–styrene–acrylate (ASA) materials are typically used. These materials utilize ethylene–propylene copolymers and polybutylacrylate as the rubber phase, respectively. Ethylene–propylene and polybutylacrylate rubbers are inherently more weatherable than polybutadiene because they are more saturated leaving fewer labile sites for oxidation (130). Even though AES and ASA polymers are more weatherable than ABS, additives are needed to stabilize the materials against outdoor photochemical degradation for prolonged periods. Additive packages for AES and ASA weatherable materials generally contain both uv absorbers and hindered amine light stabilizers. Typical outdoor applications for weatherable polymers include recreational vehicles, camper tops, and swimming pool accessories. The extremely hostile environments where these stabilized AES materials are utilized still take their toll on the materials. Over very prolonged periods of use, the surface gains a chalky appearance as the polymer degrades. Serious discoloration can also result and was found to be caused by degradation of the additives (131).

High heat ABS resins are produced by adding a third monomer to the styrene and acrylonitrile to "stiffen" the polymer backbone, thus raising the T_g. Two monomers used commercially for this purpose are α-methylstyrene (132) and *N*-phenylmaleimide (133).

Not only are ABS polymers useful engineering plastics, but some of the high rubber compositions are excellent impact modifiers for poly(vinyl chloride) (PVC). Styrene–acrylonitrile-grafted butadiene rubbers have been used as modifiers for PVC since 1957 (134).

New Rubber-Modified Styrene Copolymers. Rubber modification of styrene copolymers other than HIPS and ABS has been useful for specialty purposes. Transparency has been achieved with the use of methyl methacrylate as a comonomer; styrene–methyl methacrylate copolymers have been successfully modified with rubber. Improved weatherability is achieved by modifying SAN copolymers with saturated, aging-resistant elastomers (135).

Inorganic-Reinforced Styrene Polymers. Glass reinforcement of PS and SAN markedly improves their mechanical properties. The strength, stiffness, and fracture toughness are generally at least doubled. Creep and relaxation rates are significantly reduced and creep rupture times are increased. The coefficient of

thermal expansion is reduced by more than half, and generally, response to temperature changes is minimized (136). Normally, ca 20 wt% glass fibers, eg, 6 mm long, 0.009 mm dia, E-glass, can be used to achieve these improvements. PS, SAN, HIPS, and ABS have been used with glass reinforcement.

Four approaches are currently available for producing glass-reinforced parts. These include use of preblended (reinforced molding compound; blending of reinforced concentrates with virgin resin), a direct process, in which the glass is cut and weighed automatically and blended with the polymer at the molding machine, and general inplant compounding (123). The choice of any of these processes depends primarily on the size of the operation and the corresponding economics.

Reinforcement of PS with inorganic materials other than glass has been under intense study in recent years. The inorganic materials of highest interest have a lamellar (layered) structure with at least one dimension in the nanometer scale range. Hence, addition of these inorganic materials to polymers form what are called nanocomposite materials. Many natural and synthetic lamellar inorganic materials are commercially available. The molecular structures of these materials vary widely. The biggest challenge encountered when blending nanolayered inorganic with hydrophobic polymers like PS is to end up with the inorganic nanolayers separated and evenly dispersed throughout the polymer matrix. The grouping of the layers of lamellar pieces can generally be visualized as a cabbage-like or book-like structure in which, for the purpose of making a nanocomposite, the task is to scatter the leaves or book pages uniformly throughout the polymer matrix (Fig. 19). The dimensions of the individual lamellae are on the nanometer scale and are important for enhancement of polymer physical properties.

Several approaches for the exfoliation of platelets exist in producing the PS nanocomposite. The actual mixing of the inorganic with PS can take place via compounding or by introducing it into the polymerization process. The approaches include (*1*) using the inorganic material with no modification, (*2*) chemical treatment of the inorganic material surface to alter hydrophilicity or to attach reactive functional groups, (*3*) use of compatibilizers/surfactants when mixing, (*4*) copolymerization styrene with a polar comonomer (ie, maleic anhydride) to make PS more compatible with the polar inorganic material, (*5*) physical manipulation of inorganic material (ie, freeze-drying or ball milling) (Fig. 20), and (*6*) use of polymerization mechanism to do the work of exfoliating the platelets.

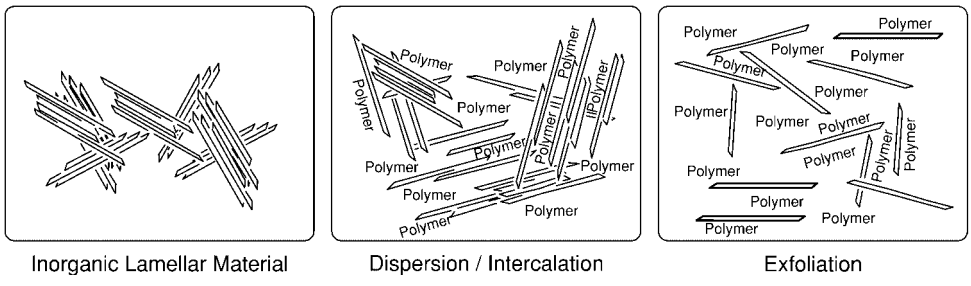

Fig. 19. Illustration of dispersed/intercalated platelets and exfoliated platelets.

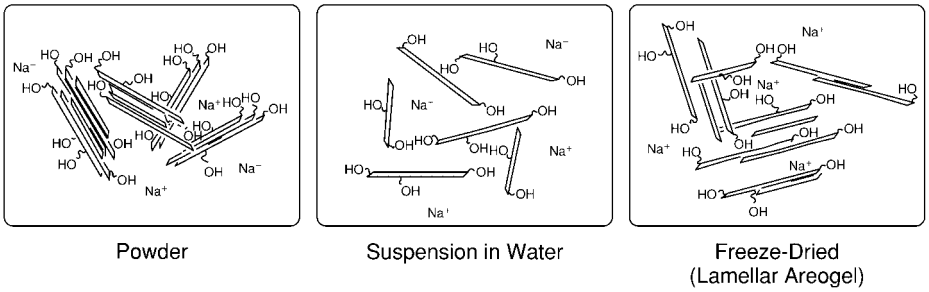

Fig. 20. Use of freeze-drying to separate lamellae.

There are advantages and disadvantages to these approaches. Method 1 is simple; however, unless working with a highly polar polymer, exfoliation and dispersion of the mismatched systems is unlikely without using a great deal of energy to mechanically separate and disperse the layered material. Methods 2–4 require the addition of compatibilizing additives, and have been shown to be quite effective. Use of these additives often results in compromising the physical properties of the parent polymer system, and benefits that might be provided by the inorganic platelets can easily be outweighed by the addition of these extra materials. Use of these additives can also add substantial cost to the composite system. Approach 5 is a useful tool when used in combination with the other approaches, but when used alone, it is difficult to obtain fully exfoliated dispersions. Using the polymerization mechanism to exfoliate the platelets (method 6) is generally not as straightforward as the other methods; however, it can be an ideal way to exfoliate and disperse platelets without the use of unwanted additives or the added expense of compounding approaches.

The synthesis of a PS/Montmorillanite clay nanocomposite prepared by combining methods 2 and 6 described earlier was published (137) (Fig. 21). They utilized living free-radical polymerization (LFRP) of styrene to provide exfoliated platelets in a PS matrix. Transmission electron micrographs and x-ray diffraction patterns support the idea of preparing nanocomposites via polymerization initiation.

Only recently have some elegant approaches for the synthesis of finely dispersed composites been reported in the academic literature (137,138). The styrene-based systems were SAN, ABS, and PS. Blends of these materials were prepared either by compounding with organically modified inorganic materials or by mixing organically modified (with or without an additional compatibilizer) with monomer prior to polymerization. Physical properties of the composites were also examined in several reports, and some changes in modulus and T_g reported. Many of these studies focused on attempts to disperse these ionic inorganic materials in the incompatible organic polymer systems. Good dispersions were obtained in some cases; however, complete exfoliation of the inorganic lamellar systems was generally not obtained. As a result, only intercalated products were made. Having exfoliated platelets of the proper aspect ratio and in the correct alignment in the polymer matrix should provide the maximum impact on physical properties; however, dispersing such a material in relatively nonpolar systems, such as styrenic polymers, remains a challenge.

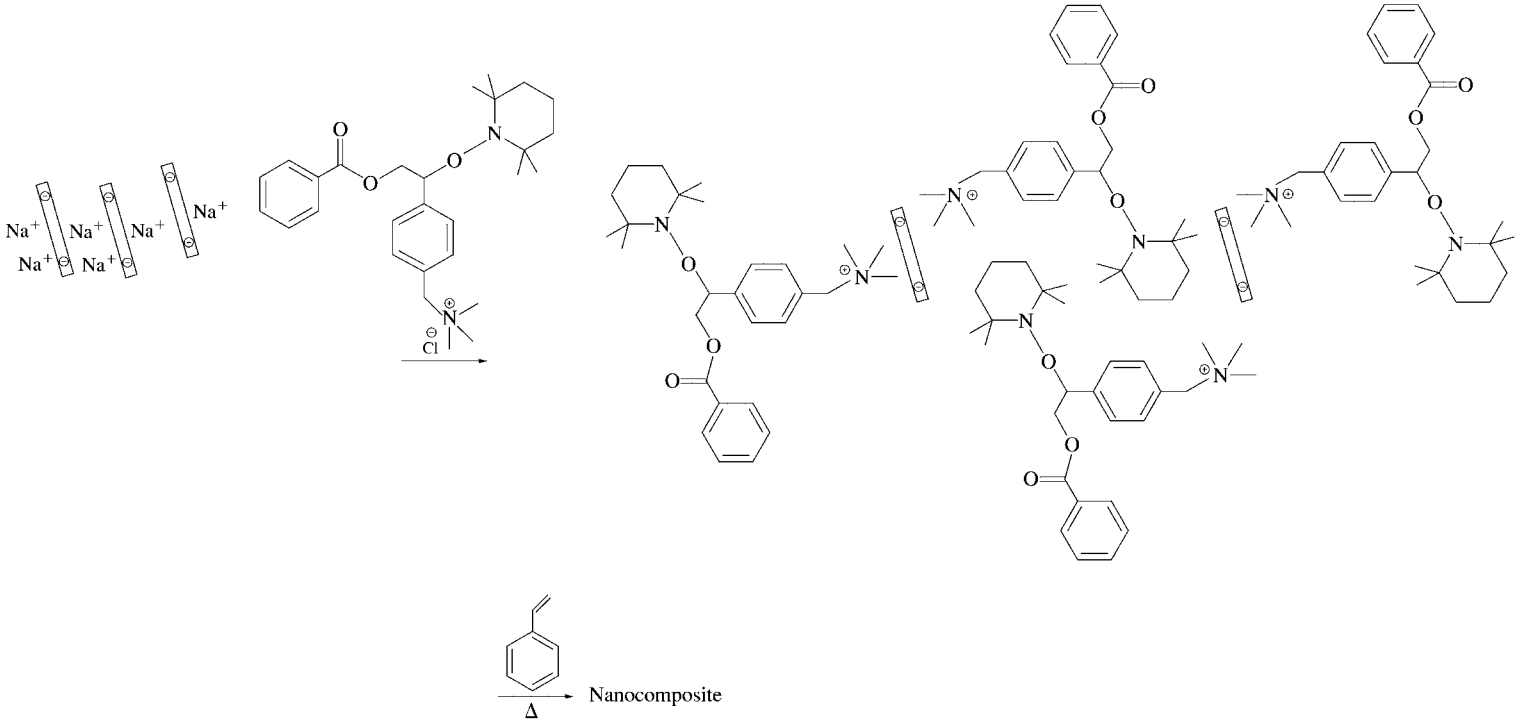

Fig. 21. LFRP of styrene to produce nanocomposites.

Degradation

Like almost all synthetic polymers, styrene plastics are susceptible to degradation by heat, oxidation, uv radiation, high energy radiation, and shear. However, in normal use, only uv radiation imposes any real limit on the general usefulness of these plastics (139,140). Thus, it is generally recommended that the use of styrene plastics in outdoor applications be avoided.

Thermal Degradation. Typically, PS loses about 10% of its molecular weight when it is fabricated. A significant amount of research has been carried out to determine the nature of the "weak links" in PS (141–144). Various initiation of degradation mechanisms have been proposed: (*1*) chain-end initiation (unzipping), (*2*) random scission initiation, and (*3*) scission of weak links in the polymer backbone. It has been suggested that chain-end initiation is the predominant mechanism at 310°C while random scission produces stable molecules. Evidence for weak link scissions comes mainly from studies showing loss of molecular weight vs. degradation time. These plots usually show a rapid initial drop in molecular weight indicating initial rapid weak link scission. However, the picture is also complicated by the fact that the mechanism of degradation is temperature-dependent. It appears that weak link scissions taking place at high temperatures initiate depolymerization while at lower temperatures, scissions simply cause a decrease in molecular weight. In any case, a clear difference in thermal stability has been shown between PS produced using a peroxide initiator and PS made without an initiator polymerization. Figure 22 shows the Arrhenius activation

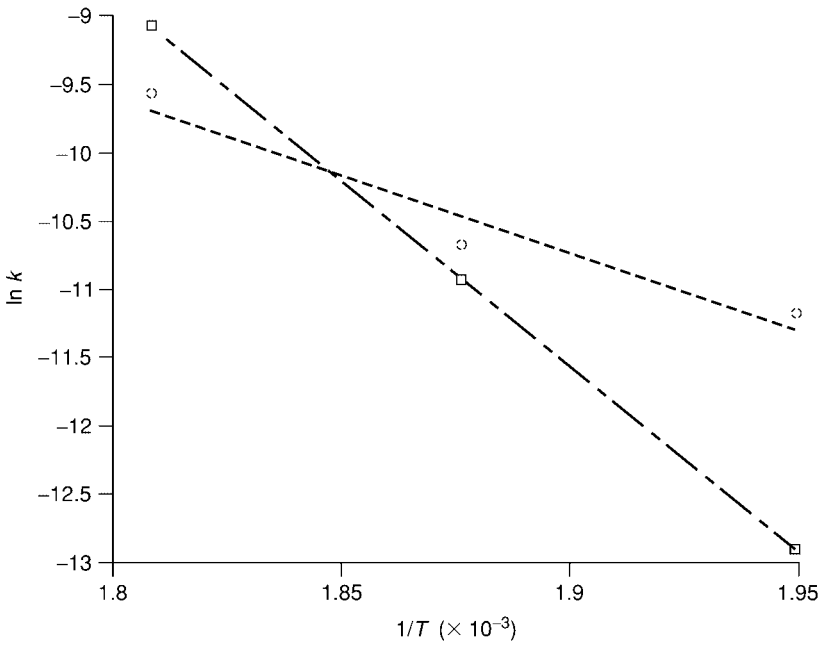

Fig. 22. Comparison of thermal stability of the PS backbone made with and without peroxide initiator ––○–– Peroxide initiated $E_a = 94.6$ kJ/mol (22.6 kcal/mol); -□—No initiator added $E_a = 226$ kJ/mol (54 kcal/mol).

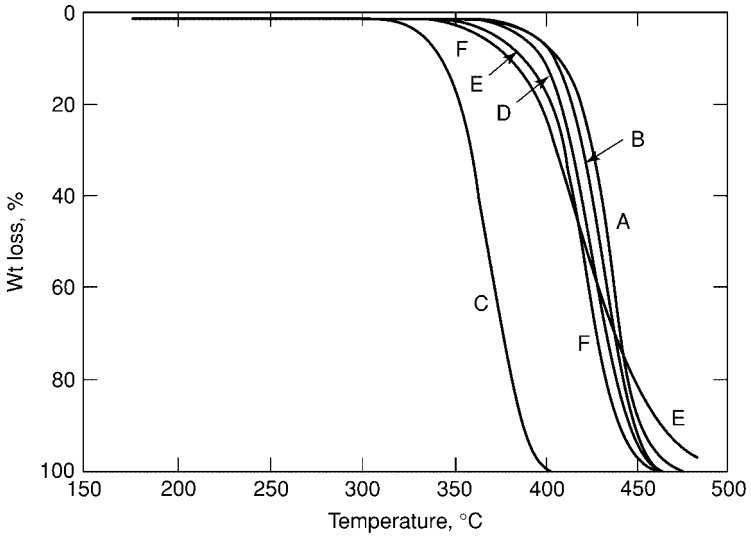

Fig. 23. Thermogravimetric analysis of polymers and copolymers of styrene in nitrogen at 10°C/min. A, PS; B, poly(vinyl toluene); C, poly(α-methylstyrene); D, poly(styrene*co*-acrylonitrile), 71.5% styrene; E, poly(styrene*co*-butadiene), 80% styrene; F, poly(styrene*co*-methylstyrene), 75% styrene.

energy for chain scission in PS made with and without a peroxide initiator. This difference in stability of the resins is likely due to the initiator derived fragments that remain in the polymer after isolation.

Poly(α-methylstyrene) unzips to monomer exclusively. Figure 23 is a comparison of the thermal stability of several copolymers. Thermal-oxidative degradation of PS occurs much faster, leading to additional volatile components consisting of aldehydes and ketones, yellowing of the polymer with a very dramatic drop in molecular weight, and some cross-linking. Rates and yields are highly oxygen- and temperature-sensitive. Figure 24 shows the magnitude of oxidative attack on PS and the extent to which an antioxidant can protect the polymer.

Environmental Degradation. In the past several years, PS has received much public and media attention. Polystyrene has been described by various environmental groups as being nondegradable, nonrecyclable, toxic when burned, landfill-choking, ozone-depleting, wildlife-killing, and even carcinogenic. These misconceptions regarding PS have resulted in boycotts and bans in various localities. Actually, PS comprises less than 0.5% of the solid waste going to landfills (Fig. 25) (145).

The approach which the plastics industry has taken in managing plastics waste is an integrated one of source reduction, recycling, incineration for energy recovery, reduction of litter, development of photodegradable plastics for specific litter prone applications, the development of biodegradable plastics, and increasing public awareness of the recyclability and value of PS. The balance of these approaches varies from year to year depending upon public concerns, political pressures, legislation, technology development, and the development of an understanding of the actual contribution of plastics to total solid waste generation.

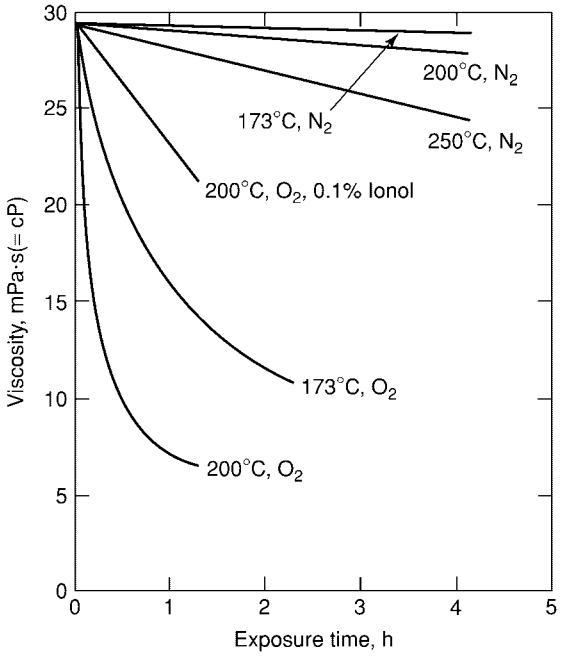

Fig. 24. Thermal and thermooxidative degradation of PS.

Currently, recycling is being the most heavily researched and developed. The National Plastics Recycling Company (NPRC) was established in 1989 through the combined efforts of the top eight U.S. PS producers (ie, Huntsman, Dow, Polysar, Fina, Arco, Mobil, Chevron, and Amoco). Its charter is to facilitate plastic recycling with the ultimate objective of recycling 25% of the PS produced in the United States each year (146).

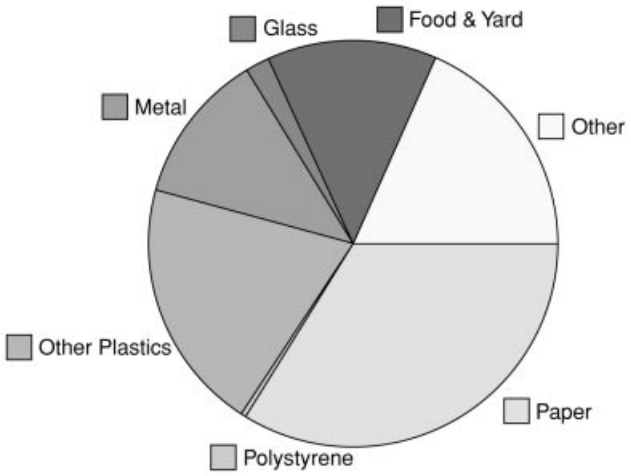

Fig. 25. Approximate composition of solid waste going into landfills in the United States (145)

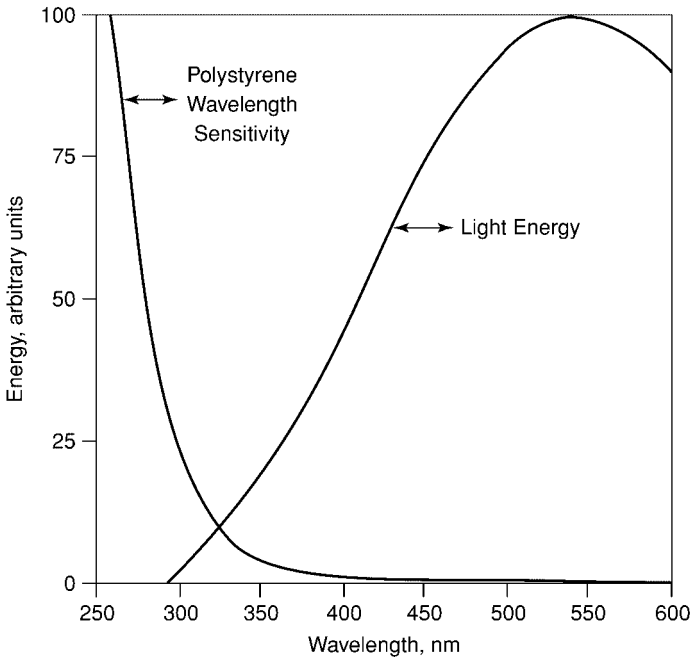

Fig. 26. Energy of the solar spectrum vs the wavelength sensitivity of PS.

Photodegradation. Natural sunlight emits energy only in wavelengths above 290 nm. Therefore, any polymer that does not absorb light energy at wavelengths above 290 nm should not be photodegradable. The activation spectrum of PS versus the intensity of the solar spectrum is shown in Figure 26. Since PS degradation is activated by radiation at wavelengths above 290 nm, it is quite photodegradable and must be stabilized by the addition of uv-absorbing additives if it is to be used in outdoor applications where durability is important.

Even though PS is naturally quite photodegradable, there have been considerable efforts to accelerate the process to produce photodegradable PS (147–152). The approach is to add photosensitizers (typically ketone-containing molecules), which absorb sunlight (eg, benzophenone). The absorbed light energy is then transferred to the polymer to cause backbone scission via an oxidation mechanism (Fig. 27). Photodegradable PS would be useful in litter prone applications (eg, fast food packaging).

A more effective approach to enhancing the rate of photodegradation of PS is to copolymerize styrene with a small amount of a ketone-containing monomer. Thus, the ketone groups are attached to the polymer during its manufacture (Fig. 28) (147,149).

Attaching the ketone groups to the polymer backbone is more efficient, on a chain scission/ketone bases, because some of the light energy that the pendant ketone absorbs leads directly to chain scission via the Norrish type II mechanism, as well as photooxidation via the Norrish type I mechanism (Fig. 29) (149).

A key problem with the manufacture of photodegradable PS containing low levels of methyl vinyl ketone and methyl isopropenyl ketone is their human

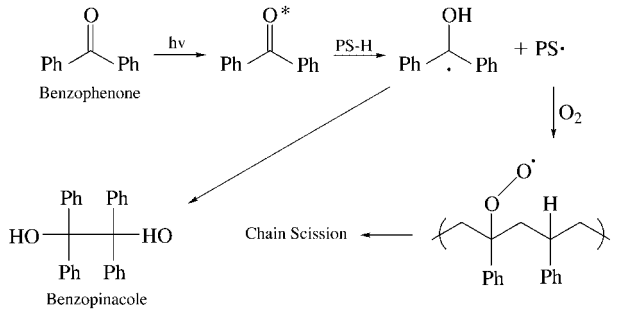

Fig. 27. The chemistry of molecular weight breakdown of PS during outdoor exposure.

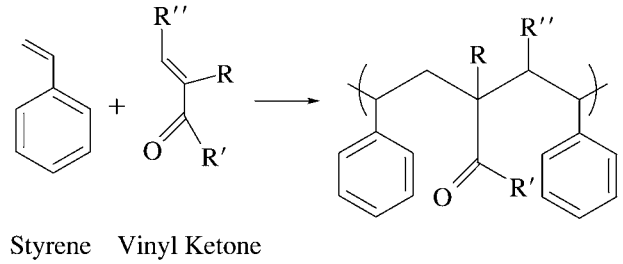

Fig. 28. Incorporation of photosensitive ketone groups into PS during manufacture.

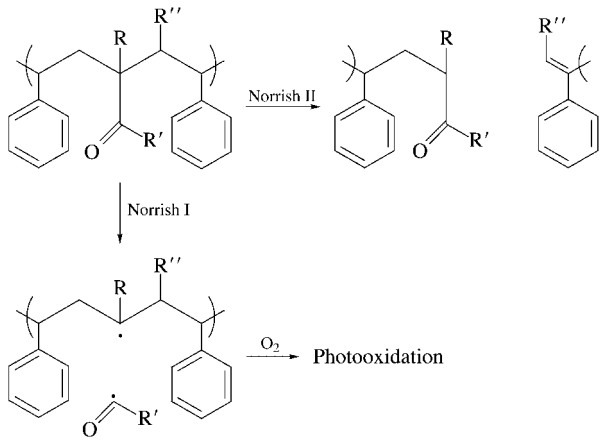

Fig. 29. Polystyrene backbone scission resulting from sunlight exposure of PS containing attached ketone groups.

toxicity. This problem has been solved by adding the ketoalcohol intermediate, formed during the vinyl ketone manufacture, to the styrene polymerization and generating the vinyl ketone *in situ*. (Fig. 30) (151,152).

A concern in the use of photodegradable PS is the environmental impact of the products of photooxidation. However, photodegraded PS is expected to be more susceptible to biodegradation because the molecular weight has been reduced,

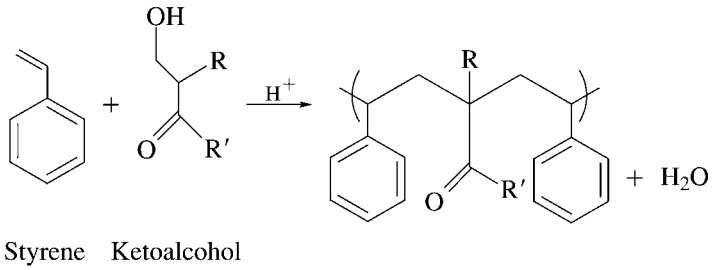

Fig. 30. Manufacture of photodegradable PS via *in situ* vinyl ketone process.

the PS chains have oxidized end groups, the incorporation of oxygen as alcohol and ketone groups has increased the hydrophilicity of the PS fragments, and the surface area has increased (153–155).

Biodegradation. Polystyrene is inherently resistant to biodegradation mainly because of its hydrophobicity. Efforts have been made to enhance the biodegradability of PS by inserting hydrolyzable linkages (eg, ester and amide) into its backbone. This was accomplished by adding monomers to the polymerization, which are capable of undergoing ring-opening copolymerization (Fig. 31) (156).

Environmental Effect of Blowing Agents. Until the mid-1980s, the most common blowing agents for extruded PS foams were chlorofluorocarbons (CFCs). However, when these materials were shown to contribute to the ozone depletion problem, there became a considerable effort to find alternative blowing agents for the manufacture of extruded PS foam. Most of the research has focused on the development of carbon dioxide foaming technology for PS (157). By contrast, PS bead foam uses hydrocarbon blowing agents (eg, pentane). Hydrocarbon blowing agents are extremely flammable and add volatile organic compounds to the atmosphere. In Europe, all PS foam is manufactured using carbon dioxide as the blowing agent.

Polymerization

Styrene and most derivatives are among the few monomers that can be polymerized by all four distinct mechanisms, ie, anionic, cationic, free-radical, and

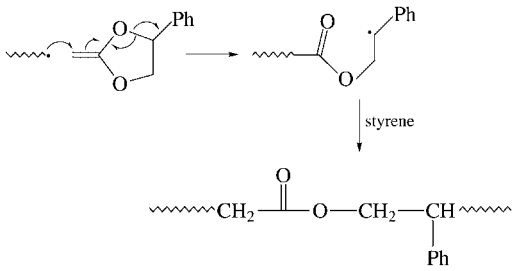

Fig. 31. Preparation of biodegradable PS by incorporating ester linkages into the backbone via ring-opening copolymerization of styrene with a cyclic ketene acetal.

Ziegler–Natta. These include processes dependent on electromagnetic radiation, which is usually a free-radical mechanism, or high energy radiation, which is either a cationic or free-radical mechanism depending on the water content of the system. All mechanisms, other than Ziegler–Natta, generally yield polymers with a high degree of random placement of the phenyl group relative to the backbone, ie, the polymers are classified as atactic and amorphous. Anionically made PS is usually atactic and amorphous, but in some cases, eg, at low temperatures, iPS has been prepared.

Each of the mechanisms used to polymerize styrene has its own unique advantages/disadvantages as summarized below.

Anionic:

Initiation, propagation, and termination steps are sequential resulting in the formation of narrow polydispersity ($M_w/M_n < 1.1$); termination step is controlled allowing control of end-group structure; polymerization feed must be purified.

Cationic:

High molecular weight polymers are difficult to make because of the instability of polystyrylcarbocation giving fast termination; polymerization feed must be purified.

Free-Radical:

Initiation, propagation, and termination steps are simultaneous resulting in the formation of broad polydispersity ($M_w/M_n > 2$); multiple termination paths lead to a variety of end groups; polymerization feed need not be purified.

Ziegler–Natta:

Metal complexes allowing stereospecific polymerization resulting in the formation of high melting crystalline tactic PS; polymerization feed must be purified.

Free-radical polymerization is the preferred industrial route because: (*1*) monomer purification is not required (158) and (*2*) initiator residues need not be removed from polymer as they have minimal effect on polymer properties. The exceptions are the styrene–butadiene block copolymers and very low molecular weight PS. These polymers are manufactured using anionic and cationic polymerization chemistry, respectively (159). Analytical standards are available for PS prepared by all four mechanisms (see INITIATORS).

Free Radical. The styrene family of monomers are almost unique in their ability to undergo spontaneous or thermal polymerization merely by heating to

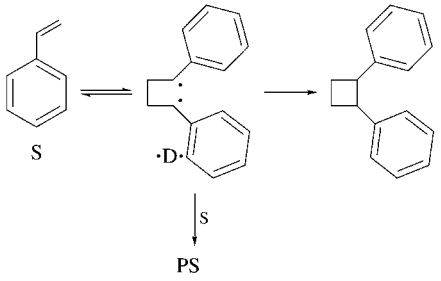

Fig. 32. Flory mechanism for spontaneous initiation of styrene polymerization

>100°C. Styrene in essence acts as its own initiator. The mechanism by which this spontaneous polymerization occurs has been studied extensively and has challenged researchers for over 50 years. Two mechanisms explaining spontaneous styrene polymerization have been proposed and supported by considerable circumstantial evidence. The oldest mechanism (160) involves a bond-forming reaction between two molecules of styrene to form a 1,4-diradical (·D·) (Fig. 32). Evidences favoring this mechanism include (*1*) the identification of *cis* and *trans* 1,2-diphenylcyclobutanes as major dimers (161,162), and (*2*) the large differences between spontaneous and chemically initiated (azobisisobutyronitrile) styrene polymerizations in the presence of the free-radical scavenger 1,1′-diphenyl-2-picrylhydrazyl (DPPH). The rate of consumption of DPPH is 25 times faster than that expected from the rate of polymerization measurements. This difference was explained by the spontaneous formation of ·D·, many of which become self-terminated before initiating polymer radicals (163). However, experiments to test the mechanism showed that there was no significant difference in the molecular weight of PS initiated by monoradicals compared with the spontaneously initiated polymerizations taken to the same monomer conversion (164).

The second mechanism (Fig. 33) (165) involves the Diels–Alder reaction of two styrene molecules to form a reactive dimer (DH) followed by a

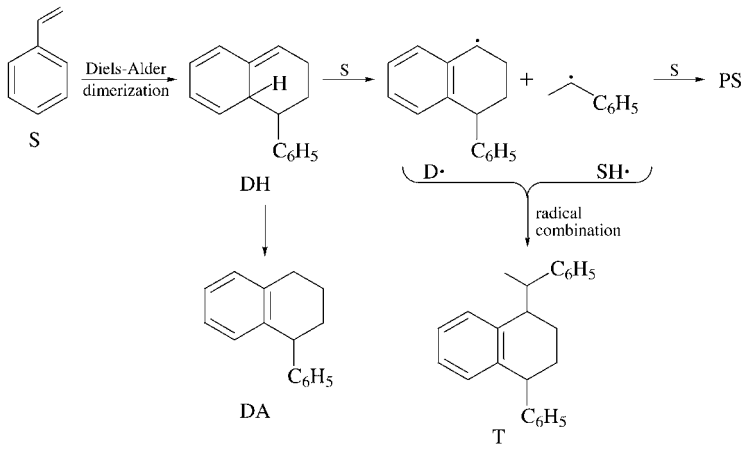

Fig. 33. Mayo mechanism for spontaneous initiation of styrene polymerization.

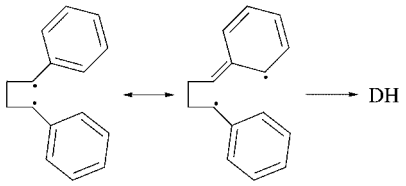

Fig. 34. Formation of the Mayo Dimer via the Flory Diradical.

molecular-assisted homolysis (MAH) between the DH and another styrene molecule. The Mayo mechanism has been generally preferred even though critical reviews (162,166) have pointed out that the mechanism is only partially consistent with the available data. Also, the postulated intermediate DH has never been isolated. Evidences supporting the mechanism include kinetic investigations (167,168), isotope effects (166), and isolation/structure determination of oligomers (166,169). Even though the reactive dimer intermediate DH has never been isolated, the aromatized derivative DA has been detected in PS (169). Also, D· has been indicated as an end group in PS using ^{1}H NMR and uv spectroscopy (170).

The Flory and Mayo proposals could be combined by the common diradical ·D·, which collapses to either DH or 1,2-diphenylcyclobutane (Fig. 34). Nonconcerted Diels–Alder reactions are permissible for two nonpolar reactants (171).

The spontaneous polymerization of styrene was studied in the presence of various acid catalysts (172) to see if the postulated reactive intermediate DH could be intentionally aromatized to form inactive DA. The results showed that the rate of polymerization of styrene is significantly retarded by acids (eg, camphorsulfonic acid) accompanied by increases in the formation of DA. This finding gave further confirmation for the intermediacy of DH since acids would have little effect on the cyclobutane dimer intermediate in the Flory mechanism.

A potentially important commercial benefit of adding an acid catalyst to the spontaneous free-radical polymerization of styrene is that a significant shift results in the rate/molecular weight curve for PS. This shift is most pronounced at high molecular weights allowing formation of high molecular weight PS at a much faster polymerization rate (Fig. 35). An explanation for this phenomenon is that the intermediate DH has a high chain-transfer constant (ie, ∼10) (173). Addition of acid immediately causes DH to aromatize, thus lowering its concentration and hence decreasing its availability to participate in chain-transfer processes. Also, the main mechanism of termination is chain coupling (174), the rate of which is most affected by radical concentration. Since the polymerization temperature can be raised in the presence of acid without increasing free-radical concentration, the propagation rate is increased relative to termination rate, thereby raising the molecular weight.

The addition of a fugitive acid such as camphorsulfonic acid to styrene polymerizations contaminates the polymer with a substance that could lead to corrosion of equipment being used to process the polymer. To solve this problem, Dow researchers added vinyl functional sulfonic acids (eg, 2-sulfoethyl methacrylate) to the polymerization (175). The acid then becomes copolymerized into the polymer, thus immobilizing it. Also, they found that the addition of as low as 10 ppm

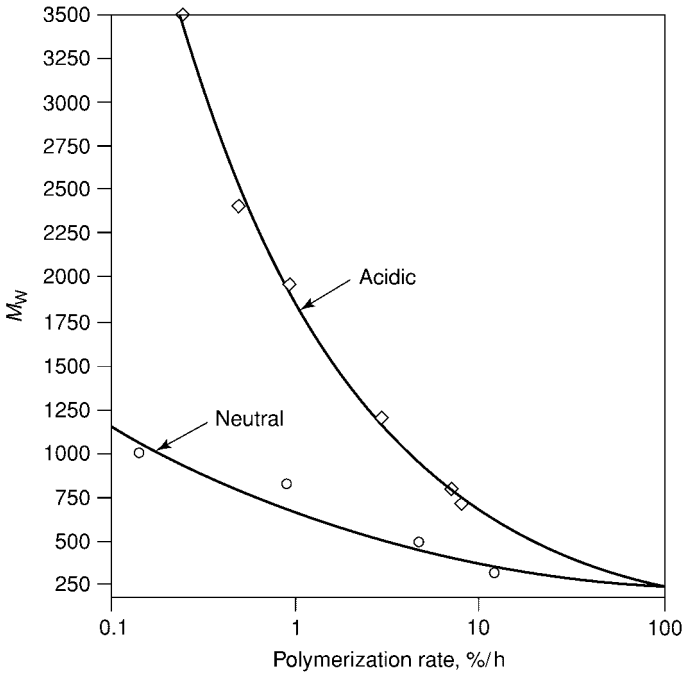

Fig. 35. Polymerization rate vs molecular weight relationship for spontaneous bulk styrene polymerization under neutral and acidic conditions.

of 2-sulfoethyl methacrylate significantly increases the production rate of high molecular weight PS (176).

Polystyrene produced by the spontaneous initiation mechanism is typically contaminated by dimers and trimers (1–2 wt%). These oligomers are somewhat volatile and cause problems during extrusion (vapors) and molding (mold sweat) operations. The use of chemicals to generate initiating free radicals significantly reduces the formation of oligomers. Oligomer production is reduced because the polymerization temperature can be lowered to slow down the Diels–Alder dimerization reaction. A wide range of free-radical initiators are available. They differ mainly in the temperature at which each generates free radicals at a useful rate. Typically, in continuous bulk polymerization processes it is best to polymerize styrene at about the 1-h half-life temperature of the initiator it contains to maximize initiator efficiency.

Initiators that have been utilized to initiate styrene polymerization can be generally categorized into three types: peroxides, azo, and carbon–carbon (177). Peroxides are thermally unstable and decompose by homolysis of the O—O bond, resulting in the formation of two oxy radicals. Azo compounds decompose by concerted homolysis of the N—C bonds on either side of the azo linkage, resulting in extrusion of nitrogen gas and the formation of two carbon-centered radicals. Carbon–carbon initiators decompose by homolysis of a sterically strained C—C bond, resulting in the formation of two carbon-centered radicals. The radicals initiate styrene polymerization and end up attached to the chain ends and may have an effect upon polymer stability (178–181).

Since most of the bulk PS reactors were originally designed to produce spontaneously initiated PS in the 100–170°C temperature range, the peroxide initiators used generally have 1-h half-lives in the range of 90–140°C. If the peroxide decomposes too rapidly, a run-away polymerization could result, and if it decomposes too slowly, peroxide exits the reactor. Since organic peroxides are significantly more expensive than styrene monomer (5–20×), it is economically prudent to choose an initiator that is highly efficient and is entirely consumed during the polymerization.

Another economically driven objective is to utilize initiators that increase the rate of polymerization of styrene to form PS having the desired molecular weight. The commercial weight-average molecular weight (M_w) range for GPPS is 200,000–400,000. For spontaneous polymerization, the M_w is inversely proportional to polymerization rate (Fig. 36).

The main reason that the M_w decreases as the polymerization temperature increases is the increase in the initiation and termination reactions leading to a decrease in the kinetic chain length (Fig. 37). At low temperature, the main termination mechanism is polystyryl radical coupling, but as the temperature increases, radical disproportionation becomes increasingly important. Termination by coupling results in higher M_w PS than any of the other termination modes.

There are typically several different product grades produced in a single-polymerization reactor, and transitioning between these products in the minimum time maximizes production yield. Most PS producers rely on the use of kinetic modeling and computer simulation to aid in the manufacture of PS to minimize

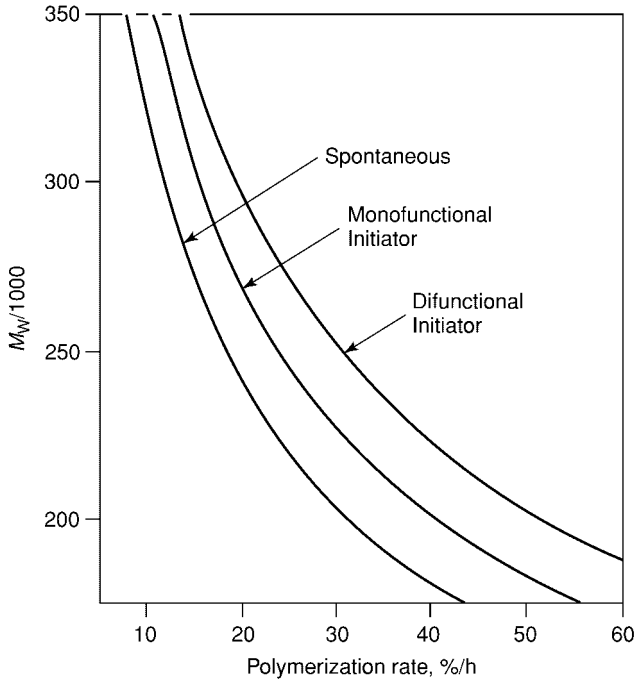

Fig. 36. Polymerization rate for PS using different types of initiators.

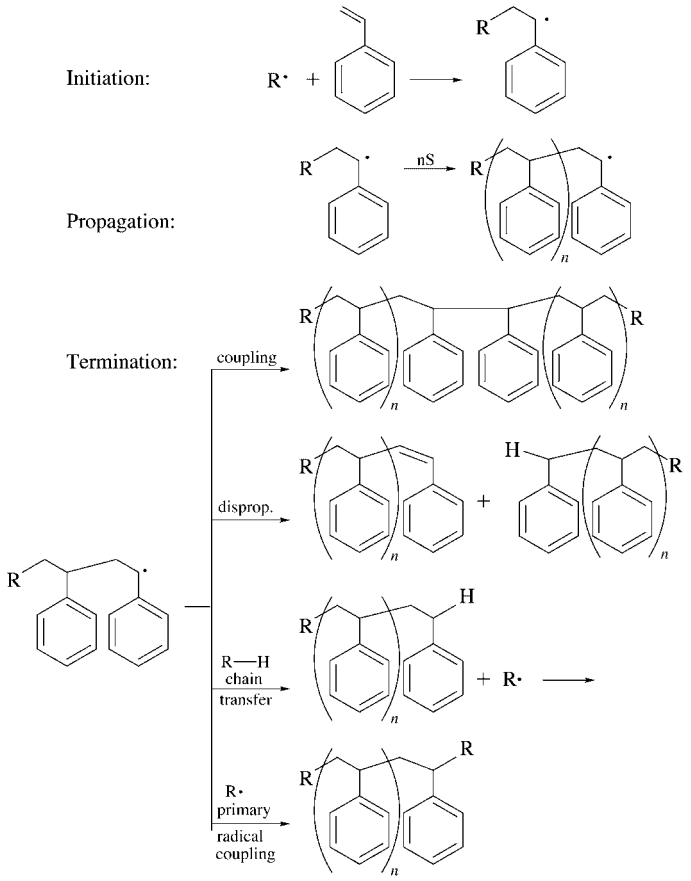

Fig. 37. General chemistry of free-radical styrene polymerization.

transition time between product grades. Kinetic models have been developed for styrene polymerization without added initiators (182–184), using one monofunctional (185–189), two monofunctional initiators with different half-lives (190), symmetrical difunctional (**4**), (191) and (**5**), (**6**), (192) and the unsymmetrical difunctional initiators (**7**), (193,194) and (**8**) (195,196). These models clearly show the polymerization rate advantage of using initiators for the manufacture of PS using continuous bulk polymerization processes (Fig. 36).

One of the key reasons for the polymerization rate advantage of using difunctional initiators is their theoretical ability to form initiator fragments, which can initiate polymer growth from two different sites within the same fragment, ultimately leading to "double-ended PS." If double-ended PS chains are produced, given that the main mechanism of termination is chain coupling, it is clear why higher M_w PS can be produced at faster rates using difunctional initiators (197). One of the goals of PS researchers has been the discovery of an initiator that truly initiates only double-ended PS chains. Because the main mechanism of termination is radical coupling, the production of pure double-ended chains would lead to the formation of ultrahigh molecular weight PS because termination by chain

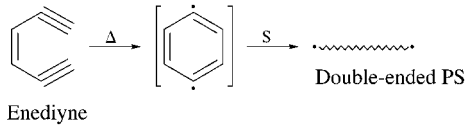

Fig. 38. Double-ended PS initiated by diradical formed during Bergman Cyclization.

coupling would only lead to a higher molecular weight double-ended chain. There have been many attempts to develop initiators that form only diradicals. However, the discovery of diradicals that efficiently initiate styrene polymerization is a challenge (198). Dow researchers recently discovered that the *p*-phenylene diradical formed during "Bergman Cyclization" of certain enediynes can initiate double-ended PS, but commercialization of these initiators remains a challenge (Fig. 38) (199). To date, the only clear demonstration of double-ended PS has been with difunctional LFRP initiators (200).

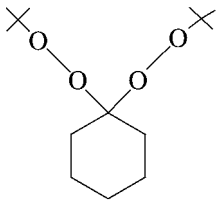

4

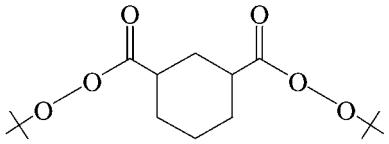

5

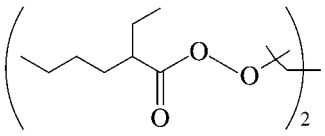

6

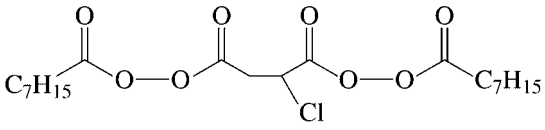

7

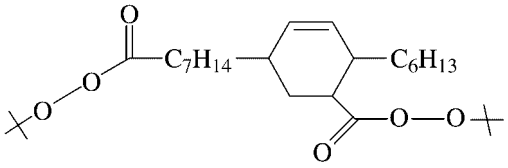

8

Below 80°C, radical combination is the primary termination mechanism (201). Above 80°C, both disproportionation and chain transfer with the Diels–Alder dimer are increasingly important. The gel or Trommsdorff effects, as manifested by a period of accelerating rate concomitant with increasing molecular weight, is apparent at below 80°C in styrene polymerization; although, subtle changes during the polymerization at higher temperature may be attributed to variation of the specific rate constants with viscosity (201,202).

In some cases, inhibition of polymerization can be regarded as a special type of chain transfer. This is of importance in commercial-scale operations involving styrene storage for extended periods. The majority of inhibitors are of the phenolic/quinone family. All of these species function as inhibitors only in the presence of oxygen. 4-*tert*-Butylcatechol (TBC) at 12–50 ppm is the most universally used inhibitor for protecting styrene. At ambient conditions and with a continuous supply of air, TBC has a half-life of 6–10 weeks (203). The requirement of oxygen causes complex side reactions, resulting in significant oxidation of the monomer, which causes yellow coloration especially in the vapor phase. An inert gas blanket reduces this problem and flammability hazards, but precautions must be taken to ensure an adequate level of dissolved oxygen in the liquid phase. Another family of inhibitors is that characterized by the N—O bond; these do not seem to require oxygen for effectiveness. They include a variety of nitrophenol compounds, hydroxylamine derivatives, and nitroxides (204,205). Nitric oxides are particularly useful. The unpaired electron associated with the N—O bond is very stable and yet nitroxides couple with carbon-centered radicals at diffusion-controlled rates. The alkoxyamines produced when nitroxides couple with styryl radicals are thermally labile. At elevated temperatures (generally >100°C), the C—O bond dissociates back to the precursor radicals in equilibrium with the alkoxyamine. Thus, if alkoxyamines are added to styrene, they can initiate polymerization. The nitroxide moiety is retained on the propagating chain-end and effectively supresses the termination mechanisms (ie, polystyryl radical coupling, chain transfer, and disproportionation) typical of normal free-radical polymerization. The result is that narrow polydispersity PS is produced. Once the unreacted styrene is removed from the nitroxide-terminated PS and a second monomer is added, a block copolymer can be produced.

Other miscellaneous compounds that have been used as inhibitors are sulfur and some sulfur compounds, picrylhydrazyl derivatives; carbon black, and some soluble transition-metal salts (206). Both inhibition and acceleration have been reported for styrene polymerized in the presence of oxygen. The complexity of this system has been clearly demonstrated (207). The key reaction is the alternating copolymerization of styrene with oxygen to produce a polyperoxide, which

Table 4. Chain-Transfer Constants (K_{ct}) in Free-Radical Styrene Polymerization

Compound	K_{ct}	T,°C
Benzene	0.00002	100
Toluene	0.00005	100
Ethylbenzene	0.0002	100
Isopropylbenene	0.0002	100
α-Methylstyrene dimer	0.3	120
l-Dodecanethiol	13	130
l,l-Dimethyl-l-decanethiol	1.1	120
l-Hexanethiol	15	100

above 100°C decomposes to initiating alkoxy radicals. Therefore, depending on the temperature, oxygen can inhibit or accelerate the rate of polymerization.

Chain Transfer in Free-Radical Styrene Polymerization. The concept of chain transfer is depicted in Figure 37. Chain-transfer agents are occasionally added to styrene to reduce the molecular weight of the polymer, although for many applications this is unnecessary as polymerization temperature alone is generally sufficient to achieve molecular weight control. Some typical chain-transfer agents for styrene polymerization are listed in Table 4. The chain-transfer agents of commercial significance are α-methylstyrene dimer, terpinolene, dodecane-1-thiol, and 1,1-dimethyldecane-1-thiol. Chain transfer to styrene monomer has been reported, but recent work strongly suggests that this reaction is negligible and transfer with the Diels–Alder dimer is the actual inherent transfer reaction (208,209). Chain transfer to PS has received some attention, but experiments indicate that it is minimal (210,211). If it did occur at a significant extent, then the polymer would be branched. The chain-transfer constants of several common solvents and chain-transfer agents are shown in Table 4.

High levels of chain-transfer agents can be used to control the termination process. If the chain-transfer agent has a functional group attached to it, the functional group ends up becoming attached to the end of the PS chain. If the functionalized chain-transfer agent operates by donating an H-atom to the polystyryl radical, the functional group ends up becoming attached to only one end of the PS chain. However, this technique does not quantitatively functionalize the polymer chains because not all chains get initiated by the functionalized chain-transfer agent fragment formed by loss of the H-atom. However, if both the initiator and the chain-transfer agent contain the functional group (F), high purity one-end functional PS can be produced (Fig. 39) (212).

Another approach to control end-group structure is the use of chain-transfer agents that operate by an addition–fragmentation mechanism. This approach can lead to the formation of PS having functional groups at both ends if both the initiating and terminating fragments contain functional groups (Fig. 40).

Recently, it was found that the common chain-transfer agent α-methylstyrene dimer operates by an addition–fragmentation mechanism (Fig. 41) (213).

The use of addition–fragmentation chain-transfer agents also places a reactive double bond on one end of the polymer chain and thus yields a macromonomer.

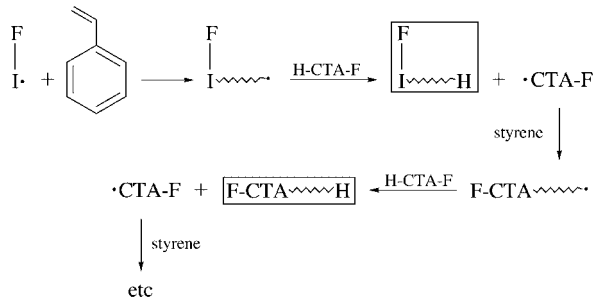

Fig. 39. Preparation of mono-end-functional PS using both a functionalized initiator and a functionalized chain-transfer agent (CTA).

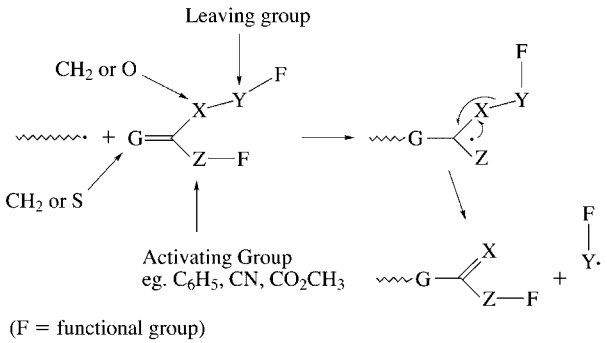

Fig. 40. Generic addition–fragmentation chain-transfer structure and the mechanism of action.

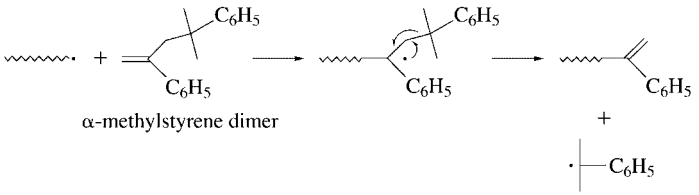

Fig. 41. Mechanism of action of α-methylstyrene dimer.

Copolymerization of the chain-end double bond with more styrene leads to branched PS.

Ionic. Instead of a neutral unpaired electron, styrene polymerization can proceed with great facility through a positively charged species (cationic polymerization) or a negatively charged species (anionic polymerization). The polymerization reaction is more sensitive to impurities than the free-radical system, and pretreatment of the monomer is generally required (214). *n*-Butyllithium (NBL) is the most widely used initiator for anionic polymerization of styrene. In solution, it exists as six-membered aggregates, and a key step in the initiation sequence is dissociation yielding at least one isolated molecule.

If the initiation reaction is very much faster than the propagation reaction, then all chains start to grow at the same time, and since there is no inherent termination step (living polymerization), the statistical distribution of chain lengths is very narrow. The average molecular weight is calculated from the mole ratio of monomer-to-initiator sites. Chain termination is usually accomplished by adding proton donors, eg, water or alcohols, or electrophiles such as carbon dioxide.

Anionic polymerization, if carried out properly, can truly be a living polymerization (215). Addition of a second monomer to polystyryl anion results in the formation of a block polymer with no detectable free PS. This technique is of considerable importance in the commercial preparation of styrene–butadiene block copolymers, which are used either alone or blended with PS as thermoplastics.

Anionic polymerization offers very fast polymerization rates because of the long lifetime of polystyryl carbanions. Early research focused on this attribute, most studies being conducted at short reactor residence times ($<$1 h), at relatively low temperatures (10–50°C), and in low chain-transfer solvents (typically benzene) to ensure that premature termination did not take place. Also, relatively low DPs were typically studied. Continuous commercial free-radical solution polymerization processes to make PS, on the other hand, operate at relatively high temperatures ($>$100°C), at long residence times ($>$1.5 h), utilize a chain-transfer solvent (ethylbenzene), and produce polymer in the range of 1000–1500 DP.

Two companies (Dow and BASF) have devoted significant research efforts to develop continuous anionic polymerization processes for PS. However, to date no PS is produced commercially using these processes. Dow researchers utilized conventional free-radical polymerization reactors of the CSTR-type (216–220) to study the anionic polymerization of styrene while BASF focused upon continuous reactors of the linear-flow-type (221). In an anionic CSTR process, initiation, propagation, and termination occur simultaneously and thus the polydispersity of the resulting PS is $\sim$2. A chain-transfer solvent (ethylbenzene) and relatively high temperatures (80–140°C) were also used. Under these conditions, the chain transfer to solvent (CTS) is extremely high since the high monomer conversions ($>$99%) achieved under steady-state operation results in a large ratio (typically, 500:1) of solvent to monomer. The result of high CTS is that very high yields of PS based on NBL (the most costly raw material) and PS having high clarity (low color) are produced (Fig. 42). Under very stringent feed purification conditions, as high as an 8000% yield based on NBL initiator (158) can be achieved. According to Figure 42, without high levels of CTS, it would be impossible to make a PS having sufficient clarity to meet the current color requirements to be sold as "prime" resin (with no CTS, 640 ppm of NBL is required to produce a PS of 1000 DP).

One of the key benefits of anionic PS is that it contains much lower levels of residual styrene monomer than free-radical PS (222). This is because free-radical polymerization processes only operate at 60–80% styrene conversion, while anionic processes operate at $>$99% styrene conversion. Removal of unreacted styrene monomer from free-radical PS is accomplished using continuous devolatilization at high temperature (220–260°C) and vacuum. This process leaves about 200–800 ppm of styrene monomer in the product. Taking the styrene to a lower level requires special assisted devolatilization processes such as steam stripping (223).

The most recent process research aimed at anionic PS is that of BASF. Unlike the Dow process, they utilize CPFR with virtually no backmixing to make narrow

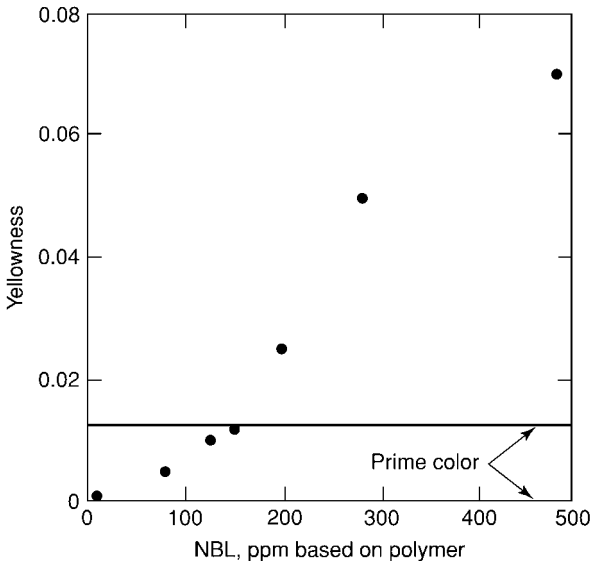

Fig. 42. Polystyrene color vs amount of *n*-butyllithium (NBL) consumed for its production in a CSTR.

polydispersity resins. In the Dow CSTR anionic process, the fast polymerization rate achieved with anionic polymerization is not a problem because the polymerization exotherm is controlled by the rate of monomer addition to the reactor; that is, the reactor is operated in a monomer-starved condition. However, in CPFR, the rate of polymerization of NBL-initiated styrene polymerization far exceeds the ability to remove heat resulting in run-away polymerization. This problem was recently solved by Asahi (224) and BASF with the addition of electron deficient metal alkyls (eg, dibutylmagnesium, diethylzinc, and triethylaluminum) to assist the butyl lithium initiator (225,226). Addition of metal alkyls accomplish two things: (*1*) the propagation rate is slowed and (*2*) the polystyryl lithium chain end is stabilized to high temperatures. The rate of the polymerization can actually be slowed to match the rate typically observed during free-radical polymerization of styrene by the addition of the proper amount of metal alkyl (Fig. 43). As the conversion of monomer to polymer proceeds, the viscosity rapidly increases forcing the need to finish the polymerization at high temperatures to be able to handle the high viscosity. It is well known that at temperatures $>100^{\circ}$C, PS lithium is unstable and decomposes by elimination of lithium hydride, resulting in the formation of dead polymer. The presence of electron deficient metal alkyls increases the thermal stability of the polystyryl chain ends so that polymerization up to high conversion and temperatures can be achieved.

The mechanism (226) involves the formation of a metal complex or aggregate between the lithium and the electron deficient metal. Styrene then inserts in the complex. This hypothesis is supported by the change in uv spectrum as the Li/Mg ratio changes. There is a shift of the λ_{max} to lower wavelength as the Mg/Li ratio approaches unity. As the Mg/Li ratio is increased to >1, the λ_{max} shifts back until at 20/1, the λ_{max} returns to match that of pure polystyryl lithium.

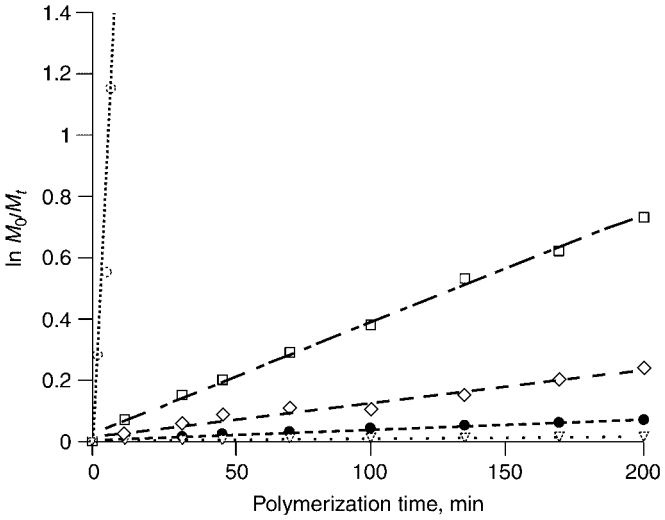

Fig. 43. Propagation rate retarding effect of adding dibutylmagnesium to butyllithium initiated anionic polymerization of styrene. ···○··· Lithium alone; -□—Mg/Li = 0.8; —◇—Mg/Li = 2; ––●–– Mg/Li = 4; ···▽··· Mg/Li = 20.

Continuous anionic polymerization, conducted above the ceiling temperature (61°C), is also useful for making thermally stable styrene-*co*-α-methylstyrene (SAMS) having high α-methylstyrene (AMS) content. Preparation of SAMS having >20 wt% of AMS units using bulk free-radical polymerization leads to very slow polymerization rates, low molecular weight polymer, and the formation of high levels of oligomers. The preparation of SAMS using an anionic CSTR polymerization reactor operating at 90–100°C allows the production of SAMS having up to about 70 wt% AMS units (Fig. 44) (227). By conducting the polymerization above the ceiling temperature, no AMS polyads of more than two units are possible. SAMS copolymers having polyads of greater than two units in length are thermally unstable (228).

Cationic polymerization of styrene can be initiated either by strong acids, eg, perchloric acid, or by Friedel-Crafts reagents with a proton-donating activator, eg, boron trifluoride or aluminum trichloride, with a trace of a protonic acid or water. Cationic polymerization of styrene can also be initiated using heterogeneous acid catalysis such as acidic clays and strong acid ion exchange resins. The solvent again plays an important role, and chain-transfer reactions are very common where the reactants are polymer, monomer, solvent, and counterion. As a result, high molecular weights are more difficult to achieve and molecular weight distributions are often comparable to those obtained from free-radical polymerizations. Commercial use of cationic styrene polymerization is reported only where low molecular weight polymers are desired (110). In recent years, considerable advances have taken place with regard to cationic polymerization of styrene. Its use in making block copolymers and even living cationic polymerizations have been reported (229).

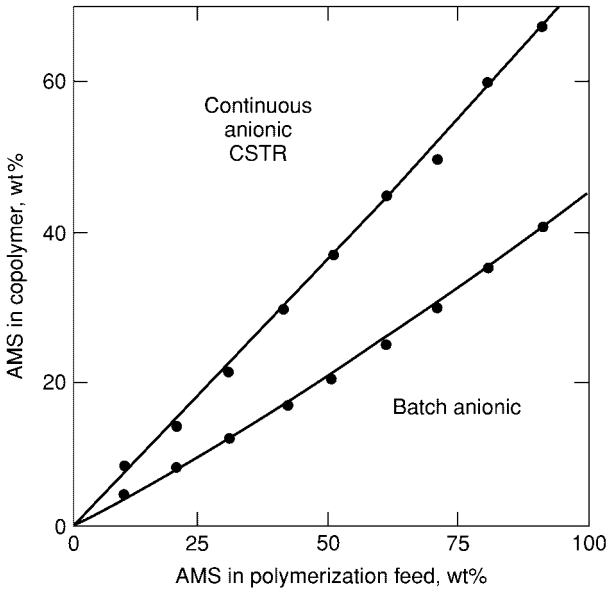

Fig. 44. Comparison of continuous (CSTR) and batch anionic production of SAMS.

Ziegler–Natta. Ziegler–Natta-initiated styrene polymerization yields stereoregular tactic PS. The tacticity can be isotactic (phenyl rings *cis* to each other) or syndiotactic (phenyl rings *trans* to each other) depending upon the initiator structure (230). Currently, all commercially important styrenic plastics are amorphous, since the vast excess of these polymers is made by a free-radical mechanism. However, Dow Chemical and Idemitsu Petrochemical Companies are working together to commercialize crystalline sPS. Dow and Idemitsu are currently manufacturing sPS using a bulk polymerization process. Since the sPS crystallizes as it forms, the polymerization process is very challenging because it requires mixing and removing the heat of polymerization from a sticky solid. Proper reactor design is required to keep the sticky mass from solidifying. The properties of sPS are quite different from atactic PS because of its crystallinity (mp = 270°C). Since sPS must be fabricated above its melting point and the polymer decomposes at 300°C, there is a very narrow fabrication temperature range. This problem is improved by copolymerizing a small amount of comonomer (eg, *p*-methylstyrene) into the polymer to lower the crystalline melting point. Because of its crystallinity, sPS finds utility in applications requiring heat resistance and solvent resistance (231) (see SYNDIOTACTIC POLYSTYRENE).

Living Free-Radical Styrene Polymerization. The requirements for a polymerization to be truly "living" are that the propagating chain-ends must not terminate during the polymerization. If the initiation, propagation, and termination steps are sequential (ie, all of the chains are initiated and then propagate at the same time without any termination), then monodisperse (ie, M_w/M_n = 1.0) polymer is produced. In general, anionic polymerization is the only mechanism that yields truly living styrene polymerization and thus monodisperse

PS. However, significant research has been conducted with the goal of achieving "living" styrene polymerization using cationic, free-radical, and Ziegler–Natta mechanisms.

Since Otsu first proposed living free-radical polymerization (LFRP) in 1982, (232,233) there has emerged a multitude of examples (234–242). However, significant controversy exists over the nature of the living chain-end and whether the process can really be called "living." Instead, terms such as pseudo-living, quasi-living, resuscitatable, stable free-radical-mediated, and dormant, have been used to better describe the process. Currently, most researchers prefer to use the term controlled radical polymerization. The process generally involves the addition of relatively stable free radicals to the polymerization. The growing polystyryl radicals are intercepted and terminated by coupling with the stable radicals thereby minimizing termination by chain transfer and the coupling of polystyryl radicals with themselves. Prior to the discovery of LFRP, stable free radicals were only added to styrene as polymerization inhibitors. They acted as radical scavengers to stop the propagation process. However, the bond formed between the polystyryl radical and some stable freeradical is somewhat labile, and styrene can insert into the bond once it is activated by heat or photolysis. The main evidences used to support the livingness of the polymerization are the increase of molecular weight with monomer conversion, the formation of narrow polydispersity PS, and the ability to prepare block copolymers. Normally, free-radical polymerizations show relatively flat molecular weight versus conversion plots. Although no one has yet demonstrated the preparation of truly monodisperse ($M_w/M_n=1.0$) PS using LFRP, polydispersities approaching 1.05 have been reported for very low molecular weight ($M_w < 20{,}000$) PS prepared in the presence of stable nitroxy radicals.

A variant of the LFRP of styrene is called atom transfer radical polymerization (ATRP). In ATRP the initiator is an activated halide. The halogen–carbon bond is broken by transfer of the halogen from the chain end to a chelated transition metal (eg, copper, iron, or ruthenium). After the resulting polystyryl radical adds a few monomer units, the halogen transfers back onto the chain-end. This process repeats itself many times resulting in the formation of PS having a controlled molecular weight. If at some point a second monomer is added to the polymerization, block copolymers are produced. Although the chemistry is potentially low in cost due to the nature of the low cost of the initiators and metal catalysts, there is a serious drawback; ie, the transition-metal catalyst is difficult to remove from the final polymer. Since the presence of traces of transition metals tend to promote degradation of polymers, some means must be developed for the easy elimination of the catalyst residues from the polymer before ATRP becomes a commercial reality.

Currently, most of the LFRP research is focused on the use of nitroxides as the stable freeradical. The main problems associated with nitroxide mediated radical polymerizations (NMRP) are slow polymerization rate and the inability to make high molecular weight narrow polydispersity PS. This inability is likely due to side reactions of the living end leading to termination rather than propagation (243). The polymerization rate can be accelerated by the addition of acids or anhydrides to the process (244). The mechanism of the accelerative effect of the acid is not certain. Another problem with nitroxides is that they work well for vinylaromatic monomers, but not for acrylate and diene monomers. This has

greatly limited their use for making styrene containing block copolymers. A way around this problem is to make the nonstyrene block using some other chemistry and then place an alkoxyamine group on one of the chain-ends. The alkoxyamine functional polymer is then dissolved in styrene and heated to >100°C where the alkoxyamine functional polymer becomes a macroinitiator for the styrene polymerization (245). There are several examples of the tandem polymerization concept, including the preparation of polymethylmethacrylate (PMMA) via normal radical polymerization using an alkoxyamine functional azoinitiator (**9**). Subsequently, styrene polymerization is initiated using the alkoxyamine functional PMMA (**10**) as a macroinitiator to make S-MMA block copolymer (**11**). The synthetic scheme is displayed in Figure 45.

The successful application of NMRP to the synthesis of pure block copolymers requires that the termination processes that typically take place during free-radical polymerization (ie, radical coupling, chain transfer, and disproportionation) be virtually eliminated.

There have been two approaches to the study of the NMRP of styrene: (*1*) *in situ* formation of the NMRP initiator (Fig. 46) (246,247) and (*2*) presynthesis of the initiator (200,248).

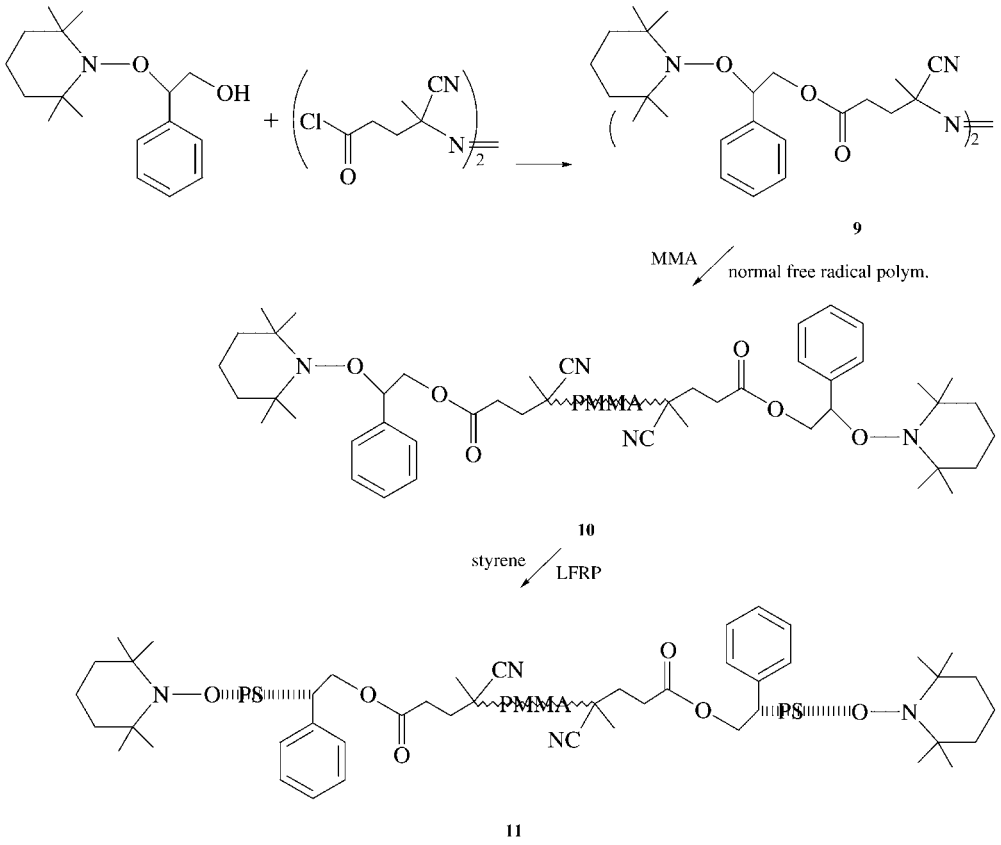

Fig. 45. Normal-living tandem polymerization approach to make styrenic block copolymers.

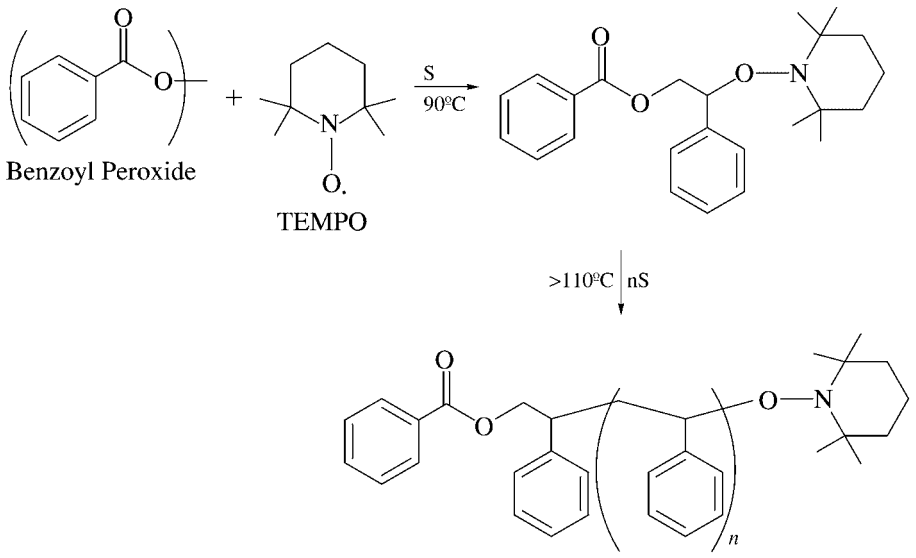

Fig. 46. *In situ* synthesis of alkoxyamine initiator during nitroxide mediated radical polymerization (NMRP) of styrene.

The *in situ* approach leads to the formation of multiple nitroxide initiating species and there is not perfect stoicheometry between the initiating and mediating species. With the presynthesis approach, a pure compound can be used to initiate polymerization which should lead to "cleaner chemistry." However, it has been believed that excess nitroxy radicals is important to achieve narrow polydispersity and good end-group purity (249).

There has been debate over the extent that NMRP eliminates termination processes. The thermal stability of a small molecule (**12**) that models the propagating chain-end of the NMRP of styrene has been synthesized and studied (250). Thermolysis of (**12**) in an ESR spectrophotometer showed continuous formation of 2,2,6,6-tetramethylpiperdinyloxy (TEMPO). Analysis of the residue left in the ESR tube showed decomposition products consisting primarily of styrene. They went on to study the kinetics of the decomposition and found that (**12**) decomposes in the temperature range utilized for NMRP of styrene at a rate comparable to the styrene conversion rate. Based on this observation, they concluded that end-group purity achieved by NMRP of styrene should decrease with both M_n and monomer conversion. They further concluded that this termination process would likely seriously limit the ability of NMRP for the preparation of high molecular weight (>100,000) PS having a narrow polydispersity. These conclusions have been disputed by other research groups who have attempted to prove that NMRP chemistry virtually eliminates all termination processes. These claims are supported by measuring the amount of nitroxyl moiety on the terminal chain-end. Both NMR (251) and nitrogen analyses (252) have been utilized to determine the nitroxyl content of PS made using NMRP. However, these techniques are not very sensitive and provide only an approximation of the level of nitroxide groups in the polymer. Further, it has not been conclusively established that the nitroxide

is at the chain terminus. Furthermore, because of the insensitivity of these analytical techniques, TEMPO-end capped PS samples to be analyzed have always had molecular weights <10,000. Most researchers have reported levels of nitroxide on the terminal chain end at >90% (251). The quality of nitroxide-mediated polymerization is directly linked to maintenance of alkoxyamine functionality on the PS chain end during the polymerization.

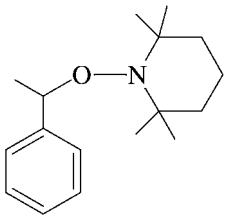

12

The level of alkoxyamine on the PS chain end during the polymerization up to high conversions and molecular weight has been measured (253). A very sensitive gpc-uv analysis technique was used to precisely quantitate the level of chromophore attached to polymers (254). They compared the end-group purity of PS made by the *in situ* and presynthesis of initiator approaches, as well as demonstrating the impact of excess nitroxide on nitroxide end-group yield. The gpc-uv technique for polymer end-group analysis requires that the initiator/mediator be tagged with a chromophore having a unique absorbance; that is, absorb at a wavelength at which PS is totally transparent (>280 nm). The chromophore chosen for study was the phenylazophenyl chromophore because of its intense absorption at >300 nm. The chromophore was attached to either the initiating or terminating fragment of the alkoxyamine initiator allowing direct quantitative comparison of both the initiating and terminal ends of PS initiated/mediated using these materials. The data show that the number of polymer chains having chromophores attached to a chain-end decreases with the number-average molecular weight (M_n). This trend is not as dramatic if the chromophore is attached to the initiating radical. M_n and styrene conversion are directly proportional. Therefore, it follows that chain-end purity also decreases rapidly with monomer conversion. This was predicted from earlier work on the thermal decomposition of a small molecule which models the dormant end during NMRF (250). Polystyrene having both a M_n >10,000 and at the same time >90% of one of its chain-ends having a chromophore were never obtained. This data has significant implications for those trying to use NMRP to make functionalized polymers and block copolymers; that is, it is impossible to make polymers having perfect structures by using this chemistry. Therefore, unless you are willing to accept styrenic polymers having some defects in the structure, this chemistry should not be used. However, this chemistry may be the best way to make certain block copolymers even though the structure produced is not perfect. For example, S-*co*-S-*alt*-MA copolymers have been synthesized using NMRP (255). At the present time, no alternative chemistry for making these block copolymers exists.

To date, no one has yet commercialized any polymers produced using an LFRP process, although several companies are aggressively evaluating the

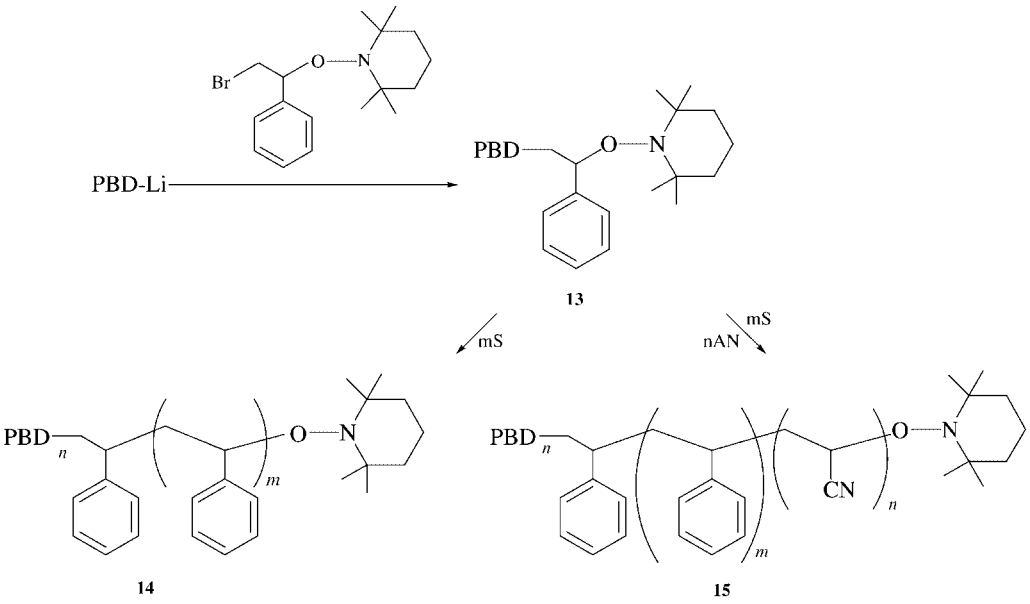

Fig. 47. Dow *in situ* block copolymer process for making HIPS/ABS toughened (256).

potential of the chemistry for commercial use. One of the applications of highest potential volume is the preparation of styrene–butadiene block copolymers *in situ* during the manufacture of HIPS (256). In this process (Fig. 47), butadiene is polymerized to PB using conventional anionic chemistry. Normally, after the polymerization is complete, the resulting polybutadienyl lithium (PB-Li) is terminated by the addition of a proton donor (an alcohol) to quench the carbanion. However, in the tandem process, a species capable of initiating LFRP that is connected to a group capable of terminating PB-Li is added to terminate the PB rubber (257). This results in the formation of PB that has an LFR functional group on one of its chain ends (**13**). The LFR-functionalized PB is then dissolved in styrene. The rubber styrene solution is then pumped into a typical continuous bulk PS reactor. During the polymerization process, the LFR-functionalized PB acts as a macroinitiator, resulting in the formation of a styrene–butadiene block polymer (**14**) *in situ*, simultaneously with the formation of PS. The final product is a blend of PS and a styrene–butadiene block rubber. The resulting HIPS product has properties similar to HIPS made by polymerizing a solution of styrene containing a styrene–butadiene block rubber (**14**). The same chemistry can be used to make ABS resins where the rubber phase ends up being a SAN–butadiene block copolymer (**15**).

Recently, a universal alkoxyamine initiator (**16**) was reported that allows LFRP of monomers other than styrene. This new alkoxyamine was discovered utilizing high speed combinatorial synthesis techniques. It has been used to make styrene–butadiene, S–BA, and S-MMA block copolymers directly without the need for tandem polymerization techniques (258).

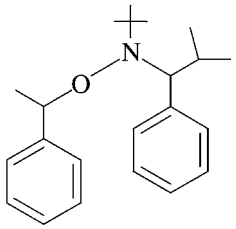

16

The newest LFRP system involves reversible addition fragmentation chain transfer (RAFT) (259). PS, PMA, and PMMA having a polydispersity of <1.3 and block copolymers containing these monomers have been produced utilizing this novel chemistry. The initiators are either thioesters or thiocarbonates (260). The RAFT process is shown in Figure 48.

Amazingly, CSIRO researchers (261) used the RAFT chemistry to make an S-nBA-S triblock copolymer having an M_n of 162,000 and a polydispersity of 1.16. This was accomplished using a difunctional RAFT reagent (thiocarbonate (**17**)). The chemistry is depicted in Figure 49.

Copolymerization. Styrene spontaneously copolymerizes with many other monomers. The styrene double bond is electronegative because of the donating effect of the phenyl ring. Monomers that have electron withdrawing substituents (eg, acrylonitrile, maleic anhydride) tend to most readily copolymerize with styrene because their electropositive double bonds are attached to the electronegative styrene double bond. Spontaneous copolymerization experiments of many different monomer pair combinations indicate that the mechanism of initiation changes with the relative electronegativity difference between the monomer pairs (262).

Copolymerization makes possible dramatic improvements in one or more properties. There is a vast amount of literature on styrene-containing copolymers

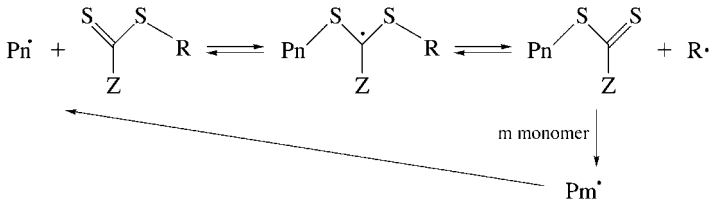

Fig. 48. Reversible addition fragmentation chain transfer (RAFT) process developed by CSIRO researchers.

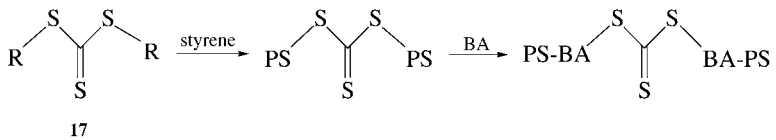

17

Fig. 49. Synthesis of S-BA block copolymers using the RAFT process.

Table 5. Free-Radical Copolymerization Reactivity Ratios for the Monomer Pairs

Monomer 2	r_1	r_2	T, °C
Acrylonitrile	0.4	0.04	60
Butadiene	0.5	1.40	50
m-Ethyl methacrylate	0.54	0.49	60
m-Divinylbenzene	0.65	0.60	60

[a] Monomer 1 = Styrene

(263). The reactivity ratios for the monomer pairs are listed in Table 5. Styrene–acrylonitrile (SAN) copolymers are large-volume thermoplastics with improved mechanical properties and heat and solvent resistance with some loss of color stability (see ACRYLONITRILE AND ACRYLONITRILE POLYMERS). The disparity of reactivity ratios shown in Table 5 implies an unequal insertion rate of the monomers into the copolymer; Figure 50 illustrates manifestations of this effect. Most SAN copolymers are manufactured at or near the azeotrope or crossover point (A in Fig. 50) to avoid significant drift in composition (Fig. 51) (264,265). SAN copolymers having as little as a 4 wt% difference in acrylonitrile content are not miscible (73). Therefore, the preparation of SAN under conditions where composition drift can occur leads to haze. Reactors have been designed to overcome composition drift problems on a commercial scale (266). All SAN copolymers produced in the United States are made in a mass or solution continuous process. The greater tendency of these copolymers to develop yellow coloration requires more attention to techniques of polymerization and devolatilization (267–270). The discoloration

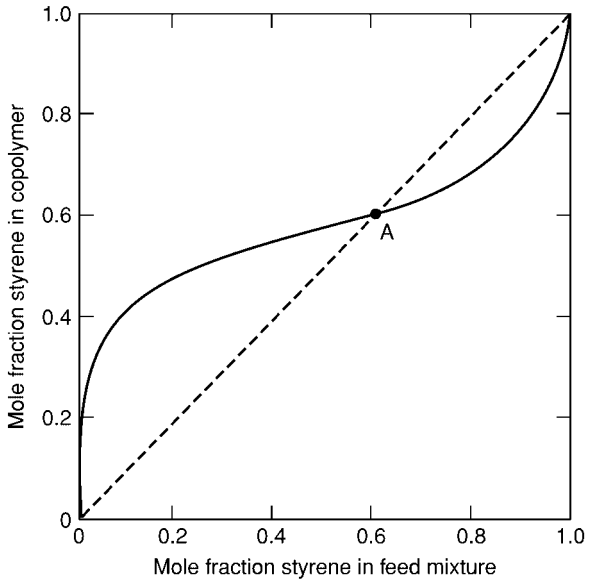

Fig. 50. Relationship between feed composition and copolymer composition of styrene acrylonitrile copolymerization.

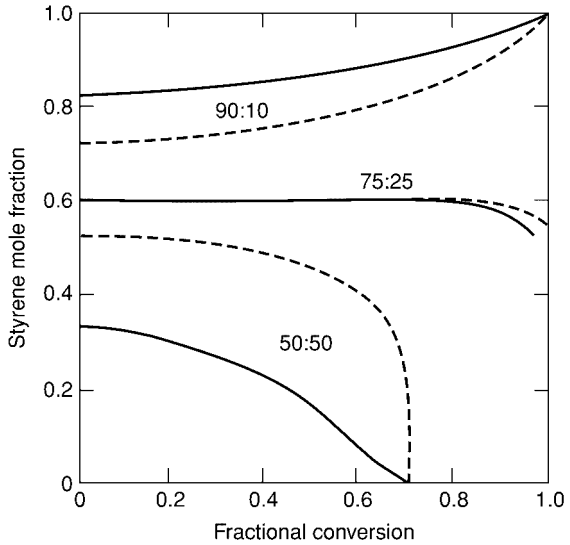

Fig. 51. Drift in monomer composition (—) and copolymer composition (—) with conversion for three initial monomer mixtures; ratios are based on wt%.

mechanism has been linked to both acrylonitrile sequence distribution in the polymer backbone (271) and the thermal decomposition of oligomers (272–275).

Copolymers with butadiene, ie, those containing at least 60 wt% butadiene, are an important family of rubbers. In addition to synthetic rubber, these compositions have extensive uses as paper coatings, water-based paints, and carpet backing. Because of unfavorable reaction kinetics in a mass system, these copolymers are made in an emulsion polymerization system, which favors chain propagation and disfavors termination (276). The result is economically acceptable rates with desirable chain lengths. Usually, such processes are run batchwise in order to achieve satisfactory particle-size distribution.

Styrene–maleic anhydride (SMA) copolymers are used where improved resistance to heat is required. Processes similar to those used for SAN copolymers are used. Because of the tendency of maleic anhydride to form alternating copolymers with styrene, composition drift is extremely severe unless the polymerization is carried out in CSTR reactors having high degrees of backmixing.

Divinylbenzene copolymers with styrene are produced extensively as supports for the active sites of ion-exchange resins and in biochemical synthesis. About 1–10 wt% divinylbenzene is used, depending on the required rigidity of the cross-linked gel, and the polymerization is carried out as a suspension of the monomer-phase droplets in water, usually as a batch process. Several studies have been reported recently on the reaction kinetics (277,278).

Polymerization of styrene in the presence of PB rubber yields a much tougher material than PS. Although the material is usually opaque and has a somewhat lower modulus, the gain in impact resistance has placed this plastic in very wide commercial usage. The polymerization is complex because the rubber has sufficient reactivity, ie, at the allylic hydrogen and addition to 1,2-vinyl units, to graft and cross-link and the polymerization system is comprised of two phases.

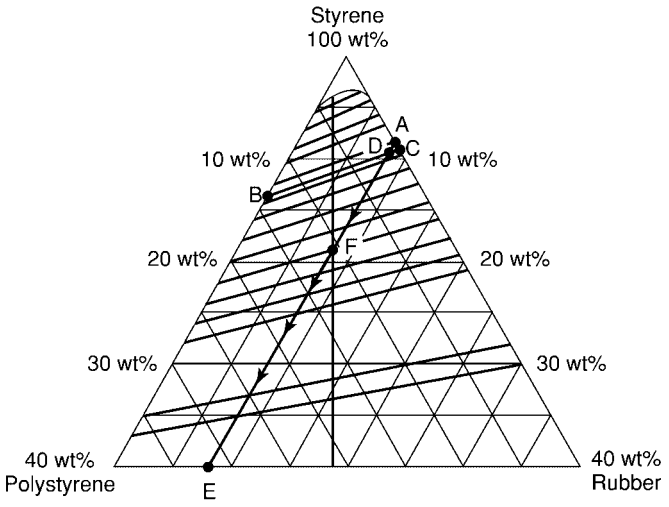

Fig. 52. Ternary phase diagram for the system styrene PS–PB rubber.

The graft copolymer of PS on polybutadiene acts as an emulsifier, stabilizing the dispersion against coalescence. Events taking place during this polymerization can be followed with the ternary phase diagram shown in Figure 52. For a feed mixture made up of 8 wt% rubber in styrene (point A) on an increment of conversion to PS (to D), phase separation occurs. Small droplets of styrene/PS, which are stabilized by the graft copolymer, are dispersed in the styrene/polybutadiene solution. The composition of the two phases is given by points B and C for the PS-rich phase and polybutadiene-rich phase, respectively. The phase-volume ratio, ie, rubber phase/PS phase, is given by the ratio DB/DC. As the reaction proceeds along the line AE, the phase composition and phase-volume ratio can be read from the tie lines. Larger droplets of PS solution form and the small, original ones remain. When the phase-volume ratio is about unity (point F), provided there is sufficient shearing agitation, the larger PS-containing droplets, which have mostly coalesced into large pools, become the continuous phase and polybutadiene-containing droplets are dispersed therein (279,280). However, the latter contain the small, original PS particles as occlusions. The particle size and size distribution are largely controlled by the applied shear rate during and after phase inversion, the viscosity of the continuous phase, the viscosity ratio of the two phases, and the interfacial tension between the phases (81,279). The viscosity parameters depend on phase compositions, polymer molecular weights, and temperatures; the interfacial tension is largely controlled by the amount and structure of the graft copolymer available at the particle surface. Phase-contrast micrographs of this phase-inversion sequence, wherein the PS phase is dark, are shown in Figure 53. If shearing agitation is insufficient, then phase inversion does not occur and the product obtained is an inter network of cross-linked rubber with PS, and its properties are much inferior. The morphology of the dispersed rubber phase remains much as formed after phase inversion, unless there is a step change in phase concentration by, eg, blending streams. Rubber-phase volume, including the occlusions, largely controls performance; for example, Table 6 illustrates Izod impact strength dependence (281).

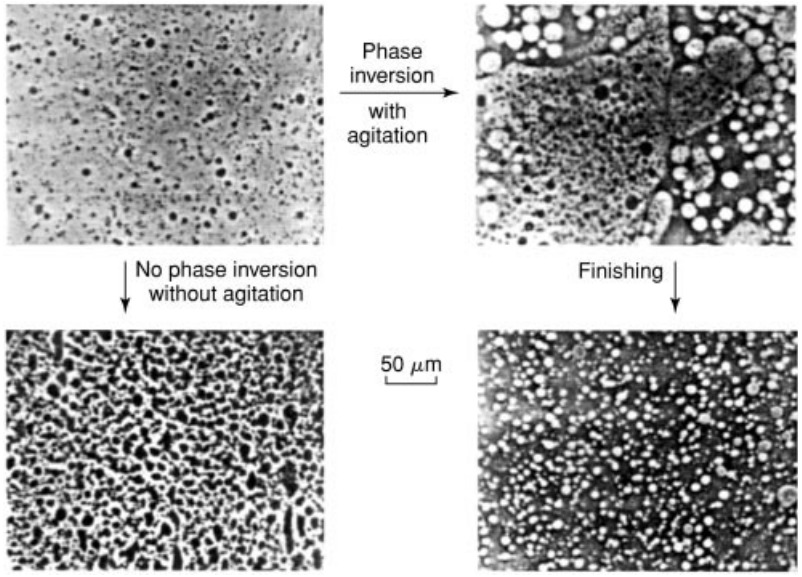

Fig. 53. Phase-contrast photomicrographs showing particle formation via phase inversion.

Once the desired particle size and morphology with sufficient graft to provide adequate adhesion between the rubber particles and the PS phase have been achieved, the integrity of the particle must be protected against deformation or destruction during fabrication by cross-linking of the polybutadiene chains. These chemical changes taking place on the rubber begin with polymerization. Either anionic or Ziegler–Natta-polymerized polybutadiene is used at 5–10 wt% styrene. If peroxide initiators are used, about half of the rubber is grafted by the time phase inversion occurs; less is grafted in the absence of peroxides (282).

Hydrogen abstraction by alkoxy radicals at any of the allylic sites yields a site for styrene polymerization, resulting in a graft (282,283). Model studies based on styrene–butadiene block copolymers show a strong influence of graft structure on particle morphology (81,82). The double bonds in polybutadiene are much less

Table 6. Dependence of Izod Impact Strength on Rubber Particle Size

Rubber particle weight average dia., μm	Izod impact strength[a], J/m[b]
0.6	48
0.8	53
1.0	64
1.5	75
2.0	91
2.5	93
3.0	99
3.5	100

[a] ASTM D256.56.
[b] To convert J/m to ft·lbf/in., divide by 53.38.

reactive than those in styrene, but as conversion exceeds ca 80% and temperature approaches or exceeds 200°C, copolymerization through the polybutadiene (1,2 units) chain seems to occur and leads to cross-linking and, hence, gel formation (284).

Since the extent of grafting of PS onto PB has such a profound effect on the properties of HIPS, there has been a significant amount of research carried out to develop an understanding of the grafting process and also the development of ways to increase the extent of grafting (60,285–288).

Commercial Polymerization Processes

Polymerization. There are two problems in the manufacture of PS: removal of the heat of polymerization (ca 700 kJ/kg (300 Btu/lb)) of styrene polymerized and simultaneously handling a partially converted polymer syrup with a viscosity of ca 10^5 mPa (= cP). The latter problem strongly aggravates the former. A wide variety of solutions to these problems have been reported. For the four mechanisms described earlier, ie, free radical, anionic, cationic, and Ziegler–Natta, several processes can be used. Table 7 summarizes the processes that have been used to implement each mechanism for liquid-phase systems. Free-radical polymerization of styrenic systems, primarily in solution, is of principal commercial interest. Suspension processes are declining in importance (289,290). Emulsion processes have been reviewed (291). The historical development of styrene polymerization processes has been reviewed (289,292,293).

Two types of reactors are used for continuous solution polymerization. The first is the continuous plug-flow reactor (CPFR), approximating in the ideal case a plug-flow reactor, and the second is the continuous-stirred tank reactor (CSTR), which ideally is isotropic in composition and temperature (see REACTOR TECHNOLOGY). The CPFR usually involves conductive heat transfer to many tubes through which a heat-transfer fluid flows. Multiple temperature zones can easily be achieved in a single reactor; agitation is provided by a rotating shaft with arms down the central axis of the tubular vessel. Reactors of this type operate for long periods and handle very high viscosity partial polymers with reliable heat-transfer coefficients. CSTRs are either of the recirculated coil configuration and rely upon conduction to the cooled jacket for heat removal or are ebullient making use primarily of evaporative cooling to achieve temperature control. The limitation

Table 7. Process vs Mechanism for Styrene Polymerization

	Mechanism			
Process	Free radical	Anionic	Cationic	Zeigler
Mass/bulk	Used for all styrene plastics	Yes	Yes	
Solution	Used for all styrene plastics	Styrene–butadiene block copolymers	Yes	Yes
Suspension	Used for all styrene plastics			
Precipitation	Yes			
Emulsion	Used for styrene–butadiene latices and ABS plastics			

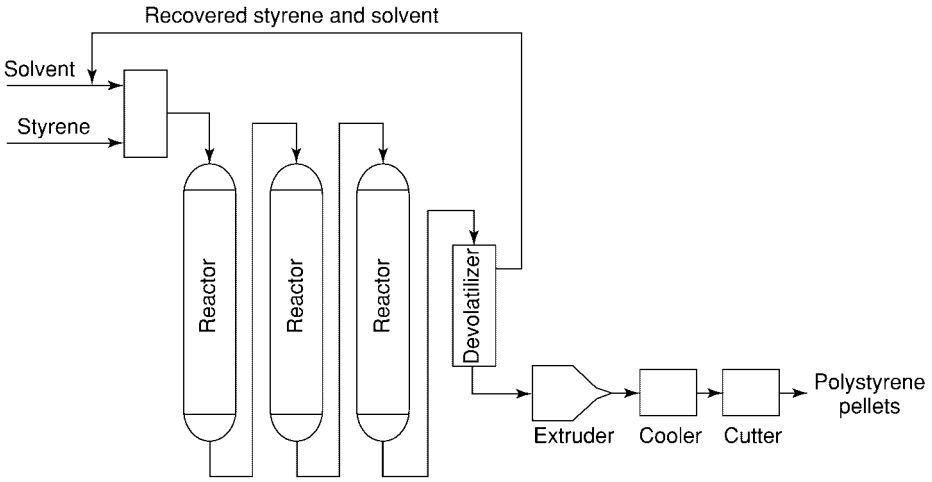

Fig. 54. Typical continuous plug-flow reactor (CPFR) polymerization process.

of this reactor occurs at high viscosity, when the rate of vapor disengagement is exceeded by the rate of vapor generation and the ability to mix in the condensed vapor. Typically, this limit occurs at 60–70 wt% solids. Figures 54 and 55 illustrate typical processes based on these two types of reactors. Most GPPS is manufactured in the United States in such facilities. The CPFR process (Fig. 54) typically uses up to 20 wt% ethylbenzene mainly to reduce viscosity, but also to eliminate reactor fouling. The three reactors may each be subdivided into three temperature-control zones, which allows for flexible control of the molecular weight distribution of the polymer as well as optimum output per reactor volume. Temperatures are 100–170°C. At ca 80 wt% solids, the partial polymer is heated from 180°C to 240°C before being devolatilized upon entering a vacuum tank. The recovered solvent and monomer are continuously recycled to the feed. The molten polymer leaves the vacuum tank and is stranded, cooled, and chopped into pellets for shipping. The CSTR process (Fig. 7) differs in that it is typically a single reactor and, therefore,

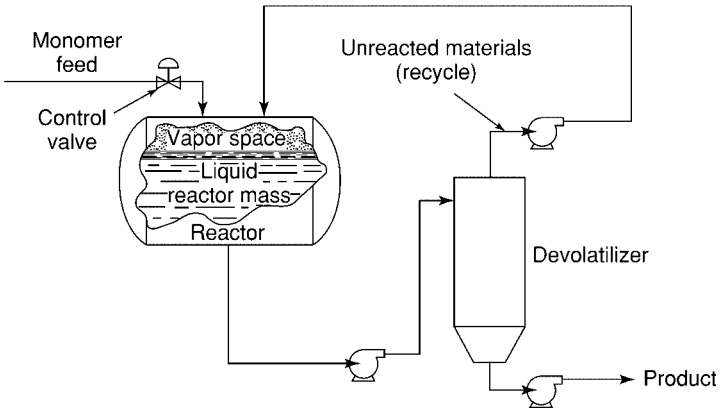

Fig. 55. Typical CSTR polymerization process.

involves a single temperature zone and operates at ca 60 wt% solids, requiring a large polymer heater to achieve adequate devolatilization (294,295). The need for a large polymer heater to achieve adequate devolatilization can be eliminated by adding a CPFR after the CSTR to carry the conversion to high solids.

There has been some research aimed at continuously converting monomer completely to polymer using reactive extrusion (296). However, this process has not yet been commercialized.

Rubber-modified PS manufacture places several additional demands: (*1*) dissolving ca 5–10 wt% polybutadiene in styrene, often a 10- to 20-h process; (*2*) shear conditions to achieve phase inversion and the desired particle size for a given product; (*3*) control of phase compositions to produce the desired particle morphology; and (*4*) sufficient time and temperature at the end of the process to achieve the necessary cross-linking, gel formation, and swelling index. Graft copolymer formation occurs throughout the polymerization, and sufficient amount of graft copolymer for phase stability is necessary at phase inversion. In the case of a CPFR system (Fig. 54), only addition of a rubber dissolver is needed to meet these requirements. For a CSTR-based system (Fig. 55), multiple reactors in series are required to avoid rapid shifts in phase compositions on mixing of one reactor effluent with the next reaction contents with loss of desirable morphology (297,298). Figure 56 shows a multizone CSTR reactor system. Phase inversion and particle sizing is accomplished in the first-stage reactor with the effluent entering a single-tank, baffled reactor operating as five stages with a common vapor space. An alternative is three CSTR reactors in series, followed by an adiabatic reactor to achieve high solids content (297). The multiple stages are necessary to achieve favorable

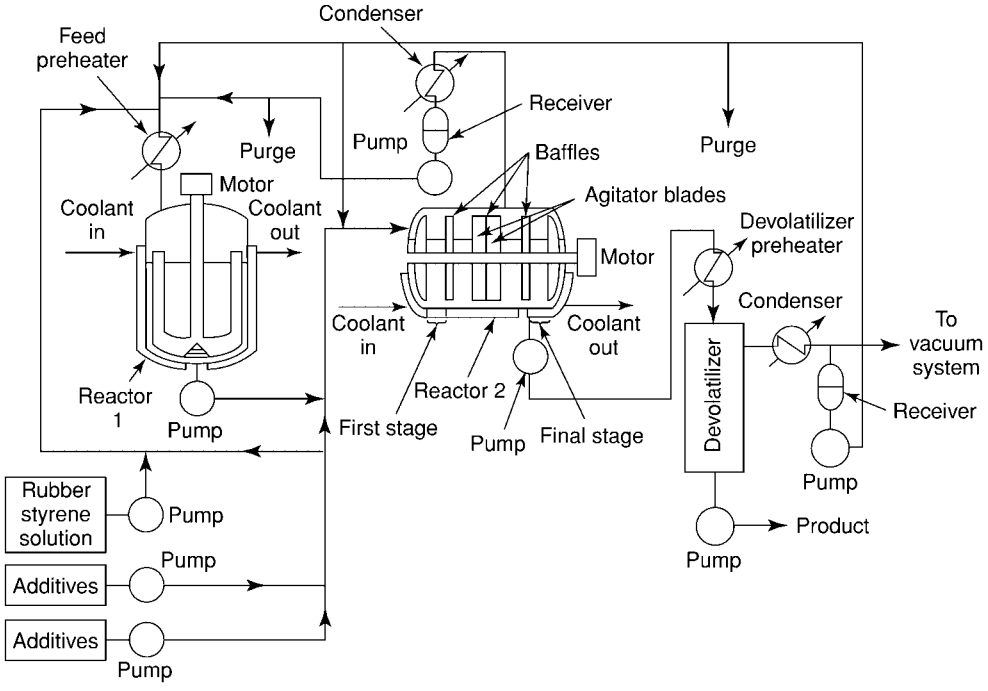

Fig. 56. Typical staged CSTR process for HIPS.

rubber-particle morphology with CSTRs; CPFR systems inherently avoid sudden phase-composition changes, unless severe internal backmixing is allowed to occur.

Generally, phase inversion and particle sizing occurs in the first reactor. Grafting rate is highest initially, and the amount formed is adequate to stabilize the particles. The shear field in the reactor is critical to the control of particle size as well as to meet the minimum shear rate for phase inversion, without which the product consists of a continuous cross-linked rubber network with markedly inferior properties (279,280). After the particles are formed and sized, only gentle agitation is applied to aid heat transfer without disturbing the particle structure. Conditions that produce the desired PS-phase molecular weight are used. Prior to devolatilization, the partial polymer is heated to ca 200°C to cross-link the rubber chains in order to protect the rubber particles from the very high shear fields during fabrication. Stranding, cooling, and chopping into pellets follows.

Polybutadiene rubbers are used almost exclusively as reinforcing agents for styrenic plastics. The very low glass-transition temperature (−80°C or lower) gives good low temperature properties, and the allylic hydrogen atom and weakly active double bonds can provide the desired degree of grafting and cross-linking. Other rubbers have been used; acrylates, ethylene–propylene–diene rubbers, polyisoprene, and polyethylene have been reported, but with limited commercial success because of their low chemical reactivity, not withstanding their acceptable glass-transition temperature (299).

Devolatilization. Current bulk polymerization processes convert styrene to about 80%. The polymer syrup exits the polymerization reactor at about 170°C. The most common devolatilization technology involves increasing the temperature of the syrup to >230°C by passage through a heat exchanger connected to a vacuum tank. The syrup foams, forming strands which fall into a vacuum tank at 5–10 mm Hg as they exit the heat exchanger. An equilibrium of styrene in the polymer and in the vapor phase takes place, which is dependent upon the temperature and the pressure in the tank. Figure 57 shows the vapor–polymer equilibrium partitioning data (calculated) for styrene in PS at various levels of vacuum (one-stage devolatilizer) (300). Typically, devolatilizers operate at ca 230–240°C and 5–10 mm Hg. Therefore, the level of residual styrene monomer left in the polymer is typically in the range of 300–500 ppm. If the polymer temperature is increased to greater than 240°C, polymer degradation begins to take place resulting in the formation of styrene monomer. Asahi researchers have solved this problem by stabilizing the polymer against unzipping by the addition of a special stabilizer (**18**), thus allowing higher temperature devolatilization to be carried out (301).

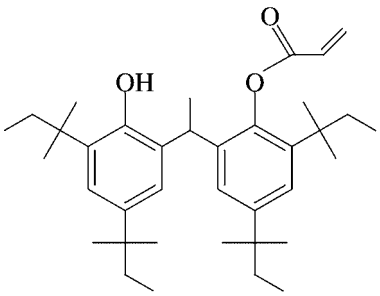

18

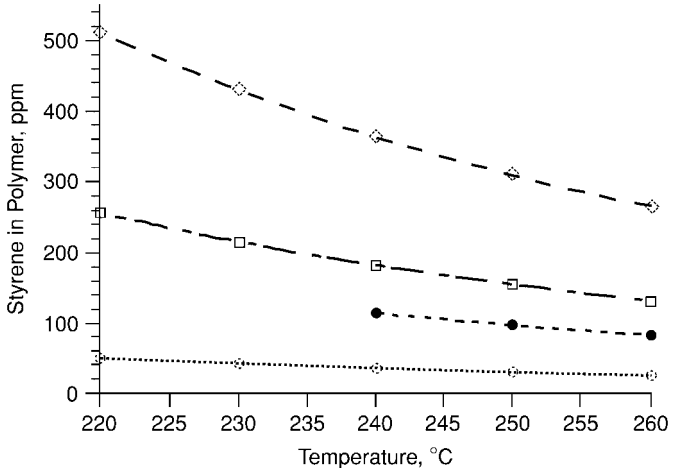

Fig. 57. Vapor-polymer equilibrium partitioning data for styrene in PS vs temperature and pressure. ···○··· 133.3 Pa; -□—667 Pa;—◇—1.33 kPa; --●-- 667 Pa + 10% water. To convert Pa to mm Hg, divide by 133.3.

Some foods packaged in PS are extremely sensitive to taste (eg, chocolate chip cookies). These sensitive applications require PS having residual styrene monomer levels below 200 ppm. It is not feasible to consistently lower the styrene level to <200 ppm without special techniques.

A new technology for lowering residuals in PS being commercialized by Dow is centrifugal devolatilization in a rotating packed bed (302,303). The basic concept involves pumping the molten PS into the center of an evacuated spinning rotor packed with metal mesh. Centrifugal force quickly pushes the polymer through the high surface area mesh where it coats the metal and volatiles quickly diffuse from the thin polymer film. The centrifugal force continues to force the polymer out of the metal mesh packing against the exterior surface of the centrifuge having a circumferential set of die holes. After being extruded from the die holes, the polymer strands are cut into pellets as the rotor rotates past a slowly moving, continuous knife blade. A drawing of the centrifugal devolatilizer is shown in Figure 58.

A very effective way to get residual styrene monomer levels below equilibrium is to replace the styrene in the vapor phase with something else. Generally, it is preferred that the material in the vapor phase be condensable, nontoxic, low cost, easily separable from the recycle, and inert (eg, water). However, simply bleeding the replacement material into the vapor space of the devolatilizer would still require significant residence time to reach equilibrium. A way to expedite the equilibrium process is to mix the replacement material with the molten polymer (304). Then as the material vaporizes in the molten polymer, it nucleates bubbles stripping styrene from the polymer while creating a vapor phase composed mainly of the stripping material. Stripping materials that have been used include nitrogen, (305), methanol (306), and water (307).

Another technique to expedite the transport of the volatile components from the molten polymer is to increase the number and rate of bubbles formed (308).

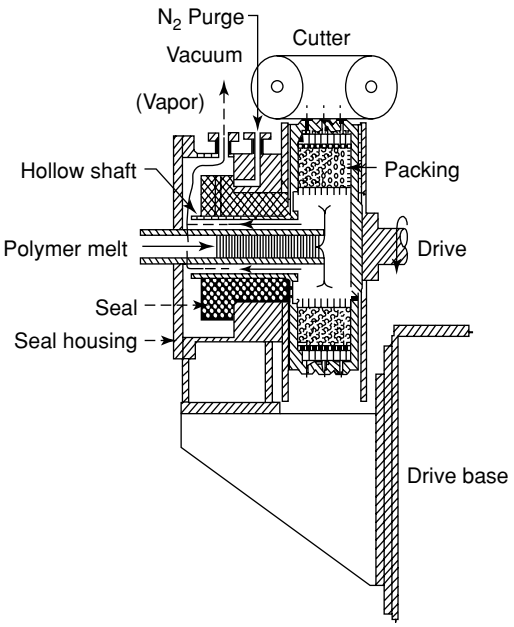

Fig. 58. Drawing of centrifugal devolatilizer being used by Dow.

Techniques that have been used to increase the number of bubbles and their rate of formation (nucleation) are the addition of chemical nucleating agents (309) and ultrasound (310). Nucleation of bubbles in the molten polymer can help expedite achievement of equilibrium in conventional falling strand devos. However, this facilitation mechanism can not get below equilibrium and thus has marginal value.

Chemically Removing Residual Monomer. Some researchers have tried to lower the level of residual styrene monomer by chemical means. The idea of adding something to molten PS that scavenges residual styrene monomer has been the subject of extensive R&D efforts over the past several decades. However, there is an inherent difficulty in this concept; that is, small molecules in very low concentration must diffuse together, find each other, and couple together in a viscous polymer. The obvious way to overcome this difficulty is to use the scavenger in higher than stoicheometric concentration. This introduces several new problems including contamination of the polymer with a new material and increased raw material costs. Styrene scavenger compounds that have been patented include unsaturated fatty acids (311) and aldehydes (312), sulfonyl hydrazides (313), cyclopentadienes (311), K-resin (314), peroxides (315), and terpenes (316).

Another option for lowering residual styrene monomer is to carry the polymerization up to high conversion. Typically, continuous bulk polymerization processes produce partial polymer syrups at about 65–80% solids. The unreacted styrene that remains is removed by evaporation. If the solids content of the polymer could be taken higher, the level of residual styrene in the polymer would be lower, especially when using a one-stage devolatilizer. In suspension polymerization, devolatilization is not even required because styrene is polymerized to $>$99.9% monomer conversion. If it were possible to polymerize styrene to very high

conversion in bulk polymerization processes, significantly lower residual styrene monomer could be achieved. Because of viscosity constraints, bulk polymerization reactors cannot operate at >80% solids. To achieve >99% monomer conversion while maintaining the solids <80% would require high levels of solvent. The problem with solvents is chain transfer. Going above 95% conversion in ethylbenzene results in an exponential increase in polydispersity due primarily to chain transfer effects. A high conversion bulk styrene polymerization process resulting in the formation of low residual PS has been patented, which solves the viscosity problem and allows going to >99.9% solids by finishing the polymerization off in an extruder (317). Extruders are not very effective heat exchangers, yet are designed for handling high viscosity materials. Thus, Kelly carried out the polymerization of pure styrene monomer without the use of a solvent in a conventional polymerization reactor to normal solids levels and then fed the partial polymer into an extruder where he finished off the polymerization. He used a mixture of initiators having different half-lives so that radicals were continuously generated. Recently, free-radical polymerization of styrene directly in an extruder using 1 wt% peroxide initiator was analyzed (318). They were not successful in making PS having a molecular weight >100,000. They got around this problem by attaching a prepolymerization reactor to the front end of the extruder to polymerize to 25% solids to make high M_w PS. The low M_w PS then made in the extruder giving them a bimodal PS. The conversion they achieved in the extruder was 98–99%.

A final technique that has been utilized to chemically remove residual styrene in PS is radiation treatment. Both beta (e-beam) and gamma radiation have been tried. E-beam appears to be the most effective form of radiation and is most suitable for continuous use (319,320). The e-beam ruptures C—H bonds, resulting in the formation of PS radicals. These radicals are very reactive and scavenge unreacted monomer. However, if no styrene is in the vicinity of the PS radical, it can do other things such as couple with another PS radical or react with oxygen. Currently, electron beam treatment of polymers is used commercially for elastomer cross-linking (wire/cable coatings) but not for monomer reduction.

Polystyrene treated with 1–4 Mrad of e-beam radiation at temperatures between 25 and 200°C shows an optimum irradiation temperature between 80 and 150°C (Fig. 59). It is interesting that all dosages tested have a temperature range for maximum effectiveness, which drifts toward lower temperature as the dosage increases (321). At all temperatures studied, weight-average molecular weight increases with e-beam dose (Fig. 60) (321).

Fabrication.

Injection Molding. There are two basic types of injection-molding machines in use: the reciprocating screw and the screw preplasticator (322). Their simple design, uniform melt temperature, and excellent mixing characteristics make them the preferred choice for injection molding. Machines with shot capacities up to 25 kg for solid injection-molded parts and 65 kg for structural foam parts are available (323,324). Large solid moldings include automotive dash panels, television cabinets, and furniture components. One-piece structural foam parts weighing 35 kg or more are molded for increased rigidity, strength, and part weight reduction (325) (see PLASTICS PROCESSING).

The injection-molding process is basically the forcing of melted polymer into a relatively cool mold where it freezes and is removed in minimum time. The shape

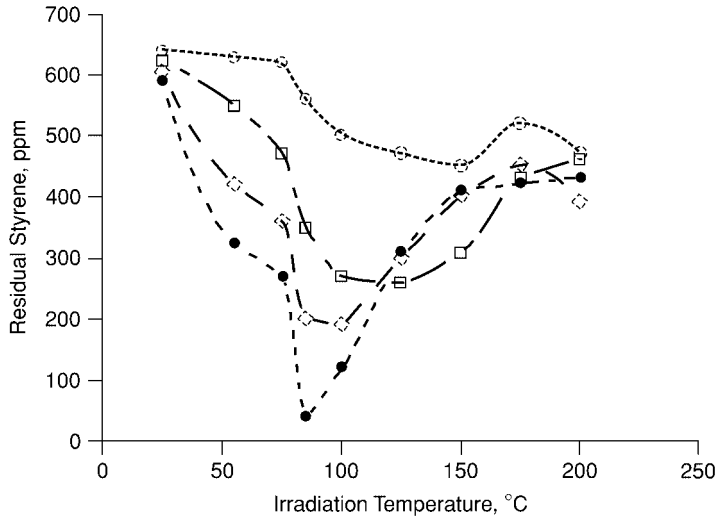

Fig. 59. Performance of different e-beam doses vs temperature (321). --○-- 10 kGy; -□—20 kGy; -◇—30 kGy; --●-- 40 kGy. To convert kGy to Mrad, divide by 10.

of a molding is defined by the cavity of the mold. Quick entry of the material into the mold followed by quick setup results in a significant amount of orientation in the molded part. The polymer molecules and, in the case of heterogeneous rubber-modified polymers, the rubber particles tend to be highly oriented at the surface of the molding. Orientation at the center of the molding tends to be significantly less because of the relaxation of the molten polymer.

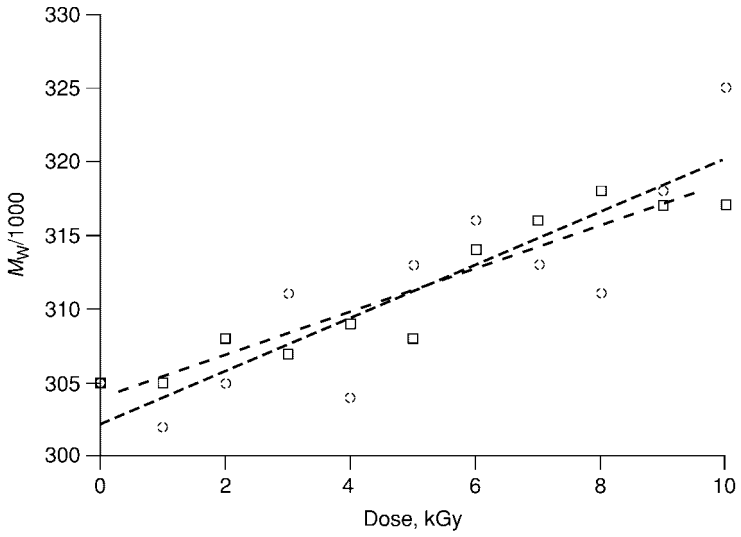

Fig. 60. Effect of dose on M_w at ambient and elevated temperature (321). --○-- 25°C; -□—85°C. To convert kGy to Mrad, divide by 10.

The anisotropy that develops during the molding operation is detrimental to the performance of the fabricated part in several ways. First, highly oriented moldings, which form particularly if low melt temperatures are used, exhibit good gloss, have an abnormally narrow use temperature range causing early warping, and, perhaps most importantly, tend to be brittle even though the material is inherently capable of producing tough parts (326). However, this development of polymer orientation during molding can also be used to advantage, as in the case of rotational orientation during the molding operation (327).

The achievement of isotropic moldings is also important when the molded part is to be decorated, ie, painted, metallized, etc Highly oriented parts that have a high frozen-in internal stress memory tend to give rise to rough or distorted surfaces as a result of the relaxing effect of the solvents and/or heat. For electroplating ABS moldings, it is particularly important to obtain isotropic moldings. Isotropy can be achieved by the use of a high melt temperature, a slow fill speed, a low injection pressure, and a high mold temperature (127,128,328,329).

Injection molding of styrene-based plastics is usually carried out at 200–300°C. For ABS polymers, the upper limit may be somewhat less, since these polymers tend to yellow somewhat if too high a temperature and/or too long a residence time are imposed.

To obtain satisfactory moldings with good surface appearance, contamination, including that by moisture, must be avoided. For good molding practice, particularly with the more polar styrene copolymers, drying must be part of the molding operation. A maximum of 0.1 wt% moisture can be tolerated before surface imperfections appear.

For achieving appropriate economics, injection-molding operations are highly automated and require few operating personnel (322). Loading of the hopper is usually done by an air-conveying system; the pieces are automatically ejected, and the rejects and sprues are ground and reused with the virgin polymer. Also, hot probes or manifold dies are used to eliminate sprues and runners.

Extrusion. Extrusion of styrene polymers is one of the most convenient and least expensive fabrication methods, particularly for obtaining sheet, pipe, irregular profiles, and films. Relatively small extruders, eg, 11.5 cm diameter, can produce well over 675 kg/h of polymer sheet. Extrusion is also the method for plasticizing the polymer in screw injection-molding machines and is used to develop the parison for blow molding. Extrusion of plastics is also one of the most economical methods of fabrication, since it is a continuous method involving relatively inexpensive equipment. The extrusion process has been studied in great detail (330,331). Single-screw extruders work extremely well with styrene-based plastics. Machines are available with *L*/*D* (length-to-diameter) ratios of 36:1 or more. Some of the longer *L*/*D* extruders are used with as many as three vent zones for removal of volatiles, often eliminating the necessity for predrying as is practiced with hygroscopic materials, eg, SAN and ABS. Where venting is inadequate, these polymers must be predried to a maximum moisture content of 0.03–0.05 wt% to obtain high quality sheet (see FILMS AND SHEETING).

Many rubber-modified styrene plastics are fabricated into sheet by extrusion primarily for subsequent thermoforming operations. Much consideration has been given to the problem of achieving good surface quality in extruded sheet (332,333).

Excellent surface gloss and sheet uniformity can be obtained with styrene-based polymers.

Considerable work has been done on mathematic models of the extrusion process, with particular emphasis on screw design. Good results are claimed for extrusion of styrene-based resins using these mathematical methods (331,334).

With the advent of low cost computers, closed-loop control of the extrusion system has become commonplace. More uniform gauge control at higher output rates is achievable with many commercial systems (335,336).

Lamination of polymer films, both styrene-based and other polymer-types, to styrene-based materials can be carried out during the extrusion process for protection or decorative purposes. For example, an acrylic film can be laminated to ABS sheet during extrusion for protection in outdoor applications. Multiple extrusion of styrene-based plastics with one or more other plastics has grown rapidly in the last 10 years.

Thermoforming and Orientation. Thermoforming of HIPS and ABS extruded sheet is of considerable importance in several industries. In the refrigeration industry, large parts are obtained by vacuum-forming extruded sheet. Vacuum forming of HIPS sheet for refrigerator-door liners was one of the most significant early developments promoting the rapid growth of the whole family of HIPS. When a thermoplastic polymer film or sheet is heated above its glass-transition temperature, it can be formed or stretched. Under controlled conditions, new shapes can be controlled; also, various amounts of orientation can be imparted to the polymer film or sheet for altering its mechanical behavior.

Thermoforming is usually accomplished by heating a plastic sheet above its softening point and forcing it against a mold by applying vacuum, air, or mechanical pressure. On cooling, the contour of the mold is reproduced in detail. In order to obtain the best reproduction of the mold surface, carefully determined conditions for the plastic-sheet temperature, ie, heating time and mold temperature, must be maintained.

Several modifications of thermoforming plastic sheet have been developed. In addition to straight vacuum forming, there are vacuum snapback forming, drape forming, and plug-assist-pressure-and-vacuum forming. Some combinations of these techniques are also practiced. Such modifications are usually necessary to achieve more uniform wall thickness in the finished deep-draw sections. Vacuum forming can also be continuous by using the sheet as it is extruded. An example of this technology is practiced with several high speed European lines in operation in the United States. Precise temperature conditioning allows carefully controlled levels or orientation in the finished part (337).

Thermoforming is perhaps the process with the lowest unit cost. Examples of thermoformed articles are refrigerator-door and food-container liners, containers for dairy products, luggage, etc Some of the largest formed parts are camper/trailer covers and liners for refrigerated-railroad-car doors (338).

Orientation of styrene-based copolymers is usually carried out at temperatures just above T_g. Biaxially oriented films and sheet are of particular interest. Such orientation increases tensile properties, flexibility, toughness, and shrinkability. PS produces particularly clear and sparkling film after being oriented biaxially for envelope windows, decoration tapes, etc Oriented films and sheet of

styrene-based polymers are made by the bubble process and by the flat-sheet or tentering process. Fibers and films can be produced by uniaxial orientation (339) (see FILMS AND SHEETING).

Blow Molding. Blow molding is a multistep fabrication process for manufacturing hollow symmetrical objects. The granules are melted and a parison is obtained by extrusion or by injection molding. The parison is then enclosed by the mold, and pressure or vacuum is applied to force the material to assume the contour of the mold. After sufficient cooling, the object is ejected.

Styrene-based plastics are used somewhat in blow molding but not as much as linear PE and PVC. HIPS and ABS are used in specialty bottles, containers, and furniture parts. ABS is also used as one of the impact modifiers for PVC. Clear, tough bottles with good barrier properties are blow-molded from these formulations.

Polystyrene or copolymers are used extensively in injection blow molding. Tough and craze-resistant PS containers have been made by multiaxially oriented injection-molded parisons (340). This process permits the design of blow-molded objects with a high degree of controlled orientation, independent of blow ratio or shape.

Additives. Processing aids, eg, plasticizers and mold-release agents (see ABHERENTS), are often added to PS. Even though PS is an inherently stable polymer, other compounds are sometimes added to give extra protection for a particular application. Rubber-modified polymers containing unreacted allylic groups are very susceptible to oxidation and require carefully considered antioxidant packages for optimum long-term performance. Ziegler–Natta-initiated polybutadiene rubbers are especially sensitive in this respect, since they often contain organocobalt residues from the catalyst complex. For food-contact applications, the additives must be FDA approved. Important additives used in styrene plastics are listed in Table 8.

Economic Aspects

Most of the styrene monomer manufactured globally goes into the manufacture of PS and its copolymers; thus the price of the two tend to parallel each other (Fig. 61).

Polystyrene is a global product with North America, Western Europe, and the Pacific consuming most of the world's production (Fig. 62). The global PS production capacity generally parallels the demand for the material (Fig. 63). However, the trend over the last 15 years has been toward narrowing the gap between capacity and demand in an effort to maximize the profitability of the business.

Characterization

Four modes of characterization are of interest: chemical analyses, ie, qualitative and quantitative analyses of all components; mechanical characterization, ie, tensile and impact testing; morphology of the rubber phase; and rheology at

Table 8. Additives Used in Styrene Plastics

Type	Compounds	Examples	Amount (wt%)	Comments
Plasticizers	Mineral oil		<4	all cause loss of heat-distortion temperature
	Phthalate esters			
	Adipate esters			
Mold-release agents agents	Steric acid		0.1	Many mold-release agents cause yellowness of haze
	Metal sterates			
	Sterate esters			
	Silicones			
	Amide waxes		3	
Antioxidants	Alkylated phenols	Ionol	1	Synergism sometimes achieved with multiple use
	Phosphite esters	Tris(nonylphenyl) phosphite	1	
	Thioesters	Dilaurylthio-dipropionate	1	
Antistatic agents	Quaternary ammonium compounds		2	
uv stabilizers	Benzotriazoles	Tinuvin P	0.25	
	Benzophenones			
Ignition supression agents	Halogenated compounds			Synergism sometimes achieved with multiple use
	Antimony oxide			
	Aluminum oxide			
	Phosphate esters			

a range of shear rates. Other properties measured are stress-crack resistance, heat-distortion temperatures, flammability, creep, and others depending on the particular application (341).

Since plastics are almost invariably modified with one or more additives, there are three components of chemical analysis: the high molecular weight portion, ie, the polymer; the additives, ie, plasticizer and mold-release agent; and the residuals remaining from the polymerization process. The high molecular weight portion is best characterized using gpc which gives molecular weight and polydispersity information. If the gpc is equipped with a diode-array detector, chromophores responsible for polymer discoloration can be located (177). The additives in the polymer are best characterized by extracting them from the polymer and analyzing the extract using high performance liquid chromatography (342). Figure 5 illustrates typical molecular weight distribution curves from gpc, and Figure 64

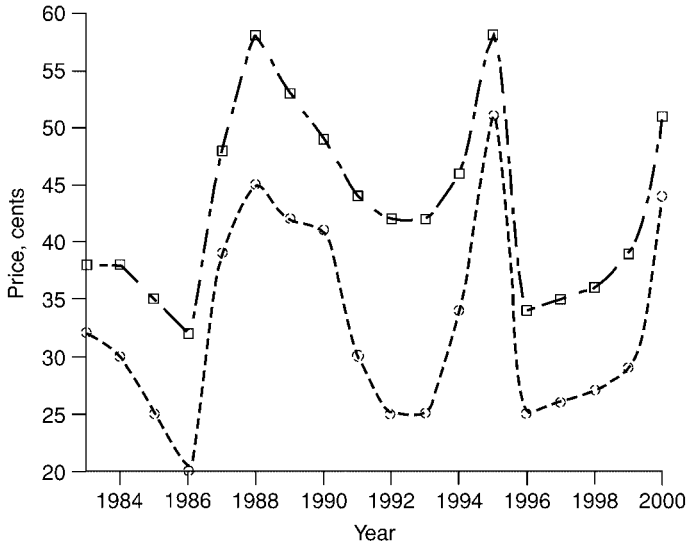

Fig. 61. Historical comparison of styrene monomer and GPPS pricing. ···○··· Styrene monomer; -□—Polystyrene.

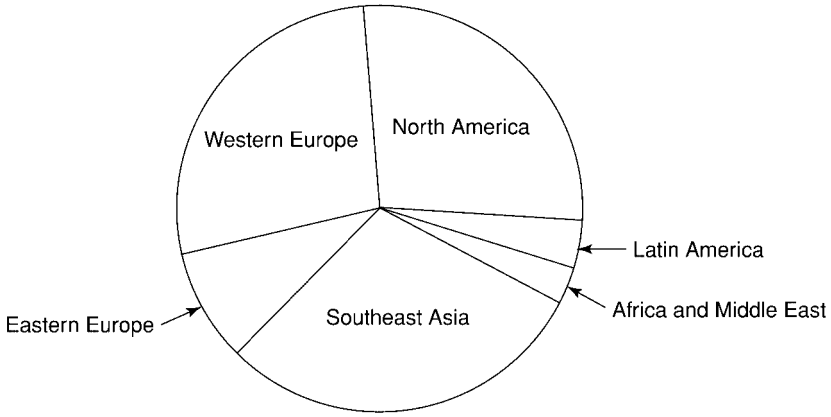

Fig. 62. Global consumption of PS by geographical area (145).

shows a capillary gas chromatogram for determining residuals. Chemical characterization techniques utilized for styrenic polymers are summarized in Table 9. Mechanical testing is carried out according to the methods listed in Table 10.

Rubber particle-size distribution is usually measured with a Coulter counter or directly from electron photomicrographs (110,343); the latter also gives details of particle morphology. Rheological studies are made with a modified tensile tester with capillary rheometer (ASTM D1238-79) or with the powerful Rheometrics mechanical spectrometer (344). For product specifications, a simple melt-flow test is used (ASTM D1238 condition G) with a measurement of the heat-distortion

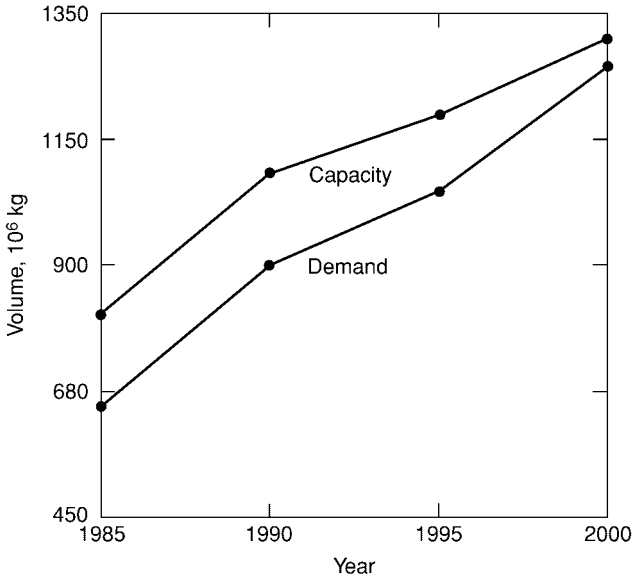

Fig. 63. Global demand vs capacity for PS since 1985 (145).

temperature (ASTM D1525). These two tests, with solution viscosity as a measure of molecular weight, have been used historically to characterize PS. However, molecular weight distribution and residuals analyses, in general, have replaced them.

Health and Safety Factors

In pellet form, styrene-based plastics have a very low degree of toxicity (345). Under normal conditions of handling and use, they should pose no unusual problems from ingestion, inhalation, or eye or skin contact. Heating of these polymers usually results in the release of some vapors. The vapors contain some styrene [TLV = 100 ppm (1974); human detection, 5–10 ppm] and, in the case of styrene–acrylonitrile copolymers, some acrylonitrile [TLV = 2 ppm (1978)] as well as very low levels of degraded and oxidized hydrocarbons and additives. The warning properties of styrene and any oxidized organics are such that the vapors normally can be detected by humans at very low levels, and hazardous concentrations are usually irritating and obnoxious. Nevertheless, adequate ventilation should be provided.

Styrene polymers burn under the right conditions of heat and oxygen supply. This can occur even when they are modified by addition of ignition-suppression chemicals. Once ignited, these polymers may burn rapidly and produce a dense black smoke. Combustion products from any burning organic material should be considered toxic. Ignition temperatures of several styrenic polymers are listed in Table 11. Fires can be extinguished by conventional means, ie, water and water fog.

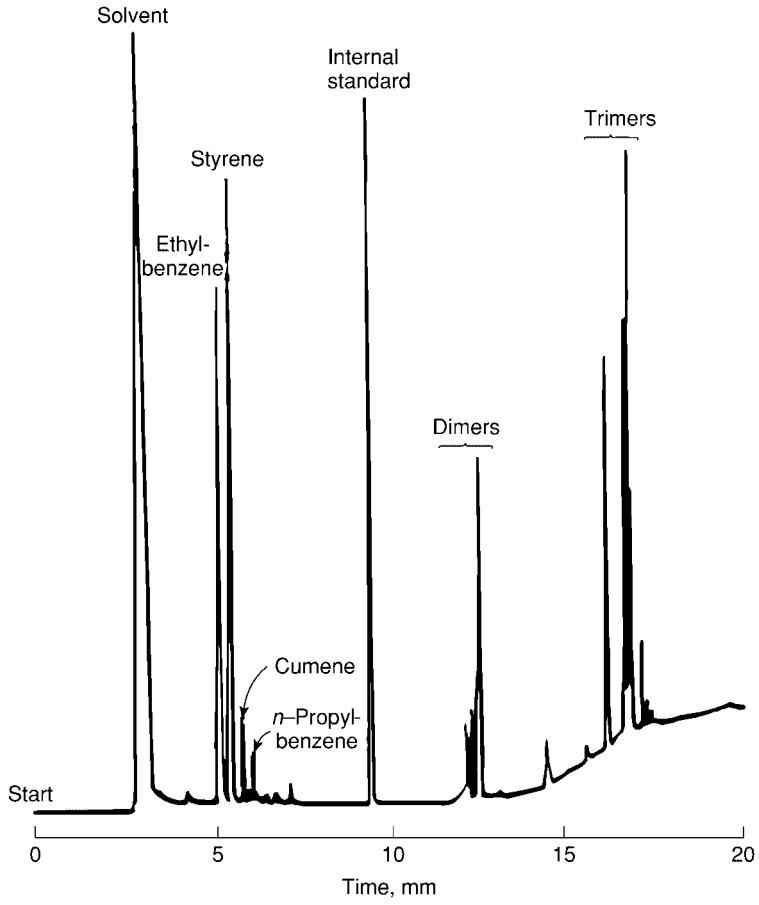

Fig. 64. Capillary gas chromatogram showing residuals in PS.

Table 9. Chemical Characterization Techniques[a]

High molecular weight component		Additive		Residuals	
Variable	Method	Variable	Method	Variable	Method
Molecular weight	Solution viscometry	Mineral oil	gc/hplc	Styrene	gc
Molecular weight distribution	gpc	Phthalate esters	gc	Solvents	gc
Copolymer composition	ir	Stearates	ir	Oligomers	gc
Rubber content	ir	Other	hplc		
Graft yield	solubility				

[a]gpc = gel-permeation chromatography; gc = gas chromatography; hplc = high performance liquid chromatography; ir = infrared analysis.

Table 10. Mechanical Tests on PS

Test	ASTM method
Stress–strain	
Tensile	D638
Compression	D695
Flexural	D790
Impact	
Izod	D256
Dart	D3029
Hardness	D785
Creep	D2990

Table 11. Ignition Temperatures and Burnhing Rates of Styrene-Based Polymers[a]

Polymer	Minimum flash-ignition temperature, °C	Minimum self-ignition temperature, °C	Burning rate[b], cm/s
Polystyrene			
General–purpose	345–360	488–496	<0.06
Rubber–modified	385–399	435–474	<0.06
Styrene–acrylonitrile copolymer	366	454	<0.06
Acrylonitrile–butadiene–styrene	404	>404	<0.06

[a]Test specimens for burning rate data were 1.27 × 15.24 × 0.318 cm^3. Descriptions of burning rate and other flammability characteristics developed from small-scale laboratory testing do not reflect hazards presented by these or any other materials under actual fire conditions.
[b]In a horizontal position.

Uses

PS Foams. The early history of foamed PS is given in Reference 346 and the theory of plastic foams is discussed in Reference 347. Dow became the first to commercially manufacture PS-extruded foam board for home insulation under the trade name Styrofoam (348). Foamable PS beads were developed in the 1950s by BASF under the trademark of Styropor (349–351). These beads, made by suspension polymerization in the presence of blowing agents such as pentane or hexane, or by post-pressurization with the same blowing agents, have had an almost explosive growth, with 200,000 metric tons used in 1980. Some typical physical properties of PS foams are listed in Table 12 (see FOAMED PLASTICS). Some believe that there are unlimited new opportunities for the development of new foam materials (352).

The following are commercially significant foamed PSs. Extruded planks and boards in the density range of 29 kg/m^3 and largely flame retardant are used for low temperature thermal insulation, buoyancy, floral display, novelty, packaging, and construction purposes. Foamed boards and shapes from foaming-in-place (FIP) beads (density 16–32 kg/m^3) are used for packaging, buoyancy, insulation, and numerous other applications. Batch molding of boards and shapes as well as automated molding of continuous planks are used. Extruded foamed PS sheet

Table 12. Characteristics Properties of Some Polystyrene Foams

Property	Styrofoam[a], extruded	Bead, board-molded	Foam sheet	ASTM
Density, kg/m^3[b]	35	32	96	
Compressive strength, kPa[c]	310	207–276	290	D1621
Tensile strength, kPa[c]	517	310–379	2070–3450	D1623
Flexural strenght, MPa[d]	1138	379–517		D790
Thermal conductivity, W/(m·K)[e]	0.030	0.035	0.035	C177
Heat distortion, °C	80	85	85	

[a]Registered trademark of The Dow Chemical Co.
[b]To convert kg/m^3 to lb/ft^3, multiply by 0.0624.
[c]To convert kPa to psi, multiply by 0.145
[d]To convert MPa to psi, multiply by 145.
[e]To convert W/(m·K) to (Btu·in.)/(h·ft·^{2}°F), multiple by 6.933.

17 mm thick with densities of 64–160 kg/m^3 are used largely in packaging applications. Extremely fine cell size is required for texture and strength. Special nucleating agents are employed for this purpose, eg, polymers of styrene and maleic anhydride, citric acid–sodium bicarbonate mixtures, and talc (353). High density (35–64 kg/m^3) extruded planks are used for heavy-duty structural applications. Styrene copolymer foams containing, eg, acrylonitrile for gasoline resistance are made either by extrusion or from beads. High density (480–800 kg/m^3) injection-molded objects are made from mixtures of FIP beads and PS granules or more commonly HIPS or ABS with a chemical blowing agent, eg, azodicarbonamide. These moldings have a high density skin of essentially PS and a foamed core. Foamable ABS systems, eg, laminates with ABS skins and a heat-foamable core, are used for structural applications, as in car body parts (354). Of growing commercial significance is coextruded, foam-core ABS pipe (355,356). Reducing the density of the foam core by up to one-half and using a chemical blowing agent results in about a 20% overall pipe weight and raw material usage reduction. Syntactic foams are combinations of foamable beads, eg, expandable PS or SAN copolymers. These are mixed with a resin, usually thermosetting, which has a large exotherm during curing, eg, epoxy or phenolic resins (357). The mixture is then placed in a mold and the exotherm from the resin cure causes the expandable particles to foam and forces the resin to the surface of the mold. A typical example is expandable PS in a flexible polyurethane-foam matrix used in cushioning applications (358). Sandwich panels are made either by foaming beads between the skin materials or by adhering skins to planks cut to precise dimensions. Foamed PS beads are admixed with concrete for lightweight masonry structures (359).

Extruded Rigid Foam. In addition to low temperature thermal insulation, foamed PSs are used for insulation against ambient temperatures in the form of perimeter insulation and insulation under floors and in walls and roofs. The upside-down roof system, in which foamed plastic such as Styrofoam plastic foam is applied above the tar-paper vapor seal, thereby protecting the tar paper from extreme thermal stresses that cause cracking, has been patented (360). The foam is covered with gravel or some other wear-resistant topping (see ROOFING MATERIALS).

In addition to such thermal-insulation uses in buildings, there is a potentially tremendous new area in the form of highway underlayment to prevent frost damage. Damage to roadways, roadbeds, and airfields because of frost action is a costly and aggravating problem. Conventional treatments to prevent such damage are expensive and unreliable. During the 1960s, an improved and more economical solution to the problem was developed (361). It is based on the use of thermal insulation to reduce the heat loss in the frost-susceptible subgrade soil so that no freezing occurs. Many miles of insulated pavements have been built in the United States, Canada, Europe, and Japan. The concept has proved valid, and the performance of extruded PS foam has been completely satisfactory. It is expected that the use of this concept will continue to grow as natural road-building materials continue to become more scarce and expensive and as the weight and speed of land and airborne vehicles continue to increase.

A 2.54-cm Styrofoam plastic foam with thermal conductivity of ca 0.03 W/(m·K) [(0.21 Btu·in.)/(ft·h·°F)] is equivalent to 61 cm of gravel. Any synthetic foam having compressive strength sufficiently high and thermal conductivity sufficiently low is effective. However, the resistance of PS-type foams to water, frost damage, and microorganisms in the soil makes them especially desirable. An interesting and important application of this concept was the use of Styrofoam in the construction of the Alaska Pipeline. In this case, the foam was used to protect the permafrost.

Rigid Foam from FIP Beads. Expandable PS (EPS) has been in wide use in packaging since its introduction. Applications range from pallet shipping containers for computer terminals to material-handling stacking trays to packages for fresh fruits and vegetables. Expandable PS serves as a cushioning material, a package insert for blocking and bracing, a flotation item, or as insulation.

The basic resin for EPS is in the form of beads that are expanded to a desired density before molding. Densities for packaging parts typically are 20–40 kg/m^3. Once expanded, the beads are fused in a steam-heated mold to form a specific shape. Most parts are molded of standard white resins, although several pastel colors are available.

Converters who manufacture EPS parts and components for packaging are called shape molders. Others who mold large billets, eg, measuring 0.6 × 1.2 × 2.4 m, are called block molders. The package user can obtain EPS parts without the benefits of a mold; parts can be fabricated from billets by hot-wire cutting. Whether molded or fabricated, EPS packages and their components are typically designed by careful consideration of the compression and cushioning properties of expanded PS (362).

A large number of factors that influence the foaming of foamable PS beads, eg, the molecular weight of the polymer, polymer type, blowing-agent type and content, and bead size, have been analyzed (363). It is suggested that at least part of the pentane blowing agent is present in microvoids in the glassy PS. Thus, the density of beads containing 5.7 wt% *n*-pentane is 1080 kg/m^3, compared to a value of 1050 kg/m^3 for pure PS beads and compared with a calculated density of 1020 kg/m^3 for a simple mixture in which *n*-pentane is dissolved in the PS. If all of the pentane were in voids, the calculated density would be 1120 kg/m^3. About 60% of the pentane is held in voids, with the balance presumably dissolved. *n*-Pentane present in voids has a reduced vapor pressure, which depends on the effective

Table 13. Loss of Isopentane from Foaming-in-Place Chlorostyrene Beads[a] in Open Storage, wt%[b]

	After 20 h		After 300 h	
Temperature,°C	Polystyrene	Poly(chlorostyrene)	Polystyrene	Poly(chlorostyrene)
25	18	1.3	40	10
50	38	12	72	33
80	48	24	80	54

[a] 420-mm beads.
[b] Initial concentration of isopentane = 6 wt%.

microcapillary diameter. Dissolved *n*-pentane in PS will also have a reduced vapor pressure, by an amount depending on the thermodynamic interaction between solvent and polymer.

An unspecified experimental styrene copolymer, possibly with acrylonitrile, shows a greatly reduced tendency to lose blowing agent on aging at 23°C (363). FIP beads from chlorostyrene likewise have a greatly enhanced ability to retain blowing agent as indicated in Table 13. The higher heat distortion of this polymer requires steam pressures of 210–340 kPa (30–50 psi) for blowing.

Various other factors that influence the foaming of PS, especially cross-linking, are described (359). In Reference 359, foaming is discussed as a viscoelastic process in which there is competition between the blowing pressure, which increases with temperature, and the thinning and rupture of cell walls with consequent collapse of the foam. The presence of cross-links reduces the tendency for cell-wall rupture. Figure 65 shows foam volumes attained as a function of temperature for various amounts of divinylbenzene. The effects of temperature and cross-linking on the kinetics of foaming is also discussed in Reference 359.

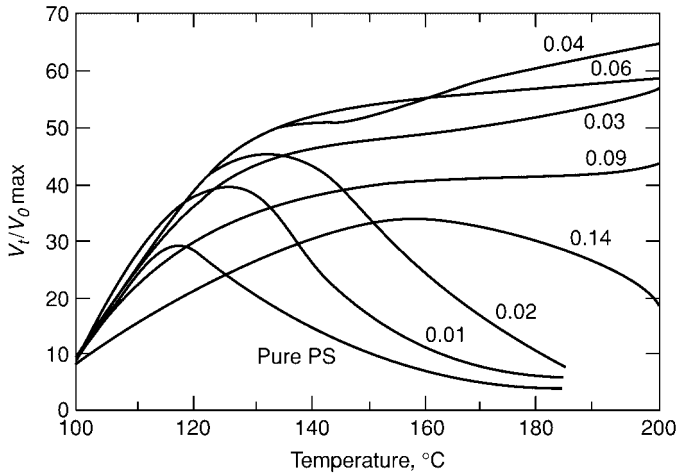

Fig. 65. Maximum foaming volume of styrene divinylbenzene copolymers containing 8.8 wt% CO_2 as a function of divinybenzene content and temperature. Numeral beside curve indicates wt% divinylbenzene. V_t/V ratio of final volume to initial volume at temperature t. Adapted from Ref. 362.

Another important factor affecting the foaming of PS beads is the differential rate of diffusion of *n*-pentane compared to steam and air. It is estimated that the quantity of *n*-pentane normally used is sufficient to produce a foaming volume of 30-fold and hence a foam density of no more than 32 kg/m^3. However, the steam and/or air that diffuses into the beads contributes to further expansion, so that foaming volumes of 60-fold or more are commonly achieved. This aspect of diffusion has been discussed in some detail (364). In cycle foaming in air, beads are allowed to equilibrate with air after each heat-foaming step through a series of stages. Foaming volumes of 200:1 have been achieved in this manner, with densities down to 3.2–4.8 kg/m^3.

Lightweight concrete is made from prefoamed EPS beads, Portland cement, and organic binders. Precast shapes are being used to provide structural strength, thermal insulation, and sound deadening.

Polystyrene as a Raw Material for Rigid Thermoplastic Foams. The low cost of PS and its high thermal stability, which provides good recycle efficiency, as well as the possibility of using low cost blowing agents, are important to the use of PS in rigid thermoplastic foams. The heat-distortion point of ca 80°C (in contrast to 65°C for PVC foam) permits its use in most construction applications. The low sensitivity of the polymer to moisture is another important factor.

Because of all of the aforementioned and possibly for other reasons, PS has been the dominant material used in rigid thermoplastic foams. Poly(vinyl chloride) is economical and has good physical properties and is flame retarding, but it has marginal heat-distortion properties for some uses and does not readily lend itself to the continuous extrusion process used for PS foam. So far, no FIP beads system based on PVC has been perfected. This could well be a result of its high vapor barrier compared to PS. Polyethylene is too permeable to retain a blowing agent and hence is ruled out as a FIP bead material, but it is commercially significant as extruded foam.

Flame Retardants. The growing use of PS foams in the construction industry has provided impetus for continuing research on flame-retardant additives (see FLAME RETARDANTS). Organic bromine compounds, eg, or pentabromomonochlorocyclohexane, have long been used for this purpose in extruded PS foam. Use of injection-molded structural foams, based on HIPS and ABS and containing flame-retardant additives, has grown rapidly since the late 1970s. A typical additive system to impart the required flame-retardant properties is bis(pentabromophenyl) oxide and a synergist, eg, antimony trioxide. Because of environmental concerns over the use of halogenated flame-retardant chemicals, research is currently focusing upon the development of halogen-free systems. Phosphorous containing compounds are currently the most heavily researched alternative.

Foamed Sheet. PS foamed sheet is used for foamed trays, egg cartons, disposable dinnerware, and packaging. Foam sheet manufacturing techniques, manufacturers' logistics, and markets are described in Reference 365. Choice of the correct blowing agent for foam sheet is critical in determining ultimate density and physical properties. Further, the choice of blowing agent may be dictated by safety considerations, eg, flammability of hydrocarbons, or environmental concerns, eg, chlorofluorocarbons (366).

Table 14. Gas and Water Vapor Permeabilities of PS Films[a]

Composition	Oxygen	CO_2	Water
Unmodified PS	3.50	14.00	1600
72:28 styrene-*stat*-acrylonitrile	0.09	4.62	2900

[a]Gas permeability units = $(cm^3 \cdot cm)/(10^{10}\ cm^2 \cdot s \cdot kPa)$.

Oriented PS Film and Sheet. Oriented PS film, in addition to having the lowest cost of any of the rigid plastic materials, offers a high degree of optical clarity, high surface gloss, and excellent dimensional stability (particularly with regard to relative humidity) and is heat shrinkable. It is not a barrier film; in fact, one of its largest uses, that of packaging field-fresh produce, depends upon its being highly permeable to oxygen and water vapor (see Table 14).

PS films have been the subject of several reviews (367–370).

Although PS is normally considered a rather brittle material, biaxial orientation imparts some extremely desirable properties, particularly in regard to an increase in elongation. Thus, the 1.5–2% of elongation normally associated with unoriented PS can become as high as 10%, depending on the exact conditions of preparation (371,372).

Several methods have been utilized in preparing biaxially oriented PS film. The bubble process is used commercially. The high softening point, coupled with the tendency of oriented film to shrink above 85°C, makes heat sealing difficult. Solvent, adhesive, and ultrasonic sealing are used in most applications. Scratch resistance, impact strength, and crease resistance are low. Although the bubble process superficially resembles the common bubble process for making polyethylene, polypropylene, and Saran film, there are a number of substantive differences, and the PS process is considerably more difficult to achieve. In the case of polyethylene, for example, crystallinity stabilizes the blown bubble, whereas with a true thermoplastic, eg, PS, one must stabilize the blown film by cooling below the T_g. This involves extremely careful control of temperature in the blowing process.

As a general rule of thumb, there is an economic break-even point at ca 0.08 mm, which coincides with the defined difference between film and sheet. Film is made more economically by the bubble method and sheet by the tenter-frame method. The exact thickness for break-even depends on technological improvements, which can be made in both processes, in the degree of control which is used in regulating them and in quality requirements.

PS film contains no plasticizers, absorbs negligible moisture, and exhibits exceptionally good dimensional stability. It does not become brittle with age nor distort when exposed to low or high humidity. Excellent machinability, ie, ability to pass through packaging machinery at high speeds and to be cut and sealed, etc, clarity, and stability are central factors in the use of oriented PS in window envelopes. These same characteristics have also led to applications of film for window cartons. An antifog film 0.025–0.032 mm thick has been used extensively for the windows of cartons for bacon. Substantial amounts of film are also employed as sheet protectors and as inserts in wallets. A thickness of 0.060–0.130 mm is customary for these applications. PS film can be printed by means of flexographic,

rotogravure, and silk-screen methods. A lamination of reverse-printed film and paper has been used for an attractive, high sparkle package for hand soap. The film is an excellent base for metallizing because of the almost complete absence of volatiles. Oriented PS film is also widely used for lamination to PS foamed sheet for preprinted decoration and/or property enhancement (373).

For PS sheet, the use responsible for its rapid growth is in meat trays, where the merchandising value is important, ie, the transparency of the package, as well as its resistance to moisture and dimensional stability. A smaller but growing use is as a photographic-film base where dimensional stability at all humidities and low gel count are both important. The thermoplastic nature of PS and the memory effects built into it through biaxial orientation make it especially suitable for packaging applications. It must be processed under pressure rather than by vacuum-forming equipment to avoid the shrinkage, which would otherwise result from the high level of orientation.

Important uses of PS are as windows in envelopes, etc, as mentioned earlier, and as produce overwrap. High optical clarity is required for mechanised reading of characters through envelope windows, a significant technological trend which is certain to enhance the use of PS film. In regard to produce overwrap, the transmission characteristics of PS for water vapor and oxygen coincide more or less with the metabolic requirements of the produce being packaged, eg, lettuce, so that in addition to giving mechanical protection to something like a head of lettuce, the produce is able to metabolize in a normal manner (374). Low cost and high optical clarity are important. In addition, the feel of PS film gives an impression of crispness as far as the product is concerned. PS film also has potential use as a type of synthetic paper (see PULP, SYNTHETIC). GPPS must be treated so that it is opaque, and this can take the form of either pigmentation, mechanical abrasion, or a surface treatment, eg, a chemical etch. HIPS is reasonably opaque. PS film can be given a suitable coating, eg, a latex-clay coating, of the kind that is used on ordinary paper for the purpose of achieving a good printable surface. There are several general discussions of gas permeabilities in plastic films (6,8,9,375,376) (see BARRIER POLYMERS).

BIBLIOGRAPHY

"Styrene Polymers" in *EPST* 1st ed., Vol. 13, pp. 128–447, by R. F. Boyer, H. Keskkula, and A. Platt, The Dow Chemical Company; "Styrene Polymers" in *EPSE* 2nd ed., Vol. 16, pp. 1–246, by E. R. Moore and co-workers, The Dow Chemical Company.

1. M. Hocking, *Science* **251**, 504 (1991).
2. A. E. Platt and T. C. Wallace, in M. Grapon, ed., *Encyclopedia of Chemical Technology*, Vol. **21**, John Wiley & Sons, Inc., New York, 1983, pp. 801–847.
3. D. Schrader, in J. Brandrup and E. H. Immergut, eds., *Polymer Handbook*, 4th ed., John Wiley & Sons, Inc., New York, 1999, pp. V-91–96.
4. W. W. Graessley, *Adv. Polym. Sci.* **16**, 3 (1974).
5. M. Szwarc, M. Levy, and Milkovich, *J. Am. Chem. Soc.* **78**, 2656 (1956).
6. H. Keskkula, G. M. Simpson, and F. L. Dicken, *Soc. Plast. Eng. Prepr. Ann. Tech. Conf.* **12** XV-2, (1966).
7. F. J. Furno, R. S. Webb, and N. P. Cook, *Prod. Eng.* **35**, 87 (1964).
8. W. E. Brown, *International Plastics Congress, 1966*, N.V. t'Raedthuys, Utrecht, Netherlands, 1967.

9. R. L. Bergen and W. E. Wolstenholme, *SPE J.* **16**, 1235 (1960).
10. G. B. Jackson and J. L. McMillan, *SPE J.* **19**, 203 (1963).
11. S. G. Turley and H. Keskkula, *Polym. Eng. Sci.* **7**, 1 (1967).
12. W. E. Brown, *Performance of Plastics in Building, No. 1004*, Building Research Institute, Inc., Washington, D.C., 1963.
13. R. McFedries Jr., *Plast. World* **24**, 34 (1963).
14. E. Scalco, T. W. Huseby, and L. L. Blyler Jr., *J. Appl. Polym. Sci.* **12**, 1343 (1968).
15. E. H. Andrews, in J. V. Schmitz, and W. E. Brown, eds., *Testing of Polymers*, Vol. **4**, Wiley-Interscience, New York, 1969, p. 237.
16. W. H. Haslett Jr. and L. A. Cohen, *SPE J.* **20**, 246 (1964).
17. U.S. Pat. 4585825 (1986), M. A. Wesselmann (to The Dow Chemical Company).
18. J. Roovers, *Macromolecules* **17**, 1196 (1984).
19. C. Bazuin, A. Eisenberg, and M. Kamal, *J. Polym. Sci., Part B: Polym. Phys.* **24**, 1155 (1986).
20. M. Hara, P. Jar, and J. A. Sauer, *Polymer* **32**, 1622 (1991).
21. C. B. Bucknall, *Adv. Polym. Sci.* **27**, 121 (1978).
22. E. J. Kramer, *Adv. Polym. Sci.* **52/53**, 1 (1983).
23. A. M. L. Magalhaes and R. J. M. Borggreve, *Macromolecules* **28**, 5841 (1995).
24. R. A. Bubeck and co-workers, *Mater. Sci.* **26**, 6249 (1991).
25. N. C. Liu and W. E. Baker, *Polym. Eng. Sci.* **32**, 1695 (1992).
26. S. J. Wu, *J. Appl. Polym. Sci.* **35**, 549 (1988).
27. E. Piorkowska, A. S. Argon, and R. E. Cohen, *Macromolecules* **23**, 3838 (1990).
28. Y. Okamoto, and co-workers, *Macromolecules* **24**, 5639 (1991).
29. A. Hall and I. Burnstein, *J. Mater. Sci.* **29**, 6523 (1994).
30. D. B. Priddy, *Adv. Polym. Sci.* **114**, 69 (1994).
31. M. A. Bellinger, J. A. Sauer, and M. Hara, *Polymer* **35**, 5478 (1994).
32. M. A. Bellinger, J. A. Sauer, and M. Hara, *Macromolecules* **27**, 1407 (1994).
33. N. Ishihara and co-workers, *Macromolecules* **19**, 2464 (1986).
34. A. J. Pasztor, B. G. Landes, and P. J. Karjala, *Thermochemica. Acta* **177**, 187 (1991).
35. U.S. Pat. 2287188 (1942) L. A. Matheson and R. F. Boyer (to The Dow Chemical Company).
36. R. L. Miller and L. E. Nielsen, *J. Polym. Sci.* **55**, 643 (1961).
37. D. Allan and co-workers, *Macromolecules* **27**, 7621 (1994).
38. *Modern Plastics Encyclopedia 1968–69*, Vol. **45**, 1968, p. 43.
39. J. Eichhorn, *J. Appl. Polym. Sci.* **8**, 2497 (1964).
40. U.S. Pat. 3324076 (1967), M. E. EIder, R. T. Dickerson, and W. F. Tousignant (to The Dow Chemical Company).
41. M. Hayashi, K. Kojima, and A. Hirao, *Macromolecules* **32**, 2425 (1999).
42. H. Iatrou, J. W. Mays, and N. Hadjichristidis, *Macromolecules* **31**, 6697 (1998).
43. D. Knauss and co-workers, *Macromolecules* **33**, 3557 (2000).
44. R. P. Quirk and Y. Tsai, *Macromolecules* **31**, 8016 (1998).
45. N. G. Vasilenko and co-workers, *Macromol. Chem. Phys.* **199**, 889 (1998).
46. M. Weissmueller and W. Burchard, *Macromol. Chem. Phys.* **200**, 541 (1999).
47. M. Xenidou and N. Hadjichristidis, *Macromolecules* **31**, 5690 (1998).
48. S. Delassus and co-workers, *Macromolecules* **27**, 1307 (1994).
49. A. Deffieux and M. Schappacher, *Macromol. Symp.* **132**, 45 (1998).
50. K. Matyjaszewski and co-workers, *Macromolecules* **32**, 6526 (1999).
51. R. P. Quirk and co-workers, *Macromol. Symp.* **118**, 89 (1997).
52. Y. Tezuka, H. Imai, and T. Shiomi, *Macromol. Chem. Phys.* **198**, 627 (1997).
53. D. J. Groves and co-workers, *Polymer* **39**, 3877 (1998).
54. M. A. Hempenius and co-workers, *Macromolecules* **31**, 2299 (1998).
55. D. Ferri and P. Lomellini, *J. Rheol. (N.Y.)* **43**, 1355 (1999).

56. J. F. Tassin and co-workers, *Rheol. Ser.* **5**, 37 (1996).
57. D. B. Priddy and M. Pirc, *ACS Polym. Prepr.* **29**, 340 (1988).
58. R. E. Drumright, P. E. Kastl, and D. B. Priddy, *Macromolecules* **26**, 2246 (1993).
59. J. C. Bevington and C. J. Dyball, *Polymer* **16**, 938 (1975).
60. B. Howell and co-workers, *ACS Polym. Prepr.* **40**, 73 (1999).
61. E. Niki and Y. Kamiya, *J. Org. Chem.* **38**, 1403 (1973).
62. E. Niki and Y. Kamiya, *J. Chem. Soc. Perkin. Trans.* **1975**, 1221 (1975).
63. U. Stimming and C. Durning, *Macromolecules* **26**, 3271 (1993).
64. E. Trommsdorff, H. Kohle, and P. Lagally, *Makromol. Chem.* **1**, 169 (1947).
65. S. Zhu and A. Hamielec, *Makromol. Chem., Macromol. Symp.* **69**, 247 (1993).
66. U.S. Pat. 4376847 (1983), T. Matsubara and co-workers.
67. U.S. Pat. 5191040 (1993), K. Izumida and R. Okumura.
68. L. Tung and co-workers, *J. Polym. Sci., Polym. Chem. Ed.* **19**, 2027 (1981).
69. U.S. Pat. 5455321 (1995), C. Cummings and P. Hathaway (to The Dow Chemical Company).
70. S. Tinetti and co-workers, *J. Appl. Polym. Sci.* **64**, 683 (1997).
71. U.S. Pat. 5034485 (1991), W. Tong and D. Priddy (to The Dow Chemical Company).
72. C. J. Hawker, *Angew. Chem., Int. Ed. Engl.* **34**, 1456 (1995).
73. G. E. Molau, *J. Polym. Sci., Polym. Phys. Ed.* **3**, 1007 (1965).
74. J. Kressler and co-workers, *Macromol. Rapid Commun.* **16**, 631 (1995).
75. U.S. Pat. 3265765 (1966), G. Holden and R. Milkovich (to Shell).
76. U.S. Pat. 4267284 (1981), A. G. Kitchen (to Phillips).
77. G. E. Molau, *J. Polym. Sci., Polym. Chem. Ed. 3*, **1267**, 4235 (1965).
78. J. Moacanin, G. Holden, and N. W. Tschoegl, *J. Polym. Sci., Polym. Symp.* **26**, 1 (1969).
79. G. Reiss, *J. Macrotool. Sci. Phys.* **B17**, 355 (1980).
80. R. Xie and co-workers, *Macromolecules* **27**, 3444 (1994).
81. A. Echte, *Angew. Makrotool. Chem.* **58/59**, 175 (1977).
82. H. Feng, Z. Feng, and L. Shen, *Macromolecules* **27**, 7840 (1994).
83. J. Stock and R. Stadler, *Makromol. Chem., Macromol. Symp.* **76**, 127 (1993).
84. M. R. Ambler, *Chromatogr. Sci. Ser.* **19**, 29 (1981).
85. T. Guo and W. Yang, *J. Damage Mech.* **2**, 364 (1993).
86. H. L. Hsieh, *CHEMTECH* **11**, 626 (1981).
87. U.S. Pat. 3336267 (1967), R. I. Zimmerman and W. E. O'Connor (to The Dow Chemical Company).
88. U.S. Pat. 3231524 (1966), D. W. Simpson (to The Dow Chemical Company).
89. M. Barsacchi and co-workers, *Angew. Chem., Int. Ed. Engl.* **30**, 989 (1991).
90. E. Drent, J. A. M. van Broekhoven, and M. J. Doyle, *J. Organomet. Chem.* **417**, 235 (1991).
91. Eur. Pat. Appl. 416815 (1991), J. Stevens and co-workers (to The Dow Chemical Company).
92. S. Betso and co-workers, *Annu. Tech. Conf.—Soc. Plast. Eng.* **58**, 3012 (2000).
93. H. Chen and co-workers, *Annu. Tech. Conf.—Soc. Plast. Eng.* **58**, 1838 (2000).
94. C. Park and G. Clingerman, *Annu. Tech. Conf.—Soc. Plast. Eng.* **54**, 1887 (1996).
95. U.S. Pat. 6090359 (2000), D. A. Hucul (to The Dow Chemical Company).
96. M. Gehlsen and co-workers, *J. Polym. Sci., Part B: Polym. Phys.* **33**, 1527 (1995).
97. R. H. Boundy, R. F. Boyer, and S. Stoesser, *Styrene, Its Polymers, Copolymers and Derivatives*, Reinhold Publishing Corp., New York, 1952. ACS, Monograph No. 115.
98. H. W. McCormick, *J. Polym. Sci.* **25**, 488 (1957).
99. U.S. Pat. 3206445 (1965), H. Volk (to The Dow Chemical Company).
100. U.S. Pat. 3340238 (1967), W. E. Smith and H. Volk (to The Dow Chemical Company).
101. U.S. Pat. 3011918 (1961), L. H. Silvernail and M. W. Zembal (to The Dow Chemical Company).

102. G. E. Molau and H. Keskkula, *J. Polym. Sci., Polym. Chem. Ed.* **4**, 1595 (1966).
103. S. Strella, in E. Baer, ed., *Engineering Design for Plastics*, Reinhold Publishing Corp., New York, 1964, pp. 795–814.
104. R. F. Boyer, *Polym. Eng. Sci.* **8**, 161 (1968).
105. C. B. Bucknall, *Toughened Plastics*, Applied Science Publishers, London, 1977.
106. H. Willersinn, *Makromol. Chem.* **101**, 297 (1966).
107. C. B. Bucknall and R. R. Smith, *Polymer* **6**, 437 (1965).
108. J. A. Schmitt, *J. Appl. Polym. Sci.* **12**, 533 (1968).
109. H. Keskkula, S. G. Turley, and R. F. Boyer, *J. Appl. Polym. Sci.* **15**, 351 (1971).
110. K. Kato, *J. Electron Microsc.* **14**, 220 (1965).
111. D. A. Walker, in Ref. 38, p. 334.
112. H. Keskkula and P. A. Traylor, *J. Appl. Polym. Sci.* **11**, 2361 (1967).
113. R. J. Williams and R. W. A. Hudson, *Polymer* **8**, 643 (1967).
114. Ger. Pat. 3002394 (1981), K. Jung and co-workers (to Roehm).
115. *Properties and Processing of K-Resins BDS Polymer, Technical Service Memorandum 245*, Phillips Petroleum Co.
116. K. Knoll and N. Niessner, *Macromol. Symp.* **132**, 231 (1998).
117. A. Argon and co-workers, *J. Polym. Sci., Polym. Phys. Ed.* **19**, 253 (1981).
118. H. Feng and co-workers, *Macromolecules* **27**, 7830 (1994).
119. F. Haaf and co-workers, *J. Sci. Ind. Res.* **40**, 659 (1981).
120. L. Nielsen and R. Landel, *Mechanical Properties of Polymers and Composites*, Marcel Dekker, Inc., New York, 1994.
121. O. Gebizlioglu and A. Argon, and R. Cohen, *Adv. Chem. Ser.* **211**, 259 (1986).
122. C. H. Basdekis, *ABS Plastics*, Reinhold Publishing Corp., New York, 1964.
123. *Br. Plast.* **38**, 708 (Dec. 1965).
124. H. Keskkula, G. Simpson, and F. Dicken, *Soc. Plast. Eng. Prepr. Annu. Tech. Conf.* **12**, XV-2 (1966).
125. G. M. Kraynak, *Soc. Plast. Eng. Annu. Tech. Conf.* **13**, 896 (1967).
126. Vacuum Metallizing Cycolac, Technical Report P135, Borg-Warner Corp., Chicago, 1980.
127. E. N. Hildreth, *Modern Plastics Encyclopedia*, Vol. **43**, 1966, p. 1991.
128. K. Stoeckhert, *Kunststoffe* **55**, 857 (1965).
129. *Mod. Plast.* **45**, 84 (Aug. 1968).
130. N. L. Maecker and D. B. Priddy, *J. Appl. Polym. Sci.* **42**, 21 (1991).
131. B. Bell and co-workers, *J. Appl. Polym. Sci.* **54**, 1605 (1994).
132. U.S. Pat. 4874829 (1989), C. E. Schwier and W. C. Wu (to The Dow Chemical Company).
133. U.S. Pat. 5091470 (1992), H. Wolsink, J. Plommer, and T. Traugott (to The Dow Chemical Company).
134. U.S. Pat. 2802809 (1957), R. A. Hayes (to Firestone).
135. E. Zahn, *Appl. Polym. Syrup.* **11**, 209 (1969).
136. W. E. Brown, J. D. Striebel, and D. C. Fuccella, *Automotive Engineering Congress*, Paper 680059, Jan. 8, 1968.
137. M. Weimer and co-workers, *J. Am. Chem. Soc.* **121**, 1615 (1999).
138. J. Bergman and co-workers, *Chem. Comm.* **21**, 2179 (1999).
139. C. H. Bamford and C. F. M. Tipper, eds., *Chemical Kinetics*, Vol. **14**, Elsevier Scientific Publishing Co., New York, 1975.
140. N. Grassie, ed., *Developments in Polymer Degradation*, Vols. **1** and **2**, Applied Science Publishers, London, 1977.
141. M. Guaita, O. Chiantore, and L. Costa, *Polym. Degrad. Stab.* **12**, 315 (1985).
142. O. Chiantore, M. Guaita, and N. Grassie, *Polym. Degrad. Stab.* **12**, 141 (1985).
143. G. G. Cameron, W. A. Bryce, and L. T. McWalter, *Eur. Polym. J.* **20**, 563 (1984).
144. R. S. Lehrle, R. E. Peakman, and J. C. Robb, *Eur. Polym. J.* **18**, 517 (1982).

145. J. R. Stoppert, *PS Deserves More Respect, Houston, Tex.*, 1991.
146. G. A. Mackey, R. C. Westphal, and R. Coughanour, in R. J. Ehrig, ed., *Plastics Recycling*, Hanser, Munich, 1992.
147. K. Sikkema and co-workers, *Polym. Degrad. Stab.* **38**, 119 (1992).
148. K. Sikkema and co-workers, *Polym. Degrad. Stab.* **38**, 113 (1992).
149. M. Hanner and co-workers, *Polym. Degrad. Stab.* **39**, 235 (1993).
150. U.S. Pat. 5187249 (1993), V. A. Dais and D. B. Priddy (to The Dow Chemical Company).
151. J. O'Brien, P. Smith, and D. Priddy, *Polym. Degrad. Stab.* **39**, 69 (1993).
152. U.S. Pat. 5194527 (1993), J. O'Brien, K. Sikkema, and D. Priddy (to The Dow Chemical Company).
153. J. Potts and co-workers, *Polym. Sci. Technol.* **3**, 61 (1973).
154. J. Guillet, M. Heskins, and L. Spencer, *Polym. Mater. Sci. Eng.* **58**, 80 (1988).
155. S. Karlsson, O. Ljungquist, and A. Albertsson, *Polym. Degrad. Stab.* **21**, 237 (1988).
156. W. J. Bailey, *Polym. J.* **17**, 85 (1985).
157. PCT Int. Appl. WO 9322371 (1993), G. Welsh, B. Dalke, and E. Lee (to The Dow Chemical Company).
158. D. B. Priddy and M. Pirc, *J. Appl. Polym. Sci.* **40**, 41 (1990).
159. U.S. Pat. 4087599 (1978), J. M. Roe and D. B. Priddy (to The Dow Chemical Company).
160. P. J. Flory, *J. Am. Chem. Soc.* **59**, 241 (1937).
161. W. A. Pryor, *ACS Symp. Ser.* **69**, 33 (1978).
162. W. Brown, *Makromol. Chem.* **128**, 130 (1969).
163. N. Barr and co-workers, *Eur. Polym. J.* **14**, 245 (1978).
164. K. E. Russel and A. Tobolsky, *J. Am. Chem. Soc.* **76**, 395 (1954).
165. F. R. Mayo, *J. Am. Chem. Soc.* **90**, 1289 (1968).
166. W. A. Pryor and L. Lasswell, *Adv. Free-Radical Chem.* **5**, 27 (1975).
167. F. R. Mayo, *J. Am. Chem. Soc.* **75**, 6133 (1953).
168. R. R. Hiatt and P. D. Bartlett, *J. Am. Chem. Soc.* **81**, 1149 (1959).
169. R. Kaiser and co-workers, *Angew. Makromol. Chem.* **12**, 25 (1970).
170. Y. Chong, E. Rizzardo, and D. Solomon, *J. Am. Chem. Soc.* **105**, 7761 (1983).
171. J. Mulzer and co-workers, *Chem. Ber.* **121**, 2231 (1988).
172. W. Buzanowski and co-workers, *ACS Polym. Prep.* **32**, 220 (1991).
173. W. Pryor and J. Coco, *Macromolecules* **3**, 500 (1970).
174. D. Hensley, S. Goodrich, H. Harwood, and P. Rinaldi, *Macromolecules* **27**, 2351 (1994).
175. U.S. Pat. 5962605 (1999), D. Priddy and V. Dais (to The Dow Chemical Company).
176. U.S. Pat. 5948874 (1999), W. Pike and D. Priddy (to The Dow Chemical Company).
177. D. B. Priddy, *Adv. Polym. Sci.* **111**, 69 (1994).
178. G. Moad, D. Solomon, and R. I. Willing, *Macromolecules* **21**, 855 (1988).
179. J. McKellarand and N. F. Allen, *Photochemistry of Man Made Polymers*, Applied Science Publishers, London, 1978.
180. H. Susuki, Y. Tanaka, and Y. Ishii, *Sen'i Gakkaishi* **35**, 296 (1979).
181. D. Bellus and co-workers, *J. Polym. Sci., Part C* **22**, 629 (1969).
182. A. D. Schmidt and W. H. Ray, *Chem. Eng. Sci.* **36**, 1401 (1981).
183. J. W. Hammer, T. A. Akramov, and W. A. Ray, *Chem. Eng. Sci.* **36**, 1897 (1981).
184. K. Ito and T. Aoyama, *Eur. Polym. J.* **23**, 955 (1987).
185. L. Blavier and J. Villermaux, *Chem. Eng. Sci.* **39**, 101 (1984).
186. C. H. Bamford, *Polymer* **31**, 1720 (1990).
187. J. Bogunjoko and B. W. Brooks, *Makromol. Chem.* **184**, 1603 (1983).
188. K. Y. Hsu and S. A. Chen, *Polym. Eng. Sci.* **24**, 1253 (1984).
189. F. L. Marten and A. E. Hamielec, *J. Appl. Polym. Sci.* **27**, 489 (1982).
190. K. J. Kim and K. Y. Choi, *Polym. Eng. Sci.* **31**, 333 (1991).
191. M. A. Villalobos, A. E. Hamielec, and P. E. Wood, *J. Appl. Polym. Sci.* **42**, 629 (1991).
192. K. Y. Choi, W. R. Liang, and G. D. Lei, *J. Appl. Polym. Sci.* **35**, 1562 (1988).

193. K. J. Kim, W. Liang, and K. Y. Choi, *Ind. Eng. Chem. Res.* **28**, 131 (1989).
194. K. J. Kim and K. Y. Choi, *Chem. Eng. Sci.* **44**, 297 (1989).
195. K. J. Kim and K. Y. Choi, *Chem. Eng. Sci.* **43**, 965 (1988).
196. K. Y. Choi and G. D. Lei, *AIChE J.* **33**, 2067 (1987).
197. V. R. Kamath, *Mod. Plast.* **58**, 106 (1981).
198. E. Toplikar and co-workers, *Polym. Bull. (Berlin)* **39**, 37 (1997).
199. U.S. Pat. 5618900 (1997), R. Drumright and co-workers (to The Dow Chemical Company).
200. I. Li and co-workers, *Macromolecules* **29**, 8554 (1996).
201. J. C. Bevington, H. W. Melville, and R. P. Taylor, *J. Polym. Sci.* **12**, 449 (1954).
202. A. V. Tobolsky, C. E. Rogers, and R. D. Brickman, *J. Am. Chem. Soc.* **28**, 1277 (1960).
203. *Form No. 115-575-79, The Dow Chemical Company*, Midland, MI, 1979.
204. U.S. Pat. 4177110 (1979), J. M. Watson (to Cosden).
205. U.S. Pat. 4086147 (1978), J. M. Watson (to Cosden).
206. M. H. George, in G. E. Ham, ed., *Vinyl Polymerization*, Marcel Dekker, Inc., New York, 1967, pp. 186–188.
207. A. A. Miller and F. R. Mayo, *J. Am. Chem. Soc.* **78**, 1017 (1956).
208. O. F. Olaj, H. F. Kauffmann, and J. W. Breitenback, *Makromol. Chem.* **178**, 2707 (1977).
209. Ref. 3, pp. 11–61.
210. E. Niki and Y. Kamiya, *J. Org. Chem.* **38**, 1403 (1975).
211. E. Niki and Y. Kamiya, *J. Chem. Soc. Perkin Trans.* **1975**, 1221 (1975).
212. U.S. Pat. 4910274 (1990), D. B. Priddy (to The Dow Chemical Company).
213. Y. Watanabe and co-workers, *Chem. Lett. (Japan)* **1975**, 1089 (1993).
214. D. B. Priddy and M. Pirc, *J. Appl. Polym. Sci.* **40**, 41 (1990).
215. M. Szwarc, *Carbanions, Living Polymers and Electron Transfer Processes*, Wiley-Interscience, New York, 1968.
216. D. B. Priddy, M. Pirc, and B. J. Meister, *Polym. React. Eng.* **1**, 343 (1993).
217. D. B. Priddy and M. Pirc, *J. Appl. Polym. Sci.* **37**, 1079 (1989).
218. D. B. Priddy and M. Pirc, *J. Appl. Polym. Sci.* **37**, 393 (1989).
219. D. B. Priddy and M. Pirc, *ACS Polym. Prepr.* **29**, 340 (1988).
220. U.S. Pat. 4859748 (1989), D. Priddy and M. Pirc (to The Dow Chemical Company).
221. R. Thiele, *Chem. Eng. Technol.* **17**, 127 (1994).
222. Ger. Pat. 4235980 (1994), F. Brandstetter, H. Gausepohl, and R. Thiele (to BASF).
223. U.S. Pat. 3773740 (1973), T. T. Szabo (to Union Carbide).
224. Jpn. Pat. 11116613 (1999), K. Ebara (to Asahi).
225. A. Deffieux and co-workers, *ACS Polym. Prepr.* **41**, 1386 (2000).
226. P. Desbois and co-workers, *Macromol. Chem. Phys.* **200**, 62 (1999).
227. U.S. Pat. 4647632 (1987), D. B. Priddy (to The Dow Chemical Company).
228. D. B. Priddy, T. D. Traugott, and R. H. Seiss, *J. Appl. Polym. Sci.* **41**, 383 (1990).
229. K. Miyashita and co-workers, *Macromolecules* **27**, 1093 (1994).
230. R. Campbell, T. Newman, and M. Malanga, *Macromol. Symp.* **97**, 151 (1995).
231. U. Koch-Reuss, *Kunststoffe* **88**, 1139 (1998).
232. T. Otsu, M. Yoshida, and T. Tazaki, *Makromol. Chem., Rapid Commun.* **3**, 133 (1982).
233. T. Otsu and M. Yoshida, *Makromol. Chem., Rapid Commun.* **3**, 127 (1982).
234. T. Otsu and A. Kuriyama, *Polym. Bull.* **11**, 135 (1984).
235. T. Otsu and A. J. Kuriyama, *Macromol. Sci., Chem.* **A21**, 961 (1984).
236. T. Otsu, *Kobunshi* **37**, 248 (1988).
237. T. Otsu, T. Tazaki, and M. Yoshioka, *Chem. Express* **5**, 801 (1990).
238. E. Rizzardo, *Chemistry in Australia* **Jan-Feb**, 32 (1987).
239. B. R. Smirnov, *Vysokomol. Soedin., Ser.* **A32**, 583 (1990).

240. D. Mardare and K. Matyjaszewski, *ACS Polym. Prepr.* **35**, 778 (1994).
241. M. Georges and co-workers, *Macromolecules* **26**, 2987 (1993).
242. K. Endo, K. Murata, and T. Otsuk, *Macromolecules* **25**, 5554 (1992).
243. I. Li and co-workers, *ACS Polym. Prepr.* **36**, 469 (1995).
244. M. Georges and co-workers, *ACS Polym. Prepr.* **35**, 870 (1994).
245. I. Li and co-workers, *Macromolecules* **30**, 5195 (1997).
246. M. Saban and co-workers, *Macromolecules* **28**, 7032 (1995).
247. M. Georges and co-workers, *Macromol. Symp.* **88**, 89 (1994).
248. C. Hawker, *J. Am. Chem. Soc.* **116**, 11185 (1994).
249. R. Veregin and co-workers, *Macromolecules* **29**, 2746 (1996).
250. I. Li and co-workers, *Macromolecules* **28**, 6692 (1995).
251. T. Fukuda and co-workers, *Macromolecules* **29**, 6393 (1996).
252. S. Hammouch and J. Catala, *Macromol. Rapid Commun.* **17**, 149 (1996).
253. Y. Zhu and co-workers, *ACS Symp. Ser.* **685**, 214 (1998).
254. D. B. Priddy, *Mater. Eng. (N.Y.)* **1995**, 9, 629 (1995).
255. D. Benoit and co-workers, *Macromolecules* **33**, 1505 (2000).
256. U.S. Pat. 5721320 (1998), D. Priddy and I. Li (to The Dow Chemical Company).
257. S. Kobatake and co-workers, *Macromolecules* **30**, 4238 (1997).
258. C. Hawker and co-workers, *Polym. Mater. Sci. Eng.* **80**, 90 (1999).
259. Y. Chong and co-workers, *Macromolecules* **32**, 2071 (1999).
260. R. Mayadunne and co-workers, *Macromolecules* **32**, 6977 (1999).
261. E. Rizzardo and co-workers, *ACS Symp. Ser.* **768**, 278 (2000).
262. H. K. Hall, *Angew. Chem. Int. Ed. Engl.* **22**, 440 (1983).
263. Ref. 3, pp. II-303–II-333.
264. G. E. Molau, *J. Polym. Sci., Part B* **3**, 1007 (1965).
265. H. J. Karam, in K. Solc, ed., *Polymer Compatibility and Incompatibility*, MMI Press, Midland, MI, 1981.
266. A. W. Hansen and R. L. Zimmermann, *Ind. Eng. Chem.* **49**, 1803 (1957).
267. Ger. Pat. 2138176 (1971) (to BASF).
268. U.S. Pat. 4243781 (1981), R. W. Kent Jr. (to The Dow Chemical Company).
269. U.S. Pat. 4268652 (1981), R. W. Kent Jr. (to The Dow Chemical Company)
270. U.S. Pat. 4206293 (1980), R. L. Kruse (to Monsanto).
271. D. B. Priddy, *Adv. Polym. Sci.* **121**, 123 (1995).
272. E. Stark and co-workers, *J. Macromol. Sci., Macromol. Rep.* **A29**, 1 (1992).
273. D. Allan and co-workers, *Macromolecules* **26**, 6068 (1993).
274. B. Bell and co-workers, *Macromolecular Reports* **A29**, 1 (1992).
275. D. Hasha and co-workers, *Macromolecules* **25**, 3046 (1992).
276. F. Miller, in R. R. Meyers and J. S. Long, eds., *Treatise on Coatings*, Vol. **1**, Part 2, Marcel Dekker, Inc., New York, 1968, pp. 1–57.
277. O. Okay and co-workers, *Macromolecules* **28**, 2728 (1985).
278. O. Okay, *Polymer* **35**, 796 (1994).
279. G. F. Freeguard, *Br. Polym. J.* **6**, 205 (1974).
280. U.S. Pat. 2694692 (1954), J. L. Amos, J. L. McCurdy, and O. R. McIntire (to The Dow Chemical Company).
281. U.S. Pat. 4214056 (1980), R. E. Lavengood (to Monsanto).
282. A. Brydon, G. M. Burnett, and G. G. Cameron, *J. Polym. Sci. Chem. Ed.* **11**, 3255 (1973); *J. Polym. Sci. Chem. Ed.* **12**, 1011 (1974).
283. T. Kotaka, *Makromol Chem.* **177**, 159 (1976).
284. D. J. Stein, G. Fahrbach, and H. Adler, *Adv. Chem. Ser.* **142**, 148 (1975).
285. C. Chen, *Polym. Eng. Sci.* **40**, 441 (2000).
286. PCT Int. Appl. 9832797 (1998), M. Demirors and co-workers (to The Dow Chemical Company).

287. R. Guerrerro-Santos, H. Harwood, and D. Priddy, *ACS Polym. Prepr.* **40**, 75 (1999).
288. D. Priddy and co-workers, *ACS Polym. Prepr.* **40**(2), 73 (1999).
289. R. H. Simon and D. C. Chappelear, *ACS Symp. Ser.* **104**, 71 (1979).
290. R. B. Bishop, *Practical Polymerization for PS*, Cahners Books, Boston, 1971.
291. D. C. Blackley, *Emulsion Polymerization—Theory and Practice*, Applied Science Publishers, London, 1975.
292. J. L. Amos, *Polym. Eng. Sci.* **14**, 1 (1974).
293. R. F. Boyer, *J. Macromol. Sci. Chem.* **A15**, 1411 (1981).
294. U.S. Pat. 3884766 (1975), W. G. Bir and J. Novack (to Monsanto).
295. U.S. Pat. 3966538 (1976), C. G. Hagberg (to Monsanto).
296. W. Michaeli, H. Hocker, U. Berghaus, and W. Frings, *J. Appl. Polym. Sci.* **48**, 871 (1993).
297. U.S. Pat. 4011284 (1977), G. Gawne and C. Ouwerkerk (to Shell).
298. U.S. Pat. 3903202 (1975), D. E. Carter and R. H. M. Simon (to Monsanto).
299. E. Martuscelli, R. Palumbo, and M. Kryszewski, *Polymer Blends*, Plenum Press, New York, 1980.
300. C. Chen, *Polym.-Plast. Technol. Eng.* **33**, 55 (1994).
301. Jpn. Pat. 9143320 (1997), H. Sasaki, K. Yoshida, and A. Shichizawa (to Asahi).
302. U.S. Pat. 4940472 (1990), R. Hay and A. Dowell (to The Dow Chemical Company).
303. U.S. Pat. 4952672 (1990), E. Moore and R. Hay (to The Dow Chemical Company).
304. K. Ravindrassath and R. Mashelkar, *Chem. Eng. Sci.* **43**, 429 (1988).
305. C. Yang and co-workers, *AIChE J.* **43**, 1874 (1997).
306. U.S. Pat. 3987235 (1976), S. Fujimoto (to The Dow Chemical Company).
307. U.S. Pat. 5380822 (1995), J. Skilbeck (to Novacor).
308. R. Albalak, Z. Tadmor, and Y. Talmon, *AIChE J* **36**, 1313 (1990).
309. R. Albalak, Z. Tadmor, and Y. Talmon, *Mater. Res. Soc. Symp. Proc.* **237**, 181 (1992).
310. U.S. Pat. 5468429 (1995), T. Li, I. Tung, and D. Yu.
311. S. Nagai, A. Ueda, and H. Ikezawa, *Makromol. Chem.* **182**, 1669 (1981).
312. U.S. Pat. 4275175 (1981), I. Gomez (to Monsanto Co.).
313. U.S. Pat. 4124658 (1978), P. Camerman (to Cosden).
314. U.S. Pat. 5185400 (1993), R. Farrar, D. Hartsock, and F. Mueller (to Phillips).
315. Brit. Pat. 1330896 (1973), P. Blakemore (to Monsanto).
316. U.S. Pat. 4221905 (1980), E. Tokas (to Monsanto Co.).
317. U.S. Pat. 5274029 (1993), J. Kelley.
318. A. van der Goot and L. Janssen, *Adv. Polym. Technol.* **16**, 85 (1997).
319. Eur. Pat. Appl. 479560 (1992), H. Abe and co-workers, (to Sumitomo).
320. R. Derbyshire, *Radiat. Phys. Chem.* **14**, 333 (1979).
321. PCT Int. Appl. 9948931 (1999), D. Priddy and M. Demirors (to The Dow Chemical Company).
322. J. Lignon, *Mod. Plast.* **57**, 317 (1980).
323. C. Milacron, *Mod. Plast.* **57**, 332 (1980).
324. *Hoover Universal Sales Literature, HV 450, Manchester, Mich.*
325. *Plastics Design Forum, 22 (May/June 1980).*
326. H. Keskkula and J. W. Norton Jr., *J. Appl. Polym. Sci.* **2**, 289 (1959).
327. K. J. Cleereman, *SPE J.* **23**, 43 (Oct. 1967).
328. P. A. M. Ellis, *Plast. Inst. Trans. J.* **35**, 537 (1967).
329. H. R. Jacobi, *Screw Extrusion of Plastics*, Life Books Ltd., London, 1963.
330. J. F. T. Pittman and R. Sander, *Int. Polym. Process.* **9**, 326 (1994).
331. H. Shidara and M. M. Denn, *J. Non-Newtonian Fluid Mech.* **48**, 101 (1993).
332. J. Fredos, ed., *Plastic Engineering Handbook*, Van Nostrand Reinhold Co., Inc., New York, 1976.
333. E. P. Weaver, *Polym. Eng. Sci.* **6**, 172 (1966).

334. C. Guerrero and P. J. Carreau, *J. Polym. Eng.* **12**, 155 (1993).
335. R. W. Brand and R. L. Keiks, *Plast. Technol.* **37** (Feb. 1972).
336. N. Fountas, *Plast. World* **37**, 40 (Nov. 1979).
337. U.S. Pat. 4039609 (1977), A. W. Thief and H. Hell (to Bellaplast).
338. *Cycolac Brand, ABS Polymers Sales Bulletin, Marbon Chemical Division of Borg-Warner Corp., Chicago, 1980.*
339. W. R. R. Park and J. Conrad, *Encyclopedia of Polymer Science and Technology*, Vol. **2**, Wiley-Interscience, New York, 1965, p. 339.
340. K. Cleereman, W. Schrenk, and L. Thomas, *SPE J.* **24**, 27 (1968).
341. R. Bubeck and co-workers, *Polym. Eng. Sci.* **21**, 624 (1981).
342. N. Skelly and co-workers, *Polym. Mater. Sci. Eng.* **59**, 23 (1988).
343. D. E. James, *Polym. Eng. Sci.* **8**, 241 (1968).
344. T. Shimada, P. Horng, and R. Porter, *J. Rheol.* **24**, 78 (1980).
345. *Product Stewardship-Styrene Plastics, Form. No. 304-109-1280, The Dow Chemical Company. Midland, MI, 1980.*
346. R. N. Kennedy, in R. J. Bender, ed., *Handbook of Foamed Plastics*, Lake Publishing Co., Libertyville, 111, 1965.
347. K. C. Frisch and J. H. Saunders, *Plastic Foams*, Vol. **1**, Part 1, Marcel Dekker, Inc., New York, 1972.
348. K. Suh and R. Skochdopole, *Kirk-Othmer Encyclopedia of Chemical Technology*, 3rd ed., Vol. **11**, 1980. pp. 82–126.
349. U.S. Pat. 2681321 (1954), F. Stasny and R. Gaeth (to BASF).
350. U.S. Pat. 2744291 (1956), F. Stasny and K. Buchholtz (to BASF).
351. U.S. Pat. 2787809 (1957), F. Stasny (to BASF).
352. L. Rubens, *J. Polym. Sci., Polym. Symp.* **72**, 241 (1985).
353. U.S. Pat. 3231524 (1966), D. W. Simpson and C. H. Pottenger (to The Dow Chemical Company).
354. D. C. Wollard, Paper presented at the *12th Annual SPI Conference*, Washington, D.C., Oct. 16–18, 1967.
355. F. R. Bush and G. C. Rollerson, Paper presented at the *38th SPE-ANTEC*, New York, 1980.
356. U.S. Pat. 4249875 (1981), E. Hart and R. Rutledge (to Cosden).
357. Low Temperature Systems, Form No. 179-2086-77, The Dow Chemical Company, Midland, MI, 1977.
358. B. Brooks and L. G. Rey, *J. Cell. Plast.* **9**, 232 (1973).
359. L. C. Rubens, *J. Cell. Plast.* **1**, 3 (1965).
360. U.S. Pat. 3411256 (1968), J. B. Best (to The Dow Chemical Company).
361. U.S. Pat. 3250188 (1966), G. A. Leonards (to The Dow Chemical Company).
362. R. L. Chatman, *Package Eng.* **26**, 56 (1981).
363. A. R. Ingram and H. A. Wright, *Mod. Plast.* **41**, 152 (Nov. 1963).
364. S. J. Skinner, S. Baxter, and P. J. Grey, *Plast. Inst. Trans. J.* **32**, 180 (1964).
365. R. Martino, *Mod. Plast.* **55**, 34 (1978).
366. J. G. Burt, *J. Cell. Plast.* **15**, 158 (1979).
367. O. Sweeting, ed., *Science and Technology of Polymer Films*, Vols. **1** and **2**, Wiley-Interscience, New York, 1968/1969.
368. J. Pinsky, Ref. 347, Vol. **2**.
369. W. R. R. Park, ed., *Plastics Film Technology*, Reinhold Publishing Corp., New York, 1969.
370. C. Saikaishi, *Jpn. Chem. Quart.* **1**, 49 (1968).
371. W. R. R. Park and J. Conrad, in N. M. Bikales, ed., *Encyclopedia of Polymer Science and Technology*, Vol. **2**, Wiley-Interscience, New York, 1968.
372. H. J. Karam, Ref. 347, Vol. **1**, pp. 227–253.

373. *Lamination of Trycite Plastic Films to PS Foam Sheet*, Bulletin No. 500-898-79, The Dow Chemical Company, Midland, Mich., 1979.
374. C. R. Scott, F. J. Butt, and J. Eichhorn, *Mod. Packag.* **38**, 135 (1965).
375. H. Yasuda, H. Clark, and V. Stannett, in N. M. Bikales, ed., *Encyclopedia of Polymer Science and Technology*, Vol. **9**, Wiley-Interscience, New York, 1968, pp. 794–807.
376. C. E. Rogers, in E. Baer, ed., *Engineering Design for Plastics*, Reinhold Publishing Corp., New York, 1964, pp. 609–688.

DUANE PRIDDY
Dow Chemical Company

STYRENE–BUTADIENE COPOLYMERS

Introduction

Styrene–butadiene (SB) copolymers represent one of the largest and most diverse group of polymers in use today. This has come about due to the wide range of properties that can be obtained by modification of styrene–butadiene ratio as well as other material characteristics. Copolymers that contain low levels of styrene, high in butadiene content, show elastomeric behavior, and copolymers that are styrene-rich show thermoplastic behavior. This way SB copolymers can exhibit material performance characteristics ranging from pure elastomeric, as in car tire and other flexible applications, to full thermoplastic, as in injection-molded transparent medical devices. This ability to span such large performance regimes has been a key reason for their widespread use. The other factor that has been critical to the success of SB copolymers has been the commercial availability of the monomers, styrene and butadiene. This article focuses on elastomeric and thermoplastic versions of SB copolymers. In addition to these, SB latex is also used in coatings and paint applications. SB latex is not covered here.

Monomers

Butadiene. Global consumption of butadiene monomer in 1996 was 7.5 million metric tons (1). The largest use of butadiene was for styrene–butadiene rubber, representing 28% of the total volume. Butadiene is manufactured in several different ways. The key industrial processes include recovery of butadiene from ethylene production as a by-product and dehydrogenation using either the

Encyclopedia of Polymer Science and Technology. Copyright John Wiley & Sons, Inc. All rights reserved.

Houdry process or the oxidative dehydrogenation of *n*-butenes. Finally in some Asian countries, butadiene is also produced from ethanol.

Styrene. Global consumption of styrene monomer in 1998 was 17.9 million metric tons (2). While polystyrene was the largest outlet, SB copolymers (including latexes) consumed a total of 1.95 million metric tons. Styrene monomer is produced by two processes. Ethylbenzene dehydrogenation is the most widespread process used for styrene manufacture, followed by the propylene oxide coproduct route.

Styrene–Butadiene Rubber (SBR)

Introduction of automobiles brought with it the need for materials suitable for tire manufacture. In early 1900s, natural rubber was the material of choice. During the World War I restricted access to natural rubber started development programs in Germany. One of the polymers, polydimethylbutadiene, was used for a short while. Further research between two world wars led to the development of Buna S by I.G. Farben (a new company formed by combining Bayer, BASF, and Huls of Germany in 1933). The new rubber incorporated styrene (S stands for Styrol, German name for styrene, in Buna S), improving the performance dramatically. Similarly as U.S. access to natural rubber became restricted during the World War II, a government sponsored research program, known as Government Rubber-Styrene (GR-S), was started. All the rubber producers were organized under the consortium of American Rubber Manufacturers and were overseen by the newly set up Office of Rubber Reserve. The primary product was Buna S.

After the second world war, the United States became aware of the new developments in cold SBR production, which was superior to Buna S type rubbers, and subsequently most of the production facilities in the United States were converted to run the cold SBR process. Cold SBR has become the standard process for emulsion-based SBR production across the globe.

Developments in the anionic polymerization of butadiene were adopted for manufacture of solution SBR. While the emulsion process gave primarily 1,4-cis microstructure in the final product, the solution process gave a lower level of 1,4-cis level, typically around 45%. Furthermore the cis content as well as 1,2-vinyl content could be modified. In addition, better control of branching and molecular weight distribution attainable with anionic process made solution SBR suitable for tire applications, challenging the established use of cold SBR. Developments in the anionic process also led to new copolymer structures in which blocks of polybutadiene can be coupled to blocks of polystyrene, generating a unique class of polymers. Developments in SB block copolymers led to new materials which were thermoplastic in character, unlike SBR which is an elastomer. Solution-processes-based thermoplastic SB block copolymers form the basis of the transparent impact polystyrene (TIPS) as well as the other block copolymers used in plastics modification. The block copolymers of styrene and butadiene are the subject of the second part of this article.

Polymerization Process

Butadiene and styrene can be copolymerized in a number of ways. Both ionic and free-radical initiations can be used for this purpose. This fact is reflected in

industrial production of SBRs. Initially the free-radical process was entirely based on hot emulsion processes utilizing a polymerization temperature of 50°C. Later developments showed that much improvement can be made to the product if the polymerization temperature can be lowered to around 5°C. As a result the "cold" emulsion process became the process of choice. Today the cold emulsion process accounts for the larger portion of the emulsion SBR market. Introduction of cold emulsion process and advances in anionic polymerization have demonstrated even further advantages, leading to the introduction of the solution process. The solution SBR products make up a smaller part of the consumption but their volume is increasing.

Cold SBR. Cold SBR is produced by the emulsion process (3–12). In the emulsion process an emulsion of monomers (styrene and butadiene) is formed in water by the help of an emulsifying agent, usually a soap (13). The monomers in the emulsion are polymerized by a water-soluble initiator fragment, a free radical generated from a hydroperoxide (3) or from an oxidation reduction process. As the free radical enters the emulsion droplet, a micelle, it polymerizes the monomers present.

Emulsion polymerization can be divided into three distinct phases (14) (see Fig. 1). In the nucleation stage, phase I, a free radical is generated (6,15) from the initiating species in the water phase. The most commonly used initiators are the redox systems such as persulfate with ferrous ion (16,17).

$$S_2O_8^{2+} + Fe^{2+} \rightarrow Fe^{3+} + SO_4^{2-} + SO_4^{-\cdot}$$

The free radical then has the possibility to react with monomer dispersed in the system in several states, the most significant of which is micelles (18). Micelles are monomer droplets stabilized by the emulsifying agent. An emulsifying agent contains both oil-soluble and water-soluble parts in its molecular structure, and hence forms the interphase between the water and the dispersed monomeric phase. At the start of phase I, a typical system contains 10^{18} micelles/mL and the initiation rate is around 10^{13} radicals/(mL·s). As the radicals enter the particles, the polymerization proceeds in the usual manner at a rate r_p with a propagation rate constant k_p and the monomer concentration $[M]$ in the particle (3–5,9).

$$r_p = k_p[M]$$

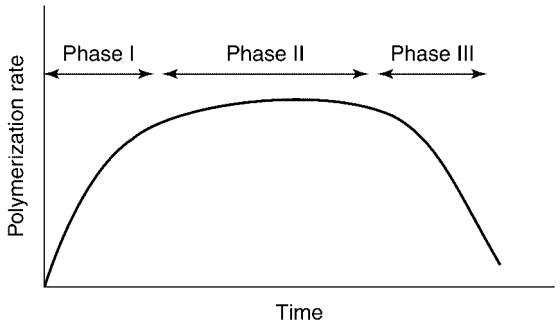

Fig. 1. Three distinct polymerization phases for emulsion polymerization of styrene and butadiene.

As the polymerization continues and monomer is converted to the polymer, the growing micelles continue to absorb more and more emulsifying agent from the medium. As the emulsifier concentration starts to decrease in the reaction medium, there comes a time when the emulsifier concentration falls below a critical micelle concentration. Micelles are formed and maintained only if the emulsifier concentration is above this critical level. The conversion of monomer is typically 15–20% in the first phase.

The growth stage of the process, phase II, starts with micelles becoming polymer particles with a thin layer of surfactant on its surface. At this stage the polymer particles are swollen with monomer that has diffused from the monomer droplets to polymer particles. Major part of the polymerization reaction takes place at the growth stage. The polymerization reaches a steady state inside the swollen polymer particles (10,11). The growth stage ends when most of the monomer is converted to polymer, reaching a conversion level of around 65%. As the monomer concentration drops, the rate of polymerization decreases dramatically as given in Figure 1.

The final stage, phase III, is characterized by complete disappearance of monomer droplets. If the steady state is not maintained by fresh monomer diffusion into the polymer particles, the polymerization rate declines. The unreacted monomer continues to polymerize at a declining rate. If this process is allowed to continue, onset of gelation can take place through chain transfer to polymer.

Rate of polymerization R_p is given by

$$R_p = k_p[M][P\cdot]$$

where $[P\cdot]$ is the concentration of active particles. $[P\cdot]$ is usually expressed as

$$[P\cdot] = \frac{10^3 N' n}{N_A}$$

where N' is the number of particles (including micelles), n is the average number of radicals per micelle plus particles, and N_A is the Avogadro number. Finally, expressing R_p in its usual units of moles per liter-second gives

$$R_P = \frac{10^3 N' n}{N_A} k_P[M]$$

The number-average degree of polymerization, X_n, in emulsion polymerization is dependent on the rate r_i at which primary radicals enter a polymer particle:

$$r_i = \frac{R_i}{N}$$

where R_i is the rate of initiation. In most cases the rate of initiation is same as the rate of termination r_t. This is because as soon as a new radical enters the particle the termination takes place immediately by biradical coupling reaction. Then the

number-average degree of polymerization, X_n, is

$$X_n = \frac{r_p}{r_i} = \frac{Nk_p[M]}{R_i}$$

Emulsion polymerization has some unique advantages in comparison to solution or bulk polymerization processes. Most of the advantages are due to the unique polymerization kinetics, such as ability to make high molecular weight monomers at faster polymerization rates. Presence of water enables good temperature control, easy heat removal, and gives lower viscosity.

Selection of components for the emulsion polymerization process is critical. Initiator system, emulsifier, chain transfer agents play a significant role in kinetics of polymerization and in defining the properties of the final product.

A simplified process diagram of cold SBR production facility is given in Figure 2 (19,20). The process can be divided into four units:

(1) Feed preparation and clean up
(2) Polymerization
(3) Coagulation
(4) Drying and packaging

Primary function of feed preparation section is to remove impurities from butadiene and styrene monomer. Both monomers contain an inhibitor as

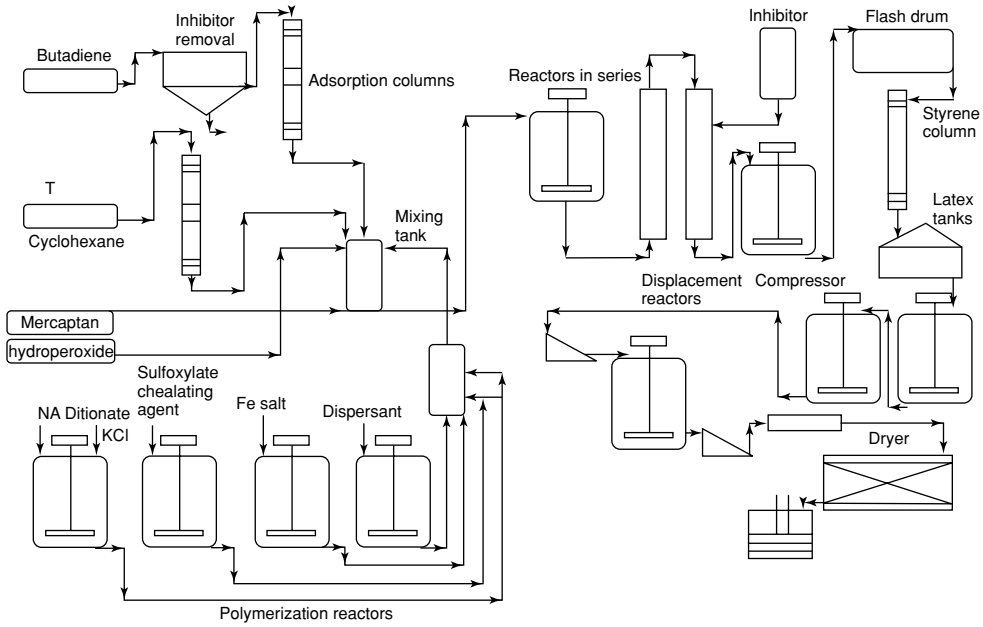

Fig. 2. Process layout showing main components of "cold" emulsion SBR process.

supplied (inhibitors are added to monomers to stop any premature polymerization during transport and storage) and it must be removed by washing with NaOH solution. Following this, water is removed from the monomer stream. Inhibitor and other oxygenated species are removed by passing styrene monomer through an activated alumina column. Other raw materials such as chain transfer agents, usually *t*-dodecyl mercaptan (or other mercaptans), hydroperoxide such as *p*-methane hydroperoxide, a solution of potassium chloride, sodium dithionate (oxygen scavenger), reducing agent such as sodium formaldehyde sulfoxylate, ferrous sulfate heptahydrate, are prepared in the feed preparation section. Similarly a solution of soaps, usually a mixture of two or more, is also prepared in the feed section.

The polymerization section consists of a series of polymerization reactors jacketed to remove the heat of polymerization. Initially the polymerization reactors are charged with deaerated water and the reactants fed to the reactor. As the polymerization reaction takes place, the heat generated is removed to maintain a reaction temperature of around 5°C, and hence the term "cold" SBR process. Once the desired level of conversion is reached in the displacement reactors, a short stopper is added to terminate the reaction. Then the unreacted monomers are removed by flashing the heated latex. All the unreacted monomers are fed into a recycle tank and returned to the start of the process (13). The latex is then fed to blending tanks to obtain the desired specification and to make the product uniform. Also, at this stage, slightly off-spec material can be blended in.

In the coagulation section, the water is separated from the polymer by chemical means and a slurry of the rubber crumb is obtained. The slurry is then filtered and washed several times. Finally the crumb is further dewatered in an expeller, dried in an expander dryer, and sent to the finishing section.

The finishing section consists of baler, film wrapper, and packaging unit.

Solution SBR Process. Solution SBR is based on the anionic process (19,21–25). There are some key differences between emulsion SBR and solution SBR processes, that form the bases for the differences between the two product groups. In the free-radical polymerization process, a polymer chain is initiated by the initiator fragment. In a fraction of a second, several thousand monomers units are added to the growing chain. The polymer chain then terminates through one of three mechanisms: (*1*) through a coupling reaction with another radical; (*2*) through disproportionation, where an electron is transferred from one radical to another; or (*3*) through a chain transfer reaction. Termination leads to a dormant polymer molecule which remains inactive until the end of the polymerization process.

In anionic polymerization, the initiator, typically alkyl lithium, initiates the polymerization process and rapidly reacts with the available monomer molecules. Then the active polymer chains remain active for the duration of the polymerization process. They will continue to polymerize any additional monomer that may be added to the system. The growing polymer chains must be deactivated specifically by the addition of a deactivator at the end of the process.

By far the most common initiator for copolymerization of styrene and butadiene is butyl lithium. Once the polymerization process is initiated, the tendency of the anionic species to add to butadiene or styrene monomer will be different. The polybutadienyl anion prefers to react with another butadiene monomer rather

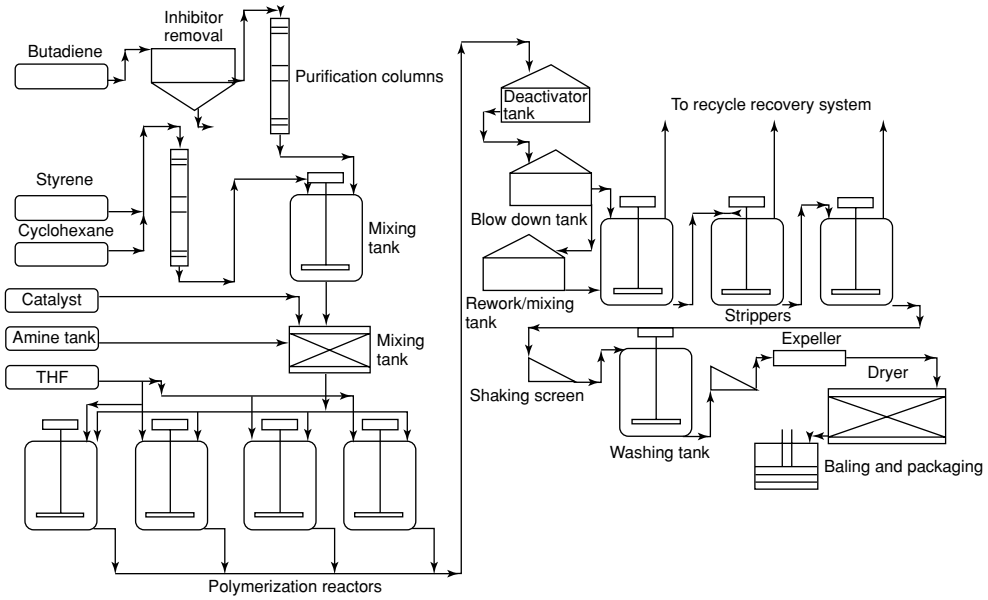

Fig. 3. Process layout showing main components of solution SBR process.

than a styrene monomer. In fact styrene can be used as a solvent for the anionic polymerization of butadiene if the polymerization reaction is terminated as soon as the butadiene monomer is depleted. If special precautions are not taken, a block copolymer of butadiene and styrene will be obtained. Especially in tire applications, it is very important to have a random copolymer. Special additives must be employed to assure random distribution of styrene units in the copolymer (26).

Solution SBR processes are based on anionic polymerization using butyl lithium initiator. A process flow diagram of the solution SBR process is given in Figure 3, showing major parts of the process. Detailed description of the process has been compiled from the information contained in a series of patents issued to major SBR producers (19,21–25).

The process is made up of three main stages:

(1) Feed preparation and clean up
(2) Polymerization
(3) Finishing

As butyl lithium initiator is very sensitive to water, inhibitor, oxygenated species, and active hydrogen-containing impurities, very stringent feed purification procedures must be carried out. Failure to have high purity will lead to deactivation of the most expensive raw material, butyl lithium [currently around $44/kg (19)]. Trace amounts of water from purified butadiene are removed by passing through a molecular sieve column. Styrene is purified by passing through an alumina column.

The polymerization section consists of a series of continuously stirred tank reactors (24,25). The solvent (25) (usually cyclohexane) and monomers are fed into the reactor and an initiator as well as a randomizer [usually tetrahydrofuran (THF)] is added. The function of the randomizer is to make sure that no blocks are formed from a single monomer (Hall, Oxolanyl Cyclic Acetals as Anionic Polymerization Modifiers #68). This is because the reactivity ratios of the monomers are not ideal. Usually the reaction temperature is kept less than 110°C to prevent deactivation of the growing chain ends (25). Once polymerization is complete, alcohol is added to terminate the polymerization reaction and the polymer solution is transferred to holding tanks to be blended to increase uniformity. Subsequent steps of washing and filtering remove all the unreacted monomers, THF, and other chemicals.

The finishing section consists of drying, bailing, wrapping, and weighing. The polymer is dried in two steps, then passed through a lump breaker to break any gels, and eventually packaged to the desired specification.

Because of the significant difference in polymerization characteristics, emulsion and solution processes produce SBR with a different balance of properties. These differences are a result of the molecular structure, branching, molecular weight distribution, and microstructure. In general, the solution SBR process provides a higher capability to modify the molecular parameters.

Some of the key advantages of solution SBR over emulsion SBR are molecular weight and molecular weight distribution control, low levels of branching, lower levels of contaminants, and higher degree of control over molecular topology. These characteristics provide improved performance to end-use applications as in tire manufacture. Solution SBR can lead to better balance between treadwear, traction, and rolling resistance. These three are the key properties that a tire manufacturer will aim to optimize (26).

The solution SBR process can control the molecular weight distribution and branching very effectively. During emulsion process the polymer chains grow in a very short while and then terminate, whereas in the solution process the growing chains are active until the monomers are consumed or a terminating agent is added. As a result the chains produced in solution process tend to be uniform in length whereas emulsion process leads to a broad distribution as chains that grow at different times in the process tend to have different molecular weight. The branching is a random process in the emulsion SBR route whereas it must be specifically incorporated by introducing branching agents during the solution process.

The monomeric unit in polybutadiene can exist in three distinct forms: 1,4-cis, 1,4-trans, and 1,2-vinyl (see Fig. 4). The relative portions of each one of these

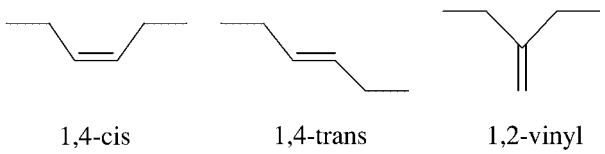

Fig. 4. Different types of microstructure for polybutadiene.

microstructures have a strong influence on the final properties of the polymer. Both the solution SBR and emulsion SBR processes give similar levels of 1,4 structures. Emulsion process gives a 1,2-vinyl level of about 20%. Depending on the specifics of the process, the solution process can give anywhere from about 8 to 60%.

Processing of SBR

SBR as manufactured, is an elastomeric material that requires further processing to convert it to a final article for end use. The processing accomplishes three key objectives. First of all it gives the article its final shape, then it incorporates additives that are required by the targeted end use, and finally causes cross-linking of the rubber. Without cross-linking, the rubber will not be usable, as it is a soft "gummy" material that would not retain its shape during use.

Typical processing of SBR is done in two stages (27). In the first stage, non-reactive components are mixed with the rubber to obtain a good dispersion. At this stage, to prevent any cross-linking, the cross-linking agents and accelerators are not added. The first-stage processing is called nonproductive stage as no cross-linking occurs at this stage. SBR (and optionally, a second rubber) is mixed with additives such as fillers, oils, antioxidants, stabilizers, and antiozonants, as well other specific additives. Fillers are added to "extend" the rubber. By far the most common filler is carbon black. Their function is usually to reduce the cost of the overall formulation and also to improve physical properties such as tensile strength. The carbon black fillers come in standard forms (28). A list of most common fillers and their function is given in Table 1. A large number of other components are used in the manufacture of SBR articles.

Oil extenders include naphthenic, aromatic, and parafinic oils. Their function is to soften the rubber for processing. Other processing oils include castor and tall oils as well as low molecular weight resins.

Once the nonproductive stock is mixed in an internal mixer in the second-stage cross-linking agents, accelerators are added to the nonproductive stock, which can then be shaped into final form and cured. The curing process is a chemical cross-linking reaction that builds bonds between rubber molecules.

SBR contains active double bonds on the polymer backbone. Cross-linking reactions are carried out by generating free radicals which react to form content bonds. Without the help of acceleration this reaction requires long times and high temperatures. By proper choice of activators and accelerators both the curing temperature and curing speed can be tailored for a given application.

By far the largest volume of SBR goes into automobile tires, representing some 80% of the total volume (30). In addition to tires, many other applications from gaskets to hoses also use SBRs. The single most important property of SBRs is their glass-transition temperature T_g. For tire applications T_g must be in a certain range, typically -70 to -50°C. Proper choice of T_g is important for control of friction and traction. If the T_g is too high, the rubber can loose its rubbery properties at low temperatures. On the other hand, too low a T_g can also cause problems. At very low T_g's, the traction at wet roads and moderate temperatures can suffer. In general, lower the T_g, better the treadwear. Tire manufacturers must

Table 1. Different Classes of Materials Used in SBR Processing and Their Function

Class	Compound	Function
Fillers	Carbon black	Reinforcing filler improves physical properties and reduces cost
	Calcium carbonate	Reduces cost and increases tensile strength. Both reinforcing (small particle) and nonreinforcing [coarse (29)] types exist
	Clay	Reduces cost and increases tensile strength
	Silica	Improves physical properties
Processing aids	Naphthenic/aromatic/ paraffinic oil	Extender (for softening of rubber)
	Castor/tall oil	Improves elongation
Vulcanization agents	Sulfur	Cross-linking
	Disulfide organic hydroperoxides	Fast accelerator, low temperature curing
	Tetramethylthiuram	Low sulfur cross-linking
Accelerators	Mercaptobenzothiazole dithiocarbomates	Fast accelerator, low temperature curing
Accelerators and activators	Zinc oxide, stearic acid diethanolamine	Cross-linking
Antioxidants	Phenolics	Nonstaining stabilizers
	Phosphites	Good stabilizers for SBR
Antiozonants	Diaryl-phenylene diamine	Low cost antiozonant

balance many compiling requirements of traction, wear, and rolling resistance by proper selection of T_g for this application. T_g has a strong influence on the hysterisis imparting rolling resistance and fuel consumption.

Two key variables that influence glass-transition temperature are styrene content and percentage of 1,2-vinyl in the microstructure. For emulsion process, the relationship between T_g and styrene content is as follows (31):

$$T_g = -78 + \frac{128S}{1.0 - 0.5S}$$

where S is the weight fraction of styrene in the copolymer.

Similarly for 1,2-vinyl content, the following relationship holds:

$$T_g = [1/(0.00578 - 0.0031S - 0.00212V + 0.00212VS)] + 273$$

where V is the weight fraction of 1,2-vinyl units in the butadiene portion of the copolymer. These equations are valid only for emulsion SBRs. In the case of solution SBR, some of the styrene units are present as short block and are not truly random copolymers.

Specifications, Testing, and Environmental Aspects

SBRs are characterized at different stages of their manufacture and use, utilizing several types of test procedures. During the manufacturing stage of the rubber, a series of tests are carried out to establish solids content (conversion), molecular weight, and chemical composition. Conversion is measured by just removing solvent and unreacted monomers, while chemical composition can be measured by either ir spectroscopy or by titration. The molecular weight and molecular weight distribution are determined by gel permeation chromatography.

Once the polymers are manufactured further characterization takes place prior to processing or during the process itself. The two key properties that are critical are T_g and Mooney viscosity. The most convenient way to measure the T_g is by differential scanning calorimeter. Mooney viscosity is an industry specific test procedure that is used for assessing the processability of the rubber. Mooney viscosity (ASTM D1646) is measured by rotation of a disk inside a cavity under pressure. This equipment does not measure the viscosity, but rather the torque required to rotate the disk at 100°C at a rate of 2 rpm. The results are usually given as

$$50 - \mathrm{ML}1 + 4(100^{\circ}\mathrm{C})$$

where 50-ML is the viscosity number, L indicates the larger of two rotor diameters used (other one being a smaller one for higher viscosity rubbers), 1 is the time in minutes that the specimen is preheated, 4 is the time in minutes after starting the motor at which the reading is taken, and 100°C indicates the temperature of the test.

In recent years dynamic mechanical testing has become an important means in correlating the performance of tires to molecular structure. Especially *tan delta* (ratio of elastic modulus to viscous modulus) has been used for understanding rolling resistance, skid resistance, and wear (26).

During the manufacturing process, primary health and environmental concerns relate to emissions and exposure. In most countries there are strict regulations concerning exposure to styrene and butadiene monomers. In the United States the exposure limits for styrene monomer is set at a time waited average of 50 ppm. The same value for butadiene is 10 ppm. During the processing, the breakdown of additives is a major concern. Use of secondary amines are regulated in some countries through monitoring of volatile nitrosamine generation. One of the primary environmental concerns for the rubber industry is the growing mountains of used tires. No significant outlet has been found for the recycling of the rubber in tires.

Styrene–Butadiene Block Copolymers

Emulsion and solution SBRs are made up of butadiene and styrene units that are randomly distributed along the polymer backbone. In the case of free-radical-polymerization-based emulsion process, the radical center randomly polymerizes both the styrene and butadiene units. The frequency by which these monomers

are incorporated into the growing polymer chain is determined by the reactivity ratios and the concentration of the monomers. In free-radical polymerizations the growing polymer chains have very short life spans in the order of less than a second. This eliminates any possibility of using sequential monomer addition techniques to make block copolymers. The only way to make block copolymers in the free-radical process is through incorporation of active sites into the polymer backbone which at a later stage is activated by heat or radiation in the presence of another monomer as indicated below.

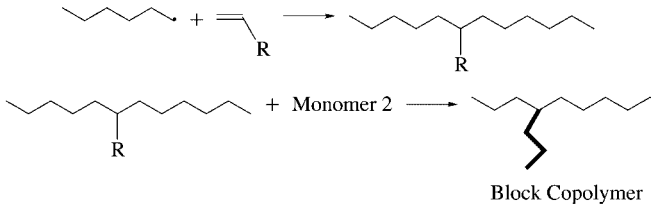

This route has been used extensively to make several types of block copolymers that cannot be made by anionic polymerization techniques. Systems where R is a peroxide group (32,33), diazo groups (34), hydroperoxide groups (35), or living free-radical groups (29,35) are used. Even though this route to block copolymers has been extensively investigated academically, no significant industrial application has been developed. Recent advances in living free-radical polymerizations indicate that this route might be more suitable for industrial use.

Industrially the most significant route to block copolymerization of styrene and butadiene is through anionic polymerization. The living nature of the anionic polymerization makes it possible to produce block copolymers of styrene and butadiene mostly through sequential addition of monomers.

Properties of Block Copolymers. Random copolymers of styrene and butadiene form homogeneous, one-phase systems showing typical characteristics of a single-phase polymer, such as a single T_g. In contrast the block copolymers of styrene and butadiene are two phase systems, with distinct domains of polybutadiene and polystyrene. As long as polystyrene domains are over 6000 amu in molecular weight, a two-phase system develops (36). The actual morphology of the block copolymer depends on the weight ratio of styrene and butadiene in the copolymer (Fig. 5). At low levels of styrene, a continuous polybutadiene phase develops with small spherical structures of polystyrene dispersed in the system (Fig. 6). As the styrene content of the block copolymer increases, spherical inclusions of polystyrene become elongated into cylindrical structures, becoming platelets at higher styrene levels (15–45%). At about 45% styrene level, co-continuous structures develop with alternating layers of polystyrene and polybutadiene.

The nature of SB block copolymers is defined by the weight ratio of styrene and butadiene. Those that contain more than 50 wt% butadiene are elstomers showing distinct elastomeric behavior. Industrially most polymers of this type contain 10–40 wt% styrene. As the styrene content increases the elastomeric nature of the block copolymer decreases. If the styrene content is above 50 wt% then a thermoplastic resin is obtained. These materials have the typical properties of

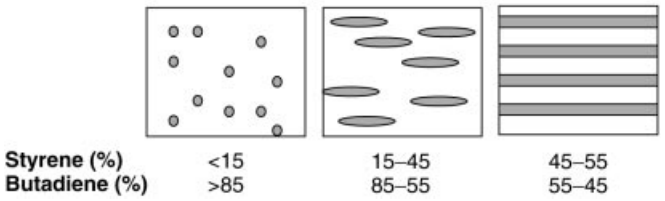

Fig. 5. Dependence of copolymer morphology on copolymer ratio in block copolymers of styrene.

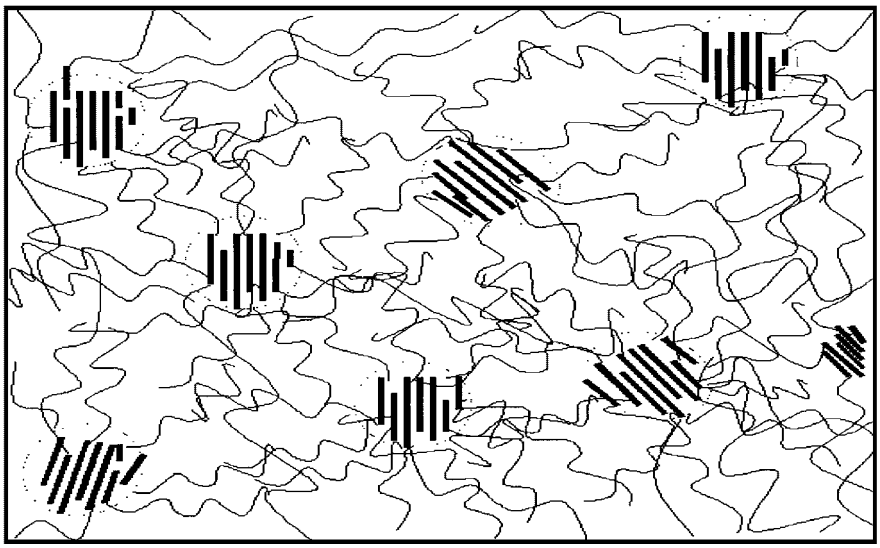

Fig. 6. A graphical representation of SB block copolymer structure at ambient temperature, with styrene content of 15% or less. Polystyrene phase (dark short lines) is presented as spherical domains dispersed in polybutadiene phase.

thermoplastic resins. As the styrene content approaches 100%, the resins become similar to high impact polystyrene (HIPS).

Manufacturing Process for Block Copolymers. Manufacturing of block copolymers is similar to solution SBR process, as they both use anionic polymerization. For elastomeric block copolymers the process is similar to solution SBR process. This is because the same feed purification and reactor layout is needed for producing elastomeric SBR polymers. The main difference between the solution SBR process and block copolymer production process is due to the fact that the styrene monomer distribution in the solution process is random while in block copolymers styrene is present as blocks (sequences of styrene monomer forming a polystyrene segment). In the process styrene and butadiene monomers are charged to the reactors at the same time. In the block copolymer process, first the butadiene segment is polymerized in the absence of styrene monomer. As the conversion of butadiene monomer nears completion, styrene monomer is added. Depending on the actual sequence, the transition from butadiene to styrene

segment can be graded, whereby the concentration of monomer units in the backbone changes from pure butadiene to a mixture of styrene and butadiene, eventually becoming pure styrene. These types of copolymers are referred to as tapered block copolymers. A short transition from butadiene to styrene units can also be achieved by making sure that all the butadiene is reacted prior to addition of styrene. In the case of triblock copolymers (SBS), two techniques are employed for manufacture. In the first case a sequential addition of monomers is used. First, styrene is polymerized until completion, followed by addition of butadiene and polymerization to completion. At the final stage, additional styrene monomer is added to form the triblock structure (Fig. 7). The second method is based on the use of bifunctional anionic initiators (37,38). With this type of initiator, the butadiene segment is produced first, followed by addition of styrene. As the bifunctional initiator grows the polymer from both ends, a triblock copolymer is obtained with two monomer addition steps versus the tri monomer addition steps of the monofunctional initiator case. Alternatively a coupling agent can also be used to produce SBS block copolymers with two steps of monomer addition (39,40). Elastomeric block copolymers can be finished in a manner similar to solution SBR if styrene content is relatively low. At above 25–30% styrene content the block copolymer looses its rubbery nature and becomes a relatively tough, difficult to bale product. At around 40% styrene content the product is powdery and cannot be baled easily. In the case of elastomeric block copolymers, unreacted monomers and solvent can be removed by steam stripping (41).

In the literature, many routes to synthesis of block copolymers are given, but on commercial scale, only the anionic solution process is used. In the case of solution SBR great care is taken to assure random distribution of monomeric units. In block copolymers great care is taken to assure that the butadiene and styrene units exist as blocks. The thermoplastic block copolymers, especially those with

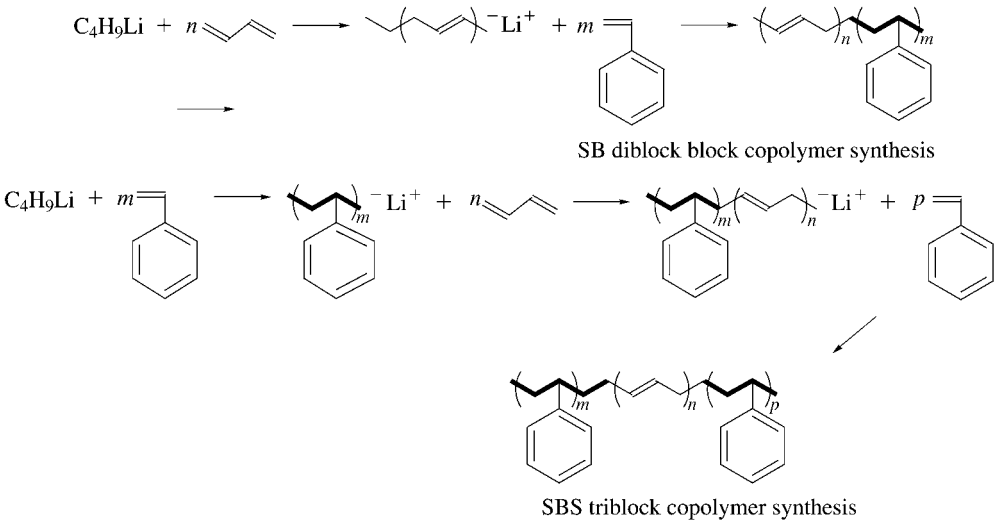

Fig. 7. Synthesis of triblock copolymers (S–B–S) with sequential monomer addition.

styrene contents above 65 wt%, can be finished with conventional thermoplastic finishing equipment.

The feed preparation and reactor sections of thermoplastic block copolymer production process are similar to the solution SBR process (36,39,40,42–45). Styrene, butadiene, and solvent are purified by distillation, followed by passing the reactants and solvent over alumina columns and molecular sieves (Fig. 8).

Thermoplastic Block Copolymers. Most well-known thermoplastic block copolymers are the K-Resin family (36,46) (Phillips Petroleum Co.). These contain about 27% butadiene in a star-block form (Fig. 9).

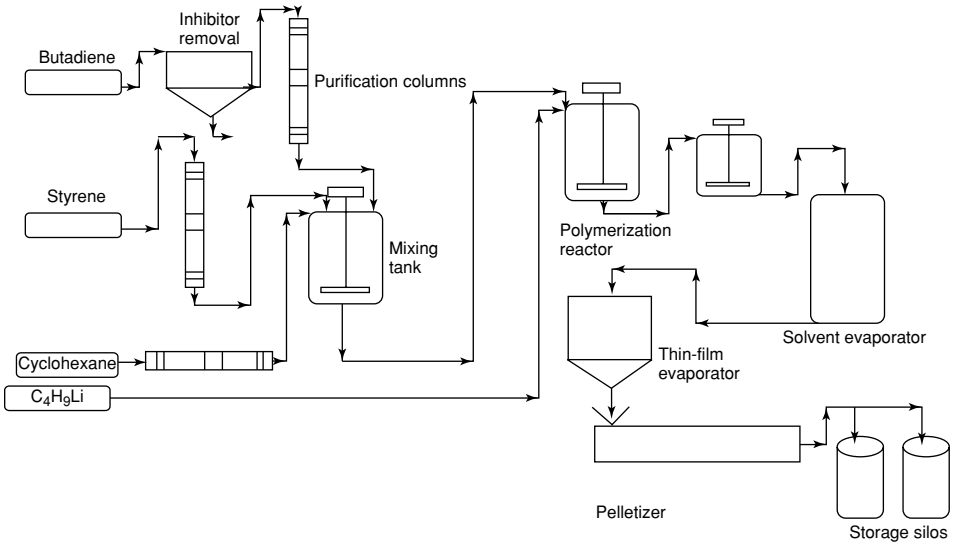

Fig. 8. Process layout showing main components of solution SB block copolymer manufacturing process.

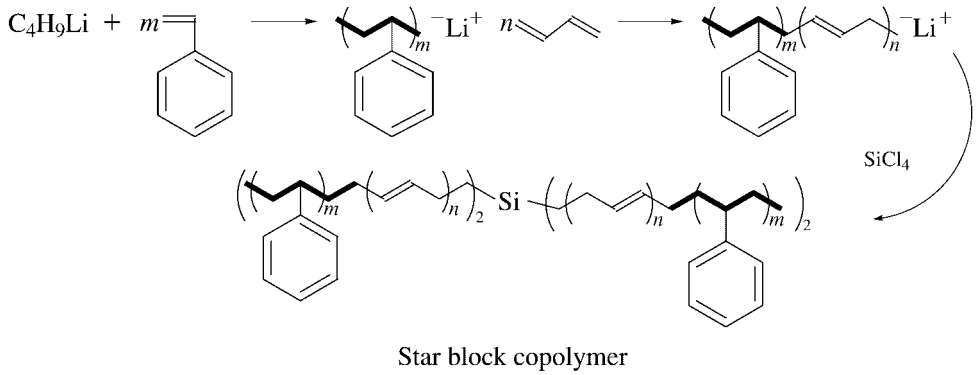

Fig. 9. Synthesis of star-block copolymers.

K-Resin is made up of a star-block copolymer where the inner polybutadiene segments are of about the same molecular weight while the outer polystyrene segments are of different molecular weight (47). This enables accurate control of polybutadiene segment thickness, ensuring improved clarity. To achieve optimum clarity, the polybutadiene segment thickness must be about one-tenth of the wavelength of visible spectrum or less (see ELASTOMERS, THERMOPLASTIC).

Processing of Block Copolymers. Elastomeric block copolymers contain blocks of styrene units that form hard segments below the glass-transition temperature of polystyrene. In most uses they do not need to be cured as the hard polystyrene segments act as cross-linking units below the glass-transation temperature of polystyrene (48,49). The block copolymers are seldom used in their pure form for fabrication of end-use articles. Most of the time they will be blended with other rubbers. By far the largest use of these types of block copolymers is for impact modification of polystyrene where they are blended with a polystyrene resin in a compounder or an extruder. They are also used in the manufacture of special grades of HIPS, mostly high gloss types, for injection molding or as a gloss layer for the co-extrusion of HIPS. One of the critical issues for thermoplastic SB block copolymer processing is cross-linking of the rubber phase. Special care must be taken to ensure processing temperatures do not exceed 240°C (51). If higher temperatures are needed, then the residence time must be minimized. Formation of cross-linked rubber is particularly important for the extrusion thermoforming process as these processes generate large amounts of recycle which is then blended with the virgin resin. In this way certain portions of the resin can end up going through the processes several times, further increasing the chances of gel formation. Presence of gel is detrimental to thermoformed articles as they cause significant problems in the appearance and wall thickness distribution for the thermoformed articles.

Economic Aspects and Use

Block copolymers of styrene and butadiene are extensively used in blends as well as neat products. Most of the blends are made with polystyrene resins, where addition of block copolymer improves the toughness of otherwise brittle polystyrene. Such materials find widespread use in food packaging, from yogurt cups to polystyrene film used for food packaging. Some volume of copolymer is also used as an impact modifier in the manufacture of specialty grades HIPS.

Block copolymers containing 20–40% styrene are also useful as impact modifiers for ignition-resistant HIPS as well as other polystyrene resins. Kraton® rubbers are available from Shell Chemical Co. and Vector® rubbers are available from Dexco Polymers (a joint venture between The Dow Chemical Co. and The Exxon Chemical Co.). Both grades are used extensively for this purpose as are other similar products from other suppliers. Kraton rubbers are usually triblock copolymers of SBS type. The center block is polybutadiene with terminal blocks of polystyrene (49–51). By far the largest use of block copolymers is in the form of TIPS resins. There are a number of suppliers, with Phillips Petroleum and BASF

Table 2. Properties of K-Resin Grades KR01 and KR03 from Philips Petroleum Co.

Property	ASTM test method	KR01	KR03
Density, g/cm^3	D1505	1.01	1.01
Melt flow rate, g/10 min	D1238	8	8
Tensile yield strength 50 mm/min, MPa[a]	D638	30	26
Elongation to break, %	D638	20	160
Flexural yield strength, MPa[a]	D790	44	34
Flexural modulus, MPa[a]	D790	1492	1414
Heat deflection temperature 1.8-MPa fiber stress, °C	D638	77	73
Izod impact strength 3.2-mm specimen, notched, J/m[b]	D252	22	41
Hardness, Shore D	D2740	75	65
Vicat softening point, °C	D1525	93	87
Light transmission, %		90	90

[a]To convert MPa to psi, multiply by 145.
[b]To convert J/m to ft·lbf/in., divide by 53.38.

being the largest producers. Phillips Petroleum product is supplied under the trade name K-Resin, with several grades for extrusion and injection molding (51). BASF also supplies a number of grades under the trade name Styrolux. Clarity, toughness, and rigidity are the key combinations for TIPS, making the product very desirable for both extrusion-thermoforming and injection-molding applications. In most cases the TIPS resins are blended with polystyrene depending on the toughness requirements of the final formulation. Properties of two grades of K-Resin are given in Table 2 (51) (see ELASTOMERS, THERMOPLASTIC).

Most significant environmental issues with respect to block copolymer synthesis relate to manufacturing process, taste and odor issues in end use, and solid waste in final disposal of these polymers. Manufacturing process issues relate to industrial hygiene, exposure, and volatile organic emissions. In end use, block copolymer/polystyrene blends tend to have taste and odor issues, especially for sensitive food packaging applications.

BIBLIOGRAPHY

1. F. Stahl, CEH Marketing Research Report, SRI International, 1999.
2. K.-L. Ring, *Chemical Economics Handbook*, SRI International, 1999.
3. D. C. Blackley, *Emulsion Polymerization*, Applied Science Publishers Ltd., London, 1975.
4. J. L. Gardon, in C. E. Schildknecht and I. Skeist, eds., *Polymerization Processes*, Wiley-Interscience, New York, 1977.
5. J. L. Gardon, in F. Millich and C. E. Carraher Jr., eds., *Interfacial Synthesis*, Marcel Dekker, Inc., New York, 1977, Chapt. "9".
6. W. D. Harkins, *J. Am. Chem. Soc.* **69**, 1428 (1947).
7. R. G. Gilbert and D. H. Napper, *J. Chem. Soc., Faraday Trans. 1* **70**, 391 (1974).

8. B. S. N. Hawkett, D. H. Napper, and R. G. Gilbert, *J. Chem. Soc., Faraday Trans. 1* **71**, 2288 (1975).
9. B. S. N. Hawkett, D. H. Napper, and R. G. Gilbert, *J. Chem. Soc., Faraday Trans. 1* **73**, 690 (1977).
10. W. V. Smith and R. W. Ewart, *J. Chem. Phys.* **16**, 592 (1948).
11. W. V. Smith, *J. Am. Chem. Soc.* **70**, 3695 (1948).
12. J. Ugelstad and F. K. Hansen, *Rubber Chem. Technol.* **49**, 536 (1976).
13. U.S. Pat. 5,583,173 (1996), R. Gujarathi and co-workers (to Goodyear Tire & Rubber Co.).
14. M. Morton and P. P. Salatiello, *J. Polym. Sci.* **8**, 111 (1951).
15. W. V. Smith and R. W. Edwart, *J. Chem. Phys.* **16**, 592 (1948).
16. I. M. Kolthoff and A. I. Medalic, *J. Polym. Sci.* **6**, 189 (1951).
17. E. M. Verdurmen, J. M. Geurts, and A. L. German, *Makromol. Chem.* **195**, 641 (1994).
18. G. Odian, *Principles of Polymerization*, John Wiley & Sons, Inc., New York, 1981, pp. 319–337.
19. S. Naqvi, PEP Review 96-5, Styrene–Butadiene Rubber, SRI International, 1998.
20. K. Othmer, *Encyclopeda of Chemical Technology*, 4th ed., 1997.
21. U.S. Pat. 5,100,965 (1992), W. L. Hsu and co-workers (to Goodyear Tire & Rubber Co.).
22. U.S. Pat. 5,448,003 (1995), W. L. Hsu (to Goodyear Tire & Rubber Co.).
23. U.S. Pat. 5,578,542 (1996), D. F. Lawson and co-workers (to Bridgestone).
24. U.S. Pat. 5,625,017 (1997), K. Morita and co-workers (to Bridgestone).
25. EP 0768323A1 (1996), A. Nakayama and co-workers (to Bridgestone).
26. U.S. Pat. Appl. No. US97-9107252 (1997), R. J. Zimmer and co-workers (to Goodyear Tire & Rubber Co.).
27. M. Morton, *Rubber Technology*, 3rd ed., Van Nostrand Reinhold Co., Inc., New York, 1987.
28. *The Synthetic Rubber Manual*, 12th ed., International Institute of Synthetic Rubber Producers, Inc., Houston, Tex., 1992, pp. 19–28.
29. D. B. Z. Y. Priddy, B. A. Howell, D. Meunier, J. Lyons, and M. Demirors, in *Book of Abstracts, 218th ACS National Meeting*, New Orleans, Aug. 22–26, 1999.
30. *Japan Chemical Week* **38**, 2 (1977).
31. L. A. Wood, *J. Polym. Sci.*, **28**, 319 (1958).
32. W. A. L. H. Hahn, *Macromol. Chem.* **16**, 50 (1955).
33. N. G. Gaylord, *Interchem. Rev.* **15**, 91 (1957).
34. W. A. F. A. Hahn, *Macromol. Chem.* **21**, 77 (1956).
35. M. Demirors, in *218th ACS National Meeting*, 1999, American Chemical Society, New Orleans.
36. U.S. Pat. 3,639,517 (1972), A. G. Kitchen and co-workers (to Philips Petroleum).
37. EPO 25,942 (1981), H. Hoecker and co-workers (to BASF).
38. U.S. Pat. 4,861,742 (1989), K. Bronstert and co-workers (to BASF).
39. PCT Int. Appl. 89/10,378 (1989), E. Lanza and co-workers (to Labofina).
40. U.S. Pat. 4,845,173 (1989), N. Yoshida and co-workers (to Sumitomo).
41. Japan Kokai 1-182308 (1989), T. Shiraki and co-workers (to Asahi Chemical Industry).
42. U.S. Pat. 4,427,837 (1984), L. H. Tung and co-workers (to Dow Chemical Co.).
43. Japan Kokai 64-56712 (1989), T. Shiraki and co-workers (to Asahi Chemical Industry).
44. U.S. Pat. 4,148,771 (1979), L. L. Nash (to Phillips Petroleum).
45. U.S. Pat. 4,431,777 (1984), L. H. Tung and co-workers (to Dow Chemical Company).
46. *K-Resin, Technical Brochure No. 1381-88-A02, Phillips 66 Company, Pasadena, Tex.*
47. G. Kraus and co-workers, *J. Polym. Sci., Part A-2* **9**, 1839 (1971).
48. *Kraton Thermoplastic Rubber*, Technical Brochure No: SC198-89, Shell Chemical Co., Oak Brook, Ill., 1989.

49. *Kraton Thermoplastic Rubber, Typical Properties*, Technical Brochure No. SC-68-90, Shell Chemical Co., Chicago, Ill., 1990.
50. *Kraton Thermoplastic Rubber, Processing and Fabricating Kraton Thermoplastic Rubber*, Technical Brochure No. SC-455-90, Shell Chemical Co., Oak Brook, Ill., 1990.
51. *K-Resin: Properties and Processing*, Technical Brochure No. 490-91-A02, Philips Petroleum, Houston, Tex., 1991.

MEHMET DEMIRORS
Dow Chemical Company

SULFUR–CONTAINING POLYMERS

Introduction

In the last decade of the twentieth century, sulfur-containing polymers have increasingly come into attention because of their interesting properties that make them useful in a wide range of applications. They can be used as high performance engineering plastics, chemically stable ion-exchange membranes in electromembrane processes, proton-conducting electrolytes, and optical, optoelectronic, and photochemical materials. Some polymers are employed in biomedical applications, eg, sulfopolymers as biomembranes and blood-compatible materials, and polysulfates and polysulfonetes as antithrombotic or antiviral agents. The presence of sulfur, particularly in the form of disulfide bridges, plays an important role in biopolymers.

The purpose of this review is mainly to present recent advances in the area of sulfur-containing polymers that may not yet have commercial applications. Nevertheless, older but still significant material has been included at the beginning of the discussion of each class (see also POLY(ARYLENE SUFIDE)S; POLYSULFIDES; POLYSULFONES).

Poly(monosulfide)s

Polymers containing a monosulfide linkage in both the main chain and the pendent group are the subject of many detailed studies. A few reviews of the synthesis and properties of all types of polymers have been published (1–4); the nearest one covering polymer with sulfur in the main chain appeared in 1992 (3). Polysulfides with controlled and well-defined structures are easily prepared.

Encyclopedia of Polymer Science and Technology. Copyright John Wiley & Sons, Inc. All rights reserved.

Nevertheless, the only commercial poly(monosulfide) is Ryton [Philips Petroleum Co., poly(thio-1,4-phenylene) more frequently referred to as poly(*p*-phenylene sulfide) or poly(phenylene sulfide) (PPS)].

Much effort has been devoted to preparing aromatic compounds in view of their significance as reactive intermediates for the synthesis of high performance linear aromatic polymers by ring-opening polymerization (ROP) (5). In an attempt to develop a novel synthetic method for the preparation of high molecular weight poly(thioarylene)s, macrocyclic aromatic sulfides and disulfides have been intensively prepared (6–14). The coordination chemistry of macrocyclic polysulfides has also received considerable attention during the past years. The thiacrown ether polymer ligands can be used as ion-exchange resins, metal ion adsorbents, and polymeric phase-transfer catalysts (15,16). Molecular systems in which tetrathiafulvalene is incorporated into macrocycles with supplementary donor atoms are potential electroactive cation sensors (17). The π-conjugated polymers have been extensively studied because of their attractive electronic properties.

Aliphatic Poly(monosulfide)s. High molecular weight polymers may be obtained easily by ring-opening chain-growth polymerization of the smaller rings (episulfides with three and four atoms, thiiranes, and thietanes, respectively) (3,4). Nevertheless, polymers with larger aliphatic groups have been prepared only by step-growth polymerization (1,3).

The most important here have been the addition of dithiols to diolefins (3,18) and the condensation of alkali metal sulfides or dithiolates with dihalides (3,19).

In the last decade, only a few new wholly aliphatic or mixed aliphatic–aromatic poly(monosulfide)s have been reported.

A series of poly(oxyalkylene)s such as poly[oxy((alkylthio)methyl)ethylene] (**1**), poly[oxy((alkylthio)methyl)ethylen-*co*-oxyethylene], and poly[oxy-2,2-bis((alkylthio)methyl)trimethylene] containing (alkylthio)methyl side groups were prepared from corresponding chloromethyl compounds with sodium alkanethiolates, using *N*,*N*-dimethylacetamide (DMAc) as a solvent and tetrabutylphosphonium bromide (tetra-*n*-butylphosphonium bromide) [3115-68-2] as a phase-transfer catalyst at 25 or 140°C (20). This substitution reaction gave 100% conversion with little, if any, backbone cleavage. The obtained (alkylthio)methyl-substituted polymers [intrinsic viscosities ([η]) from 1.10 to 2.68 dL/g and glass-transition temperatures (T_g) from −6 to −71°C] were successfully oxidized under mild conditions to highly polar (alkylsulfonyl)methyl-substituted poly(oxyalkylene)s (eg, **2**). The effectiveness and simplicity of these reactions make it possible to synthesize copolymers with chloro- and thioether, and/or sulfone side groups; this opens unlimited possibilities for making new polymers for various applications, including liquid crystalline polymers (21).

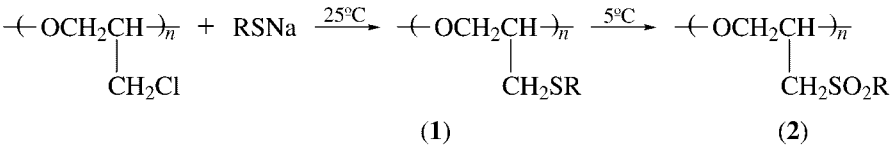

(**1**) (**2**)

R = CH_3, $(CH_2)_xCH_3$ (where x = 1, 2, 3, 4), $CH(CH_3)_2$

The novel partially crystalline polymer (**3**) with number-average molecular weight (M_n) of up to 5700 was prepared under various conditions by catalyzed self-condensation of 3-hydroxypropyl methoxycarbonylethyl sulfide (**4**) or 3-hydroxypropyl carboxyethyl sulfide (**5**) (22). The degree of crystallinity, melting temperature (T_m), T_g, and temperature of initial decomposition (T_d) were 36–46%, 37–47°C, −61 to −70°C, and 164–260°C, respectively. The monomers (**4**) and (**5**) were prepared by an addition of methyl 3-mercaptopropionate and 3-mercaptopropionic acid with allyl alcohol [107-18-6] catalyzed by AIBN [2,2′-azobis(2-methylpropionitrile), azobisisobutyronitrile, azodiisobutyrodinitrile, 2,2′-azobis(2-methylpropanenitrile), α,α'-azodiisobutyronitrile, 2,2′-azobis(isobutyronitrile), 2,2′-dicyano-2,2′-azopropane, Porofor-57, 2,2′-dimethyl-2,2′-azodipropionitrile, 2,2(-azobis(2-methylpropionitrile))] [78-67-1].

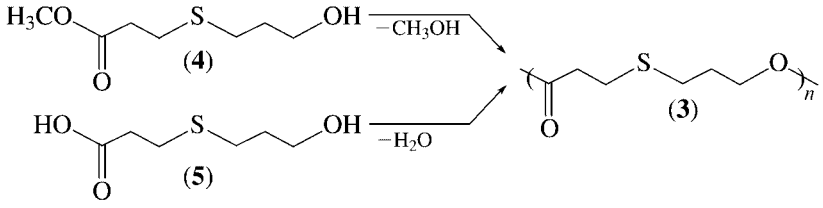

An addition of conjugate 1,4-benzenedithiol (A) to 1,4-divinylbenzene (1,4-diethenylbenzene, *p*-divinylbenzene) (B) [105-06-6] was investigated in detail in the presence of the AIBN initiator in toluene at 75°C (23). It was found that the polymerization proceeded without an induction period, to give a white polymer with a high molecular weight [weight-average molecular weight (M_w) = 110,000] in ∼90% yield for 2 h. In addition, it was confirmed by ^{1}H nmr, ir, and the sulfur contents that the polymer had an alternating structure of A and B units.

The synthesis and radical addition behavior of optically active cysteine-based monomers with mercapto and olefin groups have also been studied (24). *N*-4-vinylbenzoyl-L-cysteine methyl ester polymerized satisfactorily to afford the corresponding polysulfide (with M_n in the range of 7000–23,000) in good yields.

A novel one-pot synthesis of sulfur-containing polymers including poly(monosulfide)s (polythioethers), poly(disulfide)s, polythioesters, and polythiourethanes from a five-membered cyclic dithiocarbonate (5-phenoxymethyl-1,3-oxathiolane-2-thione) and diamines has been examined. Polythioethers with M_n = 2600–17,700 were obtained by condensation of *in situ* forming dithiol with α,α'-dibromo-*p*-xylene [623-24-5] (25). A synthesis by using a bifunctional five-membered cyclic dicarbonate and benzylamine [100-46-9] has also been reported (26).

High temperature solution condensation of 4,4′-bis(mercaptomethyl)biphenyl (MMB) (**88d**) or 4,4′-dimercaptobiphenyl (4,4′-biphenyldithiol) (MB) with various aliphatic and aromatic–aliphatic dihalogen hydrocarbons has been studied in detail. Polymers with reduced viscosity

(η_{red}) = 0.18–0.54 dL/g and in ~78–99% yield were obtained under optimum conditions. Their characteristics were T_m = 104–248°C from MMB, 215–345°C from MB and T_d = 230–270°C from MMB, 290–340°C from MB. All the polymers showed good chemical resistance. Some mechanical and electrical properties of the selected polymers were examined (27).

Poly(arylene sulfide)s. The best-known polymer in this class is PPS (**6**). The commercial product produced from dichlorobenzene and sodium sulfide (Na_2S) by polymerization in a polar solvent, eg, *N*-methyl-2-pyrrolidinone (NMP) [872-50-4], contains up to a few percent of disulfide linkages.

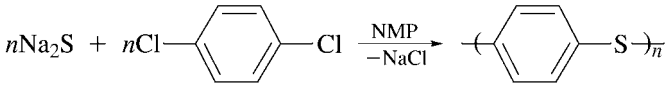

(**6**)

Linear PPS is a crystalline material with T_m ~285°C and T_g = 85°C for a degree of polymerization of ~200. PPS shows a rather good chemical and thermal resistance (T_d = 370°C) and finds a wide range of applications as a high performance thermoplastic with excellent mechanical properties (3,28,29).

The main types of preparation of poly(arylene sufide)s can broadly be classified into electrophilic and nucleophilic reactions; the latter are much more developed. In addition, many other polycondensation, oxidation, irradiation, or electroinitiated reactions were developed for the synthesis of various aromatic or aromatic–aliphatic materials (3).

Ring-Opening Polymerization (ROP). Free-radical ROP of various macrocyclic oligomers containing an aromatic sulfide linkage has recently been intensively studied as a new facile route to obtaining high performance thermoplastic polymers. The advantageous aspects of ROP over the conventional condensation methods are the elimination of solvents, the absence of by-products, and the rapid formation of high molecular weight polymers in high yields. Another noticeable attractive feature in using cycles is their much lower melt viscosity compared with that of the polymers, which facilitates reactive injection molding (14).

It was found that heating cyclic oligomers which contain an aromatic sulfide linkage in the presence of elemental sulfur or an aromatic disulfide, eg, 2,2′-dithiobis(benzothiazole) (MBTS, 2-mercaptobenzothiazole disulfide, etc) [120-78-5] readily yields high molecular weight polymers by ROP which proceed via a free-radical mechanism (8). The free-radical nature of the polymerization was confirmed by electron spin resonance (esr) spectroscopy. Melt polymerization of the cyclic hexakis(thio-1,4-phenylene) gave only a low molecular weight polymer (12,14,30) whereas that of a lower melting mixture of cyclic oligomers (**7**) led to the formation of highly crystalline high molecular weight poly(thio-1,4-phenylene), which is compared with that of commercial PPS. Other macrocycles, eg, (**8**), also gave high polymers (M_n ~30,000) (8).

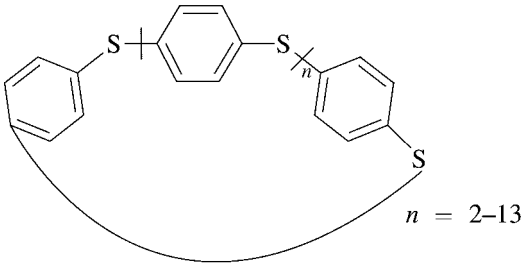

(**7**)

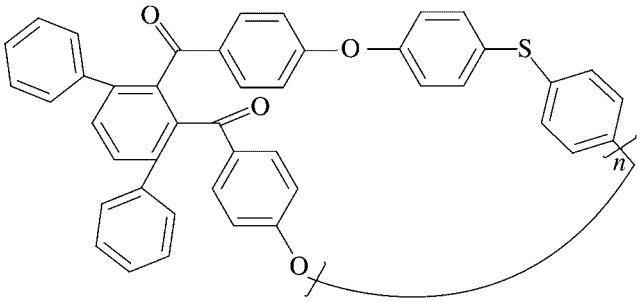

(**8**)

Free-radical ROP of cyclic oligo(thioarylene)s (**9**) in the presence of a small amount of an initiator (elemental sulfur or MBTS) in melt at 300°C has been studied (14).

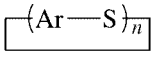

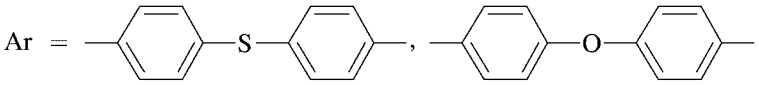

(**9**)

Linear poly(thioarylene)s obtained (yield 91–100%) were rather low-molecular-weight polymers (M_n = 1500–2100 with polydispersity 2.2–3.1). Their T_ms were 195–250°C, temperatures of the 10% weight loss (T_{d10}) ~490°C.

Other Methods. The electrophilic reaction of sulfur dichloride (SCl_2) or sulfur chloride (S_2Cl_2) with phenyl sulfide (diphenyl sulfide, diphenylthioether, 1,1′-thiobisbenzene) [139-66-2] in dichloromethane [75-09-2] solution at room temperature was studied in the presence of various catalysts (31). The resulting oligomeric products contained a linear structure linked by sulfide and disulfide bonds. It was found that SCl_2 showed higher reactivity than S_2Cl_2. The quantitative yield was achieved among other things with a catalyst, such as Fe, $SnCl_4$, $TiCl_4$, or $ZnCl_2$. An Fe catalyst gave a white product containing no elemental sulfur.

It has been reported that tris(2,2′-bipyridine)ruthenium(II) chloride catalyzed the photooxidative polymerization of diaryl disulfides by O_2, by which poly(thioarylene)s were efficiently prepared. The polymerization proceeded through the electrophilic reaction of the sulfonium cation which was produced selectively by the photoredox system. The ruthenium(II) complex provided the first photocatalytic system for the polymerization of diphenyl disulfide. The linear structures of the obtained polymers were confirmed (32).

Linear perfluorinated PPS was successfully prepared in 100% yield by the new method condensation of the corresponding fluorinated aryl sulfoxide via the poly(arylenesulfonium salt) as a precursor (33). The polymer had a significantly higher T_m (373°C) than that of PPS (285°C). The contact angle measurements showed that the surface energy of the polymer ($\sigma_s = 41$ mN/m) is comparable to those of poly(ethylene terephthalate) [25038-59-9] and polystyrene [9003-53-6]. High molecular weight PPS is also synthesized by this method.

New aromatic poly(monosulfide)s (**10**) (34) containing a 1,3,5-triazine ring were readily prepared with moderate yields by the aromatic nucleophilic substitution polymerization of 2,4-dichloro-1,3,5-triazine derivatives with bis(4-mercaptophenyl) sulfide (4,4′-thiodibenzenethiol) [19362-77-7] under mild conditions in the presence of a base in tetrahydrofuran (THF) [109-99-9] solution or in the *o*-dichlorobenzene/water two-phase system by using phase-transfer catalyst. The resulting polymers showed highly crystalline structures and high thermal stability (T_d ~330–410).

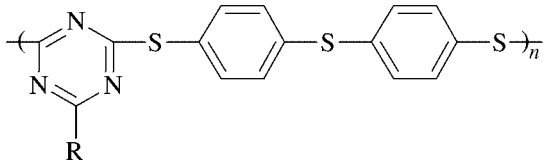

R = C_6H_5, C_6H_5NH, $C_6H_5(CH_3)N$,$(C_6H_5)_2N$, C_6H_5O, C_6H_5S

(**10**)

Preliminary investigations of the thermal polymerization reactions of newly obtained cyclic aromatic disulfides with *p*-diiodobenzene [624-38-4] and dibromobenzene [26249-12-7], or bis(4-bromophenyl) ether (4,4′-dibromodiphenylether, bis-*p*-bromophenyl ether, *p,p*′-dibromodiphenyl ether) [2050-47-7] as a new alternative approach to PPS and other polysulfides have been reported (9). The reactions were carried out in diphenyl ether solution at 270°C giving polymers with ~96% yield.

Macrocyclic Polythioethers. During the past decade, intensive studies have taken place of the complexation of transition metal ions with crown thioether ligands, mainly 1,4,7-trithiacyclononane (9S3) (**11**) as well as 1,4,7-trithiacyclodecane (10S3) (**12**), 1,4,7,11,14,17-hexathiacycloeicosane (20S6) (**13**), and 1,4,7,10,13,16,-hexathiacyclooctadecane (18S6) (**14**), and many articles (35–42), including reviews (35–39), dealing with the coordination chemistry of these ligand systems have been published. The crown thioether complexes of the soft

metal ions exhibit unusual stereochemical, spectroscopic, and electrochemical properties, such as the ability to stabilize uncommon oxidation states including Pd(III), Pt(III), Au(II), and Rh(II), the ability to force metals ions into unusual geometries such as octahedral Rh(I) and Au(III), the formation of metal–carbon bonds, and the ability to activate carbon–hydrogen bonds in ring-opening reactions (41).

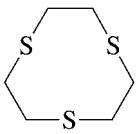

(**11**)

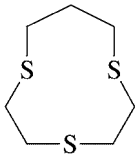

(**12**)

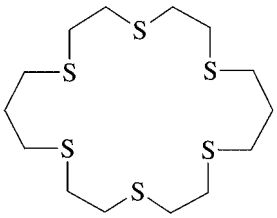

(**13**)

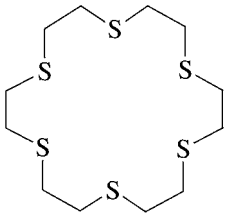

(**14**)

The thiacrown ether monomers (**15**) were polymerized and copolymerized with styrene [100-42-5] and *N*-vinyl-2-pyrrolidinone (*N*-vinyl-2-pyrrolidone, *N*-vinylpyrrolidone, 1-vinyl-2-pyrrolidone, 1-vinyl-2-pyrrolidinone, vinylbutyrolactam, etc) [88-12-0] by radical polymerization, giving the thiacrown ether polymer ligands which had binding selectivity for Ag(I) and Hg(II) ions. These polymers are likely to be efficient sorbents for the heavy metal ions under industrial conditions, since they can be used repeatedly under acidic conditions (15,16).

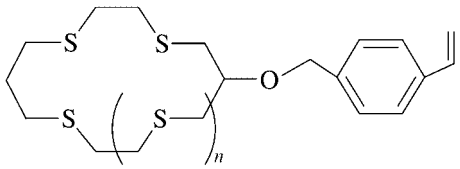

$n = 1$ or 3

(**15**)

A new method has been reported of the synthesis of thiocrowned and oxothiocrowned 1,3-dithiole-2-thiones from the key starting compound of 4,5-bis(benzylthio)-1,3-dithiole-2-thione. Intramolecular phosphite coupling reaction yielded the new tetrathiafulvalene (TTF) [31366-25-3] derivatives incorporated into thiacrown as well as oxathiacrown ether macrocycles in moderate yields. This procedure permits the isolation of asymmetric sulfur/oxygen donors not accessible by other methods (43). TTF-containing macrocycles with sulfur and selenium soft donor atoms were obtained by using a similar method (17). The cyclic voltammograms of these TTFs were discussed.

Polythiophenes. Polythiophene and its alkyl derivatives are the first class of conducting polymers with a good stability toward oxygen and moisture (3,44–46) (see ELECTRICALLY-CONDUCTING POLYMERS). High molecular weight polymers are successfully produced by the chemical oxidations (Lewis acid), the organometallic coupling (chemical), and the electropolymerization methods. Good-quality films are afforded by electropolymerization.

The synthesis of 3-(perfluoro)-thiophenes and 3-(polyfluoro)-thiophenes as precursors to electrically conductive polymers has been reported (47–53). The incorporation of a significant percentage of fluorine into the polymer is anticipated to allow greater control over its oxidation potential and provide better long-term chemical and thermal stability in the electrochemical environment over that of the nonfluorinated polythiophene analogs.

The novel functionalized polythiophenes, poly[3-(6-hydroxyhexyl)thiophene] and poly(3-octanethio-2,2′-bithiophene), have been used as selective coating materials for quartz crystal microbalance (QCM) sensors. These Langmuir–Blodgett film coated QCM sensors are useful in detecting heavy metal ions in aqueous solution, which are major pollutants in wastewater (54).

Tetrathiafulvalene Polymers. TTF and its derivatives form highly conductive anisotropic (quasi one-dimensional) charge-transfer complexes and radical cation salts. To obtain materials with three-dimensional conductivity, good processability, and film-forming properties, the polymeric forms of TTF are prepared. TTF can be incorporated into the polymer backbones via condensation to polyesters, polyamides, polyurethanes, and polysulfonates (55).

Several main-chain and side-chain TTF polymers have been synthesized via a multistep synthesis (55). They combine the unique properties of high molecular weight polymers, such as processability, with the outstanding electron-donating properties of TTF systems. Doping the polyurethane-type polymer (**16**) with 2,3,5,6-tetrafluoro-7,7,8,8-tetracyanoquinodimethane led to a free-standing, processable film exhibiting a moderately high electrical conductivity

of 8×10^{-4} S·cm^{-1}, which is comparable to iodine-doped nonordered polythiophene.

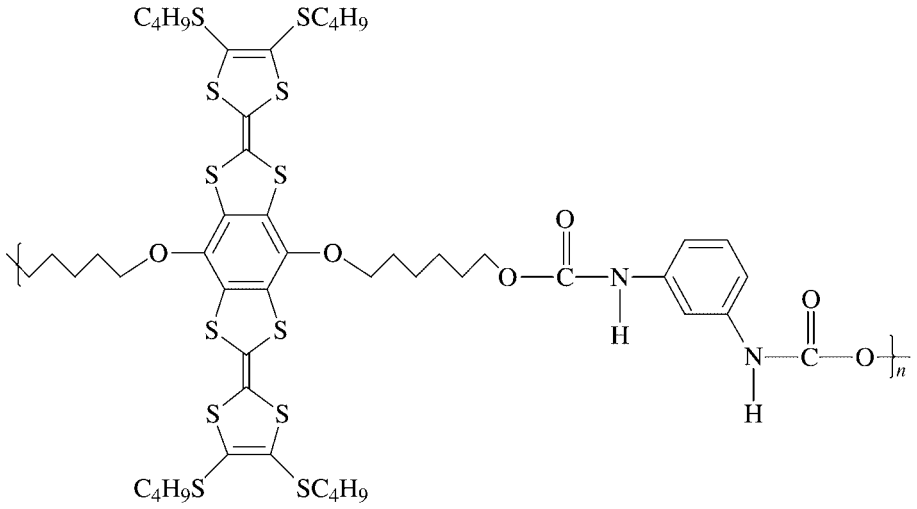

(**16**)

The synthesis of a fully conjugated, planar, and sulfur-rich TTF polymer, which should increase the dimensionality of the conduction process in the doped state, was also reported (55).

Conjugated Polymers. Sulfur-containing conjugated polymers have played a major role in the development of temperature-stable thermoplastic materials and in the search for materials being suitable as active components of optoelectronic and photonic devices. The new synthetic approaches to these polymers, including poly(phenantrolinebisthiazole), poly(phenylene sulfide-phenyleneamine) (PPSA), poly(tetrathiafulvalene), sulfur-containing [n]acenes, and donor-acceptor substituted poly(phenylenevinylene), were presented in a review article in 1997 (56). Two different strategies have been taken. The first one comprises the synthesis of suitably functionalized monomeric building blocks, which can be easily polymerized by common polymerization methods; the second one is based on novel methods of carbon–carbon and carbon–sulfur bond formation.

High molecular weight PPSA (M_n = 150,000) (**17**) and poly(phenylene sulfide–phenyleneamine–phenyleneamine) (PPSAA) (M_n = 68,000) (**18**) have been synthesized in high yields via their poly(sulfonium) cations through the acid-induced condensation reaction (57,58). These novel polymers represent the first hybrid structures of PPS and polyaniline (PAni). Both polymers are structurally well-defined and exhibit exceptional solubility in many solvents, including THF, *N*,*N*-dimethylformamide (DMF) [68-12-2], dimethylsulfoxide (DMSO) [67-68-5], and NMP, contrary to PPS and PAni. The electronic properties of polymer (**19**) that define this material as a prominent candidate for efficient hole-transport ability in light-emitting diodes (LEDs) have already been studied.

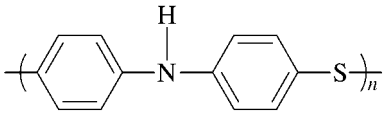

(**17**)

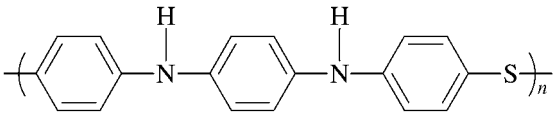

(**18**)

The first π-conjugated TTF polymer composed entirely of vinylogous, linearly fused TTF moieties was achieved by oxidative polymerization of 2-5-di(benzylidene)-1,3,4,6-tetrathiapentalene (59).

The syntheses of the first sulfonio-bridged, *p*-phenylene ladder oligomers (**44**) that have a planar ribbon-type structure have also been reported (60).

Poly(monosulfide ketone)s. Aromatic poly(monosulfide ketone)s [poly (thioether ketone)s] have been investigated in view of their potential use as high performance thermoplastics.

Poly(*p*-phenylene sulfide ketone) (**19**) (61) was prepared under different conditions by polymerization of 4,4′-difluorobenzophenone [345-92-6] (**20**) with sodium sulfide (Na_2S). Since the reaction involves nucleophilic aromatic substitution, it should be facilitated in aprotic polar solvents by increased dianion reactivity. A high molecular weight polymer [inherent viscosity (η_{inh}) = 0.95 dL/g] was obtained in solution of *N*-cyclohexyl-2-pyrrolidinone (*N*-cyclohexyl-2-pyrrolidone, 1-cyclohexyl-2-pyrrolidinone, 1-cyclohexyl-2-pyrrolidone, cyclohexyl-2-pyrrolidone, CHP) [6837-24-7], using freshly crystallized and dehydrated Na_2S. The polymer was high melting, $T_m = 335^\circ C$ and $T_g = 152^\circ C$.

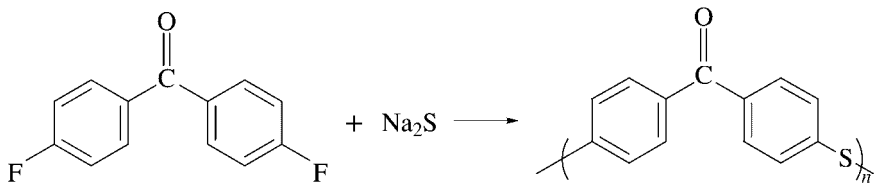

(**20**) (**19**)

Random copoly(*p*-phenylene sulfide sulfone/ketone)s were easily prepared in high yield (~95–99%) by the solution (NMP) condensation of sodium hydrosulfide (NaSH) with bis(4-chlorophenyl) sulfone (4,4′-dichlorodiphenyl sulfone) [80-07-9] and 4,4′-dichlorobenzophenone [98-98-2]. Copolymers with sulfone/ketone molar ratios > 25:75 were amorphous, whereas those with ratios ≤ 25:75 were crystalline. These materials form tough, creaseable films and exhibit a linear increase in the T_g from 144 to 215°C, with increasing sulfone content (62).

A series of poly(thioether ketone)s or poly(thioether ether ketone)s (η_{inh} = 0.1–0.73 dL/g) were synthesized by condensation of aromatic dicarboxylic acids with aryl compounds containing ether or sulfide structures using phosphorous pentoxide/methanesulfonic acid as the condensing agent and solvent. The polymers showed T_{d10} in the range of 420–485°C in air and nitrogen atmospheres (63).

Poly(thioether ketone)s (**21**) (η_{inh} = 0.3–0.54 dL/g, tetrachloroethane, 0.5%) were also prepared in good yield (92–94%) from masked bisthiophenol (**22**) and difluoro-compounds (**23**) such as 4,4′-difluorobenzophenone [345-92-6] (**23a**) or 1,3-bis(4-fluorobenzoyl)benzene (**23b**) by solution (NMP) polymerization in the presence of $KHCO_3$. The polymers showed T_g = 106–121°C and excellent thermal stability (T_{d10} ~460–515°C in N_2 and air). This novel method eliminates the problem associated with the conventional procedure in handling the unstable bisthiophenol monomers (64).

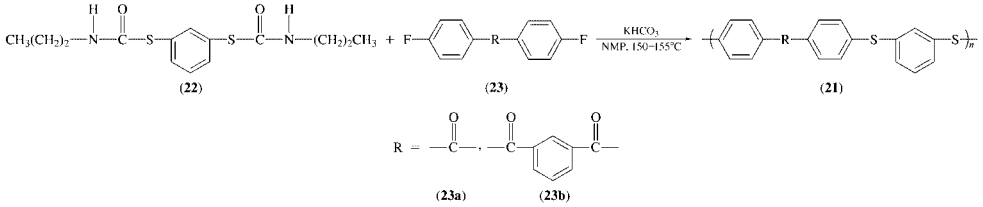

A series of high molecular weight poly(thioether ketone)s (M_n = 55,000–100,000), eg, (**24**) and (**25**), have successfully been prepared from bis(4-mercaptophenyl) ether (4,4′-dimercaptodiphenyl ether) or bis(4-mercaptophenyl) sulfide (4,4′-dimercaptodiphenyl sulfide) by reaction with a series of ketone-activated aromatic fluoro-compounds in the presence of anhydrous K_2CO_3. The polymers are amorphous and soluble in common organic solvents. They show T_gs from 154 to 251°C and excellent thermal stability [temperatures of 5% weight loss (T_{d5}) even above 500°C] (65).

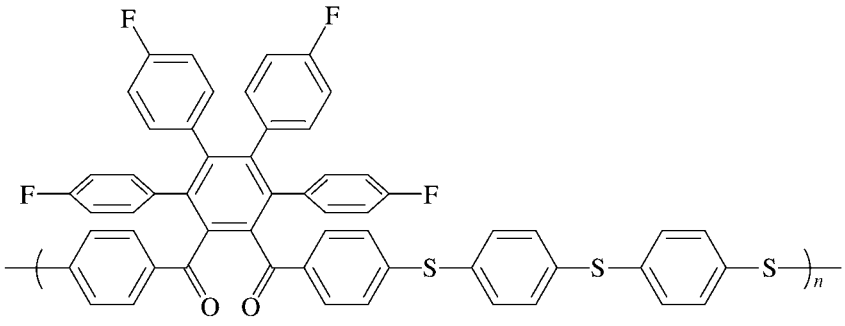

(**24**)

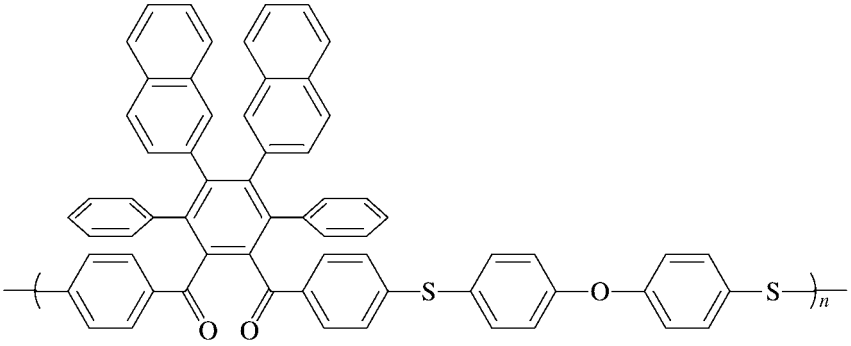

(**25**)

Optically active poly(γ-ketosulfide)s have also been the subject of detailed studies. Different routes to both aliphatic (66,67) and aromatic (68–70) polymers and their chirooptical properties have been described.

Poly(disulfide)s

During the last several decades, aliphatic poly(polysulfide)s, including poly(disulfide)s, have been extensively investigated because of their interesting properties resulting from the presence of polysulfide linkages. The properties such as good resistance to solvents and hydrocarbon fuels, resistance to dissolution for linear polymers and to swelling for cross-linked polymers, as well as generally good low temperature properties have given them a particular position among specialty elastomers. The Thiokol Co. in the United States marketed the first synthetic polysulfide rubber under the trade name Thiokol A [poly(ethylene tetrasulfide)]. Rohm and Haas now produces and distributes Thiokols. Aliphatic poly(disulfide)s, eg, Thiokol D [poly(ethyl ether disulfide], have also been produced commercially (71,72). There are several reviews of the synthesis and properties of this class of polymers (2,3,73,74) (see POLYSULFIDES).

In the last decade, extensive efforts have been devoted to the synthesis of cyclic oligomers as precursors for the preparation of high molecular weight polymers by ROP. Although it is routine to prepare aliphatic poly(disulfide)s by ROP (75), little attention has been given to the ROP study of cyclic (aromatic disulfide)s (3,76).

A series of cyclic (aromatic disulfide) oligomers have been synthesized in high yields by a copper-catalyzed oxidation with oxygen of arenedithiols in DMAc solution (10). The aryl groups contained moieties such as isopropylidene, ketone, sulfone, ether, thioether, and phenylphosphine oxide groups. In general, these cyclic oligomers with up to nine repeating units were soluble in common organic solvents and had sharp melting points. Contrary to earlier-described cyclization reactions, which were run over 16 h under high dilution conditions, this one was complete in 3–4 h at room temperature (10).

The ROP reaction of the cyclic oligomers mixture (**26**) derived from 2,2-bis(4-mercaptophenyl)propane (4,4′-isopropylidene bisthiophenol) was studied in both diphenyl ether solution and melt without adding any catalyst. It was found that

ROP began at ~150°C in solution and at ~200°C in melt. It may be supposed that the reaction is initiated by forming upon heating the radical species of (26). The highest molecular weight polymers (**27**) (M_n = 64,000–88,000) were formed at 200°C with conversion of cycles ~80% in solution and ~98% in melt. A ^{13}C nmr study indicated that structurally regular polymers were formed below 250°C (77).

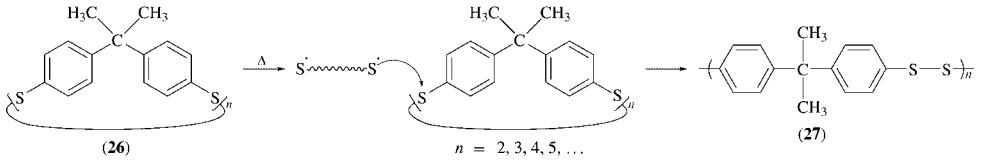

Earlier attempts of ROP without adding any catalyst were performed on some cyclic bis(arylene tetrasulfide)s upon heating (78) and 1,2,3-trithiane [3325-33-5] upon standing at room temperature (77). Some cyclic (arylene) disulfides were already prepared earlier by using iodine or DMSO as oxidizing agent, mainly to study their structural geometry and their potential for complexation (79–84).

A new easier approach to cyclic poly(aliphatic disulfide)s by catalytic transformation of thiiranes by (thiirane)$W(CO)_5$ complexes has been studied (85,86). For this purpose, the new thiirane complexes such as $W(CO)_5$(thiirane) (c1), $W(CO)_5$(*cis*-dimethylthiirane) (c2), and $W(CO)_5$(*trans*-dimethylthiirane) (c3) were prepared and characterized. It was found that c1, as $W(CO)_5$(NCMe) (87) used earlier, transforms free thiirane (thiacyclopropane, ethylene sulfide) [420-12-2] (**28**) into a mixture of cyclic poly(disulfide)s (**29**), and ethylene, catalytically; the compound (**29a**) was the major product (~66%). Also, *cis*- and *trans*-dimethylthiirane were catalytically transformed by c2 and c3 with the formation of small amounts of cyclic disulfides. The mechanism of these reactions has been proposed.

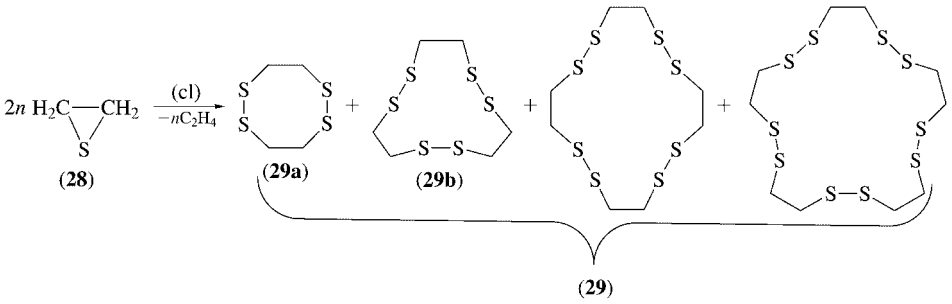

Cyclic disulfides have been shown to exhibit a variety of antimicrobial properties (85,88). The compounds 1,2,5,6-tetrathiacyclooctane (**29a**) and 1,2,5,6,9,10-hexathiacyclododecane (**29b**) were tested for antimicrobial activity, using a standard disk diffusion assay. The compound (**29a**) exhibited moderate antimicrobial activity toward *Escherichia coli*.

Contrary to the extensive studies on the coordination properties of polythioether macrocycles (35–42), little information is available about cyclic

poly(disulfide)s. The first reaction which was performed with compound (**29a**) and $Ru_3(CO)_{12}$ led to the formation of two isomers of $Ru_3(CO)_7(\mu\text{-}SCH_2CH_2S)_2$, which contained bridging ethanedithiolate ligands formed by cleavage of both of the disulfide S—S bonds (89). Attempts to prepare complexes of (**29a**) and (**29b**) without cleavage of disulfide bonds were performed by reaction with CuI in acetonitrile [75-05-8] (90). Two new compounds obtained in yields of 75 and 61%, respectively, were characterized crystallographically. They exhibited interesting extended structures in the solid state that were created by the formation of bridging ligands involving η^2-coordination of the cyclic disulfides.

An interesting new approach to poly(disulfide)s with a variety of main-chain structures by one-pot oxidation polymerization of dithiols forming *in situ* from monofunctional (25) and bifunctional (91) five-membered cyclic dithiocarbonates and diamines or amines, respectively, has recently been reported. Polymers with M_n up to ~20,000 and a good yield (up to 98%) were obtained. The starting dithiocarbonates can be easily synthesized by incorporation of CS_2 into epoxides in the presence of metal halides under mild conditions (92,93).

Other oxidation processes leading to poly(disulfide)s, namely the electrochemical (anodic) oxidation of Bunte salts (bisthiosulfates) (94) as well as oligomerization and cyclization of 1,2-ethanedithiol [540-63-6] by selenium dioxide [7446-08-4] or iodine, have also been studied (95).

Poly- and copoly(disulfide)s as electroactive materials have been used successfully in the lithium/poly(ethylene oxide)/(solid redox polymerization electrodes) (Li/PEO/SRPE) battery system (96). The high level of performance of these polymeric materials in thin-film Li/PEO batteries demonstrates the versatility of the SRPE and indicates that such batteries may be useful for a wide range of applications.

Water-insoluble ethylenic poly(disulfide)s (**30**) were prepared, for the first time, by the treatment of dithiocyanates (**31**) with KOH and $K_3Fe(CN)_6$ in aqueous solution, and characterized. These simple-structure polymers become semiconductive upon chemical doping (97).

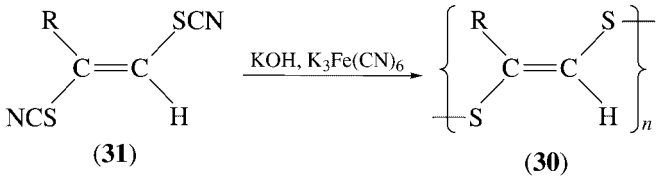

(**31**) (**30**)

R = H, $CH_3(CH_2)_3$, C_6H_5

The importance of disulfide bridges in peptides and proteins is well known, and many elegant ways to form these structures have been reported (98,99). In contrast, the corresponding "trisulfide" variants reflect a rather newly appreciated area of chemical and biological interest (100).

Sulfonium Polymers. Polysulfonium salts have been extensively studied because of the versatile possibilities of their application. They can be used as ion-exchange resins, polymer supports in peptide synthesis, polymeric reagents, and

conducting materials (101). The poly(sulfonium cation) is chemically stable and soluble in common solvents, such as acetone, acetonitrile, or protic acid. These properties are applicable to the modification of the polymer in a homogeneous solution under moderate conditions.

There have been reports of examples of polymers with sulfonium salt moieties applied as a catalyst to organic reactions (102) and precursors of such polymers as PPS (103–107), perfluorinated PPS (33), poly(*p*-phenylene vinylene) (PPV) (108–111) and its derivatives (112), as well as PPSA and PPSAA (57,58).

For example, the high molecular weight PPS (**32**) (M_w > 200,000) was synthesized via soluble poly[methyl-4-(phenylthio)phenylsulfonium cation] (**33**) through oxidative polymerization of methyl-4-(phenylthio)phenyl sulfoxide (**34**). The polymerization process carried out in trifluoromethanesulfonic acid (triflic acid, CF_3SO_3H) [1493-13-6] and in the presence of P_2O_5 as dehydrate agent at room temperature for 24 h quantitatively produced the high molecular weight polymer (**33**) which was converted, also quantitatively, to PPS (**32**) by nucleophilic demetylation in pyridine [110-86-1] (104,105). The polymerization of (**34**) in sulfuric acid, particularly at elevated temperature and extended reaction time, resulted in a slight sulfonation on the phenylene ring in the polymer chain.

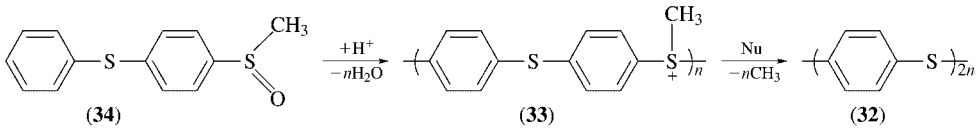

(**34**) (**33**) (**32**)

The highly sulfonated polysulfonium salt (**35**) synthesized by the polymerization of (**34**) in the presence of SO_3 can be converted by nucleophilic demethylation with aqueous KCl to the highly sulfonated PPS (**36**) exhibiting excellent proton conductivity (113).

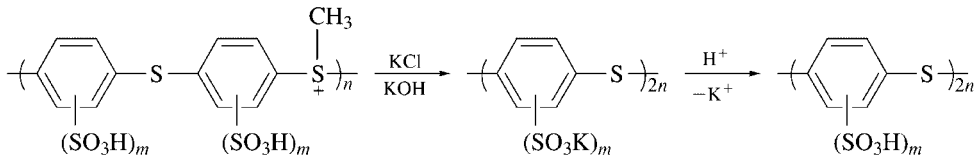

(**35**) (**36**)

Poly(arylenesulfonium salt)s are employed as new polymeric alkylation reagents because, after the dealkylation, they are converted to insoluble PPS that can easily be removed from the reaction mixture (114,115).

Thiophenium salt derivatives can be utilized as powerful alkylating reagents because of their remarkable instability in nucleophilic solvents (116,117). In order to investigate a similar application of poly(thiophenium salt)s, new polymers

having pendent *S*-alkyldibenzothiophenium salt moieties have been, for the first time, synthesized and characterized (118–120). Two synthetic routes to polymer (**37**) were investigated: the polymer reaction of poly(2-vinyldibenzothiophene) (**38**) with methyl iodide [74-88-4] and silver tetrafluoroborate [14104-20-2] carried out in 1,2-dichloroethane [107-06-2] at room temperature, and the radical polymerization of a vinyl monomer bearing dibenzothiophenium moieties, ie, 5-methyl-2-vinyldibenzothiophenium tetrafluoroborate (**39**), carried out in acetonitrile with an AIBN catalyst at 60°C. The former method gave the polymer in 96% yield with 71% substitution of the methyldibenzothiophenium tetrafluoroborate units, whereas the latter in 88% yield with 79% substitution. The analogous polymer with 63% substitution was also prepared by the polymer reaction of poly[2-(*p*-vinylbenzyl)dibenzothiophene] (120). The attempts of demethylation showed that the complete demethylation of the dibenzothiophenium units in polymer (**37**) was achieved at 80°C for 48 h by the reaction in acetonitrile (119). In addition, it was found that thermal decomposition of the polysulfonium polymers obtained took place in two steps; the first step was associated with demethylation. These properties suggest the possibility of utilizing these polymers as an alkylating reagent and an initiator of the cationic polymerization.

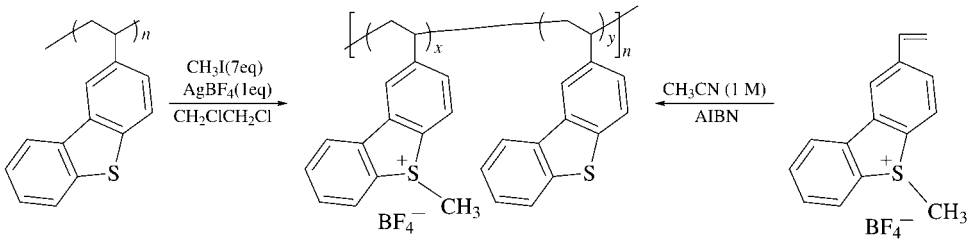

(**38**) (**37**) (**39**)

Attention has been paid to the polysulfonium salts as a new type of photochemical polymeric materials (121,122). Several kinds of poly(arylenesulfonium salt)s having methyl (**40**) propyl (**41**), and phenyl substituents (**42**, **43**) including a novel class of polyelectrolites having triphenylsulfonio groups in the main chain (**42**, **43**) were synthesized in yield up to 100% by the sulfoxide-acid system reaction from the corresponding alkyl and aryl sulfoxide monomers (105,107,115,122).

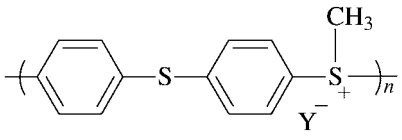

Y = CF_3SO_3, PF_6

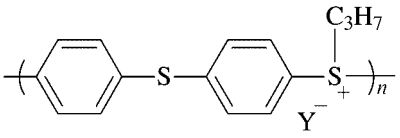

$Y = CF_3SO_3, PF_6, AsF_6, SbF_6$

(**41**)

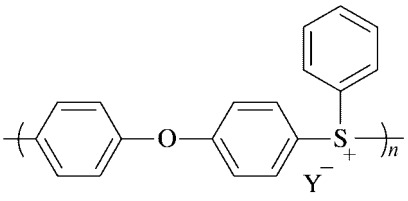

$Y = CF_3SO_3, PF_6$

(**42**)

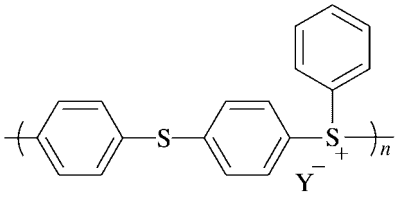

$Y = CF_3SO_3, PF_6$

(**43**)

They showed good solubility in protic acids, including formic acid [64-18-6], sulfuric acid, and CF_3SO_3H and polar organic solvents, including methanol, acetonitrile, DMF, DMSO, etc. The photochemical reactivities of the resulting polymeric sulfonium salts, eg, photolysis (photodegradation), photoinitiated polymerization, and quantum yields, were investigated in detail with comparison to those of the corresponding monomeric compounds. It was found that the photoirradiation of ultraviolet light at the π–π^* transition band resulted in the selective degradation of the polymer to the corresponding aryl or alkyl sulfide monomer. The photodegradation was accompanied by proton generation, which could be useful for the photoinitiated polymerization of epoxy compounds. The polymeric sulfonium salts were more effective than the monomeric ones because of a larger extinction coefficient at the irradiation wavelength (122).

The synthesis of the first sulfonio-bridged, *p*-phenylene ladder oligomers (**44**) that have a planar ribbon-type structure have been reported (60).

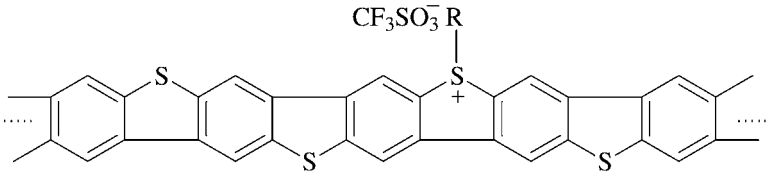

R = CH_3, $CH_3(CH_2)_5$

(**44**)

The oligomers are soluble in formic acid, sulfuric acid, and CF_3SO_3H but insoluble in common organic solvents, including methanol, acetone, acetonitrile, and chloroform. In the presence of an extended π-conjugation, two-dimensional planar structures have electronic advantages, for example, as a lower bandgap material (123).

Poly(sulfonic acid)s and Their Derivatives. Polymers substituted by sulfo groups have a wide range of applications because of their unusual properties. Water-soluble polymers are used as emulsifiers, flocculants, thickeners, tanning agents, wetting or cleaning agents, etc. They are also applied in the paint industry and in dye manufacturing (124,125). Introduction of the sulfo groups into fibers (eg, polyester fiber by using sodium-5-sulfo-dimethylisophthalate as ionic comonomer) (126) improves dyeability and imparts antistatic properties. Another important area of application is in construction engineering, eg, concrete technology as high range water reducers (superplasticizers). Lignosulfates, sulfonated melamine-formaldehyde and naphthalene-formaldehyde condensates are typical superplasticizers used commercially (127,128). Poly(3-alkylsulfonate thiophene)s (129), sulfonatoalkoxy-substituted poly(*p*-phenylene) (130), highly sulfonated PPS (113), and PAni (131) are water-soluble conductive polymers. The polyelectrolyte block copolymers, eg, poly(alkyl methacrylate)-*b*-poly(sulfonated glycidyl methacrylate) (132) and poly(ethylethylene)-*b*-poly(styrenesulfonate) (133), were found to be effective stabilizers in emulsion polymerization. Insoluble polymers are used as ion-exchange resins and they find application as membrane materials, eg, Nafion (DuPont, a sulfonated perfluoropolymer) (134,135). A great demand for chemically stable ion-exchange membranes for electromembrane processes, such as electrodialysis, polymer electrolyte membrane electrolysis, and polymer electrolyte fuel cells, has, in the past years, stimulated investigations dealing with the developing of the sulfonation process of thermally and chemically stable engineering plastics.

Sulfopolymers are employed in biomedical systems. Much effort has been expended to improve blood-contacting biomaterials, eg, segmented polyurethanes, and develop various polysulfates and polysulfonates as antithrombotic or antiviral agents.

Sulfo groups (as a free acid, salt, or ester) can be introduced into polymers by homo- or copolymerization of monomers containing sulfo groups, or by direct sulfonation of the polymer.

Poly(sulfonic acid)s. There are many reports on the sulfonation of commercially available, high performance engineering plastics, including

poly(*p*-phenylene) (PPP) (130), Udel [Union Carbide, poly(ether ether sulfone)] (136,137), poly(oxy-1,4-phenyleneoxy-1,4-phenylenecarbonyl-1,4-phenylene) [poly(phenylene ether ether ketone) (PEEK)] (138–144), and PPS (103,113,145–148), etc. (see POLYSULFONES; ENGINEERING THERMOPLASTICS, OVERVIEW).

The sulfonation of PEEK (**46**) in concentrated sulfuric acid or in its mixture with methanesulfonic acid [75-72-2] gives polymeric material which is soluble in organic solvents, eg, DMF (138), and good membranes with interesting properties were obtained by processing from these solutions (139–142).

The sulfonation reaction of several kinds of commercially available poly(aryl ether ketone)s with various ether/carbonyl group ratio (0.67–2.0) (**45**, **46**, **47**, and **48**) by mixtures of sulfuric acid and oleum was studied (143). It appeared that with decreasing amounts of ether links in the polymer backbone the sulfonation is hindered, and to obtain products with the same degree of sulfonation, the SO_3 concentration of the reaction mixture has to be increased. Depending on the polymer structure, polymers with contents of sulfonate groups $\sim$1.2–2.0 meq·g^{-1} polymer were well soluble in DMF or NMP. The cationic exchange membranes with permselectivities >96% and electrical resistances <2 Ω·cm^{-2} from the polymers with a high degree of sulfonation were produced. The electrical and mechanical properties of these membranes compare very well with other membrane materials.

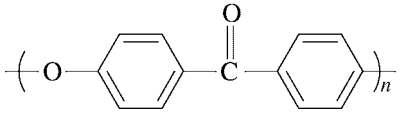

(**45**)

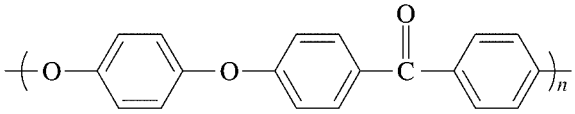

(**46**)

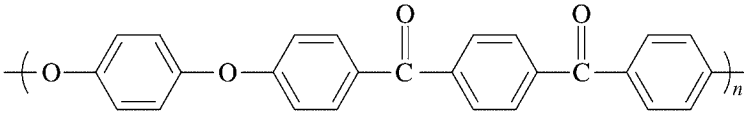

(**47**)

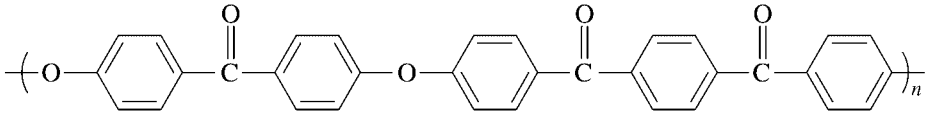

(**48**)

The electrical properties of the thermostable PEEK (**49**) and poly(4-phenoxybenzoyl-1,4-phenylene) (PPBP) (**50**) sulfonated with sulfuric acid and containing 65 mol% sulfonic acid have been studied and compared (144). Sulfonated

PPBP showed much higher and more stable proton conductivity than that of sulfonated PEEK, which is in agreement with the strong water absorption of the former polymer, as a consequence of the presence of the flexible pendent side chains. These properties may be important for future design and development of fuel cells based on polymer electrolytes.

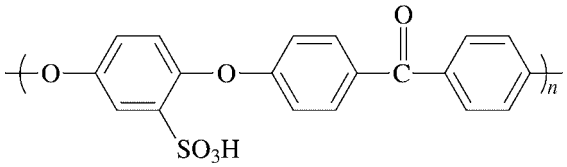

(**49**)

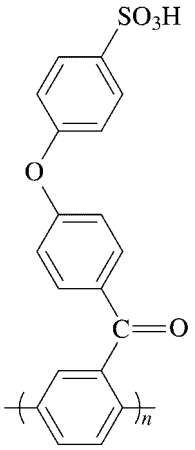

(**50**)

A new process has been developed for the sulfonation of the chemically stable engineering polymer polysulfone Udel (**51**) (137). This multistep sulfonation process described in equation (1) consists of the following steps: lithiation of the polymer at −50 to −80°C, gassing with SO_2, oxidation of the formed polymeric sulfinate with H_2O_2, NaOCl, or $KMnO_4$, and final ion-exchange of the lithium salt of the sulfonic acid in aqueous HCl. By this method the sulfonic acid group is inserted into the more hydrolysis-stable diarylsulfone part of molecule, contrary to conventional electrophically sulfonation which it undergoes at position ortho to the ether bridge of the bisphenol A [2,2-bis(4-hydroxyphenyl)propane, *p*,*p*′-isopropylidenebisphenol, dian, etc] [80-05-7] part (135). The resulting polymer (**52**) has been characterized in terms of ion-exchanges group content, conductivity, and hydrolytic stability. Membranes made from (**52**) showed good conductivity, good permselectivity (>90%), and good hydrolytic stability in 1 *N* HCl and water at temperatures of up to 80°C. This new sulfonation method can be applied to all the polymers which form soluble lithium salts.

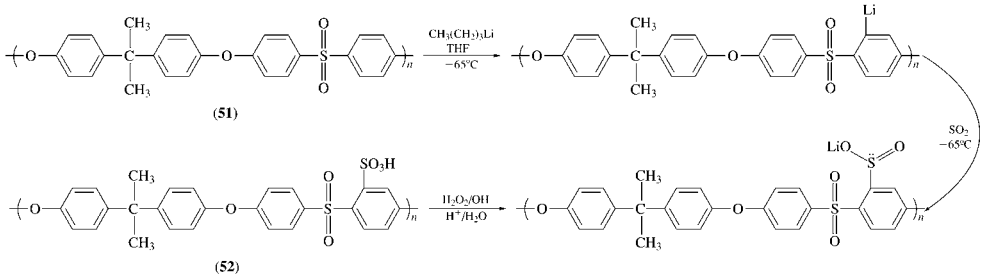

(1)

Alternative potential materials for preparation of cation-exchange membranes are sulfonated poly(phenylquinoxaline)s (**53**) (149), which were produced by polymeric reaction sulfonation of poly(phenylquinoxaline)s (**54**) or by synthesis from monomers, directly in the sulfonating medium (eq. 2). In both cases, sulfonation was carried out in a sulfuric acid/oleum mixture (4:1) at 125°C. High strength thermally stable films showing high hydrolytic stability were cast from the solution of (**53**) in DMF. Polymers (**53**) can also be processed by compression molding.

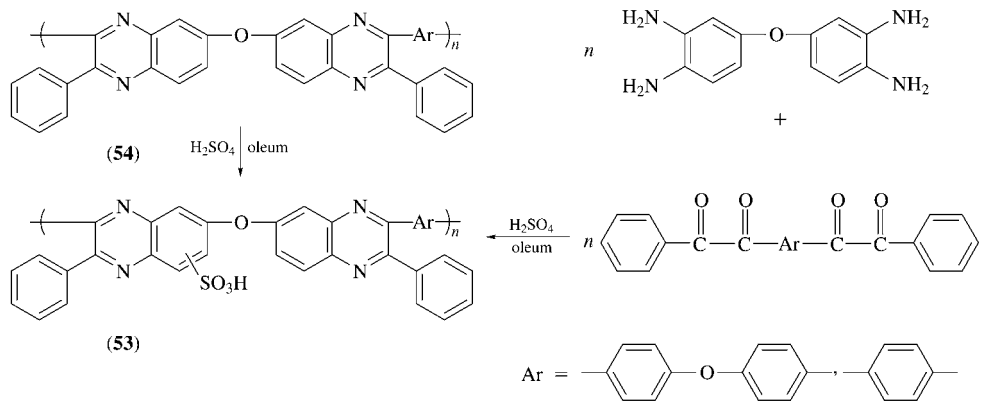

(2)

Earlier attempts to prepare highly sulfonated PPS by sulfonation with SO_3 were unsuccessful; the formation of only lightly sulfonated polymers (up to 0.5 sulfonic acid groups per phenylene, *m*) accompanied by the formation of ladder or cross-linked structures because of the stringent reaction conditions took place (145–148). The highly sulfonated PPS (*m* up to 2.0) (**36**) was successfully prepared by the polymerization of methyl-4-(phenylthio)phenyl sulfoxide (**34**) in sulfuric acid via polysulfonium salt as a soluble precursor (113). The sulfonation can be controlled by the reaction time, the temperature, and/or the addition of SO_3. The sulfonated polymer (**36**), unlike the nonsubstituted polymer, is soluble in water and methanol, and can form a transparent film. It was found that (**36**) exhibits a good water affinity and an excellent proton conductivity of up to 4.5×10^{-2} S·cm^{-1} at 80°C.

Membranes made from homogeneously sulfonated polystyrene exhibited proton conductivity equal to that of Nafion, with methanol permeability about 70% smaller than for this ionomer. This is attractive particularly in relation to the methanol fuel cell technology (150).

Other proton-exchange membranes bearing sulfonic acid groups were produced by radiation-induced grafting of styrene onto fluorinated polymers and subsequent sulfonation (151–161). Membranes produced from, eg, the high radiation resistance commercial poly(tetrafluoroethylene-*co*-hexafluoropropylene) films having degrees of grafting of 16% and above showed proton conductivity of the magnitude of $10^{-2}\ \Omega^{-1}\cdot cm^{-1}$ at room temperature, and thermal stability at temperatures up to 290°C under an oxygen atmosphere (151).

A new type of amphiphilic polymer blend comprising polystyrene (PS), poly(ethylene oxide) (PEO), and microspheres of cross-linked polystyrene sulfonic acid (PSSA) was prepared by solution blending and followed by casting. The ir and the differential scanning calorimetry (dsc) studies showed that besides providing protons, PSSA plays a role in enhancing the miscibility of PS and PEO. The influence of the mixing extent between PS and PEO on the proton conductivity has also been studied (162).

The first water-soluble, electroactive, self-doped sulfonatoalkoxy-substituted PPP, poly[2,5-bis(3-sulfonatopropoxy)-1,4-phenylene-*alt*-1,4-phenylene] (**55**), was synthesized from 1,4-benzenediboronic acid [4612-26-4] (**56**) and the disodium salt of 1,4-dibromo-2,5-bis(3-sulfonatopropoxy)benzene (**57**) by the homogeneous Suzuki coupling method (130). The polymer purified by dialysis of an aqueous solution was composed exclusively of 1,4-linkages. The ability to utilize a variety of bis(boronic acids) in this polymerization with sulfonate containing aryl halides will lead to a high degree of structural control of the optoelectronic properties of these water-soluble polymers.

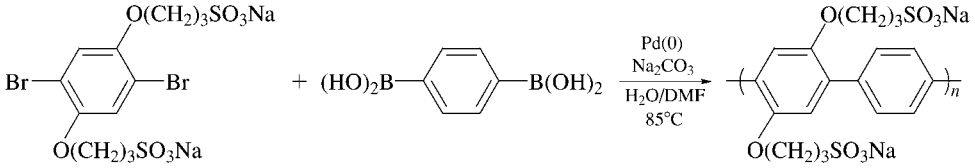

(**57**) (**56**) (**55**)

As a new approach to sulfonated polymers, sulfonation of oligo(2-propenyloxy)methyloxyirane by SO_2 in presence of amines has been studied (163). It was shown that, depending on the reaction conditions, oligomeric sulfo acid or its derivatives (**58**) as well as crown polysulfonic acid (**59**) can be synthesized. Crown polysulfonic acid is produced by the copolymerization of SO_2 with double bonds of unsaturated oligomer.

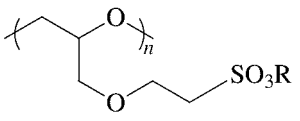

R = H, K, Na, Li, NHR_3^1; R^1 = organic radical

(**58**)

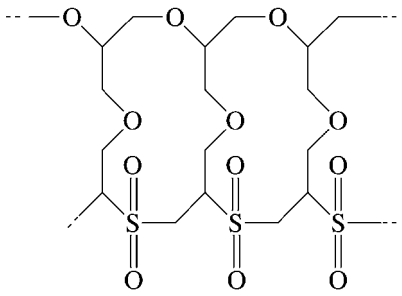

(**59**)

The synthesis, characterization, and some properties of novel unimolecular micelles of hydrophobically modified sodium polysulfonates as well as their potential utility for novel photochemical systems have been reviewed (164).

A novel series of water-soluble amphoteric cyclocopolymers containing the pH-responsive hydrophobic monomer, *N,N*-diallyl-*N*-methylamine [2424-01-3], and the sulfobetaine monomer, 3-(*N,N*-diallyl-*N*-methylammonio)-propanesulfonate, have been prepared in 0.5 *M* NaCl aqueous solution (pH 4.0), using 2-hydroxy-1-[4-(hydroxyethoxy)phenyl]-2-methyl-1-propanone (Irgacure 2959) as the free-radical photoinitiator (165). Equilibrium dialysis experiments demonstrated that they could be utilized to control the sequestration of organic foulants and thus have potential application as polymeric surfactants in micellar-enhanced ultrafiltration processes for water purification.

Numerous copolymers based on the ionizable monomer 2-(acrylamido)-2-methylpropanesulfonate (AMPS, 2-methyl-2-[(1-oxo-2-propenyl)amino]-1-propanesulfonic acid) [15214-89-8] and mainly vinyl or acryl comonomers were prepared and characterized because of their various application possibilities. Some of them are mentioned below.

Micelle-forming materials obtained by radical copolymerization of sodium salt of AMPS with 9-vinylphenanthrene and 1-vinylpyrene (AIBN, THF solvent, 60°C) can be used as media for photosensitized electron transfer in aqueous systems (166). Reactive microgels obtained by copolymerization of AMPS with *N,N′*-methyleneacrylamide are suitable for the immobilization of biological materials (167).

Copolymers synthesized by a sodium persulfate-initiated free-radical solution polymerization of acrylamide and AMPS (at different pH values) as a new type of super-absorbent polymer have been studied in terms of swelling or viscosity behavior in water (168).

The reaction of fluoroalkanoyl peroxides with AMPS or AMPS and the comonomers such as trimethylvinylsilane and methyl methacrylate gives novel fluoroalkylated end-capped homo- or copolymers which are able to form gels both in water and organic polar solvents such as methanol, ethanol, DMF, and DMSO under noncross-linked conditions. These AMPS polymer hydrogels have a strong metal ion binding power. Moreover, they are potent and selective inhibitors of the human immunodeficiency virus type 1 (HIV-1) replication in cell culture. One of these gelling polymers was found to possess antibacterial activity against *Staphylococcus aureus* (169).

Copolymers synthesized from AMPS and lauryl methacrylamide in different mole ratios were characterized and used as separation media in electrokinetic chromatography (170).

The new polyacrylic fibers (OHIS, Skopje) contain incorporated AMPS, which gives new and improved dyeing properties to the fiber. It can be dyed in more brilliant hues compared to Malon fiber with itaconic acid as an acidic comonomer (171).

Thermoassociative water-soluble copolymers containing AMPS and poly(ethylene oxide) [25322-68-3] grafts can be applied in the oilfield industry as thickening agents functioning at elevated temperatures (172,173).

A new water-soluble sulfonated phenolic resin as a potential superplasticizer was prepared from formaldehyde, phenol, and sodium bisulfite ($NaHSO_3$) through a four-step reaction procedure. It was found that this resin could reduce the water content and improve the workability and compressive strength of concrete. The best results were obtained for concrete containing 2 wt% resin, which are comparable with commercial superplasticizers (128,174–176).

Wholly aromatic ionic polyesters such as poly(sulfo-*p*-phenylene terephthalate), poly(sulfo-*p*-phenylene bromoterephthalate), and poly(sulfo-*p*-phenylene nitroterephthalate) containing sulfonate pendent groups have been synthesized, for the first time, by an interfacial condensation procedure from commercially available hydroquinonesulfonic acid potassium salt and terephthaloyl chloride, 2-bromoterephthaloyl chloride or 2-nitroterephthaloyl chloride, respectively (177). It was found that nitro-substituted polyester forms lyotropic liquid crystalline solutions in the wide range of DMSO/water solvent mixtures (15, 30, 50, and 70 vol%), in DMF/water (50 vol%), and in pure water and DMF. Because of their decomposition upon heating at high temperature, these polyesters do not show thermotropic liquid crystal transitions in solid state.

Other lyotropic liquid crystalline polyesters based on poly(sulfo-*p*-phenylene nitroterephthalate) as well as poly(sulfo-*p*-phenylene nitroterephthalamide) have been reported (178).

Biomedical Applications. Considerable effort has been focused on the modification of segmented polyurethanes as biomaterials to improve their blood-contacting behavior, eg, preventing the occurrence of thrombosis and thromboembolization. The incorporation of the functional sulfonate groups representing key structural elements of the anticoagulant bioactive molecule, heparin [9005-49-6] (179), is a less difficult type of modification than the incorporation of the molecule itself. The various segmented polyurethanes containing sulfonate groups in the hard (180–186) and soft segment (187,188) were synthesized and characterized in order to investigate their anticoagulant effects as the consequence of the platelet

adhesion. From this study it appears that incorporation of sulfonate ions into polyurethanes directly affects the blood-contacting response of these materials. However, the effect can be beneficial or deleterious, and it appears to be dependent on the molecular location of the ions and the structure of the polymer.

The effects of the polysulfonic acid derivative 4-*t*-butylcalix[8]arene-*p*-sulfonic acid (GL 522-Y-1, Genelabs, Redwood City, Calif., U.S.) (**60**) on thrombosis *in vivo* and haemostasis *in vitro* have been investigated. On the basis of its unique antithrombotic properties, GL 522-Y-1 seems to open a new pathway in the field of antithrombotics; so far it was primarily developed as an antiviral drug (189).

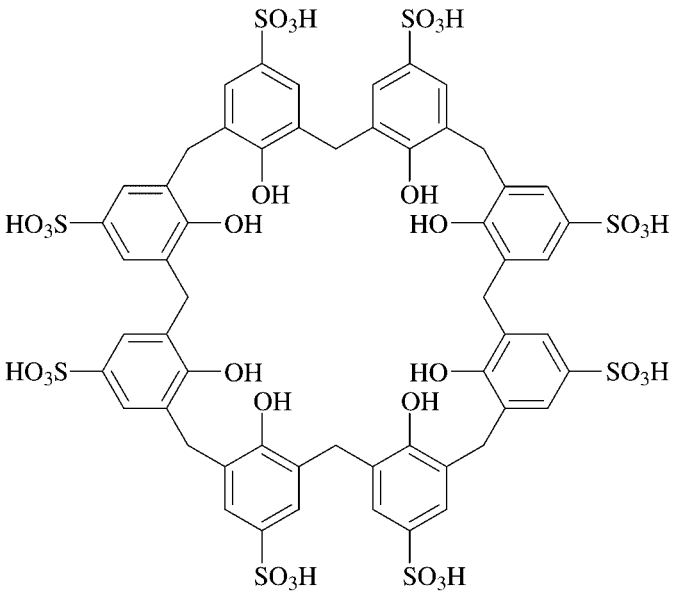

(**60**)

In the past few years, several compounds have been described that exhibit marked activity against respiratory syncytial virus (RSV) *in vitro* (190). Among the most potent and selective RSV inhibitors are various polyanionic substances, including polysulfonates (eg, poly(vinylsulfonate), poly(styrenesulfonate), poly(acrylamidomethylpropanesulfonate), sulfonated derivatized dextrans, etc) and polysulfates (virus adsorption). They have significantly higher selectivity index than Ribavirin (1-β-D-ribofuranosyl-1,2,4-triazole-3-carboxamide, Tribavirin; Virazole; Viramid; RTCA; Vilona; Virazid, etc) [36791-04-5], which is the only antiviral agent approved for the treatment of RSV infections.

Polysulfonates. Aromatic polysulfonates having the sulfonate ester group in the main chain possess good physical, chemical, electrical, and thermal properties. Their characteristics are high softening and melting temperatures, thermal stability of up to 300°C, resistance to alkali, acids, and oils, and solubility in halogenated aliphatic hydrocarbons. They can be processed by molding, extruding, injection molding, as well as casting from solution. These polymeric materials can be useful as coatings and adhesives (3,191). High molecular weight

polysulfonates are easily obtained by step-growth polymerization reaction of aromatic diphenols with aromatic disulfonyl dichlorides using phase-transfer catalyst (3,191–193). Wholly aliphatic polysulfonates are prepared by ROP of cyclic sulfonates (3).

Catalyzed (benzyltriethylammonium chloride [56-37-1]) interfacial condensation of aromatic-(poly)cycloaliphatic diphenols and their bromoderivatives, including 4,4′-(1-cyclohexylidene)diphenol, 4,4′-(2-norbolidene)diphenol, 4,4′-(1-cyclohexylidene)-di-(2,6-dibromophenol), and 4,4′-(2-norbolidene)-di-(2,6-dibromophenol) with various aromatic dichlorides was studied in detail (191,194). Depending on the reaction conditions and the monomer used, the low crystalline polymers (with η_{red} ~0.2–1.7 dL/g and softening range of 160–310°C) soluble in halogenated aliphatic and aromatic hydrocarbons and DMF were obtained. They exhibited hydrolytical stability to both mineral acids and bases at room temperature and good thermal stabilities of up to 290–360°C.

More recently, similar polysulfonates, eg, (**61**) and (**62**), prepared by conventional interfacial condensation using water-chloroform as an interface, alkali as an acid acceptor, and cetyltrimethylammonium bromide [57-09-0] as an emulsifier have thoroughly been studied (195–206). In general, the polymers possess good solubility in common solvents, good acid and alkali resistance, thermal stabilities of up to 355°C, and tensile strength of up to ~20 MPa (199).

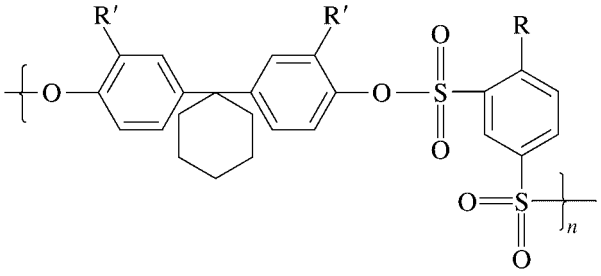

$R = H, R' = H; R = CH_3, R' = H; R = R' = CH_3$

(**61**)

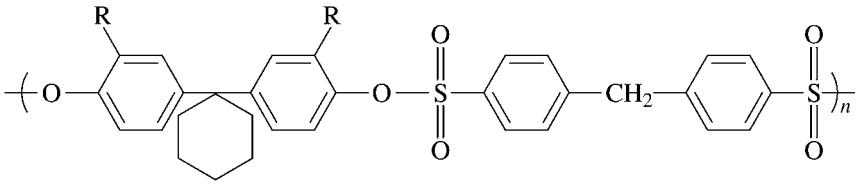

$R = H, CH_3$

(**62**)

The tests of biological activities showed that polysulfonates exhibit good or moderate antibacterial activities against *Escherichia coli*, *Staphylococcus citrus*, *Aspergillus niger* and *Aspergillus awamori*, *Becillus megaterium*, etc (195–198,

200). Acoustic (ultrasonic) studies of these polysulfonates have been performed in chlorinated and aprotic solvents in order to understand their structures as well as polymer–solvent and polymer–polymer interactions (202–206).

Polysulfonates with reactive pendent chloromethyl groups (**63**) can be synthesized by solution polymerization of bisepoxides (**64**) with disulfonyl chlorides (**65**) (207).

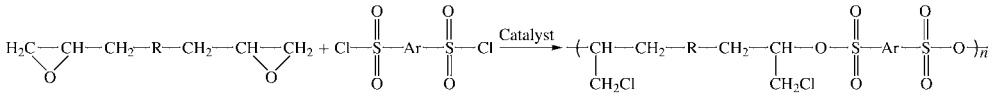

(64) (65) (63)

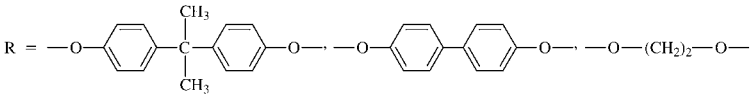

(64a) (64b) (64c)

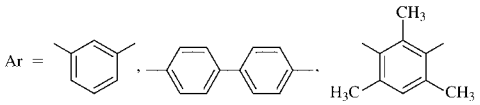

(65a) (65b) (65c)

The examination of the effect of various reaction conditions on the polymerization of (**64a**) with (**65a**) showed that the polymer with the highest molecular weight (M_n = 16,000) and good yield (95%) was obtained in 2,4-dichlorotoluene [95-73-8], using tetra-*n*-butylphosphonium bromide [3115-68-2] as a catalyst at 130°C for 24 h. From among other polymers prepared under optimum conditions, those based on (**64c**) showed low molecular weights.

Polysulfates

Polysulfates are widely studied because of their potential biomedical applications. Heparin, a naturally occurring sulfated polysaccharide, has antithrombogenic properties and is used in cardiovascular surgery (179,208). Polysulfates in general, and sulfated polysaccharides in particular, are active against a wide variety of enveloped viruses (209,210).

Various polysulfates, eg, heparin, dextran sulfate, mannan sulfate (**66**), galactan sulfate, xylomannan sulfate, polyacetal polysulfate, poly(vinylalkoholsulfate) (**67**), and poly(acrylic acid vinylalcoholsulfate), are the most potent and selective RSV inhibitors (190).

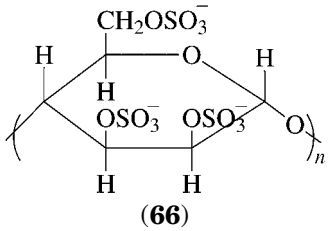

(**66**)

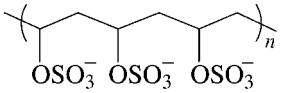

(**67**)

Heparin and other sulfated polysaccharides extracted from sea algae were found to be potent and selective inhibitors of the HIV-1 replication in cell culture as well as various enveloped viruses, including viruses that emerge as opportunistic pathogens (eg, herpes simplex virus and cytomegalovirus) in immunosuppressed [eg, AIDS (the acquired immune deficiency syndrome)] patients. As potential anti-HIV drug candidates, sulfated polysaccharides offer a number of promising features (209,210).

A major commercial sulfated polysaccharide is carrageenan [9000-07-1], used in ice cream and other food products (see GUMS).

Polythiocarbonates

In general, polythiocarbonates are polymers containing the structural units (**68**) with one to three sulfur atoms and unit (**69**). They are mainly prepared by ROP of the corresponding cyclic monomers, eg, ethylenethiocarbonate (1,3-dioxolan-2-thione) [20628-59-5] or 1,3-oxathiolane-2-thione, or by condensation reactions involving dithiols and adequate difunctional coupling compounds. The synthesis and properties of many kinds of polythiocarbonates were reviewed in 1992 (3).

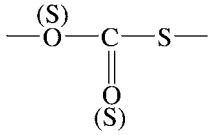

(**68**)

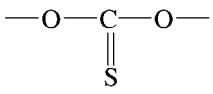

(**69**)

Poly(monothiocarbonate)s (**70**) (211–214), (**71**) (215), (**72**) (216), and (**73**) (217) containing oxythiocarbonyloxy linkages (**69**) are prepared from thiophosgene (carbon chlorosulfide, thiocarbonylchloride, carbonothioic dichloride) [463-71-8] and corresponding diphenols under phase-transfer conditions with quaternary ammonium and phosphonium salts as catalysts. The influence of the structure of the bisphenols and the nature of the catalyst on yields and η_{inh} have been studied. Under optimum conditions, polymers in ~90–97% yields and η_{inh} up to 1.8 (**70**), 0.09 (**71**), 0.24–0.63 (**72**), and 0.24–0.36 dL/g (**73**) (0.5 g/dL, $CHCl_3$, at 25°C) were obtained.

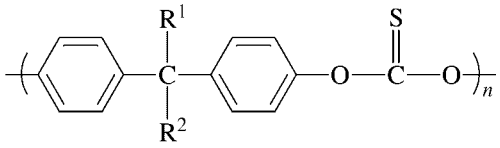

$R^1 = H, CH_3, C_2H_5$

$R^2 = H, CH_3, C_2H_5, CH_3(CH_2)_2, (CH_3)_2CH, —CH_2CH(CH_3)_2, C_6H_5$

(**70**)

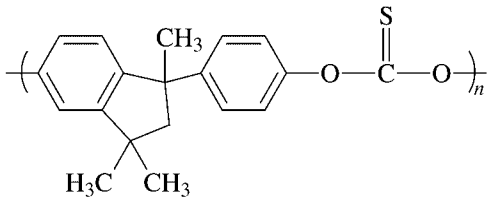

(**71**)

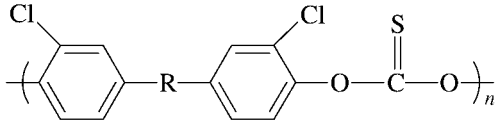

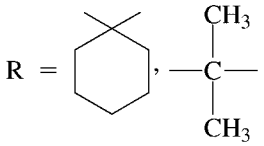

(**72**)

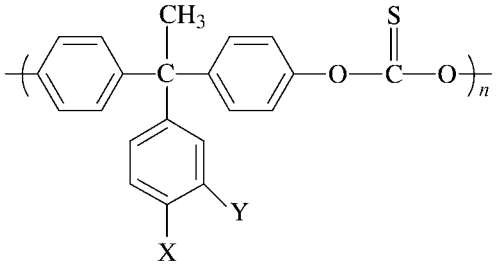

X = Cl, Y = H; X = H, Y = Cl; X = Y = Cl

(**73**)

The synthesis of related poly(ester-thiocarbonate)s containing the ester group in the main chain (218,219) and in the side chain (220) as well as poly(amide-thiocarbonate)s containing the amide group in both the main (221) and side (222) chains under phase-transfer conditions have also been reported. It has been shown that this technique can be effective to prepare polythiocarbonates derived from diphenols containing Si or Ge, bis(4-hydroxyphenyl)-dimethyl-germane, bis(4-hydroxyphenyl)-diphenyl-germane, bis(4-hydroxyphenyl)-dimethyl-silane, and bis(4-hydroxyphenyl)-diphenyl-silane (223).

Thermogravimetric (TG) investigations exhibited that the thermal stability of this family of polythiocarbonates is in general lower than that of corresponding polycarbonates (224–226). The solution properties (dipole moment and partial specific volume) and chain flexibility of different polymers have been studied (227–233).

Polymers containing thiocarbonylthio —S—CO—S— and oxycarbonylthio —O—CO—S— linkages (**68**) were prepared by catalyzed interfacial condensation of aliphatic dithiols, including 1,3-propanedithiol, 1,4-butanedithiol, and 1,6-hexanedithiol (3,234), or aromatic dithiols such as 1,3-dimercaptobenzen (1,3-benzenedithiol) [626-04-0] and 2,2-bis(4-mercaptophenyl)propane (BMP) (3, 235,236) with phosgene or bisphenol A bis(chloroformate) [2024-88-6] (235), respectively.

Polymers synthesized from phosgene and dithiols with BTEAC (benzyltriethylammonium chloride) [56-37-1] as phase-transfer catalyst have low $[\eta]$ (up to 0.16 dL/g) and relatively low yields (~70%). This result can be attributed to the low reactivity of the thiochloroformate groups —SCOCl, which derive from the reaction of the thiol groups with phosgene. Using the catalyst DMAP (4-dimethylaminopyridine) [1122-58-3] instead of BTEAC significantly increased molecular weight of the resulting polymers (236).

Polymers with bisphenol A moieties were obtained in high yields and with high molecular weights, particularly those obtained by using DMAP as catalyst and based on BMP (M_w = 180,000) (**74**) (236). They exhibited T_g = 58–90 and 154°C for aliphatic and aromatic dithiol BMP, respectively. Coupled block copolymers (**75**) containing both carbonate and thiocarbonate groups synthesized under the same conditions of phase-transfer catalysis in high yields (up to 95%) from the above-mentioned dithiols and bisphenol A polycarbonate oligomers were high molecular weight polymers, particularly those based on BMP (**75a**) (M_w = 170,000). Their T_gs were 124–158°C (234,236).

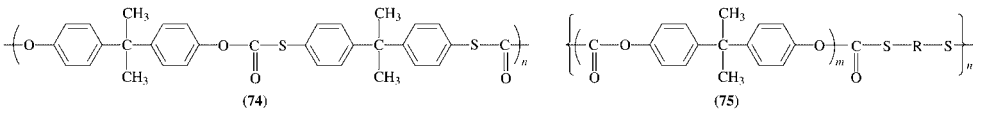

(74)

(75)

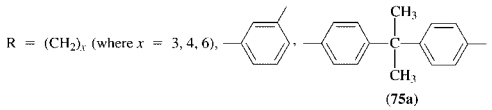

(75a)

On the basis of the TG analysis, all these polythiocarbonates are, in general, less thermally stable polymers compared with the corresponding polycarbonates

(236,237). The high refractive indices observed make these polymers, particularly poly(dithiocarbonate)s, potentially interesting for optical applications (ie, lenses and optical fibers) (238).

It has been reported that five-membered cyclic dithiocarbonates (**76**) undergo selective ROP with initiators such as $CF_3SO_3CH_3$ [333-27-7] and $CF_3SO_3C_2H_5$ [425-75-2] through the cyclic carbenium cation (**77**) leading to the formation of the corresponding poly(dithiocarbonate)s (**78**) with thiocarbonylthio linkages (239–241).

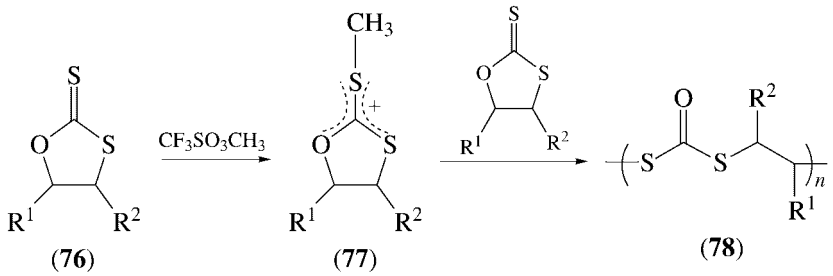

(**76**) (**77**) (**78**)

R^1 = CH_3, CH_2CH_3, CH_2Cl, $CH_2OC_6H_5$

R^2 = H

The first example of the controlled living cationic ROP of the five-membered cyclic dithiocarbonate (**79**) based on the neighboring group participation initiated with CF_3SO_3H or $CF_3SO_3CH_3$ has also been demonstrated (234). This new concept of living polymerization may be applied to the design of well-defined novel functional polymers.

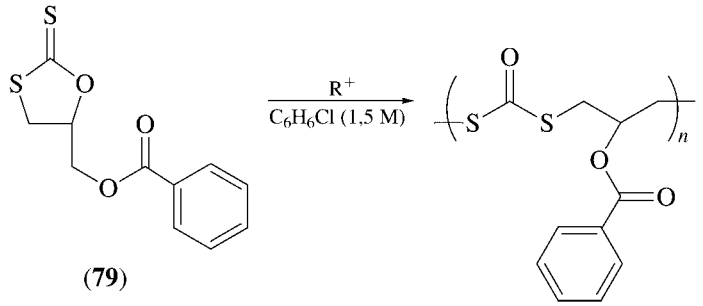

(**79**)

The high molecular weight polymethacrylate (**80**) (M_n above 100,000) bearing five-membered cyclic dithiocarbonate groups in the side chain can easily be prepared by AIBN-catalyzed homopolymerization of 5-(methacryloyloxy)methyl-1,3-oxathiolane-2-thione (**81**) (DMSO, 60°C); however the formation of some cross-linked products takes place (243). To avoid the cross-linking reaction, the comonomer methyl methacrylate and more diluted conditions were used.

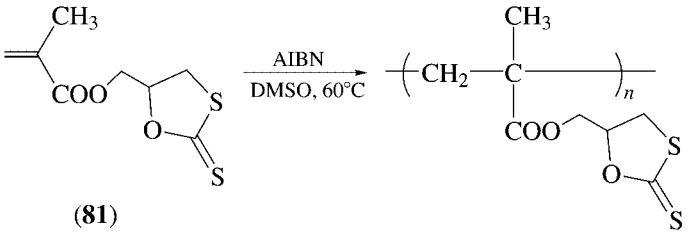

(**81**) (**80**)

A novel monomer (**81**) was synthesized by the reaction of glycidyl methacrylate [106-91-2] and CS_2 in the presence of LiBr in THF solution at room temperature in 93% yield. The attempts to synthesize polymer (**80**) by polymer reaction of poly(glycidyl methacrylate) with CS_2 were unsuccessful because of the formation of the cross-linking gels. When the copolymer (**82**) (glycidyl methacrylate/methyl methacrylate = 39/61, M_n = 80,000 with polydispersity 1.71) was allowed to react with CS_2 in THF solution and LiBr as catalyst, the yellowish polymer (**83**) (M_n = 114,000 with polydispersity = 5.08) was obtained without cross-linking, soluble in many common organic solvents (243); polymer (**80**) was soluble only in DMSO and DMF. These materials are potentially the most versatile reactive polymers which react with amines to afford a polymethacrylate bearing a thiol group in the side chain as well as potential optical materials, heavy metal-affinity polymers, and photo-reactive polymers.

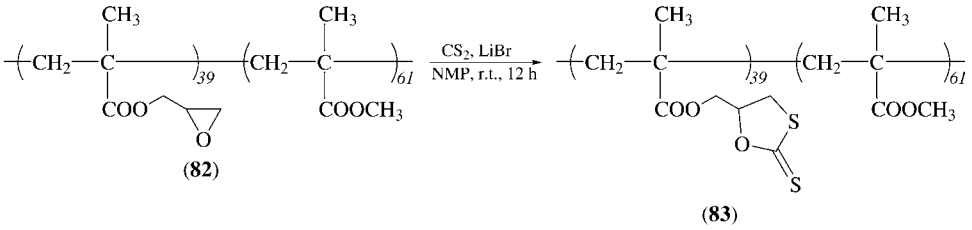

(**82**) (**83**)

The first cationic polymerization of the sulfur-containing spiro ortocarbonates (**84**) under various initiators both in chlorobenzene [108-90-7] or dichloroethane solution and in the absence of a solvent has been studied (244). The low molecular weight poly(thioether-monothiocarbonate)s (**85**) (M_n = 700–2500 with polydispersity = 3.2–7.8) were obtained. The polymerization is believed to occur via a controlled tandem double ring-opening mechanism. Monomers (**84**) were synthesized via a two-step procedure from 1,1-dichloro-1-diphenoxymethane (**86**) and 1,3-propanediol [504-63-2] (**87**). The relative hydrolytic stability of these monomers is greater than their oxygen analogues.

Polythioesters

Contrary to their oxygen counterparts polyesters, polythioesters were not commercialized and their research interest has decreased in the last few years. This

can partly be due to a more difficult and expensive approach to starting materials, eg, acid dichlorides and dithiols as well as the instability of polymers against alkalis. The synthesis and properties of the polythioesters are reviewed in References 2, 3, and 245.

Interfacial condensation of the two series of dithiols (**88**), aromatic (**88a**) and (**88b**) (246–251) or aliphatic–aromatic (**88c**) and (**88d**) (252–256) with various diacid dichlorides (**89**), aliphatic (**89a**) and isomeric phthaloyl chlorides (**89b**), (**89c**), and (**89d**) has been studied in detail as a continuation of an earlier-undertaken systematic study of linear polythioesters. High molecular weight polymers (**90**) (η_{red} up to ~2.5 dL/g) in good yields (up to ~99%) were obtained under optimum conditions. They were characterized in terms of structures, chemical and thermal resistance, and some mechanical and electrical properties. In general, polymers exhibit a good thermal resistance of up to 450°C. They are resistant to diluted alkali or mineral acids, but decompose when treated with concentrated reagents. Polymers derived from isophthaloyl chloride [99-63-8] (**89c**) and terephthaloyl chloride [100-20-9] (**89d**) are insoluble in common organic solvents, high melting (above 200°C, some even 300°C) and thermal-stable (up to 300–450°C) materials showing good mechanical properties.

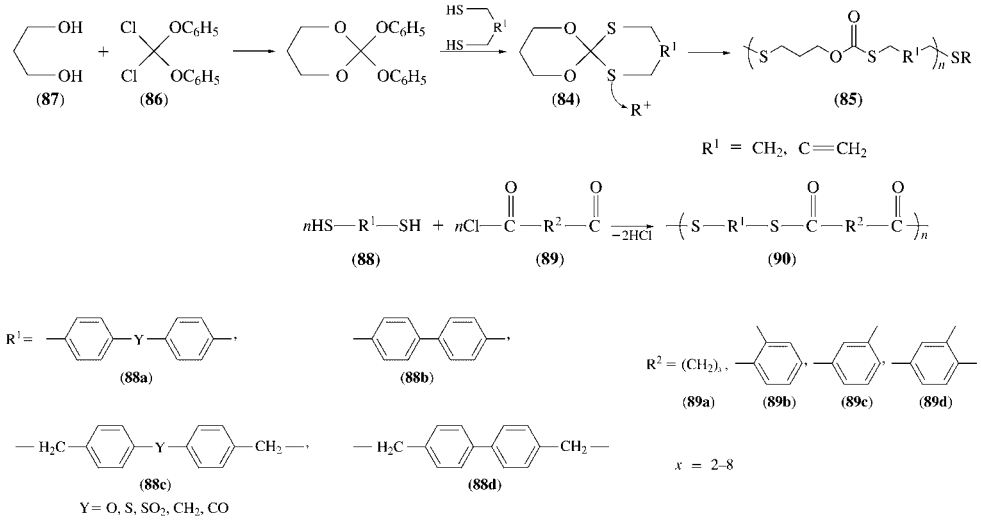

The low temperature solution polymerization of MMB (**88d**) with selected aliphatic and aromatic diacid dichlorides under optimum conditions produced significantly lower molecular weight polymers or copolymers (η_{red} ~0.2–0.6 dL/g) in up to 96% yield (257).

Polythioesters (**91**) have been prepared by condensation of terephthaloyl (**89d**) or succinyl chloride [543-20-4] (**92**) with a dithiol (**93**) generated *in situ* from bifunctional five-membered cyclic dithiocarbonate (**94**) and benzylamine [100-46-9] (**95**) in THF solution at room temperature (26). The polymers with M_n = 5100–8200 or 2900 were obtained in the presence of triethylamine [121-44-8] or pyridine [110-86-1], respectively in ~90% yields. Their T_gs were 51–76°C.

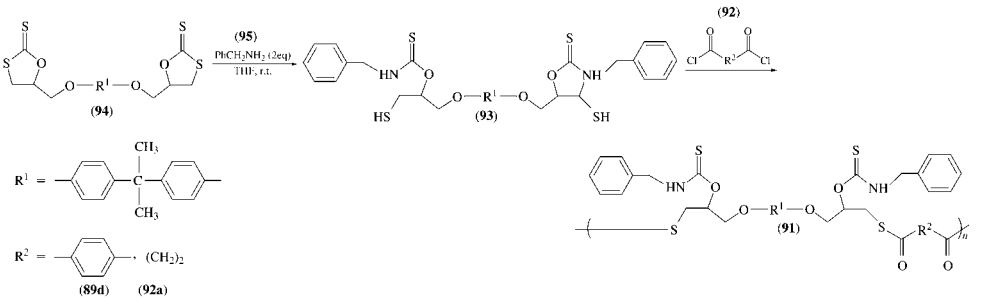

It has been reported that the novel bifunctional thiomethacrylates (**96**), which have refractive indices of 1.6 and larger, are very important and useful monomers for high index cross-linkers for optical plastics (258).

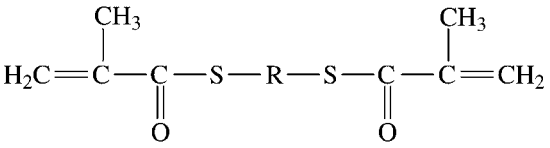

$$R = CH_2CH_2, —(CH_2CH_2Y)_nCH_2\,CH_2— \quad \text{where } Y = O, S; n = 1, 2, 3$$

Transparent resins with light weight, a high refractive index, large Abbe number, and excellent impact strength can be produced by using these good copolymerizable (eg, with styrene and acrylonitrile) cross-linking thiomethacrylates. Monomers can be prepared in high yields (84–93%) by phase-transfer catalyzed (tri-*n*-octylmethylammonium chloride [5137-55-3]) interfacial condensation of dithiols and methacryloyl chloride in the chloroform/(H_2O, KOH) system plus inhibitor.

Polythioacetals

Earlier studies on polythioacetals, mainly aliphatics, revealed limited possibilities to utilize these materials as potential industrial thermoplastics because of their instability in the molten state as well as an offensive odor of some monomers and degradation products (2,259–261). Aromatic polythioacetals (262–264) and thiacrown ethers bearing thioacetal linkages (36,37,262,265–267) have recently received increasing attention.

Various macrocycles, eg, **97**, **98**, **99**, **100**, and **101**, have been extensively studied in terms of the synthesis, properties, and complexation behavior.

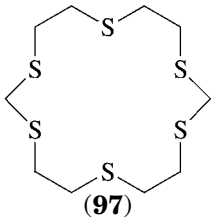

(**97**)

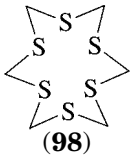

(**98**)

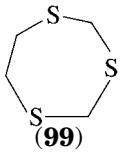

(**99**)

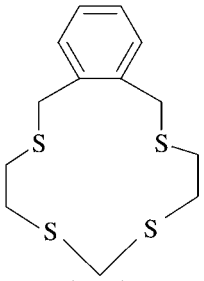

(**100**)

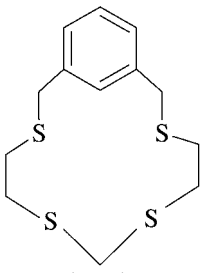

(**101**)

They can be prepared in roughly 50–75% yields by two different synthetic routes described in equations (3) and (4), for example, the synthesis of 1,3,6,9,11,14-hexathiacyclohexadecane (16S6) (**97**) (267). It should be noted, however, that for many cycles the only practical method of synthesis is method (4). Thus, the cycles (**100**) and (**101**) were prepared by the reaction cyclization of the *in situ* generated bis cesium salt of 3,5-dithiaheptane-1,7-dithiol with

α,α'-dibromo-*o*-xylene [91-13-4] or α,α'-dibromo-*m*-xylene [626-15-3] in 52 and 63% yield, respectively (266).

$$2NaSCH_2CH_2SCH_2CH_2SNa + 2BrCH_2Br \xrightarrow{\text{ethanol}} (\mathbf{97}) + 4NaBr \quad (3)$$

$$HSCH_2CH_2SCH_2SCH_2CH_2SH + ClCH_2CH_2SCH_2SCH_2CH_2Cl \xrightarrow{Cs_2CO_3/DMF} (\mathbf{97}) \quad (4)$$

It has been found that acid-catalyzed condensation of 2,2′-thiodiethanethiol [3570-55-6] (**102**) with carbonyl compounds (or equivalents thereof) carried out in solution can, under chosen conditions, lead to good yields to thiocrown ethers containing thioacetal units (262). A detailed examination of a prototype reaction of (**102**) with benzaldehyde [100-52-7] (**103**) showed that depending on the reaction conditions, a different distribution of the products [monomer (**104**), dimer (**105**), and polymer (**106**) of $M_n = 11{,}250$ with polydispersity = 1.9] is achieved. Products (**104**), (**105**), and (**106**) with maximum yields 87, 62, and 99% respectively, can be obtained.

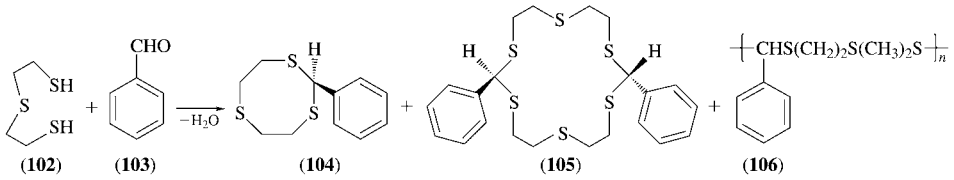

(**102**) (**103**) (**104**) (**105**) (**106**)

High molecular weight linear polymers with M_n ~9000–27,600 in up to 70% yield (after repeated reprecipitation from $CHCl_3$/ethyl ether) can be obtained by acid-catalyzed (*p*-toluenesulfonic acid [104-15-4]) solution (dichloromethane) polymerization of various aromatic aldehydes such as benzaldehyde and its *p*-substituted (CH_3O–, CH_2=$CHCH_2O$–, Cl-) derivatives with aliphatic dithiols such as 1,6-hexanedithiol [1191-43-1], 3,6-dioxaoctane-1,8-dithiol [14970-87-7], tetramethylene bis(3-mercaptopropionate), or aromatic dithiol bis(4-mercaptophenyl) ether (263). Nevertheless, the formation of some cyclic side products took place, which have been isolated and identified. Polyrotaxane structures were also found under special conditions (eg, at a shorter reaction period). The linear polymers exhibited $T_g = -31$ to $-13°C$ (from aliphatic dithiols) and 82°C (from aromatic dithiol) and T_d above 200°C. In contrast, the bulk polymerization catalyzed by HPF_6 [16940-81-1] generated *in situ* has produced well-defined thioacetal structure polymers in high yield up to 90% but with low molecular weights of $M_n = 2300$–5700.

Polysulfoxides

Polysulfoxides are polymers containing high reactivity sulfoxide groups towards the free-radical or ionic center and so they are used as functional polymers. Polysulfoxides are a catalyst for reactions conducted under phase-transfer conditions

(268–270). Poly(sulfinyl acrylate)s exhibit some biological activity (271,272). Membranes bearing sulfoxide moieties are permeable, particularly to polar compounds (273,274). Aliphatic polysulfoxides having sulfoxide groups in the main chain can be used as novel polymeric oxidizing reagents, compatibilizers, and polymer solvents. These novel aprotic polar polymers can also be expected to become novel reactive polymers (18,275). The chiral polysulfoxides can be utilized as stationary phases of chiral hplc column and as polymer reagents (276).

Polysulfoxides with sulfoxide group in the side chain are obtained by polymerization of monomers containing a sulfoxide group linked to the unsaturated carbon–carbon bond via aromatic or aliphatic units (**107**) (268,269,271,272,277). They are also synthesized by a Michael-type addition of dithiols to diolefins with a double bond activated by an adjacent sulfoxide group (274,278). Both methods were successfully applied to preparation of copolymers (274,277).

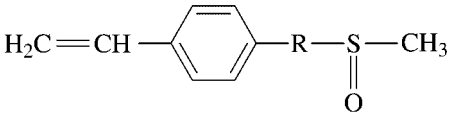

(**107**)

Polysulfoxides containing the sulfoxide group in the main chain are mainly synthesized by controlled oxidation of polysulfides using various oxidizing agents, including nitric acid, *tert*-butyl hydroperoxide [75-91-2], hydrogen peroxide [7722-84-1], peracids, or bromine, but it is difficult to avoid some sulfone formation (3). Poly(phenylene sulfoxide) of M_n ~8000 (279) and poly(*p*-phenoxyphenyl sulfoxide) of $M_n = 4800$ (280) containing no sulfone groups were obtained using nitric acid or hydrogen peroxide, respectively, as oxidizing agent. More recently, the selective and quantitative oxidation of atactic poly(propylene sulfide) to its corresponding sulfoxide was conducted by using *m*-chloroperbenzoic acid, hydrogen peroxide, or bromine under stoichiometric conditions either in homogeneous solution or in two-phase process (281).

Earlier reports dealing with oxidation of aliphatic polysulfides to polysulfoxides (19,281) contain no information about the properties of the resulting polysulfoxides.

The synthesis, properties, and application of aliphatic polysulfoxides with a methylene chain between sulfur atoms of various length (**108**) have been reported (18).

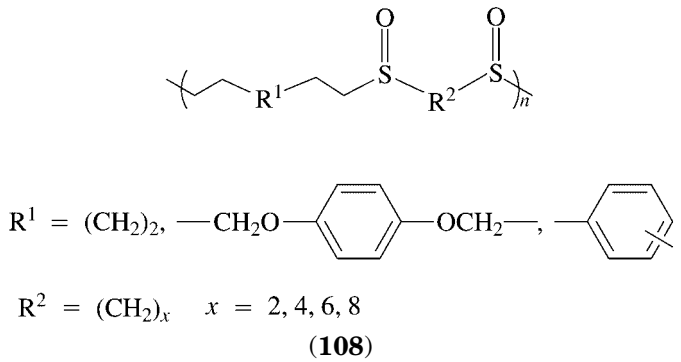

(**108**)

Polymers of M_n = 1600–6500 with polydispersity ~1.2–2.8 were prepared by addition of diolefins with dithiols and the following two-phase oxidation of the resulting polydisulfides. The effective oxidation (up to 92% of sulfoxide units) of polysulfides was conducted by using aqueous hydrogen peroxide in chloroform with or without heating. The formation of polysulfoxides was strongly supported by spectroscopic analysis. Poly(hexamethylene sulfoxide) obtained in this way was subject to Swern oxidation of primary or secondary alcohols, in which 1-octanol [111-87-5] and 6-undecanol [23708-56-7] were oxidized to give 1-octanal [124-13-0] and 6-undecanone [927-49-1], respectively, in quantitative yields (18).

The miscibility of aliphatic polysulfoxides (**109**) and (**110**) (T_g: 125°C, 7°C) with other commodity polymers was examined by comparing T_gs of the mixture of these polymers with T_gs of the original polymers by dsc. It was found that these polysulfoxides had good miscibility with poly(2-methyl-2-oxazoline) and/or poly(*N*-vinylpyrrolidinone) (275).

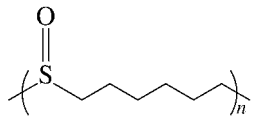

(**109**)

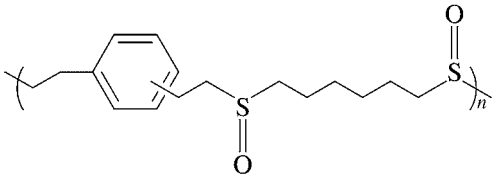

(**110**)

The novel highly optically active polysulfoxides (**111**) and (**112**) (276) with chiral sulfonyl groups in the main chain were prepared by asymmetric oxidation of corresponding polysulfides by using chiral *N*-sulfonyloxaziridine. The polysulfoxide with the enantiomeric excess (ee) of up to 91% was obtained in good chemoselectivity when the reaction was carried out with one equivalent of (−)-*N*-sulfonyloxaziridine (**113**) in chloroform at room temperature followed by reflux.

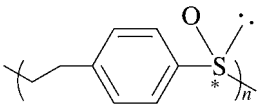

(**111**)

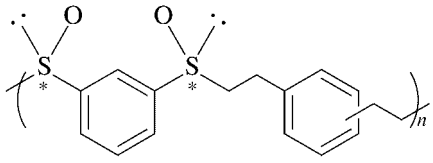

(**112**)

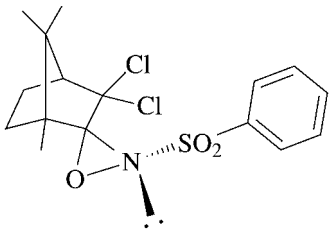

(**113**)

This asymmetric oxidation is the first example of introduction of chirality in good enantioselectivity into the main chain of a polymer by the polymer reaction, that is, the first example of the control of "tacticity" by polymer reaction. An earlier paper (282) described the synthesis of the liquid crystalline polymers having sulfoxide groups with low enantiomeric excess (25% ee). Another synthetic route to optical active polysulfoxides is the polymerization of optically active vinyl sulfoxides (283,284).

Polythiourethanes

Polythiourethanes (polythiocarbamates), the analogues of polyurethanes in which the ethereal or carbonyl oxygen atom of the urethane group has been replaced by sulfur [unit (**114**) and (**115**), respectively] are a relatively little-known class of polymers.

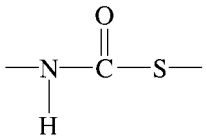

(**114**)

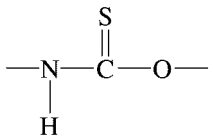

(**115**)

Polymers containing units (**114**) can be prepared by step-growth polymerization of diisocyanates with dithiols or bischlorothioformates with diamines. Early reports on the synthesis of these polymers concerned the melt polymerization of decamethylene diisocyanate [4538-39-0] and 1,10-decanedithiol [1191-67-9] (285,286).

Later, both the methods have been studied and compared, the addition reaction of various diisocyanates and dithiols carried out in chlorobenzene/*o*-dichlorobenzene solution with tri-*n*-propylamine [102-69-2] and DABCO (1,4-diazabicyklo[2.2.2.]octane, triethylene diamine, 2,2′-diazabicyclo[2.2.2]octane, TED, BACO) [280-57-9] as catalyst (eq. 5) and interfacial condensation of

various diamines and bischlorothioformates in the $CHCl_3/H_2O,Na_2CO_3$ system (eq. 6) (287).

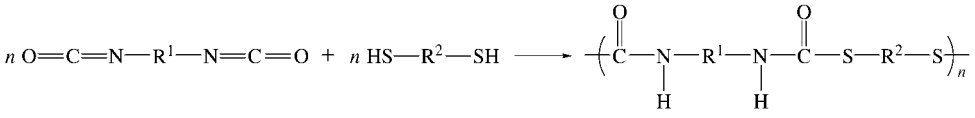

(5)

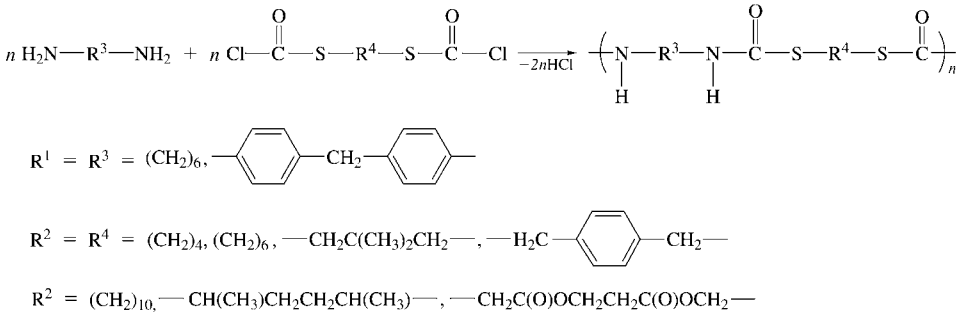

(6)

In general, the diisocyanate method was found to produce a higher yield (47–87% vs 31–73%) of the lower molecular weight polymers (η_{inh} 0.14–0.33 vs 0.30–1.20 dL/g) than that by the bischlorothioformate method. Polythiourethanes were found to be highly insoluble, odorless white powders which tend to decompose in light, in hot solvents, and in aqueous base. They melt somewhat higher than their oxygen analogues, but are less thermally stable. Some polymers form the pliable films from DMF solution.

Polythiourethanes (**116**) and (**117**) have been prepared by polymerization of the corresponding diisocyanates, HDI (hexamethylene diisocyanate, 1,6-diisocyanatohexane, 1,6-hexamethylene diisocyanate, hexamethylene-1,6-diisocyanate, HMDI, etc) [822-06-0], MDI (methylene diphenyl diisocyanate, 4,4′-diphenylmethane diisocyanate, diphenylmethane-4,4′-diisocyanate, methylene bis(*p*-phenylene isocyanate), etc] [101-68-8], or 2,6-TDI (toluene-2,6-diisocyanate, 2,6-tolylene diisocyanate, 2,6-toluene diisocyanate, etc) [91-08-7] with dithiols which were formed *in situ* from monofunctional (25) or bifunctional (26) five-membered cyclic dithiocarbonates and various diamines or benzylamine [100-46-9], respectively. The reactions were carried out in THF or THF/DMAC solution with triethylamine [121-44-8] as catalyst at room temperature. The polymers in yield of 74–100% with $M_n = 6000–17{,}200$ were obtained; their T_gs were 45–89°C. Contrary to common polythiourethanes showing low solubility even in highly polar organic solvent such as DMF and DMSO, these polymers are soluble in common organic solvents, including acetone and THF.

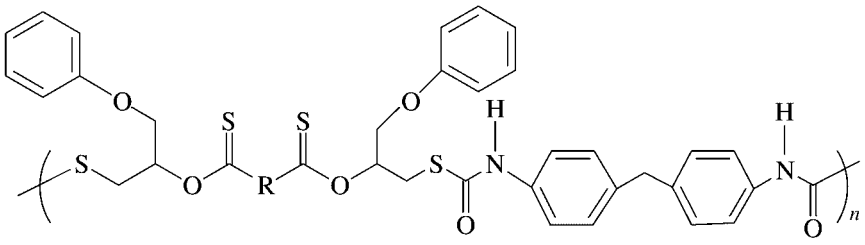

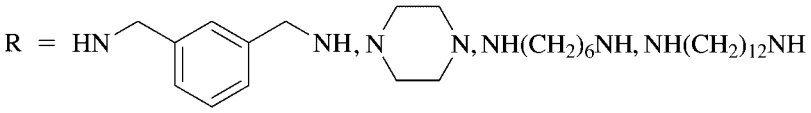

(**116**)

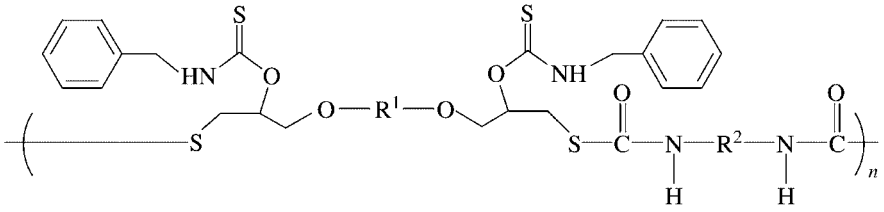

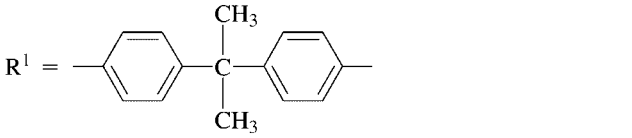

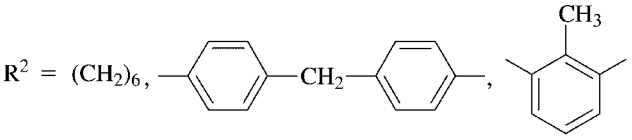

(**117**)

The SH- and NCO-terminated linear thiourethane telechelics containing units (**114**) (M_n = 520–610) were synthesized by DABCO-catalyzed addition reaction of 3,6-dioxaoctane-1,8-dithiol [14970-87-7] with various diisocyanates, including HDI, the mixture of 2,4,4-trimethylhexamethylene diisocyanate [15646-96-5] and 2,2,4-trimethylhexamethylene diisocyanate [6938-22-0], and isophorone diisocyanate [4098-71-9]. It has been shown that NCO-terminated prepolymers can be transformed into telechelics with olefinic end groups by treating with allyl alcohol [107-18-6], 2-hydroxyethyl methacrylate, or diallylamine [124-02-7] (288).

Polythiourethanes (**118**) containing units (**115**) bearing thiol groups were prepared in yield of up to 96% by the addition reaction of bifunctional five-membered cyclic dithiocarbonates (**119**) with diamines (**120**) carried out at room temperature in THF solution (93).

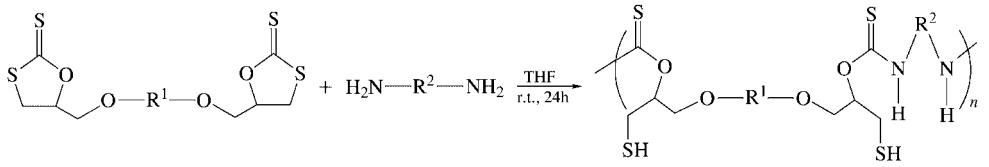

(**119**) (**120**) (**118**)

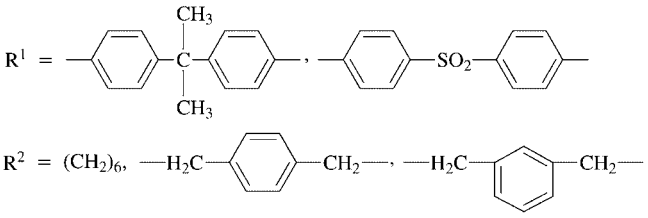

Their characteristics (after protection of the thiols group by acetylation) are M_n = 5700–12,000 with polydispersity = 1.38–1.65, T_{d10} = 216–248°C, T_g = 45–73°C, and the ability to form transparent films. Thus, polythiourethanes may be used as reactive polymers bearing the thiol groups which are sensitive to radical sources and applied to optical materials.

Polyesters Containing Sulfur Linkages

Among the thiopolyesters, polymers of linear structure containing S atoms in the main chain occupy the main position. They may find wide application as non-volatile plasticizers for such polymers as poly(vinyl chloride) and rubber modifiers. They are also useful for modifying or plasticizing elemental sulfur, which may be reacted with them by heating a mixture of the sulfur and polyester to produce such useful products as caulking compounds and compositions for striping or marking highways and other surfaces (289–294). Hydroxyl-terminated aliphatic–aromatic thiopolyesters are used as poliol components in the synthesis of high elasticity polyurethane elastomers (293,295,296). Some thiopolyesters with S atom in the side chain are used as intermediates in the synthesis of the polymers containing free thiol groups that might be of considerable usefulness as reducing agents in the thiol-disulfide system (297).

Linear thiopolyesters containing sulfur in the main chain were synthesized by step-growth polymerization of monothio- and dithiocarboxylic acids or their esters with diols and thiodiols mainly by using melt methods.

The earliest reports on thiopolyesters concern the syntheses of the low molecular weight polymers from the diethyl ester of thiodivaleric acid and some polymethylene diols (298), thiodiacetic acid [123-93-3] and 2,2′-thiodiethanol

[111-48-8] (299), and dimethyl ester of the 4,4′-thiodibenzoic acid or alkylenedithiodibenzoic acids and some polymethylene diols (300). The highly resistant high molecular weight polymers (M_n ~20,000) from 3,6-dithiaoctanedioic or 3,5-dithiaheptanedioic acid and fluorine-containing diols have also been described (301). All these reactions were carried out in melt at temperatures in the range of 160–250°C, at the first stage at atmospheric pressure and next under reduced pressure (130–400 Pa).

A few years later, various mainly aliphatic monothiopolyesters (**121**) and dithiopolyesters (**122**) (289,290) with M_n up to 10,000 were obtained by melt polymerization of the various monothio- and dithiocarboxylic acids, including 3,3′-thiodipropionic acid [111-17-1], thiodiisobutyric acid, 2,2′-dithiodiacetic acid [505-73-7], 3,3′-dithiodipropionic acid [1119-62-6], 4,4′-dithiodibutyric acid [2906-60-7], 7,7′-dithiodiheptanoic acid, 8,8′-dithiodioctanoic acid, and 4,4′-dithiodibenzoic acid with diols, including 1,2-ethanediol [107-21-1], 1,6-hexanediol [629-11-8], and 1,4-benzenedimethanol [589-29-7]. The process was typically carried out in the presence of nitrogen at temperatures 170–190°C for monothio products and 150–180°C for dithio products in two stages. First the diacid was heated with small excess of diol at atmospheric pressure. In the next stage, the low molecular weight polyester obtained earlier was submitted to transesterification by heating under reduced pressure (26–70 Pa) in the presence of a catalyst (PbO) and inhibitor of cross-linking 4-*tert*-butylcatechol [PTBC, 4-*tert*-butylpyrocatechol, TBC, 4-(1,1-dimethylethyl)-1,2-benzenediol, tertiary-butylcatechol)] [98-29-3].

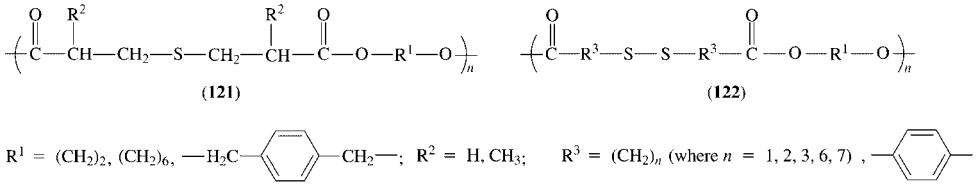

(**121**) (**122**)

R^1 = $(CH_2)_2$, $(CH_2)_6$, —H_2C—C$_6$H$_4$—CH_2—; R^2 = H, CH_3; R^3 = $(CH_2)_n$ (where n = 1, 2, 3, 6, 7), —C$_6$H$_4$—

Some of these novel thiopolyesters were used for modifying or plasticizing elemental sulfur. In this order, thiopolyesters were heated with elemental sulfur in amounts of 10–90 wt% at a temperature range of 150–250°C, until a clear melt was obtained. The resulting polyester–sulfur compositions (PSC) showed tensile strength from 0.5 to 10 MPa and elongation at break from 17 to 240%. Their tensile strength was improved by adding such fillers as glass wool and poly(ethylene terephthalate) fiber or by using cross-linked thiopolyesters. The best results in terms of color and flexibility for the wide range of 10–90% sulfur used were achieved by using 3,3′-thiodipropionic acid.

In the last decade, extensive and systematic studies were undertaken of the synthesis structure, properties, and application of linear thiopolyesters (**123**) prepared by melt polymerization from various new aliphatic–aromatic thiodicarboxylic acids and aliphatic diols as well as aliphatic–aromatic bis[4-(2′-hydroxyethylthiomethyl)phenyl]methane (EM) (291–296,302,303).

Thiodiacids (**124**), including diphenylmethane-4,4′-bis(methylthioacetic acid) (**124a**), diphenylmethane-4,4′-bis(methylthiopropionic acid) (**124b**),

naphthalene-1,4-bis(methylthioacetic acid) (**124c**), naphthalene-1,5-bis(methylthioacetic acid) (**124d**), and benzophenone-4,4′-bis(methylthioacetic acid) (**124e**) (T_m = 167, 149, 156, 189, 116°C, respectively) were prepared from suitable dimercapto compounds by condensation with monochloroacetic acid [79-11-8] or 3-chloropropionic acid [107-94-8] in 10–20% aqueous solution of NaOH.

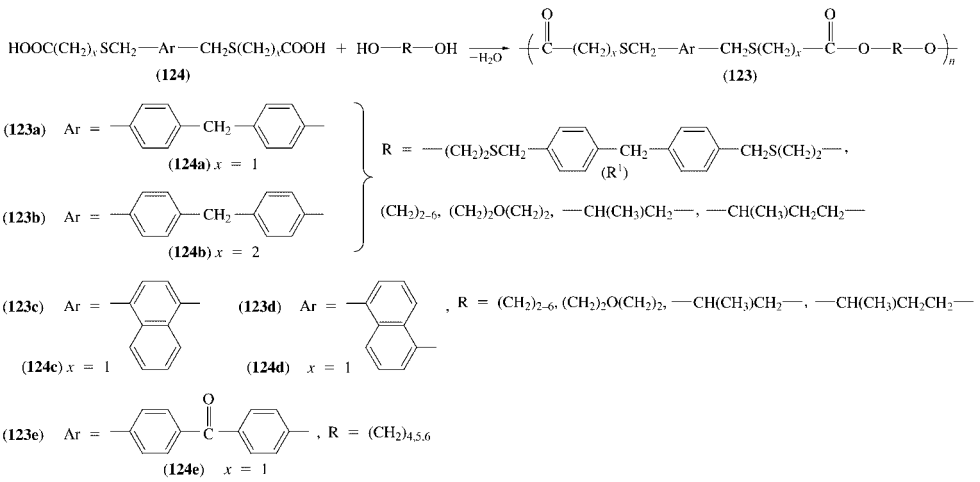

The kinetics of these esterification reactions was studied at 150, 160, and 170°C. Reaction rate constants and activation parameters from carboxyl group loss were determined using classical methods. The kinetic studies revealed that the rate of the reaction with (**124a**) was more than two times that with (**124b**) (293,303,304). From the two naphthalene-derived acids, (**124c**) showed a greater reactivity than (**124d**) (295). Thiopolyesters (M_n up to 10,000) are thick oils, waxy solids, or solids; (**123b**) and (**123d**) showed a large tendency to crystallize at room temperature. The relatively low T_gs (∼−30 to −10°C) were shown by (**123a**) and (**123b**) derived from aliphatic diols.

New PSC (291–294) with increased tensile strength in the form of thermoplastic rubber-like materials with sulfur cross-linked structure were obtained by heating thiopolyester (**123a**) or (**123b**) derived from 1,2-ethanediol [R = $(CH_2)_2$], 2,2′-oxydiethanol [111-46-6] [R = $(CH_2)_2O(CH_2)_2$], or EM (R = R^1) with 20–80% elemental sulfur at the temperature of about 220°C for 15–25 min. Depending on the nature of the thiopolyester and the amount of sulfur used, products with various degrees of hardness and elasticity characterized by tensile strength and elongation at break in the range of 0.4–21 MPa and 2–340%, respectively, were obtained. A cross-linking effect increasing the tensile strength of the PSC was achieved by introduction of diphenylmethane units with active methylene groups in the polymer chain. The formation of sulfur bridges of thiopolyesters involving these methylene groups was confirmed by solid-state ^{13}C nmr spectroscopy using cross-polarization magic-angle spinning (CP/MAS) and total sideband suppression (TOSS) techniques.

Some hydroxyl-terminated thiopolyesters (**123**) were used for preparing thiopoly(ester-urethane)s (293,295,296) (see next section). The novel thiopolyesters (**123e**) (M_n of 2000–2600), because of their structures incorporating benzophenone units, may also be considered as new diol components of uv-autopolymerizable polyurethane-(meth)acrylate oligomers.

Thiopolyester (**125**) from 4,4′-thiodiphenol [bis(4-hydroxyphenyl) sulfide, 4-hydroxyphenyl sulfide] [2664-63-3] (**126**), and adipoyl chloride [111-50-2] (**127**) was synthesized by both solution and interfacial condensation, as well as thiocopolyesters from (**126**), (**127**), and bisphenol-A (BPA) by interfacial condensation (305). Thiopolyester (**125**) under optimum interfacial polymerization conditions (tetrachloroethane as organic phase, tetra-*n*-butylammonium bromide [1643-19-2] as a phase transfer catalyst) showed a considerably higher specific viscosity value (1.64) than the polymer obtained in solution (0.18); it was a rather brittle material. Comonomer BPA was introduced into the polymer (**125**) chain in order to improve the toughness. Copolymer with the highest yield (93%) and the highest M_n (20,500) was obtained at the molar ratio (**126**)/BPA = 60/40. Its tensile strength was ~44 MPa. Polymers (**126**) with a content above 60 mol% showed a high barrier for oxygen permeability, especially the homopolymer (1.30×10^{-15} $cm^2 \cdot s^{-1} \cdot Pa^{-1}$).

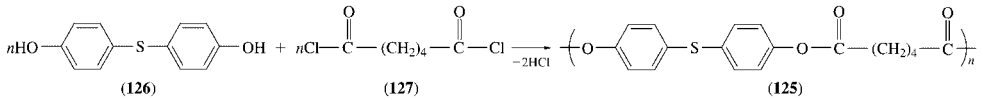

(**126**) (**127**) (**125**)

Few thiopolyesters with S atom in the side chain have been reported. The low-molecular-weight polymer (**128**) (297) with side benzylthiomethyl chains was successfully prepared by the condensation of 2-benzylthiomethyl-1,4-butanediol (**129**) with adypoil chloride (**127**) in refluxing benzene. Attempts to obtain a polymer with free thiol groups through debenzylation did not bring satisfactory results because of the simultaneous degradation of the polymer.

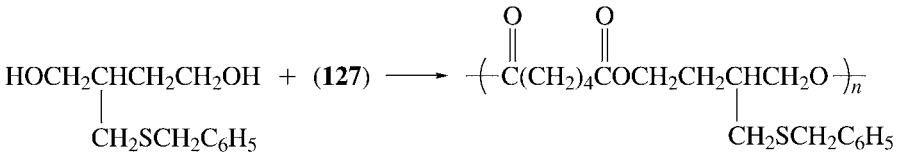

(**129**) (**128**)

Related polymers (**130**), also relatively low molecular weights (M_n up to 4400) and tolylmethylthiomethyl or naphthylmethylthiomethyl side chains, were obtained by uncatalyzed and catalyzed melt condensation of diacids (**131**), *p*-tolylmethylthiomethylsuccinic acid (**131a**), or 1-naphthylmethylthiomethylsuccinic acid (**131b**) with 2,2′-oxydiethanol (**132**) (306). Polymers showed thermal stabilities of up to ~220 or 280°C, respectively.

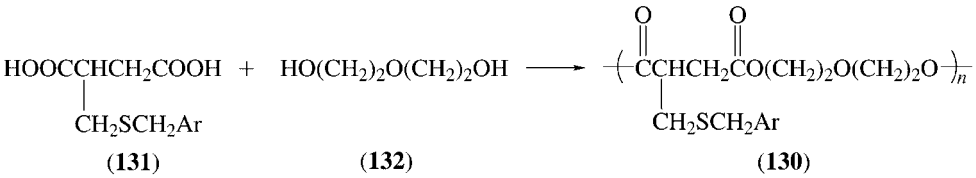

(131) (132) (130)

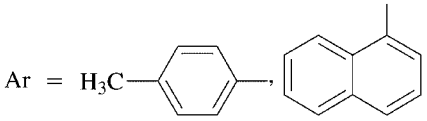

(131a) (131b)

Poly(3-hydroxyalkanoate) (**133**) (307) with a thiophenoxy group at the end of the side chain was obtained from *Pseudomonas putida* 27N01, a newly isolated bacterial strain, using 11-thiophenoxyundecanoic acid as the sole carbon source.

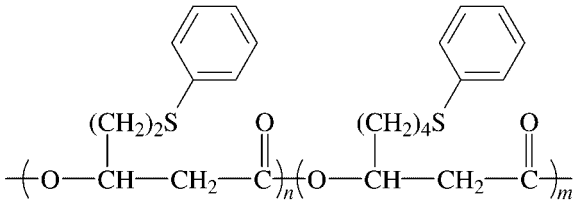

(**133**)

The polymer (M_n = 81,000 with polydispersity = 1.8, T_g = 4°C) had a white cream color and was elastomeric. This is the first report of poly(3-hydroxyalkanoates) containing a sulfur atom in the structure produced from bacteria. It may be supposed that (**133**) will usher in a new era of bacterial polymers.

Polyurethanes Containing Sulfur Linkages

Earlier studies (297) on the synthesis of thiopolyurethanes were attempted with the aim of obtaining polymers containing free sulfhydryl groups, which are compounds of considerable interest for a variety of reasons, eg, as reducing agents in the thiol-disulfide systems.

Thiopolyurethanes (**134**) with sulfur in side chain ([η] ~0.1–0.3 dL/g) prepared by solution (benzene) polymerization of the diol (**129**) with diisocyanates (**135**), HDI (**135a**), MDI (**135b**), or 2,4-TDI (2,4-toluene diisocyanate, 2,4-tolylene diisocyanate, 2,4-diisocyanatotoluene, etc) [584-84-9] (**135c**), were used as the polymeric intermediates for the synthesis of these polymers. The benzyl groups were successfully removed from polymer (**134a**) with sodium in a mixed solvent of liquid ammonium and *n*-propylamine [107-10-8], giving polymer (**136**).

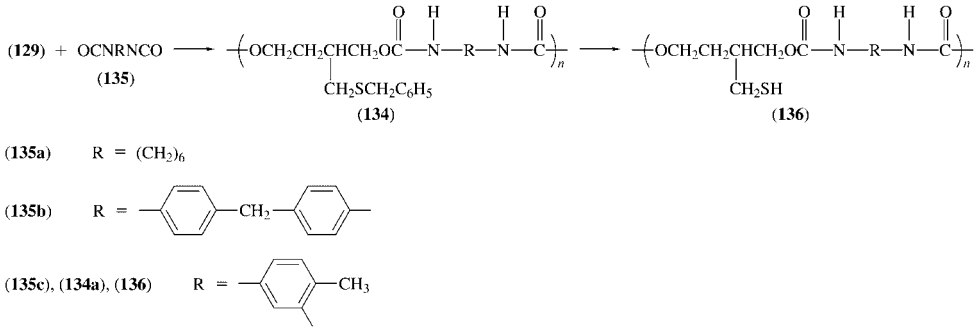

The analogous thiopolyurethanes with the side tolylmethylthiomethyl or naphthylmethylthiomethyl chains (306) were obtained from 2-(*p*-tolylmethylthiomethyl)-1,4-butanediol (TB) or 2-(1-naphthylmethylthiomethyl)-1,4-butanediol and HDI or Izocyn T-80 [TDI-80, the mixture of 2,4-TDI (80 wt%) and 2,6-TDI (20 wt%)] by solution (benzene) polymerization in the presence of di-*n*-butyltin dilaurate (DBTDL) [77-58-7] as catalyst. The polymer based on TB and HDI (η_{red} = 1.17 dL/g) was a high elasticity thermoplastic elastomer with tensile strength of 2.2 MPa and elongation at break of 780%.

The growing interest in polyurethane elastomers because of their unique properties, as well as in sulfur-containing polymers, prompted scientists in the last decade to undertake studies on the synthesis and properties of a novel class of thiopolyurethanes containing thioether linkages in the main chain, derived from various new diol components as aliphatic–aromatic simple thiodiols (308–314) and linear thiopolyester diols (293,295,296).

High elasticity thermoplastic thiopoly(ester-urethane)s of general structure (**137**) were prepared from newly obtained hydroxyl-terminated thiopolyesters (**123c**, **123d**, **123e** with R = $(CH_2)_{4,5,6}$ and **123a**, **123b** with R = (R^1); M_n = 1600–2900) and HDI (**135a**) or MDI (**135b**) at the ratio of NCO/OH = 1 or 1.05 by melt polymerization at temperature ~130°C in the presence of DBTDL as catalyst, when a less reactive HDI was used. Their characteristics were η_{red} ~0.4–1.1 dL/g (1,1,2,2-tetrachlorethane [79-34-5], 0.5–1%), T_gs from −1 to 18°C, tensile strength of 0.6–12 MPa, elongation at break of 500–1400%, and good thermal (up to 220–260°C) and chemical resistance. Polymers from (**123d**) showed the highest tensile strength, whereas those from (**123b**) the lowest T_gs. Thiopolyurethanes from (**123a**) and (**123b**) containing diphenylmethane units with active methylene groups are new, potentially peroxide-curable polymers.

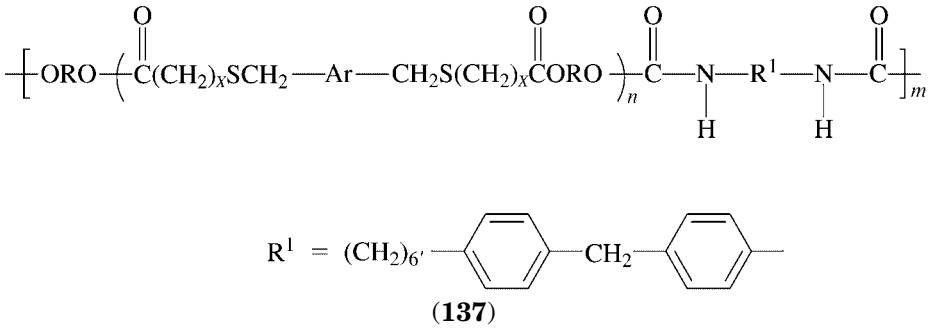

(**137**)

The DBTDL-catalyzed step-growth solution and melt polymerization reaction of the low melting thiodiols (**138**) with HDI (**135a**) at NCO/OH ratio = 1.05 produced thermoplastic nonsegmented thiopolyurethanes (**139a**) (309) and (**139b**) (308) showing partially crystalline structure (T_gs below 40°C, T_ms = 47–124°C). Higher molecular weight polymers (η_{red} = 0.63–1.24 dL/g, tetrachloroethane, 0.5–1%) were obtained by solution (DMF) polymerization. They showed tensile strength in the range of 16–50 MPa and thermal stability of up to 230–240°C.

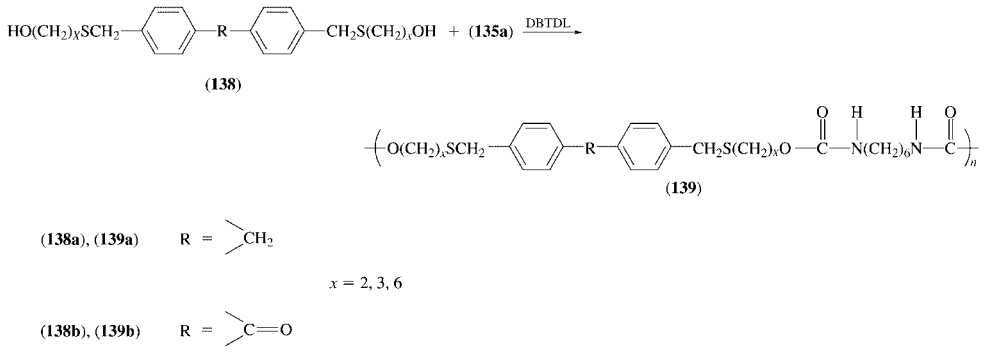

Thiodiols (**138b**) (315) (T_m = 38–76°C), including 4,4′-bis(2-hydroxyethylthiomethyl)benzophenone (x = 2), 4,4′-bis(3-hydroxypropylthiomethyl) benzophenone (x = 3), and 4,4′-bis(6-hydroxyhexylthiomethyl)benzophenone (x = 6) and thiodiols (**138a**) (309) (T_m = 68–78°C), including bis[4-(2-hydroxyethylthiomethyl)phenyl]methane (x = 2), bis[4-(3-hydroxypropylthiomethyl) phenyl]methane (x = 3), and bis[4-(6-hydroxyhexylthiomethyl)phenyl]methane (x = 6) were prepared by condensation reaction of the corresponding dithiols 4,4′-bis(mercaptomethyl)benzophenone or bis[4-(mercaptomethyl)phenyl]methane with 2-chloroethanol [107-07-3], 3-chloro-1-propanol [627-30-5], or 6-chloro-1-hexanol [2009-83-8], respectively, in 10% aqueous solution of sodium hydroxide.

Segmented thiopolyurethanes prepared from thiodiol (**138b**) with x = 6 (308) and all thiodiols (**138a**) (310,311) as chain extenders, HDI (**135a**), and 20–80 mol% poly(tetramethylene oxide) (PTMO) [24979-97-3] of M_n = 1000 as the soft segment by one-step process in the same conditions as for nonsegmented polymers were thermoplastic elastomers (except those based on 20% PTMO) showing partially crystalline structure. The polymers exhibited definite T_gs (−70 to −60), nearly independent of the hard segment content up to 50 wt% (40–80 mol% PTMO), indicating the existence of mainly microphase-separated soft and hard segments. Higher molecular weight polymers (M_n = 12,000–45,000 with polydispersity ∼2–4) were produced by the melt polymerization process. They showed tensile strength of 6–17 MPa and elongation at break of 140–680%. In each of the series, the increased PTMO soft-segment content decreased hardness, modulus of elasticity, and tensile strength, whereas elongation at break increased.

Because their structures incorporate diphenylmethane units with active methylene groups, polymers from (**138a**) are new, potentially peroxide-curable,

HDI-based thipolyurethanes, whereas polymers from (**138b**) containing benzophenone units may find use as interesting modifiers of photosensitive polyurethane resins.

Studies on the synthesis and properties of the linear nonsegmented thiopolyurethanes based on thiodiol containing atom S attached directly to aromatic ring bis[4-(2-hydroxyethylthio)phenyl] ether (**140**) ($T_m = 94°C$) under melt and solution polymerization conditions at the NCO/OH ratio = 1 showed that these polymers are brittle, hard, or rubber-like solids unsoluble and nonfusible up to 300°C from MDI (**135b**) (312), melting at ~245°C from 2,4-TDI (**135c**) (314), and soluble in DMF and DMSO at heating and melting at ~215°C from HDI (**135a**) (313). Their T_gs were 43–52°C. All the polymers were thermally stable up to 230–270°C. The introduction of comonomer 1,6-hexanediol significantly decreased T_m and T_g, and increased the solubility of the copolymers.

The synthesis and properties of the thermoplastic segmented thiopolyurethanes derived from thiodiol (**140**), 2,4-TDI (**135c**), and 20–80% PTMO of $M_n = 650$ and 1000 under one-step solution (DMF) and melt polymerization conditions (the ratio of NCO/OH = 1, DBTDL as catalyst) have also been reported (314). The most interesting are high molecular weight polymers (η_{red} = 1.42–2.30 dL/g) obtained by melt polymerization from PTMO of $M_n = 1000$. They are rubber-like products easily soluble in organic solvents and showing high adhesion to many substrates; these polymers may be useful as glues.

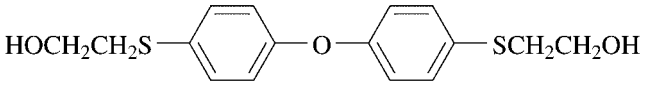

(**140**)

The reactions of some aliphatic thiodiols as 2,2′-thiodiethanol [111-48-8] or 4,4′-thiodibutanol with HDI were investigated many years ago (316).

Polysulfoximines

The chemical and physical properties of the polysulfoximines are of particular interest because of their rigid and unsymmetrical structure (**141**) and the polymers can be considered as new, potentially high-performance, engineering plastics. In recent years, the first preliminary studies on the synthesis and properties of this novel class of sulfur-containing polymers have been reported (317–320).

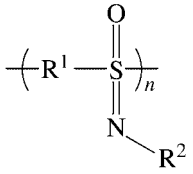

R^2 = H, alkyl, allyl, aryl, acyl, sulfonyl, etc.

(**141**)

The self-condensation of sulfonoimidoyl chlorides such as *N*-tosyl (Ts) derivative of the benzene- and 4-phenoxybenzene-sulfonimidoyl chloride (**142**) utilizing a catalytic ($AlCl_3$ or $FeCl_3$) Friedel–Crafts reaction has been studied as a way to produce these polymers. It has been found that the reaction of the former compound yielded no polymeric product, whereas that of (**142**) produced exclusively methanol-insoluble polymer (**143**) of $M_n = 14{,}500$ with polydispersity = 1.45 in 80% yield (317).

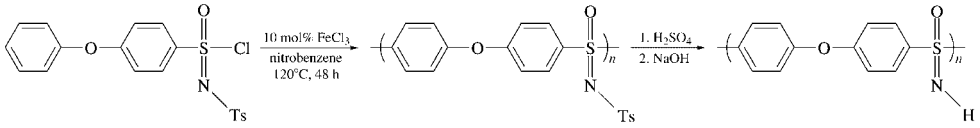

(**142**) (**143**) (**144**)

The treatment of (**143**) with concentrated sulfuric acid followed by neutralization with NaOH at room temperature gave the corresponding polymer (**144**) containing the "free" sulfoximine moiety and with M_n nearly equal to that of (**143**); the T_gs of (**143**) and (**144**) were almost equal, namely 335 and 333°C, respectively. Polymer (**144**) was much more thermally stable than (**143**) and its thermal stability (20 wt% loss temperature ~550°C) is comparable to that of poly(ether-sulfone).

BIBLIOGRAPHY

"Sulfur-Containing Polymers" in *EPST* 1st ed., Vol. 13, pp. 448–477, by E. J. Goethals, Rijksuniversiteit Gent; "Sulfur-Containing Polymers" in *EPSE* 2nd ed., Vol. 16, pp. 246–368, by A. Duda and S. Penczek, Polish Academy of Sciences.

1. N. G. Gaylord, ed., *Polyethers, Part III: Polyalkylene Sulfides and Other Polythioethers*, Wiley-Interscience, New York, 1962, Chapts. "12–14".
2. E. J. Goethals, in A. Sonning and P. S. Magee, eds., *Topics in Sulfur Chemistry*, Vol. **3**, G. Thieme Publishers, Stuttgart, 1977, p. 1.
3. N. Spassky, M. Sepulchre, and P. Sigwalt, in H. R. Kricheldorf, ed., *Handbook of Polymer Synthesis, Part B*, Marcel Dekker, Inc., New York, 1992, p. 991, Chapt. "16".
4. P. Sigwalt and N. Spassky, in K. J. Ivin and T. Saegusa, eds., *Ring-Opening Polymerization*, Elsevier Applied Science, New York, 1984, p. 603.
5. D. J. Brunelle, in D. J. Brunelle, ed., *Ring-Opening Polymerization: Mechanism, Catalysis, Structure, Utility*, Hanser, New York, 1993, Chapt. "11".
6. M. L. Kaplan and W. D. Reents Jr., *Tetrahedron Lett.* **23**, 373 (1982).
7. J. Franke and F. Vögtle, *Tetrahedron Lett.* **25**, 3445 (1984).
8. Y.-F. Wang, K. P. Chan, and A. S. Hay, *Macromolecules* **28**, 6371 (1995).
9. Y. Ding and A. S. Hay, *Macromolecules* **29**, 4811 (1996).
10. Y. Ding and A. S. Hay, *Macromolecules* **29**, 6386, (1996).
11. Y. Ding and A. S. Hay, *Macromolecules* **30**, 2527, (1997).
12. D. A. Zimmerman, J. L. Koenig, and H. Ishida, *Polymer* **37**, 3111 (1996).
13. Y.-F. Wang and A. S. Hay, *Macromolecules* **29**, 5050 (1996).
14. E. Tsuchida and co-workers, *Macromolecules* **31**, 6469 (1998).
15. M. Tomoi and co-workers, *Makromol. Chem.* **184**, 2431 (1983).
16. K. Yamashita and co-workers, *React. Funct. Polym.* **31**, 47 (1996).
17. M. Wagner and co-workers, *J. Chem. Soc., Perkin Trans 1* **16**, 1995 (1996).

18. T. Oyama, J. Ozaki, and Y. Chujo, *Polym. Bull.* **38**, 379 (1997).
19. C. Marco and co-workers, *Macromolecules* **16**, 95 (1983); C. Marco and co-workers, *Makromol. Chem.* **185**, 1255 (1984).
20. J.-C. Lee, M. H. Litt, and C. E. Rogers, *Macromolecules* **30**, 3766 (1997).
21. J.-C. Lee, M. H. Litt, and C. E. Rogers, *Macromolecules* **31**, 2440 (1998).
22. Y.-K. Lee and co-workers, *Kobunshi Ronbunshu* **55**, 49 (1998).
23. E. Kobayashi, R. Kuribayashi, and S. Aoshima, *Polym. Advan. Technol.* **6**, 394 (1995).
24. H. Kudo, F. Sanda, and T. Endo, *Macromolecules* **32**, 8370 (1999).
25. W. Choi and co-workers, *Macromol. Chem. Phys.* **199**, 1909 (1998).
26. W. Choi, F. Sanda, and T. Endo, *J. Polym. Sci., Part A: Polym. Chem.* **36**, 1189 (1998).
27. W. Podkościelny and B. Tarasiuk, *Angew. Makromol. Chem.* **234**, 145 (1996); B. Tarasiuk, W. Podkościelny, and W. Majewski, *Angew. Makromol. Chem.* **251**, 13 (1997).
28. U.S. Pat. 3354129 (Nov. 21, 1963), J. T. Edmonds Jr. and H. W. Hill Jr. (to Phillips Petroleum Co.).
29. L. C. Lopez and G. L. Wilkes, *J. Macromol. Sci., C: Rev. Macromol. Chem.* **29**, 84 (1989).
30. D. A. Zimmerman and H. Ishida, Abstracts of MacroAkron'94, July 11–15, 1994, p. 160.
31. K. Miyatake and co-workers, *Polym. Advan. Technol.* **3**, 401 (1992).
32. K. Yamamoto and co-workers, *Phosphorus Sulfur* **120/121**, 407 (1997).
33. K. Miyatake and co-workers, *Macromolecules* **31**, 403 (1998).
34. S. Kondo and co-workers, *J. Macromol. Sci., A: Pure Appl. Chem.* **33**, 811 (1996).
35. A. J. Blake and M. Schröder, in A. G. Sykes, ed., *Advances in Inorganic Chemistry*, Vol. **35**, Academic Press, New York, 1990, p. 2.
36. S. R. Cooper, *Acc. Chem. Res.* **21**, 141 (1988).
37. S. R. Cooper, in S. R. Cooper, ed., *Crown Compounds: Toward Future Applications*, VCH Publishers, New York, 1992, Chapt. "15".
38. S. R. Cooper and S. C. Rawle, *Struct. Bonding (Berlin)* **72**, 1 (1990).
39. M. Schröder, *Pure Appl. Chem.* **60**, 517 (1988).
40. G. J. Grant and co-workers, *Inorg. Chim. Acta* **244**, 73 (1996).
41. G. J. Grant and co-workers, *Inorg. Chim. Acta* **246**, 31 (1996).
42. G. J. Grant and co-workers, *Inorg. Chim. Acta* **274**, 192 (1998).
43. M. Wagner, S. Zeltner, and R.-M. Olk, *Liebigs Ann.* **4**, 551 (1996).
44. Ref. 3, p. 1353, Chapt. "21".
45. G. Tourillon, in T. A. Skotheim, ed., *Handbook of Conducting Polymers*, Vol. **1**, Marcel Dekker, Inc., New York, 1986, Chapt. "9".
46. J. Roncali, *Chem. Rev.* **92**, 711 (1992).
47. S. K. Ritter and co-workers, *J. Fluorine Chem.* **93**, 73 (1999).
48. M. Yoshida and co-workers, *Bull. Chem. Soc. Jpn.* **61**, 3549 (1988).
49. W. Büchner and co-workers, *J. Electroanal. Chem.* **227**, 355 (1990).
50. W. Büchner and co-workers, *J. Fluorine Chem.* **59**, 301 (1992).
51. A. El Kassmi and co-workers, *J. Electroanal. Chem.* **326**, 357 (1992).
52. M. Lemaire and co-workers, *New J. Chem.* **14**, 359 (1990).
53. S. K. Ritter, R. E. Noftle, and A. E. Ward, *Chem. Mater.* **5**, 752 (1993).
54. S. C. Ng and co-workers, *Langmuir*, **14**, 1748 (1998).
55. S. Frenzel and co-workers, *J. Mater. Chem.* **5**, 1529 (1995).
56. S. Frenzel, C. Kübel, and K. Müllen, *Phosphorus Sulfur* **120/121**, 77 (1997).
57. J. Leuninger and co-workers, *Macromolecules* **31**, 1720 (1998).
58. J. Leuninger and co-workers, *Synth. Met.* **101**, 681 (1999).

59. H. Muller and co-workers, *Chem. Commun.* **15**, 1407 (1999).
60. A. Haryono and co-workers, *Macromolecules* **32**, 3146 (1999).
61. V. R. Durvasula, F. A. Stuber, and D. Bhattacharjee, *J. Polym. Sci., Part A: Polym. Chem.* **27**, 661 (1989).
62. D. R. Senn, *J. Polym. Sci., Part A: Polym. Chem.* **32**, 1175 (1994).
63. M. Ueda, T. Abe, and M. Oda, *J. Polym. Sci., Part A: Polym. Chem.* **30**, 1993 (1992).
64. Z. Y. Wang and A. S. Hay, *Polymer* **33**, 1778 (1992).
65. Y. Ding and A. S. Hay, *Pure Appl. Chem. A* **34**, 405 (1997).
66. L. Angiolini, C. Carlini, and E. Salatelli, *Makromol. Chem.* **193**, 2883 (1992).
67. L. Angiolini, C. Carlini, and E. Salatelli, *Polymer* **34**, 3778 (1993).
68. L. Angiolini and co-workers, *Polymer* **36**, 1071 (1995).
69. L. Angiolini and co-workers, *Gazz. Chim. Ital.* **126**, 69 (1996).
70. L. Angiolini and co-workers, *J. Polym. Sci., Part A: Polym. Chem.* **34**, 2999 (1996).
71. M. B. Berenbaum and I. R. Panek, in Ref. 1, p. 43.
72. S. M. Ellerstein and E. R. Bertozzi, *Encyclopedia of Chemical Technology*, Vol. **19**, Wiley-Interscience, New York, 1987, p. 814.
73. K. Kishore and K. Ganesh, *Adv. Polym. Sci.* **121**, 81 (1994).
74. D. E. Vietti, in G. Allen and J. C. Allen, eds., *Comprehensive Polymer Science*, Vol. **5**, Pergamon Press, New York, 1989, p. 533.
75. R. C. Thomas and L. J. Reed, *J. Am. Chem. Soc.* **78**, 6146 (1956).
76. J. Houk and G. M. Whitesides, *Tetrahedron* **45**, 91 (1989).
77. Y. Ding and A. S. Hay, *Polymer* **38**, 2239 (1997).
78. N. A. Hiatt, *Polym. Prepr. (Am. Chem. Soc., Div. Polym. Chem.)* **13**, 594 (1972).
79. C. Marschalk and J. P. Niederhauser *Bull. Soc. Chim. Fr.* 147 (1952).
80. L. Field, W. D. Stephens, and E. L. Lippert Jr., *J. Am. Chem. Soc.* **83**, 4783 (1961).
81. D. T. Wong and C. S. Marvel, *J. Polym. Sci.* **14**, 1637 (1976).
82. M. S. Raasch, *J. Org. Chem.* **44**, 2629 (1979).
83. F. R. Bottino and co-workers, *J. Chem. Soc., Perkin Trans. 1* **18**, 199 (1981).
84. N. B. Pahor and co-workers, *Gazz. Chim. Ital.* **110**, 227 (1980).
85. R. D. Adams, J. A. Queisser, and J. H. Yamamoto, *J. Am. Chem. Soc.* **118**, 10674, (1996).
86. R. D. Adams and co-workers, *Organometallics* **16**, 1430 (1997).
87. M. H. Goodrow and W. K. Musker, *Synthesis* (6) 457 (1981); M. H. Goodrow, M. M. Olmstead, and W. K. Musker, *Tetrahedron Lett.* **23**, 3231 (1982); G. Crank and M. I. H. Makin, *Aust. J. Chem.* **37**, 2331 (1984).
88. V. St. Georgiev, *Med. Res. Rev.* **10**, 371 (1990).
89. R. D. Adams and J. H. Yamamoto, *J. Cluster Sci.* **7**, 643, (1996).
90. R. D. Adams, M. Huang, and S. Johnson, *Polyhedron* **17**, 2775 (1998).
91. W. Choi and co-workers, *J. Polym. Sci., Part A: Polym. Chem.* **36**, 79 (1998).
92. N. Kihara, Y. Nakawaki, and T. Endo, *J. Org. Chem.* **60**, 473 (1995).
93. T. Moriguchi and T. Endo, *Macromolecules* **28**, 5386 (1995).
94. A. Orzeszko, A. Czerwinski, and Z. Kazimierczuk, *J. Polym. Mater.* **14**, 21 (1997).
95. W. Amaratunga, J. Milne, and A. Santagati, *J. Polym. Sci., Part A: Polym. Chem.* **36**, 379 (1998).
96. M. M. Doeff and co-workers, *J. Electrochem. Soc.* **139**, 2077 (1992).
97. M. Giffard and co-workers, *J. Chem. Res. (S)* 126 (1993).
98. L. Field, in S. Oae, ed., *Organic Chemistry of Sulfur*, Plenum, New York, 1977, p. 303.
99. D. Andreu and co-workers, in M. W. Pennington and B. M. Dunn, eds., *Methods in Molecular Biology: Peptide Synthesis Protocols*, Vol. **35**, Humana, Totowa, N.J., 1994, p. 91.
100. L. Chen and co-workers, *J. Med. Chem.* **40**, 864 (1997).

101. M. F. Hoover, *J. Macromol. Sci., Chem.* **4**, 1327 (1970).
102. S. Kondo and co-workers, *Makromol. Chem., Rapid Commun.* **9**, 625 (1988).
103. K. Miyatake and co-workers, *Macromolecules* **29**, 6969 (1996).
104. K. Yamamoto and co-workers, *J. Am. Chem. Soc.* **115**, 5819 (1993).
105. E. Tsuchida, E. Shouji, and K. Yamamoto, *Macromolecules* **26**, 7144 (1993); E. Tsuchida, K. Yamamoto, and E. Shouji, *Macromolecules* **26**, 7389 (1993).
106. E. Tsuchida and co-workers, *Angew. Chem., Int. Ed. Engl.* **35**, 2843 (1996).
107. E. Shouji and co-workers, *Chem. Lett.* **43**, 403 (1994).
108. R. O. Garay and R. W. Lenz, *J. Polym. Sci., Part A: Polym. Chem.* **30**, 977 (1992).
109. J. D. Stenger-Smith, R. W. Lenz, and G. Wegner, *Makromol. Chem.* **190**, 3005 (1989).
110. J. M. Machado and co-workers, *J. Polym. Sci., Part B: Polym. Phys.* **27**, 199 (1989).
111. R. Lenz and co-workers, *J. Polym. Sci., Part A: Polym. Chem.* **26**, 3241 (1988).
112. B. Winkler, L. Dai, and A. W.-H. Mau, *Chem. Mater.* **11**, 704 (1999).
113. K. Miyatake and co-workers, *Macromolecules* **30**, 2941 (1997).
114. E. Shouji and co-workers, *Polym. Advan. Technol.* **5**, 109, 507 (1994).
115. A. Haryono and co-workers, *Macromolecules* **31**, 1202 (1998).
116. D. N. Kevill and S. W. Anderson, *J. Org. Chem.* **56**, 1845 (1991).
117. T. Umemoto, *Chem. Rev.* **96**, 1757 (1996).
118. O. Shimomura and co-workers, *J. Polym. Sci., Part A: Polym. Chem.* **35**, 2813 (1997).
119. O. Shimomura and co-workers, *J. Polym. Sci., Part A: Polym. Chem.* **36**, 1779 (1998).
120. O. Shimomura and co-workers, *React. Funct. Polym.* **40**, 29 (1999).
121. E. Tsuchida and co-workers, *Chem. Commun.* 2091 (1996).
122. A. Haryono, K. Miyatake, and E. Tsuchida, *Macromol. Chem. Phys.* **200**, 1257 (1999).
123. J. Roncali, *Chem. Rev.* **97**, 173 (1997).
124. J. A. Kent, *Riegel's Handbook of Industrial Chemistry*, 8th ed., Van Nostrand Reinhold Co., Inc., New York, 1983.
125. K.-M. Chen and H.-J. Liu, *J. Appl. Polym. Sci.* **34**, 1879 (1987).
126. B. R. Rao and K. V. Datye, *Text. Chem. Color.* **28**, 17 (1996).
127. S. Mindess and J. F. Young, *Concrete*, Prentice Hall, Englewood Cliffs, N.J., 1981.
128. K.-C. Hsu, S.-D. Chen, and N. Su, *J. Appl. Polym. Sci.* **76**, 1762 (2000).
129. A. D. Patil and co-workers, *J. Am. Chem. Soc.* **109**, 1858 (1987).
130. A. D. Child and J. R. Reynolds, *Macromolecules* **27**, 1975 (1994).
131. X.-L. Wei and co-workers, *J. Am. Chem. Soc.* **118**, 2545 (1996).
132. L. Leemans and co-workers, *Macromolecules* **24**, 5922 (1991).
133. H. Müller and co-workers, *Macromolecules* **30**, 2288 (1997).
134. A. Eisenberg, B. Hird, and R. B. Moore, *Macromolecules* **23**, 4098 (1990).
135. S. A. Perusich, P. Avakian, and M. Y. Keating, *Macromolecules* **26**, 4756 (1993).
136. A. Noshay and L. M. Robeson, *J. Appl. Polym. Sci.* **20**, 1885 (1976).
137. J. Kerres, W. Cui, and S. Reichle, *J. Polym. Sci., Part A: Polym. Chem.* **34**, 2421 (1996).
138. M. T. Bishop and co-workers, *Macromolecules* **18**, 86 (1985); X. Jin and co-workers, *Br. Polym. J.* **17**, 4 (1985); Ch. Bailly and co-workers, *Polymer* **28**, 1009 (1987).
139. Eur. Pat. 331298 (Oct. 12, 1989), B. N. Hendy (to Imperial Chemical Industries Plc.).
140. Brit. Pat. 2216134 (Oct. 4, 1989), M. J. Peer (to Paterson Candy International Ltd.).
141. Eur. Pat. 286091 (Oct. 12, 1988), S. Ch. Williams and co-workers (to Union Carbide Corp.).
142. Eur. Pat. 277834 (Aug. 10, 1988), J. E. Tomaschke, A. J. Testa, and J. G. Vouros (to Hydranautics).
143. H.-H. Ulrich and G. Rafler, *Angew. Makromol. Chem.* **263**, 71 (1998).
144. T. Kobayashi and co-workers, *Solid State Ionics* **106**, 219 (1998).

145. L. Giuffre and co-workers, *Hydrogen Energy* **8**, 419 (1983).
146. E. Montoneri and co-workers, *Int. J. Polym. Mater.* **11**, 263 (1987).
147. E. Montoneri, *J. Polym. Sci., Part A: Polym. Chem.* **27**, 3043 (1989).
148. P. Hruszka, J. Jurga, and B. Brycki, *Polymer* **33**, 248 (1992).
149. N. M. Belomoina and co-workers, *Vysokomol. Soedin. Ser. B* **38**, 355 (1996).
150. N. Carretta, V. Tricoli, and F. Picchioni, *J. Membrane Sci.* **166**, 189 (2000).
151. M. M. Nasef and co-workers, *J. Appl. Polym. Sci.* **78**, 2443 (2000).
152. S. Sugiyama and co-workers, *React. Polym.* **21**, 187 (1993).
153. X. Zhli-Li and co-workers, *Radiat. Phys. Chem.* **22**, 939 (1983).
154. S. Holmberg and co-workers, *J. Mater. Chem.* **6**, 1309 (1996).
155. S. Holmberg, J. Näsman, and F. Sundholm, *Polym. Adv. Technol.* **9**, 121 (1998).
156. H. P. Brack and co-workers, *Polym. Sci. Eng.* **77**, 368 (1998).
157. M. M. Nasef and co-workers, *J. Appl. Polym. Sci.* **73**, 2095 (1999).
158. M. M. Nasef and co-workers, *J. Appl. Polym. Sci.* **76**, 1 (2000).
159. M. V. Rouilly and co-workers, *J. Membr. Sci.* **81**, 89 (1993).
160. M. M. Nasef, H. Saidi, and H. M. Nor, *J. Appl. Polym. Sci.* **76**, 220 (2000).
161. M. M. Nasef, H. Saidi, and M. A. Yarmo, *J. Appl. Polym. Sci.* **77**, 2455 (2000).
162. L. Hong and N. P. Chen, *J. Polym. Sci., Part B: Polym. Phys.* **38**, 1530 (2000).
163. B. A. Trofimov and co-workers, *Vysokomol. Soedin. Ser. B* **41**, 543 (1999).
164. Y. Morishima, *Trends Polym. Sci.* **2**, 31 (1994).
165. R. S. Armentrout and C. L. McCormick, *Macromolecules* **33**, 2944 (2000).
166. Y. Itoh, Y. Morishima, and S. Nozakura, *J. Polym. Sci., Polym. Chem. Ed.* **20**, 467 (1982).
167. Y. Huang, U. Seitz, and W. Funke, *Makromol. Chem.* **186**, 273 (1985).
168. F. Rosa, J. Bordado, and M. Casquilho, *Cell. Polym.* **16**, 175 (1997).
169. H. Sawada and co-workers, *J. Mater. Chem.* **8**, 1517 (1998).
170. W. Shi, C. J. Watson, and C. P. Palmer, *J. Chromatogr. A* **905**, 281 (2001).
171. B. Mangovska, G. Bogoeva-Gaceva, and I. Jordanov, *Tekstil* **49**, 131 (2000).
172. F. LAlloret and co-workers, *Rev. I. Fr. Petrol.* **52**, 117 (1997).
173. F. LAlloret, D. Hourdet, and R. Audebert, *Colloid Polym. Sci.* **273**, 1163 (1995).
174. K.-C. Hsu and Y.-F. Lee, *J. Appl. Polym. Sci.* **57**, 1501 (1995).
175. K.-C. Hsu and Y.-F. Lee, *J. Mater. Sci.* **31**, 5787 (1996).
176. S.-D. Chen, C.-H. Hwang, and K.-C. Hsu, *Cem. Concr. Res.* **29**, 255 (1999).
177. J. Lin and co-workers, *Macromolecules* **25**, 7107 (1992).
178. D. T. B. Hannah and D. C. Sherrington, *J. Mater. Chem.* **7**, 1985 (1997).
179. M. Jozefowicz and J. Jozefonvicz, *Pure Appl. Chem.* **56**, 1335 (1984); P. Hovingh, M. Piepkorn, and A. Linker, *Biochem. J.* **237**, 537 (1986).
180. T. G. Grasel and S. L. Cooper, *J. Biomed. Mater. Res.* **23**, 311 (1989).
181. A. Z. Okkema, S. A. Visser, and S. L. Cooper, *J. Biomed. Mater. Res.* **25**, 1371 (1991).
182. J. H. Silver, J. W. Marchant, and S. L. Cooper, *J. Biomed. Mater. Res.* **27**, 1443 (1993).
183. J. H. Silver and co-workers, *Biomaterials* **13**, 339 (1992).
184. J. P. Santerre and co-workers, *J. Biomed. Mater. Res.* **26**, 39 (1992).
185. G. A. Skarja and co-workers, *J. Biomed. Mater. Res.* **34**, 427 (1997).
186. G. A. Skarja and J. L. Brash, *J. Biomed. Mater. Res.* **34**, 439 (1997).
187. A. Takahara and co-workers, *J. Biomed. Mater. Res.* **25**, 1095 (1991).
188. L. L. Yung, F. Lim, and S. L. Cooper, *Trans. Soc. Biomater.* **18**, 78 (1995).
189. P. Radziwon and co-workers, *Haemostasis* **28**, 86 (1998).
190. E. De Clercq, *Int. J. Antimicrob. AG.* **7**, 193 (1996).
191. M. Podgórski and W. Podkościelny, *J. Appl. Polym. Sci.* **34**, 639 (1987).
192. Y. Imai, M. Ueda, and M. Ii, *Makromol. Chem.* **179**, 2085 (1978).

193. Y. Imai, M. Ueda, and M. Ii, *Kobunshi Ronbunshu (Japan)* **35**, 807 (1978); *Chem. Abstr.* **90**, 87899e (1979).
194. M. Podgórski, *Ann. Univ. Mariae Curie-Sklodowska, Sect. AA: Chem.* **44/45**, 59 (1989–1990) (in Polish).
195. M. M. Kamani and P. H. Parsania, *J. Polym. Mater.* **12**, 217 (1995).
196. M. M. Kamani and P. H. Parsania, *J. Polym. Mater.* **12**, 223 (1995).
197. J. A. Desai, U. Dayal, and P. H. Parsania, *J. Macromol. Sci., A: Pure Appl. Chem.* **33**, 1113 (1996).
198. A. R. Shah, S. Sharma, and P. H. Parsania, *J. Polym. Mater.* **14**, 1 (1997).
199. K. M. Rajkotia, M. M. Kamani, and P. H. Parsania, *Polymer* **38**, 715 (1997).
200. F. D. Karia and P. H. Parsania, *Eur. Polym. J.* **35**, 121 (1999).
201. F. D. Karia and P. H. Parsania, *J. Polym. Mater.* **16**, 161 (1999).
202. F. D. Karia and P. H. Parsania, *Eur. Polym. J.* **36**, 519 (2000).
203. A. R. Shah and P. H. Parsania, *J. Polym. Mater.* **14**, 33 (1997).
204. K. M. Rajkotia, S. Baluja, and P. H. Parsania, *Eur. Polym. J.* **33**, 1005 (1997).
205. M. M. Kamani and P. H. Parsania, *J. Polym. Mater.* **13**, 191 (1996).
206. J. A. Desai and P. H. Parsania, *J. Polym. Mater.* **13**, 79 (1996).
207. S. Minegishi, A. Kameyama, and T. Nishikubo, *J. Polym. Sci., Part A: Polym. Chem.* **36**, 249 (1998).
208. C. H. Cholakis and M. Sefton, in S. W. Shalaby, A. S. Hoffman, B. O. Ratner, and T. A. Horbett, eds. *Polymers as Biomaterials*, Plenum Press, New York, 1984, p. 305.
209. E. De Clercq, *Biomed. Pharmacother*. **50**, 207 (1996).
210. M. Witvrouw and E. De Clercq, *Gen. Pharmacol.* **29**, 497 (1997).
211. L. H. Tagle and co-workers, *Makromol. Chem.* **186**, 915 (1985).
212. L. H. Tagle, F. R. Diaz, and P. Riveros, *Polym. J.* **18**, 501 (1986).
213. L. H. Tagle, F. R. Diaz, and N. Valdebenito, *Polym. Bull.* **18**, 479 (1987).
214. L. H. Tagle, F. R. Diaz, and P. Salas, *J. Macromol. Sci. Chem. A* **26**, 1321 (1989).
215. L. H. Tagle, F. R. Diaz, and M. L. Jimenez, *Polym. Bull.* **28**, 645 (1992).
216. L. H. Tagle, F. R. Diaz, and R. Fuenzalida, *J. Macromol. Sci., A: Pure Appl. Chem.* **31**, 283 (1994).
217. L. H. Tagle, F. R. Diaz, and C. Margozzini, *Polym. Bull.* **25**, 319 (1991).
218. L. H. Tagle and co-workers, *Int. J. Polym. Mater.* **20**, 159 (1993).
219. L. H. Tagle, F. R. Diaz, and Y. H. Cisternas, *Bol. Soc. Chil. Quim.* **39**, 279 (1994) (in Spanish).
220. L. H. Tagle, F. R. Diaz, and A. Donso, *J. Macromol. Sci., A: Pure Appl. Chem.* **33**, 1643 (1996).
221. L. H. Tagle, F. R. Diaz, and A. Godoy, *Polym. Bull.* **36**, 717 (1996).
222. L. H. Tagle and co-workers, *Polym. Bull.* **39**, 9 (1997).
223. L. H. Tagle and co-workers, *J. Macromol. Sci., Pure Appl. Chem.* **37**, 997 (2000).
224. L. H. Tagle and F. R. Diaz, *J. Therm. Anal.* **38**, 2385 (1992).
225. L. H. Tagle, F. R. Diaz, and C. Margozzini, *J. Therm. Anal.* **36**, 2521 (1990).
226. L. H. Tagle and F. R. Diaz, *Int. J. Polym. Mater.* **28**, 187 (1995).
227. L. Gargallo and co-workers, *Eur. Polym. J.* **23**, 571 (1987).
228. L. Gargallo and co-workers, *Eur. Polym. J.* **24**, 1119 (1988).
229. L. Gargallo and co-workers, *J. Appl. Polym. Sci.* **35**, 1103 (1998).
230. M. J. Fabre and co-workers, *Polymer* **33**, 194 (1992).
231. M. F. Rey-Stolle and co-workers, *Eur. Polym. J.* **33**, 295 (1997).
232. M. F. Rey-Stolle and co-workers, *Polym. Int.* **46**, 93 (1998).
233. J. Mogin and co-workers, *Eur. Polym. J.* **28**, 187 (1992).
234. C. Berti, E. Marianucci, and F. Pilati, *Makromol. Chem.* **189**, 1323 (1988).
235. C. Berti, E. Marianucci, and F. Pilati, *Polym. Bull. (Berlin)* **14**, 85 (1985).

236. M. Bandiera and co-workers, *Makromol. Chem.* **194**, 2453 (1993).
237. G. Montaudo and co-workers, *J. Polym. Sci., Part A: Polym. Chem.* **27**, 2277, 2657 (1989).
238. E. Marianucci and co-workers, *Polymer* **35**, 1564 (1994).
239. W. Choi and co-workers, *J. Polym. Sci., Part A: Polym. Chem.* **35**, 3853 (1997).
240. W. Choi, F. Sanda, and T. Endo, *Macromolecules* **31**, 2454 (1998).
241. W. Choi, F. Sanda, and T. Endo, *Heterocycles* **52**, 125 (2000).
242. W. Choi, F. Sanda, and T. Endo, *Macromolecules* **31**, 9093 (1998).
243. N. Kihara, H. Tochigi, and T. Endo, *J. Polym. Sci., Part A: Polym. Chem.* **33**, 1005 (1995).
244. M. K. Bromley and D. H. Solomon, *Polymer* **40**, 6539 (1999).
245. H. G. Bührer and H. G. Elias, *Adv. Chem. Ser.* **129**, 105 (1973).
246. W. Podkościelny and B. Tarasiuk, *Angew. Makromol. Chem.* **207**, 173 (1993).
247. W. Podkościelny, and W. Rudź, *Eur. Polym. J.* **29**, 69 (1993).
248. W. Podkościelny and W. Rudź, *J. Appl. Polym. Sci.* **47**, 1523 (1993).
249. W. Podkościelny and D. Wdowicka, *J. Appl. Polym. Sci.* **30**, 1579 (1985).
250. W. Podkościelny, and A. Kultys, *J. Polym. Sci., Polym. Chem. Ed.* **22**, 2265 (1984).
251. W. Podkościelny and A. Kultys, *Ann. Univ. Mariae Curie-Sklodowska, Sect. AA: Chem.* **46/47**, 9 (1995) (in Polish); *Chem. Abstr.* **125**, 196549c (1996).
252. W. Podkościelny and B. Tarasiuk, *Angew. Makromol. Chem.* **204**, 139 (1993).
253. W. Podkościelny and W. Rudź, *Eur. Polym. J.* **29**, 1115 (1993).
254. W. Podkościelny and W. Rudź, *J. Appl. Polym. Sci.* **53**, 815 (1994).
255. W. Podkościelny, H. Maziarczyk, and D. Wdowicka, *Ann. Univ. Mariae Curie-Sklodowska, Sect. AA: Chem.* **52/53**, 39 (1998) (in English); *Chem. Abstr.* **131**, 214656r (1999).
256. W. Podkościelny and M. Podgórski, *Angew. Makromol. Chem.* **241**, 135 (1996).
257. W. Podkościelny, B. Tarasiuk, and E. Poździk, *Ann. Univ. Mariae Curie-Sklodowska, Sect. AA: Chem.* **46/47**, 73 (1995) (in Polish); *Chem. Abstr.* **125**, 222626x (1996).
258. T. Matsuda and co-workers, *J. Macromol. Sci., A: Pure Appl. Chem.* **37**, 239 (2000).
259. E. J. Goethals, *J. Macromol. Sci. Rev.* **2**, 73 (1968).
260. W. H. Sharkey, *Adv. Polym. Sci.* **17**, 74 (1975).
261. W. H. Sharkey, in A. V. Tobolsky, ed., *Chemistry of Sulfides*, Wiley-Interscience, New York, 1967, p. 205.
262. H. Xianming, R. M. Kellogg, and F. van Bolhuis, *J. Chem. Soc., Perkin Trans. 1* **6**, 707 (1994).
263. S. Sensfuss, *Angew. Makromol. Chem.* **234**, 191 (1996).
264. M. Kakimoto, T. Seri, and Y. Imai, *Polym. J. (Tokyo)* **19**, 1303 (1987).
265. J. J. H. Edema and co-workers, *Tetrahedron* **48**, 8065 (1992).
266. J. J. H. Edema and co-workers, *J. Org. Chem.* **58**, 5282 (1993).
267. B. de Groot and S. J. Loeb, *Inorg. Chem.* **28**, 3573 (1989).
268. S. Kondo, K. Ohta, and K. Tsuda, *Makromol. Chem., Rapid Commun.* **4**, 145 (1983); S. Kondo and co-workers, *Makromol. Chem.* **186**, 1 (1985).
269. J. A. Davies and A. Soop, *Makromol. Chem., Rapid Commun.* **4**, 777 (1983).
270. K. Udipi, *Polym. Prepr. Am. Chem. Soc. Div. Polym. Chem.* **28**, 217 (1987).
271. H. G. Batz, V. Hofmann, and H. Ringsdorf, *Makromol. Chem.* **169**, 323 (1973); V. Hofmann, H. Ringsdorf, and G. Muacevic, *Makromol. Chem.* **176**, 1929 (1975).
272. V. Hofmann and H. Ringsdorf, *Makromol. Chem.* **181**, 351 (1980).
273. E. Klein and co-workers, *Biopolymers* **10**, 647 (1971).
274. K. Imai and co-workers, *Makromol. Chem., Rapid Commun.* **6**, 413 (1985).
275. T. Oyama, J. Ozaki, and Y. Chujo, *Polym. Bull.* **40**, 503 (1998).
276. T. Oyama and Y. Chujo, *Macromolecules* **32**, 7732 (1999).

277. K. Ogura and co-workers, *J. Macromol. Sci. Chem.* **17**, 1371 (1982).
278. Y. Imay, A. Asamidori, and M. Ueda, *Makromol. Chem., Rapid Commun.* **1**, 659 (1980).
279. Belg. Pat. 644780 (Sept. 7, 1964), H. A. Smith (to The Dow Chemical Company).
280. T. Fujisawa, M. Kakutani, and N. Kobayashi, *Polym. Lett.* **9**, 91 (1971).
281. C. Orgeret-Ravanat and J. C. Galin, *Makromol. Chem.* **189**, 2017 (1988).
282. A. S. Angeloni and co-workers, *Makromol. Chem.* **191**, 2787 (1990).
283. J. E. Mulvaney and R. A. Ottaviani, *J. Polym. Sci., Part A-1* **8**, 2293 (1970).
284. F. Toda and K. Mori, *J. Chem. Soc., Chem. Commun.* (14), 1059 (1986).
285. U.S. Pat. 2284896 (June 2, 1942), W. E. Hanford and D. F. Holmes (to E. I. du Pont de Nemours & Co., Inc.).
286. U.S. Pat. 2284637 (June 2, 1942), W. E. Catlin (to E. I. du Pont de Nemours & Co., Inc.).
287. E. Deyer and D. W. Osborne, *J. Polym. Sci.* **47**, 349, 361 (1960).
288. E. Klemm and C. Stöckl, *Makromol. Chem.* **192**, 153 (1991).
289. U.S. Pat. 3459787 (Aug. 5, 1969), W. E. Weesner (to Research Co.).
290. U.S. Pat. 3513133 (Apr. 19, 1970), W. E. Weesner.
291. A. Kultys and W. Podkościelny, *J. Appl. Polym. Sci.* **49**, 1615 (1993).
292. A. Kultys, *J. Polym. Sci., Part A: Polym. Chem.* **35**, 2231 (1997).
293. A. Kultys, *J. Polym. Sci., Part A: Polym. Chem.* **37**, 835 (1999).
294. Pol. Pat. 168785 (Apr. 30, 1996), A. Kultys and W. Podkościelny (to Mariae Curie-Sklodowska University).
295. A. Kultys, W. Podkościelny, and S. Pikus, *J. Polym. Sci., Part A: Polym. Chem.* **36**, 2359 (1998).
296. A. Kultys, *J. Polym. Sci., Part A: Polym. Chem.* **38**, 3977 (2000).
297. C. G. Overberger and H. Aschkenasy, *J. Am. Chem. Soc.* **82**, 4357 (1960).
298. R. E. Wilfong, *J. Polym. Sci.* **54**, 385 (1961); V. V. Korshak and S. V. Vinogradova, *Zh. Ob. Khim.* **26**, 732 (1956).
299. J. Colonge and P. Stuchlik, *Bull. Soc. Chim. Fr.* **17**, 832 (1950).
300. Brit. Pat. 604075 (June 28, 1948), A. R. Lowe (to Imperial Chemical Industries Ltd.); U.S. Pat. 2727881 (Dec. 20, 1955), J. R. Caldwell and J. W. Wellman (to Eastman Kodak Co.).
301. G. C. Schweiker and P. Robitschek, *J. Polym. Sci.* **24**, 33 (1957).
302. A. Kultys and W. Podkościelny, *J. Appl. Polym. Sci.* **39**, 715 (1990).
303. A. Kultys, *J. Polym. Sci., Part A: Polym. Chem.* **35**, 547 (1997).
304. A. Kultys and W. Podkościelny, *Ann. Univ. Mariae Curie-Sklodowska, Sect. AA: Chem.* **48/49**, 117 (1995) (in English); *Chem. Abstr.* **126**, 251479c (1997).
305. H. Hirano and M. Tanaka, *Angew. Makromol. Chem.* **267**, 57 (1999).
306. A. Kultys and W. Podkościelny, *J. Appl. Polym. Sci.* **61**, 1781 (1996).
307. Y. Takagi and co-workers, *Macromolecules* **32**, 8315 (1999).
308. A. Kultys, W. Podkościelny, and S. Pikus, *J. Polym. Sci., Part A: Polym. Chem.* **37**, 4140 (1999).
309. A. Kultys, W. Podkościelny, and W. Majewski, *J. Polym. Sci., Part A: Polym. Chem.* **38**, 1767 (2000).
310. A. Kultys, W. Podkościelny, and D. Wdowicka, in *World Polymer Congress IUPAC Macro 2000*, Warsaw, Poland, July 9–14, 2000. Book of Abstracts, Vol. 1, p. 94, 2000.
311. A. Kultys and S. Pikus, *J. Polym. Sci., Part A: Polym. Chem.* **39**, 1773 (2001).
312. D. Wdowicka and W. Podkościelny, *Iran. Polym. J.* **5**, 175 (1996).
313. D. Wdowicka, W. Podkościelny, and H. Maziarczyk, *Iran. Polym. J.* **6**, 253 (1997).
314. D. Wdowicka, W. Podkościelny, and A. Kultys, *Iran. Polym. J.* **9**, 97 (2000).
315. W. Podkościelny and A. Kultys, *Angew. Makromol. Chem.* **246**, 71 (1997).
316. O. Bayer, *Angew. Chem.* **59A**, 257 (1947).

317. T. Takata, K. Nakamura, and T. Endo, *Macromolecules* **29**, 2696 (1996).
318. T. Takata, K. Nakamura, and T. Endo, *Polym. Prepr. Jpn.* **43**, 392 (1994).
319. T. Takata, K. Nakamura, and T. Endo, *Polym. Prepr. Jpn.* **42**, 1949 (1993).
320. T. Takata, *Phosphorus Sulfur* **120**, 405 (1997).

ANNA KULTYS
Maria Curie-Sklodowska University

SURFACE PROPERTIES

Introduction

The design of the interface between a polymer and another material has become a key aspect in many important industrial technologies because the associated interfacial properties are often crucial to the success of the application. The properties of polymer interfaces are highly dependent on the nature of the material with which it is in contact. Three types of interfaces must generally be considered: polymer–air, polymer–liquid, and polymer–solid. In reality, the properties at these interfaces do not change suddenly; instead there is a region of property gradients referred to as the "interphase" between the two coexisting phases. The polymer–air interphase is commonly referred to as a surface and is the subject of this review.

In the case of the polymer–air interphase, the usual goal of applications is to control how another material sticks to or spreads over the polymer. Many polymer applications require surfaces that have so-called nonstick properties. Classic examples include Teflon or other fluorocarbon coated fry pans touted to have nonstick properties and waxes that keep an automotive finish looking cleaner and shinier by inhibiting water from spreading dirt over the finish. There are, on the other hand, an equal number of applications where the surface must provide strong adhesion. A polymeric automobile body panel, for example, requires a surface that promotes the spreading and adhesion of various paints and finishes. Furthermore, the resulting coating applied must present a host of surface properties including scratch resistance, smoothness, and gloss, or the automobile will not be marketable.

Encyclopedia of Polymer Science and Technology. Copyright John Wiley & Sons, Inc. All rights reserved.

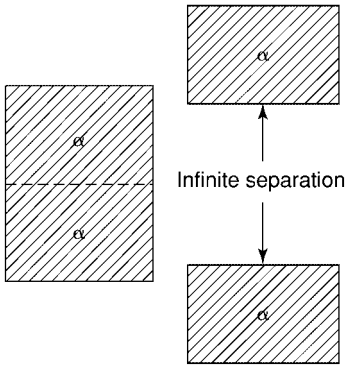

Fig. 1. Creation of two interphases from a bulk material.

Thermodynamics of the Interphase

The single most important property of a polymeric interphase is its interfacial tension. This property describes the energy required to create the interphase and can be readily defined through classical thermodynamics. The *interfacial tension* γ for a polymer–air interface (ie, the surface tension) is generally defined in terms of the work required to reversibly divide and separate a material into two parts, as depicted in Figure 1. The work required to perform the separation is called the work of cohesion, W_c, and provides an operational definition for the surface tension:

$$\gamma \equiv W_c/2 \tag{1}$$

This paradigm is not strictly valid for polymers because one cannot create this division without cutting through or breaking polymer chains. However, it is useful in illustrating the general properties of polymer interfaces. In fact, the reverse process of joining two polymers to annihilate two surfaces does provide a reasonable representation of the origin of polymer interfacial tension. In any case, the creation of a polymer surface of area A therefore requires the addition of surface free energy in the amount γA.

The thermodynamic definition of surface tension follows directly from this construction. In the presence of a surface, the total Gibbs free energy includes the normal bulk free energy terms and this new surface free energy term

$$G = H - TS + \gamma A \tag{2}$$

where G is the Gibbs free energy, S is entropy, T is temperature, and H is enthalpy. The surface tension then has the thermodynamic definition

$$\gamma \equiv \left(\frac{\partial G}{\partial A}\right)_{T,P} \tag{3}$$

With this new definition, classical thermodynamic manipulations can be applied to yield a variety of useful expressions defining properties such as the entropy of interface formation per unit area

$$\Delta S = -\frac{d\gamma}{dT} \tag{4}$$

and the enthalpy of interface formation per unit area

$$\Delta H = \gamma - T\frac{d\gamma}{dT} \tag{5}$$

The molecular origin of interfacial tension γ can also be understood through the paradigm represented by Figure 1. It is well known that molecules have mutually attractive intermolecular forces due to the combined effects of dispersive, dipole, induced dipole, and hydrogen bonding interactions. At short distances, however, Born repulsive forces result from the overlap of molecular orbitals. These two forces balance at the equilibrium separation distance r_0, setting the conditions that control the density at that temperature. The dependence of interaction forces on the separation distance is embodied in potential energy function such as the Lennard–Jones 6–12 potential shown in Figure 2, where the additive effects of short-range repulsion and longer-range attraction are evident.

In general, interaction potentials for each type of interaction lead to net forces that follow an inverse square law, and when taken collectively result in a cohesive energy expression of the form

$$W_c = (A/12\pi)\left(r_0^{-2} - r^{-2}\right) \tag{6}$$

where r is the separation distance and A is the Hamaker constant representing the cumulative strength of all types of interactions. If the separation distance is extended to infinity, and the paradigm of Figure 1 and equation (1) are applied, a relation between the macroscopic interfacial tension and the strength of molecular interactions becomes apparent:

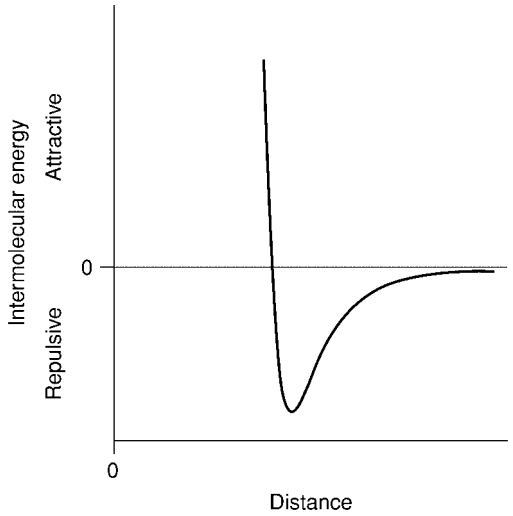

Fig. 2. A typical intermolecular potential energy diagram.

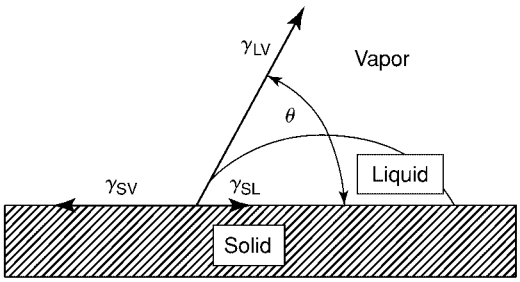

Fig. 3. The definition of the contact angle for a nonwetting liquid in contact with a solid.

$$\gamma = A/24\pi r_0^2 \tag{7}$$

The surface tension of a polymer has an important influence on the degree to which a liquid or molten polymer will wet or spread across it. A liquid in contact with a solid will exhibit a *contact angle* that is defined as the angle between the tangent to the surface of the sessile drop from the air/liquid/solid contact point and a line through the base of the liquid where it contacts the solid, as depicted in Figure 3. The equilibrium contact angle θ results from the balance of three interfacial forces described by the Young's equation (1).

$$\gamma_{SV} = \gamma_{SL} + \gamma_{LV}\cos\theta \tag{8}$$

The term γ_{SV} is the surface tension of the solid material in equilibrium with its vapor, γ_{LV} is the surface tension of the liquid material in equilibrium with its vapor, and γ_{SL} is the interfacial tension between the solid and liquid materials. Complete, spontaneous wetting occurs when $\theta = 0^\circ$, or when the spreading coefficient λ defined below is greater than or equal to zero:

$$\lambda = \gamma_{SV} - \gamma_{SL} - \gamma_{LV} \geq 0 \tag{9}$$

If a heterogeneous surface is treated as consisting of two domains, Cassie's equation can be applied as follows (2):

$$\cos\theta_c = f_1\cos\theta_1 + f_2\cos\theta_2 \tag{10}$$

where θ_c is the observed contact angle, θ_1 and θ_2 are the pure component contact angles of components 1 and 2 respectively, and f_1 is the surface fraction of component 1.

Homopolymer Surface Tension

Surface tension values for high polymers range from about 20 mN/m for highly hydrophobic materials such as poly(dimethyl siloxane) and polyfluorocarbons, to about 45 dynes/cm for polar materials such as some polyesters and polyamides.

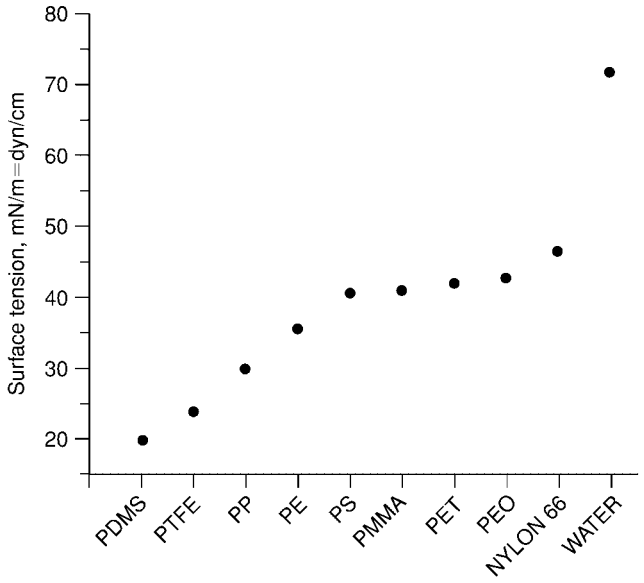

Fig. 4. Surface tension of a variety of polymers compared to that of water.

For comprehensive listings of experimental surface tension values for a wide variety of polymers, the reader is referred to several excellent references 3,4–5. The surface tension of even the most polar polymers generally fall well below that of water (as shown in Figure 4) so that in terms of surface tension, polymers should be considered at best only mildly hydrophilic. Polymers are low surface energy materials in comparison with other classes of materials by virtue of their low mass density and consequently a low interaction density, as is demonstrated in Table 1, which shows typical values for a range of different types of materials.

Table 1. Surface Tensions of Different Types of Materials[a]

Material	Temperature, °C	Surface tension, mN/m (=dyn/cm)
Aluminum (mp = 660°C)	660	873
Gold (mp = 1064°C)	1064	1130
Silicon (mp = 1450°C)	1450	725
Sodium chloride	801	114
Soda-lime glass	900	330
Titanium carbide	600	280
Graphite	720	230
Aluminum oxide	1850	950
Poly(dimethyl siloxane)	20	20.4
Poly(ethylene oxide)	20	42.9
Poly(ethylene terephthalate)	20	44.6

[a]Ref. 3.

Empirical Prediction. To this point, surface tension has been described in terms of an operational definition, a thermodynamic definition, and through its molecular origin. In practice, however, these three approaches do not constitute any pragmatic means for estimating usable values for the surface tension of polymers. The literature pertaining to homopolymer surface tension is thus replete with empirical methods for estimating this important parameter. The basis of these methods, however, is the fundamental behavior presented above. Consideration of the origin of surface forces shows clearly that any empirical expression for polymer surface tension must consider both the spatial density of interactions present and the strength of those interactions.

Group contribution methods for the estimation of polymer surface tension are cast in terms of these two factors. The strength of the interactions is represented by the dispersive solubility parameter δ^{d}, which can be calculated from tabulated values of dispersive molar attraction constants F_i according to (6)

$$\delta^{\mathrm{d};} = \sum_i F_i / v \tag{11}$$

where v is the molar volume of the unit or molecule under consideration. The surface tension for the polymer backbone can then be estimated from an empirical relationship that is reasonably successful for nonpolar polymers (5):

$$\gamma = 0.2575 \delta^2 \rho^{-1/3} \tag{12}$$

The strength of interactions is represented by the solubility parameter δ in $(\mathrm{cal/mL})^{1/2}$ and ρ is the density in g/mL. This formula predicts surface tensions that are within 5–10% of measured values (3), based upon two experimental parameters that are readily available for a large number of polymers. In the case of poly(dimethyl siloxane), the group contribution prediction for the backbone, 20.9 mN/m, compares well with the value 20.4 ± 0.07 mN/m estimated by extrapolation of experimental data to infinite molecular weight (7).

Group contribution methods are also useful because they can be applied to calculate surface tensions for a portion of the polymer molecule, for example a polymer chain end, for which there is no reliable method for direct experimental measurement. For end groups, one of several empirical relationships developed for low molecular weight compounds of various types can be employed, for example (8).

$$\gamma = 0.07147 v^{1/3} (\delta^{\mathrm{d}})^2 \tag{13}$$

Molecular Weight Dependence. Empirical expressions have also been developed to describe the molecular weight dependence of surface tension. Early expressions proposed by Wu (3)

$$\gamma^{1/4} = \gamma_\infty^{1/4} - k_{\mathrm{s}} / M \tag{14}$$

and by LeGrand and Gaines (9)

$$\gamma = \gamma_\infty - k_e/M^{2/3} \tag{15}$$

provide reasonable representations of polymer surface tensions but cannot be readily distinguished from each other by most sets of experimental data. Here, M is the number-average molecular weight, γ_∞ is the surface tension at infinite molecular weight, and k_s and k_e are proportionality constants. Theoretical considerations lead to a general expression for the molecular weight dependence of form

$$\gamma = \gamma_\infty - k/M^x \tag{16}$$

Lattice calculations (10) predict that the power law dependence varies continuously from $x = 2/3$ for low molecular weights to $x = 1$ for high molecular weights. Off-lattice Monte Carlo simulations (11) predict that $x = 1$ in the limit of high molecular weight. These predictions, however, do not take into account situations where the end group is chemically distinct from the polymer backbone. It has been proposed that k could be modified to take into account the difference in surface energies between the polymer backbone and the end group (3). It has been proposed that the value of x varies between 1/2 and 1, depending on the strength of the attractive interaction between the end group and the surface (12). When the attraction is weak, the chains are ideal and the surface concentration of end groups varies as $2/x$. For intermediate attractive forces, all end groups within a thickness equivalent to the radius of gyration are trapped at the surface, leading to $1/x^{1/2}$ dependence. For strong attraction, the chains become stretched and the additional elastic forces give rise to a surface concentration of end groups that is also proportional to $1/x^{1/2}$. Lattice calculations have been used to show that the exponent x for surface-active end groups was also approximately equal to 1/2, as opposed to 1 for the case of no surface segregation (13). Experimental studies of end functional polymers (7) showed that the surface tension was best modeled with an inverse dependence on molecular weight, ie $x = 1$. This was the only model that gave consistent values of γ_∞, extrapolated from high molecular weight data, for all the different end group types. Careful examination of these experimental data shows that the value of x changes over different ranges of molecular weight, from unity for high molecular weights to lower values for intermediate molecular weights, consistent with the results of the simulations.

Theories of Homopolymer Surface Tension. More rigorous expressions for predicting polymer surface tension have been derived from equations of state for polymers. Corresponding states principles have been employed to derive expressions for surface tensions in terms of characteristic equation of state parameters and the associated reduced temperature, pressure, and volume. One proposed expression is of the form (14)

$$\gamma = 0.095 P^{*^{2/3}} T^* / \tilde{V}^{2.1} \tag{17}$$

where P, T, and V are the pressure, temperature, and volume respectively. The asterisks indicate characteristic parameters obtained from an equation of state and

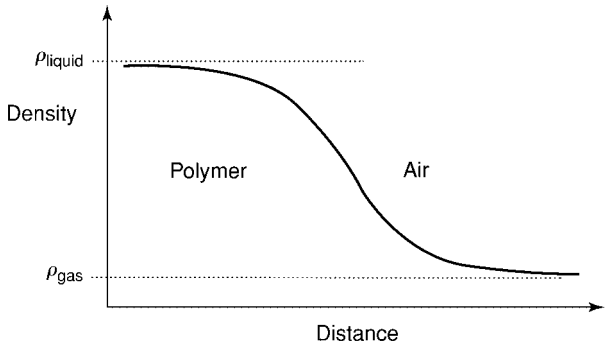

Fig. 5. The density gradient at a polymer–air interface.

the tilde indicates a parameter reduced by the characteristic parameter. A modification (15) of this treatment produces a better representation of experimental data; however the theory has two additional adjustable parameters that cannot be determined a priori.

The most successful theoretical approaches produced to date are based upon the generalized van der Waals square gradient approach (16,17). The approach considers the effects of the density gradient across a polymer–air interface, as depicted in Figure 5. The length scale of the surface gradient is normally of the order of 1 nm. Because the reduced free energy density is dependent on both reduced temperature and reduced density, it will generally vary through the interface in a manner represented in Figure 6. The double tangent construction sets the

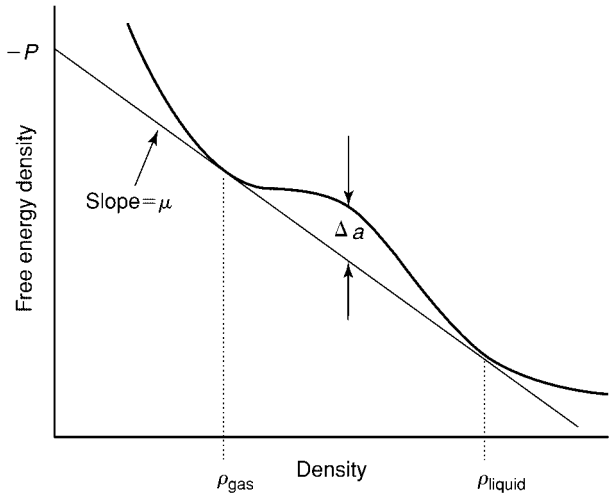

Fig. 6. Schematic representation of the surface excess free energy Δa as a function of density. The double tangent construction defines the densities of the equilibrium coexisting phases, ρ_{gas} and ρ_{liquid}. The slope of the double tangent construction is equal to the chemical potential m. Δa for a particular density is defined as the difference between the free energy density curve and the double tangent line.

chemical potentials equal for the two coexisting phases represented by the minima at reduced densities $\tilde{\rho}_{\text{gas}}$ and $\tilde{\rho}_{\text{gas}}$. The reduced surface tension is related to the excess reduced free energy density $\tilde{\Delta}$, defined in Figure 6, integrated across the surface density gradient

$$\tilde{\gamma} = 2\int_{-\infty}^{\infty} \{\tilde{\kappa}\,\Delta\tilde{\alpha}[\tilde{\rho}(z)]\}^{1/2} \mathrm{d}z \tag{18}$$

A change of variables produces a more convenient integration

$$\tilde{\gamma} = 2\int_{\tilde{\rho}_{\text{gas}}}^{\tilde{\rho}_{\text{liquid}}} (\tilde{\kappa}\,\Delta\tilde{\alpha})^{1/2} \mathrm{d}\tilde{\rho} \tag{19}$$

The square gradient coefficient $\tilde{\kappa}$ is defined by

$$\tilde{\kappa} = \frac{-\mathrm{d}\tilde{\kappa}_1}{\mathrm{d}\tilde{\rho}} + \tilde{\kappa}_2 \tag{20}$$

where the first term on the right-hand side is related to the interaction potential and assumes a value of 0.5 for purely dispersive interactions. The second term arises from nonlocal entropy effects (18) and is equal to $\tilde{T}/24\tilde{\rho}$. Equation (19) furnishes a means of determining the surface tension by a straightforward integration of an equation of state that describes $\Delta\tilde{\alpha}(\tilde{\rho},\tilde{T})$.

The use of compressible lattice fluid theory for $\Delta\tilde{\alpha}(\tilde{\rho},\tilde{T})$ in equation (19) gives a reasonable representation of both the molecular weight and temperature dependence of surface tension for poly(dimethyl siloxane) (19) as shown in Figure 7. The agreement becomes even better if the correction term $\tilde{\kappa}_2$ for surface entropy effects is included, but the value of the first square gradient coefficient must be adjusted slightly to 0.55 from the mean field value of 0.5 to achieve the excellent degree of correspondence illustrated. The use of the Flory, Orwall, and Vrij equation of state in relation 19, with equation of state parameters defined locally to provide better representation of density data, provides predictions within 1% of experiment (20). The molecular weight dependence predicted by this approach also follows equation (16), with a value of $x = 1$ for high molecular weights and a value of 2/3 for intermediate molecular weights.

It has been shown that the lattice fluid model including the nonlocal entropy effects reproduced experimental data over a wide range of temperatures (21). The reduced surface tensions for many different polymers formed a master curve when plotted against reduced temperature according to the relation

$$\tilde{\gamma} = 0.6109 - 0.6725\tilde{T} - 0.1886\tilde{T}^2 \tag{21}$$

as shown in Figure 8. This figure and Figure 7 illustrate that, over small temperature ranges, surface tension varies almost linearly with temperature, consistent with the typical linear dependence of density on temperature observed for polymers. The temperature coefficient of surface tension for polymers (3) generally falls in the range 0.05–0.07 mN/m-dyn/(cm·°C).

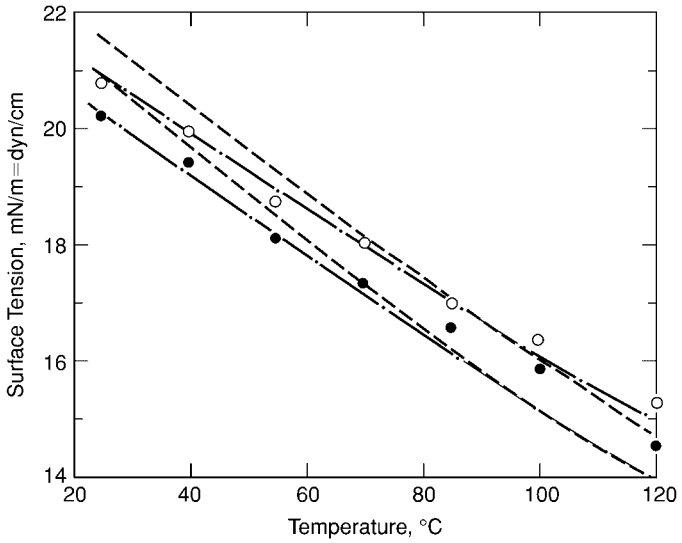

Fig. 7. Comparison of experimental surface tensions for 75,000 molecular weight PDMS (open circles) and 3900 molecular weight PS (filled circles), with the predictions of square gradient theory. The dashed lines are for $\tilde{\kappa} = 0.55$ and the dashed-dotted line is for $-\mathrm{d}\tilde{\kappa}_1/\mathrm{d}\rho = 0.40$ including the effects of nonlocal entropy effects. After Reference 19.

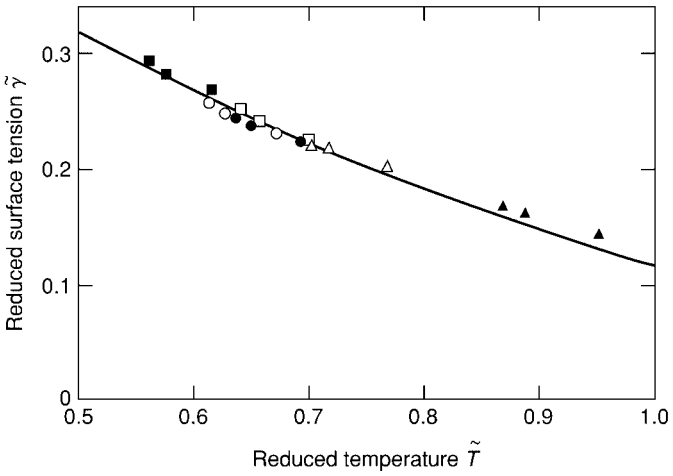

Fig. 8. Reduced surface tension versus reduced temperature of polymers. Solid line is Poser Sanchez theory with $\tilde{\kappa} = 0.55$. ○ Branched polyethylene; ● linear polyethylene; □ polyisobutylene; ■ polystyrene; △ poly(vinylacetate); ▲ poly(dimethyl siloxane). From Ref. 21.

Surface Segregation Effects

Most commercial polymer resins that are currently available are complex multiconstituent systems that have been formulated to simultaneously optimize a number of desirable bulk properties. The formulations might include plasticizers,

antioxidants and uv stabilizers, toughening agents, compatibilizers, lubricants, extenders, fillers and other additives. The presence of minute concentrations of additives in the bulk polymer can often dominate the properties of the surface of the material as a result of surface segregation effects. That is, there is a driving force for components of lower surface energy to preferentially adsorb at the surface, thereby decreasing the surface energy of the overall system. Surface segregation is an almost universal phenomenon that occurs in miscible as well as immiscible multicomponent systems and has been well documented for polymer blends (22,23), copolymers (24), and polymer solutions (25). Perfluorinated hydrocarbons and silicones have some of the lowest surface energies known, and relatively small amounts blended into a homopolymer matrix can reduce the surface tension markedly (26,27).

Surface segregation can occur with or without the formation of a separate phase at the surface. The latter is a process that is sometimes referred to as *blooming*. If a surface phase is present, the situation reverts back to wetting of one material by another. The case to be considered here is when the mixture is a true solution. When a component i of a miscible mixture adsorbs preferentially at the surface, it affects a change in the surface energy equivalent to $\gamma_i \, \mathrm{d}A_i$, where $\mathrm{d}A_i$ is the surface area occupied by type i molecules and γ_i is the surface tension. In order to relocate the molecule in the interphase, it must demix from the bulk phase, requiring an increase of $n_i \, \mathrm{d}\mu_i$ in the bulk chemical potential energy, where n_i is the mole fraction of species i in the bulk phase and $\mathrm{d}\mu_i$ is its chemical potential change. For the overall system to come to equilibrium, there is a net balance of the bulk and surface energy changes for all p components, represented by the classical Gibbs–Duhem relation (at constant T and P), modified for the influence of an interphase

$$\sum_{i=1}^{p} n_i \mathrm{d}\mu_i = \sum_{i=1}^{p} \gamma_i \mathrm{d}A_i \tag{22}$$

Further manipulation of this relationship leads to the classic Gibbs adsorption isotherm:

$$-\mathrm{d}\gamma = \sum_i \Gamma_i \mathrm{d}\mu_i \tag{23}$$

where the surface excess of species i is defined as $\Gamma_i = n_i/A$.

Relations 22 and 23 emphasize that the surface composition of a typical multicomponent polymer may differ drastically from that of the bulk, even for a true solution. Lower surface energy components adsorb preferentially at the surface, thereby lowering the overall surface tension of the mixture. In terms of adhesion, the manifestation of surface segregation is a generally weaker interface, since lowering the surface energy will decrease the thermodynamic work of adhesion.

In practice, the process of surface segregation offers a convenient means to modify polymer surfaces by intentional segregation of a particular additive to the surface. Surface-active additives, which may generally be termed macrosurfactants, usually lower the surface energy and are subsequently used widely to create release surfaces on polymeric substrates.

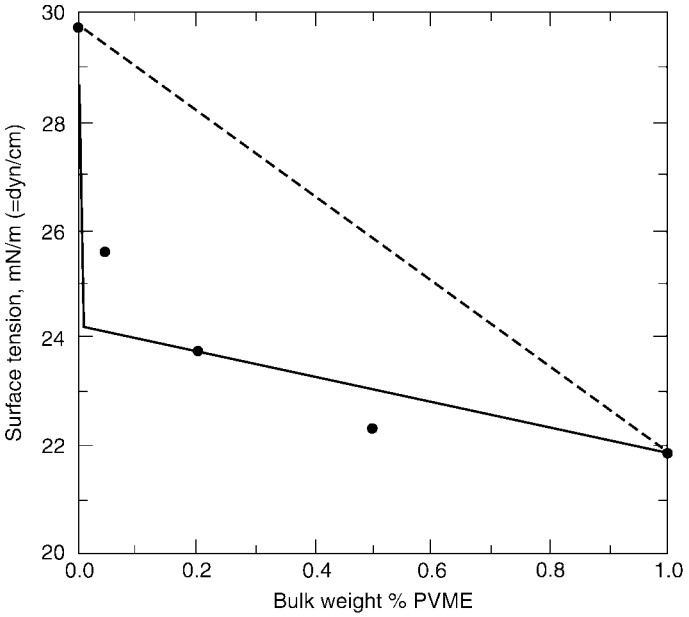

Fig. 9. Surface tension for blends of PVME and PS. From Ref. 23.

Binary Polymer Blends. Miscible polymer blends have proven to be important model systems for the study of surface segregation, and their surface properties have already been studied in some detail. Originally, surface segregation for these systems was evidenced by surface tension measurements (23), wherein the addition of small amounts of the lower surface energy constituent was found to bring about an incommensurably large decrease in the surface tension as shown in Figure 9, similar to the well-known behavior of surfactants. The surface tension can be directly related to the free energy of the system and serves as an important thermodynamic characterization of the surface state.

The characterization of surface structure for miscible blends is a more formidable task, requiring techniques that are sensitive to the composition of the blend within several nanometers of the surface. X-ray photoelectron spectroscopy (xps) provided the first direct and quantitative evaluation of surface composition and surface composition gradients for miscible polymer blends of poly(vinyl methyl ether) (PVME) and polystyrene (PS) (22,23). Since that time, the situation has changed dramatically with the advance of theory and the application of exciting new experimental techniques to this problem. In addition to xps and pendant drop tensiometry (22,23), forward recoil spectroscopy (28), neutron (29) and x-ray reflectivity (30), secondary ion mass spectroscopy (either dynamic or time-of-flight-static) (31,32), and attenuated total reflectance Fourier transform infrared spectroscopy (33–35), have been applied successfully to study surface segregation. The advent of these new tools has enabled a multitechnique experimental approach toward careful examination of the validity of current surface segregation theories (36–39).

The surface composition and near surface gradient structure of miscible binary homopolymer blends are determined by a balance between the surface energy

driving force for segregation and the exchange free energy that is associated with near surface demixing. At equilibrium, this balance represents a minimum in the overall free energy. This situation can be readily treated by mean field theories based upon the generalized van der Waals square gradient framework (40,41). If the interactions are sufficiently short-range in nature, the surface free energy for a planar interface with sharp density gradient is given by (37)

$$\gamma = \gamma_s(\phi_b) + \int_{\phi_b}^{\phi_s} [\gamma_s^{'} + 2(\kappa \Delta F)^{1/2}] d\phi \tag{24}$$

where ϕ_s and ϕ_b are the surface and bulk volume fractions of the blend component with lower surface free energy, and γ_s and F are the contributions to the free energy of a unit area of surface and a unit volume of the uniform bulk mixture, respectively. The term $\Delta F = F(\phi) - F(\phi_b^-) - (\phi - \phi_b^-)(\partial F/\partial \phi)_b$ is the free energy cost to exchange composition in the near surface gradient, which eventually balances with the free energy decrease, $\gamma_s^{'} = \partial \gamma_s / \partial \phi$, associated with the lowering of surface energy upon adsorption of the low surface energy polymer at the surface. In the weak segregation limit, the square gradient coefficient κ, which is related to the nature of the interaction potential, takes the form

$$\kappa = a^2/[36\phi(1-\phi)] \tag{25}$$

The polymers are assumed to be symmetric, with identical statistical segment lengths a.

The effect of the surface is represented by a bare surface energy, which depends only on the boundary surface volume fraction, and is defined by

$$\gamma_s(\phi_s) = -\gamma_1 \phi_s \frac{1}{2} \gamma_2 \phi_s^2 \tag{26}$$

where γ_1 is a chemical potential favoring one component at the surface, and γ_2 represents the loss of interactions between components because the presence of the surface. Bond counting arguments lead to the approximation that $\gamma_2 \cong 4b\chi$, where χ and b are the interaction parameter and unit lattice dimension [ie, equivalent to the statistical segment length a, respectively, from Flory–Huggins theory (42)]. The surface energy difference between the two pure components is $\Delta\gamma = \gamma_1 - \frac{1}{2}\gamma_2$.

The exchange free energy ΔF can be calculated from the Flory–Huggins form for the free energy of mixing (42)

$$F(\phi_A) = [\phi_A/N_A]\ln\phi_A + [(1-\phi_A)/N_B]\ln(1-\phi_A) + \phi_A(1-\phi_A)\chi \tag{27}$$

where N_A and N_B are the number of lattice units per chain for the two blend components A and B, respectively.

The surface composition is obtained by minimizing the surface tension (eq. (24)) with respect to the surface composition, yielding the boundary condition

$$-\gamma_s = \pm 2(\kappa \Delta F)^{1/2}|_{\phi=\phi_s} \tag{28}$$

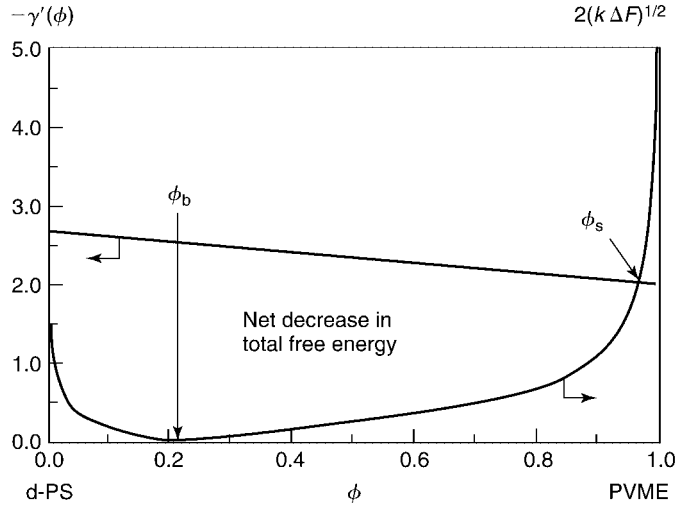

Fig. 10. Phase portrait for a blend of PVME and PS for a bulk concentration of 0.21. The surface concentration is the point at which the surface tension reduction $-\gamma'(\phi)$ equals the increase in free energy $2(k\Delta F)^{1/2}$, associated with demixing to create the surface excess of PVME.

The possibility of two signs results from the taking of a square root, but the correct sign is easily resolved as the only physically realistic solution. Equation (28) is useful in demonstrating the qualitative and quantitative aspects of the surface segregation phenomenon, through the construction of so-called *phase portraits*. A phase portrait is simply a graphical representation of the concentration dependence of the two terms in equation (28). The surface composition can be read directly off of this graph as the concentration at which the two contributions are equal, as depicted in Figure 10.

The surface composition gradient can also be readily calculated from this theory, since $d\phi/dz = 2(\kappa\,\Delta F)^{1/2}$, leading to

$$\phi(z) = -\int_{\phi_b}^{\phi_s} (\kappa/\Delta F)^{1/2} d\phi \tag{29}$$

It is evident from relations 28 and 29 that, using experimentally measured values for the binary interaction parameter, the statistical segment length and the surface energy difference between the blend components, the surface composition, and the surface concentration profile can be calculated. Simulated profiles have a form that closely approximates an exponential decay of the type

$$\phi(z) \cong \phi_b + (\phi_s - \phi_b)\exp(-z/\xi) \tag{30}$$

The surface gradient is conveniently characterized by the surface decay length ξ, which is equivalent to the bulk correlation length as $z \to \infty$. The decay length is relatively small in the strong segregation limit, but can become very large (eg, 10–20 nm) when concentration fluctuations grow near the critical point.

The majority of experimental data has been measured for two blend systems: PS/PVME, and isotopic blends of PS and poly(perdeutero-styrene). The surface compositions for PS/PVME blends were found to scale directly with the surface energy difference between the constituents (23), showing that the latter factor dominates the surface behavior, a result that might be expected for these nearly athermal blends with large surface energy differences (The PS/PVME system has an interaction parameter estimated to be -0.0011 and can be considered as effectively athermal). The square gradient theory with the Flory–Huggins free energy of mixing provides a reasonable representation of the surface tension behavior, but overestimates the surface composition at low PVME contents (43), especially when compared to literature xps data on surface composition gradients (22,23). The latter study (43) proposed that configurational entropy effects due to PVME chains flattening out at the surface and/or effects related to the concentration dependence of the Flory interaction parameter within the interphase may give rise to the discrepancies. The behavior of the isotopic blends is more complicated, since the surface energy difference and the interaction enthalpy for these blends are small. Here, there is a delicate balance between the surface energy reduction and the loss in chemical potential due to surface demixing, and it has been predicted that either component may segregate to the surface, depending on the molecular weight. Again, however, the theory tends to overestimate the observed surface composition. For an excellent general discussion of surface segregation in isotopic blends see Ref. 44. Blends of hydroxylated-PS with PVME have also been studied (33), where it was concluded that the surface segregation behavior was dominated by the bulk thermodynamics as a result of hydrogen bonding between hydroxyl groups on PS and the PVME ether linkage. The lack of significant surface segregation of PVME in these systems was attributed to the enthalpy of mixing (ie, about 3 J/cm^3) that opposes demixing of the PVME.

End-Functional Polymers. End-functional polymers are interesting model systems through which to explore the effects of functional groups on polymer surface and bulk properties (45). The generalized van der Waals approach cannot be easily adapted to treat the surface properties of heterogeneous polymers such as end-functional polymers and co-polymers. Here the incompressible lattice model (45) is the preferred approach. This model was first extended in 1988 (47) to study the surface properties of end-functional polymers and random copolymers, and a similar approach was applied to examine the structure of polymers confined between two plates (11). The theory was extended to consider the surface properties of α,ω-functional poly(dimethyl siloxane) and was found to provide excellent predictions of the molecular weight dependence of surface tension for a variety of different end groups, as demonstrated in Figure 11.

The inputs are the polymer chain length and the surface interaction parameter between end groups and repeat units (or between different monomers in the case of a copolymer)

$$\chi_s = \frac{(\gamma_e - \gamma_r)}{kT} \tag{31}$$

The subscripts e and r refer to the end group and repeat unit respectively. The effects of the bulk interaction parameter between the two components can be

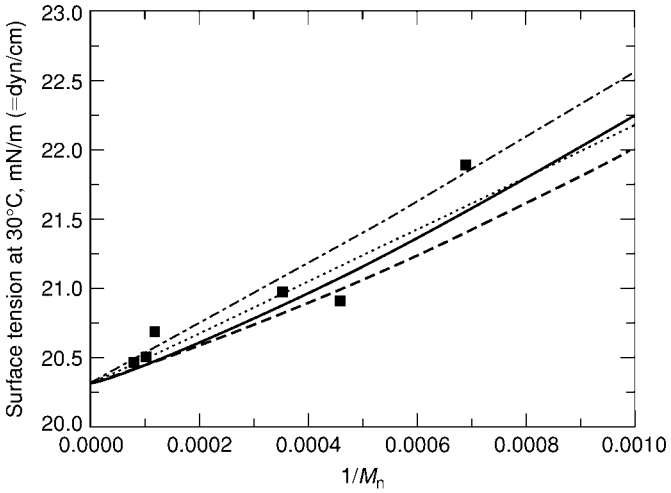

Fig. 11. Surface tension for amine-terminated PDMS (squares) as a function of $1/M_n$. The two thicker lines represent predictions from the lattice model calculations, assuming various group additivity expressions to calculate the surface interaction parameter. The two thinner lines are predictions that neglect end group segregation effects. From Ref. 7.

included at the cost of additional complexity. The lattice theory yields a table of values for the composition $\phi_{1,1}$ of component 1 in the first lattice layer as a function of χ_s, and chain length. The surface tension can readily be calculated from this table according to the relation

$$\gamma = \phi_{1,1}\gamma_1 + (1 - \phi_{1,1})\gamma_2 \tag{32}$$

where the subscripts 1 and 2 refer to the two components, eg, end group and repeat unit. If information on the pure component surface tensions is not available, they may be estimated by the group contribution methods described by equations (11–13).

The lattice model can also be used to obtain the composition depth profile of end groups at the surface. Typical profiles are shown in Figure 12. The profiles exhibit two characteristic length scales. There is an initial zone of segregation that is one lattice layer in thickness (of the order of 1 nm). The zone has an excess of end functional groups when χ_s is negative, and a depletion of end functional groups when χ_s is positive. Following the initial zone of excess or depletion, there is a second region of depletion or excess, respectively, that decays back to the bulk composition over a length scale that is related to the overall chain dimensions. A slight surface excess of end groups is predicted even when χ_s is zero as a result of the entropic preference for locating chain ends at a surface. Angle-dependent x-ray photoelectron spectroscopy measurements have documented the expected depletion zone for end-functional poly(dimethyl siloxane) with positive χ_s (49).

Several studies (50–52), have demonstrated the existence of a surface excess of fluorinated end groups for fluorosilane-terminated PS (PS-F), a system with negative χ_s. Typical behavior for these materials is shown in Table 2, which lists

Table 2. Surface Properties of PS-F

Material	M_n by gpc, g/mol	Functionality	Surface tension,[a] mN/m (=dyn/cm)	Surface fraction of end groups
PTFE			18.2 (22)	
5K PS-F	5,300	0.89	19.9	0.87
11K PS-F	10,900	0.78	22.1	0.72
25K PS-F	25,000	0.85	24.1	0.58
148K PS-F	148,000	1.00	29.7	0.19
PS			32.4 (42.1)	

[a]Parentheses indicate literature values.

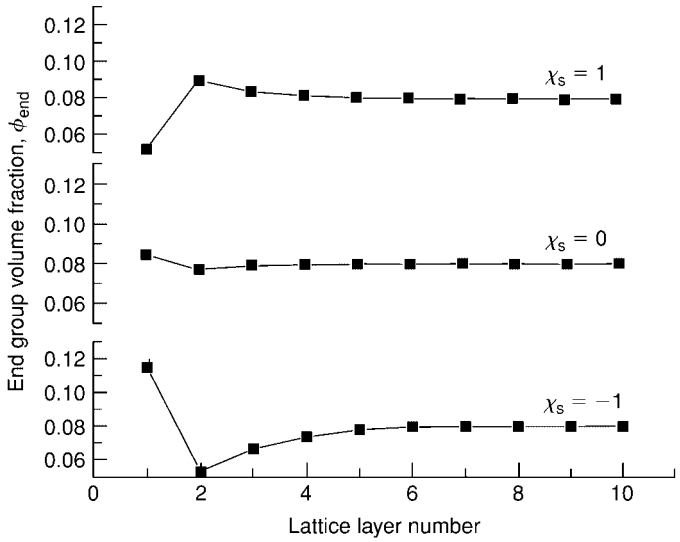

Fig. 12. End group concentration depth profiles for a chain with 11 monomers as a function of the surface interaction profile. Adapted from Ref. 48.

surface energies and compositions as a function of molecular weight determined by contact angle analysis (53,54) of solid samples at room temperature. The surface tension can be adjusted anywhere between that of poly(tetrafluoroethylene) (PTFE) and PS by changing the molecular weight (ie, the fraction of fluorinated end groups). The power law coefficient for the scaling of polymer surface tension with molecular weight for this system increased with molecular weight. Experimental end group concentration depth profiles for these polymers determined by with negative χ_s agree well with predicted depth profiles (55).

Studies on blends of PS with fluorocarbon-terminated PS (PS-F) documented that the low energy end group in neat PS-F adsorbed preferentially at the surface, and that PS-F is surface active in the PS matrix (56). Adsorption of the end-fluorinated PS at the styrene surface can be used as an effective means to control the wetting and dewetting properties of PS (57). A paper (58) to appear shows that xps surface composition depth profiles for these blends (53,54) compare well to the predictions of a new lattice model calculation that is an extension of the previous lattice model (48).

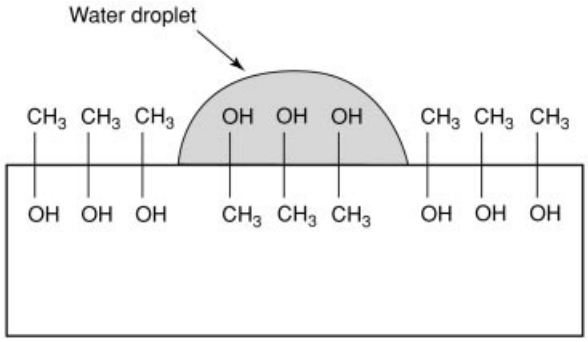

Fig. 13. Schematic diagram representing the Holly–Refojo concept (59) of surface reorganization of a functional polymer surface.

Reorganization of Heterogeneous Polymer Surfaces. The significance of the surface structure of end-functional polymers becomes apparent when considering the stability of functional polymer surfaces. The surfaces of functional and heterogeneous polymers are known to reorganize readily when exposed to water, for example as depicted in Figure 13 (59). The driving force for the phenomena is the minimization of the interfacial free energy. At an air-polymer interface, low energy hydrophobic components are favored as they lower the interfacial tension.

When the polymer is contacted with water, hydrophilic components are preferred at the water-polymer interface and the surface attempts to reconfigure to locate high energy hydrophilic components at the interface. The reorganization of end-functional PSs shown in Figure 14 (53,60) typifies this behavior. The water

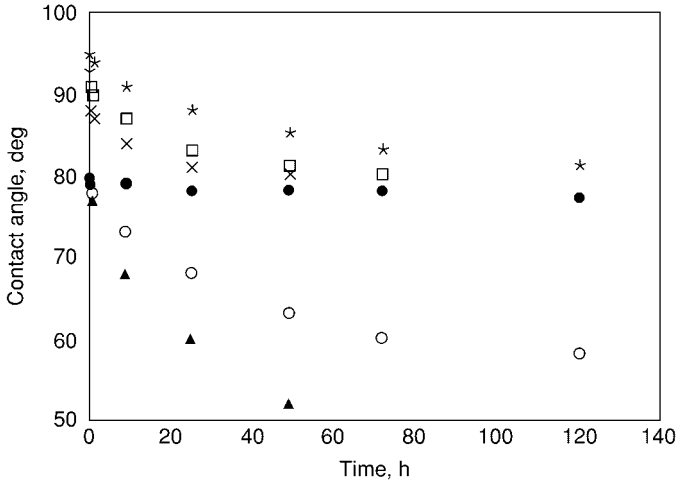

Fig. 14. Water contact angle data illustrating the reorganization of end-functional polystyrenes in the glassy state. The number in the sample designation refers to the molecular weight in thousands; PS is polystyrene, PS-F is fluorosilane-terminated polystyrene, and PS-COOH is carboxylic acid-terminated polystyrene. ● 100K PS; ✶ 5K PS-F; □ 10K PS-F; × 25K PS-F; ▲ 6.5K PS-COOH; ○ 10K PS-COOH. From Ref. 60.

contact angles for PS-Fs are initially high because of a surface excess of the lower energy fluorosilane end groups (ie, χ_s is negative), but asymptote toward the value for unmodified PS when exposed to water vapor. The low energy component (ie, the fluorosilane end group) is favored at the air–polymer interface, while the highe nergy component, in this case the PS backbone, is favored at the water–polymer interface. Conversely, the water contact angle for carboxylic acid-terminated PS starts out at the value for unmodified PS because of a surface depletion of end groups, but decreases with time when exposed to water vapor as the carboxylic acid groups relocate to the surface. The reorganization process occurs even in the glassy state because it requires movement of the end groups over distances equivalent to only one or two lattice layers, consistent with the structure of excess and depletion layers illustrated in Figure 11. The temperature dependence of the process is Arrhenius in nature, demonstrating that surface reorganization necessitates only local chain motion to occur (53).

Copolymers. Random (61), block (62–64), and graft copolymers (65,66) have all been shown to be effective in reducing surface tension, though configurational constraints limit the segregation of the copolymer sequences to the interface compared to blends of identical composition as demonstrated in Figure 15. For block copolymers (see Fig. 16), surface activity increases with block length and an increasing difference in the relative surface activity of the blocks. (63,64)

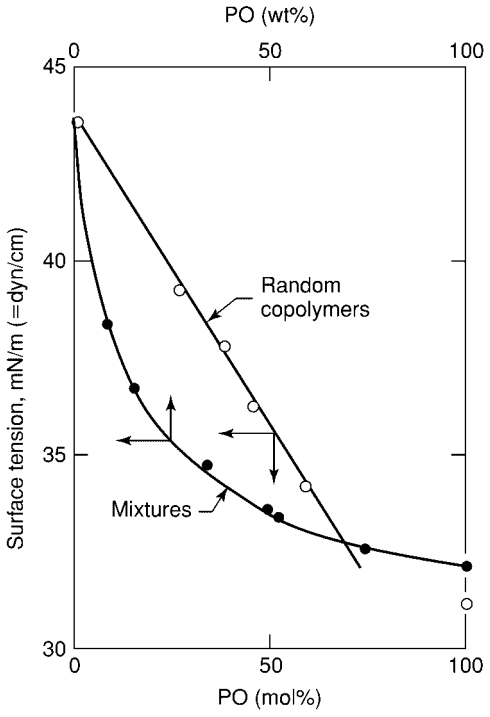

Fig. 15. A comparison of surface tension for blends and random copolymers composed of the same two monomers, polyethylene oxide and polypropylene oxide (PO). From Ref. 63.

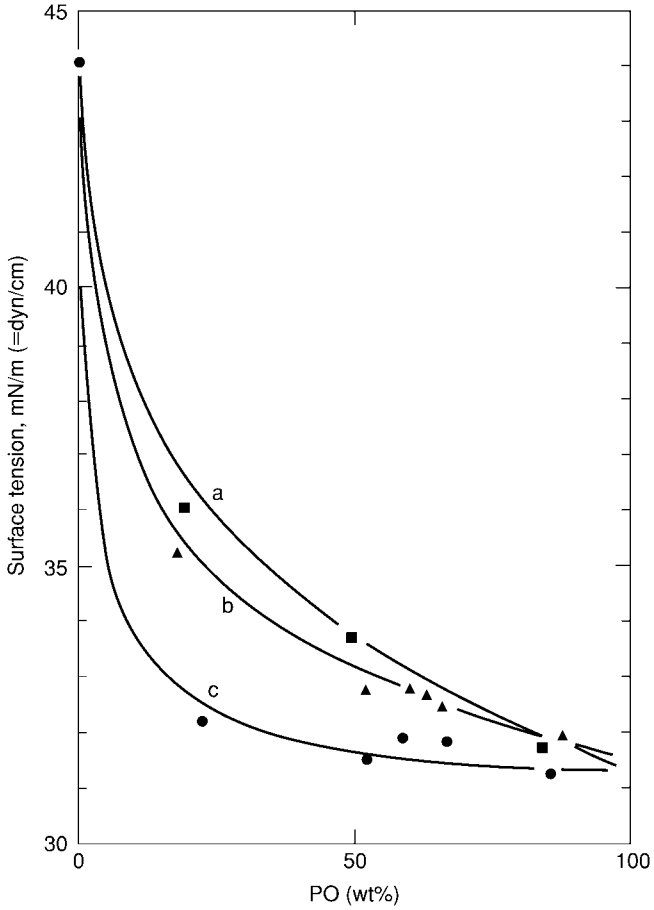

Fig. 16. The effect of sequence length on the surface tension of triblock copolymers with ethylene oxide mid-blocks and propylene oxide end-blocks. The mid-block lengths are (**a**) 16, (**b**) 30, and (**c**) 56. From Ref. 63.

For a block copolymer system where the differences in surface energy between the two components is less, wetting constraints can lead to surface heterogeneity (62). For the same composition, block copolymers, segregate more effectively to the surface than graft copolymers, which in turn are more surface active than random copolymers, though problems with microphase separation are reduced for random copolymers (61). Other chain architectures have been investigated and also been shown to be surface active (67).

Copolymers can also be used as additives to reduce surface tension. It is well known, for example, that poly(styrene-*b*-dimethyl siloxane) copolymers, PS-b-PDMS, adsorb at the surface of PS, with the low surface energy PDMS block located at the surface (68,69). The resultant PDMS-enriched surface exhibits release properties toward most substrates. The rate of migration of the block copolymers from the bulk phase to the surface (Fig. 17), however, can be very slow, depending on the bulk composition (70).

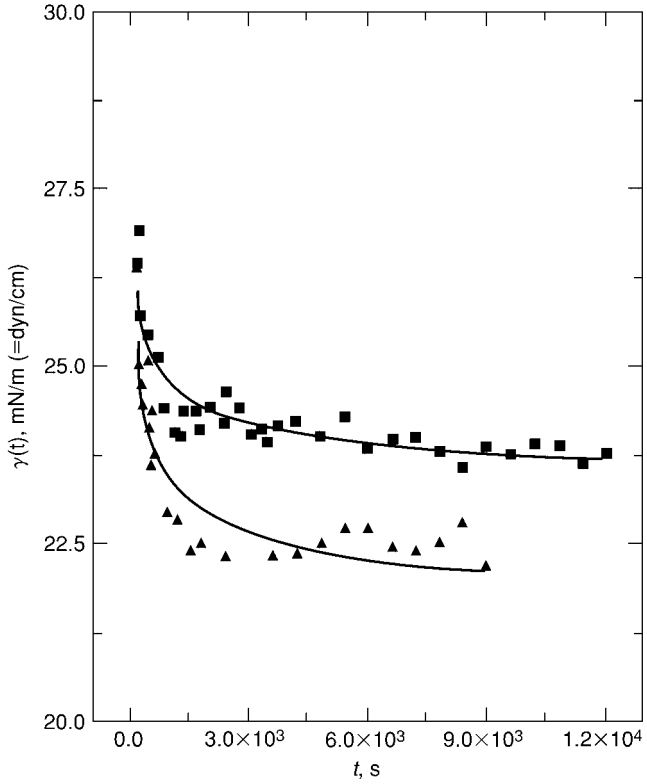

Fig. 17. Time dependence of surface tension (82) for PS-b-PDMS block copolymers added to a PS matrix as a function of bulk copolymer concentration. ■ $\phi_0=2.2\times10^{-3}$; ▲ $\phi_0=5.0\times10^{-3}$.

Surface-active block copolymer can also be employed to carry a functional group or payload to the surface of a polymer matrix. PS-b-PDMS, wherein the silicone block was terminated with a silane group, was used to create smart surfaces with selective adhesion properties (71). When the block copolymer adsorbed at the surface of PS substrates, the silane group was presented to the surface. Adhesion was observed only toward polymer coatings that could react with the silane group, that is, polymers containing vinyl functionality.

Surface Tension Measurement

Surface tensions of polymeric fluids or melts may be measured by a variety of direct techniques, with those based upon analysis of the shape of axisymmetric fluid drop profiles (3,72) the most versatile and popular. Discussions of the relative advantages and disadvantages of each technique are presented in Reference 3. Several drop geometries are possible as shown in Figure 18. The shape of these drops is governed by the Bashforth–Adams equation

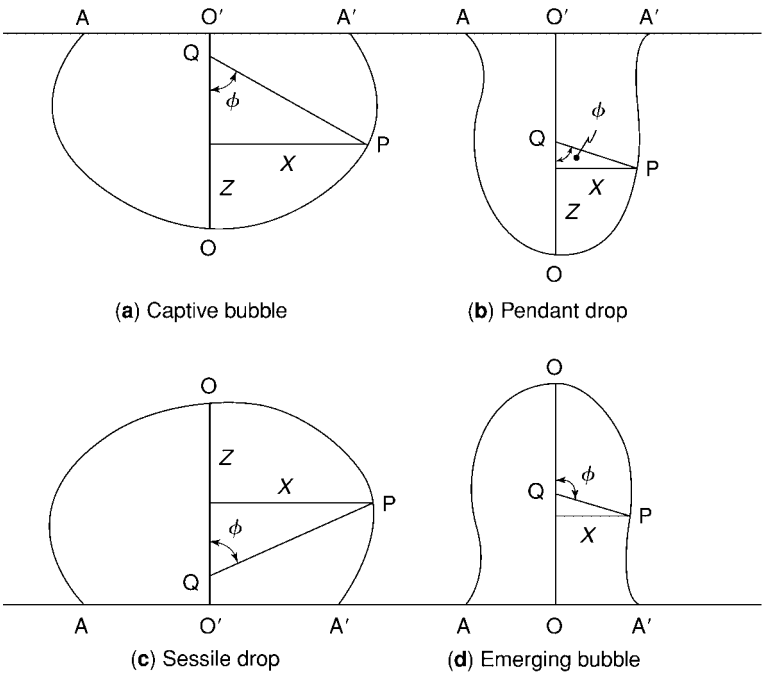

Fig. 18. Drop geometries employed in the measurement of surface tension. From Ref. 3.

$$2+\beta\left(\frac{z}{b}\right)=\frac{1}{R/b}+\frac{\sin\phi}{x/b} \tag{33}$$

where b is the radius of curvature at the drop apex, R is the principal radius in the plane of the axis of symmetry, x and z are the horizontal and vertical positions on the drop profile, respectively, and β is the shape factor defined as

$$\beta=\frac{b^2\rho g}{\gamma} \tag{34}$$

In modern techniques (19), the image of a molten polymer drop is collected by video imaging methods, and the drop profile is then obtained by application of edge detection algorithms. The shape of the drop is regressed to equation (33) to obtain a value for β and consequently for γ. For high molecular weight, viscous polymers, the time to reach an equilibrium drop shape may be limiting and other techniques may be preferred. In addition, the drop analysis techniques require knowledge of the polymer density at the temperature of the surface tension determination, which may not be readily available.

The Wilhelmy plate technique (73,74), does not require density data and can sometimes reach equilibrium much faster than the drop profile methods. This technique involves immersion of a solid plate, typically glass or platinum into the

fluid. If the fluid wets the plate, the downward force on the plate, measured by a microbalance, is

$$F = p\gamma\cos\theta - \rho g A d \tag{35}$$

where p is the perimeter of the plate, A its cross-sectional area, θ is the contact angle, and d the immersion depth. If the contact angle is zero, ie, the fluid wets the plate, a plot of F/p against d has a slope of $\rho gA/p$ and extrapolates to γ at $d = 0$. An excellent refinement of the method that involves the use of a glass thread as the plate (75), provides accurate polymer surface tensions with rapid equilibration times, even for high molecular weights.

The surface tension of a solid polymer or an inorganic substrate is difficult to measure directly and is generally estimated by indirect methods based upon equation (8). Fox and Zisman, for example, demonstrated that for solid polymers (76–78) and other substrates (79), an empirical linear relationship existed between the surface tensions γ_{SV} of a homologous series of liquids and the cosine of their contact angles on a particular substrate (see Fig. 3). When extrapolated to zero contact angle, the data produced a value for γ_C, a parameter referred to as the critical surface tension. The utility of this parameter is that spontaneous wetting should occur for all fluids with surface tensions less than γ_C. While many investigators equate γ_C directly with the surface tension γ_{SV}, of the solid, Zisman was careful in emphasizing that it is only an empirical parameter that in some way reflects the overall behavior of γ_{SV}. Critical surface tensions (3) for nonpolar fluorocarbon polymers are as low as 16 dyn/cm and those for polar polymers, such as polyacrylonitrile, are as high as 50 dyn/cm.

The theory of fractional polarity combined with Young's equation provides another means of estimating the surface tension of the solid (3). Application of the harmonic mean approximation leads to the relation

$$\gamma_{LV}(1-\cos\theta) = 4\left[\frac{\gamma_s^d\gamma_{LV}^d}{\gamma_s^d+\gamma_{LV}^d} + \frac{\gamma_s^p\gamma_{LV}^p}{\gamma_s^p+\gamma_{LV}^p}\right] \tag{36}$$

where γ^d represents the dispersive contribution to the surface tension, and γ^p the polar component of the surface tension. The total surface tension γ is given by

$$\gamma = \gamma^d + \gamma^p \tag{37}$$

The harmonic mean equation is generally considered to be applicable to low surface tension materials such as organic polymers and liquids. If γ^d and γ^p are known for two liquids, and the contact angles of those liquids on the solid of interest are measured, equation (36) produces two simultaneous equations that can be solved to find the surface tension and polarity of a solid polymer surface. Numerous assumptions have been made in developing the theory of fractional polarity. For example, it ignores the possibility of induced polarity at the interface between polar and nonpolar materials (80). These assumptions limit the application of equation (36) to systems where at least one and preferably both of the

components is relatively nonpolar. The theory breaks down when interfacial interactions lead to molecular rearrangements at the interface between solid and liquid. In addition it was found that pairs of liquids with similar dispersive and polar components of surface tension gave unreasonable results for the substrate surface tension calculated by the harmonic mean method (81).

BIBLIOGRAPHY

"Surface Properties" in *EPST* 1st ed., Vol. 13, pp. 533–551, by H. Schonhorn, Bell Telephone Laboratories, Inc.; "Interfacial Properties" in *EPSE* 2nd ed., Vol. 8, pp. 237–279, by J. T. Koberstein, University of Connecticut.

1. T. Young, *Trans. Roy. Soc.* **95**, 65 (1805).
2. A. B. D. Cassie, *Discuss. Faraday Soc.* **3**, 11 (1948).
3. S. Wu, *Polymer Interface and Adhesion*, Marcel Dekker, Inc., New York, 1982.
4. S. Wu, in J. Brandrup and E. H. Imergut, eds., *Polymer Handbook*, 3rd ed., John Wiley & Sons, Inc., New York, 1989, pp. VI/411–VI/434.
5. S. Wu, in D. R. Paul and S. Newman, eds., Vol. **1**, *Polymer Blends*, Academic Press, Inc., New York, 1978, pp. 243–293.
6. C. M. Hansen, *J. Paint Technol.* **39**, 104 (1967).
7. C. J. Jalbert and co-workers, *Macromolecules* **21**, 2980 (1988).
8. J. H. Hildebrand, and R. L. Scott, *Solubility of Nonelectrolytes*, Van Nostrand Reinfold Co., Inc., Princeton, N.J., 1950.
9. D. G. LeGrand and G L. Gaines Jr., *J. Colloid Interface Sci.* **31**, 162 (1969).
10. D. N. Theodorou, *Macromolecules* **21**, 1411 (1988).
11. S. K. Kumar, M. Vocatello, and D. Y. Yoon, *Macromolecules* **23**, 2189 (1990).
12. P. G. de Gennes, *Acad. Sci.* **307** 1841 (1988)
13. D. N. Theodorou, *Macromolecules* **21**, 1422 (1988).
14. G. Patterson and A. K. Rastogi, *J. Phys. Chem.* **74**, 1076 (1970).
15. G. T. Dee and B. B. Sauer, *Polymer* **36**, 1673 (1995).
16. J. W. Cahn, *J. Chem. Phys.* **30**, 1121 (1959).
17. C. I. Poser and I. C. Sanchez, *Macromolecules* **14**, 361 (1981).
18. K. M. Hong and J. Noolandi, *Macromolecules* **14**, 1223 (1981).
19. Q. S. Bhatia and co-workers, *J. Colloid Interface Sci.* **106**, 353–359 (1985).
20. B. B. Sauer and G. T. Dee, *J. Colloid Interface Sci.* **162**, 25 (1994).
21. I. C. Sanchez, *Physics of Polymer Surfaces and Interfaces*, Butterworth–Heinemann, Boston, 1992.
22. D. H. Pan and W. M. Prest, *J. Appl. Phys.* **58**, 2861 (1985).
23. Q. S. Bhatia, D. H. Pan, and J. T. Koberstein, *Macromolecules* **21**, 2166 (1988).
24. R. L. Schmidt and co-workers, *Macromolecules* **18**, 2675 (1985).
25. G. J. Gaines Jr., *J. Chem. Phys.* **73**, 3143 (1969).
26. L. J. Gerenser and co-workers, *Langmuir* **1**, 305 (1985).
27. M. K. Bennet, *Polym. Eng. Sci.* **17**, 450 (1977).
28. R. A. L. Jones and co-workers, *Phys. Rev. Lett.* **62**, 280 (1989).
29. R. A. L. Jones and co-workers, *Europhys. Lett.* **12**(1), 41 (1990).
30. M. Stamm, G. Reiter, and K. Kunz, *Physica B* **173**, 35, 1991.
31. X. Zhao and co-workers, *Macromolecules* **24**, 5991 (1991).
32. Q. S. Bhatia and M. C. Burrell, *Surf. Interf. Anal.* **15**, 388 (1990).
33. J. M. G. Cowie, B. G. Devlin, and I. J. McEwen, *Polymer* **34**, 501 (1993).
34. J. M. G. Cowie, B. G. Delvin, and I. J. McEwen, *Macromolecules* **26**, 5628 (1993).
35. J. M. G. Cowie, B. G. Delvin, and I. J. McEwen, *Polymer* **34**, 4130 (1993).

36. H. Nakanishi and P. Pincus, *J. Chem. Phys.* **79**, 977 (1983).
37. I. Schmidt and K. Binder, *J. Phys. (Paris)* **46**, 1631 (1985).
38. A. Hariharan and S. K. Kumar, *Macromolecules* **23**, 3584 (1990).
39. A. Hariharan, S. K. Kumar, and T. P. Russell, *Macromolecules* **24**, 4909 (1991).
40. J. D. van der Waals, *Z. Phys. Chem.* **13**, 657 (1894).
41. J. W. Cahn, *J. Chem. Phys.* **66**, 3367 (1977).
42. P. J. Flory, *Principles of Polymer Chemistry*; Cornell University Press, Ithaca, N.Y., 1971.
43. C. Forrey, M.S. Thesis, *Surface Properties of PS/PVME Blends*, University of Connecticut, 2001.
44. R. A. L. Jones and R. W. Richards, *Polymers at Surfaces and Interfaces*, University Press, Cambridge, U.K. 1999, Chapt. "5".
45. J. T. Koberstein, *Series on Directions in Condensed Matter Physics: Polymer Surface, Interfaces and Thin Films*, World Scientific Publishing, Singapore, 2000, pp. 115–181.
46. J. M. M. H. Scheutjens and G. J. Fleer, *J. Chem. Phys.* **83**, 1619 (1979).
47. D. N. Theordorou, *Macromolecules* **21**, 2197 (1988).
48. C. A. Jalbert and co-workers, *Macromolecules* **30**, 4481 (1997).
49. C. A. Jalbert and co-workers, *Macromolecules* **27**, 2409 (1994).
50. J. F. Elman and co-workers, *Macromolecules* **27**, 5341 (1994).
51. M. O. J. Hunt and co-workers, *Macromolecules* **26**, 4854 (1993).
52. S. Affrossman and co-workers, *Macromolecules* **27**, 1588 (1994).
53. C. A. Jalbert, Ph.D. Dissertation, *Surface and Interfacial Segregation in End Functionalized Polymers*, University of Connecticut, 1993.
54. R. Mason and co-workers, *Adv. Colloid Interface Sci.* **94**, 1 (2001).
55. P. A. O'Rourke Muisener, Ph.D. Dissertation, *The Molecular Design of Functional Polymer Surfaces*, University of Connecticut, 2001; P. A. O'Rourke Muisener, J. T. Koberstein, and S. Kumar, *Macromolecules*, in press.
56. T. F. Schaub and co-workers, *Macromolecules* **29**, 3982 (1996).
57. C. Yuan, M. Ouyang, and J. T. Koberstein, *Macromolecules* **32**, 2329 (1999).
58. P. A. V. O'Rourke Muisener and co-workers, *Macromolecules*, in press.
59. F. J. Holly and M. F. Refojo in J. D. Andrade, ed., *ACS Symposium Series No. Hydrogels for Medical and Related Applications*, American Chemical Society, Washington, D.C., 1976, pp. 252–266.
60. J. T. Koberstein, *MRS Bull.* **21**, 16 (1996).
61. J. Hoepken and M. Moeller, *Macromolecules* **25**, 1461 (1992)
62. H. R. Thomas and J. J. O'Malley, *Macromolecules* **12**, 323 (1979)
63. A. K. Rastogi and L. E. St. Pierre, *J. Colloid Interface Sci.* **31**, 168 (1969).
64. A. K. Rastogi and L. E. St. Pierre, *J. Colloid Interface Sci.* **35**, 16 (1971).
65. P. Jannasch, *Macromolecules* **31**, 1341 (1998).
66. J. Wang and co-workers, *Macromolecules* **30**, 1906 (1997).
67. A. Mueller, T. Kowalewski, and K. L. Wooley, *Macromolecules* **31**, 776 (1998).
68. W. Hu, J. T. Koberstein, J. P. Lingelser, and Y. Gallot, *Macromolecules* **28**, 5209 (1995).
69. X. Chen and J. Gardella, *Macromolecules* **27**, 3363 (1994).
70. D. Cho, C. Jalbert, and J. T. Koberstein, *Macromolecules* **33**, 5245–5251 (2000).
71. J. T. Koberstein and co-workers, *J. Adhesn.* **66**, 229–249 (1998).
72. S. H. Anastasiadis and co-workers, *J. Colloid Interface Sci.* **199** 55 (1987).
73. L. Wilhelmy, *Ann. Phys.* **119**, 177 (1863).
74. R. H. Dettre and R. E. Johnson Jr., *J. Colloid Interface Sci.* **21**, 367 (1966).
75. B. B. Sauer and N. V. DiPaolo, *J. Colloid Interfae Sci.* **144**, 527 (1991).
76. H. W. Fox and W. A. Zisman, *J. Colloid Sci.* **5**, 514 (1950).
77. H. W. Fox and W. A. Zisman, *J. Colloid Sci.* **7**, 109 (1952).
78. H. W. Fox and W. A. Zisman, *J. Colloid Sci.* **7**, 428 (1952).

79. W. A. Zisman, in R. F. Gould, ed. *Advances in Chemistry Series No. 43*, American Chemical Society, 1964, p. 1.
80. J. R. Dann, *J. Colloid Interface Sci.* **32**, 302 (1970).
81. D. H. Kaelble, *J. Adhesn.* **2**, 66 (1970).
82. W. C. Hu, Ph.D. Dissertation, *Interfacial Activities of Block Copolymers in Immiscible Homopolymer Blends*, University of Connecticut, 1993.

JEFFREY T. KOBERSTEIN
Columbia University

SUSPENSION (OR PRECIPITATION) POLYMERIZATION.

See HETEROPHASE POLYMERIZATION.

SYNDIOTACTIC POLYSTYRENE

Introduction

Syndiotactic polystyrene (sPS) is a relatively new material discovery in semicrystalline polymers with a high melting point and rapid crystallization rate, which makes it possible to injection mold the material. The stereospecific polymerization was made possible by the combination of a transition metal catalyst with weakly coordinating cocatalysts, such as methylaluminoxane. The excellent balance of mechanical, electrical, solvent resistance, and dimensional stability properties combined with a relatively low price (based on styrene monomer) have made this material a competitor to existing engineering plastics. The products also have excellent heat performance and are finding application in automotive (under the hood), electrical, and electronic connector systems.

Structure, Crystallinity, and Physical Properties

Syndiotactic polystyrene, as generally polymerized with monocyclopentadienyl catalysts, has a high percentage of rrrr pentad structure. The ^{13}C nmr chemical shift for the phenyl-1 carbon and backbone methylene carbon are approximately 145.3 and 44.9 ppm, respectively (1,2). In general these polymers are found to be greater than 99% pure in syndiotactic structure as defined by nmr. sPS can be further purified of any atactic polystyrene (aPS) developed during the polymerization procedure by extraction with solvents such as methyl ethyl ketone (MEK).

The syndiotactic configuration of the backbone and the high degree of stereoregularity give rise to a semicrystalline polymer, which is able to crystallize at a high rate (3,4), and form well-structured spherulitic morphology when quiescently

Encyclopedia of Polymer Science and Technology. Copyright John Wiley & Sons, Inc. All rights reserved.

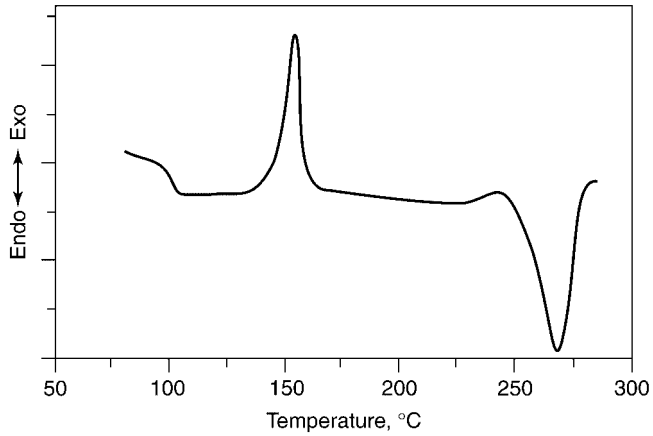

Fig. 1. Differential scanning calorimetry of homopolymer sPS. Sample was prepared by heating first to 320°C then quickly cooled to room temperature, and then scanned at a heating rate of 20°C/min.

crystallized from the melt (5–7). Peak crystallization rates of 7×10^{-2} at 180°C (isothermal) have been measured (3). Although sPS maintains its 100°C glass-transition temperature for the amorphous phase, its relatively high melting point (peak at ~ 270°C, Fig. 1) (8) and high crystallization rate, along with high modulus, good electrical properties, and solvent resistance make it useful as an engineering plastic material. The equilibrium melting point has been measured between 287 and 292°C using Hoffman–Weeks techniques (9,10), and the heat of fusion for 100% crystalline sPS was measured as 53.2 J/g (8).

Table 1 gives the general physical properties of unfilled sPS homopolymer.

From the melt it is now well established that sPS crystallizes primarily in an all-trans (T_4) form (α-form) with a planar zigzag backbone structure (11, 12) (see Fig. 2). A second (β-form) structure (T_2G_2) is also present, but under normal crystallization conditions the level of this structure is quite low (13–15). Calculations of the ultimate elastic modulus of the α-form sPS crystal are as high as 83 GPa (16). Experimentally, using x-ray diffraction, this has been reported at 86 GPa (12.5×10^6 psi) (17). The stiffness of the crystalline sPS is due primarily to intrachain interactions involving bond bending and stretching. The applied stress

Table 1. Physical Properties of Unfilled sPS Homopolymer

Properties	Value	Test method
Melting point, °C	270	dsc
Glass-transition temperature, °C	100	dsc
Visual appearance	White opaque	
Density, g/cm^3	1.05	ISO 1183B
Water absorption (24 h, 50% RH),%	0.01	ASTM D570
Dielectric constant at 1–1000 kHz	2.6	ASTM D150
Dissipation factor at 100 kHz	0.0002	ASTM D150
Volume resistivity, Ω·cm	1.0×10^{17}	ASTM D257

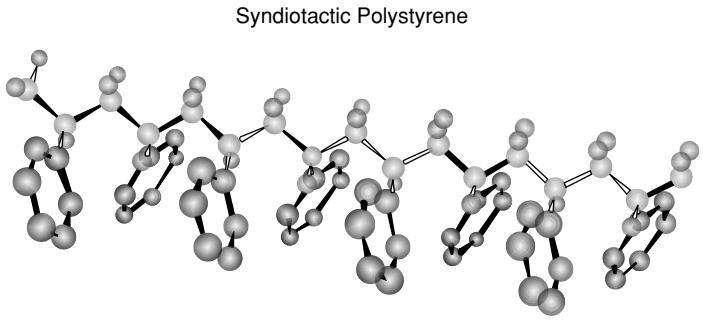

Fig. 2. Planar zigzag structure of sPS.

to the backbone through the all-trans structure is carried through these bending and stretching modes, with these energy terms increasing the most under the applied stress. In addition, the bulky phenyl groups prevent very close interchain packing of the molecules in the crystal. In fact, the density of the crystalline phase of sPS is very close to that of the amorphous phase at ambient temperature and pressure and is essentially the same as that of atactic amorphous polystyrene. A volume/temperature experiment for aPS and sPS is shown in Fig. 3. At 10-MPa pressure the specific volume of the two structures below T_g is almost identical. Above T_g the crystalline sPS domains have a lower density than the liquid phase

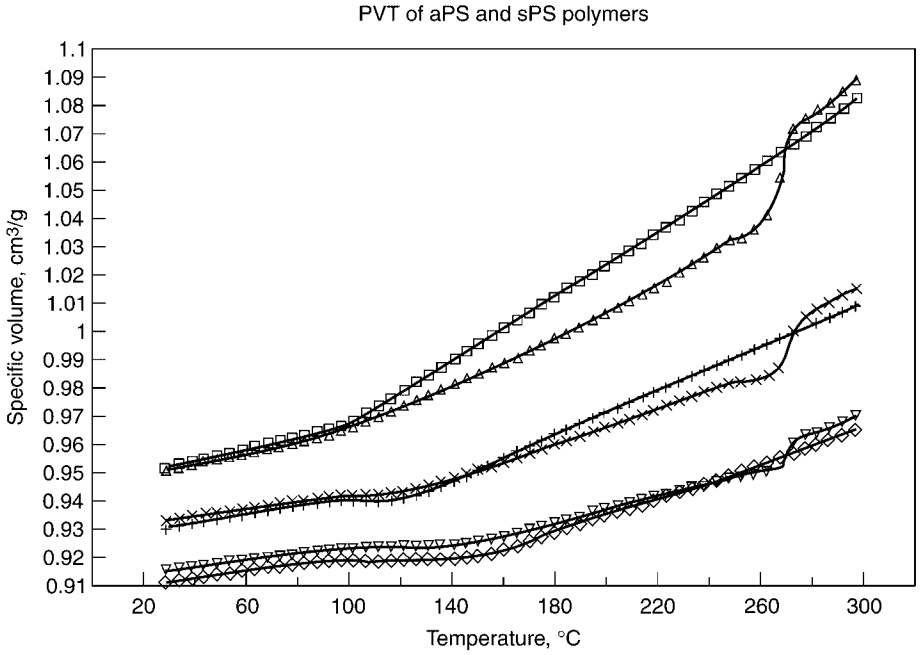

Fig. 3. Pressure/volume/temperature curves for sPS and aPS at 10, 100, and 200 MPa. □ 10 MPa aPS; + 100 MPa aPS; ◇ 200 MPa aPS; Δ 10 MPa sPS; × 100, MPa sPS; ▽ 200 MPa sPS. To convert MPa to psi, multiply by 145.

aPS, which is a very unusual property leading to improved fabricating properties for sPS. This all stems from a relatively high average cross-sectional area 70 $Å^2$ (0.7 nm^2) for each molecule of sPS because of the bulky nature of the phenyl rings. Polyethylene cross-sectional area by comparison is only 18 $Å^2$ (0.18 nm^2) (16). This high cross-sectional area leads to considerable space between polymer chains even in the crystalline phase and therefore to lower density.

Crystallized from the melt, sPS forms a crystalline morphology of well-ordered spherulites nucleated homogeneously. In neat noncontaminated sPS with 20–50°C/min cooling rates from the melt the spherulites formed are approximately 7–10 μm in diameter. Lamella thickness is generally 8–15 nm (7). It is a typical practice to add nucleators to the material to improve its apparent overall crystallization rate (18). These nucleated materials show smaller well-impinged spherulitic structures of about 2 μm in diameter. Crystallization kinetics of the bulk unnucleated polymer has been measured by several techniques and shows a dependence on molecular weight with a broad maximum rate between 190 and 240°C (3,4). When measured in a dsc experiment with a cooling rate of 10°C/min the unnucleated sPS will show a maximum for the crystallization peak of 234–236°C. Nucleated with certain organic salts [such as aluminum *p*-tert-butyl benzoate (pTBBA)] this maximum is shifted to 247–249°C (19).

Mechanical Properties

Failure and deformation mechanisms have been studied and published for sPS and have been compared to aPS (20). The semicrystalline sPS material fails with a slow, controlled crack growth while aPS fails with considerable crazing and some yield. Micrographs of fracture surfaces show that the spherulites are relatively stable structures, and it is the material at the interface of spherulites that draws and fails. A mechanism of constrained crazing and void coalescence is proposed with the spherulites themselves acting as the stress concentrators for the initiation of failure. The damage zone is then highly confined to the interspherultic regions of the semicrystalline morphology. Fig. 4 shows typical stress–strain behavior of sPS. The lack of change in Poisson's ratio for sPS is a further evidence of the lack of yielding mechanisms available in the stiff sPS material. Higher impact sPS products can be obtained using styrene–ethylene/butene–styrene block copolymers (21) or polyolefin elastomers (22) as dispersed phase toughening aids. These are added during the extrusion compounding of the formulated products. The basic mechanical properties of unfilled sPS are given in Table 2.

Reinforcement materials (such as glass fibers) or filler materials are generally compounded into sPS in order to take advantage of the high melting point and high modulus of the base resin. The addition of a well-dispersed, chemically coupled glass fiber above the percolation threshold volume creates a unique material. In general, these products are 30 and 40 wt% glass-filled products. The tensile strength of glass-filled sPS is increased to 100–130 MPa with a modulus from 7500 to 11,000 MPa. Impact properties, such as Gardner impact, are shown to be 4–7 J and notched impact strengths are 70–120 J/m. Table 3 gives typical physical and mechanical properties for commercial formulations of sPS including impact modified and ignition resistant formulations.

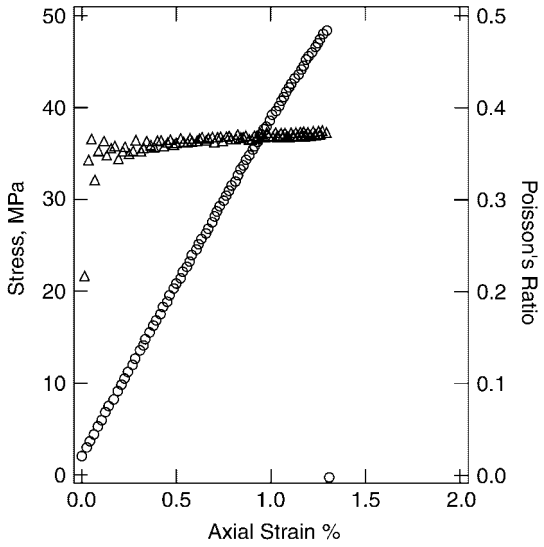

Fig. 4. Example of the tensile dilatometry results for injection molded sPS (349 kg/mol) at 23°C (20). ○ Stress; Δ Poisson's ratio. To convert MPa to psi, multiply by 145.

Table 2. Mechanical Properties of Unfilled sPS Homopolymer

Properties	Value	Test method
Tensile strength at yield, MPa[a]	41	ISO R527
Tensile modulus, MPa[a]	3450	ISO R527
Elongation at break,%	1.3	ISO R527
Flexural strength, MPa[a]	71	ISO 178
Flexural modulus, MPa[a]	3950	ISO 178
Izod impact (notched at 23°C), J/m[b]	10	ISO 180

[a]To convert MPa to psi, multiply by 145.
[b]To convert J/m to ft·lbf/in., divide by 53.38.

Solubility and Solvent Resistance

At room temperature there are no known solvents for sPS. Under ambient conditions of temperature and pressure the amorphous regions can be swollen with good solvents for aPS such as toluene, benzene, tetrahydrofuran, or dichloroethane. Chlorinated aromatics (such as trichlorobenzene, TCB) will dissolve sPS at temperatures above the glass-transition temperature (>100°C). Typically a 5–10 wt% solution can be prepared by heating the polymer with TCB at 160°C, with agitation. This solvent is generally used for solution viscosity or gel permeation chromotography.

The excellent solvent resistance of the base sPS material is useful in many applications for the formulated product. Table 4 shows the basic solvent resistance data for commercial products (23).

Table 3. Physical and Mechanical Properties of Commercial Grade Formulated sPS Products[a]

Properties	ASTM method	30% glass	40% glass	30% glass, impact modified	30% glass, ignition resistant	40% glass, ignition resistant, impact modified
Tensile strength, MPa[b]	D638	121	132	105	97	122
Tensile modulus, MPa[b]	D638	10,000	11,170	7,580	9,650	10,340
Elongation, %	D638	1.5	1.5	3.4	1.8	1.8
Flexural strength, MPa[b]	D790	167	185	163	137.9	188
Flexural modulus, MPa[b]	D790	10,000	10,480	7,930	10,340	12,760
Notched izod impact, J/m[c] (23°C)	D256	96	112	117	70	91
Notched izod impact, J/m[c] (−18°C)	D256	96	112	96	70	91
Gardner impact (23°C), J	D3029	4.2	4.9	4.0		
Gardner impact (−29°C), J	D3029	5.2	5.2	7.3		
Vicat softening point, °C	D1525	263	263	263	263	263
Deflection temperature @ 1.82 MPa, °C	D648	249	249	232	227	240
Deflection, °C temperature @ 0.45 MPa[b]	D648	263	263	263	263	263
Coefficient of linear thermal expansion, 10^{-6} cm/cm·°C)	D696	38.7	31.5	42.3	30.5	25.2
Dielectric constant	D150	3.1	3.1	3.1	3.1	3.1
Dielectric strength, kV/mm	D149	23.6	23.6	23.6	23.6	23.6
Dissipation factor	D150	0.0002	0.0002	0.0002	0.001	0.001
Specific gravity	D792	1.25	1.32	1.21	1.41	1.47
Water absorption, % (24 h, 50% RH)	D570		0.01	0.01	0.01	0.01
Mold shrinkage, cm/cm	D955		0.0015–0.0025	0.003–0.004	0.025–0.035	0.001–0.002

[a]Ref. 23.
[b]To convert MPa to psi, multiply by 145.
[c]To convert J/m to ft·lbf/in., divide by 53,38

Table 4. General Solvent Resistance Properties for sPS Formulations[a]

Solvent	General performance
Acids	Excellent
Bases	Excellent
Glycols (antifreeze)	Excellent
Automotive oils	Good
Chlorinated hydrocarbons	Poor
Aromatic hydrocarbons	Fair
Aliphatic hydrocarbons	Good
Gasoline	Fair
Alcohols	Excellent
Salt solutions	Excellent
Water and hot water	Excellent

[a]Ref. 23.

Polymerization

The development of coordinative polymerization of olefins during the second half of the twentieth century has been one of the most important achievements in polymer chemistry. Extensive studies have been carried out on the heterogeneous polymerizations of ethylene and propylene (24–26). Controlling the stereochemistry of polypropylene is of critical importance for the control of polymer properties. The introduction of methylaluminoxane (MAO) was a significant development in homogeneous coordinative polymerization of olefins (27,28). By utilizing MAO as a cocatalyst, metallocene catalysts exhibited outstanding polymerization activities. Furthermore, the structure of the metallocene complex could be modified to yield changes in polymer stereoregularity, molecular weight, and molecular weight distribution (29–31). Metallocenes, together with the MAO cocatalyst, have allowed the synthesis of highly stereoregular polypropylene (32,33), polyethylene with improved rheological properties (34), and ethylene copolymers with high comonomer incorporation (35).

Indeed, Ishihara and co-workers succeeded in the first preparation of sPS through activation of a transition metal complex with MAO (36,37). Typically, Group IV metallocene complexes have been used as catalysts for the polymerization of sPS. Of these, the monocyclopentadienyl-type complexes of titanium have been found to give the highest polymerization activity based on transition metal (38,39). Subsequent to the development of MAO as the sPS cocatalyst, it has been found that highly electrophilic activators, such as the tetrakis(pentafluorophenyl) borate type, can be used as cocatalysts for the production of sPS (40,41).

The syndiotacticity of sPS results from the homogeneous coordinative polymerization process (1,42). Styrene monomer complexes at a vacant coordination site on the transition metal, typically titanium, and inserts into a titanium carbon or hydride bond (Fig. 5). In the case of the growing polymer chain, the insertion occurs via cis-addition with secondary insertion so that the titanium is attached to the carbon bearing the phenyl substituent (43). Chain transfer occurs typically via β-hydride elimination, forming a titanium hydride, or via reaction with an

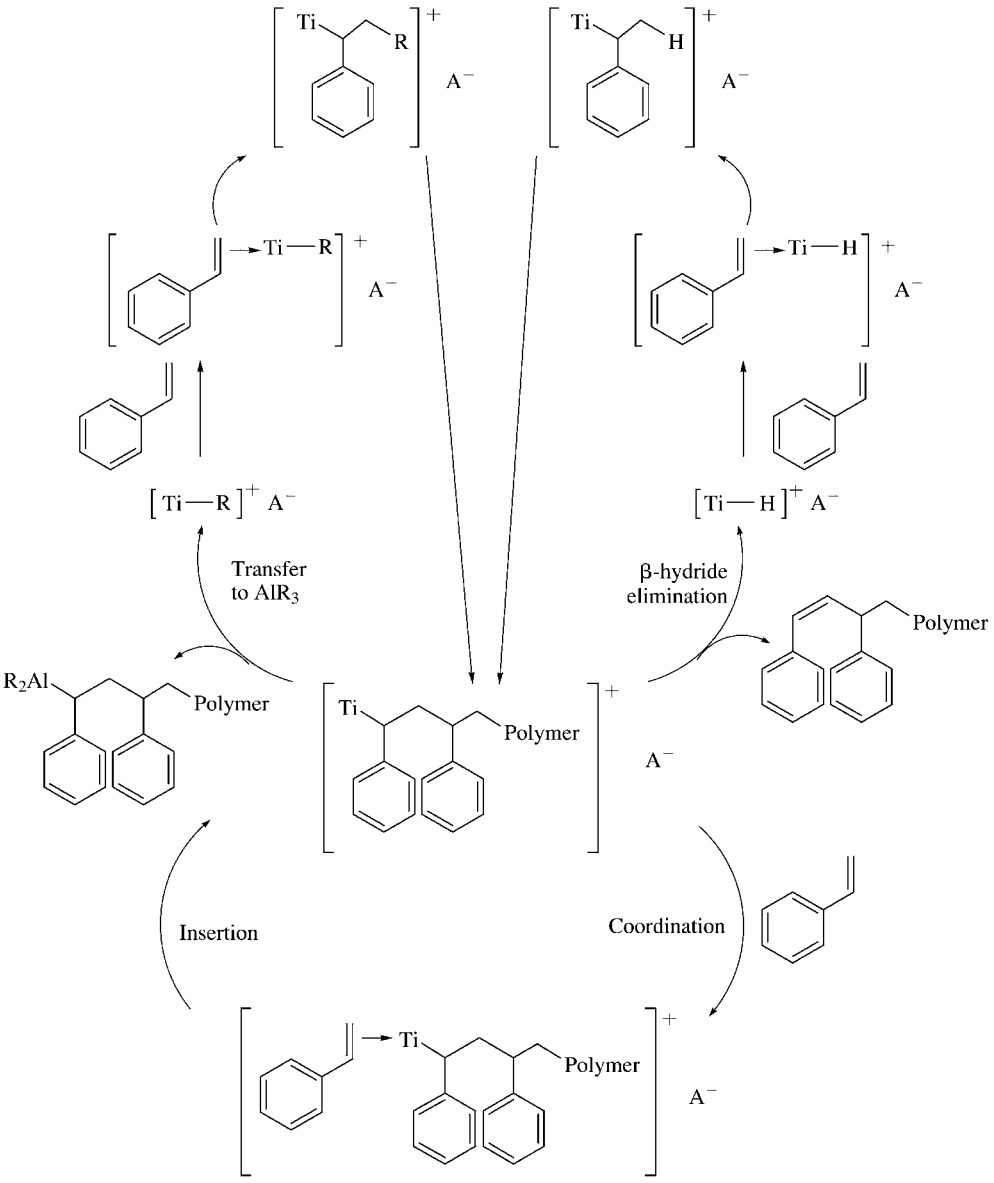

Fig. 5. Generalized schematic of sPS polymerization mechanism. Ligands on titanium omitted for clarity. A^- represents counterion, such as MAO or borate type.

aluminum alkyl species, forming a titanium alkyl (44,45). In either case, reinsertion by styrene monomer generates a new growing polymer chain at the titanium site. The characteristic backbone defects in sPS were analyzed by ^{13}C nmr spectroscopy in order to establish the mechanism of syndiospecificity (46). The defect structures were found to be consistent with a chain-end control mechanism in which the last monomer added to the growing polymer chain directs the insertion of the next monomer added to the chain.

Transition Metal Complexes. The transition metal is the site of the homogeneous coordinative polymerization of sPS and can consequently influence the polymerization activity, polymer molecular weight, and syndiospecificity, as well as other parameters. Various transition metals have been tested and reported for the polymerization of styrene monomer to sPS (1,39). Syndiotactic stereospecificity is observed for $TiCl_4$, $TiBr_4$, $Ti(OCH_3)_4$, $Ti(OC_2H_5)_4$, $[C_5H_5]TiCl_3$, $[C_5H_5]2TiCl_2$, $[(CH_3)_5C_5]TiCl_3$, $[(CH_3)_5C_5]_2TiCl_2$, $[C_5H_5]ZrCl_3$, and $Ti(acac)_2Cl_2$ (acac = acetylacetonate). Polymerization with the following catalysts leads to atactic materials: $ZrCl_4$, $[C_5H_5]_2ZrCl_2$, $[C_5H_5]_2HfCl_2$, $Nb(OC_2H_5)_5$, $Ta(OC_2H_5)_5$, $Cr(acac)_3$, $Co(acac)_3$, and $Ni(acac)_2$. Titanium complexes are more active than other transition metals for syndiotactic polymerization of styrene.

The catalytic activity of titanium complexes varies significantly with the ligands bonded to the titanium. Among those complexes active for sPS polymerization, monocyclopentadienyl-type complexes of titanium yield the highest polymerization activity based on titanium. For substituted cyclopentadienyl complexes, the polymerization activity decreases in the following order (1,47): $[(C_2H_5)(CH_3)_4C_5]Ti(OCH_3)_3 - 100 > [(CH_3)_5C_5]Ti(OCH_3)_3 - 95 > [(CH_3)_4HC_5]Ti(OCH_3)_3 - 64 > [((CH_3)_3Si)_2H_3C_5]Ti(OCH_3)_3 - 12 > [C_5H_5]Ti(OCH_3)_3 - 5$. Electron-releasing substituents on the cyclopentadienyl ligand generally yield complexes with higher polymerization activities, suggesting stabilization of the active site by the electron-donating ligands. However, pendant donor ligands, such as aminoalkyl (48), methoxyethyl (49), or even phenethyl (50), on the cyclopentadienyl ring result in lower polymerization activities. It is possible that these pendant donors hinder coordination or insertion of the styrene molecule. Furthermore, coordination of the pendant donor to MAO may occur, causing destabilization of the active site.

Biscyclopentadienyl complexes and bridged metallocene complexes of titanium show lower polymerization activities than the monocyclopentadienyl complexes (39). The catalytic activity and syndiospecificity for bridged metallocenes does increase by decreasing the bite-angle (51). Although ansa-monocyclopentadienyl-amido titanium complexes are essentially inactive for homopolymerization of styrene, efficient sPS formation with nonbridged amido cylcopentadienyl complexes of titanium has been reported (52).

Other cyclopentadienyl-type ligands on titanium have been investigated for their effect on polymerization of styrene monomer to sPS. Indenyltitanium trichloride has been reported to be a significantly more active catalyst than cyclopentadienyltitanium trichloride (53). This has spawned additional work on substituted indenyl complexes (54,55), benzindenyl complexes (56), and cyclopentaphenanthrene titanium derivatives (57). Several non-cyclopentadienyl complexes of titanium have been investigated for the polymerization of sPS. These have included benzamidinate ligands (58), bridged bisphenolato ligands (59), and pyrazoylborate ligands (60). While these complexes do yield sPS, the activities are lower than those of the monocyclopentadienyl-type complexes.

For the monocyclopentadienyl complexes of titanium, $[(CH_3)_5C_5]Ti(X)_3$, the polymerization activities decrease in the following order for the ancillary ligand X: $OCH_3 - 100 > OC_6H_5 - 98 > Cl - 45 >$ O-*t*-$C_4H_9 - 11 >$ O-*i*-$C_3HF_6 - 4$ (1). The bulky *tert*-butylalkoxide and the electron-withdrawing alkoxide cause a decrease in conversion, which may be due to a decrease in the number of active sites for

polymerization. Increased activity for the trifluoride monometallocene titanium complexes, X = F, relative to the analogous trichlorides has been reported (61). Similar results have been reported for indenyl and substituted indenyl complexes of titanium (62).

Several investigations of supported catalysts for the polymerization of sPS have been reported (63–66). Generally, two approaches have been evaluated for preparing a supported catalyst system for sPS. Either a homogeneous catalyst, such as $(C_5H_5)TiCl_3$, is attached to a solid support and activated by MAO or the MAO cocatalyst is attached to a support followed by reaction with the metallocene. Under certain conditions, high activity and syndiotacticity have been reported for these supported catalyst systems (67).

Cocatalysts. The MAO cocatalyst, basically a reaction product of (TMA) and water, was critical in the discovery of sPS (68). Prior to the introduction of MAO, the homogeneous metallocene, $(C_5H_5)_2TiCl_2$, activated with an aluminum alkyl species yielded only aPS with low activity (38). While the exact characterization of MAO has not been achieved analytically, it has generally been accepted to have an oligomeric structure with the molecular formula $(CH_3AlO)_n$ (69,70). Currently, MAO is believed to act as a cocatalyst by alkylation of the titanium catalyst and abstraction of a ligand from the catalyst. The active species formed by this process is a titanium(III) cationic species in combination with an MAO counterion (39). Evidence for a titanium(III) cationic active species in styrene polymerization with MAO activation has been obtained by esr spectroscopy (71).

In sPS polymerizations, the polymer yield can be affected by the properties of the MAO cocatalyst, such as its molecular weight and residual TMA content. The catalytic activity has been reported to increase with increasing MAO molecular weight, reaching high activity with a molecular weight in the range of approximately 500 (72). Because of the nature of the preparation of MAO, it usually contains residual TMA, which can vary with the synthesis. The residual TMA generally decreases the activity of the catalyst system (1); however, the effect is dependent upon the catalyst. In the case of $(C_5H_5)TiCl_3$ and $Ti(OC_2H_5)_4$ as catalysts, the polymerization activity is reduced by TMA in molar ratios of TMA/MAO from about 0.5 to 2 (73). The activity of the catalyst system can also depend significantly upon molar ratio of MAO/Ti (Fig. 6). The results, however, are also dependent upon the catalyst used in the polymerizations. The polymer yield, with $[(CH_3)_5C_5]Ti(OR)_3$ as the catalyst, increased with increasing MAO/Ti molar ratio, reaching a maximum at a ratio of approximately 300–500 to 1 (47).

In addition to MAO, boron compounds based on tris(pentafluorophenyl)boron and its derivatives, typically dimethylanilinium tetrakis(pentafluorophenyl) borate, have been used as cocatalysts for sPS polymerizations (40,41). Although MAO has been used in large molar excesses relative to the titanium complex, the boron compounds may be used in roughly equimolar amounts to the titanium catalyst. The boron cocatalyst reacts with a titanium alkyl species, either by protonation in the case of dimethylanilinium tetrakis(pentafluorophenyl)borate or by alkyl group abstraction in the case of tris(pentafluorophenyl)boron, to generate a titanium cationic species with a borate counterion (74–76). The esr spectral evidence has been reported for these systems, supporting a titanium(III) cationic active species (76).

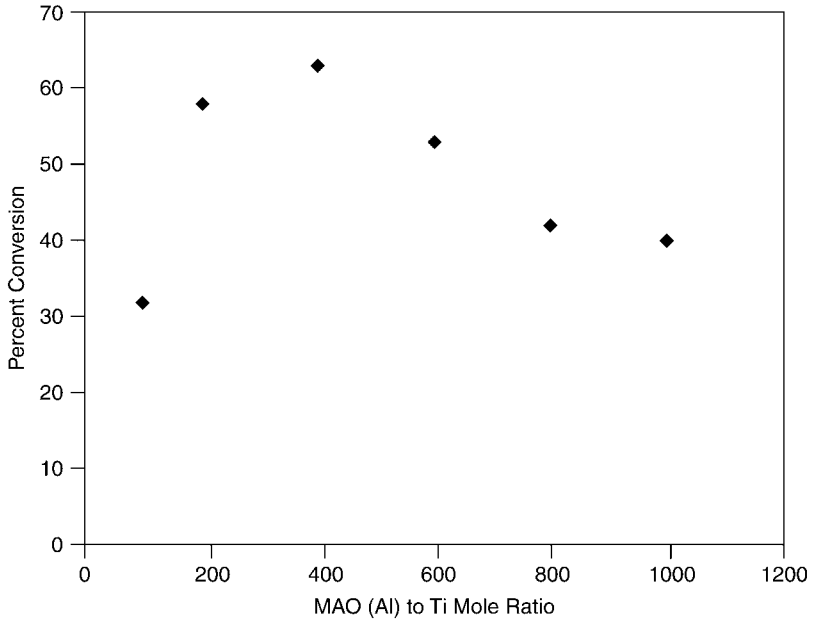

Fig. 6. Percent conversion to sPS as a function of MAO-to-titanium mole ratio for $[(CH_3)_5C_5]Ti(OCH_3)_3$ (47).

The polymerization activity of tris(pentafluorophenyl)boron has been reported to be higher than that of dimethylanilinium tetrakis(pentafluorophenyl) borate with $[(CH_3)_5C_5]Ti(CH_3)_3$ as the catalyst (77). It was proposed that the dimethylaniline coordinates to the active site and decreases the polymerization activity. The use of dimethylanilinium tetrakis(pentafluorophenyl)borate with triisobutylaluminum (TIBA) and $[(CH_3)_5C_5]Ti(CH_3)_3$ as the catalyst has been reported to yield high activity for sPS polymerization (74).

Additives. Certain additives may be included with the catalyst system of the transition metal catalyst and MAO or borate cocatalyst in order to improve the polymerization activity or perhaps to adjust a polymer property into a useful range. Activators that have been reported for sPS polymerization include aluminum alkyls, hydrogen, and organometallic compounds of tin and zinc.

Aluminum alkyls that have been investigated in catalyst systems for sPS polymerization include TMA, triethylaluminum (TEA), and TIBA (1,73,78). In conjunction with $[(CH_3)_5C_5]TiCl_3$ and MAO, the polymerization activity increases with the addition of aluminum alkyl in the following order: TMA < TEA < none < TIBA (Table 5). Aluminum alkyls can act as both reducing agents and alkylating agents for the titanium catalyst. In this case, the polymerization activity is decreased by the strong reducing agents, TMA and TEA.

Hydrogen is a well-known chain transfer agent in classical Ziegler–Natta heterogeneous polymerization and also causes a decrease in molecular weight when used in sPS polymerization (79). Additionally, as shown in Fig. 7, hydrogen significantly improves catalyst efficacy in sPS polymerization (80,81). The activation by hydrogen in sPS polymerization may be due to reactivation of dormant polymerization sites.

Table 5. Relative Polymerization Activities of Aluminum Alkyls with the Catalyst System $[(CH_3)_5C_5]TiCl_3$/MAO[a]

Aluminum alkyl	Relative activity	M_w
None	100	750,000
TMA	13	64,000
TEA	23	84,000
TIBA	560	580,000

[a]Ref. 1.

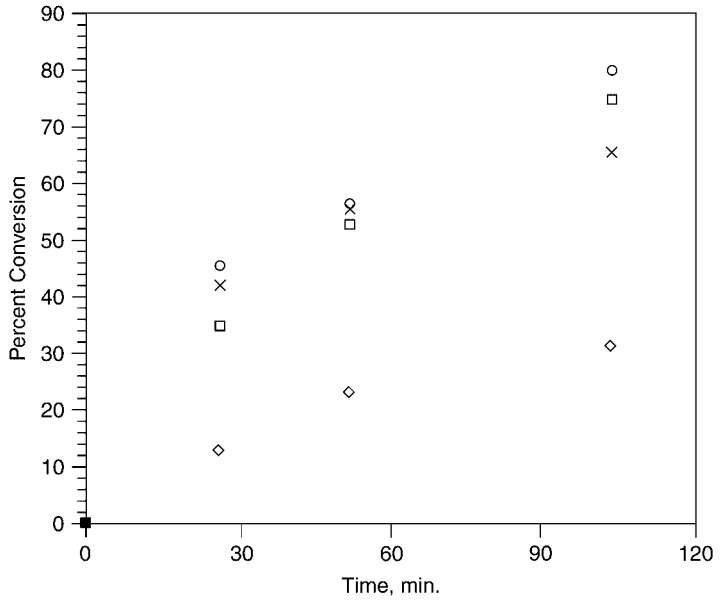

Fig. 7. Effect of hydrogen pressure on conversion for $[(CH_3)_5C_5]Ti(OCH_3)_3$/MAO catalyst system (80). ◇ no H_2; □ 13.8 kPa H_2; ○ 41.4 kPa H_2; × 55.2 kPa H_2. To convert kPa to mm Hg, multiply by 7.5.

Two other activators have been investigated for sPS catalyst systems. Tetraphenyltin, when added to the titanium and MAO catalyst system, has been reported to significantly improve the yield of sPS and cause an increase in the sPS molecular weight (82). It was proposed that mixed aluminum–tin sites may form in the MAO structure, which could affect the active site formation. The influence of diphenylzinc on the metallocene MAO catalyst system for sPS polymerization has been reported for titanium and zirconium (83).

Molecular Weight Control. Chain transfer under the usual sPS polymerization conditions occurs primarily via β-hydride elimination or chain transfer to aluminum alkyl (Fig. 5). For the $(C_5H_5)Ti(OC_4H_9)_3$/MAO catalyst system at low monomer concentration, it has been reported that the rate of β-hydride elimination is 76 times faster than chain transfer to MAO (84). Additional evidence for β-hydride elimination as the main mechanism of chain transfer has been reported from analysis of the *tert*-butylcyclopentadienyltitanium trichloride catalyst

for sPS polymerization (45). Increasing the polymerization temperature significantly decreases the polymer molecular weight, presumably by increasing the rate of β-hydride elimination (1).

However, sPS molecular weight may also be decreased by the addition of external additives, such as aluminum alkyls or hydrogen. The effect on the molecular weight depends upon the titanium catalyst but aluminum alkyls (TMA, TEA, or TIBA) are all effective at decreasing the sPS molecular weight (Table 5) (1,73). Hydrogen, in addition to increasing the catalyst efficiency, is effective as a chain transfer agent in reducing the sPS molecular weight (79–81).

Copolymerization. Polymerization of various ring-substituted styrene monomers using the characteristic sPS catalyst system $(C_5H_5)TiCl_3$/MAO yielded the corresponding syndiotactic substituted polystyrenes (38,85). Electron releasing substituents, tertiary-butyl or methyl, gave higher conversions than styrene monomer, which in turn gave higher conversion than electron withdrawing substituents, such as fluorine or chlorine. Therefore, syndiospecific copolymers of styrene with alkyl-substituted styrenes have been conveniently prepared and their physical properties studied (86–88). The copolymers exhibit a random incorporation of the comonomers in the polymer backbone. Indeed, for syndiotactic poly(styrene-*co*-*p*-methylstyrene), as the content of *p*-methylstyrene (pMS) is increased, the melting point decreases regularly from the value for sPS homopolymer. Furthermore, the lower crystallization temperatures and the breadth of the crystallization peaks by dsc suggest a slower crystallization rate for the copolymers relative to sPS.

Several reports have been published on the copolymerization of styrene and olefins, ie ethylene or butadiene, utilizing the typical sPS catalyst system. The results have depended on the specific catalyst and polymerization conditions. It has been reported that the copolymerization of styrene and ethylene with $(C_5H_5)TiCl_3$ and MAO yielded a mixture of polyethylene and sPS (89,90). An alternating copolymerization using the borane based catalyst system $[(CH_3)_5C_5]Ti(CH_2C_6H_5)_3/B(C_6F_5)_3$ has also been reported (91). No evidence of stereoregularity was found in the copolymer. The products of copolymerization of styrene and ethylene using the catalyst system $(C_5H_5)Ti(OC_6H_5)_3$/MAO have been analyzed (92), leading to the conclusion that the polymer was a random copolymer. However, the polymerization results were influenced by the nature of the MAO, the TMA content, and the polymerization conditions. Copolymerization of styrene and butadiene has been reported with the $[C_5H_5]TiCl_3$/MAO catalyst system (93). Under certain polymerization conditions, block copolymers of sPS–polybutadiene are obtained without appreciable contamination by the homopolymers. dsc and ^{13}C nmr spectroscopy were used to confirm the block structure.

Laboratory Polymerization Techniques. Syndiotactic polymerization of styrene monomer must be carried out under inert atmosphere taking utmost care to exclude oxygen, water, and other polar impurities. The monomer and any solvent must be free of oxygen, water, and polar impurities. Styrene is typically distilled from calcium hydride and stored under inert atmosphere. Alternatively, styrene is conveniently purified prior to polymerization by sparging with nitrogen or argon and passing through activated alumina (94). Furthermore, it has been reported that removal of phenylacetylene from styrene monomer via hydrogenation is beneficial for higher catalyst activity (95).

The sPS polymerization has been reported using several different laboratory scale polymerization techniques. Slurry polymerization, using a diluent such as iso-octane, is particularly convenient since the polymer precipitates from the nonsolvent as a finely divided solid (47,96). Bulk polymerization has often been reported in small laboratory reactors (97). However, in this case, a solid mass forms at low conversions as the polymer crystallizes from the polymerizing mixture. Diffusion, heat transfer, and reactor fouling may be concerns with bulk polymerization of sPS. Suspension polymerization of sPS has also been reported utilizing a perfluorinated hydrocarbon in which both the monomer and polymer are insoluble (98). Beads of sPS are obtained in good yield with kinetics similar to bulk polymerization.

Commercial Processes. Several processes have been reported in the patent literature for the production of sPS. A continuous polymerization process was disclosed using a self-cleaning type reactor comprising kneading elements arranged on rotating shafts (99,100). sPS could be produced efficiently without adhesion of the polymer to the reactor or the agitator. By distributing the catalyst addition along the axis of the reactor, improved temperature control and productivity was claimed (101). Additionally, a second stirred vessel could be added as a secondary reactor to prolong the polymerization times.

Another continuous process has been disclosed for the production of sPS in which monomer and catalyst are introduced into a reactor containing previously added fluidized sPS particles (102–104). Temperature control is achieved by partial evaporation of the monomer. A similar process was disclosed in which a nonsolvent was evaporated in order to control the polymerization temperature (105).

A different type of process has been disclosed in which sPS is produced by dispersion polymerization (106–108). A special block copolymer based on polybutadiene is used as the dispersant. The advantages of this process include being able to produce sPS in conventional stirred reactors at low viscosity with improved productivity and without reactor fouling.

Processing

Syndiotactic polystyrene formulated products are generally injection molded into useful parts for automotive, electrical, electronic, medical, and other market applications (109,110). The melt viscosity of sPS at normal processing temperatures is very low, especially in comparison to other engineering thermoplastic polymers. Syndiotactic polystyrene rheology allows it to flow in to very thin molds at relatively low pressure, and crystallize quickly with low warpage providing for fast cycle times. Table 6 shows the mold shrinkage data typical for formulated commercial products. Since sPS has very low moisture absorbance, there are no additional changes in part dimension with humidity.

Syndiotactic polystyrene will strain-induce crystallize, as well as quiescently crystallize as discussed previously. Furthermore, under certain conditions, it may also be quenched to the amorphous state. In injection molded parts, these processes may lead to skin/core differences in morphology that can be observed (111,112). With higher temperature molds ($>150^{\circ}$C) the parts are generally fully

Table 6. Typical Mold Shrinkage for Formulated sPS Commercial Products[a]

Formulation Type	Flow shrinkage,%	Cross-flow shrinkage,%
30% glass filled (GF)	0.2–0.4	0.5–0.9
40% glass filled (GF)	0.1–0.3	0.4–0.9
30% GF, impact modified (IM)	0.1–0.3	0.2–1.0
30% GF, ignition resistant (IR)	0.27–0.37	Not available
30% GF, IR, IM	0.15–0.3	0.7–0.9
40% GF, IR, IM	0.1–0.2	0.6–0.8

[a]Ref. 23.

crystallized to the first 10 μm of the surface. Fig. 8 shows a plot of percent crystallinity as a function of distance from the surface of the mold for sPS with a mold temperature of 105°C and increasing level of nucleator (pTBBA). The low crystallinity at the surface leads to higher absorbance of good solvents such as benzene. Fig. 9 illustrates the effect of mold temperature and nucleator level on the ability of molded parts to imbibe solvent (benzene). It is clear that low crystallinity at the surface correlates to higher levels of benzene up-take and is consistent with the fact that a skin/core structure is present. Syndiotactic polystyrene is generally nucleated in commercial formulations and molded at higher mold temperatures in applications where solvent resistance is critical.

Syndiotactic polystyrene can also be extruded into sheet, quenched quickly, and then tentered to form biaxially oriented film. It can also be thermoformed

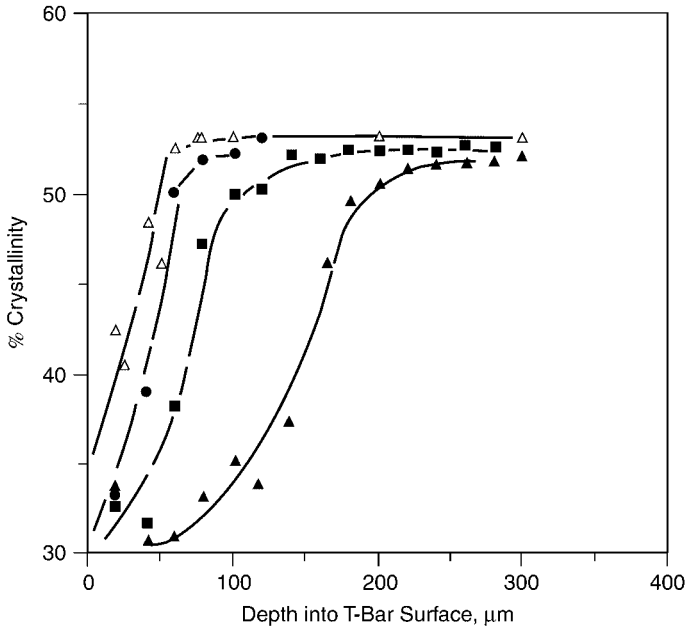

Fig. 8. Plot of percent crystallinity versus depth for tensile bars injection molded with a mold temperature of 105°C. ▲ 0.1 % Al p-TBBA; ■ 0.3% Al p-TBBA; • 1.0% Al p-TBBA; Δ 1.3% Al p-TBBA.

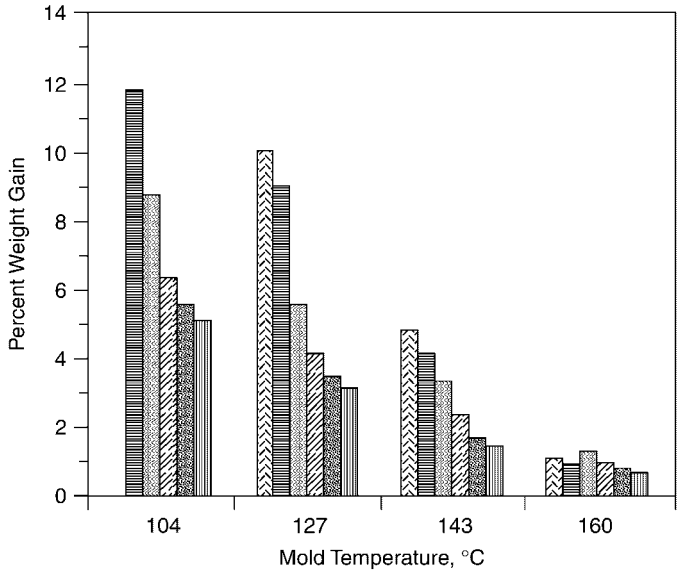

Fig. 9. Benzene absorption (wt. gain after 24-h immersion). Injection molded tensile bars at various mold temperatures and nucleator (Al p-TBBA) levels. Control; 0.1; 0.3%; 0.6%; 1.0%; 1.3%.

from the quenched sheet to form cups, bowls, and other parts. In this case unfilled (neat) or in some cases a low level copolymer (such as pMS) can be used to decrease the quiescent crystallization rate allowing for thicker sheets and films to be made. The copolymer made with pMS disrupts the crystallization of homopolymer sPS such that the melting point is decreased. Fig. 10 shows the peak melting point as

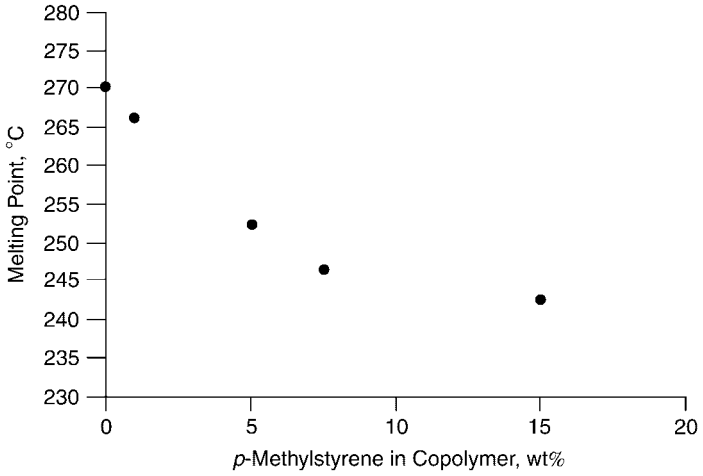

Fig. 10. Plot of melting point (as determined by dsc) versus the level of pMS in a syndiotactic copolymer with styrene.

a function of pMS content in the polymer. The decrease in melting point is a result of smaller crystallites and thinner lamellae. At pMS contents greater than 20% it is very difficult to crystallize the copolymer even with long annealing times.

Economic Aspects

Syndiotactic polystyrene is manufactured by Dow Chemical Company in Germany at announced capacity of 36,400 t/year. Idemitsu Petrochemical Company also manufactures sPS in Japan at approximately 5000 t/year. Compounding to the formulated products is done around the world at many locations. Pricing varies by formulation and product but is generally 3.30–5.50/kg at this time.

BIBLIOGRAPHY

1. N. Tomotsu and co-workers, *J. Mol. Catal. A: Chem.* **128**, 167 (1998).
2. T. H. Newman and M. T. Malanga, in *Proc. 4th SPSJ Int. Polymer Conf.*, Yokohama, Japan, (1992), p. 27.
3. R. D. Wesson, *Polym. Eng. Sci.* **34**, 1157 (1994).
4. S. Cimmino and co-workers, *Polymer* **32**, 1080 (1991).
5. E. L. Thomas, *Chemtracts Macromol. Chem.* **1**(2), 118–120 (1990).
6. O. Greis and co-workers, *Polymer* **30**, 590 (1989).
7. L. C. Lopez and co-workers, *Polymer* **36**, 2331 (1995).
8. A. J. Pasztor Jr., B. G. Landes, and P. J. Karjala, *Thermochim. Acta* **177**, 187 (1991).
9. J. Arnauts and H. Berghmans, *Polym. Commun.* **31**, 343 (1990).
10. N. V. Gvozdic and D. J. Meier, *Polym. Commun.* **32**, 493 (1991).
11. C. De Rosa and co-workers, *J. Polym. Sci., Part B: Polym. Phys.* **29**, 265 (1991).
12. B. G. Landes, M. T. Malanga, and B. P. Thill, *Adv. X-Ray Anal.* **33**, 433 (1990).
13. G. Guerra and co-workers, *Macromolecules* **23**, 1539 (1990).
14. V. Vittoria, A. R. Filho, and F. DeCandia, *J. Macromol. Sci., B: Phys.* **30**, 155 (1990).
15. V. Vittoria, R. Susso, and F. DeCandia, *J. Macromol. Sci., B: Phys.* **28**, 419 (1989).
16. Z. Sun, R. J. Morgan, and D. N. Lewis, *Polymer* **33**, 725 (1992).
17. Y. Chatani and co-workers, *Polym. Prepr. Jpn.* **37**, 1179 (1988).
18. U.S. Pat. 5322869 (June 21, 1994) K. Yamasaki and co-workers, (to Idemitsu Kosan Co., Ltd.).
19. Z. Sun, *Unpublished work of The Dow Chemical Company*, 1995.
20. M. A. Jones and co-workers, *J. Appl. Polym. Sci.* **64**, 673 (1997).
21. U.S. Pat. 5391603 (Feb. 21, 1995), T. Wessel, B. Thill, and Y. B. Huang (to The Dow Chemical Company).
22. U.S. Pat. 6063872 (May 16, 2000), K. Nichols, J. Warakomski, and D. Bank (to The Dow Chemical Company).
23. R. Brentin, D. Bank, and M. Hus, in *Proc. Reg. Tech. Conf., Eastern New England Product Design and Development Div., Soc. Plast. Eng.*, Boston, Oct. 16–18, 1996.
24. J. Boor Jr., *Ziegler–Natta Catalyst and Polymerization*, Academic Press, New York, 1979.
25. J. C. W. Chien, *Coordination Polymerization*, Academic Press, New York, 1975.
26. K. Soga and T. Shiono, *Prog. Polym. Sci.* **22**, 1503 (1997).
27. A. Andresen and co-workers, *Angew. Chem., Int. Ed. Eng.* **15**, 630 (1976).

28. H. Sinn and W. Kaminsky, *Adv. Organomet. Chem.* **18**, 99 (1980).
29. J. Huang and G. L. Rempel, *Prog. Polym. Sci.* **20**, 459 (1995).
30. W. Kaminsky, *Angew. Makromol. Chem.* **223**, 101 (1994).
31. A. L. McKnight and R. M. Waymouth, *Chem. Rev.* **98**, 2587 (1998).
32. H. H. Brintzinger and co-workers, *Angew. Chem., Int. Ed. Eng.* **34**, 1143 (1995).
33. O. Olabisi, M. Atiqullah, and W. Kaminsky, *J. Macromol. Sci., C: Rev. Macromol. Chem. Phys.* **37**, 519 (1997).
34. G. M. Benedikt and B. L. Goodall, eds., *Metallocene-Catalyzed Polymers: Materials, Properties, Processing and Markets*, Plastics Design Library, Norwich, N.Y., 1998.
35. S. S. Reddy and S. Sivaram, *Prog. Polym. Sci.* **20**, 309 (1995).
36. N. Ishihara and co-workers, *Polym. Prepr. Jpn.* **35**, 240 (1986).
37. N. Ishihara and co-workers, *Macromolecules* **19**, 2465 (1986).
38. N. Ishihara, M. Kuramoto, and M. Uoi, *Macromolecules* **21**, 3356 (1988).
39. R. Pó and N. Cardi, *Prog. Polym. Sci.* **21**, 47 (1996).
40. U.S. Pat. 5066741 (Nov. 19, 1991), R. E. Campbell Jr. (to The Dow Chemical Company).
41. C. Pellecchia and co-workers, *Makromol. Chem., Rapid Commun.* **13**, 265 (1992).
42. A. Zambelli, C. Pellecchia, and A. Proto, *Macromol. Symp.* **89**, 373 (1995).
43. C. Pellecchia and co-workers, *Makromol. Chem., Rapid Commun.* **8**, 277 (1987).
44. A. Zambelli and co-workers, *Macromolecules* **20**, 2035 (1987).
45. D. J. Dunclf and co-workers, *Macromolecules* **29**, 6399 (1996).
46. T. H. Newman and M. T. Malanga, in *Proc. 4th SPSJ Int. Polymer Conf.*, 1992, p. 27.
47. R. E. Campbell Jr., T. H. Newman, and M. T. Malanga, *Macromol. Symp.* **97**, 151 (1995).
48. M. S. Blais, J. C. W. Chien, and M. D. Rausch, *Organometallics* **17**, 3775 (1998).
49. P. Foster, M. D. Rausch, and J. C. W. Chien, *J. Organomet. Chem.* **527**, 71 (1997).
50. J. C. Flores and co-workers, *Organometallics* **15**, 4944 (1996).
51. M. L. H. Green and N. Ishihara, *J. Chem. Soc., Dalton Trans.* **5**, 657 (1994).
52. P.-J. Sinneman, T. P. Spaniol, and J. Okuda, *J. Organometal. Chem.* **598**, 179 (2000).
53. T. E. Ready and co-workers, *Macromolecules* **26**, 5822 (1993).
54. P. Foster, J. C. W. Chien, and M. D. Rausch, *Organometallics* **15**, 2404 (1996).
55. Y. Kim, B. H. Koo, and Y. Do, *J. Organometal. Chem.* **527**, 155 (1997).
56. P. Foster, M. D. Rausch, and J. C. W. Chien, *J. Organometal. Chem.* **571**, 171 (1998).
57. N. Schneider, M.-H. Prosenc, and H.-H. Brintzinger, *J. Organometal. Chem.* **545/546**, 291 (1997).
58. J. C. Flores, J. C. W. Chien, and M. D. Rausch, *Organometallics* **14**, 1827 (1995).
59. J. Okuda and E. Masoud, *Macromol. Chem. Phys.* **199**, 543 (1998)
60. U.S. Pat. 5237069 (Aug. 17, 1993), T. H. Newman (to The Dow Chemical Company).
61. W. Kaminsky and co-workers, *Macromolecules* **30**, 7647 (1997).
62. G. Xu and E. Ruckenstein, *J. Polym. Sci., Part A: Polym. Chem.* **37**, 2481 (1999).
63. K. Soga and H. Nakatani, *Macromolecules* **23**, 957 (1990).
64. K. Soga, R. Koide, and T. Uozumi, *Macromol. Chem., Rapid Commun.* **14**, 511 (1993).
65. J.-H. Yim and co-workers, *Eur. Polym. J.* **32**, 1381 (1996).
66. J. Xu and co-workers, *Macromol. Rapid Commun.* **18**, 875 (1997).
67. V. Pasquet and R. Spitz, *Macromol. Chem. Phys.* **200**, 1453 (1999).
68. N. Ishihara and M. Kuramoto, *Stud. Surf. Sci. Catal.* **89**, 339 (1994).
69. S. Psynkiewicz, *Polyhedron* **9**, 429 (1990).
70. M. R. Mason and co-workers, *J. Amer. Chem. Soc.* **115**, 4971 (1993).

71. J. C. W. Chien, Z. Salajka, and S. Dong, *Macromolecules* **25**, 3199 (1992).
72. N. Tomotsu, M. Kuramoto, M. Taksuchi, and H. Maezawa, in *Metallocenes '96, Proc. Int. Congr. Metallocene Polym.*, Vol. 2, 1996, p. 179.
73. R. Pó, N. Cardi, and L. Abis, *Polymer* **39**, 959 (1998).
74. H. Kucht and co-workers, *App. Organomet. Chem.* **8**, 393 (1994).
75. A. Grassi, A. Zambelli, and F. Laschi, *Organometallics* **15**, 480 (1996).
76. A. Grassi and co-workers, *Macromolecules* **30**, 1884 (1997).
77. C. Pellecchia and co-workers, *Macromol. Chem., Rapid Commun.* **13**, 265 (1992).
78. Q. Wu, Q. Gao, and S. Lin, *J. Appl. Polym. Sci.* **70**, 765 (1998).
79. Eur. Pat. 0659775 (Dec. 22, 1994), S. Ikeuchi and N. Tomotsu (to Idemitsu Kosan Co.).
80. U.S. Pat. 5468818 (Nov. 21, 1995), T. H. Newman and K. K. Borodychuk (to The Dow Chemical Company).
81. K. Yokota and co-workers in W. Kaminsky, ed., *Metalorganic Catalysts for Synthesis and Polymerization*, Springer-Verlag, Berlin, 1999, p. 435.
82. R. Pó, R. Santi, and N. Cardi, *J. Polym. Sci., Part A: Polym. Chem.* **37**, 1053 (1999).
83. F. M. Rabagliati and co-workers, *Polym. Bull.* **39**, 693 (1997).
84. J. C. W. Chien and Z. Salajka, *J. Polym. Sci., Part A: Polym. Chem.* **29**, 1253 (1991).
85. A. Grassi and co-workers, *Macromolecules* **22**, 104 (1989).
86. N. Cardi and co-workers, *Macromol. Symp.* **102**, 123 (1996).
87. H. Nakatani and co-workers, *Polymer* **38**, 4751 (1997).
88. R. Thomann and co-workers, *Macromolecules* **30**, 8401 (1997).
89. P. Aaltonen and co-workers, *Macromolecules* **27**, 3136 (1994).
90. P. Aaltonen and J. Seppala, *Eur. Polym. J.* **30**, 683 (1994).
91. C. Pellecchia and co-workers, *Macromolecules* **29**, 1158 (1996).
92. G. Xu and S. Lin, *Macromolecules* **30**, 685 (1997).
93. A. Zambelli and co-workers, *Macromol. Chem. Phys.* **201**, 393 (2000).
94. Eur. Pat. 0662465 (July 24, 1990), H. Teshima, M. Kuramoto, and M. Takeuchi (to Idemitsu Kosan Co.).
95. U.S. Pat. 5064918 (Nov. 12, 1991), M. T. Malanga (to The Dow Chemical Company).
96. U.S. Pat. 5252693 (Oct. 12, 1993), N. Ishihara, M. Kuramoto, and M. Uoi (to Idemitsu Kosan Co.).
97. T. H. Newman and M. T. Malanga, *J. Macromol. Sci, A: Pure Appl. Chem.* **34**, 1921 (1997).
98. U.S. Pat. 4950724 (Aug. 21, 1990), M. T. Malanga and T. H. Newman (to The Dow Chemical Company).
99. Eur. Pat. 389939 (Oct. 3, 1990), J. H. Siddall (to The Dow Chemical Company).
100. U.S. Pat. 5254647 (Oct. 19, 1993), K. Yamamoto and co-workers (to Idemitsu Kosan Co.).
101. Eur. Pat. 584646 (Nov. 8, 1993), H. Ase, K. Ishikawa, and H. Imabayashi (to Idemitsu Kosan Co.).
102. U.S. Pat. 5037907 (Aug. 6, 1991), H. Imabayashi and co-workers (to Idemitsu Kosan Co.).
103. U.S. Pat. 5306790 (Apr. 26, 1994), H. Imabayashi, K. Ishikawa, and Y. Ishida (to Idemitsu Kosan Co.).
104. U.S. Pat. 5484862 (Jan. 16, 1996), J. H. Siddall and D. A. Beaudoin (to The Dow Chemical Company).
105. Jpn. Pat. 07025906 (Jan. 27, 1995), S. Baba and co-workers (to Idemitsu Petrochemical Co.).
106. Eur. Pat. 643102 (Mar. 15, 1995), B. Gunesin, M. Lux, and G. E. McKee (to BASF AG).
107. WO 9830613 (July 16, 1998), J. Wünsch and M. Schneider (to BASF AG).
108. WO 9964483 (Dec. 16, 1999), J. Wünsch and W. Anselmann (to BASF AG).

109. D. Bank, T. E. Wessel, and J. Kolb, SAE Technical Paper Series, #93088, 1993.
110. W. E. Burk, C. E. Peterson, N. A. Rotstein, and R. P. Brentin, in *Proc. of the EIC/EMCW Tech. Conf.*, Oct. 1999, p. 1101.
111. L. Lopez and co-workers, *Polymer* **36**, 2331 (1995).
112. Y. Ulcer and co-workers, *J. Appl. Polym. Sci.* **60**, 669 (1996).

MICHAEL MALANGA
THOMAS H. NEWMAN
Dow Chemical Company

TETRAFLUOROETHYLENE POLYMERS. See PERFLUORINATED POLYMERS.

TRANSITIONS AND RELAXATIONS. See GLASS TRANSITION; VISCOELASTICITY

ULTRAHIGH MW PE. See ETHYLENE POLYMERS, HDPE.

URETHANE POLYMERS. See POLYURETHANES.

VINYL FLUORIDE POLYMERS (PVF)

Introduction

The base unit of poly(vinyl fluoride) (PVF) is shown by structure (**1**). DuPont first commercialized a film based on PVF under the trade mark Tedlar in 1961 and is the only known supplier of this polymer.

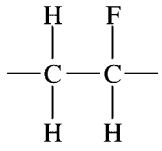

1

PVF homopolymers and copolymers have excellent resistance to sunlight degradation, chemical attack, water absorption, and solvent, and have a high solar energy transmittance rate. These properties have resulted in the utilization of PVF film and coating in outdoor and indoor functional and decorative applications. These films have found use where thermal stability, outdoor durbility, stain resistance, adherence, and release properties are required. PVF has a greater tendency to crystallize than poly(vinyl chloride). It is stable at high temperature, which is important in many of its applications.

Vinyl fluoride can be polymerized into homopolymers and copolymers with the aid of a free-radical generating catalyst (initiator), usually under high pressure. Ziegler–Natta-type catalysts can be used to prepare vinyl fluoride polymers at lower temperatures and pressures.

Encyclopedia of Polymer Science and Technology. Copyright John Wiley & Sons, Inc. All rights reserved.

Monomer

Properties. Vinyl fluoride [75-02-5] (VF), CH_2=CHF (fluoroethene), is a colorless gas at ambient conditions with an ether-like odor. VF is insoluble in water under atmospheric pressure but dissolves slightly in some alcohols and ketones, such as ethanol and acetone. Tables 1–5 (1) provide data for physical, thermodynamic, and transport properties of VF.

Other than polymerization into homo- and copolymers, VF is used for the introduction of fluorine atoms into organic compounds and polymers, eg, by grafting into fibers. The net consequence of fluorine incorporation is increased chemical and

Table 1. Physical Properties of Vinyl Fluoride

Property	Value
Molecualr weight	46.046
Boiling point, °C	−72.0
Freezing point, °C	−160.5
Critical temperature, °C	54.7
Critical pressure, MPa[a]	5.1
Critical density, g/cm^3	0.320
Vapor pressure at 21°C, MPa[a]	2.5
Liquid density at 21°C, g/cm^3	0.636

[a]To convert MPa to atm, multiply by 10.

Table 2. Estimated Thermodynamic Properties of Vinyl Fluoride

		Heat capacity, J/(g · K)[a]	
Temperature, °C	Latent heat of vaporization, J/(g · K)[a]	Saturated liquid	Saturated vapor at 0.1 MPa[b]
−28.9	171.8	2.02	0.93
−17.8	161.5	2.05	0.95
−6.7	151.2	2.09	0.98
4.4	140.1	2.13	1.00
15.6	128.0	2.27	1.03
26.7	114.2	2.72	1.05

[a]To convert J to cal, divide by 4.184.
[b]To convert MPa to atm, multiply by 10.

Table 3. Solubility of Vinyl Fluoride in Organic Solvents

Solvent	Solubility of cm^3 VF gas in 1-cm^3 solvent	Henry's law constant at, 30°C, 0.1 MPa[a]
Ethyl alcohol	4	
Diethyl ether	5.5	
Adipontrile	4	50.8
Propionitrile	10	32.9
Acetonitrile	10.5	41.9
Butyrolactone	5.2	57.0
Dimethyl formamide	8.9	33.4

[a]To convert MPa to atm, multiply by 10.

Table 4. Solubility of Vinyl Fluoride in Water

Vinyl fluoride pressure in water,[a] MPa[b]	g/100 g Water		
	27°C	79°C	100°C
0.86		0.3	
1.75		0.5	0.4
2.75	1.1		
3.43	1.5	0.9	0.8
6.87		1.5	1.5

[a]Vinyl fluoride forms a hydrate at 15.6°C and 2.22 MPa.
[b]To convert MPa to atm, multiply by 10.

Table 5. Estimated Thermal Conductivity and Viscosity of Vinyl Fluoride

Property	Liquid, saturated	Vapor, saturated at 0.1 MPa[a]
Thermal conductivity, kW/(m · K) at		
−28.9°C		10.28
−17.8°C	122.6	11.11
−6.7°C	124.2	11.98
4.4°C	127.6	12.76
15.6°C	143.9	13.35
26.7°C	172.9	14.02
Viscosity, Pa · s[b] at		
−28.9°C	0.031	0.0093
−17.8°C	0.022	0.0096
−6.7°C	0.019	0.0100
4.4°C	0.016	0.0104
15.6°C	0.015	0.0108
26.7°C	0.014	0.0112

[a]To convert MPa to atm, multiply by 10.
[b]To convert Pa · to P, multiply by 10.

thermal stability, decreased solubility, and enhanced resistance to degradation by light. The useful range of application of grafted article at lower temperatures is also improved.

Flammability. Interstate Commerce Commission has classified VF as a flammable gas. It is flammable in air between concentrations of 2.6 ± 0.5 and 21.7 ± 1.0 vol% of VF. Mixtures of air and VF have been reported to ignite at a minimum temperature of 400°C (2).

Preparation. The first preparation of VF dates back to 1901 and the reaction of zinc with 1,1-difluoro-2-bromoethane [359-07-9] (3). Phenylmagnesium bromide in ether and potassium iodide solution can replace the metal for dehalogenation (4,5). Most approaches to VF synthesis have employed reactions of acetylene [74-86-2] with hydrogen fluoride (HF) either directly (5–8) or utilizing a catalyst (6,9–13) based on mercury or aluminum (6,9,12,14). In another process, an acetylene/HF mixture is passed over a mercuric chloride or fluoride catalyst, which also produces vinylidene fluoride and difluoroethane as by-products (10). Another synthesis (11) consists of two steps in which 1,1-difluoroethane (DFE) is

formed by adding HF to acetylene, followed by pyrolytic dehydrofluorination of DFE over an aluminum salt catalyst. Vinyl fluoride is purified by removing hydrofluoric acid in soda-lime towers and by scrubbing of acetylene in ammoniacal CuCl. Oxygen is removed by distillation.

Vinyl fluoride can be made by the reaction of ethylene [74-85-1] with HF in the presence of a palladium and $CuCl_2$ catalyst (14). A mixture of HF and $CH_2{=}CH_2$ at a 2:1 ratio, containing 35% oxygen, is passed over the catalyst at 240°C, producing VF with a 20% conversion of ethylene and 92% selectivity.

Other routes of preparation include catalytic pyrolysis of DFE (15–18); dehydrochlorination of 1-fluoro-2-chloroethanes at 500°C in the presence of ethylene dichloride, with a 15% conversion and 100% selectivity (19–23); catalytic reaction of DFE with acetylene (24,25), where VF is produced by simultaneous dehydrofluorination of CF_2HCH_3 and hydrofluorination of C_2H_2 in the presence of catalyst. An optimal yield of 77.5% is obtained at a temperature of 340°C at a 2.1:1 ratio of DFE to acetylene, and ferric oxide–cadmium oxide–aluminum oxide catalyst with a ratio of 8:4:88 (25). Another procedure involves halogen exchange of vinyl chloride [75-01-4] with HF (26–28). Highest yields were reported at 370–380°C with a two-component catalyst system, containing 96% γ-Al_2O_3 and 4% Cr_2O_3 with a vinyl chloride-to-HF ratio of 1:3 (28).

Hydrogen fluoride addition to acetylene and fluorination of vinyl chloride are the most likely commercial routes for the preparation of VF (29), although most details have not been published. Commercial VF is stabilized with terpenes such as *d*-limonene to inihibit autopolymerization.

Polymer

Properties. The physical, chemical, and electrical properties of a poly(vinyl fluoride) [24981-14-4] (PVF) film are shown in Table 6.

PVF is a semicrystalline polymer with a planar zigzag chain configuration (30). The degree crystallinity depends on the polymerization method and the thermal history of the polymer; reported values range from 20 to 60% (31). The significant variation of the degree of crystallinity is thought to be primarily a function of defect structures. Wide-line nmr and x-ray diffraction studies show the unit cell to contain two monomer units and have the dimensions of $a = 0.857$ nm, $b = 0.495$ nm, and $c = 0.252$ nm (32). Similarity to the phase I crystal form of poly(vinylidene fluoride) suggests an orthorhombic crystal (33).

The relationship of polymer structure to melting point and degree of crystallinity has been the subject of a number of studies. Head-to-head regio irregularities in PVF are known (31,34,35) and the concentration of such units has been suggested as the source of variations in melting point (36–38). Commercial PVF contains approximately 12% head-to-head linkages by ^{19}F nmr and displays a peak melting point of about 190°C (37,39–41). Both nmr and ir studies have shown PVF to be atactic (31,34,35,37,42–45) and, as such, variations in stereoregularity are not thought to be a contributor to variations in melting point.

PVF with controlled amounts of head-to-head units varying from 0 to 30% have been prepared (37,39) by using a chlorine substituent to direct the course of polymerization of chlorofluoroethylenes and then reductively dechlorinating the

Table 6. Properties of Poly(vinyl fluoride) Film

Property	Value	ASTM test method[a]
Bursting strength, kPa[b]	200–450[c]	D774
Coefficient of friction with metal density, g/cm^3	0.18–0.21	D1894-78
	1.38–1.72	Weighted samples
Impact strength, kJ/m[d]	43–90	D3420-80
Refractive index, $n^{20}{}_{\mathrm{D}}$	1.46	D542; Abbe refractometer
Tear strength, kJ/m[d]		
Propagated	6–22	D1922-67
Initial	129–196	D1004-66
Tensile modulus, MPa[e]	44–110	D882
Ultimate elongation, %	115–250	D882
Ultimte yield strength, MPa[e]	33–41	D882
Linear coefficient of expansion, cm/(cm · C)	0.00005	Air oven, 30 min
Useful temperature range, °C		
Continuous use	−70 to +107	
Short cycle (1–2 h)	175	
Zero strength	260–300	Hot bar
Thermal conductivity, 1°C/cm, W/(m · K)		
At −30°C	0.14	
At 60°C	0.17	
Self-ignition temperature, °C	390	D1929
Solar energy transmittance, 359–2500 nm, %	90	E427-71
Chemical resistance after 1-year immersion at 25°C in acids (10%), bases (10%), or solvents	No visible effect	
Chemical resistance after 2-h immersion at boiling temperature in acids (10%), bases (10%), or solvents	No visible effect	
Electrical[f]		
Corona endurance, h at 60 Hz, 40 V/μm, h	2.5–6.0	D2275
Dielectric constant		D150-81
1 MHz at 23°C	6.2–7.7	
1 MHz at 100°C	10.9–12.6	
1 Hz at 23°C	8.5–8.2	
1 Hz at 100°C	14–13	
Dielectriici strength		
Short-term ac, kV/μm	0.08–0.13	
Short-term dc, kV/μm	0.15–0.19	
Dissipation factor		D150-81
1 MHz at 23°C	0.17–0.28	
1 MHz at 100°C	0.09–0.21	
1 kHz at 23°C	0.019–0.019	
1 kHz at 100°C	0.21–0.067	
Volume resistivity, GΩ · m		D150-81
At 23°C	2000–700	
At 100°C	0.7–2	
Surface resistivity, GΩ · m		D257
At 23°C	60,000–20,000	
At 100°C	7–20	

Table 6. (Continued)

Property	Value	ASTM test method[a]
Permeability		
Moisture absorption, %	0.5	D570-81
Moisture vapor transmission,[g] nmol/($m^2 \cdot s^h$) at 7.0 kPa,[i] 39.5°C	4.65–29.4	E96-58T
Gas permeability, nmol/(m · s · GPa)[j] at 98 kPa,[i] 23°C		D1434
Carbon dioxide	22.4	
Helium	302	
Hydrogen	117	
Nitrogen	0.5	
Oxygen	6.6	
Vapor permeability,[k] nmol/(m^2 · s) [l]		E96, modified
Acetic acid at 23°C	4.9	
Acetone at 23°C	1570	
Benzene at 23°C	13	
Carbon tetrachloride at 23°C	3.9	
Ethyl acetate at 23°C	138	
Hexane at 23°C	10	
Water at 39.5°C	22	

[a]Unless otherwise stated.
[b]To convert kPa to psi, multiply by 0.145.
[c]Range dependent on composition and tensile modification.
[d]To convert kJ/m to ft · lbf/in., divine by 0.534 (see ASTM D256).
[e]To convert MPa to psi, multiply by 145.
[f]When range of electrical properties is given, the first value refers to 54.8-μm transparent film, and the second vlaue to 54.8-μm white pigmented film.
[g]Measurements made on films of nominal 25-μm thickeness.
[h]To convert nmol/(m^2 · 5) to g/(m^2 · d), multiply by 1.94.
[i]To convert kPa to mm Hg, multiply by 7.5.
[j]To convert nmol/(m · s · GPa) to (cc · mL)/(m · d · atm), multiply by 7.7.
[k]At partial pressure of vapor at given temperature.
[l]To convert nmol/(M^2 · s) to g/(m^2 · d), multiply by 1.94 and by the density.

products with tributyltin hydride. This series of polymers shows melting point distributions ranging from about 220°C for purely head-to-tail polymer down to about 160°C for polymer containing 30% head-to-head linkages. This study, however, does not report the extent of branching in these polymers. Further work has shown that the extent of branching has a pronounced effect upon melting temperature (40,41). Change of polymerization temperature from 90 to 40°C produces a change in branch frequency from 1.35 to 0.3%, while the frequency of monomer reversals is nearly constant (12.5 ± 1%). The peak melting point for this series varies from 186°C (polymerization at 90°C to 206°C polymerization at 40°C).

PVF displays several transitions below the melting temperature. The measured transition temperatures vary with the technique used for measurement. T_g(L) (lower) occurs at −15 to −20°C and is ascribed to relaxation, free from restraint by crystallites. T_g(U) (upper) is in the 40–50°C range and is associated

with amorphous regions under restraint by crystallites (46). Another transition at −80°C has been ascribed to short-chain amorphous relaxation and one at 150°C associated with premelting intracrystalline relaxation.

PVF has low solubility in all solvents below about 100°C (44). Polymers with greater solubility have been prepared using 0.1% 2-propanol polymerization modifier and were characterized in *N*,*N*-dimethylformamide solution containing 0.1 *N* LiBr. M_n ranged from 76,000 to 234,000 (osmometry), and M_s from 143,000 to 654,000 (sedimentation velocity). Sedimentation velocity molecular weights can be related to intrinsic viscosity, using the Mark–Houwink equation:

$$\eta = KM^a$$

Using an a value of 0.80, which is typical of an extended polar polymer in good solvent, K is determined to be 6.52×10^{-5} (47).

The conformational characteristics of PVF are the subject of several studies (33,48). The rotational isomeric state (RIS) model has been used to calculate mean square end-to-end distance, dipole moments, and conformational entropies. ^{13}C nmr chemical shifts are in agreement with these predictions (49). The stiffness parameter (δ) has been calculated (50) using the relationship between chain stiffness and cross-sectional area (51). In comparison to polyethylene, PVF has greater chain stiffness, which decreases melting entropy, ie, $(\Delta S)_m$=8.58 J/(mol·K) [2.05 cal/(mol·K)] versus 10.0 J/(mol·K) [2.38 cal/(mol·K)].

A solubility parameter of 24.5–24.7 $MPa^{1/2}$ [12.0–12.1 $(cal/cm^3)^{1/2}$] has been calculated for PVF using room temperature swelling data (52). The polymer lost solvent to evaporation more rapidly than free solvent alone when exposed to air. This was ascribed to reestablishment of favorable dipole–dipole interactions within the polymer. Infrared spectral shifts for poly(methyl methacrylate) in PVF have been interpreted as evidence of favorable acid–base interactions involving the H from CHF units (53). This is consistent with the greater absorption of pyridine than of methyl acetate, despite a closer solubility parameter match with methyl acetate.

PVF is more thermally stable than other vinyl halide polymers. High molecular weight PVF is reported to degrade in an inert atmosphere, with concurrent HF loss and backbone cleavage occurring at about 450°C (54,55). In air, HF loss occurs at about 350°C, followed by backbone cleavage around 450°C.

More recent work reports the onset of thermal degradation at lower temperatures and provides a clearer picture of the role of oxygen (56–58). In the presence of oxygen, backbone oxidation and subsequent cleavage reactions initiate decomposition. In the absence of oxygen, dehydrofluorination eventually occurs, but at significantly higher temperatures.

PVF is transparent to radiation in the uv, visible, and near-ir regions, transmitting 90% of the radiation from 350 to 2500 nm. Radiation between 7,000 and 12,000 nm is absorbed (59). Exposure to low dose γ irradiation produces cross-links in PVF and actually increases tensile strength and etching resistance, whereas the degree of crystallinity and melting point are reduced (60). PVF becomes embrittled upon exposure to electron-beam radiation of 10 MGy (10^9 rad), but resists breakdown at lower doses. It retains its strength at 0.32 MGy (32×10^6 rad) while poly(tetrafluoroethylene) is degraded at 0.02 MGy (2×10^6 rad) (61).

Polymerization

VF undergoes free-radical polymerization in both head-to-head and head-to-tail configurations. Typically, commercial PVF contains 10–12% of inverted head-to-head and tail-to-tail units (62). VF is more difficult to polymerize than other vinyl halides (60) because of the high electronegativity of fluorine, which is the most electronegative element. Low boiling point (−72°C) and high critical temperature (54.7°C) of VF necessitate high pressure polymerization similar to that required for polyethylene.

The first polymerization involved heating a saturated solution of VF in toluene at 67°C under 600 MPa (87,000 psi) for 16 h (63). In a later procedure, benzoyl peroxide was used to initiate polymerization (9,64). The product was a polymer with a density of 1.39 g/cm^3, which was soluble in hot dimethylformamide, chlorobenzene, and other solvents. A wide variety of initiators and polymerization conditions have been explored (64–66). Examples of bulk (30,31) and solution (65,67–69) polymerizations exist; however, aqueous suspension or emulsion methods are generally preferred (64,70–79). VF volatility dictates that moderately high pressures would be required. Photopolymerizations, usually incorporating free-radical initiators, are also known (64,67,68,80).

The course of VF polymerizations is dominated by the high energy and hence high reactivity of the propagating VF radical. The fluorine substituent provides little resonance stabilization, leading to a propagating intermediate which is indiscriminate in its reactions. Monomer reversals, branching, and chain-transfer reactions are common. The reactivity of the VF radical limits the choice of polymerization medium, surfactants, initiators, or other additives and makes impurity control important. Species which can participate in chain transfer or incorporate in the polymer can depress molecular weight or degrade the thermal stability characteristics of the final polymer.

The combination of triisobutylborane [1116-39-8] and oxygen has been used to polymerize VF at reduced temperature and pressure (81). Polymerization temperature was varied from 0 to 85°C, with a corresponding drop in melting point from about 230°C (polymerization at 0°C) to about 200°C (polymerization at 85°C). This dependence of melting temperature, and degree of crystallinity, has been interpreted in terms of variations in the extent of monomer reversals during polymerization (82).

VF can be polymerized by a number of techniques, including suspension, bulk, and emulsion polymerizations in batch and continuous modes. Graft and radiation-induced polymerizations of VF have also been reported.

Suspension Polymerization. In this technique, liquid VF is suspended in water with the help of a dispersion stabilizer (70). Polymerization is initiated by an organic peroxide such as diisopropyl peroxydicarbonate below the critical temperature of VF (71,72). The reaction can also be initiated by uv light and ionizing radiation (64,73). VF dispersions are usually stabilized by water-soluble polymers such as cellulose derivatives, eg cellulose ester and sodium carboxymethylcellulose, and poly(vinyl alcohol). Inorganic salts such as magnesium carbonate, barium sulfate, and alkylsulfoacids are also used.

Polymerization is also reported in the presence of a nonionic surfactant (74) using 0.5–3.0 wt% monoalkylphenyl ether of poly(ethylene glycol)s as dispersing

agent in water and 0.5–2.5 wt% diisopropyl peroxydicarbonate as initiator. Polymer yield of 12–21 wt% are obtained in 14–18 h at 30–40°C. Radiation-initiated suspension polymerization of VF in water yields PVF soluble in solvents such as dimethylformamide (73). Increased dosages of radiation give lower molecular weight polymers. Thermal stability of PVF deteriorates with an increase in the concentration of dispersing agent.

In a modified suspension polymerization, the pressure requirements are reduced. The reaction is conducted with azo catalysts (75) at 25–100°C and pressures of 2.5–10 MPa (25–100 atm) over 18–19 h. A stainless steel reactor is flushed with nitrogen charged with 150 parts acetylene-free VF, 150 parts deoxygenated distilled water, and 0.150 parts 2,2′-azobisisobutyronitrile. The reactor is heated to 70°C for 1 h, agitated, and held at 8.2 MPa (82 atm) for 18 h. The product, 75.8 parts of PVF, is collected in the form of a white cake (64). Continuous polymerization of VF is based on the modified suspension process (76).

Bulk Polymerization. In the bulk polymerization, VF is polymerized by a peroxide initiation. In an example (67), a glass ampule is filled with VF containing 6.5×10^{-2} mol/L of di-*tert*-butyl peroxide. The ampule was irradiated by uv light from a mercury lamp below 25°C. A highly porous polymer, insoluble in VF, at conversions over 90% is obtained.

Emulsion Polymerization. VF can be readily polymerized by the emulsion method at highly reduced pressures and lower temperatures as compared to the suspension technique (77). Polymerization in an aqueous emulsion facilitates the process control and the removal of reaction heat, increases the molecular weight of the resin (74), and permits high rates of reaction and high yields.

Emulsifiers such as fatty alcohol sulfates, alkane sulfonates, alkali salts of fatty acids, and others are slightly to marginally effective (77). Fluorinated surfactants, particularly perfluorinated carboxylic acids containing seven or eight fluorine atoms, are specially effective in maintaining a high rate of polymerization after about 40% conversion. Fluorinated surfactants are characterized by low values of critical concentration of micelle formation (74). They are thermally and chemically stable, and their incorporation does not impair the PVF properties.

In a typical example (77), 200 parts water, 100 parts VF, 0.6 parts of a perfluorinated carboxylic acid, 0.2 parts ammonium persulfate, and 3 parts water glass ($Na_2O/SiO_2 = 1{:}3.3$) are introduced into a stirred autoclave. The mixture is heated to 46°C, the pressure is brought to 4.3 MPa (42.5 atm), and held for 8 h. Addition of an electrolyte precipitates a white powdery PVF at 95% yield.

Radiation-Induced Polymerization. Exposure to uv radiation in the absence of free radicals does not polymerize VF, but decomposes it into acetylene and HF (83,84). Radiation can be used in the presence of initiators (64), which decomposes into free radicals. The first reported photopolymerization of VF in the presence of benzoyl, lauroyl, or acetyl peroxide resulted in a 36% yield after 2 days at 27°C under 254-nm irradiation (64).

The rate data in radiation-induced bulk polymerization of VF reveal a heterophase process (80). Polymerization is conducted at γ-ray dosage rates of 0.13–1.0 Gy/s (13–100 rad/s) using ^{60}Co source. The rate of polymerization at 38°C is proportional to the dosage rate to the power 0.42. Gas-phase polymerization of VF with γ-ray has been studied in the range of 0.1–1.0 Gy/s (10–100 rad/s). Polymerization rate increases sharply with the increase in dosage, leading

to generation of active sites in the polymer chain and branches. Radiation polymerization of VF dissolved in solvents such as tetrachloromethane leads to chain transfer and incorporation of solvent in the polymer. VF can also be polymerized in plasma.

Graft Polymerization. The most effective method for graft polymerization of VF is radiation polymerization (80). VF has been grafted to low density polyethylene, polyisobutylene, and polyamides (85–87). The density of the graft copolymers is higher than that of the starting homopolymer. Typically, VF is brought in contact with the polymer simultaneously with irradiation.

Grafting to cellulose in the absence of solvent (87) is initiated by γ-rays by means of a ^{60}Co source. The polymer-to-monomer ratio has only a minor effect on the PVF content, which is in the range of 2–5 wt%. In the presence of solvents that cause swelling of cellulose (mercerization), the PVF content increases dramatically. At a radiation of 30 kGy (3 Mrad) in the presence of dimethylformamide, the PVF content of the graft copolymer is 26.6%; in its absence it is 4.1%.

Rot resistance of cellulose improves greatly as a result of PVF grafting (87). Some of the changes that VF grafting imparts to the polymers include a reduction in solubility in solvents, enhancement of thermal stability, increased water and oil repellency, hightened resistance to acids, and increased light stability.

Adhesion, processibility, and dyeability of PVF have been improved by grafting with other monomers (80). Styrene, methyl methacrylate, vinyl acetate, and vinylidene chloride have been grafted to PVF films by using ^{60}Co γ-rays or an electron accelerator.

Continuous Polymerization. A process for continuous polymerization of VF in aqueous medium has been described (76,78). A mixture of VF, water, and a water-soluble catalyst is stirred at 50–250°C and 15–100 MPa (150–1000 atm). A small amount of a monoolefin (C_1–C_3) is continuously introduced into the reactor to inhibit the bulk polymerization of VF to low molecular weight polmer. The water-soluble catalyst generates free radicals, which initiate the polymerization. Catalysts include ammonium persulfate, organic peroxides, and water-soluble azo initiators. In a two-stage continuous polymerization the polymer particles formed in the first stage act as nucleation sites for the second reaction zone (88).

Effect of Polymerization Variables. The polymerization variables include temperature, pressure, medium, impurities, telogen, and catalyst (initiator) (64–66).

Temperature. The polymerization has a significant effect on the molecular weight of PVF. Molecular weight generally decreases as the polymerization temperature is raised, because of a more rapid chain termination and increased branching (65,89). Initiator efficiency reaches a maximum and falls off as temperature is increased (Fig. 1).

Pressure. Polymerization of VF requires high pressures (64). The rate of polymerization and the intrinsic viscosity of the polymer increase (Fig. 2) when pressure is increased. Initiators, such as benzoyl peroxide, are generally consumed more efficiently at higher pressures. Some azo initiators do not respond to pressure in the same way.

Medium. Water is the best medium for the polymerization of VF; organic solvents have also been used. However, chain transfer to solvents leads to a sharp drop in molecular weight (65,68), and hence thermostability decreases. The PVF

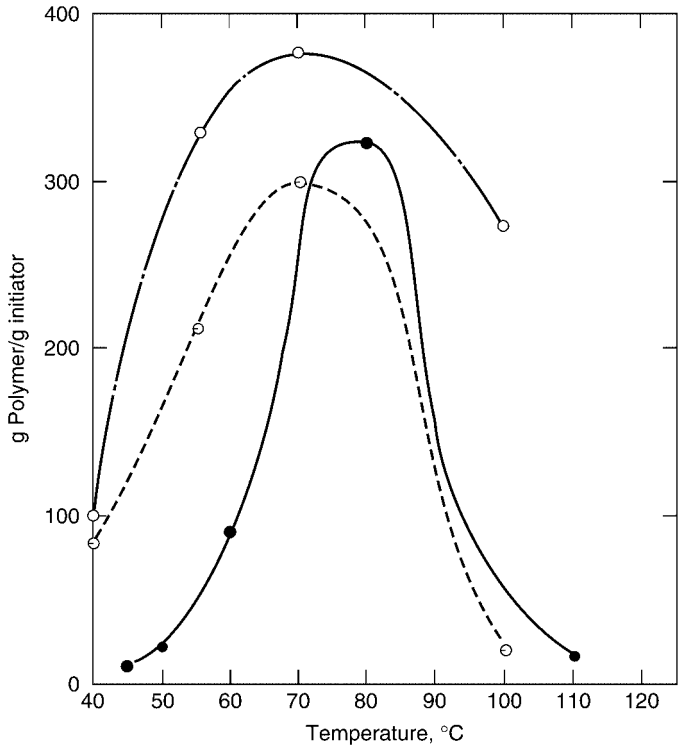

Fig. 1. Polymer yield as a function of temperature. —, 10 MPa (100 atm), 0.2% AIBN;—, 25 MPa (250 atm), 0.1% benzoyl peroxide; ——, 25 MPa (250 atm), 0.1% AIBN. From Ref. 63.

obtained is usually soluble in the solvents at the temperatures used for the polymerization reaction. A mixture of tert-butyl alcohol and water results in a high molecular weight and a high polymerization rate.

Impurities. Oxygen, acetylene, and DFE are among the impurities most likely found in VF. Oxgen up to 135 ppm appears to increase the yield, but 500 ppm inhibits the reaction slightly (65). Benzoyl peroxide at 90-MPa (900-atm) pressure is used to initiate the polymerization. At 1000-ppm acetylene content in VF, polymerization is accelerated with over 99% conversion to a highly cross-linked polymer. An increase in acetylene concentration from 0.5 to 1.0% reduced the rate by two-thirds in radiation-initiated polymerization of PVF (80). The presence of 2% acetylene reduced the yield of a low molecular weight PVF to 3%. The product was brittle and readily soluble in cyclohexane (65). VF containing up to 2.5% DFE gives a normal polymer yield; the properties of the film produced from the polymer are not affected.

Telogen. The melt viscosity of PVF can be best controlled by a chain-terminating compound (telogen), such as isopropyl alcohol or 1,3-dioxolane; toughness is not affected.

Catalysts and Initiators. The type of free-radical initiator (65) employed can have a profound effect on PVF properties, such as thermal stability and wettability.

Table 7. Melting Point and Degree of Crystallinity of Poly(vinyl fluoride) Obtained at Various Polymerization Temperatures[a,b]

Polymerization temperature, °C	Melting point, °C	Degree of crystallinity,[c] %(±2)
85	197–205	37
40	205–215	44
30	218–225	45
20	222–230	45
10	220–235	48
0	225–235	50

[a]Ref. 86.
[b]Polymerization pressure, 30 MPa (300 atm); alkylboron catalyst.
[c]From the heat of fusion (differential scanning calorimeter) and the averaged $\Delta H_u = 7.5$ kJ (1.8 kcal) per monomer unit.

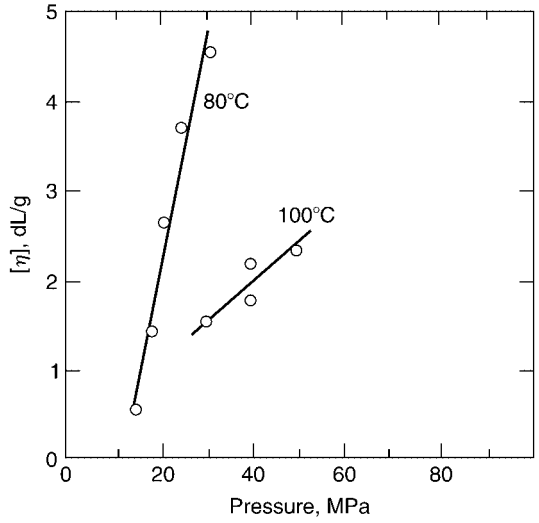

Fig. 2. Effect of polymerization pressure on intrinsic viscosity; 0.2% benzoyl peroxide initiator in aqueous medium. From Ref. 63. To convert MPa to atm, multiply by 10.

The polymer yield depends on the initiator and reaction pressure (Fig. 1). Useful water-soluble initiators include salts of inorganic peracids, organic peroxides containing hydrophilic groups, alkali metal salts of carboxylic azonitriles, and inorganic acid salts of azoamidines (76) (Table 7).

In general, polymers prepared at higher temperature tend to have low molecular weight and appear to be more branched. Increasing the initiator concentration reduces initiator efficiency and molecular weight, as evidenced by a drop in the intrinsic viscosity of the polymer.

Ziegler–Natta and Other Catalysts. Ziegler–Natta-type catalysts are used to polymerize VF. The catalysts are a mixture of transition-metal halides (titanium halides) and trialkylaluminum (triethylaluminum). Originally, olefins were polymerized by Ziegler–Natta catalysts to polymers with a high melting point, crystalline structure, and a high degree of stereoregularity

(Table 7). In an early application, VF was polymerized with a catalyst composed of diethylaluminum bromide–titanium tetrachloride–carbon tetrachloride (82). A Ziegler–Natta system based on vanadyl acetylacetonate and AlR(OR)Cl compounds gives good yields (82) at polymerization temperatures up to 50°C. A modified catalyst prepared from vanadium oxytrichloride, triisobutylaluminum, and tetrahydrofuran was found to be the most effective Ziegler–Natta system (90). However, the activity of VF with this catalyst system is much lower than that of vinyl chloride. A polymerization at low temperature and pressure utilized a triisobutyl boron catalyst activated by oxygen (82). In a similar method, oxygen was replaced by hydrogen peroxide, and polymerization was carried out in water (91). The initiator system, $AgNO_3$–tetraethyllead, is used for the polymerization of VF in dimethyl sulfoxide (69). Dimethyl sulfoxide permits the polymerization to proceed for longer periods than do other solvents by complexing of silver ions.

Copolymerization

Copolymers of VF with vinylidene fluoride [75-38-7] and tetrafluoroethylene [116-14-3] also have been prepared with this initiation system. VF tends toward alternation with tetrafluoroethylene and incorporates preferentially in copolymerization with vinylidene fluoride [see PERFLUORINATED POLYMERS, POLYTETRAFLUOROETHYLENE; VINYLIDENE FLUORIDE POLYMERS].

More recently, interpolymers of VF have been reported with tetrafluoroethylene and other highly fluorinated monomers such as hexafluoropropylene, perfluorobutylethylene, and perfluoroethylvinylether (92,93). Polymerization reaction took place in an aqueous medium using an initiator consisting of water-soluble organic azo compounds or salts inorganic peracids, examples of which include 2,2′-azobis(2-amidinopropane) dihydrochloride and ammonium persulfate. Reaction conditions were relatively mild at temperature of 60–100°C and pressure of 1–12 MPa in the absence of any surfactant.

Copolymers of VF and a wide variety of other monomers have been prepared (9,81,82,94–98). The high energy of the propagating VF radical strongly influences the course of these polymerizations. VF incorporates well with other monomers that do not produce stable free radicals, such as ethylene and vinyl acetate, but is sparingly incorporated with more stable radicals such as acrylonitrile [107-13-1] and vinyl chloride. An Alfrey-Price Q value of 0.010 ± 0.005 and an e value of 0.8 ± 0.2 have been determined (99). The low value of Q is consistent with little resonance stability and the e value is suggestive of an electron-rich monomer.

Reactivity Ratio. An extensive study covers copolymerization of various monomers with VF over a range of compositions with alkylboron or Ziegler–Natta catalysts (66). Copolymerization was carried out at 30°C in ethyl acetate or methylene chloride. Figure 3 shows the monomer–copolymer composition curves in the alkylboron-initiated copolymerization of VF with a number of monomers. The reactivity ratios given in Tables 8 and 9 indicate random arrangements of monomer units for VF–vinylidene fluoride (VF2) copolymer and formation of alternating units for VF–TFE (C_2H_4) copolymer (100).

Table 8. Reactivity Ratios in the Copolymerization of Vinyl Fluoride (M_1) at 30°C with Ziegler–Natta Catalysts[a]

Catalyst	M_2	r_1	r_2	r_1r_2
Isobutylisopropoxyaluminum chloride–vanadylbisacetylacetonate (2:1)	Vinyl chloride	0.07 ± 0.002	9 ± 1	0.63
	Vinylidene fluoride	4.2 ± 0.4	0.18 ± 0.02	0.75
	Hexafluoropropene	1.1 ± 0.05	0	0
Triisobutylaluminum–tetraisopropoxytitanium (3:1)	Hexafluoropropene	25 ± 5	0.04 ± 0.02	1.0

[a]Ref. 86.

Table 9. Reactivity Ratios in the Copolymerization of Vinyl Fluoride (M_1) at 30°C with B(i-C_4H_9)$_3$ Catalyst[a]

M_2	r_1	r_2	r_1r_2
CH_2=CH_2	0.3 ± 0.03	1.7 ± 0.1	0.51 ± 0.08
CH_2=CHCl	0.05 ± 0.005	11.0 ± 1	0.55 ± 0.10
CH_2=CF_2	5.5 ± 0.5	0.17 ± 0.03	0.93 ± 0.20
CF_2=CF_2	0.27 ± 0.03	0.05 ± 0.02	0.013 ± 0.007
CFCl=CF_2	0.18 ± 0.02	0.006 ± 0.02	0.011 ± 0.005
CF_3CF=CF_2	1.01 ± 0.01	0	0
CF_3CF=CFH (cis)	0.9 ± 0.05	0	0
cyclo-C_4F_6	3 ± 0.06	0	0
CH_2=$CHOCOCH_3$	0.16 ± 0.01	2.9 ± 0.2	0.46 ± 0.05
CH_2=CHCN	$\sim 1 \times 10^{-3}$	24 ± 2	~ 0.024

[a]Ref. 86.

Fabrication and Processing

Commercial PVF is insoluble at room temperature because of the large number of hydrogen bonds and high degree of crystallinity. Some latent solvents solvate PVF at temperatures above 100°C. PVF is converted to thin films and coatings. Processing of PVF, eg, by melt extrusion, depends on latent solvation of PVF in highly polar solvents and its subsequent coalescence. An example is plasticized melt extrusion of PVF into thin films (101). Pigments, stabilizers, plasticizers, and other additives can be incorporated in the film by dispersing them with the polymer in the latent solvent. The solvent is recovered by evaporation after extrusion. The extruded film can be biaxially oriented to varying degrees.

PVF can be applied to substrates with solvent-based or water-borne dispersions, or by powder-coating techniques. Viscosity modifiers are often needed to obtain a coatable dispersion. Dispersions can be applied by spraying, reverse roll coating, dip coating, and centrifugal casting. Other methods include casting on a continuous belt, extrusion into a hot liquid (102), and dipping a hot article into the dispersion (103).

Adherability of the film may be enhanced by its treatment with flame, electric (corona) discharge, boron trifluoride gas, activated gas plasma, dichromate sulfuric acid, and a solution of alkali metal in liquid ammonia (104–107). A

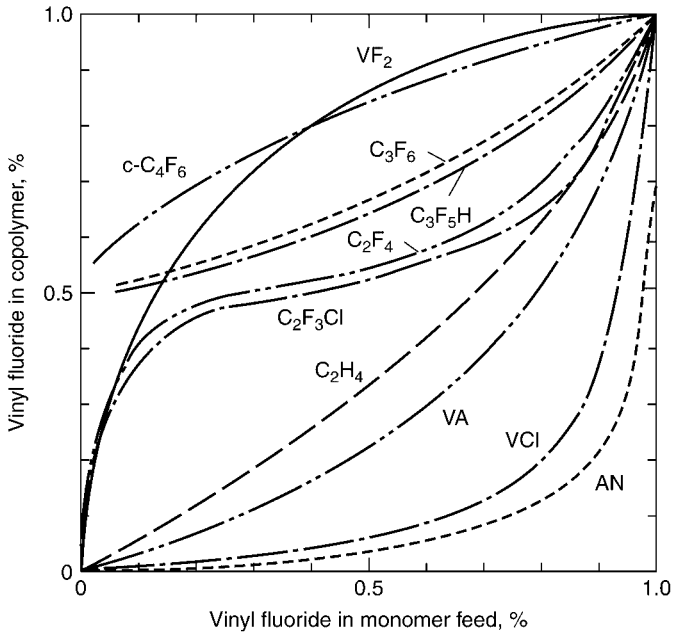

Fig. 3. Monomer–copolymer composition in the copolymerization of vinyl fluoride at 30°C with $O_2/B(i\text{-}C_4H_9)_3 = 0.5$ initiator (based on total monomer charged) and ethyl acetate as solvent. Comonomers: vinyl chloride (VCl), acrylonitrile (AN), vinyl acetate (VA), chlorotrifluoroethylene, ethylene, tetrafluoroethylene, *cis*-1-hydropentafluoropropene (C_3F_5H), hexafluoropropene (C_3F_6), hexafluorocyclobutene (c-C_4F_6), and vinylidene fluoride (VF_2). From Ref. 86.

coating of polyurethane, an alkyl polymethacrylate, or a chlorinated adhesive can be applied to PVF surfaces to enhance adhesion (102,108,109).

Economic Aspects

PVF is available from DuPont both as transparent and pigmented films and as a resin under the trademark Tedlar PVF film. Films are available in nonoriented and oriented grades in several tensile modifications and thicknesses, with either adherable or nonadherable release-grade surfaces. Nonorieted films exhibit extensive conformability to various shapes. PVF films are available in single layer and integrated multilayers where the top layer of the latter is clear and the bottom layer may possess aesthetic effects such as color, metalic appearance, or pearlescence. The 2000 prices ranged from $30 to $73 per kg. Prices for specially tailored films were significantly higher.

Health and Environment

A number of studies and reviews of the toxicological effects of exposure to VF have been conducted (110–112). A 1995 report (113) by International Agency for Research on Cancer (IARC) has evaluated the preceding data for VF and a classification of "probably carcinogenic to humans" was assigned to VF. In 1998,

American Conference of Government Industrial Hygienist (ACGIH) classified VF as an A2 carcinogen defined as "suspected human carcinogen." These classifications are based only on animal data since sufficient epidemiology data do not exist. The oncogenic potential of VF has been studied in male and female rats and mice that were administered VF via inhalation. Exposure concentrations ranged from 0 to 2500 ppm for 6 h/day, 5 days/week for up to 2 years (94). Under the conditions of this study, VF was found carcinogenic, similar to other monohaloethylenes, at concentrations of 25 ppm or greater. Mice were more susceptible than rats to the carcinogenic effects of VF and were found to metabolize VF more readily than rats or humans (114). A metabolite of VF is the suspected carcinogenic species. VF is metabolized to the suspected carcinogenic intermediate at a rate approximately one-fifth that of vinyl chloride (115–119).

VF is flammable in air between the limits of 2.6 and 22 vol%. Minimum ignition temperature for VF and air mixtures is 400°C. A small amount (<0.2%) of terpenes is added to VF so as to prevent spontaneous polymerization. The U.S. Department of Transportation has classified the inhibited VF as a flammable gas.

The self-ignition temperature of PVF film is 390°C. The limiting oxygen index (LOI) for PVF is 22.6% (120), which can be raised to 30% in antimony oxide-modified film (121). HF and a mixture of aromatic and aliphatic hydrocarbons (122) are generated from the thermal degradation of PVF. Toxicity studies, ie survival and time to incapacitation, of polymers, cellulosics (123,124), and airplane interior materials (125) expose mice to pyrolysis products and show PVF thermal degradation products to have relatively low toxicity.

Uses

The uses of PVF depend on its weatherability, strength over a wide range of temperatures, and inertness toward a wide variety of chemicals, corrosives, and staining agents. It finds wide use as a protective or decorative coating. It can be applied as a preformed film in a laminating step or from a dispersion in a coating step. It may be transparent or pigmented in a variety of colors. PVF film is laminated to cellulosics, flexible vinyls, plastics, rubbers, and resin-impregnated felt. These laminated products are applied to exterior wall panels for buildings (126,127), highway sound barriers (128), automobile trim, truck and trailer siding (129), vinyl awnings, backlit signs (130), pipe covering (131), stain-resistant wall coverings, and aircraft cabin interiors (132,133).

On metal or plastics, PVF surfaces serve as a primer coat for painting, eg, automobile parts, or where improved adhesion is desired (134). Because of its moisture impermeability and wide operating temperature range, PVF film is used to fabricate bags to contain glass-fiber mats for insulating exterior airplane walls and cargo space, and air conditioning ducts. PVF has long been used to construct bags for sampling gases (135).

Fiber-reinforced panels covered with PVF have been used for greenhouses. Transparent PVF film is used as the cover for flat-plate solar collectors (136) and photovoltaic cells (qv) (137). White PVF pigmented film is used as the bottom surface of photovoltaic cells. Nonadhering film is used as a release sheet in plastics processing, particularly in high temperature pressing of epoxy resins for circuit boards (138–140) and aerospace parts. Dispersions of PVF are coated on the exterior of steel hydraulic brake tubes and fuel lines for corrosion protection.

BIBLIOGRAPHY

"Vinyl Fluoride Polymers" in *EPST* 1st ed., Vol. 14, pp.522–540, by F. S. Cohen, Polaroid Corp. and Paul Kraft, Stauffer Chemical Co.; "Vinyl Fluoride Polymers" in *EPSE* 2nd ed., Vol. 17, pp. 468–491, by D. Brasure and S. Ebnesajjad, E. I. du Pont de Nemours & Co., Inc.

1. DuPont Techical Bulletin DP-6, E. I. du Pont de Nemours & Co., Inc., Wilmington, Del., 1969.
2. DuPont Techical Bulletin JD-39, E. I. du Pont de Nemours & Co., Inc., Wilmington, Del., 1961.
3. F. Swarts, *Bull. Clin. Sci. Acad. Roy. Belg.* **7**, 383 (1901); F. Swarts, *J. Chem. Soc. Abstr.* **82**, 129 (1902).
4. F. Swarts, *Bull. Clin. Sci. Acad. Roy. Belg.* **7**, 728 (1901).
5. U.S. Pat. 1425130 (Aug. 8, 1922), H. Plauson (to Plauson's Ltd.).
6. U.S. Pat. 2118901 (May 31, 1938), J. Soll (to I. G. Farbenindustrie AG).
7. A. V. Grossee and C. B. Linn, *J. Am. Chem. Soc.* **64**, 2289 (1942).
8. A. L. Henne, *Organic Reactions*, Vol. **2**, John Wiley & Sons, Inc., New York, 1944.
9. U.S. Pat. 2419010 (Apr. 15, 1947), D. D. Coffman and T. A. Ford (to E. I. du Pont de Nemours & Co., Inc.).
10. U.S. Pat. 2437307 (Mar. 9, 1948), L. F. Salisburg (to E. I. du Pont de Nemours & Co., Inc.).
11. U.S. Pat. 2674632 (Apr. 1, 1954), B. F. Skiles (to E. I. du Pont de Nemours & Co., Inc.).
12. U.S. Pat. 3178483 (Apr. 13, 1965), C. M. Christy and G. Teufer (to E. I. du Pont de Nemours & Co., Inc.).
13. U.S. Pat. 3607955 (Sept. 21, 1971), L. E. Gardner (to Phillips Petroleum Co.).
14. Jpn. Pat. 77 122310 (Oct. 14, 1977), T. Kuroda and T. Yamamoto (to Onoda Cement Co., Ltd.).
15. U.S. Pat. 2442993 (June 8, 1948), O. W. Cass (to E. I. du Pont de Nemours & Co., Inc.).
16. U.S. Pat. 2461523 (Feb. 15, 1949), D. D. Coffman and R. D. Cramer (to E. I. du Pont de Nemours & Co., Inc.).
17. US Pat. 5880315 (Mar. 9, 1999), V. N. M. Rao and M. A. Subramanian (to E. I. du Pont de Nemours & Co., Inc.).
18. US Pat. 6034289 (Mar. 7, 2000), F. J. Christoph, G. W. Coulston, and V. N. M. Rao, (to E. I. du Pont de Nemours & Co., Inc.).
19. U.S. Pat. 3621067 (Nov. 16, 1971), J. Hamersma (to Atlantic Richfield Co.).
20. Jpn. Pat. 46 21607 (71 21607) (June 18, 1971), B. Tatsutani and co-workers (to Electro Chemical Industrial Co., Ltd.).
21. U.S. Pat. 3642917 (Feb. 15, 1972), J. Hamersma (to Atlantic Richfield Co.).
22. Jpn. Pat. 47 11728 (72 11728) (Apr. 12, 1972), B. Tatsutani and co-workers (to Electro Chemical Industrial Co., Ltd.).
23. Jpn. Pat. 51 13123 (76 13123) (Apr. 26, 1976), B. Ryutani and co-workers (to Electro Chemical Industrial Co., Ltd.).
24. U.S. Pat. 3317619 (May 2, 1967), T. E. Hedge (to Diamond Shamrock Corp.).
25. T. S. Sirlibaev and co-workers, *Zh. Prikl. Khim.* **58**, 1666–1668 (1985).
26. Jpn. Pat. 47 11726 (72 11726), (Apr. 12, 1972), B. Tatsutani, I. Kobayashi, and K. Yamamoto (to Electro Chemical Industrial Co., Ltd.).
27. T. S. Sirlibaev, A. Akramkhodzhaev, A. A. Yul'chibaev, and K. U. Usmanov, *Synthesis of Vinyl Fluoride and 1,1-Difluoroethane from Vinyl Chloride, Deposited Document, VINITI 48575, Commonwealth of Independent States*, 1975.
28. T. S. Sirlibaev and co-workers, *Uzb. Khim. Zh.* (1), 29–31 (1980).
29. Vinyl Fluoride and Vinyl Bromide Industrial Hygiene Survey Report, Report for National Institute For Occupational Safety and Health, work performed by Tractor Jitco,

Inc., under Contract No. 210-75-0064, PB80-190150, U.S. Department of Commerce, Cincinnati, Ohio, R. E. Bales, Rept. No. C-79-111, 1978.
30. G. Natta, *Makromol. Chem.* **35**, 94 (1960).
31. M. Goerlitz and co-workers, *Angew. Makromol. Chem.* **29/30**(371), 137 (1973).
32. G. Natta, I. W. Bassi, and G. Allegra, *Atti Acad. Naz. Lincei Cl. Sci. Fis. Mat. Natur. Rend.* **31**, 350–356 (1961).
33. J. B. Lando, H. G. Olf, and A. Peterlin, *J. Polym. Sci., Part A-1* **4**, 941–951 (1966).
34. G. Caporiccio, E. Strepparola, and D. Sianesi, *Chim. Ind. (Milan)* **52**, 28–36 (1970).
35. C. W. Wilson III and E. R. Santee Jr., *J. Polym. Sci., Part C* **8**, 97–112 (1965).
36. D. Sianesi and G. Caporiccio, *J. Polym. Sci., Part A-1* **6**, 335 (1968).
37. R. E. Cais and J. M. Kometani, *Polymer* **29**, 168–172 (1988).
38. J. L. Koenig, and J. J. Mannion, *J. Polym. Sci., Part A-2* **4**, 401–414 (1966).
39. R. E. Cais and J. M. Kometani, in J. C. Randall, ed., *NMR and Macromolecules*, American Chemical Society, Washington, D.C., 1984. ACS Symposium Series. No. 247, p. 153.
40. G. Zerbi and G. Cortili, *Spectrochim. Acta* **26**, 733–739 (1970).
41. R. F. Boyer, *J. Polym. Sci., Part C* **50**, 189–242 (1975).
42. M. L. Wallach and M. A. Kabayama, *J. Polym. Sci., Part A-1* **4**, 2667–2674 (1966).
43. A. E. Tonelli, *Macromolecules* **13**, 734–741 (1980).
44. A. E. Tonelli, F. C. Schiling, and R. E. Cais, *Macromolecules* **14**, 560 (1982).
45. H. Tianbai, *Yingyong Huaxue (Chinese J. Appl. Chem.)* **2**, 15–18 (1985).
46. R. F. Boyer, and R. L. Miller, *Macromolecules* **10**, 1167–1169 (1977).
47. A. Chapira, Z. Mankowski, and N. Schmitt, *J. Polym. Sci., Part A-1* **20**, 1791–1796 (1982).
48. F. M. Fowkes and co-workers, *J. Polym. Sci., Part A-1* **22**, 547–566 (1984).
49. D. Raucher and M. Levy, *J. Polym. Sci., Part A-1* **17**, 2675–2680 (1979).
50. G. Montaudo and co-workers, *J. Polym. Sci., Part A-1* **24**, 301–316 (1986).
51. M. L. O'Shea, C. Morterra, and M. J. D. Low, *Mater. Chem. Phys.* **25**, 501 (1990).
52. B. F. Mukhiddinov and co-workers, *Dokl. Akad. Nauk SSSR*, **316**, 165–168 (1991).
53. W. E. Farneth, M. T. Aronson, and R. E. Uschold, *Macromolecules* **26**(18), 4765 (Feb. 1993).
54. Technical Information Bulletin TD-31, E. I. du Pont de Nemours & Co., Inc., Wilmington, Del., 1979.
55. Y. Rosenberg and co-workers, *J. Appl. Polym. Sci.* **45**, 783 (1992).
56. R. Timmerman and W. Greyson, *J. Appl. Polym. Sci.* **6**, 456 (1962).
57. U.S. Pat. 2953818 (Sept. 27, 1960), L. R. Bartron (to E. I. du Pont de Nemours & Co., Inc.,).
58. U.S. Pat. 3723171 (Mar. 27, 1973), O. Fuchs (to Dynamite Nobel AG).
59. U.S. Pat. 4645692 (Feb. 24, 1987), E. Vassiliou (to E. I. du Pont de Nemours & Co., Inc.,).
60. U.S. Pat. 4988540 (Jan. 29, 1991), R. F. Davis, C. G. Bragaw, and T. P. Cancannon (to E. I. du Pont de Nemours & Co., Inc.,).
61. U.S. Pat. 3139470 (June 30, 1964), R. S. Prengle and R. L. Richards Jr. (to E. I. du Pont de Nemours & Co., Inc.,).
62. F. M. C. Lin, *Chain Microstructure Studies of Poly(vinyl fluoride) by High Resolution NMR Spectroscopy*, Ph.D. Dissertation, University of Akron, 1981.
63. H. W. Starkweather, *J. Am. Chem. Soc.* **56**, 1870 (1934).
64. A. E. Newkirk, *J. Am. Chem. Soc.* **68**, 2467 (1946).
65. G. H. Kalb and co-workers, *J. Appl. Polym. Sci.* **4**, 55 (1960).
66. D. Sianesi and G. Caporiccio, *J. Polym. Sci., Part A-1* **6**, 335 (1968).
67. D. Raucher and M. Levy, *J. Polym. Sci.* **13**, 1339–1346 (1975).
68. T. S. Sirlibaev and I. Tirkashev, *Uzb. Khim. Zh.* **2**, 40–42 (1983).

69. D. Raucher and co-workers, *J. Polym. Sci.* **17**, 2825–2832 (1979).
70. Jpn. Pat. 74 027108 (July 15, 1974), H. Iwamichi and Y. Adachi (to Electro Chemical Industries Co., Ltd.).
71. U.S. Pat. 3627744 (Dec. 14, 1971), R. A. Bonsall and B. Hopkins (to Monsanto Co.).
72. Jpn. Pat. 74 028907 (July 30, 1974), S. Yashida, K. Tamaiima, and H. Kurovama (to Electro Chemical Industries Co., Ltd.).
73. V. G. Klaydin and co-workers, *Zh. Prikl. Khim.* **56**, 462–465 (1983).
74. A. K. Gafurov and co-workers, *Sb. Nauchn. Tr. Tashk. Gos. Univ. im. V. I. Lenina* **667**, 16–23 (1981).
75. U.S. Pat. 2510783 (June 6, 1950), F. L. Johnston (to E. I. du Pont de Nemours & Co., Inc.).
76. U.S. Pat. 3129207 (Apr. 14, 1964), V. E. James (to E. I. du Pont de Nemours & Co., Inc.).
77. Brit. Pat. 1161958 (Aug. 20, 1969), J. G. Frielink (to Deutsche Solvay-Werke Gesellschaft mit Beschrankter Haftung).
78. U.S. Pat. 3265678 (Aug. 9, 1966), J. L. Hecht (to E. I. du Pont de Nemours & Co., Inc.).
79. US Pat. 5229480 (Jul. 20, 1993) R. E. Uschold (to E. I. du Pont de Nemours & Co., Inc.)
80. K. U. Usmanov and co-workers, *Russ. Chem. Rev.* **46**, 462–478 1977; trans. from *Usp. Khim.* **46**, 878–906 (1977).
81. G. Natta and co-workers, *J. Polym. Sci., Part A-1* **3**, 4263 (1965).
82. D. Sianesi and G. Caporiccio, *J. Polym. Sci., Part A-1* **6**, 335 (1968).
83. A. K. Trobridge and K. R. Jennings, *Trans. Farady Soc.* **61**, 2168 (1965).
84. E. R. Sirkin and G. C. Pimentel, *J. Phys. Chem.* **88**, 1833–1840 (1984).
85. M. K. Asamov and co-workers, *Vysokomol. Soedin. Ser. A.* **28**, 1584–1588 (1986).
86. K. U. Usmanov and co-workers, *Khim. Volokna* (6), 15–17 (1979).
87. K. U. Usmanov and co-workers, *J. Polym. Sci., Part A-1* **9**, 1459–1462 (1971).
88. Brit. Pat. 1077728 (Aug. 2, 1967), J. L. Hecht and C. T. Hughes (to E. I. du Pont de Nemours & Co., Inc.).
89. A. K. Gafurov and co-workers, *Vysokomol. Soedin. Ser. B.* **20**, 383–387 (1978).
90. R. N. Haszeldine and co-workers, *Polymer* **14**, 221 (1973).
91. U.S. Pat. 3645998 (1972), Y. Likubo and co-workers (to Onoda Cement Co., Ltd.).
92. WO 98/46657, *International Patent Application* (Pub. Date Oct. 22, 1998) inventor R. E. Uschold (applicant E. I. du Pont de Nemours & Co., Inc.).
93. WO 98/46658, *International Patent Application* (Pub. Date Oct. 22, 1998) inventor R. E. Uschold (applicant E. I. du Pont de Nemours & Co., Inc.).
94. U.S. Pat. 2406717 (Aug. 27, 1946), C. A. Thomas (to Monsanto Chemical Co.).
95. U.S. Pat. 2847401 (Aug. 12, 1958), E. W. Gluesenkamp and J. D. Calfee (to Monsanto Chemical Co.).
96. U.S. Pat. 3057812 (Oct. 9, 1962), J. R. Straughan, R. Stickl Jr., and W. F. Hill Jr. (to Union Carbide Corp.).
97. F. Z. Yusupbekova and co-workers, *Uzb. Khim. Zh.* (3), 47–51 (1987).
98. R. E. Cais and J. M. Kometani, *Polymer* **29**, 168–172 (1988).
99. T. Alfrey and C. C. Price, *J. Polym. Sci.* **2**, 101 (1947).
100. D. E. Brasure, in M. Grayson, ed., *Kirk-Othmer Encyclopedia of Chemical Technology*, 3rd ed., Vol. **11**, John Wiley & Sons, Inc., New York, 1980, pp. 57–64.
101. U.S. Pat. 2953818 (Sept. 27, 1960), L. R. Bartron (to E. I. du Pont de Nemours & Co., Inc.).
102. U.S. Pat. 3723171 (Mar. 27, 1973), O. Fuchs (to Dynamite Nobel AG).
103. U.S. Pat. 4645692 (Feb. 24, 1987), E. Vassiliou (to E. I. du Pont de Nemours & Co., Inc.).

104. U.S. Pat. 3145242 (Aug. 18, 1964), W. L. Bryan (to E. I. du Pont de Nemours & Co., Inc.).
105. U.S. Pat. 3274088 (Sept. 20, 1966), L. E. Wolinski (to E. I. du Pont de Nemours & Co., Inc.).
106. U.S. Pat. 3122445 (Feb. 25, 1964), R. O. Osborn (to E. I. du Pont de Nemours & Co., Inc.).
107. C. A. L. Westerdahl and co-workers, Activated Gas Plasma Surface Treatment of Polymers for Adhesive Bonding, Part III, Technical Report 4279, Picatinny Arsenal, Dover, N.J., 1972.
108. U.S. Pat. 4215177 (July 29, 1980), A. Strassel (to Produits).
109. U.S. Pat. 3880690 (Apr. 29,1975), O. Fuchs (to Dynamite Nobel AG).
110. M. S. Bogdanffy, G. T. Makovec, and S. R. Frame, *Fund. App. Toxicol.* **26**, 223–238, 1995.
111. *Fed. Regist.* **56**, 23228 (1991).
112. G. L. Kennedy Jr., *Crit. Rev. Toxicol.* **21**(2), 149–170, 1990.
113. *IARC Monograph Series*, Vol. **63**, International Agency for Research on Cancer, 1995, pp. 467–475.
114. S. Cantoreggi and D. K. Keller, *Toxicol. Appl. Pharmacol.* **143**(1), 130–139, 1997.
115. M. E. Andersen, *Neurobehav. Toxicol. Teratol.* **3**, 383 (1981).
116. M. E. Andersen, *Drug Metab. Rev.* **13**, 799 (1982).
117. J. G. Filser and H. M. Bolt, *Arch. Toxicol.* **42**, 123 (1979).
118. H. M. Bolt, *Arbeitsmed. Sozialmed. Praventivmed*. **15**, 49 (1980).
119. H. M. Bolt, R. J. Laib, and K. P. Klein, *Arch. Toxicol.* **47**, 71 (1981).
120. C. P. Fennimore and F. J. Martin, *Combust. Flame* **10**, 135 (1966).
121. U.S. Pat. 3963672 (June 15, 1976), D. E. Brasure (to E. I. du Pont de Nemours & Co., Inc.).
122. I. N. Einhorn and co-workers, Final Report, FRC/UU-41, ETEC 75-022, NASA Contract No. NAS2-8244, National Technical Information System (NTIS), Springfield, Va., Dec. 14, 1974.
123. C. H. Hilado and co-workers, *J. Combust. Toxicol.* **3**, 157 (1976).
124. C. H. Hilado and co-workers, *J. Combust. Toxicol.* **3**, 270 (1976).
125. J. C. Spurgeon, Report No. FAA-RD-78-131, Federal Aviation Administration Contract No. 181-521-100, NTIS, Springfield, Va., Nov. 1978.
126. R. D. Leaversuch, *Mod. Plast.* **64**, 52 (July 1987).
127. V. M. Cassidy, *Mod. Met.* **41**, 36 (May 1985).
128. *Public Works* **III**, 78 (1980).
129. *DuPont Mag.* **82**, 8–11 (Mar.–Apr. 1988).
130. *DuPont Mag.* **82**, 13 (May–June 1988).
131. *Energy Managmt. Tech.* **8**, 22–23 (July–Aug. 1984).
132. R. A. Anderson and G. A. Johnson, *J. Fire Flammabil.* **8**, 364–381 (1977).
133. U.S. Pat. 5137775 (Aug. 11, 1992), S. Ebnesajjad and R. F. Davis (to E. I. du Pont de Nemours & Co., Inc.).
134. Tedlar, Du Pont Technical Bulletin TD-40, E. I. du Pont de Nemours & Co., Inc. Wilmington, Del., Feb. 1988.
135. J. C. Pau, J. E. Knoll, and M. R. Midgett, *J. Air Waste Manage. Assoc.* **41**, 1095–1097 (1991).
136. B. Baum and M. Binette, Report DOE/CS/35359-T1 (DE84011488), U.S. Department of Energy Contract No. AC04-78CS35359, NTIS, Springfield, Va., June 1983.
137. R. S. Sugimura, D. H. Otth, R. G. Ross Jr., J. C. Arnett, and G. T. Samuelson, IEEE Conference Report, IEEE, New York, Oct. 21–25, 1985.
138. G. L. Schmutz, *Circuits Mfg.* **23**, 51 (Apr. 1983).

139. J. L. Wilson, C. L. Long, D. L. Mathews, and M. L. Wilson, BDX-613-1657, U.S. Department of Energy Contract No. EY-76-C-04-0613, NTIS, Springfield, Va., Jan. 1978.
140. Jpn. Pat. 62 214939 (Jan. 21, 1987), S. Suzuki and S. Onari (to Matsushita Electric Works).
141. U.S. Pat. 2419009 (Apr 15, 1947), D. D. Coffman and T. A. Ford (to E. I. du Pont de Nemours & Co., Inc.,).

SINA EBNESAJJAD
DuPont Fluoro Products

VINYLIDENE CHLORIDE POLYMERS

Introduction

Vinylidene chloride (VDC) copolymers were among the first synthetic polymers to be commercialized. Their most valuable property is low permeability to a wide range of gases and vapors (see BARRIER POLYMERS). From the beginning in 1939, the word Saran has been used for copolymers with high VDC content, and it is still a trademark of The Dow Chemical Co. in some countries. Sometimes the names Saran and poly(vinylidene chloride) (PVDC) are used interchangeably. This can lead to confusion because, although Saran includes the homopolymer, only copolymers have commercial importance. The homopolymer, ie, PVDC, is not commercially used because it lacks the thermal stability required for processing.

The principal solution to fabrication difficulties is copolymerization. Three types of comonomers are commercially important: vinyl chloride; acrylates, including alkyl acrylates and alkyl methacrylates; and acrylonitrile. When extrusion is the method of fabrication, other solutions include formulation with plasticizers, stabilizers, and extrusion aids plus applying improved extrusion techniques. The literature on VDC copolymers through 1994 has been reviewed (1,2).

Monomer

Properties. Pure vinylidene chloride [75-35-4] (1,1-dichloroethylene) is a colorless, mobile liquid with a characteristic sweet odor. Its properties are summarized in Table 1. Vinylidene chloride is soluble in most polar and nonpolar organic solvents. Its solubility in water (0.25 wt%) is nearly independent of temperature at 16–90°C (5).

Encyclopedia of Polymer Science and Technology. Copyright John Wiley & Sons, Inc. All rights reserved.

Table 1. Properties of VDC Monomer[a,b]

Property	Value
Molecular weight	96.944
Odor	Pleasant, sweet
Appearance	Clear, liquid
Color (APHA)	0–10
Solubility of monomer in water at 25°C, wt%	0.25
Solubility of water in monomer at 25°C, wt%	0.035
Normal boiling point, °C	31.56
Freezing point, °C	−122.56
Flash point, °C	
Tag closed cup	−28
Tag open cup	−16
Flammable limits in air (ambient conditions), vol%	6.5–15.5
Autoignition temperature, °C	513[b]
Latent heat of vaporization, ΔH°_v, kJ/mol[c]	
At 25°C	26.48 ± 0.08
At normal boiling point	26.14 ± 0.08
Latent heat of fusion at freezing point, ΔH_m, J/mol[c]	6514 ± 8
Heat of polymerization at 25°C, ΔH_p, kJ/mol[c]	−75.3 ± 3.8
Heat of combustion, liquid monomer at 25°C, ΔH_c, kJ/mol[c]	1095.9
Heat of formation	
Liquid monomer at 25°C, ΔH_f, kJ/mol[c]	−25.1 ± 1.3
Gaseous monomer at 25°C, ΔH_f, kJ/mol[c]	1.26 ± 1.26
Heat capacity	
Liquid monomer at 25°C, C_p, J/(mol·K)[c]	111.27
Gaseous monomer at 25°C, C_p, J/(mol·K)[c]	67.03
Critical temperature, T_c, °C	220.8
Critical pressure, P_c, MPa[d]	5.21
Critical volume, V_c, cm^3/mol	218
Liquid density, g/cm^3	
−20°C	1.2852
0°C	1.2499
20°C	1.2137
Index of refraction, n_D	
10°C	1.43062
15°C	1.42777
20°C	1.42468
Absolute viscosity, mPa·s (=cP)	
−20°C	0.4478
0°C	0.3939
20°C	0.3302
Vapor pressure,[e] at T°C	$\log P_{kPa} = 6.1070 - 1104.29/(T = 237.697)$

[a] Refs. 3 and 4.
[b] Inhibited with methyl ether of hydroquinone.
[c] To convert J to cal, divide by 4.184.
[d] To convert MPa to atm, divide by 0.101.
[e] P measured from 6.7 to 104.7 kPa. To convert kPa to mm Hg, multiply by 7.5 (add 0.875 to the constant to convert $\log_{kPa}$ to $\log_{mmHg}$).

Manufacture. Vinylidene chloride monomer can be conveniently prepared in the laboratory by the reaction of 1,1,2-trichloroethane [79-00-5] with aqueous alkali:

$$2\ CH_2ClCHCl_2 + Ca(OH)_2 \longrightarrow 2\ CH_2{=}CCl_2 + CaCl_2 + 2\ H_2O$$

Other methods are based on bromochloroethane [25620-54-6], trichloroethyl acetate [625-24-1], tetrachloroethane [79-34-5], and catalytic cracking of trichloroethane (6). Catalytic processes produce hydrogen chloride as by-product, rather than less valuable salts, but yields of VDC have been too low for commercial use of these processes. However, good results have been reported with metal-salt catalysts (7–9).

Vinylidene chloride is prepared commercially by the dehydrochlorination of 1,1,2-trichloroethane with lime or caustic in slight excess (2–10%) (5,10). A continuous liquid-phase reaction at 98–99°C yields ~90% VDC. Caustic gives better results than lime. Vinylidene chloride is purified by washing with water, drying, and fractional distillation. It forms an azeotrope with 6 wt% methanol (11). Purification can be achieved by distillation of the azeotrope, followed by extraction of the methanol with water. An inhibitor is usually added at this point. Commercial grades contain 200 ppm of the monomethyl ether of hydroquinone (MEHQ). Many other inhibitors for the polymerization of VDC have been described in patents, but MEHQ is the one most often used. The inhibitor can be removed by distillation or by washing with 25 wt% aqueous caustic under an inert atmosphere at low temperatures.

For many polymerizations, MEHQ need not be removed; instead, polymerization initiators are added. Vinylidene chloride from which the inhibitor has been removed should be refrigerated in the dark at −10°C, under a nitrogen atmosphere, and in a nickel-lined or baked phenolic-lined storage tank. If not used within 1 day, more inhibitor should be added.

Health and Safety Factors. Vinylidene chloride is highly volatile and, when free of decomposition products, has a mild, sweet odor. Its warning properties are ordinarily inadequate to prevent excessive exposure. Inhalation of vapor presents a hazard, which is readily controlled by observance of precautions commonly taken in the chemical industry (4). A single, brief exposure to a high concentration of VDC vapor, eg, 2000 ppm, rapidly causes intoxication, which may progress to unconsciousness on prolonged exposure. The LC_{50}/4 h in rats is 6350 ppm. However, prompt and complete recovery from the anesthetic effects occurs when the exposure is for short duration. A single, prolonged exposure and repeated short-term exposures can be dangerous, even when the concentration of the vapor is too low to cause an anesthetic effect. Such exposure may produce organic injury to the kidneys and liver. For repeated exposures, the vapor concentration of VDC should be much lower. The American Conference of Governmental Industrial Hygienists threshold limit value of 5 ppm has been established to provide an adequate margin of safety.

Vinylidene chloride is hepatotoxic, but does not appear to be a carcinogen (12–17). Pharmacokinetic studies indicate that the behavior of vinyl chloride and vinylidene chloride in rats and mice is substantially different (18). No unusual health problems have been observed in workers exposed to VDC monomer over

varying periods (19). Because VDC degrades rapidly in the atmosphere, air pollution is not likely to be a problem (20). Worker exposure is the main concern. As such, personal monitoring can be done using passive dosimeters. Refer to the dosimeter supplier for collection and analysis details.

The liquid is irritating to the skin after only a few minutes of contact. The inhibitor MEHQ may be partly responsible for this irritation. Inhibited VDC is moderately irritating to the eyes. Contact causes pain and conjunctival irritation, and possibly some transient corneal injury and iritis. Permanent damage, however, is not likely.

Peroxide Formation. In the presence of air or oxygen, uninhibited VDC forms a violently explosive complex peroxide at temperatures as low as 40°C. Decomposition products of VDC products are formaldehyde, phosgene, and hydrochloric acid. A sharp, acrid odor indicates oxygen exposure and probable presence of peroxides. This is confirmed by the liberation of iodine from a slightly acidified dilute potassium iodide solution. Formation of insoluble polymer may also indicate peroxide formation. The peroxide adsorbs on the precipitated polymer, and separation of the polymer may result in an explosive composition. Any dry composition containing more than ~15 wt% peroxide detonates from a slight mechanical shock or from heat. Vinylidene chloride that contains peroxides may be purified by being washed several times, either with 10 wt% aqueous sodium hydroxide solution at 25°C or with a fresh aqueous solution of 5 wt% sodium bisulfite. Residues in vessels containing VDC should be handled with great care, and the peroxides should be destroyed with water at room temperature.

Copper, aluminum, and their alloys should not be used in handling VDC. Copper can react with acetylenic impurities to form copper acetylides, whereas aluminum can react with VDC to form aluminum chloralkyls. Both compounds are extremely reactive and potentially hazardous.

Polymerization

Vinylidene chloride polymerizes by both ionic and free-radical reactions. Processes based on the latter are far more common (21). Vinylidene chloride is of average reactivity when compared with other unsaturated monomers. The chlorine substituents stabilize radicals in the intermediate state of an addition reaction. Because they are also strongly electron-withdrawing, they polarize the double bond, making it susceptible to anionic attack. For the same reason, a carbocation intermediate is not favored.

The 1,1-disubstitution of chlorine atoms causes steric interactions in the polymer, as is evident from the heat of polymerization (see Table 1) (22). When corrected for the heat of fusion, the heat of polymerization is significantly less than the theoretical value of −83.7 kJ/mol (−20 kcal/mol) for the process of converting a double bond to two single bonds. The steric strain apparently is neither important in the addition step because VDC polymerizes easily, nor is it sufficient to favor depolymerization. The estimated ceiling temperature for PVDC is about 400°C.

Homopolymerization. The free-radical polymerization of VDC has been carried out by solution, slurry, suspension, and emulsion methods. Solution polymerization in a medium that dissolves both monomer and polymer has been

investigated (23). The kinetic measurements lead to activation energies and frequency factors in the normal range for free-radical polymerizations of olefinic monomers. The kinetic behavior of VDC is abnormal when the polymerization is heterogeneous (24). Slurry polymerizations are usually used only in the laboratory. They can be carried out in bulk or in common solvents, eg, benzene. Poly(vinylidene chloride) is insoluble in these media and separates from the liquid phase as a crystalline powder. The heterogeneity of the reaction makes stirring and heat transfer difficult; consequently, these reactions cannot be easily controlled on a large scale. Aqueous emulsion or suspension reactions are preferred for large-scale operations. Slurry reactions are usually initiated by the thermal decomposition of organic peroxides or azo compounds. Purely thermal initiation can occur, but rates are very low (25).

Bulk Polymerization. The spontaneous polymerization of VDC, so often observed when the monomer is stored at room temperature, is caused by peroxides formed from the reaction of VDC with oxygen. Very pure monomer does not polymerize under these conditions. Irradiation by either uv or γ rays (24,26) also induces polymerization of VDC.

The heterogeneous nature of the bulk polymerization of VDC is apparent from the rapid development of turbidity in the reaction medium following initiation. The turbidity results from the presence of minute PVDC crystals. As the reaction progresses, the crystalline phase grows and the liquid phase diminishes. Eventually, a point is reached where the liquid slurry solidifies into a solid mass. A typical conversion–time curve is shown in Figure 1 for a mass polymerization

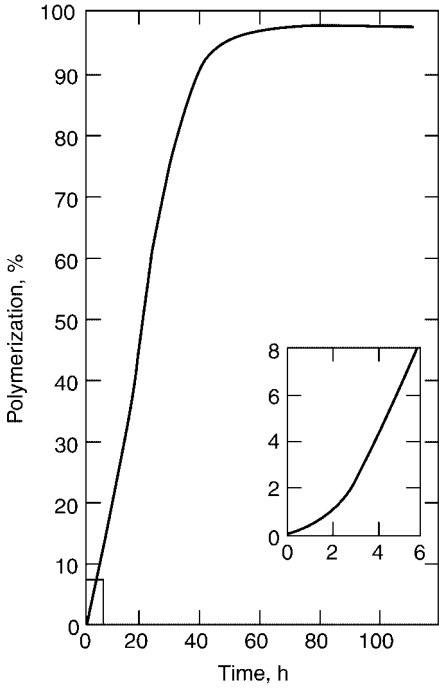

Fig. 1. Bulk polymerization of VDC at 45°C, with 0.5 wt% benzoyl peroxide as initiator (27).

catalyzed by benzoyl peroxide. The first stage of the reaction is characterized by rapidly increasing rate, which levels off in the second stage to a fairly constant value. This is often called the steady-state region. Throughout the first two stages, monomer concentration remains constant because the polymer separates into another phase. In the third stage, there is a gradual decrease in rate to zero as the monomer supply is depleted. Because the mass solidifies while monomer is still present (usually at conversions below 20%), further polymerization generates void space. The final solid, therefore, is opaque and quite porous. A similar pattern of behavior is observed when VDC is polymerized in solvents, eg, benzene, that do not dissolve or swell the polymer. In this case, however, the reaction mixture may not solidify if the monomer concentration is low.

Heterogeneous polymerization is characteristic of a number of monomers, including vinyl chloride and acrylonitrile. A completely satisfactory mechanism for these reactions has not been determined. This is true for VDC also. Earlier studies have not been broad enough to elucidate the mechanism (24,28,29). Morphologies of as-polymerized poly(vinyl chloride) (PVC) and polyacrylonitrile (PAN) are similar, suggesting a similar mechanism.

The morphology of as-polymerized PVDC is quite different (29). Nearly spherical aggregates form in the PVC and PAN systems, whereas anisotropic growth takes place in the PVDC case. The difference in morphology may be a consequence of the relative rates of polymerization and crystallization. Poly(vinylidene chloride) is unique because polymerization and crystallization probably occur nearly simultaneously. It has been reported that the average lifetime of a growing radical (τ_s) is between 0.1 and 10 s (30). The half-time ($t_{1/2}$) for crystallization of PVDC copolymers in monomer was measured to be about 1 s at 60°C and about 0.01 s at 90°C (31). This information is important for developing an understanding of a mechanism that includes a contribution from a surface reaction which has the potential for autoacceleration.

Emulsion Polymerization. Emulsion and suspension reactions are doubly heterogeneous; the polymer is insoluble in the monomer and both are insoluble in water. Suspension reactions are similar in behavior to slurry reactions. Oil-soluble initiators are used, and so the monomer–polymer droplet is like a small mass reaction. Emulsion polymerizations are more complex. Because the monomer is insoluble in the polymer particle, the simple Smith–Ewart theory does not apply (32).

A kinetic model for the particle growth stage for continuous-addition emulsion polymerization has been proposed (33). Below the monomer saturation point, the steady-state rate of polymerization, R_p, depends on the rate of monomer addition, R_a, according to the following reciprocal relationship:

$$\frac{1}{R_p} = \frac{1}{K} + \frac{1}{R_a}$$

where K depends on the number of particles and the propagation rate constant. A later study explored the kinetics of emulsion polymerization of nonswelling and swellable latex particles to define the locus of polymerization (34). There are no significant differences between the behavior of swelling and nonswelling emulsion particles and neither follows Smith–Ewart kinetics. The results indicate strongly that polymerization takes place at the particle–water interface or in a surface layer on the polymer particle.

Redox initiator systems are normally used in the emulsion polymerization of VDC to develop high rates at low temperatures. Reactions must be carried out below ~80°C to prevent degradation of the polymer. Poly(vinylidene chloride) in emulsion is also attacked by aqueous base. Therefore, reactions should be carried out at low pH.

Ionic Mechanisms. The instability of PVDC is one of the reasons why ionic initiation of VDC polymerization has not been used extensively. Many of the common initiators are sufficiently basic so as to promote E2 elimination of hydrogen chloride as the polymer is being formed. For example, butyllithium polymerizes VDC by an anionic mechanism, but the product is a low molecular weight, discolored polymer having a low chlorine content (35). Cationic polymerization of VDC seems unlikely in view of its structure (36). Some available data, however, suggest the possibility. In the low temperature, radiation-induced copolymerization of VDC with isobutylene, reactivity ratios vary markedly with temperature, indicating a change from a free-radical mechanism (37). Coordination complex catalysts may also polymerize VDC by a nonradical mechanism. Again, this speculation is based on copolymerization studies. Poly(vinylidene chloride) telomers can be prepared by using chlorine as the initiator and chain-transfer agent (38,39). Plasma polymerization of VDC in a radio-frequency glow discharge yields cross-linked polymer, which is partially degraded (40).

Copolymerization. The importance of VDC as a monomer results from its ability to copolymerize with other vinyl monomers. Its Q value equals 0.22 and its e value equals 0.36. It most easily copolymerizes with acrylates, but it also reacts, more slowly, with other monomers, eg, styrene, that form highly resonance-stabilized radicals. Reactivity ratios (r_1 and r_2) with various monomers are listed in Table 2. Many other copolymers have been prepared from monomers for which the reactivity ratios are not known. The commercially important copolymers include those with vinyl chloride (VC), acrylonitrile (AN), or various alkyl acrylates, but many commercial polymers contain three or more components, of which VDC is the principal one. Usually one component is introduced to improve the processibility or solubility of the polymer; the others are added to modify specific use properties. Most of these compositions have been described in the patent literature, and a list of various combinations has been compiled (41). A typical terpolymer might contain 90 wt% VDC, with the remainder made up of AN and an acrylate or methacrylate monomer.

Table 2. Reactivity of VDC (r_1) with Important Monomers (r_2)[a]

Monomer	r_1	r_2
Styrene	0.14	2.0
Vinyl chloride	3.2	0.3
Acrylonitrile	0.37	0.91
Methyl acrylate	1.0	1.0
Methyl methacrylate	0.24	2.53
Vinyl acetate	6	0.1

[a]Ref. 42.

Bulk copolymerizations yielding high VDC-content copolymers are normally heterogeneous. Two of the most important pairs, VDC–VC and VDC–AN, are heterogeneous over most of the composition range. In both cases and at either composition extreme, the product separates initially in a powdery form; however, for intermediate compositions, the reaction mixture may only gel. Copolymers in this composition range are swollen but not completely dissolved by the monomer mixture at normal polymerization temperatures. Copolymers containing more than 15 mol% acrylate are normally soluble in the monomers. These reactions are therefore homogeneous and, if carried to completion, yield clear, solid castings of the copolymer. Most copolymerizations can be carried out in solution because of the greater solubility of the copolymers in common solvents.

During copolymerization, one monomer may add to the copolymer more rapidly than the other. Except for the unusual case of equal reactivity ratios, batch reactions carried to completion yield polymers of broad composition distribution. More often than not, this is an undesirable result.

Vinylidene chloride copolymerizes randomly with methyl acrylate and nearly so with other acrylates. Very severe composition drift occurs, however, in copolymerizations with vinyl chloride or methacrylates. Several methods have been developed to produce homogeneous copolymers regardless of the reactivity ratio (42). These methods are applicable mainly to emulsion and suspension processes where adequate stirring can be maintained. Copolymerization rates of VDC with small amounts of a second monomer are normally lower than its rate of homopolymerization. The kinetics of the copolymerization of VDC and VC has been studied (43–46).

Studies of the copolymerization of VDC with methyl acrylate (MA) over a composition range of 0–16 wt% showed that near the intermediate composition (8 wt%), the polymerization rates nearly followed normal solution polymerization kinetics (47). However, at the two extremes (0 and 16 wt% MA), copolymerization showed significant autoacceleration. The observations are important because they show the significant complexities in these copolymerizations. The autoacceleration for the homopolymerization, ie, 0 wt% MA, is probably the result of a surface polymerization phenomenon. On the other hand, the autoacceleration for the 16 wt% MA copolymerization could be the result of Trommsdorff and Norrish-Smith effects.

Copolymers of VDC can also be prepared by methods other than conventional free-radical polymerization. Copolymers have been formed by irradiation and with various organometallic and coordination complex catalysts (26,41,48–51). Graft copolymers have also been described (52–56).

Polymer Structure and Properties

Chain Structure. The chemical composition of PVDC has been confirmed by various techniques, including elemental analysis, x-ray diffraction analysis, degradation studies, and infrared (ir), Raman, and nuclear magnetic resonance (nmr) spectroscopy. The polymer chain is made up of VDC units added head-to-tail:

$$—CH_2CCl_2—CH_2CCl_2—CH_2CCl_2—$$

Because the repeat unit is symmetrical, no possibility exists for stereoisomerism. Variations in structure can occur only by head-to-head addition, branching, or degradation reactions that do not cause chain scission, including such reactions as thermal dehydrochlorination, which creates double bonds in the structure to give, for example, $-CH_2CCl_2CH_2{=}CClCH_2CCl_2-$ and a variety of ill-defined oxidation and hydrolysis reactions that generate carbonyl groups.

The ir spectra of PVDC often show traces of unsaturation and carbonyl groups. The slightly yellow tinge of many of these polymers comes from the same source; the pure polymer is colorless. Elemental analyses for chlorine are normally slightly lower than the theoretical value of 73.2%.

The high crystallinity of PVDC indicates that no significant amounts of head-to-head addition or branching can be present. This has been confirmed by nmr spectra (57). Studies of well-characterized oligomers having degrees of polymerization (DP) of 2–10 offer further nmr evidence (38), ie, a single peak from the methylene hydrogens. Either branching or another mode of addition would produce nonequivalent hydrogens and a more complicated spectrum. However, nmr cannot detect small amounts of such structures. The ir and Raman spectra can also be interpreted in terms of the simple head-to-tail structure (58,59).

Molecular weights of PVDC can be determined directly by dilute solution measurements in good solvents (60). Viscosity studies indicate that polymers having DP from 100 to more than 10,000 are easily obtained. Dimers and polymers having DP < 100 can be prepared by special procedures (38). Copolymers can be more easily studied because of their solubility in common solvents. Gel-permeation chromatography studies indicate that molecular weight distributions are typical of vinyl copolymers.

Crystal Structure. The crystal structure of PVDC is fairly well established. Several unit cells have been proposed (61). The unit cell contains four monomer units with two monomer units per repeat distance. The calculated density, 1.96 g/cm^3, is higher than the experimental values, which are 1.80–1.94 g/cm^3 at 25°C, depending on the sample. This is typically the case with crystalline polymers because samples of 100% crystallinity usually cannot be obtained. A direct calculation of the polymer density from volume changes during polymerization yields a value of 1.97 g/cm^3 (62). If this value is correct, the unit cell densities may be low.

The repeat distance along the chain axis (0.468 nm) is significantly less than that calculated for a planar zigzag structure. Therefore, the polymer must be in some other conformation (63–65). Based on ir and Raman studies of PVDC single crystals and normal vibration analysis, the best conformation appears to be $\theta_\phi\theta_{\phi'}$, where the skeletal angle θ is 120°, and the torsional angle $\phi(\phi'$ of opposite sign) is 32.5°. This conformation is in agreement with theoretical predictions (66).

The melting temperature T_m of PVDC is independent of molecular weight above DP = 100. However, as shown in Figure 2, it drops sharply at lower molecular weights. Below the hexamer, the products are noncrystalline liquids.

The properties of PVDC (Table 3) are usually modified by copolymerization. Copolymers of high VDC content have lower melting temperatures than PVDC. Copolymers containing more than ~15 mol% acrylate or methacrylate are amorphous. Substantially more AN (25%) or VC (45%) is required to destroy crystallinity completely.

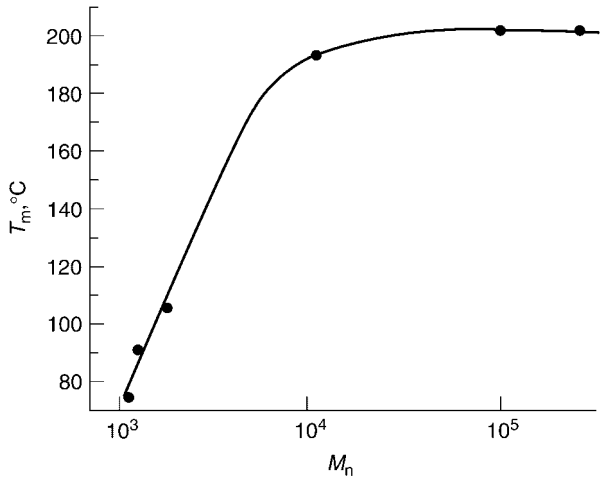

Fig. 2. Crystalline melting temperatures of PVDC (38).

The effect of different types of comonomers on T_m varies. VDC–MA copolymers more closely obey Flory's melting-point depression theory than do copolymers with VC or AN. Studies have shown that for the copolymers of VDC with MA, Flory's theory needs modification to include both lamellar thickness and surface free energy (67). The VDC–VC and VDC–AN copolymers typically have severe composition drift; therefore most of the comonomer units do not belong to crystallizing chains. Hence, they neither enter the crystal as defects nor cause lamellar thickness to decrease, and so the depression of the melting temperature is less than expected.

The glass-transition temperature T_g, of VDC copolymers has been studied extensively (68,69). The effect of various comonomers on the T_g is shown in Figure 3. In every case, T_g increases with the comonomer content at low comonomer levels, even in cases where the T_g of the other homopolymer is lower. The phenomenon has been observed in several other copolymer systems as well (71). In these cases, a maximum T_g is observed at intermediate compositions. In others, where the T_g of the other homopolymer is much higher than the T_g of

Table 3. Properties of PVDC

Property	Best value	Reported values
T_m, °C	202	198–205
T_g, °C	−17	−19 to −11
Transition between T_m and T_g, °C	80	
Density at 25°C, g/cm^3		
Amorphous	1.775	1.67–1.775
Unit cell	1.96	1.949–1.96
Crystalline		1.80–1.97
Refractive index (crystalline), n_D	1.63	
Heat of fusion, ΔH_m, J/mol[a]	6275	4600–7950

[a]To convert J to cal, divide by 4.184.

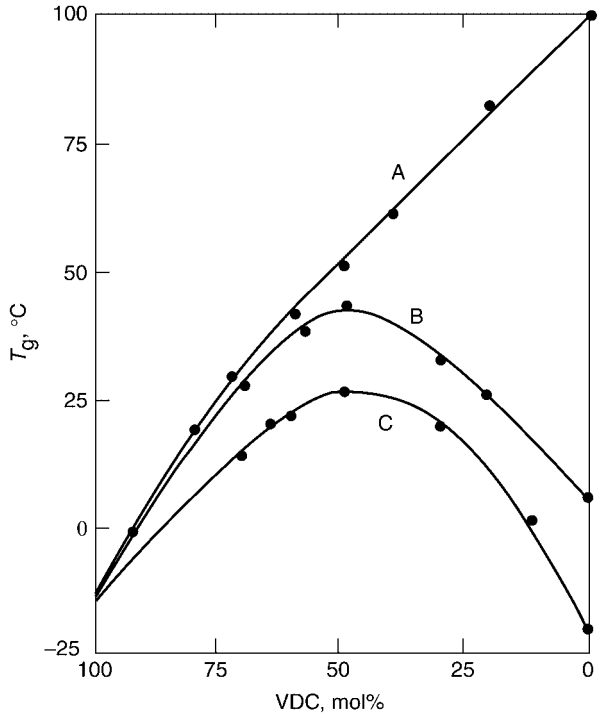

Fig. 3. Effect of comonomer structure on the glass-transition temperature of VDC copolymers (71), where A represents AN; B, MA; and C, EA.

PVDC, the glass-transition temperatures of the copolymers increase over the entire composition range. The T_g increases most rapidly at low AN levels but changes the slowest at low VC levels. This suggests that polar interactions affect the former, but the increase in T_g in the VDC–VC copolymers may simply result from loss of chain symmetry. Because of these effects, the temperature range in which copolymers can crystallize is drastically narrowed. Crystallization induction times are prolonged, and subsequent crystallization takes place at a low rate over a long period of time. Plasticization, which lowers T_g, decreases crystallization induction times significantly. Copolymers having lower glass-transition temperatures also tend to crystallize more rapidly (72).

Crystallization curves have been determined for 10 mol% acrylate copolymers of varying side-chain length. Among the acrylate copolymers, the butyl acrylate copolymer has a T_g of 8°C; the octyl acrylate, −3°C; and the octadecyl acrylate, −16°C. The rates of crystallization of these copolymers are inversely related to the glass-transition temperatures. Apparently, the long alkyl side chains act as internal plasticizers, lowering the melt viscosity of the copolymer even though the acrylate group acts to stiffen the backbone.

The maximum rates of crystallization of the more common crystalline copolymers occur at 80–120°C. In many cases, these copolymers have broad composition distributions containing both fractions of high VDC content that crystallize rapidly and other fractions that do not crystallize at all. Poly(vinylidene chloride)

probably crystallizes at a maximum rate at 140–150°C, but the process is difficult to follow because of severe polymer degradation. The copolymers may remain amorphous for a considerable period of time if quenched to room temperature. The induction time before the onset of crystallization depends on both the type and amount of comonomer; PVDC crystallizes within minutes at 25°C.

Recrystallization of a copolymer having 15 wt% VC has been found to be nucleated by material that survives the melting process plus new nuclei (72). The maximum crystallization rate occurred at 100°C; the maximum nucleation rate at 10°C. Attempts to melt all the polymer led to degradation that interfered with recrystallization.

Orientation or mechanical working accelerates crystallization has a pronounced effect on morphology. Crystals of uniaxially oriented filaments are oriented along the fiber axis (61). The long period (lamellar thickness), as determined by small-angle x-ray scattering, is 7.6 nm and decreases with comonomer content. The fiber is 43% crystalline and has a melting temperature of 195°C and an average crystal thickness of 4.5 nm. The crystal size is not greatly affected by comonomer content, but both crystallinity and melting temperature decrease with increasing comonomer.

Copolymerization also affects morphology under other crystallization conditions. Copolymers in the form of cast or molded sheets are much more transparent because of the small spherulite size. In extreme cases, crystallinity cannot be detected optically, but its effect on mechanical properties is pronounced. Before crystallization, films are soft and rubbery, with low modulus and high elongation. After crystallization, they are leathery and tough, with higher modulus and lower elongation.

Copolymers of VDC and MA have been studied by x-ray techniques (73). For example, the long period (lamellar thickness) for an 8.5 wt% MA copolymer was found to be 9.2 nm by small-angle x-ray scattering. The unit cell is monoclinic, with $a = 0.686$ and $c = 1.247$ nm by wide-angle x-ray scattering.

Significant amounts of comonomer also reduce the ability of the polymer to form lamellar crystals from solution. In some cases, the polymer merely gels the solution as it precipitates rather than forming distinct crystals. At somewhat higher VDC content, it may precipitate in the form of aggregated, ill-defined particles and clusters.

Morphology and Transitions. The highly crystalline particles of PVDC precipitated during polymerization are aggregates of thin lamellar crystals (74). The substructures are 5–10 nm thick and 100 or more times larger in other dimensions. In some respects, they resemble the lamellar crystals grown from dilute solution (75–77). The single crystals are better characterized than the as-polymerized particles. They are highly branched, with branching angles of 65–70°; the angle appears to be associated with a twin plane in the crystal (78).

Melting temperatures of as-polymerized powders are high, ie, 198–205°C as measured by differential thermal analysis (dta) or hot-stage microscopy (74). Two peaks are usually observed in dta curves: a small lower temperature peak and the main melting peak. The small peak seems to be related to polymer crystallized by precipitation rather than during polymerization.

As-polymerized PVDC does not have a well-defined T_g because of its high crystallinity. However, a sample can be melted at 210°C and quenched rapidly to

an amorphous state at $< -20^{\circ}C$. The amorphous polymer has a glass-transition temperature of $-17^{\circ}C$ as shown by dilatometry (68). Glass-transition temperature values of -19 to $-11^{\circ}C$, depending on both method of measurement and sample preparation, have been determined.

Once melted, PVDC does not regain its as-polymerized morphology when subsequently crystallized. The polymer recrystallizes in a spherulitic habit. Spherulites between crossed polarizing plates show the usual Maltese cross and are positively birefringent. The size and number of spherulites can be controlled. Quenching and low-temperature annealing generate many small nuclei that, on heating, grow rapidly into small spherulites. Slow crystallization at higher temperatures produces fewer but much larger spherulites. The melting temperature and degree of crystallinity of recrystallized PVDC also depend on crystallization conditions. The melting temperature increases with crystallization temperature, but the as-polymerized value cannot be achieved. There is no reason to believe that even these values indicate the true melting point of PVDC; it may be as high as $220^{\circ}C$. Slow, high temperature recrystallization and annealing experiments are not feasible because of the thermal instability of the polymer (79). Other transitions in PVDC have been observed by dynamic mechanical methods.

Solubility and Solution Properties. Poly(vinylidene chloride), like many high melting polymers, does not dissolve in most common solvents at ambient temperatures. Copolymers, particularly those of low crystallinity, are much more soluble. However, one of the outstanding characteristics of VDC polymers is resistance to a wide range of solvents and chemical reagents. The insolubility of PVDC results less from its polarity than from its high melting temperature. It dissolves readily in a wide variety of solvents above $130^{\circ}C$ (79). However, it should be noted that significant degradation accompanies dissolution of the polymer in polar, aprotic solvents at these temperatures.

The polarity of the polymer is important only in mixtures having specific polar aprotic solvents. Many solvents of this general class solvate PVDC strongly enough to depress the melting temperature by more than $100^{\circ}C$. Solubility is normally correlated with cohesive energy densities or solubility parameters. For PVDC, a value of 20 ± 0.6 $(J/cm^3)^{1/2}$ [10 ± 0.3 $(cal/cm^3)^{1/2}$] has been estimated from solubility studies in nonpolar solvents. The value calculated from Small's relationship is 20.96 $(J/cm^3)^{1/2}$ [10.25 $(cal/cm^3)^{1/2}$]. The use of the solubility parameter scheme for polar crystalline polymers such as PVDC has limited value. A typical nonpolar solvent of matching solubility parameter is tetrahydronaphthalene. The lowest temperature at which PVDC dissolves in this solvent is $140^{\circ}C$. Specific solvents, however, dissolve PVDC at much lower temperatures. A list of good solvents is given in Table 4. The relative solvent activity is characterized by the temperature at which a 1 wt% mixture of polymer in solvent becomes homogeneous when heated rapidly.

Poly(vinylidene chloride) also dissolves readily in certain solvent mixtures (80). One component must be a sulfoxide or *N*,*N*-dialkylamide. Effective cosolvents are less polar and have cyclic structures. They include aliphatic and aromatic hydrocarbons, ethers, sulfides, and ketones. Acidic or hydrogen-bonding solvents have an opposite effect, rendering the polar aprotic component less effective. Both hydrocarbons and strong hydrogen-bonding solvents are nonsolvents for PVDC.

Table 4. Solvents for PVDC[a]

Solvents	T,[b] °C
Nonpolar	
1,3-Dibromopropane	126
Bromobenzene	129
1-Chloronaphthalene	134
2-Methylnaphthalene	134
o-Dichlorobenzene	135
Polar aprotic	
Hexamethylphosphoramide	−7.2
Tetramethylene sulfoxide	28
N-Acetylpiperidine	34
N-Methylpyrrolidinone	42
N-Formylhexamethyleneimine	44
Trimethylene sulfide	74
N-*n*-Butylpyrrolidinone	75
Diisopropyl sulfoxide	79
N-Formylpiperidine	80
N-Acetylpyrrolidinone	86
Tetrahydrothiophene	87
N,*N*-Dimethylacetamide	87
Cyclooctanone	90
Cycloheptanone	96
Di-*n*-butyl sulfoxide	98

[a]Ref. 79.
[b]Temperature at which a 1 wt% mixture of polymer in solvent becomes homogeneous.

As-polymerized PVDC is not in its most stable state; annealing and recrystallization can raise the temperature at which it dissolves (76). Low crystallinity polymers dissolve at a lower temperature, forming metastable solutions. However, on standing at the dissolving temperature, they gel or become turbid, indicating recrystallization into a more stable form.

Copolymers having enough VDC content to be quite crystalline behave much like PVDC. They are more soluble, however, because of their lower melting temperatures. The solubility of amorphous copolymers is much higher. The selection of solvents in either case varies somewhat with the type of comonomer. Some of the more common types are listed in Table 5. Solvents that dissolve PVDC also dissolve the copolymers at lower temperatures. The identification of solvents that dissolve PVDC at low temperatures makes possible the study of dilute solution properties. Both light-scattering and intrinsic-viscosity studies have been reported (60). Intrinsic viscosity–molecular weight relationships for the three solvents investigated ($[\eta]$ in dL/g) are

(1) $[\eta] = 1.31 \times 10^{-4} M_\omega^{0.69}$ N-Methylpyrrolidinone (MP)
(2) $[\eta] = 1.39 \times 10^{-4} M_\omega^{0.69}$ Tetramethylene sulfoxide (TMSO)
(3) $[\eta] = 2.58 \times 10^{-4} M_\omega^{0.65}$ Hexamethylphosphoramide (HMPA).

Table 5. Common Solvents for VDC Copolymers

Solvents	Copolymer type	Temperature, °C
Tetrahydrofuran	All	<60
2-Butanone	Low crystallinity	<80
1,4-Dioxane	All	50–100
Cyclohexanone	All	50–100
Cyclopentanone	All	50–100
Ethyl acetate	Low crystallinity	<80
Chlorobenzene	All	100–130
Dichlorobenzene	All	100–140
Dimethylformamide	High acrylonitrile	<100

The relative solvent power (HMPA > TMSO > MP) agrees with solution-temperature measurements. The characteristic ratio C_∞ is about 8 ± 1, which is slightly larger than that of a similar polymer, polyisobutylene.

The dilute solution properties of copolymers are similar to those of the homopolymer. The intrinsic viscosity–molecular weight relationship for a VDC–AN copolymer (9 wt% AN) is $[\eta] = 1.06 \times 10^{-4} M_\omega^{0.72}$ (81). The characteristic ratio is 8.8 for this copolymer.

An extensive investigation of the dilute solution properties of several acrylate copolymers has been reported (78). The behavior is typical of flexible-backbone vinyl polymers. The length of the acrylate ester side chain has little effect on properties.

Intrinsic viscosity–molecular weight relationships have been obtained for copolymers in methyl ethyl ketone. The value for a 15 wt% ethyl acrylate (EA) copolymer is $[\eta] = 2.88 \times 10^{-4} M_\omega^{0.6}$.

Earlier work characterized the molecular weights of PVDC and VDC copolymers by using the absolute viscosity of a 2 wt% solution in *o*-dichlorobenzene at 140°C. The exact correlation between this viscosity value and molecular weight is not known. Gel-permeation chromatography is the preferred method for characterizing molecular weight; studies of copolymers have been reported (82,83).

Mechanical Properties. Because PVDC is difficult to fabricate into suitable test specimens, very few direct measurements of its mechanical properties have been made. In many cases, however, the properties of copolymers have been studied as functions of composition, and the properties of PVDC can be estimated by extrapolation. Some characteristic properties of high VDC content, unplasticized copolymers are listed in Table 6. The performance of a given specimen is sensitive to morphology, including the amount and kind of crystallinity, as well as orientation. Tensile strength increases with crystallinity, whereas toughness and elongation decrease. Orientation, however, improves all three properties. The effect of stretch ratio applied during orientation on properties of VDC–VC monofilaments is shown in Table 7.

The dynamic mechanical properties of VDC–VC copolymers have been studied in detail. The incorporation of VC units in the polymer results in a drop in dynamic modulus because of the reduction in crystallinity. However, the glass-transition temperature is raised; therefore, the softening effect observed at room

Table 6. Mechanical Properties of High VDC Content Copolymers

Property	Range
Tensile strength, MPa[a]	
Unoriented	34.5–69.0
Oriented	207–414
Elongation, %	
Unoriented	10–20
Oriented	15–40
Softening range (heat distortion), °C	100–150
Flow temperature, °C	>185
Brittle temperature, °C	−10 to 10
Impact strength, J/m[b]	26.7–53.4

[a]To convert MPa to psi, multiply by 145.
[b]To convert J/m to ft·lbf/in., divide by 53.38 (see ASTM D256).

temperature is accompanied by increased brittleness at lower temperatures. These copolymers are normally plasticized in order to avoid this. Small amounts of plasticizer (2–10 wt%) depress T_g significantly without loss of strength at room temperature. At higher levels of VC, the T_g of the copolymer is above room temperature and the modulus rises again. A minimum in modulus or maximum in softness is usually observed in copolymers in which T_g is above room temperature. A thermomechanical analysis of VDC–AN and VDC–MMA (methyl methacrylate) copolymer systems shows a minimum in softening point at 79.4 and 68.1 mol% VDC, respectively (84).

In cases where the copolymers have substantially lower glass-transition temperatures, the modulus decreases with increasing comonomer content. This results from a drop in crystallinity and glass-transition temperature. The loss in modulus in these systems is therefore accompanied by an improvement in low temperature performance. However, at low acrylate levels (<10 wt%), T_g increases with comonomer content. The brittle points in this range may therefore be higher than that of PVDC.

Table 7. Effect of Stretch Ratio on Tensile Strength and Elongation of a VDC–VC Copolymer[a,b]

Stretch ratio	Tensile strength, MPa[c]	Elongation, %
2.50:1	235	23.2
2.75:1	234	21.7
3.00:1	303	26.3
3.25:1	268	33.1
3.50:1	316	19.2
3.75:1	330	21.8
4.00:1	320	19.7
4.19:1	314	16.2

[a]Ref. 84.
[b]Average of five determinations, using the Instron test at 5 cm/min.
[c]To convert MPa to psi, multiply by 145.

The long side chains of the acrylate ester group can apparently act as internal plasticizers. Substitution of a carboxyl group on the polymer chain increases brittleness. A more polar substituent, eg, an *N*-alkylamide group, is even less desirable. Copolymers of VDC with *N*-alkylacrylamides are more brittle than the corresponding acrylates even when the side chains are long (85). Side-chain crystallization may be a contributing factor.

Barrier Properties. Vinylidene chloride copolymers are unique in that they have low permeability to a wider range of gases and liquids than other polymers. VDC copolymers are "barrier polymers" in a broad sense. Historically, the operating definition of a barrier polymer meant having an oxygen permeability less than 1.0 (cm^3(STP)·mil)/(100 $in.^2$·day·atm) [2.0 nmol/(m·s·GPa)]. A more useful descriptor for a barrier polymer is related to the application. A barrier polymer would have a set of permeabilities for important molecules sufficiently low to satisfy the containment needs. Some polymers have low permeability to gases. Others have low permeability to water. Still other polymers have low permeability to flavor/aroma/solvent (F/A/S) molecules. However, only rarely does a single polymer have low permeability in more than one category. VDC copolymers have low permeability in all three categories (see BARRIER POLYMERS).

The good barrier properties of VDC copolymers are a consequence of crystallinity and low free volume in the amorphous phase. The symmetric nature of the VDC unit in the polymer leads to nested packing that is adequate for crystallization and that leaves very little "dead" volume in the amorphous phase. Both polyisobutylene and PVDC have unusually low permeability to water compared to their monosubstituted counterparts, polypropylene and PVC (86). The values listed in Table 8 include estimates for the completely amorphous polymers. The estimated value for highly crystalline PVDC was obtained by extrapolating data for copolymers.

The effect of copolymer composition on gas permeability is shown in Table 9. The inherent barrier in VDC copolymers can best be exploited by using films containing little or no plasticizers and as much VDC as possible. However, the permeabilities of even completely amorphous copolymers, eg, 60 wt% VDC–40 wt% AN or 50 wt% VDC–50 wt% VC, are low compared to that of other polymers. The primary reason is that the diffusion coefficients for molecules in VDC copolymers

Table 8. Comparison of the Permeabilities of Various Polymers to Water Vapor[a]

	Density, g/mL		Permeability[b]	
Polymer	Amorphous	Crystalline	Amorphous	Crystalline
Ethylene	0.85	1.00	200–220	10–40
Propylene	0.85	0.94	420	
Isobutylene	0.915	0.94	90	
Vinyl chloride	1.41	1.52	300	90–115
Vinylidene chloride	1.77	1.96	30	4–6

[a] Refs. 42,86 and 87.

[b] In g/(h·100 m^2) at 7.1 kPa (53 mm Hg) pressure differential and 39.5°C for a film 25.4 μm (1 mil) thick.

Table 9. Effect of Composition on the Permeability of Various Gases through VDC Copolymers[a]

Polymer	Gas	T, °C	P, nmol/(m·s·GPa)[b]
PVDC	O_2	25	<0.04
	N_2	25	<0.02
	CO_2	25	<0.10
90/10 VC	He	25	2.23
	H_2	25	2.54
	O_2	25	0.14
	N_2	25	0.03
	CO_2	25	0.98
	H_2S	30	0.10
85/15 VC	He	34	10
	O_2	25	0.40
	CO_2	20	2.0
70/30 VC	O_2	25	0.36
50/50 VC	O_2	25	1.2
80/20 AN	O_2	25	0.14
	N_2	25	0.02
	CO_2	25	0.35
60/40 AN	O_2	25	0.71
	N_2	25	0.09
	CO_2	25	1.6

[a]Ref. 88.
[b]To convert nmol/(m·s·GPa) to $(cm^3 \cdot cm)/(cm^2 \cdot s \cdot kPa)$, divide by 4.46×10^{12}.

are very low. This factor, together with the high crystallinity and the low solubility coefficients for many gases in VDC copolymers, results in very low permeabilities. A change from PVDC to a copolymer containing 40 wt% AN or 50 wt% VC increases the permeability 10-fold but has little effect on the solubility coefficient.

The addition of a more polar comonomer, eg, AN, increases the water vapor transmission rate more than the addition of a less polar comonomer, eg, VC, when other factors are constant. For the same reason, AN copolymers are more resistant to penetrants of low cohesive energy density. All VDC copolymers, however, are very impermeable to aliphatic hydrocarbons. Comonomers that lower T_g and increase the free volume in the amorphous phase increase permeabilities more than other comonomers. Higher acrylates are examples of this phenomenon. Plasticizers increase permeabilities for similar reasons.

The effects of plasticizers and temperature on the permeabilities of small molecules in a typical VDC copolymer have been studied thoroughly. Data for oxygen permeability are contained in Figure 4. The oxygen permeability doubles with the addition of about 1.7 phr (parts per hundred of resin) of common plasticizers or a temperature increase of about 8°C (89). The moisture (water) vapor transmission rate (MVTR or WVTR) doubles with the addition of about 3.5 phr of common plasticizers (90). The dependence of the WVTR on temperature is a little more complicated. Water vapor transmission rate is commonly reported at a constant difference in relative humidity and not at a constant partial pressure

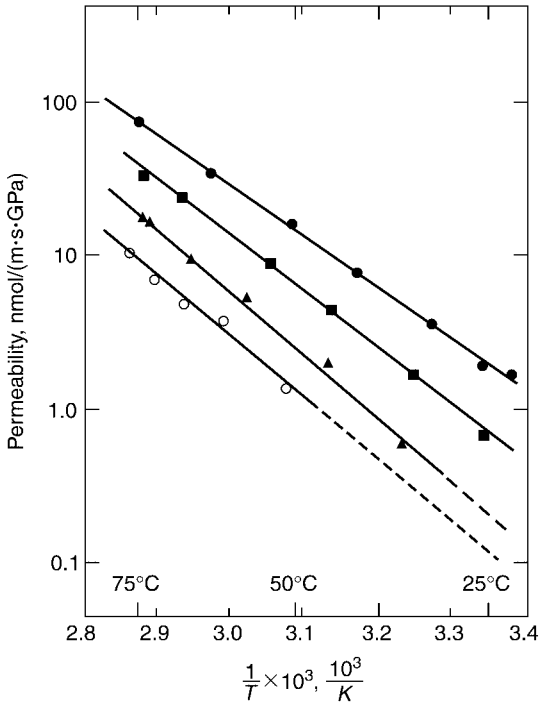

Fig. 4. Oxygen permeability in a VDC copolymer film at selected levels of plasticizer (Citroflex A-4). Plasticizer level in parts per hundred of resin (phr); ●, 7.2 phr; ■, 4.9 phr; ▲, 2.7 phr; and ○, 0.5 phr. To convert nmol/(m·s·GPa) to $(cm^3 \cdot mil)/(100\ in.^2 \cdot d \cdot atm)$, divide by 2.

difference. Hence, WVTR is a mixed term that increases with increasing temperature because both the permeability and the partial pressure at constant relative humidity increase. Carbon dioxide permeability doubles with the addition of about 1.8 phr of common plasticizers, or a temperature increase of 7°C (91).

Table 10 contains a comparison of the permeabilities of small molecules for several common polymers. The oxygen permeability is an important property for food packaging. In some cases the relative humidity is an important environmental variable. The oxygen permeability is not affected by humidity for VDC copolymers, nitrile barrier resins, poly(vinyl chloride), polystyrene, and polyolefins. The oxygen permeabilities of most nylons are increased modestly by increasing humidity, and the oxygen permeability of poly(ethylene terephthalate) is decreased modestly by increasing humidity. In contrast, the ethylene–vinyl alcohol copolymers (EVOH) are very sensitive to humidity. At low humidity, the oxygen permeabilities of EVOH are quite low. However, at the high humidity encountered in food packaging, the oxygen permeabilities of EVOH are much higher. Small changes in humidity can cause large changes in the oxygen permeabilities. Hence the data in tables need to be used carefully.

The data in Tables 11, 12, 13 describe VDC copolymers as good barriers for both gases and water. They are also good barriers to F/A/S molecules. This property for polymers has become more important since more sophisticated foods

Table 10. Barrier Properties of Polymers[a]

Polymer	Gas permeability at 23°C, nmol/(m·s·GPa)[b]			WVTR[c], nmol/(m·s)[d]
	O_2	N_2	CO_2	
High barrier vinylidene chloride copolymers	0.04–0.3	0.01–0.1	0.1–0.5	0.02–0.1
Nitrile barrier resin	1.6	—	6	1.0–1.2
Nylon-6,6; nylon-6	2–5	—	3–9	1.5–5.5
Polypropylene	300	60	1200	0.06–0.2
Poly(ethylene terephthalate)	10–18	2–4	30–50	0.4–0.7
Polylactide	90	—	375	5.1
Rigid poly(vinyl chloride)	10–40	—	40–100	0.2–1.3
High density polyethylene	300	—	1200	0.1
Low density polyethylene	500–700	200–400	2000–4000	0.2–0.4
Polystyrene	500–800	80–120	1400–3000	0.5–3.0
Ethylene vinyl alcohol				
32 mol% ethylene				
0% RH	0.02	0.002	0.09	0.9[e]
100% RH	2.3	—	—	—
44 mol% ethylene				
0% RH	0.18	0.015	0.8	0.3[e]
100% RH	1.3	—	—	—

[a] Refs. 92–94.
[b] To convert nmol/(m·s·GPa) to (cm^3·mil)/(100 $in.^2$·d·atm), divide by 2.
[c] WVTR = water vapor transmission rate at 90% RH and 38°C.
[d] To convert nmol/(m·s) to (g·mil)/(100 $in.^2$·d), multiply by 4.
[e] 40°C.

are being packaged in plastics. The permeation of F/A/S molecules differs from the permeation of small molecules in some important ways. The diffusion coefficient D for F/A/S molecules is typically 10^2–10^5 times smaller. These molecules move slower because they need to find larger openings in the polymer. The solubility coefficient S is typically 10^2–10^6 times larger. This is related to higher boiling

Table 11. Diffusion Coefficients and Solubility Coefficients of Selected Penetrants in Polymers at 75°C[a]

Penetrant	Polymer	D, m^2/s	S, kg/(m^3·Pa)
Oxygen	Poly(ethylene terephthalate)	3×10^{-13}	9.8×10^{-7}
Oxygen	High density polyethylene	1.7×10^{-11}	6.6×10^{-7}
Oxygen	VDC copolymer	1.5×10^{-14}	3.5×10^{-7}
Carbon dioxide	Acrylonitrile copolymer	1.0×10^{-13}	1.6×10^{-6}
Carbon dioxide	Poly(vinyl chloride)	8.9×10^{-13}	3.4×10^{-6}
Carbon dioxide	VDC copolymer	1.4×10^{-14}	1.1×10^{-6}
d-Limonene	High density polyethylene	7.0×10^{-14}	0.3
d-Limonene	VDC copolymer	3.0×10^{-18}	0.6
Methyl salicylate	Nylon-6	2.1×10^{-17}	0.9
Methyl salicylate	VDC copolymer	5.8×10^{-16}	0.3

[a] Ref. 95.

Table 12. Transport of *trans*-2-Hexenal in Barrier Films at 75°C

Film	Condition	Permeability P, MZU[a]	Diffusivity D, m^2/s
VDC copolymer[b]	Dry	4500	4.4×10^{-15}
VDC copolymer	90/0[c]	4100	3.9×10^{-15}
EVOH[d]	dry	2300	1.6×10^{-14}
EVOH	90/0[c]	98,000	7.2×10^{-13}

[a]To convert MZU (10^{-20} kg·m)/(m^2·s·Pa) to nmol/(m·s·GPa), divide by 9.8.
[b]Dow experimental resin XU32024.13.
[c]90% RH on the upstream side, 0% RH on the downstream side.
[d]44 mol% ethylene.

temperatures. Table 11 compares the D and S of large and small molecules in several polymers. A low D and a high S may mean that the principal mechanism for flavor loss is its being lost into the package wall (also known as scalping).

Humidity does not affect the permeability, diffusion coefficient, or solubility coefficient of F/A/S molecules in VDC copolymers. Studies using *trans*-2-hexenal and *d*-limonene are compared in Table 12. The transport in an EVOH copolymer is strongly plasticized by humidity.

Table 13. Examples of Permeation of Flavor and Aroma Compounds in Selected Polymers[a] at 25°C[b], Dry[c]

Flavor/aroma compound	Permeability P, MZU[d]	Diffusivity D, m^2/s	Solubility S, $kg/(m^3 \cdot Pa)$
Vinylidene chloride copolymer			
Ethyl hexanoate [123-66-0] ($C_8H_{16}O_2$)	570	8.0×10^{-18}	0.71
Ethyl 2-methylbutyrate [7452-79-1] ($C_7H_{14}O_2$)	3.2	1.9×10^{-17}	1.7×10^{-3}
d-Limonene [5989-27-5] ($C_{10}H_{16}$)	32	3.3×10^{-17}	9.7×10^{-2}
Ethylene–vinyl alcohol copolymer			
Ethyl hexanoate	0.41	3.2×10^{-18}	1.3×10^{-3}
Ethyl 2-methylbutyrate	0.30	6.7×10^{-18}	4.7×10^{-4}
d-Limonene	0.5	1.1×10^{-17}	4.5×10^{-4}
Low density polyethylene			
Ethyl hexanoate	4.1×10^6	5.2×10^{-13}	7.8×10^{-2}
Ethyl 2-methylbutyrate	4.9×10^5	2.4×10^{-13}	2.3×10^{-2}
d-Limonene	4.3×10^6	—	—
High density polyethylene			
d-Limonene	3.5×10^6	1.7×10^{-13}	2.5×10^{-1}
Polypropylene			
Ethyl hexanoate	8.7×10^4	3.1×10^{-15}	2.8×10^{-1}
d-Limonene	1.6×10^4	7.4×10^{-16}	2.1×10^{-1}

[a]Refs. 96–100.
[b]Values for VDC copolymer and EVOH copolymer are extrapolated from higher temperatures.
[c]Permeation in the VDC copolymer and the polyolefins is not affected by humidity; the permeability and diffusion coefficient in the EVOH copolymer can be as much as 1000 times greater with high humidity.
[d]To convert MZU (10^{-20} kg·m)/(m^2·s·Pa) to nmol/(m·s·GPa), divide by molecular weight of permeant/10.

Table 13 contains some representative data for the permeation of F/A/S molecules. VDC copolymers are good barriers to the migration of F/A/S molecules. Dry EVOH copolymers are also good barriers to the migration of F/A/S molecules. However, polyolefins are not good barriers to F/A/S molecules. The fact that most glassy polymers are good barriers to the migration of F/A/S molecules is not shown in this table.

Degradation Chemistry. Vinylidene chloride polymers are highly resistant to oxidation, permeation of small molecules, and biodegradation, which makes them extremely durable under most use conditions. However, these materials are thermally unstable and, when heated above about 120°C, undergo degradative dehydrochlorination. Furthermore, the homopolymer degrades with rapid evolution of hydrogen chloride within a few degrees of its melting temperature (200°C). For this reason, the superior characteristics of the homopolymer cannot be exploited. As a consequence, the copolymers of VDC with vinyl chloride, alkyl acrylates or methacrylates, acrylonitrile or methacrylonitrile, rather than the homopolymer, have come to commercial prominence. Such copolymers have often served as substrates for a study of the degradation reaction (101–104).

The thermal degradation of VDC copolymers occurs in two distinct steps. The first involves degradative dehydrochlorination via a chain process to generate poly(chloroacetylene) sequences (103,105). Subsequent Diels–Alder-type condensation between conjugated sequences affords a highly cross-linked network, which, upon further dehydrochlorination, leads to the formation of a large-surface-area, highly absorptive carbon (1,106). The initial dehydrochlorination occurs at moderate temperatures and is a typical chain process involving distinct initiation, propagation, and termination phases (107,108). Initiation is thought to occur via carbon–chlorine bond scission promoted by a defect structure within the polymer. An effective defect site in these polymers is unsaturation (105). Introduction of a random double bond produces an allylic dichloromethylene unit activated for carbon–chlorine bond scission. Initiation by the thermally induced cleavage of this bond, followed by propagation by successive dehydrochlorination along the chain, ie, the so-called unzipping reaction, can then proceed readily (Fig. 5).

The thermal stability of these polymers is decreased by pretreatment with uv irradiation (109), electron-beam irradiation (110), and basic solvents or reagents (111,112); by an atmosphere of oxygen (109,113–116) or nitric oxide (109); and by the presence of peroxide linkages within the polymer (113,117), residues of emulsifying agents (113), organometallic initiator residues (113), ash from a previous decomposition (113), peroxide initiator residues (109–113,117–120), or metal ions (121). All the foregoing are sufficient to introduce random double bonds into the polymer structure. This can be demonstrated by examination of the treated sample by uv and ir spectroscopic methods (110). Prolonged treatment of the polymer with basic reagents leads to more extensive dehydrohalogenation (121–126). In fact, electrolysis of a solution of tetra(*n*-butyl)ammonium perchlorate in *N*,*N*-dimethylformamide generates a basic medium, presumably containing the formamide radical anion, capable of degrading the polymer (127). High energy radiation from a variety of sources may induce damage of several kinds, including carbon–carbon bond cleavage (109). A prominent radiation-induced process is carbon–chlorine bond scission followed by elimination of hydrogen chloride

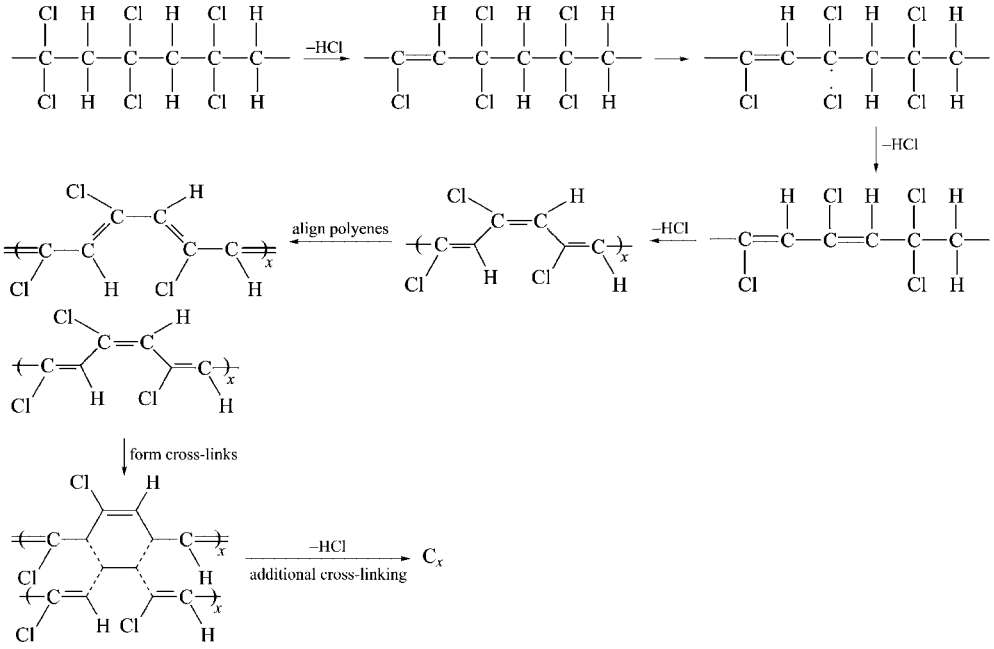

Fig. 5. Schematic of the degradation of PVDC to carbon.

(128,129). Property changes other than a decrease in thermal stability may arise as a consequence of high energy irradiation (130,131).

The principal steps in the thermal degradation of VDC polymers are formation of a conjugated polyene sequence followed by carbonization.

$$\left(CH_2{-}CCl_2\right)_n \xrightarrow{\text{fast, }\Delta} \left(CH{=}CCl\right)_n + n\,HCl \xrightarrow{\text{carbonization, slow, }\Delta} 2n\,C + n\,HCl$$

On being heated, the polymer gradually changes color from yellow to brown and finally to black. Early in the reaction, the polymer becomes insoluble, which indicates that cross-linking has occurred. The temperature of melting decreases, and the presence of unsaturation may be detected by spectroscopic (uv, ir, nmr) methods. The polymer eventually becomes infusible, and the crystal structure as detected by x-ray diffraction disappears even though the gross morphology is retained (132). The presence of carbon radicals can be detected by electron spin resonance (esr) measurements. If the temperature is raised substantially above 200°C, aromatic structures are formed. Finally, at very high temperatures (>700°C), complete carbonization occurs.

The first of these reactions, ie, the loss of the first mole of hydrogen chloride, has had the greatest impact on the end use of VDC polymers and has been the most studied and well characterized. The propensity of these polymers to undergo degradation is influenced by a wide variety of factors, including physical changes in the solid (annealing effects) and the method of preparation and purity of the polymer. The most stable polymers are those produced by bulk polymerization at low temperature with the use of a nonoxygen initiator. In general, the stability of

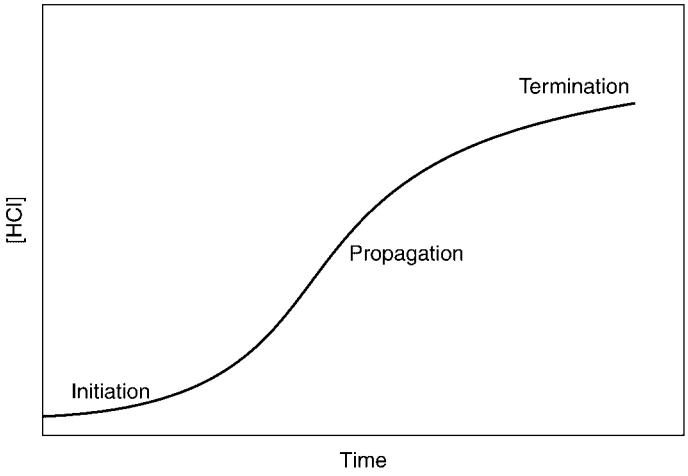

Fig. 6. Hydrogen chloride evolution for the thermal degradation of a typical VDC polymer.

the polymer reflects the method of preparation, with bulk > solution > suspension ≫ emulsion (133). In the absence of elevated temperatures, suspending agents, polar solvents, redox initiators, etc, a more perfect polymer structure is formed, ie, one containing a minimum level of unsaturation.

The impact of a less defective structure may be seen in Figure 6, which depicts hydrogen chloride evolution for the thermal degradation of a typical VDC polymer. Initiation of degradation occurs at activated allylic sites within the polymer, but initiation does not occur simultaneously at all sites. Therefore, early in the reaction, hydrogen chloride evolution increases as a function of time as initiation occurs at more and more sites. In other words, unzipping is started in an increasing number of chain segments. This gives rise to the acceleratory induction period characteristic of VDC copolymer degradation. When a greater number of initiation sites are present within the polymer, ie, at higher levels of unsaturation, the rate of hydrogen chloride evolution during the initiation phase of the degradation is greater. After unzipping has begun in all chains containing defect structures, hydrogen chloride production is essentially first order until termination by completion or other means becomes a prominent reaction. Undoubtedly, some random double-bond initiation continues to occur during propagation. However, during this period termination is roughly in balance with initiation. As the rate of termination significantly exceeds that of initiation, deceleration of degradation is observed (105,108,109). An accurate representation of the dehydrochlorination reaction over the entire range of degradation may be achieved using a kinetic expression containing two constants (107,134).

Since the low temperature degradation, ie, that which occurs at process temperatures, involves only dehydrochlorination of VDC sequences, mass loss reflecting evolution of hydrogen chloride provides a convenient means of monitoring polymer decomposition. Thus, thermogravimetry analysis (tga) is an appropriate method for assessing the degradation characteristics of VDC polymers (135,136). Rate constants may be obtained as the slopes of the appropriate linear portions of a plot of $\ln[w_\infty - w_0)/(\mathrm{w}_\infty - w_\mathrm{t})]$ versus time. The variable w_∞ is the weight of

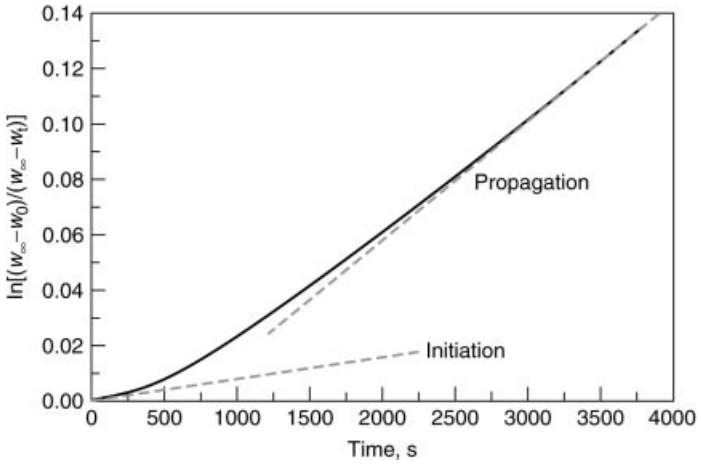

Fig. 7. Thermal degradation of a typical VDC polymer.

the sample at infinite time (t_∞) taken as that weight which would remain after 37.62% of the initial VDC component weight (corresponding to the complete loss of 1 mole of hydrogen chloride per VDC unit in the copolymer). The variable w_0 is the weight at time zero (t_0), ie, the time at which the first point was recorded, and w_t is the weight at any time t during the run. This is illustrated for a typical VDC polymer in Figure 7.

Initiation rate constants (k_i) for the degradation may be obtained by least-squares analysis of the linear segment of the early portion of this plot. Propagation rate constants (k_p) may be obtained in a similar manner from data obtained later in the run when propagation has become the dominant reaction. This is illustrated in Figures 8 and 9. Table 14 shows the rate constants obtained in this manner for the degradation of VDC/butyl acrylate copolymers.

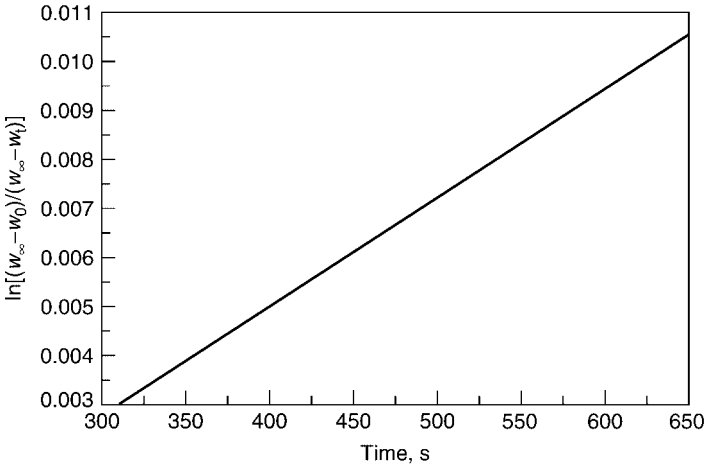

Fig. 8. Initiation rate constant (k_i) for the thermal degradation of a typical VDC polymer.

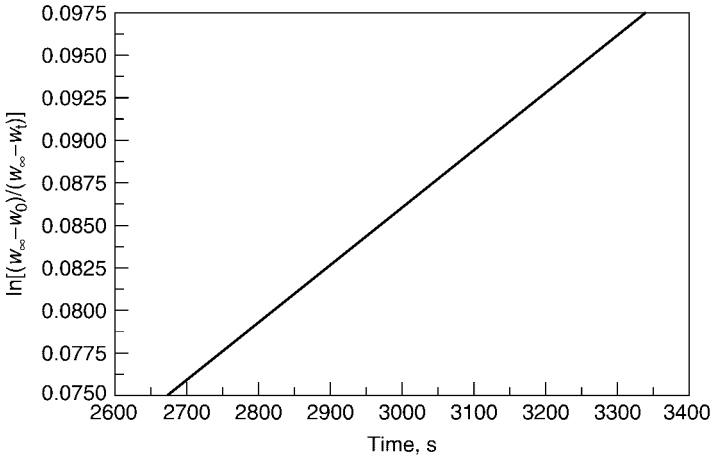

Fig. 9. Propagation rate constant (k_p) for the thermal degradation of a typical VDC polymer.

Much evidence has been accumulated to establish the radical nature of the degradation reaction (1). Prominent components of this include slight inhibition of the reaction by certain radical scavengers and changes in the esr spectrum of a sample undergoing degradation (137,138). Both suggest that radical intermediates are generated during the degradation. The exact nature of the chain-carrying species is made more apparent from the results of degradation in bibenzyl solution (103,105). Bibenzyl is an efficient radical scavenger that is converted to stilbene on interaction with a radical. Stilbene can be readily quantitated by gas–liquid partition chromatography. For the degradation of typical VDC polymers, the ratio of hydrogen chloride evolved to stilbene produced is approximately 35:1 (103,105). This is in sharp contrast to the 2:1 ratio expected for trapping of chlorine atoms with perfect efficiency and suggests that the propagating species is a radical pair that does not dissociate appreciably. Thus propagation most probably occurs by a radical chain process in which the chain-carrying species is a radical pair that decomposes to alkene and hydrogen chloride without dissociation.

Table 14. Rate Constants for the Thermal Degradation of Vinylidene Chloride/Butyl Acrylate Copolymers at 180°C

Butyl acrylate, wt%[a]	k_i, 10^{-5} s^{-1}[b]	k_p, 10^{-5} s^{-1}[b]
0	3.02 ± 0.09	8.75 ± 0.14
4	4.48 ± 0.004	8.34 ± 0.28
8	2.83 ± 0.25	6.73 ± 0.01
12	2.76 ± 0.03	5.35 ± 0.18
18	2.45 ± 0.25	4.08 ± 0.05
20	2.21 ± 0.005	3.74 ± 0.33

[a]Weight percent of monomer loaded.
[b]Averages of at least two determinations.

To some extent, the stability of VDC polymers is dependent on the nature of the comonomer present. Copolymers with acrylates degrade slowly (139,140). Apparent degradation propagation rates decrease somewhat as the acrylate content of the copolymer increases (139). The polyene sequences generated by dehydrochlorination are limited in size by the level of acrylate incorporation; that is, the acrylate molecules act as stopper units for the unzipping reaction. The impact of this chain-stopping is that the termination rate for higher acrylate content polymers is greater than for those containing smaller amounts of acrylate. Therefore, initiation and termination rates are in balance for a shorter portion of the overall reaction period. Despite the suggestion that the presence of a hydrogen-rich pendant might serve as a source of hydrogen atoms to disrupt degradation propagation (113), there is no apparent relationship between the degradation rate and the size of the alkyl portion of the acrylate comonomer (140,141).

Copolymers with AN or MA undergo degradation more readily. In addition, the degradation is more complex than that observed for acrylate copolymers. Acrylonitrile copolymers release hydrogen cyanide as well as hydrogen chloride; products of thermal degradation of MA copolymers contain methyl chloride in addition to hydrogen chloride (102,104,142,143). In both cases, degradation apparently begins in VDC units adjacent to comonomer units (142,143).

The degradation of VDC polymers in nonpolar solvents is comparable to degradation in the solid state (103,138,144,145). However, these polymers are unstable in many polar solvents (146). The rate of dehydrochlorination increases markedly with solvent polarity. In strongly polar aprotic solvents, eg, hexamethylphosphoramide, dehydrochlorination proceeds readily (144,147). This reaction is clearly unlike thermal degradation and may well involve the generation of ionic species as intermediates.

Polymers of high VDC content are reactive toward strong bases to yield elimination products and toward nucleophiles to yield substitution products. Agents capable of functioning as both a base and a nucleophile react with these polymers to generate a mixture of products (124,148–151). Weakly basic agents such as ammonia, amines, or polar aprotic solvents accelerate the decomposition of VDC copolymers. Amines function as bases to remove hydrogen chloride and introduce unsaturation along the polymer mainchain which may serve as initiation sites for thermal degradation. The overall effectiveness of a particular amine for dehydrohalogenation may be dependent on several factors, including inherent basicity, degree of steric hindrance at nitrogen, and compatibility with the polymer (152–154). Phosphines are more nucleophilic but less basic than amines. However, phosphines also promote dehydrohalogenation rather than displacement of allylic chlorine (155).

Amines can also swell the polymer, leading to very rapid reactions. Pyridine, for example, would be a fairly good solvent for a VDC copolymer if it did not attack the polymer chemically. However, when pyridine is part of a solvent mixture that does not dissolve the polymer, pyridine does not penetrate into the polymer phase (111). Studies of single crystals indicate that pyridine removes hydrogen chloride only from the surface. Kinetic studies and product characterizations suggest that the reaction of two units in each chain-fold can easily take place; further reaction is greatly retarded either by the inability of pyridine to diffuse into the crystal or by steric factors.

Aqueous bases or nucleophiles have little impact on VDC polymers, primarily because the polymer is not wetted or swollen by water. However, these polymers do slowly degrade in hot concentrated aqueous sodium hydroxide solution (121).

Lewis acids, particularly transition-metal salts, strongly promote the thermal degradation of VDC polymers (121,138,156–166,166,167). The rate of initiation of degradation is greatly enhanced in the presence of metal ions (159). The metal ion (or other Lewis acid) coordinates chlorine atoms, making them much better leaving groups. This facilitates the introduction of initial double bonds, which act as defect sites from which degradative dehydrohalogenation may propagate. Care must be taken to avoid metal ions, particularly precursors of iron chloride, during the preparation and processing of VDC polymers.

Copolymers of VDC that are free of impurities do not degrade at an appreciable rate in the absence of light below 100°C. However, when exposed to uv light, these polymers discolor (168). Again, the primary reaction seems to be dehydrochlorination. Hydrogen chloride is evolved and cross-linking occurs (109). Polyene sequences of narrow sequence length distribution are often formed (169–171). These function as initiation sites for subsequent thermal degradation (109). Laser-induced photochemistry may be used for the generation of polyene structures uncomplicated by cross-linking and graphitization (172,173). Laser-promoted dehydrohalogenation has some characteristics in common with the corresponding thermal process. Long-lived carbon radicals are formed, and the propagation of the dehydrochlorination reaction apparently proceeds via an allylic carbon radical, chlorine atom pair (173). Similar structures may be generated by chemical means (150,151,174). Other photodegradation processes, eg, hydroperoxide formation at the methylene groups, probably also occur but are less important for these polymers than is polyene formation (158).

Stabilization. The stabilization of VDC polymers toward degradation is a highly developed art and is responsible for the widespread commercial use of these materials. Although the mode of action is often not understood, some general principles of effective stabilization have been established (175). The ideal stabilizer system should

(1) absorb or combine with evolved hydrogen chloride irreversibly under conditions of use, but not strip hydrogen chloride from the polymer chain;
(2) act as a selective uv absorber;
(3) contain a reactive dienophilic moiety capable of preventing discoloration by reacting with and disrupting the color-producing conjugated polymer sequences;
(4) possess nucleophilicity sufficient for reaction with allylic dichloromethylene units;
(5) possess antioxidant activity so as to prevent the formation of carbonyl groups and other chlorine-labilizing structures;
(6) be able to scavenge chlorine atoms and other free radicals efficiently;
(7) chelate metals, eg, iron, to prevent chlorine coordination and the formation of metal chlorides.

Acid acceptors are of two general types: alkaline-earth oxides and hydroxides (176) or salts of weak acids, such as barium or calcium fatty acid salts; and

epoxy compounds, such as epoxidized soybean oil or glycidyl ethers and esters. Epoxidized oils are less effective for the stabilization of VDC polymers than for other halogenated polymers (160). The function of these materials as plasticizers and processing lubricants is probably responsible for modest improvements in processing stability. Effective light stabilizers have a chemical structure which imparts exceptional conjugative stability and very good uv absorption properties. The principal compounds of commercial interest are derivatives of salicylic acid, resorcylic acid, benzophenone, and benzotriazole. The typical hindered amine light stabilizers cannot be used in this application since they are sufficiently basic so as to promote dehydrohalogenation. This introduces allylic dichloromethylene units into the polymer mainchain, which act as initiation sites for thermal degradation. Consequently, satisfactory processing of the polymer in the presence of these additives is not possible. Examples of dienophiles that have been used are maleic anhydride and N-substituted maleimides (177).

Antioxidants are generally of two types: those that react with a free radical to stop a radical chain, that is, to scavenge chlorine atoms or peroxy radicals; and those that reduce hydroperoxides to alcohols. Phenolic antioxidants, eg, 2,6-di-*tert*-butyl-4-methylphenol and substituted bisphenols, are of the first type. Because the chain-carrying species for the degradative dehydrochlorination is a tight chlorine atom, carbon radical pair that does not dissociate appreciably during the reaction, the effectiveness of these agents is limited (161). The second type is exemplified by organic sulfur compounds and organic phosphites. The phosphites, ethylenediaminetetraacetic acid [60-00-4] (EDTA), citric acid [77-92-9], and citrates, can chelate metals. The ability of organic phosphites to function as antioxidants and as chelating agents illustrates the dual role of many stabilizer compounds. It is common practice to use a combination of stabilizing compounds to achieve optimum results (168). In addition, stabilization packages usually contain lubricants and other processing aids that enhance the effectiveness of the stabilizing compounds. The presence of these agents is particularly important to minimize the shearing component of degradation during extrusion and other processing steps (163).

Metal carboxylates have been considered as nucleophilic agents capable of removing allylic chlorine and thereby affording stabilization (162). Typical PVC stabilizers, eg, tin, lead, cadmium, or zinc esters, actually promote the degradation of VDC polymers. The metal cations in these compounds are much too acidic to be used with VDC polymers. An effective carboxylate stabilizer must contain a metal cation sufficiently acidic to interact with allylic chlorine and to facilitate its displacement by the carboxylate anion, but at the same time not acidic enough to strip chlorine from the polymer mainchain (163,167). Copper(II) carboxylates may have the balance of cation acidity and anion reactivity required to function as effective stabilizers for VDC polymers. This is reflected in Figure 10, which illustrates increasing stability of a typical VDC copolymer as it is aged at 150°C in the presence of copper(II) formate.

Vinylidene chloride polymers containing stabilizing features have been prepared. More generally, these have been polymers containing comonomer units with functionality that can consume evolved hydrogen chloride such that good radical scavenging sites are exposed (164,165,178,179).

For example, copolymers containing 4-isopropylphenyl acrylate display greater thermal stability than do the corresponding polymers containing simple

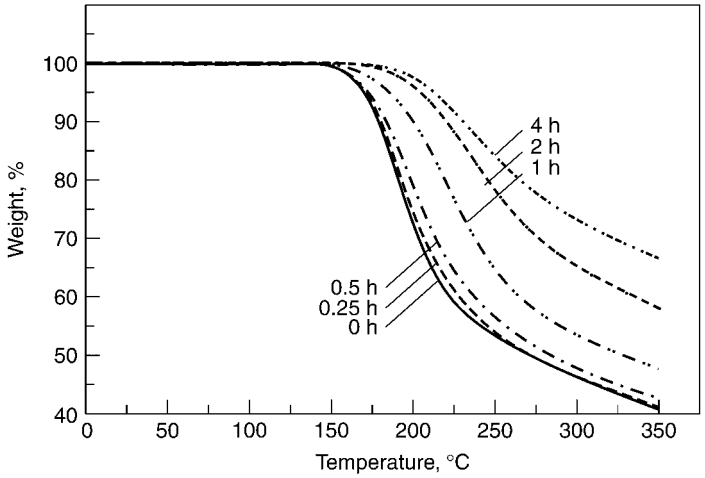

Fig. 10. Thermal degradation of a VDC/MPA (5 mol%) copolymer aged at 150°C in the presence of 5 wt% copper(II) formate for 0.25, 0.50, 1.0, 2.0, and 4.0 h.

alkyl acrylates as comonomer (164). This is illustrated in Figure 11. Stability of the copolymer increases as the level of the comonomer containing the *t*-cumyl group, capable of scavenging chlorine atoms, increases. A more quantitative reflection of this effect is provided by the rate constants displayed in Table 15. It may be noted that the magnitude of the initiation rate constant k_i decreases by a factor of 2 as the isopropylphenyl acrylate content of the polymer is increased from 0 to 5 mol%.

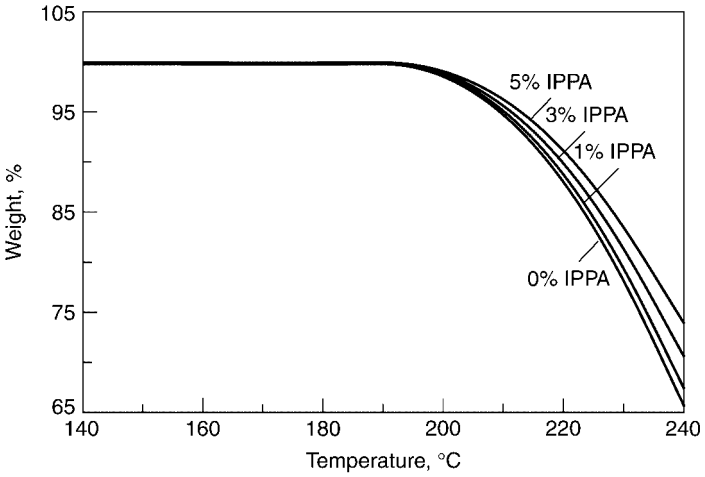

Fig. 11. Thermal degradation of vinylidene chloride/4-isopropylphenyl acrylate copolymers.

Table 15. Rate Constants for the Degradation of Vinylidene Chloride/4-Isopropylphenyl Acrylate Copolymers at 140°C

IPPA, mol%	k_i, 10^{-7} s^{-1}[a]	k_p, 10^{-7} s^{-1}[a]
0.0	3.02 ± 0.09	8.75 ± 0.14
1.0	4.48 ± 0.004	8.34 ± 0.28
3.0	2.83 ± 0.25	6.73 ± 0.01
5.0	2.76 ± 0.03	5.35 ± 0.18

[a] Averages of at least two determinations; average deviation $\leq \pm 0.10$.

Commercial Methods of Polymerization and Processing

Processes that are essentially modifications of laboratory methods and that allow operation on a larger scale are used for commercial preparation of VDC polymers. The intended use dictates the polymer characteristics and, to some extent, the method of manufacture. Emulsion polymerization and suspension polymerization are the preferred industrial processes. Either process is carried out in a closed, stirred reactor, which should be glass-lined and jacketed for heating and cooling. The reactor must be purged of oxygen, and the water and monomer must be free of metallic impurities to prevent an adverse effect on the thermal stability of the polymer.

Emulsion Polymerization. Emulsion polymerization is used commercially to make VDC copolymers. In some applications, the resulting latex is used directly, usually with additional stabilizing ingredients, as a coating vehicle to apply the polymer to various substrates. In other applications, the polymer is first isolated from the latex before use. When the polymer is not used in latex form, the emulsion/coagulation process is chosen over alternative methods. The polymer is recovered in dry powder form, usually by coagulating the latex with an electrolyte, followed by washing and drying. The principal advantages of emulsion polymerization are twofold. First, high molecular weight polymers can be produced in reasonable reaction times, especially copolymers with VC. The initiation and propagation steps can be controlled more independently than in the suspension process. Second, monomer can be added during the polymerization to maintain copolymer composition control.

The disadvantages of emulsion polymerization result from the relatively high concentration of additives in the recipe. The water-soluble initiators, activators, and surface-active agents generally cause the polymer to have greater water sensitivity, poorer electrical properties, and poorer heat and light stability. These agents promote degradative dehydrochlorination during polymerization.

A typical recipe for batch emulsion polymerization is shown in Table 16. A reaction time of 7–8 h at 30°C is required for 95–98% conversion. A latex is produced with an average particle diameter of 100–150 nm. Other modifying ingredients may be present, eg, other colloidal protective agents such as gelatin or carboxymethylcellulose, initiator activators such as redox types, chelates, plasticizers, and stabilizers; and chain-transfer agents.

Commercial surfactants are generally anionic emulsifiers, alone or in combination with nonionic types. Representative anionic emulsifiers are the sodium

Table 16. Recipe for Batch Emulsion Polymerization[a]

Ingredient	Parts by weight
Vinylidene chloride	78
Vinyl chloride	22
Water	180
Potassium peroxysulfate	0.22
Sodium bisulfite	0.11
Aerosol MA,[b] 80 wt%	3.58
Nitric acid, 60 wt%	0.07

[a] Ref. 180.
[b] Aerosol MA (American Cyanamid Co.) = dihexyl sodium sulfosuccinate.

alkylaryl sulfonates, the alkyl esters of sodium sulfosuccinic acid, and the sodium salts of fatty alcohol sulfates. Nonionic emulsifiers are of the ethoxylated alkylphenol type. Free-radical sources other than peroxysulfates may be used, eg, hydrogen peroxide, organic hydroperoxides, peroxyborates, and peroxycarbonates. Many of these are used in redox pairs, in which an activator promotes the decomposition of the peroxy compound. Examples are peroxysulfate or perchlorate activated with bisulfite, hydrogen peroxide with metallic ions, and organic hydroperoxides with sodium formaldehyde sulfoxylate. The use of activators causes the decomposition of the initiator to occur at lower reaction temperatures, which allows the preparation of a higher molecular weight polymer within reasonable reaction times. This is an advantage, particularly for copolymers of VDC with VC. Oil-soluble initiators are usually effective only when activated by water-soluble activators or reducing agents.

To ensure constant composition, the method of emulsion polymerization by continuous addition is employed. One or more components are metered continuously into the reaction. If the system is properly balanced, a steady state is reached in which a copolymer of uniform composition is produced (181). A process of this type can be used for the copolymerization of VDC with a variety of monomers. A flow diagram of the apparatus is shown in Figure 12; a typical recipe is shown in Table 17. The monomers are charged to the weigh tank A, which is kept under a nitrogen blanket. The emulsifiers, initiator, and part of the water are charged to tank B; the reducing agent and some water to tank C. The remaining water is charged to the reactor D, and the system is sealed and purged. The temperature is raised to 40°C and one tenth of the monomer and initiator charges is added, and then one tenth of the activator is pumped in. Once the reaction begins, as indicated by an exotherm and pressure drop, feeds of A, B, and C are started at programmed rates that begin slowly and gradually increase. The emulsion is maintained at a constant temperature during the run by cooling water that is pumped through the jacket. When all components are in the reactor and the exotherm begins to subside, a final addition of initiator and reducing agent completes the reaction.

Suspension Polymerization. Suspension polymerization of VDC is used commercially to make molding and extrusion resins. The principal advantage of the suspension process over the emulsion process is the use of fewer ingredients that might detract from the polymer properties. Stability is improved and water

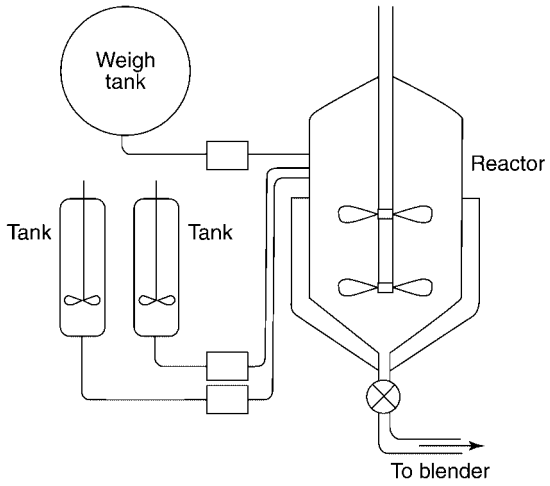

Fig. 12. Apparatus for continuous-addition emulsion polymerization of a VDC–acrylate mixture (181).

sensitivity is decreased. Extended reaction times and the difficult preparation of higher molecular weight polymers are disadvantages of the suspension process compared to the emulsion process, particularly for copolymers containing VC.

A typical recipe for suspension polymerization is shown in Table 18. At a reaction temperature of 60°C, the polymerization proceeds to 85–90% conversion in 30–60 h. Unreacted monomer is removed by vacuum stripping; then it is condensed and reused after processing. The polymer is obtained in the form of small [150–600 μm (30–100 mesh)] beads, which are dewatered by filtration or centrifugation and then dried in a flash dryer or fluid-bed dryer. Suspension polymerization involves monomer-soluble initiators, and polymerization occurs inside suspended monomer droplets, which form by the shearing action of the agitator and are prevented from coalescence by the protective colloid. It is important that the initiator be uniformly dissolved in the monomer before droplet formation. Unequal distri-

Table 17. Recipe for Emulsion Polymerization by Continuous Addition[a]

Ingredient	Parts by weight
Vinylidene chloride	468
Comonomer	52
Emulsifiers	
Tergitol[b] NP 35	12
Sodium lauryl sulfate, 25 wt%	12
Initiator ammonium peroxysulfate	10
Sodium metabisulfite ($Na_2S_2O_5$), 5 wt%	10
Water	436

[a]Ref. 181.
[b]Nonionic wetting agent produced by Union Carbide.

Table 18. Recipe for Suspension Polymerization[a]

Ingredient	Parts by weight
Vinylidene chloride	85
Vinyl chloride	15
Deionized water	200
400 mPa·s (=cP) methyl hydroxypropylcellulose	0.05
Lauroyl peroxide	0.3

[a]Ref. 182.

bution of initiator causes some droplets to polymerize faster than others, leading to monomer diffusion from slow-polymerizing to fast-polymerizing droplets. The fast-polymerizing droplets form polymer beads that are dense, hard, glassy, and extremely difficult to fabricate because of their inability to accept stabilizers and plasticizers. Common protective colloids that prevent droplet coalescence and control particle size are PVC, gelatin, and methylcellulose. Organic peroxides, peroxycarbonates, and azo compounds are used as initiators for VDC suspension polymerization.

The batch-suspension process does not compensate for composition drift, whereas constant-composition processes have been designed for emulsion or suspension reactions. It is more difficult to design controlled-composition processes by suspension methods. In one approach (183), the less reactive component is removed continuously from the reaction to keep the unreacted monomer composition constant. This method has been used effectively in VDC–VC copolymerization, where the slower reacting component is volatile and can be released during the reaction to maintain constant pressure. In many other cases, no practical way is known for removing the slower reacting component.

Economic Aspects

Vinylidene chloride monomer is produced commercially in the United States by The Dow Chemical Co. and PPG Industries. The monomer is produced in Europe by Imperial Chemical Industries, Ltd. and Solvin. The monomer is produced in Japan by the Asahi Chemical Co., Kureha Chemical Industries, and Kanto Denka Kogyo Co. Commercial suppliers of VDC copolymers include The Dow Chemical Co. in the United States and Solvin in Europe. Asahi Chemical Co. and Kureha Chemical Industries are suppliers of VDC resins in Japan. Additional manufacturers of exclusively VDC latexes include W. R. Grace and Rohm & Haas in the United States, and Scott-Bader in Europe. Local suppliers of VDC resins have also been reported in Russia and the People's Republic of China.

Although Saran is a generic name for VDC copolymers in the United States, it is a Dow trademark in most foreign countries. Other trademarks include Daran (W. R. Grace) and Serfene (Rohm & Haas) in the United States; Diofan and Ixan (Solvin) and Polyidene (Scott-Bader) in Europe; and Kurehalon (Kureha) in Japan. In addition, B. F. Goodrich Chemicals (GEON) and Avecia (Haloflex) supply nonbarrier VDC copolymers.

Applications

Melt Processing. Vinylidene chloride copolymers are melt processed via a variety of fabrication techniques. These include molding, monofilament fiber extrusion, monolayer blown film extrusion, multilayer cast- and blown-film extrusion, and multilayer sheet extrusion. There are a number of elements of melt processing and melt-processing equipment that are common to all of these fabrication techniques (184–187). These include proper equipment design and materials of construction, proper and accurately controlled operating conditions, and a properly formulated resin.

Because of their high crystalline melting point, VDC copolymers are generally melt fabricated near their thermal stability limits. Products of degradation are corrosive to equipment and given sufficient time will generate a char or carbon. Also, at temperatures of about 130°C and above, a number of metals, including iron, zinc, copper, and aluminum, catalyze the degradation of VDC resins. As a consequence the correct materials of construction are essential for melt processing VDC resins. High nickel alloys that are both corrosion resistant and do not catalyze resin degradation are preferred for all surfaces that are in direct contact with the polymer melt. For example, the extruder barrel liner may be made from Xaloy 306 or other high nickel, low iron containing alloy. Extruder screws may be made from Duranickel 301 with Colmonoy 56 flight lands. Other parts in direct contact with polymer melt should also be made out of Duranickel or similar material. Instruments such as melt thermocouples or pressure transducers could be Hastelloy C.

Degradation of VDC resins is a product of time at temperature. Both of these aspects should be controlled to optimize melt-processing performance. Extruders in the range of 18:1 to 24:1 length-to-diameter ratio are commonly used. Melt channels should be designed with a smooth flow pattern to minimize dead spots where polymer may degrade excessively or permit carbon buildup. The clearance between the screw tip and the extruder nosepiece should be minimized. Screen packs are also not recommended for melt-processing VDC resins. Proper instrumentation, including multiple melt thermocouples and pressure transducers, amperage or torque measurement for the extruder, and accurate screw speed measurement, is also critical.

Heat management is an important factor in melt-processing VDC resins. Screw design (188) and resin formulation combine to affect the amount of heat generated during melting and the eventual melt temperature. Vinylidene chloride polymer powders exhibit a relatively high level of frictional heating and also contain a large amount of entrained air (189). Screws are typically designed to be low work to minimize frictional and viscous heating. They must also be designed to eliminate air entrapment. Screws greater than 6.35-cm (2.5-in.) diameter for VDC resin processing also generally have two-zone cooling capability for further heat management.

Vinylidene chloride resins for melt processing are generally supplied formulated or unformulated. Formulated resins may be melt processed as supplied or with some additional additives. Unformulated resins require additives prior to melt processing. Processing additives for VDC resins include plasticizers, lubricants, and other process aids designed to control heat generation and residence

time in melt processing. Patent literature cites a wide variety of lubricants and processing aids, including acids, esters, amides, and metal salts of fatty acids; polyolefins or polyolefin waxes; and inorganic stabilizers such as magnesium hydroxide or tetrasodium pyrophosphate (190). Some of these processing aids are common to PVC melt processing as well. However, it should also be noted that some PVC melt-processing additives are incompatible with VDC resins and will actually degrade melt-processing performance.

Molding. Molded articles were among the earliest applications for VDC copolymers (184,191). Vinylidene chloride–vinyl chloride copolymers were originally developed for thermoplastic molding applications, and small amounts are still used for this purpose. When properly formulated with plasticizers and heat stabilizers, the resins can be fabricated by common methods, eg, injection, compression, or transfer molding. Conventional or dielectric heating can be used to melt the polymers. Rapid hardening is achieved by forming in heated molds to induce rapid crystallization. Cold molds result in supercooling of the polymer. Because the interior of the molded part remains soft and amorphous, the part cannot be easily removed from the mold without distortion. Mold temperatures of up to 100°C allow rapid removal of dimensionally stable parts. The range of molding temperatures is rather narrow because of the crystalline nature of the resin and thermal sensitivity. All crystallites must be melted to obtain low polymer melt viscosity, but prolonged or excessive heating must be avoided to prevent dehydrochlorination.

The metal parts of the injection molder, ie, the liner, torpedo, and nozzle, that contact the hot molten resin must be of the noncatalytic, corrosion-resistant type previously described. The injection mold need not be made of noncatalytic metals; any high grade tool steel may be used because the plastic cools in the mold and undergoes little decomposition. However, the mold requires good venting to allow the passage of small amounts of acid gas as well as air. Vents tend to become clogged by corrosion and must be cleaned periodically.

Molded parts of VDC copolymers are used to satisfy the industrial requirements of chemical resistance and extended service life. They are used in such items as gasoline filters, valves, pipe fittings, containers, and chemical process equipment. Complex articles are constructed from molded parts by welding; hot-air welding at 200–260°C is a suitable method. Molded parts have good physical properties but lower tensile strength than films or fibers, because crystallization is random in molded parts. Higher strength is developed by orientation in films and fibers. Physical properties of a typical molded VDC copolymer plastic are listed in Table 19.

Monofilament Fiber Extrusion. Monofilament fiber extrusion was another early application for VDC resins (184,191,193). Monofilament applications have included automotive seat covers, window screens, and upholstery fabrics, where the durability and ease of cleaning were important. Fabrics made from VDC copolymer monofilaments are still used today in applications such as filter fabrics, light screens, greenhouse covers, pool or bath fabrics, and shoe insoles (194). Such fabrics claim excellent resistance to flame, chemicals, uv light, moisture, and microbial attack.

Vinylidene chloride copolymer monofilaments typically range from 0.15- to 1.5-mm (0.006- to 0.06-in.) diameter. To produce these monofilaments, a molten

Table 19. Properties of Resin for Injection-Molding Applications[a]

Typical resin properties	Test method	Value
Ultimate tensile strength, MPa[b]	ASTM D638	24.1–34.5
Yield tensile strength, MPa[b]	ASTM D638	19.3–26.2
Ultimate elongation, %	ASTM D638	160–240
Modulus of elasticity in tension, MPa[b]		345–552
Izod impact strength, J/m[c] of notch	ASTM D256	21.35–53.38
Density, g/cm^3	ASTM D792	1.65–1.72
Hardness, Rockwell M	ASTM D785	50–65
Water absorption, % in 24 h	ASTM D570	0.1
Mold shrinkage, cm/cm (injection-molded)	ASTM D955	0.005–0.025
Limiting oxygen index, %	ASTM D2863	60.0[d]
UL-94	UL-94 Test	V–O[d]

[a]Ref. 191.
[b]To convert MPa to psi, multiply by 145.
[c]To convert J/m to ft·lbf/in. of notch, divide by 53.38.
[d]The results of small-scale flammability tests are not intended to reflect the hazards of this or any other material under actual fire conditions.

VDC copolymer extrudate is quenched to about room temperature in a supercooling tank to produce an amorphous polymer strand (184,191,193). This strand is then wrapped several times around smooth take-off rolls, and then wrapped several times around orienting rolls, which operate at a higher speed than the take-off rolls. The difference in roll speeds produces mechanical stretching, orienting the filament along the longitudinal axis while the polymer is crystallizing. A typical stretch ratio for this process is about 400%. The orientation process increases the fiber strength from about 55 MPa (8000 psi) to as high as 414 MPa (60,000 psi). Much of the increased tensile strength is obtained as the stretch ratio approaches 400%. Heat treatment may be used during or after stretching to affect the degree of crystallization and control the physical properties of the oriented filaments.

Monolayer Blown-Film Extrusion. One of the major applications for VDC resins is monolayer film produced via a blown-film extrusion process. Previously, VDC copolymer film extrusion was limited to just a few experts in the field. However, over the last several years, production of VDC-containing films has greatly expanded (195,196). Monolayer VDC copolymer blown-film lines are now commercially available from a number of manufacturers and a considerable number of lines have been recently installed around the world, particularly in the People's Republic of China.

Figure 13 illustrates a monolayer blown-film process for VDC resin. In this process (185,197–200) a tube of molten VDC resin is extruded downward and is immediately quenched in a cold-water supercooling bath. This bath cools the polymer melt to create a leathery polymer tube which is essentially amorphous VDC copolymer. The low temperature of the bath also controls nucleation of the crystallites and thus impacts the subsequent film-formation processes. After the supercooling bath, the amorphous tube is passed through a warming or reheat bath. This bath increases the resin temperature, which in turn will make the film more pliable and increase the rate of crystallization propagation during the

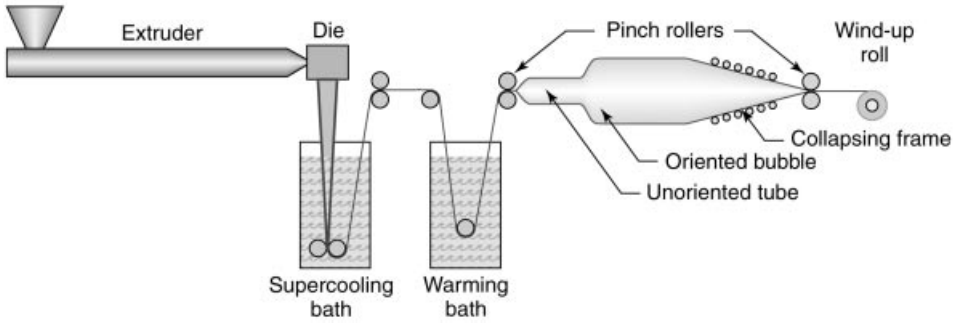

Fig. 13. Monolayer blown-film process for VDC resins (196).

subsequent film-blowing process. Exiting the warming bath, the tube passes through two sets of pinch rolls, which are arranged so that the second set of rolls travels faster than the first set. Between the two sets, air is injected into the tube to create a bubble that is entrapped by the pinch rolls. The entrapped air bubble remains stationary while the extruded tube is oriented as it passes around the bubble. In this manner, orientation is produced simultaneously in both the transverse and the longitudinal directions.

As the tube expands and orients, the amorphous polymer begins to crystallize rapidly, eventually limiting the diameter of the bubble. Adding additional air to the bubble at this point will only lengthen the bubble but will not change its overall diameter. Crystallization rate and thus bubble diameter or "blow up ratio" is controlled by a number of factors, including temperatures of the supercooling and warming baths, room temperature, polymer composition, and amount and type of plasticizer additives. These parameters as well as variables such as extrusion rate, die diameter, die gap, and drawdown ratio are combined to make a wide variety of film types and sizes. Films produced via this process generally have some shrink properties, which in many cases are advantageous. Where shrink is not desirable, films can be preshrunk via controlled heat application prior to the winding process.

Monolayer blown-film processes generally use a VDC–VC copolymer. Such resins have the combination of performance properties and optimum crystallization rate necessary for this process. Resins are generally formulated with plasticizers, lubricants, and other additives to affect performance during the extrusion process as well as in the final film applications.

Applications for VDC copolymer monolayer films fall into three major categories: household wrap, food and medical packaging, and industrial films. Food packaging includes packaging of processed meats, cheese and other dairy products, and bakery goods. Packaging types include film overwraps, shrinkable films, chub packaging, and unit packaging. Performance attributes of VDC copolymer films that are important to these applications include high barrier to oxygen, water, and other permeating molecules; clarity; resistance to fats and oils; dimensional stability; ability to be sealed and printed; and ability to withstand retort and microwave oven temperatures. Typical film properties are shown in Table 20.

Table 20. Physical Properties of PVDC Copolymer Films[a]

Properties[b]	Overwrap film	Chub packaging film A	Chub packaging film B	Unit packaging film A	Unit packaging film B	High barrier packaging film	Test methods
Average thickness, μm[c]	15	25	25	51	152	25	—
Yield, m^2 film/kg resin[d]	38	23	23	12	4	23	Calculated
Water vapor transmission rate at 90% RH and 38°C, nmol/(m·s)[e]	0.09	0.09	0.1	0.06	0.06	0.01	Permatran W
Oxygen transmission at 100% RH and 23°C, nmol/(m·s·GPa)[f]	2.6	2.6	3.8	2.9	2.9	0.16	ASTM D3985-81
Ultimate tensile strength, MPa[g]							ASTM D882-81
MD	76	97	83	111	111	83	
TD	124	138	117	133	95	128	
Ultimate elongation,%							ASTM D882-81
MD	75	90	90	95	80	100	
TD	55	60	75	80	70	50	
2% secant modulus, MPa[g]							ASTM D882-81
MD	690	690	607	690	655	1103	
TD	621	593	530	615	615	965	
Unrestrained shrink, 10 min at 100°C in air,%							ASTM D1204
MD	16	16	20	8	12	6	
TD	9	9	11	4	7	4	
Haze,%	1	5	5	3	3	2.5	ASTM D1003-61 (77)
45° gloss	115	92	90	105	105	110	ASTM D2457-60 (77)
Clarity,%	86	65	52	73	73	80	ASTM D1746-70 (78)
Film block, unconditioned, g	114	—	—	—	—	—	ASTM D3354-89
Film cling, unstretched, g	65	—	—	—	—	—	ASTM D4649-87
Kinetic coefficient of friction, film-to-metal	—	0.29	0.30	0.30	0.30	—	ASTM D1894

[a]Ref. 201.
[b]MD is machine direction; TD is transverse direction.
[c]To convert μm to mil, divide by 25.6.
[d]To convert m^2 film/kg resin to $in.^2$ film/lb resin, multiply by 704.
[e]To convert nmol/(m·s) to (g·mil)/(100 $in.^2$·d), multiply by 4.
[f]To convert nmol/(m·s·GPa) to (cc·mil)/(100 $in.^2$·d·atm), divide by 2.
[g]To convert MPa to psi, multiply by 145.

Multilayer Cast- and Blown-Film Extrusion. A significant application for VDC copolymer resins is in the construction of multilayer film and sheet (202,203). This permits the design of a packaging material with a combination of properties not obtainable in any single material. A VDC copolymer layer is incorporated into multilayer film for perishable food packaging because it provides a barrier to oxygen. A special high barrier resin is supplied specifically for this application. Typically, multilayer packaging films contain outer layers of a tough, low cost polymer such as high density or linear low density polyethylene with VDC copolymer as the core layer. Cast and blown films are produced on conventional film lines with one extruder and die designed to handle the heat-sensitive nature of VDC resin. The properties of a 0.05-mm (39-mil) multilayer cast film are listed in Table 21.

Multilayer films are produced by both cast- and blown-film coextrusion. One of the key enabling technologies in the manufacture of these multilayer films has been preencapsulation of the VDC resin (205). Preencapsulation means that the VDC resin extrudate is completely encapsulated with a more thermally stable polymer, such as an ethylene–vinyl acetate copolymer, prior to entering the coextrusion die. Using this technique, the VDC resin is not directly exposed to the

Table 21. Physical Properties[a] of a Multilayer Barrier Film[b] and a Polyethylene Film[c]

Property[d]	Multilayer film	Polyethylene film	Test method
Yield tensile strength, MPa[e]			ASTM D882-61T
MD	14	12.1	
TD	13	9.7	
Ultimate tensile strength, MPa[e]			ASTM D882-61T
MD	24	20.0	
TD	17	17	
Tensile modulus, MPa[e]			ASTM D882-61T
MD	170	180	
TD	150	180	
Elongation, %			ASTM D882-61T
MD	400	325	
TD	400	550	
Elmendorf tear strength, g			ASTM D1922
MD	800	325	
TD	650	250	
Gas transmission at 24°C, nmol/(m^2·s·GPa)[f]			ASTM D1434-63
Oxygen	6.6×10^4	1.6×10^7	
Carbon dioxide	11.1×10^4	10.0×10^7	
Nitrogen	0.8×10^4	0.8×10^7	
Water vapor transmission at 95% RH and 38°C, nmol/(m·s)[g]	2000	6400	ASTM E96-63T

[a] Refs. 202 and 204.
[b] 0.05-mm total thickness with layers of polyethylene, adhesive, and vinylidene chloride copolymer.
[c] 0.05-mm polyethylene, 0.921 g/cm^3 density.
[d] MD is machine direction; TD is transverse direction.
[e] To convert MPa to psi, multiply by 145.
[f] To convert nmol/(m^2·s·GPa) to cm^3/(100 $in.^2$·d·atm), divide by 7.9×10^4.
[g] To convert nmol/(m·s) to g/(100 $in.^2$·d), divide by 1×10^4.

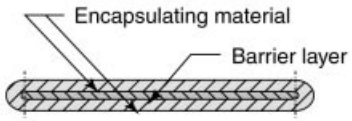

Fig. 14. Multilayer cast film showing a VDC copolymer barrier layer surrounded by a less thermally sensitive encapsulating material, such as ethylene–vinyl acetate (205). The edges are trimmed.

large surface area of the multilayer extrusion die, eliminating a greater potential for carbon formation and subsequent problems. Upon entering the die the encapsulated VDC resin is combined with other polymer layers, including tie and skin layers, to create the multilayer film.

The application of encapsulation technology to flat dies and cast film coextrusion is fairly easy to envision. As shown in Figure 14, the encapsulating material completely surrounds the VDC resin. When the edges are trimmed, a flat film with a continuous barrier layer is produced.

Blown-film coextrusion presents the added difficulty of obtaining a continuous barrier layer. A die with a crosshead mandrel is preferred over a die with a spiral mandrel, because the spiral mandrel tends to lead to long residence time in the spirals. A standard crosshead mandrel, however, results in a weld line where the barrier layer is not continuous. As shown in Figure 15, this problem is solved by providing an overlap of the barrier layer at the weld line (206). Although the barrier layer is not continuous across the weld line, sufficient overlap will create a tortuous path for permeation, and the barrier properties will be maintained

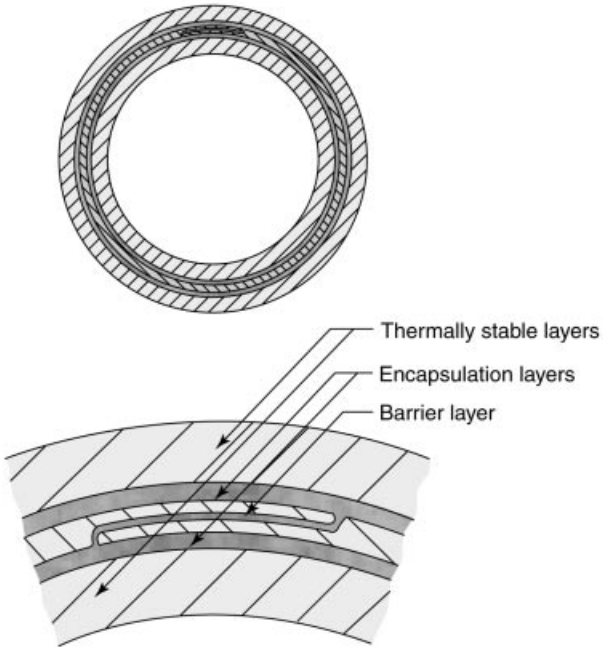

Fig. 15. Multilayer blown film with enlarged view showing overlap of barrier layer (206).

across the weld. This technology has only been recently applied to large blown-film dies. Five- to seven-layer blown-film dies up to 51-cm (20-in.) diameter have been demonstrated using this technology (207–210). These new blown-film dies also incorporate temperature isolation techniques that allow VDC resins to be coextruded with resins such as nylon that require much higher melt temperatures. Similar to the monolayer films, multilayer films are used predominately in food packaging and medical applications.

Multilayer Sheet Extrusion. Rigid containers for food packaging can be made from coextruded sheet that contains a layer of a barrier polymer (211–213). A simple example is a sheet with five layers that has a total thickness of about 1.3 mm (50 mil). The outermost layers might be polypropylene, polyethylene, polystyrene, high impact polystyrene (HIPS), or other nonbarrier polymer having good mechanical properties. The innermost barrier layer is about 125 μm (5 mil) of a VDC copolymer. Adhesive layers connect the outer layers and the barrier layer. This coextruded sheet can be formed into containers by any of several techniques, including solid-phase pressure forming and melt-phase forming. The final container has a total wall thickness of about 500 μm (20 mil) and a barrier layer that is about 50 μm (2 mil) thick. Such a container is capable of protecting oxygen-sensitive foods at ambient temperatures for a year or more. These containers are lightweight, microwavable, nonbreakable, and attractive. More sophisticated containers may have more than five layers and improved economics by including a layer of scrap or recycled polymers in the structure.

Lacquer Resins. Vinylidene chloride copolymers have several properties that are valuable in the coatings industry: excellent resistance to gas and moisture vapor transmission, good resistance to attack by solvents and by fats and oils, high strength, and the ability to be heat-sealed (214,215). These characteristics result from the highly crystalline nature of the very high VDC content of the polymer, which ranges from ~80 to 90 wt%. Minor constituents in these copolymers generally are vinyl chloride, alkyl acrylates, alkyl methacrylates, acrylonitrile, methacrylonitrile, and vinyl acetate. Small concentrations of vinylcarboxylic acids, eg, acrylic acid, methacrylic acid, or itaconic acid, are sometimes included to enhance adhesion of the polymer to the substrate. The ability to crystallize and the extent of crystallization are reduced with increasing concentration of the comonomers; some commercial polymers do not crystallize. The most common lacquer resins are terpolymers of VDC–MMA–AN (216,217). The VDC level and the MMA–AN ratio are adjusted for the best balance of solubility and permeability. These polymers exhibit a unique combination of high solubility, low permeability, and rapid crystallization (218).

Acetone, methyl ethyl ketone, methyl isobutyl ketone, dimethylformamide, ethyl acetate, and tetrahydrofuran are solvents for VDC polymers used in lacquer coatings; methyl ethyl ketone and tetrahydrofuran are most extensively employed. Toluene is used as a diluent for either. Lacquers prepared at 10–20 wt% polymer solids in a solvent blend of two parts ketone and one part toluene have a viscosity of 20–1000 mPa·s (=cP). Lacquers can be prepared from polymers of very high VDC content in tetrahydrofuran–toluene mixtures and can be stored at room temperature. Methyl ethyl ketone lacquers must be prepared and maintained at 60–70°C or the lacquer forms a solid gel. It is critical in the manufacture of polymers for a lacquer application to maintain a fairly narrow compositional distribution in the polymer to achieve good dissolution properties.

The lacquers are applied commercially by roller coating, doctor and dip coating, knife coating, and spraying. Spraying is useful only with lower viscosity lacquers, and solvent balance is important to avoid webbing from the spray gun. Solvent removal is difficult from heavy coatings, and multiple coatings are recommended where a heavy film is desired. Sufficient time must be allowed between coats to avoid lifting of the previous coat by the solvent. In the machine coating of flexible substrates, eg, paper and plastic films, the solvent is removed by ir heating or forced-air drying at 90–140°C. Temperatures of 60–95°C promote the recrystallization of the polymer after the solvent has been removed. Failure to recrystallize the polymer leaves a soft, amorphous coating that blocks or adheres between concentric layers in a rewound roll. A recrystallized coating can be rewound without blocking. Handling properties of the coated film are improved with small additions of wax as a slip agent and of talc or silica as an antiblock agent to the lacquer system. The concentration of additives is kept low to prevent any serious detraction from the vapor transmission properties of the VDC copolymer coating. For this reason, plasticizers are seldom, if ever, used.

A primary use of VDC copolymer lacquers is the coating of films made from regenerated cellulose or of board or paper coated with polyamide, polyester, polypropylene, poly(vinyl chloride), and polyethylene. The lacquer imparts resistance to fats, oils, oxygen, and water vapor (219). These coated products are used mainly in the packaging of foodstuffs, where the additional features of inertness, lack of odor or taste, and nontoxicity are required. Vinylidene chloride copolymers have been used extensively as interior coatings for ship tanks, railroad tank cars, and fuel storage tanks, and for coating of steel piles and structures (220,221). The excellent chemical resistance and good adhesion result in excellent long-term performance of the coating. Brushing and spraying are suitable methods of application.

The excellent adhesion to primed films of polyester combined with good dielectric properties and good surface properties makes VDC copolymers very suitable as binders for iron oxide pigmented coatings for magnetic tapes (222–224). They perform very well in audio, video, and computer tapes.

Vinylidene Chloride Copolymer Latex. Vinylidene chloride copolymers can be made in emulsion, and then isolated, dried, and used as coating or extrusion resins. Stable latices have been prepared and can be used directly for coatings (225–230). The principal applications for these materials are as barrier coatings on paper products and, more recently, on plastic films. The heat-seal characteristics of VDC copolymer coatings are equally valuable in many applications. They are also used for paints and as binders for nonwoven fabrics (231). Special VDC copolymer latices are used for barrier laminating adhesives, and the use of VDC copolymers in flame-resistant carpet backing is well known (232–235). VDC latices can also be used to coat poly(ethylene terephthalate) bottles to retain carbon dioxide (236).

Poly(vinylidene chloride) latices can be easily prepared by the same methods but have few uses because they do not form films. Copolymers of high VDC content are film-forming when freshly prepared but soon crystallize and lose this desirable characteristic. Because crystallinity in the final product is very often desirable, eg, in barrier coatings, a significant developmental problem has been to prevent crystallization in the latex during storage and to induce rapid

Table 22. Properties of a Typical Barrier Latex

Properties	Value
Total solids, wt%	54–56
Viscosity at 25°C, mPa·s (=cP)	25
pH	2
Color	Creamy white
Particle size, nm	ca 250
Density, g/cm^3	1.30
Mechanical stability	Excellent
Storage stability	Excellent
Chemical stability	Not stable to di- or trivalent ions

crystallization of the polymer after coating. This has been accomplished by using the proper combination of comonomers with VDC.

Most VDC copolymer latices are made with varying amounts of acrylates, methacrylates, and acrylonitrile, as well as minor amounts of vinylcarboxylic acids, eg, itaconic and acrylic acids. Low foam latices having high surface tension are prepared with copolymerizable sulfonate monomers (233,235–237). The total amount of comonomer ranges from about 8 wt% for barrier latices to as high as 60 wt% for binder and paint latices. The properties of a typical barrier latex used for paper coating are listed in Table 22. Barrier latices are usually formulated with antiblock, slip, and wetting agents. They can be deposited by conventional coating processes, eg, with an air knife (238,239).

Coating speeds in excess of 305 m/min can be attained. The latex coating can be dried in forced-air or radiant-heat ovens (240,241). Multiple coats are applied, particularly in paper coating, to reduce pinholing (242). A precoat is often used on porous substances to reduce the quantity of the more expensive VDC copolymer latex needed for covering (243). The properties of a typical coating are listed in Table 23.

Vinylidene Chloride Copolymer Foams. Low density, fine-celled VDC copolymer foams can be made by extrusion of a mixture of VDC copolymer and a blowing agent at 120–150°C (244). The formulation must contain heat stabilizers, and the extrusion equipment must be made of noncatalytic metals to prevent accelerated decomposition of the polymer. The low melt viscosity of the VDC copolymer formulation limits the size of the foam sheet that can be extruded.

Expandable VDC copolymer microspheres are prepared by a microsuspension process (245). The expanded microspheres are used in reinforced polyesters, blocking multipair cable, and in composites for furniture, marble, and marine applications (246–249). Vinylidene chloride copolymer microspheres are also used in printing inks and paper manufacture (250).

Vinylidene Chloride Copolymer Ignition-Resistant Applications. The role of halogen-containing compounds in ignition and flame suppression has been studied for many years (251–256). Vinylidene chloride copolymers are an abundant source of organic chlorine, eg, often above 70 wt%. Vinylidene chloride emulsion copolymers are used in a variety of ignition-resistant binding applications (257,258). Powders dispersible in nonsolvent organic polymer intermediates, eg, polyols, are used for both reinforcement and ignition resistance in polyurethane

Table 23. Film Properties of VDC Copolymer Latex

Property	Value
Water vapor transmission at 38°C and 95% RH, nmol/(m·s)[a]	0.012[b]
Grease resistance	Excellent
Scorability and fold resistance	Moderate
Oxygen permeability at 25°C, nmol/(m·s·GPa)[c]	0.07
Heat sealability[d]	Good
Light stability	Fair
Density, g/cm^3	1.60
Color	Watery white
Clarity	Excellent
Gloss	Excellent
Odor	None

[a]To convert nmol/(m·s) to (g·mil)/(100 in.^{2}·d), multiply by 4.
[b]Values 0.37 g/(24 h·100 in.^{2}) for 0.5 mil.
[c]To convert nmol/(m·s·GPa) to (cm^3·mil)/(100 in.^{2}·d·atm), divide by 2.
[d]Face-to-face.

foams. Vinylidene chloride copolymer powder is also used as an ignition-resistant binder for cotton batt (259–261).

The halogenated polymers generate significantly more smoke than polymers that have aliphatic backbones, even though the presence of the halogen does increase the limiting oxygen index. Heavy-metal salts retard smoke generation in halogenated polymers (261,262). A VDC emulsion copolymer having a high AN graft can be used to make ignition-resistant acrylic fibers (263). A rubber-modified VDC copolymer combines good ignition resistance with good low temperature flexibility (264,265). The rubber-modified VDC copolymer has been evaluated in wire coating where better ignition resistance and lower smoke generation are needed.

Materials are also blended with VDC copolymers to improve toughness (265–268). Vinylidene chloride copolymer blended with ethylene–vinyl acetate copolymers improves toughness and lowers heat-seal temperatures (269,270). Adhesion of a VDC copolymer coating to polyester can be achieved by blending the copolymer with a linear polyester resin (271).

BIBLIOGRAPHY

"Vinylidene Chloride Polymers" in *EPST* 1st ed., Vol. 14, pp. 540–579, by R. A. Wessling and F. G. Edwards, The Dow Chemical Company; "Vinylidene Chloride Polymers" in *EPSE* 2nd ed., Vol. 17, pp. 492–531, by R. A. Wessling, D. S. Gibbs, P. T. DeLassus, The Dow Chemical Company; B. A. Howell, Central Michigan University.

1. R. A. Wessling, *Polyvinylidene Chloride*, Gordon & Breach, New York, 1977.
2. R. A. Wessling and co-workers, in J. I. Kroschwitz, ed., Kirk-Othmer: Encyclopedia of Chemical Technology, 4th ed., Vol. **24**, John Wiley & Sons, Inc., New York, 1997, pp. 882–923.
3. *Vinylidene Chloride Monomer Safe Handling Guide*, No. 00-6339-88-SAI, The Dow Chemical Co., Midland, Mich., 1988.

4. L. G. Shelton, D. E. Hamilton, and R. H. Fisackerly, in E. C. Leonard, ed., *Vinyl and Diene Monomers, High Polymers*, Vol. **24**, Wiley-Interscience, New York, 1971, pp. 1205–1282.
5. P. T. DeLassus and D. D. Schmidt, *J. Chem. Eng. Data* **26**, 274 (1981).
6. U.S. Pat. 2,238,020 (Apr. 8, 1947), A. W. Hanson and W. C. Goggin (to The Dow Chemical Co.).
7. U.S. Pat. 3,760,015 (Sept. 18, 1973), S. Berkowitz (to FMC Corp.).
8. U.S. Pat. 3,870,762 (Mar. 11, 1975), M. H. Stacey and T. D. Tribbeck (to Imperial Chemical Industries, Ltd.).
9. U.S. Pat. 4,225,519 (Sept. 30, 1980), A. E. Reinhardt III (to PPG Industries).
10. P. W. Sherwood, *Ind. Eng. Chem.* **54**, 29 (1962).
11. U.S. Pat. 2,293,317 (Aug. 18, 1942), F. L. Taylor and L. H. Horsley (to The Dow Chemical Co.).
12. P. L. Viola and A. Caputo, *Environ. Health Perspect.* **21**, 45 (1977).
13. C. C. Lee and co-workers, *J. Toxicol. Environ. Health* **4**, 15 (1978).
14. V. Ponomarkov and L. Tomatis, *Oncology* **37**, 136 (1980).
15. R. D. Short and co-workers, EPA Report, No. PB281713, Environmental Protection Agency, Washington, D.C., 1977.
16. T. R. Blackwood, D. R. Tierney, and M. R. Piana, EPA Report, No. PB80-146442, Environmental Protection Agency, Washington, D.C., 1979.
17. J. M. Norris, *personal communication*, The Dow Chemical Co., Midland, Mich., 1982.
18. M. J. McKenna, P. G. Watanabe, and P. J. Gehring, *Environ. Health Perspect.* **21**, 99 (1977).
19. M. G. Ott and co-workers, *J. Occup. Med.* **18**, 735 (1976).
20. J. Hushon and M. Kornreich, EPA Report, No. PB280624, Environmental Protection Agency, Washington, D.C., 1978.
21. G. Talamini and E. Peggion, in G. E. Ham, ed., *Vinyl Polymerization*, Vol. **1**, Marcel Dekker, Inc., New York, 1967, Part 1, Chapt. "5".
22. P. J. Flory, *Principles of Polymer Chemistry*, Cornell University Press, Ithaca, N.Y., 1953, Chapt. "6".
23. W. H. Stockmayer, K. Matsuo, and G. W. Nelb, *Macromolecules* **10**, 654 (1977).
24. J. D. Burnett and H. W. Melville, *Trans. Faraday Soc.* **46**, 976 (1950).
25. C. E. Bawn, T. P. Hobin, and W. J. McGarry, *J. Chem. Phys.* **56**, 791 (1959).
26. W. J. Burlant and D. H. Green, *J. Polym. Sci.* **31**, 227 (1958).
27. R. C. Reinhardt, *Ind. Eng. Chem.* **35**, 422 (1943).
28. W. I. Bengough and R. G. W. Norrish, *Proc. R. Soc. London, Ser. A* **218**, 149 (1953).
29. R. A. Wessling and I. R. Harrison, *J. Polym. Sci., Part A-1,* **9**, 3471 (1971).
30. G. Odian, *Principles of Polymerization*, John Wiley & Sons, Inc., New York, 1981, Chapt. "3".
31. B. E. Obi and co-workers, *J. Polym. Sci, Part B: Polyms. Phys.* **33**, 2019–2032 (1995).
32. J. L. Gardon, in C. E. Schildknecht, ed., *Polymerization Processes*, John Wiley & Sons, Inc., New York, 1977, Chapt. "6".
33. R. A. Wessling, *J. Appl. Polym. Sci.* **12**, 309 (1968).
34. R. A. Wessling and D. S. Gibbs, *J. Macromol. Sci., A: Chem.* **7**, 647 (1973).
35. A. Konishi, *Bull. Chem. Soc. Jpn.* **35**, 197 (1962).
36. A. Konishi, *Bull. Chem. Soc. Jpn.* **35**, 193 (1962).
37. A. P. Sheniker and co-workers, *Dokl. Akad. Nauk SSSR* **124**, 632 (1959).
38. D. R. Roberts and R. H. Beaver, *J. Polym. Sci., Polym. Lett. Ed.* **17**(3), 155 (1979).
39. B. A. Howell, A. M. Kelly-Rowley, and P. B. Smith, *J. Vinyl. Tech.* **11**, 159 (1989).
40. A. R. Westwood, *Eur. Polym. J.* **7**, 377 (1971).
41. J. F. Gabbett and W. Mayo Smith, in G. E. Ham, ed., *Copolymerization*, John Wiley & Sons, Inc., New York, 1964, Chapt. "10".

42. J. Brandrup and E. H. Immergut, eds., *Polymer Handbook*, 2nd ed., John Wiley & Sons, Inc., New York, 1975.
43. K. Matsuo and W. H. Stockmayer, *Macromolecules* **10**, 658 (1977).
44. W. I. Bengough and R. G. W. Norrish, *Proc. R. Soc. London, Ser. A* **218**, 155 (1953).
45. C. Pichot, Q. T. Pham, and J. Guillot, *J. Macromol. Sci., Chem.* **12**, 1211 (1978).
46. C. Pichot and Q. T. Pham, *Eur. Polym. J.* **15**, 833 (1979).
47. B. E. Obi, *Technical data*, The Dow Chemical Company, Midland, MI, 1995.
48. N. Yamazaki and co-workers, *Polym. Prepr. (Am. Chem. Soc., Div. Polym. Chem.)* **5**, 667 (1964).
49. A. Konishi, *Bull. Chem. Soc. Jpn.* **35**, 395 (1962).
50. B. L. Erusalimskii and co-workers, *Dokl. Akad. Nauk SSSR* **169**, 114 (1966).
51. Brit. Pat. 1,119,746 (July 10, 1968) (to Chisso Corp.).
52. Can. Pat. 798,905 (Nov. 12, 1968), R. Buning and W. Pungs (to Dynamit Nobel Corp.).
53. U.S. Pat. 3,366,709 (Jan. 30, 1968), M. Baer (to Monsanto Co.).
54. U.S. Pat. 3,509,236 (Apr. 28, 1970), H. G. Siegler, R. B. Oberlar, and W. Pungs (to Dynamit Nobel Aktiengeselfichaft Co.).
55. U.S. Pat. 3,655,553 (Apr. 11, 1972), R. C. DeWald (to Firestone Tire and Rubber Co.).
56. M. Pegoraro, E. Beati, and J. Bilalov, *Chim. Ind. Milan* **54**, 18 (1972).
57. T. Fisher, J. B. Kinsinger, and C. W. Wilson, *Polym. Lett.* **5**, 285 (1967).
58. M. Meeks and J. L. Koenig, *J. Polym. Sci., Part A-1* **9**, 717 (1971).
59. S. Krimm, *Fortschr. Hochpolym. Forsch.* **2**, 51 (1960).
60. K. Matsuo and W. H. Stockmayer, *Macromolecules* **8**, 660 (1975).
61. K. Okuda, *J. Polym. Sci., Part A* **2**, 1749 (1964).
62. E. J. Arlman and W. M. Wagner, *Trans. Faraday Soc.* **49**, 832 (1953).
63. M. M. Coleman and co-workers, *J. Macromol. Sci., Phys.* **15**, 463 (1987).
64. M. S. Wu and co-workers, *J. Polym. Sci., Polym. Phys. Ed.* **18**, 95 (1980).
65. M. S. Wu and co-workers, *J. Polym. Sci., Polym. Phys. Ed.* **18**, 111 (1980).
66. R. H. Boyd and L. Kesner, *J. Polym. Sci., Polym. Phys. Ed.* **19**, 393 (1981).
67. B. E. Obi, P. T. DeLassus, and E. A. Grulke, *Macromolecules* **27**, 5491–5497 (1994).
68. R. F. Boyer and R. S. Spencer, *J. Appl. Phys.* **15**, 398 (1944).
69. K. H. Illers, *Kolloid Z.* **190**, 16 (1963).
70. R. A. Wessling and co-workers, *Appl. Polym. Symp.* **25**, 83 (1974).
71. N. W. Johnston, *Rev. Macromol. Chem. C* **14**, 215 (1976).
72. G. R. Riser and L. P. Witnauer, *Polym. Prepr. (Am. Chem. Soc., Div. Polym. Chem.)* **2**, 218 (1961).
73. B. G. Landes, P. T. DeLassus, and I. R. Harrison, *J. Macromol. Sci. B* **22**, 735 (1984).
74. R. A. Wessling, J. H. Oswald, and I. R. Harrison, *J. Polym. Sci., Polym. Phys. Ed.* **11**, 875 (1973).
75. I. R. Harrison and E. Baer, *J. Colloid Interface Sci.* **31**, 176 (1969).
76. R. A. Wessling, D. R. Carter, and D. L. Ahr, *J. Appl. Polym. Sci.* **17**, 737 (1973).
77. A. F. Burmester and R. A. Wessling, *Bull. Am. Phys. Soc.* **18**, 317 (1973).
78. M. Asahina, M. Sato, and T. Kobayashi, *Bull. Chem. Soc. Jpn.* **35**, 630 (1962).
79. R. A. Wessling, *J. Appl. Polym. Sci.* **14**, 1531 (1970).
80. R. A. Wessling, *J. Appl. Polym. Sci.* **14**, 2263 (1970).
81. M. L. Wallach, *Polym. Prepr. (Am. Chem. Soc., Div. Polym. Chem.)* **10**, 1248 (1969).
82. A. Revillion, B. Dumont, and A. Guyot, *J. Polym. Sci., Polym. Chem. Ed.* **14**, 2263 (1976).

83. A. Revillion, *J. Liq. Chromatogr.* **3**, 1137 (1980).
84. G. S. Kolesnikov and co-workers, *Izu. Akad. Nauk SSSR Otd. Khim. Nauk* 731 (1959).
85. E. F. Jordan and co-workers, *J. Appl. Polym. Sci.* **13**, 1777 (1969).
86. S. W. Lasoski, *J. Appl. Polym. Sci.* **4**, 118 (1960).
87. S. W. Lasoski and W. H. Cobbs, *J. Polym. Sci.* **36**, 21 (1959).
88. H. J. Bixler and O. S. Sweeting, in O. J. Sweeting, ed., *The Science and Technology of Polymer Films*, Vol. **2**, Wiley-Interscience, New York, 1971, Chapt. "1".
89. P. T. DeLassus, *J. Vinyl Technol.* **1**, 14 (1979).
90. P. T. DeLassus and D. J. Grieser, *J. Vinyl Technol.* **2**, 195 (1980).
91. P. T. DeLassus, *J. Vinyl Technol.* **3**, 240 (1981).
92. *Introduction to Barrier Polymer Performance*, No. 190-333-1084, The Dow Chemical Co., Midland, Mich., 1984.
93. *Permeability of Polymers to Gases and Vapors*, No. P302-336-79, The Dow Chemical Co., Midland, Mich., 1979.
94. *Kuraray EVAL Resin*, No. 6-1000-605, Kuraray Co., Ltd., Osaka, Japan, 1986.
95. P. T. DeLassus, in Proceedings of COEX America, Scotland, 1986, p. 187.
96. P. T. DeLassus, in J. I. Kroschwitz, ed., Kirk-Othmer: Encyclopedia of Chemical Technology, 4th ed., Vol. **3**, John Wiley & Sons, Inc., New York, 1992, pp. 931–962.
97. G. Strandburg, P. T. DeLassus, and B. A. Howell, in S. A. Risch and J. H. Hotchkiss, eds., *Food and Packaging Interactions II* (ACS Symposium Series No. 473), American Chemical Society, Washington, D.C., 1991, pp. 133–148.
98. P. T. DeLassus and co-workers, in J. H. Hotchkiss, ed., *Food and Packaging Interactions* (ACS Symposium Series No. 365), American Chemical Society, Washington, D.C., 1988, Chapt. "2", pp. 11–27.
99. P. T. DeLassus, G. Strandburg, and B. A. Howell, *TAPPI J.* **71**(11), 177–181 (1988).
100. G. Strandburg, P T. DeLassus, and B. A. Howell, in W. J. Karos, ed., *Barrier Polymers and Structures* (ACS Symposium Series No. 423), American Chemical Society, Washington, D.C., 1990, pp. 333–350.
101. R. F. Boyer, *J. Phys. Colloid Chem.* **51**, 80 (1947).
102. G. M. Burnett, R. A. Haldon, and J. N. Hay, *Eur. Poly. J.* **4**, 83 (1968).
103. B. A. Howell and P. T. DeLassus, *J. Polym. Sci., Polym. Chem. Ed.* **25**, 1967 (1987).
104. U.S. Pat. 3,321,417 (May 23, 1967) (to Union Carbide Corp.); N. L. Zutty and F. J. Welch, *J. Polym. Sci., Part A* **1**, 2289 (1963).
105. B. A. Howell, *J. Polym. Sci., Polym. Chem. Ed.* **25**, 1981 (1987), and references cited therein.
106. R. R. Lagasse and J. L. Schroeder, *Mater. Res. Soc. Symp. Proc.* **371**, 432 (1995).
107. J. D. Danforth, *Polym. Prepr.* **21**, 140 (1980).
108. J. D. Danforth, in P. O. Klemchuk, ed., *Polymer Stabilization and Degradation*, American Chemical Society, Washington, D.C., 1985, Chapt. "20", and references cited therein.
109. D. H. Everett and D. J. Taylor, *Trans. Faraday Soc.* **67**, 402 (1971).
110. D. Vesely, *Ultramicroscopy* **14**, 279 (1984).
111. I. R. Harrison and E. Baer, *J. Colloid Interface Sci.* **31**, 176 (1969).
112. D. R. Roberts and A. L. Gatzke, *J. Polym. Sci., Polym. Chem. Ed.* **16**, 1211 (1978).
113. B. Dolezel, M. Pegoraro, and E. Beati, *Eur. Polym. J.* **6**, 1411 (1970).
114. T.-H. Hsieh, *Polym. J.* **31**, 948 (1999).
115. T.-H. Hsieh and K.-S. Ho, *J. Polym. Sic., Part A: Polym. Chem.* **37**, 2035 (1999).
116. R. J. Pasek, D. P. Y. Chang, and A. D. Jones, *Hazard. Waste Hazard. Mater.* **13** 23 (1996).

117. P. Pendleton, B. Vincent, and M. L. Hair, *J. Colloid Interface Sci.* **80**, 512 (1981).
118. R. D. Bohme and R. A. Wessling, *J. Appl. Polym. Sci.* **16**, 1961 (1972).
119. A. Crovato-Arnaldi and co-workers, *J. Appl. Polym. Sci.* **8**, 747 (1964).
120. G. M. Burnett, R. A. Haldon, and J. N. Hay, *Eur. Polym. J.* **3**, 449 (1967).
121. R. A. Wessling, *Am. Chem. Soc. Div. Org. Coat. Plast. Chem. Pap.* **34**, 380 (1976).
122. F. F. He and H. Kise, *J. Polym. Sci., Polym. Chem. Ed.* **21**, 1972 (1983).
123. D. H. Davies, *J. Chem. Soc. Faraday Trans. 1* **72**, 2390 (1976).
124. E. Tsuchido and co-workers, *J. Polym. Sci., Part A* **2**, 3347 (1964).
125. S. S. Barton and co-workers, *Trans. Faraday Soc.* **67**, 3534 (1971).
126. S. S. Barton, J. R. Dacey, and B. H. Harrison, *Am. Chem. Soc. Div. Org. Coat. Plast. Chem. Pap.* **31**, 768 (1971).
127. Y. V. Konotsur, G. S. Shapoval, and A. A. Pud, *Theor. Exp. Chem.* **33**, 150 (1997).
128. B. A. Howell, S. I. Ahmed, and D. E. Beyer, *Polym. Prepr. (Am. Chem. Soc., Div. Polym. Chem.)* **42**, 868 (2001).
129. A. L. Evelyn and co-workers, in J. L. Duggan and I. L. Morgan, eds., *Application of Accelerators in Research and Industry*, AIP Press, New York, 1997, pp. 933–936.
130. A. K. Srivastava and H. S. Virk, *Indian J. Pure Appl. Phys.* **37**, 713 (1999).
131. A. M. Shaban, *Mater. Lett.* **22**, 309 (1995).
132. A. Bailey and D. H. Everett, *J. Polym. Sci., Part A-2* **7**, 87 (1969).
133. B. A. Howell and co-workers, in Proceedings of 28th North American Thermal Analysis Society Meeting, 2000, p. 283–286.
134. R. Simon, *Polym. Degr. Stab.* **43**, 125 (1994).
135. B. A. Howell, *Thermochim. Acta* **148**, 375 (1989).
136. B. A. Howell, *Thermochim. Acta* **134**, 207 (1988).
137. G. M. Burnett, R. A. Haldon, and J. N. Hay, *Eur. Polym. J.* **3**, 449 (1967).
138. D. E. Agostini and A. L. Gatzke, *J. Polym. Sci., Polym. Chem. Ed.* **11**, 649 (1973).
139. B. A. Howell, P. T. DeLassus, and C. Gerig, *Polym. Prepr.* **28**, 278 (1987).
140. S. Collins and co-workers, *Polym. Degrad. Stab.* **66**, 87 (1999).
141. B. A. Howell, Z. Ahmed, and S. I. Ahmed, *Thermochim. Acta* **357**, 103 (2000).
142. P. L. Kumler and co-workers, *Macromolecules* **22**, 2994 (1989).
143. V. Rossbach and co-workers, *Angew. Makromol. Chem.* **40/41**, 291 (1974).
144. D. H. Grant, *Polymer* **11**, 581 (1970).
145. D. L. C. Jackson and W. S. Reid, *Nature* **162**, 29 (1948).
146. B. A. Howell and P. B. Smith, *J. Polym. Sci., Polym. Phys. Ed.* **26**, 1287 (1988).
147. D. H. Davies and P. M. Henheffer, *Trans. Faraday Soc.* **66**, 2329 (1970).
148. E. Tsuchida and co-workers, *J. Polym. Sci., Part A* **2**, 3347 (1964).
149. S. S. Barton and co-workers, *Trans. Faraday Soc.* **67**, 3534 (1971).
150. S. E. Evsyukov, S. Paasch, and B. Thomas, *Ber. Bunsen-Ges.* **101**, 837 (1997).
151. T. Danno, K. Murakami, and R. Ishikawa, in AIP Conf. Proc., 1999, p. 486.
152. B. A. Howell and H. Liu, *Thermochim. Acta* **212**, 1 (1992).
153. B. A. Howel and F. M. Uhl, *Thermochim. Acta* **357**, 113 (2000).
154. B. A. Howell and F. M. Uhl, *Polym. Prepr.* **39**, 663 (1998).
155. B. A. Howell and B. B. S. Sastry, in Proceedings of 22nd North American Thermal Analysis Society Meeting, 1993, pp. 122–127.
156. U.S. Pat. 3,852,223 (Dec. 3, 1974), R. D. Bohme and R. A. Wessling (to The Dow Chemical Co.).
157. A. Ballistreri and co-workers, *Polymer* **22**, 131 (1981).
158. S. Gopalkrishnan and W. H. Starnes Jr., *Polym. Prepr.* **30**, 201 (1989).
159. B. A. Howell and J. R. Keeley, *Thermochim. Acta* **272**, 131 (1996).
160. B. A. Howell and co-workers, *Thermochim. Acta* **166**, 207 (1990).
161. B. A. Howell, M. F. Debney, and C. V. Rajaram, *Thermochim. Acta* **212**, 115 (1992).

162. S. R. Betso and co-workers, *J. Appl. Polym. Sci.* **51**, 781 (1994).
163. B. A. Howell and C. V. Rajaram, *J. Vinyl Tech.* **15**, 202 (1993).
164. B. A. Howell and co-workers, *Polym. Adv. Tech.* **5**, 485 (1994).
165. B. A. Howell and co-workers, *Thermochim. Acta* **272**, 139 (1996).
166. J. Ozaki, T. Watanabe, and Y. Nishiyama, *J. Phys. Chem.* **97**, 1400 (1983).
167. B. A. Howell and A. Q. Campbell, *Thermochim. Acta* **340**, 231 (1999).
168. L. A. Matheson and R. F. Boyer, *Ind. Eng. Chem.* **44**, 867 (1952).
169. G. Oster, G. K. Oster, and M. Kryszewski, *J. Polym. Sci.* **57**, 937 (1962).
170. M. Kryszewski and M. Mucha, *Bull. Acad. Pol. Sci. Ser. Sci. Chim. Geol. Geogr.* **13**, 53 (1965).
171. Y. Izumi, S. Kawanishi, N. Takagi, S. Honda, and T. Yamamoto, *Bull. Chem. Soc. Jpn.* **71**, 2459 (1998).
172. H. Niino and A. Yabe, *J. Polym. Sci., Part A: Polym. Chem.* **36**, 2483 (1998).
173. A. Yabe, *Phys. Chem. Mater. Low-Dimens. Struct.* **21**, 75 (1999).
174. R. R. Lagasse and J. L. Schroeder, *Mater. Res. Soc. Symp. Proc.* **371** 431 (1995).
175. U.S. Pat. 4,418,168 (Nov. 29, 1983), E. H. Johnson (to the Dow Chemical Co.).
176. B. A. Howell, F. M. Uhl, and D. Townsend, *Thermochim. Acta* **357**, 127 (2000).
177. B. A. Howell and J. Zhang, *Polym. Prepr. (Am. Chem. Soc., Div. Polym. Chem.)* **42**, 880 (2001).
178. B. A. Howell, D. A. Spears, and P. B. Smith, in Proceedings of the 24th North American Thermal Analysis Society Meeting, San Fransico, 1995.
179. B. A. Howell and B. Pan, *Thermochim. Acta* **357**, 119 (2000).
180. U.S. Pat. 3,033,812 (May 8, 1962), P. K. Isacs and A. Trofimow (to W. R. Grace & Co.).
181. D. M. Woodford, *Chem. Ind. (London)* **8**, 316 (1966).
182. U.S. Pat. 2,968,651 (Jan. 17, 1961), L. C. Friedrich Jr., J. W. Peters, and M. R. Rector (to The Dow Chemical Co.).
183. U.S. Pat. 2,482,771 (Sept. 27, 1944), J. Heerema (to The Dow Chemical Co.).
184. W. C. Goggin and R. D. Lowrey, *Ind. Eng. Chem.* **34**, 327 (1942).
185. A. T. Widiger and R. L. Butler, in O. J. Sweeting, ed., *The Science and Technology of Polymer Films*, Wiley-Interscience, New York, 1971, pp. 333–339.
186. *Saran Polymers for Barrier Packaging*, Form No. 190-00445-992, The Dow Chemical Co., Midland, Mich., 1996.
187. Z. Li and Y. Peng, *Suliao* **27**(2), 40–43 (1998).
188. S. R. Jenkins and co-workers, in 1998 Polymers, Laminations and Coating Conference, Book 2, TAPPI Press, Atlanta, 1989, p. 501.
189. M. A. Spalding and co-workers, *Polym. Eng. Sci.* **35**, 1907 (1995).
190. U.S. Pat. 5,006,368 (Apr. 9, 1991), P. T. Louks (to The Dow Chemical Co.).
191. C. E. Schildknecht, *Vinyl and Related Polymers*, John Wiley and Sons, Inc., New York (1952).
192. *Saran Resins*, No. 190-289-79, The Dow Chemical Co., Midland, Mich., 1979.
193. E. D. Serdynsky, in H. F. Mark, S. M. Atlas, and E. Cernia, eds., *Man-Made Fibers: Science and Technology*, Vol. **3**, Wiley-Interscience, New York, 1968, pp. 317–322.
194. *Product Literature*, Fugafil-saran GmbH & Co., 2001.
195. S. Jenkins and J. Naumovitz, *Packed with Performance*, Vol. **3**, The Dow Chemical Co., Midland, Mich., May 1999.
196. D. Zuo, *Shanghai Chem. Ind.* **22**(6), 40–43 1997.
197. W. R. R. Park, *Plastics Film Technology*, Van Nostrand Reinhold Company, Newy York, 1969.
198. J. H. Briston, *Plastics Films*, 3rd ed., Longman Scientific & Technical, Essex, England, 1988.

199. C. J. Benning, *Plastics Films for Packaging*, Technomic Publishing Co., Lancaster, Pa., 1989, p. 31.
200. H. Tamber, in PVDC Films, Plast-Ex '98 Technical Conference, 1998.
201. *Technical Datasheets*, Form No. 190-(00481 through 00487)-01, The Dow Chemical Co., Midland, Mich., 2001.
202. D. L. Roodvoets, in P. F. Bruin, ed., *Packaging with Plastics*, Gordon & Breach, New York, 1974, p. 85.
203. *SARANEX Barrier Medical Films*, Form No. 500-01814-1199, The Dow Chemical Co., Midland, Mich., 1999.
204. *SARANEX Coextruded Barrier Film*, Form No. 500-01923-0401, The Dow Chemical Co., Midland, Mich., 2001.
205. U.S. Pat. 4,643,927, (Feb. 17, 1987), R. A. Luecke (to The Dow Chemical Co.)
206. U.S. Pat. 4,842,791, (Jun. 27, 1989), G. E. Gould and R. A. Luecke (to The Dow Chemical Co.)
207. H. Tamber, in Advanced Technology Seminar, Macro Engineering & Technology Inc., Mississauga, Ontario, Canada, Sept. 1999.
208. *Can. Plast.* **59**(9), 17 (2000).
209. H. Tamber, "Barrier Films Containing PVDC/EVOH in Food & Medical Packaging Applications," in *Specialty Plastics Films 2000*, 16th Annual World Congress, on Global Film Resins, Markets, Applications, Zurich, Macro Engineering & Technology Inc., 2000.
210. *Plast. Technol.* **47**(1), 13 (2001).
211. *Rigid Coextruded Plastic Barrier Containers for Unrefrigerated Foods*, Form No. 190-337-1084, The Dow Chemical Co., Midland, Mich., 1984.
212. W. J. Schrenk and S. A. Marcus, in K. M. Finlayson, ed., *Plastic Film Technology*, Vol. **1**, Technomic Publishing Co., Lancaster, Pa., 1989, pp. 1–11.
213. R. J. Macy, in Ref. 211, pp. 220–226.
214. S. F. Roth, in American Chemical Society Chemical Marketing Economic Division Symposium (N.Y.), American Chemical Society, Washington, D.C., 1976, p. 29.
215. *Saran F Resin*, Technical Bulletin, The Dow Chemical Co., Horgen, Switzerland, 1969.
216. U.S. Pat. 3,817,780 (June 18, 1974), P. E. Hinkamp and D. F. Foye (to The Dow Chemical Co.).
217. U.S. Pat. 3,879,359 (Apr. 22, 1975), P. E. Hinkamp and D. F. Foye (to The Dow Chemical Co.).
218. U.S. Pat. 4,097,433 (June 27, 1978), W. P. Kane (to E. I. du Pont de Nemours & Co., Inc.).
219. U.S. Pat. 2,462,185 (Feb. 22, 1949), P. M. Hauser (to E. I. du Pont de Nemours & Co., Inc.).
220. W. W. Cranmer, *Corros. Houston* **8**(6), 195 (1952).
221. R. L. Alumbaugh, *Mater. Prot.* **3**(7), 34, 39 (1964).
222. U.S. Pat. 3,144,352 (Aug. 11, 1964), J. P. Talley (to Ampex Corp.).
223. U.S. Pat. 3,865,741 (Feb. 11, 1975), F. J. Sischka (to Memorex Corp.).
224. U.S. Pat. 3,894,306 (July 1, 1975), F. J. Sischka (to Memorex Corp.).
225. L. J. Wood, *Mod. Packag.* **33**, 125 (1960).
226. R. F. Avery, *Tappi J.* **45**, 356 (1962).
227. A. D. Jordan, *Tappi J.* **45**, 865 (1962).
228. B. J. Sauntson and G. Brown, *Rep. Prog. Appl. Chem.* **56**, 55 (1972).
229. P. S. Bryant, in European Flexographic Technical Association Barrier Coatings and Laminations Seminar, Vol. 1, Manchester, U.K., 1977, p. 7.
230. G. H. Elschnig and co-workers, *Pop. Plast.* **17**(2), 19 (1972).

231. U.S. Pat. 3,787,232 (Jan. 22, 1974), B. K. Mikofalvy and D. P. Knechtges (to B. F. Goodrich Co.).
232. R. G. Jahn, *Adhes. Age* **20**(6), 37 (1977).
233. U.S. Pat. 3,946,139 (Mar. 23, 1976), M. Bleyle and co-workers (to W. R. Grace & Co.).
234. U.S. Pat. 3,850,726 (Nov. 26, 1974), D. R. Smith and H. Peterson (to A. E. Staley Co.).
235. U.S. Pat. 3,617,368 (Nov. 2, 1971), D. S. Gibbs and R. A. Wessling (to The Dow Chemical Co.).
236. P. T. DeLassus, D. L. Clarke, and T. Cosse, *Mod. Plast.* **60**, 86 (Jan. 1983).
237. Brit. Pat. 1,233,078 (May 26, 1971), H. Gould and J. A. Zaslowsky (to Alcolac Chemical Co.).
238. G. H. Elschnig and A. F. Schmid, *Pop. Plast.* **17**(3), 36 (1972).
239. G. H. Elschnig and A. F. Schmid, *Pop. Plast.* **17**(4), 17 (1972).
240. G. H. Elschnig and A. F. Schmid, *Pop. Plast.* **17**(6), 17 (1972).
241. G. H. Elschnig and A. F. Schmid, *Paintindia* **22**(6), 22 (1972).
242. F. C. Caruso, in Proceedings of Test. Pap. Synth. Conf., TAPPI, Atlanta, Ga., 1974, p. 167.
243. E. A. Chirokas, *Tappi J.* **50**, 59A (1967).
244. U.S. Pat. 3,983,080 (Sept. 28, 1976), K. S. Suh, R. E. Skochdopole, and M. E. Luduc (to The Dow Chemical Co.).
245. U.S. Pat. 3,615,972 (Oct. 26, 1971), D. S. Morehouse and R. J. Tetreault (to The Dow Chemical Co.).
246. D. S. Morehouse and H. A. Walters, *SPE J.* **25**, 45 (1969).
247. T. E. Cravens, *Am. Chem. Soc. Div. Org. Coat. Plast. Chem. Pap.* **33**, 74 (1973).
248. R. C. Mildner and co-workers, *Mod. Plast.* **47**(5), 98 (1970).
249. T. F. Anderson, H. A. Walters, and C. W. Glesner, *J. Cell. Plast.* **6**(4), 171 (1970).
250. *Mater. Plast. Elastomer* **10**, 468 (Oct. 1980).
251. D. L. Chamberlain, in W. C. Kuryla and A. J. Papa, eds., *Flame Retardancy of Polymeric Materials*, Vol. **2**, Marcel Dekker, Inc., New York, 1973, pp. 109–168.
252. D. W. Van Krevelen, *Polymer* **16**, 615 (1975).
253. L. G. Imhoff and K. C. Stueben, *Polym. Eng. Sci.* **13**, 146 (1973).
254. E. R. Larsen, *J. Fire Flamm. Fire Ret. Chem.* **1**, 4 (1974).
255. E. R. Larsen, *J. Fire Flamm. Fire Ret. Chem.* **1**, 2, 5 (1974).
256. R. C. Kidder, in Proceedings of Fire Retardant Chemicals Association Semiannual Meeting, 1977, pp. 45–51.
257. J. Knightly and J. C. Bax, in Proceedings of the European Conference on Flammability Fire Retardance, 1979, pp. 75–83.
258. J. R. Goots and D. P. Knechtges, *Polym. Plast. Technol. Eng.* **5**, 131 (1975).
259. C. V. Neywick, R. E. Yoerger, and R. F. Peterson, *J. Cell. Plast.* **16**, 171 (1980).
260. U.S. Pat. 4,232,129 (Nov. 4, 1980), D. S. Gibbs, J. H. Benson, and R. T. Fernandez (to The Dow Chemical Co.).
261. U.S. Pat. 4,002,597 (Jan. 11, 1977), E. D. Dickens (to B. F. Goodrich Co.).
262. U.S. Pat. 4,055,538 (Oct. 25, 1977), W. J. Kronke (to B. F. Goodrich Co.).
263. U.S. Pat. 4,186,156 (Jan. 29, 1980), D. S. Gibbs (to The Dow Chemical Co.).
264. *Plast. Technol.* **26**(1), 13 (1980).
265. U.S. Pat. 4,206,105 (June 3, 1980), O. L. Stafford (to The Dow Chemical Co.).
266. U.S. Pat. 4,239,799 (Dec. 16, 1980), A. S. Weinberg (to W. R. Grace & Co.).
267. U.S. Pat. 3,840,620 (Oct. 8, 1974), R. Gallagher (to Stauffer Chemical Co.).
268. U.S. Pat. 3,513,226 (May 19, 1970), T. Hotta (to Kureha Kagaku Kogyo Kabushiki Kalsha Co.).
269. U.S. Pat. 3,565,975 (Feb. 23, 1971), F. V. Goff, F. Stevenson, and W. H. Wineland (to The Dow Chemical Co.).

270. U.S. Pat. 3,558,542 (Jan. 26, 1971), J. W. McDonald (to E. I. du Pont de Nemours & Co., Inc.).
271. U.S. Pat. 3,896,066 (July 22, 1975), R. O. Ranck (to E. I. du Pont de Nemours & Co., Inc.).

R. A. WESSLING
D. S. GIBBS
B. E. OBI
D. E. BEYER
The Dow Chemical Company
P. T. DELASSUS
Valparaiso University
B. A. HOWELL
Central Michigan University

VINYLIDENE FLUORIDE POLYMERS

Introduction

Poly(vinylidene fluoride) [24937-79-9] is the addition polymer of 1,1-difluoroethene [75-38-7], commonly known as vinylidene fluoride and abbreviated VDF or VF_2. The formula of the repeat unit in the polymer is $-[CH_2–CF_2]_n-$. The preferred acronym for the polymer is PVDF, but the abbreviation PVF_2 also is used frequently. (Note: PVF is the accepted acronym for poly(vinyl fluoride), $-[CH_2\text{-}CHF]_n-$.) The history and development of PVDF technology has been reviewed (1). This article deals only with *thermoplastic* VDF-based polymers having greater than 50 wt% VDF, and not *fluoroelastomeric* copolymer versions, which have significant levels of fluoro-comonomers to impart rubber-like properties and usually less than 50 wt% VDF. (see FLUOROCARBON ELASTOMERS).

Since the commercialization of this linear fluoropolymer in the mid-1960s, the applications have expanded until the production of the monomer VDF and polymer PVDF reached significant tonnages at the end of the twentieth century, albeit with essentially the same producers during the last decade. The worldwide PVDF market in 2000 was about 21,000 t according to several industry sources. PVDF usage is expected to grow at an average of about 6% for all fluoropolymers during the first decade of the twenty-first century (2). Several manufacturers (see Table 1) have announced that there would be significant capacity increases between 2000 and 2005. Applications are increasing rapidly in China and Southeast Asia as well as Japan and Korea with a high growth projection for the next few years in these areas.

The production of VDF and PVDF requires significant investment in corrosion-resistant pyrolysis reactors and low temperature distillation columns

Encyclopedia of Polymer Science and Technology. Copyright John Wiley & Sons, Inc. All rights reserved.

Table 1. Manufacturers of VDF and PVDF[a]

Producers and country of production	Trademarks
Alventia LLC–USA	
Joint venture – Solvay and Dyneon; VDF monomer only, starting 2000	
Atofina[b]–France, USA	KYNAR, KYNAR 500, KYNAR FLEX, KYNAR Superflex, KYNAR Powerflex, HYLAR
www.atofina.com (Paris)	
www.atofinachemicals.com (USA)	
Largest capacity VDF and PVDF producer; expansion underway 2002	
Ausimont–USA	
www.ausimont.com	
Large capacity VDF and PVDF	
Daikin–Japan	NEOFLON
Minimal production PVDF resins; VDF-based coating resins use trademark	
Dyneon–USA, Germany	DYNEON, HOSTAFLON
www.dyneon.com	
Not currently a PVDF producer; produces TFE-based polymers with VDF as comonomer at low content	
Creanova[c]–Germany	DYFLOR
www.creanovainc.com	
Very small amounts PVDF available	
Kirova–CHEPETSKY Khimichesky Kombinat–Russia	FLUOROPLAST
Small capacity PVDF	
Kureha Chemical Company–Japan	KF POLYMER
www.kureha.co.jp	
Moderate PVDF capacity—expansion underway for 2001	
Solvay–Belgium, USA	SOLEF
www.solvay.com	VIDAR
Large capacity Europe; USA production 2000	

[a]Locations and capacities of production sites may be found in the following reference: K.-L. Ring, A. Leder, M. Ishikawa- Yamaki, SRI International Chemical Economics Handbook Marketing Report, Dec. 1998; http://ceh.sric.sri.com/Reports/580.0700/index.html.
[b]Formerly Elf Atochem.
[c]Subsidiary of Degussa-Hüls, formerly Hüls America.

for the monomer; high pressure polymerization reactors and associated finishing equipment; and special environmental and waste handling processes. Raw material costs for the overall process of feedstock to monomer and polymer are high, depending upon the processes, but reflect to a large extent the pricing of anhydrous hydrogen fluoride, which is involved in the various manufacturing processes for VDF. Also the processes for the monomer and polymer are energy intensive. It is for these reasons that several manufacturers of PVDF have extra production capacity for VDF monomer to supply not only their internal PVDF polymer needs

but also to provide the large quantities needed by the manufacturers of VDF-based fluoroelastomers.

The demand for PVDF has been driven by a number of factors: (*1*) a unique set of properties, (*2*) the ease and versatility in processing and fabricating, (*3*) over 30 years of proven performance under various and severe thermal, chemical, radiation, weathering environments and (*4*) the need for special attributes. For example, PVDF parts are subjected to superheated steam temperatures in some chemical processes. It is used also in strong acid, chlorine, bromine, and ultrapure water systems as well as in special applications where fire resistance is required. And PVDF has been used extensively during the last 30 years in nuclear radiation environments because unlike most plastics it cross-links, retaining mechanical integrity, rather than degrades. In one of the major applications worldwide, there is now over 30 years exposure of thin PVDF-based paint coatings on monumental structures and skyscrapers documenting the durability of these coatings to protect metal from corrosion, retaining essentially the original appearance features.

During the 1990s, there has been much activity in polymerization, scientific studies, and application development related to PVDF. Many copolymer variations and compounds of PVDF have been introduced by the polymer manufacturers and their immediate resin customers. This article will reference selected recent scientific and technology advances and focus upon property profiles and uses of the various PVDF grades available. A prior encyclopedia article (3) provides extensive references to the earlier studies. Detailed information on the properties and applications is given by the PVDF manufacturers at their websites. When the term *pvdf* is used to search the *Chemical Abstracts* databases from 1992, there are approximately 500 citations per year, about half of which are patents. Hence, the freedom to operate or utilize PVDF in any application by a new user should be verified by a careful check of the patent literature. In addition, producers of PVDF should be consulted regarding proposed medical applications, especially related to body invasive or implant technology.

PVDF is a partially crystalline, linear hydrofluorocarbon polymer that contains 59.4 wt% fluorine and 3 weight percent hydrogen. The high level of intrinsic crystallinity, typically near 60%, confers stiffness and tough, creep resistant properties. Incorporation of various fluorinated comonomers at low levels, typically about 5–10 wt% but as much as 20 wt% in some cases, enhances the flexibility of PVDF by reducing the crystallinity, which, in general, also reduces the end use temperature ratings. Commercial processes involve polymerization in emulsion or suspension using free-radical initiators. The spatial arrangement of the alternating CH_2 and CF_2 groups along the polymer chain and the strong dipole moment of the CF_2 accounts for the unique polarity, unusually high dielectric constant, complex polymorphism, and high piezoelectric and pyroelectric activity of the polymer when processed appropriately (4–6).

PVDF has the characteristic resistance of fluoropolymers to harsh chemical, thermal, ultraviolet, weathering, and oxidizing or high energy, ionizing radiation environments. The chemical resistance of this hydrofluorocarbon polymer is not as broad as exhibited by perfluoropolymers because the somewhat acidic hydrogen atoms along the chain are reactive in strongly basic media, leading to the formation of fluoride salt by-products (7,8). This chemical susceptibility has, in fact,

been turned to advantage in preparing PVDF samples for adherence to a variety of substrates as well as introducing reactive functionality for chemical grafting; the mechanism of the surface chemistry has been studied (9).

PVDF homopolymers and copolymers with various fluoroolefins have a wide range of applications including wire and cable products, electronic devices, chemical process equipment, use as a weather-resistant binder for exterior architectural finishes, and many specialized uses such as a stable binder for electroactive constituents in electrochemical cells. The polymer is readily melt-processed without processing aids or stabilizers using conventional molding or extrusion equipment; porous membranes are cast from solutions; and coatings are deposited from dispersions of PVDF using latent solvents, which solubilize the polymer at elevated temperatures, along with other additives to enhance the appearance, properties, and function. Certain grades of PVDF are used extensively for fluid handling components which convey high purity chemicals and ultrapure water because the resins may be fabricated easily into parts that have very low levels of extractable ionic or organic species and also very smooth surfaces that inhibit microbial fouling.

PVDF exhibits an unusual compatibility with other polymers having strong polar groups or carbonyl groups. This miscibility aspect has led to the development of many alloys and mixed systems for coatings, membranes, and extruded products.

In summary, PVDF fulfills special requirements in a variety of niche applications because of its unique characteristics. Hence, the broad and growing usage of this polymer is understandable. VDF usage also is increasing in other fluoropolymer and fluoroelastomer applications.

Monomer

Preparation. The principal industrial route to VDF involves dehydrochlorination of 1-chloro-1,1-difluoroethane (HCFC-142b) [75-68-3]. The principal producers are ATOFINA and Solvay in Europe and the United State and Ausimont and Alventia in the United States. Many patents exist for this and other similar preparative routes based upon dehydrohalogenation of various chlorofluorohydrocarbons or related compounds. Research efforts have escalated because the HCFC production will be curtailed in the mid-2000 period as a result of environmental concerns. Kureha (Japan) announced that their expansion would involve production of VDF from 1,1-difluoroethane (HFC-152a).

Properties. VDF is a colorless, flammable, and nearly odorless gas that has a very low boiling point like other small molecules with fluorine bonds. The physical properties are listed in Table 2. It is usually polymerized above its critical temperature and pressure, typically at pressures well above 3 MPa (30 atm), and approaching 10 MPa (100 atm) in some commercial processes; the polymerization is highly exothermic. Considering the flammability limits, caution must be exercised in any handling system.

Storage and Shipment. VDF (HFC-1132a) can be stored or shipped in gas cylinders or high-pressure tube trailers without polymerization inhibitors. Terpene and quinone inhibitors, however, may be used as a safety element where

Table 2. Physical Properties of VDF, $CH_2{=}CF_2$

	Units/conditions	Value
Molecular weight	Da	64.038
Boiling point	°C	−84
Freezing point	°C	−144
Vapor pressure	kPa @ 21°C	3683
Critical pressure	kPa	4434
Critical temperature	°C	30.1
Critical density	kg/m^3	417
Explosive limits	vol% in air	5.8–20.3
Heat of formation	kJ/mol @ 25°C	−345.2
Heat of polymerization	kJ/mol @ 25°C	−474.21
Water solubility	cm3/100 g @ 25°C/10 kPa	6.3

there might be uncertain environmental storage conditions. Liquid VDF can cause frostbite upon contact with the skin.

Health and Safety Factors. The combustion products are toxic. The OSHA website www.osha-slc.gov/ChemSamp_data/CH_275620.html provides the following information and full definitions of each classification code for environmental exposure and health factors as of year-end 2000.

Classification	Ratings	Comment
ACGIH TLV	500-ppm TWA	Not classifiable as a human carcinogen
NIOSH REL	1-ppm TWA; 5-ppm ceiling (15 min)	
IARC	Group 3	Not classifiable as to its carcinogenicity to humans

Uses. The variety of fluoropolymers and fluoroelastomers incorporating VDF in the main chain is extensive. The commercially important thermoplastic copolymers are based upon hexafluoropropylene HFP (10,11) chlorotrifluoroethylene (CTFE) (12,13) and co- or ter-polymers with tetrafluoroethylene (14). Telomerization of VDF to form fluorinated oligomers by radical addition has been reviewed (15).

Polymerization

VDF and other fluoromonomers are polymerized usually in aqueous medium in either emulsion or suspension. VDF polymerization in nonaqueous media is an active research area. VDF can copolymerize with fluorinated and some nonfluorinated monomers. Several aspects of VDF copolymerization with an array of fluorinated and nonfluorinated monomers have been reviewed (16,17); the reactivity ratios along with the Q and e parameters, which are measures of reactivity and polarity, respectively, have also been compiled. The interest in these

copolymers centers upon introducing functionality in the PVDF chain for subsequent reactions.

Only emulsion and suspension polymerization of VDF are commercially practiced because water provides a sufficient heat sink for the large heat release associated with VDF polymerization. Only one VDF-copolymer with nonfluorinated comonomers, maleic monoesters, and allyl glycidal ethers has been commercialized for battery applications (18); all other reported VDF-copolymers with nonfluorinated olefins have been laboratory or patent examples (3).

Polymerization procedures, temperature, pressure, recipe ingredients, monomer feeding strategy, and post-polymerization processing are variables that influence product characteristics and quality (19–26). The variety of commercial VDF-copolymers has been reviewed (27). VDF–HFP copolymers having decreased extractable oligomers and improved solution clarity and processability, especially important to lithium ion battery applications, have been claimed (28).

The degree of polymerization of commercial PVDF ranges from 1000 to 2500 VDF units. During radical-initiated polymerization, the "head-to-tail" addition of monomer units predominates where the "head" is $-CF_2\cdot$ and the "tail" is $-CH_2\cdot$. Reversed monomeric addition leading to "head-to-head" ($-CF_2-CF_2-$) and "tail-to-tail" ($-CH_2-CH_2-$) or so-called defect structures occurs. Commercial grades exhibit a wide range of 3–7 mol% defect structures as determined usually by nmr (29). The level increases with increasing polymerization temperature (30). The defect linkages affect significantly the crystallization processes and ultimate morphology (31,32).

In the emulsion process, a water-soluble *perfluorinated*-emulsifying agent is used to avoid radical scavenging reactions during polymerization and produce stable latex with a desired solid content. Typically, perfluoroalkylcarboxylate salts are cited in many VDF polymerization process patents. VDF can be polymerized without surfactant similar to conventional monomers (33,34), but only at low solid contents. Both inorganic peroxy compounds [eg, persulfates] and organic peroxides [eg, percarbonates (21)] may be employed as initiators. Other initiator systems such as a redox system (35) or a combination of fluoroaliphatic sulfinate and bromate (36) can also initiate VDF polymerization. Operating pressures can range from 1 to 20 MPa (10–200 atm) and temperature from 10 to 130°C. In a typical recipe, the polymer particles are solid and partial crystalline with diameters ranging from 100 to 250 nm depending upon the surfactant level. Particles are formed in the early stage by a homogeneous nucleation mechanism since VDF is in the vapor state. Various chain-transfer agents can be used such as chlorofluorohydrocarbons, fluorohydrocarbons, esters, and mercaptans.

VDF and suitable comonomers can be polymerized as a microemulsion where fluorinated oil-in-water microemulsion and fluorinated surfactant are present (37–39). The core-shell structure of these self-assembling systems and their distinctive polymerization features along with the range of particle size distribution have been reported (40).

Colloidal dispersants such as cellulose derivatives or vinyl alcohol are generally used in suspension polymerization of VDF to prevent coalescence and agglomeration of particles during polymerization. The polymerization pressure is similar to that of emulsion polymerization. Organic oil-soluble initiators such as peroxides, peroxycarbonates, or peroxypivalates are used depending upon

polymerization temperature, which ranges from 20 to 110°C (41–46). The molecular weight is regulated using oil-soluble chain-transfer agents such as dialkyl ethers and dialkyl carbonates. The reactor product is a slurry of suspended particles, usually spheres 15 to 120-μm diameter (41,43).

A suspension polymerization can be carried out using a radical photoinitiator with uv–visible light. Thus, photogeneration of radicals allows a lowering of the polymerization temperature (40). Lowering the polymerization temperature reduces the number of defect structures in PVDF.

Alloys of PVDF and PVDF copolymers with acrylic polymers are produced by a multistage aqueous dispersion polymerization. These intimately mixed polymer particles have found various industrial applications; particularly, in the waterborne high performance coasting application. In the early stages of the polymerization, the fluoropolymer portion is produced under standard condition with 50- to 150-nm particles. In a later stage, acrylic monomers are added to the reactor in the presence of persulfates under atmospheric pressure. The final morphology of the alloy, which ranges from a core-shell to an inter-penetrated structure to an intimate blend morphology, depends upon the composition of the fluoropolymer particles, the acrylic type, and the feed schedule (47–53).

The nonaqueous media used for VDF polymerization is either fluorocarbons or carbon dioxide under high pressure conditions. Fluorocarbons (54,55) and partially fluorinated hydrocarbons with no significant chain-transfer activities (56) are reported to be a suitable media for VDF polymerization.

VDF polymerization technology based upon super critical or liquid carbon dioxide as polymerization media has been reported (57–62). This technology offers an advantage in the polymer isolation step where a clean dry polymer is produced simply by depressurization. The residual monomer(s) and CO_2 can be recycled back to the reactor. PVDF is not soluble in CO_2 (58–60) and as a result, additional polymeric stabilizers are required to produce stable particles. Adequate CO_2 density for polymerization requires pressure significantly higher (typically $>$100 bar) than a conventional emulsion polymerization.

Telomerization of VDF in methanol with *tert*-butyl peroxide as the initiator is reported; polymerization kinetics along with telomer characterization are discussed (63). Microwave-stimulated, low pressure plasma polymerization of VDF gives a polymer film that is less than 10 μm thick (64). Highly regular PVDF polymer with minimized head-to-head addition was synthesized (65). Perdeuterated PVDF has also been prepared and described (66). The effectiveness of 1,1,1-trifluoro-2,2-dichloroethane (HCFC-123) as a chain transfer agent producing thermally stable PVDF in emulsion polymerization has been claimed (67).

Polymer Properties

Compared to the softer and mechanically less robust perfluorocarbon polymers, PVDF has high mechanical strength, abrasion resistance, and excellent resistance to both creep under long-term stress and fatigue upon cyclic loading (68,69). It also has excellent thermal stability and resists damage from most chemicals and solvents as well as from ultraviolet and high energy radiation. Typical design properties are shown in Table 3 for the homopolymers. The resin form is not

Table 3. Design Properties of PVDF Homopolymers[a]

Properties	Value or description
Appearance in film form	Transparent to translucent
Melting transitions, crystalline, °C	155–192
Specific gravity	1.75–1.80
Refractive index, n_D at 25°C	1.42
Mold shrinkage, average %	2–3
Flammability	Self extinguishing, no dripping
Tensile strength, MPa[b]	
25°C	42–58.5
100°C	34.5
Elongation at break, %	
25°C	50–100
100°C	200–500
Yield point, MPa[b]	
25°C	38–52
100°C	17
Creep % 25°C / 13.79 MPa[b], 10,000 h	2–4
Compressive strength, 25°C, MPa[b]	55–90
Modulus of elasticity, 25°C, GPa[c]	
In tension	1.0–2.3 (145–334 E3)
In flexure	1.1–2.5 (160–362 E3)
In compression	1.0–2.3 (145–334 E3)
Izod impact, 25°C, J/m[d]	
Notched	75–235
Unnotched	700–2300
Durometer hardness, Shore D scale	77–80
Heat distortion temperature, °C	
@ 0.455 MPa (psi)	140–168 (20.3–24.4 E3)
@ 1.82 MPa (psi)	80–128 (11.6–18.6 E3)
Abrasion resistance, Tabor CS-17 @ 0.5 kg load, mg/1000 cycles	17.6
Coefficient of sliding friction to steel	0.14–0.17
Thermal coefficient of linear expansion, °C	0.7–1.5 E −4
Thermal conductivity, 25–160°C, W/(m·K)	0.17–0.19
Specific heat, J/(kg·K)	1255–1425
Water absorption, %	0.04
Moisture vapor permeability @ 1 mm thickness, g/(24 h)(m^2)	2.2 E −2
Radiation resistance to Co^{60}, MGy	10–12
Speed of sound, m/s	
Longitundinal	1930
Shear	775
Dielectric constant, 23°C	
1 kHz	12.2
1 MHz	8.9
1 GHz	4.7

[a]Values are ranges for the variety of *commercially* available grades or representative single point values. The values for any given test reflect the specific polymerization process and subsequent thermal/mechanical history of the sample. To assure consistent results in some tests, it is essential to anneal the samples in order to approach a thermodynamically stable morphology. See Ref. 27 for a compilation of VDF-copolymer properties.

[b]To convert MPa to psi, multiply by 145.

[c]To convert GPa to psi, multiply by 145,000.

[d]To convert J/m to ft·lbf/in., divide by 53.38.

hygroscopic and adsorption pickup is less than 0.05 wt% of surface water under ambient room conditions.

The properties of PVDF homopolymers and copolymers are sensitive to the chemical composition, molecular mass characteristics, and molecular architecture. These attributes are dictated by the polymerization method and ingredients, the method of isolation, and the thermal/mechanical history during isolation and subsequent processing.

From a composition viewpoint, the choice of initiator and chain-transfer agent determines end groups that affect thermal stability. These ingredients also dictate molecular mass characteristics involving the distribution of chain lengths and the molecular weight affecting processing and, ultimately, those properties related to the morphology of the solid polymer. The processing, morphology, properties, and end use performance are affected by the branching, cross-linking, differences in the content of defect structures, and other chain irregularities which exist in the PVDF polymers prepared under different conditions and ingredients. A 1999 study contrasts two commercial PVDF polymers based upon different polymerization chemistries (70), revealing differences in end groups and other properties related to composition.

Several of the key properties of PVDF homopolymers and copolymers depend upon the crystalline content and type of crystalline structure. The polymer chains involve long sequences of VDF units and can exist in several conformations. Figure 1 shows the alpha, beta, and gamma forms. The thermodynamically more stable alpha form involves a crankshaft configuration of the chain, which minimizes the steric interference between fluorine atoms along the chain. The beta form places the fluorines along one face of the chain, which is in a zigzag conformation. The gamma form is essentially a distortion of the alpha, where periodically one of the "cranks" is twisted out of the main chain geometry. Two other forms have been identified under very special conditions (71), but these so-called delta and epsilon forms are not typical of the structures existing in normal production or fabrication of parts. The effect of molecular weight and chain end groups on crystal forms of PVDF oligomers has been studied by several techniques (72) with interesting conclusions about the effect of the size of end groups upon conformational disorder in the crystals. A complex morphology involving the alpha and gamma forms occurs and dominates the spherulitic characteristics of the PVDF when the melted polymer is allowed to solidify at temperatures near the melting point (73). The reorganization rate of metastable crystals in PVDF and HFP-copolymers is dependent upon molecular weight (74).

Amorphous PVDF regions have a density of 1.68 (75), the alpha and gamma polymorphs 1.92 and 1.93, respectively, and the beta polymorphs 1.97 g/cm^3 (76). The density of the homopolymer PVDF cooled quickly from the melt is 1.76–1.78 g/cm^3. The melt density of PVDF homopolymers and VDF/HFP-copolymers is approximately 1.45–1.48 g/cm^3 at 230°C and 1 bar (77), ie a volumetric shrinkage factor of almost 20% occurs in cooling from the melt to the solid.

Depending upon the conditions, the linear PVDF chain configurations crystallize into spherulites that are lamellae of polymer chain segments. The alpha configuration is the thermodynamically stable form and predominates in the solid when molten PVDF is cooled. The beta configuration occurs in mixtures with carbonyl functional polymers or when a PVDF film sample is stretched. The gamma

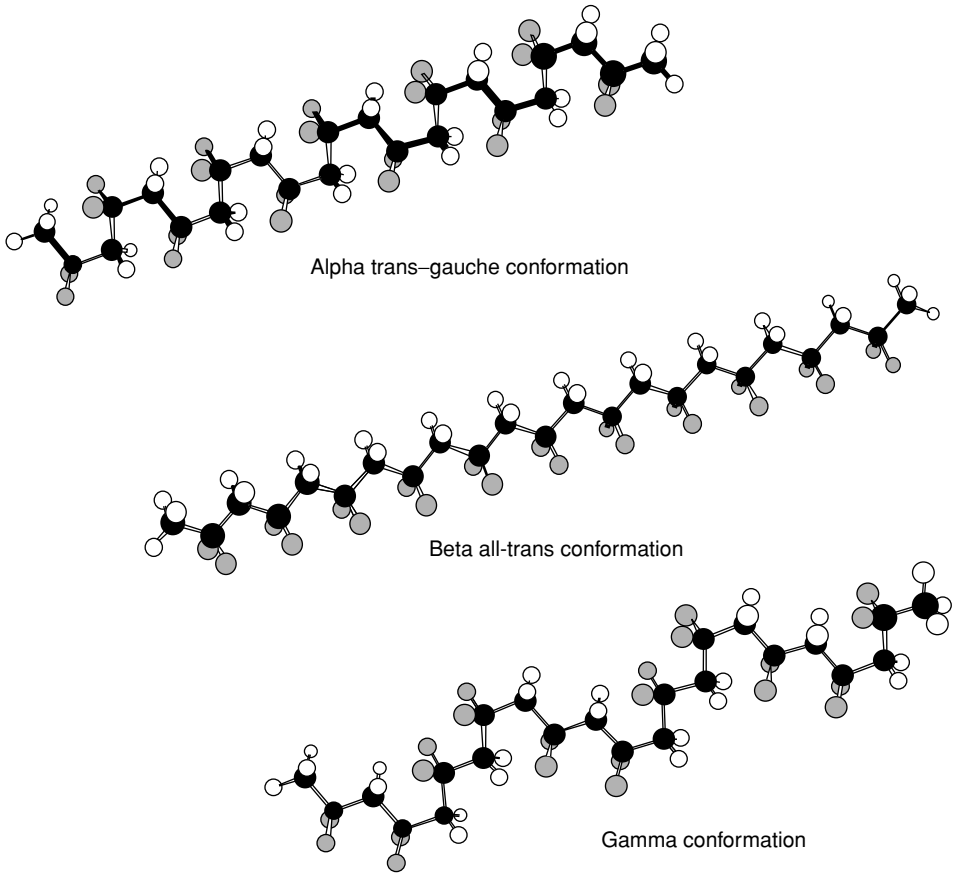

Fig. 1. Main polymorphs of PVDF.

form will develop when solid PVDF is exposed to certain chemicals. The heat of crystallization is high ranging from 50 to 58 J/g. The rates of crystallization are not only dependent upon backbone chain conformation dynamics, but also reflect the polymerization technique, which determines defect structures and end groups as well as molecular mass characteristics. PVDF crystallization may be nucleated by a variety of agents. In the absence of nucleating agents, emulsion PVDF samples show small crystallites developing slowly from the molten state compared to suspension polymer samples, which will show rapid development of very large crystallites under the same thermal conditions (rate of cooling and hold times at temperatures).

Many of the performance related properties (Table 3) in a given application (Table 4) depend upon the crystalline characteristics of the part. Interestingly, the content of defect structures determines the crystalline form; in the range of 11–14% levels, the beta form develops, whereas the alpha predominates at either extreme of this range (71,73,106). A detailed review of the effects of crystallization conditions upon the phases and morphology includes a summary of crystallographic, infrared, and thermal studies as well as related scanning electron

Table 4. Applications Profile for PVDF Homopolymers and Copolymers in Key Markets

Market applications	PVDF attributes	Comments
Coatings and paints	Solution characteristics are related to chemical composition and method of polymerization. Some processes utilize dispersions of PVDF particles with latent solvents to solubilize the PVDF at temperatures above ambient room conditions	Differences in solution behavior are exhibited by the various PVDF grades because of intrinsic chain composition (defect structures, end groups, comonomers, etc) and molecular mass characteristics
Binder for long lasting, weather resistant finishes for metals (primed galvanized steel, aluminum) used on sidings, roofing tiles, and other building components (78,79)	Photostability and resistance to radical attack. Film forming at reasonable temperatures. Long term weathering protection achieved at 25-μm film thickness.	These organosol paint formulations utilize inorganic pigments and < 30 wt% acrylic polymers, which enhance adhesion and confer other important attributes for a successful product. Major application worldwide. Thirty years of demonstrated weathering resistance (81). Often referenced as "architectural coatings"
	Formability of coated metal dependent upon coating application and storage conditions. (80)	Powder coating versions have been developed (82,83)
Decorative films for lamination to surfaces; automotive trim applications; aircraft interior surfaces in-mold lining processes (84)	Resistance to weather and chemicals; thermoformable; stain resistance; cleanability. Ability to solvent cast very thin, pigmented formulations onto carrier films, creating extremely smooth surfaces. Extruded films also	Becoming a major U.S. application. Two major film manufacturers. Both homopolymers and copolymer grades utilized to make films (85)
Corrosion resistant coatings tank liners (86)	Chemical resistant and ease of forming relatively thick coatings from liquid systems. Extruded PVDF tubing and sheet; easily thermoformed. Bead welding with PVDF rod to form seamless joints in liners	Primer coating and several applications of liquid system necessary to build to 1–2 mm thickness; drying temperatures around 250°C. Copolymer grades usually used for extruded tank lining sheets for lining tanks

Chemical processing equipment (25)	Note that PVDF may be adequate for high pH environments in applications where the surface degradation and fluoride leaching is not problematic, eg, alkaline waste streams (87)	Differences in chemical stress resistance are related to the different crystal structure of suspension and emulsion PVDF, the latter usually showing better performance
Flexible tubing for deep sea oil transport, (88)	Special PVDF grades are available (ATOFINA) having cold temperature flexibility important to installation conditions, high temperature chemical resistance	Major application. Hot, sulfurous oil at high pressure is a harsh chemical environment. Long service life requirement. Worldwide application
Packing for distillation towers	Chemical resistance, ease of molding complex shapes	Preferred over metal in many chemical processes because of corrosion issues with metals
High purity water systems; semiconductor facilities; pharmaceutical systems	Very low ionic and organic extractables; smooth surfaces inhibit microbial fouling. Operations at 90°C and in ozonated water (89)	Major application for special grades processed in special equipment to achieve low contamination resin
Piping for chemicals	Chemical resistance to strong acids and oxidizers; relatively high temperature stability	Pipe linings and solid pipe products. In one process, a solid PVDF tube with a wall thickness of several mm is hammered to a slightly smaller diameter than original, inserted into steel pipe, and allowed to relax to a tight fit, exemplifying the toughness of PVDF.
Pumps and instrument parts (90)	Chemical resistance at high temperatures Ease of molding complex shapes	Nonporous nature compared to PTFE parts High modulus reinforced compounds available from compounders

Table 4. (Continued)

Market applications	PVDF attributes	Comments
Fuel handling systems including underground storage tank systems and automotive fuel lines (91,92)	Very low permeation by hydrocarbons and oxygen containing additives achieved as a very thin barrier layer, typically about 50–250 μm	In general, these products are composites of less expensive polymers with the PVDF layer incorporated as an inner liner or embedded barrier
Electrical and Electronic	Note: High dielectric constant and dielectric loss factor are factors to be considered in any application	PVDF is not suitable as a primary insulation on AC power wiring because of absorption of the electromagnetic field and heating
Jacketing of cables for plenum areas including signaling, communication, and power lines	Flexible PVDF grades with additives as jackets on plenum cables have passed the severe UL910 modified Steiner tunnel test to qualify the products as low smoke and flame propagating assemblies meeting strict specifications	Another major application area for flexible PVDF copolymers only in the United State at this time. European and rest of the world specifications based upon fire testing may lead to further markets worldwide based upon this technology
Insulating compounds for jacketing wire and cable assemblies, cathodic protection, industrial power control systems, high temperature wiring	Radiation cross-linking improves toughness and abrasion resistance in these applications. PVDF copolymer responds readily to electron beam irradiation (93,94)	The compounds usually are mixtures of polymers and additives with PVDF being the major portion. It is the PVDF susceptibility to efficient cross-linking that allows economical processing rates
Speciality Applications		
Microporous membranes	PVDF is one of the few fluoropolymers that can be processed in solution. See Ref. 95 for a typical process and references to past technology	The technology involves casting a PVDF solution onto a surface covered with a nonsolvent, followed by special processing of the paper-like sheet. Extensive literature and patents
Toners	Triboelectric characteristics allowing charging of the carbonaceous powder. Thermoplastic nature important to fusion process. See Ref. 96 for a leading reference	PVDF is an essential ingredient at low levels in almost all commercial toners for photocopiers and many laser printers

Fishing lines and nets, Musical strings (97)	No water absorption; invisible in water; high knot strength; high specific gravity	Japanese application almost exclusively. Nylon monofilaments blended with PVDF have high knot strength and improved surface smoothness (98). Blends with polyethylene fibers (99)
Processing aid for polyolefins	PVDF copolymers at <1000 ppm in typical blown film applications is effective in reducing melt fracture and allowing increased extrusion rates	Developing market for PVDF in competition with established fluoroelastomer products
Monofilament for fabrics used in filtering wood pulp during bleaching	Chemical resistance to bleaching agents and other paper mill process chemicals	PVDF fabric replaced perforated stainless steel 25 years ago because of operational issues with metal corrosion
Lithium ion batteries; separators; electrode binder, (100–102)	Electrochemical stability at over 4 V is key property; high purity; solution casting; ability to cast thin electrodes from very high (>80%) carbon formulations	Relatively new application developing during late 1990s. Several hundred tons market in 2000, mainly in Japan
Piezo- and pyroelectric transducers for motion sensors, hydrophones, audio devices, etc; supercapacitors (103); electrolytic capacitors (104); aircraft interior sound control	Orientation under high electrical fields of the beta crystallites in thin films achieves high sensitivity to changes in shape because of pressure (piezo) or temperature (pyro). Considered a ferroelectric material because the remnant polarization is stable. Piezo film for active cancellation of noise in sound absorbing foam laminate	Very small volume application with significant impact over the years in the development of sensitive devices for military as well as security applications. Major research efforts since 1970s for this reason. Russian facilities had significant PVDF development efforts during the cold war “Foam-smart skin” concept (105)

microscopic evidence (5). The crystallization behavior of a mixture of PVDF samples, one with a low and the other a high content of defect structures, led to the interesting observation that the blended mixture crystallized faster than crystals formed in the individual samples (107), again emphasizing the importance of defect structures in affecting the properties of PVDF.

The complicated PVDF chain dynamics and the strong thermodynamic driving force to crystallize confer a complex set of intrinsic transitions as a function of temperature, which ultimately are reflected in the physical properties and behavior under various test conditions. The heat of fusion is approximately 100 J/g and depends upon the level of defects in the sample. Thermodynamic data for the amorphous and crystalline PVDF are tabulated at the website web.utk.edu/~athas/databank/vinyl/pvf2

The glass transition (T_g) of the amorphous PVDF regions is in the range of -40 to -30°C, depending upon the sample and test method. Other sub-T_g transitions have been studied recently by dielectric relaxation spectroscopy (108). These studies also indicate correlations with other techniques and identify a 50°C molecular chain transition as probably related to the amorphous region at the surfaces of crystals (109). Permeation characteristics are very sensitive to these transitions as well as the usual environmental parameters (110). Water molecules trapped in the amorphous regions are monomeric, not associated and clustered as in the liquid state (111).

The crystalline content in homopolymer PVDF samples that solidify quickly from the molten state is typically near 50%, increasing with time to higher levels approaching as a maximum 70%, again dependent upon the method of preparation and finishing. Because of the high crystallinity, the hardness or resistance to indentation of solid PVDF samples is retained up to within 10–15°C of the softening and melting transition region. Copolymers of VDF show lower levels of crystallinity (25–40%) depending upon the level of the comonomer and the method of preparation.

Unlike most crystalline polymers, PVDF exhibits thermodynamic compatibility with other polymers (112). Blends of PVDF and poly(methyl methacrylate) (PMMA), are miscible over a wide range of compositions (113–115). A variety of analytical techniques indicates specific hydrogen bonding between the oxygen of the carbonyl group and the acidic hydrogens along the PVDF chain (116). The same phenomenon explains the types of effective solvents for PVDF: cyclohexanone, dimethylsulfoxide, dimethylacetamide, phosphate esters, and other liquids with carbonyl functionality. Generally, the morphology of the polymer blends becomes even more complex than for the homopolymer PVDF because the polar or hydrogen-bonding interactions are not strong enough to overcome the strong thermodynamic driving force for PVDF crystallization. Studies indicate that the beta PVDF chain conformation develops in blends with acrylic polymers (116,117). Recently, blends with polymers containing imide moieties have been claimed (118). Ternary blends of PMMA, poly(vinyl acetate), and PVDF have been studied as a completely miscible system (119). Addition of 10–30 wt% PMMA improves the transparency of the PVDF films or coatings in the uv–visible spectrum. The relationship between the optical transmission and compatibility of PVDF/PMMA blends is reported (120); in general, films of the blends with at least 15 wt% PMMA are very transparent (>90% transmissivity).

Fabrication and Processing

PVDF is available commercially in a wide range of melt flow rates and with various additives to enhance processing or end use properties. A variety of forms are available—latex and fine powders from emulsion processes and granules from either suspension or emulsion processes.

In melting processes, it is essential to consider the full range of shear rate characteristics of the polymer. Moreover, polymerization techniques have been developed which make different versions of the same composition and polymerization ingredients behave rheologically differently. The rheological characteristics specified for a given commercial PVDF grade should be a consideration in developing a melt-based process to produce parts. Figure 2 shows the different shear behavior of two homopolymer PVDF samples prepared by polymerization with different recipes. Hence, a process such as fusion of powders to a contiguous film requires Newtonian flow at zero shear conditions (curve A), which is achieved by a narrow molecular weight distribution and low molecular weight mass. A high speed extrusion generally would proceed with less surface fracture or melt instabilities given a broad molecular weight distribution or shear-thinning melt, which is sample B, having a high molecular weight mass.

Both homopolymers and copolymers may be shaped from the molten state without extrusion aids or thermal stabilizers. A broad operating window exists for melt processing between the points when crystallites begin to melt and the onset of thermal decomposition. Figure 3 superimposes the thermal gravimetric analysis (tga) curve and the differential scanning calorimeter (dsc) graph for the melting phenomenon. Conventional equipment is used in processing molten PVDF. Longevity of equipment can be extended with special alloys on surfaces that contact the melt, but usually are not necessary.

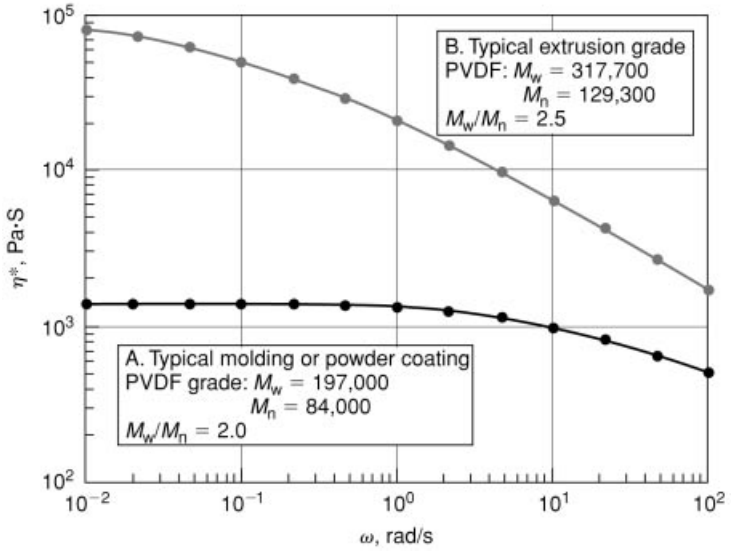

Fig. 2. Rheological profiles for two commercial PVDF grades. The melt rheology converges at high shear rates above 100 rad/s.

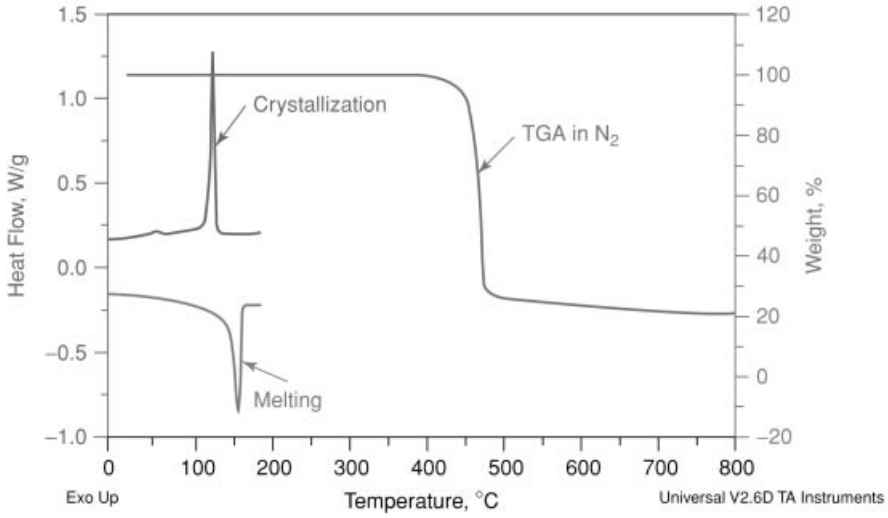

Fig. 3. Thermal gravimetric analysis and differential scanning calorimetry of a PVDF homopolymer.

All the common extrusion and molding techniques can be used to process PVDF into shapes. Typical molding temperatures in the cylinder and nozzle are 180–240°C for injection types, and for molds are 50–90°C. As a crystalline polymer, it shows relatively high mold shrinkage of about 3%, reflecting the high degree of crystallization and the difference between the solid and molten densities as mentioned earlier. In most cases, it is prudent to develop appropriate post-forming annealing cycles, typically 15°C or more above the crystallization temperature (Table 3), to stabilize the parts. Hence, the design of molds requires careful considerations of final part tolerances before cutting metal.

PVDF is not hazardous under typical melt processing conditions. At temperatures approaching 300°C, the onset of a thermal degradation will be evident as a darkening of the resin. This discoloration arises from the dehydrofluorination reaction forming the conjugated polyene structures that absorb strongly in the visible spectrum. It is helpful, in fact, as a very sensitive indicator of overheating. Immediate remedial action should be taken to reduce the heat. At temperatures well above 300°C and approaching 350°C, thermal decomposition accelerates, leading to release of hydrogen fluoride. The tga curve (Fig. 3) shows that the decomposition is essentially quantitative with respect to carbonaceous residue and hydrogen fluoride evolution at about 400°C.

Before ingredients are added to PVDF to make compounds, a thorough laboratory study should be conducted in properly vented ovens at temperatures that might be encountered in the range of operating conditions. Certain additives such as titanates and silicates catalyze the thermal decomposition of molten PVDF at temperatures lower than typical for the natural resin, leading to dangerously high pressures in the equipment because of by-product gases. Generally, metal oxides catalyze degradation at high processing temperatures, eg, the oxides of titanium, manganese, and iron. Resin producers should be consulted for melt processing

recommendations whenever additives are utilized in compounds. Frequently, the compounds include an acid-scavenging agent like zinc or calcium oxide to react with any hydrogen fluoride that might form during processing.

Coextrusion and lamination processes have been described extensively in the patent literature. The technology usually involves multilayer structures utilizing, as an adhesive layer, a compound of PVDF with another material, which provides the bonding to the substrate. In this way, the full benefits of a thin film of PVDF may be realized (121). Another approach using acrylic alloys with PVDF sometimes achieves adherence to various substrates without the "tie layer" necessary for the pure PVDF film (122). The full breadth of options available by these technologies to protect surfaces with weatherable PVDF surfaces has been reviewed (123). Surface PVDF layers on polyolefins has been a particular technology of interest with respect to suitable finishes in cost effective parts for exterior automotive and agricultural equipment applications (124).

Powder grades usually are used whenever compounds are prepared in order to achieve homogeneity of the blends. Latex grades are utilized in some applications where it is possible to dry and fuse the material under conditions producing a coating upon the substrate, typically fabrics.

Solid PVDF parts may be joined by various fusion methods; the manufacturers should be consulted for recommendations. Fusion methods are preferred over solvent joints because the strength is much greater and for the ease in preparation. Vibration welding has been practiced. Because of the high dielectric loss, ie absorption of microwave electromagnetic radiation, rf-induction heating methods have been used to soften or melt PVDF parts. Welds may be particularly susceptible to stress cracking in strongly basic solutions where discoloration develops as a result of dehydrofluorination (7,8).

Economic Aspects

The extensive use of PVDF has developed in spite of the relatively high price and specific gravity compared to the commodity nonfluoroplastic polymers and the widely known thermoplastic engineering resins. Compared to all other common fluoropolymers, PVDF is the least expensive on a volume basis. Over the last decade the market pricing of standard PVDF grades has remained remarkably constant around $14–15/kg. See www.plasticstechnology.com for updated pricing comparisons.

Health and Safety Factors

PVDF is nontoxic, odorless, and has no taste. Extraction testing has led to a listing with the FDA as being suited to single use contact with food (125); this applies to both homopolymer and copolymers with low content of HFP (<20 wt%). Various manufacturers have qualified specific grades with appropriate agencies and standards organizations for a variety of applications including potable water systems, home construction, medical applications, food contact, and packaging. Some of the agencies or standards involved are the U.S. Department of Agriculture, 3A Sanitary Standards, Food & Drug Administration, National Sanitation Founda-

tion, U.S. *Pharmacopeia* USP Class 6, and others. See the producers websites for specific applications having the appropriate approvals.

PVDF powders are not explosive, but the MSDS guidelines for personal protective equipment should be followed. The powder is not removed readily by dry cleaning; it should be brushed from dark clothing. Storage of large quantities of PVDF should adhere to local regulations regarding possible hazards in fire environments.

Uses

The major applications of PVDF are summarized in Table 4. Since the 1996 version of this encyclopedia series (3), an increasing interest has developed in the use of PVDF as a binder and polymeric separator in lithium ion batteries. The literature since 1998 also has numerous references to the use of PVDF in fuel cells, eg, in membranes (102) and electrodes (126); it is a technology anticipated to become a significant factor in electrical vehicles before 2010. These two technology areas, both of which reflect the electrochemical stability and chemical resistance attributes of PVDF, may lead to major applications for PVDF. In a related application area, the use of PVDF films for electrostatic capacitors is being investigated because it has a very high DC current breakdown voltage (770 MV/m) and a large maximum energy density capability (28.9 J/cm). Both attributes are related to the very high dielectric constant (Table 3) (103). Note that some PVDF grades are more suited to this application by virtue of purity than others are because ionic impurities lead to dielectric breakdown at relatively low voltages.

Several Japanese patent applications since 1992 discuss the processing technology necessary to manufacture monofilaments for fishing lines and nets or other monofilament applications, which must have extremely high tensile strength and knot strength (127). It is claimed that PVDF monofilaments are not visible to the fish in seawater (refractive index $\approx$ 1.31 compared to 1.42 for homopolymer PVDF).

Since the original Timmerman patent in 1964 (128) on the radiation response of PVDF, the use of PVDF in wire and cable applications has increased dramatically with electron beam irradiation as the key process step to cross-link the PVDF compounds for higher temperature capability (93,94). In general, the copolymers cross-link more efficiently than homopolymer grades. A certain PVDF homopolymer, which is polymerized at high temperatures with organic peroxides, seems to be an exception among the various homopolymer grades. Presumably, because of the particular polymerization process, this resin has been used as insulation on signal wiring since the late 1970s; it can be extruded at very high rates and cross-links more readily under ebeam irradiation than other homopolymer grades. PVDF polymers cannot be considered a generic grouping like polyethylene, which according to density or polymerization catalyst have essentially the same properties. PVDF properties and suitability for any given application are a sensitive function of the polymerization and isolation methods of the polymer, which differ for each producer.

Table 3 indicates the excellent radiation resistance to 61 Mev beta emissions from cobalt-60. A process to etch "tracks" of high energy, heavy nuclei in PVDF films has been developed in order to make nuclear track microfilters (129).

Another recent advance in PVDF technology involves coating applications using the acrylic–fluoropolymer lattices which are produced by sequential polymerizations (see as given earlier). Initial reports indicate improved paint properties than heretofore produced by mixing and blending techniques (130).

As space exploration, development of speciality military and oceanic equipment, and advances in telecommunication equipment and connection systems evolve during the next millennium, the use of PVDF will expand because of its unique set of properties and useful functions in various designs. In addition, the ease of processing by a variety of techniques into complex shapes and relatively simple and straightforward fabrication methods will be significant factors in choosing PVDF for these future applications.

BIBLIOGRAPHY

"Vinylidene Fluoride Polymers" in *EPST* 1st ed., Vol. 14, pp. 600–610, by J. Dohany, A. A. Dukert, and S. S. Preston II, Pennwalt Corp.; "Vinylidene Fluoride Polymers" in *EPSE* 2nd ed., Vol. 17, pp. 532–548, by J. E. Dohany and J. S. Humphrey, Pennwalt Corp.

1. J. E. Dohany in R. B. Seymour and G. S. Kirshenbaum, eds., *High Performance Polymers: Their Origin and Development*, Elsevier Science Publishing Co., New York, 1986, p. 287.
2. C. K. Brennen, in *Fluoropolymer 2000*, Conference Sponsored by the ACS Division of Polymer Chemistry, Oct. 15–18, 2000.
3. J. E. Dohany, in J. I. Kroschwitz, ed., *Encyclopedia of Chemical Technology*, 4th ed., Vol. **11**, Wiley-Interscience, New York, 1994 p. 694.
4. B.-J. Jungnickel, *Polymeric Materials Encyclopedia*, CRC Press, New York, Vol. **11**, 1996 pp. 7115–7127.
5. R. Gregório Jr. and co-workers, Ref. 4, pp. 7128–7138.
6. H. A. Nalwa, Inc., *Ferroelectric Polymers (Chemistry, Physics, and Applications)*, Marcel Dekker, Inc., New York, 1995.
7. P. Hinksman, D. H. Isaac, and P. Morrissey, *Polym. Degrad. Stab.* **68**(2), 299–305 (2000).
8. P. Maccone, G. Brianti, and V. Arcella, *Polym. Eng. Sci.* **40**(3), 761–767 (2000).
9. G. J. Ross and co-workers, *Polymer* **41**(5), 1685–1696 (2000).
10. U.S. Pat. 3178399 (Apr. 13, 1965), E. S. Lo (to 3M Co.).
11. Eur. Pat. Appl. 456019 (Nov. 13, 1991), L. A. Barber (to Elf Atochem North America, Inc.).
12. U.S. Pat. 4851479 (July 25, 1989), J. Blaise and P. Kappler (to Elf Atochem SA).
13. U.S. Pat. 4472557 (Sept. 18, 1984), C. Kawashima and T. Yasumura (to Central Glass Co., Ltd.).
14. Brit. Pat. 827308 (Feb. 3, 1960) (to 3M Co.).
15. B. Ameduri and B. Boutevin, *Organofluorine Chemistry: Fluorinated Alkenes and Reactive Intermediates*, Springer, Berlin, 1997, pp. 165–233; Top. Curr. Chem. Vol. **192**,
16. B. Ameduri and B. Boutevin, *J. Fluorine Chem.* **104**, P53–62 (2000)
17. B. Ameduri and co-workers, *Macromolecules* **32**, 4544–4550 (1999).
18. Eur. Pat. Appl. EP 751157 B1 (July 14, 1999), H. Ikashio, K. Horie, and F. Suzuki (to Kureha KKKK).
19. U.S Pat. 4076929 (Feb. 29, 1978), J. Dohany (to Pennwalt Corp.).
20. U.S Pat. 4128517 (Dec. 5, 1978), N. Kydonieus (to Pennwalt Corp.).
21. U.S Pat. 4360652 (Nov. 23, 1982), J. Dohany (to Pennwalt Corp.).

22. U.S Pat. 4569978 (Feb. 11, 1986), L. Barber (to Pennwalt Corp.).
23. World Pat. 9838242 (Aug. 3, 1998), R. Wille and M. Burchill (to Elf Atochem North America, Inc.).
24. Eur. Pat. Appl. 456019 (Nov. 13, 1991), L. Barber (to Atochem North America, Inc.).
25. D. A. Seiler, in J. Scheirs, ed., *Modern Fluoropolymers*, John Wiley & Sons, Inc., New York, 1997, p. 487.
26. G. Hougham, K. Johns, P. E. Cassidy, and T. Davidson, *Fluoropolymers: Synthesis and Properties*, Plenum Press, New York, 1999.
27. C. Tournut, in J. Scheirs, ed., *Modern Fluoropolymers*, John Wiley & Sons, Inc., New York, 1997, p. 577.
28. World Pat. WO 9838687 (Sept. 3, 1998), R. A. Wille and M. T. Burchill (to Elf Atochem North America, Inc.).
29. S. Russo and co-workers, *Polymer* **34**, 4777 (1993).
30. M. Gorlitz and co-workers, *Angew. Makromol. Chem.* **29/30**, 137 (1973).
31. K. Tashiro, in H. Nalwa, ed., *Ferroelectric Polymers (Chemistry, Physics, and Applications)*, Marcel Dekker, Inc., New York, 1995, pp. 97–99.
32. P. Maccone, G. Brinati, and V. Arcella, *Polym. Eng. Sci.* **40**, 761–767 (2000).
33. T. F. McCarthy and co-orkers, *J. Appl. Polym. Sci.* **70**, 2211–2225 (1998).
34. P. Bonardelli, G. Moggi, and S. Russo, *Makromol. Chem. Suppl.* **10**11, 11–23 (1985).
35. World Pat. 9717381 (June 15, 1997), T. F. McCarthy, Y. Chen, and E. J. Raional (to Allied Signal Inc.).
36. World Pat. 9702300 (July 23, 1997), W. B. Farnham and co-workers (to E. I. du Pont de Nemours and Co., Inc.).
37. Eur. Pat. 722882 (May 22, 1996), J. Abusleme and A. Chittofrati (to Ausimont S.P.A., Italy).
38. Eur. Pat. Appl. 816397 (Jan. 7, 1998), G. Brinati, P. Lazzari, and V. Arcella (to Ausimont S.P.A.).
39. Eur. Pat. 570762 (Nov. 24, 1993), V. Arcella and co-workers (to Ausimont S.P.A.).
40. E. Giannetti, A. Chittofrati, and A. Sanguineti, *Chim. Ind. (Milan)* **79**, 611–618 (1997).
41. Eur. Pat. 526216 (Feb. 3, 1993), H. Wakamori, F. Suzuki, and K. Horie (to Kureha Chemical Industry Co., Ltd.).
42. Eur. Pat. 423097 (April 17, 1991), Lasson (to Solvay et Cie.).
43. Eur. Pat. 417585 (Oct. 20, 1991), Lasson (to Solvay et Cie.).
44. Jpn. Pat. 87286707 (Nov. 12, 1987), K. Ihara, Y. Noda, and T. Amano (to Daikin Industries, Ltd.).
45. Eur. Pat. 215710 (Mar. 25, 1987), J. Blaise (to ATO CHEM SA).
46. Fr. Pat. 2542319 (Apr. 14, 1984), J. Dumoulin (to Solvay et Cie.).
47. Eur. Pat. 695766 (June 7, 1996), J. Abusleme, P.A. Guarda, and P.R. De (to Ausimont S.P.A.).
48. World Pat. 9921921 (May 6, 1999), N. Tsuda, and co-workers (to Daikin Industries, Ltd.).
49. World Pat. 9903900 (Jan. 28, 1999), S. Gaboury and X. F. Drujon (to Elf Atochem North America, Inc.).
50. Jpn. Pat. 08170045 (July 2, 1996), K. Nishiwaki, T. Shimizu, and M. Kato (to Japan Synthetic Rubber Co. Ltd.).
51. Eur. Pat. 360575 (Mar. 28, 1990), M. Kato and co-workers (to Japan Synthetic Rubber Co., Ltd.).
52. Ger. Pat. 2952457 (July 3, 1980), K. Kido, F. Suzuki, and K. Kushida (to Kureha Chemical Industry Co., Ltd.).
53. U.S Pat. 4141873 (Feb. 27, 1982), J. Dohany (to Pennwalt Corp.).
54. World Pat. 0047641 (Aug. 17, 2000), H. Saito and co-workers (to Daikin Industries, Ltd.).

55. Ger. Pat. 1806427 (May 16, 1969), D. P. Carlson (to E. I. du Pont de Nemours & Co., Inc.).
56. World Pat. 9948937 (Sept. 30, 1999), R. Kruger, G. Heilig, and C. Sommerfeld (to Bayer Aktiengesellschaft).
57. Eur. Pat. 964009 (Dec. 15, 1999), P. D. Brothers (to E. I. du Pont de Nemours & Co. Inc.).
58. P. A. Charpentier and co-workers, *Macromolecules* **32**, 5973–5975 (1999).
59. B. J. Briscoe and co-workers, *J. Polym. Sci., Part B: Polym. Phys.* **36**, 2435–2447 (1998).
60. C. A. Mertdogan, T. P. DiNoia, and M. A. McHugh, *Macromolecules* **30**, 7511–7515 (1997).
61. World Pat. 9628477 (Sept. 19, 1996), J. M. DeSimone and T. Romack (to University of North Carolina at Chapel Hill).
62. U.S. Pat. 5674957 (Oct. 7, 1997), J. M. Desimone and T. Romack, (to University of North Carolina at Chapel Hill).
63. B. Ameduri and co-workers, *Polym. Prepr. (Am. Chem. Soc., Div. Polym. Chem.)* **39**, 816–817 (1998).
64. Eur. Pat. 403915 (Dec. 27, 1990), J. Kammermaier and G. Rittmayer (to Siemens AG).
65. U.S. Pat. 4438247 (Mar. 20, 1984), R. E. Cais (to AT&T Technology).
66. R. E. Cais and J. M. Kometani, *Macromolecules* **17**, 1887 (1984).
67. Eur. Pat. Appl. EP 655468 (May 31, 1995), V. Arcella and co-workers (to Ausimont S.P.A.).
68. P. E. Bretz, R. W. Hertzberg, and J. A. Manson, *Polymer* **22**, 1272–1278 (1981).
69. S. Castagnet, J.-L. Gacougnolle and P. Dang, *Mater. Sci. Eng. A* **276**(1/2), 152–159 (2000).
70. S. M. Jo and co-workers *Polymer (Korea)* **23**, 800–808 (1999)
71. A. J. Lovinger, *Macromolecules* **15**, 40 (1982).
72. P. Herman and co-workers, *Polymer* **38**(7), 1677–1683 (1997).
73. R. Gregorio and R. C. Capitao, *J. Mater. Sci.* **35**, 299–306 (2000).
74. L. Judovits and S. M. Dounce, in *57th Annu. Tech. Conf.—Soc. Plast. Eng.*, Vol. 2, 1999, pp. 2334–2339.
75. K. Nakagawa and Y. Ishida, *Koloid Z. Z. Polym.* **251**, 103 (1973).
76. R. Hasagawa and co-workers, *Polym. J.* **3**, 600 (1972).
77. N. Mekhilef, *J. Appl. Polym. Sci.* **80**, 230–241 (2001).
78. R. A. Iezzi, *Modern Fluoropolymers*, John Wiley & Sons, Inc., New York, 1997, 271–299.
79. J. Scheirs, S. Burks, and A. Locaspi, *Trends Polym. Sci.* **3**(3), 74–81 (1995).
80. K. Kawanishi, *Hyomen Gijutsu* **48**(8), 811–814 (1997).
81. J. L. Perillion and E. J. Bartoszek, *Eur. Coatings J.* 277–283 (Apr. 1995).
82. U.S. Pat. 5739202 (Apr. 14, 1998), R. L. Pecsok (to Pennwalt Corp.).
83. U.S. Pat. 6063855 (May 16, 2000), R. L. Pecsok and J. E. Dohany (to Pennwalt Corp.).
84. Jpn. Pat. 09193237 A2 (July 29, 1997), M. Hattori, H. Yamada, and I. Ishii (to Mitsubishi Chemical Ind. Ltd.).
85. World Pat. WO 9640449 (Dec. 19, 1996), M. D. Flynn and K. Truog (to Avery Dennison Corp.).
86. G. A. Glein, in *Semicond. Pure Water Chem. Conf., 15th (UPW & Chemical Proceedings)*, Balazs Analytical Laboratory, 1996, pp. 125–136.
87. P. Hinksman, D. H. Isaac, and P. Morrissey, *Polym. Degrad. Stab.* **68**, 299–305 (2000).
88. F. Dawans, J. Jarrin, T. Lefevre, and M. Pelisson, in *Proceedings of 1986 Offshore Technology Conference*, Paper No.: OTC-5231, Houston, Tex. May 1986; *API Recommended Practice 17B*: Recommended Practice for Flexible Pipe, 2nd ed., Section 6.2.2, "Polymer Materials," American Petroleum Institute, Washington, D.C., 1998.

89. T. H. Meltzer, *Pharm. Technol.* **21**(3), 90–98 (1997).
90. D. Knight, *Chem. Eng.* **104**(4), 151 (1997).
91. Eur. Pat. Appl. EP 673762 A2 (Sept. 27, 1995), S. Roeber, H. Jadamus, and H. Ries (to Hüls Aktiengesellschaft).
92. EP 729830 (Sept. 4 1996), S. Roeber and H. Ries (to Hüls Aktiengesellschaft).
93. B. J. Lyons, in J. Scheirs, ed., *Modern Fluoropolymers*, John Wiley & Sons, Inc., New York, 1997, p. 335.
94. WO 2000017889 A1 (Mar. 30, 2000), G. H. Rodway (to Raychem Ltd.).
95. U.S. Pat. 6013688 (Jan. 11, 2000), M. M. Pacheco and J. F. Pacheco (to Corning Costar Corp.).
96. J. M. Crowley, C. Snelling, and D. Mashtare, *J. Imaging Sci. Technol.* **40**, 285–290 (1996).
97. JP 09146541 A2 (June 6, 1997), H. Ueba (to Kureha Gosen).
98. JP 10331033 (Dec. 15, 1998), Y. Yamamoto (to Furukawa Electric Co., Ltd.).
99. JP 2000017518 A2 (Jan. 18, 2000), T. Soga (to Mitsubishi Chemical Ind.).
100. U.S. Pat. 5540741 (July 30, 1996), A. Godz and co-workers (to Bell Communications Research, Inc.).
101. T. Nagatomo, C. Ichikawa, and O. Omoto, *J. Electrochem. Soc.* **134**, 305 (1987).
102. PSSA/PVDF Polymer Electrolyte Membranes for CH_3OH Fuel Cells, NASA Tech Briefs, June 1999, p. 54.
103. B. E. Conway, *Electrochemical Supercapacitors*, Kluwer Academic/Plenum Publishers, New York, 1999, p. 669.
104. M. Ishikawa, M. Morita, and Y. Matsuda, in *Proc.—Electrochem. Soc. 96-25 (Electrochemical Capacitors II)* 1997, pp. 325–335
105. C. Guigou and C. R. Fuller, in *Proc. SPIE-Int. Soc. Opt. Eng. (Industrial and Commercial Applications of Smart Structures Technologies)* 3044, pp. 68–78 (1997).
106. K. E. Cais and N. J. Sloane, *Polymer* **24**, 179 (1983).
107. J. Datta and A. K. Nandi, *Polymer* **39**, 1921–1927 (1998).
108. A. Korzhenko, F. Beaume, and B. Ernst, in *Proceedings of the 28th North American Thermal Analysis Society*, Oct. 2000, pp. 184–191.
109. Z. Liu, P. Marechal, and R. Jerome, *Polymer* **38**(19), 4925–4929 (1997).
110. S. Lee and K. S. Knaebel, *J. Appl. Polym. Sci.* **64**(3), 455–492 (1997).
111. H. Kusanagi, *Chem. Lett.* (7), 683–684 (1997).
112. D. R. Paul and J. W. Barlow, *J. Macromol. Sci., C: Rev. Macromol. Chem.* **18**, 109 (1980).
113. J. S. Noland and co-workers, *Adv. Chem. Ser.* **99**, 15 (1971).
114. J. Mijovic, H.-L. Luo, and C. D. Han, *Polym. Eng. Sci.* **22**, 234 (1982).
115. H. Yoshida, *J. Therm. Anal.* **49**(1), 101–105 (1997).
116. K. J. Kim, Y. J. Cho, and Y. H. Ho, *Vib. Spectrosc.* **9**(2), 147–59 (1995).
117. N. Tsutsumi, M. Terao, and T. Kiyotsukuri, *Polymer* **34**(1), 90–4 (1993).
118. U.S. Pat. 5959022 (Sept. 9, 1999), S.-C. Lin and S. J. Burks (to Ausimont Inc.).
119. Q. Guo, *Eur. Polym. J.* **32**, 1409–1413 (1996).
120. H. Horibe and F. Baba, *Nippon Kagaku Kaishi* **2**, 115–120 (2000).
121. U.S. Pat. 4317860 (Mar. 2, 1982), A. Strassel (to Atochem).
122. J. S. Humphrey and B. Simkin, in *Society of Plastics Engineers Vinyl RETEC 97*, Oct. 15, 1997.
123. D. Silagy, P. Bussi, and G. Marot, *J. Fluorine Chem.* **104**(1), 79–86 (2000).
124. Jpn. Pat. 08336937 A2 (Dec. 24, 1996), T. Ogura and co-workers (to Japan Synthetic Rubber Co. Ltd.).
125. *PVDF homopolymer: "Articles or component of articles intended for repeated use in contact with food", 21 CFR 177.2510; VDF copolymers: "Rubber articles intended for repeated use in food contact applications," 21 CFR 177.2600.*

126. U.S. Pat. 5783325 (July 21, 1998), I. Cabasso, Y. Yuan, and X. Xu (to The Research Foundation of New York).
127. Jpn. Pat. 9291215 (Mar. 24, 1990), Nishikawa, H. Nakada, and T. Sato (to Toray K.K.); Jpn. Pat. 10052199 (Feb. 24 1998), Y. Nakano, S. Ohira, and T. Mizuno (to Kureha Chem. Co.); Jpn. Pat. 11012850 (Jan. 19, 1999), K. Amano and M. Okano (to Toray Monofilament Co.); Jpn. Pat. 2000192327 (July 11, 2000), K. Amano and co-workers (to Toray Monofilament Co.).
128. U.S. Pat. 3142629 (July 28, 1964), R. Timmerman (to Radiation Dynamics).
129. C. D. Zhao, P. Vater, and R. Brandt, *Nucl. Tracks Radiat. Meas.* **19**, 829–832 (1991).
130. R. Iezzi, S. Gaboury, and K. Wood, *Acrylic—Fluoropolymer Mixtures and Their Use in Coatings*, Elsevier Science S. A., Ireland, 2000, pp. 1–4, 53–58. Progress in Organic Coatings, Vol. **40**.

J. S. HUMPHREY
R. AMIN-SANAYEI
Atofina Chemicals Inc.

VISCOELASTICITY

Introduction: Perspectives on the Fundamentals of Polymer Viscoelasticity

Viscoelasticity is a phenomenon that has been known since the middle of the nineteenth century when workers such as Weber (1), the Kohlrausches (2), and others were interested in using natural fibers, such as silk, to hold needles in measuring devices such as ammeters. They found hysteretic and time-dependent effects that were difficult to explain fully and to characterize. Later, Boltzmann (3) developed his superposition principle and linear viscoelasticity began to have a formal framework for understanding the phenomenology of the inelastic effects observed earlier (4). While other early pioneers such as Andrade (5) and Zener (6) observed anelasticity or viscoelasticity in metals, the real impetus for understanding viscoelasticity came with the commercial development in the middle of the twenieth century of high molecular weight polymers. One reason for this is that polymers exhibit non-Newtonian behavior in the melt state, which is attributable to both elastic effects and shear-rate-dependent viscosity. This leads to important time and rate effects during the processing of polymers. In addition, once processed, polymers are generally used at less than 200 K from the glass-transition temperature. Hence, even in the "solid-like" state, polymeric materials exhibit time- and frequency-dependent mechanical (and other) properties that have been categorized as viscoelastic. In the current work, the linear and nonlinear viscoelastic responses of polymers from both phenomenological and molecular views are surveyed. An overview of the viscoelastic behavior of polymers in solution, melt, glassy, and semicrystalline states is provided.

Material Functions—Linear Viscoelasticity. One of the most important aspects of both the phenomenological and the molecular theories of

Encyclopedia of Polymer Science and Technology. Copyright John Wiley & Sons, Inc. All rights reserved.

viscoelasticity is the ability to characterize the *material functions*. The material functions are the properties that allow one to relate the stress response to a strain (deformation) history and vice versa through a *constitutive* equation. In linear viscoelasticity theory, generally isotropic descriptions are dealt with; that is, the properties are the same in all directions. However, a material may be anisotropic and still have properties that vary with the direction of the test (7). Here only the isotropic case is considered and it is recognized that straight forward extensions can be made to the anisotropic case. In addition, only homogeneous materials, for which the properties are the same at all points within the material, only are discussed.

Stress and Strain Definitions. As remarked, the material functions relate the stress and strain responses of the material through a constitutive equation. For the elastic material, there is no time dependence and the relationships are relatively simple. In the case of linear viscoelasticity, equations that take into account the time history of the stresses or strains are required. First, stress and strain are defined.

The infinitesimal strain tensor is defined in various ways; here the notation of Timoshenko and Goodier (8) is adopted in terms of the displacements u_i of a material element and as depicted in Figure 1a.

$$\varepsilon_{ij} = \frac{1}{2}\left(\frac{\partial u_i}{\partial x_j} + \frac{\partial u_j}{\partial x_i}\right) \tag{1}$$

and the full strain matrix in terms of the ε_{ij} is written as

$$\varepsilon_{ij} = \begin{bmatrix} \varepsilon_{11} & \varepsilon_{12} & \varepsilon_{13} \\ \varepsilon_{21} & \varepsilon_{22} & \varepsilon_{23} \\ \varepsilon_{13} & \varepsilon_{23} & \varepsilon_{33} \end{bmatrix} \tag{2}$$

Similarly, the stress tensor can be defined in terms of the forces acting on the faces of an element and these are given by the following expression (see Fig. 1b):

$$\sigma_{ij} = \begin{bmatrix} \sigma_{11} & \sigma_{12} & \sigma_{13} \\ \sigma_{21} & \sigma_{22} & \sigma_{23} \\ \sigma_{13} & \sigma_{23} & \sigma_{33} \end{bmatrix} \tag{3}$$

Note that when $i \neq j$, it is common to write the shear strain $\gamma_{ij} = 2\varepsilon_{ij}$ and shear stress $\tau_{ij} = \sigma_{ij}$. In addition, $\gamma_{ij} = \gamma_{ji}$ and $\tau_{ij} = \tau_{ji}$.

Elastic Material Functions. The material functions that are used here for an isotropic, elastic material are the shear modulus G, the extensional modulus E, the bulk modulus K, and the Poisson's ratio ν. However, any two of these provides the full set of information needed to describe such a material, as they are not all independent. For simple deformations, the definitions of these moduli are

$$\begin{gathered} \text{Extensional modulus: } E = \frac{\sigma_{11}}{\varepsilon_{11}} \\ \text{Bulk modulus: } K = \frac{P}{\varepsilon_v} \quad \textit{where} \quad \mathrm{P} = \frac{\sigma_{11} + \sigma_{22} + \sigma_{33}}{3} \quad \text{and} \quad \varepsilon_v = \varepsilon_{11} + \varepsilon_{22} + \varepsilon_{33} \\ \text{Poisson's ratio: } \nu = \frac{\varepsilon_{11}}{\varepsilon_{22}} \end{gathered} \tag{4}$$

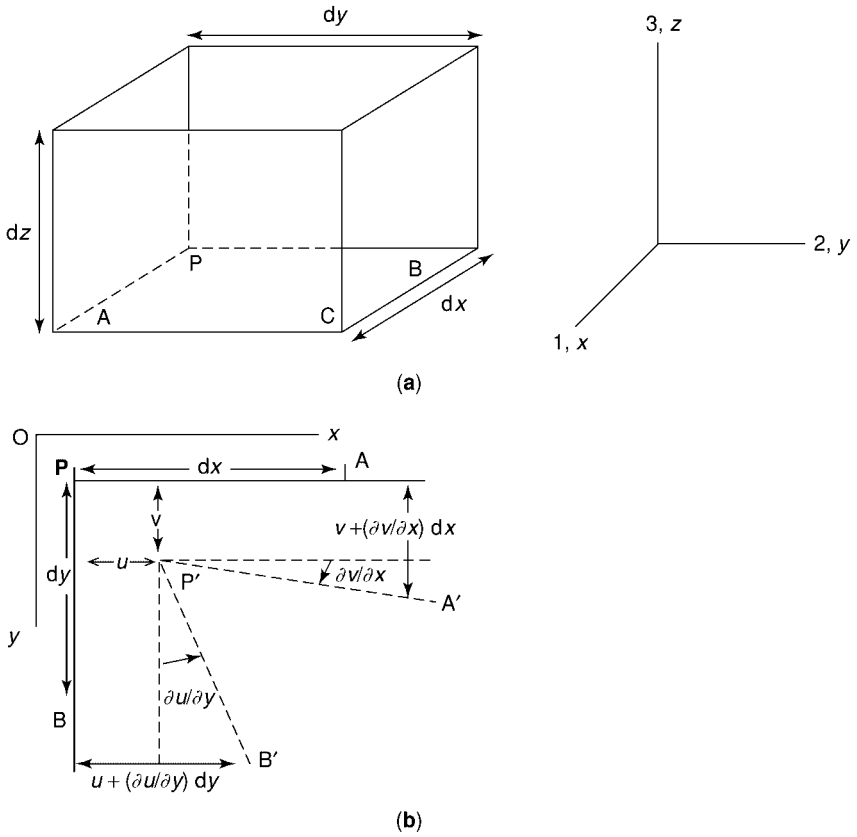

Fig. 1. (**a**) Three-dimensional depiction of elementary material point (dx, dy, dz) and the two-dimensional sketch of the displacements in the x and y directions of the cube that define the strains. The displacement of the point P has components u, v, w, and the displacement in the x direction of a nearby point A is $u+\partial u/x$; and the increase in length of PA due to a deformation would be $(\partial u/\partial x)$ dx, making the unit elongation in the x direction $\partial u/\partial x$. Similarly, unit elongations in the y and z directions would be given by $\partial v/\partial y$ and $\partial w/\partial z$. After Timoshenko (8). (**b**) Considering the distortions of the angular elements PA and PB in this two-dimensional depiction, the displacements of the point A in the y direction and of B in the x direction are given by $v+(\partial v/\partial)$ dx and $u+(\partial u/\partial y)$ dy, respectively. The small angles in the figure (distortion of the P′B′ and P′A′ relative to PB and PA) are given by $\partial v/\partial x$ and $\partial u/\partial y$. Hence, it is seen that the original right angle APB distorts to A′P′B′ by an amount $(\partial v/\partial x + \partial u/\partial y)$, which is the shearing strain between the planes xz and yz. After Timoshenko (8). (**c**) Representation of the components of stress acting on an elementary cube. After Timoshenko (8).

And the relations between the moduli are

$$G = \frac{E}{2(1+v)}$$
$$K = \frac{E}{(1-2v)} \tag{5}$$
$$E = \frac{9KG}{3K+G}$$

and one more constant referred to as the Lamé constant λ is defined as

$$\lambda = \frac{vE}{(1+v)(1-2v)} \tag{6}$$

The ways in which the moduli are obtained through experimental measurements are discussed subsequently. Still working with an elastic material, one can now define the relationships between the stresses and the strains. In this case, this is the linear elastic constitutive relation:

$$\sigma_{ij} = \lambda \delta_{ij} \varepsilon_{kk} + 2G\varepsilon_{ij} \tag{7}$$

where δ_{ij} is the Kronecker delta. For simple geometries of deformation, such as those used in experiments, equation 7 can be simplified as

$$\begin{gathered} \text{Simple extension: } \sigma_{11} = \lambda \varepsilon_{kk} + 2G\varepsilon_{11} = E\varepsilon_{11} \\ \text{Simple shear: } \sigma_{12} = \tau_{12} = \lambda \varepsilon_{kk}(0) + 2G\varepsilon_{12} = G\gamma_{12} \end{gathered} \tag{8}$$

Hence, one can relate the stresses to any applied state of strain. Furthermore, the strains can be determined as functions of the applied stresses. Note that, in general, the theory of elasticity does not demand the development of compliance functions, which relate strains to stresses, as they are the inverse of the moduli. In the case of viscoelasticity, this is not so, and both modulus and compliance functions are developed in the next section.

The Viscoelastic Material Functions. In linear viscoelasticity, the moduli discussed for the elastic case can be recast as time- or frequency-dependent functions. The same is true for the compliance functions that are discussed here. For simplicity, consider the shear modulus G which becomes $G(t)$ or $G^*(\omega)$ in the case of the viscoelastic material. An important point here is that the viscoelastic modulus functions all exhibit time (frequency) dependence. Hence, one will have functions for $K(t)$ and $E(t)$ [or, eg, $G(t)$ and $\nu(t)$] and these are required in the case of a three-dimensional strain or stress field.

The general approach to discussing linear viscoelasticity comes from the Boltzmann superposition principle represented as a *hereditary* integral. For the shear stress as a function of shear strain, one obtains

$$\tau_{12}(t) = \int_0^t G(t-t') \frac{\mathrm{d}\gamma_{12}}{\mathrm{d}t'} \mathrm{d}t' \tag{9}$$

and for the strain as a function of the stress,

$$\gamma_{12}(t) = \int_0^t J(t-t') \frac{\mathrm{d}\tau_{12}}{\mathrm{d}t'} \mathrm{d}t' \tag{10}$$

Here it is emphasized that the definition of the elastic compliance $J = 1/G$ is not valid for the viscoelastic compliance $J(t)$ used in equation 10. Rather it is the complex compliance $J^*(\omega) = 1/G^*(\omega)$. In addition, all the linear viscoelastic functions can be related one to the other. Full discussion of these relationships can be found in Ferry (9) and Tschoegl. (10).

As shown above, the material functions and the constitutive equation determine the relationships between the stresses and the applied deformations or vice versa. Hence, understandings of both the material functions and the form of the constitutive law are important to successful use of our current knowledge of the viscoelastic behavior of polymers. The material functions alone can give much insight into molecular viscoelasticity and the general time-dependent behavior of the material. Combined with the constitutive laws (eqs. 9 and 10), the material functions give a predictive capability of material performance in arbitrary loading histories. The next section first discusses these aspects of the material functions, using simple mechanical analogues that give some sense of viscoelastic behavior. This is followed by examples of the Boltzmann superposition represented in equations 9 and 10. Finally, the meaning of linear viscoelastic behavior is discussed as a potential means to gain insight into molecular behavior in polymers.

Mechanical Analogues.

The Maxwell Model. In the above development, discussion moves from elastic behavior to viscoelastic descriptions of material behavior. In a simple sense, viscoelasticity is the behavior exhibited by a material that has both viscous and elastic elements in its response to a deformation or load. In early days, this was often represented by elastic or viscous mechanical elements combined in different ways (9–12). The simplest models are two element models that contain a viscous element (dashpot) and an elastic element (spring). The dashpot is assumed to follow a Newtonian fluid constitutive law in which the stress is related directly to the strain rate by the following expression:

$$\tau_{12} = \eta_0 \, \dot{\gamma}_{12} \tag{11}$$

and the spring is assumed to be linearly elastic:

$$\tau_{12} = G\gamma_{12} \tag{12}$$

and when they are combined in series to form a *Maxwell* model the response is the combined response of the two elements. The Maxwell model is represented in the insert in Figure 2.

Now, imagine deforming the Maxwell model by applying a constant strain to it at a time $t = 0$. The deformation is held constant and the stress is monitored. Figure 2 shows the mechanical response of the Maxwell model to an applied deformation. The first (early time) response is that the "material" responds only elastically because the viscous damper initially behaves rigidly (at infinite rate of strain). The total deformation of the element remains constant, but it redistributes itself between the spring and the dashpot. This results in *stress relaxation* that occurs exponentially with time:

$$G(t) = \frac{\tau_{12}(t)}{\gamma_{12}} = G\mathrm{e}^{-t/\lambda} \tag{13}$$

And the reader is reminded that the stress is relaxing at constant strain. Furthermore, equation 13 allows one to introduce the concept of a relaxation time

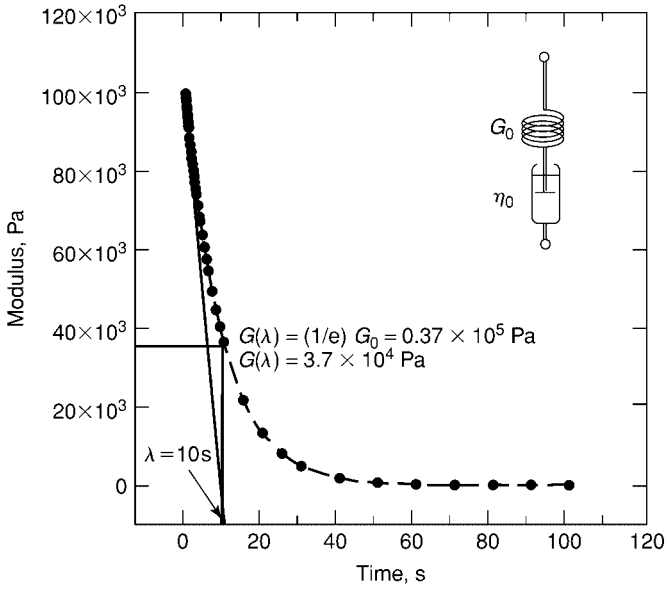

Fig. 2. Relaxation of the modulus in a stress relaxation experiment for a Maxwell element (insert). The construction shows two ways in which the relaxation time λ can be determined.

$$\lambda = \frac{\eta_0}{G} \tag{14}$$

that is, the characteristic time for the stress in the Maxwell element to decay to 1/e of its initial value (see Fig. 2). (Note the use of the symbol λ as the relaxation time and not the Lamé constant given previously. Also, τ is often used as the symbol to represent the relaxation time, but τ is used here for the shear stress.)

The Kelvin–Voigt Model. The other two-element mechanical model for viscoelasticity is the Kelvin–Voigt model in which the spring and dashpot are in parallel. In this model, the deformation or *creep* response to the imposition of a constant load is illustrated. In this instance a constant load is applied at $t = 0$ and the deformation is monitored. The Kelvin–Voigt model and its response are illustrated in Figure 3. The material property of interest in this case is the *creep compliance* $J(t)$ and it is written as

$$J(t) = \frac{\gamma_{12}(t)}{\tau_{12}} = \frac{1}{G}(1 - e^{-t/\lambda}) \tag{15}$$

And, now, the characteristic time λ is referred to as the *retardation time* because of the retarded elasticity of the material. That is, initially the load is carried by the viscous dashpot and then redistributes until, at long times, the load is carried fully by the elastic spring. Figure 3 shows the response to a loading history in which the load is applied for 100 s and then reduced to zero. Both the creep strain $\gamma(t)$ and the recoverable strain are depicted in the figure. The recoverable compliance would be obtained from the recoverable strain and the applied stress as

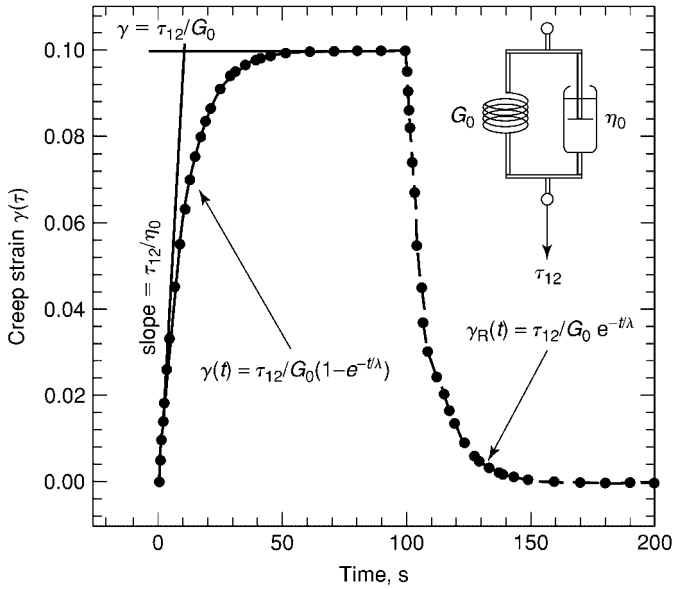

Fig. 3. Creep and recovery response for a Kelvin–Voigt model (insert).

$J_R(t) = \gamma_R(t)/\tau_{12}$, but only when the material has reached its equilibrium response is this a material property.

The Burgers Model. As a preview to the viscoelastic behavior of polymers, we next consider the four-element Burgers model that captures a "minimum" set of behaviors that is seen in polymeric materials and as discussed here (13). The insert in Figure 4 shows the Burgers model as a Maxwell model in series with a Kelvin–Voigt model. As shown in Figure 4, upon application of a constant stress τ_{12} for a time t_1 followed by its removal, the model captures the following aspects of polymer viscoelasticity:

(1) "Instantaneous" elasticity or elastic recovery (spring element G_1)
(2) Molecular "slip" (viscous element η_1)
(3) "Entropic" or rubbery elasticity (spring G_2)
(4) "Retarded" elasticity (Kelvin–Voigt element G_2 is retarded by η_2)

Polymers, as seen later, show more complex viscoelastic behaviors than does the Burgers model, but the essentials are in the Burgers model. The "instantaneous" elasticity can be thought of as the "glass-like" response; the molecular "slip" is the terminal response, as the long polymer molecules slide past each other and disentangle; the entropic elasticity occurs because of the long chains being entangled like a three-dimensional network of "entropic springs"; and the retarded elasticity occurs because of the resistance of the polymer melt to the

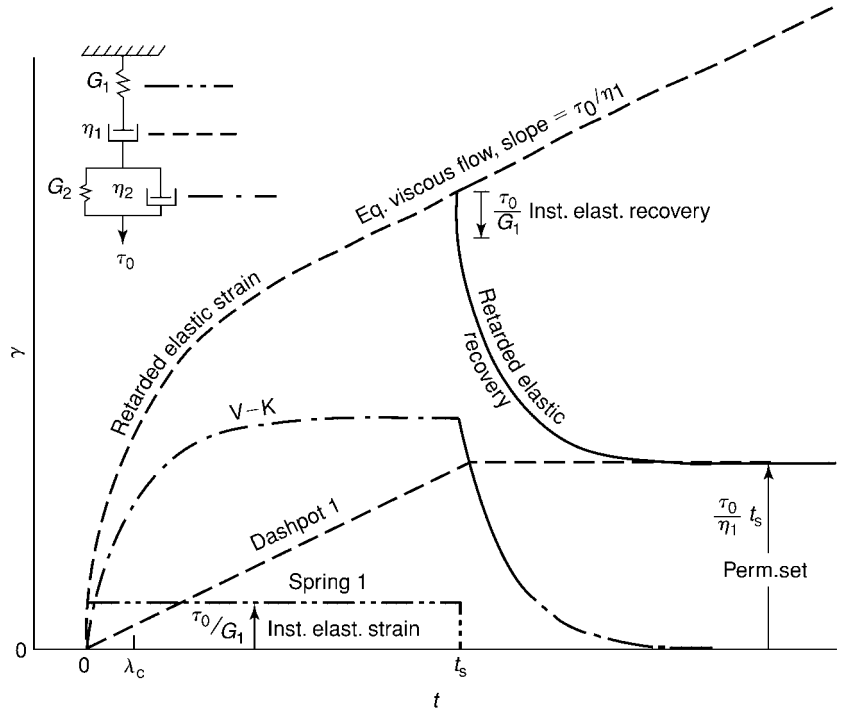

Fig. 4. Creep and recovery response for a Burgers model (insert), showing the four regions of "polymer-like" viscoelastic response as discussed in text. After Rosen (13), with permission.

forces applied by the spring. The equation for the creep compliance of the Burgers model is

$$J(t) = \frac{1}{G_1} + \frac{1}{G_2}(1 - e^{-t/\lambda}) + \frac{t}{\eta_1} \tag{16}$$

where $\lambda = \eta_2/G_2$. Upon unloading, the *recoverable compliance* $J_R(t)$ is

$$J_R(t) = J(t) - \frac{t}{\eta} \tag{17}$$

Note that equation 17 is the general equation for the recoverable compliance regardless of the model. Figure 4 gives a simplified sense of what the various aspects of polymer viscoelastic behavior are, although the actual behavior is more complex.

General Models. Clearly, one can add up springs and dashpots in a great number of ways. It is common practice to use either a generalized Maxwell model or a generalized Kelvin–Voigt model. The generalized Maxwell model, which is simply a set of Maxwell elements in parallel, is shown in Figure 5a. The generalized Kelvin–Voigt model, which is a set of Kelvin–Voigt elements in series, is shown

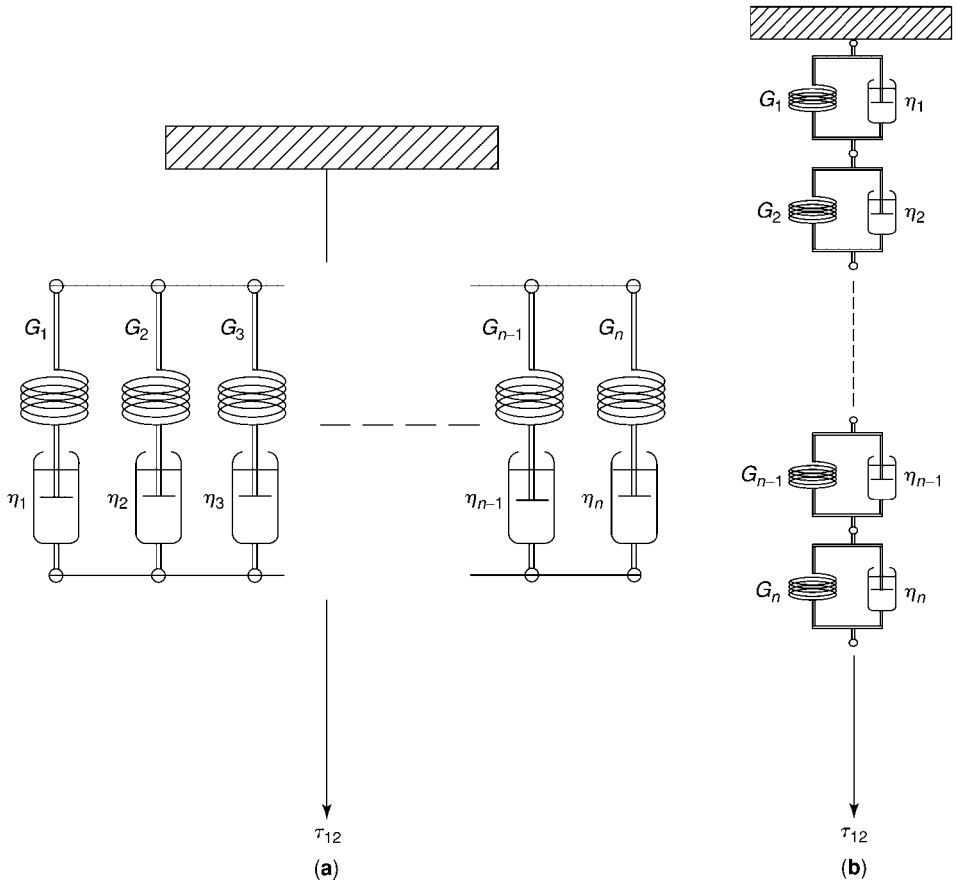

Fig. 5. (**a**) The generalized Maxwell model. (**b**) The generalized Kelvin–Voigt model.

in Figure 5b. The choice of model is primarily a matter of convenience because it is possible to find a *conjugate* Maxwell model to any Kelvin–Voigt model and vice versa (10). However, the moduli are most easily described with the Maxwell model and the equations for these are

$$G(t) = G_0 + \sum_{i=1}^{N} G_i \mathrm{e}^{-t/\lambda_i}$$

$$G'(\omega) = G_0 + \sum_{i=1}^{N} \frac{G_i \omega^2 \lambda_i^2}{1 + \omega^2 \lambda_i^2} \tag{18}$$

$$G''(\omega) = \sum_{i=1}^{N} \frac{G_i \omega \lambda_i}{1 + \omega^2 \lambda_i^2}$$

and the compliances are most easily described using the generalized Kelvin–Voigt model:

$$J(t) = J_g + \sum_{i=1}^{N} J_i(1 - e^{-t/\lambda_i}) + \frac{t}{\eta_0}$$

$$J'(\omega) = J_g + \sum_{i=1}^{N} \frac{J_i \omega^2 \lambda_i^2}{1 + \omega^2 \lambda_i^2} \tag{19}$$

$$J''(\omega) = \sum_{i=1}^{N} \frac{J_i \omega \lambda_i}{1 + \omega^2 \lambda_i^2} + \frac{\eta_0}{\omega}$$

The equation sets 18 and 19 provide a means of fitting experimental data to an arbitrary accuracy. It is important to remark, however, that the problem of actual fitting of data, while easier today than in the past because of the prevalence of high speed personal computers and commercial software, is nontrivial, and the reader who is interested in details of the treatments should refer to the appropriate literature (14–19).

Interrelationships among the Viscoelastic Material Functions. There is a continuing disagreement within the molecular viscoelasticity community about which of the above methods should be used to characterize a material (20). In fact, if one can obtain the zero shear rate viscosity and any of the other functions, these methods are all equivalent. The issue, however, revolves around the fact that some features that appear in the dynamic modulus disappear if the compliance is used as the function to represent the data and vice versa. Also, some measurements are more or less dominated by the viscosity contribution. As a result, some problems of misinterpretation of data could be averted if workers who prefer modulus representations would calculate the compliances. In addition, those who measure the compliance should calculate the moduli in order to provide the data in the format that is more common in the field because of the large number of commercial instruments that obtain dynamic moduli. The advent of modern software packages that make the interrelationships easily calculated makes this dispute seem to go away. The pathways to determine the different material functions, one from the other, are shown in Figure 6.

Boltzmann Superposition and Linear Behavior.

The Phenomenology of the Linear Theory of Viscoelasticity. One of the powers of the linear viscoelasticity theory is that it is predictive. The constitutive law that comes from Boltzmann superposition theory requires simply that the material functions discussed above be known for a given material. Then, for an arbitrary stress or deformation history, the material response can be obtained. In addition, the *elastic–viscoelastic correspondence principle* can be used so that boundary value problems such as beam bending, for which an elastic solution exists, can be solved for linear viscoelastic materials as well. Both of these subjects are treated in this section.

Boltzmann Superposition and the Constitutive Law for Linear Viscoelasticity. The underlying assumption of the Boltzmann superposition principle is that responses to loads or deformations applied to a material at different times are linearly additive. This set of assumptions leads to the constitutive laws of linear viscoelasticity theory which can be considered as a linear response theory. For discussion purposes, consider a Maxwell material that is subjected to a two-step deformation history. The history is such that a deformation $\gamma_1 = \Delta\gamma_1$

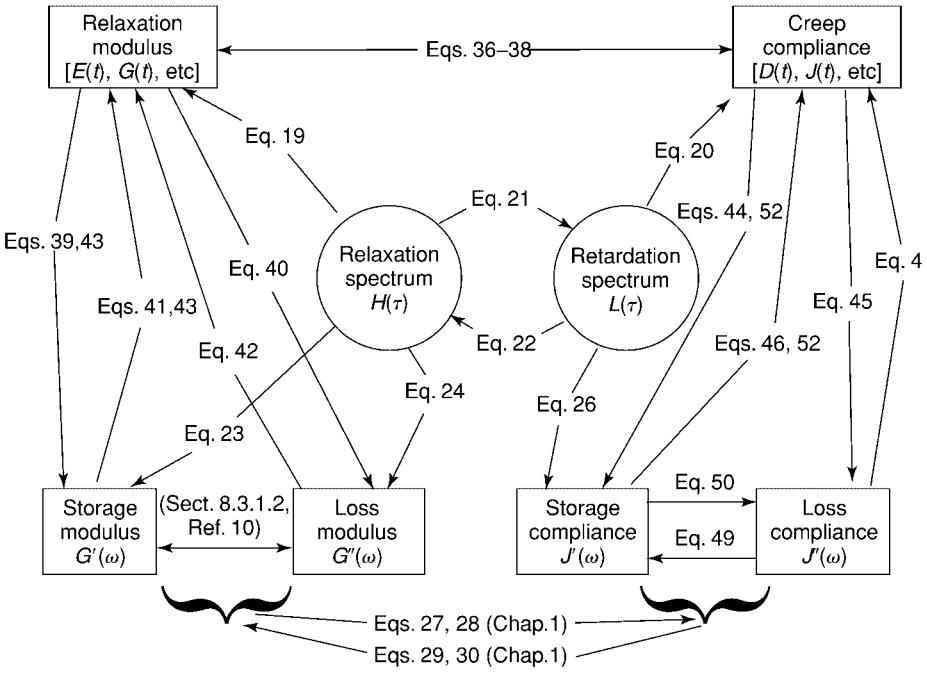

Fig. 6. Chart showing the paths to interrelate the linear viscoelastic material functions. Equation numbers refer to Chapter 3 of Ferry's book (9) unless otherwise indicated. Determination of $G'(\omega)$ from $G''(\omega)$ and $J'(\omega)$ from $J''(\omega)$ and vice versa comes from the Kramer–Kronig relation and is discussed in Tschoegl (10).

is applied at a time $t = 0$ and an additional deformation $\Delta\gamma_2$ is applied at a time t_1 so that $\gamma_2 = \gamma_1 + \Delta\gamma_2$. This can be carried on for as many steps as desired, as depicted in Figure 7a. The stress response to this deformation history is written as

$$\tau(t) = \sum_{i=1}^{N} \Delta\sigma_i(t - t_i') = \sum_{i=1}^{N} \Delta\gamma_i G(t - t_i') \tag{20a}$$

For $N = 2$

$$\tau(t) = \Delta\sigma_1(t - t_1') + \Delta\sigma_2(t - t_2') \tag{20b}$$

but $t'_1 = 0$ and $t'_2 = t_1$; therefore

$$\begin{aligned} \tau(t) &= \Delta\sigma_1(t) + \Delta\sigma_2(t - t_1) = \Delta\gamma_1 G(t) + \Delta\gamma_2 G(t - t_1) \\ &= \gamma_1 G(t) + (\gamma_2 - \gamma_1) G(t - t_1) \end{aligned} \tag{20c}$$

Figure 7b illustrates the way in which the responses add for a two-step history in which each step has the same magnitude. Equation 20a is the general form and is the discrete form of the linear superposition principle cast as a simple shear. It shows the simple linear additivity of the responses. A similar equation

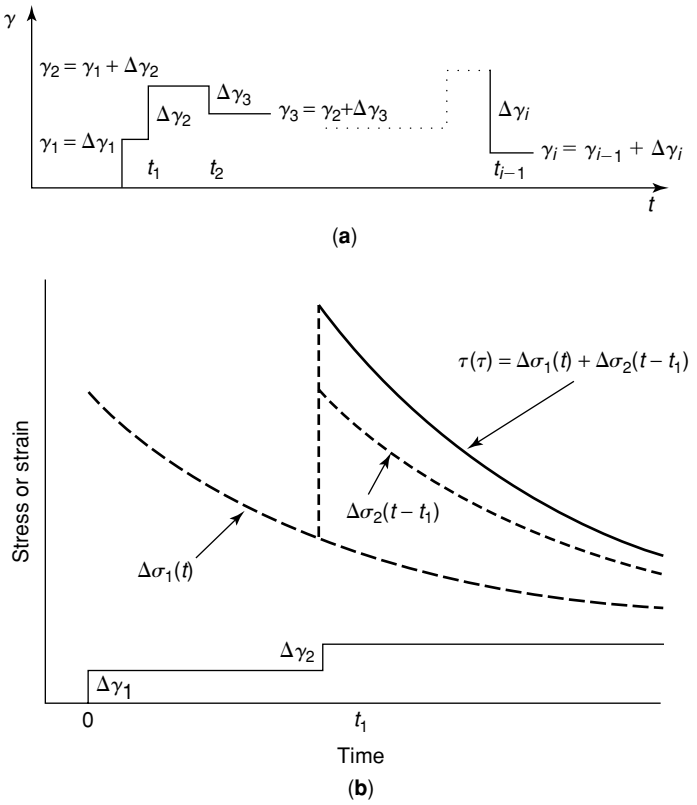

Fig. 7. (**a**) General step-strain deformation history relevant to Boltzmann-type linear superposition. (**b**) Schematic of stress additivity of responses for a Maxwell model in a two-step strain history (see text for discussion).

could be written for the strain response in terms of the stresses for a creep history. The equations can easily be generalized to include the full range of strains and stresses discussed in the next section. Furthermore, the responses can be written in terms of *hereditary integrals*:

$$\tau(t) = \int_0^t G(t - t')\frac{\mathrm{d}\gamma}{\mathrm{d}t'}\mathrm{d}t' \tag{9}$$

$$\gamma(t) = \int_0^t J(t - t')\frac{\mathrm{d}\tau}{\mathrm{d}t'}\mathrm{d}t' \tag{10}$$

Equations 9 and 10 can be solved for arbitrary strain (stress) histories to obtain the material stress (strain) response. Solution for the step-deformations requires use of the "unit Heaviside function" and is discussed in detail by Tschoegl (10) and by Findley, Onaran and co-workers. (21) Wineman and Rajagopal (22) deal with the step-strains, using Riemann–Stieltjes integrals. Other histories are more directly solvable. Also, in the linear theory the limits on the integral can be written from 0 to t rather than from $-\infty$ to t (9,10,21,22).

The final point of the current section is to illustrate that linear viscoelasticity can give rise to what looks like a "nonlinear" response. The typical example comes for a constant rate of deformation experiment. If a generalized Maxwell model is assumed, the material can be subjected to a constant rate of strain and a stress–strain curve can be plotted. As shown in Figure 8a, even though the theory behind equations 20a (or eqs. 9 and 10) is completely linear, one observes that the stress–strain response appears to be nonlinear. This is an illustration of the practicality of understanding viscoelasticity and of understanding the complex time-dependent behavior of polymeric materials. In addition, the linearity of the responses is illustrated in Figure 8b, where all the curves from Figure 8a collapse to a single curve when $\tau/(d\gamma/dt)$ vs $\gamma/(d\gamma/dt)$, (22) is plotted.

Elastic–Viscoelastic Correspondence Principle. One of the difficulties in working with time-dependent materials is solving for their response in actual conditions. For example, a composite aircraft wing might be considered as a viscoelastic beam subjected to bending moments (see Fig. 9). The problem can be solved by applying the viscoelastic constitutive equations to the problem, but in many instances this approach is tedious. Fortunately, it was shown that many classes of viscoelastic boundary-value problems can be solved if the elastic solution is known (23). This is referred to as the *elastic–viscoelastic correspondence principle*. One substitutes the Laplace transform of the viscoelastic material functions for their elastic counterparts into the elastic solution. Inversion of the Laplace transform gives the time-dependent response of the material. In the case of the pure bending of the beam just mentioned, the elastic solution for the displacements, stresses, and deflection can be written as follows (21):

$$\begin{aligned} \text{Strain:} \quad & \varepsilon(t) = -\frac{M(t)y}{E_e I} \\ \text{Stress:} \quad & \sigma(t) = -\frac{M(t)y}{I} \\ \text{Deflection:} \quad & \frac{d^2 w(x,t)}{dx^2} = \frac{M(t)}{E_e I} \end{aligned} \tag{21}$$

where $M(t)$ is the applied moment, y is the beam half thickness, I is the moment of inertia of the beam, and E_e is the elastic modulus. In the case of the viscoelastic beam, we first take the Laplace transform for the time-varying parameters and then substitute $s\hat{E}(s)$ for E_e. Then (see Ref. 21)

$$\begin{aligned} \text{Strain:} \quad & \hat{\varepsilon}(s) = -\frac{\hat{M}(s)y}{s\hat{E}(s)I} = -\frac{y}{I}\hat{J}(s)s\hat{M}(s) \\ \text{Stress:} \quad & \hat{\sigma}(s) = -\frac{\hat{M}(s)y}{I} \\ \text{Deflection:} \quad & \frac{d^2 w(x,s)}{dx^2} = \frac{\hat{M}(s)}{s\hat{E}(s)I} = \frac{\hat{J}(s)s\hat{M}(s)}{I} \end{aligned} \tag{22}$$

Note that the relationships between the viscoelastic compliance and the relaxation modulus are given by

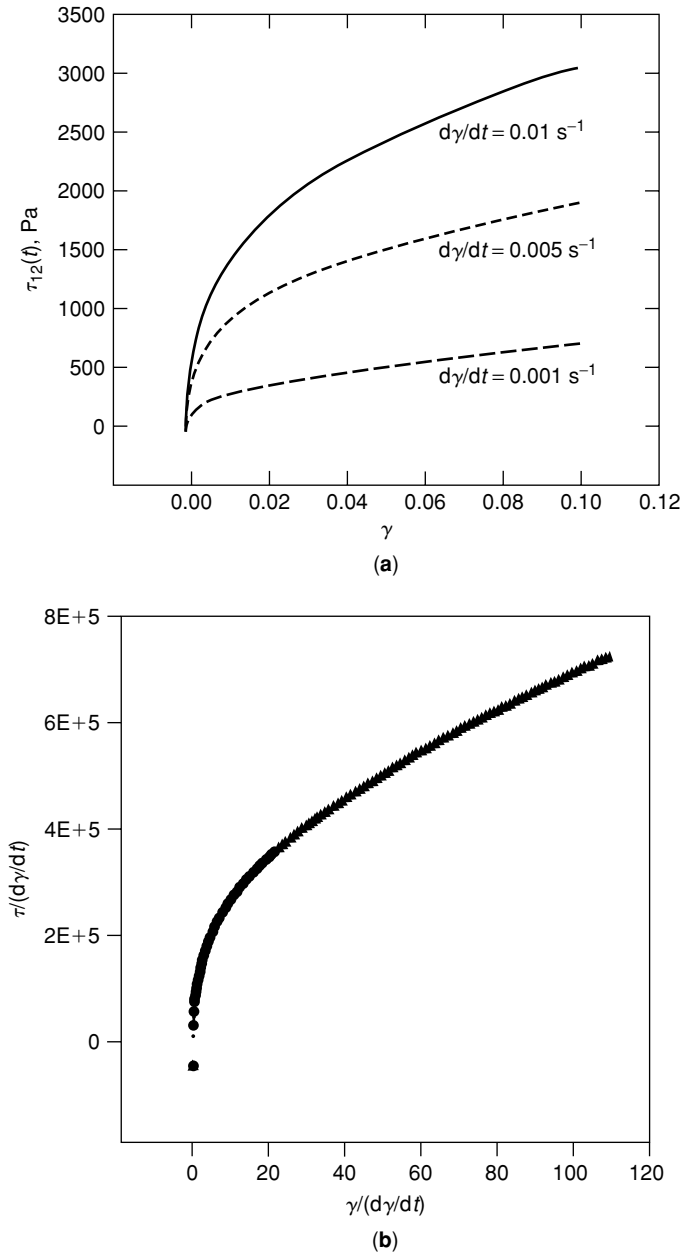

Fig. 8. (**a**) Stress–strain plot for a generalized Maxwell model to different strain rates, as depicted in figure. Plot shows "nonlinear" stress–strain behavior in spite of material model (Maxwell) following laws of linear viscoelasticity (see text). (**b**) Stress and strain data from different strain rates given in (**a**) divided by strain rate $d\gamma/dt$, demonstrating that material model follows linear viscoelasticity (see text).

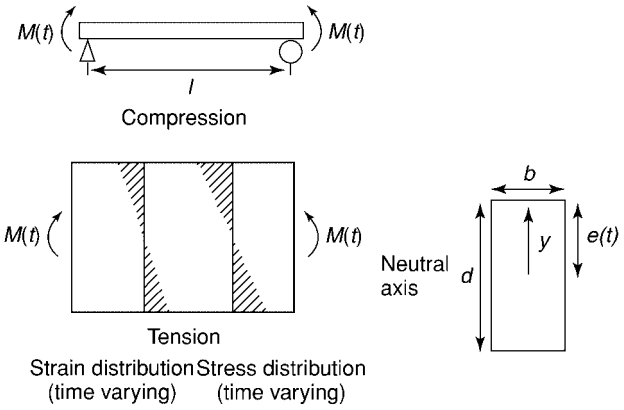

Fig. 9. Schematic of the beam-bending problem. After Findley et al. (21).

$$s\hat{E}(s) = \frac{1}{s\hat{J}(s)} \tag{23}$$

Inversion of equation 22, using the convolution transform, gives

$$\begin{aligned} \varepsilon(t) &= -\frac{y}{I}\int_0^t J(t-t')\frac{\mathrm{d}M(t)}{\mathrm{d}t'}\mathrm{d}t' \\ \sigma(t) &= -\frac{M(t)}{I} \\ \frac{\mathrm{d}^2 w(x,t)}{\mathrm{d}x^2} &= \frac{1}{I}\int_0^t J(t-t')\frac{\mathrm{d}M(t)}{\mathrm{d}t'}\mathrm{d}t' \end{aligned} \tag{24}$$

And integration of the hereditary integrals for strain and deflection gives the solution to any applied history of the moment $M(t)$. A note of caution, however, arises for mixed conditions in which the interface between the stress and the displacement boundaries is not constant. In such cases the elastic–viscoelastic correspondence principle is not applicable and the solutions become more difficult (21).

Finally, this section concludes by noting that Schapery (7,24) has shown that when the material properties are changing very slowly, an approximate solution can be obtained by substituting the viscoelastic moduli for their elastic counterparts. This will be justified in some instances. The reader should examine the literature for further consideration of the limitations of these approaches. Also, the advent of commercial finite element codes that have linear viscoelastic material elements makes the solution of such problems more routine.

Linear Viscoelastic Behavior of Polymeric Materials

General Regimes of Response. Polymeric materials exhibit a very rich set of viscoelastic responses. The responses observed depend upon the state of the

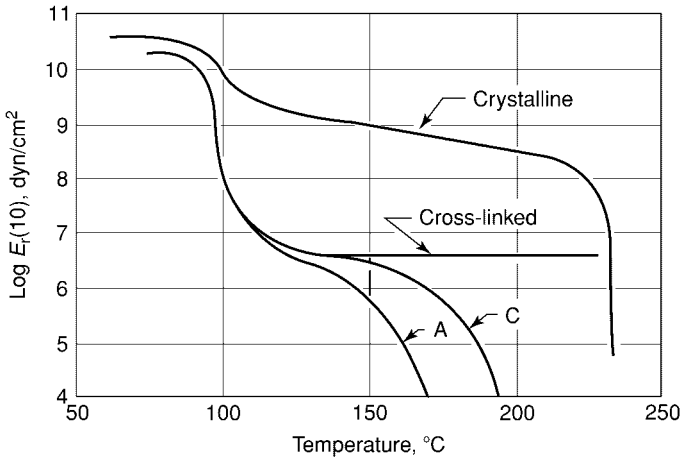

Fig. 10. The relaxation modulus (at 10 s) for a polymer measured as a function of temperature. Curves labeled A and C depict amorphous, linear polymers with the molecular weight of A being less than that of C. The cross-linked polymer is also amorphous, but cannot flow. The crystalline polymer behaves differently because it is "reinforced" by crystalline domains. After Tobolsky (25).

polymer and on its structure. The material can be in an amorphous state if it is a glass, a rubber, a melt, or a solution. In addition, the material can be semicrystalline in that crystallites partially fill or reinforce the otherwise amorphous material. Figure 10 illustrates a plot of the relaxation modulus vs T; it indicates schematically the sort of responses that are observed for an amorphous polymer as a function of temperature. Also shown is the sort of response to be obtained in a semicrystalline polymer over the same temperature range. At low temperatures, one observes a behavior that for both structures is the same as that of a high modulus material. As the glass temperature T_g is approached the amorphous material undergoes a dramatic drop in modulus by several orders of magnitude. The modulus of the semicrystalline material changes significantly, but not nearly as much. Following the modulus drop associated with the glass temperature, the amorphous polymer can exhibit a rubbery plateau due to the *entanglement network* formed by the long-chain molecules. If the molecules are not long enough the entanglement plateau will be weak or nonexistent. In the same temperature regime the semicrystalline polymer exhibits a long and slow reduction of modulus. As temperature increases, the amorphous polymer undergoes terminal flow due to the disentanglement of the molecules while the semicrystalline polymer continues changing slowly. Above the melting point of the semicrystalline polymer its modulus drops dramatically because the material has become an amorphous polymer at a temperature well above the terminal flow region. In the next sections these behaviors are discussed in more detail.

Behavior in the Amorphous State. Polymer behavior in the amorphous state can be divided into two categories: the glassy state and the fluid state. The former applies to polymers below the glass transition and is generally dominated by the segmental or local movements of the polymer chains. The fluid state of the

amorphous polymer is dominated by long-range motions of the polymer chains and the eventual onset of entanglements that give rise to very interesting viscoelastic properties. This section first describes the viscoelastic behavior of the polymer in the glassy state and through the glass temperature. This is followed by a section on the fluid-state properties that are dominated by the long-chain nature of the polymer.

Time–Temperature Superposition. In Figure 10 one observes that the viscoelastic relaxation modulus at a single time or frequency (*isochrones*) shows dramatic changes as temperature increases (25). It turns out that such behavior can be described within the context of a model which is referred to as *time–temperature superposition* or *thermo-rheological simplicity* (9,10,25). The fundamental concept here is that the relaxation times introduced above for, eg, a generalized Maxwell model, all exhibit the same temperature dependence. When thermo-rheological simplicity is valid, one can replace each λ_i in equations 18 and 19 by $a_T\lambda_i$ where the *shift factor* a_T represents the amount that the relaxation time λ_i is changed in going from some reference temperature T_R to the current temperature T. That is

$$a_T = \frac{\lambda_i(T)}{\lambda_i(T_R)} \tag{25}$$

When equation 25 is valid, it is possible to make measurements of the viscoelastic functions over a range of, say four logarithmic decades of time (frequency), at multiple temperatures and use the data to create *reduced* or *master* curves that span many more decades in time (frequency). This is useful for determining the polymer's behavior at longer or shorter times (lower or higher frequencies or rates) that would be extremely difficult to do otherwise. This can be important in both processing applications where rates can be very high and in long-term durability applications where unreasonably long times might otherwise be required to obtain test data. Figure 11 shows the actual data that were obtained for a polymeric material over a limited time range, but at multiple temperatures (25). Figure 12 shows the data reduced to a master curve using time–temperature superposition. As discussed below, the reduced curve in Figure 12 can also be related to the observed temperature dependence of the modulus depicted schematically in Figure 10.

Figure 13 shows the data for the shift factors as log a_T vs T (26). The description of the shift factors as a function of temperature is very important both for ease of application of the method to actual material behavior and because it has implications for the physical understanding of the behavior of polymeric materials. In the next three sections, the temperature dependence of the viscoelastic properties is discussed by examining the temperature dependence of the shift factors.

Properties near the Glass Temperature. In Figure 10 the curve for the amorphous polymer exhibits a behavior in which the modulus at low temperatures changes slowly as temperature increases. As the temperature approaches the glass temperature T_g, however, the modulus begins to change rapidly, dropping by up to 3 orders of magnitude, as the T_g is traversed. This is related to the changing relaxation times. Figure 12 shows a similar behavior, but now with time. At short

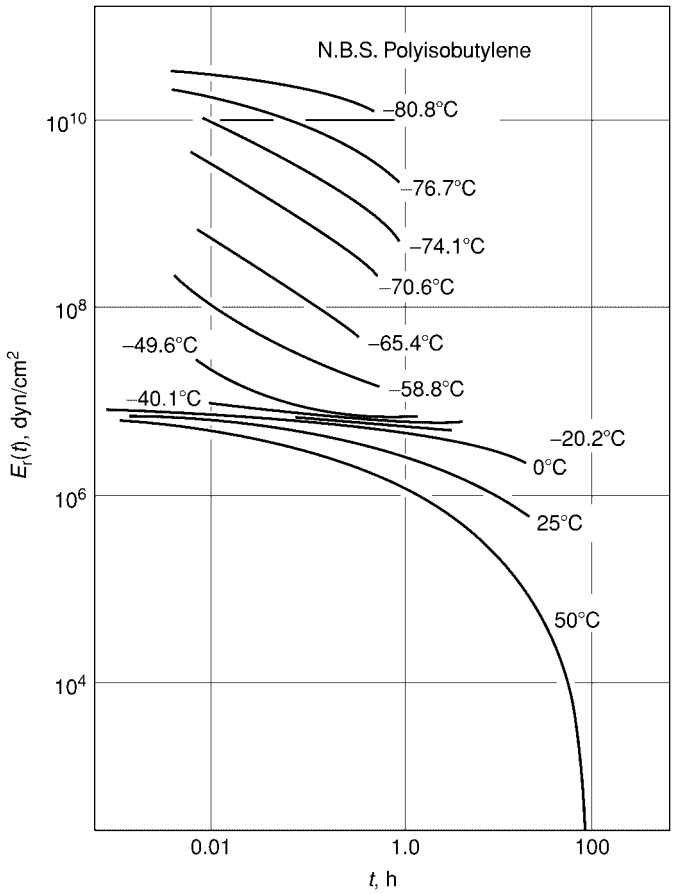

Fig. 11. Stress relaxation isotherms for a polyisobutylene amorphous polymer. After Tobolsky (25).

times, the material response changes slowly and as a glass "transition" time is approached begins to drop rapidly by the same 3 orders of magnitude. In fact, the time–temperature superposition principle allows one to go from curves in temperature space to curves in time (or frequency) space and vice versa.

When the shift factors for the relaxation times are plotted as in Figure 13, an important type of behavior is seen. Here it is observed that the shift factors increase dramatically as the temperature decreases. In fact, if one extrapolates the behavior, there is a singularity point that is reached that is about 50 K below the nominal glass temperature determined from other test methods (such as dsc). This rapid increase of the material shift factor also corresponds (eq. 25) to a rapid increase in the relaxation times as the temperature is decreased. Hence, the glass temperature is approached because the mobility in the polymer becomes so slow that, in normal experimental time scales, the molecules cannot respond to the mechanical solicitation and the material exhibits nearly solid-like properties [imagine the glassy poly(methyl methacrylate) (PMMA) that makes

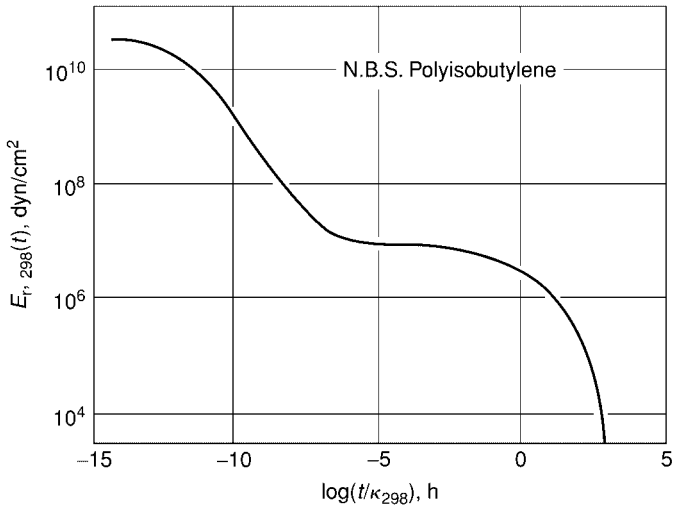

Fig. 12. Master curve generated by applying time–temperature shifting to the data given in Figure 11. (Note that $\kappa_{298} = 1/a_T$.) After Tobolsky (25).

up aircraft windows. The T_g of PMMA is about 110°C]. There are two equations that are commonly used to describe the shift factor behavior and these are discussed later. First the relationship between the viscosity and the shift factor is discussed.

The viscosity is related to the relaxation modulus through the following equation (9):

$$\eta_0 = \int_{-\infty}^{\infty} tG(t)\mathrm{dln}t \tag{26}$$

(for a Maxwell element, this would translate into $\eta_0 = G\lambda$). When the modulus is proportional to temperature T and density ρ (as in the case of rubber elasticity) the shift factor can be determined from viscosity measurements:

$$a_T = \frac{\eta_{0,T}\rho_{T_R}T_R}{\eta_{0,T_R}\rho_T T} \tag{27}$$

Hence, when the shift factor is increasing rapidly, this implies that the viscosity is also increasing rapidly.

One equation used to describe the rapid increase of the viscosity with decreasing temperature is the Vogel–Fulcher equation (27,28):

$$\eta_0 = A\mathrm{e}^{B/(T - T_\infty)} \tag{28}$$

where A is a prefactor and T_∞ is the temperature at which the viscosity extrapolates to an infinite value. Note that when $T_\infty = 0$ K, equation 28 reverts to an Arrhenius form and B would have the meaning of an activation energy (E_a/R). Equations 28 and 27 can be used together to obtain the shift factor a_T. Also, a

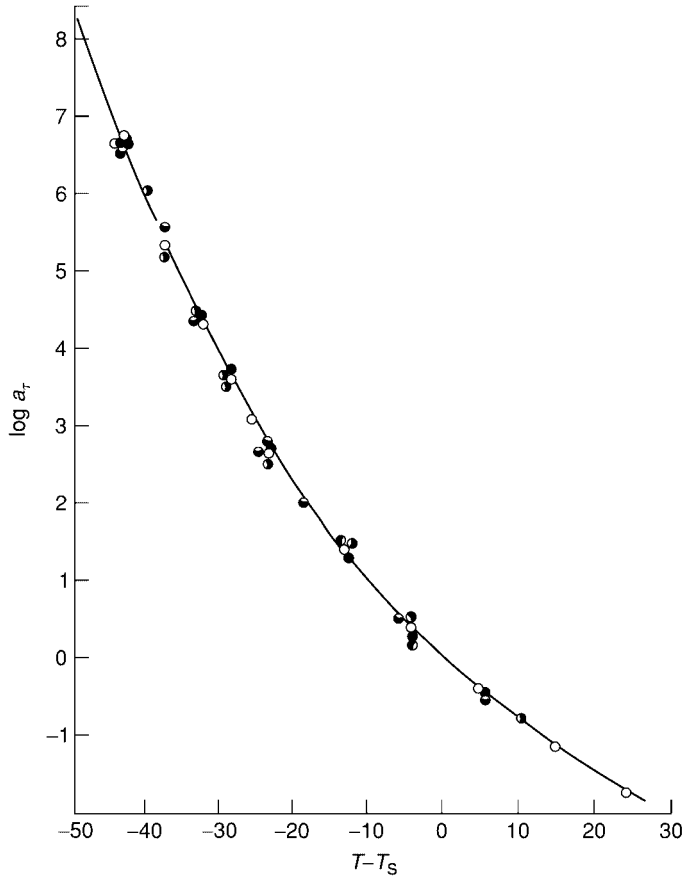

Fig. 13. Time–temperature shift factors for poly(α-methyl styrene). $T_{ref} = 204^{\circ}$C. After Fujimoto et al. (26), with permission.

similar form to equation 28 can be used to represent the temperature dependence of the relaxation times.

The other equation that is often used to describe the dependence of the shift factors on temperature is the Williams, Landel, and Ferry (WLF) equation (29):

$$\log a_T = \frac{C_1(T - T_R)}{C_2 + T - T_R} \tag{29}$$

where C_1 and C_2 are constants. The singularity in the shift factor occurs when $C_2 = -(T - T_R)$, and when $T_R = T_g$ this value is approximately 50 K, ie, the singularity occurs some 50 K below the nominal glass temperature. When $T_R = T_g$, the Vogel–Fulcher and WLF equations are related by the following expressions (9):

$$\begin{aligned} C_1 &= \frac{B}{T_g - T_\infty} \\ C_2 &= T_g - T_\infty \\ 2.303 C_1 C_2 &= B \end{aligned} \tag{30}$$

Note that for many polymers the values of the WLF parameters are close to the so-called universal values, which are $C_1 = 17.44$ and $C_2 = 51.6$ K when $T_R = T_g$. (When no other information is available, the "universal" values for C_1 and C_2 can make useful approximations to actual behavior.)

In discussing the temperature dependence of the shift factors in polymers, it is essential that a distinction be made between the segmental relaxations and the terminal relaxations. The reason for this can be seen in Figure 10 where there are two regions of rapid change in properties. The first occurs in the vicinity of the glass temperature and is due to increasing segmental or local mobility. The second occurs after the rubbery plateau and is related to the terminal relaxations that occur because of chain disentanglement in the fluid state. These two processes are now known to generally show different temperature dependences and one should be clear which relaxations are relevant in any particular situation (30–32).

Figure 13 shows the rapid increase of the shift factors (or viscosity) as T_g is approached from above. As noted previously, the point of singularity is approximately 50 K below the T_g. However, as the glass temperature is traversed, the material response does not continue to follow the WLF curve, rather it falls away from it, as shown in Figure 14 (33–35). The reasons for this are involved with the nature of the glass-transition event and the fact that the molecular mobility has become extremely low in the vicinity of the glass temperature (9,25,28,36,37). As a result, as the temperature changes, the molecules do not have enough time to relax into their equilibrium state and a glass is formed. Glasses are nonequilibrium materials and the sub-T_g behaviors are determined very much by this (36–40). Regardless of this fact, the response below T_g does not follow the WLF behavior. It can, however, follow time–temperature superposition, but with a less dramatic dependence of the shift factors on the temperature, as is seen in Figure 14. In Figure 14 there are three lines for the shift factors below T_g. In this instance, it is due to the physical aging (40) that accompanies the evolution of the nonequlibrium glass toward its equilibrium state.

Viscoelastic Relaxation Properties far below the Glass Temperature. As one moves below the glass-transition temperature, the relaxation behavior of the amorphous polymer becomes more and more sluggish as the thermal energy available to stimulate molecular motion becomes smaller. This behavior is seen in the schematic of Figure 10. However, below the glass temperature, polymers often exhibit other relaxation responses that are referred to as sub-T_g relaxations (9,41–44). A typical example is shown in Figure 15 where the dynamic responses of a series of poly(n-alkyl methyl methacrylates) as a function of temperature are shown. The reader can see that G' ($\omega = 1$ Hz) shows a smeared out "step" in response at low temperatures (approximately 0°C in the PMMA). The PMMA shows a broad peak at the same temperature in tan δ. This relaxation is referred to as the β-relaxation (relative to the α-relaxation of the glass temperature). Some

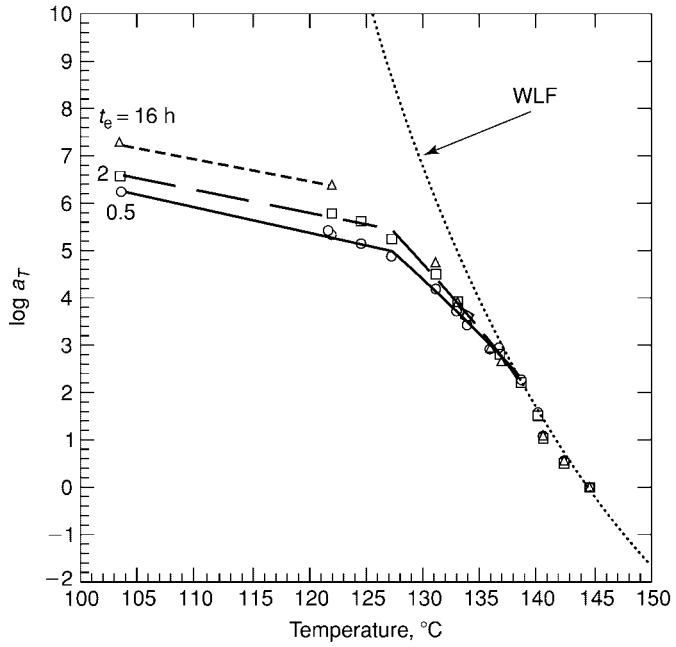

Fig. 14. Plot of shift factor (logarithm) vs T for polycarbonate, illustrating the change in behavior away from the WLF-type of temperature dependence as T_g is traversed. Also, because the glassy state is a nonequilibrium state, the material "ages." The curves at 0.5, 2, and 16 h represent the results at these aging times. After Pesce et al (33).

materials exhibit a γ-relaxation at even lower temperatures, as seen for the poly(n-butyl methacrylate) and poly(n-propyl methacrylate). The sub-T_g relaxations can affect other material properties, although the relationship between linear viscoelastic properties and, eg, failure is complicated and simple relationships not generally universal.

One important aspect of the sub-T_g relaxations is that they generally exhibit different temperature dependences than does the main glassy relaxation. The result is that time–temperature superposition is not usually valid when there is a strong sub-T_g relaxation in the polymer. An example of this is the behavior shown for poly(ethylene naphthalate) in Figure 16, where one can see that time–temperature shifting of creep data does not collapse the data to a single curve because this material has a strong β-relaxation that is not far from the glass temperature (45).

Finally, it is worth noting that the sub-T_g relaxations are often attributed to side-group motions on the polymer chain. A good example is the changing relaxation strength and position in the series of n-alkyl methacrylates that was presented in Figure 15 (44). There it is shown that both the α and the β relaxations shift systematically as the side-chain length increases from $n = 1$ (methyl) to $n = 4$ (butyl). Note, however, that the α-relaxation shifts more strongly than does the β-relaxation with increasing side-group length.

Viscoelastic Response far above the Glass Temperature: T_g The Fluid State. From Figure 10 or Figure 12 one can see the fluid state response of the

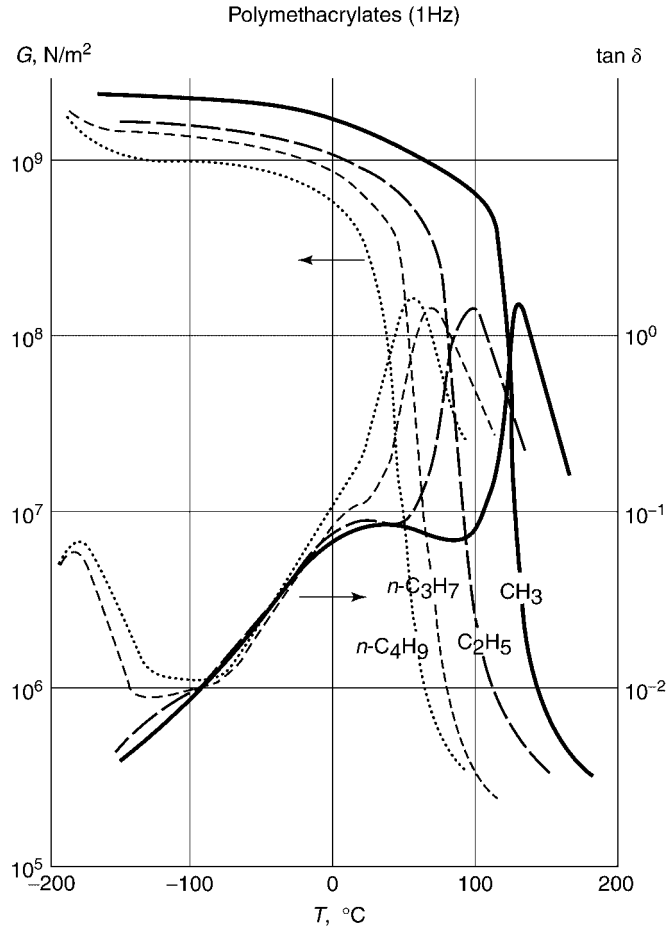

Fig. 15. Dynamic modulus and loss tangent (at 1 Hz) of a series of n-alkyl methacrylates showing how side groups change the α and β transitions. After Heijboer (44).

polymer. This is the portion of the curve at long times or high temperatures from the rubbery plateau to the end of relaxation where the polymer would take the shape of whatever container held it, ie, it is a liquid. There are several fundamental aspects to polymer behavior in this region. On the rubbery plateau, the polymer chains behave as if they were part of a three-dimensional network and their response can be described from modern rubber elasticity theories. This behavior is beyond the scope of the current review and the reader is referred to the literature for further information (46–50). At long enough times, however, the polymer chains have the opportunity to slip out of the entanglement points and the relaxation behavior seen in the terminal response regime results. The current paradigm for the viscoelastic response of polymers in this terminal flow regime is the reptation theory given by de Gennes (51) and Doi and Edwards (52–56). According to this model, the entanglement field can be represented by a tube through which the chain "reptates" along the chain direction. This is schematicized in

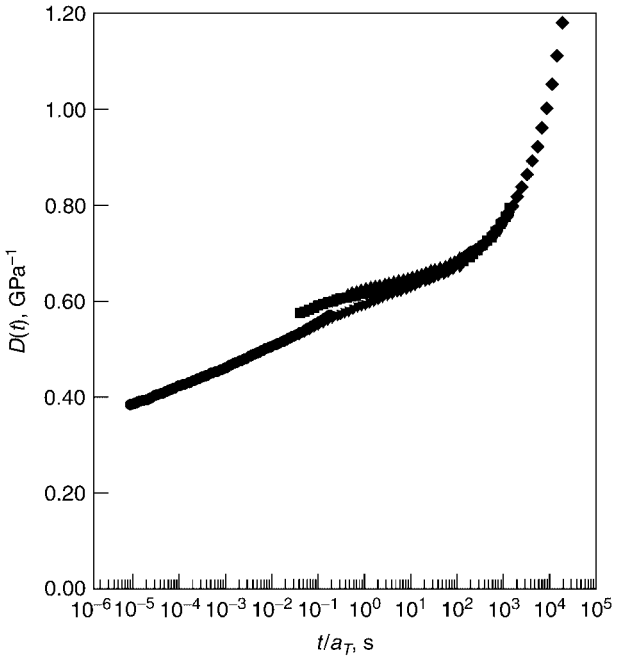

Fig. 16. Reduced curve of creep compliance vs time for PEN showing lack of time–temperature superposition (see text for discussion). ● 30°C; ▼ 50°C; ■ 80°C; ◇ 100°C. After Cerrada and McKenna (45).

Figure 17, where one can see (a) the topology of a chain in a fixed network and (b) the primitive path defined by the tube.

Before describing the reptation theory quantitatively, we first examine part of the rich set of behaviors that any theory of polymer chain dynamics in the melt state needs to be able to describe. One of the most interesting aspects of polymer melt and solution behavior is that once the material is well entangled, the viscoelastic behavior is quasi-universal. First, the zero shear rate viscosity η_0 is observed to vary with the molecular weight to a very strong power (9,57):

$$\eta_0 = AM^{\alpha} \tag{31}$$

where A is an empirical prefactor and M is the molecular weight. In fact, the observed power law dependence seems to follow very well the weight average molecular weight. This power law exponent α is generally found to be approximately 3.4. The variation of viscosity with molecular weight is shown in Figure 18 for a number of polymers from the classic work of Berry and Fox (57). The molecular weight axis also includes the concentration effect discussed shortly. The very strong molecular weight dependence of the viscosity is still not fully understood, although reptation theory has provided a very large step toward understanding.

According to the reptation theory, the dramatic slowing down of the motion of long polymer chains can be considered as similar to the motion of a chain

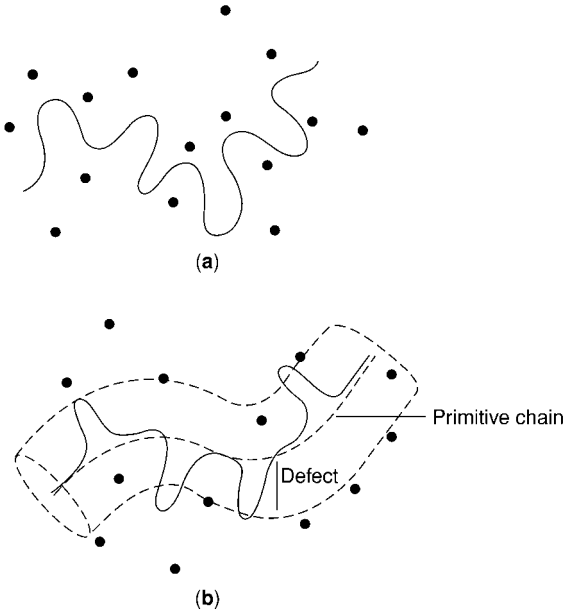

Fig. 17. Schematic of a polymer chain confined in (**a**) a fixed network of obstacles and (**b**) the primitive path representation of the same constraints as a tube. After Doi and Edwards (56), with permission.

through a network, as represented by the tube in the Doi–Edwards (DE) model. The network chains of the tube walls prevent the polymer chain from lateral motion (or at least reduce lateral motion) with the result that the chain is forced to move along the contour of the tube. The chain's Brownian movement causes it to slide back and forth within the tube until it eventually disengages. Quantitative analysis of the chain's diffusive properties leads to the estimation that the viscosity-molecular weight exponent $\alpha = 3.0$ rather than the observed 3.4. The reasons for this have been variously attributed to different mechanisms such as "primitive path" fluctuations (58), "constraint release (59)," tube fluctuations (60), and others that provide a means for the viscosity to crossover from a 3.4 power law dependence on molecular weight to a purely reptative behavior at extremely high molecular weights (61–64). There is only one set of data currently available that really bears relevance to the question of such crossover behavior and that is based on a single data point that falls well off of the 3.4 line for a polybutadiene of 1.65×10^7 g/mol molecular weight (65).

In addition to the large molecular weight dependence of the viscosity, another aspect of the chain dynamics of polymers in the terminal region is the observation that the relaxation spectrum is very broad. One measure of the breadth of the relaxation spectrum is the product of the rubbery plateau value G^0_N and the steady-state recoverable compliance J^0_e. The predicted and observed values for polymer melts are

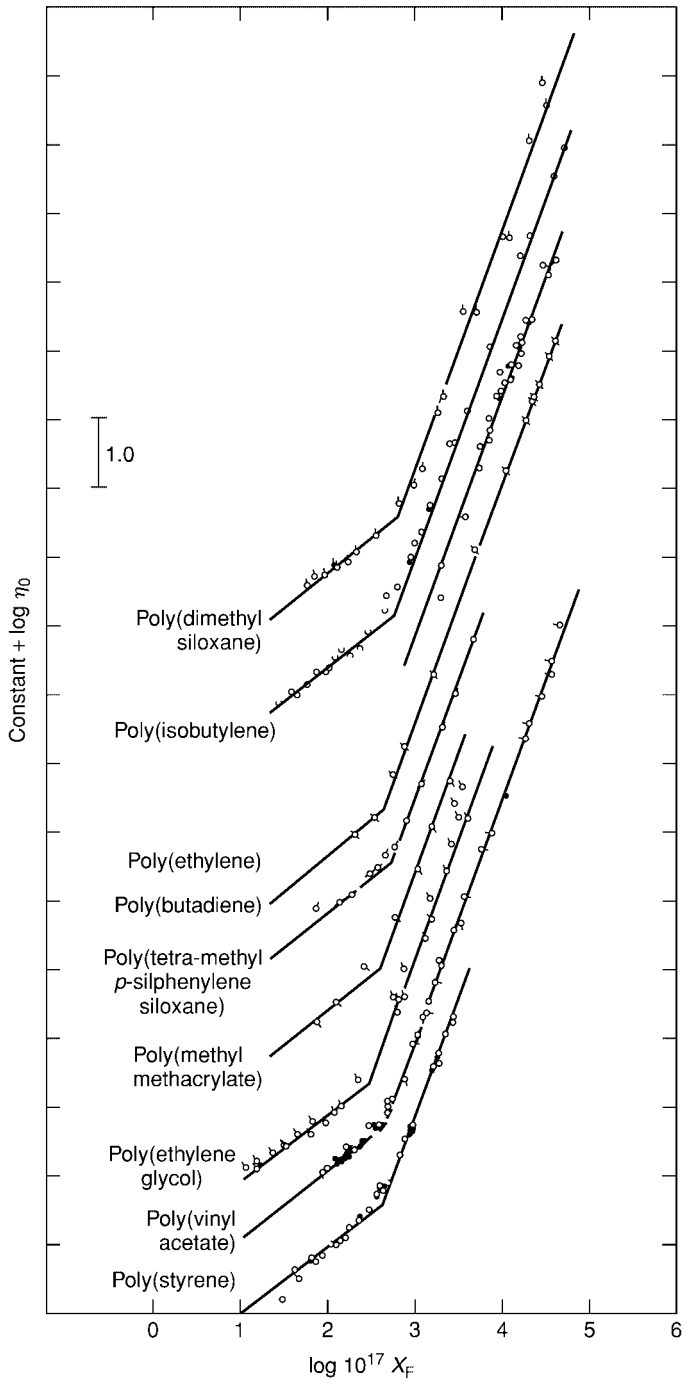

Fig. 18. Double logarithmic representation of the viscosity vs scaled molecular weight for a series of polymers, showing the change from a weak (nearly linear) dependence of viscosity on molecular weight to the entangled regime where $\eta_0 \propto M^{3.4}$. After Berry and Fox (57), with permission.

$$\begin{aligned} J_e^0 G_N^0 &\approx 2.0(\text{observed}) \\ J_e^0 G_N^0 &= 1.2(\text{reptation}) \end{aligned} \tag{32}$$

Hence, the reptation theory does not predict a broad enough relaxation spectrum and current modifications of the theory seem insufficient to describe the full range of observed viscoelastic behavior of polymer melts. Reptation theory is still the paradigm for polymer chain dynamics and provides tremendous insight into material behavior. However, as described, there are still pieces of the puzzle of polymer molecular viscoelasticity that remain to be elucidated.

Behavior of Concentrated Solutions. Another aspect of polymer chain dynamics that is important to their understanding is their behavior in entangled solution. This is particularly so because the reptation theory does not explicitly deal with the effects of concentration on the tube diameter and resulting chain dynamics. However, there are several aspects to the effects of the interactions between small molecule "solvents" or "plasticizers" that are important. The first effect is the observation that the glass-transition temperature of the material is changed, generally to lower temperatures (9,37). For the segmental relaxation, this can be reasonably well accounted for by a time–concentration superposition principle (9,66) similar to the time–temperature superposition discussed above. In the event that one is dealing with the plasticization and the segmental relaxation, the major effect is that the T_g is decreased. The other parameters in the WLF or Vogel–Fulcher equations are less impacted. The reader is directed to the extensive treatment of the problem by Ferry (9) in terms of the free-volume model of dynamics for further information.

On the other hand, the impact of the solvent as one moves into the entanglement regime is different from the simple shift in T_g, although this change is also important for understanding the behavior. The other factor that occurs is that the entanglement density decreases (perhaps the tube diameter gets larger) and the plateau modulus and steady-state recoverable compliance both change dramatically with concentration. When we work with the polymer concentration ϕ, we find that $G^0{}_N$ and $J^0{}_e$ vary as

$$G_N^0 \propto \phi^{2-2.25} \quad \text{and} \quad J_e^0 \propto \phi^{-(2-2.25)} \tag{33}$$

In Figure 18 the viscosities were found to scale as approximately $\phi^{3.4}$—the same as the molecular weight. At the same time, it has been reported (67) that the viscosity can vary by as much as ϕ^5. This difference in apparent behavior depends somewhat on the polymer–solvent system, the temperature of test relative to T_g, and whether or not the data are corrected to a constant "distance" from the glass temperature. The reason stems from the simple relation between viscosity and the relaxation modulus given in equation 26, which for a simple Maxwell model would be

$$\eta_0 = G_N^0 \lambda \tag{34}$$

Because the characteristic relaxation times λ_i vary in a way that is determined by the concentration dependence of the glass temperature, equation 34 combined

with equation 33 indicates that the method of data analysis will determine the scaling behavior observed for the viscosity as a function of concentration. When one is well above the glass transition, the λ_i can follow a dependence as strong as ϕ^3, then equation 34 with equation 33 would give (68)

$$\eta_0 \propto G_N^0 \lambda \propto \phi^2 \phi^x$$
$$\text{For } x = 3: \eta_0 \propto \phi^5 \tag{35}$$
$$\text{For } x = 1.4: \eta_0 \propto \phi^{3.4}$$

Hence, description of the dynamics of the polymer–solvent system demands complete specification of both the complex T_g–concentration relationship and the temperature(s) of test. Importantly, unlike the case of time–temperature superposition, the shift factors for the relaxation times and the viscosity will not be the same. The latter will scale, as does the viscosity, as in equation 35. However, the relaxation times themselves will scale with a much weaker concentration dependence.

Viscoelastic Response of Semicrystalline Polymers. Figure 10 illustrated the general response of the semicrystalline polymer as a function of temperature. For the amorphous polymer it was possible to show the response as a function of time (or frequency) as in Figure 12 because of time–temperature superposition principles. Unlike the amorphous polymer, the viscoelastic response of the semicrystalline polymers cannot generally be treated using time–temperature superposition. There are several reasons for this. First, the crystallites in the material may exhibit relaxations that have different temperature dependences than the amorphous phase. This would clearly lead to a breakdown of thermorheological simplicity. In addition, the amorphous phase in the semicrystalline polymer may be changed by the presence of the crystallites. This has been referred to as a rigid amorphous phase or a constrained phase. The impact of the constraint is to change the temperature dependence of the relaxation response of the constrained amorphous material relative to that of the unconstrained material. The result is that, again, time–temperature superposition does not describe the material. Figure 19 shows the viscoelastic behavior of a semicrystalline material at several temperatures (25). Tobolsky (25) made the important observation that these curves are not superimposable by simple shifting procedures. The result is that for the semicrystalline polymers, determination of the full thermo-viscoelastic response of the material can be a very time-consuming task because the ability to extrapolate outside the testing range of times or frequency is limited.

Nonlinear Viscoelastic Behavior of Polymeric Materials

General Regimes of Response. The nonlinear viscoelastic response of polymers, of course, follows some of the same classifications as does the linear response. Hence, the behavior above the glass temperature and into the terminal zone is fluid behavior, and often follows time–temperature superposition. The phenomenology of polymer melts and solutions is commonly described by

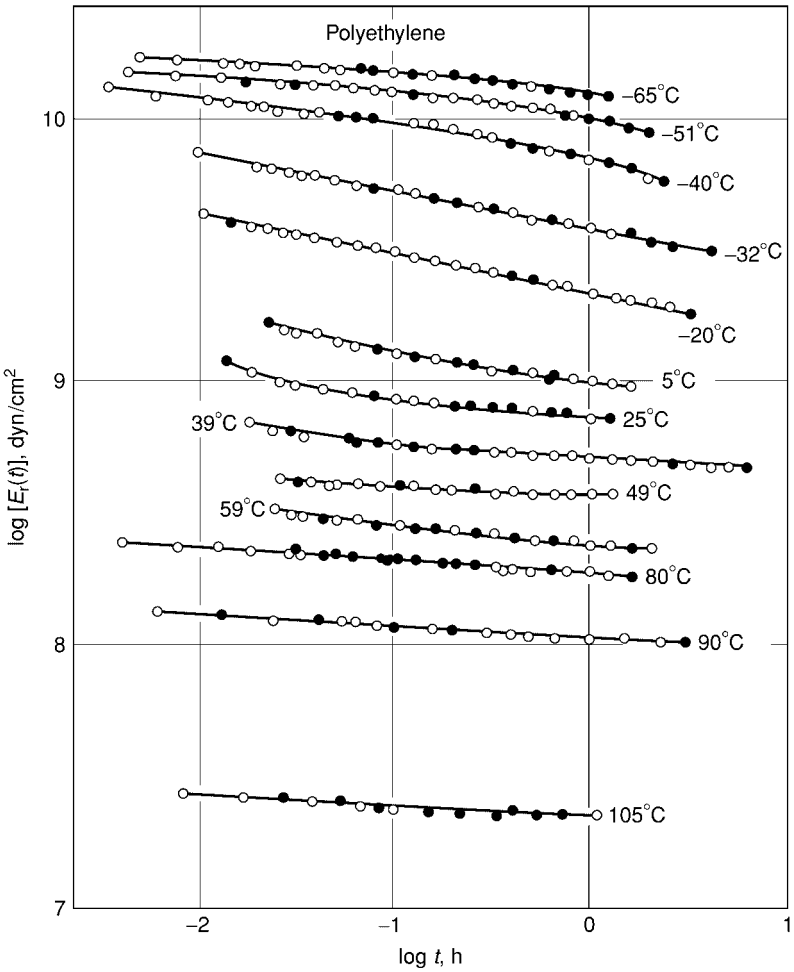

Fig. 19. Relaxation response of polyethylene in isothermal conditions, illustrating that time–temperature superposition does not generally describe the behavior of semicrystalline polymers. After Tobolsky (25).

constitutive laws that relate the stress and strain histories to each other (59,69). A brief description of the K-BKZ model (70–72) is provided as it seems to capture most of the behaviors of polymer melts and solutions subjected to large deformations or high deformation rates. At the same time the nonlinear form of the reptation model is introduced, which in early versions reduced to the K-BKZ constitutive law.

Below the glass temperature, the nonlinear viscoelastic response of polymeric materials has been much less widely studied than has the behavior of melts and solutions. One reason for this is the lack of an adequate theory of behavior. Therefore the discussion about amorphous materials below the glass temperature focuses on recent measurements of the nonlinear response as well as

attempts to apply some of the formalisms that have been applied in the melt and solution states to the behavior of glassy polymers. Finally, the behavior of semicrystalline polymers can be even more complicated and this is discussed briefly.

Behavior of Entangled Polymer Melts and Solutions: Steady-State Behavior. Before discussing the constitutive law given by the K-BKZ theory, it is important to discuss the nonlinear behavior of polymers that is observed. One such behavior is that in steady state, ie, when the material response has quit changing after the application of a stress or deformation rate. For such a situation and recalling that a Newtonian fluid follows a viscosity law in which the stress is proportional to the strain rate

$$\tau = \eta_0 \, \dot{\gamma} \tag{36}$$

where η_0 is the viscosity coefficient. While many small molecule fluids follow expression 36 extremely well, polymeric liquids exhibit *shear thinning* behavior and the viscosity is a function of the shear rate. Typical behavior is exhibited in Figure 20, where viscosity is a function of the shear rate (73). At low shear rates, one observes a Newtonian plateau, followed by a powerlaw region. After the power law region, there is some evidence that at very high shear rates there is a second Newtonian plateau where the viscosity again becomes independent of the shear rate. The power law regime can be described by an empirical equation (74):

$$\begin{aligned} \tau &= K(\dot{\gamma})^n \\ \eta &= \frac{\tau}{\dot{\gamma}} = K(\dot{\gamma})^{n-1} \end{aligned} \tag{37}$$

A possibly better description of the behavior comes from the modified Cross equation (75), particularly if there is a second Newtonian plateau:

$$\eta(T, \dot{\gamma}) = \frac{\eta_0(T)}{1 + [C\eta_0(T)\,\dot{\gamma}]^{1-n}} \tag{38}$$

This equation has the advantage of having the temperature dependence in it explicitly. When the shear-rate-dependent viscosity follows the same temperature dependence, such as WLF, as does the zero shear rate viscosity, then equation 38 is a reasonable approximation to the observed behavior. Otherwise, this is just an estimate. Figure 21 illustrates the fitting of equation 38 to some typical shear-rate-dependent data (74,76).

In addition to the observations in shear that have just been discussed, there is considerable interest in the elongational response in polymeric fluids. The elongational or Trouton viscosity η_E is three times the zero shear rate viscosity in the linear viscoelastic range. However, its behavior is more complex and, as shear rates get higher, the viscosity can even go through a maximum with increasing shear rate as illustrated in Figure 22 (77).

Behavior of Entangled Polymer Melts and Solutions: Transient Response. While the steady-state response of polymers in shear and elongational flows is of much interest, there are also many instances in which the transient response is

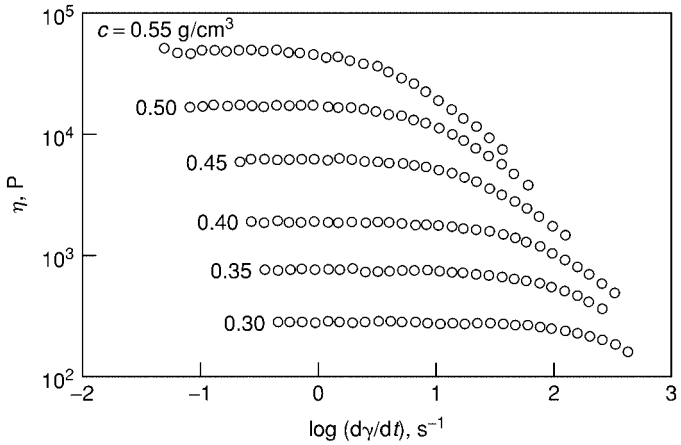

Fig. 20. Double logarithmic representation of viscosity vs. shear rate for polymer solutions having indicated concentrations. Plot illustrates shear thinning of entangled polymers as shear rate increases. After Graessley et al. (73), with permission. To convert Pa·s to P, multiply by 10.

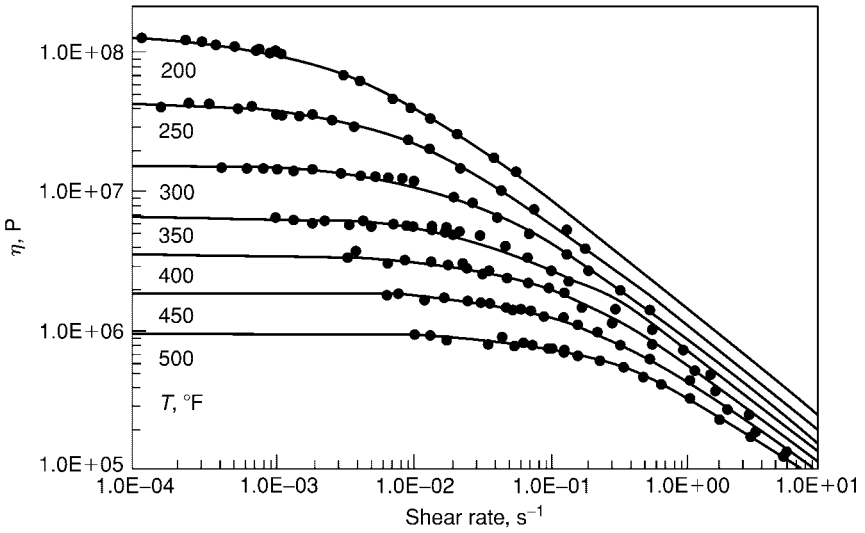

Fig. 21. Shear-rate dependence of the viscosity of a polyisobutylene material, illustrating the fit provided by equation 38. After Rosen (74), with permission. To convert Pa·s to P, multiply by 10.

important because not all processes attain steady state. There are two important transient responses in the nonlinear regime of behavior. These are the stress relaxation response in which the deformation is held constant and the stress evolution with time is followed. This was discussed above for the linear viscoelastic case. In addition, the response to a constant rate of deformation can be an important transient response to study. Also note that creep experiments are sometimes used to characterize the nonlinear response of polymeric fluids and these will also be discussed briefly.

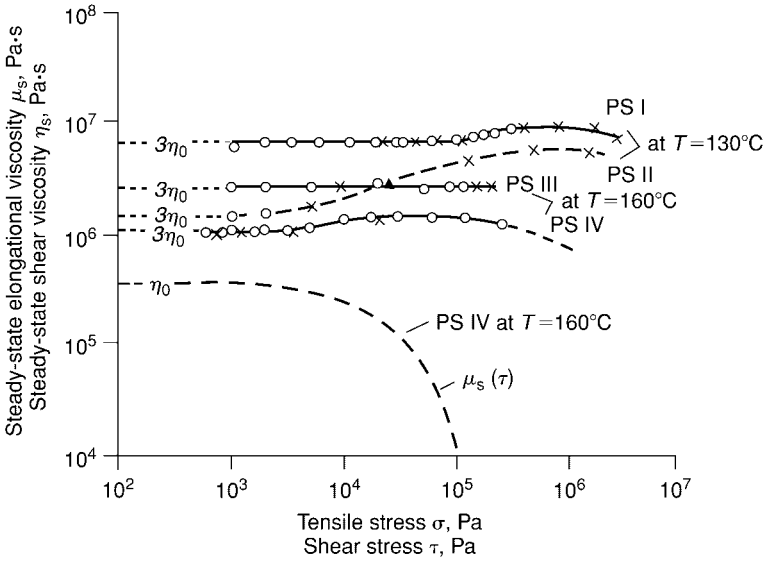

Fig. 22. Elongational viscosity as a function of shear rate for several polystyrene samples. O σ_0 = constant; X ε_0 = constant After Münstedt (77), with permission.

Transient Response: Stress Relaxation. In single-step stress relaxation experiments, the observation is that the response of a polymeric fluid becomes very deformation dependent, ie, it becomes nonlinear. Unlike the case of a linear viscoelastic response, the stress required to maintain a constant deformation is no longer simply proportional to the applied strain. Figure 23 shows the nonlinear response as log $G(\gamma, t)$ vs log t (78). As can be seen, when the strain is larger than about 0.50, the modulus begins falling onto different lines depending on the strain. In Figure 24 *isochronal* data are shown for a polymer solution as log τ_{12} vs log γ (79). If the material were linear, the plots at the different times (isochrones) would be straight with a slope of unity. This is the behavior that one observes in the limit of small strains, as indicated in the figure by the lines of slope unity at the lower deformation levels. Deviations from unity arise when the response is nonlinear; that is, the value of the modulus is a function of the strain. Finally, another way in which to consider the nonlinear behavior is to look at a plot of the relaxation modulus at different times vs the strain. A normalized form of such a plot is shown for a polymer solution in Figure 25 (80). Here, were the material response linear, the data would collapse to a line that was a constant, independent of the strain magnitude. The actual nonlinear behavior that is observed is commonly described in terms of the damping function in the Doi–Edwards model and is described subsequently.

Transient Response: Constant Rate of Deformation. The constant rate of deformation response of the linear viscoelastic material was discussed above. From that discussion, the stress-deformation response looks nonlinear even when the material is linear viscoelastic. For the nonlinear material the response will not be simply described by the linear viscoelastic laws. However, the curves will look similar at low strain rates. At higher strain rates, a stress overshoot is observed,

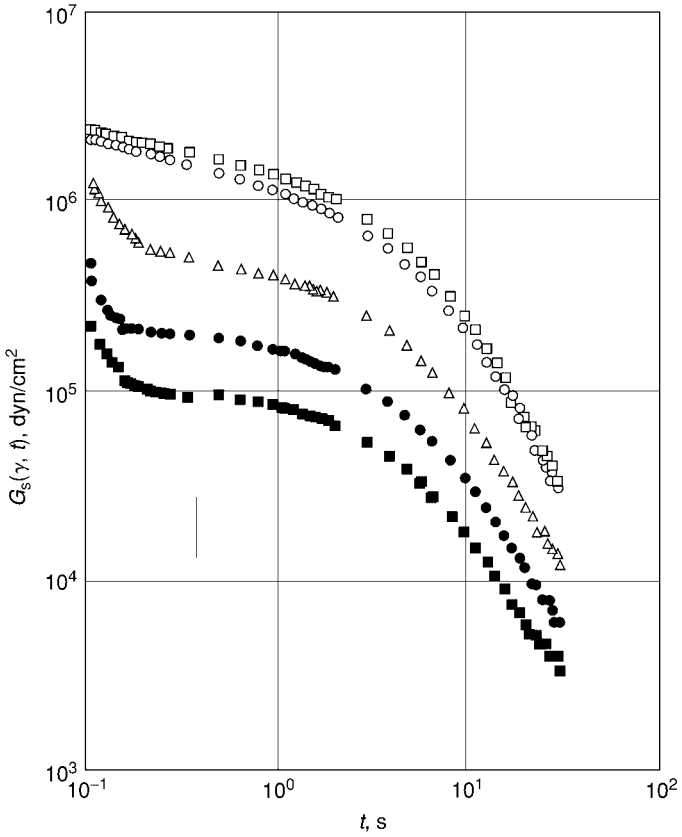

Fig. 23. Stress relaxation modulus of a concentrated polybutadiene solution subjected to increasing shear strains. From top to bottom: $\gamma = 0.333$, 0.667, 1.33, 2.00, and 2.67. After Vrentas and Graessley (78), with permission.

which cannot occur for the linear viscoelastic material. Figure 26 shows the effect of increasing the strain rate on the transient stress–time response (which is related to the strain) for a polymer solution (81). As seen, the stress overshoot becomes weaker with decreasing strain rates (when the material response may be linearly viscoelastic); however, as strain rate increases, there is an onset of a stress overshoot where the early time stress goes through a maximum before settling down to its steady-state value (from which the strain-rate-dependent viscosity would be obtained).

Transient Response: Creep. The creep behavior of the polymeric fluid in the nonlinear viscoelastic regime has some different features from what were found with the linear response regime. First, there are no ready means of relating the creep compliance to the relaxation modulus as was done in the linear viscoelastic case. In fact, the relationship between the relaxation properties and the creep properties depends entirely on the exact constitutive relationship chosen for the response of the material, and numerical inversion of the specific constitutive law is ordinarily necessary to predict creep response from the relaxation

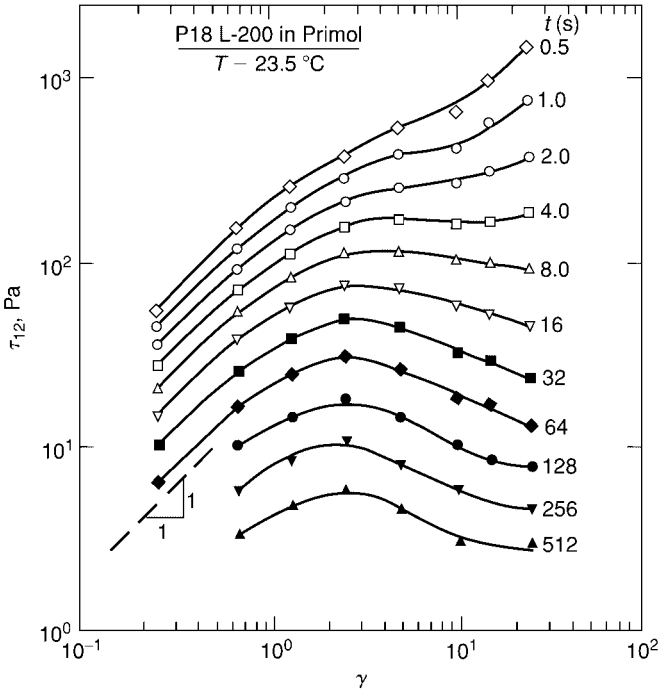

Fig. 24. Double logarithmic representation of the shear stress vs the shear strain for a polymer solution and for different isochrones, as indicated. After McKenna and Zapas (79).

behavior (or vice versa). For most cases, the material properties that appear in the constitutive equations are written in terms of the relaxation response. We discuss this subsequently in the context of the K-BKZ model.

Constitutive Description of Polymer Melt Behavior: K-BKZ and DE Descriptions. Although there are many nonlinear constitutive models that have been proposed, the focus here is on the K-BKZ model because it is relatively simple in structure, can be related conceptually to finite elasticity descriptions of elastic behavior, and because, in the mind of the current author and others (82), the model captures the major features of nonlinear viscoelastic behavior of polymeric fluids. In addition, the reptation model as proposed by Doi and Edwards provides a molecular basis for understanding the K-BKZ model. The following sections first describe the K-BKZ model, followed by a description of the DE model.

The K-BKZ Constitutive Model.

Finite Elasticity Theory: Classical Theory. The finite elasticity theories available today are very powerful and well developed from a phenomenological perspective. Because the K-BKZ (70–72) has the form of a time-dependent finite elasticity (it was developed as a "perfect elastic fluid") it is useful to briefly outline the basics of finite elasticity theory here. In the initial sections of this article, the stress and strain tensors were discussed, and it was noted that the constitutive relationships that arise between the stress and the strain include material parameters called moduli. When a material is classified as *hyperelastic* then the moduli are related to derivatives of the free energy function (often the Helmholtz free

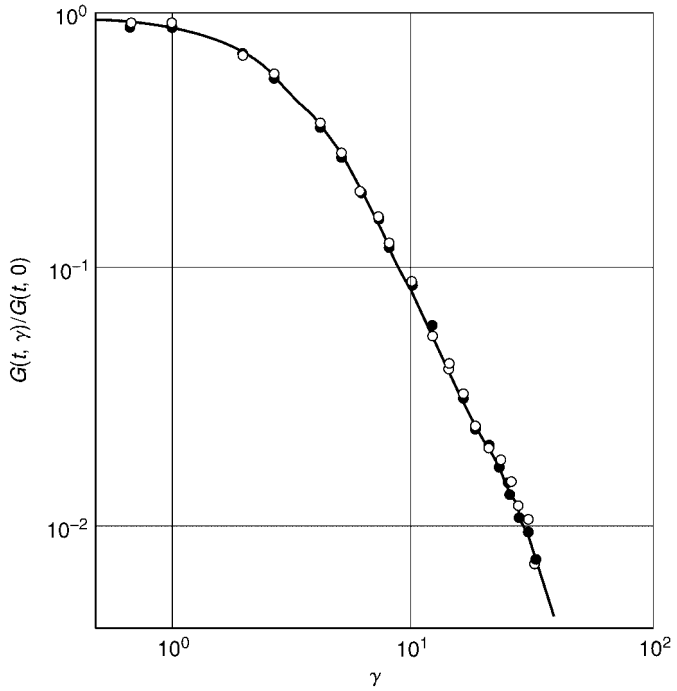

Fig. 25. Reduced nonlinear stress relaxation modulus as a function of strain for a polymer solution. This plot illustrates the strongly nonlinear or strain-dependent behavior of entangled polymers. After Osaki et al. (80), with permission.

energy) with respect to appropriate measures of the strains or deformations (83). Because here large deformations are discussed, there may be multiple possible choices for the actual deformation measurement used. In the discussion that follows, one uses the formalism developed in which the deformations are treated in the context of the Left Cauchy–Green deformation tensor B_{ij} and the free energy function $W(I_1, I_2, I_3)$ is treated as a function of the invariants of the deformation tensor. The material parameters are, then, written as derivatives of the free energy function (or strain energy density function) with respect to the invariants I_i of B_{ij}. The constitutive relationship between the stresses and deformations is then written in terms of these functions (83–86):

$$\sigma_{ij} = \frac{2}{I_3^{1/2}}\left[\left(\frac{\partial W}{\partial I_2}I_2 + \frac{\partial W}{\partial I_3}I_3\right)\Big/ + \frac{\partial W}{\partial I_1}B_{ij} - \frac{\partial W}{\partial I_2}I_3 B_{ij}^{-1}\right] \tag{39}$$

where I is the identity tensor. The invariants of B_{ij} are written in terms of the principal stretches $\lambda_i = 1 + \varepsilon_{ii}$ as

$$\begin{aligned} I_1 &= \lambda_1^2 + \lambda_2^2 + \lambda_3^2 \\ I_2 &= \frac{1}{\lambda_1^2} + \frac{1}{\lambda_2^2} + \frac{1}{\lambda_3^2} \\ I_3 &= \lambda_1^2\lambda_2^2\lambda_3^2 \end{aligned} \tag{40}$$

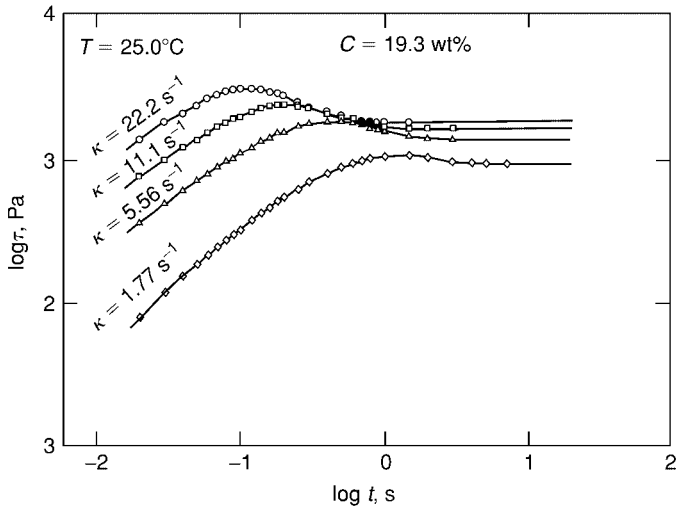

Fig. 26. Effect of strain rate on the stress-time (double logarithmic plot) behavior for a concentrated polymer solution, showing the increasing strength of the stress overshoot phenomenon with increasing strain rate. After Zapas and Phillips (81), with permission.

Note here that the λ_i's are stretches and not relaxation times as used previously. Also note that for polymer melts and solutions, the shear response function (shear modulus) is several orders of magnitude smaller than is the bulk modulus. Therefore, these materials can be treated as *incompressible*. For the linear case, the incompressibility assumption has $K \to \infty$ or $\nu \to 0.5$. Here, $I_3 = 1$ and the constitutive law for the incompressible material becomes

$$\sigma_{ij} = -p\delta_{ij} + \frac{\partial W}{\partial I_1} B_{ij} - \frac{\partial W}{\partial I_2} B_{ij}^{-1} \tag{41}$$

where p is an indeterminate hydrostatic pressure that arises because of the incompressibility condition and δ_{ij} is the Kronecker delta.

Referring to Figure 27, one can solve for the stresses in simple extension. First, the stretches are given by

$$\begin{gathered} \lambda_1 = 1 + \varepsilon_{11} \\ \lambda_2 = \lambda_3 = 1 + \varepsilon_{22} \\ \lambda_2 = \lambda_3 = \frac{1}{\lambda_1^{1/2}} (\text{because of incompressibility}) \end{gathered} \tag{42}$$

Because the material is incompressible, the stresses are only determined within an indeterminate pressure. Therefore, to represent the actual experimental conditions, it is recognized that the *principal stress difference* $\sigma_{11} - \sigma_{22}$ is being

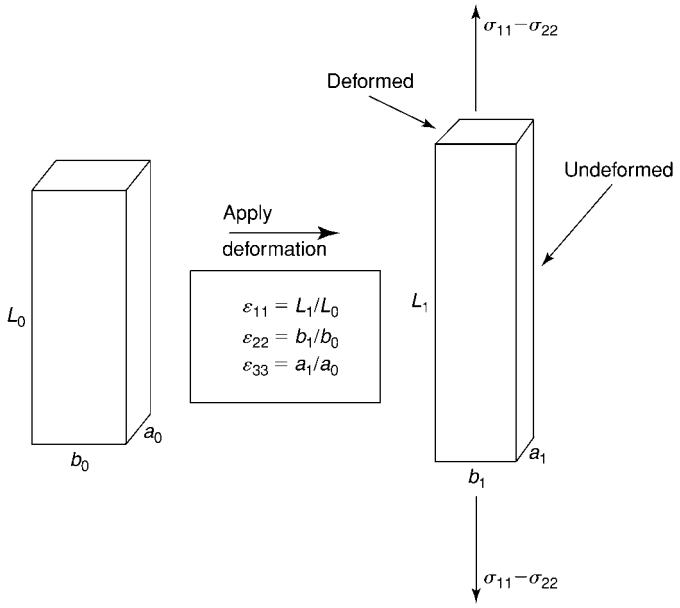

Fig. 27. Schematic of the simple extension geometry.

measured, and this is given as

$$\begin{aligned}\sigma_{11}-\sigma_{22} &= \frac{\partial W}{\partial I_1}(B_{11}-B_{22}) - \frac{\partial W}{\partial I_2}\left(B_{11}^{-1}-B_{22}^{-1}\right)\\ &= \frac{\partial W}{\partial I_1}\left(\lambda_1^2-\lambda_2^2\right) - \frac{\partial W}{\partial I_2}\left(\lambda_1^{-2}-\lambda_2^{-2}\right)\\ &= \frac{\partial W}{\partial I_1}\left(\lambda_1^2-\lambda_1^{-1}\right) - \frac{\partial W}{\partial I_2}\left(\lambda_1^{-2}-\lambda_1\right)\\ &= \left(\lambda_1^2-\lambda_1^{-1}\right)\left(\frac{\partial W}{\partial I_1}+\frac{1}{\lambda_1}\frac{\partial W}{\partial I_2}\right)\end{aligned} \tag{43}$$

The simple stress-deformation response given by equation 43 shows the strong nonlinearity that arises when the stress–strain curve for a typical rubber is plotted, even when the material is *Neo-Hookean* or *Mooney–Rivlin*, meaning that the values of $\partial W/\partial I_1 = W_1 = C_1$ and $\partial W/\partial I_2 = W_2 = C_2$ are constants. For the Neo-Hookean material, $W_1 = C_1$ and $W_2 = 0$. For the Mooney–Rivlin material (87,88), $W_1 = C_1$ and $W_2 = C_2$. Figure 28 shows plots of the stress-deformation behavior for a Neo-Hookean rubber and for a Mooney–Rivlin rubber. The figure shows that in spite of the fact that the material parameters are constants, there is a strong nonlinear response due to the geometry of deformation, ie, the $[\lambda^2 - \lambda^{-1}]$ and $1/\lambda$ terms in equation 43. Also, from equation 43 one can readily see from where the concept of the Mooney–Rivlin material arose. Dividing the equation by

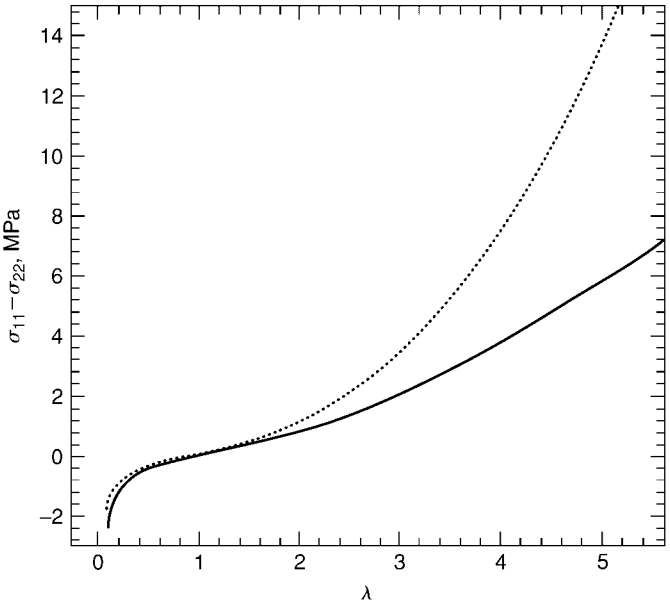

Fig. 28. Stress-stretch response for a Neo-Hookean rubber compared with that of a Mooney–Rivlin material. (————) Neo-Hookean: $C_1 = 0.24$ MPa; (· · · · ·). Mooney–Rivlin: $C_1 = 0.16$ MPa, $C_2 = 0.08$ MPa.

$[\lambda^2 - \lambda^{-1}]$, one obtains

$$\sigma_R = \frac{\sigma_{11} - \sigma_{22}}{\lambda_1^2 - \lambda_1^{-1}} = \frac{\partial W}{\partial I_1} + \frac{1}{\lambda_1}\frac{\partial W}{\partial I_2} \tag{44}$$

where σ_R is referred to as the reduced stress. For Mooney–Rivlin behavior, a plot of σ_R vs $1/\lambda_1$ gives a straight line of slope C_2 and intercept C_1. Real rubber often shows near to Mooney–Rivlin behavior in extension, but deviates in compression. For the Neo-Hookean material, the reduced stress is a constant. Figure 29a shows the calculations for the general behavior of σ_R vs $1/\lambda_1$ for the Neo-Hookean and Mooney–Rivlin materials. Figure 29b shows experimental results for two typical cross-linked rubbers, and it is seen that neither the Neo-Hookean nor the Mooney–Rivlin model would describe the behaviors exhibited (89–91). The reader is referred to reviews of various proposed strain energy functions (89,92,93) for further information.

Another important aspect of finite elasticity theory is the ability to measure the strain energy function derivatives $W_1 = \partial W/\partial I_1$ and $W_2 = \partial W/\partial I_2$. Penn and Kearsley (94) showed how this is done using data from torsional experiments. An interesting aspect about torsion in finite deformations is that in order to maintain the cylinder at a constant length, it is necessary to apply normal forces at the ends of the cylinder. If the cylinder is left unrestrained, it will lengthen in an effect referred to as the Poynting (95) effect, first observed early in the last century in experiments with metal wires. When a cylinder of length L is twisted by an amount

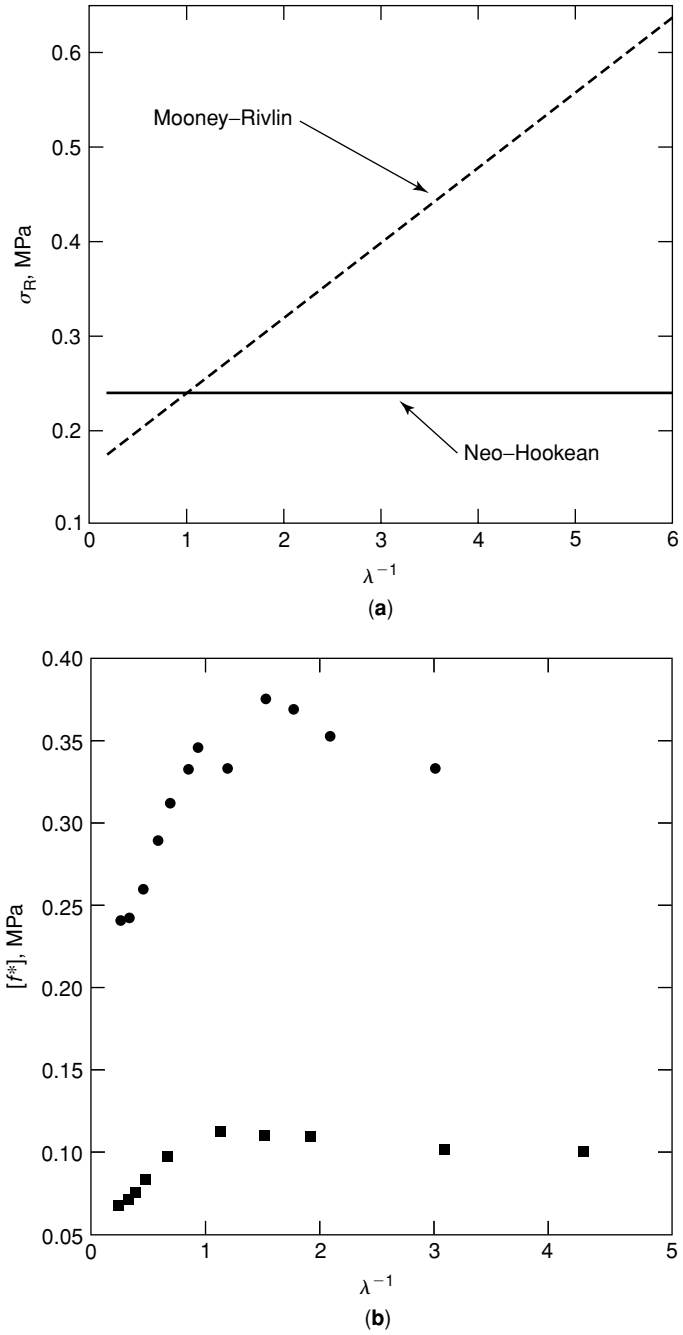

Fig. 29. (**a**) Reduced stress plot for the Neo-Hookean and Mooney–Rivlin materials of Figure 28. (**b**) Reduced stress plot for natural rubber and a polydimethylsiloxane (PDMS) rubber as indicated. Plot illustrates that actual rubber behavior may be Mooney–Rivlin-like in tension ($\lambda^{-1} < 1$), but not in compression.● Natural rubber; ■ PDMS. Plot from Han et al. (89), natural rubber data from Ref. 90, and PDMS data form reference 91.

ψ per unit length ($\psi = \theta/L$, where θ is the angle of twist) the magnitude of the torque (moment) M and the normal force N are given by the following expressions:

$$T = 4\pi\psi \int_0^R (W_1 + W_2) r^3 \mathrm{d}r \tag{45}$$

$$N = -2\pi\psi^2 \int_0^R (W_1 + 2W_2) r^3 \mathrm{d}r \tag{46}$$

where R is the cylinder radius. By differentiating each expression with respect to the limits of integration after an appropriate variable change, Penn and Kearsley (90) showed that W_1 and W_2 can be expressed as simple algebraic expressions in the torques and normal forces measured at different angles of twist, ie, deformations:

$$W_1 + W_2 = \frac{1}{4\pi\psi R^4}\left(3T + \psi\frac{\mathrm{d}t}{\mathrm{d}\psi}\right) \tag{47}$$

$$W_1 + 2W_2 = \frac{-1}{\pi\psi^2 R^4}\left(N + \psi^2\frac{\mathrm{d}N}{\mathrm{d}\psi^2}\right) \tag{48}$$

Figure 30 shows typical torque and normal force measurements for a natural rubber sample as functions of the deformation (as ψR) in a double logarithmic plot (96). The data for T, N, and their derivatives can then be obtained and used in equations 47 and 48 to solve for W_1 and W_2. Figure 31 shows typical data for the values of W_1 and W_2 as functions of deformation for a cross-linked natural rubber obtained from such measurements (94,97). Importantly, these values are related to the *damping function* of the DE model discussed subsequently. They represent the deformation dependence of the shear modulus in this instance.

Finite Elasticity Theory: The VL Representation. While the above description of the finite deformation behavior of elastic materials is very powerful, the limitation on it is that the material parameters W_1 and W_2 need to be determined in each geometry of deformation of interest. Hence, the torsional measurements described above only give values of $W_1(I_1, I_2)$ and $W_2(I_1, I_2)$ for the condition of shear (torsion is a nonhomogeneous shear) and that condition is $I_1 = \mathrm{I}_2 = 3 + \gamma^2$. More measurements need to be made to obtain the parameters in extension, compression, etc. However, in 1967, Valanis and Landel (98) proposed a strain energy function that, rather than being a function of the invariants, is a function of the stretches λ_i. The function was assumed to be separable in the stretches as

$$\hat{w}(\lambda_1, \lambda_2, \lambda_2) = w(\lambda_1) + w(\lambda_2) + w(\lambda_3) \tag{49}$$

Then, for example, in simple extension, the stress–deformation relationship becomes

$$\sigma_{11} - \sigma_{22} = \lambda_1 w'(\lambda_1) - \lambda_2 w'(\lambda_2) \tag{50}$$

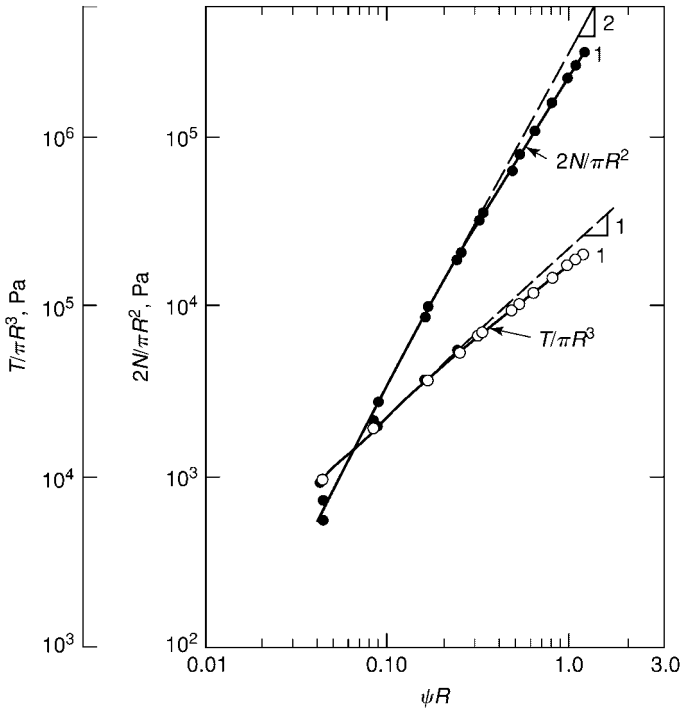

Fig. 30. Torque and normal forces (scaled by sample geometry) vs strain at outer edges of cylinder for a natural rubber sample subjected to torsional deformations. After McKenna and Zapas (96).

and it becomes a matter, for any deformation to determine the values of $w'(\lambda_i)$ and these can be obtained in any geometry of deformation. Thus, the inconvenience of performing large numbers of experiments in multiple geometries of deformation is avoided. There has been a considerable effort to establish the validity of the Valanis–Landel (VL) form of strain energy function (98–102) and it is generally found to be a very good representation of the material behavior, although some discrepancies have been observed. Some special forms of the VL function, such as the Ogden model (103,104), have been found to be very useful and are commonly used in commercial finite element modeling of rubber behavior.

Because of this usefulness it is important to have relatively simple experiments available to obtain the VL function. Kearsley and Zapas (97) have shown that either simple extension combined with simple compression or torsion with normal force measurements can be used to obtain the VL function. Valanis and Landel (98) used pure shear measurements. The equations for the torsional measurements arise from the relationship between $w'(\lambda)$ and W_1 and W_2 given by

$$w'(\lambda) - \frac{w'(1)}{\lambda} = \frac{2}{\lambda}(\lambda^2 - 1)\left(W_1 + \frac{1}{\lambda^2}W_2\right) \tag{51}$$

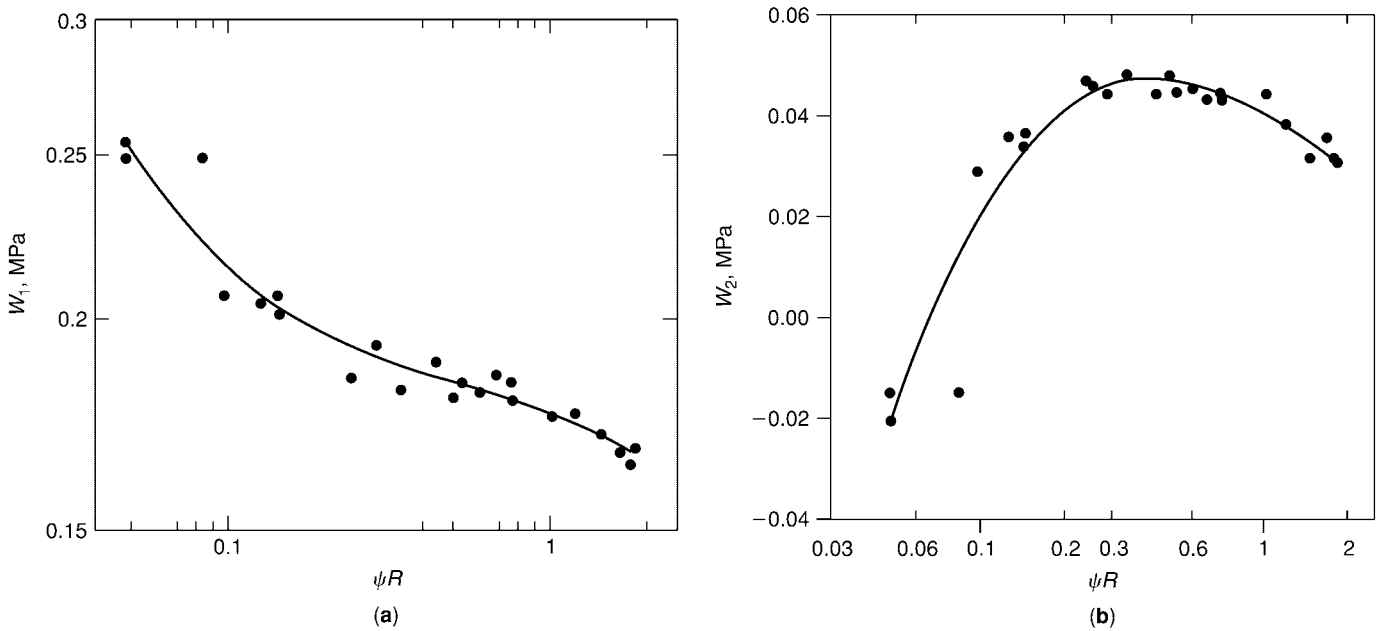

Fig. 31. (**a**) W_1 vs strain for a natural rubber material. (**b**) W_2 vs strain for a natural rubber material. Data of Penn and Kearsley (94) given in Kearsley and Zapas (97).

and the values of λ are determined from the twists of the cylinder by

$$\text{For} \quad \lambda > 1 : \lambda_{\max} = \frac{1}{2}\left[(\psi^2 R^2 + 4)^{1/2} + \psi R\right] \tag{52}$$

Thus, from torque and normal forces in torsional experiments, the VL function derivative can be obtained. Typical data for natural rubber are presented in Figures 30, 31, 32. The figures illustrate the sequence that would be used to obtain the VL function. First, obtain torque and normal force data (Fig. 30) and use equations 47 and 48 to obtain the strain energy function derivatives W_1 and W_2 (some typical results shown in Fig. 31). Finally, data of the sort shown in Figure 31 are used to obtain the VL function derivative $w'(\lambda)$. Figure 32 shows such data obtained from torsional measurements on natural rubber samples cross-linked to different extents (102).

In the case of extension and compression data, Kearsley and Zapas (97) developed a recursive method to determine the VL function from stress–strain data similar to those presented in Figure 28. The advantage in using extension and compression data rather than torsional data is that higher values of λ can be reached.

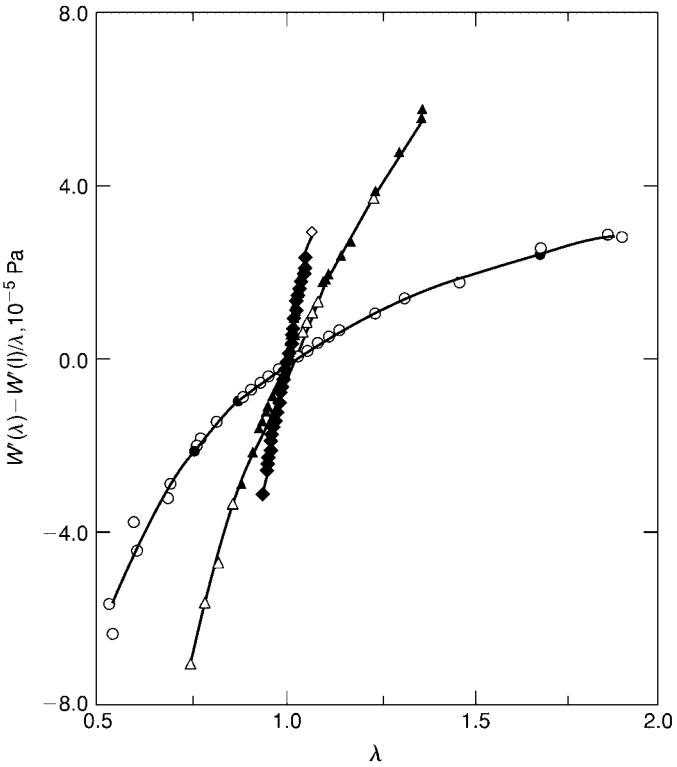

Fig. 32. The VL function (98) derivative vs stretch for natural rubber samples cured with 1, 5, and 15 parts per hundred dicumyl peroxide, as indicated. The VL function was obtained from torque and normal force measurements. ○ APHR1; △ APHR5;◇ APHR15. After McKenna et al. (102).

Finally, the power of finite elasticity theory is that once the material properties [W_1 and W_2 or $w'(\lambda)$] are known, the stresses in any deformation field can be calculated. There is an extensive literature on ways to represent the material functions and, in fact, commercial finite element codes use finite elasticity theory in calculations that can be important in applications that range from the stresses in automobile tires (105) to those in earthquake bearings for large buildings (106). One feature of the K-BKZ theory to be discussed next is that it retains the structure of finite elasticity theory and includes time-dependent properties of the viscoelastic materials that were discussed in the earlier sections of this article.

The K-BKZ Theory: Model. The K-BKZ model was developed in the early 1960s by two independent groups. Bernstein, Kearsley, and Zapas (70) of the National Bureau of Standards (now the National Institute of Standards and Technology) first presented the model in 1962 and published it in 1963. Kaye (71), in Cranfield, U.K., published the model in 1962, without the extensive derivations and background thermodynamics associated with the BKZ papers (82,107). Regardless of this, only the final form of the constitutive equation is of concern here. Similar to the idea of finite elasticity theory, the K-BKZ model postulates the existence of a strain potential function $U(I_1, I_2, t)$. This is similar to the strain energy density function, but it depends on time and, now, the invariants are those of the *relative* left Cauchy–Green deformation tensor $\boldsymbol{B}_{t,ij}$. The relevant constitutive equation is

$$\sigma_{ij}(I_1,I_2,t) = -p\delta_{ij} + \int_{-\infty}^{t} \{U_1(I_1,I_2,t-t')B_{t,ij}(t,t') - U_2(I_1,I_2,t-t')B_{t,ij}^{-1}(t,t')\}\mathrm{d}t' \tag{53}$$

Also note that the hydrostatic pressure is indeterminate because the K-BKZ is an incompressible material model. As in finite elasticity theory, the material parameters need to be obtained and, in principle, the stress response to any deformation history can be obtained. Unlike linear viscoelasticity, the integration must be carried out from $-\infty$ to t, which can lead to difficulties in numerical computer codes. This aspect of the K-BKZ theory has been discussed by (62) Larson, among others.

The relative deformation tensor $\boldsymbol{B}_{t,ij}$ assumes that the current material *configuration* (the configuration at time t) is the reference configuration. This idea is important as it is common in fluid models because fluids have no natural reference configuration while solids do. Hence, for example, the relative deformations in simple extension become

$$\lambda_{t,1} = \frac{\lambda_1(t)}{\lambda_1(t')}; \lambda_{t,2} = \frac{\lambda_2(t)}{\lambda_2(t')}; \lambda_{t,3} = \frac{\lambda_3(t)}{\lambda_3(t')} \tag{54}$$

and the invariants of $\boldsymbol{B}_{t,ij}$ are similar to those for the elastic material, but in terms of the relative deformations

$$I_1(t,t') = \left[\frac{\lambda_1(t)}{\lambda_1(t')}\right]^2 + \left[\frac{\lambda_2(t)}{\lambda_2(t')}\right]^2 + \left[\frac{\lambda_3(t)}{\lambda_3(t')}\right]^2$$

$$I_2(t,t') = \left[\frac{\lambda_1(t')}{\lambda_1(t)}\right]^2 + \left[\frac{\lambda_2(t)}{\lambda_2(t')}\right]^2 + \left[\frac{\lambda_3(t)}{\lambda_3(t')}\right]^2 \tag{55}$$

$$I_3(t,t') = 1 = \left\{\left[\frac{\lambda_1(t)}{\lambda_1(t')}\right]\left[\frac{\lambda_2(t)}{\lambda_2(t')}\right]\left[\frac{\lambda_3(t)}{\lambda_3(t')}\right]\right\}^2$$

The utility of the K-BKZ theory arises from several aspects of the model. First, it does capture many of the features, described below, of the behavior of polymeric melts and fluids subjected to large deformations or high shear rates. That is, it captures many of the nonlinear behaviors described above for steady flows as well as behaviors in transient conditions. In addition, unlike the more general *multiple integral* constitutive models (108,109), the experimental data required to determine the material properties are not overly burdensome. In fact, the information required is the single-step stress relaxation response in the mode of deformation of interest (72). If one is only interested in, eg, simple shear, then experiments need only be performed in simple shear and the exact form for $U(I_1, I_2, t)$ need not be obtained. Furthermore, because the structure of the K-BKZ model is similar to that of finite elasticity theory, if a full three-dimensional characterization of the material is needed, some of the simplifying aspects of finite elasticity theories that have been developed over the years can be applied to the behavior of the viscoelastic fluid description provided by the K-BKZ model. One such example is the use of the VL form (98) of the strain energy function discussed above (110). The next section shows some comparisons of the material response predicted by the K-BKZ theory with actual experimental data.

The K-BKZ Theory: Comparison with Experiment. The first data required to test the K-BKZ model is single-step stress relaxation data to determine the material parameters of interest. This is best seen from the following example for a simple shearing history. From equation 49, the shear stress for a simple shear deformation can be expressed as (see Ref. 72)

$$\sigma_{i,j}(t) = \int_{-\infty}^{t} -K_*[\gamma(t) - \gamma(t'), t - t']\mathrm{d}t' \tag{56}$$

where $\gamma(t) - \gamma(t')$ is the relative strain and K_* is the partial derivative of the relaxation function $K[\gamma(t) - \gamma(t'), t - t']$ with respect to the second (time) argument. For the single-step stress relaxation history in which $\gamma(t) = 0$ for $t<0$ and $\gamma(t) = \gamma$ for $t > 0$, equation 52 reduces to

$$\sigma_{ij}(t) = \int_{-\infty}^{0} -K_*[\gamma, t - t']\mathrm{d}t' \tag{57}$$

Defining $\xi = t - t'$ and performing a change of variables, equation 57 can be evaluated as

$$\sigma_{ij}(t) = \int_{\infty}^{t} K_*(\gamma, \xi)\mathrm{d}\xi = K(\gamma, t) - K(\gamma, \infty) \tag{58}$$

and because the material is a fluid, $K(\gamma, \infty) = 0$. Therefore, the shear stess is simply equal to its relaxation function $K(\gamma, t)$ for an applied shear strain of γ. As suggested by equations 56, 57, 58, one need not actually determine the values of $U_i(I_1, I_2, t)$ when the experiments of interest are always of the same geometry.

Also, because of the structure of the K-BKZ theory, torsional measurements can also be analyzed in a fashion similar to equation 58. Recall Figure 24, which depicts the single-step stress relaxation responses for a concentrated polymer solution in a torsional (parallel plate) experiment as isochronal plots of stress vs strain on double-logarithmic axes. It is worth noting that in the moderate strain regime, these data look similar to the elastic data of Figure 30. But, at large strains the curves go through a maximum. This is undoubtedly because the solutions can be deformed to a much greater magnitude than can the cross-linked rubber.

Once the single-step data are known, then integration of equation 56 (or eq. 53) for different strain histories leads to predictions for the material response in any deformation history of interest. A very powerful method of evaluating constitutive equations is the double-step strain history in which the second-step response should be able to be predicted by the model in question. Figure 33 shows the set of two-step histories that is dealt with here and subsequently. Figures 34,

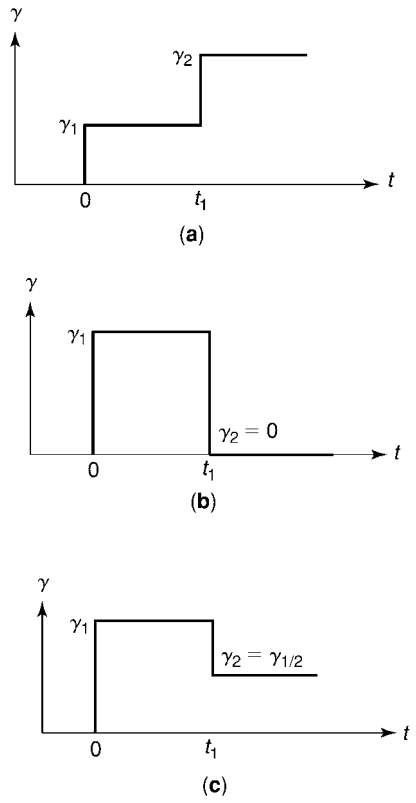

Fig. 33. Two-step strain histories. (**a**) Step-up, (**b**) step to zero deformation, and (**c**) half-step deformation histories.

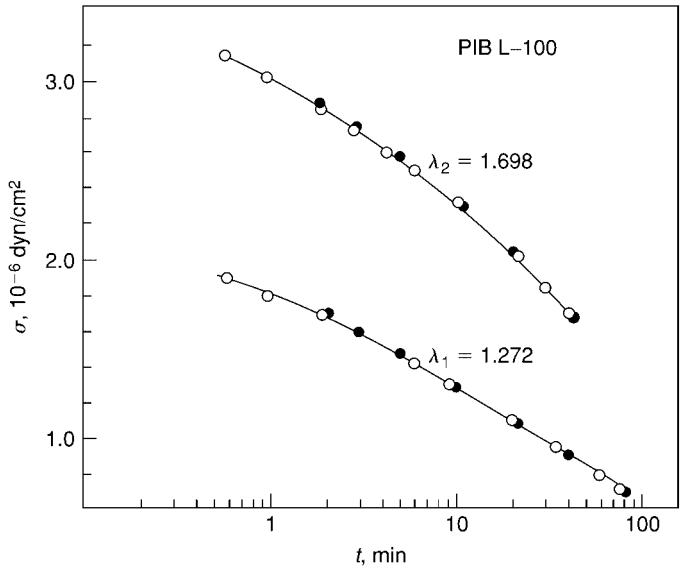

Fig. 34. Comparison of K-BKZ predictions (filled circles) with experimental data (open circles) for step-up experiment in uniaxial extension for a polyisobutylene material. After Zapas and Craft (111), with permission.

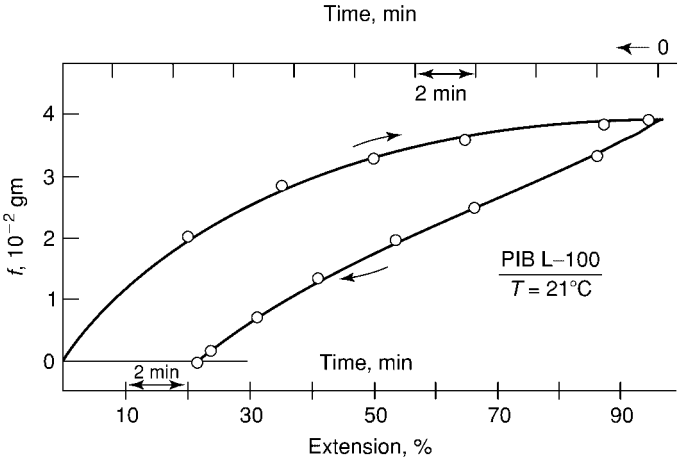

Fig. 35. Comparison of K-BKZ predictions (open circles) with experimental data (solid line) for a constant rate of strain (load–unload) history for a polyisobutylene material. After Zapas and Craft (111), with permission.

35, 36, 37, 38 show comparisons between K-BKZ predictions and the experimental data for two-step stress relaxation experiments (111), constant rate of loading and unloading experiments, creep and recovery experiments, relaxation after steady shearing flow at different shear rates, and superposition of small deformations on large ones; this last being a multiple-step experiment that could be treated as a three-step case (79) As seen, these experiments show excellent agreement

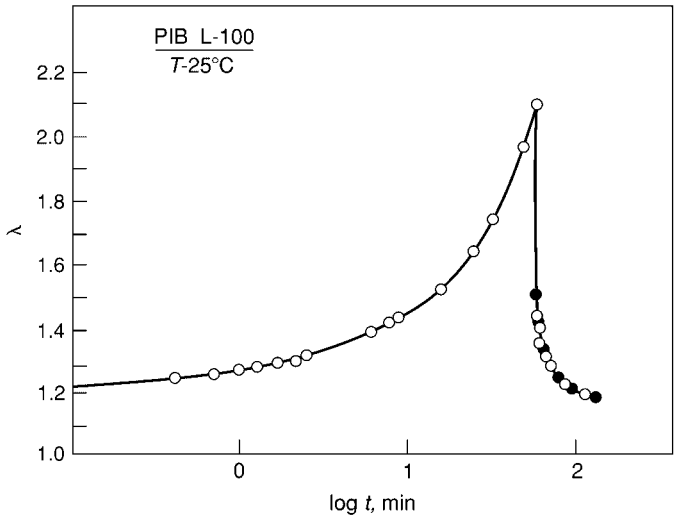

Fig. 36. Comparison of K-BKZ predictions (filled circles) with experimental data (open circles) for creep and recovery for a polyisobutylene material. After Zapas and Craft (111), with permission.

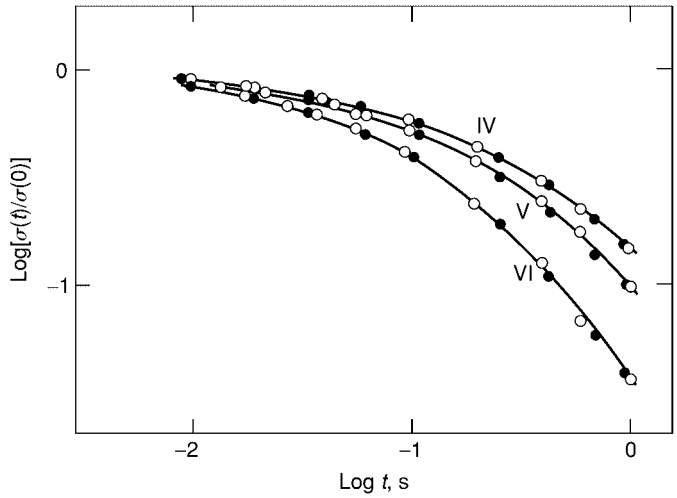

Fig. 37. Comparison of K-BKZ predictions (filled circles) with experimental data (open circles) for relaxation after a steady shearing flow. (IV) 0.177 s^{-1}; (V) 1.11 s^{-1}; (VI) 5.56 s^{-1}. After Zapas and Craft (111), with permission.

between the theory and the experiment, indicating the power of the model. Another interesting aspect of the K-BKZ theory is the predictions it makes for the normal stress responses in the so-called *half-step deformation history* in which the second step is $\frac{1}{2}$ the magnitude of the first, as depicted in Figure 33c. For any two-step history, the shear and normal stress difference responses (or torque and

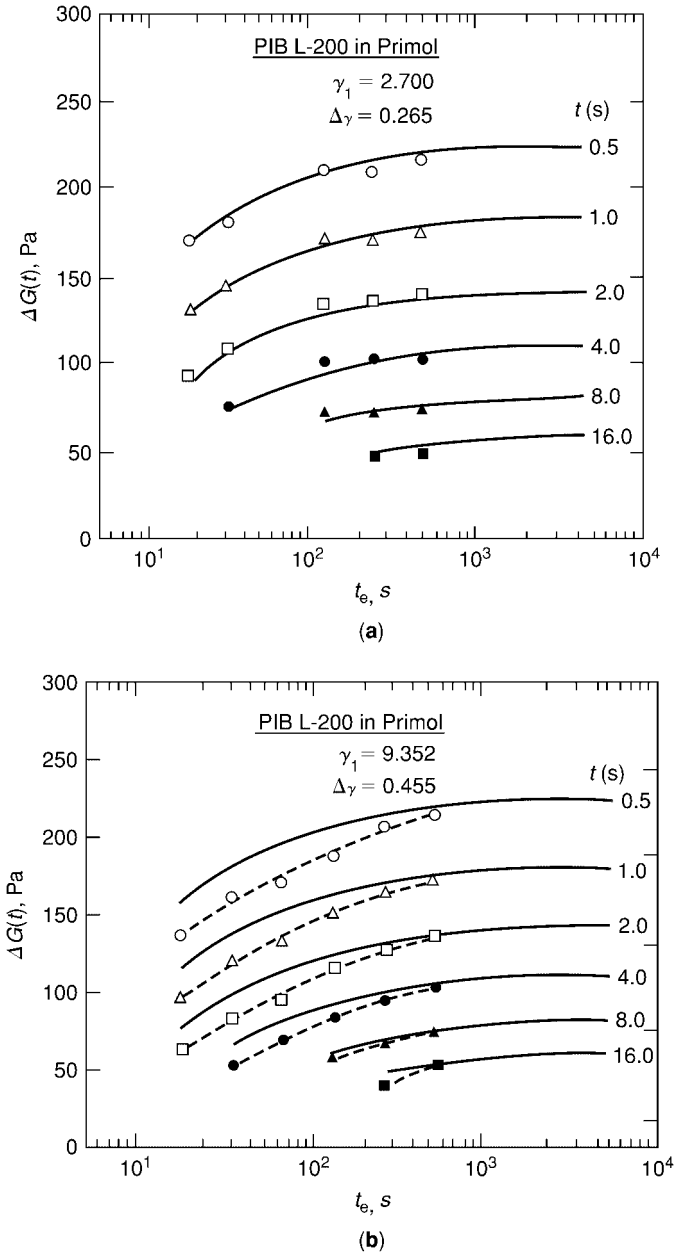

Fig. 38. Comparison of the K-BKZ predictions (lines) with data for the incremental modulus response to a small strain $\Delta\gamma$ superimposed on a large strain γ as a function of time t_e elapsed after the imposition of the large strain. Part (**a**) shows excellent agreement between the theory and experiment for $\gamma = 2.7$, while part (**b**) shows moderate deviations at small t_e values when $\gamma_1 = 9.4$. After McKenna and Zapas (79).

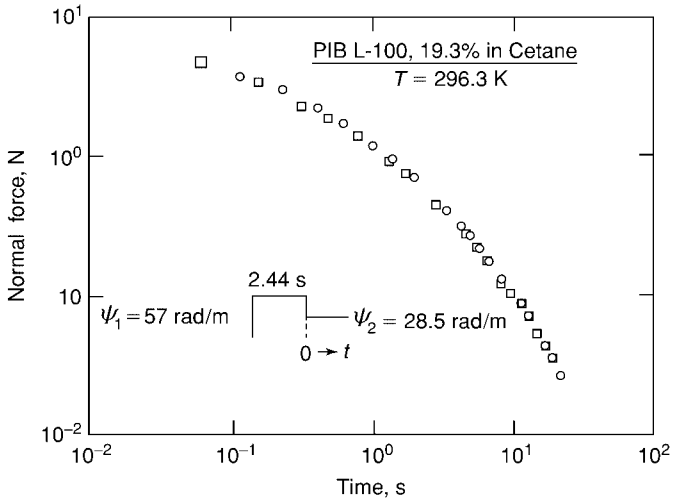

Fig. 39. Comparison of the K-BKZ prediction (squares) for the "half-step" normal stress response with the experimental behavior (open circles) for a polyisobutylene solution. After McKenna and Zapas (113).

normal force responses) can be written as (72,112–117)

$$\begin{aligned} \sigma_{12}(t-t_1) &= K(\gamma_2,t) + K(\gamma_2-\gamma_1,t-t_1) - K(\gamma_2-\gamma_1,t) \\ \sigma_{22}(t-t_1) - \sigma_{22}(t-t_1) &= H_1(\gamma_2,t) + H_1(\gamma_2-\gamma_1,t-t_1) - H_1(\gamma_2-\gamma_1,t) \\ \sigma_{22}(t-t_1) - \sigma_{33}(t-t_1) &= H_2(\gamma_2,t) + H_2(\gamma_2-\gamma_1,t-t_1) - H_2(\gamma_2-\gamma_1,t) \end{aligned} \tag{59}$$

where $K(\gamma, t)$ is the single-step stress relaxation response of the shear (or torque) and $H_i(\gamma, t)$ is that of the i^{th} principal stress difference (or normal force). On substituting torque T and normal force N for a torsional experiment into equations 59, one would see that the torque response is an odd function of the strain $[T(-\gamma) = -T(\gamma)]$ and the normal force is an even function of strain $[N(-\gamma) = N(\gamma)]$. Then, for the special $\frac{1}{2}$-step history where $\gamma_1 = 2\gamma$, the torque and normal force responses become

$$\begin{aligned} T(\psi_2,t-t_1) &= 2K(\psi_2,t) - K(\psi_2,t-t_1) \\ N(\psi_2,t-t_1) &= H(\psi_2,t-t_1) \end{aligned} \tag{60}$$

which means that the torque response depends upon the full deformation history. On the other hand, the normal force response depends only upon the time after the first step $(t - t_1)$, ie, is independent of the duration of the first step and would be equal to the magnitude of the response to a single-step deformation to a torsion magnitude of Ψ_2. Figure 39 provides the experimental evidence that this is, indeed, the behavior followed by a polyisobutylene solution. Subsequent data, however, indicate that this may not be universally true (115–117). This is discussed subsequently.

The data shown thus far describing the success of the K-BKZ theory were, generally, such that the stress never changed sign. However, it turns out that

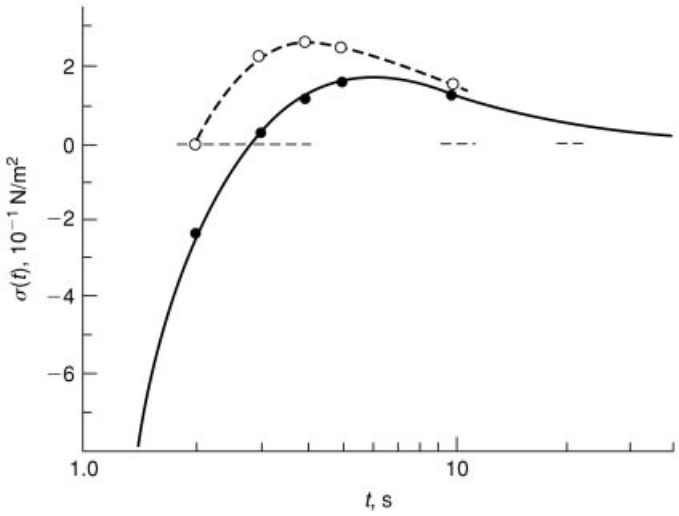

Fig. 40. Comparison of the "half-step" shear stress response predicted by the K-BKZ theory (open circles) with the experimental data (filled circles) for a polyisobutylene solution. After Zapas (118), with permission.

in *stress-reversing* flows, the K-BKZ theory seems not to work as well (62,82,107, 112,114,116,118). Figure 40 shows the shear stress response for a polyisobutylene solution in the half-step history just discussed. The response is clearly not in agreement with the K-BKZ theory prediction. Also, in some flows, predicting the pure shear behavior, which has an extensional component to it, is not consistent with the simple shear predictions (119) .

The Doi–Edwards Theory. Much of the excitement that came during the early years of the Doi–Edwards (DE) tube model (52–56) for reptation of polymer chains revolved about the fact that the use of the *independent alignment* assumption resulted in a special form of the K-BKZ model. Hence, much of the machinery that was developed in the 1960s and early 1970s to test the K-BKZ model could be implemented to test the DE model. The next sections discuss the molecular basis of the DE model, the independent alignment assumption, and how well monodisperse polymers follow the DE version of the K-BKZ model.

The Molecular Description. The fundamentals of reptation theory are best understood with the general *coarse-grained* models of a single polymer chain. If one considers the linear polymer chain to be composed of m monomers and also considers the *Rouse* approximation (120) that there are no hydrodynamic interactions [in concentrated solutions and melts this is a very good approximation (9,63)] and that the chain assumes a *Gaussian* conformation, the chain can be divided into N submolecules, each containing g monomers. The average size a of the submolecule in the Gaussian conformation is related to the step length b of the monomer (63):

$$a^2 = gb^2 \tag{61}$$

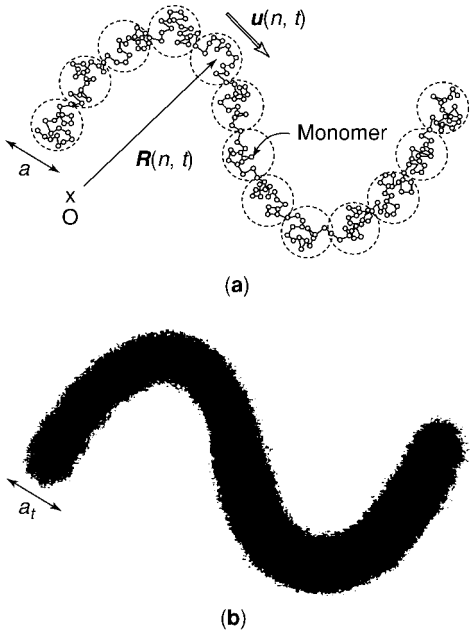

Fig. 41. Schematic representation of a real chain (**a**) and a coarse-grained chain (**b**). In the real chain depiction the small beads connected by rods are the monomeric segments and the circles represent the submolecules of the coarse-grained chain. Part (b) represents the hypothetical time-exposure photograph. After Watanabe (63), with permission.

The real chain is coarse-grained in both time and space, by dividing it into submolecules. Figure 41a shows the Rouse chain and Figure 41b illustrates a hypothetical experiment (63) in which the molecule is photographed with an exposure time t_0. When the time t_0 is large, the chain looks like a fuzzy thread with a width a_t because of the chain motion in the time interval of the "photograph." The dynamics of this Rouse chain are considered as the motion of a string of Gaussian submolecules in a viscous medium. The friction coefficient ζ on the submolecule or bead is given by

$$\zeta = g\zeta_0 \tag{62}$$

where ζ_0 is the monomeric friction coefficient. It is assumed that the force acting on a bead is represented by a Gaussian spring with a spring constant κ given by

$$\kappa = \frac{3k_B T}{a^2} \tag{63}$$

where k_B is the Boltzmann constant and T is the absolute temperature. The time-evolution of the position $\boldsymbol{R}(n,t)$ of the nth submolecule (bead) can be obtained by considering the forces acting on the the bead: frictional $\boldsymbol{F}_f$, elastic (entropic) $\boldsymbol{F}_e$,

and Brownian $\boldsymbol{F}_B$. For large N (long chains) the equation can be written as (121)

$$-\zeta\left[\frac{\partial R(n,t)}{\partial t}\right]+\kappa\frac{\partial^2 R(n,t)}{\partial n^2}+F_B(n,t)=0 \tag{64}$$

The first and second terms represent the frictional force $\boldsymbol{F}_f(n, t)$ and the elastic force $\boldsymbol{F}_e(n, t)$, respectively. The Brownian force $\boldsymbol{F}_B$ is modeled as white noise (56, 63).

Solution of equation 64 permits the determination of the dynamic properties of the chain (56,63). For this paper, the results are given for the polymer melt or concentrated solution, not for the single chain contributions to a dilute solution. The reader is referred to References 56 and 63 for more details. The properties of interest are

$$\text{Relaxation modulus: } G(t)=\frac{vk_BT}{N}\sum_{p=1}^{N}\exp\left(\frac{-2tp^2}{\lambda_{R,G}}\right) \tag{65}$$

where $\lambda_{R,G}$ is the longest relaxation time for the Rouse chain, given by

$$\lambda_{R,G}=\frac{\zeta a^2N^2}{3\pi^2k_BT} \tag{66}$$

Note that v is the number density of Rouse segments in chains of N segments in length and that are monodisperse. The index p is the eigenmode from the solution to the equation of motion. Furthermore, equation 65 is the equation for a special form of the generalized Maxwell model having constant coefficients $G_i = vk_BT$ (see eq. 18). The relaxation times are given by $\lambda_{R,G}/2p^2$.

The *zero shear rate viscosity* is calculated from (56)

$$\eta_0=\frac{v\zeta\alpha^2N}{36} \tag{67}$$

and the *steady-state (recoverable) compliance* is calculated from

$$J_s=\frac{1}{\eta_0^2}\int_0^\infty tG(t)\mathrm{d}t=\frac{2}{5vk_BT}=\frac{2M}{5\rho RT} \tag{68}$$

where ρ is the density and M is the molecular weight. Although the Rouse model was derived for dilute solutions in which there is no hydrodynamic interaction, it seems to best describe the behavior of concentrated solutions and melts that are disentangled. This is particularly so for the viscosity, which at low molecular weights seems to follow the first power prediction given by equation 67 (recall Fig. 18 at low molecular weights). Also, the equilibrium recoverable compliance of short-chain melts (both linear and cyclic) seems to follow the correct

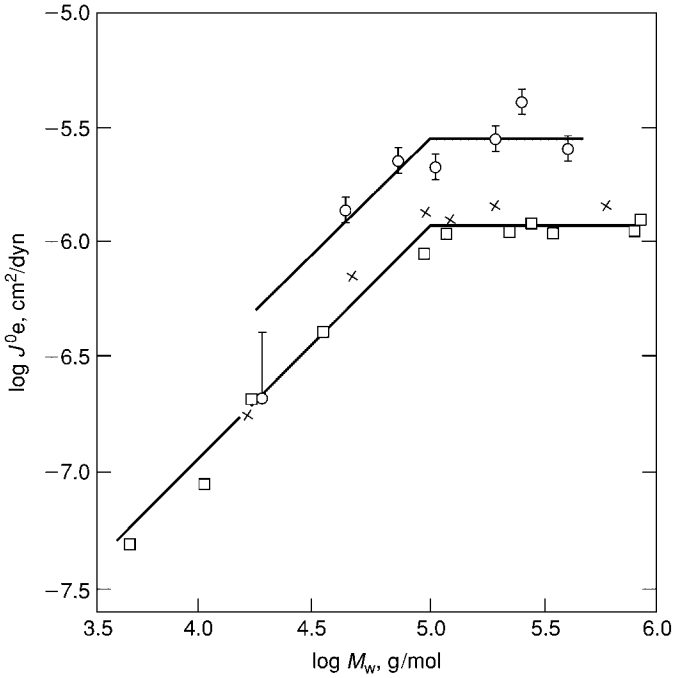

Fig. 42. Double logarithmic representation of the steady-state (recoverable) compliance as a function of molecular weight for linear (squares and crosses) and cyclic (circles) polystyrenes melts. After McKenna et al. (122).

scaling with molecular weight, as shown in Figure 42. However, once the chains get long enough to be entangled, the Rouse-like behavior no longer holds. After entanglement begins, the viscosity follows the very strong $M^{3.4}$ behavior seen in Figure 18 and the steady-state (recoverable) compliance becomes constant as seen in Figure 42 (122). It is here that a model is needed that goes beyond the Rouse model and includes entanglement effects. As noted above, the reptation model of de Gennes (51) and Doi and Edwards (52–56) is the current paradigm for polymer dynamics in the entangled state. Essentially, the DE tube model of reptation is a Rouse chain that moves through a tube that acts as a mean field of constraint. Figure 43 illustrates the movement of the chain in a tube, where the Brownian dynamics of the chain causes it to move about in the original tube until it completely disengages and the new surroundings form a new tube. Here we consider the model at length scales greater than the tube diameter a, which has been identified (57) with the (mean) distance between entanglements or a Rouse submolecule of the size of the entanglement spacing. The important parameters are the number of monomers m_e in the *entanglement segment*, the tube diameter, the friction coefficient ζ for the entanglement segment, and the number of segments in the chain N. The trajectory of bond vectors of the entanglement segments coincides with the tube axis that is referred to as the *primitive path*. These are related to the physical chain by (63)

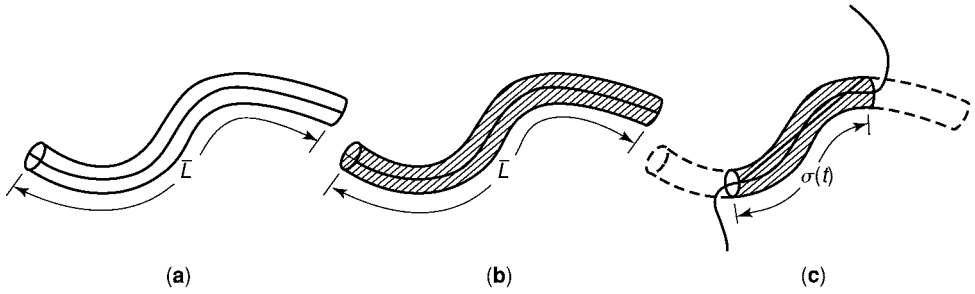

Fig. 43. Schematic of stress relaxation of a chain in the tube in the DE model for small deformations. (**a**) Prior to deformation, the tube has its equilibrium conformation. (**b**) Immediately after the deformation, the entire tube is deformed. At small strains, the contour length of the tube is unchanged. (**c**) At a later time t, the chain has partially escaped from the tube and remains partially confined by the deformed tube. The average of the contour length $\sigma(t)$ of this part of the tube is equal to $L\mu_{\text{rep}}(t)$. After Doi and Edwards (56), with permission.

$$\begin{aligned} \text{Tube diameter:} a &= m_{\text{e}}^{1/2} b \\ \text{Friction factor:} \zeta &= m_{\text{e}} \zeta_0 \\ \text{Number of segments:} N &= \frac{m}{m_{\text{e}}} \end{aligned} \tag{69}$$

where b is the effective step length of the monomer, m is the number of monomers in the chain or the degree of polymerization, and ζ_0 is the monomeric friction factor. Note that, with the exception of N, the parameters in equation 69 are independent of chain length.

In the equilibrium conformation the centerline of the tube represents a random walk with a step length that corresponds to the tube diameter. If the tube is treated as a system of slip links through which the chain can pass, the mean field of the surrounding chains results in an equivalent tensile force $\boldsymbol{F}_{\text{eq}}$ that acts on the chain ends (63,121):

$$F_{\text{eq}} = \frac{3k_{\text{B}}T}{a} \tag{70}$$

This force acts to constrain the lateral motion of the chains (tube constraints) and the average contour length of the tube coincides with the equilibrium tube length $\boldsymbol{L}_{\text{eq}}$:

$$L_{\text{eq}} = Na = \frac{R_{\text{e}}^2}{a} \tag{71}$$

where $R_{\text{e}}{}^2$ is the mean-square end-to-end distance of the unperturbed chain.

According to the DE model, the tube is fixed in space and, at equilibrium, the contour length is constant $L = L_{\text{eq}}$. This results in all entanglement segments moving together back and forth within the tube and along the tube axis. Hence, the motion is equivalent to one-dimensional diffusion within the tube along the tube axis. If one defines the position along the tube as a segment number (given by s/a, where s is the segment position), one can write an equation for the evolution

of the position $\boldsymbol{R}(n, t)$ and the unit bond vector of the nth entanglement segment $\boldsymbol{u}(n, t)$:

$$R(n,t+\Delta t)=R(n+\Delta n,t),u(n,t+\Delta t)=u(n+\Delta n,t) \tag{72}$$

where $\Delta \boldsymbol{n}$ is a normalized (by a) stochastic sliding distance and $\Delta \boldsymbol{t}$ is the time for the chain to slide this distance. Then, the Rouse chain in the tube has a curvilinear motion with a diffusion coefficient $\boldsymbol{D}_c$ that is obtained from the stochastic sliding process (61):

$$\langle \Delta n\rangle = 0, \langle \Delta n^2\rangle = \frac{2D_c}{a^2}\Delta t, \quad \text{and} \quad D_c = \frac{k_B T}{N\zeta} \tag{73}$$

The rapid motion of the entanglement segments at the chain (and tube) ends allows these to have their equilibrated configuration:

$$u = a\tilde{u}_{eq}(\text{at the chain ends}) \tag{74}$$

where $\tilde{u}_{eq}$ is an isotropically distributed unit vector.

The coarse-grained chain just discussed can be used to describe reptation dynamics at spatial scales $> a$ and time scales greater than the time $\Delta t*(a)$ for the chain to move (reptate) a distance a (63):

$$\Delta t^*(a) = \frac{Na^2\zeta}{2k_B T} \tag{75}$$

The dynamic properties for the reptation model just described are obtained by solving the equations 71, 72, 73, 74 and the linear viscoelastic properties are solved from the relationship between the stress and the chain orientation function (63). Without going into detail, the results for times longer than the tube equilibration time but shorter than the reptation time are

$$G(t) = G_N \mu_{rep}(t) \tag{76a}$$

where

$$G_N = \frac{4}{5}\upsilon N k_B T \tag{76b}$$

and

$$\mu_{rep} = \sum_{p=\text{odd}} \frac{8}{p^2\pi^2}\exp\left(-\frac{tp^2}{\lambda_{rep}}\right) \tag{76c}$$

with

$$\lambda_{rep} = \frac{\zeta N^3 a^2}{\pi^2 k_B T} \tag{76d}$$

In equation 76a the reptation time λ_{rep} is the time for the chain to escape from the tube (orientation relaxation occurs from the end to the center of the chain). G_N is the entanglement plateau modulus (this value is slightly different from that implied from rubber elasticity of an entangled network) and $\mu_{rep}(t)$ is a normalized relaxation modulus for the reptation process. In this time regime, equation 76a implies that the modulus is separable into a time function and a modulus function. This becomes important in discussing the nonlinear response, which is done, in more detail, below. Some other viscoelastic functions from the DE tube model of reptation are

$$\eta_0 = \frac{\pi^2 G_N \lambda_{rep}}{12} \tag{77}$$

$$J_s = \frac{6}{5G_N} = \frac{6}{5} J_N \tag{78}$$

At this point the reptation theory makes some strong predictions about the viscoelastic response in the linear regime, viz, the viscosity varies as N^3 and the ratio of ${J_s}^0/G_N = 6/5 = 1.2$. Note that the molecular weight dependence of the viscosity has already been discussed above, and recall that, experimentally, the viscosity varies as $N^{3.4}$. In addition, the ratio ${J_s}^0/G_N$ is observed experimentally to be in the range of 2–2.5. In spite of these failings, the reptation model is very powerful. The next section examines the stress response to deformation histories in the nonlinear range.

The DE Constitutive Equations. The DE model (52–56) made a major breakthrough in polymer viscoelasticity in that it provided an important new molecular physics based constitutive relation (between the stress and the applied deformation history). This section outlines the DE approach that built on the reptation-tube model developed above and gave a nonlinear constitutive equation, which in one simplified form gives the K-BKZ equation (70,71). The model also inspired a significant amount of experimental work. One should begin by looking at the calculation of the stresses for a material at times longer than the time it takes for the tube to equilibrate, ie, times in the reptation regime.

Doi and Edwards (56) calculate the stress considering how the conformation of the primitive chain $\boldsymbol{R}(s, t)$ is changed by the macroscopic deformation. First, one needs to know the stress equation in terms of the chain conformation, and then how the chain conformation (orientations) changes with the macroscopic deformation field. The stress equation is developed as follows:

$$\sigma_{\alpha\beta}(t) = \frac{v}{N}\left\langle \int_0^L F(t) u_\alpha(s,t) u_\beta(s,t) \mathrm{d}s \right\rangle \tag{79}$$

where $\boldsymbol{u}(s, t) = \partial \boldsymbol{R}(s, t)/\partial s$ is the unit vector tangent to the primitive chain and $F(t)$ is the tensile force acting on the primitive chain. In the equilibrium state

$$F_{eq} = \frac{3k_B T}{Na^2} L \tag{80}$$

and in the nonequilibrium state

$$F(t) = \frac{3k_B T}{Na^2} L(t) \tag{81}$$

where $L(t)$ is the tube contour at time t and L is its equilibrium value. From equations 79, 80, 81 the relationship between the stress, the contour length, and the changing chain orientation is obtained as

$$\sigma_{\alpha\beta} = \frac{3vk_B T}{N^2 a^2} \left\langle \int_0^{L(t)} L(t) \left[u_\alpha(s,t) u_\beta(s,t) - \frac{1}{3}\delta_{\alpha\beta} \right] \mathrm{d}s \right\rangle \tag{82}$$

It is now necessary to develop the equations for the relationship between the macroscopic deformations and the chain orientations. Doi and Edwards assume that the deformation is affine, ie, the primitive chain deforms in the same way as the macroscopic deformation field. Thus, a point $\boldsymbol{R}(s, -0)$ on the primitive chain is displaced as

$$R(s, -0) \rightarrow E \cdot R(s, -0) \tag{83}$$

where $\boldsymbol{E}$ is the deformation gradient tensor and its components are written as

$$E_{\alpha\beta} = \frac{\partial r'_\alpha}{\partial r_\beta} \tag{84}$$

where r′ is the coordinate in the deformed state and $\boldsymbol{r}$ is the coordinate in the undeformed state. (Note that this is similar to the definitions used earlier in defining the strains and relative deformations.)

Doi and Edwards then derive expressions for the changing contour length and change in the orientation of the primitive path. The development is beyond the scope of the current article. The important expression is that for the chain orientation tensor $\boldsymbol{Q}$ as a function of the macroscopic deformation gradient tensor:

$$Q_{\alpha\beta}(E) = \frac{\left\langle \frac{(E\cdot u)_\alpha (E\cdot u)_\beta}{|E\cdot u|} \right\rangle_0}{\langle |E\cdot u| \rangle_0} - \frac{1}{3}\delta_{\alpha\beta} \tag{85}$$

Then it is possible to determine the response of the “reptation” material to single-step stress relaxation strain histories at large deformations. The relaxation of the tube contour length $L(t)$ takes place on the time scale of the longest Rouse time of the chain in the tube and reorientation takes place over the reptation time scale λ_{rep} as the chain disengages from the tube. This is shown schematically in Figure 44. Therefore, the relaxation for times greater than the equilibration time (the Rouse time for a free chain) takes place in two steps. In the time scale during

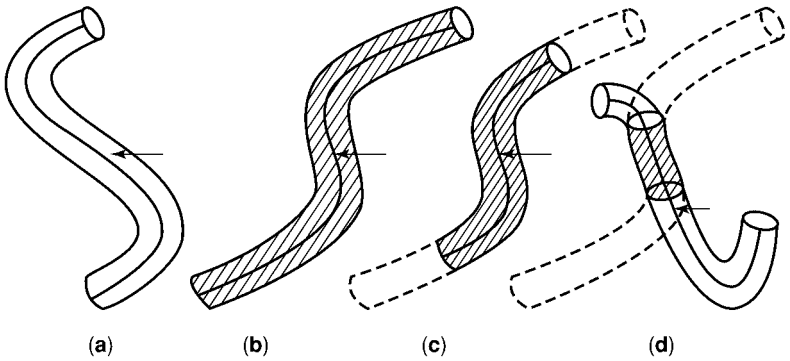

Fig. 44. Schematic of the stress relaxation process after a large step in deformation. (**a**) Equilibrium conformation of the tube prior to deformation. (**b**) Immediately after deformation, the primitive chain has been affinely deformed. (**c**) After the time λ_R, the primitive chain retracts along the tube and recovers its equilibrium contour length ($t \cong \lambda_R$). (**d**) After the time λd the primitive chain leaves the deformed tube by reptation ($t \cong \lambda_d$). After Doi and Edwards (56), with permission.

which the tube recovers its original contour length (contour length relaxation),

$$\sigma_{\alpha\beta}(t) = G_e\{1 + [\alpha(E) - 1]\exp(-t/\lambda_R)\}^2 Q_{\alpha\beta}(E), \lambda_e \le t \le \lambda_R$$
$$\text{where} \quad G_e = \frac{15}{4} G_N \quad \text{and} \quad \alpha(E) = \langle |E \cdot u| \rangle_0 \tag{86}$$

For the time after the tube has regained its original contour length, the chain begins to disengage from the tube via the reptation mechanism. The relaxation response during this time is

$$\sigma_{\alpha\beta}(t) = G_e Q_{\alpha\beta}(E) \mu_{rep}(t), t > \lambda_R \tag{87}$$

where $\mu_{rep}(t)$ is given as the relaxation function for reptation in equation 76a. Combining equations 86 and 87 one obtains the relaxation function for the two-step process:

$$\sigma_{\alpha\beta}(t) = G_e Q_{\alpha\beta}(E)\{1 + [\alpha(E) - 1]\exp(-t/\lambda_R)\}^2 \mu_{rep}(t), t > \lambda_e \tag{88}$$

For a simple shearing deformation, $\alpha(E) = \alpha(\gamma)$ and $Q_{\alpha\beta}(E) = Q_{\alpha\beta}(\gamma)$. In the linear (small deformation) regime one finds

$$\sigma(\gamma) = \left\langle \left(1 + 2\gamma u_x u_y + \gamma^2 u_y^2\right)^{1/2} \right\rangle_0 = 1 + \frac{2}{15}\gamma^2 + O(\gamma^4)$$
$$Q_{xy}(\gamma) = \frac{1}{\alpha(\gamma)} \left\langle \frac{(u_x + \gamma u_y) u_y}{\left(1 + 2\gamma u_x u_y + \gamma^2 u_y^2\right) \mathrm{k}^{1/2}} \right\rangle = \frac{4}{15}\gamma + O(\lambda^3) \tag{89}$$

and the stress response (eq. 88) becomes

$$\sigma_{xy}(t) = \frac{4}{15}\gamma G_e \mu_{rep}(t) + O(\gamma^3) \tag{90}$$

which is the linear viscoelastic response to a single-step stress relaxation history.

For larger deformations, equation 88 is used. For convenience the nonlinear relaxation modulus is defined as

$$G(\gamma,t) = \frac{1}{\gamma}\sigma_{xy}(t,\gamma) \tag{91}$$

Then, equations 88 and 91 give the following expression for the nonlinear modulus:

$$\begin{aligned} G(\gamma,t) &= G_e \frac{Q_{xy}(\gamma)}{\gamma}\{1+[\alpha(\gamma)-1]\exp(-t/\lambda_R)\}^2 \mu_{rep}(t) \\ &= h\ (\gamma) G(t)\{1+[\alpha(\gamma)-1]\exp(-t/\lambda_R)\}^2 \end{aligned} \tag{92}$$

Here $G(t)$ is the linear viscoelastic modulus and $h(\gamma)$, the *damping function* in shear is introduced. For small γ, the linear response is recovered. As γ increases, we see another relaxation in $G(\gamma, t)$ at short times that corresponds to the relaxation of the contour length. Figures 45 and 46 show the expected relaxation

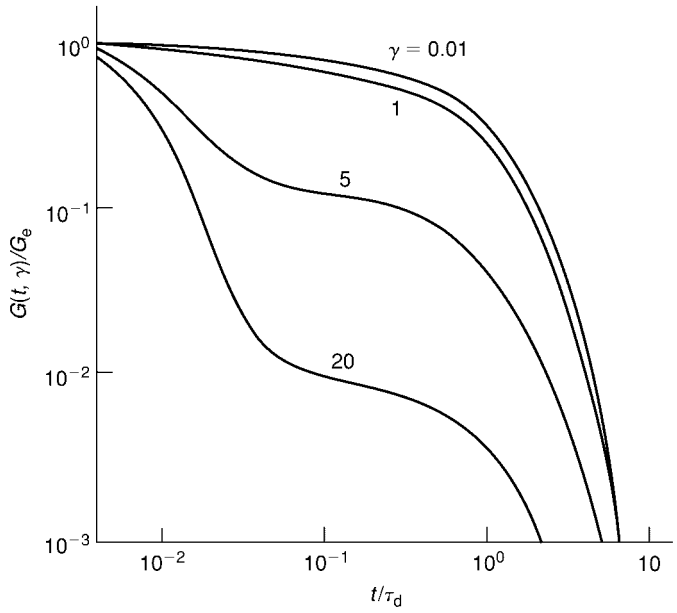

Fig. 45. Theoretical curve for the nonlinear relaxation modulus $G(t, \gamma)$ [$= G(\gamma, t)$] at different values of γ as indicated in the figure. The plot is for the case of $\lambda_d/\lambda_R = 100$. After Doi and Edwards (56), with permission.

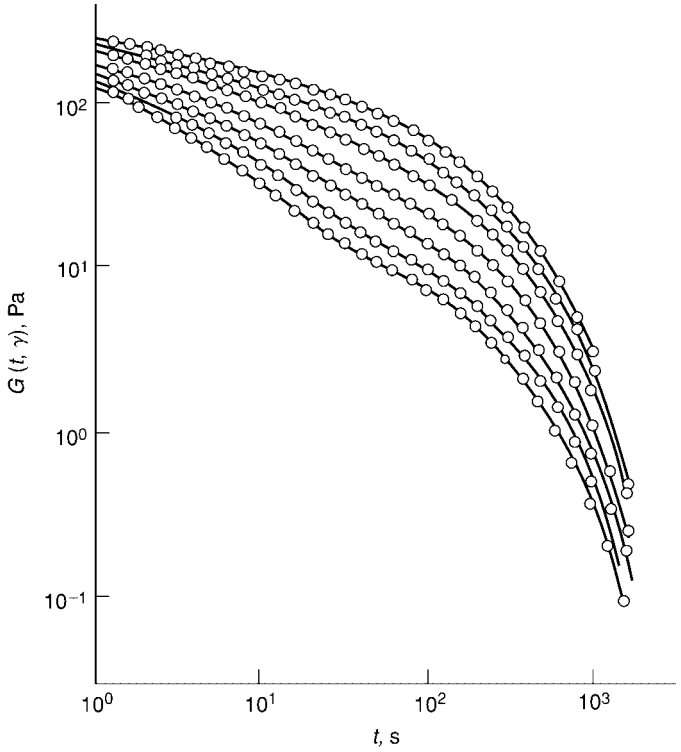

Fig. 46. Nonlinear relaxation modulus $G(t, \gamma)$ [$= G(\gamma, t)$] for a solution of polystyrene in chlorinated biphenyl ($\phi = 0.06$ g/cm^3) at 30°C. From top to bottom, shear strains γ are 0.57, 1.25, 2.06, 3.04, 4.0, 5.3, and 6.1. After Osaki et al. (123), with permission.

behavior and that obtained experimentally for a high molecular weight polymer in solution. The theoretical curves show more nearly exponential decays for both mechanisms than is seen in the actual data, which has a broader relaxational behavior. This is a well-known weakness of the DE model that is related to the relaxation function being nearly exponential in nature (the longest relaxation time is widely separated from the next time which also has a lower intensity).

In examining the single-step stress relaxation behavior of the DE model, one can also look at the normal stress responses in shearing experiments. The first and second normal stress differences are $N_1(\gamma, t)$ and $N_2(\gamma, t)$ respectively. The relevant equations are (56)

$$N_1(\gamma,t) = \frac{Q_{xx}(\gamma) - Q_{yy}(\gamma)}{Q_{xy}(\gamma)}\sigma_{xy}(\gamma,t)$$
$$N_2(\gamma,t) = \frac{Q_{yy}(\gamma) - Q_{zz}(\gamma)}{Q_{xy}(\gamma)}\sigma_{xy}(\gamma,t) \tag{93}$$

and since

$$Q_{xx}(\gamma) - Q_{yy}(\gamma) = \gamma Q_{xy}(\gamma) \tag{94}$$

$N_1(\gamma, t)$ can be written as

$$N_1(\gamma,t) = \gamma\sigma_{xy}(\gamma,t) \tag{95}$$

This relation, which also results from the K-BKZ model, is referred to as the Lodge–Meissner relationship (124) and results for materials with a finite elastic modulus at zero time.

The framework for examining arbitrary deformation histories for the "reptation" fluid has now been established and one can obtain a constitutive law for the stress response to arbitrary deformation histories. While the DE model can provide a more general constitutive equation than that to be developed now, the more general form requires numerical solution. The approximation known as the *independent alignment assumption* (IA) results in a closed form solution that gives a special case of the K-BKZ theory developed previously.

First, consider a simplification in which it is assumed that the contour length of the primitive chain remains at the equilibrium length L under the imposed deformation. This assumes an inextensible primitive chain and is seen as a reasonable approximation for slow flows or long times. Then, the deformation of the primitive chain is given by considering that the segment in the middle of the chain changes position affinely as

$$R'(0) = E \cdot R(0) \tag{96}$$

where $R(s)$ is the primitive chain conformation before deformation and $R'(s)$ is that after deformation. The primitive chain segments go from $-L/2$ to $L/2$; hence the middle is at 0.

Then the segment s' lies on the curve $E \cdot R(s)$ so that

$$R'(s') = E \cdot R(s) \tag{97}$$

s' is the contour length along the curve $E \cdot R(s'')$ from $s'' = 0$ to $s''=s$:

$$s' = \int_0^s |E \cdot u(s'')| \mathrm{d}s'' \tag{98}$$

Combination of equations 96, 97, 98 gives the transformation

$$u'(s') = \frac{E \cdot u(s)}{|E \cdot u(s)|} \tag{99}$$

Because s and s' are not equal to each other, the general constitutive equation becomes very complicated and requires numerical solution. The independent alignment approximation allows us to ignore this difference. Then, with $s' = s$ the transformation equation 99 becomes

$$u'(s) = \frac{E \cdot u(s)}{|E \cdot u(s)|} \tag{100}$$

The consequences of this approximation have been extensively investigated and the results are outlined here. In terms of the orientation tensor, the IA approximation in a single-step stress relaxation experiment in simple shear is given by

$$\begin{aligned} Q_{xy}^{\mathrm{IA}}(\gamma) &= \frac{1}{5}\gamma(\gamma \ll 1) \\ Q_{yy}^{\mathrm{IA}}(\gamma) - Q_{zz}^{\mathrm{IA}}(\gamma) &= -\frac{2}{35}\gamma^2(\gamma \ll 1) \end{aligned} \tag{101}$$

and the damping function is then given by

$$h^{\mathrm{IA}}(\gamma) = \frac{Q_{xy}^{\mathrm{IA}}(\gamma)}{\gamma/5} \tag{102}$$

which is not very different from the more general $h(\gamma)$ introduced earlier (eq. 91) over a wide range of γ (56).

Without derivation, note that Doi and Edwards developed expressions for the probability distribution function for the chain as well as the relationship between the stress and the chain orientations to arrive at an evolution equation for the stress to the chain orientation process, which is a function of the macroscopic deformations. The resulting constitutive equation is

$$\sigma_{\alpha\beta}(t) = G_{\mathrm{e}} \int_{-\infty}^{t} \left(\frac{\partial \psi(t-t')}{\partial t'} \right) Q_{\alpha\beta}^{\mathrm{IA}}[E(t,t')]\mathrm{d}t' \tag{103}$$

where $\psi(t) = \mu_{\mathrm{rep}}(t)$ is the DE relaxation function given previously. This equation is equivalent to a special form of the K-BKZ model discussed above. Note, however, that the deformation measure is somewhat different. [The reader should see Wagner and Schaeffer (125) for further discussion of the DE strain measures relative to classic strain measures.] A relaxation function $\phi_{\alpha\beta}(t, E)$ can be defined as

$$\begin{aligned} \phi_{\alpha\beta}(E,t) &= G_{\mathrm{e}} \int_{-\infty}^{0} \left(\frac{\partial \psi(t-t')}{\partial t'} \right) Q_{\alpha\beta}^{\mathrm{IA}}(E)\mathrm{d}t' \\ &= G_{\mathrm{e}} \psi(t) Q_{\alpha\beta}^{\mathrm{IA}}(E) \end{aligned} \tag{104}$$

which is the single-step stress relaxation response to the deformation represented by $Q_{\alpha\beta}{}^{\mathrm{IA}}(E)$. Then, the stress response to an arbitrary flow history is given by

$$\sigma_{\alpha\beta}(t) = \int_{-\infty}^{t} \left(\frac{\partial \phi(E,t-t')}{\partial t'} \right)_{E=E(t,t')} \mathrm{d}t' \tag{105}$$

This has the same form as the K-BKZ model described above and where the function $\phi(E, t)$ has the meaning of $K(I_1, I_2, t)$ for any given deformation (see eqs. 56, 57, 58, 59, 60). This result was a very important aspect of the DE model's success because of the broad success of the K-BKZ continuum model

that had already been established. The next sections examines some of the data that were specifically generated to test the validity of the DE model constitutive equation.

Comparison with Experiment. Of particular importance in comparing the DE model with nonlinear rheological experiments is the fact, already noted above, that the relaxation function in the linear viscoelastic regime is not broad enough to capture the actual behavior of polymers. This resulted in two important trends in the experimental tests of the DE work. First, because the K-BKZ work, eg, in two-step deformation histories, had been mostly performed on commercial polymers of broad molecular weight distribution, the tests of DE focused primarily on monodisperse polymers that were anionically polymerized. (Later developments (15,18,126–128) lead to use of broader molecular weight distributions but these will not be treated here.) Hence, much work was done, particularly by Osaki (123,129–133) and co-workers, in different two-step deformation histories where both the shear and normal stress differences could be obtained. Also, more recent work by the Venerus and Burghardt groups (115–117,134,135) has further expanded on the Osaki work. The second development was that much effort was expended to compare the form of the damping function that was measured with that given by the DE model, part of which was discussed above.

Single-Step Stress Relaxation Experiments. The damping function of the DE equation has already been compared with some of the Osaki data (Figs. 45 and 46). Here two other aspects of the Osaki work are emphazied. At long times, when the material response is dominated by the chain disengaging from the tube, the DE model gives a response that is refered to as *time–strain separable*. The possibility of time–strain separability in the response of polymer relaxation behavior was originally used by Zapas and Craft (111). Empirically, time–strain separability can be expressed by the following (see also eqs. 76a and 90):

$$G(\gamma,t) = h(\gamma)g(t) \tag{106}$$

where $h(\gamma)$ is referred to as the *shear damping function* discussed above and $g(t)$ would be a linear viscoelastic relaxation response. Osaki (123) showed that the time–strain separability appears to be valid after some characteristic time the called τ_k (now time and not stress). This is shown in Figure 47, which is a plot of $G(\gamma, t)/h(\gamma)$. If time–strain separability were valid over all times, the curves at different strains would have collapsed onto a single curve. In Figure 47 it is observed that the curves do not collapse until after the time τ_k. Unfortunately, it is not currently possible to uniquely attribute τ_k to any of the times discussed above for the tube model. It is, however, common to attribute τ_k to the finite time required for the molecule to retract along its contour length.

Another interesting aspect of the work done by Osaki was the demonstration that $h(\gamma)$ is not a universal function. Rather, it seems to depend on the number of entanglements M/M_e. The reptation theory expectation for the actual behavior in concentrated solution has been variously interpreted and there is not general agreement on the expected behavior. However, the data shown in Figure 48 are important for the understanding of polymer molecular viscoelasticity and were obtained within the important framework provided by the DE theory. From

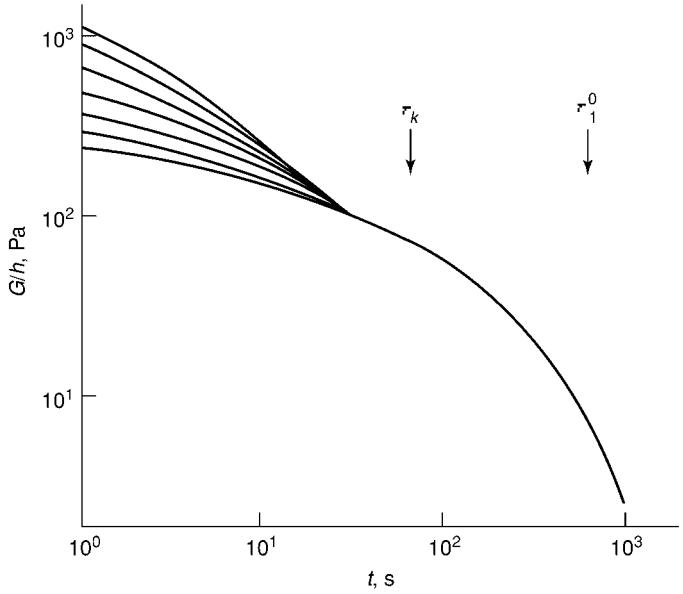

Fig. 47. Reduced relaxation modulus $G(t, \gamma)/h(\gamma)$ [$= G(\gamma, t)/h(\gamma)$] derived from data of Figure 46. The curves for $\gamma > 1.25$ shift vertically by an amount $-\log h(\gamma)$ so that they superpose in the long time regime. $\tau^0{}_1$ represents the longest relaxation time and τ_k represents the time below which superposition is not possible. After Osaki et al. (123), with permission.

Figure 48 it is seen that the damping function depends on M/M_e and on concentration. Subsequently Osaki and co-workers (123) stated that "the quantity $h(\gamma)$ scarcely varies with molecular weight or concentration." A still later work by Osaki (136), however, again shows a disagreement between experimental data and the universal $h(\gamma)$ for polystyrene solutions. In addition, Wagner and Schaeffer (119,125,137) have extensively studied the form of the universal damping function and found that it is inadequate for the description of polydisperse polymer melts.

Two-Step Stress Relaxation Experiments. As discussed above in the context of the K-BKZ model, the two-step stress relaxation experiment is a very important tool in the assessment of constitutive relations. The same has been true in the use of the two-step experiment to assess the DE model. Here, the tests in the context of the independent alignment assumption are first examined. The important aspect of the experiments performed by Osaki and co-workers is that (123,129–133) the work was performed on monodisperse polymers. The work of Venerus and Burghardt, which is further built on the work of Osaki, will also be discussed. Finally, a proposed form of constitutive model that goes beyond the independent alignment assumption and gives a tractable set of predictions for the double-step experiments is examined.

Here three types of two-step experiment are viewed and the reader is asked to recall Figure 33. The figure shows the step-up (a), the step to zero (b), and the half-step (c) histories. Both the torque and normal force responses are examined.

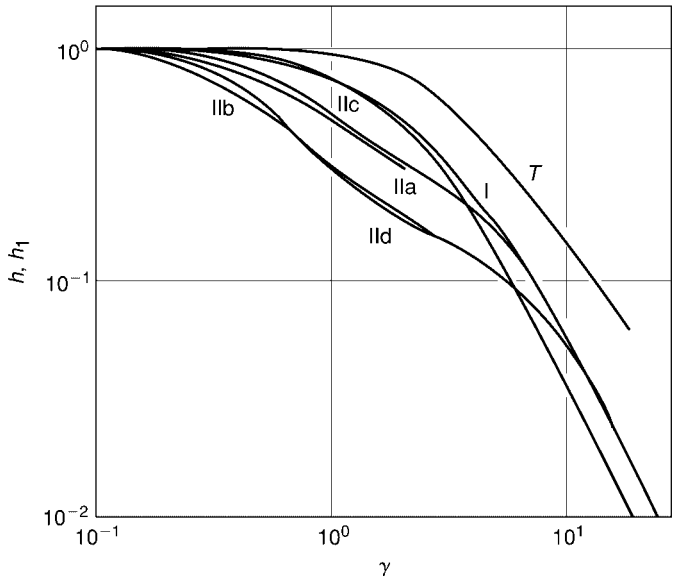

Fig. 48. Strain-dependent functions $h(\gamma)$ and $h_1(\gamma)$. The heavy line represents the DE damping function and the light lines represent experimental results $[h_1(\gamma)]$ for polystyrene solutions. For type I sample, $\phi M < 10^6$ (g·Da)/cm^3 and for type II samples $\phi M > 10^6$ (g·Da)/cm^3. For IIa, $M = 3.10 \times 10^6$ Da and $\phi = 0.329$ g/cm^3. For IIb, $M = 5.53 \times 10^6$ Da and $\phi = 0.221$ g/cm^3. For IIc and IId, $M = 7.62 \times 10^6$ Da and $\phi = 0.176$ and 0.221 g/cm^3, respectively. T is for a broad molecular weight distribution sample in which $M_w = 1.10 \times 10^6$ Da and $M_w/M_n = 4$ and $\phi = 0.21$ g/cm^3. After Osaki and Kurata (130), with permission.

In addition, because much of the data in the literature include comparisons with the DE model both with and without independent alignment, the equations for the form of the DE model that Doi proposed by suppressing the independent alignment assumption are presented. Here the results are referred to as DE-NIA. In this case for two-step stress relaxation histories recall equations 59 (DE-IA or K-BKZ)

$$\begin{aligned} \sigma_{12}(t) &= K(\gamma_2,t) + K(\gamma_2-\gamma_1,t-t_1) - K(\gamma_2-\gamma_1,t) \\ \sigma_{22}(t) - \sigma_{22}(t) &= H_1(\gamma_2,t) + H_1(\gamma_2-\gamma_1,t-t_1) - H_1(\gamma_2-\gamma_1,t) \\ \sigma_{22}(t) - \sigma_{33}(t) &= H_2(\gamma_2,t) + H_2(\gamma_2-\gamma_1,t-t_1) - H_2(\gamma_2-\gamma_1,t) \end{aligned} \tag{59}$$

and compare these with the DE-NIA equations:

$$\begin{aligned} \sigma_{12}(t) &= A(\beta)K(\gamma_2,t) + K(\gamma_2-\gamma_1,t-t_1) - [A(\beta)+B(\alpha_2,\beta)]K(\gamma_2-\gamma_1,t) \\ \sigma_{22}(t) - \sigma_{22}(t) &= A(\beta)H_1(\gamma_2,t) + H_1(\gamma_2-\gamma_1,t-t_1) - [A(\beta)+B(\alpha_2,\beta)]H_1(\gamma_2-\gamma_1,t) \\ \sigma_{22}(t) - \sigma_{33}(t) &= A(\beta)H_2(\gamma_2,t) + H_2(\gamma_2-\gamma_1,t-t_1) - [A(\beta)+B(\alpha_2,\beta)]H_2(\gamma_2-\gamma_1,t) \end{aligned} \tag{107}$$

where

$$A(\beta)=\frac{4\beta\cos(\frac{\pi\beta}{2})}{\pi(1-\beta^2)},\ B(\alpha_2,\beta)=\frac{\pi^2(1-\beta)^3}{12(\alpha_2-\beta)}\quad\text{for}\quad\beta<1$$

$$A(\beta)=\frac{4\cos(\frac{\pi}{2\beta})}{\pi(1-\beta^{-2})},B(\alpha_2,\beta)=0\quad\text{for}\quad\beta\geq 1 \tag{108}$$

$$\beta=\left(\frac{3+\gamma_2^2}{3+\gamma_1^2}\right)^{1/2},\ \alpha_2=\left[1+(\gamma_1-\gamma_2)^2\right]^{1/2}$$

As seen in the next paragraphs, the DE-NIA equations sometimes do better and sometimes worse than the DE-IA or K-BKZ equations. Also note that in all instances the measured single-step relaxation function is used rather than the theoretical DE function, which as already discussed is too narrow to capture the full breadth of the relaxation response of entangled polymers.

Step-Up. Figure 49 shows the response for a two-step history in which the second step is approximately the same magnitude as the first step, ie, $\gamma_2=2\gamma_1$. The results are from Osaki's work (138) on polystyrene solutions and illustrate that both the shear stress response and the normal stress response are well represented with the DE independent alignment approximation (ie, the K-BKZ equations). This result is similar to what was found previously for the K-BKZ model (Fig. 34) (138).

Step to Zero Deformation. Figures 50 and 51 show the response for a two-step history in which one first applies a step strain γ_1 for some time t_1 and then returns

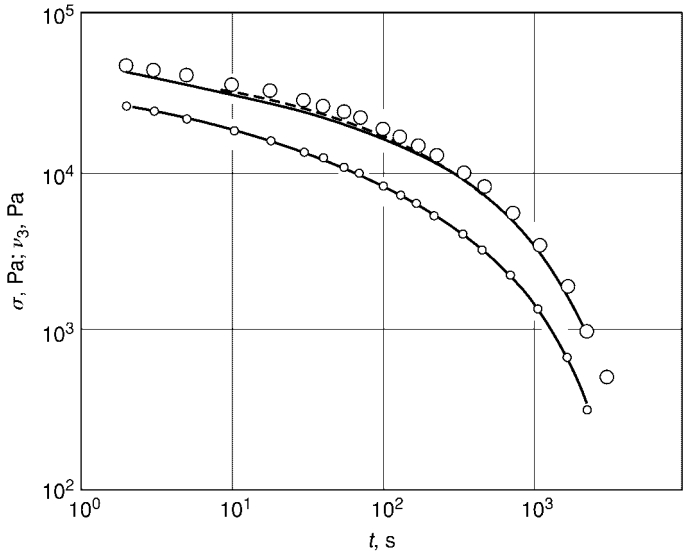

Fig. 49. Shear stress σ (○) and normal stress ν_3 (○) responses to a two-step "step-up" type of deformation history with $\gamma_1=1.47$ and $\gamma_2=2.90$ for a concentrated polystyrene solution. The solid lines are the predictions for the K-BKZ or DE-IA equations and the dashed lines are for the DE-NIA equations. After Osaki and et al. (138), with permission.

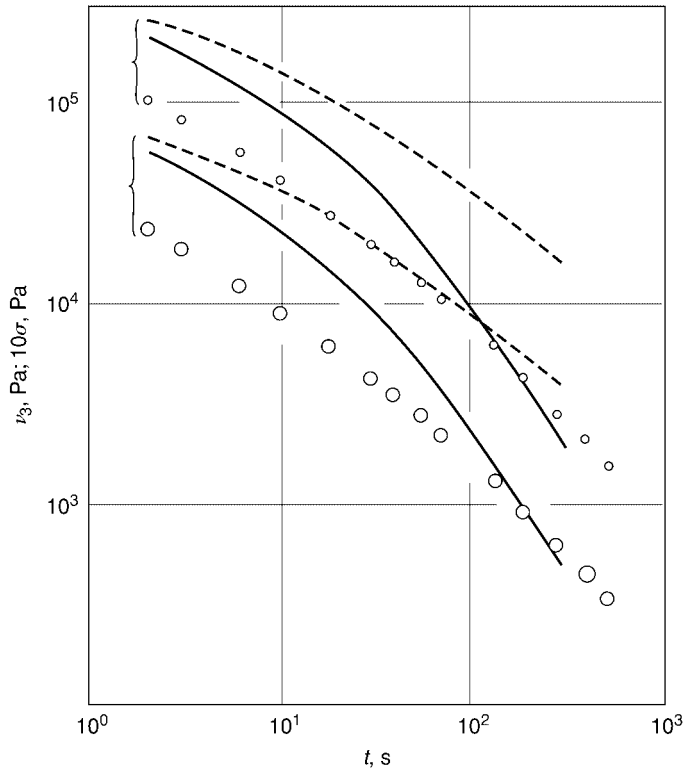

Fig. 50. Shear stress σ (○) and normal stress ν_3 (○) responses to a two-step "step to zero" type of deformation history with $\gamma_1 = 2.89$ and $\gamma_2 = 0$ for a concentrated polystyrene solution. Duration of the first step was $t_1 = 20$ s. The solid lines are the predictions for the K-BKZ or DE-IA equations and the dashed lines are for the DE-NIA equations. After Osaki et al. (138), with permission.

the material to zero deformation, $\gamma_2 = 0$. The results are, again, from Osaki (138). Figure 50 shows the results when the first step duration $t_1 = 20$ s, and it is seen that both the shear and normal stress responses are poorly represented by either the DE model with independent alignment (solid lines) or the predictions without the independent alignment assumption (dashed lines). Figure 51 shows that when t_1 gets longer ($t_1 = 200$ s) the agreement between theory and experiment improves. Also, note that both theoretical curves also begin to approach each other, as might be expected because the models are fading memory models and at very long times, the step back to zero should become equivalent to the single-step response.

Half-Step Deformation. In the discussion of the K-BKZ model, the half-step deformation was covered. Here two sets of data that go beyond what was described above are discussed. First, in the Osaki data shown in Figure 52, it is seen that the DE model with independent alignment fits the shear stress response, but not the normal stress response. Also, the theory without the independent alignment assumption does not fit the shear data. The normal stress deviation from the model prediction is interesting, as this was a "special" history for which the K-BKZ and

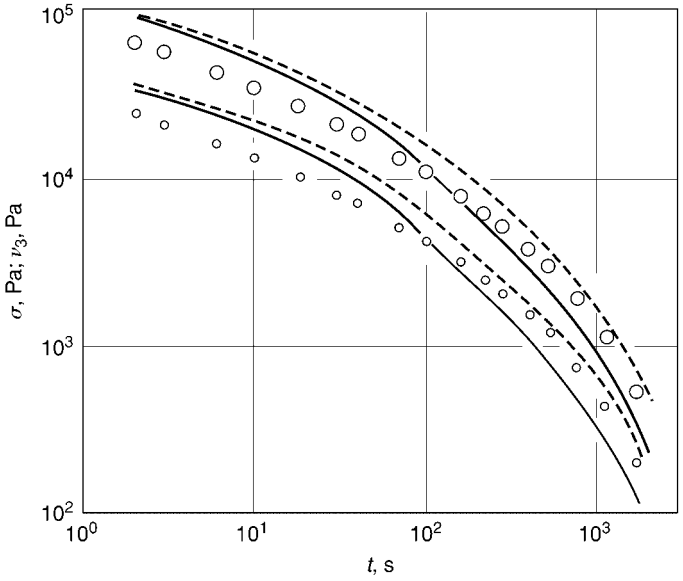

Fig. 51. Shear stress σ (○) and normal stress ν_3 (○) responses to a two-step "step-to zero" type of deformation history with $\gamma_1 = 2.89$ and $\gamma_2 = 0$ for a concentrated polystyrene solution. Duration of the first step was $t_1 = 200$ s. The solid lines are the predictions for the K-BKZ or DE-IA equations and the dashed lines are for the DE-NIA equations. After Osaki et al. (138), with permission.

DE-IA models both predicted that the normal stress response is independent of the duration of the first step (and equal to a single-step experiment with magnitude $\gamma_2 = \gamma_1/2$). Figure 52 shows that for the polystyrene solution, the single-step response for the normal stress is only in agreement with the single-step response at long times. Interestingly, Osaki's data (138) showed that the normal stress response was independent of the duration of the first step, although not equal to the single-step response. Figures 53 and 54 show a set of half-step data from Burghardt and Brown (111). The shear stress theory is not shown for comparison, but it is seen that the shear stresses go negative and then become positive, going through a maximum before joining what would be the single-step relaxation at very long times. On the other hand the normal force responses for the different values of t_1 are very interesting because they seem to become independent of the duration of the first step at a characteristic time. At short times, deviations occur. Hence, the original findings of McKenna and Zapas that the normal force response is independent of the duration of the first step, seems to only be confirmed for long times. Osaki associated this time with the value of τ_k discussed previously and where time-strain separability is applicable. An interesting aspect of this is that the observation that the normal stresses in the half-step history can independent of the duration of the first step is also observed for some polymer glasses (112–114), as discussed subsequently.

Nonlinear Viscoelastic Response of Solid-like Polymers. The study of the nonlinear viscoelastic response of solid or solid-like polymers is one that has

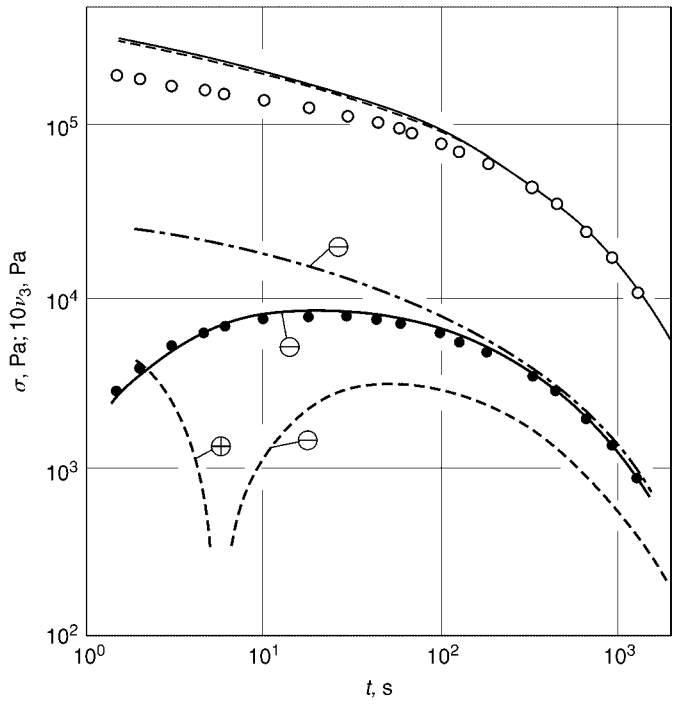

Fig. 52. Shear stress σ (○) and normal stress ν_3 (○) responses to a two-step "half-step" type of deformation history with $\gamma_1 = 2.89$ and $\gamma_2 = 1.45$ for a concentrated polystyrene solution. Duration of the first step was $t_1 = 20$ s. The solid lines are the predictions for the K-BKZ or DE-IA equations and the dashed lines are for the DE-NIA equations. Dashed-dotted line is the single-step shear stress response for $\gamma = 1.45$. After Osaki et al. (138), with permission.

been relatively neglected. One reason is that there is no real molecular framework for the description of these materials, particularly when they are amorphous. The other reason is that many workers in the field have adopted the framework of metal plasticity and then made modifications to try to adapt it to, for example, the fact that amorphous polymers do not readily admit to treatment with the physics of dislocations. In the case of semicrystalline polymers, the crystalline phase may, in some instances, succumb to a plasticity treatment, (139) but the full description of the nonlinear response requires treatment of a two-phase system. The following sections treat the problem of nonlinear behavior of solid or solid-like polymers as a problem in viscoelasticity. Primarily amorphous, glassy polymers are chosen. There are several reasons for these choices. First, the semicrystalline polymers are very complicated, as discussed briefly above, and our physical understanding of their linear viscoelastic response is still somewhat limited because of the complex interactions between amorphous and crystalline phases. Hence, while some progress has been made in dealing with the yield response of polyethylene (140,141) it is unclear how general the models are to other materials. This leaves one with the amorphous, glassy polymers. Here,

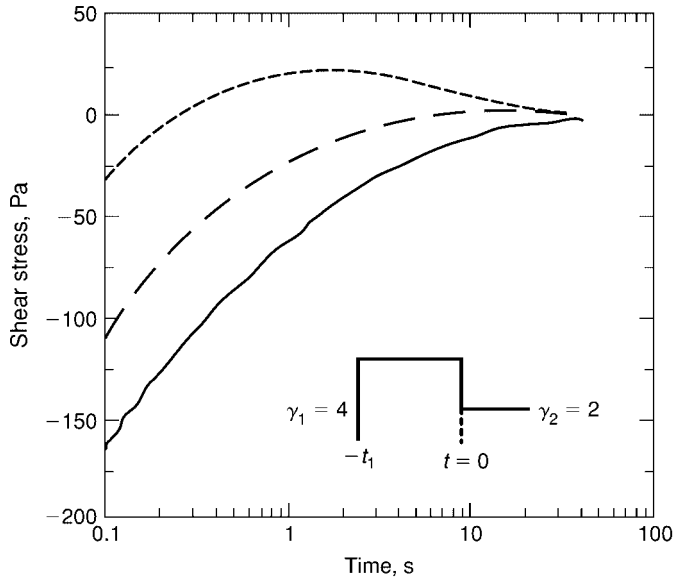

Fig. 53. Shear stress response to "half-step" type of deformation history for a concentrated polystyrene solution and for different values of the first step duration t_1. Dotted line; $t_1 =$ 1 s; dashed line; $t_1 = 4$ s; solid line; $t_1 = 16$ s. After Brown and Burghardt (134), with permission.

because the materials seem to follow time-temperature superposition in many instances, (9,33–35,40,142) there is a reasonable likelihood that a viscoelasticity framework is a good one with which to treat them. In addition, most work has focused on *post-yield* behavior, a regime to which plasticity in metals seems (inappropriately in this author's mind) applicable. With this in mind, therefore, it becomes important to investigate the *sub-yield* behavior of amorphous materials because it is the sub-yield behavior that is the precursor to yielding behavior. The latter cannot be understood until the former is. The following section deals with the K-BKZ framework and adapts it to the present investigations of the viscoelastic response of glassy polymers. Several other viscoelastic frameworks that have been, or are being, used in the study of amorphous polymers are also discussed.

The K-BKZ Framework. The above sections dealt with the K-BKZ framework for describing the nonlinear constitutive response of polymeric fluids. While the K-BKZ theory was developed for incompressible fluids, polymeric glasses are compressible in that the bulk modulus and the shear modulus are of the same order of magnitude. However, in the first work described here only torsional behavior is examined, which is nearly volume conserving (143–145). Hence, there may be reason to think that the incompressible framework is justifiable. Some aspects of compressibility are also examined and these are adapted to one instance of extension and compression behavior. Other constitutive models are also analyzed.

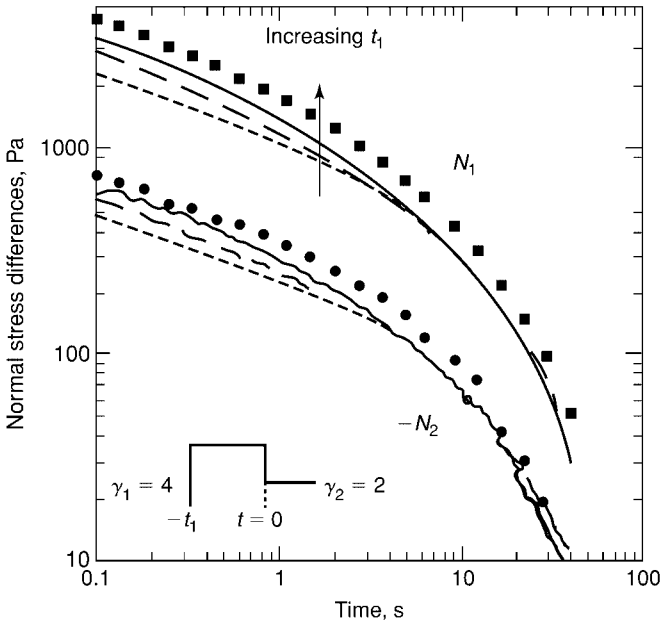

Fig. 54. Normal stress response to "half-step" type of deformation history for a concentrated polystyrene solution and for different values for the first step duration t_1. Dotted line: $t_1 = 1$ s; dashed line: $t_1 = 4$ s; solid line: $t_1 = 16$ s. Symbols represent single-step response for $\gamma = 2.0$. After Brown and Burghardt (134), with permission.

Torsional Experiments. The geometry and equations for torsion of an elastic cylinder are presented above. For the viscoelastic K-BKZ material, the equations look similar. For isochronal values of the strain potential function, one can define what looks like a time-dependent strain-energy function $W_i(I_1, I_2, t)$:

$$W_i(I_1,I_2,t) = \frac{\partial W(I_1,I_2,t)}{\partial I_i} = \int_{-\infty}^{t} \frac{\partial U(I_1,I_2,t-t')}{\partial I_i} \mathrm{d}t' \tag{109}$$

Then, isochronal values $W_i(I_1, I_2, t)$ can be used to characterize the stress relaxation behavior of solid cylinders and, similar to the behavior found for rubber, the strain energy function derivatives can be determined for different materials. There is relatively little work in this area, but the results are intriguing. Figure 55 shows the isochronal torque and normal force responses for a polycarbonate material subjected to maximum strains of approximately 0.10 at the outside radius of the cylinder. This strain is just below the yield point of the polycarbonate in torsion. These data have a similar appearance to the rubber data shown in Figure 31 at small strains (the torque follows ψR and the normal force follows $\psi^2 R^2$), but as the strain increases toward $\psi R = 0.1$, there is a strong softening in the responses as yield is approached. In the case of the rubber samples, such softening does not occur even for strains as high as $\psi R = 2.0$. The time-dependent equivalent of equations 47 and 48 can be used to analyze the torque and normal forces so as to determine the values of $W_1(I_1, I_2, t)$ and $W_2(I_1, I_2, t)$. Such data are shown for a PMMA material in Figure 56 and for the polycarbonate in Figure 57.

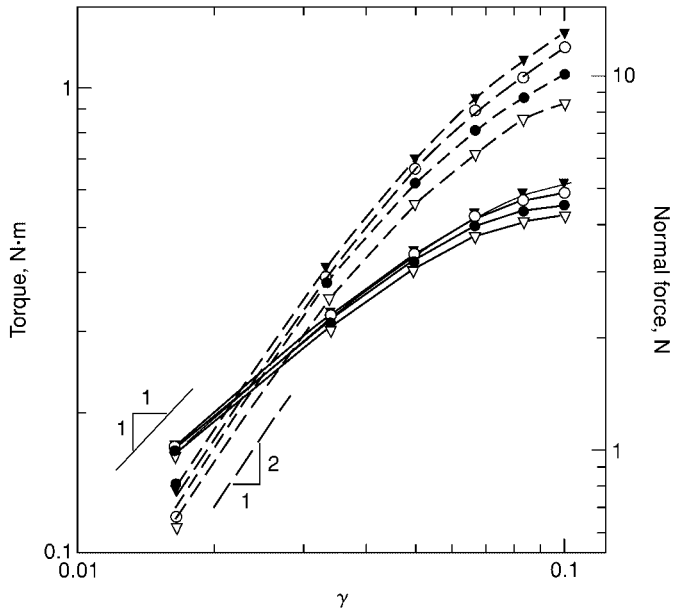

Fig. 55. Torque and normal force responses for a glassy polycarbonate material in stress relaxation conditions. *Isochrones*: ▼ 1 s; ○ 10 s; ● 100 s; ▽ 1000 s. After Pesce and McKenna (146).

Figure 58 shows the isochronal VL function behavior for the polycarbonate as a function of the stretch λ. Clearly, the behavior is very different for the material below the glass transition, that is the solid-like or glassy polycarbonate, than it is for the rubbery material in Figure 32.

Although this approach seems useful, unlike the rubbery polymers, the glassy polymers are compressible materials in the sense that the ratio of the bulk and shear moduli is near unity, rather than being in the neighborhood of 100–1000 for the rubber. This means that the forces to cause shape changes (distortions or shears) in the rubber are much smaller than those required to cause volume changes, while these forces are of approximately the same magnitudes in the glassy polymer. Hence, incompressible theory describes very well the behavior of the rubbery material, but does not obviously apply to the polymer glass. The next section examines the material compressibility issues and the extension of the VL function to the compressible case.

Issues of Material Compressibility. There is a full theory of compressible and nonlinear viscoelastic materials that would be equivalent to the compressible finite deformation elasticity theory described above (eq. 39), but more complicated because of the need to develop an expansion of the time-dependent strain potential function as a series of multiple integrals (108,109). One such formalism is discussed briefly under Lustig, Shay and Caruthers Model. Here a simplified model that is based upon the K-BKZ framework with a VL-like kernel function (98) is examined.

One important issue in dealing with the nonlinear viscoelastic response of materials is the amount of data needed to determine the material parameters

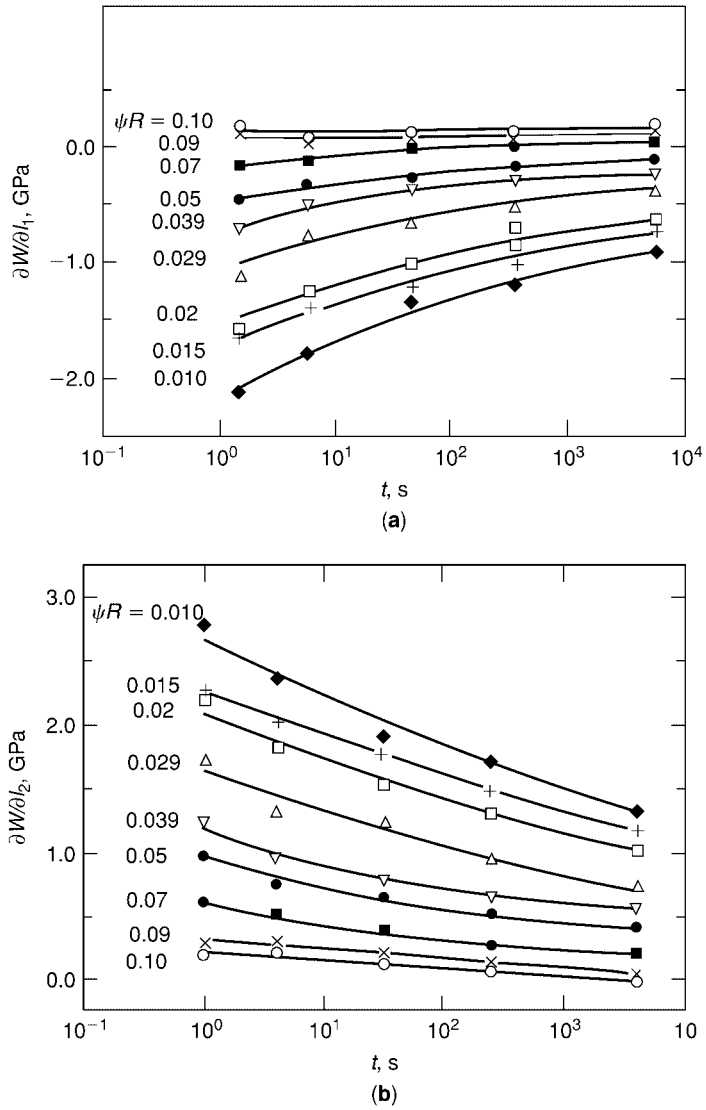

Fig. 56. Values of the time and strain-dependent strain energy function derivatives $\partial W/\partial I_1$ and $\partial W/\partial I_2$ for a glassy PMMA determined from torque and normal force measurements in single-step stress relaxation torsional experiments. After McKenna (114).

in the models. As noted above, even the general finite elasticity theory requires significant work to obtain the material parameters over the full three-dimensional deformation space. This is one reason that the VL framework is so attractive, when it works. Therefore, it is of interest to investigate whether or not the model can be extended to include compressibility. Pesce and McKenna (146) performed torsional tests on polycarbonate as described above. They then asked whether the VL function could be used to predict the tension and compression responses

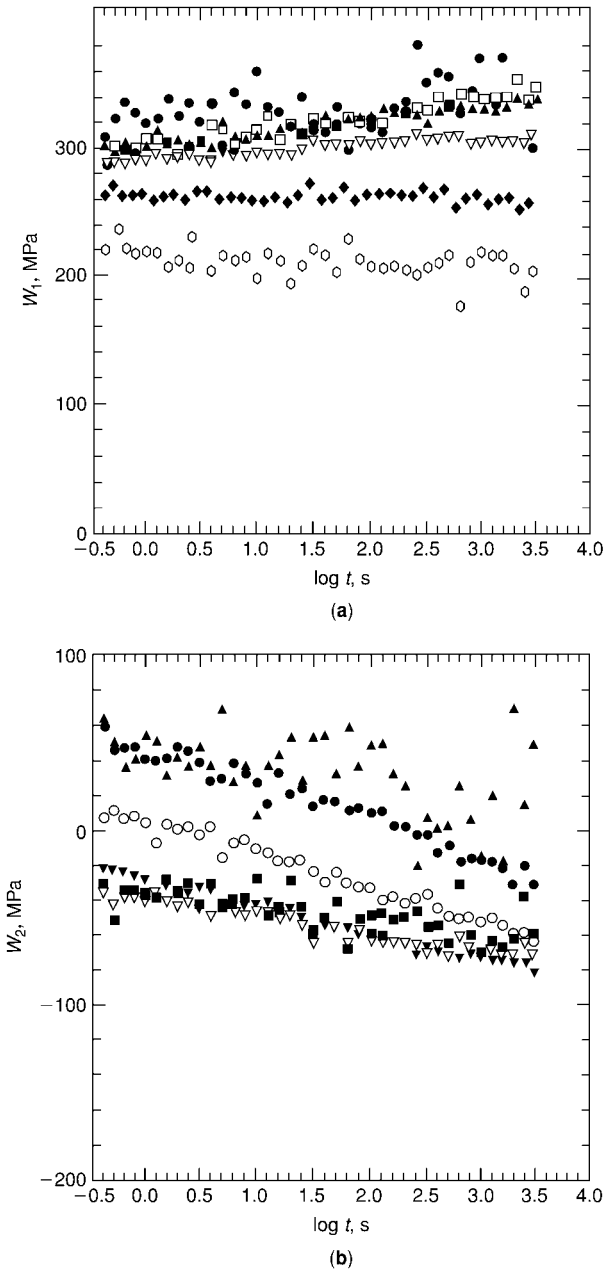

Fig. 57. Values of the time and strain-dependent strain energy function derivatives $W_1 = \partial W/\partial I_1$ and $W_2 = \partial W/\partial I_2$ for a glassy polycarbonate determined from torque and normal force measurements in single-step stress relaxation torsional experiments. (a) γ:● 0.017; □ 0.033; ▲ 0.050; ▽ 0.067;◇ 0.083; ○ 0.10. (b) γ: ▲ 0.017;● 0.033; ◦ 0.050; ▼ 0.067; ▽ 0.083; ■ 0.10. After Pesce and McKenna (146).

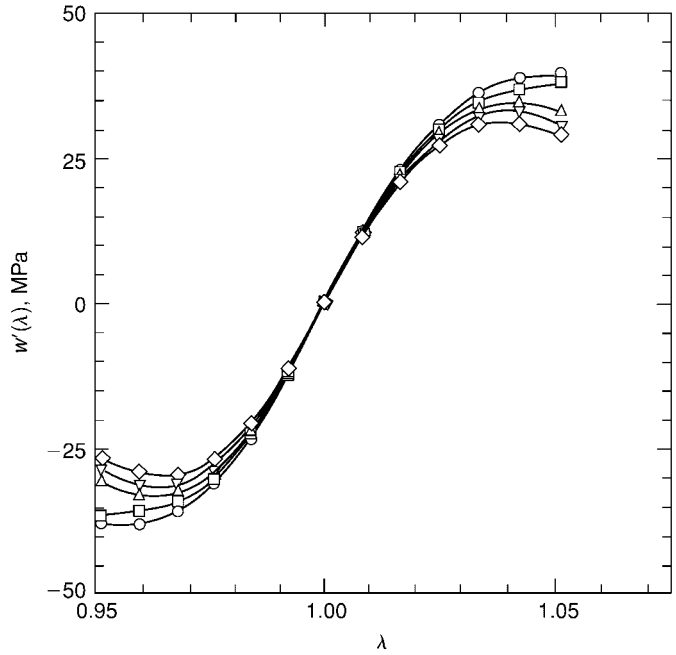

Fig. 58. The VL Valanis-Landel (98) function derivative as a function of deformation for polycarbonate as determined from data of Figures 55 and 57. ○ 0.3 s; □ 3.2 s; Δ 32 s; ∇ 320 s; ◇ 3000 s. After Pesce and McKenna (146).

of the material. An important assumption in their approach was that the VL function determined from the torsional measurements using equations 45, 46,47, 48, 49, 50, 51 (described immediately above) could be used to predict uniaxial data. When the incompressible equations 50 were applied to try to estimate the uniaxial stress-deformation data (isochronal), these equations did not work. However, upon considering the compressibility of the material good agreement with the data could be obtained. Taking, now, the strain energy density function [assumed to be separable as in the VL function (98)], one obtains

$$\hat{w}(\lambda_1,\lambda_2,\lambda_3) = w(\lambda_1) + w(\lambda_2) + w(\lambda_3) + f(\lambda_1\lambda_2\lambda_3) \tag{110}$$

where the volume $v = \lambda_1\lambda_2\lambda_3$ and the function $f(\lambda_1\lambda_2\lambda_3)$ represents the extra volume-dependent term beyond that incorporated implicitly in the principal stretches. Writing the constitutive equation for the principal stress (here the stress differences are not used), one obtains

$$\sigma_i = \frac{1}{\lambda_j\lambda_k}\left\{\frac{\partial\hat{w}}{\partial\lambda_i}\right\} \tag{111}$$

For a uniaxial deformation (extension or compression) in direction 1 and under normal ambient conditions (where $\sigma_2 = \sigma_3 \approx 0$) one can write

$$\sigma_1 = \frac{1}{\lambda_2\lambda_3}\left[\frac{\partial w}{\partial \lambda_1}\left(\frac{\partial f}{\partial v}\right)\left(\frac{\partial v}{\partial \lambda_1}\right)\right] \tag{112a}$$

$$\sigma_2 = \frac{1}{\lambda_1\lambda_3}\left[\frac{\partial w}{\partial \lambda_2} + \left(\frac{\partial f}{\partial v}\right)\left(\frac{\partial v}{\partial \lambda_2}\right)\right] \approx 0 \tag{112b}$$

Solution of equation 112b gives the relation

$$\left(\frac{1}{\lambda_1\lambda_3}\right)\left(\frac{\partial w}{\partial \lambda_2}\right) = -\frac{\partial f}{\partial v} \tag{113}$$

which when substituted into equation 112b gives the following expression for σ_1, which is similar to the equation for the principal stress differences for the incompressible material:

$$\sigma_1 = \frac{1}{\lambda_2\lambda_3} w'(\lambda_1) - \frac{1}{\lambda_1\lambda_3} w'(\lambda_2) \text{or} v\sigma_1 = \lambda_1\lambda_2\lambda_3\sigma_1 = \lambda_1 w'(\lambda_1) - \lambda_2 w'(\lambda_2) \tag{114}$$

Pesce and McKenna (140) applied equation 114 with the VL function obtained from torsional data and successfully described the uniaxial data for the same polycarbonate material to within approximately 15% up to the yield point (140). The results are shown in Figure 59. Importantly, the successful description required both a knowledge of $w'(\lambda)$ and the actual values of the lateral contraction of the material—the equivalent in the nonlinear range of the Poisson's effect in linear elasticity (or viscoelasticity).

Although the compressible VL function shows promise for the description of the response of glassy polymers in the nonlinear deformation regime, further work is required to establish the generality of the approach and how far it can be extended into the post-yield region.

Other Constitutive Model Descriptions. The above work describes a relatively simple way to think of nonlinear viscoelasticity, viz, as a sort of time-dependent elasticity. In solid polymers, it is important to consider compressibility issues that do not exist for the viscoelastic fluids discussed earlier. In this penultimate section of the article, other approaches to nonlinear viscoelasticity are discussed, hopefully not abandoning all simplicity. The development of nonlinear viscoelastic constitutive equations is a very sophisticated field that we will not even attempt to survey completely. One reason is that the most general constitutive equations that are of the multiple integral forms are cumbersome to use in practical applications. Also, the experimental task required to obtain the material parameters for the general constitutive models is fairly daunting. In addition, computationally, these can be difficult to handle, or are very CPU-time intensive. In the next sections, a class of single-integral nonlinear constitutive laws that are referred to as reduced time or material clock-type models is disscused. Where there has been some evaluation of the models, these are examined as well.

The fundamental concept of the material clock or reduced time is similar to the principle described above in the discussion of time–temperature superposition. In the mechanical constitutive models, however, the change in the stress or

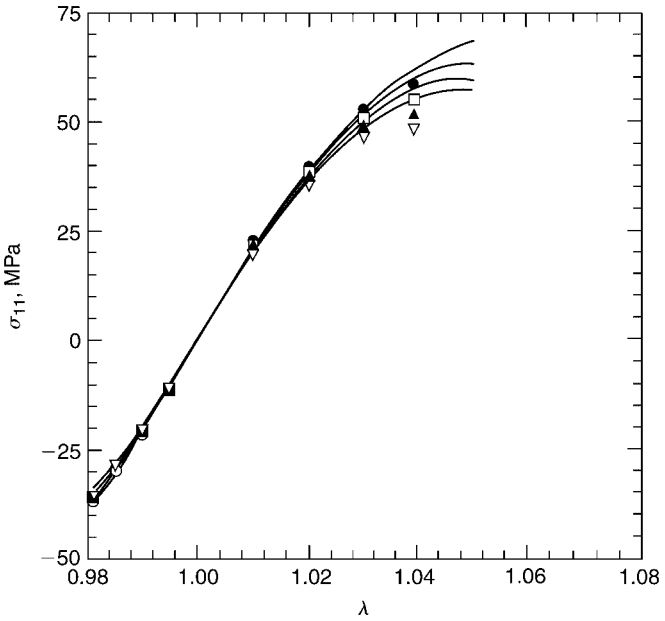

Fig. 59. Comparison between the experiment (points) and predictions (lines) from equation 114 for stress-deformation response of polycarbonate in uniaxial extension and compression.● 3.2 s; □ 32 s; ▲ 320 s; ▽ 3000 s. After Pesce and McKenna (146).

deformation induces a shift in the material relaxation time. The fact that the time depends on the state of stress (or strain) or on its history leads to additional nonlinearities in behavior from what is expected with, eg, the K-BKZ model. Physical explanations for the shifting material time are often based on free-volume ideas that are often invoked to explain time–temperature superposition. In addition, entropy changes have been invoked as have stress-activated processes.

The Schapery Model. One of the earliest models of the nonlinear viscoelastic response of polymers to use the concept of a reduced time is due to Schapery (147–149). The model is based on thermodynamic considerations and has a form similar to the Boltzmann superposition principal described previously. The model time dependences, except for the shift factors, are the same as those obtained in the linear response regime. Hence, the model is relatively easy to implement and to determine the relevant material parameters. It results in a generalization of the generalized superposition principal developed by Leaderman (150).

While the model can be formulated for three-dimensional stresses and strain states, here only the uniaxial deformation is dealt with. It is important to add that the model has both a creep formalism and a relaxation formalism. The relevant equations are presented in the next paragraphs. In addition, although this is a nonlinear theory, it is a small strain theory.

In creep experiments the equation is given as

$$\varepsilon(t) = g_0 D_0 \sigma + g_1 \int_0^t \Delta D(\psi - \psi') \frac{\mathrm{d}g_2\sigma}{\mathrm{d}t} \mathrm{d}t' \tag{115}$$

where D_0 is the zero time compliance, ΔD is the time-dependent part of the compliance, and the g_i's are material parameters. The material clock arguments are written as

$$\psi = \int_0^t \frac{\mathrm{d}\varsigma}{a_\sigma[\sigma(\varsigma)]} \quad \text{and} \quad \psi' = \int_0^{\mathrm{t}'} \frac{\mathrm{d}\varsigma}{a_\sigma[\sigma(\varsigma)]} \tag{116}$$

where a_σ is the stress shift factor.

A similar set of equations describes the stress relaxation behavior (stress as a function of strain):

$$\sigma(t) = h_\mathrm{e} E_e \varepsilon + h_1 \int \Delta E(\phi - \phi') \frac{\mathrm{d}h_2 \varepsilon}{\mathrm{d}t'} \mathrm{d}t' \tag{117}$$

Here E_e is the equilibrium modulus (infinite time modulus), ΔE is the time-dependent part of the model, and h_e and h_1 are material parameters. The reduced time arguments ϕ and ϕ' are written as

$$\phi = \int_0^t \frac{\mathrm{d}\varsigma}{a_\varepsilon[\varepsilon(\varsigma)]} \quad \text{and} \quad \phi' = \int_0^{t'} \frac{\mathrm{d}\varsigma}{a_\varepsilon[\varepsilon(\varsigma)]} \tag{118}$$

Here, note, that a_ε is the strain shift factor.

Figure 60 illustrates two-step creep and recovery data at different stresses for a reinforced polymer along with the predictions from the Schapery creep

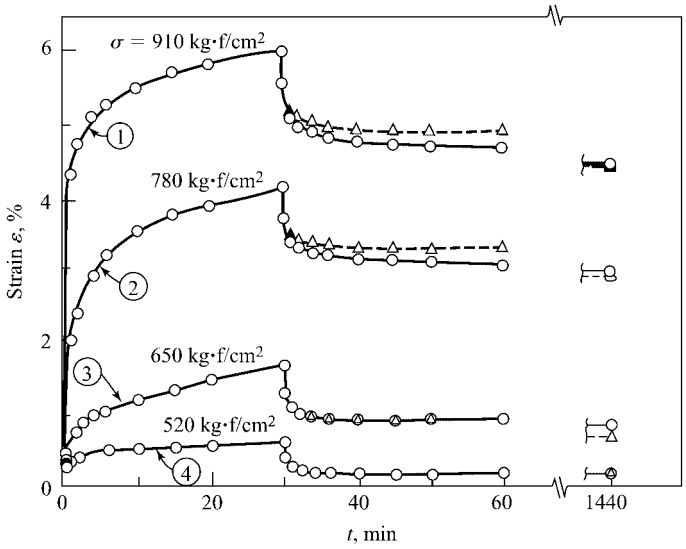

Fig. 60. Comparison of experimental (circles) creep and recovery behavior of a glass-reinforced phenolic resin with the predictions from the Schapery (147–149) nonlinear viscoelastic model. ○ Experimental Data; Δ Predicted Recovery Data (Nonlinear Theory). After Schapery (147), with permission.

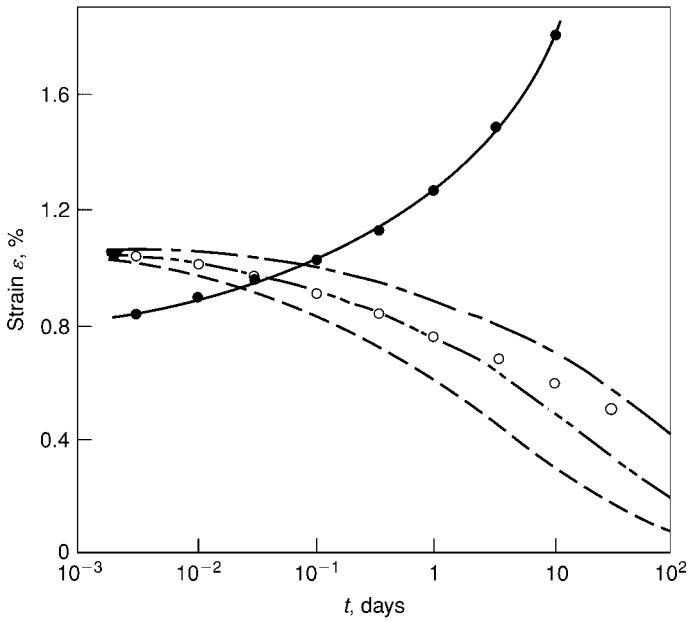

Fig. 61. Comparison of experimental (circles) creep and recovery behavior of a nitrocellulose material with the predictions from the Schapery (147–149) nonlinear viscoelastic model using different stress shift factors, as indicated. Exp. Creep Strain;—○— Exp. Recovery Strain; —— Case 1, $a_\sigma{}^{-1} = 1$;—-—Case 2, $a_\sigma{}^{-1} = 23.15$; —-Case 3, $a_\sigma{}^{-1} = 4.1$. After Schapery (147), with permission.

formulation and those obtained from simply applying a modified form of the Boltzmann superposition principle. Without going into the details of the procedures of obtaining all the parameters, it is clear that the model captures much of the observed nonlinear response, while the modified Boltzmann rule does not. (Note that the modified Boltzmann rule simply assumes additivity of responses, but without the linearity assumptions.) Figure 61 shows the creep and recovery data for a nitrocellulose film and with different values of the shift factor a_σ to try to describe the second (recovery) step. Here there is less of an agreement between the theory and the data, yet the trends are captured. In cases where materials, such as reinforced polymer matrix composites, exhibit strongly nonlinear behavior at very small strains, this set of models has been very useful (151–154). Also note that in certain deformation histories, the model can reduce to a K-BKZ type of expression and the data presented in Figure 34 was successfully described by the Schapery model (even though the deformations are fairly large).

The Zapas Strain-Clock Model and the Bernstein–Shokooh Stress-Clock Model. Although the K-BKZ theory has been highly successful, as discussed above, it also had some flaws, which lead to attempts to modify the model by incorporating material clock or reduced time concepts. In one form, Zapas introduced a strain-clock (118), ie, a change in the time scale that depended on the strain history. While the model is fully three-dimensional, for simplicity, consider

only the equations for the simple shearing case:

$$\sigma_{12}(t) = \int \{[\gamma(t) - \gamma(t')]G_*[\gamma(t) - \gamma(t'), \Phi(t,t')]\}\ \Phi\ [\gamma(t), \gamma(t'), t - t']\mathrm{d}t' \tag{119}$$

and the material time $\Phi(t, t')$ is written as

$$\Phi(t,t') = \Phi[\gamma(t), \gamma(t'), t - t'] = \int \Phi\ [\gamma(t), \gamma(\xi), t - \xi]\mathrm{d}t' \tag{120}$$

The strain-clock term (eq. 120) is a function of the entire deformation history. McKenna and Zapas used the strain-clock formalism to describe the torsional response of a PMMA material in two-step strain histories (112). The difficulty arises because the determination of material parameters requires at least the data for both the first and second step responses. Furthermore, McKenna and Zapas also assumed that the clock-form for the torque response and for the normal force response was the same. Their results were consistent with this assumption, as shown in Figure 62. However, that work also indicates that considerable experimental data are required to use the model—a constant issue in nonlinear viscoelasticity. One other interesting thing that came from the work of McKenna and Zapas (112–114) was the verification of equation 60 for the normal force. This is seen in Figure 63, where the normal force response after the half-step history is plotted against the duration of the first step for two different isochrones. As seen, for times beyond 1677 s and for both short and long isochrones, the response is both independent of the duration of the first step and the same as if the material had

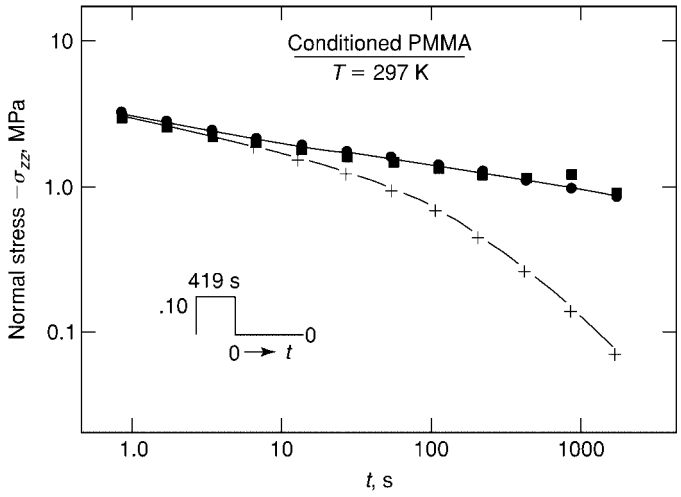

Fig. 62. Normal force response in "step to zero" type of deformation history for a PMMA polymer glass, showing the comparison between the experimental data (filled squares), the K-BKZ model predictions (crosses), and the predictions (filled circles) from the Zapas strain-clock model (118). Note that the clock terms for the normal force response were determined by fitting the shear stress response in the same experiment. After McKenna and Zapas (112).

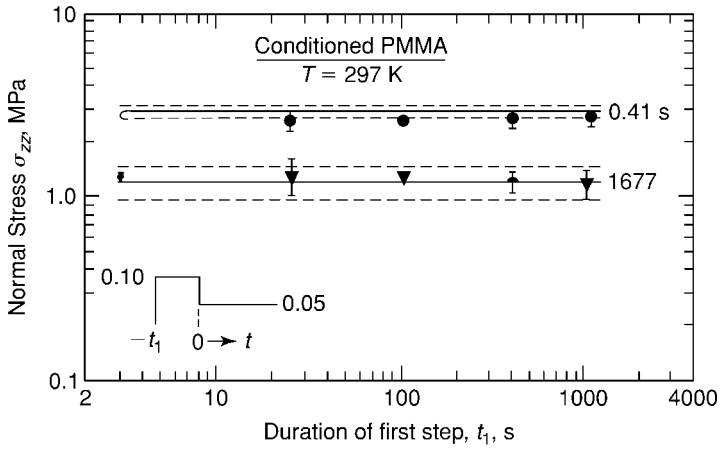

Fig. 63. "Half-step" normal force response in a PMMA polymer glass, showing that the normal force response is independent of the duration t_1 of the first step. Points are data from the second step response for $\gamma = 0.05$ after a step to $\gamma = 0.10$. Lines are data from a single-step experiment at $\gamma = 0.05$. (Solid lines: mean; dashed lines: single standard deviation). Time values of 0.41 and 1677 s are isochronal values after the imposition of the step in the deformation. After McKenna and Zapas (113).

been subjected to a step only to γ_2. The other point of import here is that, while the normal stress is following equation 60, the shear response is dramatically different. In fact, the strain-clock model fits the data, but the "reversing stress" nature of the deformation leads to a similar deviation from K-BKZ-type behavior as was seen in the polymer solution. This is shown in Figure 64. The reader is also reminded that polymer solutions seem to follow this response only at long times ($t > \tau_k$).

While the strain-clock version of the K-BKZ model seems capable of describing fairly complex nonlinear behavior, it is, at least, an inconvenient model to use. The stress-clock model of Bernstein and Shokool (155) has two features that could make it very useful. It takes less data to determine the material properties (under certain conditions) and, in the relatively small deformation regime, it can be inverted between creep and stress relaxation.

The equations in simple shear can be written as

$$\sigma_{12}(t) = \int_{-\infty}^{t} \{G_*[\gamma(t) - \gamma(t'), \beta(t,t')] b_\sigma(t')\} \mathrm{d}t' \tag{121}$$

where b_σ is the stress shift factor. The reduced time $\beta(t, t')$ is written as

$$\beta(t,t') = \int_{t'}^{t} b_\sigma(s) \mathrm{d}s \tag{122}$$

An interesting aspect of the Bernstein–Shokooh model is that the structure of the nonlinear equations is somewhat different from either the Schapery model or the Zapas strain-clock model. In the Bernstein–Shokooh model, the

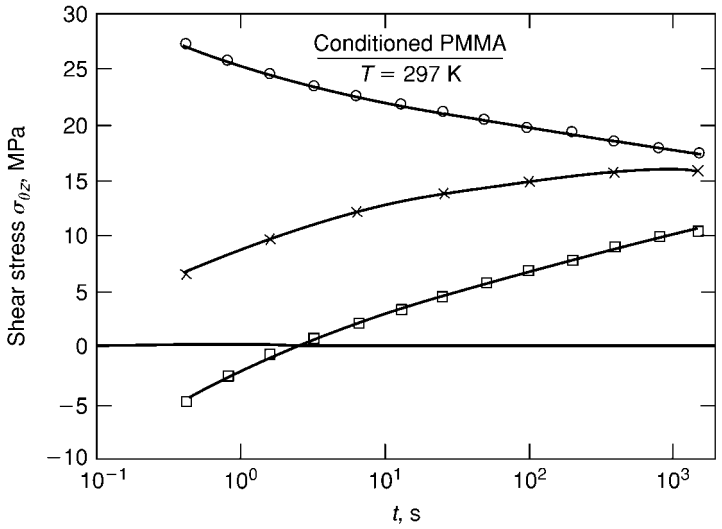

Fig. 64. "Half-step" shear stress response for a PMMA glass. Circles represent single-step stress relaxation response at $\gamma = 0.05$; crosses, K-BKZ prediction; and open squares, experimental data for second step of $\gamma = 0.05$ after a first step of $\gamma = 0.10$ having a duration $t_1 = 419$ s. After McKenna (114).

nonlinearity is set up by having the stress response to a deformation history depend also on the stress through the stress shift factor b_σ. Hence, in equation 121 there are stress terms on both sides of the equation. For the other models, including those discussed subsequently, the stresses or deformations are isolated on either side of the equation. For example, in the Schapery stress relaxation formulation (eq. 117) the stress depends on the strain and a strain-dependent material clock. Examination of equations 115 and 119 provides a similar type of conclusion for the Schapery creep formulation or the K-BKZ strain-clock equation. Hence, one might expect that the stress-clock formulation of Bernstein and Shokooh might capture a different sort of material nonlinearity from the other models. To this author's knowledge, the only other set of equations that provides a similar type of nonlinear response comes in the field of *structural recovery or physical aging* of glassy materials. The so-called Tool–Narayanaswamy–Moynihan and Kovacs–Aklonis–Hutchinson–Ramos models have been very successful to describe the kinetics of structural recovery. (The reader is referred to the relevant literature for further examination of these equations (156–160). See also AGING, PHYSICAL).

There has been relatively little testing of the Bernstein–Shokooh model. Penn did some work to describe the nonlinear response of aluminum, but this, however, was not published (161). Pesce and McKenna did some two-step stress relaxation experiments in torsion (162) using polycarbonate as the material. The results, one of which is shown in Figure 65, indicated that the model is better than the K-BKZ model, but does not perfectly describe the material response for polycarbonate.

The Knauss–Emri Model. There have been several works in the literature in which volume- or *free-volume*-dependent clocks were used to describe the

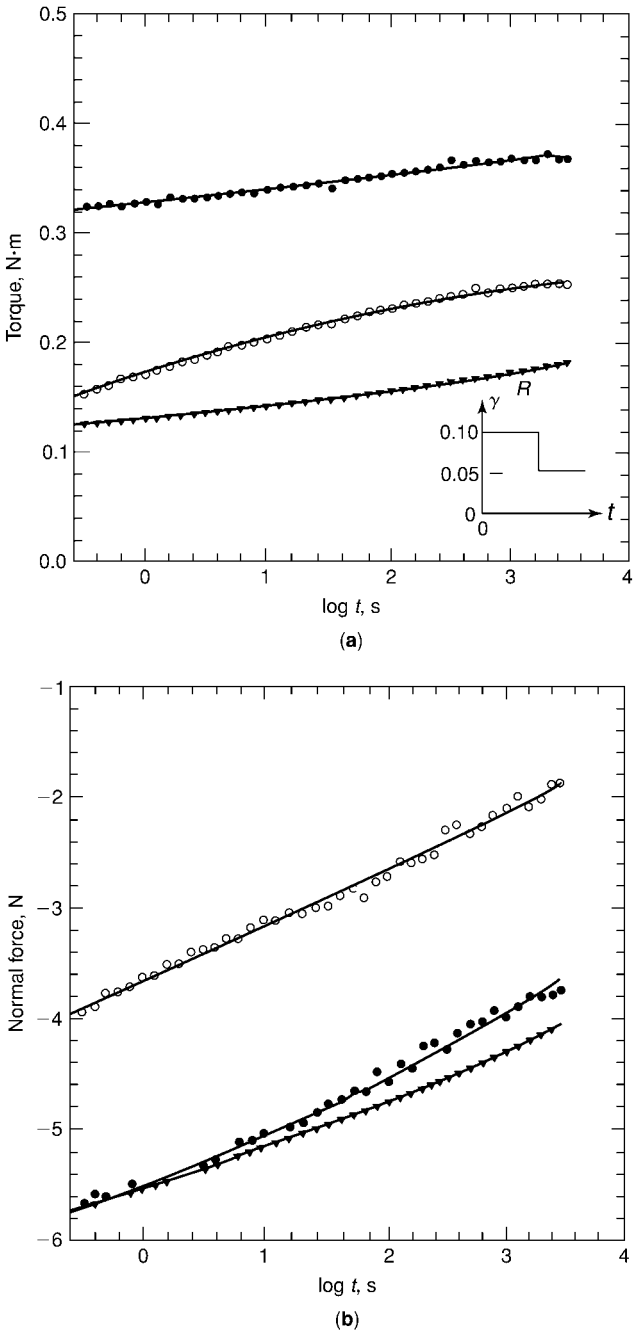

Fig. 65. "Half-step" torque (**a**) and normal force (**b**) responses for a polycarbonate glass comparing the experimental data (open circles) with the K-BKZ equation (closed circles) and the Bernstein–Shokooh stress-clock model (155) modified to an energy clock (inverted triangles) predictions. After Pesce and McKenna (162).

nonlinear viscoelastic response of polymeric glasses. The chief success among these is the Knauss–Emri model (163) in which the reduced time was defined in terms of a shift factor that depended on temperature, stress, and concentration of small molecules in such a way that the responses depended on the free volume induced by each of these parameters. For an isothermal single phase and homogeneous material, the equations are

$$\begin{aligned} S_{ij} &= 2\int_{-\infty}^{t} G(Z - Z')\frac{\partial \varepsilon_{ij}}{\partial t'}\mathrm{d}t' \\ \kappa_{ii} &= 3\int_{-\infty}^{t} K(Z - Z')\frac{\partial \varepsilon_{\mathrm{v}}}{\partial t'}\mathrm{d}t' \end{aligned} \tag{123}$$

where Z is the reduced time, S_{ij} are the deviatoric stresses, κ_{ii} is the first stress invariant, $G(t)$ and $K(t)$ are material functions, and ε_v is the dilatational strain. The dilatational strain is related to the bulk creep compliance $M(t)$ and determines the reduced time as

$$\begin{aligned} Z(t) - Z(t') &= \int_{\mathrm{t}'}^{t} = \frac{\mathrm{d}s}{\phi[\varepsilon_v(s)]} \\ \varepsilon_v(t) &= \frac{M(t)^* \mathrm{d}\kappa_{kk}}{3} \end{aligned} \tag{124}$$

where the asterisk denotes a Stieltjes convolution operation.

The Knauss–Emri model captures some of the nonlinear stress relaxation response of materials and looks like linear viscoelasticity in the reduced time variables, and hence is relatively straightforward to implement. However, the observation that material nonlinearities occur in shearing deformations as well as in compression, where the free-volume mechanisms predict decreasing mobility suggest that the model is limited in its usefulness (164,165).

The Lustig–Shay–Caruthers Model. In the past several years there has been a serious effort at the Purdue University School of Chemical Engineering under the direction of J.M. Caruthers (166–170) to adapt one such formalism to the problem of glassy materials. The formalism is that of Rational Mechanics (171) or Rational Thermodynamics, and here the Caruthers group's contributions in this area are examined briefly.

The thermoviscoelastic model is an extension of the original ideas of Coleman (171) and Noll (109) for a nonequilibrium thermodynamics referred to in the literature as *rational mechanics* or *rational thermodynamics*. Historically this approach has been controversial for a variety of reasons beyond the scope of this article. However, one very important issue in the development and uses of the rational mechanics framework has been the need to deal with multiple integral expansions of the relevant response functions and the inherent complexity that arrives in dealing with such representations. The advantage of Lustig–Shay–and Caruthers model (170) is its ability to truncate the multiple integrals and arrive at single integral representations of the material behavior. This leads to a very attractive and tractable set of equations for describing the material response. Because the single integral forms are of themselves insufficient to describe the

observed nonlinear response of glass-forming materials, a reduced time much as used in the models presented above, that depends on the configurational entropy has been introduced (170). Hence, one starts with the assumption that there exists a free energy potential functional that is time-dependent. Appropriate differentiation of the functional results in volume, enthalpy, and mechanical responses that contain sufficient information to predict strongly nonlinear behavior from laboratory determined linear viscoelastic response functions.

The detailed development that is followed is beyond the scope of this article. Here simply note that they followed a rigorous approach, beginning with a representation of the time-dependent "free energy" function $\Psi(t)$ and through appropriate simplifications and differentiations arrived at a set of equations for the entropy and stress as functions of the thermal and mechanical histories. The fluid form of the model through, single integral terms, is given by the following equations for the stress and entropy. Significantly, note that an important aspect of the model is that all the material parameters are related to response functions obtained from linear viscoelastic measurements, PVT measurements, and heat capacity measurements:

Stress:

$$\begin{aligned} T(t) = &- P^{(\infty)} I + \frac{\rho}{\rho_{\mathrm{R}}} \int_{-\infty}^{t} G_{\Delta}[I_3(t), \theta(t), t^* - \xi^*][\frac{\mathrm{d}C_t(\xi)}{\mathrm{d}\xi} - \frac{1}{3} I \frac{\mathrm{d}I_{t1}(\xi)}{\mathrm{d}\xi}]\mathrm{d}\xi \\ &+ \frac{\rho}{\rho_R} I \int_{-\infty}^{t} \frac{1}{2} K_{\Delta}[I_3(t), \theta(t), t^* - \xi^*] \frac{\mathrm{d}I_{t1}(\xi)}{\mathrm{d}\xi} \mathrm{d}\xi \\ &+ \frac{\rho}{\rho_{\mathrm{R}}} I \int_{-\infty}^{t} 2\rho_{\mathrm{R}} A_{\Delta}[I_3(t), \theta(t), t^* - \xi^*] \frac{\mathrm{d}\theta(\xi)}{\mathrm{d}\xi} \mathrm{d}\xi \end{aligned} \tag{125}$$

$$\begin{aligned} \eta(t) = \eta^{(\infty)}[I_3(t), \theta(t)] &- \int_{-\infty}^{t} A_{\Delta}[I_3(t), \theta(t), t^* - \xi^*] \frac{\mathrm{d}I_{t1}(\xi)}{\mathrm{d}\xi} \mathrm{d}\xi \\ &- \int_{-\infty}^{t} 2C_{\Delta}[I_3(t), \theta(t), t^* - \xi^*] \frac{\mathrm{d}\theta(\xi)}{\mathrm{d}\xi} \mathrm{d}\xi \end{aligned} \tag{126}$$

where P is the pressure and η is the entropy. The superscript ∞ implies the equilibrium value. ρ is the density and ρ_{R} is its value in the undeformed, reference state. I is the identity tensor, I_3 is the third absolute strain invariant of the deformation tensor (related to the volume change), $C_t(\tau)$ is the relative right Cauchy–Green strain tensor, and $I_{t1}(\tau)$ is the first relative strain invariant of $C_t(\tau)$. Note that in the Caruther's group the notation is that θ is the absolute temperature. The K_{Δ} term is the relaxation function for the bulk modulus, G_{Δ} is the shear modulus relaxation function, A_{Δ} is a constant volume thermal stress function, and C_{Δ} is the constant volume heat capacity divided by temperature. Finally, the reduced time $t*$ is defined by

$$t^* = \int_0^t \frac{\mathrm{d}\xi}{a(\xi)} \tag{127}$$

where $a(\xi)$ is a generalized shift factor that is taken to depend on the configurational entropy following the Adam–Gibbs (172) relationship:

$$\log a = M\left[\frac{1}{\eta_c \theta} - \frac{1}{\eta_{cr}\theta_r}\right] \tag{128}$$

where M is a constant, η_c and η_{cr} are the configurational entropy in the current and reference states respectively, and θ and θ_r are the temperature and reference temperature respectively. The configurational entropy can be calculated from the experimental heat capacity data, assuming that it is approximately equal to the total. The reader is referred to McWilliams (169) for further discussion. Also, note that Hodge (160) has discussed this form of shift factor in the Tool–Narayanaswamy-Moynihan equations for enthalpy recovery.

The Lustig–Shay–Caruthers model has, to date, been primarily used to estimate volume and enthalpy responses in glassy materials (see AGING, PHYSICAL)—a subset of the viscoelastic behaviors seen in solid-like or glassy polymers and not covered in this article. However, recent work between the Purdue group and Sandia National Laboratories (173) has made great strides in implementing the model into finite element codes as well as defining limits on the forms of some of the functions. The model, when finally published, will require full evaluation. At this point, the current author thinks that it will be an important contribution to the understanding of the nonlinear viscoelastic behavior of polymeric glasses.

Plasticity and Viscoplasticity and Other Models. As discussed above, the alternative representation of the nonlinear viscoelastic response of polymers is that of plasticity and viscoplasticity. In some respects, these models could be recast as viscoelastic models and they would be equivalent to some of the models discussed above. However, the perspective that glassy polymers are really fluids and do follow time–temperature superposition is lost with these models. Hence, the physical interpretation of material parameters, in this author's opinion, becomes very questionable. Therefore, only references to the major papers on polymer plasticity and viscoplasticity are given (174–177).

In addition, there are other viscoelastic models that are not dealt with here. Again, the references are provided for the reader's information (178–184).

BIBLIOGRAPHY

"Viscoelasticity" in *EPST* 1st ed., Vol. 14, pp. 670–717, by J. D. Ferry, University of Wisconsin; "Viscoelasticity" in *EPSE* 2nd ed., Vol. 17, pp. 587–665, by F. R. Schwarzl, University of Erlangen – Nürnberg.

1. W. Weber, Ueber die Elasticität der Seidenfäden *Pogg. Ann. Physik.* **4**, 247–257 (1835).
2. R. Kohlrausch, Theorie des Elektrischen Rückstandes in der Leidener Flasche *Annalen der Physik und Chemie von J. C. Poggendorff* **91**, 179–214 (1854); F. Kohlrausch, Ueber die elastische Nachwirkung bei der Torsion *Annalen der Physik und Chemie von J. C. Poggendorff* **119**, 337–369 (1863).
3. L. Boltzmann, Zur Theorie der Elastischen Nachwirkung *Sitzungsber. Akad. Wiss. Wien. Mathem.-Naturwiss. Kl.* **70**, 275–300 (1874).
4. H. Markovitz, Boltzmann and the Beginnings of Linear Viscoelasticity *Trans. Soc. Rheol.* **21**, 381–398 (1977).

5. E. N. da C. Andrade, A Theory of the Viscosity of Liquids. Part I *Phil. Mag.* **17**, 497–511 (1934); E. N. da C. Andrade, A Theory of the Viscosity of Liquids. Part II *Phil. Mag.* **17**, 698–732 (1934).
6. C. Zener, *Elasticity and Anelasticity of Metals*, University of Chicago Press, Chicago, 1948.
7. R. A. Schapery, in G. P. Sendeckyj, ed., *Composite Materials*, Vol. **2**: *Mechanics of Composite Materials* Academic Press, Inc., New York, 1974, Chapt. "4", pp. 85–168.
8. S. P. Timoshenko and J. N. Goodier, *Theory of Elasticity*, 3rd ed., McGraw-Hill, New York, 1970.
9. J. D. Ferry, *Viscoelastic Properties of Polymers*, 3rd ed., John Wiley and Sons, Inc., New York, 1980.
10. N. W. Tschoegl, *The Phenomenological Theory of Linear Viscoelastic Behavior*, Springer Verlag, Berlin, 1989.
11. A. J. Staverman and F. Schwarzl, in H. A. Stuart, ed., *Die Physik der Hochpolymeren. Vierter Band. Theorie und Molekulare Deutung Technologischer Eigenschaften von Hochpolymeren Werkstoffen*, Springer-Verlag, Berlin, 1956, Chapt. "1", pp. 1–125 (In English).
12. H. Leaderman, in F. R. Eirich, ed. *Rheology, Vol. 2: Theory and Applications*, Academic Press, Inc., New York, 1958, pp. 1–62.
13. S. L. Rosen, *Fundamental Principles of Polymeric Materials*, 2nd ed., Wiley-Interscience, New York, 1993.
14. H. H. Winter, Analysis of Dynamic Mechanical Data-Inversion into a Relaxation-Time Spectrum and Consistency Check *J. Non-Newt. Fl. Mech.* **68**, 225–239 (1997).
15. D. W. Mead, Determinations of Molecular Weight Distributions of Linear Flexible Polymers from Linear Viscoelastic Material Functions *J. Rheol.* **38**, 1797–1827 (1994).
16. G. A. Carri and H. H. Winter, Mapping of the Relaxation Patterns of Polymer Melts with Linear Flexible Molecules of Uniform Length *Rheol. Acta* **36**, 330–344 (1997).
17. M. Baumgaertel and H. H. Winter, Interrelation Between Continuous and Discrete Relaxation-Time Spectra *J. Non-Newt. Fl. Mech.* **44**, 15–36 (1992).
18. W. H. Tuminello, Molecular Weight Distributions of Tetrafluoroethylene-Hexafluoropropylene Copolymers *Polym. Eng. Sci.* **29**, 645–653 (1989).
19. S. W. Park and R. A. Schapery, Methods of Interconversion between Linear Viscoelastic material Functions. Part. I.–A Numerical Method Based on Prony Series *Int. J. Solids and Struct.* **36**, 1653–1675 (1999).
20. D. J. Plazek, Don't Cry for Me Charlie Brown or with Compliance Comes Comprehension *J. Rheol.* **44**, 831–841 (2000).
21. W. N. Findley, J. S. Lai, and K. Onaran, *Creep and Relaxation of Nonlinear Viscoelastic Materials with an Introduction to Linear Viscoelasticity*, North Holland, New York, 1976.
22. A. S. Wineman and K. R. Rajagopal, *Mechanical Response of Polymers*, Cambridge University Press, New York, 2000.
23. E. H. Lee, Stress Analysis in Viscoelastic Bodies *Quart. Appl. Math.* **13**, 183 (1955).
24. R. A. Schapery, Approximate Methods of Transform Inversion for Viscoelastic Stress Analysis in *Proc. 4th Int. Cong. Appl. Mech.*, Vol. 2, ASME, New York, 1962, p. 1075.
25. A. V. Tobolsky, *Properties and Structure of Polymers*, John Wiley and Sons, Inc., New York, 1967.
26. T. Fujimoto, M. Ozaki, and M. Nagasawa, Stress Relaxation of Monodisperse Poly-α-methylstyrene *J. Polym. Sci., Part A-2* **6**, 129–140 (1968).
27. H. Vogel, Das Temperaaturabhängigkeitsgesetz der Viskosität Flüssigkeiten *Phys. Z.* **22**, 645–646 (1921).

28. G. S. Fulcher, Analysis of Recent Measurements of the Viscosity of Glasses *J. Am. Ceram. Soc.* **8**, 339–355 (1925).
29. M. L. Williams, R. F. Landel, and J. D. Ferry, The Temperature Dependence of Relaxation Mechanisms in Amorphous Polymers and Other Glass-forming Liquids *J. Am. Chem. Soc.* **77**, 3701–3706 (1955).
30. D. J. Plazek, X. D. Zheng, and K. L. Ngai, Viscoelastic Properties of Amorphous Polymers. 1 Different Temperature Dependences of Segmental Relaxation and Terminal Dispersion *Macromolecules* **25**, 4920–4924 (1992).
31. P. G. Santangelo and C. M. Roland, Temperature Dependence of Mechanical and Dielectric-Relaxation in Cis-1,4-Polyisoprene *Macromolecules* **31**, 3715–3719 (1998).
32. R. Zorn, G. B. McKenna, L. Willner, D. Richter, Rheological Investigations on Polybutadienes with Different Microstructures over a Large Temperature Range *Macromolecules* **28**, 8552–8562 (1995).
33. J.-J. Pesce, J. M. Niemiec, M. Y. Chiang, C. L. Schutte, C. R. Schultheisz, and G. B. McKenna in M. Negahban, ed., Characterization of Polymers in the Glass Transition Range: Time-Temperature and Time-Aging Time Superposition in Polycarbonate in *Current Research in the Thermo-Mechanics of Polymers in the Rubbery–Glassy Range*, American Society of Mechanical Engineers, New York, AMD-Vol. **203**, 1995, pp. 77–88.
34. H. G. Merriman and J. M. Caruthers, Nonlinear Stress Relaxation of a Styrene-Butadiene Random Copolymer *J. Polym. Sci., Polym. Phys. Ed.* **19**, 1055–1071 (1981).
35. P. A. O'Connell and G. B. McKenna, Large Deformation Response of Polycarbonate: Time-Temperature, Time-Aging Time and Time Strain Superposition *Polym. Eng. Sci.* **37**, 1485–1495 (1997).
36. G. W. Scherer, *Relaxation in Glass and Composites*, Krieger Publishing Co., Malabar, Fla., 1992.
37. C. A. Angell K. L. Ngai, G. B. McKenna, P. F. McMilllan and S. W. Martin, Relaxation in Glassforming Liquids and Amorphous Solids *J. Appl. Phys.* **88**, 3113–3157 (2000).
38. A. J. Kovacs, Transition Vitreuse dans les Polyméres Amorphes. Etude Phénoménologique *Fortschritte der Hochpolymeren-Forschung* **3**, 394–507 (1963).
39. G. B. McKenna, in C. Booth and C. Price, eds., *Comprehensive Polymer Science, Vol. 2: Polymer Properties*, Pergamon Press, Oxford, 1989, pp. 311–362.
40. L. C. E. Struik, *Physical Aging in Polymers and Other Amorphous Materials*, Elsevier, Amsterdam, 1976.
41. L. P. Chen, A. F. Yee, and E. J. Moskala, The Molecular Basis for the Relationship Between the Secondary Relaxation and Mechanical Properties of a Series of Polyester Copolymer Glasses *Macromolecules* **32**, 5944–5955 (1999).
42. W. C. Child Jr. and J. D. Ferry, Dynamic Mechanical Properties of Poly-n-Butyl Methacrylate *J. Colloid. Sci.* **12**, 327–341 (1957).
43. A. K. Rizos, L. Petihakis, K. L. Nagi, J. H. Wu, and A. F. Yee, A Dielectric-Relaxation Study of the Gamma-Relaxation in Tetramethylbisphenol-A Polyearbonate Plasticized by Tris(2-Ethylhexyl) Phosphate *Macromolecules* **32**, 7921–7924 (1999).
44. J. Heijboer, in J. A. Prins, ed., *Physics of Non-Crystalline Solids*, North-Holland, Amsterdam, 1965, pp. 231–254.
45. M. L. Cerrada and G. B. McKenna, Stress Relaxation of Poly(ethylene Naphthalate): Isothermal, Isochronal and Isostructural Responses *Macromolecules* **33**, 3065–3076 (2000).
46. L. R. G. Treloar, *The Physics of Rubber Elasticity*, 3rd ed., Clarendon Press, Oxford, 1975.
47. J. P. Cohen Addad, ed., *Physical Properties of Polymeric Gels*, John Wiley and Sons, Inc., New York, 1996.
48. F. Horkay and G. B. McKenna, in J. E. Mark, ed., *Physical Properties of Polymers Handbook*, AIP Press, Woodbury, N. Y., 1996, pp. 379–400.

49. J. E. Mark and B. Erman, ed., *Elastomeric Polymer Networks*, Prentice Hall, Englewood Cliffs, N. J., 1992.
50. G. B. McKenna and J. A. Hinkley, Mechanical and Swelling Behavior of Well Characterized Polybutadiene Networks *Polymer* **27**, 1368–1376 (1986).
51. P. G. de Gennes, Reptation of a Polymer Chain in the Presence of Fixed Obstacles *J. Chem. Phys.* **55**, 572–579 (1971).
52. M. Doi and S. F. Edwards, Dynamics of Concentrated Polymer Systems Part 1. Brownian Motion in the Equilibrium State *J. Chem. Soc., Faraday Trans. 2* **74**, 1789–1801 (1978).
53. M. Doi and S. F. Edwards, Dynamics of Concentrated Polymer Systems Part 2.–Molecular Motion under Flow *J. Chem. Soc., Faraday Trans. 2* **74**, 1802–1817 (1978).
54. M. Doi and S. F. Edwards, Dynamics of Concentrated Polymer Systems Part 3.–The Constitutive Equation *J. Chem. Soc., Faraday Trans. 2* **74**, 1818–1832 (1978).
55. M. Doi and S. F. Edwards, Dynamics of Concentrated Polymer Systems Part 4,–Rheological Properties *J. Chem. Soc. Faraday Trans. 2* **75**, 38–54 (1979).
56. M. Doi and S. F. Edwards, *The Theory of Polymer Dynamics*, Oxford Science Publishers, Oxford, 1986.
57. G. C. Berry and T. G. Fox, The Viscosity of Polymers and Their Concentrated Solutions *Adv. Polym. Sci.* **5**, 261–357 (1968).
58. M. Doi and N. Y. Kuzuu, Rheology of Star Polymers in Concentrated Solutions and Melts *J. Polym. Sci., Polym. Lett. Ed.* **18**, 775–780 (1980).
59. W. W. Graessley, Entangled Linear, Branched and Network Polymer Systems *Adv. Polym. Sci.* **47**, 68–117 (1982).
60. M. Doi, Explanation for the 3.4 Power Law for Viscosity of Polymeric Liquids on the Basis of the Tube Model *J. Polym. Sci., Polym. Lett. Ed.* **19**, 265–273 (1981).
61. R. G. Larson, *The Structure and Rheology of Complex Fluids*, Oxford University Press, New York, 1999.
62. R. G. Larson, *Constitutive Equations for Polymer Melts and Solutions*, Butterworths, London, 1988.
63. H. Watanabe, Viscoelasticity and Dynamics of Entangled Polymers *Prog. Polym. Sci.* **24**, 1253–1403 (1999).
64. W. W. Graessley, The Entanglement Concept in Polymer Rheology *Adv. Polym. Sci.* **16**, 1–179, (1974).
65. R. H. Colby, L. J. Fetters, and W. W. Graessley, Melt Viscosity-Molecular Weight Relationship for Linear Polymers *Macromolecules* **20**, 2226–2237 (1987).
66. W. G. Knauss and V. H. Kenner, On the Hygrothermal Characterization of Polyvinyl Acetate *J. Appl. Phys.* **51**, 5131–5136 (1980).
67. T. W. Dewitt, H. Markovitz, F. J. Padden, Jr., and L. J. Zapas, Concentration Dependence of the Rheological Behavior of the Polyisobutylene-Decalin System *J. Colloid Sci.* **10**, 174–188 (1955).
68. R. W. Rendell, K. L. Ngai, and G. B. McKenna, Molecular Weight and Concentration Dependences of the Terminal Relaxation Time and Viscosity of Entangled Polymer Solutions *Macromolecules* **20**, 2250–2256 (1987).
69. C. W. Macosko, *Rheology: Principles, Measurements, and Applications*, VCH Publishers, New York, 1994.
70. B. Bernstein, E. A. Kearsley, and L. I. Zapas, A Study of Stress Relaxation with Finite Strain *Trans. Soc. Rheol.* **7**, 391–410 (1963).
71. A. Kaye, Non-Newtonian Flow in Incompressible Fluids. Part I. A General Rheological Equation of State, Note No. 134, College of Aeronautics, Cranfield, 1962, pp. 1–4.
72. B. Bernstein, Time Dependent Behavior of an Incompressible Elastic Fluid. Some Homogeneous Deformation Histories *Acta Mech.* **2**, 329–354 (1966).

73. W. W. Graessley, R. L. Hazleton, and L. R. Lindeman, The Shear Rate Dependence of Viscosity in Concentrated Solutions of Narrow Distribution Polystyrene *Trans. Soc. Rheol.* **11**, 267–285 (1967).
74. S. L. Rosen, *Fundamental Principles of Polymeric Materials*, 2nd ed., Wiley-Interscience, New York, 1993 pp. 252–253.
75. H. C. Tseng, C. A. Heiber, K. K. Wang, H. H. Chiang, and G. E. Grant, Analysis of Rheological Data from an Automated Injection-Molding Capillary Rheometer in ANTEC '85, Society of Plastics Engineers, 1985, pp. 716–719.
76. D. M. Best, *Prediction of Polymer Melt Processing Behavior*, Thesis, Carnegie Institute of Technology (now Carnegie Mellon Institution), 1969.
77. H. Münstedt, Dependence of the Elongational Behavior of Polystyrene Melts on Molecular Weight and Molecular Weight Distribution *J. Rheol.* **24**, 847–867 (1980).
78. C. M. Vrentas and W. W. Graessley, Study of Shear Stress Relaxation in Well-Characterized Polymer Liquids *J. Rheol.* **26**, 359–371 (1982).
79. G. B. McKenna and L. J. Zapas, The Superposition of Small Deformations on Large Deformations: Measurements of the Incremental Modulus for a Polyisobutylene Solution *J. Polym. Sci., Polym. Phys. Ed.* **23**, 1647–1656 (1985).
80. K. Osaki, N. Bessho, T. Kojimoto, and M. Kurata, Experimental Tests of a Few Constitutive Models for Polymer Solutions Based on Birefringence Data in Time-Dependent Fields *J. Rheol.* **24**, 125–144 (1980).
81. L. J. Zapas and J. C. Phillips, Nonlinear Behavior o Polyisobutylene Solutions as a Function of Concentration *J. Rheol.* **25**, 405–420 (1981).
82. R. I. Tanner, From A to (BK)Z in Constitutive Relations *J. Rheol.* **32**, 673–702 (1988).
83. D. C. Leigh, *Nonlinear Continuum Mechanics*, McGraw-Hill, New York, 1968.
84. W. Prager, *An Introduction to Mechanics of Continua*, Ginn and Co., Boston, 1961.
85. O. H. Varga, *Stress–Strain Behavior of Elastic Materials. Selected Problems of Large Deformation*, wiley-Interscience, New York, 1966.
86. A. S. Lodge, *An Introduction to Elastomer Molecular Theory*, Bannatek Press, Madison, Wis., 1999.
87. M. Mooney, A Theory of Large Elastic Deformation *J. Appl. Phys.* **11**, 582–592 (1940).
88. R. S. Rivlin, Large Elastic Deformations of Isotropic Materials. I. Fundametal Concepts *Phil. Trans. R. Soc. London, Ser. A*, **240**, 459–525 (1948).
89. W. H. Han, F. Horkay, and G. B. McKenna, Mechanical and Swelling Behaviors of Rubber: A Comparison of Some Molecular Models with Experiment *Math. Mech. Solids* **4**, 139–167 (1999).
90. R. S. Rivlin and D. W. Saunders, Large Elastic Deformations of Isotropic Materials. VII. Experiments on the Deformation of Rubber *Phil. Trans. R. Soc. London, Ser. A* **243**, 251 (1951).
91. H. Pak and P. J. Flory, Relationship of Stress to Uniaxial Strain in Corsslinked Poly(dimethyl siloxane) over the Full Range from Large Compression to High Elongation *J. Polym. Sci., Polym. Phys. Ed.* **17**, 1845 (1979).
92. M. Gottlieb and R. J. Gaylord, Experimental Tests of Entanglement Models of Rubber Elasticity: 1. Uniaxial Tension Compression *Polymer* 1644–1646 (1982).
93. M. Gottlieb and R. J. Gaylord, Experimental Tests of Entanglement Models of Rubber Elasticity: 2. Swelling *Macromolecules* **17**, 2024–2030 (1984).
94. R. W. Penn and E. A. Kearsley, The Scaling Law for Finite Torsion of Elastic Cylinders *Trans. Soc. Rheol.* **20**, 227–238 (1976).
95. J. H. Poynting, On the Changes in he Dimensions of a Steel Wire when Twisted, and on the Pressure of Distortional Waves in Steel *Proc. R. Soc. London, Ser. A* **86**, 534–561 (1912).
96. G. B. McKenna and L. J. Zapas, Experiments on the Small Strain Behavior of Crosslinked Natural Rubber. Part I. Torsion *Polymer* **24**, 1495–1501 (1983).

97. E. A. Kearsley and L. J. Zapas, Some Methods of Measurement of an Elastic Strain Energy Function of the Valanis–Landel Type *J. Rheol.* **24**, 483–500 (1980).
98. K. C. Valanis and R. F. Landel, A Strain Energy Function of a Hyperelastic Material in Terms of the Extension Ratios *J. Appl. Phys.* **38**, 2997–3002 (1967).
99. H. Vangerko and L. R. G. Treloar, The Inflation and Extension of Rubber Tube for Biaxial Strain Studies *J. Phys. D: Appl. Phys.* **11**, 1969–1978 (1978).
100. D. G. Jones and L. R. G. Treloar, The Properties of Rubber in Pure Homogeneous Strain *J. Phys. D: Appl. Phys.* **8** 1285–1304 (1975).
101. J. Glucklich and R. F. Landel, Strain Energy Function of Styrene Butadiene Rubber and the Effect of Temperature *J. Polym. Sci.* **15**, 2185–2199 (1978).
102. G. B. McKenna, K. M. Flynn, and Y.-H. Chen, Experiments on the elasticity of Dry and Swollen Networks: Implications for the Frenkel Flory-Rehner Hypothesis *Macromolecules* **22**, 4507–4512 (1989).
103. R. W. Ogden, Large deformation Isotropic Elasticity–On the Correlation of Theory and Experiment for Incopressible Rubberlike Solids *Proc. R. Soc. London, Ser. A* **326**, 565–584 (1972).
104. E. H. Twizell and R. W. Ogden, Non-Linear Optimization of the Material Constants in Ogden's Stress Deformation Function for Incompressible Isotropic Elastic Materials *J. Austral. Math. Soc., Ser. B* **24**, 424–434 (1983).
105. G. Karami, H. Zohari, and E. Setoudeh, Stress Disribution Change in Bias Tires Due to Changes in Cord Angle–A Finite Element Analysis *Kautsh. Gummi Kunstst.* **51**, 450–454 (1998).
106. G. L. Bradley, P. C. Chang, and G. B. McKenna, Rubber Modeling Using Uniaxial Test Data *J. Appl. Polym. Sci.*, in press.
107. R. I. Tanner, *Rheology: An Historical Perspective*, Elsevier, Amsterdam, 1998.
108. B. D. Coleman, Thermodynamics of Materials with Memory *Arch. Ration. Mech. Anal.* **17**, 1–46 (1964).
109. W. Noll, A Mathematical Theory of the Mechanical Behavior of Continuous Media *Arch. Ration. Mech. Anal.* **2**, 197–226 (1958).
110. V. Rouiller and G. B. McKenna, *Society of Plastics Engineers, in ANTEC '98*, Vol. II, 1998, pp. 2138–2143.
111. L. J. Zapas and T. Craft, Correlation of Large Longitudinal Deformations with Different Strain Histories *J. Res. Natl. Bur. Stand. (U.S.)* **69A**, 541–546 (1965).
112. G. B. McKenna and L. J. Zapas, Nonlinear Viscoclastic Behavior of Poly(methyl methacrylate) in Torsion *J. Rheol.* **23**, 151–166 (1979).
113. G. B. McKenna and L. J. Zapas, The Normal Stress Response in Nonlinear Viscoelastic Materials-Some Experimental Findings *J. Rheol.* **24**, 367–377 (1980).
114. G. B. McKenna, in K. L. Ngai and G. B. Wright, eds., Measurement of the Torque and Normal Force in Torsion in the Study of the Thermoviscoelastic Properties of Polymer Glasses in *Relaxations in Complex Systems*, U.S. Government Printing Office, NTIS, Springfield, Virginia, 1985, pp. 129–144.
115. D. C. Venerus and H. Kahvand, Doi Edwards Theory Evaluation in Double-Step Strain Flows *J. Polym. Sci., Part B: Polym. Phys.* **32**, 1531–1542 (1994).
116. D. C. Venerus and H. Kahvand, Normal Stress Relaxation in Reversing Double Step Strain Flows *J. Rheol.* **38**, 1297–1315 (1994).
117. D. C. Venerus, E. F. Brown, and W. R. Burghardt, The Nonlinear Response of a Polydisperse Polymer Solution to Step Strain Deformations *Macromolecules* **31**, 9206–9212 (1998).
118. L. J. Zapas, in H. H. Kausch, J. A. Hassell, and R. I. Jaffee, eds., Nonlinear Behavior of Polyisobutylene Solutions in *Deformation and Fracture of High Polymers*, Plenum, New York, 1974, pp. 381–395.

119. M. H. Wagner and J. Schaeffer, Assessment of Nonlinear Strain Measures for Extensional and Shearing Flows of Polymer Melts *Rheol. Acta* **33**, 506–516 (1994).
120. P. E. Rouse, A Theory of the Linear Viscoelastic Properties of Dilute Solutions of Coiling Polymers *J. Chem. Phys.* **21**, 1272–1980 (1953).
121. T. C. B. McLeish, in M. E. Cates and M. R. Evans, eds., Rheology o Linear and Branched Polymers in *Soft and Fragile Matter. Nonequilibrium Dynamics, Metastability and Flow*, Institue of Physics, London, 2000, pp. 79–111.
122. G. B. McKenna, B. J. Hostetter, A. Hadjichristides, L. J. Fetters and D. J. Plazek, A Study of the Linear Viscoelastic Properties of Cyclic Polystyrenes Using Creep and Recovery Measurements *Macromolecules* **22**, 1834–1852 (1989).
123. K. Osaki, K. Nishizawa, and M. Kurata, Material Time Constant Characterizing the Nonlinear Viscoelasticity o Entangled Polymer Systems *Macromolecules* **15**, 1068–1071 1982,
124. A. S. Lodge and J. Meissner, On the Use of Instantaneous Strains, Superposed on Shear and Elongational Flows of Polymeric Liquids, to Test the Gaussian Network Hypothesis and to Estimate Segment Concentration and its Variation During Flow *Rheol. Acta.* **11**, 351–352 (1972).
125. M. H. Wagner and J. Schaeffer, Nonlinear Strain Measures for General Biaxial Extension of Polymer Melts *J. Rheol.* **36**, 1–27 (1992).
126. J. des Cloiseaux, Double Reptation vs. Simple Reptation in Polymer Melts *Europhys. Lett.* **5**, 437–442 (1988).
127. S. T. Milner, Relating the Shear-Thinning Curve to the Molecular Weight Distribution in Linear Polymer Melts *J. Rheol.* **40**, 305–315 (1996).
128. C. Tsenoglou, Molecular Weight Polydispersity Effects on the Viscoelasticity of Entangled Linear-Polymers *Macromolecules* **24**, 1762–1767 (1991).
129. K. Osaki, S. Kimura, and M. Kurata, Relaxation of Shear and Normal Stresses in Step-Shear Deformation of a Polystyrene Solution. Comparison with the Predictions of the Doi–Edwards Theory *J. Polym. Sci., Polym. Phys. Ed.* **19**, 517–527 (1981).
130. K. Osaki and M. Kurata, Experimental Appraisal of the Doi–Edwards Theory for Polymer Rheology Based on the Data for Polystyrene Solutions *Macromolecules* **13**, 671–676 (1980).
131. K. Osaki, Y. Einaga, M. Kurata, N. Yamada, and M. Tamura, Stress Relaxation of Polymer Solutions under Large Strain: Application of Double-Step Strain *Polym. J.* **5**, 283–287 (1973).
132. K. Osaki and M. Kurata, Stress Relaxation of a Polymer Solution in Double-Step Shear Deformations: A Separate Evaluation of the Stress Components due to Entangled Segments of Different Orientations *J. Polym. Sci., Polym. Phys. Ed.* **20**, 623–632 (1982).
133. Y. Einaga, K. Osaki, M. Kurata, S. Kimura, and M. Tamura, Stress Relaxation of Polymer Solutions under Large Strain *Polym. J.* **2**, 550–552 (1971).
134. E. F. Brown and W. R. Burghardt, First and Second Normal Stress Difference Relaxation in Reversing Double-Step Strain Flows *J. Rheol.* **40**, 37–54 (1996).
135. E. F. Brown, W. R. Burghardt, H. Kahvand, and D. C. Venerus, Comparsion of Optical and Mechanical Measurements of Second Normal Stress Difference Relaxation Following Step-Strain *Rheol. Acta* **34**, 221–234 (1995).
136. K. Osaki, H. Watanabe, and T. Inoue, Damping Function of the Shear Relaxation Modulus and the Chain Retraction Process of Entangled Polymers *Macromolecules* **29**, 3611–3614 (1996).
137. M. H. Wagner and J. Schaeffer, Rubbers and Polymer Melts: Universal Aspects of Nonlinear Stress-Strain Relations *J. Rheol.* **37**, 643–661 (1993).

138. K. Osaki, S. Kimura, and M. Kurata, Relaxation of Shear and Normal Stresses in Double-Step Shear Deformations. A Test of the Doi–Edwards Theory for Polymer Rheology *J. Rheol.* **25**, 549–562 (1981).
139. Z. Bartczak, A. S. Argon, and R. E. Cohen, Deformation Mechanisms and Plastic Resistance in Single-Crystal-Textured High Density Polyethylene *Macromolecules* **25**, 5036–5053 (1992).
140. N. W. Brooks, M. Ghazali, R. A. Duckett, R. A. Unwin, and I. M. Ward, Effects of Morphology on the Yield Stress of Polyethylene *Polymer* **40**, 821–825 (1999).
141. N. W. J. Brooks, R. A. Duckett, and I. M. Ward, Modeling of Double Yield Points in Polyethylene Temperature and Strain Rate Dependence *J. Rheol.* **39**, 425–436 (1995).
142. P. A. O'Connell and G. B. McKenna, Arrhenius-type Temperature Dependence of the Segmental Relaxation below T_g *J. Chem. Phys.* **110**, 11054–11060 (1999).
143. R. S. Duran and G. B. McKenna, A Torsional Dilatometer for Volume Change Measurements on Deformed Glasses: Instrument Description and Measurements on Equilibrated Glasses *J. Rheol.* **34**, 813–839 (1990).
144. T. T. Wang, H. M. Zupko, L. A. Wyndon, and S. Matsuoka, Dimensional and Volumetric Changes in Cylindrical Rods of Polymers Subjected to a Twist Moment *Polymer* **23**, 1407–1409 (1982).
145. R. Pixa, V. LeDû, and C. Wippler, Dilatometric Study of Deformation Induced Volume Increase and Recovery in Rigid PVC *Colloid Polym. Sci.* **266**, 913–920 (1988).
146. J.-J. Pesce and G. B. McKenna, Prediction of the Sub-Yield Extension and Compression Responses of Glassy Polycarbonate from Torsional Measurements *J. Rheol.* **41**, 929–942 (1997).
147. R. A. Schapery, On the Characterization of Nonlinear Viscoelastic Materials *Polym. Eng. Sci.* **9**, 295–310 (1969).
148. R. A. Schapery, A Theory of Nonlinear Thermoviscoelasticity Based on Irreversible Thermodynamics *Proc. 5th U.S. National Congress of Applied Mechanics*, ASME, New York, 1966, pp. 511–530.
149. R. A. Schapery, Further Development of a Thermodynamic Constitutive Theory: Stress Formulation, Report AA & ES 69–72, Purdue University, Lafayette, Ind., 1969.
150. H. Leaderman, *Elastic and Creep Properties of Filamentous Materials and Other High Polymers*, The Textile Foundation, Washington, D.C., 1943.
151. G. C. Papanicolaou, S. P. Zaoutsos, and A. H. Cardon, Prediction of the Nonlinear Viscoelastic Response of Unidirectional Fiber Composites *Compos. Sci. Technol.* **59**, 1311–1319 (1999).
152. M. E. Tuttle and H. F. Brinson, Prediction of the Long-Term Creep Compliance of General Composite Laminates *Exp. Mech.* **26**, 89–109 (1986).
153. H. Poon and M. F. Ahmad, A Finite-Element Constitutive Update Scheme for Anisotropic Viscoelastic Solids Exhibiting Nonlinearity of the Schapery Type *Int. J. Numer. Methods Eng.* **46**, 2027–2041 (1999).
154. R. A. Schapery, Nonlinear Viscoelastic Solids *Int. J. Solids Struct.* **37**, 359–366 (2000).
155. B. Bernstein and A. Shokooh, The Stress Function in Viscoelasticity *J. Rheol.* **24**, 189–211 (1980).
156. A. Q. Tool, Relation Between Inelastic Deformability and Thermal Expansion of Glass in Its Annealing Range *J. Am. Ceram. Soc.* **29**, 240–253 (1946); A. Q. Tool, Viscosity and the Extraordinary Heat Effects in Glass *J. Res. Natl. Bur. Stand. (U.S.)* **37**, 73–90 (1946).
157. O. S. Narayanaswamy, A Model of Structural Relaxation in Glass *J. Am. Ceram. Soc.* **54**, 491–498 (1971).
158. C. T. Moynihan, P. B. Macedo, C. J. Montrose, P. K. Gupta, M. A. DeBolt, J. F. Dill, B. E. Dom, P. W. Drake, A. J. Esteal, P. B. Elterman, R. P. Moeller, H. Sasabe, and J. A.

Wilder, Structural Relaxation in Vitreous Materials *Ann. N.Y. Acad. Sci.* **279**, 15–35 (1976).
159. A. J. Kovacs, J. J. Aklonis, J. M. Hutchinson, and A. R. Ramos, Isobaric Volume and Enthalpy Recovery of Glasses. II. A Transparent Multiparameter Model *J. Polym. Sci., Polym. Phys. Ed.* **17**, 1097–1162 (1979).
160. I. M. Hodge, Enthalpy Relaxation and Recovery in Amorphous Materials *J. Non-Cryst. Solids* **169**, 211–266 (1984).
161. R. W. Penn, *National Bureau of Standards, unpublished*.
162. J. J. Pesce and G. B. McKenna, in M. C. Boyce, ed., *Mechanics of Plastics and Plastic Composites vols. MD–68 and AMD–215, 1995*, ASME, New York, pp 309–336 1995.
163. W. G. Knauss and I. J. Emri, Nonlinear Viscoelasticity Based on Free Volume Consideration *Comput. Struct.* **13**, 123–128 (1981).
164. G. B. McKenna, On the Physics Required for the Prediction of Long Term Performance of Polymers and Their Composites *J. Res. NIST* **99**, 169–189 (1994).
165. H. Lu and W. G. Knauss, The Role of Dilatation in the Nonlinearly Viscoelastic Behavior of Pmma under Multiaxial Stress States *Mech. Time-Dependent Matls.* **2**, 307–334 (1999).
166. J. M. Caruthers, Ph.D. Dissertations, School of Chemical Engineering, Purdue University, Lafayette, Ind.
167. S. R. Lustig, *A Continuum Thermodynamics Theory for Transport in Polymer/Fluid Systems*, Ph.D. Dissertation, School of Chemical Engineering, Purdue University, Lafayette, Ind., 1989.
168. D. M. Colucci, *The Effect of Temperature and Deformation on the Relaxation Behavior in the Glass Transition Region*, Ph.D. Dissertation, School of Chemical Engineering, Purdue University, Lafayette, Ind., 1995.
169. D. S. McWilliams, *Study of the Effect of Thermal History on the Structural Relaxation and Thermoviscoelasticity of Amorphous Polymers*, Ph.D. Dissertation, School of Chemical Engineering, Purdue University, Lafayette, Ind., 1996.
170. S. R. Lustig, R. M. Shay, and J. M. Caruthers, Thermodynamic Constitutive Equations for Materials with Memory on a Material Time Scale *J. Rheol.* **40**, 69–106 (1996).
171. B. D. Coleman, On Thermodynamics, Strain Impulses, and Viscoelasticity *Arch. Ration. Mech. Anal.* **17**, 230–254 (1964).
172. G. Adam and J. H. Gibbs, On the Temperature Dependence of Cooperative Relaxation Properties in Glass Forming Liquids *J. Chem. Phys.* **43**, 139–146 (1965).
173. J. M. Caruthers, *Purdue University and D. B. Adolf and R. S. Chambers of Sandia National Laboratories, unpublished*.
174. E. M. Arruda and M. C. Boyce, Evolution of Plastic Anisotropy in Amorphous Polymers during Finite Straining *Int. J. Plast.* **9**, 697 (1993).
175. C. G'Sell and J. J. Jonas, Yield and Transient Effects During the plastic Deformation of Solid Polymers *J. Mater. Sci.* **16**, 1956–1974 (1981); C. G'Sell, H. El Baril, J. Perez, J. Y. Cavaillé and G. P. Johari, Cavaillé and G.P. Johari, Effect of Plastic Deformation on the Microstructure and Properties of Amorphous Polycarbonate *Mater. Sci. Eng., A* **110**, 223–229 (1989).
176. E. Oleynik, S. N. Rudnev, O. B. Salamatina, and V. A. Topolkaraev, Stressed Polymer Glasses-Formation, Microstructure and Properties of Local Plastic Transformations *Makromol. Chem. Macromol. Symp.* **53**, 77–80 (1992).
177. M. C. Boyce, D. M. Parks, and A. S. Argon, Large Inelastic Deformation of Glassy Polymers, Part 1: Rate-Dependent Constitute Model *Mech. Mater.* **7**, 15–33 (1988).
178. T. A. Tervoort, E. T. J. Klompen, and L. E. Govaert, A Multi-Mode Approach to Finite, Three Dimensional, Nonlinear Viscoelastic Behavior of Polymer Glasses *J. Rheol.* **40**, 779–797 (1996).

179. A. I. Leonov, Nonequilibrium thermodynamics and rheology of viscoelastic polymer media *Rheol. Acta* **15**, 85–98 (1976).
180. E. Krempl and K. Ho, in R. A. Schapery, ed., An Overstress Model for Solid Polymer Deformation-Behavior Applied to Nylon-66 in *Time Dependent and Nonlinear Effects in Polymers and Composites*, ASTM STP-**1357**, W Conshohocken: American Society Testing and Materials (Series: American Society for Testing and Materials Special Technical Publication, Vol **1357**) 2000, pp. 118–137.
181. W. K. Waldron and A. S. Wineman, Shear and Normal Stress Effects in Finite Circular Shear of a Compressible Non-linear Viscoelastic Solid *Int. J. Nonlinear Mech.* **31**, 345–369 (1996).
182. K. S. Cho and S. Y. Kim, A Thermodynamic theory on the Nonlinear Viscoelasticity of Glassy Polymers, 1. Constitutive Equation *Macromol. Theory Simul.* **9**, 328–335 (2000).
183. Z. P. Bazant and C. Huet, Thermodynamic Functions for Ageing Viscoelasticity: Integral Form without Internal Variables **36**, 3993–4016 (1999).
184. A. Drozdov, On Constitutive Laws for Aging Viscoelastic Materials at Finite Strains *Eur. J. Mech. A—Solids* **12**, 305–324 (1993).

GREGORY B. MCKENNA
Texas Tech University

WEATHERING

Introduction

The resistance of polymeric materials to weathering is a very important factor in their use in outdoor applications that depend on their durability. *Weathering* of a polymeric material may be defined as irreversible changes in its chemical and physical properties in a direction which is usually to the detriment of its usefulness. Changes in appearance and mechanical properties result from modification of the chemical structure of the material by its complex interaction with the environmental elements, primarily solar radiation, heat/cold, moisture (solid, liquid, and vapor), oxygen, and pollutants. Although all weather factors play a very important role in the deteriorating effect of the environment on polymeric materials, the actinic radiation of the sun is the critical factor because it initiates the reactions that lead to degradation. Testing the weatherability of polymeric materials is an essential step in development of new and improved products and in ascertaining that production lots meet the specified requirements. Most polymeric products require stabilization against the effects of the environment to obtain reasonable serviceability. In some applications, weatherability tests are carried out to assure that the materials degrade rapidly after their intended use in order to protect the environment.

The destructive effect of the weather varies with geographic location, season, time of day, cloud cover, and exposure orientation because of variations in the critical weather factors with these conditions. Different weather conditions can also be encountered in individual years. Therefore, outdoor tests in one location during a specific time interval cannot be expected to provide information on either absolute durabilities or stability rankings of materials under various service conditions. Tests are commonly carried out in environments that have the most

Encyclopedia of Polymer Science and Technology. Copyright John Wiley & Sons, Inc. All rights reserved.

severe conditions, such as subtropical or desert climates, in order to determine resistance to the worst conditions. As a result of the progressive improvement over the years in the durability of polymeric materials for outdoor applications, it is now impractical in many cases to screen potential new formulations by standard outdoor weathering tests, even those that provide severe environmental conditions. Therefore, accelerated outdoor weathering techniques and laboratory accelerated tests simulating the effects of natural weathering are required for development of weatherable formulations as well as for quality control and specification tests. Laboratory tests have the advantage of allowing control of the three main test parameters, ie, radiation, heat, and moisture, for more consistent stability evaluations and for research studies on the effect of these parameters. Development of valid laboratory accelerated tests requires measurement of the critical weather factors in the end-use environment and determination of their effects on the polymeric materials.

Weather Factors and Their Effect on Polymeric Materials

Solar Radiation. Solar radiation on the earth's surface consists of energy received both directly from the solid angle of the sun's disk and diffusely reflected by the atmosphere. The diffuse component is strongly influenced by atmospheric conditions and is generally a large fraction of the total radiation, particularly in the uv region because of the greater scattering of the shorter wavelengths (1). For this reason, the spectral power distribution (SPD) of the diffuse component differs from that of the solar beam in that it contains a higher intensity of short wavelength radiation. Thus, the type of exposure that materials receive depends on their orientation. Samples positioned for maximum direct beam exposure receive less short wavelength radiation than those positioned for maximum exposure to sky radiation.

The hemispherical (direct plus diffuse) solar spectral irradiance incident on a 37°-tilted surface facing the equator at an air mass of 1.5 and turbidity of 0.27, which is representative of average conditions in the 48 contiguous states of the United States, is shown in Figure 1 (2). It is referred to as "U.S. Standard

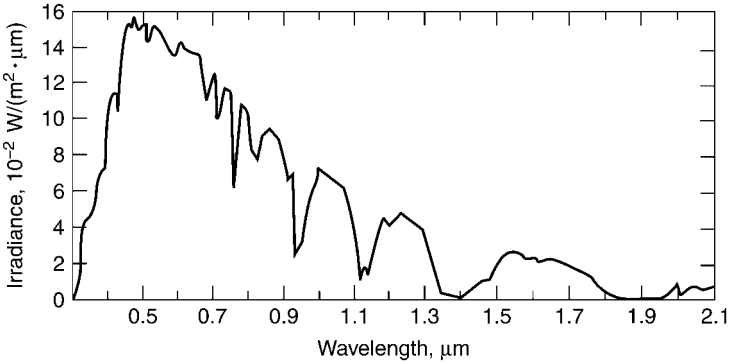

Fig. 1. Hemispherical solar spectral irradiance incident on a 37°-tilted surface facing the equator (air mass 1.5, albedo 0.2, turbidity 0.27, ozone 3.4 mm, precipitable water 14.2 mm). Based on data in Table 1 of ASTM G159-98 2. Courtesy of the American Society for Testing and Materials.

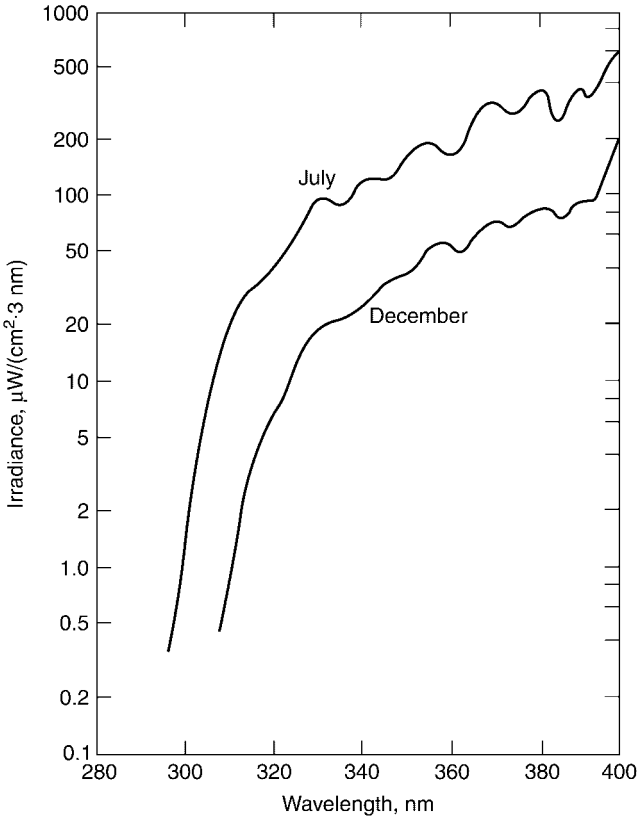

Fig. 2. Seasonal variation of direct normal solar uv spectral irradiance at 41° north latitude at noon under clear sky conditions 3. Courtesy of the American Institute of Physics.

Atmosphere." The spectral energy ranges from about 298 nm in the uv region to about 2500 nm in the near-infrared (nir) region. Both the quantity and quality of solar radiation vary with time of day, season, altitude, geographical location, and atmospheric conditions. The shorter the wavelength, the more sensitive it is to these variables. Thus, the uv portion (298–400 nm), the portion that has the largest actinic effect on most materials, varies from less than 1% to about 5% of total solar radiation. The seasonal effect of the angle of the sun on the uv SPD of direct normal solar radiation is shown in Figure 2 (3). At 41° north latitude, the short wavelength cut-on shifts from below 300 nm in the summer to about 310 nm in the winter. At all latitudes, the altitude of the sun, and thus total solar irradiance, is highest at solar noon.

Because of the small percentage of uv present in the full solar spectrum, changes in this important component cannot be detected in measurements of total solar radiation. Therefore, commercial outdoor testing facilities measure and monitor the irradiance of the uv portion alone, both total uv and narrow spectral bands of the uv, in addition to total solar radiation. Total solar uv radiation (TUVR) is typically measured between 295 and 385 nm. Irradiance is reported in watts/square meter (W/m^2) and radiant exposure, ie, irradiance integrated over time, is reported in megajoules/square meter (MJ/m^2). The average 12-month

TUVR radiant exposure is reported to be 308 MJ/m^2 at a 5° angle in a subtropical climate and 333 MJ/m^2 at latitude angle in a desert climate (4).

Spectral Effects of Solar Radiation: Activation Spectra. It is generally an accepted fact that uv radiation has a greater deteriorating effect than visible radiation on most polymeric materials. Since only radiation absorbed by a material can cause damage, and colorless materials do not absorb visible radiation, they are degraded solely by uv radiation. However, colored polymeric materials, which absorb in both the uv and visible regions, are generally degraded more severely by the uv portion of solar radiation. Dissociation of chemical bonds, a prerequisite to the chemical reactions that result in changes in appearance and mechanical properties, depends on the energies of the photons absorbed in relation to the energies of the chemical bonds. Because uv radiation has higher energy photons, it is capable of breaking stronger and more types of bonds. However, all wavelengths, whether in the uv or visible region, are not equally destructive. Degradation is wavelength specific because both absorption of radiation and its capability of breaking chemical bonds vary with wavelength. Generally, the shorter the wavelength, the more strongly it is absorbed by polymeric materials and the higher the energy of the photons. The amount of energy absorbed as a function of wavelength depends on the relative intensities of the incident wavelengths and on the absorption properties of the material.

The wavelength sensitivity of a material to a specific light source, referred to as its activation spectrum, depends on the spectral absorption properties of the material, the spectral emission properties of the light source, and the quantum efficiencies of degradation by the absorbed wavelengths. It is a graphical representation of the relative damage caused by individual spectral regions of the radiation source. The activation spectrum must be determined experimentally since quantum efficiencies cannot be predicted from fundamental principles. It generally does not equate with the spectral energy absorbed by a material. Two main techniques have been used to obtain activation spectra. One is based on the effects of narrow bands of the radiation from a polychromatic source isolated by using either interference filters or a spectrograph. The other is based on the use of uv/visible transmitting sharp cut-on glass filters to define the effects of individual spectral regions of the source while the material is exposed to all wavelengths longer than the cut-on of the filter. The techniques and the applications of activation spectra to stabilization and stability testing of polymeric materials are described and illustrated by examples in the *Handbook of Polymer Degradation*, 2nd ed. (5), and other publications (6–9).

Data obtained by both techniques on the same polymeric materials exposed to borosilicate-glass-filtered xenon arc radiation are shown in Table 1. The materials are unstabilized, commercial types. The spectral regions of the source that cause the largest change in the measured properties of the materials are listed in the column labelled "Max. Change." Although many of the samples used for the two techniques were manufactured at different times and therefore were not identical, the activation spectra are in relatively good agreement. Except for materials showing sensitivity to xenon arc radiation shorter than 300 nm, solar radiation can be expected to produce similar activation spectra based on comparable data obtained for some of the materials (5). The data show the wide range of spectral sensitivities of the different polymeric materials to solar simulated radiation

Table 1. Activation Spectra Maxima Based on Borosilicate Glass Filtered Xenon Arc Radiation

		Filter technique		Spectrographic technique	
Polymer	Measured change	Mils	Max. change, nm	Mils[a]	Max. change, nm
Acrylonitrile–butadiene–styrene	Yellowing	100	340–360	10	330
	Bleaching	100	>380	10	380–400
	Impact strength	100	350–380[b]	—	—
	Impact strength	100	>380[c]	—	—
Nylon-6 7	uv, modulus	—	—	?	390, 450
Polyamides 8 (aromatic)	Yellowing and tensile strength	—	—	?	360, 370, 414[d]
Polyarylate	Yellowing	3	350	—	—
		60	385	—	—
Polycarbonate	uv @ 340 nm	28	<300, 310–340	4.5	295, 310–340
	Yellowing	28	<300, 310–340	4.5	295, 310–340
Polyethylene	Yellowing	—	—	4	310
	C=O	—	—	4	340
Polyethylene-naphthalate 9	Yellowing and ir, modulus	—	—	5	370–380
Polypropylene	uv	—	—	15	295, 330, 370
	C=O	10	320	15	340–380
	Tensile strength	60	320–350[a]	—	—
	Tensile strength	60	360–380[b]	—	—
Polystyrene	Yellowing	125	300–330	125	319
Polysulfone	uv @ 330 nm	1	310	1	305
	Yellowing	1	320	1	310–320
	C=O, OH	—	—	1	330
Polyurethane (aromatic)	Yellowing	—	—	?	350–415[e]
Poly(vinyl chloride)	Yellowing	40	300–320	2	308–325[e]

[a]Question mark indicates unknown thickness.
[b]Short exposure.
[c]Extended exposure.
[d]Films and fibers.
[e]Various samples.

and the variation with type of degradation measured. While wavelengths shorter than 350 nm are responsible for most of the optical changes in many of the polymers, mechanical changes in the same polymers and optical changes in others are caused by wavelengths longer than 350 nm, often extending into the visible region. The wavelength sensitivity of polypropylene and acrylonitrile–butadiene–styrene based on change in mechanical properties, shifted to longer wavelength with increase in exposure. As exposure progresses, impurities are produced that are capable of absorbing longer wavelength uv radiation. In these polymers, the uv radiation of the filtered xenon arc is absorbed only by the impurities. In aromatic type polymers, the form in which they are tested has a very significant effect on the

activation spectrum. Thus, the 60-mil plaque of polyarylate is yellowed by longer wavelengths of solar-simulated radiation than the 3-mil film; the peak shifts from 350 to 385 nm with increase in thickness.

Temperature. Temperature differences in various climatic zones of the earth are responsible to a large extent for the variations in weathering. The areas exposed to the greatest solar irradiance are also those exposed to the highest temperatures. Both are usually highest near the equator and decrease with increasing latitude. Elevated temperatures can significantly influence the destructive effects of light on polymeric materials by accelerating the rate of the secondary reactions following the primary photochemical step of bond breakage and by altering these reaction processes. For example, the increase with temperature in rate of oxygen diffusion and rates of reactions of free radical fragments can alter the main mechanism of degradation. Because of differences among materials in the effect of temperature on the secondary reactions, the stability ranking of materials may change with increase in temperature.

Physical stresses result from temperature differences between the surface and bulk of polymeric materials caused by the low thermal conductivity and heat capacity of these materials. Daily and seasonal temperature cycling can cause mechanical stress in composite systems, such as between a coating and a substrate or between coating layers, because of mismatch in the thermal expansion coefficients. It often results in cracking and loss of adhesion of the coating. Even the most brittle materials will not fail in the absence of stress (10). Temperature and its cycles are also closely linked to water in all of its forms. Increase in temperature accelerates hydrolysis reactions, while reduction in temperature results in condensation as dew on the material. Freeze/thaw cycling or thermal shocks due to cool rain hitting hot, dry surfaces will induce mechanical stress which can cause structural failures in some systems, or accelerate degradation already initiated.

Daily averages and extremes of air temperature are important measurements made to quantify temperature conditions during exposure of specimens to natural weathering. However, the temperatures that materials attain is higher than that of the surrounding atmosphere. The surface temperature of exposed materials depends on the amount of radiation absorbed, the emissivity of the specimen, thermal conduction within the specimen, and exchange of heat with the surroundings through conduction and convection. A large portion of the absorbed radiation is converted to heat, and the amount absorbed is closely linked to color, with white materials absorbing only about 20% of the incident energy and black about 90%. Thus, the darker the color, the higher the temperature. Surface temperatures have been reported to reach 77°C in exposed plastic specimens (11) and 120°C inside a closed automobile exposed to sunlight (12).

Since it is not practical to measure the surface temperature of individual test specimens, black panel and white panel temperature sensors are used to represent maximum and minimum temperatures attained, respectively, by samples. The panels are thin metal substrates (stainless steel or anodized aluminum) treated on the front surface with a black or white coating that has good resistance to weathering. A thermocouple or other type of temperature sensor is attached to the center of the front or back side, preferentially the latter. The substrate can be either uninsulated, allowing ambient air to circulate on the front and back for maximum cooling, or insulated on the back to simulate specimens exposed on a

solid backing. Typically, temperatures measured by insulated black panel temperature sensors are 3–12°C higher than those by the uninsulated black panels, depending on the level of irradiance, temperature, air flow, and construction of the sensor.

Moisture. All materials used outdoors are exposed to the influence of moisture which, in combination with solar radiation, contributes significantly to the weathering of many polymeric materials. The form and amount of moisture vary widely, depending on the geographic area and ambient temperature. Moisture can take the form of humidity, dew, rain, frost, snow, or hail. The span of time over which precipitation occurs and the time the sample surface is exposed to wetness are more important in weathering of materials than the total amount of precipitation. The penetration depth of moisture into the material, and thus the influence on weathering, is substantially greater when the total amount of precipitation is distributed over a longer time period.

Moisture contributes to the weathering of polymeric materials both by reacting chemically in hydrolytic processes and by imposing mechanical stresses when it is absorbed or desorbed (10). It can also act as a solvent or carrier, eg, in leaching away plasticizers or in transporting dissolved oxygen. Examples of chemical reactions of water are hydrolysis reactions of labile bonds such as those of polyesters, polyamides, and poly(ether) urethanes and its promotion of chalking of titanium dioxide (TiO_2) pigmented coatings and building products exposed to solar radiation. Chalking results from the release of TiO_2 particles at the surface when the organic binder is degraded by the hydroxyl and perhydroxyl free radicals formed in the reaction between water, oxygen, and the titanium and hydroxyl ions produced on exposure of the pigment to uv radiation. Experience shows that chalking is most prevalent when moisture at the surface is highest; little to no chalking occurs in dry environments.

Cycling of moisture in the form of humidity or liquid water creates mechanical stresses in many materials. Absorbed water, by expanding the volume of the surface layers, results in compressive stresses on the outside and tensile stresses in the bulk. Reduction in volume of surface layers during drying is resisted by the hydrated inner layers, creating bulk compressive and surface tensile stress gradients. Cracking and loss of adhesion of coatings results. Water absorption is a diffusion controlled process, which may take weeks or months to reach equilibrium in thick forms of polymeric materials because of the slow diffusion rates. Solar radiation has a pronounced effect on the humidity-induced stresses because of the formation of polar or hydrophilic groups, which increase the tendency of the material to absorb moisture. Further, many photochemical aging processes initiated by solar radiation cause embrittlement of the surface, thus enhancing the tendency to crack under tensile stresses during the drying period. These are examples of the combined action of different weathering factors. High relative humidity levels in conjunction with heat, as, eg, in tropical and subtropical climates, often promote microbial growth. Mold, mildew, and other microbiological and botanical agents can play a significant role in material degradation, although they may not be generally thought of as weathering factors.

Commercial exposure facilities typically measure two main types of moisture: relative humidity and wet time. Measurements of relative humidity by a shaded device, such as a wet bulb/dry bulb or solid-state sensor enclosed in a

ventilated shelter, indicate the amount of water vapor in the air mass relative to its maximum capacity at the ambient temperature. *Wet time* is the amount of time liquid water is present on the surface of the material because of condensation and precipitation. It is measured either by increase in electrical conductivity of a cotton muslin wick when it is wet by rain or by the electrical potential developed in a moisture sensing galvanic cell described in ASTM G84 (13).

Oxygen. Photo-oxidation reactions, initiated by solar radiation in combination with oxygen, account for most polymer failures that occur during outdoor exposure. The penetration of oxygen into the polymer is a critical factor and is related to its rate of diffusion, which depends on the temperature, polymer type, and morphology. The importance of oxygen in the weathering process is evidenced by the fact that photo-oxidation in polymers that only weakly absorb uv, such as polyolefins, is significantly reduced toward the center of thick samples because of the limited supply of oxygen. It has been shown that oxygen diffusion and not uv radiation becomes the rate controlling process in photo-oxidation of polypropylene and polyethylene plaques at a depth at which the rate of oxygen consumption is greater than the rate at which it can be replenished from the environment (14–17). Oxygen can promote degradation in several ways:

(1) Reaction with the free radicals formed as a result of bond cleavage by solar radiation produces peroxy radicals. The latter propagate radical chain reactions that multiply the destructive effect of the radiation manifold;
(2) Reaction with sensitizers, such as ketones and certain dyes, excited by radiation to their triplet states, results in the excited singlet state of oxygen, a very reactive form of the molecule. Singlet oxygen is responsible for the rapid deterioration of many materials, particularly those with conjugated unsaturation such as natural rubber and synthetic elastomers;
(3) Oxygen can also increase the amount of solar radiation absorbed by conjugated unsaturated hydrocarbons through formation of a complex with these structural components.

Atmospheric Pollutants. Ozone is present in the earth's atmosphere both as a result of uv photolysis of oxygen in the upper atmosphere and as a result of reaction between terrestrial solar radiation and atmospheric pollutants such as nitrogen oxides and hydrocarbons from automobile exhausts. It is a powerful oxidant that can react rapidly with elastomers and other unsaturated polymeric materials to cause stiffening and cracking, particularly under mechanical stress. Other common air pollutants include sulfur oxides, hydrocarbons, nitrogen oxides, and particulate matter such as sand, dust, dirt, and soot. Some of these may react directly with organic materials, but have a much more severe effect in combination with other weather factors.

Acid rain is an important consequence of pollutants generated by modern industrial societies and has been shown to damage both organic and inorganic materials exposed to the environment. However, dilute sulfuric acid is formed only when sulfur dioxide (SO_2) and water on the surface of materials is exposed to solar radiation. It causes rapid discoloration when it reacts with pigments as well as cross-linking (10) and embrittlement (18) of polymers. The results of the action of acidic pollutants and radiation on automotive coatings has been described (19).

Acid rain enhances hydrolytic degradation and thus is an important factor in weathering of polymeric materials in which the mechanism includes hydrolysis. Acids have also been shown to interfere with the use of hindered amine light stabilizers (HALS) to improve the light stability of acrylic urethane clearcoats. It is believed that acids may reduce the effectiveness of HALS by reacting to form salts, which are then washed out of the coating. While acids generally act synergistically with radiation to accelerate the effects of weathering, acid precipitations can also slow the aging processes in polymers (20).

Outdoor Weathering Tests

Outdoor weathering tests are commonly characterized as "natural" or "accelerated." Ideally, "natural" weathering would be the result of exposure of a material in its actual intended location and orientation. The term is, however, generally used for outdoor exposure on fixed angle racks in locations and orientations that maximize the effects of weathering components, particularly solar radiation. Since these exposures will generally produce higher degradation rates than the normal end-use environments of the material, they are actually outdoor accelerated tests. In this article, "natural" exposures are divided into "static" exposure tests at fixed positions and "dynamic" exposure tests in which sample orientations are changed during the test, or in which the sun is tracked. "Accelerated" outdoor exposures include techniques that further increase either temperature or solar irradiance or both. Practices for natural and accelerated outdoor weathering of polymeric materials are described in ASTM D1435 (4) and ASTM D4364 (21), respectively.

Most natural and accelerated outdoor weathering tests in the United States are carried out in either (or both) south Florida or central Arizona. These have the two most important "benchmark" environments where materials typically fail fastest because of intensification of the weather elements responsible for degradation. South Florida has a subtropical climate with higher levels of the three critical weathering factors, solar radiation, temperature, and moisture, than are present in most end-use environments. The climate is particularly destructive to materials sensitive to moisture. A number of studies have shown that the south Florida climate has a twofold or higher weathering rate for coatings compared to that in central Europe. The central Arizona desert has become a worldwide recognized standard exposure environment for testing in a climate typical of the hot and dry conditions of the desert, having summer solar radiant exposures and temperatures that are higher than those in south Florida. The large daily and summer-to-winter temperature swings also differentiate Arizona from south Florida environments. Other test sites are in tropical and temperate climates, industrial areas, and salt air locations. The main criterion in selection of the test site is the sensitivity of the material to moisture and the type of climate in which it will be used. Often, the same materials are tested in several different climates.

Because of seasonal and year-to-year climatological variability of outdoor conditions, repeated testing during different seasons and over a period of at least 2 years is usually recommended. Results of tests conducted for less than 12 months will often depend on the particular season of the year in which they begin. In order to take into account the variability of weather, the performance of test materials

should be evaluated in comparison with that of one or more control materials having similar composition and construction and known performance rather than in terms of absolute changes. The use of two control materials, one having good durability and one having poor durability, and at least two, preferably three, replicate specimens of each test and control material is recommended.

Static Exposures. Outdoor static weathering tests can take numerous forms. Some of the variables include tilt angle, unbacked or backed exposure with various types of backing material, under glass exposure, additional wetting, and other special conditions, all of which influence the critical weathering factors. The variables of static outdoor exposures are described in detail in ASTM G7 (22) and ASTM G24 (23). The particular test variables chosen depend on the application of the material and should generally simulate the worst case in-service conditions as closely as possible. Materials used with a backing should be exposed with a similar type backing to provide higher temperatures and longer wetness times than unbacked exposures. In some cases, the backing is painted black to increase surface temperature and degradation rates. Materials intended for applications indoors or in enclosures behind specific types of glass, such as in automotive interiors, require weathering tests simulating conditions found in their specific end-use environment. Because of variation in specimen temperature and time of wetness due to location of a specimen on the exposure rack and the type or color of adjacent specimens, controls and test specimens should be placed on a single test panel or on test panels adjacent to each other.

The direction and angle of the exposed samples, measured from the horizontal, influence the amount of total radiant energy received, the quality and quantity of uv and temperature, and the time of wetness. The 45° angle is the most widely used, probably because many of the early exposure tests were carried out at temperate latitudes at which this angle was considered to be the fixed angle for optimum solar radiation for the whole year. However, in both temperate and tropical zones, exposures at 0°–20° angles contain a higher proportion of the diffuse component of incident solar radiation and therefore higher annual doses of short wavelength uv than exposures at higher angles of inclination (24,25). At 0° (horizontal) and 5° angles, samples are exposed to essentially the entire sky dome and experience higher temperatures and longer time of wetness and thus more rapid deterioration. The 5° angle is preferable because it provides for some drainage to reduce ponding and to allow some of the dirt to be washed off by rain. It is used extensively by the automotive industry for exterior applications, such as surface coatings, and may be used as an alternate to horizontal exposures for items such as indoor–outdoor carpeting, artificial turf, and roofing materials.

Samples experience maximum annual total solar radiation at an angle equal to the latitude of the exposure station, and higher annual uv radiant exposure at latitude angle minus 10°, at which they receive more diffuse radiation. At the lower angle, specimens are nearly perpendicular to the sun's radiation during the summer months when the uv content is highest (26). The 90° angle is used to simulate in-service applications of construction materials such as sidings, windows, door profiles, and automotive components, eg, doors and seat backs. However, it provides significantly lower radiant exposure, temperature, and time of wetness than a 45° or smaller angle. Therefore, the rate of degradation is usually slower for many samples exposed at this than at other fixed angles.

Dynamic Exposures. While the incidence of critical weather parameters can be modified by the setting of the static exposure angle, at any one angle it is not optimum for all seasons. Several dynamic exposure techniques have been developed to further optimize the annual radiant exposure and temperature of specimens. One consists of changing exposure orientation with seasonal changes of the sun's path. However, compared with fixed angle exposures of less than 90° in Florida and Arizona, the maximum increase in annual solar radiant exposure is only about 12% (27). In a study using this technique applied to exposure of a coating in Florida, no appreciable acceleration in degradation was obtained compared with 5° south exposure (28).

Another type of dynamic exposure uses the *Track Rack*, an equatorial mount, which is a motor-driven, follow-the-sun rack designed to maintain noontime conditions from sunrise to sunset by keeping the sample surface at a constant near-normal angle to the direct solar beam. It is often combined with variable angle exposure, but is mainly applicable to arid environments such as central Arizona where the direct beam component of solar radiation is high. Its efficiency is low in subtropical environments where the diffuse portion of solar radiation is a significant portion of the total irradiance. The option of adding water spray to Track Rack exposures provides a combination of three of the critical weather factors, increased radiant exposure, temperature, and moisture, which can significantly accelerate degradation rates of many materials over static exposures.

Accelerated Weathering Exposures. In spite of optimization of weather factors by site selection, type of backing, exposure angle, and follow-the-sun exposures, long periods of outdoor testing are required to establish the durability of modern materials. Options available for further accelerating natural weathering tests include black box enclosures for higher panel temperatures and longer wetness time than open or backed exposures and Fresnel reflectors for increased irradiance. Any major intensification of weather factors over those present under end-use conditions must be used with caution to avoid changing the types and mechanisms of degradation or altering stability rankings because of differences among materials in their response to intensified stress factors.

Black Box Exposures. The black box test was developed to simulate the air heat-sink characteristics of an automotive body and thus provide the high temperatures encountered by the surface coatings, vinyl rooftops, and decorative trim on automobiles exposed to direct sunlight. Details of the black boxes and test procedures are given in ASTM G7 (22), ASTM D4141 (29), and SAE J1976 (30). The test panels form the top surface of an open aluminum box painted with flat black paint on the outside. The box is typically positioned at 5° from the horizontal, facing the equator, but can be positioned at any angle. The insulating effect of the warmed air trapped in the box dampens out temperature variations caused by passing clouds, intermittent breezes, etc. Black box exposures also maintain surface condensation longer after daybreak, thus providing greater probability of interactions between irradiance and moisture than in other types of exposures.

Black Box under Glass Exposures. These tests were designed to simulate and accelerate the effect of interior automotive conditions. Air temperatures in the box may exceed 80°C under conditions of high outside ambient air temperature and solar irradiance. Exterior nonglass surfaces are painted flat black and interior surfaces are left unpainted. The specimens, supported on a rack in a plane parallel

to the glass cover at a distance of at least 75 mm (3 in.), can be unbacked, or backed with either expanded aluminum or a solid backing such as plywood. Liquid water is prevented from accumulating on the specimen's surface by the cover glass, and blowers inside the box circulate enclosed air for better temperature distribution. The box is typically covered with "single strength" window glass that is 2–2.5 mm thick. The requirements for under glass exposures, described in ASTM G24 (23), include exposure of new glass for at least 3 months prior to installation in test cabinets to reduce variability in test results because of rapid reduction in short wavelength uv transmission during initial exposure. After the initial pre-aging period, the glass is suitable for at least 60 months of use. Because of variability between different lots of glass, the relative performance of materials is best determined by testing them at the same time behind the same lot of glass.

Heated Black Box. The heated black box is most useful for exposures conducted in the late fall, winter, and early spring when it produces significantly higher panel temperatures than those produced by the black box. It is equipped with heaters and blowers to heat the inside air to a specified temperature during daytime hours. Heating of the backside of the panels with warm air reduces the daily variability of specimen temperatures. The heater is turned off at night to allow specimens to cool down for formation of condensation and thus for simulation of in-service conditions.

The CTH Glas-Trac™ (Controlled Temperature and Humidity, Under Glass, Sun Tracking). This equipment was designed primarily to determine the durability of automotive interior materials in an outdoor weathering chamber covered with automotive side window glass and incorporating temperature and humidity control. It combines a heated black box covered with 3-mm-thick clear tempered safety glass and a two-axis tracking system, which maintains the specimen surface perpendicular to the sun's rays from morning to evening for maximum solar irradiance. The glass cover is interchangeable with various windshield types. The exposure cabinet is controlled at $70 \pm 5^{\circ}$C air temperature during daylight hours and at $38 \pm 5^{\circ}$C air temperature/$75 \pm 10\%$ relative humidity during nighttime hours. Exposures are timed in MJ/m^2 of total uv (295–385 nm). Details of the test are given in SAE J2230 (31).

Fresnel Reflector. The maximum acceleration of aging processes in outdoor weathering is obtained by exposure on a Fresnel-reflector panel rack that provides high intensity solar radiation by following the sun and reflecting the sun's rays from an array of 10 flat mirrors onto a single target area of the test material. A blower forces air across the target to cool the test specimens and generally limits sample surface temperatures to about 15°C above the maximum temperature of equatorially mounted samples exposed to unconcentrated normal incidence radiation. Testing of samples exceeding 13 mm (0.5 in.) in thickness is not recommended because the cooling may not be sufficient for such samples. Periodic spraying with deionized water is designed to simulate and accelerate the results of conventional testing in semihumid subtropical and temperate regions. Nighttime spray cycles simulate rain and dew. Tests carried out in the absence of a programmed moisture cycle are intended to simulate conventional exposure testing in desert, arid, and semiarid regions. The test can be used to intensify either direct exposures or those behind glass. Descriptions of the device and guidelines for its use are given in ASTM D4364 (21) and ASTM G90 (32).

Since the device only concentrates the direct rays of the sun and not the diffuse radiation, it requires clear atmospheric conditions with little moisture, such as is prevalent in Arizona. The solar flux is approximately eight times as high as on an equatorial mount without mirrors, but acceleration factors over conventional outdoor tests based on elapsed time to a predetermined change in property have been reported to vary from 2 to 11 for various polymer types and compositions (11). The effectiveness of the Fresnel-reflector accelerated weathering machines depends on the quantity and quality of the uv in the direct beam component of solar radiaton. The acceleration factor will be small for materials that are degraded primarily by short solar uv wavelengths because of the deficiency of the machine in this region compared with global solar radiation. This is due to exclusion by the solar concentrator of diffuse solar radiation, which contains much of the short wavelength solar uv, and to lower reflectance of the mirrors at short wavelengths. The acceleration factor will also vary with the material tested because all materials are not affected equally by increased irradiance and temperature. Thus, the stability rankings may differ from that of natural exposure. Good correlations as well as discrepancies have been reported between Fresnel-reflector exposures and standard outdoor tests based on stability ranking of polymeric materials (28,33–37).

Timing of Exposures. Methods of "timing" outdoor weathering tests include (*1*) calendar basis—exposure for a specified number of days, months, or years; (*2*) radiant exposure basis—exposure to a specified level of solar radiant energy in a specified wavelength region based on hemispherical radiation measurements at the same tilt and azimuth angle as the test specimens; and (*3*) property change in a weathering reference material (WRM)—exposure until a specified property change has occurred in a weathering reference material exposed at the same time. Timing on a calendar basis has been the most widely used method of evaluating stabilities because of its simplicity. However, timing based on radiant exposure can reduce seasonal and year-to-year variations in weathering due to inconsistent conditions of total solar and solar uv irradiance. Timing based on property change in a WRM can reduce variations in weathering due also to other weather factors, provided its response to all factors is similar to the response of the test materials.

Studies have shown that better correlations are obtained among exposures made at different times when timing is based on incident solar uv radiation rather than on incident total solar radiation (33,38–43). Timing based on only the portion of solar uv that is responsible for the damage, ie, on the actinic portion identified by the activation spectrum of the material, should further improve correlations. Further, since all actinic wavelengths are not equally destructive, the optimum method of timing should be on the basis of "effective" radiant exposure H_{Eff}. The latter can be determined by using the activation spectrum to weight the incident radiation in accordance with equation (1).

$$E_{\mathrm{Eff}} = \sum_{\lambda_1}^{\lambda_2} E_0(\lambda) \frac{[\Delta(\lambda)]}{[\Delta(\lambda_{\mathrm{max}})]} \tag{1}$$

where E_{Eff} is the effective irradiance, $E_0(\lambda)$ is the incident irradiance at a specified wavelength, $\Delta(\lambda_{\mathrm{max}})$ is the property change at the wavelength of the activation spectrum peak, and $\Delta(\lambda)$ is the property change at a specified wavelength.

The irradiance at the wavelength corresponding to the peak of the activation spectrum ($\Delta(\lambda_{max})$) is normalized to 1.0 and irradiances at other wavelengths are multiplied by the fractional sensitivities obtained from the activation spectrum. The sum is the "effective" irradiance. The effective radiant exposure H_{Eff} is obtained by multiplying the total radiant exposure H_{Total} by the ratio of the effective irradiance divided by the total irradiance (eq. (2)).

$$H_{Eff} = \frac{E_{Eff}}{E_{Total}} H_{Total} \tag{2}$$

Laboratory Accelerated Weathering Tests

Laboratory accelerated weathering devices have been used for more than 80 years with increasing importance concomitant with the development of more weatherable materials and the need to determine in a short time the effects of natural exposures over prolonged periods. The importance of these devices lies in their ability to accelerate the weathering processes under controlled and reproducible conditions. They are particularly useful in research and development of new polymeric formulations. They are also used for quality control and specification testing. However, their application to prediction of service life under use conditions is still under development (see section on Laboratory Accelerated Versus Natural Weathering).

These devices have the unique requirement of accelerating and also simulating the effects of the natural environment. In some cases, simulation of a specialized environment is required as, eg, extreme climates or the miniclimate of the interior of an automobile. Appropriate acceleration techniques require knowledge of material-specific sensitivities to the weathering factors since validity of the tests requires that the results correlate with the effects of natural exposure, ie, that the chemical and physical changes induced in materials are similar and the stabilities of materials are correctly ranked. These requirements can only be realized if the critical weather factors in the environment are appropriately intensified so that the complex interactions of their effects are reproduced. Although the variability of weathering factors in nature precludes an exact representation of the actual conditions, the least that should be achieved is simulation of the full spectral actinic radiation of the natural source by the laboratory test source and appropriate irradiance, temperature, and moisture conditions. The ability to control the latter factors is now included in the basic design of most laboratory accelerated weathering devices.

The single most important consideration when conducting laboratory accelerated weathering tests is the SPD of the radiation source. Simulation of the incident wavelengths and relative intensities of terrestrial solar radiation is critical to simulation of the degradation caused by exposure to natural weather conditions. Both the absorption of light, which is a prerequisite to degradation, and bond breakage, the primary photochemical step following absorption of light, are wavelength dependent. The wavelengths absorbed and the fraction of the incident radiation absorbed at each wavelength are determined by the relation between the absorption properties of the material and the SPD of the light source. The

importance of simulating the SPD of the full solar uv is shown in Table 1 by the large differences in solar uv wavelengths to which different types of polymers are sensitive. Also, it is now an established fact that differences between the artificial and natural sources in the ratios of intensities of long versus short wavelength uv will change the mechanism of degradation of some aromatic type polymers and distort the antagonistic reactions caused by these spectral regions (see section on Effect of SPD of Radiation Source on Weathering). A close match to the short wavelength cut-on of solar radiation is essential when testing polymers such as polycarbonate or isophthalate based esters and others which are particularly sensitive to small changes in radiation in this region. However, the SPD of some light sources commonly used in artificial weathering devices has very little resemblance to the SPD of hemispherical solar radiation on the earth's surface, referred to as "daylight."

Carbon Arcs. Figure 3 compares the representative uv/visible emission of two types of carbon arc sources with daylight measured at noon at a 26°-tilt angle in Miami, Fla., during the spring equinox. The enclosed carbon arc uses solid and cored electrodes burning within a semisealed borosilicate glass globe that provides optical filtering of the short wavelength uv radiation and an oxygen-deficient atmosphere to enhance the efficiency of the arc. The SPD differs significantly from that of solar radiation in both the uv and visible regions. It has two long wavelength uv cyanogen emission bands that give much more intense radiation than daylight in this region and it has much weaker intensity than daylight below 350 nm and in the visible region. The enclosed carbon arc has a much weaker effect than solar radiation on materials that absorb only short wavelength uv radiation,

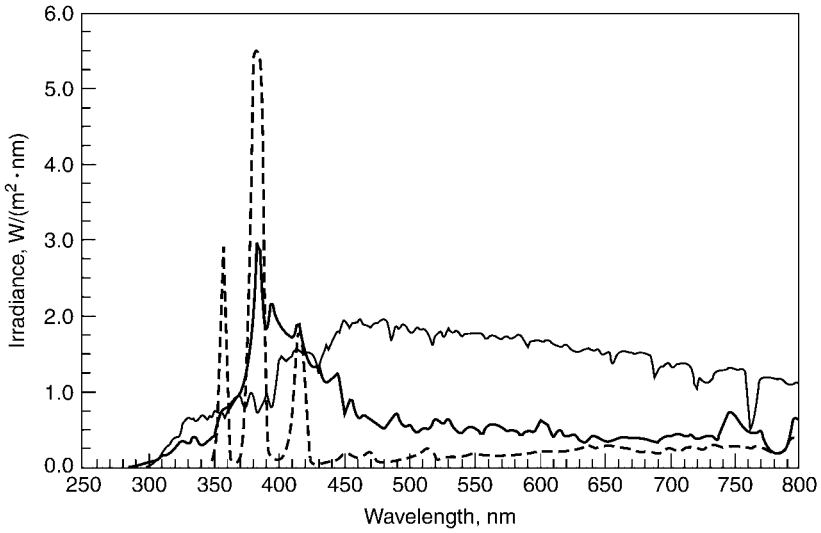

Fig. 3. Spectral power distributions of the enclosed carbon arc, the open flame carbon arc with Corex D filters, and noon daylight in Miami, Fla. at 26° south exposure during the spring equinox 5. Courtesy of Atlas Electric Devices, Reprinted with permission of Marcel Dekker, Inc. —— Daylight (Miami, Fla.); - - - - - - enclosed carbon arc; ▬▬ open flame carbon arc.

but a stronger effect on materials that also absorb long wavelength uv radiation. Therefore the stability ranking of materials that differ in uv absorption characteristics can be expected to be distorted by this source compared with exposure to daylight. Procedures for using enclosed carbon arc devices for exposure of polymeric materials are given in ASTM Standards D5031 (44), D6360 (45), and G153 (46).

The open flame carbon arc (also referred to as the Sunshine carbon arc) uses copper coated electrodes in an open flame type lamp operating in a free flow of air. The unfiltered arc emits a significant amount of short wavelength uv radiation below the solar cut-on. The SPD in Figure 3 represents the emission through Corex D® borosilicate glass filters, commonly used to improve simulation of daylight in this region. Although the filtered arc emits some wavelengths below the solar cut-on, in contrast to the enclosed carbon arc it gives a much better match to daylight in the region below 360 nm and deviates less at wavelengths longer than 360 nm. Other types of sharp cut-on glass filters can be substituted for the Corex D filters to more closely match the solar cut-on as well as to simulate daylight through window glass. When the open flame carbon arc is used without the glass filters for faster testing, reversals in stability rankings are often obtained compared with outdoor testing because of the excessive amount of high energy radiation below the solar cut-on. The latter can also cause differences in mechanism and type of degradation. Procedures for using the filtered open flame carbon arc devices for exposures of polymeric materials are given in ASTM Standards D822 (47), D1499 (48), and G152 (49).

Both types of carbon arc devices have capabilities for periodic water spray on the samples and condensation during a dark period as well as for humidity and temperature control. Both carbon arc technologies typically require daily replacement of the carbon rods, cleaning of the filters or globes, and their periodic replacement because of change in their transmission characteristics with exposure to uv radiation. There is a large volume of historical data using carbon arcs, and a number of test methods still specify their use, but this technology is largely being replaced with xenon arc systems.

Xenon Arcs. Laboratory accelerated weathering tests advanced significantly with the introduction of xenon arc devices in the 1950s in Europe and the 1960s in the United States. The properly filtered xenon arc more closely simulates terrestrial solar radiation in both the uv and visible regions than any other artificial test source. It has become established worldwide as the radiation source for optimum simulation of terrestrial solar radiation. The SPD of the water cooled xenon arc filtered with a coated infrared absorbing (CIRA) quartz inner cylinder and a soda lime glass outer cylinder is compared in Figure 4 with noon daylight in Miami, Fla., measured at a 26°-tilt angle during the spring equinox. Since the irradiance of the xenon arc can be adjusted with the voltage setting, the SPD is presented in relation to that of daylight by normalization of the two at 560 nm. The filtered xenon arc emission closely matches the spectrum of solar radiation in the uv and visible spectral regions, as well as in the region of the solar cut-on. The CIRA cylinder screens out about 50% of the 800- to 1000-nm radiation, thus reducing the excessive energy of the xenon arc compared with daylight in this region and reducing the heat it causes in materials that absorb this radiation. Other filters are used with the xenon arc to simulate exposure to daylight through window

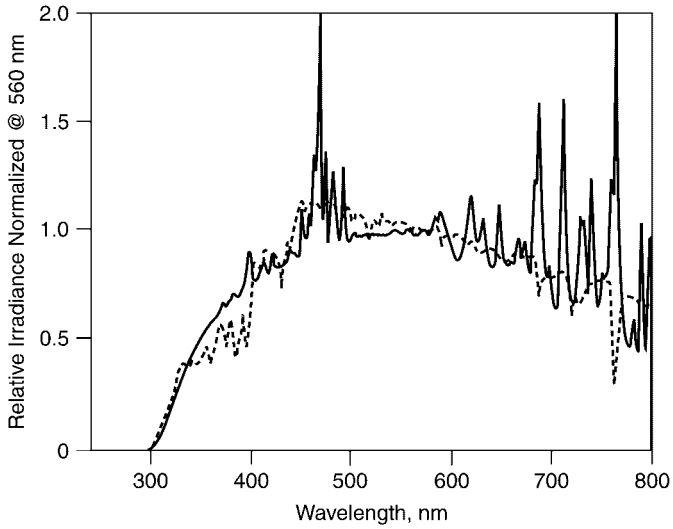

Fig. 4. Spectral power distributions of the water-cooled xenon arc with CIRA quartz inner and soda lime glass outer filters and noon daylight in Miami, Fla. at 26° south exposure during the spring equinox 5. Courtesy of Atlas Electric Devices, Reprinted with permission of Marcel Dekker, Inc. ——— Xenon, CIRA/soda lime filters; ····· Daylight (Miami, Fla.).

glass for applications in which this is required. Procedures for exposure of polymeric materials in xenon arc weathering devices are given in ASTM Standards D2565 (50), D4459 (51), and G155 (52).

Unlike carbon arc exposure devices, which have minimal control over the radiation intensity, modern xenon arc devices control irradiance through electrical power management. Two related xenon arc systems have been developed: air-cooled and water-cooled. The type of cooling has some influence on the overall design and on the optical filtering system, but has a negligible effect on the SPD of the radiation. The uv radiation absorbed by any glass filters used with exposure sources cause "solarization" of the filters, resulting in decrease in their optical transmission, which is greater the shorter the wavelength. Deposition of some of the electrode material on the inside of the quartz envelope also decreases transmission. The automatic light monitoring and control systems of xenon arc devices can compensate for this to a large degree, but not completely, until such time as the lamps and filters need replacing. Xenon arc devices have capabilities for temperature control and either periodic water spray or water immersion of the samples during exposure. Some devices can also provide condensation during the dark periods and control of relative humidity during both light and dark periods.

Fluorescent Ultraviolet Lamps. The emission properties of two types of fluorescent uv lamps, UVB-313 and UVA-340, are shown in Figure 5 in comparison with the same daylight spectrum shown in previous figures. All fluorescent uv lamps are deficient in long wavelength uv radiation and, except for a few mercury emission lines in the visible region, lack the visible and nir energy present in daylight and xenon arc radiation. Thus, they are not suitable for testing materials that are sensitive to these spectral regions. Compared with stability ranking

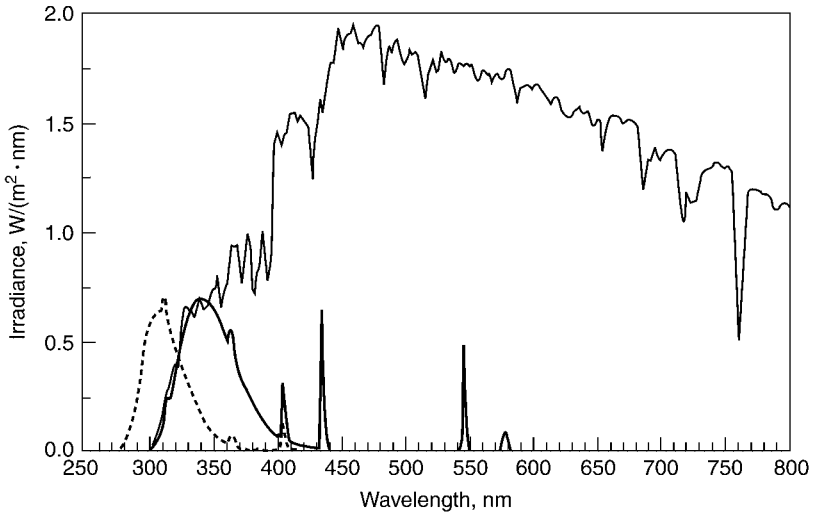

Fig. 5. Spectral power distributions of fluorescent UVB-313 lamps, fluorescent UVA-340 lamps, and noon daylight in Miami, Fla. at 26° south exposure during the spring equinox 5. Courtesy of Atlas Electric Devices, Reprinted with permission of Marcel Dekker, Inc. —— Daylight (Miami, Fla.); ····· UVB-313; ▬▬ UVA-340.

by daylight, reversals have been reported for colored materials exposed to these lamps as well as to the fluorescent UVA-351 lamps, which emit somewhat longer wavelength uv (53). The UVB-313 lamps were previously commonly used because they provided rapid tests of the sensitivity of polymeric materials to uv radiation owing to the high flux of short wavelengths below the solar cut-on. However, because of the excessive short wavelength radiation, exposures to these lamps often caused reversals in stability rankings of polymers and errors in the performance of stabilizers compared with outdoor tests. These highly energetic wavelengths can initiate different mechanisms and types of degradation than the wavelengths present in solar radiation.

Since the UVB-313 type lamps generally cannot predict the outdoor performance of polymeric materials (54–56), the UVA-340 lamps are gradually replacing them in tests on polymers that are mainly sensitive to wavelengths in the 300- to 330-nm region. These lamps match the cut-on and short wavelength spectral irradiance of solar radiation quite well in this region. However, in addition to the lack of actinic effects on materials sensitive to long wavelength uv and visible radiation, heating of colored materials by absorbed visible radiation is absent. Therefore, in contrast to the temperature variations of differently colored materials exposed to a source that emits visible radiation, all materials attain the same (ambient) temperature. Thus, stability rankings will differ from those based on exposure to solar or solar-simulated radiation. Also, the mechanical stresses resulting from the heating and cooling of the absorbing surface layer are absent, resulting in reduced tendency to crack. For all these reasons, it is important to simulate the full SPD of the source to which the materials will be exposed under use conditions.

The fluorescent uv sources are typically incorporated into fluorescent uv/condensation devices in which dark periods with condensation are alternated with periods of uv radiation. The temperature is generally controlled at different levels during each of these periods. The devices may also incorporate periodic water spray on the front surface of the samples during exposure to radiation, but do not control relative humidity. Some of the modern types of these devices have capabilities for irradiance control. Procedures for exposing polymeric materials in devices with fluorescent uv lamps are given in ASTM Standards D4329 (57), D4587 (58), and G154 (59).

Metal Halide Lamps. The uv emission curve of the borosilicate filtered HMI metal halide lamp is shown in Figure 6 compared with the emission curves of daylight and filtered xenon arc radiation. It has a multiline spectrum which can be considered to be a continuum for purposes of material testing. It gives a relatively good simulation of terrestrial solar radiation in the uv region above 300 nm, but requires additional filtering of the short wavelength radiation for better simulation of daylight. Their high efficiency and low infrared output, which eliminates the need for water cooling, makes these sources ideally suited for use in large scale multiple source arrays and effective in thermal loading studies. However, metal halide lamps have technical problems which make them difficult to use in weathering systems. One is the dependence of the SPD of the radiation on the temperature of the lamp, thus requiring as constant a temperature as possible in the vicinity of the lamp. Because of the effect of temperature on the

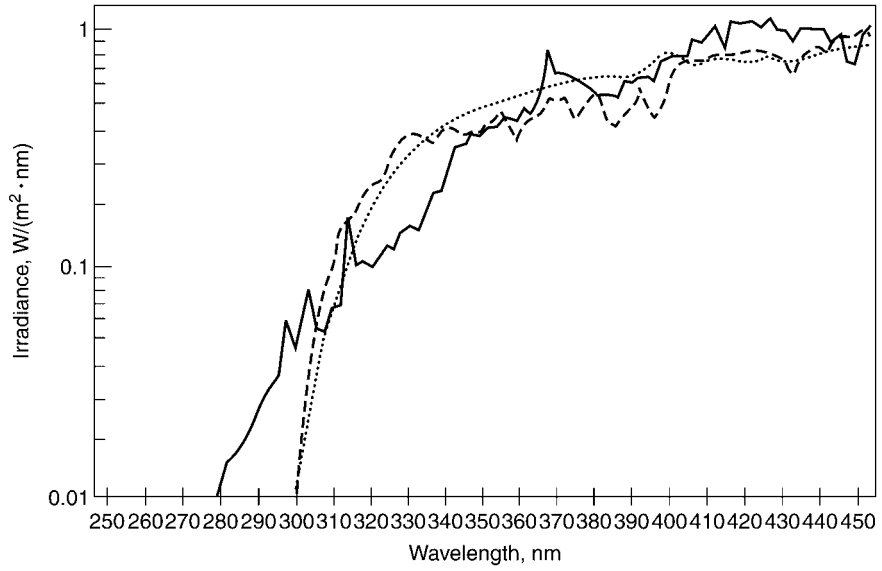

Fig. 6. Spectral power distributions of the water-cooled xenon arc with CIRA quartz inner and soda lime glass outer filters, the filtered HMI metal halide lamp, and daily average of optimum daylight in Miami, Fla. measured at normal incidence during the vernal equinox under clear sky conditions. Courtesy of Atlas Electric Devices, Reprinted with permission of Hanser Gardner Publications, Inc. —— Filtered HMI metal halide; - - - - - - average optimum daylight; · · · · · Xenon, CIRA/soda lime filters.

SPD, the latter changes with change in power. Therefore, the ability to alter the level of irradiance by changing the power is limited to about 5–10%. Reduction in irradiance is accomplished either by the use of close-meshed wire filters or by increase in the distance between the lamp and the sample. The other problem is the variation in SPD from one lamp to another of the same type. It is remedied by measuring the SPD of each lamp and selecting one that is applicable.

Effect of SPD of the Radiation Source on Weathering. The wavelengths responsible for degradation of a specific polymeric material vary with the SPD of the radiation source. Differences between the laboratory accelerated test source and the natural source in the wavelengths that degrade a material, which are identified by the activation spectra (see section on Spectral Effects of Solar Radiation: Activation Spectra), can have the following consequences (53):

(1) The screening requirements of the material will differ and thus the type of uv absorber required will differ. For example, activation spectra data showed that yellowing of a polyarylate film is caused mainly by 310- to 340-nm radiation when it is exposed to fluorescent UVB lamps, but by 335- to 365-nm radiation when it is exposed to solar radiation. Thus, this artificial test source cannot provide valid data on the protective effectiveness of the additive against solar radiation.

(2) The predominant mechanism of degradation of many polymeric materials will differ if the relative intensities of short to long wavelengths responsible for degradation differ. Studies have shown that short uv wavelengths of solar radiation absorbed by the structural components of some aromatic type polymers cause photolytic reactions which lead to photo-Fries rearrangements, while longer uv wavelengths, absorbed by impurities such as hydroperoxides and unsaturated carbonyl groups, initiate photo-oxidation reactions involving free radicals.

(3) If the predominant mechanism of degradation varies with the test source, the effectiveness of stabilizers such as free radical scavengers and excited state quenchers that act by interfering with the mechanism of degradation will differ. For example, HALS can only protect polycarbonate and aromatic polyurethane against the mechanism initiated by long wavelength uv. They are ineffective against the degradation caused by short wavelength uv. Therefore, evaluation of the performance of HALS in these polymers by using a radiation source that primarily emits short wavelengths will give misleading information on their ability to protect the polymers against solar radiation. Significant differences have also been shown among various types of exposures in the protection by HALS against photo-oxidation of acrylic melamine coatings.

(4) The amount of surface versus bulk degradation, yellowing versus bleaching, bond scission versus cross-linking, chalking versus cracking and crazing in TiO_2 pigmented systems, and other diverse types of degradation will differ if the relative intensities of short versus long actinic wavelength radiation differs.

(5) Because of differences among polymeric materials in their absorption properties and in their response to the absorbed radiation, differences between

light sources in harmful wavelengths can alter the stability ranking of materials.

Irradiance in Laboratory Weathering Tests. One of the most obvious ways to shorten test time is to increase the irradiance level. However, increase in irradiance is limited by its effect on the stability ranking of materials and the mechanism of degradation. Since all materials are not affected equally by increase in irradiance, the stability ranking of materials can change with the irradiance level. The dependence of rate of degradation on irradiance level is complex. It varies with the type of material, formulation, including type of stabilizer, and wavelength of light. For most materials, the degradation rate is not a linear or other simple function of irradiance. Thus, doubling the intensity does not necessarily double the rate of degradation. For example, rates of photo-oxidation of polypropylene have been shown to be proportional to various fractional powers of the light intensity ranging from the square root to the first power (60). The distance from the surface at which oxygen diffusion becomes the rate-limiting process in photo-oxidation reactions differs with irradiance level because of its effect on oxygen depletion. The quantum yield of degradation, ie, the amount of degradation for a specific number of photons absorbed, often decreases with increasing irradiance. In a free radical process, this is partly explained by the "cage effect." Because of the higher concentrations of free radicals formed at higher irradiance levels, the likelihood of recombination is increased and reaction with oxygen and other molecules is reduced.

In many modern laboratory accelerated test devices, the irradiance in watts per square meter (W/m^2) in a specified spectral range is photometrically monitored and the lamp power is automatically adjusted to maintain constant irradiance. In xenon arc devices, it is commonly controlled at either 340 nm, referred to as "narrow band control" or over the full uv, 300–400 nm, referred to as "broad band control." In some cases, control includes the full uv and visible range, 300–800 nm. Most standard weathering tests currently specify an irradiance of 0.35 or 0.55 $W/(m^2 \cdot nm)$ measured at 340 nm, with the higher irradiance being increasingly more widely adopted. The irradiance of 0.35 $W/(m^2 \cdot nm)$ represents the daily average of irradiance measured during daylight hours under optimum conditions in Miami, ie, at normal incidence under clear sky conditions during the vernal equinox. It is half the peak irradiance of 0.68 $W/(m^2 \cdot nm)$ measured at solar noon. The irradiance level of 0.55 $W/(m^2 \cdot nm)$ at 340 nm is more representative of the type of exposures samples receive in Miami or Arizona for 3 or 4 h before and after noon. The irradiance integrated over time is the radiant exposure in Joules per square meter which may be automatically monitored. Test duration is often specified in terms of radiant exposure rather than in chronological time.

Temperature in Laboratory Weathering Tests. The temperature of materials can have a significant influence on the effect of the absorbed uv radiation by increasing the rate of secondary reactions. While degradation can be accelerated by testing at temperatures higher than materials are exposed to under use conditions, caution must be exercised to avoid obtaining unrealistic test data. Some reactions that take place at higher temperatures will generally occur at only a very low rate, or not at all, at lower temperatures. For example, specific secondary reactions may occur only at higher temperatures because of increased

rate of decomposition of hydroperoxides or increased rate of diffusion of oxygen or of free radicals formed in primary processes. Often, a different degradation mechanism is triggered at a specific temperature. Change in degradation mechanism precludes simulation of the effects of natural exposures. Since the effect of temperature varies with type of polymer and its formulations, temperatures different than those encountered in end-use environments can distort the stability rankings of materials in addition to causing unrealistic aging behavior.

In most weathering devices, the approximate temperature of dark colored specimens is simulated and regulated with the use of a black panel sensor of either the uninsulated or insulated type described in ASTM G151 (61). It serves to control the air temperature which, in combination with the surface heat caused by absorbed radiation, provides the black panel temperature specified in the test method. The heat due to absorbed radiation depends on the visible and infrared absorption properties of the materials as well as on the SPD and irradiance of the source. Generally, the black panel temperature that specified is the maximum temperature that dark samples attain under use conditions. Currently, the highest black panel temperature specified is 89°C during the light-only period in a xenon arc device used for tests on automotive interior materials such as seat covers and dashboards (62).

Moisture in Laboratory Weathering Tests. Moisture, in combination with radiation, is often a key contributor to the weathering of polymeric materials, either by participating in the chemical reactions resulting from exposure to light or by imposing mechanical stresses. The influence of moisture on weathering of polymeric materials was discussed in the section on Outdoor Weathering. The processes of photoinitiated oxidation and hydrolysis are interrelated, with high humidity enhancing photooxidative degradation. For example, in a study on the effect of relative humidity (RH) on the photodegradation of an acrylic melamine coating, both the rate and magnitude of chain scission and oxidation were shown to increase with increase in RH (63). While some polymers are themselves sensitive to moisture, often the moisture sensitivity of formulation ingredients can have a significant effect on weathering in the presence of moisture. For example, some plasticizers in PVC can be hydrolyzed under hot humid conditions by traces of the hydrogen chloride released on exposure of PVC to uv radiation, resulting in significant loss in elongation.

Moisture can be provided in laboratory accelerated weathering devices in the form of water spray, condensation, immersion, or humidity. The type of moisture present can influence the type and rate of degradation. Many test procedures include more than one type of moisture. Commonly, the front surface of samples is periodically sprayed with cool, deionized water simultaneous with exposure to light. This imparts a thermal shock to the samples, but does not simulate natural weather conditions in which rain is unaccompanied by exposure to radiation. The formation of condensation on samples during the dark period is an effective means of simulating nighttime conditions in an environment with high moisture content, such as in Florida. It is accomplished by providing high humidity conditions while cooling the back of the samples with ambient air or a water spray. High humidity can be as effective as liquid water. In many devices, during light or dark periods without water spray, relative humidity is automatically controlled to a specified level by moistening the air using either the evaporation or atomization technique.

In devices in which wetting is by immersion, the sample is immersed in water while the surface is exposed to light. Since water absorption by polymers from a humid atmosphere or by direct wetness is a diffusion-controlled process, the frequency and duration of the exposure to moisture is often a critical parameter. Weathering processes can be accelerated by more frequent swelling and contraction than occurs in practice. The length of the required wet period depends on the water diffusion coefficient and water absorption capacity of the material as well as on its thickness. Rain, humidity periods, or both ranging up to hours may be required for some polymeric types.

Stability Evaluations and Exposure Duration. Evaluations of new materials and formulations are commonly based on stability ranking, ie, comparison between changes produced in the test material and in a control material of known durability exposed at the same time. Exposure of at least three replicates of the test and control specimens is recommended to allow analysis of variance in order to determine the significance of performance differences. Periodic evaluation of test and control materials should be made to compare rates and direction of property changes as a function of exposure time or radiant exposure. Since extent of degradation is usually not a linear function of exposure, ideally stability should be evaluated in terms of the time or radiant exposure required to produce a defined property change in a material. When exposing for a single period, the latter should be selected to give the largest performance difference between test materials. The minimum exposure period should be that necessary to produce a substantial change in the property of interest in the least stable material being evaluated.

Generally, tests for quality control and specification requirements are based on a pass/fail criteria after a specified test time or radiant exposure. The pass/fail evaluation should be based on the statistically determined combined reproducibility of the test exposure and property measurement. In the absence of statistical information, performance requirements should be based on stability ranking in comparison to a control material. Timing may be based on a specified change of color in a weathering reference material, such as the AATCC Blue Wool Lightfastness Standards used in AATCC Test Methods 16, 16A, and 16C (64). However, these reference materials are only applicable to tests that have a minimum of moisture and low heat because of their sensitivity to these factors. Change in color of test specimens compared to that of the standards has also been used to rank the lightfastness of specimens.

Laboratory Accelerated Versus Natural Weathering

Laboratory accelerated weathering tests have played an important role in development of polymeric materials with highly improved weatherability. However, since all stresses present in an outdoor exposure cannot be simulated in a laboratory accelerated test, the latter cannot replace natural exposure. It is a complimentary technique, the usefulness of which largely depends on how closely it reproduces the chemistry and weathering effects caused by the slower outdoor exposures. Thus, correlation is a fundamental issue which must be considered when selecting a laboratory accelerated weathering method. It depends on reasonably representing

the critical weather factors, ie, radiation, heat, and moisture, in the service environment and accelerating their effects without distorting the type and mechanism of degradation and stability ranking. Studies have shown that appropriate laboratory accelerated tests have the potential of providing information to predict lifetimes by natural weathering. However, before drawing any final conclusions concerning the ability of a polymer to withstand the outdoor environment based on artificial weathering tests, it is necessary to validate the results by conducting outdoor exposure tests for a reasonable length of time.

Correlation. The term correlation refers to the ability of the accelerated test to produce results that agree with real-time outdoor exposures. However, the term "results that agree" as applied to weathering tests, has various meanings, which are generally unspecified. *Correlation* often refers to the ability of different types of weathering tests to rank the performance of a series of materials in the same way, ie, *rank correlation*. Since rankings of materials can vary with the amount of radiant exposure, correlation should be determined at an optimum exposure period (54). Correlation has also been based on the similarity in type(s) of degradation caused by different types of exposure. In some cases, correlation is based either on qualitative comparison of the profiles of the graphed data on property change versus time or radiant exposure, or on a linear regression analysis of the data. "Timing" exposures in terms of only the actinic portion of the radiant exposure should provide a better basis for comparison between laboratory accelerated tests and outdoor exposures (see section on Timing of Exposures).

In order to provide a reliable early evaluation of the weatherability of a polymeric material, ideally the laboratory accelerated test should satisfy all correlation criteria when compared with results of natural weathering. However, any accelerated weathering test, either artificial or natural, only approximates the field exposure conditions. Nevertheless, the closer the simulation of the natural balance of all important weathering factors by the accelerated test, the better the correlation that will be achieved with outdoor tests and end-use service results. When the balance of weather factors is altered, the balance between the various reactions that constitute the weathering processes can change. Because of the synergistic effects of the weather factors and the complex nature of the weathering processes, acceleration by intensification of one factor alone can distort failure modes and stability ranking of materials. Additionally, conditions that give good correlation with one exposure site for one type and form of material and formulation do not necessarily assure good correlation for other materials and may not be applicable to other sites. Often, good correlation between sites is not attained because of differences in exposure conditions at different outdoor sites. The extent of correlation between two types of tests may also depend on the property measured as the criterion of degradation.

In many cases, poor correlation with outdoor test results can be attributed to inadequate simulation of the SPD of the natural source. However, when using an appropriately filtered xenon arc source at an acceptable irradiance level, lack of correlation can be due to other factors that are not adequately simulated. These may be the dry/wet cycle, type of wetting, temperature and its variations, humidity conditions during exposure to the radiation source, the light/dark cycle, and atmospheric pollutants. For some materials, lack of a dark period can preclude correlation with natural exposures. Just as the season in which the outdoor

weathering test is started can affect the test results, in laboratory tests, whether the samples are exposed first to a dry period with radiation or to a wet, dark period can alter the type of degradation and stability rankings. Factors that can interfere with correlation between laboratory accelerated tests and natural exposures are described in ASTM G151 (61). In many of the test standards, exposure specifications are arbitrary and the critical weather factors are not adequately optimized to accelerate and also simulate the effects of natural exposure. Automotive weathering tests based on SAE J1885 (62) for interior materials and SAE J1960 (65) for exterior components that utilize the xenon arc and include a dark period with condensation are an attempt to more closely simulate end-use conditions. While they do not always provide acceptable correlation with outdoor tests, they have generally been an improvement over tests that lack these parameters. Simulation of the atmospheric acid precipitations in outdoor exposures has also been shown to improve correlations based on stability ranking and type of degradation for various types of polymeric materials including sealants and automotive clearcoats (19,20,66,67).

Acceleration Factors. The term correlation is often erroneously used to describe the relation between test times for the laboratory test and outdoor weathering. The appropriate term is *acceleration factor*, which is the time to failure (or change in property) under natural exposure divided by the time to failure (or change in property) by the accelerated test, both evaluated by the same criterion of degradation. Acceleration over "real time" weathering can be accomplished in several ways: (*1*) by continuous exposure to the critical weather factors, uninterrupted by the diurnal cycle, seasonal variations, and weather conditions; (*2*) by exposure to irradiance levels that are only encountered during optimum conditions outdoors; and (*3*) by setting temperatures, relative humidity, and thermal and moisture cycles to high stress levels, but not more than the maximum under end-use conditions. The acceleration factor is meaningful only if the laboratory test does not cause unnatural failure modes or distort stability ranking of the test materials. Accelerated laboratory test conditions that provide correlation with outdoor exposure, generally have an acceleration factor between 2 and 10. Unfortunately, the greater the acceleration, the poorer the correlation.

Acceleration factors are material dependent and can be significantly different for each material and for different formulations of the same material. Therefore, it is erroneous to attempt to establish a single acceleration factor for a laboratory accelerated test to be used to predict lifetimes under natural weather conditions for a variety of materials and formulations. Because of the complex nature of the interaction of the combined weather stresses with a material, there is presently no simple way to estimate the acceleration factor for a material. Increase in irradiance cannot be equated with acceleration of degradation. For most polymeric materials, the rate of degradation is not simply a linear function of the level of irradiance. Also, it does not take into account the effect of temperature, moisture, and other weather factors. Thus, there is no substitute for determining the acceleration factor for a given material experimentally.

The acceleration factor depends not only on the laboratory accelerated test, but also on the geographical, seasonal, and environmental conditions of outdoor exposure. Further, variability in rate of degradation in both laboratory accelerated and natural exposures can have a significant effect on the acceleration factor

calculated. Therefore, the latter should be based on a sufficient number of exterior and laboratory accelerated exposures and at least two, preferably three, replicate specimens in each test so that time to failure in each can be analyzed statistically. Standardizing test conditions with a reference material such as polystyrene in devices that provide for control of weather factors can improve reproducibility of laboratory tests. Often when problems related to reproducibility in the results of accelerated weathering occur, they can be traced to differences in the samples, either because of differences in polymer batches or because of nonuniformity among the test specimens. Even specimens cut from the same sheet often vary significantly. Poor reproducibility in weathering among specimens from the same production lot can be due to the nonuniform distribution of stabilizers or uv absorbing impurities that initiate the degradation. Thus, aliphatic type polymers are particularly prone to this problem since only the impurities in these polymers are capable of absorbing terrestrial solar radiation. Ultraviolet absorbing impurities are also largely responsible for the degradation of many aromatic type polymers by solar radiation and thus for nonreproducibility in weathering of these test specimens as well. Preparation of samples and their treatment during storage can also have a substantial effect on the test results.

Evaluation of Weathering Effects. The particular test method used to evaluate weathering effects depends on the type of polymer and the appearance or mechanical property most important in its application. Appearance changes include discoloration, gloss loss, haze, crazing, chalking, and other visual effects. Some of the appearance changes are measured photometrically, while others are commonly assessed subjectively by visual inspection. The image analysis technique has recently been shown to provide objective and quantitative evaluation of weathering effects on surface morphology (68). The most frequently used criteria for assessing the weather resistance of polymer products that will be subjected to mechanical stress are tensile (or flexural) strength, elongation, impact strength, hardness, and elastic modulus. These techniques and others are described in several reviews on the subject (69,70). The specific criteria used to determine the effects of weathering can significantly influence the acceleration factor and correlation between the laboratory accelerated test and outdoor weathering.

Weathering of polymeric materials proceeds from the irradiated surface inward. Therefore, except for surface effects, changes become evident only after prolonged exposure when degradation has penetrated a sufficient distance into the material. Since degradation is essentially a surface phenomenon, the effects of weathering can be detected sooner by methods that measure surface features than by methods that measure changes in mechanical properties. However, all of these macroscopic property changes require exposure in laboratory accelerated devices for an impractical length of time when evaluating weatherabilities of products designed for useful lifetimes of more than 5 years. An alternative to further intensifying exposure conditions in order to shorten test time is evaluation of weathering effects by sensitive analytical tests that detect molecular (chemical) changes. These are precursors to the macroscopic property changes and thus are indicators of the gross changes long before the latter are manifested. The methods include uv and ir spectral changes, analysis of chemical groups such as carboxyls, hydroperoxides, and free radicals, and measurements of fluorescence and chemiluminescence (69,71–73). The surface-oriented techniques are particularly sensitive

to weathering effects. The value of these methods lies in the extent to which the changes measured are related to the macroscopic changes of the polymers.

Lifetime Predictions. Laboratory accelerated tests have been used primarily for research and development and qualifications of materials, but the ultimate goal is to use them to predict long-term performance under normal use conditions. However, the prediction of service life based on data obtained under accelerated test conditions is still largely an unsolved weathering problem because it is not a simple task. The most direct approach is to determine an acceleration factor relating the exposure time required in the accelerated test device with the time required under natural weathering conditions to produce the same property change. For the reasons given in the section on Acceleration Factors, the acceleration factor must be determined for each type and formulation of a polymeric material and varies with the type of property change measured. A practical proposal for using this approach is to determine the acceleration factor during the early stages of weathering using a sensitive analytical technique for measuring chemical changes (74,75). Assuming the chemical changes and their relation to the macroscopic property changes are the same for the accelerated test and natural exposure, the slower changes measured only by the accelerated test are extrapolated to time to failure outdoors using the acceleration factor. A curve-fitting method to determine the "acceleration shift factor" (ASF) has been developed (76). to account for changes in the relation between accelerated and natural exposure with progression of weathering. The technique requires that the profiles of the graphed property change versus exposure are similar for the two types of exposures. Regression analysis is another technique for deducing lifetimes by natural weathering from lifetimes obtained by laboratory accelerated tests. It is based on measurements of property changes as a function of exposure by both types of tests. It depends on good linear relations over the period measured or finding the mathematical expression between property change and exposure that gives a linear relationship (77). However, the same limitations exist as those inherent in using acceleration factors.

There have been many other empirical approaches to predict service life from accelerated test results, some based on relations between change in polymer properties and exposure variables (78). A simple empirical method of estimating lifetimes by comparison with control materials has recently been proposed (79). The method consists of exposing the test materials in the laboratory accelerated test device simultaneously with several control materials with similar composition and construction to the test material and having a range of failure times outdoors. It requires, as do all service life methods, that the accelerated test produce the same failure modes as natural exposure. In addition, rank correlation between the two exposures should be very high. If these conditions prevail and the service life of the control materials is well defined, the service life of the test material can be bracketed by two control materials.

A variety of techniques based on scientific principles have been also investigated for prediction of weatherabilities. Studies have included mathematical modeling of the effects of weather factors on the degradation process based on data obtained by varying stress levels in laboratory accelerated tests. Various forms of exponential expressions have been used to quantitatively describe the kinetic relations between weather factors and change in properties of polymeric

materials (80–82). It was shown that an approach referred to as the concept of "exposure parameters" was able to successfully predict 2–3 years of outdoor performance of a large number of materials based on several months of accelerated testing (81,82). It has the potential for predicting long-term outdoor weatherability at any location on the basis of accelerated indoor tests using appropriate local weather factors. Mathematical modeling using reliability-based analyses, in which weathering is characterized by frequency of failures, is currently being investigated (83). It requires laboratory accelerated tests on numerous replicate specimens so that life distribution information can be extracted and translated to service life predictions. Valid prediction by either of these mathematical modeling techniques requires accurate data on natural weather conditions, reliable laboratory test data, and considerable experimental effort.

BIBLIOGRAPHY

"Weathering" in *EPST* 1st ed., Vol. 14, pp. 779–795, by J. E. Clark, National Bureau of Standards; "Weathering" in *EPSE* 2nd ed., Vol. 17, pp. 796–827, by N. D. Searle, Consultant, Plastics and Chemicals.

1. N. Robinson, *Solar Radiation*, Elsevier Science Publishing Co., Inc., New York, 1966, pp. 161–195, Chapt. "5".
2. *ASTM G159-98, Annual Book of ASTM Standards, Vol. 14.04, American Society for Testing and Materials, West Conshohocken, Pa.*, 2000.
3. R. C. Hirt and co-workers, *J. Opt. Soc. Am.* **50**, 704–713 (1960).
4. *ASTM D1435-99, Annual Book of ASTM Standards, Vol. 8.01, American Society for Testing and Materials, West Conshohocken, Pa.*, 2000.
5. N. D. Searle, in S. H. Hamid, ed., *Handbook of Polymer Degradation*, 2nd ed., Marcel Dekker, Inc., New York, 2000, pp. 605–643, Chapt. "16".
6. N. D. Searle, in A. V. Patsis, ed., *Int. Conf. on Advances in the Stability and Controlled Degradation of Polymers*, Vol. **1**, Technomic Publishing Co., Lancaster, Pa., 1989, pp. 62–74.
7. N. D. Searle, in D. Kockott, ed., *Int. Sympos. on Natural and Accelerated Weathering of Organic Materials*, Essen, Germany, Sept. 28–29, 1987, Part B, Atlas SFTS BV, Lochem, the Netherlands, 1988, pp. 1–15.
8. L. D. Johnson, W. C. Tincher, and H. C. Bach, *J. Appl. Polym. Sci.* **13**, 1825–1832 (1969).
9. R. M. Fischer and co-workers, *Polym. Mater. Sci. Eng.* **83**, 136–139 (2000). ACS National Meeting, Aug. 20–24, 2000.
10. M. E. Nichols and C. A. Darr, *ACS Symp. Ser.* **722**, 333–353 (1999).
11. B. L. Garner and P. J. Papillo, *Ind. Eng. Chem. Prod. Res. Dev.* **1**, 249–253 (1962).
12. D. Clauson, in *75th Annual IFAI Convention*, Nov. 1987, Industrial Fabrics Assoc. Int'l, St. Paul, Minn., 1988, pp. 96–110 (Preprint).
13. *ASTM G84-99, Annual Book of ASTM Standards, Vol. 3.02, American Society for Testing and Materials, West Conshohocken, Pa.*, 2000.
14. G. C. Furneaux, K. J. Ledbury, and A. Davis, *Polym. Degrad. Stab.* **3**, 441–432 (1980–1981).
15. A. V. Cunliffe and A. Davis, *Polym. Degrad. Stab.* **4**, 17–37 (1982).
16. G. E. Schoolenberg, J. C. M. deBruijn, and H. D. F. Meijer, in *Proc. 14th Int. Conf. on Advances in Stabilization and Degradation of Polymers*, Lucerne, 1992, p. 25.
17. G. Yanai, A. Ram, and J. Miltz, *J. Appl. Polym. Sci.* **59**, 1145–1149 (1996).
18. D. Patil, R. D. Gilbert, and R. E. Fornes, *J. Appl. Polym. Sci.* **41**, 1641–1650 (1990).

19. U. Schulz and P. Trubiroha, in R. J. Herling, ed., *Durability Testing of Nonmet-tallic Materials*, American Society for Testing and Materials, West Conshohocken, Pa., 1996, pp. 106–120. ASTM STP 1294.
20. P. Trubiroha and U. Schulz, *Polym. Polym. Composites* **5**, 359–367 (1997).
21. *ASTM D4364-94, Annual Book of ASTM Standards, Vol. 8.03, American Society for Testing and Materials, West Conshohocken, Pa.*, 2000.
22. *ASTM G7-97, Annual Book of ASTM Standards, Vol. 14.04, American Society for Testing and Materials, West Conshohocken, Pa.*, 2000.
23. *ASTM G24-97, Annual Book of ASTM Standards, Vol. 14.04, American Society for Testing and Materials, West Conshohocken, Pa.*, 2000.
24. M. M. Quayyum and A. Davis, *Polym. Degrad. Stab.* **6**, 201–209 (1984).
25. H. H. G. Jellinek, *Aspects of Degradation and Stabilization of Polymers*, Elsevier, Amsterdam, 1978, Chapt. "3".
26. G. C. Newland, R. M. Schulken Jr., and J. W. Tamblyn, *Mater. Res. Stand.* **3**, 487–488 (1963).
27. *Data supplied by South Florida Test Services, Inc., Miami, Fla*.
28. M. P. Morse, in G. G. Schurr, ed., *Permanence of Organic Materials*, American Society for Testing and Materials, West Conshohocken, Pa., 1982, pp. 43–66. ASTM STP 781.
29. *ASTM D4141–95, Annual Book of ASTM Standards, Vol. 6.01, American Society for Testing and Materials, West Conshohocken, Pa.*, 2000.
30. *SAE J1976, 1998 SAE Handbook, Vol. I, Society of Automotive Engineers, Warrendale, Pa.*, 1998.
31. *SAE J2230, 1998 SAE Handbook, Vol. I, Society of Automotive Engineers, Warrendale, Pa.*, 1998.
32. *ASTM G90-98, Annual Book of ASTM Standards, Vol. 14.04, American Society for Testing and Materials, West Conshohocken, Pa.*, 2000.
33. G. A. Zerlaut and M. L. Ellinger, *J. Oil Col. Chem. Assoc.* **64**, 387–397 (1981).
34. G. A. Zerlaut, in W. E. Brown, ed., *Testing of Polymers*, Vol. **4**, Wiley-Inter-science, New York, 1969, pp. 10–34.
35. R. J. Martinovich and G. R. Hill, in M. R. Kamal, ed., *Weatherability of Plastic Materials*, Wiley-Interscience, New York, 1967, pp. 141–154. Appl. Polym. Symp. No. 4.
36. J. B. Howard and H. M. Gilroy, *Polym. Eng. Sci.* **9**, 286–294 (1969).
37. C. R. Caryl, in W. E. Brown, ed., Ref. 34, 1969, pp. 379–397.
38. G. A. Zerlaut, in W. D. Ketola and D. Grossman, eds., *Accelerated and Outdoor Durability Testing of Organic Materials*, American Society for Testing and Materials, West Conchohocken, Pa., 1994, pp. 3–26. ASTM STP 1202.
39. G. A. Zerlaut, M. W. Rupp, and T. E. Anderson, in *Proceedings of SAE International Congress*, Detroit, Feb. 1985. Paper 850378.
40. R. W. Singleton, R. K. Kunkel, and B. S. Sprague, *Text. Res. J.* **35**, 228–237 (1965).
41. R. W. Singleton and P. A. C. Cook, *Text. Res. J.* **39**, 43–49 (1969).
42. G. A. Zerlaut, in Ref. 28, pp. 10–34.
43. B. Zahradnik, and B. Juriaanse, in *ANTEC '84, 42nd Annual Technical Conference*, 1984, pp. 397–400 (Preprint).
44. *ASTM D5031-96, Annual Book of ASTM Standards, Vol. 6.01, American Society for Testing and Materials, West Conshohocken, Pa.*, 2000.
45. *ASTM D6360-99, Annual Book of ASTM Standards, Vol. 8.03, American Society for Testing and Materials, West Conshohocken, Pa.*, 2000.
46. *ASTM G153-00a, Annual Book of ASTM Standards, Vol. 14.04, American Society for Testing and Materials, West Conshohocken, Pa.*, 2000.
47. *ASTM D822-96, Annual Book of ASTM Standards, Vol. 6.01, American Society for Testing and Materials, West Conshohocken, Pa.*, 2000.

48. *ASTM D1499-99, Annual Book of ASTM Standards, Vol. 8.01, American Society for Testing and Materials, West Conshohocken, Pa.*, 2000.
49. *ASTM G152-00a, Annual Book of ASTM Standards, Vol. 14.04, American Society for Testing and Materials, West Conshohocken, Pa.*, 2000.
50. *ASTM D2565-99, Annual Book of ASTM Standards, Vol. 8.02, American Society for Testing and Materials, West Conshohocken, Pa.*, 2000.
51. *ASTM D4459-99, Annual Book of ASTM Standards, Vol. 8.03, American Society for Testing and Materials, West Conshohocken, Pa.*, 2000.
52. *ASTM G155-00a, Annual Book of ASTM Standards, Vol. 14.04, American Society for Testing and Materials, West Conshohocken, Pa.*, 2000.
53. N. D. Searle, in Ref. 38, pp. 52–67.
54. R. M. Fischer, SAE Tech. Paper Ser. No. 841022, West Coast Int'l Mtg. & Expos., San Diego, Ca., 1984, Society of Automotive Engineers, Warrendale, Pa., 1984, pp. 1–9.
55. H. H. McEwan and L. A. Simpson, Tech. Serv. Rept. D9187GC, Tioxide Group, Plc., London, 1985.
56. D. R. Bauer, M. C. Paputa Peck, and R. O. Carter III, *J. Coat. Technol.* **59**(755), 103–109 (1987).
57. *ASTM D4329-99, Annual Book of ASTM Standards, Vol. 8.03, American Society for Testing and Materials, West Conshohocken, Pa.*, 2000.
58. *ASTM D4587-91, Annual Book of ASTM Standards, Vol. 6.01, American Society for Testing and Materials, West Conshohocken, Pa.*, 2000.
59. *ASTM G154-00a, Annual Book of ASTM Standards, Vol. 14.04, American Society for Testing and Materials, West Conshohocken, Pa.*, 2000.
60. T. M. Kollmann and D. G. M. Wood, *Polym. Eng. Sci.* **20**, 684–687 (1980).
61. *ASTM G151-2000, Annual Book of ASTM Standards*, Vol. 14.04, American Society for Testing and Materials, West Conshohocken, Pa., 2000.
62. *SAE J1885, 1998 SAE Handbook*, Vol. I, Society of Automotive Engineers, Warrendale, Pa., 1998.
63. T. Nguyen and co-workers, *Polym. Mater. Sci. Eng.* **83**, 118–119 (Aug. 2000).
64. *AATCC Technical Manual*, Vol. **63**, American Association of Textile Chemists and Colorists, Research Triangle Park, N.C., 1988, pp. 33–42.
65. *SAE J1960, 1998 SAE Handbook*, Vol. I, Society of Automotive Engineers, Warrendale, Pa., 1998.
66. U. Schulz, P. Trubiroha, T. Boettger, and H. Bolte, in *8th Int. Conf. on Durability of Building Materials and Components*, May 30–June 3, 1999.
67. K. M. Wernstahl and B. Carlsson, *J. Coat. Technol.* **69**(865), 69–75 (1997).
68. F. Lee, B. Pourdeyhimi, and J. Martin, in J. D. Evans and W. D. Ketola, eds., *Durability 2000: Accelerated and Outdoor Weathering Testing*, American Society for Testing and Materials, West Conchohocken, Pa., 2000, pp. 15–34. ASTM STP 1385.
69. N. D. Searle, in J. M. Fitzgerald, ed., *Analytical Photochemistry and Photochemical Analysis: Solids, Solutions and Polymers*, Marcel Dekker, Inc., New York, 1971, pp. 249–336, Chapt. "9".
70. Ref. 25, Chapt. "5".
71. J. L. Gerlock and co-workers, *J. Coat. Technol.* **57**, 37–46 (1985).
72. G. A. George and M. Ghaemy, *Polym. Degrad. Stab.* **33**, 411–428 (1991).
73. V. Dudler, Th. Bolle, and G. Rytz, *Polym. Degrad. Stab.* **60**, 351–365 (1998).
74. D. R. Bauer, J. L. Gerlock, and R. A. Dickie, *Prog. Org. Coat.* **15**, 209–221 (1987).
75. J. L. Gerlock, D. F. Mielewski, and D. R. Bauer, *Polym. Degrad. Stab.* **20**, 123–134 (1988).
76. J. A. Simms, *J. Coat. Technol.* **59**(748), 45–53 (1987).
77. F. Gugumus, in *Symposium on Polymer Stabilization and Degradation: Problems, Techniques and Applications*, Manchester, England, Sept. 1985 (Preprint).

78. R. P. Brown, *Polym. Test.* **14**, 403–414 (1995).
79. R. M. Fischer and W. D. Ketola, in S. H. Hamid, ed., Ref. 5, 2000, pp. 645–669, Chapt. "17".
80. J. E. Clarke and J. A. Slater, NBS Technical Report No. 10116, National Bureau of Standards, Washington, D.C., Oct. 1969.
81. M. R. Kamal, *Polym. Eng. Sci.* **6**, 333–340 (1966).
82. M. R. Kamal and R. Saxon, in M. R. Kamal, ed., Ref. 35, 1967, pp. 1–28.
83. J. W. Martin, S. C. Saunders, F. L. Floyd, and J. P. Wineburg, *Federation Series on Coatings Technology*, Federation of Societies for Coating Technology, Blue Bell, Pa., 1996, pp. 1–34.

NORMA D. SEARLE
Chemical Consultant

ACOUSTIC PROPERTIES

Introduction

Sound speed and sound absorption measurements in polymers are useful both as a probe of the molecular structure of polymers and as a source of engineering design properties. As a molecular probe, acoustic properties are related to such structural factors as the glass transition (qv), cross-link density, morphology (qv), and chemical composition. Thus, acoustic measurements can be used as a measure of any of these factors, or at least to monitor changes that may occur as a function of time, temperature, pressure, or some other variable. As a source of engineering properties, acoustic measurements are used for applications such as the absorption of unwanted sound and the construction of acoustically transparent windows.

A few terms and their units should be defined because not all authors use these terms in the same way.

Acoustic refers to a periodic pressure wave. The term is synonymous with *sonic* and includes waves in the audio frequency range (ie, those that can be heard by the human ear) as well as those above the audio range (*ultrasonic* and *hypersonic*) and below the audio range. Acoustic measurement is a form of dynamic mechanical measurement, though sometimes the latter term is reserved for low frequency (see also DYNAMIC MECHANICAL PROPERTIES).

Absorption is a measure of the energy removed from a sound wave as a result of conversion to heat as the wave travels through the polymer. Absorption is synonymous with *dissipation* and is related to dynamic mechanical terms: damping, loss factor, and loss tangent. Absorption is a material property, usually given the

Encyclopedia of Polymer Science and Technology. Copyright John Wiley & Sons, Inc. All rights reserved.

symbol α, expressed in units of dB/cm, where a decibel (dB) is a unit based on ten times the common logarithm of the ratio of two acoustic energies. Alternatively, the natural logarithm can be used, in which case the units of α are Np/cm, where 1 Neper (Np) is equal to 8.686 dB. It is sometimes convenient to consider the amount of absorption for a specimen thickness equal to one wavelength, λ. This quantity $\alpha\lambda$ has units of dB (or Np). In contrast to absorption, the term *attenuation* includes energy loss due to scattering and reflection as well as absorption. Also, attenuation, in units of dB, is not a material property, but depends on specimen thickness and experimental configuration.

Frequency is the reciprocal of the period of the sound wave. Frequency f is expressed in Hertz (Hz), which is defined as one cycle per second. Sometimes frequencies are expressed in terms of radians. Since there are 2π radians in one cycle, the radian or circular (angular) frequency is given by $\omega = 2\pi f$.

Wavelength, λ (meters), is the distance between successive pressure (stress) peaks of the sound wave, and is the spatial periodicity of the wave. Frequency and wavelength are defined for a sinusoidal, harmonic (single-frequency) sound wave. More complicated, transient sound signals can be expressed as a superposition of harmonic waves with different frequencies.

Sound speed is a scalar quantity: the magnitude of the sound velocity vector. Sound speed will be denoted by v in this article, although c is sometimes used in the literature. Units of sound speed are meters per second (m/s).

This article covers the use of acoustics as a molecular probe of polymer structure and describes various acoustic applications of polymers. Enough theory and experimental details are given to make the presentation understandable, but the emphasis is on the experimental results for polymers. Most of the presentation is for small-amplitude waves in solid polymers. References to some specialized topics are given (see also MECHANICAL PROPERTIES; TEST METHODS).

Theory

This section covers the basic principles and governing equations for the experimental results that follow. Only the conclusions are presented here; the derivations are available in the references. Most of the presentation applies to linear wave propagation, ie, where Hooke's law is valid.

In an unbounded isotropic solid, two types of sound waves can be propagated. In the first type, called a longitudinal wave, the polymer vibrates in the direction of wave propagation. In the second type, called a shear wave, the polymer motion is perpendicular to the direction of propagation. Longitudinal waves are sometimes called dilatational, compressional, or irrotational waves. Shear waves are sometimes called distortional, isovoluminous, or transverse waves. These two types of waves propagate independently of one another and are the only two types possible in an unbounded solid.

Associated with each of the two modes of propagation, there is a sound speed and an absorption. Thus, four parameters are required to specify the acoustic properties of a solid isotropic polymer: longitudinal speed, shear speed, longitudinal absorption, and shear absorption.

Elastic Constants. One of the purposes of measuring sound speeds is to determine the elastic constants of the polymer. Longitudinal sound speed v_l, and shear sound speed v_s are related to elastic constants by

$$v_l = \left[\left(K + 4G/3 \right) / \rho \right]^{1/2} \tag{1}$$

$$v_s = (G/\rho)^{1/2} \tag{2}$$

where K is the adiabatic bulk modulus (equal to the reciprocal of the adiabatic compressibility), G is the shear modulus, and ρ is the polymer density. Equations 1 and 2 are strictly valid only when absorption is low. The absorption corrections have been given (1); the analysis proceeds by making the moduli complex, with the real part equal to the modulus and the imaginary part proportional to absorption.

For an isotropic solid, there are only two independent elastic constants. These two can be taken to be K and G as above, but it is sometimes convenient to use other elastic constants, such as Young's modulus E and Poisson's ratio σ. These constants can be calculated from K and G using the standard relations

$$E = 3G/\left(1 + G/3K\right) \tag{3}$$

$$\sigma = 0.5 - \mathrm{E}/6\mathrm{K} \tag{4}$$

When the lateral dimensions of the specimen are much greater than the wavelength, a longitudinal wave is propagated, as in equation 1. When the lateral dimensions are much less than the wavelength, an extensional wave is propagated. For such a wave, the sound speed is given by

$$v_{ext} = (E/\rho)^{1/2} \tag{5}$$

This type of propagation is most often encountered in the lower frequency range and is an alternative method to equation 3 for determining E.

In a liquid, shear stresses cannot be supported and the only type of wave that is propagated is a bulk wave:

$$v_b = (K/\rho)^{1/2} \tag{6}$$

Other definitions of elastic constants are sometimes used (2). The Lame constants λ and μ are related to K and G in the following manner:

$$\mu = G \tag{7}$$

$$\lambda = K - 2G/3 \tag{8}$$

Other elastic constants are defined starting from the generalized Hooke's law relation between stress σ and strain ε:

$$\sigma_i = C_{ij}\varepsilon_j \tag{9}$$

where $i, j = 1, \ldots, 6$ and the C_{ij} are the elastic stiffness constants. The number of independent constants in the 6×6 C_{ij} matrix depends on the crystal symmetry of the specimen. In the most anisotropic case, there are 21 independent elastic stiffness constants or elastic moduli. As the crystal structure becomes more symmetric, the number of independent constants decreases. For a cubic crystal, there are three independent constants, and for an isotropic solid only two, C_{11} and C_{12}. The C_{ij} matrix in this case is specified by

$$C_{11} = C_{22} = C_{33} = \lambda + 2\mu = K + 4G/3 \tag{10}$$

$$C_{12} = C_{13} = C_{23} = C_{21} = C_{31} = C_{32} = \lambda = K - 2G/3 \tag{11}$$

$$C_{44} = C_{55} = C_{66} = (C_{11} - C_{12})/2 = \mu = G \tag{12}$$

All other terms are zero. In a liquid, there is only one elastic constant K. Note that most polymeric solids are isotropic, either because they are amorphous or because they are polycrystalline, with a random orientation of the crystallites (see AMORPHOUS POLYMERS; SEMICRYSTALLINE POLYMERS).

In comparing elastic constants measured acoustically with those obtained in a static (very low frequency) test, note that acoustic values are measured under adiabatic conditions, while static values are isothermal. The two types of bulk modulus measurements are related by the standard thermodynamic relation

$$\frac{K}{K_T} = \frac{C_p}{C_v} = 1 + \frac{TV\alpha^2 K}{C_p} \tag{13}$$

where K and K_T are the adiabatic and isothermal bulk moduli, C_p and C_v are the specific heat capacities at constant pressure and volume, T is absolute temperature, and α is the cubic thermal expansion coefficient (3). (It is unfortunate that the same symbol α is also used for absorption; in context, there should be no confusion.) For shear modulus

$$G_S = G_T = G \tag{14}$$

ie, the adiabatic and isothermal moduli are equal. This result follows from the fact that shear deformation occurs at constant volume. The magnitude of K/K_T is on the order of 1.1 for polymers, and increases as the temperature is raised above the glass-transition temperature (4). This effect is more pronounced in polymers than in metals.

In addition to the adiabatic or isothermal difference, acoustically determined elastic constants of polymers differ from static values because polymer moduli are frequency-dependent. The deformation produced by a given stress depends on how long the stress is applied. During the short period of a sound wave, not as much strain occurs as in a typical static measurement, and the acoustic modulus is higher than the static modulus. This effect is small for the bulk modulus (on the order of 20%), but can be significant for the shear and Young's modulus (a factor of 10 or more) (5,6).

Strain dependence should also be considered when comparing acoustically measured elastic constants with statically measured values. As an example, for polyethylene at room temperature, the modulus is independent of strain up to a strain of about 10^{-4} (7). Beyond this point, the modulus decreases as the strain increases. Typically, acoustic measurements are made in the strain range 10^{-6}–10^{-9}, where the moduli are strain-independent, but static measurements often exceed the linear strain limit (8).

Sound Absorption. The absorption of sound in polymers can be high, in certain ranges of temperature and frequency, up to four orders of magnitude higher than typical for metals. The mechanisms of the high absorption are various molecular structural relaxation processes involving motion of the entire long molecular chains, or of selected short molecular segments. Second-order transitions (9) are associated with the various molecular relaxation processes, where a given molecular relaxation motion fully participates in the thermodynamic response of the polymer at temperatures above the transition temperature, and does not participate (is "frozen") at temperatures below the transition temperature.

The average time required for the specific molecular motion is an important parameter of the relaxation process. This time is called the relaxation time, τ, and it is a function of temperature and pressure. When the frequency of the dynamic stress (acoustic or vibration) is in the range of $1/\tau$, the strains in the polymer lag the applied stress, because of structural molecular relaxation, which leads to conversion of mechanical energy to heat, and to damping of the acoustic wave (or mechanical vibration). This type of mechanical response of the polymer is called *viscoelastic behavior* (see VISCOELASTICITY). At low frequencies, $f \leq 1/\tau$, the molecules have time to respond to the applied stress and the structural molecular relaxation completely follows the applied stress. Therefore, stress and strain are in phase and mechanical energy loss is low. The sound speeds, and elastic constants, in this frequency region are denoted by the subscript 0. At high frequencies, $f \geq 1/\tau$, the period of the applied stress is too short for the given molecular relaxation process to occur. Stress and strain are again in phase, sound absorption is low, and the sound speeds and elastic constants in this frequency range are denoted by the subscript ∞. The high frequency sound speeds are greater than the low frequency values, because of increased stiffness of the polymer at high frequencies (no molecular relaxation). It follows from the above discussion that sound speeds and elastic moduli of a polymer are frequency dependent in temperature (and pressure) ranges where a transition occurs. Also, at frequencies $f \approx 1/\tau$ there is a peak in the sound absorption per wavelength, $\alpha\lambda$.

The glass transition (qv), in the amorphous portions of the polymer, is the transition that dominates the acoustic properties of many polymers. At temperatures below the glass-transition temperature, T_g, or at frequencies $\geq 1/\tau_g$, the sound speeds have "glassy" values. At temperatures above T_g, or at frequencies $\leq 1/\tau_g$ the mechanical response of the polymer is 'rubbery.' (As shown in Figs. 1 and 2.)

The discussion that follows, of sound propagation in a lossy polymer, is limited to the case where the stress–strain relation in the polymer is linear. The effect of loss mechanisms on the mechanical response of polymers is included by modifying the stress–strain relations (eq. 9). At small strains, at which the behavior of the polymer is linear, the stress–strain relations are modified according to the

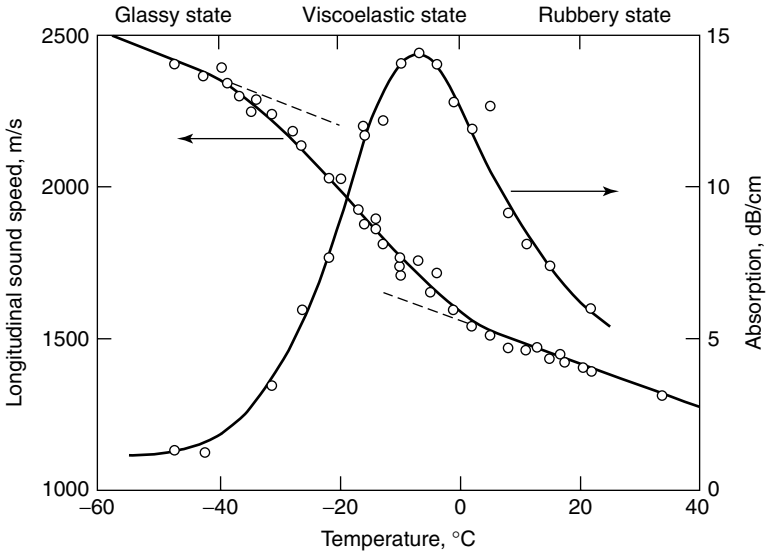

Fig. 1. The glass transition for poly(carborane siloxane)—longitudinal sound speed and absorption vs temperature at 1 MHz. Adapted from Ref. 49.

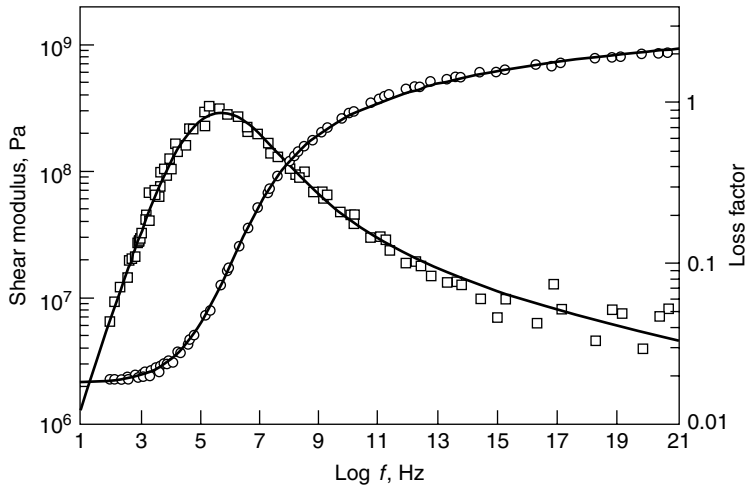

Fig. 2. The glass transition for a polyurethane (PTMG2000/MDI 3/BDO/DMPD)—shear modulus(○) and loss factor(□) vs frequency at room temperature. Adapted from Ref. 50.

Boltzman Superposition Principle (3,10). This principle states that the stress at a given point in the polymer is a function of the entire strain history at that point. Therefore, to each strain term in equation 9 is added an integral that represents contributions to the stress at a given time from strain increments at earlier times.

For example, the stress–strain relation for shear strain in an isotropic material is $\sigma = G\varepsilon$. For a viscoelastic material this relation is modified as follows:

$$\sigma(t) = G_\infty \varepsilon(t) - \int_0^\infty M(\Delta t)\varepsilon(t - \Delta t)\, \mathrm{d}\Delta t \tag{15}$$

where $\sigma(t)$ and $\varepsilon(t)$ are the shear stress and strain, at a given point in the material, at time t, and G_∞ is the high frequency (instantaneous) shear modulus. $M(\Delta t)$ is an 'after-effect,' at time t, of the strain at time $(t-\Delta t)$. Physically $M(\Delta t)$ is a relaxation function, since it describes the relaxation of molecular process excited by an imposed strain. Other stress–strain relations are modified similarly.

The Boltzman Superposition Principle is one starting point for inclusion of structural relaxation losses. An equally valid starting point is to include in equation 9 time derivatives (first-order and higher) of stress and strain. It can be shown that this approach is equivalent to the above integral representation (10). Finally, modified stress–strain relations, to describe viscoelastic response, have also been formulated using fractional derivatives (11).

A characteristic feature of viscoelastic response is the phase lag between the strain and the applied stress, due to the loss mechanisms. This phase difference is described by defining complex wave numbers, sound speeds, and elastic moduli, as follows. The relations that follow are developed specifically for a shear wave propagating through an absorbing polymer. Similar relations can be developed for longitudinal and extensional waves. Sound signals are either single-frequency (harmonic) waves, or transient signals that can be represented as a superposition of harmonic waves of different frequencies. A harmonic wave is a particularly simple case of wave motion, since in this case all quantities (stress, strain, particle displacement, etc) vary harmonically, at the same frequency. When the modified stress–strain relations are used to derive the equation for sound wave motion, the solution for a progressive, plane, harmonic wave is (11,12),

$$p = p_0\, e^{-\alpha_s x}\, e^{i(k_s' x - \omega t)} \tag{16}$$

where p is the acoustic pressure at distance x from the reference point where the pressure is p_0, $k_s' = 2\pi/\lambda_s$ is the real part of the shear wave number, where λ_s is the shear wavelength, and α_s is the sound attenuation coefficient, for shear waves, in nepers per meter. From equation 16 it follows that sound attenuation can be formally included in the wavenumber by defining a complex wavenumber,

$$k_s^* = k_s^{'} + i k_s^{''} = k_s^{'} + i\alpha_s \tag{17}$$

The expression for the shear wave now has the same form, $p = p_0 \exp[i(k_s{}^* x - \omega t)]$, as in a lossless medium. The complex wavenumber defines a complex sound speed for the material as follows:

$$v_s^* = \frac{\omega}{k_s^*} \tag{18}$$

The propagation of the wave as a function of space and time is still determined by the phase velocity, v_s, which is related to the real part of the wavenumber, $v_s = \omega/k_s{}'$.

The elastic moduli of a lossy material are also complex quantities. The relation between the complex shear wave speed and the complex shear modulus is

the same as the relation between the corresponding real quantities (eq. 2),

$$G^* = G' - iG'' = \rho v_s^{*2} \tag{19}$$

From equations 17–19 it follows that the sound attenuation coefficient is related to the complex elastic modulus,

$$\left(k_s'^2 - \alpha_s^2\right) + i(2k_s'\alpha_s) = \frac{\rho\omega^2}{G'(1+r^2)}(1+ir) \tag{20}$$

where r is called the loss factor, and is the ratio of the imaginary to the real part of the modulus,

$$r = \tan\delta = \frac{G''}{G'} \tag{21}$$

Equations 18–20 can be solved for the real and imaginary parts of the complex shear modulus (1),

$$G' = \rho v_s^2(1-r^2)/(1+r^2)2 \tag{22}$$

$$G'' = 2\rho v_s^2 r/(1+r^2)2 \tag{23}$$

A material is characterized as low loss when the attenuation per wavelength, $\alpha\lambda$, is small, $\alpha\lambda \ll 1$ or $\alpha \ll k'$. Then the loss factor is small, $r \ll 1$, and the above relations simplify to

$$k_s'^2 = \frac{\rho\omega^2}{G'} \quad \text{and} \quad \alpha_s\lambda_s = \pi r \tag{24}$$

where the shear wavelength $\lambda_s = 2\pi/k_s'$. Equation 24 is an approximation that overestimates G' by 40% when $\tan\delta = 1$, and by 1% when $\tan\delta = 0.1$. From the above equations it follows that the complex modulus is closely related to the sound speed and absorption. In particular, the frequency dependence of the real part of the elastic modulus (G') is similar to the frequency dependence of the corresponding sound phase velocity (v_s). Also, the frequency dependence of the loss factor, $\tan\delta$, is similar to the frequency dependence of $\alpha\lambda$, as shown in Figures 1 and 2.

Techniques for measuring the complex sound speeds and moduli of polymers are described in the section on test methods. The data shows that the real and imaginary components of the elastic moduli are frequency dependent. The frequency dependence is strongest for materials with high values of the loss factor r. Materials with frequency-dependent elastic moduli are called *dispersive*, and measurements and theory show that sound absorption mechanisms lead to *dispersion*. The real and imaginary part of an elastic modulus are related by the Kramers–Kronig relations, which are presented in the next section.

Kramers–Kronig Relations. The Kramers–Kronig (KK) relations are derived from the basic causality condition that the output strain cannot precede the input stress in any physical material (13–15). These relations apply to the complex, frequency-dependent elastic moduli of any material, and relate the real and imaginary components of the modulus. For example, for the complex shear modulus, $G^*(\omega) = G'(\omega) + iG''(\omega)$, the Kramers–Kronig relations are

$$G'(\omega) - G_\infty = \frac{1}{\pi} PV \int_{-\infty}^{+\infty} \mathrm{d}\omega' \, \frac{G''(\omega')}{(\omega' - \omega)} \tag{25}$$

$$G''(\omega) = -\frac{1}{\pi} PV \int_{-\infty}^{+\infty} \mathrm{d}\omega' \, \frac{G'(\omega') - G_\infty}{(\omega' - \omega)}$$

where PV is the principal value of the integral and G_∞ is the high frequency ($\omega \to \infty$) modulus. Similar relations hold for the complex bulk modulus, $K^*(\omega)$. The KK relations are significant to the acoustic designer because they show that it is not possible to select the modulus (G') and the loss factor ($\tan \delta = G''/G'$) of a material independently. The KK relation can also be used to check the consistency of experimental data. Lack of agreement between the measured loss factor and that calculated from the modulus is an indication of some experimental error. Likewise, an analytical model for a complex modulus must obey KK in order to be a physically meaningful relation.

A useful, approximate local version of the KK relation was developed by O'Donnel and co-workers (14). This approximation relates the attenuation coefficient α to the frequency derivative of the phase velocity, $\mathrm{d}v/\mathrm{d}\omega$, as follows:

$$\alpha(\omega) = \frac{\pi \omega^2}{2c^2} \frac{\mathrm{d}v}{\mathrm{d}\omega} \tag{26}$$

Equation 26 applies both to shear and longitudinal waves, where α and v are related to the real and imaginary parts of the appropriate modulus by equations 22 and 23. Examples of application of the KK relations are given in References (16) and (17). The KK relations are particularly useful for discussion of the acoustical and mechanical behavior of polymers in the viscoelastic state. In this state polymers have a high loss factor, and are used for underwater sound attenuation and for vibration damping. Equation 26 shows the trade-offs that have to be made in choosing a viscoelastic material for any specific sound attenuation or vibration damping applications. For example, it follows from equation 26 that, for shear waves, a high value of α_s requires a large $\mathrm{d}v_s/\mathrm{d}\omega$ in the viscoelastic region, which points to a material with a large relaxation strength $(G_\infty – G_0)/G_0$ and a narrow range of relaxation times. However, experience shows that in materials where the viscoelastic region occurs over a narrow range of frequencies the relaxation times, and therefore $\alpha_s(\omega)$, are strongly temperature dependent.

Equation of State. An equation of state in this context is a relation between pressure, volume, and temperature in a polymer, or a relation between any two of these variables holding the third constant. Frequently, these equations

involve the bulk modulus. Given the equation of state of a polymer, one can correlate much experimental data and extrapolate to high pressure, where measurement is difficult.

By making reasonable assumptions about the form of the intermolecular potential, it was possible to calculate bulk modulus as an analytic function of volume (18). The calculation agrees fairly well with experimental data, and with the assumption that volume is the primary factor determining bulk modulus and, by extension, sound speed.

The Gruneisen parameter is widely used in polymer equation-of-state calculations. Bulk modulus is primarily a function of volume. The volume of a polymer can be changed by varying either the pressure or the temperature, leading to two equivalent expressions for the Gruneisen parameter γ:

$$\gamma = \frac{1}{2}\left(\frac{\partial K}{\partial p}\right)_T \tag{27}$$

$$\gamma = -\frac{1}{2\alpha}\left(\frac{\partial \ln K}{\partial T}\right)_p \tag{28}$$

For solid polymers, equations 27 and 28 give approximately the same value (19).

The Gruneisen parameter also plays a role in nonlinear acoustics, and it has been shown that there is a relation between the Gruneisen parameter and ultrasonic absorption: the larger γ is, the higher the absorption (19).

Transitions. In polymer science, a change from one state to another is a transition. An important transition is the glass to rubber transition. Processes occurring at temperatures below the glass transition are called secondary transitions, even if it is not known what the two states are. The transition is identified as such through its effect on some physical property, like dynamic mechanical damping. In acoustics, processes of this type are generally called relaxations (see GLASS TRANSITION; VISCOELASTICITY).

Acoustic properties vary with frequency. Assuming this behavior can be described by a single time called the relaxation time, the frequency dependence of either longitudinal or shear waves is given by

$$v^2 = v_0^2 + \left(v_\infty^2 - v_0^2\right)\frac{\omega^2\tau^2}{1+\omega^2\tau^2} \tag{29}$$

$$\frac{\alpha\lambda}{\pi} = \frac{\left(v_\infty^2 - v_0^2\right)\omega\tau}{v_0^2 + v_\infty^2\omega^2\tau^2} \approx \frac{v_\infty^2 - v_0^2}{v_\infty^2}\frac{\omega\tau}{1+\omega^2\tau^2} \tag{30}$$

where the subscripts 0 and ∞ refer to low and high frequency limiting values, respectively, and τ is the relaxation time (20). Note that $\alpha\lambda$ is a maximum for $\omega\tau = 1$. This absorption peak is identified with a particular relaxation process or transition in the polymer.

It is generally assumed that the temperature dependence of the relaxation time is of the Arrhenius form:

$$\tau = \tau_0 \exp\left(\Delta H/RT\right) \tag{31}$$

where ΔH is the activation energy for the relaxation process, R is the gas constant, and τ_0 is a constant. Since $\tau = 1/\omega = 1/2\pi f$ at the absorption maximum, an Arrhenius plot of $\ln f$ vs $1/T$ has a slope of $-\Delta H/R$. Each point on the plot is the reciprocal temperature of the absorption peak for a given logarithmic measurement frequency. Arrhenius plots are a particularly revealing way of examining acoustic data and interpreting results in terms of molecular structure. If the Arrhenius plot is not a straight line, it is assumed that ΔH is a function of temperature.

A significant result in equations 29 and 30 is that the acoustic properties depend only on the product $\omega\tau$, not on either variable separately. Since τ is a function of temperature, as shown in equation 31, the results of changing frequency are indistinguishable from those of changing temperature (neglecting any changes in ν_0 and ν_∞). The applicability of time–temperature superposition directly follows from the form of these equations. The analytic form of the temperature dependence of the relaxation time is, however, not specified in equations 29 and 30.

The discussion so far has been limited to the single relaxation time model. In polymers, however, the measured absorption and sound speed vs frequency curves are much broader than predicted by the single relaxation time model. This observation is interpreted to mean that there is a continuous distribution of relaxation times in polymer relaxation. There has been considerable analysis of various empirical distributions of relaxation times (21). Arrhenius plots are still valid in this case, but the activation energy is interpreted as an average value. Because of the distribution of relaxation times in polymers, measurements over a broad frequency range (several decades) are required to map out a given relaxation. Experimentally, it is difficult to cover such a wide range of frequencies without using several different pieces of equipment. Acoustic measurements are then sometimes supplemented with dielectric measurements. The governing equations are strictly analogous and, in many cases, dielectric and acoustic data can be displayed on the same Arrhenius plot. A full discussion is given in Reference 21.

Hysteresis Absorption. In the vicinity of a polymer transition, the absorption vs frequency at first increases, and then decreases. In a region removed from a transition, however, absorption typically increases linearly with frequency. This behavior is referred to as hysteresis absorption and is observed in both crystalline and amorphous polymers, and also in such materials as metals and rocks. An absorption proportional to frequency can be expressed as $\alpha = cf = c\nu/\lambda$, or $\alpha\lambda =$ a constant, ie, absorption per wavelength independent of frequency is another way of describing hysteresis absorption.

It is generally assumed that the description of polymer properties requires a continuous distribution of relaxation times. Numerous forms of the distribution function have been assumed, often for mathematical simplicity or on the basis of physical intuition. It has been found that a fractional power law distribution of relaxation times of the form τ^{-m} leads to hysteresis absorption with $\alpha\lambda = m\pi/2$ (Np), when $m \leq 1$ (3). The disadvantage of this model is that attempts to justify this distribution of relaxation times on a molecular basis quantitatively have not been successful. Mathematically, almost any experimental result can be expressed in terms of a distribution of relaxation times, but there may not be any physical significance to the distribution.

It has been suggested that the origin of the hysteresis absorption is in the time delay of reorienting the polymer among the large number of metastable

equilibrium positions possible (8). The magnitude of the hysteresis absorption should depend on free volume because of two competing effects: the number of segments that reorient themselves decreases with decreasing volume, and the fraction of these segments that does not return to their original orientation increases with decreasing free volume. The second effect generally dominates, and the hysteresis absorption increases with decreasing free volume. The form of the volume dependence of the hysteresis absorption was originally assumed to be a simple linear dependence (8), but is probably more complicated (22).

Inhomogeneous Media. The inhomogeneities considered here are on the macroscopic rather than microscopic scale. The first topic considered is layered media. To begin with, consider a flat boundary between two media of different acoustic properties. When an acoustic wave traveling through one medium encounters at normal incidence the boundary with another medium, some of the acoustic energy is reflected and some transmitted (12). The sound power transmission coefficient T is given by

$$T = \frac{4Z_1Z_2}{(Z_1 + Z_2)^2} \tag{32}$$

where the subscripts refer to the two media, and the acoustic impedance Z is given by

$$Z = \rho v \tag{33}$$

Thus, the transmission properties depend on the impedance match of the two media. For a flat plate in a liquid medium

$$\frac{1}{T} = \cos^2 k_2 l + \frac{1}{4}\left(\frac{Z_2}{Z_1} + \frac{Z_1}{Z_2}\right)^2 \sin^2 k_2 l \tag{34}$$

where $k = \omega/v$, subscript 2 refers to the plate, subscript 1 refers to the liquid, and l is the thickness of the plate (12). The extension of these results to multiple layers of plane parallel plates at oblique angles of incidence, including the effect of absorption, has been considered by several authors (23,24). Some work has been done to determine polymer properties from the acoustic properties of plate transmission (25). Reflections from multiple concentric cylinders (26) and from spheres (27) have also been examined.

Another class of inhomogeneous materials of increasing practical importance is fiber-reinforced composites (qv). Usually the matrix is a polymer, such as epoxy. The reinforcement may be polymeric, such as Kevlar, or nonpolymeric, ie, glass, steel, or graphite. For a unidirectional composite with transverse isotropy, there are five independent elastic constants or moduli: C_{11}, C_{13}, C_{33}, C_{44}, and C_{66}, (28,29). Absorption measurements are particularly difficult to make on such composites. Frequently, the measured attenuation has a significant contribution as a result of scattering from the reinforcement; this is sometimes referred to as geometric dispersion.

Foamed materials can be considered to be the opposite of fiber reinforcement (see CELLULAR MATERIALS). In a foam, the gas inclusions make the matrix softer

and weaker. The introduction of even small amounts of air into a polymer can have a dramatic effect on acoustic properties. One approach to modeling the effect of a small air content ϕ on the acoustic properties of a rubber is to use Kerner's theory of composites (30):

$$K = K_0(1-\phi)/(1+3K_0\phi/4G_0) \tag{35}$$

$$G = 3G_0(1-\phi)/(3+2\phi) \tag{36}$$

$$\rho = \rho_0(1-\phi) \tag{37}$$

where the subscript 0 refers to solid rubber and the Poisson's ratio of rubber is assumed to be one-half. Longitudinal and shear sound speeds can be calculated from these equations. Absorptions can be included by making the moduli complex. In addition to Kerner's model, other models for polymer composites with microscopic inclusions have been developed (31–33). One application of such composites is for absorption of underwater sound (34). Also, this type of composite can be used as a sound-absorbing lining, at ultrasonic frequencies, in immersion tanks (35).

Nonlinear Wave Propagation. It is assumed that most acoustic measurements are made in the linear wave propagation region, ie, where Hooke's law applies. Polymers as a class, however, are more nonlinear than other solids. Nonlinear wave propagation is therefore significant in some cases.

Extensive studies of nonlinear propagation in fluids have been made (36). Although derived for fluids, the results have been applied to a number of solid polymers (37,38). In these studies, the isentropic equation of state for pressure p, in terms of density ρ, is expanded to the form

$$p - p_0 = A[(\rho-\rho_0)/\rho_0] + (B/2)[(\rho-\rho_0)/\rho_0]^2 + \cdots \tag{38}$$

The quantity B/A is the parameter of nonlinearity. From thermodynamic evaluations,

$$\frac{B}{A} = 2\rho_0 v\left(\frac{\partial v}{\partial p}\right)_T + \frac{2v\alpha T}{\rho_0 C_p}\left(\frac{\partial v}{\partial T}\right)_p \tag{39}$$

where α is the thermal-expansion coefficient. The extension of this analysis to solids involves third-order elastic constants (39). There are few measurements of third-order elastic constants for polymers. One method for determining these constants is to measure the velocities of longitudinal and shear waves in the material as a function of various applied static stresses. Hughes and Kelly (40) give the following values for polystyrene: $\ell = -18.9 \pm 0.3$, $m = -13.3 \pm 0.3$, $n = -10.0 \pm 0.1$, in units of GPa. It is found that the third-order elastic constants are related to the Gruneisen parameter. Relationships have also been found between B/A and the Gruneisen parameter (41). This is another manifestation of the fact that the Gruneisen parameter is a fundamental measure of the nonlinear behavior of a polymer.

One particular interest in nonlinear propagation in polymers is for what is known as a parametric sonar. In this application, two colinear high frequency

beams of slightly different frequency are propagated through a medium. In a perfectly elastic medium, the two waves would propagate indefinitely without interacting. In a real medium containing nonlinearity, however, there is an interaction that produces waves with the sum and difference frequencies of the two beams. Thus, a low frequency beam is generated with the highly directional character of a high frequency beam. Polymers are particularly attractive in this application because of their high nonlinearity and high absorption. Hence, the efficiency of the frequency conversion is high, and the high frequency source components are absorbed relatively quickly while the low frequency difference wave propagates much further (37).

Additive Properties. It is reasonable to assume that different chemical groups should contribute differently to the macroscopic properties of polymers. Rigid aromatic groups would be expected to raise the elastic modulus (and sound speed), while flexible aliphatic groups would be expected to lower the modulus. A quantitative expression of this idea is known as the method of additive properties and has been extensively developed and reviewed by Van Krevelen (42). In this method it is assumed that various polymer properties are determined solely from the additive contributions of their constituent groups. The groups are assumed to have unique properties that are independent of their environment. The uniqueness assumption has proven to be valid in many cases.

The simplest example of additive properties states that the molar mass M of a polymer is the sum of the molar masses of the component groups in the repeat unit. A similar equation holds for the molar volume and leads to an expression for the polymer density,

$$M = \sum N_i M_i, \quad \rho = \frac{\sum N_i M_i}{\sum N_i V_i} \tag{40}$$

where M_i is the mass of the ith component group, N_i is the number of such groups in the repeat unit, and V_i is the molar volume of the ith component group.

As applied to sound speed, the method of additive properties begins with work on liquids, where it was empirically found that

$$R = V v^{1/3} \tag{41}$$

where V is molar volume, ν is sound speed, and R is a constant, for each liquid, known as Rao's constant or the molar sound speed (43). R is an additive property, but ν is not. Since a liquid cannot support a shear stress, the sound speed in a liquid can be calculated by equation 6, so that, in terms of modulus, Rao's rule (eq. 41) can be written as

$$R = V(K/\rho)^{1/6}, \quad K = (M/V)(R/V)^6 \tag{42}$$

In applying Rao's rule to solid polymers, it should be kept in mind that the longitudinal sound speed (eq. 1) includes not only a bulk modulus term, but also a shear modulus term that must be taken into account (5). This has been done for both linear and cross-linked polymers (44–47). Van Krevelen has named the additive variable for bulk modulus the Rao function, U_R, and for shear modulus the

Table 1. Group Contributions to U_H and U_R

Group	U_H, $(cm^3/mol)(cm/s)^{1/3}$	U_R, $(cm^3/mol)(cm/s)^{1/3}$
—CH_2—	880	675
—$CH(CH_3)$—	1,875	1,650
—$CH(C_6H_5)$—	4,900	4,050
—CHCl—	1,725	1,450
—$C(CH_3)(COOCH_3)$—	4,220	3,650
—C_6H_5—$C(CH_3)_2$—C_6H_5—	11,000	8,700
—O—	400	300
—OCOO—	1,575	1,200
—CONH—	1,750	1,400

Hartmann function, U_H. The bulk and shear moduli can then be calculated from the equations,

$$K = (M/V)(U_R/V)^6 \quad \text{and} \quad G = (M/V)(U_H/V) \tag{43}$$

Group contributions to U_R and U_H for some common molecular groups, taken from Van Krevelan (42), are listed in Table 1. The bulk and shear moduli for various polymers calculated using the values from Table 1 are in good agreement with experimental values (42). Sound speeds can be predicted from the calculated elastic moduli and densities.

A limitation of the above method is that some of the required group properties are not available. This is particularly a hindrance when trying to predict the properties of polymers with novel compositions. To overcome this limitation, a new additive contribution method has been developed (48) in which the polymer properties are expressed in terms of topological variables or connectivity indices. In this method properties are determined primarily from the summation of contributions of atoms and bonds instead of groups. The pertinent properties of the handful of elements found in most polymers have been determined, allowing for the prediction of properties for most polymers having a known structure.

Sound as a Molecular Probe

Acoustic measurements have been employed as a molecular probe of polymer structure to study different aspects of molecular structure: transitions, curing (UV, visible light, thermal) (qv), density, and chemical composition in both synthetic and biological polymers.

Transitions.

Glass Transition. The acoustic properties of polymers, when plotted over broad ranges of frequency and temperature, are usually dominated by the glass transition. Typical data are shown in Figures 1 (49), and 2 (50). The change in slope of the sound speed at about −40°C is independent of frequency and is equal to the dilatometric value of T_g. This method of determining T_g has been applied to a number of polymers (51–53). The change in slope at −40°C occurs as a result of

the discontinuity in the thermal expansion coefficient and the strong dependence of modulus on density. The value of T_g determined in this manner is dependent on the density, but independent of frequency. It is important to keep in mind the difference between the glass-transition temperature, T_g, which is a fixed number, and the glass transition, which is a process that occurs at different temperatures depending on the frequency of the measurement.

Figure 1 shows the variation, in the glass-transition region, of the longitudinal sound speed and absorption with temperature at a fixed frequency, for poly(carborane siloxane). Figure 2 shows the real part of the shear modulus and the loss factor as a function of frequency, at a fixed temperature, for a polyurethane. From equation 24 it follows that the variation of the shear sound speed and absorption is similar. The longitudinal sound speed changes from ∼1500 m/s in the rubbery state to ∼2300 m/s in the glassy state. The change in the shear sound speed in the polyurethane is from ∼50 to ∼900 m/s. The large change in the shear sound speed through the glass-transition region is typical for polymers.

In small amounts, crystallinity raises T_g by limiting the motions of the amorphous regions. As the degree of crystallinity increases, the glass transition, which occurs only in the amorphous regions of the polymer, tends to be masked and may even be difficult to determine, as in the case of polyethylene. At the glass transition of an amorphous polymer, some 10–50 repeat units become free to move in cooperative thermal motion of individual chain segments, involving large-scale rearrangements of the chain backbone. Below the glass transition, these large-scale motions become frozen and cannot occur. Major changes in many physical properties, including acoustic properties, take place at the glass transition (16).

Most studies of glass transition have focused on the absorption. By repeating the measurements of Figure 1 at higher frequencies, an Arrhenius plot of the log of test frequency vs reciprocal temperature of peak absorption can be made, yielding an activation energy of about 100 kJ/mol; this is a typical value for glass transitions, albeit on the low side. A compilation of literature data for seven semicrystalline polymers has been given (54). An example of the results for polytetrafluoroethylene is shown in Figure 3. For the glass (ie α) transition, the activation energy is 700 kJ/mol, the highest value in this group. Note that an Arrhenius plot, such as Figure 3, is a convenient way to keep track of multiple transitions in a given polymer and in correlating data from various sources and various experimental techniques. Acoustic measurements over a limited range of temperature and frequency may indicate a relaxation, but it is not always clear what mechanism is producing the effect. A plot like Figure 3 is very useful in identifying the relaxation.

In the case of isotactic polypropylene, two glass transitions were found acoustically—as well as by using other techniques (55). It was shown that whereas the crystalline phase is isotactic, the amorphous phase, which gives rise to the glass transitions, includes atactic as well as isotactic chains. The atactic amorphous phase has the lower T_g.

Through consideration of Arrhenius plots of the glass transition of 14 polymers, the empirical observation was made that the lines for the various polymers all seemed to converge in one of two regions: 10^8 Hz for the more sterically restricted polymers, and 10^{18} Hz for sterically nonrestricted polymers (56). This

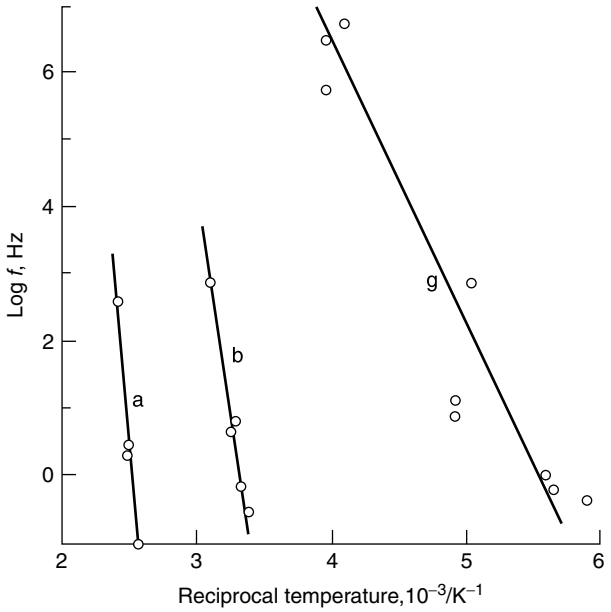

Fig. 3. Arrhenius plot for α, β, and γ transitions in polytetrafluoroethylene.

observation shows that there is a direct relation between dilatometric T_g and activation energy: the higher the T_g, the higher the activation energy. In addition to the data discussed (54,56), an even more complete summary of acoustic data on solid polymers has been compiled (57).

The glass transition provides the behavior that has the most practical significance. Secondary transitions are too small to have much effect and polymers are not generally practical to use at their melting point. The glass transition shows a large change through the transition and can be used both above and below the transition. The glass transition is a second-order phase transition, in which the primary thermodynamic functions are continuous but their first derivatives are discontinuous. For example, the specific heat capacity vs temperature is continuous through the glass transition but the derivative of the specific heat is discontinuous. The sound speeds and elastic moduli are continuous but their derivatives are discontinuous.

The most successful phenomenological model of the frequency dependence of the elastic constants around the glass transition is the Havriliak–Negami (HN) model (58)

$$(G - G_\infty)/(G_0 - G_\infty) = 1/(1 + (i\omega\tau)^\alpha)^\beta \tag{44}$$

where G_0 is the relaxed modulus (the rubbery modulus in this case), G_∞ is the unrelaxed modulus (the glassy modulus in this case), τ is the average relaxation time, and α and β are dimensionless parameters with values between 0 and 1 that, roughly, describe the width and asymmetry of the glass transition.

One application of the HN equation is that one can demonstrate an empirical relation between the height and width of the loss factor peak at the glass transition. Using measured properties of a number of polyurethanes and calculations using equation 44, it was shown (59) that high loss factor peaks are narrow and broad peaks are low. A simple relation was found between the height and width of the peak in shear sound absorption per wavelength, $\alpha_s\lambda$, as a function of frequency—namely, the product of height times width is a constant equal to 1.5 decades of frequency. These relations are important in design of polymer treatments for sound absorption and vibration damping. An example of the above relations is shown in Figure 4.

It is commonly observed that the temperature and frequency dependence of polymer relaxations are related. This is expressed qualitatively as the time–temperature superposition principle, or the frequency–temperature equivalence,

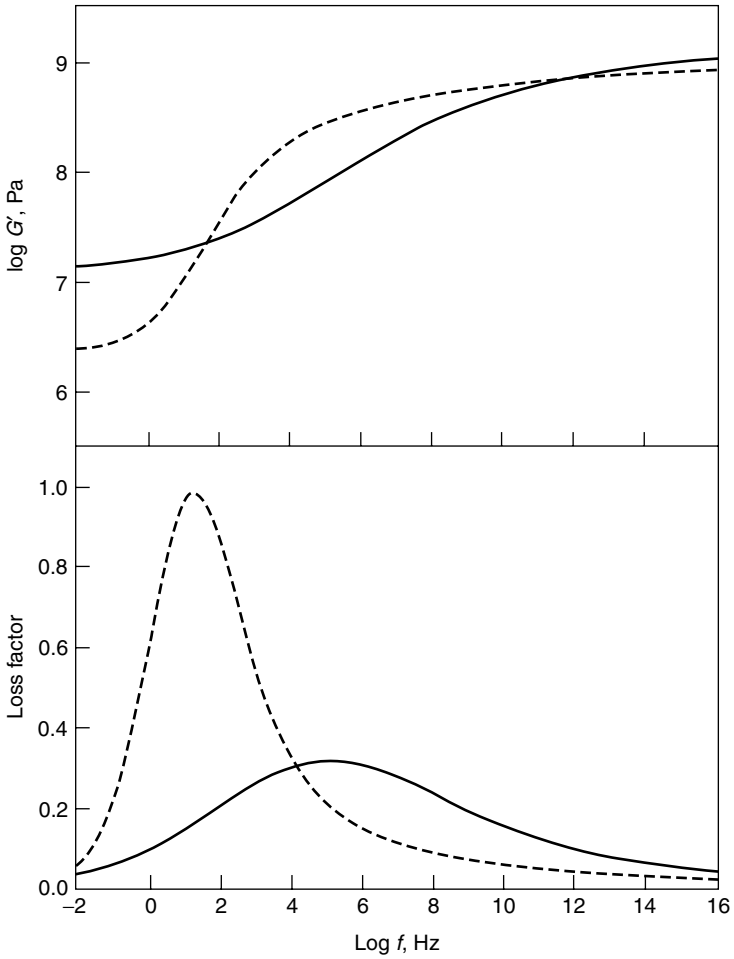

Fig. 4. Phase-separated polyurethane (solid line) compared with phase-mixed polyurethane (dashed line). The shear modulus and the loss factor are plotted as a function of frequency, through the glass-transition region. From Ref. 50.

or the method of reduced variables. A mathematical way to describe this behavior is to note that if the dispersion relation for the relaxation [eqs. 29,30, and 44] depends on frequency and temperature only through the product of frequency and a function of temperature, $\omega\tau(T)$, then the effect of a change in frequency is indistinguishable from a change in temperature. In other words, a measurement at low temperature is equivalent to a measurement at high frequency and a measurement at high temperature is equivalent to a measurement at low frequency—"equivalent" meaning that the same elastic constants and sound speeds are obtained. A material for which this equivalence holds is called thermorheologically simple. Polymers are thermorheologically simple to a greater or lesser extent. The principle is extremely useful as it allows a wide frequency range to be obtained by simply changing temperature; a frequency range that would be obtained directly only with great difficulty, if at all. A plot of modulus vs log frequency, such as Figure 2, is called a master curve.

The relation between temperature and frequency dependence is described by a function known as the shift factor, defined as the change in log frequency that is equivalent to a change in temperature. The most common analytical form of this equation is the WLF equation (3,60)

$$\log a_{\mathrm{T}} = -\frac{c_1(T - T_0)}{c_2 + (T - T_0)} \tag{45}$$

where a_{T} is the change in log frequency due to a change in temperature from a reference temperature T_0 to a measurement temperature T, and c_1 and c_2 are constants for a given polymer and reference temperature. [An extensive listing of c_1 and c_2 values is given by Ngai and Plazek (61).] This equation has been found to apply in general to polymers above their glass-transition temperatures. Below the glass-transition temperature, the Arrhenius equation has been found to be applicable (21)

$$\log a_{\mathrm{T}} = \frac{\Delta H}{R}\left(\frac{1}{T} - \frac{1}{T_0}\right) \tag{46}$$

where ΔH is the activation energy and R is the gas constant. The combination of a master curve and a shift factor curve then contains all of the temperature- and frequency-dependence information for the given polymer.

As the temperature of a polymer is raised through the glass-transition of a polymer, the moduli and sound speeds change from the high value of the glassy state to the low value of the rubbery state. There has been considerable study of the relation of the glass-transition temperature to the molecular structure of the polymer, which then relates to the elastic constants of the polymer. Examples include molecular weight, polarity, and steric effects (62). T_{g} increases asymptotically with increasing molecular weight according to the relation (63)

$$T_{\mathrm{g}} = T_{\mathrm{g},\infty} - A/M_{\mathrm{n}} \tag{47}$$

where $T_{\mathrm{g},\infty}$ is the glass-transition temperature at infinite molecular weight, A is a constant for each polymer, and M_{n} is the number-average molecular weight. The

presence of polar groups in the polymer increases the T_g. For example, poly(*cis*-1,4-isoprene) (natural rubber), with the chemical structure $-CH_2CH{=}C(CH_3)CH_2-$, has a glass-transition temperature of $-73^\circ C$ while polychloroprene (neoprene), with the chemical structure $-CH_2CH{=}C(Cl)CH_2-$, has a T_g of $-50^\circ C$. The substitution of a chlorine atom for a methyl group (with comparable size) raises the transition temperature. A correlation has been observed between the log of the average relaxation time τ in the HN equation and the reciprocal of the glass-transition temperature (64).

Secondary Transitions. Most acoustic studies of polymer transitions have been of the glass transition, but some work has been done on secondary transitions, ie, those occurring below the glass transition. One transition that has received a fair amount of study is the β relaxation in polycarbonate (65). The transition has an activation energy of 40 kJ/mol and arises from a combination of phenylene and heteroatom motion. This value, one-half to one-third the value for a glass transition, is typical of secondary transitions which involve smaller segments of the polymer. This study also found a correlation that often, but not always, exists between acoustic and dielectric measurements. The two sets of data fall on the same line and sometimes cover complementary frequency ranges. Activation energies for some secondary transitions are even smaller. The δ relaxation in poly(ethyl methacrylate), owing to ester ethyl group rotation, has an activation energy of only 9 kJ/mol (66). A study of the activation energy for the δ relaxation in polychlorotrifluoroethylene showed it to be 30 kJ/mol, and possibly associated with an uncoiling of the polymer chain. This work emphasized the usefulness of pressure as a complementary variable to temperature and frequency in the study of molecular relaxations in polymers (67).

Most of the polymers discussed so far have been linear and either amorphous or semicrystalline. The γ transition in some cross-linked epoxies is similar to that of linear polymers (68). The activation energy is 40 kJ/mol and is due to the motion of the glycol ether group.

In a detailed discussion of secondary transitions in glassy, amorphous polymers, it is shown that the β transition in polymethacrylates is caused by motion of the entire $-COOR$ group (69). This same study notes that the Arrhenius plot lines for secondary transitions of various polymers all converge to a common frequency, about 10^{13} Hz; this is the same type of empirical behavior observed for the glass transition (56).

Melting Transition. The final transition to be considered is the melting transition. Measurements at 12 MHz on linear polyethylene show that there is an absorption peak in the vicinity of the melting point and that the sound speed decreases rapidly in this region (70). Other studies show that the absorption peak does not shift with frequency and therefore is not a relaxational process (71); this type of behavior can indicate a fluctuation mechanism. The loss factor can be high in the molten region, but the shear modulus is very low. Therefore, polymers are not generally used in the molten state for damping applications.

Curing. Early measurements on polyesters, phenolic, and melamine polymers made during the curing process showed a significant rise in sound speed as the materials passed from the uncured stage, through the gel stage, to the fully cured condition (72). Absorption increased during the gel stage and then dropped in the fully cured stage (see GEL POINT). Increasing the cure temperature

increases the final sound speed and decreases the final absorption. Later work on epoxies has emphasized the difficulty in making such measurements because of temperature changes caused by the reaction exotherm, the increase of T_g, as curing proceeds, and the viscoelastic nature of the epoxies (73).

Most cure studies are done on solid polymers that have undergone various cure cycles. One study focused on the γ relaxation in diamine-cured epoxies (74). This relaxation is due to the motion of the glycol ether group, $-CH_2CHOHCH_2O-$, and is common to epoxies made with different resins and curatives. An advantage of the acoustic method is that the measurements can be made below T_g, so that the measurement process does not alter the molecular structure being measured. It was found that the absorption curve increased in height, width, and temperature as the cure temperature was raised. The activation energy was found to be dependent on the degree of cure, increasing from about 60 kJ/mol during the early stages of cure to as much as twice that value (depending on the curative) in the postcured state, as a result of steric hindrance (75).

In a curing study on resole-type phenolic, no correlation between sound speed and curing temperature was found, but both longitudinal and shear absorption decreased as the cure temperature increased (76). This behavior was related to a transition in the phenolic at about 70°C.

Another study considered the effect of cross-link density on the acoustic properties of some diamine-cured aliphatic epoxy polymers (77,78). In this case, the cross-link density was varied by altering the chain length of the aliphatic curative. The acoustic properties in the vicinity of the glass transition were found to shift—unaltered in shape—by an amount equal to the glass-transition temperature. Thus, a plot of sound speed and absorption vs $T-T_g$ gave universal curves for all polymers. In contrast, it has been shown that when the cure temperature and time are varied for another epoxy system, not only does the molecular relaxation shift, but there are also structural changes (79). Also, ultrasonic systems have been developed to monitor the cure of epoxy resins and to characterize the cure state. This is done by measuring the ultrasonic signal velocity and ultrasonic attenuation throughout the cure process (80,81).

Density. For organic liquids, it is observed that the higher the density, the higher the sound speed. Similar behavior is found with solid polymers. For polyethylene, a plot of extensional sound speed vs density is shown in Figure 5 (82). The data appear to be well represented by a straight line, though Rao's relation for liquids (eq. 41) would suggest that $v^{1/3}$ should be plotted, rather than v. The scatter in the data is such that it is inconclusive whether the linear or the cubic relation gives the best result (5,83). In the polyethylene studies, the chemical composition of the polymer was the same. Different densities resulted primarily from different degrees of crystallinity. Another study considered variations in chemical composition and plotted longitudinal sound speed vs density for 14 different polymers (52). Good correlation was found, except for the halogenated polymers. In a study of resole-type phenolic, it was found that the longitudinal sound speed correlated with density not only at room temperature, as the other studies had found, but also as a function of temperature, all on the same plot (76).

From a practical point of view, it is important to remember the correlation between sound speed and density when comparing data from different sources for the same polymer. As can be seen from Figure 5, even small changes in density

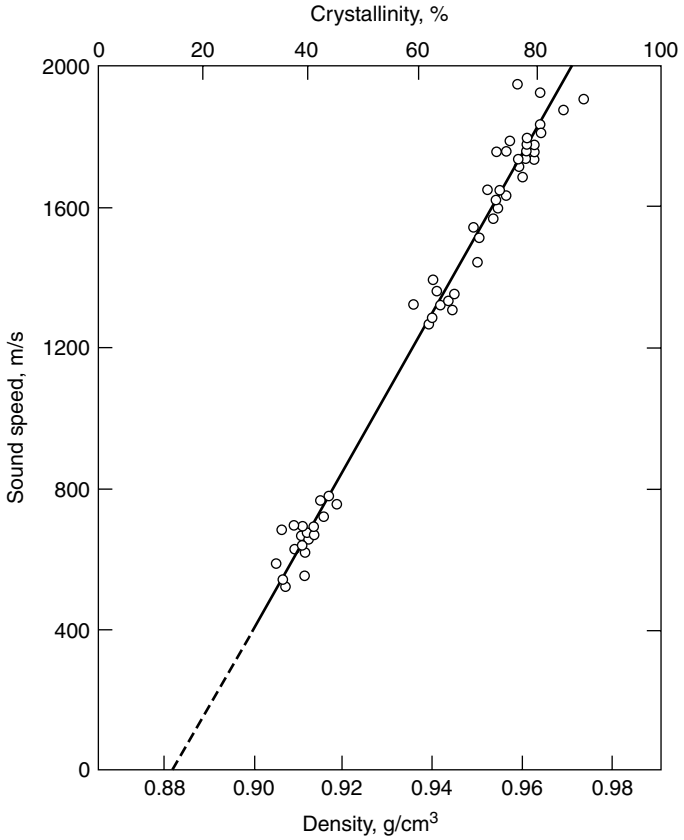

Fig. 5. Extensional sound speed vs density and crystallinity for polyethylene.

produce large changes in sound speed. This type of behavior was mentioned previously in connection with the effect produced in the vicinity of the glass transition. Also, because of the direct relation between density and crystallinity, sound speed measurements provide a means of measuring or monitoring polymer crystallinity.

From a fundamental point of view, sound speed can be said to depend primarily on volume because of the volume dependence of the intermolecular potential. Any mechanism that changes the volume of the polymer will change the sound speed by an amount determined by the volume change, and not by the mechanism producing the volume change. This is true for such diverse mechanisms as degree of crystallinity, branching, cross-linking, and temperature and pressure changes.

Sound Speed. A number of studies have been made on the effect of variations in molecular structure on sound speed. Replacing the hydrogen atoms in polyethylene with fluorine atoms lowers the sound speed, in line with the expectation that there will be a reduction in intermolecular attraction due to the larger size of the fluorine atoms (53). In this case, the sound speed also decreases because the polymer density increases. Similarly, in a series of poly(alkyl methacrylates), the sound speed decreases as the alkyl side-chain length increases (84). Again, there is a volume increase that reduces the intermolecular attraction.

The introduction of a phenylene group into an epoxy polymer structure raises the sound speed. These polymers and other phenylene-containing polymers, such as polycarbonate, polysulfone, and poly(ether sulfone), all have relatively high sound speeds (65). The aromatic ring imparts a conformational rigidity to the backbone structure of these polymers, which is responsible for the high sound speed.

So far, the molecular variations discussed were made in homopolymers. A number of studies have been made on multiple-component systems, either chemical combinations such as copolymers or physical combinations such as plasticized polymers. As an example of the former, the sound speed in copolymers of methyl methacrylate and methacrylic acid increases in a regular manner as the mole fraction of methacrylic acid increases (85).

Several studies have been made of the effect of various plasticizers (qv) on poly(vinyl chloride) (86–88). In addition to shifting the glass transition, the plasticizers lower the sound speed. Since the sound speed in the plasticizers is less than that in poly(vinyl chloride), this is not surprising. Water can be considered as a plasticizer. Its effect on poly(methyl methacrylate) is the lowering of sound speed expected from a plasticizer (89).

The sound speed in polymer blends (qv) varies with composition in a manner similar to that in copolymers. For blends of polystyrene and poly(vinyl methyl ether), the sound speed increases as the weight percent of the higher-sound-speed polystyrene increases, but the relation may not be linear because of phase inversion caused by polymer incompatibility (90) (see COMPATIBLITY). The effect of carbon black (qv) on sound speed in rubber is more complicated than in blends, but the qualitative effect is to increase the sound speed (91). In contrast, the addition of iron oxide to rubber decreases the sound speed (92). In this case, the higher density of the filler dominates, rather than the higher modulus. A decrease in sound speed is also observed when voids are present (79). In this case, the lower modulus of the voids dominates, rather than the lower density.

Additive Properties. Many of the studies cited have considered the effect on the sound speed, of substituting one component for another or an aromatic for an aliphatic. One is thus led to the possibility that there is a certain sound speed associated with each chemical component. This is indeed the case, as was first demonstrated for liquids, and then for solid polymers.

For liquids, it was empirically found that the Rao constant R of equation 41 was an additive property, which was expressed in terms of individual atom values (43). Since the measurements also showed that aromatic compounds have higher sound speed than aliphatic compounds, an R value was also assigned to the carbon–carbon double bond. It was later pointed out that better results are found by considering bonded atom groups such as C—H, C—C, O—H, etc (93). A further refinement was to use radical increments, $-CH_3$, $-CH_2-$, $-C_6H_5$, etc (94).

In an extensive account of the application of the method of additive properties to numerous polymer properties, component values determined from measurements on organic liquids were used and good agreement between predicted and measured sound speeds were found (42). This approach has now been applied to numerous linear polymers (45,46,95).

Results have also been obtained for the density and bulk modulus of crosslinked epoxies (44). Agreement is about the same as for linear polymers. Finally,

shear modulus has been related to an additive property (47). These results, along with the additive results for density and bulk modulus, show how both longitudinal and shear sound speeds are related to molecular components.

Biological Polymers. Although biopolymers are structurally and morphologically different from the polymers discussed so far, biopolymers are similar in their long-chain polymeric nature. Also, many of the techniques of studying other polymers apply to biopolymers. Perhaps the most common observation on the acoustic properties of biopolymers is that the absorption is a linear function of frequency, ie, a hysteresis absorption (96,97). Because of its appearance in very different biopolymers, hysteresis is presumed to arise whenever there is a broad spectrum of relaxation times (96), perhaps through the same mechanism postulated for other polymers (97).

In measurements on liver tissue, the absorption was found to be high, compared with blood, and sensitive to variation of protein structure (96). By making measurements on tissue that had successively more extensive destruction of the gross tissue structure, it was found that the absorption is largely independent of cellular and subcellular structure. Absorption occurs primarily at the macromolecular level. A comprehensive compilation of ultrasonic properties of mammalian tissues that gives absorption results for 30 different tissue types has been prepared (98). One conclusion of this work was that since tissue condition or preparation or both may influence ultrasonic properties, *in vivo* measurements should be encouraged. Most measurements in biopolymers have been made with longitudinal waves, but some data are available for shear sound speed and absorption (99). Some progress has been made in characterizing the pathological state of a tissue in a study that also examines hysteresis absorption and presents a theory in terms of a distribution of relaxation times (100).

The dynamic elastic properties of soft tissues, and methods of measurement (including acoustic techniques) are reviewed by Sarvazyan (101). The corresponding review for hard tissues is given by Lees (102). Propagation of acoustic waves in human tissue is of interest because acoustic waves, both at audio and ultrasonic frequencies, are widely used in medicine for imaging and identification of tumors. Recently, nuclear magnetic resonance techniques have been developed for imaging the propagation of shear waves in biopolymers (103).

Applications

In this section, results of acoustic measurements that are used directly in some applications are presented without molecular interpretation.

Sound Speed. Representative sound speeds measured at room temperature, ambient pressure, and at frequencies in the MHz range are given in Table 2, taken from various sources (49,76,85,87,104–106,108,109). (Abbreviations for polymers listed in Table 2 are given in Tables 3 and 4.). The longitudinal speeds vary from about 1000 to 3000 m/s, a range intermediate between that of metals (3000–6000 m/s) and that of liquids (900–1500 m/s). Shear speeds vary from about 700 to 1400 m/s, a range lower than the 1600 – 3300 m/s range for metals. Densities are also listed in Table 2 because the speed in a given polymer varies with density. Owing to the usual variations from batch to batch of polymer,

Table 2. Sound Speeds[a] for Various Polymers

	Density, g/cm^3	Longitudinal, speed v_1, m/s	Shear speed v_s, m/s	Ref.[b]
General polymers[c]				
Poly(methacrylic acid)	1.285	3350		85
Phenolic polymer	1.22	2840	1320	76
Epoxy polymer	1.205	2820	1230	
Polyhexamethyleneadipamide	1.147	2710	1120	
Polycaprolactam	1.146	2700	1120	
Poly(methyl methacrylate)	1.191	2690	1340	
Polypropylene	0.913	2650	1300	
Polyphenylquinoxaline	1.209	2460	1130	76
Polyoxymethylene	1.425	2440	1000	
Polyethylene, high density	0.957	2430	950	
Polystyrene	1.052	2400	1150	
Poly(vinyl chloride)	1.3916	2376		87
Poly(vinyl butyral)	1.107	2350		
Polysulfone	1.24	2297		104
Poly(phenylene oxide)	1.08	2293		104
Polycarbonate	1.19	2280		104
Poly(ethylene oxide)	1.208	2250		
Poly(4-methyl-1-pentene)	0.835	2180	1080	105
Polyurethane, polyether-based	1.104	2130		49
Poly(acrylonitrile–butadiene–styrene)	1.023	2040	830	105
Polyethylene, low density	0.922	1970		
Poly(vinylidene fluoride)	1.779	1930	775	
Polyurethane, polybutadiene-based	1.008	1660		49
Poly(carborane siloxane)	1.041	1450		
Polytetrafluoroethylene	2.177	1380		
Polydimethylsiloxane	1.045	1020		
Epoxy polymers[d]				
DGEBA/DETA	1.190	2910		106
DGEBA/TETA	1.184	2810		106
BDGE/MPDA	1.227	2579		77
DGEBA/D	1.162	2520		107
BDGE/PDA	1.179	2423		77
BDGE/HDA	1.152	2301		77
BDGE/DDA	1.094	2033		77
DGEPG/TETA	1.116	1561		106
DGEPG/DETA	1.108	1561		106
Urethane polymers[d]				
PTMG650/TDI/TMAB	1.118	1744		108
PTMG650/TDI/MBOCA	1.119	1717		108
PTMG1000/TDI/TMAB	1.089	1632		108
PTMG1000/TDI/MBOCA	1.085	1606		108
PTMG2000/TDI/TMAB	1.047	1545		108
PTMG2000/TDI/MBOCA	1.045	1547		108
PTMG2692/TDI/TMAB	1.035	1523		108
PTMG2692/TDI/MBOCA	1.035	1523		108
Filled polymers				
DGEBA/TETA/39% glass spheres	1.050	2879		106
Poly(vinyl chloride) + DOP	1.290	2120		87
Poly(isobutylene–isoprene) + carbon	1.130	1973		
Polychloroprene + carbon	1.420	1720		
1,2-Polybutadiene + carbon	1.100	1567		
cis-1,4-Polyisoprene + carbon	1.120	1524		

[a] Measurements made at room temperature, ambient pressure, and frequencies in the MHz range.
[b] Taken from Ref. 109 except as noted.
[c] See Table 3.
[d] See Table 4.

Table 3. Trade Names of Some Common Polymers

ABS	Generic abbreviation for a terpolymer of acrylonitrile, butadiene, and styrene
Cycolac	Poly(acrylonitrile–butadiene–styrene) or ABS (Marbon)
Delrin	Poly(methylene oxide) or polyformaldehyde (DuPont)
Kel-F	Poly(chlorotrifluoroethylene) (3M)
Kynar	Poly(vinylidene fluoride) (Pennwalt)
Lexan	Polycarbonate (General Electric)
Lucite	Poly(methyl methacrylate) (ICI)
Marlex	Polyethylene (and other polymers) (Phillips Petroleum)
Mylar	Poly(ethylene terephthalate) (DuPont)
Nylon	Generic description of a polyamide, including nylon-6 (polycaprolactam) and nylon-6,6 (polyhexamethylene adipamide)
Plexiglas	Poly(methyl methacrylate) (Rohm & Haas)
Teflon	Poly(tetrafluoroethylene) (DuPont)
TPX	Poly(4-methyl-l-pentene) (Mitsui)
Zytel	Poly(hexamethylene adapamide) or nylon-6,6 (DuPont)

Table 4. Abbreviations for Epoxy and Polyurethane Polymers

BDGE	Butanediol diglycidyl ether
BEPD	2-Butyl-2-ethyl-1,3-propanediol
D	Tri(2-ethyl hexoate) salt of tri(dimethyl amino methyl) phenol
DDA	Dodecanediamine
DEPD	2,2-Diethyl-1,3-propanediol
DETA	Diethylenetriamine
DGEBA	Diglycidyl ether of bisphenol A
DMPD	2,2-Dimethyl-1,3-propanediol
DOP	Dioctylphthalate
EMPD	2-Ethyl-2-methyl-1,3-propanediol
HDA	Hexanediamine
MBOCA	Methylene bis(*o*-chloroaniline)
MDI	4,4′-Diphenylmethane diisocyanate
MDIL	Modified MDI (liquid)
MPDA	*m*-Phenylene diamine
PDA	Propanediamine
PPG	Polypropylene glycol
PTMG	Poly(tetramethylene ether) glycol
PTMAB	Poly(tetramethylene diaminobenzoate)
RDGE	Resorcinol diglycidyl ether
TDI	Toluene diisocyanate
TETA	Triethylenetetramine
TMAB	Trimethylene-bis-*p*-aminobenzoate
Z	Aromatic eutectic mixture of methylene dianaline, MPDA, and phenyl glycidyl ether
13BDO	1,3-Butanediol
14BDO	1,4-Butanediol

Table 5. Temperature Dependence of Sound Speeds[a]

Polymer	$-dv_l/dT$, m/(s·K)	$-dv_s/dT$, m/(s·K)	Ref.
Polysulfone	1.38		104
Polystyrene	1.5	4.4	110
Poly(phenylene oxide)	1.52		104
Poly(methyl methacrylate)	2.5	2.0	109
Polyphenylquinoxaline	3.0	1.3	76
Polycarbonate	3.58		104
Poly(acrylonitrile–butadiene–styrene)	4.1	1.5	105
Poly(4-methyl-1-pentene)	4.2	1.8	105
Phenolic polymer	7.1	4.0	76
Polyethylene, high density	9.6	6.8	109
Polypropylene	15.0	6.7	109

[a]Measurements made in the vicinity of room temperature, at ambient pressure, and at frequencies in the MHz range.

the sound speeds given in Table 2 can easily differ by 1% or more from other measurements.

Table 2 is representative of the variation in speeds found from one polymer type to another. Considerable variations within one type can also occur. For example, within a series of epoxy polymers (47,77), the longitudinal speed can vary from 2000 to 3000 m/s. For poly(vinyl chloride), plasticizers (87) can lower the longitudinal speed from 2380 to 1490 m/s. The variation of sound speed with density (crystallinity) has already been mentioned (82) and is illustrated in Figure 5.

Many sound speed measurements in polymers have been made as a function of temperature, usually over a range of 100 K or less. Qualitatively, the speeds decrease as the temperature increases. Except in the vicinity of a transition, the decrease is usually linear and of greater magnitude than for metals. Representative values of the rate of decrease of sound speeds with temperature are given in Table 5. Measurements were made over a 300-K temperature range for poly(ethylene terephthalate) (111) and for styrene–butadiene–styrene block copolymers (112). Measurements for a series of polyimides were made over a 600-K range (113).

Cryogenic temperature measurements of both longitudinal and shear speeds have been made for many polymers. For polyethylene, polytetrafluoroethylene, polyformaldehyde (acetal resin), and polyamides (114,115) at low temperature, there is a plateau in the temperature dependence where sound speed becomes independent of temperature. All relaxation processes have become frozen out. For poly(methyl methacrylate), however, there is no plateau (116). Even at very low temperature, the methyl group attached to an ether link can rotate. Fluoropolymers also exhibit more complicated behavior (117). Some measurements in the range 0.2–2 K on two epoxy polymers indicate a peak rather than a plateau (118).

Measurements as a function of frequency are not common because of the experimental difficulties. Most data are available only at three or four frequencies

Table 6. Absorptions for Various Polymers[a]

Polymer	Longitudinal absorption, dB/cm	Shear absorption, dB/cm	Ref.
Poly(methyl methacrylate)	1.4	4.3	8
Poly(4-methyl-1-pentene)	1.4	6.7	105
Polyethylene, high density	3.3	25.0	8
Polyphenylquinoxaline	3.5	15.0	76
Phenolic polymer	4.1	19.0	76
Poly(ethylene oxide)	7.1		8
Polyurethane, polyether-based	7.5		49
Polyurethane, polybutadiene-based	9.1		49

[a]Measurements made at room temperature. ambient pressure, and a frequency of 2 MHz.

covering about one decade. Qualitatively, the speeds increase as the frequency increases. Longitudinal measurements on vulcanized rubber compounds at five frequencies from 0.04 to 10 MHz are available (119), as well as longitudinal and shear results for a nitrile–butadiene vulcanizate at 2, 5, and 10 MHz (120). By using time–temperature superposition, longitudinal and shear measurements at 0.5, 1, and 2 MHz as a function of temperature on an epoxy polymer have been extended to a very wide frequency range (121).

Measurements as a function of pressure are available in a few cases. Qualitatively, the speed increases as the pressure increases. Most studies have only gone as high as 200 MPa. Measurements have been made on polystyrene (122), poly(methyl methacrylate) (122), polyethylene (122), polyisobutylene (123), natural rubber vulcanizate (124), plasticized poly(vinyl chloride) (125), and polychlorotrifluoroethylene (67). Other measurements have been made up to 300 MPa for high density polyethylene (126), and up to 500 MPa for poly(methyl methacrylate) (127). Finally, measurements to 1 GPa have been made for polystyrene (126) and poly(methyl methacrylate) (128). For the latter, $dv_l/dp = 2.66$ m/(s·MPa) and $dv_s/dp = 1.07$ m/(s·MPa).

Absorption. Representative sound absorptions measured at room temperature, ambient pressure, and a frequency of 2 MHz are given in Table 6. The longitudinal absorptions vary from 1 to 10 dB/cm and the shear absorptions vary from 4 to 25 dB/cm. These values are higher than for metals. The measurements in Table 6 were not made near the glass transition; much higher values are found near the glass transition. For one epoxy, the peak longitudinal absorption at 2 MHz was 30 dB/cm (77). Rubber compounds typically have the highest peak absorptions. At 10 MHz, peak longitudinal absorptions vary from 150 dB/cm for butadiene–styrene rubber to 450 dB/cm for butyl rubber (91,119). Absorption measurements are sensitive not only to the temperature and frequency of the test, but also to the state of the polymer owing to such factors as plasticization (86,88,89,93) and crystallinity (71).

Absorption measurements as a function of temperature have been made over moderate temperature ranges for a variety of polymers, including vulcanized rubbers (91,119,120), poly(methyl methacrylate) (128), poly(4-methyl-l-pentene) (105), poly(acrylonitrile–butadiene–styrene) (ABS) (105), epoxy polymers (47,77),

polyphenylquinoxaline (76), phenolic polymer (76), fluoropolymers (53), polycarbonate (65), polysulfone (65), and poly(ether sulfone) (65). Measurements over a wide temperature range have been made for polyethylene (70) and polyimides (113).

Measurements as a function of frequency indicate hysteresis behavior when not in the vicinity of a transition (8,128). By using time–temperature superposition, a wide range of frequencies covering the glass transition of natural rubber has been obtained (124). Other frequency measurements, covering less than one decade, have been made for various polymers (65,89,91,120).

Measurements as a function of pressure have been made in a few cases. For poly(methyl methacrylate) (128), the hysteresis shear absorption at 1 GPa is about one-fourth of that at ambient pressure. For plasticized poly(vinyl chloride) (125), polyisobutylene (123), and natural rubber vulcanizate (124), upon the application of pressure, the glass transition peak shifts to higher temperature with a lower but broader peak.

Elastic Constants. For the polymers listed in Table 2 for which both longitudinal and shear sound speeds are given, the elastic constants have been calculated at room temperature, ambient pressure, and a frequency of 2 MHz; these are listed in Table 7. The moduli values are approximately 1 order of magnitude lower than those for metals. The range of Poisson's ratio values is somewhat higher than that for metals. A review of elastic properties of polymers is given by Hartmann (130).

In addition to the measurements given in Table 7, other data are available, including polyethylene as a function of density (crystallinity) (5); natural rubber vulcanizate compressibility as a function of temperature, pressure, and frequency (124); bulk and shear moduli as a function of temperature for various polymers (47, 53,131,132); and the pressure and temperature dependence of the bulk modulus of poly(methyl methacrylate) (128) and polystyrene (110).

Table 8 gives values of the real part of the extensional modulus (eqs. 3 and 5) and the loss factor. The values for most of the polymers are outside the glass-transition region, while the values for polyurethanes are typical of the glass-transition region. The high values of tan δ are of interest for sound absorption and for vibration damping.

Data on the frequency dependence of elastic moduli was obtained by Lagakos co-workers (129), who used different techniques to determine the Young's modulus E' both at kHz and at MHz frequencies. Their values for the frequency derivative of E' are given, for selected polymers, in Table 9. These values are typical for the region outside the glass transition.

In addition to chemical composition, the morphology of the polymer also affects the elastic constants. For example, the moduli of crystalline regions of a polymer are different from the amorphous regions of the same chemical composition. Also, especially in the polyurethanes, the degree of microphase separation influences elastic constants. In this case there are soft segments and hard segments (not necessarily crystalline) that are mixed or separated to varying degrees and this affects the elastic constants. An example is shown in Figure 4, where a phase-separated polyurethane (PTMG1000/MDI 3/BDO) is compared with a phase-mixed polymer (PTMG1000/MDI 3/DMPD). The data in this figure illustrates the general trend that a phase-mixed polyurethane will have low rubbery

Table 7. Elastic Constants for Various Polymers[a]

Polymer	Density, g/cm^3	Bulk modulus K', GPa	Shear modulus G', GPa	Young's modulus E', GPa	Poisson's ratio σ	Ref.[b]
General polymers						
Phenolic polymer	1.22	7.02	2.13	5.79	0.36	76
Epoxy polymer	1.184	7.13	1.83	5.05	0.38	
Polyhexamethylene adipamide	1.147	6.53	1.43	3.99	0.40	
Polycaprolactam	1.146	6.45	1.43	4.00	0.40	
Poly(methyl methacrylate)	1.191	6.49	2.33	6.24	0.34	
Polypropylene	0.913	4.37	1.54	4.13	0.34	
Polyphenylquinoxaline	1.209	5.21	1.54	4.20	0.37	76
Polyoxymethylene	1.425	6.59	1.43	4.01	0.40	
Polyethylene, high density	0.957	4.54	0.91	2.55	0.41	
Polystyrene	1.052	4.21	1.39	3.76	0.35	
Poly(4-methyl-l-pentene)	0.835	2.67	0.97	2.61	0.34	105
Poly(acrylonitrile–butadiene–styrene)	1.023	3.33	0.70	1.96	0.40	105
Poly(vinylidene fluoride)	1.779	5.18	1.07	3.00	0.40	
Polycarbonate	1.194	4.57	0.99	2.77	0.40	129
Poly(vinyl chloride)	1.386	5.41	1.59	4.34	0.37	129
Polysulfone	1.236	4.92	1.05	2.94	0.40	129
Poly(phenylene oxide)	1.073	3.86	1.07	2.94	0.37	129
Polytetrafluoroethylene	2.18	2.79	1.16	3.06	0.32	114
Epoxy polymers						
RDGE/PDA	1.2711	8.65	2.64	7.19	0.36	47
RDGE/MPDA	1.3023	8.23	2.62	7.11	0.36	47
RDGE/HDA	1.2299	7.88	2.14	5.89	0.38	47
DGEBA/PDA	1.1844	7.28	1.97	5.42	0.38	47
DGEBA/MPDA	1.2033	6.78	2.00	5.46	0.37	47
DGEBA/HDA	1.1595	6.52	1.69	4.67	0.38	47
RDGE/DDA	1.1667	6.38	1.29	3.63	0.41	47
DGEBA/Z	1.202	6.27	1.81	4.95	0.37	121
DGEBA/DDA	1.1255	5.34	1.15	3.22	0.40	47
Filled polymers						
Polyester + water	1.042	2.94	0.44	1.26	0.43	
Polyepoxide + glass spheres	0.718	2.57	1.18	3.07	0.30	
Polyepoxide + glass spheres	0.793	2.40	0.83	2.23	0.35	
Polyepoxide + glass spheres	0.691	2.14	0.95	2.48	0.31	

[a]Measurements made at room temperature, ambient pressure, and at frequencies in the range 1–2 MHz.
[b]Taken from Ref. 109 except as noted.

modulus and a phase-separated polyurethane will have a high rubbery modulus. The glassy modulus is about the same in both cases. Associated with the low rubbery modulus is a high, narrow loss peak, while a low, broad loss peak is associated with the high rubbery modulus.

Elastic constants for unidirectional fiber composites with transverse isotropy have been measured for some composites (qv) with an epoxy matrix. Depending

Table 8. Extensional Modulus and Loss factor at Room Temperature[a]

Polymer	ρ, g/cm^3	E', GPa	tan δ	f_{av}, kHz	Ref.
General polymers at various frequencies					
Polyethylene	0.964	3.58		9	82
Polyethylene	0.907	0.27		3	82
Poly(2,6-dimethyl-1,4-phenylene oxide)	1.06	2.39	0.01	10	133
Poly(ethylene terephthalate)	1.380	2.70	0.01	0.1	111
Poly(ethylene terephthalate)	1.335	1.77	0.02	0.1	111
Polyurethanes at 1 kHz					
1 PPG777/3 MDIL/1 14BDO	1.170	1.17	0.22		134
1 PTMG1000/3 MDI/2 BEPD	1.106	0.47	0.41		50
1 PTMG1000/3 MDI/2 EMPD	1.119	0.38	0.42		50
1 PPGI000/3 MDIL/1 14 BDO	1.154	0.34	0.67		134
1 PTMG2000/6 MDI/4 DMPD	1.108	0.30	0.47		50
1 PTMG1000/3 MDI/2 DMPD	1.123	0.29	0.55		50
1 PTMG1000/3 MDI/2 DEPD	1.073	0.18	0.76		50
1 PTMGI000/3 MDI/1 14BDO	1.139	0.10	0.26		50
1 PTMG1430/3 MDI/1 14BDO	1.105	0.044	0.14		50
1 PPG2000/3 MDIL/1 14BDO	1.101	0.016	0.39		134
1 PTMG1000/4 MDI/3 DMPD	1.092	0.009	0.55		50
1 PTMG2000/3 MDI/2 BEPD	1.064	0.009	0.37		50
1 PTMG650/2 TDI/1 PTMAB	1.087	0.009	0.47		135
1 PTMG2000/3 MDI/2 DMPD	1.074	0.009	0.35		50
1 PTMG1000/2 TDI/1 PTMAB	1.073	0.007	0.27		135

[a]Data for the polyurethanes is in the viscoelastic region of the glass transition.

Table 9. Frequency Derivatives of Young's Moduls

Polymer	ρ, g/cm^3	$dE'/d\log f$, GPa/decade	Ref.
Poly(methyl methacrylate)	1.187	0.509	129
Polypropylene	0.901	0.469	129
Poly(tetrafluoroethylene)	2.160	0.145	129
Polyethylene	0.951	0.116	129
Poly(methylene oxide)	1.424	0.099	129
Poly(hexamethylene	1.141	0.097	129
Polysulfone	1.236	0.069	129
Polycarbonate	1.194	0.047	129
Polystyrene	1.048	0.037	129

on whether glass fibers (28) or carbon fibers (qv) (29) are used, C_{11} varies from 40 to 300 GPa and C_{12} is only about 5 GPa. The other elastic constants are generally intermediate. For the most part, the elastic constants are fiber-dominated.

The Gruneisen parameter, used in equation-of-state calculations, has been determined from acoustic measurements in a number of cases. For high density polyethylene (126), the Gruneisen parameter was calculated from the pressure dependence of the sound speed. It was found that γ varied from 3.5 to 5.5 over the

temperature range −55 to 15°C, in good agreement with the room temperature value of 5.1 found from the temperature dependence of the acoustically determined bulk modulus (109). For poly(methyl methacrylate) and polystyrene, little temperature dependence was found, both polymers having $\gamma \sim 4$. Other measurements of γ using the temperature dependence of the bulk modulus include 7.6 for phenolic polymer (76), 4.4 for polyphenylquinoxaline (76), 5.1 for poly(4-methyl-l-pentene) (105), 7.2 for poly(acrylonitrile–butadiene–styrene) (105), 5.2 for poly(methyl methacrylate) (128), 4.4 for polystyrene (110), and 11.0 for isotactic polypropylene (109).

Underwater Acoustics. Acoustically transparent materials are used in a number of underwater applications, including transducer windows, sonar domes, potting compounds, and hydrophone support structures. A commonly used class of material for these purposes is called Rho-C rubber (BF Goodrich trademark), because the impedance, $Z = \rho c$ (where c is sound speed), matches that of water. A disadvantage of Rho-C rubber is that it does not possess structural rigidity. A material sometimes used when rigidity is required is poly(acrylonitrile–butadiene–styrene). Transmission loss measurements from 100 kHz to 2 MHz, at room temperature, show that a 2-mm-thick sheet of ABS has a transmission loss at normal incidence that averages 1 dB (136). This is slightly higher than that for the rubber, but still low enough for most applications. ABS has more angle dependence than Rho-C rubber and thus does not have quite as large a field of view. Another rigid window material is poly(4-methyl-l-pentene), which, because of its low density (0.835 g/cm^3), has an impedance closer to seawater than does ABS. The calculated transmission loss for poly(4-methyl-l-pentene) is less than for ABS at normal incidence, but greater than ABS for incident angles greater than about 45° (105). Another approach to acoustically transparent structural materials is the combination of more or less flexible epoxy polymers with different types of microballoons (106). Sound speeds varying from 2890 to 1560 m/s are obtained. Many trade-offs are possible, depending on the transmission loss and rigidity required.

Acoustic lenses are used in applications such as high resolution sonar and underwater imaging for salvage, as well as for medical imaging, materials inspection systems, and ultrasonic microscopy. Three types of lenses are common: (*1*) single refractive element, liquid-filled lens, (*2*) single-element thin solid lens, and (*3*) two-element athermal solid lens (a low sound speed and high sound speed material in contact designed so that the focal length is independent of temperature over a wide range). The liquid lenses are limited to an angular resolution of 0.5° and have a temperature-dependent focal length. For single-element thin solid lenses of polyhexamethyleneadipamide, polyethylene, and polystyrene, as well as two-element athermal lenses of poly(phenylene oxide)–polydimethylsiloxane, beam widths on the order of 0.35° over a 30° field of view can be obtained (137). Even higher angular resolution has been achieved using a four-element solid lens, consisting of two doublets of polystyrene–polydimethylsiloxane (138). For this lens, a resolution of 0.2° over a 20° field of view with good temperature properties was obtained. Multilayer systems have potential use for both acoustic windows and lenses. Transmission loss measurements and calculations for one-, two-, and three-layer systems utilizing various polymers have been made (23,24).

Anechoic (echo-reducing) coatings to reduce tank-wall reflections are needed in many underwater acoustic test facilities. One effective design utilizes butyl

rubber loaded with metal particles (usually aluminum flakes) prepared so that the final product contains small gas pockets surrounding the particles (139). Even more effective than thin sheets of this material is a gradual transition from water to coating in the form of cones of the coating material. Although thicker than the sheets, the cone structure gives more than 25 dB echo reduction from 20 kHz to 1 MHz at normal incidence. Coatings for the 2–7 MHz range of interest in materials inspection and medical applications have made use of polydimethylsiloxane loaded with ferric oxide (a dense filler) and microballoons (both glass and phenolic) (135), as well as paraffin wax and polychloroprene (140).

For a parametric sonar receiver in water, the insertion of a polydimethylsiloxane cylinder in front of the receiver improved the parametric conversion gain by 20 dB and reduced the beam width by a factor of 2–3 (37).

Miscellaneous. Vibration damping is typically effected with a polymer used in the vicinity of the glass transition. Different temperature and frequency ranges are covered by using different homopolymers, blends, copolymers, plasticizers (qv), and other fillers. The application of time-temperature superposition to damping materials has been demonstrated for various polymers (141). One way of achieving a very broad transition region is through the use of interpenetrating polymer networks (142). The structure of interpenetrating polymer networks, and their acoustic and damping properties are reviewed in Reference 143. Data on the complex shear and Young's moduli for various commercial damping treatments are presented by Nashif co-workers (144). Closed-cell polyurethane foams (145) and solution blends (146) also have potential for broad application. See Reference 147 for a comprehensive review of this application (see also CELLULAR MATERIALS).

Airborne noise applications include acoustically transparent open-cell polyurethane foam (148) for use as a microphone windscreen, and acoustically absorbing polyurethane foam (149) for noise abatement. Polyester-based foam has superior mechanical properties and acoustical absorption, but poor humid aging. Polyether-based foam has better humidity resistance and is inexpensive, but has less absorption.

Also, some studies have been done on the effect of insonification on polymerization reactions. In one case, it was found that insonification produced a rapid increase in conversion during free-radical polymerization of methyl methacrylate (150).

A class of polymer materials that has extensive applications in acoustics and vibrations is that of electroactive polymers. In these polymers there is coupling between mechanical deformation and electric fields. An applied stress produces both strains and charge separation, which leads to an output voltage between opposite surfaces of the polymer. Conversly, an applied electric field produces strains in the polymer. The induced strain has a linear and a quadratic term in the applied electric field. The linear term is characteristic of piezoactive response and the quadratic term corresponds to electrostrictive response.

Examples of polymers that have a piezoactive response are poled poly(vinylidene fluoride) (PVDF) (151) and its copolymers with trifluoroethylene co(VDF-TrFE) (152), and the family of odd nylons (153) (see PIEZOELECTRIC POLYMERS). These are partially crystalline materials in which the crystalline regions have a permanent electric dipole moment. These polymers show ferroelectric switching behavior indicating that after poling they have a net

polarization. The piezoelectrically induced strain, linear in the field, for the fluorinated polymers is up to 0.3% for fields of 30 V/μm (0.8 kV/mil). Recent extensive measurements of the piezoactive coefficients for PVDF, including temperature and frequency dependence, are given in Reference 154. Applications of PVDF and copolymers include (155) high frequency loudspeakers, transducers (single and arrays) for generating and receiving ultrasound (for nondestructive testing and medical imaging), and acoustically transparent, small (point) size hydrophones for imaging underwater ultrasonic fields (156,157). Also, PVDF transducers are used as industrial acoustic and vibration sensors (154).

The strain dependence for electroded polymers that is quadratic in the field consists of two terms: one a Maxwell stress due to the attraction of free surface charge on the electrodes, and the other electrostriction, which is a change of dielectric function with strain (158), related to dipole moments induced by the applied electric field. This quadratic term occurs for all materials and does not require a permanent polar moment. A large ambient electrostriction of 4% strain has been reported for irradiated copolymers of VDF/TrFE (159), terpolymers of VDF/TrFE/CTFE (160), and for polyurethanes (161). For the case of the fluorinated copolymers the irradiation or the addition of the third monomer for the terpolymers is hypothesized to create defects and decrease the size of correlation of the polarization regions, allowing the dipoles more freedom to respond to the electric field. This results in large dielectric constants on the order of 80 (159). An electrostrictive strain of 4% deformation for polyurethanes has been measured by both optical (161,162) and capacitance methods (161,163). The frequency range for the electrostrictive response is found up to 1 kHz for polyurethanes. A space charge distribution is indicated as the electrostrictive mechanism for these polymers (164). The fluorinated terpolymers and copolymers are highly crystalline and can impart a higher stress than that of these lower-modulus urethane elastomers. Other dielectric elastomer systems that have been shown to have large electric field coupling yielding strains of 100% are acrylics and silicones. These polymers have a low modulus and their deformation has been shown to be accounted for by the quadratic Maxwell stress term (165). The design and performance of an underwater flextensional projector transducer based on an electrostrictive copolymer of VDF/TrFE is described by Z. Y. Cheng and co-workers (166).

Electrets are another type of electrically active polymer. These are materials that contain embedded electrical charges (155). Electret films are extensively used as membranes in microphones. The embedded electrical charges in the electret film eliminate the need to supply an external d-c bias voltage to the microphone.

Test Methods

A comprehensive review of measurement techniques is presented by Capps (167), who also gives data for the complex Young's modulus for a range of polymers. This data includes the rubbery, transition, and glassy regions, and parameters for time–temperature superposition (eq. 45). The measurement techniques fall broadly into three categories: wave propagation methods, resonance methods, and forced-vibration nonresonance methods. The resonance and forced-vibration

techniques are designed to measure directly the complex Young's and shear moduli, and the acoustic properties of the polymer are calculated from this data.

Wave-Propagation Methods.

Immersion Technique. A test method known as the immersion technique will be described in some detail. Other test methods will then be discussed in contrast to this method. The immersion technique is relatively simple to use and provides both longitudinal and shear sound speeds and absorption over a range of temperatures, generally in the MHz frequency range, to 1% accuracy in sound speed.

In this method, acoustic waves are generated by a piezoelectric transducer, which converts an oscillating electric field to a mechanical oscillation. Detection of acoustic waves that have traveled through a polymer specimen is done with the same type of transducer. Depending on its use, a transducer is called a transmitting transducer (transmitter) or receiving transducer (receiver). Common transducer materials are quartz and various polycrystalline ceramics, such as lead zirconate titanate (PZT), polarized in a strong electrostatic field.

Measurements are made by sending acoustic pulses, typically less than 1 ms duration, through a specimen. Pulses, rather than continuous waves, are used because it is easy to determine the time it takes for a pulse to go through a specimen by looking for the beginning of the pulse. In the immersion technique, the specimen, transmitter, and receiver are all immersed in a liquid. Pulses are sent from one transducer to the other both with and without the specimen in the path of the sound beam. From the changes in the detected signal when the specimen is removed, the speed and absorption can be calculated.

The specimen is in the shape of a circular or rectangular slab. When a specimen of lateral dimensions several times the acoustic wavelength is supported with its face perpendicular to the path of the sound beam, longitudinal waves are generated in the specimen (119,125,168). A variation of this method is to hold the specimen at an angle to the sound beam. In this way, both longitudinal and shear waves are generated in the specimen. If the angle at which the specimen is held is greater than the critical angle, the longitudinal wave is totally internally reflected and only the shear wave is propagated (29,86).

In a typical immersion apparatus, when making shear measurements, the specimen is rotated with respect to fixed transducers to obtain shear waves. In the apparatus described here, the transducers are rotated about the fixed specimen (109,169). Eight specimens are mounted on the periphery of a circle and are moved into and out of the path of the sound beam. Especially when making measurements as a function of temperature, it saves time when eight specimens are immersed at once.

PZT transducers, 2.5 cm in diameter, are used in this apparatus. The larger the transducer diameter at a given frequency, the better collimated the acoustic beam (170). In this case, at 1 MHz, the diffraction attenuation is negligible and specimen alignment is not critical. The resonant frequency of the transducer is proportional to its thickness, 0.25 cm, and is 0.75 MHz. The maximum output of the transducer is at its resonant frequency, but it can be operated below resonance without much loss, and can be operated at harmonics of the resonant frequency to obtain higher frequency measurements. In this manner, the apparatus has been

used to make measurements over the frequency range 0.1–10 MHz, though most of the data are taken at 2 MHz.

An ideal immersion liquid has a very low sound speed, is liquid over a wide temperature range, and is safe. A low viscosity silicone fluid was chosen for this apparatus. This liquid can be used to make measurements over the temperature range −50 to 150°C.

For measurements of the longitudinal speed the specimen is oriented with its face perpendicular to the sound beam. With the specimen between the transducers, the detected pulse is displayed on the oscilloscope and the position, for example, of the first peak of the pulse is noted. The specimen is then removed from the path of the sound beam. Since the speed in the immersion liquid is less than the speed in the polymer, the signal will take a longer time to reach the receiver, and the pulse will move to the right on the oscilloscope screen when the specimen is removed. The difference in transit times t for the specimen and for an equal thickness of liquid is determined from this shift in position. For a specimen of thickness L, the transit time is L/v_l, where v_l is the longitudinal speed of the specimen. The transit time through an equal thickness of liquid is L/v_{liq}, where v_{liq} is the speed in the liquid. Therefore,

$$\Delta t = L/v(\mathrm{liq}) - L/v_l \tag{48}$$

so that v_{l} can be calculated, since v_{liq} in this case (49,109) is given by

$$v(\mathrm{liq}) = 976 - 2.5(T - 25) \tag{49}$$

for v_{liq} in m/s and T in °C.

Shear speed is measured by rotating the transducers so that the sound beam strikes the specimen at an angle. At off-normal incidence, both shear and longitudinal waves are generated. When both waves are present, they overlap in the received signal and are difficult to separate. However, if and only if $v_{\mathrm{liq}} < v_{\mathrm{l}}$, there is a critical angle beyond which there is total internal reflection of the longitudinal wave, and only the shear wave propagates through the specimen. It is for this reason that a low sound speed immersion liquid is desirable. Shear speed v_{s} is calculated in a manner similar to that for v_{l}. The procedure is more involved only because the path length through the specimen is somewhat greater than the specimen thickness (109).

Longitudinal absorption is found by comparing the amplitude of the received signal with no specimen in place to that of the signal with a specimen held perpendicular to the sound beam. The amplitude will be less with the specimen in place, both because the absorption in the polymer is greater than in the liquid and because some of the sound energy is reflected when it strikes the specimen. The amount of reflection can be calculated so that the absorption can be determined (109). Shear absorption proceeds in a similar manner (109). Immersion apparatuses can be used to measure sound speeds to an accuracy of 1% or better, and absorption to 10% or better.

Delay Rod Techniques. In the delay rod technique, the acoustic path of liquid between the transducers and the specimen in the immersion apparatus is replaced with solid rods of quartz or metal (120). The purpose of the delay

rods (also called buffer rods) is to give enough separation between pulses that the complete pulse can be sent by the transmitter before the beginning of the pulse arrives at the receiver. This technique eliminates stray r-f pickup by the receiver. A very thick specimen could be used for the same purpose, but polymers are generally highly absorbing, so that thin specimens are necessary in order to detect the transmitted signal. Since there is no liquid to freeze, this technique has been used down to liquid helium temperature (114,115).

Two problems are encountered with the delay rod technique. First, there must be a good bond between the transducers and the delay rods and also between the delay rods and the specimen. Second, shear measurements cannot be made with the same transducers used for longitudinal measurements. Various bonding agents have been used. For longitudinal waves, silicone liquid, stopcock grease, and glycerin have been successfully used. For shear waves, which are more highly damped, the problem is more critical. A low molecular weight poly(α-methylstyrene) liquid and mixtures of phthalic anhydride and glycerol are effective. All of these bonding agents have the advantage of being relatively easy to remove so that the transducer can be recovered intact. An epoxy bond can give good coupling, but is difficult to remove.

Longitudinal and shear measurements are made separately with different sets of transducers. Quartz transducers are often used. Quartz crystals produce different types of vibrations depending on how they are cut. An X-cut quartz crystal is used for generating longitudinal waves. Y-cut or AC-cut quartz crystals are used to generate shear waves.

Speed and absorption measurements can be made in a similar manner to those in the immersion technique or by using a null method (114). In this method, the pulse input to the transmitter is split in two. The pulse that has traversed the specimen is then mixed with an out-of-phase signal directly from the pulsed oscillator. By properly delaying and attenuating the direct signal, a null is obtained. Using this technique, an accuracy of 0.5% in speed can be obtained.

Multiple Echo Techniques. In multiple echo techniques, pulses of sound that traverse the specimen are partially reflected at the face of the specimen and bounce back and forth with continually diminished amplitude. From the time it takes for the echo to travel from one face to the other and the reduction in its amplitude during this trip, the speed and absorption can be calculated. Since the pulse must make several trips through the specimen, this technique cannot be used for highly absorbing materials. On the other hand, the technique is very accurate.

In one version of this technique (171) that has been successfully applied to polymers (124), two transducers are bonded directly onto the specimen. Two independently controlled pulses are applied to the transmitter. The first pulse generates a series of signals at the receiver corresponding to the directly transmitted signal and its subsequent echoes. The second pulse generates a similar set of signals. The second pulse is then delayed and attenuated so that the envelope of the directly transmitted signal coincides with that of the first echo of the first pulse. By adjusting the frequency of the measurement, the coincident signals can be made to interfere destructively and cancel each other out. The required frequency depends on the transit time through the specimen and allows accurate determination of the transit time. Absorption is obtained from the

attenuation required to match the amplitude of the direct pulse with the first echo. Sound speed measurements can be made to an accuracy of 0.1% and absorption to ±1 dB.

Another version of the multiple echo technique (172,173) that has been used to make very accurate sound speed measurements in polymers makes use of a single transducer bonded directly to the specimen (110). Pulses are reflected from the opposite face and return as echoes to the front face. By adjusting the pulse repetition rate, an echo from a later pulse can be made to overlap a multiple echo from an earlier pulse. When the repetition rate is adjusted to obtain an in-phase condition, constructive interference will result in a maximum amplitude in the superimposed signals. A value of sound speed accurate to 0.05% can be obtained by observing several repetition rates that yield an in-phase condition at the transducer resonant frequency and by repeating the measurements at some other frequency, eg, 10% below resonance, and on other specimens that differ only in thickness.

Laser Ultrasonics. Ultrasonic waves can be both generated and detected in solids using lasers. Laser ultrasonic systems have been developed for measuring the velocity and attenuation of ultrasound in materials. A high-power pulsed laser is used to generate a broadband ultrasonic pulse, and the time of flight and amplitude of this pulse are measured at one or more points on the material, using a low power, continuous laser (174). The advantages of the laser system are

(1) The system is noncontact, so it does not load the sample and can be configured for fast scanning of the sample surface.
(2) The sound generation/detection regions are small, and the system can be modeled as a point source/point receiver system.
(3) The ultrasonic signals are broadband and the sound speed and attenuation are measured over a range of frequencies.

A disadvantage of the laser system is its relatively low generation and detection efficiency.

Brillouin Scattering. The scattering of light by sound waves, a phenomenon first suggested by Brillouin, has become a practical tool with the advent of the laser. Sound waves are present in solids as a result of collective thermal vibrations, called thermal acoustic phonons. Since the phonons have a velocity relative to the photons, the scattered light is Doppler-shifted by an amount directly proportional to the sound speed. Brillouin scattering is observed for both longitudinal and transverse (shear) phonons. The Brillouin scattered lines are, to a first approximation, Lorentzian in shape. The width of the line is related to the phonon lifetime, or absorption coefficient. Brillouin scattering is thus a method of measuring sound speed and absorption in the 1–10-GHz frequency range.

Measurements of Brillouin scattering using a Fabry–Perot interferometer have been made on poly(methyl methacrylate) and poly(vinyl chloride) as a function of temperature through the glass transition (175). Only longitudinal measurements were obtained with this arrangement; shear waves could not be detected. Improved measurement methods using multiple-pass Fabry–Perot interferometry have been demonstrated for polystyrene (176), poly(4-methyl-1-pentene) (177), and several other amorphous polymers (178).

Through the use of thin films 0.1–0.3 mm thick, Brillouin scattering was measured in nontransparent polymers, such as polyethylene and poly(ether sulfone) (179). This technique is also useful for studying shear waves in polymers.

Surface Acoustic Waves. All of the discussion so far has dealt with the propagation of acoustic waves in bulk polymers. In addition to longitudinal and shear waves, however, a surface or Rayleigh wave, called a surface acoustic wave, can also be propagated.

A surface acoustic wave probe for polymers has been developed (180). Periodic distortions in piezoelectric substrates are induced by application of r-f energy to sets of interdigitated electrodes laid down on the substrate by standard photolithographic and etching techniques. There are 50 finger pairs, each finger 1 miL wide, with 2 miL spacings between adjacent fingers. This device has a wavelength of 100 μm and an operating frequency of about 32 MHz. The probe has been used to detect melting, glass, and secondary transitions in thin films of various polymers.

Low Frequency Techniques. For measurements below about 100 kHz, different test methods have been developed. Progressive wave techniques have been used to measure waves in rubber rods or strips. The specimen must be sufficiently long so that there are no reflections from the end of the specimen. An electromechanical shaker is used to excite one end of the specimen and a phonograph needle pickup is moved along the length of the specimen. From the amplitude vs distance measurement, the absorption is calculated. From the phase difference between shaker and pickup, the speed is calculated. This type of apparatus is generally used to measure extensional waves, governed by Young's modulus, over a frequency range from 100 Hz to 40 kHz (181). A modification of this technique has been used to measure torsional waves, governed by the shear modulus, over a frequency range from 1 to 8 kHz (182). Since these measurements must be repeated at each frequency, this method is time consuming. The method is also limited in accuracy and the range of materials that can be measured.

A pulse technique for the kilohertz frequency range is described in Reference 17. In this method the sample was immersed in a large water-filled tank, and a large area projector and hydrophone were used, operated in a pulse mode. The longitudinal sound speed and absorption were determined from measurements of signal amplitude and time of flight. Measurements were made on a polyurethane rubber sample, $35 \times 35 \times 5.2$ cm, over the range 12.5–75 kHz and 3.9–39.6°C. (The water-filled tank is also designed to operate at pressures up to 100 psi.) Also, the dynamic shear modulus was measured, using a rheometer, and the dynamic bulk modulus was determined from the longitudinal and shear measurements.

Resonance Techniques. Resonance methods (183–185) are used for measurements below about 100 kHz. The complex modulus (usually Young's or shear) is determined over a limited frequency range at a number of fixed temperatures, usually over one to three decades of frequency and over the useful temperature range of the material. From the measured data, reduced frequency plots at constant temperature are generated by the application of the time–temperature principle (3). In these plots, the real and imaginary parts of the complex modulus are plotted over many decades of frequencies, typically, as many as six or more decades of frequency than were actually measured.

Resonance techniques have been extensively used to find polymers with high loss factors, for sound absorption and vibration-damping applications, and to

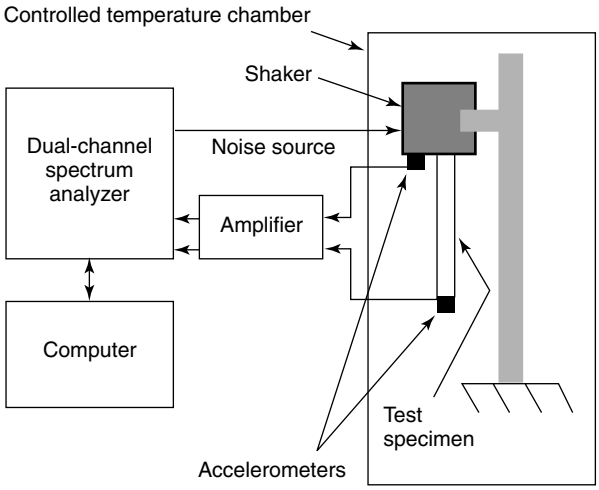

Fig. 6. Schematic diagram for the resonance apparatus.

determine relations between acoustic and elastic properties and molecular composition and morphology.

The complex dynamic Young's modulus can be determined from the response of a bar-shaped test specimen in a forced-resonance method (186). A shaker drives one end of the specimen (nominally 100 × 6 × 6 mm). Miniature accelerometers are used to measure the driving point acceleration at the shaker and the response of the test specimen as shown in Figure 6. The output signals from the accelerometers are analyzed by a dual-channel fast Fourier transform spectrum analyzer. The analyzer determines the acceleration ratio and phase difference of the two accelerometers, and also provides a random noise source to drive the shaker over a frequency range of 25 Hz to 20 kHz. The measured data are always sampled and rms-averaged at least 8 times, for low noise data, and up to 256 times, for noisy data. The displayed amplitude ratio versus frequency goes through a number of resonant peaks from which the sound speed (governed by the Young's modulus) and absorption (loss factor) are computed. The measurements are made over a temperature range of −60 to 70°C at 5° intervals.

The acceleration at selected locations on the sample can also be measured using a laser Doppler vibrometer (LDV) (187). The advantage of the LDV is that it is a noncontact measurement and does not disturb the vibration of the sample. Reference 187 describes a measurement setup that operates in the frequency range 500–2500 Hz, temperature range 0–40°C, and at pressures up to 500 psi.

Forced-Vibration Nonresonance Methods. In the forced, nonresonant method (183,188) sensors are used to measure the drive force and resulting displacement at one end of the sample. The complex modulus (shear or Young's) is determined from the amplitude ratio and relative phase of the force to the displacement. There are similarities between the resonance and nonresonance techniques. The complex modulus is measured over a limited frequency range at a number of fixed temperatures, and the time–temperature superposition principle is used

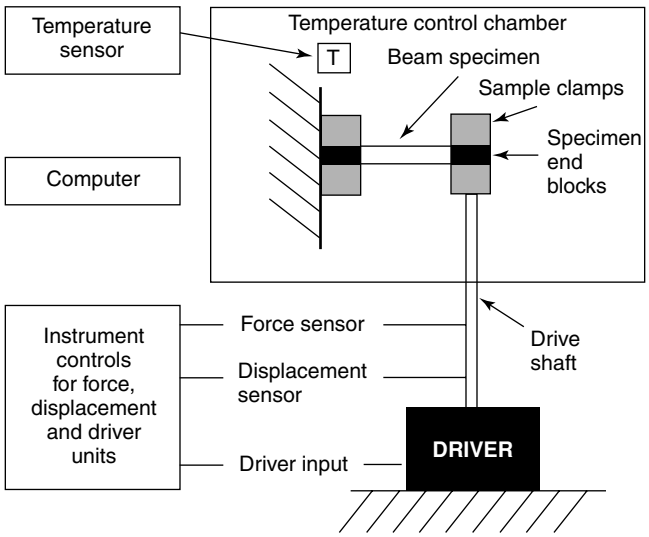

Fig. 7. Schematic diagram for the single cantilever beam apparatus for measurement of the complex Young's modulus. (A forced vibration nonresonance method.)

to generate a plot of the complex modulus over many decades of frequency. The applications of the data are similar.

In a forced, nonresonant method, the complex dynamic Young's modulus can be determined from the response of a beam mounted in a single-cantilever fixture (188) as shown in Figure 7. A thin sample (nominally $1.2 \times 10 \times 3$ mm) is clamped at both ends. One end is attached to a shaker through a driveshaft. The force and displacement are measured at the driven end at fixed frequencies. The low frequency/low mass bending solution is used together with the measured input impedance to infer the Young's modulus and loss factor. Sixteen discrete frequencies from 0.01 to 200 Hz are available, with an operating temperature range from -100 to 300°C.

BIBLIOGRAPHY

"Sound Absorption" in *EPST* 1st ed., Vol. 12, pp. 700–724, by R. S. Moore, Bell Telephone Laboratories, Inc.; "Acoustic Properties" in *EPST* 2nd ed., Vol. 1, pp. 131–160, by B. Hartmann, U.S. Naval Surface Weapons Center.

1. R. S. Marvin and J. E. McKinney, in W. P. Mason, ed., *Physical Acoustics*, Vol. **II**, Academic Press, New York, 1965, Pt. B, pp. 165–229.
2. W. P. Mason, *Physical Acoustics and the Properties of Solids*, Van Nostrand, Princeton, N.J., 1958.
3. J. D. Ferry, *Viscoelastic Properties of Polymers*, 3rd ed., John Wiley & Sons, Inc., New York, 1980.
4. R. W. Warfield, D. J. Pastine, and M. C. Petree, *Appl. Phys. Lett.* **25**, 638 (1974).
5. J. Schuyer, *J. Polym. Sci.* **36**, 475 (1959).
6. D. J. Pastine, *J. Chem. Phys.* **49**, 3012 (1968).
7. L. E. Nielsen, *Mechanical Properties of Polymers*, Van Nostrand, Princeton, N.J., 1962, p. 64.

8. B. Hartmann and J. Jarzynski, *J. Appl. Phys.* **43**, 4304 (1972).
9. H. B. Callen, *Thermodynamics*, John Wiley & Sons, Inc., New York, 1960, pp. 124–127.
10. R. M. Christensen, *Theory of Viscoelasticity*, Academic Press, New York, 1971.
11. F. Mainardi, in A. Guran, A. Bostrom, O. Leroy, and G. Maze, eds., *Acoustic Interactions with Submerged Elastic Structures, Part 4*, World Scientific Publishing Co., Singapore, 2002, pp. 97–161.
12. L. E. Kinsler, A. R. Frey, A. B. Coppens, and J. V. Sanders, *Fundamentals of Acoustics*, 4th ed., John Wiley & Sons, Inc., New York, 2000.
13. A. I. Beltzer, *Acoustics of Solids*, Springer-Verlag, Berlin, 1988.
14. M. O'Donnel, E. T. Jaynes, and J. G. Miller, *J. Acoust. Soc. Am.* **69**, 696–701 (1981).
15. K. R. Waters, M. S. Hughes, J. Mobley, G. H. Brandenburger, and J. G. Miller, *J. Acoust. Am.* **108**, 556–563 (2000).
16. E. Balizer, and J. V. Duffy, *Polymer* **33**, 2114–2122 (1992).
17. P. H. Mott, C. M. Roland, and R. D. Corsaro, *J. Acoust. Soc. Am.* **111**, 1782–1790 (2002).
18. M. G. Broadhurst and F. I. Mopsik, *J. Chem. Phys.* **52**, 3634 (1970).
19. B. Hartmann, *Acustica* **36**, 24 (1976).
20. T. A. Litovitz and C. M. Davis, in W. P. Mason, ed., *Physical Acoustics*, Vol. **II**, Academic Press, Inc., New York, 1965, Pt. A, pp. 281–349.
21. N. G. McCrum, B. E. Read, and G. Williams, *Anelastic and Dielectric Effects in Polymeric Solids*, John Wiley & Sons, Inc., New York, 1967.
22. R. Kono and H. Yoshizaki, *J. Appl. Phys.* **47**, 531 (1976).
23. D. L. Folds and C. D. Loggins, *J. Acoust. Soc. Am.* **62**, 1102 (1977).
24. W. Madigosky and R. Fiorito, *J. Acoust. Soc. Am.* **65**, 1105 (1979).
25. R. Fiorito, W. Madigosky, and H. Uberall, *J. Acoust. Soc. Am.* **69**, 897 (1981).
26. L. Flax and W. G. Neubauer, *J. Acoust. Soc. Am.* **61**, 307 (1977).
27. T. Hasegawa and Y. Watanabe, *J. Acoust. Soc. Am.* **63**, 1733 (1978).
28. J. E. Zimmer and J. R. Cost, *J. Acoust. Soc. Am.* **47**, 795 (1970).
29. R. E. Smith, *J. Appl. Phys.* **43**, 2555 (1972).
30. E. H. Kerner, *Proc. Phys. Soc. London, Sect. B* **69**, 808 (1956).
31. W. M. Madigosky and K. P. Scharnhorst, in R. D. Corsaro and L. H. Sperling, eds., *Sound and Vibration Damping with Polymers*, (ACS Symposium Series 424), ACS Press, Washington, D.C., 1990, pp. 229–300.
32. A. M. Baird, F. H. Kerr, and D. J. Townend, *J. Acoust. Soc. Am.* **105**, 1527–1538 (1999).
33. R. Lim and R. H. Hackman, *J. Acoust. Soc. Am.* **87**, 1076–1103 (1990).
34. J. Jarzynski, in R. D. Corsaro and L. H. Sperling, eds., *Sound and Vibration Damping with Polymers*, (ACS Symposium Series 424), ACS Press, Washington, D.C., 1990, pp. 49–62.
35. R. D. Corsaro, J. D. Klunder, and J. Jarzynski, *J. Acoust. Soc. Am.* **68**, 655 (1980).
36. R. T. Beyer, *Nonlinear Acoustics*, Acoustical Society of America (American Institute of Physics), New York, 1999.
37. R. D. Corsaro and J. Jarzynski, *J. Acoust. Soc. Am.* **66**, 895 (1979).
38. W. M. Madigosky, I. Rosenbaum, and R. Lucas, *J. Acoust. Soc. Am.* **69**, 1639 (1981).
39. J. H. Cantrell Jr., M. A. Breazeale, and A. Nakamura, *J. Acoust. Soc. Am.* **67**, 1477 (1980).
40. D. S. Hughes, and J. L. Kelly, *Phys. Rev.* **92**, 1145–1149 (1953).
41. B. Hartmann, *J. Acoust. Soc. Am.* **65**, 1392 (1979).
42. D. W. Van Krevelen, *Properties of Polymers*, 3rd ed., Elsevier, Amsterdam, 1990.
43. M. R. Rao, *J. Chem. Phys.* **9**, 682 (1941).
44. B. Hartmann and G. F. Lee, *J. Appl. Phys.* **51**, 5140 (1980).
45. G. V. Reddy, S. Chattopadhyay, Y. P. Singh, and R. P. Singh, *Acustica* **48**, 347 (1981).
46. S. Bagchi and R. P. Singh, *Acustica* **51**, 68 (1982).
47. B. Hartmann and G. Lee, *J. Polym. Sci., Polym. Phys. Ed.* **20**, 1269 (1982).

48. J. Bicerano, *Prediction of Polymer Properties*, Marcel Dekker, New York, 1993.
49. B. Hartmann and J. Jarzynski, *J. Polym. Sci., Part A-2* **9**, 763 (1971).
50. J. V. Duffy, G. F. Lee, J. D. Lee, and B. Hartmann, in R. D. Corsaro, and L. H. Sperling, eds., *Sound and Vibration Damping with Polymers*, (ACS Symposium Series 424), ACS Press, Washington, D.C., 1990, pp. 281–300.
51. R. N. Work, *J. Appl. Phys.* **27**, 69 (1956).
52. Y. Wada and K. Yamamoto, *J. Phys. Soc. Jpn.* **11**, 887 (1956).
53. S. F. Kwan, F. C. Chen, and C. L. Choy, *Polymer* **16**, 481 (1975).
54. Y. Wada, *J. Phys. Soc. Jpn.* **16**, 1226 (1961).
55. Y. Wada, Y. Hotta, and R. Suzuki, *J. Polym. Sci., Part C* **23**, 583 (1968).
56. A. F. Lewis, *J. Polym. Sci., Polym. Lett. Ed.* **1**, 649 (1963).
57. D. W. Phillips and R. A. Pethrick, *J. Macromol. Sci., Rev. Macromol. Chem.* **16**, 1 (1977).
58. S. Havriliak, and S. Negami, in R. F. Boyer, ed., *Transitions and Relaxations in Polymers*, Wiley Interscience, New York, 1966, pp. 99–117. J. Polym. Sci., Part C, No. 14.
59. B. Hartmann, G. F. Lee, J. D. Lee, and J. J. Fedderly, *J. Acoust. Soc. Am.* **101**, 2008–2011 (1997).
60. M. L. Williams, R. F. Landel, and J. D. Ferry, *J. Am. Chem. Soc.* **77**, 3701 (1955).
61. K. L. Ngai, and D. J. Plazek, in J. E. Mark, ed., *Physical Properties of Polymers Handbook*, American Institute of Physics, New York, 1996, pp. 341–362.
62. B. Hartmann, in R. D. Corsaro, and L. H. Sperling, eds., *Sound and Vibration Damping with Polymers*, (ACS Symposium Series 424), American Chemical Society Press, Washington, D.C., 1990, pp. 23–45.
63. T. G. Fox, and P. J. Flory, *J. Appl. Phvs.* **21**, 581 (1950).
64. B. Hartmann, G. F. Lee, J. D. Lee, J. J. Fedderly, and A. E. Berger, *J. Appl. Polym. Sci.*, **60**, 1985–1993 (1996).
65. D. W. Phillips, A. M. North, and R. A. Pethrick, *J. Appl. Polym. Sci.* **21**, 1859 (1977).
66. K. Shimizu, O. Yano, Y. Wada, and Y. Kawamura, *J. Polym. Sci., Polym. Phys. Ed.* **11**, 1641 (1973).
67. G. A. Samara and I. J. Fritz, *J. Polym. Sci., Polym. Lett. Ed.* **13**, 93 (1975).
68. I. L. Perepechko and L. A. Kvacheva, *Polym. Sci., USSR* **13**, 142 (1971).
69. J. Heijboer, *Int. J. Polym. Mater.* **6**, 11 (1977).
70. R. K. Eby, *J. Acoust. Soc. Am.* **36**, 1485 (1964).
71. N. A. Bordelius and V. K. Semenchenko, *Sov. Phys. Acoust.* **16**, 519 (1971).
72. A. G. H. Dietz, E. A. Hauser, F. J. McGarry, and G. A. Sofer, *Ind. Eng. Chem.* **48**, 75 (1956).
73. E. P. Papadakis, *J. Appl. Phys.* **45**, 1218 (1974).
74. R. G. C. Arridge and J. H. Speake, *Polymer* **13**, 443 (1972).
75. R. G. C. Arridge and J. H. Speake, *Polymer* **13**, 450 (1972).
76. B. Hartmann, *J. Appl. Polym. Sci.* **19**, 3241 (1975).
77. B. Hartmann, *Polymer* **22**, 736 (1981).
78. B. Hartmann, *Ann. N. Y. Acad. Sci* **371**, 308 (1981).
79. L. G. Bunton, J. H. Daly, I. D. Maxwell, and R. A. Pethrick, *J. Appl. Polym. Sci.* **27**, 4283 (1982).
80. S. R. White, P. T. Mather, and M. J. Smith, *Polym. Eng. Sci.* **42**, 51–67 (2002).
81. J. Dorighi, S. Krishnaswamy, and J. Achenbach, *Res. Nondestr. Eval.* **9**, 13–24 (1997).
82. P. D. Davidse, H. L. Waterman, and J. B. Westerdijk, *J. Polym. Sci.* **59**, 389 (1962).
83. A. Levene, W. J. Pullen, and J. Roberts, *J. Polym. Sci., Part A* **3**, 697 (1965).
84. A. M. North, R. A. Pethrick, and D. W. Phillips, *Polymer* **18**, 324 (1977).
85. I. L. Pavlinov, I. B. Rabinovich, V. Z. Pogorelko, and A. V. Ryabov, *Polym. Sci., USSR* **10**, 1471 (1968).
86. Y. Maeda, *J. Polym. Sci.* **XVIII**, 87 (1955).

87. N. V. Karyakin, L. B. Rabinovich, and V. A. Ul'yanov, *Polym. Sci., USSR* **11**, 3159 (1969).
88. G. W. Paddison, *Polym. Eng. Sci.* **14**, 382 (1974).
89. A. S. Gilbert, R. A. Pethrick, and D. W. Phillips, *J. Appl. Polym. Sci.* **21**, 319 (1977).
90. D. J. Hourston and I. D. Hughes, *Polymer* **19**, 1181 (1978).
91. A. W. Nolle and S. C. Mowry, *J. Acoust. Soc. Am.* **20**, 432 (1948).
92. P. Hatfield, *Br. J. Appl. Phys.* **1**, 252 (1950).
93. R. T. Lagemarm and J. E. Corey, *J. Chem. Phys.* **10**, 759 (1942).
94. G. Natta and M. Baccaredda, *J. Polym. Sci.*, **IV**, 533 (1949).
95. P. C. Bandyopadhyay, A. K. Maity, T. K. Chaki, and R. P. Singh, *Acustica* **50**, 75 (1982).
96. H. Pauly and H. P. Schwan, *J. Acoust. Soc. Am.* **50**, 692 (1971).
97. P. M. Gammell, D. H. LeCroissette, and R. C. Heyser, *Ultrasound Med. Biol.* **5**, 269 (1979).
98. S. A. Goss, R. L. Johnston, and F. Dunn, *J. Acoust. Soc. Am.* **64**, 423 (1978).
99. E. L. Madsen, H. J. Sathoff, and J. A. Zagzebski, *J. Acoust. Soc. Am.* **74**, 1346 (1983).
100. C. M. Sehgal and J. F. Greenleaf, *J. Acoust. Soc. Am.* **72**, 1711 (1982).
101. A. Sarvazyan, in M. Levy, H. E. Bass, and R. R. Stern, eds., *Handbook of Elastic Properties of Solids, Liquids, and Gases*, Vol. **3**, Academic Press, New York, 2001, pp. 107–127.
102. S. Lees, in M. Levy, H. E. Bass, and R. R. Stern, eds., *Handbook of Elastic Properties of Solids, Liquids, and Gases*, Vol. **3**, Academic Press, New York, 2001, pp. 148–208.
103. P. J. McCracken, T. E. Oliphant, J. F. Greenleaf, and R. L. Ehman, in M. Levy, H. E. Bass, and R. R. Stern, eds., *Handbook of Elastic Properties of Solids, Liquids, and Gases*, Vol. **1**, Academic Press, New York, 2001, pp. 109–120.
104. D. L. Folds, *J. Acoust. Soc. Am.* **52**, 426 (1972).
105. B. Hartmann, *J. Appl. Phys.* **51**, 310 (1980).
106. R. E. Montgomery, F. J. Weber, D. F. White, and C. M. Thompson, *J. Acoust. Soc. Am.* **71**, 735 (1982).
107. H. J. Sutherland, and R. Lingle, *J. Appl. Phys.* **43**, 4022–4026 (1972).
108. C. M. Thompson, and W. L. Heimer II, *J. Acoust. Soc. Am.* **77**, 1229–1238 (1985).
109. B. Hartmann and J. Jarzynski, *J. Acoust. Soc. Am.* **56**, 1469 (1974).
110. D. L. Lamberson, J. R. Asay, and A. H. Guenther, *J. Appl. Phys.* **43**, 976 (1972).
111. L. L. Perepechko and V. A. Grechishkin, *Polym. Sci., USSR* **15**, 1139 (1973).
112. M. Shen, V. A. Kaniskin, K. Biliyar, and R. H. Boyd, *J. Polym. Sci., Polym. Phys. Ed.* **11**, 2261 (1973).
113. I. L. Perepechko, A. Mirzokarimov, V. V. Rodionov, and V. D. Vorob'ev, *Polym. Sci., USSR* **16**, 1910 (1974).
114. I. L. Perepechko and V. E. Sorokin, *Sov. Phys. Acoust.* **18**, 485 (1973).
115. P. D. Golub and L. I. Perepechko, *Sov. Phys. Acoust.* ∼**0**, 22 (1974).
116. P. D. Golub and L. I. Perepechko, *Sov. Phys. Acoust.* **19**, 391 (1974).
117. V. Ye. Sorokin and L. L. Perepechko, *Polym. Sci. USSR* **16**, 1915 (1974).
118. D. S. Matsumoto, C. L. Reynolds Jr., and A. C. Anderson, *Phys. Rev. B* **19**, 4277 (1979).
119. D. G. Ivey, B. A. Mrowca, and E. Guth, *J. Appl. Phys.* **20**, 486 (1949).
120. A. W. Nolle and P. W. Sieck, *J. Appl. Phys.* **23**, 888 (1952).
121. H. J. Sutherland, *J. Appl. Phys.* **49**, 3941 (1978).
122. D. S. Hughes, E. B. Blankenship, and R. L. Mims, *J. Appl. Phys.* **21**, 294 (1950).
123. H. Singh and A. W. Nolle, *J. Appl. Phys.* **30**, 337 (1959).
124. J. E. McKinney, H. V. Belcher, and R. S. Marvin, *Trans. Soc. Rheol.* **IV**, 347 (1960).
125. A. Zosel, *Kolloid Z.* **213**, 121 (1966).
126. Y. Wada, A. Itani, T. Nishi, and S. Nagai, *J. Polym. Sci., Part A-2* **7**, 201 (1969).
127. J. Gielessen and J. Kopplemann, *Z. Kolloid*, **172**, 162 (1960).
128. J. R. Asay, D. L. Lamberson, and A. H. Guenther, *J. Appl. Phys.* **40**, 1768 (1969).

129. N. Lagakos, J. Jarzynski, J. H. Cole, and J. A. Bucaro, *J. Appl. Phys.* **59**, 4017–4031 (1986).
130. B. Hartmann, in M. Levy, H. E. Bass, and R. R. Stern, eds., *Handbook of Elastic Properties of Solids, Liquids, and Gases*, Vol. **3**, Academic Press, New York, 2001, pp. 51–68.
131. R. Kono, *J. Phys. Soc. Jpn.* **16**, 1580 (1961).
132. E. Morita, R. Kono, and H. Yoshizaki, *Jpn. J. Appl. Phys.* **7**, 451 (1968).
133. S. de Petris, V. Frosini, E. Butta, and M. Baccaredda, *Makromol. Chem.* **109**, 54–61, (1967).
134. B. Hartmann, and G. F. Lee, *J. Non-Cryst. Solids* **131–133**, 887–890, (1991).
135. B. Hartmann, J. V. Duffy, G. F. Lee, and E. Balizer, *J. Appl. Polym. Sci.* **35**, 1829–1852 (1988).
136. L. C. Adair and R. L. Cook, *J. Acoust. Soc. Am.* **54**, 1763 (1973).
137. D. L. Folds, *J. Acoust. Soc. Am.* **53**, 826 (1973).
138. D. L. Folds and J. Hanlin, *J. Acoust. Soc. Am.* **58**, 72 (1975).
139. W. S. Cramer and T. F. Johnston, *J. Acoust. Soc. Am.* **28**, 501 (1956).
140. R. C. Chivers, A. D. Smith, and P. R. Filmore, *Ultrasonics* **19**, 125 (1981).
141. D. L. G. Jones, *J. Sound Vib.* **33**, 451 (1974).
142. J. A. Grates, D. A. Thomas, E. C. Hickey, and L. H. Sperling, *J. Appl. Polym. Sci.* **19**, 1731 (1975).
143. R. B. Fox, and co-workers, in R. D. Corsaro and L. H. Sperling, eds., *Sound and Vibration Damping with Polymers*, (ACS Symposium Series 424), ACS Press, Washington, D.C., 1990, pp. 359–456.
144. A. D. Nashif, D. I. G. Jones, and J. P. Henderson, *Vibration Damping*, Wiley-Interscience, New York, 1985.
145. A. C. F. Chen and H. L. Williams, *J. Appl. Polym. Sci.* **20**, 3403 (1976).
146. D. J. Hourston and I. D. Hughes, *J. Appl. Polym. Sci.* **26**, 3487 (1981).
147. J. C. Snowdon, *J. Acoust. Soc. Am.* **66**, 1245 (1979).
148. K. Matsuzawa and M. Ochi, *J. Acoust. Soc. Am.* **68**, 212 (1980).
149. Y. Imai and T. Asano, *J. Appl. Polym. Sci.* **27**, 183 (1982).
150. K. F. O'Driscoll and A. U. Sridharan, *J. Polym. Sci., Polym. Chem. Ed.* **11**, 1111 (1973).
151. R. G. Kepler, in H. S. Nalwa, ed., *Ferroelectric Polymers Chemistry, Physics, and Applications*, Marcel Dekker, New York, 1995, p. 183.
152. T. Furukawa, *Phase Transitions* **18**, 143 (1989).
153. B. A. Newman, P. Chen, K. D. Pae, and J. I. Scheinbeim, *J. Appl. Phys.* **51**, 5161 (1980).
154. Y. Roh, V. V. Varadan, and V. K. Varadan, *IEEE Trans. Ultrason. Ferroelectr. Freq. Control* **49**, 836–847 (2002).
155. G. M. Sessler, and J. E. West, in G. M. Sessler, ed., *Electrets*, 2nd ed., Springer-Verlag, New York, 1987, pp. 347–381,
156. P. C. Beard, A. M. Hurrell, and T. N. Mills, *IEEE Trans. Ultrason Ferroelectr Freq. Control* **47**, 256–264 (2000).
157. B. Fay, G. Ludwig, C. Lankjaer, and P. A. Lewin, *Frequency response of PVDF needle-type hydrophones, Ultrason. Med. Biol.* **20**, 361–366. (1994).
158. J. A. Stratton, *Electromagnetic Theory*, McGraw-Hill, New York, (1941).
159. Q. M. Zhang, V. Bharti, and X. Zhao, *Science* **280**, 836 (1998).
160. H. Xu, Z.-Y. Cheng, D. Olson, T. Mai, Q. M. Zhang, and G. Karvanos, *Appl. Phys. Lett.* **78**, 2360 (2001).
161. M. Zhenyi, J. Scheinbeim, J. Lee, and B. Newman, *J. Pol. Sci., b, Pol. Phys.* **32**, 2721 (1994).
162. F. Guillot, J. Jarzynski, and E. Balizer, *J. Acoust. Soc. Am.* **110**, 2980 (2001).
163. Y. M. Shkel, and D. Klingenberg, *J. Appl. Phys.* **88**, 415 (1998).
164. J. Su, Q. M. Zhang, and R. Y. Ting, *Appl. Phys. Lett.* **71**, 386 (1997).

165. R. Perine, R. Kornbluh, Q. Pei, and J. Joseph, *Science* **287**, 836 (2000).
166. Z. Y. Cheng, T.-B. Xu, Q. Zhang, R. Meyer, D. Van Toll, and J. Hughes, *IEEE Trans. Ultrason. Ferroelectr. Freq. Control* **49**, 1312–1320 (2002).
167. R. N. Capps, *Elastomeric Materials for Acoustical Applications*, Naval Research Laboratory, Washington D.C., (1989).
168. H. J. McSkimin and P. Andreatch Jr., *J. Acoust. Soc. Am.* **49**, 713 (1971).
169. B. Hartmann, in R. A. Fava, ed., *Polymers, Part C: Physical Properties, (Methods of Experimental Physics, Vol. 16)* Academic Press, New York, 1980, pp. 59–90.
170. H. Seki, A. Granato, and R. Truell, *J. Acoust. Soc. Am.* **28**, 230 (1956).
171. J. Williams and J. Lamb, *J. Acoust. Soc. Am.* **30**, 308 (1958).
172. H. J. McSkimin, *J. Acoust. Soc. Am.* **33**, 12 (1961).
173. H. J. McSkimin and P. Andreatch, *J. Acoust. Soc. Am.* **34**, 609 (1962).
174. S. Guilbaud, and B. Audoin, *J. Acoust. Soc. Am.* **105**, 2226–2235, (1999).
175. D. A. Jackson, H. T. A. Pentecost, and J. G. Powles, *Mol. Phys.* **23**, 425 (1972).
176. E. M. Brody, C. J. Lubell, and C. L. Beatty, *J. Polym. Sci., Polym. Phys. Ed.* **13**, 295 (1975).
177. J. Krliger, L. Peetz, and M. Pietralla, *Polymer* **19**, 1397 (1978).
178. G. D. Patterson, *J. Polym. Sci., Polym. Phys. Ed.* **15**, 455 (1977).
179. G. D. Patterson, *J. Polym. Sci., Polym. Phys. Ed.* **14**, 143 (1976).
180. J. A. Groetsch III, and R. E. Dessy, *J. Appl. Polym, Sci.* **28**, 161 (1983).
181. W. M. Madigosky and G. F. Lee, *J. Acoust. Soc. Am.* **66**, 345 (1979).
182. W. S. Cramer, *J. Polym. Sci.* **XXVI**, 57 (1957).
183. J. J. Dlubac, G. F. Lee, J. V. Duffy, R. J. Deigan, and J. D. Lee, in R. D. Corsaro L. H. Sperling, eds., *Sound and Vibration Damping with Polymers*, (ACS Symposium Series 424), ACS Press, Washington, D.C., 1990, pp. 49–62.
184. W. M. Madigosky and G. F. Lee, *J. Acoust. Soc. Am.* **73**, 1374 (1983).
185. S. L. Garrett, *J. Acoust. Soc. Am.* **88**, 210–221 (1990).
186. ANSI S2.22–1998, Resonance Method for Measuring the Dynamical Mechanical Properties of Viscoelastic Materials.
187. R. L. Willis, L. Wu, and Y. H. Berthelot, *J. Acoust. Soc. Am.* **109**, 611 (2001).
188. S. ANSI,23–1998, Single Cantilever Beam Method for Measuring the Dynamic Mechanical Properties of Viscoelastic Materials.

JACEK JARZYNSKI
Georgia Institute of Technology
EDWARD BALIZER
JEFFRY J. FEDDERLY
GILBERT LEE
U.S. Naval Surface Warfare Center

ACRYLAMIDE POLYMERS.

See Volume 1.

ACRYLIC (AND METHACRYLIC) ACID POLYMERS.

See Volume 1.

ACRYLIC ELASTOMERS, ETHYLENE-ACRYLIC.

See ETHYLENE-ACRYLIC ELASTOMERS.

ACRYLIC ESTER POLYMERS. See Volume 1.

ACRYLONITRILE AND ACRYLONITRILE POLYMERS.
See Volume 1.

ACRYLONITRILE–BUTADIENE–STYRENE POLYMERS.
See Volume 1.

ADDITIVES. See Volume 1.

ADHESION. See Volume 1.

ADHESIVE COMPOUNDS. See Volume 1.

ADSORPTION

Introduction

When a multicomponent system is exposed to an interface, there is a change in the concentration profile at the interfacial region. If the concentration of one or more of the components at interface increases, then these components are said to adsorb at that interface and the phenomenon is known as *adsorption*. Conversely, when there is a decrease in the concentration of one or more of the components at the interface the phenomenon is called *depletion*.

The extent of adsorption is quantified by the term *surface excess*, which has dimensions of mass/unit area. Figure 1 illustrates the concentration of the adsorbed species as a function of distance from the interface. The shaded area in Figure 1 is defined as surface excess. Mathematically it can be defined as follows:

$$\Gamma = \int_0^\infty [c(z) - c(\infty)]\, \mathrm{d}z$$

where $c(z)$ is the concentration at a distance z from the interface and $c(\infty)$ is the bulk concentration. Surface excess can be positive, zero, or negative.

Polymer Adsorption. The driving force for adsorption typically is the enthalpic interaction between the interface and the polymer segments. Exceptions include aqueous solutions near hydrophobic substrates. In that case, the driving force may include the hydrophobic interaction between water and the surface. The enthalpic interactions may be of various forms such as hydrogen bonding, interfacial tension, van der Waals attraction, polar interactions, and electrostatic attractions. This enthalpic interaction is offset by the loss in conformational entropy

Encyclopedia of Polymer Science and Technology. Copyright John Wiley & Sons, Inc. All rights reserved.

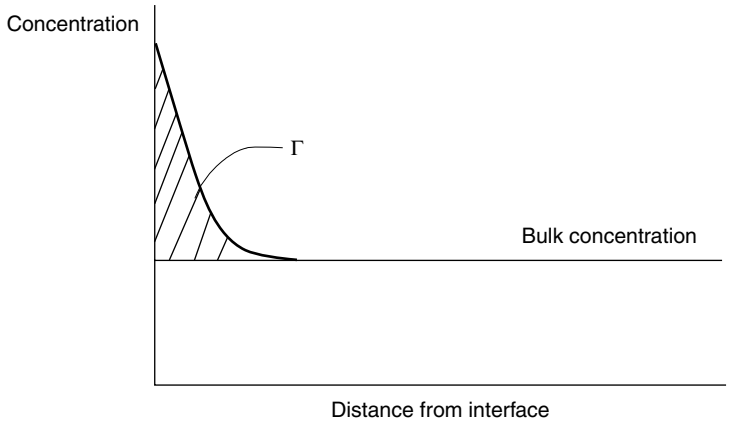

Fig. 1. Concentration profile of an adsorbed layer.

due to localization of the adsorbed molecules at the interface. A balance of these two effects thus controls the extent of adsorption of a species.

Since a single chain is composed of many monomeric units, even a weakly attractive interaction between a monomeric unit and the interface gets amplified. For example, the surface–segment interaction energy for polystyrene on silica is of the order of 1.8 kT (1). If there are 100 monomeric units per chain that interact with the substrate, the net energy of interaction will be of the order of 180 kT. Because of such strong energetic interactions, polymer adsorption differs significantly from the phenomenon of small-molecule adsorption. Once adsorbed, a chain cannot easily desorb from the surface because that would require all the 100 monomeric units to leave the surface simultaneously. Consequently, the desorption rates of adsorbed chains into pure solvent are extremely slow and quite often the adsorption is irreversible. This leads to another salient feature seen in polymer adsorption, ie saturation of the surface at extremely small bulk polymer concentrations.

In the presence of an interface the conformation of the adsorbed chain gets modified. The structure of adsorbed polymer chains is defined by "trains," "loops," and "tails" (2), as shown in Figure 2. The segments of the chain that are in physical contact with the interface are called trains. Loops and tails are the parts of

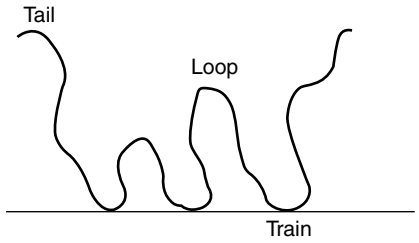

Fig. 2. Structure of an adsorbed polymer chain.

the chain that are not in direct contact with the interface. Loops are the portions of the chain between two trains, while tails are the parts that incorporate the chain ends. The presence of a train segment increases the enthalpic gain upon adsorption and the loops and tails reduce the entropic penalties upon adsorption. The equilibrium structure attained by the adsorbed chain will be a balance between these two forces. However, the structure of the adsorbed chain often does not reach thermodynamic equilibrium during the course of adsorption measurements because of the high energy barrier that has to be overcome for rearrangements in the adsorbed layer.

Techniques to Study Polymer Adsorption

The typical adsorbed amount in the case of polymer adsorption at a surface is of the order of 1–5 mg/m^2. Techniques needed to study adsorption have to be sensitive enough to detect the adsorbed mass. To increase the surface area and to improve the sensitivity of measurements, adsorption studies are done on dispersed particles where the surface area-to-volume ratio is high. Advances in instrumentation in the recent years have also resulted in the development of sensitive techniques that allow researchers to directly investigate adsorbed polymer layers on planar surfaces. In measurements of this type, the contribution from the molecules in the bulk is of the same order of magnitude as, if not lesser than, the contribution from the adsorbed layer, and it is possible to accurately account for the bulk contributions. These measurements provide important insights into the aspects of structure and dynamics of adsorbed polymers that could not be measured using dispersed particles.

Measurements on Dispersions.

Concentration Measurements. In the case of dispersed particles, the change in concentration (ΔC) of a known volume (V) of supernatant solution before and after adsorption is measured using techniques such as UV–vis and IR absorption spectroscopy. The surface excess is then related to the change in concentration as

$$\Gamma = \frac{\Delta C V}{A}$$

A is the surface area of the adsorbent. The accuracy of these measurements is limited by two factors: the sensitivity of the method used to measure ΔC and the accuracy in measuring the surface area of the adsorbent.

Scattering Techniques. The thickness of adsorbed layers can be determined using light, X-ray, and neutron scattering techniques (3). Quasi-elastic light scattering measurements on dispersion of particles measure the diffusion coefficients of particles in the dispersion. The size of these particles is related to the diffusion coefficient by the Stokes–Einstein equation. This measurement is performed on the dispersion with and without the adsorbed polymer. The difference in the radii in the two measurements is the thickness of the adsorbed layer. In these measurements it should be ensured that the particles in the dispersion are monodisperse and that there is no flocculation. In X-ray and neutron

measurements, the scattering intensity is measured as a function of the scattering angle, and the data can be modeled to determine thickness and volume profile of the adsorbed polymer chains. The experimental conditions are chosen such that the particles are invisible in the medium, so that only the adsorbed layer contributes to the scattering. This technique is called "contrast matching." In neutron scattering this is achieved by varying the isotopic composition of the solvent, while in X-ray scattering contrast matching is achieved by changing the atomic composition of the solvent. X-ray and neutron scattering can also be used to study adsorption in porous substrates.

Nuclear Magnetic Resonance (NMR) and Electron Spin Resonance (ESR). Nuclear magnetic resonance methods (4) can detect the changes in the mobility of adsorbed segments of the chain. The spin–spin relaxation time (T_2) and the spin–lattice relaxation time (T_1) are determined by the structure of the material and its state of motion. In liquids (mobile state) T_2 is almost equal to T_1. However, in the case of solids T_2 becomes very long. This difference in the behavior of T_2 due to components of the chain being in the liquid-like state (composed of loops and trains) and in the solid-like state (composed of trains) is used to estimate the fraction of the chain present in the form of trains. This fraction is called the bound fraction. Similarly, the solvent relaxation time can be used to estimate the bound fraction. The average solvent relaxation time is affected by the rate of exchange of the solvent molecules between the surface and the bulk. The presence of polymer segments on the surface can increase or decrease this rate of exchange. If the presence of train segments affects this exchange rate, the change in the solvent relaxation time can be used to estimate the bound fraction on the surface. Also, using high resolution NMR, it is possible to resolve the chemical shifts due to changes in the electronic environment of the chain segments near the interface. Using this shift, one can estimate the bound fraction in the adsorbed layer.

Electron spin resonance (5) measures the difference in the relaxation process between the segments in the loops and trains. The spectra of an adsorbed layer is deconvoluted into contributions from the loops, the tails, and the trains of the adsorbed layer by comparison with the spectra obtained in solution or melt state (mobile components) and on adsorbed oligomers at low temperatures (immobile components). It is also possible to measure the rotational correlation time of the mobile and immobile segments. The drawback of this technique is that a label has to be attached to the polymer and this might change the adsorption behavior of the chain.

Measurements on Flat Surfaces. The advantage of using flat surfaces is that adsorption measurements can be performed under well-defined conditions of surface energies and known surface area. The drawback is the increased sensitivity required of the measurement techniques.

Quartz Microbalance and Direct Microbalance Techniques. These methods provide direct measurements of the adsorbed mass. The vibration frequency of a quartz single crystal is very sensitive to the mass of the crystal. Upon adsorption, the vibration frequency shifts to lower values and the changes in the frequency can be related to the adsorbed mass. The surface excess can be determined by dividing the adsorbed mass by the surface area (6). Another method to directly measure the surface excess is the microbalance technique. In this technique, the

surface excess is estimated from the change is mass of a substrate of known surface area due to adsorption. Using microbalances capable of detecting changes of the order of 10^{-4} mg, researchers have been able to measure adsorbed amounts as low as 0.2 mg/m^2 (7).

Evanescent Wave/Spectroscopic Techniques. When a beam of light propagating in a medium of refractive index n_1 is incident on another medium of lower refractive index n_2, it will be completely reflected if the angle of incidence is greater than $\sin^{-1}(n_2/n_1)$. This phenomenon is called *total internal reflection*. Under these conditions, at the interface there exists an exponentially decaying evanescent electric field that can probe molecules that are present in the interfacial region. The penetration depth of this electric field can be determined by the wavelength of light, the incident angle, and the two refractive indices. This phenomenon is used in combination with FTIR spectroscopy to study adsorption on surfaces (8). The advantage of this technique is that *in situ* measurements can be performed, and changes in the adsorbed layer can be measured as a function of time. Typically, the penetration depth of the evanescent wave is much larger than the thickness of the adsorbed layer, and there can be a significant contribution to the absorbance from the bulk solution that has to be properly subtracted.

The same principles of total internal reflection can also be used to excite fluorescent chromophores attached to the polymer chain (9). The emitted fluorescence can be used to estimate the surface excess. In addition to subtracting the background signal, fluorescence quenching in the adsorbed layers may also have to be considered while estimating the adsorbed amount. The disadvantage of this technique is that the polymer chains have to be labeled with fluorescence molecules and that might influence the adsorption process.

Besides the adsorbed amount, it is also possible to measure the bound fraction of an adsorbed chain using IR spectroscopy. In order to do so there should be some distinguishable change in the features of the unbound and bound segments. Often there is a change in the absorption bands of functional groups upon adsorption to a substrate. This change in the IR spectra is due to physical and chemical interactions of the polymer with the substrate. For example, when poly(methyl methacrylate) adsorbs on an oxidized silicon substrate the carbonyl peak shifts to a lower wave number because of hydrogen bonding between the carbonyl and surface silanol groups (10). This change in the peak position can be experimentally resolved, and with proper calibration it is possible to estimate the bound fraction. Another method used to obtain structural information of the adsorbed layer is based on IR dichroism (11), where the ratio of absorption of p- and s-polarized components of light is measured. The dichroic ratio is defined as $D = A_z/A_x$, where A_z and A_x are the adsorptions parallel and perpendicular to the surface normal, respectively. For an isotropic chain, the dichroic ratio has a value of 1; however, if the dipole moments in the chain are preferentially oriented parallel to the surface, D is smaller than 1.

It is also possible to study exchange kinetics of the adsorbed polymers using these techniques. In the case of IR spectroscopy, exchange between deuterated and hydrogenated polymer chains at the surface can be studied as a function of time. From the rate of change in the specific absorption bands one can estimate the time constant for exchanging a chain in the solution with one on the surface. In the same way it is possible to study the kinetics of one species displacing another adsorbed

species on the surface. Similarly, fluorescence spectroscopy can be used as an alternate technique to study absorption kinetics. The fluorescent label is attached to one of the species, providing a contrast between the two adsorbing chains. The exchange kinetics is studied by monitoring the changes in the fluorescence signal as a function of time. Alternately, exchange kinetics at the surface can also be studied by fluorescence correlation spectroscopy (FCS) and fluorescence photobleaching recovery (FPR) techniques (12).

Reflectometry. Techniques described in this section are sensitive to the concentration profile of the adsorbed polymer chains. Optical reflectivity measurements are sensitive to changes in the refractive index in the adsorbed layer. Similarly, X-ray reflectivity is sensitive to the change in electron density in the adsorbed layer and neutron reflectivity is sensitive to the variation in the scattering length density in the adsorbed layer. In the last two cases it is possible to define an effective refractive index for the system. The variation of this refractive index in the adsorbed layer is used to obtain the concentration profile.

Ellipsometry is an optical technique that measures the changes in amplitude and phase of *s*- and *p*-polarized light upon reflection (13). These changes are related to the refractive index of the substrate and the thickness and refractive index of the adsorbed polymer layer. In order for this technique to work one needs a system with a high refractive index contrast between the surface and the adsorbed layer. By measuring these changes for different wavelengths of light and at different incident angles one can also determine the concentration profile of the adsorbed layer. Since this is an *in situ* measurement, ellipsometry can also be used to study adsorption kinetics as a function of time (14).

In the case of X-ray and neutron methods, the reflectivity is measured as a function of incident angle. The reflectivity data is then modeled as being made up of a number of layers varying in refractive index to determine the concentration profile (15). In the case of neutron reflectivity, the contrast can be provided using deuterated solvents. X-ray reflectivity is also most commonly used to study the thickness of dry films or adsorption at the air–liquid interface.

Hydrodynamic Measurements. Hydrodynamic methods rely on the fact that the flow of solvent past a surface having adsorbed polymers is different from the flow of solvent past an uncovered surface. The thickness measured in this technique is called the hydrodynamic thickness. The difference in pressure drop between a coated and uncoated capillary under identical flow conditions can be used to estimate hydrodynamic film thickness (16).

Surface Force Measurements. Another method to measure the thickness of adsorbed layers is by the surface force apparatus (SFA) (17). In this method two freshly cleaved mica sheets are glued to the surfaces of two crossed cylindrical lenses. Polymer chains are then allowed to adsorb on the mica sheets. In order to measure the thickness of the adsorbed layers the two cylinders are brought in contact and the force between them is measured as a function of separation. The onset of the repulsive force associated with compression of the adsorbed layer can be related to the thickness of the adsorbed layer. On the other hand, in the event of bridging between the adsorbed layers the force will be attractive. Recent advances in the instrument have made it possible to probe the effect adsorption has on the flow of fluid past a surface (18).

Adsorption at Solid–Liquid Interfaces

Adsorption of Homopolymers.

Adsorption Isotherms. Because of the strong tendency of polymer chains to adsorb at attractive surfaces, the surface gets saturated at very small bulk concentrations. Adsorption isotherms of this nature are known as "high affinity isotherms." The adsorption isotherm of polymer chains adsorbing on solid substrates depends on the polymer molecular weight, solvent quality, and polymer–surface interactions. Figure 3a illustrates the adsorption isotherms for polymer chains in a good solvent as a function of concentration. The surface excess

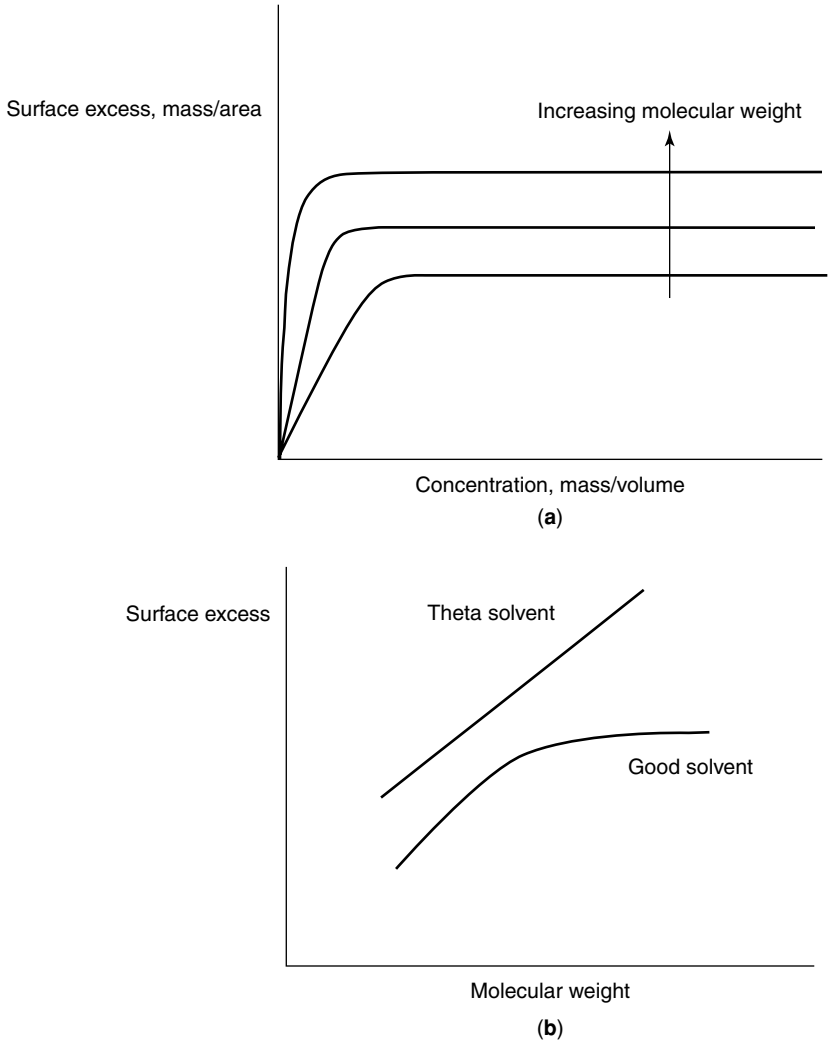

Fig. 3. (**a**) High affinity adsorption isotherm; (**b**) molecular weight dependence of surface excess.

saturates rapidly with increase in concentration of polymer chains in solution. Initially, the surface excess increases with an increase in molecular weight but at high enough molecular weights, the surface coverage becomes independent of molecular weight, as illustrated in Figure 3b. The adsorbed amount is higher in the case of a theta solvent as compared to a good solvent and it increases continuously as a function of molecular weight (19).

The shape of the isotherm is influenced by the average molecular weight as well as the molecular weight distribution of the adsorbing polymer. At low molecular weights and for polymers showing a broad molecular weight distribution, the isotherm displays a more rounded profile, while in the case of a narrow molecular weight distribution and large molecular weights a sharp profile is observed. In a solution containing polymers of two different molecular weights, the low molecular weight polymer will adsorb first because of faster diffusion constants in the solution. However, the higher molecular weight polymer will eventually displace the lower molecular weight polymer at the surface (20).

Adsorption from a solution containing chains of different sizes depends on the concentration of the polymer chains in the solution. If the adsorbing chains have a broad molecular weight distribution, the smaller chains will adsorb at the surface only when the bulk concentration is extremely small. Under these conditions the surface is not saturated and it can accommodate chains of all sizes. On increasing the bulk concentration the surface gets saturated and the smaller chains begin to be displaced by the larger chains. Thus, the larger chains will predominantly populate a completely covered surface. This is a consequence of the fact that the total loss of translational entropy per unit mass when high molecular weight chains adsorb is lower, as compared to shorter chains, while the change in the enthalpy per unit mass is the same. Thus, the change in total free energy upon adsorption is lower for longer chains in comparison to the shorter ones.

Structure of Adsorbed Polymers. As seen in Figure 2, the structure of the adsorbed chain can be described in terms of loops, tails, and trains (1). The relative fractions of loops, tails, and trains in an adsorbed chain depend upon the strength of interactions between the monomeric units and the interface, polymer concentration, and molecular weight.

Experimentally, it is not possible to distinguish between the segments that form loops and segments that form tails. However, theories such as the Scheutjens–Fleer theory (21) provide information regarding the structure of the adsorbed chains. According to this theory, train segments dominate the structure of adsorbed low molecular weight polymers. With increase in molecular weight, the fraction of segments forming loops and tails increases at the expense of the segments participating in trains. The fraction of the chain in loops increases continuously with the size of the chain; however, after an initial increase, the fraction of the chain in tails remains more or less constant.

The average length of the tail in an adsorbed polymer is predicted to increase with molecular weight and this dependence becomes stronger as the solution concentration increases. On increasing the bulk concentration, the fraction of the chain present in the tail is also predicted to increase at the expense of the fraction of monomers in loops.

The bound fraction, defined as $p = \Gamma_{tr}/\Gamma$ (Γ_{tr} is the surface excess of polymer in physical contact with the substrate), can be experimentally measured and has been known to vary from 0.2 to 0.8 (22). The bound fraction strongly depends on

the solvent quality, the polymer–surface interaction, and the surface coverage. In a good solvent the bound fraction remains constant when the surface is unsaturated. This corresponds to the adsorption from dilute solutions. However, in concentrated solutions when the surface is saturated, the bound fraction starts to decrease. This suggests that chains initially have a flat conformation but as the surface gets populated the chains begin to form loops and tails (23). The bound fraction also increases when the interaction between the chain and the surface increases or when the solvent quality decreases.

For adsorbed homopolymers the average density (or concentration of chain segments) decays monotonically with the distance (z) from the surface. Neutron reflectivity and small-angle neutron scattering have experimentally measured the segment density of the adsorbed layer. Scaling arguments suggest that the segment density scales as $z^{-4/3}$ (24) in good solvents, whereas mean field calculations predict that the segment density scales as z^{-2} (25). These predictions are valid only in the limit that the chains are extremely large. Experimental results obtained so far are in qualitative agreement with these predictions; however, there seems to be no agreement on the value of the exponent (26,27).

Thickness of Adsorbed Layers. Since the adsorbed layer is heterogeneous in the distribution of segments, the experimentally measured thickness will depend upon the structural aspect of the adsorbed chain that the technique measures. For example, hydrodynamic techniques are sensitive to the contributions from tail segments. On the other hand, ellipsometry is sensitive to the trains and loops of an adsorbed layer. As the tails are much longer than the loops, the hydrodynamic thickness is larger than those measured by optical techniques. The structure of the adsorbed layer changes with the solvent quality, surface coverage, and size of the adsorbing molecule; therefore, all of the above parameters will influence the value of the measured thickness. For example, since the tail length increases strongly with the chain size, the hydrodynamic thickness shows a stronger dependence on the molecular weight as compared to the thickness obtained by ellipsometry. Also because of the fact that chains adopt flat conformations at low surface coverage, the hydrodynamic thickness will be lower at low surface coverage, but will increase strongly with increasing surface coverage (21).

Thickness measurements on adsorbed layers have found that the thickness of the adsorbed layer exhibits a power law dependence on the molecular weight. However, the value of the exponent has been reported to vary from 0.4 to 0.7. The value of the exponent depends upon the technique and the polymer–solvent system being studied (28). In the case of adsorption from a theta solvent, the thickness of the adsorbed layer varies as $M^{0.5}$ (29).

Dynamics of Adsorbed Chains. In solution, conformation interconversions in a polymer chain occur in microsecond time scales. At a surface, because of adsorption of train segments the time frame for conformational rearrangements of adsorbed macromolecules is increased to hours. The nonequilibrium nature of the adsorbed layer is strongly evident in the exchange kinetics of adsorbed polystyrene molecules (30,31). The exchange time constants depend on the duration of time that the adsorbed chains are allowed to stay on the surface before being displaced. In order to explain this behavior, it is suggested that the adsorbed chains continuously relax toward an equilibrium state by increasing the bound fraction. The time required to reach an equilibrium conformation can be of the order of days. The direct IR measurements of bound fraction in poly(methyl methacrylate) and

poly(dimethyl siloxane) also suggest that the bound fraction increases with time (32,33).

An interesting feature of adsorbed polymers is that the chains do not desorb from the surface when exposed to the pure solvent. This apparent irreversibility of adsorption arises from the fact that the activation energy required to remove a chain from a surface is extremely high. However, it is possible to replace an adsorbed chain with a displacer molecule that has a higher affinity for the surface (34).

If the exchange is governed by surface energetics, the surface excess of the initially adsorbed polymer decays exponentially with time. The time constant for exchange of an equilibrated layer in this case increases exponentially with the molecular weight of the adsorbed molecules. However, this is true only for a chemically homogeneous surface. In the case of a chemically heterogeneous surface the exchange time constant shows a power law dependence on the molecular weight (30).

If the exchange is governed by diffusion away from the surface, then a stretched–exponential type of behavior $\Gamma(t) = \Gamma(0)\ \exp[-(t/\tau)^{\beta}]$ is observed for the decay in the surface excess of the initially adsorbed polymer. The value of the exponent β can vary between 0 and 1, depending on the rate of readsorption and the bulk diffusion rates (35,36). If diffusion is slow and the chain exhibits a strong tendency to readsorb, β will have a small value ($\beta < 1/2$). The time constant for exchange in this case scales as D^{-1}, where D is the diffusion coefficient of the polymer chain in the matrix of adsorbed chains.

Adsorption of Copolymers. In the case of adsorption of copolymers the structure and extent of adsorption depend on the type of copolymer involved. Figure 4a is a schematic of the type of structures that adsorbed copolymers might adopt.

In block copolymers (qv), the block that is preferentially adsorbed is called the anchor while the nonadsorbing block is called the buoy. In this case the adsorbed structure is affected by the nature of the solvent and the relative sizes of the blocks.

In a solvent that selectively solubilizes one of the blocks, when the chain adsorbs, the anchor collapses to form a dense layer, while the buoy stretches out to form a brush-like structure. Adsorption in this case is decided by the competition between van der Waals attraction between the anchor and the substrate and repulsive interactions between the buoys. This is referred to as the "van der Waals brush regime" (37).

If the solvent is nonselective, the anchor has a swollen structure similar to an adsorbed homopolymer. In the case of adsorption of an AB block copolymer from nonselective solvents there are two possible cases (38): The first is referred to as the "buoy" regime, in which the anchor are small and adsorption is dominated by repulsive interactions between the buoys. Increasing the length of the anchor will increase the amount adsorbed. The second case is called the "anchor" regime, in which the anchor layer is saturated and the buoys are small in size. Here, increasing the length of the anchor block will not increase the adsorbed amount.

A major difference between adsorption of homopolymers and block copolymers is that in the case of block copolymers, the proportion of trains and loops are small as compared to the tails. Consequently, the volume profile in block copolymers exhibits a parabolic decay with distance (39,40). In the case of random

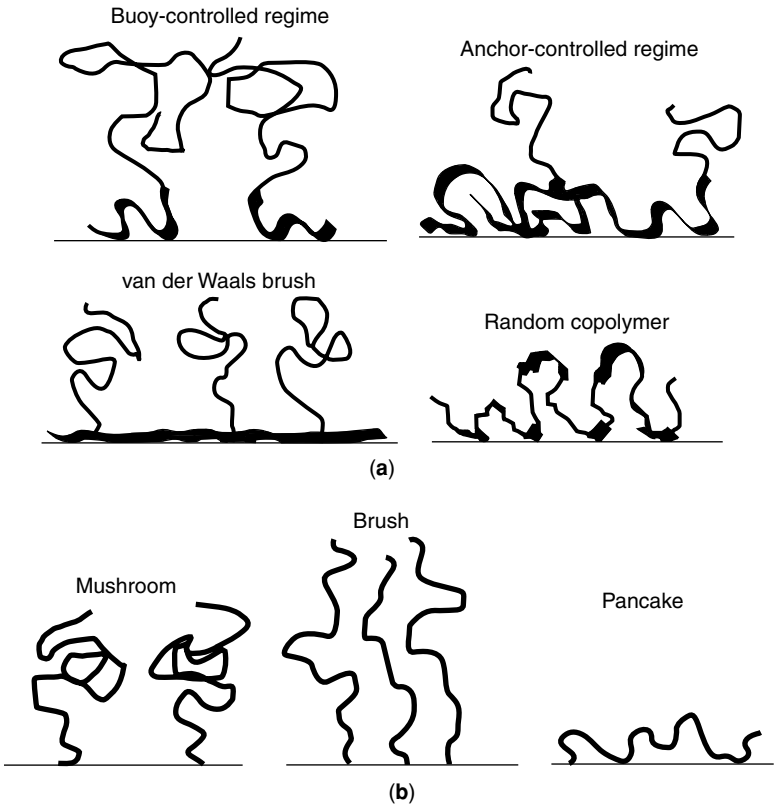

Fig. 4. (**a**) Adsorption of copolymers at a surface; (**b**) end functionalized polymers at a surface.

copolymers, in addition to the solvent quality and size, the adsorption behavior is determined by the composition and distribution of the monomers along the chain. For a truly statistical copolymer the adsorption behavior can be expected to be between the behaviors of the two homopolymers (41).

Adsorption of End Functionalized Chains. Terminally attached polymer chains (42) are a special case of adsorption because the end groups may be permanently grafted to the surface. The reason for this kind of behavior is the formation of strong bonds between the end group and the surface. If the bond is chemical in nature the adsorption is called chemisorption. In the case of physisorption, the interaction between the end group and the surface strongly outweighs the solvent–surface and solvent–end group interaction.

Figure 4b is a schematic of the various structures that terminally adsorbed chains can adopt at the interface. The structure of these attached chains depends on the surface coverage, solvent quality, and the polymer–surface interaction. If the latter interaction is extremely weak the chain gets repelled from the surface, forming a "mushroom" type structure at low surface coverages. If the polymer–surface interaction is strong enough then at low surface coverage the polymer adopts a flat conformation called a "pancake." At large surface coverages, the chains stretch to form a structure known as a "brush."

The degree to which the chains extend is controlled by the excluded volume interactions between the chains and the entropic penalty due to stretching. The extension of the mushroom structure normal to the surface is of the order of $2R_g$, where R_g is the size of the chain in the bulk, while in the case of an extended brush it is much longer. For a fixed surface coverage the thickness of the adsorbed layer increases linearly with chain length. If the chain length is fixed the thickness has a power law dependence on the grafting density (43).

Measurements of the structure of these chains when the polymer does not adsorb on the surface indicate that the volume fraction profile is parabolic at high surface coverages. Changing the solvent conditions causes a dramatic change in the volume profile, which changes from being parabolic in good solvents to being block-like in bad solvents (44).

Adsorption of Polyelectrolytes. The presence of charges on the surface or on the polymer chain affects the adsorption behavior of polymers. When the polymer is uncharged but the surface is charged, the surface attracts counterions that can prevent the polymer from adsorbing. This interaction can be screened by addition of salt, but the effect of the salt is not very significant.

In the adsorption of polyelectrolytes, columbic interactions play a significant role. These interactions can exist between the chain and the surface as well as between the ions on the chain. Addition of salt causes these interactions to be screened and therefore the salt concentration has a significant impact on the adsorption behavior. When adsorption occurs on an uncharged surface the adsorbed amount increases with an increase in salt concentration. When the salt concentration is low the adsorbed chains are predominantly flat and the adsorbed amount does not depend significantly on the length of the molecule. At high salt concentrations the polyelectrolyte adsorption is similar to the adsorption of uncharged homopolymers exhibiting similar structural features such as loops and tails. Under these conditions the adsorbed amount does increase as a function of molecular weight. Similarly, when the polyelectrolyte adsorbs on a surface having the same charge, no adsorption is seen until a critical salt concentration after which the adsorbed amount starts to increase. When the surface is oppositely charged and the polymer has a strong interaction with the surface, the polyelectrolyte adsorption increases with salt concentration provided that the chain is highly charged (45). However, if the chain is not highly charged, increasing the salt concentration reduces the electrostatic interaction between the chain and the surface, reducing adsorption. Increasing the salt concentration may also reduce the solvent quality and will result in an increase in adsorption. Also, if the counterions start adsorbing on the surface, they will displace the adsorbed polyelectrolyte chains (46). Using scaling arguments it has been shown that the thickness of the adsorbed layer is a nonmonotonic function of the surface charge density (47).

A sequential adsorption of anionic and cationic charged polyelectrolytes also leads to formation of stable multilayers (48). Upon adsorption, the charged groups present in the adsorbed chains may overcompensate the charges present on the surface, resulting in a change in its polarity. Now the surface can attract another oppositely charged polyelectrolyte molecule. By sequentially using anionic and cationic polyelectrolytes it is possible to form a multilayer whose stability can be controlled by the polymer charge and the ionic strength. It has been shown that very stable multilayers are formed with high charge content and in the presence of low ionic strength (49).

Adsorption at Liquid–Liquid Interfaces

An example of adsorption of this kind is the adsorption occurring at the oil–water interface. The driving force for adsorption in this case is the minimization of the interfacial tension between the two interfaces. Typically, random copolymers or block copolymers, in which the monomeric units are preferentially solvated in either of the two phases, adsorb readily at the interface. In the case of homopolymers, adsorption occurs either if the polymer is soluble in both the phases or if the polymer has functional groups that can reduce the interfacial tension. Thus, both poly(ethylene oxide) and poly(methyl methacrylate) readily adsorb at the toluene–water interface. The former is soluble in both the phases while the latter has polar side groups that effectively screen the interactions between toluene and water. However, because of its hydrophobic nature polystyrene does not adsorb at the same interface (50).

One of the simplest methods to study adsorption at the oil water interface is to measure the variation of interfacial tension as a function of concentration. If the polymer used for adsorption is monodisperse, then the Gibbs equation (51) may be used to estimate the surface excess. However, if the polymer is polydisperse, this method will give erroneous values of the surface excess because the larger molecules will tend to adsorb preferentially, and the equation is unable to account for this adsorption behavior. As a result, most of the data available in the literature report the change in the interfacial tension as a function of concentration without attempting to convert it into an adsorbed amount. Apart from interfacial tension measurements, other techniques such as total internal reflection fluorescence microscopy (52) and scintillation measurements from radiolabeled polymers (53) have also been used to measure the adsorption at the liquid–liquid interface.

The thickness of adsorbed layers at liquid interfaces has been experimentally studied using neutron reflectivity (54). The structure of the adsorbed polymer at the liquid–liquid interface depends on the nature of the polymer and the interaction of the segments with the two phases. For example, if a diblock copolymer adsorbs at an oil water interface, the chain will partition itself in the two phases such that the block that is preferentially solvated by water will be in the aqueous phase, while the block that is preferentially solvated by oil remains in the organic phase. This results in the chains stretching at the interface, and the adsorbed layer becomes thick. On the other hand, if a random copolymer having the same composition as the diblock copolymer were to be adsorbed at the same interface, the interfacial thickness would be smaller because the unfavorable interactions between the parts of the copolymer and the two phases would localize the chain at the interface.

Adsorption at Air–Liquid and Polymer–Polymer Interfaces

The structure of adsorbed chains at the air–liquid interface is similar to that at the solid–liquid interface. Adsorption at air–liquid interface has been studied by ellipsometry (54), X-ray and neutron reflectivity (55,56), surface tension measurements (57), X-ray evanescent wave-induced fluorescence (58), and Langmuir trough techniques (55). Neutron reflectivity measurements indicate that in the

case of homopolymers the segment density decreases as $z^{-4/3}$, which is consistent with scaling predictions for homopolymers at the solid–liquid interface (55).

Another interface of interest is the interface between two polymers. Adsorption at this interface is important from the point of compatibilization in blends. The structure of block copolymers at the interface can be studied using neutron reflectivity. By selective deuteration it is possible to distinguish between the blocks and the homopolymer chains. The measurements indicate that the block copolymer partitions itself in the two immiscible phases, and the segments joining the blocks are distributed over the interfacial region (59).

Applications of Polymer Adsorption

The phenomenon of polymer adsorption has applications in the areas of colloidal science, tribology, separation science, adhesion, nanotechnology, and medicine. Here, we summarize some recent applications of adsorbed polymers.

Flocculation and Stabilization of Colloids. When two surfaces covered with adsorbed polymers are brought in contact with each other they may experience strong repulsive or attractive forces. The interaction forces depend on solvent quality, surface coverage, and segment–surface interactions. In poor solvents or on sparsely coated surfaces the force can be attractive. For sparsely coated surfaces, chain segments from one surface get adsorbed onto the other surface, resulting in bridging. In the removal of suspended fine solids in wastewater treatment it is advantageous to bring particles together, and here bridging-induced flocculation or other attractive forces are useful. In a good solvent and in the case where the surface is completely saturated with adsorbing chains, the force is repulsive. This phenomenon is known as *steric repulsion*. Colloidal particles that tend to coagulate can be stabilized by addition of extremely small amounts of polymer as stabilizers. This technique is commonly used in stabilizing inks, cosmetics, processed food, lubricants, etc (60).

Friction and Lubrication. Steric repulsive forces also exist between two surfaces that are covered by polymer brushes. The onset of repulsive forces coincides with the touching of two brush-coated surfaces. This distance can be controlled by the molecular weight of the polymer chain. Interestingly, in the case of brushes the friction coefficient is very low. This offers an ideal situation where the surfaces can sustain a large normal force with very little resistance to sliding and may find applications as friction modifiers (61). The development of chemical grafting technique in the last five years offer possibilities to create micron-thick brush layers and may offer a more robust approach for practical applications (62).

Polymer Structure and Characterization. In separation science, the phenomenon of adsorption coupled with size-exclusion chromatography (SEC) has been applied to rapidly separate and characterize polymers. In this technique, called full adsorption–desorption/SEC coupling (FAD/SEC), all the components of a polymer blend are initially adsorbed onto an adsorbent. Then each component is displaced using a suitable small-molecule displacer and sent into the SEC column to characterize their size and mass distribution. This approach also finds application in characterizing copolymers having complex architecture (63).

Nanotechnology. In the past 10 years, layer-by-layer deposition has emerged as an important technique to prepare tailored polymer thin films. In this technique oppositely charged polyelectrolytes are adsorbed on a charged surface in a sequential manner. It is possible to incorporate a number of features in these films by varying the functional groups in the adsorbing polymers. For example, by incorporating electrooptical moieties in the multilayer it is possible to form nonlinear optical devices. Similarly, by incorporating silica and submicron-sized metallic spheres one can obtain arrays for photonic band gap applications. It is also possible to obtain two- or three-dimensional structures by the same technique, making it an attractive alternative to conventional photoresist-based lithography (64).

Biomaterials. Adsorbed polymers find many applications as surface modifiers in biomedical applications. By choosing a combination of hydrophobic and hydrophilic copolymers, surfaces can be modified to make them biocompatible (65) (see BIOMOLECULES AT INTERFACES). In the area of tissue engineering (qv), adsorbed layers with specific amino acid sequences can be used to promote cell adhesion and proliferation. The recent developments in the design of biochips to analyze specific DNA molecules also take advantage of this technology. Polymer adsorption on patterned surfaces can be used to mimic pattern recognition. This effect can be used to develop sensors and molecular-scale separation processes (66).

BIBLIOGRAPHY

"Adsorption" in *EPST* 1st ed., Vol. 1, pp. 551–567, by R. Ullman, Ford Motor Co.; "Adsorption" in *EPSE* 2nd ed., Vol. 1, pp. 577–594, by A. Silberberg, The Weizmann Institute of Science.

1. G. P. Van der Beek, M. A. Cohen Stuart, G. J. Fleer, and J. E. Hofman, *Langmuir* **5**, 1180 (1989).
2. E. Jenkel and B. Rumbach, *Elektrochem* **55**, 612 (1951).
3. G. J. Fleer, M. A. Cohen Stuart, J. M. H. M. Scheutjens, T. Cosgrove, and B. Vincent, *Polymers at Interfaces*, Chapman and Hall, London, 1993, pp. 69–72, 80–87.
4. T. Cosgrove and P. C. Griffiths, *Adv. Colloid Interface Sci.* **42**, 175 (1992)
5. Y. Imamura and H. Sakai, *Bull. Chem. Soc. Jpn.* **60**, 1261 (1987).
6. T. Z. Fu, U. Stimming, and C. J. Durning, *Macromolecules* **26**, 3271 (1993).
7. H. Terashima *J. Colloid Interface Sci.* **212**, 100 (1999).
8. D. J. Kuzmenka and S. Granick, *Colloids Surf.* **31**, 105 (1988).
9. V. A. Rebar and M. M. Santore, *J. Colloid Interface Sci.* **178**, 29 (1996).
10. B. J. Fontana and J. R. Thomas, *J. Phys. Chem.* **65**, 480 (1962).
11. E. P. Enriquez and S. Granick, *Colloids Surf. A* **113**, 11 (1996).
12. N. L. Thompson, T. P. Burghardt, and D. Axelrod, *Biophys. J.* **33**, 435 (1981).
13. R. M. Azzam and N. M. Bashara, *Ellipsometry and Polarized Light*, North Holland, Amsterdam, (1989).
14. T. Pankewitsch, P. Vanhoorne, R. Jerome, and M. Stamm, *Macromolecules* **28**, 6986 (1995).
15. T. P. Russell, *Mater. Sci. Res.* **5**, 171 (1990).
16. Ref. 3, pp. 67–69.
17. J. N. Israelachvili, R. K. Tandon, and L. R. White, *J. Colloid Interface Sci.* **78**, 430 (1980).
18. A. Dhinojwala and S. Granick, *Macromolecules* **30**, 1079 (1997).

19. Ref. 3, p. 270.
20. Z. Fu and M. M. Santore, *Macromolecules* **31**, 7014 (1998).
21. Ref. 3, pp. 241–249.
22. A. Takahashi and M. Kawaguchi, *Adv. Polym. Sci.* **46**, 1 (1982).
23. Z. Fu and M. M. Santore, *Langmuir* **13**, 5779 (1997).
24. P. G. De Gennes, *Adv. Colloid Interface Sci.* **27**, 189 (1987).
25. Ref. 3, pp. 146–147.
26. L. Auvray and J. P. Cotton, *Macromolecules* **20**, 202 (1987).
27. T. Cosgrove, T. G. Heath, K. Ryan, and T. L. Crowley, *Macromolecules* **20**, 2879 (1987).
28. Ref. 3, pp. 261–265.
29. H. Gebhard and E. Killmann, *Angew. Makromol. Chem.* **53**, 171 (1976).
30. P. Frantz and S. Granick, *Phys. Rev. Lett.* **66**, 899 (1991).
31. P. Frantz and S. Granick, *Macromolecules* **27**, 2553 (1994).
32. H. E. Johnson and S. Granick, *Macromolecules* **23**, 3367 (1990).
33. I. Soga and S. Granick, *Macromolecules* **31**, 5450 (1998).
34. M. A. Cohen Stuart, G. J. Fleer, and J. M. H. M. Scheutjens, *J. Colloid Interface Sci.* **97**, 526 (1984).
35. J. F. Douglas, H. E. Johnson, and S. Granick, *Science* **262**, 2010 (1993).
36. Y. Wang, R. Rajagopalan, and W. L. Mattice, *Macromolecules* **28**, 7058 (1995).
37. C. Marques, J. F. Joanny, and L. Leibler, *Macromolecules* **21**, 1051 (1988).
38. C. M. Marques and J. F. Joanny, *Macromolecules* **22**, 1454 (1989).
39. Ch. Toprakcioglu, L. Dai, and M. A. Ansarifar, *J. Macromol. Sci., A: Pure Appl. Chem.* **29**(Suppl. 2), 139 (1992).
40. T. Cosgrove, T. G. Heath, J. S. Phipps, and R. M. Richardson, *Macromolecules* **24**, 94 (1991).
41. Ref. 3, pp. 321–340.
42. S. T. Milner, *Science* **251**, 4996 (1991).
43. P. Auroy, L. Auvray, and L. Leger, *Phys. Rev. Lett.* **66**, 719 (1991).
44. A. Karim, S. K. Satija, J. F. Douglas, J. F. Ankner, and L. J. Fetters, *Phys. Rev. Lett.* **73**, 3407 (1994).
45. S. A. Sukhishvili, A. Dhinojwala, and S. Granick, *Langmuir* **15**, 8474 (1999).
46. Ref. 3, pp. 346–350.
47. A. V. Dobrynin, A. Deshkovski, and M. Rubinstein, *Phys. Rev. Lett.* **84**, 3101 (2000)
48. G. Decher, and J. D. Hong, *Makromol. Chem., Makromol. Symp.* **46**, 321 (1991).
49. N. G. Hoogeveen, M. A. Cohen Stuart, G. J. Fleer, and M. R. Bochmer, *Langmuir* **12**, 3675 (1996).
50. H. F. Huber and C. Thies, *J. Polym. Sci., Polym. Phys.* **8**, 71 (1970).
51. R. Teppner, S. Bae, K. Haage, and H. Motschmann, *Langmuir* **15**, 7002 (1999).
52. R. Y. Ofoli and G. Arivalagan, *Langmuir* **16**, 4279 (2000).
53. J. B. Schlenoff and R. Wang, *Macromolecules* **31**, 494 (1998).
54. J. S. Phipps, J. M. Richardson, T. Cosgrove, and A. Eaglesham, *Langmuir* **9**, 3530 (1993).
55. O. Theodoly, R. Ober, and C. E. Williams, *Eur. Phys. J. E* **5**, 51 (2001).
56. L. T. Lee, O. Guiselin, B. Farnoux, and A. Lapp, *Macromolecules* **24**, 2518 (1991).
57. R. Ober, L. Paz, C. Taupin, P. Pincus, and S. Boileau, *Macromolecules* **16**, 50 (1983).
58. S. W. Barton, L. Bosio, R. Cortes, and F. Rondelez, *Europhys. Lett.* **17**, 401 (1992).
59. T. P. Russell, S. H. Anastasiadis, A. Menelle, G. P. Felcher, and S. K. Satija, *Macromolecules* **24**, 1575 (1991).
60. J. Israelachvili, *Intermolecular and Surface Forces*, Academic Press, Inc., London, 1992, pp. 289–303.
61. J. Klein, Y. Kamiyama, H. Yoshizawa, J. N. Israelachvili, G. H. Fredrickson, P. Pincus, and L. J. Fetters, *Macromolecules* **26**, 5552 (1993).
62. M. Biesalski and J. Ruehe, *Macromolecules* **32**, 2309 (1999).
63. D. Berek and S. H. Nguyen, *Macromolecules* **31**, 8243 (1998).

64. P. T. Hammond, *Curr. Opin. Coll. Interface Sci.* **4**, 430 (2000).
65. N. B. Holland, Y. Qiu, M. Ruegsegger, and R. E. Marchant, *Nature* **392**, 799 (1998).
66. A. J. Golumbfskie, V. S. Pande, and A. K. Chakraborty, *Proc. Natl. Acad. Sci. U. S. A.* **96**, 11707 (1999).

ASHWIN RAO
ALI DHINOJWALA
The University of Akron

AGING, PHYSICAL. See VOLUME 1.

ALKYD RESINS. See VOLUME 1.

AMINO RESINS AND PLASTICS. See VOLUME 1.

AMORPHOUS POLYMERS

Introduction

Amorphous materials are characterized by the absence of a regular three-dimensional arrangement of molecules; ie, there is no long-range order. However, a certain regularity of the structure exists on a local scale denoted as short-range order. For low molecular weight amorphous materials the structure is characterized with respect to the short-range order of the centers of the molecules as well as the orientational order of the molecular axes. For the case of long-chain amorphous materials it is necessary to specify an additional structural parameter, namely the conformation (1) of the chain which depends predominantly on the intramolecular interactions along the chain (see CONFORMATIONS AND CONFIGURATION).

The structure however is not static but changes continuously as a result of thermally driven orientational and translational molecular motions. The time scale of these motions may consist of a few nanoseconds up to several hundred years. The structure of the amorphous state as well as its time-dependent fluctuations can be analyzed by various scattering techniques such as x-ray, neutron, and light scattering. The static properties (structure) are probed by coherent elastic scattering methods, whereas the time-dependent fluctuations are investigated by inelastic and quasi-elastic neutron scattering, and dynamic light scattering.

Scattering Methods for the Study of Static and Dynamic Properties

X-ray experiments use radiation with a wavelength in the range $10^{-1} - 1$ nm (see X-RAY SCATTERING). The energy of x-rays is so high that all electrons are excited. The electric field of the incoming wave induces dipole oscillations in the atoms.

Encyclopedia of Polymer Science and Technology. Copyright John Wiley & Sons, Inc. All rights reserved.

The accelerated charges generate secondary waves that add up at large distances to the overall scattering amplitude. All secondary waves have the same frequency, but they may have different phases caused by the different path lengths. Because of the high frequency it is only possible to detect the scattering intensity, the square of the scattering amplitude, and its dependence on the scattering angle. Neutron scattering (qv) experiments allowed for measurements of polymer conformations at large scales, which were not feasible with x-rays. Neutrons interact with the nuclei of the atoms whereas x-rays interact with the electrons. The interaction with matter is different, but the problem of interfering secondary waves is the same. Instead of the electron density the scattering length density is dealt with. The essential fact in neutron scattering is the pronounced difference in the scattering amplitude between hydrogen and deuterium, which is important for the variation of the contrast between the particles and the matrix. Quasi-elastic neutron and light scattering experiments measure the correlation function of the conformational fluctuations of the macromolecules at a given length scale. Neutron scattering monitors the segmental mobility of a polymer chain in the nanometer and nanosecond region, whereas light scattering reflects translational diffusion of the whole polymer coil.

This article describes the present state of knowledge regarding the structure of amorphous polymers as obtained from scattering techniques and the corresponding dynamic properties from a structural point of view. A detailed knowledge of the structure is very important because the thermal, mechanical, viscoelastic, optical, and even electrical properties are strongly governed by the structure and its temporal fluctuations.

In order to describe the static structure of the amorphous state as well as its temporal fluctuations, correlation functions are introduced, which specify the manner in which atoms are distributed or the manner in which fluctuations in physical properties are correlated. The correlation functions are related to various macroscopic mechanical and thermodynamic properties. The pair correlation function $g(\boldsymbol{r})$ contains information on the thermal density fluctuations, which in turn are governed by the isothermal compressibility $\kappa_T(T)$ and the absolute temperature for an amorphous system in thermodynamic equilibrium. Thus the correlation function $g(\boldsymbol{r})$ relates to the static properties of the density fluctuations. The fluctuations can be separated into an isobaric and an adiabatic component, with respect to a thermodynamic as well as a dynamic point of view. The adiabatic part is due to propagating fluctuations (hypersonic sound waves) and the isobaric part consists of nonpropagating fluctuations (entropy fluctuations). By using inelastic light scattering it is possible to separate the total fluctuations into these components.

Knowledge of the density and orientational correlation functions is not sufficient to characterize the structure completely, since different structures can give rise to identical correlation functions. Therefore it is necessary to assume models. A complete description of the structure requires that the spatial arrangement of the chain elements, the chain conformation, be known. Usually, average values of the conformation (2) such as the mean square radius of gyration or the mean square end-to-end distance are determined. Direct structure measurements involve the interaction between electromagnetic radiation and the substance in question. A full description of the system will require information about both its

static and dynamic properties. Structure information about the time-averaged or static state is obtained from elastic scattering experiments; ie, the scattered intensity is integrated over all frequencies. Time-dependent or dynamic structures, on the other hand, can be studied with inelastic scattering techniques; ie, the scattered intensity is analyzed with respect to the frequency. The mathematical tool which is used to relate the scattering function $S(q, \omega)$ with properties of the system is a Fourier or Laplace transformation. The system in real space is characterized by correlations between various physical properties (eg, particle densities, distances between atoms, orientations, fluctuations in the local dielectric tensor, pressure and entropy fluctuations) in terms of the corresponding correlation functions.

The theoretical analysis of the scattered spectrum was first presented by Komarov and Fisher (3) and Pecora (4) independently in 1963. In 1964 the spectrum of laser light scattered by dilute solutions of polystyrene latex spheres was observed (5) and was found to exhibit a lineshape in good agreement with theory. In a typical scattering experiment (6) a monochromatic beam of radiation is incident on the material; the wave vector is denoted as $\boldsymbol{k}_0$ and the frequency by ω_0. The scattered radiation is recorded as a function of the scattering angle and frequency shift ω, where

$$\boldsymbol{q} = \boldsymbol{k}_1 - \boldsymbol{k}_0 \quad \text{with} \quad |\boldsymbol{q}| = \frac{4\pi n}{\lambda} \sin(\theta/2) \tag{1}$$

$\boldsymbol{k}_1$ is the wave vector of the scattered radiation, ω_1 the frequency, and λ the wavelength.

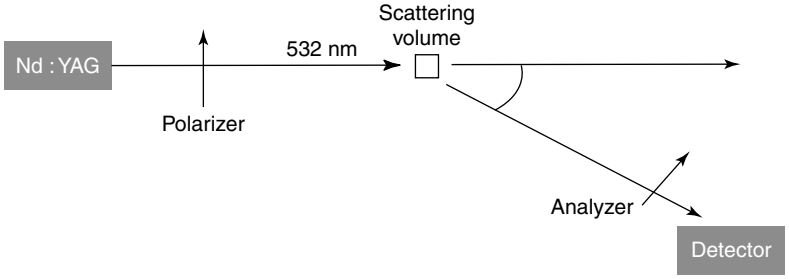

The distribution of the scattered radiation as a function of $\boldsymbol{q}$ contains information about the distribution of atoms or molecules on a molecular level, provided that the wavelength of the radiation used is of the order of magnitude of the interatomic spacings. This is the case for neutron and x-ray scattering, whereas in the case of light scattering only integral properties of the structure can be analyzed because of the large wavelength involved. It is worth mentioning that one characteristic property of elastic scattering is its coherence. Thus spatial information is contained in the phases, and the scattered intensity is determined by the interference of the scattered waves in front of the detector. Consequently, if q is a characteristic correlation length in a polymeric system, the obtained information is an ensemble average over distances of the order of q^{-1}. A polarized light scattering experiment with wavelengths 2–3 orders of magnitude longer than neutron wavelengths, observes averages over much longer correlation lengths. By correctly chosen q-range, local or global features of the polymers can be studied (7).

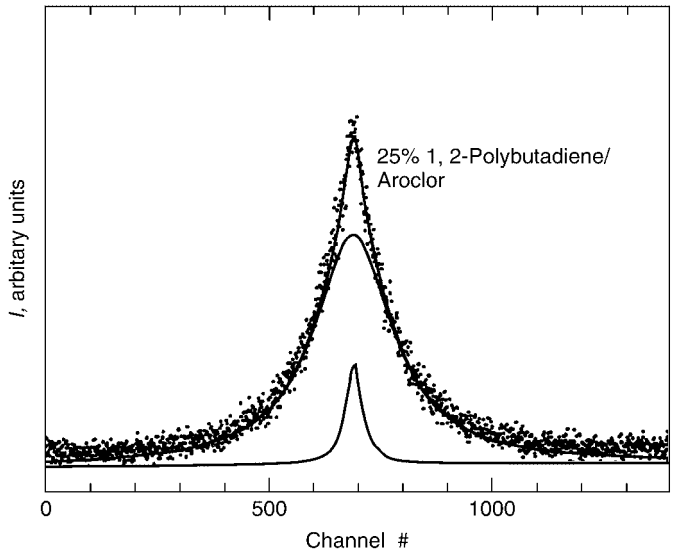

Fig. 1. Depolarized Rayleigh spectra of 1,2-polybutadiene in Aroclor at 353 K. The depolarized spectra were fit to either one or a sum of two Lorentzian functions plus a baseline, considering the overlap of neighboring orders. The integrated intensity is proportional to the effective optical anisotropy γ_{eff}^2.

The method of light scattering with different techniques (8) can cover a wide dynamic range from 10^5 up to 10^{-12} s. With Fabry–Perot interferometry the Rayleigh–Brillouin (9) and depolarized spectra (10,11) can be frequency analyzed to reveal the effects of segmental (12) and orientational (13) fluctuations between 10^{-8} and 10^{-12} s. At longer time scales the scattered light can be analyzed by the photon correlation spectroscopy (pcs) technique. The polarization of the scattered light and the scattering vector $\boldsymbol{q}$, which determines the wavelength of the observed fluctuations, selects and characterizes the observed motion. Figure 1 shows a typical depolarized Rayleigh spectrum (14) of 1,2-polybutadiene in Aroclor at 353 K. The depolarized spectra were fit to either one or a sum of two Lorentzian functions plus a baseline, considering the overlap of neighboring orders. The integrated intensity is proportional to the effective optical anisotropy γ_{eff}^2 and is given by following the expression:

$$I_{\text{VH}} = Af(n)\rho^*\gamma_{\text{eff}}^2 \tag{2}$$

where A is a constant, $f(n)$ is the product of the local field correction and the geometrical factor $1/n^2$, with n being the refractive index and ρ^* is the number density of the solute. Figure 2 shows depolarized intensity correlation functions for a poly(styrene-*b*-1,4-isoprene) block copolymer (15) in the disordered state. The total molecular weight M_n of the copolymer is 3930 and the molecular weight of the polystyrene (PS) block is 2830. The primary contribution to the spectra comes from the local segmental motion of the PS in the copolymer and the dispersion broadens with decreasing temperature, which is evident by inspection of the curves in Figure 2.

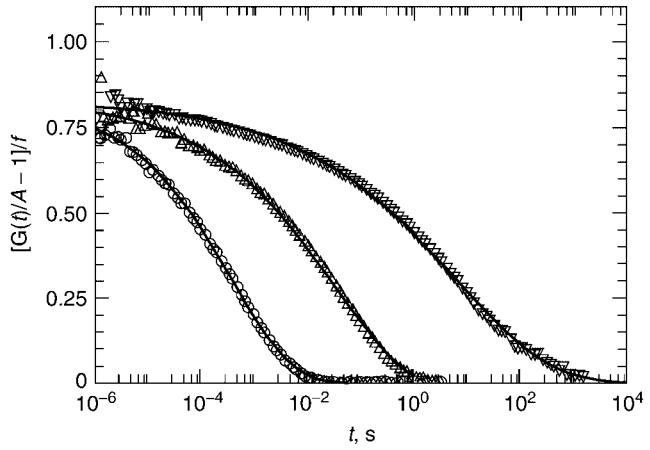

Fig. 2. Depolarized intensity correlation functions for the poly(styrene-*b*-1,4-isoprene) block copolymer. Solid curves are the KWW fits to the data and the β parameters used in the fits are given in the inset. The total molecular weight of the copolymer is $M_n = 3930$ and the molecular weight of the PS block is equal to 2830. The primary contribution to the spectra comes from the local segmental motion of the PS in the copolymer and the dispersion broadens with decreasing temperature. ○ $\beta = 0.38$ at 323 K; △ $\beta = 0.30$ at 303 K; ▽ $\beta = 0.25$ at 287 K.

The structure of the amorphous state is subjected to time-dependent variations, because of the existence of translational and/or orientational motions of both the individual segments and the chain as a whole (16). These motions couple to the light since they induce variations of the local dielectric constant $\varepsilon(\boldsymbol{r}, t)$ or the local polarizability $\alpha(\boldsymbol{r}, t)$. Inelastic and quasi-elastic scattering measurements allow the determination of the time laws according to which these motions occur (17). The particular motion detected by the light scattering technique depends on the polarization of the scattered light and on the scattering vector $\boldsymbol{q}$, which gives the wavelength of the observed fluctuations. Light scattering depends on the directions of the polarizations of the scattered radiation and the incident radiation. Provided that the incident and scattered light are polarized with the electric vector at right angles to the plane containing $\boldsymbol{k}_1$ and $\boldsymbol{k}_0$, VV scattering is observed. Frequency shifts are detectable in the case of light scattering, and thus, temporal fluctuations of the structure can be determined. Individual photons may be scattered with a slight frequency shift. The magnitude and sign of the frequency shift depend on the velocity and the direction with respect to the incident radiation in which an individual particle is moving. This frequency shift is referred to as the *Doppler effect*. The free motion of the particles (macromolecules) in solution is a thermal diffusion with no net transport and therefore no net exchange in energy between the system and the incident light. The scattered light thus consists of a narrow Lorentzian spectrum of frequencies symmetrically broadened because of the random Brownian motion of the particles, and centered at the incident frequency of the laser. The time-correlation function and the frequency-dependent power spectrum are related by Fourier transform. This is usually referred to as quasi-elastic light scattering (qels), a technique allowing one to extract dynamical information about the system, ie, the diffusion coefficient. Because of the large

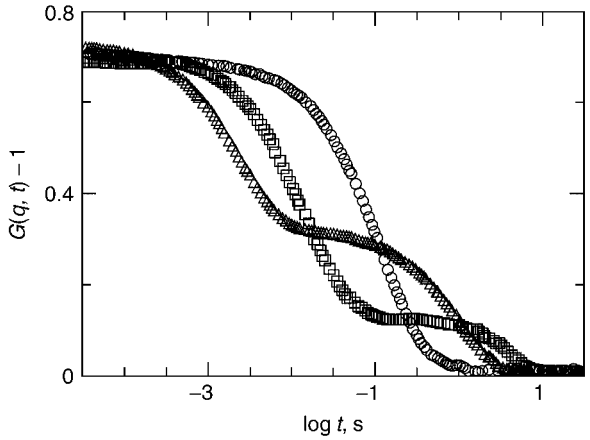

Fig. 3. Experimental intensity correlation functions in the VV configuration for a low molecular weight (PS/PI) polymer blend. Two diffusive decay rates are essentially observed in the VV configuration; however, close to the critical point the faster rate dominates. ○ 315 K (VV); □ 328 K (VV); △ 348 K (VV).

wavelength of the incident light, one sees only integral structural properties, averaged over long distances. The so-called depolarized (18) (VH) light scattering (dls), where V and H indicate a vertical and horizontal direction of the polarization of the incident and scattered light relative to the scattering plane, is related to fluctuations of the anisotropy of the polarizability tensor. Thus, reorientational motions of individual optically anisotropic molecules or collective motions of such molecules may be analyzed by dls (19).

The light scattering spectrum obtained in the VV configuration contains both the anisotropic component and an isotropic one, which is related to local density fluctuations, giving rise to fluctuations of the polarizability or the dielectric constant. In most cases the anisotropic contribution is much smaller than the isotropic one; therefore, the VV scattering measures the density fluctuations (isotropic part) directly. Figure 3 shows experimental correlation functions in the VV configuration for a low M_w polystyrene/polyisoprene (PS/PI) blend, and Figure 4 shows the corresponding depolarized experimental correlation functions (20). Two diffusive decay rates are essentially observed in the VV configuration (Fig. 3); however, close to the critical point the faster rate dominates. The relaxation mode that is shown in the VH scattering geometry is due to double scattering induced by composition fluctuations.

The quantities measured in light scattering spectroscopy are either the autocorrelation function of the electric field $C(t) = \langle \boldsymbol{E}(t) \cdot \boldsymbol{E}(0) \rangle$ or its Fourier transform, the spectrum of the scattered light $I(\omega)$, by using the Fabry–Perot interferometer.

$$I(\omega) = \frac{1}{2\pi} \int_{-\infty}^{+\infty} \mathrm{e}^{-i\omega t} C(t)\, \mathrm{d}t \tag{3}$$

The correlation function $C_{\mathrm{aniso}}(\boldsymbol{q}, t)$ of the total scattered field from undiluted polymers is given by

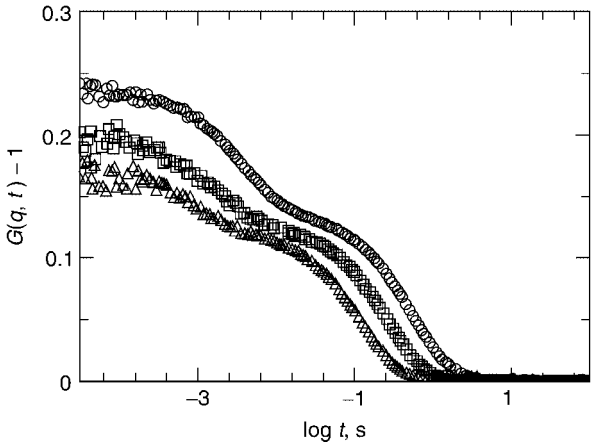

Fig. 4. Depolarized intensity correlation functions for the (PS/PI) polymer blend of Figure 3. The relaxation mode that is shown in the VH scattering geometry is due to double scattering induced by composition fluctuations. △ 353 K (VH); □ 343 K (VH); ○ 333 K (VH).

$$C_{\text{aniso}}(\boldsymbol{q},t)=\left\langle \sum_{m,n}^{N}\sum_{i,j}^{N_s}\alpha_{yz}^{(n)}(j,t)\alpha_{yz}^{(m)}(i,0)\exp\left\{i\boldsymbol{q}\cdot\left[\boldsymbol{r}_j^{(n)}(t)-\boldsymbol{r}_j^{(m)}(0)\right]\right\}\right\rangle \tag{4}$$

where N is the number density of the polymer, and N_s is the number of scatterers per molecule. The angular brackets denote an ensemble average. According to the above equation two mechanisms are generally responsible for VH scattering: segmental orientation combined in the subscript yz and segmental center of mass motion in the exponent term. Alternatively, these two modes are not always statistically independent and frequently even reflect other motions such as overall molecular orientation and coherent internal Rouse–Zimm modes for rigid and flexible coils respectively. On the other hand the correlation function of the isotropic component of the scattered light can be written in the form

$$C_{\text{iso}}(\boldsymbol{q},t)=\alpha^2\left\langle \sum_{m,n}^{N}\sum_{i,j}\exp\left\{i\boldsymbol{q}\cdot\left[\boldsymbol{r}_j^{(n)}(t)-r_j^{(m)}(0)\right]\right\}\right\rangle \tag{5}$$

In contrast to the correlation function of the anisotropic component, only the segment center of mass motion affects the isotropic scattering component. However, because of intra- and interchain interactions in bulk polymers there is no rigorous calculation of the general expressions in equations 4 and 5. Only the Rayleigh–Brillouin spectrum of a viscoelastic fluid, which is determined by the high frequency part of the density fluctuations in equation 5, has an analytical form (21). A spectrum has been computed using a generalized relaxation equation. The polarized scattering is governed by thermal density fluctuations, which, from a thermodynamic point of view, can be separated into an adiabatic and an isobaric component. The adiabatic component gives rise to longitudinal hypersonic waves. The isobaric component I_R causes a nonpropagating thermal diffusive mode. The

translational motion of the segments associated with the isotropic light scattering produces thermally induced longitudinal sonic waves, the nonpropagating thermal diffusive mode, and a localized motion. The first two fluctuations give rise to the shifted Brillouin doublet (22,23) I_B at frequencies $+\omega_s$ and $-\omega_s$ and to the central Rayleigh line. The line width of the unshifted central line, the Rayleigh line, is determined by the thermal conductivity. The intensity ratio, the so-called Landau–Placzek (LP) ratio, is given in the simplest case by the ratio of the specific heats C_P and C_V.

$$\frac{I_R}{2I_B} = \langle C_P/C_V \rangle - 1 \tag{6}$$

In viscous fluids, however, a coupling occurs between internal and external modes of freedom and translational motions. This structural relaxation process, characterized by a frequency ω_e, influences both the central line as well as the Brillouin doublet, depending on the frequency of this relaxation relative to the frequency of the hypersonic waves. In principal three different cases must be considered:

(1) The so-called fast relaxation limit in which $\omega_e \gg \omega_s$. In this case the structural relaxation gives rise to a broad background scattering in the frequency scale, leaving the Rayleigh–Brillouin spectrum nearly unchanged.

(2) The intermediate relaxation limit in which $\omega_e \cong \omega_s$. The two frequencies are of the same order of magnitude and the structural relaxation contributes heavily to the line width of the Brillouin lines. The relaxation processes can be resolved by means of the Fabry–Perot interferometry (24). Figure 5

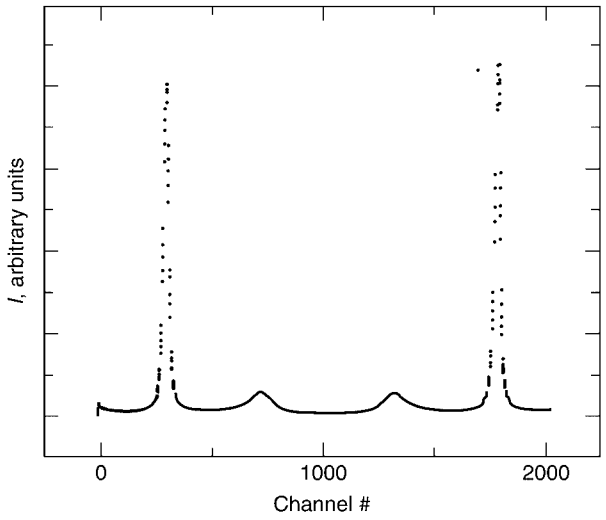

Fig. 5. Polarized Rayleigh–Brillouin spectrum of amorphous PnHMA taken with a Burleigh plane Fabry–Perot interferometer using a free spectral range of 12.4 GHz at 295 K. The two Brillouin peaks are shifted from the incident frequency by the product of the wave vector $\boldsymbol{q}$ and the sound velocity u. The line width of the Brillouin peaks is related to the attenuation of the sound waves. • PnHMA.

visualizes a polarized Rayleigh–Brillouin spectrum of amorphous poly(*n*-hexyl methacrylate) taken with a Burleigh plane Fabry–Perot interferometer using a free spectral range of 12.4 GHz at 295 K. The two Brillouin peaks are shifted from the incident frequency by the product of the wave vector $\boldsymbol{q}$ and the sound velocity u. The line width of the Brillouin peaks is related to the attenuation of the sound waves.

(3) The slow relaxation limit in which $\omega_e \ll \omega_s$. The structural relaxation leads to an additional central line, the so-called Mountain peak (25,26), the width of which can be determined by pcs (27). Thus, structural relaxation processes taking place close to the glass-transition temperature can be investigated by this technique.

The dynamics of slowly varying thermal density fluctuations has been studied by means of pcs (28,29) in the frequency range between 10^{-3} and 10^{7} Hz for several polymeric systems in the molten state as well as in the glassy state. The measured intensity autocorrelation function $C(\boldsymbol{q}, t)$ is related to the normalized time correlation function $g^{(1)}(\boldsymbol{q}, t)$ by

$$C(q,t) = A\left[1 + f\left|\alpha g^{(1)}(q,t)\right|^2\right] \tag{7}$$

where f is the instrumental factor, calculated by means of a standard, a is the fraction of the total scattered intensity associated with the process under investigation with correlation times longer than 10^{-7} s, and A is the baseline. For the pcs measurements near T_g, fluctuations in density and orientation are strongly coupled and hence the relaxation times obtained are indistinguishable. Experimentally only those components with relaxation times longer than 10^{-7} s (frequencies $<$ 0.1 MHz) will be observed by pcs. It was found that, in general, the observed correlation functions are highly nonexponential and have been fitted to the empirical Kohlraush–Williams–Watts (KWW) function

$$g^{(1)}(t) = \exp\left[-(t/\tau)^{\beta}\right] \quad \text{with} \quad 0 < \beta \leq 1 \tag{8}$$

and for concentration fluctuations it is written as

$$g^{(1)}(q,t) = \exp\left[-(t/\tau)^{\beta}\right] \quad \text{with} \quad 0 < \beta \leq 1 \tag{9}$$

Using the KWW function the mean relaxation time is given by

$$\langle\tau\rangle = \int_{-\infty}^{+\infty} g^{(1)}(t)\,\mathrm{d}t = \frac{\tau}{\beta}\Gamma(\beta^{-1}) \tag{10}$$

where $\Gamma(\beta^{-1})$ is the Gamma function. $g^{(1)}(t)$ is related to the longitudinal compliance (30,31) $D(t)$ by

$$\alpha g^{(1)}(t) = \left[D_0 - D(t)\right]/D_\infty \tag{11}$$

and

$$D(t) = D_\infty + (D_0 - D_\infty)\int_{-\infty}^{+\infty} L(\ln\tau)(1 - e^{-1/\tau})\, d\ln\tau \tag{12}$$

The depolarized spectrum is dominated by local fluctuations of the optical anisotropy owing to an overall orientation of stiff molecules, local motions of optically anisotropic segments or internal Rouse–Zimm modes for flexible chain molecules. The depolarized spectrum thus reflects dynamics of collective molecular orientation when the interaction between translation and rotation can be neglected.

Density Fluctuations—Excess Scattering at Low *q*

From statistical fluctuation theory (32), the static structure factor is given by

$$\lim_{q\to 0} S(q) = \langle \delta N^2 \rangle = V\rho^2 k_B T \beta_T(T) \tag{13}$$

where $\delta N\,(=N - \langle N\rangle)$ is the fluctuation in the number of particles in the scattering volume V, ρ is the average number density, and β_T is the isothermal compressibility $[-1/V(\partial V/\partial P)_T]$. The total density fluctuation in an arbitrary volume is given by

$$\Psi_T \frac{\langle \delta N^2 \rangle}{\langle N \rangle} = e k_B T \beta_T(T) \tag{14}$$

According to the above equation, the density fluctuations should have a temperature dependence similar to that of $\beta_T(T)$, which is discontinuous at T_g. However, it has been shown earlier (33–42) that it is only the temperature coefficient of the density fluctuations which is discontinuous at T_g.

The density fluctuations defined above can be obtained experimentally in two ways: (*1*) from the measured compressibility data using equation 14, or (*2*) from small-angle x-ray scattering (saxs), using the extrapolating intensity at $q = 0$ (33–42):

$$\lim_{q\to 0} I(q) = n^2 k_B T \beta_T(T) \tag{15}$$

where n is the average electron density. Then, the particle density fluctuation is given by

$$\frac{\langle \delta N^2 \rangle}{\langle N \rangle} = \frac{I(0)}{nZ} \tag{16}$$

where Z is the number of electrons per particle.

Two examples are discussed below where the measured density fluctuations are compared with the calculated ones from the compressibility data. In Figure 6,

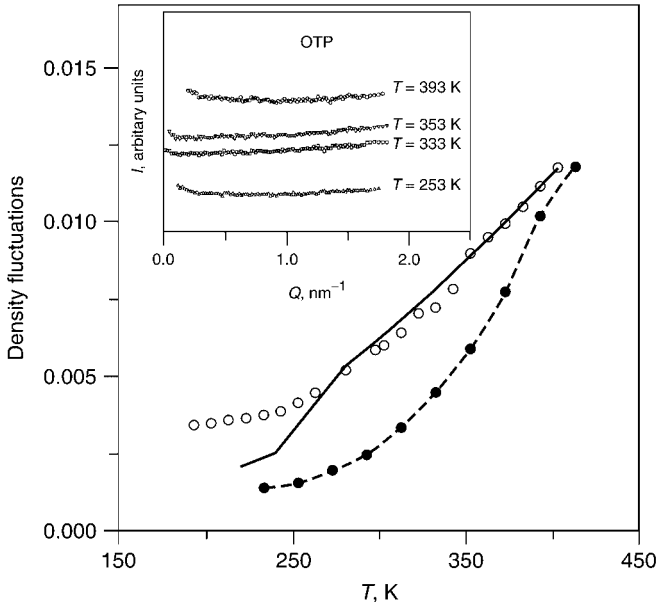

Fig. 6. Density fluctuation in OTP measured by saxs (○). The solid line gives the calculated density fluctuations from the measured isothermal compressibility. Filled symbols gives the propagating density fluctuations calculated from the Brillouin shift in a Rayleigh–Brillouin experiment. The inset shows typical saxs curves obtained with a conventional Kratky saxs camera.

the density fluctuations are shown for the glass-forming liquid *ortho*-terphenyl (OTP), and in Figure 7 for two polymers with slightly different backbone structures; bisphenol A polycarbonate (BPA-PC) and tetramethyl-bisphenol A polycarbonate (TMPC) (42). In both cases, at $T > T_g$, there is a good agreement between the measured and calculated density fluctuations but at $T < T_g$, the former exceed the latter by a factor of 2. Below T_g, the density fluctuation can be described as $\rho k_B T \beta_T(T_g)$, where $\beta_T(T_g)$ is the compressibility obtained from pressure–volume–temperature (PVT) measurements in a comparable time scale with $I(0)$, without, however, displaying a leveling-off to a constant value. The much higher density fluctuations below T_g result from the non-equilibrium nature of the glass and the contribution of frozen-in fluctuations (33–42).

The free-volume fluctuation model (43) which is based on the average free volume and its fluctuations has been successful in describing such differences in density fluctuations of different polymers as well as to explain the suppression of the intensity of sub-glass processes in polymer/additive systems. According to the model, the free volume is assumed to have a Gaussian distribution characterized by two parameters: (*1*) the average free volume $\langle V \rangle$ and (*2*) the distribution of free volume, which is given by the variance $\langle \delta V^2 \rangle^{1/2}$ of the distribution $P(\delta V)$. The saxs measurements allow the direct evaluation of the density fluctuation and the average free volume can be estimated from the position of the "amorphous halo" as obtained from wide angle x-ray scattering (waxs). Figure 8 gives a schematic of the distribution $P(\delta V)$ of the density fluctuations in glassy BPA-PC and TMPC

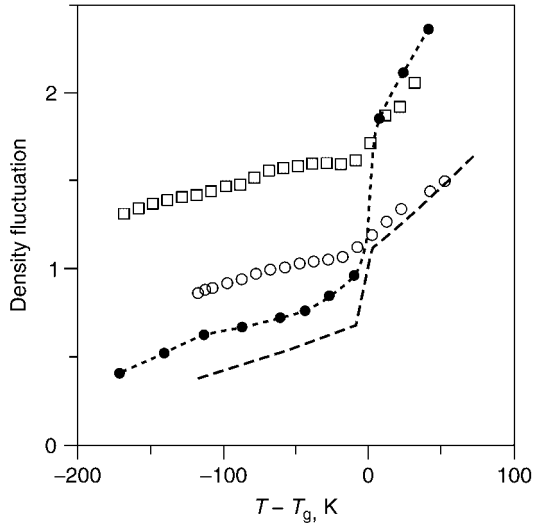

Fig. 7. Density fluctuations, measured by saxs, for BPA-PC (○) and TMPC (□) as a function of $T-T_g$. The dotted line is the calculated density fluctuation of TMPC from the isothermal compressibility data of this study obtained in a PVT experiment. The dashed line represents the calculated density fluctuation of BPA-PC from the literature compressibility data.

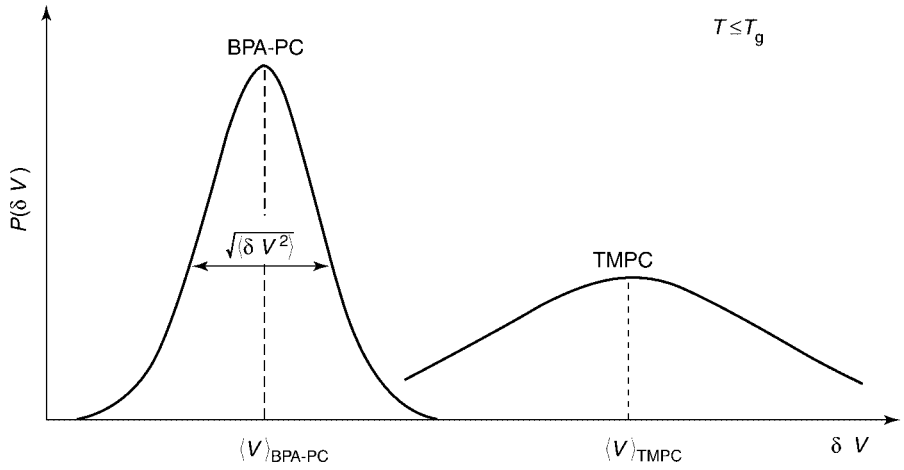

Fig. 8. Schematic of the distribution $P(\delta V)$ of the density fluctuations in glassy BPA-PC and TMPC, according to the free-volume fluctuation model.

according to the free-volume fluctuation model. Peak positions and widths are determined by the average free volume and by its fluctuations, respectively. This is a nice example of a system where $\langle V\rangle$ and $\langle \delta V\rangle$ are determined to be different against the assumed "universality." This variance reflects on the structural units; in TMPC the methyl substitution causes less efficient packing as compared to BPA-PC.

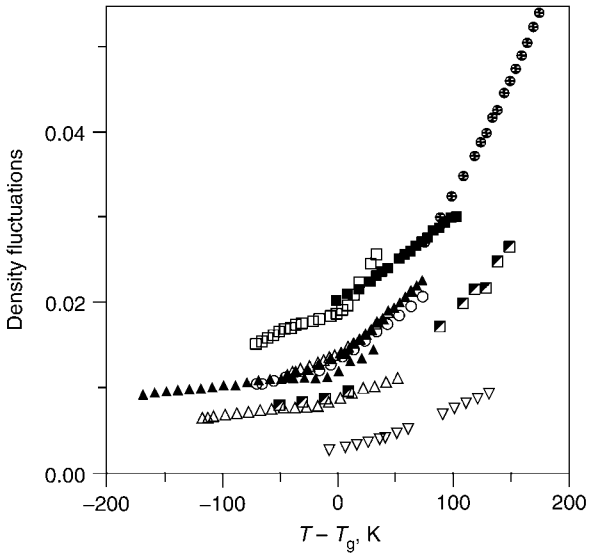

Fig. 9. Density fluctuations of some glass-forming liquids and polymers as a function of temperature difference from T_g. ▽ BKDE; △ BPA-PC; ▲ TMPC; □ OTP; ○ poly(cyclohexyl methacrylate) (PCHMA); ▲ poly(*n*-butyl methacryalte); ■ poly(*n*-hexyl methacrylate); □ poly(methyl methacrylate) (PMMA); • polybutadiene.

In Figure 9, the measured density fluctuations from a variety of polymers and glass-forming liquids are compared. The amount of density fluctuations at the glass transition is typically about 1%; however, the results shown (Fig. 9) indicate considerable variation among the different polymers and glass-forming liquids investigated. Typically, glass-forming liquids possess the lowest fluctuations and in some cases (mainly within the poly(*n*-alkyl metacrylate) series, ie, for poly(methyl methacrylate) (PMMA), poly(*n*-butyl methacryalate) (PnBMA), poly(*n*-hexyl methacrylate) (PnHMA), the measured density fluctuation above the glass transition exceeds the calculated one from the PVT measurements on identical samples. The higher contribution of density fluctuations can have different origins, such as "contamination" from concentration fluctuations (ie, additives) or contribution from short-range intersegmental density fluctuations. Additives alone, however, should be in high concentrations (44) to explain the observedbehavior.

The evaluation of density fluctuations using equation 14 or 16, conceals the relative contribution of propagating and static components in the measured total density fluctuations. To overcome this difficulty one can evaluate the contribution of the propagating density fluctuations from the temperature dependence of the phonon peak obtained in the Rayleigh–Brillouin experiment (44). This is based on the notion that the propagating density fluctuations are determined from the thermal-diffuse scattering (tds) near the origin of the reciprocal space, as in the case of crystalline solids. Then in the limit $q \to 0$, this contribution is given by

$$\Psi_S = \left.\frac{\langle \delta N^2 \rangle}{\langle N \rangle}\right|_{\text{phonon}} = \rho k_B T \beta_S(T) \tag{17}$$

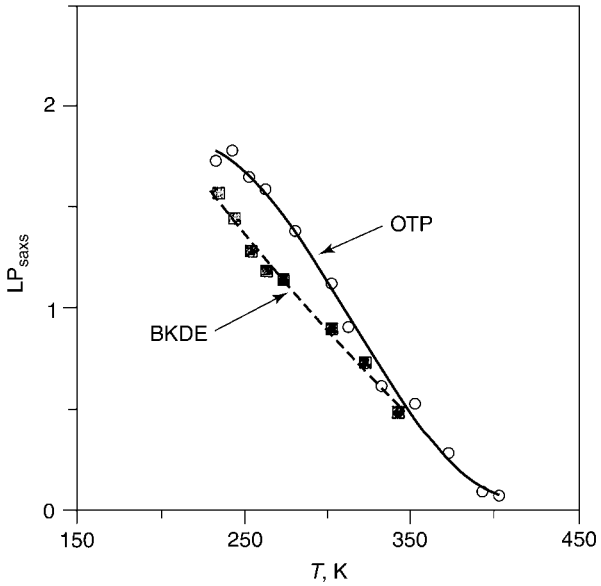

Fig. 10. LP intensity ratio obtained from the measured compressibilities of OTP (○) and BKDE (■).

where $\beta_S(T)$ is now the adiabatic compressibility ($\beta_S = 1/\rho^* u^2$, ρ^* is the mass density and u is the sound velocity) evaluated at the frequency ω_{phonon}. The ratio of the total to the propagating fluctuations defines an "x-ray" LP ratio (44):

$$R_{LP} = \frac{\Psi_T}{\Psi_S} - 1 = \frac{\beta_T}{\beta_S} - 1 \tag{18}$$

which is readily obtained in a Rayleigh–Brillouin experiment from the intensities of the central (I_C) and shifted Brillouin lines (I_B) as $I_C/2I_B$. The temperature dependence of the LP ratio for two glass-forming liquids, OTP and BKDE [1,1-di(4′-methoxy-5′ methyl-phenyl)cyclohexane] (45), is shown in Figure 10 and is in good agreement with the values predicted for relaxing liquids.

On the basis of the saxs results obtained within the shown q-range, one would assume that the density fluctuations of OTP and BKDE (equivalently called BMMPC) behave as one would expect from equilibrium statistical mechanics. However, one can notice a slight increase of $I(q)$ at low q, which finds its counterpart at the much higher $I(q)$ at the smaller q values accessible by light scattering (ls). In order to use both sets of data (ls and saxs) in a common plot, an effective compressibility $k_B T \beta_T$ is defined, which is obtained from saxs as I/n^2 and from ls by using (45):

$$\frac{R_i(q)}{\pi^2/\lambda^4(\rho * \partial\varepsilon/\partial\rho *)^2} = k_B T \beta_T \tag{19}$$

where $R_i(q)$ is the isotropic Rayleigh ratio [$R_i(q) = R_{VV}(q) - (4/3)R_{VH}$]. The results, in the form of relative density fluctuations, are shown in Figure 11 for BMMPC.

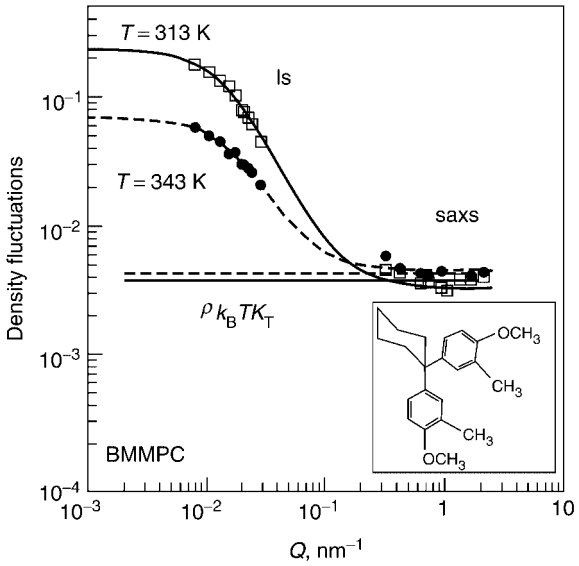

Fig. 11. Relative density fluctuations of BMMPC measured by light scattering (ls) and saxs at two temperatures: T_g + 52 K and T_g + 82 K. The curves are obtained by fitting with the Ornstein–Zernike function.

For the description of the shape of the static scattering function one can try to use the Ornstein-Zernike function:

$$S(q) = \frac{S(0)}{1 + \xi_{OD}^2 q^2} \tag{20}$$

where ξ_{OD} is the static correlation length. For OTP and BMMPC, very large correlation lengths up to 180 nm at temperatures T_g + 40 K are obtained. On the basis of the distinct scattering feature, which violates the thermodynamic law (eq. 13), these fluctuations are called long-range density fluctuations in contrast to the normal density fluctuations detected by conventional-laboratory saxs measurements.

The essential contribution of Fischer and co-workers was not only to show the existence of long-range density fluctuations in static experiments (46–48) (which was known from earlier static light scattering measurements), but also to demonstrate the existence of a new ultraslow hydrodynamic process (ie, $\Gamma \sim q^2$) in pcs, with relaxation rates Γ about $10^{-4} - 10^{-7}$ lower than those associated with the α-process at a given temperature (45,49), and to study the associated kinetics (50). These effects are caused by long-range density fluctuations indicating a nonhomogeneous distribution of free volume and the appearance of the ultraslow mode is a result of the redistribution of free volume in space. A model has been proposed (45,49), which describes the long-range density fluctuations as a result of the coexistence of molecules with two different dynamic states, and a particular molecule and its surrounding can pass over from the “solid-like” state into the “liquid-like” state on a time scale which is given by the ultraslow mode.

Order in Amorphous Polymers and the Associated Dynamics

It is well known (51–53) that the waxs spectra of semicrystalline samples display sharp diffraction peaks whose intensity and width reflect the frequency and periodicity, respectively, of some characteristic distances obtained using Bragg's law: $d = 2\pi/q^*$. Today, there is consensus that "amorphous" polymers are not completely amorphous but they possess a reasonable degree of local order. For example, the presence of a scattering peak in x-ray diffraction patterns (called *amorphous halo*) implies the existence of fluctuations in electron density distribution within the sample. Although there is not a known one-to-one correspondence between peak position and size of the corresponding density fluctuations, the Bragg equation, $\lambda = 2d \sin\theta$, may still be applied to an amorphous halo position to provide an equivalent Bragg size for the density fluctuation. Hence, in amorphous polymers the *equivalent* Bragg spacings are discussed. It has been shown that the position of the amorphous halo varies systematically within the same family of polymers and that it is correlated with the cross-sectional area of the polymer chain in the crystal (53).

As an example of regularity in the diffraction patterns, the waxs spectra for different polycarbonates of bisphenol A (54) are shown in Figure 12. The figure shows different diffraction patterns starting from the monomer ($x = 1$, which is crystalline), the pentamer ($x = 5$), and other oligomers up to the bulk. It is interesting to note that there is a correlation of the most intense reflection in the crystalline monomer with the amorphous halo in the BPA polymers and that the first sharp diffraction peak gets broader as one moves from the pentamer to the polymer.

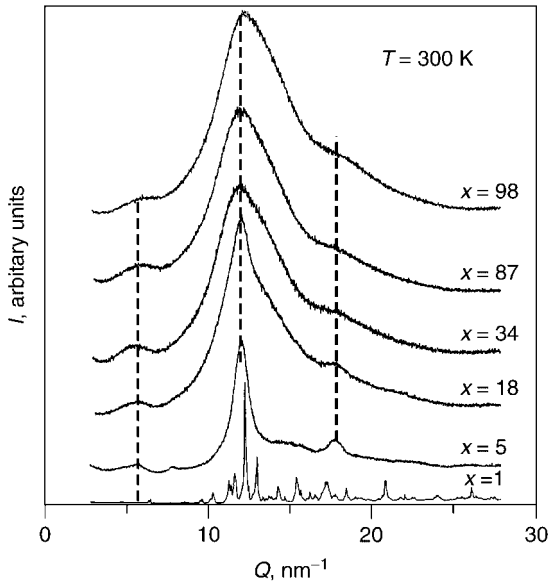

Fig. 12. Waxs spectra of different polycarbonates of bisphenol A starting from the monomer ($x = 1$), to the pentamer ($x = 5$), to the polymer. Notice the sharp diffraction maxima in the monomer (crystalline) and the broader patterns on the polymeric substances.

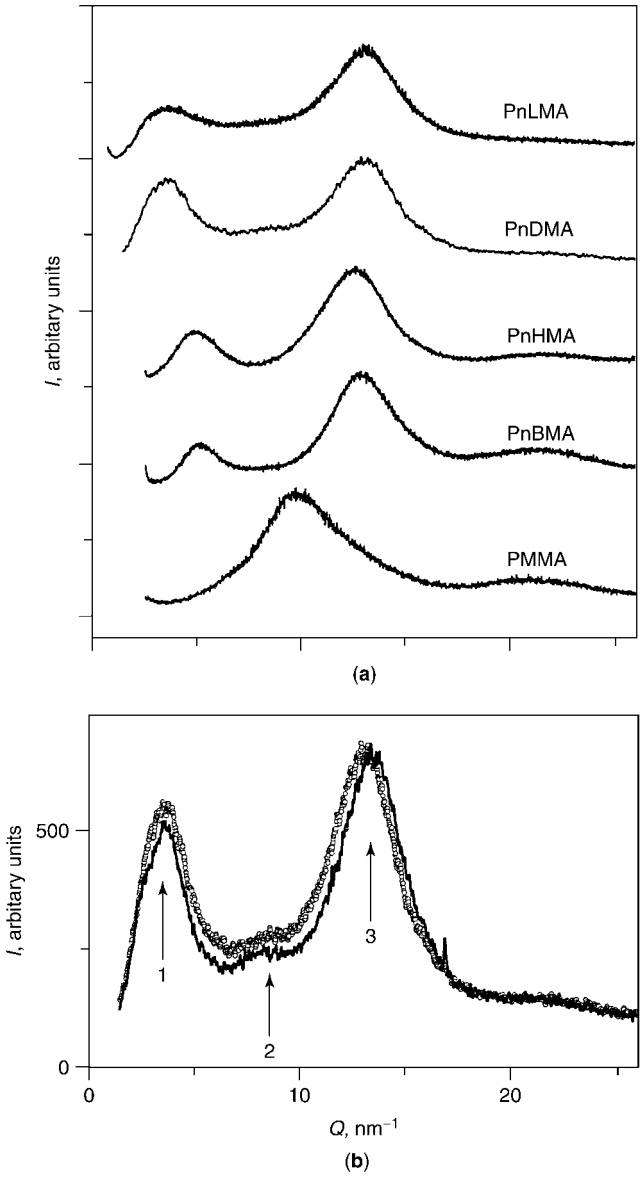

Fig. 13. (**a**) Waxs spectra of a series of poly(n-alkyl methacrylates) shown at 293 K. Notice the development of the LVDW peak which shifts to lower Q values with increasing alkyl side chain. (**b**) Waxs spectra for PnDMA shown at two temperatures as indicated. Arrows show the positions of the three main peaks in the spectra. ○ $T = 293$ K; —— $T = 223$ K.

Another class of polymers with interesting intersegmental structure and packing properties are the poly(n-alkyl methacrylates) (55,56). Figure 13 gives the waxs pattern of PMMA, PnBMA, PnHMA, PnDMA, and PnLMA. With the exception of PMMA, the waxs spectra for poly(n-alkyl methacrylates) show three peaks (arrows 1, 2, and 3 in Fig. 13b). The peak at high q, with an equivalent

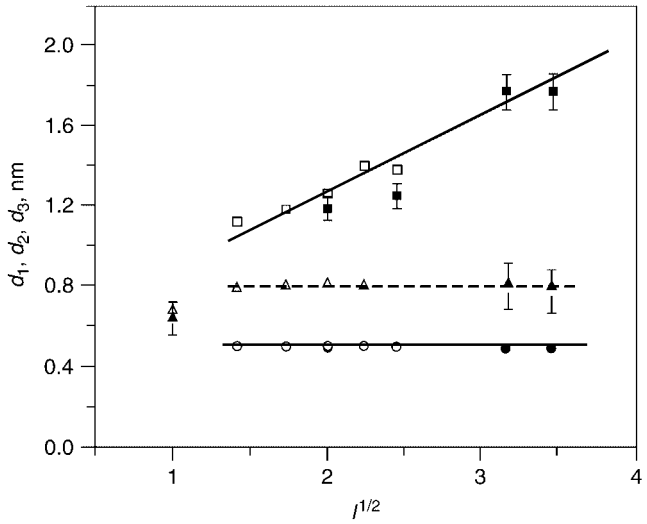

Fig. 14. Equivalent Bragg spacings as a function of the number of carbon atoms (l) on the alkyl chain. Lines are linear fits to the data. Notice the pronounced l-dependence of d_1. • d_3; ▲ d_2; ■ d_1.

Bragg spacing of about 0.5 nm, corresponds to the van der Waals (VDW) contacts of atoms and is known as the VDW peak. The temperature variation of this peak reflects mainly the thermal expansion of the system. The peak at low q, which is usually referred as the low van der Waals (LVDW) peak, is found to have a systematic dependence in the number (l) of carbon atoms on the alkyl side chain. Figure 14 displays the dependence of the three peaks on $l^{1/2}$ for a series of poly(n-alkyl methacrylates), with l in the range $1 \leq l \leq 12$ at 293 K. The LVDW peak, with corresponding distances from 1.0 to 1.8 nm, reflects mainly the average distance between adjacent backbones, which is an increasing function of the number of carbon atoms l on the alkyl side chain. The l-dependence of d_1 can be parameterized as $d_1 = d_0 + sl^{1/2}$, with $d_0 \approx 0.7$ nm and $s \approx 0.385$ nm/CH2. The intermediate peak (Peak #2), which is more difficult to obtain, is also plotted in Figure 14. Its position corresponds to the main peak in PMMA which, in contrast to the rest of the series, does not exhibit an LVDW peak. This feature of PMMA has been discussed in the literature earlier (51).

In the past, there has been a continuous effort to correlate specific dynamic properties, such as the boson peak, the separation of the segmental (α-) from the subglass (β-) process, and the fragility with the structure of amorphous polymers. More specifically, a correlation between the low frequency peak in the Raman spectra and the properties of the first sharp diffraction peak was shown to exist (57,58). Herein the relation of the structure factor with the dynamic property of fragility is recalled (55). The temperature dependence of the relaxation times of various members of the series of poly(n-alkyl methacrylates) is shown in Figure 15. Despite the fact that the "fragility" is usually defined for homogeneous systems, whereas here the monomer itself is intrinsically heterogeneous, one can still compare $\tau(T)$ from different samples. For this purpose one can employ the usual "fragility plot" where the relaxation times are plotted as a function of reduced temperature

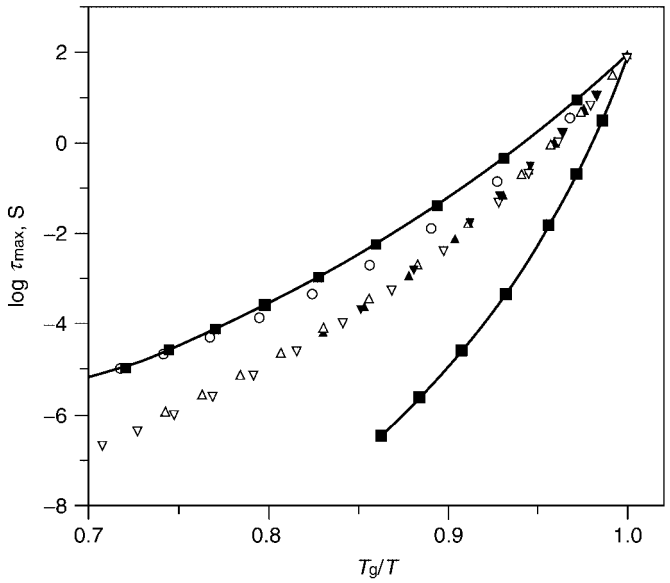

Fig. 15. T_g-scaled plot of the segmental relaxation times of PMMA (♦), PnEMA (▲), PnBMA (△), PnHMA (▼), PnNMA (▽), PnDMA (■), and PnLMA (○). The T_g is operationally defined here as the temperature at which the segmental relaxation time is 100 s. There is change in the nature of the glasses when going from PMMA to the higher member of the series, which reflects in the change from "fragile" to "strong" behavior.

(Fig. 15). Furthermore, to facilitate the comparison, the *glass-transition temperature* T_g is operationally defined as a temperature corresponding to the most probable relaxation time of 100 s. There is a pronounced variation of the curvature or the "steepness index" which is defined as

$$m = \frac{\mathrm{d}\log\tau}{\mathrm{d}(T_g/T)} \tag{21}$$

which is evaluated near T_g, in going from PMMA (with $m \sim 92$) to poly(n-decyl methacrylate) (PnDMA) ($m \sim 36$). The variation in m implies a change from "fragile" to "strong" liquids, which occurs within the same family of polymers only by increasing the length of the side chain with the addition of a CH_2 unit.

The dynamic behavior within the class of poly(n-alkyl methacrylates) possess the natural question as to whether this dynamic richness reflects on the structural changes, and if so, on what length scale. In other words, are the observed dynamic changes from "fragile" to "strong" reflected on the structural changes? Earlier studies already revealed a correlation between the monomer structure and the degree of intermolecular cooperativity (59). The correlation is shown in Figure 16, where both the steepness index m and the position of the LVDW peak is shown as a function of l. In doing so one is directly comparing a dynamic with a structural property. There is a nice correlation between the two quantities, which shows that the observed dynamic changes from "fragile" to "strong" occur by reorganizations at the intersegmental distances, which are enlarged by increasing l. The above is

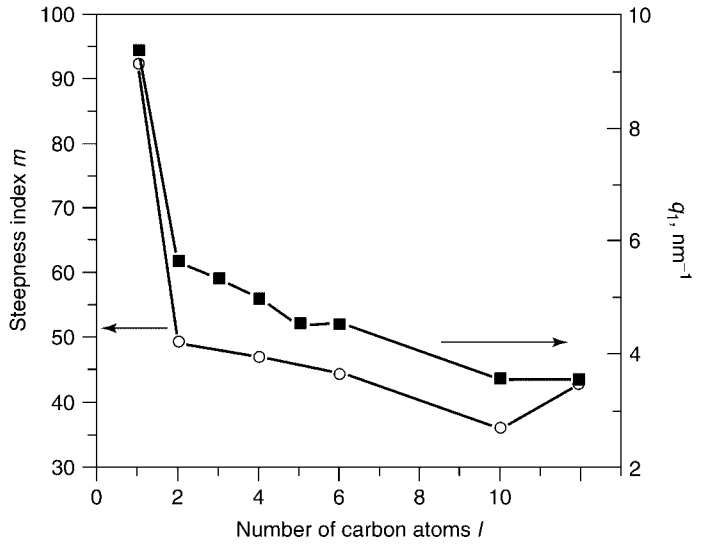

Fig. 16. Steepness index m [$=\mathrm{d}\log\,\tau/\mathrm{d}(T_g/T)$], extracted from the initial slopes in the previous figure, plotted as a function of the number of carbon atoms (l) on the side chain of poly(n-alkyl methacrylates). In the same plot the dependence of the LVDW peak in the waxs spectra Q_1 is shown. There is a one-to-one correspondence between the structural properties and the steepness index, which implies the relation of the fragility to the intersegmental correlations.

one example where the static structure factor influence the dynamic properties within a series of polymers.

Temperature Dependence of the Amorphous State

All linear and most branched amorphous polymers are liquids. In the realm of continuum mechanics a material is a liquid if it flows. Nonrecoverable deformation resulting from applied tractions are proportional to the time of the created stresses, which are also proportional to or functions of the strain rate. They are liquid-like flow deformations. Also stresses in liquids caused by applied shear strains decay to zero with time. Most amorphous polymers are highly viscous and markedly viscoelastic. This time- and frequency-dependent mechanical behavior is dependent on molecular structure and weight, temperature, pressure, and concentration. Many of these polymers have no crystalline solid state because there are stereochemical variations along their molecular chain-like backbones. This lack of long-range regularity in the molecular structure precludes an assembly with the long-range order, which is the essence of the crystalline state. In other words irregular molecules cannot crystallize. On the other hand even some polymers with stereoregular chains, such as polycarbonate, do not crystallize readily because of exceedingly low rates of nucleation.

Upon cooling with consequent molecular crowding the mobility of molecular segments diminishes. Ultimately the local mobility becomes so low that the short-range order that exists does not achieve its more compact equilibrium

structure in the time allowed by the imposed cooling rate. The rate of decrease of volume with temperature upon further cooling diminishes in a usually narrow temperature range in comparison to that due to the change in magnitude of anharmonic vibrations alone. The liquid structure is thus kinetically "frozen in" and the liquid is called a glass. The intersection of the equilibrium volume–temperature line with the glass line defines the glass temperature T_g. Most often T_g is called the glass-transition temperature implying a thermodynamic change in state. Below T_g the material is said to be in the glassy state. However no change in state occurs. The amorphous material is still in the liquid state albeit with an enormous viscosity (above 10^{11} Pa·s; 10^{12} P) and extremely long relaxation and retardation times. A glass is therefore a viscoelastic liquid with a specific volume which is greater than its equilibrium value. A volume–temperature cooling curve for high molecular weight polyisobutylene (NBS PIB) is shown in Figure 17, where the decrease in the thermal contraction coefficient α in the neighborhood of T_g is clearly seen (60). The dependence of $T_g(q)$ upon the rate of cooling q is illustrated in Figure 18, where cooling curves for polystyrene (PS) were obtained at rates ranging from 2°C/min to 1°C/day (61). When held isothermally and

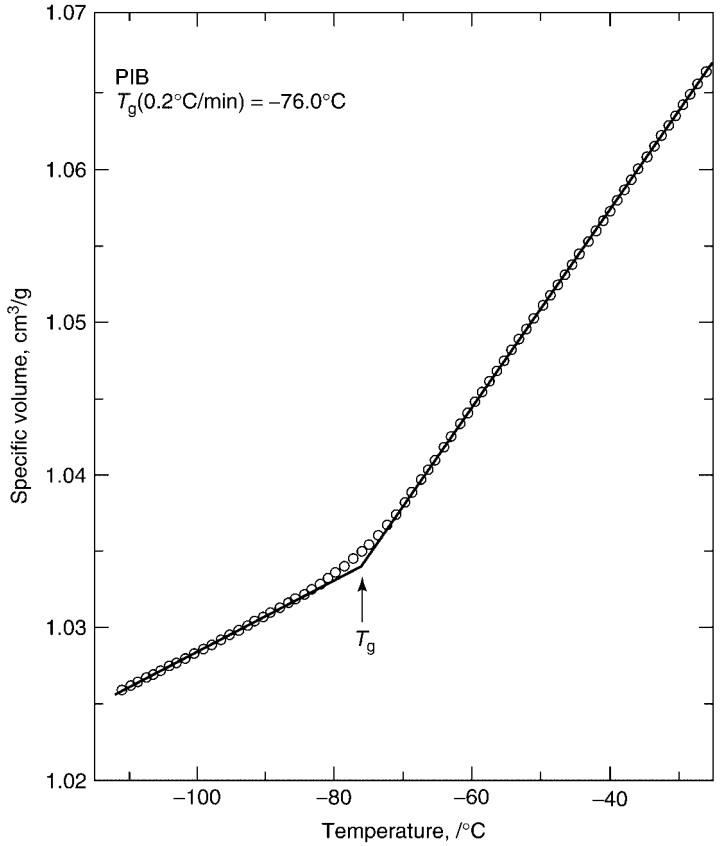

Fig. 17. Dilatometric cooling curve at 0.2°C/min for PIB obtained using the differential gas dilatometer (60).

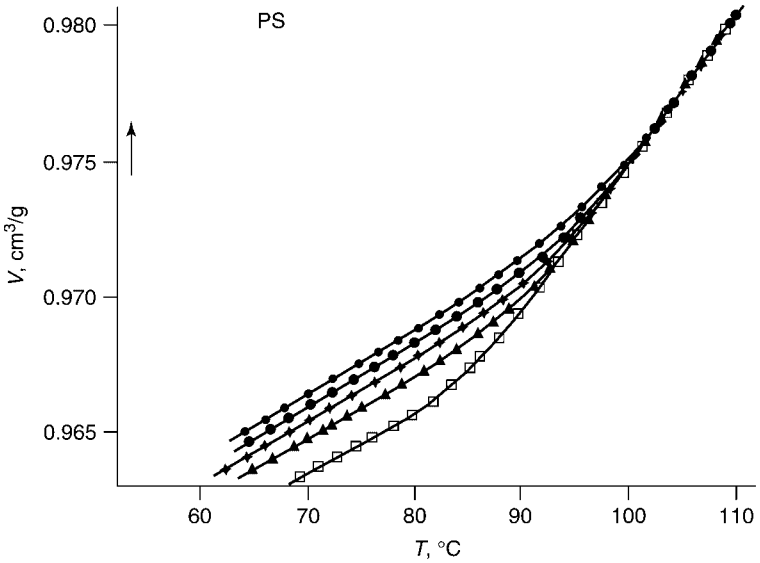

Fig. 18. Volume–temperature curves obtained at different rates of cooling q for PS encompassing the glass temperature $T_g(q)$ (61). – q, K/h: —●— 120; —○— 30; —◆— 6; —△— 1.2; —□— 0.042.

isobarically below T_g, the volume decreases with time toward its equilibrium value. This process is called physical aging, during which kinetic properties slow down enormously and brittleness increases. The above comments on T_g and glasses are not restricted to amorphous polymers, since all amorphous materials organic, inorganic, polymeric, and nonpolymeric will become glassy (rigid, highly viscous, and usually brittle) upon cooling if crystallization does not intervene.

Materials with molecular networks, such as cross-linked elastomers and crystalline polymers, do not flow and so are classified as viscoelastic solids. Shear stresses do not decay to zero with time, ie, equilibrium stresses can be supported. Above T_g, such amorphous materials are still classified as solids, but most of their physical properties such as thermal expansivity, thermal conductivity, and heat capacity are liquid-like.

Viscoelastic Behavior of Amorphous Materials

The stress σ in an ideally elastic materials is uniquely related to a specific strain γ, $\sigma = G\gamma$ (where G is the shear modulus), whereas the stress in a Newtonian fluid is uniquely related to the rate of strain, $\dot{\gamma} = d\gamma/dt$,

$$\sigma = \eta\dot{\gamma} \tag{22}$$

Such behavior is approximated over limited ranges. The energy input to deform an ideal elastic body is entirely recoverable. In other words, the mechanical energy is conserved. The energy input to deform a Newtonian fluid is completely dissipated into heat. None of the deformation is recoverable. Most materials are measurably

viscoelastic where the energy of deformation is partially dissipated into heat. Their mechanical response is consequently a function of time and frequency. Because of the time or frequency dependence, when mechanical measurements are made, it is necessary to hold one of the pertinent variables constant to obtain characterizing functions. The three most common measurements involve creep, stress relaxation, and dynamic (sinusoidal) deformation. Isothermal measurements are necessary, since although isochronal temperature scans may be considered easier, during such scans time-scale shifts and magnitudes of compliance or rigidity can change simultaneously. Isothermal results separate the two variables (62) (see VISCOELASTICITY).

Creep. In the creep experiment a constant stress σ_0 is created in a previously relaxed specimen at some starting time, and the resulting strain $\gamma(t)$ is followed as a function of the ensuing time. Given a sufficiently long time of creep, the velocity of creep will decelerate to zero if a viscoelastic solid is being measured or to a finite constant value if a viscoelastic liquid is being measured. Some time after an apparent constant velocity is reached, in the latter case, viscoelastic steady state is achieved. Then the stress can be made equal to zero by removing all tractions on the specimen and a portion of the deformation will be recovered; again, as a function of time. The portion that is permanent deformation reflects the contribution of viscous flow to the total deformation accumulated during creep. Since a viscoelastic solid does not flow, by definition, all of its creep deformation is recoverable. When the strains or the strain rates are sufficiently small, the creep response will be linear. In this case, when the time-dependent strain is divided by the constant stress, a unique creep compliance curve results; that is, at each time there is only one value for this ratio, which is the compliance; ie, $\gamma(t)/\sigma_0 \equiv J(t)$. Two sources of error that are most specifically deleterious to creep recovery is not reaching steady state before removing the stress (a nonunique curve results), and the presence of friction and other sources of residual stress. Ultimately, in recovery measurements, instrumental disturbances determine the longest time of valid measurement.

Stress Relaxation. The decaying stress is measured as a function of the time after a sudden "instantaneous" strain γ_0 is applied to a previously relaxed sample in the stress relaxation measurement. The stress $\sigma(t)$ eventually drops to an equilibrium finite value for a viscoelastic solid and to zero for a viscoelastic liquid. Sources of uncertainty that are particularly serious in stress relaxation are (*1*) the determination of applied small strains if the sample is glassy or crystalline, since the linear range of response may be exceeded even at a strain of 1% and (*2*) the difficulty in measuring the attendant stress over the required 4–6 orders of magnitude in the softening dispersion. Stress relaxation and creep often cover the same kind of time scale range, 0.1 s to 10 h or a day. Measurements extending for months to years have been carried out, but are not common. The stress relaxation modulus $G(t) \equiv \sigma(t)/\gamma_0$.

Dynamic Mechanical Measurements. Dynamic mechanical measurements yield either the complex modulus, $G^*(\omega) = G'(\omega) + iG''(\omega)$, or the complex compliance, $J^*(\omega) = J'(\omega) - iJ''(\omega)$.

Sinusoidal stresses or strains of constant frequency are applied to a sample until a steady sinusoidal strain or stress results, with a fixed phase angle between the input and the output. Most often only about two cycles are required

to establish steady conditions. The greatest errors are obtained when the system phase angle of measurement is near 0, 90, or 180°. In some forced oscillation measurements the uncertainty of the loss modulus G'' becomes great when phase angle of the system approaches 0 and 180°, and G', the storage modulus, usually cannot be accurately determined when the material phase angle is near 90°. Dynamic moduli or compliances can be calculated without ambiguity from most sinusoidal measurements, but to avoid confusion in an already cluttered nomenclature it has become traditional to only calculate compliances from creep and moduli from stress relaxation. Dynamic measurements are the measurement of choice if information at equivalently short times is desired, since such measurements are possible at a megacycle and higher, but creep or stress relaxation measurements at times shorter than a millisecond are not possible. The circular frequency ω (in radians per second) should be associated with the reciprocal of the time t.

Questions concerning further experimental details including many on linear and nonlinear flow measurements can often be answered in References 62–68.

Significant Variables

Temperature Dependences. Each and every group of molecular mechanisms contributing to viscoelastic behavior has its own temperature-dependent rate. This is usually recognized except for behavior observed high above the T_g of amorphous polymers, where a single temperature dependence of time or frequency shifts is usually reported. The temperature dependence of the terminal zone of response, reflecting viscous flow and long-range recoverable deformation, was first reported to be different from that observed in the softening dispersion (the glassy to rubbery zone) in PS (69) and later in PVAc [poly(vinyl acetate)] (70). Numerous other examples have since been recognized (71,72). An example from atatic polypropylene (aPP) is given in Figure 19 (30,71–75).

There is evidence that the softening dispersion which extends from the glassy level ($J_g \approx 10^{-9}$ Pa^{-1}) to the rubbery level (J_g 10^{-5} Pa^{-1}) of compliance has three contributions (segmental, sub-Rouse, and Rouse modes) (76–79). Reducing data to a common extended curve by shifting them along the time or frequency scale to obtain a wider range of characterization is only legitimate when all of the contributions from molecular mechanisms to deformations have the same temperature dependence. Therefore, curves of viscoelastic functions reflecting the presence of more than one mechanism cannot be validly superposed to yield accurate predictions. Such data is considered thermorheologically complex. The presence of multiple temperature dependences is also observed in permitivity and dynamic light scattering measurements. An example of the reduction of the recoverable compliance curves of PIB shown in Figure 20 is seen in Figure 21 (78). The apparent success of the reduction is shown to be illusory with data taken over a wider frequency range. This is seen in Figure 22, where loss tangent curves [$\tan \delta = J''/J' = G''/G'$ (1)] presented at four temperatures from −74.2 to −35.8°C (78,80) reveal the presence of two groups of viscoelastic mechanisms which shift along the time-scale differently with temperature.

In addition to temperature time-scale shifts, which are attributed to changes in the relative or fractional free volume (62), the magnitude of the compliance or

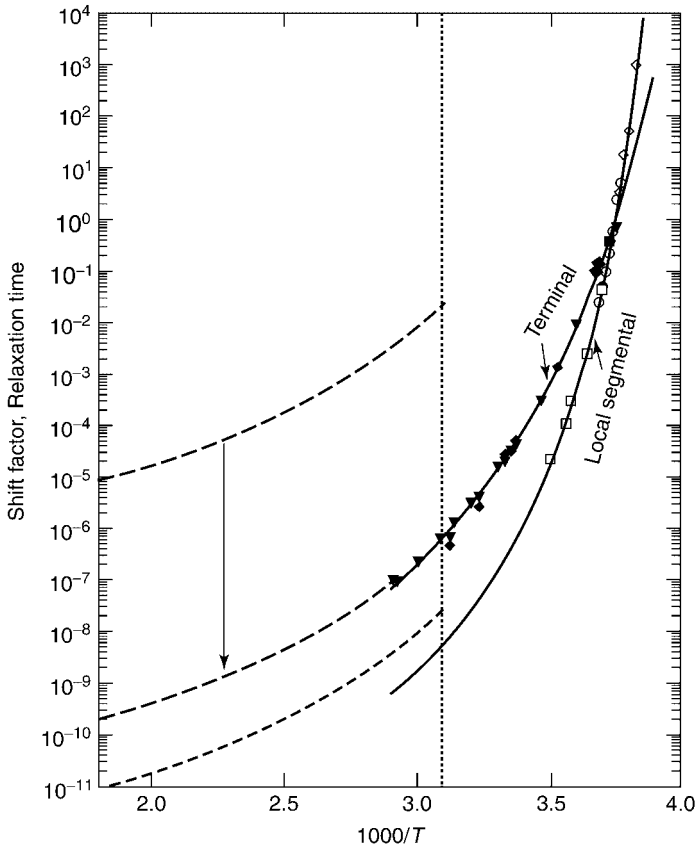

Fig. 19. Temperature dependence of the shift factors of the viscosity (▼), terminal dispersion (⧫), and softening dispersion (◊) of app from Ref. 73. The temperature dependence of the local segmental relaxation time determined by dynamic light scattering (□) (30) and by dynamic mechanical relaxation (○) (74). The two solid lines are separate fits to the terminal shift factor and local segmental relaxation by the Vogel–Fulcher–Tammann–Hesse equation. The uppermost dashed line is the global relaxation time τ_R, deduced from nmr relaxation data (75). The dashed curve in the middle is τ_R after a vertical shift indicated by the arrow to line up with the shift factor of viscosity (73). The lowest dashed curve is the local segmental relaxation time τ_{seg} deduced from nmr relaxation data (75).

modulus can change. The kinetic theory of rubber-like elasticity suggests that the entropically based modulus contribution to the viscoelastic response should increase in direct proportion to the absolute temperature. Correspondingly the reciprocal of the steady-state recoverable compliance should be directly proportional to the absolute temperature. In Figure 23 this can be seen to be true at temperatures that are greater than $2T_g$, but between $1.2T_g$ and $2T_g$; J_s (identified in the figure as J_e) is essentially independent of temperature. At still lower temperatures a strong decrease of J_s is seen (81).

Molecular Weight and Distribution Dependences. The influences of molecular weight and its distribution on the viscous flow (82) viscoelastic behavior

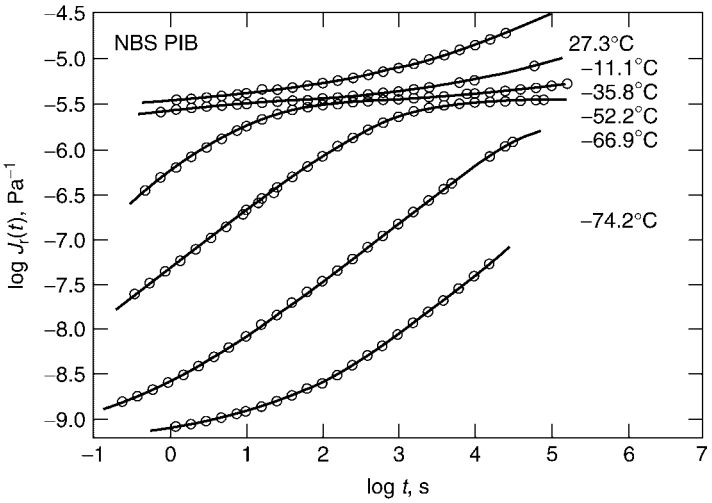

Fig. 20. Double-logarithmic plot of the recoverable compliance $J_r(t)$ of the National Bureau of Standards (NBS) PIB sample measured as a function of time at six temperatures as indicated.

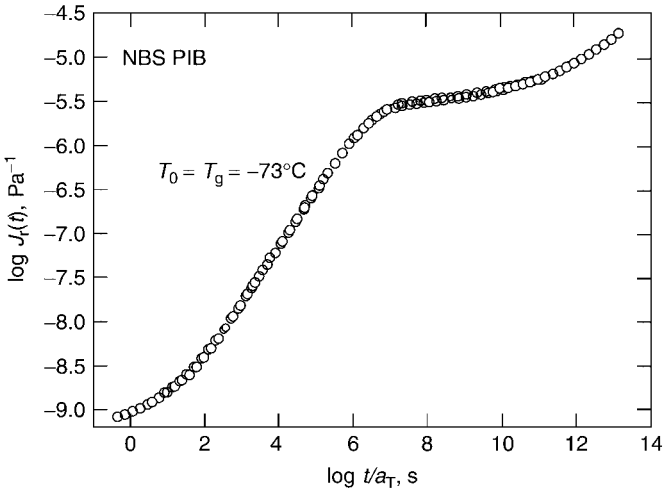

Fig. 21. Data from Figure 20 reduced to a common curve at the reference temperature T_0 of −73°C.

of amorphous polymers (83) have been reviewed. The flow behavior of bulk amorphous polymers and their concentrated solutions has been rationalized (82). Also, the basis for analyzing the viscosity as the product of two factors has been documented:

$$\gamma = F\zeta \tag{23}$$

where F is the structure factor, which depends on the polymer chain length (molecular weight) and branching, and ζ is the friction factor per chain atom,

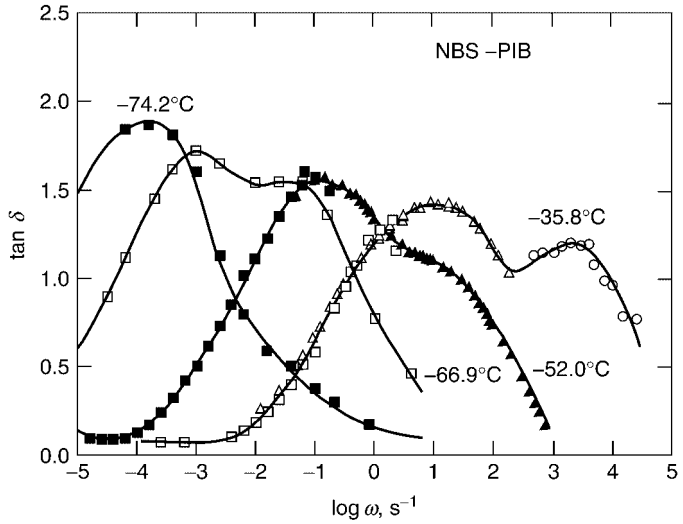

Fig. 22. tan δ as a function of actual frequencies at several temperatures for NBS PIB. The data were obtained by using several instruments spanning the frequency range as shown in the abscissa. The high frequency data at $-35.8°C$ (○) are from Ref. 80. The rest of the data were obtained by a combination of creep compliance and dynamic modulus measurements.

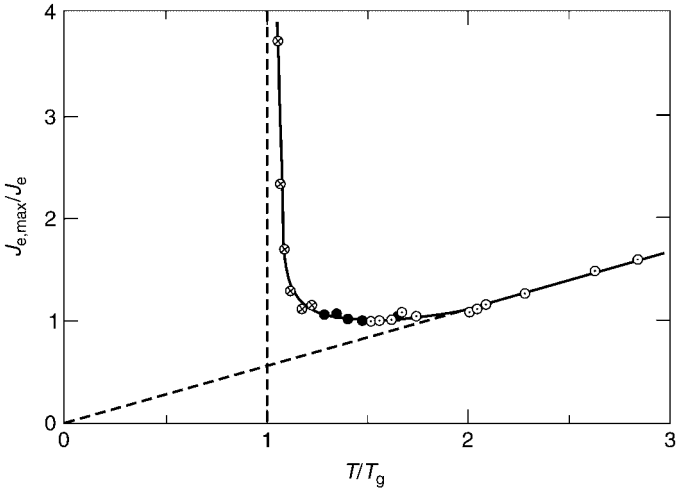

Fig. 23. Normalized reciprocal steady-state recoverable compliance $J_{e,max}/J_e$ for three polymers, poly(dimethyl siloxane), PIB, and PS, versus the reduced temperature T/T_g; T_g is the glass temperature and the normalized compliance $J_{e,max}$ is the largest experimentally indicated value which appears to occur at $T/T_g \approx 1.5$. The broken line through the origin indicates the expected kinetic theory result for a rubber-like modulus. ◎ poly(dimethyl siloxane); • PIB; ⊗ PS.

which depends principally on temperature. The latter is influenced by the molecular weight through the variation of the glass temperature. Holding the number-average molecular weight M_n constant so that T_g does not change while varying the weight-average molecular weight M_w at constant temperature, as was

done in References 83 and 84, ζ can be held constant so that the molecular weight dependence can be determined. It was found that at low molecular weights, F is proportional to the molecular weight in accord with Bueche's theory (85). Above a critical molecular weight M_c, the dependence increases to a proportionality of $M^{3.4}$ (82,83,86). This behavior appears to be universal and independent of the chemical nature of the polymer.

For polymers with broad molecular weight distributions the viscosity appears to be a function of the weight-average molecular weight M_w. This relationship fails for extreme binary blends with molecular weight ratios of 8 (87), 27 (88), and 380 (89). The blend data fall substantially below the curve determined for narrow distribution polymers.

Viscoelastic Behavior of Narrow Molecular Weight Distribution Polymers

The variations of the viscoelastic behavior of narrow molecular weight distribution amorphous polymers can most readily be seen in the broadening of the retardation spectrum $L(\lambda)$, as shown in Figure 24 (90). $L(\lambda)$, where λ is the retardation time, characterizes the contribution to the creep compliance $J(t)$, the dynamic storage compliance $J'(\omega)$, and the dynamic loss compliance $J''(\omega)$ according to the following relations (62):

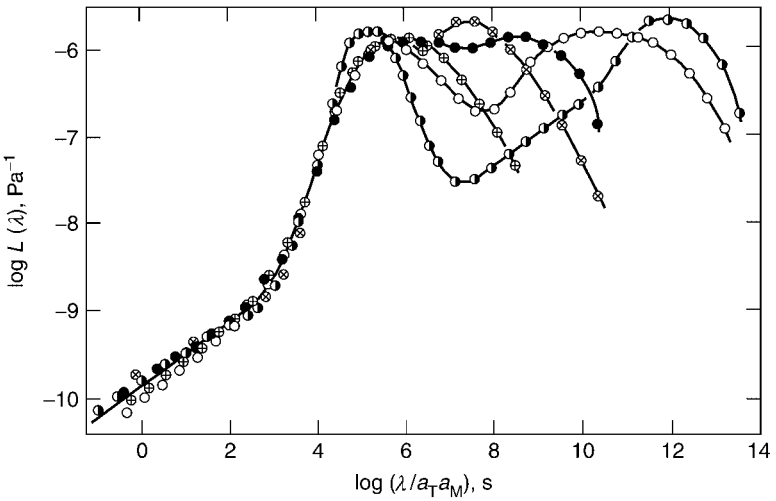

Fig. 24. Bilogarithmic plot of the retardation spectra $L(\lambda)$ of PS with narrow molecular weight distribution as functions of the reduced retardation time $\lambda_r = \lambda/a_T\, a_M$, where a_T is the temperature reduction factor and a_M is the molecular weight reduction factor [the latter reflects the change in $T_g(M)$]. The molecular weights and symbols for the various PSs are 4.7×10^4, A25, ⊕; 9.4×10^4, M102; ⊗; 1.9×10^5, L2, •; 6.0×10^5, A19, ○; and 3.8×10^6, F380, ◑. The reference temperature $T_0 = 100°C$ and the reference molecular weight $M_0 = 1.9 \times 10^5$.

$$J(t) = J_g + \int_{-\infty}^{\infty} L(1 - e^{-t/\lambda}) d\ln\lambda + \frac{t}{\eta} \tag{24}$$

$$J'(\omega) = J_g + \int_{-\infty}^{\infty} \left(\frac{L}{1+\omega^2\lambda^2}\right) d\ln\lambda \tag{25}$$

$$J''(\omega) = \int_{-\infty}^{\infty} \left(\frac{L\omega\lambda}{1+\omega^2\lambda^2}\right) d\ln\lambda + \frac{1}{\omega\eta} \tag{26}$$

The integrals involving L deal only with recoverable deformation, which for the most part reflects molecular orientation from various mechanisms. Permanent deformations are accounted for by the terms containing the viscosity coefficient η. From equation 24 it can be seen that the long-time limiting recoverable compliance is

$$J_s = J_r(\infty) \equiv \lim_{t\to\infty} \left[J(t) - t/\eta\right] = J_g + \int_{-\infty}^{\infty} L d\ln\lambda \tag{27}$$

Thus the steady-state recoverable compliance J_s is the sum of the glassy compliance and the limiting delayed compliance,

$$J_d = \int_{-\infty}^{+\infty} L d\ln\lambda \tag{28}$$

The recoverable shear creep compliance $J_r(t) = J(t) - t/\eta$, but to obtain $J_r(t)$ over an appreciable range of time-scale in the terminal (long-time) zone of response the recoverable deformation must be measured directly, after achieving steady state in a creep measurement, and subsequently setting the stress to zero. Since the measurement of recovery is a zero-stress experiment, extensive recovery cannot be determined with instruments that employ ball-bearing to support the moving element. Air-bearing instruments are also severely limited. With a magnetically levitated moving element an optimized range of measurement is achieved. The steady-state recoverable compliance of a viscoelastic liquid in elongation may not be measurable even under the weightless condition of outer space because of the interference of surface tension. In oscillatory measurements of dynamic compliances or moduli the interference of friction can be avoided with wire supports.

Equation 24 indicates that the strains arising from different molecular mechanisms add simply in the compliances and in principle can be separated. On the other hand, the stresses do not add and the different mechanisms cannot be easily resolved in modulus functions. In solution the solvent and the polymer contributions are also seen to be additive, as shown below. To understand the somewhat esoteric viscoelastic functions this additivity is helpful. It should also be noted that there are only two functions that do not contain contributions involving viscous flow, which obscure the recoverable responses which are largely, if not completely,

due to molecular orientations. They are the storage compliance J' and the recoverable creep compliance $J_r(t)$.

Near T_g, molecular mobilities are so small that the times required to achieve steady state become enormous. To avoid this dilemma, it has been proposed that steady-state could be achieved in creep at higher temperatures in a short time and would be maintained with cooling to the neighborhood of T_g so long as the stress was held constant (31). This tactic appears to work and is extremely useful.

In Figure 24 (90) the lowest molecular weight, narrow distribution PS depicted as A25 ($M = 47{,}000$) has only two contributions, (*1*) at short times a common linear portion between log λ_r of -1 and 3 with a slope of 1/3 and it is followed by (*2*) a symmetrical peak centered at log $\lambda_r = 6$. The short-time region reflects the presence of Andrade creep in which the recoverable creep compliance is a linear function of $t^{1/3}$. An alternative description by a generalized Andrade creep with t^{β_α}, with β_α not necessarily equals to 1/3 and varies from one polymer to another, is possible. Actually such a generalized Andrade creep is the short-time part of the

$$J_\alpha(t) = J_g + (J_{e\alpha} - J_g)\left\{1 - \exp\left[1 - (t/\tau_\alpha)^{1-n_\alpha}\right]\right\} \tag{29}$$

where $0 < (1 - n_\alpha) \leq 1$ and $(1 - n_\alpha)$ is to be identified with β_α (72,91). The steady-state compliance $J_{e\alpha}$ is the part of J_d contributed by the local segmental motion, also called the α-relaxation. As to be discussed later in sections on Dielectric Spectroscopy and Photon Correlation Spectroscopy, the time correlation function of the α-relaxation of amorphous polymers can be analyzed to have the stretched exponential form $\exp[-(t/\tau_\alpha)^{\beta_\alpha}]$, similar to equation 8, and β_α varies from polymer to polymer. For example, PS and PIB have β_α equal to 0.36 and 0.55 respectively.

The retardation spectrum of $J_\alpha(t)$ from equation 29 has the τ^{β_α} dependence at a short retardation time τ (notice that λ has been used earlier to denote retardation times), and also exhibits the peak as exhibited by the nonpolymeric glass-formers (see Fig. 29 to be introduced later). $J_{e\alpha}$ has been determined only for low molecular weight polymers and is approximately $J_{e\alpha} \approx 4.0 J_g$ for PS (92) and $J_{e\alpha} \approx 5.0 J_g$ for poly(methylphenyl siloxane) (93).

The increase in the compliance contributed by the area under the symmetrical peak overwhelms the Andrade or the generalized Andrade contribution and increases until a rubbery level is reached at about 10^{-6} cm^2/dyn (10^{-5} Pa^{-1}). This increase in compliance is attributed to the polymer chain modes, first successfully described by Rouse (94). His theory was extended by Ferry, Landel, and Williams from a dilute solution theory to one dealing with the viscoelastic properties of undiluted polymers (95) (see VISCOELASTICITY). However, the extended Rouse model has limitations. It has been recognized (96) that by taking the short-time limit of the extended Rouse modes contribution to the modulus, one obtains $G(0) = \upsilon NkT = \upsilon \rho RT/M$, where N is the number of molecules per cm^3 and υ is the number of submolecules per chain (62). The number of monomers in a submolecule, z, is given by P/υ, where P is the number of monomers in a polymer chain. For a polymer of molecular weight 150,000 and a density of 1.5 g/cm^3 and by assuming that the smallest submolecule that can be still be Gaussian consists of five monomer units (ie, $z = 5$), it was found that $G(0) = 7.5 \times 10^6$ Pa [$J(0) = 1.3 \times 10^{-7}$ Pa^{-1}]. This value is about 2 orders of magnitude smaller (larger) than the experimentally determined value of

the glassy modulus G_g (glassy compliance J_g) which typically falls in the neighborhood of 10^9 Pa (10^{-9} Pa^{-1}). Thus the extended Rouse model cannot account for the short-time portion of the glass–rubber dispersion of entangled polymers because here the modulus (compliance) decreases (increases) continuously from about 10^9 Pa (10^{-9} Pa^{-1}) to the plateau modulus of about 10^5 Pa (10^{-5} Pa^{-1}). These deficiencies of the extended Rouse model are not surprising because, after all, according to the model the submolecule is the shortest length of chain which can undergo relaxation and the motions of shorter segments within the submolecules are ignored. The Gaussian submolecular model of Rouse can, at best, account only for viscoelastic behavior in the longer relaxation time portion of the glass–rubber softening dispersion. Thus the extended Rouse model has to be augmented by the molecular mechanisms involving chain units smaller than the submolecule but larger than the local segmental motion, which we called the sub-Rouse modes. Clear evidences of sub-Rouse modes were found by viscoelastic measurement (78,79) and by dynamic light scattering (27,29) in PIB. The high frequency peak or shoulder of tan δ as a function of frequency in Figure 6 is caused by the sub-Rouse modes. The softening dispersion thus has three contributions: (*1*) the local segmental motion responsible for $J(t)$ from $J_g \approx 10^{-9}$ Pa^{-1} up to about $J_{s\alpha} \approx 5 \times 10^{-9}$ Pa^{-1}, (*2*) the sub-Rouse modes from $J_{s\alpha}$ up to somewhere near $J_{sR} \approx 10^{-7}$ Pa^{-1}, and (*3*) the modified Rouse modes from $J_{sR} \approx 10^{-7}$ Pa^{-1} up to the plateau level. These estimates may vary for polymers with very different chemical structures.

Although the local segmental relaxation does not show up in Figure 22, other supplementary data indicate that all three groups of viscoelastic mechanism—local segmental, sub-Rouse, and Rouse modes—all have different temperature shift factors. For the Rouse and the sub-Rouse modes this fact was shown first by creep compliance measurements in PS in the softening dispersion (72,98) long before sub-Rouse modes were clearly resolved in PIB (Fig. 22) and the term used. It has been confirmed in PS by dynamic modulus measurements. Examples are the data on PS obtained (99) using an inverted forced oscillation pendulum and some unpublished data (72,100) on PS and TMPC (tetramethyl BPA polycarbonate) using a commercial instrument, and in PIB (101). These data are partly reproduced in a review (72). The lack of reduction of the data is clear from the dependence of the shape of the tan δ peak with temperature of measurement and occurs over a frequency region that corresponds to compliances in the range from 10^{-5} Pa^{-1} down to about 10^{-7} Pa^{-1}. Narrowing of the softening dispersion of PMMA and PVAc with decreasing temperature was found by comparing the data obtained (102) at higher temperature (higher frequency) with that obtained (103) at lower temperature (longer times). This behavior can be considered to be unusual because viscoelastic spectra usually are seen to broaden with falling temperature. All the abnormal behaviors described in this paragraph follow as consequences of the shift factors of local segmental relaxation, the sub-Rouse modes, and the Rouse modes having decreasing sensitivity to temperature in this order, as found directly in PIB (79,97). As temperature is decreased, time–temperature superposition fails because the separations between the three groups of viscoelastic mechanisms are decreased, a phenomenon which is appropriately called *encroachment* (72,79).

As the molecular weight increases a second long-time peak develops in $L(\lambda)$, reflecting a rubber-like plateau in $J_r(t)$ which increases in length. The spectrum

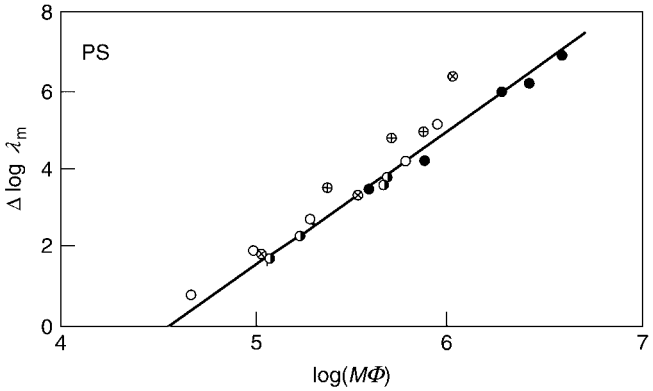

Fig. 25. Length of entanglement rubbery plateau as measured by the separation of the peaks of the retardation spectra on the logarithmic time-scale, $\Delta \log \lambda_m$, as a funciton of the logarithm of the product of the molecular weight M and the volume fraction of the polymer, Φ. • Blends (89); ◑ blends (104); ○ monodisperse (105); ⊗ TCP solution (106); ⊕ (107,108).

seen in Figure 24 for the highest molecular weight PS sample F380 (3.8×10^6) has two additional long-time features 3) a second Andrade region and 4) a terminal symmetrical peak, centered at $\log \lambda_r \cong 12$. The length of the plateau seen in $\log J_r(t)$ is measured by the time separation of the two peaks in $L(\lambda_r)$, $\Delta \log \lambda_m$. The length of the plateau can be seen to increase with the 3.4 power of the molecular weight, just as the viscosity. In fact the length of the plateau goes to zero at the viscosity critical molecular weight ($M_c \approx 35{,}000$) as seen in Figure 25, where λ denotes the retardation time (89). Since the rubber-like plateau is attributed to the presence of a transient entanglement network of the polymer chains, it is clear that the entanglements manifest themselves at the same molecular weight in viscous and recoverable deformations with the same degrees of enhancement with increasing molecular weight. Although Figure 24 was derived from the reduced curve obtained by time–temperature superposition of isothermal recoverable creep compliance data, actually the two shift factors of terminal dispersion and the local segmental relaxation do not have the same temperature dependence in a common temperature range above T_g (Fig. 19). None of the three mechanisms in the softening dispersion have the same temperature dependence for their shift factors. Therefore, the shift factor a_T used to obtain master curve for polymers by time–temperature superposition, as given in Figures 21 and 24, is actually a combination of the individual shift factors of the several different viscoelastic mechanisms. At low temperatures, a_T is principally determined by the shift factor of the local segmental mode. With increasing temperature, in turn a_T is principally determined by the shift factors of the sub-Rouse modes, the Rouse modes, modes in the plateau, and the terminal modes. Hence, it is wrong to assume that a_T describes the temperature dependence of *any* or *all* of the viscoelastic mechanisms.

Applying the kinetic theory of rubber-like elasticity (62,109) to the entanglement network one can determine the molecular weight between entanglements M_e from the plateau compliance J_N or plateau modulus G_N (62);

$$J_N = G_N^{-1} = M_e/\rho RT \tag{30}$$

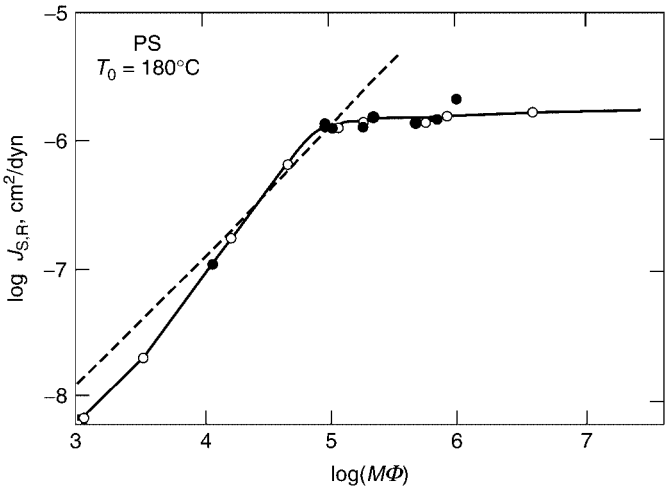

Fig. 26. Reduced steady-state compliances $J_{s,r}$ for PSs with narrow molecular weight distributions plotted logarithmically as a function of the product of the molecular weight M and the volume fraction of polymer, Φ. The dashed line represents the prediction of the modified Rouse theory. The solvent in the solutions is TCP. • $J_{s,r}$(solution) = $J_s\ \Phi^2\ T/T_0$; ○ $J_{s,r}$(bulk) = J_s.

where ρ is the density, T is the absolute temperature (K), and R is the gas constant. At high molecular weights $M \gg M_c$ the steady-state recoverable compliance J_s has been reported to be 2–10 times larger than J_N (83). Reported values for J_s have to be accepted with caution because the dependence of J_s is far more sensitive to the molecular weight distribution than to the molecular weight. The results for $J_s(M)$ reported in Reference 105 are shown in Figure 26, where at low molecular weights J_s is amazingly close to the first power dependence predicted by the modified Rouse theory (94,95) with no adjustable parameters. At higher molecular weights, $M > 3M_c$, and J_s becomes independent of molecular weight. This surprising behavior was first reported by Tobolsky and co-workers (110). Results from nine studies on PS show that the published values vary by up to a factor of 5 (111).

It has been shown (112) that molecular weight blends with low concentrations of high molecular components can exhibit J_s values that are nearly 20 times greater than those shown by any of the monodisperse components. Trace amounts of high molecular tails in low molecular weight polymers can enhance the J_s by more than a 1000-fold (105). The recoverable compliance of a polymer with close to a random molecular weight distribution can be more than 10 times higher than that of a narrow distribution sample with the same number-average molecular weight M_n (113).

Long-chain branching, in particular narrow distribution, star-branched polymers (chains joined at a common center) also enhances the steady-state recoverable compliance J_s. It has been shown (114) that four- and six-arm star PS do not show the molecular weight independence at high molecular weight as seen with linear polymers. J_s continues to increase with the first power of the molecular weight; ie, the Rouse prediction continues unabated at the highest molecular weights measured.

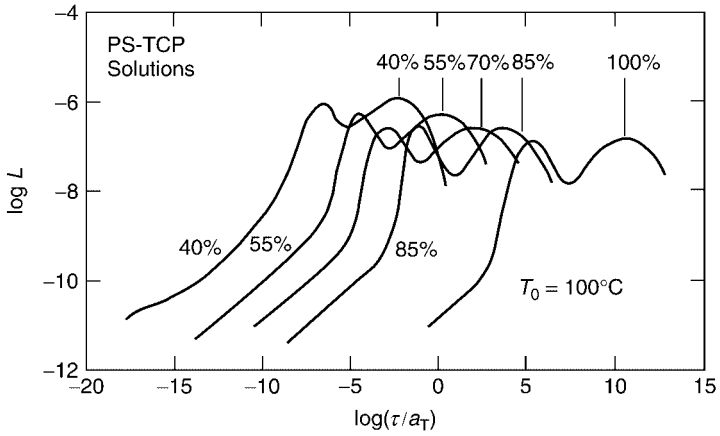

Fig. 27. Logarithmic plot of retardation spectra against reduced time for the more concentrated solutions (40% and above) of PS PC-6A (in TCP) and of the undiluted polymer. In all cases the reference temperature T_0 is 100°C.

Concentration Dependence. The effect of diluent on the viscoelastic behavior of a polymer is profound and complicated. The first and most dramatic effect is the usual strong decrease in the glass temperature T_g, which happens because the T_g of the solvent is usually much lower than that of the polymer, since T_g is tied to the local mobility of the molecules; ie, the local mobility determines when liquid structure rearrangements cannot keep up with the imposed *rate of cooling*. Thereafter the specific volume of the liquid is greater than its equilibrium value. The rearrangements needed to obtain the required local molecular packing are kinetically arrested. Contraction continues with cooling at a diminished rate only because of the reduction in the magnitude of the anharmonic molecular vibrations. Therefore, with increasing diluent concentration, at a given temperature, one obtains solutions that are further above their T_g. Hence molecular mobility is greater because of the larger relative free volume, and the viscoelastic functions $J(t)$, $G(t)$, and $G^*(\omega)$ are found at increasingly shorter times or higher frequencies. This shift toward shorter times with increasing diluent concentration can be seen in Figures 27 and 28 (107,108). The retardation spectra for a narrow molecular weight distribution PS ($M = 860{,}000$) and seven solutions in tricresyl phosphate (TCP) are presented. The spectrum for the bulk polymer is compared with those of the four most concentrated solutions (40, 55, 70, and 85 wt% of PS) at 100°C in Figure 27. The severe shifts to shorter reduced times t/a_T are due to the decrease of T_g. The four lowest concentrations 1, 25, 10, 25, and 40 wt% of PS are compared at −30°C in Figure 28, which shows the shift to shorter times, but the other two effects are most clearly seen at the lower concentrations, although they are present at all concentrations. The separation of the two major peaks diminishes with decreasing polymer concentration, reflecting the shortening rubber-like plateau. With dilution the overlap of the polymer chain coils diminishes and therefore the number of intermolecular entanglements per molecule decreases. With dilution the concentration of viscoelastic elements decreases and each element supports a greater observed compliance. Finally, it should be appreciated that the

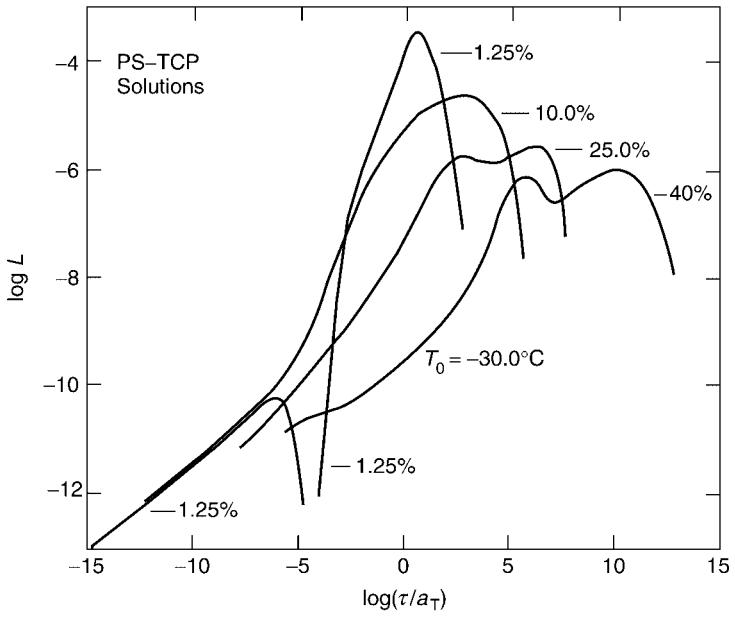

Fig. 28. Logarithmic plot of retardation spectra against reduced time for the less concentrated solutions (40% and less) of PS PC-6A (in TCP) and of the undiluted polymer. In all cases the reference temperature T_0 is −30°C.

solvent manifests its independent contribution to the deformation, especially at the lowest polymer concentrations. The spectrum for the 1.25% solution is split into two peaks. Measurements on the pure solvent identified the peak at short times to be due to the solvent. Hence the second sharp peak is the polymer peak. The fact that the polymer and solvent molecule motions influence one another, but contribute additively but separately to the deformation, is the reason for the manifestation of two observed T_g's in some of the solutions (107,108).

The Glass Temperature, A Material Characterizing Parameter

For the glass temperature to be a material characterizing parameter it must be determined by cooling from equilibrium (see GLASS TRANSITION). Heating measurements yield an approximation to the fictive temperature of the starting glassy materials, which is a function of its thermal history below T_g. The glass-transition temperature is therefore a specimen characterizing parameter and a unique function of the rate of cooling. It has been shown (115) that local segmental motions contribute both to the glassy Andrade creep region and to liquid structural relaxation. It is therefore reasonable to expect that for a given rate of cooling the local mobility which determines the T_g departure from an equilibrium liquid structure has to be the same for all amorphous materials. It has consequently been established that at T_g the retardation function, at short times, in the region of the time scale attributed to local segmental motions is the same functionally

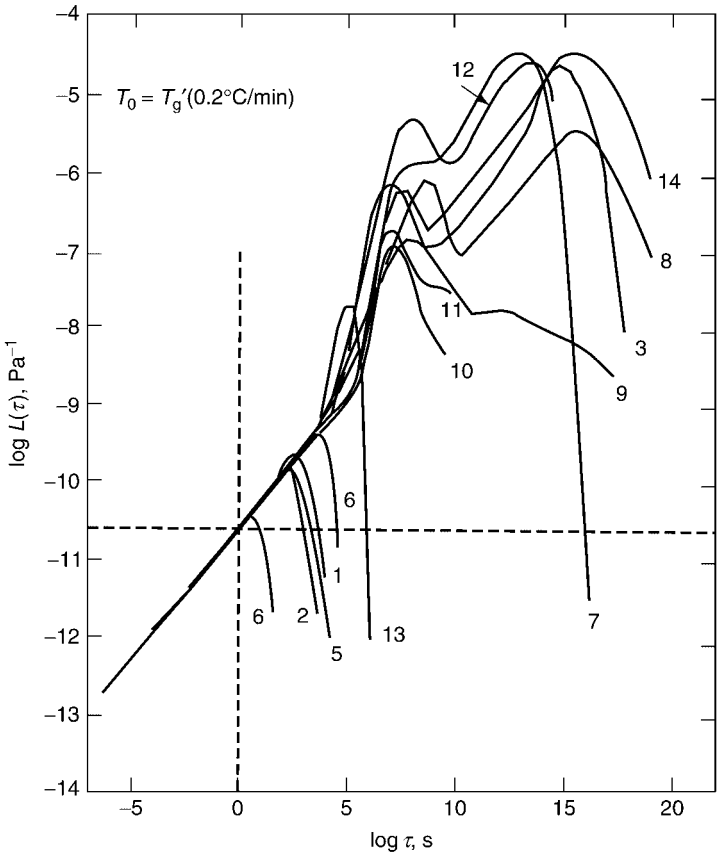

Fig. 29. Superposition of the retardation spectra at short times for 1) 6PE; 2) Aroclor 1248; 3) polypropylene; 4) TCP; 5) OTP; 6) $Tl_2SeAs_2Te_3$; 7) PS Dylene 8; 8) PIB; 9) Viton 10A; 10) EPON 1004/DDS; 11) EPON 1007/DDS; 12) PB/Aroclor 1248 Soln; 13) Se 14) PVAc.

and in position for many amorphous materials including nonpolymeric, organic glass-formers, inorganic glasses, and polymers. Figure 29 shows the common viscoelastic behavior between log τ of -6 to $+1$, where τ is the reduced retardation time. To obtain close superposition, T_g's measured at a cooling rate of 0.2°C/min were adjusted by up to 2°C, which is thought to reflect the usual magnitude of uncertainty (60). It is at longer times that the structural differences of the materials manifest themselves. In the region of Andrade creep dominance $L(\tau)$ was calculated by Thor Smith to be (116)

$$L(\tau) = 0.246\beta_A\tau^{1/3} \tag{31}$$

where β_A is the Andrade coefficient (117) in

$$J_r(t) = J_A + \beta_A t^{1/3} \tag{32}$$

In the short-time regime the constant J_A in equation 32 is equal to the glassy compliance J_g. From Figure 29, at $\tau = 1$ s, $L(\tau)$ is 2.24×10^{-12} cm^2/dyn (or is 2.24×10^{-11} Pa^{-1}). Therefore, the temperature at which $\beta_A = 9.10 \times 10^{-12}$ cm^2/(dyn·s$^{1/3}$) is T_g ($Q = 0.2^\circ$C/min, where Q is the rate of cooling).

Although the short-time compliance data of diverse amorphous materials can be represented by Andrade creep (eq. 32), the reason for such a "universal" behavior is unclear. The alternative description of the local segmental contribution by equation 29 with $(1-n_\alpha) \equiv \beta_\alpha$ not necessarily equal to 1/3 and its value dependent on the material itself offers a different possibility. The generalized Andrade creep

$$J_r(t) = J_g + Bt^{1-n_\alpha} \tag{33}$$

which is the short-time limit of equation 29, will replace equation 32 and be used to fit the data at short times and determine J_g in the process.

Dependence of Viscoelastic and Dynamic Properties on Chemical Structure

It was recognized already in the early days of viscoelastic measurements that the time or frequency dependence of the softening zone can vary considerably with the chemical structure of the polymer. As early as in 1956 it was found that the softening dispersions of PIB and PS contrast sharply (118,119). The glassy compliance (modulus) and the plateau compliance (modulus) are similar for PIB and PS, but the width of the glass–rubber softening dispersion of PIB is several decades broader in time or frequency than that of PS. In a 1991 review (120) it was remarked that the origin of this difference is still not clear. From the discussion in previous sessions and results summarized in a review (71,72), the other differences in viscoelastic properties of PIB and PS include the lesser differences between the temperature dependences of the three viscoelastic mechanisms in the softening dispersion of the former (71,72,79). The terminal dispersion as well as the $M^{3.4}$ molecular weight dependence of the viscosity of monodisperse entangled linear polymers does not depend on chemical structure of the repeat units. Nevertheless, the difference between the temperature dependences of the terminal dispersion (or the viscosity) and the local segmental motion is significantly less in PIB than in PS.

Dielectric relaxation and photon correlation spectroscopic measurements (to be discussed later) have found that the stretched exponential time correlation function of the α-relaxation of amorphous polymers, $\exp[-(t/\tau_\alpha)^{\beta_\alpha}]$, has β_α that varies from polymer to polymer. For example, PS and PIB have β_α equal to 0.36 and 0.55 respectively. It was recognized that this difference in the stretched exponent β_α of PIB and PS is the origin of their contrasting viscoelastic properties (72,79, 121,122).

Low Molecular Weight Amorphous Polymers. The most spectacular observations of breakdown in time–temperature superposition occur in low molecular weight polymers. The effect was first seen in PS by creep and recovery measurement (105). The recoverable compliance $J_r(t)$ for a 3400 Da molecular weight PS undergoes a dramatic change in shape of the recoverable compliance

curve as the temperature is lowered toward T_g. At the same time the steady-state recoverable compliance J_s decreases 30-fold down to a value which is only about five times J_g. This was confirmed by complex shear modulus measurements of Gray, Harrison and Lamb (123). The viscoelastic anomalies found in low molecular weight PSs are general phenomena because they are also found in other polymers. These include polypropylene glycol (124), poly(methylphenyl siloxane) (125), and selenium, a natural polymer (126,127). An example is shown by $J_r(t)$ data of a near monodisperse poly(methylphenyl siloxane) with molecular weight of 5000 Da plotted against the logarithm of the reduced time t/a_T. The origin of the effect has been traced (122) to the stronger temperature dependence of the shift factors of the local segmental modes, the sub-Rouse modes, and the Rouse modes in this order, ie, encroachment of the local segmental mode toward the two longer time mechanisms (122). Confirmation of this explanation was provided by dielectric relaxation in polypropylene glycol and in PI (126,128).

Dynamic Properties of Amorphous Polymers Probed by Other Techniques

Besides viscoelastic measurements described above, there are a variety of techniques that can probe the dynamic and viscoelastic properties of amorphous polymers. Their advantages and disadvantages as compared with shear viscoelastic measurements in elucidating the dynamic properties become clear in the following sections.

Dielectric Spectroscopy. Dielectric experiments obtain the permittivity $\varepsilon'(\omega)$ and loss $\varepsilon''(\omega)$ of materials that has a permanent dipole moments over a wide range of frequency (129,130). The complex dielectric permittivity $\varepsilon^*(\omega) = \varepsilon'(\omega) - i\varepsilon''(\omega)$ is given by the one-sided Fourier transform of the normalized dipole moment autocorrelation function $\phi(t) = \langle M(0) \cdot M(t)\rangle / \langle M^2(0)\rangle$ as

$$\left[\varepsilon^*(\omega) - \varepsilon_\infty\right] / (\varepsilon_0 - \varepsilon_\infty) = \int_0^\infty \exp(-i\omega t') \left[-\mathrm{d}\phi(t')/\mathrm{d}t'\right] \mathrm{d}t' \tag{34}$$

where ε_0 and ε_∞ are the low and high frequency limit of $\varepsilon'(\omega)$, respectively.

By a combination of commercial instruments, the wide frequency range $10^{-4} < f = \omega/2\pi < 10^{10}$ Hz is accessible to probe the molecular motions. The technique usually probes only the local segmental relaxation (often called the primary or α-relaxation in dielectric relaxation) and the secondary (β, γ, ...) relaxations exclusively. For a few polymers such as polypropylene glycol and PI that have a component of the dipole moment parallel to the polymer chain backbone, additional relaxation processes due to some normal modes that correspond to the mechanical terminal zone, are dielectrically active (126,128,131–133). The α-loss peak has an asymmetrically skewed shape with a width which can be much larger than a Debye peak given by $\varepsilon'' \propto \omega\tau/(\omega^2\tau^2 + 1)$. The degree of departure from the Debye peak varies from polymer to polymer. The two parameter Cole–Davidson (134) and the three parameter Havriliak–Negami (HN) (135) empirical functions have often been used to fit the experimental data because these two are empirical functions of the frequency and are very convenient for fitting experimental data.

An equally popular empirical function of frequency is obtained from equation 34 with $\phi(t)$ given by the KWW function (136,137)

$$\phi(t) = \exp\left[-(t/\tau)^{1-n_\alpha}\right] \tag{35}$$

with $0 < (1 - n_\alpha) \equiv \beta_\alpha < 1$. The KWW function has two parameters as compared with three parameters in the HN equation. As a consequence, the HN function always provides a better fit to the data than does the KWW function. Nevertheless the KWW function has been found to give an adequate fit (with ubiquitous deviation at high frequencies) to the dielectric data and is often used in current literature. It is also popular with theoreticians for the construction of models to explain the non-Debye behavior of the α-relaxation process. The popularity is probably due to the fact that it has only two parameters, the KWW exponent $1-n_\alpha$ that controls both the width and the degree of skewness and τ corresponds approximately to the most probable correlation time. Irrespective of the choice of the empirical function used to fit the dielectric dispersion, the frequency of the dielectric loss maximum determines the most probable frequency of the local segmental motion. In contrast to viscoelastic measurements, the Rouse modes and the modes in the terminal zone are usually not observed. Thus the α-relaxation is the dominant contribution to $\varepsilon^*(\omega)$ and its dispersion or $1-n_\alpha$ can be easily determined. The dielectric dispersions of small molecular glass-formers including salol, toluene, bromopentane, propylene carbonate, glycerol, propylene glycol are temperature-dependent (138), with $1-n_\alpha$ increasing with increasing temperature and in some cases approaches unity (ie, Debye relaxation) at high temperatures. There are also some evidences that the dielectric dispersion of the α-relaxation of amorphous polymers also narrows with increasing temperature; however, apparently $1-n_\alpha$ is not close to unity even at high temperatures where the α-relaxation time is of the order of 10^{-10} s. An example is PVAc (139,140). This difference between small molecular glass-former and amorphous polymers is due to the presence of bonded interaction between repeat units in the polymer chains (141,142). In fact, the local segmental mode of a polymer chain already has dispersion broader than the Debye relaxation as shown by dielectric relaxation measurement of dilute solution of PVAc in a solvent (143).

Photon Correlation Spectroscopy. Photon correlation spectroscopy (pcs) is one among several light scattering techniques reviewed in the beginning of this article. The technique is sensitive to density fluctuations as well as concentration fluctuations (125,144,145) and obtains directly the autocorrelation functions in the time domain. It has been suggested that pcs data correspond to the longitudinal compliance (146). The local segmental mode is the main contributor to density fluctuation and is featured exclusively in the data taken by pcs, although in addition the sub-Rouse modes have also been seen in PIB (27,31). Most pcs studies on bulk polymers as well as nonpolymeric glass-forming liquids have shown that the KWW functions are adequate representations of the experimental time-correlation functions for the density fluctuations. Thus the KWW function that fits the pcs data gives directly the dispersion of the α-relaxation. The KWW exponent $1-n_\alpha$ characterizing the dispersion varies from polymer to polymer. For example, PS has the smaller value of 0.36 (23,29), PIB has the larger value of 0.55 (27,31),

and poly(methylphenyl siloxane) has the intermediate value of 0.45 (125). Since pcs, dielectric relaxation, and shear mechanical relaxation or compliance measure different dynamic variables and different correlation functions, it is not surprising that dispersion parameter $1 - n_\alpha$ and the effective relaxation or retardation time τ_α determined by the three techniques can be different (147–150).

Besides pcs, other light scattering techniques including Brillouin scattering and Fabry–Perot interferometry described in previous sections have been applied to probe the dynamics of polymers at higher frequencies than the more conventional techniques. Interpretations of the results from these techniques are still subjects of controversy and are not discussed here.

Ultrasonic Attenuation. The frequency range of this technique is of the order of 1 MHz. The attenuation α of the longitudinal waves is related to the longitudinal loss modulus M'' by $M'' = 2\alpha\rho u^3/\omega$, and the longitudinal storage modulus M' by $M' = \rho u^2$, where ρ is the density and u is the ultrasonic velocity. For an example of the use of this techniques, see References 151 and 152.

Nuclear Magnetic Resonance Techniques. Several experimental techniques stemming from the basic principles of nuclear magnetic resonance (qv) were developed in the last decade, which probe relaxation as local as the primary local segmental motion and the secondary relaxation and as extensive as diffusion of the entire chain. Some of these techniques and representative data have been reviewed (153) and are not discussed further here. However, in Figure 30 the local segmental relaxation correlation time τ_c of high molecular weight PS is shown as a function of temperature obtained by two-dimensional exchange nmr (154,155) up to long times exceeding 100 s, and compared with the shift factor $a_{T,S}$ from time–temperature superposition of recoverable creep compliance $J_r(t)$ curves of another high molecular weight PS (PS-A25) in the glass–rubber softening region described earlier (105). Only the fits to the data of τ_c and $a_{T,S}$ by the William–Landel–Ferry (WLF) equation (156) are given. The nmr τ_c has the same temperature dependence as $a_{T,S}$ in the temperature range below 384 K, where $a_{T,S}$ is determined principally by measurements of $J_r(t) < 10^{-7}$ Pa^{-1} and reflects the shift factors of the local segmental motion, $a_{T,\alpha}$, and the sub-Rouse modes, $a_{T,sR}$. Above 384, τ_c starts to exhibit stronger temperature dependence than $a_{T,S}$. Between approximately 384 and 407 K, $a_{T,S}$ is determined by curves with $J_r(t)$ larger than 10^{-7} Pa^{-1} and consist of Rouse modes and possibly some shorter time modes in the plateau. Thus the nmr data gives another proof that the local segmental relaxation time has stronger temperature dependence than the Rouse modes (71,72). Above approximately 407 K, the creep compliance data is contributed entirely by the terminal viscoelastic mechanism, which has exactly the same temperature dependence as the viscosity shift factor $a_{T,\eta}$ shown also in Figure 30. It is unsurprising that the extrapolation of $a_{T,S}$ to this high temperature regime shows a different (weaker) temperature dependence than the actual shift factor for the viscosity. More important is that the nmr data τ_c of the local segmental relaxation time τ_α clearly has stronger temperature dependence than the viscosity in the *entire* temperature range shown in Figure 30.

Quasi-elastic Neutron Scattering. Coherent and incoherent inelastic neutron scattering are unique experimental techniques to characterize molecular motions on a time scale between 10^{-14} and 10^{-8} s. The continued development of high resolution inelastic scattering techniques in the past two decades (157–159) enables measurement of the dynamic structure factor $S(Q, \omega)$ and the

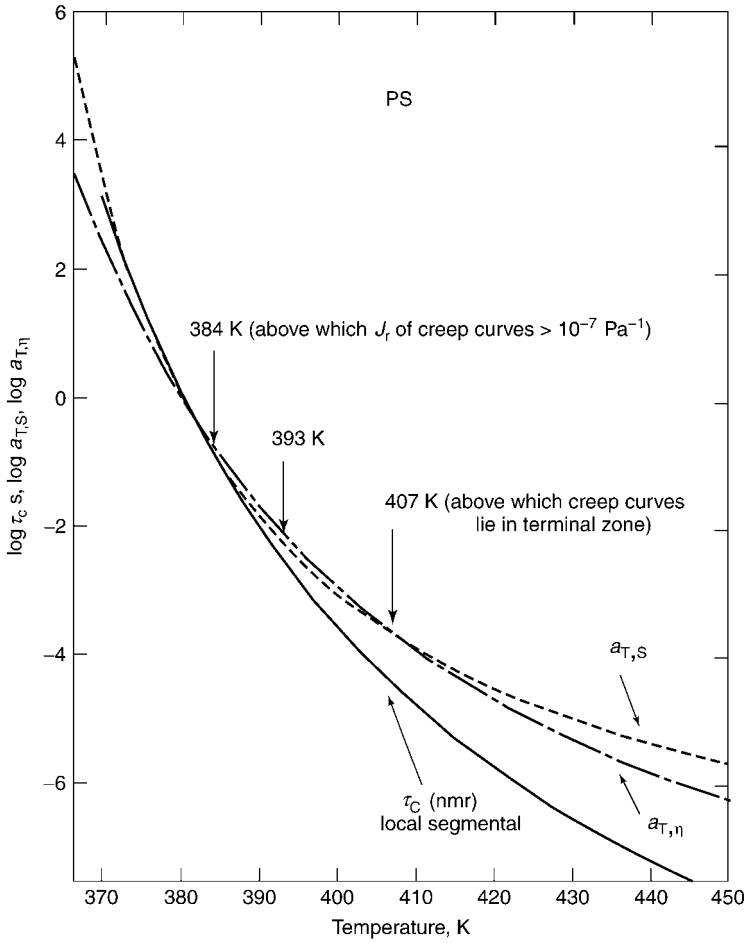

Fig. 30. The local segmental relaxation correlation time τ_c of high molecular weight PS as a function of temperature obtained by two-dimensional exchange nmr (154,155) up to long times exceeding 100 s, and compared with the shift factor $a_{T,S}$ from time–temperature superposition of recoverable creep compliance $J_r(t)$ curves of another high molecular weight PS (PS-A25) in the glass–rubber softening region (105). Only the fits to the data of τ_c (——) and $a_{T,S}$ (– – – –) by the WLF equation are given. The viscosity shift factor $a_{T,\eta}$ is also shown (– – – – –). The nmr τ_c clearly has stronger temperature dependence than the viscosity in the *entire* temperature range. There is also good agreement between the temperature dependence of τ_c and $a_{T,S}$ at temperatures below 384 K where $a_{T,S}$ becomes sequentially the shift factor of first the sub-Rouse modes and second the local segmental modes as temperature is decreased toward T_g.

intermediate scattering function $S(Q, t)$ in the typical Q (momentum transfer) range of $0.01\ nm^{-1} < Q < 0.5\ nm^{-1}$, suitable for the study of the local segmental motion in polymers. $S(Q, t)$ is related to the density–density correlation function. The advantage of quasi-elastic neutron scattering (QENS) is the information on the Q-dependence. Also partial replacement of hydrogen atoms by deuterons in the repeat units of the polymer let the experimenter select the location of the motion to be studied by the technique. The disadvantage is the presence of scattering by anharmonic vibrations and faster processes, which make the extraction of

the part of the data related to local segmental relaxation difficult. Consequently, at present interpretation of QENS data is unclear and controversial, and is not discussed here.

Enthalpy and Heat Capacity Relaxation. The conventional techniques based on differential scanning calorimetry by which enthalpy relaxation is measured at different cooling and heating rates is discussed elsewhere in the encyclopedia by others. Extensive review of the subject can be found in Reference 160. Measurements of heat capacity and entropy of polymers as a function of temperature are well documented and the data can be found in Reference 161. Frequency-dependent heat capacity spectroscopy has been developed (162,163) and application to study the local segmental dynamics of polymers has been made (163).

Positronium Annihilation Lifetime Spectroscopy. Positron annihilation lifetime spectroscopy (pals) is primarily viewed as technique to parameterize the unoccupied volume, or so-called free volume, of amorphous polymers. *In vacuo*, the ortho-positronium (o-Ps) has a well-defined lifetime τ_3 of 142 ns. This lifetime is cut short when o-Ps is embedded in condensed matter via the "pick-off" mechanism whereby o-Ps prematurely annihilates with one of the surrounding bound electrons. The quantum mechanical probability of o-Ps "pick-off" annihilation depends on the electron density of the medium, or the size of the heterogeneity. Typically the heterogeneity is assumed to be a spherical "cavity" (164,165) so that τ_3 can be easily related to an average radius R ($R_0 = R + \Delta R$) of the nanopore:

$$\tau_3 = \frac{1}{2}\left[1 - \frac{R}{R_0} + \frac{1}{2\pi}\sin\left(\frac{2\pi R}{R_0}\right)\right] \tag{36}$$

Novel studies on zeolites (165–167) confirm the validity of this approach and find ΔR, the o-Ps penetration depth into the electron cloud surrounding the cavity, to be nearly constant ($\Delta R \approx 0.161$ nm). For amorphous polymers, it is understood that spherical nanopores are a first-order approximation at best. Nevertheless, pals is widely used for the structural characterization of the unoccupied volume in glassy materials. There are many works on pals studies of amorphous polymers. Only some of the more recent works are cited here (168–170).

Pressure Dependence of Polymer Dynamics. Pressure is one of the essential thermodynamic variables that control the structure and the associated dynamics of polymers and glass-forming systems. The pressure dependence of the viscoelastic relaxation times is of paramount importance because hydrostatic pressure is encountered in polymer processing. Dielectric spectroscopy was among the first dynamic techniques to take advantage of pressure through the recognition of the fact that the dynamic state of a glass-forming system can only be completely defined if T and P are specified. This observation motivated studies of the effect of pressure on the dielectric α- and β-processes in a number of systems in the early 1960s (171–174). The main concern in these pioneering studies was to unravel the effect of pressure on separating mixed processes.

However, since then and until only recently, the lack of a versatile experimental setup has put a halt in these studies and made pressure, for a number of years, the "forgotten" variable. During the past 20 years, polymer chemistry has produced an unparalleled number of polymeric compounds with unmatched physical properties ranging from polymer blends with a well-defined thermodynamic

state to block copolymers with well-controlled nanostructures. Moreover, the interest in traditional fields such as polymer crystallization has been rejuvenated through the possibility of new experimental probes and novel synthesis. Pressure, however, was not applied up until recently in systems where the thermodynamic state of the system is of importance.

Herein an example of current interest is provided, where the thermodynamic state of the system play a dominant role in polymer dynamics. The example consists of studying the effect of pressure on the local and global chain dynamics (175,176).

The effect of pressure on the local segmental dynamics and on sub-T_g relaxations has been studied in detail (172–174). It was found that pressure exerts a stronger influence on the segmental as compared to the local sub-T_g relaxations and is the right variable if a separation of the two modes is needed. On the other hand, the effect of pressure on the global chain dynamics that control the flow regime and thus of interest in polymer processing only recently has started to be explored.

Herein the results of recent studies (175,176) are reviewed, treating the effect of pressure on the segmental and chain dynamics as a function of polymer molecular weight. The polymer is PI, which has been extensively studied before as a function of temperature for different molecular weights. Being a Type-A polymer (according to Stockmayers classification) it has components of the dipole moment both parallel and perpendicular to the chain, giving rise, respectively, to end-to-end vector and local segmental dynamics. The aim is to investigate the effect of P on M_e. This question is not only of fundamental importance but has industrial implications as well (ie, in polymer processing). For this purpose five *cis*-PIs have been used: PI-1200, PI-2500, PI-3500, PI-10600, and PI-26000, with the numbers indicating number-average molecular weights and with polydispersity of less than 1.1. The entanglement molecular weight of PI is 5400; thus the first three samples are not entangled.

The molecular weight dependence of the segmental and longest normal modes are shown in Figure 31 in the different samples as a function of pressure, at 320 K. Notice that the segmental modes (through the higher apparent activation volume) exhibit a stronger P-dependence than the corresponding normal modes. At any given P, the longest normal mode times exhibit a weak molecular weight dependence for $M < M_e$ ($\tau \sim M^2$) and a stronger dependence for $M > M_e$ ($\tau \sim M^{3.4}$). Notice the additional molecular weight dependence for the smaller molecular weights due to chain-end effects. Nevertheless, increasing pressure does not change significantly the picture from atmospheric pressure and this signifies that there is a minor, if any, dependence of M_e on P.

The main results can be summarized as follows. The spectral shape of the normal modes and of the segmental mode is invariant under variation of T and P. However, both time–temperature superposition and time–pressure superposition of the entire spectrum fails because of the higher sensitivity of the segmental mode to T and P variations, respectively. The former has been discussed in earlier sections (71,72,79,126,128). The latter results from the higher activation volume for the segmental mode. The activation volume of the segmental mode for the different molecular weights exhibits a strong T-dependence and scales as $T-T_g$. Lastly, M_e does not show a significant P-dependence.

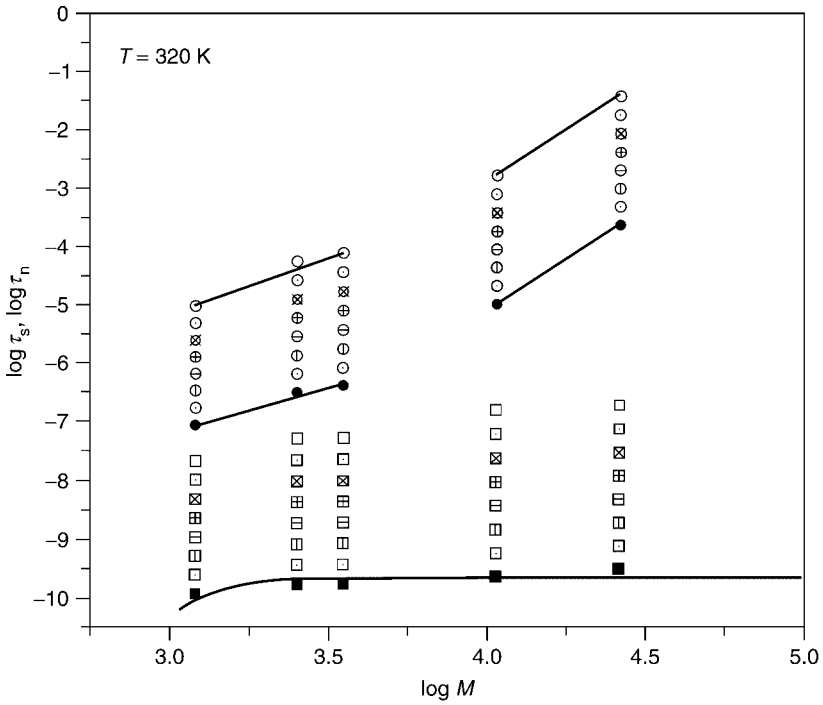

Fig. 31. Molecular weight dependence of the segmental (□) and longest normal mode (○) for the five PIs investigated, plotted for different pressures at 320 K. The shortest time corresponds to the data at 1 bar and the rest are interpolated data shown at intervals of 0.5 kbar. The line through the segmental times at atmospheric pressure is a guide for the eye.

BIBLIOGRAPHY

"Amorphous Polymers" in *EPSE* 2nd ed., Vol. 1, pp. 789–842, by I. Voight-Martin, Johannes Gutenberg Universität, and J. Wendorff, Deutsches Kunststoff-Insititut.

1. P. J. Flory, *Statistical Mechanics of Chain Molecules*, John Wiley & Sons, Inc., New York, 1969.
2. P. G. de Gennes, *Scaling Concepts in Polymer Physics*, Cornell University Press, Ithaca, NY, 1979.
3. L. I. Komarov and I. Z. Fisher, *Soviet Phys. JETP* **16**, 1358 (1963).
4. R. Pecora, *J. Chem. Phys.* **40**, 1604 (1964).
5. H. Z. Cummins, N. Knable, and Y. Yeh, *Phys. Rev. Lett.* **12**, 150 (1964).
6. B. Chu, *Laser Light Scattering*, Academic Press, Inc., New York, 1974.
7. B. J. Berne and R. Pecora, *Dynamic Light Scattering*, John Wiley & Sons, Inc., New York, 1976.
8. W. Brown, *Light Scattering: Principles and Development*, Clarendon Press, Oxford, 1996.
9. G. Floudas, A. K. Rizos, W. Brown, and K. L. Ngai, *Macromolecules* **27**, 2719 (1994).
10. A. K. Rizos, R. M. Johnsen, W. Brown, and K. L. Ngai, *Macromolecules* **28**, 5450 (1995).
11. H. C. Anderson and R. Pecora, *J. Chem. Phys.* **54**, 2584 (1971).
12. A. K. Rizos, G. Fytas, and J. C. Roovers, *J. Chem. Phys.* **97**, 6925 (1992).
13. A. K. Rizos, G. Fytas, T. P. Lodge, and K. L. Ngai, *J. Chem. Phys.* **95**, 2980 (1991).
14. A. K. Rizos and K. L. Ngai, *Macromolecules* **27**, 7076 (1994).

15. A. K. Rizos and K. L. Ngai, *Macromolecules* **31**, 6217 (1998).
16. M. Doi and S. F. Edwards, *The Theory of Polymer Dynamics*, Oxford Science Publications, Oxford, 1986.
17. K. Zero and R. Pecora, *Dynamic Light Scattering, Applications of Photon Correlation Spectroscopy*, Plenum Press, New York, 1985.
18. C. H. Wang, *Mol. Phys.* **41**, 541 (1980).
19. A. K. Rizos and K. L. Ngai, *Phys. Rev. B* **46**, 8126 (1992).
20. A. K. Rizos, *Polymer* **37**, 5743 (1996).
21. C. H. Wang, *Spectroscopy of Condensed Media*, Academic Press, Inc., New York, 1985.
22. G. D. Patterson, *J. Polym. Sci., Polym. Phys. Ed.* **14**, 741 (1976); *J. Polym. Sci., Polym. Phys. Ed.* **15**, 579 (1977).
23. G. D. Patterson, in R. Pecora, ed., *Dynamic Light Scattering*, Academic Press, Inc., New York, 1986, Chapt. "6", p. 260.
24. L. Giebel G. Meier, G. Fytas, and E. W. Fischer, *J. Polym. Sci. Phys.* **15**, 579 (1992).
25. R. D. Mountain, *J. Res. Nalt. Bur. Stand. (U.S.)* **70A**, 207 (1966).
26. R. D. Mountain, *Rev. Mod. Phys.* **38**, 205 (1966).
27. A. K. Rizos, T. Jian, and K. L. Ngai, *Macromolecules* **28**, 517 (1995).
28. G. D. Patterson, *J. Non-Cryst. Sol.* **31**, 109 (1978).
29. G. D. Patterson, C. P. Lindsey, and J. R. Stevens, *J. Chem. Phys.* **70**, 643 (1979).
30. G. Fytas and K. L. Ngai, *Macromolecules* **21**, 804 (1988).
31. K. L. Ngai, D. J. Plazek, and A. K. Rizos, *J. Polym. Sci., Polym. Phys. Ed.* **35**, 599 (1997).
32. A. Guinier, *X-ray Diffraction*; W. H. Freeman and Co., New York, 1963.
33. J. H. Wendorf and E. W. Fischer, *Kolloid Z. Z. Polym.* **251**, 876 (1973,).
34. J. H. Wendorf and E. W. Fischer, *Kolloid Z. Z. Polym.* **251**, 884 (1973).
35. J. Rathjie and W. Ruland, *Colloid Polym. Sci.* **254**, 358 (1976).
36. W. Wiegand and W. Ruland, *Progr. Colloid Polym. Sci.* **66**, 355 (1979).
37. J. J. Curro, and R.-J. Roe, *J. Polym. Sci.* **21**, 1785 (1983).
38. R.-J. Roe, *J. Chem. Phys.* **79**, 936 (1983).
39. R.-J. Roe and J. J. Curro, *Macromolecules* **16**, 428 (1983).
40. J. J. Curro and R.-J. Roe, *Polymer* **25**, 1424 (1984).
41. R.-J. Roe and H.-H. Song, *Macromolecules* **18**, 1603 (1985).
42. G. Floudas, T. Pakula, M. Stamm, and E. W. Fischer, *Macromolecules* **26**, 1671 (1993).
43. E. W. Fischer et al. *Makromol. Chem.* **12**(suppl.), 189 (1985).
44. G. Floudas, T. Pakula, and E. W. Fischer, *Macromolecules* **27**, 917 (1994).
45. E. W. Fischer, *Physica A* **201**, 183 (1993).
46. E. W. Fischer, Ch. Becker, J.-U. Hagenau, and G. Meier, *Progr. Colloid Polym. Sci.* **80**, 198 (1989).
47. B. Gerharz, G. Meier, and E. W. Fischer, *J. Chem. Phys.* **92**, 7110 (1990).
48. E. W. Fischer, G. Meier, T. Rabenau, A. Patkowski, W. Steffen, and W. J. Thonnes, *J. Non-Cryst. Solids* **131–133**, 134 (1991).
49. E. W. Fischer, A. Patkowski, and E. Eckstein, *Macromol. Symp.* **124**, 1 (1997).
50. T. Kanaya, A. Patkowski, E. W. Fischer J. Seils, H. Glaser, and K. Kajia, *Acta Polym.* **45**, 137 (1994).
51. L. R. Miller, R. F. Boyer, and J. J. Heijober, *Polym. Sci., Polym. Phys. Ed.* **22**, 2021 (1984).
52. G. R. Mitchell, in S. E. Keinath, R. L. Miller, and J. K. Rieke, eds., *Order in Amorphous Polymers*, Plenum Press, New York, 1987.
53. R. L. Miller and R. F. Boyre, *J. Polym. Sci., Polym. Phys. Ed.* **22**, 2043 (1984).
54. G. Floudas, unpublished results (2001).
55. G. Floudas and P. Stepanek, *Macromolecules* **31**, 6951 (1998).
56. G. Floudas, P. Placke, P. Stepanek, W. Brown, G. Fytas, and K. L. Ngai, *Macromolecules* **28**, 6799 (1995).

57. A. P. Sokolov A. Kisliuk, M. Soltwisch, and D. Quitmann, *Phys. Rev. Lett.* **69**, 1540 (1992).
58. L. Borjesson A. K. Hassan, J. Swenson, and L. M. Torell, *Phys. Rev. Lett.* **70**, 1275 (1993).
59. R. Bohmer, K. L. Nagi, C. A. Angell, and D. J. Plazek, *J. Chem. Phys.* **99**, 4201 (1993).
60. C. A. Bero, Universal Creep Behavior of Amorphous Materials Near Their Glass Temperature, Ph. D. dissertation, University of Pittsburgh, 1994.
61. R. Greiner and F. R. Schwarzl, *Rheol. Acta* **23**, 378 (1984).
62. J. D. Ferry, *Viscoelastic Properties of Polymers*, 3rd ed., John Wiley & Sons, Inc., New York, 1980.
63. D. J. Plazek, *Methods of Experimental Physics*, Vol. **16**, Part C: Polymers, Academic Press, Inc., New York, 1990, Chapt. "11".
64. R. W. Whorlow, *Rheological Techniques*, 2nd ed., E. Harwood, New York, 1992.
65. A. A. Collyer, ed., *Techniques in Rheological Measurement*, Chapman and Hall, London, 1993.
66. A. A. Collyer and D. W. Clegg, eds. *Rheological Measurement*, Elsevier Applied Science, London, 1988.
67. B. E. Read and G. D. Dean, *The Determination of Dynamic Properties of Polymers and Composites*, John Wiley & Sons, Inc., New York, 1978.
68. A. You, Malkin, A. A. Ashadsky, V. V. Kovriga, and A. E. Chalykh, *Experimental Methods of Polymer Physics*, Prentice-Hall, Inc., Englewood Cliffs, N.J., 1983.
69. D. J. Plazek, *J. Phys. Chem.* **69**, 3480–3487 (1965).
70. D. J. Plazek, *Polymer J.* **12**, 43–53 (1980).
71. K. L. Ngai and D. J. Plazek, in J. E. Mark, ed., *Physical Properties of Polymer Handbook*, AIP Press, Woodbury, N.Y., 1996, Chapt. "25".
72. K. L. Ngai and D. J. Plazek, *Rubber Chem. Techol., Rubber Rev.* **68**, 376 (1995); D. J. Plazek, *J. Rheol.* **40**, 987 (1996).
73. D. L. Plazek and D. J. Plazek, *Macromolecules* **16**, 1469 (1983).
74. P. G. Santangelo, C. M. Roland, and K. L. Ngai, *Macromolecules* **29**, 3651 (1996).
75. X. Qiu, N. E. Moe, M. D. Ediger, and L. J. Fetters, *J. Chem. Phys.* **113**, 2918 (2000).
76. E. Donth and K. Schneider, *Acta Polym.* **36**, 273–278 (1985).
77. P. G. Santangelo, K. L. Ngai, and C. M. Roland, *Macromolecules* **26**, 2682–2687 (1993).
78. D. J. Plazek I. C. Chay, K. L. Ngai, and C. M. Roland, *Macromolecules* **28**, 6432–6436 (1995).
79. K. L. Ngai, D. J. Plazek, and A. K. Rizos, *J. Polym. Sci., Part B: Polym. Phys.* **35**, 599–614 (1997).
80. E. R. Fitzgerald, L. D. Grandine, and J. D. Ferry, *J. Appl. Phys.* **24**, 640, 911 (1953)
81. D. J. Plazek and A. J. Chelko Jr., *Polymer* **18**, 15–18, (1977).
82. G. C. Berry and T. G Fox, *Adv. Polym. Sci.* **5**, 261–357 (1968).
83. W. W. Graessley, *Adv. Polym. Sci.* **16**, 1–179 (1974).
84. V. R. Allen and T. G Fox, *J. Chem. Phys.* **41**, 337–343 (1964).
85. F. Bueche, *Physical Properties of Polymers*, Wiley-Interscience, New York, 1962, p. 70.
86. T. G. Fox and V. R. Allen, *J. Chem. Phys.* **41**, 344–352 (1964).
87. J. P. Montfort, G. Marin, and P. Monge, *Macromolecules* **17**, 1551 (1984).
88. H. Watanabe, T. Sakamoto, and T. Kotaka, *Macromolecules* **18**, 1008–1015 (1985).
89. D. J. Plazek, C. Seoul, and C. A. Bero, *J. Non-Cryst. Solids* **131–133**, 570–578 (1991).
90. G. C. Berry and D. J. Plazek, in D. R. Uhlmann and N. Kreidl, eds., *Glass Science and Technology*, Vol. **3**, Academic Press, Inc., New York, 1986.
91. B. E. Read, P. E. Tomlins, and G. D. Dean, *Polymer* **31**, 1204 (1990).
92. K. L. Ngai, I. Echeverria, and D. J. Plazek, *Macromolecules* **29**, 7937 (1997).
93. D. J. Plazek, C. Bero, S. Neumeister, G. Floudas, G. Fytas, and K. L. Ngai, *Colloid Polym. Sci.* **272**, 1430 (1994).
94. P. E. Rouse Jr., *J. Chem. Phys.* **21**, 1272–1280 (1953).

95. J. D. Ferry, R. F. Landel, and M. L. Williams, *J. Appl. Phys.* **26**, 359–362 (1955).
96. M. L. Williams, *J. Polym. Sci.* **62**, 57 (1962).
97. A. K. Rizos, K. L. Ngai, and D. J. Plazek, *Polymer* **38**, 6103 (1997).
98. D. J. Plazek, *J. Polym. Sci.*, Part A-2 **6**, 621 (1968).
99. J. Y. Cavaille, C. Jordan, J. Perez, L. Monnerie, and G. P. Johari, *J. Polym. Sci., Part B: Polym. Phys.* **25**, 1235 (1987).
100. R. Connelly (*unpublished*) see Ref. 72.
101. L. I. Palade, V. Verney, and P. Attené, *Macromolecules* **28**, (1995).
102. M. L. Williams and J. D. Ferry, *J. Colloid Sci.* **10**, 474 (1955).
103. D. J. Plazek, M. J. Rosner, and D. L. Plazek, *J. Polym. Sci., Part B: Polym. Phys.* **26**, 473 (1988).
104. S. J. Orbon and D. J. Plazek, *J. Polym. Sci., Polym. Phys. Ed.* **17**, 1871 (1979)
105. D. J. Plazek and V. M. O'Rourke, *J. Polym. Sci., Part A-2* **9**, 209–243 (1971).
106. N. Raghupathi, Ph.D. dissertation, University of Pittsburgh, 1975.
107. E. Riande, N. Nemoto, and M. Kurata, *J. Polym. Sci.: Symp.* **50**, 405–430 (1975).
108. D. J. Plazek, R. G. Smith, and M. Murata, *J. Polym. Sci., Polym. Phys. Ed.* **17**, 2189–2213 (1979).
109. L. R. G. Treloar, *The Physics of Rubber Elasticity*, 2nd ed., Oxford University Press, London 1958.
110. A. V. Tobolsky, J. J. Aklonis, and G. Akovali, *J. Polym. Sci.* **42**, 723–728 (1965).
111. H. Odani, N. Nemoto, and M. Kurata, *Bull. Inst. Chem. Res. Kyoto ehniv.* **50**, 117 (1972).
112. H. Leaderman, R. G. Smith, and L. C. Williams, *J. Polym. Sci.* **36**, 233–257 (1959).
113. D. J. Plazek and P. K. Agarwal, in Proc. VII Int. Cong. on Rheology, Gothenburg, Sweden, 1976, p. 488.
114. W. W. Graessley and J. Roovers, *Macromolecules* **12**, 959–965 (1979).
115. C. A. Bero and D. J. Plazek, *J. Polym. Sci., Part B: Polym. Phys.* **29**, 39–47 (1991).
116. T. Smith, Private Communication.
117. E. N. da C. Andrade, *Proc. R. Soc. London, Ser. A* **84**, 1 (1910).
118. A. V. Tobolsky, *J. Appl. Phys.* **27**, 673 (1956).
119. J. D. Ferry, in H. A. Stuart, ed., *Die Physik der Hochpolymeren*, Vol. **IV**, Springer-Verlag, Berlin, 1956, p. 389, Figure VI. 13.
120. J. D. Ferry, *Macromolecules* **24**, 5237 (1991).
121. D. J. Plazek, X. D. Zheng, and K. L. Ngai, *Macromolecules* **25**, 4920 (1992).
122. K. L. Ngai, D. J. Plazek, and C. Bero, *Macromolecules* **26**, 1065 (1993).
123. R. W. Gray, G. Harrison, and J. Lamb, *Proc. R. Soc. London, A Ser.* **356**, 77 (1977).
124. J. Cochrane, G. Harrison, J. Lamb, and D. W. Phillips, *Polymer* **21**, 837 (1980).
125. D. J. Plazek, C. Bero, S. Neumeister, G. Floudas, G. Fytas, and K. L. Ngai, *Colloid Polym. Sci.* **272**, 1430 (1994).
126. D. J. Plazek, A. Schönhals, E. Schlosser, and K. L. Ngai, *J. Chem. Phys.* **98**, 6488 (1993).
127. K. M. Bermatz, Viscoelastic Properties of Inorganic Glasses, Ph.D. dissertation, University of Pittsburgh, 2000.
128. K. L. Ngai, A. Schönhals, and E. Schlosser, *Macromolecules* **25**, 4915 (1992).
129. N. G. McCrum, B. E. Read, and G. Williams, *Anelastic and Dielectric Effects in Polymeric Solids*, John Wiley & Sons, Inc., London, 1967.
130. G. Williams, *Adv. Polym. Sci.* **33**, 60 (1979).
131. M. E. Baur and W. H. Stockmayer, *J. Chem. Phys.* **43**, 4319 (1965).
132. K. Adachi and T. Kotaka, *Prog. Polym. Sci.* **18**, 585 (1993).
133. D. Boesse, D. F. Kremer, and L. J. Fetters, *Macromolecules* **23**, 1826 (1990).
134. D. W. Davidson and R. H. Cole, *J. Chem. Phys.* **18**, 1417 (1950); *J. Chem. Phys.* **19**, 1484 (1951).
135. S. Havriliak and S. Negami, *J. Polym. Sci., Polym. Symp.* **14**, 89 (1966).

136. R. Kohlrausch, *Pogg. Ann. Phys.* **12**, 393 (1847); *Pogg. Ann. Phys.* IV **56**, 79 (1954).
137. G. Williams and D. C. Watts, *Trans. Faraday Soc.* **66**, 80 (1971).
138. K. L. Ngai, *J. Non-Cryst. Solids* **7**, 275 (2000).
139. R. Nozaki and S. Mashimo, *J. Chem. Phys.* **84**, 3575 (1986).
140. F. Stickel, Untersuchung der Dynamik in niedermolekularen Flüssigkeiten mit Dielektrischer Spectroscopie, Ph.D. dissertation, Johannes Gutenburg University, Mainz, Germany, Shaker, Aachen, 1995.
141. C. K. Hall and E. Helfand, *J. Chem. Phys.* **77**, 3275 (1982).
142. R. W. Rendell and K. L. Ngai, *J. Non-Cryst. Solids* **131–133**, 942 (1991).
143. S. Mashimo, H. Nakamura, and A. Chiba, *J. Chem. Phys.* **76**, 6342 (1982); S. Mashimo and A. Chiba, *Polym. J.* **5**, 41 (1973).
144. G. Fytas, Th. Dorfmueller and B. Chu, *J. Polym. Sci., Polym. Phys. Ed.* **22**, 1471 (1981); K. L. Ngai and G. Fytas, *J. Polym. Sci., Polym. Phys. Ed.* **24**, 1683 (1986).
145. G. Fytas, G. Floudas, and K. L. Ngai, *Macromolecules* **23**, 1104 (1990).
146. C. H. Wang and E. W. Fischer, *J. Chem. Phys.* **82**, 632 (1985).
147. K. L. Ngai, S. Mashimo, and G. Fytas, *Macromolecules* **21**, 3030 (1988).
148. H. Takeuchi and R. J. Roe, *J. Chem. Phys.* **94**, 7446, 7458 (1991).
149. R. J. Roe, D. Rigby, H. Furuya, and H. Takeuchi, *Comp. Polym. Sci.* **2**, 32 (1992).
150. K. L. Ngai, *J. Chem. Phys.* **98**, 7588 (1993).
151. I. Alig, F. Stieber, A. D. Bakhramov, Yu. S. Manucharov, and V. A. Solovyev, *Polymer* **30**, 842 (1989).
152. G. Floudas, G. Fytas, and I. Alig, *Polymer* **32**, 2307 (1991).
153. K. Schmidt-Rohr and H. W. Spiess, *Multidimensional Solid State NMR and Polymers*, Academic Press, Inc., London, 1994.
154. H. W. Spiess, *J. Non-Cryst. Solids* **131–133**, 766 (1991).
155. S. Kauffmann, S. Wefing, D. Schaefer, and S. W. Spiess, *J. Chem. Phys.* **93**, 197 (1990).
156. M. L. Williams, R. F. Landel, and J. D. Ferry, *J. Am. Chem. Soc.* **77**, 3701 (1955).
157. F. Mezei, *J. Non-Cryst. Solids* **131–133**, 317 (1991).
158. F. Frick, R. Zorn, D. Richter, and B. Farago, *J. Non-Cryst. Solids* **131–133**, 169 (1991).
159. D. Richter, A. J. Dianoux, W. Petry, and J. Teixeria Springer Proc. In Physics, Vol. **37**: eds. *Dynamics of Disordered Materials*, Springer, Berlin, 1989.
160. I. Hodge, *J. Res. Natl. Inst. Stand. Technol.* **102**, 195 (1997).
161. http://web.utk.edu/~athas/databank/intro.html.
162. N. O. Birge, *Phys. Rev. B* **34**, 1631 (1986).
163. J. Korus et al. *Thermochim. Acta* **304/305**, 99 (1997); M. Beiner et al. *Macromoleules* **29**, 5183 (1996).
164. S. J. Tao, *J. Chem. Phys.* **56**, 5499 (1972).
165. M. Eldrup, D. Lightbody, and J. N. Sherwood, *Chem. Phys.* **63**, 51 (1981).
166. H. Nakanishi and H. Ujihira, *J. Phys. Chem.* **86**, 4446 (1982).
167. H. Nakanishi, S. J. Wang, and Y. C. Jean, in S. C. Sharma, ed., Proc. Positron Annihilation in Liquids, World Scientific Publishers, Singapore, 1987, p. 292.
168. H. A. Hristov, B. A. Bolan, A. F. Yee, L. Xie, and D. W. Gidley *Macromolecules* **29**, 8507 (1996).
169. A. Uedono, T. Kawano, S. Tanigawa, M. Ban, M. Kyoto, and T. Uozumi, *J. Polym. Sci., Part B: Polym. Phys.* **35**, 1601 (1997).
170. J. Bartos, P. Bandzuch, O. Sausa, K. Kristiakova, J. Kristiak, T. Kanaya, and W. Jenninger, *Macromolecules* **30**, 6906 (1997); J. Bartos and J. Kristiak, *J. Non-Cryst. Solids* **235–237**, 293 (1998).
171. G. Williams, *Adv. Polym. Sci.* **33**, 60 (1979).
172. H. Sasabe and S. Saito, *J. Polym. Sci.*, Part A-2 **6**, 1401 (1968).
173. H. Sasabe and S. Saito, *J. Polym. Sci.*, Part A-2 **6**, 1401 (1968).
174. G. Wiliams, *Trans. Faraday Soc.* **60**, 1548 (1964); *Trans. Faraday Soc.* **60**, 1556 1964.

175. G. Floudas and T. Reisinger, *J. Chem. Phys.* **111**, 5201 (1999).
176. G. Floudas, C. Gravalides, T. Reisinger, and G. J. Wegner, *J. Chem. Phys.* **111**, 9847 (1999).

K. L. NGAI
Naval Research Laboratory
G. FLOUDAS
University of Ioannina
Foundation for Research and Technology-Hellas, Institute of Electronic Structure and Laser
D. J. PLAZEK
University of Pittsburgh
A. K. RIZOS
University of Ioannina
Foundation for Research and Technology-Hellas, Institute of Electronic Structure and Laser
University of Crete

ANIONIC POLYMERIZATION

Introduction

This article describes the general aspects of anionic polymerization of vinyl, carbonyl, and heterocyclic monomers. Polymerizations involving multicomponent catalyst systems (coordinated anionic polymerization) are not discussed. Anionic polymerization is a chain reaction polymerization in which the active species is formally an anion, ie, an atom or group with a negative charge and an unshared pair of electrons. Anions can be considered to be the conjugate bases of the corresponding acids, as shown in the following equation. The stability and reactivity of anionic species can be deduced from pK_a values for the equilibria depicted in this equation for the corresponding conjugate acid. The more acidic conjugate acids (lower pK_a values) are associated with a correspondingly more stable anionic species.

$$\mathrm{A{-}H} \overset{K_a}{\rightleftharpoons} \mathrm{A^-} + \mathrm{H^+} \qquad (1)$$

In general, these anions are associated with a counterion, typically an alkali metal cation. The exact nature of the anion can be quite varied depending on the structure of the anion, counterion, solvent, and temperature. The range of possible species is depicted in terms of a Winstein spectrum of structures as shown in equation 2 for a carbanionic chain end (R^-). In addition to the aggregated (**1**) and unassociated (**2**) species, it is necessary to consider the intervention of free ions (**5**) and the contact (**3**) and solvent-separated (**4**) ion pairs; Mt^+ represents a metallic counterion such as an alkali metal cation (1). In hydrocarbon media, species (**1–3**) would be expected to predominate. Polar solvents tend to shift the Winstein

Encyclopedia of Polymer Science and Technology. Copyright John Wiley & Sons, Inc. All rights reserved.

spectrum to the right, ie, toward more reactive, less associated, more ionic species. With respect to the nature of the bonding in organoalkali metal compounds, it is generally agreed that the carbon–alkali metal bond is ionic for sodium, potassium, rubidium, and cesium. For carbon–lithium bonds, however, there is disagreement regarding the relative amount of covalent versus ionic bonding (1–3). One unique aspect of anionic polymerization is that the reactive propagating species are not transient intermediates. Carbanions and organometallic species can be prepared and investigated independently of the polymerization process. These species can also be characterized during the polymerization.

$$\underset{1}{(RMt)_n} \rightleftharpoons \underset{2}{n\,RMt} \rightleftharpoons \underset{3}{R^-,Mt^+} \rightleftharpoons \underset{4}{R^-//\,Mt^+} \rightleftharpoons \underset{5}{R^-} + Mt^+ \qquad (2)$$

Living Anionic Polymerization

A *living polymerization* is a chain polymerization that proceeds in the absence of the kinetic steps of termination and chain transfer (4,5). For living anionic polymerization of vinyl monomers, the propagating species is a carbanion associated with the corresponding counterion, as shown in the scheme below. Living polymerizations provide versatile methodologies for the preparation of macromolecules with well-defined structures and low degrees of compositional heterogeneity. Using these methodologies it is possible to synthesize macromolecular compounds with control of a wide range of compositional and structural parameters including molecular weight, molecular weight distribution, copolymer composition and microstructure, stereochemistry, branching, and chain-end functionality. Anionic polymerization is the archetype of a living polymerization and it embodies the following defining characteristics of living polymerizations (6).

(1) *Initiation*

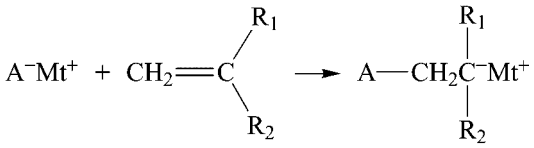

(2) *Propagation*

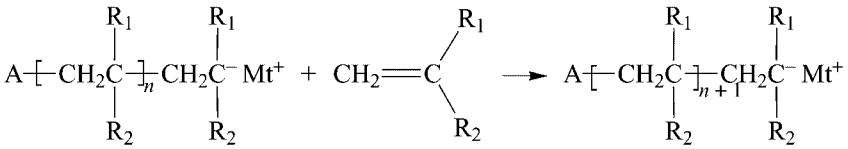

(3) *Deliberate termination* (no spontaneous termination)

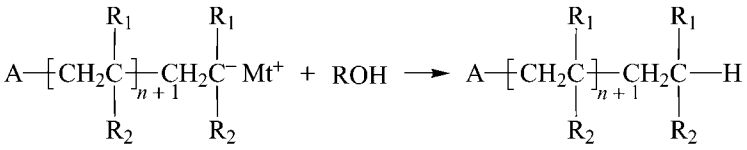

Molecular Weight. The number-average molecular weight (M_n) in living anionic polymerization is a simple function of the stoichiometry and the degree of conversion of the reaction since one polymer is formed for each initiator molecule. The expected number-average molecular weight can be calculated, as shown in equation 3, as a function of conversion.

$$M_n = \text{grams of monomer consumed/moles of initiator} \tag{3}$$

From a practical point of view, polymers can be prepared with predictable molecular weights ranging from $\approx 10^3$ to $> 10^6$ g/mol using living anionic polymerizations. The ability to predict and control molecular weight depends critically on the absence of significant amounts of terminating species that react with the initiator, decrease the effective number of molecules of initiator, and thus increase the observed molecular weight relative to the calculated molecular weight.

Molecular Weight Distribution. In principle, it is possible to prepare a polymer with a narrow molecular weight distribution (Poisson distribution) by using living polymerization when the rate of initiation is competitive with or faster than the rate of propagation (5,7). This condition ensures that all of the chains grow for essentially the same period of time. The relationship between the polydispersity and the degree of polymerization for a living polymerization is shown in equation 4:

$$X_w/X_n = 1 + \left[X_n/(X_n+1)^2\right] \approx 1 + (1/X_n) \tag{4}$$

The second approximation is valid for high molecular weights. The Poisson distribution represents the ideal limit for termination-free polymerizations. Thus, it is predicted that the molecular weight distribution will become narrower with increasing molecular weight for a living polymerization system. Broader molecular weight distributions are obtained using less active initiators, with mixtures of initiators or with continuous addition of initiator as involved in a continuous flow, stirred tank reactor. Thus, living polymerizations can form polymers with broader molecular weight distributions. It has been proposed that a narrow molecular weight distribution (monodisperse) polymer should exhibit $M_w/M_n \leq 1.1$ (8).

Block Copolymers. One of the important aspects of living polymerizations is that since all chains retain their active centers when the monomer has been consumed, addition of a second monomer will form a diblock copolymer (9–11). Sequential addition of monomer charges can generate diblocks such as A—B, triblocks such as A—B—A, A—B—C, and even more complex multiblock structures. In principle, each block can be prepared with controlled molecular weight and narrow molecular weight distribution.

Chain-End Functionalized Polymers. In principle, the propagating carbanionic center that remains at the end of the polymerization can react with a variety of electrophilic species to incorporate functional groups (—X) at the chain end, as shown in equation 5 (12–14):

$$P^- + X—Y \text{ (electrophilic reagent)} \longrightarrow P—X + Y^- \quad (5)$$

Methods have been reported and tabulated for the synthesis of a diverse array of functional end groups.

An alternative methodology for the synthesis of functionalized polymers using living anionic polymerization is the use of functionalized initiators (15,16). If a functional group (or a suitably protected functional group) is incorporated into the initiator, then that functional group will be at the initiating end of every polymer molecule, as shown below:

(1) *Initiation*

$$X—I^- + M \longrightarrow X—I—M^-$$

(2) *Propagation*

$$X—I—M^- + n\,M \longrightarrow X—I—\left[M\right]_n—M^-$$

(3) *Termination*

$$X—I—\left[M\right]_n—M^- \longrightarrow X—P$$

where X is the functional group in the initiating species $X—I^-$ and X—P is the α-functionalized polymer. In principle, this method can quantitatively produce functionalized polymers with controlled molecular weights and narrow molecular weight distributions.

Star-Branched Polymers. An extension of the concept of controlled termination reactions is the ability to prepare star-branched polymers by post-polymerization reactions with multifunctional linking reagents as shown in equation 6, where L is a linking agent of functionality n (17–20):

$$n\,P^* + L \longrightarrow (P)_nL \quad (6)$$

For example, termination of a living anionic polymerization with a tetrafunctional electrophile such as silicon tetrachloride will produce a four-armed star polymer as shown in equation 7. Given that PLi is a well-defined living polymer, a branched polymer with a predictable, well-defined structure will be formed from the linking reaction.

$$4\,PLi + SiCl_4 \longrightarrow (P)_4Li + 4\,LiCl \quad (7)$$

A variety of linking agents with variable functionalities have been described and tabulated in the literature (11,18,19).

General Considerations

Monomers. Two broad types of monomers can be polymerized anionically: vinyl, diene, and carbonyl-type monomers with difunctionality provided by one or more double bonds; and cyclic (eg, heterocyclic) monomers with difunctionality provided by a ring that can open by reaction with nucleophiles. For vinyl monomers, there must be substituents on the double bond that can stabilize the negative charge that develops in the transition state for monomer addition, as shown in equation 8:

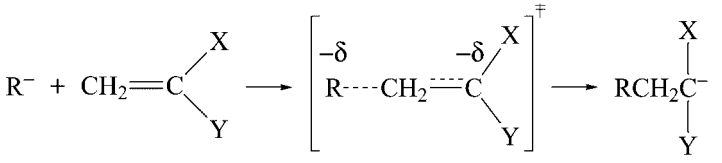

(8)

These substituents must also be stable to the anionic chain ends; thus, relatively acidic, proton-donating groups (eg, amino, hydroxyl, carboxyl, acetylene functional groups) or strongly electrophilic functional groups that can react with bases and nucleophiles must not be present or must be protected by conversion to a suitable derivative. In general, substituents that stabilize the negative charge by anionic charge delocalization render vinyl monomers polymerizable by an anionic mechanism. Such substituents include aromatic rings, double bonds, as well as carbonyl, ester, cyano, sulfoxide, sulfone, and nitro groups. The general types of monomers that can be polymerized anionically without the incursion of termination and chain-transfer reactions include styrenes, dienes, methacrylates, vinylpyridines, aldehydes, epoxides, episulfides, cyclic siloxanes, lactones, and lactams. Monomers with polar substituents such as carbonyl, cyano, and nitro groups often undergo side reactions with initiators and propagating anions; therefore, controlled anionic polymerization to provide high molecular weight polymers is generally not possible. Many types of polar monomers can be polymerized anionically, but do not produce living, stable, carbanionic chain ends. These types of polar monomers include acrylonitriles, cyanoacrylates, propylene oxide, vinyl ketones, acrolein, vinyl sulfones, vinyl sulfoxides, vinyl silanes, halogenated monomers, ketenes, nitroalkenes, and isocyanates.

The simplest vinyl monomer, ethylene, although it has no stabilizing moiety, can be polymerized by an anionic mechanism using butyllithium complexed with *N*,*N*,*N*′,*N*′-tetramethylethylenediamine (TMEDA) as a complexing ligand. The conversion of a double bond to two single bonds provides the energetic driving force for this reaction. Because of the insolubility of the crystalline, high density polyethylene formed by anionic polymerization, the polymer precipitates from solution during the polymerization.

Solvents. The choice of suitable solvents for anionic polymerization is determined in part by the reactivity (basicity and nucleophilicity) of initiators and propagating anionic chain ends. For styrene and diene monomers, the solvents of

choice are alkanes and cycloalkanes, aromatic hydrocarbons, and ethers; the use of alkenes has also been described, although chain transfer can occur. Aromatic hydrocarbon solvents provide enhanced rates of initiation and propagation relative to the alkanes; however, chain transfer reactions can occur with alkylated aromatic solvents, eg, toluene.

Polar solvents such as ethers and amines react with organometallic initiators, as well as propagating polystyryl and polydienyl carbanions, to decrease the concentration of active centers (21–23). The rate of reaction with ethers decreases in the order Li > Na > K. For example, dilute solutions of poly(styryl)lithium in tetrahydrofuran (THF) at room temperature decompose at the rate of a few percent each minute. Alkyllithium initiators also react relatively rapidly with ethers; the order of reactivity of organolithium compounds with ethers is tertiary RLi > secondary RLi > primary RLi > phenyllithium > methyllithium > benzyllithium (21). An approximate order of reactivity of ethers toward alkylithium compounds is dimethoxyethane, THF > tetrahydropyran> diethyl ether> diisopropyl ether. Tertiary amines can also react with alkyllithium compounds. The importance of these reactions can be minimized by working at lower temperatures (eg, $<0^{\circ}$C); it is also advisable to use only the minimum amounts of ethers and other Lewis bases required as additives.

For less reactive anionic chain ends such as those involved in the propagation of heterocyclic monomers, a wider range of solvents can be utilized. For example, dipolar aprotic solvents such as dimethylsulfoxide (DMSO), *N*,*N*-dimethylformamide (DMF), and hexamethylphosphoramide (HMPA) can be used for polymerizations of epoxides.

Initiation

A useful guide to choose an appropriate initiator for anionic polymerization of a given monomer is that the initiator should have a reactivity (stability) similar to that of the propagating anionic species (23,24). If the initiator is too reactive, then side reactions are promoted. If the initiator is relatively unreactive, the initiation reaction may be slow or inefficient.

The stabilities of anionic initiators can be deduced from the pK_a values of the corresponding conjugate acids as shown in equation 1 (25). Monomer reactivity in anionic polymerization can be categorized in terms of the stability of the anions formed by nucleophilic addition or ring opening as deduced from the pK_a values for the conjugate acids of these anions. Thus, those monomers that form the least stable anions, ie, have the largest values of pK_a for the corresponding conjugate acids, are the least reactive monomers in anionic polymerization; in turn, these less reactive monomers require the use of the most reactive, organometallic initiators as shown in Table 1. Initiators can be classified in terms of their mechanisms of initiation: (*1*) initiation by electron transfer (alkali and alkaline-earth metals and radical anions) and (*2*) nucleophilic addition. The following sections discuss each of these initiator types.

Initiation by Electron Transfer.

Alkali Metals. The direct use of alkali metals and alkaline-earth metals as initiators for anionic polymerization of diene monomers as first reported in 1910

Table 1. Relationships between Monomer Reactivity, Carbanion Stability, and Suitable Initiators[a,b]

Monomer type	pK_a DMSO	pK_a H_2O	Initiators[c]
Ethylene	56		RLi
Dienes	44		NH_2^-, RLi, RMt
Styrenes	43		Naphthalene radical anions[d], cumyl K, Mt
Acrylonitrile	32		RMgX
Alkyl methacrylates	30–31	27–28	Fluorenyl$^-$, Ar_2RC^-, ketyl radical anions[e]
Vinyl ketones	26	19	
Oxiranes	29–32	16–18	RO^-
Thiiranes	17	12–13	
Nitroalkenes	17	10–14	
Siloxanes		10–14	RO^-, OH^-
Lactones	12	4–5	RCO_2^-
Cyanoacrylates	11		HCO_3^-, H_2O
Vinylidene cyanide	11	11	

[a] Ref. 24.
[b] pK_a of the conjugate acid of the anionic propagating intermediate.
[c] Mt refers generally to alkali metals (Li, Na, K, Rb, Cs).
[d] For example, naphthalene radical anion$^{\bullet -}$ $Li^+/Na^+/K^+$.
[e] $Ar_2CO^{\bullet -}$.

is primarily of historical interest because these are uncontrolled, heterogeneous processes (4). One of the most significant developments in anionic vinyl polymerization was the discovery reported in 1956 by Stavely and co-workers (26) at Firestone Tire and Rubber Co. that polymerization of neat isoprene with lithium dispersion produced high *cis*-1,4-polyisoprene, similar in structure and properties to *Hevea* natural rubber. This discovery led to the development of commercial anionic solution polymerization processes using alkyllithium initiators.

The mechanism of the anionic polymerization of styrenes and 1,3-dienes initiated by alkali metals has been described in detail (27). Initiation is a heterogeneous process occurring on the surface of the metal (Mt) by reversible transfer of an electron to adsorbed monomer (M), as shown in the following scheme:

$$\mathrm{Mt} + \mathrm{M} \rightleftharpoons \mathrm{Mt}^+, \mathrm{M}^{\cdot -}$$

$$2\ \mathrm{Mt}^+, \mathrm{M}^{\cdot -} \longrightarrow \mathrm{Mt}^+, {}^-\mathrm{M}\text{—}\mathrm{M}^-, \mathrm{Mt}^+$$

$$\mathrm{Mt}^+, {}^-\mathrm{M}\text{—}\mathrm{M}^-, \mathrm{Mt}^+ + n\ \mathrm{M} \longrightarrow \mathrm{Mt}^+, {}^-\mathrm{M}\text{—}\left[\mathrm{M}\right]_n\text{—}\mathrm{M}^-, \mathrm{Mt}^+$$

The initially formed radical anions ($M^{\bullet -}$) rapidly dimerize to form dianions. Monomer addition to these dianions forms adsorbed oligomers that desorb and continue chain growth in solution. Unlike homogeneous anionic initiation processes with organometallic compounds, this heterogeneous initiation reaction continues to generate new active chain ends during the course of the subsequent propagation reactions. Consequently, there is little control of molecular weight, and relatively broad molecular weight distributions have been reported for the

soluble polymer obtained from these bulk polymerizations (M_w/M_n = 3–10) (28); formation of a high degree of branching and gel content (45%) have also been reported for these processes (26,28).

Alkali metals can dissolve in solvating media such as ethers and amines to form blue solutions of solvated electrons. In the presence of strongly complexing ligands such as crown ethers or cryptands, electrides (complexed alkali cation and electron) or nuclides (complexed alkali cation and alkali metal anion) can be formed as shown below (29):

$$2\ Mt \overset{\text{crown ether or cryptand}}{\rightleftharpoons} [Mt^+]Mt^- \text{ (Nuclide)}$$

$$Mt \overset{\text{crown ether or cryptand}}{\rightleftharpoons} [Mt^+]e^- \text{ (Electride)}$$

Nuclides have been shown to react with monomers such as styrene and methyl methacrylate to form intermediate dianions that are rapidly protonated by the solvent THF to form the monoanion initiating species, as shown below (30,31):

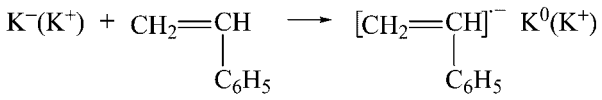

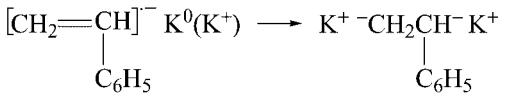

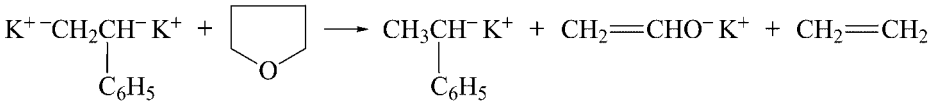

For the nuclide-initiated polymerization of methyl methacrylate, although there was good agreement between calculated and observed molecular weights, the molecular weight distributions were broad (M_w/M_n = 1.2–1.6) (31).

Radical Anions. Many aromatic hydrocarbons react reversibly with alkali metals in polar aprotic solvents to form stable, homogeneous solutions of the corresponding radical anions, as shown in equation 9 (4,27).

$$M + Ar \rightleftharpoons Ar^{\cdot -}Mt^+ \text{ (Mt = Li, Na, K, Rb, Cs)} \quad (9)$$

Radical anions can only be formed efficiently in polar aprotic solvents such as THF and glymes. Aromatic radical anions such as sodium naphthalene react with monomers such as styrene by reversible electron transfer to form the corresponding monomer radical anions, as shown in the following scheme (R = H):

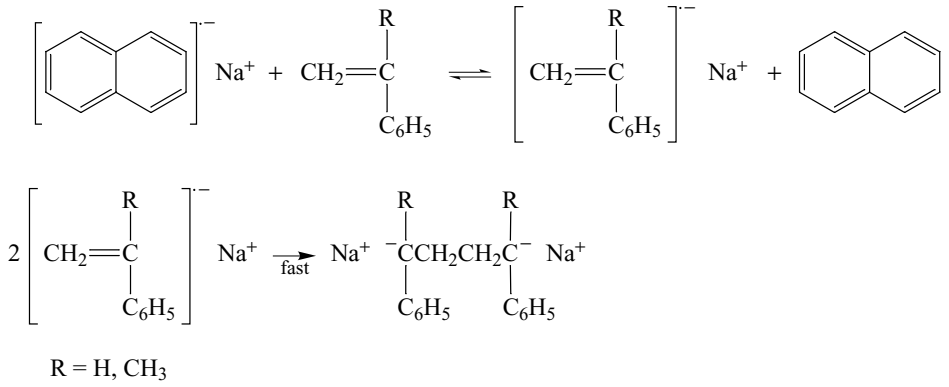

R = H, CH_3

Although the equilibrium between the radical anion of the monomer and the aromatic radical anion lies far to the left because of the low electron affinity of the monomer, this is an efficient initiation process because the resulting monomer radical anions rapidly undergo tail-to-tail dimerization reactions with rate constants that approach diffusion control.

The reactions of monomers with aromatic radical anions or directly with alkali metals can be used to prepare oligomeric dianionic initiators from monomers such as α-methylstyrene that have accessible ceiling temperatures ($T_c = 61^\circ C$) (32), as shown in the above scheme (R = CH_3). Dimers or tetramers can be formed depending on the alkali metal system, temperature, and concentration.

Monomers that can be polymerized with aromatic radical anions include styrenes, dienes, epoxides, and cyclosiloxanes. For epoxides and cyclosiloxanes, the mechanism of initiation involves nucleophilic addition of the radical anion to these monomers, as shown below, in contrast to the electron transfer mechanism occurring for hydrocarbon monomers (see previous scheme).

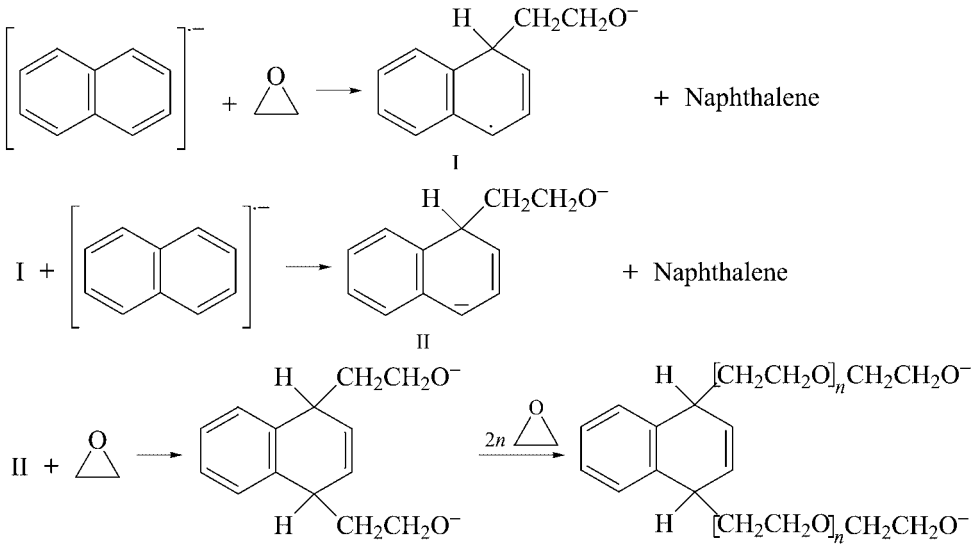

Initiation by Nucleophilic Addition.

Alkyllithium Compounds. Although anionic polymerization of vinyl monomers can be effected with a variety of organometallic compounds, alkyllithium compounds are the most useful class of initiators (1,21,24,33). A variety of simple alkyllithium compounds are readily available commercially in hydrocarbon solvents such as hexane and cyclohexane. They can be prepared by reaction of the corresponding alkyl chlorides with lithium metal.

Alkyllithium compounds are generally associated into dimers, tetramers, or hexamers in hydrocarbon solution (2,21). The degree of association is related to the steric requirements of the alkyl group; ie, the degree of association decreases as the steric requirements of the alkyl group increase.

The relative reactivities of alkyllithiums as polymerization initiators are intimately linked to their degree of association, as shown below, with the average degree of association in hydrocarbon solution, where known, indicated in brackets after the alkyllithium (2,23,33):

(1) *Styrene polymerization*:

Menthyllithium [2] > *s*-C_4H_9Li [4] > *i*-C_3H_7Li [4–6] > *i*-C_4H_9Li > *n*-C_4H_9Li [6] > *t*-C_4H_9Li [4]

(2) *Diene polymerization*:

Menthyllithium [2] > *s*-C_4H_9Li [4] > *i*-C_3H_7Li [4–6] > *t*-C_4H_9Li [4] > *i*-C_4H_9Li > *n*-C_4H_9Li [6]

In general, the less associated alkyllithiums are more reactive as initiators than the more highly associated species.

Alkyllithium initiators are primarily used as initiators for polymerizations of styrenes and dienes (see Table 1). They effect quantitative, living polymerization of styrenes and dienes in hydrocarbon solution. In general, these alkyllithium initiators are too reactive for alkyl methacrylates and vinylpyridines (see Table 1). *n*-Butyllithium is used commercially to initiate anionic homopolymerization and copolymerization of butadiene, isoprene, and styrene with linear and branched structures. Because of its high degree of association (hexameric), *n*-butyllithium-initiated polymerizations are often effected at elevated temperatures (>50°C) to increase the rate of initiation relative to propagation and thus to obtain polymers with narrower molecular weight distributions (34).

sec-Butyllithium is used commercially to prepare styrene—diene block copolymers because it can initiate styrene polymerization rapidly as compared to propagation so that even polystyrene blocks with relatively low molecular weights (10,000–15,000 g/mol) can be prepared with stoichiometric control and narrow molecular weight distributions.

Alkyllithiums react quite differently with cyclic sulfides compared to the normal nucleophilic ring-opening reaction with epoxides (35,36). Ethyllithium reacts with 2-methylthiacyclopropane to generate propylene and lithium ethanethiolate. The resulting lithium ethanethiolate is capable of initiating polymerization of 2-methylthiacyclopropane.

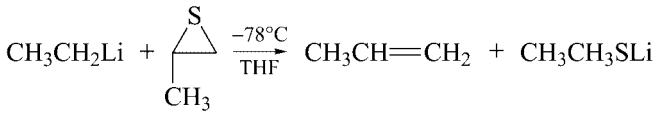

(10)

In contrast, ethyllithium reacts with 2-methylthiacyclobutane to form an alkyllithium product that is capable of initiating polymerization of styrene.

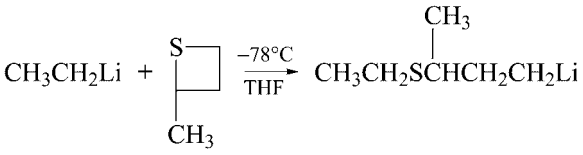

(11)

Organoalkali Initiators. In general, the simple organoalkali metal derivatives other than lithium are not soluble in hydrocarbon media. However, higher homologues of branched hydrocarbons are soluble in hydrocarbon media. The reaction of 2-ethylhexyl chloride and sodium metal in heptane produces soluble 2-ethylhexylsodium (37). This initiator copolymerizes mixtures of styrene and butadiene to form styrene—butadiene copolymers with high (55–60%) vinyl microstructure (38,39).

Cumyl potassium ($pK_a \approx 43$ based on toluene) is a useful initiator for anionic polymerization of a variety of monomers, including styrenes, dienes, methacrylates, and epoxides. This carbanion is readily prepared from cumyl methyl ether, as shown in equation 12, and is generally used at low temperatures in polar solvents such as THF.

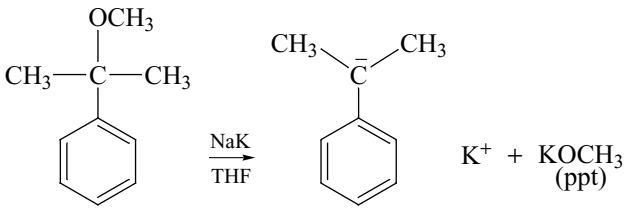

(12)

Difunctional Initiators. Aromatic radical anions, such as lithium naphthalene or sodium naphthalene, are efficient difunctional initiators (see scheme under Radical Anions). However, the need to use polar solvents for their formation limits their utility for diene polymerization since the unique ability of lithium to provide high 1,4-polydiene microstructure is lost in polar media. The methodology for preparation of hydrocarbon-soluble, dilithium initiators is generally based on the reaction of an aromatic divinyl precursor with 2 moles of butyllithium. Unfortunately, because of the tendency of organolithium chain ends in hydrocarbon solution to associate and form electron-deficient dimeric, tetrameric, or hexameric aggregates, most attempts to prepare dilithium initiators in hydrocarbon media have generally resulted in the formation of insoluble, three-dimensionally associated species (40).

The reaction of *m*-diisoproprenylbenzene with 2 moles of *t*-butyllithium in the presence of 1 equiv of triethylamine in cyclohexane at −20°C has been reported to form pure diadduct without oligomerization (eq. 13) (41). This initiator in the presence of 5 vol% of diethyl ether for the butadiene block has been used to prepare well-defined poly(methyl methacrylate)-*block*-polybutadiene-*block*-poly(methyl methacrylate).

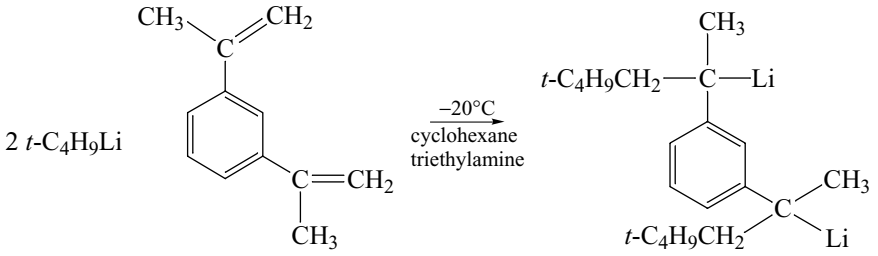

(13)

The reaction of pure *m*-divinylbenzene with *sec*-butyllithium in toluene at −49°C in the presence of triethylamine ($[(C_2H_5)_3N]/[Li] = 0.1$) has been reported to produce the corresponding dilithium initiator in quantitative yield (42). Polymerization of butadiene with this initiator in toluene at −78°C produced well-defined polybutadiene with high 1,4-microstructure (87%).

A useful, hydrocarbon-soluble, dilithium initiator has been prepared by the dimerization of 1,1-diphenylethylene with lithium in cyclohexane in the presence of anisole (15 vol%) as shown in equations 14 and 15 (43). Although the initiator was soluble in this mixture, it precipitated from solution when added to the polymerization solvent (cyclohexane or benzene). Therefore, the dilithium initiator was chain extended with approximately 30 units of isoprene to generate the corresponding soluble oligomer. This initiator was used to prepare well-defined polystyrene-*block*-polyisoprene-*block*-polystyrene and poly(α-methylstyrene)-*block*-polyisoprene-*block*-poly(α-methylstyrene) triblock copolymers with >90% 1,4-microstructure by sequential monomer addition.

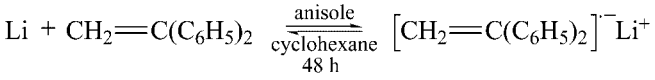

(14)

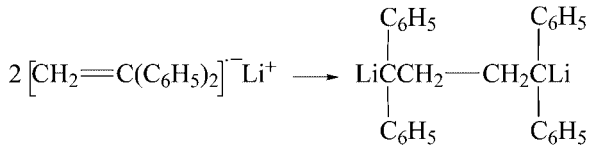

(15)

The addition reaction of 2 mol of *sec*-butyllithium with 1,3-bis(1-phenylethenyl)benzene (eq. 16) proceeds rapidly and efficiently to produce the corresponding dilithium species that is soluble in toluene or in cyclohexane (24,44). Although this dilithium initiator is useful for the preparation of homopolymers

and triblock copolymers with relatively narrow molecular weight distributions, it is necessary to add a small amount of Lewis base or ≥2 equiv of lithium alkoxide (eg, lithium *sec*-butoxide) to produce narrow, monomodal molecular weight distributions.

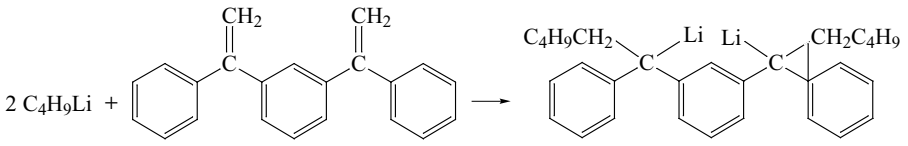

(16)

Functionalized Initiators. Alkyllithium initiators that contain functional groups provide versatile methods for the preparation of end-functionalized polymers and macromonomers (15,16). For a living anionic polymerization, each functionalized initiator molecule will produce one macromolecule, with the functional group from the initiator residue at one chain end and the active anionic propagating species at the other chain end. However, many functional groups such as hydroxyl, carboxyl, phenol, and primary amine are not stable in the presence of reactive dienyllithium and styryllithium chain ends. Therefore, it is necessary to convert these functional groups into suitable derivatives, ie, protected groups, that are stable to the carbanionic chain ends and that can be removed readily after the polymerization. Examples of protected functional initiators include the hydroxyl-protected initiators, 1-lithium-6-(1-ethoxyethoxy)hexane, 6-(*t*-butyldimethylsiloxy)hexyllithium, and 3-(*t*-butyldimethylsiloxy)propyllithium, as well as a primary amine-protected initiator, 4-*bis*(trimethylsily)aminophenyllithium (45).

1,1-Diphenylmethylcarbanions. The carbanions based on diphenylmethane ($pK_a = 32$) (see Table 1) are useful initiators for vinyl and heterocyclic monomers, especially alkyl methacrylates at low temperatures (46). 1,1-Diphenylalkyllithiums can also efficiently initiate the polymerization of styrene and diene monomers that form less stable carbanions. Diphenylmethyllithium can be prepared by the metalation reaction of diphenylmethane with butyllithium or by the addition of butyllithium to 1,1-diphenylethylene, as shown in equation 17. This reaction can also be utilized to prepare functionalized initiators by reacting butyllithium with a substituted 1,1-diphenylethylene derivative. Addition of lithium salts such as lithium chloride, lithium *t*-butoxide, or lithium 2-(2-methoxyethoxy)ethoxide with 1,1-diphenylmethylcarbanions and other organolithium initiators has been shown to narrow the molecular weight distribution and to improve the stability of active centers for anionic polymerization of both alkyl methacrylates and *t*-butyl acrylate (47,48).

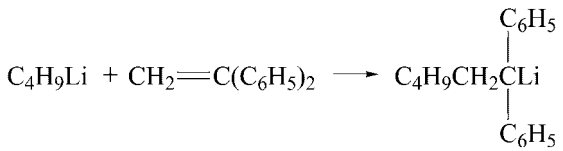

(17)

Fluorenyl Carbanions. Salts of fluorene ($pK_a \approx 23$) are more hindered and less reactive than many other organometallic initiators. Fluorenyl carbanions can be readily formed by metalation of fluorenes with alkali metal derivatives, as shown in equation 18. Carbanion salts of 9-methylfluorene are preferable to fluorene, since the latter generate chain ends that contain reactive, acidic fluorenyl hydrogens that can participate in chain transfer reactions. Fluorenyl salts are useful initiators for the polymerization of alkyl methacrylates, epoxide, and thiirane monomers.

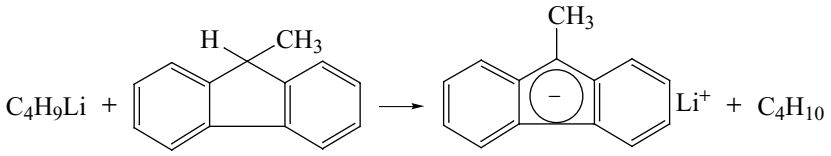

(18)

Styrene and Diene Monomers

Kinetics of Polymerization.

Initiation Kinetics. The mechanism of initiation of anionic polymerization of vinyl monomers with alkyllithium compounds and other organometallic compounds is complicated by association and cross-association phenomena in hydrocarbon solvents and by the presence of a variety of ionic species in polar media (4,27,33,49). The kinetics of initiation are complicated by competing propagation and the occurrence of cross-association of the alkyllithium initiator with the propagating organolithium (50). Thus, only the initial rates provide reliable kinetic data.

Typical kinetics of the initiation reaction of *n*-butyllithium with styrene in benzene exhibit a first-order dependence on styrene concentration and approximately a one-sixth-order dependence on *n*-butyllithium concentration, as shown in equation 19.

$$R_i = k_i(K_d/6)^{1/6}[C_4H_9Li]_o^{1/6}[M] \tag{19}$$

Since *n*-butyllithium is aggregated predominantly into hexamers in hydrocarbon solution, the fractional kinetic order dependency of the initiation process on the total concentration of initiator has been rationalized on the basis that unassociated *n*-butyllithium is the initiating species and that it is formed by the equilibrium dissociation of the hexamer as shown below:

$$(n\text{-}C_4H_9Li)_6 \overset{K_d}{\rightleftharpoons} 6\ n\text{-}C_4H_9Li \tag{20}$$

$$n\text{-}C_4H_9Li + CH_2{=}CH(C_6H_5) \xrightarrow{k_i} n\text{-}C_4H_9{-}CH_2CHLi(C_6H_5) \tag{21}$$

The kinetic order for *sec*-butyllithium-initiated polymerization of styrene is close to 0.25 in benzene solution; this result is also consistent with initiation by unassociated *sec*-butyllithium, since *sec*-butyllithium is associated predominantly into tetramers in benzene solution.

The frequent coincidence of the fractional order with the degree of association supports the postulate that the initiating species is a small amount of reactive monomeric alkyllithium in equilibrium with the much larger concentration of the unreactive aggregated species. However, the correctness of this interpretation, ie, direct dissociation to monomeric, unassociated species, has been questioned (33). The experimentally observed energies of activation, eg, 75 kJ/mol (18 kcal/mol) for *n*-butyllithium initiation of styrene polymerization (51), appear to be too low to include the enthalpy of complete dissociation of the aggregates, which is estimated to require approximately 452 kJ/mol (108 kcal/mol) (52). An alternative is the incomplete or stepwise dissociation of the aggregate, for example, as shown in equations 22–25 for hexamers; equation 25 plus equation 24 would apply for tetramers.

$$(RLi)_6 \rightleftharpoons (RLi)_5 + RLi \tag{22}$$

$$(RLi)_6 \rightleftharpoons (RLi)_4 + (RLi)_2 \tag{23}$$

$$(RLi)_2 \rightleftharpoons 2\,RLi \tag{24}$$

$$(RLi)_4 \rightleftharpoons 2\,(RLi)_2 \tag{25}$$

In aliphatic solvents the inverse correspondence between reaction order dependence for alkyllithium and degree of organolithium aggregation is not observed (49). In addition, the rates of initiation in aliphatic solvents are several orders of magnitude less than in aromatic solvents. Most reaction orders for alkyllithium initiators in aliphatic solvents are close to unity. These results suggest that in aliphatic solvents the initiation process may involve the direct addition of monomer with aggregated organolithium species (eq. 26) to form a cross-associated species.

$$(RLi)_n + M \longrightarrow [(RLi)_{n-1}(RMLi)] \tag{26}$$

The formation of cross-associated species would be expected to complicate the kinetics and lead to variable reaction orders as a function of conversion. The observation of pronounced induction periods has been ascribed to the enhanced reactivity of the mixed (ie, cross-associated) aggregated species. The effects of cross-association provide at least a partial explanation for the discrepancies reported in the literature for the kinetic order dependencies on alkyllithium initiator concentration; thus, only in the initial stages is it likely that a detailed interpretation of the mechanism is possible.

Lewis bases and alkali metal alkoxides have been used as additives to modify the initiation reaction with alkyllithium compounds. In the presence of THF, the

initiation reaction kinetics of styrene with *sec*-butyllithium exhibit a first-order dependence on alkyllithium concentration. Lewis bases such as ethers and amines, when present in amounts comparable to the initiator concentration, dramatically increase the relative rate of initiation of styrene and diene polymerizations relative to propagation.

The effect of lithium alkoxides on alkyllithium-initiated polymerizations is important because these salts are ubiquitously present to some extent as impurities formed by the reactions with oxygen (13) (eq. 27) and hydroxylic impurities (eq. 28). In fact, it is common practice to utilize excess butyllithium, ie, more than the stoichiometric amount required to generate the required molecular weight, to scavenge impurities in the solvent and monomer feed.

$$RLi + O_2 \longrightarrow R{-}R + RO_2R + ROOH + ROH \quad (27)$$

$$RLi + R'OH \longrightarrow R{-}H + R'OLi \quad (28)$$

The effects of lithium alkoxides on the rates of alkyllithium-initiation reactions depend on the solvent, the monomer, the alkoxide structure, the alkyllithium initiator, and the ratio of [RLi]/[LiOR′] (49,50). For *n*-butyllithium initiation of styrene in cyclohexane, the rate of initiation is increased at low relative concentrations of added lithium alkoxide [t-C_4H_9OLi]/[C_4H_9Li]< 0.5). At a ratio of 1/1, the rate is essentially the same as the control without alkoxide; beyond this ratio, the rate decreases continuously with increasing relative concentration of lithium alkoxide. In aromatic solvents, the initiation rate decreases with increasing relative concentrations of lithium alkoxide. Lithium alkoxides generally accelerate the rate of initiation by alkyllithiums (*n*-butyllithium and *sec*-butyllithium) for isoprene in hexane.

Propagation Kinetics. The kinetics of propagation for styrene and diene monomers in hydrocarbon solvents with lithium as the counterion is complicated by chain-end association (49,50,53). The kinetics of propagation can be investigated independently of initiation so that complications from cross-association with the initiator are absent. The reaction order dependence of the propagation rate on active center concentration is independent of the identity of the hydrocarbon solvent, aromatic or aliphatic, although the relative propagation rates, under equivalent conditions, are faster in aromatic versus aliphatic solvents.

Styrene Monomers. The anionic propagation kinetics for styrene (S) polymerization with lithium as counterion is relatively unambiguous. The reaction order in monomer concentration is first order as it is for polymerization of all styrene and diene monomers in heptane, cyclohexane, benzene, and toluene. The reaction order dependence on total chain-end concentration, $[PSLi]_o$, is one-half as shown in equation 29:

$$R_p = -d[S]/dt = k_{obs}[PSLi]_o^{1/2}[S] \quad (29)$$

The observed one-half kinetic order dependence on chain-end concentration is consistent with the fact that poly(styryl)lithium is predominantly associated into

dimers in hydrocarbon solution. If the unassociated poly(styryl)lithium is the reactive entity for monomer addition, a simple dissociative mechanism can be invoked (equations 30 and 31). This mechanism leads to the kinetic equation shown in equation 32.

$$(\mathrm{PSLi})_2 \overset{K_\mathrm{d}}{\rightleftharpoons} 2\ \mathrm{PSLi} \tag{30}$$

$$\mathrm{PSLi} + \mathrm{S} \xrightarrow{K_\mathrm{p}} (\mathrm{PS})\mathrm{SLi} \tag{31}$$

From equations 30 and 31, it can be seen that the observed rate constant for propagation, k_{obs}, is actually a composite of the propagation rate constant, k_p, and the equilibrium constant for dissociation of the dimeric aggregates, K_d, raised to the one-half power (eq. 32).

$$\begin{aligned} R_\mathrm{p} &= -\,\mathrm{d[S]}/\mathrm{d}t = k_\mathrm{p}[\mathrm{PSLi}][\mathrm{S}] \\ &= k_\mathrm{p}(K_\mathrm{d}/2)^{1/2}[\mathrm{PSLi}]_\mathrm{o}^{1/2}[\mathrm{S}] \\ &= k_\mathrm{obs}[\mathrm{PSLi}]_\mathrm{o}^{1/2}[\mathrm{S}] \end{aligned} \tag{32}$$

The measurement of the dissociation constants of the aggregates is difficult because of the low concentration of the unassociated species; thus, it is generally not possible to obtain directly a value for the propagation rate constant k_p (see, however, Refs. 54–56).

In contrast to this simple interpretation, the kinetic order dependence on chain-end concentration for propagation of styrene and *o*-methoxystyrene in toluene with alkyllithium initiators varies from 0.62 to 0.66 (56). Furthermore, recent neutron scattering data indicate that poly(styryl)lithium in benzene solution exhibits concentration-dependent degrees of aggregation involving predominantly dimers and tetramers, as well as small amounts of large-scale aggregates (57). These results suggest that the actual mechanism of propagation may be much more complicated than that depicted in equations 30 and 31 (see, however, Ref. 58).

A comparison of the observed propagation rate constants for styrene polymerization with different alkali metal counterions is shown in Table 2. Poly(styryl)sodium was presumably associated into dimers since kinetic orders of one-half were observed for the rate dependence on the active chain-end concentration. Poly(styryl)potassium exhibits intermediate behavior; dependence on chain-end concentration was one-half order at higher concentrations, but first order at low concentrations. Poly(styryl)rubidium and poly(styryl)cesium exhibit first-order dependencies on chain-end concentrations which is consistent with unassociated chain ends in cyclohexane. The counterion dependence is $K^+ > Rb^+ > Cs^+ \gg Li^+$ in cyclohexane and $K^+ > Na^+ > Li^+$ in benzene. The interpretation of these results is complicated by the fact that the complex observed rate constants (k_{obs}) reflect both the fact that the dissociation constant for the dimers increases with increasing cation size (no association for rubidium and cesium) and also the fact that the requisite energy associated with charge separation in the transition state would be less for the larger counterions.

Table 2. Kinetic Parameters for Styrene Propagation in Hydrocarbon Solvents[a]

Counterion	Solvent	Temperature, °C	$[k_p(K_D/n)^{1/n}]$ (k_{obs}), $L^{1/n}/(mol^{1/n}\cdot s)$
Lithium	Benzene	30	1.55×10^{-2}
Lithium	Cyclohexane	40	2.4×10^{-2}
Sodium	Benzene	30	17×10^{-2}
Potassium	Benzene	30	180×10^{-2}
Potassium	Cyclohexane	40	30
Rubidium	Cyclohexane	40	22.5[b]
Cesium	Cyclohexane	40	19[b]

[a]Ref. 49.

[b]Propagation rate constant presumably for the unassociated species (see eq. 32); first-order dependence on active chain-end concentration observed.

Diene Monomers. The delineation of the mechanism of propagation of isoprene and butadiene in hydrocarbon solution with lithium as counterion is complicated by disagreement in the literature, regarding both the kinetic order dependence on chain-end concentration and the degree of association of the chain ends, as well as by apparent changes in kinetic reaction orders with chain-end concentration (53). For butadiene and isoprene propagation, reported reaction order dependencies on the concentration of poly(dienyl)lithium chain ends include 0.5, 0.33, 0.25, and 0.167. Kinetic studies of isoprene propagation with lithium as counterion in hydrocarbon solvents showed that the kinetic order dependence on chain-end concentration changed from 0.5 to either 0.25 or 0.17 as the chain-end concentration was varied from 10^{-2} to 10^{-6} mol/L (53,59,60). Comparison of these kinetic orders with the degrees of association of the poly(dienyl)lithium chain ends is complicated by the lack of agreement regarding the predominant degree of association of these species in hydrocarbon solution. Predominant degrees of association of both 2 and 4 have been reported by different research groups using the same techniques, ie, concentrated solution viscometry and light scattering (61–64). Recent evaluation of the association states of poly(butadienyl)lithium chain ends in benzene by small-angle neutron scattering, as well as both dynamic and static light scattering, indicates that dimeric and tetrameric aggregates are in equilibrium with higher order aggregates ($n > 100$) (65,66).

Relative Reactivities of Styrene and Dienes. The relative reactivities of dienes *versus* styrenes depend on the chain-end concentrations because of the differences in kinetic order dependencies on chain-end concentration. The relative rates of propagation at [PLi] $= \approx 10^{-3}$ M are in the order styrene > isoprene > butadiene. However at [PLi] $\leq \approx 10^{-4}$ M, isoprene propagates faster than styrene (53).

Effects of Lewis Bases. The addition of small amounts of Lewis bases such as ethers and tertiary amines generally increases the rate of propagation in alkyllithium-initiated polymerizations. These Lewis bases decrease the average degree of association of the polymeric organolithium aggregates as determined by concentration solution viscosity measurements. In contrast, addition of strongly coordinating Lewis bases such as N,N,N',N'-tetramethylethylenediamine and pentamethyldiethylenetriamine can either increase or decrease the reaction rate for alkyllithium propagation of isoprene relative to hydrocarbon solution, depending on the chain-end concentration (67). This situation arises from the

different reaction order dependencies on chain-end concentration, ie, 0.3 in hydrocarbon solution compared to 1.1 for the stoichiometric Lewis base complexes. The addition of lithium alkoxides generally decreases the rate of propagation, while addition of other alkali metal alkoxides increases the rate of polymerization in hydrocarbon solution.

Polar Solvents. A change in the reaction medium from hydrocarbon to polar solvent causes changes in the nature of the alkali metal carbanions that can be interpreted in terms of the Winstein spectrum of ionic species, as shown below (68,69). Thus, in addition to the aggregated (**1**) and unassociated (**2**) species that can exist in hydrocarbon solution, in polar solvents it is necessary to consider the intervention of free ions (**5**) and the contact (**3**) and solvent-separated (**4**) ion-paired carbanion species, as shown below:

$$\begin{array}{ccccccccc} (RMt)_n & \rightleftharpoons & n\,RMt & \rightleftharpoons & R^-,Mt^+ & \rightleftharpoons & R^- \,//\, Mt^+ & \rightleftharpoons & R^- + Mt^+ \\ \mathbf{1} & & \mathbf{2} & & \mathbf{3} & & \mathbf{4} & & \mathbf{5} \\ \downarrow k_1[M] & & \downarrow k_2[M] & & \downarrow k_3[M] & & \downarrow k_4[M] & & \downarrow k_5[M] \end{array} \qquad (33)$$

In general, as the polarity and solvating ability of the medium increases, more ionic species (a shift in the Winstein spectrum from left to right) are formed. In addition, each different chain-end species can react with monomer with its own unique rate constant.

In weakly polar solvents such as dioxane ($\varepsilon = 2.21$), the kinetics of styrene propagation exhibit pseudo-first-order kinetics as illustrated in equation 34, where k_{obs} is the observed pseudo-first-order rate constant, k_p is the propagation rate constant, and $[PS^-Mt^+]$ represents the concentration of carbanionic chain ends that does not change for a living polymerization.

$$-d[S]/dt = k_{obs}[S] = k_p[PS^-Mt^+][S] \qquad (34)$$

The values of k_p can be obtained by plotting k_{obs} versus $[PS^-Mt^+]$. The order of reactivity [rate constants in brackets are in units of L/(mol·s)] of alkali metal counterions is Li [0.9] < Na [3.4–6.5] < K [20–34] < Cs [5–24] (27). The trend of increasing reactivity with increasing ionic radius, as also observed in hydrocarbon solution, has been taken as evidence for contact ion pairs as the reactive propagating species. Similar behavior has been observed for isoprene polymerization in diethyl ether ($\varepsilon = 4.34$); the propagation rate constant assigned to the lithium contact ion pair is 3.2 L/(mol·s) (70).

In more polar solvents such as THF ($\varepsilon = 7.6$), a concentration dependence was observed for the plots of k_{obs} versus $[PS^-Mt^+]$; ie, k_p exhibits a linear dependence of $1/[PS^-Mt^+]^{1/2}$ (27). This dependence has been interpreted in terms of the participation of both ion pairs and free ions as active propagating species, as shown below:

$$\begin{array}{ccccc} R^-,Mt^+ & \overset{K_{diss}}{\rightleftharpoons} & R^- & + & Mt^+ \\ \downarrow k_{\pm}[M] & & \downarrow k_-[M] & & \end{array} \qquad (35)$$

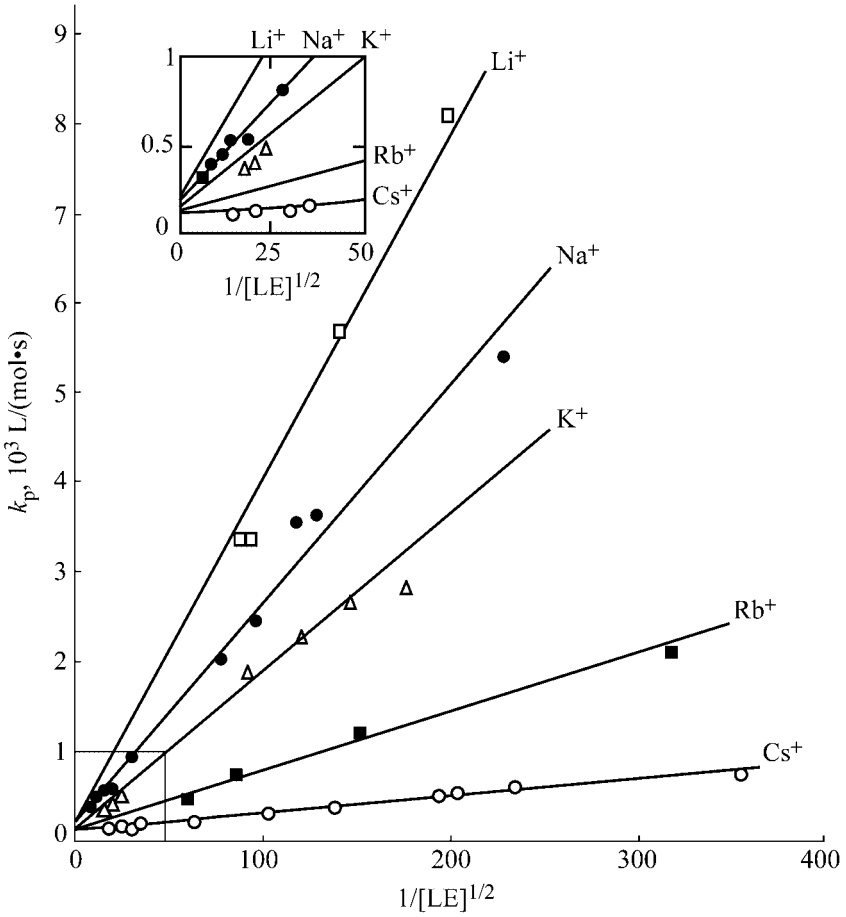

Fig. 1. Plots of the propagation constant k_p for salts of living polystyrene in THF vs $1/[LE]^{1/2}$. □ Li^+; ● Na^+; △ K^+; ■ Rb^+; ○ Cs^+. $T = 25°C$. From Ref. 27; reprinted by permission of Springer-Verlag.

where $k_\pm$ is the propagation rate constant for the ion pair species, k_- is the propagation rate constant for the free ion, and K_{diss} is the equilibrium constant for dissociation of ion pairs to free ions. The corresponding expression for k_p is shown below, recognizing that this k_p is only an apparent propagation rate constant.

$$k_p = k_\pm + k_- K_{diss}^{1/2}/[P^- Mt^+]^{1/2} \tag{36}$$

Plots of the apparent propagation rate constant versus $1/[P^- Mt^+]^{1/2}$ are shown in Figure 1. From this figure it can be deduced that the slopes of the lines decrease as the cation size increases from lithium to cesium. Since k_- is independent of the cation, the variation of the slope with counterion reflects a decrease in K_{diss} as the counterion size increases. This is consistent with independent measures of the dissociation constants for free ion formation from both conductometric and

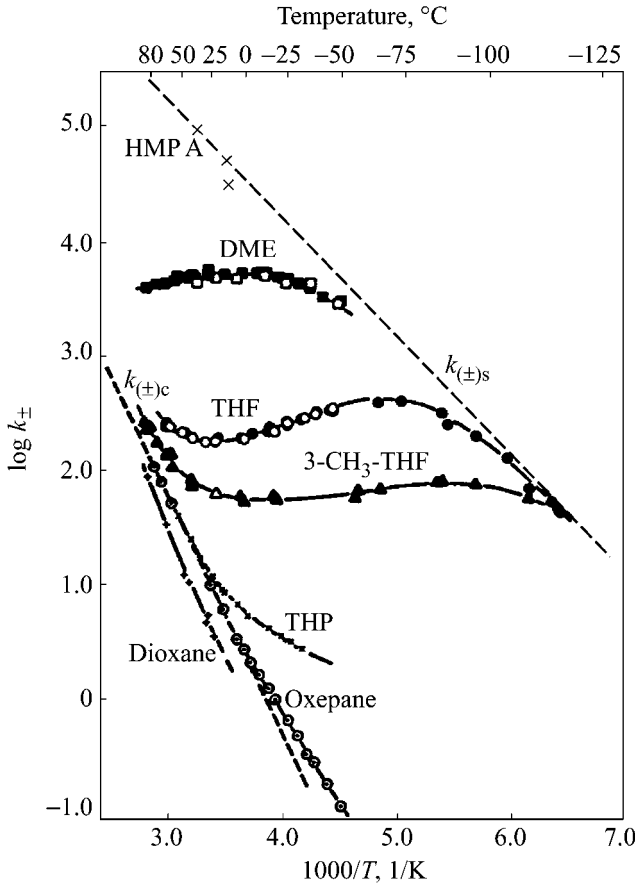

Fig. 2. Arrhenius plots of the propagation constants of ion pairs of poly(styryl)sodium in various solvents. The curves approach a common assymptote at low temperatures, interpreted as a linear Arrhenius plot referring to the propagation constant of solvent-separated ion pairs, and the curves approach again a common assymptote at high temperatures, interpreted as a linear Arrhenius plot referring to the propagation constant of tight ion pairs. From Ref. 27; reprinted by permission of Springer-Verlag.

kinetic studies. Figure 1 also shows that the intercepts, that represent $k_{\pm}$, also decrease with increasing cation size. Values of the propagation rate constant for free styryl anions are relatively insensitive to solvent; values for k_{-} of 0.65×10^5 and 1.3×10^5 L/(mol·s) have been reported at 25°C in THF (27). Corresponding values of $k_{\pm}$ vary from 160 L/(mol·s) for lithium to 22 L/(mol·s) for cesium ion in THF at 25°C. Similar results have been obtained for cumyl potassium-initiated polymerization of butadiene in THF; k_{-} had a value of 4.8×10^4 L/(mol·s) and $k_{\pm}$ was <1 L/(mol·s) at 0°C (71).

Although normal Arrhenius behavior was observed for k_{-}, anomolous increases of $k_{\pm}$ with decreasing temperature were observed in polar solvents such as THF and dimethoxyethane (glyme), as shown in Figure 2 (27). These results have been explained in terms of a temperature-dependent equilibrium between contact and solvent-separated ion pairs, as shown below:

Table 3. Ion Pair Rate Constants for Anionic Polymerization of Poly(styryl)sodium in Ethereal Solvents and the Equilibrium Constant and Thermodynamic Parameters for Ion Pair Equilibrium

Solvent	k_c, L/(mol·s)	k_s, 10^4 L/(mol·s)	$K_{c/s}$ (25°C)	ΔH, kJ/mol[a]	ΔS, J/(mol·K)[a]
DME[b]	12.5	5.5	0.13	−23	−94
THF	34	2.4	2.25×10^{-3}	−27	−142
3-CH_3-THF[c]	20	12.4	5.8×10^{-4}	−21	−134
THP[d]	10.7	5.3	1.3×10^{-4}	−12.6	−117
Dioxane	5.5	—	$<10^{-5}$	—	—

[a]To convert J to cal, divide by 4.184.
[b]1,2-Dimethoxyethane.
[c]3-Methyltetrahydrofuran.
[d]Tetrahydropyran.

$$\underset{\text{contact}}{R^-,Mt^+} \underset{}{\overset{K_{c/s}}{\rightleftharpoons}} \underset{\text{solvent-separated}}{R^-//\ Mt^+}$$

$$\downarrow k_c[M] \qquad \downarrow k_s[M]$$

This equilibrium shifts from the less reactive contact ion pair to the more reactive solvent-separated ion pair as temperature is decreased because the contribution from the unfavorable (negative) entropy of dissociation ($T\Delta S$) decreases and the enthalpy of dissociation is negative. As shown in Table 3, the values of k_c and k_s are not much dependent upon solvent, but the equilibrium constants $K_{c/s}$ are very dependent on the polarity of the solvent. These results also provide a rationalization for the effect of counterion on $k_\pm$ shown in Figure 1. Smaller cations such as lithium interact more strongly with solvent and form significant amounts of more reactive solvent-separated ion pairs.

Termination Reactions. The categorization of a given polymerization system as living is based on results obtained on the laboratory time scale, ie, the absence of chain-termination or chain-transfer reactions occurring within the normal time required to complete the polymerization and carry out any subsequent chemical reactions with the active carbanionic polymer chain ends (6). In fact, the amount of spontaneous termination reactions in typical alkyllithium-initiated polymerizations of styrene and diene monomers depends on time, temperature, and whether polar additives are present (22,72,73).

Polymeric organolithium compounds exhibit good stability in hydrocarbon solution at ambient temperatures and for short periods of time at elevated temperatures (22,72). The principal mode of decomposition is loss of lithium hydride (β-hydride elimination) to form a double bond at the chain end, as illustrated below for poly(styryl)lithium.

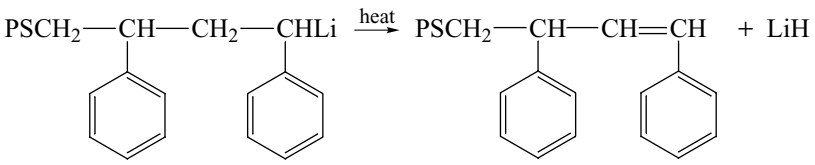

(37)

Poly(styryl)lithium exhibits good stability over the duration of the polymerizations and beyond, ie, days, at ambient temperatures in hydrocarbon media. However, at elevated temperatures, it is observed that the initial uv absorption at 334 nm decreases and a new absorption is observed at 450 nm, assigned to a 1,3-diphenylallyllithium species as shown below (22):

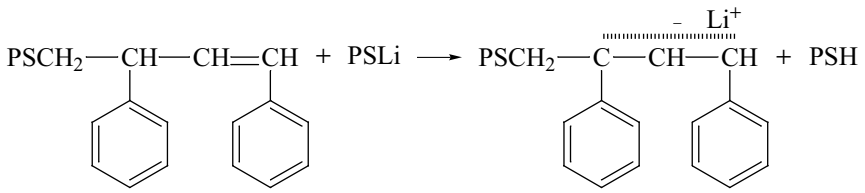

(38)

The rate constant for spontaneous decomposition was reported to be 4×10^{-5} s^{-1} at 65°C in cyclohexane (22,74). Analogous decomposition reactions have been observed for poly(styryl)sodium. The thermal stability of poly(α-methylstyryl)lithium is much lower than that of poly(styryl)lithium. The observed half-lives for spontaneous termination are 5 h and a few minutes at 25 and 60°C, respectively (75). However, the chain ends were stabilized with respect to spontaneous decomposition by the addition of TMEDA. The relative thermal stability of styryl carbanionic chain ends follows the order K $\gg$ Na $>$ Li for the alkali metal counterions.

The carbanionic active centers based on 1,3-butadiene and isoprene, with lithium as counterion, generally possess good stability in hydrocarbon solvents at ambient temperatures. However, poly(dienyl)lithiums undergo complex decomposition reactions upon prolonged storage or heating at elevated temperatures. Poly(butadienyl)lithium in ethylbenzene exhibits an absorption maximum at 300 nm, which gradually decreases in intensity with the formation of absorption tails between 350 and 500 nm (22). Approximately 20% of the active centers were destroyed in less than 3 h at 100°C in ethylbenzene (76). The apparent first-order rate constant for decomposition of poly(butadienyl)lithium in hexane was estimated to be 1.9×10^{-5} s^{-1} at 93°C and a chain-end concentration of 2.2 mequiv of poly(butadienyl)lithium per 100 g of solution (25 wt% polymer) (74). The corresponding first-order rate constant for chain-end decomposition of poly(isoprenyl)lithium at 93°C was estimated to be 6.7×10^{-5} s^{-1} (74). Although the differences are not large, the relative order of increasing stabilities of chain ends toward thermal degradation is poly(α-methylstyryl)lithium $\ll$ poly(styryl)lithium $<$ poly(isoprenyl)lithium $<$ poly(butadienyl)lithium as estimated by chain-end titration data.

Size exclusion chromatography (sec) analyses of the thermal decomposition products of poly(dienyl)lithiums in heptane at 80°C have shown that the chain-end decomposition is accompanied by formation of species which have double and triple the molecular weight of the original living polymer (77). After heating for 46 h at 80°C in heptane, a 12 wt% yield of coupled products was observed for poly(isoprenyl)lithium; after heating for 27 h at 80°C in heptane, a 19wt% yield of coupled products was observed for poly(butadienyl)lithium. The following reactions illustrate the type of reactions proposed to explain the formation of dimeric products:

$$\underset{\text{Active, uncoupled}}{PCH_2{-}CH{=}CH{-}CH_2Li} \xrightarrow{\text{heat}} \underset{\text{Inactive, uncoupled}}{PCH{=}CH{-}CH{=}CH_2} + LiH \tag{39}$$

$$P'Li + PCH{=}CH{-}CH{=}CH_2 \longrightarrow \underset{\text{Active, coupled}}{PCH(Li){-}CH{=}CH{-}CH_2{-}P'} \tag{40}$$

$$\underset{\text{Li}}{PCH(Li){-}CH{=}CH{-}CH_2{-}P'} \xrightarrow{\text{heat}} LiH + \underset{\text{Inactive, coupled}}{PCH{=}CH{-}CH{=}CH{-}P'} \tag{41}$$

Evidence also suggests that athermal metalation of the backbone can occur as shown below:

$$PBDLi + P{-}CH_2{-}CH{=}CH{-}CH_2{-}P \longrightarrow PBDH + \underset{\text{Li}}{P{-}CH(Li){-}CH{=}CH{-}CH_2{-}P} \tag{42}$$

It would be expected that this in-chain metalation coupled with elimination of lithium hydride would lead to in-chain diene units which would have even more reactive allylic hydrogens for further metalation–elimination–coupling sequences that would promote thermal decomposition, branching, and ultimately gel formation.

Polymeric organolithium compounds exhibit limited stability in ether solvents analogous to alkyllithium compounds. Living carbanionic polymers react with ether solvents such as THF in a pseudo-first-order decay process and the rate decreases in the order Li > Na > K. For example, a 10^{-5} M solution of poly(styryl)lithium in THF at 25°C exhibited a rate of decay of a few percent per minute, but poly(styryl)cesium was found to be exceptionally stable (78). Metalation and decomposition reactions can also occur in the presence of amines such as TMEDA.

Chain-Transfer Reactions. Chain-transfer reactions to polymeric organoalkali compounds can occur from solvents, monomers, and additives that have pK_a values lower or similar to those of the conjugate acid of the carbanionic chain end (72). Relatively few monomers that undergo anionic polymerization exhibit chain transfer to monomer. Chain transfer has been well documented for the anionic polymerization of 1,3-cyclohexadiene. The chain-transfer constant (k_{tr}/k_p) was calculated to be 2.9×10^{-2} at 20°C and 9.5×10^{-3} at 5°C in cyclohexane (79). Although chain transfer would be expected for *p*-methylstyrene, controlled polymerizations can be effected when the temperature is maintained at room temperature or below. The observations of broad molecular weight distributions and a low molecular weight tail by sec analysis have provided evidence for chain transfer during the anionic polymerization of *p*-isopropyl-α-methylstyrene (80).

The kinetics of chain transfer to ammonia have been investigated for potassium amide-initiated polymerization of styrene in liquid ammonia at −33.5°C.

The calculated chain-transfer constant (k_{tr}/k_p) was 2.34×10^{-4} (81). The chain-transfer reaction of poly(styryl)lithium with toluene at 60°C was investigated during the polymerization of styrene with the use of ^{14}C-labeled toluene. The calculated chain-transfer constant (k_{tr}/k_p) was 5×10^{-6} (82). A much larger chain-transfer constant ($k_{tr}/k_p = 1.28 \times 10^{-4}$) was found for analogous transfer from toluene to poly(styryl)sodium. Chain-transfer reactions are promoted by Lewis bases. A chain-transfer constant of 0.2 was reported for the telomerization of butadiene initiated by metallic sodium in a toluene/tetrahydrofuran mixture at 40°C (83). Significant chain-transfer effects have also been reported for alkyllithium-initiated polymerizations using alkenes as solvents. Allenes and alkynes act as modifiers in alkyllithium-initiated polymerizations that have the effects of lowering rates of reaction and polymer molecular weights. Although these carbon acids can terminate chain growth, the ability of the resulting metalated chain-transfer product to reinitiate chain growth has only been demonstrated for 1,2-butadiene (84).

Polar Monomers

Polar Vinyl Monomers. The anionic polymerization of polar vinyl monomers is often complicated by side reactions of the monomer with both anionic initiators and growing carbanionic chain ends, as well as chain-termination and chain-transfer reactions. However, synthesis of polymers with well-defined structures can be effected under carefully controlled conditions. The anionic polymerizations of alkyl methacrylates and 2-vinylpyridine exhibit the characteristics of living polymerizations under carefully controlled reaction conditions and low polymerization temperatures to minimize or eliminate chain-termination and chain-transfer reactions. The proper choice of initiator for anionic polymerization of polar vinyl monomers is of critical importance to obtain polymers with predictable, well-defined structures. As an example of an initiator that is too reactive, the reaction of methyl methacrylate (MMA) with *n*-butyllithium in toluene at −78°C produces approximately 51% of lithium methoxide by attack at the carbonyl carbon (85).

Methyl Methacrylate. The most generally useful initiator for anionic polymerization of MMA and related compounds is 1,1-diphenylhexyllithium which is formed by the quantitative and facile addition of butyllithium with 1,1-diphenylethylene (DPE) (eq. 17) (46). Using this initiator in THF at −78°C, it is possible to polymerize MMA to obtain polymers and block copolymers with predictable molecular weights and narrow molecular weight distributions. Controlled polymerizations are not effected in nonpolar solvents such as toluene, even at low temperatures. Other useful initiators for polymerization of MMA are oligomers of (α-methylstyryl)lithium whose steric requirements minimize attack at the ester carbonyl group in the monomer. These initiators are also useful for the polymerization of 2-vinylpyridine (see METHACRYLIC ESTER POLYMERS).

The principal termination reaction in the anionic polymerization of MMA is a unimolecular backbiting reaction with the prepenultimate ester group to form a six-membered ring, β-keto ester group at the chain end, as shown below:

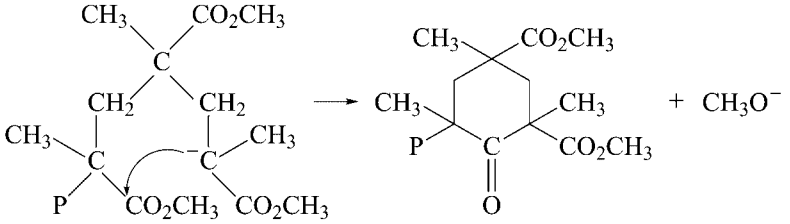

The rate of this backbiting reaction decreases with increasing size of the counterion.

A dramatic development in the anionic polymerization of acrylate and methacrylate monomers was the discovery that by addition of lithium chloride it was possible to effect the controlled polymerization of *t*-butyl acrylate (86). Thus, using oligomeric (α-methylstyryl)lithium as initiator in THF at -78°C, the molecular weight distribution (M_w/M_n) of the polymer was 3.61 in the absence of lithium chloride but 1.2 in the presence of lithium chloride ([LiCl]/[RLi] = 5). In the presence of 10 equiv of LiCl, *t*-butyl acrylate was polymerized with 100% conversion and 95% initiator efficiency to provide a polymer with a quite narrow molecular weight distribution ($M_w/M_n = 1.05$). More controlled anionic polymerizations of alkyl methacrylates are also obtained in the presence of lithium chloride. Other additives, which promote controlled polymerization of acylates and methacrylates, include lithium *t*-butoxide, lithium (2-methoxy)ethoxide, and crown ethers (47,48). The addition of lithium chloride also promotes the controlled anionic polymerization of 2-vinylpyridine.

The kinetics of anionic polymerization of MMA are complicated by chain-end association effects and the involvement of both free ions and ion pairs as propagating species. Lithium ester enolates are highly aggregated even in THF; association numbers range from 2.3 to 3.5 (87). Because of chain-end association, a dependence of propagation rate constants on chain-end concentration has been observed for lithium and sodium counterions. The propagation rate constant for the free ions at -75°C in THF is 4.8×10^5 L/(mol·s) (88). The propagation rate constants for ion pairs vary in the order Cs $\approx$ K $\approx$ Na $\gg$ Li. This is consistent with the conclusion that contact ion pairs are the predominant propagating species. The ion pair rate constants for lithium and potassium as counterions in THF at -40°C are 100 and 750 L/(mol·s), respectively (89).

The kinetic effects of lithium chloride on anionic polymerization of alkyl acrylates and methacrylates have been carefully examined (47,48,90,91). Added lithium chloride decreases the rate of propagation but has little effect on the rate of termination. In the absence of lithium chloride, free ions as well as associated and unassociated species can participate in the propagation event. By a common ion effect, the role of free ions is minimized by addition of lithium chloride. In the absence of lithium chloride, the rate of interconversion between tetameric aggregates, dimeric aggregates, and unassociated ion pairs is slow relative to propagation resulting in broader molecular weight distributions. Lithium chloride decreases the amount of aggregated species and forms cross-associated complexes with the lithium ester enolate ion pairs. Most important, the equilibration among these lithium chloride cross-aggregated species is fast relative to propagation so that narrow molecular weight distributions can be obtained.

Heterocyclic Monomers. A variety of heterocyclic monomers can be polymerized by anionic ring-opening polymerizations. The types of anionically polymerizable heterocyclic monomers include oxiranes (epoxides), thiacyclopropanes, thiacyclobutanes, lactones, lactides, lactams, anhydrides, carbonates, and siloxanes (92). Among these heterocyclic monomers, the anionic polymerizations of epoxides have been examined most extensively.

Ethylene Oxide. The anionic polymerization of ethylene oxide is complicated by association phenomena and the participation of ion pair and free ion intermediates in the propagation reactions (see POLYETHERS). Simple lithium alkoxides are strongly associated into hexamers and tetramers even in polar media such as THF and pyridine (93). As a consequence, lithium alkoxides are unreactive as initiators for the anionic polymerization of oxiranes. Association effects can be minimized by effecting polymerizations in alcohol media or in dipolar aprotic solvents.

The potassium hydroxide-initiated polymerization of ethylene oxide in alcoholic solvents such as diethylene glycol produces low molecular weight polyols ($M_w \approx 600$–700) with broad molecular weight distributions because of chain-transfer reactions with alcohol that occur throughout the polymerization, as shown below (98):

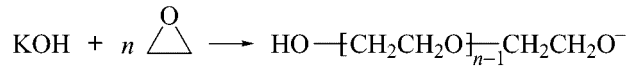

(43)

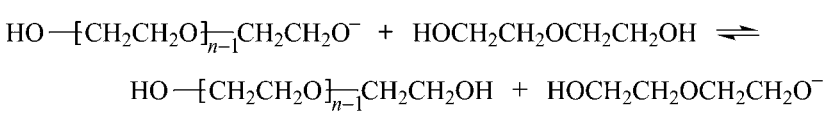

(44)

"Living polymerizations with reversible chain transfer" (6) can be effected for alkoxide-initiated polymerizations of ethylene oxide in the presence of alcohol ([ROH]/[NaOR] $\approx$ 10) in solvents such as dioxane (95,96). Narrow molecular weight distributions are obtained because, although there is formally a chain-transfer reaction between OH-ended polymers and alkoxide-ended polymers, the equilibrium between these two types of chain ends is rapid and reversible such that all chains participate uniformly in chain growth as described in Reference 97.

Association phenomena and the presence of both ion pairs and free ions as propagating species complicate the kinetics of sodium alkoxide-initiated polymerizations of ethylene oxide even in dipolar aprotic solvents such as HMPA ($\varepsilon = 26$). However, living polymerizations occur in dipolar aprotic solvents and in ethers such as THF, although the rates are much slower in ethers. The rates of propagation increase with increasing radius of the cation. The rates of propagation of ethylene oxide are also accelerated in the presence of cation complexing agents such as crown ethers and cryptands. Although the cryptated ion pairs are somewhat less reactive than the uncomplexed ion pairs, cryptands promote dissociation of the ion pairs to form free ions that are 70 times more reactive than the ion pairs (98). Because of the concentrated charge on oxygen, contact ion pairs predominate. The propagation rate constants in THF at 20°C for the cesium ion pair and

the free ion are 7.3 and 100 L/(mol·s) (98). An optimized, living polymerization procedure utilized *N*-carbazolylpotassium as initiator in THF at 20°C in the presence of crown ether (4,7,13,16,21,24-hexaoxa-1,10-diazabicyclo[8.8.8]hexacosane); narrow molecular weight distribution polymers with controlled molecular weights as high as 266,000 g/mol could be obtained (99).

Propylene Oxide. The anionic ring-opening polymerizaton of propylene oxide is much slower than the analogous polymerization of ethylene oxide (see POLYETHERS). The propagation rate constant at 40°C in neat propylene oxide is 1.9×10^{-4} L/(mol·s) (100). The anionic ring-opening polymerization of propylene oxide using hydroxide or alkoxide initiators is not a living polymerization. Chain transfer to monomer competes with propagation to limit the maximum molecular weight attainable and to broaden the molecular weight distribution, as shown below.

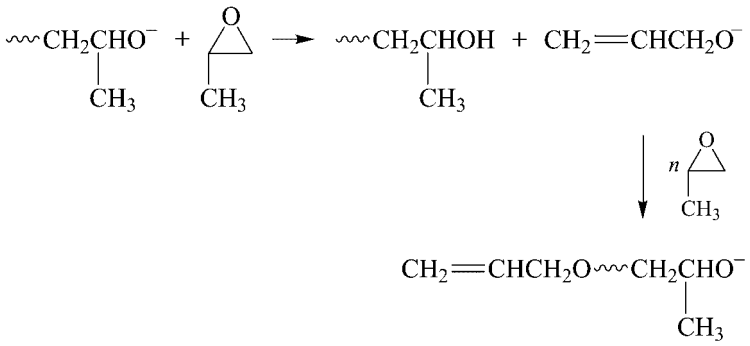

Thus, chains are formed that have the unsaturated allyloxy end group. The chain-transfer constant (k_{tr}/k_p) is approximately 0.01; thus, the molecular weight attainable is theoretically limited to approximately 6×10^3 g/mol (101). However, molecular weights as high as 13,000 g/mol have been obtained for polymerization of neat propylene oxide with potassium as counterion in the presence of 18-crown-6 ether. Under these conditions, chain-transfer constants as low as 8×10^{-4} have been reported (102). This is due to the rapid equilibration between hydroxyl-ended chains and alkoxide-ended chains, that ensures uniform growth of all chains even after chain transfer, as shown below:

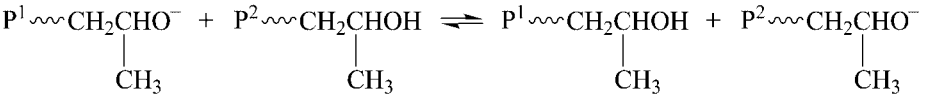

However, chain transfer to monomer will still broaden the molecular weight distribution and prevent molecular weight control even when reversible chain transfer among growing species occurs. This rapid and reversible chain transfer is used to prepare branched polypropylene oxide polymers. Initiation of propylene oxide polymerization with an alkali metal alkoxide and a triol such as glycerol will produce the corresponding polypropylene oxide with an average functionality of three.

The anionic polymerization of propylene oxide initiated by potassium alkoxide or hydroxide occurs predominantly (95%) by cleavage of the O—CH_2 bond. For bulk polymerization at 80°C, approximately 4% head-to-head placements occur.

However, there is no stereocontrol in this alkoxide-initiated ring opening and the resulting polymer is nontactic (103).

Chain-transfer reactions to monomer occur with other homologues of propylene oxide. The reactivity of higher epoxides decreases as expected on the basis of steric hindrance effects on nucleophilic attack at the oxirane carbons.

Propylene Sulfide. The anionic polymerization of propylene sulfide is a living polymerization that proceeds in the absence of termination and chain transfer (96) (see POLY(ALKYLENE SULFIDE)S). The regiochemistry of addition corresponds to regular head-to-tail addition without detectable amounts of head-to-head or tail-to-tail additions. The polymer stereochemistry is nontactic. The kinetics of propagation of propylene sulfide initiated by carbazylsodium in THF at chain-end concentrations $<10^{-3}\ M$ are not complicated by chain-end association effects. The reported propagation rate constants for contact ion pairs and free ions at -40°C were 1×10^{-3} and 1.7 L/(mol·s), respectively (96). The ion pair rate constants for the corresponding [2.2.2]cryptate-solvated sodium thiolate were more than two times larger than the corresponding free ion rate constants in THF at -39°C (98).

Lactones.

β-Propiolactone. The anionic polymerizations of the β-lactones and ε-lactones have been extensively investigated (104). Living characteristics are observed for the polymerization of β-propiolactone using a dibenzo-18-crown-6 ether complex of sodium acetate as the initiator in dichloromethane (105). Depending on the reactivity of the initiator, either acyl–oxygen cleavage or alkyl–oxygen cleavage can occur to form the corresponding alkoxide or carboxylate anions, respectively, as illustrated below for initiation with potassium methoxide that results in both modes of ring opening.

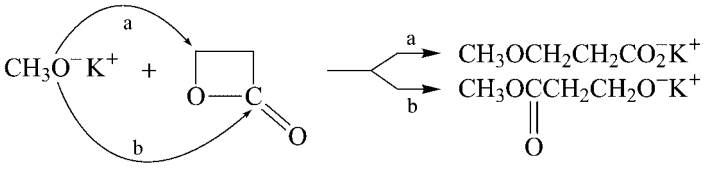

(45)

Only alkyl–oxygen cleavage is observed for initiation with potassium acetate. Regardless of the initiator, all propagating species eventually become carboxylate anions because in each subsequent propagation step a fraction of the alkoxide anions are converted to carboxylate anions. The kinetics of these polymerizations are complex. Both complexed ion pairs and free ions are involved in the propagation reactions and the free ion rate constants depend on monomer concentration. The relative reactivity of complexed ion pairs and free ions is temperature-dependent. Above the inversion temperature of -35°C, free ions are more reactive than ion pairs, but below this temperature, the ion pairs are more reactive. At 30°C in DMF, the observed (average) propagation rate constant is 0.13 L/(mol·s) (106). The anionic polymerization of α,α-dialkyl-β-propiolactones such as pivalolactone (α,α-dimethyl-β-propiolactone) initiated with carboxylate anions exhibits the main characteristics of living polymerizations.

ε-Caprolactone. The anionic polymerization of ε-lactones, especially ε-caprolactone, is generally complicated by intramolecular cyclization reactions and redistribution reactions that prevent control of molecular weight and lead to

broader molecular weight distributions (104). Alkoxides and not carboxylates are active initiators for polymerization of ε-caprolactone consistent with the identification of the alkoxide anion as the propagating species, as shown below:

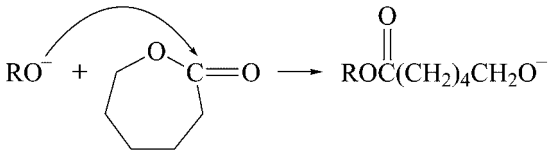

(46)

Chain-end association complicates the kinetics of polymerization. Evidence for aggregation of lithium and sodium alkoxides, but not for potassium alkoxides, in THF has been found. The propagation rate constants in THF at 20°C for the free ions and ion pairs are 3.5×10^2 and 4.8 L/(mol·s) (107). The anionic polymerization of ε-caprolactone leads to the formation of considerable amounts of oligomers as by-products. In dilute solution no high polymer is formed. In bulk polymerization, more than one-third of the equilibrium distribution of products are oligomers that have been identified to be cyclic (see eq. 47). The intermolecular analogue of this reaction (transesterification) leads to scrambling of the polymer molecular weights and a molecular weight distribution that broadens with time.

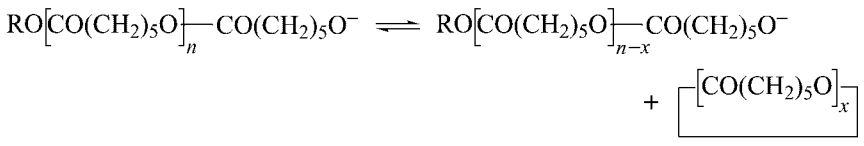

(47)

Polymerizations with lithium as counterion minimize backbiting reactions at short reaction times.

Cyclic Carbonates. Aliphatic, cyclic carbonates such as 5,5-dimethyl-1,3-diox-2-one can be polymerized using alkyllithium compounds as initiators in hydrocarbon solution to high molecular weight polymers (108,109). Ring-chain equilibration is promoted at long reaction times and in THF as solvent. At −10°C in toluene, *sec*-butyllithium-initiated polymerization of 5,5-dimethyl-1,3-diox-2-one proceeds via a lithium alkoxide-propagating species to form high molecular weight polymer ($M_n \approx 100{,}000$ g/mol) with only small amounts of a cyclic oligomer fraction after 1 h.

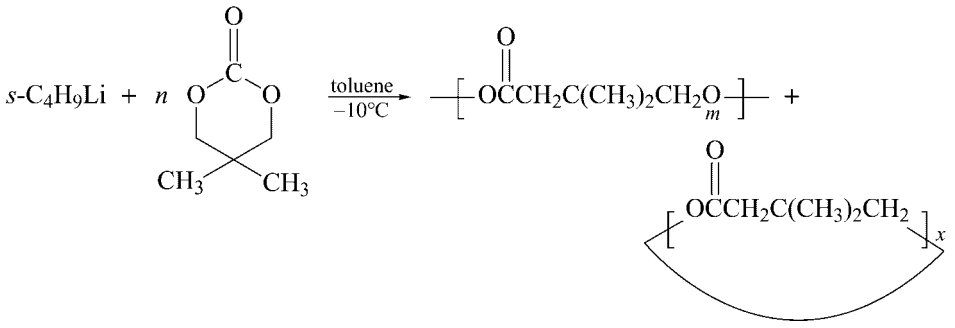

(48)

Efficient methods for the synthesis of cyclic bisphenol-A polycarbonates have provided a practical technology for the rapid synthesis of high molecular weight bisphenol-A polycarbonates by anionic ring-opening polymerization, as shown below (108). A mixture of cyclic oligomers ($M_w \approx 1300$) was polymerized with lithium stearate for 0.5 h at 300°C to yield the corresponding linear polymer with M_w = 300,000 and M_w/M_n = 2.4 (110). Rapid chain–chain equilibration occurs under these conditions. Other useful anionic polymerization initiators include lithium phenoxide, lithium phenylacetate, and sodium benzoate. Diphenylcarbonate can be used as a chain-transfer agent to control the molecular weight.

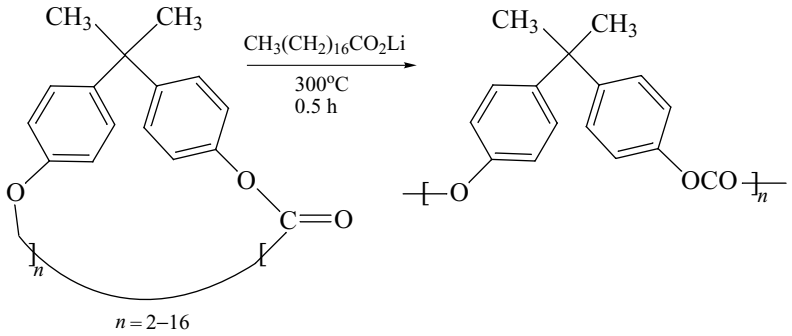

(49)

Siloxanes. A variety of bases, eg, hydroxides, alkoxides, phenolates, and silanolates, are effective initiators for the anionic polymerization of hexamethyl cyclotrisiloxane (D_3) and octamethyl cyclotetrasiloxane (D_4) (111). The heat of polymerization for the cyclic oligomers in the series from the tetramer (D_4) to the decamer (D_{10}) is approximately zero and the only driving force is a small positive entropy [approx 5.8 J/(mol SiO groups·K)] (112). The trimer D_3 is unique in having a slightly exothermic heat of polymerization of 19.6 kJ/mol (3.5 kcal/mol) (113). The growing polymer for D_4 polymerization is in equilibrium with the monomer (2% at 140°C) as well as with various kinds of oligomers and cyclic polymers (10–15%); a Gaussian distribution of linear polymers is obtained. The concentrations of each of the various cyclics ($n > 15$) are in accord with the Jacobsen–Stockmayer cyclization theory (114). The mechanism of polymerization can be described as an equilibration among these various components; in addition to reaction with the monomer, the growing silanolate chain ends react with all siloxane bonds via intramolecular cyclization and intermolecular chain transfer, as shown below:

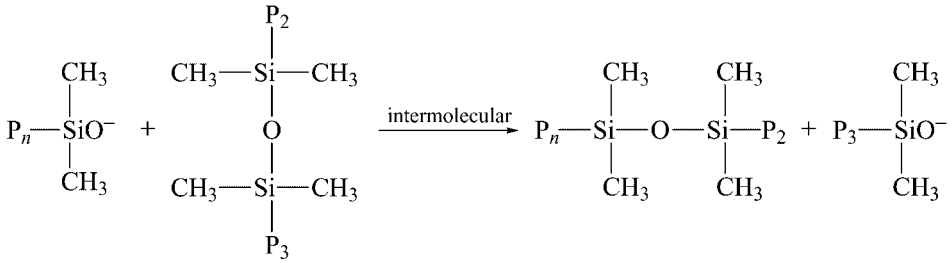

(50)

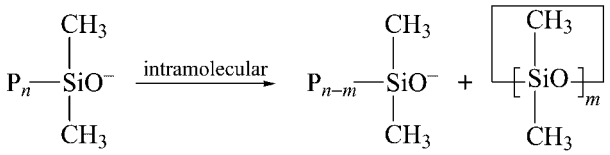

(51)

In contrast to the polymerization of D_4, the anionic polymerization of D_3 with lithium as counterion is a living polymerization which produces polydimethylsiloxanes with well-defined structures. Useful initiators include lithium silanolates or the product from the reaction of 3 moles of butyllithium with D_3 in hydrocarbon solvent, as shown below. It is noteworthy that no polymerization occurs in the absence of a Lewis base promoter such as THF, glymes, DMSO, or HMPA.

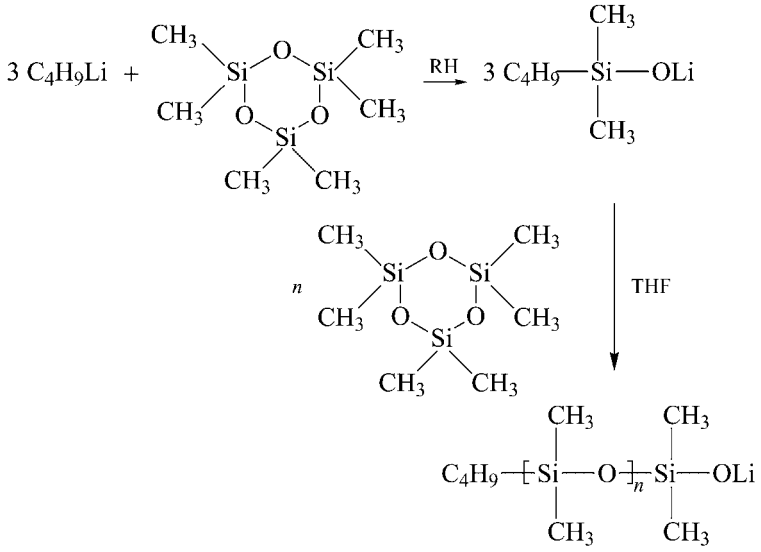

The kinetics of polymerization of cyclosiloxanes are complicated by chain-end association. Complexation of counterions with cryptands disrupts the aggregates. For the lithium [2.1.1]cryptand complex in aromatic solvent at 20°C, the propagation rate constants for D_3 and D_4 are 1.4 and 4×10^{-3} L/(mol·s), respectively (98) (see SILICONES).

Stereochemistry

Polydienes.

Polydienes in Hydrocarbon Solvents. One of the most important synthetic and commercial aspects of anionic polymerization is the ability to prepare polydienes with high 1,4-microstructure using lithium as the counterion in hydrocarbon solution (115,116). The key discovery was reported in 1956 by scientists at the Firestone Tire and Rubber Co., that polyisoprene produced by lithium metal-initiated anionic polymerization had a high (>90%) *cis*-1,4 microstructure analagous to

natural rubber (26). In general, conjugated 1,3-dienes [CH_2=C(R)–CH=CH_2] can polymerize to form four isomeric microstructures as shown below:

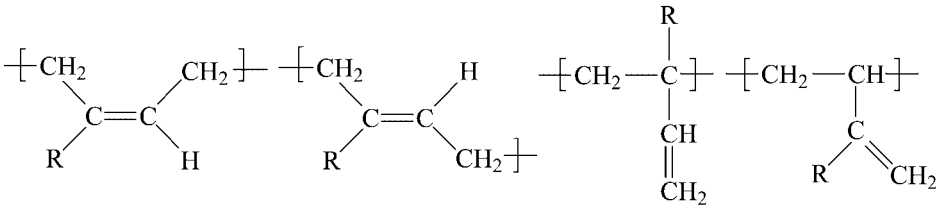

cis-1,4 *trans*-1,4 1,2 3,4

R = H (butadiene; 1,2 = 3,4); R = CH_3 (isoprene)

The stereochemistry of the anionic polymerization of isoprene and butadiene depends on the counterion, monomer concentration, chain-end concentration, solvent, temperature, and the presence of Lewis base additives (see BUTADIENE POLYMERS; ISOPRENE POLYMERS). The effect of counterion on polybutadiene stereochemistry is illustrated by the data in Table 4, which shows that lithium is unique among alkali metal counterions in producing polybutadiene with high 1,4 microstructure. Similar results have been reported for the stereochemistry of the anionic polymerization of isoprene (see Table 5) except that the stereochemistry with lithium as the counterion in neat isoprene is 94% *cis*-1,4 and 6% 3,4 compared with 35% *cis*-1,4, 52% *trans*-1,4, and 13% 1,2 for analogous polymerization of butadiene. From the data in Table 6, it is possible to delineate the effects of monomer concentration, chain-end concentration, monomer concentration, and solvent. The highest *cis*-1,4 microstructures are obtained in the absence of solvent, ie, with neat monomer, at low concentrations of initiator ($\approx 10^{-6}$ *M*). High *cis*-1,4 enchainment is also favored by the use of aliphatic versus aromatic solvents at low concentrations of initiator; however, the total amount of 1,4 microstructure (cis + trans) is relatively insensitive to solvent and chain-end concentration. In general, temperature is not an important variable for polydienes prepared in hydrocarbon solution, with lithium as the counterion; however, relatively large effects of pressure have been reported.

A comprehensive hypothesis has been proposed to explain the effects of the concentrations of active chain ends and monomer on polydiene microstructure

Table 4. Effect of Counterion on Polybutadiene Microstructure for Neat Polymerizations[a]

		Microstructure (%)		
Counterion	Temperature, °C	*cis*-1,4	*trans*-1,4	1,2
Lithium	70	35	52	13
Sodium	50	10	25	65
Potassium	50	15	40	45
Rubidium	60	7	31	62
Cesium	60	6	35	59

[a]Ref. 117.

Table 5. Effect of Counterion on Polyisoprene Microstructure for Neat Polymerizations[a]

		Microstructure (%)			
Counterion	Temperature, °C	*cis*-1,4	*trans*-1,4	1,2	3,4
Lithium	25	94	—	—	6
Sodium	25	—	45	7	48
Potassium	25	—	52	8	40
Rubidium	25	5	47	8	39
Cesium	25	4	51	8	37

[a]Refs. 117 and 118.

Table 6. Microstructure of Polydienes in Hydrocarbon Media Using Organolithium Initiators

			Microstructure (%)			
Initiator concentration, *M*	Solvent	Temperature, °C	*cis*-1,4	*trans*-1,4	3,4	Reference
Polyisoprene						
6×10^{-3}	Heptane	−10	74	18	8	119
1×10^{-4}	Heptane	−10	84	11	5	
8×10^{-6}	Heptane	−10	97	—	3	
5×10^{-6}	Heptane	25	95	2	3	120
9×10^{-3}	Benzene	20	69	25	6	121
5×10^{-6}	Benzene	25	72	20	8	120
1×10^{-2}	Hexane	20	70	25	5	121
1×10^{-5}	Hexane	20	86	11	3	
3×10^{-3}	None	20	77	18	5	
8×10^{-6}	None	20	96	—	4	
			cis-1,4	*trans*-1,4	1,2	
Polybutadiene						
8×10^{-6}	Benzene	20	52	36	12	
5×10^{-1}	Cyclohexane	20	53[a]		47	122
1×10^{-5}	Cyclohexane	20	68	28	4	121
3×10^{-2}	Hexane	20	30	60	8	
2×10^{-5}	Hexane	20	56	37	7	
3×10^{-3}	None	20	39	52	9	
5×10^{-6}	None	20	86	9	5	

[a]Total 1,4 content (cis + trans).

(123). Based on studies with model compounds and the known dependence of polydiene microstructure on diene monomer (D) and chain-end concentrations as shown in Table 6, the mechanistic hypothesis shown below was advanced.

$$\sim\sim\text{cis}^* + \text{D} \xrightarrow{k_p^{cis}} \sim\sim\text{cis,cis}^*$$

$$k_1 \rightleftharpoons k_{-1}$$

$$\sim\sim\text{trans}^* + \text{D} \xrightarrow{k_p^{trans}} \sim\sim\text{trans,cis}^*$$

It was proposed that isomerization of the initially formed cis form of the active chain end occurs competitively with monomer addition at each step of the reaction (123,124). Thus, when the concentration of monomer is high relative to the chain-end concentration, the first-order isomerization of the cis form does not compete effectively with monomer addition. However, at low concentrations of monomer relative to chain ends, the isomerization does compete and significant amounts of the trans form will be in equilibrium with the cis form.

The kinetic order dependence on the active chain-end concentration is approximately 0.25 for diene propagation, while the kinetic order dependence on the active chain end concentration is approximately one for cis–trans isomerization of the chains ends (53,116). Thus, while the unassociated chain ends add monomer, isomerization of the chain ends occurs in the aggregated state. Since aggregation is favored by increasing chain-end concentrations, high 1,2 microstructure is observed (47% for butadiene) for high chain-end concentrations ([PBDLi] = $\approx 0.1\,M$) and high *cis*-1,4 microstructure (86% for butadiene) is obtained at low chain-end concentrations ($\approx 10^{-6}\,M$).

The microstructure of anionic polymerization of other poly(1,3-diene)s with lithium as counterion in hydrocarbon media is also predominantly 1,4 (115). However, higher amounts of *cis*-1,4 microstructures are obtained with more sterically hindered diene monomers. Thus, using conditions which provide polyisoprene with 70% *cis*-1,4, 22% *trans*-1,4, and 7% 3,4 microstructure, 2-*i*-propyl-1,3-butadiene and 2-*n*-propyl-1,3-butadiene provide 86% and 91% *cis*-1,4 enchainment, respectively. Both 2-phenyl-1,3-butadiene (92% *cis*-1,4) and 2-(triethylsilyl)-1,3-butadiene (100% *cis*-1,4) also exhibit high *cis*-1,4 enchainment.

Polydienes Polar Solvents. In polar media, the unique, high 1,4 stereospecificity, with lithium as counterion, that is observed in hydrocarbon media is lost and large amounts of 1,2-poly(butadiene) and 3,4-poly(isoprene) enchainments are obtained (see Tables 7 and 8). Tables 7 and 8 show that there is a tendency toward higher 1,4 content with increasing size of the counterion in polar media. The highest 1,2 content in polybutadiene and the highest amounts of 1,2 and 3,4 enchainments in polyisoprene are obtained with lithium and sodium. The highest 1,4 enchainments are observed for cesium as counterion in polar media. Higher 1,4 contents are also obtained in less polar solvents such as dioxane.

There are several important structural differences for polydienyl anions in polar media versus hydrocarbon solvents: (*1*) chain ends are generally not associated into higher aggregates in polar media compared to hydrocarbon; (*2*) the charge distribution of unsymmetrical allylic anions is a function of solvent, counterion, and temperature; (*3*) the kinetic and equilibrium distribution of chain-end configurations can vary with solvent and counterion; (*4*) the distribution of contact ion pairs, solvent-separated ion pairs, and free ions can vary with solvent, counterion, and temperature.

Using the relationship that the chemical shift per electron corresponds to 114 ppm/electron, the calculated charge distributions for neopentylallyl-alkali metal **I** and neopentylmethylallyl-alkali metal **II** compounds have been calculated and the results are shown in Table 9 (131).

Table 7. Effects of Polar Solvents on Polybutadiene Microstructure[a,b]

			Microstructure (%)		
Solvent	Counterion	Temperature, °C	*cis*-1,4	*trans*-1,4	1,2
THF	Lithium	0	6	6	88
THF	Lithium	−78	~0	8	92
THF	Sodium	0	6	14	80
THF	Sodium	−78	~0	14	86
THF	Potassium	0 or −78	5	28	67
$(C_2H_5)_2O$	Lithium	0	8	17	75
$(C_2H_5)_2O$	Sodium	0	7	23	70
$(C_2H_5)_2O$	Potassium	0	11	34	55
Dioxane	Lithium	15	—	13	87
Dioxane	Sodium	15	—	15	85
Dioxane	Potassium	15	—	45	55
Dioxane	Cesium	15	—	59	41
Dioxane	Free ion	15	—	22	78

[a]Refs. 125 and 126.
[b]Free ion formation was suppressed for the measurements in THF and $(C_2H_5)_2O$ by the addition of tetraphenylboride salts (triphenylcyanoboron for potassium).

Table 8. Effects of Polar Solvents on Polyisoprene Microstructure

			Microstructure (%)					
		Temperature,			Total 1,4 content			
Solvent	Counterion	°C	*cis*-1,4	*trans*-1,4	(cis + trans)	1,2	3,4	Reference
THF	Lithium	30			12	29	59	127
THF	Sodium	0			11	19	70	128
DME[a]	Li, Na, K, Cs	15			24–26	28–33	44–48	129
$(C_2H_5)_2O$	Lithium	20			35	13	52	130
$(C_2H_5)_2O$	Sodium	20			17	22	61	
$(C_2H_5)_2O$	Potassium	20			38	19	43	
$(C_2H_5)_2O$	Cesium	20			52	16	32	
Dioxane	Lithium	15	3	11		18	68	126
Dioxane	Potassium	15	4	32		14	50	
Dioxane	Free ion	15	<1	24		32	44	

[a]1,2-Dimethoxyethane.

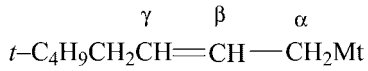

I

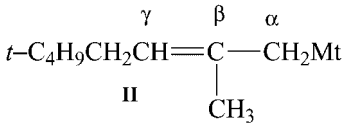

II

Compounds **I** and **II** can be regarded as models for butadienyl and isoprenyl carbanionic chain ends, respectively. The data in Table 9 show that while the negative charge is more localized on the alpha (α) carbon in hydrocarbon solution for the lithium derivatives, in polar media there is less charge on the alpha (α) carbon

Table 9. Calculated Charges on Allyl Carbon Atoms of Neopentylallyl- and Neopentylmethylallyl-alkali Metal Compound[a]

Counterion	Solvent	Calculated charges on allylic carbon atoms			∑(total)
		α	β	γ	
Neopentylallyl-alkali metal (**I**)					
Li	C_6H_6	0.79	−0.13	0.22	0.88
	THF	0.69	−0.15	0.40	0.94
Na	THF	0.65	−0.12	0.49	1.02
K	THF	0.59	−0.11	0.53	1.01
Rb	THF	0.55	−0.11	0.53	0.97
Cs	THF	0.51	−0.12	0.52	0.91
Neopentylmethylallyl-alkali metal (**II**)					
Li	C_6H_6	0.80	−0.14	0.19	0.85
	THF	0.73	−0.15	0.34	0.92
Na	THF	0.69	−0.12	0.38	0.95
K	THF	0.61	−0.09	0.44	0.96
Rb	THF	0.58	−0.09	0.47	0.96
Cs	THF	0.54	−0.10	0.45	0.89

[a]Ref. 131.

and more charge on the gamma (γ) carbon in all allyl organoalkali compounds. The presence of more negative charge on the gamma (γ) carbon provides a partial explanation for the formation of predominantly side-chain vinyl microstructure in polar media; however, lithium with the least charge on the gamma carbon gives the highest 1,2 enchainment and cesium with high charge on the gamma carbon gives the highest 1,4 enchainment. It has been suggested that a highly solvated lithium cation in ether solvents, which is situated closer to the alpha carbon in the allylic anion, may block reaction with monomer at this position and lead to preferential attack at the less hindered gamma position to form 1,2-butadiene units (132).

Sterically hindered, 2-alkyl-substituted dienes form high 1,4 microstructure in polar media as well as in hydrocarbon media (115). Butyllithium-initiated polymerization of 2-isopropyl-1,3-butadiene in diethyl ether produces a polymer with 81% *cis*-1,4 and 19% *trans*-1,4 microstructure. Similarly, >90% 1,4 microstructure is observed in THF for butyllithium-initiated polymerization of 2-triethylsilyl-1,3-butadiene, 2-trimethoxysilyl-1,3-butadiene, 1-phenyl-1,3-butadiene,1-pyridyl-1,3-butadiene, and 2-phenyl-1,3-butadiene.

Polar Modifier Effects. Small amounts of Lewis base additives in hydrocarbon media can exert dramatic effects on polydiene microstructure as shown by the data in Table 10. Lewis bases which interact most strongly with lithium produce the highest amount of 1,2 microstructure. For example, there is a correlation between the enthalpies of interaction of Lewis bases with polymeric organolithium compounds and the ability of these bases to promote 1,2 enchainment (136). The highest vinyl contents for polybutadiene are obtained with the most strongly coordinating ligands such as the bidentate bases, TMEDA and DIPIP (bispiperidinoethane). To obtain significant amounts of vinyl microstructure with

Table 10. Effects of Temperature and Concentration of Lewis Base on Vinyl Content of Polybutadiene in Hexane

		1,2 Microstructure (%)				
Base	[Base]/[Li]	5°C	30°C	50°C	70°C	Reference
Triethylamine	30	—	21	18	14	133
	270	—	37	33	25	
Diethyl ether	12	—	22	16	14	
	180	—	38	29	27	
Tetrahydrofuran	5	—	44	25	20	
	85	—	73	49	46	
Diglyme	0.1	—	51	24	14	
	0.8	—	78	64	40	
N,*N*,*N*′,*N*′-Tetramethylethylenediamine	0.6	—	73	47	30	
	0.4	78	—	—	—	134
	6.7	85	—	—	—	
	1.14	—	76	61	46	133
Bispiperidinoethane	0.5	91	50	44	21	135
	1	99.99	99	68	31	

weak donor-type bases such as diethyl ether and triethylamine, they must be present in large amounts relative to lithium. In contrast, the strongly coordinating bases produce high vinyl polybutadiene microstructure at low base to lithium atom ratios (R = [Base]/[Li] = 1–2).

An interesting effect of Lewis bases on diene microstructure is the fact that in the presence of strongly coordinating bases such as TMEDA, 1,2 units are observed for polyisoprene. For example, the microstructure of polyisoprene formed in the presence of TMEDA ([TMEDA]/[Li] = 1) in cyclohexane corresponds to 21% 1,4, 12% 1,2, and 67% 3,4 (137). The formation of 1,2 units requires the formation of the less stable 1,4 chain ends versus 4,1 chain ends as shown in equation 52:

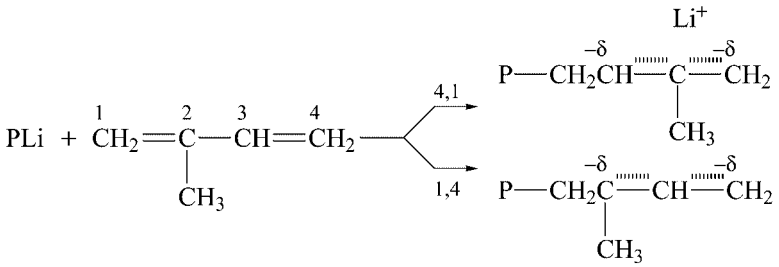

(52)

With lithium as counterion in neat monomer or in hydrocarbon solvent, no 1,2 enchainment is detected (see Tables 5 and 6).

Another interesting and surprising phenomenon observed in alkyllithium-initiated polymerization of butadiene in the presence of TMEDA is that cyclization to form in-chain vinylcyclopentane units (up to 60%) is observed

when the butadiene monomer is introduced into the reactor at low rates (eq. 53) (138).

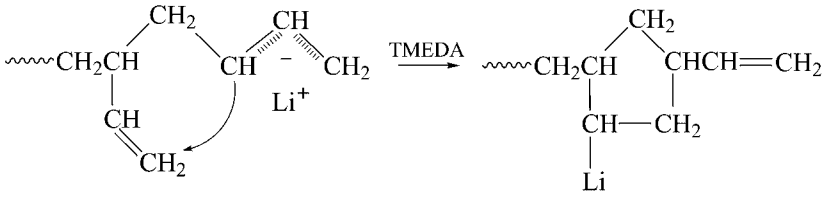

(53)

Under such conditions, propagation does not effectively compete with cyclization; similar results are obtained with bispiperidinoethane. With respect to the mechanistic requirements for this type of cyclization, it was reported that batch polymerization in THF/TMEDA (92/2, v/v) at 0°C showed no evidence of these cyclic units although the vinyl content was almost 90%. This reaction forms a relatively unstable 2° alkyllithium from a resonance-stabilized allylic lithium, which would appear to be energetically unfavorable. However, it should be noted that this process also converts a π bond into a more stable σ bond as in any vinyl polymerization. The generality of this cyclization process in monomer-starved systems was demonstrated by showing that significant amounts of cyclization are observed using sodium as counterion in the presence of TMEDA and also with lithium complexed only with THF.

The ability to prepare polydienes with variable microstructures is an important aspect of alkyllithium-initiated anionic polymerization. The main consequence of the change in microstructure is that the glass-transition temperatures of the corresponding polymers are higher for polymers with more side-chain vinyl microstructure. For example, the glass-transition temperature of polybutadiene is an almost linear function of the % 1,2 configuration in the chain as shown in Figure 3 (139). Thus, while *cis*-1,4-polybutadiene has a glass-transition temperature of −113°C, 1,2-polybutadiene has a glass-transition temperature of −5°C (140). This has practical consequences because polybutadienes with medium vinyl contents (eg, 50%) have glass-transition temperatures ($\approx$ −60°C) and properties which are analogous to styrene–butadiene rubber. Analogously, the glass-transition temperature of *cis*-1,4-polyisoprene is approx −71°C, a polyisoprene with 49% 3,4 enchainment exhibited a T_g of −36°C (141).

Methacrylate Stereochemistry. Like the anionic polymerization of dienes, the anionic polymerization of alkyl methacrylates, especially MMA, is dependent on the counterion, solvent, and to a certain extent temperature (116,142,143). In general, the stereochemistry of the anionic polymerization of alkyl methacrylates in toluene solution with lithium as the counterion is highly isotactic (68–99%) and the isotacticity increases with the steric requirements of the alkyl ester group as shown in Table 11. Isospecificity for polymerizations in toluene is also observed for alkyl sodium initiators (67% mm), but not for potassium or cesium alkyls in toluene. Sterically hindered Grignard reagents, in particular *t*-butylmagnesium bromide or isobutylmagnesium bromide prepared in ether, provide controlled, living polymerizations and highly isotactic polymers (86.7 and 92.5% mm, respectively), provided that excess magnesium bromide is present to shift the Schlenk

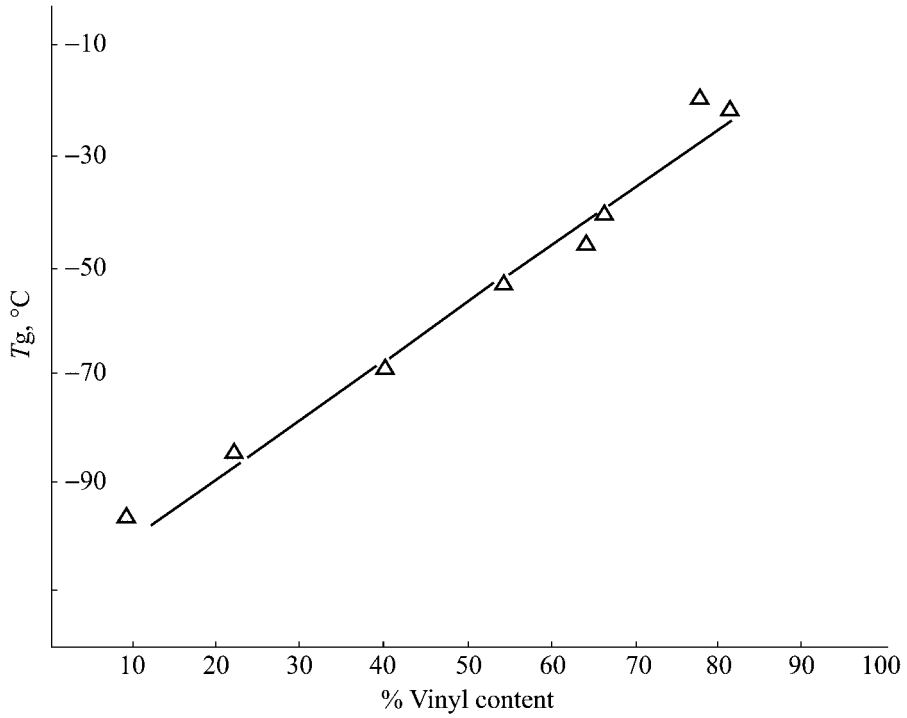

Fig. 3. Variation of T_g with vinyl (1,2) content for polybutadiene. From Ref. 139; reprinted by permission of Plenum Press.

equilibrium (eq. 54) in favor of RMgBr.

$$R_2Mg + MgX_2 \rightleftharpoons 2\ RMgX \tag{54}$$

In contrast, using di-*t*-butylmagnesium, prepared in ether, PMMA was obtained with predominantly syndiotactacity (79% rr). Highly isotactic PMMA is obtained for ether-free dibenzylmagnesium-initiated polymerization in toluene. Ate-type complexes of *t*-butyllithium with trialkylaluminums ([Al]/[Li] $\geq$ 2) effect living and highly syndiotactic ($\geq$90% rr) polymerization of MMA in toluene. Analogous complexes of *t*-butyllithium with (2,6-di-*t*-butyl-4-methylphenoxy)diisobutylaluminum ([Al]/[Li] $\geq$ 1) at 0°C in toluene generate PMMA with predominantly syndiotactic placements (71–75% rr). In contrast, the ate complex of *t*-butyllithium with bis(2,6-di-*t*-butylphenoxy)methylaluminum forms predominantly heterotactic PMMA (67.8% mr) and poly(ethyl methacrylate) (87.2% mr at −78°C; 91.6% mr at −95°C).

As shown in Table 12, in polar media highly syndiotactic PMMA is formed for free ions and with lithium and sodium as counterions; for sodium, syndiospecificity is observed only in more polar solvents such as dimethyoxyethane or in the presence of strongly solvating ligands such as cryptands. Lithium is the smallest alkali metal cation and the most strongly solvated; the equilibrium constants for formation of free ions and solvent-separated ion pairs are largest for lithium and

Table 11. Stereochemistry of Anionic Polymerization of Alkyl Methacrylates in Toluene Solution

Alkyl ester	Initiator	Temperature, °C	Microstructure (Triads, %) mm	mr	rr	Reference
CH_3	DPHLi[a]	−78	86	10	4	85
	C_4H_9Li		68	19	13	
	Amyl-Na		67	25	9	144
	Octyl-K		39	36	25	145
	Fluorenyl-Cs		6	50	44	
	t-$C_4H_9Li/(C_2H_5)_3Al$[b]		0	10	90	146
C_2H_5	DPHLi[a]		89	10	1	144
tC_4H_9	C_4H_9Li	−70	90	5	5	147
$(C_6H_5)_2CH$	C_4H_9Li	−78	99	1	0	148
$(C_6H_5)_3C$	C_4H_9Li		96	2	2	
CH_3	t-C_4H_9MgBr		96.7	3	0.3	149
	n-C_4H_9MgBr		11	15.3	73.7	
	i-C_4H_9MgBr		92.5	5.4	2.1	
	$(t\text{-}C_4H_9)_2Mg$		1.4	19.2	79.4	
	$(C_6H_5CH_2)_2Mg$	−70	63	24	13	150
	t-C_4H_9Li/Al(BHT)-$(iB)_2$[c]	0	2	26	72	151
	t-C_4H_9Li/$Al(ODBP)_2$-CH_3[d]	−78	11.6	67.8	20.6	152

[a] 1,1-Diphenylhexyllithium.
[b] [Al]/[Li] ≥ 2.
[c] t-Butyllithium/(2,6-di-t-butyl-4-methylphenoxy)diisobutylaluminum ([Al]/[Li] ≥ 1).
[d] t-Butyllithium/bis(2,6-di-t-butyl-phenoxy)methylaluminum ([Al]/[Li] ≥ 2).

smallest for cesium. Since cesium and potassium have a tendency to form heterotactic placements, it is proposed that contact ion pairs result in predominantly heterotactic placements while solvent-separated ion pairs and free ions form predominantly syndiotactic placements in polar media. These results are general for a variety of alkyl methacrylates; even diphenylmethyl methacrylate gives 87% syndiotactic triads in THF with lithium as counterion at −78°C. However, the exception is trityl methacrylate which forms 94% isotactic triads under the same conditions and also in toluene.

A variety of stereoregulating mechanisms have been invoked to explain the stereochemistry of anionic polymerization of alkyl methacrylates (158–160). As discussed earlier (161), although syndiotactic diads are thermodynamically slightly favored over isotactic diads, the free-energy differences are so small that the formation of stereoregular chains must be kinetically controlled. The kinetic control arises from the differences in free energies of activation ($\Delta\Delta G^{\neq} = \Delta G_{iso}{}^{\neq} - \Delta G_{syndio}{}^{\neq}$) with respect to addition of a monomer unit to form an isotactic versus a syndiotactic diad. Relatively small activation energy differences can lead to large differences in the stereochemistry of propagation. Thus, a change in free energy of activation difference of only 5.4 kJ/mol (1.3 kcal/mol) can change the stereochemistry from 50/50 = iso/syndio to 90/10 = iso/syndio. Since only limited tools are available to predict or understand the physical and chemical basis of such factors as solvation, particularly those associated with small energy differences of

Table 12. Stereochemistry of Anionic Polymerization of Alkyl Methacrylates in Polar Solvents

Alkyl ester group	Counterion	Solvent	Temperature, °C	Microstructure (Triads, %) mm	mr	rr	Reference
CH_3	Li	THF	−85	1	15	84	153
			−45	1	22	77	89
		THP	−35	6	32	62	154
		DME	−57	1	16	83	89
		Dioxane	13	10	35	55	154
	Na	THF	−51	4	38	58	155
		THP	−47	22	52	26	89
		DME	−55	2	21	77	156
		[222], DME	−98	1	19	80	89
	K	THF	−60	9	52	39	153
		Dioxane	13	14	56	30	154
	Cs	THF	−53	5	52	42	157
		DME	−66	3	37	60	156
	Free ion	DME	−98	1	20	79	89
	Mg[a]	THF	−78	0.2	9.6	90.2	143
$(C_6H_5)_2CH$	Li	THF	−78	2	11	87	148
$(C_6H_5)_3C$				94	4	2	
$(CH_3)_3C$	Li		−40	12	49	39	89
	Na		−48	6	65	29	
	Cs		−42	4	51	45	
	Radical		−55	4	17.5	78.5	143

[a] Polymerization initiated by n-C_4H_9MgBr in the presence of 2 equiv of TMEDA.

this order of magnitude, it is prudent to limit phenomenological interpretations of these stereochemical effects. Thus, any explanation of the predominantly syndiotactic polymerization stereochemistry in THF with lithium as the counterion (84% rr at −85°C) is tempered by the fact that the stereochemistry for the free-radical polymerization of MMA is also highly syndiotactic (78.5% at −55°C) (139). Many factors such as polar monomer coordination and interaction of the counterion with the chain end and with the penultimate groups have been invoked to explain the formation of isotactic polymers in non-polar media. The coordination of the penultimate ester group with the lithium ester enolate group at the chain end would dictate a meso placement. This simple picture, however, does not take into account the fact that these lithium ester enolates are highly associated in hydrocarbon solution and in polar media such as THF (87).

The control of PMMA stereochemistry is important because the glass-transition temperature of PMMA strongly depends on the microstructure (143). The measured T_g for 99% mm PMMA is reported to be 50°C, and the T_g for PMMA with 96–98% rr triads is 135°C. To obtain a PMMA with higher upper use temperature, polymers with the highest syndiotactic microstructure are required.

Styrene Stereochemistry. The effect of counterion, solvent, and temperature on the stereochemistry of anionic polymerization of polystyrene is shown in Table 13. The principal conclusion is that the stereoregularity of polystyrenes

Table 13. Stereochemistry of Polystyrenes Prepared with Anionic Initiators[a]

			Stereochemistry		
Counterion	Solvent	Temperature, °C	mm	mr	rr
Li	THF	−78	0.10	0.32	0.58
		20	0.12	0.37	0.51
	Toluene	−20	0.13	0.42	0.45
		20	0.07	0.41	0.52
K	THF	−78	0.09	0.34	0.57
Cs	THF	−78	0.14	0.35	0.51
Na	Toluene	10	0.15	0.40	0.45
K			0.22	0.37	0.41
Rb			0.21	0.44	0.35
Cs			0.24	0.41	0.35

[a]Refs. 162 and 163.

prepared by anionic polymerization is predominantly syndiotactic and that the stereoregularity is surprisingly independent of the nature of the cation, the solvent and the temperature, in contrast to the sensitivity of diene stereochemistry to these variables.

When small amounts of water were deliberately added to butyllithium in hydrocarbon solution, it was possible to prepare polystyrene with as much as 85% polymer that was insoluble in refluxing methyl ethyl ketone and identified as isotactic polystyrene by x-ray crystallography (164). Isotactic polystyrene (10–22% crystalline) can be prepared when lithium *t*-butoxide is added to *n*-C_4H_9Li initiator and the polymerization in hexane (styrene/hexane = 1) is effected at −30°C (165). This polymerization becomes heterogeneous and is quite slow (after 2–5 days, 50% monomer conversion; 20–30% conversion to isotactic polymer).

Vinylpyridines. The stereochemistry of anionic polymerization of 2-vinylpyridine is predominantly isotactic for most polymerization conditions as shown by the data in Table 14 (166). The coordination of the penultimate pyridyl nitrogen with the magnesium ester enolate at the chain end has been invoked to

Table 14. Stereochemistry of Poly(2-vinylpyridine)s Prepared with Anionic Initiators[a]

			Stereochemistry		
Counterion	Solvent	Temperature, °C	mm	mr	rr
Li	Toluene	−78	0.69	0.21	0.10
[b]	THF	−78	0.44	0.44	0.12
[c]			0.56	0.36	0.08
			0.26	0.51	0.23
Mg	Toluene	25	0.76	0.18	0.06
	THF	25	0.37	0.56	0.07
Rb	THF	−78	0.50	0.36	0.14

[a]Ref. 166.
[b]$[LiB(C_6H_5)_4]/[I] = 2.0$.
[c]Poly(4-vinylpyridine).

explain the high meso triad content for initiation by Grignard-type reagents in hydrocarbon solution. The absence of this interaction for 4-vinylpyridine results in almost atactic polymer stereochemistry.

Copolymerization

Relatively few comonomer pairs undergo anionic copolymerization to incorporate significant amounts of both monomers into the polymer chains (167). In general, the comonomer that is most reactive (lowest pK_a value for the conjugate acid of the propagating anion; see Table 1) will be incorporated to the practical exclusion of the other comonomer. Comonomer pairs that can be effectively copolymerized include styrenes with dienes and methacrylates with acrylates, ie, comonomer pairs with similar reactivity.

Anionic copolymerizations have been investigated by applying the classical Mayo–Lewis treatment that was originally developed for free-radical chain reaction polymerization (168). The copolymerization of two monomers (M_1 and M_2) can be uniquely defined by the following four elementary kinetic steps, assuming that the reactivity of the chain end (M_1^- or M_2^-) depends only on the last unit added to the chain end; ie, there are no penultimate effects.

$$\sim\sim M_1^- + M_1 \xrightarrow{k_{11}} \sim\sim M_1 — M_1^- \tag{55}$$

$$\sim\sim M_1^- + M_2 \xrightarrow{k_{12}} \sim\sim M_1 — M_2^- \tag{56}$$

$$\sim\sim M_2^- + M_2 \xrightarrow{k_{22}} \sim\sim M_2 — M_2^- \tag{57}$$

$$\sim\sim M_2^- + M_1 \xrightarrow{k_{21}} \sim\sim M_2 — M_1^- \tag{58}$$

From these four basic kinetic equations, the Mayo–Lewis instantaneous copolymerization equation can be derived as shown below:

$$\frac{d[M_1]}{d[M_2]} = \frac{[M_1](r_1[M_1]+[M_2])}{[M_2](r_2[M_2]+[M_1])} \tag{59}$$

where $r_1 = k_{11}/k_{12}$ and $r_2 = k_{22}/k_{21}$ and $d[M_1]/d[M_2]$ represents the instantaneous copolymer composition. The monomer reactivity ratios r_1 and r_2 represent the relative reactivity of each growing chain end for addition of the same monomer compared to crossover to the other monomer. Representative monomer reactivity ratios for anionic copolymerizations are listed in Table 15. The applicability of standard copolymerization theory to anionic polymerization has been considered in detail. Equations 55–58 represent an oversimplification since the chain ends are aggregated in hydrocarbon solution and there is a spectrum of ion pairs and free ions in polar media.

In most copolymerizations, $r_1 \neq r_2$ and one monomer is preferentially incorporated into the initially growing polymer. This leads to a depletion of the

Table 15. Anionic Copolymerization Parameters in Hydrocarbon Solution with Alkyllithium Initiators

M_1	M_2	Solvent	Temperature, °C	r_1	r_2	Reference
Butadiene	Styrene	None	25	11.2	0.04	169
		Benzene	25	10.8	0.04	
		Cyclohexane	25	15.5	0.04	
		Hexane	0	13.3	0.03	
			25	12.5	0.03	
			50	11.8	0.04	
		THF	−78	0.04	11.0	
			0	0.2	5.3	
			25	0.3	4.0	
		Diethyl ether	25	1.7	0.4	
		Triethylamine	25	3.5	0.5	
		Anisole	25	3.4	0.3	
		Diphenyl ether	25	2.8	0.1	
	Isoprene	Hexane	20	2.72	0.42	170
	1,1-Diphenylethylene	Benzene	40	54	∼0	171
		THF	0	0.13	∼0	
Isoprene	Styrene	Benzene	30	7.7	0.13	172
		Toluene	27	9.5	0.25	173
		Cyclohexane	40	16.6	0.046	174
		THF	27	0.1	9	175
	1,1-Diphenylethylene	Benzene	40	37	∼0	176
		THF	0	0.12	∼0	
Styrene	1,1-Diphenylethylene	Benzene	30	0.7	∼0	177
		THF	30	0.13	∼0	

preferentially incorporated monomer in the feed and the composition of the copolymer formed changes with conversion. For systems undergoing continuous initiation, propagation, and termination, the resulting compositional heterogeneity is intermolecular; ie, the copolymer formed initially is different from the copolymer formed at the end of the reaction. However, in living anionic copolymerization, all of the compositional heterogeneity arising from the disparity in monomer reactivity ratios is incorporated into each growing polymer chain.

Tapered Block Copolymers. The alkyllithium-initiated copolymerizations of styrene with dienes, especially isoprene and butadiene, have been extensively investigated and illustrate the important aspects of anionic copolymerization. As shown in Table 15, monomer reactivity ratios for dienes copolymerizing with styrene in hydrocarbon solution range from approximately 8 to 17, while the corresponding monomer reactivity ratios for styrene vary from 0.04 to 0.25. Thus, butadiene and isoprene are preferentially incorporated into the copolymer initially. This type of copolymer composition is described as either a *tapered block copolymer* or a *graded block copolymer*. The monomer sequence distribution can be described by the structures below:

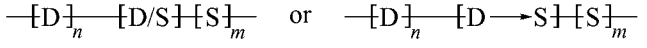

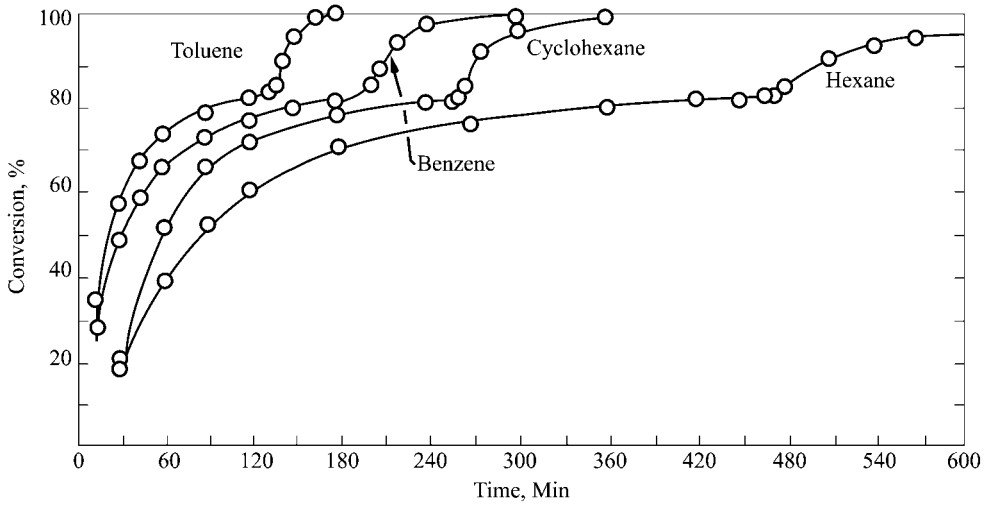

Fig. 4. Copolymerization of butadiene and styrene in different solvents at 50°C. Parts of butadiene/styrene/solvent/*n*-butyllithium = 75/25/1000/0.13 (2.0 mmol). From Ref. 50; reprinted by permission of the Rubber Division of the American Chemical Society.

First there is a diene-rich block; a middle block follows, which is initially richer in butadiene with a gradual change in composition until eventually it becomes richer in styrene; a final block of styrene completes the structure. For a typical copolymerization of styrene and butadiene (25/75, wt/wt), the solution is initially almost colorless, corresponding to the dienyllithium chain ends and the rate of polymerization is slower than the hompolymerization rate of styrene, as shown in Figure 4. The homopolymerization rate constants for styrene, isoprene, and butadiene are 1.6×10^{-2} $L^{1/2}/(mol^{1/2}\cdot s)$, 1.0×10^{-3} $L^{1/4}/(mol^{1/4}\cdot s)$, and 2.3×10^{-4} $L^{1/4}/(mol^{1/4}\cdot s)$, respectively (49). After approximately 70–80% conversion, the solution changes to orange-yellow, which is characteristic of styryllithium chain ends. At the same time, the overall rate of polymerization increases (inflection point). Although the percent conversion at which the inflection point is observed does not appear to depend on solvent, the time to reach this percent conversion is quite solvent-dependent, as shown in Figure 4. Analysis of the copolymer composition indicates that the total % styrene in the copolymer is less than 5% up to approximately 75% conversion (see Fig. 5) (50). When these samples are analyzed by oxidative degradation by ozonolysis, polystyrene segments (corresponding to polystyrene blocks in the copolymer) are recovered only after the inflection point is reached as shown in Figure 5. For a 75/25 (wt/wt) feed mixture of butadiene/styrene, 80% of the styrene is incorporated into the tapered block copolymer as block styrene.

The kinetics of copolymerization provide an explanation for the copolymerization behavior of styrenes with dienes. One useful aspect of living anionic copolymerizations is that stable carbanionic chain ends can be generated and the rates of their crossover reactions with other monomers measured independently of the copolymerization reaction. Two of the four rate constants involved in copolymerization correspond at least superficially to the two homopolymerization reactions

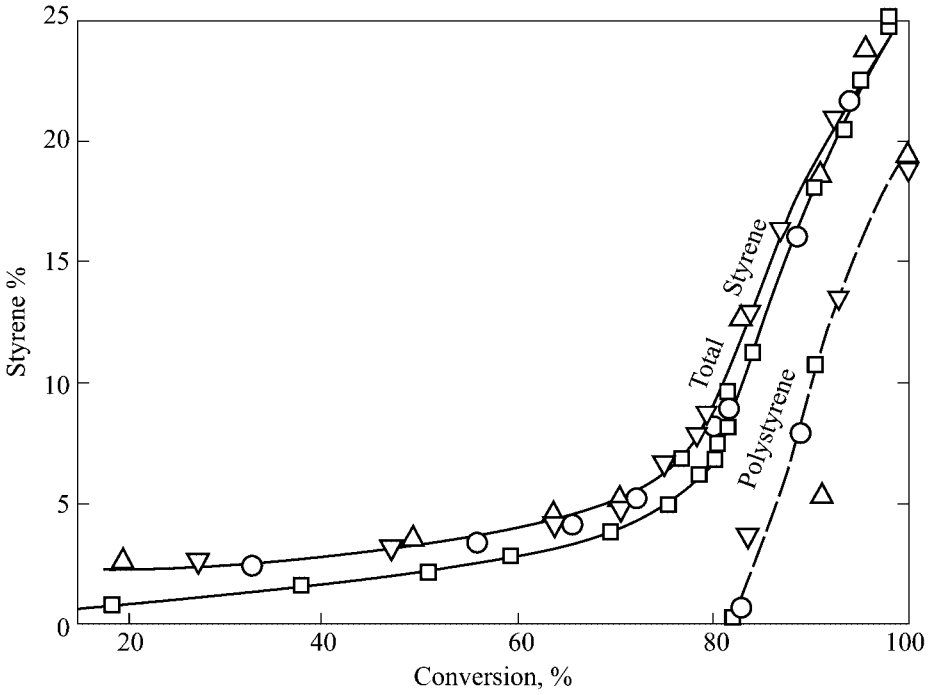

Fig. 5. Copolymerization of styrene from butadiene–styrene (75/25) at 50°C. □ Hexane; Δ cyclohexane; ∇ benzene; ○ toluene. From Ref. 50; reprinted by permission of the Rubber Division of the American Chemical Society.

of butadiene and styrene, eg, k_{BB} and k_{SS}, respectively. The other two rate constants can be measured independently as shown in equations 60 and 61:

$$\text{PSLi} + \text{Butadiene} \xrightarrow{k_{SB}} \text{PS—BDLi} \tag{60}$$

$$\text{PBDLi} + \text{Styrene} \xrightarrow{k_{BS}} \text{PBD—SLi} \tag{61}$$

Kinetic results of a number of independent kinetic studies can be summarized as follows for styrene–butadiene copolymerization (49,178):

$$\underset{[1.1 \times 10^{2}\text{L/(mol·s)}]}{k_{SB}} \gg \underset{[4.5 \times 10^{-1}\text{L/(mol·s)}]}{k_{SS}} > \underset{[8.4 \times 10^{-2}\text{L/(mol·s)}]}{k_{BB}} > \underset{[6.6 \times 10^{-3}\text{L/(mol·s)}]}{k_{BS}}$$

This kinetic order contains the expected order of homopolymerization rates, ie, $k_{SS} > k_{BB}$. The surprising result is that the fastest rate constant is associated with the crossover reaction of the poly(styryl)lithium chain ends with butadiene monomer (k_{SB}); conversely, the slowest reaction rate is associated with the crossover reaction of the poly(butadienyl)lithium chain ends with styrene monomer (k_{BS}). Similar kinetic results have been obtained for styrene–isoprene copolymerization.

In polar media, the preference for diene incorporation is reduced as shown by the monomer reactivity ratios in Table 15. In THF, the order of monomer reactivity ratios is reversed compared to that in hydrocarbon media. The monomer reactivity ratios for styrene are much larger than the monomer reactivity ratio for dienes.

The counterion also has a dramatic effect on copolymerization behavior for styrene and dienes (38). It is particularly noteworthy that the monomer reactivity ratios for styrene ($r_S = 0.42$) and butadiene ($r_B = 0.30$) are almost equal for copolymerization in hydrocarbon at 30°C using an organosodium initiator; however, butadiene is incorporated predominantly as vinyl units (60% 1,2). In contrast, initial styrene incorporation is observed for analogous organopotassium initiators ($r_S = 3.3$) and butadiene ($r_B = 0.12$).

Tapered butadiene–styrene copolymers are important commercial materials because of their outstanding extrusion characteristics, low water absorption, good abrasion resistance, and good electrical properties. Tapered block copolymers are used for wire insulation and shoe soles (after vulcanization) as well as for asphalt modification (179).

Random Styrene–Diene Copolymers. Random copolymers of butadiene (SBR) or isoprene (SIR) with styrene can be prepared by addition of small amounts of ethers, amines, or alkali metal alkoxides with alkyllithium initiators. Random copolymers are characterized as having only small amounts of block styrene content. The amount of block styrene can be determined by ozonolysis or, more simply, by integration of the ^{1}H nmr region corresponding to block polystyrene segments (δ = 6.5–6.94 ppm) (180). Monomers reactivity ratios of $r_B = 0.86$ and $r_S = 0.91$ have been reported for copolymerization of butadiene and styrene in the presence of 1 equiv of TMEDA ([TMEDA]/[RLi] = 1) (181). However, the random SBR produced in the presence of TMEDA will incorporate the butadiene predominantly as 1,2 units. At 66°C, 50% 1,2-butadiene microstructure will be obtained for copolymerization in the presence of 1equiv of TMEDA (134). In the presence of Lewis bases, the amounts of 1,2-polybutadiene enchainment decreases with increasing temperature.

In general, random SBR with a low amount of block styrene and low amounts of 1,2-butadiene enchainment (<20%) can be prepared in the presence of small amounts of added potassium or sodium metal alkoxides. Using 0.2 equiv of sodium 2,3-dimethyl-2-pentoxide, the monomer reactivity ratios for alkyllithium-initiated SBR were found to be $r_B = 1.1$ and $r_S = 0.1$ (182). The resulting copolymer had only 5% block styrene and 18% 1,2-vinyl microstructure. The unique copolymerization behavior in these mixed alkali metal alkoxide/organolithium systems may be due to the formation of cross-associated adducts.

Commercial anionically prepared, random SBR polymers (solution SBR) prepared by alkyllithium-initiated polymerization typically have 23% *cis*-1,4, 49% *trans*-1,4, and 28% vinyl microstructure compared to 10% *cis*-1,4, 70% *trans*-1,4, and 20% vinyl microstructure for emulsion SBR with the same comonomer composition. Solution SBRs typically have branched architectures to eliminate cold flow. Compared to emulsion SBR, solution random SBRs require less accelerator and give higher compounded Mooney viscosity, lower heat buildup, increased resilience, and better retread abrasion index (179). Terpolymers of styrene, isoprene, and butadiene have been prepared using a chain of single-stirred reactors, whereby the steady-state concentration of each monomer and Lewis base

modifier at any degree of conversion can be controlled along the reactor chain (183).

BIBLIOGRAPHY

"Anionic Polymerization" in *EPST* 1st ed., Vol. 2, pp. 95–137, by C. G. Overberger, Polytechnic Institute of Brooklyn; J. E. Mulvaney, University of Arizona; and A. M. Schiller, American Cyanamid Co.; "Anionic Polymerization" in *EPSE* 2nd ed., Vol. 2, pp. 1–43, by S. Bywater, National Research Council of Canada.

1. H. L. Hsieh and R. P. Quirk, *Anionic Polymerization: Principles and Practical Applications*, Marcel Dekker, Inc., New York, 1996, Chapt. "3".
2. Ref. 1, Chapt. 1.
3. A.-M. Sapse and P. V. R. Schleyer, eds., *Lithium Chemistry: A Theoretical and Experimental Overview*, Wiley-Interscience, New York, 1995.
4. M. Szwarc, *Carbanions, Living Polymers and Electron Transfer Processes*, Wiley-Interscience, New York, 1968.
5. Ref. 1, Chapt. 4.
6. R. P. Quirk and B. Lee, *Polym. Int.* **27**, 359 (1992).
7. P. J. Flory, *J. Am. Chem. Soc.* **62**, 1561 (1940).
8. L. J. Fetters, in J. I. Kroschwitz, ed., Encyclopedia of Polymer Science and Engineering, 2nd ed., Vol. **10**, John Wiley & Sons, Inc., New York, 1987, p. 19.
9. G. Riess, G. Hurtrez, and P. Bahadur, in J. I. Kroschwitz, ed., *Encyclopedia of Polymer Science and Engineering*, Vol. **2**, John Wiley & Sons, Inc., New York, 1985, p. 324.
10. Ref. 1, Chapt. 12.
11. R. P. Quirk, D. J. Kinning, and L. J. Fetters, in S. L. Agarwal, ed., *Comprehensive Polymer Science, Vol. 7: Specialty Polymers and Polymer Processing*, Pergamon Press, Oxford, 1989, p. 1.
12. Ref. 1, Chapt. 11.
13. R. P. Quirk, in S. L. Aggarwal and S. Russo, eds., *Comprehensive Polymer Science*, First Supplement, Pergamon Press, Elmsford, N.Y., 1992, p. 83.
14. A. Hirao and M. Hayashi, *Acta Polym.* **50**, 219 (1999).
15. R. P. Quirk, S. H. Jang, and J. Kim, *Rubber Chem. Technol.* **69**, 444 (1996).
16. A. O. Patil, D. N. Schulz, and B. M. Novak, eds., *Functional Polymers: Modern Synthetic Methods and Novel Structures* (ACS Symposium Series 704), American Chemical Society, Washington, D.C., 1998, Chapts. "1, 4–6", 8.
17. J. Roovers, in Ref. 9, 2nd ed., p. 478.
18. Ref. 1, Chapt. 13.
19. M. Pitsikalis and co-workers, *Adv. Polym. Sci.* **135**, 1 (1998).
20. K. Ishizu and S. Uchida, *Prog. Polym. Sci.* **24**, 1439 (1999).
21. B. J. Wakefield, *The Chemistry of Organolithium Compounds*, Pergamon Press, New York, 1974.
22. M. D. Glasse, *Prog. Polym. Sci.* **9**, 133 (1983).
23. Ref. 1, Chapt. 5.
24. R. P. Quirk and V. M. Monroy, in J. I. Kroschwitz, ed., *Kirk-Othmer Encyclopedia of Chemical Technology*, 4th ed., Vol. **14**, John Wiley & Sons, Inc., New York, 1995, p. 461.
25. Ref. 1, Chapt. 2.
26. F. W. Stavely and co-workers, *Ind. Eng. Chem.* **48**, 778 (1956).
27. M. Szwarc, *Adv. Polym. Sci.* **49**, 1 (1963).

28. E. W. Duck and J. M. Locke, in W. M. Saltman, ed., *The Stereo Rubbers*, Wiley-Interscience, New York, 1977, p. 139.
29. M. J. Wagner and J. L. Dye, *Annu. Rev. Mater. Sci.* **23**, 223 (1993).
30. M. Szwarc, Z. Jedlinski, and H. Janeczek, *Macromolecules* **30**, 4498 (1997).
31. H. Janeczek, Z. Jedlinski, and I. Bosek, *Macromolecules* **32**, 4503 (1999).
32. K. J. Ivin and W. K. Busfield, in J. I. Kroschwitz, ed., *Encyclopedia of Polymer Science and Engineering*, Vol. **12**, John Wiley & Sons, Inc., New York, 1988, p. 555.
33. Ref. 1, Chapt. 6.
34. H. L. Hsieh and O. F. McKinney, *Polym. Lett.* **4**, 843 (1966).
35. M. Morton, R. F. Kammereck, and L. J. Fetters, *Br. Polym. J.* **3**, 120 (1971).
36. M. Morton and R. F. Kammereck, *J. Am. Chem. Soc.* **92**, 3217 (1970).
37. A. A. Arest-Yakubovich and co-workers, *Polym. Int.* **37**, 165 (1995).
38. B. I. Nakhmanovich and co-workers, *Macromol. Rapid Commun.* **17**, 31 (1996).
39. A. A. Arest-Yakubovich, in M. E. Volpin, ed., *Chemistry Reviews*, Vol. **19**, Part 4, Harwood, Basel, 1994, p. 1.
40. F. Bandermann, H.-D. Speikamp, and L. Weigel, *Makromol. Chem.* **186**, 2017 (1985).
41. Y. S. Yu and co-workers, *Macromolecules* **29**, 2738 (1996).
42. R. D. Sanderson, A. H. A. Roediger, and G. J. Summers, *Polym. Int.* **35**, 263 (1994).
43. L. J. Fetters and M. Morton, *Macromolecules* **2**, 453 (1969).
44. R. P. Quirk and J.-J. Ma, *Polym. Int.* **24**, 197 (1991).
45. D. N. Schulz, J. C. Sanda, and B. G. Willoughby, in J. E. McGrath, ed., *Anionic Polymerization: Kinetics, Mechanisms, and Synthesis* (ACS Symposium Series 166), American Chemical Society, Washington, D.C., 1981, p. 427.
46. R. P. Quirk and co-workers, *Adv. Polym. Sci.* **153**, 67 (2000).
47. P. Vlcek and L. Lochmann, *Prog. Polym. Sci.* **24**, 793 (1999).
48. C. Zune and R. Jérôme, *Prog. Polym. Sci.* **24**, 631 (1999).
49. S. Bywater, in C. H. Bamford and C. F. H. Tipper, eds., *Comprehensive Chemical Kinetics, Vol. 15: Non-Radical Polymerization*, Elsevier, New York, 1976, p. 1.
50. H. L. Hsieh and W. H. Glaze, *Rubber Chem. Technol.* **43**, 22 (1970).
51. D. J. Worsfold and S. Bywater, *Can. J. Chem.* **38**, 1891 (1960).
52. G. Graham, S. Richtsmeier, and D. A. Dixon, *J. Am. Chem. Soc.* **102**, 5759 (1980).
53. Ref. 1, Chapt. 7.
54. R. N. Young and co-workers, *Polym. Int.* **33**, 217 (1994).
55. S. Bywater, *Polym. Int.* **38**, 325 (1995).
56. L. J. Fetters, J. S. Huang, and R. N. Young, *J. Polym. Sci., Part A: Polym. Chem.* **34**, 1517 (1996).
57. J. Stellbrink and co-workers, *Macromolecules* **31**, 4189 (1998).
58. S. Bywater, *Macromolecules* **31**, 6010 (1998).
59. S. Bywater and D. J. Worsfold, in T. E. Hogen-Esch and J. Smid, eds., *Recent Advances in Anionic Polymerization*, Elsevier, New York, 1987, p. 109.
60. H. Sinn, C. Lundborg, and O. T. Onsager, *Makromol. Chem.* **70**, 222 (1964).
61. M. Morton and co-workers, *Macromolecules* **3**, 327 (1970).
62. D. J. Worsfold and S. Bywater, *Macromolecules* **5**, 393 (1972).
63. L. J. Fetters and M. Morton, *Macromolecules* **7**, 552 (1974).
64. A. Hernandez and co-workers, *Makromol. Chem., Rapid Commun.* **1**, 75 (1980).
65. L. J. Fetters and co-workers, *Macromolecules* **28**, 4996 (1995).
66. J. Stellbrink and co-workers, *Macromolecules* **32**, 5321 (1999).
67. S. Dumas, J. Sledz, and F. Schue, in Ref. 43, p. 463.
68. Ref. 1, Chapt. 3.
69. S. Winstein and co-workers, *J. Am. Chem. Soc.* **76**, 2597 (1954).

70. C. J. Dyball, D. J. Worsfold, and S. Bywater, *Macromolecules* **12**, 819 (1979).
71. A. Garton and S. Bywater, *Macromolecules* **8**, 697 (1975).
72. Ref. 1, Chapt. 8.
73. M. Fontanille, in G. C. Eastmond, A. Ledwith, S. Russo, and P. Sigwalt, eds., *Comprehensive Polymer Science, Vol. 3: Chain Polymerization I*, Pergamon Press, Elmsford, N.Y., 1989, Chapt. "27", p. 425.
74. W. J. Kern and co-workers, *J. Appl. Polym. Sci.* **16**, 3123 (1972).
75. D. Ades, M. Fontanille, and J. Leonard, *Can. J. Chem.* **60**, 564 (1982).
76. F. Schue and co-workers, *Makromol. Chem., Macromol. Symp.* **67**, 213 (1993).
77. W. Nentwig and H. Sinn, *Makromol. Chem., Rapid Commun.* **1**, 59 (1980).
78. D. N. Bhattacharyya and co-workers, *J. Phys. Chem.* **69**, 612 (1965).
79. B. Francois and X. F. Zhong, *Makromol. Chem.* **191**, 2743 (1990).
80. J. Leonard and S. L. Malhotra, *J. Macromol. Sci., A: Chem.* **11**, 2087 (1977).
81. W. C. E. Higginson and N. S. Wooding, *J. Chem. Soc.* 760 (1952).
82. A. L. Gatzke, *J. Polym. Sci., Part A-1* **7**, 2281 (1969).
83. S. Kume and co-workers, *Makromol. Chem.* **84**, 137 (1965).
84. J. E. Puskas, *Makromol. Chem.* **194**, 187 (1993).
85. K. Hatada, T. Kitayama, K. Fumikawa, K. Ohta, and H. Yuki, in Ref. 43, p. 327.
86. R. Fayt and co-workers, *Macromolecules* **20**, 1442 (1987).
87. V. Halaska and L. Lochmann, *Coll. Czech. Chem. Commun.* **38**, 1780 (1973).
88. G. Löhr and G. V. Schulz, *Eur. Polym. J.* **10**, 121 (1974).
89. A. H. E. Müller, in Ref. 59, p. 205.
90. M. Janata, L. Lochmann, and A. H. E. Müller, *Makromol. Chem.* **194**, 625 (1993).
91. M. Janata, L. Lochmann, and A. H. E. Müller, *Makromol. Chem.* **191**, 2253 (1990).
92. D. J. Brunelle, ed., *Ring-Opening Polymerization: Mechanisms, Catalysis, Structure, Utility*, Hanser, New York, 1993.
93. V. Halaska, L. Lochmann, and D. Lim, *Coll. Czech. Chem. Commun.* **33**, 3245 (1968).
94. F. E. Bailey Jr. and H. G. France, in J. A. Moore, ed., *Macromolecular Syntheses, Collective*, Vol. **1**, John Wiley & Sons, Inc., New York, 1977, p. 289.
95. G. Gee, W. C. E. Higginson, and G. T. Merrall, *J. Chem. Soc.* 1345 (1959).
96. S. Boileau, in G. C. Eastmond, A. Ledwith, S. Russo, and P. Sigwalt, eds., *Comprehensive Polymer Science, Vol. 3: Chain Polymerization*, Part I, Pergamon Press, Oxford, 1989, p. 467.
97. P. J. Flory, *J. Am. Chem. Soc.* **62**, 1561 (1940).
98. S. Boileau, in Ref. 45, p. 283.
99. C. D. Eisenbach and M. Peuscher, *Makromol. Chem., Rapid Commun.* **1**, 105 (1980).
100. J. Ding, C. Price, and C. Booth, *Eur. Polym. J.* **27**, 891 (1991).
101. C. Price, *Acc. Chem. Res.* **7**, 294 (1974).
102. J. Ding and co-workers, *Eur. Polym. J.* **27**, 895 (1991).
103. T. Tsuruta and Y. Kawakami, in Ref. 96, p. 489.
104. R. Jérôme and Ph. Teyssie, in Ref. 96, p. 501.
105. S. Slomkowski and S. Penczek, *Macromolecules* **9**, 367 (1976).
106. A. Hofman, S. Slomkowski, and S. Penczek, *Makromol. Chem.* **185**, 91 (1984).
107. S. Slomkowski and A. Duda, in Ref. 92, p. 114.
108. D. J. Brunelle, in Ref. 92, p. 309.
109. H. Keul, R. Bacher, and H. Höcker, *Makromol. Chem.* **187**, 2579 (1986).
110. D. J. Brunelle and T. G. Shannon, *Macromolecules* **24**, 3035 (1991).

111. T. C. Kendrick, B. M. Parbhoo, and J. W. White, in G. C. Eastmond, A. Ledwith, S. Russo, and P. Sigwalt, eds., *Comprehensive Polymer Science, Vol. 4: Chain Polymerization*, Part II, Pergamon Press, Oxford, 1989, p. 459.
112. J. B. Carmichael and R. Winger, *J. Polym. Sci., Part A* **3**, 971 (1965).
113. B. Hardman and A. Torkelson in J. I. Kroschwitz, ed., *Encyclopedia of Polymer Science and Engineering*, 2nd ed., Vol. **15**, John Wiley & Sons, Inc., New York, 1989, p. 204.
114. H. Jacobson and W. H. Stockmayer, *J. Chem. Phys.* **18**, 1600 (1950).
115. Ref. 1, Chapt. 9.
116. S. Bywater, in Ref. 96, Chapt. 28, p. 433.
117. F. C. Foster and J. L. Binder, Advances in Chemistry Series No. 19, American Chemical Society, Washington, D.C., 1957, p. 26.
118. A. V. Tobolsky and C. E. Rogers, *J. Polym. Sci.* **40**, 73 (1959).
119. W. Gerbert, J. Hinz, and H. Sinn, *Makromol. Chem.* **144**, 97 (1971).
120. M. M. F. Al-Jarrah, R. L. Apikian, and E. Ahmed, *Polym. Bull.* **12**, 433 (1984).
121. M. Morton and J. R. Rupert, in F. E. Bailey Jr., ed., *Initiation of Polymerization*, (ACS Symposium Series 212), American Chemical Society, Washington, D.C., 1983, p. 284.
122. S. Bywater, D. J. Worsfold, and G. Hollingsworth, *Macromolecules* **5**, 389 (1972).
123. D. J. Worsfold and S. Bywater, *Macromolecules* **11**, 582 (1978).
124. W. Gerbert, J. Hinz, and H. Sinn, *Makromol. Chem.* **144**, 97 (1971).
125. S. Bywater, Y. Firat, and P. E. Black, *J. Polym. Sci., Polym. Chem. Ed.* **22**, 669 (1984).
126. R. Salle and Q. T. Pham, *J. Polym. Sci., Polym. Chem. Ed.* **15**, 1799 (1977).
127. S. Bywater and D. J. Worsfold, *Can. J. Chem.* **45**, 1821 (1967).
128. Unpublished work of S. Bywater quoted in Ref. 112.
129. A. Essel and Q. T. Pham, *J. Polym. Sci., Part A-1* **10**, 2793 (1972).
130. C. J. Dyball, D. J. Worsfold, and S. Bywater, *Macromolecules* **12**, 819 (1979).
131. S. Bywater and D. J. Worsfold, *J. Organometal. Chem.* **159**, 229 (1978).
132. S. Bywater, in Ref. 45, p. 71.
133. T. A. Antkowiak and co-workers, *J. Polym. Sci., Part A-1* **10**, 1319 (1972).
134. R. Werbowyj, S. Bywater, and D. J. Worsfold, *Eur. Polym. J.* **22**, 707 (1986).
135. A. F. Halasa, D. F. Lohr, and J. E. Hall, *J. Polym. Sci., Polym. Chem. Ed.* **19**, 1357 (1981).
136. R. N. Young, R. P. Quirk, and L. J. Fetters, *Adv. Polym. Sci.* **56**, 1 (1984).
137. P. Bres and co-workers, *Macromolecules* **19**, 1325 (1986).
138. A. R. Luxton and co-workers, *Polymer* **22**, 382 (1981).
139. S. L. Aggarwal, T. G. Hargis, R. A. Livigni, H. J. Fabris, and L. F. Marker, in J. Lal and J. E. Mark, eds., *Advances in Elastomers and Rubber Elasticity*, Plenum, New York, 1986, p. 17.
140. I. G. Hargis, R. A. Livigni, and S. L. Aggarwal, in A. Whelan and K. S. Lee, eds., *Developments in Rubber Technology—4*, Elsevier, Essex, U.K. 1987, p. 1.
141. J. M. Widmaier and G. C. Meyer, *Macromolecules* **14**, 450 (1981).
142. H. Yuki and K. Hatada, *Adv. Polym. Sci.* **31**, 1 (1979).
143. K. Hatada, T. Kitayama, and K. Ute, *Prog. Polym. Sci.* **13**, 189 (1988).
144. W. Fowells and co-workers, *J. Am. Chem. Soc.* **89**, 1396 (1967).
145. K. Hatada and co-workers, *Polym. J.* **12**, 55 (1980).
146. T. Kitayama and co-workers, *Makromol. Chem.* **15**(Suppl.) 167 (1989).
147. T. Tsuruta, T. Makimoto, and H. Kanai, *J. Macromol. Sci.* **1**, 31 (1966).
148. H. Yuki and co-workers, *Polym. J.* **1**, 36 (1970).
149. K. Hatada and co-workers, *Polym. J.* **18**, 1037 (1986).
150. A. Soum, N. D'Accorso, and M. Fontanille, *Makromol. Chem., Rapid Commun.* **4**, 471 (1983).

151. D. G. Ballard and co-workers, *Macromolecules* **25**, 5907 (1992).
152. T. Kitayama, T. Hirano, and K. Hatada, *Polym. J.* **28**, 61 (1996).
153. H. Jeuck and A. H. E. Müller, *Makromol. Chem., Rapid Commun.* **3**, 121 (1982).
154. J. P. Pascault and co-workers, *Eur. Polym. J.* **10**, 1107 (1974).
155. V. Warzelhan, H. Höcker, and G. V. Schulz, *Makromol. Chem.* **181**, 149 (1980).
156. R. Kraft and co-workers, *Makromol. Chem., Rapid Commun.* **1**, 363 (1980).
157. A. H. E. Müller, H. Höcker, and G. V. Schulz, *Macromolecules* **10**, 1086 (1977).
158. A. H. E. Müller, in Ref. 45, p. 440.
159. B. L. Erusalimskii, *Mechanisms of Ionic Polymerization*, Consultants Bureau, New York, 1986, p. 223.
160. G. Odian, *Principles of Polymerization*, 3rd ed., Wiley-Interscience, New York, 1991, p. 659.
161. P. Pino and U. W. Suter, *Polymer* **17**, 977 (1976).
162. S. Suparno and co-workers, *Polym. J.* **13**, 313 (1981).
163. S. Raynal, *Polym. J.* **15**, 585 (1983).
164. D. J. Worsfold and S. Bywater, *Makromol. Chem.* **65**, 245 (1963).
165. L. Cazzaniga and R. E. Cohen, *Macromolecules* **22**, 4125 (1989).
166. A. H. Soum and T. E. Hogen-Esch, *Macromolecules* **18**, 690 (1985).
167. Ref. 1, Chapt. 10.
168. F. R. Mayo and C. Walling, *Chem. Rev.* **46**, 191 (1950).
169. L.-K. Huang, Ph.D. dissertation, University of Akron, Akron, Ohio, 1979; quoted in Ref. 184.
170. D. J. T. Hill and co-workers, *Polym. Bull.* **9**, 292 (1983).
171. H. Yuki and Y. Okamoto, *Bull. Chem. Soc. Jpn.* **43**, 148 (1970).
172. S. L. Agarwall, R. A. Livigni, L. F. Marker, and T. J. Dudek, in J. J. Burke and V. Weiss, eds., *Block and Graft Copolymers*, Syracuse University Press, Syracuse, N.Y. 1973, p. 157.
173. Y. L. Spirin and co-workers, *Polym. Sci. USSR* **3**, 233 (1962).
174. D. J. Worsfold, *J. Polym. Sci., Part A-1* **5**, 2783 (1967).
175. A. A. Korotkov, S. P. Mitzengendler, and K. M. Aleyev, *Polym. Sci. USSR* **3**, 487 (1962).
176. Y. Yuki and Y. Okamoto, *Bull. Chem. Soc. Jpn.* **42**, 1644 (1969).
177. H. Yuki and co-workers, *Bull. Chem. Soc. Jpn.* **40**, 2659 (1967).
178. R. Ohlinger and F. Bandermann, *Makromol. Chem.* **181**, 1935 (1980).
179. Ref. 1, Chapt. 17.
180. V. D. Mochel, *Rubber Chem. Technol.* **40**, 1200 (1967).
181. Y. Y. Melenevskaya and co-workers, *Vysokomol. Soedin., A* **21**, 2008 (1979); *Polym. Sci. USSR* **21**, 2215 (1979).
182. R. P. Quirk, Y. Lee, and J.-P. Zhou, *Polym. Prep. (Am. Chem. Soc., Div. Polym. Chem.)* **41**(1), 129–130 (2000).
183. A. F. Halasa and co-workers, *Eur. Rubber J.* **172**, 36 (June 1990); *Rubber Plastics News* **19**, 63 (May 26, 1990).
184. M. Morton, *Anionic Polymerization: Principles and Practice*, Academic Press, Inc., New York, 1983, p. 142.

GENERAL REFERENCES

H. L. Hsieh and R. P. Quirk, *Anionic Polymerization: Principles and Practical Applications*, Marcel Dekker, Inc., New York, 1996.
M. Morton, *Anionic Polymerization: Principles and Practice*, Academic Press, Inc., New York, 1983.

M. Szwarc, *Carbanions, Living Polymers and Electron Transfer Processes*, Wiley-Interscience, New York, 1968.
M. Szwarc, *Ionic Polymerization Fundamentals*, Hanser, Cincinnati, Ohio, 1996.
D. J. Brunelle, ed., *Ring-Opening Polymerization: Mechanisms, Catalysis, Structure, Utility*, Hanser, Munich, 1993.
Comprehensive Polymer Science, Vol. 3: Chain Polymerization, Part I, Pergamon Press, Oxford, 1989.

RODERIC P. QUIRK
The University of Akron

ANTIFOAMING AGENTS. See VOLUME 1.

ANTIOXIDANTS

Introduction

Antioxidants are used to retard the reaction of organic materials, such as synthetic polymers, with atmospheric oxygen. Such reaction can cause degradation of the mechanical, aesthetic, and electrical properties of polymers; loss of flavor and development of rancidity in foods; and an increase in the viscosity, acidity, and formation of insolubles in lubricants. The need for antioxidants depends upon the chemical composition of the substrate and the conditions of exposure. Relatively high concentrations of antioxidants are used to stabilize polymers such as natural rubber and polyunsaturated oils. Saturated polymers have greater oxidative stability and require relatively low concentrations of stabilizers. Specialized antioxidants which have been commercialized meet the needs of the industry by extending the useful lives of the many substrates produced under anticipated conditions of exposure. In 2000, approximately 227,000 t (500 million pounds) of antioxidants were sold in polymer applications, with a value of $1.3 billion (1). On average, the growth rate of antioxidants is around 4%, roughly tracking the growth of the global polymer markets (2).

Mechanism of Uninhibited Autoxidation

The mechanism by which an organic material (RH) undergoes autoxidation involves a free-radical chain reaction is shown below (3–5):

Initiation

$$RH \rightarrow \text{Free radicals, eg, } R\cdot, ROO\cdot, RO\cdot, HO\cdot \quad (1)$$

$$ROOH \rightarrow RO\cdot + OH\cdot \quad (2)$$

Encyclopedia of Polymer Science and Technology. Copyright John Wiley & Sons, Inc. All rights reserved.

$$2\,ROOH \rightarrow RO\cdot + ROO\cdot + H_2O \quad (3)$$

$$ROOR \rightarrow 2\,RO\cdot \quad (4)$$

Propagation

$$R\cdot + O_2 \rightarrow ROO\cdot \quad (5)$$

$$ROO\cdot + RH \rightarrow ROOH + R\cdot \quad (6)$$

Termination

$$2\,R\cdot \rightarrow R{-}R \quad (7)$$

$$ROO\cdot + R\cdot \rightarrow ROOR \quad (8)$$

$$2\,ROO\cdot \rightarrow \text{Nonradical products} \quad (9)$$

Initiation. Free-radical initiators are produced by several processes. The high temperatures and shearing stresses required for compounding, extrusion, and molding of polymeric materials can produce alkyl radicals by homolytic chain cleavage. Oxidatively sensitive substrates can react directly with oxygen, particularly at elevated temperatures, to yield radicals.

It is virtually impossible to manufacture commercial polymers that do not contain traces of hydroperoxides. The peroxide bond is relatively weak and cleaves homolytically to yield radicals (eqs. 2 and 3). Once oxidation has started, the concentration of hydroperoxides becomes appreciable. The decomposition of hydroperoxides becomes the main source of radical initiators.

The absorption of (uv) light produces radicals by cleavage of hydroperoxides and carbonyl compounds (eqs. 10–12)

$$ROOH \xrightarrow{h\nu} RO\cdot + OH\cdot \quad (10)$$

$$R{-}\overset{\overset{O}{\|}}{C}{-}R \xrightarrow{h\nu} R{-}\overset{\overset{O}{\|}}{C}\cdot + R\cdot \quad (11)$$

$$R{-}\overset{\overset{O}{\|}}{C}\cdot \rightarrow R\cdot + CO \quad (12)$$

Most polymer degradation caused by the absorption of uv light results from radical-initiated autoxidation.

Direct reaction of oxygen with most organic materials to produce radicals (eq. 13) is very slow at moderate temperatures. Hydrogen-donating antioxidants

Table 1. Dissociation Energies of Carbon–Hydrogen Bonds[a]

R—H	D_{R-H}, kJ/mol[b]	Bond type
$CH_2{=}CHCH_2{-}H$	356	Allylic
$(CH_3)_3C{-}H$	381	Tertiary
$(CH_3)_2CH{-}H$	395	Secondary

[a]Ref. 8.
[b]To convert kJ to kcal, divide by 4.184.

(AH), particularly those with low oxidation–reduction potentials, can react with oxygen (eq. 14), especially at elevated temperatures (6).

$$RH + O_2 \longrightarrow R\cdot + HO_2\cdot \quad (13)$$

$$AH + O_2 \longrightarrow A\cdot + HO_2\cdot \quad (14)$$

Propagation. Propagation reactions (eqs. 5 and 6) can be repeated many times before termination by conversion of an alkyl or peroxy radical to a nonradical species (7). Homolytic decomposition of hydroperoxides produced by propagation reactions increases the rate of initiation by the production of radicals.

The rate of reaction of molecular oxygen with alkyl radicals to form peroxy radicals (eq. 5) is much higher than the rate of reaction of peroxy radicals with a hydrogen atom of the substrate (eq. 6). The rate of the latter depends on the dissociation energies (Table 1) and the steric accessibility of the various carbon–hydrogen bonds; it is an important factor in determining oxidative stability (8).

Polybutadiene and polyunsaturated fats, which contain allylic hydrogen atoms, oxidize more readily than polypropylene, which contains tertiary hydrogen atoms. A linear hydrocarbon such as polyethylene, which has secondary hydrogens, is the most stable of these substrates.

Autocatalysis. The oxidation rate at the start of aging is usually low and increases with time. Radicals, produced by the homolytic decomposition of hydroperoxides and peroxides (eqs. 2–4) accumulated during the propagation and termination steps, initiate new oxidative chain reactions, thereby increasing the oxidation rate.

Metal-Catalyzed Oxidation. Trace quantities of transition metal ions catalyze the decomposition of hydroperoxides to radical species and greatly accelerate the rate of oxidation. Most effective are those metal ions that undergo one-electron transfer reactions, eg, copper, iron, cobalt, and manganese ions (9). The metal catalyst is an active hydroperoxide decomposer in both its higher and its lower oxidation states. In the overall reaction, two molecules of hydroperoxide decompose to peroxy and alkoxy radicals (eq. 5).

$$ROOH + M^n \longrightarrow ROO\cdot + M^{(n-1)+} + H^+ \quad (15)$$

$$ROOH + M^{(n-1)+} \longrightarrow RO\cdot + M^{n+} + OH^- \quad (16)$$

$$2\,ROOH \longrightarrow ROO\cdot + RO\cdot + H_2O$$

Termination. The conversion of peroxy and alkyl radicals to nonradical species terminates the propagation reactions, thus decreasing the kinetic chain length. Termination reactions (eqs. 7 and 8) are significant when the oxygen concentration is very low, as in polymers with thick cross sections where the oxidation rate is controlled by the diffusion of oxygen, or in a closed extruder. The combination of alkyl radicals (eq. 7) leads to cross-linking, which causes an undesirable increase in melt viscosity and molecular weight.

Radical Scavengers

Hydrogen-donating antioxidants (AH), such as hindered phenols and secondary aromatic amines, inhibit oxidation by competing with the organic substrate (RH) for peroxy radicals. This shortens the kinetic chain length of the propagation reactions.

$$\mathrm{ROO\cdot} + \mathrm{AH} \xrightarrow{k_{17}} \mathrm{ROOH} + \mathrm{A\cdot} \qquad (17)$$

$$\mathrm{ROO\cdot} + \mathrm{RH} \xrightarrow{k_{6}} \mathrm{ROOH} + \mathrm{R\cdot}$$

Because k_{17} is much larger than k_6, hydrogen-donating antioxidants generally can be used at low concentrations. The usual concentrations in saturated thermoplastic polymers range from 0.01 to 0.05%, based on the weight of the polymer. Higher concentrations, ie, ca 0.5–2%, are required in substrates that are highly sensitive to oxidation, such as unsaturated elastomers and acrylonitrile-butadiene-styrene (ABS).

Hindered Phenols. Even a simple monophenolic antioxidant, such as 2,6-di-*tert*-butyl-*p*-cresol [128-37-0] (**1**), has a complex chemistry in an autooxidizing substrate as seen in Figure 1 (10).

Stilbenequinones such as compound **5** absorb visible light and cause some discoloration. However, upon oxidation phenolic antioxidants impart much less color than aromatic amine antioxidants and are considered to be nondiscoloring and nonstaining.

The effect substitution on the phenolic ring has on activity has been the subject of several studies (11–13). Hindering the phenolic hydroxyl group with at least one bulky alkyl group in the ortho position appears necessary for high antioxidant activity. Nearly all commercial antioxidants are hindered in this manner. Steric hindrance decreases the ability of a phenoxyl radical to abstract a hydrogen atom from the substrate and thus produces an alkyl radical (14) capable of initiating oxidation (eq. 17).

$$\mathrm{A\cdot} + \mathrm{RH} \longrightarrow \mathrm{AH} + \mathrm{R\cdot} \qquad (18)$$

Replacing a methyl with a tertiary alkyl group in the para position usually decreases antioxidant effectiveness. The formation of antioxidants such as compound (**4**) by dimerization is precluded because all benzylic hydrogen atoms are replaced by methyl groups. A strong electron-withdrawing group on the aromatic ring, such

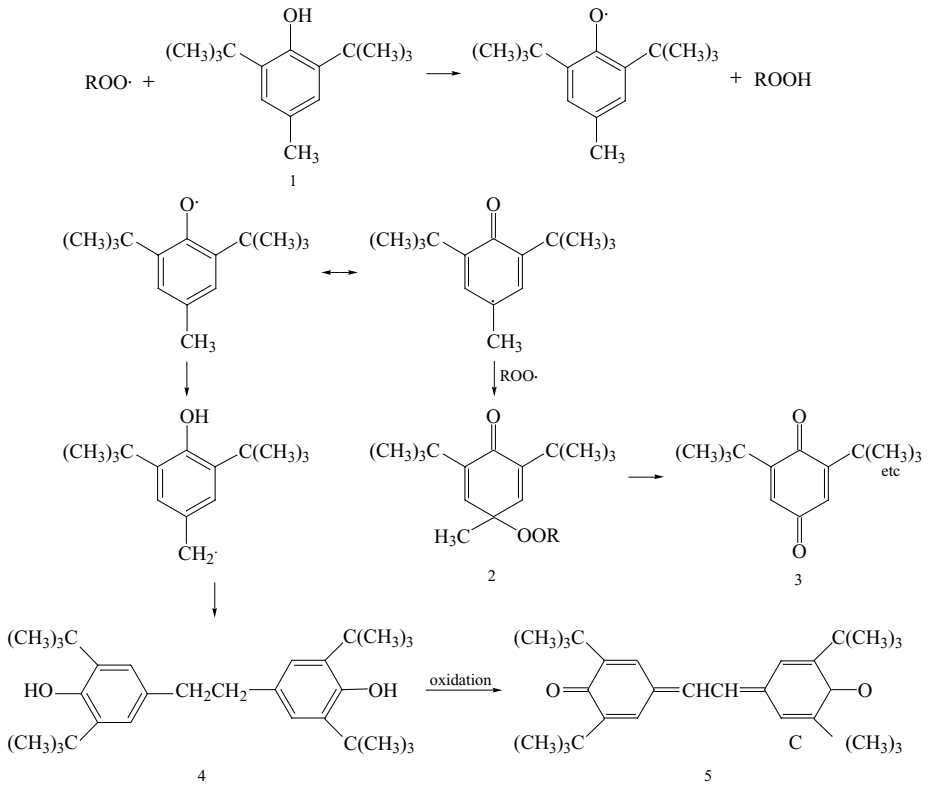

Fig. 1. Chemical transformations of 2,6-di-*tert*-butyl-*p*-cresol in an oxidizing medium (10).

as cyano or carboxy, decreases the ability of the phenol to donate its hydrogen atom to a peroxy radical of the substrate and reduces antioxidant effectiveness.

The usefulness of a hindered phenol for a specific application depends on its radical-trapping ability, its solubility in the substrate, and its volatility under test conditions. Table 2 shows the importance of volatility to stabilizer performance. Equimolar quantities of alkyl esters (**6**) of 3,5-di-*tert*-butyl-4-hydroxyhydrocinnamic acid were evaluated in polypropylene at 140°C, using two different procedures (15). When tested in an airstream, only the octadecyl ester(**6**) (where $n = 18$) was effective in stabilizing the polymer. Under these conditions, the lower homologues were lost by volatilization. The oxygen-uptake test, carried out in a closed system that minimizes evaporative loss, showed that homologues were effective to varying degrees. The differences in effectiveness can probably be attributed to differences in the solubility of various homologues in the amorphous phase of the polypropylene. When dodecane, a liquid in which all the compounds are soluble, was used as a substrate instead of polypropylene, the antioxidant activities were relatively close.

Introducing long aliphatic chains into a stabilizer molecule decreases volatility and increases solubility in hydrocarbon polymers. This improves performance; however, it also increases the equivalent weight of the active

Table 2. Influence of Antioxidant (6) Volatility on Effectiveness at 140°C

		Time to failure in PP, h		Time to failure in dodecane, h
n^a	$t_{1/2}$, h^b	O_2 uptake	Airstream	
1	0.28	95	2	25
6	3.60	312	2	23
12	83.0	420	2	20
18	660.0	200	165	20

[a] *n* in

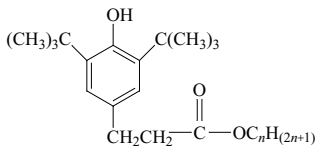

(**6**)

[b] Antioxidant half-life in polypropylene exposed to a nitrogen stream at 140°C.

moiety. Di-, tri-, and polyphenolic antioxidants combine relatively low equivalent weights with low volatility. Commercially important di-, tri-, and polyphenolic stabilizers include 2,2′-methylenebis(6-*tert*-butyl-*p*-cresol) [85-60-9] (**7**), 1,3,5-trimethyl-2,4,6-tris(3′5′-di-*tert*-butyl-4-hydroxybenzyl)benzene [1709-70-2] (**8**), and tetrakis[methylene(3,5-di-*tert*-butyl-4-hydroxyhydrocinnamate)]methane [6683-19-8] (**9**).

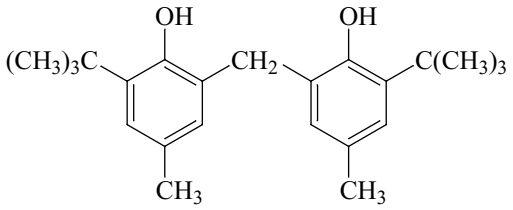

(**7**)

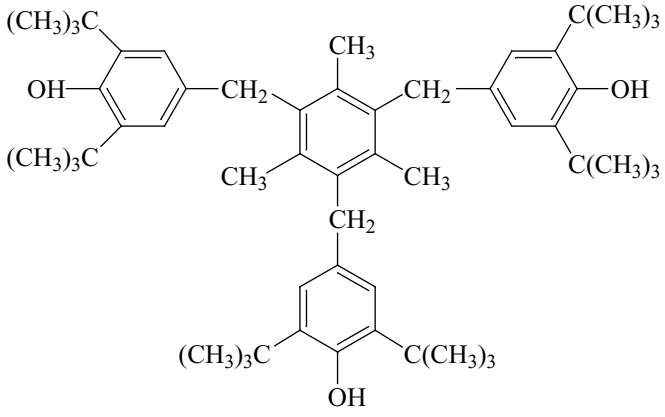

(**8**)

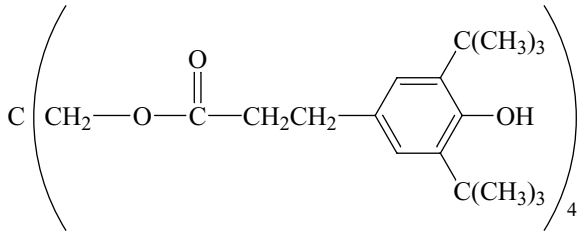

(**9**)

Aromatic Amines. Antioxidants derived from *p*-phenylenediamine and diphenylamine are highly effective peroxy radical scavengers. They are more effective than phenolic antioxidants for the stabilization of easily oxidized organic materials, such as unsaturated elastomers. Because of their intense staining effect, derivatives of *p*-phenylenediamine are used primarily for elastomers containing carbon black (qv).

N,*N*′-Disubstituted-*p*-phenylenediamines, such as *N*-phenyl-*N*′-(1,3-dimethylbutyl)-*p*-phenylenediamine [793-24-8] (**10**), are used in greater quantities than other classes of antioxidants. These products protect unsaturated elastomers against oxidation as well as ozone degradation (see RUBBER CHEMICALS).

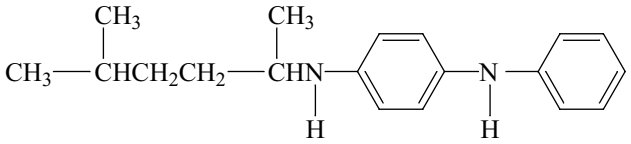

(**10**)

Low concentrations of alkylated paraphenylenediamines, such as *N*,*N*′-di-*sec*- butyl-*p*- phenylenediamine [69796-47-0], are added to gasoline to inhibit oxidation.

Figure 2 shows some of the reactions of aromatic amines that contribute to their activity as antioxidants and to their tendency to form highly colored polyconjugated systems.

Alkylated diphenylamines **11** and derivatives of both dihydroquinoline (**12**) and polymerized 2,2,4-trimethyl-1,2-dihydroquinoline [26780-96-1] (**13**) develop less color than the *p*-phenylenediamines and are classified as semistaining antioxidants. Derivatives of dihydroquinoline are used for the stabilization of animal feed and spices.

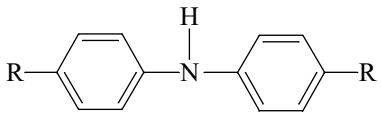

(**11**)

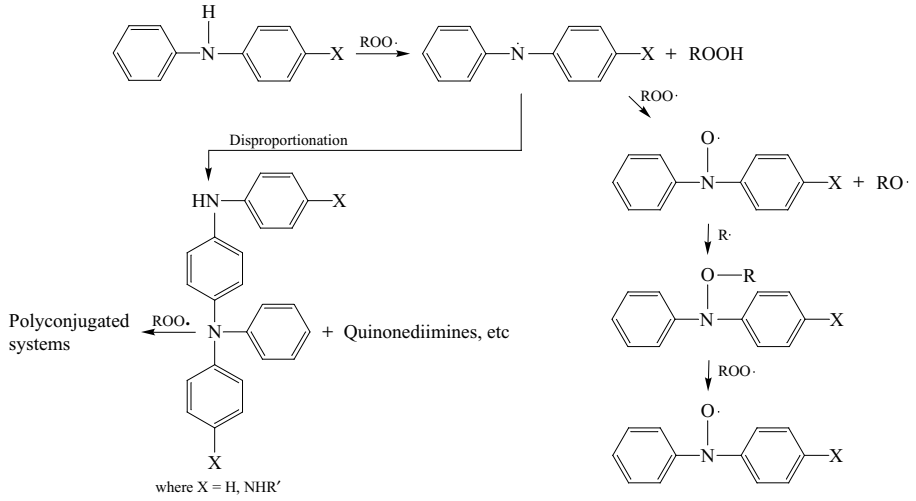

Fig. 2. Oxidation of aromatic amine antioxidants (**10**).

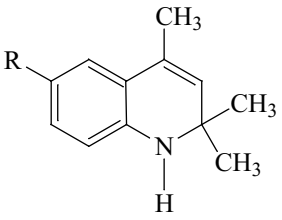

(**12**)

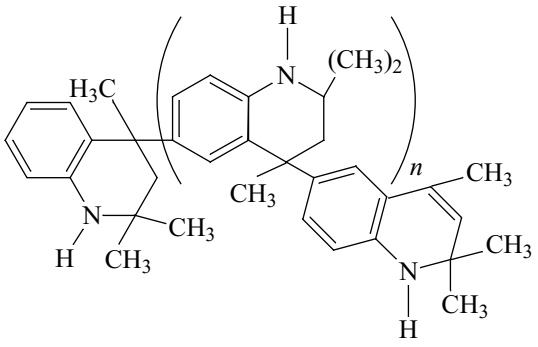

(**13**)

4,4′-Bis(α,α-dimethylbenzyl)diphenylamine [1008-67-1] (**14**) has only a slight tendency to stain and has been recommended for use in plastics as well as elastomers.

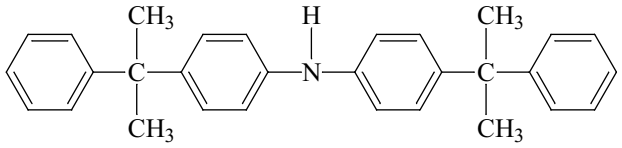

(**14**)

Hindered Amines. Hindered amines are extremely effective in protecting polyolefins and other polymeric materials against photodegradation. They usually are classified as light stabilizers rather than antioxidants.

Most of the commercial hindered-amine light stabilizers (HALS) are derivatives of 2,2,6,6-tetramethylpiperidine [768-66-1] (**15**) (16).

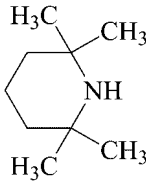

(**15**)

These stabilizers function as light-stable antioxidants to protect polymers. Their antioxidant activity is explained by the following sequence (17):

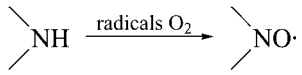

(19)

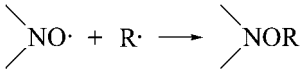

(20)

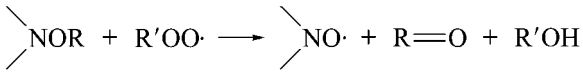

(21)

According to this mechanism, hindered-amine derivatives terminate propagating reactions (eqs. 5 and 6) by trapping both the alkyl and peroxy radicals. In effect, NO competes with O_2, and NOR competes with RH. Since the nitroxyl radicals are not consumed in the overall reactions, they are effective at low concentrations.

Hydroxylamines. A relatively new stabilizer chemistry, commercially introduced in 1996, (18) based on the hydroxylamine functionality, can serve as a very powerful hydrogen-atom donor and free-radical scavenger (19), as illustrated in Figure 3.

This hydroxylamine chemistry is extremely powerful on an equivalent weight basis in comparison with conventional phenolic antioxidants and phosphite melt-processing stabilizers. In terms of its free-radical scavenger capability, however, it is more effective during melt-processing of the polymer, but not during long-term thermal stability (ie, below the melting point of the polymer). This is quite interesting because of the similarity between the type of free-radical scavenging chemistry that hydroxylamines and phenols are both capable of providing. However, the temperature range is different. This is discussed further below.

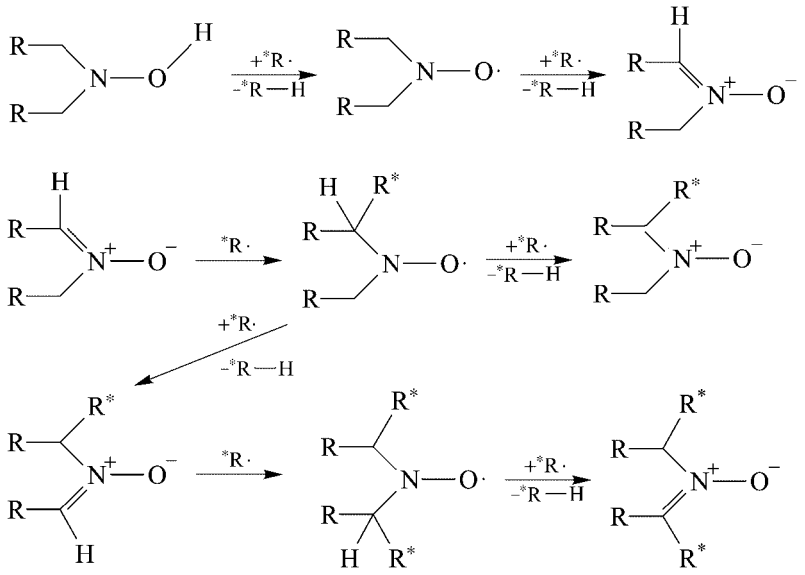

Fig. 3. Free Radical Decomposition Mechanism for Hydroxylamines. $*R^{\bullet}$= alkyl ($R^{\bullet}$), alkoxy ($RO^{\bullet}$), or peroxy ($ROO^{\bullet}$) type radicals.

The only commercial hydroxylamine product used in polyolefins and other selected polymers is a product of a process based on the oxidation of bis-tallow amine [14325-92-2].

There is a similar commercially available product based on related chemistry. It is a product of a process based on the oxidation of methyl-bis-tallow amine [204933-93-7]. The oxidation product of methyl-bis-tallow amine is a trialkylamineoxide, a precursor to hydroxylamine stabilization chemistry. The trialkylamineoxide is converted to a hydroxylamine and a long-chain olefin during the initial melt compounding of the polymer by a Cope elimination reaction, as shown below.

$$R_2(CH_3)N^+—O^- + \text{Heat} \longrightarrow R(CH_3)N—OH + R—CH{=}CH2$$

Benzofuranones. In 1997, a fundamentally new type of chemistry was introduced, which not only inhibits the autoxidation cycle, but attempts to shut it down as soon as it starts (20). The exceptional stabilizer activity of this class of benzofuranones is due to the ready formation of a stable benzofuranyl radical by donation of the weakly bonded benzylic hydrogen atom (see Fig. 4).

The resonance stabilized benzofuranyl (lactone) radicals can either reversibly dimerize or react with other free radicals. Model experiments have demonstrated that this class of chemistry behaves as a powerful hydrogen atom donor and are also effective scavengers of carbon-centered and oxygen-centered free radicals (21) (see Fig. 5).

While the sterically hindered phenols react preferentially with oxygen-centered radicals such as peroxy and alkoxy, rather than with carbon-centered radicals, benzofuranones can scavenge both types of radicals. Accordingly, a benzofuranone can be repeatedly positioned at key locations around the autoxidation

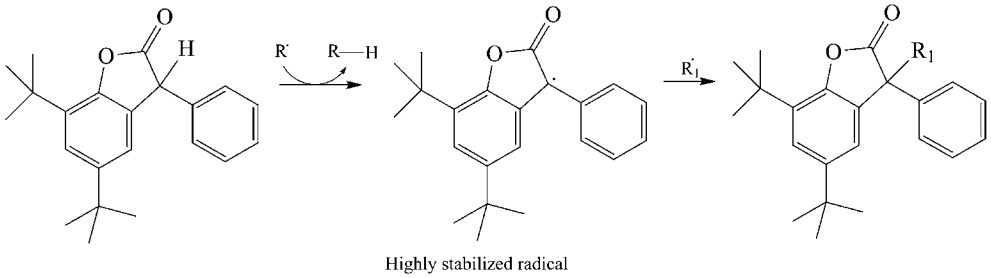

Fig. 4. Proposed Stabilization Mechanism of Arylbenzofuranones. R• = Carbon- or Oxygen-Centered Radical.

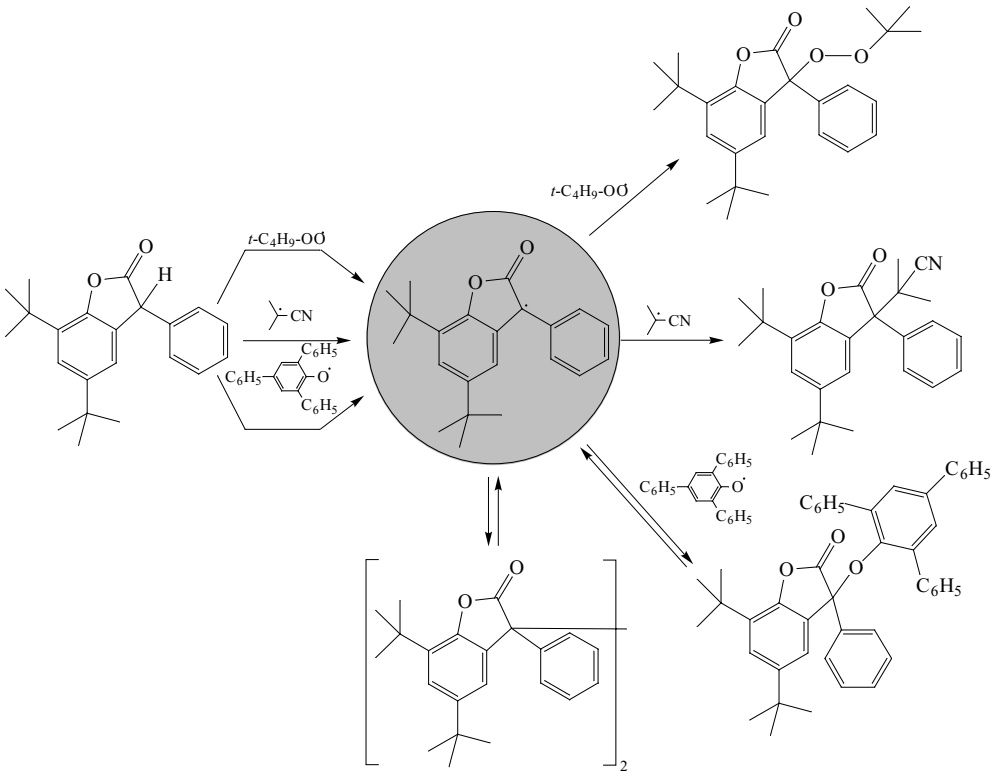

Fig. 5. Carbon-centered free-radical trapping reactions with benzofuranones.

cycle to inhibit the proliferation of free radicals. In addition, the scavenging of carbon-centered radicals is representative of a mode of stabilization that is more like "preventive maintenance," compared with more traditional stabilizers such as phenols and phosphites, which operate in something more like a "damage control" mode.

Benzofuranones are similar to hydroxylamines in that on an equivalent weight basis, they are more powerful than conventional phenolic antioxidants or phosphite-based melt-processing stabilizers. Once again it should be noted

that even though benzofuranones are capable of providing free-radical scavenging chemistry similar to phenolic antioxidants, the effective temperature domain is typically above the melting point of the polymer, eg, during melt-processing (similar to hydroxylamines). This will be discussed further below.

Peroxide Decomposers

Thermally induced homolytic decomposition of peroxides and hydroperoxides to free radicals (eqs. 2–4) increases the rate of oxidation. Decomposition to nonradical species removes hydroperoxides as potential sources of oxidation initiators. Most peroxide decomposers are derived from divalent sulfur and trivalent phosphorus.

Divalent Sulfur Derivatives. A dialkyl ester of thiodipropionic acid (**16**) is capable of decomposing at least 20 mol of hydroperoxide (22). Some of the reactions contributing to the antioxidant activity of these compounds are shown in Figure 6 (23,24).

According to Figure 6, hydroperoxides are reduced to alcohols, and the sulfide group is oxidized to protonic and Lewis acids by a series of stoichiometric reactions.

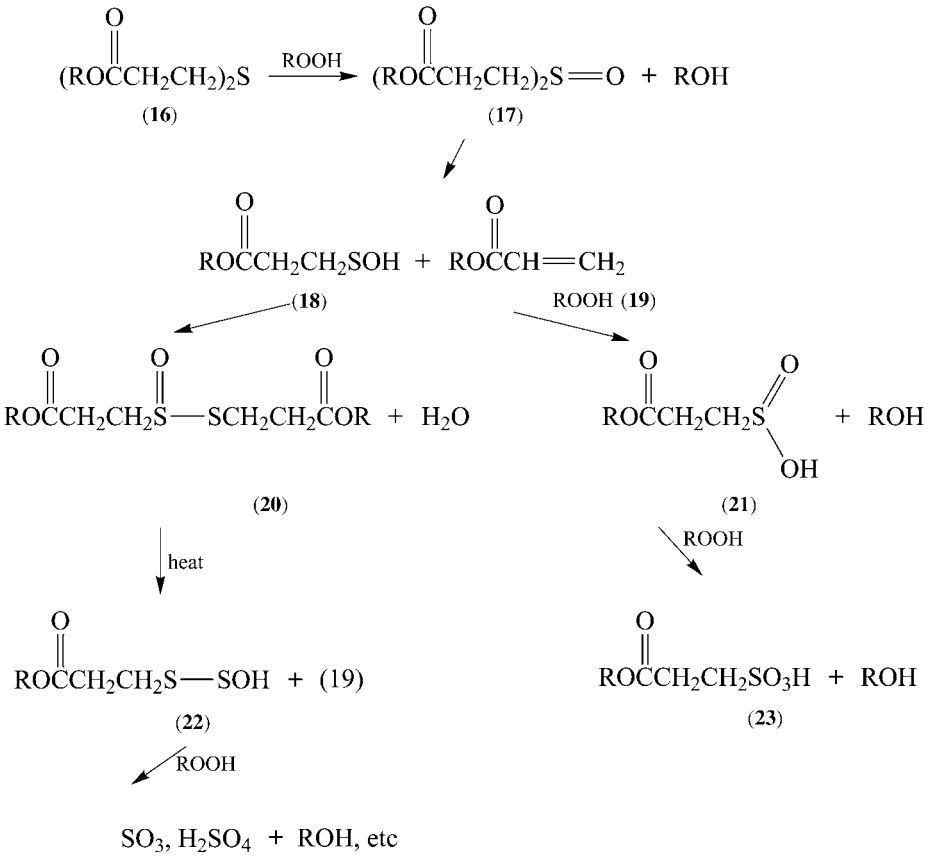

Fig. 6. Decomposition of hydroperoxides by esters of thiodipropionic acid (18).

The sulfinic acid (**21**), sulfonic acid (**23**), sulfur trioxide, and sulfuric acid are capable of catalyzing the decomposition of hydroperoxides to nonradical species.

When used alone at low temperatures, dialkyl thiodipropionates are rather weak antioxidants. Synergistic mixtures with hindered phenols, however, are highly effective at elevated temperatures and are used extensively to stabilize polyolefins, ABS, impact polystyrene, and other plastics.

Esters of thiopropionic acid tend to decompose at high processing temperatures, and their odor makes them unsuitable for some food-packaging applications.

Trivalent Phosphorus Compounds. Trivalent phosphorus compounds reduce hydroperoxide to alcohols:

$$\mathrm{ROOH} + \mathrm{PR'_3} \longrightarrow \mathrm{ROH} + \mathrm{O{=}PR'_3} \qquad (22)$$

These compounds are used most frequently in combination with hindered phenols for a broad range of applications in rubber and plastics. They are also able to suppress color development caused by oxidation of the substrate and the phenolic antioxidant. Unlike phenols and secondary aromatic amines, phosphorus-based stabilizers generally do not develop colored oxidation products.

Esters of phosphorous acid derived from aliphatic alcohols and unhindered phenols, eg, tris-nonylphenylphosphite (**24**), hydrolyze readily and special care must be taken to minimize decomposition by exposure to water or high humidity. The phosphorous acid formed by hydrolysis is corrosive to processing equipment, particularly at high temperatures.

The hydrolysis of phosphites is retarded by the addition of a small amount of a base such as triethanolamine. A more effective approach is the use of hindered phenols for esterification. Relatively good resistance to hydrolysis is shown by two esters derived from hindered phenols: tris(2,4-di-*tert*-butylphenyl)phosphite [31570-04-4] (**25**) and tetrakis(2,4-di-*tert*-butylphenyl)4,4′-biphenylenediphosphonite [38613-77-3] (**26**). A substantial research effort over the last decade to develop hydrolytically stable phosphites while retaining the excellent hydroperoxide decomposing activity has resulted in the introduction of a number of new commercial products such as the dicumyl phosphite [154862-43-8].

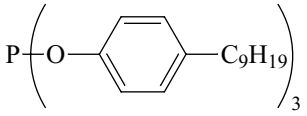

(**24**)

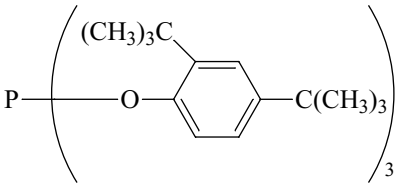

(**25**)

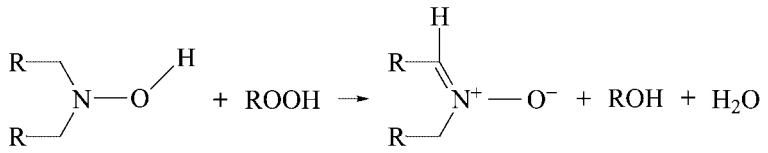

Fig. 7. Hydroperoxide Decomposition Mechanism for Hydroxylamines. R: mixture of long chain alkyl groups; $C_{16}H_{33}$, $C_{18}H_{37}$, $C_{20}H_{42}$, and $C_{22}H_{45}$.

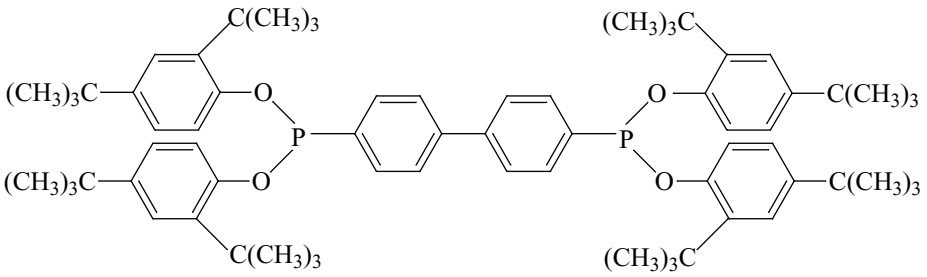

(**26**)

Hydroxylamines. As mentioned above, hydroxylamines are very effective as free-radical scavengers. They are also noted for their ability to decompose hydroperoxides (25); this is shown in equation 21 and illustrated in Figure 7.

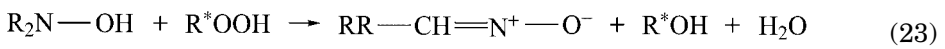

(23)

Hydroxylamines serve as a sequential source of hydrogen atoms, reducing hydroperoxides to their corresponding alcohol. In the course of this reaction, the hydroxylamine is converted to a nitrone.

Metal Deactivators

The ability of metal ions to catalyze oxidation can be inhibited by metal deactivators (26). These additives chelate metal ions and increase the potential difference between their oxidized and reduced states. This decreases the ability of the metal to produce radicals from hydroperoxides by oxidation and reduction (eqs. 15 and 16). Complexation of the metal by the metal deactivator also blocks its ability to associate with a hydroperoxide, a requirement for catalysis (27).

Examples of commercial metal deactivators used in polymers are oxalyl bis(benzylidene)hydrazide [6629-10-3] (**27**), *N*,*N*′-bis-(3,5-di-*tert*-butyl-4-hydroxyhydrocinnamoyl)hydrazine [32687-78-8] (**28**), 2,2′-oxamidobisethyl (3,5-di-*tert*-butyl-4-hydroxyhydrocinnamate) [70331-94-1] (**29**), *N*,*N*′-(disalicylidene)-1,2-propanediamine [94-91-7] (**30**), ethylenediaminetetraacetic acid [60-00-4] (**31**) and its salts, and critic acid (**32**) (Fig. 8).

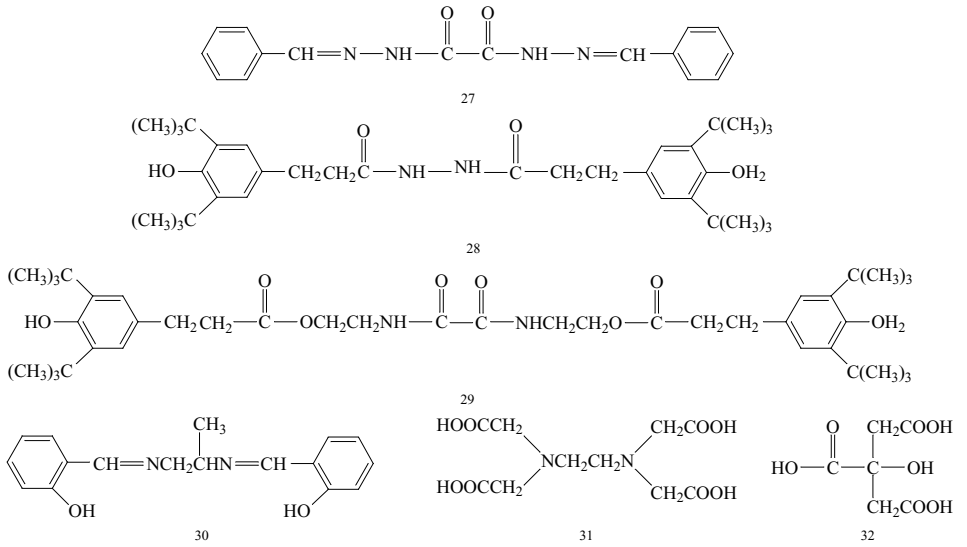

Fig. 8. Commercial metal deactivators.

Effective Temperatures for Antioxidants

As mentioned above, certain types of antioxidants provide free-radical scavenging capability, albeit over different temperature ranges. Figure 9 illustrates this in a general fashion for representative classes of antioxidants, over the temperature range of 0–300°C.

As a representative example, hindered phenols are capable of providing long-term thermal stability below the melting point of the polymer, as well as melt-processing stability above the melting point of the polymer. Most (if not all) hindered phenols are useful across the entire temperature range.

Thiosynergists, in combination with a hindered phenol, contribute to long-term thermal stability, primarily below the melting point of the polymer. In extreme cases where peroxides have built up in the polymer, thiosynergist can be shown to have a positive impact during melt processing. This, however, is not the norm, and this type of melt-processing efficacy has been left out of the figure.

Hindered amines, commonly thought of as being useful for uv stabilization, are also useful for long-term thermal stability below the melting point of the polymer. This effectiveness is due to the fact that hindered amines work by a free-radical scavenging mechanism, but they are virtually ineffective at temperatures higher than 150°C. Therefore, hindered amines, when used as a reagent for providing long-term thermal stability, should always be used in combination with an effective melt-processing stabilizer.

Phosphites, hydroxylamines, and lactones are most effective during melt-processing, either through free-radical scavenging or hydroperoxide decomposition. They are not effective as long-term thermal stabilizers. These type of stabilizers also help with long-term thermal stability. By sacrificing themselves during melt processing, they lessen the workload on the phenolic

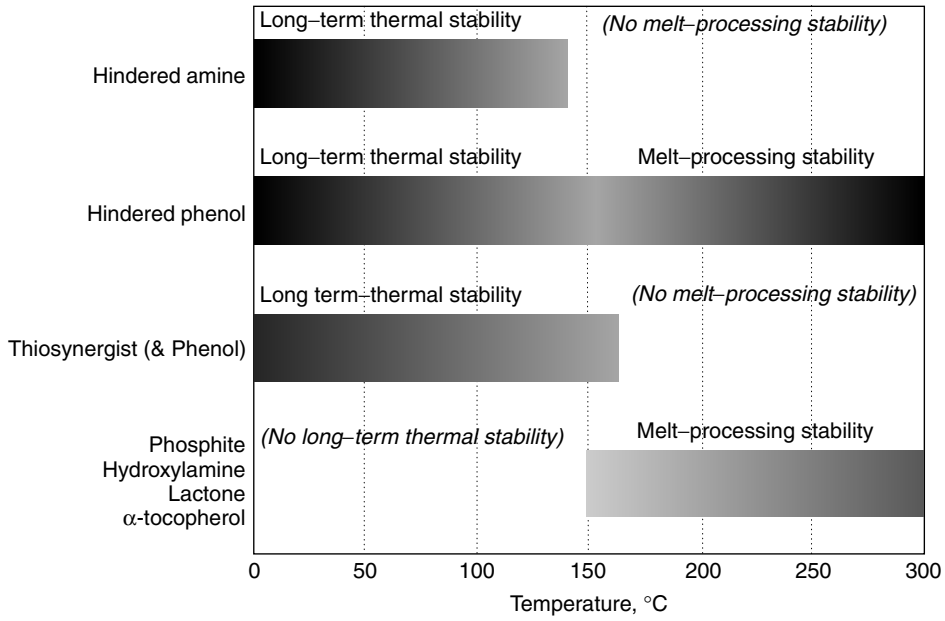

Fig. 9. General representation of effective temperature ranges for selected types of antioxidants.

antioxidant, allowing more to remain intact to help with long-term thermal stability.

One anomaly that should be pointed out is the hindered phenols based on tocopherols. Even though tocopherols, such as Vitamin E [10191-41-01], fall into the general class of hindered phenols, they behave more as melt-processing stabilizers, and less as reagents for providing long-term thermal stability, at least with regard to polymer stabilization.

Antioxidant Blends

In practical application, it is reasonable to use more than one type of antioxidant in order to meet the requirements of the application, such as melt-processing stability as well as long-term thermal stability. The most common combination of stabilizers used, particularly in polyolefins, are blends of a phenolic antioxidant and a phosphite melt-processing stabilizer. Another common combination is a blend of a phenolic antioxidant and a thioester, especially for applications that require long-term thermal stability. These common phenol-based blends have been used successfully in many different types of end-use applications. The combination of phenolic, phosphite, and lactone moieties represents an extremely efficient stabilization system since all three components provide a specific function.

For color-critical applications requiring "phenol-free" stabilization, synergistic mixtures of hindered amines (for both uv stability as well as long-term thermal

stability) with a hydroxylamine or benzofuranone (for melt processing), with or without a phosphite, can be used to avoid discoloration typically associated with the overoxidation of the phenolic antioxidant (28). The use of "phenol-free" stabilization systems is very effective in color-critical products, such as polyolefin films and fibers, as well as selected thermoplastic olefin (TPO) applications.

Synergist Mixtures of Antioxidants

A mixture of antioxidants that function by different mechanisms might be synergistic and provide a higher degree of protection than the sum of the stabilizing activities of each component. The most frequently used synergistic mixtures are combinations of radical scavengers and hydroperoxide decomposers.

Typically, blend titration experiments are performed at a set loading of additives, starting with 100% of Component A and 0% of Component B. A series of formulations are designed to shift to the other extreme with 0% Component A and 100% Component B. By measuring a series of performance parameters, the optimum ratio of A to B can be determined. This type of work is time consuming, but in the end, the optimum ratio is identified with real data. If three or more components are being assessed at the same time, statistically designed experiments are often useful in terms of sorting out the data.

Antagonistic Mixtures of Antioxidants

Mixtures of antioxidants can also work against each other. Chemistries that interfere with each other may not necessarily be obvious until the evidence is presented. For example, to ensure long-term thermal stability and good light stability, one might use a combination of a phenolic antioxidant and a divalent sulfur compound for thermal stability and a hindered amine for light stability.

Unfortunately, the oxidation products of the sulfur compound can be quite acidic and can complex the hindered amine as a salt, preventing the hindered amine from entering into its free-radical scavenging cycle. This antagonism has been generally known for quite a while (29) and has been discussed (30).

Other types of antagonistic chemistry often involve relatively strong acids or bases (either Bronstead or Lewis) that can interact with the antioxidants in such a way as to divert them into transformation chemistries that have nothing to do with polymer stabilization.

Application of Antioxidants in Polymers

Nearly all polymeric materials require the addition of antioxidants to retain physical properties and to ensure an adequate service life. The selection of an antioxidant system is dependent upon the polymer and the anticipated end use.

Polyolefins. Low concentrations of stabilizers ($<0.01\%$) are often added immediately to polyethylene and polypropylene after synthesis and prior to isolation so as to retard oxidation of the polymer before they are exposed to sources

Table 3. Synergism between a Hindered Phenol and a Thiosynergist[a]

Additive, %		
Radical scavenger[b]	Hydroperoxide decomposer[c]	Induction period, days
0.0	0.3	4
0.1	0.0	16
0.1[d]	0.3[d]	45

[a]Ref. 21.
[b]Tetrakis[methylene(3,5-di-*tert*-butyl-4-hydroxyhydrocinnamate)]methane.
[c]Dilauryl thiodipropionate.
[d]Mixture.

of oxygen or air (see ETHYLENE POLYMERS; PROPYLENE POLYMERS). Higher concentrations are added downstream during the conversion of the reactor product to a pelletized form. The antioxidant components and concentrations are selected by the manufacturer to yield general-purpose grades, or can be optimized to meet a specific end-use application.

In downstream applications, these polymers can be subjected to temperatures as high as 300°C, during cast film extrusion and thin-wall injection molding. In these type of demanding applications, processing stabilizers are used to decrease both the change in viscosity (molecular weight) of the polymer melt and the development of color. A phosphite, such as tris(2,4-di-*tert*-butylphenyl)phosphite (**25**) or bis(2,4-di-*tert*-butylphenyl)pentaerythritol diphosphite [26741-53-7], in combination with a phenolic antioxidant such as octadecyl 3,5-di-*tert*-butyl-4-hydroxyhydrocinnamate (**6**), may be used. Concentrations usually range from 0.01 to 0.5% depending on the polymer and the severity of the processing conditions. For long-term exposure, a persistent antioxidant such as tetrakis[methylene(3,5-di-*tert*-butyl-4-hydroxyhydrocinnamate)]methane (**9**), at a concentration of 0.1–0.5%, may be added to the base stabilization package.

A sulfur-containing synergistic mixture can be used to obtain an extended service life at a decreased cost.

The synergistic effect of a hydroperoxide decomposer, eg, dilauryl thiodipropionate [123-28-4] (**33**), and a radical scavenger, eg, compound **9**, in protecting polypropylene during an oxygen-uptake test at 140°C is shown in Table 3.

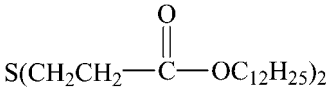

(**33**)

The sum of the individual activities of these antioxidants was 20 days, whereas a mixture of the two stabilizers protected the polymer for 45 days (31).

Oligomeric-HALS are effective thermal antioxidants for polypropylene. Thus 0.1% of *N*,*N*′-bis(2,2,6,6-tetramethyl-4-piperadinyl)-1,6-hexanediamine polymer, with 2,4,6-trichloro-1,3,5-triazine and 2,4,4-trimethyl-2-pentaneamine [70624-18-9] (**34**) (Fig. 10 & Table 4), protects polypropylene multifilaments against oxidation when exposed at 120°C in a forced-air oven for 47 days (32). The simple hindered phenol 3,5-di-*tert*-butyl-4-hydroxytoluene [128-37-0] (0.1%) affords protection for only 14 days.

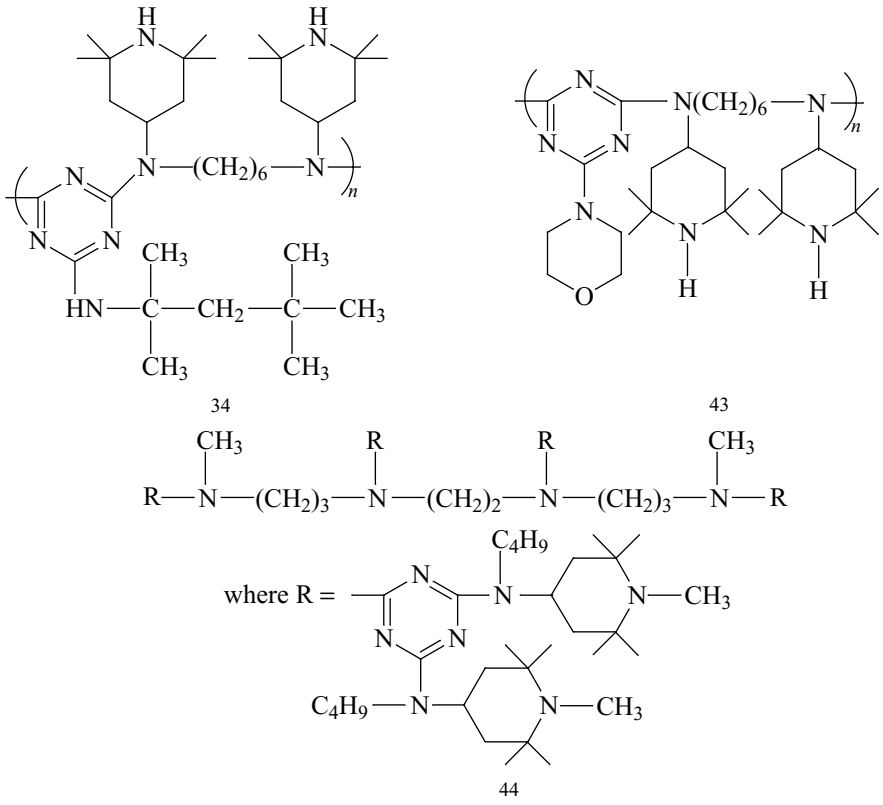

Fig. 10. Hindered 1,6-hexanediamine antioxidants.

The stabilization of polyolefins used to insulate copper conductors requires the use of a long-term antioxidant plus a copper deactivator. Both compounds **28** and **29** are bifunctional antioxidants that have built-in metal deactivators. Compound **27** is an effective copper deactivator as part of an additive package that includes an antioxidant.

Polyamides. Because of their excellent mechanical properties at high temperatures, polyamides, particularly mineral and glass-filled grades, are finding increased usage in demanding applications such as automotive (under-the-hood) applications (see POLYAMIDES, PLASTIC). Only a few publications dealing with stabilization of polyamides are found in the literature (33). The aliphatic polyamides differ in their structure, PA 6,6, PA 6, PA 4,6, PA 11, and PA 12 being the most common types. The oxidative stability of the various types is dependent on the density of the amorphous phase and the degree of crystallinity because these two factors control oxygen migration into the polymer matrix (34). Aromatic polyamides are rather insensitive to oxidative degradation.

The traditional stabilization system for aliphatic polyamides are copper salts. Typical systems are based on low levels of copper (<50 ppm) and iodide or bromide salts (35). The mechanism of stabilization is not well understood but may be due to hydroperoxide decomposition initiated by metal ions (36). These systems

Table 4. Commonly Used Antioxidants[a] by Class

Chemical name	CAS registry no.	Suggested substrates[b]	Suppliers
Monophenols			
α-Tocopherol	[10191-41-01]	PO, PUR	Ciba SC, BASF
2,6-Di-*tert*-butyl-4-methylphenol	[128-37-0]	PA, PES, PO, POM, PUR, PVC, RU, PS	Great Lakes, Merisol, PMC, Crompton
Octadecyl-3,5-di-*tert*-butyl-4-hydroxycinnamate	[2082-79-3]	CE, PA, PO, PUR, PVC, PS	Ciba SC, Crompton, Great Lakes, GE Specialty
Isooctyl-3,5-di-*tert*-butyl-4-hydroxycinnamate	[126-43-61-0]	PUR	Ciba SC, Crompton
Bisphenols			
2,2′-Methylenebis(4-methyl-6-*tert*-butylphenol)	[119-47-1]	CE, PA, POM, PUR, PVC, RU, PS	Cytec, RT Vanderbilt, Great Lakes, Ferro
2,2′-Methylenebis(4-ethyl-6-*tert*-butylphenol)	[88-24-4]	PA, PO, PVC	Cytec
4,4′-butylidenebis(6-*tert*-butyl-3-methylphenol)	[85-60-9]	CE, EVA, PA, PES, PO, PVC, RU, PS	Flexsys
N,*N*′-Hexamethylene bis(3,5-di-*tert*-butyl-4-hydroxyhydrocinnamide)	[23128-74-7]	PA, PES, PA, RU	Ciba SC, Great Lakes
1,6-Hexamethylenebis(3,5-di-*tert*-butyl-4-hydroxyhydrocinnamate)	[35074-77-2]	CE, PES, PO, POM, PUR, PVC, PS	Ciba SC
Benzenepropanoic acid, 3-(1,1-dimethylethyl)-4-hydroxy-5-methyl-,2,4,8,10-tetraoxaspiro[5.5] undecane- 3,9-diylbis(2,2-dimethyl-2,1-ethanediyl) ester[c]	[90498-90-1]		Sumitomo
Triethyleneglycol bis(3,5-di-*tert*-butyl-4-hydroxyhydrocinnamate)	[36443-68-2]	PA, POM, PVC, PS	Ciba SC, Great Lakes
Calcium bis[*O*-ethyl(3,5-di-*tert*-butyl-4-hydroxybenzyl)]-phosphonate	[65140-91-2]	PO, RU	Ciba SC
Polyphenols			
1,3,5-Trimethyl-2,4,6-tris(3′,5′-di-*tert*-butyl-4′-hydroxybenzyl)-benzene	[1709-7-2]	CE, PA, PES, PO, POM, PVC, RU, PS	Albemarle, Ciba SC, Great Lakes, Sigma 3V
3:1 Condensate of 3-methyl-6-*tert*-butylphenol with crotonaldehyde	[1843-03-4]	CE, PA, PES, PO, POM, PUR, PVC, RU, PS	ICI Americas

Table 4. (Continued)

Chemical name	CAS registry no.	Suggested substrates[b]	Suppliers
Tetrakis[methylene(3,5-di-*tert*-butyl-4-hydroxyhydrocinnamate)methane	[6683-19-8]	CE, PA, PES, PO, POM, PVC, PS	Ciba SC, Great Lakes, Crompton, GE Specialty Chem
1,3,5-Tris(3,5-di-*tert*-butyl-4-hydroxybenzyl) isocyanurate	[27676-62-6]	CE, PA, PES, PO, POM, PVC, PS	Ciba SC, RT Vanderbilt, Great Lakes Chem, Sigma 3V
3,5-Di-*tert*-butyl-4- hydroxy-hydrocinnamic triester with 1,3,5-Tris(2-hydroxyethyl)-*s*-triazine-2,4,6-(1*H*,3*H*,5*H*)trione	[34137-09-2]	CE, PA, PO, PUR, PVC, RU, PS	Ciba SC, RT Vanderbilt
1,3,5-Tris(4-*tert*-butyl-3-hydroxy-2,6-dimethylbenzyl)-*s*-triazine-2,4,6-(1*H*, 3*H*,5*H*)trione	[40601-76-1]	CE, PA, PES, PO, POM, PUR, PVC, RU, PS	Cytec, Ciba SC, Great Lakes Chem
Bis[3,3-bis(4-hydroxy-*tert*-butylphenyl)butanoic acid], Glycol ester	[32509-66-3]	CE, PA, PES, PO, POM, PVC, PS	Clariant
Butylated reaction product of *p*-cresol and dicyclopentadiene	[31851-03-3]	CE, PA, PES, PO, POM, PVC, RU, PS	Goodyear
Phenolics with dual functionality			
4,4′-Thiobis(6-*tert*-butyl-3-methylphenol)	[96-69-5]	PA, PES, PO, PVC, RU, PS	Flexsys, Sumitomo
4,4′-Thiobis(2-methyl-6-butylphenol)[c]	[96-66-2]	PO, RU	Albemarle
Thiodiethylene bis(3,5-di-*tert*-butyl-4-hydroxycinnamate)	[41484-35-9]	CE, PA, PO, PUR, PVC, RU, PS	Ciba SC, Great Lakes
4,6-Bis(octylthiomethyl)-*o*-cresol	[110553-27-0]	RU, PS	Ciba SC
Reaction product of nonylphenol, dodecanethiol, and formaldehyde	[188793-84-2]	RU, PS	Goodyear
2,4-Bis(*n*-octylthio-6-(4-hydroxy-3,5-di-*tert*-butylanilino)-1,3,5-triazine	[991-84-4]	RU, PS	Ciba SC
2-(1,1-dimethylethyl)-6-[3-(1,1-dimethylethyl)-2-hydroxy-5-methylphenyl]methyl-4-methylphenylacrylate	[61167-58-6]	PS	Sumitomo, Ciba SC

Metal deactivators			
N,*N*′-Bis(3,5-di-*tert*-butyl-4-hydroxyhydrocinnamoyl)hydrazine	[32687-78-8]	PA, PO, RU	Ciba SC, Great Lakes
2,2′-Oxamidobisethyl(3,5-di-*tert*-butyl-4-hydrocinnamate)	[70331-94-1]	PA, PO, RU	Crompton
Oxalic acid, bis(benzylidenehydrazide)[c]	[6629-10-3]	PA, PO, RU	Eastman
Arylamines			
4,4′-Bis(dimethylbenzyl)-diphenylamine	[10081-67-1]	RU, PO, PS, PUR	Crompton
N-Phenyl-α-naphthylamine	[90-30-2]	PA, PES, PO, RU	Bayer, Flexsys, RT Vanderbilt
N-Phenyl-*N*′-isopropyl-*p*-phenylenediamine	[101-72-4]	RU	Bayer, Flexsys, RT Vanderbilt, Crompton
Polymerized 2,2,4-trimethyl-1,2-dihydroquinoline[c]	[26780-96-1]	RU	Flexsys, RT Vanderbilt, Crompton
Octylated diphenylamine	[68411-46-1]	RU, PUR	Ciba SC, Crompton, Great Lakes, RT Vanderbilot
Thioethers			
Didodecyl-3,3′-thiodipropionate	[123-28-4]	PA, PO, RU	Cytec, Crompton, Evans Chemetic
Distearyl-3,3′-thiodipropionate	[693-36-7]	PA, PO, RU	Cytec, Crompton, Evans Chemetic
Pentaerythritol tetrakis(3-dodecylthio)propionate	[29598-76-3]	PA, PO	Crompton
S,*S*′-Distearyl disulfide	[2500-88-1]	PA, PO, RU	Clariant
Phosphites/phosphonites			
Tris nonylphenylphosphite	[26523-78-4]	CE, PES, PO, PUR, PVC, RU, PS	Crompton, GE Specialty, Dover
Tris(2,4-di-*tert*-butylphenyl)phosphite	[31570-04-4]	CE, PES, PO, PUR, PS	Ciba SC, GE Specialty, Great Lakes, Crompton
Distearyl pentaerythritoldisphosphite	[3806-34-6]	CE, PES, PO, PUR, PS, RU	GE Specialty

Table 4. (Continued)

Chemical name	CAS registry no.	Suggested substrates[b]	Suppliers
Bis(2,4-di-*tert*-butylphenyl)pentaerythritol diphosphite	[26741-53-7]	CE, PES, PO, PUR, PS, RU	GE Specialty, Ciba SC, Great Lakes
2,4,6-Tri-*tert*-butylphenyl-2-butyl-2-ethyl-1,3-propanediol phosphite	[161717-32-4]	PO, PS	GE Specialty
Bis(2,4-dicumylphenyl)pentaerythritol diphosphite	[154862-43-8]	CE, PES, PO, PUR, PS, RU	Dover
Tetrakis(2,4-di-*tert*-butylphenyl)-4,4′-biphenylenediphosphonite	[119345-01-6]	CE, PES, PO, PUR, PS, RU	Clariant, Ciba SC, Great Lakes
Hindered amines			
Poly[6-[(1,1,3,3-tetramethylbutyl)amino]-1,3,5-triazine-2,4-diyl][(2,2,6,6-tetramethyl-4-piperidinyl)imino]-1,6-hexanediyl[(2,2,6,6-tetramethyl-4-piperidinyl)imino]	[71878-19-8]	PO, EVA	Ciba SC
Poly[6-[1-morpholino]-1,3,5-triazine-2,4-diyl][2,2,6,6-tetramethyl-4-piperidinyl)imino]-1,6-hexanedityl[(2,2,6,6-tetramethyl-4-piperidinyl)imino]	[82451-48-7]	PO, EVA	Cytec
Butanedioic acid, dimethyl ester, polymer with 4-hydroxy-2,2,6,6-tetramethyl-1-piperidine, ethanol	[65447-77-0]	PO, EVA	Ciba SC
7-Oxa-3,20-diazadispiro[5.1.11.2]heneicosan-21-one, 2,2,4,4-tetramethyl-, hydrochloride, reaction products with epichlorohydrin, hydrolyzed, polymerized	[202483-55-4]	PO, EVA	Clariant

1,3-Propanediamine, *N*,*N*″-1,2-ethanediylbis-, polymer with 2,4,6-trichloro-1,3,5-triazine, reaction products with *N*-butyl-2,2,6,6-tetramethyl-4-piperidinamine	[136504-96-6]	PO, EVA	Sigma 3V
1,3,5-Triazine-2,4,6-triamine, *N*,*N*-1,2-ethane-diyl-bis[(4,6-bis[butyl(1,2,2,6,6-pentamethyl-4-piperidinyl)amino]-3,1-propanediyl)]bis(*N*′,*N*′-dibutyl-*N*′,*N*′-bis(1,2,2,6,6-pentamethyl-4-piperidinyl)	[106990-43-6]	PO, EVA	Ciba SC
Siloxanes and silicones, methyl-hydrogen, reaction products with 2,2,6,6-tetramethyl-4-(2-propenyloxy)piperidine	[182635-99-0]	PO, EVA	Great Lakes
Processing stabilizers			
2(3*H*)-Benzofuranone, 5,7-bis(1,1-dimethylethyl)-3-hydroxy, reaction products with *o*-xylene	[181314-48-7]	PO, PUR	Ciba SC
1-Octadecanamine, *N*-hydroxy-*N*-octadecyl	[123250-74-8]	PO, RU	Ciba SC
Di (rape oil)alkyl-*N*-methylamine oxide	[204933-93-7]	PO, RU	GE Specialty

[a]FDA regulated unless otherwise indicated. Regulated by the U.S. Food and Drug Administration as an indirect food additive under Title 21 of the U.S. Code of Federal Regulations (21 CFR), Part 175 (Adhesives and Coatings) and/or Part 177 (Polymers).
[b]CE: cellulosics; EVA: ethylene–vinyl acetate copolymers; PA: polyamides; PES: polyesters; PO: polyolefins; POM: polyoxymethylenes; PUR: polyurethanes, polyols; RU: rubber; PS: polystyrenes; PVC: poly(vinyl chloride).
[c]Not FDA regulated.

are effective in polyamides whereas in other polymers, such as polyolefins, small amounts of oxidized copper can often act as prodegradants. Good dispersion of the copper is critical to good performance. Since copper salts are water soluble, they can be leached from the polymer in certain applications (eg aqueous dye baths), leading to reduced efficacy and environmental issues. Aromatic amines are effective long-term stabilizers, but because of their discoloring nature, their use is limited to carbon black-filled systems. Phenolic antioxidants when added during the polycondensation reaction, contribute to improved initial color and long-term thermal stability, particularly at lower end-use temperatures. The relative merits of the various stabilization systems are shown in the following table:

Antioxidant system	Advantages	Disadvantages
Copper/halogen salts	Best performance at elevated temperatures (>150°C)	Discoloration
	Very low levels required	Leaching in aqueous environment Must be well dispersed
Aromatic amines	Good long-term thermal stabilizer performance	Discoloration
		Needs high concentration
Phenolics	Best performance at lower temperatures when copper salts cannot be used	Less effective at high temperature conditions such as under-the-hood
	Good initial and long-term color performance	

Styrenics. Unmodified styrenics such as crystal polystyrene are relatively stable, and under most end-use conditions it is not necessary to add antioxidants (see STYRENE POLYMERS). Low levels (0.1%) of a hindered phenolic antioxidant are added to protect the polymer during repeated processing of scrap. Styrene-acrylonitrile (SAN) copolymers discolor during processing above 220°C (see ACRYLONITRILE POLYMERS). While this is primarily a nonoxidative process related to the acrylonitrile comonomer, the color can be suppressed to some extent through the addition of a combination of a phenolic antioxidant and a phosphite (37). High impact polystyrene (HIPS) is more susceptible to oxidative degradation because of the presence of an unsaturated butadiene rubber phase. Antioxidants can be added either during the manufacturing process to protect the rubber phase during polymerization and monomer stripping or postpolymerization. Color and impact properties are typically better if the antioxidant is added during polymerization, but care must be taken to avoid adverse effects on the kinetics through interaction with the peroxide catalysts. This is particularly problematic if phosphites are added. Acrylonitrile–butadiene–styrene (ABS) is a graft copolymer produced primarily in an emulsion process followed by a compounding step in which the high rubber content polymer is blended with SAN in various ratios to achieve the desired end-use properties. Antioxidants are required during the coagulation and drying steps to protect the high rubber content particles. The best performance is achieved through the use of a combination of hindered phenol (0.25%) and thioester synergist (0.5%) (38). The stability of the finished ABS is directly related to the butadiene content (39).

Polyesters. Poly(ethylene terephthalate), PET, requires little to no antioxidant during thermal processing. In some cases, phosphites are added to improve the color of regrind. During polycondensation, pentavalent phosphorus compounds such as triphenylphosphate or trimethylphosphate may be added. These additives form complexes with the transesterification catalyst residues (manganese, tin, zinc), yielding a polymer with reduced hydroxyl end groups. This affords better hydrolytic stability during end use and reduced discoloration prior to the condensation reaction (40). Poly(butylene terephthalate), PBT, because of its higher hydrocarbon content, is more susceptible to oxidative degradation than PET. The combination of a phenolic antioxidant (0.05–0.10%) and a phosphite (0.1%) is typically used to stabilize PBT (see POLYESTERS, THERMOPLASTIC).

Polycarbonate. Polycarbonate, PC, is susceptible to photo-oxidation, and antioxidants are necessary to maintain the low color and high transparency critical to its end-use applications (see POLYCARBONATES). Phosphites (0.1%) are used to minimized color development during processing. It has been shown that the inherent stability of PC is related to the level of phenolic end groups (41). These levels can increase as a result of humidity-induced hydrolysis catalyzed by acid. The phosphite chosen must be very stable to avoid the generation of catalytic amounts of phosphorus acids.

Polyacetal. Polyacetals thermally decompose by an acid-catalyzed depolymerization process starting at the chain ends (see ACETAL RESINS). The polymer structure is stabilized by end capping and introducing comonomers to interrupt the unzipping. The process is autocatalytic since the liberated formaldehyde is easily oxidized to formic acid, which is a prodegradant. Formaldehyde scavengers and phenolic antioxidants are typically used in polyacetal formulations (42).

Polyurethanes. The oxidative stability of polyurethanes (PURs) is highly dependent on the chemical nature of both the polyol component and the isocyanate. Thus, PUR derived from a polyester polyol is typically more stable than one derived from a polyether polyol (see POLYURETHANES). The methylene group adjacent to the ether linkage in polyether polyols is easily oxidized to hydroperoxides during storage. If not inhibited, decomposition of these built-up hydroperoxides can occur catastrophically during the highly exothermic reaction of the polyol and the isocyanate. Blends of a hindered phenol (0.2%) and an aromatic amine (0.1%) are typically used as storage stabilizers in polyether systems providing PUR foams with excellent color. Similar systems are used in polyester polyols, but at lower use levels (43).

Elastomers. Polyunsaturated elastomers are sensitive to oxidation. Stabilizers are added to the elastomers prior to vulcanization to protect the rubber during drying and storage. Nonstaining antioxidants such as butylated hydroxytoluene (**1**), 2,4-bis(octylthiomethyl)-6-methylphenol [110553-27-0], 4,4′-bis(α,α-dimethylbenzyl)diphenylamine (**14**), or a phosphite such as tris(nonylphenyl)phosphite (**24**) may be used in concentrations ranging from 0.01 to 0.5%.

Staining antioxidants such as *N*-isopropyl-*N*′-phenyl-*p*-phenylenediamine [101-72-4] (**35**) are preferred for the manufacture of tires. These potent antioxidants also have antiozonant activity and retard stress cracking of the vulcanized rubber. Carbon black, used in tires for reinforcement, hides the color developed by the antioxidant. According to use requirements, up to 3% of an amine antioxidant having antiozonant activity is added prior to vulcanization.

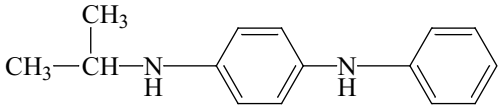

(**35**)

When staining tendencies of the substituted paraphenylene diamines cannot be tolerated, semistaining amine antioxidants are used to provide some protection to the elastomers. The semistaining antioxidants include polymerized compounds **13** and compound **14**. These compounds, however, provide no protection against ozone.

Antioxidants resistant to extraction by lubricants and gasoline are preferred for the stabilization of elastomers used in automotive applications such as gaskets and tubing. Aromatic amine antioxidants such as *N*-phenyl-*N*′-(*p*-toluenesulfonyl)-*p*-phenylenediamine [100-93-6] (**36**), with low solubility in hydrocarbons, are extracted slowly from elastomers and are used for these applications.

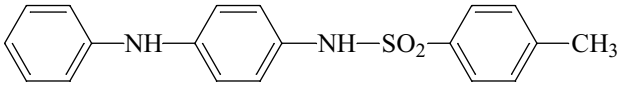

(**36**)

Binding the antioxidant chemically to the elastomer chain by copolymerization or grafting is a better solution to this problem. The addition of *N*-(4-anilinophenyl)methacrylamide [22325-96-8] (**37**) to a polymerization recipe for nitrile butadiene rubber (NBR) produces a polymer with a built-in antioxidant resistant to extraction (44).

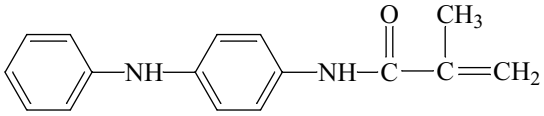

(**37**)

Raw NBR containing 1.5% of the built-in antioxidant retained 92% of its original resistance to oxidation after exhaustive extraction with methanol. NBR containing a conventional aromatic amine antioxidant (octylated diphenylamine) retained only 4% of its original oxidative stability after similar extraction.

It is also possible to graft an aromatic amine antioxidant bearing a sulfhydryl group on to the backbone of an elastomer.

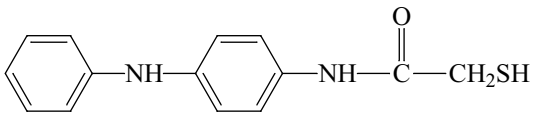

(**38**)

When 4-(mercaptoacetamido)diphenylamine [60766-26-9] (**38**) is added to EPDM rubber and mixed in a torque rheometer for 15 min at 150°C, 87% of it

chemically binds to the elastomer (45). The mechanical and thermal stress placed on the polymer during mixing ruptures the polymer chain, producing free radicals that initiate the grafting process.

Poly(vinyl chloride). While reasonably stable with respect to oxidative degradation, PVC is very susceptible to thermal degradation. Protection of PVC from thermal degradation leading primarily to dehydrohalogenation reactions is out of the scope of this article. Some additives, used primarily as HCl scavengers, also have antioxidant properties. Aralkylphosphites, in particular, are used as components of thermal stabilizing mixtures which also exhibit antioxidant properties, leading to improved resin color.

Fuels and Lubricants. Gasoline and jet-engine fuels contain unsaturated compounds that oxidize on storage, darken, and form gums and deposits. Radical scavengers such as 2,4-dimethyl-6-*tert*-butylphenol [1879-09-0], 2,6-di-*tert*-butyl-*p*-cresol (**1**), 2,6-di-*tert*-butylphenol [128-39-2], and alkylated paraphenylene diamines are used in concentrations of about 5–10 ppm as stabilizers.

The catalytic activity of copper as an oxidant in fuels and lubricants can be inhibited by the use of a metal deactivator such as *N*,*N*′-disalicylidene-1,2-diaminopropane (**30**) at a concentration of 5–10 ppm.

Lubricants for gasoline engines are required to withstand harsh conditions. The thin films of lubricants' coating on piston walls are exposed to heat, oxygen, oxides of nitrogen, and shearing stress. Relatively high concentrations of primary antioxidants and synergists are used to stabilize lubricating oils. Up to 1% of a mixture of hindered phenols, of the type used for gasoline, and secondary aromatic amines, such as alkylated diphenylamine and alkylated phenyl-α-napththylamine, are used as the primary antioxidants. About 1% of a synergist, zinc dialkyldithiophosphonate, is added as a peroxide decomposer. Zinc dialkyldithiophosphates (**39**) are cost-effective multifunctional additives. They interrupt oxidative chains by trapping radicals by electron donation, decompose peroxides, and serve as a corrosion and wear inhibitors.

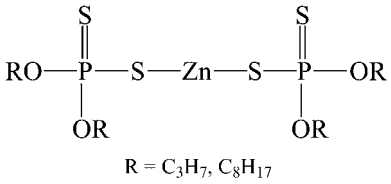

R = C_3H_7, C_8H_{17}

(**39**)

Both zinc and phosphorus deactivate the catalysts used to control emissions and governmental regulations limit their concentrations to below 0.1%.

Test Methods

Polymers. There are a variety of test methods available for monitoring the oxidative stability in the polymer as it is exposed to different types of stresses. These changes can be physical or aesthetic. Physical transformations of

the polymer might involve changes in molecular weight, molecular weight distribution, or crystallinity. Aesthetic transformations of the polymer might involve changes such as discoloration or changes in the surface appearance due to microscopic cracks which affect gloss.

These changes can be measured using simple testing equipment and procedures described in ASTM methods (eg, tensile strength, impact resistance, color development, oxidative induction time, oven aging).

Estimation of oxidative stability under conditions of use is more difficult to measure. To decrease the time required for oxidative failure, specimens are exposed at temperatures higher than those anticipated in use. Oven aging the polymer at temperatures below the melting point of the polymer is a method for assessing the long-term thermal stability of a given substrate. A range of test temperatures can be used to create an Arrhenius plot as test temperature (°C or K) vs time to failure (eg, embrittlement, or 50% retention of tensile strength or elongation). If the apparent activation energy remains constant, a plot of the logarithm of failure time against the reciprocal of the absolute temperature results in a straight line. Extrapolation to temperature of use provides an estimate of failure time.

Because of different reactions and the raw materials used, the apparent activation energy of the overall process can deviate considerably from linearity, and an extrapolation can lead to serious errors in estimating failure time (46).

Representative measures of aesthetic properties would include color development, loss of gloss, increase in haze, chalking, loss of surface smoothness, exudation and/or blooming of additives or low molecular weight polymer, and staining.

To assess the retention of physical or aesthetic properties, it is important to understand that increasing surface area-to-volume ratio increases susceptibility to oxidation as does the rate of loss of the antioxidant by volatilization (47).

In the past, oxygen-uptake measurements at elevated temperatures were used to determine oxidation resistance. Today, other types of testing, such as oxidative induction time (OIT), by differential scanning calorimetry or chemiluminescence, are used.

For oxygen-uptake experiments, the time required to absorb a specified volume of oxygen is an indication of failure when the change in the rate of oxygen absorption is not sufficient to permit an accurate measurement of the induction period. However, the amount of oxygen absorbed and the loss of desired properties must be correlated. This type of test is not reliable for estimating service life under conditions in which the polymer is exposed to air movement.

Oxidative induction time or oxidative induction temperature experiments are used to assess the relative oxidative stability of the polymer. The experiments are typically conducted under severe testing conditions, typically at elevated temperatures (significantly above the melting point of the polymer) using oxygen as the oxidant. It should be noted that this method is not useful for predicting long-term thermal stability; however, these methods can be useful for quickly assessing the relative potency of different types of stabilizer systems (48).

For chemiluminescence experiments, the procedure is similar to the aforementioned OIT experiments, in that the time to catastrophic oxidation of the

polymer is measured; in this case, below the melting point of the polymer. During this catastrophic oxidation, there are certain chemistries that take place which result in chemiluminescence. The amount of light that is given off during this process is measured by a charge-coupled device. This method, developed over the last decade, can provide useful information about the oxidative stability of the polymer in much shorter time period than conventional oven aging, but under more realistic oxidative environment in comparison with oxidative induction time (49).

Lubricants. A sequence of tests has been devised to evaluate antioxidants for use in automotive crankcase lubricants. The Indiana Stirring Oxidation Test (ISOT) JISK2514 is an example of a laboratory screening test. The oil is stirred at 165.5°C in the presence of air. Copper and iron strips are used as metal catalysts. The development of sludge, viscosity, and acidity are determined periodically. Failure time is determined when the development of acidity requires 0.4 mg KOH/g for neutralization. Formulated lubricants are then evaluated for performance in engines (see Oldsmobile Sequence III D) (50). Candidate lubricants containing the antioxidants are tested in fleets of automobiles for thousands of miles. As described above for polymers, modified oxygen uptake tests can also be used with lubricants to measure oxidative stability (51).

The effectiveness of antioxidants as preservatives for fats and oils is evaluated by determining the rate of peroxide development using the active oxygen method (52). The development of a rancid odor is used to evaluate the stability of food items (Schaal oven stability test) (53).

Ancillary Properties

In reality, there is more to antioxidants than providing stability to the polymer by quenching free radicals and decomposing hydroperoxides. Other key issues besides rates of reactivity and efficiency include performance parameters such as volatility, compatibility, color stability, physical form, taste or odor, regulatory issues associated with food contact applications, and polymer performance vs cost (54).

Volatility. Most additives are melt compounded into the polymer after the polymerization stage. The melt compounding and downstream conversion (into shaped articles) processing steps represent significant heat histories. Storage of the product can also be quite warm in certain climates. It is important that the antioxidant, as well as its transformation products that may also provide stability, does not volatilize from the polymer. Many commercial antioxidants have been designed with higher molecular weights to address this issue.

Compatibility. Antioxidants should be soluble in the polymeric matrix. If they are not soluble, they should at least migrate or diffuse slowly. If the solubility limit of the antioxidant in the polymer is exceeded, exudation will occur. Exudation or blooming involves the migration of the additive out of the polymer matrix onto the surface as a very thin film. Blooming of the antioxidant can diminish surface gloss, create stickiness, eliminate blocking (cling) of film surfaces to one another and negatively affect printability.

Color Stability. It is important that antioxidants do not provide unwanted color because of the transformation chemistries associated with preventing oxidation. Some antioxidants are prone to forming color by their very nature, while other antioxidants discolor only when they have been overoxidized. Pigments can be used to mask the subtle changes in the base color of the polymer.

Physical Form. Because of hazards associated with dusting, many antioxidants are now being offered commercially in dust-free forms, such as granules or pellets. Liquid or molten antioxidants are another interesting alternative, as long as they are compatible in the polymer matrix. Still, some polymer manufactures need the additives as fine powders in order to achieve good premixing with their reactor product before melt compounding into the traditional pellet form.

Taste and Odor. For applications that involve food contact, home or personal use, taste and odor are key issues. The human nose is very sensitive, more so than some analytical instruments, able to detect some compounds at the parts per billion (ppb) level.

Health and Safety Factors

Safety is assessed by subjecting the antioxidant to a series of animal toxicity tests, eg, oral, inhalation, eye, and skin tests. Mutagenicity tests are also carried out to determine possible or potential carcinogenicity. Granulated and liquid forms of antioxidants are receiving greater acceptance to minimize the inhalation of dust and to improve flow characteristics.

A number of antioxidants are regulated by the U.S. Food and Drug Administration (FDA) as indirect additives for polymers used in food contact applications (primarily food packaging) under Title 21 of the U.S. Code of Federal Regulations (21CFR), Part 175 (Adhesives and Coatings) and/or Part 177 (Polymers). Acceptance is determined by subchronic or chronic toxicity in more than one animal species and by the concentration expected in the diet, based on the amount of the additive extracted from the polymer by solvents that simulate food in their extractive effects. Materials are regulated by the FDA for use in plastics contacted by food stuffs to ensure a minimum risk to the consumer. Broad FDA regulation is increasingly a requirement for the successful introduction of a new antioxidant.

Cost Effectiveness

The point in using an antioxidant is to choose the appropriate type and level to adequately stabilize the polymer for a particular end-use application.

For example, if the material is a nondurable good, such as bags and food wrap, the type and concentration of antioxidant is chosen to minimize unnecessary costs associated with stabilizing the polymer. The antioxidant should be able to provide stabilization for the initial melt compounding and processing into the finished article. It is important to consider that scrap from the melt compounding needs to be recycled, and unexpected shutdowns and start-ups may occur.

On the other hand, if the material is a durable good, such as geomembranes, insulation for wire and cable, or gas and water transmission pipes, the type and concentration of the phenolic antioxidant is chosen to meet the long service-life criteria. The costs associated with this type or level of antioxidant is worth the additional value of the final product.

Commercial Antioxidants. Table 4 includes the main classes of antioxidants sold in the United States and the supplier's suggested applications. Some of these are mixtures rather than single components. This is especially true of alkylated amines and alkylated phenols. The extent of alkylation and the olefins used for alkylation can vary among manufacturers. Table 4 is not a complete listing of available antioxidants in the United States.

BIBLIOGRAPHY

"Antioxidants" in *EPST* 1st ed., Vol. 2, pp. 171–197, by G. C. Maassem, R. T. Vanderbilt Co., and R. J. Fawcett and W. R. Cornell, The B. F. Goodrich Co.; "Antioxidants" in *EPSE* 2nd ed., Vol. 2, pp. 73–91, by M. Dexter, Ciba-Geigy Corp.

1. *Chem. Eng. News* 21 (Dec. 4, 2000).
2. *Chem. Mark. Reporter* 7 (June 19, 2000).
3. L. Bolland, *Q. Rev. London* **3**, 1 (1949).
4. L. Bateman, *Q. Rev. London* **8**, 147 (1954).
5. U. Ingold, *Chem. Rev.* **61**, 563 (1961).
6. R. Shelton and W. L. Cox, *Rubber Chem. Technol.* **27**, 671 (1954).
7. Barnard, L. Bateman, J. I. Cunneen, and J. F. Smith, in L. Bateman, ed., *Chemistry and Physics of Rubber-Like Substances*, Maclaren, London, 1963, p. 593.
8. A. Kerr, *Chem. Rev.* **66**, 465 (1966).
9. J. Chalk and J. F. Smith, *Trans. Faraday Soc.* **53**, 1214 (1957).
10. P. Pospisil, in E. Scott, ed., *Developments in Polymer Stabilization*, Vol. **1**, Applied Science Publishers, Ltd., London, 1979, pp. 6–11.
11. C. Nixon, H. B. Minor, and G. M. Calhoun, *Ind. Eng. Chem.* **48**, 1874 (1956).
12. H. Rosenwald, J. R. Hoatson, and J. A. Chenicek, *Ind. Eng. Chem.* **41**, 162 (1950).
13. I. Wasson and W. M. Smith, *Ind. Eng. Chem.* **45**, 197 (1953).
14. G. Scott, *Atmospheric Oxidation and Antioxidants*, Elsevier, Amsterdam, the Netherlands, 1965, p. 109.
15. G. Scott, *J. Appl. Polym. Sci.* **35**, 131 (1979).
16. J. Galbo, in Encyclopedia of Polymeric Materials, CRC Press, Inc., Boca Raton, Fla., 1996, pp. 3616–3623.
17. P. Klemchuk and M. E. Gande, *Makromol. Chem., Macromol. Symp.* **28**, 117–144 (1989).
18. D. Horsey, in *Additives '96*, Houston, Feb. 1996.
19. P. A. Smith and S. E. Gloyer, *J. Org. Chem.* **40**, 2508–2512 (1975).
20. C. Kröhnke, in *Polyolefins 10, Conference*, Houston, Feb. 1997.
21. P. Nesvadba and C. Kröhnke, in *Additives '97, 6th Int. Conf.*, New Orleans, Feb. 1997.
22. R. Shelton, in W. L. Hawkins, ed., *Polymer Stabilization*, Wiley-Interscience, New York, 1972, pp. 97–98.
23. G. Scott, ed., *Development in Polymer Stabilization*, Vol. **4**, Applied Science Publishers, Ltd., London, 1981, pp. 16–17.

24. C. Armstrong, M. J. Husbands, and G. Scott, *Eur. Polym. J.* **15**, 241 (1979).
25. H. E. DeLaMare, G. M. Coppinger, *J. Org. Chem.* **28**, 1068–1070 (1963).
26. J. Chalk and J. F. Smitth, *Trans. Faraday Soc.* **53**, 1235 (1957).
27. P. Klemchuk and M. E. Gande, *Makromol. Chem., Macromol. Symp.* **28**, 83 (1989).
28. R. E. King III, in *SPE Polyolefins RETEC*, Houston, Feb. 2001.
29. K. B. Chakraborty and G. Scott, *Chem. Ind.* 237 (1978).
30. K. Kikkawa and Y. Nakahara, *Polym. Degrad. Stab.* **18**, 237 (1987).
31. Rysavy, *Kunststoffe* **60**, 118 (1970).
32. A. Tozzi, G. Cantatore, and F. Masina, *Text. Res. J.* **48**, 434 (1978).
33. B. Brassat and H. J. Buuysch, *Kuntststoffe* **70**, 833 (1980).
34. P. Gijsman, D. Tummers, and K. Janssen, *Polym. Degrad. Stab.* **49**, 121 (1995).
35. M. I. Kohan, *Nylon Plastics Handbook*, Carl Hanser Verlag, Munich, 1995, pp. 58–59, 441.
36. K. Janssen, P. Gijsman, and D. Tummers, *Polym. Degrad. Stab.* **49**, 127 (1995).
37. F. Gugumus, in H. Zweifel, ed., *Plastics Additives Handbook*, 5th ed., Carl Hanser Verlag, Munich, 2001.
38. H. Zweifel, *Stabilization of Polymeric Materials*, Springer-Verlag, Berlin, 1998, pp. 88–90.
39. T. Hirai, *Jpn. Plast.* (Oct. 1970).
40. U. Gold, *Chem. Rev.* **61**, 85 (1961).
41. C. A. Pryde and M. Y. Hellmann, *J. Appl. Polym. Sci.* **25**, 2573 (1980).
42. F. R. Stohler and K. Berger, *Angew. Makromol. Chem.* **176/177**, 327 (1990).
43. S. M. Andrews, Paper presented at the "*Sixty Years of Polyurethanes" Int. Symp.*, University of Detroit, Mercy, 1998.
44. E. Meyer, R. W. Kavchik, and F. J. Naples, *Rubber Chem. Technol.* **46**, 106 (1973).
45. G. Scott and Setoudeh, *Polym. Degrad. Stab.* **5**, 81 (1983).
46. H. Hansen and co-workers, *Org. Coat. Plast. Prepr.* **34**, 97 (1974).
47. P. Gysling, *Adv. Chem. Ser.* **85**, 239 (1968).
48. J. R. Pauquet, R. V. Todesco, and W. O. Drake, in *42nd International Wire & Cable Symposium*, Nov. 1993.
49. S. W. Bigger and co-workers, *Polym. Prepr.* **42**, 375 (2001).
50. *ASTM Bull.* 19103 (1990).
51. D. Chasan, in J. Pospisil and P. P. Klemchuk, eds., *Oxidation Inhibition in Organic Materials*, Vol. **I**, CRC Press, Inc., Boca Raton, Fla., 1990, pp. 291–326.
52. Technical Data Bulletin ZG-159c, Eastman Chemical Products, Inc., Kingsport, Tenn., Mar. 1985.
53. Technical Data Bulletin ZG-194c, Eastman Chemical Products, Inc., Kingsport, Tenn., Oct. 1987.
54. R. E. King III, in Encyclopedia of Polymeric Materials, CRC Press, Inc., Boca Raton, Fla., 1996, pp. 306–313.

GENERAL REFERENCES

Refs. 14, 22, and 49 are good general references.
M. Dexter, in J. I. Kroschwitz, ed., Encyclopedia of Chemical Technology, 4th ed., Vol. **3**, Wiley-Interscience, New York, 1992, pp. 424–447.

W. Voigt, *Die Stabilisierung der Kunstoffe Gegen Licht and Warme*, Springer-Verlag, Heidelberg, 1966.
K. Schwarzenbach, in H. Zweifel, ed., *Plastics Additives Handbook*, Hanser, Munich, 2000, pp. 1–137.
J. Pospisil and P. P. Klemchuk, eds., *Oxidation Inhibition in Organic Materials*, Vols. **I** and **II**, CRC Press, Inc., Boca Raton, Fla., 1990.

MARTIN DEXTER
RICHARD W. THOMAS
ROSWELL E. KING III
Ciba Specialty Chemicals

ANTIOZONANTS.

See RUBBER CHEMICALS.

ATOMIC FORCE MICROSCOPY.

See Volume 1.

ATOM TRANSFER RADICAL POLYMERIZATION.

See LIVING RADICAL POLYMERIZATION.

ATRP.

See LIVING RADICAL POLYMERIZATION.

BARRIER POLYMERS

Introduction

Barrier polymers can be broadly defined as macromolecules having the ability to significantly restrict the passage of gases, vapors, and liquids. Since all polymers restrict the transport of penetrants to some degree and the barrier performance of polymers to different penetrants depends on a variety of factors, it is difficult to provide a concise, objective definition. In a practical sense, however, the definition of a barrier polymer depends upon the end-use requirements, and a material that provides sufficient barrier for a particular application can be considered to be a barrier polymer for that purpose. In the present discussion, polymers that have resistance to transport of gases, vapors, and liquids as one of their key attributes will be considered to be barrier polymers.

Polymers have found wide acceptance as alternatives to traditional materials such as glass, paper, and metals, in food, beverage, and other packaging industries. A key characteristic of glass and metals as packaging materials is their total barrier to transport of gases and vapors. While polymers can provide an attractive balance of properties such as flexibility, toughness, light weight, formability, and printability, they do allow the transport of gases and vapors to some extent. Unfortunately, an inexpensive, recyclable polymeric material possessing high barrier properties to every gas or vapor in addition to good mechanical, thermal, and optical properties is not available. For this reason, the selection of a barrier polymer for a particular application typically involves tradeoffs between permeation, mechanical, and aesthetic properties as well as economic and recycling considerations. Additionally, there is an ongoing interest in optimizing property sets of barrier polymers to provide an efficient and economical method for packaging and for extending the shelf life of packaged foods and beverages.

Encyclopedia of Polymer Science and Technology. Copyright John Wiley & Sons, Inc. All rights reserved.

This article discusses various types of barrier polymers and structures, their permeability characteristics and the underlying phenomena involved, measurement techniques, ways to predict and improve barrier properties, and current as well as potential future applications for barrier polymers.

Fundamentals of Permeation in Polymers

The permeability coefficient, or simply permeability, characterizes the steady-state rate of mass transport of penetrant molecules through polymers. In a dense polymer film, the permeability P is defined as the molar flux of penetrant through the polymer relative to a fixed coordinate system N_A normalized by the film thickness L and the difference between the upstream (p_2) and downstream (p_1) partial pressures (1):

$$P = \frac{N_A L}{(p_2 - p_1)} \tag{1}$$

Accordingly, permeability has dimensions of quantity of penetrant (either mass or moles) times thickness divided by area, time, and pressure. Several units have been used to report permeability of gases and water vapor in the literature. In the United States, a commonly used unit for permeability of gases in barrier polymers is $(cm^3(STP)\cdot mil)/(100\ in.^2\cdot day\cdot atm)$. Table 1 provides conversion factors for several permeability units, including the SI unit $(mol\cdot m)/(m^2\cdot s\cdot Pa)$, which is commonly preferred in technical encyclopedias.

The steady-state transport properties of water vapor in barrier polymers are characterized by water vapor transmission rate (WVTR). The dimensions of WVTR are quantity of water transmitted through a film times thickness divided by area and time, and a common unit for WVTR is $(g\cdot mil)/(100\ in.^2\cdot day)$. Table 2 provides conversion factors for some WVTR units, including the SI unit $(mol\cdot m)/(m^2\cdot s)$. WVTR can be converted to water vapor permeability by dividing by the water partial pressure difference (which can be calculated from the specified relative humidity and temperature).

Penetrant transport through polymers is described by the so-called solution-diffusion model (1). According to this model, permeation through a flat sheet or film occurs in three steps: penetrant dissolves into the upstream (ie, the high partial pressure or high thermodynamic activity) side of the film, diffuses through the film, and desorbs from the downstream (ie, the low partial pressure or low thermodynamic activity) side of the film. The rate-limiting step in this process is diffusion through the film. In one dimension, penetrant diffusion through a polymer typically follows Fick's law:

$$N_A = -D\frac{dC}{dx} \tag{2}$$

where D is the effective diffusion coefficient for the penetrant in the polymer and dC/dx is the local concentration gradient of the penetrant.

When the downstream side penetrant partial pressure and concentration are negligible relative to those on the upstream face of the film, using Fick's law of

Table 1. Table of Common Gas Permeability Units with Conversion Factors[a]

Given	To obtain: Barrer	$\frac{\text{cc·cm}}{\text{cm}^2\text{·s·cm Hg}}$	$\frac{\text{cc·cm}}{\text{cm}^2\text{·s·atm}}$	$\frac{\text{cc·cm}}{\text{cm}^2\text{·s·Pa}}$	$\frac{\text{mol·cm}}{\text{cm}^2\text{·s·cm Hg}}$	$\frac{\text{mol·m}}{\text{m}^2\text{·s·Pa}}$	$\frac{\text{cc·mil}}{100\ \text{in.}^2\text{·day·atm}}$	$\frac{\text{cc·20}\mu\text{m}}{\text{m}^2\text{·day·atm}}$
Barrer	1	1.00×10^{-10}	7.60×10^{-9}	7.501×10^{-14}	4.461×10^{-15}	3.346×10^{-16}	1.668×10^{2}	3.283×10^{3}
$\frac{\text{cc·cm}}{\text{cm}^2\text{·s·cm Hg}}$	1.00×10^{10}	1	76	7.501×10^{-4}	4.461×10^{-5}	3.346×10^{-6}	1.668×10^{12}	3.283×10^{13}
$\frac{\text{cc·cm}}{\text{cm}^2\text{·s·atm}}$	1.316×10^{8}	1.316×10^{-2}	1	9.869×10^{-6}	5.87×10^{-7}	4.403×10^{-8}	2.195×10^{10}	4.32×10^{11}
$\frac{\text{cc·cm}}{\text{cm}^2\text{·s·Pa}}$	1.333×10^{13}	1.333×10^{3}	1.013×10^{5}	1	5.948×10^{-2}	4.461×10^{-3}	2.224×10^{15}	4.377×10^{16}
$\frac{\text{mol·cm}}{\text{cm}^2\text{·s·cm Hg}}$	2.241×10^{14}	2.241×10^{4}	1.703×10^{6}	16.81	1	7.501×10^{-2}	3.738×10^{16}	7.359×10^{17}
$\frac{\text{mol·m}}{\text{m}^2\text{·s·Pa}}$	2.988×10^{15}	2.988×10^{5}	2.271×10^{7}	2.241×10^{2}	13.33	1	4.984×10^{17}	9.81×10^{18}
$\frac{\text{cc·mil}}{100\ \text{in.}^2\text{·day·atm}}$	5.996×10^{-3}	5.996×10^{-13}	4.557×10^{-11}	4.497×10^{-16}	2.675×10^{-17}	2.007×10^{-18}	1	19.68
$\frac{\text{cc·20}\mu\text{m}}{\text{m}^2\text{·day·atm}}$	3.046×10^{-4}	3.046×10^{-14}	2.315×10^{-12}	2.285×10^{-17}	1.359×10^{-18}	1.019×10^{-19}	5.08×10^{-2}	1

[a]Given permeability in the units shown in one element of the first column, convert it to the units shown in one element of the first row by multiplying the original permeability by the factor at the intersection of the row and column of interest. For example, a value of 2 (cc·20 μm)/(m^2·day·atm) is equal to (2 × 0.0508) or 0.1 (cc·mil)/(100 in.^{2}·day·atm). In this table and throughout the article cc (or cm^3) has been used to denote cubic centimeters of gas as measured at standard temperature and pressure (STP) conditions, which are 0°C and 1 atm.

Table 2. Table of Common WVTR Units with Conversion Factors[a]

Given	To obtain		
	$\frac{\text{mol·m}}{\text{m}^2\text{·s}}$	$\frac{\text{g·mil}}{100\ \text{in.}^2\text{·day}}$	$\frac{\text{g·cm}}{\text{m}^2\text{·day}}$
$\frac{\text{mol·m}}{\text{m}^2\text{·s}}$	1	3.95×10^{9}	1.55×10^{8}
$\frac{\text{g·mil}}{100\ \text{in.}^2\text{·day}}$	2.53×10^{-10}	1	3.94×10^{-2}
$\frac{\text{g·cm}}{\text{m}^2\text{·day}}$	6.45×10^{-9}	25.4	1

[a]Given a WVTR value in units shown in one element of the first column, convert it to the units shown in one element of the first row by multiplying the original WVTR value by the factor at the intersection of the row and column of interest. For example, a value of 2 (g·cm)/(m^2·day) is equal to (2 × 25.4) or 50.8 (g·mil)/(100 $in.^2$·day).

diffusion (eq. 2), permeability can be expressed as product of the effective diffusion coefficient D and the solubility coefficient S, which is the ratio of the equilibrium penetrant concentration in the polymer at the upstream side of the film divided by the penetrant partial pressure or activity in the contiguous phase (1):

$$P = D \times S \tag{3}$$

According to equation 2, the diffusion coefficient is a kinetic term characterizing the mass flux of penetrant through a polymer film in response to a concentration gradient (1). Diffusion coefficients have units of (length)^2/time, and are often expressed in cm^2/s. The solubility or partition coefficient is a thermodynamic factor that links the equilibrium penetrant concentration in the polymer, C, with the penetrant partial pressure contiguous to the polymer surface, p (1):

$$C = S \times p \tag{4}$$

When the penetrants of interest are vapors, liquids, or solids, the partial pressure is often replaced by penetrant activity. For an ideal gas, penetrant activity is equal to the ratio of penetrant partial pressure to its saturation vapor pressure (1). For nonideal systems thermodynamic models must be used to estimate penetrant activity (2).

The diffusion process of penetrants in polymers can be broadly classified into two categories: Fickian (which obeys the Fick's law of diffusion) and non-Fickian. Penetrants in rubbery polymers and at low activities in glassy polymers typically exhibit Fickian behavior (3). The signature of Fickian diffusion in a thin polymer film contacted on both faces with a constant partial pressure (or activity) of penetrant is a weight increase due to penetrant absorption that is initially a linear function of the square root of the contact time and then asymptotically approaches a fixed equilibrium value (3). For Fickian diffusion-controlled kinetics of penetrant transport in a plane film whose thickness (L) is much smaller than its width or length, the time required to reach steady state in a permeation experiment, t_{SS}, is given by (3):

$$t_{ss} = \frac{L^2}{D} \tag{5}$$

The diffusion coefficients of large penetrants (eg, flavor and aroma compounds) in barrier polymers, which can be of the order of 10^{-14} cm^2/s or less, coupled with a typical film thickness of 10 μm result in extremely large time scales (over 3 years) to reach steady-state transport. Hence, over the shelf life of packaged products (typically of the order of several months), flavor and aroma compounds may never achieve equilibrium or steady-state conditions. In such cases, the steady-state permeability does not provide sufficient information to predict package shelf life. As discussed later, more detailed knowledge of penetrant solubility and diffusivity is required to accurately predict migration of such compounds.

In glassy polymers, deviations from Fickian behavior can occur. These deviations are generally believed to arise as a consequence of the finite rate of polymer structure reorganization in response to penetrant-induced swelling during the sorption–diffusion process (4). An example of so-called non-Fickian diffusion behavior is the penetrant sorbing into the polymer in two stages, an initial Fickian-like stage followed by a protracted, slow drift toward the final equilibrium sorption value (5). In such cases, the time required to achieve steady-state transport may be much higher than that predicted based on equation 5. This type of diffusion behavior is often observed when organic vapors at relatively high activity sorb into amorphous glassy polymers (6). For example, toluene vapors exhibit Fickian diffusion behavior in amorphous poly(vinyl chloride) (PVC) films at activities up to 0.4 and show increasingly non-Fickian behavior at higher activities (7).

Mechanism of Penetrant Transport in Dense Polymers

The rate-limiting step for penetrant diffusion is the creation of transient "gaps" in the polymer matrix via local scale polymer segmental dynamics involving several polymer chains (8). Penetrant molecules vibrate inside local cavities in the polymer matrix at frequencies much higher than the frequency of polymer chain motion required to open a gap of sufficient size to accommodate the penetrant. These steps are shown schematically in Figure 1. In Figure 1a, a penetrant molecule is shown dissolved in a polymer matrix. The penetrant vibrates inside a gap or molecular scale cavity in the polymer matrix at very high frequency (ca 10^{12} vibrations/s or 1 vibration/ps) (8). The polymer molecules do not occupy the entire volume of the polymer sample. Because of packing inefficiencies and polymer chain molecular motion, some of the volume in the polymer matrix is empty or "free" and this so-called free volume is redistributed continuously as a result of the random, thermally stimulated molecular motion of the polymer segments (1).

In Figure 1b, local polymer segmental motion has opened a connecting channel between two free-volume elements in the polymer matrix and the penetrant molecule can, as a result of its own Brownian motion, explore the entire corridor between the initial free-volume element which it occupied and the second free-volume element which is connected to it via the opening of a transient gap in the polymer matrix. Eventually, local segmental motion of the polymer segments closes the connection between the two free-volume elements and if the penetrant happens to be away from its original position, as shown in Figure 1c, when the gap in the polymer matrix is closed, the penetrant will be trapped in another free-volume element in the polymer matrix and will have executed a diffusion step. The

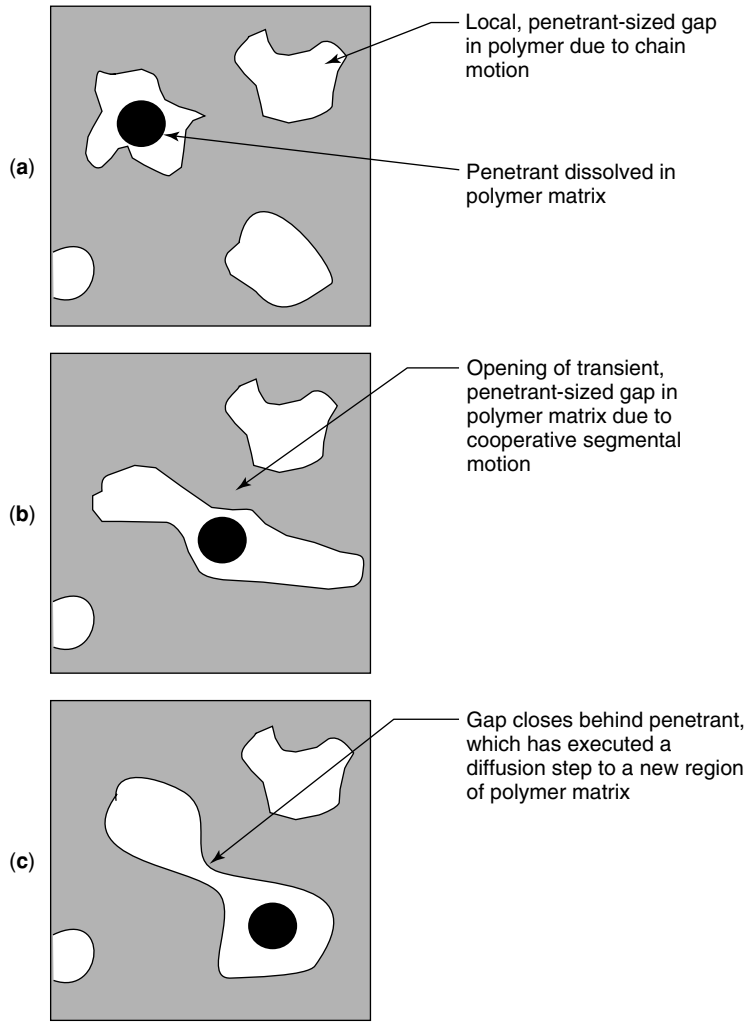

Fig. 1. Schematic depicting mechanism of penetrant transport in polymers (8).

process shown in Figure 1 has been called the "Red Sea" mechanism of penetrant transport in polymers (8).

Figure 2 shows a schematic of two polymer chains undergoing coordinated local segmental motion as a result of random, thermally stimulated movements of the polymer chains to open a gap between the polymer chains of sufficient size to permit passage of a penetrant molecule from one free-volume element to another (9). This schematic emphasizes that the polymer segmental motion is the rate-controlling step in penetrant diffusion.

Figure 3 provides a very simplistic schematic of the molecular processes involved in the local segmental motions of polymers that contribute to the formation of transient gaps in the polymer matrix important for penetrant diffusion. This figure shows what is believed to be a typical example of intramolecular cooperative local segmental motion of the polymer backbone of a polyethylene chain. This

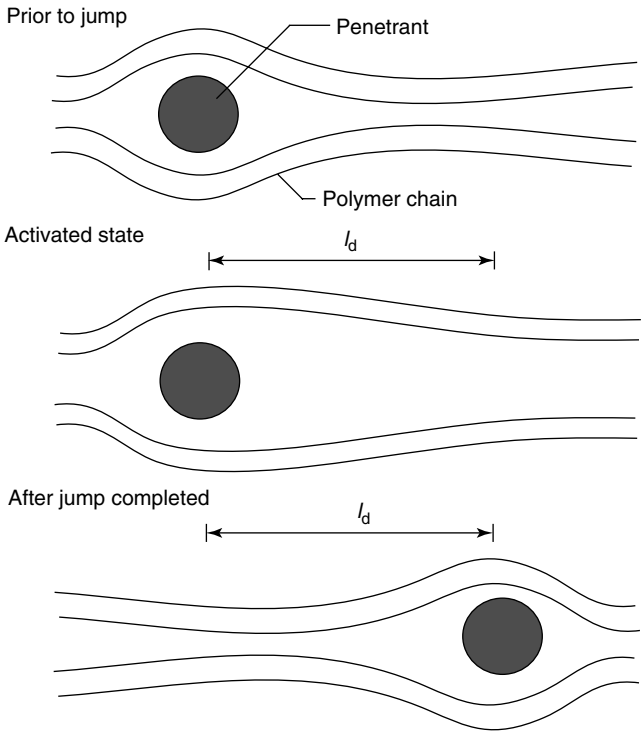

Fig. 2. Schematic depicting polymer chain position before, during, and after a diffusion step by a penetrant molecule (9).

so-called crankshaft motion requires the cooperation of several adjacent ethylene units and can act to create gaps in the polymer matrix of sufficient size to accommodate small penetrant molecules. It should be emphasized that the detailed understanding of the molecular level motions in polymers that contribute to diffusion is evolving rapidly as a result of more detailed atomistic simulation of penetrant transport in polymers. As a result, more realistic descriptions of the important molecular processes for penetrant diffusion in polymers should be expected in the near future.

The motion of polymer segments to produce a gap of sufficient size to accommodate a penetrant molecule is much slower than the vibration of the penetrant in a gap in the polymer matrix. For example, computer simulations of oxygen diffusion in a polyimide reveal that the oxygen molecules execute a diffusion step approximately once every nanosecond (1 ns = 1000 ps) (10). The rate of production of gaps of sufficient size to accommodate penetrant molecules decreases with increasing size of the penetrant. That is, there are fewer gaps produced per unit time in a polymer matrix of sufficient size to accommodate methane (kinetic diameter = 0.38 nm), for example, than there are for hydrogen (kinetic diameter = 0.289 nm).

Computer simulation results of diffusion in poly(2,6-dimethyl-1,4-phenylene oxide) (PPO) have been reported (11). Figures 4 and 5 present the results for the displacement of an oxygen molecule and a nitrogen molecule, respectively, as a

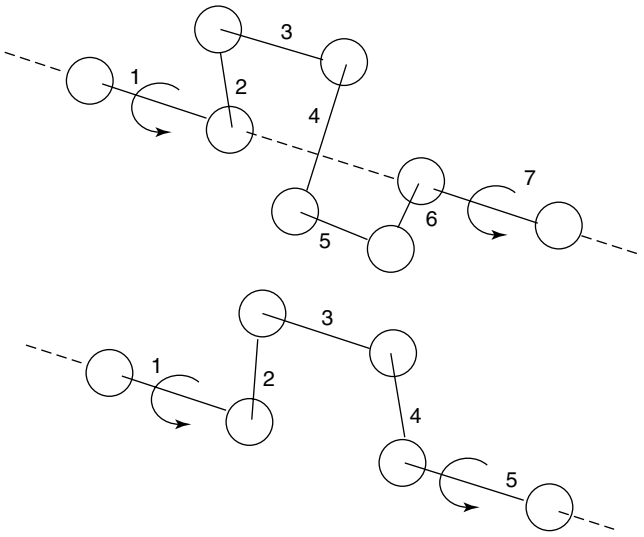

Fig. 3. Crankshaft motion—An example of local segmental dynamics in polyolefins. Each ball represents, for example, a methylene (ie, CH_2) unit in PE and the solid lines represent the covalent chemical bonds between neighboring CH_2 groups. Such molecular motions are believed to be important in providing pathways for diffusion of small molecules in polymers. The crankshaft motion requires the simultaneous rotation of several contiguous methylene units about bonds 1 and 7 or bonds 1 and 5 (9).

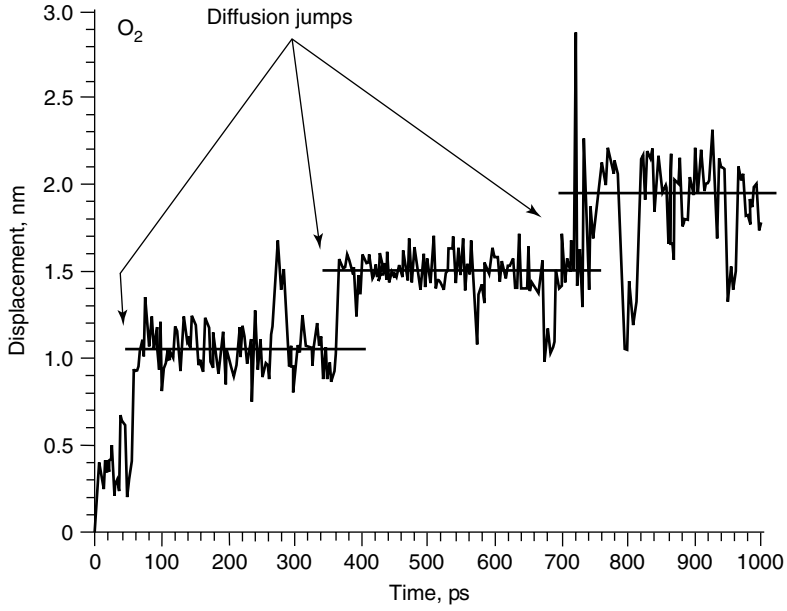

Fig. 4. Computer simulation of the displacement of an oxygen molecule in poly(2,6-dimethyl-1,4-phenylene oxide) as a function of time (11).

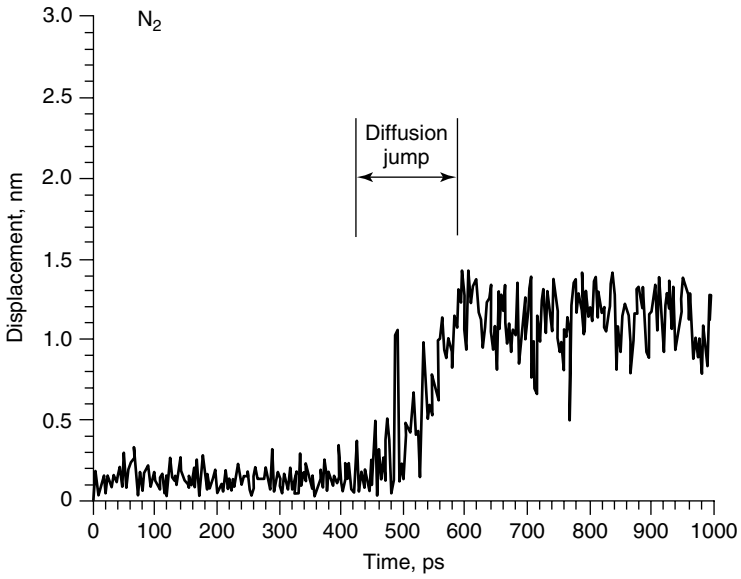

Fig. 5. Computer simulation of the displacement of a nitrogen molecule in poly(2,6-dimethyl-1,4-phenylene oxide) as a function of time (11).

function of time. There is about one diffusion jump for oxygen (kinetic diameter = 0.346 nm) every 300–350 ps but only one diffusion step for nitrogen (kinetic diameter = 0.364 nm) over the entire 1000 ps duration of the computer simulation (11). The oxygen molecule spends most of its time rattling within a small cage (or free-volume element) with average displacements of the order of 0.2 nm or so. The diffusion jumps occurring approximately every 300–350 ps involve displacements of the oxygen atom of the order of 0.4–0.5 nm. As shown in Figure 5, the diffusion jump length for nitrogen is longer (approximately 1 nm) and the jumps occur less frequently. However, these results are obtained for very short periods of time owing to computational limitations, and very long simulations would be required to generate precise estimates of jump lengths and jump frequencies. Because of the extremely demanding computational resources required for such molecular-level simulations, they are only now becoming possible for small molecule migration in relatively permeable polymers. As yet, computers are not fast enough to provide realistic simulations of phenomena such as migration of large flavor molecules in high barrier polymers.

Factors Affecting Permeability, Diffusivity, and Solubility

Free Volume. The dependence of penetrant transport properties on chain packing in polymers is often described using correlations involving the *fractional free volume* (FFV) of polymers. FFV is the fraction of volume in a polymer that is available to assist in penetrant transport, and does not include volume occupied by polymer molecules and volume in the polymer matrix that is otherwise unavailable

for penetrant transport. It is often estimated using group contribution methods. One popular method for estimating FFV is based on the following expression (1):

$$\mathrm{FFV} = \frac{V - V_0}{V} \tag{6}$$

where V is the polymer specific molar volume and V_0 is the so-called occupied volume that is not available to assist in penetrant transport. The occupied volume is usually estimated by Bondi's method as follows (12):

$$V_0 = 1.3V_\mathrm{w} \tag{7}$$

where V_w is van der Waals volume of the molecule. A good estimate of V_w can be obtained from bond radii, van der Waals radii of constituent atoms, and geometric factors. Bond radii are nearly constant from one molecule to another since the same chemical bond will always have the same radius. The most complete list of V_w values is available in the compilation given in Reference 13. The dependence of diffusion coefficients on FFV can be expressed as (14):

$$D = A \exp\left(\frac{-B}{\mathrm{FFV}}\right) \tag{8}$$

where A and B are empirical constants. The higher the FFV, the larger the diffusion coefficient. Figure 6 shows the effect of free volume on gas diffusion coefficients in a series of substituted polysulfones (15).

The dependence of solubility on FFV is usually weaker than that of diffusivity, especially in amorphous polymers (16). Therefore, permeability often follows a similar dependence on free volume as penetrant diffusivity. Attempts have been made to correlate FFV of polymers with gas permeability (17,18). As shown in Figure 7 (17), a nearly linear correlation was found to exist between the logarithm of oxygen permeability coefficients and the inverse of FFV in several families of amorphous, glassy polymers and high barrier liquid crystalline polymers. Many barrier polymers are glassy materials, since their use temperature is below their glass-transition temperature. In glassy polymers, which are nonequilibrium materials, free volume can be altered to some extent by the processing history of the sample (19). For instance, higher rates of cooling create higher free volume in the glassy state, and vice versa. A more effective way to alter free volume is to vary the chemical structure by, for example, adding or removing pendant groups on the polymer backbone (19). The presence of polar groups with low specific volumes can reduce the free volume (and hence, penetrant diffusion coefficients) by facilitating more efficient packing of the polymer chains due to stronger interactions between them (19). For example, barrier polymers such as polyacrylonitrile (PAN) and poly(vinyl alcohol) (PVOH) have polar pendant groups, which lead to strong energetic interactions between the polymer chains, efficient polymer chain packing, low free volume, and, in turn, low permeability coefficients.

Free volume in polymers can be measured using probes such as electrochromic, photochromic, and fluoroscent probes, as well as xenon nuclear magnetic resonance, small-angle x-ray scattering, density measurements, and positron

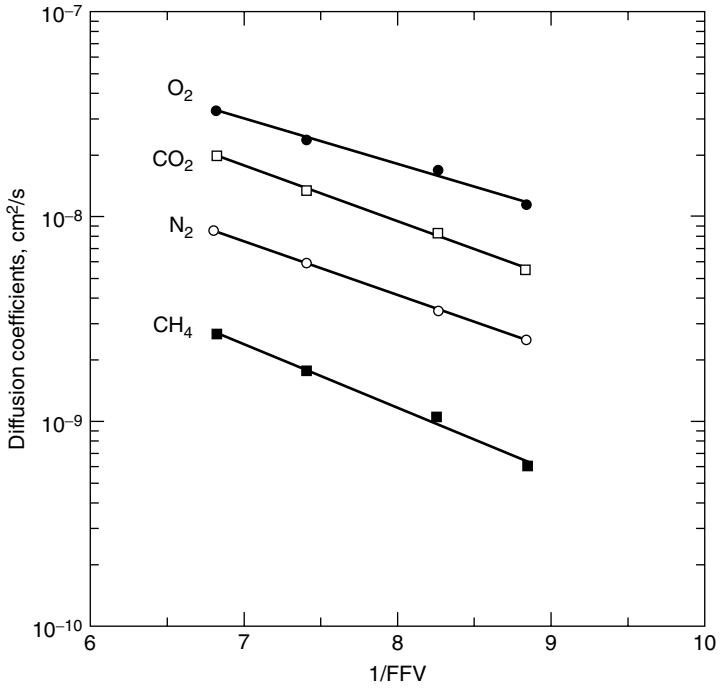

Fig. 6. Correlation of gas diffusion coefficients with inverse of polymer fractional free volume in a series of substituted polysulfones (15).

annihilation lifetime spectroscopy (pals) (20). Each method has its strengths and limitations, and a simple, direct measure of FFV is not available. The pals technique has, however, emerged in the past several years as a valuable nondestructive probe of free volume in polymers (20,21). PALS uses orthoPositronium (oPs) as a probe of free volume in the polymer matrix. oPs resides in regions of reduced electron density, such as free-volume elements, that typically range in radius from 0.2 to 0.4 nm. This range of cavity radii compares well with nonbonded interatomic distances in polymers and molecular radii of diffusing penetrants (20). PALS permits an estimate of both the size and concentration of free-volume elements in the polymer matrix. Transport properties of barrier polymers, copolymers, and polymer blends have been well correlated with FFV as measured by pals (20–26).

Temperature. The temperature dependence of permeability and diffusivity are usually modeled using Arrhenius equations of the following forms (1):

$$P = P_0 \exp\left(\frac{-E_p}{RT}\right) \tag{9}$$

$$D = D_0 \exp\left(\frac{-E_D}{RT}\right) \tag{10}$$

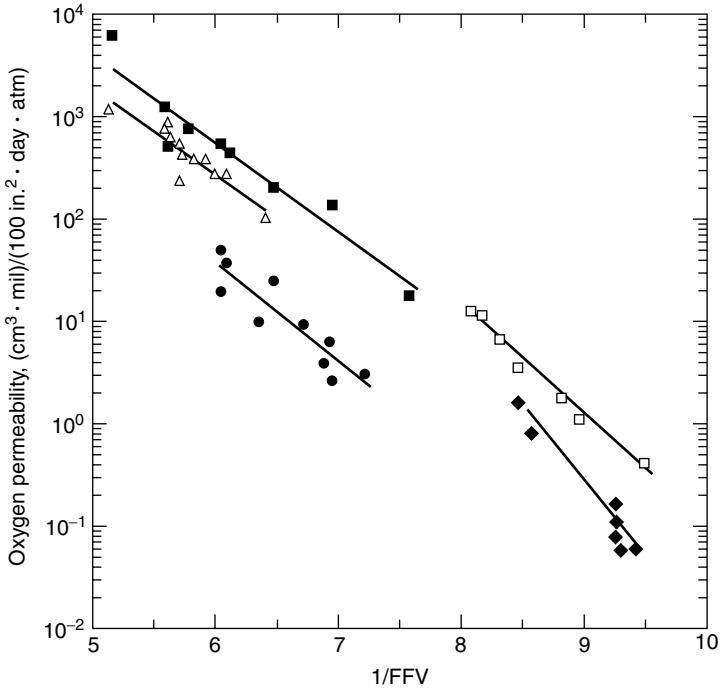

Fig. 7. Correlation of oxygen permeability with inverse of polymer fractional free volume for several families of amorphous, glassy, and liquid crystalline polymers (17). ■ Polystyrene (35°C), △ polycarbonates (35°C), ● polyesters (30°C), □ polyamides (25°C), ◇ liquid crystalline polymers (35°C).

where E_p and E_D are activation energies for permeation and diffusion, and P_0 and D_0 are preexponential factors. The effect of temperature on solubility is usually expressed by a van't Hoff relationship (1):

$$S = S_0 \exp\left(\frac{-\Delta H_S}{RT}\right) \tag{11}$$

where S_0 is a preexponential factor and ΔH_s is the heat of sorption of penetrant in the polymer. Since steady-state permeability is the product of diffusivity and solubility, the activation energy of permeation can be defined as the sum of activation energy of diffusion and the heat of sorption (1):

$$E_p = E_d + \Delta H_S \tag{12}$$

E_d is always positive; ΔH_s is often positive for light gases (such as H_2, O_2, and N_2), but can be negative for larger, more soluble penetrants (such as C_3H_8 and C_4H_{10}). For polymers such as low density polyethylene (LDPE) and poly(vinyl chloride) (PVC), E_p is always positive (1). Therefore, permeability increases with increasing temperature. To illustrate this behavior, Figure 8 shows the effect of temperature on oxygen permeability of four widely used barrier polymers (27).

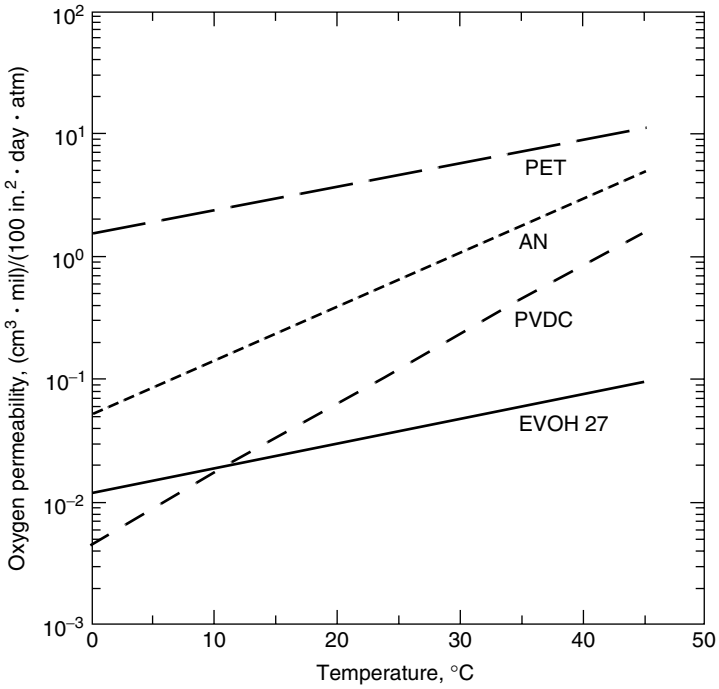

Fig. 8. Effect of temperature on oxygen permeability at 75% RH. PET is poly(ethylene terephthalate), AN is an acrylonitrile–styrene copolymer, PVDC is vinylidene chloride–vinyl chloride copolymer (coextrusion resin grade), and EVOH 27 is ethylene vinyl alcohol copolymer containing 27 mol% ethylene (27).

At temperatures far from the transition temperatures (eg, glass-transition temperature and melting point) the Arrhenius relationship (eq. 10) is obeyed, and with a known activation energy of diffusion, E_D, the diffusion coefficient of a penetrant in a polymer can be estimated at any temperature. In cases where E_D is not reported, it can be estimated using a known correlation (28,29) between D_0 and E_D:

$$\ln D_0 = a\frac{E_D}{RT} - b \tag{13}$$

where a and b are independent of penetrant type. The parameter a is independent of polymer type and has a universal value of 0.64 (30). b has a value of 9.2 [$-\ln(10^{-4}$ cm^2/s)] for rubbery polymers (ie, polymers above their T_g) and 11.5 [$-\ln(10^{-5}$ cm^2/s)] for glassy polymers (ie, polymers below their T_g) (13). Equation 13 is often referred to as a "linear free-energy" relation. Similar relations between D_0 and E_D are observed for viscosity of organic liquids, molten salts, and metals (31) and for first-order chemical reaction kinetics (32), which are also activated processes described by the Arrhenius equation. Additionally, common barrier polymers such as poly(ethylene terephthalate) (PET) and polycarbonate

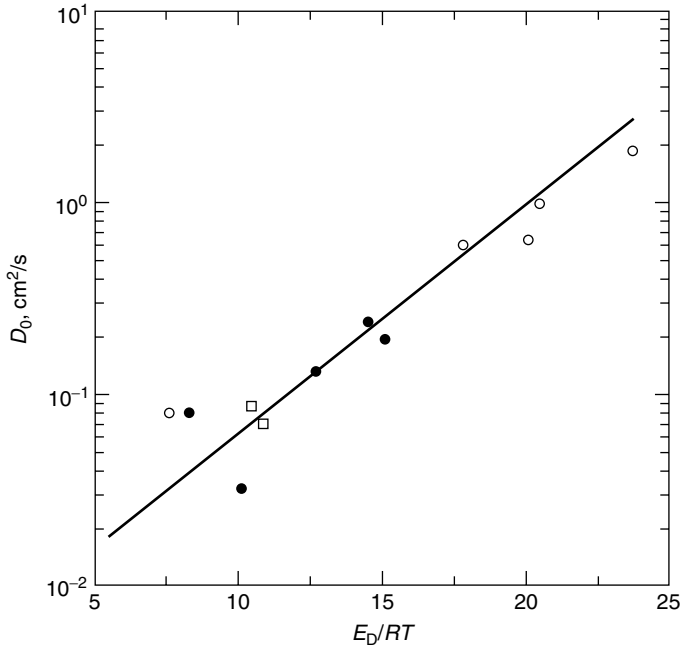

Fig. 9. Correlation of D_0 with E_D/RT for various penetrants in glassy polymers (33). ○ Poly(ethylene terephthalate), ● bisphenol-A polycarbonate, □ tetramethyl bisphenol-A PC.

(PC) are known to follow this relation both above and below the glass-transition temperature, as shown in Figure 9 (33). Combining equations 10 and 13 gives

$$D = \exp\left[-b - \left(1 - \alpha\right) \frac{E_D}{RT} \right] \tag{14}$$

On the basis of a single value of the diffusion coefficient at one temperature, E_D can be estimated from equation 14. This equation can then be used to estimate the diffusion coefficient at other temperatures, provided that the two temperatures do not traverse thermal transitions (such as glass transition) and the polymer morphology is otherwise unchanged.

Chemical Structure. The presence of polar groups on or in polymer chains often increases chain rigidity, which can increase glass-transition temperature and improve mechanical properties, and increases packing density (1). Conventional barrier polymers, such as PAN, have very low gas permeability as a result, in part, of restricted chain mobility due to the presence of polar groups. Polymer chain interactions can be quantified in terms of cohesive energy density (CED), and CED has a strong influence on penetrant diffusion. CED of a polymer is the square of its solubility parameter and characterizes the strength of attraction (or interactions) between the polymer chains. It can be estimated using group contribution techniques (13). In a simple model of penetrant diffusion in polymers, the activation energy for diffusion is directly proportional to the CED of a polymer

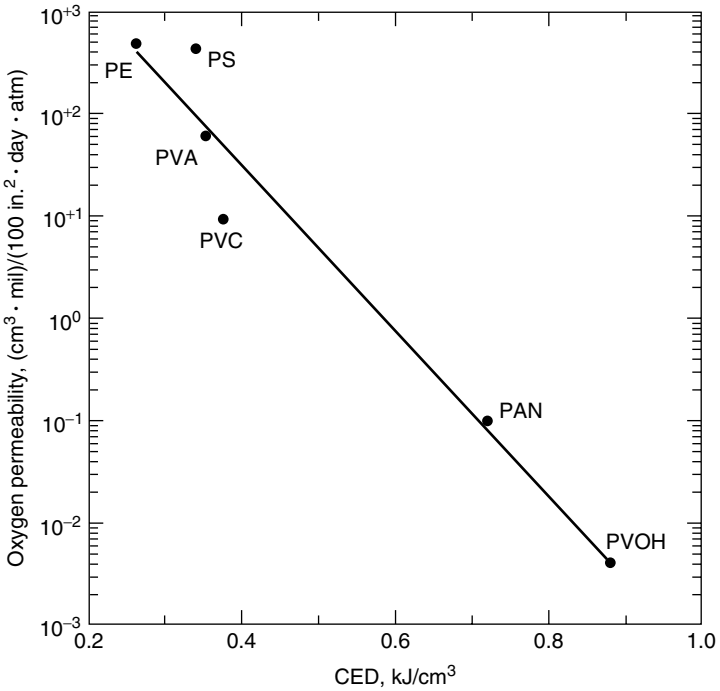

Fig. 10. Correlation of oxygen permeability (23°C, 0% RH) with CED for six barrier polymers: PE, PS, PVA, PVC, PAN, PVOH (36,37).

(34). On the basis of this model and the linear free-energy relation (35), the logarithm of penetrant diffusion coefficients should decrease linearly with increasing CED. Solubility of relatively nonpolar penetrants usually has a weaker dependence on CED than diffusivity, and hence, the logarithm of permeability should decrease linearly with increasing CED. As shown in Figure 10, a nearly linear correlation was found between oxygen permeability and CED of barrier polymers with permeability values ranging over 5 orders of magnitude (36,37).

Penetrant diffusivity, and hence permeability, can also be decreased by adding substituents to the polymer chain that reduce chain flexibility. Bulky side groups or rigid linkages such as aromatic groups decrease chain flexibility and hence reduce penetrant diffusion coefficients. Flexible linkages, such as ether or methylene groups, produce the opposite effect (1). Several methods are used to characterize chain flexibility (1). The glass-transition temperature is a measure of long range or bulk molecular motion, and high T_g materials are usually rigid and inflexible. Sub-T_g relaxations are another indication of molecular motion, and correlations of O_2 and CO_2 permeability with sub-T_g relaxations have been observed within a family of amorphous polyesters and copolyesters (38). However, the exact nature of molecular motions which control penetrant diffusion are complex and unclear, and hence T_g and sub-T_g relaxations do not, in general, provide predictive correlations with penetrant diffusivity (1).

Changes in molecular structure of the polymer often affect more than one factor influencing permeability and the net effect can be difficult to anticipate.

For example, addition of bulky side groups can stiffen the polymer chains, which is expected to reduce the diffusion coefficients. However, the same modification could also decrease chain packing in the amorphous phase and reduce the level of crystallinity in the polymer, which are expected to increase the diffusion coefficients (39). The net result of these competing effects can be difficult to predict a priori.

Crystallinity. Increasing crystallinity in a polymer generally decreases gas permeability (16) (see SEMICRYSTALLINE POLYMERS). Crystallinity influences both solubility and diffusion coefficients. For most polymers and penetrants of interest, crystalline regions, which are much more dense and well ordered than amorphous regions, preclude penetrant sorption, thereby reducing penetrant solubility. Additionally, the presence of impermeable crystallites in a polymer matrix acts as barriers to diffusion, increasing the path length for diffusion and, in some cases, increasing chain rigidity, which also reduces diffusion coefficients (16). Although crystallite size, shape, and orientation do not usually influence solubility in polymers significantly, these factors can be important in penetrant diffusion. The effect of crystallinity on penetrant diffusion can be expressed using the following model (39):

$$D = \frac{D_a}{\tau\beta} \tag{15}$$

where D_a is the penetrant diffusion coefficient in the amorphous polymer, τ is a geometric impedance (ie, tortuosity) factor, and β is a chain immobilization factor. Impermeable crystalline regions force penetrants to follow a tortuous pathway through the permeable amorphous regions. This effect is captured by the factor τ, which is the ratio of the average distance traveled by a penetrant molecule to the thickness of the sample (39). τ can be a complex function of crystalline content as well as crystallite size, shape, and orientation (16,40). Crystallites can also restrict segmental mobility by acting as physical cross-links. This effect is taken into account by the factor β and is generally more pronounced in flexible rubbery polymers such as polyethylene (PE). In glassy polymers such as PET, the inherent rigidity of the chain backbone imposes more impedance to chain mobility than the crystallites and hence, β is one (16) (see AMORPHOUS POLYMERS).

A two-phase model is often used to describe penetrant solubility in a semicrystalline polymer (41):

$$S = S_a\phi_a \tag{16}$$

where S_a is solubility coefficient in the amorphous regions of the polymer and ϕ_a is amorphous phase volume fraction. This model assumes that the solubility of the crystalline regions is zero, and that the presence of crystallites does not change the amorphous phase solubility coefficient. For polymers used in barrier packaging applications, the assumption of zero solubility in the crystalline regions is generally accurate (42). The second assumption that the amorphous phase solubility is independent of crystalline content is not necessarily obeyed, particularly in glassy polymers, whose state of amorphous phase structural organization may be influenced significantly by common processing protocols (eg, orientation, stretching,

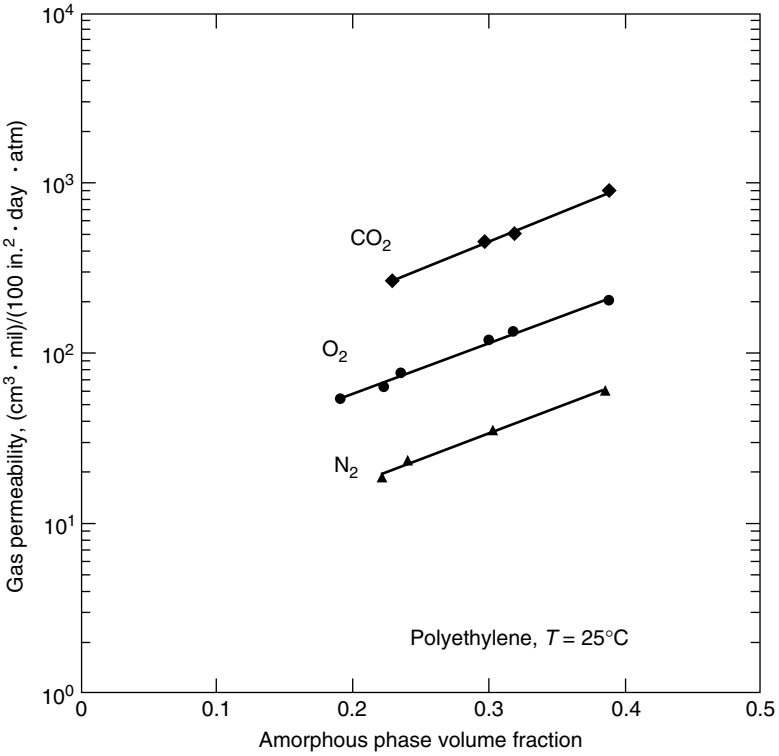

Fig. 11. Effect of crystalline content on gas permeability in PE at 25°C and 0% RH (47).

annealing, and contact with crystallization-inducing agents) (43–46). Nevertheless, the simplest and most commonly used model for the effect of crystallinity on steady-state permeability is based on these assumptions and is expressed by the following relationship:

$$P = (S_a \phi_a)\left(\frac{D_a}{\tau\beta}\right) \tag{17}$$

Figure 11 shows the effect of crystallinity on gas permeability in PE at 25°C. Permeability decreases with increasing crystallinity primarily because of decreasing diffusion coefficients. The effect of crystallinity is more pronounced on tortuosity factor τ than the chain immobilization factor β (47). In glassy polymers, the most widely used approximations for τ and β are $\tau = {\phi_a}^{-1}$ and $\beta = 1$. Introducing these values into the above equation yields $P = P_a {\phi_a}^2$, where P_a is the amorphous phase permeability.

In certain polymers, the simple assumptions of the two-phase model do not hold. For example, poly(4-methyl-1-pentene) (PMP), which is a highly permeable polymer, has a very low density crystal structure, and hence, penetrant molecules can sorb into its crystalline phase (42). In PET, it has been observed that the presence of crystalline regions increased the concentration of sorption sites in the

amorphous regions remaining in the polymer after crystallization (41). Others have recently examined this phenomenon in PET in more detail (48,49). It has been reported (43) that exposing amorphous PET to a strongly sorbing penetrant at high activity results in penetrant-induced crystallization. This process affects the amorphous phase penetrant solubility of PET, resulting in a marked increase in overall solubility with increasing crystallinity. For example, acetaldehyde solubility in PET increased by more than 300% as a result of penetrant-induced crystallinity of about 36 wt% (43). This effect was attributed to the creation of microvoids in the polymer as a by-product of penetrant-induced crystallization (43). Evidence for microvoid formation in PET due to exposure to strongly sorbing penetrants has been presented in studies investigating solvent treatments to improve the dyeability of PET yarns (44), and in studies investigating the effect of crystallizing liquids on the morphology of PET (45,46). For example, it has been reported that dye uptake in PET fibers exposed to dimethylformamide (DMF) was four to five times higher than in unexposed fibers (44). The dye diffusion coefficient was also more than 2 orders of magnitude higher in the DMF-exposed samples than in the unexposed samples (50).

Chain Orientation. Stretching or drawing of polymer films can improve mechanical properties, and under certain conditions, barrier properties (see FILMS, ORIENTATION). The degree of chain orientation achieved is dependent on the draw ratio and other process conditions (16). Orientation is usually characterized by birefringence and quantified by the Herman's orientation function f (51):

$$f = \frac{1}{2}(3\cos^2\theta - 1) \tag{18}$$

where θ is the average angle between the polymer chain axis and the draw direction.

Depending on the mode of deformation and the physical processes that occur during orientation, permeability may either increase or decrease with increasing orientation (16). Impermeable polymer crystallites may become oriented into plate-like structures during deformation, and this process generally decreases penetrant diffusivity by increasing tortuosity (16). In addition, drawing of semicrystalline polymers can improve barrier properties through stress-induced crystallization and orientation of the remaining amorphous phase. Hence, the reduction in permeability caused by orientation of crystallizable polymers can be greater than that in noncrystallizable polymers (16). The dramatic effect of orientation is supported by oxygen permeability data for PET in the literature. A 4 $\times$ biaxial orientation (ie, draw ratio = 4 in each axis) decreased the permeability of oxygen in PET by a factor of about 2 (52). For other systems, however, increases in permeability upon biaxial orientation have also been reported. A vinylidene chloride (VDC)–vinyl chloride copolymer, for example, showed an increase in oxygen permeability from 0.2 (cm^3·mil)/(100 $in.^2$·day·atm) to 0.3 (cm^3·mil)/(100 $in.^2$·day·atm) upon 2.5 $\times$ biaxial orientation (53). The permeability increase was attributed to microvoid development during orientation of the polymer chains after crystallinity was fully developed. Table 3 shows the effect of orientation on oxygen permeability of semicrystalline and amorphous barrier polymers (53). In semicrystalline VDC copolymer and nylon MXD-6 polymers, under the conditions studied, the orientation process results in a slight increase in oxygen permeability

Table 3. Effect of Orientation on Oxygen Permeability Characteristics of Semicrystalline and Amorphous Barrier Resins[a]

Barrier polymer resins	Oxygen permeability,[b] $(cm^3 \cdot mil)/(100\ in.^2 \cdot day \cdot atm)$
Semicrystalline resins	
VDC copolymer[c]	
Compression molded film	0.20 ± 0.02
Extrusion cast film	0.20 ± 0.01
Biaxially oriented – 2.5 ×	0.30 ± 0.01
Aromatic Nylon MXD-6[d]	
Extrusion cast	0.37 ± 0.09
Biaxially oriented – 2 ×	0.39
Amorphous resins	
Amorphous Nylon Selar PA 3426[e]	
Extrusion cast film	1.40 ± 0.31
Uniaxially oriented – 2.5 ×	1.14 ± 0.07
Biaxially oriented – 2.5 ×	1.01 ± 0.01
Polyacrylic-imide XHTA-50A[f]	
Extrusion cast	3.12 ± 0.17
Uniaxially oriented – 2 ×	2.95 ± 0.04
Uniaxially oriented – 2.5 ×	2.84
Biaxially oriented – 2 ×	2.76 ± 0.03

[a] Ref. 53.
[b] At 23.5°C, 65% RH.
[c] Dow Chemical Company's vinylidene chloride–vinyl chloride copolymer (experimental grade XU 32009.02).
[d] Trademark of Mitsubishi Gas Chemical Co., Japan.
[e] Trademark of E. I. du Pont de Nemours & Co., Wilmington, Del.
[f] Trademark of Rohm & Haas Co., Philadelphia, Pa.

with chain orientation, whereas the reverse is true for amorphous Selar 3426 and polyacrylic-imide barrier polymers.

Penetrant Concentration (or Partial Pressure). The influence of penetrant concentration on solubility, diffusivity, and, in turn, permeability varies, depending on the penetrant–polymer system. Rubbery and glassy polymers typically show little or no concentration dependence for solubility, diffusivity, and permeability of light gases such as H_2, N_2, and O_2. Consistent with this notion, Figure 12a shows essentially no influence of pressure on H_2 permeability in PE (19). Gases such as CO_2, which are more soluble than light gases, typically have a permeability–presssure response in glassy polymers similar to that shown in Figure 12b. Permeability decreases monotonically with increasing pressure as predicted by the dual-mode sorption model (54). The magnitude of the permeability decrease depends upon the amount of so-called nonequilibrium excess volume in the polymer, which can increase with increasing T_g, the affinity of the penetrant for the nonequilibrium excess volume, and the mobility of the penetrant in the nonequilibrium excess volume relative to its mobility in the equilibrium free volume (1). The permeability of a rubbery polymer to an organic vapor often exhibits the behavior shown in Figure 12c. The monotonic increase in permeability is often due to increases in penetrant solubility with increasing pressure coupled with increases in diffusivity with increasing pressure (1). The response shown in

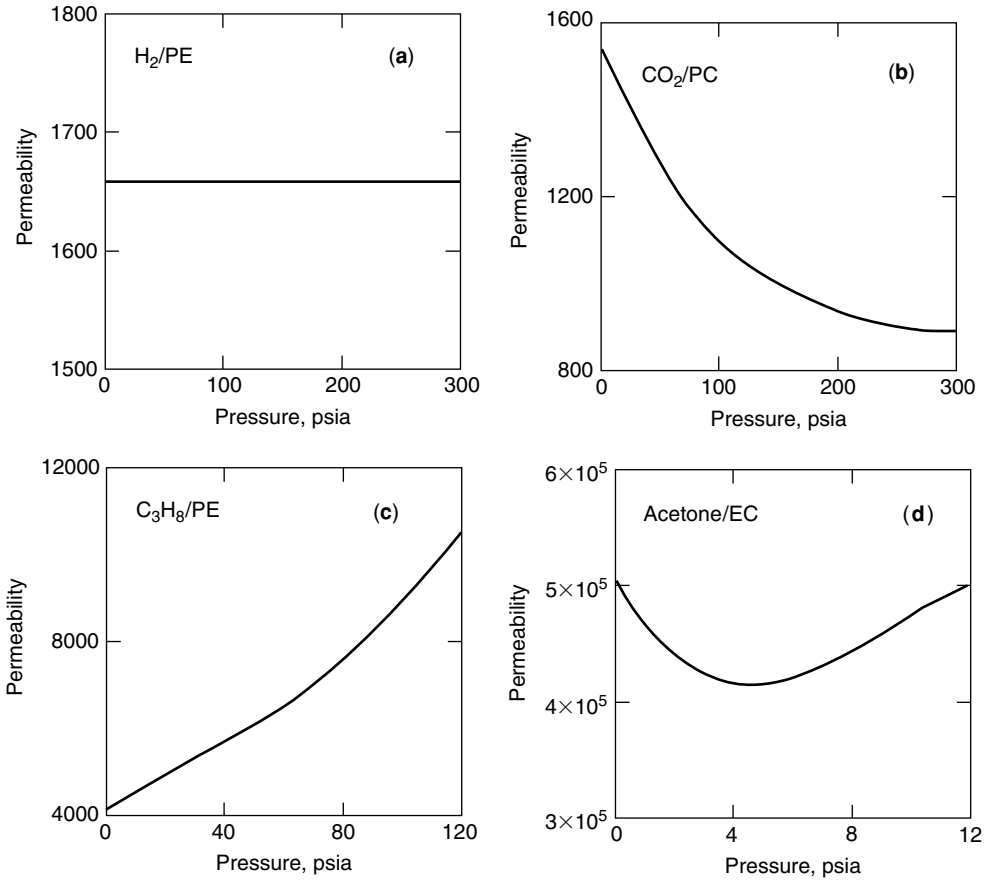

Fig. 12. Typical permeability–pressure dependence in rubbery and glassy polymers. (**a**) Hydrogen in PE at 30°C, (**b**) carbon dioxide in PC at 35°C, (**c**) propane in PE at 20°C, (**d**) acetone in ethyl cellulose (EC) at 40°C (19). The permeability values have units of $(cm^3 \cdot mil)/(100\ in.^2 day \cdot atm)$.

Figure 12d is typical for strongly interacting penetrants (eg, organic vapors) in glassy polymers at sufficiently high penetrant partial pressures. It can be viewed as a superposition of the behaviors in Figures 12b and 12c (1). The sharp increase in permeability begins as the penetrant plasticizes the polymer. Plasticization occurs when penetrant molecules dissolve in the polymer matrix at sufficient concentration to force polymer chain segment separation, thereby increasing the free volume, and in turn, facilitating polymer segmental motion. This increase in segmental mobility, which may be observed by the depression in T_g, results in an increase in penetrant diffusion coefficients and, in turn, permeability (1).

Humidity. The absorption of water can increase, decrease, or have no effect on gas permeability of barrier polymers (27). Increasing the relative humidity (RH) from 0 to 50% increases the oxygen permeability of cellophane (regenerated cellulose) by an order of magnitude, and exposure to 90% RH removes it from the class of high barriers by further increasing the permeability by more than an

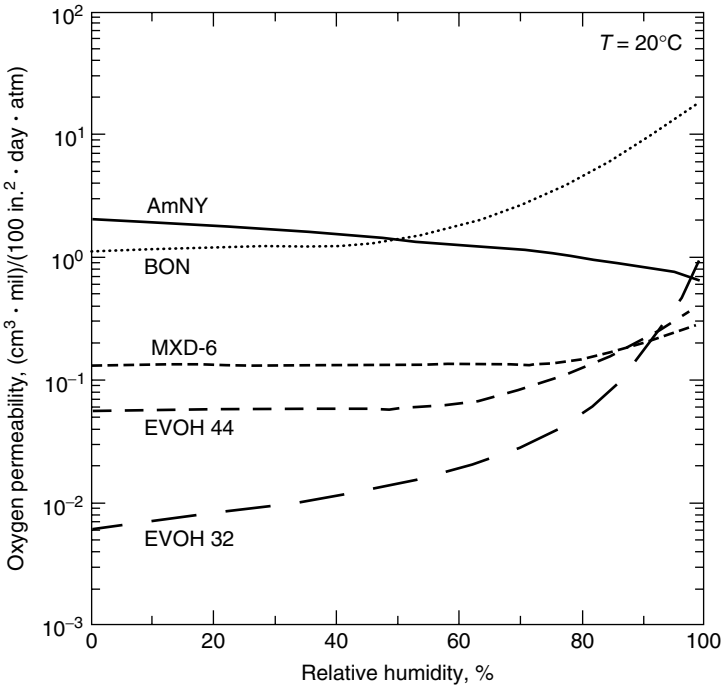

Fig. 13. Effect of relative humidity on oxygen permeability of hydrophilic barrier polymers. AmNY is amorphous nylon (Selar), BON is biaxially oriented nylon-6, MXD-6 is oriented poly(metaxylylenediamine–adipic acid), EVOH 44 and 32 are ethylene vinyl alcohol copolymers containing 44 and 32 mol% ethylene (27).

order of magnitude (27). For packaging of foods that require protection against oxygen ingress, cellophane is coated or laminated with water barriers such as polyolefins (27). Other hydrophilic barrier polymers, with the exception of certain amorphous polyamides, also lose their barrier properties with increasing RH, as shown in Figure 13. This is because water acts as a plasticizer and increases the free volume of the polymer (55). However, at low to moderate RH, amorphous polyamides and PET show slightly improved barrier properties with increasing RH (27). This behavior has been explained as the water molecules not swelling the polymer, but occupying some of the polymer free-volume sites instead, resulting in reduction in permeability of other gases (56). VDC copolymers, acrylonitrile copolymers, and polyolefins show essentially no effect of RH on gas permeability (57).

Techniques for Measuring Transport Properties

The determination of permeability, solubility, and diffusivity requires direct or indirect measurement of mass transfer under controlled conditions. The permeability of barrier polymers can be determined directly by measuring the pressure change or other physical evidence of transfer or indirectly by using an indicator of permeation, such as chemical reaction of the transferring gas with another

substance. The preferred methods of measurement differ for different classes of penetrants: light gases, water vapor, condensable vapors, and food flavor and aroma compounds.

There are two basic methods for measuring permeability: isostatic and quasi-isostatic (55). Isostatic methods employ a continuous flow on both sides of the polymer film to provide constant penetrant concentrations. Quasi-isostatic methods use a continuous flow to maintain constant penetrant concentration only on the upstream side and allow penetrant accumulation on the downstream side of the film. However, this accumulation is limited to a very low concentration, and hence the penetrant partial pressure difference can be approximated as a constant (55). Figure 14a typically shows the course of an isostatic permeability experiment for a barrier polymer film of uniform thickness exposed to constant penetrant partial pressure p on the upstream side and constant removal of penetrant that has permeated through the film to the downstream side. Using a specified initial condition (concentration in the film uniformly equal to zero) and boundary conditions (constant penetrant concentration C at the upstream side and zero penetrant concentration at the downstream side), this situation can be described by the following mathematical expression (58):

$$q = \frac{DC}{L}\left(t - \frac{L^2}{6D}\right) - \frac{2LC}{\pi^2}\sum_{n=1}^{\infty}\frac{(-1)^n}{n^2}\exp\left(\frac{-Dn^2\pi^2 t}{L^2}\right) \tag{19}$$

where q is the total mass of penetrant permeating per unit film area in time t, D is the diffusion coefficient, L is film thickness, and C is penetrant concentration at the upstream side in equilibrium with the upstream penetrant partial pressure p. When steady state is reached, t becomes large enough to make the exponential term negligibly small, and the above equation reduces to

$$q = \frac{DC}{L}\left(t - \frac{L^2}{6D}\right) \tag{20}$$

A plot of q vs t yields a straight line whose slope is the steady-state penetrant flux ($N_A = DC/L$) and whose x-axis intercept is called the time lag (t_L).

$$t_L = \frac{L^2}{6D} \tag{21}$$

The time lag can be related to the time required to achieve steady state ($t_{SS} \sim 2.7t_L$) (27). The diffusion coefficient can be calculated by rearranging the above equation (58):

$$D = \frac{L^2}{6t_L} \tag{22}$$

Permeability can be calculated from equation 1 and the steady-state flux value ($P = N_A\, L/p = DC/p$). It should be noted that for concentration-dependent diffusion coefficients, t_L will vary with the pressure difference across the polymer film, and as a result, this simple time lag analysis may yield significant

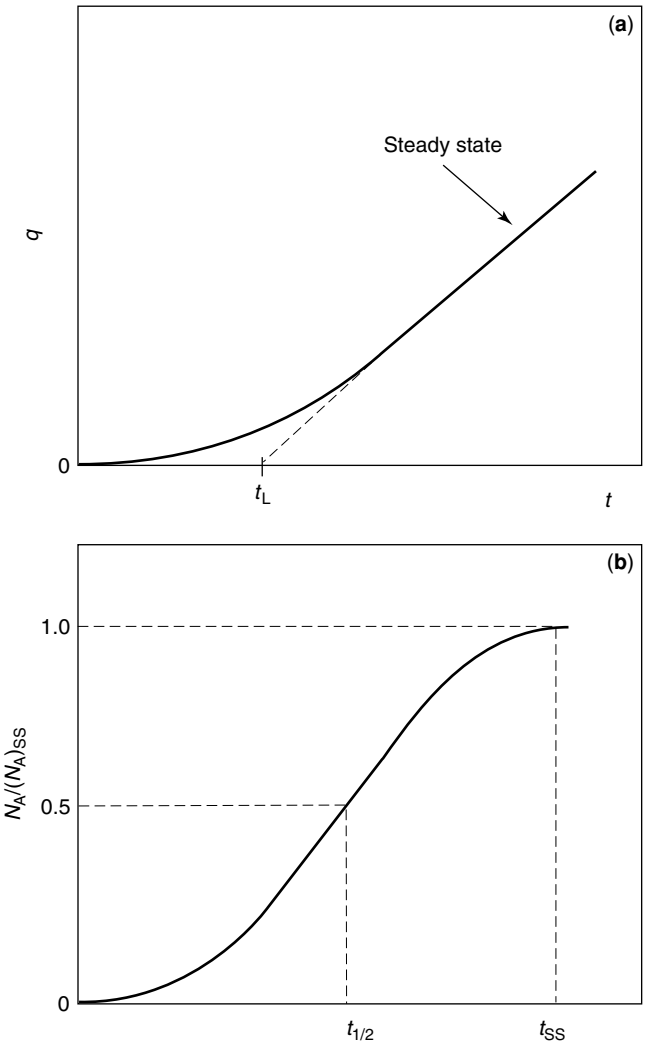

Fig. 14. (**a**) Mass of permeating penetrant per unit film area (q) as a function of time (providing a measure of time lag t_L). (**b**) Normalized penetrant flux (N_A) as a function of time (providing a measure of halftime $t_{1/2}$). t_{SS} is time required to achieve steady state.

errors in the diffusion coefficients estimated using equation 22 (58). More general expressions for the time lag have been developed by including the concentration dependence of D (59). Alternatively, a 'concentration-averaged' diffusion coefficient can be obtained by plotting normalized penetrant flux (ie, flux at any time t divided by the steady-state flux) as a function of time (Fig. 14b). The diffusion coefficient can be estimated using the following relationship (60):

$$D = \frac{L^2}{7.2t_{1/2}} \tag{23}$$

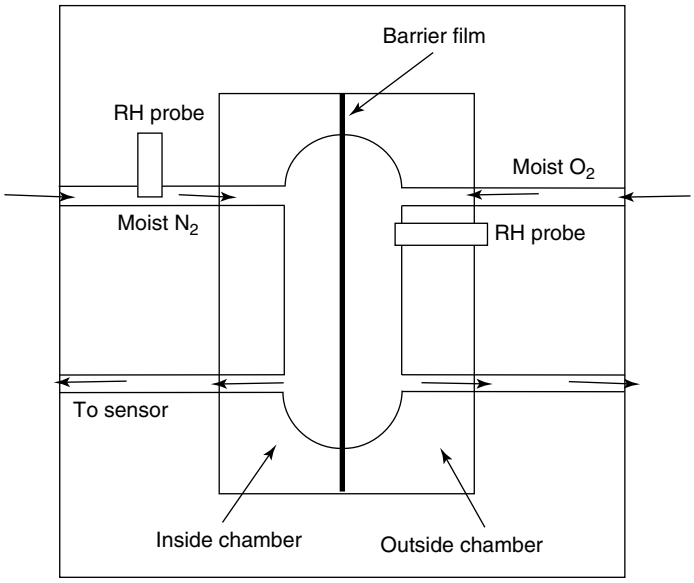

Fig. 15. A schematic of a permeation cell in the Ox-Tran (MOCON, Inc.) oxygen transmission rate measurement system (62).

where $t_{1/2}$ is the halftime (ie, time required for the penetrant flux to reach half of its steady-state value). Thus, permeability, diffusivity, and hence solubility ($S = P/D$) can be determined from a single experiment. Given the ready availability of computing power, it is now possible to use any of a variety of numerical techniques to fit the entire response and extract the desired parameters and, when applicable, their concentration dependence.

Oxygen and Carbon Dioxide Permeation. The most widely used commercial instrument for measuring oxygen transmission rates of flat films and packages is the Ox-Tran (Modern Controls Inc., Minneapolis, Minn.), and measurements are made in accordance with ASTM method D3985 (61). In this isostatic coulometric method, flat film samples are clamped into a diffusion cell, which is then purged of residual oxygen using an oxygen-free carrier gas such as N_2. The carrier gas is routed to the instrument sensor until a stable zero has been established. Pure oxygen is then introduced into the outside chamber of the diffusion cell (see Fig. 15) (62). Oxygen molecules diffusing through the film to the inside chamber are conveyed to the sensor by the carrier gas. The Ox-Tran system uses a patented coulometric sensor (Coulox) to detect oxygen transmission through both flat films and packages. This sensor provides parts-per-billion sensitivity to oxygen even in the presence of water vapor. Digital pressure and flow controls allow for RH control. Alternative instruments for measuring oxygen transmission rates include Oxygen Permeation Analyzers from Illinois Instruments Inc. (Ingleside, Ill.).

Modern Controls, Inc. (MOCON) also makes instruments for measuring carbon dioxide permeation. Their Permatran-C line of instruments uses an infrared detector to detect carbon dioxide that permeates through the test film.

Water Vapor Permeation. WVTRs can either be measured by the traditional gravimetric "cup" method (63) or by newer electronic instruments. The newer method (eg, ASTM method F1249 (64)) uses infrared detection to measure water vapor transmission through barrier films. One of the most widely used commercial WVTR systems is Permatran-W (Modern Controls Inc., Minneapolis, Minn.). The newest model of this system (Permatran-W 3/31) uses a patented modulated infrared sensor to detect water vapor transmission through flat films and packages. It provides a sensitivity in the range of parts per million. Various models are available with different temperature and RH capabilities.

Lyssy AG (Zollikon, Switzerland) also manufactures automatic water vapor permeability testers designated as the L80 line of instruments. The L80-5000 is the newest member and the fifth generation in this series.

In the traditional method (ASTM method E96) (27), a sample cell containing either a desiccant or distilled water is covered with the sample film and placed in a controlled atmosphere. Typical conditions for the desiccant method are 100°F (37.8°C) and an external RH of 90%, although the standard also allows for temperatures between 70 and 90°F (21 and 32°C) at (50 ± 2)% RH. The cell assembly is weighed periodically until steady state is reached. WVTR can be calculated from the steady-state rate of change in the weight of the cell.

Flavor and Aroma Compounds. Measurement of transport rates of flavor and aroma vapors in plastics is more complicated than that of either water vapor or light gases. Elaborate equipment and sensitive analytical devices are required to obtain reliable results. Since the transport behavior of these compounds is often strongly concentration dependent, measurements must be made in the activity range in which the compounds are present in practice. Thus, some of the major complexities include providing precisely mixed quantities of the condensable vapor in an inert carrier such as nitrogen or argon at very low concentrations, typically a few parts per million, and assuring that the concentration is maintained. Temperature must also be carefully controlled to prevent condensation on equipment surfaces (27).

As such, no single instrument has gained the widespread acceptance noted above for instruments for O_2, CO_2, and water vapor, though several methods have been used to measure transport properties of flavor and aroma compounds in barrier polymers. These include isostatic permeation techniques and gravimetric techniques (65). The permeation techniques directly yield permeability and diffusivity of flavors in barrier polymers. Solubility can then be calculated indirectly using the relation $P = D \times S$. The MAS 2000 Organic Vapor Permeation Test System (MAS Technologies Inc., Zumbrota, Minn.) is an example of a system that was commercially available for flavor permeation measurements. Mass spectrometry and flame ionization detection have also been successfully used as vapor concentration detectors (65). In contrast, gravimetric techniques permit direct and independent measurements of both solubility and diffusivity (66). It is possible to measure sorption and desorption of organic flavors in barrier polymers using sensitive gravimetric sorption instruments such as the McBain spring balance and the Rubotherm magnetic suspension balance (67–70). A schematic of a McBain spring balance assembly is shown in Figure 16. The polymer sample is suspended from a sensitive helical quartz spring inside the sorption chamber. After introducing the penetrant, the spring position relative to a fixed reference

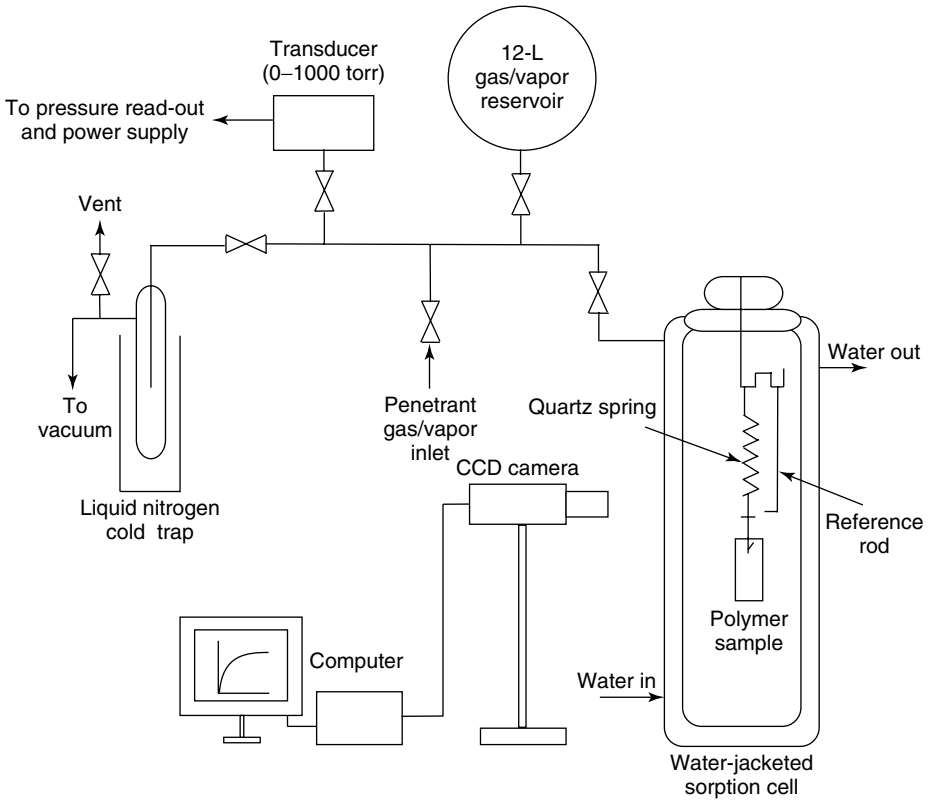

Fig. 16. A schematic of a McBain spring balance apparatus for measuring sorption and desorption of organic vapors in barrier polymers (66).

rod hanging inside the chamber is recorded using a CCD camera. From the kinetic uptake data, solubility and diffusivity values are estimated (71). Acceptable levels of agreement have been reported for solubility coefficients of ethyl acetate in LDPE, linear LDPE (LLDPE), and ionomer films obtained from gravimetric and isostatic permeation techniques (65).

Techniques for Predicting Transport Properties

Modeling Transport Properties of Gases and Condensable Vapors in Polymers. The permeation of low molecular weight gases such as O_2, N_2, CO_2 as well as large flavor and aroma compounds is an essential consideration in the selection and schematic of food packages and containers. Predictive models for permeation would minimize the number of experiments required in package material selection and development. Perhaps, more importantly, they also provide an insight into the underlying factors controlling permeation in barrier polymers.

The permachor method has been used to predict permeabilities of low molecular weight penetrants in barrier polymers (72). Although originally developed

for O_2, N_2, and CO_2, this method can be extended to other gases and vapors, provided there is no specific interaction between the penetrant and the polymer. It has been successfully used for over 60 different polymers (72). In this method, numerical values (ie, group contributions) are assigned to polymer segments. An average numerical value can then be obtained for the polymer, which is referred to as the permachor value of the polymer. A simple equation is used to relate gas permeability P to polymer permachor value π:

$$P = A\,\mathrm{e}^{-s\pi} \tag{24}$$

where A and s are temperature-dependent constants. This method also takes into account the reduction in permeability caused by the orientation of crystalline polymers using the following expressions:

$$P = \left(\frac{A}{\tau_0}\right) e^{-s\pi} \tag{25}$$

$$\tau_0 \approx \frac{1.13}{\sqrt{\phi_a}} \tag{26}$$

where τ_0 is tortuosity related to crystallite orientation and ϕ_a is the amorphous phase volume fraction. A good agreement has been reported between experimental and model predictions of O_2, N_2, and CO_2 permeability values in a variety of polymers (72). This method has also been modified for predicting liquid permeation through polymers (63). The permachor method works well for polymers and copolymers, but is not applicable to polymer blends (27). As with any group contribution method, caution should be exercised when attempting to perform predictions which are outside the data set used to generate the correlation.

Other methods for correlating gas permeability in barrier polymers with polymer molecular structure have been developed using free-volume theory (17,18,73). Group contribution techniques can be used to estimate polymer free volume from densities and intrinsic volumes of various polymer components. In the method proposed in Reference 18, polymer-specific free volume was used, which was defined as $(V-V_0)/M$, where V is specific volume, V_0 is specific occupied volume, and M is polymer molecular weight. V_0 can be calculated according to Bondi's method from van der Waals volumes of the various groups in the polymer structure (18). In this model, free volume was defined on a unit weight basis so that various molecular structures could be compared on the same weight basis. The model predicts a linear relationship between logarithm of gas permeability and the reciprocal of polymer-specific free volume. Other improvements to this model have been suggested (17,73). Gas permeability has often been correlated with FFV (as defined in eq. 6) using the following relation (73):

$$P = A\exp\left(\frac{-B}{\mathrm{FFV}}\right) \tag{27}$$

where A and B are constants for a particular gas. It has been observed that when this model is limited to a specific family of polymers, eg, polyesters and polyamides

(17), a reasonably good correlation can be obtained. However, when the correlation is broadened to include a wider range of polymer types, there is considerable scatter in the data, particularly at low values of gas permeabilities. Even though these free-volume-based models have some fundamental basis for correlating transport properties, they have the following limitations (18,73): (*1*) the assumption of solubility being independent of free volume and polymer structure is clearly an approximation, (*2*) the concept of free volume cannot capture all the factors affecting gas permeability (such as chain flexibility and CED), and (*3*) there may be errors in values of van der Waals volumes available in the literature. Attempts have been made to refine these models by introducing more empirical parameters and making them more predictive, and these efforts have resulted in significant improvements in the accuracy of the correlations (73).

Larger and more condensable penetrants, eg, flavor and aroma compounds, can have extremely low diffusion coefficients in common barrier polymers, resulting in extremely large time scales to achieve steady state. For example, *d*-limonene has diffusion coefficients of the order of 10^{-14} cm^2/s in PET (74). When coupled with a typical film thickness of 10 μm, this leads to time scale to reach steady state of more than 3 years. Hence, as noted before, over the shelf life of the packaged product (typically of the order of several months), flavor and aroma compounds may never reach steady-state transport. Therefore, independent predictions of their diffusion and solubility coefficients become necessary. Several methods have been proposed for predicting solubility coefficients. A widely used method is based on a thermodynamic approach that relates penetrant sorption to solubility parameters of the penetrant and the polymer (75). This dependence can be expressed as follows:

$$\begin{aligned} S &= S_0 \exp[(\Delta H_{vap} - \Delta H_{mix})/RT] \\ \Delta H_{mix} &= \nu_1 \phi_2 (\delta_1 - \delta_2)^2 \end{aligned} \tag{28}$$

where S_0 is a constant for a particular polymer, ν_1 is partial molar volume of the penetrant, ϕ_2 is volume fraction of polymer in the mixture, δ_1 and δ_2 are solubility parameters of penetrant and polymer respectively, and ΔH_{mix} is enthalpy change on mixing of penetrant molecules with polymer segments. The values of ν_1, δ_1, and δ_2 can be obtained from the literature (36). The enthalpy change on vaporization of the penetrant (ΔH_{vap}) can be calculated from the penetrant boiling point by using available correlations (2). Reasonably good agreements have been reported between model-predicted and experimentally observed solubility coefficients of several penetrants in vinylidene chloride–vinyl chloride copolymers and LDPE at 85 and 30°C respectively (76).

For penetrants that interact with the polymer matrix primarily via dispersion (ie, van der Waals) forces, penetrant solubility scales with measures of penetrant condensability such as penetrant boiling point, critical temperature, or the force constant in the Lennard–Jones potential model (43). The following relation between penetrant critical temperature and penetrant solubility has been derived using a classical thermodynamics model (13,77):

$$\ln S_a = N + MT_c \tag{29}$$

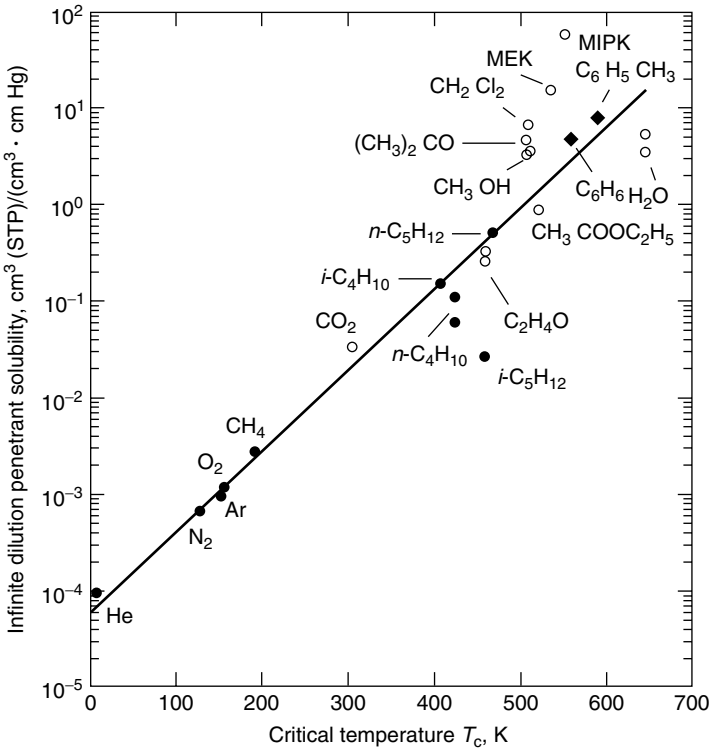

Fig. 17. Correlation of infinite dilution penetrant solubility with penetrant critical temperature in PET ((71) and unpublished data). ● Nonpolar penetrants, ○ polar and quadrupolar penetrants, ◇ aromatic penetrants. MEK is methyl ethyl ketone and MIPK is methyl isopropyl ketone. The slope $M = 0.019 \pm 0.001\ K^{-1}$ and intercept $N = -9.6 \pm 0.4$.

In this expression, N is a parameter that depends primarily on polymer–penetrant interactions and polymer free volume. T_c is the penetrant critical temperature, which is widely tabulated for many penetrants of interest (2). M is constant and has a value of approximately $0.016\ K^{-1}$ for gas dissolution in liquids and in rubbery and glassy polymers (13). While N varies from polymer to polymer, average values of -9.7 and -8.7 for rubbery and glassy polymers at 35°C, respectively, when solubility is expressed in $cm^3(STP)/(cm^3 \cdot cm\ Hg)$ have been recommended (13). Penetrants with strong dipole or quadrupole moments may be more soluble in a polar polymer matrix, such as PET, than predicted based on equation 29 (71). Although equation 29 is strictly valid for penetrant sorption in equilibrium matrixes, such as liquids or rubbery polymers, it also provides an excellent description of equilibrium solubility in glassy polymers (71). Figure 17 shows the correlation of penetrant solubility in PET with penetrant critical temperature (71). Nonpolar penetrants show excellent agreement with the model presented in equation 29 and polar or quadrupolar penetrants exhibit significant scatter around the correlation line.

Over wider ranges of critical temperature, it has been suggested that penetrant solubility coefficients may be better correlated with the square of reciprocal reduced temperature $(T_c/T)^2$ (78):

$$\ln S_a = n + m\left(\frac{T_c}{T}\right)^2 \tag{30}$$

where T is the temperature of the experiment, and m and n are the slope and intercept of the correlation line, respectively. This equation may also be derived from fundamental thermodynamic considerations (43). Other semiempirical methods, eg, UNIFAC group contribution model, have also been proposed for predicting penetrant solubility in polymers (79,80).

Several predictive and correlative methods have been developed for diffusion coefficients of penetrants in polymers. An empirical relationship has been developed for correlating diffusion coefficients with penetrant critical volume (81):

$$D_a = \frac{\tau}{V_c^{\eta}} \tag{31}$$

where D_a is amorphous phase diffusion coefficient, V_c is penetrant critical volume, and τ, η are adjustable constants. This equation has been proposed based on analogy with correlations of diffusion coefficients with critical volume of small molecules in liquids. For larger penetrants (eg, long-chain hydrocarbons), diffusion steps may occur via motion of only part of the molecule, and critical volume is not expected to capture the effective size of a penetrant unit participating in a diffusion step (43). In such cases, diffusion coefficients would be less sensitive to penetrant size than indicated in the above equation. Also, critical volume fails to capture the effect of penetrant shape on diffusion coefficients (71). Figure 18 shows a plot of D vs. V_c for PET at 25°C. Diffusion coefficients of penetrants (up to molecular weights of 100 Da) in PVC, PS (polystyrene), and PMMA [poly(methyl methacrylate)] have been correlated empirically with other measures of penetrant size, such as molecular diameter (82).

A theoretical model based on polymer free volume, temperature, and penetrant size and shape has been developed (83). According to this model, diffusion coefficients of large penetrants in amorphous rubbery polymers are given by

$$D = \frac{V_f^2}{6}\left(\frac{eRT}{M}\right)^{1/2}\left(\frac{1}{\ell_1 \mathrm{Ac}_1^2} + \frac{1}{\ell_2 \mathrm{Ac}_2^2} + \frac{1}{\ell_3 \mathrm{Ac}_3^2}\right)\exp\left(\frac{-E_D}{RT}\right) \tag{32}$$

where V_f is average free volume per polymer chain segment, e is the base of natural logarithm, M is penetrant molecular weight, ℓ_i is length of penetrant molecule along a given direction i (taken as the principal axis of inertia), Ac_i is effective penetrant molecular cross-sectional area perpendicular to the direction i, and E_D is the activation energy of diffusion. V_f can be calculated from the following equation (83):

$$V_f = V\left[0.025 + \alpha_f(T - T_{g2} + kw_1)\right] \tag{33}$$

where V is the total volume per mole of the polymer repeat unit, α_f is temperature coefficient of free-volume expansion, T_{g2} is glass-transition temperature of the polymer, k is plasticizing efficiency of the penetrant for the polymer, and w_1 is

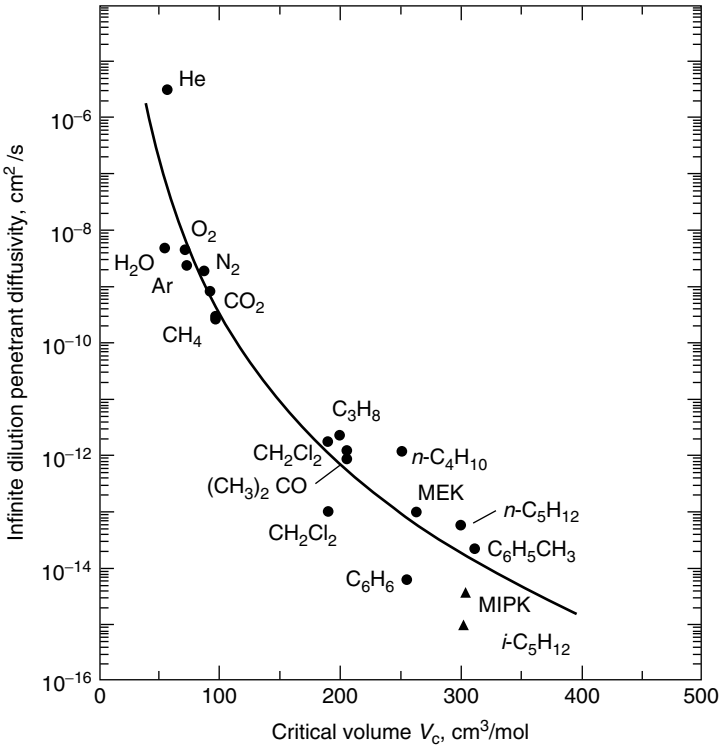

Fig. 18. Effect of penetrant size on infinite dilution, amorphous phase diffusion coefficients in PET at 25°C ((71) and unpublished data). ▲ Branched pentrants. MEK is methyl ethyl ketone and MIPK is methyl isopropyl ketone. The best-fit parameters of equation 31 are $\tau = (5.7 \pm 1.2) \times 10^8$ (cm^2/s) $(cm^3/mol)^{9.1}$ and $\eta = 9.1 \pm 0.9$.

weight fraction of the penetrant in the polymer. Equation 32 is strictly valid for large penetrants satisfying the size criterion $V_s \gg V_f$, where V_s is effective steric volume of the penetrant (83). The penetrant molecular shape dependence is represented by the three-termed expression within the parentheses of equation 32. The equation can be applied to penetrants of a wide variety of molecular shapes (83). This model has been tested using data for diffusion of plasticizers in PVC (83).

"Migration Modeling" of Polymer Additives into Packaged Foods and Beverages. One of the key applications of barrier polymers is food and beverage packaging. Several low molecular weight components, eg, monomers and oligomers, as well as additives such as lubricants, stabilizers, and plasticizers, which are necessary for processing and stability, can be present in polymers used for packaging. Hence, there exists a potential for permeation (or migration) of these additives into the food or beverage with subsequent contamination (84–86). To ensure the safety of packaged food components, the U.S. Food and Drug Administration (FDA) established a 'Threshold of Regulation' approach which sets upper limits on the additive concentrations in the food (84). Since traditional migration testing methods are time consuming, expensive, and the analysis can

be difficult (especially at low penetrant concentrations), the FDA has developed models for predicting the additive concentration in the food simulant and rate of transport of additives (84):

$$q = 2C_0\rho\sqrt{\frac{D_p t}{\pi}} \tag{34}$$

where q is total mass of permeating species per unit surface area, C_0 is initial additive concentration in the polymer, ρ is polymer density, D_p is additive diffusion coefficient, and t is the package shelf life. This equation assumes that (84) (*1*) permeation is diffusion-controlled and follows Fick's law, (*2*) no solubility-limited partitioning occurs between the polymer and the food, and (*3*) other external phase mass transfer resistances (eg, mixing, reaction with food) are negligible. The following empirical equation has been developed for predicting diffusion coefficients (84):

$$D_p = 10^4 \times \exp\left[A_p - a \times \mathrm{MW} - b\left(\frac{1}{T}\right)\right] \tag{35}$$

where D_p is additive diffusion coefficient (cm^2/s), A_p is constant for a particular polymer, MW is additive molecular weight (g/mol), and a, b are correlation constants with values of 0.01 mol/g and 10,450 K respectively. The A_p values are 9 for LDPE, −3 for PET, and 5 for HDPE and PP (84). A semiempirical model for predicting diffusion coefficients has also been developed (87):

$$\ln D_P = \ln A + \alpha\left(\mathrm{MW}\right)^{1/2} - \frac{K\left(\mathrm{MW}\right)^{1/3}}{T} \tag{36}$$

where A, α, and K are constants determined from experimental data. The diffusion coefficients follow Arrhenius-type behavior and are taken to be independent of penetrant concentration (84). These models do not explicitly account for the effect of polymer crystallinity or orientation on additive diffusion coefficients.

The approach of the European Commission (EC), on the other hand, has been to assign 'specific migration limits' to different substances with adverse toxicological properties (86). A Fickian diffusion-based model, called the Piringer migration model, which uses the 'Migratest Lite' program, has been used (85,86), and its mathematical form is given below:

$$M_t = C_0\rho L\left(\frac{\alpha}{1+\alpha}\right)\left[1 - \sum_{n=1}^{\infty} 2\alpha\left(1+\alpha\right)\left(1+\alpha+\alpha^2 q_n^2\right)\exp\left(\frac{-D_p t q_n^2}{L^2}\right)\right], \qquad \alpha = \frac{1}{K}\frac{V_F}{V_p},\ \tan q_n = -\alpha q_n \tag{37}$$

where L is film thickness, K is partition coefficient, and V_F and V_p are the volumes of food and polymer, respectively. The diffusion coefficient can be estimated from equation 35.

The sorption and transport of flavor and aroma compounds from the food simulant into the packaging walls can affect the migration of additives from the

walls into the food simulant. Neither approach (FDA or EC) takes this effect into account. In general, these migration models provide conservative estimates (from a safety viewpoint) of additive concentrations in the food simulant and their diffusion coefficients. However, there are certain cases when they can fail (84) (eg, in cases where the flavor and aroma compounds from the food simulant plasticize the polymer, or if the additive reacts either with the polymer or with the food simulant to produce a species that is not detectable), and attempts are being made to improve them.

Chemical Structures and Properties of Barrier Polymers

Barrier polymers can be broadly classified as high barrier and moderate to low barrier polymers, depending on the degree to which they restrict the passage of gases such as O_2 or CO_2 and water vapor. The boundaries between these classifications, while somewhat arbitrary, are based on the effect of the barrier properties of the polymer on the shelf life of the packaged products. This section discusses various properties of different classes of barrier polymers. The selection of a barrier polymer for a particular packaging application depends not only on its barrier properties but also on other physical properties, and a comparison of physical, mechanical, and optical properties of some commonly used barrier polymers is, therefore, presented in Table 4 (88). Permeabilities of light gases (O_2 and CO_2) and water vapor are presented in Tables 5 and 6 respectively (27), and Table 7 presents permeability, diffusivity, and solubility of flavor and aroma compounds in various high and moderate barrier polymers (63). Permeability data of light gases and water vapor in barrier polymers (93–97) are more widely available than those of flavor and aroma compounds (98–100). Proper caution should be exercised when using or comparing data from different sources since, as discussed in the previous sections, polymer permeability values depend on a wide variety of factors.

High Barrier Polymers. High barrier polymers are generally understood to be those polymers which offer a high resistance to gas transmission. There are no specific limits for the gas transmission rates, but this category comprises polymers with gas permeabilities low enough to significantly prolong the shelf life of packaged products.

Ethylene–Vinyl Alcohol Copolymers. The general structure of ethylene–vinyl alcohol (EVOH) resins is as follows (101):

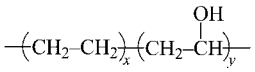

EVOH resins are random copolymers of ethylene and vinyl alcohol made by the hydrolysis of ethylene vinyl acetate copolymers (101). The leading manufacturers are Kurray (EVALCA) and Nippon Gohsei (57). In commercial grades of EVOH used in packaging, ethylene concentration ranges from 29 to 44 mol% (EVAL Co., U.S.). No additives are required in their processing as the presence of ethylene units renders the otherwise intractable vinyl alcohol melt processable in conventional molding and extrusion equipments. A high concentration of

Table 4. Physical, Mechanical, Optical, and Chemical Properties of Some Commonly Used Barrier Polymers[a]

Property	HDPE	LDPE	PP	PET	PVC	PS	PVDC	Nylon-6	EVOH
Density, g/cm^3	0.945–0.967	0.915–0.925	0.90	1.4	1.22–1.36	1.05	1.6–1.7	1.14	1.14–1.19
Glass-transition temperature, °C	−55	−25	−20	80	∼80	100	−17	50	
Yield, Pa^{-1}, 1 mil	4.1	4.2	4.4	2.9	2.8	3.8	2.4	3.5	3.3–3.5
Tensile strength, MPa	17.2–41.4	10.3–34.5	137.8–206.7	172.2–227.4	27.5–55.1	55.1–82.7	55.1–110.2	172.2–255	8.2–11.7
Tensile modulus, 1% secant, GPa	0.9	0.1–0.3	2.4	4.8	2.4–4.1	2.7–3.3	0.3–1	1.7–2	2.0–2.6
Elongation at break, %	200–600	200–600	50–275	70–130	100–400	2–30	50–100	70–120	120–280
Tear strength, kN/m[b]	—	17.5–87.5	175–263	175–350	17.5–52.5	52.5–175	0.35	87.5–140	—
Chemical resistance	Inert	Inert	Inert	Inert	Inert	Inert (except oils, greases)		Inert, sorbs water	Inert
Haze, %	3	5–10	3	2	1–2	1	1–5	1.5	1–2
Light transmission, %	—	65	80	88	90	92	90	88	90
Heat-seal temperature range, °C	135–155	120–175	90–150	135–175	135–170	120–175	120–150	120–175	175–200
Service temperature range, °F	−40 to 120	−55 to 80	5 to 120	−70 to 150	−30 to 65	−60 to 80	−15 to 135	−70 to 200	−15 to 150

[a]Ref. 88.

[b]To convert kN/m to lb/in., divide by 0.175.

Table 5. Oxygen and Carbon Dioxide Permeabilities of Various High and Moderate Barrier Polymers[a]

	Gas permeability,[b] $(cm^3 \cdot mil)/(100\ in.^2 \cdot day \cdot atm)$	
Barrier polymer	Oxygen	Carbon dioxide
EVOH, 27 mol% ethylene	0.03 (20°C)	0.04 (20°C, 65% RH)
P(VDC–AN) barrier coating	0.04	0.1
Liquid crystalline polymer[c]	0.06 (100% RH)	
EVOH, 44 mol% ethylene	0.07 (20°C)	0.2 (20°C, 65% RH)
PVDC coextrusion resin	0.10	0.25
Nylon MXD-6 oriented film	0.17	
BLOX 4000 series PHAE resin[d]	0.2 (80% RH)	
Nitrile resin	0.65	1.6
Amorphous nylon	1.2	4.0 (30°C, 80% RH)
PEN polyester[e]	1.2	
Nylon-6, biaxially oriented	2.6	5.8 (dry)
PET, 25% crystalline (bottle wall)	4.8	24
PVC, rigid	5.0	20
Nylon-6, unoriented	6.6	10.2
Aclar 33C PCTFE film[f]	7.0 (0% RH)	16 (0% RH)
PP, biaxially oriented	150	548
HDPE, molded	185	580
MDPE, molded	250	1000
PS film, oriented	365	900
LDPE, molded	498	2500

[a] Ref. 27.
[b] At 75% RH and 23–25°C except as noted.
[c] Vectra A950 LCP film (Celanese AG) (89).
[d] BLOX is a trademark of The Dow Chemical Co. (Midland, Mich.) (90).
[e] Ref. 57.
[f] Aclar is a trademark of Honeywell (Morristown, N.J.) (91).

ethylene is also recommended for thermoforming (102). At low to moderate RH, EVOH copolymers provide an excellent barrier to gases. The hydroxyl units (or OH groups) contribute strongly to increasing chain cohesive energy density and improving barrier properties, and so the greater the fraction of OH groups, the lower the permeability (103). Figure 19 shows the effect of ethylene concentration on oxygen and water vapor permeability of EVOH (27). This figure also presents permeation properties of poly(vinyl alcohol) (PVOH) [ie, fully hydrolyzed poly(vinyl acetate)] and HDPE (which has no OH groups) for comparison with the EVOH series (see VINYL ALCOHOL POLYMERS). As RH increases, the barrier properties of EVOH copolymers decrease (cf Fig. 13). The OH groups are also responsible for the hydrophilic nature of the polymer. Hence, the greater the percentage of vinyl alcohol units, the greater the influence of humidity on gas barrier properties of EVOH copolymers (27). Conversely, high proportions of ethylene units improve resistance to moisture (as shown in Fig. 13) and decrease the water vapor transmission rate, as shown in Figure 19. Moisture sensitivity can also be decreased somewhat by biaxial orientation (57). EVOH also offers very high barrier to flavor and aroma compounds and these barrier properties are not as sensitive to

Table 6. Water Vapor Transmission Rates of Various High and Moderate Barrier Polymers[a]

Barrier polymer	Water vapor transmission rate,[b] (g·mil)/(100 in^2·day)
P(VDC–AN) barrier coating	0.02
Aclar 33C PCTFE film[c]	0.025
PVDC coextrusion resin	0.09
Liquid crystalline polymer[d]	0.15 (100% RH)
PP, biaxially oriented	0.25
HDPE, molded	0.3
MDPE, molded	0.7
PVC, rigid	0.9
LDPE, molded	1.0
Nylon MXD-6 oriented film	1.2
EVOH, 44 mol% ethylene	1.4
PET, 25% crystalline (bottle wall)	1.8
Nitrile resin	4.0
EVOH, 27 mol% ethylene	5.7
PS film, oriented	7.1
Nylon-6, biaxially oriented	10
Amorphous nylon	10
Nylon-6, unoriented	15

[a]Ref. 27.
[b]At 90% RH, 37.8°C.
[c]Aclar is a trademark of Honeywell (Morristown, N.J.) (91).
[d]Vectra A950 LCP film (Celenese AG) (89).

moisture as its oxygen barrier (57). In the majority of commercial applications, EVOH is used in a multilayer structure with moisture barrier and/or structural layers on each side, a typical example being multilayer bottles with polypropylene (PP) for ketchup (57). EVOH has also been used as a flavor barrier on the inside of PE-coated paperboard containers, a typical application being packaging of orange juice, where it minimizes the loss of limonene from the juice into the PE layer (57). EVOH is used as a barrier layer in many other rigid and flexible packaging applications.

Nitrile Polymers. The general structure of nitrile copolymers is shown below (101):

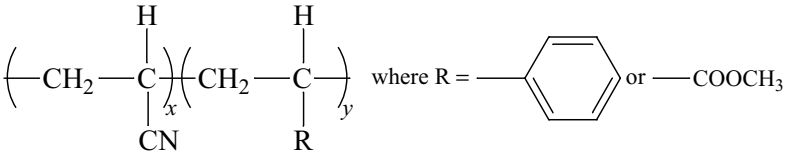

Application of PAN in packaging started in the 1960s. Despite processing difficulties, PAN was used because of its excellent barrier properties. A group of copolymers were developed in the 1970s. Comonomers are methyl acrylate and styrene at concentration up to 20 mol% (103). They are efficient oxygen barriers and have high grease and oil resistance, strength, and stiffness. Lopac (Monsanto Co.), Barex (Sohio), and Cycopac (Borg-Warner Chemicals) are three

Table 7. Permeability, Diffusivity, and Solubility Coefficients of Flavor and Aroma Compounds in Various High and Moderate Barrier Polymers (63) at 25°C and 0% RH

Flavor/aroma compound	Permeability, 10^{-22} (kg·cm)/(cm^2·s·Pa)[a]	Diffusivity, cm^2/s	Solubility, kg/(cm^3·Pa)
Ethylene vinyl alcohol copolymer[b]			
Ethyl hexanoate	0.41	3.2×10^{-14}	1.3×10^{-9}
Ethyl 2-methylbutyrate	0.3	6.7×10^{-14}	4.7×10^{-10}
Hexanol	1.2	2.6×10^{-13}	4.6×10^{-10}
trans-2-Hexenal	110	6.4×10^{-13}	1.8×10^{-8}
d-Limonene	0.5	1.1×10^{-13}	4.5×10^{-10}
3-Octanone	0.2	1.0×10^{-14}	2.0×10^{-9}
Propyl butyrate	1.2	2.7×10^{-13}	4.5×10^{-10}
Vinylidene chloride copolymer[b]			
Ethyl hexanoate	570	8.0×10^{-14}	7.1×10^{-7}
Ethyl 2-methylbutyrate	3.2	1.9×10^{-13}	1.7×10^{-9}
Hexanol	40	5.2×10^{-13}	7.7×10^{-9}
trans-2-Hexenal	240	1.8×10^{-13}	1.4×10^{-7}
d-Limonene	32	3.3×10^{-13}	9.7×10^{-9}
3-Octanone	52	1.3×10^{-14}	4.0×10^{-7}
Propyl butyrate	42	4.4×10^{-14}	9.4×10^{-8}
Dipropyl disulfide	270	2.6×10^{-14}	1.0×10^{-6}
Low density polyethylene			
Ethyl hexanoate	4.1×10^{6}	5.2×10^{-9}	7.8×10^{-8}
Ethyl 2-methylbutyrate	4.9×10^{5}	2.4×10^{-9}	2.3×10^{-8}
Hexanol	9.7×10^{5}	4.6×10^{-9}	2.3×10^{-8}
trans-2-hexenal	8.1×10^{5}		
d-Limonene	4.3×10^{6}		
3-Octanone	6.8×10^{6}	5.6×10^{-9}	1.2×10^{-7}
Propyl butyrate	1.5×10^{6}	5.0×10^{-9}	3.0×10^{-8}
Dipropyl disulfide	6.8×10^{6}	7.3×10^{-10}	9.3×10^{-7}
High density polyethylene			
d-Limonene	3.5×10^{6}	1.7×10^{-9}	2.5×10^{-7}
Menthone	5.2×10^{6}	9.1×10^{-9}	4.7×10^{-7}
Methyl salicylate	1.1×10^{7}	8.7×10^{-10}	1.6×10^{-6}
Polypropylene			
2-Butanone	8.5×10^{3}	2.1×10^{-11}	4.0×10^{-8}
Ethyl butyrate	9.5×10^{3}	1.8×10^{-11}	5.3×10^{-8}
Ethyl hexanoate	8.7×10^{4}	3.1×10^{-11}	2.8×10^{-7}
d-Limonene	1.6×10^{4}	7.4×10^{-12}	2.1×10^{-7}
Poly(ethylene terephthalate)[c]			
d-limonene	1.5	6.0×10^{-13}	

[a] To convert the permeability values to (cm^3·mil)/(100 in.^{2}·day·atm), multiply the values provided in the table by (4.98×10^{22})/MW, where MW is penetrant molecular weight (g/mol).
[b] Values have been extrapolated from higher temperatures.
[c] At 25°C; values are not expected to show any significant variations with RH (92).

commercial nitrile copolymers that have been used in packaging applications. Their compositions are shown in Table 8. Barex and Cycopac are rubber-modified for improved mechanical properties, and the barrier properties of these copolymers are relatively insensitive to moisture. Concerns about the possible migration of

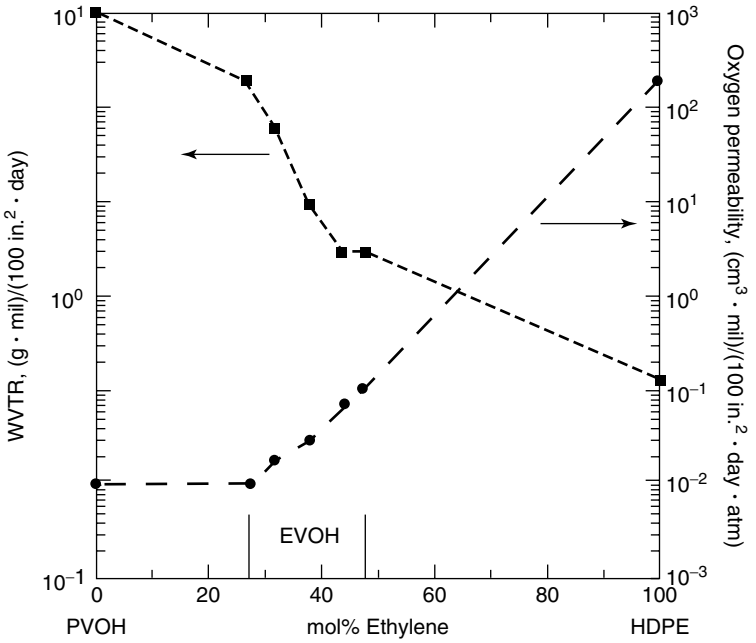

Fig. 19. Effect of ethylene content on oxygen permeability (20–23°C, 65% RH) and WVTR (40°C) of EVOH. The figure also shows data for PVOH and HDPE for comparison (27).

acrylonitrile monomer, a toxic compound (57), have limited the use of nitrile polymers in food contact applications (see ACRYLONITRILE AND ACRYLONITRILE POLYMERS).

Vinylidene Chloride Copolymers. Copolymers of VDC with vinyl chloride and acrylonitrile were among the first high barrier polymers to be widely used. During their commercial appearance in the late 1930s, they had the lowest permeabilities among plastics to gases and water vapor (103). Poly(vinylidene chloride) (PVDC) homopolymer is soluble only in hot dichlorobenzene (among common solvents) and has a melting point only a few degrees below its decomposition temperature (103). These characteristics make it difficult to fabricate by melt-processing

Table 8. Compositions of Commercial, High Barrier Nitrile Copolymers[a]

Polymer	Manufacturer[b]	Chemical composition[c]
Lopac	Monsanto Co.	70% acrylonitrile + 30% styrene
Barex	Sohio	74% acrylonitrile + 26% methyl methacrylate + 10% butadiene graft rubber
Cycopac	Borg-Warner Chemicals	74% acrylonitrile + 26% styrene + 10% butadiene graft rubber

[a]Ref. 63.
[b]Manufacture are listed from Ref. 63. However, these copolymers are now manufactured by BP Amoco Chemicals.
[c]Data from FDA regulations for corresponding materials.

techniques. Copolymers were synthesized to overcome these drawbacks. Acrylates were found to be among the most useful comonomers, along with vinyl chloride and acrylonitrile (103). By adding comonomers, the melting point can be decreased to a range of 140–175°C (as compared to 198–205°C for PVDC), thus making melt processing feasible (104). These copolymers are semicrystalline and soluble in only a limited range of solvents. The most notable attributes of VDC copolymers are their chemical resistance and extremely low permeabilities to gases and water vapor (cf Tables 5 and 6). The structure of the most widely used vinylidene chloride–vinyl chloride copolymer is shown below:

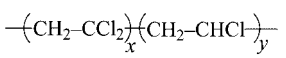

where x is 85–90 mol% (103). VDC copolymers are commercially available under a variety of trade names such as Saran (The Dow Chemical Co.), Daran (W. R. Grace), Amsco Res (Union Oil), and Serfene (Rohm and Haas) within the United States; Haloflex (Neoresins), Diofan (Solvin), Ixan (Solvin), and Polyidene (Scott-Bader) in Europe (see VINYLIDENE CHLORIDE POLYMERS). Copolymers are available in the following forms (103): (*1*) lattices of approx. 1000–1500 Å which can be applied as coatings to paper and plastic films to improve their barrier properties, (*2*) soluble resins for coating plastic films (especially cellophane) to improve their barrier properties, (*3*) melt-processable resins for extrusion, coextrusion, and molding, and (*4*) clear, transparent films for commercial packaging applications. Small amounts of processing aids and heat stabilizers are added to extrusion and molding resins.

Polyamides. The standard semicrystalline polyamides (PA) (nylon-6, nylon-6,6, etc) used in packaging have medium gas barrier properties, and their barrier properties are affected by humidity (101). However, specialty grades of polyamides with higher gas barrier properties are available. Commercial grades of Selar amorphous polyamides (AmPA) (E. I. du Pont de Nemours & Co., Wilmington, Del.), for example, exhibit good O_2 barrier and reduced dependence of gas barrier properties on RH. In fact, their gas barrier properties improve with increasing RH (cf Fig. 13). At an RH of 80% or more, their O_2 barrier is similar to that of PAN (102). Moreover, at 95–100% RH, the O_2 barrier is equivalent to that of EVOH at similar conditions, and substantially better than that of nylon-6. The amorphous nature of Selar results in a much broader range of processing conditions than those of semicrystalline nylon-6 (105). The mechanical and barrier properties of AmPA can be improved by orientation (see POLYAMIDES, PLASTICS; POLYAMIDES, AROMATIC).

Another high barrier polyamide is MXD-6 resin (Mitsubishi Gas and Chemical Co., and Toyobo, Japan), which was developed in the 1970s. It is made from the reaction of *m*-xylylenediamine and adipic acid (57):

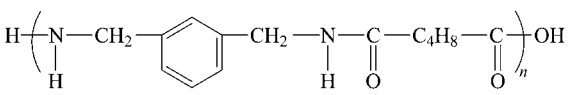

It provides improved clarity, mechanical, thermal, and barrier properties relative to standard nylons. It has better gas barrier properties than nylon-6 and PET at all humidities, and is better than EVOH at 100% RH. The barrier properties of MXD-6 are relatively unaffected by moisture up to an RH of 70% (57). Because of its cost and the lack of a domestic source, MXD-6 has found limited applications in the United States. It has a much wider market in Japan, appearing in commercial applications such as nonpasteurized plastic beer bottles and carbonated soft drink bottles (57).

Polyesters. The most widely used member of the polyester family for food and beverage packaging applications is PET (see POLYESTERS, THERMOPLASTIC). However, PET offers a moderate barrier to gases and water vapor. Poly(ethylene naphthalate) (PEN) offers a much higher barrier to gases and water vapor than PET and can be classified as a high barrier polyester.

PEN is a homopolymer of dimethyl-2,6-naphthalene dicarboxylate (NDC) and ethylene glycol (106):

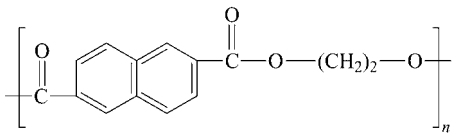

The rigid double-ring structure in the polymer backbone results in increased mechanical strength, heat stability, and barrier properties as compared to PET. As with PET, orientation produces a substantial reduction in gas permeability, and the oxygen permeability of oriented PEN is a factor of 5 lower than that of oriented PET (57). Teijin (Japan) and ICI (U.K.) have been the leaders in manufacturing PEN films. Teijin manufactures both resin and films, the latter under the trade name Teonex. Since 1990, DuPont and Teijin have had a worldwide joint venture in polyester films, including PEN. DuPont has also acquired ICI's Melinex PET film and Kaladex PEN film operations. The main disadvantages of PEN are its high cost, and unsettled sources of monomer technology and supply (57). One of the leading manufacturers of NDC, BP Amoco Chemicals (Decatur, Ala.) has developed a technology that uses *o*-xylene rather than naphthalene as the feedstock, which could reduce the manufacturing cost of PEN resin (57). Other newer NDC technologies from Kobe Steel (Japan) and Mobil Chemicals could also lead to reduced cost for PEN. Another way of addressing the price issue is by using blends or copolymers of PEN with PET. Gas and vapor permeability has been found to decrease continually as PEN is added to PET (107,108).

Liquid Crystalline Polymers. Liquid crystalline polymers, main-chain (qv) (LCPs) offer excellent thermal and chemical resistance, and exhibit very high barrier properties that are almost unmatched by existing barrier polymers (16,109,110). They also offer adequate mechanical properties for certain packaging applications (111). LCPs are very efficiently packed, highly oriented, and often semicrystalline materials. Commercially available LCPs such as Vectra (Celanese AG), Zenite (E. I. du Pont de Nemours & Co.), and Xydar (Solvay Advanced

Polymers, Alpharetta, Ga.) are aromatic copolyesters that have a significantly higher degree of chain orientation than typical polyesters such as PET (111).

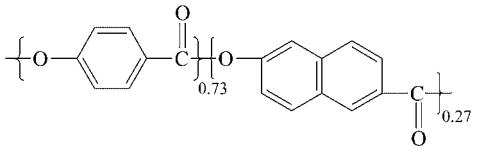

Structure of Vectra

LCPs of this kind were first introduced to the market in the 1980s. Table 9 shows a comparison of properties of biaxially oriented LCP films with those of PET films (112). Figure 20 compares barrier properties of LCPs with other barrier polymers. LCPs offer the best combination of water vapor and O_2 barrier properties among all known classes of polymers. They also offer excellent barrier to CO_2, N_2, and other gases and vapors (111). However, commercial applications of LCPs have been limited primarily because of their high cost, lack of transparency, and processing characteristics (111). One key to unlocking the potential of LCPs in barrier packaging is to be able to process thin uniform layers in coextruded multilayer structures. Recently, three-layered structures (PET–tie layer–LCP) have been coextruded (Superex Polymer, Inc., Waltham, Mass.) with a total thickness of 25–50 μm and 10–30% LCP layer thickness. This multilayer film is claimed to offer a high performance–cost ratio (111).

Poly(hydroxy amino ethers). Poly(hydroxy amino ethers) (PHAE) are a new family of high barrier epoxy-based thermoplastics. The general chemical structure of amide-containing PHAE, which are formed by the reaction of

Table 9. Comparison of Properties of Biaxially Oriented LCP and PET Films[a]

Property	Biaxially oriented LCP film[b]	Biaxially oriented PET film[c]
Tensile strength, MPa[d]	240	170
Tensile modulus, GPa[e]	12.4	3.5
Oxygen permeability[f], $(cm^3 \cdot mil)/(100 \cdot in.^2 \cdot day \cdot atm)$	0.05	4.8
Water vapor permeability,[g] $(g \cdot mil)/(100 \cdot in.^2 \cdot day \cdot atm)$	0.02	1.7
Density, g/cm^3	1.4	1.4
Upper use temperature, °C	Over 250	120
Tear resistance, kN/m[h]		
Initiation	595	35
Propagation	175–525	9–53

[a]Ref. 112.
[b]Vectra (Celanese AG) isotropic LCP film (orientation angle = 45°).
[c]Mylar (DuPont) isotropic PET film (orientation angle = 45°).
[d]To convert MPa to psi, multiply by 145.
[e]To convert GPa to psi, multiply by 145,000.
[f]Permeability value at 25°C (and unspecified RH).
[g]Permeability value at 25°C and 90% RH.
[h]To convert kN/m to lb/in., divide by 0.175.

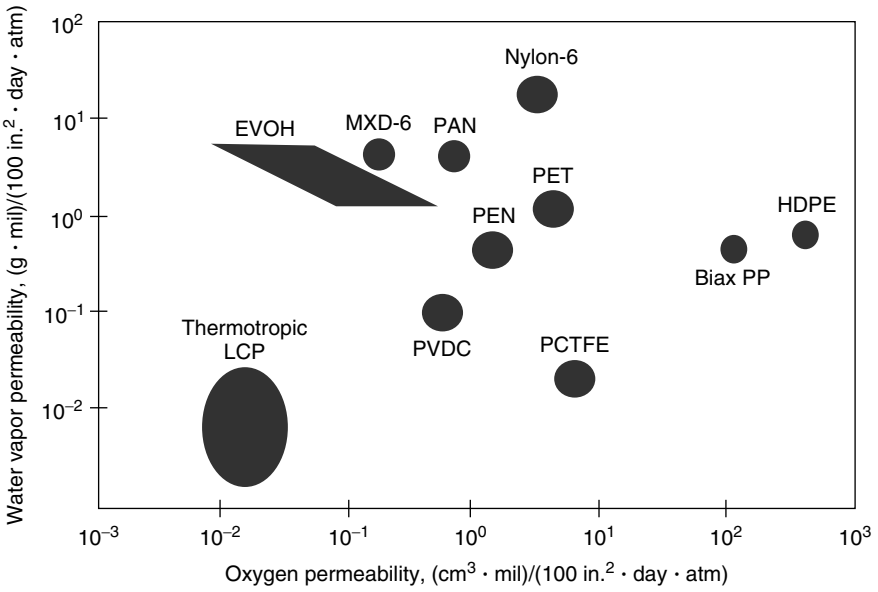

Fig. 20. A comparison of oxygen and water vapor barrier properties of various high and moderate barrier polymers at 23°C (111).

amide-containing bisphenols with aromatic diglycidyl ethers (113), is shown below:

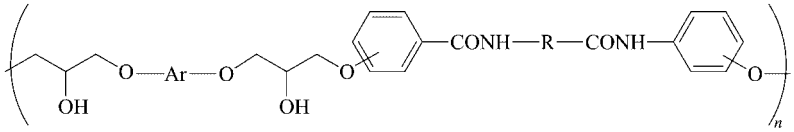

where R can be $-(CH_2)_n-$ ($n = 1, 2, 3\ldots$) or an aromatic group, and Ar designates an aromatic moiety.

These polymers are amorphous, with T_g values ranging from 90 to 133°C. They incorporate both amide and hydroxyl moieties on the chain backbone. In order to prevent cross-linking, the hydroxyl groups are generated during the polymerization of preferred amide-containing monomers (113). The presence of aromatic groups between the amide groups in the polymer backbone can result in high T_g and good barrier properties. It has also been observed that the presence of *m*-phenylene units instead of *p*-phenylene units can reduce O_2 permeabilities (as much as 30–40%) by increasing the chain packing efficiency of the polymer (113). This phenomenon is, in fact, rather general among aromatic polymers. Often, meta-linked aromatic rings in polymer backbones have lower permeability coefficients than their para-linked analogues (114,115). Lower O_2 permeabilities can also be obtained when hydrogen bonding interactions in the polymer backbone are increased either by reducing the number of nonpolar methylene units or by increasing the population density of polar amide groups (113). Unlike other hydroxyl-containing polymers such as EVOH, the barrier properties

of amide-containing PHAE improve with increasing RH (19,113). For example, a decrease in O_2 permeability from 1.4 (cm^3·mil)/(100 $in.^2$·day·atm) at 5% RH to 0.8 (cm^3·mil)/(100 $in.^2$·day·atm) at 75–80% RH has been reported. On the basis of preliminary work involving density and pals studies, it has been postulated that water molecules not only occupy free-volume elements in these materials but also enhance interchain cohesion, thus inhibiting the transport of other nonpolar gases (116).

A series of polymers from the PHAE family has recently been commercialized by Dow Chemical Co. (Midland, Mich.) under the trade name BLOX Adhesive and Barrier Resins (90,117). They offer high gas barrier properties, excellent adhesion to a variety of substrates, high optical clarity, and good mechanical properties. For example, BLOX 4000 series resins exhibit an oxygen transmission rate of 0.1 (cm^3·mil)/(100 $in.^2$·day·atm) at 23°C and 60% RH (90). The BLOX resins have found some commercial applications in barrier packaging, starch-based foam packaging, and powder coatings (117).

Polychlorotrifluoroethylene. Polychlorotrifluoroethylene (PCTFE) is a flexible thermoplastic made from fluorinated–chlorinated resins. It was first discovered in the 1950s and has been commercially produced since the 1960s (118). Its chemical structure is as shown below:

$$-\left(\mathrm{CFCl}-\mathrm{CF_2}\right)_n-$$

The key characteristics of this polymer are its high optical clarity and excellent moisture barrier properties (118). In commercial Aclar resins (Honeywell, Morristown, N.J.), the polymer is generally modified by copolymerization, resulting in a semicrystalline material with T_g of about 45°C and melting point of about 190°C (104). It shows excellent thermal and chemical stability, and high water vapor and O_2 barrier properties (120) (cf Tables 5 and 6). For example, Aclar films typically have water vapor transmission rates less than 0.04 (g·mil)/(100 in^2·day) (23°C) and oxygen transmission rates less than 14 (cm^3·mil)/(100 in^2·day) (25°C) (119). PCTFE is most widely used for producing blister packs in pharmaceutical applications (118). The moisture barrier properties can be tailored by varying the PCTFE layer thickness in coextruded multilayer structures, thereby adjusting the performance-to-cost ratio. An example of a commercial coextruded structure is Aclar NT AE-1 (Honeywell, Morristown, N.J.), which is 33 μm thick, and contains about 8.4 μm of PCTFE (118). PCTFE can also be laminated with PP, PAN, PET, HDPE, LDPE, and PVC and then formed into blister packs. Other applications of the same technology include electronic component packaging where lower moisture barrier may be acceptable, resulting in more favorable economics (118).

Moderate Barrier Polymers. Polymers in this category include polyesters, polyolefins, poly(vinyl chloride), polystyrene, and certain semicrystalline polyamides. The polymers included in this section are typically more widely available, have more manufacturers, and are less expensive than the specialty barrier resins described in the previous section.

Polyesters. Polyesters represent a class of versatile barrier plastics. PET is by far the most important member in this family from a commercial

viewpoint. It is extensively used in the food and beverage packaging industries and is especially known for its widespread use in bottles for carbonated beverages (120) (see POLYESTERS, THERMOPLASTIC). The other members in this category are poly(trimethylene terephthalate) (qv) (PTT) and Polylactide (PLA).

Poly(ethylene terephthalate). PET is a linear thermoplastic made from ethylene glycol and terephthalic acid, or ethylene glycol and dimethyl terephthalate (101). The structure of PET is shown below:

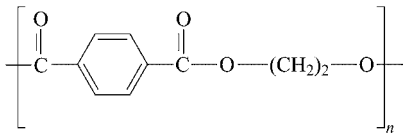

PET is used in many rigid food and beverage containers because of a good balance of physical and mechanical properties, barrier properties, processibility and formability, ecological and toxicological characteristics, and economics (121). As a result, PET bottles have virtually replaced glass packages for carbonated soft drinks in the United States. In the glassy state, it is strong, stiff, ductile, and tough. It can be oriented by stretching during molding and extrusion, which further increases its strength, stiffness, and barrier properties. One of the early drawbacks of PET was its low heat distortion temperature of 60°C (140°F), which prevented it from being used in applications requiring filling at elevated temperatures (121). However, careful heat-treatment increases the heat distortion temperature of crystalline PET containers and recently commercialized processes claim resistance to temperatures of up to 90–92°C (194–196°F) (121). It has moderate barrier properties for light gases, but is a good barrier for flavors and aroma compounds. Its barrier properties can be improved by increasing crystallinity and orientation (121). A 4× biaxial orientation of amorphous PET at temperatures near 100°C produces significant strain-induced crystallization and decreases the permeability of O_2 and CO_2 by a factor of about 2 (71).

Oriented and heat-set PET films have also found use in a broad range of flexible packaging applications because of their high strength, good barrier, high clarity, heat resistance, and good metalizability. There are more than 50 specific application areas for PET films (122). Manufacturers have met the product requirements of each of the diverse end-use markets by tailoring formulations and process conditions. For example, in the food and beverage packaging industries, many types of PET films have been developed, including metallized PET films for packaging of coffee, wine, and meats, poly(vinylidene chloride)-coated PET films for meat and cheese packaging, and coextruded multilayer PET films for heat-sealable packaging (122). Commercial manufacturers of PET films include DuPont Teijin Films (Mylar, Melinex, Tetoron) and Mitsubishi Polyester Film, LLC. (Diafoil, Hostaphan).

Poly(trimethylene terephthalate). PTT is made from the polycondensation reaction of trimethylene glycol (also called 3G) with either terephthalic acid or dimethyl terephthalate (57). Although this polymer was first synthesized in 1941, it was never commercialized because of lack of an economical source of 3G. In the

early 1990s, Shell Chemical Co. announced a catalyst breakthrough to make 3G economically by hydroformylation of ethylene oxide (57).

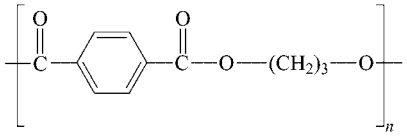

PTT is an engineering resin and has been targeted mainly toward injection-molding applications. However, there have been claims about its barrier properties (57), and it is therefore included in this article for completeness.

Because of the presence of an odd number of methylene units in the chain backbone, PTT has physical properties different from PET (57). Its O_2 permeability is about 6 $(cm^3 \cdot mil)/(100\ in.^2 \cdot day \cdot atm)$ at 0% RH, and moisture absorption rate is typically 0.03% after 24 h and 0.15% after 14 days (57). Typical properties of PTT are as follows: it has a melting point of 228°C, a T_g of 45–65°C, and can be produced with crystallinity values up to 45 wt%.

Polylactide. Polylactide (PLA) is a semicrystalline, linear thermoplastic made from lactic acid, especially as derived from corn (maize). Polylactide (qv) is new to the commercial market (123). Its applications are still being explored. However, its barrier is adequate for some food packaging uses, especially for management of flavor and aroma profiles. It can be heat sealed and thermoformed. It has a glass-transition temperature of 55–65°C. The principal manufacturer of PLA is Cargil Dow, LLC (NatureWorks).

Polyamides. This category of moderate barrier polymers includes nylon-6 and nylon-6,6. Nylon-6 is made by the polymerization of caprolactam, and nylon-6,6 is made by the reaction of hexamethylenediamine and adipic acid (101). Their chemical structures are shown below:

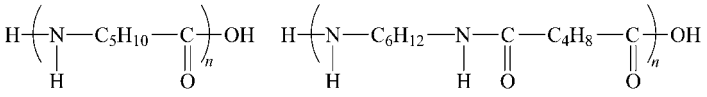

Nylon-6 Nylon-6,6

In general, nylons have good gas and aroma barrier properties, but poor moisture barrier properties (57) (cf Tables 5 and 6). Absorbed water has a plasticizing effect that leads to a reduction in tensile strength and increase in impact strength. Uniaxial and biaxial orientations can improve their flex-crack resistance, mechanical, and barrier properties (101). Biaxially oriented nylons offer better gas barrier properties, softness, and puncture resistance, compared to oriented PET, which offers better rigidity and moisture barrier properties (101). Nylons are less widely used in the packaging industry than polyolefins or PET, with the majority of the applications being blow-molded bottles (coextrusion and blending of nylon-6 with PE), for industrial and household chemical markets (57).

Polyolefins. PE and PP are two of the most widely used polymers in the food and beverage packaging industry. These polymers find use as films, moldings, coatings, adhesives, and closures (124). They are available in a wide variety of

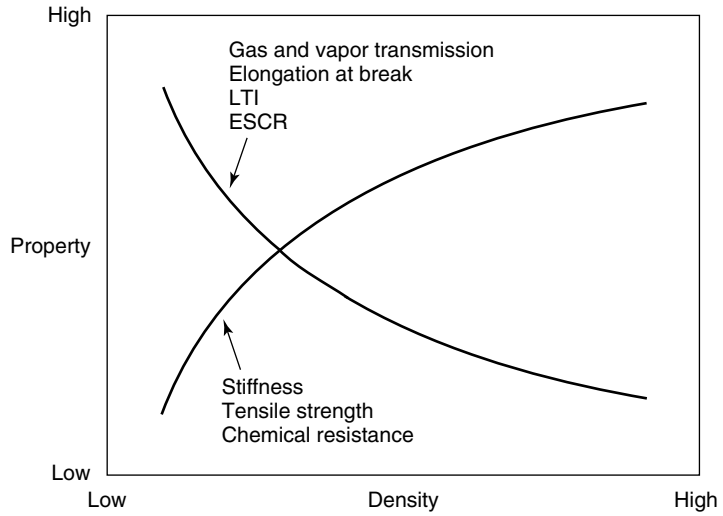

Fig. 21. Typical effect of density on various properties of PE. LTI is low temperature impact strength and ESCR is environmental stress-crack resistance (124).

types and grades. Although they have much higher permeabilities to gases than many other barrier polymers, they are very good moisture barriers (cf Tables 5 and 6).

PE, whose structure is shown below, was one of the first olefinic polymers to be used commercially in the packaging industry:

$$-\left(CH_2-CH_2\right)_n-$$

It is classified on the basis of density (see ETHYLENE POLYMERS, HDPE; ETHYLENE POLYMERS, LDPE; ETHYLENE POLYMERS, LLDPE; ETHYLENE POLYMERS, VLDPE). Figure 21 shows the effect of density on various properties of PE (124). A branched structure for low density PE (LDPE) results from exceptionally high temperature and pressure during its manufacture. It is tough, flexible, can be easily melt processed, and has good moisture barrier properties. It is a semicrystalline polymer with crystallinity typically in the range of 40%. Medium density PE (MDPE) is stronger, stiffer, and has better barrier properties than LDPE. High density PE (HDPE) is essentially unbranched and is the strongest and most rigid polymer in this family. It offers barrier properties to moisture and gases that are superior to those of LDPE and MDPE.

If unsaturated comonomers such as butene, hexene, or octene are added to the HDPE polymerization process in the presence of a stereospecific catalyst, it results in the formation of a linear polymer with short branch-like pendant groups (104). Its density is in the same range as LDPE, but the degree of branching is greatly reduced. This polymer is called linear LDPE (LLDPE) and its density depends on the amount of comonomer added. The larger the amount of the comonomer, the lower the density of the copolymer (104). LLDPE combines the

clarity and excellent heat-seal properties of LDPE with the strength and toughness of HDPE. It is often blended with LDPE in order to optimize the benefit obtained from both materials (104).

PP, whose chemical structure is shown below, can be made by the catalytic polymerization of propylene at high temperature and pressure (124):

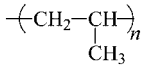

Isotactic PP (with all methyl groups on same side of the polymer chain) is the commercially desired form for packaging applications (124) (see PROPYLENE POLYMERS (PP)). The concentration of atactic PP (with irregular arrangement of methyl groups) is kept low by suitable catalysts and polymerization conditions (124). PP offers high resistance to water vapor permeation and is widely used in rigid as well as flexible food packaging applications. PP films can be oriented, which improves their barrier properties, mechanical strength, and optical properties. For example, oriented PP has about three times higher resistance to water vapor transmission than unoriented PP (27). These properties can be varied over a wide range by the choice of the manufacturing process.

Poly(vinyl chloride). Poly(vinyl chloride), also known as vinyl or PVC, is made by low pressure free-radical polymerization of vinyl chloride at temperatures in the 38–71°C range (101). Its chemical structure is shown below:

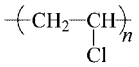

PVC is a versatile polymer that can be formulated to meet the requirements of many applications in packaging and other industries (88) (see VINYL CHLORIDE POLYMERS). Its properties can be tuned over a very wide range by incorporating comonomers, plasticizers, and other additives. When used as a rigid sheet or bottle, little modification is required, but PVC requires the addition of plasticizers to make it useful as a barrier film for flexible packaging (88). The plasticizers increase chain flexibility and reduce the processing temperature of PVC. For example, addition of 40 vol% dioctyl phthalate plasticizer reduces the T_g of PVC from 100°C to about 5°C (125). The increase in chain flexibility of plasticized PVC also results in a reduction in its gas barrier properties primarily as a result of higher diffusion coefficients in plasticized films. Figure 22 presents a comparison of diffusion coefficients of several penetrants in plasticized and unplasticized PVC films (126) (see PLASTICIZERS).

PVC has some drawbacks as a food-packaging material (88): Vinyl chloride monomer is an animal carcinogen and causes liver cancer in humans. Thus the amount of monomer in the finished polymer should be brought down to 1 ppm or less. There is concern about the toxicity of plasticizers and other additives used in PVC. Moreover, there have also been concerns that incineration of chlorine-containing plastics can possibly lead to the formation of dioxin, a chlorinated toxic molecule. Finally, the release of plasticizers over long periods of time can lead to gradual embrittlement of PVC films. However, none of these drawbacks significantly affect the functionality of PVC and it is used to make flexible films,

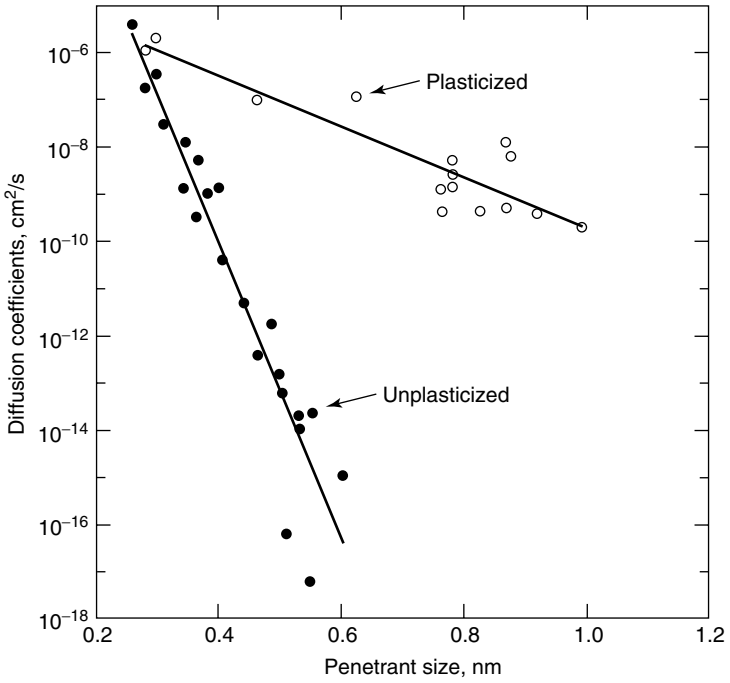

Fig. 22. Diffusion coefficients in unplasticized and plasticized PVC at 30°C as a function of penetrant molecular diameter (126).

rigid sheets, and bottles for a variety of food (eg, fresh fruits, vegetables, and poultry packaging in the United States) and nonfood packaging applications (104).

Polystyrene. Polystyrene (PS) is made by the peroxide-catalyzed bulk or suspension polymerization of styrene (101) (see STYRENE POLYMERS). The polymerization reaction takes place at low pressure and temperature in the range of 250–400°F, and the polymer chemical structure is given by

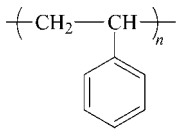

Polymer molecular weight, which affects the processing characteristics of the resin, is often in the range of 40,000–220,000; variations in molecular weight can be obtained by changing the catalysts and polymerization conditions. PS is an amorphous, clear, hard, brittle, low-strength material with poor impact resistance (101). It has low to moderate moisture and gas barrier properties (88). Copolymerization with butadiene or other rubbers increases its impact strength and decreases stiffness (88). This copolymer is commonly referred to as high impact polystyrene (HIPS). Comonomers such as α-methyl styrene can improve the heat resistance of PS by increasing the heat distortion temperature to 100°C or

higher (88). PS can be foamed by adding foaming agents such as pentane to the reaction mixture during the suspension polymerization. This so-called expanded polystyrene (EPS) is a very low density, yet highly rigid material that is used for making egg cartons, and trays for meat, poultry, and other products (88). However, EPS has poor gas barrier properties.

Improving Barrier Properties of Polymers

Barrier Structures. As mentioned in the previous sections, the principal application of barrier polymers is in the food and beverage packaging industries. Combining two or more polymers, or other materials, can achieve performance advantages not available in any of the materials taken alone. In many cases, to achieve better barrier performance, it is more efficient and economical to use a thin layer of an expensive high barrier polymer (eg, EVOH) sandwiched between layers of less expensive, moderate barrier, structural polymers (eg, PP, PET) than to increase the monolayer thickness of the moderate barrier polymer. Multilayer structures can be obtained by coextrusion, lamination, and coating. Barrier polymers may also be combined to form miscible and immiscible blends.

Multilayer Structures. Steady-state barrier properties of multilayer films can be described by their permeability, which can be calculated by treating the individual layers as resistances in series (63):

$$\frac{1}{P'} = \frac{L_t}{P_t} = \frac{L_1}{P_1} + \frac{L_2}{P_2} + \cdots + \frac{L_n}{P_n} \tag{38}$$

where P_t, L_t, and P' are permeability, thickness, and permeance of the composite structure, and P_1, P_2, ..., P_n and L_1, L_2, ..., L_n are the permeabilities and thicknesses of the individual layers. The permeability P_t (or permeance P') can be used to evaluate the performance of the composite structure for packaging applications. Figure 23 illustrates the effect of barrier layer thickness on permeability of a hypothetical two-layer sheet, the permeability of the barrier layer being 0.1 (cm^3·mil)/(100 $in.^2$·day·atm) and that of the nonbarrier layer being 100 (cm^3·mil)/(100 $in.^2$·day·atm). For moisture-sensitive polymers (eg, EVOH or nylon), it is important to use the permeability that corresponds to the effective RH that the layer will experience in the composite structure.

Coextrusion (qv) is one of the most cost-effective techniques for producing multilayer barrier polymer films (127). Although coextruded films typically have 3–7 layers, as many as 11 layers can be extruded simultaneously (128). This technique allows for the thinnest possible layers of the individual polymer resins within the structure. Resins that do not bond well can be bonded together with an adhesive 'tie' layer (128). The materials must be compatible in terms of their melt temperatures and viscosities in order to undergo simultaneous coextrusion. Figure 24 presents a comparison of processing temperatures of various commonly used barrier polymers (129). Figure 25 shows a schematic of a typical 9-layer coextruded structure. A coextrusion line will have several different extruders, each extruder responsible for supplying individual polymer resins (127).

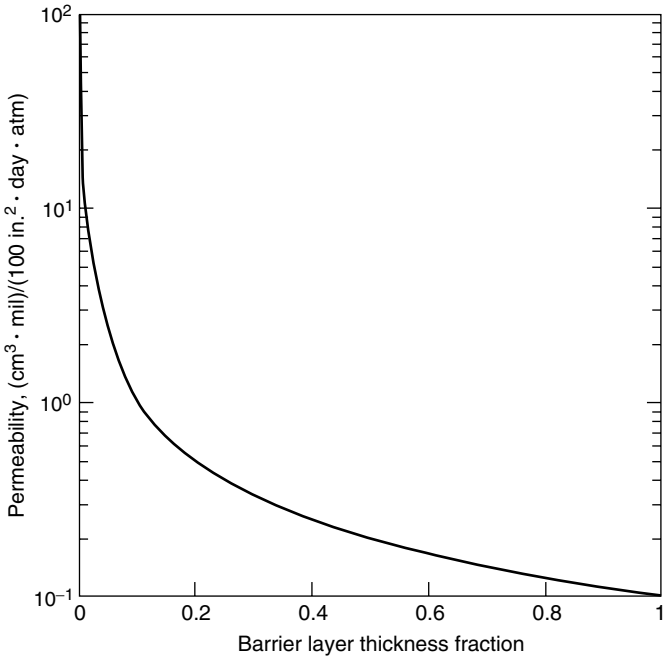

Fig. 23. Effect of thickness of barrier layer on permeability of a hypothetical two-layer barrier composite structure.

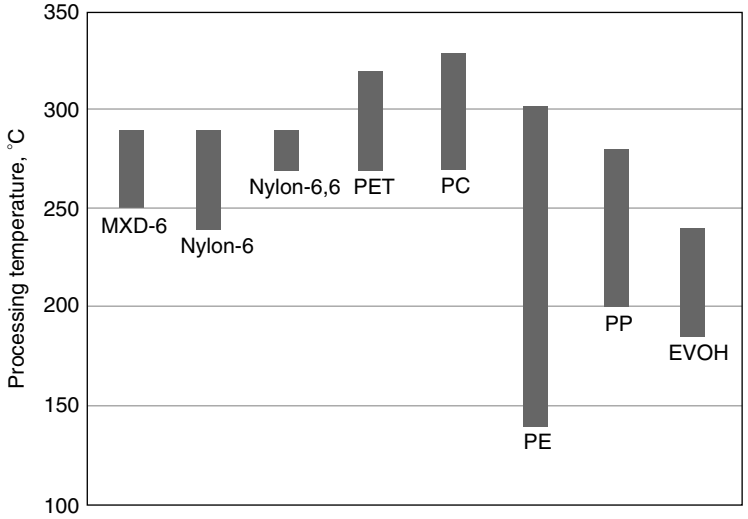

Fig. 24. A comparison of processing temperatures of various commercially used barrier polymers (129).

Coating and lamination are two additional processes for producing multilayer structures and are especially useful in applications where a nonpolymeric material is part of the structure. Coatings can be melt extrusions of a polymer onto a base film or can be made by applying solutions or dispersions of polymers to the

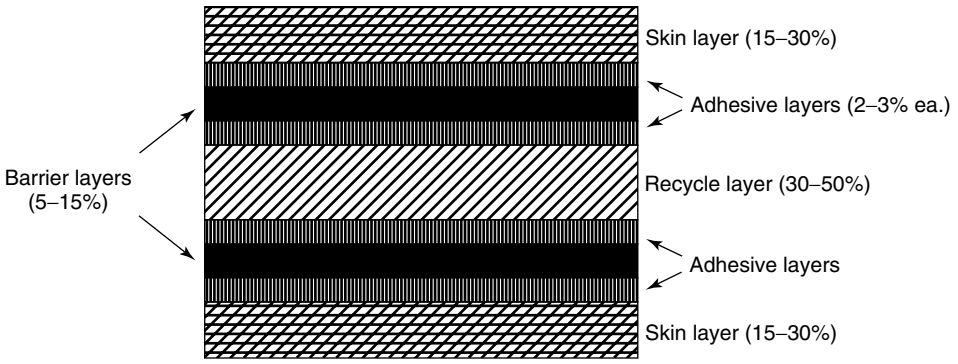

Fig. 25. An example of a typical symmetrical nine-layer coextruded barrier composite structure (128).

base film (128). Barrier polymers that resist water vapor and provide gas barrier are often laminated to paper and paperboard. Cellophane, a flexible transparent gas barrier polymer, can also be made 'moisture-proof' by coating or laminating with other polymer films (27). A commercial application of solvent coating with barrier polymers is VDC resin dissolved in a polar solvent and coated onto cellophane or PET (63). Water-based emulsion coatings of VDC are used for plastic PET beer bottles, primarily in the United Kingdom. They can typically lower O_2 permeability of PET bottles by nearly 60% (57). Several companies produce PVDC emulsions for coating films such as nylon, PE, PP, and PET to improve their O_2 and moisture barrier properties (57). In the mid-1990s, PPG Industries, Inc. introduced Bairocade external epoxy-amine organic coatings for improving barrier properties of PET bottles (130,131). It is claimed that these coatings can reduce O_2 permeability of PET bottles by a factor of 6 or more with the level of barrier improvement depending on the thickness and formulation used, and that coated bottles extend the shelf life of carbonated beverages by a factor of 3, and beer by a factor of 20 relative to uncoated bottles (131).

Another way of improving barrier properties of polymers is by coating them with thin inorganic layers (57,132,133). This can typically improve barrier properties by a factor of 100, whereas the thickness of the barrier coating applied is less than 0.5% of the base film (57). Laminations and coatings of aluminum foil or aluminum oxide on barrier polymers can provide significant improvements in gas barrier properties (57). These metallized films contain an extremely thin layer of aluminum, which not only enhances the barrier properties of the base film, but also provides a shiny metallic appearance. Because the layer is very thin, it does not appreciably affect the strength and flexibility of the base film (134). The barrier properties of metallized films can approach those of pure aluminum foil. However, unlike aluminum foil, metallized films are not subject to flex-cracking and hence, are better at maintaining their barrier properties (134). Barrier polymers that have been successfully metallized include PP, nylons, PET, and unplasticized PVC. As an example, 99% decrease in oxygen permeability and 98.5% decrease in water vapor permeability have been reported for metallized PET films as compared to unmetallized PET films (135). Metallized films are widely used in the

flexible packaging industry, an example being potato chip packages consisting of multilayer structures of oriented PP, PE, and metallized PP (136).

However, one of the main disadvantages of metallized structures is that they may not be transparent—a desirable feature for many packaging applications. In part to address this shortcoming, several alternative high barrier coating technologies, typically producing amorphous carbon or glass-like layers, are being investigated. These newer coatings have achieved limited market penetration to date, with most of the commercial activity in Europe and Japan. It is still unclear what their eventual importance will be, but these technologies are being actively pursued. Among the various glass and ceramic materials used as barrier coatings, silicon dioxide (silica) has been the most widely used (57,133). These barrier composite structures are clear, microwaveable, and recyclable. Electron-beam treatment and plasma-enhanced chemical vapor deposition (PECVD) are two of the most widely used techniques for depositing thin silica layers on barrier polymers (57,137). In the electron-beam treatment, a high energy electron-beam source is used to vaporize silica, which then precipitates onto the polymer film, forming a continuous coating as the film passes through a vacuum chamber. The resulting coatings are uniform and can be as thin as 0.04 μm. PECVD has the advantage of being able to control coating density and thickness, by changing the process variables (137). Figure 26 presents the effect of coating thickness on oxygen permeability of a PECVD silica-coated PET film (137). Barrier properties of silica-coated polymers can be superior to those of high barrier polymers such

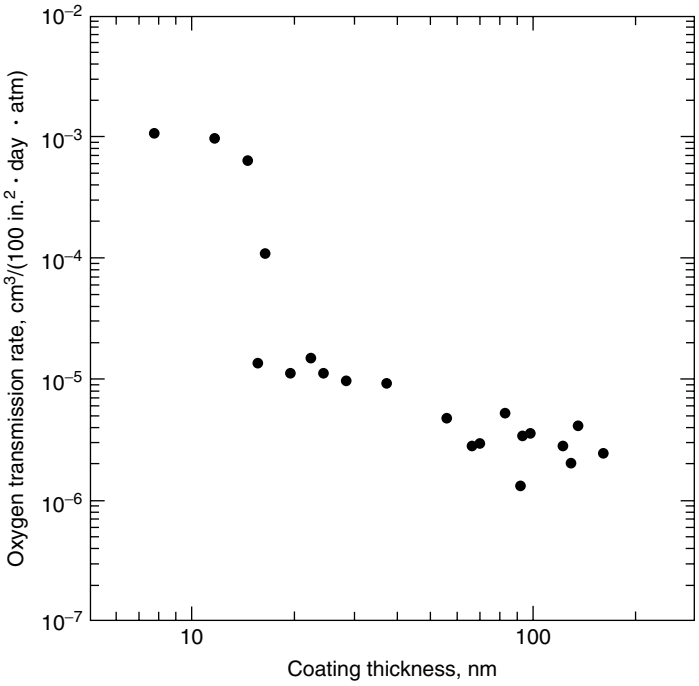

Fig. 26. Effect of plasma-deposited silica coating thickness on steady-state oxygen transmission rates (33°C, 0% RH) of PET films that have an uncoated thickness of 13 μm (137).

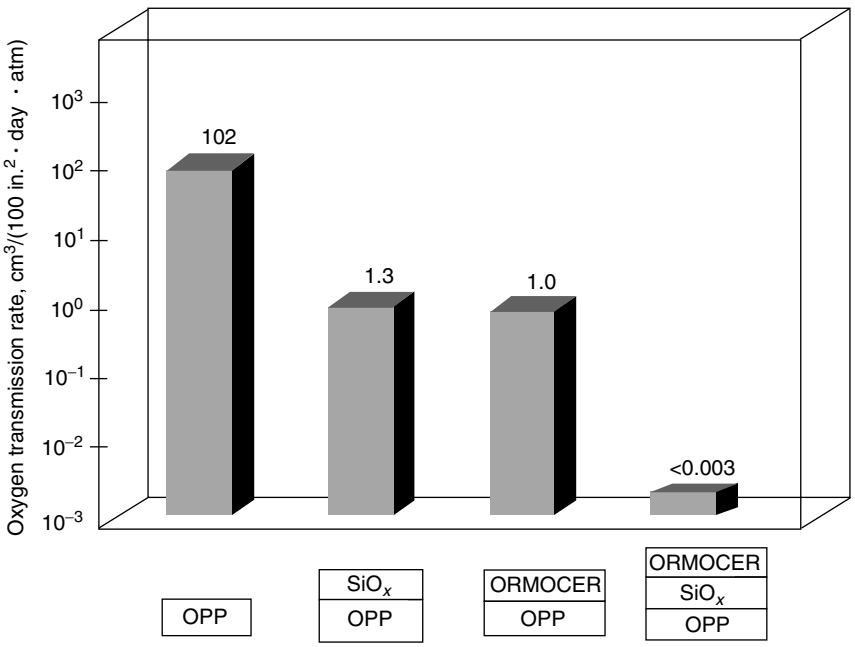

Fig. 27. Influence of ORMOCER coatings on oxygen transmission rates (OTRs) of SiO_x-coated oriented polypropylene (OPP) (OTR measured at 23°C and 70% RH) (138).

as PVDC and EVOH. Moreover, they are not influenced by moisture and temperature (57). However, because of poor adhesion and mechanical properties, for all practical applications silica-coated films have to be laminated.

Recently, inorganic–organic hybrid polymers have been developed, which can be used as laminating agents and in conjunction with silica to enhance barrier properties of polymers (138,139). An example is ORMOCER or organically modified ceramic (Fraunhofer Gesellschaft, Germany). Such materials can be used as coatings as well as high barrier laminating agents in multilayer structures. The use of ORMOCER as a top layer on silica-coated PP can significantly improve its oxygen barrier properties, as shown in Figure 27. The composite structure also offers good water vapor barrier properties. Similar improvements in barrier properties of PET have been reported (138). Figure 28 shows a comparison of O_2 and water vapor barrier properties of different barrier polymer composite structures (140).

Another potential candidate as an effective barrier coating is *diamond-like carbon* (DLC) (132). DLC refers to a group of amorphous, hard, and chemically inert materials consisting of carbon bonded partially as diamond (sp^3) and partially as graphite (sp^2) and containing 0–40% hydrogen atoms. These coatings are transparent, flexible, extremely impermeable, biocompatible, and adhere well to a wide range of polymers.

Among the most recent commercial applications of barrier polymeric containers coated with thin inorganic layers is plastic beer packaging. Glaskin (Tetra

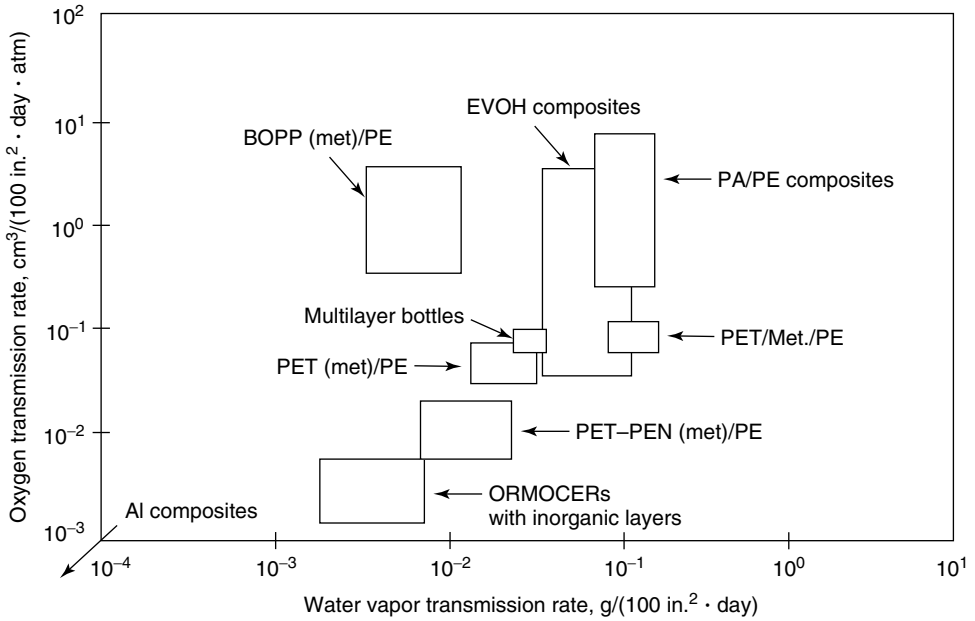

Fig. 28. A comparison of oxygen and water vapor transmission rates of various barrier polymer composite structures (140). BOPP (met) is biaxially oriented, metallized polypropylene; PET (met.) is metallized poly(ethylene terephthalate); PEN (met) is metallized poly(ethylene naphthalate); Al composites are aluminum composites.

Pak, Geneva, Switzerland) is a proprietary technology that utilizes a vacuum deposition process for coating clear, extremely thin layers of silicon oxide on the inside of blown plastic bottles (141). It offers excellent barrier properties for O_2, CO_2, and flavor compounds, and it is completely recyclable. For beer packaging, a shelf life of 6 months has been claimed using this technology. BESTPET (Barrier Enhanced Silica Coated PET) is another silica-based coating technology developed by the Coca Cola Co. (Atlanta, Ga.) in conjunction with Applied Films (Longmont, Colo.) and Krones (Nevtraubling, Germany). The exterior surface of PET bottles is coated with a thin silica layer and improvements in barrier properties of PET by a factor of at least 2 have been claimed, which results in a shelf life of over 6 months for packaged beer (142). A carbon-based high-barrier bottle coating technology is ACTIS (Amorphous Carbon Treatment on Internal Surface technology) (Sidel, France) (143). In this process, the internal surface of plastic bottles is coated with a 0.15 μm thick layer of highly hydrogenated amorphous carbon obtained from a food-safe gas (eg, acetylene) in its plasma state. This technology has been claimed to improve O_2 barrier properties of PET bottles by a factor of 30, and CO_2 barrier properties by a factor of 7. Another carbon-based DLC coating technology (Kirin Brewery, Japan) claims to improve the barrier properties of PET for O_2, CO_2, and H_2O by factors of 20, 7, and 8 respectively (142).

Miscible and Immiscible Blends. Polymer blending offers an alternative, simple, unique, and economical approach for improving barrier properties for several applications (see POLYMER BLENDS). In general, the goal is to add small

amounts of a high barrier polymer (generally more expensive) to a selected matrix polymer (generally low cost) (40). High cost polymers such as PEN and LCPs can be blended with lower cost polymers such as PET to achieve a balance of barrier properties and cost. A common objective of blending is to attenuate the deficiencies while maintaining as much as possible the desirable properties of each component. Occasionally, synergistic effects result in blend properties better than those of the individual components (40). Reactive blending is also possible, for example, with the mixing of different polyester polymers (transesterification), or polyester and nylon (polyesteramide formation) (40).

In general, polymer blends can be broadly classified as homogenous or miscible blends and multiphase or immiscible blends. The permeability coefficient P of miscible blends as well as copolymers often follows an empirical semilogarithmic additivity rule (40):

$$\ln P = \phi_1 \ln P_1 + \phi_2 \ln P_2 \tag{39}$$

where ϕ_i is volume fraction of the ith component and P_i is the component's permeability coefficient. This simple additivity rule is generally obeyed only if there are no interactions between the components. Deviations from this rule can either be positive or negative depending on the nature and magnitude of interactions (40). For example, a miscible blend of styrene–acrylonitrile copolymers (SAN) containing 9% acrylonitrile (AN) and tetramethyl bisphenol A polycarbonate (TMPC) shows negative deviations from the linear additivity rule, indicating strong polymer–polymer interactions. On the other hand, blends of SAN containing 13.5 and 28% AN, and PMMA show positive deviation from the linear additivity rule (40).

When immiscible polymers are blended, or when inorganic filler is added to a polymer matrix, it results in the formation of a dispersion of one component in a continuous matrix of the other. Figure 29 shows several schematic examples of such systems (144). Immiscible polymer blends are far more common than miscible blends (40). Barrier properties of an immiscible blend depend on the permeabilities of the individual components, their volume fractions, phase continuity, and the aspect ratio of the dispersed (or discontinuous) phase (40). The aspect ratio L/W refers to the shape of the particles in the dispersed phase. Spheres and cubes have an aspect ratio of 1, whereas platelets and rods have higher aspect ratios.

The presence of an impermeable dispersed phase lowers the permeability by increasing tortuosity. The Maxwell model can be used to calculate the permeability of a polymer blend, P, with impermeable spherical particles dispersed in a continuous phase (40):

$$P = \frac{P_{\mathrm{m}}\left(1 - \phi_{\mathrm{d}}\right)}{1 + \phi_{\mathrm{d}}/2} \tag{40}$$

where P_{m} is permeability of the continuous polymer phase and ϕ_{d} is volume fraction of the dispersed phase. Different models for permeation in a heterogeneous medium wherein the dispersed phase is impermeable and represented by

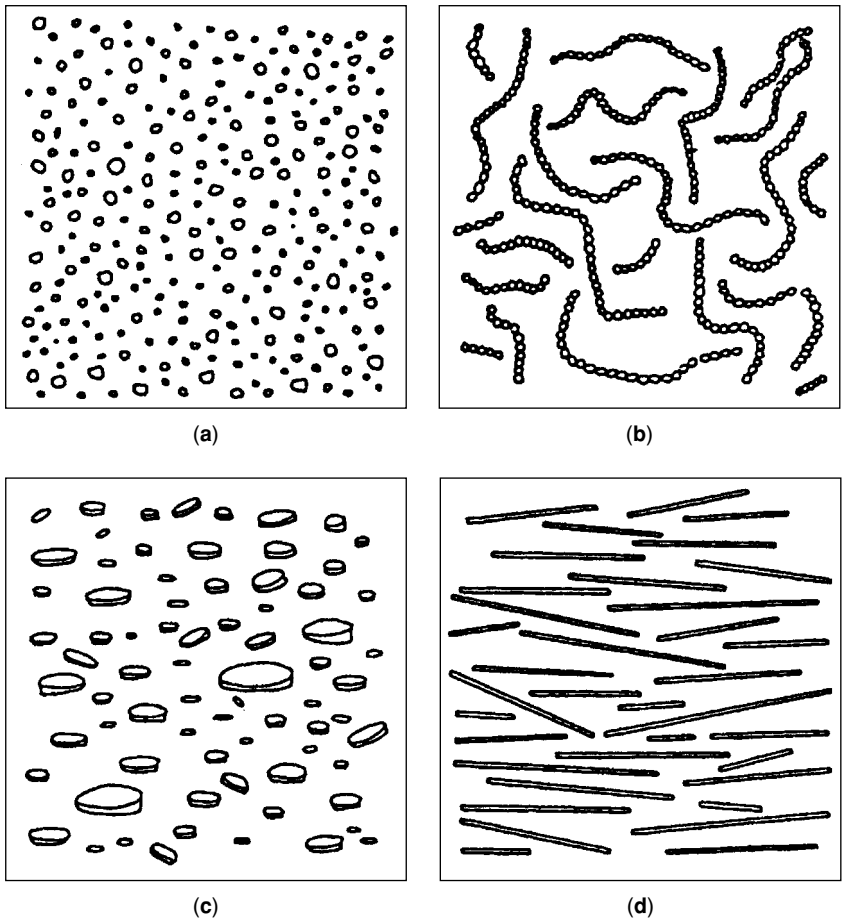

Fig. 29. Examples of heterogeneous, immiscible blends. (**a**) Random spheres in a dispersed phase, (**b**) aggregated spheres in a dispersed phase, (**c**) oriented platelets in a dispersed phase, and (**d**) oriented rods in a dispersed phase (144).

different geometrical shapes have been reviewed (144). Several modifications to the Maxwell model have been made to describe permeation behavior in platelets and ellipsoid-shaped particles dispersed in a more permeable continuous phase (40). For example, oxygen barrier properties of blends of oriented PET and EVOH have been successfully modeled with one such modification (Fricke model) (145). Robeson extended the Maxwell model by applying it to blends in which both the polymers contribute to the continuous phase (40). This model considers the practical implications of attempts to increase the barrier performance of a moderate barrier polymer by adding small amounts of a high barrier polymer to it. According to this model, a multilayer structure provides the highest barrier followed by a blend in which the high barrier polymer is the continuous phase (40).

Figure 30 shows the improvement in O_2 barrier properties of PE–EVOH blends as a function of EVOH volume fraction. Blends of PET with MXD-6 nylon

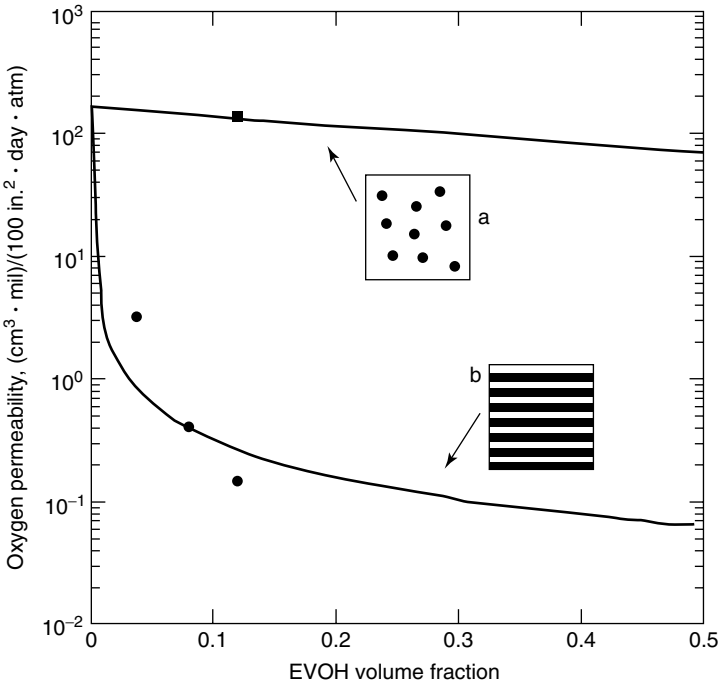

Fig. 30. Effect of EVOH content on oxygen permeability of PE–EVOH blends that exhibit (**a**) discontinuous morphology and (**b**) co-continuous lamellar morphology (40).

(Mitsubishi Gas Chemical Co.) have shown significant reduction in O_2 and CO_2 permeability coefficients relative to those of PET and are being investigated for use in plastic containers (40). PET–EVOH blends have been promoted (Kuraray Co.) for potential applications in the beverage industry (57). The transport properties of PET–LCP blends have also been studied, and Table 10 shows the reductions in permeabilities of O_2, N_2, and CO_2 that have been reported for blown films containing 2, 10, and 30 wt% LCP (146).

Polymer Nanocomposites. Polymer nanocomposites are immiscible blends made by adding nanometer-size particles to barrier polymers. Since nanometer-size grains, fibers, and plates have dramatically increased surface area compared

Table 10. Gas Permeabilities[a] of LCP–PET blends[b]

%LCP[c] in PET	CO_2 permeability	O_2 permeability	N_2 permeability
0	114.5	21.3	5.1
2	78.1	14.9	2.6
10	65.8	12.0	3.1
30	34.5	5.5	2.0

[a] $(cm^3 \cdot mil)/(100\ in.^2 \cdot day \cdot atm)$.
[b] Ref. 40.
[c] Rodrun LC3000 LCP.

to conventional-size materials, the chemistry of nanosized materials is different from other conventional materials. Polymers filled with nanometer-size particles have significantly different properties than those filled with conventional inorganic materials (147). Properties of nanocomposites such as high tensile strength can be achieved by using higher conventional filler loading, but other properties such as improved clarity cannot be duplicated by filled resins at any loading (148).

Polymer nanocomposites were developed in the late 1980s, and were first commercialized by Toyota, which used nanocomposite parts in one of its car models for several years (57). Initial developments focussed on the use of nylon resins and very fine smectite clay particles, with surface area of about 750 m^2/g, as fillers (57). Ube Industries developed its first nylon nanocomposite in 1989 for an automotive timing belt cover. They have also developed other nylon nanocomposites called nylon clay hybrids (57). More recently, novel nanocomposite nylon-6 resins developed by Honeywell Engineered Applications and Solutions (Morristown, N.J.) have been claimed to improve O_2 and CO_2 barrier properties by a factor of 3–4 (149). It has also been claimed that these nanocomposites double the heat resistance of nylon-6 and improve other mechanical properties by 30–50% (149). Others such as Nanocor, Inc. (150) are also actively developing nanocomposites for enhanced barrier performance. Commercial products are available for PP and fluoropolymers. Some of the other potential candidate polymers for nanocomposites include polyesters, PS, and ethylene vinyl acetate copolymers (57). Several polymer nanocomposites, including amorphous nylon and EVOH matrixes, intended for high barrier applications are in various stages of development.

Oxygen-Scavenging Systems. Another strategy for improving the barrier properties of polymers is the introduction of reactive groups in the polymer. These groups can reduce the transmission of penetrants such as oxygen and water vapor and the term “active barrier” is often used to describe this approach to distinguish it from “passive barrier” packages that rely on reduced permeability to decrease gas transmission. By using an oxygen scavenger, which absorbs the residual oxygen after packaging, quality changes of oxygen-sensitive foods can be minimized (151–153). Although oxygen-scavenging technology is rapidly evolving and encompasses a wide variety of chemistries, the majority of current commercial oxygen-scavenger packages probably still employ sachets that remove oxygen from the headspace via iron oxidation. Ageless (Mitsubishi Gas Chemical Co., Japan) oxygen absorbers are the most commonly used sachets that are placed inside the food package (57). If the initial oxygen concentration and oxygen permeability of the packaging polymer is known, then an oxygen scavenger can be chosen with a higher capacity than the theoretically needed capacity, and near total absence of oxygen can be maintained during the expected shelf life of the product (151). Other iron-based oxygen-scavenger sachets are ATCO (Standa Ind., France), Freshilizer (Toppan Printing Co., Japan), Vitalon (Toagosei Chem. Ind., Japan), Freshpax (Multisorb Technologies Inc., U.S.), and Sanso-cut (Finetec Co., Japan) (151).

An alternative to sachets is to incorporate the oxygen scavenger into the barrier polymer structure itself (151). An example of this strategy is Oxbar (Crown Cork and Seal, Philadelphia, Pa.), which involves cobalt-catalyzed oxidation of nylon MXD-6 polymer used in multilayer PET bottles for packaging of

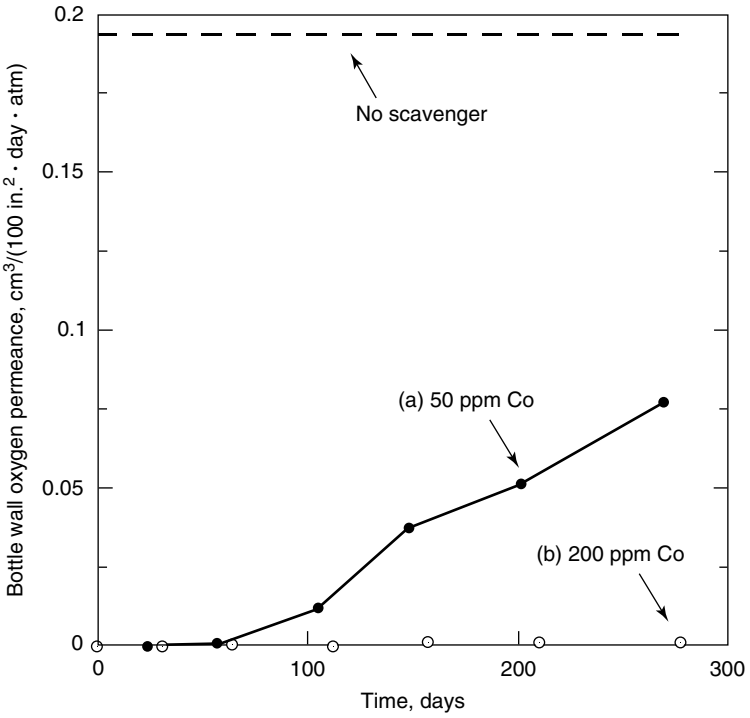

Fig. 31. Reduction in oxygen transmission rates due to oxygen scavenging in blends of PET and nylon MXD-6 (157). The measurements were made at 23°C and 50% RH. (**a**) 4 wt% MXD-6 and 50 ppm cobalt (as metal); (**b**) 4 wt% MXD-6 and 200 ppm cobalt (as metal). For comparison, the dotted line indicates oxygen permeance in the absence of cobalt catalyst (no scavenging).

beverages. Another example of a polymer-based absorber is Amosorb (BP Amoco Chemicals), which can reportedly be incorporated into various rigid and flexible packaging structures (151). This is a rapidly evolving field and several other companies have also introduced or announced oxygen-scavenging resins. Among those active in this area are EVAL Co., U.S., Kuraray Co., Japan and Darex Co., U.S., with DarEval (154); Owens-Illinois/Continental PET Technologies with CPTX-312; Honeywell International, Inc. with scavenging nylon resin (155); Cryovac with OS 1000; and Chevron Phillips Chemical Co. with their OSP scavengers (156). While the speed and capacity of oxygen-scavenging films are considerably lower than iron-based oxygen-scavenger sachets (151), oxygen ingress into the package can be reduced to very low levels with appropriately designed scavenger structures. Figure 31 presents an example of the reduction in oxygen transmission rate due to oxygen scavenging in blends of PET and nylon MXD-6 (157). Scavengers can also be incorporated into the liner of bottle closures where they can significantly reduce the ingress of oxygen into the package through the closure liner (158).

A recent study (159) has shown that incorporation of inorganic fillers as well as reactive groups in barrier polymer films can significantly improve the shelf life of packages. According to that theory, the presence of immobile reactive groups dramatically increases the *time lag* (ie, the time required to achieve steady-state permeability), but do not affect steady-state transport of penetrants across barrier polymer films. For example, in LDPE and PVDC films containing 10% flakes of mica or clay and linolenic acid as the oxygen-scavenging species, the time lag for permeation of O_2 dramatically increased by about 3 orders of magnitude to 40 h and 3 years, respectively (159).

Conclusions

Barrier polymers are widely used in food, beverage, and other packaging industries. Some of the their advantages over traditional packaging materials such as glass, paper, and metals are flexibility, light weight, toughness, versatility, and printability. The selection of a polymer for a particular packaging application depends on its barrier as well as other physical properties. A comparison of these properties and current as well as potential future applications for different types of barrier polymers has been presented. Additionally, important factors governing permeability (eg, penetrant size, polymer chemical structure, temperature, humidity) as well as ways to measure and predict permeability have also been discussed.

Unlike glass and metals, no polymer offers an infinite gas barrier. Despite this limitation, monolayer polymer structures in many instances satisfy the barrier requirements for a package. In other situations, combinations of different polymers, or polymers with inorganic materials, in the form of multilayer structures or blends, can provide cost-effective barrier for the intended shelf life of packaged products. As a result, plastic packaging is ubiquitous. Market pressures, however, drive the need for continual improvements in packaging materials. Hence, there is an ongoing interest in improving the barrier properties of polymers used in packaging, and the search for improved barrier polymers and structures is ongoing. Inorganic materials such as silicon and aluminum oxides and clays can be used to significantly enhance gas barrier and other mechanical properties of polymers. One area of recent activity is polymer nanocomposites, which involves dispersion of nanoscale barrier particles in a polymer matrix. A considerable amount of research is also being focussed on techniques for developing thin layers of inorganic coatings on barrier polymer films and containers. In addition, work in the field of oxygen-scavenging technologies (so-called active packaging systems) has resulted in several developments. While advances in these newer barrier technologies have recently opened up several commercial applications, with plastic beer packaging being perhaps the most publicized, it is much too early to accurately predict their eventual success in the market place. Constructions with established "passive" barrier polymers currently dominate the barrier packaging market, and these materials are expected to be commercially important for many years to come.

BIBLIOGRAPHY

"Barrier Polymers" in *EPST* 1st ed., Vol. 1, pp. 65–95, by S. P. Nemphos, M. Salame, and S. Steingiser, Monsanto Co.; "Barrier Polymers" in *EPSE* 2nd ed., Vol. 4 pp. 176–192, by W. A. Combellick, Goodyear Tire & Rubber Co.

1. K. Ghosal and B. D. Freeman, *Polym. Adv. Technol.* **5**, 673 (1994).
2. R. C. Reid, J. M. Prausnitz, and B. E. Poling, *The Properties of Gases and Liquids*, McGraw Hill, New York, 1988, p. 230.
3. J. Crank, *The Mathematics of Diffusion*, 2nd ed., Clarendon Press, Oxford, 1975, p. 414.
4. C. E. Rogers, in J. Comyn, ed., *Polymer Permeability*, Elsevier Applied Science, London, 1988, p. 11.
5. C. C. McDowell, B. D. Freeman, and G. W. McNeely, *Polymer* **40**, 3487 (1999).
6. A. H. Windle, in Ref. 4, p. 75.
7. A. R. Berens, *J. Appl. Polym. Sci.* **37**, 901 (1989).
8. F. Muller-Plathe, *Acta Polym.* **45**, 259 (1994).
9. W. J. Koros and M. W. Hellums, in J. I. Kroschwitz, ed., *Encyclopedia of Polymer Science and Engineering*, John Wiley & Sons, Inc., New York, 1990, Supplement Volume, p. 724.
10. D. Hofman and co-workers, *Polymer* **37**, 4773 (1996).
11. J. R. Fried, *J. Membr. Sci.* **149**, 115 (1998).
12. A. Bondi, *J. Phys. Chem.* **68**, 441 (1964).
13. D. W. van Krevelen, *Properties of Polymers: Their Correlation with Chemical Structure; Their Numerical Estimation and Prediction from Additive Group Contributions*, 3rd ed., Elsevier, Amsterdam, 1990, p. 875.
14. M. H. Cohen and D. Turnbull, *J. Chem. Phys.* **31**, 1164 (1959).
15. K. Ghosal, R. T. Chern, and B. D. Freeman, *J. Polym. Sci., Polym. Phys. Ed.* **33**, 657 (1995).
16. D. H. Weinkauf and D. R. Paul, in W. J. Koros, ed., *Barrier Polymers and Structures* (ACS Symposium Series, Vol. **423**), American Chemical Society, Washington, D.C., 1990, p. 60.
17. D. H. Weinkauf and D. R. Paul, *J. Polym. Sci., Polym. Phys. Ed.* **30**, 837 (1992).
18. W. M. Lee, *Polym. Eng. Sci.* **20**, 65 (1980).
19. A. Singh and W. J. Koros, in Permeation Processes in Barriers and Membranes: Differences and Similarities, Polymers, Laminations & Coatings Conference, San Francisco, Calif., 1998, p. 361.
20. A. J. Hill and co-workers, *Eur. Polym. J.* **32**, 843 (1996).
21. B. D. Freeman and A. J. Hill, in M. R. Tant and A. J. Hill, eds., *Structure and Properties of Glassy Polymers*, Vol. **710**, American Chemical Society, Washington, D.C., 1997, p. 306.
22. E. A. McGonigle and co-workers, *Polymer* **42**, 2413 (2001).
23. V. P. Shantarovich and co-workers, *Macromolecules* **33**, 7453 (2000).
24. J. E. Robertson, T. C. Ward, and A. J. Hill, *Polymer* **41**, 6251 (2000).
25. G. Dlubek and co-workers, *J. Phys.: Condens. Matter* **10**, 10443 (1998).
26. H. Yang and Y. C. Jean, *Mater. Sci. Forum* **255–257**, 40 (1997).
27. W. E. Brown, in W. E. Brown, ed., *Plastics in Food Packaging*, Marcel Dekker, Inc., New York, 1992, p. 292.
28. R. M. Barrer, *Trans. Faraday Soc.* **38**, 322 (1942).
29. G. J. van Amerongen, *J. Appl. Phys.* **17**, 972 (1946).
30. R. M. Barrer and G. Skirrow, *J. Polym. Sci.* **3**, 549 (1948).
31. R. M. Barrer, *Trans. Faraday Soc.* **39**, 48 (1943).

32. J. E. Leffler, *J. Org. Chem.* **20**, 1202 (1955).
33. W. J. Koros, in Ref. 16, p. 1.
34. P. Meares, *J. Amer. Chem. Soc.* **76**, 3415 (1954).
35. T. K. Kwei and W. Arnheim, *J. Chem. Phys.* **37**, 1900 (1962).
36. J. Brandrup, E. H. Immergut, and E. A. Grulke, *Polymer Handbook*, 4th ed., Wiley-Interscience, New York, 1999, p. VI–198.
37. M. Salame, in K. M. Finlayson, ed., *Plastic Film Technology*, Vol. **1**, Technomic Publishing Co., Inc., Lancaster, Pa., 1989, p. 132.
38. R. R. Light and R. W. Seymour, *Polym. Eng. Sci.* **22**, 857 (1982).
39. A. S. Michaels, W. R. Vieth, and J. A. Barrie, *J. Appl. Phys.* **34**(1), 13 (1963).
40. P. M. Subramanian and I. G. Plotzker, in D. R. Paul and C. B. Bucknall, eds., *Polymer Blends*, Vol. **2**, John Wiley & Sons, Inc., New York, 2000, p. 359.
41. A. S. Michaels, W. R. Vieth, and J. A. Barrie, *J. Appl. Phys.* **34**(1), 1 (1963).
42. A. C. Puleo, D. R. Paul, and P. K. Wong, *Polymer* **30**, 1357 (1989).
43. G. E. Serad and co-workers, *Polymer* **42**, 6929 (2001).
44. H. D. Weigmann and co-workers, *Text. Res. J.* **46**, 574 (1976).
45. H. Jameel, J. Waldman, and L. Rebenfeld, *J. Appl. Polym. Sci.* **26**, 1795 (1981).
46. H. Jameel, H. D. Noether, and L. Rebenfeld, *J. Appl. Polym. Sci.* **27**, 773 (1982).
47. A. S. Michaels and R. B. J. Parker, *J. Polym. Sci.* **61**, 53 (1959).
48. N. Qureshi and co-workers, *J. Polym. Sci., Polym. Phys. Ed.* **38**, 1679 (2000).
49. D. J. Sekelik and co-workers, *J. Polym. Sci., Polym. Phys. Ed.* **37**, 847 (1999).
50. H. D. Weigmann and co-workers, *Text. Res. J.* **47**, 745 (1977).
51. P. H. Hermans and P. Platzek, *Kolloid Z.* **88**, 68 (1939).
52. M. R. Tant and co-workers, *Polym. Mater. Sci. Eng.* **81**, 374 (1999).
53. R. Shastri, H. C. Roehrs, C. N. Brown, and S. E. Dollinger, in Ref. 16, p. 239.
54. D. R. Paul, *Ber. Bunsenges. Phys. Chem.* **83**, 294 (1979).
55. R. J. Hernandez, S. E. M. Selke, and J. D. Culter, *Plastics Packaging: Properties, Processing, Applications, and Regulations*, Hanser Gardner Publications, Inc., Cincinnati, Ohio, 2000, p. 313.
56. R. J. Hernandez, *J. Food Eng.* **22**, 495 (1994).
57. G. Strupinsky and A. L. Brody, in A Twenty-Year Retrospective on Plastics: Oxygen Barrier Packaging Materials, Polymers, Laminations & Coatings Conference, San Francisco, Calif., 1998, p. 119.
58. W. R. Vieth, *Diffusion in and through Polymers: Principles and Applications*, Oxford University Press, New York, 1991, p. 20.
59. H. L. Frisch, *J. Phys. Chem.* **62**, 401 (1958).
60. K. D. Ziegel, H. K. Frensdorff, and D. E. Blair, *J. Polym. Sci.* **7**, 809 (1969).
61. *Annual Book of ASTM Standards, Standard D3985*, Vol. 15.09, American Society for Testing and Materials, West Conshocken, Pa., 1994, p. 542.
62. *Ox-Tran® Oxygen Transmission Rate Measurement System*, MOCON, Inc., Minneapolis, Minn., 1998.
63. P. DeLassus, in J. I. Kroschwitz, ed., Encyclopedia of Polymer Science and Technology, Vol. **3**, John Wiley & Sons, Inc., New York, 1992, p. 931.
64. *Annual Book of ASTM Standards, Standard F1249*, Vol. **15.09**, American Society for Testing and Materials, West Conshocken, Pa., 1994, p. 1051.
65. C. D. Barr, J. R. Giacin, and R. J. Hernandez, *Packag. Technol. Sci.* **13**, 157 (2000).
66. C. C. McDowell, D. T. Coker, and B. D. Freeman, *Rev. Sci. Instr.* **69**, 2510 (1998).
67. P. Hernandez-Munoz, R. Gavara, and R. J. Hernandez, *J. Membr. Sci.* **154**, 195 (1999).

68. M. Moaddeb and W. J. Koros, *J. Appl. Polym. Sci.* **57**, 687 (1995).
69. B. I. Chaudhary and A. I. Johns, *J. Cell. Plast.* **34**, 312 (1998).
70. O. Pfannschmidt and W. Michaeli, in Determination of the Solubility and Diffusivity of Gases in Polymers by using a High Pressure Magnet-Suspension-Balance, Annual Technical Conference of the Society of Plastics (ANTEC), Atlanta, Ga., 1998, p. 1918.
71. S. N. Dhoot and co-workers, *J. Polym. Sci., Polym. Phys. Ed.* **39**, 1160 (2001).
72. M. Salame, *Polym. Eng. Sci.* **26**, 1543 (1986).
73. J. Y. Park and D. R. Paul, *J. Membr. Sci.* **125**, 23 (1997).
74. R. Franz, *Packag. Technol. Sci.* **6**, 91 (1993).
75. S. C. Fayoux, A. Seuvre, and A. J. Voilley, *Packag. Technol. Sci.* **10**, 145 (1997).
76. G. Strandburg, P. T. DeLassus, and B. A. Howell, in S. J. Risch and J. H. Hotchkiss, eds., *Food and Packaging Interactions II*, Vol. **473**, American Chemical Society, Washington, D.C., 1991, p. 133.
77. R. M. Barrer and G. J. Skirrow, *J. Appl. Polym. Sci.* **3**, 564 (1948).
78. S. A. Stern, J. T. Mullhaupt, and P. J. Gareis, *AIChE J.* **15**, 64 (1969).
79. S. Li and J. S. Paik, *Trans. ASAE* **39**, 1013 (1996).
80. J. S. Paik and M. A. Tigani, *J. Agric. Food Chem.* **41**, 806 (1993).
81. B. D. Freeman and I. Pinnau, in B. D. Freeman and I. Pinnau, eds., *Polymeric Materials for Gas Separations: Chemistry and Materials Science*, American Chemical Society, Washington, D.C., 1999, p. 1.
82. R. C. Mason and co-workers, *Tappi J.* **75**(6), 163 (1992).
83. C. S. Coughlin, K. A. Mauritz, and R. F. Storey, *Macromolecules* **24**, 1526 (1991).
84. T. H. Begley, *Food Addit. Contam.* **14**, 545 (1997).
85. O. Piringer and co-workers, *J. Agric. Food Chem.* **46**, 1532 (1998).
86. A. O'Brien, A. Goodson, and I. Cooper, *Food Addit. Contam.* **16**, 367 (1999).
87. W. Limm and H. C. Hollifield, *Food Addit. Contam.* **13**, 949 (1996).
88. W. A. Jenkins and J. P. Harrington, in W. A. Jenkins and J. P. Harrington, eds., *Packaging Foods with Plastics*, Technomic Publishing Co., Lancaster, Pa., 1991, p. 46.
89. *Permeability and Other Film Properties of Plastics and Elastomers*, Plastics Design Library, Norwich, N.Y., 1995, p. 143.
90. *BLOX*™ *Adhesion and Barrier Resins: Product Information*, The Dow Chemical Company, May 2001.
91. A. B. Robertson and K. R. Habermann, in M. Bakker, ed., The Wiley Encyclopedia of Packaging Technology, John Wiley & Sons, Inc., New York, 1986, p. 311.
92. J. Quezada-Gallo, F. Debeaufort, and A. Voilley, in S. J. Risch, ed., *Food Packaging: Testing Methods and Applications* (ACS Symposium Series, Vol. **753**), American Chemical Society, Washington, D.C., 1999, p. 130.
93. Ref. 89, p. 706.
94. V. T. Stannett, *Polym. Eng. Sci.* **18**, 1129 (1978).
95. R. J. Ashley, in J. Comyn, ed., *Polymer Permeability*, Elsevier Applied Science Publishers Ltd., Essex, England, 1985, Chapt. "7".
96. M. Salame, in Ref. 91, p. 48.
97. S. Pauly, in J. Brandrup and E. H. Immergut, eds., *Polymer Handbook*, 3rd ed., Wiley-Interscience, New York, 1989, p. IV–435.
98. P. T. DeLassus, in J. I. Gray, B. R. Harte, and J. Miltz, eds., *Food Product-Package Compatibility*, Technomic Publishing Co., Lancaster, Pa., 1987, p. 229.

99. J. Landois-Garza and J. H. Hotchkiss, in J. H. Hotchkiss, ed., *Food and Packaging Interactions* (ACS Symposium Series, Vol. **365**), American Chemical Society, Washington, D.C., 1988, p. 42.
100. M. G. R. Zobel, in Aroma Barrier Properties of Coextruded Films, Proceedings of 4th Annual International Conference on Coextrusion Markets and Technology, Schotland Business Research, Princeton, N.J., 1984, p. 75.
101. G. L. Robertson, in H. A. Hughes, ed., *Food Packaging: Principles and Practice*, Vol. **6**, Marcel Dekker, Inc., New York, 1993, p. 9.
102. R. Catala and R. Gavara, *Food Sci. Tech. Int.* **2**, 281 (1996).
103. Ref. 27, p. 132.
104. Ref. 55, p. 89.
105. *Selar PA Processing Guide*, E. I. du Pont de Nemours & Co., Inc., Wilmington, Del., 2001.
106. P. M. Morse, *Chem. Eng. News* 8 (Nov. 10, 1997).
107. T. M. McGee and A. S. Jones, in The Effect of Processing Parameters on Physical Properties of PET/PEN Blends for Bottle Applications, 11th Annual High Performance Blow Molding Conference: Technical Innovations in Blow Molding, Cleveland, Ohio, 1995, p. 89.
108. C. C. McDowell and co-workers, *J. Polym. Sci., Polym. Phys. Ed.* **36**, 2981 (1998).
109. G. R. Cantrell and co-workers, in C. Carfagna, ed., *Liquid Crystalline Polymers*, Pergamon Press, Oxford, 1994, p. 233.
110. N. R. Miranda and co-workers, *J. Membr. Sci.* **94**, 67 (1994).
111. R. Lusignea, *Tappi J.* **80**, 205 (1997).
112. R. Lusignea, in Flexible Multilayer Packaging with Oriented LCP Barrier Layer, Polymers, Laminations & Coatings Conference, San Francisco, Calif., 1998, p. 889.
113. D. J. Brennan and co-workers, *Macromolecules* **29**, 3707 (1996).
114. K. Ghosal and co-workers, *Macromolecules* **29**, 4360 (1996).
115. M. R. Pixton and D. R. Paul, in D. R. Paul and Y. P. Yampolskii, eds., *Polymeric Gas Separation Membranes*, CRC Press: Boca Raton, Fla., 1994, p. 83.
116. C. H. Silvis, *Trends Polym. Sci.* **5**(3), 75 (1997).
117. T. Glass, H. Pham, and M. Winkler, in New Thermoplastic Adhesive and Barrier Resins, ANTEC 2000: Plastics, The Magical Solution, Orlando, Fla., 2000.
118. W. Erickson, in New Coextruded PCTFE-Based Moisture Barrier Films for High Performance Packaging, Polymers, Laminations & Coatings Conference, San Francisco, Calif., 1998, p. 355.
119. *Aclar Fluoropolymer Films: Product Information*, Honeywell International, 2001.
120. P. T. DeLassus, D. L. Clarke, and T. Cosse, *Mod. Plast.* 86 (Jan. 1983).
121. Ref. 27, p. 125.
122. E. Werner, S. Janocha, M. Hopper, and K. Mackenzie, in J. I. Kroschwitz, ed., Encyclopedia of Polymer Science and Technology, Vol. **12**, Wiley-Interscience, New York, 1992, p. 193.
123. N. Whiteman, P. T. DeLassus, and J. Gunderson, in TAPPI Proceedings of PLC Conference, 2001.
124. Ref. 27, p. 105.
125. J. L. Throne, in Ref. 91, p. 529.
126. A. R. Berens, *Makromol. Chem., Macromol. Symp.* **29**, 95 (1989).
127. J. H. Levy, in Nylon 6 Barrier Coextrusions: A Cost-effective Packaging Route, Polymers, Laminations & Coatings Conference, San Francisco, Calif., 1998, p. 163.

128. Ref. 88, p. 11.
129. *MXD-6 Nylon Polyamide Property Brochure*, Mitsubishi Gas Chemical Co., Inc., 2001.
130. D. A. Abramowicz and P. J. Heyes, in Comparing the Performance of Barrier-Coated versus Multilayer PET Containers for Oxygen Sensitive Products, Nova-Pack Americas 2000, Orlando, Fla., 2000.
131. T. Hart, in New Effective Barrier Coating for Plastic Containers, Bev-Pak Americas '97, Directions 21, Inc., 1997.
132. D. S. Finch and co-workers, *Packag. Technol. Sci.* **9**, 73 (1996).
133. N. Inagaki, in S. J. Clarson, J. J. Fitzgerald, M. J. Owen, and S. D. Smith, eds., *Silicones and Silicone-Modified Materials*, ACS Symposium Series, Vol. **729**, Oxford University Press, Washington, D.C., 2000, p. 544.
134. Ref. 55, p. 217.
135. Ref. 101, p. 111.
136. Ref. 88, p. 195.
137. A. S. Da Silva Sobrinho, G. Czeremuszkin, M. Latreche, and M. R. Wertheimer, in W. W. Lee, R. d'Agostino, and M. R. Wertheimer, eds., *Plasma Deposition and Treatment of Polymers*, Materials Research Society Symposium Proceedings, Vol. **544**, Materials Research Society, Boston, 1998, p. 245.
138. K. H. Haas and co-workers, *Surf. Coat. Tech.* **111**, 72 (1999).
139. M. Hoffmann and co-workers, *J. Sol Gel Sci. Tech.* **1/2**, 141 (1998).
140. H. Langowski, *Kunstoffe* **90**(6), 88 (2000).
141. *Packaging World* 2 (May 2000).
142. I. Bucklow and P. Butler, *Materials World* 14 (Aug. 2000).
143. *Packaging World* 2 (June 1999).
144. R. M. Barrer, in J. Crank and G. S. Park, eds., *Diffusion in Polymers*, Academic Press, New York, 1968, p. 165.
145. K. M. Kit, J. M. Schultz, and R. Gohil, *Polym. Eng. Sci.* **35**, 680 (1995).
146. O. Motta and co-workers, *Polymer* **37**, 2373 (1996).
147. E. Petrovicova and co-workers, *J. Appl. Polym. Sci.* **78**, 2272 (2000).
148. *Polymer Nanocomposites*, Business Communications Co., Inc., Apr. 2000.
149. *Packaging World* (Nov. 6, 2000).
150. K. Kamena, in Emerging Nanocomposite Technologies for Barrier and Thermal Improvements in PET Containers, Nova-Pack Americas '99, Orlando, Fla., 1999, p. 1.
151. L. Vermeiren and co-workers, *Trends Food Sci. Tech.* **10**, 77 (1999).
152. W. Scholl, in Active Barrier Packaging: A Technology for the 21st Century, Polymers, Laminations & Coatings Conference, Atlanta, Ga., 1999, p. 671.
153. M. L. Rooney, in M. L. Rooney, ed., *Active Food Packaging*, 1st ed., Blackie Academic & Professional, Glasgow, U.K., 1995, p. 74.
154. S. Lambert, in New EVOH-Based Oxygen Scavenging Resins for Use in Co-Injected PET Bottles, Nova-Pack Europe 2000, Neuss, Germany, 2000, p. 163.
155. E. P. Socci, M. K. Akkapeddi, and D. C. Worley, in New High Barrier, Oxygen Scavenging Polyamides for Packaging Applications, ANTEC, 2001.
156. B. D. Rodgers, in New High Capacity Oxygen Scavenging Polymer For Use in Flexible Packaging, Flex-Pak Europe 2000, Amsterdam, Nov. 2000, p. 61.
157. U. S. Pat. 5,639,815 (1997), M. A. Cochran and co-workers.

158. F. N. Teumac, B. A. Ross, and M. R. Rassouli, *MBAA Tech. Q.* **27**, 122 (1990).
159. C. Yang, E. Nuxoll, and E. Cussler, *AIChE J.* **47**, 295 (2001).

SUSHIL N. DHOOT
University of Texas at Austin
BENNY D. FREEMAN
University of Texas at Austin
MARK E. STEWART
Eastman Chemical Company

BIODEGRADABLE POLYMERS, MEDICAL APPLICATIONS

Introduction

Traditional applications of synthetic polymers are mostly based on their relative inertness to biodegradation compared with natural macromolecules, such as cellulose, and proteins. Biodegradation of the polymers can occur in several ways including photodegradation, oxidation, and hydrolysis. Practically, biodegradation involves enzymatically promoted breakdown caused by living organisms, usually microorganisms, but it is now well accepted that the biodegradation can occur by hydrolysis, oxidation, or photooxidation in a biological environment. These polymers have been used in many aspects of life, eg, in environmentally friendly packaging materials (1,2), agriculture (3,4), drug delivery (5,6), gene delivery (7,8), and tissue engineering (9,10). (See CONTROLLED RELEASE TECHNOLOGY; ENVIRONMENTALLY DEGRADABLE POLYMERS; GENE-DELIVERY POLYMERS; TISSUE ENGINEERING). This article emphasizes the various biodegradable polymers obtained either synthetically or from natural resources and their uses for biomedical applications.

Factors Affecting Biodegradation

Effect of Polymer Structures. Synthetic biodegradable polymers contain hydrolyzable linkages along the polymer chain; for example, amide enamine, ester, phosphate, phosphazene, carbonate, anhydride, urea, and urethane linkages are susceptible to biodegradation by microorganisms and hydrolytic enzymes. In addition, polymers containing substituents such as benzyl, hydroxy, carboxy, methyl, and phenyl groups have been prepared in the hope that an introduction of these

Encyclopedia of Polymer Science and Technology. Copyright John Wiley & Sons, Inc. All rights reserved.

substituents might increase biodegradability (11). Among benzylated polymers, mixed results have been obtained for polyamides. Since most enzyme-catalyzed reactions occur in aqueous media, the hydrophilic–hydrophobic character of synthetic polymers greatly affects their biodegradability. A polymer containing both hydrophobic and hydrophilic segments seems to have a higher biodegradability than those polymers containing either hydrophobic or hydrophilic structures only. A series of poly(alkylene tartrate)s was found to be readily assimilated by *Aspergillus niger*. However, the polymers derived from C6 and C8 alkane diols were more degradable than the more hydrophilic polymers derived from C2 and C4 alkane diols or the more hydrophobic polymers derived from the C10 and C12 alkane diols. Among the degradable poly(α-aminoacid-*co*-ε-caproic acid)s, the hydrophilic copolyamide derived from serine was more susceptible than those containing only hydrophobic segments. For a synthetic polymer to be degradable by enzyme catalysis, the polymer chain must be flexible enough to fit into the active site of the enzyme. This aspect most likely accounts for the fact that while the flexible aliphatic polyesters are readily degraded by biological systems, the more rigid aromatic poly(ethylene terephthalate) is generally considered to be inert (12).

Effect of Polymer Morphology. Selective chemical degradation of semicrystalline polymer samples shows certain characteristic changes (13–16). During degradation, the crystallinity of the sample increases rapidly at first and then levels off to a much slower rate as the crystallinity approaches 100%. This effect is attributed to the eventual disappearance of the amorphous portions of the sample. The effect of morphology on the microbial and enzymatic degradation of poly(ε-caprolactone) (PCL), a known biodegradable polymer with a number of potential applications, has been studied (17,18). Scanning electron microscopy has shown that the degradation of a partially crystalline polycaprolactone film by filamentous fungi proceeds in a selective manner, with the amorphous regions being degraded prior to the degradation of the crystalline region. The microorganisms produce extracellular enzymes responsible for the selective degradation. This selectivity can be attributed to the less-ordered packing of amorphous regions, which permits easier access for the enzyme to the polymer chains. The size, shape, and number of crystallites all have a pronounced effect on the chain mobility of the amorphous regions and thus affect the rate of degradation. This effect has been demonstrated by studying the effects of changing orientation via stretching on the degradation (17,18).

Degradation in biological medium, cells, tissues, and body fluids proceeds differently from chemical degradation as enzymes, biological reagents in the cell organelles, and fluids are involved in the degradation process. Enzyme is able to degrade the crystalline regions faster than hydrolysis. The enzyme system shows no intermediate molecular weight material but shows a much smaller weight shift with degradation as compared to chemical degradation. This shift indicates that although degradation is selective, the crystalline portions are degraded shortly after the chain ends are made available to the exoenzyme. The lateral size of the crystallites has a strong effect on the rate of degradation because the edge of the crystal is where degradation of the crystalline material takes place, because of the crystal packing. A smaller lateral crystallite size yields a higher crystallite edge surface in the bulk polymer. Prior to the saturation of the enzyme active

sites, the rate is dependent on available substrate; therefore, a smaller lateral crystallite size results in a higher rate of degradation. The degradation rate of a PCL film is zero order with respect to the total polymer, but is not zero order with respect to the concentrations of the crystallite edge material. The drawing of PCL films causes an increase in the rate of degradation, whereas annealing of the PCL causes a decrease in the rate of degradation (19). This phenomenon is probably due to opposite changes in lateral crystallite sizes. *in vitro* chemical and enzymatic degradations of polymers, especially polyesters, were analyzed with respect to chemical composition and physical properties. It was found quite often that the composition of a copolymer giving the lowest melting point is most susceptible to degradation (19). The lowest packing order, as expected, corresponds with the fastest degradation rate.

Effect of Molecular Weight. Microorganisms produce both exoenzymes, which degrade polymers from terminal groups, and endoenzymes, which degrade polymers randomly along the chain. One might expect a large molecular effect on the rate of degradation in the ease of exoenzymes and a relatively small molecular weight effect in the case of endoenzymes. Low molecular weight hydrocarbons, however, can be degraded by microbes. They are taken in by microbial cells, "activated" by attachment to coenzyme A, and converted to cellular metabolites within the microbial cell. However, these processes do not function well (if at all) in an extracellular environment, and the plastic molecules are too large to enter the cell. This problem does not arise with natural molecules, such as starch and cellulose, because conversions to low molecular weight components by enzyme reactions occur outside the microbial cell. Photodegradation or chemical degradation may decrease molecular weight to the point that microbial attack can proceed. Hydrolytic degradation of polyesters and polyanhydrides is affected by the molecular weight as a result of differences in water accessibility to large molecular weight polymeric materials.

Effect of Radiation and Chemical Treatment. Photodegradation with UV light and the γ-irradiation of polymers generate radicals and/or ions that often lead to cleavage and cross-linking. Oxidation also occurs, complicating the situation, since exposure to light is seldom in the absence of oxygen. Generally this changes the material's susceptibility to biodegradation. Initially, one expects the observed rate of degradation to increase until most of the fragmented polymer is consumed and a slower rate of degradation should follow for the cross-linked portion of the polymer. Similarly, photooxidation of polyalkenes promotes (slightly in most cases) the biodegradation (20). The formation of carbonyl and ester groups is responsible for this change. Processes have been developed to prepare copolymers of alkenes containing carbonyl groups so that they will be more susceptible to photolytic cleavage prior to degradation. As expected, γ-ray irradiation greatly affects the rate of *in vitro* degradation of polyesters (21,22). For polyglycolide and poly(glycolide-*co*-lactide), the pH of the degradation solution decreased as the process proceeded. The change–time curves exhibit sigmoidal shapes and consist of three stages: early, accelerated, and later; the lengths of these three regions were a function of γ-irradiation. Increasing radiation dosage shortens the time of the early stage. The appearance of the drastic pH changes coincides with loss of tensile breaking strength.

Classification

On the basis of the formation, biodegradable polymers can be classified into two groups including synthetic biodegradable polymers and natural biodegradable polymers.

Synthetic Biodegradable Polymers. A representive list of synthetic biodegradable polymers is given in Table 1, which includes chemical backbone structures of these polymers. These polymers can be catagorized into two types on the basis of their backbone structures, namely (*1*) polymers with hydrolyzable backbone and (*2*) polymers with carbon backbone.

Polyester. Polyesters having hydrolyzable ester bond in their backbone are considered the best biomaterial with regard to design and performance. Among polyesters, poly(lactic acid) (PLA) can be made of the lactic acid monomers which contain an asymmetric α-carbon atom with three different isomers as D-, L-, and DL-lactic acid (see POLYLACTIDE). The physiochemical properties of optically active homopolymers poly(D-lactic acid) (PDLA) or poly(L-lactic acid) (PLLA) are the same, whereas the racemic PLA has very different characteristics (25). Racemic PLA and PLLA have glass-transition temperatures (T_g's) of 57 and 56°C respectively, but PLLA is highly crystalline with a melting temperature (T_m) of 170°C; racemic PLA is purely amorphous. The polymer characteristics are affected by the comonomer composition, the polymer architecture, and molecular weight (26). The crystallinity of the polymer, an important factor in polymer biodegradation, varies with the stereoregularity of the polymer. Sterilization using γ-irradiation decreases the polymer molecular weight by 30–40% (26). The irradiated polymers continue to decrease in molecular weight during storage at room temperature. This decline in molecular weight affects the mechanical properties and the release rate from the polymers. PLA and its copolymers with less than 50% glycolic acid content soluble in common solvents such as chlorinated hydrocarbons, tetrahydrofuran, and ethyl acetate. Poly(glycolic acid) (PGA) is insoluble in common solvents but in hexafluoroisopropanol and hexafluoroacetone sesquihydrate (HFASH). In its highly crystalline form, PGA has a very high tensile strength of 69–138 MPa (10,000–20,000 psi) and modulus of elasticity of about 6900 MPa (~1,000,000 psi). The solubility parameters were in the range of 16.2 and 16.8, which are comparable to those of polystyrene and polyisoprene (27).

A comparison study on the physicomechanical properties of several biodegradable polyesters was reported (28). The thermal properties, tensile properties, and the flexural storage modulus as a function of temperature were determined. The following polymers were compared: poly(L-lactic acid), poly(DL-lactic acid), poly(glycolic acid), poly(ε-caprolactone), poly(hydroxybutyrate) and copolymers with hydroxyvaleric acid, and poly(trimethylene carbonate). The thermal and mechanical properties of several of the polymers tested are summarized in Table 2 (28). A comprehensive review on the mechanical properties of several biodegradable materials used in orthopedic devices has been published (29). The tensile and flexural strength and modulus, as well as the biodegradation of various lactide/glycolide polymers, poly(orthoester), and polycaprolactone have been summarized in a tabular or diagram format.

Polycaprolactone. Poly(ε-caprolactones) (PCL) are synthesized by ring-opening polymerization of ε-caprolactones and are soluble in chlorinated and

Table 1. Examples of Synthetic Biodegradable Polymers[a]

Structure	Name
Polyesters	
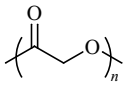	Poly(glycolic acid) (PGA)
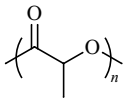	Poly(lactic acid) (PLA)
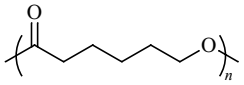	Poly(ε-caprolactone) (PCL)
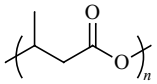	Poly(β-hydroxybutyrate)
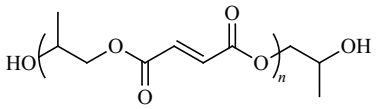	Poly(propylene-fumarate)
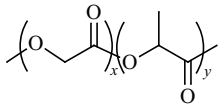	Poly(lactide-glycolide)
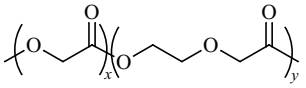	Poly(*p*-dioxane-*co*-glycolide)
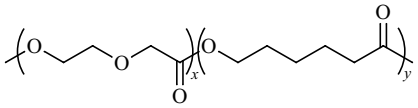	Poly(*p*-dioxane-*co*-caprolactone)
Poly(orthoesters)	
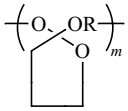	Poly(orthoester) I
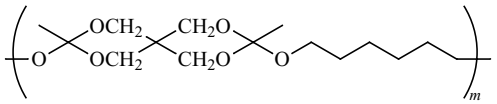	Poly(orthoester) II
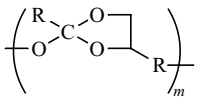	Poly(orthoester) III

Table 1. (continued)

Structure	Name
Other polyesters	
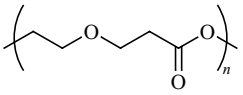	Poly(1,5-dioxipan-2-one)
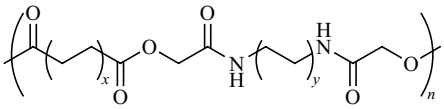	Poly(ester amide)
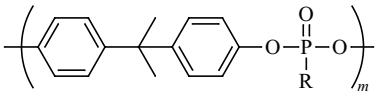	Polyphosphate ester
Polyphosphazenes	
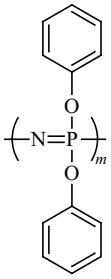	Poly(aryloxyphosphazene)
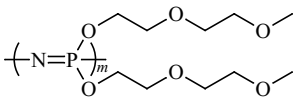	Poly(PEG-phosphazene)
Amino acid derived polymers	
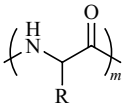	Poly(amino acid)
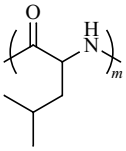	Polyleucine
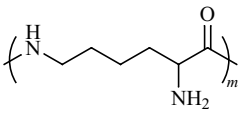	Polylysine

Table 1. (continued)

Structure	Name
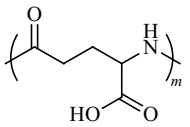	Poly(glutamic acid)
Polyanhydrides	
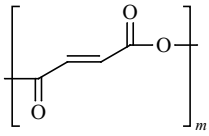	Poly(fumaric acid)
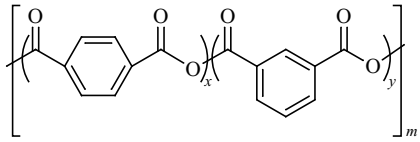	Poly(terephthalic-*co*-isophthalic acid)
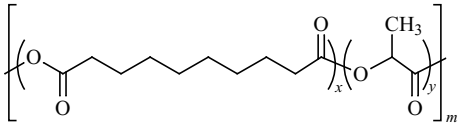	Block-poly(sebacic anhydride)-*co*-poly(lactic acid)
Polysaccharides	
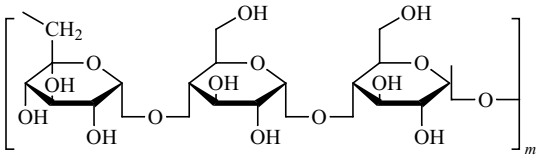	Pullulan
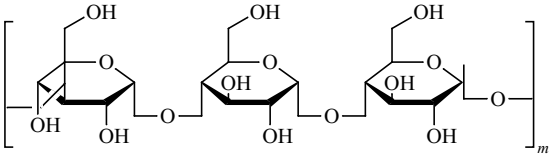	Elsinan
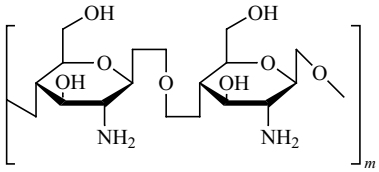	Chitosan
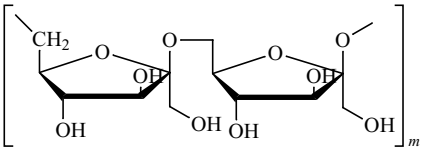	Levan

Table 1. (continued)

Structure	Name
Polyurethanes 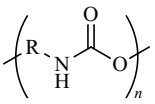	Poly(urethanes)
Poly(amide-amines) 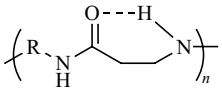	Poly(amide-enamines)
Natural polypeptides 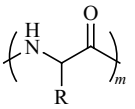	
A plasma glycoprotein belonging structurally to the keratin–myosin group. Synthesized and secreted by hepatic parenchymal cells. Essential to the clotting of blood. The molecular weight is 340,000. Soluble, but forms an insoluble gel on conversion to fibrin. Fibrin monomer is fibrinogen from which one or two peptides have been removed by means of thrombin.	Fibrinogen
Polypeptide substance comprising one third of the total protein in mammalian organisms; main constituent of skin, connective tissue, and the organic substance of bones and teeth. Different types of collagens exist.	Collagen (qv)
A heterogeneous mixture of water-soluble proteins of high average molecular weight. Derived from collagen. Swells up in water to form a gel/insoluble in organic solvents.	Gelatin (qv)

[a] The structures of polymers and description of their properties and applications can be found in either Ref. 23 or Ref. 24.

aromatic hydrocarbons, cyclohexanone, and 2-nitropropane but insoluble in aliphatic hydrocarbons, diethyl ether, and alcohols (30). The homopolymer of PCL melts at 59–64°C with a T_g of −60°C. Copolymerization with lactide increases the T_g with the increase in the lactide content in the polymer (31). The crystallinity of the polymer decreases with the increase in polymer molecular weight; polymer of weight 5000 is 80% crystalline whereas the polymer of weight 60,000 is 45% crystalline (32).

Tokiwa and Suzuki (33) have discussed the hydrolysis and biodegradation of PCL by fungi, and have shown that PCL can be degraded enzymatically. Blends of PCL and polyesters prepared from alkanediols and alkane dicarboxylic acids with natural substances such as tree bark have been molded into shaped containers for horticultural seeding plantouts (34). After 3 months of soil burial, the PCL

Table 2. Thermal and Mechanical Properties of Biodegradable Polyesters[a]

Polymer	M_w	T_g, °C	T_m, °C	Tensile strength, MPa[b]	Tensile modulus, MPa[b]	Elongation Yield, %	Elongation Break, %
Poly(lactic acid)							
L-PLA	50,000	54	170	28	1200	3.7	6.0
L-PLA	100,000	58	159	50	2700	2.6	3.3
L-PLA	300,000	59	178	48	3000	1.8	2.0
DL-PLA	107,000	51	—	29	1900	4.0	5.0
Poly(glycolic acid) (PGA)	50,000	35	210	NA	NA	NA	NA
Poly(β-hydroxybutyrate)							
PHB	370,000	1	171	36	2500	2.2	2.5
P(HB-11%HV)	529,000	2	145	20	1100	5.5	17
Poly(ε-caprolactone) (PCL)	44,000	−62	57	16	400	7.0	80
Poly(trimethylene carbonate) PTC	48,000	−15	—	0.5	3	20	160
Poly(orthoesters)							
t-CDM:1,6-HD[c] (35:65)	99,000	55	—	20	820	4.1	220
t-CDM:1,6-HD[c] (70:30)	101,000	84	—	19	800	4.1	180

[a]Taken from Ref. 28.
[b]To convert MPa to psi, multiply by 145.
[c]*t*-CDM: 1,6-HD=*trans*-cyclohexane dimethanol: 1,6-hexanediol.

containers were found to be embrittled, disintegrated, and biodegraded, which suggests that the extracellular enzymes in the soil may cleave the polymer chain prior to the assimilation of the polymer by microorganisms.

Poly(β-hydroxybutyrate). Poly(β-hydroxybutyrate) (PHB) is made by a controlled bacterial fermentation (see POLY(3-HYDROXYALKANOATES). The producing organism occurs naturally. An optically active copolymer of 3-hydroxybutyrate (3HB) and 3-hydroxyvalerate (3HV) has been produced from propionic acid or pentanoic acid by *Alcaligenes eutrophus*. PHB is characterized as having a high molecular weight (>100,000, $[\eta] > 3$ dL/g) with a narrow polydispersity and a crystallinity of around 50%. The melting point depends on the polymer composition; P(3HB) homopolymer melts at 177°C with a T_g at 9°C, the 91:9 copolymer with 4HB melts at 159°C, and the 1:1 copolymer with 3HV melts at 91°C. The PHB properties in the living cells of *A. eutrophus* were determined using X-ray and variable-temperature ^{13}C NMR relaxation studies (35). PHB is an amorphous elastomer with a T_g around −40°C in its "native" state within the granules. The biodegradation of these polymers in soil and activated sludge show the rate of degradation to be in the following order (36):

$$\text{P(3HB}-co-9\%\text{4HB)} > \text{P(3HB)} = \text{P(3HB}-co-50\%\text{3HV)}$$

Microspheres degraded slowly in phosphate buffer at 85°C and after 5 months, 20–40% of the polymer eroded under these conditions. Copolymers having a higher fraction of 3HV and low molecular weight polymers were more susceptible to hydrolysis (36).

Poly(phosphoesters). Poly(phosphoesters) are synthesized from the reaction of ethyl or phenyl phosphorodichloridates and various dialcohols including bisphenol A and poly(ethylene glycol) of various molecular weights (37). Leong and co-workers (38) have incorporated phosphoester groups into poly(urethanes). Poly(urethanes) have been used as blood-contacting biomaterials because of their having a broad range of physical properties: from hard and brittle to soft and tacky (38). Leong and co-workers has designed inert biomaterial for controlled release application by introducing phosphoester linkage in poly(urethane) (38). Introduction of phosphoester linkage does not change the mechanical properties inherent in the poly(urethanes) and provides excellent biodegradable materials.

Polycarbonates. Polycarbonates are synthesized from the reaction of dihydroxy compounds with phosgene or with bischloroformates of aliphatic dihydroxy compounds by transesterification, and by polymerization of cyclic carbonates (39). These polymers have been synthesized from carbon dioxide and the corresponding epoxides in the presence of organometallic compounds as initiators. Poly(ethylene carbonate) and poly(propylene carbonate) are linear thermoplastic polyesters of carbonic acid with aliphatic dihydroxy compounds (39). Poly(dihydropyrans) were developed for contraceptive delivery. The *in vivo* and *in vitro* release of contraceptive steroids and antimalarial agents from polymer matrices has been studied. Poly(*p*-dioxanone) is clinically used as an alternative to poly(lactide) in absorbable sutures with similar properties to poly(lactide) with the advantage of better irradiation stability during sterilization (40). This polymer has not yet been developed as a carrier for controlled drug delivery. Biodegradable polymers derived from naturally occurring, multifunctional hydroxy acids and amino acid have been investigated by Lenz and Guerin (41).

Poly(amides). The utilization of amide-based polymers, especially natural proteins, in the preparation of biodegradable matrices have been extensively investigated in recent years (42). Microcapsules and microspheres of cross-linked collagen, gelatin, and albumin have been used for dug delivery (43). The synthetic ability to manipulate amino acid sequences has seen its maturity over the last two decades with new techniques and strategies continually being introduced.

Poly(amides) such as poly(glutamic acid) and poly(lysine) and their copolymers with various amino acids have also been studied as drug carriers (41,44,45). Pseudopoly(amino acids), prepared from N-protected trans-4-hydroxy-L-proline, and poly(iminocarbonate) from tyrosine dipeptide as monomeric starting material have been reported (46–48). The properties, biodegradability, drug release, and biocompatibility of this class of polymers have been reviewed (42,46).

Polyphosphazenes. The polymers are most commonly synthesized by a substitution reaction of the reactive poly(dichlorophosphazene) with a wide range of reactive nucleophiles such as amines, alkoxides, and organometallic molecules. The reaction is carried out in general at room temperature in tetrahydrofuran or aromatic hydrocarbon solutions (49). Two different types of polyphosphazenes are of interest as bioinert materials: those with strongly hydrophobic surface characteristics and those with hydrophilic surfaces. Polycarbonates (qv) bearing fluoroalkoxy side groups are some of the most hydrophobic synthetic polymers known (50,51). Such polymers are as hydrophobic as poly(tetrafluoroethylene) (Teflon), but unlike Teflon, polyphosphazenes of this type are flexible or elastomeric, easy to prepare, and they can be used as coatings for other materials.

The uniqueness of the polyphosphazenes stems from its inorganic backbone (N=P) which with certain organic side groups can be hydrolyzed to phosphate and ammonia. Several polymer structures have been used as matrix carriers for drugs (51) or as a hydrolyzable polymeric drug, where the drug is covalently bound to the polymer backbone and released from the polymer by hydrolysis (52). A comprehensive review on the synthesis, characterization, and medical applications of polyphosphazenes was published (53).

Poly(orthoesters). Poly(orthoesters) were first designated as Chronomer and later as Alzamer (54). They were prepared by a transesterification reaction. The molecular weight of poly(orthoesters) were significantly dependent on the type of diol and catalyst used for synthesis. A linear, flexible diol like 1,6-hexanediol gave molecular weights greater than 200 kDa, whereas bisphenol A in the presence of catalyst gave molecular weights around only 10,000 kDa (55). Mechanical properties of the linear poly(orthesters) can be varied over a large range by selecting various compositions of diols. It was shown that the T_g of the polymer prepared from 3,9-diethylidene-2,4,8,10-tetraoxaspiro[5,5]undecane can be varied from 25 to 110°C by simply changing the amount of 1,6-hexanediol in trans-1,4 cyclohexane dimethanol from 100% to 0% (29). A linearly decreasing relationship between the T_g and percentage of 1,6 hexanediol is observed. One could take advantage of the above relationship in selecting the polymer for *in vivo* applications because *in vivo* the T_g of the polymer would drop because of the inhibition of water, resulting in the loss of stiffness and rigidity of the polymer.

Polyanhydrides. The majority of the polyanhydrides (qv) are prepared by melt polycondensation. The sequence of reaction involves first the conversion of a dicarboxylic acid monomer into a prepolymer consisting of a mixed anhydride of the diacid with acetic anhydride. This is achieved by simply refluxing the diacid monomer with acetic anhydride for a specified length of time. The polymer is obtained subsequently by heating the prepolymer in vacuo to eliminate the acetic anhydride (56). Almost all polyanhydrides show some degree of crystallinity as manifested by their crystalline melting points. An in-depth X-ray diffraction analysis was conducted with the homopolymers of sebacic acid (SA), bis(carboxyphenoxy)propane (CPP), bis(carboxyphenoxy)hexane (CPH), and fumaric acid, and the copolymers of SA with CPP, CPH, and fumaric acid (57). The results indicated that the homopolymers were highly crystalline and the crystallinity of the copolymers was determined, in most cases, by the monomer of highest concentration. Copolymers with a composition close to 1:1 were essentially amorphous (57). The melting point of the aliphatic–aromatic copolyanhydrides is proportional to the aromatic content. For this type of copolymers there is characteristically a minimum T_m between 5 and 20 mol% of the lower melting component (57).

The majority of polyanhydrides dissolve in solvents such as dichloromethane and chloroform. However, the aromatic polyanhydrides display much lower solubility than the aliphatic polyanhydrides. In an attempt to improve the solubility and decrease the T_m, copolymers of two different aromatic monomers were prepared. These copolymers displayed a substantial decrease in T_m and an increase in solubility than did the corresponding homopolymers of aromatic diacids (57).

Natural Biodegradable Polymers. Biopolymers formed in nature during the growth cycles of all organisms are referred to as natural polymers. Their

synthesis generally involves enzyme-catalyzed, chain-growth polymerization reactions of activated monomers, which are typically formed within cells by complex metabolic processes.

Polysaccharides. For materials applications, the principal polysaccharides of interest are cellulose and starch because of their easy and cheap resources, but increasing attention is being given to the more complex carbohydrate polymers produced by bacteria and fungi, especially to polysaccharides such as xanthan, curdlan, pullulan, and hyaluronic acid (see CARBOHYDRATE POLYMERS).

Starch. Starch thermoplastic (qv) is a polymer that occurs widely in plants. The principal crops used for its production include potatoes, corn, and rice. In all of these plants, starch is produced in the form of granules, which vary in size and somewhat in composition from plant to plant. In general, the linear polymer, amylose, makes up about 20 wt% of the granule, and the branched polymer, amylopectin, the remainder. Research on starch includes investigation of its water-adsorptive capacity, the chemical modification of the molecule, its behavior under agitation and high temperature, and its resistance to thermomechanical shear. The starch molecule has two important functional groups, the —OH group that is susceptible to substitution reactions and the C—O—C bond that is susceptible to chain breakage. By reaction of its —OH group, modification of various properties can be obtained. One example is the reaction with silane to improve its dispersion in polyethylene (58). Cross-linking or bridging of the —OH groups changes the structure into a network while increasing the viscosity, reducing water retention and increasing its resistance to thermomechanical shear. Acetylated starch does have several advantages as a structural fiber or film-forming polymer as compared to native starch. Starch acetate has an improved solubility compared to starch and is easily cast into films from simple solvents. The degree of acetylation is easily controlled by transesterification, allowing polymers to be produced with a range of hydrophobicities.

Since isocyanates are highly reactive with hydroxyl groups, they can be used to prepare a number of reactive resins that cross-link with starch. The addition of starch to isocyanate resins considerably reduced costs and improved solvent resistance and strength properties (59). Starch can be modified with nonpolar groups, such as fatty esters, before the isocyanate reaction to improve the degree of reactivity (60).

Cellulose. Cellulose (qv) is a very highly crystalline, high molecular weight polymer, which is insoluble in water and organic solvents. It is soluble in aggressive, hydrogen bond-breaking solvents such as *N*-methylmorpholine-*N*-oxide. Because of its insolubility, cellulose is usually converted into derivatives to make it more processable. The important derivatives of cellulose are reaction products of one or more of the three hydroxyl groups, which are present in each glucopyranoside repeating unit, including (*1*) ethers (61,62), eg, methyl cellulose and hydroxylethyl cellulose; (*2*) esters (63), eg, cellulose acetate and cellulose xanthate, which are used as soluble intermediates for processing cellulose into either fibre or film forms, during which the cellulose is regenerated by controlled hydrolysis; and (*3*) acetals (64), especially the cyclic acetal formed between the C2 and C3 hydroxyl groups and butyraldehyde.

Chitin and Chitosan. Chitin is a macromolecule found in the shells of crabs, lobsters, shrimps, and insects (see CHITIN AND CHITOSAN). It consists of

2-acetamide-2-deoxy-*b*-*d*-glucose through the *b*-(1-4)-glycoside linkage. Chitin can be degraded by chitinase. Chitin fibers have been utilized for making artificial skin and absorbable sutures (65). Chitin is insoluble in its native form but chitosan, the partly deacetylated form, is water-soluble. The materials are biocompatible and have antimicrobial activities as well as the ability to chelate heavy metal ions. They also find applications in the cosmetic industry because of their water-retaining and moisturizing properties. Using chitin and chitosan as carriers, a water-soluble prodrug has been synthesized (66). Modified chitosans have been prepared with various chemical and biological properties (67). *N*-Carboxymethylchitosan and *N*-carboxybutylchitosan have been prepared for use in cosmetics and in wound treatment (68). Chitin derivatives can also be used as drug carriers (69), and a report of the use of chitin in absorbable sutures shows that chitins have the lowest elongation among suture materials including chitin (70), PGA, plain catgut, and chromic catgut. The tissue reaction of chitin is similar to that of PGA (71).

Alginic Acid. Alginate is a binary linear heteropolymer containing 1,4-linked α-l-guluronic acid and β-*d*-mannuronic acid. Alginates have been studied extensively for their ability to form gels in the presence of divalent cations (72,73). Alginic acid forms water-soluble salts with monovalent cations, low molecular weight amines, and quaternary ammonium compounds. It becomes water-insoluble in the presence of polyvalent cations such as $Ca^{2+}\cdot$, $Be^{2+}\cdot$, $Cu^{2+}\cdot$, $Al^{3+}\cdot$, and $Fe^{3+}\cdot$. Alginate gels have been used widely in controlled release drug delivery systems (73). Alginates have also been used to encapsulate various herbicides, microorganisms, and cells.

Naturally Occurring Polypeptides. The proteins that have found applications as materials are, for the most part, neither soluble nor fusible without degradation and so they are used in the form in which they are found in nature. This description is especially true for the fibrous proteins wool (qv), silk (qv), and collagen (qv). All proteins are specific polymers with regular arrangements of different types of a-amino acids; so the biosynthesis of proteins is an extremely complex process involving many different types of enzymes. In contrast, the enzymatic degradation of proteins, with general-purpose proteases, is a relatively straightforward, amide hydrolysis reaction.

Gelatin. Gelatin (qv), an animal protein, consists of 19 amino acids joined by peptide linkages and can be hydrolyzed by a variety of proteolytic enzymes to yield its constituent amino acids or peptide components (74). This nonspecificity is a desirable factor in intentional biodegradation. Gelatin is a water-soluble, biodegradable polymer with extensive industrial, pharmaceutical, and biomedical uses, which has been employed for coatings and microencapsulating various drugs (75,76) and for preparing biodegradable hydrogels (77).

A method was developed to prepare a simple, flexible gelatin film-based artificial skin that could adhere to an open wound and protect it against fluid loss and infection. The approach was to mix polyglycerols, either as is or after reaction with epichlorohydrin, with commercially available gelatin and then cast films on Teflon-covered trays (78). The films were tough and adhered to open wounds spontaneously. They could be loaded with bioactive molecules, such as growth factors and antibiotics that would be released over several days. The films could be sterilized with γ-rays or prepared under sterile conditions.

Toxicity and Biocompatibility

In all the potential uses of polymeric materials, a direct contact between the polymer and biological tissues is evident; therefore, for the eventual human application of these biomedical implants and devices, an adequate testing for safety and biocompatibility of the specific polymer matrix is essential. Biocompatibility deals with how the tissue reacts to foreign materials and the ability of a material to perform with an appropriate host response in a specific application.

Poly(lactic-*co*-glycolide). Whenever a synthetic polymer material is to be utilized *in vivo*, the possible tissue–implant interactions must be taken into consideration. In the case of biodegradable matrices, not only the possible toxicity of the polymer has to be evaluated, but also the potential toxicity of its degradation products. Moreover, biocompatibility is considered as the foundation for biocompatibility of degradable polymer systems. Thus, PLLA is defined as a safe biomaterial for *in vivo* use because its degradation product L-lactic acid is a natural metabolite of the body. Even though PLGA is extensively used and represents the gold standard of degradable polymers, increased local acidity due to its degradation can lead to irritation at the site of polymer implant. Agrawal and Athanasiou (79) have introduced a technique in which basic salts are used to control the pH in local environment of PLGA implant. The feasibility of lactide/glycolide polymers for the controlled release of bioactive agents is well proven, and they are the most widely investigated biodegradable polymers for drug delivery. The lactide/glycolide copolymers have been subjected to extensive animal and human trials without any significant harmful side effects (80). However, some limited incompatibility of certain macromolecules with lactide/glycolide polymers was observed. Bezwada and co-workers (81) studied *in vitro* and *in vivo* biocompatibility and efficacy of block copolymer of poly(glycolide) and PCL in the form of Monocryl (Ethicon) sutures.

Poly(caprolactone). The biocompatibility and toxicity of poly(caprolactone) have mostly been tested in conjuction with evaluations of Capronor (Schering), which is an implantable 1-year contraceptive delivery system composed of a levonorgestrel-ethyl oleate slurry within a poly(caprolactone) capsule. In a preliminary 90-day toxicology study of Capronor in female rats and guinea pigs, except a bland response at the implant site and a minimal tissue encapsulating reaction, no toxic effects were observed (82). The Capronor-polycaprolactone contraceptive delivery system was also tested implanted in rats and monkeys (83). Based on animal clinical and physical data such as blood and urine analysis, ophthalmoscopic tests, and histopathology after necropsy, no significant differences between the test and control groups was observed. Phase I and II clinical trials with Capronor were recently carried out in different medical centers (83).

Polyphosphazenes. Biocompatibility and safety testing of polyphosphazenes by subcutaneous implantation in animals have shown minimal tissue response (84). The connection between hydrophobicity and tissue compatibility has been noted for classical organic polymers (85). Thus, these hydrophobic polyphosphazenes have been mentioned as good candidates for use in heart valves, heart pumps, blood vessel prostheses, or as coating materials for

pacemakers or other implantable devices; however, more *in vivo* testing and clinical trials are needed (53).

In their bioerosion reactions polyphosphazenes display a uniqueness that stems from the inorganic backbone, and the appropriate side groups can undergo facile hydrolysis to phosphate and ammonia. The phosphate can be metabolized and the ammonia excreted. Theoretically, if side groups attached to the polymer are released by the same process being excretable or metabolizable, then the polymer can be eroded under hydrolytic conditions without the danger of a toxic response. Polyphosphazenes of this type are potential candidates as erodible biostructural materials for sutures, or as matrices for controlled delivery of drugs (53).

Poly(orthoesters). As mentioned previously, the Chronomer poly(orthoester) material from Alza Corp. or Alzamer has been investigated as bioerodible inserts for the delivery of the narcotic antagonist naltrexone, and for the delivery of the contraceptive steroid norethisterone (86,87). *In vitro* studies have shown that good control over release of tetracycline could be achieved, and very good *in vitro* adhesion to bovine teeth demonstrated (88). However, studies in beagle dogs with naturally occurring periodontitis were not successful because ointment-like polymers with a relatively low viscosity are squeezed out of the pocket within about 1 day, despite good adhesiveness (54).

Naturally Occurring Polymers. The use of natural biodegradable polymers to deliver drugs continues to be an area of active research despite the advent of synthetic biodegradable polymers (43). Natural polymers remain attractive primarily because they are natural products of living organisms, readily available, relatively inexpensive, and capable of a multitude of chemical modifications (89). Most investigations of natural polymers as matrices in drug delivery systems have focused on the use of proteins (polypeptides or polyamides) such as gelatin, collagen, and albumin. Collagen is a major structural protein found in animal tissues where it is normally present in the form of aligned fibers. Because of its unique structural properties, collagen has been used in many biomedical applications as absorbable sutures, sponge wound dressings, composite tissue tendon allografts, injectables for facial reconstructive surgery, and as drug delivery systems especially in the form of microspheres (90).

Besides the collagen biocompatibility and nontoxicity for most tissues (91), several factors including the possible occurrence of antigenic responses, tissue irritation due to residual aldehyde cross-linking agents, and poor patient tolerance of ocular inserts have adversely influenced its use as a drug delivery vehicle (90). For example, 5-fluorouracil and bleomycin cross-linked sponges made from purified bovine skin collagen were implanted in rabbit eyes to test their posssible use in preventing fibroblast proliferation following ophthalmic surgery, resulting in a chronic inflammatory reaction elicited by the sponges even in the absence of drug (92).

Noncollagenous proteins, particularly albumin and to a lesser extent gelatin, continue to be developed as drug delivery vehicles. The exploitable features of albumin include its reported biodegradation into natural products, its lack of toxicity, and noninmunogenicity (93).

Medical Applications

Over the past decade the use of polymeric materials for the administration of pharmaceuticals and as biomedical devices has increased dramatically. Important biomedical application of biodegradable polymers is in the areas of controlled drug delivery systems (92–96) and in the form of implants and devices for fracture repairs (97–100), ligament reconstruction (101), surgical dressings (102), dental repairs, artificial heart valves, contact lenses, cardiac pacemakers, vascular grafts (103), tracheal replacements (104), and organ regeneration (105).

Biomaterials in general are used for the following purposes:

(1) to replace tissues that are diseased or otherwise nonfunctional, as in-joint replacements, artificial heart valves and arteries, tooth reconstruction, and intraocular lenses;
(2) to assist in the repair of tissue, including the obvious sutures, but also bone fracture plates and ligament and tendon repair devices;
(3) to replace all or part of the functions of the major organs, such as in haemodialysis, oxygenation (lungs), left ventricular or whole heart assistance (heart), perfusion (liver), and insulin delivery (pancreas);
(4) to deliver drugs to the body, either to targeted sites (eg, directly to a tumor) or sustained delivery (insulin, pilocarpine, contraceptives).

Biodegradable plastics have been developed as surgical implants in vascular and orthopedic surgery, as implantable matrices for the controlled long-term release of drugs inside the body, as absorbable surgical sutures, and for use in the eye (106,107).

Surgical Sutures. Tissue damage that results in a loss of structural integrity, for example, a deep cut in soft tissue or a fracture of a bone, may not be capable of unassisted self-healing. The insertion of a device to hold the tissue together may facilitate the healing process. The classic examples are the use of sutures to hold both deep and superficial wounds together. Once the healing is complete, the suture becomes redundant and can impose undesirable constraints on the healing tissues. It is preferable to remove the material from the site, either physically or by self-elimination.

Synthetic absorbable sutures were developed in the 1960s, and because of their good biocompatibility in tissues they are now widely used in tracheobronchial surgery, as well as general surgery. They are multifilament-type sutures, which have good handle ability (106). However, for continuous suturing, braided sutures with nonsmooth surfaces are not useful. Monofilament sutures have smooth surfaces and are adequate for continuous suturing. For a monofilament suture, PGA or PLA are too stiff and inflexible. The more flexible polydioxanones and polyglyconates can be used as sutures because of their lower bending moduli (108). Furthermore, copolymers of l-lactide and ε-caprolactone-poly(caprolactone-lactic acid) are bioabsorbable elastic materials and their clinical applications have been studied (109).

Bone Fixation Devices. Although metal fixation in fracture treatment for undisturbed bone healing is a successful procedure, cortical bone and steel have

very different mechanical properties. The elasticity constant of bone is only 1/10 of implanted steel while tensile strength is 10 times lower (110). Thus, the removal of metal implants can result in weakened bone with a danger of refracture. Biodegradable implants can meet the dynamic processes of bone healing, decreasing the mechanical strength of the material. After months, the entire material will disappear and no secondary surgery will be required. PGA, PLA, polydioxanone, and PHB have potential roles in this area. For clinical applications, polydioxanone was recommended for ligament augmentation, for securing a ligament suture, as a kind of internal splinting suture, and as a kind of internal splinting to allow for early motion of the extremities after an operation (108,109).

Biodegradable polymers are useful for many other applications. A marrow spacer can help to save autologous bone material. A plug for closing the bone marrow is employed for endoprosthetic joint replacement. Fibers are used for filling large bone defects without mechanical loads (110).

Vascular Grafts. Many studies have been undertaken to develop acceptable small diameter vascular prostheses. Niu and co-workers (111) designed small diameter vascular prostheses with incorporated matrices that can be absorbed into a growing anastomotic neointima. It was pointed out that a gelatin–heparin complex when adequately cross-linked, could simultaneously function as a temporary antithrombogenic surface and as an excellent substructure for an anastomotic neointima.

Adhesion Prevention. Tissue adhesion after surgery occasionally causes serious complications. Materials that prevent tissue adhesion should be flexible and tough enough to provide a tight cover over the traumatized soft tissues, and should be biodegradable and reabsorbable after the injured tissue is completely regenerated. Matsuda and co-workers (112,113) developed photocurable mucopolysaccharides for a newly designed tissue adhesion prevention material that meets numerous requirements such as nonadherent surface characteristics, biocompatibility, biodegradability in accordance with the wound healing rate, and nontoxicity. Mucopolysaccharides (hyaluronic acid and chondroitin sulphate) partially functionalized with photoreactive groups, such as cinnamate or thyamine, were subjected to UV irradiation to produce water-insoluble gels via intermolecular photodimerization of the photoreactive groups (113). Photocured films with lower degrees of substitution, which had high water swellability and flexibility, prevented tissue adhesion and exhibited enhanced biodegradability. It was suggested that these newly designed mucopolysaccharide gels may aid injured tissue repair in a bioactive manner.

Artificial Skin. For healing burns, skin substitutes or wound dressings made of biodegradable polymeric materials have recently been developed. Until now, most of the commercially developed artificial skins have utilized biodegradable polymers such as collagen (114), chitin, and poly-l-leucine (115,116) which are enzymatically degradable polymers. Recently, Koide and co-workers (117) developed a new type of biomaterial for artificial skin, in the form of a sponge, by combining fibrillar collagen (F-collagen) with gelatin. The sponge was physically and metabolically stabilized by introducing cross-links. Although several types of collagen-based artificial skins have been developed (118–120), some undesirable characteristics of native collagen were noticed (121), such as inducing rod-like shapes in fibroblasts and enhancing the expression of collagenase genes

in fibroblasts. F-collagen with gelatin was found to overcome the above problems. Yasutomi and co-workers (122) developed a biosynthetic wound dressing with a drug delivery capability. This medicated wound dressing is composed of a spongy mixture sheet of chitosan-derivatized collagen, which is laminated with a gentamycin sulphate impregnated polyurethane membrane. From *In vitro* evaluation, it was shown that this wound dressing is capable of suppressing bacterial growth and minimizing cellular damage. Evaluation of this wound dressing was conducted in 80 clinical cases including superficial second-degree burns, deep second-degree burns, donor sites, and pressure sores, and achieved excellent results. The development of hybrid artificial skins is also another important target in biomedical engineering. Here, synthetic polymers and cell cultures are combined to form a synthetic–biological composite. In this case, a biodegradable polymer may be required as the template for growing cells and tissue cultures *in vivo*.

Drug Delivery Systems. Biodegradable and non-degradable polymers have been used for controlled delivery of drugs (see CONTROLLED RELEASE TECHNOLOGY). The limitations of conventional methods of drug delivery, by tablet or injection for example, are well known. As a dose is applied, the plasma levels will be raised, but these will be rapidly decreased as the drug is metabolized and will soon be below therapeutic levels. The next dose takes the plasma level high again and a cyclic pattern may be established, with most of the drug plasma levels possibly being outside the optimal range. In addition, the drug usually permeates throughout the body and it is not targeted to the location where it is specifically required. Among the many possible solutions to these problems is the use of controlled drug delivery systems (123,124), from which the drug is released at a constant, predetermined rate, and possibly targeted to a particular site. One of the most prominent approaches is that in which the drug is contained within a polymer membrane or is otherwise encapsulated in a polymer matrix, and where the drug diffuses out into the tissues following implantation, and erosion or dissolution of the polymer contributes to the release mechanism. It sounds, therefore, feasible to produce systems that allow easy and safe processing and can be injected into a body cavity without the need for surgical retrieval after completion of the release. Furthermore, the differential rates of drug delivery might be of profound interest for cases where elevated drug doses are necessary in the beginning of treatment.

BIBLIOGRAPHY

"Microbiological Degradation" in *EPST* 1st ed., Vol. 4, pp. 716–725, by W. M. Bejuki, BioSciences Information Service of Biological Abstracts; "Biodegradable Polymers" in *EPSE* 2nd ed., Vol. 2, pp. 220–243, by S. J. Huang, The University of Connecticut.

1. J. H. Han, *Food Technol.* **54**, 56 (2000).
2. I. S. Arvanitoyannis, *J. Macromol. Sci., Rev. Macromol. Chem. Phys. C* **39**, 205 (1999).
3. C. L. McCormick, *Encycl. Polym. Sci. Eng.* **1**, 611 (1985).
4. K. J. Sugimoto, *Ferment. Assoc. Jpn.* **36**, 98 (1990).

5. C. G. Pitt and A. Schindler, *Prog. Contracept. Delivery Syst.* **1**, 17 (1980).
6. T. Hayashi, *Prog. Polym. Sci.* **19**, 663 (1994).
7. R. J. Mumper and S. L. Klakamp, *Drug Targeting Delivery* **10**, 143 (1999).
8. A. Nagarsekar and H. Ghandehari, *J. Drug Targeting* **7**, 11 (1999).
9. H. W. T. Matthew, *Polymeric Biomaterials*, 2nd ed., Marcel Dekker, Inc., New York, 2002, p. 167.
10. B.-S. Kim and D. J. Mooney, *Trends Biotechnol.* **16**, 224 (1998).
11. S. J. Huang, M. Bitritto, K. W. Leong, J. Pavlisko, M. Roby, and J. R. Knox, *Adv. Chem. Ser.* **169**, 205 (1978).
12. J. E. Potts, in M. Grayson, ed., *Kirk-Othmer Encyclopeida of Chemical Technology*, (Suppl. Vol.), Wiley-Interscience, New York, 1984, p. 626.
13. Y. Udagawa, *J. Polym. Sci., Part A2* **9**, 1807 (1971).
14. G. N. Patel and A. Keller, *J. Polym Sci., Polym. Phys. Ed.* **13**, 323 (1975).
15. F. B. Khambatta, F. Warner, T. Russell, and R. S. Stein, *J. Polym. Sci., Polym. Phys. Ed.* **14**, 1391 (1976).
16. W. D. Varnell, I. R. Harnson, and S. J. J. Kosnioski, *J. Polym. Sci., Polym. Phys. Ed.* **10**, 1237 (1981).
17. C. V. Benedict, C. V. Cook, P. Jarrett, J. A. Cameron, S. J. Huang, and P. Bell, *J. Appl. Polym. Sci.* **28**, 327 (1983).
18. C. V. Benedict, J. A. Cameron, and S. J. Huang, *J. Appl. Polym. Sci.* **28**, 335 (1983).
19. G. E. Zeikov and U. S. Livshitz, *Polym. Degrad. Stab.* **17**, 65 (1987).
20. A. C. Albertsson, S. O. Anderson, and S. Karlsson, *Polym. Degrad. Stab.* **18**, 73 (1987).
21. C. C. Chu, *Polymer* **26**, 591 (1985).
22. D. F. Williams, C. C. Chu, and J. Dwyer, *J. Appl. Polym. Sci.* **29**, 1865 (1984).
23. S. W. Shalaby, ed., *Biomedical Polymers, Designed to Degrade Systems*, Hanser Publishers, New York, 1994.
24. A. J. Domb, J. Kost, and D. M. Wiseman, *Handbook of Biodegradable Polymers*, Harwood Academic Publishers, London, 1997.
25. K. A. Walter, R. Tamargo, A. Olivi, P. C. Burger, and H. Brem, *Neurosurgery* **37**, 1129 (1995).
26. L. Montanari, M. Costantini, E. C. Sigoretti, L. Valvo, M. Santucci, M. Bartolomei, P. Fattibene, S. Onori, A. Faucitano, B. Conti, and I. Genta, *J. Controlled Release* **56**, 219 (1998).
27. U. Siemann, in Proc. Int. Symp. Control. Rel. Bioact. Mater., Vol. 12, 1985, p. 53.
28. I. Engelberg and J. Kohn, *Biomaterials* **12**, 292 (1991).
29. U. Daniels, M. K. O. Chang, K. P. Andriano, and J. Heller, *J. Appl. Biomater.* **1**, 57 (1990).
30. D. E. Perrin and J. P. English, in A. J. Domb, J. Kost, and D. M. Weiseman, eds., *Handbook of Biodegradable Polymers*, Vol. **7**, Hardwood Academic Publishers, Amsterdam, the Netherland, 1997, p. 63.
31. A. Schindler, R. Jeffcoat, G. L. Kimmel, C. G. Pitt, M. E. Wall, and R. Zweidinger, *Contemp. Top. Polym. Sci.* **2**, 251 (1977).
32. C. G. Pitt, F. I. Chasalow, Y. M. Hibionada, D. M. Klimas, and A. Schindler, *J. Appl. Polym. Sci.* **26**, 3779 (1981).
33. Y. Tokiwa and T. Suzuki, *Nature* **270**, 76 (1977).
34. X. D. Feng, C. X. Song, and W. Y. Chen, *J. Polym. Sci., Polym. Lett. Ed.* **21**, 593 (1983).
35. S. R. Amor, T. Rayment, and J. K. M. Sanders, *Macromolecules* **24**, 4583 (1991).

36. H. Brandl, R. A. Gross, R. W. Lenz, and R. C. Fuller, *Appl. Environ. Microbiol.* **54**, 1977 (1988).
37. K. W. Leong, *Connect. Tissue Res.* **31**, S69 (1995).
38. K. W. Leong, Z. Zhao, and B. I. Dahiyat, *Controlled Drug Delivery* 469 (1997) (CA 127: 23619).
39. T. Kawaguchi, M. Nakano, K. Juni, S. Inoue, and Y. Yoshida, *Chem. Pharm. Bull.* **30**, 1517 (1982).
40. R. S. Bezwada, S. W. Shalaby, H. D. Newman, and A. Kafrauy, *Trans. Soc. Biomater.* **13**, 194 (1990).
41. R. W. Lenz and P. Guerin, in E. Chiellini and P. Giusti, eds., *Polymers in Medicine: Functional Polymers and Polyamides for Medical Applications of Biodegradable Polymers*, Plenum Press, New York, 1993.
42. J. Kemnitzer and J. Kohn, in A. J. Domb, J. Kost, and D. M. Weiseman, eds., *Handbook of Biodegradable Polymers*, Vol. **7**, Hardwood Academic Publishers, Amsterdam, the Netherlands, 1997, p. 251.
43. S. Bogdansky, *Drugs Pharm. Sci.* **45**, 231 (1990).
44. S. J. Huang and L.-H. Ho, *Macromol. Symp.* **144**, 7 (1999).
45. K. W. Leong, *Polym. Controlled Drug Delivery* 127 (1991) (CA 114: 192314).
46. A. Nathan and J. Kohn, in S. W. Salaby, ed., *Biomedical Polymers: Designed to Degrade Systems*, Hanser/Gardner, Cincinnati, Ohio., 1994, p. 117.
47. J. Kohn, *Trends Polym. Sci.* **1**, 206 (1993).
48. J. Kohn and R. Langer, *J. Am. Chem. Soc.* **109**, 817 (1987).
49. J. Vandorpe, E. Schacht, S. Dejardin, and Y. Lemmouchi, in A. J. Domb, J. Kost, and D. M. Weiseman, eds., *Handbook of Biodegradable Polymers*, Vol. **7**, Hardwood Academic Publishers, Amsterdam, the Netherlands, 1997, p. 161.
50. C. W. R. Wade, S. Gourlay, R. Rice, A. Hegyeli, R. Singler, and J. White, in C. E. Carraher, J. E. Sheats, and C. U. Pittman, eds., *Organometallic Polymers*, Academic Press, New York, 1978, p. 289.
51. S. Lora, G. Palma, M. Carenza, P. Caliceti, and G. Pezzin, *Biomaterials* **14**, 430 (1993).
52. H. R. Allcock and S. Kwon, *Macromolecules* **19**, 1502 (1986).
53. H. R. Allcock, in M. Chasin and R. Langer, eds., *Biodegradable Polymers as Drug Delivery Systems*, Marcel Dekker, New York, 1990, p. 163.
54. J. Heller, in A. J. Domb, J. Kost, and D. M. Weiseman, eds., *Handbook of Biodegradable Polymers*, Vol. **7**, Hardwood Academic Publishers, Amsterdam, the Netherlands, 1997, p. 99.
55. J. Heller, D. W. H. Penhale, B. K. Fritzinger, J. E. Rose, and R. F. Helwing, *Contracept. Delivery Syst.* **4**, 43 (1983).
56. A. J. Domb, S. Amselem, and M. Maniar, *Polym. Biomater.* 399 (1994).
57. A. J. Domb, O. Elmalak, V. R. Shastri, Z. Ta-Shma, D. M. Masters, I. Ringel, D. Teomim, and R. Langer, in A. J. Domb, J. Kost, and D. M. Weiseman, eds., *Handbook of Biodegradable Polymers*, Vol. **7**, Hardwood Academic Publishers, Amsterdam, the Netherlands, 1997, p. 135.
58. J. C. Huang, A. S. Shetty, and M. S. Wang, *Adv. Polym. Technol.* **10**, 23 (1990).
59. F. H. Otey, R. P. Westhoff, W. F. Kwolek, and C. L. Mehletter, *Ind. Eng. Chem. Prod. Res. Dev. Biol. Stand.* **8**, 267 (1969).
60. F. H. Otey, R. P. Westhoff, and C. L. Mehletter, *Staerke* **24**, 267 (1972).
61. S. D. Seneker and J. E. Glass, *Adv. Chem. Ser.* **248**, 125 (1996).
62. B. Rossall, *Int. Biodeterior. Bull.* **10**, 95 (1974).
63. R. M. Gardener, C. M. Buchman, R. Komark, D. Dorschel, C. Boggs, and A. W. White, *J. Appl. Polym. Sci.* **52**, 1477 (1994).

64. W. J. Bailey, *Polym. J. (Tokyo)* **17**, 85 (1985).
65. O. C. Agboh and Y. Qin, *Polym. Adv. Technol.* **8**, 355 (1997).
66. J. Hosokawa, M. Nishiyama, K. Yoshihara, and T. Kubo, *Ind. Eng. Chem. Res.* **29**, 800 (1990).
67. Q. Li, E. T. Dunn, E. W. Grandmaison, and M. F. A. Goosen, *J. Bioact. Compat. Polym.* **7**, 370 (1992).
68. S. P. C. Filho and J. Desbrieres, *Natural Polymers and Agrofibers Based Composites* 41 (2000).
69. S. Tokura, Y. Miura, Y. Uraki, K. Watanabe, I. Saiki, and I. Azuma, *Am. Chem. Soc. Div. Polym. Chem.* **31**, 627 (1990).
70. M. Tashibana, A. Yaita, H. Tamiura, K. Fukasawa, N. Nagasue, and T. Nakanura, *Jpn. J. Surg.* **18**, 533 (1988).
71. R. A. A. Muzzarelli, *Chitin in Nature and Technology*, Plenum Press, New York, 1986.
72. G. A. King, A. J. Daugulis, P. Faulkner, and M. F. A. Goosen, *Biotechnol. Prog.* **3**, 231 (1987).
73. A. A. Badwan, A. Abumalloh, E. Sallam, A. Abukalaf, and O. Jawan, *Drug Dev. Ind. Pharm.* **11**, 239 (1985).
74. S. J. Huang and K.-W. Leong, *Polym. Prepr., Am. Chem. Soc., Div. Polym. Chem.* **20**, 552 (1979).
75. Y. Tabata and Y. Ikada, *J. Controlled Release* **27**, 79 (1993).
76. Y. Tabata and Y. Ikada, *J. Pharm. Pharmacol.* **39**, 698 (1987).
77. N. Yui, *Baiosaiensu to Indasutori* **56**, 537 (1998).
78. B. G. Shinde, V. S. Nithianandam, K. Kaleem, and S. Erhan, *Biomed. Mater. Eng.* **2**, 123 (1992).
79. C. M. Agrawal and K. A. Athanasiou, *J. Bio. Med. Mater. Res.* **38**, 105 (1997).
80. P. Tormala and P. Rokkanen, *Adv. Sci., Technol.* **12**, 639 (1995).
81. R. S. Bezwada, D. D. Jamiolkowski, I. L. Lee, A. Vishvaroop, J. Persivale, S. Trenka-Benthin, E. Erneta, A. Y. Surydevara, and S. Liu, *Biomaterials* **16**, 1141 (1995).
82. K. Juni and M. Nakano, *Crit. Rev. Ther. Drug Carrier Syst.* **3**, 209 (1986).
83. C. G. Pitt, in M. Chasin and R. Langer, eds., *Biodegradable Polymers as Drug Delivery Systems*, Marcel Dekker, New York, 1990, p. 71.
84. J. E. Bergshma, F. R. Rozema, R. R. M. Bos, A. W. M. Van Rozendaal, W. H. De Jong, J. S. Teppema, and C. A. P. Joziasse, *J. Mater. Sci., Mater. Med.* **6**, 715 (1995).
85. J. E. Bergshma, F. R. Rozema, R. R. M. Bos, G. Boering, W. C. de Brruijin, and A. J. Pennings, *Biomaterials* **16**, 267 (1995).
86. H. Brem, A. Kader, J. I. Epstein, R. J. Tamargo, A. Domb, R. Langer, and K. W. Leong, *Sel. Ther.* **5**, 55 (1989).
87. R. J. Tamargo, J. I. Epstein, C. S. Reinhard, M. Chasin, and H. Brem, *J. Biomed. Mater. Res.* **23**, 253 (1989).
88. L. W. Seymour, R. Duncan, J. Duffy, S. Y. Ng, and J. Heller, *J. Controlled Release* **31**, 201 (1994).
89. J. S. Kay, B. S. Litin, M. A. Jones, A. W. Fryczkowsky, M. Chvapil, and J. Herschler, *Ophthalmic Surg.* **17**, 796 (1986).
90. B. A. Rhodes, I. Zolle, J. W. Buchanan, and H. N. J. Wagner, *Radiology* **92**, 1453 (1969).
91. S. S. Davis, L. Illum, J. G. McVie, and E. E. Tomlinson, *Microspheres and Drug Therapy: Pharmaceutical, Immunological and Medical Aspects*, Elsevier, Amsterdam, the Netherlands, 1984.
92. J. J. Marty and R. C. Oppenheim, *Aust. J. Pharm. Sci.* **6**, 65 (1977).

93. H. Yu, Ph.D. dissertation, *Massachusetts Institute of Technology, Cambridge, Mass.*, 1988.
94. K. S. Soppimath, T. M. Aminabhavi, A. R. Kulkarni, and W. E. Rudzinski, *J. Controlled Release* **70**, 1 (2001).
95. M. Chasin, *Biomed. Appl. Synth. Biodegrad. Polym.* 1 (1995) (CA 123: 296312).
96. J. Heller, *CRC Crit. Rev. Ther. Drug Carrier Syst.* **1**, 39 (1984).
97. R. Langer, *J. Controlled Release* **16**, 53 (1991).
98. A. K. Dash and G. C. Cudworth II, *J. Pharmacol. Toxicol. Methods* **40**, 1 (1998).
99. O. Bostman and H. Pihlajamaki, *Biomaterials* **21**, 2615 (2000).
100. C. Durucan and P. W. Brown, *Adv. Eng. Mater.* **3**, 227 (2001).
101. W. L. Murphy and D. J. Mooney, *J. Periodontal Res.* **34**, 413 (1999).
102. M. C. Wake, P. K. Gupta, and A. G. Mikos, *Cell. Transplant* **5**, 465 (1996).
103. S. H. J. Mendak, R. J. Jensik, M. F. Haklin, and D. L. Roseman, *Ann. Thorac. Surg.* 38 (1984).
104. J. P. Vacanti and R. Langer, *Lancet* **354**, 132 (1999).
105. R. C. Thomson, M. C. Wake, M. J. Yaszemski, and A. G. Mikos, *Adv. Polym. Sci.* **122**, 245 (1995).
106. R. Jain, N. H. Shah, A. W. Malick, and C. T. Rhodes, *Drug Dev. Ind. Pharm.* **24**, 703 (1998).
107. R. A. Jain, *Biomaterials* **21**, 2475 (2000).
108. R. S. Bezwada, D. D. Jamiolkowski, and K. Cooper, *Drug Targeting Delivery* **7**, 29 (1997).
109. T. Nakamura, S. Hitomi, T. Shimamoto, S. H. Hyon, S. Watanabe, and Y. Shimizu, in A. Pizzoferrato, P. G. Machetti, A. Ravaglioli, and A. J. C. Lee, eds., *Biomedicals and Clinical Applications*, Elsevier Science, Amsterdam, the Netherlands, 1987, p. 759.
110. K. E. Rehm, in Proc. 4th Int. Conf. on Biomaterials, Denkendorf, 1992, p. 163.
111. S. Niu, H. Kurumatani, S. Satoh, K. Kanda, T. Oka, and K. Watanabe, *ASAIO Trans.* **39** M750 (1993).
112. T. Matsuda, M. J. Moghaddam, H. Miwa, K. Sakurai, and F. Iida, *ASAIO Trans.* **38**, M154 (1992).
113. T. Matsuda, H. Miwa, M. J. Moghaddam, and F. Iida, *ASAIO Trans.* **39**, M327 (1993).
114. C. Artandi, *CHEMTECH* 476 (1981).
115. Y. Kuroyanagi, E. Kim, M. Kenmochi, K. Ui, H. Kageyama, M. Nakamura, A. Ikeda, and N. Shioya, *J. Appl. Biomater.* **3**, 153 (1992).
116. Y. Kuroyanagi, E. Kim, and N. Shioya, *J. Burn Care Rehabil.* **12**, 106 (1991).
117. M. Koide, K. Osaki, J. Konishi, K. Oyamada, T. Katamura, and A. Takahasi, *Biomed. Mater. Res.* **27**, 79 (1993).
118. I. V. B. Annas, J. F. Bruke, *J. Bimed. Mater. Res.* **14**, 65 (1980).
119. C. J. Doillon, C. F. Whyne, S. Brandwein, and F. H. Silver, *J. Biomed. Mater. Res.* **20**, 1219 (1986).
120. S. T. Boyce, D. J. Christian, and J. F. Hansbrough, *J. Biomed. Mater. Res.* **22**, 939 (1988).
121. K. Yoshizato, A. Makino, and K. Nagayoshi, *Biomed. Res.* **9**, 33 (1988).
122. Y. Yasutomi, N. Nakakita, N. Shioya, and Y. Kuroyanagi, *Burn Inj.* **19**, 102 (1993).

123. J. Kopecek, *Biomaterials (Guildford, Engl.)* **5**, 19 (1984).
124. M. Asano, M. Yoshida, H. Omichi, and H. Yamanaka, *Maku* **17**, 216 (1992).

NEERAJ KUMAR
AVIVA EZRA
TIRTSA EHRENFROIND
MICHAL Y. KRASKO
ABRAHAM J. DOMB
The Hebrew University of Jerusalem

BIOMOLECULES AT INTERFACES

Introduction

Many biomolecules are amphiphilic, that is, possess certain regions that interact favorably, and others that interact less favorably, with an aqueous solvent. As such, these biomolecules tend to reside at the interfacial region separating an aqueous phase from another phase of matter. The process of interfacial attachment is referred to as "adsorption"; "adsorbed molecules" or "adsorbates" are terms describing molecules having undergone adsorption (qv). The principal forces leading to adsorption have been identified; these are the ionic, van der Waals, hydrogen bonding, donor/acceptor, and solvation interactions (1). Attachment by a chemical bond is also possible. Proteins, peptides, amino acids, polysaccharides, lipids, and nucleic acids are examples of biological molecules known to adsorb at solid–liquid, liquid–liquid, and/or liquid–vapor interfaces. To fully understand a biomolecule, one must understand its behavior at relevant interfaces, for it is the rare biomolecule not exhibiting a strong tendency to adsorb!

Many examples of biomolecules at interfaces come from nature. Membrane proteins—a term describing those spanning the cell membrane—actually reside at two interfaces (intracellular matrix–cell membrane and extracellular matrix–cell membrane) and serve to regulate transport into and out of cells. Plasma proteins—those existing in blood—attach to the surface of an unrecognized material and initiate the clotting cascade. Other examples come from technological applications. The above-mentioned clotting process unfortunately occurs onto medical implants as well. Interfacial adsorption is ubiquitous during bioprocessing applications; this can have the deleterious effects of vessel fouling and product structural alteration. Adsorption is one common mechanism by which bioseparations are conducted and biocatalysts are immobilized. Adsorbed protein layers are known to have a strong influence on living cells; this effect is exploited in tissue engineering and cellular bioreactors. Finally, both the fabrication of, and detection using, biosensors involve biomolecules residing at interfaces.

Encyclopedia of Polymer Science and Technology. Copyright John Wiley & Sons, Inc. All rights reserved.

The purpose of this article is to introduce, expand interest in, and grow awareness of, the field of biomolecules at interfaces. Motivation for study in any field is typically driven by either application or curiosity. Workers investigating biomolecules at interfaces are fortunate in that numerous important technological applications exist together with several intriguing and perplexing (and for the most part unsolved!) intellectual curiosities. In most areas of science and engineering, important advances accompany the close interplay between theoretical prediction and experimental measurement. Biomolecules at interfaces is no exception, and a summary of key theoretical tools and experimental methods comprises the subsequent two sections. Note that no attempt is made toward an exhaustive coverage of biomolecule/interface systems. The reader is also invited to consult other excellent reviews related to this topic (1–3).

Technological Applications

A number of important technological applications motivate the study of biomolecules at interfaces. In this section, discussion focuses on important examples in two areas: biomaterials and biosensors.

Biomaterials. Biomaterials find important application as medical implants and tissue engineering substrates. In each case, clinical or scientific effectiveness strongly depends on the behavior of interfacial biomolecules. Other articles in this encyclopedia discuss various aspects of biomaterials. In this section, important aspects dealing with adsorbed biomolecules are briefly presented.

Medical Implants. The insertion of medical implants serving as teeth, bones, skin, blood vessels, and even organs has become commonplace. A universal problem concerns unwanted biological responses; these may be thrombogenic, inflammatory, immunological, or infectious (4–6). It is now well established that protein adsorption precedes and directs these unfavorable events. For example, it is the plasma protein fibrinogen that is thought to initiate thrombogenesis. A small conformational change in the adsorbed fibrinogen is now known to cause platelet adhesion and subsequent aggregation; these events are followed by fibrin formation (6).

Not surprisingly, focus has been directed toward preventing protein adsorption altogether or promoting adsorption of "passivating" proteins (ie those known not to trigger subsequent biological responses). A preeminent strategy for preventing initial protein adsorption involves the grafting of hydrophilic polymer chains to a material surface. Polyethylene oxide (PEO) is particularly effective in this capacity (7–17). The originally suggested mechanism by which PEO prevents protein adsorption involved hydrodynamic currents due to the motion of the grafted chains (7). Subsequent theoretical work has shown that proteins residing within reach of the polymeric brush reduce the conformational freedom of the grafted chains; the polymer layer thus provides an entropic barrier to adsorption (18–25). Very recent work has also demonstrated the importance of the conformational freedom of the individual PEO monomeric units to the prevention of protein adsorption (17).

An alternative to the complete prevention of protein adsorption is the controlled placement of certain biomolecules that act against thrombogenesis. One

natural choice is heparin, an anticoagulant. A number of studies suggest that surfaces with grafted heparin show a diminished thrombogenic response (26,27), but controversy remains as to whether the mechanism is due to heparin-catalyzed antithrombin deactivation of coagulation proteases (28) or to a suppressed adsorption of cell adhesion proteins (29). In addition, although success has been achieved with heparin-coated surfaces, results are not uniformly favorable (30).

Tissue Engineering Substrates. Tissue Engineering (qv) is a field of biomedical study in which techniques are sought to create functional replacements for diseased human tissues and organs (31–36). Successful tissue engineering offers the potential for considerable prolongation of the length and quality of human life. Additionally, it has been estimated that the availability of engineered tissues could reduce expenses related to tissue loss and end-state organ failure by $400 billion per year (31). The key issue in tissue engineering is the availability of materials onto which cells attach, spread, grow, differentiate, and eventually organize to form a desired tissue. Reasoning that the presence of an artificial material would tend to inhibit cellular activity, early efforts were directed toward developing biologically inert materials. The current view, however, is one of a material possessing chemical/biological sequences and patterns capable of signaling and controlling the cellular response (32,37). Materials promoting a natural response, inducing a supernormal response, and/or inhibiting a naturally occurring (but unwanted) response are needed to engineer replacement human tissues.

Tissues or cells typically interact with a biomaterial indirectly through a layer of adsorbed protein. Certain matrix proteins are known to promote cell attachment and growth. One example is fibronectin, a large, extracellular glycoprotein whose constituent modules contain binding sites for a wide range of biomolecules and biological units (38). Its cell-binding site, consisting of the tripeptide amino acid sequence argenine–glycine–asperigine (RGD), is known to bind to the integrin proteins located within the cell membrane; this triggers events that ultimately induce the adhesion, spreading, and growth of cells. Thus, one strategy toward biomaterials for tissue engineering applications is to attach to the biomaterial surface, either chemically or physically, a layer of matrix protein (39–48).

An important alternative to the surface placement of entire proteins is the direct attachment of the cell-binding peptide sequences, such as the RGD sequence in fibronectin (32,37,49–59). This is an example of a "biomimetic" strategy, ie one that mimics biology. Advantages over direct placement of proteins are the greater degree of control of peptide density, spatial arrangement, and orientation and the diminished risk of the material triggering an immune response (37). Disadvantages include the need for additional chemical surface modification (one must generally attach the peptide units and grafted linear polymer chains such as PEO to ensure that proteins do not adsorb and cover the peptides) and the loss of biological signaling from other peptide sequences on the proteins. A number of successes have been reported and it is safe to say that this is currently the most actively researched approach to develop biomaterials as tissue engineering substrates.

Biosensors. A biosensor is an analytical device for the detection of a target biomolecule (60–63). Although many variations are possible, all biosensors combine a detector, where a biological recognition event takes place, with a transducer, which produces an output signal from the recognition event. A biosensor

must be selective for the target molecule in a mixture of structurally similar species. Robustness, cost, size, and real-time measurement capability are additional factors governing the effectiveness of a given biosensing configuration. A number of clinical and biomedical applications are envisioned, but to date the most successful examples of commercialization are the glucose detectors used in the management of diabetes. Other important applications are found in food production, environmental monitoring, and defense/security.

A biosensor's detector typically consists of chemical receptors attached or "immobilized" to a material surface (typically the transducer surface). These are often themselves biomolecules. Detection involves an interaction between these immobilized molecules and biomolecules from solution that approach the detector surface. In this sense, both the fabrication of, and detection using, biosensors involve biomolecules at interfaces.

Biosensor Fabrication. A crucial step in biosensor fabrication is the immobilization of chemical receptors. Chemical receptors may be of two types: catalytic or affinity. In both cases, the target molecule binds specifically to a chemical receptor. In the former, the binding event triggers a measurable change in the transducer. In the latter, the specific binding event leads to a catalyzed chemical reaction, often involving the target molecule itself. The presence of the catalyzed reaction product(s) then triggers a measurable change in the transducer. An important example is the catalytic glucose sensor, in which an oxidation of glucose takes place by immobilized glucose oxidase to gluconic acid and hydrogen peroxide. Hybrid biosensors, in which both catalytic and affinity receptors are utilized, are also possible.

The principal methods for the immobilization of chemical receptors are (*1*) physical adsorption to a solid surface, (*2*) chemical adsorption (covalent attachment) to the surface, (*3*) affinity binding to physically or chemically bound species, and (*4*) entrapment within a matrix. Since physical adsorption relies on relatively weak forces (van der Waals, ionic, solvation, donor/acceptor), molecules placed in this way may detach over time and/or exhibit nonuniform biological activity because of a distribution of surface orientations/conformations. However, this method is clearly the simplest of the four and therefore often finds use. An example is the popular enzyme-linked immunosorbent assay (ELISA) used in medical diagnostics.

A more robust and controllable means of surface attachment is through a covalent bond. Large biomolecules such as proteins typically possess a number of functional groups capable of chemical binding; these include amino, carboxyl, sulfhydryl, phenolic, thiol, and imidizol groups. The best choice for preserving biological activity and optimizing accessibility of the receptor's active site is often a functional group far from the active site. Suitable complementary reactive groups are available on some surfaces (for example, hydroxyl groups on silica), but in many cases, surface modification is needed. A popular means of surface modification is to employ self-assembled monolayers (SAMs) (64). SAMs are closely packed, (approximately) vertically aligned alkane chains residing at an interface. Through chemically functionalized termini, the tailoring of physical and chemical properties of the surface is possible. Chemical immobilization results from a reaction between a specific functional group at a SAM molecule terminus and a biomolecule. (In some cases, a bifunctional reagent is used to achieve the coupling.) A SAM may be placed onto a surface by the Langmuir–Blodget method

(65), via reaction of silanes with a metal oxide surface (66), or via reaction of alkane thiols, alkane sulfides, or alkane disulfides with a metal surface (67,68). Another popular means of surface modification is through a grafted polysaccharide gel (69). Attachment occurs via straightforward chemistry, beginning with an EDC/NHS modification of the polysaccharide layer (70) followed by coupling of an amine, thiol, or aldehyde group on the protein with an NHS ester. The result is a three-dimensional film of receptor molecules.

Affinity binding offers a level of control over receptor molecule orientation and conformation that can significantly exceed that of either physical or chemical attachment. Typically, monoclonal antibodies (IgGs) specific to a region of the receptor molecule away from the active site are used. Binding constants are very high, typically in the range of 10^9–$10^{12}\ M^{-1}$. The antibody itself may be attached physically, chemically, or via specific linkages between its F_c (constant) region and a preadsorbed Protein A or G molecule (71). Additionally, the antibody may be chemically modified via an attached biotin group; in this case, specific binding occurs between the biotin and a complementary site on a molecule of preadsorbed avidin or streptavidin (72,73).

Finally, biomolecules may be immobilized via entrapment within a polymer gel matrix. A number of polymers may be used, eg cellulose acetate (74), poly(vinyl alcohol) (75), and polypyrrole (76). Although high density biomolecule films are possible, a drawback is gradual leakage. This may be alleviated somewhat by cross-linking the biomolecules via chemical reaction. In the case of proteins or peptides, this may be achieved via glutaraldehyde, a reagent that couples with lysine amino acids.

Biosensor Detection. As mentioned above, detection occurs via a measurable change in the biosensor's transducer. Binding of a target molecule to an immobilized chemical receptor may bring about measurable changes that are electrochemical, electrical, thermal, magnetic, optical, or piezoelectric. The principles behind some of these mechanisms are further described in the section entitled Experimental Methods. Additional information can be obtained from a recent review (62).

Intellectual Challenges

A number of experimental observations concerning biomolecules at interfaces are at first glance quite puzzling. Many of them stem from a tendency of these (typically) large molecules to display an adsorptive behavior dependent on history. One example from the literature concerns the adsorption of human serum albumin onto synthetic hydroxyapatite (77). In a series of experiments, the concentration of bulk protein to which hydroxyapatite particles were exposed was varied and the adsorbed amount measured. As shown in Figure 1, when the adsorbed density versus concentration in solution (ie the adsorption isotherm) is plotted (Fig. 1), one finds a significant dependence on the "concentration trajectory," ie on the concentrations to which the surface was exposed at earlier times. Another example is the stepwise adsorption of cellulose onto silica (78). In this experiment, a sample is alternately exposed to solutions of increasing or decreasing cellulose concentration (between each concentration, a rinse is conducted in cellulose-free solution). As shown in Figure 2, it is found that the adsorption isotherm differs, depending

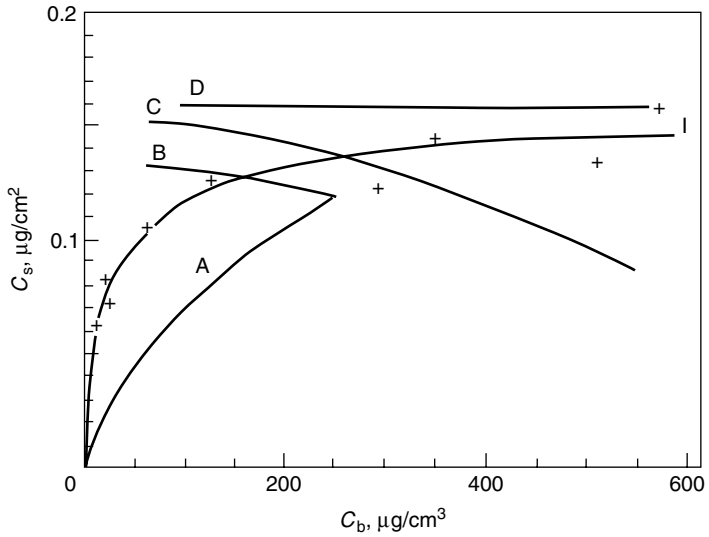

Fig. 1. The concentration of human serum albumin adsorbed to hydroxyapatite particles versus bulk protein concentration along several concentration "trajectories." Curve A: a gradual increase in bulk protein concentration via flow of 0.066 g/L protein solution into chamber of particles. Curve B: a gradual decrease in bulk protein concentration via flow of buffer solution without protein. Curve C: a protein concentration of 0.695 g/L for 30 min followed by a gradual decrease in bulk protein concentration via flow of buffer solution. Curve D: a protein concentration of 0.858 g/L for 8 h followed by a gradual decrease in bulk protein concentration via flow of buffer solution. Curve I: Protein concentrations corresponding to the horizontal axis for 8 h. Taken with permission from Ref. 77.

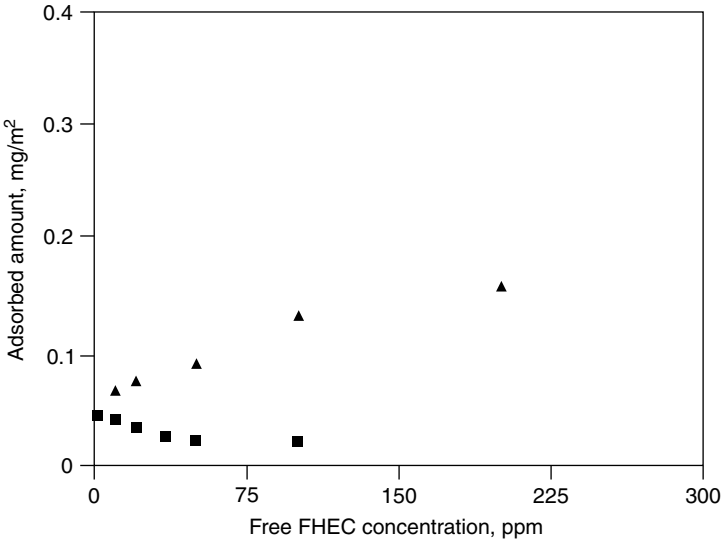

Fig. 2. The density of hydroxyethylcellulose adsorbed to silica versus bulk concentration for a series of alternating 40-min exposures to pure buffer and biopolymer solutions. Curves representing progressively increasing (squares) and decreasing (triangles) concentrations are shown. Taken with permission from Ref. 78.

upon whether the steps are of increasing or decreasing concentration. In fact, the adsorbed density increases with solution concentration only along the decreasing series. A final example is the multistep kinetic measurement of fibronectin onto silica–titania (79). As in the previous example, a surface is alternately exposed to a protein solution and an otherwise identical solution containing no protein. As shown in Figure 3, when the time between the first and second adsorption step is short, the rates of adsorption along both steps are roughly identical. However, when a longer time period separates the two steps, the rate of adsorption during the second step greatly exceeds—for a given amount of adsorbed protein—the rate during the initial step.

These features may be explained by considering two interesting features of biomolecular adsorption (features also exhibited by many synthetic macromolecules): (*1*) the presence of irreversibility and (*2*) the presence of post-adsorption "relaxation" events on a time scale exceeding that of adsorption. Irreversibility is demonstrated in Figure 4, where the kinetics of cytochrome P450 adsorption to a lipid bilayer are shown (80). One sees that replacement of the protein solution by an identical solution without protein results in only a fraction of the adsorbed molecules leaving the surface, the others being essentially irreversibly adsorbed. The insensitivity of isotherm D in Figure 1 to dilution can be explained by irreversible adsorption occurring at the initial (highest) concentration. The history-dependent behavior observed in Figures 2 and 3 can be explained by post-adsorption relaxation mechanisms. The decreasing nature of the ascending concentration branch of Figure 2 may be explained by the presence of post-adsorption conformational changes. These changes lead to a flatter, more elongated adsorbed molecule and are favored when the rate of adsorption is slow, as occurs when the bulk concentration is low. In contrast, when the rate of adsorption is high, relaxation to the flatter structure is sterically blocked by molecules adsorbing at neighboring positions. If the same type of post-adsorption event occurred in the system whose kinetics are displayed in Figure 3, one would find a decreased rate of adsorption during the second step because of the greater surface area covered by the more conformationally altered molecules. Instead, the increased second-step adsorption rate is caused by another type of post-adsorption structural change: clustering or aggregation among the adsorbed molecules. This event opens up space on the surface in much the same way as clustering furniture in the corner of a room opens space for a social gathering.

The history dependence engendered by the slow rate, relative to that of initial attachment, of subsequent relaxation events (eg internal conformational changes, aggregation with other adsorbed molecules) renders challenging the theoretical treatment of biomolecules (as well as many synthetic macromolecules) at interfaces. Nonequilibrium methods must generally be employed, but these are less well developed than their equilibrium counterparts. The quest for a theoretical description is therefore a daunting one; progress along this front is the topic of the next section.

Theoretical Approaches

The ultimate objective in any physical science is often to understand a system or phenomenon quantitatively, that is, within the framework of a mathematical

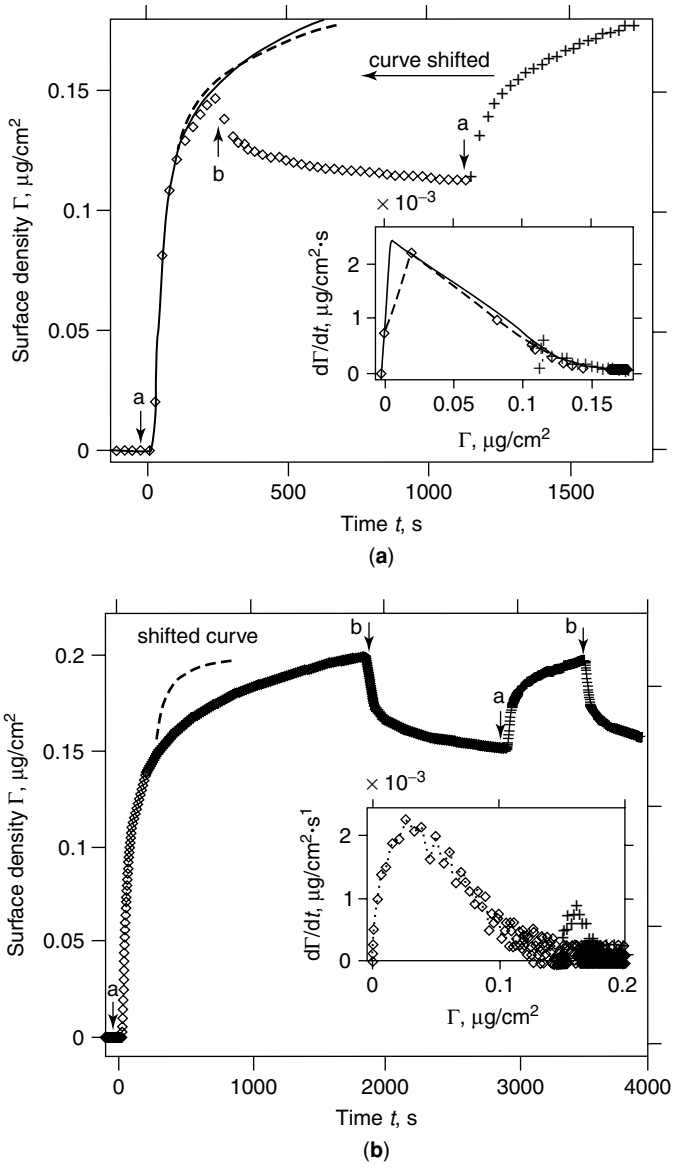

Fig. 3. The density of fibronectin adsorbed to silica–titania versus time for a multistep experiment in which exposure to a flowing solution of 0.05 g/L protein concentration is interrupted by exposure to a flowing solution without protein. (**a**) A short initial adsorption step and rinse. (**b**) A longer initial adsorption step and rinse. Taken with permission from Ref. 79.

model. Attempts to model biomolecules at interfaces—where, as mentioned above, history-dependent behavior is rampant—fall principally along five lines. The first and simplest is the site description in which interfacial behavior is modeled as the filling of discrete adsorption sites at the interface. Borrowing heavily from theories on gas adsorption, many closed-form mathematical models are available. A second is the particle description in which the biomolecule is approximated by

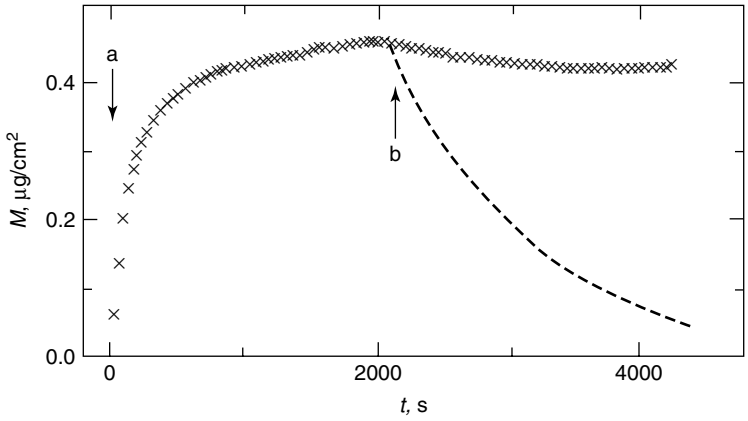

Fig. 4. The density of cytochrome P450 adsorbed to a lipid bilayer versus time. Points A and B denote the onset and termination of exposure to the protein solution and the dashed line represents the expected curve assuming first-order kinetics and fully reversible adsorption. Taken with permission from Ref. 80.

a simple geometric object whose adsorption behavior is governed by a few lumped phenomenological parameters. A third is the colloidal approach combining the simple particle geometry with an explicit, continuum approach to the forces of interaction. A fourth is the polymer description, in which the chain-like structure of most biomolecules (linear sequence of amino acids in proteins and peptides, linear sequence of nucleic acids in DNA and RNA) is used to justify a treatment using theoretical methods developed for synthetic polymers. Finally, a fifth is the atomistic description in which the detailed molecular architecture of the biomolecule is taken into account. A molecular force field is invoked and the energy from the biomolecule–surface interactions is summed. (Solvent molecules are often implicit.) Of course, the level of detail within each of these approaches varies according to the system and the objectives of study. Generally, the particle description is preferred for modeling systems of all but infinitely dilute surface densities.

Site Description. The adsorption of biomolecules at an interfacial region can be modeled as the filling of discrete surface sites. Although such models are more appropriate for gas adsorption, their mathematical simplicity has made them convenient and frequently used tools for modeling biomolecular adsorption as well. The most well known is the Langmuir model, in which fully reversible adsorption occurs onto noninteracting sites. The kinetic expression is

$$\frac{d\Gamma}{dt} = k_a c_s \left(1 - \frac{\Gamma}{\Gamma_{max}}\right) - k_d \Gamma \tag{1}$$

where Γ is the adsorbed density, t is the time, k_a is the intrinsic adsorption rate, c_s is the concentration of adsorbing species in solution at the surface, Γ_{max} is the density of adsorbed species when all surface sites are filled, and k_d is the intrinsic rate of desorption. The solution to equation 1 is

$$\frac{\Gamma(t)}{\Gamma_{max}} = \frac{Kc_s}{1+Kc_s}\left[1 - e^{-(k_a c_s/\Gamma_{max} + k_d)t}\right] \tag{2}$$

where $K = k_a/k_d$.

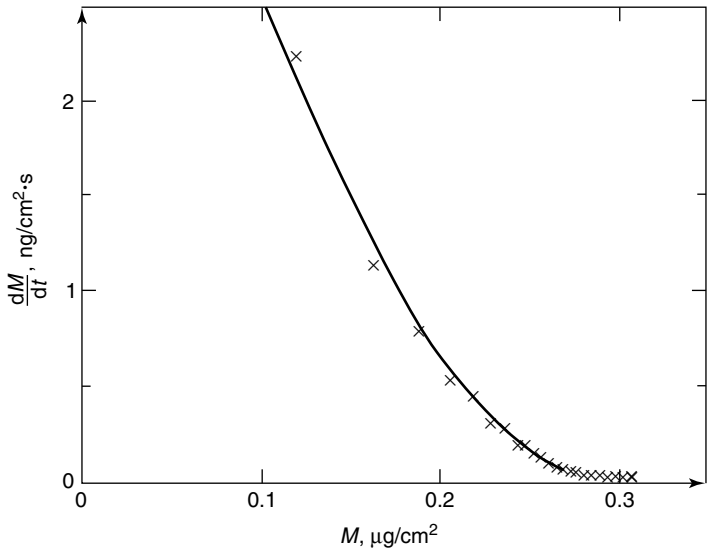

Fig. 5. The rate of adsorption of transferrin onto silica–titania versus adsorbed amount. Taken with permission from Ref. 81.

A consideration of Figure 4 demonstrates the inadequacy of the Langmuir approach to most biomolecular systems. For one, the saturation is approached much more slowly than the exponential behavior predicted by equation 2. Secondly, by setting c_s=0, equation 1 would predict a complete desorption during a rinse. Instead, desorption of only a small fraction of the adsorbed molecules results. Finally, equation 1 predicts a linear relationship between adsorption rate and adsorbed amount. In fact, most systems demonstrate a nonlinear relationship. An example is shown in Figure 5 for transferrin adsorption onto silica–titania (81). Despite these and other drawbacks, the Langmuir model continues to find use in a number of instances.

Extensions to account for experimentally observed features of biomolecular adsorption have appeared. For example, the case of adsorption followed by subsequent "spreading" has been treated in the context of a Langmuir approach (82,83). Other examples are models employing interactions between molecules on neighboring sites (or sets of sites in cases of multiple occupancy). Two-dimensional protein ordering or aggregation has been modeled using hexagons adsorbing to a hexagonal lattice (84) and tetramers adsorbing to a square lattice (85). A model additionally considering surface site heterogeneity has also appeared (86).

Particle Description. If the adsorption rate reflects the amount of available surface for adsorption, then the nonmonotonic decrease in adsorption rate with adsorbed density of Figure 5 may be interpreted as being due to the filling of a continuous surface by geometric objects. This result is not surprising; when one considers that the greater size of most biomolecules compared to the expected distance between surface attachment sites, adsorption essentially occurs onto a continuum. Such an approach to biomolecular adsorption is called a particle description and, through its more realistic treatment of surface exclusion effects, represents an improvement over a site description. At first thought, modeling a

complicated biological molecule as a simple geometric object (eg sphere, ellipsoid) seems a ridiculous oversimplification. After all, millennia of evolution have produced biomolecules of exquisite complexity. However, unlike synthetic molecules, certain biomolecules (eg proteins) possess a unique folded three-dimensional structure (many are crystallizable!) and so long as the interfacial perturbation is not too great, may keep this structure and behave, to a first approximation, as a rigid object. (Of course, a large interfacial perturbation may cause the biomolecule to unfold to a degree where a polymer description becomes more appropriate.) In fact, the particle description is able to predict many interesting features of biomolecular adsorption (an important example of this is shown in Figure 5).

When adsorption is completely irreversible, the particle description reduces to the random sequential adsorption (RSA) model (87–89). An RSA process is one in which hard objects are added randomly and sequentially to a surface at a given rate and in which any object placed in a position so as to overlap with another object is immediately removed. The governing kinetic equation is

$$\frac{\mathrm{d}\Gamma}{\mathrm{d}t} = k_{\mathrm{a}} c_{\mathrm{s}} \Phi \tag{3}$$

where Φ is the fractional surface available for adsorption. For line segments adsorbing to an infinite line, an analytical solution is available (90,91). In higher dimensions, analytical solutions have been elusive. However, exact theoretical treatment is possible in the limits of low and high surface coverage. At low surface coverage, Φ may be expressed as a power series in surface coverage (92):

$$\Phi = 1 + A_1\theta + A_2\theta^2 + \cdots \tag{4}$$

where θ is the fraction of the surface covered by the vertically projected area of the particles. At high surface coverage, the time evolution of the size distribution of isolated regions of empty space may be deduced and related to the overall rate of adsorption. This gives

$$\Phi = Ct^{-\nu} = (\theta_\infty - \theta)^{\frac{\nu}{\nu - 1}} \tag{5}$$

where C is a constant, θ_∞ is the surface coverage approached as $t \to \infty$, and ν is an exponent whose value depends on the particle geometry. For example, in the case of a disk, $\nu = 3/2$ (93,94); while for an elongated, convex 2-D object, $\nu = 4/3$ (95). A reasonable approximate expression for Φ valid at all times is found in the form of a Pade approximant (92):

$$\Phi \approx \frac{(\theta_\infty - \theta)^{\frac{\nu}{\nu - 1}}}{1 + B_1\theta + B_2\theta^2 + \cdots} \tag{6}$$

where the coefficients B_i are evaluated in terms of the known A_is by matching the first few terms in the θ expansion of equation 6 with those in the θ expansion of equation 4.

Most biomolecular adsorption systems exhibit only partial irreversibility (see, eg, Fig. 4). The RSA model may be extended to include desorption and post-adsorption structural changes. In this case, one must write at least two kinetic

equations (one for each structure or "state" of the adsorbed molecule) (96–102):

$$\frac{d\Gamma_\alpha}{dt} = k_a c_s \Phi_\alpha - k_d \Gamma_\alpha - k_s \Gamma_\alpha \Psi_{\alpha\beta} \tag{7}$$

$$\frac{d\Gamma_\beta}{dt} = k_s \Gamma_\alpha \Psi_{\alpha\beta} \tag{8}$$

In equations 7 and 8, Γ_α and Γ_β are the adsorbed densities of molecules in their initial and surface-altered structures, Φ_α is the fractional available area for adsorbed molecules in their initial state, $\Psi_{\alpha\beta}$ is the probability that an adsorbed molecule in its initial state has available area around it sufficient to allow for a conversion to the surface-altered state, and k_s is the intrinsic rate of structural alteration. (Extensions are straightforward to cases of several adsorbed states.) Theoretical approximations to the functions Φ_α and $\Psi_{\alpha\beta}$ have been made in cases of (*1*) purely irreversible adsorption ($k_d = 0$, no surface diffusion) using methods analogous to those used to derive equations 4–6 (97), and (*2*) high surface mobility using the equilibrium-scaled particle method (101,102). Simulations have also been performed (96,98–100). Nonuniform or time-dependent rate constants have also been incorporated in these expressions (99,100,103) and an extension accounting for protein clustering has been developed (104,105). A model combining the site and particle descriptions has been proposed (106). A complete description of the adsorption process may be obtained by coupling equations 7 and 8 to bulk transport equations (107).

Another particle description is the molecular mean field treatment in which the free energy of a system of molecules near to an interfacial region is expressed as a functional of the density distribution (108). This approach was inspired by the single-chain mean-field method developed to study the behavior of grafted polymer layers. The equilibrium adsorbate density distribution is just that which minimizes the free-energy functional subject to certain excluded volume constraints. The system's dynamics may also be determined through a generalized diffusion equation; the diffusive flux is proportional to the chemical potential gradient, and the position-dependent chemical potential is determined as the functional derivative of the (nonequilibrium) free energy with respect to density. Although more computationally intensive than the particle methods discussed above, the major advantages of this method are the straightforward extensions to mixtures, multiple conformational states, realistic intermolecular potentials, and the presence of grafted polymer layers (20–25,109).

A brief mention is merited for models treating biomolecular (typically protein) adsorption in the presence of tethered polymer chains. Early efforts utilized the Alexander–de Gennes theory to describe the steric repulsion felt by proteins near the polymer layer in its "brush" regime (18). Although results are qualitatively correct, this approach requires the chains to be longer than those used experimentally, so quantitative applicability is limited. A subsequent effort employed a self-consistent field approach, but again only long chains were considered (19). The treatment of systems with chain lengths closer to those of experiment became possible through the single-chain mean-field theory (20–25). This theory allows for the incorporation of detailed molecular structure for both polymer and protein and has been used to accurately predict the long- and short-time adsorptive properties of biomaterials containing grafted polymer chains (24,110).

Colloidal Description. A colloidal approach combines the simple particle geometry with an explicit, continuum approach to the forces of interaction (111–113). At the heart of this approach is a treatment of electrostatics via the Poisson equation,

$$\nabla^2\phi = -\frac{\rho(\vec{r})}{\varepsilon} \tag{9}$$

where ϕ is the electric potential, ρ is the charge density, and ε is the dielectric permittivity. Within a solid adsorbent or a (assumed rigid) protein, the charge density distribution results from the presence of immobile charged species. In solution, the charge density distribution results from dissolved ionic species, which may be assumed to be distributed in a Boltzmann manner,

$$\rho_i(\vec{r}) = \rho_{i,\text{bulk}} z_i \exp\left(-z_i e\phi(\vec{r})/k\text{T}\right) \tag{10}$$

where $\rho_{i,\text{bulk}}$ is the bulk density of ionic species i, z_i is its valence, e is the elementary charge, k is the Boltzmann constant, and T is the absolute temperature. The resulting electric potential—which for all but the simplest geometries must be determined numerically—is used to calculate the total interaction energy

$$U_{\text{elec}} = \sum_i z_i e\phi(\vec{r}_i) \tag{11}$$

where the sum runs over all charges in the system. (The sum becomes an integral in the case of a continuous charge distribution.)

Colloidal approaches also frequently account for van der Waals interactions, ie interactions due to fluctuating dipoles. For atomic species, these interactions vary as distance to the minus sixth power. For protein/surface systems modeled via a colloidal description, this $1/r^6$ dependence is integrated over the volumes of the interacting bodies. The result is the product of a Hamaker constant, which depends upon material properties, and a term dependent on the system's geometry. In addition, forces related to solvation (114) and donor/acceptor (115) affects may also be included.

Although not amenable to predictions of irreversibility or conformational change, colloidal approaches have been successful in predicting qualitative trends in—and, to a certain extent, quantitative values of—equilibrium constants in the case of fully reversible adsorption at low surface coverage (116–120). In many cases, simple protein geometries and charge distributions suffice. In other cases, such as when adsorption is controlled by charged patches (121,122), more realistic models must be used. An accounting of protein–protein interactions to allow for a finite surface coverage has also been made (123–126).

The colloidal approach has also been applied to the adsorption of DNA on to a charged surface (127,128).

Polymer Description. A lattice model heteropolymer (129–131) provides a simple yet instructive description of a protein molecule. In general, the coarse graining is such that each segment represents a portion of the protein (ie many amino acids). In the simplest case, two types of segments are present; these may be thought of as polar and hydrophobic (132–138). In other cases, a distribution

of segmental interactions is employed (139–143). The minimalist nature of this model allows for efficient sampling of conformational space via simulation (for chains of less than 20 segments, exact enumeration of all conformations is possible). Despite its apparent simplicity, for a proper choice of segment–segment nearest-neighbor interaction strength, this model is capable of exhibiting the essential physics of protein folding (eg coil–globule and globule–folded transitions and the presence of a glass transition). Of particular importance have been 27 segment models in which certain sequences fold into a unique $3 \times 3 \times 3$ cubic structure (134,136–143). Recently, uniquely folding sequences have been studied at liquid–solid (99,144–146) and liquid–liquid (147) interfaces. An interesting observation has been the initial continuous transition of the model protein to an unfolded, fully flattened state followed by an activated transition to a partially refolded, less-flattened state (145,146). Proteins modeled as shorter chains, where exact enumeration is possible, have also been studied at the liquid–solid interface (148,149).

Other lattice polymer efforts have been based on the self-consistent field theory of Scheutjens and Fleer (150,151). This approach differs from previously posed statistical theories for chain molecules in that the partition function is expressed in terms of the distribution of chain conformations rather than the distribution of segment densities. The equilibrium distribution of chain (ie model protein) conformations is thus calculable. Quantities predicted using this approach include the force between parallel plates coated with protein (152,153), the adsorption isotherm (154,155), and the segmental density distribution (154–157).

A simple yet instructive model for determining general features of certain biomolecules at interfaces is the random heteropolymer description (158–174). A random heteropolymer is defined as one whose sequence of monomers follows a statistical distribution. A collection of random heteropolymers is therefore an example of a quenched–annealed system, that is, one in which certain degrees of freedom are fixed and follow a known distribution (in this case, the heteropolymer sequence) and others equilibrate with respect to these fixed degrees of freedom (in this case, the spatial distribution of the segments). Special methods developed for treating such systems (175) are therefore applicable and have been useful in determining properties of single (160) and sets of (162,164) adsorbed chains.

Clearly, nucleic acids are also amenable to a polymer description. Theoretical (176) and simulation (177,178) methods have been used to determine the structure, dynamics, and thermodynamics of nucleic acid chains on surfaces.

Atomistic Description. Molecular modeling at the atomistic level has become commonplace. The dual challenges of accurate potential force field description and efficient configurational sampling have been met to a degree where predictive capabilities now exist for many single- and multicomponent systems of simple molecules. The extension of these methods to biomolecules, and more specifically to biomolecules at interfaces, presents a challenge because of the size and complexity of these molecules. However, some attempts to calculate physical properties of atomistically modeled biomolecules at interfaces have appeared (see Molecular modeling (structure, molec. graphics)).

Early efforts were essentially static calculations of the interaction energy between a rigid protein and a surface (112,114,121,179–181). Pairwise atomistic potential energy descriptions were used to calculate the van der Waals and electrostatic contributions. In the case of hydrophobic surfaces, solvation energies

were estimated from partition coefficients of the individual amino acids between aqueous and organic phases (114,180). Some of these studies treated the electrostatic interactions in a colloidal manner (112,121). The calculated energies for various geometries were helpful in understanding chromatographic behavior. Similar calculations of individual amino acids on self-assembled monolayers have also been conducted with the hope of uncovering trends useful for predicting behavior of entire protein molecules (182).

Molecular dynamics (MD) is a method in which Newton's equations of motion are solved for a molecular system obeying a differentiable potential function. A few efforts at modeling proteins at interfaces using MD have appeared (183–187). Obviously, these studies provide dynamic as well as thermodynamic information on biomolecules at interfaces. Systems studied have included lysozyme and myoglobin on polyethylene glycol (183), cytochrome c on hydrophilic and hydrophobic self-assembled monolayers (184), leucine enkephalin near a crystalline polyethylene surface (185), thermal hysteresis proteins on ice (186), and lysozyme on polyvinylimidazole (187).

Experimental Methods

Progress in any field requires information on the state of well-defined systems as a function of conditions. Advancement is thus intimately linked to the availability of experimental probes capable of providing accurate and detailed information. Important metrics of biomolecules at interfaces include the interfacial composition; distributions in molecular orientation, molecular spatial arrangement, and intramolecular conformation; and biological activity. In this section, several experimental techniques probing the physical properties of biomolecules at interfaces are introduced; these are grouped into optical, piezoelectric, and scanning probe methods. Further details can be found in other excellent reviews (62,188,189).

Optical Methods. Optical methods involve directing polarized monochromatic light toward the solid–liquid interface and measuring a response, eg the polarity or intensity of reflected or emitted light. Various schemes have been proposed, as described below, and these allow for the determination of adsorbed-layer thickness, density, and composition as well as information on internal conformation. Principal advantages of optical experimental probes include nondestructiveness and the capability of continuous, real-time measurements.

Reflection-based methods (190–194) involve measuring the reflection of polarized light at the interface between two optical media. In fact, two reflections are measured: one for the electric field component perpendicular to the plane of incidence (transverse electric or *s*-wave) and one for the electric field component parallel to the plane of incidence (transverse magnetic or *p*-wave). At a certain angle of incidence (the Brewster angle), the *p*-wave reflection vanishes and around this angle, the reflectivity, or square of the amplitude of the *p*-wave reflection, and ellipticity, or ratio of *p*- and *s*-wave reflections, become very sensitive to interfacial heterogeneity, as brought about eg by adsorption of biomolecules. By assuming the adsorbed layer to be uniform in refractive index, both its thickness and refractive index may be determined. By further assuming a linear dependence of refractive index on concentration, the adsorbed density is calculable (195).

Optical waveguide methods (188,196–198) are based on the phase shift associated with multiple interfacial reflections: when either the *s*- or *p*-wave undergoes a total phase shift equal to an integral multiple of 2π upon one complete traversal of a planar, dielectric waveguide sandwiched between media of lower refractive index, a standing wave is excited in the waveguiding film. Because of their dependence on reflection, the phase shifts are sensitive to interfacial heterogeneity—and the thickness, refractive index, and density of an adsorbed biomolecular layer can be readily determined.

When light traversing an optically dense medium approaches an interface with a more optically rare medium at an angle exceeding a critical value, $\theta_{crit} = \sin^{-1}(n_{rare}/n_{dens})$, a total internal reflection occurs and an evanescent wave of exponentially decaying intensity penetrates the rarer medium. This phenomenon is at the heart of certain spectroscopic methods used to probe biomolecules at interfaces (199). In total internal reflection fluorescence (TIRF) spectroscopy (200–202), the evanescent wave excites fluorescent probes attached to the biomolecules, and detection of the emission associated with their decay provides information on the density, composition, and conformation of adsorbed molecules. In fourier transform infrared attenuated total reflection (FTIR-ATIR) spectroscopy (203,204), the evanescent wave excites certain molecular vibrational degrees of freedom, and the detected loss in intensity due to these absorbances can provide quantitative data on density, composition, and conformation.

Surface plasmon resonance (SPR) (205–209) is an optical method in which the *p*-wave of incident light excites a propagating, nonradiative charge density oscillation at a metal–dielectric interface. The resonant condition is the matching of the wave vector component of the *p*-wave parallel to the interface to the wave vector of the surface plasmon. The latter is sensitive to the optical properties of a fluid or adlayer near the interface, so by monitoring changes in the angular distribution of the intensity of reflected light, physical properties of adsorbed species may be determined.

Piezoelectric Methods. A *piezoelectric crystal* is one in which a mechanical stress induces an electric current. Conversely, application of an alternating voltage to a piezoelectric crystal induces a vibration. The frequency of oscillation is extremely sensitive to the mass contacting the crystal, and it is the frequency shift due to adsorption that is the basis for piezoelectric methods (210). A quartz crystal microbalance (QCM) (211–214) consists of a thin disk of (piezoelectric) crystalline quartz sandwiched between thin-film metal electrodes. Upon application of an alternating voltage, the crystal undergoes thickness shear mode vibration. The mass adsorbed to the electrode surface—here, unlike in the optical methods described above, the mass includes trapped solvent—is simply proportional to the frequency shift. In addition, the dissipation of energy following voltage removal, as measured by the decay of the oscillation amplitude, is a sensitive measure of the viscoelastic properties of an adsorbed layer. QCM thus provides a valuable complement to optical methods through information concerning conformation (via the amount of trapped solvent in an adsorbed film) and rigidity (via the film viscoelastic response).

Scanning Probe Methods. Scanning probe methods (215–217) involve probing a solid surface with a very sharp tip and measuring its deflection or other physical change in order to create a topographical image or to determine a surface force profile. Two common methods for imaging biomolecules at interfaces

are contact-mode and tapping-mode atomic force microscopy. In the former, the tip is scanned over the surface while remaining essentially in contact with the surface or adsorbed species. In the latter, the probe oscillates as it scans and only in the "valley" of each oscillation does it contact the substrate. An advantage to the tapping-mode method is the elimination of shear forces capable of damaging soft samples (eg biomolecules) that can diminish image resolution. Atomic force microscopy in force–distance mode provides information on the intramolecular, intermolecular, and molecule–surface forces. The experiment involves directing the tip (often coated with biomolecules) toward the surface and measuring the resulting force as a function of tip–surface distance. The capability to extract information from individual molecules is the principal advantage to scanning probe methods; in contrast, optical and piezoelectric methods give information on the collective properties of an adsorbed layer.

Conclusions

Biomolecules at interfaces continues to be a challenging and important subject of basic research and biotechnological development. Despite intense investigation for several decades, a number of significant challenges remain, including the complete prevention of protein adsorption onto blood-contacting biomaterials, the controlled placement of biologically active molecules on sensing and tissue engineering substrates, and the quantitative prediction of events occurring as biomolecules approach and reside at the interfacial region. Recent experimental developments, particularly those in optical, scanning probe, and piezoelectric instrumentation—and advances in statistical–mechanical modeling, interatomic force field development, and computational power—are converging to provide new insights, at an unparalleled rate, in order to meet these and other emerging challenges.

BIBLIOGRAPHY

1. C. A. Haynes and W. Norde, *Colloids Surf., B* **2**, 517 (1994).
2. M. Malmsten, *J. Colloid Interface Sci.* **207**, 186 (1998).
3. M. Malmsten, ed., *Biopolymers at Interfaces*, Vol. **75**, Surfactant Science Series, Marcel Dekker, Inc., New York, 1998.
4. J. D. Andrade and V. Hlady, *Adv. Polym. Sci.* **79**, 1 (1986).
5. L. P. Tang and J. W. Eaton, *Am. J. Clin. Pathol.* **103**, 466 (1995).
6. W. J. Hu, J. W. Eaton, and L. P. Tang, *Blood* **98**, 1231 (2001).
7. Y. Mori, S. Nagaoka, H. Takiuchi, T. Kikuchi, N. Noguchi, H. Tanzawa, and Y. Noishiki, *Trans. Am. Soc. Artifi. Intern. Organs* **28**, 459 (1982).
8. H. Jacobs, D. Grainger, T. Okano, and S. W. Kim, *Artif. Organs* **12**, 506 (1988).
9. J. H. Lee, J. Kopecek, and J. D. Andrade, *J. Biomed. Mater. Res.* **23**, 351 (1989).
10. M. Amiji and K. Park, *Biomaterials* **13**, 682 (1992).
11. M. Amiji and K. Park, *J. Biomater. Sci.—Polym. Ed.* **4**, 217 (1993).
12. J. M. Courtney, N. M. K. Lamba, S. Sundaram, and C. D. Forbes, *Biomaterials* **15**, 737 (1994).
13. J. H. Lee, H. B. Lee, and J. D. Andrade, *Prog. Polym. Sci.* **20**, 1043 (1995).
14. J. D. Andrade, V. Hlady, and S. I. Jeon, *Hydrophilic Polymers: Performance with Environmental Acceptance*, American Chemical Society, Washington, D.C., 1996, p. 51.

15. A. S. Hoffman, *J. Biomater. Sci.—Polym. Ed.* **10**, 1011 (1999).
16. D. Leckband, S. Sheth, and A. Halperin, *J. Biomater. Sci.—Polym. Ed.* **10**, 1125 (1999).
17. A. R. Halperin and D. E. Leckband, *C. R. Acad. Sci. Ser. IV—Phys. Astrophys.* **1**, 1171 (2000).
18. S. I. Jeon, J. H. Lee, J. D. Andrade, and P. G. Degennes, *J. Colloid Interface Sci.* **142**, 149 (1991).
19. G. Subramanian, D. R. M. Williams, and P. A. Pincus, *Macromolecules* **29**, 4045 (1996).
20. I. Szleifer, *Physica A* **244**, 370 (1997).
21. I. Szleifer, *Curr. Opin. Solid State Mater. Sci.* **2**, 337 (1997).
22. I. Szleifer, *Biophys. J.* **72**, 595 (1997).
23. M. A. Carignano and I. Szleifer, *Colloids Surf., B—* **18**, 169 (2000).
24. J. Satulovsky, M. A. Carignano, and I. Szleifer, *Proc. Natl. Acad. Sci. U.S.A.* **97**, 9037 (2000).
25. I. Szleifer and M. A. Carignano, *Macromol. Rapid Commun.* **21**, 423 (2000).
26. M. Fukutomi, S. Kobayashi, K. Niwaya, Y. Hamada, and S. Kitamura, *Artif. Organs* **20**, 767 (1996).
27. S. Svenmarker, E. Sandstrom, T. Karlsson, E. Jansson, S. Haggmark, R. Lindholm, M. Appelblad, and T. Aberg, *Eur. J. Cardio-Thorac. Surg.* **11**, 957 (1997).
28. J. Sanchez, G. Elgue, J. Riesenfeld, and P. Olsson, *J. Biomed. Mater. Res.* **29**, 655 (1995).
29. N. Weber, H. P. Wendel, and G. Ziemer, *Biomaterials* **23**, 429 (2002).
30. R. Blezer, B. Fouache, G. M. Willems, and T. Lindhout, *J. Biomed. Mater. Res.* **37**, 108 (1997).
31. R. Langer and J. P. Vacanti, *Science* **260**, 920 (1993).
32. J. A. Hubbell, *Bio/Technology* **13**, 565 (1995).
33. J. Kohn, *MRS Bull.* **21**, 18 (1996).
34. A. Curtis and M. Riehle, *Phys. Med. Biol.* **46**, R47 (2001).
35. Y. Tabata, *Drug Discov. Today* **6**, 483 (2001).
36. S. Lalan, I. Pomerantseva, and J. P. Vacanti, *World J. Surg.* **25**, 1458 (2001).
37. J. A. Hubbell, *Curr. Opin. Biotechnol.* **10**, 123 (1999).
38. J. R. Potts and I. D. Campbell, *Matrix Biol.* **15**, 313 (1996).
39. J. G. Steele, B. A. Dalton, G. Johnson, and P. A. Underwood, *Biomaterials* **16**, 1057 (1995).
40. M. Mrksich, C. S. Chen, Y. N. Xia, L. E. Dike, D. E. Ingber, and G. M. Whitesides, *Proc. Natl. Acad. Sci. U.S.A.* **93**, 10775 (1996).
41. C. D. Tidwell, S. I. Ertel, B. D. Ratner, B. J. Tarasevich, S. Atre, and D. L. Allara, *Langmuir* **13**, 3404 (1997).
42. C. H. Thomas, C. D. McFarland, M. L. Jenkins, A. Rezania, J. G. Steele, and K. E. Healy, *J. Biomed. Mater. Res.* **37**, 81 (1997).
43. A. J. Garcia, P. Ducheyne, and D. Boettiger, *Tissue Eng.* **3**, 197 (1997).
44. K. Webb, K. Caldwell, and P. A. Tresco, *Crit. Rev. Biomed. Eng.* **28**, 203 (2000).
45. G. Rainaldi, P. Filippini, A. Ferrante, P. L. Indovina, and M. T. Santini, *J. Biomed. Mater. Res.* **55**, 104 (2001).
46. R. Biran, K. Webb, M. D. Noble, and P. A. Tresco, *J. Biomed. Mater. Res.* **55**, 1 (2001).
47. C. R. Nuttelman, D. J. Mortisen, S. M. Henry, and K. S. Anseth, *J. Biomed. Mater. Res.* **57**, 217 (2001).
48. M. Balcells and E. R. Edelman, *J. Cell. Physiol.* **191**, 155 (2002).
49. W. G. Dai and W. M. Saltzman, *Biotechnol. Bioeng.* **50**, 349 (1996).
50. S. P. Palecek, J. C. Loftus, M. H. Ginsberg, D. A. Lauffenburger, and A. F. Horwitz, *Nature* **385**, 537 (1997).
51. S. M. Cannizzaro, R. F. Padera, R. Langer, R. A. Rogers, F. E. Black, M. C. Davies, S. J. B. Tendler, and K. M. Shakesheff, *Biotechnol. Bioeng.* **58**, 529 (1998).

52. K. M. Shakesheff, S. M. Cannizzaro, and R. Langer, *J. Biomater. Sci.—Polym. Ed.* **9**, 507 (1998).
53. G. B. Fields, J. L. Lauer, Y. Dori, P. Forns, Y. C. Yu, and M. Tirrell, *Biopolymers* **47**, 143 (1998).
54. N. Patel, R. Padera, G. H. W. Sanders, S. M. Cannizzaro, M. C. Davies, R. Langer, C. J. Roberts, S. J. B. Tendler, P. M. Williams, and K. M. Shakesheff, *FASEB J.* **12**, 1447 (1998).
55. J. L. Myles, B. T. Burgess, and R. B. Dickinson, *J. Biomater. Sci.—Polym. Ed.* **11**, 69 (2000).
56. R. A. Quirk, W. C. Chan, M. C. Davies, S. J. B. Tendler, and K. M. Shakesheff, *Biomaterials* **22**, 865 (2001).
57. R. A. Stile and K. E. Healy, *Biomacromolecules* **2**, 185 (2001).
58. B. K. Mann, A. S. Gobin, A. T. Tsai, R. H. Schmedlen, and J. L. West, *Biomaterials* **22**, 3045 (2001).
59. D. J. Irvine, A. V. G. Ruzette, A. M. Mayes, and L. G. Griffith, *Biomacromolecules* **2**, 545 (2001).
60. C. R. Lowe, B. Hin, D. C. Cullen, S. E. Evans, L. D. G. Stephens, and P. Maynard, *J. Chromatogr.* **510**, 347 (1990).
61. M. P. Byfield and R. A. Abuknesha, *Biosens. Bioelectron.* **9**, 373 (1994).
62. A. F. Collings and F. Caruso, *Rep. Prog. Phys.* **60**, 1397 (1997).
63. P. J. O'Connell and G. G. Guilbault, *Anal. Lett.* **34**, 1063 (2001).
64. T. Wink, S. J. vanZuilen, A. Bult, and W. P. vanBennekom, *Analyst* **122**, R43 (1997).
65. G. G. Roberts and C. W. Pitt, *Langmuir–Blodgett Films*, Elsevier, Amsterdam, 1982/1983.
66. J. Sagiv, *J. Am. Chem. Soc.* **102**, 92 (1980).
67. R. G. Nuzzo and D. L. Allara, *J. Am. Chem. Soc.* **105**, 4481 (1983).
68. M. D. Porter, T. B. Bright, D. L. Allara, and C. E. D. Chidsey, *J. Am. Chem. Soc.* **109**, 3559 (1987).
69. S. Howell, M. Kenmore, M. Kirkland, and R. A. Badley, *J. Mol. Recognit.* **11**, 200 (1998).
70. J. M. Lee, H. H. L. Edwards, C. A. Pereira, and S. I. Samii, *J. Mater. Sci.: Mater. Med.* **7**, 531 (1996).
71. J. Turkova, *J. Chromatogr., B* **722**, 11 (1999).
72. P. S. Stayton, S. Freitag, L. A. Klumb, A. Chilkoti, V. Chu, J. E. Penzotti, R. To, D. Hyre, I. Le Trong, T. P. Lybrand, and R. E. Stenkamp, *Biomol. Eng.* **16**, 39 (1999).
73. P. S. Stayton, K. E. Nelson, T. C. McDevitt, V. Bulmus, T. Shimoboji, Z. Ding, and A. S. Hoffman, *Biomol. Eng.* **16**, 93 (1999).
74. H. Gunasingham, P. Y. T. Teo, Y. H. Lai, and S. G. Tan, *Biosensors* **4**, 349 (1989).
75. J. H. Liu, M. Y. Chen, and M. T. Lin, *J. Appl. Polym. Sci.* **40**, 2161 (1990).
76. Y. Kajiya, H. Sugai, C. Iwakura, and H. Yoneyama, *Anal. Chem.* **63**, 49 (1991).
77. M. J. Mura-Galelli, J. C. Voegel, S. Behr, E. F. Bres, and P. Schaaf, *Proc. Natl. Acad. Sci. U.S.A.* **88**, 5557 (1991).
78. V. A. Rebar and M. M. Santore, *Macromolecules* **29**, 6262 (1996).
79. C. Calonder, Y. Tie, and P. R. Van Tassel, *Proc. Natl. Acad. Sci. U.S.A.* **98**, 10664 (2001).
80. J. J. Ramsden, *Chem. Soc. Rev.* **24**, 73 (1995).
81. J. J. Ramsden, *Phys. Rev. Lett.* **71**, 295 (1993).
82. I. Lundstrom, *Prog. Colloid Polym. Sci.* **70**, 76 (1985).
83. M. Wahlgren, T. Arnebrant, and I. Lundstrom, *J. Colloid Interface Sci.* **175**, 506 (1995).
84. V. P. Zhdanov and B. Kasemo, *Proteins* **40**, 539 (2000).
85. P. Zhdanov, F. Hook, and B. Kasemo, *Proteins* **43**, 489 (2001).
86. W. J. Ceyrolles, P. Viot, and J. Talbot, *Langmuir* **18**, 1112 (2002).
87. J. W. Evans, *Rev. Mod. Phys.* **65**, 1281 (1993).

88. P. Schaaf, J. C. Voegel, and B. Senger, *Ann. Phys. (Paris)* **23**, 1 (1998).
89. J. Talbot, G. Tarjus, P. R. Van Tassel, and P. Viot, *Colloids Surf., A* **165**, 287 (2000).
90. A. Renyi, *Publ. Math. Inst. Hung. Acad. Sci.* **3**, 109 (1958).
91. A. Renyi, *Sel. Trans. Math. Stat. Prob.* **4**, 205 (1963).
92. P. Schaaf and J. Talbot, *Phys. Rev. Lett.* **62**, 175 (1989).
93. Y. Pomeau, *J. Phys. A: Math. Gen.* **13** L193 (1980).
94. R. H. Swendsen, *Phys. Rev. A* **24**, 504 (1981).
95. J. Talbot, G. Tarjus, and P. Schaaf, *Phys. Rev. A* **40**, 4808 (1989).
96. P. R. Van Tassel, P. Viot, G. Tarjus, and J. Talbot, *J. Chem. Phys.* **101**, 7064 (1994).
97. P. R. Van Tassel, J. Talbot, G. Tarjus, and P. Viot, *Phys. Rev. E* **53**, 785 (1996).
98. P. R. Van Tassel, P. Viot, and G. Tarjus, *J. Chem. Phys.* **106**, 761 (1997).
99. V. P. Zhdanov and B. Kasemo, *Proteins* **30**, 177 (1998).
100. V. P. Zhdanov and B. Kasemo, *J. Chem. Phys.* **109**, 6497 (1998).
101. A. P. Minton, *Biophys. J.* **76**, 176 (1999).
102. M. A. Brusatori and P. R. Van Tassel, *J. Colloid Interface Sci.* **219**, 333 (1999).
103. J. Talbot, *Adsorpt.—J. Int. Adsorpt. Soc.* **2**, 89 (1996).
104. A. P. Minton, *Biophys. Chem.* **86**, 239 (2000).
105. A. P. Minton, *Biophys. J.* **80**, 1641 (2001).
106. X. Z. Jin, N. H. L. Wang, G. Tarjus, and J. Talbot, *J. Phys. Chem.* **97**, 4256 (1993).
107. C. Calonder and P. R. Van Tassel, *Langmuir* **17**, 4392 (2001).
108. F. Fang and I. Szleifer, *Biophys. J.* **80**, 2568 (2001).
109. M. A. Carignano and I. Szleifer, *Mol. Phys.* **100**, 2993 (2002).
110. T. McPherson, A. Kidane, I. Szleifer, and K. Park, *Langmuir* **14**, 176 (1998).
111. K. A. Sharp and B. Honig, *Annu. Rev. Biophys. Biophys. Chem.* **19**, 301 (1990).
112. B. J. Yoon and A. M. Lenhoff, *J. Phys. Chem.* **96**, 3130 (1992).
113. C. M. Roth and A. M. Lenhoff, in M. Malmsten, ed., *Biopolymers at Interfaces*, Marcel Dekker, Inc., New York, 1998, p. 89.
114. D. R. Lu, S. J. Lee, and K. Park, *J. Biomater. Sci.—Polym. Ed.* **3**, 127 (1991).
115. C. Calonder, J. Talbot, and J. J. Ramsden, *J. Phys. Chem. B* **105**, 725 (2001).
116. J. Stahlberg, B. Jonsson, and C. Horvath, *Anal. Chem.* **64**, 3118 (1992).
117. C. M. Roth and A. M. Lenhoff, *Langmuir* **11**, 3500 (1995).
118. J. Stahlberg and B. Jonsson, *Anal. Chem.* **68**, 1536 (1996).
119. C. M. Roth, K. K. Unger, and A. M. Lenhoff, *J. Chromatogr. A* **726**, 45 (1996).
120. N. BenTal, B. Honig, R. M. Peitzsch, G. Denisov, and S. McLaughlin, *Biophys. J.* **71**, 561 (1996).
121. D. Asthagiri and A. M. Lenhoff, *Langmuir* **13**, 6761 (1997).
122. C. J. van Oss, A. Docoslis, W. Wu, and R. F. Giese, *Colloids Surf., B* **14**, 99 (1999).
123. M. R. Oberholzer, J. M. Stankovich, S. L. Carnie, D. Y. C. Chan, and A. M. Lenhoff, *J. Colloid Interface Sci.* **194**, 138 (1997).
124. M. R. Oberholzer, N. J. Wagner, and A. M. Lenhoff, *J. Chem. Phys.* **107**, 9157 (1997).
125. M. R. Oberholzer and A. M. Lenhoff, *Langmuir* **15**, 3905 (1999).
126. S. Ravichandran and J. Talbot, *Biophys. J.* **78**, 110 (2000).
127. R. Menes, P. Pincus, R. Pittman, and N. Dan, *Europhys. Lett.* **44**, 393 (1998).
128. C. Fleck, R. R. Netz, and H. H. von Grunberg, *Biophys. J.* **82**, 76 (2002).
129. K. A. Dill, S. Bromberg, K. Z. Yue, K. M. Fiebig, D. P. Yee, P. D. Thomas, and H. S. Chan, *Protein Sci.* **4**, 561 (1995).
130. M. Karplus and A. Sali, *Curr. Opin. Struct. Biol.* **5**, 58 (1995).
131. V. S. Pande, A. Y. Grosberg, and T. Tanaka, *Rev. Mod. Phys.* **72**, 259 (2000).
132. H. S. Chan and K. A. Dill, *Annu. Rev. Biophys. Biophys. Chem.* **20**, 447 (1991).
133. R. Miller, C. A. Danko, M. J. Fasolka, A. C. Balazs, H. S. Chan, and K. A. Dill, *J. Chem. Phys.* **96**, 768 (1992).
134. E. I. Shakhnovich and A. M. Gutin, *Proc. Natl. Acad. Sci. U.S.A.* **90**, 7195 (1993).
135. H. S. Chan and K. A. Dill, *J. Chem. Phys.* **100**, 9238 (1994).

136. N. D. Socci and J. N. Onuchic, *J. Chem. Phys.* **101**, 1519 (1994).
137. A. M. Gutin, V. I. Abkevich, and E. I. Shakhnovich, *Proc. Natl. Acad. Sci. U.S.A.* **92**, 1282 (1995).
138. N. D. Socci and J. N. Onuchic, *J. Chem. Phys.* **103**, 4732 (1995).
139. E. I. Shakhnovich and A. M. Gutin, *Nature* **346**, 773 (1990).
140. E. Shakhnovich, G. Farztdinov, A. M. Gutin, and M. Karplus, *Phys. Rev. Lett.* **67**, 1665 (1991).
141. D. K. Klimov and D. Thirumalai, *Phys. Rev. Lett.* **76**, 4070 (1996).
142. D. K. Klimov and D. Thirumalai, *Proteins* **26**, 411 (1996).
143. D. K. Klimov and D. Thirumalai, *J. Chem. Phys.* **109**, 4119 (1998).
144. V. P. Zhdanov and B. Kasemo, *Phys. Rev. E: stat. Phys., Plasmas, Fluids, Relat. Interdiscip. Top.* **56**, 2306 (1997).
145. V. P. Zhdanov and B. Kasemo, *Proteins* **42**, 481 (2001).
146. V. Castells, S. Yang, and P. R. Van Tassel, *Phys. Rev. E: stat. Phys., Plasmas, Fluids, Relat. Interdiscip. Top.* **65**, 031912 (2002).
147. R. E. Anderson, V. S. Pande, and C. J. Radke, *J. Chem. Phys.* **112**, 9167 (2000).
148. M. R. Wattenbarger, H. S. Chan, D. F. Evans, V. A. Bloomfield, and K. A. Dill, *J. Chem. Phys.* **93**, 8343 (1990).
149. H. S. Chan, M. R. Wattenbarger, D. F. Evans, V. A. Bloomfield, and K. A. Dill, *J. Chem. Phys.* **94**, 8542 (1991).
150. J. M. H. M. Scheutjens and G. J. Fleer, *J. Phys. Chem.* **83**, 1619 (1979).
151. J. M. H. M. Scheutjens and G. J. Fleer, *J. Phys. Chem.* **84**, 178 (1980).
152. G. Belfort and C. S. Lee, *Proc. Natl. Acad. Sci. U.S.A.* **88**, 9146 (1991).
153. E. Dickinson, V. J. Pinfield, D. S. Horne, and F. A. M. Leermakers, *J. Chem. Soc., Faraday Trans.* **93**, 1785 (1997).
154. F. A. M. Leermakers, P. J. Atkinson, E. Dickinson, and D. S. Horne, *J. Colloid Interface Sci.* **178**, 681 (1996).
155. E. Dickinson, D. S. Horne, V. J. Pinfield, and F. A. M. Leermakers, *J. Chem. Soc., Faraday Trans.* **93**, 425 (1997).
156. E. Dickinson, V. J. Pinfield, and D. S. Horne, *J. Colloid Interface Sci.* **187**, 539 (1997).
157. J. M. P. van den Oever, F. A. M. Leermakers, G. J. Fleer, V. A. Ivanov, N. P. Shusharina, A. R. Khokhlov, and P. G. Khalatur, *Phys. Rev. E: stat. Phys., Plasmas, Fluids, Relat. Interdiscip. Top.* **65**, 041708 (2002).
158. T. Cosgrove, N. A. Finch, and J. R. P. Webster, *Macromolecules* **23**, 3353 (1990).
159. C. M. Marques and J. F. Joanny, *Macromolecules* **23**, 268 (1990).
160. J. F. Joanny, *J. Phys. II* **4**, 1281 (1994).
161. L. Gutman and A. K. Chakraborty, *J. Chem. Phys.* **101**, 10074 (1994).
162. L. Gutman and A. K. Chakraborty, *J. Chem. Phys.* **103**, 10733 (1995).
163. L. Gutman and A. K. Chakraborty, *J. Chem. Phys.* **105**, 7842 (1996).
164. L. Gutman and A. K. Chakraborty, *J. Chem. Phys.* **104**, 7306 (1996).
165. S. Srebnik, A. K. Chakraborty, and E. I. Shakhnovich, *Phys. Rev. Lett.* **77**, 3157 (1996).
166. D. Bratko, A. K. Chakraborty, and E. I. Shakhnovich, *Comput. Theor. Polym. Sci.* **8**, 113 (1998).
167. A. K. Chakraborty and D. Bratko, *J. Chem. Phys.* **108**, 1676 (1998).
168. S. Srebnik, A. K. Chakraborty, and D. Bratko, *J. Chem. Phys.* **109**, 6415 (1998).
169. A. J. Golumbfskie, V. S. Pande, and A. K. Chakraborty, *Proc. Natl. Acad. Sci. U.S.A.* **96**, 11707 (1999).
170. X. Chatellier and J. F. Joanny, *Eur. Phys. J. E* **1**, 9 (2000).
171. S. Srebnik, *J. Chem. Phys.* **112**, 9655 (2000).
172. A. Naidenov and S. Nechaev, *J. Phys. A: Math. Gen.* **34**, 5625 (2001).
173. V. A. Brazhnyi and S. Stepanow, *Eur. Phys. J. B* **27**, 355 (2002).
174. S. Stepanow and A. L. Chudnovskiy, *J. Phys. A: Math. Gen.* **35**, 4229 (2002).
175. S. F. Edwards and P. W. Anderson, *J. Phys. F.* **5**, 965 (1975).

176. R. R. Netz and J. F. Joanny, *Macromolecules* **32**, 9013 (1999).
177. N. Pernodet, V. Samuilov, K. Shin, J. Sokolov, M. H. Rafailovich, D. Gersappe, and B. Chu, *Phys. Rev. Lett.* **85**, 5651 (2000).
178. Y. S. Velichko, K. Yoshikawa, and A. R. Khokhlov, *Biomacromolecules* **1**, 459 (2000).
179. D. R. Lu and K. Park, *J. Biomater. Sci.—Polym. Ed.* **1**, 243 (1990).
180. S. J. Lee and K. Park, *J. Vac. Sci. Technol., A* **12**, 2949 (1994).
181. V. Noinville, C. Vidalmadjar, and B. Sebille, *J. Phys. Chem.* **99**, 1516 (1995).
182. R. A. Latour and C. J. Rini, *J. Biomed. Mater. Res.* **60**, 564 (2002).
183. K. Lim and J. N. Herron, in J. M. Harris, ed., *Poly(ethylene glycol) Chemistry: Biotechnical and Biomedical Applications*, Plenum Press, New York, 1992, p. 29.
184. D. J. Tobias, W. Mar, J. K. Blasie, and M. L. Klein, *Biophys. J.* **71**, 2933 (1996).
185. A. M. Bujnowski and W. G. Pitt, *J. Colloid Interface Sci.* **203**, 47 (1998).
186. J. D. Madura, K. Baran, and A. Wierzbicki, *J. Mol. Recognit.* **13**, 101 (2000).
187. S. Ravichandran, J. D. Madura, and J. Talbot, *J. Phys. Chem. B* **105**, 3610 (2001).
188. J. J. Ramsden, *Q. Rev. Biophys.* **27**, 41 (1994).
189. P. B. Garland, *Q. Rev. Biophys.* **29**, 91 (1996).
190. P. Schaaf, P. Dejardin, and A. Schmitt, *Revue De Physique Appliquee* **20**, 631 (1985).
191. P. Schaaf, P. Dejardin, and A. Schmitt, *Revue De Physique Appliquee* **21**, 741 (1986).
192. M. Malmsten, *J. Colloid Interface Sci.* **166**, 333 (1994).
193. L. Heinrich, E. K. Mann, J. C. Voegel, and P. Schaaf, *Langmuir* **13**, 3177 (1997).
194. H. Elwing, *Biomaterials* **19**, 397 (1998).
195. J. A. de Feijter, J. Bejamins, and F. A. Veer, *Biopolymers* **17**, 1759 (1978).
196. P. M. Nellen, K. Tiefenthaler, and W. Lukosz, *Sens. Actuators* **15**, 285 (1988).
197. W. Lukosz, *Sens. Actuators, B* **29**, 37 (1995).
198. J. Voros, J. J. Ramsden, G. Csucs, I. Szendro, S. M. De Paul, M. Textor, and N. D. Spencer, *Biomaterials* **23**, 3699 (2002).
199. N. J. Harrick, *Internal Reflection Spectroscopy*, John Wiley & Sons, Inc., New York, 1967.
200. N. L. Thompson and D. Axelrod, *Biophys. J.* **33**, A183 (1981).
201. R. A. Vanwagenen and J. D. Andrade, *Fed. Proc.* **41**, 1483 (1982).
202. B. K. Lok, Y. L. Cheng, and C. R. Robertson, *J. Colloid Interface Sci.* **91**, 87 (1983).
203. K. K. Chittur, *Biomaterials* **19**, 357 (1998).
204. A. R. Hind, S. K. Bhargava, and A. McKinnon, *Adv. Colloid Interface Sci.* **93**, 91 (2001).
205. B. Liedberg, C. Nylander, and I. Lundstrom, *Sens. Actuators* **4**, 299 (1983).
206. S. Lofas, M. Malmqvist, I. Ronnberg, E. Stenberg, B. Liedberg, and I. Lundstrom, *Sens. Actuators, B* **5**, 79 (1991).
207. B. Liedberg, C. Nylander, and I. Lundstrom, *Biosens. Bioelectron.* **10**, R1 (1995).
208. J. Homola, S. S. Yee, and G. Gauglitz, *Sens. Actuators, B* **54**, 3 (1999).
209. L. M. Lechuga, A. Calle, and F. Prieto, *Quim. Anal.* **19**, 54 (2000).
210. G. Z. Sauerbrey, *Z. Physics* **155**, 206 (1959).
211. M. Rodahl, F. Hook, A. Krozer, P. Brzezinski, and B. Kasemo, *Rev. Sci. Instrum.* **66**, 3924 (1995).
212. M. Rodahl, F. Hook, and B. Kasemo, *Anal. Chem.* **68**, 2219 (1996).
213. C. K. O'Sullivan and G. G. Guilbault, *Biosens. Bioelectron.* **14**, 663 (1999).
214. C. K. O'Sullivan, R. Vaughan, and G. G. Guilbault, *Anal. Lett.* **32**, 2353 (1999).
215. G. Binnig, C. F. Quate, and C. Gerber, *Phys. Rev. Lett.* **56**, 930 (1986).
216. J. Jahanmir, B. G. Haggar, and J. B. Hayes, *Scanning Microsc.* **6**, 625 (1992).
217. H. G. Hansma and L. Pietrasanta, *Curr. Opin. Chem. Biol.* **2**, 579 (1998).

PAUL R. VAN TASSEL
Wayne State University

BIOTECHNOLOGY APPLICATIONS. See Volume 1.

BLOCK COPOLYMERS. See Volume 1.

BLOCK COPOLYMERS, TERNARY TRIBLOCK. See Volume 1.

BLOWING AGENTS. See CELLULAR MATERIALS.

BLOW MOLDING. See Volume 1.

BULK AND SOLUTION POLYMERIZATIONS REACTORS

Introduction

This article discusses polymerization reactors where the continuous phase is a solution of a polymer in its own monomer or in a solvent. When the low molecular weight species is primarily monomer, the reaction is a bulk polymerization; and when it is a solvent, the reaction is a solution polymerization. This distinction has little practical importance. The important consideration is that a high viscosity polymer solution is the continuous phase and is in contact with the reactor walls and the agitator. In contrast, suspended-phase polymerizations (such as emulsion, dispersion, and suspension) and gas-phase polymerizations have a low viscosity continuous phase (see HETEROPHASE POLYMERIZATION).

Table 1 lists representative bulk and solution polymerizations. All these polymerizations give a polymer-rich continuous phase that, at the end of the reaction, will have a viscosity $10^4 - 10^7$ times higher than the feed solution. Laminar flow is the norm. Heat and mass transfer coefficients are much lower than is common in the chemical industry, and specialized equipment is often necessary.

The manner in which viscosity increases with conversion has a strong influence on reactor design. Polymerizations with long chain lives, such as condensation and anionic polymerizations increase chain length and viscosity slowly. When half the monomer has reacted, the number-average chain length will be about 2 and the viscosity of the mixture will be about twice that of the pure monomer. Polymerizations with short chain lives, as is typical of free-radical and transition-metal catalyses, yield high molecular weight polymers from the onset. A mixture containing 50% monomer by weight might contain a polymer with an

Encyclopedia of Polymer Science and Technology. Copyright John Wiley & Sons, Inc. All rights reserved.

Table 1. Representative Bulk and Solution Polymerizations

Polymer	Type of polymerization	Process	Reaction medium	Heat of reaction, kJ/mol[a]	Reaction exotherm, K	By-product to be removed
Polyethylene	Vinyl addition	High pressure	Solution of polyethylene in ethylene	95.0	1610	Heat
High density Polyethylene	Vinyl addition	Solution	Solution of polyethylene in hexane	95.0	1610	Heat
Poly(vinyl chloride)	Vinyl addition	Bulk	Polymer-rich phase in contact with a (suspended) vinyl chloride phase	95.8	730	Heat
Polystyrene	Vinyl addition	Bulk	Solution of polystyrene in styrene and ethyl benzene	69.9	320	Heat
PMMA	Vinyl addition	Bulk	Solution of polymer in methyl methacrylate	56.5	270	Heat
Nylon-6	Ring opening	Bulk	Solution of polymer in caprolactam	15.9	68	None
Polysulfone	Condensation	Solution	Solution of polymers and monomers in monochlorobenzene with a suspended NaCl phase	25.1	24	NaCl
Polycarbonate	Condensation	Interfacial	Polymer solution in methylene chloride in contact with an aqueous NaOH phase	0	0	HCl (as NaCl)
Poly(butylene terephthalate)	Condensation	Bulk	Polymer solution in diglycol terephthalate	0	0	Ethylene glycol

[a]To convert kJ/mol to kcal/mol, divide by 4.184.

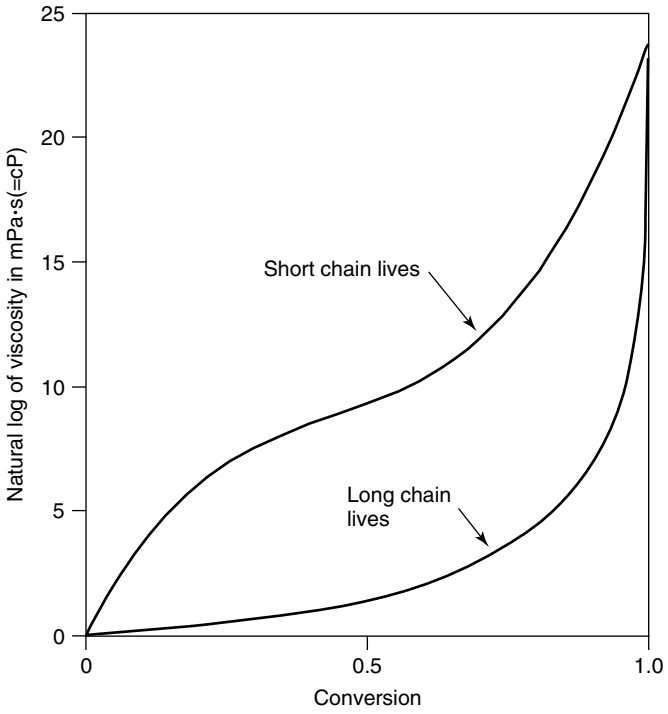

Fig. 1. Representative curves of viscosity as a function of conversion for short and long chain lives. The end point in both cases is a number-average chain length of 1000 and 0.1% residual monomer.

average chain length of 1000 and a viscosity that is 10^4 times that of the monomer. Figure 1 illustrates the difference between short and long chain lives for a polymerization that starts and ends at the same points but proceeds by different mechanisms.

There are three key design issues in bulk and solution polymerizations:

(1) Removing the heat of polymerization. This is applicable mainly to vinyl addition polymerizations.
(2) Achieving adequate stoichiometry and by-product removal to obtain high molecular weight polymers. This is applicable mainly to condensation polymers.
(3) Achieving desired copolymer composition distributions.

Managing the Reaction Exotherm

For vinyl addition and diene polymerizations, heat removal is a primary concern. The reaction exotherm listed in Table 1 is the heat of polymerization divided by the specific heat of the polymer. It is a fictitious quantity for energetic polymerizations since bonds break and the polymer reaches a ceiling temperature well before

Table 2. Methods for Temperature Control

Method for controlling temperature	Example system
React to low conversion	High pressure polyethylene
Dilute with solvent	Solution polyethylene
Dilute with dead polymer	PMMA casting
Adiabatic reactors	Nylon-6 casting
Boiling CSTRs	Polystyrene bulk continuous
Cold feed to a CSTR	PMMA bulk continuous
CSTRs with heat transfer to jackets or internal coils	Specialty polymers in small reactors
Flow inside a single tube	High pressure polyethylene
Shell-and-tube reactors	Solution polyethylene
Stirred-tube reactors	Polystyrene bulk continuous

the full exotherm is realized, but it provides a rough measure of the difficulty of controlling the reaction temperature.

The vinyl addition polymers undergo polymerization by opening a double bond in a substituted ethylene molecule. The energy release is 50–100 kJ/mol. The reaction exotherm varies over a broader range since it depends on the mass of the substituted groups. Thus ethylene and vinyl chloride polymerizations have the same heat of reaction per mole but very different exotherms due to the relative mass of the monomers. The vinyl addition polymerizations are too energetic to allow adiabatic polymerizations, except in very special cases. Heat removal is a dominant consideration in reactor design. In sharp contrast, a condensation polymer such as poly(ethylene terephthalate) is formed by a series of ester exchange reactions where the bonds being made and broken have nearly the same energy. Adiabatic polymerizations are possible for such polymers, and heat may even be added to evaporate the condensation by-product. Conversion is typically limited by by-product removal.

Table 2 lists various methods that have been used to control the temperature in bulk and solution polymerizations. All these processes continued to be practiced industrially but some would no longer be chosen for new construction.

Reaction to low conversion and the use of large amounts of solvent are conceptually similar. The high pressure process for low density polyethylene limits conversion to about 15%. This reduces the exotherm to about 250°C. A similar result is achieved in the solution process for high density polyethylene, where the conversion of monomer is high but the reactor contains about 85% solvent. Both processes rely on supplemental cooling by sensible heat transfer to tube walls. The high pressure uses a single tube and is “once through” with respect to polymer. The solvent process employs a shell-and-tube heat exchanger in a recycle loop.

Figure 2 shows the reaction exotherm for the semi adiabatic batch polymerization of a methyl methacrylate casting system. The methyl methacrylate monomer has been diluted with dead polymer to limit the exotherm and to increase the viscosity of the casting syrup. The polymerizing mass undergoes a glass transition and polymerization stops before the temperature reaches the atmospheric boiling point of methyl methacrylate, thus avoiding bubbles in the cast

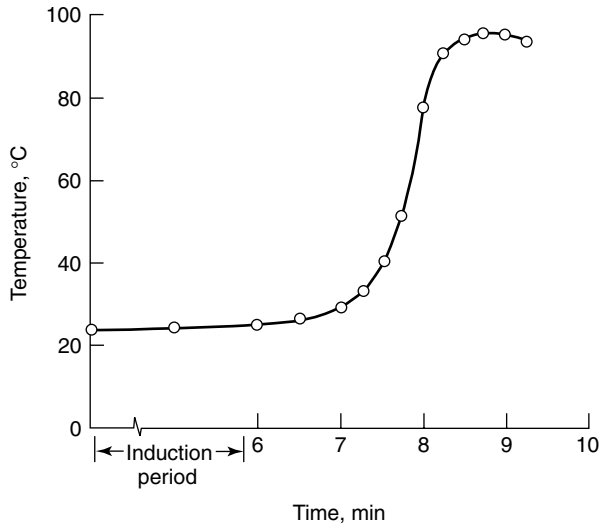

Fig. 2. Reaction exotherm for a methyl methacrylate casting system.

product. A less energetic polymerization such as that for polycaprolactam can be cast in large parts without need for dilution with dead polymer.

Continuous-flow stirred-tank reactors (CSTRs) can be cooled in three ways. The most elegant method is to allow boiling of the monomer or solvent so that the heat of reaction is removed in an overhead condenser. The pressure in the vessel is set to give the desired temperature. The condensate can be returned to the vessel or recycled back to the feed. This process is commonly used for polystyrene. Chilling the feed is another means for managing the exotherm in a CSTR. Refrigeration to -40°C has been used for the bulk, continuous polymerization of PMMA. Laboratory reactors and small-scale industrial reactors can be cooled using jackets or internal coils, but this method scales up poorly.

Removing Chemical By-products

Most condensation polymerizations are reversible and become limited by equilibrium unless the condensation by-product is removed. Spontaneous removal occurs when the by-product is insoluble in the reaction medium. The low solubility of NaCl in organic solvents means reactions like those for polysulfone and phenoxy (ie a high molecular epoxy) proceed irreversibly with the chain length depending only on the reaction time and initial stoichiometry. Phenol–formaldehyde condensations are limited both by the initial stoichiometry and by the formation of by-product water. Dual limitations are difficult to satisfy when a high molecular weight polymer is desired, and it is common to change the chemistry so that the stoichiometric limitation is eliminated. If poly(ethylene terephthalate) were made by the direct condensation of its two monomers, terephthalic acid and ethylene glycol, exact stoichiometry and removal of by-product water would both be needed to achieve high molecular weights. The standard industrial process uses

a preliminary esterification and separation to obtain a self-condensing monomer, diglycol terephthalate. The monomer has inherently perfect stoichiometry, but its polymerization is strictly limited by the presence of by-product ethylene gycol. By-product removal is easy when the viscosity is low. A typical process has one or two stirred tanks in series that remove ethylene glycol in overhead condensers. The effluent from the last stirred tank is fed to a specially designed reactor that approximates piston flow (also known as plug flow). It is typically a twin-screw device machine that exposes the now viscous polymer solution to vacuum while moving it forward.

Copolymerization

Random Copolymerization. Bulk and solution polymerizations are well suited to copolymerization where a second or third monomer is added to achieve desired physical properties. Minor amounts of an alpha-olefin, such as 1-butene or 1-hexene, are copolymerized with ethylene to control crystallinity and density, producing linear low density polyethylene. A second diol is used to control crystallinity in poly(ethylene terephthalate). Examples are the two monomers used in substantially equal quantities, styrene/acrylonitrile polymers and ethylene/propylene rubbers. The need in all these examples is to achieve a uniform distribution of the various monomers within a polymer chain and between chains produced at different points or times in the reactor. Batch and tubular reactors are poorly suited to this task because the monomers react at different rates. When the chain life is short, molecules formed early and late in the polymerization will have different average compositions. When the chain life is long, a substantial composition difference can exist within individual molecules. These problems can be avoided by using a continuous-flow stirred tank or the functionally equivalent loop reactor. A loop reactor that consists of a pump, heat exchanger, and recycle piping provides the same mixing environment as a stirred tank but is more easily scaled up when heat must be transfer through the vessel walls. Boiling CSTRs also scale well for heat transfer purposes. In either geometry, ie a conventional tank with an internal agitator or the loop reactor, entering feed is rapidly mixed and distributed throughout the vessel to provide a chemically uniform environment.

Block Copolymerization. A polymerization with long chain lives can be used to make block copolymers (qv). An important commercial example is styrene/butadiene blocks produced by anionic polymerization (qv). A solution polymerization is done in a batch reactor, starting with one of the two monomers. That monomer is reacted to completion and the second monomer is added while the catalytic sites on the chains remain active. This produces a block copolymer of the AB form. Early addition of the second monomer produces a tapered block. If the second monomer is reacted to completion and replaced by the first monomer, an ABA triblock is obtained. This process is not easily converted to continuous operation because polymerizations inside tubes rarely approach the piston-flow environment that is needed to react one monomer to completion before adding the second monomer. Designs using static mixers (also known as motionless mixers) are a possibility.

Kinetic Models

A process model for any type of polymerization must begin with a kinetic model. Condensation polymerizations have relatively simple kinetics. The forward reaction is typically modeled as a second-order reaction with respect to the end groups, using a single rate constant assumed to be independent of chain length. The reverse reaction is also modeled as second order. Addition polymerizations are more complex, consisting of initiation, propagation, chain transfer, and termination steps. The mathematics are understood but the necessary constants are rarely published. A significant exception is the classic kinetic study by Hui and Hamielec (1) on styrene polymerization that, with minor modifications, has had wide industrial use and serves as a prototype for similar studies.

The gel effect is a special phenomenon encountered in free-radical polymerizations, that can have a major effect on reactor design. As the polymerization proceeds, the viscosity of the reaction mix increases. The diffusivity of all molecular species decreases, but chain entanglements cause the diffusivity of long polymer molecules to decrease to a much greater extent than the monomer. The initiation rate is unaffected when a chemical initiator is used and is largely unaffected even for thermal initiation. Propagation involves a small molecule reacting with a growing chain and continues at a reasonable rate. However, the termination step involves interactions between two large molecules so that the termination rate decreases significantly at high conversion. The concentration of free radicals increases, as do the total polymerization rate and the average chain length. This leads to still larger reductions in the termination rate and to an autoaccelerating reaction that can be almost explosively fast. Poly(methyl methacrylate) provides the classic example of the gel effect. The autoacceleration shown in Figure 1 is due to the combined effects of the exotherm and chain entanglements. A commercial process for polystyrene uses a single stirred tank operated at about 70 wt% polymer. The entire vessel operates in the gel region and thus has a very high volume productivity.

Tubular Reactors

Polymerizations in tubular reactors have been extensively studied. Most results are proprietary, although quite comprehensive models for the polymerization of styrene in a tube are available in the literature. Tubular reactor models combine the equations for diffusion, reaction, and heat transfer. They are coupled with the equations of motion owing to the dependence of viscosity on temperature and composition. The non-Newtonian nature of the polymer solution is of secondary importance. The resulting set of simultaneous equations is readily solved on a computer. Results depend on a large number of parameters that are specific to each polymerization, but the following generalizations are possible:

(1) The low velocities near the tube wall give higher polymer concentrations and higher viscosities. This further lowers velocities near the wall and increases velocities near the centerline. In extreme cases, hydrodynamic instabilities

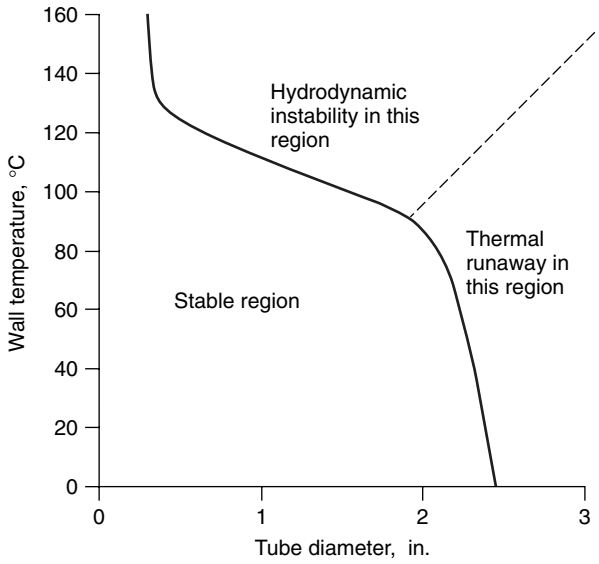

Fig. 3. Stability diagram for the thermally initiated bulk polymerization of styrene with an inlet temperature of 135°C.

lead to oscillations and the jetting of unreacted monomer down the center of the tube.

(2) The heat of polymerization distorts the temperature profile. When there is cooling at the walls, the maximum temperature will occur at an intermediate radial position. For energetic polymerizations, there is a maximum tube diameter beyond which a runaway becomes inevitable.

(3) Tube-to-tube instabilities can arise when multiple tubes are fed in parallel from a single pressure source. If extra polymerization should occur in one tube, the flow through that tube will decrease, leading to still more polymerization. When the feed stream is relatively inviscid, it cannot displace polymer from a tube and the tube plugs.

Figure 3 shows a stability diagram for a bulk styrene polymerization. Performance is governed by four variables: the monomer inlet temperature, the tube diameter, the wall temperature, and the mean residence time in the tube. Figure 3 shows the effects of wall temperature and tube diameter for plausible values of the other variables. Very small tubes are stable for any wall temperature. Intermediate size tubes are subject to hydrodynamic instability and large tubes are subject to thermal runaway. The maximum conversion for a tube larger than 0.95 cm is 20% and is achieved in a 5-cm tube.

The instabilities possible in tubular reactors have had a major influence on the process design. A model of the high pressure process for polyethylene is available in the literature (2) and there are even more sophisticated proprietary models. The highpressure process for polyethylene uses a single tube about 4.5 cm in diameter and several miles long to avoid thermal runaway and tube-to-tube

instabilities. Hydrodynamic problems still exist, and some plants have used a forced oscillation to alleviate them. The discharge valve on the reactor is quickly opened and closed every few minutes, temporarily lowering the discharge pressure from about 240 to 69 MPa (35,000 to 10,000 psi) and causing a sudden surge in flow that redistributes the polymer in the tube.

For most polymerizations starting from monomer, tubular reactors have been avoided because of the various stability problems. They can be used in recycle loops where the per-pass conversion is low, in solution polymerizations with large amounts of solvent, and in post- or finishing reactors intended to drive a polymerization to completion. Shell-and-tube designs with as many as 1000 tubes are used in polystyrene processes where they also serve as devolatilization preheaters. The entering polymer solution has a concentration of about 70%, and its viscosity is high enough to avoid tube-to-tube instabilities.

Kenics-type static mixers have been used as inserts in tubular reactors. Compared to an open tube operated at the same pressure drop, the static mixer gives about 40% more heat transfer. Stand-alone mixer reactors of the Koch or Sultzer SMR type have been used as post-reactors and devolatilization preheaters. The polymer flows through the shell side of the SMR and the heat transfer fluid flows inside tubes that have been strategically placed to promote radial mixing of the polymer. One bulk polystyrene process used the SMR as in a recycle loop as the first reactor, but the capital cost is high compared to alternatives such as a boiling CSTR or a proprietary stirred-tube reactor.

Some tubular reactors have internal agitation. These include conventional single- and twin-screw extruders used for grafting (eg maleation) or other modification reactions that start with a prepolymerized feed. They can provide a surprisingly uniform reaction environment but are extremely expensive in terms of reactor volume. Economics limit residence times to a few minutes and so they are rarely used for polymerizations starting from monomer. Specialized designs are used as polyester finishing reactors, and they are now able to produce the high molecular weights needed for blow-molded bottles, eliminating the previous need for solid-state polymerization.

Conveyor belt and moving web reactors give a piston-flow reaction environment. The polymer layer is usually thin enough so that heat transfer is not a serious issue, but the confinement of vapors to meet environmental requirements can be expensive. Thus waterborne or condensation polymerizations without by-products (eg polyurethanes) are preferred. Ultraviolet and electron beam curing is common. Applications include photographic and xerographic films, breathable fabrics, coated abrasives, and printed films, as well as polymers manufactured on belt flakers.

Stirred-Tank Reactors

Conventional stirred tanks are commonly used for both batch and continuous polymerizations. Normal design practice is to use pitched blade turbines, with impeller to tank diameter ratios of 40–70%, for viscosities up to 10 Pa·s (100 P) and sometimes up to 100 Pa·s. Helical ribbon and sometimes anchor agitators

are used for viscosities of from 10 to 1000 Pa·s, and intermeshing, dual impellers are used for the highest viscosities. Jacket heating or cooling is used for small reactors and for start-ups. Boiling reactors have overhead condensers. Typically, the condensed monomer or solvent is simply returned to the upper surface of the liquid, but is sometimes sprayed over the vapor dome to dissolve any polymer that might polymerize there. A modern polystyrene process consists of a CSTR followed by several stirred-tube reactors in series (3). The stirred-tube reactor is nonboiling and uses internal coils to remove the heat of polymerization. The design scales poorly, and it seems that these reactors have reached their maximum size. Productivity increases are achieved by putting several of them in series. Other nonboiling reactors use an external circulation loop with a shell-and-tube heat exchanger in the loop. In some processes, the stirred tank has been eliminated and the heat exchanger provides most of the reactor volume.

An important design criterion for a stirred-tank reactor, whether batch or continuous, is that the mixing time must be short compared to the reaction half-life. Correlations for mixing time are available in the literature. They range from a few seconds in laboratory glassware to a few minutes in industrial reactors. A secondary criterion for continuous-flow stirred tanks is that the circulation rate must be a large multiple of the net throughput. This criterion ensures that the residence time distribution approximates the exponential distribution of an ideal CSTR. A ratio of 10:1 is normally adequate for this purpose. Some loop reactors have been designed with recycle ratios of 100:1, but this was done to achieve better heat transfer and shorter mixing times.

Solvent Recovery

Removal of solvent including any unreacted monomer is a necessary step in most bulk and solvent polymerizations. One possible method is antisolvent coagulation. The polymer solution is contacted with large quantities of another solvent that is compatible with the original solvent but not with the polymer. When done correctly, the process gives a suspension of nontacky, microporous particles of polymer that are substantially free of solvent. The particles are collected by filtration or centrifugation and are further dried. Antisolvent coagulation is the standard preparative tool of the research chemist but is rarely used industrially because the separation and recycle streams are so large. It is common for the flow rate of stream containing the combined solvents to be more than 50 times that of the polymer stream.

Devolatilization removes volatile components by exposure to heat and vacuum. Single- and twin-screw extruders are commonly used for this purpose, and wiped-film evaporators are used for low volume, specialty polymers. All these devices generate surface area by a combination of mechanical milling and foaming, but generation of surface area by foaming scales up more easily than mechanical generation. Flash devolatilization (qv) relies exclusively on foaming and is the preferred method for high volume polymers.

BIBLIOGRAPHY

"Bulk Polymerization" in *EPST* 1st ed., Vol. 2, pp. 642–666, by H. Ringsdorf, Universitat Marburg; "Bulk Polymerization" in *EPSE* 2nd ed., Vol. 2, pp. 500–514, by E. B. Nauman, Rensselaer Polytechnic Institute; "Solution Polymerization" in *EPSE*, 2nd ed., Vol. 15, pp. 402–418, by G. Swift and K. A. Hughes, Rohm & Haas.
"E. B. Nauman, *Chemical Reactor Design, Optimization and Scaleup*, McGraw-Hill, New York, 2002, Chapts. 8 and 13.
1. A. W. Hiu, and A. E. Hamielac, *J. Appl. Poly. Scim.* **16**, 749 (1972).
2. S. K. Gupta, A. Kumar, and M. V. G. Krishnamurthy, *Polym. Eng. Sci.* **25**, 37–47 (1985).
3. C.-C. Chen, *Polym. Eng. Sci.* **40**, 441–464 (2000).

E. BRUCE NAUMAN
Rensselaer Polytechnic Institute

BUTADIENE POLYMERS

Introduction

1,3-Butadiene was first prepared in 1863, and its conjugated structure was proposed in 1886 (1,2). However, the ability of butadiene to polymerize was not recognized until almost 50 years later when, in 1909, a rubbery polymer was first reported as being prepared from butadiene via thermal polymerization (3). Shortly thereafter, the more controlled polymerization of butadiene initiated by sodium metal was reported in 1911 (4). During this time period, a sharp rise in natural rubber prices prompted the Bayer Corp. to develop methyl rubber from 2,3-dimethylbutadiene. Though interest in synthetic rubber faded after World War I, in 1926 a rise in price of natural rubber prompted the German company I. G. Farbenindustrie to resume research on the sodium-initiated polymerization of butadiene. This work eventually led to the German commercialization of two synthetic rubbers: Buna 32 and Buna 115 (from *bu*tadiene and *na*trium). Concurrently, in the 1920s research on the emulsion polymerization of butadiene was being carried out in Germany and the United States. The first butadiene–styrene copolymer prepared from an emulsion polymerization (Buna S) at I. G. Farbenindustrie proved to be superior to polybutadiene (5). From this work, Buna-N, a copolymer of butadiene and acrylonitrile, was developed for its solvent and oil resistance. Although the products of this work were inferior to natural rubber, their technology, with considerable modification and improvement, formed the basis for synthetic rubber production (GR-S and GR-N) in the United States. Under the government-established Rubber Reserve in World War II, GR-S and SBR became a general-purpose rubber with an annual production of ca 717,700 t in 1945.

Encyclopedia of Polymer Science and Technology. Copyright John Wiley & Sons, Inc. All rights reserved.

Butadiene Monomer

1,3-Butadiene, $CH_2{=}CH{-}CH{=}CH_2$, is the simplest conjugated diene, and its structure has received much theoretical attention because of its symmetry and simplicity (6). Heats of hydrogenation and combustion reveal that the stabilization contributed by the conjugation of the double bonds is 12.5–14.6 kJ/mol (3–3.5 kcal/mol) (7). Electron diffraction reveals a planar molecule with bond lengths C=C, 0.1337 nm; C–C, 0.1483 nm; and C–H, 0.1082 nm; the bond angles are C=C–C 122.4° and C=C–H 119.8° (8). The values for the C–C bond lengths predicted by valence bond approximations are in close agreement with these observed figures (9). The C–C single bond between the two double bonds is shorter than the usual 0.154 nm of an isolated single C–C bond. Some of the proposed explanations for this shortened bond, which indicates some double bond character, can be expressed in polar resonance or terminal diradical structures with some long bond or interaction between the end carbons. However, because the energies of these structures are high, molecular orbital calculations indicate that there is little resonance in the ground state and that the bond lengths are determined by the state of hybridization of carbon (10). The resistance to rotation about the central bond is attributed to π-conjugation and leads to two conformers, the nonpolar *s-trans* and polar *s-cis* form as seen in the conformational equation (1).

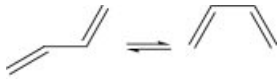

(1)

Although at dry ice temperature the *s-cis* form predominates (11), chemical (12) and spectroscopic (13,14) evidence suggests that *s-cis*-butadiene is present to the extent of only 3% at room temperature. The energy difference between the two forms has been variously determined as 7.1 ± 2.1 kJ/mol (1.7 ± 0.5 kcal/mol) (15) and 9.6 kJ/mol (2.3 kcal/mol) (16).

The ultraviolet spectrum of gaseous butadiene is highly complex, but the origin of each of the transitions in the 230–135 nm region has been identified (17). In hexane solution butadiene absorbs at λ_{max} 217 nm, $\epsilon = 21{,}000$ (18). The bathochromic effect of conjugation is evident upon comparison with those values for ethylene, λ_{max} 170 nm, $\epsilon = 17{,}000$ in the vapor (19).

The infrared spectrum has been recorded in the gaseous (20), liquid (20,21), and solid states. Raman spectra (14,22) are also available. Rotational constants have been calculated from the pure rotational Raman spectrum (23).

The complex proton magnetic resonance spectrum of 1,3-butadiene has been analyzed, and the calculated spectrum for this AA′BB′CC′ system has been determined (24,25). The temperature-sensitive coupling constant for the protons on carbons 2 and 3 suggests an equilibrium between the predominant *s-trans* conformer and a skewed conformer having out-of-plane double bonds (25). The comparatively simple ^{13}C spectrum shows little effect of conjugation on the chemical shifts of the carbons (26).

The microwave spectrum has been examined in an effort to detect the *s-cis* conformer (27). The appearance potentials and relative abundances of the

Table 1. Physical and Thermodynamic Properties of 1,3-Butadiene

Property	Value	Reference
Molecular weight	54.09	30
Boiling point, °C		
At 101.3 kPa[a]	−4.413	31
At 200 kPa	14.44	31
At 245 kPa	21	32
Melting point, °C	−113	32
Freezing point in air at 101.3 kPa, °C	−108.915	31
Density at saturation pressure, g/mL		
At 20°C	0.6211	
At 25°C	0.6149	31
Pressure coefficient of boiling point at 101.3 kPa, °C/Pa	4.502	31
Vapor pressure of liquid at 21°C, kPaa	24.5	
Molar volume at 20°C, liquid, mL/mol	87.08	31
Critical temperature, °C	152	31
Critical pressure, MPab	4.33	31
Critical density, g/mL	0.245	31
Critical volume, mL/g	4.09	31
Critical PV/RT	0.271	31
Enthalpy of combustion ΔH_c^0, at 25°C, 101.3 kPa, all gases, kJ/molc	−137.65	31
Enthalpy of formation ΔH_f^0, at 25°C, gas, kJ/mol	6.393	31,33
Entropy S^0, at 25°C, J/(mol·K)c	15.92	31
Free energy of formation ΔF_f^0, at 25°C, gas, kJ/mol	8.607	31
Heat content function $(H_o^0 - H_o^0)/T$, at 25°C, J/(mol·K)	2.906	31,33
Free energy function $(F^0 - H_o^0)/T$, at 25°C, J/(mol·K)	−13.02	31,33
Entropy S^0, at 25^0, for the ideal gas state, J/(mol·K)	15.92	31,33
Enthalpy $H^0 - H_o^0$, at 25°C, for the ideal gas state, J/mol	866.54	31,33
Heat capacity C_p^0, for the ideal gas state, at 25°C, mJ/(g·K)	77.56	31,33
Surface tension at 20°C, mN/m (=dyn/cm)	13.41	34
Solubility parameter, $(J/m^3)^{1/2}$	14.5×10^3	35
Flash point, °C	−76.1	32
Lower explosion limit, %	2.0	31
Upper explosion limit, %	11.5	31
Autoignition temperature, °C	420	31
Vapor density, g/L	1.87	31

[a]To convert kPa to mm Hg, multiply by 7.5.
[b]To convert MPa to psi, multiply by 175.
[c]To convert J to calories, divide by 4.184.

principal ions from the mass spectrum (28) of butadiene, as well as x-ray data for the crystalline material (29), have been reported.

Physical Properties. At room temperature 1,3-butadiene is a highly reactive, colorless gas with a mildly aromatic odor (30). Physical properties are given in Table 1. Plots of heat of vaporization, vapor pressure, vapor and liquid heat capacity, liquid density, surface tension, and vapor and liquid viscosity are available as functions of temperature (32), as are plots of vapor and liquid thermal conductivity and heat of formation and free energy of formation of the gaseous butadiene (36). The vapor pressure of butadiene in Pascals

Table 2. Solubility of Butadiene in Organic Solvents at 20°C[a]

Solvent	Butadiene, vol%
Acetone	65
Benzene	66.3
Dichloromethane	91.4
Amyl acetate	115.3

[a]Ref. 37.

can be calculated at any temperature in degrees Celsius by using the Antoine equation:

$$\log P = A - \frac{B}{C + t}$$

with the constants $A = 9.74022$ (6.85941 for mm Hg), $B = 935.531$, and $C = 239.554$ (31).

Butadiene is soluble in organic solvents such as ethanol, diethyl ether, acetone, benzene, and hexane (Table 2) (38). Solubilities in liquid ammonia, methanol, *n*-octane, toluene, xylene, ethylene glycol, acetone (39), and water (40,41) have been reported.

Reactions. Because of the rich chemistry associated with conjugated diene structures, the reactivity of 1,3-butadiene has been studied extensively. However, the hundreds of polymers and copolymers described in the literature represent by far the most important commercial uses for butadiene.

Butadiene and atmospheric oxygen form an explosive polyperoxide (42,43). At 50°C the liquid-phase reaction is independent of oxygen pressure between 5.33 and 120 kPa (40 and 900 mm Hg). Below an oxygen pressure of 5.33 kPa (40 mm Hg) the oxidation rate decreases with decreasing oxygen pressure; increased temperature and free-radical initiators accelerate the reaction. The polyperoxide is composed of equal amounts of 1,4- and 1,2-butadiene units separated by peroxide, $-O_2-$, units. It is only slightly soluble in butadiene and accumulates as a second phase in neat butadiene.

Butadiene dimerizes by a Diels–Alder reaction thereby forming mainly 4-ethenylcyclohexene (4-vinylcyclohexene) (eq. (2)). In this dimerization reaction, butadiene acts as both diene and dienophile. The dimerized product is always present in butadiene unless freshly distilled. Although this reaction occurs spontaneously, selective catalysts based upon nitrosyliron compounds do exist (44). Vinylcyclohexene is a starting material for plasticizers and antioxidants. It should be noted that this reaction also gives smaller amounts of 1,2-divinylcyclobutane and 1,5-cyclooctadiene (45).

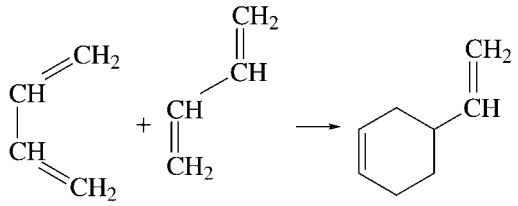

(2)

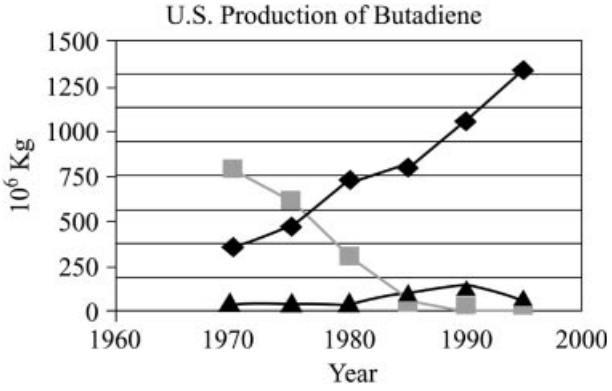

Fig. 1. Butadiene manufacture in the United States. —◆—, Co-produced; —■—, On-purpose; —▲—, Other.

Manufacture.

Ethylene Coproduction. Historically, butadiene was first prepared in pilot plant quantities via an uneconomical electric arc process. However, the primary source of butadiene in the world today is as a by-product of thermal pyrolysis of hydrocarbon feedstocks in ethylene production. In the United States, production of coproduct butadiene exceeded that of "on-purpose" butadiene for the first time in 1977 and by 1990 high cost on-purpose butadiene production was essentially eliminated in the United States (Fig. 1) (46,47). In 1996, the total US production of butadiene was 1.75 million, 93% of which was co-produced (47). Steam cracking of hydrocarbons yields varying amounts of butadiene, depending on the nature of the feedstock, the volume of ethylene produced, and the severity of the cracking operations (48–50). For example, when feedstocks are switched from atmospheric gas oils and napthas to propane and butane, yields of butadiene drop by as much as 60% (51).

An analysis of the typical by-products in the C_4 stream derived from cracking a full-range Middle East naphtha is given in Table 3. The range reflects composition at medium and high severity during steam cracking.

Table 3. Typical Composition of a Crude C_4 Stream[a]

Component	Wt%
C_3 hydrocarbons	0.3
Butanes	6.5–3.4
1-Butene	16.0–13.7
cis-2-Butene	5.3–4.8
trans-2-Butene	6.6–5.8
Isobutene	27.4–22.2
1,3-Butadiene	37.0–47.5
Acetylenes	0.4–1.8
C_5 hydrocarbons	0.5

[a]Ref. 48.

A spike in crude oil prices in late 1999 and 2000 has led many steam-cracking operations to switch from heavy to light feedstocks, resulting in lower yields of butadiene. This factor, combined with historically poor investment economics for added butadiene extraction capacity, should lead to tight butadiene supplies through 2004 when additional extraction capacity is expected to become fully on-line. Further expansion of butadiene extraction capacity in North America will be limited by crude butadiene supplies unless new domestic ethylene capacity is added (52).

In addition, dehydrogenation of *n*-butane or *n*-butene also affords butadiene. For example, the Houdry process for conversion of *n*-butane to butadiene requires temperatures of about 620°C and involves passing *n*-butane over a fixed bed reactor containing a chromium–alumina catalyst. Single-pass conversions reach only 30–40% requiring multiple recycling passes of unreacted intermediate butylenes and *n*-butane. The other primary means of dehydrogenation is conducted by passing a preheated stream of *n*-butene, steam, and air over fixed bed reactors containing a heterogenous autoregenerative catalyst. Bismuth molybdate catalysts have been studied in this process (53), but patents suggest that zinc ferrite catalysts have been used commercially (54–57). Nickel phosphate and Li–Sn–P catalysts have been patented by Phillips (58,59).

Other techniques for the preparation of butadiene have also been used commercially, including the aldol condensation of acetaldehyde and the reaction of acetylene and formaldehyde. However, these processes are no longer employed commercially. Both India and the former USSR have developed ethanol-based production of butadiene (60–64). While these routes have a major advantage in terms of low capital and operational costs, raw material costs are prohibitive in most areas (47). Such plants are only viable in areas where there is little domestic petroleum but abundant ethanol supply.

Purification. For polymerization, butadiene that is at least 99 mol% pure is required. Although alkynes are the most troublesome impurities, separation of the butadiene from other C_4 products is also necessary. Simple fractional distillation is effective for removing the light (C_3) and heavy (C_5) ends from butadiene, but not for removing the various C_4 species because of the closeness of the boiling points to each other and to butadiene. Further complicating purification, butadiene forms azeotropes with *n*-butane and 2-butene. The most widely used recovery systems are extraction with aqueous cuprous ammonium acetate (CAA) and solvent extractions with furfural, acetonitrile, dimethylformamide, dimethylacetamide, or *N*-methylpyrrolidinone (65,66).

Cuprous ammonium acetate extraction. Butadiene is purified by aqueous CAA extraction in a liquid–gas countercurrent process developed by Exxon (67–69). The cuprous salt forms a soluble addition complex with butadiene, which is decomposed by heat; thus the process is adaptable to countercurrent multistage equipment. Typically, the C_4 hydrocarbon mixture with a butadiene content of 30–40% contacts the CAA solution in a countercurrent fashion in a series of mixer–settlers. Cooling to ca −15°C is required to promote complex formation. The more saturated hydrocarbons, butanes, and butenes are first removed by distillation. Butadiene is released from the complex by further heating to 80°C. After ammonia is removed by washing with water, distillation produces butadiene that is 98–99% pure. Acetylenes and allenes are extracted with the butadiene but must

be removed; acetylenes can lead to foaming and plugging by polymer formation (70–76).

Solvent extraction. This purification method is based on the alteration of the relative volatilities of the C_4 hydrocarbons by selective solvents. The volatilities follow the order of the boiling points. 1-Butene (bp = −6.3°C), for example, is more volatile than butadiene (bp = −4.4°C); *n*-butane (bp = −0.5°C) is less volatile. Selective solvents change this order, making the impurities more volatile than butadiene. Hence, separations become easier. Furfural (77), acetonitrile (78), *N*,*N*-dimethylformamide (79), *N*,*N*-dimethylacetamide (80), and *N*-methylpyrolidinone (81) appear to be most widely used (82). β-Methoxyproprionitrile (78), dimethylsulfoxide (83), and *N*-acetylmorpholine (84) have also been studied. The commercial processes generally do not require prehydrogenation. They employ countercurrent extraction of the C_4 stream where the butanes and butenes are removed at the top, and the butadiene-rich solvent at the bottom. The butadiene is stripped from the solvent and further purified by fractional distillation. The butadiene is at least 99% pure and contains a few ppm acetylenes.

Specifications and Standards. Commercial polymerization-grade butadiene is at least 99% pure; higher purity grades up to 99.86% are available from specialty gas suppliers (85). A representative specification and analysis is given in Table 4. A pure grade has been analyzed for hydrocarbon impurities by gas chromatography (see Table 5).

Health and Safety.

Toxicity. Short-term exposure to <1000 ppm butadiene has not been associated with significant adverse acute effects; however, higher levels may cause eye irritation or transient nervous system depressant effects. The International Agency for Research in Cancer assessed human and laboratory cancer data, and judged there to be limited evidence in humans for cancer, sufficient evidence in animals, and an overall qualification as a "2A" chemical (probably carcinogenic to humans) (89). The monograph cites several studies of rubber and monomer

Table 4. Specification and Analysis of 1,3-Butadiene[a] Inhibited with *p-tert*-butylcatechol (ASTM D1157)

	Specification	Analysis	ASTM Standard
Appearance	Clear and free of suspended matter		
Conjugated diene, as 1,3-butadiene, min wt%	99.0	99.1	
Acetylenes, α, as vinylacetylene, max ppm	500	150	D1020
Butadiene dimer, max wt%	0.2	0.01	D2426
Nonvolatile matter, max wt%	0.1	0.01	D1025
C_5 hydrocarbons, max wt%	0.05	0.01	
Carbonyl, as acetaldehyde, max ppm	50	<20	D1089
Acetylenes, vinyl, max ppm	10	0–5	D2593
Peroxides, as hydrogen peroxide, max ppm	10	nil	D1022
Sulfur, as H_2S, max ppm	10	nil	D1072

[a]Ref. 86.

Table 5. Impurities in High Purity 1,3-Butadiene

Impurity[a]	Concentration, ppm[b]	Impurity[a]	Concentration, ppm[b]
Methane	10	Neopentane	N/A
Ethane	7	Butane	210
Ethylene	12	1-Butene	5500
Acetylene	0.3	Isobutene	2500
Cyclopropane	0.4	1,2-Butadiene	N/A
Propane	5	*cis*-2-Butene	270
Propene	46	*trans*-2-Butene	390
Propadiene	70	1-Butyne	N/A
Propyne	13	1-Butene-3-yne	N/A
Isobutane	61		

[a]Ref. 87.
[b]Ref. 88.

production workers, some of which contain suggestive evidence for leukemogenic activity for butadiene. However, there is uncertainty of butadiene's association with leukemia because of inconsistent findings in data between studies (lymphosarcomas vs leukemias, decreased cancer risk association with longer employment, other chemical factors implicated in etiology). Support for a lack of human carcinogenicity for butadiene despite positive mouse findings (multiple tissues at low exposures) is that the mouse enzymatically transforms the chemical to mutagenic and carcinogenic metabolites (eg, butadiene diepoxide) whereas rats and humans are less prone to do so (90). The US EPA considers butadiene a "probable human carcinogen" (91). The potential for butadiene to cause mutations in rodents is known, while effects associated with reproductive and/or developmental functions are currently under investigation.

Butadiene had previously been considered nontoxic (92). It is mildly narcotic when inhaled at concentrations below 2%. At higher concentrations it has anesthetic effects that can cause respiratory paralysis and death (93). Butadiene is an irritant of the eyes and upper respiratory tract; contact of the liquid with the skin may have frostbite-like effects.

Occupational Guidelines. US OSHA has set an 8-h time-weighted average air standard for occupational settings of 1 ppm, and 5 ppm for a 15 min short-term exposure limit (94). The ACGIH has established a threshold limit value of 2 ppm for butadiene, and considers the chemical a "suspected human carcinogen." An odor threshold for the chemical is reported as 1.0–1.6 ppm in air (95). Potential nonoccupational exposures to the public occur as a result of the presence of butadiene in combustion gases (fossil fuels, tobacco smoke).

Handling and Storage. Butadiene is dangerous because of its explosiveness when mixed with air (38). Because of the high vapor pressure of the liquid, it must be kept under pressure. Butadiene reacts with air to form explosive peroxides and must be inhibited. Peroxides or rusty iron surfaces may initiate the formation of "popcorn" polymer which can plug pipelines. Butadiene material fires are fought like other hydrocarbon fires, with carbon dioxide or dry chemical extinguishers. Safe handling and storage require careful exclusion of oxygen, thorough grounding of all equipment, and avoidance of excessive temperatures in closed vessels.

Inhibited butadiene of polymerization purity is available in cylinders (3.8–454 L), tank cars, tank trucks, and pipelines (96,97). The cylinders may be shipped by motor or rail freight (98). Containers are subject to regulations of the Department of Transportation and must be labeled "Flammable Gas" (96). Butadiene is usually stored in bulk under refrigeration rather than pressure in order to suppress formation of the dimer 1-vinylcyclohexene (99). Smaller quantities in cylinders under pressure should be kept away from sources of ignition and heat.

Polymer Structure

Microstructure refers to the disposition of the double bonds present in the polymer chain and macrostructure refers to long chain features such as extent of branching, molecular weight, and molecular weight distributions.

Polybutadiene Microstructure. Butadiene polymerizes by addition. Having two double bonds, it forms a variety of polymer structures. One of these, known as the vinyl or 1,2-type, results from addition across just one of the double bonds (eq. 3).

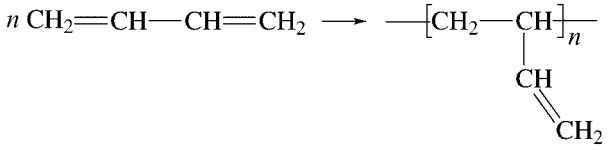

(3)

Actually, three vinyl structures are possible: the isotactic (**1**), in which all the vinyl groups are attached to a backbone carbon with the same spatial arrangement, either the D or L isomer; the syndiotactic (**2**), in which the vinyl groups are attached to backbone carbons with alternating D and L configuration; and the atactic with a random mixture of the D and L isomers.

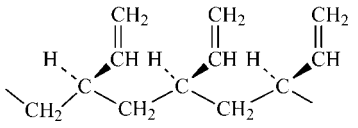

isotactic polybutadiene

(**1**)

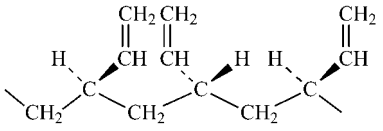

syndiotactic polybutadiene

(**2**)

A second type of structure arises by 1,4 addition when both double bonds participate. The resulting double bond in the polymer backbone permits two 1,4

structures, the *cis*-1,4 (or Z) (**3**) and the *trans*-1,4 (or E) (**4**) isomers. In the absence of side chains, there is no tacticity that can arise from 1,4-addition.

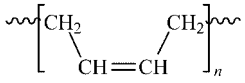

cis-1,4 isomer

(**3**)

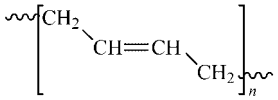

trans-1,4 isomer

(**4**)

In an actual polymer it is possible to have any or all of the several forms in a single chain. The structures indicated have all been synthesized individually, as well as in various mixtures, to give polymers with a preponderance of either 1,2- or 1,4 units.

The microstructure of polybutadienes has been determined by infrared (100–102) and Raman spectroscopy (103). The 965 cm^{-1} band is due to trans double bonds; the 740 cm^{-1} band to cis double bonds in polymers of high cis content, shifting to 725 cm^{-1} for low cis; and the 911 cm^{-1} band is due to the vinyl double bonds.

Sequence and tacticity information can be obtained from both ^{1}H and ^{13}C nmr spectra; ^{1}H is most useful at high fields where separations of peaks are sufficient to allow determination of cis, trans, and vinyl contents from both the olefinic and aliphatic resonance peaks (104). Spin decoupling of the olefinic peaks gives triad distributions of the cis and trans isomers (105). At low fields, determination of only 1,2- and 1,4 units is possible because of the severe overlapping of the resonances. The ^{13}C nmr spectrum of a polybutadiene contains two groups of resonances arising from aliphatic and olefinic carbons (106,107). Microstructures (108), sequence distribution (107), and tacticity of the vinyl units can be determined (109,110).

The glass-transition temperature (T_g) and the melting point (T_m) of polybutadienes are microstructure-dependent (Table 6).

cis-1,4, *trans*-1,4, and vinyl polybutadiene microstructures are well understood in terms of conditions influencing their formation during polymerization and the effect of the population distribution and tacticity of these microstructures on the thermal properties of the polymer. However, literature cites another microstructure inherent to polybutadiene that is not as well understood. Certain polymerization conditions favor formation of a cyclic structure in the growing polymer chain during anionic polymerization. Unlike polysiloxane polymerizations in which a percentage of macrocyclic polymer is regularly formed (115), or post-conversion reactions which cyclize polyisoprene (116), this cyclic form of polybutadiene appears to form during normal anionic polymerization reactions. This structure was mentioned in the anionic polymerization of poly(2-phenylbutadiene) as the authors noted lower levels of unsaturation than

Table 6. Glass-Transition Temperature and Melting Temperatures of Selected Polybutadienes

Polybutadiene	T_g, °C	T_m, °C[a]
cis-1,4-	−106[b]	2
trans-1,4-	−107[b]	
Form I		97
Form II		145
Syndiotactic 1,2-	−28[c]	156
Isotactic 1,2-		126
Atactic, 1,2-	−4[c]	
11% 1,2-	−94[d]	None

[a]Ref. 111.
[b]Ref. 112.
[c]Ref. 113.
[d]Ref. 114.

expected, and found evidence for five-membered rings using ozonolysis/mass spectroscopy techniques (117). Most early work citing the cyclic structure involves methods producing low molecular weight polybutadiene oils and resins (118,119). These references discuss possible polymerization conditions conducive for cyclic structure formation, including monomer-starved conditions and elevated temperatures. Several subsequent publications developed these ideas further and proposed a backbiting mechanism that involves the two penultimate monomeric groups in the chain (120,121). Noting that the polymerization conditions in these references involve polar modification, it would appear that relatively high vinyl levels are inherent to the formation of cyclic polybutadiene. The most in-depth work to date involves nuclear magnetic resonance analysis of commercially available polybutadiene resins and develops evidence for vinyl-substituted cyclopentane units as part of the polymer backbone (122,123). Experimental evidence included in these references cites a range of incorporation of cyclic structure between 0 and 45% by weight. In-depth polymerization studies to elucidate the thermodynamic and kinetic conditions favoring this structure formed by anionic polymerization techniques have not been published, and the contribution to glass-transition temperature and other thermal properties of cyclic polybutadiene elastomers has not been established.

Many references exist for cyclic diene structures formed during certain cationic polymerizations (124–127). The exact mechanism involved in the formation of the ladder-like fused ring structure has yet to be determined.

The sequence distribution of two copolymerizing monomers depends on the catalyst or initiator used, the method of polymerization, and the concentration and reactivities of the monomers. Reactivity ratios for many monomer pairs have been measured for free-radical, anionic, and coordination polymerization of butadiene (128).

Polybutadiene Macrostructure. Macrostructure refers to the molecular weight, molecular weight distribution, and extent of branching in a polymer. Branch sites along a polymer backbone can be either comb-like short-chain random branching (in the case of polybutadiene, most often derived from grafting reactions), random long-chain branching, or highly branched dendritic structures

(129). Often the nature and extent of branching and the breadth of the molecular weight distribution is dependent on the catalyst/initiator system and polymerization conditions.

Free-Radical Polymerization. The highly reactive nature of radical species results in polymerization products with high levels of branching. The relative levels of recombination and disproportionation termination reactions determines the breadth of the molecular weight distribution. Chain-transfer agents also affect the macrostructure of the polymer.

Ziegler–Natta Polymerization. The macrostructure of Ziegler–Natta polybutadiene varies considerably and is most dependent on the metal catalyst's ability to undergo chain-transfer events. Typically, early transition metals are less likely to participate in metal-hydride elimination chain-transfer reactions than the more electron-rich late transition metals (130). This phenomenon allows early metal systems, such as titanium, to catalyze the formation of polymers with narrow molecular weight distributions and low branching. Conversely, nickel systems are dominated by chain-transfer reactions and therefore generate polybutadienes with very large molecular weight distributions. Cobalt, also a late transition metal, catalyzes the formation of branched polybutadiene presumably by reinsertion of a terminated conjugated diene end group. Another factor controlling the macrostructure of Ziegler–Natta polybutadiene is the propensity of the catalyst to chain transfer to the aluminum co-catalyst. This type of chain-transfer reaction is dominant in neodymium systems leading to linear polymers but with broad molecular weight distributions.

Anionic Polymerization. Complementing the diversity in microstructure inherent to anionic chemistry, living anionic polymerization based on alkali metal alkyl initiating systems can also afford a wide range of macrostructural possibilities for polybutadiene products.

Batch polymerization methods can produce narrower molecular weight distributions than continuous processes (131), resulting in materials with lower hysteresic properties. Low vinyl polybutadiene can be produced with either linear or branched macrostructure. Polymerizations of polybutadiene performed at moderate temperatures produce linear chains in comparison to high temperature processes which give rise to random thermal branching. Divinylbenzene is a difunctional monomer that is commonly added to promote long-chain branching. This common cold-flow-reducing agent effectively incorporates into the polymer chain to generate a macromonomer that can further polymerize to give long-chain branching (132). Coupling agents of various functionality can be added at full conversion to produce star polymers with enhanced rheological properties (133,134). These branched materials not only have greatly reduced cold flow, but can also offer improved high shear mixing and extruding properties over more linear counterparts (135,136).

In contrast to the inherent linearity exhibited by unmodified low vinyl polybutadiene polymerized at moderate temperature, medium to high vinyl polybutadiene produced in continuous systems have the tendency to be highly branched. The common use of alkali metal alkoxides with or without additional polar modifiers to increase the vinyl content results in a superbasic system with a high tendency to metallate the polymer chain (137–141). The metallated site can reinitiate in the presence of continuously fed monomer and produce random

long-chain branching (142,143). Proper design of the continuous polymerization process or choosing initiator/alkali metal alkoxide/polar modifier systems with decreased superbasic activity can reduce the overall levels of branching (144,145).

Synthesis of Polybutadiene

Free-Radical Polybutadiene. Free-radical emulsion polymerization of butadiene has yet to gain commercial importance. Unlike emulsion styrene–butadiene copolymers, which exhibit excellent abrasion resistance, crack-growth resistance, and easy processing (146), emulsion polybutadiene does not perform as well in typical rubber applications as its solution counterpart. The main difference between these two types of rubber stems from the lack of T_g control in the free-radical polymerization process. The indiscriminate nature of free-radical chain propagation results in a polybutadiene containing a mixture of 1,4- and 1,2-microstructure (147). Although the cis/trans ratio of the 1,4-enchainment can be controlled with temperature, the total vinyl content remains constant between 15 and 20% (Table 7). In most cases, the resulting polybutadiene will have a T_g near -80°C, which is a full 20° higher than that of high *cis*-polybutadiene produced with Ziegler–Natta catalysts (qv).

Another drawback of emulsion polybutadiene is the rapid formation of gel during the polymerization. In order to avoid significant quantities of gel it is necessary to terminate the polymerization below 60% conversion. In this fashion, as monomer concentration is depleted, the reaction of a growing chain with the backbone of another chain can be avoided. One material that actually takes advantage of the rapid recombination of growing chains in a free-radical polymerization is hydroxytelechelic polybutadiene (HTPB). HTPB is typically prepared in a butanol solvent with the use of hydrogen peroxide as an initiatior (149–156). Termination of growing chains via primary radical recombination results in the formation of dihydroxy functional polybutadienes. Molecular weights are limited, but nevertheless a market exists for oligomers of both carboxytelechelic and hydroxytelechelic polybutadienes. Advances in controlled radical polymerization techniques (157–161) have led to a number of recent studies covering hydroxy radical initiated butadiene polymerizations (162,163).

Ziegler–Natta Polybutadiene. Ziegler–Natta polybutadiene is the generic name given to materials produced from polymerization catalysts based on transition metals (see ZIEGLER–NATTA CATALYSTS). These catalysts follow a

Table 7. Effect of Temperature on the Microstructure of Emulsion Polybutadienes[a]

Polymerization temp, °C	*cis*-1,4, %	*trans*-1,4, %	1,2, %
−33	5.4	78.9	15.6
5	13.0	69.9	16.5
50	19.0	62.7	18.8
70	20.8	59.4	19.8

[a]Ref. 148.

coordination polymerization mechanism and typically employ insoluble metal halides or soluble metal carboxylates in conjunction with aluminum alkyl co-catalysts (164,165). The commercial success of Ziegler–Natta type polymerizations is related to the ability of this broad class of catalyst to afford *stereoregular* polybutadienes. All the three types of possible microstructure for polybutadiene—1,4-*cis*, 1,4-*trans*, and 1,2-vinyl—can be achieved in near 100% regularity with the appropriate metal catalyst. The most significant of these materials being high *cis*-polybutadiene. This polymer, with a T_g below -100°C, has very good abrasion resistance, high resilience, and low heat buildup and is used in many tire-related applications. Such properties have made *cis*-polybutadiene the second largest volume synthetic rubber, behind only emulsion SBR (146).

cis-1,4-Polybutadiene. At least four different metal catalysts have been commercialized for the production of *cis*-polybutadiene, namely, titanium, cobalt, nickel, and most recently neodymium. Each of these catalysts generate polymers that vary in microstructure, such as cis content, as well as in macrostructure, which includes molecular weight, molecular weight distribution, and degree of branching. The end user must consider both the microstructure and macrostructure obtained with each catalyst system when optimizing an elastomer for a given application (166).

Titanium Catalysts. The titanium catalyst was the first system to be commercialized in the 1950s by Phillips Petroleum (167). Generally, titanium-catalyzed polybutadiene is characterized by its low branch content and narrow molecular weight distribution leading to good tensile properties and fatigue resistance but poor processibility (168,169). The catalyst is comprised of a titanium halide precursor and an aluminum alkyl co-catalyst. The most studied system consists of treating titanium tetraiodide with three to eight equivalents of triisobutyl aluminum (TIBA) in an aromatic solvent at 30°C. This results in polymerization of butadiene to *cis*-polybutadiene having a cis content greater than 90% (170,171). Polymer molecular weight is inversely dependent on catalyst concentration with high molar mass polymers being obtained at low catalyst levels. To prepare materials that are easily processed, approximately 1–2 millimoles of titanium tetraiodide per hundred grams of monomer (mmphm) is required (172). The catalyst is heterogeneous, and although catalyst activity is sensitive to the Al/Ti ratio, the overall cis content is only slightly affected. The cis content is, however, very sensitive to the type of halogen employed in the polymerization. As Table 8 shows, the cis content drops significantly as iodide is replaced with more electronegative halides. The dependence of microstructure on halide is apparent for all of the cis-specific transition metal catalysts except neodymium. A number of alternative

Table 8. Cis Content %, as a Function of Metal Halide and Transition Metal in Polybutadiene Polymerization[a]

Transition Metal	I	Br	Cl	F
Titanium	93	87	75	35
Cobalt	50	91	98	93
Nickel	10	80	85	98
Neodymium	97	97	96	96

[a]Refs. 173 and 174.

catalysts to the classic binary titanium system exist, including combinations of $TIBA/I_2/TiCl_4$ (175–177) $(C_2H_5)_2$ $AlI/TiCl_4$ (178), $(C_2H_5)_3Al/TiCl_4/TiI_4$ (179,180), and $DIBAlH/AlI_3/TiCl_4$ (181). The $TIBA/I_2/TiCl_4$ systems used in a molar ratio of 8:1.5:1 has been optimized for conversion, molecular weight, and *cis*-1,4-content and has been used in the commercial production of *cis*-polybutadiene (182,183).

Cobalt Catalysts. The preparation of high *cis*-polybutadiene with cobalt catalysts was first disclosed by B. F. Goodrich and is characterized by a high degree of branching and good processibility (184). By analogy to the titanium halide catalysts, early cobalt work focused on $CoCl_2$ as the catalyst precursor. Unlike titanium, the use of trialkyl aluminum species does not lead to an active catalyst. Instead, an alkyl aluminum *halide* must be employed as co-catalyst in these systems (185–191). Moreover, maximum activity appears to be linked to the Lewis acidity of the co-catalyst. For example, the use of aluminum ethyl sesquichloride $[Al_2(C_2H_5)_3Cl_3]$ in place of diethyl aluminum chloride results in a more active catalyst. Increasing the strength of the Lewis acid even further, by using ethyl aluminum dichloride or aluminum trichloride, results in competitive gel formation. The balance of activity and gel content has been achieved through the use of water as a third catalyst component. Maximum activity is achieved when water is added at approximately 10 mol% to the diethyl aluminum chloride (192). Above this concentration, water begins to act as a catalyst poison retarding the rate of polymerization. Presumably the water is reacting with $(C_2H_5)_2AlCl$ to generate the Lewis acidic ethylchloroaluminoxane $[O(AlC_2H_5Cl)_2]$ (193). Degree of branching, as a measure of solution viscosity at equal molecular weight, decreases with increasing water content.

Catalyst systems based on $CoCl_2$ are heterogeneous in nature and require catalyst levels as high as 10 mmphm in order to achieve good conversion. Much lower levels are used when soluble cobalt salts are employed. These salts include pyridine adducts of $CoCl_2$, cobalt octanoates, cobalt acetylacetonates, and cobalt versatates in the plus two or three oxidation state. When soluble salts are utilized, catalyst levels can drop to as low as 0.01 mmphm of cobalt with Al/Co ratios of 100–1000/1. Typical cis contents range from 95 to 98%. Catalyst activity and molecular weight are also dependent on the solvent used for polymerization. Benzene is the solvent of choice resulting in the most active polymerizations (194); however, mixtures of aromatic and aliphatic solvents are used in production plants in an effort to reduce the amount of benzene emissions (195). Molecular weight must also be regulated in these systems through the use of a chain-transfer agent. Suitable transfer agents are those that regulate molecular weight without adversely affecting the rate of chain propagation and polymer microstructure. For the cobalt systems hydrogen, ethylene, propylene, and allenes such as 1,2-butadiene are all effective regulators (196).

Nickel Catalysts. Nickel-catalyzed high *cis*-polybutadiene, first developed by Bridgestone (197–199), is typically less branched than commercial cobalt polybutadiene but exhibits an equally high cis content of 98%. The polymer is also characterized by a large molecular weight distribution of 4–5 giving the material good processibility. The commercial process utilizes a soluble nickel(II)carboxylate, aluminum trialkyl, and a halogen source (200). Of these three components, the process is most dependent on the choice of halogen. As was seen in Table 5, use of nickel-iodide yields mostly *trans*-polybutadiene while Br, Cl,

and F all favor cis polymerization (201–203). Initially boron trifluoride etherate was used as a halogen source but later hydrogen fluoride was also implemented in large-scale production (204). Catalyst activity is similar to the cobalt system, with reasonable rates and molecular weights being achieved with 0.01 mmphm nickel. Typical Al/Ni ratios are 10–50/1 with an F/Al ratio of 2–3/1. Unlike the cobalt system, chain transfer readily competes with propagation in the nickel system resulting in broad molecular weight distributions. Maximum molecular weights are achieved during the first 50% of conversion and then level off for the remainder of the polymerization (205). The final molecular weight is inversely dependent on catalyst levels. Alternatively, to obtain low molecular weights an olefin containing molecular weight modifier such as 1-butene or 1,5-hexadiene may be used when low catalyst levels are employed. Studies with nickel octanoate have shown that microstructure is a function of molecular weight (206). As the molecular weight increases the cis content increases at the expense of both the trans and vinyl; the amount of trans is always about twice the amount of vinyl. At 10,000 M_n the cis content increases to over 90% and at 100,000 M_n or more, cis content is $>$96%. Recent advances have also been made in the control of nickel polybutadiene macrostructure, resulting in the commercial availability of a branched, improved processing material (207).

Because of the unique ability of nickel to readily form stable metal-allyl complexes, many mechanistic studies of this system have been undertaken. From these, it is clear that nickel allyl species are indeed involved in the coordination polymerization of polybutadiene (208–212). Whether generated *in situ* or added directly as catalyst, the type of polymer produced from π allyl NiX complexes is determined by the nature of X, electron-donating or accepting additives, and the transition metal. The chloride complex gives cis polymer, the iodide trans, and the bromide a mixed microstructure (213). Catalytic activity is low and yields are poor with the latter catalysts. Complexes of more electronegative anions, such as trichloroacetate and trifluoroacetate, exhibit high catalytic activity and afford polymers of very high cis contents (214). Electron-donating additives, such as oxygen, ethers, alcohols, and phosphites, tend to inhibit π-allyl polymerization and increase the trans content. On the other hand, electron-accepting additives, such as tin and titanium halides, metal salts, and iodine, increase the activity of π-allyl nickel halides. π-Allyl nickel chloride retains the high cis microstructure in the polymer with most added metal salts. Iodide complexes of these electron acceptors produce high cis polymers, rather than the expected trans polymer.

It is also clear that in many instances the stereoregular outcome of monomer insertion is dependent on the initial mode of monomer coordination and rate of anti-syn allyl isomerization. For example, in a now classic experiment (215–217), the polymerization of butadiene with π-allyl nickel(II)trifluoroacetate in the absence of an external ligand yields high *cis*-polybutadiene. Upon addition of a trialkylphosphite, however, the stereo control is completely reversed and *trans*-polybutadiene is formed. One explanation put forth to explain this behavior is that in the absence of a ligand the incoming monomer can bind to the metal in an η^4-cis configuration (218,219). This bonding mode will result in the formation of a syn-allyl upon migration of the growing polymer chain and subsequently a cis configuration in the polymer. Conversely, if a ligand is present, the incoming monomer will favor η^2-monodentate complexation. Migration of the growing

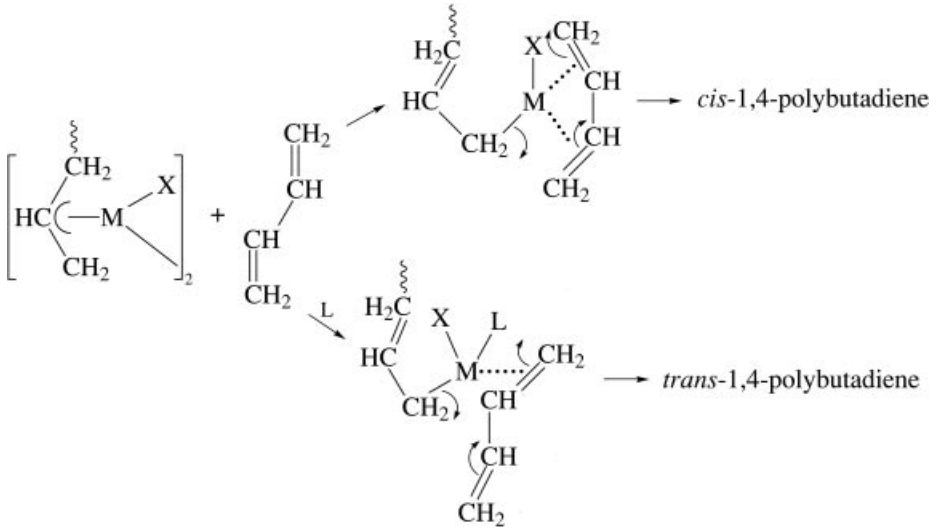

Fig. 2. Coordination and insertion mechanisms leading to *cis*- and *trans*-1,4-polybutadiene.

polymer into this bond will result in the generation of an anti-allyl leading to trans polymer (Fig. 2). The mechanism is, however, dependent on the assumption that no isomerization from η^3-syn-allyl to η^3-anti-allyl occurs or that η^4-trans coordination of butadiene is not favored (220,221). A comparison of the mechanism of isolated nickel-allyl catalyzed diene polymerization with the traditional Ziegler–Natta nickel system has been reviewed (222).

Neodymium Catalysts. The most recent catalyst system developed for the commercial production of high *cis*-polybutadiene is based on the rare earth metal neodymium. Although it was recognized in the 1960s that lanthanide catalysts, in general (223–225), and neodymium, in particular, were viable *cis*-polybutadiene catalysts, it was not until the 1980s that the process was commercialized (226–229). Polymer produced from this class of catalyst is characterized by a linear macrostructure and a very high cis content of greater than 98% giving the rubber excellent abrasion and fatigue performance. The linearity of the material, coupled with high molecular weight, makes this rubber more difficult to process than the other high cis polymers. This problem has been addressed and there are now versions of neodymium polybutadiene available, which contain long chain branches reducing cold flow and improving processability while maintaining a high cis microstructure (230,231).

The chemistry of the neodymium catalyst has very recently been reviewed (233,234), and although the resulting polymer is similar to other high *cis*-polybutadienes the change from a transition metal based system (Ti, Co, Ni) to a lanthanide metal with valance *f*-electrons creates striking differences in the polymerization chemistry. There are two main types of catalyst systems (235). The first is a ternary system based on soluble neodymium carboxylates in conjunction with a trialkylaluminum cocatalyst and a halogen source (236,237). The second system is a binary catalyst comprising of an insoluble neodymium halide

complexed with three equivalents of a Lewis base such as alcohols, amines, or phosphonates and a trialkylaluminum (238–240). In general, the two systems behave similarly; however, the homogeneous ternary system appears to have gained acceptance commercially (241). As with the transition metal based systems, a halogen must be present for high cis-polymerization; however, any halogen will suffice (172). Chloride and bromide derivatives make more active catalysts but the cis content is equally high for fluoride or iodide complexes. Typical catalyst concentrations are between 0.10 and 0.30 mmphm Nd, placing the activity of these systems between titanium on the low side and cobalt or nickel on the high side. Branched trialkylaluminum and dialkylaluminum hydrides used in an Al/Nd ratio of 10–40/1 in conjunction with two to three equivalents to Nd of a halide source such as diethylaluminum chloride or *tert*-butylhalides treated with a branched long-chain neodymium carboxylate give the highest activity (242). Polymer molecular weight is inversely proportional to overall catalyst levels as well as aluminum alkyl concentration. As the aluminum to Nd ratio increases, the molecular weight of the polymer decreases (243). This effect is most pronounced for diisobutylaluminum hydride, and in light of the fact that typical chain-transfer agents such as hydrogen, olefins, and 1,2-butadiene are ineffective in this system (244), aluminum hydrides are often used as molecular weight regulators. Another difference between the Nd catalysts and Ti, Co, or Ni, is that Nd is more efficient in hydrocarbon solvents than in aromatics (245). Presumably, benzene can compete with monomer for open coordination sites on the large *f*-block metal through η^6-coordination. Enhanced reactivity in hydrocarbon solvents makes this class of catalysts very amenable to commercial solution polymerization.

trans-1,4-Polybutadiene. Polybutadiene with a high trans microstructure is a crystalline resin-like material with a melt temperature of 95°C for the alpha form and 145° for the beta form. A number of metal catalysts have been used to prepare high *trans*-polybutadiene including vanadium (246–249), titanium (250–252), cobalt (253), nickel (254,255), neodymium (256,257), and rhodium (258). As is the case for the cis specific catalyst, these trans systems are typically comprised of an insoluble metal halide or soluble metal carboxylate in conjunction with an aluminum alkyl co-catalyst. In general, trans catalysts are less active than cis catalysts.

Vanadium Catalysts. The vanadium system is heterogeneous in nature and combines VCl_3 with triethylaluminum in an Al/V ratio of 2–10/1 to achieve a 99% *trans*-polybutadiene (259,260). Formation of high molecular weight polymer coupled with the highly crystalline nature of the material causes the polymer to precipitate during the polymerization. Encapsulation of active catalyst in the insoluble polymer particles can be a conversion-limiting occurrence. From a process standpoint, dispersion of the heterogeneous catalyst particles becomes a very important issue. Along these lines, mixed metal systems of VCl_3 with $TiCl_3$ in a 1:4 ratio have been found to create a highly dispersed active trans catalyst (261).

Cobalt Catalysts. Cobalt catalysts have the advantage of being readily available as soluble metal salts. Combining cobalt carboxylates with diethyl aluminum chloride in the presence of a Lewis base such as triethylamine at an Al/Co/NR_3 ratio of 10:1:10 results in reasonable conversion of butadiene to polybutadiene with a 95% trans content (253). Control of microstructure is possible through changes

in catalyst concentration and make-up allowing for a range of trans contents from 72 to 95% with the rest of the polymer being made up of mostly 1,2-vinyl.

Nickel Catalysts. The use of a Lewis base to convert an otherwise cis catalyst into a trans catalyst has already been demonstrated for nickel (212–214). Similarly, the cis-specific nickel catalyst can also be converted into a trans catalyst by replacing Ni–F complexes with Ni–I. Polymers obtained from these systems can have up to 97% trans content (262).

Neodymium Catalysts. Neodymium catalysts are known to polymerize butadiene to *trans*-polybutadiene in the absence of a halogen source. For example, when $Nd(versatate)_3$ is treated with magnesium dialkyl in a critical ratio of 1:10, a polymer with 90–95% trans content is obtained (256). Molecular weights are typically below 100,000 and the catalyst must be used at levels above 0.25 mmphm to obtain reasonable conversion. More recently, a trans-specific system has been described in which a neodymium phosphate is treated with four equivalents of butyl lithium, yielding a high trans polymer in good conversion (257). Interestingly, a neodymium halide species treated with tributylphosphate and dibutyl magnesium also yielded high *trans*-polybutadiene (263).

Rhodium Catalysts. An extremely interesting system for the production of high *trans*-1,4-polybutadiene is based on a rhodium catalyst used in an emulsion-type aqueous polymerization (258,264). In a typical recipe, rhodium(III)nitrate or rhodium(III)chloride is shaken in the presence of water, sodium dodecylbenzenesulfonate, and butadiene achieving 99% *trans*-1,4-polybutadiene, albeit in low conversion (265). The polymerization is very dependent on the emulsifier present, with the most active catalysts being generated from long-chain alkyl sulfates or aryl sulfonates (266). In the absence of an aluminum alkyl co-catalyst, the dependence on the sulfonate group may arise from the need for rhodium alkyls to form from the migration of an Rh-sulfonate bond (267). The kinetics of this system has been explored (268,269) and a very thorough review exists (270).

1,2-Polybutadiene. Unlike *cis*- and *trans*-1,4-polybutadiene, high vinyl 1,2-polybutadiene has a chiral center which can exist in one of three different stereochemically related forms. The material can either be atactic, leading to an amorphous elastomer, or it can be isotactic or syndiotactic, both of which are crystalline. The elastomeric amorphous form has found utility in tire tread applications (271) and although certain molybdenum (272) coordination catalysts can produce this material, commercialization has focused on anionic alkali metal initiators modified with Lewis bases. Of the two crystalline forms, isotactic 1,2-polybutadiene with a melting temperature of 126°C is the most elusive isomer. A few chromium systems based on soluble salts and aluminum alkyls have been reported to give 45% of the isotactic polymer in a mixture of the atactic isomer (273,274).

Most Ziegler–Natta catalysts for high vinyl 1,2-polybutadiene yields syndiotactic polymer with a melting temperature that ranges between 90 and 220°C depending on the degree of crystallinity. The microstructure of this material was first recognized by Natta (272) in 1955 and can be prepared with cobalt (275–280), vanadium (281), molybdenum (282,283), chromium (274,284), and titanium (285) salts treated with aluminum alkyl co-catalysts.

A high melting (>200°C) material and a low melting material (90°C), both produced from cobalt catalysts, have been commercialized by Ube

Industries (286) and Japan Synthetic Rubber Co. (JSR) (287) respectively. The high melting polymer is made from a preformed cobalt octoate/triisobutylaluminum/butadiene/carbon disulfide catalyst formed in a ratio of 1:3:20:1 and charged at a level between 0.1 and 0.2 mmphm. High crystalline material having greater than 98% 1,2-microstructure is obtained with a melt temperature of 195–205°C. Use of other modifiers such as diethyl fumarate results in a lower degree of crystallinity and a melt temperature of 150°C (288). The very low melting syndiotactic 1,2-polybutadiene from JSR utilizes a cobalt–phosphine catalyst system. The catalyst is generated by treating bis(triphenylphosphine)cobalt dibromide with triisobutlyaluminum in the presence of water in a ratio of 1:20:10. Typically, the polymer has 90% 1,2-microstructure and a melt temperature of 90°C. Mechanistic studies aimed at uncovering the differences in these systems have been described (289,290).

A very unique system for the polymerization of syndiotactic 1,2-polybutadiene with varying degrees of crystallinity and melts ranging from 120 to 190°C has been disclosed by The Goodyear Tire & Rubber Co (291). In this example, cobalt octoate treated with butadiene, triisobutylaluminum, and carbon disulfide has been shown to polymerize butadiene in an emulsion polymerization. This example represents a rare case of a Ziegler–Natta polymerization process tolerant of water. The lack of reactivity towards water could be due to the formation of an impenetrable capsule of crystalline polymer around the cobalt catalyst. In this fashion, only the lipophilic butadiene is able to diffuse into the region of active catalyst.

Frontiers of Ziegler–Natta Catalysts. There are a number of areas of Ziegler–Natta polybutadiene research that have attracted recent attention. These include the use of new co-catalysts, metallocene, or single-site catalysts, and development of supported Ziegler–Natta catalysts for gas-phase polymerization. Much of this work can be tied to the discovery by Kaminsky and Sinn (292–294) that methylaluminoxane (MAO) acts as an extremely efficient co-catalyst in metallocene-catalyzed ethylene polymerization. Examination of MAO in Ziegler–Natta type conjugated diene polymerization includes work on catalysts such as vanadium (295,296), titanium (297–299), cobalt (300–302), nickel (298,303,304), and neodymium (305–307). In certain cases, the use of MAO in place of traditional trialkylaluminum co-catalysts has resulted in the formation of highly active cis catalysts even in the absence of a halogen source. The use of MAO with homogeneous metallocene catalysts for butadiene polymerization has focused mainly on cyclopentadienyltitanium trichloride systems (298,299,309–311). Although this system has comparable activity to traditional Ziegler–Natta catalysts, the overall cis content is only 80%. Unlike the plastics industry where metallocenes and well-defined single-site catalysts have rapidly gained commercial success, the use of these systems for polybutadiene production has not, as of yet, matured. However, one area that is certain to be dominated by this class of catalyst is the area of gas-phase polymerization. In-roads to such a process for high *cis*-polybutadiene have been made by Bayer through the use of an inorganic supported neodymium allyl/MAO complex (312). Similarly, supported cyclopentadienyltitanium complexes, also activated with MAO, have been used for the gas-phase polymerization of high *trans*-polybutadiene (313). Nickel (314) and cobalt (315) systems have also been disclosed.

Anionic Polybutadiene. Anionic polymerization (qv) is perhaps the most versatile technology for producing polybutadiene in terms of microstructural and macrostructural control. The relative stability of the anionic propagating center allows for excellent control and manipulation of the conformation of enchained monomeric units and the overall structure of the polymer backbone. Coordination catalyst technologies are best employed if highly stereospecific and/or highly tactic microstructures are desired. Although high *trans*-1,4- and high *cis*-1,4-polybutadiene elastomers can be produced by a variety of Ziegler–Natta technologies (316), a wider range of thermal and rheological properties can be realized with anionic polymerization systems resulting in a broader range of applications for this technology.

As mentioned previously, during World War I, alkali metals were investigated early in the search for a suitable elastomeric substitute for natural rubber. German and Russian researchers used sodium metal to polymerize dienes (317,318), but these materials proved ill-suited for tire applications. An alkali metal catalyst was later developed by Firestone researchers (319), which was used to produce *cis*-1,4-polybutadiene on a commercial scale. Alkyl lithium initiators have since been utilized to produce very high molecular weight polybutadienes with approximately 70% *cis*-1,4 structures. Lithium-based initiators produce the lowest vinyl content and highest 1,4-enchainment when compared to the other alkali metals. These properties were desired when efforts to emulate natural rubber dominated synthetic rubber research. Presently, research efforts have shifted focus from low vinyl products to higher vinyl, higher glass-transition temperature materials. This shift follows a trend toward higher performance tires with improved traction and handling characteristics, while not sacrificing wear and fuel economy properties. Anionically prepared polybutadienes with elevated vinyl contents and controlled long-chain branching characteristics can be used in many applications when a balance between traction and fuel economy is desired.

Anionic polymerization of 1,3-butadiene allows for a wide range of heterotactic vinyl enchainment levels. The structures obtained in hydrocarbon solvents with alkali metal initiators are shown in Table 9. Lithium polybutadiene maintains the lowest vinyl, highest 1,4 content possible via anionic polymerization. The microstructure produced via a free-radical emulsion polymerization is provided as a reference.

Polar modifiers are most often employed to control the level of vinyl structures formed during living lithium-based anionic polymerization processes in nonpolar solvents. Relatively small amounts of added polar modifier, based on the

Table 9. Microstructure of Alkali Metal Initiated Polybutadienes[a]

Catalyst or condition	*cis*-1,4, %	*trans*-1,4, %	1,2, %
Lithium	35	52	13
Sodium	10	25	65
Potassium	15	40	45
Rubidium	7	31	62
Cesium	6	35	59
Emulsion	18	64	18

[a]Refs. 320 and 321.

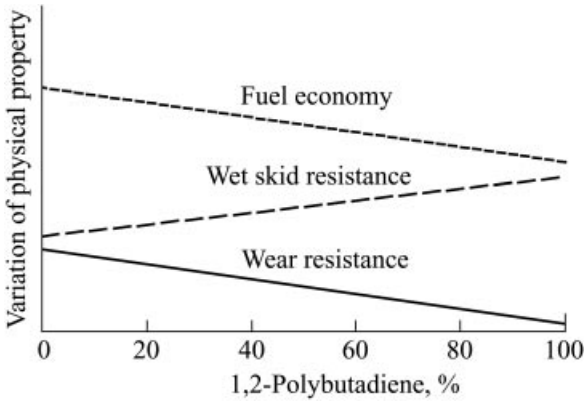

Fig. 3. Glass-transition temperature as a function of vinyl content.

stoichiometry of anionic propagating centers, can have profound vinyl-directing effects (322,323). The vinyl content correlates directly to the glass-transition temperature, as seen in Figure 3 (271) and in other references (324,325). Higher modifier to chain-end ratios produce higher vinyl levels. The vinyl-directing strength of most polar modifiers can also be a function of polymerization temperature (326).

Increased polymerization temperatures decrease the vinyl-directing strength and result in lower glass-transition temperatures for the product. In commercially produced polybutadiene, the vinyl content can be controlled by the choice of polar modifier, its relative concentration to the propagating centers, and the polymerization temperature. Polybutadiene products with elevated vinyl contents can be made at normal polymerization temperatures (50–100°C) with many conventional polar modifiers, including tetrahydrofuran (327), chelating diamines (328), bi-1,3-dioxanes (329), bisdipiperidinoethane (330), and alkyl ethers derived from tetrahydrofurfuryl alchohols (331). Recently, with varying success, attempts have been made to model the vinyl-directing strengths of polar modifiers based on a number of parameters (332,333).

Polymerization propagation rate constants for unmodified lithium systems have a fractional order dependence on chain-end concentration and are relatively slow when compared to modified systems. The dienyl-lithium chain end has a tendency to aggregate in hydrocarbon solutions (334), and give lower polymerization rates. The order of aggregation is reported to be dependent on factors such as chain-end concentration (335,336), monomer concentration, temperature, and solvent (337). The use of polar modification not only increases vinyl contents, but generally interferes with aggregation and drives the equilibrium to monomeric chain-end species with subsequent increases in the polymerization rates.

In addition to the use of specific Lewis bases to influence the vinyl content of products formed via anionic polymerizations, the use of alkali metal alkoxide salts in lithium polymerizations can also affect the ratio of vinyl enchainment (338). Salts of lithium have little to no effect on microstructure at typical molecular weights and commercial polymerization temperatures, while those of sodium, potassium, and rubidium increase the vinyl content significantly. The addition of

polar solvents into these anionic systems also increases the vinyl content of the product.

Commercial lithium-based anionic polybutadienes at typical molecular weights and polymerization temperatures, regardless of polar modification, have *cis*-/*trans*-1,4 ratios of approximately 0.5–0.7. Higher cis contents can be attained for unmodified polybutadiene in solution at very low initiator concentrations (very high molecular weights) or in neat monomer (339). High *trans*-1,4 structure can also be promoted in lithium-based systems. The use of barium salts with lithium can produce elevated *trans*-1,4 content relative to *cis*-1,4 at lower temperatures (340,341). Other systems that produce *trans*-1,4 products include complexes of dibutylmagnesium or alkyl lithium and potassium salts (342,343). The products of these systems, polymerized in hydrocarbon solvents, displayed both a soluble high vinyl fraction and an insoluble high *trans*-1,4 fraction.

Low Vinyl Polybutadiene. Typical glass-transition temperatures range between −95 and −80°C for commercial unmodified to slightly modified lithium polybutadiene (10–30% vinyl). These products are made by a variety of producers via living anionic initiators resulting in amorphous polybutadiene of 10% vinyl, 35% *cis*-1,4, and 55% *trans*-1,4 structure. Several review articles and books describing the anionic polymerization to make low vinyl polybutadiene have been published (323,327,344,345). These materials generally show good wear properties because of the low glass-transition temperatures when compounded in tire formulations. Hysteresis is generally lower than higher vinyl products but remains a function of the long-chain branching content. Low vinyl polybutadienes do have lower green strengths than the high *cis*-1,4 Ziegler–Natta catalyzed products, because of a lack of strain crystallization. However, where amorphous characteristics are desired, optimally compounded carbon black stock prepared with lithium polybutadiene shows very little difference in performance compared to the Ziegler–Natta catalyzed high cis-1,4 material. It is believed that the essential requirement is a high overall 1,4 content regardless of whether it is primarily cis or more equally distributed between cis and trans. High *cis*-1,4-polybutadienes (Ziegler–Natta) do show improved tack and process more easily, primarily because of macrostructural differences including broader molecular weight distributions and higher branching levels.

Medium and High Vinyl Polybutadiene. Many tire performance properties are closely related to the glass-transition temperature of the polymer system used (324,325,346). As the glass-transition temperature is increased, wet and dry traction is increased, but abrasion resistance is compromised (347). Again, hysteretic properties are more a function of macrostructure than glass-transition temperature. Figure 4 depicts the trends in tire performance properties as a function of polybutadiene vinyl content (271).

An interest in the medium to high vinyl polybutadienes has been encouraged by rising styrene monomer prices. Medium vinyl polybutadienes of similar T_g offer an alternative to poly(styrene–butadiene) copolymers in the tire industry and can also be used in other applications, including shoe soles, conveyer belts, and other engineered rubber products (348). Commercial medium vinyl materials typically display glass-transition temperatures in the −75 to −55°C range (35–55% vinyl). The vinyl content is increased relative to low vinyl polybutadiene by polar modification of the living anionic chain end.

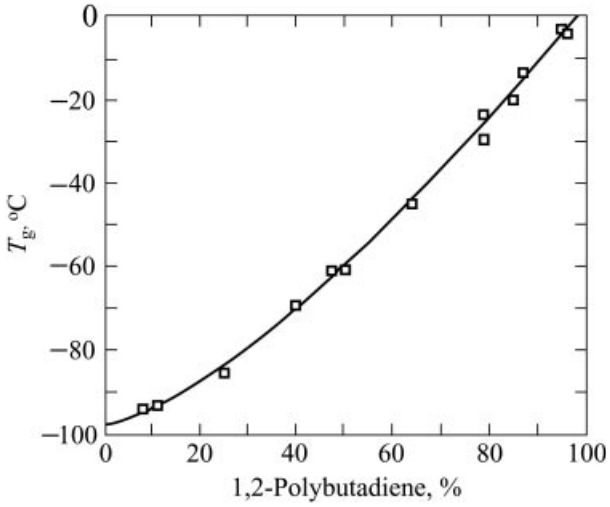

Fig. 4. Tire performance properties as a function of vinyl content.

Amorphous high vinyl polybutadienes (>70% vinyl) have glass-transition temperatures higher than −40°C (349). These materials are typically made with lithium initiators combined with a mixed alkali metal alkoxide and/or polar modifier system. As a result, commercial high vinyl polybutadienes are typically quite branched but display excellent traction properties. These materials are most often used in silica-filled tire applications.

Functionalization. Anionically prepared polybutadiene offers the unique advantage of near quantitative chain-end functionalization. Through a variety of functional initiating and/or terminating agents, a variety of reactive moieties can be attached to the polymer termini (350). For example, there are several methods available that introduce hydroxyl groups at both the α- and ω-chain ends (351,352). In addition, functional initiators can be utilized to provide hydroxyl, amine, and tin functionality (353). Cyclic amine functionalization at either termini can provide hysteresis improvements in carbon black filled compounds (354,355). The polymer macrostructure can also be modified by adding functional linking agents such as tin (or silicon) tetrachloride. Tin-coupled polymers give benefits in processing and have been reported to also decrease compound hysteresis (356–358). Using a combination of functional initiators and terminators, polybutadienes containing two types of end groups can be synthesized (359), enabling greater control of post-conversion polymer chemistries.

Cationic Polymerization. Like anionic polymerization, cationic polymerization is an addition reaction involving a relatively stable ionic propagating species. Cationic polymerization proceeds by an attack on the monomer by an electrophilic species, resulting in heterolytic cleavage of a double bond producing a carbocation. In the case of olefins, the carbocation is of the carbenium form. The most complete reference to date acknowledging the importance of cationic polymerization chemistry is a 1975 book (360).

Early research demonstrated that 1,3-butadiene can be polymerized by strong organic acids (361) or Lewis acids at low temperatures (361–363). Typical

microstructures were primarily *trans*-1,4 linkages with the remainder being mostly vinyl. For the synthesis of low molecular weight oils and resins, aliphatic ethers were used in conjunction with metal halide/hydrogen halide mixtures (364).

Later studies reported polybutadiene produced from combinations of diethyl aluminum chloride and various salt hydrates in benzene at 20°C (125). These same studies highlighted the disagreement between theoretical unsaturation amounts and that which were actually found. An intramolecular backbiting mechanism producing pendent cyclohexene groups was postulated. An overview of many papers proposing that cationically polymerized diene monomers by a mixed initiating system of magnesium bromide/titanium tetrachloride in benzene produced cyclized structures was published in 1969 (365). Structures inferred by infrared spectroscopy included cyclic ladder units alternating with linear *trans*-1,4 segments that generate a heat-stable form of cyclopolybutadiene (126,366). Similar studies using highly acidic alkyl aluminum chloride/titanium tetrachloride mixtures in *n*-heptanes produced insoluble polymer (367). The insolubility was attributed to either cross-linking or a ladder-like structure comprised of joined rings.

These cyclic structures were found to be inherent to most cationically polymerized dienes in nonpolar solvents (368). It has been reported that these cyclic structures could also be produced by typical cationic polymerization in the presence of ubiquitous proton-donating impurities, chain-transfer reactions (to monomer and aromatic solvents), and more conventional elimination reactions (369).

In contrast, high molecular weight soluble cationically polymerized polybutadiene products can be produced with relatively high rates with the ion pair $(C_2H_5)_2Al^+$ $C_2H_5AlCl_3^-$ in conjunction with cobalt. By mixing either $(C_2H_5)_2AlCl$ with C_2H_5AlCl or $(C_2H_5)_3Al$ with $AlCl_3$, this ion pair can produce high *cis*-1,4 microstructures (>90%) (370).

It should be noted that the only cationically polymerized butadiene product commercialized is DuPont's Budium®, which is an oligomeric resin used for tin-can linings. This product is produced using $BF_3{\cdot}(C_2H_5)_2O/H_2O$ in hexane at low temperature (371).

Polymerization Processes

Polybutadiene can be prepared by a number of processes, including bulk, solution, suspension, emulsion, and gas-phase polymerizations. Of the commercially significant polymerization processes, production of polybutadiene by solution technologies are the most predominant. The relative popularity of these processes follow the limitations dictated by the chemistries most practiced when producing polybutadiene commercially, including Ziegler–Natta, anionic, free-radical, and single-site technologies. Several of the more commercially relevant processes are outlined in detail below.

Solution Polymerization Process. Solution polymerization processes are often used when polymerization thermodynamics are largely exothermic, as in the case of polybutadiene. The solvent not only acts as a diluent, but also allows for efficient transfer of the heat of polymerization to a heat sink. Given the proper

choice of solvent, lower solution viscosities can also be maintained. Polybutadiene polymerizations can be carried out in aliphatic, cycloaliphatic, or aromatic solvents. Chain transfer to solvent may be a concern, as are impurities inherent to the solvent feed stream. Solution polymerization systems may be either batch or continuous in operation, with the broadness of the molecular weight distribution dependent on the configuration used. Ziegler–Natta and anionic polymerization technologies are the most common types used in solution polybutadiene production. Commercial high *cis*-polybutadiene can be made via either technology in solution systems, though Ziegler–Natta systems predominate by a wide margin. High *trans*-polybutadiene can also be produced by Ziegler–Natta catalysts. High vinyl elastomeric materials are typically produced via anionic solution polymerization.

Ziegler–Natta solution polymerization processes are very sensitive to impurities. Both the monomer and solvent streams must be well purified. Carbonyl and acetylenic impurities, common in crude monomer streams, must be removed along with the common polymerization inhibitor *tert*-butylcatechol. Molecular weight control is often accomplished by the addition of chain-transfer agents in certain Ziegler–Natta systems.

In anionic solution systems the feed stocks are typically dried over various types of dessicants because the systems are sensitive to water contamination. When using continuous anionic solution polymerization systems, it is necessary to employ low (ppm) concentrations of a chain-transfer agent in order to discourage gelation and fouling; 1,2-butadiene is often used for this purpose in commercial applications. Alkyl-lithium-initiated polybutadiene is less prone to contain gel and does not contain the heavy metal catalyst residues associated with Ziegler–Natta catalyzed products.

The polybutadiene produced by solution processes must be adequately desolvated in order to maintain low residual monomer and solvent in the product. Steam stripping is often employed in commercial processes in order to recover the solvent for recycling, followed by mechanical drying (extruder) and/or hot air drying of the wet polymer crumb.

Emulsion Polymerization. The free-radical polymerization of butadiene in a homogeneous system results in chain lengths that are too short for high quality elastomers. If the free-radical concentration in homogeneous media is high enough to give a useful reaction rate, it is also high enough to favor termination reactions or monomer depletion before high molecular weights are achieved.

In contrast to homogeneous free-radical systems, emulsion free-radical polymerization affords high propagation rates and high molecular weight products of elastomeric quality (372,373). The propagating radical chains are somewhat physically isolated and thus prevented from recombining as rapidly as they would in solution or bulk media. The emulsion process allows convenient temperature control, which is advantageous in the highly exothermic polymerization of butadiene (1.4 kJ/g). Heat removal and temperature control are considerably more difficult at high reaction rates in viscous solution or bulk processes.

A typical emulsion system contains water, monomer(s), initiator, emulsifier (soap), and a molecular weight modifier. Upon vigorous stirring, an emulsion consisting of monomer droplets dispersed in an aqueous phase is formed. The aqueous

phase contains the initiators, dispersed monomer droplets, and micelles formed from the emulsifier. Primary initiation centers, formed in the aqueous phase, diffuse into the micelles where polymerization proceeds (374,375). The polymer particle formed within the micelle then tends to absorb monomer from the surrounding aqueous phase because the monomer in the vicinity of the polymer particle has been consumed by polymerization. Continued uptake of monomer results in growth of the polymer particle at the expense of the monomer droplets. As the polymer particles grow, the emulsifier adsorbs on the increasing surface area and eventually leads to the disappearance of micellar soap as well as the monomer droplet phase. Relatively little polymer is believed to form in the aqueous phase or in the monomer droplet phase.

In a continuous process, butadiene, soap, initiator, and activator (an auxiliary initiating agent) are pumped continuously from storage tanks through a series of agitated reactors at such a rate that the desired degree of conversion is reached at the last reactor. A terminator is added, the latex warmed with steam, and the unreacted butadiene flashed off. After addition of an antioxidant, the latex is coagulated by the addition of brine, followed by dilute sulfuric acid or aluminum sulfate. The coagulated crumb is washed, dried, and baled for shipment.

Gas-Phase Polymerization Processes. Gas-phase polymerization is the newest process in development for the commercial polymerization of conjugated dienes. Although primarily utilized for the polymerization of ethylene and propylene monomers, commercial gas-phase processes are being extended to include the manufacture of polybutadiene. Many polymer manufacturers have reported researching gas-phase processes for diene monomers, and several have established significant patent portfolios including Amoco, Bayer, Exxon, Mitsui, and Union Carbide. To date, Bayer appears to be closest to commercializing a gas-phase process for producing polybutadiene rubber (376,377).

The purported benefits of gas-phase technology include the reduction in overall waste streams, including no waste water, lower solid waste, and reduced overall emissions. Solvent recycling is no longer necessary, and costly polymer product isolation and drying steps are not required. Products are typically isolated from the reactor as powder or crumb. Production costs have the potential to be significantly lower than either solution or emulsion technologies.

The chemistries utilized in gas-phase technologies employ the same Ziegler–Natta (314,315) and single-site (metallocene) catalysts (313) described in the processes included below. In gas-phase systems, however, the catalysts are generally solid-supported, but produce the same range of polybutadiene microstructures inherent to the nonsupported catalyst. Several patents also include anionic polymerization systems as useful in gas-phase processes (378). Kinetic modeling work has also been done to better predict the gas-phase polymerization behavior of 1,3-butadiene (379).

Economic Aspects

The economics of polybutadiene production are characterized by overcapacity on a global basis. Total world capacity increased by 649,000 t from 1995 to 1999; however, actual production increased by only 167,000 t during this same period

Table 10. Global Capacity and Production for Polybutadiene by Region—1999[a]

	Capacity	Production	Net trade	Consumption
United States	675	600	51	544
Western Europe	498	332	−53	385
Japan	344	290	116	191
Other	1463	880	−118	837
Total	*3019*	*2102*	*0*	*1957*

[a]Ref. 380.

Table 11. Major Producers of Polybutadiene Elastomers[a]

Company and plant location	Annual capacity as of January 2000, 10^3 t	World capacity, %
Russian companies	395	13
Bayer AG (Canada, France, Germany, and United States)	448	15
Chinese producers	341	12
The Goodyear Tire & Rubber Co. (United States)	230	8
Michelin (France)	220	7
Enichem (Italy and United Kingdom)	145	5
Bridgestone/Firestone (Japan and United States)	134	5
Korea Kumho Petrochemical Co., Ltd. (Republic of Korea)	167	6
Other	882	29
Total	*2962*	*100*

[a]Ref. 380.

resulting in a drop in global capacity utilization from 82 to 70% (380). Global production figures are tabulated in Table 10. Major polybutadiene producers are listed in Table 11.

The average annual growth rate in consumption between 1990 and 1999 was 2.0% per year on a global basis. However, because of an unusual increase of natural rubber prices in 1994, polybutadiene use in tires in the United States increased by 6.1% per year from 1994 to 1996 (380). This was, however, followed by the return of natural rubber prices to their historic norm and a resulting decrease in polybutadiene use in tires. During the period from 1996 to 1999, tire shipments increased by 4.3% whereas polybutadiene use in tires lagged behind—increasing at only 2.5% per year (380). While the combination of predominately small cars, radial tires, and low car sales drastically reduced butadiene production in the early 1980s, in the 1990s this was followed by a significant market shift to larger vehicles, sport-utility vehicles (SUV), and high performance tires. Of the trends in consumer demand, only high mileage tires demand high levels of polybutadiene in the tread compound. High performance tires require higher T_g materials and SUV tires place traction and durability demands on compounds that cannot be met by polybutadiene.

The portion of polybutadiene going into nontire applications continues to increase. Between 1980 and 1999, the portion of polybutadiene consumed in tire

Table 12. Typical U.S. List Prices, $/kg, for Selected Grades of Polybutadiene[a, b]

	Clear rubber grade	Clear plastics grade	Oil extended 37.5 phr oil[c]	Oil-black masterbatch[d]
Jan. 1982	1.49–1.65	1.53–1.67	1.54	1.10
Oct. 1989	1.49–1.76	1.53–1.80	1.69	1.23
Jan. 1993	1.49–1.76	1.53–1.80	1.67	1.21
Jan. 1996	1.71–1.94	1.75–1.94	1.90	1.39–1.50
Feb. 2000	1.69–1.96	1.72–1.96	1.85–1.94	1.39–1.50

[a]Ref. 380.
[b]Prices are FOB Gulf Coast manufacturing plant, freight collect, for truckload and car quantities.
[c]Parts of highly aromatic oil.
[d]Contains 77 parts per hundred of resin (phr) of N-302 or N-303 carbon black and 53 phr of highly aromatic oil.

applications decreased by 11–67% of world production. Use of polybutadiene in high impact polystryene modification and ABS resin manufacture account for 15–20% of global demand (380,381). Polybutadiene used in these applications must be essentially gel free and colorless. The remaining markets for polybutadiene are divided among industries including golf balls and footwear and assorted industrial products including, but not limited to, conveyor belts, v-belts, seals, gaskets, and wire insulation. In the mid 1990s the number of rounds of golf played in the United States increased at roughly a 10% annual rate (380). However, this rate of growth has not been sustained in the latter part of the 1990s and into the 2000s with total rounds of golf being flat in recent years. Despite a leveling off in rounds of golf played in the latter part of the 1990s and into 2000, changes in ball construction, including the predominance of solid core over wound core golf balls, has maintained stability in this market segment.

Prices typically vary depending on the market segment and grade of polymer sold. Typical United States prices are given in Table 12.

BIBLIOGRAPHY

"Butadiene Polymers" in *EPST* 1st ed., Vol. 2, pp. 678–754, by W. M. Saltman, The Goodyear Tire & Rubber Company; "Butadiene Polymers" in *EPSE* 2nd ed., Vol. 2, pp. 537–590, by David P. Tate and T. W. Bethea, Firestone Tire & Rubber Company.

1. E. Caventou, *Ann.* **127**, 93 (1863).
2. H. E. Armstrong and A. K. Miller, *J. Chem. Soc.* **49**, 80 (1886).
3. E. G. M. Törnqvist, in J. P. Kennedy, and E. G. M. Tönqvist, eds., *Polymer Chemistry of Synthetic Elastomers*, Part I (Vol. XXIII of High Polymers: A Series of Monographs on the Chemistry, Physics, and Technology of High Polymeric Substances) Wiley-Interscience, New York, 1968, p. 57.
4. C. H. Harries, *Ann.* **383**, 157 (1911).
5. U.S. Pat. 1,938,731 (Dec. 12, 1933), W. Boch and E. Tschunker (to I. G. Farbenindustrie).
6. W. J. Bailey, in E. C. Leonard, ed., *Vinyl and Diene Monomers*, Part 2 (Vol. XXIV of High Polymers: A Series of Monographs on the Chemistry, Physics, and Technology of High Polymeric Substances), Wiley-Interscience, New York, 1971.

7. G. W. Wheland, *Resonance in Organic Chemistry*, John Wiley & Sons, Inc., New York, 1955, Chapt. "3".
8. A. Almenningen, O. Bastiansen, and M. Traetteberg, *Acta. Chem. Scand.* **12**, 1221 (1958).
9. W. T. Dixon, *Tetrahedron* **18**, 875 (1962).
10. M. J. S. Dewar and H. N. Schmeising, *Tetrahedron* **11**, 96 (1960).
11. R. S. Rasmussen, D. D. Tunnicliff, and R. R. Brattain, *J. Chem. Phys.* **11**, 432 (1943).
12. W. B. Smith and J. L. Massingill, *J. Am. Chem. Soc.* **83**, 4301 (1961).
13. M. J. S. Dewar and S. D. Worley, *J. Chem. Phys.* **49**, 2454 (1968).
14. D. A. C. Compton, W. O. George, and W. F. Maddams, *J. Chem. Soc., Perkin Trans.* **2**, 1666 (1976).
15. E. B. Reznikowa, V. I. Tyulin, and V. M. Tatevskii, *Opt. Spektrosk.* **13**, 364 (1962).
16. J. G. Aston and co-workers, *J. Chem. Phys.* **14**, 67 (1946).
17. R. McDiarmid, *J. Chem. Phys.* **64**, 514 (1976).
18. H. H. Jaffe and M. Orchin, *Theory and Applications of Ultraviolet Spectroscopy*, John Wiley & Sons, Inc., New York, 1962, p. 228.
19. L. C. Jones Jr. and L. W. Taylor, *Anal. Chem.* **27**, 228 (1955).
20. C. W. Haas, ed., *Catalog of Selected Infrared Spectral Data*, American Petroleum Institute Research Project 44, Thermodynamic Research Center, Texas A&M University, College Station, Tex., 1978.
21. Yu. N. Panchenko and Yu. A. Pentin, *Zavod. Lab.* **33**, 1156 (1967).
22. Y. Udagawa and co-workers, *J. Raman Spectrosc.* **1**, 341 (1973).
23. G. W. Hills and W. J. Jones, *J. Chem. Soc., Faraday Trans.* **2**, 827 (1975).
24. R. T. Hobgood Jr. and J. H. Goldstein, *J. Mol. Spectrosc.* **12**(1), 76 (1964).
25. A. L. Segra, L. Zetta, and A. DiCorato, *J. Mol. Spectrosc.* **32**, 296 (1969).
26. R. A. Friedel and H. L. Retcofsky, *J. Am. Chem. Soc.* **85**, 1300 (1963).
27. D. R. Lide Jr., *J. Chem. Phys.* **37**, 2074 (1962).
28. J. L. Franklin, and A. Mogenis, *J. Phys. Chem.* **71**, 2820 (1967).
29. J. V. Smith, ed., *X-Ray Powder Data File, Sets 1–5 (Revised), ASTM Special Technical Publication 48-J, American Society for Testing Materials, Philadelphia, Pa., 1960, File No. 3-0347*.
30. M. Windholz, ed., *The Merck Index*, 10th ed., Merck & Co., Inc., Rahway, NJ, 1983, p. 1480.
31. F. O. Rossini, K. S. Pitzer, R. L. Arnett, R. M. Braun, and G. C. Pimentel, *Selected Values of Physical and Thermodynamic Properties of Hydrocarbons and Related Compounds*, American Petroleum Institute Research Project 44, Carnegie Press, Pittsburgh, Pa., 1953.
32. R. W. Gallant, *Hydrocarbon Process. Pet. Refiner* **44**(10), 151 (1965).
33. J. E. Kilpatrick and co-workers, *J. Res. Natl. Bur. Stand.* **42**, 225 (1949).
34. R. R. Dreisbach, ACS Advances in Chemistry Series No. 22: *Physical Properties of Chemical Compounds, Vol. II*, American Chemical Society, Washington, D.C., 1959.
35. H. Burrell, in J. Brandrup, and E. H. Immergut, eds., *Polymer Handbook*, 2nd ed., John Wiley & Sons, Inc., New York, 1975, p. IV–341.
36. C. L. Yaws, *Chem. Eng.* **83**(5), 107 (Mar. 1, 1976).
37. *Butadiene*, Petro-Tex Chemical Corp., Houston, Tex., 1957.
38. R. C. Weast, ed., *Handbook of Chemistry and Physics*, 64th ed., CRC Press, Inc., Boca Raton, Fla., 1983, p. C-184.
39. H. Hannart, M. Haccuria, and M. P. Mathieu, *Ind. Chim. Belge* **2**, 156 (1967).
40. F. A. Bovey, I. M. Kolthoff, A. I. Medalia, and E. J. Meehan, *Emulsion Polymerization* (Vol. IX of High Polymer: A Series of Monographs on the Chemistry, Physics, and

Technology of High Polymeric Substances), Interscience Publishers, New York, 1955, p. 156.
41. C. D. McAuliffe, *Am. Chem. Soc. Div. Pet. Chem. Prepr.* **9**, 275 (1964).
42. D. G. Hendry, F. R. Mayo, and D. Schuetzle, *Ind. Eng. Chem. Prod. Res. Dev.* **7**(2), 136 (1962).
43. D. G. Hendry and co-workers, *Ind. Eng. Chem. Prod. Res. Dev.* **7**(2), 145 (1962).
44. I. Tkatchenko, *J. Organomet. Chem.* **124**, C39 (1977).
45. J. A. Berson, P. B. Dervan, and R. Malherbe, *J. Am. Chem. Soc.* **98**, 5937 (1976).
46. H. L. Fisher, in G. S. Whitby, ed., *Synthetic Rubber*, John Wiley & Sons, Inc., New York, 1954, Chapt. "5".
47. J. G. Lacson, *Butadiene Elastomers*, Chemical Economics Handbook, SRI International, Menlo Park, Calif., Apr. 2000.
48. J. A. Philpot, *Europ. Chem. News Chemscope* 15 (Oct. 17, 1975).
49. T. B. Baba and J. R. Kennedy, *Chem. Eng.* **83**(1), 116 (1976).
50. R. E. Haney, in Ref. 6 Chapt. "2".
51. Ethylene, Report No. 29C, Process Economics Program, SRI International, Menlo Park, Calif., 1985.
52. *Chemical Market Rep.* **259**(17), 15.
53. C. L. Thomas, *Catalytic Processes and Proven Catalysts*, Academic Press, New York, 1970.
54. U.S. Pat. 3,778,488 (Dec. 11, 1978), L. J. Croce and L. Bajars (to Petro-Tex Chemical Corp.).
55. Ger. Offen. 2,539,217 (Mar. 11, 1976), J. R. Baker (to Petro-Tex Chemical Corp.).
56. Ger. Offen. 2,539,238 (Mar. 11, 1976), H. F. Christmann and E. J. Miklas (to Petro-Tex Chemical Corp.).
57. U.S. Pat. 4,020,120 (Apr. 26, 1977), H. F. Christmann and E. J. Miklas (to Petro-Tex Chemical Corp.)
58. U.S. Pat. 4,044,066 (Aug. 23, 1977), D. L. Ripley (to Petro-Tex Chemical Corp.).
59. U.S. Pat. 3,732,327 (May 8, 1973), E. W. Pitzer (to Phillips Petroleum Co.).
60. U.S. Pat. 3,026,360 (Mar. 20, 1962), S. K. Lachowicz (to Distillers Co., Ltd.).
61. A. Talalay and M. Magat, *Synthetic Rubber from Alcohol*, Interscience Publishers, New York, 1945.
62. S. K. Bhattacharyya, N. D. Ganguly, B. N. Avasthi, A. K. Kar, and V. Shankar, Symposium on *Fluidization Related Processes*, Kharagpur, India, 1964, p. 241.
63. S. K. Bhattacharyya and S. K. Sanyal, *J. Catal.* **7**(2), 152 (1967).
64. S. K. Bhattacharyya, N. D. Ganguly, and B. N. Avasthi, *Kinet. Katal.* **6**(1), 144 (1965).
65. J. Urbanski, *Przem. Chem.* **56**(3), 129 (1977).
66. T. Reis, *Petro/Chem. Eng.* **41**(8), 12 (1969).
67. E. G. Curphey, *Ind. Chem.* **35**, 423 (1959).
68. W. J. Brack and M. R. Beychok, *Pet. Refiner* **36**, 294 (1957).
69. U.S. Pat. 3,296,329 (Jan. 3, 1967), G. Z. Moore (to El Paso Products Co.).
70. U.S. Pat. 2,566,135 (Aug. 28, 1951), C. E. Morrell, and M. W. Swaney (to Standard Oil Development Co.).
71. U.S. Pat. 2,566,136 (Aug. 28, 1951), C. E. Morrell (to Standard Oil Development Co.).
72. U.S. Pat. 2,566,137 (Aug. 28, 1951), C. E. Morrell and M. W. Swaney (to Standard Oil Development Co.).
73. U.S. Pat. 2,847,487 (Aug. 12, 1958), W. N. Kestner, W. C. Kohfeld, and S. N. Eubank (to Esso Research and Engineering Co.).
74. U.S. Pat. 2,985,697 (May 23, 1961), R. P. Cahn (to Esso Research and Engineering Co.).

75. U.S. Pat. 3,017,442 (Jan. 16, 1962), N. N. Hochgraf (to Esso Research and Engineering Co.).
76. U.S. Pat. 3,192,282 (June 29, 1965), C. E. Porter (to Esso Research and Engineering Co.).
77. J. W. Hobbs, R. S. Josephson, and H. L. Rogers, *Oil Gas J.* **73**(3), 76 (1975).
78. G. D. Davis, E. C. Makin Jr., and C. H. Middlebrooks, *Adv. Chem. Ser.* **97**, 215 (1970).
79. H. Hebel and M. Kaspereit, *Chem. Tech. (Leipzig)* **23**, 419 (1971).
80. U.S. Pat. 3,769,217 (Oct. 30, 1973), R. Bannister, G. W. Harris, and J. F. Boston (to Union Carbide Corp.).
81. U. Wagner and H. M. Weitz, *Ind. Eng. Chem.* **62**(4), 43 (1970).
82. T. Reis, *Petro/Chem. Eng.* **41**(8), 12 (1969).
83. Ger. Offen. 2,009,177 (Sept. 10, 1970), P. Mikitenko, G. Cohen, and J. Durandet (to Institute Francais du Petrole des Curburants et Lubrifiants).
84. Ger. Offen. 1,916,255 (Oct. 8, 1970), G. Preusser, M. Schulze, and K. Richter (to Heinrich Koppers, GmbH).
85. *Matheson Tri-Gas Online Catalog*, www.mathesongas.com (Sept. 15, 2001).
86. *Specifications Butadiene*, Exxon Chemical Co., Houston, Tex., 1973.
87. A. DiCorcia, R. Samperi, and G. Capponi, *Chromatographia* **10**, 554 (1977).
88. A. DiCorcia and R. Samperi, *J. Chromatogr.* **107**(1), 99 (1975).
89. IARC Monographs on the Evaluation of Carcinogenic Risks to Humans, *Monograph #71, IARC*, Lyon, France, 1999, pp. 109–225,
90. J. A. Bond, Himmelstein, M. W. et al, *Toxicology* **113**, 48–54 (1996).
91. "Butadiene" in *Integrated Risk Information System. US Environmental Protection Agency*, website http://www.epa.gov/iris 2001.
92. L. M. Miller, Investigation of Selected Potential Environmental Contaminants: Butadiene and its Oligomers. Report 1978, EPA-560/2-78-008, Science Information Service Organization, Franklin Research Center, Philadelphia, Pa.
93. H. W. Gerarde, in D. W. Fassett and D. D. Irish, eds. *Industrial Hygiene and Toxicology, Vol II: Toxicology*, Wiley-Interscience, New York, 1963, p. 1205.
94. US Occupational, Safety, and Health Administration, website http://www.osha.gov/, 2001.
95. 2000 Threshold Limit Values and Biological Exposure Indices Handbook, American Conference of Governmental Industrial Hygienists, Cincinnati, Ohio, 2000.
96. Code of Federal Regulations, Title 49, Transportation, *Office of the Federal Register, National Archives and Records Service, General Services Administration, Washington, D.C., Parts 106–180, Spring* 1999.
97. Office of Pipeline Safety, 2000 Code of Federal Regulations, Parts 190–199. http://ops.dot.gov/cfr2000.html.
98. Handling C_4 Hydrocarbons, *Petro-Tex Chemical Corp., Houston, Tex.*
99. *Butadiene Product Stewardship*, Shell Chemical Co., Houston, Tex.
100. J. L. Binder, *J. Polym. Sci.*, Part A **1**, 47 (1963).
101. J. L. Binder, *J. Polym. Sci.*, Part A **3**, 1587 (1965).
102. R. S. Silas, J. Yates, and V. Thornton, *Anal. Chem.* **31**, 529 (1959).
103. S. W. Cornell and J. L. Koenig, *Rubber Chem. Technol.* **43**, 322 (1970).
104. E. R. Santee Jr., R. Chang, and M. Morton, *J. Polym. Sci., Polym. Lett. Ed.* **11**, 449 (1973).
105. E. R. Santee Jr., V. D. Mochel, and M. Morton, *J. Polym. Sci., Polym. Lett. Ed.* **11**, 453 (1973).
106. K. F. Elgert, G. Quack, and B. Stuetzel, *Polymer* **15**, 612 (1974).
107. K. F. Elgert, G. Quack, and B. Stuetzel, *Polymer* **16**(3), 154 (1975).

108. J. L. Guerry, *Rev. Gen. Caoutch. Plast.* **54**(575), 103 (1977).
109. V. D. Mochel, *J. Polym. Sci.*, Part A-1 **10**, 1009 (1972).
110. K. F. Elgert, G. Quack, and B. Stutzel, *Makromol. Chem.* **175**, 1955 (1974).
111. G. H. Stempel, in Ref. 35, p. V-1.
112. W. S. Bahary, D. I. Sapper, and J. H. Lane, *Rubber Chem. Technol.* **40**, 1529 (1967).
113. W. A. Lee and R. A. Rutherford, in Ref. 35, p. III–139.
114. A. E. Oberster, T. C. Bouton, and J. K. Valaitis, *Angew. Makromol. Chem.* **29/30**, 291 (1973).
115. J. A. Semlyen, ed., *Cyclic Polymers*, Elsevier Applied Science Publishers, London, 1986.
116. D. B. Patterson, D. H. Beebe, and J. La, in C. E. Carraher and co-workers, eds., *Modification of Polymers*, Plenum Press, New York, 1983, p. 383.
117. R. J. Ambrose and W. L. Hergenrother, *Macromolecules* **5**, 275 (1972).
118. U.S. Pat. 3,678,121 (July 18, 1972), B. J. McElroy and J. H. Merkley (to Lithium Corp. of America).
119. U.S. Pat. 3,966,961 (June 29, 1976), A. F. Halasa (to Firestone Tire and Rubber Co.).
120. J. Oziomek and S. Futamura, *Abstracts of the Papers of the American Chemical Society* **172**, 152 (1976).
121. P. Aukett and A. R. Luxton, *J. Oil Colour Chem. Assoc.* **60**, 173 (1977).
122. G. Quack and L. J. Fetters, *Macromolecules* **11**, 369 (1978).
123. A. R. Luxton and co-workers, *Polymer* **22**, 382 (1981).
124. W. Cooper, in P. H. Plesch, ed., *The Chemistry of Cationic Polymerization*, Macmillan, New York, 1963, p. 353.
125. E. I. Tinyakova and co-workers, *Dokl. Akad. Nauk SSSR* **144**, 592 (1969).
126. N. G. Gaylord and co-workers, *J. Polym. Sci., A* **2**, 3969 (1964).
127. M. Stolka, J. Vodehnal, and I. Kössler, *J. Polym. Sci., A* **2**, 3987 (1964).
128. Ref. 35, p. II-105ff.
129. G. Odian, *Principals of Polymerization*, 3rd ed., John Wiley & Sons, Inc., New York, 1991, p. 17.
130. J. P. Collman, L. S. Hegedus, J. R. Norton, and R. G. Finke, *Principles and Applications of Organotransition Metal Chemistry*, University Science Books, Mill Valley, Calif., 1987.
131. H. Fahti, A. E. Hamielec, and E. J. Davison, *Polym. React. Eng.* **4**, 243 (1996).
132. U.S. Pat. 3,280,084 (Oct. 18, 1966), R. P. Zelinski and H. L. Hsieh (to Phillips Petroleum Co.).
133. R. P. Zelinski and C. F. Wofford, *J. Polym. Sci.*, Part A-3 93 (1965).
134. U.S. Pat. 3,281,383 (Oct. 25, 1966), R. P. Zelinski and H. L. Hsieh (to Phillips Petroleum Co.).
135. G. Kraus, in W. M. Saltman, ed., *The Stereo Rubbers*, Wiley Interscience, New York, 1978.
136. A. Ghijsels and H. J. M. A. Mieras, *J. Polym. Sci., Polym. Phys.* **11**, 1849 (1973).
137. A. Modrini, *Adv. Carbanion Chem.* **1**, 1 (1992).
138. L. Lochmann and J. Trekoval, *Collect. Czech. Chem. Comm.* **15**, 585 (1988).
139. L. Lochmann and D. Lim, *J. Organomet. Chem.* **28**, 153 (1971).
140. R. Pi and co-workers, *J. Organomet. Chem.* **306**, C1 (1986).
141. B. Nakhmanovich, I. Zolotareva, and A. Arest-Yakubovich, *Macromol. Chem. Phys.* **200**, 2015 (1999).
142. J. C. Falk and co-workers, *Rubber Chem. Technol.* **46**, 1044 (1973).
143. D. P. Tate and co-workers, *J. Polym. Sci.*, Part A-1 **9**, 139 (1971).
144. M. Kerns, Z. Xu, and S. Christian, Paper presented at the ACS Rubber Division Meeting, Sept. 1999. Paper #158

145. S. K. Henning and M. L. Kerns, Paper presented at Deutsche Kautschuk Tagung 2000, Sept. 2000.
146. D. Threadingham and co-workers, Rubber, 3. Synthetic, in *Ulmann's Encyclopedia of Industrial Chemistry (electronic edition)*, 6th ed., New York: Wiley-VCH Verlag GmbH, Weinheim, Germany, 2001.
147. G. Moad and D. H. Solomon, *The Chemistry of Free Radical Polymerization*, Elsevier Science Ltd., Oxford, 1995, pp. 159–161.
148. J. L. Binder, *Ind. Eng. Chem.* **46**, 1727 (1954).
149. K. Jankova and co-workers, *J. Appl. Polym. Sci.* **64**, 2491 (1997).
150. Bulg. Pat. 41,562 (1985), K. Jankova and co-workers.
151. U.S. Pat. 3,714,110 (1973) J. A. Verdol and R. W. Ryan.
152. D. M. French, *Rubber Chem. Technol.* **42**, 71 (1969).
153. U.S. Pat. 2,228,791 (1974) (to Atlantic Richfield Co.).
154. J. C. Brosse, M. Bonnier, and G. Legeay, *Makromol. Chem.* **183**, 303 (1982).
155. J. C. Brosse, M. Bonnier, and G. Legeay, *Makromol. Chem.* **182**, 3457 (1981).
156. J. C. Brosse and co-workers, *Adv. Polym. Sci.* **81**, 169 (1987).
157. D. Mardare and K. Matyjaszewski, *Macromolecules* **27**, 645 (1994).
158. K. Matyjaszewski, ed., American Chemical Society Symp. Series: *Controlled Radical Polymerization*, Washington, 1998, p. 685.
159. M. K. Georges, G. K. Hamer, and N. A. Listigovers, *Macromolecules* **31**, 9087 (1998).
160. S. Kobatake and co-workers, *Macromolecules* **32**, 10 (1999).
161. D. Benoit and co-workers, *Macromolecules* **33**, 363 (2000).
162. J. L. Pradel, B. Ameduri, and B. Boutevin, *Macromol. Chem Phys.* **200**, 2304 (1999).
163. J. L. Pradel and B. Boutevin, B. *J. Polym. Sci.*, Part A **38**, 3293 (2000).
164. Ph. Teyssie, P. Hadjiandreou, M. Julemont, and R. Warin, in R. P Quirk, ed., *Transition Metal Catalyzed Polymerizations Ziegler–Natta and Metathesis Polymerization*, Cambridge University Press, Cambridge, UK, 1988, p. 639.
165. W. Cooper, in W. M. Saltman, ed., *The Stereo Rubbers*, John Wiley & Sons, Inc., New York, 1977, p. 21.
166. N. R. Kumar, A. K. Chandra, and R. Mukhopadhyay, *Int. J. Polym. Mater.* **34**, 91 (1996).
167. GB Pat. 848 065 (1956) (to Phillips Petroleum Co.).
168. W. Cooper and co-workers, *J. Polym. Sci.* **50**, 159 (1961).
169. J. F. Henderson, *J. Polym. Sci.*, Part C **4**, 233 (1963).
170. Belg. Pat. 551,851 (May 27,1957), R. P. Zelinski and D. R. Smith (to Phillips Petroleum Co.).
171. W. M. Saltman and T. H. Link, *Ind. Eng. Chem. Prod. Res. Dev.* **3**(3), 199 (1964).
172. Ref. 165, p. 24.
173. H. L. Hsieh and H. C. Yeh, *Rubber Chem. Technol.* **58**, 117 (1985).
174. M. C. Throckmorton, *Kaut. Gummi. Kunstst.* **22**, 293 (1969).
175. U.S. Pat. 3,205,213 (Sept. 7, 1965), R. S. Stearns and A. Fono (to Firestone Tire & Rubber Co.).
176. U.S. Pat. 3,375,239 (Mar. 26, 1968), W. J. Trepka and C. A. Uraneck (to Phillips Petroleum Co.).
177. U.S. Pat. 3,449,312 (June 10, 1969), R. J. Minchak (to Goodrich-Gulf Chemicals).
178. L. H. Howland and co-workers, *Ind. Eng. Chem.* **44**, 762 (1952).
179. Brit. Pat. 865,337 (Apr. 12, 1961) (to Phillips Petroleum Co.).
180. P. H. Moyer and M. H. Lehr, *J. Polym. Sci.*, Part A **3**, 217 (1965).
181. W. Marconi and co-workers, *J. Polym. Sci.*, Part A **3**, 735 (1965).
182. U.S. Pat. 3,220,998 (Nov. 30, 1965), D. E. Berger (to Phillips Petroleum Co.).

183. *Hydrocarbon Process.* **56**, 199 (1977).
184. BE 543,292 (1955), S. E. Horne (to Goodrich Gulf).
185. M. Gippin, *Ind. Eng. Chem. Prod. Res. Dev.* **1**, 32 (1962).
186. M. Gippin, *Rubber Chem. Technol.* **35**, 1066 (1962).
187. C. Longiave and R. Castelli, *J. Polym. Sci.*, Part C **4**, 387 (1963).
188. W. Cooper, D. E. Eaves, and G. Vaughan, *Makromol. Chem.* **67**, 229 (1963).
189. Belg. Pat. 573,680 (1957).
190. Belg. Pat. 575,671 (1958) (to Goodrich-Gulf Chem. Inc.).
191. Belg. Pat. 579,689 (1958) (to Shell Int. Res.).
192. Ref. 165, p. 29.
193. M. Gippin, *Ind. Eng. Chem., Prod. Res. Dev.* **1**, 32 (1962).
194. G. J. Van Amerongen, ACS Advances in Chemistry Series No. 52, American Chemical Society, Washington, D.C., 1966, Chapt. "11", p. 136.
195. P. Cass and co-workers, *J. Polym. Sci.*, Part A **39**, 2244 (2001).
196. C. Longiave, R. Castelli, and M. Ferraris, *Chim. Ind. (Milan)* **44**, 725 (1962).
197. U.S. Pats. 3,170,905, 3,170,906, and 3,170,907 (Feb. 23, 1965), K. Ueda and co-workers (to Bridgestone Tire Co., Ltd.).
198. U.S. Pat. 3,178,403 (Apr. 13, 1965), K. Ueda and co-workers, (to Bridgestone Tire Co., Ltd.).
199. T. Yoshimoto and co-workers, *Makromol. Chem.* **139**, 73 (1970).
200. S. Kitagawa and Z. Harada, *Jap. Chem. Q* **IV-1**, 41 (1968).
201. L. Porri and co-workers, *J. Polym. Sci.*, Part C **16**, 2525 (1967).
202. V. A. Kormer and co-workers, *J. Polym. Sci.*, Part C **16**, 4351 (1969).
203. J. F. Harrod and L. R. Wallace, *Macromolecules* **2**, 449 (1969).
204. M. C. Throckmorton and F. S. Farson, *Rubber Chem. Technol.* **45**, 268 (1972).
205. T. Yoshimoto and co-workers, *Makromol. Chem.* **139**, 61 (1970).
206. W. M. Saltman and L. J. Kuzma, *Rubber Chem. Technol.* **46**, 1055 (1973).
207. U.S. Pat. 5,451,646 (1995), K. F. Castner (to The Goodyear Tire and Rubber Co.).
208. P. W. Jolly and G. Wilke, *Organic Synthesis*, Vol. **II**, Academic Press, New York, 1975, Chapt. "IV".
209. M. Julémont and Ph. Teyssié, in R. Ugo, ed., *Aspects of Homogeneous Catalysis: A Series of Advances*, Vol. **4**, Reidel Publishing Co., Dordrecht, the Netherlands, 1981, p. 99ff.
210. F. Dawans and Ph. Teyssié, *Ind. Eng. Chem. Prod. Res. Dev.* **10**, 261 (1971).
211. A. Yamamoto and T. Yamamoto, *J. Polym. Sci., Macromol. Rev.* **13**, 161 (1978).
212. G. W. Parshall, *Homogeneous Catalysis*, John Wiley & Sons, Inc., New York, 1980, pp. 54–56.
213. L. Porri, G. Natta, and M. C. Gallazzi, *J. Polym. Sci., Polym. Symp.* **16**, 2525 (1967).
214. F. Dawans and Ph. Teyssié, *J. Polym. Sci., Polym. Lett.* **7**, 111 (1969).
215. J. C. Marechal, F. Dawans, and Ph. Teyssié, *J. Polym. Sci., Polym. Chem.* **8**, 1993 (1970).
216. Ph. Teyssié and F. Dawans, in Ref. 165, p. 79.
217. J. P. Durand, F. Dawans, and Ph. Teyssié, *J. Polym. Sci.*, Part B **5**, 785 (1967).
218. Ph. Teyssié, M. Julémont, J. M. Thomassin, E. Walckiers, and R. Warin, in J. C. W. Chien, ed., *Coordination Polymerization*, Academic Press, Inc., New York, 1975, p. 327.
219. M. C. Gallazzi, A. Giarrusso, and L. Porri, *Makromol. Chem. Rapid Commun.* **2**, 59 (1981).
220. J. Furukawa, *Acc. Chem. Res.* **13**(1), 1 (1980).
221. H. Yasuda, K. Tatsumi, and A. Nakamuto, *Acc. Chem. Res.* **18**, 120 (1985).

222. R. Taube and co-workers, *Makromol. Chem., Macromol. Symp.* **66**, 245 (1993).
223. U.S. Pat. 3,297,667 (1967), W. von Dohlen and co-workers (to Union Carbide).
224. U.S. Pat. 3,676,411 (July 11, 1972), M. C. Throckmorton and W. M. Saltman (to The Goodyear Tire & Rubber Co.).
225. U.S. Pat. 3,794,604 (Feb. 26, 1974), M. C. Throckmorton and R. E. Mournighan (to The Goodyear Tire and Rubber Co.).
226. U.S. Pat. 4,242,232 (Dec. 30, 1980), U.S. Pat. 4,260,707 (Apr. 7, 1981), G. Sylvester, J. Witte, and G. Marwede (to Bayer AG).
227. U.S. Pat. 4,699,960 (Oct. 13, 1987), S. Gordini, A. Carbonaro, and S. Spina (to Enichem Elastomeri, SpA).
228. U.S. Pat. 4,444,903 (Apr. 24, 1984), A. Carbonaro, D. Ferraro, and M. Bruzzone (to Enoxy Chimica).
229. J. Witte, *Angew. Makromol. Chem.* **94**, 119 (1981).
230. U.S. Pat. 4,990,573 (Feb. 5, 1991), P. Andreussi, R. Bianchi, and M. Bruzzone (to Enichem).
231. U.S. Pat. 5,567,784 (Oct. 22, 1996), W. Wieder, D. Kuhlmann, and W. Nentwig (to Bayer AG).
232. L. Porri and co-workers, *ACS Symp. Ser.* **749**, 15 (2000).
233. F. Cabassi, S. Italia, G. Ricci, and L. Porri, in R. P. Quirk, ed., *Transition Metal Catalyzed Polymerization*, Cambridge University Press, Cambridge, UK, 1988, p. 655.
234. N. G. Marina and co-workers, *Polym. Sci. USSR* **26**, 1251 (1984).
235. L. Porri and A. Giarrusso, in G. C. Eastmond, A. Ledwith, S. Russo, and P. Sigwalt, Eds., *Comprehensive Polymer Science*, Part II, Vol. **4**, Pergamon Press, Oxford, 1989, p. 53.
236. R. P. Quirk and co-workers, *Polymer* **41**, 5903 (2000).
237. A. Pross and co-workers, *Angew. Makromol. Chem.* **211**, 89 (1993).
238. H. Iovu and co-workers, *Eur. Polym. J.* **33**, 811 (1997).
239. H. Iovu and co-workers, *Eur. Polym. J.* **35**, 335 (1999).
240. J. H. Yang and co-workers, *Macromolecules* **15**, 230 (1982).
241. D. J. Wilson, *J. Polym. Sci.*, Part A **33**, 2505 (1995).
242. D. J. Wilson, *Polymer*, **34**, 3504 (1993).
243. J. B. Nickaf, R. P. Burford, and R. P. Chaplin, *J. Polym. Sci.*, Part A **33**, 1125 (1995).
244. U.S. Pat. 4,663,405 (May 5, 1987), M. C. Throckmorton (to The Goodyear Tire and Rubber Co. and Enichem).
245. G. Ricci, G. Boffa, and L. Porri, *Makromol. Chem. Rapid Commun.* **7**, 355 (1986).
246. U.S. Pat. 2,977,349 (Mar. 28, 1961), C. E. Brockway and A. F. Ekar (to Goodrich–Gulf Chemicals, Inc.).
247. G. J. Van Amerongen, ACS Advances in Chemistry Series No. 52, Americal Chemical Society, Washington, D.C., Chapt. "11", p. 136.
248. G. Natta and co-workers, *Chim. Ind. (Milan)* **40**, 362 (1958).
249. G. Natta, L. Porri, and A. Mazzei, *Chim. Ind. (Milan)* **41**, 116 (1959).
250. N. G. Gaylord, T. K. Kwei, and H. F. Mark, *J. Polym. Sci.* **42**, 417 (1960).
251. G. Natta and co-workers, *Chim. Ind. (Milan)* **41**, 398 (1959).
252. A. Mazzei and co-workers, *Chim. Ind. (Milan)* **45**, 528 (1963).
253. W. Cooper, D. E. Eaves, G. Vaughan, G. Degler, and R. Hank, Advances in Chemistry Series No. 52, American Chemical Society, Washington, D.C., 1966, p. 46.
254. L. Porri, G. Natta, and M. C. Gallazzi, *J. Polym. Sci., Polym. Symp.* **16**(5), 2525 (1967).
255. Ph. Teyssié and F. Dawans, in Ref. 165, Chapt "3".
256. D. K. Jenkins, *Polymer* **26**, 147 (1985).
257. U.S. Pat. 6,018,007 (Jan. 25, 2000), T. J. Lynch (to Bridgestone Co.).

258. R. E. Rinehart and co-workers, *J. Am. Chem. Soc.* **83**, 4864 (1961).
259. Ref. 165, p. 40.
260. N. N. Sigaeva and co-workers, *Polym. Sci., Ser. A* **42**, 831 (2000).
261. G. J. van Amerongen, *Adv. Chem. Ser.* **52**, 136 (1966).
262. Ref. 165, p. 44.
263. N. G. Marina and co-workers, *Polym. Sci., Ser. B* **39**, 34 (1997).
264. A. J. Canale and co-workers, *Chem. Ind.* 1054 (1962).
265. R. E. Rinehart and co-workers, *J. Am. Chem. Soc.* **84**, 4145 (1962).
266. M. Morton, I. Piirma, and B. Das, *Rubber Plast. Age* **46**, 404 (1965).
267. D. C. Blackley and R. K. Matthan, *Br. Polym. J.* **2**, 25 (1970).
268. Ph. Teyssié and R. Dauby, *Polym. Lett.* **2**, 413 (1964).
269. R. E. Rinehart, *Polym. Prepr.* **7**, 556 (1966).
270. D. C. Blackley, *Emulsion Polymerization*, Applied Science Publishers, Ltd., London, 1975, pp. 529–553.
271. A. F. Halasa and J. M. Massie, in J. I. Kroschwitz, ed., *Kirk-Othmer Encyclopedia of Chemical Technology*, 4th ed., Vol. **8**, John Wiley and Sons, Inc., New York, 1991.
272. G. Natta, *Makromol. Chem.* **16**, 213 (1955).
273. G. Natta and co-workers, *Chim. Ind. (Milan)* **41**, 12 (1959).
274. C. E. H. Bawn and co-workers, *Polymer* **5**, 419 (1964).
275. E. Susa, *J. Polym. Sci., Polym. Symp.* **4**, 399 (1963).
276. M. Iwamoto and S. Yuguchi, *J. Polym. Sci., Polym. Lett.* **5**, 1007 (1967).
277. U.S. Pat. 4,051,308 (Sept. 27, 1977), A. F. Halasa (to Firestone Tire & Rubber Co.).
278. Y. Takeuchi, A. Sekimoto, and M. Abe, in R. D. Deanin, ed., American Chemical Society Symposium Series, Vol. **4**: New Industrial Polymers, American Chemical Society, Washington, D.C., 1974.
279. H. Ashitaka and co-workers, *J. Polym. Sci., Polym. Chem. Ed.* **21**, 1853 (1983).
280. H. Ashitaka, K. Jinda, and H. Ueno, *J. Polym. Sci., Polym. Chem. Ed.* **21**, 1951 (1983).
281. G. Natta, *J. Polym. Sci.* **48**, 219 (1960).
282. G. Natta, *Nucleus (Paris)* **4**(2), 97 (1963); G. Natta, *Nucleus (Paris)* **4**(3), 211 (1963).
283. Z. Hongbing, L. Ying, Z. Chongqi, F. Ruliang, *China Syn. Rubber Ind.* **22**, 205 (1999).
284. Eur Pat. 962471 (1999), S. Luo (to Bridgestone Corp.).
285. G. Natta, L. Porri, and A. Carbonaro, *Makromol. Chem.* **77**, 126 (1964).
286. N. K. Mori, T. Taketomi, and F. Imaizumi, *Nippon Kagaku Kaishi* **11**, 1982 (1975).
287. S. Otsuka, K. Mori, and M. Kawakanni, *Kogyo Kagaku Zasshi* **67**, 1652 (1964).
288. C. Longiave and R. Castelli, *J. Polym. Sci.*, Part C **4**, 387 (1964).
289. H. Ashitaka, K. Jinda, and H. Ueno, *J. Polym. Sci., Polym. Chem. Ed.* **21**, 1989 (1983).
290. H. Ono and T. Kato, *J. Polym. Sci.*, Part A **38**, 1083 (2000).
291. U.S. Pat. 4,429,085 (Aug. 12, 1984), J. N. Henderson and co-workers (to The Goodyear Tire and Rubber Co.).
292. A. Andersen and co-workers, *Angew. Chem., Int. Ed. Engl.* **15**, 630 (1976).
293. H. Sinn and co-workers, *Angew. Chem., Int. Ed. Engl.* **19**, 396 (1980).
294. W. Kaminsky and co-workers, *Makromol. Chem., Rapid. Commun.* **4**, 417 (1983).
295. G. Ricci, S. Italia, C. Comitani, and L. Porri, *Polym. Commun.* **32**, 514 (1991).
296. G. Ricci, S. Italia, and L. Porri, *Macromol. Chem. Phys.* **195**, 1389 (1994).
297. Ital. Pat. 1241100 (Dec. 29, 1993), G. Ricci and co-workers.
298. L. Oliva and co-workers, *Makromol. Chem., Rapid Commun.* **11**, 519 (1990).
299. G. Ricci and co-workers, *J. Organomet. Chem.* **451**, 67 (1993).
300. M. Takeuchi, T. Shiono, and K. Soga, *Polym. Int.* **29**, 209 (1992).

301. P. Cass and co-workers, *J. Polym. Sci.*, Part A **39**, 2256 (2001).
302. P. Cass and co-workers, *J. Polym. Sci.*, Part A **37**, 3277 (1999).
303. K. Endo and Y. Yamanaka, *Macromol. Rapid. Commun.* **20**, 312 (1999).
304. K. Endo, Y. Uchida, and Y. Matsuda, *Macromol. Chem. Phys.* **197**, 3515 (1996).
305. L. Porri, A. Giarrusso, and G. Ricci, *Makromol. Chem., Macromol. Symp.* **66**, 231 (1993).
306. D. Wilson, *Polym. Int.* **39**, 235 (1996).
307. L. Porri and co-workers, *Polym. Prepr. (Am. Chem. Soc., Div. Polym. Chem.)* **39**, 214 (1998).
308. A. Miyazawa, T. Kase, and K. Soga, *J. Polym. Sci.*, Part A **37**, 695 (1999).
309. A. Zambelli and C. Pellecchia, *Catalyst Design for Tailor-Made Polyolefins*, Elsevier, New York, 1994, p. 209.
310. G. Ricci, C. Bosisio, and L. Oliva, *Macromol. Chem., Rapid Commun.* **17**, 789 (1996).
311. A. Peluso, R. Improta, and A. Zambelli, *Macromolecules* **30**, 2219 (1997).
312. U.S. Pat. 5,958,820 (Sept. 28, 1999), R. Taube and co-workers, (to Bayer AG).
313. W. Kaminsky and C. Strübel, *Macromol. Chem. Phys.* **201**, 2519 (2000).
314. U.S. Pat. 6,004,677 (Dec. 21, 1999), K. J. Cann, M. A. Apecetche, and M. Zhang (to Union Carbide Chemicals and Plastics Technology Co.).
315. U.S. Pat. 5,879,805 (Mar. 9, 1999), M. Brady and K. J. Cann (to Union Carbide Chemicals and Plastics Technology Co.).
316. W. Cooper in W. M. Saltman, ed., *The Stereo Rubbers*, Wiley-Interscience, New York, 1977.
317. F. E. Matthews and E. H. Strange, *J. Chem. Soc. Ind.* **30**, 1398 (1911).
318. U.S. Pat. 1,058,056 (Apr. 8, 1913), C. Harries (to Farbenfabriken Bayer A.G.).
319. F. W. Stavely and co-workers, *Ind. Eng. Chem.* **48**, 778 (1956).
320. F. C. Foster and J. L. Binder, ACS Advances in Chemistry Series, Vol. **19**: *Handling and Uses of Alkali Metals*, American Chemical Society, Washington, D.C., 1957, p. 26.
321. A. W. Meyer, R. R. Hampton, and J. A. Davison, *J. Am. Chem. Soc.* **74**, 2294 (1952).
322. T. A. Antkowiak and co-workers, *J. Appl. Polym. Sci.* **10**, 1319 (1972).
323. H. L. Hsieh and R. P. Quirk, *Anionic Polymerization*, Marcel Dekker, Inc., New York, 1996, p. 217.
324. E. W. Duck, *Eur. Rubber J.* **155**(12), 38 (1973).
325. E. W. Duck and J. M. Locke, *J. Inst. Rubber Ind.* **2**, 223 (1968).
326. A. W. Langer, *Polym. Prepr.* **7**(1), 132 (1966).
327. M. Morton, *Anionic Polymerization: Principals and Practice*, Academic Press, New York, 1983.
328. C. C. Chang, J. W. Miller Jr., and G. R. Schorr, *J. Appl. Polym. Sci.* **39**, 2395 (1990).
329. S. Bywater, D. J. Worsfold, and P. E. Black, *Makromol. Chem. Suppl.* **15**, 31 (1989).
330. A. F. Halasa, D. F. Loh, and J. E. Hall, *J. Polym. Sci., Polym. Chem. Ed.* **19**, 1357 (1981).
331. W. L. Hsu, A. F. Halasa, and T. T. Wetli, *Rubber Chem. Technol.* **71**, 62 (1998).
332. D. Hesterwerth, D. Beckelmann, and F. Bandermann, *J. Appl. Polym. Sci.* **73**, (1999).
333. Y. Dachuan, J. Guantai, and L. Meizhu, *J. Polym. Mater.* **4**, 227 (1987).
334. L. J. Fetters and co-workers, *Macromolecules* **28**, 4996 (1995).
335. H. S. Makowski and M. Lynn, *J. Macromol. Chem.* **1**, 443 (1966).
336. A. Hernandez and co-workers, *Makromol. Chem., Rapid Commun.* **1**, 75 (1980).

337. M. Morton, L. J. Fetters, and E. E. Bostick, *J. Polym. Sci.*, Part C **1**, 311 (1963).
338. H. L. Hsieh and C. F. Wofford, *J. Polym. Sci.*, Part A-1 **7**, 449 (1969).
339. Ref. 323, p. 201.
340. S. L. Aggarwal, T. G. Hargis, R. A. Livigni, H. J. Fabris, and L. F. Marker, in J. Lal and co-workers, eds., *Advances in Elastomers and Rubber Elasticity*, Plenum, New York, 1986, p. 17.
341. I. G. Hargis, R. A. Livigni, and S. L. Aggarwal, in J. Mark and co-workers, eds., ACS Symposium Series **193**: *Synthesis and Properties of Diene Elastomers with Controlled Structure*, American Chemical Society, Washington, D.C., 1982, p. 73.
342. D. B. Patterson and A. F. Halasa, *Macromolecules* **24**, 1583 (1991).
343. D. B. Patterson and A. F. Halasa, *Macromolecules* **24**, 4489 (1991).
344. M. Morton and L. J. Fetters, *Rubber Chem. Technol.* **48**, 359 (1975).
345. L. E. Foreman, in J. P. Kennedy and co-workers, eds., *Polymer Chemistry of Synthetic Elastomers*, Part II, Vol. **6**, Interscience Publishers, New York, 1969, p. 491.
346. H. E. Railsback and R. P. Zelinski, *Kaut. Gummi Kunst.* **25**, 254 (1972).
347. C. Yong and G. T. Jin, *Rubber Ind.* **43**, 744 (1996).
348. J. R. Haws, L. L. Nash, and M. S. Wilt, *Rubber and Plast. Age* 107 (June 1975).
349. A. W. Langer Jr., *Am. Chem. Soc., Div. Chem. Prepr. No. 1* **7**, 132 (1966).
350. R. P. Quirk and co-workers, *Macromol. Chem., Macromol. Symp.* **32**, 47 (1990).
351. U.S. Pat. 3,055,952 (Sept. 25, 1962), E. J. Goldberg (to E. I. du Pont de Nemours & Co.).
352. U.S. Pat. 3,175,997 (Mar. 30, 1965), H. L. Hsieh (to Phillips Petroleum Co.).
353. R. P. Quirk and S. H. Jang, *Rubber Chem. Technol.* **69**, 444 (1996).
354. U.S. Pat. 5,552,499 (Sept. 3, 1996), T. Kitamura and co-workers (to Bridgestone Co.).
355. U.S. Pat. 6,025,450 (Feb. 15, 2000), D. F. Lawson and co-workers (to Bridgestone Co.).
356. C. A. Uraneck and J. N. Short, *J. Appl. Polym. Sci.* **14**, 4421 (1970).
357. F. Tsutsumi, M. Sakakibara, and N. Oshima, *Rubber Chem. Technol.* **63**(1), 8 (1990).
358. V. Ruiz Santa Quiteria, C. A. Sierra, J. G. Fatou, C. Galán, and L. Fraga, 148th Rubber Division Meeting, American Chemical Society, Cleveland, OH, Oct. 17, 1995. Paper Number 78.
359. M. Pitsikalis and N. Hadjichristidis, *Macromolecules* **28**, 3904 (1995).
360. J. P. Kennedy, *Cationic Polymerization of Olefins: A Critical Inventory*, John Wiley and Sons, Inc., New York, 1975.
361. C. S. Marvel and co-workers, *J. Polym. Sci.* **6**, 483 (1951).
362. T. E. Ferrington and A. V. Tobolsky, *J. Polym. Sci.* **31**, 25 (1958).
363. W. S. Richardson, *J. Polym. Sci.* **13**, 325 (1954).
364. F. Runge and R. Aust, *Chem. Technol. (Berlin)* **9**, 701 (1957).
365. N. G. Gaylord and M. Svestka, *J. Polym. Sci.*, Part B **7**, 55 (1969).
366. N. G. Gaylord and co-workers, *J. Am. Chem. Soc.* **85**, 641 (1963).
367. N. G. Gaylord, I. Kössler, and M. Stolka, *J. Macromol. Sci., Chem.* **A2**, 421 (1968).
368. B. Matyska and co-workers, *Collection Czech. Chem. Commun.* **30**, 2569 (1965).
369. Ref. 360, p. 159.
370. Ref. 360, p. 163.
371. L. A. Eldib, *Hydrocarbon Process. Pet. Refiner* **42**, 164 (1963).
372. D. C. Blackley, *Emulsion Polymerization*, John Wiley & Sons, Inc., New York, 1975.
373. J. Ugelstad and F. K. Hansen, *Rubber Chem. Technol.* **49**, 536 (1976).
374. W. D. Harkins, *J. Am. Chem. Soc.* **69**, 1428 (1947).
375. W. D. Harkins, *J. Polym. Sci.* **5**, 217 (1950).
376. *Eur. Chem. News* **1682**, 28 (1995).
377. M. Roberts, *Chem. Week* **21**, 22 (1995).

378. U.S. Pat. 6,071,847 (June 6, 2000), W. M. Cole and co-workers (to Bridgestone Co.)
379. J. Ling and co-workers, *Polymer* **41**, 8703 (2000).
380. J. G. Lacson, *Polybutadiene Elastomers*, Chemical Economics Handbook, SRI International, Menlo Park, Calif., Apr. 2000.
381. Monthly NR/SR Report, The Rubber Manufacturers Association, Inc.

MICHAEL KERNS
STEVEN HENNING
MICHAEL RACHITA
Goodyear Tire and Rubber Company

BUTYL RUBBER

Introduction and Background

Isobutylene has been of interest since the early days of synthetic polymer research when Friedel Crafts catalysts were used to prepare elastic materials. Isobutylene polymers of commercial importance include homopolymers and copolymers containing small amounts of isoprene or *p*-methylstyrene. Currently, chlorinated and brominated derivatives of butyl(poly[isobutylene-*co*-isoprene]) have the highest sales volume.

Isobutylene was first observed to polymerize in 1873 but high molecular weight polymers were not made until work at I. G. Farben in Germany established that molecular weight increases with decreasing polymerization temperature. Polyisobutylene was synthesized at -75°C using BF_3 as a catalyst. However, as the polymer was saturated, it could not be cross-linked into a rubbery network and no commercial uses were found (1).

Poly[isobutylene-*co*-isoprene] or butyl rubber was synthesized in 1937 at the Standard Oil Development Co., forerunner of ExxonMobil Chemical Co. (2). The first sulfur-curable copolymer was prepared in ethyl chloride over an aluminum chloride catalyst with 1,3-butadiene as the comonomer; however, it was soon found that isoprene was a better comonomer and that methyl chloride was a better polymerization diluent. During World War II, the natural rubber supply to the United States was drastically curtailed, boosting the production of synthetic rubber. The commercial production of butyl rubber in 1943 was an enormous scientific and engineering achievement given the very early state of the art and complexity of this technology.

The discovery of butyl rubber was, in fact, the discovery of the limited-functionality elastomers. Unlike natural rubber and polybutadiene, which have

Encyclopedia of Polymer Science and Technology. Copyright John Wiley & Sons, Inc. All rights reserved.

reactive sites on every monomer unit, the unsaturation in butyl rubber is widely spaced along a saturated, flexible hydrocarbon chain. The principle of limited functionality has been subsequently used in other elastomers, eg, ethylene–propylene terpolymers and chlorosulfonated polyethylene. Halogenated butyl rubber was first synthesized at Goodrich (3). A brominated butyl rubber was commercialized via a small-scale batch method in 1954 starting from *N*-bromosuccinimide and butyl rubber. The product was withdrawn in 1969. Following the withdrawal of Goodrich bromobutyls from the market, Polymer Co. of Canada developed the commercial process using elemental bromine, which is the currently used commercial process. Chlorinated butyl rubber was developed at ExxonMobil and commercialized in 1961. It is made by the continuous chlorination of a solution of butyl rubber (4). Currently, brominated butyl rubber is also manufactured by a similar continuous-solution process.

The first use for butyl rubber was as inner tubes, whose air-retention characteristics contributed significantly to the safety and convenience of tires. Good weathering, ozone resistance, and oxidative stability have led to applications in mechanical goods and elastomeric sheeting. Automobile tires were manufactured for a brief period from butyl rubber, but poor abrasion resistance curtailed this development.

Halogenated butyl rubber greatly extended the usefulness of butyl rubber by providing much higher vulcanization rates and improving the compatibility with highly unsaturated elastomers, such as natural rubber and styrene–butadiene rubber (SBR). These properties permitted the production of tubeless tires with chlorinated or brominated butyl innerliners. The retention of air pressure (5) and low intercarcass pressure (6) extended tire durability.

Polyisobutylene is produced in a number of molecular weight grades and each has found a variety of uses. The low molecular weight liquid polybutenes have applications as adhesives, sealants, coatings, lubricants, and plasticizers, and for the impregnation of electrical cables (7). Moderate molecular weight polyisobutylene was one of the first viscosity-index modifiers for lubricants (8). High molecular weight polyisobutylene is used to make uncured rubbery compounds and as an impact additive for thermoplastics.

Process Chemistry

Butyl rubber is prepared from 2-methylpropene [115-11-7] (isobutylene) and 2-methyl-1,3-butadiene [78-79-5] (isoprene). Isobutylene with a purity of >99.5 wt% and isoprene with a purity of >98 wt% are used to prepare high molecular weight butyl rubber. Water and oxygenated organic compounds are minimized by feed purification systems because these impurities interfere with the cationic polymerization mechanism. Copolymers of isobutylene can also be prepared from mixed C_4 olefin containing streams that contain *n*-butene. These copolymers are generically known as polybutenes.

Isobutylene Polymerization Mechanism. The carbocationic polymerization of isobutylene and its copolymerization with viable comonomers like isoprene and *p*-methylstyrene is mechanistically complex (9–11). The initiating system is typically composed of two components: an initiator and a Lewis

acid coinitiator. Typical Lewis acid coinitiators include $AlCl_3$, (alkyl)$AlCl_2$, BF_3, $SnCl_4$, $TiCl_4$, etc. More recently uncommon Lewis acid such as methylaluminoxane (MAO) (12,13) and specifically designed weakly coordinating Lewis acids such as $B(C_6F_5)_3$ (14,15) have been used as Lewis acids in initiating systems for isobutylene polymerization. Common initiators include Brønsted acids such as HCl, RCOOH, H_2O, alkyl halides, eg, $(CH_3)_3CCl$, $C_6H_5(CH_3)_2Cl$, esters, ethers, peroxides, and epoxides. More recently, transition-metal complexes, such as metallocenes and other single-site catalyst systems, when activated with weakly coordinating Lewis acids or Lewis acid salts, have been used to initiate isobutylene polymerization (16). In the initiation step, isobutylene reacts with the Lewis acid coinitiator–initiator pair to produce a carbenium ion. Additional monomer units add to the formed carbenium ion in the propagation step. Temperature, solvent polarity, and counterions affect the chemistry of propagation. These reactions are fast and highly exothermic. The propagation rate constant has been determined to be around 10^8 L/(mol · s), essentially diffusion-limited (17,18). Polymerizations at low temperature give extremely high polymerization rates in either hydrocarbon or halogenated hydrocarbon solvents. Isoprene is copolymerized mainly by trans-1,4-addition (>90%), and to a lesser extent by either 1,2-addition (19,20) or as a branched 1,4-addition product (21). The propagation proceeds until chain transfer or termination occurs.

In the chain-transfer step, the carbenium ion chain end reacts with isobutylene, isoprene, or a species with an unshared electron pair, ie, RX, solvents, counterion, and olefins. Reaction with these species terminates the growth of this macromolecule and permits the formation of a new chain. The activation energy of chain transfer is larger than propagation, thus the molecular weight of the polymer is strongly influenced by the polymerization temperature. Lower temperatures lead to higher molecular weight polymer. As comonomers exhibit their own chain-transfer characteristics, the presence of comonomer can also influence the final molecular weight of a copolymer. Higher isoprene contents typically lower the molecular weight of prepared butyl rubber (22,23). Termination results from the irreversible destruction of the propagating carbenium ion and discontinuance of the kinetic chain. Termination reactions include the collapse of the carbenium ion–counterion pair, hydride abstraction from comonomer, formation of dormant or stable allylic carbenium ions, or by reaction of the carbenium ion with nucleophiles, eg alcohols or amines. The reactivity ratios are strongly affected by the polymerization conditions (Table 1). A laboratory procedure for the preparation of butyl rubber is described in Reference 34.

Fundamental rate constants for the initiation, propagation, chain-transfer, and termination steps in the polymerization process are difficult to measure because of the rapid rate of reaction. However, recent work (35) has shown that the propagation rate constant is of the order of 6×10^8 L/(mol · s).

Studies of the living cationic polymerization of isobutylene and copolymerization with isoprene have begun (36,37). The living copolymerization of isobutylene and isoprene has so far produced a random copolymer with narrow molecular weight distribution and a well-defined structure. For example, the BCl_3/cumyl acetate polymerization system in methyl chloride or methylene chloride at -30°C provides for copolymers with 1–8 mol% trans-1,4-isoprene units and M_n between 2000 and 12,000 with a M_w/M_n of under 1.8. The advent of living polymerization

Table 1. Copolymerization Reactivity Ratios of the Isobutylene/Isoprene System[a]

Initiating system	Solvent	T,°C	r_1	r_2	Reference
$AlCl_3$	CH_3Cl	−103	2.5 ± 0.5	0.4 ± 0.1	24
$EtAlCl_2$	CH_3Cl	−100	2.17	0.5	25
$AlCl_3$	CH_3Cl	−90	2.3		26
$EtAlCl_2 + Cl_2$	CH_3Cl	−35	2.5		27
$AlCl_3$	EtCl	−95	2.26	0.38	28,29
$EtAlCl_2$	EtCl	−90	2.27	0.44	28,29
$EtAlCl_2$	CH_3Cl 88%/hexane 12%	−80	2.15	1.03	30
$EtAlCl_2$	CH_3Cl 50%/hexane 50%	−80	1.90	1.05	30
$EtAlCl_2$	CH_3Cl 12%/hexane 88%	−80	1.17	1.08	30
$EtAlCl_2$	Hexane 100%	−80	0.80	1.28	30
$AlCl_3$	C_5/CH_2Cl_2	−70	1.56 ± 0.19	0.95 ± 0.17	31,32
$AlCl_3$	CH_3Cl	−80	1.6		33

[a]Ref. 24.

of isobutylene has brought about the preparation of a large number of new isobutylene-based materials.

High molecular weight copolymers of isobutylene and isoprene have been prepared at temperatures 40–50°C higher than is commercially practiced using metallocene and single-site initiators (12–16). Newer Lewis acids like methylaluminoxane and weakly coordinating anions or their salts like $B(C_6F_5)_3$ or $R^+[B(C_6F_5)_4]^-$ also prepare high molecular weight copolymers at these higher temperatures (12–16).

Modification of Butyl Rubbers.

Halobutyls. Chloro- and bromobutyls are commercially the most important derivatives. The halogenation reaction is carried out in hydrocarbon solution using elemental chloride and bromine (equimolar with the enchained isoprene). The halogenation is fast and proceeds mainly by an ionic mechanism. The structures that may form include the following:

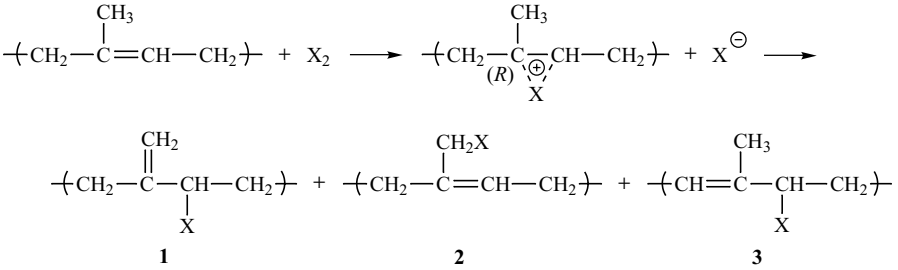

(1)

Normally structure **1** is dominant (>80%) (38,39). More than one halogen atom per isoprene unit can also be introduced. However, the reaction rates for excess halogens are lower and the reaction is complicated by chain fragmentation (40).

Other Derivatives. Various other derivatives have appeared on the market or reached the market development stage. Conjugated-diene butyl is obtained by the controlled dehydrohalogenation of halogenated butyl rubber (41). The product

can be cross-linked with peroxide or exposure to radiation. Free-radical grafting with vinyl monomers, eg styrene, can be used in a graft cure, leading to a transparent rubber with a T_g of about -59°C. Carboxy-terminated polyisobutylene useful in forming networks with epoxies or aziridine has been prepared from high molecular weight butyl rubber or a poly(isobutylene-*co*-piperylene) [26335-67-1] copolymer (42). The resulting carboxy-terminated polymers are viscous liquids. High molecular weight isobutylene–cyclopentadiene rubbers containing up to 40% cyclopentadiene were produced and developed by ExxonMobil (43) and were recently reexamined by Daelim (43). Highly branched polyisobutylene are prepared by use of an appropriately designed initiator that is also a comonomer in the polymerization (44).

Isobutylene–Isoprene–Divinylbenzene Terpolymers. A partially cross-linked terpolymer of isobutylene, isoprene, and partially reacted divinyl benzene is commercially available from Rubber Division, Bayer Inc., Canada. The residual vinyl functionality may be cross-linked with peroxides, a treatment that would normally degrade conventional butyl rubbers. This material is used primarily in the manufacture of sealant tapes and caulking compounds (45).

Liquid Butyl Rubber. Degradation of high molecular weight butyl rubber by extrusion at high shear rates and temperatures produces a liquid rubber with a viscosity average molecular weight (M_v) between 20,000 and 30,000. The relatively low viscosity aids in formulating high solids compounds for use in sealants, caulks, potting compounds, and coatings. Resulting compounds can be poured, sprayed, and painted.

New Materials.

Star-Branched (SB) Butyl. Butyl rubbers have unique processing characteristics because of their viscoelastic properties and lack of crystallization of compounds on extension. They exhibit both low green strength and low creep resistance as a consequence of high molecular weight between entanglements. To enhance the strength of uncured traditional butyl rubber a relatively high molecular weight is required. Increasing molecular weight also causes an increase in relaxation time along with high viscosity. In such situations it is usually helpful to broaden the molecular weight distribution, but this is difficult to accomplish in conventional butyl rubber polymerization. Physical blending of low and high molecular weight polymer can also provide broader molecular weight distributions, but it results in other processing problems such as high extrudate swelling in flow-through shaping dies.

SB butyl has a bimodal molecular weight distribution with a high molecular weight branched mode and a low molecular weight linear component. The polymer is prepared by a conventional carbocationic copolymerization of isobutylene and isoprene at low temperature, but in the presence of a polymeric branching agent. The high molecular weight branched molecules are formed during the polymerization via a graft-from or a graft-onto mechanism. A graft-from reaction takes place when a macroinitiator/macrotransfer reagent, such as hydrochlorinated poly(styrene-*co*-isoprene) or chlorinated polystyrene, is used. A graft-onto reaction takes place when a multifunctional terminating agent, eg, poly(styrene-*co*-butadiene), is employed as the branching agent. In general, the SB butyl has 10–20% high molecular weight branched molecules, which have a random comblike structure with 20–40 butyl branches. Although this is not a true star topology,

it approaches a star structure since the branching agent is relatively short and the branching density is relatively high, ie, the molecular weight between branching points is low compared to the segment length of the butyl branches. SB butyl rubbers offer a unique balance of viscoelastic properties, resulting in significant processability improvements. Dispersion in mixing and mixing rates are improved. Compound extrusion rates are higher, die swell is lower, shrinkage is reduced, and surface quality is improved. The balance between green strength and stress relaxation at ambient temperature is improved, making shaping operations such as tire building easier. Several grades of ExxonMobil SB butyl polymers including copolymer, chlorinated, and brominated copolymers are now commercially available.

Brominated Poly(isobutylene-co-p-methylstyrene). *para*-Methylstyrene [622-97-9] (PMS) can be readily copolymerized with isobutylene via classical carbocationic copolymerization using a strong Lewis acid, eg, $AlCl_3$ or alkyl aluminum in methyl chloride, at low temperature. The copolymer composition is very similar to the feed monomer ratio because of the similar copolymerization reactivity ratios, ie, $r_1 = 1$ and $r_2 = 1.4$, under commercial polymerization conditions. These new high molecular weight copolymers encompass an enormous range of properties, from polyisobutylene-like elastomers to poly(*p*-methylstyrene)-like tough, hard plastic materials with T_gs above 100°C, depending on monomer ratio. A highly reactive and versatile benzyl bromide functionality, $C_6H_5CH_2Br$ can be introduced by the selective free-radical bromination of the benzyl group in the copolymer. The brominated copolymer can be cross-linked with a variety of cross-linking systems. This new functionalized copolymer preserves polyisobutylene properties, low permeability, and unique dynamic response, while adding the behavior of inertness to ozone, a property similar to ethylene–propylene rubbers. Copolymers with PMS below 10 mol% are most useful for elastomeric applications because the T_gs are near −60°C. Several grades of the brominated copolymer (Exxpro Polymers) are available from ExxonMobil (46,47).

The benzyl bromide in the brominated copolymer can also be easily converted by nucleophilic substitution reactions to a variety of other functional groups and graft copolymers as desired for specific properties and applications (47). Ionomers (48), grafted copolymers (49), radiation-cured rubbers (50), and rubber-toughened nylons (51) are a few examples of the derivatives and functions that modification of brominated poly(isobutylene-*co*-*p*-methylstyrene) can offer.

Thermoplastic Elastomers. With the structural control inherent in living polymerization, new block copolymers (qv) containing polyisobutylene are now possible (36). ABA triblock copolymers (A = polymethyl vinyl ether, B = polyisobutylene) that provide morphologies capable of exhibiting properties of an elastomer at use temperature, while processing like a thermoplastic, have been made from polyisobutylene and several styrenic derivatives (52–58) (see ELASTOMERS, THERMOPLASTIC). As thermoplastic elastomers, these materials offer other advantages owing to the intrinsic properties of polyisobutylene, namely low permeability and low dynamic modulus. More recently, star block copolymers of the A_2B_2 type have been prepared and exhibit unique physical properties (59). Many more architecturally designed polyisobutylenes are possible through living polymerization techniques. Kuraray Inc., Japan, commercially test-marketed polyisobutylene–polystyrene block copolymers. Also, Kaneka Inc., Japan, produce Epion, a functionalized polyisobutylene.

Manufacturing

Most of the butyl polymers made commercially are produced by copolymerizing isobutylene and isoprene in precipitation processes that use methyl chloride as the diluent and a catalyst system comprising a Lewis Acid and an alkyl halide. The Lewis acid used in many of the commercial butyl rubber plants is aluminum chloride, which is low cost, a solid, and soluble in methyl chloride. Aluminum alkyls are now becoming popular because they simplify catalyst preparation and have been shown to increase monomer conversion.

The manufacture of butyl rubber, poly(isobutylene-*co*-*p*-methylstyrene) (Exxpro backbone) and high molecular weight polyisobutylene (Vistanex) requires a complex manufacturing process consisting of feed purification, feed blending, polymerization, slurry stripping, and finishing. A schematic flow diagram (Fig. 1) shows the major units in a butyl plant.

An alternative solution process, developed in Russia, uses a C_5–C_7 hydrocarbon as solvent and an aluminum alkyl halide as the initiator. The polymerization is conducted in scraped surface reactors at -90 to $-50^{\circ}C$. The solution process avoids the use of methyl chloride, which is an advantage when butyl rubber is to be halogenated. However, the energy costs are higher than for the slurry process because of the higher viscosity of the polymer solution. Consequently, it is unlikely that the well-established slurry process will be displaced.

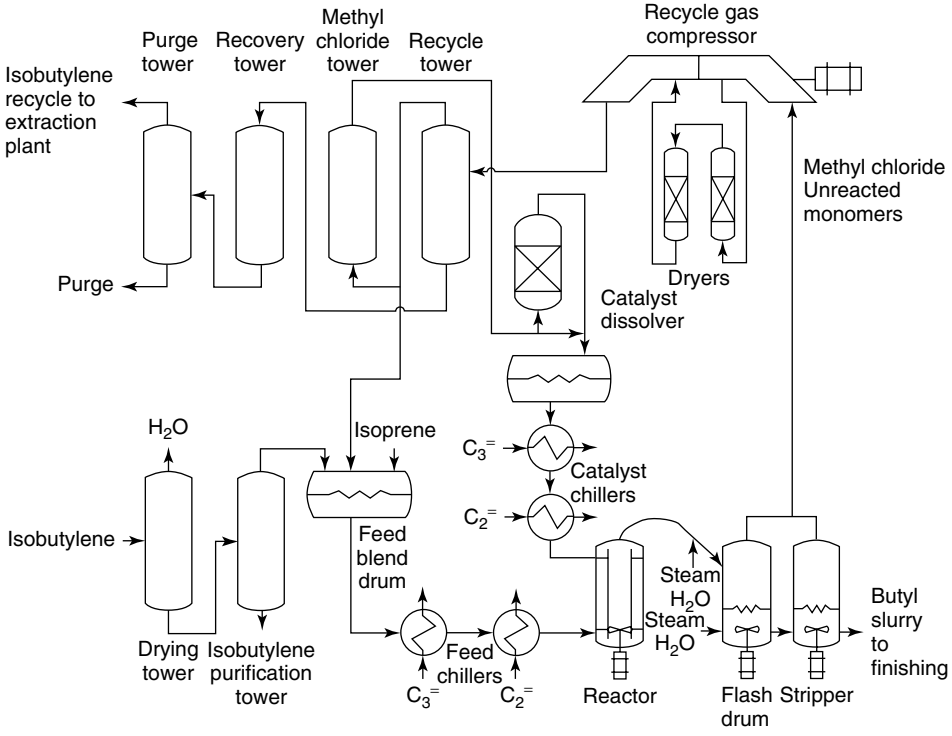

Fig. 1. Butyl plant flow plan.

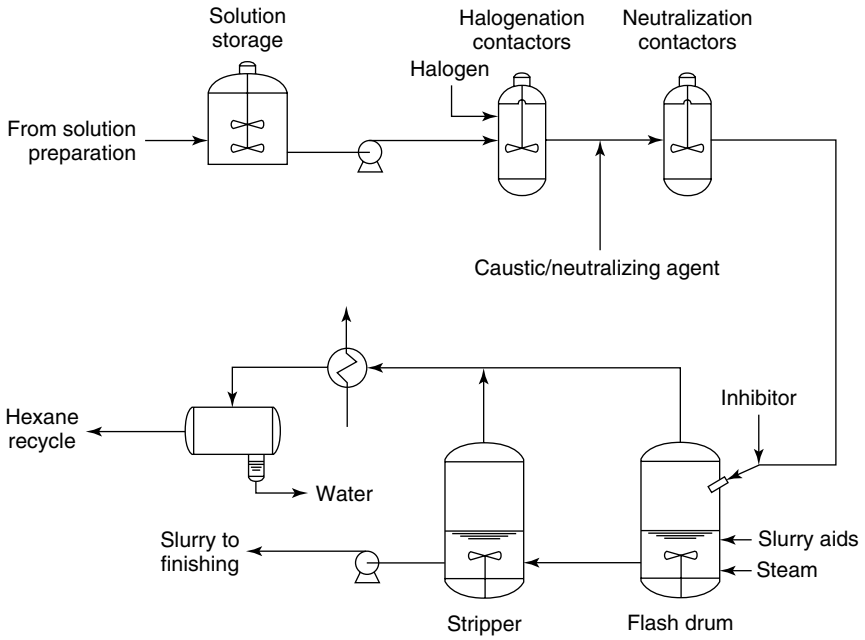

Fig. 2. Block diagram of halogenation.

The manufacture of halobutyl rubbers such as Bromobutyl, Chlorobutyl, and Exxpro [bromopoly(isobutylene-*co*-*p*-methylstyrene)] requires a second chemical reaction: the halogenation of the polymer backbone. This can be achieved in two ways, the finished polymer produced in the butyl plant can be dissolved in a hydrocarbon solvent such as hexane or pentane, or a solvent replacement process can be used to dissolve the polymer from the slurry leaving the reactor. A schematic flow diagram of the halogenation process is shown by Figure 2.

Monomer Purification. To make high molecular weight polymers with good isobutylene conversion and good reactor service factor, the feed must be pure and dry. We must start with high quality isobutylene (>99%), dry it, and remove other olefins, eg butene-1, butene-2, propene, and oxygenated hydrocarbons such as dimethyl ether and methanol. A number of commercial processes are available for production of the required high purity isobutylene. An extraction process based on sulfuric acid has been developed by several companies (60,61) and is used extensively. Significant quantities of isobutylene are also produced by dehydration of *tert*-butyl alcohol (62). The highest purity isobutylene is produced by MTBE (methyl-*t*-butyl ether, [1634-04-4]) decomposition plants. This process starts with the selective reaction of dilute isobutylene in a C_4 stream with methanol over an acid ion-exchange resin, eg, Amberlyst 15, to form MTBE. This ether is produced mainly as a high octane blending component for low lead gasoline. Catalytic decomposition at 170–200°C and 600 kPa (5.9 atm) over a fixed-bed acid catalyst, eg, $SiO_2Al_2O_3$ or Amberlyst 15, produces high purity isobutylene (63–65).

The isobutylene is then dried by azeotropic distillation and purified in a super-fractionating distillation column to reduce the butenes to less than 1000 ppm. Note that if water is not removed it will cause icing in the feed chillers and this will lead to a poor reactor service factor.

The purified isobutylene is then blended with a recycled methyl chloride stream containing a low level of isobutylene (∼5%). Finally, the comonomer, isoprene or *p*-methylstyrene, is added. In this blending process, control of the ratio of comonomer to isobutylene is very important. This is because it has a significant impact on the composition of the polymer produced, the conversion of monomer, and the stability of reactor operation. For these reasons, a combination of both an analyzer and a mass balance control can be used to maintain the composition of the feed blend. The feed blend contains 20–40 wt% of isobutylene and 0.4–1.4 wt% of isoprene or 1–2 wt% of *p*-methylstyrene, depending on the grade of butyl rubber to be produced; the remainder is methyl chloride.

Polymerization. Catalyst solution is produced by passing pure methyl chloride through packed beds of granular aluminum chloride at 45°C. The concentrated solution formed is diluted with additional methyl chloride to which a catalyst activator is added and the solution later stored. The feed blend and catalyst solutions are chilled to −100 to −90°C in a series of heat exchangers before entry to the reactor.

The cold feed and catalyst are introduced continuously to a reactor comprising a central vertical draft tube surrounded by concentric rows of cooling tubes. The reactors have an aspect ratio of 28 (length) to 8 (diameter) and contain an axial flow pump located at the bottom of the draft tube that circulates the slurry through the cooling tubes. The reactor is constructed with 3.5 or 9 wt% nickel steel, or alloys that have adequate impact strength at the low temperature of the polymerization reaction. The production of high molecular weight butyl requires a polymerization temperature below −135°F (−90°C) and the reaction is exothermic, generating 0.82 MJ/kg (350 Btu/lb) of polymer. This requires a two-stage refrigeration system that uses boiling propylene or propane and ethylene as the refrigerants. In some plants ammonia is used in the first stage of the refrigeration process.

The reactors are the epicenter of all butyl plants and are mechanically complex. The operation of the remainder of the plant is dictated by the reactors. Essentially, the reactors are stirred tanks that contain a heat exchanger to keep them cold.

In the reactor, polymer chains are initiated by the catalyst and propagate in solution. Chain propagation occurs in microseconds but the overall reaction rate is controlled by the slower initiation sequence. As individual polymer molecules are formed they precipitate to produce a fine milky slurry of sub–micron-size particles. These particles grow in the reactor by accreting new polymer chains and by agglomeration.

The polymer slurry circulates through the reactor tubes, and boiling liquid ethylene in the reactor jackets keeps the reactor contents cold. The butyl polymerization process is complex because of the combination of low temperature operation, polymer slurry formation, and difficulty in directly measuring polymer quality. To achieve high molecular weight, the reaction temperature must be kept low to reduce the amount of chain transfer. In the slurry process, the viscosity

is relatively low, and good heat transfer can be achieved. To maintain a stable slurry, the temperature must be kept below the glass-transition temperature, T_g, of polyisobutylene (−68°C) and, as the slurry is shear-thinning, there must be a high level of shear. The axial flow pump that provides a high degree of circulation in the reactor achieves this.

One of the common theories to explain fouling in a butyl reactor is that rubber particles in the reactor slurry are not completely glassy because of diluent and monomers in the surface layer. This causes them to be sticky as well as agglomerating, and the particles will stick to the heat-transfer surfaces in the reactor. This causes the heat-transfer resistance to increase and the slurry temperature to warm. Eventually, this warming can cause the slurry to destabilize and the viscosity to increase rapidly. Ultimately, this could lead to plugging, which requires extended solvent washing to clean the reactor. Therefore, production in a reactor is stopped every 2–4 days for solvent washing. This forces a cyclical multireactor operation in which some reactors are producing polymer while others are being washed to remove rubber fouling. Typical runs are from 18 to 60 h, depending on feed purity, slurry solids concentration, and production rate.

The production rate is 2.0–4.5 t/h, depending on feed rate, monomer concentration in the feed, and monomer conversion. The conversion of isobutylene and isoprene typically ranges from 75–95% and 45–85%, respectively, depending on the grade of butyl rubber being produced. The molecular weight of the polymer produced is set by the ratio of chain-making to chain-terminating processes. In commercial plants the molecular weight and composition of the polymer formed are controlled by the concentration of monomers in the reactor liquid phase and the amount of terminating or transfer species present to interrupt chain growth. The slurry composition depends on the monomer content of the feed stream and the extent of monomer conversion. In practice, the flow rate and the composition of catalyst to the reactor is the principal operating variable; reactor residence time is often in the range 30–60 min.

The original reactor design, known as the draft tube reactor, has been used commercially since the initial development of butyl in the 1940s. An improved design in which the draft tube is replaced by additional tubes and the circulation pump is redesigned has recently been proposed (66).

In addition to these changes to the mechanical design of the reactor, improvements to the polymerization chemistry and diluent have been investigated in the last decade. Examples are the use of supercritical carbon dioxide (67) and the use of aluminum alkyls in the catalyst system (68).

Halogenation. Chlorinated and brominated butyl rubber can be produced in the same plant in blocked operation. However, there are some differences in equipment and reaction conditions. A longer reactor residence time is required for bromination because of the slower reaction rate compared to chlorination. Separate facilities are needed to store and meter the individual halogens to the reactor. Additional facilities are required because of the complexity of stabilizing bromobutyl rubber.

The halogenation process begins with the preparation of a hexane solution of butyl rubber with the desired molecular weight and unsaturation. Slurry from a butyl polymerization reactor is dissolved (69–71) by transferring it into a drum containing hot liquid hexane that rapidly dissolves the fine slurry particles.

Hexane vapor is added to flash methyl chloride and unreacted monomers overhead for recovery and recycle. The solution of butyl in hexane passes to a stripping column where the final traces of methyl chloride and monomers are removed. The hot solution is brought to the desired concentration for halogenation, typically 20–25 wt% in an adiabatic flash step.

Alternatively, bales of finished butyl rubber are chopped or ground to small pieces and conveyed to a series of agitated dissolving vessels or to a large vessel divided into multiple stages. Solutions containing 15–20% polymer can be prepared in 1–4 h depending upon temperature, particle size, and agitation. This method has the advantage of being independent from the butyl polymerization process but requires storage and careful inventory control between the two stages of the process. This process also requires two finishing operations: one to produce dry butyl backbone, the second to finish the halobutyl product. Investment costs for the two dissolving processes are similar, but energy costs for the dissolving process can be higher.

Halogenation is the second major chemical reaction in the production of halobutyl polymers. It is usually carried out by adding bromine liquid or chlorine vapor to a solution of rubber in hydrocarbon solvent (hexane or pentane), which is often referred to as cement. The cement must be essentially free of monomers, or low molecular weight toxic species will be formed during the chlorine or bromine reactions. The halogenation of the butyl backbone is an ionic-substitution reaction in which the halogen is added to the cement stream in a well-mixed reactor (eq. 1). This reaction is unusual for polymers where it's more typical for the bromine to add across the double bond.

Insufficient mixing will lead to poor distribution of the halogen on the polymer, which can cause the product cure characteristics to be unsatisfactory. Another potential problem is the vigorous reaction of liquid chlorine with hydrocarbon. This leads to complete breakdown of some of the polymer, producing carbon and HX. This causes the polymer to be gray rather than the normal off-white and the product properties to be adversely affected.

For both chloro- and bromobutyl rubber two isomers are formed as shown in equation 1. The ratio of these isomers must be carefully controlled in order to keep consistent product properties.

The by-product from this reaction, HX, is normally reacted with aqueous caustic solution to give a soluble salt. Incomplete neutralization will leave HX in the rubber, and subsequent reactions during the drying process can destabilize the polymer. The key to good neutralization is good mixing of the halogen and cement. Further improvements to the neutralization process can be achieved by the addition of a surfactant (72).

Because of the generation of HCl or HBr, the maximum efficiency for halogen usage in this process is 50%. An improvement in efficiency can be achieved by adding hydrogen peroxide to the process to convert the acid back to halogen (73).

The bromination reaction required to produce Exxpro requires a free-radical reaction because there is no unsaturation in the backbone. The bromine and a free-radical initiator are added to the cement, mixed well, and then passed through a series of stirred tank reactors where the chain reaction shown by equation 2 occurs.

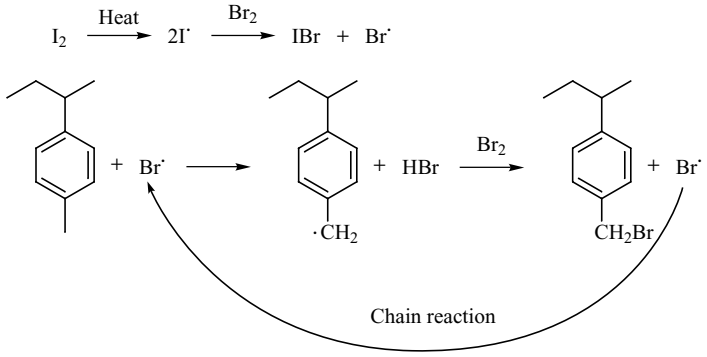

(2)

An alternative process is bulk-phase halogenation (74–76). Dry butyl rubber is fed into a specially designed extruder reactor and contacted in the melt phase with chlorine or bromine vapor. By-product halogen acids are vented directly, avoiding the need for a separate neutralization step. Halogenated rubbers comparable in composition and properties to commercial products can be obtained.

Finishing. The halogenated rubber solution then passes into a vertical drum where the solvent is flashed and stripped by steam and hot water. Calcium stearate is added to the slurry in this drum to prevent polymer agglomeration. A second vessel in series provides additional residence time for the solvent to diffuse from the rubber and be vaporized. The final solvent content and the steam usage for solvent removal depend on the conditions in each vessel. Typically, the lead flash drum is operated at 105–120°C and 200–300 kPa (29–43.5 psi). Conditions in the final stripping stage are 101°C and 105 kPa (15 psi). The hexane can be reduced to 0.5–1.0 wt% with a steam usage of 2.0–2.5 kg/kg rubber.

The resultant polymer/water slurry is kept agitated and then screened to separate the bulk water from the rubber. The polymer is then dried in a series of extrusion dewatering and drying steps to a final moisture content of <0.3 wt%. Antioxidants and stabilizers, eg, BHT and epoxidized soybean oil, protect against dehydrohalogenation and are added in the final extrusion step. Fluid-bed conveyors and/or airvey systems are used to cool the product to an acceptable packaging temperature. The resultant dried product is in the form of small "crumbs," which are subsequently weighed and compressed into 75-lb bales for wrapping in polyethylene film and packaged into wooden or metal crates or cardboard containers.

Structure, Properties, and Product Applications of Isobutylene-Based Polymers

Molecular Structure.

Polyisobutylene. Isobutylene polymerizes in a regular head-to-tail sequence to produce a polymer having no asymmetric carbon atoms. The two pendant methyl groups bonded to alternative chain atoms in polyisobutylene (PIB) produce steric crowding, for which a partial relief is achieved by a distortion of the methylene carbon to 124° as compared to 110° for the tetrahedral carbon (73,74).

Methyl crowding is further alleviated by distorting the dihedral angle, leading to a splitting of the trans-rotational isomer by about 25° (73–75). The splitting of the trans isomer in two equivalent states is a special feature of PIB, not observed in its vinyl analogue, and has significant impacts on its local chain-segment dynamics (76). The additional fast trans-to-trans skeletal relaxation process in PIB results in a faster segmental motion and a lower glass-transition temperature despite the fact that PIB is a sterically strained and crowded macromolecule (76). The glass-transition temperature of PIB is about −70°C (77). It is an amorphous elastomer in the unstrained state. On extension at room temperature, PIB of high molecular weight crystallizes into crystals of an 8/3 helix with an alternating distorted trans-gauche structure (78). One chain end of PIB is typically unsaturated because of chain-transfer and termination mechanisms. Molecular weights could range from several hundred to several millions. There is no long-chain branching unless special synthesis methods are employed. The molecular weight distribution is commonly the most probable with $M_w/M_n = 2.0$.

Polybutenes. Copolymerization of mixed isobutylene and 1-butene containing streams with a Lewis acid catalyst system yields low molecular weight copolymers, from several hundreds to a few thousand, that are clear, colorless, and viscous liquids. The chain ends are unsaturated and are often chemically modified to provide a certain functionality (79,80).

Butyl Rubber. In butyl rubber, isoprene is enchained predominantly (90–95%) by 1,4-addition and head-to-tail arrangement (81–84). The remaining minor isoprene species may be interpreted spectroscopically either as 1,2-enchained (83,84) or as branched species from 1,4-addition (85). Depending on the grade, the unsaturation in butyl rubber is between 0.5 and 3 mol%. The glass-transition temperature of butyl rubber is about −65°C (86). With the low content of isoprene and a near-unity reactivity ratio between isoprene and isobutylene (87), a random distribution of enchained isoprene monomer in butyl rubber is achieved. The molecular weight distribution in butyl rubber is mostly with M_w/M_n of 3–5.

Halogenated Butyl Rubber. Halogenation at the isoprene site in butyl rubber proceeds by a halonium ion mechanism leading to the formation of a predominated exomethylene alkyl halide structure in both chlorinated and brominated rubbers (88,89). Upon heating, the exo allylic halide rearranges to give an equilibrium distribution of exo and endo structures (90–92). Halogenation of the unsaturation has no apparent effects on the butyl backbone and on the butyl glass-transition temperature. However, cross-linked halobutyl rubbers do not crystallize on extension as a result of the backbone irregularities introduced by the halogenated isoprene units.

Star-Branched (SB) Butyl. Introduction of a branching agent of styrene–butadiene–styrene (SBS) block copolymer during cationic polymerization of butyl leads to a SB butyl that, in general, contain 10–15% of star polymers, with remaining linear butyl chains (93,94). SB butyl is a reactor blend of linear polymers and star polymers, where the star molecules were synthesized during polymerization by cationic grafting of propagating linear butyl chains onto the branching agent (95). In the solid state, these star polymers aggregate to form ∼30-nm-diameter spherical domains separated by about 90 nm and covered by about 6 vol% (96,97). It was proposed that these domains consist of predominantly the styrene–butadiene–styrene branching agent (96). A much broader molecular

weight distribution is achieved in SB butyl with M_w/M_n greater than 8. Halogenation of SB butyl results in the same halogenated structure in the linear butyl chains and in the linear butyl chain arms of the star fraction as that in the halogenated butyl. Unreacted butadiene blocks of the SBS branching agent were 100% brominated and 60% chlorinated after halogenation (98).

Brominated Poly(isobutylene-co-p-methylstyrene). Copolymerization of isobutylene with *para*-methylstyrene (PMS) produces a saturated copolymer backbone with randomly distributed pendant *para*-methyl-substituted aromatic rings. During radical bromination after polymerization, some of the substituted *para*-methyls are converted to bromomethyls for vulcanization and functionization (99,100). Brominated poly(isobutylene-*co*-*p*-methylstyrene) polymers are saturated terpolymers containing isobutylene, 1–6 mol% PMS, and 0.5–1.5 mol% BrPMS (brominated *para*-methylstyrene). Their T_gs increase with increasing PMS content and is around -60°C. The molecular weight distribution of brominated poly(isobutylene-*co*-*p*-methylstyrene) is narrow, with M_w/M_n less than 3 (99).

Physical Properties.

Permeability. Primary uses of polyisobutylene and isobutylene copolymers of butyl, halobutyl, SB butyl, and brominated poly(isobutylene-*co*-*p*-methylstyrene) in elastomeric vulcanized compounds rely on their properties of low air permeability and high damping. In comparison with many other common elastomers, polyisobutylene and its copolymers are notable for their low permeability to small-molecule diffusants as a result of their efficient intermolecular packing (101–103) as evidenced by their relative high density (density of 0.917 g/cm^3). This efficient packing in isobutylene polymers leads to their low fractional free volumes and low diffusion coefficients for penetrants (101). In combination with the low solubilities of small-molecule diffusants in isobutylene polymers, low permeability values for small molecules, such as He, H_2, O_2, N_2, CO_2, and others, are observed in isobutylene polymers as compared with other elastomers (104).

As shown in Figure 3, diffusion coefficients of nitrogen in both various diene rubbers and in butyl rubber increase with increasing differences between the measurement temperature and the corresponding rubber's glass-transition temperature. However, although the rate of increase in diffusion coefficient with $T-T_g$ is about the same between diene rubbers and butyl rubber, the absolute values of diffusion coefficient in butyl rubber are significantly less than that of diene rubbers. Considering isobutylene, copolymers discussed contain only small amounts of comonomers besides isobutylene, their temperature-dependent permeability values follow the same curve in Figure 3 for butyl rubber. With brominated poly(isobutylene-*co*-*p*-methylstyrene) having the highest T_g among isobutylene copolymers, it has the corresponding lowest permeability value at room temperature among isobutylene copolymers (105).

Dynamic Damping. Polyisobutylene and isobutylene copolymers are high damping at 25°C, with loss tangents covering more than eight decades of frequencies even though their T_gs are less than -60°C (106,107). This broad dispersion in PIB's dynamic mechanical loss modulus is unique among flexible-chain polymers and is related to its broad glass–rubber transition (108). The narrowness of the glass–rubber transition, as defined by the steepness index, for PIB is 0.65, which is much smaller than most polymers. In addition, PIB has the most symmetric

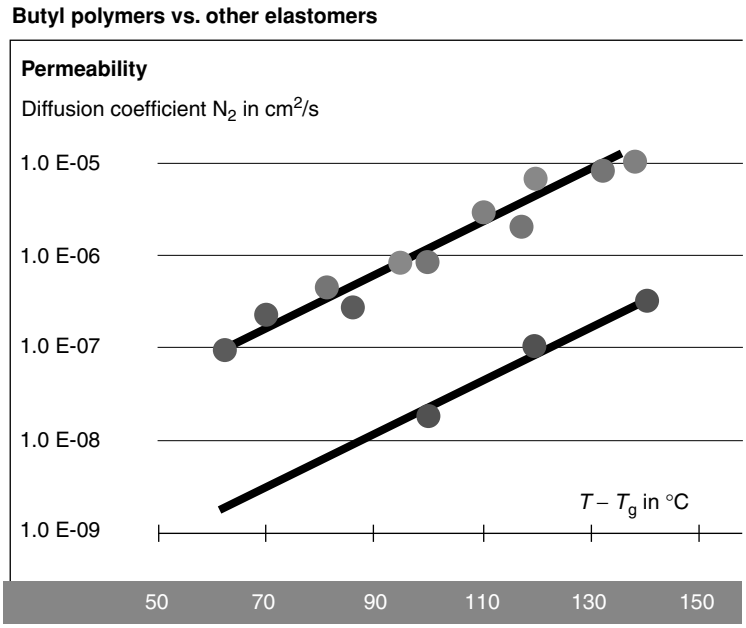

Fig. 3. Diffusion coefficients of nitrogen in diene rubbers and in butyl rubber as a function of $T - T_g$ (Data from Ref. 104). ■ Chloroprene rubber (neoprene); ■ styrene butadiene rubber; ■ natural rubber; ■ nitrile butadiene rubber; ■ butyl rubber.

and compact monomer structure among amorphous polymers, which minimizes the intermolecular interactions and contributes to its unique viscoelastic properties (109,110). As a result, a separation in time scale between the segmental motion and the Rouse modes is broader in glass–rubber transition, leading to the appearance of the sub-Rouse mode (108,109). In Rouse's theory, a polymer chain is represented as a sequence of equivalent Gaussian submolecules. The Rouse mode refers to motions of these submolecules, and sub-Rouse mode involves motions of chain units smaller than these submolecules. Considering the differences in temperature dependencies of these motions, the glass transitions of PIB and its copolymers are thermo-rheological complexes and they do not follow time–temperature superposition (108,111). PIB and its copolymers have high entanglement molecular weights (112) and corresponding low plateau moduli which, in turn, contribute to their high tack or self-adhesion in the uncross-linked state. Entanglement molecular weight of PIB is about 9000 as compared with 1300 for polyethylene, 1700 for ethylene–propylene copolymer, 2000 for 1,4-polybutadiene, 3000 for styrene–butadiene copolymer, and 6100 for hevea rubber.

Chemical Properties. PIB is a saturated hydrocarbon where the unsaturated chain ends could undergo reactions typical of a hindered olefin. These end groups are used, particularly in low molecular weight materials where plenty of chain ends are available, as a route to functionization, such as the introduction of amine groups to PIB for producing dispersants for lubricating oils. As for butyl rubbers, their in-chain unsaturations could be attacked by atmospheric-ozone-leading degradation and, hence, require protection by antioxidants (113).

Chlorobutyls are thermally more stable than bromobutyls. Upon thermal exposure up to 150°C, no noticeable decomposition took place in chlorobutyl except for some allylic chlorine rearrangement, whereas the elimination of HBr occurred in bromobutyl concurrently with isomerization to produce conjugated dienes that subsequently degrade (91,92). Brominated poly(isobutylene-*co*-*p*-methylstyrene), without any unsaturation, is the most thermally stable isobutylene copolymer. In addition, the strong reactivity of the benzylic bromine functionality in brominated poly(isobutylene-*co*-*p*-methylstyrene) with nucleophiles allows functionization and grafting in addition to its uses for vulcanization (99,100). Polyisobutylene and its copolymers, including butyl, halobutyl, and brominated poly(isobutylene-*co*-*p*-methylstyrene), are readily soluble in nonpolar solvents where cyclohexane is an excellent solvent, benzene is a moderate solvent, and dioxane is a nonsolvent (114).

Elastomeric Vulcanizates. As with almost all rubbers, the applications of isobutylene copolymers in rubber goods require compounding and subsequent vulcanization, or cross-linking. During compounding, various fillers, processing aids, plasticizers, tackifiers, curatives, and antidegradants are added.

Fillers. Filler addition is a common practice in rubber industries to stiffen and strengthen amorphous rubbers. In addition to the reinforcement, fine and particulate fillers, most notably carbon black, suppress elasticity of gum rubbers and render better processability, such as less die swell, less shrinkage, less melt fracture, and less nerve (or less elastic spring-back in uncured state) (115). Physical interactions between carbon blacks and rubber are strong but can yield upon stressing. The effects of carbon black on properties of butyl, halobutyl, and brominated poly(isobutylene-*co*-*p*-methylstyrene) rubbers are similar to that of other elastomers. As particle size decreases with a corresponding increase in specific surface area, the strength, modulus, hardness, viscosity, and damping of carbon-black-filled vulcanized rubbers increase (116,117). Tensile strength, in general, is raised to a maximum with carbon black content and then decreases at higher loading. For butyl rubber, this maximum tensile strength is obtained at 50–60 phr (part per hundred of rubber) of carbon black.

Beyond filler addition in rubbers, elastomeric behavior can be tailored by proper blending of filled elastomers. Major reasons for the usage of blends are to reduce compound cost, to improve processability, and to enhance final product performance (118). But, in this case, selective filler partition may alter the blend morphology and produce significant changes in blend properties. Elastic and fracture properties, such as resilience, tear strength, and fatigue resistance, of rubber blends have been found to depend strongly on filler phase distribution (119,120). Carbon aggregates were known to preferentially reside in the polymer with higher unsaturation, lower viscosity, and higher polarity, generally in that order of significance (121). Hence, a preferential filler partition into the diene rubber phase, such as BR and SBR, in diene rubber blends with butyl rubber was found (122,123). However, with the strong interactions between allylic bromine or benzylic bromine in bromobutyl and in brominated poly(isobutylene-*co*-*p*-methylstyrene), respectively, and carbon blacks (124), the opposite in terms of preferential filler partition into the bromobutyl or brominated poly(isobutylene-*co*-*p*-methylstyrene) phases in their blends with high diene rubbers was indicated (125,126).

Mineral fillers are used for light-colored rubber compounds for cost reduction and physical improvement. In butyl and halobutyl, alkaline fillers, such as calcium silicates, and hygroscopic fillers can strongly retard cure, while acid clays can accelerate cure. Silicas provide maximum reinforcement among mineral fillers but they promote compound stiffness and strongly affect cure rates by their absorption of curatives. Clays are less reinforcing and calcined clay is particularly suited for pharmaceutical stopper applications for its purity, low water content, and particle size uniformity. Talc is semireinforcing and improves resistance to fragmentation during needle penetration and withdrawal in pharmaceutical closures. Nonreinforcing fillers, such as calcium carbonate, are added to lower compound cost without affecting cure. Strong reductions in permeability in black or light-colored compounds of isobutylene copolymers could be achieved by adding small percents (less than 5 wt%) of exfoliated high-aspect-ratio atomic-thickness sheets of layered mineral, such as organonanoclays, without significant compromises in flexibility (127–129). The alignment of the nanoclay leads to a nematic-phase morphology and introduces torturosity for the diffusants, resulting in the lowering in permeability (130).

Plasticizers and Processing Aids. Petroleum-based oils are commonly used as plasticizers to lower compound viscosity and to improve processability and low temperature properties but with an increase in compound air permeability. Plasticizers are selected for their compatibility with isobutylene polymers and for their low temperature properties. Butyl rubber has a solubility parameter that is similar in value to that of polybutene, and paraffinic and naphthenic oils for which they are preferred. Although not to be considered as solvating agents, paraffin waxes and low molecular weight polyethylene are added for improved processing. For an improvement in low temperature flexibility, ester-type plasticizers, such as adipates and sebacates, can be used. In addition to functioning as a plasticizer, Struktol 40 MS can enhance filler dispersion and cure adhesion to high diene rubber substrates. Materials such as mineral rubber and asphaltic pitch have also been used for this dual function.

Other Ingredients. Other compound ingredients include tackifiers, flame retarders, odorants, and lubricants. Hydrocarbon tackifier resins improve the tack of unvulcanized compounds without any side reactions but are less effective than the phenolic type. However, phenol-formaldehyde tackifier resins react with halobutyl through their methylol groups, leading to premature cure. Hindered phenolic antioxidants added during manufacture of butyl and halobutyl prevent oxidation during their finishing, storage, and usage. These antioxidants also improve the resistance of vulcanized butyl and halobutyl compounds to ozone cracking. Additional stabilization against dehydrohalogenation at elevated temperature is required for halobutyls (26,131). Calcium stearate is used in chlorobutyl and a combination of calcium stearate and an epoxidized soybean oil is applied in bromobutyl to prevent dehydrohalogenation. No antioxidants or other stabilizers are added in brominated poly(isobutylene-*co*-*p*-methylstyrene).

Vulcanization. Vulcanization or curing in isobutylene polymers introduces chemical cross-links via reactions involving either allylic hydrogen or allylic halogen in butyl or halobutyl, respectively, or benzylic bromine in brominated poly(isobutylene-*co*-*p*-methylstyrene) to form a polymer network. In butyl

and halobutyl, most vulcanizates have about 1×10^{-4} mol of cross-links per cm^3, or about 250 backbone carbon atoms between cross-links.

Butyl. The basic curing agent for butyl rubber is elemental sulfur, with the formation of sulfide cross-links. Because of the low unsaturation in butyl rubbers, sulfur accelerators, such as thiurams or dithiocarbamates, are required to obtain acceptable rates and states. To activate accelerators and to stabilize cross-links already formed, butyl compounds require zinc oxide. Sulfur cross-links rearrange at elevated temperatures as a result of their low bonding energy that could lead to creep and permanent set in strained butyl at high temperatures. The resin cure in butyl rubber is based on the reaction of the methylol groups in the phenol-formaladehyde resin with allylic hydrogen in butyl, usually with a Lewis acid catalyst, to yield carbon–carbon cross-links that are thermally stable. Resin cure is preferred in butyl tire-curing bladders for their required thermal fatigue stability.

Halobutyl. The basic curing agent for halobutyl is zinc oxide, with the formation of carbon–carbon cross-links by alkylation catalyzed by a zinc halide produced after dehydrohalogenation of halobutyl (90,91,132). The ease of halogen elimination is the main difference between chlorobutyl and bromobutyl during curing where the bromobutyl cures faster (133). Esterification occurs at the halogen site in the presence of stearic acid. As a result, stearic acid accelerates cure rate and lowers the cure state. The zinc oxide cure is sensitive to acidic and basic compounding ingredients. In general, acids accelerate cure while bases retard. Water is a strong retarder because it complexes with reactive intermediates. In some applications, such as special pharmaceutical stoppers, the absence of zinc is mandatory. On the baseis of the strong reactivity between amine and allylic halogen (134), diamines can be used as the curative. While regular butyl undergoes molecular weight breakdown in the presence of peroxide, halobutyl can be cross-linked with organic peroxides. The best cure rate and optimal properties are achieved with a suitable co-agent, such as *m*-phenylene bismaleimide, at high temperatures.

Brominated Poly(isobutylene-co-p-methylstyrene). Using mainly zinc oxide and stearic acid, the cross-linking of brominated poly(isobutylene-*co*-*p*-methylstyrene) involves the formation of carbon–carbon bonds through Friedel–Crafts alkylation coordinated by a zinc complex (135,136). Unlike halobutyls, brominated poly(isobutylene-*co*-*p*-methylstyrene) cures extremely slowly with zinc oxide alone. A nucleophilic agent, such as zinc stearate, is needed to promote rapid displacement of benzyl bromide. The zinc stearate can be added directly or can be formed during vulcanization through the reaction of zinc oxide and stearic acid. In cases where faster cure is desired, dinucleophilic substitution using dinucleophiles, such as diamines, is the method of choice.

Uses. The polyisobutylene portion of the isobutylene copolymers, such as butyl, halobutyl, and brominated poly(isobutylene-*co*-*p*-methylstyrene), imparts chemical and physical characteristics that make them highly useful in a wide variety of applications. The low degree of permeability to gases accounts for the largest uses of butyl and halobutyl rubbers, namely as inner tubes and tire innerliners. These same properties are also of importance in air cushions, pneumatic springs, air bellows, accumulator bags, and pharmaceutical closures. The thermal stability of butyl rubber makes it ideal for rubber tire-curing bladders, high

temperature service hoses, and conveyor belts for hot material handling. With the added thermal stability in brominated poly(isobutylene-*co*-*p*-methylstyrene), it has made inroads in applications of bladders and curing envelopes.

Isobutylene-based polymers exhibit high damping and have uniquely broad damping and shock absorption ranges in both temperature and frequency. Molded rubber parts from butyl and halobutyl find wide applications in automobile suspension bumpers, exhaust hangers, and body mounts.

Blends of halobutyl or brominated poly(isobutylene-*co*-*p*-methylstyrene) with high diene rubbers are used in tire sidewalls and tread compounds (137–139). In sidewalls, ozone resistance, crack cut growth, and appearance are critical to their performance. Properly formulated blends with high diene rubbers that exhibit phase cocontinuity yield excellent sidewalls (140). The property balance for tire tread compounds can be enhanced by the incorporation of a more damping halobutyl or brominated poly(isobutylene-*co*-*p*-methylstyrene) rubber phase (141). Improvements in wet-, snow-, and ice-skid resistances and in dry traction without compromises in abrasion resistance and rolling resistance for high performance tires can be accomplished by using bromobutyl or brominated poly(isobutylene-*co*-*p*-methylstyrene) up to 30 phr in tread compounds (142).

Blends of isobutylene polymers with thermoplastic resins are used for toughening of these compounds (143,144). High-density polyethylene and isotactic polypropylene are often modified with 5–30 wt% of PIB. In some cases, a halobutyl phase is cross-linked as it is dispersed in the plastic phase to produce a highly elastic compound that is processable in thermoplastic molding equipment (145,146). The strong reactivity of the benzylic bromine group in brominated poly(isobutylene-*co*-*p*-methylstyrene) with amines during blending of brominated poly(isobutylene-*co*-*p*-methylstyrene) with polyamides results in surface-reactive compatibilization that suppresses coalescence and leads to extremely fine dispersions in these blends (147). Combining the low permeability values of both polyamides and brominated poly(isobutylene-*co*-*p*-methylstyrene), dynamic vulcanized thermoplastic blends of polyamides with brominated poly(isobutylene-*co*-*p*-methylstyrene) have been demonstrated to be suitable for tire innerliner applications (148–151).

Polybutenes enjoy extensive uses as adhesives, caulks, sealants, and glazing compounds. They are also used as plasticizers in rubber formulations with butyl, SBR, and natural rubber. In linear low density polyethylene (LLDPE) blends, they induce cling to stretch-wrap films. Polybutenes when modified at their chain-end unsaturations with polar functionality are widely employed in lubricants as dispersants. Blends of polybutene with polyolefins produce semisolid gels that can be used as potting and electrical-cable filling materials.

It should be noted that proper compounding and formulation are critical to the successful uses of all elastomer materials. It is recommended that the suppliers be contacted for information.

Health and Safety Factors

Polyisobutylene, isobutylene–isoprene copolymers, and isobutylene-*p*-methylstyrene copolymers are considered to have no chronic hazards associated

Table 2. Annual Butyl and Halogenated Butyl Rubber Production Capacity (YE 2002)

Producer	Products	Capacity, 10^3 t
ExxonMobil Chemical Co.		
Baton Rouge, La.	Halobutyl rubbers	143
Baytown, Tex.	Butyl rubber	27
	Halobutyl rubbers and Exxpro	75
Notre Dame de Gravenchon, France	Butyl rubber	54
Fawley, U.K.	Halobutyl rubbers	97
Japan Butyl Co., Ltd.[a]		
Kawasaki, Japan	Butyl rubber	78
Kashima, Japan	Halobutyl rubbers	52
Bayer (152)		
Sarnia, Ontario, Canada	Butyl, halobutyl rubbers	140
Zwijndrecht, Belgium	Butyl, halobutyl rubbers	115
CIS (152)		
Nizhnekamsk, Russia	Butyl rubbers	60
Togliati, Russia	Butyl rubbers	35
Sinopec (152)		
Yanshan, P.R. China	Butyl rubbers	30

[a]Jointly owned with Japan Synthetic Rubber Co., Ltd.

with exposure under normal industrial use. Some grades can be used in chewing-gum base and are regulated by the FDA in 21 CFR 172.615. Vulcanized products prepared from butyl rubber or halogenated butyl rubber may contain small amounts of toxic materials as a result of the particular vulcanization chemistry. Although many vulcanizates are inert, eg, zinc oxide cured chlorobutyl is used extensively in pharmaceutical stoppers, specific recommendations should be sought from suppliers.

Economic Aspects

Table 2 shows the manufacturing capacity for the world's major butyl and halobutyl polymers manufacturers. In addition to ExxonMobil Chemical and Bayer, during the last 10 years, butyl rubber produced at both Nizhnekamsk and Togliati has been sold throughout the world. Also, in the last 5 years, Sinopec has started to produce butyl polymers at its Yanshan plant in the People's Republic of China. All of the world's butyl plants use the more efficient slurry process except for the Togliati plant, which uses the solution process.

Manufacturing capacity has continued to expand in the last decade to keep up with the increasing demand due to expanding car sales and the growth in popularity of sports–utility vehicles, particularly in the United States. Apart from the economic downturns in 1992 and 2001, Figure 4 shows the worldwide sales of halobutyl polymers increasing steadily at approximately 4% per year. The widespread use of halobutyl innerliners in the tires of both passenger cars and light trucks accounts for most of these sales, although there is a small market for pharmaceutical stoppers. For most of the decade, halobutyl manufacturing plants have been running well above 85% capacity.

Fig. 4. Worldwide halobutyl sales. Halobutyl, worldwide; Halobutyl, Americas.

In the 1990s, sales of regular butyl polymers have not seen the same rate of growth as halobutyl. The majority of sales are to inner tube and tire bladder applications and, except for trucks and in some developing countries, these markets have been overtaken by the more popular tubeless tire. The introduction of the Russian and Chinese manufacturers has also dampened demand and not until the early 2000s has there been significant growth. Figure 5 shows the sales of regular butyl polymers during the past decade.

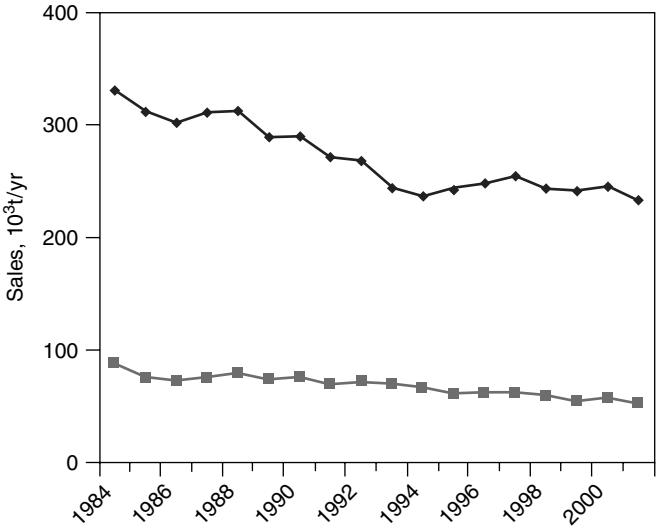

Fig. 5. Worldwide butyl sales. Regular butyl, worldwide; Regular butyl, Americas.

BIBLIOGRAPHY

"Butylene Polymers" in *EPST* 1st ed., Vol. 2, pp. 754–795, by D. J. Buckley, Esso Research and Engineering Company; "Isobutylene Polymers" in *EPSE* 2nd ed., Vol. 8, pp. 423–448, by Edward N. Kresge, Ralph H. Schatz, and H.-C. Wang, Exxon Chemical Co.

1. E. G. M. Tornqvist, in J. P. Kennedy and E. G. M. Tornqvist, eds., *Polymer Chemistry of Synthetic Elastomers*, Part 1, John Wiley & Sons, Inc., New York, 1968, p. 76.
2. R. M. Thomas, I. E. Lightbown, W. J. Sparks, P. K. Frolich, and E. V. Murphree, *Ind. Eng. Chem.* **32**, 1283–1292 (1940).
3. R. T. Morrissey, *Rubber World* **138**, 725 (1955).
4. F. P. Baldwin, *Rubber Chem. Technol.* **52**, 677 (1979).
5. D. Coddington, *Rubber Chem. Technol.* **59**, 905 (1979).
6. S. A. Banks, F. Brzenk, J. A. Rae, and C. S. Hua, *Rubber Chem. Technol.* **38**, 158 (1965).
7. Bulletin 12-K, Amoco Chemical Corp. Chicago, Ill.
8. Ref. 2, p. 209.
9. K. Matyjaszewski, ed., *Cationic Polymerizations*, Marcel Dekker, Inc., New York, 1996.
10. J. P. Kennedy and M. Marechal, *Carbocationic Polymerization*, John Wiley & Sons, Inc., New York, 1982.
11. P. H. Plesch and A. Gandini, *The Chemistry of Polymerization Process*, Monograph 20, Society of Chemical Industry, London, 1966.
12. A. Lisovskii, E. Nelkenbaum, V. Volkis, R. Semiat, and M. S. Eisen, *Inorg. Chim. Acta* **334**, 243 (2000).
13. U.S. Pat. 5,668,232 (Sept. 16, 1997), G. Langstein, D. Freitag, M. Lanzendörfer, and K. Weiss (to Bayer, AG).
14. T. D. Shaffer and J. R. Ashbaugh, *J. Polym. Sci., Part A: Polym. Chem.* **35**, 329 (1997).
15. S. Jacob, P. Zhenglie, and J. P. Kennedy, *Polym. Bull.* **41**, 503 (1998).
16. M. C. Baird, *Chem. Rev.* **100**, 1471 (2000).
17. M. Roth and H. Mayr, *Macromolecules* **29**, 6104 (1996).
18. H. Schlaad, Y. Kwon, L. Sipos, R. Faust, and B. Charluex, *Macromolecules* **33**, 8225 (2000).
19. D. M. Cheng, I. J. Gardner, H.-C. Wang, C. B. Fedrick, and A. H. Dekmezian, *Rubber Chem. Technol.* **63**, 265 (1990).
20. J. E. Puskas and C. Wilds, *Rubber Chem. Technol.* **67**, 329 (1994).
21. J. L. White, T. D. Shaffer, C. J. Ruff, and J. P. Cross, *Macromolecules* **28**, 3290 (1995).
22. J. P. Kennedy and R. M. Thomas, *Polymerization and Polycondensation Processes* (Advances in Chemistry Series 34), American Chemical Society, Washington, D.C., 1962, p. 111.
23. Ref. 22, p. 326
24. U.S. Pat. 2,356,128 (1944), R. M. Thomas and W. J. Sparks.
25. J. P. Kennedy and N. H. Canter, *J. Polym. Sci., Part A1* **5**, 2455 (1967).
26. S. Cesca, P. Giusti, P. L. Magagnini, and A. Priola, *Makromol. Chem.* **176**, 2319 (1975).
27. S. Cesca, A. Priola, M. Bruzzone, G. Ferraris, and P. Giusti, *Markromol. Chem.* **176**, 2339 (1975).
28. J. Bandrupt and E. H. Immergut, eds., *Polymer Handbook*, 3rd ed., John Wiley & Sons, Inc., New York, 1989.
29. Polymer Corp., private communication.
30. W. A. Thaler and J. D. Buckley Jr., *Rubber Chem. Technol.* **49**, 960 (1976).
31. C. Corno, A. Priola, G. Spallanzani, and S. Cesca, *Macromolecules* **17**, 37 (1984).
32. J. P. Kennedy and I. Krishenbaum in E. C. Leonard, ed., *Vinyl and Diene Monomers, Part 2*, New York, 1971, Chapt. 3, p. 691.
33. J. E. Puskas, M. Verhelst, P. Collart, and J. B. Schmidt, *Kautsch. Gummi Kunstst.* **48**, 866 (1995).

34. E. N. Kresge, R. H. Schatz, and H.-C. Wang, in J. I. Kroschwitz, ed., *Encyclopedia of Polymer Science and Engineering*, Vol. **8**, 2nd ed., John Wiley & Sons, Inc., New York, 1987, pp. 423–448.
35. M. Roth and H. Mayr, *Macromolecules* **29**, 6104–6109 (1996).
36. B. Ivan and J. P. Kennedy, *Designed Polymers by Carbocationic Macromolecular Engineering: Theory and Practice*, Hanser Publishers, Munich, 1991.
37. R. Faust, A. Fehervari, and J. P. Kennedy, *Br. Polym. J.* **19**, 379 (1987).
38. R. Vukov, *Rubber Chem. Technol.* **57**, 275 (1984).
39. A. Van Tongerloo and R. Vukov, in Proceedings of the International Rubber Conference, Venice, 1979, p. 70.
40. F. P. Baldwin and co-workers, *Rubber Plast. Age* **42**, 500 (1960).
41. F. P. Baldwin and I. J. Gardner, *Chemistry and Properties of Cross-Linked Polymers*, Academic Press, Inc., New York, 1977, p. 273.
42. F. P. Baldwin and co-workers, *Adv. Chem. Ser.* **91**, 448 (1969).
43. U.S. Pat. 5,883,207 (Mar. 16, 1999), H. K. Youn, B. W. Hwang, C. S. Chu, Y. S. Chung, G. S. Han, Y. H. Yeom, C. J. Lee, M. K. Jun, and K. D. Park (to Daelim Industrial Co., Ltd.).
44. U.S. Pat. 6,156,859 (Dec. 5, 2000), G. Langstein, W. Obrecht, J. E. Puskas, O. Nuyken, and K. Weiss (to Bayer AG).
45. J. Walker, G. J. Wilson, and K. J. Kumbhani, *J. Inst. Rubber Ind.* **8**, 64 (1974).
46. U.S. Pat. 5,162,445 (Nov. 10, 1992), K. W. Powers and H.-C. Wang (to Exxon Chemical Co.).
47. H.-C. Wang and K. W. Powers, *Elastomerics* **124**, 14 and 22 (1992).
48. P. Arjunan, H.-C. Wang, and J. A. Olkusz, *Functional Polymers*, (ACS Symposium Series 704), American Chemical Society, Washington, D.C., 1998, pp. 199–216.
49. U.S. Pat. 5,548,029 (Aug. 20, 1996), K. W. Powers, H.-C. Wang, T.-C. Chung, A. J. Dias, and J. A. Olkusz (to Exxon Chemical Patents, Inc.).
50. U.S. Pat. 5,824,717 (Oct. 20, 1998), N. A. Merrill, H.-C. Wang, and A. J. Dias (to Exxon Chemical Patents, Inc.).
51. T. Yu, H.-C. Wang, K. W. Powers, A. F. Yee, and D. Li, *Polym. Prepr. (Am. Chem. Soc., Polym. Chem. Div.)* **33**, 622 (1992).
52. U.S. Pat. 4,946,899 (Aug. 7, 1990), J. P. Kennedy, J. E. Puskas, G. Kaszas, and W. G. Hager (to The University of Akron).
53. G. Kaszas, J. E. Pusaks, J. P. Kennedy, and W. G. Hager, *J. Polym. Sci., Polym. Chem. Ed. A* **29**, 427 (1991).
54. M. Gyor, Z. Fodor, and H.-C. Wang, *J. Macromol. Sci., A: Pure Appl. Chem.* **31B**, 2055 (1994).
55. X. Cao, L. Sipos, and R. Faust, *Polym. Bull.* **45**, 121 (2000).
56. D. Li and R. Faust, *Macromolecules* **28**, 4893 (1995).
57. J. E. Puskas, G. Kaszas, J. P. Kennedy, and W. G. Hager, *J. Polym. Sci., Polym. Chem. Ed. A* **30**, 41 (1992).
58. J. P. Kennedy, S. Midha, and Y. Tsunogae, *Macromolecules* **26**, 429 (1993).
59. Y. C. Bae and R. Faust, *Macromolecules* **31B**, 2480 (1998).
60. G. T. Baumann and M. R. Smith, *Hydrocarbon Process. Pet. Refiner.* **33**(5), 156 (1954).
61. A. M. Valet and co-workers, *Hydrocarbon Process. Pet. Refiner.* **41**(5), 119 (1962).
62. H. Kroper, K. Schlomer, and H. M. Weitz, *Hydrocarbon Process. Pet. Refiner.* **48**(9), 195 (1969).
63. U.S. Pat. 3,665,048 (Jan. 14, 1970), H. R. Grane and I. E. Katz (to Atlantic Richfield Co.).
64. V. Fattore and co-workers, *Hydrocarbon Process.* **60**(8), 101 (1981).
65. Belg. Pat. 882,387 (July 16, 1980), L. A. Smith Jr. (to Chemicals Research and Licensing Co.); Ger. Pat. 2,534,544 (Feb. 12, 1976), R. Tesei, V. Fattore, and F. Buonomo (to SNAM Piogetti SpA).

66. U.S. Pat. 5,417,930 (May 23, 1995), M. F. McDonald, D. J. Lawrence, and D. A. Williams (to Exxon Chemical Inc.).
67. T. Pernecker, and J. P. Kennedy, *Polym. Bull. (Berlin)* **33**(1), 13–19 (1994); *Polym. Bull. (Berlin)* **32**(5/6), 537–543 (1994).
68. Eur. Pat. 0 344 021 A2 (Jan. 22, 1992), K. W. Powers and H.-C. Wang (to Exxon Chemical).
69. U.S. Pat. 3,023,191 (Feb. 27, 1962), B. R. Tegge, F. P. Baldwin, and G. E. Serniuk (to Esso L Research & Engineering Co.).
70. U.S. Pat. 2,940,960 (June 14, 1960), B. R. Tegge and co-workers (to Esso Research & Engineering Co.).
71. U.S. Pat. 3,257,349 (June 21, 1966), J. A. Johnson Jr. and E. D. Luallin (to Esso Research & Engineering Co.).
72. U.S. Pat. 5,286,804 (Feb. 15, 1994), R. N. Webb, K. W. Powers, H.-C. Wang, M. F. McDonald, J. V. Fusco, and H. F. VanBrackle.
73. U.S. Pat. 5,681,901 (Oct. 28,1997), N. F. Newman.
74. U.S. Pat. 4,384,072 (May 17, 1983), N. F. Newman and R. C. Kowalski (to Exxon Research & Engineering Co.).
75. U.S. Pat. 4,573,116 (Apr. 23, 1985), R. C. Kowalski, W. M. Davis, and L. Erwin (to Exxon Research & Engineering Co.).
76. U.S. Pat. 4,548,995 (Oct. 22, 1985), R. C. Kowalski and co-workers (to Exxon Research & Engineering Co.).
77. L. A. Wood, *Rubber Chem. Technol.* **49**, 189 (1976).
78. G. Allegra, E. Benedetti, and C. Pedone, *Macromolecules* **3**, 727 (1970).
79. *Bulletin 12-M, Amoco Chemical Corp.*, Chicago, Ill., 1990.
80. I. Puskas, E. M. Banas, and A. G. Nerhein, *J. Polym. Sci., Polym. Symp.* **56**, 191 (1976).
81. C. Y. Chu and R. Vukov, *Macromolecules* **18**, 1423 (1985).
82. I. Kuntz and K. D. Rose, *J. Polym. Sci., Part A: Polym. Chem.* **27**, 107 (1989).
83. D. M. Cheng, I. J. Gardener, H.-C. Wang, C. B. Frederick, and A. H. Dekmezian, *Rubber Chem. Technol.* **63**, 265 (1990).
84. J. E. Puskas and C. Wilds, *Rubber Chem. Technol.* **67**, 329 (1994).
85. J. L. White, T. D. Shaffer, C. J. Ruff, and J. P. Cross, *Macromolecules* **28**, 3290 (1995).
86. H.-C. Wang, unpublished data, 1990.
87. J. P. Kennedy and E. Marechal, *Carbocationic Polymerization*, John Wiley & Sons, Inc., New York, 1982.
88. U.S. Pat. 5,162,445 (Nov. 10, 1992), K. W. Powers, H.-C. Wang, T.-C. Chung, A. J. Dias, and J. A. Olkusz (to Exxon Chemical).
89. R. M. Thomas and W. J. Sparks, in G. S. Whitby, ed., *Synthetic Rubber*, John Wiley & Sons, Inc., New York, 1954, Chapt. 24.
90. C. C. Chu and R. Vukov, *Macromolecules* **18**, 1423 (1985).
91. R. Vukov, *Rubber Chem. Technol.* **57**, 284 (1984).
92. J. S. Parent, D. J. Thom, G. White, R. A. Whitney, and W. Hopkins, *J. Polym. Sci., Part A: Polym. Chem.* **39**, 2019 (2001).
93. U.S. Pat. 5,071,913 (Dec. 10, 1991), K. W. Powers, H.-C. Wang, D. C. Handy, and J. V. Fusco (to Exxon Chemical).
94. H.-C. Wang, K. W. Powers, and J. V. Fusco, in *ACS Rubber Division Meeting*, Mexico City, Mexico, May, 1989.
95. I. Duvdevani, L. Gursky, and I. J. Gardener, in ACS Rubber Division Meeting, Mexico City, Mexico, May, 1989.
96. L. L. Ban, I. Duvdevani, and H.-C. Wang, in ACS Rubber Division Meeting, Las Vegas, May, 1990.
97. A. H. Tsou, unpublished data, 2000.
98. H.-C. Wang and I. Duvdevani, unpublished data, 1990.

99. H.-C. Wang and K. W. Powers, in ACS Rubber Division Meeting, Toronto, Canada, May, 1991.
100. Ref. 88.
101. R. H. Boyd and P. V. Krishna Pant, *Macromolecules* **24**, 6325 (1991).
102. P. V. Krishna Pant and R. H. Boyd, *Macromolecules* **25**, 494 (1992).
103. P. V. Krishna Pant and R. H. Boyd, *Macromolecules* **26**, 679 (1993).
104. G. J. van Amerongen, *Rubber Chem. Technol.* **37**, 1065 (1964).
105. G. E. Jones, unpublished data, 2001.
106. E. R. Fitzgerald, L. D. Grandine Jr., and J. D. Ferry, *J. Appl. Phys.* **24**, 650 (1953).
107. J. D. Ferry, L. D. Grandine Jr., and E. R. Fitzgerald, *J. Appl. Phys.* **24**, 911 (1953).
108. D. J. Plazek, I.-C. Chay, K. L. Ngai, and C. M. Roland, *Macromolecules* **28**, 6432 (1995).
109. D. J. Plazek and K. L. Ngai, *Macromolecules* **24**, 1222 (1991).
110. A. K. Rizos, K. L. Ngai, and D. J. Plazek, *Polymer* **38**, 6103 (1997).
111. K. L. Ngai and D. J. Plazek, *Rubber Chem. Technol.* **68**, 376 (1995).
112. J. D. Ferry, *Viscoelastic Properties of Polymers*, 3rd ed., John Wiley & Sons, Inc., New York, 1980.
113. J. F. S. Yu, J. L. Zakin, and G. K. Patterson, *J. Appl. Polym. Sci.* **23**, 2493 (1979).
114. R. A. Orwoll, *Rubber Chem. Technol.* **50**, 451 (1977).
115. J.-B. Donnet, R. C. Bansal, and M. J. Wang, eds., *Carbon Black*, 2nd ed., Marcel Dekker, Inc., New York, 1993.
116. A. R. Payne, *J. Appl. Polym. Sci.* **7**, 873 (1963).
117. M. Morton, ed., *Rubber Technology*, 3rd ed., Chapman and Hall, London, 1995.
118. E. T. McDonel, K. C. Baranwal, and J. C. Andreis, in D. R. Paul and S. Newman, eds., *Polymer Blends*, Vol. **II**, Academic Press, New York, 1978, Chap. 19.
119. W. M. Hess and V. E. Chirico, *Rubber Chem. Technol.* **50**, 301 (1977).
120. W. M. Hess, P. C. Vegvari, and R. A. Swor, *Rubber Chem. Technol.* **58**, 350 (1985).
121. J. E. Callan, W. M. Hess, and C. E. Scott, *Rubber Chem. Technol.* **44**, 814 (1971).
122. E. M. Dannenberg, *Rubber Chem. Technol.* **48**, 410 (1975).
123. A. M. Gessler, *Rubber Chem. Technol.* **41**, 1494 (1969).
124. K. Yurekli, R. Krishnamoorti, M. F. Tse, K. O. McElrath, A. H. Tsou, and H.-C. Wang, *J. Polym. Sci., Part B: Polym. Phys.* **39**, 256 (2001).
125. A. H. Tsou and W. H. Waddell, *Kautschuk Gummi Kunststoffe* **55**, 382 (2002).
126. A. H. Tsou, G. E. Zheng, and M. C. Boyce, *J. Polym. Sci., Part B: Polym. Phys.* (submitted).
127. E. P. Giannelis, *Adv. Mater.* **8**, 29 (1996).
128. U.S. Pat. 5,576,372 (Nov. 19, 1996), E. N. Kresge and D. J. Lohse (to Exxon Chemical).
129. U.S. Pat. 5,883,173 (Mar. 16, 1998), C. W. Elspass, D. G. Peiffer, E. N. Kresge, D.-T. Hsieh, J. J. Chludzinski, and K. S. Liang (to Exxon Research & Engineering).
130. A. A. Gusev and H. R. Lusti, *Adv. Mater.* **13**, 1641 (2001).
131. F. P. Baldwin, D. J. Buckley, I. Kuntz, and S. B. Robinson, *Rubber Plas. Age* **42**, 500 (1961).
132. I. Kuntz, R. L. Zapp, and R. J. Pancirov, *Rubber Chem. Technol.* **57**, 813 (1984).
133. R. L. Zapp and A. A. Oswald, *Rubber Chem. Technol.* **48**, 860 (1978).
134. J. S. Parent, G. D. F. White, R. A. Whitney, and W. Hopkins, *Macromolecules* **35**, 3374 (2002).
135. J. M. Frechet, R. Bielski, H.-C. Wang, J. V. Fusco, and K. W. Powers, *Rubber Chem. Technol.* **66**, 98 (1993).
136. R. Bielski, J. M. Frechet, J. V. Fusco, K. W. Powers, and H.-C. Wang, *J. Polym. Sci., Part A* **31**, 755 (1993).
137. E. T. McDonel, K. C. Baranwal, and J. C. Andries, in D. R. Paul and S. Newman, eds., *Polymer Blends*, Vol. **2**, Academic Press, Inc., New York, 1978, Chapt. 19.
138. J. E. Rogers and W. H. Waddell, *Rubber World* **219**, 24 (1999).

139. K. O. McElrath and A. L. Tissler, in ACS Rubber Division Meeting, Anaheim, May, 1997.
140. A. H. Tsou, I. Duvdevani, and K. O. McElrath, *Rubber Chem. Technol.* (in press).
141. W. H. Waddell, J. H. Kuhr, and R. R. Poulter, in ACS Rubber Division Meeting, Cleveland, October, 2001.
142. W. H. Waddell, R. C. Napier, and R. R. Poulter, *Kautschuk Gummi Kunststoffe* **54**, 1 (2001).
143. J. M. Willis, B. D. Favis, and J. Lunt, *Polym. Eng. Sci.* **30**, 1073 (1990).
144. E. Kresge, *Rubber Chem. Technol.* **64**, 469 (1991).
145. R. C. Puydak and D. R. Hazelton, *Plast. Eng.* **44**, 27 (1988).
146. U.S. Pat. 5,051,477 (Sept. 24, 1991), B. Wenderoth, F. Schuetz, S. Brand, H. Sauter, E. Ammerman, and G. Lorezn (to BASF Atiengesellschaft).
147. U.S. Pat. 6,013,727 (Jan. 11, 2000), R. Dharmarajan, R. C. Puydak, H.-C. Wang, K. W. Powers, T. C.-C. Chi, and D. R. Hazelton (to Exxon Chemical).
148. EP Pat. 0857761A1 (Aug. 12, 1998), J. Watanabe (to Yokohama Rubber Co.).
149. EP Pat. 0722850B1 (May 6, 1999), H. Takeyama (to Yokohama Rubber Co.).
150. EP Pat. 0969039A1 (Jan. 5, 2000), J. Watanabe (to Yokohama Rubber Co.).
151. U.S. Pat. 6,359,071 (Mar. 19, 2002), J. Watanabe (to Yokohama Rubber Co.).
152. International Institute of Synthetic Rubber Producers, Inc., *Worldwide Rubber Statistics*, 2001.

ROBERT N. WEBB
TIMOTHY D. SHAFFER
ADDY H. TSOU
ExxonMobil

CARBOCATIONIC POLYMERIZATION

Introduction

Cationic polymerization is a chain-growth reaction where the active center is positively charged. In the case of *carbocationic polymerization*, the active center is a carbenium ion. The term *cationic* polymerization also covers polymerizations where the active center contains a heteroatom (eg, oxonium, sulfonium, ammonium, or phosphonium ion); these are not included in this chapter. The focus will be on carbocationic polymerization.

In order to get a perspective about the importance of *carbocationic* polymerization in polymer science and engineering, its positioning in the overall picture needs to be considered. The estimated total volume of polymers produced commercially by *cationic* polymerization is around 3–3.5 million tons per annum (1). This constitutes about 3% of the total synthetic polymer market. Polymers produced commercially by *carbocationic* polymerization make up about 2% of the total polymer market. On the basis of these numbers, *carbocationic* polymerization appears to be insignificant.

The main products are poly- and oligoisobutylenes, poly(butenes), hydrocarbon resins, and poly(vinyl ethers)—these will be discussed in more detail under Industrial Carbocationic Processes. Estimated worldwide production capacities are listed in Table 1.

It can be seen that isobutylene-based products are the most important; they range from viscous oils to high molecular weight elastomers, such as butyl and halobutyl rubbers (see BUTYL RUBBER). The latter exemplify most strikingly the practical importance of *carbocationic polymerization*. Butyl and halobutyl rubbers are used as inner tubes or inner liners in vehicle tires, because of their exceptional impermeability toward gases and moisture (3,4). Had butyl and halobutyl

Encyclopedia of Polymer Science and Technology. Copyright John Wiley & Sons, Inc. All rights reserved.

Table 1. Worldwide Production Capacities of Commercially Produced Carbocationic Polymers[a]

Polymer	Thousand Metric Tons/year
Isobutylene-based elastomers (butyl, halobutyl)	760
Polybutenes	650
Polyisobutylenes	100
Resins	
C_9 + indene–coumarone	350
C_5 + dicyclopentadiene	274
Vinyl aromatics	128
Polyterpenes	25–30
Poly(vinyl ethers)	20–25

[a]Ref. 2.

rubbers not been discovered, we would have to pump up our car and bicycle tires daily as the air would escape through the rubbers used to build the body of these tires. Butyl and halobutyl rubbers have very high damping properties and therefore are used in machinery mounts to reduce vibration; unique examples include dampeners for bridges and foundations for earthquake-resistant buildings. They also have outstanding oxidative, environmental, and chemical stability, rendering them suitable for applications as industrial rubber goods, seals, adhesives, condenser caps, and pharmaceutical stoppers. An interesting application is chewing gums (considered essential by our children as any parent can testify). Emerging applications of polyisobutylene-based rubbers include biomedical implants that could save lives (5). These examples highlight the importance of carbocationic polymerization.

This article discusses the most important aspects of carbocationic polymerization, with references to more detailed information for specialists.

Historical Background

Carbocations are extremely reactive. Because of their high reactivity, identification or direct observation of carbocations is extremely difficult—although they are the intermediates of many organic reactions. The existence of carbocations became generally accepted in the 1920s and 1930s through the work of Whitmore, Ingold, and Meerwein (6). Analytical proof was first given by Olah in 1963 (7,8). Reacting SbF_5 and alkyl halides in "superacid" media, he was able to prepare carbocations stable enough for ^1H NMR characterization. He proposed to use the term *carbenium ion* for classical trivalent sp^2 carbocations (such as CH_3^+) and *carbonium ion* for the pentavalent carbocation (CH_5^+) (7,8). This nonclassical entity has a two-electron, three-center-bound pentacoordinated carbon; ammonium (NH_4^+), oxonium (R_3O^+), or sulfonium (R_3S^+) ions can be considered as similar "nonclassical" structures.

The first example of carbocationic polymerization, the resinification of turpentine oil by sulphuric acid (9), dates back a couple of centuries. Other examples

from the 1800s include the polymerization of pinene with $SnCl_4$ and BF_3 (10), turpentine with BF_3 (11), and styrene and isobutylene with sulphuric acid (11,12).

Hunter and Yohe laid out the first mechanism of carbocationic polymerization in 1933 (13). According to their proposal, the metal halide–monomer interaction leads to the formation of a "zwitterion" (the German word *zwitter* stands for "between"):

$$MtX_n + CH_2{=}C(CH_3)_2 \rightarrow MtX_n^- {-}CH_2{-}(CH_3)_2C^+$$

Polymerization then proceeds by reaction of monomer with the carbenium ion. In this system, the metal halide was considered the "catalyst." For thermodynamic reasons, this mechanism was criticized (14,15) and later abandoned as Polanyi's school put forth the idea of coinitiation on the basis of the study of the isobutylene–$TiCl_4$ system (16). Polanyi suggested that the true initiator in this system would be derived from the reaction between a cationogen such as water, and $TiCl_4$, the coinitiator (eq. 1):

$$TiCl_4 + H_2O + CH_2{=}C(CH_3)_2 \rightarrow CH_2{-}(CH_3)_2C^+TiCl_4OH^- \quad (1)$$

This reaction can be written in a more generalized form (eq. 2):

$$MtX_n + I{-}B + CH_2{=}C(CH_3)_2 \rightarrow I{-}CH_2{-}(CH_3)_2C^+MtX_nB^- \quad (2)$$

where I represents the true initiating species, such as a proton or carbenium ion, and B represents a basic group, eg, a hydroxide or a halide. The metal halide coinitiators are still called "catalysts" in the industry, as the processes used today were originally developed many decades ago. It would be helpful to all if the scientifically accepted terms were more commonly used.

Classical carbocationic polymerization is very rapid and therefore difficult to control, and is riddled with side reactions and incomplete monomer conversion. In contrast, *living* (or *controlled*) carbocationic polymerization opened new avenues for macromolecular engineering, ie, the design and synthesis of well-defined structures with efficient processes (17–20).

Monomers for Carbocationic Polymerizations

The most common monomers in carbocationic polymerization are alkenes, often termed "vinyl" monomers. Carbocationic polymerization of vinyl monomers proceeds by the electrophilic attack of the initiating and/or propagating carbenium ion on the double bond of the monomer. In order to sustain the chain reaction of propagation in competition with termination or transfer reactions, the carbenium ion has to be sufficiently stable and the monomer has to be sufficiently nucleophilic to ensure long enough lifetime of the active center to propagate.

Stability of Carbenium Ions. In terms of thermodynamic stability, carbenium ions can be ranked on the basis of gas-phase hydride affinity, heats of ionization, ionization equilibrium in solution, and S_N1-solvolysis rate (21). The "stability scales" obtained by these different methods correlate reasonably well

Table 2. Ranking of Carbenium Ions by Stability

Carbenium ion	$\Delta_R H^0$, kJ/mol (R—H → $R^+ + H^-$)[a]	log k (R—Cl, EtOH, 25°C)[b]
CH_3^+	1306	—
$CH_3—CH_2^+$	1143	—
$CH_3—CH^+—CH_3$	1034	−10.8
$Ar—CH_2^+$	—	−9.4
$(CH_3)_3C^+$	963	−7.1
$Ar—CH^+—CH_3$	963	−6.8
$(CH_3)_3—CH_2—C(CH_3)_2^+$	—	−5.6
$(CH_3)_2C{=}CH—CH_2^+$	940	−4.6
$Ar—C(CH_3)_2^+$	921	−3.4
$CH_3—O—Ar—CH^+—CH_3$	—	−1.7
$(Ar)_3C^+$	—	0.8
$[CH_3—O—Ar]_2—CH^+$	—	1.8

[a] Hydride affinity of carbocations (21). Original data from Ref. 22.
[b] Solvolysis rate constant of the corresponding alkyl chlorides in ethanol (21). Original data from Ref. 23.

(21). Table 2 lists selected carbenium ions in order of increasing stability, along with their hydride affinity and the solvolysis rate constants of the corresponding alkyl halides.

It can be seen that as the stability of carbenium ions increases as a result of inductive or resonance effects, their reactivity (electrophilicity) decreases.

Nucleophilicity of Monomers. Figure 1 shows cationically polymerizable monomers in order of increasing nucleophilicity. The numbers listed are nucleophilicity parameters (N) developed by Mayr (24,25). N values were derived by measuring the rate of reaction between diarylcarbenium ions and various monomers using UV–vis spectroscopy and are discussed more later in this article.

Optimum combination of carbocation stability and monomer nucleophilicity is necessary for effective polymerization. Indeed, isobutylene positioned in the middle of both the carbocation stability and monomer nucleophilicity scales can be polymerized effectively to yield high molecular weight polymers, while the other monomers listed above mostly yield low molecular weight products by carbocationic polymerization.

Examples of Active Monomers. A vinyl monomer can undergo carbocationic polymerization only if the double bond is the most basic site of the monomer. For example, acrylates and vinyl acetate cannot be polymerized cationically

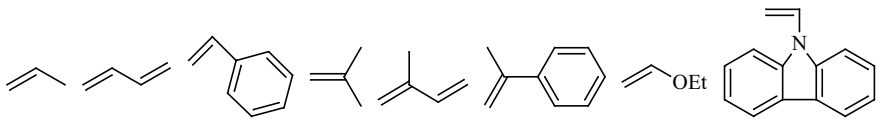

N: −2.63 −1.15 0.78 1.07 1.12 2.39 3.9 5.02

Fig. 1. Ranking of monomers by nucleophilicity.

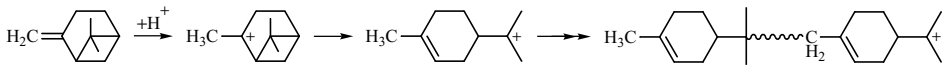

Fig. 2. Release of steric hindrance by isomerization in the carbocationic polymerization of β-pinene.

because the carbonyl oxygen of the ester group is more basic than the vinyl group. If the stability of the chain-carrier carbenium ion forming from a particular monomer is too high or too low, it cannot undergo carbocationic polymerization; *N*-vinyl amines readily react with cationic initiators, but the formation of stable ammonium salts prevents their polymerization. Alkyl vinyl ethers can be polymerized readily, although the oxygen is certainly more basic than the vinyl group. However, in this case protonation of the vinyl group leads to the formation of a carbocation stabilized via charge delocalization. Another example of these n,π-donor monomers is *N*-vinylcarbazole. In these monomers the combination of an unsaturation with an electron-donating heteroatom leads to very easy polymerization (26); the monomers are highly nucleophilic and form very stable carbenium ions (see Table 2 and Fig. 1) As a consequence, their polymerization can be initiated by initiators that would be inefficient with less-reactive monomers. However, the high stability of their carbenium ions restricts their ability to copolymerize with monomers of lower nucleophilicity. Ethylene, propene, or *n*-butenes only give oligomers because of the low stability/high reactivity of the corresponding carbenium ions. Hydride transfer from oligomers prevents the formation of high molecular weight product. For example, the primary cation formed from ethylene will abstract a hydride ion from the secondary carbon of the oligomer.

In addition to carbocation stability and monomer nucleophilicity, steric factors are also important. For example 1,1-diphenylethylene, a very reactive monomer can only be dimerized, because of the formation of a sterically buried carbenium ion (27). Other monomers that cannot be polymerized to high polymers because of steric congestion in the transition state are 2,4,4-trimethyl-1-pentene, 1,2-diphenylethylene (stilbene), 3-methylindene, and 2-methylenenorbornane.

In some monomers, such as β-pinene (Fig. 2) or methylene–norbornene, isomerization of the initially formed carbenium ion helps overcome the steric restriction (27,28):

Monomers containing more than one double bond (conjugated or nonconjugated dienes and trienes) with similar reactivity lead to ill-defined mixtures of cyclized, branched, or cross-linked polymers (27).

Monomers active in carbocationic polymerization have been periodically reviewed over the years (26–30). Isobutylene remains the monomer with optimum combination of nucleophilicity, carbocation stability, and steric factors, yielding high molecular weight elastomers.

Initiating Systems

Carbocationic polymerization can be initiated by a wide variety of chemical and physical methods. Examples are initiation by Brönsted acids, Lewis acids, Lewis

acids in combination with a proton or carbenium ion source, stable carbenium ions, UV or γ-irradiation, photochemical reactions, and the application of a high electric field.

The inverse relationship between stability and reactivity of carbenium ions plays an important role in the initiation step. In order to achieve high initiator efficiency, it is essential to match the stability of the propagating carbenium ion with that of the initiating species. For instance, *primary* and *secondary* alkyl halides were found to have low initiation efficiency in the polymerization of isobutylene coinitiated by $(C_2H_5)_2AlCl$ at $-50^\circ C$, because of the high reactivity and hence short lifetime of the corresponding ions compared with the growing *tertiary* carbocation (31). Better initiation efficiency was achieved using *tert*-butylchloride, because of the positive inductive and hyperconjugative stabilizing effect of the three methyl groups. However, further stabilization of the carbenium ion by aryl groups resulted in decreasing initiation efficiency. Hundred percent initiation efficiency was achieved when 2-chloro-2,4,4-trimethyl pentane was used in conjunction with $TiCl_4$ (32). This can be explained with the effect of *back-strain*. The solvolysis rate of 2-chloro-2,4,4-trimethyl pentane was found to be 21 times higher than that of *tert*-butylchloride, attributed to back-strain, ie, the release of steric strain during rehybridization from sp^3 to sp^2 (33). On the basis of the relative rates of reactions between selected alkyldiphenyl carbenium ions and *tertiary* carbocations with allylsilanes, the 2,4,4,6,6-pentamethyl-2-heptyl cation was a perfect match for a polyisobutylene cation with 33 repeat units (34).

The stability and nucleophilicity of the counteranion (sometimes called "gegenion," based on the German equivalent word) is equally important in the initiation step as well as in the subsequent propagation, chain-transfer, and termination steps. Detailed reviews of various initiating systems are available (15,35–37). The most important initiating systems will be discussed briefly.

Brönsted Acids. The ability of Brönsted acids to initiate carbocationic polymerization is strongly dependent on their acidity (pK_a value), the basicity and nucleophilicity of the counteranion derived from the Brönsted acid, and the stability of the carbenium ion formed from the monomer (37). Highly nucleophilic counteranions will result in the formation of covalent bonds between anion and cation, preventing polymerization. Highly basic counteranions will promote chain transfer by proton elimination. Strong Brönsted acids, such as trifluoromethane sulfonic acid (triflic acid) or perchloric acid, are capable of polymerizing most of the cationically active monomers. The kinetic order of the initiation reaction with respect to the acid is typically higher than one, indicating the involvement of additional acid molecules in the initiation step (38). Weaker Brönsted acids such as hydrogen halides can only polymerize monomers, yielding very stable carbenium ions, such as *N*-vinylcarbazole (39,40). Although the pK_a values of trichloro- or trifluoroacetic acid are higher than those of hydrogen halides, they can readily polymerize monomers such as styrene derivatives or cyclopentadiene (37). The likely reason for this is the participation of a second acid molecule in the ionization step and/or in the stabilization of the counteranion (eq. 3):

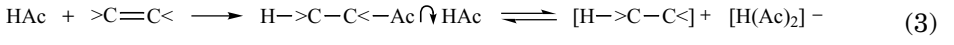

(3)

Lewis Acids. Certain Lewis acids or their mixtures are capable of initiating carbocationic polymerization in the absence of a cation or proton source. This type of initiation is called direct initiation. Hunter and Yohe (13) proposed the formation of zwitterions. The more accepted mechanism is auto-ionization of a Lewis acid dimer, followed by its addition to the monomer (eq. 4):

$$Mt_2X_{2n} \rightleftharpoons MtX^+_{n-1}MtX^-_{n+1} + >C{=}C< \rightarrow [MtX_{n-1}{-}>C{-}C<]^+[MtX_{n+1}]^- \qquad (4)$$

Auto-ionization of dimer Lewis acids was first suggested by Korshak and Lebedev (41). Friedel–Crafts metal halide Lewis acids show various degrees of association in hydrocarbons. Aluminum halides can form dimers and trimers (42), but $TiCl_4$ was shown to be monomeric in CH_2Cl_2 (43). The low temperature polymerization of isobutylene in *n*-heptane initiated by $AlBr_3$ is an example of auto-ionization (44). Other possible mechanisms have been postulated for direct initiation, such as formation of the carbenium ion by the interaction of a halogenated solvent with the Lewis acid, electron transfer from the monomer to the Lewis acid, and allylic hydride transfer; for a summary see Reference 45. Recently, direct initiation of isobutylene polymerization by haloboration of the monomer was demonstrated (46).

Another example of direct initiation is the initiation of vinyl ethers or styrenes by iodine (eq. 5). In this case the initiator is formed *in situ* by the addition of iodine to the double bond (47).

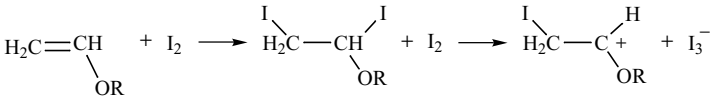

(5)

It has also been suggested that the elimination of HI from the monomer–iodine adduct, followed by hydro-iodization of another monomer, supplies the real initiator (48); this proposal is represented in Fig. 3 for styrene.

Because of these consecutive steps, initiation by iodine is slow. Purposeful addition of HI with I_2 leads to significantly better initiation and, in the case of *t*-butyl vinyl ether, living polymerization (49).

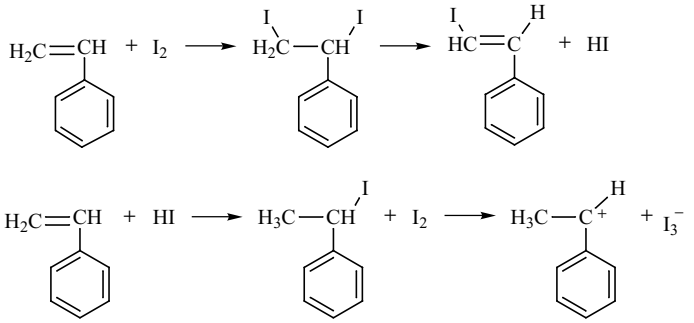

Fig. 3. Initiation of the carbocationic polymerization of styrene by I_2.

Combination of Lewis acids with proton or cation sources (moisture, Brönsted acids, alkyl or aralkyl halides, esters, ethers, peroxides, or epoxides) results in a significantly more efficient initiating system. The wide variety of cation sources available allows close matching of the stability of the initiating and growing carbenium ions, a prerequisite for high initiator efficiencies and the synthesis of polymers with controlled structure. This type of initiation can be written in a general form as follows:

Ionization

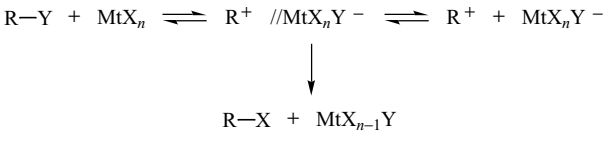

(6)

Initiation

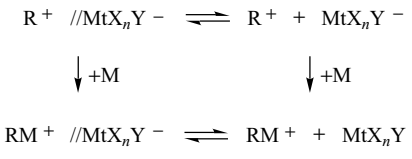

(7)

where $R^+//MtX_{n+1}^-$ and R^+ represent paired and free ions, respectively. The above equilibria are strongly dependent on the nucleophilicity of the Y group, the strength of the Lewis acid, the stability of the carbenium ion, the stability/nucleophilicity of the counteranion, and the type of the polymerization medium used. The strength of a Lewis acid generally increases with increasing atomic number within the same group ($BCl_3 < AlCl_3 < GaCl_3$), with the oxidation state ($SnCl_2 \ll SnCl_4$), and with ligands in the following order: aryl, alkyl, $\ll$ carboxyl, alkoxyl < I < Br < Cl < F (50).

The ion pairs or free ions can either initiate polymerization as shown in the second set of equilibria, or "collapse," with the counteranion forming covalent species as indicated by the downward arrow in the first equilibrium. This latter reaction could lead to counteranion exhange as shown, deactivating the initiating system because of the decreased Lewis acidity of the $MtX_{n-1}Y$ formed (eg, when halide ligands are replaced with alkoxy, hydroxyl, or carboxyl groups) or the formation of inactive R—X species (eg, formation of R—F in case of R—X/BF_3 or SbF_5 systems).

Initiation rate constants (ie, the rate constant of addition of the initiating carbocations to the monomer as shown in the set of equilibria in eq. 7) were determined for a large number of monomers using carbocations derived from the reaction of diaryl and substituted diarylmethyl chlorides with various Lewis acids (21). As indicated by the reaction scheme shown in equation 7, initiation can occur with the participation of solvent-separated ion pairs or free ions. According to Mayr's results, paired and free carbenium ions have identical reactivity and the reaction rates are independent of the nature of the counteranion. Rate constants were found to increase only slightly with increasing solvent polarity

($k_{CH_3NO_2}/k_{CHCl_3} = 4.8$). A careful review of published carbocationic polymerization rate constants (51) also found small differences (one order of magnitude) between $k^{+/-}$ and k^+. The magnitude of and differences between $k^{+/-}$ and k^+ as well as the very high rate constants of carbocationic isobutylene and styrene polymerizations coinitiated by Lewis acids, reported by Mayr (24) and Faust (52), are debated (53).

Initiation by Organometallic Complexes. Considering the industrial importance of isobutylene and the difficulties associated with the processes necessary to produce high molecular weight polyisobutylene-based polymers (eg, low temperature, methyl chloride diluent), it is not surprising that considerable efforts have been made to find catalyst systems capable of polymerizing isobutylene by coordination mechanism. This goal so far has not been achieved. It has repeatedly been shown that isobutylene can easily be polymerized using Ziegler–Natta-type catalysts or cationic metallocene complexes, but the polymerization mechanism remained carbocationic in nature. For a review of these efforts see Reference 54. Nevertheless, these research efforts had some important outcomes. They underscored the importance of counteranions in chain termination and/or transfer processes (55–61) and led to the synthesis of isobutylene/ethylene copolymers by insertion polymerization (62,63).

It has been shown that initiating systems with non- or weakly coordinating counteranions produce higher molecular weight polyisobutylene than do "conventional" initiating systems at the same temperature. The classical example is γ-ray-induced polymerization of isobutylene (see next section), but certain solid-phase initiating systems yielded similarly high molecular weight polyisobutylenes (64). This was attributed to the reduction/elimination of counteranion-assisted chain termination and/or transfer processes. Organometallic or metallocene-based initiating systems with non- or weakly coordinating counteranions such as $B(C_6F_5)_4^-$, $R{-}B(C_6F_5)_3^-$, and $HO{-}B(C_6F_5)_3^-$ (55–61) also led to molecular weights similar to that obtainable by γ-ray or solid-phase–induced isobutylene polymerization (64). It was suggested that these systems polymerize via "counteranion-unencumbered" carbocations.

Essentially alternating isobutylene/ethylene copolymers were prepared using (dimethylsilyl)(tetramethylcyclopentadienyl)(cyclododecylamido)dimethyltitanium activated with tetrakis(pentafluorophenyl)borate, triphenylmethyltetrakis(pentafluorophenyl)borate, or MAO (62,63). Since the reactivities of cations derived from ethylene and isobutylene are vastly different (ethylene yields only oligomers by carbocationic mechanism), this copolymerization most likely proceeds by insertion mechanism. This is further supported by the absence of PIB homopolymer, and the absence of IB–IB diads as demonstrated by ^1H NMR analysis of copolymers with as high as 45 mol% IB content. This indirectly confirms that IB will not homopolymerize to high polymers by insertion mechanism.

Initiation by Electromagnetic Radiation. In this type of initiation electromagnetic radiation such as light, γ-radiation, high energy electrons, or high intensity electric fields induces carbocationic polymerization. Activation by γ-radiation and high energy electrons used to be the most investigated of these methods (65), but recently photoinitiation has generated a lot of interest.

In initiation by γ-radiation, the first step is the formation of radical cations, which then react with the monomer forming the initiating carbocation together

with free radicals:

$$M \xrightarrow{\gamma\text{-radiation}} M^{+\cdot} + e^{-}$$

$$M^{+\cdot} + M \longrightarrow M^{+} + M^{\cdot} \qquad (8)$$

The cation is more reactive than the free radical, thereby dominating the initiation reaction. Radical cations can also be formed by high energy electrons, vacuum UV radiation, high intensity electric fields, or anodic oxidation of the monomer. Nuclear chemical initiation involves the use of tritium; this method produced very high molecular weight polyisobutylenes and polystyrenes (65).

Photoinitiation. Photoinitiation has been very popular in recent years. This also proceeds through the formation of radical cations. One example is the polymerization of isobutylene initiated by illuminating a quiescent heptane solution of the monomer containing VCl_4 or $TiCl_4$ (66). Interestingly, charge-transfer interaction between electron-rich donor monomers (*N*-vinylcarbazole, vinyl anthracene, or vinyl ethers) and strong electron acceptors (tetracyanoethylene, *o*- or *p*-chloranil, maleic anhydride) can lead to carbocationic polymerization even in the absence of light (67).

Crivello discovered a fundamentally different type of photoinitiation (68). He showed that onium salts, such as diaryl iodonium (**1**), initiate cationic polymerization of a wide

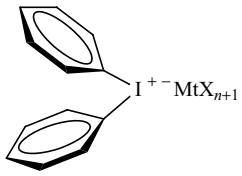

(**1**)

variety of monomers: olefins, *N*-vinylcarbazole, alkyl vinyl ethers, epoxides, or lactams. The photoexcitation of the salt leads to heterolytic and homolytic cleavage of the carbon–iodine bond. Further reaction of the aryl cations and aryl iodide cation radicals with solvents, monomers, or impurities leads to the formation of the ultimate initiating species, $HMtX_n$. Triarylsulfonium salts are also effective in this type of initiation. These initiators are currently used in applications such as printing inks, stereolithography, holographic recording, and microelectronic photoresists. An alternative initiating system is based on allylic onium salts (eg allylthiophenium, allylpyridinium salts), which in conjunction with radical initiators can lead to thermal or photoinitiated carbocationic polymerization (69).

Polymerization Media

Solvents. The polymerization medium is a very important element in carbocationic polymerization. Although generally the term "polarity" is used to characterize solvents/diluents in carbocationic polymerization, it is ill-defined and

oversimplifies the role of the polymerization medium. In the literature, solvents are almost exclusively characterized by their dielectric constant. The use of dielectric constant to describe solvent effects is based on Born and Bjerrum's simple theoretical approach to ion–solvent interaction, and on the equation derived later by Laidler and Eyring for the dependence of ion–molecule interactions on the reaction medium (70–72). The application of this "hard spheres in continuum" model is limited to large ions, which remain practically unsolvated. As this model completely ignores the structural aspects of solvent interaction and the charge redistribution within and between solute and solvent, it fails to describe most of the experimental findings (73).

The more advanced, dynamic coordination or functional approach considers the solute–solvent or ion–solvent interactions as a result of electron pair donor–acceptor interactions, and inductive and mesomeric effects. According to this theory, the equilibrium between nonionized species and solvent-separated ion pairs is a function of the dynamic electron pair acceptor and donor properties of the solvent, not simply their "static" polarity (73,74). Ionization may be affected by a nucleophilic attack of a donor (D) or by an electrophilic attack of an acceptor (A) directed to the substrate R—Y. The strong donor–acceptor interactions first lead to charge redistribution between and within the molecules (pile-up and spill-over effects), and ultimately to the heterolytic scission of the covalent R—Y bond (eq. 8):

$$D_m \curvearrowright R{-}Y \curvearrowright A_z \rightleftharpoons [RD_m]^+ \quad [YA_z]^- \tag{8}$$

where the arrows (↷)indicate the coordinative interactions between molecules, and subscripts m and z refer to the number of donor and acceptor molecules participating in this reaction. In carbocationic polymerization this simple ionization scheme is further influenced by coordinative interaction between R—Y (initiator) and the Lewis acid MtX_n:

$$D_m \curvearrowright R{-}Y \curvearrowright MtX_n \curvearrowright A_z \rightleftharpoons [RD_m]^+ \quad [Y\,MtX_n\,A_z]^- \tag{9}$$

The ion pairs shown in equation 9 may subsequently undergo electrolytic dissociation leading to the formation of "free" ions. The separation of the ions is primarily dependent on the dielectric constant of the solvent. According to this dynamic view of solvent–solute interactions, in addition to the static dielectric constant, a measure of electron acceptor and electron donor ability is required to interpret the role of solvents in ionic polymerizations. The empirical acceptor and donor numbers (AN and DN), developed by Gutmann, provide a good measure of electron pair accepting and donating ability of solvents. These parameters were used to describe solvent effects in carbocationic polymerization (75). From this approach it is clear that solvents with high electron acceptor and low electron donor properties are required for carbocationic polymerization. Indeed, solvents most frequently used for carbocationic polymerization have low DN and high AN (see Table 3). At the same time, the electron-pair–accepting ability of the solvent should not exceed that of the monomer.

Ionization and dissociation equilibria during initiation and propagation can be shifted by the adjustment of the electron-pair–accepting ability of the solvent

Table 3. Dielectric, Electron Acceptor, and Donor Properties of Solvents[a] Used for Carbocationic Polymerization

Solvent	ε (20°C)	AN	DN
n-Hexane	1.89	0	0
Cyclohexane	2.02	0	0
Benzene	2.28	8.2	0
CH_2Cl_2	9.08	20.4	0
$CHCl_3$	4.81	23.1	0
CCl_4	2.24	8.6	0
1,2-dichloroethane	10.36[b]	16.7	0
Nitromethane	35.9	20.5	2.7
Nitrobenzene	34.82[b]	14.8	4.4

[a]Ref. 76.
[b]25°C.

or solvent mixture used. Solvents with high dielectric constant should be selected for shifting the equilibria in the direction of greater ionization and/or dissociation. This will be discussed in more detail in the Controlled Carbocationic Polymerization section.

The use of liquid and supercritical CO_2 as an alternative, environmentally friendly or "benign" solvent should be mentioned here. De Simone reported the first examples of carbocationic polymerization in liquid and supercritical CO_2. Vinyl ethers and oxetane containing fluorinated side chains yielded low molecular weight products (77). Kennedy reported the carbocationic polymerization of isobutylene in supercritical and liquid CO_2 (78), also yielding low molecular weight polymer. Butyl rubber was reportedly produced in liquid CO_2/hexane mixture (79). However, it seems that the initial excitement surrounding liquid and supercritical CO_2 as alternative solvents for polymerization has disappeared.

Temperature. In terms of temperature, the first consideration in carbocationic polymerization—as in any enthalpy-driven chain reaction—is the ceiling temperature T_c. T_c is the limiting temperature above which the rate of depropagation exceeds the rate of propagation at a given monomer concentration:

$$M_n^+ + M \underset{k_{dp}}{\overset{k_p}{\rightleftharpoons}} M_{n+1}^+ \tag{10}$$

The reaction temperature therefore must be below the T_c of the monomer at that concentration. This typically is not a problem since the synthesis of high molecular weight polymers by carbocationic polymerization often requires low temperatures (−80 to −100°C). The rationale is that chain-breaking reactions that have higher activation energy than propagation may be "frozen out" at low temperatures. Interestingly, Mayr argues that in the carbocationic polymerization of certain monomers (isobutylene, styrene), k_p is in the diffusion-limiting range; thus propagation itself proceeds virtually without activation energy (24). The dielectric constant of solvents increases with decreasing temperature, yielding more charge separation and higher reactivity at lower temperatures. This could result in negative apparent activation energies of propagation observed in some carbocationic polymerizations (80–85).

Kinetics and Mechanisms of Carbocationic Polymerizations

The elementary reactions in carbocationic polymerization are initiation, propagation, termination, and chain transfer. The formation of a high molecular weight polymeric product requires that the rate of propagation R_p be much higher than the rates of chain-breaking reactions

$$\mathrm{DP}_n = R_p \Big/ \left(\sum R_i + \sum R_{tr} \right) \tag{11}$$

where DP_n stands for the number-average degree of polymerization, and R_i and R_p stand for the rates of initiation and propagation. In addition, the rate of initiation R_i must be equal to or higher than the rate of termination during the entire process, or initiation must be completed in the early stages of the process and the rate of irreversible termination must be zero or very small. If low molecular weight oligomeric products are required, the chain-breaking processes should be fast relative to propagation (26).

The kinetics and mechanism of carbocationic polymerization are difficult to study, owing to the high reactivity of the carbocations. Monomer consumption can be monitored by dilatometry, gravimetric sampling, or on-line techniques such as UV–vis (86) or FTIR monitoring (87,88). Very fast reactions can be followed by stop-flow techniques (89). Adiabatic calorimetry has been used extensively, although admittedly this technique is not kinetically rigorous. In the case of very fast reactions (eg, the carbocationic polymerization of isobutylene and styrene under certain conditions), it may be physically impossible to remove the polymerization heat fast enough to maintain isothermal conditions in a laboratory batch reactor, thus kinetic investigations in these systems must be viewed with caution. This chapter will discuss general aspects of the kinetics and mechanisms of carbocationic polymerizations.

Initiation. Mechanistic and kinetic aspects of the initiation step in carbocationic polymerizations have been discussed under Initiating Systems. It should be emphasized here that the overall rate of initiation is usually influenced by a series of consecutive and competitive reactions such as those shown in equations 6 and 7. The rate of initiation, ie, the rate of addition of the initiating carbocations to the monomer must be clearly differentiated from the overall rate. Measuring the initiator consumption under polymerization conditions is often very difficult, especially when very low initiator concentration is used to obtain high molecular weight polymers. In addition, the rate constant of initiation can only be deduced from initiator consumption data when the exact mechanism of the initiation and the active-center concentration is known independently. More often than not, these are debated. The so-called diffusion clock method employs competitive experiments: between the reaction of the monomer with *in situ* generated carbocations, and the reaction of these carbocations with a reference nucleophile reacting with a known rate constant (90). Using this method, $k_i = 6 \times 10^8$ $\mathrm{dm^3/mol/s}$ was obtained in isobutylene oligomerization initiated with 2-chloro-2,4,4-trimethyl pentane/$TiCl_4$ (91). This value is in excellent agreement with that

calculated from the linear free energy relationship introduced by Mayr (92),

$$\log k = s(N + E) \tag{12}$$

where N is the nucleophilicity parameter and $\boldsymbol{s}$ is the slope of the log k vs E (electrophilicity) plot. $E(An_2CH^+)$ was set 0 and $\boldsymbol{s}$(2-methyl-1-pentene) was set 1.0 and N corresponds to the intercept of the correlation line with the abscissa (log $k = 0$). Detailed discussion of this novel method is not possible here, but this approach could serve as a foundation to design effective initiators, especially for controlled carbocationic polymerization.

Propagation. Cationic polymerizations with carbenium ion chain carriers are almost exclusively limited to vinyl monomers; notable exceptions include the polymerization of strained rings such as 1,1-dimethylcyclopropane (93), shown in equation 13.

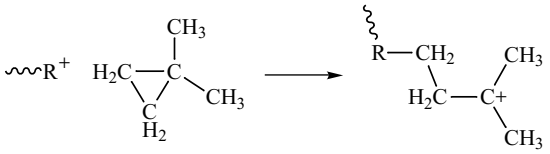

(13)

Carbocationic polymerization of vinyl monomers proceeds by repeated electrophilic addition of the monomer to the growing carbenium ion, following Markovnikov's rule, which leads to the formation of regular head-to-tail polymers (Fig. 4).

In general, carbocationic polymerizations are highly exothermic ($-\Delta H$ = 80−120 kJ/mol), owing to the formation of a C—C single bond from a π-bond. Similar to most other chain-growth polymerizations, carbocationic polymerizations are enthalpy driven; the entropy loss of about −120 J/mol/K related to the loss of freedom in mobility of the polymer chain must be counterbalanced by the enthalpy change $\Delta G = \Delta H - T\Delta S \leq 0$.

The open transition state—sp^2-hybridized carbocations—has low stereoselectivity, thus mostly atactic polymers are formed (94). At the same time, reportedly the very first synthetic stereoregular polymer was an isotactic poly(isobutyl vinyl ether) prepared by carbocationic polymerization initiated with $BF_3/O(C_2H_5)_2$ at −78°C (95). Other examples of stereoregular crystalline polymers synthesized by homogeneous and heterogeneous carbocationic polymerization are polymers of vinyl ether derivatives, and 2,5-dimethyl styrene or α-methylstyrene (95–100). Stereoregular vinyl ether polymers have also been synthesized using

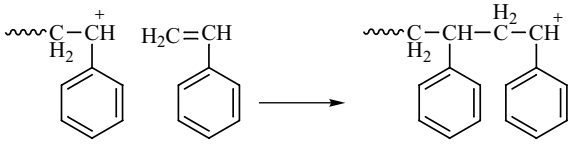

Fig. 4. Head-to-tail addition in carbocationic polymerization.

Table 4. Propagation Rate Constant of Various Monomers in Bulk Polymerization

Monomer	Temperature, °C	k_p dm^3/mol/s	Reference
Isobutylene	0	1.5×10^8	110
Isoprene	0	2×10^3	111
Cyclopentadiene	−78	5.8×10^8	112
Styrene	15	3×10^6	113
Styrene	20	2.5×10^7	114
Styrene	30	4×10^8	115
α-Methylstyrene	0	4×10^6	113
α-Methylstyrene	23.3	4×10^7	114
Ethyl vinyl ether	0	3.5×10^7	116
Isopropyl vinyl ether	0	9×10^5	117
tert-Butyl vinyl ether	0	5×10^4	117
Isobutyl vinyl ether	30	3×10^5	113
Isobutyl vinyl ether	0	4×10^4	118

solid-supported catalysts, metal oxides, and modified Ziegler–Natta catalysts (101–107). Several mechanisms have been suggested to account for the formation of stereoregular polymers in carbocationic polymerization. One suggested mechanism involves an sp^3-hybridized transition state due to coordination with the counteranion (108). Others suggested ring structures forming at the end of the growing chain (98,109). Controlling the microstructure of polymers synthesized by carbocationic polymerization may be one of the most challenging areas of future research (94).

In general, carbocationic homopolymerization is characterized by low activation enthalpy, low concentration of active species (10^{-8}–10^{-5} mol/dm^3), high propagation rate constants (10^3–10^8 dm^3/mol/sec), and short lifetime of the carbenium ion (94). Table 4 lists propagation rate constants determined in bulk carbocationic polymerization of various monomers initiated by γ-radiation, electron pulse, or field ionization techniques.

High propagation rates and low concentration of active species renders kinetic measurements/calculations difficult and leaves plenty of room for debate concerning the mechanism and kinetics of carbocationic polymerizations. Kinetic evaluation is further hampered by the coexistence of covalent species with ion pairs and "free" ions as originally suggested by Winstein (119) for reactions involving cationic intermediates:

$$\underset{\text{covalent}}{\text{R—X}} \rightleftharpoons \underset{\text{ion pairs}}{\text{R}^+\text{X}^-} \rightleftharpoons \underset{\text{contact or tight}}{\text{R}^+\text{//X}^-} \rightleftharpoons \underset{\text{solvent-separated or loose ion pairs}}{\text{R}^+ + \text{X}^+} \quad \underset{\text{free ions}}{}$$

Ions termed "free" may be involved in electrostatic interactions with the counteranion, or in similar interactions limiting their "freedom," but in relative terms these effects are long-range interactions. Similar to anionic polymerization, both free carbocations and ion pairs are capable of polymerization. However, the difference between their reactivity is significantly smaller than in the case of anionic polymerization. As mentioned before, it was recently suggested that in fact there is no difference between $k_p{}^+$ and $k_p{}^{+/-}$ (21) – this is currently debated and needs

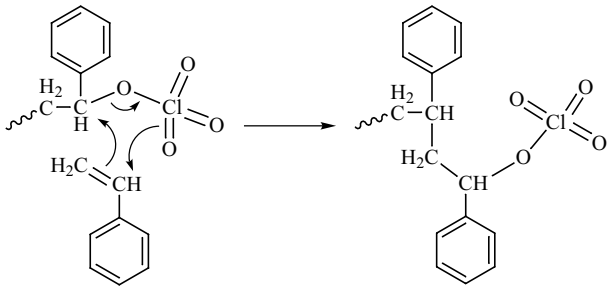

Fig. 5. "Pseudocationic" mechanism proposed for the polymerization of styrene initiated by perchloric acid.

close examination. In anionic polymerization, the k_p of the free ions can be three orders of magnitude higher than that of the tight ion pairs (120). In contrast, the $k_p^+/k_p^{+/-}$ ratio in perchloric acid–initiated polymerization of styrene was measured to be 20 at −80°C, and only 8 at −60°C (121). This difference between the $k_p^+/k_p^{+/-}$ ratios in cationic and anionic polymerization is related to the bulkiness of the counteranion in cationic polymerization. The interionic distance of contact or tight ion pairs in carbocationic polymerization is closer to that of the solvent-separated ion pairs of anionic polymerization (122). Determination of k_p^+ and $k_p^{+/-}$ in cationic systems is very difficult because of the extremely low concentration of the active species. By spectroscopic techniques (NMR, UV) only the most stable carbenium ions can be detected under polymerization conditions.

The existence of a dynamic equilibrium between dormant (covalent) and active (ionic) species in controlled carbocationic polymerizations had been debated for years. It has been argued that under certain conditions, polarized covalent species can directly react with monomer; examples are the "pseudocationic" mechanism proposed for the polymerization of styrene initiated by perchloric acid (123,124) (Fig. 5) or the "two-component group transfer polymerization" proposed for the polymerization of isobutylene initiated by the dicumylacetate/BCl_3 system (125) (Fig. 6). Recent results and theoretical considerations support the now generally accepted view that the true active species are ions, and the dormant species serve as a reservoir from which the propagating ion pairs are formed (126–131). The existence of a dynamic equilibrium between dormant and active species and the ability to suppress the formation of free ions made possible the synthesis of polymers with controlled molecular architecture via carbocationic polymerization.

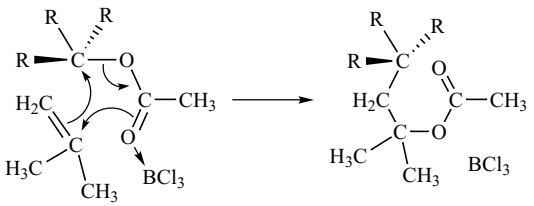

Fig. 6. "Two-component group transfer polymerization" proposed for the polymerization of isobutylene initiated by the dicumylacetate/BCl_3 system.

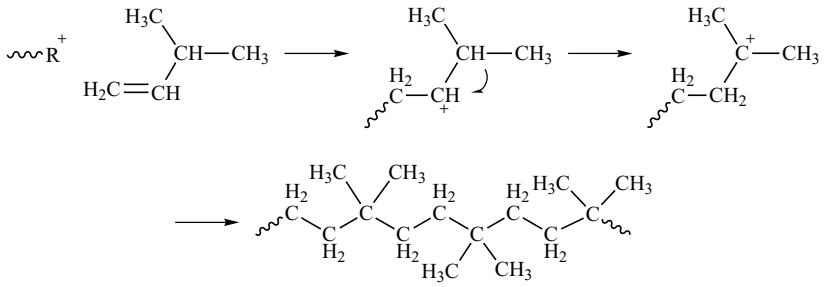

Fig. 7. Hydride shift in the polymerization of 3-methyl-1-butene, yielding crystalline stereoregular polymer.

This equilibrium can be compared to the equilibrium between active propagating chains and ion-pair agglomerates in anionic polymerization—such aggregates have not been found in carbocationic polymerizations.

Carbenium ions are inherently reactive species and can readily undergo side reactions. These side reactions can be part of the propagation step or lead to the termination of the polymeric and/or kinetic chain. For example, the propagating chain end may rearrange to an energetically more favored structure prior to the next propagation step, as in the isomerization polymerization of β-pinene (see Fig. 2). The isomerization step may involve hydride or methide shifts. An interesting example of 1,2-hydride shift is the carbocationic polymerization of 3-methyl-1-butene. Below -100°C, crystalline polymer containing 1,3 repeat units, shown in Figure 7, was obtained (132). Above this temperature, amorphous polymer containing both regular 1,2 and 1,3 repeat units formed (132). Isomerization may also lead to chain-breaking; this will be discussed in the next section.

Conjugated dienes can be readily polymerized by carbocationic techniques. In fact, cyclopentadiene is considered to be one of the more reactive carbocationic monomers (126). However, the carbocationic polymerization of conjugated dienes leads to polymers with rather unattractive physical properties owing to side reactions such as cross-linking and cyclization. Products obtained range from low molecular weight oils through tacky resins to cross-linked and brittle materials, depending on the monomer and the polymerization conditions. Loss of unsaturation has been frequently observed and it was mainly attributed to cyclization (133). For example, trans-1,4 enchainment of butadiene or isoprene can readily undergo carbocationic cyclization (134,135), as shown in Figure 8. Not surprisingly, no reports were found on the controlled carbocationic polymerization of dienes. One exception is the synthesis of polyisobutylene–polyisoprene multiblock copolymers and their use for the preparation of UV-cured transparent flexible coatings by living carbocationic polymerization using sequential monomer addition (136). Nevertheless, carbocationic copolymerizations involving dienes are very important—the industrial butyl process is a copolymerization of isobutylene with a small amount of isoprene (3,4).

Chain-Breaking Reactions. When discussing chain-breaking reactions, kinetic chain and polymer chain should be distinguished. Chain transfer involves polymer chain termination, but the kinetic chain remains unbroken. True termination breaks both the polymer and kinetic chains. The so-called reversible

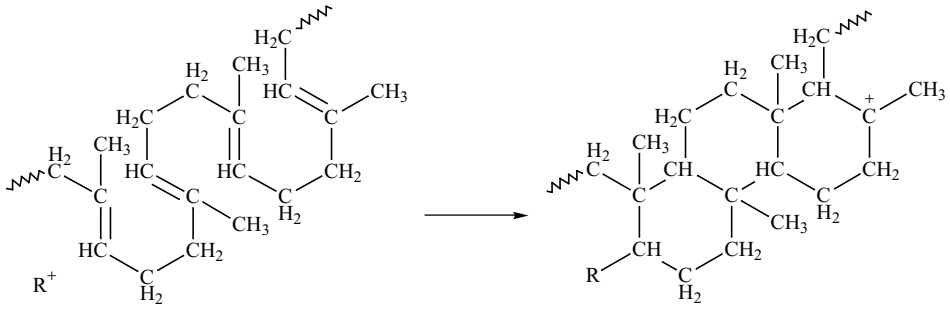

Fig. 8. Cyclization in the carbocationic polymerization of isoprene.

termination slows down the formation of the polymer without permanently terminating the kinetic chain (137). This is the key to controlled carbocationic polymerizations, which will be discussed separately in the next section. Interestingly, strong nucleophiles or electron-pair–donor compounds, which are considered to be strong terminating agents, were found to mediate controlled carbocationic polymerizations (138,139). The mechanism of the role of these additives remains unclear (140).

Termination. Termination will break the kinetic chain, yielding inactive species. Termination reactions have been classified as follows (141):

(1) Spontaneous charge neutralization
(2) Degradative transfer
(3) Reaction with nucleophiles

Spontaneous charge neutralization involves transfer of a negatively charged group from the counteranion to the carbenium ion and might lead to the formation of inactive covalent chain ends (142). An example is shown in equation 14

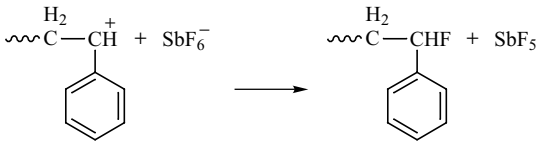

(14)

Other examples are alkylation of the chain end in alkylaluminum halide coinitiated isobutylene polymerization (143). This type of counteranion exchange can also result in the formation of a Lewis acid that is too weak to ionize the chain end, as depicted in equation 15.

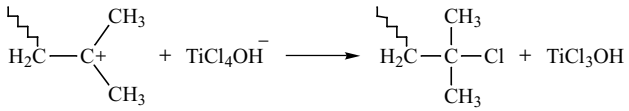

(15)

The rate of termination decreases with increasing acid strength of the counteranion (144). Counteranion stabilization by solvation will slow down termination by charge neutralization (145). Reversible termination by charge neutralization can lead to controlled carbocationic polymerization (see under Controlled Carbocationic Polymerization).

Degradative chain transfer involves the formation of carbocations too stable to propagate and will be discussed under Chain Transfer.

Nucleophilic compounds may react directly with the carbenium ion to yield an unreactive compound, or with the Lewis acid reducing its acid character. If the weakened Lewis acid is not able to activate the chain end, termination occurs. Strong bases may also abstract and trap β-hydrogens, leading to termination instead of chain transfer (146). It should be mentioned here that controlled isobutylene and styrene polymerizations yielding narrow MWD are mediated by strong nucleophiles in small concentrations. The mechanism of this effect remains controversial (147). Alcohols are regarded as strong terminating agents; but in concentrations not exceeding the concentration of the Lewis acid, they can act as initiators (148) and accelerate carbocationic polymerization (149). In addition, added alcohols and other nucleophiles can lead to a molecular weight increase. For example, the highest molecular weight of polyisobutylene achievable in the presence of ethanol was obtained at 1:1 ethanol/$AlCl_3$ concentration ratio (149). Termination may also be caused by complexation of the catalyst or coinitiator with the monomer, or occlusion of the active growing species in the precipitated polymer (150).

It was proposed that the apparent negative overall activation energies observed in carbocationic polymerizations (80–82) are the consequence of relatively high activation energies of kinetic termination reactions, compared to the activation energies of initiation and propagation (144). Kennedy and Trivedi (151) found that in the carbocationic polymerization of isobutylene the activation enthalpy difference of molecular weight is lowest under conditions when the molecular weight is controlled by termination, and highest where the molecular weight is controlled by chain transfer to monomer. Termination control occurs at low temperature, indicating that for this monomer the activation energy for transfer is higher than the activation energy for termination. In the controlled carbocationic polymerization of isobutylene initiated by $TiCl_4$-based systems, negative apparent activation energies were found, while in the case of BCl_3 slight positive values were obtained (152). This seems to contradict the reasoning that the negative apparent activation is due to exothermic ionization, ie, in systems coinitiated with strong Lewis acids the activation enthalpy of ionization is higher than that of propagation (153). BCl_3 is a stronger Lewis acid than $TiCl_4$ (154); but forms a less stable counteranion, leading to rapid termination (155).

Chain Transfer. Chain transfer is the most important chain-breaking reaction in carbocationic polymerization. It can be considered as a subcase of termination, when this latter is accompanied by reinitiation. In chain-transfer reactions the active center is "transferred" to a new site: to unreacted monomer or initiator, the preformed polymer, or the solvent. This can happen by β-proton elimination from the growing chain, or Friedel–Crafts alkylation of aromatic rings. β-Hydrogen atoms of the propagating carbenium ions are quite acidic owing to the delocalization of the positive charge. In isobutylene, vinyl ether, and styrene

polymerization β-hydrogens may carry as much as 7–12% of the positive charge (156). Loss of proton leads to the formation of an end group with an unsaturation, shown in equation 16 for styrene polymerization.

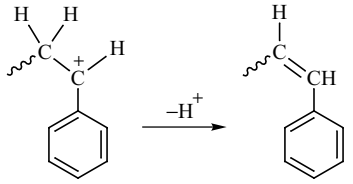

(16)

Spontaneous proton elimination is unlikely, but β-protons can be abstracted by basic compounds (solvent, counteranion, additives) in the system, including the monomer in competition with propagation (94). Mayr and co-workers (91) found that in the case of 1,2-dialkyl-substituted ethylenes, electrophilic attack on the double bond and hydride abstraction have comparable activation energies, so these systems are riddled with chain transfer, while in the case of 1,1-dialkyl and higher alkylated ethylenes the attack of carbocations at the C=C double bond is preferred.

Electrophilic aromatic substitution (Friedel–Crafts alkylation) catalyzed by acids can occur inter- or intramolecularly. Intramolecular alkylation leads to indanyl ring formation in styrene polymerization, as shown in Figure 9a. Intermolecular reactions involving two or more polymer chains lead to branching—see Figure 9b. Isomerization by hydride or alkyl transfer (157,158) leading to more stable carbenium ions can also be considered as a form of chain transfer. The protons or new active sites forming in chain-transfer reactions can initiate new chains. While the overall concentration of active sites does not change with chain transfer, polymerization kinetics may be affected, depending on the relative reactivity and concentration of the new active sites. For instance, when the new active site is very unreactive, reinitiation will be slow or may not happen. These

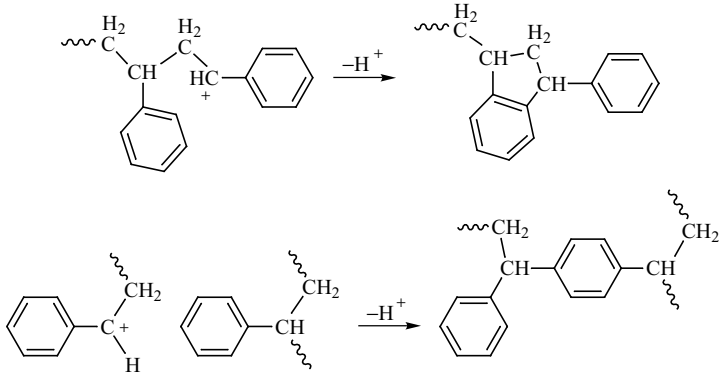

Fig. 9. (**a**) Chain transfer by intramolecular alkylation in styrene polymerization. (**b**) Chain transfer by intermolecular alkylation leading to branching in styrene polymerization.

processes are termed *degradative chain transfer* or *degradative termination*. In all cases, polymer chains are terminated, which leads to the decrease of the average molecular weight or degree of polymerization, and broadening of the molecular weight distribution. In the case of isobutylene polymerization initiated by $AlCl_3$-based systems, competition between transfer to monomer and solvent manifested itself in the so-called inversion temperature (159). At this temperature, the degree of polymerization was found to be independent of monomer concentration. In contrast, below or above this temperature, monomer concentration had an effect on the degree of polymerization; at low temperatures DP_n decreased with increasing [M], while above the inversion temperature an opposite trend was observed. It was rationalized that below the inversion temperature, the rate of transfer to monomer exceeds the rate of transfer to solvent, so increasing monomer concentration leads to a lower degree of polymerization.

Kennedy and Squires investigated termination and transfer processes in isobutylene polymerization initiated by $AlCl_3$ at $-78^\circ C$ in *n*-pentane (160) and devised a scale of termination or "poison" and transfer coefficients. Most compounds acted as both "poisons" and chain-transfer agents. In industry, chain-transfer agents are often deliberately used to control polymerization processes (161).

Kinetic evaluation of various transfer and termination processes uses an adopted form of the Mayo equation derived from the general formula

$$1/\mathrm{DP}_n = \left(\sum R_\mathrm{t} + \sum R_\mathrm{tr}\right) \Big/ R_\mathrm{p} \tag{17}$$

where DP_n stands for the number-average degree of polymerization, and R_t, R_{tr}, and R_p stand for the rates of termination, transfer, and propagation, respectively. Equation 17 defines the instantaneous DP_n, and has frequently been used to evaluate transfer and termination coefficients (in case of transfer to monomer and spontaneous termination, $C_{tr} = k_{tr}/k_p$; $C_t = k_t/k_p$) at low conversion. At high conversion, the integrated form of the equation has to be used, and depending on the complexity of the reaction, analysis may become quite complicated (162).

Copolymerization

In carbocationic homopolymerization, propagation rate constants are relatively high for all monomers, in spite of major differences in nucleophilicity (24,25). The reason for this lies in the fact that the stability of the carbenium ion formed from the corresponding monomer increases with the nucleophilicity of the monomer. This can be illustrated by comparing isobutylene, a weakly nucleophilic monomer producing a very reactive carbocation, and *N*-vinylcarbazole, a very nucleophilic monomer producing a very stable carbocation. Very high propagation rate constants were reported for both monomers (6×10^8 dm^3/mol/s for isobutylene and 1×10^7 dm^3/mol/s for *N*-vinylcarbazole at $20^\circ C$), based on model studies (25,91). However, in case of copolymerization, differences between the stability of carbenium ions and the nucleophilicity of the monomers hinder the formation of random copolymers. For example, the rate constant of addition of isobutylene monomer (1)

to a growing polymer chain with a carbocation derived from *N*-vinylcarbazole (2) would be $k_{21} = 2 \times 10^3$ dm^3/mol/s, calculated using the reference scale and method (see eq. 12) developed by Mayr (92,163). This cross-propagation constant is four to five orders of magnitude lower than the corresponding homopolymerization rate constants, rendering the copolymerization of the two monomers impossible. This is why there is no example of copolymer formation between monomers having significantly different nucleophilicity such as the isobutylene/*N*-vinylcarbazole or isobutylene/alkyl vinyl ether pairs.

The simplest copolymerization model is the terminal model, according to which the reactivity of the growing chain is determined by the last (terminal) monomer unit. In this case two reactivity ratios (r_1 and r_2) are sufficient to describe the instantaneous composition of a binary copolymer:

$$\frac{d[M_1]}{d[M_2]} = \frac{[M_1]}{[M_2]} \frac{r_1[M_1] + [M_2]}{r_2[M_2] + [M_1]} \tag{18}$$

where $r_1 = k_{11}/k_{12}$, $r_2 = k_{22}/k_{21}$ and k_{11} and k_{22} are the propagation rate constants of the homopolymerization and k_{12} and k_{21} of the cross-propagation steps. Reference 164 provides a good summary of the methods available for the determination of reactivity ratios as well as an excellent collection and assessment of 643 cationic copolymerization systems. On the basis of this extensive data set, it appears that the terminal model describes most of the carbocationic copolymerization systems investigated. There are few exceptions where the effect of the penultimate unit has to be considered; one example is the copolymerization of indene with 3-methylindene (165).

Table 5 lists some selected copolymerization reactivity ratios. It is clear from the data that the monomer yielding the more stable carbocation dominates the copolymerization. Considering the importance of carbocation stability, it is not surprising that in some instances reasonable correlation was obtained between $\log(1/r_1)$ and Hammett's σ or Brown's σ^+ values of the substituents of the second monomer. Examples are the copolymerization of α-methylstyrene with substituted styrenes (169) or styrene with substituted 1- and 2-phenylbutadienes (172). It is thus expected that ideal copolymerization ($r_1 = r_2 = 1$) in carbocationic systems is unlikely—the only reported ideal system is the copolymerization of

Table 5. Effect of Carbenium Ion Stability on Copolymerization Reactivity Ratios

Monomer 1	Monomer 2	Polymerization system	r_1	r_2	Ref.
Styrene	2-Vinylphenanthrene	$TiCl_4/CCl_4/0^\circ C$	0.95	8.1	166
Styrene	2-Vinylphenanthrene	$TiCl_4/CH_2Cl_2/0^\circ C$	0.3	9.3	166
4-Methylstyrene	4-Methoxystyrene	$I_2/CH_2Cl_2/0^\circ C$	0.56	11	167
4-Methylstyrene	4-Methoxystyrene	$I_2/CCl_4/0^\circ C$	0.22	28.7	166
4-Chlorostyrene	4-Methylstyrene	$TiCl_4/CH_2Cl_2/0^\circ C$	0.10	10.0	168
4-Chlorostyrene	4-Methylstyrene	$TiCl_4/CCl_4$—NOBz/$0^\circ C$	0.22	4.5	169
Styrene	α-Methylstyrene	$TiCl_4$/Tol/$0^\circ C$	0.22[a]	1.34[a]	170
Styrene	α-Methylstyrene	$TiCl_4$/NOBz/$0^\circ C$	0.20[a]	9.02[a]	170
Styrene	Isobutylene	$TiCl_4/CH_2Cl_2/-20^\circ C$	0.70[a]	2.70[a]	171

[a]Values calculated from original data using the Kelen–Tudos method as published in Ref. 164.

Table 6. Effect of Temperature on Copolymerization of Styrene; Reactivity Ratios

Monomer 2	Polymerization system	T, °C	r_1	r_2	Reference
2-Vinylphenanthrene	$TiCl_4/CH_2Cl_2$	0	0.3	9.3	166
		−40	0.4	4.7	166
		−72	0.35	2.95	166
4-Methylstyrene	$TiCl_4/CH_2Cl_2$	25°C	0.36	3.15	168
		0°C	0.60	2.9	168
		−30°C	0.48	2.5	168
trans-1-Phenyl-1,3-butadiene	BF_3OEt_2/Tol	0°C	0.7	3.3	176
		−40°C	0.7	3.0	176
		−78°C	0.74	2.6	176

isobutylene with β-pinene at −130/−120°C in ethyl chloride initiated with "H_2O"/EtAlCl combination (173). Large differences in reactivity ratios render the synthesis of polymers with uniform composition at the microscopic level difficult in carbocationic systems. This was circumvented by the so-called forced ideal copolymerization method. The comonomer mixture was fed into the reaction mixture at rates not exceeding the overall copolymerization rate. Under these conditions, α-methylstyrene/styrene or isobutylene/styrene copolymers with composition identical to the composition of the comonomer mixture were obtained (174,175).

Reaction conditions such as temperature and nature of the solvent and coinitiator can have a profound effect on the reactivity ratios (164). There are several examples in carbocationic copolymerization indicating that for $r > 1$, the reactivity ratio decreases with decreasing temperatures. Table 6 lists some selected data.

This trend is opposite to that observed in radical polymerization, in which reactivity ratios approach unity with increasing temperature; this was attributed to similar entropies of activation (177). Apparently, entropy effects cannot be neglected in carbocationic copolymerization (178).

It has been observed that in carbocationic copolymerization the molecular weight of the resulting copolymer is always lower than that of the individual homopolymers prepared under identical conditions (179). This was explained by the high k_{tr}/k_p ratio of the favored cross-propagation step (reaction of the most reactive chain end with the monomer giving the most stable carbenium ion), compared to the respective homopolymerization k_{tr}/k_p ratios (173).

Copolymerizations involving dienes such as the copolymerization of isobutylene with isoprene are important from the industrial point of view (3,4). Isoprene acts as a strong chain-transfer and terminating agent in the carbocationic polymerization of isobutylene (161), and at high concentration it leads to a crosslinked, insoluble product (180). Because of the limited composition range available for analysis, determination of the reactivity ratios in this system is rather difficult. Reactivity ratios published for the isobutylene/isoprene system are listed in Table 7.

Interestingly, controlled copolymerization was achieved in the isobutylene/2,4-dimethyl pentadiene-1,3 system, explained by the internal strain exerted by the methyl groups of the 2,4-dimethyl pentadiene-1,3 incorporated into the copolymer, and the presence of electron-pair donors forming *in situ* from the initiators (190).

Table 7. Copolymerization Reactivity Ratios of the Isobutylene (1)/Isoprene (2) System

Initiating system	Solvent	T,°C	r_1	r_2	Reference
$AlCl_3$	CH_3Cl	−103	2.5 ± 0.5	0.4 ± 0.1	181
$EtAlCl_2$	CH_3Cl	−100	2.17	0.5	182
$AlCl_3$	CH_3Cl	−90	2.3		183
$EtAlCl_2$+Cl_2	CH_3Cl	−35	2.5		184
$AlCl_3$	EtCl	−95	2.26	0.38	185
$EtAlCl_2$	EtCl	−90	2.27	0.44	185
$EtAlCl_2$	CH_3Cl 88%/hexane 12%	−80	2.15	1.03	186
$EtAlCl_2$	CH_3Cl 50%/hexane 50%	−80	1.90	1.05	186
$EtAlCl_2$	CH_3Cl 12%/hexane 88%	−80	1.17	1.08	186
$EtAlCl_2$	Hexane 100%	−80	0.80	1.28	186
$AlCl_3$	C_5/CH_2Cl_2	−70	1.56 ± 0.19	0.95 ± 0.17	187,188
$AlCl_3$	CH_3Cl	−80	1.6		189

Copolymerization studies provide a very useful tool to assess the effect of polymerization medium, coinitiator, counteranion, and additives on polymerization kinetics. However, the interpretation of results is difficult because of the interrelationships between these parameters. For examples and details see Reference 164.

Controlled Carbocationic Polymerization

Traditionally, carbocationic polymerizations have been considered uncontrollable, owing to the high reactivity of the chain carriers. Similar to radical polymerization (qv), they were treated as random processes, governed by the statistical probability of side reactions such as chain transfer and termination, relative to propagation. Real control in polymerization processes was first achieved in anionic systems (see ANIONIC POLYMERIZATION). The term "living polymerization" was introduced by Szwarc (191), although controlled polymerizations without chain-breaking processes had been observed experimentally much earlier (18,192). Similar to the history of living anionic polymerization, living conditions in carbocationic systems had been achieved experimentally as early as 1974 (193,194), before systematic research had begun to be carried out into living carbocationic conditions. The breakthrough was the successful production of high molecular weight and nearly uniform polymers with controlled carbocationic polymerization, by Kennedy's group (19). Carbocationic polymerizations reportedly exhibiting living characteristics have been called "pseudocationic," "quasiliving," then "truly living." All of these provide control over the molecular weight of the polymer, defined as the ratio of converted monomer to initiator:

$$M_n(\text{g/mol}) = \Delta M(\text{g})/I(\text{mol}) \tag{19}$$

where ΔM is the amount of monomer converted into polymer, and I is the molar amount of initiator. According to Szwarc's classical definition, in living polymerizations M_n increases linearly with conversion, and in the case of instantaneous initiation, the polymers produced in a batch reactor will have a polydispersity

described by the Poisson distribution:

$$M_w/M_n = DP_w/DP_n = 1 + 1/DP_n \tag{20}$$

where M_n and DP_n, and M_w and DP_w are the number- and weight-average MW and DP, respectively. Under controlled conditions, nearly uniform polymers can be produced at sufficiently high MWs. Since the active centers do not enter into side reactions, their concentration remains constant and the monomer consumption rate will obey a linear first-order dependency. The early experimental examples of living carbocationic polymerizations were riddled with broad molecular weight distribution, and thus were not acknowledged to be controlled polymerizations. In fact, the achievement of carbocationic living polymerization was considered to be impossible, because of the inherently high reactivity of carbocations, which tend to enter into irreversible termination and chain-transfer reactions via β-proton expulsion (142). It was then recognized that the key to controlled carbocationic polymerization was the promotion of an equilibrium between dormant and active propagating chain ends and thereby providing sufficient time for synthetic manipulations. Importance of reversible termination in order to obtain control over the polymerization was first outlined by the original "quasiliving" concept (137) (eq. 21)

$$\begin{array}{ccc} P_n & \rightleftharpoons & P_n^* \\ \text{inactive} & & \text{active} \end{array}$$

$$P_n^* + M \Longrightarrow P_{n+1^*} \tag{21}$$

Remarkably, the same key concept applies in living radical polymerizations. It has been suggested that the term "temporary deactivation" is more appropriate than "reversible termination," to emphasize control (20).

In controlled carbocationic polymerizations the initiating systems are usually Lewis acids in conjunction with a carbocation source such as an alkyl, allyl, or aralkyl halide, ester, ether, or epoxide (18). The Lewis acid coinitiators reactivate or reinitiate the inactive polymer chain to produce the active growing carbocations. The existence of the dynamic equilibrium between dormant covalent and active ionic species in carbocationic polymerizations is now generally accepted. Ligand exchange and dynamic NMR studies supported the evidence of the involvement of ionic species even in polymerizations that were thought to proceed by a "pseudocationic" or "insertion" mechanism (18). The temporary deactivation also allows for MWD control. This concept was introduced by Puskas, and co-workers (195) and is valid for all polymerization systems with temporary deactivation. According to this treatment, MWD is governed by the run length l, which is defined as the average number of monomer units incorporated into the polymer chain during a productive ionization period:

$$DP_w/DP_n = 1 + l/DP_n \tag{22}$$

This general equation reduces to the Poisson distribution when $l = 1$. The magnitude of l will define the narrowness of the MWD. At sufficiently high MW, $l = 25$ still yields $DP_w/DP_n < 1.1$. The MWD criteria for living polymerizations

can then be defined as follows:

$$DP_w - DP_n = l = \text{constant} \tag{23}$$

Since the Poisson distribution is a subcase of the general definition of MWD for $l = 1$, Poisson or very narrow MWD does not seem to be necessary in the definition of living polymerization. Living (controlled) carbocationic polymerization can be viewed as a process where the most probable distribution of monomer incorporation during an active ionization period is superimposed on a Poisson distribution of the repeating events of ionization periods. Depending on the lifetime of the active cationic species, the run length l can be $l \gg 1$, resulting in broader MWD. For instance, at $l = 50$, and at $DP_n = 50$, the MWD will be $M_w/M_n = 2$. With increasing conversion, the MWD will get progressively narrower.

The temporary deactivation process seems to protect the active species from side reactions long enough for synthetic manipulation. It is understood that chain-breaking processes might be identified in polymerizations, which are considered living today (20). The real power of controlled polymerizations in general, and controlled carbocationic polymerizations in particular, is their ability to control the polymerization process in order to design and build new polymeric structures. Since certain monomers can only be polymerized via a carbocationic mechanism, the significance of controlled carbocationic polymerization is evident. Polyisobutylene is a very important example—it has a fully saturated backbone with excellent stability and is thus a prime candidate for building model structures (Fig. 10) for systematic structure–property studies. Structure–property relationship studies are considered to be of critical importance. Hopefully, controlled carbocationic polymerization will make an important contribution in this area (196).

From an industrial point of view, controlled carbocationic polymerization has serious drawbacks. Except for block copolymer production, narrow MWD is a disadvantage, since broad distribution or polydispersity improves the physical properties and/or processability of commodity polymers (3). In controlled carbocationic polymerization, one initiator molecule produces only one polymer chain. Since the coinitiator, usually a Lewis acid such as $TiCl_4$ and BCl_3, is used in at least a tenfold excess over the initiator, the *catalyst efficiency*, a term used in industry to express the activity of the initiating system in terms of grams of polymer per grams of Lewis acid, is very poor in comparison with commercial processes (a few hundred vs several thousands). However, the ability of controlled carbocationic polymerization to produce new polymeric structures in a controlled manner may override these and other concerns. Anionic living polymerizations have long been commercialized, producing branched polybutadienes for high impact polystyrene production, styrene–isoprene–butadiene terpolymers and various functionalized

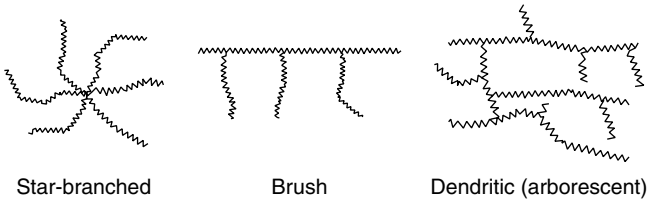

Fig. 10. Model polymer structures for structure–property relationship studies.

rubbers for tire production, and styrenic block copolymers (thermoplastic elastomers or recyclable rubbers). Under laboratory conditions, anionic polymerization is considered a difficult experimental technique (197). The relative newcomer, controlled carbocationic polymerization, is similarly viewed as a difficult-to-master method in the laboratory. In addition, it often is perceived to be inferior to living anionic polymerization. Ironically, large-scale commercial ionic polymerizations require less stringent conditions than laboratory procedures, because of the much smaller surface area-to-volume ratios. Commercial examples of controlled carbocationic polymerizations include poly(vinyl ethers) used in liquid-crystal technology (198), polystyrene–polyisobutylene–polystyrene block copolymers and functionalized polyisobutylenes, which have been test-marketed recently by Kuraray and Kaneka Co. of Japan (19). Several reviews provide detailed description of controlled carbocationic polymerization (18–20,199–201). It should be mentioned here that controlled polymerization of *p*-hydroxy styrene was also achieved in aquoeus media (202). This may prove to be a revolutionary breakthrough in controlled carbocationic polymerization.

Industrial Carbocationic Processes

There are relatively few surveys available on industrial carbocationic polymerization (1,2,203,204). In this section, the most important commercial polymers produced by carbocationic polymerization will be discussed.

Polyisobutylene. The polymerization of isobutylene by strong acids at room temperature was first reported in 1873 (12). The reaction yielded a "sticky liquid" (mainly dimers and trimers). In 1929, Otto at I.G. Farbenindustrie discovered that high molecular weight polymer could be prepared by cooling the reaction mixture with dry ice (205). Presently low, medium, and high molecular weight polyisobutylenes are produced commercially, with significantly more volume for the former two (see BUTYL RUBBER). The unique properties of polyisobutylene are low permeability, good thermal and oxidative stability, ozone resistance, chemical resistance, high hysteresis (mechanical dampening), and tack. The BASF process to produce high molecular weight polyisobutylene was developed on the basis of Otto's pioneering work. In the original process a mixture of ethylene and isobutylene was sprayed on a moving belt along with a solution of BF_3 in ethylene (206); the reaction heat was removed by the evaporation of ethylene. The original ESSO process was developed by Standard Oil of New Jersey (now known as ExxonMobil) and used methyl chloride and $AlCl_3$ to produce high molecular weight polyisobutylenes (1). These processes most likely have been modified, although the fundamentals may be the same. The molecular weight of polyisobutylenes produced by these processes ranges from few hundred thousand to few hundred million. High molecular weight PIB is used as binder in sealing tapes. It is also used to modify asphalt to improve weathering and low temperature properties as well as toughness and abrasion resistance of the mix. Polyethylene and polypropylene modified with polyisobutylene display improved barrier, flex, and stress-cracking properties. Polyisobutylene compounded into natural rubber (NR) or styrene–butadiene rubber (SBR) improves aging, cut growth, flex, and stress-cracking properties. Low (few hundred) and medium (few thousand) molecular weight polyisobutylenes are produced at higher temperatures to reduce molecular weight. BASF uses a batch

process, polymerizing isobutylene in isobutane with the CH_3OH/BF_3 initiating system. Medium molecular weight is achieved by using higher purity isobutylene and lower temperatures (−25 to −40°C, compared to −10°C for low molecular weight polymer). Infineum (a joint venture between ExxonMobil and Shell) uses a continuous process in hexane, initiating the reaction with a suspension of $AlCl_3$ in hexane and regulating molecular weight with the process temperature (1,2). Low and medium molecular weight polyisobutylenes are used as viscosity modifiers, fuel and lubricating oil additives, tack improvers in adhesive formulations, and primary binders in caulking and sealing compounds. Blending them into waxes used for paper coating reduces the penetration of the wax into the paper, and improves moisture resistance. In lubrication the main advantage of polyisobutylene is that it decomposes without residues. In the mid 1990s Shell started to commercialize an amine-functionalized low molecular weight PIB as fuel/oil additive. Emulsification of sludge particles by functionalized PIB is an important aspect of this application.

Isobutylene-Based Elastomers. Butyl elastomer is a random copolymer of isobutylene and a small amount (0.7–2.2 mol%) of isoprene. The dominant form of the incorporated isoprene is 1,4-trans. This copolymer was the first example of low unsaturation elastomers. The starting point of the development of butyl rubber was a collaborative research effort carried out by Otto (I.G. Farbenindustrie) and Thomas (Standard Oil Development Co.) in 1933–1935. Thomas suggested the use of the $AlCl_3$/ethyl chloride polymerization system, instead of BF_3/ethylene. The goal was the production of elastomers that could be cured to yield cross-linked polyisobutylene-based rubbers. First butadiene was copolymerized with isobutylene to provide the necessary double bonds for curing sites. Later butadiene was replaced by isoprene because of its higher reactivity as a comonomer, and ethyl chloride was replaced by methyl chloride as diluent because of its higher stability (207,208). Currently the $AlCl_3$-coinitiated copolymerization of isobutylene with isoprene in methyl chloride is the basic technology for the production of butyl elastomers. The first butyl plants using this technology, located in Baytown and Baton Rouge, Louisiana, and Sarnia, Canada, were constructed as part of the Synthetic Rubber Procurement program during World War II. It is interesting to note that this was the second most important program next to the Manhattan Project. Although numerous incremental process improvements were reported since World War II, production of butyl rubber is still based on the original technology (3,4). Butyl rubber is produced in a continuous slurry process at low temperatures (−90 to −100°C) using methyl chloride as diluent and a solution of $AlCl_3$ dissolved in methyl chloride as the initiating system. Small amounts of water or HCl as cationogen sources are used to promote initiation. The reactor resembles a heat exchanger, with the slurry circulating inside the pipes that are cooled by boiling ethylene in the jacket. The product is separated from the diluent and unreacted monomers by coagulating it in hot water. More detailed information can be found in References 3,4, and 203. A solution process called the "Russian process" was developed in the former Soviet Union (209). Polymerization is carried out in isopentane at around −90°C, initiated with water/alkylaluminum chloride(s).

The most important physical properties of butyl rubber are essentially the same as those of poly-isobutylene; low permeability, good chemical and thermal stability due to the low unsaturation content, and high damping. Butyl elastomers

are cross-linked (cured) with sulphur to yield cross-linked rubbers. The most important application of butyl rubbers is tire inner tubes. Other applications include tank liners, vibration dampeners, protective clothing, tire curing bladders, railway pads, wire and cable coating, belting, hoses, and chewing gum base.

Halogenation of the isoprene enchainments in butyl elastomers yields halobutyl elastomers. Reaction of the isoprene units with elementary bromine or chlorine leads to the formation of allylic halide units along the chain—a substitution as opposed to addition across the double bonds. This leads to much faster curing, which permitted the development of tubeless tires, as adhesion of halobutyl to the rest of the tire could be achieved. Halobutyls are primarily used by the tire industry to form the inner liner of the "tubeless" tire. Other applications are similar to that of butyl. Chlorobutyl is also used in pharmaceutical stoppers.

Over the years additional polyisobutylene-based elastomers were developed and commercialized. Butyl partially cross-linked with divinyl benzene with a high gel content has high resistance to cold flow (creep), improved green strength (green strength refers to the ability of a yet uncured tire to keep its shape, which relates to the 300% modulus of the raw elastomer) and elasticity, and good recovery after deformation. These properties are especially important to prevent the sag and cold flow of caulking compounds, sealants, and adhesives (210). Unlike regular butyl, it can be cured by peroxides via the unreacted pendent vinyl groups of the divinylbenzene units. Star-branched butyls are produced by the addition of polystyrene–polybutadiene block copolymer to the reactor (211). A fraction of the growing chains grafts onto the block copolymer; the star-branched portion of the final product is about 10–15 wt%, with the rest of the chains being linear. This combination leads to improved green strength, coupled with enhanced processability.

It should be noted here that commercial high molecular weight isobutylene-based elastomers are characterized by the so-called Mooney viscosity, not by molecular weight or molecular-weight distribution. This standardized low shear viscosity measurement is used to grade all synthetic and natural elastomers and rubbers (212). Interestingly, this highly prevalent method in industry is rarely ever mentioned in textbooks or encyclopedias.

Polybutenes. Polybutenes are ill-defined copolymers of isobutylene with butenes (203). They are low molecular weight (M_n = 300–2000 g/mol), clear oily or viscous liquids, with 85–95% isobutylene content. They are produced by the carbocationic polymerization of C_4 refinery stream, using $AlCl_3$ or in some cases BF_3 as coinitiator, and impurities or purposefully added HCl or H_2O as initiators. The C_4 stream is a product of crude oil distillation, containing a mixture of C_4 hydrocarbons such as isobutylene, *cis*- and *trans*-2-butenes, 1-butene, and butane. Molecular weight is controlled by temperature (-10 to $+30^\circ$C) and initiator concentration. Intensive chain-transfer reactions result in exo and endo terminal double bonds. The exo double bond is more reactive and is preferred for further functionalization with, for example, maleic anhydride or phosphorous pentasulfide. The most important use of polybutenes is in the production of lubricating oil additives. Functionalized polybutanes improve wear resistance because of their ability to emulsify small metal particles.

Hydrocarbon Resins. Hydrocarbon resins are ill-defined, low molecular weight products of the carbocationic polymerization of aliphatic or aromatic mono and diolefins, ranging from viscous liquids to high melting point thermoplastics.

These resins are generally grouped into three main categories depending on the source of the raw material (1,203,204). The indene–coumarone resins are coal tar based. Aliphatic, aromatic, and dicyclopentadiene resins are made from distillate fractions of cracked petroleum. Polyterpene resins are produced using monomers isolated from turpentine oil (α- or β-pinene) or etheral oils of lemon, orange, mandarin, or caraway (*d,l*-limonene or dipentene and *d*-limonene).

Commercial production of the coal tar based indene–coumarone (benzofuran) resins started in the early 1900s, using sulphuric acid as initiator in the temperature range of -10 to $+50^{\circ}$C. The subsequent use of $AlCl_3$ and BF_3-based initiating systems resulted in a lighter-colored product. Polymerization is carried out in bulk or naphtha. The primary use of indene–coumarone resins is in adhesives, coatings, inks, and additives for the rubber industry. Starting from the mid-1900s, petroleum-based aromatic resins gradually replaced indene–coumarone resins. Petroleum-based resins consist of aliphatic, aromatic, and dicyclopentadiene-based polymers. Aliphatic resins are produced from C_5 feed stream, a mixture of isoprene, cyclopentadiene, and piperylene (1,2-pentadiene) along with various monoolefins. Cyclodienes lead to gel formation and they are removed before polymerization. Aromatic resins are produced from C_8–C_{10} petroleum distillate fraction (styrene, α–methylstyrene, vinyl toluenes, indene, methylindene, dicyclopentadiene, cyclopentadiene/methyl–cyclopentadiene dimer, and methyl–cyclopentadiene dimer). Petroleum-based resins are produced by carbocationic or thermally induced free-radical polymerization. In the case of dicyclopentadiene resins, free-radical polymerization is the dominant mode of synthesis. The most frequently used Lewis acid carbocationic initiators are $AlCl_3$ and BF_3. $AlCl_3$ leads to higher molecular weight products, but the loss of unsaturation via cyclization is more pronounced. Frequently the Lewis acid is complexed with ethers, phenols, or aldehydes to reduce reactivity, increase solubility, and alter product properties (molecular weight, molecular weight distribution, and chain structure).

Petroleum resins have excellent tack properties, so they are used to improve tack in hot-melt and pressure-sensitive adhesive formulations, floor coverings, sealants, caulks, mastics, and rubber compounds. They are also used in printing inks as binder and protective coatings, and in paints and varnishes to improve gloss and water resistance.

Water-white resins are a recent commercial development. They are made by the homo- or copolymerization of pure vinyl aromatic monomers such as styrene or alpha-methylstyrene. Polymerization is carried out in aromatic solvents using BF_3 or complexes of BF_3 at 15–40°C. A controlled amount of water is added in order to improve initiation efficiency. The molecular weight of the product is low as a result of the extensive chain transfer processes at this temperature. Water-white resins are used where color stability is important.

The production and application of polyterpene resins are very similar to those of petroleum-based resins (1,203,204).

Poly(vinyl ethers). Homopolymers of vinyl ethers are produced via carbocationic polymerization. Polymerization is carried out either in bulk or solution using BF_3 or its complexes, $AlCl_3$, or $SnCl_4$. Commercially important poly(vinyl ethers) are made of methyl, ethyl, isobutyl, and octadecyl vinyl ethers [$T_g = -34$, -42, -19, and 50°C (1)]. Depending on their glass-transition temperature and molecular weight, commercial poly(vinyl ethers) are viscous oils, tacky resins, or

elastomeric solids. Poly(vinyl ethers) are added to pressure-sensitive adhesives in order to increase tack. They are also used as viscosity improvers in lubricants or as plasticizers in elastomers and coatings.

BIBLIOGRAPHY

"Cationic Polymerization" in *EPST* 1st ed., Vol. 3, pp. 35–59, by A. M. Eastham, National Research Council of Canada; Suppl. Vol. 2, pp. 161–197, by P. Kubisa and S. Penczek, Polish Academy of Sciences; "Cationic Polymerization" in *EPSE* 2nd ed., vol. 2, pp. 729–814, by A. Gandini and H. Cheradame, Institut National Polytechnique de Grenoble (EFP).

1. J.-P. Vairon and N. Spassky, in K. Matyjaszewski, ed., *Cationic Polymerizations: Mechanisms, Synthesis, and Application* (Plastics Engineering 35), Marcel Dekker, Inc., New York, 1996, p. 683.
2. R. J. Pazur and H.-H. Greve, in J. E. Puskas, A. Michel, and S. Barghi, eds., *Ionic Polymerizations and Related Processes* (NATO Science Series, Series. E 359), Kluwer Academic Publishers, Boston, Mass., 1999, p. 13.
3. J. Duffy and J. E. Puskas, *Synthesis of Butyl Rubber by Cationic Polymerization, in Ullmann's Encyclopedia of Industrial Chemistry*, Vol. **A23**, 6th ed., Wiley-VCH, Weinheim, 1998, p. 51.
4. E. Kresge and H.-C. Wang, *Kirk-Othmer Encyclopedia of Chemical Technology*, 4th ed., Vol. **8**, Wiley-Interscience, New York, 1993, p. 934.
5. L. Pinchuk, I. J. Khan, J. B. Martin, and G. J. Wilson, *Sixth World Biomater. Congr. Trans.* 1452 (2001).
6. R. T. Morrison and R. N. Boyd, *Organic Chemistry*, 6th ed., Prentice Hall, Englewood Cliffs, N. J., 1992, p. 191.
7. G. A. Olah, in G. A. Olah, ed., *Friedel–Crafts and Related Reactions*, Vol. **1**, Wiley-Interscience, New York, 1963.
8. G. A. Olah, *J. Am. Chem. Soc.* **94**, 808 (1972).
9. B. R. Watson, *Chem. Assays (London)*, 5th ed., Vol. III, 1789.
10. M. Deville, *Ann. Chim. Phys.* **75**, 66 (1839).
11. M. Berthelot, *Bull. Soc. Chim. Fr.* **11**, 4 (1869).
12. V. Gorianov and A. Butlerov, *Ann.* **169**, 146 (1873).
13. W. H. Hunter and R. V. Yohe, *J. Am. Chem. Soc.*, **55**, 1248 (1933).
14. P. H. Plesch, in J. C. Robb and W. F. Peaker, eds., *Progress in High Polymers*, Vol. **2**, Hiffe Books, London, 1968, p. 137.
15. A. Gandini and H. Cheradame, *Adv. Polym. Sci.* **34/35**, 1 (1980).
16. A. G. Evans, D. Holden, P. Plesch, M. Polanyi, H. A. Skinner, and M. A. Weinberger, *Nature* **157**, 102 (1946); A. G. Evans, G. W. Meadows, and M. Polanyi, *Nature* **158**, 94 (1946); P. H. Plesch, M. Polanyi, and H. A. Skinner, *J. Chem. Soc.* 257 (1947).
17. J. E. Puskas, P. Antony, C. Paulo, J. Kwon, M. Kovar, P. Norton, and V. Altstädt, *Macromol. Mater. Eng.* **286**, 565–582 (2001).
18. J. E. Puskas and G. Kaszas, *Progr. Polym. Sci.* **25**, 403–452 (2000).
19. J. P. Kennedy, *J. Polym. Sci., Part A: Polym. Chem.* **37**, 2285–2293 (1999).
20. K. Matyjaszewski and M. Sawamoto, in K. Matyjaszewski, ed., *Cationic Polymerizations: Mechanisms, Synthesis, and Application* (Plastics Engineering 35), Marcel Dekker, Inc., New York., 1996, pp. 265–380.
21. H. Mayr, in K. Matyjaszewski, ed., *Cationic Polymerizations: Mechanisms, Synthesis, and Application* (Plastics Engineering 35), Marcel Dekker, Inc., New York, 1996, p. 51.
22. D. H. Aue and M. T. Bowers, in M. T. Bowers, ed., *Gas Phase Ion Chemistry*, Vol. **2**, Academic Press Inc., New York, 1979, Chapt. "9".

23. J. P. Dau-Schmidt, PhD thesis, Medizinische Universität zu Lübeck, 1992.
24. H. Mayr, in J. E. Puskas and co-workers, eds., *Ionic Polymerizations and Related Processes* (NATO Science Series Series E, 359), Kluwer Academic Publishers, Boston, Mass., 1999, p. 99.
25. H. Schimmel, A. R. Ofial, and H. Mayr, *Macromolecules* **35**, 5454 (2002).
26. A. Gandini and H. Cheradame, *Encyclopedia of Polymer Science and Engineering*, Vol. **2**, Wiley-Interscience, New York, 1985, p. 740.
27. J. P. Kennedy and E. Marechal, *Carbocationic Polymerization*, Wiley-Interscience, New York, 1982, pp. 31–55.
28. J. P. Kennedy, *Cationic Polymerization of Olefins: A Critical Inventory*, Wiley-Interscience, New York, 1975.
29. P. H. Plesch, in J. C. Robb and W. F. Peaker, eds., *Progress in High Polymers*, Vol. **2**, Hiffe Books, London, 1968, p. 157.
30. O. Nuyken and S. Pask, in W. J. Mijs, ed., *New Methods for Polymer Synthesis*, Plenum Press, New York, 1992, p. 111.
31. J. P. Kennedy and E. G. M. Tornquist, *Polymer Chemistry of Synthetic Elastomers*, Wiley-Interscience, New York, 1968, pp. 301–307, 409–413.
32. G. Kaszas and J. E. Puskas, *Polym. React. Eng.* **2**, 251 (1994).
33. H. C. Brown and H. L. Berneis, *J. Am. Chem. Soc.* **75**, 10 (1953).
34. H. Mayr, M. Roth, and R. Faust, *Macromolecules* **29**, 6110 (1996).
35. Ref. 27, pp. 83–158.
36. G. Sauvet and P. Sigwalt, in G. Allen and J. C. Bevington, eds., *Comprehensive Polymer Science*, Vol. **3**, Pergamon Press, Oxford, 1989, p. 579.
37. K. Matyjaszewski and C. Pugh, in K. Matyjaszewski, ed., *Cationic Polymerizations: Mechanisms, Synthesis, and Application* (Plastics Engineering 35), Marcel Dekker, Inc., New York, 1996, pp. 164–189.
38. J. P. Vairon, A. Rives, and C. Bunel, *Makromol. Chem., Macromol. Symp.* **60**, 97 (1992).
39. G. D. Jones, in P. H. Plesch ed., *The Chemistry of Cationic Polymerization*, Pergamon Press, New York, 1963, p. 542.
40. M. Sawamoto, J. Fujimori, and T. Higashimura, *Macromolecules* **20**, 916 (1987).
41. V. Korshak and N. N. Lebedev, *J. Gen. Chem. U.S.S.R.* **18**, 1766 (1948).
42. T. Mole and E. A. Jeffrey, *Organoaluminum Compounds*, Elsevier, Amsterdam, 1972.
43. H. Cheradame and co-workers, *Bull. Soc. Chim. Fr.* 849 (1970).
44. M. Marek and M. Chmelir, *J. Polym. Sci., Part C* **23**, 223 (1968).
45. A. Gandini and H. Cheradame, *Adv. Polym. Sci.* **34/35**, 99–124 (1980).
46. B. Köröskenyi and R. Faust, *J. Macromol. Sci., Pure Appl. Chem. A* **36**(4), 471 (1999).
47. J. A. Ledwith and D. C. Sherrington, *Polymer* **12**, 344 (1971).
48. P. Giusti and F. Abdruzzi, *J. Polym. Sci., Part C* **16**, 3797 (1958).
49. M. Miyamoto, M. Sawamoto, and T. Higashimura, *Macromolecules* **18**, 611 (1985).
50. D. P. N. Satchell and R. S. Satchell, *Chem. Rev.* **69**, 251 (1969)
51. P. H. Plesch, *Prog. React. Kinetics* **18**, 1 (1993).
52. H. Schlaad, Y. Kwon, L. Sipos, and R. Faust, *Macromolecules* **33**, 8225 (2000).
53. P. H. Plesch, *Macromolecules* **34**, 1143 (2001).
54. M. C. Baird, *Chem. Rev.* **100**, 1471 (2000).
55. U.S. Pat. Appl. 08/234,782 (1994), T. D. Shaffer (to Exxon Chemical Co.).
56. T. D. Shaffer, in R. Faust and T. D. Shaffer, eds., *Cationic Polymerization: Fundamentals and Applications* (ACS Symposium Series No. 665), American Chemical Society, Washington, D.C., 1997, p. 96.
57. U.S. Pats. 5,439,996 (1995) and 5,448,001 (1995), M. C. Baird (to Queen's University at Kingston).
58. R. Quyourm, Q. Wang, M. C. Baird, and D. J. Gillis, *J. Am. Chem. Soc.* **116**, 6435 (1994).

59. S. Jacob, Z. Pi, and J. P. Kennedy, *Polym. Bull.* **41**, 503 (1998).
60. Z. Pi, S. Jacob, and J. P. Kennedy in J. E. Puskas and co-workers, eds., *Ionic Polymerizations and Related Processes* (NATO Science Series, Series E, 359), Kluwer Academic Publishers, 1999, p. 1.
61. A. G. Carr, D. M. Dawson, and M. Bochmann, *Macromolecules* **31**, 3184 (1998).
62. U.S. Pat. Appl. 08/803,687 (1997), T. D. Shaffer and K. R. Squire (to Exxon Chemical Co.).
63. T. D. Shaffer, J. A. Canich, and K. R. Squire, *Macromolecules* **31**, 5145 (1998).
64. Ref. 28, pp. 130–133, 1975.
65. A. Gandini and H. Cheradame, *Encyclopedia of Polymer Science and Engineering*, Vol. **2**, John Wiley & Sons, Inc., New York, 1985, p. 739.
66. M. Marek and L. Toman, *J. Polym. Sci., Polym. Symp.* **42**, 339 (1973).
67. Ref. 27, p. 124.
68. J. V. Crivello, *J. Polym. Sci., Polym. Chem.* **37**, 4241 (1999).
69. Y. Yagci, A. Onen, and I. Reetz, *Macromol. Symp.* **174**, 255 (2001).
70. M. Born, *Z. Phys.* **1**, 45 (1920).
71. N. Bjerrum and E. Larsson, *Z. Phys. Chem.* **127**, 358 (1927).
72. K. J. Laidler and H. Eyring, *Ann. N.Y. Acad. Sci.* **39**, 303 (1940).
73. V. Gutmann, *The Donor–Acceptor Approach to Molecular Interactions*, Plenum Press, New York, 1978.
74. U. Mayer, V. Gutmann, and W. Gerger, *Monatsh. Chem.* **106**, 1235 (1975).
75. J. Puskas, G. Kaszas, J. P. Kennedy, and T. Kelen, *J. Macromol. Sci., Chem., Part A* **18**, 1353–1366 (1982/1983).
76. R. Schmid, *J. Solution Chem.* **12**(2), 135 (1983).
77. M. R. Clark and J. M. DeSimone, *Macromolecules* **28**, 912 (1995).
78. Gy. Deak, T. Pernecker, and J. P. Kennedy, *Macromol. Rep. A* **32**, 969, 979, (1995).
79. U.S. Pat. 5,543,479 (1996), W. Baade, R. Heinrich, G. Langstein, T. Mülder, and J. E. Puskas (to Bayer AG).
80. A. R. Mathieson, in P. Plesch, ed., *Chemistry of Cationic Polymerization*, McMillan, New York, 1963, p. 237.
81. R. Cotrel, G. Sauvet, J. P. Vairon, and P. Sigwalt, *Macromolecules* **9**, 931 (1976).
82. M. Villesange, G. Sauvet, J. P. Vairon, and P. Sigwalt, *J. Macromol. Sci., Chem., Part A* **11**, 391 (1977).
83. R. F. Storey and K. R. Choate Jr., *Macromolecules* **30**, 4799–806 (1997).
84. Zs. Fodor, Y. C. Bae, and R. Faust, *Macromolecules* **31**, 4439–46 (1998).
85. C. Paulo, J. E. Puskas, and S. Angepat, *Macromolecules* **33**, 4634 (2000).
86. B. Charleaux, A. Rives, J.-P. Vairon, and K. Matyjaszewski, *Macromolecules* **29**, 5777 (1996).
87. J. E. Puskas, M. G. Lazendörfer, and W. E. Pattern, *Polym. Bull.* **40**, 55 (1998).
88. R. F. Storey, A. B. Donnalley, and T. L. Maggio, *Macromolecules* **31**, 1523 (1998).
89. J. P. Vairon, B. Charleux, and M. Moreau, in J. E. Puskas, and co-workers, eds., *Ionic Polymerizations and Related Processes* (NATO Science Series, Series E, 359), Kluwer Academic Publishers, Boston, Mass., 1999, p. 177.
90. H. Mayr and A. Pock, *Chem. Ber.* **119**, 2473, 2497 (1986).
91. H. Mayr, M. Roth, and G. Lang, *Cationic polymerizations; Fundamentals and Applications* (ACS Symposium Series 665), 1997, Chapt. "3", pp. 25–40.
92. H. Mayr and M. Patz, *Angew. Chem.* **106**, 990 (1994); H. Mayr, and M. Patz, *Intl. Ed. Engl.* **33**, 938 (1994).
93. A. D. Ketley, *J. Polym. Sci., Polym. Lett.* **1**, 313 (1963).
94. K. Matyjaszewski and C. Pugh, in K. Matyjaszewski, ed., *Cationic Polymerizations: Mechanisms, Synthesis, and Application* (Plastics Engineering 35), Marcel Dekker, Inc., New York, 1996, pp. 189–225.

95. C. E. Schildknecht, S. T. Gross, H. R. Davidson, J. M. Lambert, and A. O. Zoss, *Ind. Eng. Chem.* **40**, 2104 (1948).
96. S. Okamura, T. Higashimura, and H. Yamamoto, *J. Polym. Sci.* **33**, 510 (1958).
97. C. E. Schildknecht, *Ind. Eng. Chem.* **50**, 1047 (1958).
98. C. E. H. Bawn and A. Ledwith, *Q. Rev.* **16**, 361 (1962).
99. N. G. Gaylord and H. F. Mark, *Linear and Stereoregular Addition Polymers*, Interscience, New York, 1959.
100. H. Z. Friedlander and W. M. Thomas *J. Polym. Sci.* **31**, 215 (1958).
101. M. Villensange, A. Rives, C. Bunel, J. P. Vairon, M. Froeyen, M. V. Beylen, and A. Persoons, *Makromol. Chem., Macromol. Symp.* **47**, 271 (1991).
102. J. P. Vairon, A. Rives, and C. Bunel, *Makromol. Chem., Macromol. Symp.* **60**, 97 (1992).
103. M. Sawamoto, A. Furukawa, and T. Higashimura, *Macromolecules* **16**, 518 (1983).
104. S. Penczek, P. Kubisa, K. Brzezinska, and M. Basko, *Polym. Prepr.* **34**, 812 (1993).
105. W. O. Choi, M. Sawamoto, and T. Higashimura, *J. Polym. Chem., Chem. Ed.* **28**, 2923, 2937 (1990).
106. K. Matyjaszewski, *Macromolecules* **21**, 933 (1988).
107. D. P. Kelly and R. J. Spear, *Austr. J. Chem.* **31**, 1209 (1978).
108. T. Higashimura, T. Yonezawa, S. Okamura, and K. Fukui, *J. Polym. Sci.* **39**, 487 (1959).
109. D. J. Kram and K. J. Kopecki, *J. Am. Chem. Soc.* **81**, 2748 (1959).
110. F. Williams and R. B. Taylor, *J. Am. Chem. Soc.* **91**, 3728 (1969).
111. F. Williams, A. Shinkawa, and J. P. Kennedy, *J. Polym. Sci., Polym. Symp.* **56**, 421 (1976).
112. M. A. Bonin, W. A. Busler, and F. Williams, *J. Am. Chem. Soc.* **87**, 199 (1965).
113. F. Williams, K. Hayashi, K. Ueno, K. Hayashi, and S. Okamura, *Trans. Faraday Soc.* **63**, 1501 (1967).
114. M. C. C. Brendle and A. M. Ilvoas, *Br. Polym. J.* **1976**, 11 (1976).
115. K. Ueno, F. Williams, K. Hayashi, and S. Okamura, *Trans. Faraday Soc.* **63**, 1478 (1967).
116. Y. J. Chung, J. M. Rooney, D. R. Squire, and V. Stannet, *Polymer* **16**, 527 (1975).
117. V. Stannet, H. Garreau, C. C. Ma, J. M. Rooney, and D. R. Squire, *J. Polym. Sci., Polym. Symp.* **56**, 233 (1976).
118. K. Hayashi, K. Hayashi, and S. Okamura, *J. Polym. Sci., Part A1* **9**, 2305 (1971).
119. S. Winstein, E. Clippinger, A. H. Fainberg, R. Heck, and G. C. Robinson, *J. Am. Chem. Soc.* **78**, 328 (1956).
120. M. Szwarc, *Ionic Polymerization Fundamentals*, Hanser Publishers, Munich, 1996.
121. J. P. Lorimer and D. C. Pepper, *Proc. R. Soc., London, Ser. A* **351**, 551 (1976).
122. K. Matyjaszewski and C. Pugh, in K. Matyjaszewski, ed., *Cationic Polymerizations: Mechanisms, Synthesis, and Application* (Plastics Engineering 35), Marcel Dekker, Inc., New York, 1996, pp. 31.
123. A. Gandini and P. H. Plesch, *J. Chem. Soc.* **4765**, 4826 (1965).
124. P. H. Plesch, *Makromol Chem., Macromol Symp.* **13/14**, 393 (1988).
125. R. Faust and J. P. Kennedy, *J. Polym. Sci., Part A: Polym. Chem.* **25**, 1847 (1987).
126. K. Matyjaszewski, *J. Polym. Sci., Polym. Chem. Ed.* **25**, 765 (1987).
127. A. Williams, *Chem. Soc. Rev.* **23**, 93 (1994).
128. M. Szwarc, *Macromolecules* **28**, 7309 (1995).
129. D. C. Pepper, *Macromol. Chem.* **196**, 963 (1995).
130. G. Kaszas, J. Puskas, and J. P. Kennedy, *Makromol. Chem., Macromol. Symp.* **13/14**, 473 (1988).
131. G. Kaszas, J. E. Puskas, C. C. Chen, and J. P. Kennedy, *Macromolecules* **23**, 3909 (1990).
132. J. P. Kennedy, *Encyclopedia of Polymer Science and Technology*, Vol **7**, Wiley-Interscience, New York, 1967, p. 754.

133. Ref. 28, pp. 154–204.
134. N. G. Gaylord and M. Sveska, *J. Polym. Sci., Part B* **7**, 55 (1969).
135. M. Stolka, J. Vodenhal, and I. Kossler, *J. Polym. Sci., Part A* **2**, 3987 (1964).
136. J. E. Puskas, G. Kaszas, and J. P. Kennedy, *J. Macromol. Sci. Chem., Part A* **28**(1), 65 (1991).
137. J. P. Kennedy, T. Kelen, and F. Tudos, *J. Macromol. Sci., Chem. Part A* **18**, 1189 (1982–83).
138. T. Higashimura, S. Aoshima, and M. Sawamoto, *Makromol. Chem., Macromol. Symp.* **13/14**, 457 (1988).
139. G. Kaszas, J. E. Puskas, J. P. Kennedy, and C. C. Chen, *J. Macromol. Sci., Chem., Part A* **26**, 1099 (1989).
140. J. E. Puskas and G. Kaszas, *Prog. Polym. Sci.* **25**, 412 (2000).
141. Ref. 27, p. 218.
142. D. C. Pepper, *J. Polym. Sci., Polym. Symp.* **50**, 51 (1975).
143. J. P. Kennedy, *J. Org. Chem., Part A* **3**, 532 (1970).
144. R. W. Lenz, *Organic Chemistry of Synthetic High Polymers*, Wiley-Interscience, New York, 1967, pp. 514–515.
145. J. J. Throssell, S. P. Good, M. Szwarc, and V. Stannett, *J. Am. Chem. Soc.* **78**, 1122 (1956).
146. A. Gandini and H. Cheradame, *Adv. in Polym. Sci.* **34/35**, 157–161 (1980).
147. Y. Wu, Y. Tan, and G. Wu, *Macromolecules* **35**, 3801 (2002).
148. Z. Zlamal and A. Kazda, *J. Polym. Sci., Part A1* **1**, 3199 (1963).
149. A. I. Nesmelov, and co-workers, *Polym. Sci. U.S.S.R.* **30**, 2085 (1988).
150. P. H. Plesch, *Macromol. Chem.* **175**, 1065 (1974).
151. J. P. Kennedy and P. D. Trivedi, *Adv. Polym. Sci.* **28**, 113 (1978).
152. T. L. Maggio and R. F. Storey, *Polym. Prepr.* **40**, 958 (1999).
153. K. Matyjaszewski and M. Sawamoto, in K. Matyjaszewski, ed., *Cationic Polymerizations: Mechanisms, Synthesis, and Application* (Plastics Engineering 35), Marcel Dekker, Inc., New York, 1996, p. 343.
154. M. F. Lappert, *J. Chem. Soc.* **542**, 817 (1961).
155. J. P. Kennedy, S. Y. Huang, and S. C. Feinberg, *J. Polym. Sci., Polym. Chem. Ed.* **15**, 2864 (1977).
156. K. Matyjaszewski, *Makromol. Chem., Macromol. Symp.* **13/14**, 433 (1988).
157. J. P. Kennedy, J. J. Elliott, and B. E. Hudson, *Makromol. Chem.* **79**, 109 (1964).
158. R. W. Lenz, *Organic Chemistry of Synthetic High Polymers*, Wiley-Interscience, New York, 1967, p. 483.
159. J. P. Kennedy and R. M. Thomas, *J. Polym. Sci.* **46**, 233 (1960); **49**, 189 (1961); **55**, 311 (1961); J. P. Kennedy, I. Kirshenbaum, R. M. Thomas, and D. C. Murray, *J. Polym. Sci., Part A: Polym. Chem.* **1**, 789 (1963).
160. J. P. Kennedy and R. G. Squires, *J. Macromol. Sci., Part A* **1**, 995 (1963).
161. U.S. Pat. 2,781,334 (1957), L. M. Welch, H. L. Wilson, and L. B. Turner (to Esso Research and Engineering Co.).
162. J. P. Kennedy, I. Majoros, and A. Nagy, *Adv. Polym. Sci.* **1**, 112 (1994).
163. H. Mayr, T. Bug, M. F. Gotta, N. Hering, B. Irrgang, B. Janker, B. Kempf, R. Loos, A. R. Ofial, G. Remennikov, and H. Schimmel, *J. Am. Chem. Soc.* **123**, 9500 (2001).
164. Ref. 27, pp. 305–393.
165. E. Marechal, C. Bit, and P. Sigwalt, *Bull. Soc. Chim. Fr.* **1966**, 3487 (1966).
166. Ph. Blin, C. Bunel, and E. Marechal, *J. Chem. Res.* **S 206**, M 2619 (1978).
167. K. Yamamoto and T. Higashimura, *J. Polym. Sci., Polym. Chem. Ed.* **14**, 2621 (1976).
168. F. Visse and E. Marechal, *Polymer.* **26**, 485 (1974).
169. C. G. Overberger, L. H. Around, D. H. Tanner, J. J. Taylor, and T. Alfrey Jr., *J. Am. Chem. Soc.* **74**, 4848 (1952)
170. A. V. Tobolsky and R. J. Boudreau, *J. Polym. Sci.* **51**, S53 (1961).

171. Y. Imanishi, T. Higashimura, and S. Okamura, *J. Macromol. Sci., Chem., Part A1* **3**, 2455 (1965).
172. K. Hasegawa and R. Asami, *Polym. J.* **8**, 276 (1976).
173. J. P. Kennedy and T. Chou., *Adv. Polym. Sci.* **21**, 1 (1976).
174. J. E. Puskas, G. Kaszas, J. P. Kennedy, T. Kelen, and F. Tudos, *J. Macromol. Sci., Chem., Part A* **18**, 1315 (1982/1983).
175. G. Kaszas, M. Gyor, J. P. Kennedy, T. Kelen, and F. Tudos, *J. Macromol. Sci. Chem., Part A* **18**, 1367 (1982/1983).
176. R. Asami, K. Hasegawa, N. Asai, I. Moribe, and A. Doi, *Polym. J.* **8**, 74 (1976).
177. K. F. O'Driscoll, *J. Macromol. Sci., Chem.* **A3**, 307 (1969).
178. Ref. 27, pp. 349–357.
179. Ref. 27, pp. 381–386.
180. W. S. Richardson, *J. Polym. Sci.* **31**, 25 (1958).
181. U.S. Pat. 2,356,128 (1944), R. M. Thomas and W. J. Sparks (to Jasco Inc.).
182. J. P. Kennedy and N. H. Canter, *J. Polym. Sci., Part A1* **5**, 2455 (1967).
183. S. Cesca, P. Giusti, P. L. Magagnini, and A. Priola, *Makromol. Chem.* **176**, 2319 (1975).
184. S. Cesca, A. Priola, M. Bruzzone, G. Ferraris, and P. Giusti, *Makromol. Chem.* **176**, 2339 (1975).
185. J. Bandrupt and E. Immergut, eds., *Polymer Handbook*, 2nd ed., John Wiley & Sons, Inc., New York, 1975, p. II–224.
186. W. A. Thaler and J. D. Buckley Jr., *Rubber Chem. Technol.* **49**, 960 (1976).
187. C. Corno, A. Priola, G. Spallanzani, and S. Cesca, *Macromolecules* **17**, 37 (1984).
188. J. P. Kennedy and I. Krishenbaum, in E. C. Leonard, ed., *Vinyl and Diene Monomers, Part 2*, Wiley-Interscience, New York, 1971, Chapt. 3, p. 691.
189. J. E. Puskas, M. Verhelst, P. Collart, and J. B. Schmidt, *Kautsch. Gummi, Kunstst.* **48**, 866 (1995).
190. G. Kaszas, J. E. Puskas, and J. P. Kennedy, *Macromolecules* **25**, 1775–1779 (1992).
191. M. Szwarc, *Nature* **178**, 1168 (1956).
192. M. Szwarc and M. van Beylen, *Ionic Polymerization and Living Polymers*, Chapman and Hall, New York, 1993.
193. D. C. Pepper, *Makromol. Chem.* **175**, 1077 (1974).
194. A. F. Johnson and R. N. Young, *J. Polym. Sci., Polym Symp.* **56**, 211 (1976).
195. J. E. Puskas, G. Kaszas, and M. Litt, *Macromolecules* **24**, 5278 (1991).
196. C. G. Robertson, C. M. Roland, and J. E. Puskas, *J. Rheol.* **46**, 307–321 (2002); C. M. Roland, C. G. Robertson, C. Paulo, and J. E. Puskas, *J. Rheol.* **45**, 759–772 (2001); P. G. Santangelo, C. M. Roland, and J. E. Puskas, *Macromolecules* **32**, 1972–1977 (1999); C. Paulo and V. Altstädt, *Rubber Chem. Technol.* **75**, 853–863 (2002).
197. E. E. Malmstrom and C. J. Hawker, *Macromol. Chem. Phys.* **199**, 923 (1998).
198. V. Percec and D. Tomazos, *Adv. Mater.* **4**, 548 (1992).
199. M. Sawamoto, in K. Matyjaszewski, ed., *Cationic Polymerizations: Mechanisms, Synthesis, and Application* (Plastics Engineering 35), Marcel Dekker, Inc., New York, 1996, pp. 381–436.
200. J. E. Puskas and G. Kaszas, *Rubber Chem. Technol.* **69**, 462–475 (1996).
201. J. P. Kennedy and B. Ivan, *Designed Polymers by Carbocationic Macromolecular Engineering: Theory and Practice*, Hanser, Munchen, 1992.
202. K. Satoh, M. Kamigaito, and M. Sawamoto, *Polym. Prepr.* **40**, 895–896 (1999).
203. Ref. 27, pp. 464–503.
204. M. J. Zohuriaan-Mehr and H. Omidian, *J. Macromol. Sci., Rev. Macromol. Chem. Phys.* **C40**(1), 23–49 (2000).
205. U.S. Pat. 2,084,501 (1937), M. Otto and M. Mueller-Cunradi (to I. G. Farbenindustrie).
206. K. S. Whiteley, T. G. Heggs, H. Koch, R. L. Mawer and W. Immel, *Ullman's Encyclopedia of Industrial Chemistry*, 5th ed., Vol. A21, VCH Publishers, Weinheim, 1992, p. 555.

207. R. M. Thomas, *Rubber Chem. Technol.* **42**, G90 (1969).
208. Ref. 28, p. 11.
209. CA 1,019,095 (1973), N. V. Scherbakova and co-workers.
210. J. Walker, G. J. Wilson, and K. J. Kumbhani, *J. Inst. Rubber Ind*, 1 (Apr., 1974).
211. U.S. Pat. 5,071,913 (1991), K. W. Powers, H.-C. Wang, D. C. Handy, and J. V. Fusco (to Esso Research and Engineering Co.).
212. M. Morton, ed., *Rubber Technology*, 2nd ed., Van Nostrand Reinhold Co., New York, 1973, p. 92.

JUDIT E. PUSKAS
The University of Western Ontario
GABOR KASZAS
Rubber Division, Bayer Inc.

CARBOHYDRATE POLYMERS.

See Volume 9.

CELLULAR MATERIALS

Introduction

Cellular polymers, otherwise known as foamed polymers or polymeric foams, or expanded plastics, have been important to human life since primitive people began to use wood, a cellular form of the polymer cellulose. Cellulose (qv) is the most abundant of all naturally occurring organic compounds, comprising approximately one-third of all vegetable matter in the world (1). Its name is derived from the Latin word *cellula*, meaning very small cell or room, and most of the polymer does indeed exist in cellular form, as in wood, straws, seed husks, etc. The high strength-to-weight ratio of wood, good insulating properties of cork and balsa, and cushioning properties of cork and straw have contributed both to the incentive to develop and to the background knowledge necessary for development of the broad range of cellular synthetic polymers in use.

The first cellular synthetic plastic was an unwanted cellular phenol–formaldehyde resin produced by early workers in this field. The elimination of cell formation in these resins, as given by Baekeland in his 1909 heat and pressure patent (2), is generally considered the birth of the plastics industry. The first commercial cellular polymer was sponge rubber, introduced between 1910 and 1920 (3). Most plastic polymers can be foamed. However, a relative few have commercial significance, such as polystyrene, polyolefins, poly(vinyl chloride), polyimides, and polyurethanes.

Cellular polymers have been commercially accepted in a wide variety of applications since the 1940s (4–13). The total usage of foamed plastics in the United States has risen from 1.4×10^6 t in 1982 to 2.2×10^6 t in 1992 and has been projected to rise to about 3.1×10^6 t in 2002 (14).

Encyclopedia of Polymer Science and Technology. Copyright John Wiley & Sons, Inc. All rights reserved.

Classification

A cellular plastic has been defined as a plastic of which the apparent density is decreased substantially by the presence of numerous cells dispersed throughout its mass (15). In this article the terms *cellular plastic*, *foamed plastic*, *expanded plastic*, and *plastic foam* are used interchangeably to denote all two-phase gas–solid systems in which the solid is continuous and composed of a synthetic or natural polymer.

The gas phase in a cellular polymer is distributed in voids, pores, or pockets called cells. If these cells are interconnected in such a manner that gas can pass from one to another, the material is termed *open-celled*. If the cells are discrete and the gas phase of each is independent of that of the other cells, the material is termed *closed-celled*.

The nomenclature of cellular polymers is not standardized; classifications have been made according to the properties of the base polymer (16), the methods of manufacture, the cellular structure, or some combination of these. The most comprehensive classification of cellular plastics, proposed in 1958 (17), has not been adopted and is not consistent with some of the common names for the more important commercial products.

One ASTM test procedure has suggested (18) that foamed plastics be classified as either rigid or flexible, a flexible foam being one that does not rupture when a $20 \times 2.5 \times 2.5$-cm piece is wrapped around a 2.5-cm mandrel at a uniform rate of 1 lap per 5 s at 15–25°C. Rigid foams are those that do rupture under this test. This classification is used in this article.

In the case of cellular rubber, the ASTM uses several classifications based on the method of manufacture (19,20). These terms are used here. Cellular rubber is a general term covering all cellular materials that have an elastomer as the polymer phase. Sponge rubber and expanded rubber are cellular rubbers produced by expanding bulk rubber stocks and are open-celled and closed-celled, respectively. Latex foam rubber, also a cellular rubber, is produced by frothing a rubber latex or liquid rubber, gelling the frothed latex, and then vulcanizing it in the expanded state.

The term structural foam has been defined as flexible or rigid foams produced at greater than about 320 kg/m^3 density having holes in a foamed core rather than a typical lower density structure of pentagonal dodecahedron type (21). Integral foams are also structural foams having a foamed core that gradually decreases in void content to solid skins (22).

Theory of the Expansion Process

Foamed plastics can be prepared by a variety of methods. The most important process, by far, consists of expanding a fluid polymer phase to a low density cellular state and then preserving this state. This is the foaming or expanding process. Other methods of producing the cellular state include leaching out solid or liquid materials that have been dispersed in a polymer, sintering small particles, and dispersing small cellular particles in a polymer. The latter processes are relatively straightforward processing techniques but are of minor importance.

The expansion process consists of three steps: creating small discontinuities or cells in a fluid or plastic phase; causing these cells to grow to a desired volume; and stabilizing this cellular structure by physical or chemical means.

Initiation and Growth of Cells. The initiation or nucleation of cells is the formation of cells of such size that they are capable of growth under the given conditions of foam expansion. The growth of a hole or cell in a fluid medium at equilibrium is controlled by the pressure difference (ΔP) between the inside and the outside of the cell, the interfacial surface tension (γ), and the radius r of the cell:

$$\Delta P = 2\frac{\gamma}{r} \tag{1}$$

The pressure outside the cell is the pressure imposed on the fluid surface by its surroundings. The pressure inside the cell is the pressure generated by the blowing agent dispersed or dissolved in the fluid. If blowing pressures are low, the radii of initiating cells must be large. The hole that acts as an initiating site can be filled with either a gas or a solid that breaks the fluid surface and thus enables the blowing agent to surround it (23–26).

During the time of cell growth in a foam, a number of properties of the system change greatly. Cell growth can, therefore, be treated only qualitatively. The following considerations are of primary importance: (*1*) the fluid viscosity is changing considerably, influencing both the cell growth rate and the flow of polymer to intersections from cell walls, leading to collapse; (*2*) the pressure of the blowing agent decreases, falling off less rapidly than an inverse volume relationship because new blowing agent diffuses into the cells as the pressure falls off according to equation 1; (*3*) the rate of growth of the cell depends on the viscoelastic nature of the polymer phase, the blowing agent pressure, the external pressure on the foam, and the permeation rate of blowing agent through the polymer phase; and (*4*) the pressure in a cell of small radius r_2 is greater than that in a cell of larger radius r_1. There is thus a tendency to equalize these pressures either by breaking the wall separating the cells or by diffusion of the blowing agent from the small to the larger cells. The pressure difference ΔP between cells of radii r_1 and r_2 is shown in equation 2.

$$\Delta P = 2\gamma\left(\frac{1}{r_2} - \frac{1}{r_1}\right) \tag{2}$$

Stabilization of the Cellular State. The increase in surface area corresponding to the formation of many cells in the plastic phase is accompanied by an increase in the free energy of the system; hence the foamed state is inherently unstable. Methods of stabilizing this foamed state can be classified as chemical, eg, the polymerization of a fluid resin into a three-dimensional thermoset polymer, or physical, eg, the cooling of an expanded thermoplastic polymer to a temperature below its second-order transition temperature or its crystalline melting point to prevent polymer flow.

Chemical Stabilization. The chemistry of the system determines both the rate at which the polymer phase is formed and the rate at which it changes from a

viscous fluid to a dimensionally stable cross-linked polymer phase. It also governs the rate at which the blowing agent is activated, whether it is due to temperature rise or to insolubilization in the liquid phase.

The type and amount of blowing agent governs the amount of gas generated, the rate of generation, the pressure that can be developed to expand the polymer phase, and the amount of gas lost from the system relative to the amount retained in the cells.

Additives to the foaming system (cell growth-control agents) can greatly influence nucleation of foam cells, either through their effect on the surface tension of the system, or by acting as nucleating sites from which cells can grow. They can influence the mechanical stability of the final solid foam structure considerably by changing the physical properties of the plastic phase and by creating discontinuities in the plastic phase that allow the blowing agent to diffuse from the cells to the surroundings. Environmental factors such as temperature and pressure also influence the behavior of thermoset foaming systems.

Physical Stabilization. In physically stabilized foaming systems the factors are essentially the same as for chemically stabilized systems, but for somewhat different reasons. Chemical composition of the polymer phase determines the temperature at which foam must be produced, the type of blowing agent required, and the cooling rate of the foam necessary for dimensional stabilization. Blowing agent composition and concentration controls the rate at which gas is released, the amount of gas released, the pressure generated by the gas, escape or retention of gas from the foam cells for a given polymer, and heat absorption or release owing to blowing agent activation.

Additives have the same effect on thermoplastic foaming processes as on thermoset foaming processes. Environmental conditions are important in this case because of the necessity of removing heat from the foamed structure in order to stabilize it. The dimensions and size of the foamed structure are important for the same reason.

Manufacturing Processes

Cellular plastics and polymers have been prepared by a wide variety of processes involving many methods of cell initiation, growth, and stabilization. The most convenient method of classifying these methods appears to be based on the cell growth and stabilization processes. According to equation 1, the growth of the cell depends on the pressure difference between the inside of the cell and the surrounding medium. Such pressure differences may be generated by lowering the external pressure (decompression) or by increasing the internal pressure in the cells (pressure generation). Other methods of generating the cellular structure are by dispersing gas (or solid) in the fluid state and stabilizing this cellular state, or by sintering polymer particles in a structure that contains a gas phase.

Foamable compositions in which the pressure within the cells is increased relative to that of the surroundings have generally been called expandable formulations. Both chemical and physical processes are used to stabilize plastic foams from expandable formulations. There is no single name for the group of cellular plastics produced by the decompression processes. The various operations used to

Table 1. Methods for Production of Cellular Polymers

Type of polymer	Extrusion	Expandable formulation	Froth foam	Compression mold	Injection mold	Sintering
Cellulose acetate[a]	X					
Epoxy resin[b]		X	X			
Phenolic resin		X				
Polyethylene[a]	X	X		X	X	X
Polystyrene	X	X			X	X
Silicones		X				
Urea–formaldehyde resin			X			
Urethane polymers[b]		X	X		X	
Latex foam rubber			X			
Natural rubber	X	X		X		
Synthetic elastomers	X	X		X		
Poly(vinyl chloride)[a]	X	X	X	X	X	
Ebonite				X		
Polytetrafluoroethylene						X

[a]Also by leaching.
[b]Also by spray.

make cellular plastics by this principle are extrusion, injection molding, and compression molding. Either physical or chemical methods may be used to stabilize products of the decompression process.

A summary of the methods for commercially producing cellular polymers is presented in Table 1. This table includes only those methods thought to be commercially significant and is not inclusive of all methods known to produce cellular products from polymers.

Expandable Formulations.

Physical Stabilization Process. Cellular polystyrene [9003-53-6], the outstanding example, poly(vinyl chloride) [9002-86-2], copolymers of styrene and acrylonitrile (SAN copolymers [9003-54-7]), and polyethylene [9002-88-4] can be manufactured by this process.

Polystyrene. There are two types of expandable polystyrene processes: expandable polystyrene for molded articles and expandable polystyrene for loose-fill packing materials.

Expandable polystyrene for molded articles is available in a range of particle sizes from 0.2 to 3.0 mm, and in shapes varying from round beads to ground chunks of polymer. These particles are prepared either by heating polymer particles in the presence of a blowing agent and allowing the blowing agent to penetrate the particle (27) or by polymerizing the styrene monomer in the presence of blowing agent (28) so that the blowing agent is entrapped in the polymerized bead. Typical blowing agents used are the various isomeric pentanes and hexanes, and mixtures of these materials (29).

The fabrication of these expandable particles into a finished cellular-plastic article is generally carried out in two steps (30–33). First the particles are

expanded by means of steam, hot water, or hot air into low density replicas of the original material, called prefoamed or preexpanded beads. After proper aging, enough of these prefoamed beads are placed in a mold to just fill it; the filled mold is then exposed to steam. This second expansion of the beads causes them to flow into the spaces between beads and fuse together, forming an integral molded piece. Stabilization of the cellular structure is accomplished by cooling the molded article while it is still in the mold. The density of the cellular article can be adjusted by varying the density of the prefoamed particles.

Expandable polystyrene for loose-fill packaging materials is available in various sizes and shapes varying from round disks to S-shaped strands. These particles can be prepared either by deforming the polystyrene under heat and impregnating the resin with a blowing agent in an aqueous suspension (34) or by the extrusion method with various die orifice shapes (35). The expansion of these particles into a product is usually carried out in two or three expansions by means of steam with at least one day of aging in air after each expansion (36). Stabilization is accomplished by cooling the polymer phase below its glass-transition temperature during the expansion process.

Poly(vinyl chloride). Cellular poly(vinyl chloride) can be produced from several expandable formulations as well as by decompression techniques. Rigid or flexible products can be made depending on the amount and type of plasticizer used (37).

Polyethylene. Because polyethylene has a sharp melting point and its viscosity decreases rapidly over a narrow temperature range above the melting point, it is difficult to produce a low density polyethylene foam with nitrogen or chemical blowing agents because the foam collapses before it can be stabilized. This problem can be eliminated by cross-linking the resin before it is foamed, which slows the viscosity decrease above the melting point and allows the foam to be cooled without collapse of cell structure.

Cross-linking of polyethylene can be accomplished either chemically or by high energy radiation. Radiation cross-linking is usually accomplished by X-rays (38) or electrons (39,40). Chemical cross-linking of polyethylene is accomplished with dicumyl peroxide (41), di-*tert*-butyl peroxide (42), or other peroxides. Radiation cross-linking (43) is preferred for thin foams, and chemical cross-linking for the thicker foams.

Expandable polyethylene foam sheet can be made by a four-step process: (*1*) mixing of polyethylene, chemical blowing agent, and cross-linking agent (in the case of chemical cross-linking) at low or medium temperature [examples of decomposable blowing agents used for expandable polyethylene are azodicarbonamide, 4,4′-oxybis(benzenesulfonyl hydrazide), and dinitrosopentamethylene-tetramine] (29); (*2*) shaping at low or medium temperature; (*3*) chemical cross-linking at medium temperature or radiation cross-linking; and (*4*) heating and expanding at high temperature. Expansion of the cross-linked, expandable polyethylene sheet can be accomplished either by floating the sheet on the surface of a molten salt bath at 200–250°C and heating from above with IR heaters or by circulating hot air, or by expanding in the mold with high pressure steam.

Liquid Chemical Stabilization Processes. This method is more versatile and thus has been used successfully for more materials than the physical

stabilization process. Chemical stabilization is more adaptable for condensation polymers than for vinyl polymers because of the fast yet controllable curing reactions and the absence of atmospheric inhibition.

Polyurethane Foams. The most important commercial example of the chemical stabilization process is the production of polyurethane foams, which began in the mid-1950s. Depending on the choice of starting materials and processing techniques, it is possible to generate a wide variety of foams for such diverse uses as wood replacement in decorative cabinetwork or all-foam mattresses; to insulate portable coolers or for ultrasoft furniture cushions; as a sprayed-on insulating foam for pipes; or molded seat cushions for cars. Excellent summaries of the chemistry and technology of these polymers have been published (7,44,45) (see POLYURETHANES).

The urethane-forming ingredients in a polyurethane foam formulation are the isocyanate (**1**) and the polyol (**2**) as shown in equation 3.

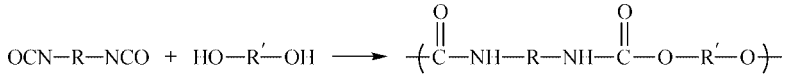

(3)

Another useful reaction is the reaction of water with isocyanate to generate CO_2 and urea groups that modify the polymeric structure. This vigorous reaction is also a prime source of exothermic heat to drive equation 3 to completion.

$$OCN{-}R{-}NCO + 2\ HOH \rightarrow NH_2{-}R{-}NH_2 + 2\ CO_2 \quad (4)$$

Further reaction of the active hydrogens on nitrogen in the urethane groups (**3**) can occur with additional isocyanate (**1**) at higher temperatures to cause formation of allophanate structures. The active hydrogens in urea groups can also react with additional isocyanate to form disubstituted ureas, which can still further react with isocyanate to form biurets (7).

The urethane-forming reaction (eq. 3) is known as the gelling reaction since it is the primary means of polymerizing the starting materials into long-chain polymer networks. The CO_2-forming reaction is known as the blowing reaction because of its contribution of CO_2 as an *in situ* blowing agent. The amount of blowing reaction is controlled by the water level of the formulation. The gelling and blowing reaction rates are determined by the catalyst choices. Typically, tertiary amines are used to foster the blowing reaction and organometallics are used to promote gellation although both contribute to both reactions. Urethane reactions often use a combination of catalysts to achieve the desired reactivity balance. Additional blowing may be obtained through the use of an auxiliary blowing agent such as methylene chloride, CFC-11, or HCFC-141b. On the basis of the Montreal protocol on climate change, the previous blowing agents are being phased out and the current blowing agents in use or under consideration include hydrocarbons such as isopentane, HFC-245fa, HFC-365mfc, and CO_2 (46).

Silicone surfactants are used to assist in controlling cell size and uniformity through reduced surface tension and, in some cases, to assist in the solubilization

of the various reactants (47,48). Recently, non-silicone lower cost surfactants for rigid polyurethane foams have been developed by Dow with the tradename Vorasurf and are based on copolymers of butylene oxide and ethylene oxide (49).

The foam process may be described as follows: the materials are metered in appropriate quantities into a mixing chamber and thoroughly mixed. Tiny air (or gas) bubbles are generated in the liquid to effect nucleation. After a short induction period the blowing agents begin to diffuse into and enlarge the tiny nucleation bubbles, causing a creamy appearance. The period from mixing to this point is known as the cream time, which is normally about 6–15 s for flexible foams. As more blowing agents are generated the foaming mixture continues to expand and becomes more viscous as the polymerization occurs in the liquid phase. The total number of bubbles remains constant during the foam rise. The reduction of surface tension by the surfactant stabilizes the tender foaming mixture to prevent coalescing of the bubbles.

About 100–200 s after mixing, the blowing reaction ceases but the gelling reaction continues, strengthening the struts of the foam, cells. The thin cell walls of a flexible foam then burst (blow-off) and the gases are released throughout the foam which has polymerized sufficiently to prevent collapse. The period from mixing to full rise (with blow-off in flexible foams) is known as rise time. The polymerization continues until the foam has gelled, usually 20–120 s after rise time. Loss of surface tackiness is known as tack free time. Rigid foams display a gel time prior to full rise. Additional cure time is necessary to achieve full polymer physical properties. This is a time–temperature characteristic that may vary from hours to days in duration.

The physical properties of the final foam can be varied broadly by controlling the degree of cross-linking in the final polymer as well as the structure of R and R′ in (**1**) and (**2**). The average molecular weight between cross-links is generally 400–700 for rigid polyurethane foams, 700–2500 for semirigid foams, and 2500–20000 for flexible foams (7). The structure of the diisocyanate is limited to some six or eight commercially available compounds (7). For this reason the variation between cross-links is controlled primarily by the polyol (**2**); it is common to use the equivalent weight (the ratio of molecular weight to hydroxyl units) as a criterion for the expected foam rigidity. The equivalent weights of polyhydroxy resins used for rigid foams are less than 300, for semirigids between 70 and 2000, and for flexibles between 500–3000.

Two general types of processes have been developed for producing polyurethanes on a commercial scale: the one-shot process and the prepolymer process. In the one-shot process, which is most widely used today, all primary streams (some of which may be premixed) are delivered to the foam mixing head at once for mixing and dispensing. In the prepolymer process the polyhydroxy component first reacts with isocyanate as shown in equation 5 to form an isocyanate-terminated molecule, which can ultimately react with water to liberate CO_2 for foaming and obtain chain linkage via the urea groups. Use of excess isocyanate results in the formulation of an isocyanate/polyol adduct, which contains a quantity of free isocyanate as well as a structured prepolymer. This adduct may be used as the source of isocyanate in a conventional system using additional polyol, catalysts, blowing agents, etc.

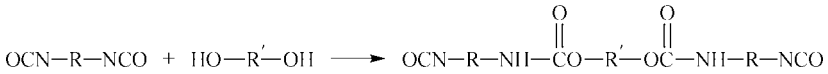

(5)

The foam-forming ingredients are carefully metered to obtain the proper ratio of reactants, thoroughly mixed by either mechanical or impingement means, then applied as a liquid, a spray, or a froth with subsequent expansion and curing.

Polyisocyanurates. The isocyanurate ring formed by the trimerization of isocyanates is known to possess high thermal and flammability resistance as well as low smoke generation during burning (50–53). Cross-linking via the high functionality of the isocyanurates produces a foam with inherent friability. Modification of the isocyanurate system with a longer chain structure such as that of polyether polyols or terephthalate-based polyester polyols increases the abrasion resistance of the resultant foam. Aluminum foil-faced sheets of modified isocyanurate-based foams are now widely used as an insulation material. The manufacturing process for isocyanurate foams is similar to that for rigid polyurethane foams (see ISOCYANATE-DERIVED POLYMERS).

Polyphenols. Another increasingly important example of the chemical stabilization process is the production of phenolic foams (54–57) by cross-linking polyphenols (resoles and novolacs) (see PHENOLIC RESINS). The principal features of phenolic foams are low flammability, solvent resistance, and excellent dimensional stability over a wide temperature range (54), so that they are good thermal-insulating materials.

Most phenolic foams are produced from resoles and acid catalyst; suitable water-soluble acid catalysts are mineral acids (such as hydrochloric acid or sulfuric acid) and aromatic sulfonic acids (58). Phenolic foams can be produced from novolacs but with more difficulty than from resoles (54). Novolacs are thermoplastic and require a source of methylene group to permit cure. This is usually supplied by hexamethylenetetramine (59).

A typical phenolic foam system consists of liquid phenolic resin, blowing agent, catalyst, surface-active agent, and modifiers. Various formulations and composite systems (60–62) can be used to improve one or more properties of the foam in specific applications, such as insulation properties (58,63–66), flammability (67–69), and open cell (70–73) quality.

Several manufacturing processes can be used to produce phenolic foams (54, 74): continuous production of free-rising foam for slabs and slab stock similar to that for polyurethane foam (65,75); foam-in-place batch process (56,76); sandwich paneling (58,77,78); and spraying (65,79).

Other Materials. Foams from epoxy resins (54,55,80,81), silicone resins (26,55,82,83), and polyimides (84,85) can also be formed by a chemical stabilization process. In certain applications such as aircraft, ships, and railway, specific properties such as high temperature performance and low smoke generation are demanded. As such foam attributed like high temperature resistance while maintaining strength in all directions, inherent fire resistance and chemical resistance are required. For many advanced structural composites, ROHACELL (trademark of Rohm, GmbH, Darmstadt, Germany) closed-cell rigid structural foam produced from polymethacrylimide (PMI) by cured foam molding process serves as core

material (85). Its chemistry allows the material to have self-extinguishing characteristics and service conditions at room temperature as well as in high temperature and high pressure.

Decompression Expansion Processes.

Physical Stabilization Process. Cellular polystyrene, cellulose acetate, polyolefins, and poly(vinyl chloride) can be manufactured by this process.

Polystyrene. The extrusion process for producing cellular polystyrene and copolymers of styrene is probably the oldest method utilizing physical stabilization in a decompression expansion process (86). A solution of blowing agent in molten polymer is formed in an extruder under pressure. This solution is forced out through an orifice onto a moving belt at ambient temperature and pressure. The blowing agent then vaporizes and causes the polymer to expand. The polymer simultaneously expands and cools under such conditions that it develops enough strength to maintain dimensional stability at the time corresponding to optimum expansion. The stabilization is due to cooling of the polymer phase to a temperature below its glass-transition temperature by the vaporization of the blowing agent, gas expansion, and heat loss to the environment. Polystyrene foams produced by the decompression process are commercially offered in the density range of 23–53 kg/m^3 (1.4–3.3 lb/ft^3) as well as at higher densities (87).

The extrusion of expandable polystyrene beads or pellets containing pentane blowing agent was originally used to produce low density foam sheet (88,89). The current method is to extrude polystyrene foam in a single-screw tandem line or twin-screw extruder and produce foam sheet by addition of pentane or fluorocarbon blowing agents into the extruder (90,91). For sheet thicknesses of less than 500 μm (20 mil), the blown-bubble method is normally used. This method involves blowing a tube from a round or annular die, collapsing the bubble, and then slitting the edges to obtain two flat sheets. For greater sheet thicknesses the sheet is pulled over a sizing mandrel and slit to obtain a flat sheet. Cooling of the expanded material by the external air is necessary to stabilize the foam sheet with a good skin quality.

Cellular polystyrene can also be produced by an injection-molding process. Polystyrene granules containing dissolved liquid or gaseous blowing agents are used as feed in a conventional injection-molding process (92). With close control of time and temperature in the mold and use of vented molds, high density cellular polystyrene moldings can be obtained.

Cellulose Acetate. The extrusion process has also been used to produce cellular cellulose acetate (93) in the density range of 96–112 kg/m^3 (6–7 lb/ft^3). A hot mixture of polymer, blowing agent, and nucleating agent is forced through an orifice into the atmosphere. It expands, cools, and is carried away on a moving belt.

Polyolefins. Cellular polyethylene, polypropylene, and their copolymers are prepared by both extrusion and molding processes. High density polyolefin foams in the density range of 320–800 kg/m^3 are prepared by mixing a decomposable blowing agent with the polymer and feeding the mixture under pressure through an extruder at a temperature such that the blowing agent is partially decomposed before it emerges from an orifice into a lower pressure zone. Simultaneous expansion and cooling take place, resulting in a stable cellular structure owing to rapid crystallization of the polymer, which increases the modulus of the polymer enough to prevent collapse of cell structure (23,33,94). This process is widely used

in wire coating and structural foam products. These products can also be produced by direct injection of inert gases into the extruder (95,96).

Low density polyethylene foam products (thin sheets, planks, rounds, tubes) in the range of 32–160 kg/m^3 (2–10 lb/ft^3) have been prepared by an extrusion technique using various gaseous fluorocarbon blowing agents (97,98). The techniques are similar to those described earlier for producing extruded polystyrene foam planks and foam sheets.

Thermoplastic Structural Foams. Structural foams having an integral skin, cellular core, and a high strength-to-weight ratio are formed by means of injection molding, extrusion, or casting, depending on product requirements (99,100,100). The two most widely used injection molding processes are the Union Carbide low pressure process (102) and the USM high pressure process (103).

In the low pressure process, a short shot of a resin containing a blowing agent is forced into the mold, where the expandable material is allowed to expand to fill the mold under pressures of 690–4140 kPa (100–600 psi). This process produces structural foam products with a characteristic surface swirl pattern produced by the collapse of cells on the surface of molded articles.

In the high pressure process, a resin melt containing a chemical blowing agent is injected into an expandable mold under high pressure. Foaming begins as the mold cavity expands. This process produces structural foam products with very smooth surfaces since the skin is formed before expansion takes place.

Extruded structural foams are produced with conventional extruders and a specially designed die. The die has an inner, fixed torpedo located at the center of its opening, which provides a hollow extrudate. The outer layer of the extrudate cools and solidifies to form solid skin; the remaining extrudate expands toward the interior of the profile. One of the most widely used commercial extrusion processes is the Celuka process developed by Ugine–Kuhlmann (104).

Large structural foam products are produced by casting expandable plastic pellets containing a chemical blowing agent in aluminum molds on a chain conveyor. After closing and clamping the mold, it is conveyed through a heating zone, where the pellets soften, expand, and fuse together to form the cellular products. The mold is then passed through a cooling zone. This process produces structural foam products with uniform, closed-celled structures but no solid skin.

Poly(vinyl chloride). Cellular poly(vinyl chloride) is prepared by many methods (105), some of which utilize decompression processes. Unlike the typical process used for thermoplastic resins where the melt is heated to a temperature considerably above its second-order transition temperature so the resin can flow, poly(vinyl chloride) requires the assistance of a plasticizer to fuse into a plastisol resin. This process is used because the poly(vinly chloride) resin is susceptible to thermal degradation.

The fusion of a dispersion of poly(vinyl chloride) resin in a plasticizer provides a unique type of physical stabilization process. The viscosity of a resin–plasticizer dispersion shows a sharp increase at the fusion temperature. In such a system expansion can take place at a temperature corresponding to the low viscosity; the temperature can then be raised to increase viscosity and stabilize the expanded state.

Extrusion processes have been used to produce high and low density flexible cellular poly(vinyl chloride). A decomposable blowing agent is usually blended

with the compound prior to extrusion. The compounded resin is then fed to an extruder where it is melted under pressure and forced out of an orifice into the atmosphere. After extrusion into the desired shape, the cellular material is cooled to stabilize it and is removed by a belt.

Another type of extrusion process involves the pressurization of a fluid plastisol at low temperatures with an inert gas. This mixture is subsequently extruded onto a belt or into molds, where it expands (106,107). The expanded dispersion is then heated to fuse it into a dimensionally stable form.

Injection molding of high density cellular poly(vinyl chloride) can be accomplished in a manner similar to extrusion except that the extrudate is fed for cooling into a mold rather than being maintained at the uniform extrusion cross-section.

Microcellular Foams. Two notable methods to produce microcellular foams include gas supersaturation in combination with an extrusion process developed by MIT/Trexel (108) and the continuous extrusion process by Dow (109). These processes promote a high level of nucleation, which can result in cell sizes as small as 5 μm.

Polymer Chemical Stabilization Processes. Cellular rubber and ebonite are produced by chemical stabilization processes. Most elastomers can be made into either open-celled or closed-celled materials. Natural rubber, SBR, nitrile rubber, polychloroprene, chlorosulfonated polyethylene, ethylene–propylene terpolymers, butyl rubbers, and polyacrylates have been successfully used (110–112).

Cellular Rubber. This material is an expanded elastomer produced by expansion of a rubber stock, whereas latex foam rubber is produced from a latex. The following general procedure applies to production of cellular rubbers from a variety of types of rubber (110). A decomposable blowing agent, along with vulcanizing systems and other additives, is compounded with the uncured elastomer at a temperature below the decomposition temperature of the blowing agent. When the uncured elastomer is heated in a forming mold, it undergoes a viscosity change, as shown in Figure 1. The blowing agent and vulcanizing systems are chosen to yield open-celled or closed-celled cellular rubber. Although inert gases such as nitrogen have been pressurized into rubber and the rubber then expanded upon release of pressure, the current cellular rubbers are made almost entirely with decomposable blowing agents as exemplified by sodium bicarbonate [144-55-8], 2,2′-azobisisobutyronitrile [78-67-1], azodicarbonamide [123-77-5],

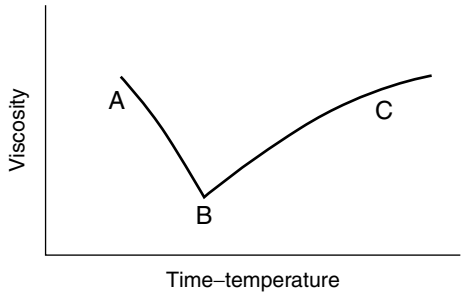

Fig. 1. Viscosity of cellular rubber stock during a production cycle (110).

4,4′-oxybis(benzenesulfonyl hydrazide) [80-51-3], and dinitrosopentamethylenetetramine [101-25-7]. The compound named is the most important commercial compound in its particular class.

To produce open-celled cellular rubber the blowing agent is decomposed just prior to point A in Figure 1 so that the gas is released at the point of minimum viscosity. As the polymer expands, the cell walls become thin and rupture; however, the connecting struts have developed enough strength to support the foam. This process is ordinarily carried out in one step inside a mold under pressure.

The timing for blowing agent decomposition is more critical in making closed-celled cellular rubber; it must occur soon enough after point A to cause expansion of the elastomer but far enough past point A to allow the cell walls to become strong enough not to rupture under the blowing stress. The expansion of closed-celled rubber is often carried out in two main steps: a partial cure is carried out in a mold that is a reduced-scale replica of the final mold; removed from this mold, it expands partly toward its final form. It is then placed in an oven to complete the expansion and cure.

A continuous extrusion process, as well as molding techniques, can be used as the thermoforming method. A more rapid rate of cure is then necessary to ensure the cure of the rubber before the cellular structure collapses. The stock is ordinarily extruded at a temperature high enough to produce some curing and expansion and then oven-heated to complete the expansion and cure.

A unique process for chemical stabilization of a cellular elastomer upon extrusion has been shown for ethylene–propylene rubber: the expanded rubber obtained by extrusion is exposed to high energy radiation to cross-link or vulcanize the rubber and give dimensional stability (113). EPDM is also made continuously through extrusion and a combination of hot air and microwaves or radio frequency waves, which both activate the blow and accelerate the cure.

Cellular Polyurethane. Polyurethane structural foam produced by reaction injection molding (RIM) is a rapidly growing product that provides industry with the design flexibility required for a wide range of applications. This process is more efficient than conventional methods in producing large-area, thin-wall, and load-bearing structural foam parts. In the RIM process, polyol and isocyanate liquid components are metered into a temperature-controlled mold that is filled 20–60%, depending on the density of structural foam parts (114). When the reaction mixture then expands to fill the mold cavity, it forms a component part with an integral, solid skin and a microcellular core. The quality of the structural part depends on precise metering, mixing, and injection of the reaction chemicals into the mold.

Cellular Ebonite. Cellular ebonite is the oldest rigid cellular plastic. It was produced in the early 1920s by a process similar to the processes described for making cellular rubber. The formulation of rubber and vulcanizing agent is changed to produce an ebonite rather than rubber matrix (115).

Dispersion Processes. In several techniques for producing cellular polymers, the gas cells are produced by dispersion of a gas or liquid in the polymer phase followed, when necessary, by stabilization of the dispersion and subsequent treatment of the stabilized dispersion. In frothing techniques, a quantity of gas is mechanically dispersed in the fluid polymer phase and stabilized. In another method, solid particles are dispersed in a fluid polymer phase, the dispersion

stabilized, and then the solid phase dissolved or leached, leaving the cellular polymer. Still another method relies on dispersing an already cellular solid phase in a fluid polymer and stabilizing this dispersion. This results directly in cellular polymers called syntactic foams.

Frothing. The frothing process for producing cellular polymers is the same process used for making meringue topping for pies. A gas is dispersed in a fluid that has surface properties suitable for producing a foam of transient stability. The foam is then permanently stabilized by chemical reaction. The fluid may be a homogeneous material, a solution, or a heterogeneous material.

Latex Foam Rubber. Latex foam rubber was the first cellular polymer to be produced by frothing. (*1*) A gas is dispersed in a suitable latex; (*2*) the rubber latex particles are caused to coalesce and form a continuous rubber phase in the water phase; (*3*) the aqueous soap film, breaks owing to deactivation of the surfactant in the water, breaking the latex film, and causing retraction into the connecting struts of the bubbles; (*4*) the expanded matrix is cured and dried to stabilize it.

The earliest frothing process developed was the Dunlop process, which made use of chemical gelling agents, eg, sodium fluorosilicate, to coagulate the rubber particles and deactivate the soaps. The Talalay process, developed later, employs freeze-coagulation of the rubber followed by deactivation of the soaps with carbon dioxide. The basic processes and a multitude of improvements are discussed extensively in Reference (3). A discussion more oriented to current use of these processes is given in Reference (116).

Latex rubber foams are generally prepared in slab or molded forms in the density range 64–128 kg/m^3 (4–8 lb/ft^3). Synthetic SBR latexes have replaced natural rubber latexes as the largest-volume raw material for latex foam rubber. Other elastomers used in significant quantities are polychloroprene, nitrile rubbers, and synthetic *cis*-polyisoprene (116).

One method (117) of producing cellular polymers from a variety of latexes uses primarily latexes of carboxylated styrene–butadiene copolymers, although other elastomers such as acrylic elastomers, nitrile rubber, and vinyl polymers can be employed.

Urea–Formaldehyde Resins. Cellular urea–formaldehyde resins can be prepared in the following manner: an aqueous solution containing surfactant and catalyst is made into a low density, fine-celled foam by dispersing air into it mechanically. A second aqueous solution consisting of partially cured urea–formaldehyde resin is then mixed into the foam by mechanical agitation. The catalyst in the initial foam causes the dispersed resin to cure in the cellular state. The resultant hardened foam is dried at elevated temperatures. Densities as low as 8 kg/m^3 can be obtained by this method (118).

Polyurethanes. Polyurethane foam systems have also been frothed using both low boiling dissolved materials and whipped-in air or other gas. Rigid polyurethane foam systems using a previously mixed polyol, surfactant, and catalyst system pressurized in a container with blowing agent are used for froth discharge into pour-in-place cavity filling (119). Flexible polyurethane foam is mechanically frothed by whipping dry gas such as air into the combined polyol and isocyanate. The thick, creamy froth is then doctored onto a carpet or textile back to form a variety of coatings ranging from a very thin unitary to a 1.8-cm-thick resilient foam (120).

Syntactic Cellular Polymers. Syntactic cellular polymer is produced by dispersing rigid, foamed, microscopic particles in a fluid polymer and then stabilizing the system. The particles are generally spheres or microballoons of phenolic resin, urea–formaldehyde resin, copolymers of vinylidene chloride and acrylonitrile (121), glass, or silica, ranging 30–120 μm diameter. Commercial microballoons have densities of approximately 144 kg/m^3 (9 lb/ft^3). The fluid polymers used are the usual coating resins, eg, epoxy resin, polyesters, and urea–formaldehyde resin.

The resin, catalyst, and microballoons are mixed to form a mortar, which is then cast into the desirable shape and cured. Very specialized electrical and mechanical properties may be obtained by this method but at higher cost. This method of producing cellular polymers is quite applicable to small-quantity, specialized applications because it requires very little special equipment.

In a variation on the usual methods for producing syntactic foams (122,123), expandable polystyrene or styrene–acrylonitrile copolymer particles (in either the unexpanded or prefoamed state) are mixed with a resin (or a resin containing a blowing agent) which has a large exotherm during curing. The mixture is then placed in a mold and the exotherm from the resin cure causes the expandable particles to foam and squeeze the resin or foamed matrix to the surface of the molding. A typical example is Voraspan, expandable polystyrene in a flexible polyurethane foam matrix (124). These foams are finding acceptance in cushioning applications for bedding and furniture.

Other Processes. Some plastics cannot be obtained in a low viscosity melt or solution that can be processed into a cellular state. For these cases two methods have been used to achieve the needed dispersion of gas in solid: sintering of solid plastic particles and leaching of soluble inclusions from the solid plastic phase.

Sintering has been used to produce a porous polytetrafluoroethylene (10). Cellulose sponges are the most familiar cellular polymers produced by the leaching process (125). Sodium sulfate crystals are dispersed in the viscose syrup and subsequently leached out. Polyethylene (126) or poly(vinyl chloride) can also be produced in cellular form by the leaching process. The artificial leather-like materials used for shoe uppers are rendered porous by extraction of salts (127) or by designing the polymers in such a way that they precipitate as a gel, with many holes (128).

Phase Separation. Microporous polymer systems consisting of essentially spherical, interconnected voids, with a narrow range of pore and cell-size distribution have been produced from a variety of thermoplastic resins by the phase-separation technique (129). If a polyolefin or polystyrene is insoluble in a solvent at low temperature but soluble at high temperatures, the solvent can be used to prepare a microporous polymer. When the solutions, containing 10–70% polymer, are cooled to ambient temperatures, the polymer separates as a second phase. The remaining nonsolvent can then be extracted from the solid material with common organic solvents. These microporous polymers may be useful in microfiltrations or as controlled-release carriers for a variety of chemicals.

A recent aproach to microporous foams involves the polymerization of high internal-phase water in oil emulsions (130). These flexible, hydrophilic open-celled foams are suitable for absorption of aqueous fluids and are being

considered as a replacement for the absorbent cores in absorbent articles such as diapers.

Properties of Cellular Polymers

The mechanical properties of rigid foams vary considerably from those of flexible foams. The tests used to characterize these two classes of foams are, therefore, quite different, and the properties of interest from an application standpoint are also quite different. In this discussion the ASTM definition of rigid and flexible foams given earlier is used.

Several countries have developed their own standard test methods for cellular plastics, and the International Organization for Standards (ISO) Technical Committee on Plastics TC-61 has been developing international standards. Information concerning the test methods for any particular country or the ISO procedures can be obtained in the United States from the American National Standards Institute. The most complete set of test procedures for cellular plastics, and the most used of any in the world, is that developed by the ASTM; these procedures are published in new editions each year (131). There have been several reviews of ASTM methods and others pertinent to cellular plastics (26,54,132–134).

The properties of commercial rigid foamed plastics are presented in Table 2. The properties of commercial flexible foamed plastics are presented in Table 3. The definition of a flexible foamed plastic is that recommended by the ASTM Committee D 11. The data shown demonstrate the broad ranges of properties of commercial products rather than an accurate set of properties on a specific few materials. Specific producers of foamed plastics should be consulted for properties on a particular product (139–141,149–152).

The properties that are achieved in commercial structural foams (density $>$ 0.3 g/cm^3) are shown in Table 4. Because these values depend on several structural and process variables, they can be used only as general guidelines of mechanical properties from these products. A good engineering guide has been published (100).

Structural Variables. The properties of a foamed plastic can be related to several variables of composition and geometry often referred to as structural variables.

Polymer Composition. The properties of foamed plastics are influenced both by the foam structure and, to a greater extent, by the properties of the parent polymer. The polymer phase description must include the additives present in that phase as well. The condition or state of the polymer phase (orientation, crystallinity, previous thermal history), as well as its chemical composition, determines the properties of that phase. The polymer state and cell geometry are intimately related because they are determined by common forces exerted during the expansion and stabilization of the foam.

Density. Density is the most important variable in determining mechanical properties of a foamed plastic of given composition. Its effect has been recognized since foamed plastics were first made and has been extensively studied.

Cell Structure. A complete knowledge of the cell structure of a cellular polymer requires a definition of its cell sizes, cell shapes, and the location of each cell in the foam.

Table 2. Physical Properties of Commercial Rigid Foamed Plastics[a]

	ASTM test	Cellulose acetate[b]		Polystyrene									Polyurethane			
															Isocyanurate	
Property	Phenolic[c]			Extruded plank[b,d]			Expanded plank[e,f]		Extruded sheet		PVC[g]		Polyether[h]		Bun[g]	Laminate[i]
Density, kg/m[j]		96–128	32–64	35	53	16	32	80	96	160	32	64	32–48	64–128	32	32.000
Mechanical properties																
Compressive strength, kPa[k] at 10%	D1621	862	138–620	310	862	90–124	207–276	586–896	290	469	345	1035	138–344	482–1896	210	117–206
Tensile strength, kPa[k]	D1623	1172	138–379	517		145–193	310–379	1020–1186	2070–3450	4137–6900	551	1207	138–482	620–2000	250	248–290
Flexural strength, kPa[k]	D790	1014	172–448	1138		193–241	379–517				586	1620	413–689	1380–2400		
Shear strength, kPa[k]	C273	965	103–207	241			241				241	793	138–207	413–896	180	117.000
Compression modulus, MPa[l]	D1621	38–90		10.3			3.4–14				13.1	35	2.0–4.1	10.3–31		
Flexural modulus, MPa[l]	D790	38		41			9.0–26				10.3	36	5.5–6.2	5.5–10.3		
Shear modulus, MPa[l]	C273		2.8–4.8	10.3			7.6–11.0				6.2	21	1.2–1.4	3.4–10.3		1.700
Thermal properties																
Thermal conductivity, W/(m·I)	C177	0.045–0.046	0.029–0.032	0.030		0.037	0.035	0.035	0.035	0.035	0.023		0.016–0.025	0.022–0.030	0.054	0.019
Coefficient of linear expansion, 10^{-5}/°C	D696		0.9	6.3	6.3	5.4–7.2	5.4–7.2	5.4–7.2					5.4–7.2	7.2	7.2	
Max service temperature, °C		177	132	74		74–80	74–80	74–80	77–80	80			93–121	121–149	149	149.000
Specific heat, kJ/(kg·K)[m]	C351			1.1									ca 0.9	ca 0.9	ca 0.9	
Electrical properties																
Dielectric constant	D1673	1.12	1.19–1.20	< 1.05	< 1.05	1.02	1.02	1.02	1.27000	1.28000			1.05	1.1	1.4	
Dissipation factor		20	0.028–0.031	< 0.0004	< 0.0004	0.0007	0.0007	0.0007	0.00011	0.00014			13.05	18.2		
Moisture resistance																
Water absorption, vol %	C272	4.5	13–51	0.02	0.05	1–4	1–4	1–4								
Moisture vapor transmission, g/(m)·GPa)[n]	E96			35		<120	35–120	23–35	86	56	15		35–230	50–120		230.000

[a] Data on epoxy resins can be found in Ref. 135; on urea–formaldehyde resins, Ref. 136.
[b] Ref. 16.
[c] Refs. 137 and 138.
[d] Refs. 16 and 139.
[e] Refs. 138 and 140.
[f] Ref. 141.
[g] Ref. 142.
[h] Ref. 143.
[i] Ref. 144.
[j] To convert kg/m^3 to lb/ft^3, multiply by 0.0624.
[k] To convert kPa to psi, divide by 6.895.
[l] To convert MPa to psi, multiply by 145.
[m] To convert kJ/(kg·K) to Btu/(lb·F), divide by 4.184.
[n] To convert GPa to psi, multiply by 145,000.

Table 3. Physical Properties of Commercial Flexible Foamed Plastics

Property	ASTM test	Expanded NR[a,b]		Expanded CR[a,b]	Expanded SBR[b]	Latex foam rubber	Polyethylene-extruded plank[c]			Polyethylene sheet		Polypropylene			Polyurethane							Silicone	
															Standard cushioning[f]		Carpet underlay[g]	High resilience type[h,i]		PVC[j]			
										Extruded[c]	Cross-linked[d]	Unmodified[e]	Modified[e]	Sheet[d]								Liquid[k]	Sheet[f]
Density, kg/m^3[b]		56	320	192	72	80	35	96	144	43	26–28	64–96	64–96	10	16	24	34	26	40	112	96	272	160
Cell structure		Closed	Closed	Closed	Closed	Open	Closed	Closed	Closed	Closed	Closed	Closed	Closed		Open	Open	Open	Open	Open	Closed	Open	Open	Open
Compressive strength 25% deflection, kPa[l]	D3574, D3575			52			48	124	360			550	206	4.8	4.4	5.7	15.7	1.9	4.6				
Tensile strength, kPa[l]	D3574		206	758	551	103	138	413	690	41		830	344		88	118	258	79	103	24	3.4	36 at 20%	
Tensile elongation, %	D3574			500		310	60	60	60	276	276–480	1100	1380	138–275	160	205	135	200	160		220	227	310
Rebound resilience, %	D3574					73				50		25	75			40		65	62				
Tear Strength, (N/M)^m × 10^2	D3574						10.5	26	51	26					3.3	4.4	3.7	2.6	2.4				
Max. service temperature, °C		70	70	70	70		82	82	82	82	79–93	135	135	121								350	260
Thermal conductivity, W/(m·K)	C177	0.036	0.043	0.065	0.030		0.053	0.058	0.058	0.040–0.049	0.036–0.040	0.039	0.039	0.039						0.040		0.078	0.086

[a] NR = natural rubber, CR = chloroprene rubber.
[b] Ref. 131.
[c] Ref. 162.
[d] Ref. 135.
[e] Ref. 163.
[f] Ref. 164.
[g] Ref. 165.
[h] Ref. 166.
[i] Ref. 167.
[j] Ref. 168.
[k] To convert kg/m^3 to lb/ft^3, multiply by 0.0624.
[l] To convert kPa to pai, multiply by 0.145.
[m] To corvert N/m to lb·f/in., divide by 1.75.

Table 4. Typical Physical Properties of Commercial Structural Foams

Property	ASTM test	ABS		Noryl[a]	Nylon[b]	PC[c]	Polyester[d]	HDPE	Polypropylene		High impact polystyrene		[e]			PVC
Glass-reinforced		no	yes	no	yes	no	30%	no	no	20%	no	20%	no	no	no	no
Density, g/cm^3		0.80	0.85	0.80	0.97	0.80	1.10	0.60	0.60	0.73	0.70	0.84	0.40	0.50	0.60	0.50
Tensile strength, kPa[f]	D1623	18,600	48,000	22,700	101,000	37,900	76,000	8,900	13,800	20,700	12,400	34,500	11,000	17,200	23,400	6,900
Compression strength, kPa[e] at 10% compression	D1621	6,900		34,500		51,700	76,000	8,900					5,500	12,400	19,300	
Flexural strength, kPa[e]	D790	25,500	82,700	41,400	172,000	68,900	137,900	18,800	22,000	41,400	31,000	58,600	22,000	31,700	41,400	
Flexural modulus, GPa[g]	D790	0.86	5.2	1.7	5.2	2.1	6.6	0.83	0.83	2.8	1.4	5.2	0.7	0.9	1.1	
Max use temperature, °C		82		96	203	132	193	110	115							

[a] Noryl is an alloy of poly(2,6-dimethyl-1,4-phenylene ether) and polystyrene.
[b] Nylon-6,6 glass-reinforced.
[c] Polycarbonate.
[d] Thermoplastic polyester.
[e] Ref. 163.
[f] To convert kPa to psi, divide by 6.895.
[g] To convert GPa to psi, multiply by 145,000.

Cell size has been characterized by measurements of the cell diameter in one or more of the three mutually perpendicular directions (153) and as a measurement of average cell volume (154,155). Mechanical, optical, and thermal properties of a foam are all dependent upon the cell size.

Cell geometry is governed predominantly by the final foam density and the external forces exerted on the cellular structure prior to its stabilization in the expanded state. In a foam prepared without such external forces, the cells tend to be spherical or ellipsoidal at gas volumes less than 70–80% of the total volume, and they tend toward the shape of packed regular dodecahedra at greater gas volumes. These shapes have been shown to be consistent with surface chemistry arguments (154,156,157). Photographs of actual foam cells (Fig. 2) show a broad range of variations in shape.

In the presence of external forces, plastic foams in which the cells are elongated or flattened in a particular direction may be formed. This cell orientation can have a marked influence on many properties. The results of a number of studies have been reviewed (54,55).

The *fraction of open cells* expresses the extent to which the gas phase of one cell is in communication with other cells. When a large portion of cells are interconnected by gas phase, the foam has a large fraction of open cells, or is an open-celled foam. Conversely, a large proportion of noninterconnecting cells results in a large fraction of closed cells, or a closed-celled foam.

The nature of the opening between cells determines how readily different gases and liquids can pass from one cell to another. Because of variation in flow of different liquids or gases through the cell-wall openings, a single measurement of the fraction of open cells does not fully characterize this structural variable, especially in a dynamic situation.

Gas Composition. In closed-celled foams, the gas is partitioned between the polymer phase and the void space. The gas dissolved in the polymer phase affects the mechanical properties. The gas in the void phase or cells can contain some of the blowing agent (called captive blowing agent), gas components of air that have diffused in, or other gases generated during the foaming process. Such properties as thermal and electrical conductivity can be profoundly influenced by the cell gas composition. In open-celled foams the presence of air exerts only a minor influence on the static properties but does affect the dynamic properties such as cushioning.

Rigid Cellular Polymers. A separate class of high density, rigid cellular polymers has grown continually since the 1970s to become significant commercially. These are the structural foams with a density >300 kg/m^3. They are treated here as a separate category of rigid foams.

Compressive strength and modulus are widely used as general criteria to characterize the mechanical properties of rigid plastic foams. Rigid cellular polymers generally do not exhibit a definite yield point when compressed but instead show an increased deviation from Hooke's law as the compressive load is increased (158,159). For precision the compressive strength is usually reported at some definite deflection (commonly 5 or 10%). The compressive modulus is reported as extrapolated to 0% deflection unless otherwise stated. Structural variables that affect the compressive strength and modulus of a rigid plastic foam are, in order of decreasing importance, plastic-phase composition, density, cell structure, and

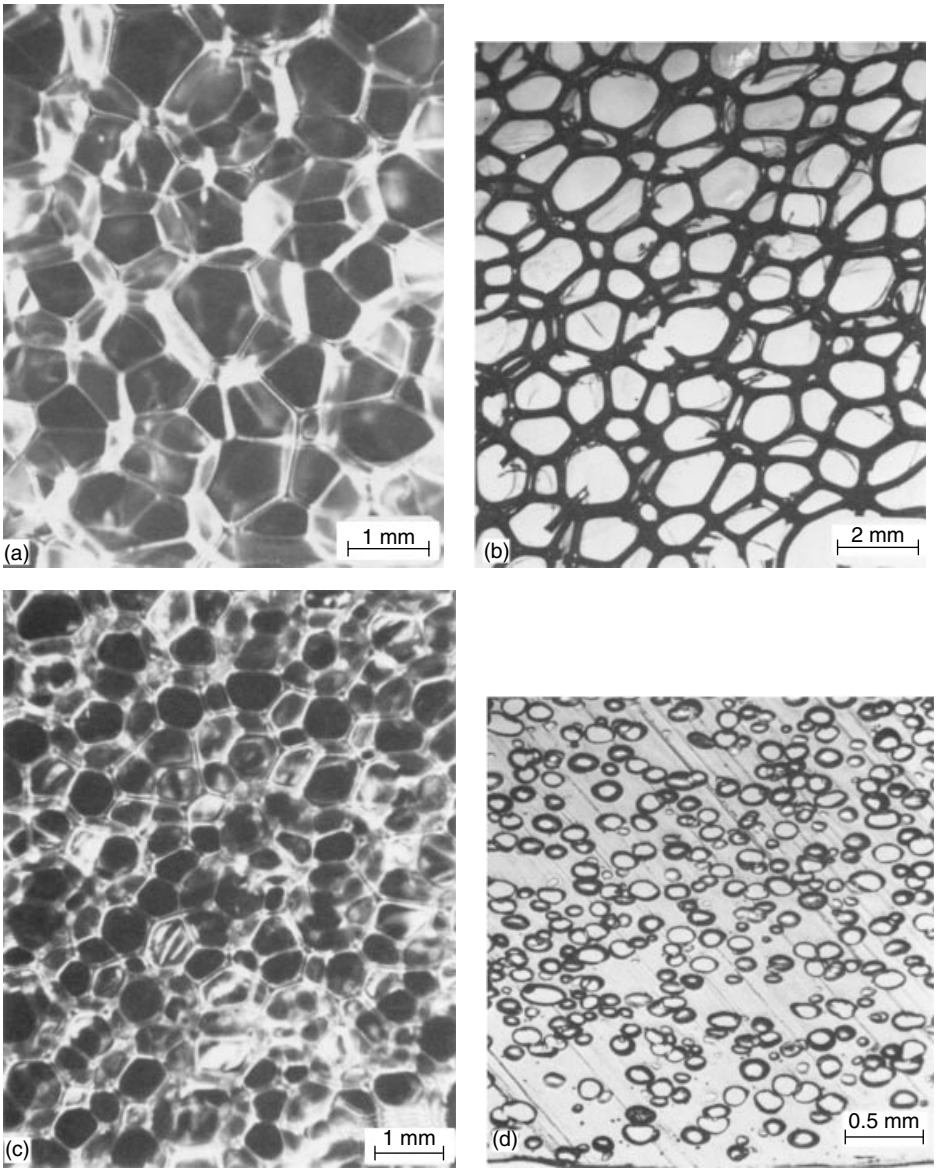

Fig. 2. Photomicrographs of foam cell structure: (**a**) extruded polystyrene foam, reflected light, 26 ×; (**b**) polyurethane foam, transmitted light, 26×; (**c**) polyurethane foam, reflected light, 12 ×; (**d**) high density plastic foam, transmitted light, 50 × (16) Courtesy of Van Nostrand Reinhold Publishing Corp.

plastic state. The effect of gas composition is minor, with a slight effect of gas pressure in some cases.

Compressive Behavior. Density and polymer composition have a large effect on compressive strength and modulus. In general, compressive strength and

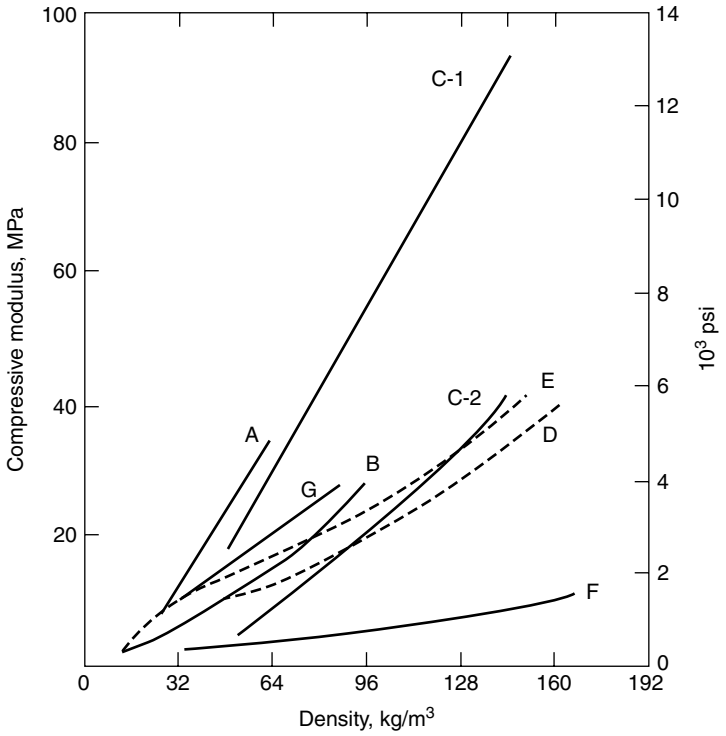

Fig. 3. Effect of density on compressive modulus of rigid cellular polymers. A, extruded polystyrene (134); B, expanded polystyrene (160); C-1, C-2, polyether polyurethane (161); D, phenol–formaldehyde (160); E, ebonite (160); F, urea–formaldehyde (160); G, poly(vinylchloride) (162). To convert kg/m^3 to lb/ft^3, multiply by 0.0624.

modulus of closed-cell low density foams may be expressed as

$$\text{Strength or modulus} = A\rho^a$$

Where A, a are constants, and ρ represents the foam density. This relationship is illustrated in Figure 3. The dependence of compressive properties on cell size has been discussed (16). The cell shape or geometry has also been shown important in determining the compressive properties (16,54,55,163,164). In fact, the foam cell structure is controlled in some cases to optimize certain physical properties of rigid cellular polymers.

Strengths and moduli of most polymers increase as the temperature decreases (165). This behavior of the polymer phase carries into the properties of polymer foams, and similar dependence of the compressive modulus of polyurethane foams on temperature has been shown (161).

Tensile strength and modulus of rigid foams have been shown to vary with density in much the same manner as the compressive strength and modulus. General reviews of the tensile properties of rigid foams are available (16,54,55, 134,166).

Those structural variables most important to the tensile properties are polymer composition, density, and cell shape. Variation with use temperature has also been characterized (167). Flexural strength and modulus of rigid foams both increase with increasing density in the same manner as the compressive and tensile properties. More specific data on particular foams are available from manufacturers' literature and in References 16,54,55,134 166. Shear strength and modulus of rigid foams depend on the polymer composition and state, density, and cell shape. The shear properties increase with increasing density and with decreasing temperature (167).

Creep. The creep characteristic of plastic foams must be considered when they are used in structural applications. *Creep* is the change in dimensions of a material when it is maintained under a constant stress. Data on the deformation of polystyrene foam under various static loads have been compiled (168). There are two types of creep in this material: short-term and long-term. Short-term creep exists in foams at all stress levels; however, a threshold stress level exists below which there is no detectable long-term creep. The minimum load required to cause long-term creep in molded polystyrene foam varies with density, ranging from 50 kPa (7.3 psi) at foam density 16 kg/m^3 (1 lb/ft^3) to 455 kPa (66 psi) at foam density 160 kg/m^3 (10 lb/ft^3).

The successful application of time–temperature superposition (169) for polystyrene foam is particularly significant in that it allows prediction of long-term behavior from short-term measurements. This is of interest in building and construction applications where load bearing and dimensional change are important.

Structural Foams. Structural foams are usually produced as fabricated articles in injection molding or extrusion processes. The optimum product and process match differs for each fabricated article, so there are no standard commercial products for one to characterize. Rather there are a number of foams with varying properties. The properties of typical structural foams of different compositions are reported in Table 4.

The most important structural variables are again polymer composition, density, and cell size and shape. Structural foams have relatively high densities (typically $>$300 kg/m^3), and cell structures similar to those in Figure 2d that are primarily composed of holes in contrast to a pentagonal dodecahedron type of cell structure in low density plastic foams. Since structural foams are generally not uniform in cell structure, they exhibit considerable variation in properties with particle geometry (100).

The mechanical properties of structural foams and their variation with polymer composition and density has been reviewed (100). The variation of structural foam mechanical properties with density as a function of polymer properties is extracted from stress–strain curves. However, because of possible anisotropy of the foam, the data must be considered as apparent data. These relations can provide valuable guidance toward arriving at an optimum structural foam, however.

Flexible Cellular Polymers. The application of flexible foams has been predominantly in comfort cushioning, packaging, and wearing apparel (142,170, 171), resulting in emphasis on a different set of mechanical properties than for rigid foams. The compressive nature of flexible foams (both static and dynamic) is their most significant mechanical property for most uses (Table 3). Other

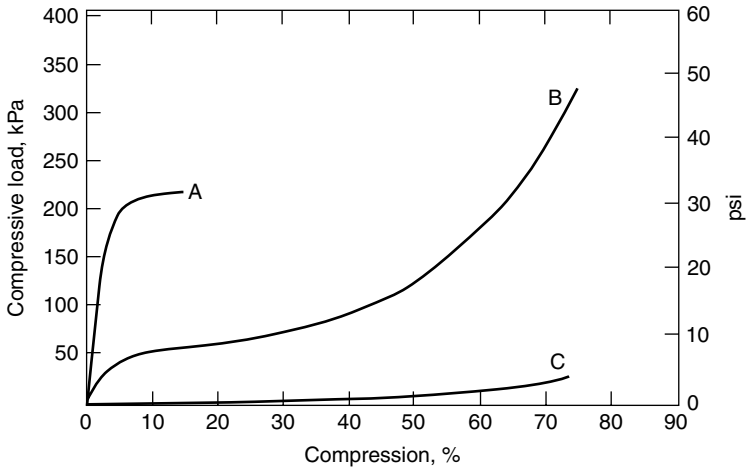

Fig. 4. Load vs compression for plastic foams (159). A, polystyrene, 32 kg/m^3; B, polyethylene, 32 kg/m^3; C, latex rubber foam, 32 kg/m^3. To convert kg/m^3 to lb/ft^3, multiply by 0.0624.

important properties are tensile strength and elongation, tear strength, and compression set. These properties can be related to the same set of structural variables as those for rigid foams.

Compressive Behavior. The most informative data in characterizing the compressive behavior of a flexible foam are derived from the entire load–deflection curve of 0–75% deflection and its return to 0% deflection at the speed experienced in the anticipated application. Various methods have been reported (3,142,172–175) for relating the properties of flexible foams to desired behavior in comfort cushioning. Other methods to characterize package cushioning have been reported. The most important variables affecting compressive behavior are polymer composition, density, and cell structure and size.

Polymer composition is the most important structural variable (Fig. 4). Although the polystyrene and polyethylene foams are approximately the same density and the open-celled latex foam significantly more dense, all three show markedly different compressive strengths. The compressive behavior of latex rubber foams of various densities (3,176) is illustrated in Figure 5. Similar relationships undoubtedly hold for vinyl and flexible polyurethane foams as well. In the case of polyurethane foams there are many variables in addition to density that heavily influence compressive behavior (26,44,55). For example the effects of reaction water content, polyol molecular weight, polymer polyol content, and isocyanate index on polymer tensile stiffness have been described (177). A further strong variation of flexible polyurethane foam compressive behavior can occur as a result of changes in the closed-cell content as measured by means of an airflow manometer described in ASTM method D3574.

Various geometric coring patterns in polyurethanes (174,178) and in latex foam rubber (179) exert significant influences on their compressive behavior. A good discussion of the effect of cell size and shape on the properties of flexible foams is contained in References (60) and (163). The effect of open-cell content in polyethylene foam is demonstrated (173).

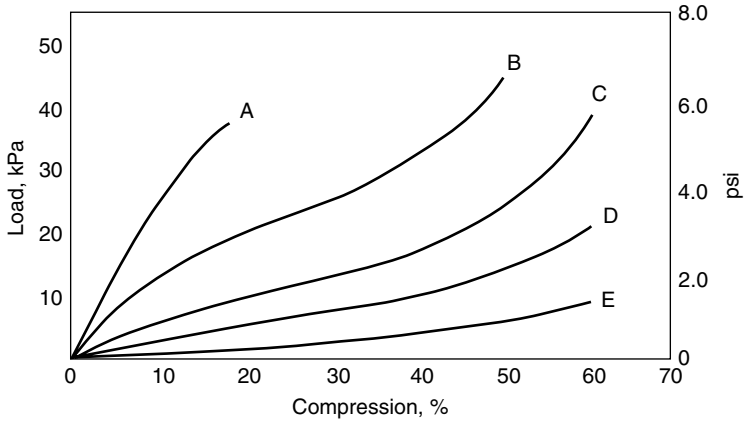

Fig. 5. Effect of load on compression for latex foams of different densities (3,173). A, 304 kg/m^3; B, 208 kg/m^3; C, 179 kg/m^3; D, 139 kg/m^3; E, 99 kg/m^3. To convert kg/m^3 to lb/ft^3, multiply by 0.0624.

Tensile Strength and Elongation. The tensile strength of latex rubber foam has been shown to depend on the density of the foam (159,180) and on the tensile strength of the parent rubber (180,181). At low densities the tensile modulus approximates a linear relation with density but increases with a higher power of density at higher densities. Similar relations hold for polyurethane and other flexible foams (166,182,183).

The tensile elongation of solid latex rubber has been shown to correlate well with the elongation of foam from the latex (181). The elongation of flexible polyurethane has been related to cell structure (183,184).

Tear Strength. A relation for the tearing stress of flexible foams that predicts linear increase in the tearing energy with density and increased tearing energy with cell size has been developed (180). Both relationships are verified to a limited extent by experimental data.

Flex Fatigue. Considerable information on the measurement and cause of flex fatigue in flexible foams has been published (185–187). Changing compressive strength and volume upon repeated flexing over long periods of time is a significant deterrent to the use of polyurethane foam in many cushioning applications. For polyurethane foams these changes have been correlated mainly with changes in chemical structure.

Compression Set. The compression set is an important property in cushioning applications. It has been studied for polyurethane foams (188,189), and has been discussed in reviews (26,55,166). Compression set has been described as flex fatigue and creep as well.

Other Properties. The thermal, electrical, acoustical, and chemical properties of all cellular polymers are of such a similar nature that the discussions of these properties cannot be separated into rigid and flexible groups.

Thermal Properties.

Thermal Conductivity. More information is available relating thermal conductivity to structural variables of cellular polymers than for any other property.

Several papers have discussed the relation of the thermal conductivity of heterogeneous materials in general (190,191) and of plastic foams in particular (135,153,161,192–194), with the characteristic structural variables of the systems.

The following separation of the total heat transfer into its component parts, even if not completely rigorous, proves valuable to understanding the total thermal conductivity k of foams:

$$k = k_s + k_g + k_r + k_c \tag{6}$$

where k_s, k_g, k_r, and k_c are the components of thermal conductivity attributable to solid conduction, gaseous conduction, radiation, and convection, respectively.

As a good first approximation (190), the heat conduction of low density foams through the solid and gas phases can be expressed as the thermal conductivity of each phase times its volume fraction. Most rigid polymers have thermal conductivities of 0.07–0.28 W/(m·K) and the corresponding conduction through the solid phase of a 32 kg/m^3 (2 lb/ft^3) foam (3 vol%) ranges 0.003–0.009 W/(m·K). In most cellular polymers this value is determined primarily by the density of the foam and the polymer-phase composition. Smaller variations can result from changes in cell structure.

Although conductivity through gases is much lower than that through solids, the amount of heat transferred through the gas phase in a foam is generally the largest contribution to the total heat transfer because the gas phase is the principal part of the total value (ca 97 vol% in a 32 kg/m^3 foam). Table 5 lists values of the thermal conductivity for several gases that occur in the cells of cellular polymers. The thermal conductivities of the halocarbon gases are considerably less than those of oxygen and nitrogen. It has, therefore, proved advantageous to prepare cellular polymers using such gases that measurably lower the k of the polymer foam. Upon exposure to air the gas of low thermal conductivity in the cells can get mixed with air, and the k of the mixture of gases can be estimated by a mixing rule such as the Riblett (eq. 7).

$$k_m = \sum_i k_i M_i^{1/3} P_i / \sum_i M_i^{1/3} P_i \tag{7}$$

where k_m is the k of the gaseous mixture; k_i, M_i, and P_i are the component thermal conductivity, molecular weight, and partial pressure, respectively. Changes in total k calculated using equations (6) and (7) with change in gas composition agree well with experimental measurements (154,194,195,198,199).

There is ordinarily no measurable convection in cells of diameter less than about 4 mm (153). Theoretical arguments have been in general agreement with this work (161,194,195). Since most available cellular polymers have cell diameters less than 4 mm, convection heat transfer can be ignored with good justification. Studies of radiation heat transfer through cellular polymers have been done (153,161,194,195,200,201).

The variation in total thermal conductivity with density has the same general nature for all cellular polymers (153,192). The increase in k at low densities is owing to an increased radiant heat transfer; the rise at high densities to an increasing contribution of k_s.

Table 5. Thermal Conductivity at 20°C, of Gases Used in Cellular Polymers[a]

Compound[b]	Thermal conductivity, W/(m·K)
Trichlorofluoromethane (CFC-11)	0.0084
Dichlorodifluoromethane (CFC-12)	0.0098
Trichlorotrifluoroethane (CFC-113)	0.0072
Dichlorotetrafluoroethane (CFC-114)	0.0104
Dichlorofluoromethane (CFC-21)	0.0112
Chlorodifluoromethane (HCFC-22)	0.0106
Difluoromethane (HFC-32)	0.0163
2-Chloro-1,1,1,2-tetrafluoroethane (HCFC-124)	0.0106
Pentafluoroethane (HFC-125)	0.0131
1,1,1,2-Tetrafluoroethane (HFC-134a)	0.0127
1,1-Dichloro-1-fluoroethane (HCFC-141b)	0.0083
1-Chloro-1,1-difluoroethane (HCFC-142b)	0.0108
Trifluoroethane (HFC-143a)	0.0137
1,1-Difluoroethane (HFC-152a)	0.0136
Dichloromethane	0.0063
Methyl chloride	0.0105
2-Methylpropane	0.0161
Carbon dioxide	0.0168
Air	0.0259

[a]Refs. 195 and 196.
[b]CFC, chlorofluorocarbon; HCFC, hydrochlorofluorocarbon.

The thermal conductivity of most materials decreases with temperature. When the foam structure and gas composition are not influenced by temperature, the k of the cellular material decreases with decreasing temperature. When the composition of the gas phase may change (ie, condensation of a vapor), then the relationship of k to temperature is much more complex (153,194,195,202).

The thermal conductivity of a cellular polymer can change upon aging under ambient conditions if the gas composition is influenced by such aging. Such a case is evidenced when oxygen or nitrogen diffuses into polyurethane foams that initially have only a fluorocarbon blowing agent in the cells (26,133,153,193–195, 202–207).

Thermal conductivity of foamed plastics has been shown to vary with thickness (201). This has been attributed to the boundary effects of the radiant contribution to heat transfer. Other modifications to the thermal conductivity of foamed plastics are directed at reducing the radiation heat transfer. Radiation heat transfer varies inversely with extinction coefficient, and two techniques are current available for moderating transmission. When the average cell size is reduced, while maintaining a constant density, the total length and surface area of struts available to absorb radiation are increased. Also by using infrared (IR) blockers radiation heat transfer can be reduced by 15 to 20%. These materials, such as carbon black particles, graphite and aluminum flakes, when included in the polymer cell walls can improve the foam thermal conductivity (208,209). As opaque materials, they make the foam less transparent to IR wavelengths where appreciable

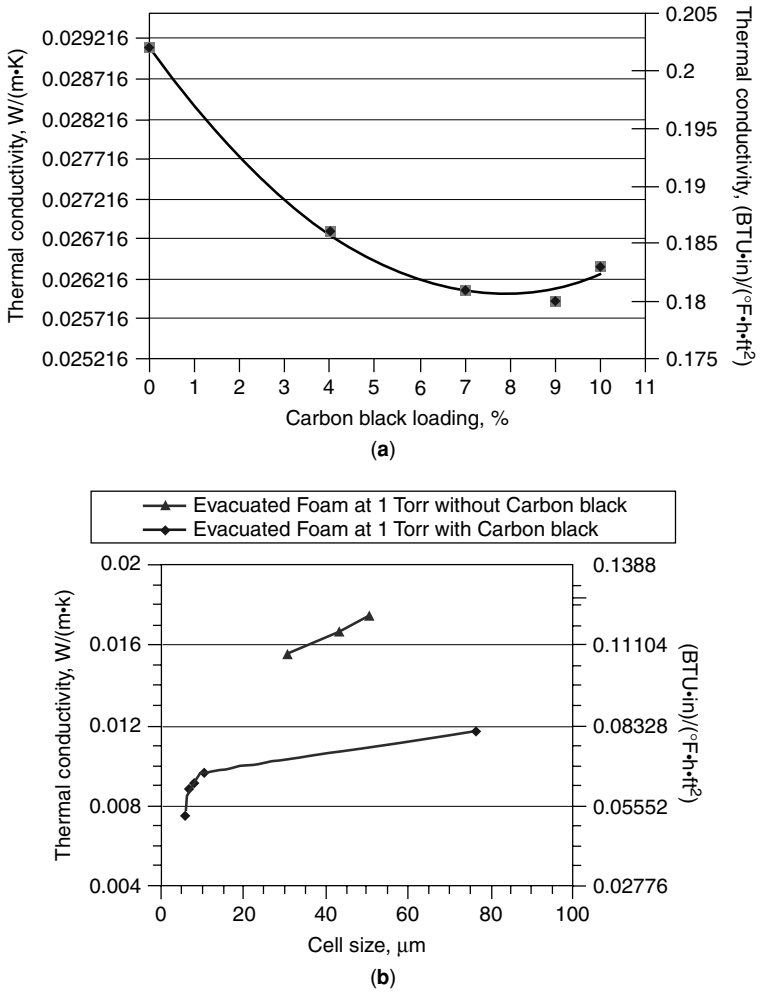

Fig. 6. (**a**) Effect of carbon black loading on thermal conductivity (209); (**b**) Effect of cell size and carbon black IR attenuator on the thermal conductivity of polystyrene foam panel core material (208).

thermal radiation is emitted at room temperature. Too large an amount of the solid filler can cause the effective conductivity to increase because solid conductivity begins to dominate (209). Figure 6a shows the effect of carbon back loading on the thermal insulation performance of polystyrene foam. Additionally, using IR-attenuating fillers in conjunction with vacuum insulation can decrease the effective thermal conductivity of foam materials (208). Figure 6b show the comparative performance of filled and unfilled foam as a function of cell size.

Specific Heat. The specific heat of a cellular polymer is simply the sum of the specific heats of each of its components. The contribution of the gas is small and can be neglected in many cases.

Coefficient of Linear Thermal Expansion. The coefficients of linear thermal expansion of polymers are higher than those for most rigid materials at ambient

temperatures because of the supercooled-liquid nature of the polymeric state, and this applies to the cellular state as well. Variation of this property with density and temperature has been reported for polystyrene foams (210) and for foams in general (16). When cellular polymers are used as components of large structures, the coefficient of thermal expansion must be considered carefully because of its magnitude compared with those of most nonpolymeric structural materials (211).

Maximum Service Temperature. Because the cellular materials, like their parent polymers (212), undergo a gradual decrease in modulus as the temperature rises rather than a sharp change in properties, it is difficult to precisely define the maximum service temperature of cellular polymers. The upper temperature limit of use for most cellular polymers is governed predominantly by the plastic phase. Fabrication of the polymer into a cellular state normally builds some stress into the polymer phase; this may tend to relax at a temperature below the heat-distortion temperature of the unfoamed polymer. Of course, additives in the polymer phase or a plasticizing effect of the blowing agent on the polymer affect the behavior of the cellular material in the same way as the unfoamed polymer. Typical maximum service temperatures are given in Tables 2, 3, and 4.

Flammability. The results of small-scale laboratory tests of plastic foams have been recognized as not predictive of their true behavior in other fire situations (213). Work aimed at developing tests to evaluate the performance of plastic foams in actual fire situations continues. All plastic foams are combustible, some burning more readily than others when exposed to fire. Some additives (134,138), when added in small quantities to the polymer, markedly improve the behavior of the foam in the presence of small fire sources. Plastic foams must be used properly, following the manufacturers recommendations and any applicable regulations.

Moisture Resistance. Plastic foams are advantageous compared with other thermal insulations in several applications where they are exposed to moisture pickup, particularly when subjected to a combination of thermal and moisture gradients. In some cases the foams are exposed to freeze–thaw cycles as well. The behavior of plastic foams has been studied under laboratory conditions simulating these use conditions as well as under the actual use conditions.

In a study (214) of the moisture gain of foamed plastic roof insulations under controlled thermal gradients, the apparent permeability values were greater than those predicted by regular wet-cup permeability measurements. The moisture gains found in polyurethane are greater than those of bead polystyrene and much greater than those of extruded polystyrene.

Moisture pickup and freeze–thaw resistance of various insulations and the effect of moisture on the thermal performance of these insulations has been reported (215). In protected membrane roofing applications the order of preference for minimizing moisture pickup is extruded polystyrene $\gg$ polyurethane $>$ molded polystyrene (215).

Water pickup values for insulation in use for 5 years were, extruded polystyrene, 0.2 vol%; polyurethane without skins, 5 vol%; and molded polystyrene; 8–30 vol%. These correspond to increases in k of 5–265%. For below-grade applications extruded polystyrene was better than molded polystyrene or polyurethane without skins in terms of moisture-absorption resistance and retention of thermal resistance. Increased water content has been related with increased thermal conductivity of the insulations (216–220).

Electrical Properties. Cellular polymers have two important electrical applications (16). One takes advantage of the combination of inherent toughness and moisture resistance of polymers along with the decreased dielectric constant and dissipation factor of the foamed state to use cellular polymers as electrical-wire insulation (94). The other combines the low dissipation factor and the rigidity of plastic foams in the construction of radar domes. Polyurethane foams have been used as high voltage electrical insulation (221).

Environmental Aging. All cellular polymers are subject to a deterioration of properties under the combined effects of light or heat and oxygen. The response of cellular materials to the action of light and oxygen is governed almost entirely by the composition and state of the polymer phase (16). Expansion of a polymer into a cellular state increases the surface area; reactions of the foam with vapors and liquids are correspondingly faster than those of solid polymer.

Foams prepared from phenol–formaldehyde and urea–formaldehyde resins are the only commercial foams that are significantly affected by water (16). Polyurethane foams exhibit a deterioration of properties when subjected to a combination of light, moisture, and heat aging; polyester-based foam shows much less hydrolytic stability than polyether-based foam (44,203,204).

A great deal of work has been done to develop additives that successfully eliminate environmental degradation (222). The best source of information on specific additives for specific foams is the individual manufacturer of the foam. The resistance to rot, mildew, and fungus of cellular polymers can be related to the amount of moisture that can be taken up by the foam (160). Therefore, open-celled foams are much more likely to support growth than are closed-celled foams. Very high humidity and high temperature are necessary for the growth of microbes on any plastic foam.

Miscellaneous Properties. Cellular polymers are useful for acoustic insulation. Sound transmission is altered only slightly because it depends predominantly on the density of the barrier (in this case, the polymer phase). Therefore by themselves cellular polymers are very poor materials for reducing sound transmission. They are, however, quite effective in absorbing sound waves of certain frequencies (160). Open-cell foams with the cells open to the surface are particularly effective. Recently, low modulus closed-cell polyolefin foams having a large cell size of >5 mm have been developed by the Dow Chemical Co with the trademark QUASH. These foams have shown unique sound absorbtion properties by utilizing the vibration of large, flexible low modulus cell windows (223). The combination of other advantageous physical properties with fair acoustical properties has led to the use of several different types of plastic foams in sound-absorbing constructions (224,225). The sound absorption of a number of cellular polymers has been reported (15,160,224,226). Cellular urea–formaldehyde and phenolic resin foams have been used to some extent in interior sound-absorbing panels and, in Europe, expanded polystyrene has been used in the design of sound-absorbing floors (227). In general, cost, flammability, and cleaning difficulties have prevented significant penetration of the acoustical tile market. The low percent of reflection of sound waves from plastic foam surfaces has led to their use in anechoic chambers (225).

The permeability of cellular polymers to gases and vapors depends on the fraction of open cells as well as the polymer-phase composition and state. The

Table 6. Market for Cellular Polymers,[a] 10^3 t

Item	1967	1982	1995[b]
	By market		
Insulation	58	261	472
Flooring	20	98	154
Other construction	9	136	288
Cushioning	52	195	336
Other furniture	40	103	175
Packaging	43	177	311
Transportation	76	140	238
Consumer	44	136	225
Bedding	18	57	113
Appliances	14	40	61
Other	68	225	408
Total	*441*	*1567*	*2781*
	By resin		
Flexible urethane	181	511	844
Rigid urethane	68	248	449
Styrene	125	410	699
Vinyl	61	232	413
Others	6	165	376
Total	*441*	*1567*	*2781*

[a]Ref. 16.
[b]Projected.

presence of open cells in a foam allows gases and vapors to permeate the cell structure by diffusion and convection flow, yielding very large permeation rates. In closed-celled foams the permeation of gases or vapors is governed by composition of the polymer phase, gas composition, density, and cellular structure of the foam (198,203,204,224,228,229).

The penetration of visible light through foamed polystyrene has been shown to follow approximately the Beer–Lambert law of light absorption (16). This behavior presumably is characteristic of other cellular polymers as well.

Comfort Cushioning. Comfort cushioning is the largest single application of cellular polymers; flexible foams are the principal contributors to this field. Historically, cushioning in particular and flexible foams in general have been the greatest volume of cellular polymers. However, the rapid growth rate of structural, packaging, and insulation applications has brought their volume over that of flexible foams during the past few years. Table 6 shows U.S. consumption of foamed plastics by resin and market (14).

The properties of greatest significance in the cushioning applications of cellular polymers are compression–deflection behavior, resilience, compression set, tensile strength and elongation, and mechanical and environmental aging; of these, compression–deflection behavior is the most important. The broad range of compressive behavior of various types of flexible foam is one of the strong points of cellular polymers, since the needs of almost any cushioning application can be met by changing either the chemical nature or the physical structure of the foam. Flexible urethanes, vinyls, latex foam rubber, and olefins are used to make

foamed plastic cushioning for automobile padding and seats, furniture, flooring, mattresses, and pillows. These materials compete with felt, fibers, innerspring, and other filling materials.

Latex foam rubber was initially accepted as a desirable comfort-cushioning material because of its softness to the touch and its resilience (equal to that of a steel spring alone but with better damping qualities than the spring).

Cellular rubber has been used extensively as shoe soles, where its combination of cushioning ability and wear resistance, coupled with desirable economics, has led to very wide acceptance. In this case the cushioning properties are of minor importance compared with the abrasion resistance and cost. Other significant cushioning applications for cellular rubbers and latex foam rubbers are as carpet underlay and as cushion padding in athletic equipment.

Thermal Insulation. Thermal insulation is the second largest application of cellular polymers and the largest application for the rigid materials. The properties of greatest importance in determining the applicability of rigid foams as thermal insulants are thermal conductivity, ease of application, cost, moisture absorption and transmission permeance, and mechanical properties (see INSULATION, THERMAL). Plastic foams containing a captive blowing agent have considerably lower thermal conductivities than other insulating materials, whereas other rigid cellular plastics are roughly comparable with the latter. Vacuum insulation panels containing rigid open-celled microcellular polystyrene foam enclosed in a nonpermeable membrane on which a vacuum has been applied have shown very low thermal conductivities (230). Super-insulating materials are made by encapsulation of a filler material inside a barrier film, aluminum foil or metallized film. These materials exhibit 5 to 7 times the R-value of typical nonvacuum insulating materials, depending on vacuum level and barrier and filler type. Uses for these vacuum insulation panels (VIP) include refrigeration and controlled-temperature shipping containers. Several key issues that have to be addressed with vacuum panel technology include the vacuum level required to achieve super insulation and functionality of the panels during use. First, the evacuated envelope must be impermeable enough to maintain the desired vacuum over the lifetime of the insulation. The envelope cannot be made of heavy metal foil, which is a good gas barrier, but can cause substantial thermal short-circuiting around the circumference of the package and severely increase the effective conductivity. Second, the ease of manufacturing panels in various shapes that lend itself to functional use. A technology based on a polystyrene foam core material seems to have resolved these issues in their commercial offering of an Instill (trademark of the Dow Chemical Company) product that combines performance with durability (230). Figure 7 shows the comparative performance of an Instill over less durable vacuum panel technologies.

Domestic Refrigeration. The very low thermal conductivity of polyurethanes plus the ease of application and structural properties of foamed-in-place materials gives refrigeration engineers considerable freedom of styling. This has resulted in an increasingly broad use of rigid polyurethane foams in home freezers and refrigerators that has displaced conventional rock wool and glass wool.

Commercial Refrigeration. Again, low thermal conductivity is important, as are styling and cost. Application methods and mechanical properties are of

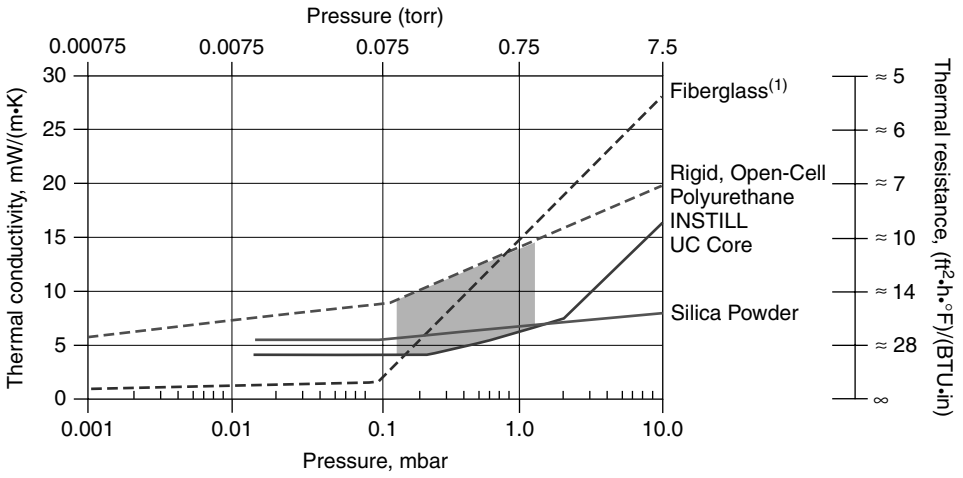

Fig. 7. Comparative performance of vacuum panel core materials (230).

secondary importance because of design latitude in this area. For example, large institutional chests, commercial refrigerators, freezers, and cold-storage areas, including cryogenic equipment and large tanks for industrial gases, are insulated with polystyrene or polyurethane foams. Polystyrene foam is still popular where cost and moisture resistance are important; polyurethane is used where spray application is required. Polystyrene foam is also widely used in load-bearing sandwich panels in low temperature space applications.

Refrigeration in Transportation. Styling is unimportant. The volume of insulation and a low thermal conductivity are of primary concern. Volume is not large, so application methods are not of prime importance. Low moisture sensitivity and permanence are necessary. The mechanical properties of the insulant are quite important owing to the continued abuse the vehicle undergoes. Cost is of less concern here than in other applications. Polystyrene foam is widely used in this application.

Residential Construction. Owing to rising energy costs, the cost and low thermal conductivity are of prime importance in wall and ceiling insulation of residential buildings. The combination of insulation efficiency, desirable structural properties, ease of application, ability to reduce air infiltration, and moisture resistance has led to the use of extruded polymeric and polyisocyanurate foam in residential construction as sheathing, as perimeter and floor insulation under concrete, and as a combined plaster base and insulation for walls.

Commercial Construction. The same attributes desirable on residential construction applications hold for commercial construction as well, but insulation quality, permanence, moisture insensitivity, and resistance to freeze–thaw cycling in the presence of water are of greater significance. For this reason cellular plastics have greater application here. Both polystyrene and polyurethane foams are highly desirable roof insulations in commercial as well as in residential construction.

Cellular polymers are also used for pipe and vessel insulation. Spray and pour-in-place techniques of application are particularly suitable, and polyurethane and epoxy foams are widely used. Ease of application, fire properties, and low thermal conductivity have been responsible for the acceptance of cellular rubber and cellular poly(vinyl chloride) as insulation for smaller pipes.

The insulating value and mechanical properties of rigid plastic foams have led to the development of several novel methods of building construction. Polyurethane foam panels may be used as unit structural components (231) and expanded polystyrene is employed as a concrete base in thin-shell construction (232).

Packaging. Because of the extremely broad demands on the mechanical properties of packaging materials, the entire range of cellular polymers from rigid to flexible is used in this application. The most important considerations are mechanical properties, cost, ease of application or fabrication, moisture susceptibility, thermal conductivity, and aesthetic appeal.

The proper mechanical properties, particularly compressive properties, are the primary requirements for a cushioning foam (233,234). The reader is referred to the following sources for more specific information: package design (235); general vibration and shock isolation (236); protective package design (237); selection of cushioning material (233,238); and characterization of cellular polymers for cushioning applications (234,236,237,239).

Creep of a cushion packaging material when subjected to static stresses for long periods of storage or shipment is also an important consideration. Polystyrene foam shows considerable creep (168) at high static loadings but that creep is insignificant under loadings in the static stress region of optimum package design (16). The ability of polystyrene foam to withstand repeated impacts has also been studied (162,240).

The low density of most cellular plastics is important because of shipping costs for the cushioning in a package. Foams with densities ranging from 4 to 32 kg/m^3 are used in this application. The inherent moisture resistance of cellular plastics is of added benefit where packages may be subjected to high humidity or water. Many military applications require low moisture susceptibility. Foamed polystyrene is used as packaging inserts and as containers such as food trays, egg cartons, and drinking cups, which require moisture resistance, rigidity, and shock resistance. Foamed polyurethane is also used as specialty packaging materials for expensive and delicate equipment.

The clean, durable, non–dust-forming character of polyethylene foam has led to its acceptance in packaging missile parts (241). Polyethylene foam sheet has also displaced polystyrene foam sheet for packaging glass bottles and containers because of its greater resiliency and tear resistance.

Antistatic protection is an important consideration within the electronic industry, and various antistatic agents are used commercially to alleviate this problem in cushion packaging materials.

Structural Components. In most applications structural foam parts are used as direct replacements for wood, metals, or solid plastics and find wide acceptance in appliances, automobiles, furniture, materials-handling equipment, and in construction. Use in the building and construction industry account for more than one-half of the total volume of structural foam applications. High impact

polystyrene is the most widely used structural foam, followed by polypropylene, high density polyethylene, and poly(vinyl chloride). The construction industry offers the greatest growth potential for cellular plastics.

The sandwich-type structure of polyurethanes with a smooth integral skin produced by the reaction injection molding process provides a high degree of stiffness as well as excellent thermal and acoustical properties necessary for its use in housing and load-bearing structural components for the automotive, business machine, electrical, furniture, and materials-handling industry.

Buoyancy. The low density, closed-celled nature of many cellular polymers coupled with their moisture resistance and low cost resulted in their immediate acceptance for buoyancy in boats and floating structures such as docks and buoys. Since each cell in the foam is a separate flotation member, these materials cannot be destroyed by a single puncture.

The combination of structural strength and flotation has stimulated the design of pleasure boats using a foamed-in-place polyurethane between thin skins of high tensile strength (242). Other cellular polymers that have been used in considerable quantities for buoyancy applications are those produced from polyethylene, polystyrene, poly(vinyl chloride), and certain types of rubber. The susceptibility of polystyrene foams to attack by certain petroleum products that are likely to come in contact with boats led to the development of foams from copolymers of styrene and acrylonitrile that are resistant to these materials (243,244).

Electrical Insulation. The substitution of a gas for part of a solid polymer usually results in large changes in the electrical properties of the resulting material. The dielectric constant, dissipation factor, and dielectric strength are all generally lowered in amounts roughly proportional to the amount of gas in the foam.

For low frequency electrical insulation applications, the dielectric constant of the insulation is ideally as low as possible (see INSULATION, ELECTRICAL). The lower the density of the cellular polymer, the lower the dielectric constant and the better the electrical insulation. Dielectric strength is also reduced at lower density; the insulation is, therefore, susceptible to breakdown from voltage surges from such sources as lightning and short circuits. Because physical properties are also diminished proportionally to density, optimum density is determined by a compromise in properties. For many applications this compromise has been at an expansion of two or three volumes, mainly because the minimum physical properties required for fabrication and use are obtained at that point. Polyolefin foams have been most used as low frequency electrical insulation; poly(vinyl chloride) and polystyrene foams are used also. Producing a completely homogenous, closed-celled foam at lower densities in high speed wire-coating apparatus is difficult.

In high frequency applications, the dissipation factor is of greater importance. Coaxial cables using cellular polyolefins have been quite successfully used for frequencies in the megahertz range and above. Cellular plastics have also been used as structural materials in constructing very large radar-receiving domes (245). The very low dissipation factor of these materials makes them quite transparent to radar waves.

Space Filling and Seals. Cellular polymers have become common for gasketing, sealing, and space filling. Cellular rubber, poly(vinyl chloride), silicone (100), and polyethylene are used extensively for gasketing and sealing of

closures in the automotive and construction trade (110). Most cellular materials must be predominantly closed-celled in order to provide the necessary barrier properties. The combination of chemical inertness, excellent conformation to irregular surfaces, and ability to be compressed to more than 50% with relatively small pressures and still function satisfactorily contribute to the acceptance of cellular polymers in these applications.

In the construction industry, cellular polymers are used as spacers and sealant strips in windows, doors, and closures of other types, as well as for backup strips for other sealants.

Miscellaneous Applications. Cellular plastics have been used for display and novelty pieces since their early development. Polystyrene foam combines ease of fabrication with light weight, attractive appearance, and low cost to make it a favorite in these uses. Phenolic foam has its principal use in floral displays. Its ability to hold large amounts of water for extended periods is used to preserve cut flowers. Cellular poly(vinyl chloride) is used in toys and athletic goods, where its toughness and ease of fabrication into intricate shapes have been valuable.

Commercial Products and Processes

Flexible Polyurethane. These foams are produced from long-chain, lightly branched polyols reacting with a diisocyanate, usually toluene diisocyanate [1321-38-] (TDI), to form an open-celled structure with free air flow during flexure. During manufacture these foams are closely controlled for proper density, ranging from 13 to 80 kg/m^3 (0.8–5 lb/ft^3), to achieve the desired physical properties and cost.

In flexible polyurethane foams, the primary blowing agent is carbon dioxide, which is formed by the reaction of water and toluene diisocyanate. Softer foams with lower densities require an auxiliary blowing agent such as HCFC-141b, or potentially HFC-245fa and HFC-365mfc, hydrocarbons, and CO_2. Since the load-bearing characteristics of the foam are of great importance to the ultimate consumer this property is also closely controlled during manufacture.

Raw Materials. Polyether polyols are used in about 90% of polyurethane foams. The elastomeric polymer is provided additional toughness in the overall polymer matrix by the presence of hard segment urea-based polymers derived from the water/isocyanate reaction (see ISOCYANATES, ORGANIC; URETHANE POLYMERS). Intermolecular hydrogen bonding plays a further role in overall foam hardness. The polyols are typically trifunctional, but di- and tetrafunctional polyols are also used. The polyol chain initiator determines the functionality of the final product; glycerol or trimethylolpropane are the most common triol initiators. Propylene oxide (PO) is then polymerized onto the initiator to form a long-chain triol with an equivalent weight of 1000–1500. PO chains are characterized by pendent methyl groups and terminal secondary hydroxyl groups that provide the lower level of reactivity used for slab foam manufacture. Ethylene oxide (EO) can be used in conjunction with PO to modify the polyether chain by reducing the pendent methyl groups. This is called a hetero polyol, with the possibility of adding a mixed PO/EO feed to form a random hetero or a batch EO feed to form a block hetero polyol. Additionally, EO can be used at the end of the polyol polymerization to produce

primary hydroxyl groups at chain termination. This is known as EO capping and results in polyols with considerably higher reactivities toward isocyanates which is the polyol type required for molded foam production.

Another type of polyol often used in the manufacture of flexible polyurethane foams contains a dispersed solid phase of organic chemical particles (246–248). The continuous phase is one of the polyols described above for either slab or molded foam as required. The dispersed phase reacts in the polyol using an addition reaction with styrene and acrylonitrile monomers in one type or a coupling reaction with an amine such as hydrazine and isocyanate in another. The solids content ranges from about 21% with either system to nearly 40% in the styrene–acrylonitrile system. The dispersed solids confer increased load bearing, and in the case of flexible molded foams also act as a cell opener.

The isocyanates used in the manufacture of flexible foam are TDI and polymeric 4,4′-methylenediphenyl diisocyanate [101-68-8] (MDI). Slab foam manufacturing is based almost entirely on TDI, which is most often supplied as a blend of 80% 2,4-isomer and 20% 2,6-isomer by weight. There have been efforts to develop slab foaming technology using polymeric MDI in place of TDI (249–251). Polymeric MDI is often used in manufacturing molded foams usually blended with TDI, often at a 4: 1 ratio of TDI to MDI by weight. The acidity and isomer distribution are key factors controlling the reactivity of these isocyanates. Foams are generally produced with a slight excess of isocyanate groups. The stoichiometric balance of a foam formulation is known as the foam index, with 100 index as the balance point and 110 index indicating 110% isocyanate equivalents compared to active hydrogen equivalents.

Catalysis of the flexible polyurethane foaming operation is accomplished through the use of tertiary amine compounds, often using two different amines to balance the blowing and gelling reactions. Organometallic compounds, usually stannous salts, are also used to facilitate gelling and promote final cure.

Hydrolyzable or nonhydrolyzable siloxane compounds provide nucleating assistance for fine, uniform cells and surface tension depression for stabilization of the expanding cell walls prior to gelation of the polymer. The slab foam cells are mostly open after ultimate foam rise and blow off. Too much surfactant or too much tin-gelation catalyst cause the foam to have a larger number of closed cells. This tight foam lets very little air pass through a cut block of foam. Tight foams are prone to shrink as the hot gas inside the closed cell cools, thus producing less pressure and volume. Molded foams often need to be crushed after demolding to mechanically open closed cells and prevent shrinkage. Surfactants must be carefully chosen for use in flexible slab, high resilience (HR) slab, and HR or hot-molded systems, since most are not interchangeable.

Fillers (qv) are occasionally used in flexible slab foams; the two most commonly used are calcium carbonate (whiting) and barium sulfate (barytes). Their use level may range up to 150 parts per 100 parts of polyol. Various other ingredients may also be used to modify a flexible foam formulation. Cross-linkers, chain extenders, ignition modifiers, auxiliary blowing agents, etc, are all used to some extent, depending on the final product characteristics desired.

Process and Equipment. The critical requirements for urethane foam dispensing equipment are accurate metering of the ingredients to the mixing chamber, adequate short-cycle mixing, and proper dispensing ability. The polyol,

isocyanate, and water must all be delivered at an accurate rate to maintain the desired stoichiometry that is essential for predicting final foam performance and properties. The other ingredients must also be precisely controlled to obtain optimum processing and performance. Thorough ingredient mixing is made more critical because the components are reactive and thus may not remain in the mixing chamber for more than a few seconds. There is also a wide range of component viscosities; low viscosity isocyanates are dispersed in fairly high viscosity polyols. Additionally the mixing head must deliver the foam ingredients in a smooth flowing manner to minimize air entrainment or splashing.

There are two basic metering/mixing systems (based on pressure) in wide use. Low pressure (less than 2000 kPa) systems use positive displacement pumps to deliver material via a heat exchanger and recycle valve to a mixing chamber with a mechanically driven impeller. High pressure (2000–20000 kPa) systems use precision high pressure pumps to deliver material via flow-adjusting valves and/or orifices to a cylindrical impingement mixing chamber. Following each use the impingement mixing chamber is cleared by advancing a piston that eliminates the need for solvent flushing as is required for low pressure machines.

The mixing head dispenses the foam in several ways depending on the particular foam production process. Flexible foam molding requires the head to be positioned over the open mold, moved in relation to the mold for the best pour pattern and to dispense material on a required quantity shot basis. After the ingredients are placed in the mold cavity the lid is closed and the mold heated. The materials foam and expand to fill the mold, then gel and cure. The mold is then opened, the foam part removed, and a fresh layer of mold release sprayed onto the mold. The foam object is crushed to enhance cell opening and then may be post-cured. The two basic processes for molding are the earlier developed hot process where the molds are subjected to a high temperature (204–371°C) and the cold process where the mold ranges from room temperature to about 120°C. The chemistry used for the cold process is called high resilience (or HR) foam system.

Flexible slab operations often use a traversing arrangement to dispense the foam ingredients back and forth on a layer of polyethylene film carried on a conveyor belt. Side papers are brought up to the edge of the film and the assembly enters a tunnel fitted with an exhaust system. The liquid foam ingredients begin to react and the foam rises to full height within 3–4.5 m after entering the tunnel. As the slab bun exits the tunnel the side papers are pulled off; the bun is then cut into appropriate lengths and delivered to a cure area. Generally a minimum of 24 h is required to cure the bun prior to cutting into blocks for shipping. This simplest form of slab foam manufacture leaves the top of the bun with a rounded cross section much like the top of a loaf of bread. This rounding introduces a waste factor during subsequent cutting of the bun into rectangular blocks for final use as furniture cushions, mattresses, etc. Starting in the late 1970s a number of patented processes were introduced to provide a square block with less wasted foam. These include side paper lifting, top smoothing, and bottom dropping, in which case the foam ingredients are fed to an overflow trough and the expanding foam is allowed to grow down instead of up.

Alternative processes are block-pouring into a large, open-topped box lined with plastic film from which the cured bun is subsequently removed, or a recently introduced vertical foaming operation. In the latter case the foam ingredients

are fed to the bottom of an enclosed trough. As the foam expands vertically it is pulled up by side conveyors. At the top of the square conveyor the foam is cut into length (usually about 2 m) and laid on its side for further curing. Since one of the large foam markets, carpet underlayment, uses long thin sections of foam, it is also desirable to generate cylinders of foam that can then be peeled using a long sharp blade. Round buns of foam are generated by proprietary techniques using conventional conveyors and also with the vertical foaming apparatus modified accordingly. Scrap foam is utilized by shredding into small pieces, adding a prepolymer glue, tumbling to mix, compressing into a mold, then curing with steam. This so-called rebond foam is prepared in a variety of density grades, then cut, sliced, or peeled to proper form for a number of applications, including carpet underlayment.

Economics. Flexible polyurethane foam is generally sold by the board foot, 1in. $\times$ 1 ft $\times$ 1 ft (0.083 ft^3 = 0.0024 m^3), in the United States. Typical densities are 18.5–32.0 kg/m^3 (1.15–2.0 lb/ft^3) for conventional foams and 40.0 kg/m^3 (2.5 lb/ft^3) for HR foam. Foam prices are usually double the cost of the chemicals for standard grades.

Applications. Carpet underlayment as just described is a substantial market. Most furniture cushioning is made from blocks of slab-produced polyurethane foam in the density range of 16–29 kg/m^3 (1.0–1.8 lb/ft^3). For passenger car seating about 90% is made by the molded foam process. A minor portion of the market, 9000–14,000 t (20–30 million pounds), uses 40 kg/m^3 (2.5 lb/ft^3) high resilient (HR) foam for higher priced furniture cushions. The furniture market for polyurethane foams grew strongly until saturation occurred around 1979. Market use now tends to reflect the current economic trends.

Consumption of polyurethane foam in bedding reached a maximum in 1978 and has since declined. The innerspring mattress has remained the standard in the United States whereas all-foam mattresses have gained a dominant market share in Europe.

Textile uses are a relatively stable area and consist of the lamination of polyester foams to textile products, usually by flame lamination or electronic heat sealing techniques. Flexible or semirigid foams are used in engineered packaging in the form of special slab material. Flexible foams are also used to make filters (reticulated foam), sponges, scrubbers, fabric softener carriers, squeegees, paint applicators, and directly applied foam carpet backing.

Rigid Polyurethane. These foams are characterized by closed-celled structure and very high compressive strength. They are produced by reacting a highly branched, short-chain polyol with an aromatic isocyanate of two or more functionality, which is often polymeric. Pour-in-place and free-rise rigid polyurethane foams usually have a density in the region of 32.0 kg/m^3 (2.0 lb/ft^3), although molded rigid foams have densities ranging up to 640 kg/m^3 (40 lb/ft^3) in structural foams. Insulation effectiveness is one of the outstanding characteristics of rigid polyurethane foams that display thermal conductivities as low as 0.017 W/(m $\cdot$ K).

Raw Materials. The highly branched, short-chain polyols used for rigid foams can be initiated from amines such as diethylenetriamine to provide five functional sites or saccharides such as sorbitol or sucrose that have 6 or 8 functional

sites, respectively. Subsequent polymerization of PO and/or EO at low levels further controls viscosity and reactivity of the resultant polyol. The level of oxide addition also contributes to the rigidity of the final foam product by controlling the molecular weight per branch point as well as influencing shrinkage resistance and moisture sensitivity. Amine-initiated polyols tend to be autocatalytic because of the tertiary amine groups residual in the molecule.

The isocyanates used with rigid foam systems are either polymeric MDI or specialty TDIs. Both contain various levels of polymerized isocyanate groups that contribute to molecular weight per cross-link and also may affect reactivity because of steric hindrance of some isocyanate positions.

Surfactants for use with rigid foams are also silicone-based but are quite different from those used for flexible foams. In this case it is more important for the surfactant to also act as a compatibilizer in assisting the intermixing of the isocyanate and polyol during the reaction period. Of course nucleation and cell stabilization during the early phase of foaming are also important functions of the surfactant. Water may also be used in rigid formulations but to a much lesser degree than in flexible foams.

Rigid polyurethane foams are normally foamed with blowing agents having low thermal conductivities and low permeability, such as CFC-11 or HCFC-141b where it is still acceptable, and potentially HFC-245fa, HFC-365mfc, hydrocarbons, and CO_2 because of regulatory pressures. Because of the closed-celled structure of these foams and the low permeability of the blowing agent, the gas is retained in the foam for a long period, providing the superior insulating properties of these products. However, as blowing agents such as hydrocarbons and CO2, which have higher thermal conductivity and permeability, are used, the long-term insulation property will be diminished.

Catalysis is usually accomplished through the use of tertiary amines such as triethylenediamine. Other catalysts such as 2,4,6-*tris*-(*N*,*N*-dimethylaminomethyl)phenol are used in the presence of high levels of crude MDI to promote trimerization of the isocyanate and thus form isocyanurate ring structures. These groups are more thermally stable than the urethane structure and hence are desirable for improved flammability resistance (248). Some urethane content is desirable for improved physical properties such as abrasion resistance.

Miscellaneous chemicals are used to modify the final properties of rigid polyurethane foams. For example, halogenated materials are used for flammability reduction, diols may be added for toughness or flexibility, and terephthalate-based polyester polyols may be used for decreased flammability and smoke generation. Measurements of flammability and smoke characteristics are made with laboratory tests and do not necessarily reflect the effects of foams in actual fire situations.

Process and Equipment. Rigid polyurethane foam processes use the same high or low pressure pumping, metering, and mixing equipment as earlier described for flexible foams. Subsequent handling of the mixture is determined by the end product desired.

Lamination. Rigid foam boardstock with a variety of facer materials is commonly used for insulation in building construction. The boardstock is produced on

a continuous basis by applying the polyurethane (or polyisocyanurate) forming mixture onto one facer sheet, allowing the mixture to begin foaming, applying the second facer on top, and passing the assembly into a fixed gap conveyor to provide heat for cure and to control thickness. This is followed by edge trimming and cutting to board length. In this manner boardstock is produced with facer materials such as kraft paper, aluminum foil, and tarpaper and a foam core thickness ranging up to 10 cm (4 in.).

Pour-in-Place. The polyurethane forming mixture can be poured into a cavity that will then be filled by the flowing, foaming reaction mixture. This method is used for such things as insulating refrigerator cabinets and filling hull cavities in boats and barges.

Molding. The reaction mixture can be discharged into a mold to flow out and fill the cavity. High density (about 320 kg/m^3 or 20 lb/ft^3) moldings can be used for decorative furniture items such as drawer fronts or clock frames. The formulation can be adjusted to produce integral foams.

Bun Stock. By pouring the reaction mixture on a continuous belt a long bun can be produced like the flexible slab foam previously described. After curing, the bun can be cut into slabs or blocks as required by the end use.

Box Foams. A measured quantity of the reaction mixture can be placed in an open-topped crate or box and allowed to foam in a free rise mode. The block is removed after gelling and is cut into end use pieces after curing.

Spray. In spray-on applications the reactive ingredients are impingement mixed at the spray head. Thickness of the foam is controlled by the amount applied per unit area, and additional coats are used if greater than 2.5-cm (1.0-in.) thickness is required. This method is commonly used for coating industrial roofs or insulating tanks and pipes.

Applications. Rigid polyurethane foam laminates for residential sheating (1.2–2.5-cm-thick with aluminum skins) and roofing board (2.5–10.0 cm thick with roofing paper skins) are the leading products, with about 45 t of liquid spray systems also in use. Metal doors insulated by a pour-in-place process constitute another substantial use.

Household refrigerator and freezer designs have been influenced by the increased cost of energy and the need to develop competitive units with comparable energy efficiency ratings. These factors have increased the use of rigid polyurethane foam as pour-in-place insulation in place of the fiber glass insulation now used in only about 30% of the market. Since CFC and now mostly HCFC blown foams have much better insulating effectiveness, the cabinet wall thickness can be reduced from the former fiber-glass-centered design. The pour-in-place cabinet insulating process is carried out in large-scale integrated operations. Commercial refrigeration applications are found in cold storage room insulation, reach-in coolers, and retail display cases. These markets are also using more insulation to offset the higher cost of energy.

The principal use of rigid foam in the transportation market is for insulation of refrigerated truck trailers and bodies as well as refrigerated rail cars. The liquid urethane ingredients are usually poured into large panels held in a fixture. These are then used as integral components: walls, roofs, or floors of the trailer or rail car. Additional uses are insulated truck bodies, recreational vehicles, and cargo containers.

Tanks, pipes, and ducts have been increasingly insulated because of the high cost of energy. For example, oil storage tanks must be kept warm to maintain a moderate viscosity for pumping. The energy required to maintain this temperature can be sharply reduced by insulating the tank with rigid polyurethane foam. This type of insulation is often spray-applied but may also be cut from boardstock.

Packaging constitutes another significant use and is often a foam-in-place operation to protect industrial equipment such as pumps or motors. Furniture articles molded from rigid foam are used in the form of decorative drawer fronts, clock cases, and simulated wooden beams. Flotation for barge repair and sport boats as well as insulation for portable coolers are a few other uses.

Economics. Rigid foam systems are typically in the range of 32 kg/m^3 (2 lb/ft^3) and, are typically about 30–40% higher in price than the pour-in-place foam systems because of differences in raw material costs and process. Unit prices for pour-in-place polyurethane packaging systems fall between the competitive expandable polystyrene bead foam and low density polyethylene foams.

Polystyrene. There are five basic types of polystyrene foams produced in a wide range of densities and employed in a wide variety of applications: (*1*) extruded polystyrene board; (*2*) extruded polystyrene sheet; (*3*) expanded bead molding; (*4*) injection-molded structural foam; and (*5*) expanded polystyrene loose-fill packaging.

Expanded polystyrene (EPS) beadboard insulation is produced with expandable polystyrene beads. These beads are produced by impregnating with 5–8% pentane and sometimes with flame retardants such as hexabromocyclododecane or pentabromomonochlorohexane. The beads are preexpanded by fabricators with steam or vacuum and then allowed to age. The preexpanded beads are fed to the steam-heated block molds where further expansion and fusion of beads take place. The molded blocks are then sliced into various sizes needed for specific applications after curing. Block densities range from 13 to 48 kg/m^3 (0.8–3 lb/ft^3), with 24 kg/m^3 (1.5 lb/ft^3) most common for cushion packaging and 16 kg/m^3 (1.0 lb/ft^3) for insulation applications.

Expanded polystyrene bead molding products account for the largest portion of the drinking cup market and are used in fabricating a variety of other products including packaging materials, insulation board, and ice chests. The insulation value, the moisture resistance, and physical properties are inferior to extruded boardstock, but the material cost is much less.

Expanded polystyrene loose-fill packaging materials are produced normally by extrusion process followed by multiple steam expansions to give low density foam shapes that resemble "S," "8," and hollow shells. They are produced with either pentane or HCF-141b or pentane/HCFC-141b-mixed blowing agents, but with the eventual phase out of HCFC-141b, pentane, or CO_2. Expandable polystyrene loose-fill packaging material is also produced by suspension polymerization process with blowing agent incorporated into the polymer during the polymerization. Recently, starch-based loose-fill packaging products have been introduced using water as the primary blowing agent. These products are used as dunnage or space-filling materials for cushion packaging. Under severe load conditions, vibrational settling may occur, resulting in a nonuniform cushioning protection throughout the package. They have good shock absorbency, excellent resiliency, and are odorless.

The light weight of these products reduces user's shipping costs and conserves energy in transportation. These products are reusable, a key property from economic, ecological, and energy conservation standpoints. Most products are available in bulk densities of 4.0–4.8 kg/m^3 (0.25–0.30 lb/ft^3).

Extruded polystyrene board was first introduced in the early 1940s by Dow Chemical Co. with the tradename Styrofoam (86,252,253). The Styrofoam process consists of the extrusion of a mixture of polystyrene and volatile liquid blowing agent expanded through a die to form boards in various sizes. The continuous boards are then passed through the finishing equipment for further sizing.

In 1979, UC Industries, a joint venture between U.S. Gypsum and Condec Corp., began manufacture of a similar extruded polystyrene foam. Its process is believed to consist of a single-screw tandem extrusion line (114.3-mm main extruder and 152.4-mm extruder as a cooler) and produce foam boardstock in a vacuum chamber connected to a barometric leg that acts as a vacuum seal (254,255). The continuous foam board coming out of a pool of water is then passed through the finishing equipment for sizing.

In 1982, Minnesota Diversified Products, Inc. started to produce a similar extruded polystyrene foam insulation. This process (256) was developed by LMP (Lavorazione Materie Plastiche) SpA, Turin, Italy, and consists of a corotating twin-screw extruder (132-mm diameter, 21:1 L/D) with a single-screw extension as a cooling section, a combination motionless mixer/homogenizer and heat exchanger, a flat die, and finishing equipment for sizing and curing.

In 1992, Dow introduced CO_2 only blown-extruded polystyrene foam with the trademark Avance in response to environmental regulations of ozone, depleting gases (ODP). Later, BASF introduced a CO_2 and ethanol blown-extruded polystyrene foam with the trademark Styrodur C. Other potential non-ODP blowing agents being used are HFC-134a, HFC-152a, HFC-245, and HFC-365 and inorganic blowing agents such as nitrogen and water.

Extruded polystyrene foam sheet is primarily produced in a single-screw tandem extrusion line consisting of a 114.3-mm (4.5-in.) primary extruder, screen changer, 152.4-mm (6.0-in.) secondary extruder as a cooler, and an annular die. Typical throughput rate for this size ranges from 340 to 450 kg (h. The sheet is normally extruded in thicknesses of about 0.4–6.5 mm, and at densities from about 50 to 160 kg/m^3. Polystyrene pellets and a nucleating agent such as talc or a combination of citric acid and sodium bicarbonate are fed to a primary extruder and melted. A blowing agent such as *n*-pentane, isopentane, HCFC-22, or HFC-152a, and inorganics such as CO_2 and water is then injected into the primary extruder and mixed with the molten polymer. The mixture is passed through a secondary extruder to cool the mixture to appropriate foaming temperature. The cooled polymer gel is then passed through an annular die at which point foaming takes place. The foam bubble is pulled over a sizing mandrel and slit to obtain a flat sheet, which is then wound into a roll for storage and curing. The cured sheet is thermoformed into a finished product by either sheet manufacturers or fabricators. The raw material cost for the foam sheet is higher than that for the foam insulation boardstock because of its higher density. On the other hand, the capital cost for the foam sheet line is lower than that for the foam board because of its simpler finishing equipment. Primary application of foam sheet is as a packaging

material in items such as disposable dishes and food containers, trays for meat, poultry and produce products, and egg cartons.

Injection-molded structural foam is used widely for high density items such as picture frames, furniture, appliances, housewares, utensils, toys, pipes, and fittings. Most of these products are produced by injection molding or profile extrusion methods from impact-modified polystyrene. Almost all high density foam products are produced with a chemical blowing agent that releases either nitrogen or carbon dioxide, typically sodium bicarbonate or azodicarbonamides. Medium density products can be produced with either a physical or chemical blowing agent, or a combination of both.

Applications. In residential sheathing insulation, fiber board and oriented strand-board are the most widely used products because of their structural strength and cost. The use of extruded and molded polystyrene foam and of foil-faced isocyanurate foam is increasing, depending on the cost, the amount of insulation required, and compatibility of insulation with other construction systems. In cavity-wall insulation, mineral wool, polyurethane, urea–formaldehyde, and fiber glass are widely used, although fiber glass batt is the most economical insulation for stud-wall construction. In mobile and modular homes, cellular plastics are used widely because of their light weight and more efficient insulation value. The foam density ranges between 23 kg/m^3 (1.4 lb/ft^3) and 40 kg/m^3 (2.5 lb/ft^3) depending on the process and blowing agent used to produce a typical 25-mm (1-in.) sheathing product.

Poly(vinyl chloride). Cellular poly(vinyl chloride) (PVC) foam is available in both flexible and rigid foams. Flexible PVC foams are primarily produced by spread coating and calendering of fluid plastisols by means of a chemical blowing agent or mechanical frothing with air. Flexible PVC foams are also made by the extrusion process. Rigid PVC foams are produced by the extrusion or injection molding processes. Blowing is achieved by a chemical blowing agent or gas injection into the extruder.

Raw Materials. PVC is inherently a hard and brittle material and very sensitive to heat; thus it must be modified with a variety of plasticizers, stabilizers, and other processing aids to form heat-stable flexible or semiflexible products or with lesser amounts of these processing aids for the manufacture of rigid products (see VINYL POLYMERS; VINYL CHLORIDE POLYMERS). Plasticizer levels used to produce the desired softness and flexibility in a finished product vary between 25 parts per hundred (pph) parts of PVC for flooring products to about 80–100 pph for apparel products (248). Numerous Plasticizers (qv) are commercially available for PVC, although dioctyl phthalate (DOP) is by far the most widely used in industrial applications because of its excellent properties and low cost. For example, phosphates provide improved flame resistance, adipate esters enhance low temperature flexibility, polymeric plasticizers such as glycol adipates and azelates improve the migration resistance, and phthalate esters provide compatibility and flexibility (257).

In addition to modifying PVC with plasticizers, it is also necessary to incorporate heat heat stabilizers (qv) into the formulation in order to scavenge the HCl evolved at the processing temperatures, thereby reducing thermal degradation of the polymer. Typical heat stabilizers used for PVC are metallic compounds of barium, cadmium, zinc, lead, and tin; lead and zinc are the most common (257).

Plasticizers containing epoxy linkages such as epoxidized soy bean oil or synergistic compounds such as dibasic lead phthalate and dibasic lead phosphite are also used to enhance heat stability. Non–lead-containing heat stabilizers are currently being developed. Other ingredients such as color pigments and fillers are added to the formulation for the desired coloration and cost reduction, respectively.

There are two principal PVC resins for producing vinyl foams: suspension resin and dispersion resin. The suspension resin is prepared by suspension polymerization with a relatively large particle size in the 30–250-μm range and the dispersion resin is prepared by emulsion polymerization with a fine particle size in the 0.2–2-μm range (257). The latter is used in the manufacture of vinyl plastisols, which can be fused without the application of pressure. In addition, plastisol-blending resins, which are fine-particle-size suspension resins, can be used as a partial replacement for the dispersion resin in a plastisol system to reduce the resin costs.

A very widely used decomposable chemical blowing agent is azodicarbonamide. Its decomposition temperature and rate of evolution of gaseous components are greatly influenced by the stabilizers containing zinc. Lead and cadmium are considered moderate activators for *p*,*p*′-oxybis(benzenesulfonyl hydrazide) (OBSH). OBSH can also be used as a blowing agent for PVC foams.

Process and Equipment.

Flexible Poly(vinyl chloride) Foam. Spread coating is usually carried out by applying a thin coating of plastisol skin coat on a release paper, which is then partially fused in a forced air convection oven in the range of 150°C to facilitate rolling and unrolling of the product. This product passes through the second coating head where a plastisol-containing suitable chemical blowing agent is applied to the plastisol-skin side of the laminate. The fabric is then adhered to the foam plastisol and passed through the final oven at 200–235°C for fusion and foaming. The paper is separated from the vinyl foam and both the paper and the product are taken away by separate winding rolls (257). The optimum oven temperatures depend on the residence time and the type of blowing agent used.

A *calender processing* is also used to produce substantial quantities of vinyl–fabric laminates. Raw materials are first blended in a Banbury mixer operated at either elevated or room temperatures to dissolve the plasticizer into the PVC resin. The blended materials are fluxed into a homogeneous mass of vinyl compound. The material is then discharged to a Banbury mill to cool the batch down. The material can now be fed to an extruder and passed through the various nips between the calender rolls to obtain a sheet of well-controlled gauge. Vinyl foam–fabric, laminates may be produced by combining a vinyl film to be used as the skin layer and a vinyl sheet containing blowing agent with fabric, and activating the blowing agent by passing through a forced air convection oven.

The *chemical expansion method* is most widely used for the manufacture of flexible PVC foam. The three general methods used to produce flexible vinyl foam (258) are (*1*) the pressure molding technique, which consists of the decomposition of the blowing agent and fusion of the plastisol in a mold under pressure at elevated temperatures, cooling the mold, removing the molded part, and post-expansion at some moderate temperature; (*2*) the one-stage atmospheric foaming method in which the blowing agent is decomposed in the hot viscosity range that lies between the gelation and complete fusion of the plastisol; and (*3*) the two-stage atmospheric

foaming method in which the blowing agent is decomposed below the gelation of the plastisol, followed by heating at high temperature to fuse the foamed resin (259).

The *mechanical process* is used to produce low density, open-celled foam by expanding the plastisol before gelation and fusion. The three general methods (258) include the Dennis process (260), elastomer process (261), and the Vanderbilt process (262,263). The Dennis process utilizes a countercurrent adsorption technique by gravity feeding of the liquid plastisol through a packed absorption column under a low pressure (<690 kPa) of carbon dioxide in order to provide the largest surface area for absorption. The chilled plastisol mixture is pumped under pressure through a nozzle or tube and foams as it comes to atmospheric pressure. The wet foam is then gelled (170–182°C) in a conventional oven for thin sections or in a high frequency oven for thick sections.

The elastomer process is very similar to the Dennis process involving a number of steps in which a gas, formerly carbon dioxide and now fluorocarbon, is mixed with a plastisol under pressure. When released to atmospheric pressure, the gas expands the vinyl compounds into a low density, open-cell foam that is then fused with heat.

The Vanderbilt process involves the mechanical frothing of air into a plastisol containing proprietary surfactants by means of an Oakes foamer or a Hobart-type batch whip. The resulting stable froth is spread or molded in its final form, then gelled and fused under controlled heat. The fused product is open-celled with fine cell size and density as low as 160 kg/m^3 (10 lb/ft^3).

Rigid Poly(vinyl chloride) Foam. The techniques that have been used to produce rigid vinyl foams are similar to those for the manufacture of flexible PVC foams. The two processes that have reached commercial importance for the manufacture of rigid vinyl foams (258) are the Dynamit–Nobel extrusion process and the Kleber–Colombes Polyplastique process for producing cross-linked grafted PVC foams from isocyanate-modified PVC in a two-stage molding process.

The Dynamit–Nobel extrusion process (264) utilizes a volatile plasticizer such as acetone that is injected into the decompression section of a two-stage screw and is uniformly dispersed in the vinyl resin containing a stabilizer. The resulting PVC foam has low density and closed cells.

The Kleber–Colombes rigid PVC foam (265,266) is produced by compression molding vinyl plastisol to react and gel the compound, followed by steam expansion. The process involves mixing, molding, and expansion. The formulation consists of PVC, isocyanate, vinyl monomers such as styrene, anhydrides such as maleic anhydride, polymerization initiators, FC-11, and nucleators. The ingredients are mixed in a Werner–Pfleiderer or a Baker Perkins type of mixer, and the resulting plastisol is molded under pressure. The initial temperature of the molds is 100–110°C, which increases to 180–200°C because of exothermic polymerization of the vinyl monomers and anhydride. The mold is cooled and the partially expanded PVC is removed and then further expanded by steam. After the water treatment, the foam is thermoset with a closed-celled structure and a relatively low thermal conductivity.

Applications. Flexible cellular poly(vinyl chloride) was developed as a comfort-cushioning material with compression–deflection behavior similar to latex rubber foam, and with the added feature of flame retardancy (37). It has a

larger compression set than either latex rubber or polyurethane foams. The fact that the plasticizer in flexible vinyl foams can migrate to the surface restricts flexible vinyl foams in some applications. Furniture and motor vehicle upholstery is the largest market for flexible vinyl foams. Because of better aesthetics (leather-like plastics), comfort, and favorable pricing, they are expected to show good growth in upholstery, carpet backing, resilient floor coverings, outerwear, footwear, luggage, and handbags. The only application for flexible vinyl foams in protective packaging applications is for stretch pallet wraps. These wraps are produced by extrusion.

Rigid vinyl foams in construction markets have grown substantially as a result of improved techniques to manufacture articles with controlled densities and smooth outer surfaces. Wood molding substitute for door frames and other wood products is an area that has grown. Rigid vinyl foams are also used in the manufacture of pipes and wires as resin extenders and in sidings and windows as the replacement of wood or wood substitutes.

Economics. The price of rubber-modified flexible PVC foam ranges between about \$2.00 and \$3.00 per board foot (\$800–1200/m^3) and that of unmodified, plasticized PVC foam is about \$0.70 and \$2.50 per board foot (\$300–\$1000/m^3) depending on the volume, thickness, and density of the product.

Polyolefins.

Polyethylene. There are three basic types of polyethylene foams of importance: (*1*) extruded foams from low density polyethylene (LPDE); (*2*) foam products from high density polyethylene (HDPE); and (*3*) cross-linked polyethylene foams. Other polyolefin foams have an insignificant volume as compared to polyethylene foams and most of their uses are as resin extenders.

Extruded low density foam produced from LDPE is a tough, flexible, and resilient closed-celled foam used in a wide variety of applications such as cushion packaging and safety components. The resiliency of this product gives excellent energy absorption so important in cushion packaging, athletic pads, flotation devices, and occupant safety applications. Unlike other resilient products, uniform energy absorption can be achieved with low density polyethylene foam over an extremely wide temperature range from −54 to 71°C. The closed-celled nature of this product leads to negligible water pickup. This is important in military packaging where outdoor tropical storage or shipments in high humidity ship holds is common or where freeze–thaw arctic storage conditions are encountered. These products are produced primarily with, isobutane and a selective permeability modifer, glycerol monostearate. The permeability modifier plays a unique role in achieving the dimensional stability of the flexible low density polyethylene foam over the wide range of temperatures because of its ability to closely match the permeability through LDPE of isobutane with that of air (267).

HDPE foam is primarily used as a high density rigid product. Shipping pallets are a rapidly growing market, at a projected growth rate of about 26% per year for the mid-1990s. Most of these products are produced by thermoforming sheet and injection molding.

Cross-linked polyethylene foams are produced by either radiation or chemical cross-linking of an extruded expandable sheet containing a chemical blowing agent. The cross-linked expandable sheet is subsequently passed over a molten

salt bath or passed through hot-air ovens. This process is somewhat complicated, expensive, and limited to the thin products in the continuous process but thicker foams can be produced in a more complicated batch process. A batch molding process utilizing expandable beads is also used to produce thicker foams. These products can be produced in a wide range of densities and thicknesses, with fine cell size, having more flexibility, higher resiliency, and better thermoforming capability than the extruded foam products from LDPE. These products also have finer texture and a softer, more resilient feel than extruded low density polyethylene foams and are used in comfort, cushioning and cushion-packaging applications.

Kanegafuchi Chemical of Japan has introduced a chemical cross-linking process for producing PE foams by the bead technique similar to EPS. These beads have been used to produce molded articles as cushioning materials, sound insulating panels, etc. Asahi-Dow and BASF have also been reported to have developed similar products.

Polypropylene. Recently the successful production of polypropylene foam plank of large crosssections has been accomplished by the Dow Chemical Co. by using a die that creates a foam product consisting of a plurality of coalesced strands or profiles (268). Among other uses, this unique structural olefinic foam STANDFOAM EA (trademark of The Dow Chemical Co.) has been successfully applied in automotive energy absorption applications (269).

Health and Safety

Flammability. Plastic foams are organic in nature and, therefore, are combustible. They vary in their response to small sources of ignition because of composition and/or additives (268). All plastic foams should be handled, transported, and used according to manufacturers' recommendations as well as applicable local and national codes and regulations.

Among the blowing agents, hydrocarbons and some of the HCFCs and HFCs are flammable and pose a fire hazard in handling at the manufacturing plants.

Atmospheric Emissions. Certain organic compounds are found to be smog-generating substances because of their high photochemical reactivity at ambient conditions. Examples include hydrocarbon, ethanol, and ethyl chloride. Since fully or partially halogenated hydrocarbons, HCFCs and HFCs, are considered to have low reactivity in the lower atmosphere (troposphere), substitution of photochemically reactive compounds for the current blowing agents may reduce ozone depletion in the stratosphere, but may have unacceptable global warming potentials (GWP). Therefore, the blowing agent interaction with the total environment needs to be considered in developing environmentally acceptable alternative blowing agents (46).

Toxicity. The products of combustion have been studied for a number of plastic foams (270). As with other organics the primary products of combustion are most often carbon monoxide and carbon dioxide, with smaller amounts of many other species, depending on product composition and test conditions.

The presence of additives or unreacted monomers in certain plastic foams can limit their use where food or human contact is anticipated. Heavy metals

can also be found in various additives. The manufacturers' recommendations or existing regulations again should be followed for such applications.

BIBLIOGRAPHY

"Cellular Materials" in *EPST* 1st ed., Vol. 3, pp. 80–130, by R. E. Skochdopole, The Dow Chemical Co.; "Cellular Materials" in *EPSE* 2nd ed., Vol. 3, pp. 1–59, by K. W. Suh and D. D. Webb, The Dow Chemical Co.

1. E. Ott, H. M. Spulin, and M. W. Grafflin, eds., *Cellulose and Cellulose Derivatives*, 2nd ed., Part I, Interscience Publishers, Inc., New York, 1954, p. 9.
2. U.S. Pat. 942,699 (Dec. 7, 1909), L. H. Baekeland.
3. E. W. Madge, *Latex Foam Rubber*, John Wiley & Sons, Inc., New York, 1962.
4. H. Junger, *Kunststoff-Rundschau* **9**, 437 (1962).
5. W. C. Goggin and O. R. McIntire, *Br. Plast.* **19**, 528 (1947).
6. A. F. Randolph, ed., *Plastics Engineering Handbook*, 3rd ed., Reinhold Publishing Corp., New York, 1960, pp. 137–138.
7. J. H. Saunders and K. C. Frisch, *Polyurethanes, Chemistry and Technology*, Vol. **I**, Wiley-Interscience, New York, 1963.
8. A. E. Lever, *Plastics (London)* **18**, 274 (1953).
9. *Plast. World*, 1 (May 1953).
10. *ETHAFOAM Brand Polyethylene Foam(bulletin)*, The Dow Chemical Co., Midland, Mich., 1980.
11. U.S. Pat. 3,058,161 (Oct. 16, 1962), C. E. Beyer and R. B. Dahl (to The Dow Chemical Co.).
12. L. Nicholas and G. T. Gmitter, *J. Cell, Plast.* **1**(1), 85 (1965).
13. T. Wirtz, paper presented at the 2nd SPI International Cellular Plastic Conference, Society of Plastics Industry, New York, Nov. 8, 1968.
14. *ITA, P.: Industry Study 485, Foam Plastics*, The Freeonia Group, Inc., May, 1993.
15. *ASTM D883-80C, American Society for Testing and Materials*, Philadelphia, Pa., 1982.
16. J. D. Griffin and R. E. Skochdopole, in E. Baer, ed., *Engineering Design for Plastics*, Reinhold Publishing Corp., New York, 1964.
17. A. Cooper, *Plast. Inst. (London) Trans.* **26**, 299 (1958).
18. *ASTM D1566-82*, Vol. 37, ASTM, Philadelphia, Pa., 1982.
19. *ASTM D1056-78*, ASTM, Philadelphia, Pa., 1982.
20. *ASTM D1055-80*, ASTM, Philadelphia, Pa., 1982.
21. K. W. Suh, in D. Klempner and K. C. Frisch, eds., *Polymeric Foams*, Hanser Publishers, New York, 1991.
22. F. Shutov, *Integral/Structural Polymer Foams*, Springer-Verlag, Berlin, 1986.
23. R. H. Hansen, *SPE J.* **18**, 77 (1962).
24. A. R. Ingram and H. A. Wright, *Mod. Plast.* **41**(3), 152 (1963).
25. K. Hinselmann and J. Stabenow, *Ver. Dtsch. Ing.* **18**, 165 (1972).
26. K. C. Frisch and J. H. Saunders, *Plastic Foams*, Vol. **1**, Part 1, Marcel Dekker, Inc., New York, 1972.
27. U.S. Pat. 2,681,321 (June 15, 1954), F. Stastny and R. Gaeth (to BASF).
28. U.S. Pat. 2,983,692 (May 9, 1961), G. F. D'Alelio (to Koppers Co.).
29. H. R. Lasman, *Mod. Plast.* **42**(1A), 314 (1964).
30. S. J. Skinner, S. Baxter, and P. J. Grey, *Trans. J. Plast. Inst.* **32**, 180 (1964).
31. Ref. 30, p. 212.

32. S. J. Skinner and S. D. Eagleton, *Trans. J. Plast. Inst.* **32**, 321 (1964).
33. K. Goodier, *Br. Plast.* **35**, 349 (1962).
34. U.S. Pat. 3,697,454 (Oct. 10, 1972), R. L. Trimble (to Sinclair Koppers).
35. U.S. Pat. 3,066,382 (Dec. 4, 1962), M. L. Zweigle and W. E. Humbert (to The Dow Chemical Co.).
36. *PELASPAN-PAC Bulletin*, The Dow Chemical Co., Midland, Mich., 1979.
37. R. J. Meyer, *SPE J.* **18**, 678 (1962).
38. Jpn. Kokai 72,43,059 (June 22, 1972), J. Morita and co-workers (to Nitto Electric Industrial Co. Ltd.).
39. Jpn. Pat. 73,04,868 (Feb. 12, 1973), S. Nakada and co-workers (to Sekisui Chemical Co. Ltd.).
40. Br. Pat. 1,333,392 (Oct. 10, 1973), S. Minami and co-workers (to Toray Industries, Inc.).
41. U.S. Pat. 3,812,225 (May 21, 1974), K. Hosoda and co-workers (to Furukawa Electric).
42. Fr. Pat. 1,446,187 (July 15, 1966), J. Zizlsperger and co-workers (to BASF).
43. A. Osakada and M. Koyama, *Jpn. Chem. Q.* **5**, 55 (1969).
44. J. H. Saunders and K. C. Frisch, *Polyurethanes, Chemistry and Technology*, Vol. **II**, Wiley-Interscience, New York, 1964.
45. G. Woods, *Flexible Polyurethane Foams*, Elsevier Applied Science Publishers Inc., New York, 1982.
46. *Handbook for the Montreal Protocol on Substances that Deplete the Ozone Layer*, 2nd ed., Ozone Secretariat, UNEP, New York, Oct. 1991.
47. F. O. Baskent and J. Pavlenyi, *Plast. Compound.* (Mar./Apr. 1983).
48. H. J. Kollmeier, H. Schator, and P. Zaeske, in Proceedings of the SPI, 26th Annual Conference, San Francisco, Technomic Publishing Co., Stamford, Conn., Nov. 1981, p. 219
49. *VORSURF 504*, technical data sheet #109-01558, The Dow Chemical Co., Midland Mich., Jan. 2002.
50. K. C. Frisch, K. J. Patel, and R. D. Marsh, *J. Cell, Plast.* **6**, 203 (1970).
51. R. Merten and co-workers, *J. Cell. Plast.* **4**, 262 (1968).
52. H. J. Papa, *Ind. Eng. Chem. Pod. Res. Dev.* **9**, 478 (1970).
53. R. H. Fish, *Proc. NASA Conf. Mater. Improved Fire Safety* **11**, 1 (1970).
54. K. C. Frisch and J. H. Saunders, *Plastic Foams*, Vol. **1**, Part 2, Marcel Dekker, Inc., New York, 1973.
55. C. J. Benning, *Plastic Foams*, Vol. **1**, Wiley-Interscience, New York, 1969.
56. H. Weissenfeld, *Kunststoffe* **51**, 698 (1961).
57. Ref. 12, p. 149.
58. U.S. Pat. 3,821,337 (June 28, 1974), E. J. Bunclark and co-workers (to Esso Research Engineering).
59. *Plastic Age*, 17th ed., Japan Plastics Industry Annual, Tokyo, 1974.
60. U.S. Pat. 3,726,708 (Apr. 10, 1973), F. Weissenfels and co-workers (to Dynamit Nobel).
61. Fr. Pat. 2,185,488 (Feb. 8, 1974), J. Dugelay.
62. U.S. Pat. 3,830,894 (Aug. 20, 1974), H. Juenger and co-workers (to Dynamit Nobel).
63. U.S. Pat. 3,807,661 (Mar. 11, 1975), P. J. Crook and S. P. Riley (to Pilkington Brothers, Ltd.).
64. U.S. Pat. 3,907,723 (Sept. 23, 1975), M. Pretot (to Certain-Teed Products Corp.).
65. Ger. Offen. 2,204,945 (Sept. 21, 1972), J. Tardy and co-workers.
66. Fr. Pat. 2,190,613 (Mar. 8, 1974), J. Tardy.
67. U.S. Pat. 3,766,100 (Oct. 16, 1973), H. A. Meyer-Stoll and co-workers (to Deutsche Texaco).

68. U.S. Pat. 3,741,920 (June 26, 1973), F. Weissenfels and co-workers (to Dynamit Nobel).
69. U.S. Pat. 3,694,387 (Sept. 26, 1972), H. Junger and co-workers (to Dynamit Nobel).
70. USSR Pat. 358,342 (Nov. 3, 1972), I. F. Ustinova and co-workers (to Kucherenko, VA, Central Scientific Research Institute of Building Structures).
71. U.S. Pat. 3,101,242 (Aug. 20, 1963), J. M. Jackson Jr. (to V. L. Smithers Manufacturing).
72. Jpn. Pat. 72,19,624 (June 5, 1972), M. Asaoka and co-workers (to Hitachi Chemical).
73. Br. Pat. 1,268,440 (Mar. 29, 1972), D. J. Rush and co-workers (to Midwest Research Institute).
74. K. Murai, *Plast. Age* **18**(6), 93 (1972).
75. V. D. Valgin and co-workers, *Plast. Massy* **1**, 28 (1974).
76. V. C. Valgin, *Europlast. Mon.* **46**(7), 57 (July 1973).
77. U.S. Pat. 3,400,183 (Sept. 3, 1968), P. I. Vidal (to Rocma Anstalt).
78. U.S. Pat. 3,214,793 (Nov. 2, 1965), P. I. Vidal (to Rocma Anstalt).
79. U.S. Pat. 3,122,326 (Feb. 25, 1964), D. P. Cook (to Union Carbide).
80. Ref. 12, p. 140.
81. *Epon Foam Spray 175, A Low Temperature Insulation (bulletin)*, Shell Chemical Co., Houston, Tex., Nov. 1963.
82. Ref. 12, p. 164.
83. H. Vincent and K. R. Hoffman, *Mod. Plast.* **40**, 418 (1962).
84. J. Gagiani, U. A. K. Sorathia, and A. L. Wilcoxson, NASA Report CR-151472, NIST Publication N77-28301 (June, 1977)
85. *ROHACELL Composite Foams (product literature)*, Richmond Aircraft Products, Norwalk, Calif. 2001.
86. U.S. Pat. 2,515,250 (July 18, 1950), O. R. McIntire (to The Dow Chemical Co.).
87. V. L. Gliniecki, Seventh Ann. Tech. Conf., Proc., SPI, New York, Apr. 24-25, 1963.
88. *Mod, Plast.* **51**(1), 36, 40 (Jan. 1974).
89. T. P. Martens and co-workers, *Plast. Technol.* **12**(9), 46 (1966).
90. D. A. Knauss and F. H. Collins, *Plast. Eng.* **30**(2), 34 (1974).
91. F. H. Collins and co-workers, *Soc. Plast. Eng. Tech. Pap.* **19**, 643 (1973).
92. L. W. Meyer, *SPE J.* **18**, 1341 (1962).
93. Ref. 12, p. 139.
94. W. T. Higgins, *Mod. Plast.* **31**(7), 99 (1954).
95. U.S. Pat. 3,251,911 (May 17, 1966), R. H. Hansen (to Bell Telephone Lab.).
96. U.S. Pat. 3,268,636 (Aug. 23, 1966), R. G. Angell Jr. (to Union Carbide Corp.).
97. U.S. Pat. 3,065,190 (Nov. 20, 1962), D. S. Chisholm and co-workers (to The Dow Chemical Co.).
98. U.S. Pat. 3,067,147 (Dec. 4, 1962), L. C. Rubens and co-workers (to The Dow Chemical Co.).
99. J. L. Throne, *J. Cell. Plast.* **12**, 264 (1976).
100. J. L. Throne and F. Shutov, in J. I. Kroschwitz, ed., *Encyclopedia of Polymer Science and Engineering*, 2nd ed., Vol. **15**, John Wiley & Sons, Inc., New York, 1985, pp. 771–797.
101. R. W. Freund and co-workers, *Plast. Technol.*, 35 (Nov. 1973).
102. U.S. Pat. 3,436,446 (Apr. 1, 1969), R. G. Angell Jr. (to Union Carbide Corp.).
103. *USM Foam Process, Technical Bulletin No. 653-A*, Farrel Co. Division, Ansonia, Conn.
104. Fr. Pat. 1,498,620 (Sept. 11, 1967), P. Botillier (to Ugine-Kuhlmann).
105. Ref. 12, p. 189.
106. U.S. Pat. 2,666,036 (Jan. 12, 1954), E. H. Schwencke (to Elastomer Chemical Co.).
107. U.S. Pat. 2,763,475 (Sept. 18, 1956), I. Dennis.

108. U.S. Pat. 4,473,665, (1985) J. E. Martini-Viedendnsky, N. P. Suh, and A. Waldmen (to Trexel Corp.)
109. U.S. Pat. 5,674,916, (1997) C. D. Shmidt, D. D. Imeokparia, and K. W. Suh (to The Dow Chemical Co.).
110. R. C. Bascom, *Rubber Age* **95**, 576 (1964).
111. A. Cooper, *Plast. Inst. Trans. J.* **29**, 39 (1961).
112. L. Spenadel, *Rubber World* **150**(5), 69 (1964).
113. U.S. Pat. 3,062,729 (Nov. 6, 1962), R. E. Skochdopole, L. C. Rubens, and G. D. Jones (to The Dow Chemical Co.).
114. J. J. Kolb, in B. C. Wendle, ed., *Engineering Guide to Structural Foam*, Technomic Publishing Co., Inc., Westport, Conn., 1976, p. 161.
115. A. Cooper, *Plast. Inst. Trans. J.* **29**, 39 (1961).
116. T. H. Rogers, Paper presented at Regional Tech. Conf., Palisades Section, Society of Plastics Engineers, New York, Nov. 1964.
117. *Dow Latex Foam Process (bulletin)*, The Dow Chemical Co., Midland, Mich.
118. *Iporka (bulletin)*, Badische Anilin- und Soda-Fabrik AG, Ludwigshafen am Rhein, Germany, July 1953.
119. T. H. Ferrigno, *Rigid Plastic Foams*, Reinhold Publishing Corp., New York, 1963, pp. 76–86.
120. T. E. Cravens, *Carpet Rug Ind.* (Oct. 1976).
121. *EXPANCEL*, Technical data sheet #1, Nobel Industries Sweden, Feb 12, 1988.
122. *Dow Low Temperature Systems (bulletin)*, 179-2086-77, The Dow Chemical Co., Midland, Mich., 1977.
123. U.S. Pat. 2,959,508 (Nov. 8, 1960), D. L. Graham and co-workers (to The Dow Chemical Co.).
124. J. B. Brooks and L. G. Rey, *J. Cell. Plast.* **9**, 232 (1973).
125. *Chem. Week* **19**(17), 43 (1962).
126. *Chem. Eng. News* **37**(36), 42 (1959).
127. U.S. Pat. 2,772,995 (Dec. 4, 1956), J. D. C. Wilson II (to E. I. du Pont de Nemours & Co., Inc.).
128. Can. Pat. 762,421 (July 4, 1967), M. E. Baguley (to Courtaulds Ltd.).
129. W. Worthy, *Chem. Eng. News*, 23 (Dec. 11, 1978).
130. U.S. Pat. 5,268,224 (Dec. 7, 1993), T. A. Thomas, K. J. Stone, G. A. Young, G. D. LaVon, and J. C. Dyer (to Procter and Gamble Corp.)
131. *1993 Annual Book of ASTM Standards*, ASTM, Philadelphia, Pa., 1993.
132. W. H. Touhey, *J. Cell. Plast.* **4**, 395 (1968).
133. C. J. Hilado, *J. Cell. Plast.* **3**, 502 (1967).
134. K. W. Suh and D. D. Webb, in J. I. Kroschwitz, ed., *Encyclopedia of Polymer Science and Engineering*, 2nd ed., Vol. **3**, John Wiley & Sons, Inc., New York, 1985, p. 1.
135. R. P. Toohy, *Chem. Eng. Prog.* **57**(10), 60 (1961).
136. C. A. Schutz, *J. Cell, Plast.* **4**(2), 37 (1968).
137. R. J. Bender, ed., *Handbook of Foamed Plastics*, Lake Publishing Co., Libertyville, Ill., 1965.
138. *Mod. Plast. Enc.* **54**, 485 (1977–1978).
139. *STYROFOAM SI Brand Plastic Foam (bulletin)*, The Dow Chemical Co., Midland, Mich., 1978.
140. Ref. 138, p. 776.
141. *Sweets Catalog File 7, Thermal and Moisture Protection*, Sweets Div., McGraw-Hill Information System Co., New York, 1978.
142. *ETHAFOAM Brand Plastic Foam (bulletin)*, The Dow Chemical Co., Functional Products and Systems Dept., Midland, Mich., 1976.

143. H. H. Lubitz, *J. Cell, Plast.* **5**, 221 (1969).
144. J. E. Knight, in Proceedings of the SPI 27th Annual Conference, Bal Harbour, Fla., Technomic Publishing Co., Stamford, Conn., Oct. 1982, p. 227.
145. W. R. Nicholson and J. E. Plevyak, Ref. 167, p. 306.
146. J. Pavlenyi and F. O. Baskent, Ref. 167, p. 295.
147. G. Woods, *Flexible Polyurethane Foams*, Elsevier Applied Science Publishers Inc., New York, 1982.
148. C. E. Lee and co-workers, *J. Cell, Plast.* **13**(1), 62 (1977).
149. Y. Landler, *J. Cell, Plast.* **3**, 400 (1967).
150. R. K. Traeger, *J. Cell, Plast.* **3**, 405 (1967).
151. H. E. Reymove and co-workers, *J. Cell. Plast.* **11**, 328 (1975).
152. *U.S. Foamed Plastics Market and Directory*, Technomic Publishing Co., Stamford, Conn., 1973.
153. R. E. Skochdopole, *Chem. Eng. Prog.* **57**(10), 55 (1961).
154. R. H. Harding, *Mod. Plast.* **37**(10), 156 (1960).
155. D. M. Rice and L. J. Nunez, *SPE J.* **18**, 321 (1962).
156. *Br. Plast.* **35**, 18 (1962).
157. A. J. deVries, *Meded. Rubber Sticht. Delft* **326**, 11 (1957); *Rec. Trav. Chim.* **77**, 81, 209, 283, 383, 441 (1958).
158. T. L. Phillips and D. A. Lannon, *Br. Plast.* **34**, 236 (1961).
159. R. E. Skochdopole and L. C. Rubens, *J. Cell, Plast.* **1**(1), 91 (1965).
160. A. Cooper, *Plast. Inst. Trans.* **26**, 299 (1958).
161. D. J. Doherty, R. Hurd, and G. R. Lester, *Chem. Ind. (London)*, 1340 (1962).
162. J. F. Hawden, *Rubber Plast. Age* **44**, 921 (1963).
163. R. H. Harding, *J. Cell. Plast.* **1**, 385 (1965).
164. R. H. Harding, *Resinography of Cellular Materials*, ASTM Technical Publication 414, ASTM, Philadelphia, Pa., 1967.
165. R. J. Corruccini, *Chem. Eng. Prog.* **53**, 397 (1957).
166. E. A. Meinecke and R. E. Clark, *Mechanical Properties of Polymeric Foams*, Technomic Publishing Co., Stamford, Conn., 1972.
167. R. M. McClintock, *Adv. Cryog. Eng.* **4**, 132 (1960).
168. W. B. Brown, *Plast. Prog.* **1959**, 149 (1960).
169. G. M. Hart, C. F. Balazs, and R. B. Clipper, *J. Cell, Plast.* **9**(3), 139 (1973).
170. J. L. Eakin, *Plast. Eng.* **34**(7), 56 (1978).
171. G. H. Smith, *Rubber Plast. Age* **44**(2), 148 (1963).
172. G. J. Bibby, *Rubber Plast. Age* **45**(1), 52 (1964).
173. *Plast, Technol.* **8**(4), 26 (1962).
174. J. H. Saunders and co-workers, *J. Chem. Eng. Data* **3**, 153 (1958).
175. R. P. Marchant, *J. Cell, Plast.* **8**(2), 85 (1972).
176. T. H. Rogers and K. C. Hecker, *Rubber World* **139**, 387 (1958).
177. C. G. Seefried and co-workers, *J. Cell, Plast.* **10**(4), 171 (1974).
178. J. M. Buist and A. Lowe, *Trans. Plast. Inst.* **27**, 13 (1959).
179. J. Talaly, *Ind. Eng. Chem.* **46**, 1530 (1954).
180. A. N. Gent and A. G. Thomas, paper presented at Prox. 7th Ann. Tech. Conf., Cellular Plastics Div., SPI, New York, Apr. 1963.
181. L. Talalay and A. Talalay, *Ind. Eng. Chem.* **44**, 791 (1952).
182. M. A. Mendelsohn and co-workers, *J. Appl. Polym. Sci.* **10**, 443 (1966).
183. E. A. Blair, *Resinography of Cellular Materials*, ASTM Technical. Publication. 414, ASTM, Philadelphia, Pa., 1967, p. 84.
184. J. H. Saunders, *Rubber Chem. Technol.* **33**, 1293 (1960).
185. B. Beals, F. J. Dwyer, and M. A. Kaplan, *J. Cell. Plast.* **1**(1), 32 (1965).
186. R. P. Kane, *J. Cell. Plast.* **1**(1), 217 (1965).

187. *Plast. Technol.* **8**(4), 26 (1964).
188. S. M. Terry, *J. Cell. Plast.* **7**(5), 229 (1971).
189. S. M. Terry, *J. Cell. Plast.* **12**(3), 156 (1976).
190. R. L. Gorring and S. W. Churchill, *Chem. Eng. Prog.* **57**(7), 53 (1961).
191. M. E. Stephenson Jr. and M. Mark, *ASHRAE J.* **3**(2), 75 (1961).
192. F. O. Guenther, *SPE Trans.* **2**, 243 (1962); A. Cunningham and co-workers, *Cell. Plast.* **7**, 1 (1988).
193. R. E. Knox, *ASHRE J.* **4**(10), 3 (1962); D. W. Reitz and co-workers, *J. Cell. Plastics* **20**, 332 (1984).
194. R. H. Harding, *Ind. Eng. Chem. Proc. Des. Dev.* **3**(2), 117 (1964);
195. J. R. Booth, in R. S. Graves and D. C. Wysocki, eds., *Insulating Materials: Testing and Applications*, ASTM 1116, ASTM, Philadelphia, Pa., 1991.
196. *Freon Technical Bulletin #B-2*, E. I. du Pont de Nemours & Co., Inc., Wilmington, Del., 1975; *Freon Technical Bulletin #AG-1*, E. I. du Pont de Nemours & Co., Inc., Wilmington, Del., 1992.
197. J. H. Perry, *Chemical Engineers Handbook*, 4th ed., McGraw-Hill Book Co., New York, 1963.
198. F. J. Norton, *J. Cell. Plast.* **3**(1), 23 (1967).
199. R. M. Lander, *Refrig. Eng.* **65**(4), 57 (1957).
200. B. K. Larkin and S. W. Churchill, *AIChE J.* **5**, 467 (1959).
201. B. Y. Lao and R. E. Skochdopole, paper presented at 4th SPI International Cellular Plastics Conference, Montreal, Canada, Nov. 1976.
202. G. A. Patten and R. E. Skochdopole, *Mod. Plast.* **39**(11), 149 (1962); I. R. Shankland, *Adv. Foam Aging* **1**, 60 (1986).
203. C. J. Hilado, *J. Cell. Plast.* **3**(4), 161 (1967).
204. I. R. Shankland, Paper presented at the International Workshop on Long Term Thermal Performance of Cellular Plastics, SPI, Canada, Oct. 1989.
205. R. R. Dixon, L. E. Edleman, and D. K. McLain, *J. Cell. Plast.* **6**(1), 44 (1970).
206. C. F. Sheffield, Paper presented at the ORNL Symposium on Mathematical Modeling of Roofs, Oak Ridge National Laboratory, Oak Ridge, Tenn., Sept. 15, 1988.
207. G. W. Ball, R. Hurd, and M. G. Walker, *J. Cell. Plast.* **6**(2), 66 (1970); D. W. Reitz and co-workers, *J. Cell. Plastics* **20**, 104 (1984).
208. U.S. Pat. 5,679,718 (Oct. 21, 1997), K. W. Suh, M. Yamada, C. D. Shmidt, and D. D. Imeokparia (to The Dow Chemical Co.).
209. W.O. 9006339 (June 14, 1990), F. Romesberg (to the Dow Chemical Co.); U.S. Pat. 5,010,112 (Apr. 23, 1991) L. R. Glicksman and co-workers; 5,373,026 (1994), A. Bartz (both to The Dow Chemical Co.)
210. L. Vahl, in Ref. 117, p. 267.
211. C. H. Wheeler, Foamed Plastics, U.S. Army Natick Labs and Committee on Foamed Plastics, U.S. Dept. Comm. Office Tech. Serv. PB Rept. 181576, Apr. 22-23, 1963, p. 164.
212. G. A. Patten, *Mater. Des. Eng.* **55**(5), 117 (1962).
213. FTC Consent Agreement, file #7323040, The Dow Chemical Co., Midland, Mich., 1974.
214. C. P. Hedlin, *J. Cell, Plast.* **13**(5), 313 (1977).
215. F. J. Dechow and K. A. Epstein, *Thermal Transmission Measurements of Insulation*, ASTM STP 660, ASTM, Philadelphia, Pa., 1978, p. 234.
216. M. M. Levy, *J. Cell. Plast.* **2**(1), 37 (1966).
217. I. Paljak, *Mater. Constr. (Paris)* **6**, 31 (1973).
218. H. Mittasch, *Plaste Kautsch*, **16**, 268 (1969).

219. J. Achtziger, *Kunststoffe* **23**, 3 (1971).
220. C. W. Kaplar, CRREL Internal Report No. 207, U.S. Army CRREL, Hanover, N. H., 1969.
221. P. J. Palmer, *J. Cell, Plast.* **9**(4), 182 (1973).
222. N. Z. Searle and R. C. Hirt, *SPE Trans.* **2**, 32 (1962).
223. *QUASH Sound Management Foam (product literature)*, Form #172-01502-3000GS, The Dow Chemical Co., (2001).
224. A. Cooper, *Plastics* **29**(321), 62 (1964).
225. *Mod, Plast.* **39**(8), 93 (1962).
226. G. L. Ball II, M. Schwartz, and J. S. Long, *Off. Dig. Fed. Soc. Paint Technol.* **32**, 817 (1960).
227. E. F. Cuddihy and J. Moacanin, *J. Cell, Plast.* **3**(2), 73 (1967).
228. C. E. Rogers, in E. Baer, ed., *Engineering Design for Plastics*, Reinhold Publishing Corp., New York, 1964.
229. *INSTILL Vacuum Insulation Core (bulletin)*, Form #174-01002-998SMG, The Dow Chemial Co., Midland, Mich., (1998).
230. S. C. A. Paraskevopoulos, *J. Cell, Plast.* **1**(1), 132 (1965).
231. *Forming Thin Shells (bulletin)*, The Dow Chemical Co., Midland, Mich., 1962.
232. R. K. Stern, *Mod. Packag.* **33**(4), 138 (1959).
233. R. G. Hanlon and W. E. Humber, *Mod. Packag.* **35**(10), 158 (1962).
234. M. Bakker, ed., *The Wiley Encyclopedia of Packaging Technology*, John Wiley & Sons, Inc., New York, 1986, p. 228.
235. R. G. Hanlon and W. E. Humbert, *Package Eng.* **7**(4), 79 (1962).
236. K. Brown, *Package Design Engineering*, John Wiley & Sons, Inc., New York, 1959.
237. A. R. Gardner, *Prod. Eng.* **34**(25), 114 (1963).
238. N. C. Hilyard and co-workers, *Mechanics of Cellular Plastics*, Macmillan Publishing Co., Inc., New York, 1982.
239. C. Kienzle, paper presented at Regional Technical Conference, Buffalo, N.Y., Society of Plastics Engineers, Inc., New York, Oct. 5, 1961, p. 93.
240. *Plast. World* 15 (Mar. 1964).
241. *Mod. Plast.* **42**(1A), 294 (1964).
242. A. R. Ingram, *J. Cell, Plast.* **1**(1), 69 (1965).
243. *TYRIL Foam 80*, technical data sheet no. 2-1, The Dow Chemical Co., Midland, Mich., Jan. 1964.
244. E. B. Murphy and W. A. O'Neil, *SPE J.* **18**, 191 (1962).
245. F. Stastny, *Baugewerbe* **19**, 648 (Apr. 1957).
246. U.S. Pat. 3,383,351 (May 14, 1968), P. Stamberger.
247. U.S. Pat. 3,652,639 (Mar. 28, 1972), L. C. Pizzini (to BASF).
248. U.S. Pat. 4,042,537 (Aug. 16, 1977), M. Dahm and co-workers.
249. S. C. Cohen and co-workers, in Ref. 51, p. 100.
250. R. J. Lockwood and co-workers, in Ref. 165, p. 196.
251. T. R. McClellan and co-workers, in Ref. 165, p. 204.
252. U.S. Pat. 2,023,204 (Dec. 3, 1935), C. G. Munters and co-workers (to C. G. Munters).
253. U.S. Pat. 3,960,792 (June 1, 1976), M. Nakamura (to The Dow Chemical Co.).
254. U.S. Pat. 3,704,083 (Nov. 28, 1972), A. L. Phipps.
255. U.S. Pat. 4,247,276 (Jan. 27, 1981), A. L. Phipps (to Condec Corp.).
256. *Proc. Eng. News*, 11 (July, 1978).
257. A. C. Werner, in Ref. 131.
258. Ref. 60, Chapt. 4.
259. C. S. Sheppard, H. N. Schnack, and O. L. Mageli, *J. Cell. Plast.* **2**, 97 (1966).

260. U.S. Pat. 2,763,475 (Sept. 18, 1956), I. Dennis.
261. U.S. Pat. 2,666,036 (Jan. 12, 1954), E. H. Schwencke (to Elastomer Chemical).
262. U.S. Pat. 3,301,798 (Jan. 31, 1967), R. R. Waterman and D. C. Morris (to R. T. Vanderbilt).
263. U.S. Pat. 3,288,729 (Nov. 29, 1966), R. R. Waterman and K. M. Deal (to R. T. Vanderbilt).
264. U.S. Pat. 3,020,248 (1962) (to Dynamit-Nobel Akt).
265. Br. Pat. 901,118 (1960) (to Kleber-Colombes).
266. Br. Pat. 993,763 (1963) (to Kleber-Colombes).
267. U.S. Pat. 3,644,230 (1972), E. W. Cronin (to Haskon, Inc.).
268. U.S. Pat. 4,824,720 (April 25, 1989) B. A. Malone (to The Dow Chemical Co.).
269. K. W. Suh, and co-workers, *Adv. Mater.* **12**(23), 1779–1789 (2000).
270. C. J. Hilado and R. W. Murphy, *Design of Buildings for Fire Safety*, ASTM Spec. Tech. Publ. STP 685, 16-105 ASTM, Philadelphia, Pa., 1979.

DANIEL D. IMEOKPARIA
KYUNG W. SUH
WILLIAM G. STOBBY
The Dow Chemical Company

CELLULOSE ETHERS

General Considerations

Alkylation of cellulose yields a class of polymers generally termed cellulose ethers. Most of the commercially important ethers are water-soluble and are key adjuvants in many water-based formulations. The most important property these polymers provide to formulations is rheology control, ie, thickening and modulation of flow behavior. Other useful properties include water-binding (absorbency, retention), colloid and suspension stabilization, film formation, lubrication, and gelation. As a result of these properties, cellulose ethers have permeated a broad range of industries including foods, coatings, oil recovery, cosmetics, personal care products, pharmaceuticals, adhesives, printing, ceramics, textiles, building materials, paper, and agriculture.

Total U.S. and worldwide consumption of purified and crude grades of cellulose ethers in 2000 was estimated at 82,500 and 371,000 t, respectively (1). The value of the world market for cellulose ethers was nearly $2.0 billion in 2000, with a projected average annual global growth rate of 2.3% between 2000 and 2005. The consumption in 2000 was approximately 83,000 t in the United States, 180,000 t in Western Europe, 26,000 t in Japan, and 82,000 t in the rest of the world. Prices for the principal products range from about $1.43/kg for crude grades of sodium carboxymethylcellulose to over $19.21/kg for purified grades of ethylcellulose.

Although many cellulose ether compositions have been synthesized since the early 1900s, only a few have gained commercial importance. Cellulose ethers first appeared in the literature in 1905 (2). By 1912, cellulose ethers compositions were patented (3–5). By the mid-1930s, methyl-, ethyl-, and benzylcelluloses were commercially available (6,7). These compositions were soluble in organic solvents.

Encyclopedia of Polymer Science and Technology. Copyright John Wiley & Sons, Inc. All rights reserved.

Water-soluble cellulose ether compositions grew rapidly through the 1950s and 1960s, and today far exceed commercial value over organic-solvent-soluble compositions. The highest volume cellulose ethers, the industry workhorses, are sodium carboxymethylcellulose, hydroxyethylcellulose, and hydroxypropylmethylcellulose. Cellulose ethers as a class compete with a host of other materials including natural gums, starches, proteins, synthetic polymers, and even inorganic clays. They provide effective performance at reasonable cost and are derived from a renewable, natural resource.

Cellulose ethers are manufactured by reaction of purified cellulose with alkylating reagents under heterogeneous conditions, usually in the presence of a base, typically sodium hydroxide, and an inert diluent. Cottonseed linter fiber and wood fiber are the principal sources for cellulose. Purified cellulose cotton linters, commonly termed chemical cottons, are generally of higher purity and higher maximum molecular weight than purified cellulose from dissolving grades of wood pulp. The base, in combination with water, activates the cellulose matrix by disrupting hydrogen-bonded crystalline domains, thereby increasing accessibility to the alkylating reagent. This activated matrix is commonly termed alkali cellulose (8–12). Other reagents may be used in combination with sodium hydroxide, such as ammonia, surfactants, phase transfer agents, or enzymes, to promote formation of a more uniformly activated cellulose matrix (13–21). The base also promotes the etherification reaction. The several purposes of the inert diluent are to suspend/disperse the cellulose, provide heat transfer, moderate reaction kinetics, and facilitate recovery of the product. The diluent may also help to distribute reagents among fibers to promote a uniform reaction (22). Crude grades of cellulose ethers, most notably sodium carboxymethylcellulose, may be made in the absence of any diluent. Reactions are typically conducted at elevated temperature, ∼50–140°C, and under nitrogen to inhibit oxidative molecular weight degradation of the polymer (23,24), if so desired. After reaction, crude grades are simply dried, ground, and packed out; purified grades require removal of by-products in a separate operation prior to drying. Various additives, such as colloidal silicas, may be added in small amounts to some products prior to drying or before packout to improve dry handling properties. Instead of dry powders, cellulose ethers are also supplied in liquid forms, either as fluidized suspensions or water solutions (25–27). In addition to these unit operations, schematically outlined in Figure 1, a molecular

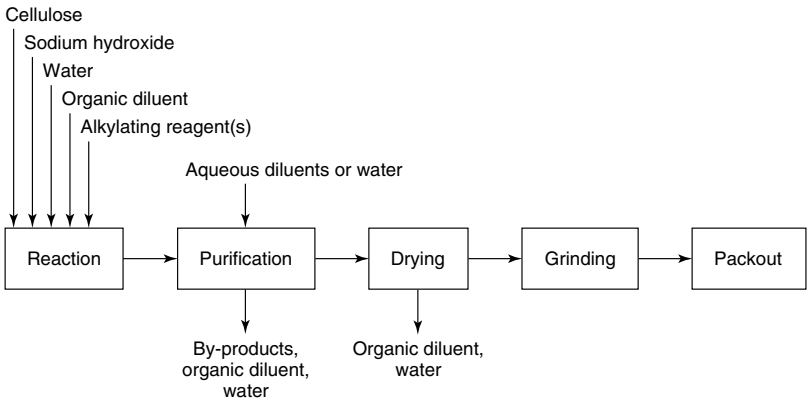

Fig. 1. Unit operations for the manufacture of purified cellulose ethers.

weight reduction operation may be included in the process at any of several points, most notably either in the reaction vessel (before, during, or after the alkylation reaction), after purification before drying, or treatment of dry material (28–30). Hydrogen peroxide is commonly used, though deliberate degradation may also be induced through controlled alkaline-catalyzed autoxidation with oxygen (air) in the reactor. Acids can also be used to cleave the cellulose chain (31,32).

An important characterization parameter for cellulose ethers, in addition to the chemical nature of the substituent, is the extent of substitution. As the Haworth representation of the cellulose polymer shows, it is a linear, unbranched polysaccharide composed of glucopyranose (anhydroglucose) monosaccharide units linked through their 1,4 positions by the β anomeric configuration.

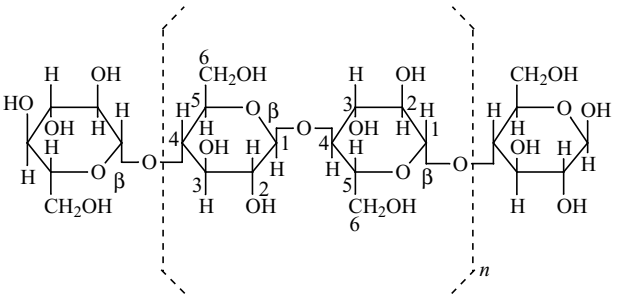

The structurally similar starch amylose polymer is linked through the α anomeric configuration. The three hydroxyl functions per anhydroglucose unit are noteworthy; these hydroxyls are the active sites for ether formation.

The extent of substitution is described as the *degree of substitution* (DS), defined as the average number of hydroxyl groups substituted per anhydroglucose unit. Excluding the terminal residues, each anhydroglucose moiety has three available hydroxyl groups for a maximum DS value of 3. In certain cases the alkylating reagent, such as an alkylene oxide, generates a new hydroxyl group upon reacting which can then further react to give oligomeric chains. The product is then characterized by its *molar substitution* (MS), the moles of reagent combined per mole of anhydroglucose unit. The ratio of MS to DS is a measure of the average chain length of the oligomeric side chains. Organo-soluble ethylcellulose has a DS of 2.3–2.8. Most water-soluble derivatives have DS values of 0.4–2.0. Hydroxyalkyl ethers have MS values typically between 1.5 and 4.0.

MS and DS values are average values, placing no significance on the formal distribution of the substituents within or among polymer chains. Substituent distribution, however, is an important molecular parameter affecting solution rheology and ultimately end use properties. A classic example is offered by sodium carboxymethylcellulose (33). Depending on reaction conditions, sodium carboxymethylcellulose (CMC) of DS ~0.80 can be made to exhibit a varying degree of solution thixotropy, the effect being dependent not so much on DS but rather on the distribution of substituents.

Thixotropic solutions are characterized by a decrease in viscosity on shearing, followed by a time-dependent increase after the shear stress is removed. A plot of shear rate versus shear stress reveals a hysteresis loop. Association among

polymer chains via electrostatic, hydrogen-bonding, or hydrophobic effects can lead to thixotropy. Carboxymethyl substituent uniformity along the polymer chain affects thixotropic behavior of CMC because regions of contiguous unsubstituted anhydroglucose units, ie, blocks, among polymer chains tend to associate through hydrogen bonding (34). The extent of blockiness is controlled by reaction conditions (34,35). Solution thixotropy is important in applications requiring suspension or stabilization of particulates.

As substituent uniformity is increased, either by choosing appropriate reaction conditions or by reaction to high degrees of substitution, thixotropic behavior decreases. CMCs of DS $\geqslant$ 1.0 generally exhibit pseudoplastic rather than thixotropic rheology. Pseudoplastic solutions also decrease in viscosity under shear but recover instantaneously after the shear stress is removed. A plot of shear rate versus shear stress does not show a hysteresis loop.

Other examples illustrating the effect of substituent distribution on properties include (*1*) enzymatic stability of hydroxyethylcellulose (HEC) (36,37), (*2*) salt compatibility of carboxymethylcellulose (38,39), and (*3*) thermal gelation properties of methylcellulose (40). The enzymatic stability of HEC is an example where the actual position of the substituents within the anhydroglucose units is considered important. Increasing substitution at the C-2 position promotes better resistance toward enzymatic cleavage of the polymer chain. Positional distribution is also a factor in the other two examples.

^{13}C NMR is one method used for the compositional and structural characterization of cellulose ethers (41–47). Other structural characterization methods are based on various chromatographic techniques (48–51). The results show that the reactivity of the three hydroxyl groups can vary significantly depending on the alkylating reagent, the type of reaction, and reaction conditions. For most cellulose ethers, substitution occurs primarily at the C-2 and C-6 hydroxyl groups (51–53).

Aside from the chemical nature of the substituent and its DS (MS) and distribution, solution viscosity, ie, polymer molecular weight, is another important characterization parameter. Generally, manufacturers supply cellulose ethers in different viscosity grades, made by choosing a cellulose furnish of appropriate molecular weight, blending celluloses of different molecular weights or by reducing the molecular weight during processing (9–11). Most manufacturers specify solution viscosity data and not polymer molecular weight in their technical literature; however, molecular weight can be estimated from the classical Mark–Houwink equation:

$$[\eta] = KM^a$$

where $[\eta]$ is intrinsic viscosity, K and a are empirically derived constants, and M is the viscosity-average molecular weight, which approximates the weight-average molecular weight, or the degree of polymerization (DP). Values of K and a for various cellulose ethers are available (54,55,123). Mark–Houwink equations for CMC and HEC in 0.02 M KH_2PO_4, pH 5.5, are given below.

$$\text{CMC: } [\eta] = 1.95 \times 10^{-2}[\text{DP}_\text{W}]^{0.83} \text{ (Ref. 54)}$$

$$\text{HEC: } [\eta] = 6.70 \times 10^{-3}[\text{DP}_\text{W}]^{0.92} \text{ (Ref. 55)}$$

Molecular weight from solution viscosity measurements represents an average value of polymer chain lengths. The distribution of chain lengths making up a polymer fraction is commonly termed molecular weight distribution (MWD), a parameter that can influence performance properties, particularly mechanical properties of films. Size exclusion chromatography (SEC), also termed gel-permeation chromatography (GPC), has been the classical method for determining MWD. However, the lack of suitable columns hindered development of aqueous SEC methods for water-soluble polymers until the 1980s. Now, because of the development of high performance packings and columns, the MWD of water-soluble cellulose ethers is a measurable parameter (56–59).

Many cellulose ethers contain mixed substituents (cellulose mixed ethers) in order to enhance or modify the properties of the monosubstituted derivative. For example, incorporation of low levels of hydroxypropyl or hydroxyethyl groups into methylcellulose increases its thermal gelation and flocculation temperatures in aqueous media. Carboxymethylation of hydroxyethylcellulose produces a product having excellent tolerance to mono- and divalent metal ions in solution but which readily cross-links with tri- or tetravalent ions to give highly viscoelastic gels. The solubility of ethylcellulose in organic aliphatic solvents is improved by incorporating hydroxyethyl moieties. The newest commercial cellulose ether composition that has gained considerable importance in the marketplace is a mixed ether, HEC modified with hydrophobic long-chain hydrocarbyl groups (60–62). The hydrophobic groups promote polymer chain association in solution, drastically altering rheology and surface activity properties.

Health and Safety Factors. No adverse toxicological or environmental factors are reported for cellulose ethers in general (33,60–73). Some are even approved as direct food additives, including purified carboxymethylcellulose, methylcellulose, hydroxypropylmethylcellulose, and hydroxypropylcellulose.

The only known hazard associated with cellulose ethers is that they may form flammable dusts when finely divided and suspended in air, a hazard associated with most organic substances. An explosion may result if suspended dust contacts an ignition source. Cloud and layer ignition temperatures generally vary between 290 and 410°C (74). Critical airborne concentrations vary depending on particle size. This hazard can be minimized largely through good housekeeping and proper design and operation of handling equipment.

Another minor hazard is that water-soluble cellulose ether powders form a slippery surface when wet; therefore, spills should be cleaned promptly to avoid slipping accidents.

Commercial Cellulose Ethers

Sodium Carboxymethylcellulose.

Properties. Sodium carboxymethylcellulose [9004-32-4] (CMC), also known as cellulose gum, is an anionic, water-soluble cellulose ether available in a wide range of substitution. The most widely used types are in the 0.7–1.2 DS range. Water solubility is achieved as the DS approaches 0.6; as the DS increases, solubility increases. The rate at which CMC dissolves depends primarily on its particle size. Finely ground material dissolves faster than coarser grades. The coarse material,

however, does not agglomerate as readily when added to water and is therefore easier to disperse. The rate of dissolution also increases with increasing substitution and decreasing molecular weight, ie, viscosity. High molecular weight grades of CMC have viscosities as high as 12,000 mPa·s (=cP) at 1% solids (as recorded on a Brookfield LVT Viscometer at 30 rpm). Lower molecular weight CMCs have viscosities in water as low as 50 mPa·s (=cP) at 4% solids.

CMC is soluble in hot and cold water. Solutions may be pseudoplastic or thixotropic depending on molecular weight, DS, and manufacturing process. High molecular weight, low DS CMCs tend to be more thixotropic. Solutions are viscosity stable at ambient temperature over a wide range of pH. In general, maximum solution viscosity and best stability are obtained at pH 7–9. Above pH 10, a slight viscosity decrease is observed. As pH is lowered below 4, viscosity may first increase and then decrease as intermolecular associations among free acid groups start affecting solubility. CMC is not soluble in organic solvents, but dissolves in mixtures of water and water-miscible solvents such as ethanol or acetone. Low viscosity CMCs are more tolerant of higher levels of organic solvents.

Monovalent cations are compatible with CMC and have little effect on solution properties when added in moderate amounts. An exception is silver ion, which precipitates CMC. Divalent cations show borderline behavior and trivalent cations form insoluble salts or gels. The effects vary with the specific cation and counterion, pH, DS, and manner in which the CMC and salt are brought into contact. High DS (0.9–1.2) CMCs are more tolerant of monovalent salts than lower DS types, and CMC in solution tolerates higher quantities of added salt than dry CMC added to a brine solution.

CMC is compatible with most water-soluble nonionic gums over a wide range of concentrations. When a solution of CMC is blended with a solution of a nonionic polymer such as hydroxyethylcellulose or hydroxypropylcellulose, a synergistic effect on viscosity is usually observed. Such blends produce solution viscosities considerably higher than would ordinarily be expected. This effect is reduced if other electrolytes are present in the system.

Some typical properties of commercial CMCs are given in Table 1.

Manufacture. Common to all manufacturing processes for CMC is the reaction of sodium chloroacetate [3926-62-3] with alkali cellulose complex represented here as R_{cell} OH:NaOH:

$$R_{cell}\ OH + NaOH + H_2O \rightarrow R_{cell}\ OH : NaOH$$

$$R_{cell} : OH + ClCH_2COO^-Na^+ \longrightarrow \underset{\text{Sodium corboxymethyle cellulose}}{R_{cell}\ OCH_2COO^-Na^+} + NaCl + H_2O$$

A by-product is sodium glycolate: [2836-32-0] (sodium hydroxyacetate):

$$ClCH_2COO^-Na^+ + NaOH \rightarrow HOCH_2COO^-Na^+ + NaCl$$

Generally, monochloroacetic acid [79-11-8] (MCA) is added to the reaction slurry containing sufficient excess sodium hydroxide to neutralize the MCA and effect its reaction. The use of esters of MCA has also been reported (75,76). Common

Table 1. Typical Properties of Purified CMC[a]

Property	Value
Powder	
Appearance	White to off-white
Assay, dry basis, min %	99.5
Moisture, max %	8.0
Browning temp., °C	227
Charring temp., °C	252
Bulk density, g/cm^3	0.75
Molecular weight, M_w	$9.0 \times 10^4 - 7.0 \times 10^5$
Solution	
Viscosity, Brookfield, 30 rpm, mPa·s (=cP)	
At 1% solids (high M_w)	~6000
At 4% solids (low M_w)	~50
sp gr, 2% at 25°C	1.0068
pH, 2%	7.5
Surface tension, 1%, mN/m (=dyn/cm)	71
Refractive index, 2% at 25°C	1.3355
Film	
Refractive index	1.515

[a]Ref. 33.

reaction diluents are isopropyl alcohol, *t*-butyl alcohol, or ethyl alcohol (77,78). Dimethoxyethane has also been reported to be effective (79). The product is isolated and washed with aqueous alcohol or acetone to remove by-product salts. Unpurified crude grades are generally prepared in the absence of diluents (80–82).

Economic Aspects. Sodium carboxymethylcellulose remains the most important of the water-soluble compositions; worldwide consumption for 200 is estimated at 179,000 t (Table 2). The projected annual growth rate from 2000 to 2005 is nominal at 1.6% globally. A declining growth rate of 3% is expected in Japan over this period, but this rate is counteracted by a projected 3% growth rate expected in the rest of the world over this same time period, excluding the United States and Western Europe.

CMC consumption declined in detergent applications, but this decline was counteracted by its increased consumption in oil and gas well drilling and its continued growth in the paper segment.

Table 2. World Supply and Demand for CMC,[a] 10^3 t

Region	Capacity[b]	Production	Consumption	Imports	Exports
United States	25.9	16.7	32.3	20.3	4.7
Western Europe	195	148	91.5	2.1	58.6
Japan	44.1	22	14.4	0.3	7.9
Canada, Latin America,[c] Asia and Others	48	NA	14.4	NA	NA
Total	*313*	*186.7*	*179.4*		

[a]In 2000 (1).
[b]Crude and purified grades expressed as 100% CMC.
[c]Mexico and Latin America account for 60% of this capacity.

In the United States, the Aqualon Division of Hercules Inc., is the largest producer, followed by Penn Carbose, Inc., and MAK Chemical Crop. Western Europe has about eight companies manufacturing CMC; the six largest are Noviant if Finland, Sweden, and the Netherlands, Akzo Nobel in Italy and the Netherlands, Aqualon Division of Hercules Inc. in France, Lamberti in Italy, and Micro Technik, Clhariant, and Wolff in Germany. Competitive pressure has precipitated mergers, acquisitions, and rationalization of CMC production facilities, leading to closure of older facilities producing technical grades and favoring modernization and capacity expansion for higher value, purified CMC products.

Noviant, previously Metsa Serla, acquired by J. M. Huber in 2001, is now the world's leading, producer, developer, and distributor of CMC, with about 33% of the world's CMC market.

Among the six CMC producers in Japan, Dai-ichi Kogyo Seiyaku Co., Ltd., Daicel Chemical Industries Ltd., and Nippon Paper Industries Co., Ltd. are the three largest. As seen in Western Europe, production of purified and semipurified grades has been increasing since 1980, reaching 87% of total production in 2000, while technical grade CMC is in a declining trend. The decline in technical grade CMC in Japan is tied to the stagnant construction industry.

In Mexico and South America, the main CMC producers are Quimica Amtex S.A., Latinoquimica S.A., and Celuflok Celuloses e Amidos Ltda, where food/purified, technical, and semipurified grades of CMC are produced.

There are at least nine CMC plants in China. Shanghai Cellulose is among the largest of these producers. The largest CMC producer in Korea is Korean Ginseng Products Co., Ltd. (KOJE). Indonesia and Thailand are among the ASEAN (Association of Southeast Asia Nations) countries producing CMC, with Risjad Brasali Chemindo PT producing purified CMC in Indonesia and Thai Cellulose Products Co., Ltd. producing CMC in Thailand.

Specifications and Standards; Test Methods. *Certain types of purified sodium* carboxymethylcellulose meet standards set by the *U.S. Code of Federal Regulations* (CFR) Title 21, Section 182.1745, substances that are generally recognized as safe (GRAS). The FDA defines the direct food additive as the sodium salt of CMC, not less than 99.5% on a dry weight basis, with a maximum substitution of 0.95 carboxymethyl groups per anhydroglucose unit, and with a minimum viscosity of 25 mPa·s (=cP) in a 2% (by weight) aqueous solution at 25°C. Food-grade cellulose gum meets these requirements. Cellulose gum may also be certified Kosher.

CMC is discloced on European food and cosmetic labels is "sodium carboxymethylcellulose." This nomenclature has caused consumer concerns through association of the name with synthetic additives. There is a proposal to allow CMC to be identified as "cellulose gum" or an equivalent name, with the expectation of increasing CMC consumption in European food and personal care product segments.

Sodium carboxymethylcellulose is listed in the current *U.S. Pharmacopoeia*. Its therapeutic applications include use of sodium carboxymethylcellulose as the primary ingredient in bulk-forming laxatives. Excipient uses include use as a suspension aid, a rheology modifier, and as a tablet binder.

Sodium carboxymethylcellulose 12 (DS 1.15–1.45 minimum) is listed in the *National Formulary* (*NF XX*) for use as a pharmaceutical aid, with similar excipient uses listed.

Table 3. Applications for CMC[a]

Industry	Application	Function
Foods	Frozen desserts	Inhibit ice crystal growth
	Dessert toppings	Thickener
	Beverages, syrups	Thickener, mouthfeel
	Baked goods	Water-binder, batter viscosifier
	Pet food	Water-binder, thickener, extrusion aid
Pharmaceuticals	Tablets	Binder, granulation aid
	Bulk laxatives	Water-binder
	Ointments, lotions	Stabilizer, thickener, film-former
Cosmetics	Toothpaste	Thickener, suspension aid
	Denture adhesives	Adhesion promoter
	Gelled products	Gellant, film-former
Paper products	Internal additive	Binder, improve dry-strength
	Coatings, sizes	Water-binder, thickener
Adhesives	Wallpaper paste	Adhesion promoter, water-binder
	Corrugating	Thickener, water-binder, suspension aid
	Tobacco	Binder, film-former
Lithography	Fountain, gumming	Hydrophilic protective film
Ceramics	Glazes, slips	Binder (promotes green strength)
	Welding rods	Binder, thickener, lubricant
Detergents	Laundry	Soil anti-re-deposition aid
Textiles	Warp sizing	Film-former, adhesion promoter
	Printing paste, dye	Thickener, water-binder

[a]Ref. 33.

Cellulose gum is the accepted term used bt the Cosmetic, Toiletry, and Fragrance Asociation, Inc., for sodium carboxymethylcellulose, and it is listed as such in the Association's *CTFA International Cosmetic Ingredient Dictionary*.

Procedures for the analysis of CMC are available in manufacturers' bulletins (33).

Uses. CMC is an extremely versatile polymer, and it has a variety of applications. A sampling of significant applications is given in Table 3. A more extensive listing can be found in Reference 33.

Hydroxyethylcellulose.

Properties. Hydroxyethylcellulose [9004-62-0] (HEC) is a nonionic polymer. Low hydroxyethyl substitutions (MS = 0.05–0.5) yield products that are soluble only in aqueous alkali. Higher substitutions (MS $\geqslant$ 1.5) produce water-soluble HEC. The bulk of commercial HEC falls into the latter category. Water-soluble HEC is widely used because of its broad compatibility with cations and the lack of a solution gel or precipitation point in water up to the boiling point. The MS of commercial HEC varies from about 1.8 to 3.5. The products are soluble in hot and cold water but insoluble in hydrocarbon solvents. HEC swells or becomes partly to mostly soluble in select polar solvents, usually those that are miscible with water.

Commercially, HEC is available in a wide range of viscosity grades, ranging from greater than 500 mPa·s (=cP) at 1% solids to less than 100 mPa·s (=cP) at 5% total solids. Because HEC is nonionic, it can be dissolved in many salt solutions that do not dissolve other water-soluble polymers. It is soluble in most 10% salt solutions and in many 50% (or saturated) salt solutions such as sodium

chloride and aluminum nitrate. As a rule, the lower substitution grades are more salt-tolerant.

HEC is soluble in both hot and cold water; however, as with most water-soluble thickeners, the particles have a tendency to agglomerate, or lump, when first wetted with water. This is especially evident when the HEC is added to water with poor agitation. Manufacturers have eliminated the problem of lumping and slow dissolving by surface treating the particles, most commonly with glyoxal [107-22-2] (83–86). When added to water, the particles completely disperse. After an initial induction period, commonly termed the delayed hydration time, the dispersed particles begin to dissolve, producing smooth, lump-free solutions. The delayed hydration time can be increased or decreased by lowering or raising, respectively, the pH. Most manufacturers supply dispersible grades.

Solutions of HEC are pseudoplastic. Newtonian rheology is approached by very dilute solutions as well as by lower molecular weight products. Viscosities change little between pH 2 and 12, but are affected by acid hydrolysis or alkaline oxidation under pH and temperature extremes. Viscosities of HEC solutions change reversibly with temperature, increasing when cooled and decreasing when warmed.

HEC is generally compatible with other cellulosic water-soluble polymers to give clear, homogeneous solutions. When mixed with an anionic polymer such as CMC, however, interactions between the two polymers may result in synergistic behavior, ie, viscosities higher than predicted and calculated. HEC has excellent compatibility with natural gums.

Some typical properties of HEC are given in Table 4.

Manufacture. Purified HEC is manufactured in diluent-mediated processes similar to those used to produce CMC, except ethylene oxide [75-21-8] is used in place of MCA (87,88):

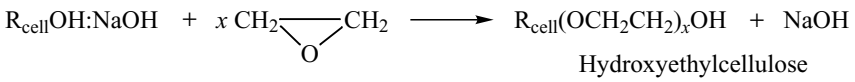

A competing reaction that consumes ethylene oxide is hydrolysis to ethylene glycol and oligomeric glycol by-products.

$$HO(CH_2CH_2O)_x^- Na^+ + H_2O \rightarrow HO(CH_2CH_2O)_xH + NaOH$$

Because of the low boiling point of ethylene oxide, reactions are generally conducted in stirred autoclaves at elevated pressures. Staged addition of caustic and ethylene oxide leads to a more uniformly substituted HEC product that is more resistant to molecular weight degradation by enzymes (89–91).

Several other modifications of HEC have been more recently reported in the literature that may find commerical utility in the future. These include modification with allyl (92), sulfoalkyl (93,94), and silyl (95) functional groups.

Table 4. Typical Properties of HEC[a]

Property	Value
Powder	
Appearance	White to light tan
Moisture, max %	5.0
Ash content (as Na_2SO_4), %	5.5
Bulk density, g/cm^3	0.6–0.75
Browning temp., °C	205–210
Molecular weight, M_w	$9 \times 10^4 - 1.3 \times 10^6$
Solution	
Viscosity, Brookfield, 30 rpm, mPa·s (=cP)	
At 1% solids (high M_w)	5000
At 5% solids (low M_w)	75
sp gr, 2%, g/cm^3	1.0033
pH	7
Surface tension, mN/m (=dyn/cm)	
MS 2.5 at 0.1%	66.8
At 0.001%	67.3
Refractive index, 2%	1.336
File	
Refractive index	1.51
Moisture content, %, at 25°C	
50% rh	6
84% rh	29

[a]Ref. 63.

Economic Aspects. A breakdown of salient 2000 world supply and demand figures for HEC is given in Table 5.

The Aqualon Division of Hercules Inc. and Union Carbide Corp., a subsidiary of the Dow Chemical Co., have manufacturing facilities is the United States and in Western Europe. Dow Chemical has an additional production facility in Brazil. Daicel Chemical Industries Ltd. and Celchem K.K. in Japan and Clariant GmbH in Europe are the only other producers of HEC.

Table 5. World Supply and Demand for HEC,[a] 10^3 t

Region	Capacity	Consumption
United States[b]	32	23.8
Western Europe[b]	43	26.6
Japan	2.2	2.1
Canada, Mexico, Latin America, Asia & Other	5.4	14.3
Total	*82.6*	*66.8*

[a]In 2000 (1).

[b]Includes hydrophobically modified hydroxyethylcellulose, ethylhydroxyethylcelluose, cationic hydroxyethylcellulose, and carboxymethylhydroxyethylcellulose.

Table 6. Applications for HEC[a]

Industry	Application	Function
Coatings	Latex paints	Thickener
	Polymer emulsions	Protective colloid
Construction	Cements, mortars	Thickener, water-binder
Paper	Coatings, sizes	Thickener, water-binder
Pharmaceuticals	Lotions, ointments	Thickener, stabilizer, water-binder
Cosmetics	Toothpastes	Thickener
	Shampoos	Thickener
	Creams, lotions	Thickener, stabilizer
Ceramics	Welding rods	Water-binder, extrusion aid
	Glazes	Water-binder (promotes green strength)

[a]Ref. 63.

Specifications and Standards; Test Methods. Although HEC is not the subject of a direct-food-additive regulation, it is included in the list of materials that are in compliance with requirements of the U.S. FDA for use in adhesives and in resinous and polymeric coatings employed on the food-contact surfaces of metal, paper, or paperboard articles, and other substrates intended for use in food packaging as specified in the U.S. CFR, Title 21, subject to the limitations and requirements of each application. HEC made dispersible by cross-linking with glyoxal is cleared only as an adhesive and as a component of paper and paperboard in contact with food. It has not been cleared as a direct food additive.

Specific grades of HEC are approved for oral and topical pharmaceutical applications as an inert ingredient. These grades of HEC meet or exceed all the requirements of the current editions of the *European Pharmacopoeia* and/or the *National Formulary* (*NF XX*).

Procedures for determing ash, moisture, solution preperation, and viscosity measurements can be found in manufactures product bulletins (63,64) and in ASTM D2364-01 (96), and in the European pharmacopoeia and/or the National Formulary (NFXX).

Uses. HEC is used as a thickener and rheology control agent, protective colloid, binder, stabilizer, suspension aid, sustained-release polymer, and a film-former in aqueous film coating. A guide to the principal uses is given in Table 6.

Mixed Ether Derivatives of HEC. Several chemical modifications of HEC are commercially available. The secondary substituent is generally of low DS (or MS), and its function is to impart a desirable property lacking in HEC.

Carboxymethylhydroxyethylcellulose (CMHEC). This is an anionic modification of HEC manufactured by Aqualon Co. Sodium carboxymethylhydroxyethylcellulose [9088-04-4] is manufactured by reaction of alkali cellulose either simultaneously or sequentially with ethylene oxide and sodium chloroacetate. Various grades, with carboxymethyl DS, CM(DS), of 0.3–0.5 and hydroxyethyl MS, HE(MS), of 0.7–2.0, are available. CMHEC has properties of both HEC and CMC. It is more compatible with salts than CMC because of the presence of nonionic hydroxyethyl groups. In saturated NaCl, only CMC with a CM(DS) $\geq$ 1.0 is completely soluble. CMHEC, on the other hand, is soluble with a CM(DS) as low as 0.3.

Table 7. Typical Properties of Mixed Ether Derivatives of HEC[a]

Property	CMHEC	Cationic HEC	EHEC	HMHEC
Powder				
Appearance	Off-white	Light yellow	Off-white	Off-white
Bulk density, g/cm^3	0.6	0.48	0.4–0.8	0.55–0.75
Ash content (as Na_2SO_4), %		3	3 (as NaCl)	10 max
Volatiles, %	6–8	7	8 max	5 max
Solution				
pH	6.5–10	7	6–7	6–8.5
Flocculation temp. in water, °C			∼65	
Surface tension, dyn/cm			∼55.00	∼62
Film				
Tensile strength, MPa[b]	69[c]	14–22[c]	45–55[d]	
Flexibility[e]		60–70[c]	25–35[d]	
Refractive index	1.530		1.49	

[a]Refs. 62,70,72, and 102.
[b]To convert MPa to psi, multiply by 145.
[c]At 50% rh.
[d]At 65% rh.
[e]MIT double folds.

CMHEC is also very tolerant of Ca^{2+} and consequently readily dissolves in seawater. Unlike HEC, CMHEC in solution may be cross-linked with trivalent cations such as Fe^{3+} and Al^{3+} to give greatly increased viscosity or three-dimensional viscoelastic gels (97).

CMHEC products are used predominantly in oil recovery applications. The high water binding capability, salt compatibility, and adsorption to clay and mineral surfaces give CMHEC ethers excellent control over high salinity fluids (98,99). Water loss in cement slurries is also reduced (100). CMHEC is also used in hydraulic fracturing fluids. Gels formed by cross-linking with multivalent cations can suspend and transport proppants into a well bore and then fracture (97,101). Some typical properties of CMHEC having a CM(DS) ∼0.3 and HE(MS) ∼0.7 are listed in Table 7.

Cationic Hydroxyethylcelluloses. These materials are primarily manufactured by Union Carbide, a subsidiary of Dow Chemical Company, and by National Starch & Chemical, a member of the ICI Group, marketed under the trade names UCARE Polymers and Celquats, respectively (70,71). The cationic substituent on the UCARE Polymer series and the Celquat SC series is 2-hydroxypropyltrimethylammonium chloride. Polyquaternium-10 is the International Nomenclature Cosmetic Ingredient (INCI) name assigned to these materials by the International Nomenclature Committee of the Cosmetic Toiletry & Fragrance Association (CTFA). National Starch & Chemical also manufactures another product under the trade-names Celquat H-100 and Celquat L-200. These materials are the reaction product of HEC with *N*,*N*-diallyl-*N*,*N*-dimethylammonium chloride. Polyquaternium-4 is the INCI name assigned to these materials.

All of these cationic polymers are substantive to the skin and hair, providing conditioning to both substrates through a combination of several mechanisms, including formation of films on these substrates that reduce moisture loss, through

repair of hair protein, and by providing antistat properties to hair. The structure of the cationic functionality, its DS (or MS), and the molecular weight of the HEC backbone affect product performance across the pH range of interest (pH 5–7). These same structural and physical characteristics affect the compatibility of these polymers with surfactants used in various shampoo, conditioner, skin cleansing, and moisturizing formulations (103). Some typical properties of Celquat resins are given in Table 7.

Hydrophobic Hydroxyethylcelluloses. These materials are produced by stepwise or simultaneous reaction of ethylene oxide and a hydrophobic alkylating reagent. Commercial products include ethylhydroxyethylcellulose [9004-58-9] (EHEC), manufactured by Akzo Nobel Berol Kemi AB under the Bermocoll trade name (72), and HEC modified with a long-chain alkyl group, generically termed HMHEC (where HM = hydrophobically modified), manufactured by the Aqualon Division of Hercules Inc. and sold under the trade name Natrosol Plus (62). These products are water-soluble.

Water-soluble EHEC is a moderate ethyl DS (∼1.0) modification of high hydroxyethyl MS (≥ 2.0) HEC. Ethyl groups lower the surface and interfacial tensions, thereby increasing surface activity. This group also modifies adsorption properties of the polymer to particulates found in many formulations such as clays, pigments, and latices. Aqueous solutions have pseudoplastic rheology. High viscosity grades are more pseudoplastic than low viscosity materials, which approach Newtonian flow behavior. Viscosities decrease reversibly with increasing temperature. Above 65°C, EHEC precipitates from solution. Salts lower the temperature at which precipitation occurs. Solution viscosities are insensitive to pH between about 3 and 11. Aqueous solutions are miscible with lower alcohols, glycols, and ketones up to equal proportions. Water-soluble EHECs are used to thicken and stabilize a variety of materials, including waterborne paints, plasters, detergents, cosmetics, and pharmaceuticals (72).

HMHEC is a modification with low levels of much longer hydrocarbon chains (hydrophobes) that not only increase surface activity but also impart associative behavior to HEC; this produces dramatic effects on solution viscosity and rheology (60,104,107). For example, an HEC with a 2% solution viscosity of 10 mPa·s (=cP) modified with ∼2.5 wt% of a C_{14}-chain hydrocarbyl moiety has a viscosity of 800 mPa·s (=cP). The effect has been attributed to micellar aggregation of the hydrophobic groups in solution (37–39). The solubility and rheological properties of HMHEC depend primarily on the molecular weight, the DS and chain length of the hydrophobe, the polymer concentration, and the composition of the aqueous media. It has been found that HMHEC is an efficient rheology control agent in latex paints (62,107). HMHEC also behaves as a polymeric coemulsifier. It can stabilize oil-in-water emulsions without the use of high HLB surfactants, enabling milder personal care and cosmetic formulations. Typical properties of an HMHEC are given in Table 7.

Hydrophobically modified ethylhydroxyethylcellulose (HMEHEC) (108), also having a long hydrocarbon chain, is also commercially available. Its properties are similar to HMHEC.

HEC modified with shorter C_2–C_6 alkyl groups produce nonassociative products that find use in building materials, such as plasters, joint compounds, and cements (109).

Methylcellulose and Its Mixed Ethers.

Properties. Methylcellulose [9004-67-5] (MC) and its alkylene oxide derivatives hydroxypropylmethylcellulose [9004-65-3] (HPMC), hydroxyethylmethylcellulose [9032-42-2] (HEMC), and hydroxybutylmethylcellulose [9041-56-9] (HBMC) are nonionic, surface-active, water-soluble polymers. Each type of derivative is available in a range of methyl and hydroxyalkyl substitutions. The extent and uniformity of the methyl substitution and the specific type of hydroxyalkyl substituent affect the solubility, surface activity, thermal gelation, and other properties of the polymers in solution.

These four MCs are available in a range of substitutions.

	Methyl DS	Hydroxyalkyl MS
MC	1.4–2.0	
HPMC	1.1–2.0	0.1–1.0
HEMC	1.3–2.2	0.06–0.5
HBMC	$\geq$1.9	$\geq$0.04

MC with a methyl DS less than about 0.6 is alkali-soluble. From about 1.6–2.4, it is water-soluble (most commercial grades); above 2.4, it is soluble in a wide variety of organic solvents. MC solutions in water start to gel at $\sim 55^{\circ}$C, independent of molecular weight. The gelation is a function of the DS, rate of heating, and type and amounts of additives such as salts. As the temperature increases, the viscosity initially decreases (typical behavior). When the gelling temperature is reached, the viscosity sharply rises until the flocculation temperature is reached. Above this temperature, the viscosity collapses. This process is reversible with temperature (110).

The mixed derivatives HEMC, HPMC, and HBMC tend to precipitate rather than gel as the temperature is increased. The higher the hydroxyalkyl substitution, the greater the tendency for precipitation. HEMCs and HPMCs tend to have higher gelation and flocculation temperatures (110). The mixed derivatives are generally more tolerant of added salts than MC itself. HPMC and HBMC are tolerant of and are soluble in some organic solvents, especially lower alcohols and glycols.

Solutions of MCs are pseudoplastic below the gel point and approach Newtonian flow behavior at low shear rates. Above the gel point, solutions are very thixotropic because of the formation of three-dimensional gel structure. Solutions are stable between pH 3 and 11; pH extremes will cause irreversible degradation. The high substitution levels of most MCs result in relatively good resistance to enzymatic degradation (36).

MC and its mixed ethers are surface-active cellulose ethers having surface tension values as low as 44 mN/m (=dyn/cm) and interfacial tension values as low as 17 mN/m (=dyn/cm) against paraffin oil.

Typical properties of MC, HPMC, HEMC, and HBMC are given in Table 8.

Manufacture. MC is manufactured by the reaction of alkali cellulose with methyl chloride (111).

$$R_{cell}OH : NaOH + CH_3Cl \rightarrow R_{cell}OCH_3 + NaCl$$

Table 8. Typical Properties of MC Ethers[a]

Property	MC	HPMC	HEMC	HBMC
Powder				
Appearance	White	White	White	White
Bulk density, g/cm^3		0.25–0.70		
Volatiles, %		8 max		
Ash content (as Na_2SO_4), %		2.5 max		
Solution				
Viscosity,[b] mPa·s (=cP)	10–15,000	5–70,000	100–70,000	
sp gr, 2% at 20°C		1.0032		
pH, 1%		5.5–9.5		
Surface tension, 0.1%, mN/m(=dyn/cm)	47–53	44–56	46–53	49–55
Interfacial tension,[c] mN/m (=dyn/cm)	19–23	17–30	17–21	20–22
Gelation temp., °C	48	54–70		49
Flocculation temp., °C	50–75	60–90	60–90	
Film				
Tensile strength, MPa,[d] 50% rh	58.6–78.6	58.6–61		
Elongation, %, 50% rh	10–15	5–10		
Softening point, °C		240		
Melting point, °C	290–305	260		
Vapor transmission, nmol/(m·s)				
Water, 37°C, 90–100% rh		520		
Oxygen, 24°C		560		

[a]Refs. 65 and 66.
[b]2% solution, Brookfield, 20 rpm.
[c]Against paraffin oil.
[d]To convert MPa to psi, multiply by 145.

The reaction is accompanied by side reactions that lead to methanol and dimethyl ether by-products.

$$CH_3Cl + NaOH \rightarrow CH_3OH + NaCl$$

$$CH_3OH + CH_3Cl + NaOH \rightarrow CH_3OCH_3 + NaCl + H_2O$$

Hydroxyalkyl modification is made by simultaneous or staged addition of an alkylene oxide, as exemplified in the following (112–115):

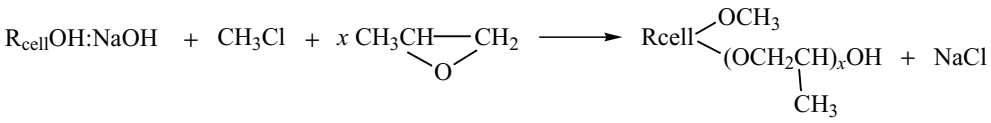

Similarly, ethylene oxide and 1,2-butylene oxide are used to make methylhydroxyethylcellulose and methylhydroxybutylcellulose, respectively.

Unlike HEC and CMC, which are purified by washing with aqueous organic solvents, MC and its hydroxyalkyl modifications are purified in hot water, where they are insoluble. Ultrafiltration techniques may be used to recover low molecular weight product from the wash water (116–118). As with other cellulose ethers, drying and grinding complete the process.

Table 9. Worldwide Supply and Demand for MC,[a] 10^3 t

Region	Capacity	Consumption	Production	Imports	Exports
United States	28.6	23.3	NA	NA	NA
Western Europe	94.4	58.8	75.2	7	23.4
Japan	12.7	8.9	12	2	5.1
Others	11.5	22.6	NA	NA	NA
Total	*147.2*	*113.6*			

[a]In 2002 (1).

Economic Aspects. A breakdown of salient figures in 2000 for the methylcelluloses is given in Table 9. The Dow Chemical Co. is the only U.S. manufacturer. They produce and market MC, HPMC, and HBMC. European producers include the Aqualon Division of Hercules Inc. in Belgium, Clariant GmbH in Germany, Dow Deutschland Inc. in Germany, Wolff Cellulosics GmbH & Co. in Germany, and Cognis Deutschland GmbH in Germany. Wolff Cellulosics GmbH plans a capacity expansion of 11,000 t in 2003 (1). Shin-Etsu Chemical Co. Ltd. and Matsumoto Yushi-Seiyaku Co., Ltd. are the two Japanese manufacturers.

Specifications and Standards; Test Methods. Premium grades of MC meet the requirements of the *U.S. Pharmacopeia – National Formulary* (U.S.P XXV-NF XX), the *European Pharmacopeia*, and the *Food Chemicals Codex IV*. MC is generally recognized as safe (GRAS), meeting the requirements of Food Additives Regulation CFR Title 21, Section 182.1480, as a multipurpose food substance in nonstandardized foods. The U.S. Department of Agriculture also allows its use in meat products, according to CFR Title 9, Section 318.7, and CFR Title 9, Section 381.147. Premium grades of some HPMCs are also approved for direct food use, meeting requirements of U.S.P. XXV, *Food Chemicals Codex IV*, and Food Additives Regulation CFR Title 21, Section 172.874, which allows their use in nonstandardized foods. Both MC and HPMC are also listed in the *Food Chemicals Codex* with their common names, "modified vegetable gum" and "carbohydrate gum," respectively. These products have also been certified Kosher.

MC and HPMC have also been authorized for use in the European food industry in a Council Directive by the European Union, and are coded E461 and E464, respectively.

MC and HPMC qualify as inert ingredients under CFR Title 40, Section 180.1001, that may be used in formulations applied to growing crops or raw agricultural products and commodities after harvest, and animals.

Analytical test methods and procedures are described in manufacturer's technical bulletins (65,66).

Uses. There are numerous applications for MC and its derivatives. Some important ones are summarized in Table 10.

Ethylcellulose and Hydroxyethylethylcellulose.

Properties. Ethyl cellulose [9004-57-3] (EC) is a nonionic, organo-soluble, thermoplastic cellulose ether, having an ethyl DS in the range of ~2.2–2.7. Actually, EC is water-soluble at DS ~ 1.2, but only those products that are thermoplastic and soluble in organic solvents are of commercial importance, because of

Table 10. Applications for MC and Its Derivatives[a]

Industry	Application	Function
Construction	Cements, mortars	Thickener, water-binder, workability
Foods	Mayonnaise, dressing	Stabilizer, emulsifier
	Desserts	Thickener
Pharmaceuticals	Tablets	Binder, granulation aid
	Formulations	Stabilizer, emulsifier
Adhesives	Wallpaper paste	Adhesive
Ceramics	Slip casts	Binder (promotes green strength)
Coatings	Latex paints	Thickener
	Paint removers	Thickener
Cosmetics	Creams, lotions	Stabilizer, thickener

[a]Refs. 65 and 66.

their ability to form tough, stable films. Above a DS of about 2.5, EC is soluble in many nonpolar solvents.

Film mechanical properties, such as tensile strength, elongation, and flexibility, depend more on the molecular weight (DP) than on substitution. Elongation and tensile strength increase to a maximum with increasing molecular weight; flexibility increases linearly.

EC is subject to oxidative degradation in the presence of sunlight or ultraviolet light, especially at elevated temperatures above the softening point. It must, therefore, be stabilized with antioxidants (67). EC is stable to concentrated alkali and brines but is sensitive to acids.

Table 11 gives typical properties for EC.

Manufacture. EC undergoes reaction with alkali cellulose in high pressure nickel-clad autoclaves. A large excess of sodium hydroxide and ethyl chloride and high reaction temperatures (up to 140°C) are needed to drive the reaction to the desired high DS values ($\geqslant$2.0). In the absence of a diluent, reaction efficiencies in

Table 11. Typical Properties of EC[a]

Property	EC
Powder	
Appearance	White
Volatiles, %	2.000
Bulk density, g/cm^3	0.3–0.35
Softening point, °C	152–162
Film	
Specific gravity	1.140
Refractive index	1.470
Tensile strength, MPa[b]	46–72
Elongation, %	7–30
Flexibility[c]	160–2000
Dielectric constant, 60 Hz	2.5–4.0

Ref. 67.
[a]To convert MPa to psi, multiply by 145.
[b]MIT double folds.

ethyl chloride range between 20 and 30%, the majority of the rest being consumed to ethanol and diethyl ether by-products.

$$R_{cell}OH : NaOH + CH_3CH_2Cl \rightarrow R_{cell}OCH_2CH_3 + NaCl + CH_3CH_2OH + (CH_3CH_2)_2O$$

Higher ethyl chloride efficiency is claimed for a process utilizing a hydrocarbon diluent coupled with stepwise addition of sodium hydroxide (119). Product work-up includes distillation to remove residual unreacted ethyl chloride, added diluent, methanol, and diethyl ether; neutralization of excess sodium hydroxide; washing in water to remove salts; drying; and grinding.

Economic Aspects. The Dow Chemical Co. and the Aqualon Division of Hercules Inc. are the only listed principal producers of EC products worldwide. Consumption has remained constant over the past several years, and it is not expected to grow in the future. Production is estimated at 5000 t/year, roughly equally divided between The Dow Chemical Co. and the Aqualon Division of Hercules Inc. As with other cellulose ethers, the price for EC varies by grade.

Specifications and Standards; Test Methods. EC is cleared for many applications in food and food contact under the Federal Food, Drug, and Cosmetic Act, as amended. Examples include binder in dry vitamin preparations for animal feed, coatings and inks for paper and paperboard products used in food packaging, and closures with sealing gaskets for food containers (44). Methods of analyses are given in ASTM D914-72 (19), *National Formulary XX*, and *Food Chemicals Codex IV*.

Uses. A summary of the applications for EC is given in Table 12.

Hydroxypropylcellulose.

Properties. Hydroxypropylcellulose [9004-64-2] (HPC) is a thermoplastic, nonionic cellulose ether that is soluble in water and in many organic solvents. HPC combines organic solvent solubility, thermoplasticity, and surface activity with the aqueous thickening and stabilizing properties characteristic of other water-soluble cellulosic polymers described herein. Like the MCs, HPC exhibits a low critical solution temperature in water.

The substitution of HPC is defined by the MS. Molar substitutions higher than approximately 3.5 are needed for solubility in water and organic solvents.

HPC is available in a number of viscosity grades, ranging from about 3000 mPa·s (=cP) at 1% total solids in water to 150 mPa·s (=cP) at 10% total solids. HPC solutions are pseudoplastic and exceptionally smooth, exhibiting little or no structure or thixotropy. The viscosity of water solutions is not affected by changes in pH over the range of 2–11. Viscosities decrease as temperature is

Table 12. Applications for EC and HEEC[a]

Industry	Application	Function
Coatings	Lacquers, varnishes	Protective film-former, additive to increase film toughness and durability, shorten drying time
Printing	Inks	Film-former
Adhesives	Hot melts	Additive to increase toughness

[a]Ref. 67.

increased. HPC precipitates from water at temperatures between 40 and 45°C. Dissolved salts and other compounds can profoundly influence the precipitation temperature (73,120).

HPC is compatible with many natural and synthetic water-soluble polymers and gums (73). Generally, blends of HPC with another nonionic polymer such as HEC yield water solutions having viscosities in agreement with the calculated value. Blends of HPC and anionic CMC, however, produce solution viscosities greater than calculated ones. This synergistic effect may be reduced in the presence of dissolved salts or if the pH is below 3 or above 10.

Like the MCs, water solutions of HPC display greatly reduced surface tension. A 0.1% solution of HPC at 25°C has a surface tension of about 44 mN/m (=dyn/cm) (and that of water is 74.1 mN/m) and interfacial tension of about 12.5 mN/m (=dyn/cm) against mineral oil. The molecular weight of the HPC has only a slight effect on the surface tension.

Examples of polar organic solvents that dissolve HPC are methanol, ethanol, propylene glycol, and chloroform. There is no tendency for HPC to precipitate as the temperature is raised. In fact, elevated temperatures improve the solvent power of organic liquids.

A low substituted hydroxypropylether of cellulose, "L-HPC" (MS = 0.2–0.4), is produced by Shin-Etsu Chemical Co., Ltd. L-HPC is insoluble, but swell in water. It is used as a binder and a distintegrant for solid medicaments.

Some typical properties of commercial high MS HPC are given in Table 13.

Manufacture. HPC is manufactured by reaction of propylene oxide [75-56-9] with alkali cellulose.

Table 13. Typical Properties of HPC[a]

Property	Value
Powder	
Appearance	Off-white
Volatiles, %	5 max
Ash content (as Na_2SO_4), %	0.2–0.5
Softening point, °C	100–150
Molecular weight, M_w	8.0×10^4–1.15×10^6
Solution	
Viscosity, Brookfield, 30 rpm, mPa·s (=cP)	
At 1% (high M_w)	2500
At 10% (low M_w)	100
Surface tension, 0.1%, mN/m (=dyn/cm)	43.6
Interfacial tension,[b] 0.1%, mN/m	12.5
Film	
Tensile strength, MPa[c]	14
Elongation, %	50
Flexibility[d] (50 μm film)	10,000
Refractive index	1.559

[a] Ref. 73.
[b] Against mineral oil.
[c] To convert MPa to psi, multiply by 145.
[d] MIT double folds.

Table 14. Applications for HPC[a]

Industry	Application	Function
Polymerization	PVC suspension polymerization	Protective colloid
Pharmaceutical	Tablets	Binder, film-former
Coatings	Paint remover	Thickener
Foods	Whipped toppings	Stabilizer
	Processed foods	Extrusion aid
Ceramics	Slip casts	Binder (promotes green strength)

[a]Ref. 73.

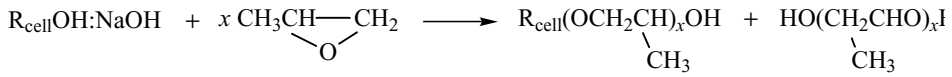

The reaction may be conducted in stirred autoclaves in the presence of hydrocarbon diluents (121,122). Like the MCs, advantage is taken of the low critical solution temperature of HPC and it is purified through multiple washings with hot water. Consequently, very low levels of residual salts and by-products are present in the final products.

Economic Aspects. The Aqualon Co. of Hercules Inc. is the only U.S. manufacturer. It is also produced in Japan by Nippon Soda Co., Ltd. Nippon Soda increased its production capacity to 1000 t at the end of 1998, to meet increasing demand from the pharmaceutical industry. Worldwide production of consumption of HPC in 2000 was estimated at 3000 t.

Specifications and Standards; Test Methods. Food-grade HPC products are manufactured for use in food and conform to the specifications for HPC set forth in CFR Title 21, Sections 121.1160 and 172.870. Food grades of HPC also conform to the specifications for HPC as listed in the current edition of the *Food Chemicals Codex* and by the Food and Agricultural Organization of the the United Nation's World Health Organization (FAO/WHO).

Pharmaceutical and cosmetic grades of HPC, as, for example, Klucel Pharm NF manufactured by the Aqualon Division of Hercules Inc. conform to the requirements of all major pharmacopeias, ie, *National Formulary* (*NF XX*), *European Pharmacopeia* (*EP*), *and Japanese Pharmacopeia (JP)*.

Toxicity testing indicates that HPC is physiologically inert (50).

Procedures for determining the ash content and moisture level, solution preparation, and viscosity measurement techniques are given in the manufacturer's literature (50).

Uses. A summary of significant uses for HPC is given in Table 14.

BIBLIOGRAPHY

"Cellulose Ethers" in *EPST* 1st ed., Vol. 3, pp. 459–549, by A. B. Savage, The Dow Chemical Company, E. D. Klug, Hercules Powder Company, and D. J. Stanonis, Plant Fibers Pioneering Research Laboratory, USDA; "Cellulose Ethers" in *EPSE* 2nd ed., Vol. 3, pp. 226–269, by E. K. Just and T. G. Majewicz, Hercules, Inc.

1. *Chemical Economics Handbook*, SRI International, Menlo Park, Calif., Nov. 2001, Section 5821.5000A.
2. W. Suida, *Montash. Chem.* **26**, 413 (1905).
3. Ger. Offen. 322,586 (July 1, 1920), O. Leuchs (to Bayer AG).
4. Fr. Pat. 462,274 (Nov. 18, 1912), H. Dreyfus; *Chem. Abstr.* **8**, 3859 (1914).
5. Brit. Pat. 12,854 (May 31, 1913), L. Lilienfield; *Chem. Abstr.* **7**, 3839 (1913).
6. D. Traill, *J. Soc. Chem. Ind. Trans.* **LIII**, 338T (1934).
7. R. E. Montonna, *Pap. Trade J. (Tappi Section)* 35 (1936).
8. J. O. Warwicker, R. Jeffries, R. L. Colbran, and R. N. Robinson, *A Review of the Literature on the Effect of Caustic Soda and Other Swelling Agents on the Fine Structure of Cotton*, Shirley Institute Pamphlet No. 93, Shirley Institute, Didsbury, Manchester, U.K., 1966.
9. T. Okano and A. Sarko, *J. Appl. Polym. Sci.* **29**, 4175–4182 (1984).
10. T. Okano and A. Sarko, *J. Appl. Polym. Sci.* **30**, 325–332 (1985).
11. H. Nishimura and A. Sarko, *J. Appl. Polym. Sci.* **33**, 855–866 (1987).
12. H. Nishimura and A. Sarko, *J. Appl. Polym. Sci.* **33**, 867–874 (1987).
13. U.S. Pat. 4,491,661 (Jan. 1. 1985), K. Bredereck, E. Togelang (to Hoechst AG).
14. U.S. Pat. 5,939,544 (Aug. 17, 1999), T. Karstens, H. Steinmeier (to Rodia Acetow AG).
15. H. Fischer, *Textilveredliung* **13**, 507 (1978).
16. Jpn. Pat. JP59075902 (Apr. 28, 1984) S. Akiva (to Daicel Chem. Ind. KK).
17. T. A. Lyubova, S. A. Kovaleva, L. G. Tokareva, Z. G. Serebtyakova, and T. P. Kartashiova, *Khim. Volokna* (5), 66–67 (1977).
18. U.S. Pat. 4,384,113 (May 17, 1983), W. H. Daly (to The Dow Chemical Company).
19. W. H. Daly, *J. Polym. Sci., Polym Lett.* **17**, 55–63 (1979).
20. Ger. Pat. DE19515439A1 (Apr. 27, 1995), J. Englehardt, W. Koch, C. Michels, F. Meister, and H. Kramer (to Wolff Walsrode).
21. PCT WO 98/38328 (Mar. 9, 1998), Y. Noguchi and M. Kamachi (to Novo Nordisk A/S).
22. H. Yokota, *J. Appl. Polym. Sci.* **30**, 263–277 (1985).
23. D. Entwistle, E. H. Cole, and N. S. Wooding, *Text. Res. J.* **XIX**, 527–624 (1949).
24. R. I. C. Michie and S. M. Neale, *J. Polym. Sci., Part A* **2**, 2063–2083 (1964).
25. U.S. Pat. 5,480,984 (Jan. 2, 1996), J. D. Angerer, J. J. Modi, and R. C. Szafranski (to Aqualon Co.).
26. U.S. Pat. 4,883,536 (Nov. 28, 1989), C. L. Burdick (to Aqualon Co.).
27. U.S. Pat. 5,228,909 (Jul. 20, 1993), C. L. Burdick and J. N. Pullig (to Aqualon Co.).
28. U.S. Pat. 2,512,338 (June 20, 1950), E. D. Klug and H. M. Spurlin (to Hercules Powder Co.).
29. U.S. Pat. 3,719,663 (Mar. 6, 1973), E. D. Klug (to Hercules Inc.).
30. U.S. Pat. 3,728,331 (Apr. 17, 1973), A. B. Savage (to The Dow Chemical Company).
31. U.S. Pat. 4,061,859 (Dec. 6, 1977), W.-J. Cheng (to The Dow Chemical Company).
32. U.S. Pat. 3,391,135 (July 2, 1968), S. Ouno, M. Tonedachi, S. Koyanagi, and K. Ito (to Shin-Etsu Chemical Industry Co., Ltd.).
33. Aqualon™ Cellulose Gum, Sodium Carboxymethylcellulose, Physical and Chemical Properties, Aqualon Co., a Hercules Inc. Co., Wilmington, Del., 1988.
34. D. J. Sikkema and H. Janssen, *Macromolecules* **22**, 364–366 (1989).
35. G. Mann, J. Kunze, F. Loth, and H.-P. Fink, *Polymer* **39**, 3155–3165 (1998).

36. M. G. Wirick, *J. Polym. Sci., Part A-1* **6**, 1705–1718 (1968).
37. J. E. Glass, A. M. Buettner, R. G. Lowther, C. S. Young, and L. A. Cosby, *Carbohydr. Res.* **84**, 245–263 (1980).
38. U.S. Pat. 4,401,813 (Aug. 30, 1983), J. L. Lowell, M. J. Nevins, K. L. G. Reid, and K. L. Walter (to NL Industries, Inc.).
39. U.S. Pat 4,525,585 (June 25, 1985), A. Taguchi and T. Ohmiya (to Diacel Chemical Industries, Ltd.).
40. S.-I. Takahashi, T. Fujimoto, T. Miyamoto, and H. Inagaki, *J. Polym. Sci., Part A* **25**, 987–994 (1987).
41. J. Reuben and H. T. Conner, *Carbohydr. Res.* **115**, 1–13 (1983).
42. J. Reuben, *Carbohydr. Res.* **157**, 201–213 (1986).
43. J. Reuben, *Carbohydr. Res.* **161**, 23–30 (1987).
44. J. Reuben and T. E. Casti, *Carbohydr. Res.* **163**, 91–98 (1987).
45. J. R. DeMember, L. D. Taylor, S. Trummer, L. E. Rubin, and C. K. Chiklis, *J. Appl. Polym. Sci.* **21**, 621–627 (1977).
46. A. Parfondry and A. S. Perlin, *Carbohydr. Res.* **57**, 39–49 (1977).
47. Y. Tezuka, K. Imai, M. Oshima, and T. Chiba, *Polymer* **30**, 2288–2291 (1989).
48. B. Lindberg, U. Linquist, and O. Stenberg, *Carbohydr. Res.* **170**, 207–214 (1987).
49. P. W. Arisz, J. A. Lomax, and J. J. Boon, *Carbohydr. Res.* **243**, 99–114 (1993).
50. P. W. Arisz, H. J. J. Kauw, and J. J. Boon, *Carbohydr. Res.* **271**, 1–14 (1995).
51. S. G. Zeller, G. W. Griesgraber, and G. R. Gray, *Carbohydr. Res.* **211**, 41–45 (1991).
52. S. P. Rowland, in N. M. Bikales, ed., *Encyclopedia of Polymer Science and Technology*, 1st ed., Suppl. Vol. **1**, Wiley-Interscience, New York, 1976, pp. 146–175.
53. A. Baar and W.-M. Kulicke, *Macromol. Chem. Phys.* **195**, 1483–1492 (1994).
54. R. A. Gelman, *J. Appl. Polym. Sci.* **27**, 2957–2964 (1982).
55. R. A. Gelman and H. G. Barth, in J. E. Glass, ed., *Water-Soluble Polymers: Beauty with Performance* (Advances in Chemistry Series, Vol. **213**), American Chemical Society, Washington, D.C., 1986, pp. 101–110.
56. H. G. Barth, *J. Chromatogr. Sci.* **18**, 409–429 (1980).
57. E. Pfannkoch, K. C. Lu, F. E. Regnier, and H. G. Barth, *J. Chromatogr. Sci.* **18**, 430–441 (1980).
58. H. G. Barth and F. E. Regnier, *J. Chromatogr.* **192**, 275–293 (1980).
59. G. Holzwarth, L. Soni, and D. N. Schulz, *Macromolecules* **19**, 422–426 (1986).
60. L. M. Landoll, *J. Polym. Sci., Polym. Chem. Ed.* **20**, 443 (1982).
61. A. C. Sau and L. M. Landoll, in J. E. Glass, ed., *Polymers in Aqueous Media* (Advances in Chemistry Series, Vol. **23**), American Chemical Society, Washington, D.C., 1989, p. 343.
62. *Natrosol® Plus—Modified Hydroxyethylcellulose*, Aqualon Co., a Hercules Incorporated Company, Wilmington, Del., 1996.
63. *Natrosol® Hydroxyethylcellulose, Physical and Chemical Properties*, Aqualon Co., a Hercules Incorporated Company, Wilmington, Del., 1987.
64. *Cellosize® Hydroxyethylcellulose*, Union Carbide Corp., New York, 1981.
65. *Methocel®*, The Dow Chemical Company, Midland, Mich., 1978.
66. *Culminal® Methylcellulose, Physical and Chemical Properties*, Aqualon Co., a Hercules Incorporated Company, Wilmington, Del., 1995.
67. *Chemical and Physical Properties of Hercules® Ethylcellulose*, Hercules Inc., Wilmington, Del., 1982.
68. *Tough Ethocel® Ethyl Cellulose Resin*, The Dow Chemical Company, Midland, Mich., 1974.

69. *Chemical and Physical Properties of Hercules® EHEC Ethylhydroxyethylcellulose*, Hercules Inc., Wilmington, Del., 1981.
70. *Celquat®, Cationic Cellulosic Polymers For Cosmetics and Toiletries*, National Starch and Chemical Corp., Bridgewater, N.J., 2002.
71. *Polymer JR For Hair Care*, Union Carbide Corp., New York., 1998.
72. *Bermocoll® Cellulose Ethers*, Berol Kemi AB, Sweden, 1977.
73. *Klucel® Hydroxypropylcellulose, Physical and Chemical Properties*, Aqualon Co., a Hercules Incorporated Company, Wilmington, Del., 1987.
74. *National Fire Codes®: A Compilation of NFPA Codes, Standards, Recommended Practices, Manuals, and Guides*, Vol. **II**, National Fire Protection Association, Md., 1987.
75. U.S. Pat. 4,525,585 (June 25, 1985), A. Taguchi and T. Ohmiya (to Diacel Chemical Industries, Ltd.).
76. U.S. Pat. 4,526,961 (July 2, 1985), E. Perplies and U. H. Felcht (to Hoechst AG).
77. U.S. Pat. 2,517,577 (Aug. 8, 1950), E. D. Klug and J. S. Tinsley (to Hercules Powder Co.).
78. U.S. Pat. 2,976,278 (Mar. 21, 1961), O. H. Paddison and R. W. Somer (to E. I. du Pont de Nemours & Co., Inc.).
79. U.S. Pat. 4,460,766 (July 17, 1984), U.-H. Felcht and E. Perplies (to Hoechst Aktiengesellschaft).
80. U.S. Pat. 2,523,377 (Sept. 26, 1950), E. D. Klug (to Hercules Powder Co.).
81. U.S. Pat. 2,553,725 (May 22, 1951), L. N. Rogers, W. A. Mueller, and E. E. Hembree (to Buckeye Chemical Oil Co.).
82. R. N. Hadar, W. F. Waldeck, and F. W. Smith, *Ind. Eng. Chem.* **44**, 2803 (1952).
83. U.S. Pat. 2,879,268 (Mar. 24, 1959), E. I. Jullander (to Mo Och Domsjo Aktiebolag).
84. U.S. Pat. 3,072,635 (Jan. 8, 1963), J. H. Menkart and R. S. Allan (to Chemical Development of Canada).
85. U.S. Pat. 3,356,519 (Dec. 5, 1967), W. C. Chambers and M. Lee (to The Dow Chemical Company).
86. Can. Pat. 947,281 (May 14, 1974), W. Patten (to Union Carbide Corp.).
87. U.S. Pat. 2,572,039 (Oct. 23, 1951), E. D. Klug and H. G. Tennent (to Hercules Powder Co.).
88. U.S. Pat. 2,682,535 (June 29, 1954), A. E. Broderick (to Union Carbide Corp.).
89. U.S. Pat. 3,313,176 (Apr. 28, 1964), E. D. Klug (to Hercules Powder Co.).
90. Can. Pat. 1,014,289 (July 19, 1977), E. D. Klug (to Hercules Inc.).
91. J. E. Glass, A. M. Buettner, R. G. Lowther, C. S. Young, and L. A. Cosby, *Carbohydr. Res.* **84**, 245 (1980).
92. U.S. Pat. 5,994,531 (Nov. 30, 1999), R. Doenges, R. Ehrler, and H. Wurm (to Clariant GmbH).
93. PCT WO 2001/09254 (Feb. 8, 2001), F. Hoehl, H. Schlesiger, and R. Kiesewetter (to Wolff Walsrode AG).
94. Jpn. Pat. Appl. 10-330401 (Dec. 15, 1998), K. Tomohito, I. Takeshi, and M. Tetsuya (to Kao Corp.)
95. A. C. Sau and T. G. Majewicz, *ACS Symp. Ser.* **476**, 265–271 (1992).
96. ASTM D2364-01, *Standard Methods for Testing Hydroxyethylcellulose*, American Society of Testing and Materials, Easton, Md., 2002.
97. U.S. Pat. 4,035,195 (July 12, 1977), T. J. Podlas (to Hercules Inc.).
98. U.S. Pat. 2,618,595 (Nov. 18, 1954), W. E. Gloor (to Hercules Powder Co.).
99. U.S. Pat. 3,284,353 (Nov. 18, 1966), J. B. Batdorf (to Hercules Powder Co.).
100. U.S. Pat. 4,433,731 (Feb. 28, 1984), J. Chatterji, B. G. Brake, and J. M. Tinsley (to Halliburton Co.).

101. U.S. Def. Publ. T103,401 (Sept. 6, 1983), T. G. Majewicz (to Hercules Inc.).
102. Hercules CMHEC 37L, Technical Bulletin VC-402C, Hercules Inc., Wilmington, Del.
103. E. D. Goddard and R. B. Hanna, *J. Am. Oil Chem. Soc.* **54**, 561–566 (1977).
104. L. Picton, L. Merle, and G. Muller, *Int. J. Polym. Anal. Characterization* **2**, 103–113 (1996).
105. U.S. Pat. 3,472,840 (Oct. 14, 1969), F. W. Stone and J. M. Rutherford Jr. (to Union Carbide Corp.).
106. U.S. Pat. 4,464,523 (Aug. 7, 1984), D. Neigel and J. Kancylarz (to National Starch and Chemical Corp.).
107. U.S. Pat. 4,228,277 (Oct. 14, 1980), L. M. Landoll (to Hercules Inc.).
108. U.S. Pat. 5,140,099 (Aug. 18, 1992), P. Bostrom, I. Ingvarsson, and K. Sundberg (to Berol Nobel AB).
109. U.S. Pat. 4,845,207 (July 4, 1989), H. E. t'Sas (to Aqualon Co.).
110. N. Sarkar, *J. Appl. Polym. Sci.* **24**, 1073–1087 (1979).
111. U.S. Pat. 4,117,223 (Sept. 26, 1978), W. Lodige, F. Lodige, J. Lucke, and E. Lipp.
112. U.S. Pat. 4,339,573 (July 13, 1982), W. Wust, H. Leischner, W. Rahse, F.-J. Carduck, and N. Kune (to Henkel Kommanditgesellschaft Aktien).
113. U.S. Pat. 4,477,657 (Oct. 16, 1984), C. P. Strange, C. D. Messelt, and C. W. Gibson (to The Dow Chemical Company).
114. U.S. Pat. 4,456,751 (June 26, 1984), C. D. Messelt and G. P. Townsend (to The Dow Chemical Company).
115. U.S. Pat. 4,650,863 (Mar. 17, 1987), U.-H. Flecht, G. Buchberger (to Hoechst AG).
116. U.S. Pat. 6,235,893 (May 22, 2001), K. C. Reibert and J. R. Conklin (to The Dow Chemical Co.).
117. U.S. Pat. 5,482,634 (Jan. 9, 1996), Y. M. Goerlach-Doht and co-workers (to The Dow Chemical Co.).
118. U.S. Pat. 5,360,902 (Nov. 1, 1994), O. Brauer and co-workers (to Wolff Walsrode AG).
119. U.S. Pat. 2,254,249 (Sept. 2, 1941), R. W. Swinehart and A. T. Maasberg (to The Dow Chemical Company).
120. E. D. Klug, *J. Polym. Sci., Part C* **36**, 491–508 (1971).
121. U.S. Pat. 3,278,521 (Oct. 11, 1966), E. D. Klug (to Hercules Inc.).
122. U.S. Pat. 3,357,971 (Dec. 12, 1967), E. D. Klug (to Hercules Inc.).
123. J. Brandrup and E. H. Immergut, *Polymer Handbook*, 3rd ed., John Wiley & Sons, Inc., New York, 1989, Section VII.

GENERAL REFERENCES

E. Ott, M. Spurlin, and M. W. Graffin, eds., *Cellulose and Cellulose Derivatives, High Polymers*, Vol. **V**, Wiley-Interscience, New York, 1954–1955, Parts I–III.

N. M. Bikales and L. Segal, eds., *Cellulose and Cellulose Derivatives, High Polymers*, Vol. **V**, Wiley-Interscience, New York, 1971, Parts IV–V.

R. L. Davidson, ed., *Handbook of Water-Soluble Gums and Resins*, McGraw-Hill, New York, 1980.

J. E. Glass, ed., *Water-Soluble Polymers: Beauty With Performance* (Advances in Chemistry Series, Vol. **213**), American Chemical Society, Washington, D.C., 1986.

J. E. Glass, ed., *Polymers in Aqueous Media: Performance through Association* (Advances in Chemistry Series, Vol. **223**), American Chemical Society, Washington, D.C., 1989.
D. Klemm, B. Philipp, T. Heinze, U. Heinze, and W. Wagenknecht, *Comprehensive Cellulose Chemistry, Vol. 2: Functionalization of Cellulose*, Wiley-VCH, Weinheim, 1998, pp. 207–302.

THOMAS G. MAJEWICZ
PAQUITA E. ERAZO-MAJEWICZ
THOMAS J. PODLAS
Hercules Inc.

CELLULOSE FIBERS, REGENERATED

Introduction

Cellulose (qv) is the natural polymer that makes up the living cells of all vegetation. It is the material at the center of the carbon cycle, and the most abundant and renewable biopolymer on the planet. Regenerated cellulose fiber producers have converted it from the fine short fibers that come from trees into the fine long fibers used in textiles and nonwovens for over a century. Regenerated cellulosics nevertheless remain unique among the mass-produced fibers because they are the only ones to use the natural polymer *directly*. Polyesters, nylons, polyolefins, and acrylics all come *indirectly* from vegetation: from the polymerization of monomers obtained from fossil fuels, which in turn are formed by the incomplete biodegradation of vegetation that grew millions of years ago.

The development of manufactured fibers is one of the great industrial successes of the twentieth century, but after 50 years of explosive growth of the original regenerated cellulosic fibers, synthetic polymer fibers now dominate the market. Natural cellulose in the form of cotton, for centuries the most important of all fibers, now takes second place to polyester. All cellulosic fibers appear relegated to little more than niches in a global textile market driven by the ready availability of cheap fossil fuels and the demand for commodity textiles. Is this relative decline of cellulose and regenerated cellulose just another example of the last stage of the growth/maturity/decline life cycle of most products or is there a possibility that, on a longer timescale, sustainable biopolymers like cellulose will prove to be a serious rival for the synthetics?

Fibers manufactured from cellulose are either *derivative* or *regenerated*. A *derivative fiber* is one formed when a chemical derivative of a natural polymer, eg, cellulose, is prepared, dissolved, and extruded as a continuous filament, and

Encyclopedia of Polymer Science and Technology. Copyright John Wiley & Sons, Inc. All rights reserved.

the chemical nature of the derivative is retained after the fiber formation process (see CELLULOSE ESTERS). A *regenerated fiber* is one formed when a natural polymer or its chemical derivative is dissolved and extruded and the chemical nature of the natural polymer is either retained or regenerated after the fiber formation process. The difficulties of making solutions of natural cellulose from which fibers can be spun has led to most fabricated cellulosic fibers being regenerated from more readily soluble derivatives of cellulose.

Originally, the word rayon was applied to any cellulose-based manufactured fiber, and therefore included the cellulose acetate fibers. However, the definition of rayon was clarified in 1951 and now includes textiles fibers and filaments composed of regenerated cellulose, excluding acetate. In Europe the fibers are now generally known as *viscose*, the term *viscose rayon* being used whenever confusion between the fiber and the cellulose xanthate solution (also called viscose—see below) is possible. (In this article the terms *regenerated cellulosics*, *rayon*, and *viscose rayon* tend to be used interchangeably.)

All synthetic fibers are produced as continuous filaments, either as yarns or tows. Yarns are fine enough to be woven or knitted directly, but cannot be intimately blended with other fibers on the principal conversion systems used for cotton and wool. For these conversion systems, staple fibers, made by cutting the much larger tows into short lengths, are needed. Tows can also be stretch-broken into slivers or tops, which can then be drawn out and twisted into spun yarns.

Denier and tex are both weight/length measures of fiber fineness: denier is the weight in grams of 9000 m of filament, yarn, or tow; tex is the weight in grams of 1000 m. For filaments, as opposed to tows or yarns, the decitex tends to be used as the measure of fineness, 1 denier being equivalent to 1.11 decitex. Filament strengths are measured in gram force/denier (gf/den) or in centiNewtons/tex (cN/tex): 1 gf/den is equivalent to 8.82 cN/tex. Occasionally, the strength of filaments is seen expressed as N/mm^2 to allow comparison with engineering materials. One N/mm^2 is equivalent to the strength in gf/den $\times$ 9 $\times$ 9.807 $\times$ the fiber specific gravity. For cellulose, the specific gravity = 1.51, so N/mm^2 = gf/den $\times$ 133.277.

History

The first successful attempt to make textile fibers from plant cellulose can be traced to George Audemars (1). In 1855 he dissolved the nitrated form of cellulose in ether and alcohol and discovered that fibers were formed as the dope was drawn into the air. These soft, strong nitrocellulose fibers could be woven into fabrics but had a serious drawback: they were explosive, nitrated cellulose being the basis of guncotton (see CELLULOSE ESTERS, INORGANIC).

Sir Joseph Swan, as a result of his quest for carbon fiber for lamp filaments (2), learned how to denitrate nitrocellulose using ammonium sulfide. In 1885 he exhibited the first textiles made from this new artificial silk, but with carbon fiber being his main theme he failed to follow up on the textile possibilities. Meanwhile Count Hilaire de Chardonnet (3) was researching the nitrocellulose route and had perfected his first fibers and textiles in time for the Paris Exhibition in 1889. There he got the necessary financial backing for the first Chardonnet silk factory

in Besancon in 1890. His process involved treating mulberry leaves with nitric and sulfuric acids to form cellulose nitrate, which could be dissolved in ether and alcohol. This collodion solution could be extruded through holes in a spinneret into warm air, where solvent evaporation led to the formation of solid cellulose nitrate filaments.

Although this first route was simple in concept, it proved slow in operation, difficult to scale up safely, and relatively uneconomical compared with the other routes. Denitration of the fibers, necessary to allow safe use wherever the fabrics may risk ignition, spoiled their strength and appearance. Nevertheless, Chardonnet earned and truly deserved his reputation as the Father of Rayon. His process was operated commercially until 1949, when the last factory—bought from the Tubize Co. in the United States in 1934 by a Brazilian company—burned down.

The second cellulosic fiber process to be commercialized was invented by L. H. Despeissis (4) in 1890 and involved the direct dissolution of cotton fiber in ammoniacal copper oxide liquor. This solvent had been developed by M. E. Schweizer in 1857 (5). The cuprammonium solution of cellulose was spun into water, with dilute sulfuric acid being used to neutralize the ammonia and precipitate the cellulose fibers. H. Pauly and co-workers (6) improved on the Despeissis patent, and a German company, Vereinigte Glanstoff Fabriken, was formed that exploited the technology. In 1901, Dr. Thiele at J. P. Bemberg developed an improved stretch-spinning system, the descendants of which survive today.

Its early commercial success owed much to the flammability disadvantages of the Chardonnet process, but competition from the viscose process led to its decline for all but the finest filament products. The process is still used, most notably by Asahi in Japan, where sales of artificial silk and medical disposable fabrics provide a worthwhile income. However, its relatively high cost, associated with the cotton fiber starting point, prevented it from reaching the large scale of manufacture achieved by the viscose rayon process.

In 1891, Cross, Bevan, and Beadle, working at Kew in the United Kingdom, discovered that cotton or wood cellulose could be dissolved as cellulose xanthate following treatment with alkali and carbon disulfide (7). The treacle-like yellow solution could be coagulated in an ammonium sulfate bath and then converted back to pure white cellulose using dilute sulfuric acid. They patented their process in 1892 without considering its fiber-making potential. In 1893 they formed the Viscose Syndicate, to grant licenses for nonfiber end uses, and the British Viscoid Co. Ltd., to exploit the process as a route to molded materials. These companies were later merged to form the Viscose Development Co. in 1902.

In another laboratory at Kew, C. H. Stearn and C. F. Topham, who had worked for Sir Joseph Swan on lamp filaments, developed the continuous filament spinning process (8) and the machinery needed to wash and collect (9,10) the yarns. A fiber-making method was outlined in 1898, and the Viscose Spinning Syndicate was formed to develop the concept into a commercial proposition.

In 1904, the Kew laboratories were visited by representatives of Samuel Courtauld & Co. Ltd., who were silk weavers looking for new raw materials and new opportunities to grow. The success and profitability of Samuel Courtauld had been built on the nineteenth-century fashion for black silk mourning crepe, and the company was planning its stock market flotation. The visitors to Kew knew that Chardonnet's process was creating a lucrative market for artificial silk in

France. They believed that Cross and Bevan's viscose route could make a similar fiber much more economically. Nevertheless, it took two attempts, the second to a changed Board of Directors after the flotation, before Courtaulds was persuaded to acquire the viscose process rights. On July 14, 1904, the Viscose Spinning Syndicate agreed to sell the viscose process rights and patents to Courtaulds for the sum of £25,000. A new factory was built and the first commercial production was started in Coventry, United Kingdom, in November 1905.

The acquisition of the rights to the viscose process became one of the most profitable investments of all time. Interest in the new fiber was intense, and growth of production capacity was exponential. By 1907, the Courtauld company was selling all the artificial silk it could produce and proceeded to expand into the U.S. market. In 1910 they formed the American Viscose Co. and in 1911 started the first U.S. viscose factory at Marcus Hook. By 1939, Courtaulds had six factories in the United States, seven in the United Kingdom, one in France, one in Canada, and joint ventures in Germany and Italy.

From 1920 to 1931, after the expiration of the viscose patents, world output increased from 14,000 to 225,000 t per year, as more than 100 companies entered the cellulose fiber field. In Europe, Vereinigte Glanstoff Fabriken (VGF, Germany), Enka (Holland), I. G. Farben (Germany), Snia Viscosa (Italy), Comptoir des Textiles Artificiels (CTA, France), Rhodiaceta (France), Tubize (Belgium), and Chatillon (Italy) were among the new starters. In the United States the new entrants included Du Pont (with help from CTA), Tubize, Chatillon, American Enka, The Industrial Fiber Corp. (later The Industrial Rayon Corp.), American Glanzstoff (later North American Rayon), and American Bemberg.

By 1941, as the first synthetic polymers were being converted into fibers (nylon and later polyester), regenerated cellulosic fiber production had risen to 1,250,000 ton. It continued to expand into the 1970s recording its highest ever annual output at 3,856,000 ton in 1973. Since then a steady decline has occurred as more and more end uses switch to the cheaper synthetic fibers based on oil valued at little more than the costs of extraction.

Applications

The original yarns were marketed as silk substitutes for use in apparel, hosiery, lace, home furnishings, ribbons, braids, and in a whole range of fabrics using blends with cotton or wool yarns. As the end uses expanded beyond silk replacement, the harsh metallic luster of the yarn proved disadvantageous, and dull "matt" fibers had to be developed. Oil dulling was invented (11) in 1926, and an improved method using titanium dioxide was developed (12) in 1929.

Commencing in the late 1930s, new developments to make very strong yarns allowed the viscose rayon to replace cotton as the fiber of choice for longer-life pneumatic tires. The pace of this line of development increased during World War II, and by the 1960s a significant part of the production of viscose yarn was for tires and industrial applications.

From 1910 onward waste filament yarn had been chopped into short lengths suitable for use on the machinery designed to process cotton and wool staples into spun yarns. In the 1930s new plants were built specifically to supply the

staple fiber markets. During World War II the production of staple matched that of filament, and by 1950, staple viscose was the most important product. The new spun-yarn outlets spawned a series of viscose developments aimed at matching the characteristics of wool and cotton more closely. Viscose rayon was, after all, silk-like. Compared with wool it lacked bulk, resilience, and abrasion resistance. Compared with cotton, it was weaker, tended to shrink and crease more easily, and had a rather lean, limp hand.

For wool outlets, coarser crimped staple fibers were developed. By the late 1960s these were widely used in the new tufted carpets, which for a period became the single largest application for the cellulosic fiber. For cotton outlets, two distinct lines of development were undertaken, the first being to boost the strength and modulus of rayon so that it could match that of cotton, and the second to alter the shape of the fiber to give bulkier, more cotton-like textures. High wet modulus (HWM) rayons of two types were developed. Staple versions of the tougher tire-yarn fibers (modal HWM fibers) were introduced for use in industrial textiles, and for blending with the rapidly growing synthetics. This class was later subdivided into the low, intermediate, and high strength variants (LWM, IWM, and HWM) as producers tuned the process to market niches. Polynosic HWM fibers with even better wet stability and higher wet modulus were introduced to blend with the better grades of cotton.

In the 1960s and 1970s, viscose producers in Europe, the United States, and Japan made various attempts to make rayon behave more like cotton in both woven fabrics and specialty papers. Avtex (U.S.) and Kurashiki Rayon (Japan) commercialized inflated–collapsed paper-making fibers. Courtaulds (U.K.) developed a range of hollow fibers, of which two were commercialized. The first, having an uncollapsed tubular shape, found worthwhile new business in thermal underwear. The other, having an unevenly collapsed tube shape and a very high absorbency, enjoyed large sales in sanitary protection products. These hollow fibers were replaced in the late 1980s by I- and Y- shaped solid fibers that performed as well as the hollow versions in the main applications.

The Viscose Process

The main raw material required for the production of viscose is cellulose (qv), a natural polymer of D-glucose (Fig. 1). The repeating monomer unit is a pair of anhydroglucose units (AGU). Cellulose and starch (qv) are identical but for the way in which the ring oxygen atoms alternate from side to side of the polymer

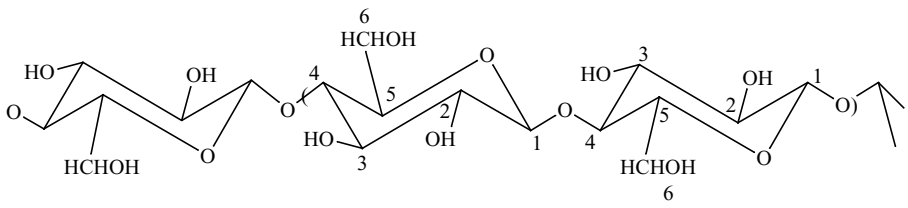

Fig. 1. Anhydroglucose units with 1–4 beta linkages as in cellulose.

chain (beta linkages) in cellulose, but remain on the same side (alpha linkages) in starch.

Cellulose is the most abundant polymer, an estimated 10^{11} t being produced annually by natural processes. Supplies for the rayon industry can be obtained from many sources; but in practice, the wood-pulping processes used to supply the needs of the paper and board industries have been adapted to make the necessary specially pure grade. Of the 3×10^8 t of wood used by the paper and board industry (13) in 1989, about 6×10^6 t were purified to provide the 2.5×10^6 t of dissolving pulp required by the viscose processes.

The trees used to make dissolving pulp are fast-growing hard or soft woods farmed specifically for their high quality pulping. For example, *Eucalyptus grandis* is farmed in relatively poor agricultural areas but grows from seedling to maturity in 7–10 years. It yields about 0.62 kg/m^2 (2500 kg/acre) per year of cellulose for fiber-making, compared with the best cotton fiber yields of 0.074 kg/m^2 (300 kg/acre) per year obtained from prime agricultural land. After sulfite or prehydrolyzed Kraft pulping, the cellulose wood fibers, liberated from the lignin (qv), pass through a sequence of purification stages, eg, chlorination; hot caustic extraction; hypochlorite, peroxide or chlorine dioxide bleaching; and cold caustic extraction.

The final properties of the rayon fiber and the efficiency of its manufacturing process depend crucially on the purity of the pulp used. High tenacity fibers need high purity pulps, and this means pulping to get up to 96% of the most desirable form of cellulose (known as alpha cellulose), and removing most of the unwanted hemicellulose and lignin. Cellulose molecular weight must be tightly controlled, and levels of foreign matter such as resin, knots, shives, and silica must be very low. Of the two main pulping processes, the sulfite route produces higher yields of lower alpha, more reactive pulp, suitable for regular staple fiber. Prehydrolyzed kraft pulps are preferred for high strength industrial yarn or modal fiber production. The highest purity pulps, up to 99% alpha cellulose, are obtained from cotton fiber. These are no longer used in viscose production but are now the main raw material for cuprammonium rayon.

The flow diagram for the viscose process is given in Figure 2. The sequence of reactions necessary to convert cellulose into its xanthate and dissolve it in soda used to be performed batchwise. Fully continuous processes, or mixtures of batch and continuous process stages, are more appropriate for high volume regular viscose staple production.

Steeping. Sheet, roll, or suitably milled flock pulp is metered into a pulper along with vigorously stirred 18% sodium hydroxide solution at 50°C. The resulting slurry, containing about 5% finely dispersed pulp, passes to a buffer tank from which it is metered to a slurry press that sieves out the swollen fiber and returns the pressings soda for concentration correction and reuse. The cellulose reacts with the soda as a complex alcohol to form the sodium salt or alk-cell.

$$\text{Cell—OH} + \text{NaOH} \rightarrow \text{Cell—ONa} + \text{H}_2\text{O} \quad (1)$$

The blanket of alk-cell leaving the slurry press is shredded, and if necessary cooled, before being conveyed to mercerizing (the ripening or aging process).

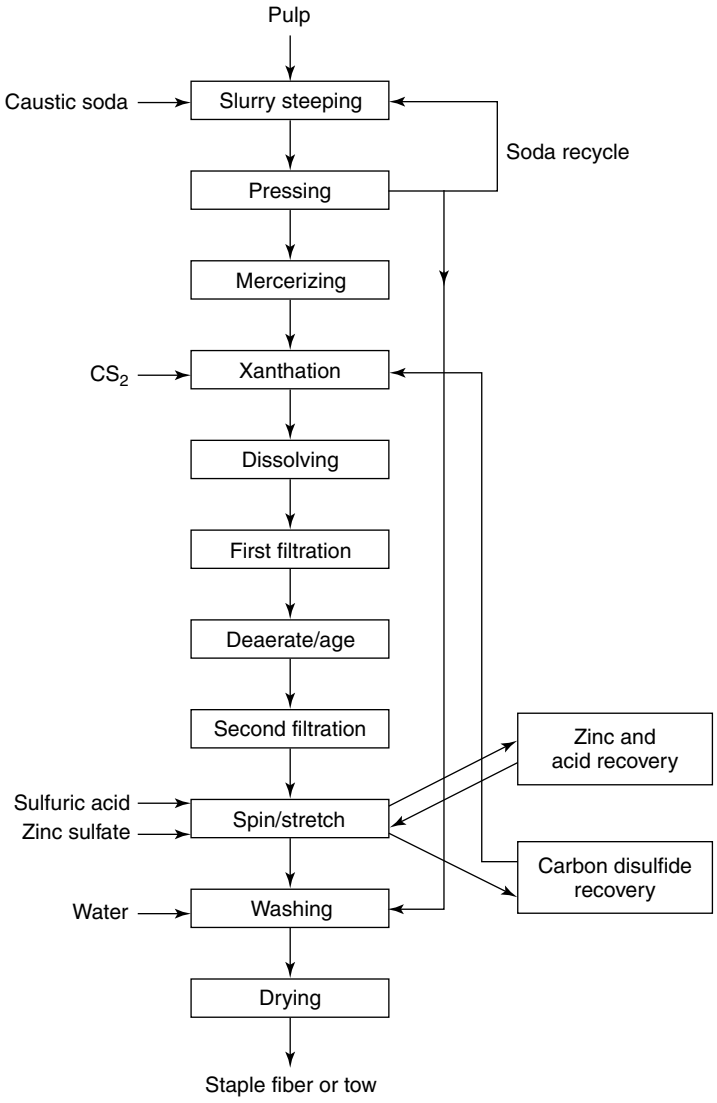

Fig. 2. The viscose process.

Hemicelluloses left over from the cellulose pulping process tend to accumulate in the steep soda, and levels of up to 3.0% are tolerable, depending on the type of fiber being produced. Equilibrium hemicellulose levels may prove to be too high for the production of stronger fibers, and in this case steps must be taken to purify the soda, eg, by dialysis, prior to reuse. In any case a proportion of the soda from the presses is filtered for later use in dissolving and washing; the steep liquor itself is corrected to the required concentration by the addition of fresh hemicellulose-free strong soda.

Mercerizing. Alk-cell mercerizing (or aging) is ideally carried out on a conveyor belt running through a temperature-and humidity-controlled tunnel. Towers, silos, cylinders, or even extended treatment in shredders are used as alternatives to belts. During mercerizing, oxidative depolymerization of the cellulose occurs, and this reduces the molecular weight to a level where the final viscose viscosity and cellulose concentration are within acceptable ranges. The optimum conditions for a given pulp depend on the details of the equipment and the cost–quality balance required by the business. The aging temperature is generally around 50°C, and the humidity is adjusted to prevent any drying of the alk-cell. Catalysts such as manganese (a few parts per million in steep liquor) or cobalt have been added to the steep soda to accelerate the aging process (14) or to allow lower temperatures to be used. Catalyzed aging on a conveyor takes 3–4 h, and at the end of the belt, the alk-cell is blown or conveyed to a fluid-bed cooler.

Whatever system is used, tight control of the aging process is essential for good quality viscose solutions, because the viscosity of the viscose depends on it. Varying viscosity can play havoc with all subsequent operations up to and including spinning. Productivity gains achieved by high-temperature or catalyzed aging tend to be accompanied by increased viscosity variability and reduced reactivity in xanthation.

Xanthation. The viscose process is based on the ready solubility of the xanthate derivative of cellulose in dilute sodium hydroxide. The reaction between alkali cellulose and carbon disulfide must therefore be as uniform as possible to avoid problems with incompletely dissolved pulp fibers that will later have to be filtered out of the viscous solution.

In theory, for regular rayon manufacture only one of the hydroxyl groups on each pair of anhydroglucose units needs to be replaced by a xanthate group, ie, the target degree of substitution (DS) is 0.5, which to achieve without waste would need 23% CS_2 on cellulose.

The desired reaction is

$$\mathrm{CellO^-\ Na^+ + CS_2 \rightarrow CellOCS_2Na} \qquad (2)$$

but side reactions between the CS_2 and the NaOH also occur, one of which is

$$\mathrm{2\ CS_2 + 6NaOH \rightarrow Na_2CO_3 + Na_2CS_3 + Na_2S + 3\ H_2O} \qquad (3)$$

It is the sodium trithiocarbonate from this side reaction that gives the viscose dope its characteristic orange color.

In addition to the cellulose xanthate [9032-37-5] forming reaction, equation 2 being reversible, cellulose can reform by

$$\mathrm{CellOCS_2Na + 2\ NaOH \rightarrow Na_2CO_2S + NaSH + CellOH} \qquad (4)$$

Clearly, free sodium hydroxide in alkali cellulose leaving the slurry presses causes problems in xanthation, and the presses have to be operated to minimize reactions 3 and 4.

Carbon disulfide [75-15-0] is a clear colorless liquid that boils at 46°C, and should ideally be free of hydrogen sulfide and carbonyl sulfide. The reaction with alkali cellulose is carried out either in a few large cylindrical vessels known as wet churns, or in many smaller hexagonal vessels known as dry churns. In the fully continuous viscose process, a Continuous Belt Xanthator, first developed by Du Pont, is used (15).

In a large wet churn operation, a weighed batch of alk-cell (5–10 t) is charged into the churn, which is then evacuated. Carbon disulfide (0.5–1 t) is admitted over a 20-min period and vaporizes in the partial vacuum. Churns are rotated slowly to encourage the solid–vapor interaction or they are stirred with a large slow-moving paddle. The reaction with alk-cell is slightly exothermic, and churns are generally cooled to maintain the temperature between 25 and 30°C. Under these conditions the xanthation reaction is completed in about 100 min and its progress can be monitored by observing the partial vacuum redeveloping as the gas is adsorbed by the solid.

About 25% of the CS_2 is wasted in side reactions (eg, reaction 3), and this means that to achieve the ideal 0.5 DS, the CS_2 charge is about 30% by weight of the cellulose. Higher charges (up to 50%) are needed for the strongest high wet modulus rayon production. Lower charges are possible if steps are taken to increase the reactivity of the alk-cell, or to suppress the undesirable side reactions, or to ensure that viscose filtration is good enough to cope with more undissolved material.

The incomplete accessibility of the cellulose molecules in alk-cell prevents complete xanthation, ie, the formation of the trixanthate, no matter how much CS_2 is used. The trixanthate would imply a DS of 3, sometimes known as a gamma value of 300 CS_2 groups per 100 AGUs. In practice, gamma values over 100 are hard to achieve in the churn, but levels up to 200 can be reached by a combination of churn addition and liquid CS_2 injection into the viscose where the cellulose accessibility is at its greatest. For regular staple production, gamma values tend to be around 50 at the churn and 30–35 at spinning.

At the end of xanthation, any remaining traces of CS_2 are flushed from the wet churn prior to, or in some cases by, admitting a charge of the dissolving or mixer soda in order to commence dissolution. For a dry churn operation, the vessel is opened to allow the golden xanthate crumbs to be discharged into a separate mixer.

Dissolution. Cellulose and its derivatives dissolve more easily in cold alkali than in hot, and the initial contact between cellulose xanthate and the mixer soda should occur at the lowest temperature possible. Two percent NaOH at no more than 10°C is admitted to the wet churn and the paddle speeded up to wet out all the crumb prior to discharge. Some of the required mixing soda charge can be retained to wash out the churn before restarting the cycle. Discharge occurs, through cutters that eliminate any large lumps of agglomerated xanthate, into the batch tank where dissolution is completed. Here it is stirred for about 2 h to allow the xanthate to dissolve. The mixing conditions are crucial. High shear mixing certainly speeds up the process but can cause local heating, which can regenerate cellulose from the xanthate.

The final composition of the solution is controlled by the ratio of xanthate to mixer soda, the concentrations of cellulose and NaOH in the xanthate, and

the concentration of NaOH in the mixer soda. For regular staple processes the cellulose/soda ratio is within the range 8.5:6.0 to 10.0:5.0, the latter tending to give lower quality viscose solutions. High quality textile yarns require a 7.5:6.5 ratio, whereas the strongest high wet modulus processes use a 6.0:6.0 ratio. Here lower cellulose concentrations are necessary to allow the use of higher molecular weights (less mercerizing), which allow higher strength development.

It is possible to add modifiers or delustrants at the dissolving stage. However, modern viscose dope plants feed several spinning machines, which are often expected to make different grades of fiber. It is therefore now more common to add the materials needed to make special fibers by injection close to the spinning machines.

Viscose Aging, Filtration, and Deaeration. After the dissolution step, the viscose cannot be spun into fibers because it contains many small air bubbles and particles. Furthermore, the degree of xanthation is too high, with too many of the xanthate groups in positions dictated by their accessibility and not in the ideal positions for uniform dissolution.

Dexanthation, and the redistribution of xanthate groups into the most favorable positions on the cellulose molecules, occurs automatically as the viscose ages. For regular staple fibers the process takes about 18 h, but for the stronger fibers, shorter times and more difficult spinning conditions have to be tolerated. During this aging process, reaction 2 goes into reverse and the xanthate groups attached to the 2- and 3- positions on the AGU (Fig. 1) hydrolyze 15–20 times as fast as those on C-6. Transxanthation occurs (16); the unoccupied C-6 hydroxyl competing with reaction 2 for the CS_2 that is leaving C-2 and C-3. The reactions favoring more spinnable viscose are in turn favored by aging for longer times at the lowest possible temperature. Cold viscoses are unfortunately much more viscous, and therefore harder to filter and deaerate.

Filtration of viscose is not a straightforward chemical engineering process. The solution of cellulose xanthate contains some easy-to-deal-with undissolved pulp fibers, and also some gel-like material that is retarded rather than removed by the filters. The viscose is unstable and tends to form more gel as it ages. Its flow characteristics make the material close to the walls of any vessel or pipe move more slowly, get older, and gel more than the mainstream viscose. So while filtration can hold back gels arising from incomplete mixing, new gels can form in the pipework after the filters.

The removal of particles that would block the spinneret holes occurs in several stages. The traditional plate-and-frame first-filters dressed with disposable multilayers chosen from woven cotton, cotton wadding, or wood pulp have now been replaced by durable nylon needlefelts that can be cleaned by automatic backwashing (17). Second filtration, usually after deaeration, is also changing to fully automatic systems with sintered steel elements that do not need manual cleaning. Third-stage filtration, close to the spinning machines, is used to provide a final polishing of viscose quality, but is only justifiable for the premium quality fibers. All processes nevertheless use small filters in each spinneret to catch any particulate matter that may have eluded, or been formed after, the main filter systems.

Continuous deaeration occurs when the viscose is warmed and pumped into thin films over cones in a large vacuum tank. The combination of the thinness

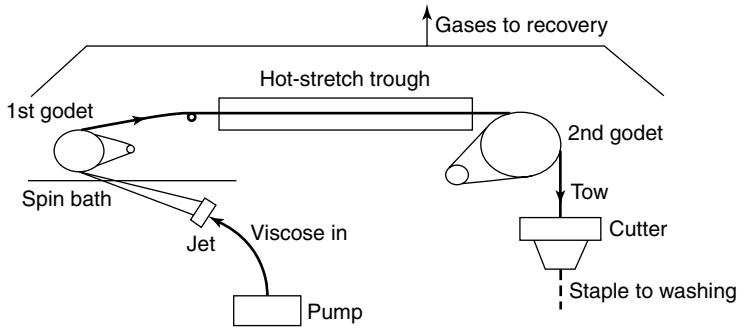

Fig. 3. One "end" of a staple fiber–spinning machine.

of the liquid film and the disruption caused by the boiling of volatile components allows the air to get out quickly. Loss of water and CS_2 lower the gamma value and raise the cellulose concentration of the viscose slightly. Older systems use batch deaeration, where the air bubbles have to rise through several feet of viscose before they are liberated.

The correct viscose age or ripeness for spinning varies according to the type of fiber being made. Ripeness can be assessed by establishing the salt concentration necessary to just coagulate the viscose dope. The preferred test uses sodium chloride (salt figure) although the alternative method (Hottenroth number) is based on ammonium chloride.

Spinning. Properly filtered and deaerated viscose of the right salt figure can be coagulated into filament by pumping it through a suitable orifice (jet or spinneret) into a coagulating bath. The forming filaments are pulled through the bath by the first godets, which in some systems also serve as an anchor against which stretch can be applied by the second godets or traction units. The assembly of pumps, spin baths, jets, godets, stretch baths, traction units, and ventilation systems is known as the spinning machine. It can take many forms depending on the type of fiber being made and the priority given to achieving a geometrically similar path for the tows from each jet. Figure 3 illustrates one end of a staple fiber–spinning machine that would have hundreds of ends making up the final tow entering the cutter.

Jets for continuous filament textile yarn are typically 1-cm-diameter gold–platinum alloy structures with 20–500 holes of 50–200-μm diameter. Tire yarn jets are also 1 cm in diameter but typically use 1000–2000 holes to give the required balance of filament and yarn denier. Staple fiber jets can have as many as 70,000 holes and can be made from a single dome of alloy or from clusters of the smaller textile or tire yarn jets. The precious metal alloy is one of the few materials that can resist the harsh chemical environment of a rayon machine and yet be ductile enough to be perforated with precision. Glass jets have been used for filament production, and tantalum metal is a low cost but less durable alternative to gold–platinum.

The basic chemistry of fiber formation is however independent of the hardware. Spin-bath liquors are mixtures of sulfuric acid (5–15%), zinc sulfate (0.05–7%), and sodium sulfate (10–28%) controlled at temperatures ranging from

30 to 60°C. They are circulated past the jets at carefully controlled rates and fully recycled. The liquid filament emerging from the jet coagulates at the interface between acid bath and alkaline viscose to form a cuticle, and later a skin, through which the rest of the coagulation and regeneration is controlled. This regeneration mechanism causes the skin–core nonuniformity, which is characteristic of regular rayon fiber cross sections.

$$2\ \text{Cell}{-}OCS_2Na + H_2SO_4 \rightarrow 2\ \text{Cell}{-}OCS_2H + Na_2SO_4 \quad (5)$$

As coagulation proceeds into the center of the forming fiber, the outside regenerates to cellulose at a rate dependent on the temperature and composition of the bath.

$$\text{Cell}{-}OCS_2H \rightarrow \text{Cell}{-}OH + CS_2 \quad (6)$$

In processes making regular staple fiber, reactions 5 and 6 occur practically simultaneously, but in high wet modulus processes, reaction 5 predominates in the spin bath, with reaction 6 occurring while stretching the filament in a hot water or steam bath. The carbon disulfide liberated in spinning and stretching can be recovered from the extracted air and from the spin-bath liquor.

Zinc salts are added to the spin bath to slow down the regeneration reaction by forming a less easily decomposed zinc cellulose xanthate intermediate. This allows greater stretch levels to be applied and results in fibers with thicker skins. There is still uncertainty as to whether the zinc cellulose xanthate gel acts by hindering acid ingress or water loss. High levels of zinc in the spin bath allow the production of tough fibers for tire reinforcement and industrial use.

Washing and Drying. In staple fiber production the filaments from all the jets on the spinning machine are combined into a few large tows and cut to length prior to washing. In filament yarn production, the yarns are kept separate and collected either as acid cakes for off-line cake washing, or wound onto bobbins after on-line washing and drying.

Again, irrespective of the hardware the chemistry is consistent. The partially regenerated fiber from the spinning machine is contaminated with sulfuric acid, zinc sulfate, sodium sulfate, carbon disulfide, and the numerous incompletely decomposed by-products of the xanthation reactions. The washing and drying systems must yield a pure cellulose fiber, suitably lubricated for the end use, and dried to a moisture level of around 10%.

The sequence of treatments is illustrated in Figure 4. Water consumption in washing is minimized by using a countercurrent liquor flow, clean water entering the system at the point where the fiber leaves, and dirty liquor leaving for chemical recovery at the point where the fiber enters.

In the staple fiber system, the tows from spinning are cut to length and sluiced onto a 30–40-m-long wire-mesh conveyor that carries the blanket of fiber through cascades of the various wash liquors. Sluicing is a critical operation because the cut lengths need to be opened just enough to allow good washing and not so much that the individual fibers entangle. Sluicing must also lay a uniformly permeable blanket of fibers several centimeters thick and a meter or so

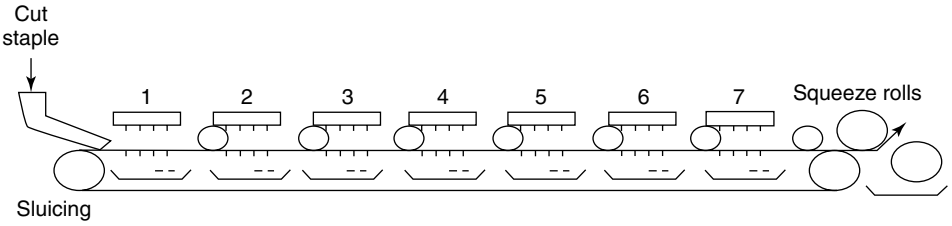

Fig. 4. Staple fiber washing sequence: 1, a *hot acid wash* (2% H_2SO_4 at 90°C) decomposes and washes out most of the insoluble zinc salts. This wash completes the regeneration of xanthate and removes as much sulfur as possible in the form of recoverable CS_2 and H_2S; 2, an alkaline sodium sulfide *desulfurization bath* solubilizes sulfurous by-products and converts them into easily removed sulfides; 3, a *sulfide wash* to remove the sulfides created in bath 2; 4, a *bleach bath* (optional) uses very dilute hypochlorite or peroxide to improve fiber whiteness; 5, a dilute acid or *sour bath* removes any remaining traces of metal ions and guarantees that any residual bleaching chemicals are destroyed; 6, a controlled-pH freshwater *final wash* removes the last traces of acid and salt prior to drying; and 7, a *finish bath* gives the fiber a soft handle for easy drying and subsequent processing.

wide because uneven laying results in uneven washing. Washing tows before cutting breaks out of the restrictions imposed by sluicing but results in the need to reoptimize processing conditions.

Cakes of textile yarn, collected in Topham boxes immediately after spinning, are processed on cake-wash machines. The cakes are wrapped in a porous paper and mounted in groups on stainless steel tubes through which the wash liquors can be forced. These tubes are mounted on a cake-wash box, which is a trolley on an overhead conveyor carrying the cakes to the different pumping stations on the machine. Each cake-wash box holds 100–200 cakes, and the permeability of each cake is critical to uniform washing. With permeability being determined largely by the degree of swelling of the fiber leaving spinning, very good control of all regeneration parameters is required to make yarn with consistent properties.

Yarn-drying procedures are far more critical than staple-drying procedures. All cellulosic fibers expand when wetted and contract on drying, the changes of size being greatest the first time the freshly made fiber is dried. If the contraction is hindered in any way, the yarn will possess a latent strain that will recover at a later stage, giving inferior weaving and dyeing. Furthermore, freshly formed regenerated cellulose undergoes a permanent change in molecular structure as it is heated, and this reduces its absorbency and hence its dye uptake.

Cakes are dried in low temperature, high humidity conditions for a long time in order to minimize strain and absorbency variability. The continuing usage of the cake system almost a century after its invention owes much to the desirable strain-free yarn arising from its washing and drying operations.

Industrial yarn uses a continuous washing and drying process based on self-advancing reels. Whereas the processing of cake yarn can take many days to complete, the continuous process is over in minutes. The process is less labor-intensive and more productive than the cake system, but the engineering and maintenance requirements are easily underestimated. It is most used for industrial yarns—still the reinforcement of choice for radial tire carcasses. For

these applications the strain built in by fast drying is no disadvantage because the yarns are expected to be at their best when bone dry. Dyeing is not required and an off-white color is tolerable. The main objective of the washing system is to remove acid and sulfur compounds that would affect the strength of the yarn during prolonged operation at high temperature.

Modified Viscose Processes. The need for ever stronger yarns resulted in the first important theme of modified rayon development and culminated—technically if not commercially—in the 0.88 N/tex (10 gf/den) high wet modulus industrial yarn process.

Tire Yarns. A method to increase the strength of viscose yarn from the 0.2 N/tex (2.2 gf/den) standard to levels needed in tires was first patented by Courtaulds in 1935 (18). By raising the zinc concentration in the spin bath to 4%, the thread could be stretched more by immersing it in a hot dilute acid bath during extension. Filament strengths increased to about 0.3 N/tex (3.3 gf/den), and the cross section became rounder, with a thicker skin than regular viscose. Pairs of these yarns were capable of being twisted into tire cords that outperformed traditional cotton cords.

The next significant strength improvement followed the 1950 Du Pont (19) discovery of monoamine and quaternary ammonium modifiers, which, when added to the viscose, prolonged the life of the zinc cellulose xanthate gel, and enabled even higher stretch levels to be used. Modifiers have proliferated since they were first patented and the list now includes many poly(alkylene oxide) derivatives (20), polyhydroxypolyamines (21–23), and dithiocarbamates (24).

Fully modified yarns had smooth, all-skin cross sections, a structure made up of numerous small crystallites of cellulose, and filament strengths around 0.4 N/tex (4.5 gf/den). They were generally known as the Super tire yarns. Improved Super yarns [0.44–0.53 N/tex (5–6 gf/den)] were made by mixing modifiers, and one of the best combinations was found to be dimethylamine with poly(oxyethylene glycol) of about 1500 mol wt (25). Ethoxylated fatty acid amines have now largely replaced dimethylamine because they are easier to handle and cost less.

The strongest fibers were made using formaldehyde additions to the spin bath while using a mixed modifier system (26–29) or using highly xanthated viscoses (50% + CS_2). Formaldehyde forms an *S*-methylol derivative with xanthate, which decomposes slowly, permitting high levels of stretch. It also reacts with the cellulose backbone to form cross-links that render the fiber high in modulus and low in extension. Unfortunately, problems associated with formaldehyde side reactions made the processes more expensive than first thought, and the inevitable brittleness that results whenever regenerated cellulose is highly oriented restricted the fibers to nontextile markets. The commercial operations were closed down in the late 1960s.

The formaldehyde approach is still used by Futamura Chemical (Japan). They make spun-laid viscose nonwovens where the hydroxymethylcellulose xanthate derivative formed from formaldehyde in the spin bath allows the fibers to bond after laying. This process was originally developed by Mitsubishi Rayon (30), who later found that the derivative was thermoplastic, and the web could be calender-bonded (120°C) prior to regeneration (31).

High Tenacity Staple Fibers. When stronger staple fibers became marketable, the tire yarn processes were adapted to suit the high productivity staple

fiber processes. Improved staple fibers use a variant of the mixed modifier approach to reach 0.26 N/tex (3 gf/den). The full 0.4 N/tex (4.5 gf/den) potential of the chemistry is unnecessary for the target end uses and difficult to achieve on the regular staple production systems.

The full potential of the mixed modifier tire yarn approach is, however, achieved in the modal or HWM (high wet modulus) staple processes using special viscose-making and -spinning systems. Courtaulds produced such fibers under the Vincel brand both in the United Kingdom and in Canada. Avtex made Avril (Fiber 40) until their closure in 1989. Lenzing still makes Modal staple in Austria. These fibers are most popular in ladies' apparel for their soft handle and easy dyeing to give rich coloration. They are made in finenesses down to 1 dtex (0.9 den) for fine yarns and hydroentangled nonwoven production (32).

Polynosic Rayons. The foregoing viscose process variants depend on the presence of zinc in the spin bath and modifiers in the viscose for their efficacy. Another strand of development began in 1952 when Tachikawa (33) patented a method for making strong, high modulus fibers that needed neither zinc nor modifier. The process was in fact related to the Lilienfeld (34) route to high strength, high modulus yarns that had failed in the 1930s because of the need for a spin bath containing 50–85% sulfuric acid. Both processes depend (33,34) on the fact that minimally aged alk-cell can, after xanthation with an excess of carbon disulfide, be dissolved at a low cellulose concentration to give very viscous viscoses containing high molecular weight cellulose. These viscoses have sufficient structure to be spun into cold, very dilute spin baths containing no zinc and low levels of sodium sulfate. The resulting gel filaments can be stretched up to 300% to give strong, round-section, highly ordered fibers, which can then be regenerated.

Toyobo's Tufcel is an excellent example of a modern polynosic fiber process, probably the most difficult viscose process to run efficiently, (35). On-line process control allows only four persons per shift to make 10,000 t/year of a variety of special fibers, including Flame Retardant, Deep Dyeing (two types), Activated Carbon Fiber, and Super Fine 0.55 dtex (0.5 denier). Alk-cell and mixing soda quality are maintained by pressings soda centrifugation, filtration, and dialysis to remove 90% of the hemicellulose. Ion-exchange membranes are used to give 50 times the life and twice the efficiency of the old dialyzer bags used in tire-yarn production. Dissolution of the 500 DP xanthate is augmented by crumb grinders on the churn outlets and by in-line homomixers, which together reduce the dissolution time from three hours to one. Spinnerets for the finer yarns have 40-μm holes, and these are protected by automatic backflush filters, removing gels down to 15-μm diameter.

The polynosic rayons enjoyed a revival of fortunes in the 1990s when the new lyocell fiber produced by Courtaulds (Tencel®)—a solvent spun fiber with polynosic properties—became popular in ladies' apparel and denim. By 2001 however the Toyobo Tufcel plant in Japan had been closed and at the time of writing, it is likely to be transferred to China where lower labor costs would allow it to compete more effectively with lyocell (see below).

Bulky Rayons. Unlike the thermoplastic synthetic fibers, viscose rayon cannot be bulked by mechanical crimping processes. Crimpers impart crimp to a regenerated cellulose fiber, but it is not a permanent crimp and will not survive wetting out.

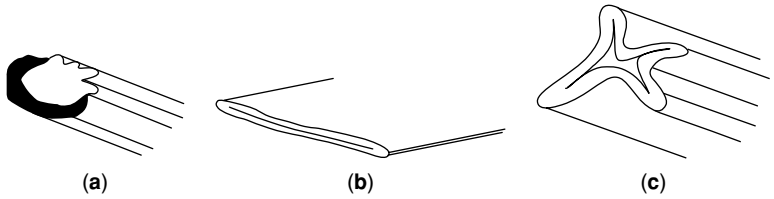

Fig. 5. Bulky rayons: (**a**) crimped rayon; (**b**) inflated–collapsed rayon; (**c**) super inflated rayon.

Permanent chemical crimp can be obtained by creating an asymmetric arrangement of the skin and the core parts of the fiber cross section. Skin cellulose is more highly ordered than core cellulose and shrinks more on drying. If, during filament formation in the spin bath, the skin can be forced to burst open to expose fresh viscose to the acid, a fiber with differing shrinkage potential from side to side is made, and crimp should be obtained (Fig. 5**a**).

Whether or not it is obtained depends on the washing mechanism allowing the shrinkage, and hence the crimp, to develop prior to the completion of regeneration. Crimp development occurs fully only in staple fiber processes, where the sluicing operation allows the cut tufts of acid tow to expand freely in ample volumes of hot liquor.

Even when crimp is fully developed it is easy to pull out (low energy) and difficult to translate into noticeably bulkier woven and knitted fabrics. It does however improve the absorbency and the cohesion of the staple (important in spun-yarn and nonwoven making) and gives a subtly different texture to woven fabrics. Coarse crimped rayon was the leading synthetic carpet fiber in Europe in the 1960s, but has since been replaced by the highly durable bulked continuous filament nylon yarns. Crimp is most important in rayon used for hygienic absorbent products.

Process conditions that favor chemical crimp formation are similar to those used for improved tenacity staple (zinc/modifier route). However, spin-bath temperature should be as high as possible (ca 60°C) and the spin-bath acidity as low as possible (ca 7%). Attempts have been made to overcome some of the leanness of high strength rayons by increasing the crimp levels. ITT Rayonier developed the Prima crimped HWM fiber (36) and made the process available to their customers. Avtex developed Avril III. Neither remain in production.

Cross-sectional modifications of a more extreme nature than skin-bursting, which nevertheless do not form crimp, have grown in importance since the early 1980s. These yield a permanent bulk increase, which can be translated into bulky fabrics without the need for special care. The first commercial staple fiber of this type was Courtaulds hollow Viloft, developed in the 1970s using a carbonate inflation technique (37).

Inflation had long been known as an intermittent problem of textile yarn manufacture. It was caused by the skin forming too quickly to allow the escape of gases liberated by the regeneration reactions, or as a result of air in the viscose at the jet. In the 1920s attempts were made to produce hollow naturally dull yarns by inclusion of gas (38) and by the addition of gas-generating agents to the

viscose (39). It was also possible to cause inflation by capturing the regenerated gases when spinning a low soda viscose (40). In 1942–1943 Du Pont used air injection to produce Bubblfil yarns as a kapok replacement for lifejackets, as thermal insulation for sleeping bags, and for aviators' uniforms.

All these early inflation processes (41) were difficult to control, and after World War II they were neglected until the 1960s. Companies in Japan, the United States, and Europe then started to develop inflated–collapsed rayons (Fig. 5**b**) for speciality papers (42) and wet-laid nonwovens.

Although none of these survived commercially for more than a few years, their development led to an increased understanding of the inflation process and the identification of conditions that could yield a continuously hollow staple fiber in large-scale production (43).

The basis of this process was the injection of sodium carbonate solution into the viscose, although direct injection of carbon dioxide gas that reacts with the viscose soda to form sodium carbonate could also be used (44). The carbonate route yielded a family of inflated fibers culminating in the absorbent multilimbed super inflated (SI) fiber (Fig. 5**c**).

In its original form (45), the fiber was intended for use in toweling where the bulk, firm handle, and high rate of wetting made it one of the few fibers that would blend with cotton without spoiling the wet texture. An even higher absorbency version was developed (46) for use in nonwovens and tampons (47), where it comfortably outperformed cotton by reexpanding like a sponge on wetting.

By the mid-1980s a different approach to the production of fine fibers with novel cross sections became possible. Noncircular spinneret holes, eg, rectangular slots, allowed the large-scale production of flat fibers down to 2.2 dtex (2 den) (Fig. 6a). These I-shaped fibers were capable of replacing the inflated hollow fibers in textile applications, providing similar levels of bulk, warmth, and handle while having a much more regular shape. They were followed by the development of solid Y- and X-shaped multilimbed fibers (48) (Fig. 6b), which performed like SI fiber but had much lower levels of water imbibition than the inflated version. Their shape and relative stiffness enabled them to absorb more fluid between, as opposed to inside, the fibers. They were therefore as absorbent in use as the inflated versions (49,50) but did not require the extra process chemicals, and were easier to wash and dry in production and use. They are the most important bulky rayons now in production.

Alloy Rayons. It is possible to produce a wide variety of effects by adding materials to the viscose dope. The resulting fibers become mixtures or alloys of

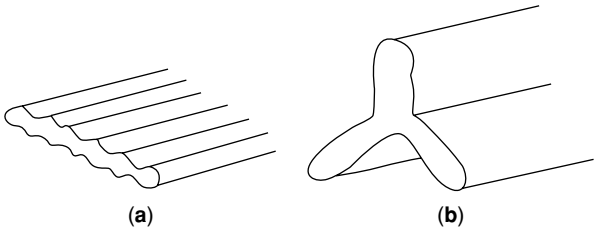

Fig. 6. (**a**) I-section rayon; (**b**) Y-section rayon.

cellulose and the other material. The two most important types of alloy arise when superabsorbent or flame-retardant fibers are made.

American Enka (51,52) and Avtex (53) both produced superabsorbent alloy rayons by adding sodium polyacrylate, or copolymers of acrylic and methacrylic acids, or sodium carboxymethylcellulose to the viscose. The resulting alloys contained about 20% of the water-soluble polymer, giving water imbibitions up to double those of the unalloyed rayons. (See SUPERABSORBENT POLYMERS). They performed particularly well in tampons, where the presence of the slippery polymer at the fiber surface encouraged wet-expansion of the compressed plug. Their use in this, the only real market that developed, declined after the Toxic Shock Syndrome outbreak (54,55) in the early 1980s. Other polymers that have formed the basis of absorbent alloys are starch (56), sodium alginate (57), poly(ethylene oxide) (58), poly(vinyl pyrrolidinone) (59), and sodium poly(acrylamido-2-methyl-2-propane sulfonic acid) (60).

Alloys of cellulose with up to 50% of synthetic polymers (polyethylene, poly(vinyl chloride), polystyrene, polytetrafluoroethylene) have also been made, but have never found commercial applications. In fact, any material that can survive the chemistry of the viscose process and can be obtained in particle sizes of less than 5 μm can be alloyed with viscose.

Flame retardancy can be obtained by adding flame-retardant chemicals to make up about 20% of the fiber weight (61). The first commercial products used tris(2,3-dibromo-1-propyl) phosphate, but the P—O bonds made these susceptible to hydrolysis by strong alkali, and the bromine increased the rate of photodegradation. The chemical was found to cause cancer in laboratory tests and in the late 1970s fell from favor (62). Propoxyphosphazine (Ethyl Corp.) retardants were later used in Avtex's PFR fiber, and a bis(5,5-dimethyl-2-thiono-1,3,2-dioxaphosphorinanyl) oxide powder (Sandoz) was the basis of later European FR fiber developments. Alloys with inorganic salts such as silicates or aluminates are possible, the salts being converted to fibrous polyacids when the cellulose is burnt off (63). This latter approach is the basis of the Visil flame-retardant fiber introduced by Kemira Oy Saeteri (64).

Cuprammonium Rayon

Asahi Chemical Industries (ACI, Japan) are now the leading producers of cuprammonium rayon. In 1990 they made 28,000 t/yr of filament and spunbond nonwoven from cotton cellulose (65). Their continuing success with a process that has suffered intense competition from the cheaper viscose and synthetic fibers owes much to their developments of high speed spinning technology and of efficient copper recovery systems. Bemberg SpA in Italy, the only other producer of cuprammonium textile fibers, was making about 2000 t of filament yarn in 1990.

The process operated by ACI is outlined in Figure 7. Bales of cotton linter are opened, cooked in dilute caustic soda, and bleached with sodium hypochlorite. The resulting highly purified cellulose is mixed with pre-precipitated basic copper sulfate in the dissolver, and 24–28% ammonium hydroxide cooled to below 20°C is added. The mixture is agitated until dissolution is complete. If necessary, air is introduced to allow oxidative depolymerization and hence a lowering of the dope viscosity.

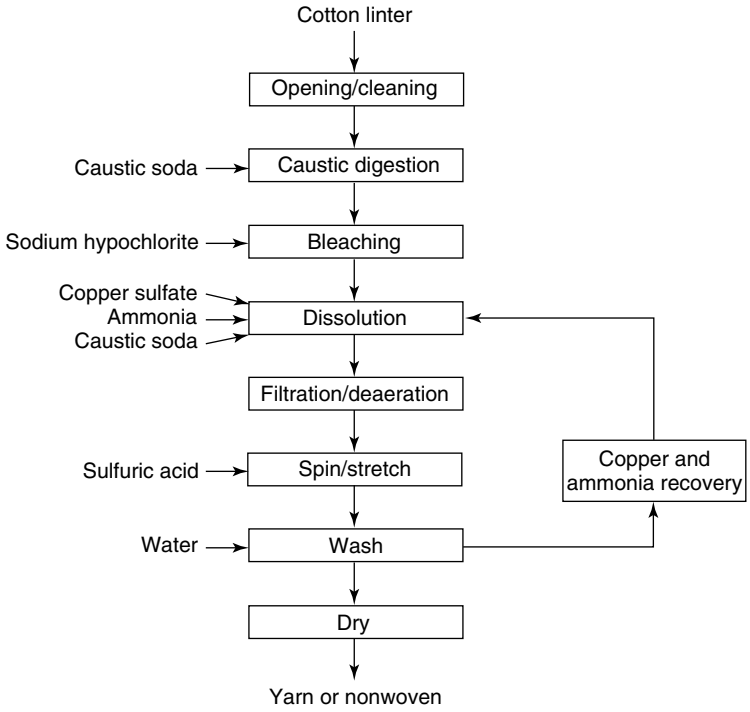

Fig. 7. The cuprammonium process.

The dark blue solution containing 5–10% of cellulose with a DP of 1000–2000 is filtered through a series of plate-and-frame filter presses using fine-mesh metal screens to remove any particles that might block the spinneret holes. It is then deaerated under vacuum and stored ready for spinning. Unlike viscose dope, the cuprammonium cellulose [9050-09-3] solution is relatively stable.

In the old classical spinning technique developed by Bemberg, the deaerated and filtered dope is extruded into a funnel-shaped glass tube through which slightly alkaline water is forced. The water carries the regenerating cellulose gel while stretching it by about 10,000% as it accelerates to the exit. The yarn then passes through a bath containing about 5% sulfuric acid, which completes the regeneration of cellulose and converts the ammonia and copper residues into their sulfates.

In the original batch process, the blue-colored yarn was collected on hanks for separate washing, lubrication, and drying treatments. The continuous process was first patented in the United States in 1934 (66) and 1935 (67), and operated by American Bemberg. This process (68) combined the batch process washing treatments in a series of tanks through which a warp of yarns (from hundreds of spinnerets) were pulled prior to drying and beaming.

The high speed continuous filament process (69) was first used for manufacturing in 1974, and this enabled the yarn production rates to be raised from 150 to 380 m/min. This system uses a pair of net conveyor belts to protect and transport an overfed warp of yarns through washing and drying. After spinning, excess bath

is stripped from the yarns by a shaking mechanism that damages the yarn less than the old comb stripper guides. In 1987, Asahi commercialized their "mark 2" high speed spinning system, which operated at 1000 m/min, and are now working on systems that will exceed 2000 m/min.

Also in 1974, ACI started the direct spinning of Bemliese nonwoven fabrics using the same conveyor belt washing technique (70). This process uses wide spinnerets and spinning cells to produce a curtain of filaments, which fall in the spinning liquor onto the conveyor. The conveyor is oscillated from side to side in order to lay the continuous fibers down in sinusoidal waves. After washing, the webs, which have strength resulting from the self-bonding nature of the fibers as spun, can be further strengthened and finished by hydroentanglement.

Almost total copper recovery needs to be achieved to meet the economic and environmental criteria for a modern cellulosic fiber process. In the basic process (71), spent spin-bath liquor was passed through ion-exchange resins and the effluent from these resins was reused in the funnels. The copper washed out of the yarn was precipitated with sodium carbonate, forming the basic copper sulfate sludge, which was reused in cellulose dissolving. Only 95% copper recovery was possible using this system. Recovery efficiencies of up to 98% were claimed for the Russian Kustanai Plant in a document (72), which also records a 99.9% recovery achieved by Japan Organo Co., Ltd. Asahi claims to have perfected copper recovery to a point where it is no longer an issue.

A high percentage of the ammonia can be recovered from the spin-bath effluent and by washing prior to the final acid bath. During acidification, remaining ammonia is converted to the sulfate and recovered when the acid wash liquor is treated with carbonate to recover the copper. Ammonia residuals in the large volumes of washwater can only be removed by distillation. Overall about 75–80% of the ammonia required to dissolve the cellulose can be recovered.

Asahi's innovations have done much to transform the cuprammonium process from an uneconomic competitor for viscose and synthetics into the fastest wet-spinning system in the world. They now claim it to be competitive both economically and environmentally with the viscose filament process.

Direct Dissolution Processes

Regenerated fibers produced via the direct dissolution of cellulose in organic solvents are generically known as lyocell fibers.

The production routes already described cope with the difficulties of making a good solution by going through an easy-to-dissolve cellulose derivative, eg, xanthate or a cellulose complex, such as cuprammonium. The ideal process, one that could dissolve the cellulose directly from ground wood, is still some way off, but since the early 1980s significant progress has been made.

There have been reviews of the early work on direct dissolution (73,74). The efforts to dissolve cellulose directly as a *base* using phosphoric, sulfuric, and nitric protonic acids, or zinc chloride, thiocyanates, iodides, and bromides as Lewis acids are recorded (73,74). With regard to cellulose acting as an *acid*, sodium zincate, hydrazine, and sodium hydroxide are listed as inorganic solvents, and quaternary ammonium hydroxides, amines, dimethylamine–DMSO mixtures, and

amine oxides as organic bases. Cellulose solutions of 16% have been achieved in lithium chloride–dimethylacetamide systems (75), and 14% solutions in dinitrogen tetroxide–dimethylformamide systems (76). Solutions of up to 14% cellulose were achieved in an extensive study of the ammonia–ammonium thiocyanate solvent system (77). The dimethylsulfoxide–paraformaldehyde system (78) is capable of dissolving a wide range of DPs without causing degradation. However, despite early promise, the problems of developing fiber production routes using these systems have, with the exception of the amine oxide route, proved insurmountable.

The cellulose-dissolving potential of the amine oxide family was first realized (79) in 1939, but it was not until 1969 that Eastman Kodak described the use of cyclic mono(*N*-methylamine-*N*-oxide) compounds, eg, *N*-methylmorpholine-*n*-oxide [7529-22-8] (NMMO), as a solvent size for strengthening paper (80) by partially dissolving the cellulose fibers.

Other patents (81,82) covered the preparation of cellulose solutions using NMMO and speculated about their use as dialysis membranes, food casings (sausage skins), fibers, films, paper coatings, and nonwoven binders. NMMO emerged as the best of the amine oxides, and its commercial potential was demonstrated by American Enka (83,84). Others (85) have studied the cellulose–NMMO system in depth; one paper indicates that further strength increases can be obtained by adding ammonium chloride or calcium chloride to the dope (86).

Both American Enka (87) and Courtaulds set up pilot-plant work in the early 1980s with the objectives of developing fiber spinning and solvent-recovery operations. The Austrian viscose producer Lenzing studied various systems (88) and commenced pilot operations on an NMMO system at the end of the 1980s. At the time of writing, only Courtaulds and Lenzing have proceeded to a commercial scale.

American Enka decided not to commercialize the process and stopped the research in 1981, probably because at that time engineering issues associated with the difficulty of avoiding exothermic reactions looked too hard to resolve economically. However when Courtaulds had demonstrated practical solutions to the many problems discovered during American Enka's early work, they (Enka that is) reentered the field with the continuous filament version of the lyocell process under their brand name "Newcell." The Akzo deal with Courtaulds involved their gaining access to Courtaulds technology in exchange for granting Courtaulds rights to use some of the key steps in the early patents mentioned above. However, Akzo–Nobel had earlier granted a lyocell license to Lenzing, the Austrian viscose fiber maker, allowing Lenzing to enter the field with a very similar process to Courtaulds. The ensuing patent litigation between Lenzing and Courtaulds was to prove costly to both companies.

Lenzing obtained a patent in the U.S.A. for a process, some aspects of which had been operated by Courtaulds for many years, and indeed were used in production at Courtaulds Tencel plant in Alabama. Courtaulds naturally objected, and applied for summary dismissal of both the U.S. and the subsequent European patent. In Europe, the Munich court would not allow the Lenzing patent to be dismissed summarily and the case went to trial. Courtaulds won, and Lenzing's European patent was disallowed, with no right of appeal. In the U.S.A., the Lenzing patent was summarily dismissed, but Lenzing appealed successfully. At this point the two companies reached a settlement out of court. The lyocell patent

estates of both companies were pooled, to be available royalty-free to both companies. The settlement only covered patented technology; there was to be no sharing of "knowhow" gained in the operation of the process, which at the time had only been commercialized by Courtaulds.

Akzo–Nobel acquired Courtaulds in 1998, and formed Acordis Fibers, bringing together in one company all the key lyocell technologies.

The Courtaulds Lyocell Process. The increasing costs of reducing the environmental impact of the viscose process coupled with the increasing likelihood that the newer cellulose solvents would be capable of yielding a commercially viable fiber process led Courtaulds Research to embark on a systematic search for a new cellulosic fiber process in the late 1970s.

The project, code-named Genesis, did not involve basic research into new solvents for cellulose so much as screening the known solvents against criteria felt to be important for the cellulosic fiber process of the future. The solvent chosen had to be recyclable at a very high level of efficiency, and hence as near to totally containable in the process as possible. It had to be safe to work with and safe in the environment in the event of any losses. It had to be able to dissolve cellulose completely without reacting with it or degrading it, and the resulting process had to be less energy-intensive than the viscose route, which was already proven to be less energy-intensive than the synthetics in an independent study (89). It was especially important to choose a system that, like the melt-spun synthetics, would not require costly gaseous- or liquid-effluent treatment systems. Finally, the process would be capable of making good textile fibers to maintain, or even extend, the cellulosics' share of the global market against fierce competition from melt-spun synthetics based on cheap but nonrenewable oil reserves.

By 1980, *N*-methyl morpholine-*n*-oxide (NMMO) was shown to be the best solvent, provided well-known difficulties associated with its thermal stability could be avoided by appropriate chemical engineering.

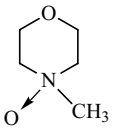

***N*-methyl morpholine-*n*-oxide (NMMO)**

(**1**)

Filaments obtained from the first single-hole extrusion experiments had promising properties, so Courtaulds committed the resources in 1982 to build a small pilot plant to test the feasibility of overcoming the solvent handling and recovery problems that had prevented earlier commercial exploitation. This system, capable of making up to 100 kg of fiber per week, met its objectives and allowed the first serious end use development to begin. Scale-up to 1000 kg/week pilot line was possible in 1984, and in 1988 a 25,000 kg/week semicommercial line was commissioned in Grimsby, United Kingdom, to allow a thorough test of the engineering and end-use development aspects. Commericalization of the fiber as Tencel followed in 1990 and rapid sales buildup, especially in Japan, led to a 16,000-t plant being built and started up in Mobile, Alabama, in 1992. A second 20,000-t factory followed in Mobile in 1995 and a third 40,000-t plant was commissioned in Grimsby in 1998.

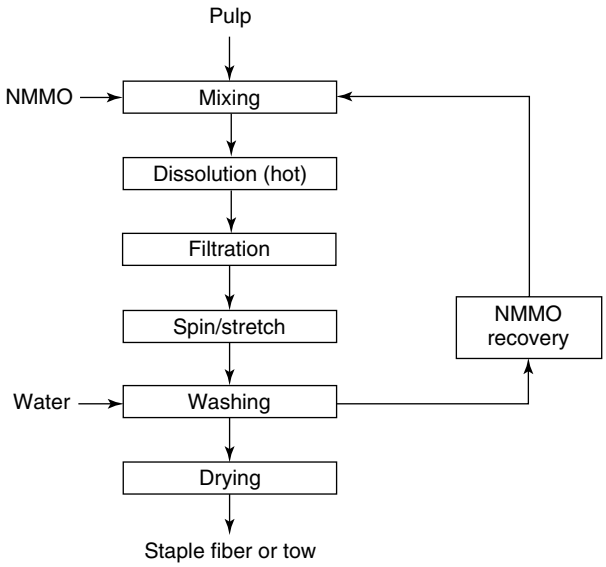

Fig. 8. Direct dissolution: Acordis Tencel process.

The Acordis system is illustrated in block, diagram form in Figure 8. Dissolving-grade woodpulp is mixed into a paste with NMMO and passes through a high temperature dissolving unit to yield a clear viscous solution. This is filtered and spun into dilute NMMO, whereupon the cellulose fibers precipitate. These are washed and dried, and finally baled as staple or tow products as required by the market. The spin-bath and wash liquors are passed to solvent recovery systems that concentrate the NMMO to the level required for reuse in dissolution.

Figure 9 is an outline flow sheet illustrating the layout of the key process steps provided courtesy of Acordis. Unlike both the viscose process and the later Lenzing Lyocell process, the fiber is washed, dried, and crimped in tow form prior to cutting. Unlike the viscose spinning process, the cellulose solution is extruded into warm air prior to immersion in the aqueous NMMO spinning solution. (This is known as dry-jet wet-spinning to distiguish it from the totally dry acetate spinning process and the totally wet viscose spinning.)

Lyocell Applications

Dry-jet wet-spinning of lyocell fiber has been described (90) as being similar to the extrusion of lyotropic rigid-rods, giving rise to a highly microfibrillar structure that is consistent across the entire cross section of the fiber—ie differing from the skin–core structure observed in viscose rayon. Wide-angle X-ray diffraction data shows lyocell to have a crystallinity of 60% (cf 40% for viscose), the celluose crystals having a a lateral dimension of about 4 nm. However, microfocus small-angle X-ray scattering (91) has recently shown a definite skin–core structure, with the thin skin having better-oriented voids than the core. This observation is more in

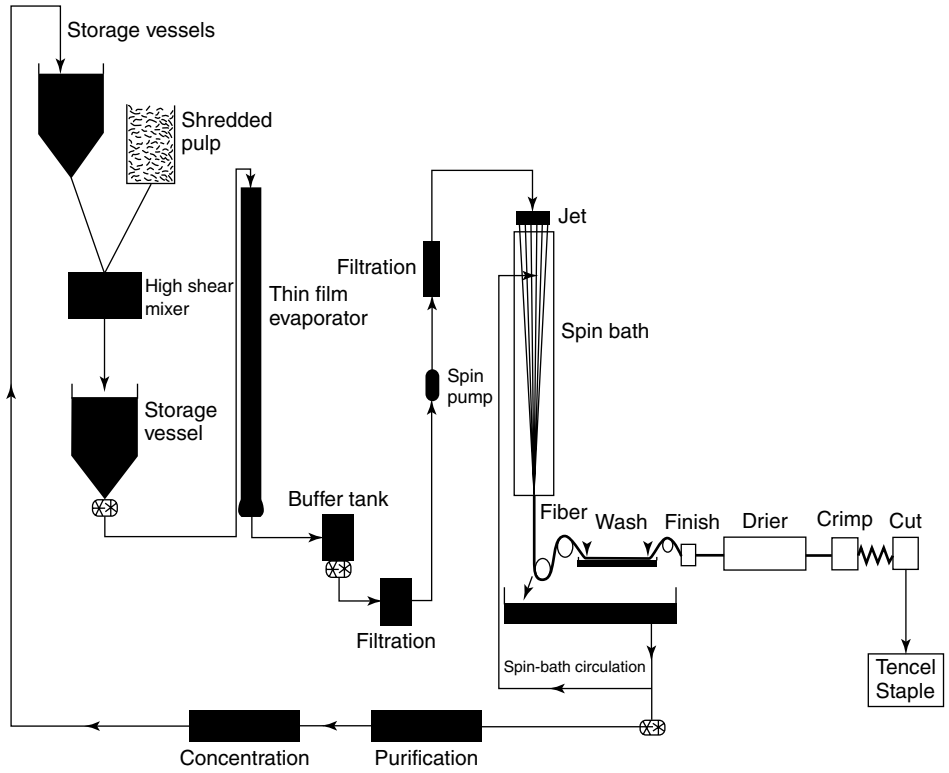

Fig. 9. Direct dissolution: Acordis Tencel Flow Diagram.

keeping with the macro observations of fibrillation in paper-making—the surface appearing to fibrillate easily—whereas breaking up the core region of the fiber proves very difficult.

The new fiber thus had physical properties (Table 1) sufficiently different from regular rayon to allow an initial market development strategy that did not erode the position of the traditional viscose fiber. The unique strength, texture, and coloration potential of the fiber enabled it to command premium prices in up-market mens' and ladies' outerwear, largely due to the fibrillation tendency being harnessed by creative finishing processes to produce "soft-touch" or "peach-skin" textures. However while premium pricing allowed the process to expand rapidly, it was only achievable while the special characteristics of lyocell were in fashion, and before the soft-touch characterisics had been developed using other cellulosics such as polynosic rayon and cotton. Furthermore the uncontrolled fibrillation that occurred when textiles made from early lyocell fibers were conventionally dyed, finished, or washed led to unacceptable fabric appearance and texture. The fibrils splitting away from the fiber surface became apparent as a frosty-looking surface that prevented the true dyed color from emerging. In extreme cases, and especially on knitted fabrics where the fibers were less tightly bound to the structure, the fibrils caused these looser fibers to entangle and form pills. Thus early lyocell had restricted potential in mass-market textiles, being confined to woven

Table 1. Properties of Selected Commercial Rayon Fibers

Property	Cuprammonium	Regular rayon	Improved rayon	Modal	Polynosic	Y-Shaped rayon[a]	Solvent spun rayon[b]
Fiber cross section							
Dry tenacity, cN/tex[c]	15–20	20–24	24–30	34–36	40–65	18–22	40–44
Extensibility at break (dry), %	7–23	20–25	20–25	13–15	8–12	17–22	14–16
Wet tenacity, cN/tex[c]	9–12	10–15	12–16	19–21	30–40	9–12	34–38
Extensibility at break (wet), %	16–43	25–30	25–35	13–15	10–15	23–30	16–18
Water imbibition, %	100	90–100	90–100	75–80	55–70	100–110	65–70
Cellulose DP[d]	450–550	250–350	250–350	300–500	550–700	250–350	550–600
Initial wet modulus[e]	30–50	40–50	40–50	100–120	140–180	35–45	250–270

[a]The Y-shaped rayon data are based on Courtaulds Galaxy fiber.
[b]The solvent-spun rayon data are based on Courtaulds Tencel fiber.
[c]To convert cN/tex to gf/den, divide by 8.82.
[d]DP = degree of polymerization.
[e]The load required to extend the wet fiber by 5% × 20.

products dyed and finished by gentle processes to lighter shades for dry-clean-only garments.

This unacceptable situation was addressed by developing production processes to allow the manufacture of lyocell fiber with minimal fibrillation tendency—even if this meant increasing process cost. This was achieved in part by altering the spinning conditions, and in part by the use of cross-linking agents in washing, to bond the fibrillar fiber structure more strongly. It was also addressed by investigating nonwoven applications for lyocell, thereby avoiding wet processing except in areas (eg paper-making and hydroentanglement) where fibrillation could be an advantage.

Several studies of its performance in nonwovens had shown it capable of yielding fabric strengths 2–3 times higher than hitherto possible with regenerated cellulosics (92,93). It appeared particularly suitable for the latest hydroentanglement systems, where its basic strength and an ability to develop a microfiber surface under the action of high pressure water jets enabled it to make very strong nonwoven fabrics having textile-like properties. The effect of high pressure water jets on lyocell fiber was first described publicly in 1989 (94). In addition to the higher fabric strengths, extensive fibrillation had occurred, making the fabrics stiffer (bonding between the fibrils). The fiber took on a chalky white appearance as bonding proceeded (light scattering from the fibrils), and absorbent capacity and wicking rates were higher than that for the higher water-imbibition viscose rayon controls: this too being an effect of the microfiber content. However the most significant alteration in properties caused by fibrillation was in the dry and wet texture of the fabrics.

Dried conventionally after hydroentanglement, hydrogen bonding between the fibrils of the highly fibrillated fibers stiffened up the fabrics, giving them an unattractive papery handle. Once rewetted, however, the material took on a suede or chamois-leather-like texture, which proved interesting to makers of durable wipes for car and window cleaning and for artificial leather, especially for shoe construction, where the inherent absorbency of the fiber could improve the comfort of leather substitutes made from, for example, splittable synthetic/lyocell blends.

Current lyocell, like the almost identical polynosic viscose rayons developed half a century ago (33), has so far proved to have similarly limited and variable potential in the fashion textile markets for which it, and the process for making it, was designed. Whether a cheaper, high-fibrillation version would improve lyocell's prospects in nonwovens is still open to debate.

Other Sovent Routes

Work on other routes to cellulosic fibers continues, some driven by a desire to identify an environmentally benign route to cellulosic fibers that can utilize the large capital investment in the viscose process equipment and hence cost less than a completely new fiber process such as lyocell.

The Finnish viscose producer Kemira Oy Saeteri collaborated with Neste Oy on the development of a carbamate derivative route. This system is based on work (95) that showed that the reaction between cellulose and urea gives a derivative easily dissolved in dilute sodium hydroxide:

$$\text{Cell—OH} + \text{NH}_2\text{—CO—NH}_2 \rightarrow \text{Cell—O—CO—NH}_2 + \text{NH}_3 \qquad (7)$$

Neste patented an industrial route to a cellulose carbamate pulp (96) that was stable enough to be shipped into rayon plants for dissolution as if it were xanthate. The carbamate solution could be spun into sulfuric acid or sodium carbonate solutions, to give that when completely regenerated had similar properties to viscose rayon's. When incompletely regenerated they were sufficiently self-bonding for use in paper-making. The process was said to be cheaper than the viscose route and to have a lower environmental impact (97). It has not been commercialized, so no confirmation of its potential is yet available.

It has been claimed that solutions containing 10–15% cellulose in 55–80% aqueous zinc chloride can be spun into alcohol or acetone baths to give fibers with strengths of 0.13–0.18 N/tex (1.5–2 gf/den). However, if these fibers were strain-dried (ie, stretched) and rewetted while under strain, strengths of 0.46 N/tex (5.2 gf/den) were achieved (98).

Asahi has been applying the steam explosion (99) treatment to dissolving pulp to make it dissolve directly in sodium hydroxide (100), and they claim (101,102) a solution of 5% of steam-exploded cellulose in 9.1% NaOH at 4°C being spun into 20% H_2SO_4 at 5°C. The apparently poor fiber properties [best results being 0.16 N/tex (1.8 gf/den) tenacity dry, with 7.3% extension] probably arise

because the fibers were syringe-extruded at 8.3 tex/filament (75 den/fil). Asahi feels that this could be the ultimate process for large-scale production of regenerated cellulose fibers.

Patents (103,104) published in February 1996 describe anisotropic cellulose solutions at concentrations up to 40% in a "solvent containing from 72 to 79 wt% of phosphorous pentoxide." Claiming a highly economical route for the production of tire yarns, the process described therein appears to be simple and elegant.

A twin-screw extruder is fed with dry fluff-pulp and the phosphoric acid solvent. The first cooled zone mixes the cellulose into the solvent and reduces the particle size, the second hotter zone starts the dissolution, and the third zone provides further blending and dissolution time, its temperature being controlled to achieve the desired reduction in cellulose DP. A final low pressure zone allows deaeration and dewatering (or the injection of additives) as necessary, and filters remove particles before spinning.

While "all available types of cellulose" can be used, dissolving pulps are preferred for best spinning and fiber properties. The solvent preparation involves mixing orthophosphoric acid with polyphosphoric acid, in a 80:20 ratio at around 50°C and then cooling and storing for several hours to arrive at the desired concentration of anhydride.

After less than 15 min in the extruder, the cellulose solution, typically containing 20% cellulose, is spun, like lyocell, through a similar-sized air gap, but into cold acetone, followed by water washing, sodium carbonate or soda neutralization, and a final water washing. Tire yarn with a breaking tenacity of 76 cN/tex, an elongation at break of 6.5%, capable of sustaining a load of 20 N/tex without extending by more than 2%, was obtained at 120 m/min spinning speed.

Michelin Research had earlier developed a process using a mixture of phosphoric and formic acids, also for tire yarns. The Akzo–Nobel process, based on phosphoric acid alone, was felt to give easier solvent recovery. A process using phosphoric acid alone (105) emerged from Michelin Research in March 1996.

Further work at Akzo–Nobel (106) showed that if extra water is injected with the solvent, or added to the anisotropic solutions described above, isotropic solutions of cellulose could be obtained at concentrations of 7–20%. A 7.6% cellulose solution could be spun to give fibers with tenacities of 18–38 cN/tex (extension at break declining from 17.4 to 8.4%) as draw ratios were increased from 60 to 150%.

One of the key requirements for making high quality high modulus fibers using the phosphoric acid approach is to keep the level of phosphorus bound to cellulose at a minimum. Allowing it to rise from the $<0.5\%$ level preferred in the above process to more than 3% by increasing the phosphorus pentoxide level in the solvent, or by increasing the storage temperature of the solvent prior to introduction of the cellulose, resulted in weaker, hard-to-handle gel fibers with very high absorbency. Akzo–Nobel therefore postulated the production of superabsorbent fibers using a variation of the phosphoric acid route (107). While the resulting patent covers conventional fiber production, perhaps in recognition of the difficulties of cleaning up such fibers, it also covers the production of fibrids by extrusion into a high shear mixer to obtain a fibrous slurry. Water absorbencies of up to 100 g/g are claimed if the fibers containing more than 6% bound phosphorus are cross-linked with ethylene glycol diglycidyl ether in a 70:30 ethanol/water mixture.

Centrifugal spinning of phosphoric acid solutions of cellulose was also explored (108), and found capable of producing mixtures of filaments with linear densities ranging from 1 to 23, and tenacities of 4 to 90 cN/tex and extensions at breakup from 1 to 15%.

In an attempt to remove the problems associated with the acetone coagulation bath, fibers were air-gap spun into aqueous salt solutions, eg up to 25% of diammonium hydrogen phosphate or potassium phosphate or 5% zinc sulphate (109). This patent also makes it clear that the corrosive nature of the solution is an issue in spinneret design.

None of the above patents address the crucial solvent recovery issues. While recovery of acetone is possible, re-creating concentrated phosphoric acid from either dilute solutions or phosphates appears as difficult as the recovery of sulphuric acid from sulphates in the viscose process. The viscose approach is of course to extract and sell the neutralization product and use fresh concentrated sulphuric acid to make up the recovery shortfall—an option that is apparently unattractive in phosphate systems.

Fiber Properties

The bulk properties of regenerated cellulose are the properties of Cellulose II, which is created from Cellulose I by alkaline expansion of the crystal structure (110,111) (see CELLULOSE). The key textile fiber properties for the most important current varieties of regenerated cellulose are shown in Table 1. Fiber densities vary between 1.53 and 1.50.

A discussion of the fiber properties is complicated by the versatility of cellulose and its conversion routes. Many of the properties can be varied over wide ranges, depending on the objectives of the producer. For instance, dry fiber strengths from less than 1 but up to 10 g/den have been made commercially, and at a given dry strength it has proved possible to vary the elongation and wet properties independently. The water imbibition of pure cellulose fibers has been varied from 45 to 450%, and the cross-sectional shape altered from circular all-skin, to multilobal collapsed tubes that reopen on wetting. Alloying adds further scope for adding properties unachievable with pure cellulose. Chemically, cellulose fibers are well endowed with reactive hydroxyl groups that render them amenable to modification by grafting, which, more so than alloying, allows the properties to be moved in the direction of synthetic polymers if the need arises. The same reactivity makes the fibers more degradable than synthetics, both chemically and biologically, although it must be said that biological degradability is easily halted by inclusion of suitable biocides.

Thermal Properties. Fibers are not thermoplastic and are stable at temperatures below 150°C, with the possible exception of slight yellowing. They begin to lose strength gradually above 170°C, and decompose more rapidly above 300°C. They ignite at 420°C and have a heat of combustion of 14,732 J/g (3.5 kcal/g).

Moisture Regain. The fibers are all highly hydrophilic, with moisture regains at 65% rh, ranging from 11 for the polynosics to 13 for regular rayon. Wetting of cellulose is exothermic, with the regenerated forms giving out 170 J/g (41 cal/g) between 40 and 70% rh, compared with 84 J/g (20 cal/g) for cotton. The

fiber structure swells as fluid is imbibed, and fiber strength and stiffness falls. The contact angle for unfinished fiber is greater than 150°.

Chemical Properties. The fibers degrade hydrolytically when contacted with hot dilute or cold concentrated mineral acids. Alkalies cause swelling (maximum with 9% NaOH at 25°C) and ultimately disintegration. They are unaffected by most common organic solvents and dry-cleaning agents. They are degraded by strong bleaches such as hypochlorite or peroxide.

Optical Properties. The fibers are birefringent. The refractive index parallel to the fiber length ranges from 1.529 for regular rayon to 1.570 for the polynosics. Refractive indexes perpendicular to the fiber length range from 1.512 (regular) to 1.531 (polynosic). Basic fibers are naturally lustrous, but can be made dull by adding opacifiers or by changing the cross-sectional shape.

Electrical. The electrical properties of the fiber vary with moisture content. The specific resistance of the fibers is around $3 \times 10^6 \Omega$/cm at 75% rh and 30°C compared with $1 \times 10^{18} \Omega$/cm for pure dry cellulose. The dielectric constant (100 kHz) is 5.3 at 65% rh and 3.5 at 0% rh. The zeta potential in water is −25 mV.

Environmental Issues: Viscose Process

As noted in the introduction, rayon is unique among manufactured fibers because it is the only one to use a natural polymer (cellulose) directly. Polyesters, nylons, polyolefins, and acrylics all come indirectly from vegetation; they come from the polymerization of monomers obtained from reserves of fossil fuels, which in turn were formed by the incomplete biodegradation of vegetation that grew millions of years ago. The extraction of these nonrenewable reserves and the resulting return to the atmosphere of the carbon dioxide from which they were made is one of the most important environmental issues of current times. Cellulosic fibers therefore have much to recommend them provided that the processes used to make them have minimal environmental impact.

Fossil Reserves. Renewable resources will become increasingly important as the planet's stocks of fossilized reserves are depleted and as governments realize that biomass can provide a truly sustainable, cost-effective source of energy and materials. The viscose route currently needs fossil reserves for energy generation but for little else.

Liquid Effluents. Recycling of acid, soda, and zinc have long been necessary economically, and the acid–soda reaction product, sodium sulfate, is extracted and sold into other sectors of the chemical industry. Acid recovery usually involves the degassing, filtering, and evaporative concentration of the spent acid leaving the spinning machines. Excess sodium sulfate is removed by crystallization and then dehydrated before sale. Traces of zinc that escape recovery are removable from the main liquid effluent stream to the extent that practically all the zinc can now be retained in the process.

Gaseous Effluents. Twenty percent of the carbon disulfide used in xanthation is converted into hydrogen sulfide (or equivalents) by the regeneration reactions. Ninety to 95% of this hydrogen sulfide is recoverable by scrubbers that yield sodium hydrogen sulfide for the tanning or pulp industries, or for conversion back to sulfur. Up to 60% of the carbon disulfide is recyclable by condensation from rich streams, but costly carbon-bed absorption from lean streams is necessary to

recover the remaining 20 + %. The technology to deal with this is becoming available, but there remains the danger that cost increases resulting from the necessary investments will make the fibers unattractively expensive compared with synthetics based on cheap nonrenewable fossil fuels.

Energy Use. Energy consumption in the xanthate process compares favorably with the synthetics. The methodology of assessing the energy usage of products and processes is currently the subject of much debate, and a standardized approach has yet to emerge. Not surprisingly, most of the published work on fibers was carried out during the last energy crises in the 1973–1981 period.

The early attempts to assess the total energy required to make baled staple fiber from naturally occurring raw materials—wood in the case of cellulosics and oil in the case of synthetics—used differing approaches and were insufficiently rigorous to allow hard conclusions to be drawn. In general, the fiber production sequence is broken into monomer making, polymer making, and fiber production, and although a variety of fibers are covered, only viscose rayon and polyester are mentioned in all of them (112–116). Tons of fuel oil equivalent per ton of fiber (TFOE/T) is the most popular unit, with rayon requiring from 1.7 to 2.4 TFOE/T and polyester requiring 2.6 to 4.2 TFOE/T.

The studies all concluded that rayon required less energy to make than polyester but there was little agreement on the magnitude of the difference. The wet-spun cellulosic fibers required more energy than melt-spun polyester for the fiber-making step, but they had no monomer energy requirement. The polymerization requirement was therefore minimal. In the case of the 1.7 TFOE/T figure for rayon, full credit was being given for the fact that the pulp mills energy needs were renewable and not dependent on fossil fuels. Pulp could be fed directly into the viscose process without incurring any transport or drying cost, and the pulp mill could be driven entirely by energy obtained from burning the parts of the tree that were not needed in the final product. This free and renewable energy was not counted.

Fiber Disposal. Cellulosic fibers, like the vegetation from which they arise, can become food for microorganisms and higher life forms; ie, they biodegrade. If necessary they burn with a rather greater yield of energy than natural vegetation. In complete biodegradation or incineration, the final breakdown products are carbon dioxide and water; these disposal methods simply recycle the cellulose to the atmospheric components from which it was made.

It is also possible to liberate and use some of the free solar energy that powered the manufacture of sugars and cellulose during photosynthesis. This can be achieved by burning or by anaerobic digestion. Slow anaerobic biodegradation occurs in all landfill sites dealing with municipal solid waste. This process generates methane from cellulose, which can be burnt to drive gas turbines. If future landfills are lined and operated with moisture addition and leachate recycling, then energy generation and the return of landfill sites to normal use can be accelerated (117).

Environmental Issues: Lyocell Process

The solvent route to rayon reinforces the inherent environmental benefits of regenerated cellulosic fibers by using a modern fiber production process which, being physical rather than chemical, reduces environmental impacts to a minimum.

N-methylmorpholine *n*-oxide (NMMO), the solvent used, is manufactured by methylation and oxidation of morpholine, which comes from a reaction between diethylene glycol and ammonia.

Apart from woodpulp (as used to make viscose rayon) it is the only significant raw material used. It does not react with the cellulose and >99% of the solvent in the dope is recovered in spinning and washing, reconcentrated and reused. It is considered to be practically nontoxic by oral or dermal route and would not be considered harmful by EEC labeling criteria. Similarly it is considered to be minimally irritating to skin and eyes by EEC criteria.

Energy Use. From an energy viewpoint, the solvent route to cellulosic fibers is identical to the viscose route up to the point where the cellulose enters the solvent. The energy content of the noncellulosic raw materials is significantly lower in the case of the solvent route, but the solvent route requires similar energy levels in dope handling, spinning, washing, and recycling. The lower water imbibition of the solvent fiber (65 vs 95%) yields savings in fiber drying and in any subsequent end-product washing and drying operations. Overall, the solvent route is capable of showing a useful economy in this important resource when compared with viscose production on the same scale.

Fossil Reserves. The ethylene glycol for NMMO manufacture currently comes via ethylene from oil refineries. However, as indicated above, the solvent recycling rate is so high that solvent usage is kept down to a few kilos per tonne of fiber, and hence fossil reserve dependence is minimal.

Gaseous Emmissions. The solvent process produces very little atmospheric emission. There are traces of volatile organic compounds associated with the solvent and the soft finish, which will leave the plant in the normal course of ventilation.

Liquid Effluents. The solvent route uses much less water than viscose, and the process effluent needs significantly less treatment.

Production and Consumption

Approximately 3 million metric tons of regenerated cellulose fibers production capacity existed in 2000 (Table 2). The leading producers of filament yarns were the Chinese state-owned factories (118,000-t capacity), Acordis in Europe (69,000 t), and the Russian plants (with 44,000 t). The leading producers of staple fiber and tow were the Chinese with 480,000 t, the Birla Group (India) with 408,000 t, Lenzing (Austria, U.S.A., and Indonesia) with 315,000 t and Acordis with 170,000-t capacity split between the United Kingdom and North America, Formosa Chemicals and Fibers Co. with 162,000 t (in Taiwan). Acordis was formed in 1998 from the fiber businesses of Courtaulds and Akzo–Nobel following the takeover of Courtaulds by Akzo, who later sold Acordis to a consortium of CVC Partners and Acordis management. (Note: since these statistics were compiled, 100,000 ton of Acordis's viscose staple fiber capacity has closed.)

Actual staple fiber consumption figures for 2001 were estimated (118) to be 1.6 million tonnes because of a sharp decline in Eastern Europe masking slight growth elsewhere (Table 3). Asian countires now account for 75% of the consumption of viscose staple in textiles, with Western Europe leading the consumption in nonwovens.

Table 2. 2000 World Capacity for Regenerated Cellulose Fibers

Fiber type	Production, 10^3 t
Industrial filament yarns	105
Textile filament yarns	390
Regular staple fiber and tow	2300
High wet modulus staple	100
Lyocell staple	100
Total	2995

Table 3. The Top 10 Consuming Countries in 2000

Country	Consumption, Ton
China	400,000
Western Europe	280,000
India	225,000
Indonesia	175,000
U.S.A	85,000
Taiwan	80,000
Turkey	60,000
Japan	55,000
Thailand	30,000
Korea	25,000

Commercial Aspects

Since the early 1980s, the viscose-based staple fibers have, like the cuprammonium and viscose filament yarns in the 1970s, ceased to be commodities. They have been repositioned from the low cost textile fibers that were used in a myriad of applications regardless of suitability, to premium priced fashion fibers delivering comfort, texture, and attractive colors in ways hard to achieve with other synthetics. They are still widely used in blends with polyester and cotton to add value, where in the 1980s they would have been added to reduce costs.

Such repositioning inevitably means reduced production volume, and this is illustrated using CIRFS data (www.cirfs.org) in Figure 10. Most capacity reductions have been in North America and especially eastern Europe. This has been offset in part by capacity increases in the Far East. Rayon is no longer a significant component of carpets, and has lost the disposable-diaper coverstock business to cheaper and more easily processed polypropylene. It has, however, gained share in health and hygiene products and is now a principal component of tampons worldwide.

Figure 11 llustrates the major share changes over the last century, this time combining the natural (mainly cotton) and regenerated cellulosics as "biopolymers".

Roughly half of the 50 million tonnes of fiber consumed annually is now made from polymers synthesized from fossil fuels.

The aesthetic, absorbency, and comfort advantages still enjoyed by the biopolymer fibers has unquestionably slowed synthetic penetration of the apparel

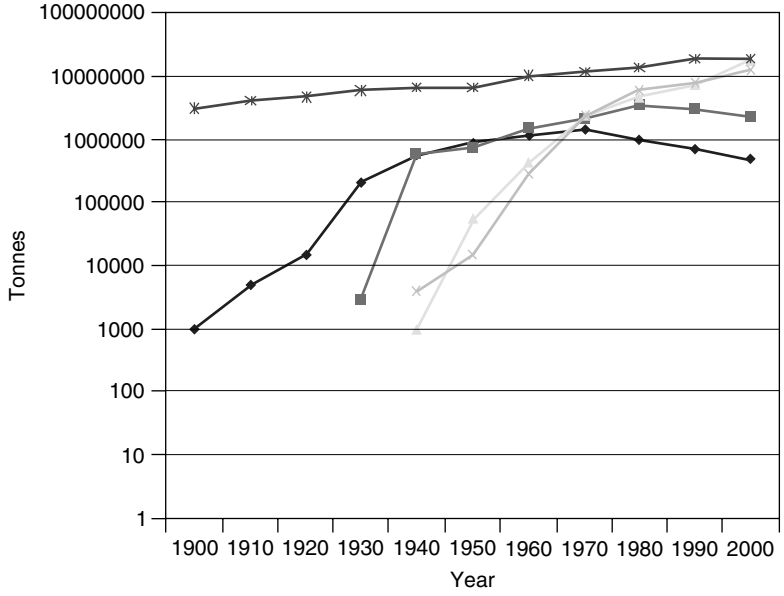

Fig. 10. World fiber production in 20th centry cf Cotton Usage—Log Scale. —◆— Cellulosic filament; —■— cellulosic staple; —✳— synthetic filament; —▲— synthetic staple, —✳— cotton.

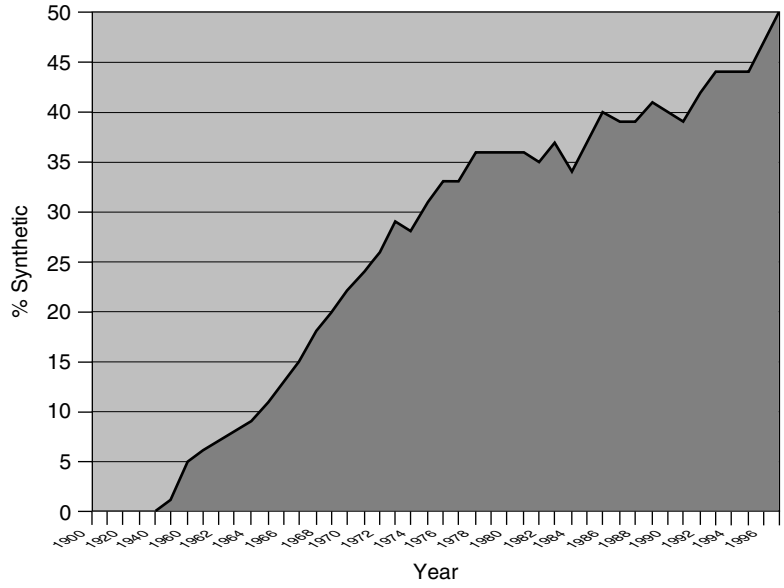

Fig. 11. Synthetics vs biopolymers in the 20th century

sector. Synthetics are used mainly for their low-cost, easy-care and durability characteristics. In the absence of fibers combining all these properties, polyester/cellulosic blends have been a most popular combination. Ratios varying between 35% cellulosic and 35% synthetic depending on the market positioning of the fabric and the relative prices of the fibers are typical.

Within the cellulosic part of the blend, rayon has to compete with cotton and can do this only

(1) when rayon prices (esp. modal or polynosic) are below cotton prices,
(2) when a fashion in a particular sector values the softness, leaness, and drape of rayon above the crisper, fuller, stiffer handle of cotton, and
(3) when the enhanced absorbency, uniformity, and processability of rayon (in this case compared with overbleached cotton at a higher price) is technically desirable, for instance in disposable nonwovens.

The lyocell process offers an environmentally acceptable way of converting natural cellulose into a premium quality rayon fiber with tensile properties approaching those of polyester. Furthermore the technology offers the potential for converting pulp to fiber on a scale and at a cost to give polyester and cotton some serious competition. The high levels of investment in the first lyocell plants necessitated launching the fiber at a premium price and therefore into the quality fashion-apparel market. This proved highly successful and led to rapid expansion up to the current capacity of around 100,000 ton. However this represents about one half of one percent of the current cellulosic fibers market, and lyocell fiber is still only available from two sources, Acordis and Lenzing.

At the time of writing, demand for lyocell has yet to increase to absorb the latest expansions, and some repositioning of the fiber in the market appears necessary.

Possible Futures

Johnson (119) argued that continued population growth and increased per capita fiber use will result in a demand for a further 70 million tonnes of fibers by 2050. With the potential for further cotton yield or hectarage increases now limited, and with the synthetics still looking unlikely to provide the comfort element of future textiles, Johnson postulates a "Cellulosics Gap" of up to 20 million tonnes.

He points out that for 60 years, cotton production has grown almost entirely because of increased fiber yield per hectare. Land area under cotton cultivation has been constant for that period, and pressure for the same top quality agricultural land will increase because of the need to feed increased population. Better irrigation, higher pesticide use, higher chemical fertilizer use, and genetic improvements achieved the cotton yield increase. In fact cotton cultivation in Russia became so intensive that despite its benign environmental image it has been the origin of environmental degradation on a massive scale (120). In the 1980s, a tonne of Central Asian cotton required approximately 800 kg of fertilizers, 100 kg of pesticides, and an aggregate of 1.5-m depth of water per square meter of growing area. In recent years cotton yield per acre has levelled off.

It is taken for granted that the implied need for an additional 50 million tonnes of synthetics could be readily provided. The predicted 20 million tonnes shortfall in absorbent or "comfort" fibers is likely to be filled by a combination of a variety of technologies:

(1) Development of more comfortable blends containing progressively less cellulosic fiber.

(2) Some increased yield of cotton per hectare from genetic engineering advances yet to be achieved.
(3) Some increased use of prime agricultural land for cotton growing.
(4) Development of low cost viscose and lyocell fibers.
(5) Development of soft flax fibers encouraged by agricultural subsidies and improved fiber-separation methods.
(6) Development of truly hydrophilic synthetics.
(7) The direct use of wood fiber in textiles.

In order for rayon to benefit from the opportunity offered by this increasing demand for fibers, the price differential between cellulosics and polyester must be reduced. The technology to achieve this does exist, but the justification for the necessary long-term investment becomes increasingly difficult as research into ever more comfortable synthetics pays off. Existing rayon plants will be unable to compete with polyester plants unless the relative costs of woodpulp and oil change dramatically in woodpulp's favour. The sustainability of cellulose and the transience of fossil reserves means that this change is likely, but not in the timeframe beloved of today's investors. In the meantime 350,000 ton/annum lyocell plants linked to a major source of low cost pulp and using a modified process to make fiber with properties similar to current viscose rayon would appear to be one of the few options for further growth of the regenerated cellulosic class of fibers.

BIBLIOGRAPHY

"Rayon" in *EPST* 1st ed., Vol. 11, pp. 810–847, by R. L. Mitchell and G. C. Daul, ITT Rayonier, Inc.; "Rayon" in *EPSE* 2nd ed., Vol. 14, pp. 45–72, by Albin Turbak, Georgia Institute of Technology.

1. Brit. Pat. 283 (Apr. 17, 1855), G. Audemars.
2. Brit. Pat. 5,978 (Dec. 31, 1883), J. W. Swan.
3. Fr. Pat. 165,349 (May 12, 1884), H. de Chardonnet.
4. Fr. Pat. 203,741 (1890), L. H. Despeissis.
5. E. Schweitzer, *J. Prakt. Chem.* **72**, 109 (1857).
6. Ger. Pat. 98,642 (1897), H. Pauly.
7. Brit. Pat. 8,700 (Apr. 8, 1893), C. F. Cross, E. J. Bevan, and C. Beadle.
8. Brit. Pat. 1,020 (Dec. 23, 1898), C. H. Stearn.
9. Brit. Pat. 23,157 (1900), C. F. Topham.
10. Brit. Pat. 23,158 (1900), C. F. Topham.
11. Brit. Pat. 273,386 (June 29, 1926), W. H. Glover and G. S. Heaven (to Courtaulds).
12. U.S. Pat. 1,875,894 (Sept. 6, 1932), J. A. Singmaster.
13. Envirocell, Eco-Profiling of Cellulose-Based Products (a study prepared for Courtaulds and others), Aug. 1990.
14. U.S. Pat. 2,542,285 (Feb. 20, 1951), R. L. Mitchell (to Rayonier Inc.).
15. H. P. von Bucher, *Tappi* **61**(4), 91 (1978).
16. A. Lyselius and O. Samuelson, *Svensk Papperstidning* **64**(5), 145 (1961).
17. L. Ivnas and L. Svensson, *Tappi* **57**(8), 115 (1974).
18. Brit. Pat. 467,500 (June 14, 1937), J. H. Givens, L. Rose, and H. W. Biddulph (to Courtaulds).
19. U.S. Pat. 2,535,045 (Dec. 26, 1950), N. L. Cox (to E. I. du Pont de Nemours & Co., Inc.).

20. U.S. Pat. 2,937,922 (May 24, 1960), R. L. Mitchell, J. W. Berry, and W. H. Wadman (to Rayonier Inc.).
21. U.S. Pat. 2,792,279 (May 14, 1957), M. R. Lytton (to American Viscose Corp.).
22. U.S. Pat. 2,792,280 (May 14, 1957), B. A. Thumm, M. R. Lytton, and J. A. Howsmon (to American Viscose Corp.).
23. U.S. Pat. 2,792,281 (May 14, 1957), C. A. Castellan (to American Viscose Corp.).
24. U.S. Pat. 2,696,423 (Dec. 7, 1954), M. A. Dietrich (to E. I. du Pont de Nemours & Co., Inc.).
25. U.S. Pat. 2,942,931 (June 28, 1960), R. L. Michell, J. W. Berry, and W. H. Wadman (to Rayonier Inc.).
26. U.S. Pat. 3,018,158 (Jan. 23, 1962), R. L. Mitchell, J. W. Berry, and W. H. Wadman (to Rayonier Inc.).
27. U.S. Pat. 3,109,698 (Nov. 5, 1963), E. Klein, H. Wise, and W. C. Richardson (to Courtaulds North America Inc.).
28. U.S. Pat. 3,109,699 (Nov. 5, 1963), W. C. Richardson (to Courtaulds North America Inc.).
29. U.S. Pat. 3,109,700 (Nov. 5, 1963), E. Klein, D. S. Nelson, and B. E. M. Bingham (to Courtaulds North America Inc.).
30. U.S. Pat. 3,718,537 (Feb. 27, 1973), A. Kawai, T. Katsuyama, M. Suzuki, and H. Ohta (to Mitsubishi Rayon Co. Ltd.).
31. U.S. Pat. 3,832,281 (Aug. 27, 1974), A. Kawai, T. Katsuyama, M. Suzuki, and H. Ohta (to Mitsubishi Rayon Co. Ltd.).
32. D. Mach, Proceedings of the 28th Dornbirn International Man Made Fibers Conference, Austria, Sept. 1989.
33. U.S. Pat. 2,592,355 (Apr. 8, 1952), S. Tachikawa.
34. U.S. Pat. 1,683,199 (Sept. 4, 1928), I. Lilienfeld.
35. T. Nagata, Proceedings of the 28th Dornbirn International Man Made Fibers Conference, Austria, Sept. 1989.
36. I. H. Welch, *Am. Text. Rep. Bull. Edn.* **AT8**, 49 (1978).
37. M. Lane and J. McCombes, *Courtaulds Challenge the Cotton Legend* (ACS Symposium Series 58), American Chemical Society, Washington, D.C., 1977, Chapt. 12.
38. Brit. Pat. 143,253 (Aug. 15, 1920), L. Drut.
39. Brit. Pat. 189,973 (Dec. 14, 1922), J. Rousset.
40. Brit. Pat. 253,954 (July 1, 1926), H. J. Heagan and F. Bayley.
41. C. R. Woodings and A. I. Bartholomew, The 23rd Man-Made Fibers Congress, Dornbirn, Austria, 1984.
42. K. L. Gray and I. A. McNab, TAPPI Plastic Paper Conference, 1970.
43. Brit. Pat. 1,283,529 (July 26, 1972), C. R. Woodings (to Courtaulds Ltd.).
44. Brit. Pat. 1,310,504 (Mar. 21, 1973), C. R. Woodings (to Courtaulds Ltd.).
45. Brit. Pat. 1,333,047 (Oct. 10, 1973), C. R. Woodings (to Courtaulds Ltd.).
46. Brit. Pat. 1,393,778 (May 14, 1975), C. R. Woodings (to Courtaulds Ltd.).
47. C. R. Woodings, *TAPPI Nonwoven Fibers Seminar*, 1979, pp. 15–28.
48. Brit. Pat. 2,208,277B (Nov. 13, 1991), A. G. Wilkes and A. I. Bartholomew (to Courtaulds plc).
49. A. G. Wilkes, Proceedings of the INDA-TEC 89 Conference, 1989.
50. C. R. Woodings, Proceedings of the Asia Nonwoven Conference, 1989.
51. U.S. Pat. 4,066,584 (Jan. 3, 1978), T. C. Allen and D. B. Denning (to Akzona Inc.).
52. U.S. Pat. 4,263,244 (Apr. 21, 1981), T. C. Allen and D. B. Denning (to Akzona Inc.).
53. U.S. Pat. 3,844,287 (Oct. 29, 1974), F. R. Smith (to FMC Corp.).
54. *T.S.S.—Assessment of Current Information and Future Research Needs*, Institute of Medicine, National Academy Press, Washington, D.C., 1982.
55. S. F. Berkley and co-workers, *JAMA* 258(7) (Aug. 21, 1987).

56. U.S. Pat. reissue 31,380 (Sept. 13, 1983), F. R. Smith (to Avtex Fibers Inc.).
57. U.S. Pat. 4,063,558 (Dec. 20, 1977), F. R. Smith (to Avtex Fibers Inc.).
58. U.S. Pat. 3,843,378 (Oct. 22, 1974), F. R. Smith (to FMC Corp.).
59. U.S. Pat. 4,179,416 (Dec. 18, 1979), F. R. Smith (to Avtex Fibers Inc.).
60. U.S. Pat. 4,242,242 (Dec. 30, 1980), T. C. Allen (to Akona Inc.).
61. B. V. Hettich, *Text. Res. J.* **54**(6), 382–390 (June 1984).
62. S. M. Suchecki, *Text. Ind.* **142**(2), 29 (1978).
63. B. V. Hettich, *50th Annual TRI Meeting*, 1980.
64. Sh. Heidari, *Chemifasern/Textilindustrie* **41–93** (Dec. 1991).
65. Y. Kaneko, *Lenzinger Ber.* **78–82** (June 1990).
66. U.S. Pat. 1,983,221 (Dec. 4, 1934), W. H. Furness (to Furness Corp.).
67. U.S. Pat. 1,983,795 (Dec. 11, 1934), W. H. Furness (to Furness Corp.).
68. U.S. Pat. 2,587,619 (Mar. 4, 1952), H. Hoffman (to Beaunit Mills Inc.).
69. U.S. Pat. 3,765,818 (Oct. 16, 1973), T. Miyazaki and co-workers (to Asahi Kasei Kogyo Kabushiki Kaisha).
70. U.S. Pat. 3,833,438 (Sept. 3, 1974), T. Kaneki and co-workers (to Asahi Kasel Kogyo Kabushiki Kalsha).
71. "Synthetic Fiber Development in Germany," *Text. Res. J.* **16**(4) (Apr. 1946).
72. U. V. Grafov and co-workers, *Khim. Volokna* (3), 63 (May–June 1976).
73. A. F. Turbak and co-workers, *A Critical Review of Cellulose Solvent Systems* (ACS Symposium Series 58), American Chemical Society, Washington, D.C., 1977.
74. A. F. Turbak, Proceedings of the 1983 International Dissolving and Speciality Pulps Conference, TAPPI, Atlanta, Ga., 1983, p. 105.
75. U.S. Pat. 4,302,252 (Nov. 24, 1981), A. F. Turbak and co-workers (to International Telephone and Telegraph Corp.).
76. U.S. Pat. 4,056,675 (Nov. 1, 1977), A. F. Turbak and R. B. Hammer (to International Telephone and Telegraph Corp.).
77. U.S. Pat. 4,367,191 (Jan. 4, 1983), J. A. Cuculo and S. M. Hudson (to Research Corp.).
78. U.S. Pat. 4,097,666 (June 27, 1978), D. C. Johnson and M. C. Nicholson (to The Institute of Paper Chemistry).
79. U.S. Pat. 2,179,181 (Nov. 7, 1939), C. Graenacher and R. Sallman (to Society of Chemical Industry in Basle).
80. U.S. Pat. 3,447,956 (June 3, 1969), D. L. Johnson (to Eastman Kodak Co.).
81. U.S. Pat. 3,447,939 (June 3, 1969), D. L. Johnson (to Eastman Kodak Co.).
82. U.S. Pat. 3,508,941 (Apr. 28, 1970), D. L. Johnson (to Eastman Kodak Co.).
83. U.S. Pat. 4,145,532 (Mar. 20, 1979), N. E. Franks and J. K. Varga (to Akzona Inc.).
84. U.S. Pat. 4,196,282 (Apr. 1, 1980), N. E. Franks and J. K. Varga (to Akzona Inc.).
85. H. Chanzy and A. Peguy, *J. Polym. Sci., Polym. Phys. Ed.* **18**, 1137–1144 (1980).
86. H. Chanzy, M. Paillet, and R. Hagege, *Polymer* **31** (Mar. 1990).
87. R. N. Armstrong and co-workers, Proceedings of the 5th International Dissolving Pulps Conference, TAPPI, Atlanta, Ga., 1980.
88. L. Lenz, *J. Appl. Polym. Sci.* **35**, 1987–2000 (1988).
89. W. C. Frith, *Energy Balance of Man-Made Fiber Production*, CIRFS, Brussels, 1980.
90. A. Coulsey and S. B. Smith, "The formation and structure of a new cellulosic fiber", *International Man-Made Fiber Conference*, Austria, 1995.
91. Moss and co-workers, *J. Appl. Polym. Sci.* **83**, 2799–2816 (2002).
92. D. A. Smith, S. D. J. Williams, and C. R. Woodings, Proceedings of the EDANA Index 87 Symposium, Geneva, 1987.
93. D. Cole and C. R. Woodings, Proceedings of the EDANA Index 90 Symposium, Geneva, 1990.
94. C. R. Woodings, Proceedings of the IMPACT89 Nonwovens Conference, Miller Freeman Publications, Amelia Island, Fla., 1989.

95. U.S. Pat. 2,134,825 (Nov. 1, 1938), J. W. Hill and R. A. Jacobson (to E. I. du Pont de Nemours & Co., Inc.).
96. Finn. Pat. 61,033 (1982), K. Ekman, O. T. Turenen, and J. I. Huttunen.
97. V. Rossi and O. T. Turenen, PIRA International Conference, Brighton, U.K., Nov. 10–12, 1987.
98. U.S. Pat. 4,999,149 (Mar. 12, 1991), L. Fu Chen (to Purdue Research Foundation).
99. T. Watanabe and co-workers, Preprint, 20th Annual Meeting of Polymer Science, Japan, 1971 p. 427.
100. K. Kamide and co-workers, *Br. Poly J.* **22**, 73–83, 121–128, 201–212 (1990).
101. K. Kamide and T. Yamashiki, *Cellulose Sources and Exploitation*, Ellis Horwood Ltd., New York, 1990, Chapt. 24.
102. K. Kamide and co-workers, *J. Appl. Polym. Sci.* **44**, 691–698 (1992).
103. WO9606208 (Feb. 29, 1996), Boerstoel, Koenders and Westerlink, (to Akzo–Nobel).
104. WO9606207 (Feb. 29, 1996), Boerstoel (to Akzo-Nobel).
105. WO9609356 (Mar. 28, 1996), Huston and co-workers (to Michelin).
106. WO9728298 (Aug. 7, 1997), Westerlink, Maatman, and Boerstoel (to Akzo–Nobel).
107. WO9730090 (Aug. 21, 1997), Westerlink, Maatman and Boerstoel, (to Akzo-Nobel).
108. WO9730196 (Aug, 21, 1997), Rusticus and Van Andel (to Akzo–Nobel).
109. WO 9830741 (July 16, 1998), Ypma, Boerstoel, and Maatman (to Akzo–Nobel).
110. A. Grobe, *Polymer Handbook*, 3rd ed., John Wiley & Sons, Inc., New York, 1989, pp. 117–170.
111. A. Sarko, *Wood and Cellulosics*, Ellis Horwood Ltd., New York, 1987, Chapt. 6.
112. Woodhead, International TNO Conference, 1976.
113. Lane and McCombes, *Text. Manuf.* 1 (1979).
114. Kogler, Proceedings of the EDANA AGM, Munich, Dec. 6, 1980.
115. Armstrong, Proceedings of the EDANA AGM, Munich, June 12, 1980.
116. Marini and Six, Proceedings of the EDANA Nonwovens Symposium, Milan, June 11, 1985.
117. Pohland and Sratakis, Controlled Landfill Management—Principles and Applications, Insight 91, Charleston, Oct. 1991.
118. F. Kogler, *Lenzinger Berichte* 81 (2002).
119. T. F. N. Johnson, World Fiber Demand 1890-2050 by Main Fiber Type. Courtaulds Fibers UK (presented to the Chinese National Textile Council), 1997.
120. *New Scientist*, (Oct. 21, 1995).
121. C. M. Deeley, *Notes for the Associateship of the Textile Institute Examination Lectures*, Sept. 14, 1959.
122. J. Dyer and G. C. Daul, *The Handbook of Fiber Science and Technology, Vol. 4: Fiber Chemistry*, Marcel Dekker, Inc., New York, 1985, Chap. 11.
123. W. Albrecht and co-workers, in *Man Made Fiber Yearbook*, CTI, Maryland, 1991, pp. 26–44.
124. D. C. Coleman, *Courtaulds: An Economic and Social History*, Vols. **2** and **3**, Clarendon Press, New York, 1980.
125. C. R. Woodings, *Regenerated Cellulose Fibers*, CRC Press, 2001, (ISBN 0-8493-1147-0), and Woodhead Publishing Ltd., 2001 (ISBN 1-85573-459-1).

CALVIN WOODINGS
Calvin Woodings Consulting Ltd.

CHITIN AND CHITOSAN. See Volume 1.

CHLOROSULFONATED POLYETHYLENE. See ETHYLENE POLYMERS, CHLOROSULFONATED.

CHLOROTRIFLUOROETHYLENE POLYMERS. See FLUOROCARBON ELASTOMERS.

CHROMATOGRAPHY, AFFINITY. See Volume 1.

CHROMATOGRAPHY, HPLC. See Volume 1.

CHROMATOGRAPHY, SIZE EXCLUSION. See Volume 1.

CHROMOGENIC POLYMERS. See THERMOCHROMIC, POLYMERS; ELECTROCHROMIC POLYMERS; PHOTOCHROMIC POLYMERS.

COATING METHODS, POWDER TECHNOLOGY

Introduction

Powder coating is a process for applying coatings on a substrate using heat fusible powders. Materials used in the process are referred to as coating powders, finely divided particles of organic polymer, either thermoplastic or thermosetting, which usually contain pigments, fillers, and other additives. After application to the substrate, the individual powder particles are melted in an oven and coalesce to form a continuous film having decorative and protective properties associated with conventional organic coatings.

The origin of powder coating technology dates back to the late 1940s when powdered thermoplastic resins were applied as coatings to metal and other substrates by flame spraying. In this process, a powdered plastic was fed through a flame spraying apparatus where the plastic particles are melted and propelled by the hot gases to the substrate. A patent issued in Great Britain to Schori Metallising Process, Ltd., in 1950 described a process for forming a coating in which powdered thermoplastics were applied to a heated substrate by dipping or rolling the heated article in the plastic powder (1). This process was difficult to practice, however, and never achieved commercial success.

A major breakthrough in powder coating occurred in the mid-1950s, when Erwin Gemmer conceived the fluidized-bed coating process, in which a heated object is dipped into a fluidized bed of powder. Gemmer was involved in developing flame spraying processes and materials in the laboratories of Knapsack-Griesheim (Hoechst), a manufacturer of specialty gases, and was searching for a more efficient method than flame spraying for coating objects with powder. The first patent applications were filed in Germany in May 1953, and the basic patent was issued

Encyclopedia of Polymer Science and Technology. Copyright John Wiley & Sons, Inc. All rights reserved.

in September 1955 (2). The first United States patent was issued in 1958 (3), and the Polymer Corp., Reading, Pa, acquired rights to the Knapsack-Griesheim patents. The Polymer Corp. mounted an aggressive effort to develop, license, and sell fluidized-bed coating technology in North America. However, acceptance of this coating process was rather slow. In 1960, the annual sales of coating powders in the United States were below 450 t, in part because of a lack of expertise in the methodology. In addition, the available powder coating materials were expensive, efficient production techniques had not been worked out, and volume of production was low.

Today, powder coating is widely accepted, with thousands of installations in the factories of original equipment manufacturers (OEMS) and custom coating job shops. It is the preferred method for coating many familiar items such as lawn and garden equipment, patio and other metal furniture, electrical cabinets, lighting, shelving and store fixtures, and many automotive components.

In the fluidized-bed coating process, the coating powder is placed in a container having a porous plate as its base. Air is passed through the plate causing the powder to expand in volume and fluidize. In this state, the powder possesses some of the characteristics of a fluid. The part to be coated, which is usually metallic, is heated in an oven to a temperature above the melting point of the powder and dipped into the fluidized bed where the particles melt on the surface of the hot metal to form a continuous film or coating. Using this process, it is possible to apply coatings ranging in thickness from about 250 to 2500 μm (10–100 mils). It is difficult to obtain coatings thinner than about 250 μm, and therefore, fluidized-bed applied coatings are generally referred to as thick-film coatings, differentiating them from most conventional paint-like thin-film coatings applied from solution or as a powder at thicknesses of 20–100 μm (0.8–4 mils).

In the electrostatic spray process, the coating powder is dispersed in an air stream and passed through a corona discharge field where the particles acquire an electrostatic charge. The charged particles are attracted to and deposited on the grounded object to be coated. The object, usually metallic and at room temperature, is then placed in an oven where the powder melts and forms a coating. Using this process it is possible to apply thin-film coatings comparable in thickness to conventional paint coatings, ie, 20–75 μm. A hybrid process based on a combination of high voltage electrostatic charging and fluidized-bed application techniques (electrostatic fluidized bed) has evolved, as well as triboelectric spray application methods. Powder coating methods are considered to be fusion-coating processes; that is, at some time in the coating process the powder particles must be fused or melted. Although this is usually carried out in a convection oven, infrared, resistance, and induction heating methods also have been used. Therefore, with minor exceptions, powder coatings are factory applied in fixed installations, essentially excluding their use in maintenance applications. Additionally the substrate must be able to withstand the temperatures required for melting and curing the polymeric powder, limiting powder coating methods to metal, ceramic, and glass (qv) substrates for the most part, although recently some plastics and wood products have been powder coated successfully.

Compared to other coating methods, powder technology offers a number of significant advantages. These coatings are essentially 100% nonvolatile, ie, no solvents or other pollutants are given off during application or curing. They are ready

to use, ie, no thinning or dilution is required. Additionally, they are easily applied by unskilled operators and automatic systems because they do not run, drip, or sag, as do liquid (paint) coatings. The rejection rate is low and the finish tougher and more abrasion resistant than that of most conventional paints. Thicker films provide electrical insulation, corrosion protection, and other functional properties. Powder coatings cover sharp edges for better corrosion protection. The coating material is well utilized: overspray can be collected and reapplied. No solvent storage, solvents dry off oven, or mixing room are required. Air from spray booths is filtered and returned to the room rather than exhausted to the outside. Moreover, less air from the baking oven is exhausted to the outside thus saving energy. Finally, there is no significant disposal problem because there is no sludge from the spray booth wash system. Any powder that cannot be reclaimed and must be discarded is not considered a hazardous waste under most environmental regulations. Although the terms coating powder and powder coating are sometimes used interchangeably, herein the term coating powder refers to the coating composition and powder coating to the process and the applied film.

Coating powders are frequently separated into decorative and functional grades. Decorative grades are generally finer in particle size and color and appearance are important. They are applied to a cold substrate using electrostatic techniques at a relatively low film thickness, eg, 20–75 μm. Functional grades are usually applied in thick films, eg, 250–2500 μm, using fluidized-bed, flocking, or electrostatic spray coating techniques to preheated parts. Corrosion resistance and electrical, mechanical, and other functional properties are more important in functional coatings.

Coating powders are based on both thermoplastic and thermosetting resins. For use as a powder coating, a resin should possess low melt viscosity, which affords a smooth continuous film; good adhesion to the substrate; good physical properties when properly cured, eg, high toughness and impact resistance; light color, which permits pigmentation in white and pastel shades; good heat and chemical resistance; and good weathering characteristics, ie, resistance to degradation by uv light, hydrolysis, and environmental pollutants. The coating powder should remain stable on storage at 25°C for at least 6 months and should possess a sufficiently high glass-transition temperature T_g so as to resist sintering on storage.

The volume of thermosetting powders sold exceeds that of thermoplastics by a wide margin. Thermoplastic resins are almost synonymous with fluidized-bed applied thick-film functional coatings and find use in coating wire, fencing, and corrosion resistant applications whereas thermosetting powders are used almost exclusively in electrostatic spray processes and applied as thin-film decorative and corrosion resistant coatings.

Thermoplastic resins have a melt viscosity range that is several orders of magnitude higher than that of thermosetting resins at normal baking temperatures (see Table 1). It is, therefore, difficult to pigment thermoplastic resins sufficiently to obtain complete hiding in thin films, yet have sufficient flow to give a smooth coating since incorporation of pigments reduces melt flow even further. In addition, thermoplastic resins are much more difficult to grind to a fine particle size than thermosetting resins, and so grinding must usually be carried out under cryogenic conditions. Because powders designed for electrostatic spraying generally have a maximum particle size of about 75 μm (200 mesh), the thermoplastic

Table 1. Physical and Coating Properties of Thermoplastic Powders[a,b]

Property	Vinyls	Polyamides	Polyethylene	Polypropylene	PVDF[c]
Melting point, °C	130–150	186	120–130	165–170	170
Preheat/postheat temperatures, °C[d]	290–230	310–250	230–200	250–220	230–250
Specific gravity	1.20–1.35	1.01–1.15	0.91–1.00	0.90–1.02	1.75–1.90
Adhesion[e]	G–E	E	G	G–E	G
Surface appearance[f]	Smooth	Smooth	Smooth	Smooth	sl OP
Gloss, Gardner 60° meter	40–90	20–95	60–80	60–80	60–80
Hardness, Shore D	30–55	70–80	30–50	40–60	70–80
Resistance[e,g]					
Impact	E	E	G–E	G	G
Salt spray	G	E	F–G	G	G
Weathering	G	G	P	P	E
Humidity	E	E	G	E	G
Acid[h]	E	F	E	E	E
Alkali[h]	E	E	E	E	G
Solvent[h]	F	E	G	E	G–E

[a]All powders require a primer and pass the flexibility test, which means no cracking under a 3-mm dia mandrel bend.
[b]From *Encyclopedia of Chemical Technology*, 4th ed.
[c]Poly(vinylidene fluoride).
[d]Typical ranges.
[e]E = excellent; G = good.
[f]OP = orange-peel effect; sl OP = slight orange-peel effect.
[g]F = fair; P = poor.
[h]Inorganic; dilute.

powders are predominant in the fluidized-bed coating process where heavier coatings are applied and a larger particle size can be tolerated. Fluidized-bed powders typically contain only about 10–15% of particles below 44 μm (325 mesh), whereas the high end of the particle-size distribution ranges up to about 200 μm (70 mesh). Most thermoplastic coating powders require a primer to obtain good adhesion and priming is a separate operation that requires time, labor, and equipment and typically involves solvents. In automotive applications, some parts are primed by electrocoating. Primers are not usually required for thermosetting powder coatings.

Thermoplastic Coating Powders

Thermoplastic resins used in coating powders must melt and flow at the application temperatures without significant degradation (see Table 1). Attempts to improve the melt flow characteristics of a polymer by lowering the molecular weight and plasticizing or blending with a compatible resin of lower molecular weight can result in poor physical properties or a soft film in the applied coating. Attempts to improve the melt flow by increasing the application temperature

are limited by the heat stability of the polymer. If the application temperature is too high, the coating shows a significant color change or evidence of heat degradation. Most thermoplastic powder coatings are applied between 200 and 300°C, well above the generally considered upper temperature limits for adequate heat stability. However, the application time is short, usually ≤5 min. The principal polymer types are based on plasticized poly(vinyl chloride) [9002-86-27] (PVC), Polyamides, plastics (qv), and other specialty thermoplastics. Thermoplastic coating powders have one advantage over thermosetting coating powders: they do not require a cure and the only heating necessary is that required to complete melting or fusion of the powder particles. Thermoplastic resins have uses in coating wire, fencing, and other applications where the process involves continuous coating at high line speeds. Typical properties of thermoplastic coating powders are given in Table 1.

PVC Coatings. All PVC powder coatings are plasticized formulations (see VINYL CHLORIDE POLYMERS). Without plasticizers (qv), PVC resin is too high in melt viscosity and does not flow sufficiently under the influence of heat to form a continuous film. Suspension and bulk polymerized PVC homopolymer resins are used almost exclusively because vinyl chloride–vinyl acetate and other copolymer resins have insufficient heat stability. A typical melt-mixed PVC coating powder formulation is given in Reference 4. Dispersion grade PVC resin is added in a postblending operation to improve fluidizing characteristics (5). Additional information on the formulation and application of PVC coating powders can be found in Reference 6. While most PVC coating powders are made by the dry-blend process, melt-mixed formulations are used where superior performance, such as in outdoor weathering applications and electrical insulation, is required (see Fig. 1). Almost all PVC powder coatings are applied by the fluidized-bed coating process. Although some electrostatic spray-grade formulations are available, they are very erratic in their application characteristics. The resistivity of plasticized PVC powders is low compared to other powder coating materials and the applied powder quickly loses its electrostatic charge. Dishwasher baskets are coated with fluidized-bed PVC powder. Other applications are various types of wire mesh and chain-link fencing. PVC coatings have a very good cost/performance balance that is difficult to match with any of the other thermoplastic materials. Properly formulated PVC powders have good outdoor weathering resistance and are used in many applications where good corrosion resistance is required. These coatings are also resistant to attack by most dilute chemicals except solvents. In addition, PVC coatings possess excellent edge coverage.

Powder coatings as a class are superior to liquid coatings in their ability to coat sharp edges and isolate the substrate from contact with corrosive environments. PVC coatings are softer and more flexible than any of the other powder coating materials. Primers used for PVC plastisols have been found generally suitable for powder coatings as well (7).

Polyamides. Coating powders based on polyamide resins have been used in fusion-coating processes from the earliest days. Nylon-11 [25587-80-9] has been used almost exclusively; however, coating powders based on nylon-12 [24937-16-4] also have been sold. The properties of these two resins are quite similar. Nylon-6 [25038-54-4] and nylon-6,6 [32131-17-2] are not used because the melt viscosities are too high.

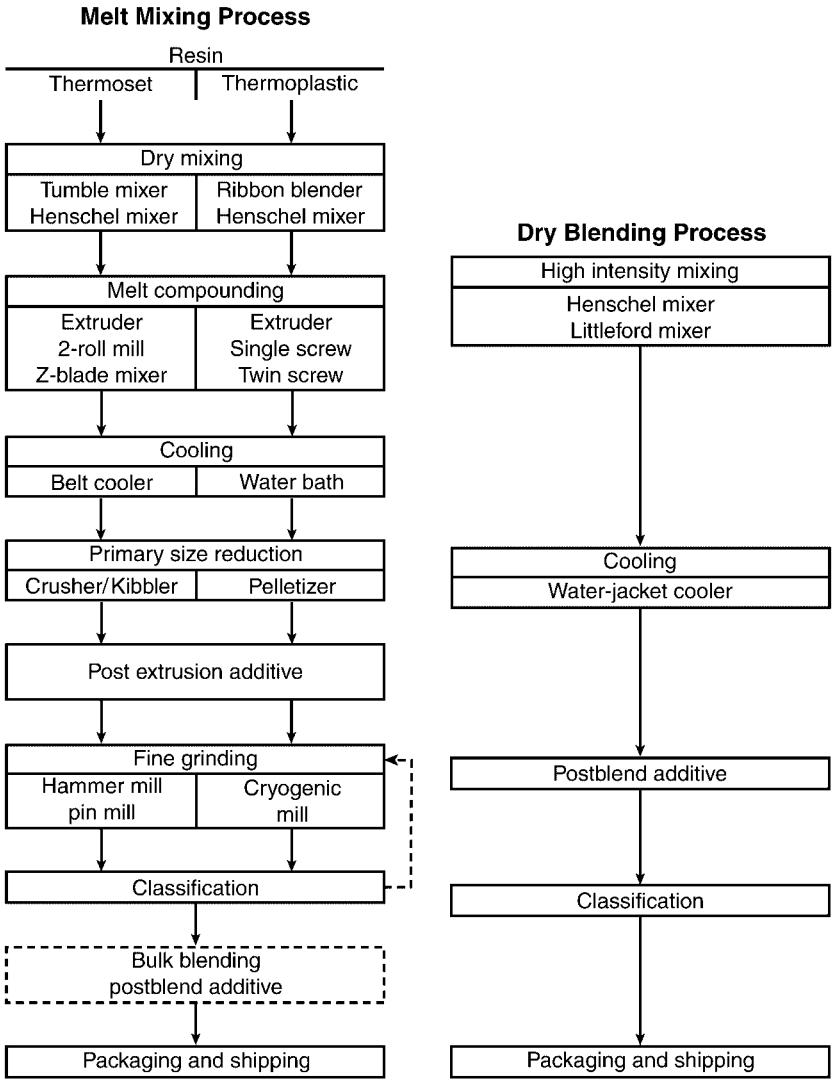

Fig. 1. Flow diagram for coating powder manufacture (adopted from *Encyclopedia of Chemical Technology*, 4th ed.).

Polyamide powders are prepared by both the melt-mixed and dry-blend process. In the latter, the resin is ground to a fine powder and the pigments are mixed in with a high intensity mixer (see Fig. 1). Melt-mixed powders have a higher gloss, eg, 70–90 on the 60° gloss meter, whereas dry-blended powders have a gloss in the range of 40–70. Because the pigment is not dispersed in the resin in the dry-blend process, it must be used at very low concentrations, usually less than 5%. Even in melt-mixed formulations, the concentration of pigment and fillers (qv) seldom exceeds about 20% of the composition (see POLYAMIDES, PLASTIC).

Nylon coating powders are available for both electrostatic spray and fluidized-bed application. Nylon coatings are very tough, resistant to scratching

and marring, have a pleasing appearance, and are suitable for food contact applications when properly formulated. These coatings are used for chair bases, hospital furniture, office equipment, knobs, handles, and other hardware. Because of expense, nylon is generally applied only to premium items. Nylon coatings have good solvent and chemical resistance and are used for dishwasher baskets, food trays, hot water heaters, plating and chemical-etching racks, and large diameter water pipes in power-generating stations. For maximum performance, a primer is used. Nylon coating powders are discussed in more detail in Reference 8.

Other Thermoplastic Coating Powders. Coating powders based on polyethylene [9002-88-4] and polypropylene [9003-07-1] have been available for many years but have achieved limited commercial success. A primary problem in using polyolefin-based powders is poor adhesion to metal. However, ethylene copolymers functionalized with acrylic acid, sold under the tradename Envelon (9), and certain grades of ionomer resins (10) have been formulated into coating powders and are enjoying some measure of commercial success. Self-adhering clear coatings based on a combination of ionomer resins and high melt index ethylene/acrylic acid copolymers are described in a recent patent (11).

Thermoplastic polyester coating powders achieved some commercial success during the mid-1980s; however, these were eventually replaced by nylon coating powders in functional coatings and thermosetting polyester coating powders in decorative applications because of lack of any unique characteristics or price advantages (see POLYESTERS, THERMOPLASTIC).

Coating powders based on poly(vinylidine fluoride) [25101-45-5] (PVDF) are available and are used in architectural applications where long-term exterior performance is required. Most are modified with thermoplastic acrylic polymers (12) or other fluoropolymer resins containing comonomers to improve melt flow and application characteristics (13). A method for preparing pigmented PVDF powders which does not require melt compounding and cryogenic grinding is described in Reference 14.

Several other thermoplastic powders are available based on specialty polymers such as ethylene–chlorotrifluoroethylene [25101-45-5], poly(phenylene sulfide) [25212-74-2], and tetrafluoroethylene–ethylene [68258-85-5] copolymers. Such powders are used in functional applications where resistance to corrosion and elevated temperatures are required. They are usually applied by fluidized-bed coating techniques but can also be applied by electrostatic techniques to a heated substrate (15). Extremely high application temperatures in the range of 250–350°C are required for these polymers because of high melting point and high melt viscosity.

Thermosetting Coating Powders

Thermosetting coating powders, with minor exceptions, are based on resins that cure by addition reactions. Thermosetting resins are more versatile than thermoplastic resins in the formulation of coating powders in that many types are available varying in melt viscosity, functional groups, and degree of functionality; numerous cross-linking agents are available, thus the properties of the applied film can be readily modified; the resin/curing agent system possess a low melt

Table 2. Physical and Coating Properties of Thermosetting Powders[a]

Property	Epoxy	Polyurethane[b]	Polyester[c]	Hybrid	Acrylic[d]
Fusion range, °C	90–200	160–220	160–220	140–210	100–180
Cure time,[e] min	1–30[f]	15–30	5–15	5–15	5–25
Storage temp, °C[g]	30	30	30	30	20
Adhesion[h]	E	G–E	G–E	G–E	G–E
Gloss, 60° meter	5–95	5–95	40–95	20–95	80–100
Pencil hardness[i]	H–4H	H–2H	H–4H	H–2H	H–2H
Flexibility[h]	E	E	E	E	F–P
Resistance[h]					
Impact	E	G–E	G–E	G–E	F
Overbake	F–P	G–E	E	G–E	G–E
Weathering	P	G–E	G–E	P–F	G–E
Acid[g]	G–E	F	G	G	F
Alkali[j]	G–E	p	F	G	P
Solvent	G–E	F	F–G	F	F

[a] Adopted from *Encylopedia of Chemical Technology*, 4th ed.
[b] Hydroxy function-blocked isocyanate cure.
[c] TGIC (triglycidyl isocyanurate)/hydlroxy, alkylamide cure.
[d] GMA (glycidyl methacrylate) type cured with DDA (dodecanedioic acid).
[e] Value is given at 160–200°C, unless otherwise indicated.
[f] At 240–135°C.
[g] Maximum value is given.
[h] E = Excellent; G = good; F = fair; P = poor.
[i] Refers to highest degree of lead hardness at which coating can be marred.
[j] Inorganic; dilute.

viscosity allowing application of thinner, smoother films and necessary level of pigments and fillers required to achieve opacity in the thin films can be incorporated without unduly affecting flow; gloss, textures, and special effects can be produced by modifying the curing mechanism or through the use of additives; and manufacturing costs are lower because compounding is carried out at lower temperatures and the resins are friable and can be ground to a fine powder without using cryogenic techniques. The properties of thermosetting coating powders are given in Table 2.

Ideally, the appearance of a powder coating should equal that of a water borne or solution coating at the normal thickness range, eg, 20–60 μm (ca 1 to >2 mils). While significant advances have been made in the formulation and application of powder coatings over the last 10 years, it is more difficult to apply powders uniformly in thin films that match the smoothness and appearance of conventional liquid finishes. However, the gap is closing rapidly. Automotive powder clear coats have been applied by BMW to several models on a production basis since 1998. As of May 2000, over 1000 car bodies per day are being powder coated on completely automated lines (but at a film thickness still higher than desired) (16).

In order to retain their particulate form and free-flow characteristics, coating powders must resist sintering or clumping during transportation, storage, and handling. To maintain these properties, the glass-transition temperature T_g, of the formulated powder must be, at a minimum, about 40°C and preferably above 50°C. In the case of epoxy resins, because of their highly aromatic backbone, the

Table 3. Melt Viscosity, T_g, and Equivalent Weight of Various Thermosetting Resins

Resin type	Equivalent weight	T_g, °C	Melt viscosity, mPa·s (=cP) at indicated temperatures	
Epoxy Resins			175°C	200°C
Type "2"	600–750	50–60	500–1000	[a]
Type "3"	700–850	55–65	1000–2000	200–400
Type "4"	850–1000	60–70	2000–3000	1000
Type "7"	1500–2500	80–85	9000–10,000	10,000
Polyester resins				
Acid functional	750–2800	50–64	–	3000–6500
Hydroxyl functional				
General Purpose	560–1870	50–55	–	3000–6000
High T_g	1400–1800	60–70	–	6500–8500
Acrylic resins				
Acid functional	750–1600	55–68	–	3000–8000
Hydroxyl functional	1250	60	–	5000
Glycidyl methacrylate	510–560	39–56	390–470	[a]

[a] Too low to measure.

necessary T_g is attained at a relatively low molecular mass. In contrast, polyester resins require linear comonomers to achieve the desired degree of flexibility leading to a lower T_g. Thus, to attain the desired T_g, higher molecular mass resins must be used resulting in higher melt viscosities (17). At an equivalent range of T_g, polyester resins have a melt viscosity about 10 times higher than for epoxy resins (see Table 3).

The main parameters affecting film formation and flow of thermosetting coating powders are surface tension and melt viscosity (18). While a high surface tension promotes the coalescence and flow of molten powder particles, a low surface tension is necessary to wet the substrate. The so-called flow control additives are used in almost all coating powders to eliminate surface defects such as craters and pinholes. A more accurate term would be "surface tension modifiers," since this is their primary effect. They are believed to function by creating a uniform surface tension at the air/surface interface of the molten coating as a result of the particle compatibility (19). The most widely used flow control additives are acrylic oligomers (20). Most are primarily based on *n*-butyl acrylate [9003-49-0] and copolymers of ethyl acrylate and 2-ethylhexyl acrylate [26376-86-3] (see ACRYLIC ESTER POLYMERS).

While there is little difference between the surface tension lowering effects of various acrylic flow additives (21), monomer composition and molecular mass can have a significant effect on the flow and orange peel of the final coating (22). The relationship between flow and melt viscosity of the binder resin(s) is more obvious. Significant efforts on the part of resin manufacturers have been made to optimize the melt viscosity of the polymers while still maintaining the required T_g. Monomer composition (23), molecular mass, and functionality (24) are among the most important variables. The degree of reactivity between the resin and the curative has a significant effect on flow and smoothness. For ideal flow and leveling of the coating, the time between melting of the powder and the start of cross-linking should be maximized. Most resins are intended for use with a

particular curing agent, and so the functionality of the resin is designed accordingly. Rapid heating of the applied powder layer, ie, high curing temperatures, results in the lowest level of melt viscosity, but also in a faster increase in viscosity once the crosslinking starts (25). Chemorheological measurements have proven useful in determining the most desirable resin/curing agent reactivity and functionality in specific thermosetting systems (26). Optimum curing conditions can be predicted based on the reaction kinetics of the coating powder (27). In addition to the chemical and rheological factors already mentioned, smoothness of the cured coating is also related to the structure of the electrostatically deposited powder layer. The initially applied powder layer is much more porous than would be expected from random close packing of particles and shows appreciable powder segregation and patterning. A comprehensive study of powder application, coalescence, and flow indicates that the orange peel, with its millimeter length scale and micron-scale amplitude, arises partly from incomplete leveling of the largest scales of unevenness originally present in the deposited powder layer (28). Previous studies have also noted the relationship between clusters or large agglomerates of particles and orange peel (29). Finer particle size powders eliminate some of the large agglomerates and result in smoother films (30), but finer particles are more cohesive, less free flowing, and more difficult to manipulate (31).

The higher degree of orange peel exhibited by powder coatings in comparison to conventional liquid coatings is a fundamental shortcoming. Determining the ultimate cause of this deficiency and correcting it will lead to even greater acceptance and use of powders in finishing processes.

Formulation. In many respects, the formulation of coating powders is similar to that for conventional paints. The resinous binder plays a major role in the basic properties of the final coating such as exterior durability, chemical resistance, flexibility and impact resistance and, to some extent, appearance. While in conventional paints, solid ingredients such as pigments and fillers are dispersed in the liquid vehicle using a mill, in coating powders, the solid ingredients are dispersed in the molten binder in an extruder. Paint dispersions must be stabilized to prevent pigment agglomeration and settling. Flooding, floating, and pigment agglomeration are not a problem in a solid binder so rheological and dispersing additives are not necessary and seldom used in coating powders. A significant formulating advantage for conventional paints is that there are few constraints on the T_g of the binder resins; they can even be liquids. In addition to the binder resin(s), curing agents, which can range from crystalline solids to polymers, flow agents, additives, pigments, and fillers are utilized in coating powders. An important formulating variable is the ratio of pigments and fillers to the binder, the pigment:binder, or P:B ratio. Typical pigment:binder ratios used in formulating various types of coating powders are listed in Table 4. In general, the P:B ratios used in coating powders are much lower than for conventional paints since there are no other liquid ingredients present to wet out the pigments. Thus the pigment volume concentration in coating powders is correspondingly lower and seldom exceeds about 25%. Higher levels of pigments or fillers significantly reduce the flow out of coating powders resulting in a rough grainy coating.

In addition to the acrylate flow control additives, silicones, primarily the polyether modified types, and fluoropolymer flow agents are also used. Care must be exercised when using powders with differing flow additives or significantly

Table 4. Pigment: Binder Ratios for Various End-Use Applications

Pigment:binder ratio	% Pigment and fillers	Approx. PVC[a]	Application
0.01–0.10	1–9	0.3–2.9	Transparent, flamboyant, clear metallic, special effects
0.1–0.2	9–17	2.9–5.7	High chroma, high DOI, automotive exterior durability, high flexibility
0.2–0.6	17–37.5	5.7–15	General purpose, appliance, furniture, fixtures, lawn and garden
0.6–1.0	37.5–50	15–23	Low cost, anticorrosive, electrical insulation, pipe coatings
1.0–1.2	50–55	23–26.5	Primers, textures, functional coatings, economy grades
>1.2	>55	>26.5	Specialized applications, zinc rich primers

[a]Pigment volume concentration (PVC) calculated using pigments and fillers having a specific gravity of 4.0.

different binder resins since cross contamination can occur resulting in loss of gloss, surface imperfections, and loss of smoothness. These incompatibilities arise from differences in the surface tension of the various powders (32). Low melting thermoplastic additives such as benzoin [119-53-9] are used in coating powders to promote bubble release and air entrapment (33). Many of the additives used in coating powders, such as uv absorbers, light and heat stabilizers, mar and slip agents, have their basis in conventional coatings. However, others, such as electrostatic or tribocharging additives and postblend additives, mixed with the finished powder to improve dry, free-flow characteristics (34) are unique to coating powders.

Many of the pigments used in conventional paints are also used in coating powders. These include inorganic pigments such as titanium dioxide, nickel/titanium rutile, iron oxides, and complex inorganic pigments. Lead and cadmium based pigments have not been used for many years in the United States and Europe and are being phased out in the rest of the world. Typical organic pigments used include phthalocyanine blues and greens, various azo types, quinacridones, carbazoles, diketo-pyrrolo pyrroles among others. In general, inorganic pigments are used to provide opacity while organic pigments are used for their chroma or saturation. Because of their high surface area and high binder demand, organic pigments cannot be used at very high levels, ie, >5–6%, before a noticeable reduction in flow and increase in orange peel of the coating starts to occur. Therefore, as a rule of thumb, the level of inorganic pigments should be maximized and the level of organic pigments minimized consistent with the requirements for opacity and chroma. As noted, even inorganic pigments, with their higher opacity and lower binder demand, are not used at as high levels in coating powders as in paints. To obtain complete opacity with a white coating powder containing 30% TiO_2 (P:B ratio = 0.46) a film thickness of 89 μm is required. The addition of only 0.001% carbon black reduces the thickness required for complete hiding to 63 μm and to 37 μm with the addition of 0.005% (35).

Fillers such as calcium carbonate, blanc fixe and barium sulfate [07727-43-7], and wollastonite [13983-17-0] are used in coating powders to modify gloss,

hardness, permeability, and other coated film characteristics, and to reduce costs (36). Clays and talcs are seldom used, except in textured coatings, because of their high binder demand and adverse affect on flow and smoothness. Silicas are usually avoided because of their abrasiveness during extrusion and grinding, with the exception of colloidal silica used as a postextrusion additive.

Matting or flattening agents are employed to control gloss, which is dependent on microscopic surface smoothness (37). Thus, nonmelting or incompatible thermoplastic resins of proper particle size such as Teflon and polypropylene are used to disrupt surface smoothness and reduce gloss (38). Similarly, incompatible waxes concentrate at the surface of the coating, also reducing gloss but resulting in a waxy feel, which is prone to showing blemishes, eg, fingerprints. Coarse grades of fillers such as barytes, calcium carbonate, or wollastonite are also used for gloss control, usually with other techniques. Curing agents having widely different reactivities cause a two-stage polymerization to occur, resulting in incompatible domains and impaired microscopic surface smoothness (39). In a similar fashion, low gloss is achieved by mixing two powders varying significantly in reactivity (40). Gloss can be controlled over a wide range using combinations of glycidyl methacrylate functional resins with acid functional polyester resins (41). In summary, there are many methods of gloss control available to the coating powder formulator covering the full range of gloss in both interior and exterior durable systems.

Special Finishes. Clear coatings are formulated using curing agents and flow additives, which have a high degree of compatibility with the resin. Conventional uv and hindered amine light stabilizers can be added to improve exterior durability. Metallic finishes can also be prepared but the metal flake must be added after the powder has already been ground to prevent break up of the metallic flakes and preserve the metallic appearance (42).

Hammertones, veins, and other special effects are prepared by the judicious addition of surface tension lowering ingredients, eg, silicones or flow control/resin master batches, usually in conjunction with a dry-blended metallic or mica-flake pigment. Textured coatings are produced by controlling the flow and particle size of the powder particles as well as with nonmelting polymers of controlled particle size. Wrinkle finishes are obtained using selected curing agents and catalysts (43).

Epoxy Coating Powders. Thermosetting coating powders based on epoxy resins [25068-38-6], $C_{15}H_{16}O_2 \cdot (C_3H_5ClO)_x$ have been used longer than any other resin system. This is because solid epoxy resins (qv) were commercially available when thermosetting coating powders were being developed and had the necessary combination of low molecular mass, T_g, and melt viscosity (see Table 3). Further, a variety of latent curing agents were also known, which allowed the development of stable, one component powders. Early efforts to develop powders based on dry-blend processing methods, such as by ball milling, were generally not commercially acceptable because the resultant coatings were low in gloss and lacked smoothness and good appearance, especially with greater than minimal levels of pigments and fillers. These problems were overcome when powders were processed by melt mixing, eg, extrusion (see Fig. 1 and related text). The earliest powders were based on dicyandiamide [461-58-4], a latent curing agent. However, these powders were too slow curing, requiring 15–30 min at 200°C to achieve full properties. A wide variety of catalysts for the dicyandiamide epoxy reaction were

evaluated, but the clear choice after several years of trial and error were imidazoles, especially 2-methyl imidazole [693-90-1]. Dicyandiamide has a high melting point and limited solubility in epoxy resins. Dicyandiamide derivatives having aromatic substitution were developed, which are more compatible with epoxy resins, easier to disperse, and more reactive while still retaining their latency. Typical of these substituted dicyandiamide derivatives are o-tolyl biguanide [93-69-6] and 2,6-xylenyl biguanide (44). Highly reactive, compatible, and low melting curatives are also prepared by reacting an epoxy resin with excess imidazole. Another class of curatives, developed somewhat later, are the linear phenolics. These have the same structure as epoxy resins but are terminated with bisphenol A [80-05-07] rather than epoxide groups and contain significant levels of free bisphenol A. Since they have a functionality of only 2, the functionality of the epoxy resin in the binder must be increased, usually by blending with an epoxidized phenol novolak resin, to give an average functionality of about 2.5–3.0. The epoxy/phenolic hydroxyl reaction is relatively slow for many applications, and so an imidazole catalyst is often included in the formulation (45). Most of these curatives are still used today in both decorative and functional epoxy coating powders and provide compositions which cure in the typical range of 10–15 min at 180–200°C or in the low temperature range of 15–20 min at 140–180°C.

Many other types of curing agents have been evaluated in formulating epoxy-based coating powders but have found use in only specialized applications. Conventional phenol or cresol novolak resin curatives impart a high degree of cross-link density but result in rather brittle coatings with undesirable color. Aromatic amines give very reactive, fast curing systems but are marginal in storage stability and their health and safety characteristics are questionable. Of course, primary aliphatic amines cannot be used because they react even at room temperature and cannot be compounded at elevated extrusion temperatures. Dihydrazides have also been evaluated but their cost/performance base can seldom justify their use. Many anhydride curing agents have been considered but only a few have found their way into commercial formulations. For a time, trimellitic anhydride [552-30-7] cured powders catalyzed with metal-organic salts were used in the formulation of very reactive, fast cure powders, such as those used for coating concrete reinforcing bars (rebars) and pipe coatings (46). However, health and safety concerns led to the decline in use of this chemistry. Benzophenone tetracarboxylic dianhydride yields highly cross-linked coatings with very good heat and chemical resistance and is used in specialized functional applications (47).

Decorative epoxy powders are used in a wide variety of applications, eg, for lighting fixtures, garden equipment, motor control cabinets, and many automotive under the hood items including coil springs, shock absorbers, mechanical parts, and even engine blocks. Low melt viscosity resins of the type “3” are most widely used in decorative applications (see Table 3). Type “4” resins and higher with a higher molecular mass and melt viscosity are more often used in functional applications such as for electrical insulation and corrosion resistance where thicker coatings are needed and a higher degree of edge coverage is necessary. Epoxy powders are used almost exclusively in rebar and pipe coatings (48). In outdoor applications, epoxy coatings chalk readily and lose gloss; however, they protect the substrate for many years. Figure 2 compares the gloss retention of epoxy coatings with other thermoset types on exterior exposure.

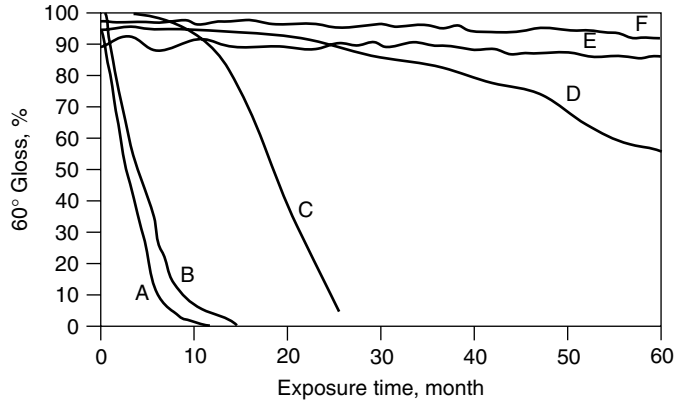

Fig. 2. Gloss retention in outdoor exposure in Florida for various powder coatings: A, epoxy; B, epoxy–polyester hybrid; C, polyester TGIC, HAA, and urethane (dark brown); D, super durable polyester TGIC, HAA, and urethane (dark brown); E, super durable polyester, clear, no light stabilizers; F, GMA acrylic, clear, light stabilized (after Ref. 49 and 50).

Epoxy–Polyester Hybrids. A major class of interior grade coating powders is based on a combination of epoxy and acid functional polyester resins. As noted, epoxy resins cured with anhydrides have desirable properties but never gained a high degree of commercial acceptance. Most anhydrides are respiratory irritants and are difficult to work with. Also, they are hygroscopic and the reactivity of coating powders cured with anhydrides varies on storage depending on the ambient humidity and the degree of conversion of the anhydride to acid. On the positive side, anhydride cured powders possess heat resistance and good color stability in contrast to the tendency for most amine cured powders to discolor on exposure to heat or exterior exposure. Therefore, programs were initiated in the research facilities of polyester resin manufacturers to develop resins which retained the desirable characteristics of anhydrides while eliminating their undesirable characteristics. This work resulted in the development of acid functional, relatively linear, saturated polyester resins specifically designed for curing bisphenol A based epoxy resins. The original resins developed had an acid number of 70–80 (equivalent weight range 700–800), and so they were used at 50:50 ratio with type "3" epoxy resins (see Table 3). The functionality is about 2.5–3, to provide good curing characteristics and cross-link density when used with the essentially bifunctional epoxy resins. Because polyester resins are less expensive than epoxy resins, higher equivalent weight polyester resins were subsequently developed which are used at a stoichiometric ratio of 60:40 and even 70:30 ratios to epoxy resin. Properties of these polyester–epoxy hybrids are similar to those of a straight epoxy, but differ in several respects. The overbake resistance (resistance to color change after extending curing) and resistance to discoloration on exposure to sunlight is superior. Because the cross-link density for hybrid coating powders is generally less than for straight epoxies, cured hybrid coatings are inferior in solvent resistance and hardness. They are also somewhat inferior in salt spray and corrosion resistance. Polyester resins, having a higher melt viscosity than epoxy resins (see Table 3), result in the hybrids having more

Table 5. 1998 Thermoset Powder Coatings Production by Resin Type[a]

Resin type	North America	Europe
Epoxy	15.0%	8.5%
Epoxy–polyester hybrid	35.7%	54.0%
Polyester–carboxyl	22.6%	29.0%
Polyester–hydroxyl	21.6%	4.0%
Acrylic and other	5.1%	4.5%
Total	*100.0%*	*100.0%*

[a]Ref. 54.

orange peel than epoxy-based coatings, especially at the higher polyester–epoxy ratios.

The reaction rate between carboxyl end groups of the polyester and the epoxide groups of the epoxy resin is generally quite slow, requiring a catalyst to obtain a practical baking time. Catalysts are frequently mixed with the polyester resin by the resin manufacturer. The ideal catalyst should exhibit good reactivity at the desired baking temperature, eg, 150–180°C, while providing good flow and shelf stability (51). Tertiary amines, amic acids, and quaternary phosphonium compounds are effective catalysts for the epoxy-carboxyl reaction (52,53).

Epoxy–polyester hybrid coatings are marginally better than straight epoxy-based coatings in gloss retention on exterior exposure (Fig. 2) but generally are not recommended for exterior applications. For the most part, applications for the hybrid powders are the same as those for decorative epoxy coating powders. The latter are being replaced by the hybrid coating powders and are increasing in market share in the United States. In Europe, hybrid coating powders are the most widely used powder type (see Table 5).

Polyester–Triglycidylisocyanurate Cured. A principal class of exterior durable powder coatings is based on acid functional, saturated polyester resins cured using triglycidylisocyanurate [02451-62-9] (TGIC) (see Fig. 2). This system was first developed in Europe in the early 1970s. The acid functional polyester resins used in TGIC-cured coating powders are similar to those used in epoxy–polyester hybrids. However, the resins for curing with TGIC have a higher equivalent weight, typically in the range of 1600–1900, and a lower degree of functionality. Thus most resins are used at a 93:7 ratio of resin to TGIC. Acid functional resins are normally prepared by a two-step process: the reaction of excess polyol and dibasic acids followed by esterification of the hydroxyl terminated resin using dibasic acids or anhydrides (55). This technique yields a resin where the functional groups are at the end of the molecule rather than occurring randomly along the polymer chain. The excellent exterior durability of polyester resins cured with TGIC is primarily a result of the nonaromatic structure of TGIC in contrast to that of the bisphenol A based epoxy resins used in polyester–epoxy hybrid coating powders. Monomer composition of the resin also plays a significant role. It is recognized that the exterior durability of polyester powder coatings is affected by factors other than resistance to uv radiation. Accumulation of moisture on the surface of the coatings, especially at elevated temperatures (darker colors), and exposure to oxygen leads to hydrolysis, oxidation, and degradation of the

resin. Environmental factors such as acid rain or alkaline bird droppings as well as cyclic heating and cooling also contribute to molecular breakdown and loss of properties. For these reasons, accelerated weather testing now frequently includes cyclic exposure to elevated temperatures and moisture as well as uv light (56).

The recent development of so-called super durable polyesters has validated the cyclic accelerated weathering approach. Super durable polyester resins are based almost exclusively on isophthalic acid while most standard resins contain terphthalic acid as well. Super durable polyesters are highly resistant to hydrolysis and degradation by uv light (57,58), which helps to account for their superior exterior durability. Compared with a standard TGIC-cured polyester powder coating in a dark color, which loses about 50% of its original gloss after about 2 years of Florida exposure, a super durable polyester cured with TGIC will last at least four times as long until the same loss of gloss occurs. Figure 2 is a plot of % gloss retained vs original level, measured on a 60° gloss meter, comparing super durable polyesters with several other types of powder coatings. Super durable polyesters are generally inferior in flexibility and impact resistance but recent advances have shown significant improvements in this regard (59).

TGIC-cured coating powders have gained a significant market share in the exterior durable market in both Europe and North America. Many buildings coated with TGIC powders in various European locations from the early 1970s and later are still in good condition, exhibiting minimal corrosion and good retention of gloss and color. In the past 10 years, some concerns have developed over health and safety issues related to TGIC, especially with regard to mutagenic characteristics. In the United States, it is generally believed the hazards are adequately addressed by the OSHA Hazard Communication Standard and the low exposure level of 0.05 mg/m^3 established (60). However, in Europe, the European Union ruled that the symbol **T** (Toxic, symbolized by a skull and crossbones) accompanied by the relevant Risk Phase R46, relating to substances considered to cause heritable genetic damage, is to be used in labeling any product containing TGIC. This requirement went into effect in June of 1998 and had the result of powder manufacturers replacing TGIC in their products. Since that time the market share of TGIC-cured polyester coating powders has decreased significantly in Europe, being largely replaced by hydroxyalkylamide-cured powders (61). Other glycidyl compounds such as a mixture of diglycidyl terphthalate [7195-44-0] and triglycidyl trimellitate [7237-83-4] (62) as well as tris(β-methyl glycidyl) isocyanurate [26147-73-3] (63) are being evaluated as TGIC replacements as well.

Polyester–Hydroxyalkylamide Cured. Hydroxyalkylamide curatives were developed in the late 1970s and early 1980s (64). Evaluation as a curative in coating powders was described in early 1991 (65). The primary commercial product is bis(*N*,*N*-dihydroxyethyl) adipamide [6334-25-4] sold under the trade name Primid XL 552 by EMS Chemie. It reacts with acid functional polyester resins by esterification and the elimination of water. The toxicological profile of this curative is benign, and it does not fall under the provisions of any current health and safety or environmental regulations. It has been shown that the ester linkage formed with Primid XL 552 and polyester resins has essentially the same characteristics as the TGIC–polyester bond (66). Practical experience has confirmed that polyester coating powders cured with Primid are essentially equivalent in weatherability and other properties to TGIC-cured powders (67).

Because the functionality of the hydroxyalkylamide curative is about 4, the functionality of the polyester resins used with them has to be designed accordingly (68).

Urethane Polyesters. In the United States the search for exterior durable coating powders led to technology based on hydroxyl functional polyester resins. The earliest curing agents evaluated were based on melamine–formaldehyde resins, such as hexa(methoxymethyl) melamine [68002-20-0], which are widely utilized as curing agents in conventional paint systems (see AMINO RESINS). Coating powders based on this chemistry suffer limitations: the melamine resin depresses the T_g of the coating powder to the point where the powder sinters during storage, especially at elevated temperatures, and the methanol generated during the curing process becomes trapped in the film, especially at thicknesses above about 50 μm, resulting in a frosty or visually nonuniform surface. An amino resin, specifically developed for use in coating powders, tetramethoxymethyl glycouril [17464-88-9], overcomes many of these disadvantages, but still requires the use of higher T_g resins and special acid catalysts (69). Coating powders based on this chemistry have not achieved a high level of commercial acceptance for general-purpose use; however, with selected catalysts, attractive wrinkle finishes are produced (70,71), which find use in special applications. Curing agents based on polyisocyanates blocked with caprolactam [00105-60-2] give an excellent combination of properties in the final film (see Table 2). Because the unblocking reaction does not start to occur until about 160°C, the powder has a chance to flow out and give a smooth uniform film prior to any substantial cross-linking. Not all of the caprolactam evolves during the curing process and some remains in the film acting as a plasticizer. Thus, urethane polyesters yield a smoother, more orange-peel-free film than the TGIC polyesters and are more preferred in the United States and Japan than in Europe (see Table 5).

The hydroxyl functional polyester resins used in this technology are similar in monomer composition to the acid functional polyesters and are based primarily on terephthalic acid [100-21-0], $C_8H_6O_4$, isophthalic acid [121-91-5], $C_8H_6O_4$, neopentylglycol [126-30-7], $C_5H_{12}O_2$, and branched using trimellitic anhydride or trimethylol propane [77-99-6]. A variety of other polylols and dibasic acids are used to modify specific resin properties such as T_g, melt viscosity, curing characteristics, and others. (72,73). Resins ranging in OH number from 30–300, equivalent weight of about 190–1870, are used in the formulation of urethane coating powders. Since the blocked isocyanate curatives are three to four times the cost of the polyester resin, the lower OH number resins are preferred for general purpose formulations, with a 50 OH number resin providing a good balance between raw material cost, physical properties, and appearance. While the higher OH number resins require higher levels of curative, the final coatings have outstanding hardness and chemical resistance. Blends of high and low OH number resins and the stoichiometric level of curative form the basis of low gloss coatings. Hydroxyl functional super durable resins, similar in monomer composition to the acid functional resins cured with TGIC, are also available. When cured with IPDI-based isocyanates, they possess exterior durability equal to that of the super durable/TGIC-based coatings (see Fig. 2). The most commonly used curing agents are trimerized isophorone diisocyanate [4098-71-9] (IPDI) ($C_{12}H_{18}N_2O_2$) blocked with caprolactam and the trimethylol propane adduct of IPDI blocked with caprolactam. Blocking agents, which unblock at lower temperatures, provide the basis for urethane powders

which cure at lower temperatures (74). New curatives have been developed which do not rely on blocking agents to mask the reactivity of the isocyanate group. Most are based on the uretdione structure, a four-membered ring formed by the reaction of isocyanate groups with each other (75). While uretdione-based curatives have been available for many years, they have high melt viscosities and require higher temperatures for curing than the blocked isocyanates. Newer versions have overcome these problems to some extent (76).

Urethane polyesters have not received widespread commercial acceptance in Europe primarily because of the caprolactam (or other blocking agents) emitted during curing. Despite the development and commercial availability of the uretdione-based curatives, which do not give off volatiles during cure, the European market for exterior grade polyester powders is still based primarily on acid functional resins (see Table 5).

Unsaturated Polyester Powders. A special class of coating powders is based on unsaturated polyester resins. They are utilized in matched metal die molding operations such as those based on sheet molding compounds and bulk molding compounds where the mold is coated with the powder prior to placing the resin charge in the mold (see POLYESTERS, UNSATURATED). The powder melts and flows on the mold surface, and when the mold is closed, the powder reacts with the molding compound forming a coating on the molded part. This process is known as in-mold coating. Unsaturated polyester resin powder coatings can provide a colored and finished exterior molded surface or a finish ready for painting. Normally, a primer/sealer must be applied to molded articles prior to painting. In addition to the unsaturated polyester resin, multifunctional resins prepared from unsaturated monomers such as triallyl cyanurate [101-37-1] or diallyl phthalate [131-17-9], suitable peroxide initiators (qv) or mixtures thereof, and mold Release Agents (qv) are used to formulate the coating powder (77).

Acrylic Powders. Coating powders based on acrylic resins have been available in Europe, the United States, and Japan since the early 1970s but have not achieved significant commercial success until recently. However, since 1997 BMW has been applying an acrylic clear-coat powder to several models and currently (2000) is powder coating over 1000 cars/day (16). Acrylic-based powders are also used in exterior trim (pigmented) and wheels (clear). The majority of clear coatings are based on a glycidyl functional methacrylic resin (GMA) cured with dodecanedioic acid [693-23-2] or a polyacid/anhydride polymer (78). Acrylic powders based on GMA resins have poor compatibility with epoxy- and polyester-based powders. If cross contamination occurs, surface defects in the form of pinholes, craters, and excessive orange peel are common.

The GMA clear coatings have outstanding exterior durability, hence their acceptance in the automotive sector (see Fig. 2). Pigmented GMA acrylic powders have not found widespread use in market areas other than automotive, eg, architectural applications. Hydroxyl functional acrylic resins cured with blocked isocyanates or uretdione-based curatives have also found use in automotive applications and their exterior durability is only somewhat less than that of the GMA acrylic powders (50). Carboxyl functional acrylic resins are also commercially available. They can be cured with TGIC for exterior applications or with bisphenol A epoxy resins. The latter combinations are sometimes called acrylic–epoxy hybrid coating powders and are noted for their excellent hardness, stain, and chemical resistance. They find use primarily in appliance coatings (79).

Recent Developments. As noted, powder coating technology has advanced to the point where powders are now routinely applied in critical automotive applications. Another market area where intense work is in progress is the development of powders having low temperature curing capabilities such that they can be used to coat wood, plastics, and other temperature sensitive substrates. A coating powder must have a high enough T_g and molecular mass so that it does not sinter on the one hand while on the other hand a low melting point and melt viscosity is desirable for low temperature application and smoothness. It is a difficult task to balance these diverse requirements. This is especially true in the case of thermally cured powders compared with uv-curable powders. In the latter case, the flow and leveling of the coating are separate from the curing reaction while with heat curable powders, cross-linking occurs even as melting and flow are in progress.

One technique for dealing with this low temperature cure/reactivity dilemma is to use a two component powder system. The resin and other binder components comprise one component and the curative and other nonreactive binder ingredients, the other (80). In the case of uv curable powders, an unsaturated polyester resin is one of the major binder components but more reactive binder components such as oligomers with high allyl functionality (81) or vinylether/ester groups (82) must also be present. Crystalline resins with reactive methacrylyl groups have also been disclosed (83). A review of photoinitiators, additives, and other components of uv-curable powders are given in References 84 and 85.

Manufacture

The vast majority of thermosetting coating powders are prepared by melt mixing. Some thermoplastic powders are also produced by this method but most are manufactured by the dry-blend process as shown in Figure 1. Production methods based on spray drying from solution (86) and precipitation from solution (87) have been evaluated but never achieved commercial success because of difficulties in solvent and/or water removal from the powders. Many types of coating powders are still manufactured in small batches, eg, 50–1500 kg, due to differences in color or chemistry, where chemical processes are not economical.

Melt Mixing. Dry ingredients, resins, curatives, additives, pigments, etc, are weighed into a batch mixer such as high-speed impeller mixers, container mixers, horizontal plow mixers, or tumble mixers where they are thoroughly blended. High-speed impeller mixers such as the Henschel give the best distributive mixing and the cycle time is relatively short, eg, 1–2 min. However, these mixers have relatively small capacity, eg, 100–300 kg, and many individual batches must be prepared for longer production runs. Horizontal plow mixers require a slightly longer mix cycle but have a larger capacity, 500–1000 kg. They also provide good distributive mixing but require longer cleaning times. Tumble mixers have a high capacity and are adequate for general purpose powders, but mixing cycles are long, 30–60 min, and distribution of ingredients is sometimes marginal. With container mixing systems, only one mixer is required and generally satisfactory distributive mixing is obtained. However many mixing containers, which become the hopper for feeding the extruder, are required as well as a mixer for each size of mixing

container. The premix is then melt-compound in a high shear extruder where the ingredients are compacted, the resin(s) melt, and individual components are thoroughly dispersed in the molten resin. These compounding machines generate sufficient heat through mechanical shear so that after start-up, little external heat needs to be supplied. Both single screw machines, with a reciprocating screw which intermeshes with fixed baffles in the barrel, such as the Buss Ko-Kneader, and twin screw extruders, primarily corotating, intermeshing types as supplied by Krupp Werner Pfleider, Baker Perkins, and others are used (see EXTRUSION). Residence time in the extruder is short, usually less than 1 min and melt temperatures low, typically 90–120°C, slightly above the melting points of the resinous components. Because of these processing conditions, very little reaction between the thermosetting components occurs. In a study carried out based on epoxy resin compositions, it was determined that 6–11% of the epoxy groups initially present reacted during extrusion (88). Significant improvements have been made in both single and twin screw extruders and for a given size machine throughput rates have increased by a factor of 3–4 over the last 10 years or so. Product quality is more consistent as a result of improved process control (89). The molten compound is cooled rapidly by passing it through water-cooled nip rolls and subsequently onto a watercooled continuous stainless steel belt or drum. The cooled compound is broken into small chips, about 10–12 mm, suitable for fine grinding. Thermosetting resins are quite friable and are usually ground to final particle size in an air classifying mill. In this grinder, a blower generates an air stream through the mill in which the product is entrained and which also serves to remove the heat of grinding. A variable speed separator controls airflow in the grinding chamber so that only the particles with the desired particle size escape. The fine powder is separated from the air stream with a cyclone separator or bag house. Powders with a finer average particle size produce smoother coatings than powders with a larger particle size. While the addition of a colloidal silica or alumina to the powder, either to the chips prior to grinding or to the ground powder, significantly improves the dry flow, handling, and transport characteristics (90), the presence of high levels of superfine particles adversely affects these same characteristics. Recent advances in grinding equipment include in-line air classifiers and baffles in the cyclone separators, which allow the production of powders with a narrower particle size distribution (91). This means that powders with a finer average particle size can be produced without a significant increase in superfine particles, ie, those below about 8–10 μm.

Dry Blending. Most plasticized PVC powders are prepared by a dry-blend process in which the plasticizers, stabilizers, pigments, and additives are absorbed on the porous PVC particles at elevated temperatures while they are being agitated in a high speed mixer (6). Other thermoplastic powders are pigmented in this fashion. Attempts to prepare thermosetting powders by a dry-blend process have proven to be unsatisfactory because of the poor wetting and dispersion of pigments and the poor appearance of the subsequent coatings.

Recent Developments. A completely new process for the manufacture of coating powders has been recently developed by the Ferro Corp. It involves solvating resinous components in supercritical gas, typically carbon dioxide (CO_2), and dispersing the pigments and other solid ingredients with an impeller or dispersion blade. After dispersion is completed, the material is hydraulically atomized

into a second vessel at a lower pressure. The CO_2 vaporizes and a combination of particles or easily grindable solid is obtained (92). A similar process for preparing coating powders is described in Reference 93. The main advantage of these processes over conventional extrusion and grinding technology is that processing temperatures are lower, eg, 40–70°C, and it is possible to form powders directly. At present, there are no powders commercially available prepared by these methods.

Another recent development is the successful application of powders from aqueous dispersions. This process is being used to apply both primer surfacers and powder clear coats to the Mercedes A Class automobiles (94). An advantage of this process is that a very fine particle size powder can be used, 100% less than 10 μm (95), and it can be applied using conventional wet spray equipment. The concept of applying powders by aqueous dispersion is not new (96) but this is the first time it has been commercially successful. Now that there are large volume applications for powder coating in the automotive sector as primer surfacers and clear coats, it is anticipated that novel methods for preparing either powders or powder dispersions utilizing efficient chemical processing methods will be developed.

Application Methods

Fluidized-Bed Coating. Fluidized-bed coating, the first significant commercial process for applying powdered polymeric materials to a substrate to form a uniform coating, is the method of choice for many applications where a heavy functional coating is required. The process is relatively simple. The main variables are the temperature of the part as it enters the fluidized bed, the mass of the part being coated, dip time, and postheat temperature. Other variables, such as motion of the part in the bed and the density and temperature of the powder in the bed, also affect the quality of the coating. The process is especially useful in coating objects having a high surface to mass ratio such as fabricated wire goods and expanded metal. Sharp edges and intersections are well covered because of the heavy film thickness, eg, 250–500 μm (10–20 mils), applied. The size of parts that can be coated is limited because the fluidized-bed container must be large enough to readily accommodate them.

Electrostatic Fluidized-Bed Coating. In an electrostatic fluidized bed, the fluidizing container and the porous plate must be constructed of a nonconductive material, usually plastic. Ionized air is used to fluidize and charge the powder. The parts to be coated are passed over the bed and charged powder is attracted to the grounded substrate. The rate of powder deposition varies significantly depending on the distance of the part from the fluidizing powder. Therefore, this process is usually utilized only when the object to be coated is essentially planar or symmetrical and can be rotated above the charged powder. Electrostatic fluidized-bed coating is an ideal method for continuously coating webs, wires, fencing, and other articles that are normally fabricated in continuous lengths and are essentially two-dimensional. In a variation of this process, two electrostatic fluid beds are arranged back to back and the continuous web of material is passed between them, coating both sides simultaneously. Millions of lineal meters of window screen have been coated using this technique (97).

Electrostatic Spray Coating. Electrostatic spray coating is the most widely utilized method for the application of powder coatings. In a typical high voltage system, powder is maintained in a fluidized-bed reservoir, injected into an air stream, and carried to the gun where it is charged by passing through a corona discharge field. The charged powder is transported to the grounded part to be coated through a combination of electrostatic and aerodynamic forces. Ideally, the powder should be projected toward the substrate by aerodynamic forces so as to bring the powder particles close to the substrate where electrostatic forces then predominate and cause the particles to be deposited. The powder is held by electrostatic forces to the surface of the substrate, which is subsequently heated in an oven where the particles fuse and form a continuous film. The processes involved are powder charging, powder transport, adhesion mechanisms, back ionization, and self-limitation. As charged powder particles and free ions generated by the high voltage corona discharge approach the powder layer already deposited, the point is reached where the charge on the layer increases until electrostatic discharge occurs. At this point, any oncoming powder is rejected and loosely adhering powder on the surface falls off. It has been demonstrated that some imperfections in the final coating are a result of defects in the powder layer (98).

The characteristic of the electrostatic spray process to form self-limiting films enables operators to apply satisfactory coatings after only brief training and instruction. It is almost impossible to create runs, drips, or sags characteristic of spray-applied liquid finishes. Furthermore, the practical design of automatic spray installations is possible. Multiple electrostatic guns mounted on reciprocators are positioned in opposition to each other in an enclosed spray booth and parts to be coated are moved between the two banks of guns where a uniform coating of powder is applied. Oversprayed powder is captured in the reclaim system and reused. Powder coating booths have been designed with interchangeable filter units to facilitate change from one powder type of color to another. A state-of-the-art automatic powder spray system using a combination of cyclone separators to reclaim the majority of overspray powder and cartridge filters to capture the remaining powder is shown in Figure 3. The cyclone units are designed for quick cleaning and are much easier to clean than a bank of cartridge filters; quick color changes are facilitated. For very short runs, the cyclone separators can be removed and oversprayed powder is not recovered.

One disadvantage of the electrostatic powder spray process using corona discharge guns is that a high voltage field is set up between the gun and the parts to be coated. Parts having deep angles or recesses are sometimes difficult to coat because of the Faraday Cage effect. One method of overcoming the Faraday Cage effect is by the use of triboelectric guns in which powder charging occurs by the frictional contact of the powder particles and the interior surface of the gun. Electrons are separated from the powder particles, which become positively charged and attracted to the substrate. Because there is no electrostatic field between the gun and the article being coated, a Faraday Cage is not developed and particles are able to more readily penetrate into recessed areas of the substrate. There are a number of commercial powder coating systems using triboelectric charging technology, but this number is quite small compared to those based on the more conventional corona guns. The powder application rate of triboelectric guns is lower than that for corona guns; additionally, powders based on a wide

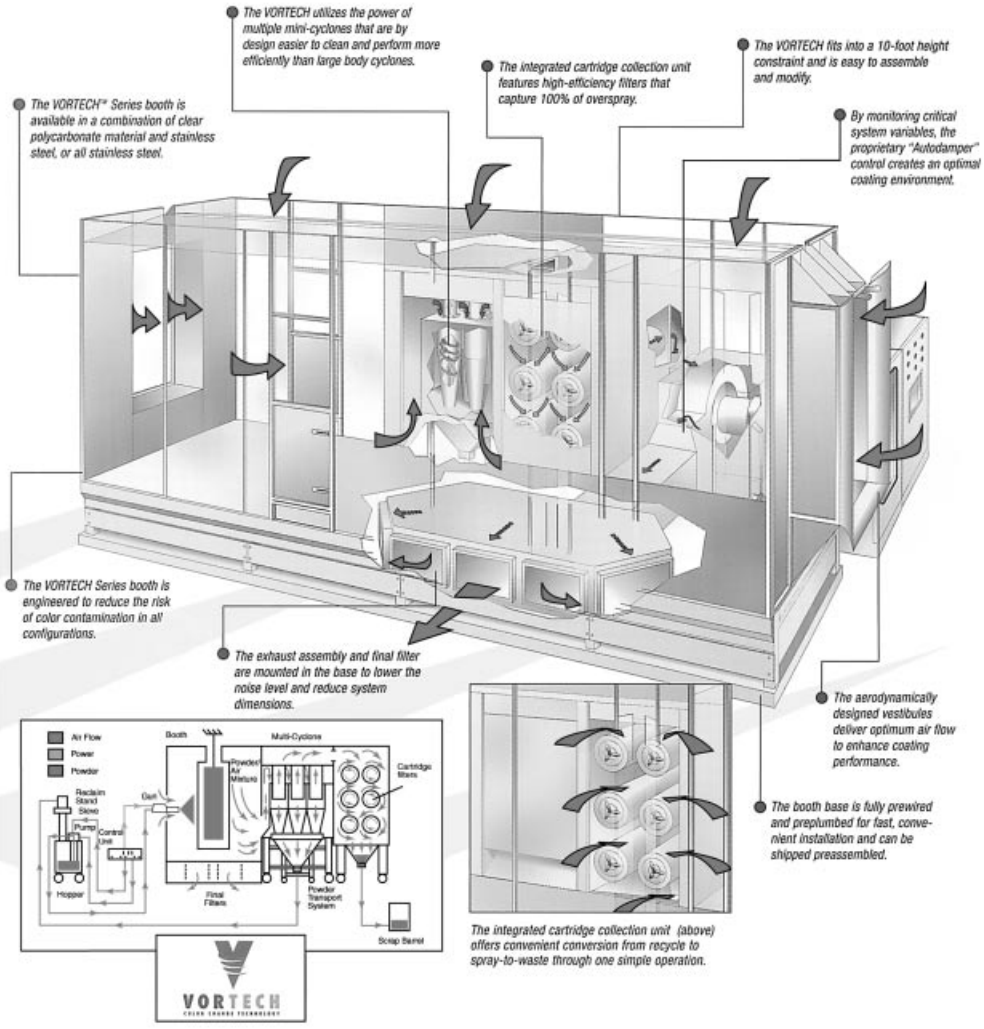

Fig. 3. Schematic diagram of an electrostatic powder spray system. Courtesy of ITW Gema.

variety of resins and formula types charge and apply readily with corona guns, whereas only certain resin systems charge well in triboelectric guns. However, additives have been developed which improve the tribocharging characteristics of powders (99).

While the basic principles of the electrostatic powder spray process have not changed, many advances in the equipment and process design have been made to improve process efficiency and quality of finish (100). Significant improvements have been made in reducing the time to change types of powders or make color changes. Much effort has gone into improving the first pass transfer efficiency, that is, the ratio of powder deposited on parts to that sprayed (101). High transfer efficiencies mean less overspray to reclaim. Less powder to reclaim means the recovery system can be reduced in size and requires less air volume and energy to

operate. Some of the means to improve transfer efficiency include programmable logic controls to adjust the motion of the guns and spray patterns for the specific parts being coated and to recognize the parts passing through the booth, shutting off powder flow when a vacancy in the line occurs or the line stops (102), sensors that detect the amount of powder in the air and modulate the air flow accordingly (103), and nonconductive spray booths and filter belts to facilitate powder reclaim (104). In the ideal case of 100% transfer efficiency, a powder reclaim system would be unnecessary and no cleanup required between color changes.

Improvements have also been made in materials. Stricter control of particle size distribution improves powder handling and transport characteristics, spray patterns, and transfer efficiency (105,106). Reduction of the superfine fraction, ie, particles below about 8–10 μm, also results in less fines in the overspray powder and less load on the reclaim system (107). More spherical powders charge more efficiently and show improved spraying characteristics (108).

Recent Developments. A major recent development is the commercial application of powders to auto bodies as primer surfacers and clear coatings. Also, specialized coating lines have been developed for the application of powders to metal blanks and coil. In the case of blank coating, sheet stock is cut and punched and coated on a flat line, using either standard or tribocharging guns. Powders are applied at a lower thickness (ca 25–40 μm) and must cure rapidly, eg, 1–2 min, to accommodate the relatively high line speeds (109). Coated blanks are shipped to the manufacturer flat, and assembled there into the final shape, eg, a refrigerator box. This eliminates an in-house coating line.

The continuous powder coating of steel coils is being carried out at a number of locations in Europe and the United Stated (110). Lines are now operating on coils 60 in. (1.52 m) wide at line speeds 250–300 ft/min (76–91 m/min) (111) and developments are in progress in which line speeds up to 1000 ft/min (305 m/min) are expected (112). Many special finishes, such as textures, hammertones, and wrinkles, are possible with powder while smooth finishes are only possible with liquid coatings. Because of the high line speeds and volume of powder applied, a novel powder charging and application system was developed (113).

Specialized application equipment has also been designed to coat the interior of can bodies (114). Powders having a finer particle size are required as well (115). A significant new powder application method has been developed utilizing photocopying and laser printing technology. Designated Electro-Magnetic Brush (EMB) Technology, it is possible to apply very thin powder coatings continuously on flat stock, either metallic or nonmetallic. Using a clear uv curable powder on a 17-in. wide EMB machine, rolls of wallpaper were coated at a thickness of 5–7 μm (0.2–0.3 mils) at a line speed of 60 m/min (197 ft/min) (116).

Hot Flocking. Several nonfluidized-bed coating methods are based on contacting a preheated substrate with powder to form a coating. Although these techniques are not widely used, for certain parts they are the preferred method of application. For example, the coating of motor stators using a thermosetting powder provides primary insulation between the core and windings. The part is preheated to about 200°C and the powder is directed from a fluidized bed using an air venturi pump, similar to those used to supply powder from the reservoir to electrostatic guns, through flexible tubes and directed at the preheated part which is rotating on a mandrel. Multiple tubes, usually in pairs in opposition to each other, are

normally used. In a similar fashion, the inside diameter of pipe can be coated by entraining powder in an airstream and blowing it through a preheated section of pipe (117). Very uniform coatings in the range of 200–300 μm can be applied by this process to provide corrosion protection for drill pipe, and water injection and gathering pipe in diameters up to ~50 cm.

Metal Cleaning and Preparation. As in any finishing operation, the surface of the object to be coated must be clean, dry, and free from rust, mill scale, grease, oil, drawing compounds, rust inhibitors, or any soil that might prevent good wetting of the surface by the coating powder. Steel should be sandblasted or centrifugally blast-cleaned to give a near white finish. Phosphate coatings are normally a pretreatment for most fabricated steel parts while nonchrome and organometallic conversion coatings are used on aluminum (118).

Economic Aspects

The worldwide market for coating powders increased at an annualized growth rate (AGR) of almost 10% during the 1990s in North America compared with a 12–13% AGR during the 1980s. Even though the rate of growth has decreased somewhat, it is estimated that powder coating represents only about 4–5% of the industrial paint market in North America. Globally, the penetration of powder coatings in the industrial paints sector is 6% with Europe leading at about 9%. By 2010, global penetration of powder coatings is expected to reach the 10% level (110).

While the primary driving force for growth during the 1980s was environmental regulations, growth during the 1990s has been driven additionally by superior performance and application economies. Powder coating is seen as an environmentally friendly technology because no solvents are present, volatile organic compounds, are absent, for the most part, venting, filtering, and solvent recovery systems are not necessary, process air is recycled, and there is little waste since most overspray powder can be collected and reused. Further, any waste generated is not classified as a hazardous waste under current regulations. Further, permits required for new coating facilities or additions to existing lines are much easier to obtain when the installation utilizes powder coating processes. Future growth will largely depend on advances in both coating materials and application technology in comparison with advances in other environmentally friendly coating methods.

The worldwide production of coating powders in 1999 is estimated at 727,100 t having a value of $803,861,000, a 6.9% increase over the quantity sold in 1998 (119) (see Table 6). This compares with a production of 236,000 t in 1989, a growth rate of over 12% per year. Europe is still the largest market, accounting for almost half, followed by North America and the Far East, each with 20%+ market share.

An indication of the growth of the powder coating in North America is reflected in the membership statistics of the Powder Coating Institute, a trade organization representing the industry. From 1987 to 2000, the number of members who manufacture coating powders increased from 5 to 28; suppliers of powder application equipment from 3 to 8; custom powder coaters from 1 to 200; and raw material suppliers from 5 to 114 (119).

Table 6. 1999 World Thermoset Powder Coatings Production[a]

	Production	
Region	Metric tons	Percent
Europe–West and East	329,100	45.3
Far East	161,585	22.2
North America	175,600	24.2
South America	29,950	4.1
Rest of World	30,865	4.2
Total	*727,100*	*100.0*

[a]Ref. 119.

Thermoset decorative coatings are by far the largest segment of coating powder production accounting for over 90% of pounds produced. Other market segments are thermoplastic powders, essentially all of which are used in fluidized-bed coating and functional thermoset powders, which find use in the pipe coating, rebar, and electrical insulation markets.

The distribution of coating powder production by resin type for several geographical areas is given in Table 5. The epoxy–polyester hybrid powder coatings account for the largest resin type in both Europe and North America. Increasing market share is mostly at the expense of the 100% epoxy-based powders, as a result of more favorable economics. In Europe, weatherable carboxyl polyesters cured with TGIC are being replaced with carboxyl functional polyesters cured with hydroxylalkylamides, other glycidyl curatives and, to some extent, urethane polyesters. While the hydroxyl functional polyester resins cured with blocked isocyanates or uretdione curatives, that is, urethane polyesters, have a significant market share in the North American market, they are still a relatively small part of the European market.

The vast majority of acrylic powders in both Europe and North America find use in the automotive industry, as clear coats for wheels and bodies and as pigmented coatings in exterior trim, "blackout" coatings, and primer surfacers.

The automotive market is the largest and fastest growing segment of the powder coating market in North America, accounting for over 16% market share, followed by appliance coatings at 15%, architectural at 3%, lawn and garden at 7%, and the balance in general metal finishing.

Test Methods

Methods for evaluating the performance of powder coatings are the same as those used for conventional coatings. Test methods for coating powders include particle size distribution, powder free flow, sintering, fluidization characteristics, and others. They have been reviewed in detail and reported in the literature (120,121). In addition, the American Society for Testing and Materials has issued a comprehensive standard that covers the most important test methods for the evaluation and characterization of powder coatings (122).

Environmental and Energy Considerations

A significant factor contributing to the growth of powder coating processes has been the proliferation of federal, state, and local environmental regulations. Starting with the Clean Air Act of 1970, which defined Hazardous Air Pollutants (HAPs), Volatile Organic Compounds (VOCs), and set standards for nationwide air quality, many additional regulations have since been enacted. In nonattainment areas, localities where pollution levels persistently exceed National Ambient Air Quality Standards, the Best Available Control Technology or Maximum Available Control Technology may be necessary to reduce the level of pollutants to that required. Powder coating installations are generally accepted as meeting these levels of control technology. States are charged with the job of achieving compliance. Permits are required by states where new finishing operations are being added to existing facilities. The presence or absence of VOCs and HAPs in coating materials has become a significant factor in the economic analysis in planning new finishing operations.

Being 100% solid materials, coating powders are essentially free of VOCs and HAPs, with the exception of trace quantities of monomers or, in some cases, solvents used in the manufacture of the raw materials (123). Caprolactam and other compounds used as blocking agents in blocked isocyanate curatives are emitted during curing. Typical levels in formulated urethane coating powders are in the range of 4–6%. While caprolactam is considered a VOC, it is not classified as an HAP. Powder coating remains the process of choice where VOCs must be reduced to the lowest possible levels, as in many OEM and automotive coating operations. Permits for additions to existing paint lines or installation of new systems are much easier to justify and obtain than when most liquid coatings are specified. In addition to the environmental advantages, the low volatile emissions of powder coatings during the baking operation has economic and energy saving advantages. Fewer air changes per hour in the baking oven are required for powder coatings than for solvent-based coatings, which saves fuel. Further, in the coating operation almost all powder is recovered and reused, resulting in higher material utilization and waste minimization. The air used in the coating booths during application is filtered and returned to the workplace atmosphere, reducing heating and cooling demands. Additionally because of the need for more sophisticated devices to control emission of VOCs in liquid systems, the capital investment to install a new powder coating line is becoming increasingly more economically favorable. The savings in material and energy costs of powder coating systems has been documented in a number of studies. An economic analysis worksheet for comparing the cost of operating a powder coating line compared with alternate systems can be found in Technical Brief #21 in Reference 121.

The only components in a coating powder which might cause the waste to be classified as hazardous are certain heavy-metal pigments sometimes used as colorants. Lead- (qv) and cadmium-based pigments (qv) are seldom used, however, and other potentially hazardous elements such as barium, nickel, and chromium are usually in the form of highly insoluble materials that seldom cause the spent powder to be characterized as a hazardous waste (124).

Health and Safety Factors

Any finely divided organic material can form ignitable mixtures when dispersed in air at certain concentrations. The most significant hazard in the manufacture and application of coating powders is the potential of a dust explosion. The severity of a dust explosion is related to the material involved, its particle size, and concentration in air at time of ignition. The *lower explosive limit* (LEL) is the lowest concentration of a material dispersed in air that explodes in a confined space when ignited. The LEL for a number of epoxy and polyester powders was measured and found to be in the range of 0.039–0.085 oz/ft^3 (39–85 g/m^3) (125). In powder coating installations, the design of the spray booth and duct work, if any, should be such that the powder concentration in air is always kept below the LEL employing a wide margin of safety. General safety considerations are detailed in Reference 126. The use of flame detection systems in all automatic powder coating installations is required. These devices must respond within 0.5 s or less to arrest all powder flow in the system. If powder ignition should occur, flame detection sensors shut down the power to the system, halting powder spraying and air flow circulation. Another element of safety for a powder coating system is the design of the booth recovery equipment. Some recovery designs utilized today, such as illustrated in Figure 3, are configured so no external venting is required. However, when traditional cyclones or dust collectors, isolated by ducting, are utilized in the coating system, a pressure relief system is necessary. If these units are not located outside the building or properly vented, explosion suppression may also be required. Furthermore, cyclones and dust collectors located inside the building should be near an outside wall and ductwork from the pressure relief vents should be directed through short runs, not exceeding 3 m when possible. Required explosion vent areas and other design considerations can be found in the literature (127). The spray guns, spray booth, duct work, dust collection and powder reclaim system, as well as the work piece, must be properly grounded (128,129).

The health hazards and risk associated with the use of powder coatings must also be considered. Practical methods to reduce employee exposure to powder such as the use of long sleeved shirts and gloves to prevent skin contact should be observed. Furthermore, exposure can be minimized by good maintenance procedures to monitor and confirm that the spray booth and dust collection systems are operating as designed. Ovens should be properly vented and operated under negative pressure so that any volatiles released during curing, eg, caprolactam, do not enter the workplace atmosphere.

In general, the raw materials used in the manufacture of powder coatings are relatively low in degree of hazard. None of the epoxy, polyester, or acrylic resins normally used in the manufacture of thermoset powder coatings are defined as hazardous materials by the OSHA Hazard Communication Standard. Most pigments and fillers used in powder coatings generally have no hazards other than those associated with particulates. Some epoxy curing agents are skin irritants; however, most of these characteristics are greatly diminished when these materials are compounded into the powder coating. In addition to being diluted, the materials are dispersed in a resinous matrix having a low degree of water solubility which appears to make them less biologically accessible. For example,

anhydrides and anhydride adducts generally elicit a strong respiratory or eye irritant response. However, when powder coatings containing anhydride-based curing agents were tested in animal exposures, the coatings were found to be nonirritating to the skin, eye, and respiratory tract (130,131). Similarly, TGIC is a skin irritant, but formulated powders containing TGIC were found not to be (132). Regulations in Europe require cautionary labeling of powders containing TGIC (see under Polyester–Triglycidylisocyanurate Cured).

Although coating powders do not appear to pose significant hazards to personnel working with them, worker exposure should nevertheless be minimized. Coating powders should be treated as Particulates Not Otherwise Classified having a Threshold Limit Value–Time Weighted Average (TLV–TWA) of 10 mg/m^3 for total particulates (133). The TLV should be maintained primarily through environmental controls. Hoods and proper ventilation should be provided during handling and application of powders. When environmental control of dust cannot be maintained below the TLV, protective equipment such as dust and fumes masks or externally supplied air respirators should be used (134).

BIBLIOGRAPHY

"Fluidized-Bed Coating" in *EPST* 1st ed., Vol. 3, pp. 808–830, by A. H. Landrock, U.S. Department of Defense, Plastics Technical Evaluation Center; "Coating Methods, Powder Coating" in *EPSE* 2nd ed., Vol. 3, pp. 575–601, by D. S. Richart, The Polymer Corp.

1. U.K. Pat. 643,691 (Sept. 27, 1950), P. G. Clements (to Schori Metallising Process, Ltd.).
2. Ger. Pat. 933,019 (Sept. 15, 1955), E. Gemmer (to Knapsack-Griesheim, AG).
3. U.S. Pat. 2,844,489 (July 22, 1958), E. Gemmer (to Knapsack-Griesheim, AG).
4. U.S. Pat. 3,640,747 (Feb 8, 1972), D. S. Richart (to the Polymer Corp.).
5. U.S. Pat. 3,264,271 (Aug. 2, 1966), H. M. Gruber and L. Haag (to the Polymer Corp.).
6. W. E. Wertz and D. S. Richart, in E. J. Wickson, ed., *Handbook of PVC Formulating*, John Wiley & Sons, Inc., New York, 1993, pp. 771–781.
7. U.S. Pat. 3,008,848 (Nov. 14, 1961), R. W. Annonio (to Union Carbide Corp.).
8. D. S. Richart, in M. I. Kohan, ed., *Nylon Plastics Handbook*, Hanser/Gardner Publications, Inc., Munich, 1995, pp. 253–269.
9. T. Glass and J. Depoy, *Paper FC91-384 presented at Finishing '91*, Sept. 23–25, 1991, Cincinnati, Ohio, sponsored by SME Dearborn, Mich.
10. *"Abcite Powder Coating Resins," DuPont Technical Bulletin*, Sept. 1996.
11. WO 98/50475 (Nov. 12, 1998), J. M. McGrath (to 3M Co.).
12. U.S. Pat. 4,770,939 (Sept. 13, 1988), W. Sietsess, T. M. Plantenga, and J. P. Dekerk (to Labofina, S.A.).
13. U.S. Pat. 5,599,874 (Feb. 4, 1997), E. Verwey, L. K. Rijkse, and M. Gillard (to Fina Research, S.A.).
14. U.S. Pat. 5,739,202 (April 14, 1998), R. L. Pecsok.
15. L. C. Stephans, *Materials Performance* **38**(6), 42–47 (1999).
16. R. Domitrz and H. Nowak, *Paint & Coat Ind.* **XVI**(5), 86–94 (May 2000).
17. M. Y. H. Chang, *Paint & Coat. Ind.* **XV**(10), 102–108 (Oct. 1999).
18. P. G. deLange, *J. Coat. Technol.* **56**(717), 23–33 (1984).
19. J. Hajas, H. Juckel, Paper presented at the *Waterborne, Higher-Solids and Powder Coating Symposium*, New Orleans, La., Feb. 10–12, 1999, University of Southern Mississippi, pp. 273–283.
20. M. A. Grolitzer, *Am. Paint & Coat. J.* **75**(46), 74–78 (Apr. 1991).

21. M. Wulf and co-workers, *Prog. Inorg. Coat.* **38**, 59–66 (2000).
22. S. A. Stachowiak, in G. D. Parfitt and A. V. Patsis, eds. *Organic Coatings Science and Technology*, Vol. **5**., Marcel Dekker, Inc., New York, 1982, pp. 67–89.
23. L. K. Johnson and W. T. Sade, *J. Coat. Technol.* **65**(826), 19–26 (1993).
24. T. Misev and E. Belder, *J. Oil Colour Chem. Assoc.* **72**(9), 363–368 (1989).
25. S. Gabriel, *J. Oil Colour Chem Assoc.* **58**, 52–61 (1975).
26. S. G. Yeates and co-workers, *J. Coat. Technol.* **68**(861), 107–114 (1996).
27. R. P. Franiau, *Paint India* **37**(9), 33–38 (1987).
28. Z. Huang, L. E. Scriven, H. T. Harris, and W. Eklund. Paper presented at *Waterborne, Higher-Solids and Powder Coatings Sumposium*, New Orleans, La., Feb. 5–7, 1997, University of Southern Mississippi, pp. 328–340.
29. V. G. Nix and J. S. Dodge, *J. Paint. Technol.* **45**(586), 59–63 (Nov. 1973).
30. J. C. Kenny, T. Ueno, and K. Tsutsui, *J. Coat. Technol.* **68**(855), 35–43 (Apr. 1997).
31. P. R. Horinka, *Ind. Paint & Powder* **71**(12), 26–30 (Dec. 1995).
32. A. J. Pekarik, Paper presented at *Powder Coating 98, Formulation & Production Conference*, Indianapolis, Ind., The Powder Coating Institute, Alexandria, Va., 1998, pp. 103–115.
33. B. E. Maxwell, R. C. Wilson, H. A. Taylor, and D. E. Williams, Paper presented at the 26th *International Conference in Organic Coatings*, Athens, Greece, 2000.
34. D. Fluck, J. Fultz, M. Darsillo, *Paint & Coat. Ind.* **XIV**(10), 214–220 (Oct. 1998).
35. K. Wolny, *"The Hiding Powder of White Powder Coatings," Kronos Technical Bulletin 6.16*, 1985.
36. D. S. Richart, *Powder Coating* **9**(1), 23–30 (Feb. 1998).
37. D. S. Richart, *Polym. Paint Colour J.* **188**(4408), 14–18 (Sept. 1998).
38. U.S. Pat. 4,242,253 (Dec. 30, 1980), M. D. Yallourakis (to E. I. duPont de Nemours & Co., Inc.).
39. U.S. Pat. 3,947,384 (Mar. 30, 1976), F. Schulde and co-workers (to Veba-Chemie AG).
40. U.S. Pat. 3,842,035, (Oct. 15, 1974), C. H. J. Klaren (to Shell Oil Co.).
41. E. Dumain, *Paint & Coatings Ind.* **XV**(9), 52–58 (Sept. 1999).
42. D. P. Chapman, Paper presented at the *18th Annual Waterborne, Higher-Solids and Powder Coating Conference*, New Orleans, La., Feb. 6–8, 1991, University of Southern Mississipi, pp. 339–346.
43. D. Foster, in *Congress Papers Powder Coating Europe 2000* (PCE 2000), Amsterdam, the Netherland (Jan. 19–21, 2000), C. R. Vincentz Verlag, Hanover, Germany, pp. 234–346.
44. U.S. Pat. 3,631,149 (Dec. 28, 1971), H. Gempeler and P. Zuppinger (to Ciba, Ltd.).
45. U.S. Pat. 4,122,060 (Oct. 24, 1978), M. Yallourakis (to E. I. du Pont de Nemours & Co., Inc.).
46. U.S. Pat. 3,477,971 (Nov. 11, 1969), R. Allen and W. L. Lantz (to Shell Oil Co.).
47. R. G. Doone, R. W. Tait, and A. P. Glaze, Paper presented at *Powder Coating '96, Formulation and Production Conference*, The Powder Coating Institute, Alexandria, Va., 1996, pp. 39–44.
48. J. Didas, *Materials Performance* **39**(6), 38–39 (June 2000).
49. Y. Merck, Paper presented at *Powder Coating 2000 Formulators Technology Conference*, The Powder Coating Institute, Alexandria, Va., 2000, pp. 101–120; Private correspondence, Y. Merck, Nov. 2000.
50. C. Bowden, D. Ostrander, and S. Miller, *Metal Finishing* **97**(5), 14–18 (May 1999).
51. R. vander Linde and E. G. Belder, in G. D. Parfitt and A. V. Patsis, eds. *Organic Coatings Science and Technology*, Vol. **5**, Marcel Dekker, Inc., New York, 1983, pp. 55–66.
52. S. P. Pappas, V. D. Kunz, and B. C. Pappas, *J. Coat. Technol*. **63**(796), 39–46 (May 1991).

53. U.S. Pat. 3,792,011 (Feb. 2, 1974), J. D. B. Smith and R. N. Kauffman (to Westinghouse Electric Corp.).
54. G. J. Bocchi, in *Congress Papers PCE 2000*, Amsterdam, the Netherlands, Jan. 19–21, 2000, C.R. Vincentz Verlag, Hanover, Germany, pp. 23–36.
55. U.S. Pat. 4,147,737 (Apr. 3, 1979), A. J. Sein and co-workers (to DSM Resins).
56. Y. Merck, in *Conference Papers "Powder Coatings What's Next*," Birmingham, U.K., Mar. 10, 1999, Paint Research Association, pp. 2–16.
57. R. R. Engelhardt, Paper presented at the *Waterborne, Higher-Solids and Powder Coating Symposium*, New Orleans, La., Feb. 24–26, 1993, University of Southern Mississippi, pp. 549–561.
58. P. Loosen and co-workers, Paper presented at *Powder Coating '96, Formulation and Production Conference*, Sept. 17, 1996, The Powder Coating Institute, Alexandria, Va., pp. 107–115.
59. Y. Merck and co-workers, *Euro. Coat. J.* 18–24 (Dec. 1999).
60. *Threshold Limit Values for Chemical Substances and Physical Agents, 2000 TLV's and BEI's*, American Conference of Governmental Industrial Hygienists (ACGIH), Cincinnati, Ohio.
61. A. Pledger, Paper presented at *Symposium on Powder Coatings*, Birmingham, U.K., Apr. 4–5, 1995, Paint Research Association, 12 pp. Paper 11.
62. EU 0 536 085 A2 (Sept. 24, 1992), J. A. Cotting (to Ciba-Giegy AG).
63. U.S. Pat. 6,114,473 (Sept. 5, 2000), S. Miyake and co-workers (to Nissan Chem. Ind. Ltd.).
64. U.S. Pat. 4,076,917 (Feb. 28, 1978), G. Swift (to Rohm & Haas Co.).
65. K. Wood and D. Hammerton, Paper presented at the *Waterborne, Higher-Solids and Powder Coating Symposium*, New Orleans, La., Feb. 6–8, 1991, University of Southern Mississippi, pp. 78–89.
66. A. Kaplan, Paper presented at the 1st *International Primid Conference*, Mar. 20–21, 1997, Flims Waldhaus, Switzerland, EMS Chimie.
67. M. Wenzler, Paper presented at the 1st *International Primid Conference*, Mar. 20–21, 1997, Flims Waldhaus, Switzerland, EMS Chimie.
68. D. Maetens and co-workers, *Euro. Coat. J.* 26–33 (May 1999).
69. W. Jacobs and co-workers, Paper presented at the *Waterborne, Higher-Solids and Powder Coating Symposium*, New Orleans, La., Feb. 26–28, 1992, University of Southern Mississippi, pp. 196–214.
70. W. Jacobs and co-workers, Paper presented at the *Waterborne, Higher-Solids and Powder Coating Symposium*, New Orleans, La., Feb. 9–11, 1994, University of Southern Mississippi, pp. 629–652.
71. U.S. Pat. 5,695,852, (Dec. 9, 1997), D. S. Richart and C. P. Tarnoski (to Morton Int., Inc.).
72. M. Y. H. Chang, *Paint & Coat. Ind.* **XV**(10), 98–108 (Oct. 1999).
73. H. B. Yokelson and co-workers, *Euro. Coat. J.* 354–369 (May 1998).
74. J. D. Pont, in *Proceedings of the Twenty-Sixth International Waterborne, Higher-Solids and Powder Coating Symposium*, New Orleans, La., Feb. 10–12, 1999, University of Southern Mississippi, pp. 232–245.
75. M. Guida and J. V. Weiss, in *Proceedings of the Twenty-Second International Waterborne, Higher-Solids and Powder Coating Symposium*, New Orleans, La., Feb. 22–24, 1995, University of Southern Mississippi, pp. 43–54.
76. H. U. Meier-Westhues, P. Thometzek, and J. J. Laas, *Farb & Lack*, **103**, 140–146 (Apr. 1997).
77. U.S. Pat. 4,873,274 (Oct. 10, 1989), F. L. Cummings and G. D. Correll (to Morton Thiokol, Inc.).
78. Eur. Pat. 0 509 393 A1 (publ. Apr. 9, 1992), D. Fink and co-workers, (to Hoechst AG).

79. D. K. Moran and M. J. M. Verlaak, Paper presented at the *Waterborne, Higher-Solids and Powder Coating Symposium*, New Orleans, La., Feb. 24–26, 1993, University of Southern Mississippi, pp. 497–507.
80. U.S. Pat. 5,907,020 (May 25, 1999), G. D. Correll and co-workers (to Morton Internation, Inc.).
81. U.S. Pat. 5,763,099 (June 9, 1998), T. A. Misev and co-workers (to DSM N.V.).
82. U.S. Pat. 5,703,198 (Dec. 20, 1997), F. Twigt and R. VanDerLinde (to DSM N.V.).
83. U.S. Pat. 5,639,560 (June 17, 1997), L. Moens and co-workers (to UCB S.A.).
84. U.S. Pat. 5,789,039 (Aug. 4, 1998), K. M. Biller and B. A. MacFadden (to Herberts Powder Coatings, Inc.).
85. R. Jahn and co-workers, in *Congress Papers – Powder Coating Europe 2000* (PCE 2000), Amsterdam, the Netherlands, Jan. 19–21, 2000, C.R. Vincentz Verlag, Hanover, Germany, pp. 309–317.
86. U.S. Pat. 3,561,003 (Feb. 2, 1971), B. J. Lanham and V. G. Hykel (to Magnavox Co.).
87. U.S. Pat. 3,737,401 (June 5, 1973), I. H. Tsou and J. W. Garner (to Grow Corp.).
88. B. Dreher, Paper presented at *XIVth FATIPEC Congress*, Budapest, June 4–9, 1978, pp. 201–207.
89. D. Mielcarek and K. Huber, Paper presented at the *Waterborne, Higher-Solids and Powder Coating Symposium*, New Orleans, La., Feb. 24–26, 1993, University of Southern Mississippi, pp. 525–535.
90. D. Fluck, J. Fultz, and M. Darsillo, *Paint & Coat., Ind.* **XIV**(10), 214–220 (Oct. 1998).
91. M. Giersemehl and G. Plihal, *Powder Handling & Processing* **11**(3) (July/Sept. 1999).
92. U.S. Pat. 5,399,597 (Mar. 21, 1995), F. Mandel, C. Green, and A. Scheibelhoffer (to Ferro Corp.).
93. U.S. Pat. 5,981,696 (Nov. 9, 1999), D. Satweeber and co-workers (to Herberts GmbH).
94. W. Kreis, *Polym. Paint Colour J.* **188**(4411), 22–24 (Dec. 1998).
95. U.S. Pat. 5,379,947 (Jan. 10, 1995), C. F. Williams and M. A. Gessner (to BASF Corp.).
96. M. Gaschke and H. Lauterbach, Paper presented at the *Waterborne, Higher-Solids and Powder Coating Symposium*, New Orleans, La., Mar. 10–12, 1980, University of Southern Mississippi.
97. G. T. Robinson, *Prod. Finish.* **16**, 42–47 (Sept. 1976).
98. V. G. Nix and J. S. Dodge, *J. Paint Technol.* **45**(586), 59 (Nov. 1973).
99. U.S. Pat. 6,113,980 (Sept. 5, 2000), H. S. Laver (to Ciba Specilty Chem. Co.).
100. S. Guscov, *Powder Coating* **11**(4), 22–31 (June 2000).
101. T. Rusk, N. Rajagopalan, and T. C. Lindsay, *Powder Coating* **11**(4), 33–42 (June 2000).
102. G. Stribling, L. Keen, and J. Trostle, in *Conference Proceedings Powder Coating '98*, Indianapolis, Ind., (Sept. 1998), The Powder Coating Institute, Alexandria, Va., pp. 229–248.
103. U.S. Pat. 6,071,348 (June 6, 2000), K. Seitz, M. Hasler, and H. Adams (to Wagner Int. AG).
104. U.S. Pat. 5,776,554 (July 7, 1998), C. R. Merritt and R. M. Thorn (to Illinois Tool Works, Inc.).
105. R. Deane, in *Congress Papers PCE 2000*, Amsterdam, the Netherlands, Jan. 19–21, 2000, C.R. Vincentz Verlag, Hanover, Germany, pp. 331–340.
106. P. R. Horinka, *Powder Coating* **6**(3), 69–75 (June 1995).
107. H. J. Lader, in *Conference Proceedings Powder Coating 94*, Cincinnati, Ohio, Oct. 11–13, 1994, The Powder Coating Institute, Alexandria, Va., pp. 254–267.
108. PCT WO 98/45356 (publ. Oct. 15, 1998), G. Kodokian (to E. I. du Pont de Nemours & Co, Inc.).
109. J. L. Quinn, *Metal Finishing* **96**(4), 10–13 (Apr. 1998).

110. F. Busato, *Congress Papers PCE 2000*, Amsterdam, the Netherlands, Jan. 19–21, 2000, C.R. Vincentz Verlag, Hanover, Germany, pp. 409–417.
111. J. N. Pennington, *Modern Metals* **56**(8), 48–53 (Sept. 2000).
112. L. J. Black, *Metal Finishing* **97**(9), 67–69 (Sept. 1999).
113. U.S. Pat. 5,695,826 (Dec. 9, 1997), E. C. Escallon (to Terronics Development Corp.).
114. Anon, *Ind. Paint & Powder* **75**(1), 20–24 (Jan. 1999).
115. U.S. Pat. 6,080,823 (June 27, 2000), L. Kiriazis (to PPG Ind. Ohio, Inc.).
116. P. H. G. Binda, in *Congress Papers PCE 2000*, Amsterdam, the Netherlands, Jan. 19–21, 2000, C.R. Vincentz Verlag, Hanover, Germany, pp. 377–391.
117. U.S. Pat. 4,243,699 (Jan. 6, 1981), J. E. Gibson.
118. P. Droniau, T. Korner, and J. Kresse, in *Congress Papers PCE 2000*, Amsterdam, the Netherlands, Jan. 19–21, 2000, C.R. Vincentz Verlag, Hanover, Germany, pp. 75–80.
119. Summary Report Worldwide Powder Coating Markets, The Powder Coating Institute, Alexandria, Va., June 2000.
120. E. Bodner, *Euro.Coat. J.* 814–832 (Nov. 1993).
121. N. Liberto, ed. *Powder Coating – The Complete Finishers Handbook*, 2nd ed., The Powder Coating Institute, Alexandria, Va., 1999, Appendix C, pp. 388–403.
122. *ASTM D3451, 1998 Annual Book of ASTM Standards*, Section 6.02, Paints, Related Coatings, and Aromatics, American Society for Testing and Materials, West Conshohocken, Pa.
123. T. Randoux and co-workers, *Euro. Coat. J.* 790–795 (Nov. 1975).
124. *"Toxicity Characteristic Leaching Procedure," Code of Federal Regulations*, 40 CFR, Part 261, Appendix II, Method 1311.
125. P. H. Dobson, *Ind. Fin.* 77–82 (Sept. 1974).
126. D. R. Scarbrough, in *Fire Protection Handbook*, 17th ed., National Fire Protection Association (NFPA), Quincy, Mass., 1989, Chapt. "2–12".
127. *Guide for Explosion Venting*, Code No. 68, NFPA, 1988.
128. *Static Electricity*, Code No. 77, NFPA, 1988.
129. *Spray Finishing Using Flammable and Combustible Materials*, Code No. 38, NFPA, 1989.
130. J. F. Fabries and co-workers, Toxicity of Powder Paints by Inhalation, Report No. 1092/RI, Dept. of Occupational Pathology, Institut National De Recherche ET De Sécurité (INRS), France, 1982.
131. *Power of Six Powder Paints to Cause Irritations and Allergies of the Skin*, INRS, May 1979.
132. *Toxicological Studies of Uralac Powder Coating Resin and Powders*, Scado B. V. (now DSM Resins), Zwolle, the Netherlands, 1979.
133. *Threshold Limit Values Biological Exposure Indices*, American Conference of Governmental Industrial Hygienists (ACGIH), Cincinnati, Ohio.
134. *OSHA Regulations*, 29 CFR, Section 1910.34.

GENERAL REFERENCES

D. A. Bate, *The Science of Powder Coatings, Vol. 1: Chemistry Formulation and Application*, Sita Technology Ltd., London, 1990.
D. A. Bate, *The Science of Powder Coatings, Vol. 2: Applications*, Sita Technology, Ltd., London, 1994.
T. Misev, *Powder Coatings – Chemistry and Technology*, John Wiley & Sons, Inc., New York, 1991.
H. Jilek, *Powder Coatings*, Fedaration of Societies for Coating and Technology, Blue Bell, Pa., 1991.

D. S. Richart, in. J. I. Kroschwitz, ed., *Encyclopedia of Chemical Technology*, 4th ed., Vol. **6**, John Wiley & Sons, Inc., New York, 1993, pp. 635–661.
N. P. Liberto, ed., *Powder Coating – The Complete Finishers Handbook*, 2nd ed., The Powder Coating Institute, Alexandria, Va., 1999.
D. Howell, *The Technology, Formulation and Application of Powder Coatings*, Vol. **1**, Sita Technology Ltd., London, 2000.

DOUGLAS S. RICHART
D.S. Richart Associates

COATING METHODS, SURVEY. See Volume 1.

COATINGS. See Volume 1.

COEXTRUSION. See Volume 2.

COLLAGEN

Introduction

Collagen is the most abundant animal protein, It is the principal protein component of all connective tissues, including skin, bone, tendon, and cartilage. All collagens play a structural and/or functional role in the extracellular matrix. As a polymer, each collagen chain has a precise, genetically determined molecular size, which may be further modified after biosynthesis by a range of secondary modification processes. Collagens are widely distributed throughout the animal kingdom, being found even in primitive species. At present, 21 distinct collagen types have been identified in humans. These vary in tissue distribution, and in the length of the triple helix and the presence of non-triple-helical interruptions. All are characterized by the triple-helical structure, which leads to a repeating Gly-X-Y amino acid sequence. This repeating motif is also found in certain other proteins from animals and bacteria, but these are not considered as collagen types as they do not have roles in the extracellular matrix.

Collagen can be commercially produced from a range of sources, with mammalian skins derived as a by-product of the food processing industry being the principal source. Various processes and modification reactions have been used to give a wide range of products. Recently, recombinant methods for collagen production have been described that may prove to be of value in the future for special applications.

Historically, collagen has been an important polymer, as it is the basis of leather and gelatin production, processes that span back several millennia. Collagen is the naturally occurring, triple-helical protein, whereas gelatin is its heat-denatured product that has distinct properties. Gelation of gelatin involves re-forming of the triple helix, but not in the same ordered phase or arrangement

Encyclopedia of Polymer Science and Technology. Copyright John Wiley & Sons, Inc. All rights reserved.

as in native collagen. Current knowledge of the complexity of the protein structure, composition, and biosynthesis has emerged principally over the last 75 years, where economically significant applications of the protein initially drove research. Most recently, studies on applications in various medical fields have proved to be of importance. An understanding of how mutations in collagen can lead to disease has also been critical in providing an understanding of this protein.

Role in the Extracellular Matrix. Collagen plays a critical and complex role in the extracellular matrix (ECM) of all connective tissues. The ECM comprises many components, including insoluble fibers, fibrils, and many different soluble proteins and glycoproteins. Other noncollagen components include various proteoglycans, hyaluronan, elastin, fibronectin, laminin, and numerous other specialized components. The main roles of the ECM are to provide tissues with their specific mechanical and physiochemical properties, and to provide a molecular scaffold with specific recognition and signaling motifs for cell attachment and migration. Although these roles are readily identified, the mechanism by which they are achieved are less obvious and the cellular regulation of biosynthesis and the control of the precise tissue organization remain poorly understood. Although individual collagen molecules may contain information that aids in self-assembly of aggregate structures, cellular interactions with the ECM strongly suggest that cells are playing the dominant role in orchestrating the complex *in vivo* assembly of tissues. Collagen, while clearly fulfilling a structural role, has now been shown to possess numerous binding sites that interact with many other molecules and cell receptors (1).

Structure

The characteristic feature of all collagens is the triple-helical structure, in which three individual polypeptide chains are wound in a coiled-coil, rope-like manner (Fig. 1). Each individual chain forms a left-handed, polyproline II like coil and these are then twisted in a right-handed manner to form the supercoiled triple-helical structure (2). The initial proposal for the triple helix motif by Ramachandran and Kartha (3) was refined by Rich and Crick (4) to eliminate certain stereochemical restrictions. This led to the proposal of two further models (RC I and RC II) that differed in their hydrogen bonding arrangements, both based on models of poly(glycine) with an additional rope twist. Subsequently, quantitative X-ray fiber diffraction data gave a detailed value for the unit twist of the molecular helix of 107.1°, which is close to that expected, 108°, for a helix with 10 units in 3 turns (5). However, there is no specific reason why a helix with a simple relationship should be formed. Later, a fiber diffraction structure of triple-helical $(Gly\text{-}Pro\text{-}Pro)_{10}$ suggested that the helical pitch may be 7/2 (6). Most recently, high resolution structures for the collagen triple helix, based on X-ray diffraction of crystals of other collagen peptides, have suggested that the 7/2 helix may be restricted to regions of very high imino acid content, whereas over the other parts of the molecule where various amino acids occupy the X- and Y-positions a 10/3 helix is present (7,8) (Fig. 2). Variations in symmetry could be important in maintaining spatial relationships between adjacent collagen molecules and in defining

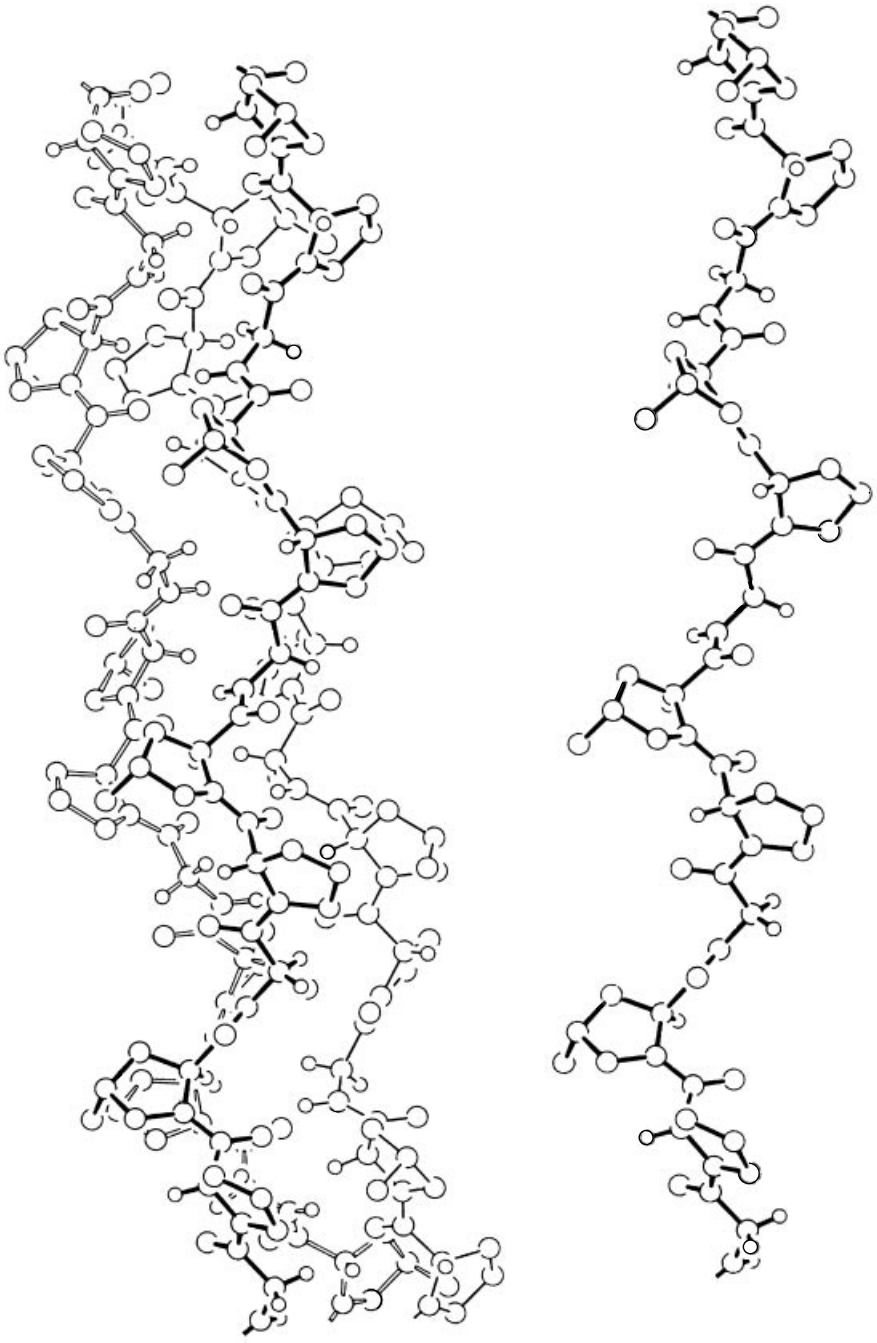

Fig. 1. The chain conformation of the collagen molecule, showing a single chain and a triple helix. Obtained through a linked atom, least-squares refinement of X-ray data obtained from dried kangaroo tail tendon. Hydrogen atoms not attached to the main chain have been omitted. From Ref. 5 with permission.

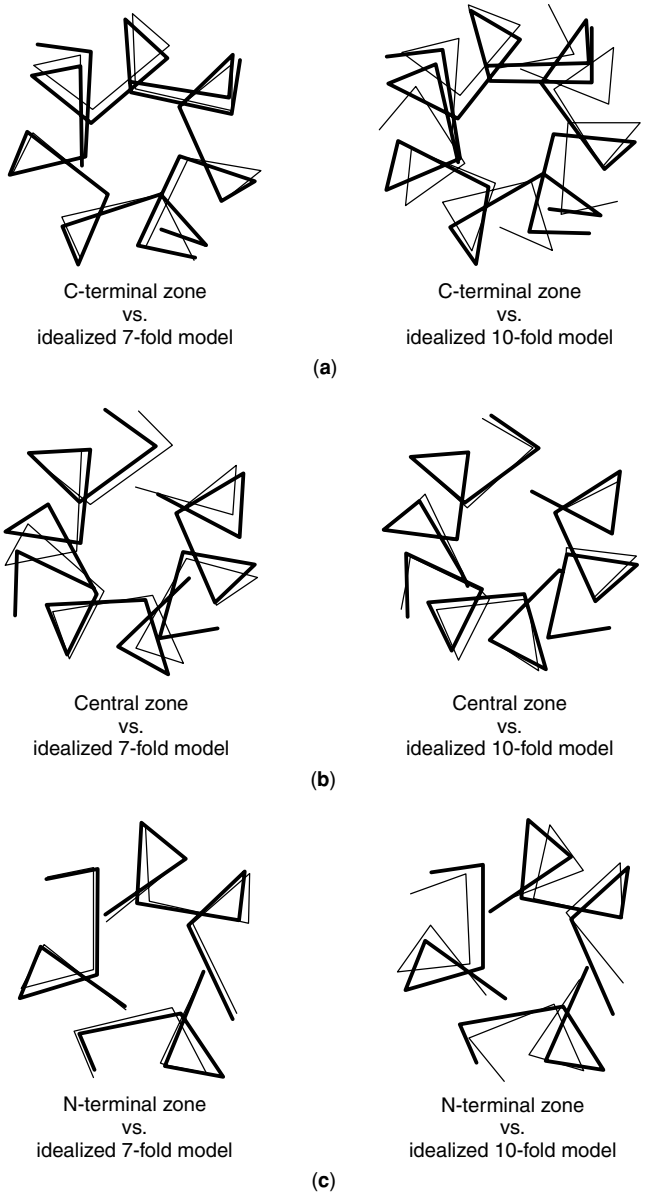

Fig. 2. Alpha carbon traces for the collagen-like peptide T3-785 (thick lines) superimposed on idealized models of 7/2 and 10/3 symmetry (thin lines), showing the variation in helical symmetry in different regions along this peptide. The central zone lacks imino acids while the terminal zones have a high imino acid content as they are Gly-Pro-Hyp repeats. From Ref. 8 with permission.

functional domains along the helix. These crystal structure data also confirmed the hydrogen bonding predicted by the RC II model. Thus, the NH of the Gly is hydrogen bonded to the C=O of the residue in the X-position along the chain through an interceding water molecule (7,9).

The triple-helical structure leads to constraints on the amino acid sequence, as every third residue is located in the close-packed center of this triple helix (5,7). Steric constraints mean that only glycine (Gly), which lacks a β-carbon atom, is small enough to fit, leading to a characteristic repeating Gly-X-Y amino acid sequence in the polypeptide chain (2). The X- and Y-positions are well exposed to solvent, with the X-position being more accessible than the Y-position (10). Either position can be occupied by any amino acid, although Gly and the aromatic amino acids tyrosine and tryptophan are rarely found. Some amino acids show a distinct preference for one position. For example, arginine is most frequently found in the Y-position, where it may provide a stabilizing influence; Phe and Leu are found preferentially in the X-position (11). Modeling studies have suggested potential electrostatic, hydrogen bonding, and steric reasons to account for these observed preferences. Overall, the imino acids proline (Pro) in the X-position and hydroxyproline (Hyp) in the Y-position are the most frequently observed, as they are critical for stabilizing the polyproline II like helix; these residues account for about 20% of the composition (11). The Hyp residues are derived from Pro by secondary modification during biosynthesis, and represent another characteristic of collagen or collagen-like sequences. The Hyp residues are more effective than Pro residues in contributing to the stability of the triple helix, although the mechanism for this observed effect is still not clear. On the one hand, it has been suggested that they contribute to stability through a hydrogen bond network that involves tightly bound water molecules. While the water molecules may or may not be important in stabilization, X-ray evidence indicates that they are an intrinsic part of the triple-helical structure (7–9). Alternatively, it has been suggested that the Hyp residues stabilize the triple helix through inductive and stereoelectronic effects (12). However, it has also been suggested that the stereochemical preferences of Pro and it analogues, such as Hyp, may be sufficient to account for the stabilization provided by Hyp (13).

The triple-helical structure has also been identified in a range of other proteins, such as macrophage scavenger receptor, mannose-binding protein, and C1q, most of which play a role in host defence mechanisms. In these cases, the triple-helical domain often exhibits ligand binding, which is key to the function of the protein (14).

Genetic Diversity and Occurrence

It was only around 1970 that it was realized that there was more than one collagen type. Thus, it was initially found that chick sternal cartilage contained a distinct collagen, termed type II (15). Shortly after, a third collagen, type III, was extracted from skin and aorta (16) and has subsequently been shown to be present in a large number of extensible tissues. Now, at least 21 distinct collagen types have been described (Table 1); however, with the completion of the human genome it is likely that this list will shortly be complete.

Each distinct collagen type has a specific chain composition, with its component chains only being found together in that particular collagen type. In some cases, the collagens are homotrimers with three identical chains, for example in type II or III collagens, whereas in other cases the collagen molecule is a heterotrimer. This can be with either two chain types, as for type I collagen, where

Table 1. Genetically Distinct Collagen Types

Type	Chain(s)	Chromosome	Molecular forms	Distribution and features
I	α1(I) α2(I)	17q21.3-q22 7q21.3-q22	[αl(I)]$_2\alpha$2(I)	Very widespread and most abundant collagen, being the main constituent of major fiber bundles, particularly in dermis, bone, ligament, and tendon
			[α1(I)]$_3$	Appears to be a minor form, found in dermis and dentin
II	αl(II)	12q13-q14	[αl(II)]$_3$	The main collagen of cartilage, where it forms the main, thin fibrils. Also found in intervertebral disk
III	αl(III)	2q24.3-q31	[αl(III)]$_3$	Often with type I, in extensible tissues such as blood vessels, dermis, and intestine. More abundant in foetal tissues
IV	αl(IV)	13q34		Located in basement membranes, with different chain combinations being associated with specific tissues
			[αl(IV)]$_2\alpha$2(IV)	Lens capsule, kidney glomerulus, aorta, bladder, etc
	α2(IV)	13q34	α3(IV)α4(IV)α5(IV)	Lung alveoli, kidney glomerulus
	α3(IV)	2q35-q37	[α5(IV)]$_2\alpha$6(IV)	Epidermis, SMC of aorta and bladder, prostate, developing intestine, colorectal mucosa
	α4(IV)	2q35-q37	[α3(IV)]$_2\alpha$4(IV)	Kidney glomerulus
	α5(IV)	Xq22	[αl(IV)]$_2\alpha$6(IV)	Seminiferous tubule
	α6(IV)	Xq22	[α3(IV)]$_2\alpha$6(IV)	Seminiferous tubule
V	αl(V)	9q34.2-q34.3	[αl(V)]$_3$	Widespread in low quantity; appears associated with type I collagen fibrils, where it may form a core filament
	α2(V)	2q24.3-q31	[αl(V)]$_2\alpha$2(V)	
	α3(V)	19p13.2	αl(V)α2(V)α3(V)	
VI	αl(VI)	21q22.3	αl(VI)α2(VI)α3(VI)	Widespread beaded filaments. Alternative spliced forms
	α2(VI)	21q22.3		
	α3(VI)	2q37		
VII	αl(VII)	3p21	[αl(VII)]$_3$	Forms anchoring filament structure that links the epithelial basement membrane to underlying fibrillar tissue
VIII	αl(VIII)	3q12-q13.1	(?)	Associated with endothelial cell layers, such as Descemet's membrane. In some tissues it forms a hexagonal lattice
	α2(VIII)	1p32.3-p34.3		

IX	αl(IX)	6q12-q14	αl(IX)α2(IX)α3(IX)	Found in cartilage and vitreous body, where it is associated with type II collagen. Can contain a GAG chain
	α2(IX)	1p32		
	α3(IX)	20q13.3		
X	αl(X)	6q21-q22	$[\alpha l(X)]_3$	A short-chain collagen, found in hypertrophic mineralizing cartilage, with a similar structure to type VIII collagen
XI	α1(XI)	1p21	α(XI)α2(Xl)α3(XI)	Forms fibrils that are associated with type II collagen in cartilage and intervertebral disc
	α2(XI)	6p21.2		
	α3(XI)	12q13-q14		
XII	αl(XII)	6q12-q13	$[\alpha l(XII)]_3$	A collagen with an interrupted triple helix associated with type I collagen fibrils
XIII	αl(XIII)	10q22	(?)	Appears to be widespread in low quantity, showing different forms because of a complex pattern of alternative splicing
XIV	αl(XIV)	8q23	$[\alpha l(XIV)]_3$	A fibril-associated collagen with an interrupted triple helix found in skin
XV	αl(XV)	9q21-q22	(?)	Is expressed in fibroblasts and smooth muscle cells; has a triple helix that is interrupted in several places
XVI	αl(XVI)	1p34-p35	(?)	Is expressed in fibroblasts and keratinocytes; has a triple helix that is interrupted in several places
XVII	αl(XVII)	10q24.3	(?)	Bullous pemphigoid antigen. At dermal–epidermal junction
XVIII	α1(XVIII)	21q22.3	(?)	Is expressed in highly vascularized tissues; has a triple helix that is interrupted in several places
XIX	α1(XIX)	6q12-q14	(?)	
XX	α1(XX)		(?)	
XXI	α1(XXI)	6p11.2–12.3	(?)	Expressed in tissues such as heart, stomach, kidney skeletal muscle, and placenta

(?)Indicates that the chain composition has note yet been determined.

Table 2. Amino Acid Compositions for Various Collagen Chains[a]

	α1(I)	α2(I)	α1(II)	α1(III)	α1(IV)	α1(VI)	α1(VII)	α1(X)
Hyp	117	113	93	144	219	34	159	74
Asp	34	33	26	28	58	71	145	12
Asn	11	12	25	24	16	28	27	13
Thr	17	22	20	15	43	39	131	24
Ser	39	30	32	45	70	52	166	26
Glu	49	55	45	48	68	68	187	22
Gln	30	42	22	26	73	40	105	22
Gly	347	351	352	367	477	156	626	174
Ala	122	106	106	94	53	72	189	36
Pro	123	115	109	96	104	56	267	69
Cys	0	0	0	2	20	19	16	1
Val	20	19	40	15	50	65	200	24
Met	7	11	5	9	30	10	17	10
Ile	7	12	17	15	58	42	55	26
Leu	21	28	33	22	84	66	207	29
Phe	15	14	13	8	46	33	39	14
Tyr	4	2	5	5	18	28	36	21
His	3	2	13	7	14	14	28	9
Lys	38	39	31	39	93	54	93	35
Arg	53	54	55	48	43	59	216	19
Trp	0	0	0	0	5	3	19	2
Residues (total)	1057	1060	1042	1057	1642	1009	2928	662
Residues (triple helix)	1014	1014	1014	1029	1268	336	1531	463

[a]Data were calculated from the amino acid sequences reported in SWISSPROT [http://www.expasy.ch/sprot/]. It has been assumed that Pro residues in the Y-position in the Gly-X-Y repeating sequence were all substantially present as 4-Hyp. Hyl and 3-Hyp are also present in small amounts in certain collagens, as determined by chemical analysis, but are not reported in this table.

the two chains are also always in the same ratio, or three different chains, as in collagen VI. Furthermore, for some collagens, for example type IV collagen, a range of different chains is found and the specific combination found is tissue-specific (17) (Table 1).

All chains are characterized by the repeating Gly-X-Y sequence motif, with the high Gly and imino acid (Pro, Hyp) content that arises from the structural constraints (2). Examination of the amino acid compositions of the chains (Table 2) shows that, although Gly content is high, it generally does not exceed the one-third ratio required by the structure, indicating that it is rarely found in the X- or Y- positions (11). In addition, there is a relatively high proportion of charged residues, consistent with the absence of a hydrophobic core as found in globular proteins. There is an excess of Lys and Arg residues compared to Asp and Glu residues, leading to a basic pI value of about 9. Typically, residues such as Trp and Cys are rarely found. A striking characteristic of collagens is the nature and extent of secondary modifications that are present. As noted above, the Hyp residues play an important role in collagen stabilization. In mammalian species, essentially every Pro in the Y-position is converted to 4-Hyp, whereas in organisms that are more primitive this is not the case. The extent of hydroxylation

provides adequate stability to meet the environmental temperature of the species (18), although the melting temperature of the collagen may be slightly lower than this (body) temperature and may vary, for example in fish, when adaptation to a higher temperature takes place. There is also a very low amount of 3-Hyp. This is found in certain chains but only in the X-position, where it is followed by a 4-Hyp in the Y-position. The other significant modification is that of Lys residues, which can be converted to hydroxylysine (Hyl) by the enzyme lysyl hydroxylase. Hyl, like Hyp, is a characteristic marker for collagens.

The lengths of individual collagen chains vary with collagen type (19,20) (Fig. 3, Table 2). Thus, the predominant collagens, type I, II, and III, termed the interstitial collagens (along with type V and XI), all have a triple-helical domain of just over 1000 residues, with short non-triple-helical domain telopeptides, that remain after the loss of propeptide domains. While type IV and VII collagens are both longer (Table 2), most collagens have shorter triple-helical segments. In some collagens, the Gly-X-Y repeat is not continuous and non-triple-helical inserts of various lengths may be present. These interruptions can be as short as a single residue, giving sequences such as -GXYGXGXY-, whereas in other cases much larger interruptions are present. The number of interruptions is also very variable between collagen types. In addition, most mature collagens retain globular domains at either or both the N- and C-terminal regions (19,20) (Fig. 3).

Each collagen type has a characteristic tissue distribution. Thus, while type I collagen is by far the most abundant, other minor collagens may be the dominant component in a specific tissue location. For example, type II collagen is the major collagen in articular cartilage, while type IV collagen plays a critical role in all basal lamina. Most collagens, such as type III collagen, are not found exclusively in a single tissue but are rather found in combination with other collagens. In particular, one group, the fibril-associated collagens with interrupted triple helices (FACIT) collagens are found associated with the interstitial collagens (27). When a particular collagen type, with its constant chain composition, is found in different tissues, it may still vary in the extent of the secondary modification that is present.

Biosynthesis and Catabolism

The majority of data on the biosynthesis and catabolism of collagens has been derived from studies on the most abundant, interstitial collagens, particularly type I collagen, but it is generally believed that most processes will be common to all collagen types (30). Overall, it is a complex process, being similar to the pattern of assembly of other multisubunit proteins, but is characterized by the involvement of a large number of specific intracellular and extracellular post-translational modification reactions (Fig. 4).

Transcription and Translation. There are at least 40 distinct genes coding for different types of collagen chains, and these are located on 15 different chromosomes, with very few of the genes in close proximity (Table 1). Transcription and mRNA processing follow the typical processes, involving 3′- and 5′-capping and 5′-methylation. This is followed by the excision of the noncoding intronic sequences. Collagen genes are composed of many intron/exon domains, requiring extensive splicing; for example, the α1(I) chain has more than 50 exons. Alternative splicing

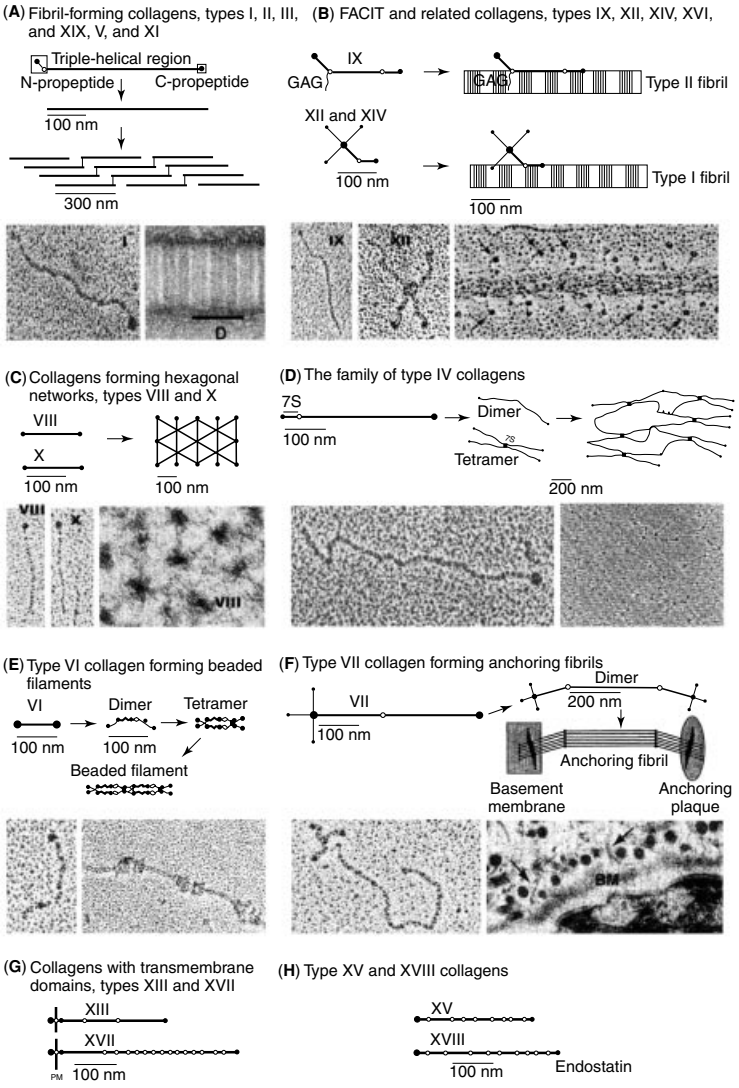

Fig. 3. Schematic illustrations of the variations in the shapes, forms, and packing of various collagen types, representing the eight classes of collagen. Closed circles indicate N- and C-terminal noncollagenous domains while open circles indicate noncollagenous domains that interrupt the triple-helical domains. GAG is glycosamino glycan and PM is plasma membrane. The assembly of groups G and H is not known. Modified from Ref. 20 with permission. Images of collagen molecules by rotary shadowing (unless stated) are included as follows: procollagen I from Ref. 21; TEM of a collagen fibril (negative staining) showing the D-period repeat, courtesy of Jacinta F. White; Type XI collagen from Ref. 22; Type XII collagen from Ref. 23; Type IX collagen decorating a type II collagen fibril, from Ref. 24; Type VIII collagen, from Ref. 25; Type X collagen, from Ref. 26; TEM of the hexagonal packing of type VIII collagen, from Ref. 27; Monomeric type IV collagen, from Ref. 22; Type IV collagen forming an interlocking network, from 28; monmeric type VI collagen, from Ref. 22; beaded filament of type VI collagen, from Ref. 27; monomeric type VII collagen, from 29; TEM showing anchoring filaments (arrows) of type VII collagen at the dermal epidermal junction, from Ref. 24; all with permission. Few published images are available for other collagen types (groups G and H).

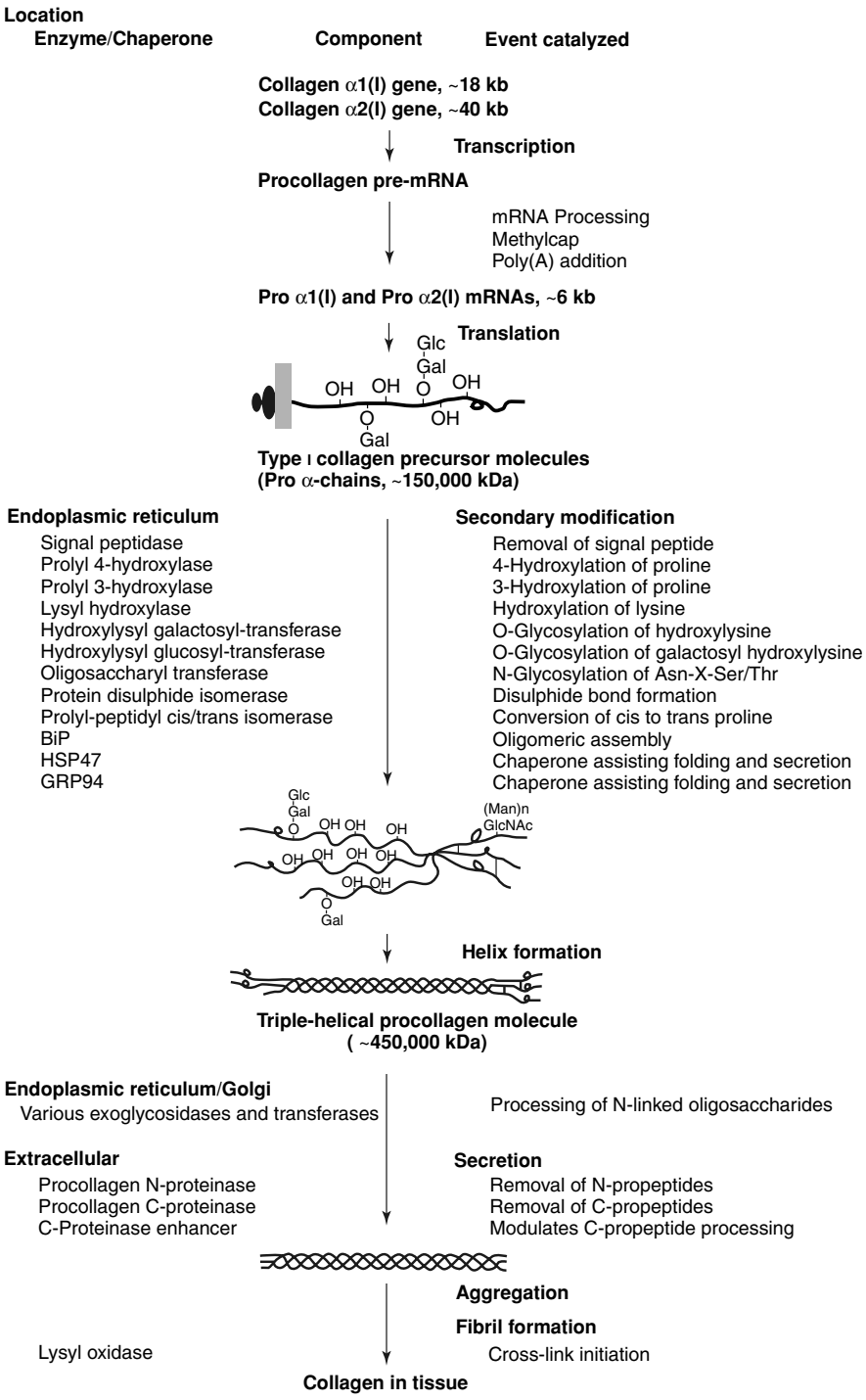

Fig. 4. The pathway for collagen biosynthesis, illustrating the major intermediates in interstitial collagen production, the main steps, and the key enzymes involved in the process. Modified from Ref. 31 with permission.

is found for some collagen types by which numerous variants can be produced. The subsequent translation products are directed into the endoplasmic reticulum (ER). This is directed by a hydrophobic N-terminal signal sequence that interacts with a signal recognition particle that binds to an ER-docking protein; release of the particle is followed by further translation. Signal peptide cleavage is achieved by a membrane peptidase (19) (Fig. 4). The product is a procollagen chain, which includes pro-domains as well as the helical domain.

Post-Translational Modifications. A wide range of intracellular modifications take place within the ER (19). The specific hydroxylation of certain Pro and Lys residues is characteristic of collagens. Lysyl hydroxylase, prolyl-4-hydroxylase, and prolyl-3-hydroxylase are similar in that they all require Fe^{2+}, 2-oxoglutarate, O_2, and ascorbate for activity (32), but differ in structure. Lysyl hydroxylase and prolyl-4-hydroxylase act on X-Lys-Gly and X-Pro-Gly sequences, while prolyl-3-hydroxylase acts on certain Pro-4-Hyp-Gly sequences. The presence of 4-Hyp is essential for the stability of the resulting collagen (33). The prolyl-4-hydroxylase is an $\alpha_2\beta_2$ tetramer, where the β-chains as a dimer also contain the independent protein disulphide isomerase activity that is important during protein, including collagen, synthesis. An alternate form of lysyl hydroxylase acts on the telopeptides. Certain Hyl residues in the helical domain are subject to further modification by glycosylation by two specific glycosidases. The first adds galactose to certain Hyl residues, the second may then add glucose to galactosyl-Hyl (34) (Fig. 4). All these enzyme modifications can only occur on the individual collagen chains before their folding into a triple helix. Asparagine N-linked glycosylation, as mannose oligosaccharide, is also present, found in the C-propeptide domain of interstitial collagens (19).

Procollagen Assembly. In cells that may be producing more than one collagen type, appropriate chain recognition and assembly are key steps in the formation of correct functional collagens. A variety of processes, including recognition at the C-terminal domains, may be involved (19). For almost all collagens, the initial interaction prior to triple helix formation is between C-propeptide domains. Folded propeptide domains are stabilized by intrachain disulphide bonds prior to trimeric association, which is followed by further interchain disulphide bond formation, all catalyzed by protein disulphide isomerase. The folding of the helical domain follows. The effectiveness and stability of this process requires Hyp formation prior to nucleation as the key step; the presence of the propeptide is not essential for nucleation. Efficient triple helix formation then requires acceleration of the rate-limiting isomerization of Pro residues to the trans form required for folding by the enzyme prolyl isomerase. The helix folding rate confirms that this isomerization process is rate-limiting (35). The overall process of folding is complex and involves the interaction of various molecular chaperones, such as HSP47 (19).

Secretion and Extracellular Processing. The secretion pathway for procollagen in part mirrors that for other extracellular proteins. Folded procollagen molecules are transported from the ER through the Golgi complex and are packaged into secretory vacuoles that release collagen from the cell surface by endocytosis. During this step, or after secretion, the interstitial procollagens are further processed by removal of the propeptide domains by specific N- and C-procollagen proteases. For other collagens, including type V collagen, pro-domains

are generally retained. For the major interstitial collagens the C-propeptide seems to be always removed, but the N-propeptide may remain, possibly to control fibril growth. Thus, quantitation of C-propeptide has been used as a measure of collagen synthesis, for example in disease states where collagen production may be altered.

Fibrillogenesis. The processes by which functional fibrils in tissues are formed from procollagen are not well understood. There is now evidence from electron microscopy that suggests that the nucleation steps that initiate fibril formation may occur within cell surface crypts (36), and that nonstaggered aggregates may be involved in this process (37), although it is possible that nucleation may occur in the matrix further from the cell.

Various *in vitro* studies on fibril formation, many utilizing pepsin- or acid-soluble collagen extracted from tissue, have identified different phases in fibril growth, including nucleation during a lag phase followed by a growth phase. These data indicated the importance of the telopeptides in fibrillogenesis (38). Subsequently, it has been suggested that the C-telopeptide binds to a specific region of a collagen fibril during the addition of new collagen molecules (39). However, probably the most significant information has been obtained from *in vitro* studies in which fibrils are formed from either pN-, pC-, or intact procollagen by addition of the specific N- and C-proteases (40). This approach leads to the formation of fibril-like moieties, but with a distinct needle-like morphology, that have the characteristic collagen D-periodic banding pattern (Fig. 3). Those formed by cleavage of pC-collagen by C-propeptidase were exclusively bipolar (41), showing a single polarity reversal in the banding pattern, and having collagen molecules oriented with amino-termini at both ends of the fibrils. The tips were not symmetric, with initial growth occurring preferentially at the sharp (α-) end compared to the blunt (β-) end.

Newly formed fibrils with characteristic D-periodicity (Fig. 5) have been isolated from various embryonic and wound repair tissues (42–44). These fibrils also

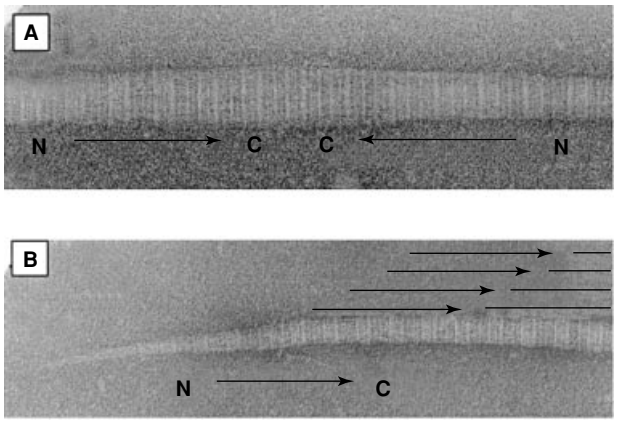

Fig. 5. TEM (negative staining) of a 9-μm fibril from 14-day wound healing tissue showing (**A**) a polarity reversal, and (**B**) a tapered end, with a schematic to illustrate the staggered overlap of individual molecules. Modified from Ref. 44 with permission.

frequently show a single polarity reversal (Fig. 5), particularly if gentle extraction methods are used (44,45), and those showing a reversal have amino-termini at both ends of these fibrils. In some cases, the regions of polarity reversal appeared to be locations where two fibril tips had come together axially. These *in vivo* derived fibrils also have distinct tapers at each end (Fig. 5), although the asymmetry observed *in vitro* is not always seen with *in vivo* samples (44). The mechanism of how these initial fibrils would grow into larger fibrils is not clear. Data suggests, perhaps, that formation of longer fibrils may occur by the fusion of small (1–10 μm) segments (42). If many small fibrils were able to axially associate, larger fibrils with multiple polarity reversals along the length would form; these, however, have not been observed. Indeed, the data on newly formed, immature fibrils contrast with those from mature tissues where polarity reversals are not observed. Lateral association of long or short fibrils provides another mechanism that may lead to thicker fibrils. Evidence suggests that this does not take place immediately, but does so later as the tissue matures (46).

In tendon, collagen type I is almost exclusively found. However, in other tissues, such as the wound repair tissue and those that are extensible, type III collagen can be a significant component along with type I collagen (47). It was of interest that immunoelectron microscopy showed that all fibrils, even at this early stage in fibril formation, were heterotypic, containing both type I and type III collagens (44). It has been suggested that other collagen types, notably type V collagen, may also be present in newly forming fibrils where they may act as a core filament. Immunoelectron microscopy has also shown the presence of type III pN-collagen in embryonic tissues, suggesting that that the N-propeptide may have a role in regulating fibril growth (48). A range of other molecules, including the small proteoglycans decorin and lumican, have also been proposed as being important in the control of fibril growth, as has hyaluronan, which is also present in large amounts in developing connective tissues (42,49). Fibrils extracted from different tissues suggest that the detailed mechanism may also be dependent on the site and function of the particular tissue. The development of knockout mice, where specific molecules that may have a role in fibril development have been deleted, should enable the role of these other molecules to be better defined.

Cross-Linking. Cross-linking is a key element in the formation of functional tissues as it provides the strength to tissues. In normal tissues, little soluble collagen can be extracted, even from young or embryonic tissues, as cross-linking occurs rapidly and provides an extensive network between all collagen molecules. The process is very specific, and is best understood for interstitial collagens (50); the extent, if any, of cross-links involving other collagen types is generally not defined.

Cross-linking is initiated by the formation of allysine and/or hydroxyallysine from specific Lys residues in the telopeptides of the interstitial collagens (Fig. 6). This step requires the action of the specific enzyme, lysyl oxidase. These aldehydes may then form initial bifunctional cross-links, termed reducible cross-links as they can be reduced by sodium borohydride. These are either aldol condensation products or aldimine or ketoamine links. The aldimine and ketoamine involve specific Lys or Hyl residues either from the telopeptides or from the helical domain of the collagen. The sites of these specific residues have been determined (Fig. 6) (50).

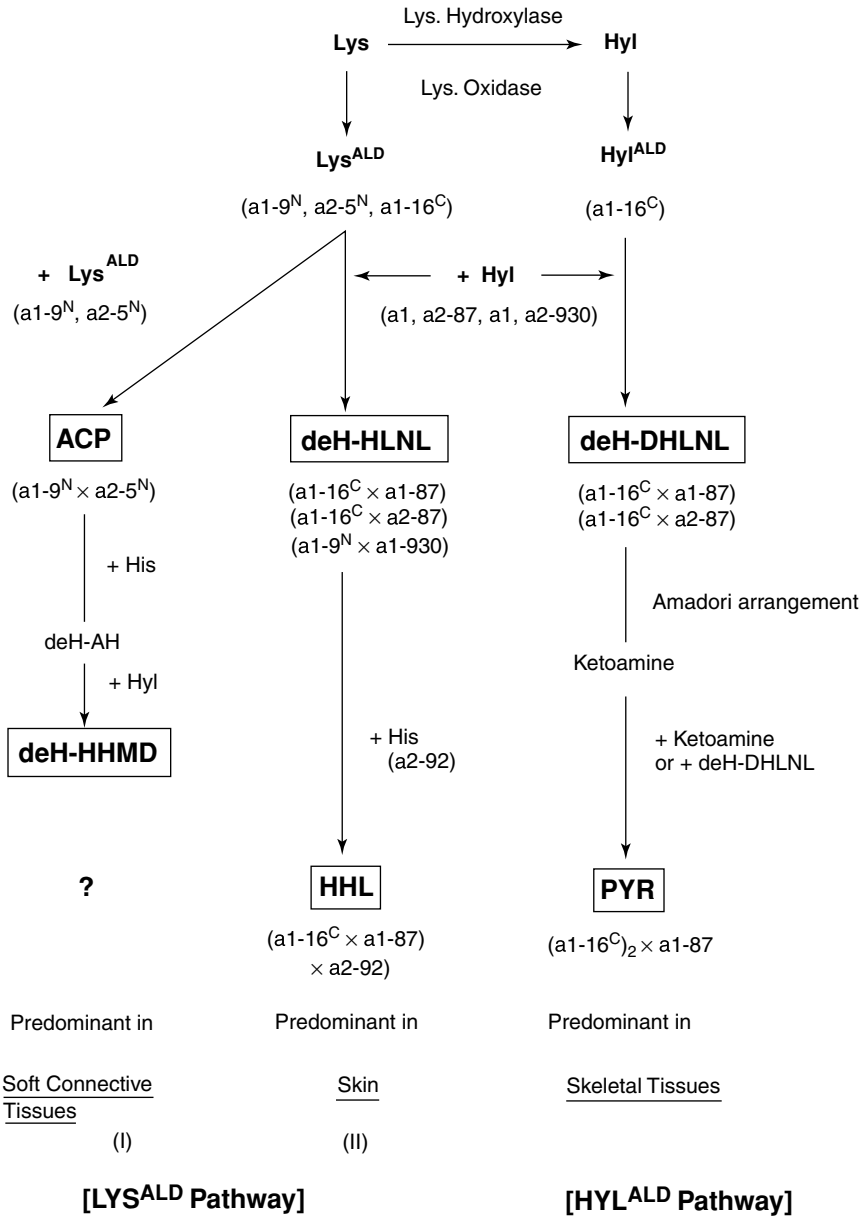

Fig. 6. The major cross-linking pathways for type I collagen. The numbers in parentheses indicate the residues involved in the cross-links, with subscripts N or C indicating telopeptide locations. Abbreviations: Lys, lysine; Hyl, hydroxylysine; LysALD, 5-amino-5-carboxypentanal (allysine); HylALD, 2-hydroxy-5-amino-5-carboxypentanal (hydroxyallysine); ACP, aldol condensation product; deH-HLNL, dehydro-hydroxylysinonorleucine; deH-DHLNL, dehydro-dihydroxylysinonorleucine; deH-HHMD, dehydro-histidinohydroxymerodesmosine; HHL, histidinohydroxylysinonorleucine; PYR pyridinoline. From Ref. 50 with permission.

As tissue ages, these initial cross-links decline in quantity as they are converted into other, more complex mature cross-links. These multifunctional cross-links are key to providing strength and stability to tissues. Despite their importance, however, the determined structures are limited (Fig. 6) and other structures may also be present. For some cross-links, such as histidinohydroxylysinonorleucine and pyridinoline, the structures are well defined and the paths to their formation well understood (Fig. 6). For others, the information is not as complete. The types and extent of cross-links vary between tissues in a specific manner (50). Finally, in addition to these specific cross-links, as tissue ages it may accumulate a range of additional cross-links that form because of nonenzymatic glycosylation of collagen (51).

Fibril and Tissue Structure. The fibrils formed by interstitial collagens have a characteristic banded pattern in electron microscopy with a repeat, the D-period, of about 65–67 nm, equivalent to about 234 amino acids (52) (Fig. 5). The individual collagen molecules are arranged in a staggered overlap structure. As each individual molecule is about 280 nm long, or 4.4 D-periods, there is a gap between the end of one molecule and the beginning of the next (Fig. 5). It is the differential stain uptake between the gap and overlap regions that gives the banding pattern in the electron microscope (52). X-ray fiber diffraction shows that the D-period repeat in tendon is 67 nm, whereas for skin and other extensible tissues it is about 65 nm, suggesting that differences in molecular packing may be present (53). Closer examination of stained fibrils shows that there is a fine structure present. This arises from the distribution of charged amino acids. Other ordered aggregates can be formed from collagen solutions—fibrous-long-spacing (FLS) and segment-long-spacing (SLS) forms—that are not found *in vivo* (52). Other collagen types show a wide range of structures. For example, the FACIT collagens associate with the interstitial collagen on the surface of the fibrils (Fig. 3). Other collagens, types IV, VI, VIII, and X, form a variety of distinct network structures, while type VII collagen forms interlocking anchoring fibrils (Fig. 3) (20). The detailed structure of these aggregate structures has generally been inferred from electron microscopy evidence. For type I collagen, however, a detailed picture of the lateral packing has now emerged from X-ray fiber diffraction data on the type I collagen tissue, rat tail tendon. These data have shown that the individual collagen molecules are packed in a quasihexagonal lattice, and that the telopeptides form a corrugated arrangement of cross-linked molecules that strengthen and stabilize the native fibril (54).

Collagen found in mature tissues is arranged into structures that form macroscopically visible fiber bundles (Fig. 7). These fiber bundles would require a mechanism whereby individual fibrils can associate and broaden to attain a functional mature tissue form (55). There is little data on the length of mature fibrils. Long fibrils (up to 1 mm) have been isolated unbroken only from echinoderms (56). Studies on mature rat tail tendon, where over 1000 fibrils were followed over 1.4 μm by serial sectioning, showed no ends, leading to an estimate for fibril length of up to 10 mm in 6-month-old tendon (57). Serial sectioning to measure the length of fibrils in 14-day chicken embryo tendon showed only one complete fibril, but the proportion of ends seen suggested that the fibrils were shorter than those found in mature tendons (58).

The amounts of different collagen types in a particular tissue may vary with location and age. For example, in skin, the amount of type III collagen is greatest

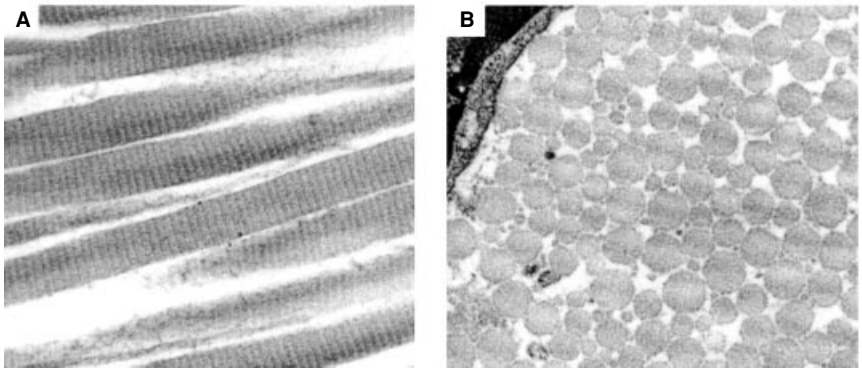

Fig. 7. TEM (positive staining) of sections of collagenous tissue, sheep cruciate ligament, showing interstitial collagen fibrils in (**A**) longitudinal and (**B**) cross sectional orientations. Photographs courtesy of Jacinta F. White.

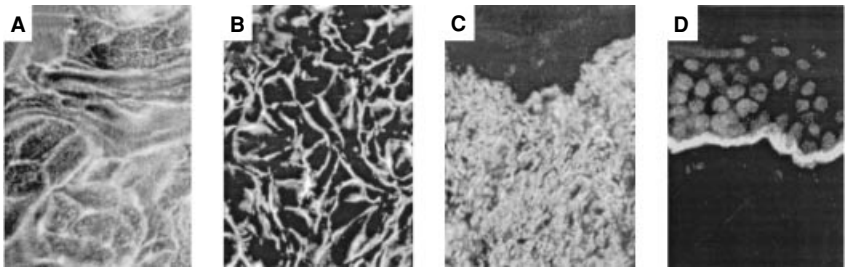

Fig. 8. Immunofluorescent examination of human skin (single sample, 22 months) for distribution of different collagen types, showing (**A**) reticular dermis examined with anti–type I collagen antibody, (**B**) reticular dermis examined with anti–type III collagen antibody, (**C**) papillary dermis examined with anti–type III antibody, and (**D**) dermal/epidermal junction examined with anti–type IV collagen antibody.

in embryonic or young tissues and is also in greater amounts in the papillary dermis compared to the reticular dermis (59). The availability of monoclonal antibodies specific to different collagen types has enabled the distribution to be readily examined (Fig. 8) (60–63).

Regulation of Collagen Biosynthesis. In order for the normal morphogenesis and differentiation processes to occur, precise temporal, spatial, and quantitative regulation of collagen biosynthesis is undoubtedly critical. The nature and extent of collagen production is sensitive to modulation by various entities, including growth factors and cytokines. Thus gene transcription is modulated by multiple, cis-acting promoters, enhancers, and silencers, which have been identified in the 5′-flanking region and within the first intron. Regulation of translation may involve sequences proximal to the translation initiation site. Various studies have suggested that the propeptide domains released during secretion and fibril formation may play a role in modulating collagen production, particularly through translational control (19).

Collagen Degradation. The rate of turnover of collagen in tissues is generally very slow, with lifetimes being estimated in years for type I collagen in bone, for type II collagen in cartilage, and for type III collagen in skin. The exception is type I collagen in periodontal ligament, which has an estimated half-life of the order of a week. However, a regulated breakdown of collagen is required for this slow turnover, as well as for wound healing, development, and tissue remodeling. The collagen in the extracellular matrix is a very stable structure, with the triple-helical domains being particularly resistant to proteolysis by typical proteases such as trypsin, chymotrypsin, and pepsin. A set of specific proteases is present in tissues—the matrix metalloproteinases (MMPs)—that are involved in the degradation of most, if not all, proteins in the ECM including collagen and collagen fragments. This set of MMPs includes at least 20 members, each with a different specificity profile, including some with collagenase and gelatinase activities (64). All these MMPs are tightly regulated, through the need for proenzyme activation to achieve activity and the presence of specific tissue inhibitors of metalloproteinases (TIMPs). The enzymes MMP-1, 8, and 13, traditionally called mammalian collagenases, break down triple-helical collagen fibrils through cleavage at a single site in a collagen molecule to give two fragments of about $\frac{3}{4}$ and $\frac{1}{4}$ of the molecular length. The cleavage site occurs in the $\alpha 1$ chain of type I collagen in the sequence -Gly(775)-Ile(776), and at an analogous sequence location in other interstitial collagen chains (65). It has been suggested that the triple helix at this location may be less tightly folded because of an imino acid deficient domain C-terminal in this site (66). After this initial cleavage a range of other enzymes, including those with activities for unfolded collagen chains and telopeptide regions are able to complete the degradation process.

Pathology. Many opportunities for molecular defects leading to disease arise for collagen because of its complex biosynthetic and catabolic pathways and the complex nature of the structural genes (19,67). The most frequently studied "collagen disease" is *Osteogenesis imperfecta* (OI). This disease occurs in a range of severities from mild to perinatal lethal and is caused by changes to type I collagen. More than 100 mutations have been characterized that involve a single base substitution leading to mutation of an obligatory glycine residue within the repeating $(\text{Gly-X-Y})_n$ motif of the collagen triple helix. In addition, a range of deletions and splicing defects has been observed that lead to similar disease outcomes. The observed consequences of replacing a Gly by a larger amino acid residue can include delayed folding, excess post-translational modification, increased intracellular breakdown, reduced secretion of collagen, abnormal fibril assembly, and a possible decrease in helical stability. Collagen mutations are generally dominant because mutant collagen chain can be incorporated into the triple helix resulting in aberrant fibril formation and function. Clinical severity for OI appears to depend on the nature of the residue replacing Gly, its location in the triple helix, and the local sequence environment around the mutation (68). Similar mutations have been observed in many other collagen types, leading to a range of diseases that reflect the tissue distribution of each particular collagen type (Table 3) (67,69).

In addition to pathological consequences arising directly from mutations to the triple-helical domain, diseases have been shown to be due to variations in the secondary modification of collagen, including defects in lysyl hydroxylase, lysyl oxidase, and N-proteinase. There is also a range of common diseases that involve

Table 3. The Involvement of Different Collagen Chains in Genetic Diseases[a]

Collagen type	Chain(s) involved	Disease
Type I	αl(I) α2(I)	Osteogenesis imperfecta
		Ehlers–Danlos syndrome types I, II, VIIA, VIIB
		Osteoporosis
Type II	αl(II)	Osteoarthrosis
		Chondrodysplasias, including
		Achondrogenesis II
		Hypochondrogenesis
		Spondyloepiphyseal dysplasia
		Spondyloepimetaphyseal dysplasia
		Kneist syndrome
		Wagner syndrome
		Stickler syndrome
Type III	αl(III)	Arterial (familial) aneurysm
		Ehlers–Danlos syndrome type IV
Type IV	α3(IV) α4(IV) α5(IV)	Alport syndrome
	α5(IV) α6(IV)	Alport syndrome(DOL, GL)
Type V	αl(V) α2(V)	Ehlers–Danlos syndrome types I and II
Type VI	αl(VI)α2(VI)α3(VI)	Bethlem myopathy
		Ullrich congenital muscular dystrophy
Type VII	αl(VII)	Dystrophic epidermolysis bullosa
Type VIII	α2(VIII)	Corneal endothelial dystrophy
Type IX	αl(IX) α2(IX) α3(IX)	Multiple epiphyseal dysplasia
		Intervertebral disc disease
		Osteoarthrosis
Type X	αl(X)	Chondrodysplasia
		Schmid metaphyseal chondrodysplasia
Type XI	α(XI)α2(Xl)α3(XI)	Nonsyndromic hearing loss
		Osteoarthrosis
		Chondrodysplasias, including
		Stickler syndrome
		Marshall syndrome
		Otospondylomegaepiphyseal dysplasia
		Weissenbacher–Zweymüller syndrome
Type XV	αl(XV)	Skeletal myopathy (possible)
Type XVII	αl(XVII)	Generalized atrophic benign epidermolysis bullosa
Type XVIII	αl(XVIII)	Knobloch syndrome

[a]Based on Ref. 20.

the metabolism or catabolism of collagen rather than mutations to the collagen genes themselves. Thus, a deficiency in ascorbic acid (vitamin C) reduces the levels of Hyp and Hyl, decreasing collagen stability and leading to scurvy. In other cases, such as the accumulation of excess type III collagen in liver fibrosis, or the decreased collagen content seen in osteoporosis, it results from changes in the balance between collagen production and degradation. Collagen degradation has also been shown to be essential for tumor growth and metastasis. Also, while collagen is normally not immunogenic, antibodies to collagen are common in patients with various diseases, such as anti–type II collagen antibodies associated with rheumatoid arthritis (70).

Isolation and Purification

The extent of purification depends on the final use of the collagen. In most cases, the other components of the ECM, such as proteoglycans and serum proteins, are removed, while if hide or skin is the collagen source the hair will also need removal. Each type of collagenous material has its own characteristic processing steps, with collagens to be used in biomedical applications having the most rigorous processing.

Collagenous Tissues. Intact collagenous tissue is used for products as diverse as leather and bioprosthetic heart valves. Thus in leather production, treatment in an alkaline solution, for example in lime, leads to tissue swelling and assists in removal of proteoglycan components, while addition of sulphide leads to removal of the hair. Prolonged alkali treatment, however, can modify the structure of the collagen, principally through loss of the amide groups from asparagine and glutamine amino acid side chains (71). On the other hand, in the preparation of bioprosthetic heart valves the extent of processing beyond trimming, attaching in a sewing ring and stabilization, usually with glutaraldehyde, is minimal as retention of collagen ultrastructure and proteoglycans may have beneficial effects on the long-term performance of the device (72,73).

Fibrillar Collagen. Fibrillar, particulate collagen is prepared either as a wet paste or a dry powder for various commercial applications. A paste is used, for example, for extrusion in casing production or for fabrication into sponges or similar devices for biomedical applications. A dry powder is used, for example, as a haemostatic agent or is reconstituted into wound dressings. The methods for production of these materials are generally of proprietary nature, but involve comminution of the tissue with possible washing or enzyme treatments to enhance purity (31).

Soluble Collagen. Very little soluble collagen can be extracted from mature tissues because of the extensive cross-linking network that is present; young or embryonic tissues provide the best yields, but these are still low. Previously, the extent of cross-linking was reduced, giving better extraction yields if the animals are made lathyritic, for example by feeding β-aminopropionitrile. For some tissues, such as rat tail tendon, aldimine cross-links are present and these can be broken by dilute acid treatment to give a soluble collagen (50) that retains its telopeptides. While this approach is useful for small-scale laboratory work, a different approach is needed for larger scale or commercial applications. The normal large-scale method is to remove the cross-links by cleaving the telopeptides with a proteolytic enzyme, utilizing the resistance of the tightly wound triple helix to proteolysis (74). The preferred enzyme is the acid protease pepsin, to which the triple helix is particularly stable, where the acidic conditions used for digestion also assist in solubilizing the collagen. Purification, for example to remove enzyme and serum digestion products, can be achieved by precipitation, for example with NaCl (75). Fractionation of different collagen types can be achieved using their differential solubility at different pH values (Table 4) (74,75). As well as NaCl, ethanol, $(NH_4)_2SO_4$, or poly(ethylene glycol) are effective precipitation agents. Although proteolysis gives a soluble product, it is normally not monomeric but rather contains a range of small oligomers as well. The oligomers are less soluble at neutral pH, this in turn providing a way of reducing their presence.

Table 4. Purification of Various Collagens by NaCl Precipitation[a]

[NaCl][b]	Neutral,[c] pH 7.5	Acid,[d] pH 2.5
0.7		I, II, III
1.2		IV, V
1.7	III	
2.4	I	
>4.0	II, V	

[a]Data from Ref. 74.
[b]Concentration (M) of NaCl required for precipitation of a given collagen type.
[c]For example, 50 mM acetic acid.
[d]For example, 1.0 M NaCl, 50 mM Tris.

Recombinant Collagen. The most recent development is the availability of recombinant collagens (76–78). This allows the production of natural human collagens that are highly pure and disease free. A recombinant process can be used to produce all types of collagens. This includes those that are of very low abundance in natural tissue and so not readily obtained in commercially practical quantities by traditional tissue extraction methods. These minor collagens may have, however, unique biological properties that are valuable for particular clinical applications. Recombinant approaches also give opportunities for the production of nonnatural molecules that may have applications as scaffolds in tissue engineering for enhancing adhesion, differentiation, and growth of specific cell types (79). These recombinant molecules could include collagens where specific sites such as the collagenase cleavage site have been deleted or modified, or novel molecules based on multiple copies of a specific functional triple-helical motif, or chimeric molecules that combine a collagen fragment together with another component, such as a growth factor (79).

Low yields of collagen have been obtained from mammalian and insect cell constructs (77). Presently, the best yields have been obtained from constructs in various yeasts such as Pichia and Saccharomyces, although constructs in plants also show promise (80). The initial advantage of the yeast system is that the key enzyme prolyl hydroxylase can be introduced in the construct, leading to stable hydroxylated collagens. This approach can now also be applied in plants (81). Although plants contain an endogenous prolyl hydroxylase, it is not active in the initial constructs. Recombinant collagens can also be produced in the milk of transgenic animals where endogenous P4H is active (82). Whichever system is used for production of recombinant collagen, the same approaches that have been successfully used for purification of soluble collagens will equally apply to the new material.

Analytical and Test Methods

Quantitation. Various standard protein analytical methods can be used for quantitation of collagen. These include determination of the total nitrogen content by Kjeldahl analysis, followed by estimation of the collagen concentration

using a conversion factor based on the known structure of collagens. This factor is dependent on the collagen type and the species of origin. However, if the sample is not pure then this method can give erroneous values because of noncollagenous nitrogen content. For fully soluble preparations with concentrations above about 2–3 mg/mL, a Biuret assay is a simple and rapid method for determining collagen concentration, although noncollagenous impurities can again give incorrect values. Amino acid analysis, however, is not as susceptible to contamination by other proteins, since this can be used to determine Hyp, which is characteristic of collagens. The amount of Tyr present can show the extent to which the telopeptides have been removed from interstitial collagens, as this amino acid is generally found only in these regions (65). However, type III collagen does contain a low level of Tyr within the helical domain. Hyp can also be determined by a specific colorimetric assay (83). Various spectroscopic techniques are also applicable for quantitation of collagen solutions. These include ORD, or CD, where determination of ellipticity allows one to determine the concentration.

Purity. A range of methods is available to assess the purity of soluble collagen preparations, but techniques to study insoluble material are limited. Determination of the refractive index of collagen dispersions using the Becke test allows an estimate of the extent of other protein impurities to be made (84). Full digestion of soluble or insoluble collagen samples with highly pure bacterial collagenase, which digests only the collagen present, allows the identification of impurities, for example by electrophoresis (see below). IR spectroscopy, which can be used to show collagen identity, also has potential for assessing the extent of denaturation in a collagen preparation as any gelatin present changes the relative intensity of the bands at 1660 and 1633 cm^{-1} (85).

Electrophoresis. Electrophoresis provides a rapid and cost-effective method for characterizing the composition and assessing the purity of soluble collagens, with various methods being available. In SDS-PAGE (86) the molecular weight distribution of individual chain components after denaturation is shown. The single-chain components, the α-chains, are the fastest moving components from intact collagens. Any significant bands moving faster than the α-chains indicate impurities or degradation products. Cross-linked chain components, for example the dimer β- and trimer γ-chains, move more slowly on the gel. Separation of $\alpha 1$(I) and $\alpha 1$(III) chains may be achieved by reduction with 2-mercaptoethanol during interrupted electrophoresis (87). SDS-PAGE is also useful for characterization of collagens by analysis of the fragments that are formed by CNBr cleavage, where the different location of Met residues in the chains leads to characteristic patterns (74). Electrophoresis can also be performed under nondenaturing conditions at acid pH, where highly porous gels allow the larger collagen molecules to migrate (88). This system does not, however, separate, the individual interstitial collagens. The stains that are used to detect collagen in each of the electrophoretic methods are not collagen-specific but stain all proteins, allowing any protein contaminants to be detected. The use of isoelectric focusing to determine collagen pI is difficult because of the poor solubility of collagen at low ionic strength at certain pH conditions. However, observation of the direction of electrophoretic mobility in native gels at different pH values can provide an indication of its net charge at a given pH. Methods for examination of collagens by capillary electrophoresis have also been described (89).

Chromatography. Gel permeation chromatography can be used to examine the heterogeneity of soluble collagen preparations (see CHROMATOGRAPHY, SEC). Large-scale, low pressure columns allow fractionation of larger quantities of material but do not have particularly good resolution. Analytical, high pressure columns, packed for example with silica-based resins, provide much better resolution, especially when used in tandem, and allow resolution of monomer through pentamer forms of collagen (90). Ion-exchange chromatography has traditionally been used for examining the chain composition of an individual collagen (74). The collagen is denatured into individual chains, either using urea or elevated temperature, and separated using, for example, a cation-exchange cellulose (eg CM-52) at pH 4.8 with elution by (and an increasing linear gradient of) NaCl. This procedure separates individual α-chains, for example from type I collagen, and also resolves various β-components. Individual chains separated by this method are then available for further detail characterization, for example by examining CNBr fragments.

Thermal Stability. Various methods have been described for determining the thermal stability of collagens, where the change in a parameter is followed with increasing temperature. These include spectral methods, such as UV spectroscopy, ORD, CD, and susceptibility to enzyme digestion, and calorimetric methods, such as differential scanning calorimetry (DSC); degraded samples will show a decrease in thermal stability. Variation in melting temperature is seen for collagens from different species, the values approximating to the upper environmental temperature experienced by an organism (18). For a given species, the different collagen types may vary in stability, with, type III collagen, for example, being more stable than type I collagen.

Immunological Methods. The availability of antibodies, particularly monoclonal antibodies that are specific for particular collagen types, or collagen chains, or even for a particular collagen type from a given species, provides a wide range of probes for collagen identification and quantitation (60–62,91). Identification can be achieved by electroblotting from gels or by slot/dot blotting of samples. If monoclonal antibodies are used, then a native gel system may be required since these antibodies are often conformation-dependent and do not work with blots from denaturing SDS-gels (88). Identification and quantitation can be achieved by a variety of ELISA-based methods. Immunohistology provides a method, by using monoclonal antibodies, of distinguishing the distributions of different collagen types in different tissues (63).

Economic Aspects and Uses

Collagen is of major economic importance. For example, it is the key component in leather production, where around 5.5 million tons of raw bovine hides on a wet salted basis are converted into various forms of leather annually. In addition, a further 600,000 t of dry sheep and goat skins are processed to leather. Leather production in turn supports a range of further manufacturing activities, including upholstery, footwear, and fashion activities. Collagen is also the raw material for gelatin production, which is worth more than US$ 1.5 billion per year, and which is a key component for many further products in, for example, the food, confectionary,

Table 5. Examples of the Use of Collagen Materials and Devices in Medical Applications

Medical area	Application
Cardiovascular surgery	Vessel replacement, heart valves
Dentistry	Periodontal attachment, alveolar ridge augmentation
Dermatology	Tissue augmentation
Dressings	Burn dressings, graft site repair, ulcer treatment
General surgery	Hernia repair, adhesion barriers, haemostats, adhesives
Neurosurgery	Nerve conduits, nerve repair, dura mater replacement
Oesophageal surgery	Augmentation
Ophthalmology	Corneal graft, vitreous replacement, retinal reattachment
Orthopaedics	Bone repair, cartilage reconstruction, ligament repair
Otology	Tympanic membrane replacement
Urology	Ureter replacement, renal repair, urinary incontinence

photographic, pharmaceutical and medical industries (see GELATIN). Collagen is also significant in biomedical applications (see below). For example, the market for bioprosthetic heart valves is worth more than US$ 100 million, while the collagen aesthetics market exceeds $50 million per year. Beyond these examples, collagen is used in a diverse range of products, including manufactured casing for the food industry, sporting and surgical gut, and cosmetics, each of which provides significant additional world markets.

Biomedical Uses. Collagen is now an important material in biomedical device applications (Table 5) and has been used successfully in a wide variety of clinical applications (31). These include areas where collagen products have been used regularly as materials of choice for specific indications for over 30 years. Two principal approaches for collagen processing are used. In one, the devices are tissue-based, where the defined shape of the tissue is retained as part of the function of the device. An important example is the bioprosthetic heart valve. In these devices, chemical fixation, typically with glutaraldehyde (92), is used to give strength and durability to the device. This processing also masks the immunogenicity of the tissue, although some sites for cell–matrix interactions may be lost. The principal drawback to this approach is the tendency for these materials to show nonspecific calcification that can impair the long-term function of the device. Various approaches have been examined to minimize or eliminate this calcification, but without full success.

The other approach is to use purified collagen. When pepsin-solubilized collagen is used, it can be purified to remove potential immunogenic contaminants (74). If required, soluble collagen can be reformed into fibrils, for example by warming a neutral-pH solution. Alternatively, comminuted collagen can be used where impurities can be removed by washing or mild proteolysis. Purified collagen can be reconstituted into the desired shape or form for the product. If necessary, the product can then be stabilized, either by a chemical fixation method such as mild glutaraldehyde treatment, or by a physical method such as dehydrothermal cross-linking. Examples include the formation of dry, stabilized collagen sheets for wound dressings, or preparation of collagen paste for soft tissue augmentation. Reconstituted products are characterized by a high biochemical purity associated

with low immunogenicity, controlled turnover (often over short time periods), controlled porosity, and retention of cell-matrix interactions that are important in biological functions in tissues. In the future, the availability of soluble recombinant collagen will lead to a further increase in medical use of collagen (77).

Although glutaraldehyde has become the predominant reagent used for stabilizing collagen products (92–94), it is seen to have certain limitations. These include its potential cytotoxicity (95), and, most importantly, its propensity to lead to unwanted calcification, particularly in bioprosthetic heart valves (96). This has led to a range of variations in the methods used, including incorporation of a range of auxiliary treatments (92–94). A range of alternative stabilizing reagents has been examined. These include other bis-aldehydes, bis-epoxides, bis-isocyanates, and bis-imidates in conjunction with simple aliphatic scaffolds, or alternative scaffolds including polyethylene oxide constructs (97). In these cases, the reagent leaves the scaffold joining the collagen molecules. Other approaches have been examined that do not introduce material into the product. In chemical approaches, such as the use of carbodiimides or acyl azides, peptide bonds are formed between the side chains of lysine and adjacent aspartic or glutamic acid residues (92). In physical methods, such as dye-mediated photooxidation (98), the mechanism is less clear. The alternative glutaraldehyde strategies and other physical and chemical methods give opportunities to produce products with a wide range of physical and biological properties (92–94).

Immunology. A fundamental issue that applies to all collagen biomedical products is the potential for an adverse immunological response to the foreign animal material. The use of recombinant human collagen has the potential to eliminate adverse responses due to the collagen, but introduces the possibility of a response to any residual material from the host organism. Collagen biomedical products are made predominantly from type I collagen, usually from bovine hides, although other collagens, such as type III collagen, may also be present in small amounts (31). The immunological responses that have been observed depend on the host species, and the form of the collagen. Thus, if the collagen still has intact telopeptides an immunodominant response is more likely, and may reflect the structural mobility of this region and the presence of tyrosine residues (69).

A large number of humans have now received soluble bovine atelocollagen implants. About 1.5% of potential patients react positively to a skin test and so are precluded from treatment (99). In these instances there is a high degree of correlation between a positive skin test and the presence of circulating anti-bovine-collagen antibodies (100). A further 1.5% of patients show a reaction after treatment. Studies on sera from these patients indicates there is no clear, single immunodominant region on the collagen molecule (101). Indeed, given the importance of the triple-helical domains in collagens, it is surprising that there are only limited reports on the nature of the epitopes being recognized. For polyclonal human sera, multiple bands have been detected after electrophoresis, although there appear to be distinct immunodominant "hotspots," particularly in α1(I)-CB6 and α2(I)-CB4 fragments (101). In mice, using a library of monoclonal antibodies to collagen type III, a clearer picture has emerged (61), showing a spread of conformational determinants along the full length of the helix.

In mice, the immunogenic determinants in collagens interact with a complex system of different types of T cells, B cells, and antigen-presenting cells, and

the nature of this response is classically T-cell-dependent (102). Identification of immune response gene(s) located in the IA or IB subregion of the major histocompatibility (H-2) locus also support a T-cell-dependent immune response to collagen in mice. The nature of the immune response gene control in humans for collagen priming and immune response is less clear.

In addition to a humoral or antibody response, collagens can also induce a cell-mediated immune response. Both native and denatured collagen can induce cellular responses in guinea pigs presensitized with only native collagen type I (103). Conversely, sensitization with denatured collagen also led to positive skin tests after challenge with native collagen (104). Clearly, the antigenic determinants involved in the cellular-type responses are different to those described for the humoral response to collagens. When collagen is used as a medical implant for soft tissue augmentation, it is this cellular type of "adverse" response that is detected in patients, and which is sometimes associated with antibody responses and extrapolated to autoimmune-type responses (69).

Health and Safety Issues

The successful use of numerous collagen products over millennia, such as leather, gelatin, and catgut sutures indicates that it is a safe material. More recently, the successful use of collagen in a wide variety of medical applications has again confirmed its general safety as a material (31). In these applications, the principal areas of risk are adverse immunological responses, either from collagen or more likely from contaminating proteins, and the possible transmission of infective organisms. Of concern is the risk of prion transmission from bovine products (bovine spongiform encephalopathy), although there is no evidence that this has occurred. On the other hand, the transmission of Creutzfeld–Jacob disease from allogenic transplants has been observed, for example via corneal transplants and from dura mater grafts.

Although collagen is regarded as a generally safe material, possible hazards can arise from the processing steps, both to workers and to the environment. For example, a range of aggressive preservatives has on occasion been used with hides and skins, and the lime and sulphide traditionally used in hide processing represent risks. In addition, agents used for stabilization, such as chromium in the tanning industry or glutaraldehyde in the biomedical industry, are potentially toxic.

BIBLIOGRAPHY

"Collagen" in *EPST* 1st ed., Vol. 4, pp. 1–16, by William F. Harrington, McCollum-Pratt Institute, Johns Hopkins University; "Collagen" in *EPSE* 2nd ed., Vol. 3, pp. 699–727, by Karl A. Piez, Collagen Corporation.

1. E. D. Hay, ed., *Cell Biology of the Extracellular Matrix*, Plenum Press, New York, 1991.
2. B. Brodsky and J. A. M. Ramshaw, *Matrix Biol.* **15**, 545 (1997).
3. G. N. Ramachandran and G. Kartha, *Nature* **174**, 269 (1954).

4. A. Rich and F. H. C. Crick, *J. Mol. Biol.* **3**, 483 (1961).
5. R. D. B. Fraser, T. P. MacRae, and E. Suzuki, *J. Mol. Biol.* **129**, 463 (1979).
6. K. Okuyama, K. Okuyama, S. Arnott, M. Takayanagi, and M. Kakudo, *J. Mol. Biol.* **152**, 427 (1981).
7. J. Bella, M. Eaton, B. Brodsky, and H. M. Berman, *Science* **266**, 75 (1994).
8. R. Z. Kramer, J. Bella, P. Mayville, B. Brodsky, and H. M. Berman, *Nat. Struct. Biol.* **6**, 454 (1999).
9. J. Bella, B. Brodsky, and H. M. Berman, *Structure* **3**, 893 (1995).
10. E. Y. Jones and A. Miller, *J. Mol. Biol.* **218**, 209 (1991).
11. J. A. M. Ramshaw, N. K. Shah, and B. Brodsky, *J. Struct. Biol.* **122**, 86 (1998).
12. S. K. Holmgren, L. E. Bretscher, K. M. Taylor, and R. T. Raines, *Chem. Biol.* **6**, 63 (1999).
13. L. Vitagliano, R. Berisio, A. Mastrangelo, L. Mazzarella, and A. Zagari, *Protein Sci.* **10**, 2627 (2001).
14. B. Brodsky and N. K. Shah, *FASEB J.* **9**, 1537 (1995).
15. E. J. Miller, *Biochemistry* **10**, 1652 (1971).
16. E. Chung and E. J. Miller, *Science* **183**, 1200 (1974).
17. M. Sundaramoorthy, M. Meiyappan, P. Todd, and B. G. Hudson, *J. Biol. Chem.* **277**, 31142 (2002).
18. B. J. Rigby and M. S. Robinson, *Nature* **253**, 277 (1975).
19. J. F. Bateman, S. Lamande, and J. A. M. Ramshaw, in W. D. Comper, ed., *Extracellular Matrix: Vol. 2, Molecular Components and Interactions*, Harwood Academic Publishers, Amsterdam, 1995, pp. 22–67.
20. J. Myllyharju and K. I. Kivirikko, *Ann. Med.* **33**, 7 (2001).
21. H. P. Bachinger, K. J. Doege, J. P. Petschek, L. I. Fessler, and J. H. Fessler, *J. Biol. Chem.* **257**, 14590 (1982).
22. R. Mayne and R. E. Burgesson, *Structure and Function of Collagen Types*, Academic Press Inc., Orlando Fla., 1987.
23. B. Dublet, S. Oh, S. P. Sugrue, M. K. Gordon, D. R. Gerecke, B. R. Olsen, and M. van der Rest, *J. Biol. Chem.* **264**, 13150 (1989).
24. S. Ricard-Blum, B. Dublet, and M. van der Rest, *Unconventional Collagens*, Oxford University Press, Oxford, 2000.
25. N. Yamaguchi, R. Mayne, and Y. Ninomiya, *J. Biol. Chem.* **266**, 4508 (1991).
26. T. M. Schmid, R. Mayne, J. J. Jeffrey, and T. F. Linsenmayer, *J. Biol. Chem.* **261**, 4184 (1986).
27. M. van der Rest and R. Garrone, *FASEB J.* **5**, 2814 (1991).
28. J. Engel and H. Furthmayr, *Methods Enzymol.* **145**, 3 (1987).
29. G. P. Lunstrum, L. Y. Sakai, D. R. Keene, N. P. Morris, and R. E. Burgeson, *J. Biol. Chem.* **261**, 9042 (1986).
30. N. J. Bulleid, *Semin. Cell Dev. Biol.* **7**, 667 (1996).
31. J. A. M. Ramshaw, J. A. Werkmeister, and V. Glattauer, *Biotechnol. Genet. Eng. Rev.* **13**, 335 (1996).
32. K. I. Kivirikko and R. Myllyla, *Methods Enzymol.* **82**, 245 (1982).
33. R. A. Berg and D. J. Prockop, *Biochem. Biophys. Res. Commun.* **52**, 115 (1973).
34. K. I. Kivirikko and R. Myllyla, *Int. Rev. Connect. Tissue Res.* **8**, 23 (1979).
35. H. P. Bachinger, P. Bruckner, R. Timpl, D. J. Prockop, and J. Engel, *Eur. J. Biochem.* **106**, 619 (1980).
36. D. E. Birk and R. L. Trelstad, *J. Cell. Biol.* **99**, 2024 (1984).
37. R. R. Bruns, D. J. Hulmes, S. F. Therrien, and J. Gross, *Proc. Natl. Acad. Sci. U. S. A.* **76**, 313 (1979).
38. A. Veis and K. Payne, in M. E. Nimni, ed., *Collagen*, Vol. **1**, CRC Press, Boca Raton, 1988, pp. 113–137.

39. D. J. Prockop and A. Fertala, *J. Biol. Chem.* **273**, 15598 (1998).
40. K. E. Kadler, Y. Hojima, and D. J. Prockop, *Biochem. J.* **268**, 339 (1990).
41. K. E. Kadler, D. F. Holmes, J. A. Trotter, and J. A. Chapman, *Biochem. J.* **316**, 1 (1996).
42. D. E. Birk, M. V. Nurminskaya, and E. I. Zycband, *Dev. Dyn.* **202**, 229 (1995).
43. D. E. Birk, R. A. Hahn, C. Y. Linsenmayer, and E. I. Zycband, *Matrix Biol.* **15**, 111 (1996).
44. J. F. White, J. A. Werkmeister, I. A. Darby, T. Bisucci, D. E. Birk, and J. A. M. Ramshaw, *J. Struct. Biol.* **137**, 23 (2002).
45. J. E. de Vente, G. E. Lester, J. A. Trotter, and L. E. Dahners, *J. Electron Microsc. (Tokyo)* **46**, 353 (1997).
46. K. E. Kadler, D. F. Holmes, H. Graham, and T. Starborg, *Matrix Biol.* **19**, 359 (2000).
47. B. Brodsky and J. A. M. Ramshaw, *Int. J. Biol. Macromol.* **16**, 27 (1994).
48. R. Fleischmajer, B. R. Olsen, R. Timpl, J. S. Perlish, and O. Lovelace, *Proc. Natl. Acad. Sci. U. S. A.* **80**, 3354 (1983).
49. P. J. Neame, C. J. Kay, D. J. McQuillan, M. P. Beales, and J. R. Hassell, *Cell. Mol. Life. Sci.* **57**, 859 (2000).
50. M. Yamauchi and G. Mechanic, in M. E. Nimni, ed., *Collagen*, Vol. **1**, CRC Press, Boca Raton, 1988, pp. 157–172.
51. D. R. Sell and V. M. Monnier, *J. Biol. Chem.* **264**, 21597 (1989).
52. A. Ruggeri and P. M. Motta, eds., *Ultrastructure of the Connective Tissue Matrix*, Martinus Nijhoff Publishers, Boston, 1984.
53. B. Brodsky and E. F. Eikenberry, *Methods Enzymol.* **82**, 127 (1982).
54. J. P. Orgel, A. Miller, T. C. Irving, R. F. Fischetti, A. P. Hammersley, and T. J. Wess, *Structure* **9**, 1061 (2001).
55. D. F. Holmes, C. J. Gilpin, C. Baldock, U. Ziese, A. J. Koster, and K. E. Kadler, *Proc. Natl. Acad. Sci. U. S. A.* **98**, 7307 (2001).
56. J. A. Trotter, J. A. Chapman, K. E. Kadler, and D. F. Holmes, *J. Mol. Biol.* **284**, 1417 (1998).
57. A. S. Craig, M. J. Birtles, J. F. Conway, and D. A. Parry, *Connect. Tissue. Res.* **19**, 51 (1989).
58. D. E. Birk and E. Zycband, *J. Anat.* **184**, 457 (1994).
59. J. A. M. Ramshaw, *Connect. Tissue Res.* **14**, 307 (1986).
60. J. A. Werkmeister, T. A. Tebb, J. F. White, and J. A. M. Ramshaw, *J. Histochem. Cytochem.* **41**, 1701 (1993).
61. J. A. Werkmeister and J. A. M. Ramshaw, *Biochem. J.* **274**(Part 3), 895 (1991).
62. J. A. Werkmeister, J. A. M. Ramshaw, and G. Ellender, *Eur. J. Biochem.* **187**, 439 (1990).
63. J. A. Werkmeister and J. A. M. Ramshaw, *Acta Derm. Venereol.* **69**, 399 (1989).
64. H. Nagase and J. F. Woessner Jr., *J. Biol. Chem.* **274**, 21491 (1999).
65. K. Kadler, *Protein Profile* **5**, 519 (1994).
66. G. B. Fields, *J. Theor. Biol.* **153**, 585 (1991).
67. D. J. Prockop and K. I. Kivirikko, *Annu. Rev. Biochem.* **64**, 403 (1995).
68. K. Beck, V. C. Chan, N. Shenoy, A. Kirkpatrick, J. A. M. Ramshaw, and B. Brodsky, *Proc. Natl. Acad. Sci. U. S. A.* **97**, 4273 (2000).
69. J. A. Werkmeister and J. A. M. Ramshaw, in D. L. Wise, ed., *Handbook of Biomaterials Engineering*, Marcel Dekker, Inc., New York, 2000, pp. 739–759.
70. L. K. Myers, G. C. Higgins, T. H. Finkel, A. M. Reed, J. W. Thompson, R. C. Walton, J. Hendrickson, N. C. Kerr, R. K. Pandya-Lipman, B. V. Shlopov, P. Stastny, A. E. Postlethwaite, and A. H. Kang, *Arthritis Rheum.* **44**, 1775 (2001).

71. E. Heidemann, *Fundamentals of Leather Manufacture*, Eduard Roether KG, Darmstadt, 1993.
72. J. M. Riddle, J. J. Jennings, P. D. Stein, and D. J. Magilligan Jr., *Scan. Electron Microsc.* 207 (1984).
73. S. L. Hilbert, L. C. Sword, K. F. Batchelder, M. K. Barrick, and V. J. Ferrans, *J. Biomed. Mater. Res.* **31**, 503 (1996).
74. E. J. Miller and R. K. Rhodes, *Methods Enzymol.* **82**, 33 (1982).
75. R. L. Trelstad, V. M. Catanese, and D. F. Rubin, *Anal. Biochem.* **71**, 114 (1976).
76. M. Nokelainen, H. Tu, A. Vuorela, H. Notbohm, K. I. Kivirikko, and J. Myllyharju, *Yeast* **18**, 797 (2001).
77. J. Myllyharju, *Methods Mol. Biol.* **139**, 39 (2000).
78. P. D. Toman, G. Chisholm, H. McMullin, L. M. Giere, D. R. Olsen, R. J. Kovach, S. D. Leigh, B. E. Fong, R. Chang, G. A. Daniels, R. A. Berg, and R. A. Hitzeman, *J. Biol. Chem.* **275**, 23303 (2000).
79. M. Hayashi, M. Tomita, and K. Yoshizato, *Biochim. Biophys. Acta.* **1528**, 187 (2001).
80. F. Ruggiero, J. Y. Exposito, P. Bournat, V. Gruber, S. Perret, J. Comte, B. Olagnier, R. Garrone, and M. Theisen, *FEBS Lett.* **469**, 132 (2000).
81. C. Merle, S. Perret, T. Lacour, V. Jonval, S. Hudaverdian, R. Garrone, F. Ruggiero, and M. Theisen, *FEBS Lett.* **515**, 114 (2002).
82. P. D. Toman, F. Pieper, N. Sakai, C. Karatzas, E. Platenburg, I. de Wit, C. Samuel, A. Dekker, G. A. Daniels, R. A. Berg, and G. J. Platenburg, *Transgenic Res.* **8**, 415 (1999).
83. G. Huszar, J. Maiocco, and F. Naftolin, *Anal. Biochem.* **105**, 424 (1980).
84. M. Jayabalan, *Leather Sci.* **32**, 140 (1985).
85. K. J. Payne and A. Veis, *Biopolymers* **27**, 1749 (1988).
86. U. K. Laemmli, *Nature* **227**, 680 (1970).
87. B. Sykes, B. Puddle, M. Francis, and R. Smith, *Biochem. Biophys. Res. Commun.* **72**, 1472 (1976).
88. J. A. M. Ramshaw and J. A. Werkmeister, *Anal. Biochem.* **168**, 82 (1988).
89. P. Chang, S. Kuan, G. Eberlein, D. Burke, and R. Jones, *J. Pharm. Biomed. Anal.* **22**, 957 (2000).
90. R. A. Condell, V. P. Hanko, E. A. Larenas, G. Wallace, and K. A. McCullough, *Anal. Biochem.* **212**, 436 (1993).
91. J. A. Werkmeister and J. A. M. Ramshaw, *J. Histochem. Cytochem.* **39**, 1215 (1991).
92. J. A. M. Ramshaw, V. Glattauer, and J. A. Werkmeister, in D. L. Wise, ed., *Handbook of Biomaterials Engineering*, Marcel Dekker, Inc., New York, 2000, pp. 717–738.
93. A. Jayakrishnan, and S. R. Jameela, *Biomaterials* **17**, 471 (1996).
94. E. Khor, *Biomaterials* **18**, 95 (1997).
95. M. Chvapil, D. Speer, W. Mora, and C. Eskelson, *J. Surg. Res.* **35**, 402 (1983).
96. G. Golomb, F. J. Schoen, M. S. Smith, J. Linden, M. Dixon, and R. J. Levy, *Am. J. Pathol.* **127**, 122 (1987).
97. U.S. Pat. 5874500 (1999), R. A. Berg, F. A. Delustro, and W. M. Rhee.
98. J. A. M. Ramshaw, L. J. Stephens, and P. A. Tulloch, *Biochim. Biophys. Acta* **1206**, (1994).
99. D. G. Wallace, J. M. McPherson, L. Ellingsworth, L. Cooperman, R. Armstrong, and K. A. Piez, in M. E. Nimni, ed., *Collagen*, Vol. **3**, CRC Press, Boca Raton, 1988, pp. 117–134.
100. D. J. Hartmann, G. Charriere, and G. Ville, *Clin. Mater.* **9**, 163 (1992).

101. L. R. Ellingsworth, F. DeLustro, J. E. Brennan, S. Sawamura, and J. McPherson, *J. Immunol.* **136**, 877 (1986).
102. H. Nowack, E. Hahn, and R. Timpl, *Immunology* **30**, 29 (1976).
103. G. Senyk and D. Michaeli, *J. Immunol.* **111**, 1381 (1973).
104. B. C. Adelmann, *Immunology* **24**, 871 (1973).

JOHN A. M. RAMSHAW
VERONICA GLATTAUER
JEROME A. WERKMEISTER
CSIRO Molecular Science

COLORANTS. See Volume 2.

COLORING PROCESSES. See Volume 2.

COMBINATORIAL METHODS FOR POLYMER SCIENCE

Introduction

Fundamental research of the synthesis and characterization of polymeric materials is driven by their use in applications including structural materials, packaging, microelectronics, coatings, biomedical materials, and nanotechnology. Current trends demand finer control of chemistry, morphology, and surface topography at the micrometer and nanometer scales. To achieve these goals, there are increasing needs for the synthesis and processing of multicomponent mixtures, composites, and thin films. However, these systems are inherently complex due to the interactions of phase transitions, microstructure, interfaces, and transport behavior that occur during synthesis and processing. The synthesis of polymers by emulsion polymerization, for example, involves colloid chemistry, micellization, transport between phases, and complex rate relationships. In the case of coatings and thin films, the mechanical and optical properties, microstructure, and phase and wetting behavior are sensitive and poorly understood functions of thickness. In addition to the complex phenomena involved in polymer synthesis and processing, there is a large variable space involving parameters whose effects often counteract one another. These include reactant composition and structure, synthetic sequence, solvent, temperature, annealing history, pressure, and thickness (eg, in films). Conventional microscopy, spectroscopy, and analytical tools for polymer synthesis and characterization were designed for one-sample-one-measurement utilization, and are suited for detailed characterization over a limited set of variable combinations. This conventional approach is preferred when the most relevant variable combinations are known a priori or can be reliably predicted from theory. However, the complex phenomena and large variable spaces present in

Encyclopedia of Polymer Science and Technology. Copyright John Wiley & Sons, Inc. All rights reserved.

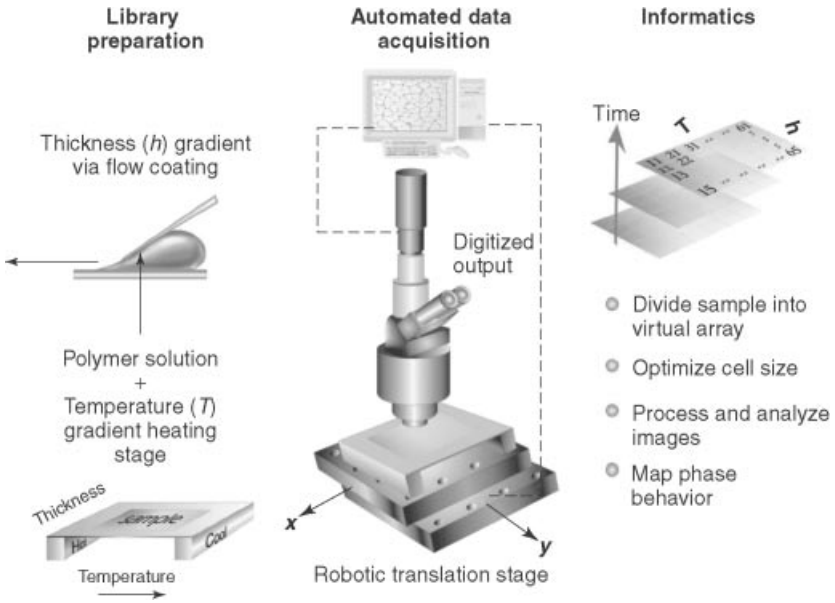

Fig. 1. Schematic of the combinatorial experimental method, as applied to the preparation of thickness and temperature gradient film libraries, high throughput screening with optical microscopy, and informatic analysis of image data as a function of temperature, thickness, and time. Adapted with permission from Ref. 22.

multicomponent, multiphase, bioactive or thin-film polymers often exceed the capabilities of current theory and conventional measurements. Therefore, a strong need exists for experimental techniques capable of highly efficient synthesis and characterization of complex polymeric systems over large numbers of variable combinations.

Combinatorial methods (CM) use experimental design, library creation, high throughput screening, and informatics to efficiently and rapidly develop new materials and measure properties over large numbers of variable combinations (Fig. 1). This is accomplished by preparing samples not one at a time, but rather as sample "libraries" containing hundreds to thousands of variable combinations each. High throughput measurements of relevant chemical and physical properties, combined with informatic data analysis, allow efficient development of structure–processing–property relationships. The benefits include efficient characterization of novel regimes of thermodynamic and kinetic behavior (knowledge discovery) and accelerated development of functional materials (materials synthesis and discovery). Although historically applied to pharmaceutical research, there is an increasing interest in applying CM to materials science, as indicated by recent reports of combinatorial methodologies for a wide range of inorganic (1–8) and organic/polymeric materials (7,9–24).

Early combinatorial *materials* research used sputtering methods to prepare composition gradient libraries for measuring the phase behavior of ternary metal alloys (20) and other inorganic materials (25). However, limitations in computing capacity and instrument automation overshadowed the benefits of combinatorial

materials' characterization until only recently. The primary limitation to *characterizing* polymers, as bulk material or films, with CM has been a shortage of techniques for preparing libraries with systematically varied composition (ϕ), morphology, physical form, thickness (h), and temperature (T). This article is a review of recent advances in applying CM to polymer synthesis and characterization. Applications of CM to the synthesis of a wide range of polymeric materials, including sensors, dendrimers, and biodegradable polymer are presented. Several novel methods developed for the preparation of T, ϕ, h, and surface energy continuous polymer film libraries are discussed. There is particular focus on the novel library preparation and high throughput screening steps, since these have been the principal limiting factors in CM development for polymers. The use of continuous gradient libraries in the measurement of fundamental properties is described for polymer blend phase behavior, block copolymer segregation, and dewetting transitions.

Combinatorial Polymer Synthesis

Despite the recent increase in combinatorial inorganic materials research (2–7,14,15), there are still relatively few studies reporting CM for the synthesis of polymeric materials. One example is the work of Brocchini and co-workers (10,11), where a 112-member combinatorial library of biodegradable polyarylates was prepared by copolymerizing all possible combinations of 14 tyrosine-based diphenols and 8 diacids. The pendant chain and backbone structures were systematically varied by the addition of methylene groups, substitution of oxygen for the methylene, and addition of branched or aromatic structures. The library products displayed diverse properties, as indicated by measurements of the glass-transition temperature T_g, air–water-contact angle (θ_w), and fibroblast proliferation during cell culture. Fibroblast proliferation was found to decrease with increased hydrophobicity except for the main-chain oxygen containing polymers that served as uniformly good growth substrates regardless of the hydrophobicity.

The results of the above study were utilized (13) to test informatic methods for designing *diverse* and *focused* combinatorial libraries. Molecular topology and genetic-algorithm-optimized quantitative structure–property relationships were used to design libraries. These techniques allowed selection of a representative subset of library members for rapid study of the entire library (a diverse subset) or concentration on a specific property of interest (a focused subset). Each monomer pair of the 112-member library was represented by a 2-D topological descriptor, used by the algorithm to select a structurally diverse and representative subset of the library. This subset was utilized to create models for the T_g and θ_w, which were tested by comparing to the T_g and θ_w of the entire library. Focused libraries of polymer structures predicted to meet certain T_g and θ_w specifications were also designed. Good agreement was reported between the calculated and experimental T_g and θ_w values, even for polymers not included in the subset library. Additionally, the focused libraries were shown to be effective in identifying polymer structures within specific T_g and θ_w ranges.

Gravert and co-workers (9) used parallel synthesis to design polymeric supports for liquid-phase organic synthesis. In this work, three polymerization

initiators containing α-nitrile diazene cores were utilized for block copolymer synthesis, while a functionalized methacrylate initiator was used to produce graft copolymers. Five vinyl monomers were used in combination with the initiators to produce approximately 50 block and graft copolymers. Copolymer products were characterized by size exclusion chromatography, nuclear magnetic resonance, and solubility in a range of solvents. Based upon this characterization, a 4-*tert*-butylstyrene-*b*-3,4-dimethoxystyrene block copolymer was selected and used successfully as a support in subsequent liquid-phase syntheses.

Takeuchi and co-workers (18) coupled combinatorial techniques with molecular imprinted polymers to develop sensors for triazine herbicides. The library consisted of a 7×7 array containing different fractions of monomers methacrylic acid (MAA) and 2-(trifluoromethyl)acrylic acid (TFMAA) with constant concentrations of the imprint molecules ametryn or atrazine. After UV-initiated polymerization, the products from the sensor library were characterized by HPLC measurement of herbicide concentration. The receptor efficiency was observed to vary with monomer type: the atrazine receptor efficiency increased with MAA composition and the ametryn receptor was enhanced by increased fractions of TFMAA. Although only monomer concentration was varied in the libraries, the authors conclude that the CM synthetic approach would be useful in analyzing other variables such as solvent, cross-linking agent, and polymerization conditions to produce optimum molecularly imprinted polymer sensors.

Dickinson and co-workers (12) reported CM synthesis of a sensor library consisting of solvatochromic dyes dissolved in polymer. Permeation of the polymer by volatile solvents induced changes in the dye's solvation environment, which were detectable by the fluorescence signal. A combination of methyl methacrylate and dimethyl(acryloxypropyl) methylsiloxane monomers was used to create two sensor libraries. A discrete library was prepared by photo-polymerizing constant concentration solutions of the dye and monomers to produce cones of polymer at different locations on the end of a fiber-optic bundle. A second, continuous library was created by adding methyl methacrylate to the copolymer monomer as UV light was scanned across the fiber-optic bundle, producing a copolymer concentration gradient across the bundle end. Both the discrete and the continuous libraries were characterized by monitoring the fluorescence response (via the fiber-optic cables) as a function of exposure to saturated organic vapors. The deposition of the library directly onto the measurement probe (fiber optic) makes this work a good example of a combined CM polymer synthesis and characterization. For the particular dye and monomer used, the fluorescence response was found to be a nonlinear function of the concentration.

Newkome and co-workers (26) report, a combinatorial strategy for synthesizing dendrimers with modified structure and surface chemistry. Mixtures of three branched isocyanate-based monomers, mixed over a wide range of compositions, were used to synthesize a combinatorial library of dendritic molecules. Based upon ^{13}C NMR spectra, the dendrimer products displayed varying degrees of peripheral heterogeneity, adjustable by controlling the ratios of the three isocyanate monomer groups. The methodology provides for the rapid modification of dendritic properties based upon the chemistry and distribution of peripheral surface groups; for example, some of the dendrimers were amphiphilic, displaying solubility in CH_3OH, H_2O, and $CHCl_3$. The degree of amphiphilicity can be

adjusted to favor solubilization in one of the solvents by varying the proportion of amino vs benzyl ether surface moieties, based upon the ratio of monomer building blocks.

Combinatorial Polymer Characterization

The previous section focused on CM studies in which the production or synthesis of new polymeric materials was the primary goal. In those examples the synthesis steps were combinatorial, but subsequent characterization steps were noncombinatorial. One exception is the fluorescent sensor libraries prepared on fiber-optic bundles, discussed above (12). In this section we describe library preparation and high throughput screening methods for the combinatorial *characterization* of both thick ($\approx$1 to $\approx$50 μm) and thin ($<$1 μm) polymer films and coatings. Here, the primary goal is not to produce new materials, but rather to use CM to measure relevant phase behavior, wetting, and microstructural properties over a large range of parameter combinations. The variables of primary importance in characterizing the physical and chemical properties of polymers in the bulk and film state include the composition in multicomponent mixtures and composites, thickness, temperature (eg, annealing, curing, melt processing), and substrate energy (γ_{so}).

While preparing polymer films and coatings libraries with variations in ϕ, h, T, and γ_{so}, we found that the deposition of films with continuous gradients in each of these properties is a convenient and practical alternative to the deposition of libraries containing discrete regimes. Of course the introduction of chemical, thickness, and thermal gradients drives nonequilibrium transport processes that will eliminate the gradients over time. The timescale and lengthscale over which gradient library measurements are valid are determined in part by the magnitude of these transport fluxes. In most cases high molecular mass ($M_w > 10{,}000$ g/mol) polymers have relatively low transport coefficients, eg, diffusivity and viscosity. (According to ISO 31–8, the term "molecular weight" has been replaced by "relative molecular mass," symbol "Mr". The conventional notation, rather than the ISO notation, has been employed for this publication.) Thus the mass transport and flow lengthscale and timescale are often orders of magnitude lower than those of the measurements, allowing properties to be measured near equilibrium.

Preparation of Polymer Coating and Thin-Film Libraries.

Thickness Gradient Libraries. A velocity-gradient knife coater (21–24), depicted in Figure 1, was developed to prepare coatings and thin films containing continuous thickness gradients. A 50-μL drop of polymer solution (mass fraction 2–5%) was placed under a knife-edge with a stainless steel blade width of 2.5 cm, positioned at a height of 300 μm and at a 5° angle with respect to the substrate. A computer-controlled motion stage (Parker Daedal) moves the substrate under the knife-edge at a constant acceleration, usually 0.5–1 mm/s^2. This causes the substrate coating velocity to gradually increase from 0 to a maximum value of 5–10 mm/s. The increase in fluid volume passing under the knife-edge with increasing substrate velocity results in films with controllable thickness gradients. Figure 2 shows h-gradients for polystyrene (PS) and blends of polystyrene/poly(vinylmethylether) (PS/PVME) films on Si substrates as a function of solution composition. Thin-film-thickness-dependent phenomena can

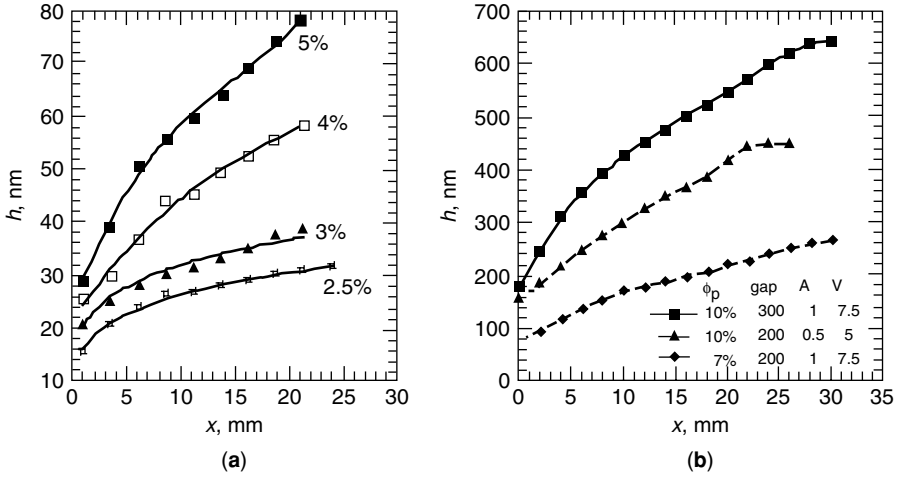

Fig. 2. (**a**) Thickness, h (nm) vs distance x (mm) for various h-gradient film libraries composed of (M_w = 1800 g/mol) on Si as a function of mass fraction PS in the toluene coating solution. (**b**) h (nm) vs x (mm) for h-gradient libraries of mass fraction 20% PS (M_w = 96,400 g/mol)/80% PVME (M_w = 119,000 g/mol) blends on Si as a function of mass fraction polymer composition in the toluene coating solution, blade substrate gap (μm), acceleration A (mm/s^2), and velocity (mm/s). Standard uncertainty in thickness is $\pm$3 nm. Figure 2a adapted with permission from Ref. 22.

be investigated from nanometers to micrometers employing several h-gradient films with overlapping gradient ranges. One can verify that the relatively weak thickness and temperature gradients do not induce appreciable flow in the polymer film over the experimental time scale (21,22). A unidirectional Navier–Stokes model for flow over a flat plate estimates lateral flow at a characteristic velocity of 1μm/h at $T = 135^\circ$C, in response to gravitational action on the thickness gradient (27). This small flow is orders of magnitude slower than the flow induced by the physical phenomena that these libraries are designed to investigate, such as dewetting (22) and phase separation (21). To check for flow, we examined thickness-gradient libraries before and after annealing at $T > T_g$, for a PS film (M_w = 1800) on Si/SiO$_x$ (22). The difference of thickness gradients across the 2 cm $\times$ 3 cm library area before and after annealing was within a standard uncertainty of $\pm$1.5 nm (22).

Composition Gradient Libraries. Three steps are involved in preparing composition gradient films: gradient mixing (Fig. 3a), gradient deposition (Fig. 3b), and film spreading (Fig. 3c). Gradient mixing utilizes two syringe pumps (Harvard PHD2000) that introduce and withdraw polymer solutions (of mass fraction $x_A = x_B$ = 0.05–0.10) to and from a small mixing vial at rates I and W, respectively. (Certain equipment and instruments or materials are identified in the article in order to adequately specify the experimental details. Such identification does not imply recommendation by the National Institute of Standards and Technology, nor does it imply the materials are necessarily the best available for the purpose.) Pump W was used to load the vial with an initial mass M_0 of solution B of $M_0 \approx 1$ g. The infusion and withdrawal syringe pumps were started simultaneously under

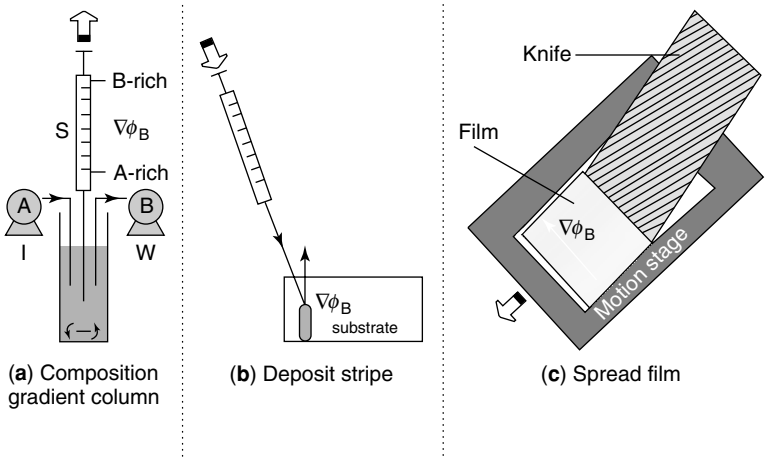

Fig. 3. Schematic of the composition gradient deposition process involving (**a**) gradient mixing, (**b**) deposition of stripe, and (**c**) film spreading. Adapted with permission from Ref. 21.

vigorous stirring of the vial solution, and a third syringe, S, was used to manually extract $\approx$50 μL of solution from the vial into the syringe needle at the rate of $S = 30$–50 μL/min. At the end of the sampling process, the sample syringe contained a solution of polymers A and B with a gradient in composition ∇x_A along the length of the syringe needle. The relative rates of I and W were used to control the steepness of the composition gradient, eg, dx_A/dt. The sample time, t_s, determines the endpoint composition of the gradient. The gradient produced by a particular combination of I, W, S, M_0, and t_s values was modeled by a mass balance of the transient mixing process, given elsewhere (21). This balance predicts that the composition gradient will be linear only if $I = (W + S)/2$, a prediction supported by FTIR measurements of composition. An 18-gauge needle long enough to contain the sample volume ensured that the gradient solution did not enter the syringe itself. This prevented turbulent mixing that might occur upon expansion of the solution from the needle into the larger diameter syringe.

Under the influence of the gradient in the syringe needle, ∇x_A, molecular diffusion will homogenize the composition. However, the timescale for molecular diffusion is many orders of magnitude larger than the sampling time. For example, consider gradient solutions of PS ($M_w = 96.4$ kg/mol, $M_w/M_n = 1.01$, Tosoh Inc.) and PVME ($M_w = 119$ kg/mol, $M_w/M_n = 2.5$) in toluene, a system used to characterize the ϕ-gradient deposition procedure (21,28). For a typical ϕ-gradient with $\Delta\phi \approx 0.025$ mm^{-1}, ϕ_{PS} and ϕ_{PVME} change negligibly by 0.004 and 0.001% in the 5-min period required for film deposition (21). [The diffusive flow rate of PS and PVME were calculated as $J = L\pi r^2 D_i \rho (d\phi_i/dx)_{max}$, where ρ is the solution density, $r = 2.3$ mm is the syringe diameter, and $L = 4.2$ mm is the length of the fluid column in the syringe. We estimate $\Delta\phi_i$ as $(Jt)/(x_p L\pi r^2\ \rho)$, where $x_p = 0.08$ is the total polymer mass fraction in solution.] Fluid flow in the sample syringe remains in the laminar regime, preventing turbulence and convective mixing, discussed elsewhere (21).

The next library preparation step (Fig. 3b) is to deposit the gradient solution from the sample syringe as a thin stripe, usually 1–2-mm wide, on the substrate. This gradient stripe was spread as a film (Fig. 3c) orthogonal to the composition gradient, using the knife-edge coater described above. After a few seconds most of the solvent evaporated, leaving behind a thin film with a gradient of polymer composition. The remaining solvent was removed under vacuum during annealing, described in the next section (T-gradient annealing). Because polymer melt diffusion coefficients D are typically of order 10^{-12} cm^2/s, diffusion in the cast film can be neglected if the lengthscale resolved in measurements is significantly larger than the diffusion length $\sqrt{Dt}$.

Composition gradient films of blends of PS/PVME and poly(D,L-lactide) (PDLA, Alkermes, Medisorb 100DL, M_w = 127,000 g/mol, M_w/M_n = 1.56)/ poly(ε-caprolactone) (PCL, Aldrich, M_w = 114,000 g/mol, M_w/M_n = 1.43) were used to test the ϕ-gradient procedure. FTIR spectra were measured with a Nicolet Magna 550 and were averaged 128 times at 4 cm^{-1} resolution. The beam diameter, 500 μm (approximate), was significantly larger than the diffusion length of 3 μm (approximate) for the experimental timescale. Films 0.3–1 μm thick were coated on a sapphire substrate and a translation stage was used to obtain spectra at various positions on the continuous ϕ-gradient.

Figure 4a shows typical FTIR spectra for a ϕ-gradient film of PS/PVME. As position is scanned along the film, a monotonic increase in PVME absorbances,

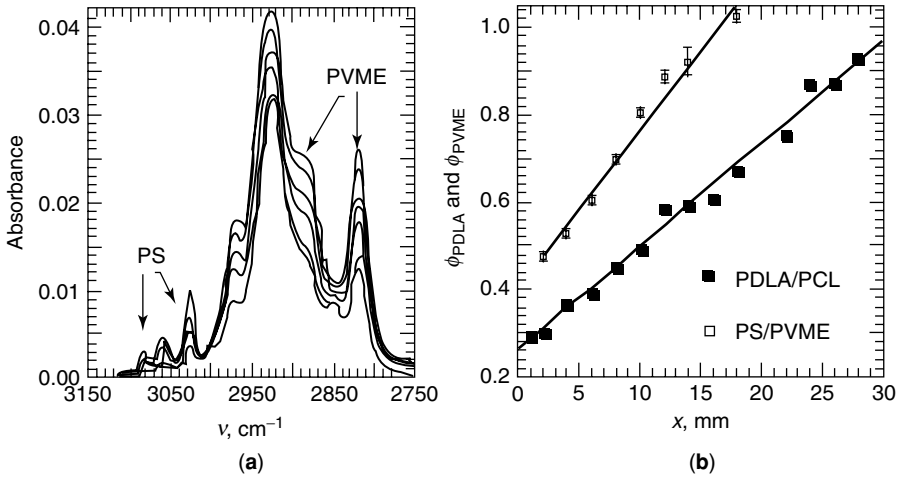

Fig. 4. (**a**) FTIR spectra at X = 2,4,8,10,14,18 mm positions along a ϕ-gradient PS/PVME library, as described in the text. PS absorptions decrease while PVME absorptions increase, monotonically, as one samples spectra across the film (increasing X (mm)). (**b**) Mass fractions ϕ_{PVME} and ϕ_{PCL} vs position x (mm) for typical PCL/PDLA and PS/PVME ϕ-gradient libraries. Composition of PS/PVME blends is calculated by calibration of the ν = 2820 cm^{-1} PVME absorption. Composition in PDLA/PCL blends is calculated by the methodology described in the text. Coating parameters were PS/PVME (I = 0.51 mL/min, W = 1.0 mL/min, S = 20 μL/min, M_0 = 1.57 mL, sample time = 94 s) and PDLA/PCL (I = 0.76 mL/min, W = 1.5 mL/min, S = 26 μL/min, M_0 = 1.5 mL, sample time = 95 s) Unless otherwise indicated by error bars, standard uncertainty is represented by the symbol size. Figure 4b adapted with permission from Ref. 21.

and a corresponding decrease in PS absorbances is observed. For the PS/PVME blend, compositions were measured based upon a direct calibration of the $\nu = 2820\ \text{cm}^{-1}$ peak by using known mixtures, yielding $\varepsilon(2820\ \text{cm}^{-1}) = (226 \pm 3)$[$\varepsilon = A/hc$, where A is the absorbance for this peak, h is the film thickness measured in micrometers, and c is the molar density of PVME in moles per liter.] For PDLA/PCL system, $\varepsilon(\nu)$ values for pure PDLA and PCL were determined over the C—H stretch regime of 2700–3100 cm^{-1}, based upon $\varepsilon_i(\nu) = A_i(\nu)/(ch)$, where A_i is the absorbance for each peak. Unknown PDLA/PCL mass fractions were determined to be within a standard uncertainty of 4% by assuming the observed spectra were linear combinations of pure PDLA and PCL spectra, eg, $A_{\text{mix}} = h(\alpha\varepsilon_{\text{PDLA}}c_{\text{PDLA}} + (1-\alpha)\varepsilon_{\text{PCL}}c_{\text{PCL}})$ and α is related to the mass fraction PDLA. Figure 4b shows typical composition gradients for PDLA/PCL blends coated from $CHCl_3$ and PS/PVME blends coated from toluene. Essentially linear gradients were obtained and the endpoints and slope agree with those predicted from mass balance (21). It is possible to create gradient films with wider composition ranges than those shown in Figure 5, by sampling the mixing vial for longer times (Fig. 4a).

Temperature Gradient Libraries. To explore a large T range, h- or ϕ-gradient films are annealed on a T-gradient heating stage, with the T-gradient *orthogonal* to the h- or ϕ-gradient. This custom aluminum T-gradient stage, shown in Figure 1, uses a heat source and a heat sink to produce a linear gradient ranging between adjustable end-point temperatures. End-point temperatures typically range from $(160 \pm 0.5)^\circ$C to $(70.0 \pm 0.2)^\circ$C over 40 mm, but are adjustable within the limits of the heater, cooler, and maximum heat flow through the aluminum

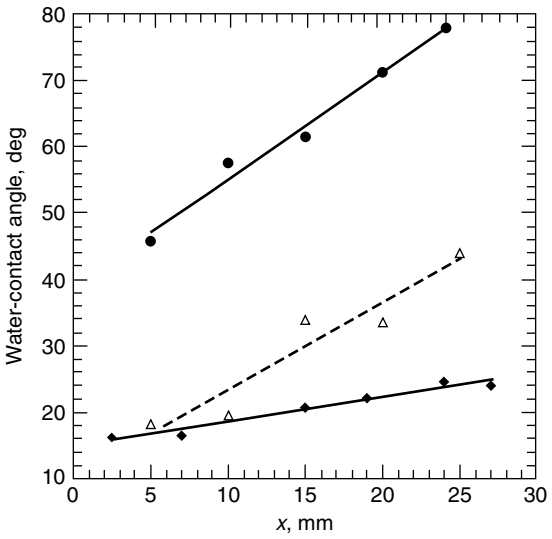

Fig. 5. Deionized water-contact angle vs position (mm) for gradient-etched SiH/Si substrates as a function of both immersion rate and Piranha solution H_2SO_4 composition. Immersion rate and mass fraction H_2SO_4 are as follows: circles, 2.0 mm/s and 30%; triangles, 0.1 mm/s and 30%; diamonds, 2.0 mm/s and 40%. Standard uncertainty in contact angle is $\pm 2^\circ$.

plate. To minimize oxidation and convective heat transfer from the substrate, the stage is sealed with an o-ring, glass plate, and vacuum pump. Each 2-D T–h or T–ϕ parallel library contains about 1800 or 3900 state points, respectively, where a "state point" is defined by the T, h, and ϕ variation over the area of a 200× optical microscope image: $\Delta T = 0.5^{\circ}$C, $\Delta h = 3$ nm, and $\Delta\phi = 0.02$. These libraries allow T, h, and ϕ-dependent phenomena, eg, dewetting, order–disorder, and phase transitions, to be observed *in situ* or postannealing with relevant microscopic and spectroscopic tools.

Surface Energy Gradients. In many polymer coating and thin-film systems, there is considerable interest in studying the film stability, dewetting, and phase behavior on substrates with surface energies varying between hydrophilic and hydrophobic extremes. Therefore, a gradient-etching procedure has been developed in order to produce substrate libraries with surface energy, γ_{s0}, continuously varied from hydrophilic to hydrophobic values (29). The gradient-etching procedure involves immersion of a passivated Si—H/Si substrate (Polishing Corporation of America) into a 80°C Piranha solution (30) at a *constant immersion rate*. The Piranha bath etches the Si—H surface and grows an oxide layer, SiO_x/SiOH, at a rate dependent on T and the volume fraction H_2SO_4 (30). A gradient in the conversion to hydrophilic SiO_x/SiOH results because one end of the wafer is exposed longer to the Piranha solution. After immersion, the wafer is withdrawn rapidly (≈10 mm/s), rinsed with deionized water, and blown dry with N_2. Typical deionized water contact angles are shown in Figure 5. By preparing several gradient substrates covering overlapping ranges of hydrophilicity, it is possible to screen a large range in surface energy, from hydrophilic ($\theta_w \approx 0^{\circ}$) to hydrophobic ($\theta_w \approx 90^{\circ}$) values of the water-contact angle.

In another procedure for varying substrate energy, developed by other authors, mixed self-assembled monolayers (SAMs) of alkanethiolates are deposited with a composition gradient (31). In this procedure, ω-substituted alkanethiolates with different terminal groups, eg, —CH_3 vs —COOH, cross-diffuse from opposite ends of a polysaccharide matrix deposited on top of a gold substrate. Diffusion provides for the formation of a SAM with a concentration gradient between the two thiolate species from one end of the substrate to another, resulting in controllable substrate energy gradients. The polysaccharide matrix is removed after a period of time, halting the diffusion process. These gradient SAM substrates were subsequently used to investigate the effect of surface energy on phase separation of immiscible polymer blends (32).

Uncertainty and Statistical Considerations of Library Measurements. A *potential drawback* of the method is that the polymer libraries are not composed of distinct sample areas, but rather have continuous gradients in ϕ, annealing T, and thicknes h. These gradients induce variance in observed properties, which is not an issue with uniform samples. Many properties measured with combinatorial libraries are obtained from microscope images (optical, fluorescent, AFM, FTIR) or spectroscopy (UV, FTIR). Thus it is important to understand how uncertainties associated with the gradients and the lateral resolution affect properties measured on the libraries. Figure 6 demonstrates how a combinatorial library is divided into a grid of "virtual" measurement sites (eg, microscope images) of lengthscale L. The T and ϕ for each measurement site is taken as the average $\langle T \rangle$ and $\langle \phi \rangle$ over the length L. Because gradients are present on the library, each

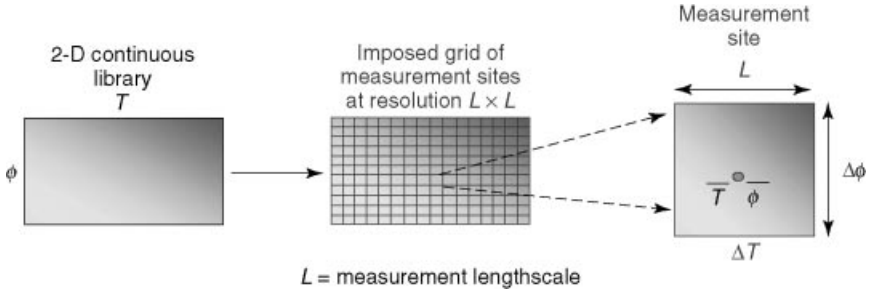

Fig. 6. Distribution of discrete measurement sites of resolution $L \times L$ over a continuous gradient library. Measurement sites have average T and ϕ with gradient variance ΔT and $\Delta\phi$.

measurement site has systematic variances, $\Delta\phi$ and ΔT, that increase as the measurement lengthscale L increases. Hence, lower measurement resolution (lower L) results in lower $\Delta\phi$ and ΔT. A typical 500 μm $\times$ 500 μm image would have reasonable variances of $\Delta\phi = 0.01$ and $\Delta T = 0.3^{\circ}$C. When measuring features within a site, the number of features sampled decreases as L decreases, causing an increase measurement uncertainty.

How to select the optimum measurement scale L, reflecting a balance between counting statistics, $\Delta\phi$ and ΔT?

The effects of these contributions on the variance about the mean of any property $\langle p\rangle$ within a measurement site is accounted for using a standard uncertainty propagation,

$$\Delta\langle p\rangle = (\partial\langle p\rangle/\partial N)\Delta N + (\partial\langle p\rangle/\partial T)\Delta T + (\partial\langle p\rangle/\partial\phi)\Delta\phi \tag{1}$$

Here $\langle p\rangle$ is a function of T, ϕ, and the number of observations made in the measurement site, $N \sim L^2$. It is assumed that the number of features (microstructures, cells, etc) can be counted exactly, so that $\Delta N = 0$. The partial derivatives can be estimated from finite difference approximations of the measured data, eg, $\partial\langle p\rangle/\partial T = [\sum p(T_{i+1},\phi_i) - \sum p(T_i,\phi_i)]/[N(T_{i+1} - T_i)]$. The values of $\Delta\phi$ and ΔT are $\Delta\phi = m_\phi L$ and $\Delta T = m_T L$, where m_T and m_ϕ are the slopes of the linear gradients, known from the library preparation procedure. Making these substitutions shows that the error propagation for property p scales as

$$\Delta\langle p\rangle \sim (m_T + m_\phi)/L \tag{2}$$

Constants have been removed from the above equation in order to reveal only the dependence on gradients and the measurement scale L. Equation 1 demonstrates that the uncertainty of any property measured on the libraries at a given ϕ and T will decrease if the measurement scale L is increased (because more features are counted) and if the magnitude of the gradients are decreased (reducing ϕ and T uncertainty). Thus the following guidelines should be followed during experimental design and data analysis: (*1*) L should be made as large as possible while still being able to resolve features of interest and (*2*) the gradient slopes should then be adjusted to attain an acceptable uncertainty (<1%) in

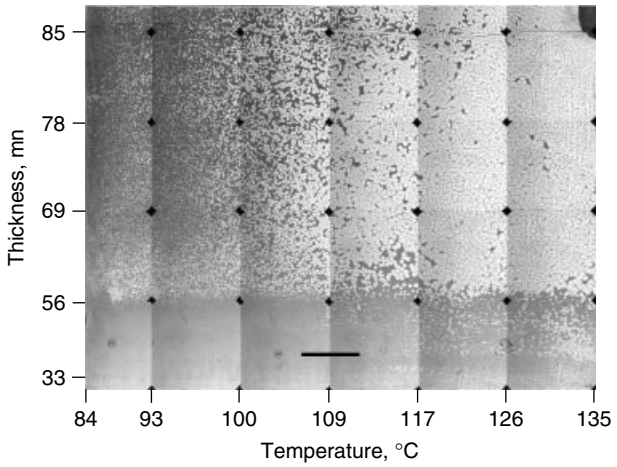

Fig. 7. Composite of optical images of a T–h combinatorial library of PS (M_w = 1800 g/mol) on silicon, $t = 2$ h, 25× magnification. Scale bar = 2.0 ± 0.1 mm. The thickness scale is a power law function (given in text), reflecting the nonlinear thickness gradient deposition procedure. Adapted with permission from Ref. 22.

the measured property. The analysis above considers only uncertainty contributions from the library gradients. Additional sources of uncertainty, arise from the measurements themselves, but these are also present for uniform conventional samples.

Fundamental Property Measurement with Combinatorial Polymer Coating and Film Libraries.

Thin-Film Dewetting. Figure 7 shows a composite of optical microscope images of a T-h library of PS (Goodyear, M_w = 1900 g/mol, M_w/M_n = 1.19) on a SiO_x/SiOH substrate (22). The thickness ranges from 33–90 nm according to $h = 33.1x^{0.30}$ ($1 < x < 28$) mm and 85°C < T < 135°C. The images, taken 2 h after initiation of dewetting, show wetted and dewetted regimes that are visible as dark and bright regions, respectively, to the unaided eye. Repeated examination of combinatorial T-h libraries at thicknesses ranging from 16–90 nm indicates three distinct thickness regimes with different hole nucleation mechanisms. For $h > 55 \pm 4$ nm, discrete circular holes in the film nucleate via heterogeneities (eg, dust) and grow at a rate dependent on T (quantification of the rate is given in Fig. 8).

Below $h \leq 55 \pm 4$ nm, there is a sharp and temperature independent transition to a regime where irregular, asymmetrical holes nucleate and grow more slowly than at $h > 55$ nm. In the regime 33 nm < h < 55 nm, the heterogeneous and capillary instability nucleation mechanisms compete. The asymmetrical holes present in this regime are surrounded by bicontinuous undulations in the film surface, with a characteristic spacing of 7 μm, as indicated by optical microscopy (22). AFM indicates a roughened surface with correlated surface undulations. A similar structure consisting of asymmetrical holes that breakup into a bicontinuous pattern at late stage, termed an "intermediate morphology," has been observed recently for 12-nm-thick films of poly(styrene-*ran*-acrylonitrile) (33). Below

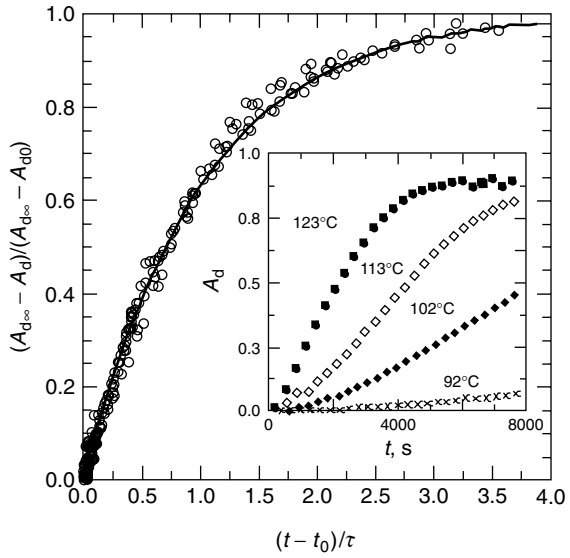

Fig. 8. T–h–t superposition of dewet area fraction data onto a universal curve, 92°C < T < 135°C, 59 nm < h < 86 nm. Inset: raw dewet area fraction vs time, $h = 79$ nm. Adapted with permission from Ref. 22.

$h \approx 33$ nm, another transition in structure and nucleation is apparent. Here, holes are nucleated by capillary instability and grow more quickly than in the region 33 nm < h < 55 nm.

Systematic studies of the temperature dependence of dewetting rates have not been reported to our knowledge. However, through its effect on viscosity, T is expected to have a strong influence on hole drainage rates. By using automated optical microscopy (Fig. 1), a 5 × 5 grid of images covering the T and h range of the library was collected every 5 min for 2 h. Automated image analysis (22) of hole area as a function of T, h, and t assays a broad range of dewetting rates in a single experiment, shown in Figure 8. The inset to Figure 8 shows the raw dewetted area fraction A_d vs t at various temperatures from the T-h library for h = 79 nm. The entire set of A_d vs t profiles for $h > 55$ nm can be fitted with $A_d = A_{d\infty} + (A_{d0} - A_{d\infty}) \exp[-(t - t_0)/\tau]$, where A_{d0} and $A_{d\infty}$ are the dewet fractions at $t = t_0$ and $t = \infty$, τ is the dewetting time constant, and t_0 is a time delay for nucleation. As shown in Figure 8, in reduced units of $(A_{d\infty} - A_d)/(A_{d\infty} - A_{d0})$ vs $(t - t_0)/\tau$, the hole drainage profiles collapse onto the universal exponential curve given above. Figure 8 contains T and h data over a large range 92°C < T < 135°C and 59 nm < h < 86 nm, and τ ranges from 2100 s (high temperatures) to 113,000 s (low temperatures). This T–h superposition for dewetting rates, previously unreported, reflects variations in the film viscosity with T and h, and could be missed altogether by relying solely upon limited numbers of samples.

Phase Behavior. Figure 9 presents a photograph of a typical temperature–composition library of the PS/PVME blend (discussed under Composition Gradient Libraries) after 90 min of annealing. As Figure 9 indicates, the lower critical solution temperature (LCST) cloud point curve can

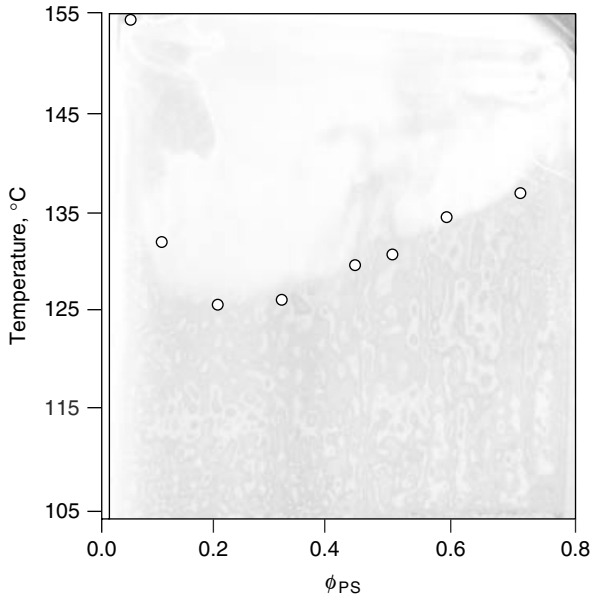

Fig. 9. Digital optical photographs of a PS/PVME T–ϕ library after 90 min of annealing, showing the LCST cloud point curve visible to the unaided eye. The library wafer dimension is 31 mm × 35 mm and the film thickness varies approximately 400–600 nm from low to high ϕ_{PS} values. White circles are light-scattering cloud points measured on separate uniform samples.

be seen with the unaided eye as a diffuse boundary separating one-phase and two-phase regions. Cloud points measured on bulk samples with conventional light scattering are shown as discrete data points and agree well with the cloud point curve observed on the library (21,34). The diffuse nature of the cloud point curve reflects the natural dependence of the microstructure evolution rate on temperature and composition. Near the LCST boundary the microstructure size gradually approaches optical resolution limits (1 μm), giving the curve its diffuse appearance. Based upon a bulk diffusion coefficient of $D \approx 10^{-17}$ m^2/s, the diffusion length ($\sqrt{Dt}$) for a $2h$ anneal is 270 nm. In Figure 9 each pixel covers about 30 μm, which is over 100 times the diffusion length, and ϕ-gradient-induced diffusion has a negligible effect on the observed LCST cloud point curve. The combinatorial technique employing T-ϕ polymer blend libraries allows for rapid and efficient characterization of polymer blend phase behavior (cloud points) in orders of magnitude less time than with conventional light scattering techniques.

Block Copolymer Segregation and Surface Morphology. The morphology of symmetric diblock copolymer thin films has been studied extensively with traditional techniques (35–48). These studies found surface induced formation of lamellae with thickness equal to the equilibrium lamellar thickness L_0 parallel to the substrate. The lamellae form smooth films when the total film thickness h is equal to an integral multiple m of L_0, $h \approx mL_0$ for one block segregating to both the substrate and air interfaces and $h \approx (m + \frac{1}{2})L_0$ for one block preferring

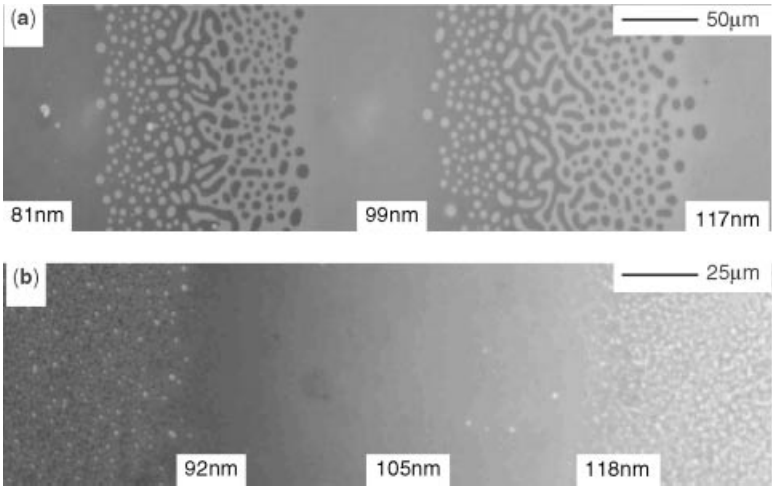

Fig. 10. (**a**) Optical micrograph of a $M_w = 26{,}000$ g/mol PS-*b*-PMMA gradient film showing the addition of two lamellae to the surface. Labels indicate $h = 4.5\ L_0$, $5.5L_0$, and $6.5L_0$ for this M_r copolymer. (**b**) Optical micrograph of a $M_w = 104{,}000$ g/mol PS-*b*-PMMA gradient film showing the change in h across the smooth region. The color change from purple to blue-green indicates a Δh of ≈25 nm across the smooth area. Standard uncertainty in thickness is ±3 nm.

the substrate and the other preferring the air interface. When h deviates from these values, holes or islands of height L_0 are found to form on the film surface so as to reduce the system energy. Although there has been significant previous investigation of these systems, almost no research on the factors controlling the lateral dimensions of these surface features has been reported. In addition, no investigation of the transition regions between the hole and island formations has been performed due to the difficulty in accurately controlling film thickness with traditional spin-coating techniques. These types of questions are ideal for CM where it is possible to produce continuous h-gradient films of symmetric diblock copolymers with various molecular masses (23,24).

Gradients in h of symmetric polystyrene-*b*-poly(methyl methacrylate) (PS-*b*-PMMA) with three different molecular masses were produced using the knife-edge flow coating technique described above. After characterization of h with UV-visible interferometry, the films were annealed at 170°C for up to 30 h to allow lamellar organization. The resulting morphologies were characterized with OM (optical microscopy) and AFM. Figure 10 presents a true color optical micrograph of a $M_w = 26{,}000$ g/mol gradient film showing morphological changes associated with the addition of two lamellae to the surface of the film. Labels denote approximate h values corresponding to $h \approx (m + \frac{1}{2})L_0$ for $m = 4$, 5, and 6. The morphology evolves from a smooth film to circular islands to a bicontinuous hole/island region to circular holes back to a smooth film from left to right in the micrograph and repeats twice. This morphology was observed to consistently repeat for h ranging from $2.0L_0$ to $6.5L_0$ for all molecular masses examined. Notably, the smooth regions of the film form a significant fraction of the morphology, corresponding to a thickness range Δh deviating significantly from an integral multiple of L_0.

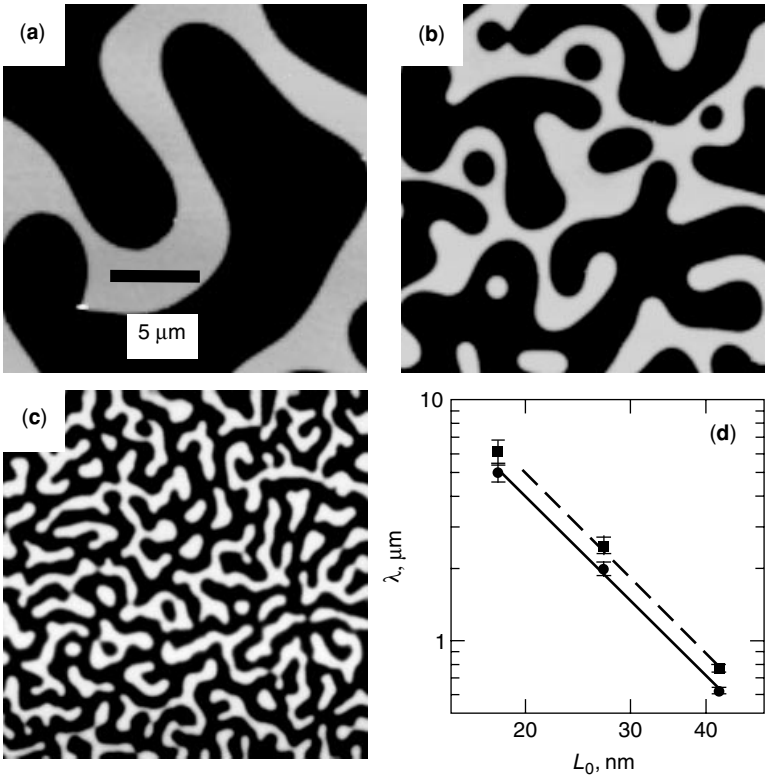

Fig. 11. AFM micrographs of PS-*b*-PMMA gradients annealed 30 h with M_w of (**a**) 26,000 g/mol, (**b**) 51,000 g/mol, and (**c**) 104,000 g/mol showing the decrease in surface feature size with increasing M_w. (Brighter regions correspond to higher topography and scale bar applies to all micrographs.) (**d**) Plot of λ vs. L_0 for samples annealed for 6 h (circle, solid line) and 30 h (square, dashed line) showing the power law dependence of λ on L_0 and M_w.

This Δh is confirmed in the optical micrograph presented in Figure 10b where the smooth region of a $M_w = 104{,}000$ g/mol PS-*b*-PMMA gradient film is displayed. The orange features on the left are holes and the yellow-green features on the right are islands and the smooth region changes color from purple to blue-green indicating an h increase. The value of Δh is $\approx 0.28 L_0$ and invariant within standard uncertainty for all M_w and h investigated. This effect is interpreted to arise from a brush-like stretching and compression of block copolymer chains in the outer lamella as the chain density varies with h. Therefore islands and holes form only when the free energy penalty of chain deformation becomes so large that the defect structures are more energetically favorable.

The lateral size of the surface patterns, which can be remarkably large when compared to L_0 or h, was also investigated using the h-gradient block copolymer film libraries. Figure 11 shows AFM micrographs of the surface of PS-*b*-PMMA gradient films with M_w of 26,000 g/mol (Fig. 11a), 51,000 g/mol (Fig. 11b), and 104,000 g/mol (Fig. 11c), annealed for 30 h at 170°C. These micrographs demonstrate that the lateral scale of the surface features decreases with increasing

M_w. This fact is quantified by obtaining 2-D Fourier transforms of the micrographs (Fig. 11d) and extracting a characteristic peak wavevector (q^*) for each M_w. Figure 11d contains a plot of $\lambda \equiv (1/q^*)$ vs L_0 for samples annealed for both 6 h and 30 h and the lines correspond to power law fits yielding the relation $\lambda\ (\mu m) \sim {L_0}^{-2.5}$ or correspondingly $\lambda\ (\mu m) \sim {M_w}^{-1.5}$. This decrease of λ with increasing M_w suggests that as M_w of the outer block copolymer layer increases, its viscoelastic nature increases the free energy cost of forming large-scale surface patterns. The large-scale pattern formation in block copolymer films is therefore tentatively ascribed to the increased surface energy required to deform the surface of the block copolymer layers with increasing M_w.

Organic Light-emitting Diodes. We also mention here two characterization studies of the optimization of organic light emitting diodes (OLEDs). Schmitz and co-workers (14–16) used a masked deposition technique to produce thickness gradients in both the organic hole transport layers and the inorganic electron transport and emitting layer. OLEDs with single-gradient and orthogonal 2-D gradient structures were produced in order to evaluate the effects of the various layer thicknesses on the device efficiency. An optimal thickness for both the hole and electron transporting layers was reported. Likewise, Gross and co-workers (17) reported the use of CM to investigate the performance of doped (oxidized) ϕ-conjugated polymers in OLEDs. In these devices the polymers serve as hole transport layers but an energy barrier for hole injection exists between the polymeric material and the inorganic anode. By varying the oxidation level of the polymer this energy barrier can be reduced to lower the device working voltage. The effect of oxidation was studied by electrochemically treating the polymer to create a continuous gradient in the oxidation level of the polymer. A gradient in thickness was created orthogonal to the gradient in oxidation to explore variations of both properties simultaneously. For this reason, this study represents a cross between both combinatorial synthesis (oxidation steps) and process characterization (thickness gradient deposition). The gradient libraries were characterized by monitoring the efficiency and onset voltage of OLEDs fabricated on the gradients.

Combinatorial Adhesion Measurements. More recently, Crosby and co-workers (49) developed a combinatorial technique that can be used to investigate adhesive interactions between a polymer and another polymer, ceramic, or metal. The primary goal in the development of this technique was to design a high throughput, parallel processing adhesion test that allowed the adhesive strength dependence on multivariable environments to be determined. This combinatorial methodology for measuring polymer adhesion is largely built upon the theory of Johnson, Kendall, and Roberts (JKR) (50), which facilitates the measurement of the adhesive forces between two contacting surfaces. In the classical use of this theory, a hemispherical lens of one material is brought into contact with a complementary substrate, and subsequently separated. Rather than using a single hemispherical lens, Crosby and co-workers (49) used an array of microlenses (Fig. 12a). During this process, the contact area and displacement of each microlens is recorded through the use of an image-acquisition system integrated with an optical microscope. With these parameters, the JKR theory can then be used to quantify the adhesion energy between the two contacting materials (51). Along each axis of the array, a gradient in different environmental parameters

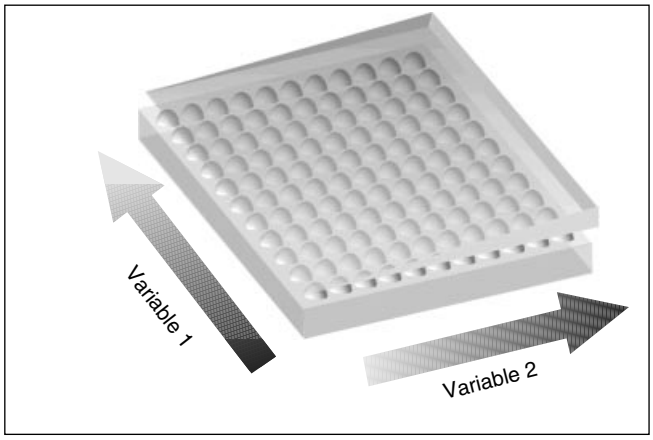

(**a**)

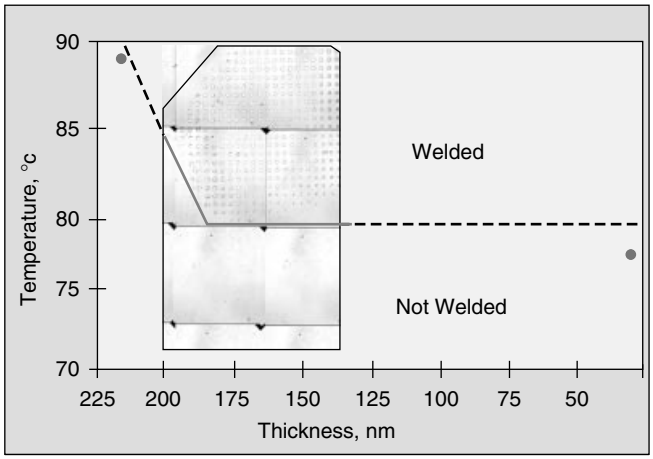

(**b**)

Fig. 12. (**a**) Schematic of microlens array used in combinatorial JKR adhesion test with two parameters varying along orthogonal axis. (**b**) Experimental results from combinatorial JKR adhesion test displaying thickness dependence of critical welding temperature for polystryrene self-adhesion. Weld spots are visible features in image. The two isolated data points were collected from independent adhesion tests. Edges of microlens array are indicated by solid black lines.

or material properties can be placed. Examples of such gradient properties are surface energy, temperature, thickness, crosslink density, blend composition, and strain. If two orthogonal gradients are placed on the array, then each microlens contact point will yield a measurement of adhesion for a unique combination of parameters. The reported microlens libraries are capable of measuring 1600 different points of adhesion within a single test.

This methodology is demonstrated by investigating the effect of thickness and temperature on the self-adhesion of PS. In this test, a microlens array was made from poly(dimethylsiloxane) (PDMS). Onto this PDMS array was floated a

thin layer of PS containing a thickness gradient. The complementary substrate for this test was a PS-coated silicon wafer with an applied temperature gradient. During contact, the PS molecules diffused across the interface to entangle and strengthen the interface, thus causing the PS coating of the PDMS microlenses to delaminate within the contact regions. This "welding" of the contact areas occurs above a critical temperature and below a critical thickness over the time scale of the test (Fig. 12b). Such measurements are useful for the microelectronics industry where adhesion of thin-polymer layers determine the integrity of electronic packaging, but the general technique will have impact on the numerous industries where adhesion plays a dominant role.

BIBLIOGRAPHY

1. E. Reddington, A. Sapienza, B. Gurau, R. Viswanathan, S. Sarangapani, E. Smotkin, and T. Mallouk, *Science* **280**, 1735 (1998).
2. X.-D. Xiang, X. Sun, G. Briceno, Y. Lou, K.-A. Wang, H. Chang, W. G. Wallace-Freedman, S.-W. Chen, and P. G. Schultz, *Science* **268**, 1738 (1995).
3. J. Wang, Y. Yoo, C. Gao, I. Takeuchi, X. Sun, H. Chang, X.-D. Xiang, and P. G. Schultz, *Science* **279**, 1712 (1998).
4. X.-D. Sun and X. X.-D. *Appl. Phys. Lett.* **72**, 525 (1998).
5. E. Danielson, J. H. Golden, E. W. McFarland, C. M. Reaves, W. H. Weinberg, and X. D. Wu, *Nature* **389**, 944–948 (1997).
6. E. Danielson, M. Devenney, D. M. Giaquinta, J. H. Golden, R. C. Haushalter, E. W. McFarland, D. M. Poojary, C. M. Reaves, W. H. Wenberg, and X. D. Wu, *Science* **279**, 837–839 (1998).
7. B. Jandeleit, D. J. Schaefer, T. S. Powers, H. W. Turner, and W. H. Weinberg, *Angew. Chem. Int. Ed.* **38**, 2494 (1999).
8. J. Klein, C. W. Lehmann, H.-W. Schmidt, and W. F. Maier, *Angew. Chem. Int. Ed.* **37**, 3369 (1998).
9. D. J. Gravert, A. Datta, P. Wentworth, and K. D. Janda, *J. Am. Chem. Soc.* **120**, 9481 (1998).
10. S. Brocchini, K. James, V. Tangpasuthadol, and J. Kohn, *J. Am. Chem. Soc.* **119**, 4553 (1997).
11. S. Brocchini, K. James, V. Tangpasuthadol, and J. Kohn, *J. Biomed. Mater. Res.* **42**, 66 (1998).
12. T. A. Dickinson, D. R. Walt, J. White, and J. S. Kauer, *Anal. Chem.* **69**, 3413 (1997).
13. C. H. Reynolds, *J. Comb. Chem.* **1**, 297 (1999).
14. C. Schmitz, P. Posch, M. Thelakkat, and H. W. Schmidt, *Phys. Chem. Chem. Phys.* **1**, 1777 (1999).
15. C. Schmitz, M. Thelakkat, and H. W. Schmidt, *Adv. Mater.* **11**, 821 (1999).
16. C. Schmitz, P. Posch, M. Thelakkat, and H. W. Schmidt, *Macromol. Symp.* **154**, 209 (2000).
17. M. Gross, D. C. Muller, H. G. Nothofer, U. Sherf, D. Neher, C. Brauchle, and K. Meerholz, *Nature* **405**, 661 (2000).
18. T. Takeuchi, D. Fukuma, and J. Matsui, *Anal. Chem.* **71**, 285 (1999).
19. N. K. Terrett, *Combinatorial Chemistry*, Oxford, Oxford, 1998.
20. K. Kennedy, T. Stefansky, G. Davy, V. F. Zackay, and E. R. Parker, *J. Appl. Phys.* **36**, 3808–3810 (1965).

21. Carson Meredith, A. Karim, and E. J. Amis, *Macromolecules* **33**, 5760–5762 (2000).
22. Carson Meredith, A. P. Smith, A. Karim, and E. J. Amis, *Macromolecules* **33**, 9747–9756 (2000).
23. A. P. Smith, Carson Meredith, J. F. Douglas, E. J. Amis, and A. Karim, *Phys. Rev. Lett.* **87**, 015503 (2001).
24. A. P. Smith, J. F. Douglas, Carson Meredith, E. J. Amis, and A. Karim, *J. Polym. Sci., Part B: Polym. Phys.* **39**, 2141 (2001).
25. J. J. Hanak, *J. Mater. Sci.* **5**, 964 (1970).
26. G. R. Newkome, C. D. Weis, C. N. Moorefield, G. R. Baker, B. J. Childs, and J. Epperson, *Angew. Chem. Int. Ed.* **37**, 307–310 (1998).
27. L. G. Leal, *Laminar Flow and Convective Transport Processes*, Butterworth-Heinemann, Boston, 1992.
28. P. J. Daivis, D. N. Pinder, and P. T. Callaghan, *Macromolecules* **25**, 170–178 (1992).
29. K. Ashley, A. Sehgal, E. J. Amis, D. Raghavan, and A. Karim, MRS 2001 Fall Meeting Proceeding, in *Polymer Interfaces and Thin Films*, in press.
30. W. Kern, ed., *Handbook of Semiconductor Wafer Cleaning Technology*, Noyes Publications, Park Ridge, N.J., 1993.
31. B. Liedberg and P. Tengvall, *Langmuir* **11**, 3821–3827 (1995).
32. J. Genzer and E. J. Kramer, *Europhys. Lett.* **44**, 180–185 (1998).
33. J. L. Masson and P. F. Green, *J. Chem. Phys.* **112**, 349 (1999).
34. Carson Meredith, A. Tona, J.-L. Sormana, A. Garcias, A. Karim, and E. J. Amis, *J. Biomed. Mater. Res.*, in Press.
35. H. Hasegawa and T. Hashimoto, *Macromolecules* **8**, 589 (1985).
36. C. S. Henkee, E. L. Thomas, and L. J. Fetters, *J. Mater. Sci.* **23**, 1685 (1988).
37. T. P. Russell, G. Coulon, V. R. Deline and D. C. Miller, *Macromolecules* **22**, 4600 (1989).
38. P. F. Green, T. M. Christensen, T. P. Russell, and R. Jerome, *Macromolecules* **22**, 2189 (1989).
39. S. H. Anastasiadis, T. P. Russell, S. K. Satija, and C. F. Majkrzak, *J. Chem. Phys.* **92**, 5677 (1990).
40. D. Ausserre, D. Chatenay, G. Coulon, and B. Collin, *J. Phys. (France)* **51**, 2571 (1990).
41. G. Coulon, D. Ausserre, and T. P. Russell, *J. Phys. (France)* **51**, 777 (1990).
42. T. P. Russell, A. Menelle, S. H. Anastasiadis, S. K. Satija, and C. F. Majkrzak, *Macromolecules* **24**, 6263 (1991).
43. P. F. Green, T. M. Christensen, and T. P. Russell, *Macromolecules* **24**, 252 (1991).
44. T. P. Russell, A. Menelle, S. H. Anastasiadis, S. K. Satija, and C. F. Majkrzak, *Macromol. Chem., Macromol. Symp.* **62**, 157 (1992).
45. A. Menelle, T. P. Russell, S. H. Anastasiadis, S. K. Satija, and C. F. Majkrzak, *Phys. Rev. Lett.* **68**, 67 (1992).
46. Z. Cai, K. Huang, P. A. Montano, T. P. Russell, J. M. Bai, and G. W. Zajac, *J. Chem. Phys.* **93**, 2376 (1993).
47. G. Coulon, J. Daillant, B. Collin, J. J. Benattar, and Y. Gallot, *Macromolecules* **26**, 1582 (1993).
48. A. M. Mayes, T. P. Russell, P. Bassereau, S. M. Baker, and G. S. Smith, *Macromolecules* **27**, 749 (1994).
49. A. J. Crosby, A. Karim, and E. J. Amis, *Am. Chem. Soc. Polym. Prepr.* **42**, 645(2001).
50. K. L. Johnson, K. Kendall, and A. D. Roberts, *Proc. R. Soc. London, Ser. A* **324**, 301–313 (1971).

51. K. R. Shull, D. Ahn, W.-L. Chen, C. M. Flanigan, and A. J. Crosby, *Macromol. Chem. Phys.* **199**, 489–511 (1998).

CARSON MEREDITH
Georgia Institute of Technology
ARCHIE P. SMITH
ALFRED J. CROSBY
ERIC J. AMIS
ALAMGIR KARIM
National Institute of Standards and Technology

COMPOSITES, FABRICATION. See Volume 2.

COMPOUNDING. See PROCESSING.

COMPUTER CONTROLLED PROCESSING. See PROCESS AUTOMATION.

CONDUCTIVE POLYMER COMPOSITES

Introduction to Electrically Conductive Adhesives

Electrically conductive adhesives (ECAs) are composites of polymeric matrices and electrically conductive fillers. Polymeric matrices have excellent dielectric properties and thus are electrical insulators. The conductive fillers provide the electrical properties and the polymeric matrix provides mechanical properties. Therefore, electrical and mechanical properties are provided by different components, which is different from metallic solders that provide both electrical and mechanical properties. ECAs have been with us for some time. Metal-filled thermoset polymers were first patented as ECAs in the 1950s (1–3). Recently, ECA materials have been identified as one of the major alternatives for lead-containing solders for microelectronics packaging applications. There are two types of conductive adhesives: anisotropically conductive adhesives (ACAs) and isotropically conductive adhesives (ICAs). Utilization of both types of conductive adhesives as lead-free alternatives for flip chip, surface mount technology (SMT), chip scale package (CSP), and ball grid array (BGA) applications are reviewed here.

Anisotropically Conductive Adhesives

Anisotropically conductive adhesives (ACAs) represent the first major division of polymer bonding agents. The anisotropic class of adhesives provides unidirectional electrical conductivity in the vertical or z-axis. This directional conductivity is achieved by using a relatively low volume loading of conductive filler (5–20 vol%) (4–6). The low volume loading is insufficient for interparticle contact

Encyclopedia of Polymer Science and Technology. Copyright John Wiley & Sons, Inc. All rights reserved.

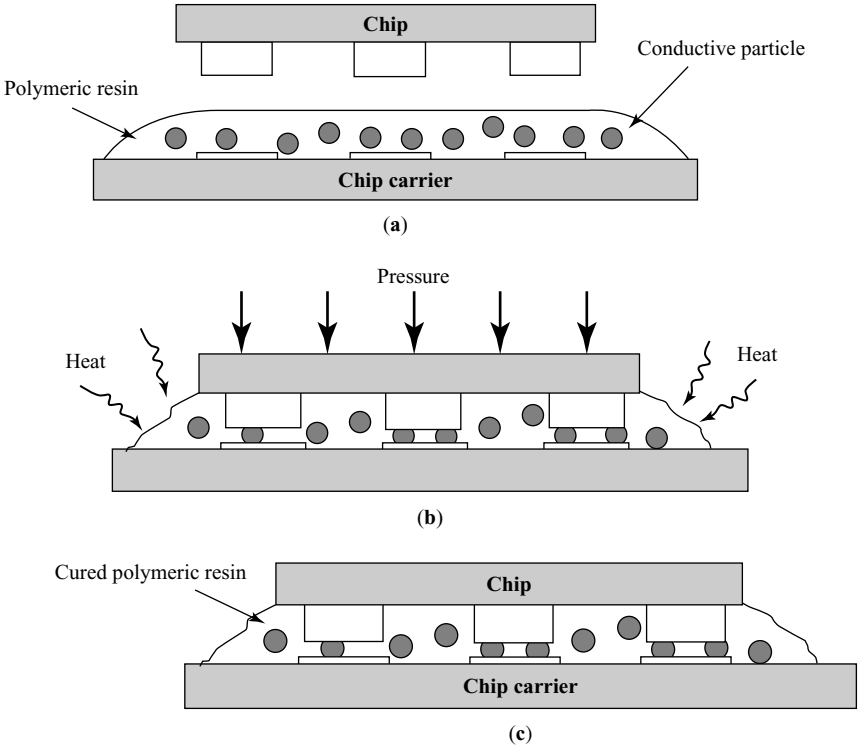

Fig. 1. A series of schematics illustrating the steps in forming an ACA joint. (**a**) Component parts: a bumped die and mating carrier with ACA spread over the surface. (**b**) Die is mounted with the carrier and held in place when cured. (**c**) Side view of the completed assembly.

and prevents conductivity in the x–y plane of the adhesive. The z-axis adhesive, in film or paste form, is interposed between the surfaces to be connected. Application of heat and pressure to this stack-up causes conductive particles to be trapped between opposing conductor surfaces on the two components. Once electrical continuity is achieved, the dielectric polymer matrix is hardened by chemical reaction (thermosets) or by cooling (thermoplastics). The hardened dielectric polymer matrix holds the two components together and helps maintain the pressure contact between component surfaces and conductive particles. A series of sketches in Figure 1 illustrates the attachment steps in achieving ACA joints.

Broadly ACAs fall into two categories: those that are anisotropically conductive before processing and those whose anisotropy arises as a result of processing. Their characteristics can be summarized as follows:

(1) Preprocessing anisotropy results from materials characterized by an ordered system of conductor elements interspersed in an adhesive matrix film. They are always in the form of tape or sheet and are evidently complicated to manufacture, requiring an adhesive film to be laser-drilled or etched then filled with conducting materials. They provide predictable contacts and are typically applied to a substrate as preforms.

(2) Postprocessing anisotropy results from materials that are a homogeneous mix of conductive fillers and adhesive matrix and that have no internal structure or order prior to processing. All adhesive pastes and some tapes fall into this category.

Adhesive Matrix. The adhesive matrix is used to form a mechanical bond at an interconnection. Both thermosetting and thermoplastic materials are used. Thermoplastic adhesives are rigid materials at temperatures below the glass-transition temperature (T_g) of a polymer. Above the T_g, polymers exhibit flow characteristics. Thus, the T_g must be sufficiently high to avoid polymer flow during the application conditions, but the T_g must be low enough to prevent thermal damage associated with chip carrier and devices during assembly. The principal advantage of thermoplastic adhesives is the relative ease with which interconnections can be disassembled for repair operations (7,8). However, thermoplastic ACAs suffer from many disadvantages. One of the most serious issues is that adhesion is not sufficient to hold the conductive particles in position, causing the contact resistance to increase after thermal shocks (7,8). Moreover, a phenomenon called spring back increases the contact resistance while the adhesive layer recovers from the stress caused by pressing of an ACA onto the components during bonding. This phenomenon, a creep characteristic exhibited by thermoplastic elastomers, occurs much after an ACA film has been heated to create the electrical joints. The contact resistance sometimes increases to more than three times the initial resistance during spring back (ie unloading) (7).

Thermosetting adhesives, such as epoxies and silicones, form a three-dimensional cross-linked structure when cured under specific conditions. Cure techniques include heat, UV light, and added catalysts. As a result of the cure reaction which is irreversible, the initial uncross-linked material is transformed into a rigid solid. The themosetting ACAs are stable at high temperatures and, more importantly, provides a low contact resistance. This results from a compressive force that maintains the conductive particles in intimate contact after the cure. That is, the shrinking caused by the cure reaction achieves a low contact resistance with long time stability. The ability to maintain strength at high temperature and robust adhesive bonds are the principal advantages of these materials. However, because the cure reaction is not reversible, rework or repair of interconnections is not an option (7,8). The choice of adhesive matrix and its formulation is critical to the long-term life properties of a composite. In practice, many options exist for the adhesive matrix. Acrylics can be used in low temperature applications (under 100°C), while epoxies are more robust and can be used at higher temperatures (up to 200°C). Polyimide is used in the harshest environments where the temperature approaches 300°C (6).

Conductive Fillers. Conductive fillers are used to provide the adhesive with electrical conductivity. The simplest fillers are metal particles such as gold, silver, nickel, indium, copper, chromium, and lead-free solders (SbBi) (6,7,9–11). The particles are usually spherical and range 3–15 μm in size for ACA applications (12). Needles or whiskers are also quoted in some patents (6).

Some ACA systems employ nonconductive particles with a thin metal coat. The core material is either plastic or glass with a metal coating consisting of gold, silver, nickel, aluminum, or chromiun. The basic particle shape of these systems is

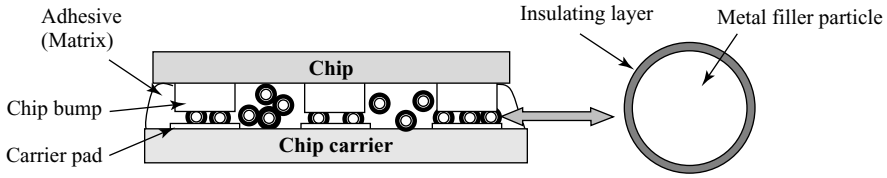

Fig. 2. Schematic depicting the cross section of an interconnection using an MCF-filled ACA.

also spherical. Plastic-cored particles deform when compressed between opposing contact surfaces, and thus provide a large contact area. Polystyrene (PS) is often selected as the core material because the coefficient of thermal expansion (CTE) of metal-coated PS beads is very close thermoset adhesives. The combination of epoxy resin and metal-plated PS beads results in a large improvement in thermal stability (7). In addition, glass can also be selected as the core material. Glass-cored particles coated with metal lead to a controlled bond-line thickness because the glass core is not deformable. Since the conductive particle size is known, the conductivity of the joint can be predicted.

To achieve fine pitch connections, a metal sphere or metal-coated plastic sphere coated with an insulating resin fillers were developed. The insulating resin layer is broken only under pressure to expose the underlying conductive surfaces, referred to as a microcapsule filler- (MCF). A higher filler loading can be achieved with MCFs for fine pitch applications, which avoid creating electrical short circuit conditions between printed circuit features (7,12). A typical cross section of an ACA interconnection with MCF material is illustrated in Figure 2.

Flip Chip Applications Using ACAs

In traditional flip chip packages, solder bumps provide electrical connections between a chip and chip carrier. To achieve high reliability, organic underfill materials are usually required to fill the gap between the chip and chip carrier. The cured underfills create a monolithic structure that evenly distributes the stress over all the material in the gap, not just on the solder connections. In the past several years, much research has been conducted to develop flip chip packages, using ACAs in place of solder bumps. The primary advantages of ACA over lead-bearing solder for flip chips include ACAs' fine pitch capability, lead-free, low processing temperature, absence of flux residue, and generally lower cost. Also, ACA flip chip technology does not require an additional underfilling process because the ACA resin acts as an underfill.

ACA flip chip technology has been employed in many applications where flip chips are bonded to rigid chip carriers (13). This includes bare chip assembly of ASICs in transistor radios, personal digital assistants (PDAs), sensor chip in digital cameras, and memory chip in lap-top computers. In all the applications, the common feature is that ACA flip chip technology is used to assemble bare chips where the pitch is extremely fine, normally less than 120 μm. For these fine applications, it is apparently the use of ACA flip chip instead of soldering which is more cost effective.

ACA flip chip bonding exhibits better reliability on flexible chip carriers because the ability of flex provides compliance to relieve stresses. For example, the internal stress generated during resin curing can be absorbed by the deformation of the chip carrier. ACA joint stress analysis conducted by Wu and co-workers indicated that the residual stress is larger on rigid substrates than on flexible substrates after bonding (14).

ACA Flip Chip for Bumped Dies.

Comparison of ACAs with Hard and Soft Fillers. Kishimoto and co-workers reported (15) ACA pastes using two different fillers: Au-coated rubber particles (soft) and nickel particles (hard). The ACAs were used to bond a flip chip with Au plated bumps to a board with copper metallization. With the application of pressure, the soft particles were brought into contact with surface pads and were deformed, which lowered this contact resistance. The hard particles, however, deformed the bumps and pads, and thus were also in intimate contact with the surfaces to help reduce this contact resistance. Their study showed that their choice of both hard and soft fillers in ACA materials had similar voltage–current behavior, and both exhibited stable contact resistance values after 1000 cycles of thermal cycling and 1200 h of 85°C/85% RH aging conditions (15).

Coated Plastic Filler. Casio developed an advanced ACA film called the Microconnector (Fig. 3) (16–18). This adhesive contains conductive particles made by coating plastic spheres with a thin layer of metal, followed by an additional 10-nm-thick layer of insulating polymeric material. The insulating layer consists of a large number of insulating micropowder particles which electrically insulate the outer surface of the spheres. The thin insulation layer is formed by causing insulating micropowder particles to adhere to the surface of the metal layer via electrostatic attraction. The base adhesive resin is thermoplastic or thermosetting,

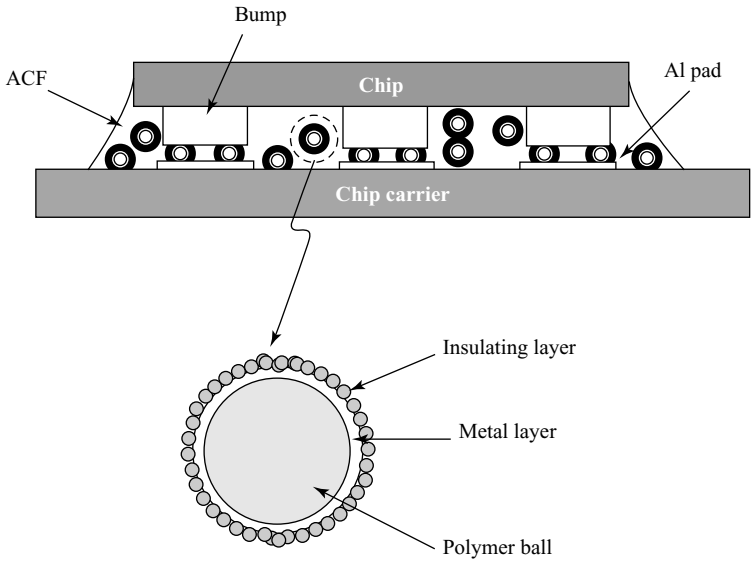

Fig. 3. Schematic depicting Casio's ACF technology – Microconnector.

producing compressive force when cured. When heat and pressure are applied during bonding, the insulating layer, which is in contact with the bump surface of an IC, is broken. However, the insulating layer remains intact on conductive particles not crushed by the bonding pads, thereby producing only *Z*-axis electrical interconnections and preventing lateral short circuit conditions. With an additional insulating layer, a fine pitch and low contact resistance can be achieved without the risk of lateral short circuiting by increasing the filler percentage (ie amount of particles per unit volume base adhesive resin or film). Casio is manufacturing pocket TVs with a liquid crystal using this material (18).

Solder Filler Systems. Unlike most commercial ACAs, where the electrical conductivity is based on the degree of mechanical contact achieved by pressing conductive particles to contact pads on board and chip bumps, solder-filled ACAs establish microscopic metallurgical interconnections. The advantage of these joints is that the metallurgical bonds that are established prevent electrical discontinuities from occurring should the adhesive polymeric matrix undergo relaxation during the operational lifetime. Therefore, solder-filled ACAs combine the benefits of both soldering and adhesive joining resulting in more reliable ACA joints. Furthermore, better electrical performance is achieved as a result of lower contact resistance established through metallurgical bonds (19).

Joints made with SnBi- and Bi-filled ACAs experience brittle intermetallic compound formation and have problems with typical conductor and coating materials such as copper, nickel, gold, and palladium (20). But Bi and BiSn are compatible with tin, lead, zinc, and aluminum. However, Zn and Al are easily oxidized, and so in practice only Sn and Pb are suitable surface finish materials for SnBi- and Bi-filled ACA applications (Fig. 4). Vuorela demonstrated that high quality interconnections were formed by metallurgical bonding SnPb-bumped chips on SnPb-coated substrates at relatively low temperature and pressure utilizing a

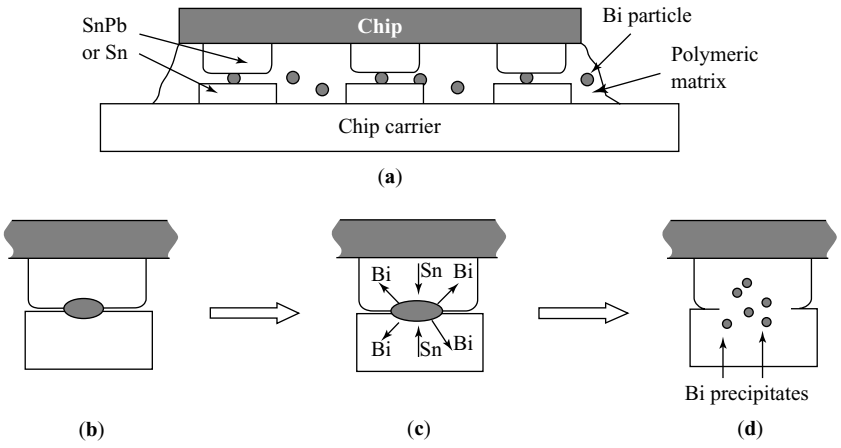

Fig. 4. Schematic illustration of the formation of electrical interconnects between a bumped chip and a mating carrier using a Bi-filled ACA. (**a**) The chip is aligned and placed on a chip carrier. (**b**) The Bi particle is deformed between a chip bump and a carrier pad when a bonding pressure is applied. (**c**) The Bi particle dissolves into the liquid lentils upon exposure of heat. (**d**) Bi diffuses into the Sn–Pb matrix and forms fine solid precipitates.

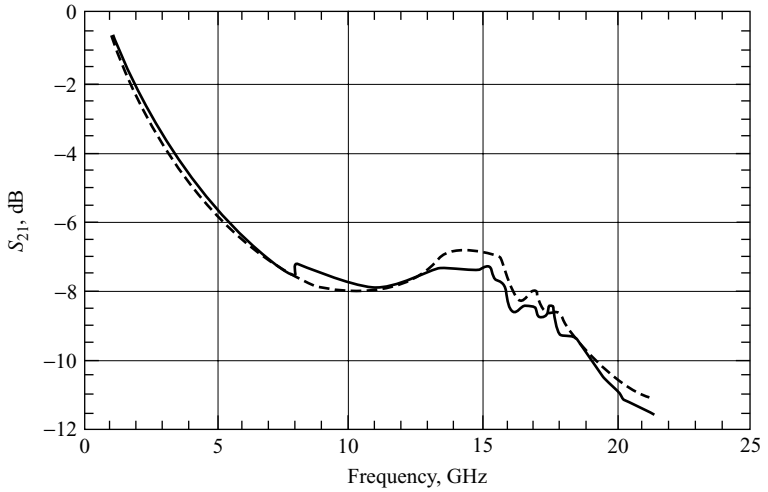

Fig. 5. ACA-bonded flip chips exhibit the same transmission coefficient, S_{21}, as solder-bonded flip chips from 1 to 21 GHz. —— Transmission: ACA; - - - - Transmission: solder.

Bi-particle-filled ACA. The ACA joints exhibited a stable resistance after 2000-h 85°C/85% RH aging or after 1000-h temperature cycle testing (−40 to 125°C). Even though this work was still preliminary, it demonstrated an interesting idea and concept. For lead-free applications, different materials such as pure Sn can be used for chip bumps and surface finish on the substrate (21).

ACA Bumped Flip Chips for High Frequency Applications. The high frequency behavior of ACA interconnections has attracted much attention in the past several years. Sihlbom and co-workers demonstrated that ACA-bonded flip chips can provide performance equivalent to solder flip chips in the frequency range of 45 MHz to 2 GHz on FR4 chip carriers and 1 to 21 GHz on a high frequency Telfon-based chip carrier (Fig. 5). The different particle sizes and materials in the conductive adhesives gave little difference in high frequency behavior of ACA joints (22,23).

Yim and co-workers developed a microwave frequency model for ACF-based flip chip joints based on microwave network analysis and *S*-parameter measurements. By using this model, high frequency behavior of ACF flip chip interconnections with two filler particles, Ni and Au-coated polymer particles, was simulated. It was predicted that Au-coated polymer-particle-filled ACF flip chip interconnections exhibited comparable transfer and loss characteristics to solder bumped flip chips up to about 13 GHz and thus they can be used for up to 13 GHz, but Ni-filled ACF joints can only be used for up to 8 GHz because the Ni particle has a higher inductance compared to the Au-coated particle. Polymeric resins with a low dielectric constant and conductive particles with low inductance are desirable for high resonance frequency applications (24).

ACA for Unbumped Flip Chips. Although ACAs are typically utilized with flip chip bumped dice, they are also used for unbumped flip chips in some cases. For unbumped flip chips, a pressure-engaged contact must be established by bringing the particles to the aluminum chip pads rather than a bump. The

pressure must be sufficient to break the oxide on the aluminum pads. A sufficient quantity of particles must be trapped in the contact pad area and remain in place during bonding and curing to achieve a reliable interconnection. In addition to maximizing the number of particles in the contact area the number of particles located between adjacent pads must be minimized so as to prevent electrical shorts. An additional factor that must be in the case of unbumped flip chips is adhesive flow during bonding and curing. It is essential to control the temperature heating to be sufficiently slow when the polymeric resin is curing so that the conductive filler particles can migrate from the chip carrier side to the chip side pad (25).

Ni/Au Coated Silver Bumps. A flip chip technology developed by Toshiba Corp. utilized an anisotropic conductive film (ACF) to attach bare unbumped chips (with Al pads) onto a printed circuit board (PCB) with bumps formed from a silver paste screen printed on the PCB (26). After curing, Ag bumps were formed (70-μm diameter, 20-μm height), which were subsequently overplated with Ni/Au. It was determined that ACF with a low CTE (28 ppm/$^\circ$C), low water absorption rate (1.3%), and that utilized a Au-plated plastic ball worked best. It was also found that Ni/Au plated Ag-paste formed bumps exhibited a smaller initial connection resistance (22 and 48 $\mu\Omega$ for Ag bumps with and without Ni/Au overplating, respectively) and a smaller connection resistance increase compared to Ag-paste formed bumps which were not overplated with Ni/Au after 1000-h accelerated thermal cycling (ATC) testing (ie the final connection resistances after aging are 294 and 717 $\mu\Omega$ for Ag bumps with and without Ni/Au overplating, respectively).

Conductive Columns. Nitto Denko Corp. developed an ACF for fine pitch flip chip applications (27). The features of this ACF were (*1*) connectability between bumpless chips and fine pitch PCB; (*2*) high electrical conductivity; (*3*) repairability (easy to peal off chips from a printed circuit board at elevated temperatures); (*4*) high reliability; and (*5*) potential storage at room temperature. There are other notable features too: (*1*) ACF is usable at pitches down to 25 μm, (*2*) the conductive elements are micrometallic columns as opposed to random-shaped particles, and (*3*) this adhesive matrix consists of a thermoplastic polymer resin, conductive columns coated with an insulator, and a high T_g polymer, which completely separates the columns from the adhesive (Fig. 6).

It is easy to change the diameter of the conductive columns in order to make the film compatible with a variety of pitches. Sn/Pb or other solder materials are plated on both the top and bottom of the conductive columns (usually copper). The plated solder on the both ends of the conductive columns melts and forms metallurgical connections between the conductive columns and metal pads on a chip and the mating chip carrier, which ensure a good connection. Figure 6a illustrates the cross section of the film structure. A rough surface, a result of plating, has the advantage of providing a good connection with the terminal pads it is in contact with. A typical terminal pad structure of a chip without bumps is shown in Figure 6b. To achieve a good connection, the height of the conductive columns must be larger than the thickness of the passivation layer (t_p). Since t_b (the distance from a Cu pad surface of the chip carrier to the passivation layer surface of the chip) is usually smaller than t_a (the distance from solder mask surface of the chip carrier to the passivation layer surface of the chip), the conductive columns will assume an inclined position during bonding if the thickness of the conductive columns

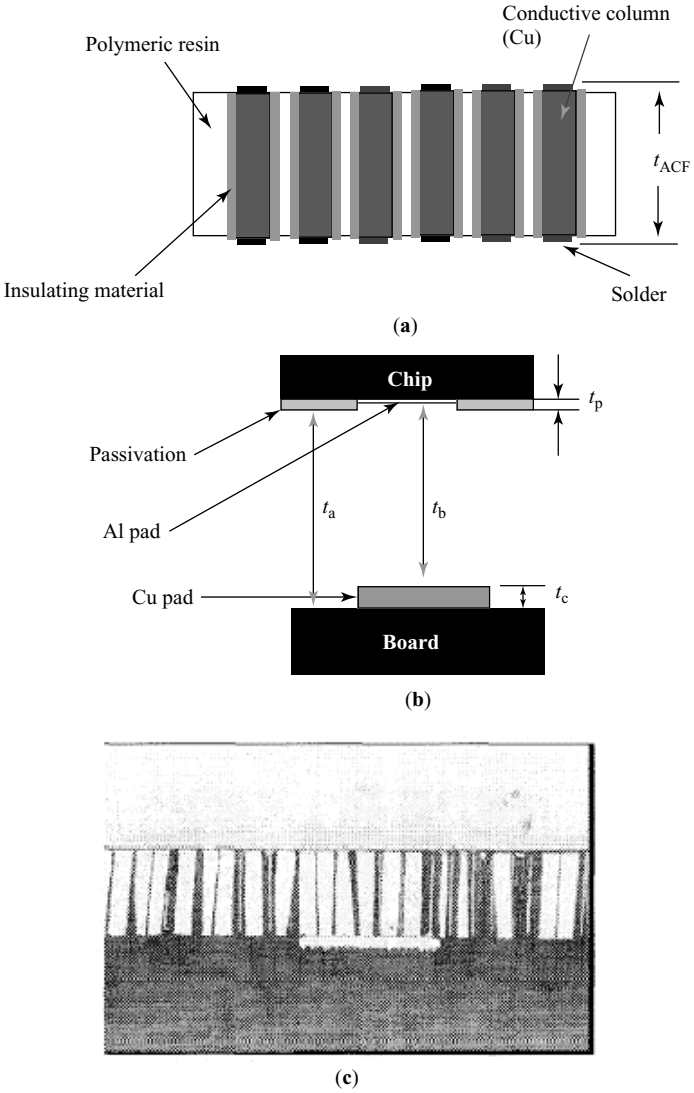

Fig. 6. Illustration of a scheme for fine pitch, flip chip interconnection. (**a**) An ACF filled with micrometallic columns. (**b**) A typical cross-sectional structure of a chip without bumps and the mating chip carrier. (**c**) A cross section of an interconnect formed between an unbumped chip and the mating chip carrier.

is larger than the ACF thickness (t_{ACF}). It is important to adjust the thickness of board or chip carrier pads and ACF thickness to achieve good connection and adhesion. Reliability results indicated that the ACF possessing an adhesive matrix with a high T_g (282°C) exhibited high reliability and the contact resistance remained unchanged after 1000 cycles of ATC testing (−25 to 125°C). Figure 6c is a photography of a cross section of a joint formed between an unbumped die and a chip carrier using this ACF flip chip interconnection method.

ACAs for CSP and BGA Applications

Area Bonding Conductive Adhesives. Aiming at the CSP application market, Merix Corp. and Auburn University collaborated to develop an ACA called *area bonding conductive (ABC) adhesives*. ABC adhesive is a two-region thermoset adhesive with ECA pads surrounded by a continuous oxide-filled dielectric adhesive to form a total area bond. Both regions are solvent-free, B-staged, nontacky epoxies supplied on a Mylar carrier release film. In contrast to conventional ACAs, conductive areas of ABC adhesive are only at bond pad locations. The assembly process for using ABC adhesives is shown in Figure 7. The ABC adhesives potentially can provide a reliable, low cost, low temperature, low pressure process for flip chip and CSP applications (28).

Au-Stud vs Electroless Ni/Au Bumps. As the demand for miniaturization has increased dramatically, concentrated efforts have been made to find cheaper alternatives to established technologies of area array solder bumps.

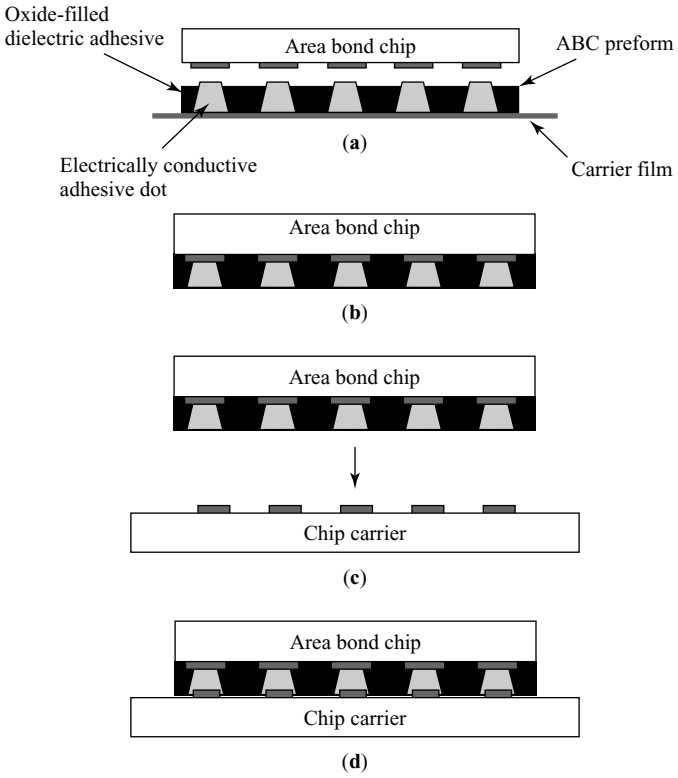

Fig. 7. Schematic depicting a flip chip assembly processing utilizing ABC adhesive. (**a**) A chip is aligned to the ABC preform which is on a carrier film. (**b**) The ABC preform is tacked to the die at 100°C and under a pressure of 150 g for 30 s, and then the carrier film is removed after the chip is cooled down. (**c**) The chip with ABC preform is aligned to a mating chip carrier (FR4 board). (**d**) The chip/ABC preform is attached to the chip carrier at 100°C and under a pressure of 150 g for 30 s, and then the package is cooled down.

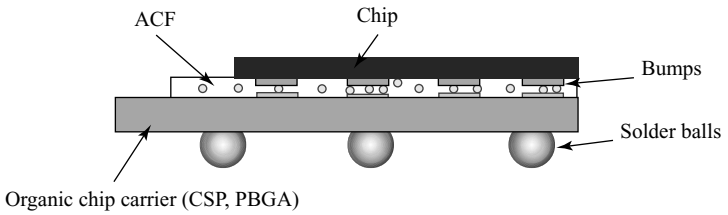

Fig. 8. Schematic depicting the side view construction of a ChipPAC CSP package that utilizes an ACF.

ChipPAC, Inc., demonstrated an alternate process/package concept covering both CSP and PBGA package formats whose construction is illustrated in Figure 8. The concept package consisted essentially of three parts: ACF, metallic bumps on the die bond pads, and an organic chip carrier (29).

Although this packaging solution was not entirely unique, reducing it to a high volume assembly and packaging process, where low cost and high reliability were key, was innovative. This configuration provides an appealing package solution, based on several factors. First, the connection can be implemented at a much finer pitch ($\sim$100 μm) compared to conventional solder bumps, and so there is a potential for a die-size reduction in flip chip IC designs that are normally implemented as multirow perimeter arrays using conventional solder bumps. Second, the ACF interconnect approach allows the use of inexpensive bumping technologies, thereby greatly reducing the wafer bumping cost portion of the overall package cost.

The combination of cured adhesive interconnection, bumps, and organic substrate provides a reliable, cost-effective flip chip CSP. It was determined that Au-stud bumps were preferable to Ni/Au bumps because of the former's compliant nature. Since the planarity control of organic chip carriers is difficult, given the nature of the material, it was simpler to change the interconnection method, ie, using Au-stud bumps. However, electroless Ni/Au bumps are still an option, if the material properties of the ACF and/or chip carrier are altered to provide compliancy.

Double-Layered ACF. Motorola developed a low cost and low profile flip chip on flex (FCOF) CSP package using ACFs (30). The package has the flexibility to utilize the existing wire-bonding pad configuration without adding prohibitive redistribution and wafer solder bumping costs, and eliminated the need for underchip encapsulation. Two types of ACF film were studied: double layer films with the second layer loaded with Ni/Au plated polystyrene–divinylbenzene (PS–DVB) spheres, and solid Ni particles. The film structure, consisting of a nonfilled and a conducting particles-filled adhesive layers, is illustrated in Figure 9. The double-layer design reduces the particle density in x–y spacing of interconnection pads, which serve to enhance the x–y plane insulation characteristics. At the same time, the double-layer film provides more adhesive volume that helps to entrap more particles on the bonding interconnection pads. Both calculated and observed values show that the number of conducting particles trapped is much higher than those in single-layer ACF. This indicate that even though particle density in a

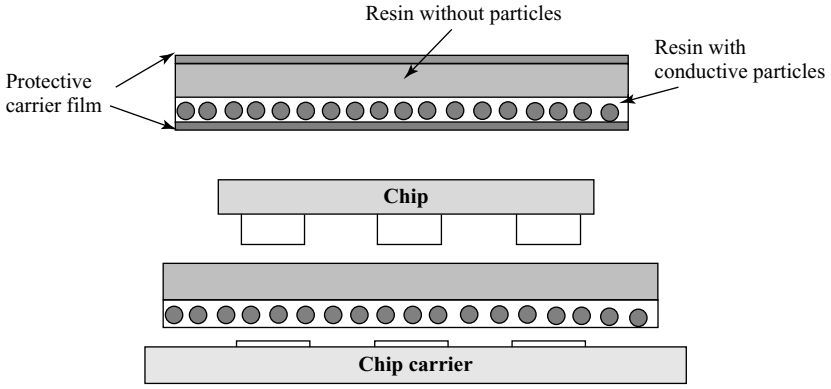

Fig. 9. Schematic of a double layer ACF.

double-layer ACF is low, conducting particles to effect electrical contact with both interconnection pads are trapped more effectively between interconnection pads in the double-layer ACF. The die has Ni/Au plated bonding pads and the chip carrier is flexible polyimide which can provide adequate compensation for the planarity differences. Its compliant nature under compressive bonding operation allows the copper traces at the bonding area to deform and compensate for nonplanarity or irregularity that exists. The ACF adhesive system provided the system with stable contact resistance after 500 cycles of liquid–liquid temperature shock (LLTS) aging (-55 to 125°C).

Ceramic Chip Carriers vs Organic Chip Carriers. A ceramic chip carrier and an organic chip carrier, whose configuration is equivalent to that of microball grid array (μBGA) style CSP and broadly representative of BGA and flip chip devices, were evaluated using ACAs with conducting particles of various sizes (31). The ceramic chip carrier has AgPd thick-film bonding pads and the organic chip carrier is a conventional PCB (1 oz Cu clad FR5 laminate) with submicron Au-coated Cu pads. It was determined that uniform conductivity and high yield were more readily achieved with organic chip carrier rather than ceramic chip carriers. This is because bonding pads on the FR5 chip carrier have better coplanarity compared to the thick-film ceramic chip carrier. ACAs with finer particles exhibited worse overall performance on both chip carriers, while ACAs with larger and polymer-cored particles exhibited better performance because the deformable polymer-cored particles compensated the gap variations between the chip bumps and the chip carriers.

SMT Applications

ACAs have been investigated as replacement for SnPb solder in surface mount (SM) attachment for fine pitch applications. The key attractive advantage is the cost effectiveness of using ACA to bond fine pitch SM components. A limitation of ACAs is the need to cure under a contact pressure. The concept of using an ACA as a solder replacement on rigid chip carriers utilizing conventional SMT

has been demonstrated by Liu and co-workers (32). Fine pitch SM components were bonded to FR4 boards with ACAs using a fine pitch bonder and then components with larger pitches were bonded with ICAs using standard SM equipment. The study demonstrated that standard surface-mounting tools could be used to assemble conductive adhesives. The connection resistance of solder-plated, plastic components (0.65 mm pitch) with ACAs bonded did not change after an accelerated temperature cycling (ATC) test conducted at −40 to 85°C. However, similar parts failed under conditions of −55 to 125°C for 1000 cycles (33). The mechanical stability problem may have been the result of an improper joint geometry, ie not optimized for ACA bonding.

Failure Mechanism

Since the adhesive matrix is a nonconductive material, interconnection joints rely to some extent on pressure to assure contact for conventional ACAs. Adhesive interconnections therefore exhibit different failure mechanisms compared to soldered connections, where the formation of intermetallic compounds and coarsening of grains are associated with the main mechanisms. Basically there are two main failure mechanisms that can affect the contacts. The first is the formation of an insulating film on either the contact areas or conductive particle surfaces. The second is the loss of mechanical contact between the conductive elements due to either a loss of adherence or relaxation of the compressive force.

Oxidation of Nonnoble Metals. Electrochemical corrosion of nonnoble metal bumps, pads, and conductive particles results in the formation of insulating metal oxides and significant increase in contact resistance. Electrochemical corrosion only occurs in the presence of moisture and metals that possess different electrochemical potentials. Humidity generally accelerates oxide formation and so too the increase in contact resistance. Reliability test results for FCOF using gold bumps and ACFs filled with Ni particles indicated that the connection resistance increased with time under elevated temperature and humidity storage conditions (34). In this case, the gold bump acts as cathode and the Ni particle as an anode. A nickel oxide, which is electrically insulating, eventually forms on the surface of the Ni particles.

Loss of Compressive Force. The compressive forces acting to maintain contact among the conductive components are partly achieved because of curing shrinkage achieved when curing the polymeric matrix of ACAs. Both the cohesive strength of the adhesive matrix and the interfacial adhesion strength between the adhesive matrix and the chip and chip carrier must be sufficient to maintain the compressive force. However, the thermal expansion of adhesives, their swelling due to moisture adsorption, and mechanical stresses due to applied loads tend to diminish this compressive force created as a result of curing. Moreover, water not only diffuses into the adhesive layer but also penetrates to the interface between adhesive and chip/chip carrier, causing a reduction in adhesion strength. As a result, the contact resistance increases and can even result in a complete loss of electrical contact (35).

Isotropic Conductive Adhesives

Percolation Theory of Conduction. Isotropic conductive adhesives (ICAs), also called as polymer solder, are composites of polymer resin and conductive fillers. The conductive fillers provide the composite with electrical conductivity through contact between the conductive particles. With increasing filler concentrations, the electrical properties of ICAs transform from an insulator to a conductor. Percolation theory has been used to explain the electrical properties of ICA composites. At low filler concentrations, the resistivities of ICAs decrease gradually with increasing filler concentration. However, the resistivity drops dramatically above a critical filler concentration, V_c, called the percolation threshold. It is believed that at this concentration, all the conductive particles contact each other and form a three-dimensional network. The resistivity decreases only slightly with further increases in the filler concentrations (36–38). A schematic explanation of resistivity change of ICAs based on percolation theory is shown in Figure 10. In order to achieve conductivity, the volume fraction of a conductive filler in an ICA must be equal to or slightly higher than the critical volume fraction. Similar to solders, ICAs provide the dual functions of electrical connection and mechanical bond in an interconnection joint. In an ICA joint (Fig. 11), the polymer resin provides mechanical stability and the conductive filler provides electrical conductivity. Filler loading levels which are too high cause mechanical integrity of adhesive joints to deteriorate. Therefore, the challenge in formulating an ICA is to maximize conductive filler content to achieve a high electrical conductivity without adversely affecting the mechanical properties. In a typical ICA formulation, the volume fraction of the conductive filler is about 25–30% (4,5).

Adhesive Matrix. Polymer matrices of ICAs are similar to ACAs. An ideal matrix for ICAs should exhibit a long shelf life (good room temperature latency), fast cure, relatively high glass-transition temperature (T_g), low moisture pickup, and good adhesion (39).

Both thermoplastic and thermoset resins can be used for ICA formulations. The main thermoplastic resin used for ICA formulations is polyimide resin. An attractive advantage of thermoplastic ICAs is that they are reworkable, eg, can

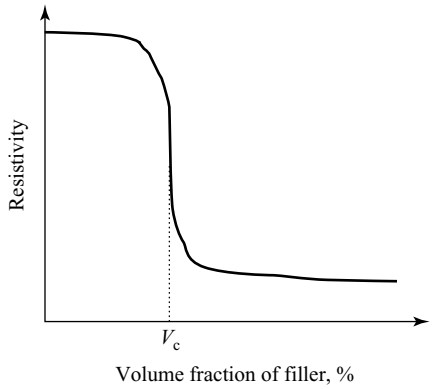

Fig. 10. Effect of filler volume fraction on the resistivity of ICA systems.

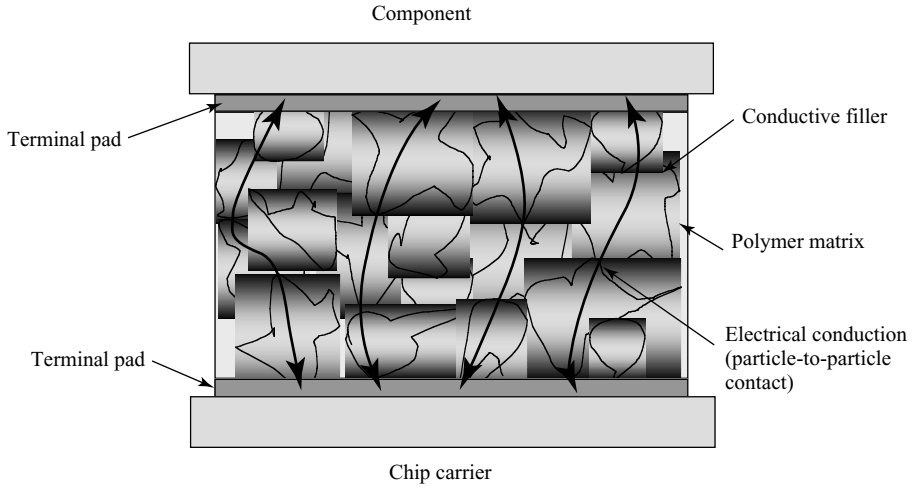

Fig. 11. Schematic that illustrates how electrical conduction paths are established by uninterrupted particle-to-particle contact between the component and chip carrier terminal pads in an ICA joint.

easily be repaired. A major drawback of thermoplastic ICAs, however, is the degradation of adhesion at high temperature. Another drawback of polyimide-based ICAs is that they generally contain solvents. During heating, voids are formed when the solvent evaporates. Most of commercial ICAs are based on thermosetting resins. Epoxy resins are most commonly used in thermoset ICA formulations because they possess superior balanced properties. Silicones, cyanate esters, and cyanoacrylates are also employed in ICA formulations (40–44).

Conductive Fillers. Because polymer matrices are dielectric materials, conductive fillers in ICA formulations provide the material with electrical conductivity. In order to achieve high conductivity, the filler concentration must be at least equal to or greater than the critical concentration predicted by percolation theory.

Pure Silver vs Ag-Coated Fillers. Silver (Ag) is by far the most popular conductive filler, although gold (Au), nickel (Ni), copper (Cu), and carbon (C) are also used in ICA formulations. Nickel and copper-based conductive adhesives generally do not have good conductivity stability because they are easily oxidized. Even with antioxidants, copper-based conductive adhesives show an increase in volume resistivity on aging, especially under high temperature and humidity conditions. Silver-plated copper has been utilized commercially in conductive inks, and should also be appreciable as a filler in adhesives. While composites filled with pure silver particles often show improved electrical conductivity when exposed to elevated temperature and humidity or thermal cycling, this is not always the case with silver-plated metals, such as copper flake. Presumably, the application of heat and mechanical energy allows the particles to make more intimate contact in the case of pure silver, but silver-plated copper may have coating discontinuities that allow oxidation/corrosion of the underlying copper and thus reduce electrical paths (4).

Particle Shape and Size. The most common morphology of conductive fillers used for ICAs is flake because flakes tend to have a large surface area, and more contact spots and thus more electrical paths than spherical fillers. The particle size of ICA fillers generally ranges from 1 to 20 μm. Larger particles tend to provide the material with a higher electrical conductivity and lower viscosity (45). A new class of silver particles, porous nano-sized silver particles, has been introduced in ICA formulations (46,47). ICAs made with this type of particles exhibited improved mechanical properties, but the electrical conductivity is less than ICAs filled with silver flakes. In addition, short carbon fibers have been used as conductive fillers in conductive adhesive formulations (36,48). However, carbon-based conductive adhesives show much lower electrical conductivity than silver-filled ones.

Silver-Copper Fillers. In 1992, a powder with a specific structure was introduced as a filler for conductive adhesives (49). A powder particle consists of two metallic components, copper and silver. Silver is highly concentrated on the particle surface and concentration gradually decreases from the surface to the inner of the particle, but always contains a small amount of silver. Conductive adhesive paste filled with this powder exhibits excellent oxidation resistance, ie can be exposed to oxygen content about 100 ppm in a nitrogen atmosphere. It also exhibits higher solderability than commercially available copper pastes, sufficient adhesion strength even after heating and/or cooling test, and least migration, almost same degree to pure copper paste (49).

Low-Melt Fillers. In order to improve electrical and mechanical properties, low-melting-point alloy fillers have been used in ICA formulations. A conductive filler powder is coated with a low-melting-point metal. The conductive powder is selected from the group consisting of Au, Cu, Ag, Al, Pd, and Pt. The low-melting-point metal is selected from the group of fusible metals, such as Bi, In, Sn, Sb, and Zn. The filler particles are coated with the low-melting-point metal which can be fused to achieve metallurgical bonding between adjacent particles, and between the particles and the bond pads that are joined using the adhesive material (50,51).

Flip Chip Applications Using ICAs

A key factor in achieving a low cost, flip chip technology is the use of ICAs. In comparison to the classical flip chip technologies, the use of ICAs for the bumping and joining provide numerous advantages:

(1) The simplification of the processing and the reduction of indexing steps by the omission of activation and purification process
(2) The smaller temperature load on elements and wiring carriers
(3) The availability of a large spectrum of possible material pairs and combinations
(4) The broad range of applicable adhesive systems and thus the selection of different processing parameters and joining characteristics
(5) Few requisites for under bump metallization (UBM) since alloy phase formation does not have to be considered

Unbumped Flip Chip Joints.

Polymer Flip Chip. Several flip chip bumping and joining techniques have been reported in the literature. Flip chips using ICAs are often called polymer flip chips (PFCs). The PFC process is a stencil printing technology in which an ICA is printed through a metal stencil to form polymer bumps on bond pads of IC devices subsequent to the UBM deposition on aluminum termination pads. The sequential processes to achieve PFC interconnects are UBM deposition, stencil printing an ICA, bump formation (ICA solidification), flip chip attach to achieve electrical connections, and underfill for enhanced mechanical and environmental integrity (52,53).

Protective Chip Pad Layer. As with virtually all flip chip processes, the Al bond pads must be protected to eliminate the formation of nonconductive aluminum oxide. This ensures a low and stable resistance at bond–bond pad interface. The PFC process utilizes an electroless plating technique, using Ni/Au or Pd, to cover the Al bond pads prior to polymer bumping. The typical metal thickness is 0.5–1.0 μm for Pd and 3.0–5.0 μm for Ni/Au.

The PFC process combines high precision stencil printing techniques with highly conductive ICAs. These polymers can be thermosetting or thermoplastic. First the polymer bumps are formed by deposition of an ICA through the metal mask directly onto the metallized bond pads on a wafer. Printed conductive adhesive bumps can offer an attractive alternative to the other bumping technologies in terms of cost and manufacturability. The printing process typically involves a screen or stencil with openings through which bumps are deposited. A screen consists of an interwoven wire mesh with an emulsion that covers the wire mesh. The emulsion is photolithographically patterned to match the bump sites. Stencils are made of metal foil. Holes for bump deposition are made by etching, electroforming (plating), or laser drilling.

During the printing process, the paste is typically dispensed some distance away from the stencil apertures. A schematic of the printing process is shown in Figure 12. Typically, the stencil is separated from a substrate by the snap-off distance. The squeegee is lowered, resulting in contact of the stencil to the substrate or wafer surface. As the squeegee moves across the stencil surface, a stable flow pattern develops in the form of a paste roll. The consequent hydrodynamic pressure developed by the squeegee pushes the paste into the patterned stencil openings. The stencil lifts away from the substrate surface with the paste remaining on the substrate.

Curing. The polymer bumps are then either fully cured or partially cured to the so-called B-stage for thermosetting polymer bumps. For thermoplastic polymer bumps, after stencil printing the solvent is removed to form solid bumps. Bump heights are typically 50–75 μm and process can accommodate pitches down to 5 mil. Bump densities of up to 80,000 bumps/wafer have been formed with excellent coplanarity.

Once the bumped wafers are diced, chips are picked from the wafers, flipped over, and then placed on and bonded to chip carriers. Different process procedures are utilized to bond thermosetting polymer bumps to similar thermoplastic bumps, as noted in Figure 13. Final processing involves a heat cure for thermosetting bumps, while thermoplastic bump connections only require in a few seconds under heat and pressure to melt the thermoplastic.

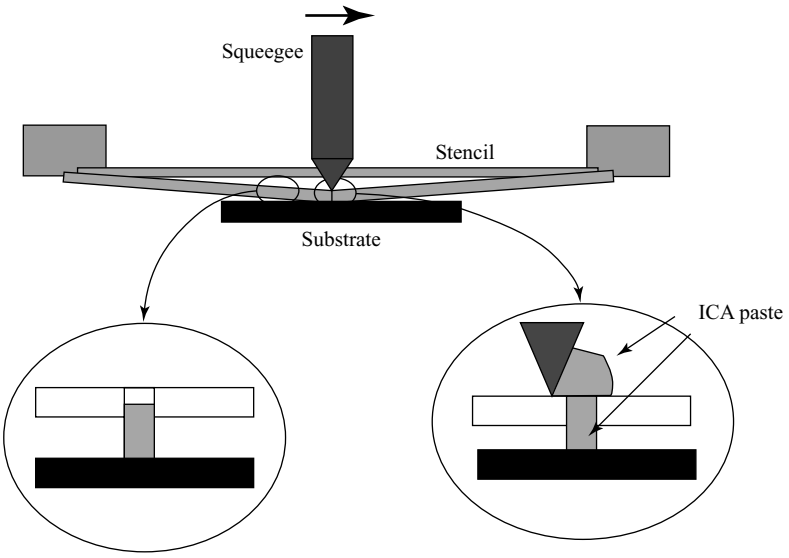

Fig. 12. Schematic depicting the ICA paste stencil printing process.

Underfill. An underfill is then injected into the gap between the chip and chip carrier and then cured to complete the flip chip process. The function of the underfill or encapsulation as it is sometimes referred to is to provide mechanical integrity and environmental protection to a flip chip assembly. Studies have demonstrated that both thermoset and thermoplastic ICAs can offer low initial joint resistances of less than 5 mΩ and stable joint resistances (Au-to-Au flip chip bonding) during all the accelerated reliability testing listed in Table 1. The reliability results have indicated that there is no substantial difference in the performance of thermoset and thermoplastic bumps and both types of polymers apparently offer reliable flip chip electrical interconnections (53).

Micromachined Bumping. A PFC bumping process is known as micromachined bumping (54,55). The bumping procedure is illustrated in Figure 14. Initially Cr/Au contact metal pads for conductive polymer bumps are deposited on Si wafers, followed by patterning a thick photoresist to create bump holes. A high aspect ratio and straight side-wall patterns are very important in shaping the conductive polymer bumps. After the lithography, thermoplastic conductive polymer material, usually thermoplastic paste filled with Ag flake, is applied by either dispensing or screen printing the paste into the bump-hole patterns. The wafer

Table 1. Accelerated Reliability Testing

Test	Condition	Time
Temperature cycle	−55 to 150°C	1000 cycle
Thermal shock	−55 to 125°C	500 cycle
Elevated temperature and humidity	85°C/85% RH	1000 h
Pressure cooker	121°C/15 psi	168 h

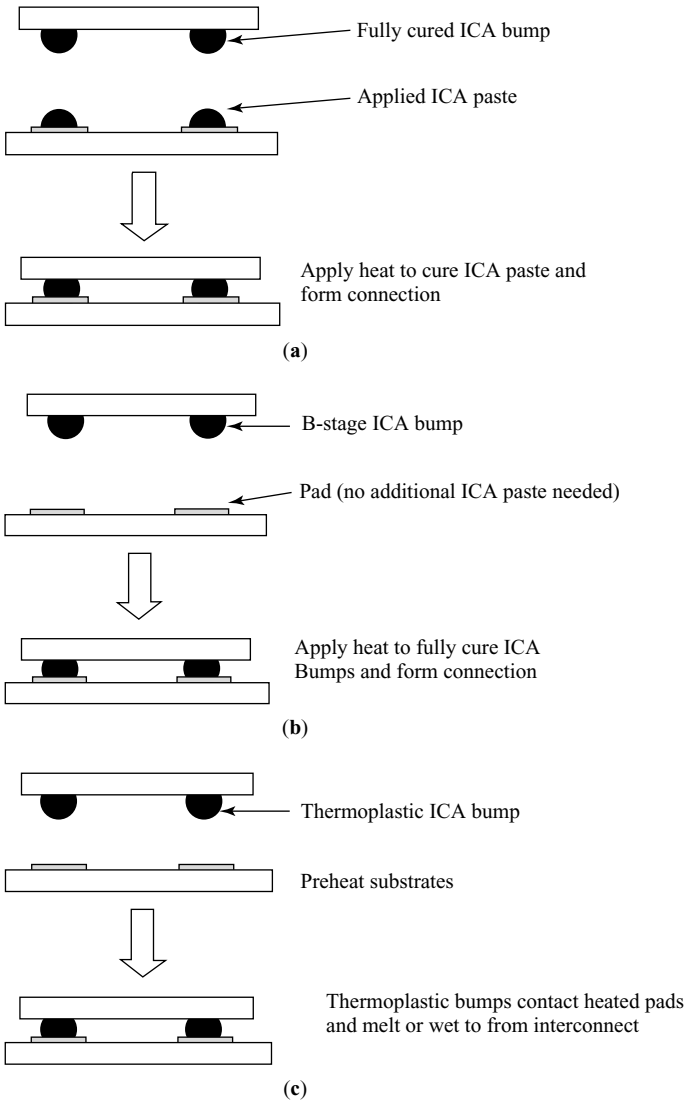

Fig. 13. Schematic illustrating various die attachment assembly processes utilizing ICAs. (**a**) Chip with cured ICA bumps mated with uncured ICA on carrier pads. (**b**) Chip with partially cured (B-staged) ICA bumps mated with bare carrier pads. (**c**) Chip with thermoplastic ICA bumps mated with bare but preheated carrier pads.

is heated in a convection oven to remove the solvent. Because of the difference in curing conditions between the thick photoresist and conductive polymer, the photoresist can be carefully stripped to expose the dried polymer bumps. Finally, the wafer is diced into individual chips.

Chips with thermoplastic bumps are placed on chip carriers and preheated to approximately 20°C above the melting point of the polymer, causing the bumps to melt onto the matching chip carrier pads. Mechanical and electrical bonds are

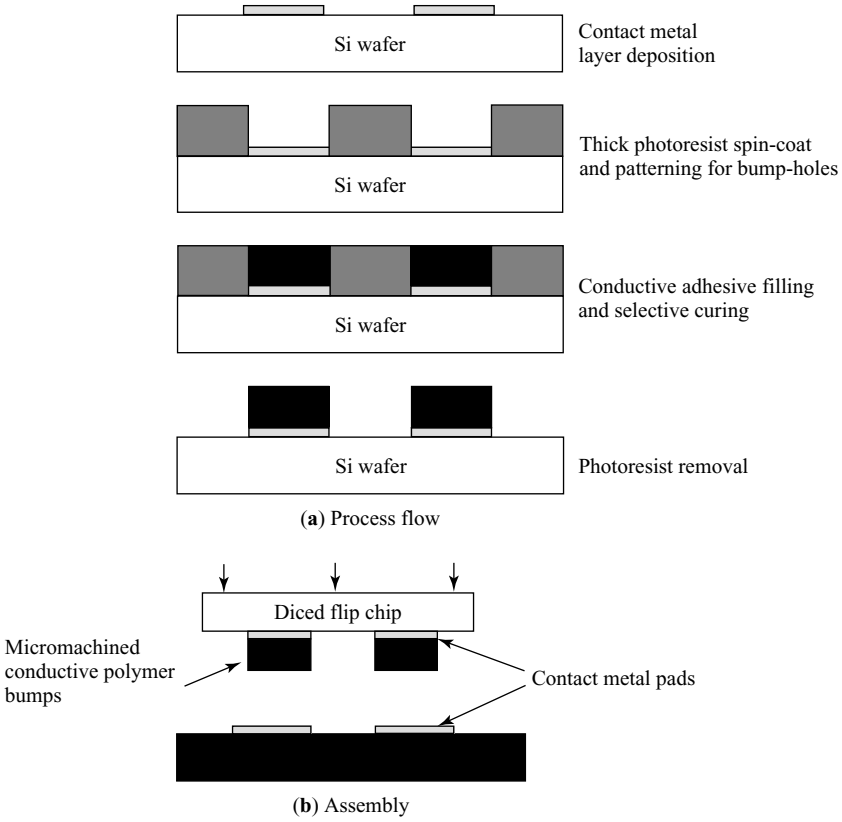

Fig. 14. Schematic depicting a flip chip technology utilizing chips with micromachined polymer bumps. (**a**) Process flow for creating micromachined polymer bumps in the wafer state. (**b**) Die attachment to a chip carrier.

established as the chip carrier cools below the polymer melting temperature. To enhance the mechanical bonding strength, a small amount of pressure can be applied by placing a weight on the chip.

This flip chip bonding technique has high potential to replace conventional solder flip chip techniques for sensor and actuator systems, optical microelectromechanical systems, optoelectronic multichip modules, and electronic system applications (55).

Metal-Bumped Flip Chip Joints. ICAs can also be used to form electrical interconnections with chips that have metal bumps. ICA materials utilize much high filler loading than ACAs to provide electrical conduction isotropically (ie in all directions) throughout the material. In order for these materials to be used for flip chip applications, they must be selectively applied to only those areas that are to be electrically interconnected. Also, the materials are not to spread during placement or curing to avoid creating electrical shorts between circuit features. Screen or stencil printing is most commonly used to precisely deposit the ICA pastes. However, to satisfy the scale and accuracy required for flip chip

bonding very accurate pattern alignment is required. To overcome this difficult requirement, Matsushita developed the transfer method (56).

Raised studs or pillars are required on either the die or the chip carrier. Matsushita uses a conventional ball bonder to form Au-stud bumps. Bumping is significantly faster than creating a complete wire bonds. A ball bumping process eliminates the need for traditional sputtering and plating processes used for standard bump formation. To prevent the bond area from becoming too large, the bumps are formed in a conical shape. The stud-bump bonding process is illustrated in Figures 15–18. The bumps are pressed level by a flat surface which adjusts both height and planarity. The ICA is selectively transferred on the bump tips by contacting the face of the die to a flat thin film of the ICA which is produced by screen printing and whose transfer thickness is controlled by changing the printed film thickness. Then the die is picked, aligned, and placed on a chip carrier. The whole assembly is exposed to heat to cure the ICA and form connections between the

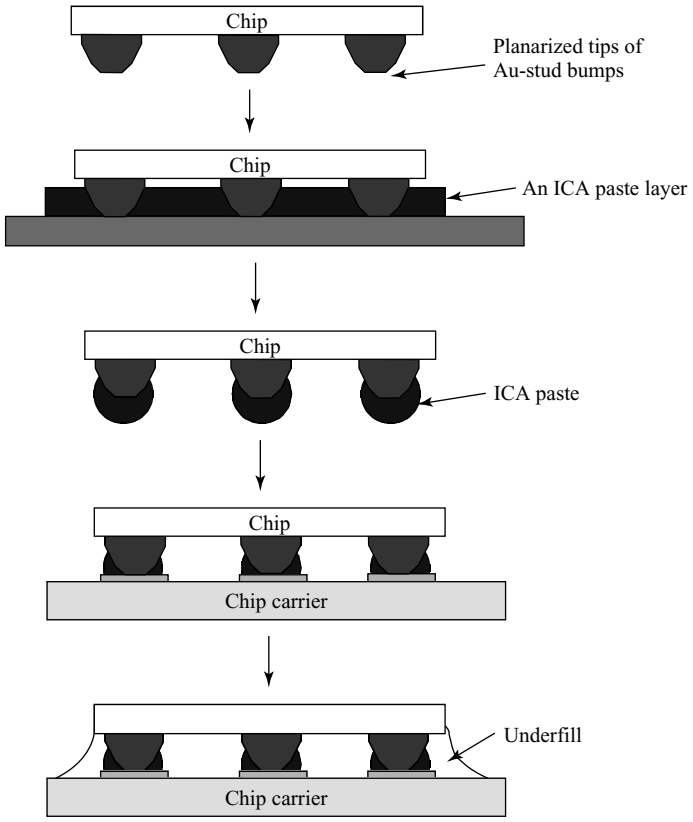

Fig. 15. Schematic of the process flow of forming joints with stud-bumped flip-chips using ICAs. (**a**) Planarize the tips of the gold-stud bumps formed with a wire bond tool. (**b**) Dip the planarized bumps into a thin layer of ICA. (**c**) Withdraw the chip leaving the bumps coated with ICA. (**d**) The chip is placed on mating pads of a chip carrier with pressure required during curing. (**e**) An underfill (an insulating adhesive) is dispensed and cured.

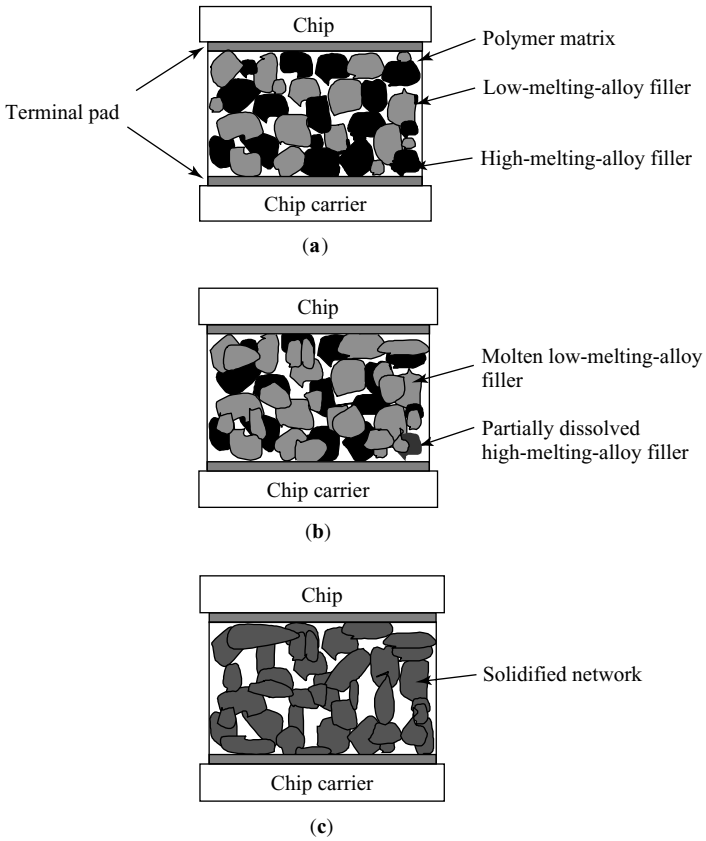

Fig. 16. Schematic of a joint formed using transient liquid phase sintering conductive adhesives. (**a**) Initial state after chip attachment and before temperature reach the melting point of the low-melting-alloy filler. (**b**) The low-melting-alloy fillers start to melt and dissolve the high-melting-alloy filler. (**c**) After the high-melting-alloy fillers are completely dissolved, the liquid metal phase solidifies and forms a three-dimensional network in the joint.

die and chip carrier. Finally, an underfill (an insulating adhesive) is dispensed between the die and the chip carrier and cured. This method offers the options of oven curing an assembly since bonding pressure is not required. A specially formulated ICA is used to avoid silver migration, containing 20% palladium in a silver–palladium alloy. This is done to avoid silver migration. A schematic of the process flow of forming joints with stud-bumped flip chips using ICAs is shown in Figure 15.

Another process for bonding a flip chip with metal bumps consists of screen printing an ICA on a chip carrier, aligning and placing the chip, curing the ICA to form bonds, and underfilling. By using this approach, SINTEF Electronics conducted a comparison study between an ICA-bonded and solder-bonded flip chips on FR4 chip carrier with Ni/Au metallization. The number of thermal cycles (-55 to 125°C) to failure for both solder and ICA flip chip circuits was compared. The study showed that stable contacts could be maintained for at least 1000–2000

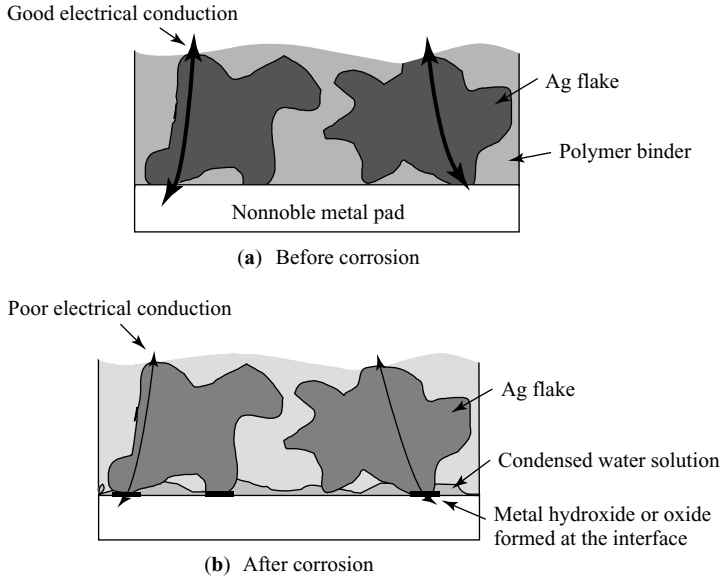

Fig. 17. Schematic depicting the effect of galvanic corrosion of a nonnoble metal pad on electrical conduction of a silver-filled ICA. (**a**) Good electrical conduction before corrosion. (**b**) Poor electrical conduction due to the formation of a metal hydroxide or oxide formation as a result of galvanic corrosion.

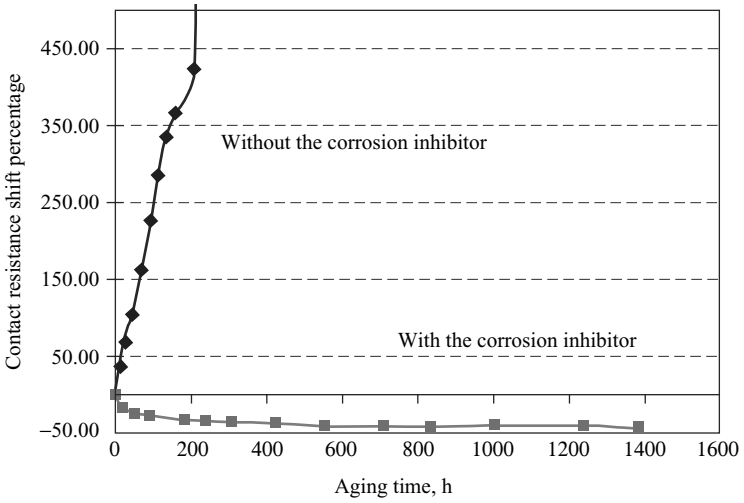

Fig. 18. Effect of a corrosion inhibitor on contact resistance between an ICA and a Sn–Pb surface with time. Aging condition: 85°C/85% RH.

cycles for ICA flip chip joints. This is comparable to the lifetime for solder flip chip joints. However, the variation among ICA samples was very high and optimization of assembly processes is needed in order to achieve more reproduciable joint resistance (57).

Other Applications of ICAs

Surface Mount Applications. Tin–lead solders (Sn–Pb) are the standard materials used to interconnect electronic components on PCBs. The most common reflow soldering process is SMT which uses tin–lead solder pastes (58–61). The pressure to reduce the industrial use of lead is growing, particularly in Europe, since it poses as a hazard to human health (62).

Thus, the use of tin–lead solder paste in SMT processes must be reduced or eliminated to both satisfy legislative actions and market-driven pressures as well. Lead-free and environmentally sound interconnect bonding processes are urgently needed. Among the possibilities are ECAs and lead-free solders (63–65). Compared to soldering technology, ECA technology can offer numerous advantages such as fewer processing steps which reduces processing cost, lower processing temperature which makes the use of heat-sensitive and low cost chip carriers possible, and fine pitch capability (64).

However, conductive adhesive technology is still in its infancy, and concerns and limitations do exist. The main limitations of commercial ICAs include lower conductivity than that of solder materials, an unstable contact resistance with nonnoble metal finished components, and poor impact performance. The electrical conductivity ($\sim 10^4\ \Omega^{-1}\cdot cm^{-1}$) of an ICA is lower than Sn–Pb solders ($\sim 10^5\ \Omega^{-1}\cdot cm^{-1}$). Although generally adequate for most electronics applications, the electrical conductivity of ICAs must be improved. Contact resistance between an ICA and nonnoble metal (such as Sn/Pb, Sn, and Ni) finished components is noted to dramatically increase with time especially under elevated temperature and humidity aging conditions (66–69). In addition, PCB assemblies are often subject to significant mechanical shock during assembly, handling, and throughout their product life. Packages cannot survive without adequate impact resistance. However, most microelectronic commercial ICAs exhibit poor impact performance. Components assembled using ICAs tend to separate from the substrate when the package experiences a sudden shock (68,70). For conductive adhesive technology to provide an acceptable solution as a solder replacement, new conductive adhesives with the desired overall properties must be developed (68). There has been a considerable effort to improve the properties of ICAs and to make them more reliable materials. These improvements are described in the following sections.

CSP Applications. Matsushita Electric Industrial Co., Ltd., developed solderless joining technologies using nickel-filled ICAs to mount a ceramic chip scale package (CSP-C) onto a FR4 board (71). Nickel was selected instead of Ag because, unlike Ag, nickel does not migrate. A significant CTE mismatch existed between the CSP-C ceramic chip carrier (CTS = 7 ppm) and the FR4 organic chip carrier (CTE = 16 ppm). This CTE mismatch resulted in large stress to be generated within the solder joints during ATC testing which resulted in early failure due to solder fatigue. ICAs usually exhibit better thermomechanical properties than solders. Also, metal-migration between joints is a great concern because the joints in a CSP area array package are arranged with a close pitch (ie in close proximity).

The packaging procedure was as follows: (*1*) the ICA was screen-printed on the area array lands of the FR4 motherboard; (*2*) the CSP-C was mounted; (*3*) and the ICA was cured to form bonds. The Ni-filled conductive adhesive demonstrated

a much higher resistance to metal migration compared to Ag-filled IACs, and equivalent to solder joints. However, the thermal fatigue life of the Ni-filled ICA joints was five times greater than comparable solder joints.

Performance of ICAs

High Frequency Performance of ICA Joints. Only very limited work has been conducted to investigate the high frequency behaviors of ICA joints. Felba and co-workers (72) investigated a formulation of ICA that performed well as a solder replacement in microwave applications. The study involved in various different adhesive base materials and several types of main (silver flakes, nickel, and graphite) and additional (soot and silver semiflake powder) filler materials. In order to assess the usefulness of a given adhesive formulation, an additional gap in the gold strip of a standard microstrip bandpass filter was made and bridged by an adhesive bonded silver jumper. Both the quality factor (Q) and loss factor (L) of the filter with the bonded jumper were measured at a frequency of 3.5 GHz in a preliminary experiment and at 3.5 and 14 GHz in a final experiment. It was determined that silver flake powders are the best filler materials for ICA for microwave applications because ICAs filled with the silver flake powders exhibit the highest Q-factor and lowest L-factor. Also, addition of soot should be avoided since it decreases the quality factor (72).

A study was made at Georgia Tech, of a flip chip test vehicle mounted on a FR4 chip carrier with a gold-plated copper transmission lines (73). The performance of eutectic Sn–Pb and ICAs were evaluated and compared using this test device. Both ICAs and eutectic Sn–Pb solder were determined to exhibit almost the same behavior at a frequency range of 45 MHz to 2 GHz and the measured transmission losses for both materials were minimal. It was also found that the S_{11} characteristics of both Sn–Pb and ICAs after exposure to 85°C/85% RH aging for 150 h did not vary from the previous signals prior to aging, but S_{12} value of the Sn–Pb joints deviated more than that of ICA joints after the aging.

Fatigue Life of ICA Joints. There have been several studies investigating the fatigue life of ICA joints. Aiming to understand the performance of ICA interconnects under fracture and fatigue loading, Constable and co-workers (74) investigated performance of ICA interconnects under fracture and fatigue loading by monitoring resistance changes (microohm sensitivity) of ICA joints during pull and fatigue testing (cyclic loading up to 1000 cycles). Observation of the fracture surface suggested that the ICA joint life depended upon the adhesive failure of the bond to the metal surface. It was observed that fracture strains for the ICAs were in the range of 20–38%, and resistance remained approximately constant in the elastic region, but the resistance started to increase rapidly as soon as the pull-force departed from linear elastic behavior. For fatigue tests, linear displacement was ramped up the preprogrammed maximum displacement and ramp back to the starting position. It was observed that the shear strain for ICA joints surviving 1000 cyclic loading was typically 10%, which is about an order of magnitude greater than solders. This suggests that using conductive adhesives may be advantageous for some flip chip. It is believed that since silver filler particles of

ICAs cannot accommodate this large strain, the silver filler particles must move relative to one another as the epoxy matrix is strained. The most common pattern of resistance change was only increased to a point corresponding to about a 70% loss in interface contact resistance before sudden failure. This was an indication that the interface crack slightly propagated into the adhesive (74).

In an effort to gain a fundamental understanding of the fatigue degradation of ICAs, Gomatam and co-workers (75) studied the behavior of ICA joints under temperature and humidity conditions. The fatigue life decreased at elevated temperature and high humidity conditions. It was also observed that the fatigue life of the ICA joints decreased considerably as the temperature cycle frequency was decreased. This effect was attributed to the fact that as the frequency was decreased, the propagating crack was exposed to higher loads for longer periods of time, effectively resulting in high creep loading (75).

Improvement of Electrical Conductivity of ICAs

Electrical conductivity of ICAs is inferior to solders (76). Even though the conductivity of ICAs is adequate for most applications, a higher electrical conductivity of ICAs is still needed. To develop a novel ICA for modern electronic interconnect applications, a thorough understanding of the materials is required.

Eliminate Lubrication Layer. An ICA is generally composed of a polymer binder and Ag-flake filler material. A thin layer of organic lubricant is present on the surface of the Ag flakes. This lubricant layer plays an important role in the performance of ICAs, including the dispersion of Ag flakes in adhesives, and the rheology of the adhesive formulations (45,76–78). The organic layer consist of a Ag salt formed between the Ag surface and the lubricant, which typically is a fatty acid such as stearic acid (78,79). This lubricant layer affects the conductivity of an ICA because it is electrically insulating (78,79). To improve conductivity, the organic lubricant layer must be partially or fully removed through the use of chemical substances that can dissolve the organic lubricant layer (78–80). However, the viscosity of an ICA paste may increase if the lubricant layer is removed. An ideal chemical substance (or lubricant remover) should be latent (does not remove the lubricant layer) at room temperature, but be active (capable of removing the lubricant layer) at a temperature slightly below the cure temperature of the polymer binder. The lubricant remover can be a solid short-chain acid, a high-boiling-point ether such as diethylene glycol monobutyl ether or diethylene glycol monoethyl ether acetate, and a polyethylene glycol with a low molecular weight (78–80). These chemical substances can improve electrical conductivity of ICAs by removing the lubricant layer on the Ag-flake surfaces and providing an intimate flake–flake contact (78,79).

Increase Shrinkage. In general, ICA pastes exhibit low electrical conductivity before cure, but the conductivity increases dramatically after they are cured. ICAs achieve electrical conductivity during the cure process, mainly through a more intimate contact between Ag flakes caused by the shrinkage of polymer binder (81). Accordingly, ICAs with a high cure shrinkage generally exhibit the best conductivity. Therefore, increasing the cure shrinkage of a polymer binder is another method for improving electrical conductivity. For ICAs based on epoxy

resins, a small amount of a multifunctional epoxy resin can be added into an ICA formulation to increase cross-linking density, shrinkage, and thus increase conductivity (81).

Apply Electric Field. The electrical conductivity of ICAs can be improved significantly by applying an electrical field before or while curing them. However, the exact reasons for this improvement are not yet clear (82).

Transient Liquid Phase Fillers. Another approach for improving electrical conductivity is to incorporate transient liquid-phase sintering metallic fillers in ICA formulations. The filler used is a mixture of a high-melting-point metal powder (such as Cu) and a low-melting-point alloy powder (such as Sn–Pb). The low-melting-alloy filler melts when its melting point temperature is achieved. The liquid phase dissolves the high-melting-point particles. The liquid exists only for a short period of time and then forms an alloy and solidifies. The electrical conduction is established through a plurality of metallurgical connections formed *in situ* from these two powders in a polymer binder. The polymer binder fluxes both the metal powders and the metals to be joined and facilitates the transient liquid bonding of the powders to form a stable metallurgical network for electrical conduction, and also forms an interpenetrating polymer network providing adhesion (Fig. 16). High electrical conductivity can be achieved using this method (83–85). The ICA joints formed include metallurgical alloying to the junctions as well as within the adhesive itself. This provides a stable electrical connection during elevated temperature and humidity aging. In addition, the ICA joints showed good impact strength due to the metallurgical interconnection between the conductive adhesive and the components. One critical limitation of this technology is that the numbers of combinations of low melt and high melt fillers are limited. Only certain combinations of two metallic fillers which are mutually soluble exist to form this type of metallurgical interconnections.

Improvement of Contact Resistance Stability

Contact resistance between an ICA (generally a Ag-flake-filled epoxy) and nonnoble metal finished components increases dramatically during an elevated temperature and humidity aging, especially at 85°C/85% RH. The National Center of Manufacturing and Science (NCMS) defined the stability criterion for solder replacement conductive adhesives as a contact resistance shift of less than 20% after aging at 85°C/85% RH conditions for 500 h (67).

Causes for Resistance Increase. Two main mechanisms, simple oxidation and corrosion of the nonnoble metal surfaces, have been proposed in the literature as the possible causes for the increase in contact resistance of ICA joints during elevated temperature and humidity aging. Simple oxidation of the nonnoble metal surfaces is claimed to be the main reason for the observed increased resistance. Corrosion is claimed to be the possible mechanism for resistance increase only by several investigators (65,66,68,86,87). One study strongly indicates that galvanic corrosion rather than simple oxidation of the nonnoble metal at the interface between an ICA and nonnoble metal is the main reason for the shift in contact resistance of ICAs (Fig. 17) (88,89). The nonnoble acts as the anode, and is reduced to a metal ion ($M - n\,e^- = M^{n+}$) because of the loss of electrons. The

noble metal acts as a cathode, and its reaction generally is $2\ H_2O + O_2 + 4\ e^- = 4\ OH^-$. Then M^{n+} combines with OH^- to form a metal hydroxide or metal oxide. As a result of this electrochemical (corrosion) process, a layer of metal hydroxide or metal oxide is formed at the interface which is electrically insulating, causing the contact resistance to increase dramatically (88,89).

Prevention. Galvanic corrosion requires the presence of moisture. An electrolyte solution must be formed at the interface before galvanic corrosion can occur. Therefore, one way to prevent galvanic corrosion at the interface between an ICA and the nonnoble metal surface is to lower the moisture pickup of the ICA. ICAs that have a low moisture absorption generally exhibit more stable contact resistance on nonnoble surfaces compared with those with high moisture absorption (90,91). Without the electrolyte, galvanic corrosion rate is very low. The electrolyte in this case is mainly from the impurity of the polymer binder (generally epoxy resins). Therefore, ICAs formulated with high purity resins should perform better.

Use of Corrosion Inhibitors. Another method of preventing galvanic corrosion is to introduce organic corrosion inhibitors into ICA formulations (89–92). In general, organic corrosion inhibitors act as a barrier layer between the metal and environment, forming a film over the metal surfaces (93–96). Some chelating compounds are especially effective in preventing metal corrosion (95). Most organic corrosion inhibitors react with the epoxy resin at a specific temperature. Therefore, if an ICA is epoxy-based, the corrosion inhibitors must not react with the epoxy resin during curing, which would cause them to be consumed and lose their effect. Organic corrosion inhibitors are thoroughly discussed in the literature (94,96). Figure 18 shows the effect of a chelating corrosion inhibitor on the contact resistance between an ICA and a Sn–Pb surface. It can be seen that this corrosion inhibitor is very effective in stabilizing the contact resistance.

Use of Oxygen Scavengers. Since oxygen accelerates galvanic corrosion, oxygen scavengers can be added into ICA formulations to slow down the corrosion rate (93). When oxygen molecules diffuse through the polymer binder, they react with the oxygen scavenger and are consumed. However, when the oxygen scavenger is completely depleted, then oxygen can again diffuse into the interface and accelerate the corrosion process. Therefore, oxygen scavengers can only delay the galvanic corrosion process. Similar to corrosion inhibitors, the oxygen scavengers used must not react with the epoxy resin at its cure temperature. The common oxygen scavengers utilized are listed below (93,97–100):

(1) hydrazine
(2) carbohydrazide
(3) hydroquinone
(4) oximes
(5) gallic acid
(6) propyl gallate
(7) hydroxylamines and related compounds
(8) dihydroxyacetone
(9) 1,2-dihydro-1,2,4,5-tetrazines
(10) erythorbic acid

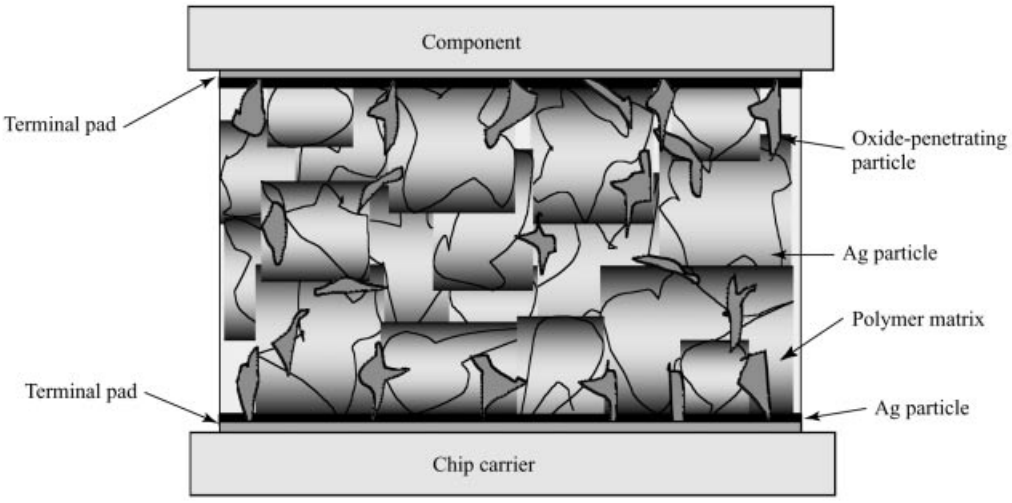

Fig. 19. Schematic depicting an ICA joint containing oxide-penetrating particles and silver filler particles.

Sharp-Edge Filler Particles. Another approach of improving contact resistance stability during aging is to incorporate some electrically conductive particles, which have sharp edges and referred as oxide-penetrating fillers, into the ICA formulations. Force must be provided to drive the oxide-penetrating particles through the oxide layer of adjoining particles and metal pads, and keep them in position. This can be accomplished by employing polymer binders that show high shrinkage when cured (Fig. 19) (101). This concept is used in Poly-Solder which has good contact resistance stability with standard surface-mounted devices (SMDs) on both solder-coated and bare circuit boards (101).

Improvement of Impact Performance

The ability to resist a performance degradation when subjected to mechanical shock is a critical property that solder replacement ICAs must possess. There are ongoing efforts to develop ICAs that exhibit acceptable impact strength, ie capable of passing the standard drop test used to evaluate the impact strength of components attached to a PCB. Among the methods are:

(1) Decrease in the filler loading to improve the impact strength (102), and reduction in the electrical conductivity of the conductive adhesives. A development was reported where conductive adhesives were formulated using low modulus resins that absorb the impact energy developed during a drop (103), but the electrical properties was not noted.
(2) Conformal coating of the SMDs to improve mechanical strength. A study demonstrated that a conformal coating improved the impact strength of conductive adhesives joints (104).

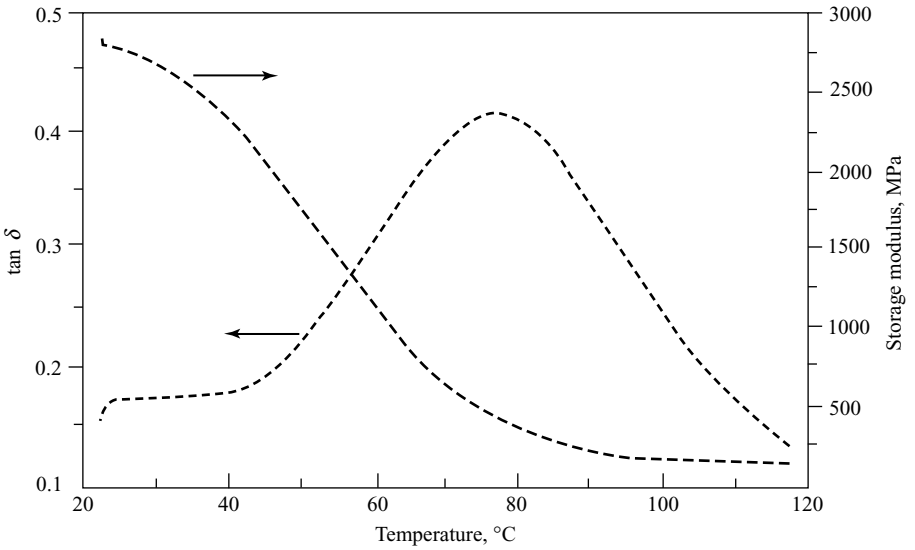

Fig. 20. Changes of tan δ and the storage modulus with temperature of an ETPU-based conductive adhesive as measured by a dynamic mechanical analyzer. To convert MPa to Psi, multiply by 145.

Epoxide-Terminated Polyurethane Systems. A class of conductive adhesives based on an epoxide-terminated polyurethane (ETPU) has been developed (105,106). This class of conductive adhesives exhibits properties typical of polyurethane materials, such as high toughness and good adhesion. The modulus and glass-transition temperature of an ICA can be adjusted by incorporating epoxy resins such as bisphenol-F epoxy resins. Conductive adhesives based on ETPU exhibit a broad loss factor (tan δ) peak with temperature changes and a high tan δ value at room temperature. The tan δ value of a material is a good indication of the damping property and impact performance of a material. In general, the higher the tan δ value, the better the damping property (impact strength) of the material. As an example, changes in tan δ and storage modulus with temperature of an ETPU-based ICA are shown in Figure 20. ICAs based on ETPU resins also exhibit a much higher loss factor over a wide frequency range compared to ICAs based on bisphenol-F epoxy resins (Fig. 21). This indicates that ICAs based on ETPU resins should exhibit good damping property and improved impact performance in a variety of electronic packages. This class of conductive adhesives has demonstrated superior impact performance and a substantial improvement in contact resistance stability with nonnoble metal surfaces, such as Sn–Pb, Sn, and Cu (105,106).

Future Challenges

Anisotropically Conductive Adhesives. Significant research has been conducted on ACAs as a potential solder replacement for some electronics packaging applications. However, many aspects of this technology must be better

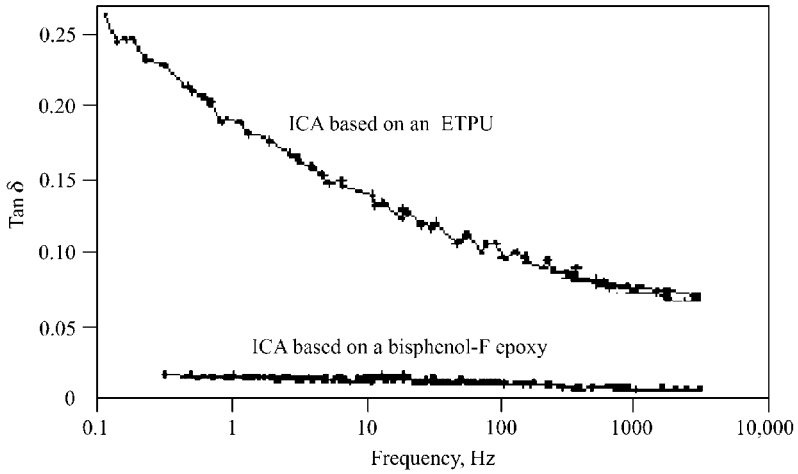

Fig. 21. The effect of frequency on the loss factor for two ICA materials.

understood before it can be widely used to replace lead-bearing solders. Some critical issues that must be addressed in the future are discussed below:

Materials Development. Develop new ACA materials that have good adhesion, high T_g, fast curing, storage stability at ambient, and stable contact resistance after various conditions frequently encountered in the field such as thermal aging and cycling, thermal shock, high temperature/high humidity/bias, etc. Also, ACAs with low CTE are required. Commercially available ACAs typically exhibit very high CTEs because of the low filler loading levels utilized. Some preliminary studies have shown that ACAs with a low CTE created by introducing nonconductive silica fillers have a lower shear strain and better contact resistance stability during thermal cycling test (107).

High Frequency Compatibility. The number of high frequency applications and utilizations are increasing rapidly; thus it is important to characterize the cross talk between particles, coupling with semiconductor devices, and other fundamental behavior of ACAs under high frequency conditions. It is also necessary to maximize the current carrying capability of ACAs at high frequency range, and after exposure to various environment tests.

Reliability. It is necessary to understand the effect of the chip carrier material on ACA join reliability. This is a key issue before ACA technology is widely utilized in manufacturing (ie in high volume and low cost applications). It is also necessary to establish failure rate prediction models for ACA joints for a wide variety of field conditions. It is essential to gain full understanding on effects of high current and high power on ACA joints, degradation, and stress relaxation of polymeric matrices; and the effects of temperature, humidity, and other environments on matrix materials and the effects of fillers.

Isotropically Conductive Adhesives. There have also been a significant number of studies to improve ICA technology. However, several critical issues associated with this technology must also be addressed before it can be used as a replacement for soldering technology:

Electrical Characteristics. The electrical conductivity of ICAs must be vastly improved since their electrical conductivity is typically 1 or 2 orders of magnitudes lower than that of solders. Silver-filled ICAs achieve their electrical conductivity through a physical contact among the Ag flaks. Because of the high particle–particle contact resistance, ICAs exhibit a high bulk resistivity. Although some preliminary work has been done to improve electrical conductivity by introducing low-melting-point alloys which form metallurgical interconnetions with the Ag flakes, additional work is necessary to achieve the desired electrical conductivity. Also, the behavior of ICA joints under high current or high power conditions, and high temperature/humidity/bias is not clear.

High Frequency Performance. The high frequency behavior of ICAs over a wide frequency range must be investigated and compared to that of solders.

Reliability. Silver-filled ICAs have a potential for silver migration, which cause electrical shorts especially in fine pitch applications. A palladium-treated silver filler exhibited a much improved antimigration characteristics compared to standard silver-filled ICAs. However, the preparation of the Pd-coated silver particles is expensive. Some low cost approaches must be developed. More comprehensive understanding of the fatigue resistance of ICA joints is required. Activities in this area have been limited and nonconclusive.

Manufacturability and Yields. Since most commercial ICAs are epoxy based, they are thermosetting materials and thus not reworkable. ICAs with reworkability must be developed by using thermoplastic or thermally degradable resins. Because of their high surface tension, SnPb solders have a self-alignment capability during solder reflow operations. However, conventional ICAs cannot self-align. Therefore, components that are bonded using ICAs require a high placement accuracy. Some preliminary research has been conducted to improve the self-alignment capability of ICAs (108,109), but much more work needs to be done.

Conductive Polymer Composites with Large Positive Temperature Coefficient

Conductive polymer composites (110,111) that contain conductive fillers such as metal powder, carbon black, and other highly conductive particles in a nonconductive polymer matrix have been widely used in electrostatic dissipation (ESD) and electromagnetic interference shielding (EMIS). A special group among electrically conductive polymer composites are conductive polymer composites that have large positive temperature coefficients (PTCs), which in some cases are called positive temperature coefficient resistance. The resistivity of this kind of composite increases several orders of magnitude in a narrow temperature range, as shown in Figure 22. The transition temperature (T_t) is defined by intersection between the tangent to the point of inflection of the resistivity versus temperature curve and the horizontal from the resistivity at 25°C (ρ_{25}). This kind of smart material can change from a conductive material to an insulating material or vice versa upon heating or cooling, respectively. The smartness of this kind of material not only lies in this large PTC amplitude (defined as the ratio of maximum resistivity at the peak or the resistivity right after the sharp increase to the resistivity at

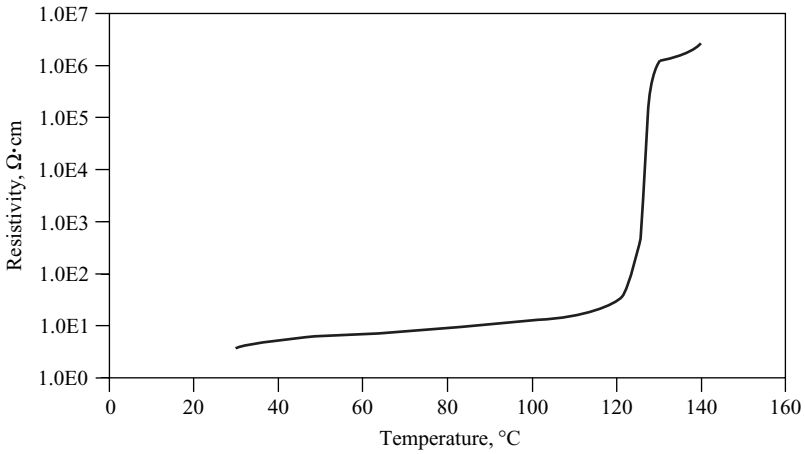

Fig. 22. Resistivity versus temperature behavior of a conductive polymer composite that has a large PTC.

25°C), but also in its reversibility, its ability to adjust the transition temperature, low temperature resistivity, and high temperature resistivity. PTC behavior in a polymer composite was first discovered by Frydman in 1945 (112), but not much attention was paid to it originally. Because Kohler obtained a much higher PTC amplitude from high density polyethylene filled with carbon black in 1961 (113), this kind of temperature-sensitive materials has aroused wide research interest and also led to many very useful applications. In this review, the general theories of PTC conductive polymer are introduced. Carbon-black-filled conductive polymer composites and their PTC behavior are discussed in more detail, in regard to the effects of fillers, the polymer matrix, processing conditions, and additives. At the end, applications of this kind of smart temperature-sensitive material are presented.

Basic Theory of Conductive Polymer Composites and PTC Behavior. The conductivity of polymer composites that contain conductive particles dispersed in a polymer matrix may result from direct contact between conductive particles and electron tunneling. The conductivity of a highly filled conductive adhesive is due to the former mechanism. Matsushige used atomic force microscopy to study the conduction mechanism in a PTC composite on a nanoscale (114). It was proposed that electron tunneling or hopping through the conductive carbon particles in the polymer matrix might be the governing mechanism for organic PTC materials.

There are two very simple mechanisms for small PTC behavior of conductive polymer composites: reduction of the contact area of neighboring conductive particles and an increase in the junction distance in electric tunneling when heated. Although the large PTC phenomenon is well known, its mechanism has not been fully understood. Different theories have been proposed (113,115,116) to explain the large PTC behavior.

Kohler (113) suggested that the PTC is due to the difference in thermal expansion of the materials. His theory was supported by some other researchers

in percolation theory (110). The conductivity of conductive polymer composites increases as the volume fraction of the conductive filler increases. For a polymer filled with conductive particles, a critical volume fraction of filler may exist, which is called the percolation volume fraction. The resistance of the conductive polymer composite whose filler volume fraction is higher than the percolation volume fraction is several orders of magnitude less than that of the composite whose filler volume faction is less than the percolation volume fraction. In the region of low filler concentration, the filler particles are distributed homogeneously in the insulating polymer matrix. There is no contact between adjacent filler particles. The resistance decreases slowly as the volume fraction of filler particles increases. As the filler concentration further increases, filler particles begin to contact other particles and agglomerate. At a certain filler concentration, the growing agglomerates form one-, two-, or three-dimensional network of the conducting phase within the insulating polymer matrix. At this range, the resistivity of the mixture shows a deep decrease to the low value of the conductive network. After the formation of the continuous conductive network, the resistivity of the mixture increases slowly because of the slightly improved quality of the conductive network as the filler content increases.

Many models have been proposed (117) to explain the electrical conductivity of mixtures composed of conductive and insulating materials. Percolation concentration is the most interesting of all of these models. Several parameters, such as filler distribution, filler shape, filler/matrix interactions, and processing technique, can influence the percolation concentration. Among these models, the statistical percolation model (118) uses finite regular arrays of points and bonds (between the points) to estimate percolation concentration. The thermodynamic model (119) emphasizes the importance of interfacial interactions at the boundary between individual filler particles and the polymeric host in the network formation. The most promising ones are the structure-oriented models, which explain conductivity on the basis of factors determined from the microlevel structure of the as-produced mixtures (120).

Because the thermal expansion coefficient of a polymer matrix is generally higher than that of the conductive particles, the volume fraction of a conductive filler in conductive polymer composite decreases as temperature increases; thus, the resistivity increases. If a conductive polymer composite is made of semicrystalline polymer as an insulator and a filler of conducting particles, whose concentration is just above the percolation volume fraction, the relatively large change in specific volume of the polymer at its melting temperature may bring the volume fraction of the conductive filler down below the critical volume fraction when the composite is heated beyond the melting temperature of the polymer crystal. Thus, the resistivity increases greatly. Kohler's theory cannot explain the very small rise in resistance exhibited by such filled polymer systems when they are strained to an amount equivalent to that found at the crystalline melting point. And the PTC amplitude should be a direct function of volume change according to Kohler's theory; however, it is not the case in reality.

Ohe proposed a more complex theory (115). He stated that PTC phenomenon could be explained by the increase of the intergrain gap among the carbon black particles caused by thermal expansion. He visualized that the distribution of the intergrain gaps in conductive composite is rather uniform at low temperature,

and the gap is small enough for extensive tunneling to occur, but the distribution at high temperature becomes random due to thermal expansion. Although the average gap distance does not change greatly, the presence of a significant amount of gap distance too large to allow electron tunneling will result in a great increase in resistance.

Meyer's theory was based on the assumption that a thin (300 Å) crystalline film of polymer is much more conductive than an amorphous film of polymer. It was shown that carbon black particles remain in the amorphous region between crystallites in a conductive composite. The high conductivity at low temperature is due to tunneling through the thin crystallite, and the PTC phenomenon is caused by a preliminary change in state of these crystallites just before the crystalline melting point that leads to a sharp reduction in the ease of tunneling and thus much higher resistivity.

Large thermal expansion during crystal melting surely contributes to a large amplitude of PTC behavior. But it contributes only to a limited level. Ohe's vision of the change from uniform distribution of carbon particle to random distribution is groundless and cannot be justified. Actually, as is shown later, cross-linking can eliminate the redistribution of carbon black after melting and stabilizes PTC behavior. PTC behavior takes place at the same time as melting, rather than before crystalline melting, as stated by Meyer. It probably is true that tunneling is easier in a crystalline region than in an amorphous region. The difference is probably due to polymer chain mobility. The work function of the conductive particle at the interface between the conductive particle and polymer matrix may increase after crystal melting due to the high mobility of the polymer chain. The same theory can explain PTC behavior in conductive polymer composites as well as the conductivity phenomenon in an ECA after curing (80). Before conductive adhesive is cured, the resin matrix has high mobility and prohibits tunneling between conductive particles. After curing, the mobility of the polymer chain is greatly reduced and thus allows tunneling between conductive particles.

Effect of Conductive Fillers on PTC Conductive Polymer. Different conductive fillers have been used as in PTC conductive polymers. Metallic powders that are stable at high temperature, such as tin, gold, and silver, were suggested as conductive fillers in PTC materials (121). In addition, ceramic powder such as tungsten carbide was also used as a filler in PTC conductive polymer composites (122). It was found that V_2O_3 has several phase transitions (110). At 160 K, it is transformed from an antiferromagnetic insulator (AFI) to a paraelectric metallic conductor (PMC), accompanied by a resistivity change from 10^5 to 10^{-2} Ω·cm. At 400 K, it changes from a PMC to a PI (paraelectric insulator) whose resistivity is $10^3 - 10^4$ Ω·cm. Most interestingly, low density polyethylene filled with V_2O_3 shows a square well in the resistivity versus temperature profile by combining a sharp NTC (negative temperature coefficient) around −110°C, and a sharp PTC around 100°C (110,123–125). A PTC transition temperature of conductive polymer composites filled with V_2O_3 was also reported in other polymer system (121,122). The T_t of a V_2O_3-filled system changes in the following manner: 100°C (low density polyethylene) < 150°C (polypropylene) < 260°C (polytetrafluoroethylene). However, the fillers mentioned before are expensive. Work has been done to develop alternative less expensive PTC conductive polymer composites. Most

of the conductive polymers for ESD and EMIS applications are thermoplastics filled with carbon black or carbon graphite because of their very low cost. Carbon black is also one of the major fillers used in so-called PTC conductive polymers (126–128).

There are several important parameters of carbon black (129): particle size (surface area), aggregate structure (carbon black particles aggregate to form a grapelike structure), porosity, crystallinity, and surface functionality. Small particle size and high structure lead to more difficult dispersion. The initial grapelike structure of carbon black formed during the manufacturing of carbon black is highly stable and can be destroyed only by very intensive processing such as grinding in a ball mill. For a given loading of carbon black, a smaller particle size would add more particles to the composite than that using carbon black of larger particle size. Thus, carbon blacks of smaller particle size would produce a composite that has a smaller separation between carbon particles (as well as the probability of more carbon particles in contact), resulting in greater conductivity. Small particle size gives a low critical volume for a carbon-black-filled polymer system (110). However, for fiberlike conductive fillers, large filler particles favor the formation of conducting paths at a low percolation concentration. High structure carbon blacks tend to produce a larger number of aggregates in contact, as well as smaller separation distances that result in greater conductivity. For a given carbon black loading, the more porous carbon black generally provides a larger number of aggregates to the composite. This results in a smaller interaggregate distance and higher conductivity. The increase in the degree of carbon black structuring is found more efficient than the increase of the specific surface of carbon black in conductive polymers. Carbon blacks that have higher oxygen content carbon particles have higher resistance. Removal of the surface oxides increases the conductivity of the original carbon black much more than heat treatment to produce graphitization. Higher graphite content in carbon black leads to higher electrical conductivity.

Although carbon black of small particles size and high aggregated structure (such as BP2000 with a average particle diameter of 12 nm manufactured by Cabot Corp.) can give polymer composites that have low resistivity, this kind of composite does not show large PTC amplitude because the aggregated structure cannot be broken down by the thermal expansion of the polymer (Fig. 23). On the contrary, a polymer composite filled with carbon black that has a large particle size and low aggregate structure (such as N660 with an average particle diameter of 70 nm manufactured by Columbia Chemicals) shows high room temperature resistivity, but high PTC amplitude (130). To obtain a PTC conductive polymer composite that has both lower room temperature resistance and high PTC transition amplitude, porous carbon black is much better than nonporous carbon black. Ueno and coworkers reported that etching a carbon black at an elevated temperature to remove the less crystalline portion and therefore to increase the surface area can improve the PTC characteristics of a conductive polymer filled with carbon black, and this material was suitable for use as a resettable fuse (126).

The PTC amplitude depends on the loading of carbon black. It was shown that for different carbon blacks, a different loading exists at which the composite has a maximum PTC amplitude (131). The carbon black concentration that gives the

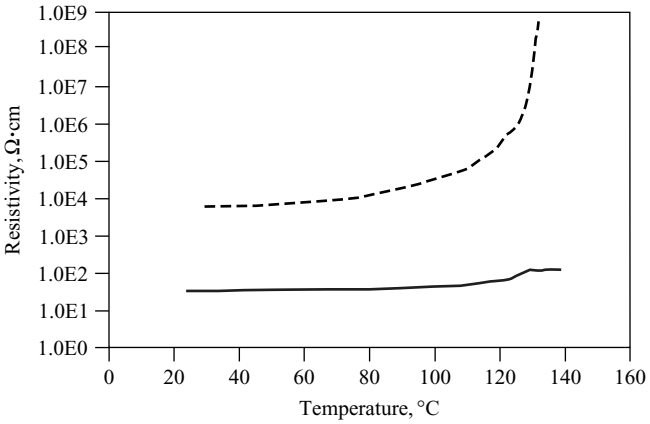

Fig. 23. Resistivity versus temperature of conductive polymer composite with different carbon blacks (the weight percentage of carbon black is 30). —— Filled with BP2000 carbon black; - - - - filled with N660 carbon black.

optimum PTC intensity can be predicted approximately from room temperature data (132).

Effect of Polymer Matrix on PTC Behavior. Polymers used as the matrix in electrically conductive polymer composites can vary from elastomers to thermoplastics and thermosets that have crystallinity varying between 0 and 80%. As mentioned in the previous section, the large PTC anomaly is due to the large thermal expansion of the polymer matrix, especially during melting of a polymer crystal. The PTC transition temperature is determined by the melting point of the polymer matrix. Because polymers that have low and high melting points are available for use in conductive polymer composites, the transition temperature can be controlled by selecting and compounding the matrix polymer for different applications that require different transition temperatures (133). A PTC conductive composite based on high density polyethylene whose melting peak temperature is 129–131°C and whose specific volume increases by approximately 10% due to melting across a narrow temperature range showed a maximum resistivity at 129–131°C (130). The transition temperature can be slightly adjusted by using a copolymer or polymer blend that has more than one homopolymer. A compound of 40 parts weight of carbon black, 60 parts of melted olefin copolymer (ethylene–ethyl acrylate copolymer), and an organic peroxide, had a T_t of 82°C (114). Another reported recipe (134) is a composite of carbon black dispersed in high density polyethylene and poly(ethylene vinyl acetate), whose T_t is 120°C. Ultrahigh molecular weight polyethylene reportedly enhanced the PTC behavior (127). Thermosetting material such as thermosetting polyester resin that was cross-linked by a free-radical reaction, was also reportedly used as a polymer matrix for a PTC conductive polymer composite (135).

The PTC amplitude depends on crystallinity. Meyer (136) showed that crystalline *trans*-polybutadiene filled with carbon black has low room temperature resistivity and a significant anomaly, whereas the amorphous *cis*-polybutadiene filled with the same amount of carbon black has much higher resistivity and no

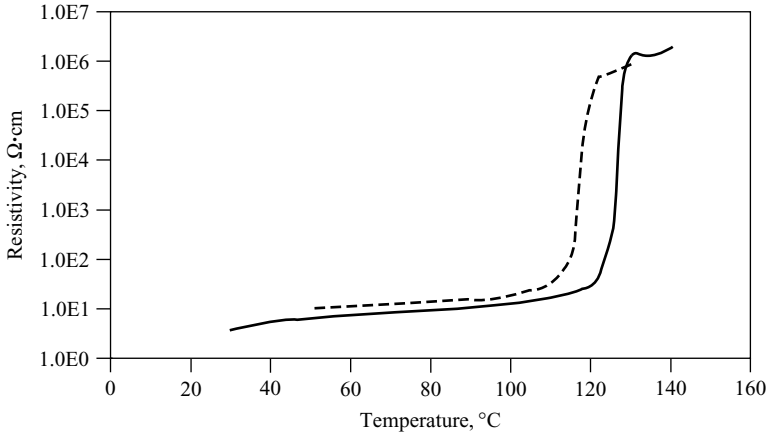

Fig. 24. Resistivity versus temperature for a PTC conductive polymer composite during heating and cooling cycles. —— Heating; - - - - cooling.

anomaly. Within a polymeric family, a polymer that is more crystalline has higher PTC amplitude. But different classes of polymers that have the same crystallinity do not exhibit identical PTC behavior and no relationship was correlated. PTC amplitude depends on polymer type. PTC amplitude increases in the following order with respect to the polymer matrix: nylon-6,6 < polypropylene < polyethylene oxide < low density polyethylene < high density polyethylene.

As mentioned before, the mechanism for the PTC anomaly in semicrystalline polymer composites is accompanied by a relatively large change in specific volume of the polymer at its melting temperature. The resistivity versus temperature curve can be well matched by the specific volume–temperature curve. Crystallization during cooling of a polymer is the reverse of melting of polymer crystal during heating. The PTC transition of this kind of smart material is reversible. During cooling, the same material shows a sharp decrease in resistivity, as shown by Figure 24. The thermal expansion of a polymer depends on its heating and cooling cycle. Because the melting temperature of a polymer crystal is always higher than the recrystallization temperature, the PTC transition of a conductive polymer composite is always higher in the heating cycle than that during the cooling cycle (110). The difference is about 18°C for polyethylene, 34°C for polyoxymethylene, and 50°C for polypropylene. Actually, all factors that affect the melting and recrystallization behavior, such as pressure and heating and cooling rates, influence the PTC behavior of a conductive polymer composite. Meyer showed that the PTC transition temperature increases and PTC amplitude decreases as the pressure increases (136).

In some conductive polymer composites, the NTC effect follows, for example, the resistivity decreases as the temperature increases further after PTC transition. The NTC effect is probably due to the reorientation, reaggregation, or reassembling of carbon black. Initially dispersed particles may become mobile in the temperature range of polymer melting to repair the broken percolation network. The measurement of resistance versus the temperature behavior of the conductive

composite was repeated for the same sample(134,137). Tang (134) observed that the PTC intensity and the base resistance decrease with thermal cycles. The reason is obviously reorganization of carbon at the high temperature.

Radiation was used to cross-link a carbon-black-filled conductive polymer composite. The NTC effect can be alleviated or reduced by cross-linking, and the PTC amplitude is stabilized (the resistance at lower temperature is stabilized) after cross-linking (110,134). The organization of carbon black is hampered in a cross-linked polymer network.

Effect of Processing Conditions and Additives. The effect of mixing time on the resistivity–temperature behavior was also investigated (134). Both the PTC effect and the reproducibility were improved greatly when the sample was mixed for a long time. It was suggested that the improvement is due to increasing absorption of the polymer on the carbon black surface and this absorption forms a polymer layer outside the carbon black particle. The room temperature resistivity increases with mixing time at constant carbon black concentration. It can also be explained that structures are broken down during mixing; thus, the resistivity increases. If the power consumption during mixing is too high, the composition would have too high resistivity at a temperature below T_g and have unsatisfactory electrical stability on aging at elevated temperature. If the power consumption is too low, it can also result in a composition that has a low PTC amplitude.

Tang (134) studied the effect of the interaction between carbon black and the polymer on electrical behavior. The absorption of polymer on the carbon black surface may be physical or chemical. The latter is caused by free-radical reaction between the polymer and carbon black, and it can occur during radiation or the preparation of the composite. In carbon-black-filled high density polyethylene, the cross-linked network of the polymer restricts the freedom of movement of carbon black. The free-radical reaction enhances the binding force between the polymer and carbon black.

Polymeric materials may be broken down under high voltage. The voltage stability of a cross-linked PTC conductive polymer is improved by incorporating a polymerizable monomer such as triallyisocyanurate before it is cross-linked (138). Antimony oxide, which does not degrade the PTC characteristics, can be used as a flame-retardant agent (121). A semiconductive inorganic substance such as silicon carbide or boron carbide was used to improve the high voltage stability (139). Alumina trihydrate can be added to a PTC conductive polymer composite to prevent dielectric breakdown, arcing, and carbon tracking under high voltage (138).

Application of PTC Conductive Polymer Composite. There are many applications for PTC conductive polymer composites, including thermistors (122), circuit protection devices (140), and self-regulating heaters (141). Because the material both heats and controls the temperature, it can be used to manufacture a self-regulating heating device. As the temperature increases, the resistance increases, and thus the power decreases. This kind of self-regulating heater can be used to prevent freezing of water and pipes used in chemical processing. It has also been used to manufacture a heater for heating a hot-melt adhesive to seal a cable splice case (142) as well as a hair curler (143). Self-regulating heaters can be

manufactured into different forms. The blanket form of PTC conductive polymer composite can allow precise temperature control across larger areas. This kind of device has been used in the repair of thermally complex aircraft structures (141,144).

Another application of PTC conductive polymers is in over-temperature and over-current protection. A device manufactured from a PTC conductive polymer composite has low resistance and much less resistance than the rest of the circuit; thus it has no influence on normal performance. But at high temperature, these devices become highly resistant or insulating; thus they dominate the circuit, reduce the current, and protect the circuit. For large abnormal current, the device can rapidly self-heat to a high resistance state, and thus reduces the current. The smartness lies in the over-temperature and over-current protection and also lies in its resettability. After the current drops and the temperature of the device decreases, the device returns to a low resistance state and allows current to pass. A resettable fuse made from a PTC conductive polymer has been on the market. This kind of resettable fuse has been used in battery chargers to terminate the charging function based on the battery temperature and protect the battery from overheating. It is also used in telecommunication equipment, computers, and power supplies.

Summary. A temperature-sensitive PTC conductive polymer composite is a true smart material. Its property can be tailored by the selecting filler, polymer matrix, and processing conditions. Its transition temperature is determined by the melting point of the polymer matrix. Its room-temperature resistivity, high temperature resistivity, and PTC transition amplitude can be adjusted by the filler and its combination with the polymer matrix. PTC transition behavior can be stabilized by cross-linking of the polymer matrix. This kind of smart material can be used in many temperature-sensitive applications such as thermistors, self-regulating heaters, and circuit protection devices.

BIBLIOGRAPHY

1. U.S. Pat. 2,774,747 (1956), H. Wolfson and G. Elliot.
2. U.S. Pat. 2,849,631 (1958), K. R. Matz.
3. U.S. Pat. 2,866,057 (1958), D. P. Beck.
4. K. Gilleo, *Soldering Surface Mount Technol.* (19), 12–17 (Feb. 1995).
5. P. G. Hariss, *Soldering Surface Mount Technol.* (20), 19–21 (May 1995).
6. A. O. Ogunjimi, O. Boyle, D. C. Whalley, and D. J. Williams, *J. Electron. Manuf.* **2**, 109–118 (1992).
7. S. Asai, U. Saruta, M. Tobita, M. Takano, and Y. Miyashita, *J. Appl. Polym. Sci.* **56**, 769–777 (1995).
8. D. D. Chang, P. A. Crawford, J. A. Fulton, R. McBride, M. B. Schmidt, R. E. Sinitski, and C. P. Wong, *IEEE Trans. Components Hybrids Manuf. Technol.* **16**, 320–326 (Dec. 1993).
9. Eur. Pat. 0 147 856 (1985), H. Ando, N. Kobayashi, H. Numao, Y. Matsubara, and K. Suzuki.

10. Eur. Pat. 0 265 077 (1987), K. Gilleo.
11. U.S. Pat. 5,136,365 (1992), R. Pennisi, M. Papageorge, and G. Urbisch.
12. H. Date, Y. Hozumi, H. Tokuhira, M. Usui, E. Horikoshi, and T. Sato, in Proceedings of ISHM'94, Bologna, Italy, Sept. 1994, pp. 570–575.
13. J. Liu, in Proceedings of 4th International Conference on Adhesive Joining and Coating Technology in Electronics Manufacturing, Helsinki, Finland, June 2000, pp. 1–15.
14. C. M. L. Wu, J. Liu, and N. H. Yeung, in Proceedings of 4th International Conference on Adhesive Joining and Coating Technology in Electronics Manufacturing, Helsinki, Finland, June 2000, pp. 101–106.
15. Y. Kishimoto and K. Hanamura, in Proceedings of 3rd International Conference on Adhesive Joining and Coating Technology in Electronics Manufacturing, Binghamton, New York, Sept. 1998, pp. 137–143.
16. U.S. Pat. 4999460 (Mar. 12, 1991) (to Casio).
17. U.S. Pat. 5123986 (June 23, 1992) (to Casio).
18. U.S. Pat. 5180888 (Jan. 19, 1993) (to Casio).
19. R. Nagle, *Int. J. Microelectron. Packag.* **1**, 187–196 (1998).
20. J. K. Kivilahti, in J. Liu, ed., *Conductive Adhesives for Electronics Packaging*, Electrochemical Publications Ltd., Port Erin, British Isles, 1999, pp. 153–183.
21. M. Vuorela, M. Holloway, S. Fuchs, F. Stam, and J. Kivilahti, in Proceedings of 4th International Conference on Adhesive Joining and Coating Technology in Electronics Manufacturing, Helsinki, Finland, June 2000, pp. 147–152.
22. R. Sihlbom, M. Dernevik, Z. Lai, J. P. Starski, and J. Liu, *IEEE Trans. Components, Packag. Manuf. Technol., Part A* **20**, 469–477 (Sept. 1998).
23. M. Dernevik, R. Sihlbom, K. Axelsson, Z. Lai, J. Liu, and P. Starski, in Proceedings of 48th IEEE Electronic Components and Technology Conference, Seattle, Washington, D.C., May 1998, pp. 1026–1030.
24. M. J. Yim, W. Ryu, Y. D. Jeon, J. Lee, J. Kim, and K. Paik, in Proceedings of 49th Electronic Components and Technology Conference, San Diego, Calif., May 1999, pp. 488–492.
25. K. Gustafsson, S. Mannan, J. Liu, Z. Lai, D. Whalley, and D. Williams, in Proceedings of 47th Electronic Components and Technology Conference, San Jose, Calif., May 1997, pp. 561–566.
26. H. Hirai, T. Motomura, O. Shimada, and Y. Fukuoka, in Proceedings of International symp on Electronic Materials and Packaging, Hong Kong, China, Nov.–Dec. 2000, pp. 1–6.
27. Y. Hotta, M. Maeda, F. Asai, and F. Eriguchi, in Proceedings of 48th IEEE Electronic Components and Technology Conference, Seattle, Washington, D.C., May 1998, pp. 1042–1046.
28. G. Connell, R. L. D. Zenner, and J. A. Gerber, in Proceedings of 47th Electronic Components and Technology Conference, San Jose, Calif., May 1997, pp. 274–278.
29. K. M. Kim, in Proceedings of 50th Electronic Components and Technology Conference, Las Vegas, Nev., May 2000, pp. 1122–1132.
30. L. Li and T. Fang, in Proceedings of 4th International Conference on Adhesive Joining and Coating Technology in Electronics manufacturing, Helsinki, Finland, June 2000, pp. 129–135.
31. A. Ogunjimi, S. Mannan, D. Whalley, and D. Williams, *IEEE Trans. Components Packag. Manuf. Technol., Part C* **19**, 257–263 (Oct. 1996).
32. J. Liu, L. Ljungkrona, and Z. Lai, *IEEE Trans. Components Packag. Manuf. Technol., Part B* **18**, 313–319 (May 1995).

33. J. Liu, *Circuit World* **19**(4), 4–15 (1993).
34. Y. C. Chan, K. C. Hung, C. W. Tang, and C. M. L. Wu, in Proceedings of 4th International Conference on Adhesive Joining and Coating Technology in Electronics manufacturing, Helsinki, Finland, June 2000, pp. 141–146.
35. H. Kristiansen and J. Liu, *IEEE Trans. Components Packag. Manuf. Technol., Part A* **21**, 208–214 (June 1998).
36. P. B. Jana, S. Chaudhuri, A. K. Pal, and S. K. De, *Polym. Eng. Sci.* **32**, 448–456 (Mar. 1992).
37. A. Malliaris and D. T. Tumer, *J. Appl. Phys.* **42**, 614–618 (1971).
38. G. R. Ruschau, S. Yoshikawa, and R. E. Newnham, *J. Appl. Phys.* **73**, 953–959 (1992).
39. J. C. Jagt, *IEEE Trans. Components Packag. Manuf. Technol., Part A* **21**, 215–225 (1998).
40. M. A. Lutz and R. L. Cole, *Hybrid Circuits* (23), 27–30 (Sept. 1990).
41. J. M. Pujol, C. Prudhomme, M. E. Quenneson, and R. Cassat, *J. Adhesn.* **27**, 213–229 (1989).
42. J. Ivan, J. Gonzales, and M. G. Mena, in Proceedings of 47th Electronic Components and Technology Conference, San Jose, Calif., May 1997, pp. 525–535.
43. I. Y. Chien and M. N. Nguyen, in Proceedings of 1994 Electronic Components and Technology Conference, San Diego, Calif., May 1994, pp. 580–584.
44. D. P. Galloway, M. Grosse, M. N. Nguyen, and A. Burkhart, in Proceedings of the IEEE/CPMT International Electronic Manufacturing Technology (IEMT) Symposium, Austin, Tex., Oct. 1995, pp. 141–147.
45. S. M. Pandiri, *Adhesiv. Age* 31–35 (Oct. 1987).
46. B. Gunther and H. Schafer, in Proceedings of the 2nd International Conference on Adhesive Joining and Coating Technology in Electronics Manufacturing, Stockholm, Sweden, June 1996, pp. 55–59.
47. S. Kotthaus, R. Haug, H. Schafer, and B. Gunther, in Proceedings of the 2nd International Conference on Adhesive Joining and Coating Technology in Electronics Manufacturing, Stockholm, Sweden, June 1996, pp. 14–17.
48. P. K. Pramanik, D. Khastgir, S. K. De, and T. N. Saha, *J. Mater. Sci.* **25**, 3848–3853 (1990).
49. A. Yokoyama, T. Katsumata, A. Fujii and T. Yoneyama, in IMC 1992 Proceedings, 1992, pp. 376–38.
50. S. K. Kang, R. Rai, and S. Purushothaman, in Proceedings of 47th Electronic Components and Technology Conference, San Jose, Calif., May 1997, pp. 565–570.
51. S. K. Kang, R. Rai, and S. Purushothaman, *IEEE Trans. Components Packag. Manuf. Technol., Part A* **21**(1), 18–22 (Mar. 1998).
52. J. Lin, J. Drye, W. Lytle, T. Scharr, R. Subrahmanyan, and R. Sharma, in Proceedings of 46th Electronic Components and Technology Conference, Orlando, Fla., May 1996, pp. 1059–1068.
53. R. H. Estes, in Proceedings of 3rd International Conference on Adhesive Joining and Coating Technology in Electronics Manufacturing, Binghamton, New York, Sept. 1998, pp. 229–239.
54. K. E. Oh, *IEEE J. Selected Top. Quantum Electron.* **5**(1), 119–126 (Jan.–Feb. 1999).
55. M. Gaynes, R. Kodnani, M. Pierson, P. Hoontrakul, and M. Paquette, in Proceedings of 3rd international Conference on Adhesive Joining and Coating Technology in Electronics Manufacturing, Binghamton, New York, Sept. 1998, pp. 244–251.
56. Y. Bessho, in Proceedings of International Microelectronics Conference, May 1990, pp. 183–189.

57. J. B. Nysaether, Z. Lai, and J. Liu, in Proceedings of 3rd International Conference on Adhesive Joining and Coating Technology in Electronics Manufacturing, Binghamton, New York, Sept. 1998, pp. 125–131.
58. H. H. Manko, *Solders and Soldering, Materials, Design, Production, and Analysis for Reliable Bonding*, 2nd ed., McGraw-Hill, New York, 1979.
59. K. Brindley and M. Judd, *Soldering in Electronic Assembly*, 2nd ed., Butterworth-Heinemann, Woburn, Mass., Mar. 1999.
60. R. Tummala, E. Rymaszeski, and A. Klopfenstein, *Microelectronics Packaging Handbook*, 2nd ed., Kluwer Academic Publishers, Boston, 1997.
61. L. P. Lambert, *Soldering for Electronic Assemblies*, Marcel Dekker, New York, Oct. 1987.
62. B. Trumble, *IEEE Spectrum* 55–60 (May 1998).
63. B. T. Alpert and A. J. Schoenberg, *Electron. Packag. Prod.* 130–132 (Nov. 1991).
64. R. Cdenhead and D. DeCoursey, *Int. J. Microelectron.* **8**(3), 14 (1985).
65. G. Nguyen, J. Williams, F. Gibson, and T. Winster, in Proceedings of International Electronic Packaging Conference, San Diego, Calif., Sept. 1993, pp. 479–486.
66. J. C. Jagt, P. J. M. Beric, and G. F. C. M. Lijten, *IEEE Trans. Components, Packag. Manuf. Technol., Part B* **18**, 292–298 (1995).
67. M. Zwolinski, J. Hickman, H. Rubon, and Y. Zaks, in Proceedings of the 2nd International Conference on Adhesive Joining and Coating Technology in Electronics Manufacturing, Stockholm, Sweden, June 1996, pp. 333–340.
68. H. Botter, in Proceedings of the 2nd International Conference on Adhesive Joining and Coating Technology in Electronics Manufacturing, Stockholm, Sweden, June 3–5, 1996, pp. 30–37.
69. C. P. Wong, D. Lu, S. Vona, and Q. K. Tong, in Proceedings of the 1st IEEE International Symposium on Polymeric Electronics Packaging, Norrkoping, Sweden, 1997, pp. 80–85.
70. J. Bolger and S. Morano, *Adhesiv. Age* 17–20 (June 1984).
71. H. Takezawa, M. Itagaki, T. Mitani, Y. Bessho, and K. Eda, in Proceedings of 4th International Symposium and Exhibition on Advanced Packaging Materials, Processes, Properties and Interfaces, Braselton, Ga., Mar. 1999, pp. 11–15.
72. J. Felba, K. P. Friedel, and A. Moscicki, in Proceedings of 4th International Conference on Adhesive Joining and Coating Technology in Electronics manufacturing, Helsinki, Finland, June 2000, pp. 232–239.
73. S. Liong, Z. Zhang, and C. P. Wong, in Proceedings of 51th Electronic Components and Technology Conference, Orlando, Fla., May 2001, pp. 1236–1240.
74. J. H. Constable, T. Kache, H. Teichmann, S. Muhle, and M. A. Gaynes, *IEEE Trans. Components Packag. Technol.* **22**(2), 191–199 (June 1999).
75. R. Gomatam, E. Sancaktar, D. Boismier, D. Schue, and I. Malik, in Proceedings of 4th International Symposium and Exhibition on Advanced Packaging Materials, Processes, Properties and Interfaces, Braselton, Ga., Mar. 2001, pp. 6–12.
76. L. Smith-Vargo, *Electron. Packag. Prod.* 48–49 (Aug. 1986).
77. E. M. Jost and K. McNeilly, in Proceedings of ISHM, Bournemouth, England, June 1987, pp. 548–553.
78. D. Lu, Q. K. Tong, and C. P. Wong, *IEEE Trans. Components Packag. Manuf. Technol., Part A* **22**, 365–371 (1999).
79. D. Lu, Q. Tong, and C. P. Wong, in Proceedings of 4th International Symposium and Exhibition on Advanced Packaging Materials, Processes, Properties and Interfaces, Braselton, Ga., Mar. 1998, pp. 256–260.

80. A. J. Lovinger, *J. Adhesn.* **10**, 1–15 (1979).
81. D. Lu, Q. K. Tong, and C. P. Wong, *IEEE Trans. Components Packag. Manuf. Technol., Part C* **22**, 223–227 (1999).
82. J. Morris and C. Cook, in Proceedings of 2nd IEEE International Symposium on Polymeric Electronic Packaging, Gothenburg, Sweden, Oct. 1999, pp. 15–26.
83. C. Gallagher, G. Matijasevic, and J. F. Maguire, in Proceedings of 47th Electronic Components and Technology Conference, San Jose, Calif., May 1997 pp. 554–560.
84. J. W. Roman and T. W. Eagar, in Proceedings of ISHM, San Francisco, Calif., Oct. 1992, pp. 52–57.
85. U.S. Pat. 5863622 (Aug. 1998), C. Gallagher, G. Matijasevic, and A. Capote.
86. K. Gilleo, *Circuits Assembly* 50–51 (1994).
87. K. Gilleo, *Circuits Assembly* 51–53 (1994).
88. D. Lu, Q. K. Tong, and C. P. Wong, *IEEE Trans. Components Packag. Manuf. Technol., Part C* **22**, 228–232 (1999).
89. Q. K. Tong, G. Fredrickson, R. Kuder, and D. Lu, in Proceedings of the 49th Electronic Components and Technology Conference, San Diego, Calif., May 1999, pp. 347–352.
90. D. Lu and C. P. Wong, *J. Appl. Polym. Sci.* **74**, 399–406 (1999).
91. D. Lu and C. P. Wong, in Proceedings of 4th International Symposium and Exhibition on Advanced Packaging Materials, Processes, Properties and Interfaces, Braselton, Ga., Mar. 1999, pp. 288–294.
92. U.S. Pat. (Mar. 1999), Q. K. Tong, A. Xiao, and D. Lu.
93. H. Leidheiser Jr., *J. Coat. Technol.* **53**(678), 29–39 (1981).
94. G. Trabanelli and V. Carassiti, in M. G. Fontana and R. W. Staehle, eds., *Advanced Corrosion Science and Technology*, Vol. **1**, Plenum Press, New York, 1970, pp. 147–229.
95. G. Trabanelli, in F. Mansfeld, ed., *Corrosion Mechanisms*, Marcel Dekker, New York, 1987, pp. 119–164.
96. O. L. Riggs Jr., in C. C. Nathan, ed., *Theoretical Aspects of Corrosion Inhibitors and Inhibition*, National Association of Corrosion Engineers, Houston, Tex., 1973, pp. 2–27.
97. P. A. Reardon, in Corrosion'86 (Paper No. 175), National Association of Corrosion Engineers, Houston, Tex., 1986.
98. M. G. Noack, in Corrosion'89 (Paper No. 436), National Association of Corrosion Engineers, Houston, Tex., 1989.
99. P. A. Reardon and W. E. Bernahl, Corrosion'87 (Paper No. 438), National Association of Corrosion Engineers, Houston, Tex., 1987.
100. S. Romaine, in Proceedings of the American Power Conference, Chicago, Ill., Apr. 1986, pp. 1066–1073.
101. U.S. Pat. 5180523 (Nov. 1989), D. Durand, D. Vieau, A. L. Chu, and T. S. Weiu.
102. S. Macathy, in Proceedings of Surface Mount International, San Jose, Calif., Aug. 1995, pp. 562–567.
103. S. A. Vona and Q. K. Tong, in Proceedings of 4th International Symposium and Exhibition on Advanced Packaging Materials, Processes, Properties and Interfaces, Braselton, Ga., Mar. 1998, pp. 261–267.
104. J. Liu and B. Weman, in Proceedings of the 2nd International Symposium on Electronics Packaging Technology, Shanghai, China, Dec. 1996, pp. 313–319.
105. D. Lu and C. P. Wong, *IEEE Trans. Components Packag., Manuf. Technol. Part C* **22**, 324–330 (1999).

106. D. Lu and C. P. Wong, *Encyclopedia of Smart Materials*, John Wiley & Sons, Inc., New York, in press.
107. M. Yim and K. Paik, *IEEE Trans. Components Packag. Manuf. Technol.* **24**(1), 24–32 (Mar. 2001).
108. J. Wu, K. Moon, and C. P. Wong, in Proceedings of 51st Electronic Components and Technology Conference, Orlando, Fla., May 2001, pp. 571–575.
109. K. Moon, J. Wu, and C. P. Wong, in Proceedings of International Symposium on Advanced Packaging Materials: Processes, Properties and Interfaces, Braselton, Ga., Mar. 2001, pp. 341–346.
110. X. Yi, G. Wu, and Y. Pan, *Polym. Int.* **44**, 117 (1997).
111. V. E. Gul, *Structure and Properties of Conducting Polymer Composites*, VSP BV, the Netherlands, (1996).
112. U.K. Pat. 604,695 (1945), E. Frydman.
113. U.S. Pat. 3,243,753 (1961), F. Kohler.
114. K. Matsushige, K. Kobayashi, N. Iwami, T. Horiuchi, E. Shitamori, and M. Itoi, *Thin Solid Films* **273**, 128 (1996).
115. K. Ohe and Y. Naito, *Jpn. J. Appl. Phys.* **10**, 99 (1971).
116. J. Meyer, *Polym. Eng. Sci.* **14**, 706 (1974).
117. F. Lux, *J. Mater. Sci.* **28**, 285 (1993).
118. R. Zallen, *The Physics of Amorphous Solids*, John Wiley & Sons, Inc., New York, 1983, Chapt. "4".
119. M. Sumita, K. Sakata, S. Asai, K. Miyasaka, and H. Nakagawa, *Polym. Bull.* **25**, 265 (1991).
120. K. Yoshida, *J. Phys. Soc. Jpn.* **59**, 4087 (1990).
121. U.S. Pat. 3,673,121, J. Meyer.
122. U.S. Pat. 5,793,276, H. Tosaka, M. Takaya, S. Moriya, H. Kobuke, and M. Hamada.
123. K. A. Hu, J. Runt, A. Safari, and R. E. Newnham, *Ferroelectrics* **68**, 115 (1986).
124. Y. Pan and G. Z. Wu, *J. Zhejiang Univ.* **4**, 613 (1994).
125. M. Narkis, A. Ram, and F. Flashner, *J. Appl. Polym. Sci.* **25**, 1515 (1980).
126. U.S. Pat. 5,171,774, A. Ueno, M. Takata, N. Yamazaki, and S. Sugaya.
127. U.S. Pat. 5,554,679, T. Cheng.
128. U.S. Pat. 5,174,924, M. Yamada, S. Isshiki, and Y. Kurosawa.
129. K. Kinoshita, *Carbon Electrochemical and Physicochemical Properties*, John Wiley & Sons, Inc., New York, (1988).
130. S. Luo and C. P. Wong, *IEEE Trans. Components Packag. Technol.* **23**, 151 (2000).
131. M. Narkis, A. Ram, and F. Flashner, *J. Appl. Polym. Sci.* **22**, 1163 (1978).
132. M. Narkis, A. Ram, and F. Flashner, *Polym. Eng. Sci.* **18**, 649 (1978).
133. U.S. Pat. 4,668,857, J. Smuckler.
134. H. Tang, Z. Y. Liu, J. H. Piao, X. F. Chen, Y. X. Lou, and S. H. Li, *J. Appl. Polym. Sci.* **51**, 1159 (1994).
135. U.S. Pat. 5,545,679, P. Bollinger Jr., D. Mueller, J. Smith, and H. Wehrli III.
136. J. Meyer, *Polym. Eng. Sci.* **13**, 462 (1973).
137. F. Geng, L. Gao, and W. Guo, *Proc. Symp. Electr. Insul. Mater.* 133 (1995).
138. U.S. Pat. 4,188,276, B. Lyons and Y. Kim.
139. U.S. Pat. 4,732,701, M. Nishii, H. Miyake, and H. Fujii.
140. A. Au, in Annual Technical Conference, Society of Plastics, Brookfield Center, Conn., 1985, pp. 412–413.
141. W. Robert, *Proc. Nat. SAMPE Symp. Exhibition* **30**, 1441 (1985).
142. U.S. Pat. 4,880,962, J. Nolf, J. Vansant, and M. Jensen.

143. U.S. Pat. 3,689,736, J. Meyer.
144. L. H. Mccarty, *Des. News* **42**(20), 108 (1986).

DAOQIANG LU
SHIJIAN LUO
C. P. WONG
Georgia Institute of Technology

CONFORMATION AND CONFIGURATION.

See Volume 2.

CONTACT LENSES.

See HYDROGELS.

CONTROLLED MICROSTRUCTURE.

See SINGLE SITE CATALYSTS.

CONFORMATION AND CONFIGURATION

Introduction

Scientists have devised many models for treating the enormous number of conformations accessible to a flexible chain molecule. Most of these models pay little attention to the real covalent structure of the chain. Therefore they are ill suited to the development of a thorough understanding of why one polymer behaves differently from another. The rotational isomeric state model is unique in that it describes the conformation-dependent properties of the chain in terms of the real covalent structure, and does so in a computationally efficient manner. The data fed into the model include structural information (lengths of bonds, angles between successive bonds, values of the preferred torsion angles) and energetic information (contributions of short-range intrachain interactions to the preferences for specific values of the torsion angles, and specific pairs of torsion angles at neighboring bonds, ie, the interdependence of the torsions). This information is processed in a manner that rapidly gives the average of chain properties, such as the mean square unperturbed end-to-end distance $\langle r^2 \rangle_0$, with the average being performed over all of the accessible conformations.

The rotational isomeric state model is not among the newer models used in polymer science. Its earliest application to polymers was reported half a century ago (1), using mathematical techniques invented 10 years earlier (2). Applications of the model to polymers received a strong boost from Flory's group in the 1960s, leading to the publication of his classic book on the subject at the end of that decade (3). Another book, published 25 years later, updates the techniques and applications (4). The literature now contains rotational isomeric state models for literally hundreds of polymers. A few hundred of the models that appeared in

Encyclopedia of Polymer Science and Technology. Copyright John Wiley & Sons, Inc. All rights reserved.

the literature up to the early 1990s have been tabulated in a standard format in lengthy reviews (5,6).

The classic use of the rotational isomeric state model is for the rationalization of the mean square unperturbed dimensions of a long-chain molecule, as measured either in dilute solution in the absence of excluded volume (ie, in a Θ solvent) or in the bulk amorphous state (7). A much simpler model for such a chain uses random flight statistics to write a temperature-independent $\langle r^2 \rangle_0$ as the product of a term N that is directly proportional to the degree of polymerization and another term $\langle L^2 \rangle$ that specifies the mean square step length of a segment.

$$\langle r^2 \rangle_0 = N \langle L^2 \rangle \tag{1}$$

The counterpart of equation (1) in the rotational isomeric state model also has a dependence on the degree of polymerization, through the use of a serial product over all n bonds in the chain.

$$\langle r^2 \rangle_0 = Z^{-1} \mathrm{F}_1 \mathrm{F}_2 \cdots \mathrm{F}_2 \tag{2}$$

Here Z is the conformational partition function, which contains information about the temperature T and the energies of all of the accessible conformations of the chain. The $\mathbf{F}_i$ are matrices that combine geometric information, namely the length of bond i, l_i, the angle between bonds i and $i+1$, θ_i, and the perferred torsion angles at bond i, ϕ_i, with the energetic information contained in Z. The rotational isomeric state model is more realistic than the freely jointed chain model because it includes temperature, different energies for the various preferred conformations, and the geometry of these conformations.

The present description of the rotational isomeric state model has several parts. First, we will describe the formulation and uses of Z, which initially restricts the focus to the thermodynamic (energetic) part of the rotational isomeric state model. Then we will describe how the structural information (l_i, θ_i, ϕ_i) is incorporated in the model. Finally, we will combine the thermodynamic and the structural information, which will take us back to equation (2). Along the way we will mention a few other properties, in addition to $\langle r^2 \rangle_0$, that can be successfully rationalized with the rotational isomeric state model. Finally, several illustrative applications will be presented.

Although developed primarily for the analysis of the conformation-dependent physical properties of flexible chain molecules in the Θ state (essentially a single-chain problem, due to the neglect of excluded volume), the rotational isomeric state model has important applications in other types of problems. It has been used for generation of detailed models for glassy atactic polypropylene at bulk density (8). The rotational isomeric state model is also instrumental in the simulation of the mixing of structurally similar polymers, as illustrated also by polypropylene, where melts of isotactic and atactic polypropylene are miscible, but melts of isotactic and syndiotactic polypropylene are immiscible (9,10). Space limitations will preclude extensive description of these more advanced applications of the rotational isomeric state model.

The Conformational Partition Function *Z*

Although not in any way restricted in application to polyethylene, it is nevertheless useful to adopt this polymer for purposes of illustration because the conformational properties of its small oligomers are likely to be known to the reader. The discussion conveniently begins with the central C—C bond in *n*-butane, CH_3CH_2—CH_2CH_3. The conformational energy, which is a continuous function of the torsion angle at this bond, has been written using the cosine of the torsion angle (11).

$$U(\phi) = 11.8 + 7.66\cos\phi + 4.64\cos 2\phi + 8.8\cos 3\phi \tag{3}$$

Here $U(\phi)$ is in $kJ \cdot mol^{-1}$ and $\phi = 0$ in the *cis* conformation. This function, which is depicted in Figure 1, has the three maxima and three minima summarized in Table 1. When the populations are distributed according to $\exp(-U(\phi)/RT)$, and T has values that are likely to be of interest, there will be a significant population of ϕ near all three minima, but the populations in the vicinity of the maxima will be very small, as shown in Figure 2. This observation suggests a simplification in which the continuous range for ϕ is approximated by a set of three discrete values corresponding to the three regions of ϕ that have significant population. These three regions are named *trans* and *gauche*$^{\pm}$ in *n*-butane. They are often abbreviated as t and $g^{\pm}$. The normalized populations of these three regions are given in the last column of Table 1. The statistical weight of g^+ (or g^-) relative to t is denoted by σ. The value of σ is temperature-dependent. It is less than 1/3 at finite T because the regions near $\phi = \pm 70^\circ$ are of higher energy than the region near $\phi = 180^\circ$. The term in parentheses in the last column of Table 1 $(1 + 2\sigma)$ is the conformational partition function (or sum of statistical weights for

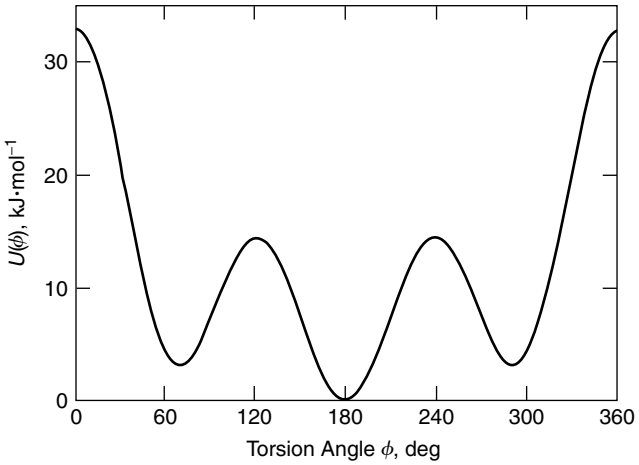

Fig. 1. Torsion potential energy function for the central C—C bond in *n*-butane. From Ref. 4. Copyright © 1994 John Wiley & Sons, Inc. Reprinted by permission of John Wiley & Sons, Inc.

Table 1. Maxima and Minima in the Torsion Potential Energy Function for the Internal C—C Bond in *n*-Butane

ϕ, deg	Maximum or minimum	U, kJ·mol^{-1}	U/kT at 300 K	Population
180	Minimum	0	0	$1(1+2\sigma)^{-1}$
$\sim(\pm 121)$	Local maximum	$\sim$14	$\sim$6	$\sim$0
$\sim(\pm 70)$	Local minimum	$\sim$3	$\sim$1	$\sigma(1+2\sigma)^{-1}$
0	Maximum	$\sim$33	$\sim$13	$\sim$0

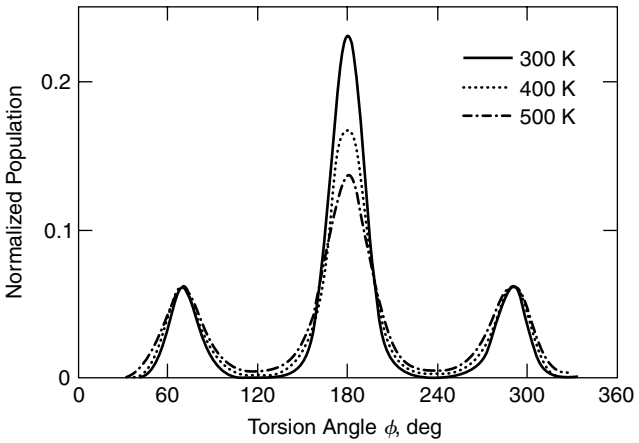

Fig. 2. Normalized populations of the torsion angle at the central C—C bond in *n*-butane at 300, 400, and 500 K. From Ref. 4. Copyright © 1994 John Wiley & Sons, Inc. Reprinted by permission of John Wiley & Sons, Inc.

all conformations) for *n*-butane in the rotational isomeric state approximation. The probability of any state is its statistical weight u_i divided by the sum of all statistical weights, ie, the conformational partition function $p_i = Z^{-1}\ u_i$, $Z = \sum u_i$.

Extension of this concept to a longer alkane suggests three conformations for each internal C—C bond, or 3^{n-2} conformations for a chain of n bonds. If the bonds were independent of one another, the conformational partition function would be $(1+2\sigma)^{n-2}$. However, interdependence of neighboring torsions destabilizes some of the conformations, with important implications for their statistical weights. The most important interdependence in the *n*-alkanes is the interaction known as the *pentane effect* because *n*-pentane is the smallest alkane in which it is seen. If the two internal C—C bonds of *n*-pentane adopt *g* states, only the two conformations with *g* states of the same sign have conformational energies near $2E_\sigma$, which is the prediction based on the assumption of independent bonds. If the *g* states are of opposite sign, however, the conformational energy is higher than this prediction by nearly 7.5 kJ·mol^{-1} because of the repulsive interaction of the terminal methyl groups in these two conformations. The conformational energy of these two conformations is $2E_\sigma + E_\omega$, with E_ω about 7.5 kJ·mol^{-1}. The conformational

partition function for *n*-pentane is not $(1 + 2\sigma)^2$, as would have been the case if the two internal bonds were independent, but is instead given by $1 + 4\sigma + 2\sigma^2 (1 + \omega)$.

The influence of the interdependence of neighboring bonds is easily incorporated in the formulation of the conformational partition function for long chains. The method employs a statistical weight matrix **U** for each bond. For bond i somewhere within a long chain, $\mathbf{U}_i$ has the following composition:

(1) The number of columns is given by the number of rotational isomeric states at bond i, ν_i;
(2) The number of rows is given by the number of rotational isomeric states at bond $i - 1$, ν_{i-1};
(3) Every element in column η contains the statistical weight required by the first-order (dependent on one torsion) interaction when bond i is in the state indexed by that column;
(4) Every element in row ξ of column η also contains the statistical weight required by the second-order (dependent on two torsions) interaction when bond i is in the state indexed by that column and bond $i - 1$ is in the state indexed by that row.

For polyethylene, the first two points specify dimensions of 3×3 for $\mathbf{U}_i$. Assuming the order of indexing of rows and columns is t, g^+, g^-, the third point specifies the presence of σ in all elements in the second and third columns. The fourth point specifies the appearance of ω in the 2,3 and 3,2 elements. Therefore the statistical weight matrix for polyethylene is the 3×3 matrix in equation (4) (12).

$$\mathrm{U}_i = \begin{bmatrix} 1 & \sigma & \sigma \\ 1 & \sigma & \sigma\omega \\ 1 & \sigma\omega & \sigma \end{bmatrix}_i \tag{4}$$

More generally, $\mathbf{U}_i$ is formulated as the product of a diagonal matrix $\mathbf{D}_i$ with dimensions given by point (*1*), and with the statistical weights for the first-order interactions on the main diagonal, in the order required by the indexing of the columns of $\mathbf{U}_i$ (13). The second-order interactions occur in a matrix $\mathbf{V}_i$ (which has dimensions given by points (*1*) and (*2*)). For polyethylene, the $\mathbf{U}_i$ in equation (4) can be generated as the product of the $\mathbf{V}_i$ and $\mathbf{D}_i$ defined in equation (5).

$$U_i = \mathrm{V}_i\mathrm{D}_i = \begin{bmatrix} 1 & 1 & 1 \\ 1 & 1 & \omega \\ 1 & \omega & 1 \end{bmatrix}_i \begin{bmatrix} 1 & 0 & 0 \\ 0 & \sigma & 0 \\ 0 & 0 & \sigma \end{bmatrix}_i \tag{5}$$

Z for *n*-butane is given by the sum of the elements in the top row of $\mathbf{U}_2$, and Z for *n*-pentane is the sum of the elements in the top row of $\mathbf{U}_2\mathbf{U}_3$. In general, the contribution of bonds 2 through $n-1$ to Z is given by the sum of the elements

in the top row of the serial product $\mathbf{U}_2\mathbf{U}_3 \cdots \mathbf{U}_{n-1}$. This sum can be extracted by appending an initial $\mathbf{U}_1$ defined as [1 0 $\cdots$ 0] and a terminal $\mathbf{U}_n$ that is a column in which all elements are 1.

$$Z = \mathrm{U}_1\mathrm{U}_2 \cdots \mathrm{U}_n \tag{6}$$

Application of this equation yields $Z = 1 + 2\sigma$ for n-butane and $Z = 1 + 4\sigma + 2\sigma^2(1 + \omega)$ for n-pentane, as expected. It correctly incorporates the first-order interaction and the pentane effect for longer chains. Interactions of higher order (depending on three or more successive bonds) are not included. This reliance on short-range (first- and second-order) interactions means that the expression cannot be expected to apply when longer range interactions play an important role, as they do under circumstances where excluded volume is important. The treatment based on short-range interactions is appropriate for the Θ state, where excluded volume is not important.

The serial product in equation (6) implies that the $\mathbf{U}_i$ need not all be identical. The only restriction on their relationship is that all pairs must be conformable for matrix multiplication. Conformability is ensured by the requirements expressed in the first two points before equation (4). Equation (6) can be used with chains in which different types of bonds are present, as in polyoxyethylene (14). It can also be used for chains in which not all bonds have the same number of rotational isomeric states, as in the polycarbonate of bisphenol A (15).

The standard operations of statistical mechanics permit extraction of useful information from Z. The temperature dependence of Z gives the amount by which the average conformational energy and conformational entropy exceed their zero values.

$$\langle E \rangle - E_0 = kT^2(\partial \ln Z/\partial T) \tag{7}$$

$$S = (\langle E \rangle - E_0)/T + k \ln Z \tag{8}$$

The probability that bond i will be in state η, denoted by $p_{\eta;i}$, is calculated with a matrix $\mathbf{U}_{\eta;i}'$ that is obtained from $\mathbf{U}_i$ by zeroing out all of the elements except those in the column indexed by state η at this bond (16).

$$p_{\eta;i} = Z^{-1}\left(\prod_{\mathrm{j}=1}^{i-1}\mathrm{U}_j\right)\mathrm{U}'_{\eta;i}\left(\prod_{k=i+1}^{n}\mathrm{U}_k\right) \tag{9}$$

Equation (9) evaluates the ratio of the sum of the statistical weights for all conformations in which bond i is in state η to the sum of the statistical weights of all conformations, ie, Z. If bond i is in the middle of a long polyethylene chain, the combination of equations (4), (6), and (9), with $\sigma = 0.543$ and $\omega = 0.087$ (as appropriate for a temperature of about 423 K), yields three $p_{\eta;i}$ that have 1 as their sum.

$$p_{t;i} = 0.596 \tag{10}$$

$$p_{g^+;i} = p_{g^-;i} = 0.202 \tag{11}$$

The t state is preferred in the melt at this temperature. The symmetry of the torsion potential energy function in equation (3) for the C—C bond in polyethylene, $U(\phi) = \mathrm{U}(-\phi)$, produces $p_{g^+;i} = p_{g^-;i}$. Knowledge of all of the $p_{\eta;i}$ is often useful in the interpretation of conformation-dependent spectral properties that have a local origin, such as the chemical shift and coupling constants in nmr spectroscopy (17).

The probability that bonds i and $i-1$ are in states η and ξ, respectively, is computed with a $\mathbf{U}_{\xi\eta;i}{}''$ that is obtained from $\mathbf{U}_i$ by zeroing out all of the elements except the single element at row ξ, column η.

$$p_{\xi\eta;i} = Z^{-1}\left(\prod_{\mathrm{j}=1}^{i-1}\mathrm{U}_j\right)\mathrm{U}''_{\xi\eta;i}\left(\prod_{k=i+1}^{n}\mathrm{U}_k\right) \tag{12}$$

The numerical values of $p_{\xi\eta;i}$ are conveniently presented in the form of a matrix that has the same dimensions as $\mathbf{U}_{\xi\eta;i}{}''$. For the same case described in equations (10) and (11), this matrix has elements with the numerical values presented in equation (13).

$$p_{\xi\eta;i} = \begin{bmatrix} 0.321 & 0.138 & 0.138 \\ 0.138 & 0.0591 & 0.00516 \\ 0.138 & 0.00516 & 0.0591 \end{bmatrix}_i \tag{13}$$

Summation of the elements in the individual columns reproduces the results in equations (10) and (11). The result $p_{tg^+;i} = p_{tg^-;i} = p_{g^+t;i} = p_{g^-t;i}$ arises from the symmetry of the torsion potential energy function and the absence of a distinguishable direction along the polyethylene chain. The interdependence of the bonds makes the probability for two successive g states dependent on the relationship of their signs, $p_{g^+g^+;i} = p_{g^-g^-;i} > p_{g^+g^-;i} = p_{g^-g^+;i}$.

Another useful probability can be derived from the previous equations. Given that there is state ξ at bond $i-1$, $q_{\xi\eta;i}$ is the probability for finding state η at bond i.

$$q_{\xi\eta;i} = p_{\xi;i}/p_{\xi\eta;i-1} \tag{14}$$

The numerical results in equation (13) specify nine values that can be presented in matrix form.

$$p_{\xi\eta;i} = \begin{bmatrix} 0.538 & 0.231 & 0.231 \\ 0.682 & 0.292 & 0.026 \\ 0.682 & 0.026 & 0.292 \end{bmatrix}_i \tag{15}$$

The sum of the three elements in each row is 1 in equation (15), whereas the sum of all nine of the elements is 1 in equation (13). The probability for conformation κ in a long chain (where κ is a subscript that uniquely defines that

conformation) is given by the product of the appropriate $p_{\eta;i}$ for bond 2 and the appropriate $q_{\xi\eta;i}$ for all subsequent bond pairs.

$$p_k = p_{\alpha;2} q_{\alpha\beta;3} q_{\beta\gamma;4} \cdots q_{\psi\omega;n-1} \tag{16}$$

Equation (16) can be employed to generate representative samples of chains for purposes such as the evaluation of the distribution function for the end-to-end distance (18).

Geometry of Individual Chain Conformations

Equation (6) writes Z as a serial product of n statistical weight matrices, one matrix for each bond in the chain. The information in Z specifies the probability for each and every conformation of the chain, via equation (16). In preparation for the computation of properties such as $\langle r^2 \rangle_0$ (where the average is over all conformations), it is desirable to formulate r^2 (for a single conformation) as a serial matrix product, just as Z was expressed as a serial matrix product in equation (6).

The end-to-end vector $\boldsymbol{r}$ for a chain is often written as a sum of bond vectors.

$$r = l_1 + l_2 + \cdots + l_n \tag{17}$$

The form adopted in equation (17) assumes that $\boldsymbol{r}$ and all of the $\boldsymbol{l}_i$ are expressed in the same coordinate system. Specification of the elements in any one of the $\boldsymbol{l}_i$ requires knowledge of the length of the bond and its orientation in the coordinate system common to all $\boldsymbol{l}_i$. The rotational isomeric state model uses a different approach. Each $\boldsymbol{l}_i$ is expressed in a local Cartesian coordinate system with axis x_i along bond i, axis y_i in the plane of bonds $i-1$ and i, with a positive projection on bond $i-1$, and z_i completing a right-handed Cartesian coordinate system. The x and y axes for the local coordinate systems of the first two bonds are depicted in Figure 3. In its own coordinate system, each $\boldsymbol{l}_i$ is easily written in terms of the length of this bond.

$$l_i = \begin{bmatrix} l_i \\ 0 \\ 0 \end{bmatrix} \tag{18}$$

The $\boldsymbol{l}_i$ can all be expressed in the coordinate system of the first bond by premultiplication by a serial product of transformation matrices, $\mathbf{T}_1 \cdots \mathbf{T}_{i-1}$, where the form of each $\mathbf{T}$ depends on the conventions adopted for expressing the bond angle and torsion angle. A common form is presented in equation (19).

$$T_i = \begin{bmatrix} -\cos\theta & \sin\theta & 0 \\ -\sin\theta\cos\phi & -\cos\theta\cos\phi & -\sin\phi \\ -\sin\theta\sin\phi & -\cos\theta\sin\phi & \cos\phi \end{bmatrix}_i \tag{19}$$

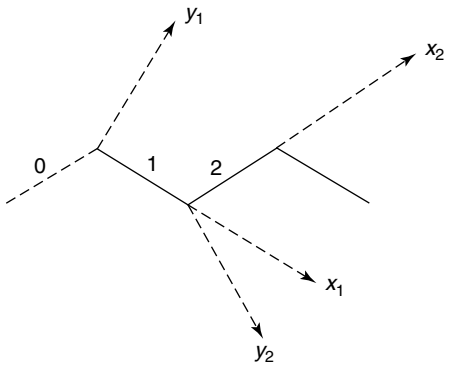

Fig. 3. The local coordinate systems defined by two consecutive bonds. From Ref. 19. Copyright © 1976 John Wiley & Sons, Inc. Reprinted by permission of John Wiley & Sons, Inc.

The torsion angle at bond i, defined as 0 for a cis placement, is denoted by ϕ_i, and the angle between bonds i and $i+1$ is θ_i. $\mathbf{T}_1$ is the special case where the undefined ϕ_1 is taken to be 180°.

With this notation, equation (17) can be written as a sum of n terms that involve $\boldsymbol{l}_i$ and $\mathbf{T}_i$.

$$r = l_1 + \mathrm{T}_1 l_2 + \mathrm{T}_1\mathrm{T}_2 l_3 + \cdots + \mathrm{T}_1\mathrm{T}_2\cdots\mathrm{T}_{n-1} l_n \tag{20}$$

This sum can be generated as a serial product of n matrices, one for each bond in the chain (20).

$$r = [\,\mathrm{T}\quad \mathrm{l}\,]_1 \begin{bmatrix} \mathrm{T} & \mathrm{l} \\ 0 & 1 \end{bmatrix}_2 \cdots \begin{bmatrix} \mathrm{T} & \mathrm{l} \\ 0 & 1 \end{bmatrix}_{n-1} \begin{bmatrix} l \\ 1 \end{bmatrix}_n \tag{21}$$

A more compact notation writes each of the matrices on the right-hand side of equation (21) as $\mathbf{A}_i$.

$$r = \mathrm{A}_1\mathrm{A}_2\cdots\mathrm{A}_\mathrm{n} \tag{22}$$

If the bond vector is replaced by the dipole moment vector for bond i, $\boldsymbol{m}_i$, an equivalent serial product of matrices produces the dipole moment for this chain.

$$\mu = [\,\mathrm{T}\quad \mathrm{m}\,]_1 \begin{bmatrix} \mathrm{T} & \mathrm{m} \\ 0 & 1 \end{bmatrix}_2 \cdots \begin{bmatrix} \mathrm{T} & \mathrm{m} \\ 0 & 1 \end{bmatrix}_{n-1} \begin{bmatrix} m \\ 1 \end{bmatrix}_n \tag{23}$$

The squared end-to-end distance is generated as a matrix product using the same information that was required for $\boldsymbol{r}$ in equation (21), but processing that information differently (20).

$$r^2 = \mathrm{G}_1\mathrm{G}_2\cdots\mathrm{G}_\mathrm{n} \tag{24}$$

The internal $\mathbf{G}_i$ are 5×5 matrices which can be written in block form with dimensions 3×3.

$$\mathrm{G}_i = \begin{bmatrix} 1 & 2l^{\mathrm{T}}\mathrm{T} & \mathrm{l}^2 \\ 0 & \mathrm{T} & \mathrm{l} \\ 0 & 0 & 1 \end{bmatrix}_i, \quad 1<i<n \tag{25}$$

$\mathbf{G}_1$ is given by the top row of $\mathbf{G}_i$, and $\mathbf{G}_n$ is given by the last column.

The squared dipole moment μ^2 is obtained by the same formalism upon substitution of $\boldsymbol{m}$ for $\boldsymbol{l}$ and m^2 for l^2.

If all of the atoms in the chain are of the same mass, the squared radius of gyration is generated as a matrix product that uses the same information required for $\boldsymbol{r}$ and r^2, but processing that information differently.

$$s^2 = (n+1)^{-2}\mathrm{H}_1\mathrm{H}_2 \cdots \mathrm{H}_{n-1}\mathrm{H}_n = (n+1)^{-2}\prod_{i=1}^{n}\mathrm{H}_i \tag{26}$$

The internal $\mathbf{H}_i$ are 7×7 matrices when written out element by element, but they can also be written in a more compact blocked form.

$$\mathrm{H}_i = \begin{bmatrix} 1 & \mathrm{G}_{\lfloor} & \mathrm{l}^2 \\ 0 & \mathrm{G} & \mathrm{G}_{\rfloor} \\ 0 & 0 & 1 \end{bmatrix}_i \tag{27}$$

Here $\mathbf{G}_{\lfloor}$ denotes the top row of $\mathbf{G}$, $\mathbf{G}_{\rfloor}$ denotes the last column of $\mathbf{G}$, $\mathbf{H}_1$ is formulated as the top row of $\mathbf{H}_i$, and $\mathbf{H}_n$ is formulated as the last column of $\mathbf{H}_n$.

Other conformation-dependent properties can be formulated in a similar manner (4,20).

Averages over All Conformations

The basis for computing the averages over all conformations is illustrated for the case of the mean square unperturbed end-to-end distance $\langle r^2 \rangle_0$ (20). Let $r_\kappa{}^2$ denote the squared end-to-end distance of conformation κ. The probability of this conformation is given by equation (16). The desired result is the weighted sum over all conformations.

$$\langle r^2 \rangle_0 = \sum p_\kappa r_\kappa^2 \tag{28}$$

The probability is the ratio of the statistical weight for conformation κ, denoted by w_κ, to the sum of the statistical weights for all conformations, Z.

$$\langle r^2 \rangle_0 = Z^{-1}\sum w_\kappa r_\kappa^2 \tag{29}$$

The w_κ is the product of statistical weights $w_{\kappa;i}$, that appear in the appropriate elements of the $\mathbf{U}_i$, and ${r_\kappa}^2$ is the serial product of $\mathbf{G}$ matrices, according to equation (25), where the appropriate ϕ_i is used in each $\mathbf{G}_i$. The $w_{\kappa;i}$ can be grouped with the appropriate $\mathbf{G}_{\kappa;i}$.

$$\langle r^2\rangle_0 = Z^{-1}\sum_\kappa \prod_{i=1}^{n} w_{\kappa;i}\mathrm{G}_{\kappa;i} \tag{30}$$

The numerator is merely the expression for Z, with each statistical weight expanded by multiplication onto the appropriate $\mathbf{G}$ matrix. Therefore the desired result is obtained by equation (2) with supermatrices that contain the geometric information in $\mathbf{G}$ and the energetic information in $\mathbf{U}$.

$$\mathrm{F}_i = \begin{bmatrix} u_{11}\mathrm{G}_{\phi_1} & \mathrm{u}_{12}\mathrm{G}_{\phi_2} & \cdots & \mathrm{u}_{1v_i}\mathrm{G}_{\phi_{v_i}} \\ \mathrm{u}_{21}\mathrm{G}_{\phi_1} & \mathrm{u}_{22}\mathrm{G}_{\phi_2} & \cdots & \mathrm{u}_{2v_i}\mathrm{G}_{\phi_{v_i}} \\ \vdots & \vdots & \ddots & \vdots \\ u_{v_{i-1}1}\mathrm{G}_{\phi_1} & \mathrm{u}_{v_{i-1}2}\mathrm{G}_{\phi_2} & \cdots & \mathrm{u}_{v_{i-1}v_i}\mathrm{G}_{\phi_{v_i}} \end{bmatrix}_i, \quad 1<i<n \tag{31}$$

The first bond is treated with $\mathbf{F}_1 = [\mathbf{G}_[\ \mathbf{0}]_1$ and a column of $i-1$ copies of $\mathbf{G}_{[n}$ is used for the last bond.

The mean square unperturbed end-to-end distance is usually reported as the dimensionless characteristic ratio, defined as the ratio of the true $\langle r^2\rangle_0$ to the value that would have been predicted for the same chain, using the freely jointed chain model (eq. (1)).

$$C_n = \langle r^2\rangle_0 / n\langle l^2\rangle \tag{32}$$

The values of C_n approach a limit as n increases if the chain is flexible. The limiting value is denoted by C_∞.

A perfectly analogous approach permits computation of $\langle \boldsymbol{r}\rangle_0$ and $\langle s^2\rangle_0$, substituting the expressions in equation (22) or equation (26) for the one in equation (24).

The FORTRAN source code for a simple yet versatile computer program for calculation of $\langle r^2\rangle_0$ by equation (2) is available in Appendix C of Reference 4. This source code, along with sample input and output files, can be downloaded from www.polymer.uakron.edu/~wlm. The program executes quickly on any modern computer that has a FORTRAN compiler.

Uses of the Expressions

This section provides several illustrative examples of questions that can be addressed with the rotational isomeric state model.

Often useful information is accessible from Z itself. For example, one can inquire into the average number of bonds in a sequence of t placements in a polyethylene melt at 450 K. The solution is obtained as the ratio of the probability of a t state to the probability for the initiation of a sequence of t states. This ratio is $p_{t;i}(p_{g^+t;i} + p_{g^-t;i})^{-1}$, where bond i is in the interior of a long chain, far enough from either end so that it is not subject to end effects. In practice, the chain might have $n = 20$ and $i = 10$. Z is computed from equation (6), using the $\mathbf{U}$ given by equation (4). The probabilities are obtained from equations (9) and (12). The ratio has a value of about 2.4, for reasonable assignment of the numerical values of E_σ and E_ω.

With the incorporation of the matrix expressions for the properties of individual chains, more information becomes accessible. For example, how sensitive are the components of $\langle \boldsymbol{r} \rangle_0$ to the interdependence of the bonds in a polyethylene melt at 140°C? Using the $\mathbf{U}$ in equation (4) with $\omega = 1$ (independent bonds) and again with $\omega = 0$ (strongly interdependent bonds), along with equation (6) for Z and a simple modification (substitution of $\mathbf{A}$ for $\mathbf{G}$) of equation (2) for $\langle \boldsymbol{r} \rangle_0$, yields, in the limit for long chains,

$$\langle r \rangle_0 = \begin{bmatrix} 0.61\text{nm} \\ 0.52\text{nm} \\ 0 \end{bmatrix} \quad \text{for interdependent bonds and}$$

$$\langle r \rangle_0 = \begin{bmatrix} 0.34\text{nm} \\ 0.29\text{nm} \\ 0 \end{bmatrix} \quad \text{for independent bonds.}$$

How quickly does C_n reach its asymptotic limit at large n? The upper curve in Figure 4 depicts the C_n calculated from the $\mathbf{U}$ in equation (4) with $\sigma = 0.43$

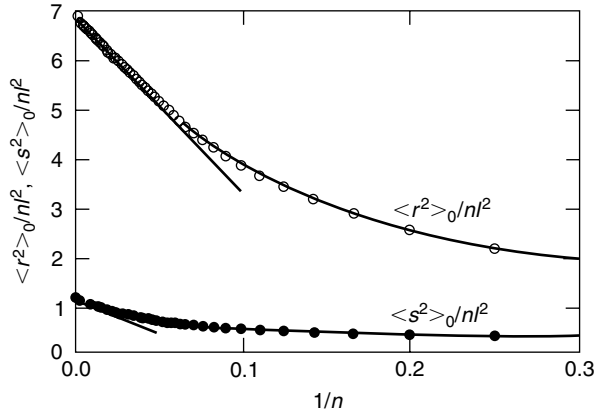

Fig. 4. The dependence of $\langle r^2 \rangle_0$ and $\langle s^2 \rangle_0$ on $1/n$ for unperturbed polyethylene chains. From Ref. 4. Copyright © 1994 John Wiley & Sons, Inc. Reprinted by permission of John Wiley & Sons, Inc.

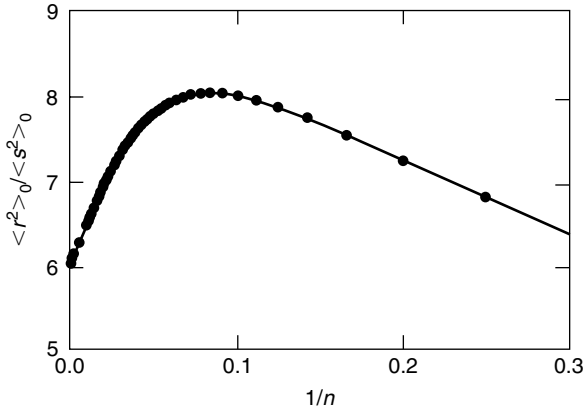

Fig. 5. The dependence of $\langle r^2\rangle_0/\langle s^2\rangle_0$ on $1/n$ for unperturbed polyethylene chains, using the data from Figure 4. From Ref. 4. Copyright © 1994 John Wiley & Sons, Inc. Reprinted by permission of John Wiley & Sons, Inc.

and $\omega = 0.034$, using Z from equation (6) and $\langle r^2\rangle_0$ from equation (2). The final approach of C_n to C_∞ is linear in $1/n$.

$$C_n = C_\alpha - a/n \tag{33}$$

Here a is a positive constant. C_n is within about 5% of C_∞ in Figure 4 when n reaches 100. The form of equation (33) is common to flexible chains, but the value of a depends on the nature of the chain, with a tendency for a to become larger as the stiffness of the chain increases.

Is the rotational isomeric state model consistent with $\langle r^2\rangle_0/\langle s^2\rangle_0 = 6$ for long flexible chains? The lower curve in Figure 4 depicts the values of $\langle s^2\rangle_0$, calculated in the same manner as the $\langle r^2\rangle_0$ in the upper curve, but with substitution of $\mathbf{H}_i$ for $\mathbf{G}_i$ and division by $(n+1)^2$, as required by equation (26). The ratio $\langle r^2\rangle_0/\langle s^2\rangle_0$ is depicted in Figure 5. It reaches 6 in the limit $n \to \infty$, but the ratio is larger than 6 at small n, because $\langle r^2\rangle_0/nl^2$ reaches its limit faster than does $\langle s^2\rangle_0/nl^2$.

The rotational isomeric state model can be used to rationalize the temperature-dependence of conformation-dependent properties, through the dependence of the statistical weights on temperature. How strong is the temperature dependence of the dimensions of the chains in a polyethylene melt, assuming that we remain above the temperature at which crystallization occurs? Calculations of $\langle r^2\rangle_0$ from equations (2), (4), and (6), assuming that the only temperature dependence is from the Boltzmann factors $\sigma = \exp(-E_\sigma/kT)$ and $\omega = \exp(-E_\omega/kT)$, yields $\partial \ln \langle r^2\rangle_0/\partial T = -0.001\ \mathrm{deg}^{-1}$.

A common use of the rotational isomeric state model is to learn how specific structural properties (at the local level) affect conformational properties at the level of a long chain. Polyisobutylene provides a good example. The bond angles in the backbone of polyisobutylene alternate between 110° (for CH_2—C—CH_2) and 124° (for C—CH_2—C). How strongly, and in what direction, does this alternation in bond angles affect the mean square dimensions of the chains in a polyisobutylene

melt? Using Z from equation (6) and $\langle r^2 \rangle_0$ from equation (2), along with the **U** and ϕ from the rotational isomeric state model for polyisobutylene described in Reference 21, replacement of the two different θ by their average ($\theta = 117^\circ$ for all bond angles) increases $\langle r^2 \rangle_0$ by 21%.

The rotational isomeric state model can also tell us how stereochemical composition affects the conformations of a chain. When selecting from isotactic and syndiotactic poly(2-vinyl pyridine), and isotactic and syndiotactic poly(*N*-vinyl carbazole), which of the four chains has the smallest and the largest unperturbed dimensions? Using the rotational isomeric state models proposed for these two polymers (22,23), the values of C_∞ at 300 K are 4.9 and 7.7, respectively, for isotactic and syndiotactic poly(2-vinyl pyridine), whereas isotactic and syndiotactic poly(*N*-vinyl carbazole) have much larger values of approximately 15 and 39, respectively. The most compact unperturbed chain is isotactic poly(2-vinyl pyridine), and the most extended chain is syndiotactic poly(*N*-vinyl carbazole).

ACKNOWLEDGMENTS

The preparation of this manuscript was supported by National Science Foundation grant DMR 9844069. The text was completed in April 2000, while WLM was on sabbatical leave at Sandia National Laboratory. He thanks Dr. John G. Curro for his hospitality during this leave.

BIBLIOGRAPHY

"Conformation and Configuration" in *EPST* 1st ed., Suppl. Vol. 1, pp. 176–195, by A. E. Tonelli, Bell Laboratories; "Conformation and Configuration" in *EPSE* 2nd ed., Vol. 4, pp. 120–144, by A. E. Tonelli, AT&T Bell Laboratories.

1. M. V. Volkenstein, *Dokl. Akad. Nauk SSSR* **78**, 879 (1951).
2. H. A. Kramers and G. H. Wannier, *Phys. Rev.* **60**, 252 (1941).
3. P. J. Flory, *Statistical Mechanics of Chain Molecules*, Wiley-Interscience, New York, 1969; reprinted with the same title by Hanser, Munich, 1989.
4. W. L. Mattice and U. W. Suter, *Conformational Theory of Large Molecules. The Rotational Isomeric State Model in Macromolecular Systems*, Wiley-Interscience, New York, 1994.
5. M. Rehahn, W. L. Mattice, and U. W. Suter, *Adv. Polym. Sci.* **131/132**, 1 (1995).
6. J. D. Honeycutt, in J. E. Mark, ed., *Physical Properties of Polymer Handbook*, American Institute of Physics, Woodbury, N. Y., 1996, p 39.
7. P. J. Flory, *J. Chem. Phys.* **17**, 303 (1949).
8. D. N. Theodorou and U. W. Suter, *Macromolecules* **18**, 1467 (1985).
9. T. Haliloglu and W. L. Mattice, *J. Chem. Phys.* **111**, 4327 (1999).
10. T. C. Clancy and co-workers, *Macromolecules* **33**, 9452 (2000).
11. A.-C. Tang, *J. Chinese Chem. Soc.* **19**, 33 (1952).
12. A. Abe, R. L. Jernigan, and P. J. Flory, *J. Am. Chem. Soc.* **88**, 631 (1966).
13. P. J. Flory, P. R. Sundararajan, and L. C. DeBolt, *J. Am. Chem. Soc.* **96**, 5015 (1974).
14. A. Abe, K. Tasaki, and J. E. Mark, *Polym. J.* **17**, 883 (1985).
15. M. Hutnik, A. S. Argon, and U. W. Suter, *Macromolecules* **24**, 5956 (1991).
16. R. L. Jernigan and P. J. Flory, *J. Chem. Phys.* **50**, 4165 (1969).
17. A. E. Tonelli, F. C. Schilling, and R. E. Cais, *Macromolecules* **15**, 849 (1982).
18. J. E. Mark and J. G. Curro, *J. Chem. Phys.* **81**, 6408 (1984).
19. A. Abe, J. W. Kennedy, and P. J. Flory, *J. Polym. Sci., Polym. Phys. Ed.* **14**, 1337 (1976).

20. P. J. Flory, *Macromolecules* **7**, 381 (1974).
21. L. C. DeBolt and U. W. Suter, *Macromolecules* **20**, 1424 (1987).
22. A. E. Tonelli, *Macromolecules* **18**, 2579 (1985).
23. A. Abe and co-workers, *Macromolecules* **21**, 3414 (1988).

WAYNE L. MATTICE
CARIN A. HELFER
The University of Akron

CONTACT LENSES. See HYDROGELS.

COORDINATION POLYMERS. See METAL-CONTAINING POLYMERS.

CREEP. See VISCOELASTICITY.

CONTROLLED RELEASE TECHNOLOGY

Introduction

For many decades, pharmaceuticals have primarily consisted of simple, fast-acting chemical compounds that are dispensed orally for the treatment of an acute disease or a chronic illness and have been mostly facilitated by drugs in various pharmaceutical dosage forms, including tablets, capsules, pills, suppositories, creams, ointments, liquids, aerosols, and injections. Even today these conventional dosage forms are the primary mode of drug administration for prescription and over-the-counter drug products. Conventional drug formulations typically provide a prompt release of drug in a bolus form. For drugs which get cleared rapidly from the body, achieving and maintaining the drug concentration within the therapeutically effective range requires a multiple dosing regimen, often more than once a day. Such an inconvenient dosing regimen leads to lack of patient compliance as well as a significant fluctuation in drug levels in the plasma (Fig. 1). The premise of administration methods that allow the patients to safely treat themselves is as significant as any other health care development, particularly in developing countries where doctors, clean syringes, sterile needles, and sophisticated treatments are few and far between (1).

Recently, several technical advancements have resulted in the development of new technologies capable of controlling the administration of a drug at a targeted site in the body in an optimal concentration-versus-time profile (2–4). The term "drug delivery" covers a very broad range of techniques used to get therapeutic agents into human body. These techniques are capable of controlling the rate of drug delivery, sustaining the duration of therapeutic activity, and/or targeting the delivery of drug to a tissue as described in various articles (5–7).

The main objective of this article is to present an overview of controlled release technology, the polymers used for controlled release therapies, as well as the

Encyclopedia of Polymer Science and Technology. Copyright John Wiley & Sons, Inc. All rights reserved.

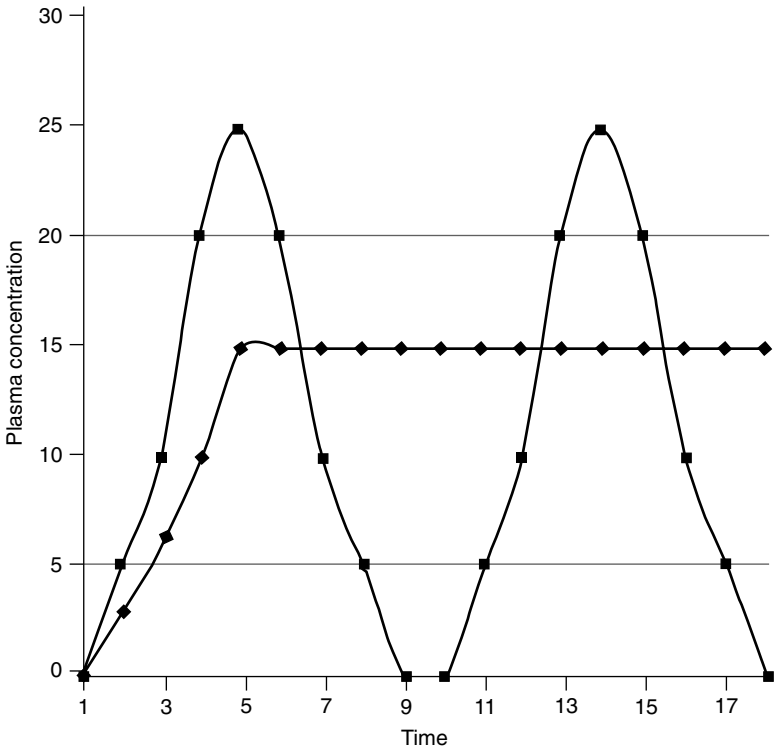

Fig. 1. Comparison of typical pharmacokinetic profiles seen for conventional vs. controled release formulations. —◆— CDR; —■— conventional; ——— toxic level; and ——— minimum therapeutic level.

strategies used for drug encapsulation and release. Furthermore, an emphasis has been laid upon the important applications of this technology in the pharmaceutical and biomedical fields.

Need of Controlled Drug Release Systems

The ways in which drugs or new biological products are administered have gained increasing attention in the past few decades. Controlled release systems provide numerous benefits over the conventional dosage forms. Conventional dosage forms, which are still predominant for the pharmaceutical products, are not able to control either the rate of drug delivery or the target area of drug administration and provide an immediate or rapid drug release. This necessitates frequent administration in order to maintain a therapeutic level. As a result, drug concentrations in the blood and tissues fluctuate widely (Fig. 1). The concentration of drug is initially high, that can cause toxic and/or side effects, then quickly fall down below the minimum therapeutic level with time elapse (1,6). The duration of therapeutic efficacy is dependent upon the frequency of administration, the half-life of the drug, and release rate from the dosage form. In contrast, controlled release

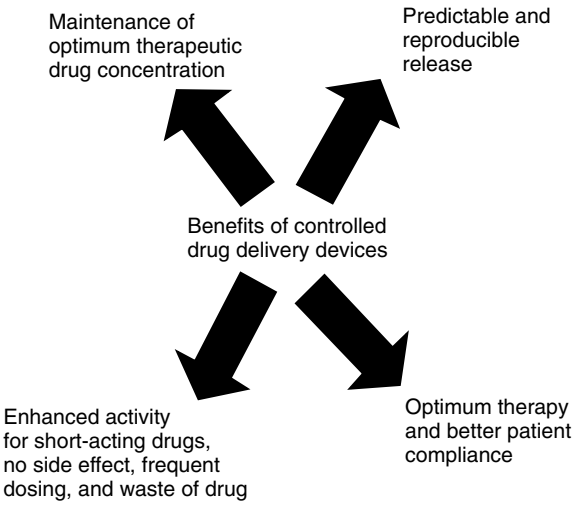

Fig. 2. Benefits of controlled release formulations.

dosage forms are not only able to maintain therapeutic levels of drug with narrow fluctuations but they also make it possible to reduce the frequency of drug administration (8). Drug concentration profile in serum depends on the preparation technology, which may generate different release kinetics resulting in different pharmacological and pharmacokinetic responses in the blood or tissues (9).

Controlled drug release formulations offer several advantages over conventional dosage forms (Fig. 2). Some of the salient features of controlled release formulations are described below.

(1) The drug is released in a controlled fashion that is most suitable for the application. The control could be in terms of onset of release (delayed vs. immediate), duration of release, and release profile itself.
(2) The frequency of doses could be reduced thereby enhancing patient compliance.
(3) The drug could be released in a targeted region. This could be achieved either by tailoring the formulation to release the drug in that particular environment or by timed release of the drug. By targeting drug release, drug efficacy could be maximized.
(4) By targeting the drug to the desired site, systemic exposure of the drug could be reduced, thereby decreasing systemic side effects (especially for toxic drugs).
(5) The drug could be protected from the physiological environment for a longer duration of time. Thus the effective residence time of the drug could be extended.

However, controlled release products do not always provide positive effects for every type of formulation design. Negative effects outweigh benefits in the following circumstances (10,11)

(1) Dose dumping
(2) Less accurate dose adjustment
(3) Increased potential for first-pass metabolism
(4) Dependence on residence time in gastrointestinal (GI) tract
(5) Delayed onset

The limitations of controlled drug release formulations (CDRFs) technology making some drugs unsuitable for formulations are as follows (12,13):

(1) There is a risk of drug accumulation in the body if the administered drug has a long half-life, causing the drug to be eliminated at a slower rate than it is absorbed.
(2) Some drugs have a narrow therapeutic index, and thus, need to administer repeatedly to maintain the serum drug level within a narrow range. Such drugs may not be feasible for CDRF.
(3) If the GI tract limits the absorption rate of the drug, the effectiveness of the CDRF is limited (for oral controlled release).
(4) If a drug undergoes extensive first-pass clearance, its controlled release formulation may suffer from lower bioavailability.
(5) The cost of CDRF may be substantially higher than the conventional form.

Especially from the point of view of the last factor, improvement of safety and efficacy of the new products alone has not been enough to justify introducing new CDRF products. Evaluation of economic benefits, costs, and quality of life impact need to be assessed.

Design of Controlled Release Systems

A controlled release system comprises a drug and the material in which the drug is loaded. This system must be biocompatible and friendly with the body. Because of this reason, selection of the drug and the polymer along with desired properties is a prime factor in designing a controlled release system to deliver the drug at the desired site of action in the body (14). Drug properties are discussed in this rection. Polymers used in controlled release and polymer fabrication with drug encapsulation are discussed in subsequent sections.

Drugs-Controlled Release. Before designing a controlled drug release system, one has to select the route of drug delivery with several considerations which include physical and chemical properties of the drug, doses of the drug, route of administrations, type of drug delivery system desired, desired therapeutic effect, physiologic release of the drug from delivery system, bioavailability of the drug at the absorption site, and pharmacodynamics of the drugs (10,15). These properties of the drug can be discussed in two ways, viz. behavior of the drug in its delivery system and behavior of the drug and its delivery system in the body. In the former part, drug properties can influence release characteristics from its delivery systems, for example, in any controlled release system, drug availability is controlled by the drug release kinetics rather than absorption, and the associated

rate constant for drug release are smaller than the absorption rate constant. To control drug release, one can employ a variety of approaches, such as, dissolution (16,17), diffusion (18,19), swelling (20,21), osmotic pressure (22,23), complexation (24), ion-exchange (25,26), and magnetic field (27,28).

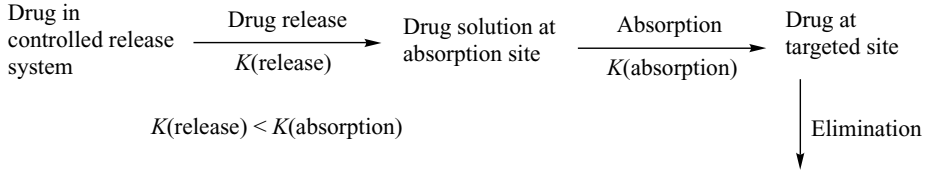

In the second part, behavior of the drug and its delivery system is extremely complex, involving the fate of drug during transit to the target area as well as its fate in the biophase. The effectiveness of the drug at its target area depends on the pharmacokinetics of the drug and its carrier in the body (29). These constraints of the drug in a controlled release system have been discussed in the subsequent subheadings.

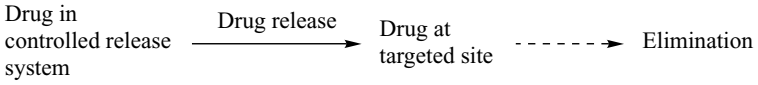

Physicochemical Properties of Drugs. Physicochemical properties of the drug affect the drug release performance of a controlled drug release system in the body (30). These properties, which include aqueous solubility, drug stability, molecular size, partition coefficient, and protein binding, may prohibit/restrict placement of drug in controlled release, restrict the route of drug administration, and significantly restrict the drug release performance for one reason or the other. Physicochemical properties can be determined from *in vitro* experiment, while biological properties are those that result from typical pharmacokinetic studies on the absorption, distribution, metabolism, and excretion characteristics of the drug and those resulting from pharmacological studies (29). Compounds with very low aqueous solubility usually suffer oral bioavailability problems because of limited GI transit time of the undisclosed particles and limited solubility at absorption site. Unfortunately, for many drugs, the site of maximum absorption is the area in which the drug is least soluble. Thus, choice of oral controlled/sustained release formulations is limited by aqueous solubility of the drug. This property may be useful for matrix-type devises where these limitations can be utilized to achieve sustained/controlled drug release; however, dissolution-limited bioavailability may occur. Partition coefficient (31) and molecular size of the drug influence not only the permeation of a drug across biological membrane but also the diffusion across or through a rate-controlling membrane or matrix (32). Drugs with extremely high partition coefficient (ie, drugs having high oil solubility) readily penetrate the membranes but are unable to proceed further, while the drug with excessive aqueous solubility, for example, low oil–water partition coefficient, cannot penetrate the membranes. Hence, a balance in the partition coefficient is needed to give an optimum flux for permeation through the biological and rate-controlling membranes.

Drug stability in biological media provides the bioavailability; for example, drugs that are unstable in the stomach can be placed in a slowly soluble form or have their release delayed until they reach the small intestine. Drug and plasma protein interaction influences the duration of drug action. It is well known that blood proteins are mostly recirculated and not eliminated; thus, drug protein binding can serve as a depot for drug producing a prolong release profile if a high degree of drug binding occurs.

Biological Properties of Drugs. At the time of designing a system, a comprehensive picture of drug deposition must be very clear and this should be based on a complete examination of pharmacological action of the drug in the *in vivo* experiments, which include adsorption, distribution, metabolism, and excretion (ADME) (Fig. 3). The pharmacological action of a drug can be correlated better with the concentration–time course of the drug (or its active metabolite) in the blood or some other biophase than with the absolute dose administered, and it involves pharmacokinetics and pharmacodynamics of a drug in the body. Pharmacokinetics facilitates predictions of time course of drug concentrations and drug action in the body (29,33), while pharmcodynamics offer a quantitative assessment of the time course of drug effect on the body after administration by any route (29,34). From a pharmacokinetics standpoint, there are two fundamental approaches to design the formulations that allow for the attainment of the desired therapeutic concentration of the drug and are maintained throughout a dosing interval (11). The first approach involves selection of the drugs that have long enough elimination half-lives to be administered infrequently. This approach can be successful if an analog from a class of biologically active drug has a long elimination half-life or can be adopted in the early stage of a new developing drug candidate to avoid a time-consuming and cost-extensive research and development program in animal/human. In the second approach, drug formulations are modified in such a way that

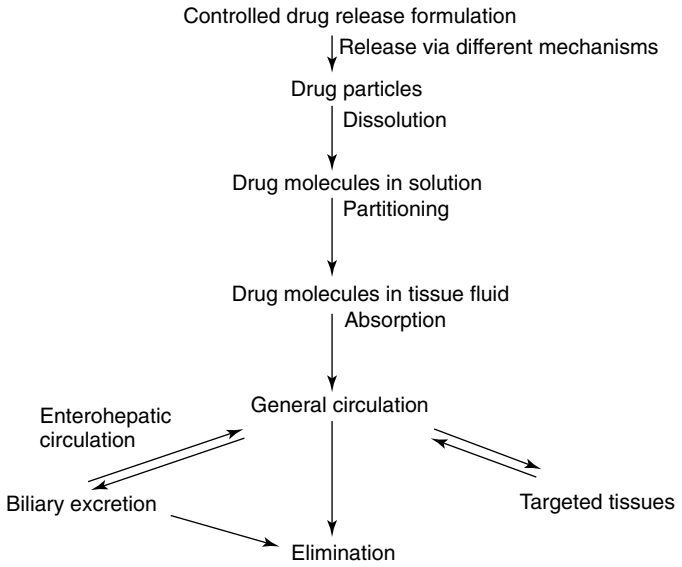

Fig. 3. Fate of drug in controllled release formulation.

the fluctuation in drug concentrations during a dosing interval is reduced. Thus, with a prior knowledge of a drug's elimination and distribution pharmacokinetics and the use of correct approach to the estimation of mean resident time (MRT) (the time a drug molecule takes to traverse through the body and that can be used to compare dosage forms), it is possible to design formulation having particular release characteristics with predictive impacts on the MRT of a drug in the body.

Pharmacodynamics of a drug has a significant impact on the design and development of sustained release products, which can also be approached by two fundamental routes. First, if pharmacokinetics of a drug is known then this can be linked to available pharmacodynamic data, resulting in a unified concept relating the kinetics of the drug (or an active metabolite) to the time course of drug effect (10,35). In the second case where pharmacokinetics of the drug cannot be defined accurately [ie, AUCs (area under the curve) cannot be accurately measured because of assay sensivity limitation] or where drug effect is apparently unrelated to concentrations, alternative approaches can be utilized. In this case, one can study the relationship of drug effect and steady-state drug concentration at various drug-dosing levels in the same individual. By using sustained release dosage forms resulting in varying release rate constants, one can derive valuable information regarding a drug product.

Each drug is characterized by its own pharmacokinetic–pharmacodynamic (PK-PD) profile (as a part of the drug-approval process) on the basis of the physicochemical properties, conformation, and other structural attributes that govern the transport within the body and across various barriers. The number and type of biological hurdles a drug has to overcome governs the design of delivery systems as well as the route of administration. Compared to the general "sigmoid" PK-PD profile for conventional molecules, the PK-PD relationship of biopharmaceuticals is complicated by short biological half-life, instability, multiple biological actions and operation of compensatory regulatory events in the body. Once the PK-PD relations have been established, plasma levels can be substituted for therapeutic effects that can aid in setting PK bioequivalence standards. In near future, one of the major objectives of CDRF technology should be to match medication delivery in time with biological rhythm (36,37). One such CDRF is Covera-HS (Pharmacia Corp; verapamil HCl) tablets, which attempts to match the body circadian rhythm for treatment of blood pressure rate (36). Covera-HS is taken at bedtime and the drug release is retarded during the sleep period (4–5 h) to achieve optimal blood levels between early morning and noon.

Factors That May Make a Drug Unsuitable for CDRF. Some drugs are not fit for controlled release because of the nature of drug action, physical limitations (large dose, duration of drug release), and alternative administration, ie, oral daily doses vs. monthly implant, etc. Drugs that are given at acute situations are usually not useful for controlled extended release, for example, tissue plasminogen activator (TPA) that is given during a heart attack to dissolve blood clotting and allow blood flow. Any delay in medication may result in death. In another example, when someone is suffering from a headache and needs immediate relief, these controlled release systems are not useful. Drugs that have a beneficial effect in the body at specific times during the day should be given only at that time, and not be delivered in large doses of controlled release formulations, which may otherwise result in unnecessary dose dumping.

Thus, the following drug properties and therapeutic requirement should be taken into account in designing a controlled release system:

(1) Drug elimination half-life
(2) Doses to be administered
(3) Therapeutic index
(4) Low solubility
(5) Route of administration
(6) Poor absorption
(7) Extensive first-pass clearance
(8) Difference in time course of circulating drug level with its pharmacological effects
(9) PD vs. PK of the drugs

Polymers in Controlled Drug Release Formulations

Polymers have been widely used to encapsulate drugs in the form of reservoir or matrix to release the drug at the proximity of the desired site (Table 1). Thus, there must be clarity about the biocompatibility, toxicity, and elimination of these polymers (38,39). Novel concepts for polymer-based controlled release systems that have emerged over the years include new polymers, new methods for drug linkages, and new processes for drug encapsulation (40). The active ingredient could be either physically entrapped into the polymer matrix by an emulsification-, atomization-, or agitation-based process or could be linked to the polymer backbone via physical or chemical bonds. The drug release is typically observed to be diffusion-controlled, polymer erosion controlled, or a combination of the two. Hence, drug release properties strongly depend on the physical and chemical properties of the polymer. Even a minor variation in the polymer structure, such as an endgroup modification, may be sufficient to modify its degradation characteristics and subsequently the drug release properties. Furthermore, different polymer properties are desired for different drugs and different applications. This has led to an intensive effort in developing novel polymeric systems for controlled release applications. Development of such novel formulations is further fueled by the growing demand for patient-friendly medicines in the pharmaceutical and biotechnology industries.

Various natural, semisynthetic, and synthetic polymers are in use as the structural backbone for both controlled release and conventional drug delivery systems (Table 1). Polymers selected in the preparation of the dosage form must comply with the following requirements:

(1) **Safety.**

Harmful/toxic impurities must be removed from polymers before their usage in CDRFs. The residual monomers, initiators, and other chemicals used in the polymer synthesis/modification must be removed after

Table 1. Polymers in Controlled Release Technology

Polymer	Controlled release mechanism	Special notes
Natural or semisynthetic		
Albumin	Dissolution	
Cellulose	Dissolution and diffusion	Binder, diluent, disintegrant
Chitin	Diffusion	
Chitosan	Dissolution	
Cellulose acetate	Osmosis	
Ethylcellulose	Osmosis	
Cellulose acetate butyrate	Osmosis	
Carboxymethylcellulose, sodium salt cross-linked	Dissolution	
Gelatin	Dissolution	
Hydroxypropylmethyl cellulose	Dissolution	Binder
Starch thermally modified	Dissolution	
Xanthan gum	Dissolution	
Collagen	Diffusion	
Guar gum		
Karana gum		Binder
Dextrin		
Sodium starch glycolate		
Methyl cellulose		Binder
Tragacanth gum		
Aliginic acid		Binder
Cellulose acetate phthalate		Entric coating material
Cellulose acetate trimelliate		Entric coating material
Poloxamer	Diffusion	
Synthetic		
Nylon		
Poly(ethylene glycol)	Dissolution	
Poly(glycolic acid)	Dissolution	
Poly(lactic acid)	Dissolution	
Poly(vinyl alcohol)	Dissolution and osmosis	
Poly(vinylpyrrolidinone), cross-linked	Dissolution	Binder
Poly(urethane)	Osmosis	
Poly(vinyl chloride), cast	Osmosis	
Poly(vinyl chloride), extruded	Osmosis	
Poly(carbonates)	Osmosis	
Poly(vinyl fluoride)	Osmosis	
Ethylene vinyl acetate	Osmosis	
Cellophane, polyethylene-coated	Osmosis	
Poly(ethylene)	Osmosis	
Ethylene-propylene copolymer	Osmosis	
Polypropylene	Osmosis	
Poly(vinyl chloride) rigid	Osmosis	
Poly(alkylcyanoacrylate)	Diffusion	
Poly(ethylene-*co*-vinyl acetate)	Diffusion	

Table 1. (Continued)

Polymer	Controlled release mechanism	Special notes
Poly(hydroxyethyl methacrylate)	Diffusion	
Poly(hydroxypropylethyl methacrylate)	Diffusion	
Poly(methyl methacrylate)	Diffusion	
Poly(vinyl alcohol-*co*-methacrylate)	Diffusion	
Polyisobutene	Diffusion	
Silicone rubber	Diffusion	
	Diffusion	

the polymerization/modification. The chemicals employed in the polymer fabrication processes (ie, additives, stabilizers, plasticizers, and catalyst residues) are carefully selected to meet regulatory requirements.

(2) **Physical and mechanical properties.**

The polymers must possess the necessary mechanical properties required for the dosage form design, such as elasticity, compactability, resistance to tensile, swelling and shear stresses, and resistance to tear and fatigue.

(3) **Biocompatibility.**

The polymer should not cause significant local irritation to the surrounding tissues. If biodegradable, then the polymer degradation by-products must be nontoxic, nonimmunogenic, and noncarcinogenic.

There are many ways to synthesize new polymers and modify existing polymers. Different monomers (for addition polymerization or condensation polymerization) may be used or existing polymers may be modified. However, only a handful of polymers are used in pharmaceutical drug delivery systems because of their commercial availability, established biocompatibility, and government registration. Table 1 is listed with the polymers used or evaluated for controlled release. Most polymers used in pharmaceutical dosage forms were not originally designed for this purpose. However, the production of new, life-saving, genetically engineered drugs (peptides and proteins), which have characteristically short half-lives, presents an opportunity for significant research in the area of polymer development in order to prolong their therapeutic effects in human body.

Polymer Fabrication and Drug Encapsulation

Encapsulation of the therapeutic agent into a polymer matrix can be brought about by a variety of methods. These methods depend on the desired fabrication of the polymer matrix. Some of the common techniques used for drug encapsulation for different polymer forms are described in this section.

Polymer Films and Rods. Polymer films can be cast by various techniques including dip coating, spin coating, hot-melt casting, and solvent casting. Typical applications for polymer films are in the medical device industry as coatings for controlled release from devices and implants such as stents. These applications require the polymer to be elastomeric to allow flexible films at micron-size thickness. The films can be casted with the drug encapsulated by homogenization/solubilization in the polymer melt/solution. The polymer film could also be extruded using a single or double screw extruder. Screw extrusion is also used to fabricate another form of polymer, ie, drug encapsulated rods/cylinders. Such extruded rods could be implanted subcutaneously to provide sustained drug delivery.

Polymer Microspheres. For applications in drug delivery, it is desired that the polymer formulation should be present as an injectable form. From this perspective, the polymer–drug combination could be fabricated as microspheres that can be suspended in an injection vehicle prior to injection. Subcutaneous or intramuscular injections are used for microspheres whereas smaller particles (in the nano range) could be injected intravenously. Microspheres can be fabricated using a variety of techniques, some of which are described below.

(1) **Spray drying.**

In spray drying the polymer and drug are dissolved in a common solvent and spray-atomized to create microspheres. This technique is useful to create particles in the size range of up to 50 μm, wherein the polymer has a sufficiently high glass-transition temperature to allow formation of discrete microparticles during atomization. The size and morphology of microparticles created using the spray drying technique depends on the nature of the polymer as well as the spray dryer operating parameters including chamber volume, flow rate, and nozzle design (41).

(2) **Solvent evaporation.**

In this technique the drug is emulsified/dispersed in the polymer solution. This emulsion/dispersion is further emulsified in a surfactant bath to allow for the formation of solid microparticles consisting of the drug encapsulated within the polymer matrix. Variations of this technique include single emulsion and double emulsion microencapsulation. Since microparticles are created during the slow evaporation of the solvent, this technique is also termed as solvent evaporation technique. Solvent evaporation/emulsification techniques are useful when the desired particle size is higher and/or when the drug is not soluble in the organic solvent (Fig. 4).

(3) **Freeze spray atomization.**

In this process a suspension of drug in an organic polymer solution is atomized into a liquid nitrogen bath. Absolute ethanol is added to extract the organic solvent. This process is particularly feasible for proteins since the protein is in a solid, less reactive form, making it less susceptible to

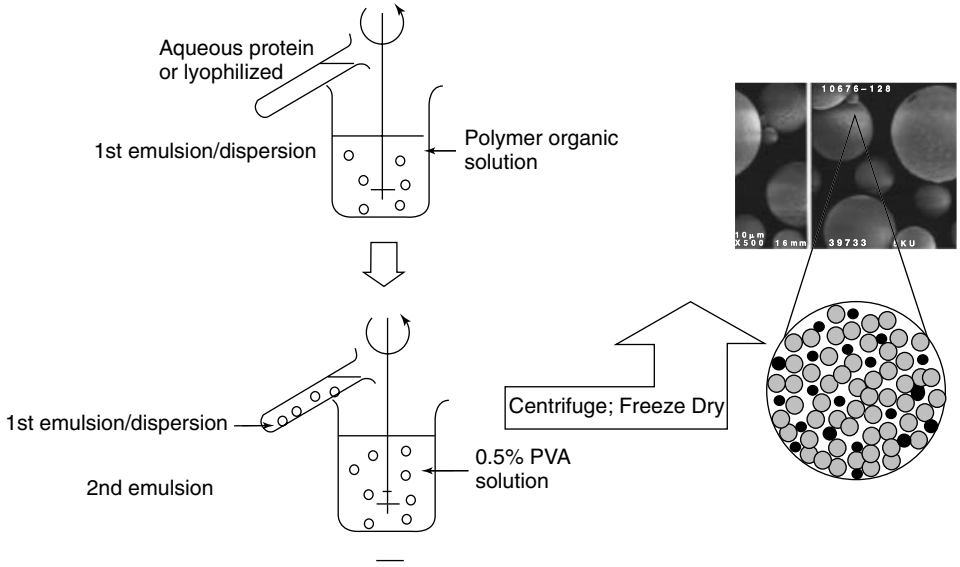

Fig. 4. Schematic representation of the emulsion-based microencapsulation processes; the single emulsion process utilizes lyophilized drug in the first step whereas the double emulsion process utilizes an aqueous solution of the drug in the first step.

damage during processing. Furthermore, the low temperature maintained throughout the process prevents thermal denaturation of the protein (42). This process has been utilized in the production of the first commercially available polymer-based sustained release protein formulation, Nutropin Depot, marketed by Genentech.

Polymer *In Situ* Gels. Drug encapsulation for injectable gels could be carried out by simple mixing of the drug into the polymer gel. To obtain sustained release, it is desirable that the polymer gel should acquire some viscosity upon injection into the body. Such *in situ* gelation characteristics could be achieved by various mechanisms such as those described below:

(1) **Temperature-induced gelation.**

Thermoreversible gelation could be obtained for ABA-type block copolymers wherein A denotes a hydrophilic segment while B denotes a hydrophobic segment. Because of the alternating block structure, such polymers undergo micellization driven by increasing temperature. The formation of micelles is thermodynamically favorable in ABA block structures, especially when the hydrophobic–hydrophilic balance is appropriately achieved. An example of such thermoreversible polymers includes PEG–PLGA–PEG (43) and Pluronics, which are ABA-type block copolymers of PEG and PPG. In each of the examples, the polymers could be engineered to be solutions at room temperature and converted into semisolid gels at body temperature.

(2) **pH-induced gelation.**

If the polymer is soluble at a certain pH and is insoluble at pH 7.4, then it would undergo pH-induced gelation on injection into the body. Examples of such polymers include synthetic polymers such as polyacrylic acid and natural polymers such as chitosan.

(3) **Solvent-induced gelation.**

Solvent-induced gelation could be obtained for a water-insoluble polymer, dissolved in a biocompatible solvent to create an injectable solution. When the solution is injected the solvent diffuses out and water from the physiological environment diffuses in. This diffusion process leads to a phase transition for the polymer as it goes from the solvent phase to a nonsolvent phase and forms a semisolid gel (44). Several factors such as polymer crystallinity, hydrophilicity, and water uptake govern the sol–gel transition and subsequently the drug release characteristics.

Classification of CDRFs

Drug delivery systems have been classified on the basis of route administration, for example, parenteral, eternal, respiratory, transdermal, and miscellaneous Flow (Fig. 5). Controlled release systems are based on the release mechanisms that may be erosion, diffusion, or chemically controlled, and thus these are classified under the heading of various categories of drug delivery. For example, under eternal drug delivery systems, release of a drug can be controlled by various mechanisms like diffusion, osmosis, or chemically controlled mechanism. In the broad way, these devices are of two types, as reservoir devices and matrix devices. The former involve the encapsulation of a drug within the polymeric shell, while the latter describe a system in which a drug is well dispersed throughout within the polymer matrix. However, on the basis of drug release mechanism, these devices can be classified into three types, as shown in Figure 6. Some examples of controlled release systems are described briefly here.

Diffusion-Controlled. Two types of diffusion-controlled systems have been used including reservoir systems (drug coated by a polymer membrane) and matrix systems (drug dispersed in a polymer matrix). In the reservoir systems, the drug is encapsulated by a polymeric membrane through which the drug is released by diffusion. This polymeric membrane is known as solution diffusion membrane (implying the mechanism of drug transport) and can be microporous or nonporous. In nonporous membrane, drug release is governed by the diffusion through polymer and thus, release can be controlled by selecting a polymer showing desirable drug solubility and diffusivity in the polymer matrix (see MEMBRANE TECHNOLOGY). In microporous membranes, pores with the size range 1.0 nm to several hundred millimeters are filled with drug permeable liquid or gel medium. Thus, diffusion of the drug through the medium in the pore will dominate the drug release process. These systems are very useful in the delivery of high molecular

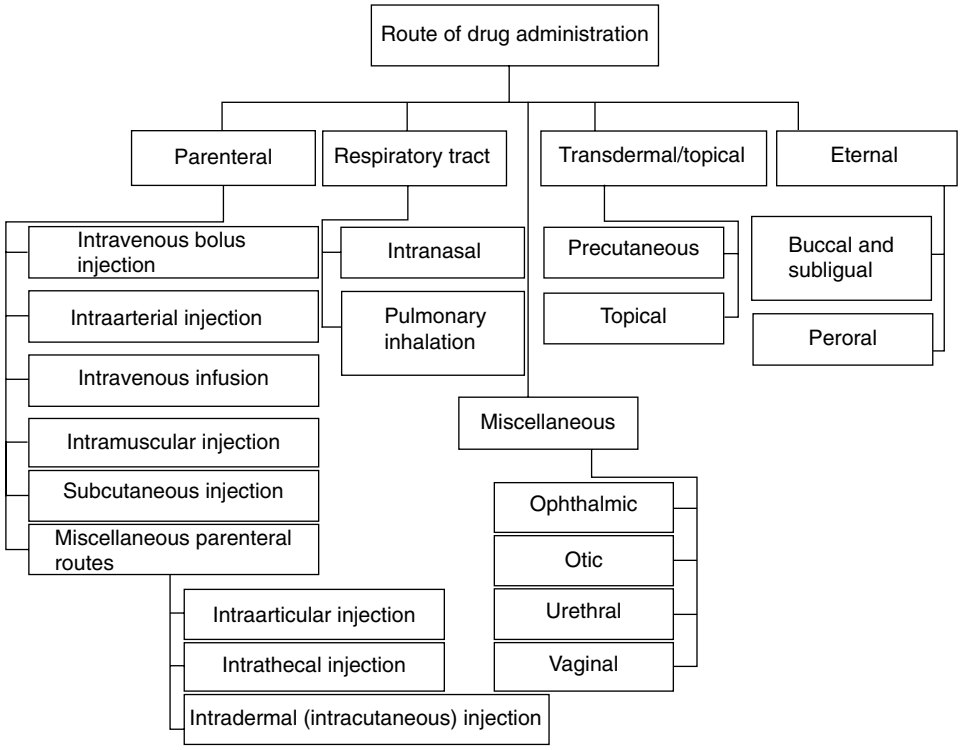

Fig. 5. Various routes of drug administration.

weight drugs such as protein and peptide drugs. Matharu and co-workers (19) reported the theoretical considerations, designing, and engineering of a "barrier coated-reservoir" type of a delivery system for theophylline using poly(vinyl alcohol) (PVA) as the coating material. After getting the desired theoretical *in vitro* release profile, *in vivo* studies were carried out on a dog model.

In monolithic systems, the drug is dissolved or dispersed homogeneously throughout the water-insoluble polymer matrix which may be microporous or nonporous (45). Monolithic systems are not suitable for zero-order release; however, it can be achieved by adjusting the physical shape of the device (46).

Dissolution-Controlled. Dissolution-controlled systems can also be classified as reservoir and matrix devices. Polymers used for these devices are generally water-soluble but water-insoluble polymers can also be used as long as they absorb water and disintegrate the drug. In reservoir devices, drug particles are coated with water-soluble polymeric membranes. The solubility kinetics of the membrane depends on the thickness of the membrane and type of the polymer used. Thus, drug release can be achieved and controlled by preparing devices with alternating layers of drug and polymeric coats or by preparing a mixture of particles which have different coating characteristics. Matrix dissolution devices are generally prepared by compressing powder mix of drug and a water-soluble or water-swellable polymer. They can also be made by casting and drying of a polymer solution containing a suitable amount of dissolved or dispersed drug. A variety of other excipient may optionally be included to aid formulation properties. The

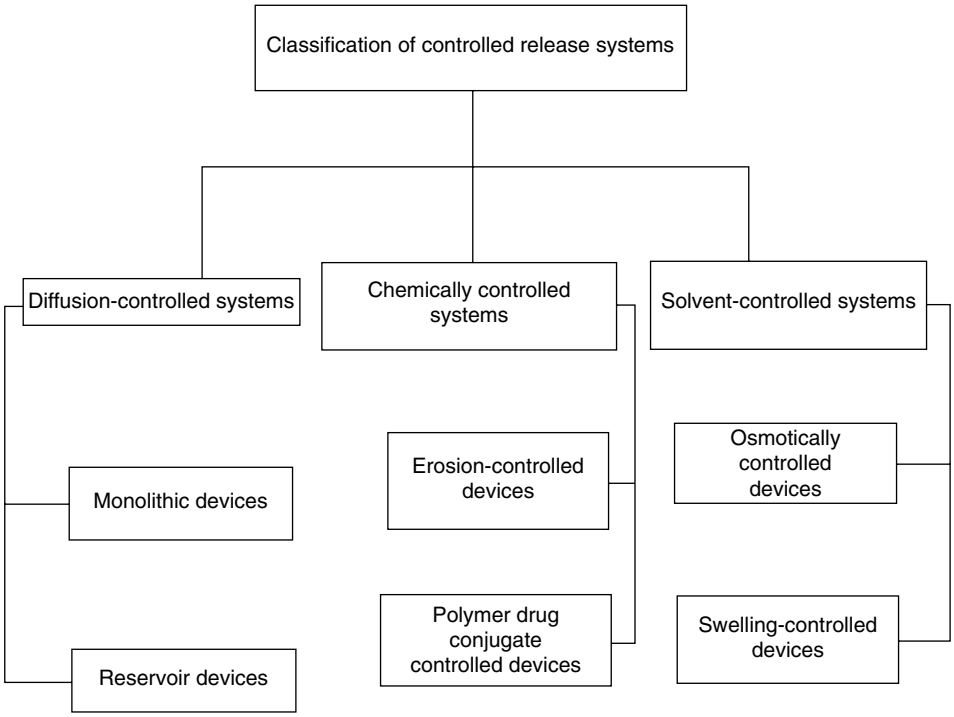

Fig. 6. Classification of controlled release systems.

influence of excipients and formulation factors on the dissolution behavior of the methyl hydroxyethyl cellulose (MHEC) tablets has been investigated (47). The use of drugs with higher solubility leads to a slight acceleration of the release because of the contribution of diffusion to the release process (caused by channels formed as a result of drug solubilization). Furthermore, alterations of the composition of the dissolution medium affect drug release.

Degradation/Erosion-Based Systems. While early research on polymer-based controlled release systems involved both degradable and nondegradable polymers, degradable polymers are preferred for parenteral drug delivery applications. Degradation of the polymer eliminates the need for a surgery to recover the spent polymer after the entire drug is released. It also reduces issues related to the long-term safety of the polymer. For biodegradable polymers, release of the drug is often intricately tied up with the polymer degradation profile. As can be seen in Figure 7, polymer degradation could be either enzymatic (facilitated by specific enzymes in the body), hydrolytic, or a combination of the two. The drug could be either physically entrapped in the polymer matrix wherein it would be released by diffusion and/or erosion of the polymer mass. Alternatively, the drug could also be chemically attached to the polymer backbone. In such a situation, the drug is released by the enzymatic/hydrolytic cleavage of the chemical bond between the polymer and the drug. A further classification of polymer degradation is established based on the polymer mass erosion patterns. If the polymer is hydrophobic then it restricts the diffusion of water into its matrix and hence polymer erosion may be restricted

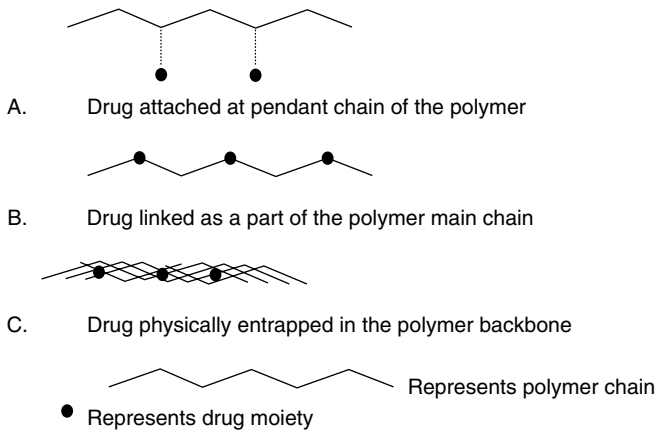

Fig. 7. Schematic representation of different embodiments of polymer-based controlled release formulations.

to the surface (as is the case for certain polyanhydrides). A more conventional case for majority of polymers including PLA and PLGA is when erosion occurs throughout the bulk of the polymer matrix (termed as *bulk erosion*). Bulk erosion is associated with a drop in pH within the interior of the matrix. While such a pH drop is detrimental to pH labile drugs, it could be utilized to stabilize certain type of basic drugs such as campothein (48).

Various diffusion models have been proposed for different scenarios and embodiments (49). Ritger and Peppas (50) proposed an empirical equation that has been successful in modeling the drug release for several formulation scenarios. This equation correlated the fraction of drug released to the time as

$$M_t/M_o = kt_n$$

M_t and M_o denote the drug release at time t and total amount of drug in the formulation respectively. The empirical coefficients k and n are related to the kinetics and diffusion mechanism respectively. When $n = 0.5$, this equation obeys Fick's law of diffusion. On the other hand, $n = 1$ denotes case II diffusion to play a prominent role. The key feature of this model is its simplicity as well as its ability to offer insights on the diffusion mechanisms based on the value of k.

Mathematical models have also been proposed to incorporate polymer degradation kinetics as an integral part of the theoretical framework explaining drug release characteristics (51). Similarly, kinetic models have been used to explain degradation profiles of the polymer. As listed in Table 2, several polymer properties play an important role in their degradation behavior.

Osmotic Delivery Systems. Osmosis-controlled devices comprises a core reservoir of drugs, with or without osmotically active salt, coated with a semipermeable membrane. The presence of salt or drug molecules creates an osmotic pressure gradient across the membrane and the diffusion of water into the device gradually forces the drug molecules out through an orifice made in the device. For a durable device, the mechanical strength of semipermeable membrane should be strong enough to resist the stress building inside the device. The drug release rate

Table 2. Important Properties of the Polymer that Influence Its Degradation Characteristics

Property	Effect on degradation kinetics
Chemical linkages	The type of hydrolytic linkage determines rate of degradation. For example, anhydride bonds are known to degrade faster than ester bonds.
Molecular weight (MW)	Higher the MW, slower is the degradation rate
Morphology	Porous forms (higher surface area) may be more susceptible to hydrolysis because of enhanced access for water penetration
Crystallinity	Higher crystallinity leads to slower degradation
Water uptake	Water uptake leads to faster degradation because of a better access for water to attack the polymer chains.
Polymerization conditions	Use of catalysts, reaction temperature, etc may affect the degradation properties of the polymer
Chain defects	Chain defects are often associated with faster degradation. Lesser the uniformity in structure, higher is the rate of hydrolysis.

from the osmotic devices, which is directly dependent on the rate of external water diffusion, can be controlled by the type, thickness, and area of the semipermeable membrane. Alza developed osmotic devices such as elementary osmotic pump system for oral administration and Alzet osmotic pump for implant. A recent review by Singh and co-workers discusses osmosis as a phenomenon for controlled drug delivery, along with the device concepts such as Rose Nelson pump, Higuchi osmotic pump, and Higuchi Theeuwes osmotic pump (52).

Ion-Exchange Systems. Polyelectrolytes have been used as cross-linker to form water-insoluble ion-exchange resins. The drug is bound to the ionic groups by salt formation during absorption and released after being replaced by appropriately charged ions in the surrounding media. For cationic drug delivery, poly(styrene sulfonic acid) and poly(acrylic acid) can be used as anionic ion-exchange resin where sulfonic and carboxylic groups make the complexes with cationic drugs and hydrogen ions and/or other cation such as sodium or potassium ions activate the release of cationic drugs by replacing them from the drug–resin complex. On the other hand, cationic ion-exchange resins like poly(dimethylamino ethyl methacrylate) have been used for the delivery of anionic drug, in which basic group namely amino or quaternary amino group makes a complex with anionic drugs. The interaction of a series of *O*-*n*-acyl propranolol prodrugs (I, R = C1–9 alkyl or CH_3C) with strong cation exchange resins has been reported and various variables that control loading and release profiles have been investigated (25). The effect of *O*-*n*-acyl chain-length on the loading and release profiles was detected by molecular size, for example, the loading was inhibited for the groups with increased size, and release rates were reduced. Again, this enables some control of release profiles but the approach was found to be most suitable for drugs that were active at low doses, which allow full use of these variations without the necessity for large amounts of resin in the delivery system. Sometimes, the

ion-exchange resins are additionally coated with a polymer film, such as acrylic acid and methacrylate copolymer or ethylcellulose, to regulate the swelling of the resin and to further control the drug release. The Pennkinetic system is an example of the devices based on these mechanism to deliver dextromethorphan from the ethylcellulose-coated poly(styrene sulfonate).

Polymeric Prodrugs. Many water-soluble polymers possess functional groups to which drug molecules can be covalently attached and thus, these polymers that have no therapeutic effect serve as drug carriers. The drug molecules are gradually released from the polymer by hydrolytic or enzymatic cleavage. If the cleavage occurs by chemical hydrolysis, the drug release depends on the nature of the covalent bonds and pH of the environment; however, it is very slow in the body. If the drug molecule is released by enzymatic hydrolysis, the release is mainly dependent on the concentration of enzymes. Thus, the exact release profile depends on the *in vivo* condition and not on the delivery system itself. To be a useful carrier, a polymer should possess certain features:

(1) The polymer should remain water-soluble even after drug loading
(2) Molecular weight of the polymer should be large enough to permit glomerular filtration but small enough to reach all cell types.
(3) Drug-carrier linkages should be stable in body fluid and yet degradable after capturing in target cells.

This can be achieved by making the linkage degradable by lisosomal enzymes, in which the polymer is nontoxic, nonimmunogenic, biocompatible, and degradable by lysosomal enzymes to be eliminated from the body after releasing drugs. Starch derivatives, dextran (53), poly(aminoacids), PVP, and poly(hydroxypropyl methacrylamide) have been used as polymeric drug carriers.

Magnetically Stimulated Systems. The two principle parameters controlling the release rates in these systems are magnetic field characteristics and mechanical properties of the polymer matrix. It was found that when the frequency of the applied field was increased from 5 to 11 Hz, the release rate of the bovine serum albumin (BSA) from ethylene vinyl acetate (EVAc) copolymer matrices rose in linear fashion (54). The mechanical properties of the polymeric matrix also affect the extent of magnetic enhancement (54). For example, the modulus of elasticity of the EVAc copolymer can be easily altered by changing the vinyl acetate content of the copolymer. The release rate enhancement induced by the magnetic field increases as the modulus of elasticity of EVAc decreases. A similar phenomenon was observed for cross-linked alginate matrices: higher release rate enhancement for less rigid matrices (55). Edlemean and co-workers. (56) also showed that enhanced release rates observed in response to an electromagnetic field (50 G, 60 Hz) applied for 4 min were independent of duration of the interval between repeated pulses.

Photostimulated Systems. Photoresponsive gels reversibly change their physical or chemical properties upon photoradiation. A photoresponsive polymer consists of a photoreceptor, usually a photochromic chromophore, and a functional part. The optical signal is captured by the photochromic molecules and then the isomerization of the chromophores in the photoreceptor converts it to a chemical

signal. Suzuki and Tanak (57) reported a phase transition in polymer gels induced by visible light, where the transition mechanism is due to the direct heating of the network polymer by light.

Ultrasonically Stimulated Systems. Kost and co-workers (58) proposed that cavitation and acoustic streaming are responsible for the augmented degradation and release of biodegradable polymers. Miyazaki and co-workers (59) speculated that the ultrasound caused increased temperature in their delivery system, which may facilitate diffusion.

Electrically Stimulated Systems. In the late 1980s, Grimshaw (60) reported four different mechanisms for the transport of proteins and neutral solutes across hydrogel membranes:

(1) Electrically and chemically induced swelling of a membrane to alter the effective pore size and permeability
(2) Electrophoric augmentation of solute flux within a membrane
(3) Electroosmotic augmentation of solute flux within a membrane
(4) Electrostatic partitioning of charged solutes into charged membranes

Kwon and co-workers (61) studied drug release from electric current sensitive polymers. Edrophonium chloride, a positively charged solute, was released in an on-off pattern from a matrix device by an electric field. The mechanism was explained as an ion exchange between positive solute and hydroxonium ion, followed by fast release of the charged solute from the hydrogel. The fast release was attributed to the electrostatic force, the squeezing effect, and the electroosmosis of the gel. However, the release of neutral solute was controlled by diffusion affected by swelling and deswelling of the gel.

Representative Applications

Controlled Release of Peptides and Proteins. Sustained release applications are especially useful for proteins/peptides because of their short half-lives (62). This concept was first utilized commercially in Lupron Depot, which was introduced as a sustained release formulation of a lutenizing hormone-releasing hormone (LHRH), leuprolide acetate, with poly(lactic acid) as the polymer (63). Following the success of Lupron Depot, other sustained release formulations of LHRH analogues have also been commercialized, including Zoladex wherein the LHRH peptide is encapsulated in PLA-extruded rods, and Trelstar depot wherein the peptide is encapsulated in PLGA polymer matrices.

Recently, a once-in-four-weeks formulation of a cyclic peptide Octreotide, encapsulated in biodegradable PLGA–glucose polymer matrix, has also been commercialized under the trade name Sandostatin LAR (Novartis Pharmacenticals Corp.) (64). In 2000, a human growth hormone sustained release formulation (Nutropin Depot) became the first polymer-based sustained release formulation of a therapeutic protein to receive marketing approval from the Food and Drug Administration. This commercialized formulation encapsulates a zinc-complexed form of recombinant human growth hormone in a PLGA matrix (41). Other therapeutic proteins that are being tested for encapsulation in polymer matrices

include bone morphogenic protein (65), erythropoietin (66), and nerve growth factor (67).

Controlled Release of Antirestenotic Agents from Stent Coatings. Stents are tiny wire scaffold-like devices, which have become the most successful and widely used innovation in interventional cardiology of the last decade. These devices are inserted inside blocked sections of coronary arteries and expanded into place using a balloon catheter in a procedure called an angioplasty. In as many as 40% of patients receiving angioplasty, a new blockage develops at the site because of scar tissue growth and inflammation, a condition referred to as restenosis. More than 500,000 Americans are treated for restenosis annually. Stents coated with a biocompatible polymer, encapsulating an antirestenotic agent, have proven to be a successful therapy to reduce or eliminate restenosis. Several drugs including cytostatic agents (Rapamune), antiproferative agent (Paclitaxel), and antiinflamatory agents have been encapsulated in micron-thick films that coat the metallic stent (68). The polymers used for this application are required to be elastic, biocompatible, and hemocompatible. Lewis and co-workers (69) demonstrated the use of phosphorylcholine-based polymers for this application. Other polymers tested for this application include polylactide and polyurethane (70).

Polymeric Systems for the Treatment of Cancer. By providing sustained release at the desired site, high doses of toxic drugs can be delivered to the site without introducing the drug into systemic circulation. This results in a major advantage for the administration of chemotherapeutic drugs, wherein the drugs can be encapsulated into polymer matrices and administered directly into the tumor area. Gliadel (Guilford Pharmaceuticals) implant is a product based on the above concept, encapsulating a chemotherapeutic agent, carmustine, into a biodegradable polymer, fabricated as a dime-sized wafer (see BIODEGRADABLE POLYMERS, MEDICAL APPLICATIONS). Several wafers are implanted by the surgeon into the brain cavity during a tumor resection surgery. By direct release of the drug in the tumor region in the brain, the problem of overcoming the blood-brain barrier is resolved. Also, high doses of the chemotherapeutic agent are delivered at the tumor site, thus making the therapy significantly more effective than systemic administration. Other chemotherapeutic agents that are also being developed as sustained release formulations include paclitaxel and cisplatin (71).

The biggest success of polymer controlled release systems in cancer therapy however has been in the area of prostate cancer treatment. This therapy is unique since it uses a hormone-suppressant rather than a chemotherapeutic agent to minimize cancer cell growth in the prostate. Several products include Lupron Depot (TAP Pharmaceuticals), Zoladex (Astra-Zeneca), and Trelstar Depot (Debio RP, Pharmacia). Lupron Depot involves PLA microspheres, Zoladex formulation is an extruded rod, whereas Trelstar depot consists of PLGA microspheres, all of which incorporate LHRH analogues.

Sustained Release of Drugs for CNS-Related Disorders. Another area of application for polymer-based controlled release technologies is for the sustained delivery of drugs for the central nervous system (CNS) related disorders. CNS-related drugs include a wide range of therapeutics including pain management agents, drugs to prevent substance abuse, as well as drugs for conditions such as schizophrenia, Parkinson's and Alzheimer's disease. Drugs such as lidocaine and bupivicaine have been studied for sustained local anesthesia at the site of surgery (72). For this application, the anesthetic agent is encapsulated

in a biodegradable polymer and injected in the proximity of the site of pain. The drug is released facilitating high concentrations at the local site, without reaching the threshold levels of systemic toxicity. In other cases such as schizophrenia, Parkinson's and Alzheimer's diseases, sustained release of the medication may reduce the chance of missed doses and aid in an effective dose regimen.

Gene Therapy. For more than two decades, researchers have been working to alleviate disease through gene therapy. In this type of treatment a gene is delivered to cells, allowing them to produce their own therapeutic proteins. Traditionally, DNA delivery systems have been classified as viral vector-mediated systems and nonviral vector-mediated systems (73). Currently, because of their highly evolved and specialized components, viral systems are by far the most effective means of DNA delivery, achieving high efficiencies (>90%) for both delivery and expression (74). The most promising nonviral gene delivery system thus far, other than the "gene gun," is the DNA vaccine application, which comprises of ionic complexes formed between DNA and polycationic liposomes (75,76) (see GENE-DELIVERY POLYMERS).

Nonviral vectors can be divided into two broad categories—physical and chemical—according to Huang. Physical methods involve taking plasmids and forcing them into cells through such means as electroporation or particle bombardment. Chemical methods use lipids, polymers, or proteins that will complex with DNA, condensing it into particles and directing it to the cells. Nonviral systems

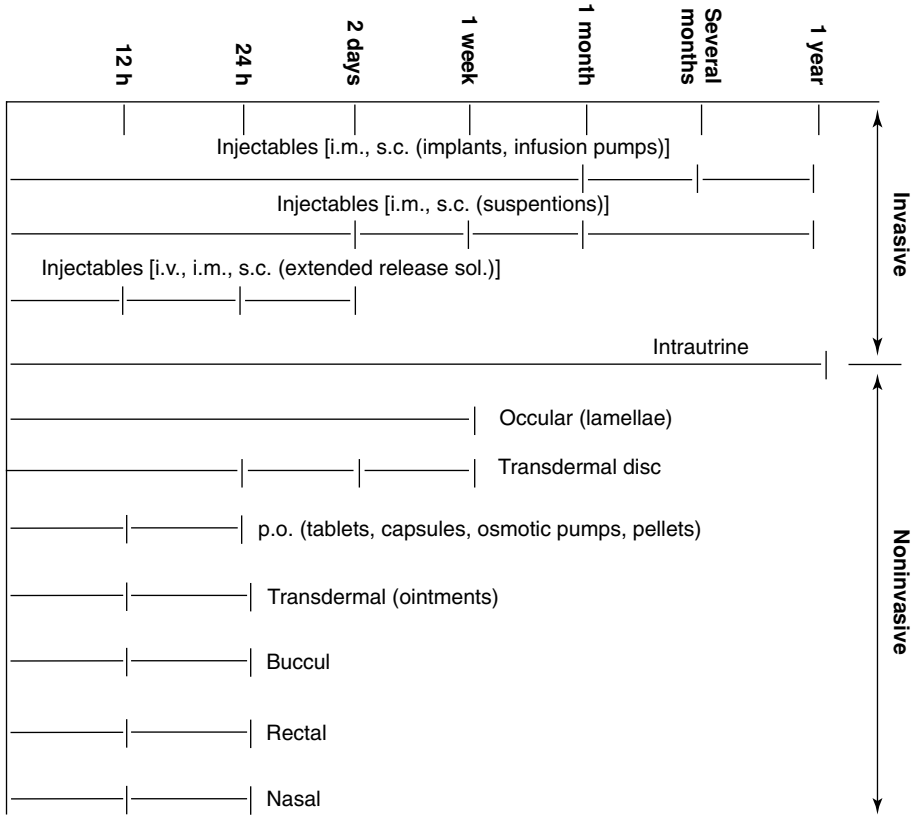

Fig. 8. Route of administration and length of action in the body.

for gene delivery have several potential advantages over viral vectors. Viruses can cause an immune response that can make repeat administrations ineffective. Nonviral vectors can also carry more DNA than viruses, allowing the delivery for larger genes. In addition, nonviral vectors are easier and less expensive to manufacture. The plasmids that are used in nonviral systems can be produced in bacteria such as *Escherichia coli*. The same production facilities can be used to manufacture a variety of plasmids incorporating different genes. Many recent reviews describe various aspects of nonviral vectors for gene therapy including different polymers and success and failure stories (77–79).

Controlled Release Systems in Market

Controlled release has gained a good impact among the various drug delivery technologies because of patient compliances, safety of drug, and minimum side effects. Various controlled release systems according to their drug availabilities, route of administration, and length of action in the body are presented in Figure 8. It had been estimated that the world pharmaceuticals sales was nearly $400 billion during the year 2000 and about 12.5% or $50 billion for drugs involving special drug delivery technology. Sales of drug delivery products are expected to more than double to $104 billion in 2005. Among them, more than 20% share goes to controlled drug release technologies. Examples of controlled release technologies available in the market place are given in Table 3.

Table 3. Some Examples of Controlled Release Products in Market

Technology	Technology name (drug)	Application	Company
Liposome-based formulations	Evacet (Doxorubicin)	Breast cancer and other cancers	Elan with acquisition of Liposome, Inc.
One-yearly drug implant	Viadur (Leuprolide)	Prostate cancer	ALZA/J&J
Biodegradable implants	Gliadel (BCNU[a])	Treatment of brain cancer	Guilford Pharmaceuticals, Inc.
Biodegradable microsphere for sustained-release for peptides/proteins	ProLease	Delivery of peptides and small molecules	Alkermes, Inc.
Time release oral drug release	Pulsincap	Drug release at predetermined time or location in the GI-tract	RP Scherer Corp.
Oral controlled release system to control the release of a specific drug	Geomatrix	Predetermined therapeutic objective for a drug	SkyePharma

[a] *N*,*N*-bis(2-chloroethyl)-*N*-nitrosourea.

BIBLIOGRAPHY

"Controlled-release Technology" in *EPSE* 2nd ed., Suppl. Vol., pp. 164–186, by Raphael M. Ottenbrite, Virginia Commonwealth University.

1. J. R. Robinson, *Control. Drug Delivery* 1 (1997).
2. W. A. Ritschel, *Methods Find. Exp. Clin. Pharmacol.* **13**, 313 (1991).
3. R. Langer, *Nature* **392**, 5 (1998).
4. S. P. Vyas, V. Sihorkar, and V. Mishra, *J. Clin. Pharm. Ther.* **25**, 21 (2000).
5. Y. W. Chien, *Novel Drug Delivery Systems: Fundamentals, Developmental Concepts and Biomedical Assessments*, Marcel Dekker, New York, 1982.
6. K. Park, *Controlled Drug Delivery: Challenges and Strategies*, American Chemical Society, Washington, D.C., 1997, pp. 629.
7. M. N. V. Ravi Kumar, N. Kumar, A. J. Domb, and M. Arora, *Adv. Polym. Sci.* **160**, 45 (2002).
8. J. Heller, *Control. Drug Delivery* 127 (1997).
9. N. B. Graham, *Chem. Ind.* 482 (1990).
10. A. Rubinstein and J. R. Robinson, *Prog. Clin. Biochem. Med.* **4**, 71 (1987).
11. W. A. Ritschel, *Drug Dev. Ind. Pharm.* **15**, 1073 (1989).
12. R. Langer, *Biomater. Artif. Cells Artif. Organs* **15**, 752 (1988).
13. H. P. Koch, *Sci. Pharm.* **59**, 85 (1991).
14. I. K. Grigor'yants, G. A. Trikhanova, A. G. Balabushevich, N. N. Tikhomirova, and N. I. Shumskaya, *Khim.-Farm. Zh.* **20**, 1250 (1986).
15. T. Nagai, *Yakugaku Zasshi* **108**, 613 (1988).
16. N. A. Peppas, *J. Biomed. Mater. Res.* **17**, 1079 (1983).
17. A. Sood and R. Panchagnula, *S.T.P. Pharm. Sci.* **9**, 157 (1999).
18. G. J. Boer and J. Kruisbrink, *Biomaterials* **8**, 265 (1987).
19. R. S. P. Matharu and J. K. Lalla, *Drug Dev. Ind. Pharm.* **20**, 1225 (1994).
20. H. B. Hopfenberg, *AIChE Symp. Ser.* **77**, 37 (1981).
21. K. V. R. Rao and K. P. Devi, *Int. J. Pharm.* **48**, 1 (1988).
22. C. Bindschaedler, R. Gurny, and E. Doelker, *J. Controlled Release* **4**, 203 (1986).
23. R. K. Verma, B. Mishra, and S. Garg, *Drug Dev. Ind. Pharm.* **26**, 695 (2000).
24. F. Chellat, M. Tabrizian, S. Dumitriu, E. Chornet, P. Magny, C. H. Rivard, and L. Yahia, *J. Biomed. Mater. Res.* **51**, 107 (2000).
25. W. J. Irwin, K. A. Belaid, and H. O. Alpar, *Drug Dev. Ind. Pharm.* **13**, 2047 (1987).
26. V. Anand, R. Kandarapu, and S. Garg, *Drug Discovery Today* **6**, 905 (2001).
27. P. K. Gupta and C. T. Hung, *Life Sci.* **44**, 175 (1989).
28. R. Langer, R. Siegel, L. Brown, K. Leong, J. Kost, and E. Edelman, *Ann. N.Y. Acad. Sci.* **446**, 1 (1985).
29. P. R. Mayer, *Control. Drug Delivery* 589 (1997).
30. V. H.-L. Lee and J. R. Robinson, *Drugs Pharm. Sci.* **6**, 71 (1978).
31. Y. W. Chien and H. J. Lambert, *J. Pharm. Sci.* **63**, 515 (1974).
32. B. G. Amsden and M. F. A. Goosen, *AIChE J.* **41**, 1972 (1995).
33. E. J. Vanhoogdalem, A. G. Deboer, and D. D. Breimer, *Clin. Pharmacokinet.* **21**, 11 (1991).
34. L. K. Paalzow and L. Sjalander-Brynne, *Adv. Drug Delivery Rev.* **33**, 235 (1998).
35. P. Gruber, M. A. Longer, and J. R. Robinson, *Adv. Drug Delivery Rev.* **1**, 1 (1987).
36. C. Young, *Pharm. Times* 19 (May 1996).
37. D. D. Breimer, *J. Controlled Release* **62**, 3 (1999).
38. R. Langer, *Acc. Chem. Res.* **33**, 94 (2000).
39. A. Domb, M. Maniar, S. Bogdansky, and M. Chasin, *Crit. Rev. Ther. Drug Carrier Syst.* **8**, 1 (1991).
40. R. A. Jain, *Biomaterials* **21**, 2475 (2000).

41. G. F. Palmieri, G. Bonacucina, P. Di Martino, and S. Martelli, *Drug Dev. Ind. Pharm.* **27**, 195 (2001).
42. O. L. Johnson, W. Jaworowicz, J. L. Cleland, L. Bailey, M. Charnis, E. Duenas, C. Wu, D. Shepard, S. Magil, T. Last, A. J. S. Jones, and S. D. Putney, *Pharm. Res.* **14**, 730 (1997).
43. B. Jeong, Y. H. Bae, and S. W. Kim, *J. Biomed. Mater. Res.* **50**, 171 (2000).
44. K. J. Brodbeck, S. Pushpala, and A. J. McHugh, *Pharm. Res.* **16**, 1825 (1999).
45. J. Heller, *FIDIA Res. Ser.* **11**, 179 (1987).
46. C. T. Laurencin, H. J. Koh, T. X. Neenan, H. R. Allcock, and R. Langer, *J. Biomed. Mater. Res.* **21**, 1231 (1987).
47. S. Zuleger and B. C. Lippold, *Int. J. Pharm.* **217**, 139 (2001).
48. A. Shenderova, T. G. Burke, and S. P. Schwendeman, *Pharm. Res.* **16**, 241 (1999).
49. J. Siepmann and N. A. Peppas, *Adv. Drug Delivery Rev.* **11**, 139 (2001).
50. P. L. Ritger and N. A. Peppas, *J. Controlled Release* **5**, 37 (1987).
51. R. P. Batycky, J. Hanes, R. Langer, and D. A. Edwards, *J. Pharm. Sci.* **86**, 1464 (1997).
52. P. Singh, V. Sihorkar, V. Mishra, B. Saravanababu, N. Venkatesan, and S. P. Vyas, *East. Pharm.* **42**, 39 (1999).
53. J. Coro, *Acta Farm. Bonaerense* **16**, 173 (1997).
54. J. Kost, R. Noecker, E. Kunica, and R. Langer, *J. Biomed. Mater. Res.* **19**, 935 (1986).
55. O. Saslawski, P. Couvrer, and N. Peppas, in J. Heller, F. Harris, H. Lohmann, H. Merkle, and J. Robinson, eds., *Controlled Release of Bioactive Materials*, Basel, 1988, p. 26.
56. E. Edelman, L. Brown, J. Taylor, and R. Langer, *J. Biomed. Mater. Res.* **21**, 229 (1987).
57. A. Suzuki and T. Tanaka, *Nature* **346**, 345 (1990).
58. J. Kost, K. Leong, and R. Langer, *Proc. Natl. Acad. Sci. U.S.A.* **86**, 7663 (1989).
59. S. Miyazaki, C. Yokouchi, and M. Takada, *J. Pharm. Pharmacol.* **40**, 716 (1988).
60. P. E. Grimshaw, A. J. Grodzinksy, M. L. Yarmush, and D. M. Yarmush, *Chem. Eng. Sci.* **104**, 827 (1989).
61. I. C. Kwon, Y. H. Bae, and S. W. Kim, *J. Controlled Release* **17**, 149 (1991).
62. S. Cohen, T. Yoshioka, M. Lucarelli, L. H. Hwang, and R. Langer, *Pharm. Res.* **8**, 713 (1991).
63. H. Okada, *Adv. Drug Delivery Rev.* **28**, 43 (1997).
64. P. H. Davies, S. E. Stewart, L. Lancranjan, M. C. Sheppard, and P. M. Stewart, *Clin. Endrocrinol.* **48**, 311 (1998).
65. J. A. Schrier and P. P. DeLuca, *Pharm. Dev. Technol.* **4**, 611 (1999).
66. K. F. Pistel, B. Bittner, H. Koll, G. Winter, and T. Kissel, *J. Controlled Release* **59**, 309 (1999).
67. X. M. Lam, E. T. Duenas, and J. L. Cleland, *J. Pharm. Sci.* **90**, 1356 (2001).
68. S. H. Lewis, H. M. van Beusekom, P. W. Serruys, and W. J. van Der Giessen, *Curr. Interv. Cardiol. Rep.* **3**, 28 (2001).
69. A. L. Lewis, Z. L. Cumming, H. H. Goreish, L. C. Kirkwod, L. A. Tolhurst, and P. W. Stratford, *Biomaterials* **22**, 99 (2001).
70. W. J. van der Giessen, A. M. Lincoff, R. S. Schwartz, H. M. van Beusekom, P. W. Serruys, D. R. Holmes Jr., S. G. Ellis, and E. J. Topol, *Circulation* **94**, 1690 (1996).
71. E. Harper, W. Dang, R. G. Lapidus, and R. I. Garver Jr., *Clin. Cancer Res.* **5**, 4242 (1999).
72. A. Paavola, P. Tarkkila, M. Xu, T. Wahlstrom, J. Yliruusi, and P. Rosenberg, *Pharm. Res.* **15**, 482 (1998).
73. E. W. Alton and D. M. Geddoes *Gene Ther.* **2**, 88 (1995).
74. A. Smith, *Nature* **49**, 807 (1995).
75. M. Cotton and E. Wagner, *Curr. Opin. Biotechnol.* **4**, 705 (1993).
76. A. Singhal and L. Huang, in J. A. Wolff ed., *GeneTherapeutics: Methods and Applications of Direct Gene Transfer*, Birkhauser, Boston, 1994.

77. S. C. De Smedt, J. Demeester, and W. E. Hennink, *Pharm. Res.* **17**, 113 (2000).
78. D. Luo and W. M. Saltzman, *Nat. Biotechnol.* **18**, 33 (2000).
79. C. Pichon, C. Goncalves, and P. Midous, *Adv. Drug Delivery Rev.* **53**, 75 (2001).

NEERAJ KUMAR
University of Tennessee Health Science Center
MAHESH CHAUBAL
Drugdel.com
A. J. DOMB
The Hebrew University of Jerusalem
RAVI KUMAR N. V. MAJETI
University of Saarland

COORDINATION POLYMERS. See METAL-CONTAINING POLYMERS.

COTTON

Introduction

The use of cotton predates recorded history. Although the actual origin of cotton is still unknown, archaeological findings indicate its use in cloth in 3000 BC. Early explorers in Peru found cotton cloth on exhumed mummies that dated to 200 BC. The first cotton mill was built in Beverly, Massachusetts, in about 1790, and in 1794 Eli Whitney was granted a patent for the invention of the cotton gin, the "engine" that separates the cotton from the seed.

Cotton culture has evolved from gathering of the lint and seed from wild plants by indigenous people to the domestication and cultivation of selected species. Cotton is both a fiber (lint) and food (cottonseed) crop. For each 45.36 kg (100 lb) of fiber produced, the plant also produces ~68.04 kg (150 lb) of cottonseed. Cotton, which only has value once the fiber and seed are separated at the gin, is perishable and must be harvested in a timely manner or the fiber and seed can deteriorate in quality and value.

Cotton fiber is the most important natural vegetable textile fiber used in spinning to produce apparel, home furnishings, and industrial products (1). In 2001, worldwide ~37% of the textile fiber consumed was cotton (2). In its marketed form, raw cotton consists of masses of fibers packaged in bales of ~85–230 kg (187–507 lb). A single kilogram (2.2 lb) of cotton may contain 200 million or more individual fibers.

Cottonseed [world's no. 3 oilseed; 26,665 tons (3)] can be fed as whole seed (16% oil, ~45% protein) to dairy cattle or crushed at a cottonseed oil mill to obtain oil [160 kg/ton (320 lb/tons)], hulls [260 kg/ton (540 lb/t)], meal [455 kg/ton (910 lb/tons)], linters [fuzz fibers $\leq$0.33 mm long; 83.5 kg/ton (167 lb/tons)], and manufacturing loss [31.5 kg/ton (63 lb/tons)] (4). The oil is used for human

Encyclopedia of Polymer Science and Technology. Copyright John Wiley & Sons, Inc. All rights reserved.

consumption; the hulls and meal are sources of vegetable protein feed for animals; and the linters are used as a chemical cellulose source and in batting for upholstered furniture and mattresses as well as for high quality paper.

The origin, development, biology/breeding, production, morphology, chemistry, physics, and utilization of cotton have been discussed in many publications (1,4–9).

Cotton fibers are seed hairs from plants of the *Malvaceae* family, the tribe *Gossypieae*, and the genus *Gossypium*. It is a warm-weather shrub or tree that grows naturally as a perennial but for commercial purposes is grown as an annual. Botanically, cotton is a fruit. The principal domesticated species of cotton of commercial importance are *hirsutum, barbadense, arboreum*, and *herbaceum*. Many different varieties of these species have been developed through breeding to produce cotton plants with improved agronomic properties and cotton fibers with improved length, strength, and uniformity. In addition to conventional breeding methods, genetic engineering is being used to produce transgenic cottons with insect resistance (eg, Bollgard; "Bt cottons" incorporting genes from *Bacillus thuringiensis* for boll worm/bud worm resistance) and herbicide tolerance [eg, bromoxynil (Buctril; "BXN cotton") and glyphosate (Roundup; "Roundup Ready cottons") tolerant cottons, which enable reduced use of herbicides] (10). In 2002, transgenic cotton varieties are ∼25–30% of the cotton grown in the world and are being grown in the United States, China, Australia, South Africa, Argentina, Mexico, India, and Indonesia. Research is underway to produce transgenic cottons with other improved agronomic traits as well as improved fiber quality properties.

Gossypium hirsutum, developed in the United States from cottons that originated in Central America and Mexico, includes all of the many varieties of American Upland cotton. Upland cottons now provide >90% of the world's production of raw cotton fiber and vary in length from ∼22 to 36 mm (7/8 to $1\frac{1}{2}$ in.) with micronaire scale [numerical values are roughly the equivalent of linear density (expressed in micrograms weight per inch of length); represents fiber surface area, used as an indicator of fiber fineness (http://www.uster.com/en/prod/main_2_0_4.htm)] ranging from 3.8 to 5.0. *G. hirsutum* is a shrubby plant that reaches a maximum height of 1.8 m (5.9 ft). and is used in apparel, home furnishings, and industrial products.

Gossypium barbadense, originally of early South American origin, has the longest staple length and is commonly referred to as "extra long staple" (ELS) cotton. It includes Sea Island, Egyptian Giza strains, American Pima, and Tanguis cottons. Sea Island is the longest and silkiest of the commercial cottons. *G. barbadense* accounts for ∼8% of current world production. ELS cotton fiber is long and fine with a staple length usually greater than 35 mm ($1\frac{3}{8}$ in.) and a micronaire <4.0. The plant grows from black usually linter-less seeds and reaches a height of 1.8–4.5 m (5.9–14.8 ft). Egypt is the major producer of ELS cotton today. Pima, an ELS, is a complex cross of Egyptian and American Upland strains and is grown in the western United States as well as South America. *G. barbadense* is used in high quality apparel, speciality yarns for lace and knitted goods, and sewing thread.

Gossypium arboreum and *Gossypium herbaceum*, known collectively as "Desi" cottons, are the other commercial species. They are the Asiatic or Old World short staple cottons. Both are of minor commercial importance but are grown in

India and Pakistan. *G. herbaceum* is also grown in China. These cottons are the shortest and coarsest cottons cultivated, ranging from 9.5 to 19 mm ($\frac{3}{8}$ to $\frac{3}{4}$ in.) and micronaire >6.0. *G. arboreum*, the tree wool of India, grows as tall as 4.5–6.0 m (14.8–19.7 ft) and includes both Indian and Asiatic varieties. Its seeds are covered with greenish gray fuzz fibers below the white lint fibers. *G. herbaceum*, the original cotton of India, averages 1.2–1.8 m (3.9–5.9 ft) in height. The fiber is grayish white and grows from a seed encased in gray fuzz fibers.

Commercial cottons are almost all white but recently there has been a renewed interest in naturally colored cottons. They have existed for >5000 years (11,12). The availability of synthetic dyes and the need for high quality, higher yielding cottons caused these cottons that are short, weak, and low yielding to almost disappear. Naturally colored cottons available today are usually shorter, weaker, and finer than regular upland cottons, but can be spun into ring and rotor yarns for some applications alone or when blended with normal white fiber (13). The color can intensify with washing and colors can vary somewhat from batch to batch (13). Colored cottons are being grown presently in the United States, Peru, China, and Australia. The amount available is very small. Shades of brown and green are the main colors available. Other colors (mauve, red) are available in Peru and some other colors are being researched. The color for brown and red-brown cotton appears to be in material bodies in the lumen. The different colors of brown and red-brown are due most likely to tannins derived from (+)-catechin (14) and some may be protein–tannin polymers. The color in green cottons is due to a lipid biopolymer (suberin) deposited between the cellulose microfibrils in the secondary wall. The brown cotton fibers (and white lint cultivars) do not contain suberin like the green cotton fibers. Green cotton fibers are chacterized by a high wax content of 14–17% of their dry weight, whereas white and brown fibers contain only 0.4–0.7% wax (14,15).

At present, cotton is grown in environments that range from arid to tropical, with long to very short growing seasons. Cotton typically requires a growing season of at least 160 days when minimum temperatures are >15°C (60°F) (7). Fairly moist and loamy soil produces the highest yields. Under normal climatic conditions, cotton seeds germinate and seedlings emerge in 7–10 days after planting. Flower buds (known as squares) appear 35–45 days later, followed by open white (Upland cotton) or creamy to dark-yellow (Pima cotton) flowers 21–25 days later. One day after the flower opens the cotton boll begins to grow rapidly, if the flower has been fertilized. Mature bolls open 40–80 days after flowering, depending on variety and environmental conditions. Within the boll are three to five divisions called locks or locules, each of which normally has seven to nine seeds that are covered with both lint and linters (Fig. 1). The linters form a short, shrubby undergrowth beneath the lint hairs on the seed. At least 13,000–21,000 fibers are attached to each seed and there are close to 500,000 fibers in each boll.

Each cotton fiber is a single cell that originates in the epidermis of the seed coat at about the time the flower opens. The fibers first emerge on the broad, or chalazal, end of the seed and progress by degrees to the sharp, or micropylar, end. As the boll matures, the fiber grows until it attains its maximum length, which averages ~2500 times its diameter (Fig. 2). During the first 3 weeks, the cell is composed of a thin wall (primary wall) that is covered with a waxy, pectinaceous material, which encloses the protoplasm or plant juices. The primary wall also

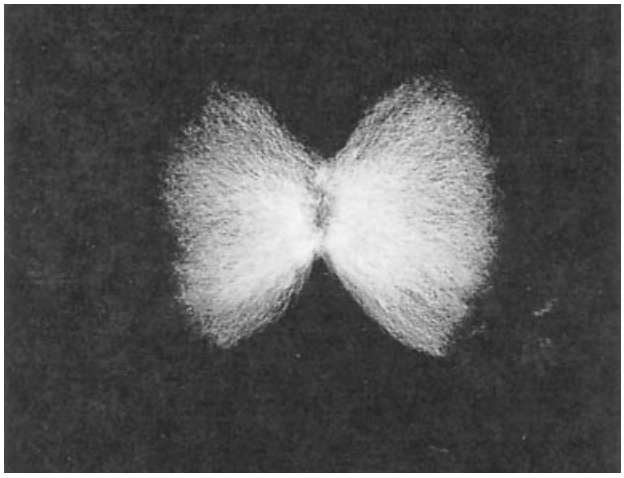

Fig. 1. Cotton butterfly with lint and linters (fuzz fibers).

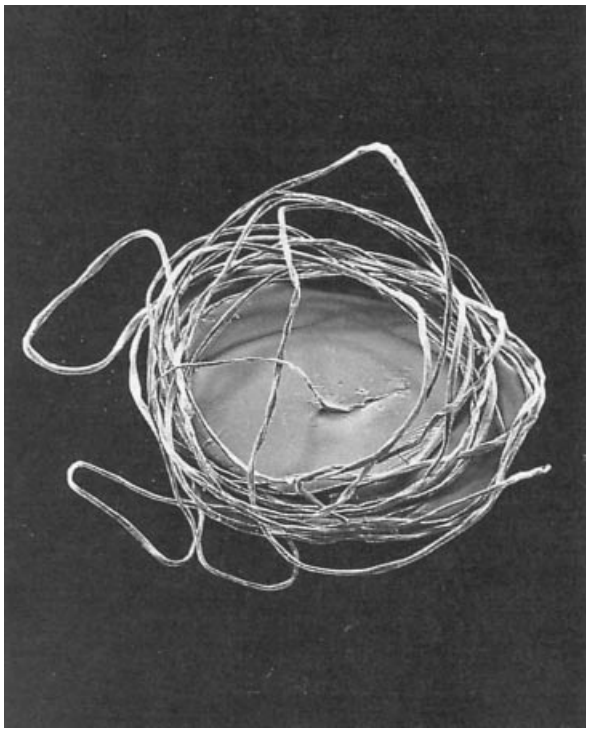

Fig. 2. Single cotton fibers, showing ratio of length to diameter.

contains protein, cellulose, and hemicellulose. In ~17–25 days after flowering (postanthesis), when the boll is half-mature, each fiber virtually attains its full length. Then layers of cellulose (qv) are deposited on the inside of the thin casing, or primary wall. The pattern of deposition is such that one layer of cellulose is formed each day in a centripetal manner until the mature fiber has developed a

thick secondary wall of cellulose from the primary wall to the lumen, or central canal. The fiber now consists of three main parts: primary wall, secondary wall, and lumen. At the end of the growing period when the boll opens, the fibers dry out. The mature cotton fiber is a dead, hollow dried cell wall tubular structure, which is collapsed, shriveled, and twisted, giving the cotton fiber convolutions. The convolutions differentiate cotton fibers from all other forms of seed hairs and are partially responsible for many of the unique characteristics of cotton.

The seed hairs of cultivated cottons are divided into two groups (fuzz fibers or linters and lint) that differ in length, width, pigmentation, and strength of adherence to the seed. The growth of linters is much the same as that of lint, but elongation is initiated about 4 days after flowering. They are usually ~0.33 cm (1.3 in.) long compared with the 2.5 cm (1 in.) average length of lint fibers and are twice as thick, or ~32 μm (Fig. 3). Their color is usually greenish-brown to gray. After lint fibers have been ginned off the seed, the linters remain. Removal of linters is usually done at the cottonseed oil mill and requires a machine similar to that used at the saw cotton gin to remove the fiber from the seed.

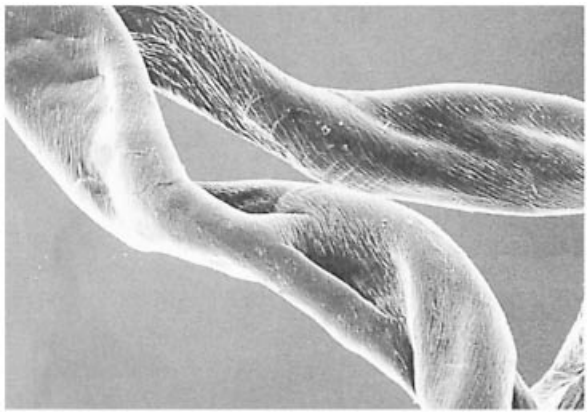

(**a**)

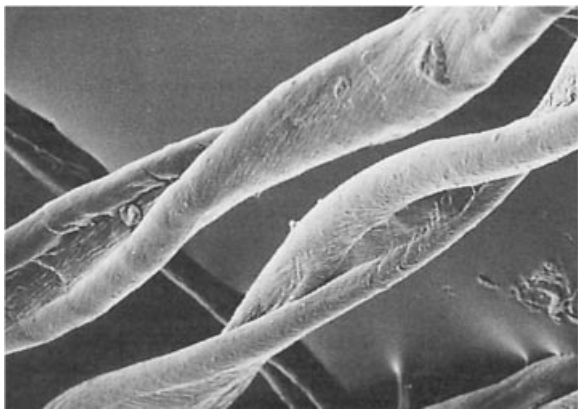

(**b**)

Fig. 3. Longitudinal view of fuzz (**a**) and lint (**b**) fibers.

Cotton Fiber Biosynthesis

During the cell elongation stage of fiber development, a primary cell wall envelopes the growing fiber. The principal components of fiber primary cell walls are pectins, hemicelluloses, cellulose, and proteins. Relatively few studies on the chemical identity and structure of fiber primary cell wall components have been conducted (16–18). In higher plants, pectins and hemicelluloses are produced in Golgi bodies and are deposited in the wall by fusion of Golgi-derived vesicles with the cell membrane. Cell wall proteins are synthesized in association with the endoplasmic reticulum and may be glycosylated in the Golgi. In contrast, the enzyme complex responsible for cellulose biosynthesis is associated with the cell membrane in structures known as rosettes.

Cellulose biosynthesis has been extremely difficult to characterize biochemically. At maturity, cotton fibers are nearly pure cellulose and should be a rich source of the enzyme cellulose synthase. Unfortunately, it has been difficult to separate a β-1,4-glucan (cellulose) producing activity from a large background of β-1,3-glucan (callose) synthesis. Progress in separating the two enzyme activities from cotton fiber has been reported recently (19); however, detailed structural information comparing the two enzymes is still lacking. With the advent of molecular genetic approaches to study genes expressed during cotton fiber development, a breakthrough has been achieved. By determining the sequence of many messenger RNA (m RNA) molecules produced by immature cotton fibers, two gene transcripts with regions similar to those found in bacterial cellulose synthases were discovered (20). These subunits of the cellulose synthase complex were named CesA1 and CesA2 and are produced concomitantly with the initiation of secondary cell wall biosynthesis in fiber (20). A third CesA gene from cotton has also been described and is expressed both during the cell elongation and secondary wall thickening stages (21). The CesA subunit alone will not produce cellulose, but genetic experiments in the model plant *Arabidopsis* link the CesA gene to cellulose biosynthesis (22). In addition, a membrane-associated cellulase gene has also been implicated in cellulose biosynthesis by induced mutations in *Arabidopsis* (23,24). It seems paradoxical that cellulase, an enzyme capable of degrading cellulose, is involved in cellulose biosynthesis. Initiation of cellulose biosynthesis in cotton fiber has been found to require sitosterol-β-glucoside as a primer (25). It has been suggested that the cellulase activity is required for cleaving the primer from the growing glucan chain. Another enzyme, sucrose synthase, colocalizes with sites of cellulose biosynthesis in cotton fiber membranes, and may function to partition substrate to the cellulose biosynthetic complex (26).

Production

About 80 countries in the world grow cotton. Planting time for cotton varies by locality, varying from February to June in the northern hemisphere; harvest time is in the late summer or early/late fall. In the western hemisphere, cotton is cultivated between about 37°N and 32°S latitude and in the eastern hemisphere, between ~47°N and 30°S.

Cultivation of cotton differs markedly from one country to another, depending upon the degree of mechanization (7). When cotton is grown and processed in a responsible manner, it does not have adverse effects on the environment, the workplace, or the consumer (1,27). In the United States cotton-breeding research as well as management and harvesting practices have increased the yields and so about 30% as much land is needed today to produce the same amount of cotton as in 1930. Through conventional cotton-breeding research, many fine-quality cotton varieties have been developed (28).

Field Preparation. Field preparation practices reflect the varied environments and production systems encountered in the various cotton-growing regions. In the United States, some form of conventional or clean tillage dominates in regions not subject to erosion. This includes incorporation of plant residues in the fall to minimize overwintering insects and food sources for disease organisms; deep tillage in either fall or spring to improve root penetration, water availability, and crop performance; ridges or beds may be formed following tillage to facilitate surface drainage, irrigation, and aeration and speed soil warming; and shallow tillage completes field preparation to enhance soil tilth and seedling growth.

Conservation tillage systems are gaining in popularity in areas subject to soil erosion. Conservation tillage, which includes minimum till, no till, and other forms of maintaining residue on the soil surface, has enabled farmers to increase their production options in response to their specific challenges. These systems became feasible with the advent of specialized equipment and new herbicide chemistry that reduce or eliminate the need for extensive tillage.

Planting. Less than 5% of the cottonseed produced is used for planting seed. Advances in equipment design and engineering have vastly improved the precision of the planting operation. Seed depth and spacing can be adjusted in response to soil, weather, geographical, and seasonal requirements. When coupled with high quality seed and state-of-the art weather forecasts, seeding rates can closely approximate final stand density.

Irrigation. Approximately 70% of the U.S. cotton is rain-grown, but western states (Arizona, California, and New Mexico) grow only irrigated cotton. The use of supplemental irrigation is increasing in some rain-grown areas of Texas, New Mexico, and the mid-south states, so that presently ~70–80% of U.S. cotton uses some form of supplemental irrigation. Whether applied down the furrow via ditches, overhead with moving pipes or below the surface in drip systems, irrigation requires close producer attention. Water demand by the crop is monitored with soil or plant-based instrumentation including calculated evapotranspiration, soil tensiometers, gypsum blocks and neutron probes, leaf pressure chambers, and infrared (IR) thermometers that measure canopy temperature. The specific technique selected reflects the production region, soil characteristics, irrigation capabilities, and management style of the individual producer. Whatever technique is employed, irrigation decisions are made to maximize production efficiency and eliminate waste.

Fertilization. Cotton normally is grown under intense production systems; many fields are planted in cotton year after year. However, in the United States in 2002 ~55–100% of cotton farmers, depending on the state, also grow other crops and have the potential for crop rotation (personal communication from D. K. Lanclos, National Cotton Council, based on a 2002 planting intentions survey).

On average, U.S. cotton is fertilized with 31 kg (68.3 lb) of nitrogen, 10 kg (22 lb) of P_2O_5, and 6.8 kg (15 lb) of K_2O (29). The type and concentration of fertilizer required for high yield depends on many factors such as soil type, previous fertilization rate, cropping system, and irrigation. Therefore, an efficient fertilization program must be based on results of soil and tissue tests and the yield desired from the crop.

Supplying nutrients according to crop demands has replaced traditional methods, as soil and tissue testing have become widespread. Nitrogen can now be metered out on an "as-needed" basis through the use of rapid and reliable soil and tissue testing methods. Unnecessary and undesirable applications are, therefore, avoided, reducing the risk of off-site discharge of nitrates. Potassium fertilization has undergone a similar evolution as application strategies are modified in light of sod characteristics and yield expectations. Soil and tissue testing, coupled with soil or foliar-applied potassium, enables growers to respond rather than anticipate crop needs. Other macronutrients, such as phosphorus, or micronutrients, such as boron, can be applied in a manner consistent with producer philosophy without compromising environmental quality.

Throughout the cotton-growing regions of the United States, the method of applying fertilizer must be tailored to the crop needs and the characteristics of the cropping system. In some production systems, fertilizer is applied during the seedbed preparation, whereas in other systems it may be applied at planting or after emergence. Combinations of preplant and post-emergence applications are common, especially for nitrogen. Foliar application is relatively new. Dilute nitrogen and phosphorus solutions are sprayed on the foliage of the plant at various times during the season, which is an attempt to match fertilizer application to the weekly needs of the plant more closely.

Crop Protection. Cotton can be affected by insects (30), weeds, diseases (31), nematodes, and mycotoxins. About 90% of the U.S. cotton uses Integrated Pest Management (IPM) practices. This approach optimizes the total pest management system by utilizing all available tools, including rotation, crop residue destruction, maximum crop competitiveness, earliness, pest scouting, action thresholds, releases of beneficial insects, sterile insect releases, and selective crop protection chemistry.

New plant protection options including new chemical, biological, and transgenic technologies coupled with good IPM schemes are helping to reduce use of broad spectrum pesticides favored in the past. Weed management (32) is a particularly exciting area as genetically engineered transgenic cotton varieties and less persistent herbicides become available. Diseases (31) and nematode pests (33) are managed by selecting tolerant or resistant cultivars and adopting specific agronomic practices that minimize their impact on cotton performance. Aflatoxin, a mycotoxin by-product (secondary metabolite) of the naturally occurring fungi, *Aspergillus flavus and parasiticus*, can be a serious food safety hazard, if it occurs on cottonseed. A potential biocontrol (competitive exclusion) method (34) for managing aflatoxin in cotton is being evaluated and developed in Arizona. Also ammoniation of the cottonseed is an effective way to eliminate the aflatoxin in seeds used for feeding (35).

Insect management (30) continues to evolve as more selective chemistry reaches commercialization, as insect-resistant trangenic cottons are introduced,

sterile insect technology evolves, and cultural practices are refined. Historically, the most destructive pests of the cotton plant in the United States are the boll weevil (36) and the bollworm/budworm complex. Insects are serious threats to the cotton industry in countries around the world. The boll weevil migrated into the United States from Mexico in around 1892 and spread over the entire cotton belt within 30 years (36). An organized effort to eradicate the boll weevil began in the United States in 1978. Using pheromone technology for trapping and detection, insect diapause control to disrupt reproduction and hibernation, and chemical control technology, the weevil is being systematically eliminated from the United States. Before the boll weevil eradication program started, the domestic cotton crop lost to the weevil was ~$200 million a year, and ~$75 million a year was spent for pesticides to control this destructive pest (37). Because of the boll weevil eradication program, this pest is on the way to being eliminated in the United States. About 33% of cotton-growing states have completed elimination of the boll weevil and ~65% are nearing completion (38).

A serious cotton insect pest in Arizona, California, New Mexico, far western Texas, and northwestern Mexico is the pink bollworm, which overwinters as diapausing (hibernating) larvae in the soil. After feeding on the late-blooming bolls, the larvae drop to the ground and hibernate for the winter, emerging as adults in the spring to lay eggs on the early cotton blooms. The eggs hatch and the new larvae bore into the fresh cotton bolls, go through molting stages, bore their way out, and drop to the ground. Throughout the growing season, the cycle repeats itself, rendering useless vast numbers of cotton plants in a single field.

For >25 years, the San Joaquin Valley of California has been protected from pink bollworm through use of a monitoring and sterile insect release program. Moths are mass-reared, irradiated to render them sexually sterile, and released onto fields where traps indicate a potential reproducing population. Chemical treatments also are effective along with other practices that include early stalk shredding, early and deep tillage, and winter irrigation that drowns diapausing larvae (39). Insect-resistant transgenic cottons are particularly effective in controlling the pink bollworm. Presently, pink bollworm eradication efforts (40) are underway in parts of the United States and northwestern Mexico.

Other insects injurious to the cotton plant include aphids, leafhoppers, lygus bugs, mites, whiteflies, fleahoppers, thrips, cutworms, and leaf miners (30). As boll weevils are being eliminated and transgenic insect protectant plants are reducing damage from bollworms, pests, which traditionally were considered secondary, are now gaining in prominance.

Harvesting

Except for the cotton gin, the introduction of the mechanical harvester has probably had a greater effect on cotton production than any other single event. Commercial mechanical harvesters were introduced into the United States after World War II and by 1955, ~23% of the U.S. cotton was mechanically harvested. Presently, >99% of the U.S. cotton crop is mechanically harvested, but ~75% of the cotton produced in the world is still hand-harvested one boll at a time (41).

When the cotton boll reaches full maturity, it begins to lose moisture and opens. As the boll opens, the drying fiber fluffs or expands outward. After the seed

cotton (linters and lint) has dropped to a moisture content of ∼12% it is ready for harvest. If the cotton is to be mechanically harvested, the plant is usually treated with a harvest-aid chemical (ie, a defoliant or desiccant) (41). A defoliant induces abscission (shedding) of foliage. The removal of leaves helps to minimize the trash harvested with the mechanical harvester and promotes faster drying of early morning dew on the lint. Defoliants should not be applied until ∼60% of the bolls are open and harvest should be delayed for 7–14 days after application. Desiccants (qv) are chemicals that induce rapid loss of water from the plant tissue and subsequent death of the tissue. The dead foliage remains attached to the plant. Harvest can begin in 3–5 days after application.

Once the plant is ready, the cotton is mechanically harvested with either a spindle picker or cotton stripper. The spindle picker selectively harvests seed cotton from open bolls. The unopened bolls are left on the plant and can be picked at a later date. The spindle picker uses a rotating tapered barbed spindle to remove the cotton from the bur (seed case). The seed cotton is wrapped around the spindle, pulled from the bur, removed from the spindle with a rubber doffer, and then transferred to a basket. Two types of cotton strippers are currently in use in the United States. The finger-type stripper uses multiple fingers made from metal angles with the vee turned up and operating at a 15°–20° approach angle with the ground. The roll-type stripper uses two 7-in. diameter (17.8-cm diameter) stripper rolls angled 30° with the ground and rotating in opposite directions. Each roll consists of three brushes and three paddles mounted in alternating sequence.

Strippers are efficient and can harvest up to 99% of the cotton from the plant. They are nonselective and remove not only the seed cotton but also the cracked and unopened bolls, the burs, and other foreign matter. The extra foreign matter requires additional cleaning at the gin.

After harvesting, the seed cotton is transported to the gin where the fiber is separated from the seed. Because the gin capacity is usually not sufficient to keep up with the harvesters, the harvested cotton is often stored in a compacted module and ginned at a later date. The type of storage or seed cotton processing may place additional constraints on the harvest process. If the seed cotton is to be placed in module storage, the cotton should not be harvested until the moisture content is 12% or less and the harvested seed cotton should be free of green plant material, such as leaves and grass.

Ginning

Gin equipment is designed to remove foreign matter, moisture, and cottonseed from raw seed cotton (42). Two types of gins are in common use—the saw gin and the roller gin. Saw gins are normally used for Upland cottons, whereas roller gins are used for the ELS (Pima) cottons. In a saw gin, the cotton enters the saw gin stand through a huller front and the saws grasp the seed cotton and draw it through widely spaced ribs. The ginning action is caused by a set of saws rotating between a second set of narrowly spaced ginning ribs. The saw teeth pass between the ribs pulling the fiber through at the ginning point. The space is too narrow for the seed to pass and so the fiber is pulled from the seed. A roller gin consists of a ginning roll (covered with a compound cotton and rubber material), a stationary

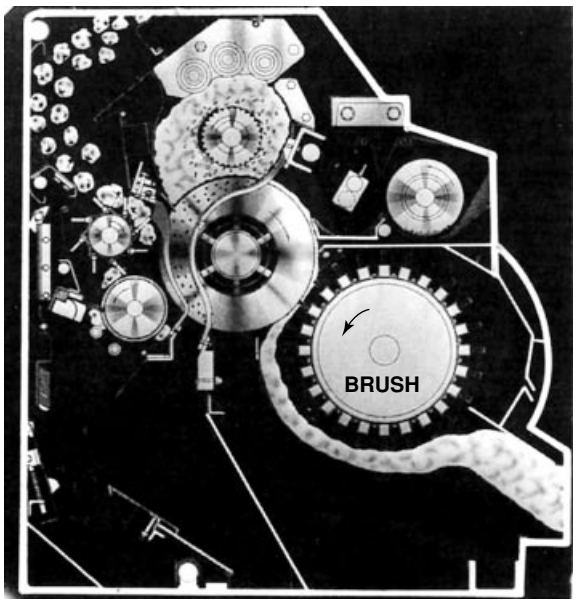

Fig. 4. A modern gin stand that separates fiber from cottonseed.

knife held against the roll, and a rotary knife. The rotating roll pulls the fiber under the stationary knife. The seeds cannot pass under the stationary knife and is separated from the fiber. The rotary knife then pushes the ginned seed away from the ginning point allowing room for more seed cotton to be ginned.

Typical types of gin equipment are cylinder cleaners, stick machines, and lint cleaners for cleaning; hot air driers for removing moisture; gin stands for separating the fiber from the cottonseed; and the bale press for packaging the lint (42). The gin stand (Fig. 4) is actually the only item of equipment required to gin cotton, the other equipment is for trash removal and drying. About 636 kg of seed cotton is required to produce a bale (~227 kg; 500 lb) of lint cotton from spindle-harvested cotton. The remainder consists of about 354-kg seed and 55-kg trash and moisture. Typical gins contain one to four individual gin stands, each rated at 6–15 bales/h. However, a few gins contain as many as eight gin stands and produce up to 100 bales/h. The greatest number [30,498] of gins existed in the United States in 1902. The majority were on plantations, and they processed 10.6 million bales (2.3×10^9 kg) of cotton (43). Since then the number of gins has declined, and the average number of bales processed per gin has increased. In 2000, a total of ~1018 active gins handled a crop of 16,742,000 bales ($\sim 3.65 \times 10^9$ kg) for an average of 16,446 bales (3.58×10^6 kg) per gin plant (44). The number of bales produced in the United States varies substantially from year to year, which places a severe financial burden on the ginning industry.

Mechanical harvesting systems were made possible by the invention of saw-type lint-cleaning systems in the early 1950s. Lint cleaners enabled gins to remove from the cotton the additional trash that resulted from mechanical harvesting. The mechanical systems reduced the harvesting period from 4–5 months to ~6–8 weeks of intensive operation. Severe congestion problems at the gin were eased

with the storage of seed cotton in 8- to 15-bale, freestanding modules. Modules avoided the massive need for wheeled trailers during the compressed harvest season. Storage of seed cotton in modules increased rapidly from the 1970s onward, accounting for >90% of the crop in 2000. At present, the average U.S. cotton ginning capacity is ~30 bales/h. A few gins process in excess of 100 bales/h (45).

Most of the U.S. gins are now operated as cooperatives or as corporations serving many cotton producers. Automatic devices do the work faster, more efficiently, and more economically than hand labor. High volume bulk seed cotton handling systems and hydraulic suction systems to remove cotton from modules, high volume trailers to get cotton into the gin, larger trailers and modules, increased processing rates for gin equipment, automatic controls, automated bale packaging and handling devices, and improved management have all increased efficiency.

After ginning, baled cotton is sampled so that grade and quality parameters can be determined (classification). The fiber quality/physical attributes affect the textile manufacturing efficiency and the quality of the finished product. Cotton bales are normally stored in warehouses in the form of highly compressed bales. The International Organization for Standardization (ISO) specifies that bale dimensions should be of length 140 cm (55 in.), width 53.3 cm (21 in.), height 70–90 cm (27.6–35.4 in.), and density of 360–450 kg/m ^{3} (22.4–28 lb/ft ^{3}) (46). Bales of cotton produced in the United States meet these dimensional standards. Bales of cotton packaged in accordance with these dimensions (ISO 8115) are not considered a flammable solid by the International Maritime Organization and the U.S. Department of Transportation for transportation purposes for vessel and other types of shipment (47,48) and are considered to present no measurable pest risk to the importing country.

Baled cotton fiber is merchandized and shipped by the merchant to the textile mill for manufacturing into products for the consumer. The seed is shipped directly for feeding to dairy cattle or to a cottonseed oil mill for crushing (49–51).

Classification/Measurement of Fiber Quality

Classification is a standardized set of procedures for measuring the quality/physical attributes of raw cotton fiber that affect the quality of finished products and/or manufacturing efficiency (52).

Classing U.S. Upland Cotton. In the United States, the quality of cotton is described (classed) in terms of color, leaf, extraneous matter, fiber length, length uniformity, strength, and micronaire according to the Official Cotton Standards (also called "universal standards") (52). Research to rapidly measure other important fiber characteristics, such as maturity, stickiness, and short fiber content, continues. The transition to all-instrument classification will be completed as soon as the technology can be developed and instruments are sufficiently refined. Practically all cotton grown in the United States is classed by the Cotton Program, AMS, U. S. Department of Agriculture (USDA), on a fee basis at the request of producers. Measurements for fiber length, length uniformity, fiber strength, micronaire (fineness), color grade, and trash are performed by precise high volume instruments (commonly referred to as "HVI" classification, see below). There are

25 official color grades (15 physical standards and 10 descriptive) for American Upland cotton, plus 5 categories of below-grade. Micronaire reading is determined by an airflow measurement. (Micronaire is often associated with maturity since usually the more mature the fiber, the larger the diameter. Such association is a gross estimation and often unreliable measure of maturity.) Classification for leaf grade, preparation, and extraneous matter are still based on subjective (classer) determinations performed by visual observation.

Classing U.S. Long Staple (Pima). Pima (ELS cotton) and Upland cotton-grade standards differ (52). The most significant difference is that the American Upland color grade is determined by instrument measurement and the American Pima color grade by trained cotton classers. Pima is naturally of a deeper yellow color than Upland cotton. The leaf content of Pima standards are peculiar to this cotton and do not match Upland standards. Because it is roller-ginned, Pima cotton's appearance is not as smooth (ie, more stringy and lumpy) as that obtained with the saw gin process. There are six official cotton grades for American Pima color and six for leaf, ranging from grade 1 (highest) to 6 (lowest). All are represented by physical standards and a descriptive standard for cotton, which is below grade.

Classing in Other Countries. The measurement of fiber quality/classing in countries other than the United States can be based on variety and growing area; appearance and visual observation; visual class and length; or classed as seed cotton, ginned by class of seed cotton, and reclassed after ginning. At present, more countries are moving to some type of automated testing system like the HVI. Differences between the U.S. classing system and those of other countries are described in the literature (1).

High Volume Instrument (HVI) Systems. Instruments to measure fiber properties have been used for a number of years, but until recently high costs and the length of time required for the tests have limited their use. However, in the mid-1960s, a cooperative effort between the USDA and instrument manufacturers began what was aimed at developing instruments that are fast enough for classification of the millions of bales of cotton produced each year. This led to the development of HVI systems. Modern HVI systems make use of the latest advances in electronic instrumentation and space-age technology to rapidly and inexpensively measure the more important fiber properties, including length, length uniformity, strength, fineness, color (including color grade), and trash.

At present, the Switzerland-based Zellweger Uster Corp. is the major HVI system manufacturer on the market. Zellweger Uster continues to advance the utilization of its cotton fiber testing technology through measurement systems specifically adapted for utilization in classing offices, gins, and mills. In recent years, other HVI system manufacturers have come into the market providing competing technologies and choices for HVI users. Schaffner Technologies of Knoxville, Tenn., Lintronics, Ltd. of Arad, Israel, and Premier Polytronics, Ltd. of Coimbatore, India are offering HVI systems at various stages of development targeted for use in gins, mills, and classification. At the end of 2001, there were some 1450 HVI systems in 70 countries.

Currently, HVI systems are providing reliable information on six characteristics of quality from a cotton sample in ~30 s that are highly related to the spinning quality and market value of the cotton. Starting with the 1991 crop year,

cotton has been required to be tested by HVI to be eligible for price supports in the United States. Information on every bale of cotton greatly improves the marketing of cotton and encourages the production of cotton with fiber properties desired by users.

Advanced Fiber Information System. The Advanced Fiber Information System (AFIS) (53–55) is a recent development that incorporates several fundamental measures into one system. AFIS measures several fiber properties that are key to predicting the ease of spinning and quality of finished product, including fiber neps (small tangles of fiber), dust, trash, fiber length, short fiber, and maturity. The measurements are unique in that individual fibers and particles (neps and dust) are automatically counted and sized. The principle of operation is that a fiber individualizer aeromechanically opens and separates the sample into single fibers that are injected into an airstream. Dust and trash particles are diverted to a filter while the airstream transports the fibers and neps past an electrooptical sensor that is calibrated to measure the specific size characteristics of the fibers and neps. The AFIS determines the average size and size distribution of neps. Measurements of dust and trash include their particle size distributions, the number of dust and trash particles per gram, and the average size of trash particles.

AFIS length measurements include percentage of short fiber content (<12.7 mm; 0.50 in.) by number and by weight; average length by number and by weight; coefficient of variation of fiber length by number and by weight; upper quartile length (75% of fibers shorter than) by weight; and the 5% length by number (95% of the fibers shorter than). Fiber maturity measurements include fiber fineness (linear density measured in millitex), the immature fiber content (% of immature fibers by number), and the average maturity ratio.

Physical Properties

Fiber length is universally accepted as the most important fiber property, because it greatly affects processing efficiency and yarn quality. The recognized reference machine method for fiber length information is the Suter–Webb Comb Sorter (56). Fibers are sorted and separated by a series of combs into length increments of 1.6 mm (0.063 in.). Each group is then weighed to determine the weight–length distribution parameters, which include the mean length of the longest half (upper-half mean) of the fibers by weight, the mean length, the percentage of the fibers <12.7 mm (0.5 in.), and the coefficient of length variation. Variations of length are unique to specific varieties of cotton and range from <2.5 cm (1 in.) for short-staple Upland varieties to 2.6–2.8 cm (1.02–1.10 in.) for medium-staple Uplands, to >2.85 cm (1.12 in.) for long-staple varieties (Pima, Egyptian, and Sea Island) (52,57).

Next to length, *fiber strength* is the most important physical property that relates to fiber and yarn quality. The recognized reference method for fiber strength is based on measurements made on bundles of parallel fibers (58). One suitable instrument, the Pressley tester, consists of a set of jaws and an inclined lever system in which an ever-increasing load is applied to the specimen until the bundle breaks. The position of the load when the bundle breaks is read from the scale and

used, together with the bundle weight, to calculate bundle strength. An alternate approach to bundle measurements is the Stelometer tester, which uses a somewhat different loading concept but still requires clamped and weighed bundles very much like the Pressley. In this case, the clamp jaws are separated by 3.2 mm (gauge length), a convention that has proven the method to be highly related to yarn strength and processing parameters. Fiber strength is expressed as breaking stress or force to break per linear density of the bundle. These units are newtons [or gram force (gf)] per linear density (tex), where 1.0 tex = 1 g/1000 m. Variations in fiber strength are also unique to specific varieties of cotton and range from 0.176 to 0.216 N/tex (18 to 22 gf/tex) for short-staple Upland varieties to 0.235–0.275 N/tex (24–28 gf/tex) for some medium-staple Uplands to 0.314–0.373 N/tex (32–38 gf/tex) for long-staple varieties (Pima, Egyptian, and Sea Island) (59).

Another important characteristic property of cotton is its *fineness*, or *linear density*, or weight per unit length. The normal units for cotton fineness are millitex (the units of tex are expressed in g/km). Fineness is directly related to the amount of cellulose in the fiber, which is a function of the fiber wall area, excluding the hollow center (lumen), and the fiber length. Variations in fiber fineness range from ∼100 mtex for fine Sea Island cotton to ∼180 mtex for a typical United States Upland variety to in excess of 300 mtex for a coarse Asian cotton (60). The term *fiber maturity* relates to the degree of development or thickening of the fiber wall relative to its outer perimeter. Recent developments in techniques for preparing excellent thin cross sections of cotton coupled with advances in computerized microscopic image analysis allow for rapid and accurate measurements of fiber wall area and perimeter (61,62). An acceptable range of maturity for mill usage is from 75 to 80%. The most commonly used measure/indicator of fiber fineness is the Micronaire reading, an airflow measurement performed on a 3.25-g test specimen, which is compressed to a specific volume in a porous chamber. Air is forced through the specimen and the resistance to the airflow is proportional to the linear density. The Micronaire reading is affected by a combination of both fiber fineness and maturity to the extent that for the same genetic variety with a constant perimeter, the Micronaire will correspond to maturity. Depending on acceptable maturity, a good range of Micronaire is between ∼3.5 and 4.8 (63).

In addition to fiber length, strength, and fineness, two other properties that have significant bearing on fiber and yarn properties are *color* and *trash* measurements, which are measured by instrumentation such as the Nickerson–Hunter Colorimeter (64) and the Shirley Non-Lint Analyzer (65).

Textile Processing

Yarn Manufacturing. Cotton is received by the textile mill in the form of highly compressed bales (∼450 kg/m^3), weighing ∼227 kg (480 lb). Although the seed and a large portion of the plant trash are removed at the gin, baled cotton still contains various forms of trash, including stem, leaf, and seed coat fragments that must be removed in the manufacturing process.

The first step in textile mill processing is opening and blending (66). Cotton properties vary considerably from bale to bale; therefore, to ensure consistency in processing efficiency and product quality, it is important that many bales be blended to produce a homogeneous mix. To do this, bales of cotton are arranged in

a "lay-down" so that sophisticated blending equipment can continuously remove some cotton from >100 bales of cotton at a time, thereby ensuring consistency of fiber properties along the length of the yarn.

After blending, the cotton is fed through a series of opening and cleaning machines containing various types of revolving beaters and sawtooth cylinders that reduce the cotton into smaller masses of less compacted tufts. Most of the dirt and heavier trash is removed through screens or grids as the cotton is tumbled, beaten, shaken, or otherwise manipulated.

The next step is carding, where the cotton is passed between two surfaces set in close proximity to each other and covered with fine brush-like wires. The surfaces move in opposite directions or in the same direction at different speeds, resulting in a combing action that separates the fibers into a fine web. Getting the cotton to this opened condition causes most of the remaining finer trash to be removed. The fine web of fibers delivered from the card is condensed into a rope-like strand called card sliver and coiled into large cans.

Fibers in card sliver are held together by the natural cohesiveness of the cotton. The fibers must now be further aligned and straightened. In a process called drawing, several strands of card sliver (usually eight) are combined to produce a single sliver of improved uniformity and fiber orientation. The drawing frame contains four or five sets of drafting rolls rotating at progressively higher speeds, that attenuate or draft the material down to approximately the original size of the card sliver. The cotton sliver is generally processed through two or three drawings to obtain maximum uniformity and parallelization of individual fibers.

Cotton is combed to produce finer, higher quality yarns and fabrics. In 1990, ~12% of the cotton processed in the United States was combed. Combing mechanically removes as much as 10–15% of the cotton as short fiber. These fibers are used in the production of lower grades of fabric. Yarns not spun from combed cotton are referred to as carded yarns. Because many of the short fibers have been removed, combed yarns are stronger and more uniform than carded yarns. However, the combing process is expensive and adds considerably to yarn costs.

The next process, roving, is an intermediate step in the preparation of the cotton exclusively for ring spinning. On the roving frame, the sliver is attenuated several times by a series of drafting rollers and a small amount of twist is added to hold the smaller mass of stock together. The product, also called roving, is then wound on a special bobbin to accommodate the creel on a ring-spinning frame.

The final process in the yarn manufacturing operation is spinning. Ring spinning is the mainstay of the textile industry and accounts for >50% of all cotton yarn produced in the United States. In ring spinning, the roving is first attenuated to the desired size through a series of drafting rollers. The strand of drafted fibers passes through a metal guide, or traveler, which revolves rapidly around a circular track, or ring, which in turn surrounds a rotating spindle and bobbin. Sufficient twist to obtain the required tensile strength is inserted by the rotation of the spindle and bobbin at speeds of up to ~20,000 rpm. Yarn is wound on the bobbin (spinning tube) by an up and down traversing of the ring. Average production rates for ring-spun yarns range from 18 to 27/m (20 to 30 yard/min).

The newer spinning methods produce yarn directly from drawing sliver, such yarns rarely, if ever, achieving the overall quality of ring, spun yarns. Rotor, or open-end spinning is a method of yarn formation that can produce coarser yarns at

three to five times the rate of ring spinning. Sliver is fed to a pinned or sawtooth-covered opening roller that rotates at a relatively high speed and individualizes the fibers. The opened fibers are then drawn via suction through a conical-shaped duct and then aligned and deposited on the inside of a rapidly revolving rotor (up to 150,000 rpm) from which they are twisted into yarn. Twist is inserted by rotation of the rotor, and the yarn is removed through a tube and wound onto a package. Rotor-spun yarns are more uniform but weaker than ring-spun yarns.

Air-jet spinning is one of the newest yarn formation techniques and can spin yarns at speeds of up to 183 m/min (200 yard/min). A conventional roller drafting system is used to reduce drawing sliver to the proper size. The drafted ribbon of fibers is then opened, twisted, and entangled by jets of compressed air as they pass through nozzle assemblies. Air-jet spun yarns tend to be weaker and harsher than those produced by ring or rotor spinning. Another new method of yarn production in limited use is friction spinning. In this process, the yarn is formed by frictional contact of the fibers with a pair of rotating perforated drums. The rotation of the drums causes the fibers to be rolled into a thread, which is then drawn off axially from the drums as a finished yarn. Production rates for this equipment can exceed 229 m/min (250 yard/min).

Fabric Manufacturing (Weaving and Knitting). Yarns manufactured in the spinning process are used to make woven or knitted fabrics. Weaving and knitting are the two pimary textile processes for manufacturing fabrics. In the modern textile industry, these processes take place on electrically powered automated machines, and the resulting fabrics go into a wide range of end uses, including apparel, home furnishings, and industrial products (67). Most woven and knitted cotton fabrics are produced from single yarns. However, for the manufacture of industrial fabrics such as canvas, it is necessary to combine, or ply twist, several strands of single yarns together to obtain increased strength and resilience. Sewing thread and cordage are also produced from multiple plies of single yarns twisted together.

The weaving process consists of interlacing straight yarns at right angles to one another. Warp yarns are supplied from a large reel, called a warp beam, mounted at the back of the weaving machine. Each warp yarn-end is threaded through a heddles harness, which is used to lift or depress the warp yarns to allow the weaving to be done.

The machine knitting process consists of interlocking loops of yarn on powered automated machines that are equipped with rows of small, hooked needles which draw formed yarn loops through previously formed loops. The hooked needles have a unique latch feature that closes the hook to easily allow the loop drawing, then opening to allow the yarn loop to slide off the needle. There are circular-knitting, flat-knitting, and warp-knitting machines.

Nonwoven Manufacturing. Cotton staple is readily processed to form carded, air laid, or carded/crossed-lapped webs that can be bonded by various techniques to form useful nonwoven materials, eg, needlepunched, spunlaced (hydroentangled), and stitch-bonded nonwovens, and resin-bonded and thermal-bonded carded fabrics (68). Many times a combination of these processes is used to produce hybrid structures and other products. Cotton's share of the nonwovens market in 2002 is 7.8% globally and 2.8% in North America (69). In 2000–2001, ~32–36 million kg (70–80 million lb) of cotton was used in North America to

produce the following nonwovens [in millions of kg (millions of lb)]: swabs [6.4–7.3 (14–16)], bandages [1.8–2.3 (4–5)], cosmetic pads [(13–15)], tampons/feminine pads [6.8–7.7 (15–17)], spunlaced wipes [1.4 (3)], surgical sponges [0.9–1.4 (2–3)], shoulder pads/glove padding [0.9–1.4 (2–3)], jewellery box pads [0.9–1.8 (2–4)], quilt bedding [0.9–1.4 (2–3)], and diapers (see NONWOVENS, STAPLE FIBER).

Chemical Composition and Morphology

The cotton fiber is a single biological cell, 15–24 μm in width and 12–60 mm (4.7–23.6 in.) in length. It has a central canal, or lumen, down its length except at the tip (70). It is tapered for a short length at the tip, and along its entire length the dried fiber is twisted frequently and the direction of twist reverses occasionally (71). These twists (referred to as convolutions) are important in spinning because they contribute to the natural interlocking of fibers in a yarn.

Raw cotton fiber after ginning and mechanical cleaning is essentially 95% cellulose [9004-34-6] (70,71) (Table 1). The noncellulose materials, consisting mostly of waxes, pectinaceous substances, and nitrogenous matter (mainly protein), are located to a large extent in the primary wall, with small amounts in the lumen (72). Analysis of the fiber for metal content (73–75) is given in Table 2. Potassium, magnesium, calcium, sodium, iron, and phosphorus are the most abundant elements; silicon, chlorine, sulfur, and boron are sometimes detected in trace amounts (73); lead and cadmiun are not detected (73); and arsenic levels in untreated cotton is usually <1 ppm (74). Knowledge of the content of metals is important to processors, because metals can contribute to problems in yarn manufacturing, bleaching, and dyeing (1).

Of the noncellulose constituents, nitrogen-containing compounds (mostly protein) normally occur in the largest amounts, almost entirely in the lumen, and are most likely protoplasmic residue left behind after the gradual drying up of the living cell. Most of the pectin in the cotton fiber is in the primary wall. Removal of the pectic substances is accomplished by scouring, which does not change the properties of the cotton greatly.

Table 1. Composition of Typical Cotton Fibers

	Composition, percent of dry weight	
Constituent	Typical	Range
Cellulose	94.0	88.0–96.0
Protein (% N $\times$ 6.25)[a]	1.3	1.1–1.9
Pectic substances	1.2	0.7–1.2
Ash	1.2	0.7–1.6
Wax	0.6	0.4–1.0
Total sugars	0.3	
Pigment	Trace	
Others	1.4	

[a]Standard method of estimating percent protein from nitrogen content (% N).

Table 2. Metal Content of Cotton[a]

Metal	Content, ppm
Potassium	2000–6500
Magnesium	400–1200
Calcium	400–1200
Sodium	100–300
Iron	30–90
Manganese	1–10
Copper	1–10
Zinc	1–10
Lead	n.d.[b]
Cadmium	n.d.
Arsenic	Trace (<1)[c]
Phosphorus	180–1000[d]

[a]Ref. 73.
[b]n.d. = not detected
[c]Ref. 74.
[d]Ref. 75.

The wax of most cottons is located principally on the fiber surface in the primary wall of the fiber and is a complex mixture of higher molecular weight lipids (1); there are some differences among varieties. The green lint cotton, as discussed earlier, contains ~14–17% wax of high melting point. Because the wax becomes established in fibers, largely if not wholly, during the first phase of development, the wax content as a percentage of the whole fiber mass decreases as the fiber maturity or degree of wall thickening increases; the finer cottons tend to have a larger percentage of wax. Wax serves as a lubricant and is essential for proper spinning of the fiber into yarn. After spinning and weaving or knitting, the wax is removed by scouring and bleaching in preparation for dyeing and finishing.

The mature cotton fiber has a primary and secondary wall, and a lumen. It also has a cuticle and a winding layer between the primary walls (Fig. 5). The cellulose of the primary wall exists as a randomly woven network of microfibrils in and on which are deposited noncellulose materials that form the primary wall. Just beneath the primary wall is the winding layer, which is also the first layer of the secondary wall. The winding layer appears to be made up of a single layer of fibrillar bundles composed of highly oriented cellulose microfibrils and oriented at an angle to the fiber axis. The main body of the fiber consists of cellulose fibrils packed tightly in a solid cylinder, which, under certain conditions of chemical swelling, can be induced to separate into more or less concentric layers. These layers seem to have a finer and more regular structure than does the winding layer, because the 20–50 secondary wall layers have cellulose microfibrils compactly aligned along the axis of the fiber (see CELLULOSE).

The gross morphology of cotton, which refers to the relatively large structural elements above, is visible in the electron microscope. The microfibrillate structure includes pores, channels, and cavities that play an important role in the chemical modification of cotton. The fibrils follow a spiral pattern and at times reverse; it is believed that regions of low strength along the length of the fiber occur close

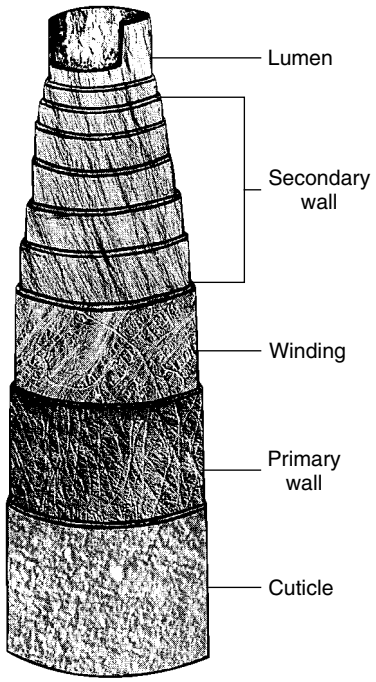

Fig. 5. Schematic diagram of cotton fiber.

to the reversal zones. Microfibrils of the secondary wall are 10–40 nm wide, and these in turn are composed of elementary fibrils (crystallites) 3–6 nm wide.

Chemical modification of the cotton fiber must be achieved within the physical framework of this rather complicated architecture. Uniformity of reaction and distribution of reaction products are inevitably influenced by rates of diffusion, swelling, and shrinking of the whole fiber, and by distension or contraction of the fiber's individual structural elements during finishing processes.

Structure and Reactivity

Chemical Structure. The raw cotton fiber produced in the bolls of the cotton plant is composed almost entirely of the polysaccharide cellulose (see CELLULOSE). Evidence from degradation of cellulose by hydrolysis, oxidation, and other chemical reactions shows that it is a $1 \rightarrow 4$ linked linear polymer of β-D-glucopyranose (Fig. 6). If degradation is extensive, cellobiose (the dimer) or glucose is produced.

The molecular cellulose chains have varying lengths. Measurements of the chain length require that cotton be in solution. Solvents for this purpose include cuprammonium hydroxide solution, phosphoric acid [7664-38-2], nitric acid [7697-37-2], quaternary ammonium bases, cadmium ethylenediamine hydroxide [14874-24-9], cupriethylenediamine hydroxide [111274-71-6] (76), *N*,*N*-dimethylacetamide [127-19-5]–lithium chloride [7447-41-8] (DMAC—LiCl), and

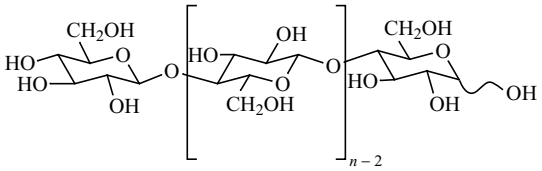

Fig. 6. Chemical structure of cellulose.

1,3-dimethyl-2-imidazolidinone [80-73-9] (DMI) and lithium chloride (77). DMAC–LiCl (27,28), when used in conjunction with gel permeation chromatography (GPC) (78,79), provides both the weight (M_w) and number average (M_n) molecular weight of cellulose in a nondegrading solvent without derivatization. Many researchers have reported weight-average molecular weights for cotton cellulose ranging from 800,000 to 900,000 (~6000 glucose residues) but results vary widely. Those reported for DMAC–LiCl (27,28) are very high (~1,500,000), which may be due to incomplete dissolution of the cotton fibers in this solvent. Cotton cellulose generally has a higher molecular weight than wood cellulose.

Molecular and Supramolecular Physical Structure. The chains of cellulose molecules associate with each other by forming intermolecular hydrogen bonds and hydrophobic bonds. They coalesce to form microfibrils also called crystallites. In cotton, the microfibrils can organize into macrofibrils 60–300 nm wide. The macrofibrils are organized into fibers. Cotton fibers have a complex, reversing, helical arrangement of macrofibrils. There are several different forms or polymorphs [cellulose I to IV and X with recent subclasses Iα and Iβ (80,81)], depending on the source and treatment. There are both different unit cells and different packing arrangements in the unit cell. Native cotton is cellulose I. It has been proposed that cotton and other commercial cellulose, such as wood and ramie, are mostly cellulose Iβ (82). The crystal structure of cellulose Iβ is fairly well understood (83). Despite this, research continues on the crystal structures of it (84) and cellulose II (85) (see CELLULOSE).

Typical one-step commercial mercerization of cotton yarn with caustic or liquid ammonia causes only partial conversion to cellulose II or cellulose III. Cotton cellulose is partially converted to cellulose II by repeated mercerization, the swelling of cellulose in strong alkali (eg, 23% NaOH), followed by rinsing and drying. Cellulose III results from treatment of cellulose with liquid ammonia (ammonia mercerization) or amines. Cellulose III can be made from either cellulose I or II. When treated with water, cellulose III can revert to its parent structure. Cellulose IV can be prepared by treating cellulose I, II, or III in glycerol at temperatures ~260°C. Conversion of the crystal form in cotton fibers to cellulose IV can be effected by heat treatment of ethylamine-treated cotton cellulose in either saturated steam or formamide with minimal fiber degradation (86). Like cellulose III, cellulose IV preparations can revert to their parent structures.

Conversion to cellulose II and cellulose III via caustic mercerization and liquid ammonia treatment are commercial textile processes that are discussed later. Figure 7 shows the characteristic diffractograms (Cu Kα radiation) of native cellulose, cellulose mercerized with sodium hydroxide, and cellulose treated with liquid ammonia.

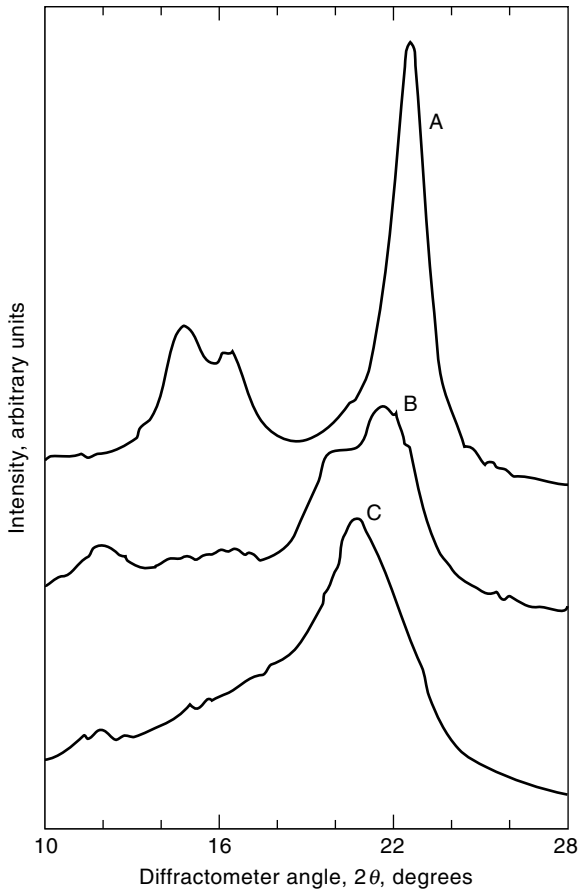

Fig. 7. X-ray diffractograms. A, native; B, NaOH mercerized; C, NH_3-treated.

Pore Structure and Affinity for Water. The cotton fiber is a porous, hydrophilic material that accounts for the comfort of cotton clothing. Moisture is retained tenaciously in cotton. The moisture absorbed from the atmosphere and held under ambient conditions is expressed either as moisture content (amount of moisture as the percentage over the oven-dried weight) or more commonly as moisture regain (amount of moisture as a percentage of the oven-dry sample). Under ordinary atmospheric conditions, moisture regain is 7–11%. Upon immersion in liquid water the cotton fiber swells and its internal pores fill with water. Pure cotton holds a substantial percentage of its dry weight in water under conditions of centrifugation. Values for the liquid water held depend on the test used. The values are ~30% for water of imbibition (87) and 50% for the water retention (88). Centrifugation conditions are less severe in the latter case.

Pores accessible to water molecules are not necessarily accessible to chemical agents. Many uses of cotton, eg, easy care fabric, depend on chemical modification to impart the desired properties. Knowledge of accessibility to dyes and other chemical agents of various sizes under water-swollen conditions is required for better control of the various chemical treatments applied to cotton textiles. The

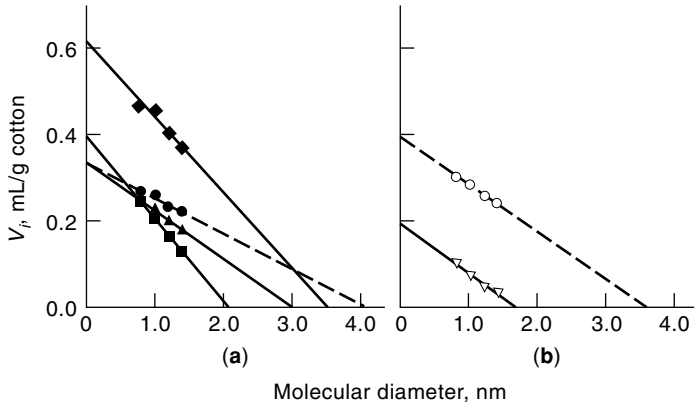

Fig. 8. Internal volume (V_i) that is accessible to sugars as functions of the cotton molecular diameters (89). (**a**) Batting: ▲ greige; ● , scoured–bleached; ♦ , caustic mercerized; ■ , liquid ammonia treated. (**b**) Fabric: ○ , scoured–bleached; ▼, cross-linked.

principle of molecular exclusion by GPC (89) has been used to assess the pore size distribution in cottons after various chemical treatments. Trends for accessibility to sugars of increasing size are depicted in Figure 8. These probes cover the range of molecular sizes of reagents generally used to modify cotton chemically.

Scouring and bleaching slightly increase the accessible internal volume, liquid ammonia treatment of the scoured–bleached cotton decreases it slightly, caustic mercerization substantially enhances accessibility, and cross-linking to impart durable press properties reduces the accessible internal pore volume substantially.

Availability of Hydroxyl Groups. The chemical structure given in Figure 6 shows the 2-OH, 3-OH, and 6-OH groups that are potential sites for the same chemical reactions that occur with common alcohols. However, the regular occurrences of intermolecular and intramolecular hydrogen bonds in the crystalline regions of cotton cellulose render the involved hydroxyl groups unavailable to chemical agents under mild reaction conditions. Chemical agents that have access to the interior pores of the cotton fiber thus find potential reactive sites unavailable for reaction. Direct information on the availabilities of 2-OH, 3-OH, and 6-OH on accessible surfaces has been obtained from chemical measurements based on the reaction of the cellulose with diethylaminoethyl chloride [2210-36-8] under mild conditions (90,91). The order of decreasing availability of hydroxyl groups in cotton is 2-OH $>$ 6-OH $\gg$ 3-OH. Specific values for the relative availability of the 3-OH and 6-OH to the 2-OH depend on the growth (92) and processing (42) history of the fiber. Data on growth and weathering are given in Table 3. Values for relative availability of hydroxyls are maintained throughout the ginning procedure but gradually increase (to $\sim$0.40 and $\sim$0.80 for 3-OH/2-OH and 6-OH/2-OH, respectively) as the fibers are subjected to the stress of processing in the greige mill (93).

Reactions for Practical Objectives

Chemical modification has assisted in building cotton's position in the market place despite the advent of synthetic fibers.

Table 3. Relative Availabilities of Hydroxyl Groups of Cotton Cellulose Throughout Growth and Weathering[a]

Days postanthesis[b]	Period	3-OH/2-OH	6-OH/2-OH
20	Growth/closed boll	0.12	0.49
27		0.05	0.59
34		0.05	0.58
41		0.05	0.59
48		0.06	0.59
62	Field weathering/open boll	0.24	0.68
83		0.30	0.75
104		0.31	0.74

[a]Ref. 41.
[b]Bolls open shortly after 48 days postanthesis.

Mercerization. One of the earliest known modifications of cotton that had commercial potential was mercerization. Traditionally, the process employed a cold concentrated sodium hydroxide (caustic soda) treatment of yarn or woven fabric followed by washing and a mild acetic acid neutralization. Maintaining the fabric under tension during the entire procedure was integral to achieving the desired properties. The resultant mercerized cotton has improved luster, dyeability, and strength. A variation of this procedure substitutes hot sodium hydroxide that is allowed to cool while the cotton remains immersed in the caustic solution. More thorough initial penetration increases the efficiency of the mercerizing process. If the cotton is allowed to shrink freely during contact with mercerizing caustic, slack mercerization takes place; this technique produces a product with greatly increased stretch (stretch cotton) that has found application in both medical and apparel fields. Effects similar to those from sodium hydroxide mercerization have been produced by exposure of the cotton to volatile primary amines or to ammonia. A procedure that uses liquid ammonia has found commercial adaptation (94). Improvements in luster and strength are similar to those achieved with sodium hydroxide mercerization, but dyeability is not enhanced. A distinct structural difference exists chemically between cotton mercerized in sodium hydroxide and that treated in liquid ammonia, particularly after nonaqueous quenching (95). With both treatments, there is increased accessibility, but differences in dye receptivity presumably result from differences in swelling loci between sodium hydroxide and liquid ammonia treatments.

Etherification. The accessible, available hydroxyl groups on the 2, 3, and 6 positions of the anhydroglucose residue are quite reactive (96) and provide sites for much of the current modification of cotton cellulose to impart special or value-added properties. The two most common classes into which modifications fall, include etherification and esterification of the cotton cellulose hydroxyls as well as addition reactions with certain unsaturated compounds to produce cellulose ethers (see CELLULOSE ETHERS). One large class of cellulose-reactive dyestuffs in commercial use attaches to the cellulose through an alkali-catalyzed etherification by nucleophilic attack of the chlorotriazine moiety of the dyestuff:

$$\text{Cellulose—O}^- + \text{Cl—Dyestuff} \rightarrow \text{Cellulose—O—Dyestuff} + \text{Cl}^-$$

Cross-linking. By far, the most important commercial modifications of cotton cellulose are those that occur through etherification. For example, commercial modification of cotton to impart durable-press, smooth drying, or shrinkage resistance properties involves cross-linking adjacent cellulose chains through amidomethyl ether linkages. This cross-linking is commonly achieved by immersing the fabric in a solution of the agent and an appropriate catalyst, removing the excess liquid by passing the fabric through squeeze rolls (pad), drying in an oven to remove the remaining water, and heating to a high temperature to effect covalent bond formation to cellulose. This sequence is called a pad-bake process. Methylene, or oligomeric, cross-links from a pad-bake formaldehyde treatment result in severe fabric strength loss. There is, however, a process for cross-linking cotton-containing garments with formaldehyde in the vapor phase that has found commercial acceptance in the uniform-rental garment market. Most reagents for cross-linking cotton cellulose are difunctional or polyfunctional amidomethylol compounds or amido compounds that have pendent hydroxyls on carbons alpha to the amido nitrogen (see AMINO RESINS). The methylol compound is generated by reaction of the amido compound with formaldehyde [50-00-0]. For example, ethyleneurea [120-9-34] reacts as follows (97).

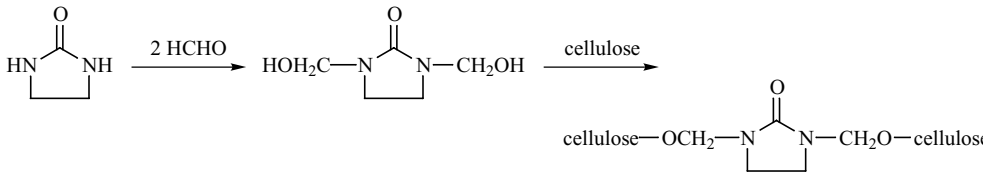

Commercially available cross-linking agents include dimethylolurea [140-95-4], dimethylolethyleneurea [136-84-5], dimethyloldihydroxyethyleneurea [1854-26-8], dimethylolpropyleneurea [3270-74-4], dimethylolalkyl carbamate, tetramethylolacetylenediurea [5395-50-6], methylolated melamine, dimethylolalkyltriazone, dimethoxymethyluron [7327-69-7], dihydroxydimethylethyleneurea [3923-79-3] (dimethylurea–glyoxal adduct), and ethyleneurea–glyoxal [107-22-2] adducts. The cross-linking proceeds via either Lewis or Brønsted acid catalysis (98) by a carbocation mechanism. Gross effects of the cross-linking are increased resiliency (manifested in wrinkle resistance, smooth drying properties, dimensional stability, and greater shape-holding properties) as well as reduced extensibility, strength, and moisture regain. These effects are observed with one cross-link per 20–25 anhydroglucose residues (99). Liquid ammonia treatment of cotton fabric, followed by cross-linking, attenuates the strength loss as well as an accompanying loss in abrasion resistance. This combination contributed to a reappearance of all-cotton fabrics in the woven shirting/sheeting market in the 1970s (100).

Resiliency. Base-catalyzed reactions of cotton cellulose with either monoepoxides or diepoxides to form cellulose ethers also result in fabrics with increased resiliency. Monoepoxides, believed to result only in cellulose hydroxyalkyl ethers or linear graft polymers (101), produce marked improvement in resiliency under wet conditions, but little improvement under ambient conditions. Difunctional

epoxides, which are capable of cross-linking cellulose, can be used to impart increased resiliency to cotton textiles under both wet and ambient conditions (102). Besides imparting resiliency through epoxide etherification, oil and water repellency can be imparted by reactions of monomeric perfluoro epoxides with cotton. Epoxide-reacted cotton also accept dyes not traditionally used for cotton. Etherification of cotton with ethyleneimine [2734-98-8] provides a means for imparting special properties to cotton; the end product depends on the attached group. The cross-linking reaction between bis(hydroxyethyl) sulfone and cellulose is another base-catalyzed etherification that produces fabrics possessing increased resiliency under both wet and ambient conditions. The earliest application of sulfone cross-links to cotton textiles was the reaction of divinyl sulfone under alkaline conditions (103). However, the hazard of working with the vinyl compound led to modifications of the sulfone agent. Vinyl groups were replaced with more stable precursors such as the β-thiosulfatoethyl, β-sulfatoethyl (104), or β-hydroxyethyl groups (105). Etherification of cotton by divinyl sulfone [77-77-0] and its precursors also forms the basis for a large class of fiber-reactive dyes with the general formula of dye-$SO_2CH{=}CH_2$ (106).

Other Cellulose Ethers. Other cotton cellulose ethers include carboxymethyl, carboxyethyl, hydroxyethyl, carbamoylethyl, cyanoethyl, sulfoethyl, and aminoethyl (aminized cotton) products. Most, with the exception of cyanoethylated and aminized cotton, are of interest in applications requiring solubility or swellability in water or alkali (107). In addition, ethers with pendent acid or basic groups have ion-exchange properties (108). Aminized cotton is of interest because it introduces basic groups onto the cotton that provide sites for attachment of acid dyes. Simultaneous aminization of cotton and dyeing with an acid dyestuff marked the first successful attempt at dye attachment to cellulose through an ether linkage (109).

Flame Resistance. The chemical treatment of cotton with fire retardants to make it flame resistant is discussed elsewhere. Numerous end uses for cotton require it to be flame-resistant. The major factors that influence ignition of cotton materials are airflow, relative humidity of the fabric, the amount of oxygen available, physical factors (geometry, density, thickness, etc), chemical factors (eg, inorganic impurities), heat source, and rate of heating. Thermal analysis studies in air and in 8.4% oxygen indicate that cotton ignites at ~360–425°C (110,111).

Although certain cellulose esters, such as the ammonium salt of phosphorylated cotton and cellulose phosphate [9015-14-9], are flame-resistant, the attachment of most currently used durable polymeric flame retardants for cotton is through ether linkage to the cellulose at a relatively low degree of substitution (DS). Nondurable flame retardants based on liquid-or vapor-phase applications of boric acid [10043-35-3] or methyl borate [121-43-7] are used in treatment of cotton batting for upholstery, bedding, and automotive cushions (112–114). Cotton carpet materials will pass the U.S. Consumer Product Safety Commission (CPSC) federal flammability test for carpets (16 CFR 1630) when cross-linked with polycarboxylic acids such as 1,2,3,4-butanetetracarboxylic acid or citric acid with sodium phosphate, sodium hypophosphite, sodium bicarbonate, or sodium carbonate catalysis (115).

Water Repellency. The development of water-repellent cellulose ethers has been reviewed (116). A typical example of a commercial etherification for

waterproofing cotton is with stearamidomethylpyridinium chloride:

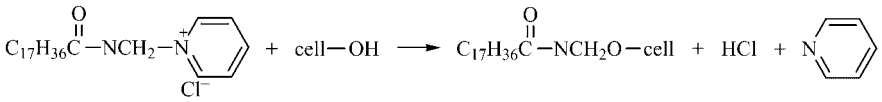

N-substituted, long-chain alkyl monomethylol cyclic ureas have also been used to waterproof cotton through etherification. Other water-repellent finishes for cotton are produced by cross-linked silicone films (117). In addition to the polymerization of the phosphorus-containing polymers on cotton to impart flame retardancy and of silicone to impart water repellency, polyfluorinated polymers have been successfully applied to cotton to impart oil repellency. Chemical attachment to the cotton is not necessary for durability; oil repellency occurs because of the low surface energy of the fluorinated surface (118).

Cyanoethylation. One of the earliest examples of etherification of cellulose by an unsaturated compound through vinyl addition is the cyanoethylation of cotton (119). This base-catalyzed reaction with acrylonitrile [107-13-1], a Michael addition, proceeds as follows:

$$CH_2{=}CHCN + Cell{-}OH \rightarrow Cell{-}OCH_2CH_2CN$$

For most textile uses, a DS <1 is desirable. Cyanoethylation can impart a wide variety of properties to the cotton fabric, such as rot resistance, heat and acid resistance, and receptivity to acid and acetate dyes. Acrylonitrile and acrylonitrile polymers (qv) has also been radiation-polymerized onto cotton with a ^{60}Co source. Microscopical examination of ultrathin sections of the product shows that the location of the polymer is within the fiber (120). Examination of the ir spectrum of cotton-containing polymerized acrylonitrile indicates that grafting occurs at the hydroxyl site of the cellulose (121). Another monomer grafted onto cellulose by irradiation is styrene polymers (qv). Chemical properties, mechanisms, and textile properties of these grafted polymers of cellulose have been summarized (122). Graft polymerization onto cotton has also been induced by both chemical (123) and photochemical (72) initiation.

Irradiation. The effects of high energy radiation (eg, gamma radiation) on cotton properties have also been investigated (124–127). Depolymerization of cellulose occurs with increasing energy absorption; carbonyl formation, carboxyl formation, and chain cleavage occur in the ratio of 20:1:1. With these chemical changes, there is a corresponding increase in solubility in water and alkali and a decrease in fiber strength. The gamma-irradiated cotton has base ion-exchange properties. Irradiation of cotton with near ultraviolet (UV) light (325–400 nm) causes formation of cellulose free radicals and mild oxidative degradation of the cotton (128). Carbonyl and carboxyl contents of the cotton cellulose increase, and DP and tensile strength decrease, with increasing time of irradiation (129). The induction of cellulose free radicals by near uv irradiation forms the basis for photofinishing with vinyl monomers to produce graft polymers on the cotton:

$$\text{Cell—H} \xrightarrow{h\nu} \text{Cell} + \text{H}\cdot$$
$$\text{Cell} + n\text{M} \longrightarrow \text{Cell—(M)}_{n-1}\text{M}\cdot$$

Another useful reaction of cotton cellulose occurs in an ionized atmosphere, which is essentially a surface reaction. Glow discharge treatment of cotton yarn in air increases water absorbency and strength (130), and surface-dependent properties of cotton fabric are drastically changed by exposure to low temperature–low pressure plasma generated by radio-frequency radiation (131). Because only a few extremely high energy electrons (10–15 eV) are generated, ambient temperature is maintained in the chamber. Light microscopy indicates a smoother surface after treatment, but scanning electron microscopy shows no change from native cotton. Spectral changes show some oxidation of the treated cotton, a decreased carbon/oxygen ratio. Free radicals similar to those produced from ^{60}Co radiation are formed. In addition, highly charged species are also formed, allowing such usually inert monomers as benzene to be polymerized onto the cotton with great capacity for bond cleavage. Plasma treatment produces an increased rate of wetting and drying and produces a highly absorbent cotton. The cohesiveness and fiber friction of cotton sliver was increased temporarily through air-trace chlorine corona treatments at 95°C and atmospheric pressure (132,133). With a 15-kV electrode voltage at a frequency of 2070 Hz, no chemical effects on the cotton could be noted. Dyeability, hand, and wettability were unaffected. The increase in cohesiveness allows the production of yarns with increased strength, abrasion resistance, and greater spinnability (134). Thus yarns of significantly lower twist can be produced with strength equal to, or higher than, untreated cotton yarns of higher twist.

Insolubilization. Insolubilization of compounds within textiles parallels the history of humanity; the direct dyeing techniques for cotton were highly advanced in the Bronze Age. With the exception of fiber-reactive dyes discussed earlier, other cotton dyes, ie, vat and sulfur, are insolubilized within the fiber after an oxidization step. Insoluble metal oxides have been used to flameproof cotton, and zirconium compounds have been insolubilized on cotton to render the fabric microbial resistant (135) or mildew resistant (136) via a mineral dyeing process (see TEXTILE FINISHING).

Insolubilization and five other methods for imparting antimicrobial properties to cotton have been described (137). These methods can all be classified under one or more of the chemical reactions of cotton cited earlier; they include fiber reactions to form metastable bonds, grafting through thermosetting agents, formation of coordination compounds, ion-exchange methods, polymer formation with possible grafting, and a regeneration process. Also a commercialized process for antibacterial cotton fabrics uses insoluble peroxide complexes of zirconyl acetate (138).

When exposed to heat, cotton fabrics increase in temperature to an extent that is proportional to their specific heats. Altering the chemical composition of the fabrics such that large amounts of heat are absorbed and released in repeatable cycles of controllable temperature ranges produces fabrics that are described as temperature adaptable. The process insolubilizes polyethylene glycols by cross-linking with methylolamides on the cotton fabric (139). As with flame-retardant cotton, attachment to the cellulose is through an ether linkage at a relatively low DS.

Esterification. There are both inorganic and organic esters of cellulose (140) (see CELLULOSE ESTERS). Of the three most common inorganic esters, cellulose nitrate [9004-70-0], phosphate, and sulfate, only cellulose sulfate [9088-06-6] is soluble in water. Cellulose sulfate attains water solubility at a DS of 3, indicating esterification of all three hydroxyl groups, whereas the sodium salt of cellulose sulfate is soluble in hot and cold water with a DS of only 0.33. Sodium cellulose sulfate is used in applications requiring suspension, thickening, stabilizing, and film-forming properties. The class of phosphonic acid and phosphoric acid dyestuffs attach to cotton through esterification by the phosphonic acid or phosphoric acid group of the dyestuff. Until recently, organic esters of cotton cellulose, with two notable exceptions, were only of academic interest, although partial esterification of cotton by fatty acids has been reported to increase resiliency (141).

Acetylation of cotton to an acetyl content slightly >21% produces a material with greatly increased resistance to fungal and microbiological degradation, in addition to tolerance of high temperatures not exhibited by native cotton; fibrous appearance and physical properties are unchanged by the acetylation. X-ray diffractograms indicate that, at this extent of substitution, only accessible (noncrystalline) regions of the cotton are involved in the acetylation (142).

In the 1960s, esterification of cotton cellulose with polycarboxylic acids to produce smooth-drying fabrics was investigated (143,144). Catalysis was by partial neutralization of the carboxyl groups. Although improvements in resiliency were obtained, the levels were not commercially acceptable. In the late 1980s, better catalyst systems were discovered for the ester cross-linking of cellulose; inorganic salts of phosphorus-containing acids were found to give ester cross-links that are durable to multiple home launderings. Because of the improved catalysis, certain tricarboxylic and tetracarboxylic acids have shown promise for commercialization (145). These acids include 1,2,3,4-butanetetracarboxylic acid [1703-58-8], tricarballylic acid [99-14-9], and citric acid [77-92-9] (146), maleic acid and itaconic acid as copolymers (147,148), and monopolymers/terpolymers of maleic acid (149). An anhydride formation mechanism has been proposed for the esterification cross-linking of cellulose. An advantage of the polycarboxylic acids in finishing for attaining durable press is that these agents do not contain formaldehyde and thus do not release formaldehyde during processing or end use. Finishes from polycarboxylic acids are superior to those from other nonformaldehyde agents mentioned earlier, such as epoxides, sulfones, acetals, and cyclic urea derivatives, because they are innocuous and are durable to home laundering.

Enzymatic Modification

The industrial use of enzymes in the textile industry (150,151) has increased substantially in recent years. Lipases, proteases, and cellulases are being used. Lipases and proteases are used to assist in cleaning textiles. Treatments involving cellulases, which hydrolyze the cellulose polymer, are relatively new and are of particular importance. Cellulases obtained from both bacterial and fungal sources are being used to give fabrics a soft hand, to give cellulosic fabric surfaces a smooth and clear appearance by removing fabric fuzz fibers ("biopolishing"), and to provide a stone-washed appearance to denim ("biostoning") (152–154). Cellulases are

also being added to detergents to maintain the color appearance of cotton cellulose fabrics by removing fabric fuzz fibers and pills that form on wear and laundering. The effectiveness of cellulase for removal of material from the fabric is dependent on the type of mechanical action during processing. This includes the abrasive action of fabric-to-fabric contact or the cascading effect of aqueous solution on the cellulosic substrate (155). One of the main reasons for using enzymes instead of other chemicals as finishing agents for cotton cellulose is that they are environmentally safer. The small catalytic quantities of enzymes that are used for finishing treatments are biodegradeable like proteins in general.

New Products

Smart Cotton-Based Wound Dressings. Cotton gauze is still a standard care item in the management of chronic wounds. However, since the time of ancient Greece, wound care and dressing strategies have primarily relied on empiricism. Smart wound dressings made from cotton gauze have more recently been designed and prepared with a rational approach based on knowledge of how destructive proteases play a role in the pathology of nonhealing wounds. Cotton gauze may be tailored to enhance the biochemistry of wound healing more effectively by designing formulations and conjugates of cotton cellulose that inhibit or neutralize destructive proteases, such as elastase, which prevent wound healing. Three approaches have been taken to develop protease fiber-inhibitors useful for chronic wounds: formulation of inhibitors on the dressing (156), synthesis of elastase recognition sequences on cotton cellulose (157), and the derivatization of cellulose with functional groups having an affinity for elastase (158). Understanding how these new cotton dressings work in accelerating healing of the chronic wound may signal a new product area of smart wound dressings that are useful in medical treatment modalities of pressure ulcers, leg ulcers, and diabetic foot sores.

Composites from Cotton. Cellulose fibers are abundant, readily available, versatile, and highly resistant to heat flow. They should be studied/evaluated as valuable starting materials for the design and development of thin low cost nonwoven composite insulation that can adhere to the walls of homes, office buildings, industrial complexes, warehouses, and tents. These applications currently cannot use fiberglass insulation within their exterior wall spaces. Cotton and other cellulosic fibers have thermal resistance similar to fiberglass. However, they do not cause immune and skin sensitivities, nor pulmonary problems that are associated with fiberglass use. Initial research on evaluating the commercial potential of cotton fibers as insulating materials involved composite nonwoven insulation materials that were made from cotton, kenaf, jute, polyester, polypropylene, sucrose-based epoxy formulations, and aluminum foil (159). The needlepunched fiber batts were rendered flame-resistant by use of inorganic reagents and urea.

Economic Aspects

Marketing/Merchandizing Raw Cotton. There are several routes by which cotton fiber in the United States changes ownership from the grower to its final destination at the spinning mill. The grower may sell cotton directly to

a spinning mill under a grower contract or the grower may sell cotton to a gin, broker, commission firm, or shipper. Some growers, after ginning their cotton, may sell through a cooperative organization or may place the cotton in a depository as collateral under the Commodity Credit Corp. Loan Program, to be either withdrawn on repayment of the loan plus interest and storage or forfeited for sale by the government. These intermediate buyers then sell the cotton to foreign or domestic mills.

World Production, Consumption, and Prices. World production, consumption, and prices are shown in Tables 4 and 5. World cotton production in 2001 was about ~90 million bales (~19.6 million metric tons; 21.6 million tons). Presently the chief cotton-growing countries of the world are China (23%), the United States (20%), India (12%), Pakistan (9%), and Uzbekistan (5%), which produced about ~70% of the world's cotton in 2000 (160). The price is widely variable because it is affected by many factors in the United States and internationally (161).

Table 4. World Cotton Production[a] [million 217.7-kg] (480-lb) bales]

Year	World	China	United States	India	Pakistan	Uzbekistan
1985[b]	80.3	19.0	13.4	9.0	5.6	7.9
1990	87.0	20.7	15.5	9.1	7.5	7.3
1995	93.0	21.9	17.9	13.2	8.2	5.7
1996	89.5	19.3	18.9	13.9	7.3	4.8
1997	91.6	21.1	18.8	12.3	7.2	5.2
1998	84.5	20.7	13.9	12.7	6.3	4.6
1999	87.4	17.6	17.0	12.2	8.6	5.2
2000[c]	88.8	20.3	17.2	10.9	8.2	4.4
2001[c]	98.2	24.4	20.3	11.9	8.3	4.8

[a]Ref. 160.
[b]A year begins Aug. 1 of the year given and ends July 31 of the following year.
[c]June 12, 2002 estimates by USDA—World Agricultural Outlook Board.

Table 5. World Cotton Consumption [million 217.7-kg (480-lb) bales] and Price of Cotton[a]

Year	World	China	United States	India	Pakistan	Turkey	Price[b]
1985[c]	75.0	18.0	6.4	7.2	2.4	2.1	49.0
1990	85.1	20.0	8.7	9.0	5.6	2.5	82.9
1995	86.0	19.7	10.6	12.0	7.2	4.4	85.5
1996	87.3	20.3	11.1	12.4	7.0	4.7	78.6
1997	87.2	19.6	11.3	12.7	7.2	5.0	72.2
1998	84.7	19.2	10.4	12.6	7.0	4.6	58.9
1999	91.9	22.2	10.2	13.5	7.7	5.6	52.9
2000[d]	92.3	23.5	8.9	13.5	8.1	5.2	57.3
2001[d]	93.3	24.5	7.6	13.2	8.5	6.0	41.4

[a]Ref. 160.
[b]A year begins Aug. 1 of the year given and ends July 31 of the following year.
[c]Cotlook, Ltd. A Index; cents/lb (Ref. 161). 2001 estimate through June 28, 2002.
[d]June 12, 2002 estimates by USDA—World Agricultural Outlook Board.

Table 6. Number of Items from a Cotton Bale (217.7 kg; 480 lb)

Women's wear	Number	Men's wear	Number	Others	Number
Dresses	274	Dress shirts (woven)	765	Diapers	3085
Jeans	249	Sport shirts (woven)	906	Sheets	249
Socks (mid-calf)	4321	Work shirts	543	Pillow cases	1256
Blouses (woven)	773	Boxer shorts	2104	Bath towels (terry)	690
Sweaters	379	Jockey shorts	2419		
Nightgowns	780	T-shirts	1217		
Slacks (woven)	415	Trousers (dress/sport)	484		
Shorts	733	Trousers (work)	374		
		Jeans	215		
		socks (mid-calf)	3557		

Uses. Cotton is used in many apparel and home furnishing items. Table 6 gives the approximate number of items that can be produced from one bale of cotton.

Health and Safety Factors

Respiratory Disease. Byssinosis is an occupational lung disease that can affect a small number of textile workers after repeated inhalation of the dust generated during the processing of cotton and some other vegetable fibers (eg, flax and soft hemp) (162–166). Byssinosis may cause progressive and disabling airway narrowing. Cotton dust, an airborne particulate matter released into the working environment as cotton is handled or processed in textile processing, is a complex mixture of botanical trash, soil, and microbiological material (ie, bacteria and fungi) (167). The etiological agent and pathogenesis of byssinosis are not known (166–168). However, control studies in experimental cardrooms suggest that endotoxin from Gram-negative bacteria is associated to some degree with worker reaction to dust (170). Appropriate engineering controls in cotton textile processing areas or washing cotton essentially can eliminate incidence of workers' reaction to cotton dust (164,165). The U.S. Occupational Safety and Health Administration (OSHA) issued revised standards for occupational exposure to cotton dust in 1985 (171) and revised the standard again in 2001 (172) to add batch-washed cotton as an acceptable way to wash cotton to eliminate worker reaction to the dust.

Skin Irritation/Dermatitis. Handling or processing of cotton does not cause skin irritation, since nothing naturally on the surface of cotton fiber is known to cause dermatitis. However, it is possible for some atypical cottons that have been treated with something not approved for use on cotton or off-grade highly microbiologically contaminated cottons to cause skin irritation.

Formaldehyde. Formaldehyde is a component of resins used to impart durable-press and other properties to cotton fabrics. It can be released in small quantities from treated cotton fabrics. Formaldehyde is classified as a "probable human carcinogen," because it has been shown to be an animal carcinogen and there is limited evidence to indicate that it is a carcinogen in humans (173). Sensory irritation of the mucous membranes of the eyes and the respiratory tract, and cellular changes in the nasal cavity are the principal noncancer effects of exposure

to low airborne concentrations of formaldehyde (173). Exposure to formaldehyde from cotton textiles is controlled by the chemical technology for low emitting formaldehyde resin technology and nonformaldehyde finishes discussed earlier and by increased ventilation in the workplace. OSHA has issued standards for control of occupational exposure to formaldehyde (174). The U.S. Consumer Product Safety Commission (CPSC) does not regulate formaldehyde in textiles because its studies did not indicate that there is an acute or chronic health problem due to formaldehyde exposures from textiles: "current evidence. . . does not indicate that formaldehyde exposure from resin treated textiles is likely to present a carcinogenic risk" (175–177).

BIBLIOGRAPHY

"Cotton" in *EPST* 1st ed., Vol. 4, pp. 244–272, by J. C. Arthur Jr., Southern Regional Research Laboratory, USDA; "Cotton" in *EPSE* 2nd ed., Vol. 4, pp. 261–284, by J. C. Arthur Jr., Consultant.

1. P. J. Wakelyn, N. R. Bertoniere, A. French, H. Zeronian, and co-workers, in M. Lewin and E. M. Pearce, eds., *Handbook of Fiber Chemistry*, 2nd ed., Marcel Dekker, Inc., New York, 1998, Chapt. "9", pp. 577–724.
2. *World Synthetic Fibres Supply/Demand* Report 2001, PCI-Fibres & Row Materials, Crawley, West Sussex, UK.
3. *Oil world Annual 2000*.
4. Cottonseed, *INFORM* **11**, 820–839 (2000); *Cottonseed and Its Products*, 9th ed., National Cottonseed Products Association, Memphis, Tenn., 1990.
5. T. M. Bell and F. E. M. Gillham, *The World of Cotton*, ContiCotton, EMR, Washington, D. C., 1989.
6. A. S. Basra, ed., *Cotton Fibers Developmental Biology, Quality Improvement' and Textile Processing*, Food Products Press, Binghamton, N.Y., 1999.
7. R. J. Kohel and C. F. Lewis, eds., *Cotton* (Agronomy No. 24), American Society of Agronomy, Crop Science Society of America, Inc., Soil Science Society of America, Inc., Madison, Wis., 1984.
8. C. B. Purves, in E. Ott, H. M. Spurlin, and M. W. Graefflin, eds., *Cellulose and Cellulose Derivatives*, 2nd ed., Pt. 1, Interscience Publishers, Inc., New York, 1954, pp. 29–53.
9. S. J. Hake, T. A. Kerby, and K. D. Hake, eds., *Cotton Production Manual, Pub. 3352*, Division of Agriculture and Natural Resources, University of California, Oakland, CA, 1996.
10. P. J. Wakelyn, J. Stewart, and co-workers, Report of the Expert Panel on Cotton and Biotechnology, International Cotton Advisory Committee (ICAC), Nov. 2000.
11. J. M. Vreeland, Proc. Beltwide Production Conf., National Cotton Council, Memphis, Tenn., 1993, pp. 1533–1536.
12. J. M. Vreeland, *Scientific. Am.* **280**(4), 112–118 (1999).
13. L. B. Kimmel and M. P. Day, *AATCC Rev.* **1**(10), 32–36 (2001).
14. U. Ryser, in Ref. 4 Chapt. 1, pp. 21–28.
15. C. M. Conrad, *Science* **94**, 113 (1941).
16. M. C. Meinert and D. P. Delmer, *Plant Physiol.* **59**, 1088 (1977).
17. H. R. Huwyler, G. Franz, and H. Meier, *Planta* **146**, 635 (1979).
18. T. Hayashi and D. P. Delmer, *Carbohydr. Res.* **181**, 273 (1988).
19. K. Kudlicka and R. M. Brown, Jr., *Plant Physiol.* **115**, 643 (1997).
20. J. R. Pear, Y. Kawagoe, W. E. Schreckengost, D. P. Delmer, and D. M. Stalker, *Proc. Natl. Acad. Sci. U.S.A.* **93**, 12637 (1995).
21. W. Laosinchai, X. Cui, and R. M. Brown Jr., *Plant Physiol.* (PGR00-002) **112**, 291 (2000).

22. T. Arioli, L. Peng, A. S. Betzner, J. Burn, W. Wittke, W. Herth, C. Camilleri, H. Hofte, J. Plazinski, R. Birch, A. Cork, J. Glover, J. Redmond, and R. E. Williamson, *Science* **279**, 717 (1998).
23. F. Nicol, I. His, A. Jauneau, S. Vernhettes, H. Canut, and H. Hofte, *EMBO J.* **17**, 5563 (1998).
24. R. Lane, A. Wiedemeier, L. Peng, H. Hofte, S. Vernhettes, T. Desprez, C. H. Hocart, R. J. Birch, T. I. Baskin, J. E. Burn, T. Arioli, A. S. Betzner, and R. E. Williamson, *Plant Physiol.* **126**, 278 (2001).
25. L. Peng, Y. Kawagoe, P. Hogan, and D. P. Delmer, *Science* 295, 147 (2002).
26. C. H. Haigler, M. Ivanova-Datcheva, P. S. Hogan, V. V. Salnikov, S. Hwang, L. K. Martin, and D. P. Delmer, *Plant Molec. Biol.* **47**, 29 (2001).
27. P. J. Wakelyn, K. Menchey, and A. G. Jordan, Cotton and Environmental Issues. Cotton—Global Challenges and the Future. Papers presented at a Technical Seminar at the 59th Plenary Meeting of the International Cotton Advisory Committee (ICAC), Cairns, Australia, Nov. 9, 2000, pp. 3–11.
28. *Cotton Varieties Planted, 1991 Crop*, U.S. Agricultural Marketing Service, Memphis, Tenn., Aug. 1991.
29. G. W. Wallingford, Paper presented at the *Southern Soil Fertility Conference*, Memphis, Tenn., Oct. 15–18, 1991.
30. E. G. King, J. R. Phillips, and R. J. Coleman, eds. *Cotton Insects and Mites: Characterization and Management* (The Cotton Foundation Reference Book Series, No. 3), The Cotton Foundation, Memphis, Tenn., 1996.
31. T. L. Kirkpatrick and C. S. Rothrock, eds. *Compendium of Cotton Diseases*, 2nd ed., APS Press, St. Paul, Minn., 2001.
32. C. G. McWhorter and J. R. Abernathy, eds., *Weeds of Cotton: Characterization and Control* (The Cotton Foundation Reference Book Series, Number Two), The Cotton Foundation, Memphis, Tenn., 1992.
33. D. Blasingame and co-workers, *Nematodes, Your Hidden Enemies: Identification and Control*, The Cotton Foundation, National Cotton Council, and Aventis CropScience, 2002.
34. P. J. Cotty, *Phytopathology* **84**, 1270–1277 (1994).
35. D. L. Park, and W. D. Price, *Rev. Environ. Contam. Toxicol* **171**, 139–175 (2001).
36. W. A. Dickerson, A. L. Brashear, J. T. Brumley, F. L. Carter, W. J. Grefenstette, and F. A. Harris, eds., *Boll Weevil Eradication in the United States Through 1999* (The Cotton Foundation Reference Book Series, No. 6), The Cotton Foundation, Memphis, Tenn., 2001.
37. G. A. Slater, *Cotton Int. (Memphis)* **43**, 90, 130, 138 (1976).
38. O. El-Lissy and W. Grefenstette, Boll Weevil Eradication in the U.S. 2001, in Proc. 2002 Beltwide Cotton Conf. (Cotton Insect Research & Control Conf.), National Cotton Council, Memphis, Tenn., 2002 [CD-ROM].
39. T. Miller, *Pesticide Outlook* **12**(2), 68–70 (2001); J. P. Dean, *Agric. Res.* **24**(12), 8 (1976).
40. *Anonymous, Pink Bollworm Eradication, National Cotton Council*, Aug. 20012001.
41. J. R. Supak and C. E. Snipes, eds., *Cotton Harvest Management: Use and Infuence of Harvest Aids* (The Cotton Foundation Reference Book Series, No. 5), The Cotton Foundation, Memphis, Tenn., 2001; M. R. Chaudhry, Harvesting and Ginning of Cotton in the World, in Proc. Beltwide Cotton Conf., Vol. 2, 1997, pp. 1617–1619.
42. W. S. Anthony and W. D. Mayfield, Managing editors, *Cotton Ginners Handbook, USDA, ARS* (Agricultural Handbook No. 503), Dec. 1994; Report of the Expert Panel on Ginning Methods, Int. Cotton Advisory Committee (ICAC), Sept. 2001.
43. U.S. Bureau of Census, *Cotton Production in the United States; Crop of 1970*, U.S. Government Printing Office, Washington, D.C., 1971.

44. USDA, National Agricultural Statistics Board Summary, Washington, D.C., May 2001.
45. W. S. Anthony, *Cotton Gin Oil Mill Press* **91**(20), 8 (1990).
46. Cotton Bales Dimensions and Density, ISO 8115, International Organization for Standardization, Switzerland, 1986.
47. U.S. Code of Federal Regulations, Vol. 49, Part 172.102 Special Provisions, 137, cotton, dry.
48. P. J. Wakelyn and S. E. Hughs, *Fire and Material* 26 (2002).
49. P. J. Wakelyn and P. J. Wan, *Oil Mill Gaz.* **106**(8), 14–22 (2001).
50. R. D. O'Brien and P. J. Wan, Cottonseed Oil Processing and Utilization, in Proc. World Conf. on Oilseed Processing and Utilization, AOCS Press, Champaign, Ill., 2001, pp. 90–140.
51. P. J. Wan and R. D. O'Brien, *Lipid Technol.* **13**(3), 61–65 (2001).
52. *The Classification of Cotton*, Agriculture Handbook 566, U.S. Department of Agriculture, Cotton Program, Agricultural Marketing Service, Washington, D.C., Revised Apr. 2001.
53. G. H. Davidonis, A. Johnson, J. A. Landivar, and K. B. Hood, *Textile Res. J.* 69, 754–759 (1999).
54. W. Zurek, M. Greszta, and I. Frydrych, *Textile Res. J.* **69**, 804–810 (1999).
55. R. S. Krowicki, O. Hinojosa, D. P. Thibodeaux, and K. E. Duckett, *Textile Res. J.* **66**, 70–72 (1996).
56. Standard Test Method for Length and Length Distribution of Cotton Fibers (Array Method), ASTM D1440-96, *Annual Book of ASTM Standards*, Vol. 07.01, ASTM, Philadelphia, Pa., 2001, pp. 345–350.
57. *2002 Buyers Guide*, Cotton Council International, Washington, D.C., 2002.
58. "Standard Test Method for Breaking Strength and Elongation of Cotton Fibers (Flat Bundle Method)", ASTM D1445-95, *Annual Book of ASTM Standards*, Vol. 07.01, ASTM, Philadelphia, Pa., 2001, pp. 360–368.
59. *Textile World Manmade Fiber Chart, Textile World*, McGraw-Hill Book Co., Inc., New York, 151(8) [magazine insert], 2001.
60. E. Lord, *Manual of Cotton Spinning, Part I, Vol. II: The Characteristics of Raw Cotton*, Textile Book Publishers, Inc., New York, 1961.
61. D. P. Thibodeaux and J. P. Evans, *Textile Res. J.* **56**, 130–139 (1986).
62. E. K. Boylston, D. P. Thibodeaux and J. P. Evans, *Textile Res. J.* **63**, 80–87 (1993).
63. E. Lord, *The Origin and Assessment of Cotton Fiber Maturity*, 2nd ed., The International Institute for Cotton, Manchester, U.K., 1982.
64. D. Nickerson, *Textile Res. J.* **21**, 33–38 (1951).
65. Standard Test Method for Non-Lint Content of Cotton, ASTM D2812-95, *Annual Book of ASTM Standards*, Vol. 07.01, ASTM, Philadelphia, Pa., 2001, pp. 663–667.
66. P. J. Wakelyn, in A. L. Ivester and J. D. Neefus, eds., *ILO Encyclopaedia of Occupational Health and Safety*, 4th ed., Chapt. "89", Textile Goods Industry, International Labour Office, Geneva, Switzerland, 1997, pp. 89.9–89.11.
67. C. Crocker, in A. L. Ivester and J. D. Neefus, eds., *ILO Encyclopaedia of Occupational Health and Safety*, 4th ed., Textile Goods Industry, International Labour Office, Geneva, Switzerland, 1997, Chapt. "89", pp. 89.21–89.23.
68. *Cotton Nonwovens: A Technical Guide*, Cotton Inc., 1997.
69. *Cotton Nonwovens: Innovations & Solutions*, Cotton Inc., 2002.
70. M. L. Rollins, *Forest Products J.* **18**(2), 91 (1968).
71. J. O. Warwicker, R. Jeffries, R. L. Colbran, and R. N. Robinson, *A Review of the Literature on the Effect of Caustic Soda and Other Swelling Agents on the Fine Structure of Cotton*, Shirley Institute Pamphlet No. 93, Didsbury, Manchester, U.K., 1966.

72. M. L. Rollins, in D. S. Hamby, ed., *The Cotton Fiber, American Cotton Handbook*, 3rd ed., Interscience Publishers, New York, 1965.
73. D. E. Brushwood and H. H. Perkins Jr., *Text. Chemist Color.* **26**(3), 32 (1994).
74. H. H. Perkins Jr., and D. E. Brushwood, *Text. Chemist Color.* **23**(2), 26–28 (1991).
75. L. N. Domelsmith, and co-workers, *Text. Res. J.* **56**(1), 14 (1986).
76. D. C. Johnson, in T. P. Nevel and S. H. Zeronian, eds., *Cellulose Chemistry and Its Applications*, Ellis Horwood, Chichester, U.K., 1985, pp. 181–201.
77. M.-A. Rousselle, Determining the Molecular Weight Distribution of Cotton Cellulose: A New GPC Solvent, *Text. Res. J.* 72 (in press).
78. J. D. Timpa, *J. Ag. Food Chem.* **39**, 270 (1991).
79. J. D. Timpa and H. H. Ramey, *Textile Res. J.* **59**, 611 (1989).
80. J. Sugiyama, T. Okano, H. Yamamoto, and F. Horii, *Macromolecules* **23**, 3196 (1990).
81. J. Sugiyama, R. Vuong, and H. Chanzy, *Macromolecules* **24**, 4168 (1991).
82. R. H. Atalla and D. L. VanderHart, *Science* **223**, 1465 (1984).
83. V. L. Finkenstadt and R. P. Millane, *Macromolecules* **31**, 7776–7783 (1998).
84. Y. Nishiyama, T. Okano, P. Langan, and H. Chanzy. *Int. J. Biol. Macromol.* **26**, 279–283 (1999).
85. P. Langan, Y. Nishiyama, and H. Chanzy. *J. Am. Chem. Soc.* **121**, 9940–9946 (1999).
86. S. H. Zeronian and H.-S. Ryu, *J. Appl. Polym. Sci.* **33**, 2587 (1987).
87. H. M. Welo, H. M. Ziffle, and A. W. McDonald, *Textile Res. J.* **22**, 261 (1952).
88. G. Jayme, *Tappi* **41**, 180A (1958).
89. N. R. Bertoniere, in J. F. Kennedy, G. O. Phillips, and P. A. Williams, eds., *Cellulose, Structural and Functional Aspects* (Series in Polymer Science and Technology), Ellis Horwood, Chichester, U.K., 1989, pp. 99–104.
90. S. P. Rowland and N. R. Bertoniere, in T. P. Nevel and S. H. Zeronian, eds., *Cellulose Chemistry and Its Applications*, Ellis Horwood, Chichester, U.K., 1985, pp. 112–137.
91. N. R. Bertoniere and S. H. Zeronian, in R. H. Attala, ed., *The Structures of Cellulose* (ACS Symposium Series 340), American Chemical Society, Washington, D.C., 1987, pp. 255–271.
92. S. P. Rowland and P. S. Howley, *J. Polym. Sci., Polym. Chem. Ed.* **23**, 183 (1985).
93. N. R. Bertoniere, P. S. Howley, S. E. Hughs, W. S. Anthony, and G. F. Ruppenicker, Proc. Beltwide Cotton Conf., Vol. 3, 1992, p. 1267.
94. Brit. Pat. 1,084,612 (Sept. 27, 1967) J. L. Karl and P. Stranger-Johannassen (to Sentralinstitutt for Industriell Forskning and Norsk Tekstilforskningsinstitutt); Brit. Pat. 1,136,417 (Dec. 11, 1968), R. M. Gailey (to J. and P. Coats, Ltd.).
95. T. A. Calamari Jr., S. P. Schreiber, A. S. Cooper, and W. A. Reeves, *Text. Chem. Color.* **3**, 235 (1971).
96. E. Heuser, *Text. Res. J.* **20**, 828 (1950); T. E. Timell, *Sven Papperstidn.* **56**, 483 (1953).
97. J. G. Frick Jr., *Chem. Technol.* **1**, 100 (1971).
98. A. G. Pierce Jr., R. M. Reinhardt, and R. M. H. Kullman, *Text. Res. J.* **46**, 420 (1976).
99. J. G. Frick Jr., B. A. Kottes Andrews, and J. D. Reid, *Text. Res. J.* **30**, 495 (1960).
100. S. A. Heap, *Colourage* **24**(7), 15 (1977).
101. J. B. McKelvey, B. G. Weber, and E. Klein, *Text. Res. J.* **29**, 918 (1959).
102. R. R. Benerito, R. J. Berni, J. B. McKelvey, and B. G. Burgess, *J. Appl. Polym. Sci., Part A* **1**, 3407 (1963).
103. U.S. Pat. 2,524,399 (Oct. 3, 1950), D. L. Schoene and V. S. Chambers (to U.S. Rubber Co.).
104. G. C. Tesoro, P. Linden, and S. B. Sello, *Text. Res. J.* **31**, 283 (1961).
105. Can. Pat. 625,790 (Aug. 15, 1961), R. O. Steele (to Rohm and Haas Co.).
106. R. H. Peters, *Textile Chemistry III, The Physical Chemistry of Dyeing*, Elsevier Scientific Publishing Co., Inc., New York, 1975, pp. 624–629.
107. L. A. Graham and C. A. Suratt, *Am. Dyest. Rep.* **67**(7), 36 (1978).
108. J. D. Guthrie, *Ind. Eng. Chem.* **44**, 2187 (1952).

109. J. D. Guthrie, *Am. Dyest. Rep.* **41**(1), P13, 30 (1952).
110. B. Miller, J. R. Martin, and R. Turner, *J. Appl. Polym. Sci.* **28**, 45–56 (1983).
111. F. Shafizadeh and Y. Sekiguchi, *Combust. Flame* **55**, 171–199 (1984).
112. N. B. Knoepfler, in V. M. Bhatnagar, ed., Proceedings of the European Conference on Flammability and Fire Retardants, Technomic Publishing Co., Westport, Conn., 1980, p. 115.
113. A. R. Horrocks, *Rev. Prog. Color.* **16**, 62–101 (1986).
114. P. J. Wakelyn, W. Rearick, and J. Turner, *Am. Dyest. Rep.* **87**(2), 13–21 (1998).
115. E. J. Blanchard, E. E. Graves, and P. A. Salame, *J. Fire Sci.* **18**, 151 (2000); W. A. Rearick, M. L. Wallace, V. B. Martin, and P. J. Wakelyn, *AATCC Rev.* **2**(2) 12–15 (2002).
116. J. T. Marsh, *An Introduction to Textile Finishing*, 2nd ed., Chapman and Hall, London, 1966, pp. 458–494.
117. C. M. Welch, J. B. Bullock, and M. F. Margavio, *Text. Res. J.* **37**, 324 (1967).
118. E. J. Grajeck and W. H. Petersen, *Text. Res. J.* **32**, 320 (1962).
119. G. C. Daul, R. M. Reinhardt, and J. D. Reid, *Text. Res. J.* **25**, 246 (1955).
120. J. C. Arthur Jr., and R. J. Demint, *Text. Res. J.* **30**, 505 (1960).
121. J. C. Arthur Jr., and R. J. Demint, *Text. Res. J.* **31**, 988 (1961).
122. J. C. Arthur Jr., and F. A. Blouin, *Am. Dyest. Rep.* **51**, 1024 (1962).
123. H. H. St. Mard, C. Hamalainen, and A. S. Cooper Jr., *Am. Dyest. Rep.* **56**(5), 24 (1967).
124. A. H. Reine, N. A. Portnoy, and J. C. Arthur Jr., *Text. Res. J.* **43**, 638 (1973).
125. F. A. Blouin and J. C. Arthur Jr., *Text. Res. J.* **28**, 198 (1958).
126. J. C. Arthur Jr., *Text. Res. J.* **28**, 204 (1958).
127. R. J. Demint and J. C. Arthur Jr., *Text. Res. J.* **29**, 276 (1959).
128. J. C. Arthur Jr., in Proceedings of the 13th Cotton Utilization Conference, ARS-S-64, U.S. Agricultural Research Service, Southern Research Center, New Orleans, La., 1975, p. 6.
129. J. C. Arthur Jr., and O. Hinojosa, *Appl. Polym. Symp.* **26**, 147 (1975).
130. R. B. Stone and J. R. Barrett Jr., *Text. Bull.* **88**(1), 66 (1962).
131. H. Z. Jung, T. L. Ward, and R. R. Benerito, *Text. Res. J.* **47**, 217 (1977).
132. W. J. Thorsen, *Text. Res. J.* **41**, 331 (1971).
133. W. J. Thorsen, *Text. Res. J.* **41**, 455 (1971).
134. D. P. Thibodeaux and H. R. Copeland, in 15th Textile Chemical Processing Conference, USDA Southern Regional Research Center, New Orleans, La., 1975, pp. 36–40.
135. C. J. Conner, A. S. Cooper, W. A. Reeves, and B. J. Trask, *Text. Res. J.* **34**, 347 (1964).
136. C. J. Conner, G. S. Danna, A. S. Cooper, and W. A. Reeves, *Text. Res. J.* **37**, 94 (1967).
137. D. D. Gagliardi, *Am. Dyest. Rep.* **51**, P49 (1962).
138. T. L. Vigo, G. F. Danna, and C. M. Welch, *Text. Chem. Color.* **9**, 77 (1977).
139. U.S. Pat. 4,851,291 (July 25, 1989), T. L. Vigo, C. M. Frost, J. S. Bruno, and G. F. Danna (to U.S. Department of Agriculture).
140. R. M. Reinhardt and J. D. Reid, *Text. Res. J.* **27**, 59 (1957).
141. J. B. McKelvey, R. J. Berni, and R. R. Benerito, *Text. Res. J.* **34**, 1102 (1964).
142. C. F. Goldthwait, E. M. Buras Jr., and A. S. Cooper Jr., *Text. Res. J.* **21**, 831 (1951).
143. D. D. Gagliardi and F. B. Shippee, *Am Dyest. Rep.* **52**, P300 (1963).
144. U.S. Pat. 3,526,048 (Sept. 1, 1970), S. P. Rowland, C. M. Welch, and M. A. F. Brannan (to U.S. Department of Agriculture).
145. C. M. Welch, C. M. Pastore and P. Keikens, eds., *Surface Characteristic of Fibers and Textiles*, Marcel Dekker, Inc., New York, 2002, pp. 1–32.
146. U.S. Pat. 4,820,307 (Apr. 11, 1989), C. M. Welch and B. K. Andrews (to U.S. Department of Agriculture).
147. H.-M. Choi, *Text. Res. J.* **62**, 614 (1992).
148. H.-M. Choi and C. M. Welch, *Am. Dyest. Rep.* **83**, 48 (1994).
149. C. Q. Yang, X. Wang, and I.-S. Kang, *Text. Res. J.* **76**, 334 (1997).

150. P. H. Nielson, and co-workers, Enzyme Applicationes, Industrial, *Kirk–Othmer Encyclopedia of Chemical Technology*, 4th ed., Vol. **9**, John Wiley & Sons, New York, 1993, pp. 567–597, 602–604.
151. S. M. Betrabet, *Colourage* **41**(5), 21 (1994).
152. D. Kochavi, T. Videbaek, and D. Cedroni, *Am. Dyest. Rep.* **37**(9), 24–28 (1990).
153. G. L. Pedersen, G. A. Screws Jr., and D. M. Cedroni, *Can. Text. J.* 31–35 (Dec. 1992).
154. L. G. Snyder, *Text. Chem. Color.* **29**(6), 27–31 (1997).
155. U.S. Pat. 5,232,851 (Aug. 3, 1993), T. Cox, P. E. Hawks, and S. A. Klahorst (to Springs Industries, Inc. and Genencor International, Inc.)
156. J. V. Edwards, A. F. Bopp, B. S. Batiste, A. J. Ullah, I. K. Cohen, R. F. Diegelmann, and S. J. Montante, *Wound Rep. Reg.* **7**, 106–118 (1999).
157. J. V. Edwards, D. Yager, A. Bopp, R. F. Diegelmann, S. Goheen, R. F. Diegelmann, S. Goheen, Cohen, and I. K. Design, in J. V. Edwards and T. L. Vigo, eds., *Bioactive Fibers and Polymers* (ACS Symposium Series 792), American Chemical Society, Washington, D.C., 2001, pp. 76–89.
158. J. V. Edwards, D. R. Yager, I. K. Cohen, R. F. Diegelmann, S. Montante, N. Bertoniere, and A. Bopp, *Wound Rep. Reg.* **9**, 50–58 (2001).
159. N. D. Sachinvala, D. L. Winson, D. V. Parikh, H. H. Solhjoo, D. Parks, T. L. Vigo, E. J. Blanchard, and N. R. Bertoniere, *Polym. Adv. Technol.* **13**, 66–79 (2002).
160. USDA-World Agricultural Outlook Board, World Agricultural Supply and Demand Estimates, various issues, 2002 (http://www.usda.gov/oce/waob/wasde/wasde.htm).
161. Food and Agricultural Policy Research Institute, University of Missouri-Columbia, FAPRI Baseline, 2002 (http://www.fapri.missouri.edu/FAPRI Publications.htm).
162. R. Rylander, R. S. F. Schilling, C. A. C. Pickering, G. B. Rooke, A. M. Dempsey, and R. R. Jacobs, *Br. J. Ind. Med.* **44**, 577–579 (1987).
163. R. R. Jacobs and P. J. Wakelyn, in Proc. Beltwide Res. Conf., National Cotton Council, Memphis, Tenn., 1998, pp. 213–220.
164. Regulatory Review of OSHA's Cotton Dust Standard ([29CFR 1910.1043]), U.S. Dept. of Labor, Office of Program Evaluation, Occupational Safety and Health Administration, Sept. 2000.
165. Washed Cotton, Current Intelligence Bulletin 56, U. S. Dept. of Health and Human Services, National Institute for Occupational Safety and Health, Aug. 1995.
166. C. A. C. Pickering, in R. R. Jacobs, P. J. Wakelyn, and L. N. Domelsmith, eds., Proceedings of the 15th Cotton Dust Research Conference, National Cotton Council, Memphis, Tenn., 1991, pp. 298–299.
167. P. J. Wakelyn, G. A. Greenblatt, D. F. Brown, and V. W. Tripp. *Am. Ind. Hyg. Assoc. J.* **37**, 22 (1976).
168. M. S. Rohrbach, in R. R. Jacobs, P. J. Wakelyn, and L. N. Domelsmith, eds., Proceedings of the 15th Cotton Dust Research Conference, National Cotton Council, Memphis, Tenn., 1991, pp. 300–306.
169. P. J. Nichols, in R. R. Jacobs, P. J. Wakelyn, and L. N. Domelsmith, eds., Proceedings of the 15th Cotton Dust Research Conference, National Cotton Council, Memphis, Tenn., 1991, pp. 307–320.
170. R. M. Castellan, S. A. Olenchock, K. B. Kingsley, and J. L. Hankinson, *New Engl. J. Med.* **317**, 605 (1987).
171. *Fed. Reg.* **50**, 51120–51179 (Dec. 13, 1985) (29 CFR 1910. 1043).
172. *Fed. Reg.* **66**, 18191–18192 (Apr. 6, 2001).
173. Formaldehyde Risk Assessment Update, Office of Toxic Substances, U.S. Environmental Protection Agency, Washington, D. C., June 11, 1991.
174. *Fed. Reg.* **52**, 46168–46312 (Dec. 4, 1987) (29 CFR 1910.1048).
175. Formaldehyde in Textiles, Briefing Package, U.S. Consumer Product Safety Commission, Washington, D. C., Dece. 30, 1983.

176. Status Report on Formaldehyde in Textiles Portion of Dyes and Finishes Project, U.S. Consumer Product Safety Commission, Jan. 3, 1984.
177. J. D. Robbins, W. P. Norred, A. Bathija, and A. G. Ulsamer, *J. Toxicol. Environ. Health* **14**, 453 (1984).

PHILLIP J. WAKELYN
The National Cotton Council of America

CREEP. See VISCOELASTICITY.

CRITICAL PHASE POLYMERIZATIONS. See Volume 2.

CRYSTALLINE POLYMERS. See SEMICRYSTALLINE POLYMERS.

CYANOACRYLIC ESTER POLYMERS. See POLYCYANOACRYLATES.

CYCLIC OLEFIN POLYMERS. See ETHYLENE-NORBORNENE COPOLYMERS.

CYCLOHEXANEDIMETHANOL POLYESTERS. See Volume 2.

CYCLOPENTADIENE AND DICYCLOPENTADIENE

Introduction

Cyclopentadiene [542-92-7] (CPD), C_5H_6, (**1**), and its more stable dimer, dicyclopentadiene [77-73-6] (DCPD), $C_{10}H_{12}$, (**2**), are the major constituents of hydrocarbon resins, cyclic olefin polymers, and a host of specialty chemicals. They can be transformed into many chemical intermediates used in the production of pharmaceuticals, pesticides, perfumes, flame retardants, and antioxidants. Because of their wide industrial uses, their chemistry has been extensively investigated and documented. Numerous reviews (1–12) have been published on the subject. The production processes and industrial uses of CPD and DCPD are summarized in Reference 13. In addition to the classical organic reactions, CPD forms organic metallic complexes, ferrocene, with transition metals (14). Some of these complexes have been established as excellent olefin polymerization catalysts. Several reviews have been published on this rapid growing field (15–19) (see SINGLE-SITE CATALYSTS).

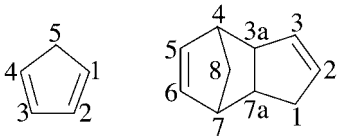

1 **2**

Encyclopedia of Polymer Science and Technology. Copyright John Wiley & Sons, Inc. All rights reserved.

Table 1. Physical Properties of Cyclopentadiene and Dicyclopentadiene

Physical properties	Cyclopentadiene	Dicyclopentadiene
Molecular weight	66.1	132.2
Bp, 101.3 kPa[a],°C	40.0	170
Mp,°C	−97.2	32
Physical form	Colorless liquid	Colorless solid
Odor	Sweet terpenic	Camphoraceous
d_4^{20}	0.8021	
d_4^{35}		0.9302
n_D^{20}	1.4440	1.5105
n_D^{35}		1.5050
Heat of combustion, kJ/mol[b]	2929	5767
Heat of vaporization, kJ/mol[b]	28.9	38.5
Heat of fusion, kJ/mol[b]	8.0	2.1
Specific heat, kJ/(kg·K)[b]	1.7	1.7
Heat of cracking, kJ/mol[b]		102.9
Spontaneous ignition point,°C		
In oxygen	510	510
In air	640	680
Dielectric constant at 40°C		2.43
Ionization energy, eV	8.5	8.8

[a]To convert kPa to mm Hg, multiply by 7.5.
[b]To convert kJ to kcal, divide by 4.184.

Physical Properties

The physical properties of CPD and DCPD are given in Table 1. DCPD, 3a,4,7,7a-tetrahydro-4,7-methano-1*H*-indene, can exist in two stereoisomers, the endo and exo forms. Because commercially available DCPD is mostly the endo isomer, the properties in Table 1 are pertinent to those of the endo isomer. Spectroscopical information on CPD and DCPD can be found in (20) (mass spectrum), and (21) (nmr spectrum). References 2 (ir, uv, and Raman spectra).

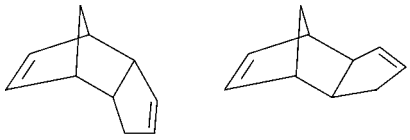

(endo DCPD) (exo DCPD)

DCPD decomposes rapidly at its normal boiling point to two molecules of cyclopentadiene. Purification of DCPD by distillation must be conducted under vacuum conditions. Figure 1 depicts the lowering of the boiling point as a function of pressure. The dimer is the form in which CPD is sold commercially.

Chemical Reactions

Cyclopentadiene is very reactive. In addition to the vast number of reactions one expects from conjugated double bond structures which include Diels–Alder addition, hydrogenation, halogen addition, etc, the highly acidic methylene group

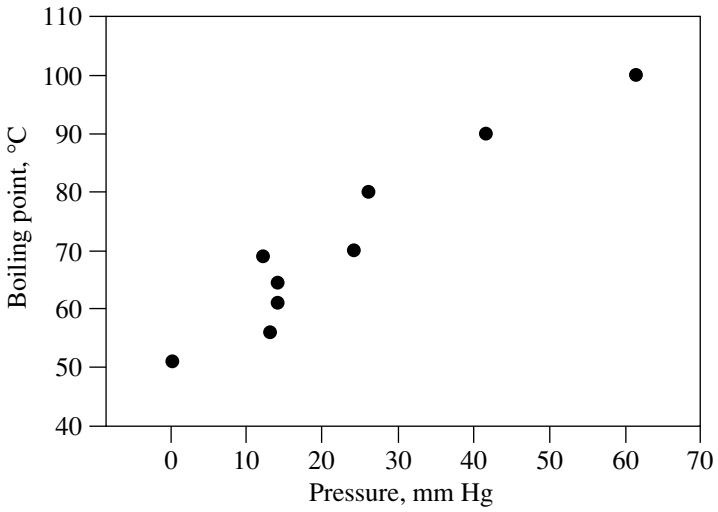

Fig. 1. Boiling point of dicyclopentadiene as a function of pressure. To convert kPa to mm Hg, multiply by 7.5.

promotes a number of condensation reactions. On the other hand, DCPD behaves like nonconjugated dienes, with the exception that the double bond in the bicycloheptene ring is more reactive than that in the five-membered ring because of the bond angle strain in the bicycloheptene ring.

Diels–Alder Addition. In Diels–Alder addition, the conjugated double bonds of CPD react with the π bond of a dienophile, a compound containing ethylenic or acetylenic unsaturation. The ethylenic or acetylenic group is added across the 1,4 position of the CPD, resulting in a bicyclo[2.2.1]heptene derivative, a cyclohexene derivative with a bridged methylene group. Because of Diels–Alder reactions, many multicyclic compounds can be synthesized with CPD as the building blocks. Examples of these reactions, which are highly exothermic 71–75 kcal/mol, are shown in Table 2.

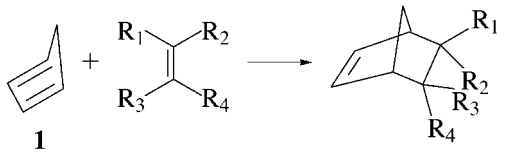

1

Both CPD and DCPD can be used in the reactions. However for the latter, the reaction needs to be carried out at temperatures above 175°C in order for the DCPD to dissociate rapidly to the CPD monomer. The rate of the reaction is strongly affected by other substituents of the dienophile. For instance, the reaction between CPD and maleic anhydride occurs spontaneously, whereas that between CPD and ethylene requires elevated temperatures and very high pressure. A long floppy chain on the dienophile is also a strong inhibitor of the reaction (22).

Diels–Alder addition is stereochemically specific (22). There is a strong tendency of most substituents of the dienophile to orient in the endo configuration in the bicycloheptene derivative formed from CPD.

Table 2. Diels–Alder Adducts from Cyclopentadiene

Dienophile	Structure of adduct
Dibasic acids and derivatives Maleic anhydride, R = H Chloromaleic anhydride, R = Cl	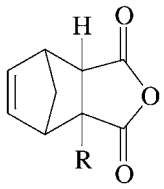
Monobasic acids Crotonic acid, R_1 = H; R_2 = CH_3 Methacrylic acid, R_1 = CH_3; R_2 = H	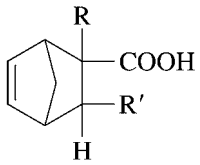
Aldehydes Acrolein, R = H Crotonaldehyde, R = CH_3	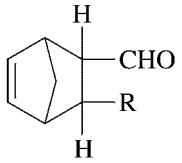
Ketones Methyl propenyl ketone (3-penten-2-one), R_1 = CH_3; R_2 = CH_3 Methyl vinyl ketone (3-buten-2-one), R_1 = H; R_2 = CH_3	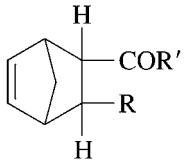
Vinyl compounds Ethylene, R = H Styrene, R = C_6H_5 Vinyl acetate, R = CH_3COO	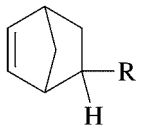
Acetylenes Acetylene, R = H Acetylenedicarbonitrile, R = CN	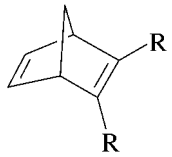
Quinones *p*-Benzoquinone	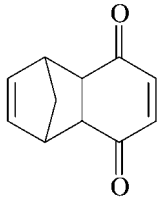

Table 2. (Continued)

Dienophile	Structure of adduct
Nitroso compounds Nitrosobenzene	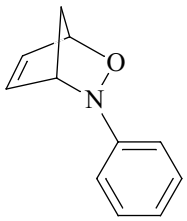
Conjugated diolefins 1,3-Butadiene, R = H	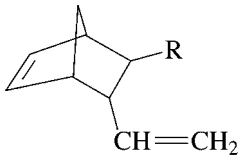

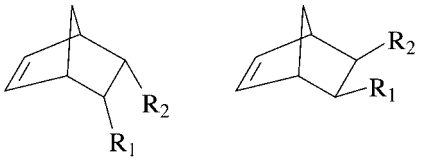

Endo Exo

With maleic anhydride as the dienophile, the reaction leads exclusively to the endo form (23) of the nadic anhydride, *endo-cis*-bicyclo[2.2.1]hept-5-ene-2,3-dicarboxylic anhydride [129-64-6] (**3**).

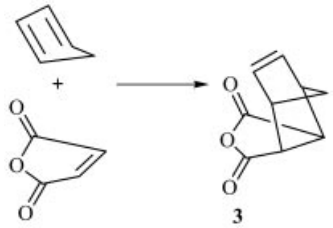

3

Polymerization. Cyclopentadiene dimerizes spontaneously and exothermally at ambient temperature to endo DCPD via the Diels–Alder addition mechanism, in which one of the CPD molecule acts as the dienophile. At temperatures above 100°C, CPD polymerizes thermally to trimers, tetramers, and higher oligomers. Since either one of the nonconjugated double bonds in an oligomer can participate in the Diels–Alder addition to the CPD to form a higher oligomer, the higher oligomers can have several structural isomers. For instance, two trimers, 3a,4,4a,5,8,8a,9,9a-octahydro-4,9:5,8-dimethanobenz-1*H*-[*f*]indene [7158-25-0] (**4**) and 1,4,4a,4b,5,8,8a,9a-octahydro-1,4:5,8-dimethano-1-*H*-fluorene [35184-08-8] (**5**), are formed in the ratio 87:13 by the addition of CPD to DCPD (24).

Table 3. Yield (wt%) of Cyclopentadiene Oligomers at Various Temperatures and Contact Times

Oligomer	14 h at 150–160°C	22 h at 170–180°C	90 h at 200°C
Tricyclopentadiene	40	50	25
Tetracyclopentadiene	10	30	45
Pentacyclopentadiene	2	5	10
Unreacted DCPD	50	10	5

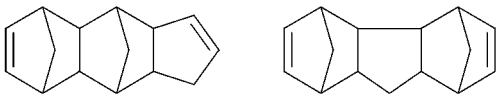

4 **5**

In contrast to DCPD, higher thermal oligomers are crystalline compounds with little odor. The yields of the oligomers at various temperatures and contact times are shown in Table 3.

In addition to thermal polymerization, CPD can be polymerized rapidly at low temperatures with the aid of Lewis acid catalysts (25). The catalysts most often used in the industry are $AlCl_3$ and BF_3, although $AlBr_3$, $TiCl_4$, $SnCl_4$, as well as alkyl aluminum chlorides are all known to be effective catalysts.

Condensation via the Methylene Group. Because of the resonance stabilization of the π electron system, the cyclopentadienyl anion forms readily from CPD after the dissociation of the acidic methylene proton. Under alkaline conditions, CPD undergoes condensation reaction with carbonyl compounds, such as ketones and aldehydes, yielding a family of highly colored fulvene derivatives (26).

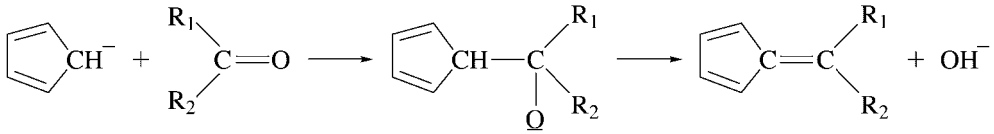

The color of the fulvenes increases with the size of R_1 and R_2 (2). The dimethylfulvene is bright yellow whereas fulvenes with aromatic substitutents are blood-red. The aldehyde condensation products are also strongly colored. Because they resinify easily, it is difficult to separate them in the pure form.

Fulvenes can be hydrogenated to the corresponding alkylated cyclopentanes in the presence of nickel or palladium catalysts. Therefore, the condensation reaction provides a convenient route for the synthesis of alkylated cyclopentanes from CPD.

Cyclopentadiene reacts with alkaline oxides and hydroxides forming the alkaline cyclopentadienyl salts. Alkaline hydroxides supported on high surface materials such as kiesclguhr and alumina are good absorbents for trace amounts of CPD contaminant in other hydrocarbons (27).

Hydrogenation. Cyclopentadiene can be hydrogenated stepwise through cyclopentene to cyclopentane in the presence of hydrogen and noble metal catalysts such as palladium (2). The heats of reaction at 82°C are as follows (28):

$$C_5H_6 + H_2 \rightarrow C_5H_8 \qquad 92.9 \text{ kJ/mol}(22.2 \text{ kcal/mol})$$

$$C_5H_6 + 2H_2 \rightarrow C_5H_{10} \qquad 212.8 \text{ kJ/mol}(50.9 \text{ kcal/mol})$$

Similarly, DCPD is hydrogenated first to the dihydro derivative and then to the tetrahydro DCPD (29). The heat of hydrogenation of the double bond of the bicycloheptene ring is 139 kJ/mol (32.2 kcal/mol) whereas that of the five-membered ring is 110 kJ/mol (26.2 kcal/mol) (30). Therefore, the former double bond is more reactive and is the first to be hydrogenated, yielding 3a,4,5,6,7,7a-hexahydro-4,7-methanoindene (**6**), one of the two possible structural isomers of the dihydro DCPD.

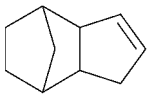

6

Oligomers of CPD can also be hydrogenated. The endo isomers of the hydrogenated products are wax-like solids. Physical properties of the hydrogenated oligomers can be found in References 30–32. Hydrocarbon resins produced by polymerization of CPD are hydrogenated to improve their color, light stability, and adhesive properties. Colorless resins obtained this way are used for demanding applications such as adhesives for transparent pressure sensitive tape.

Hydrogenation of CPD and DCPD with noble metal catalysts tends to produce a mixture of dihydro and tetrahydro derivatives. If only the dihydro derivatives are to be produced, selective hydrogenation catalysts must be used. Hydrogenation catalysts designed for the conversions of conjugated diolefins like 1,3-butadiene or isoprene to the olefins have been used for this service. These catalysts are mostly palladium metal modified with one or more promoters (33).

Oxidation. Cyclopentadiene reacts spontaneously with oxygen to form a brown, gummy substance that contains a substantial amount of peroxides. Dicyclopentadiene reacts with air slowly, yielding a gummy deposit. The gum formation in DCPD can be inhibited by the addition of 100–200 ppm by weight of antioxidants such as *t*-butylcatechol and α-naphthol. Vapor-phase catalytic oxidation of CPD over vanadium oxide at 400–525°C yields maleic anhydride, carbon dioxide, and formaldehyde. Dihydroxylcyclopentenes and tetrahydroxylcyclopentane can be prepared by treating CPD with hydrogen peroxide (34–37).

Halogenation. Halogens and hydrogen halides react readily with the conjugated double bonds of CPD, producing a series of halogenated compounds ranging from the monohalocyclopentene to tetrahalocyclopentane. 3-Chlorocyclopentene is not stable. It decomposes on standing, with resinification and the release of hydrogen chloride.

The halogenated derivatives of CPD serve as the starting points for the synthesis of a large number of organic compounds, including amines, alcohols, and thiocyanates. Of all the chloro compounds derived from CPD, only

hexachlorocyclopentadiene [77-47-4] has been used in commercial quantities. It is prepared by a liquid phase chlorination of CPD below 50°C (38). Tetrachlorocyclopentane is produced first, by chlorine addition, and is then converted to octachlorocyclopentane by catalytic chlorination over arsenious oxide or phosphorus pentachloride at 175–250°C. Octachlorocyclopentane is then dehydrochlorinated thermally to the hexachlorocyclopentadiene.

Hexachlorocyclopentadiene is the basis for a number of pesticides such as Chlorodane, Aldrin, Dieldrin, and Kepone. The production of some of these materials has been banned in many regions because of their carcinogenic properties and toxicity to wildlife. Hexachlorocyclopentadiene is also the raw material for chlorendic acid, which is used as a flame retardant (product information from Velsicol Chemical Corp.) for unsaturated polyester resins.

Alkylation. Cyclopentadiene can be multiply alkylated in high yields using alkyl halides, oxo alcohols, and Guerbet alcohols (39,40). The multiply alkylated cyclopentanes obtained by hydrogenation of the diene derivatives have been demonstrated to be useful as synthetic lubricants.

Source and Production

Steam crackers for the production of ethylene are the primary source of CPD and DCPD, although a small amount is still recovered from coal tar distillation. The amount of CPD produced depends on the feedstock to the cracker. The yield from a naphtha cracker is 6–8 times of that from a gas cracker, which uses ethane and propane feed mixture.

The cracked gas leaving the furnace section of a steam cracker contains many chemical components. They are separated by a series of fractionation columns. The bottom stream from the debutanizer column, known as the pyrolysis gasoline in the industry, contains the C5 and heavier fractions of the cracked gas. Typically, CPD plus DCPD constitute 15–25 wt% of the pyrolysis gasoline. Because CPD dimerizes readily, it is usually recovered in the form of the DCPD.

There are two ways by which DCPD can be obtained from the pyrolysis gasoline, depending on whether the pyrolysis gasoline is processed immediately after leaving the debutanizer. When the pyrolysis gasoline is processed immediately, the amount of DCPD present is small. The process scheme generally follows that depicted in Figure 2. The C5 fraction of the pyrolysis gasoline is first separated as the overhead of a depentanizer. The C5 stream is heat-soaked in a dimerizer at about 100°C. The CPD in the C5 stream is converted to DCPD. The separation of the low boiling C5 components from the DCPD is achieved by a second fractionation in which the DCPD is recovered as the bottom product. The DCPD is mainly in the endo form and has a purity of 82–90%.

If the pyrolysis gasoline is placed in storage before it is processed or if the process is supplemented with purchased pyrolysis gasoline, a significant amount of the CPD in the pyrolysis gasoline is already in the form of DCPD, since CPD dimerizes to DCPD at a rate of 9 mol%/h at 35°C. The recovery of the DCPD follows a different process scheme as shown in Figure 3. The pyrolysis gasoline is first heat-soaked in a dimerizer to convert remaining CPD to DCPD. The effluent from the dimerizer is fractionated in one or more columns where the C5–C9 components

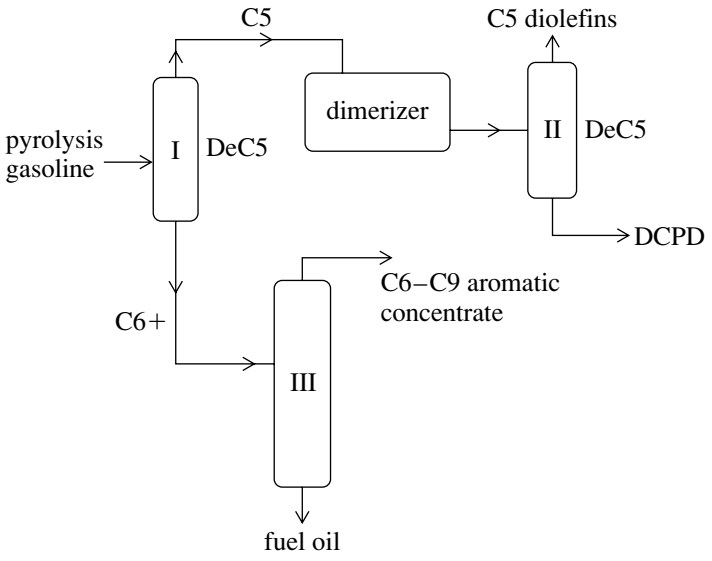

Fig. 2. Process scheme for extracting dicyclopentadiene from pyrolysis gasoline when the gasoline is processed immediately after its production in an ethylene plant.

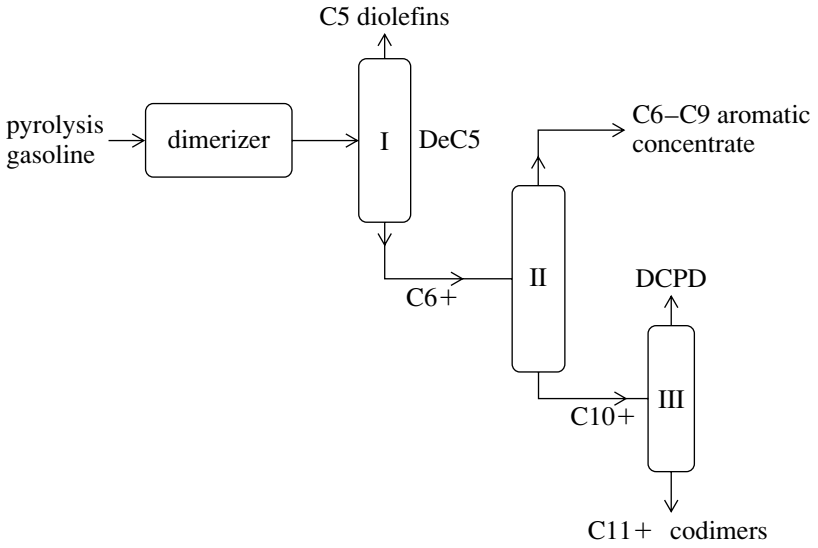

Fig. 3. Process scheme for extracting dicyclopentadiene from pyrolysis gasoline when the gasoline was in storage for an extended period of time after its production in an ethylene plant.

are separated from the C10 and heavier fractions. (Usually, this fractionation is carried out in two steps: First a CPD-lean C5 stream is produced as the overhead of a depentanizer. The bottom stream of the depentanizer is further processed in a second column which separates the C6–C9 components as the overhead while the C10 and heavier fractions become the bottom stream.) The C10 and heavier

stream, which contains 50–70% DCPD, is distilled to yield a DCPD overhead product. The purity of the DCPD is 82–95%.

The process in Figure 2 requires less demanding fractionation, but it has the disadvantage of leaving in the DCPD all the oligomers produced during the heat-soak step. The process scheme in Figure 3 also has the advantage of flexibility in adjusting the DCPD product to a desirable purity by simply varying the fractionation conditions in the last column.

High purity DCPD in the range of 98–99% is produced by thermal cracking of the lower purity DCPD. Pure CPD is separated from the crude DCPD by distillation and is redimerized in controlled conditions to avoid oligomer formation. Unreacted CPD is stripped from the high purity DCPD by mild fractionation (41).

The annual capacity of DCPD production for all grades in the United States is estimated to be in excess of 350 million pounds in 1999. The major U.S. producers are B. F. Goodrich Co., Equistar Chemicals (a joint venture of Lyondell Petrochemical, Milennium Chemicals, and Occidental Petroleum Co.), Exxon Chemical Co., Phillips Petroleum Co., Shell Oil Co., Texmark Chemicals, and Velsicol Chemical Corp. The major consumptions of DCPD in the United States are in the production of hydrocarbon and unsaturated polyester resins (80%), ethylene–propylene terpolymers (10%), reaction injection molding (5%), and miscellaneous uses (5%). The last includes flame retardants, pesticides, antioxidants, and metallocene catalyst production. The demand for DCPD will grow in a rate of 4% per year in the next several years.

Western Europe and Japan have, respectively, annual DCPD production capacities of 176 and 195 million pounds, and predicted annual growth rates of 5 and 6% (42). The major producers in Europe are Exxon, EniChem, Dow, and Shell. Nippon Zeon and JSR are the major producers in Japan.

Storage and Handling

Because CPD monomer dimerizes spontaneously at room temperature and a large quantity of heat (75 kJ/mol or 18 kcal/mol) is released in the process, material containing a substantial amount of CPD should not be stored in any sealed container without the provision of removing the heat. The rate constant of the dimerization is $1.2 \times 10^6 \exp(-16.7/RT)$ L/(mol·s) (2). Thus, the rate of reaction accelerates rapidly with increasing temperature.

Temp,°C	Dimerization rate, mol%/h
−20	0.05
0	0.5
10	1
15	1.5
20	2.5
25	3.5
30	6
35	9
40	15

Without adequate heat dissipation, runaway dimerization occurs. The resulting high temperature leads to the building up of pressure, which will eventually burst the container. Commercial quantity of CPD is usually produced, stored, and shipped in the form of the stable dimer, DCPD. Because of the high freezing point of DCPD, the material is transported in tank cars, rail cars, or barges equipped with heating elements. The heating of the DCPD must be regulated. Otherwise, excess temperature will lead to the formation of the undesirable oligomers. Exposing DCPD to even a trace amount of oxygen or rust at temperatures in excess of 100°C promotes the formation of peroxides and other oxygenates. The oxygenates degrade the quality of the DCPD because they impact undesirable color to the product. DCPD is usually stabilized with 100–200 ppm of antioxidants such as *tert*-butyl catechol to prevent gum deposit during storage.

For commercial applications, which require the CPD monomer, the CPD is obtained from DCPD by thermal cracking. The process involves distilling the DCPD at its normal boiling point (170°C) under an inert atmosphere. At 170°C, DCPD cracks at a rate of 36%/h. By maintaining the overhead temperature of the column at 41–42°C, the boiling point of CPD, an overhead condensate of pure CPD monomer can be obtained. The thermal cracking and distillation can also be accomplished by heating the DCPD in the presence of a heavy oil at about 250°C. The heavy oil functions as a solvent to minimize fouling due to resinification at high temperature. Another method of producing CPD is by cracking the DCPD in the vapor phase at 350–400°C. At these temperatures, the decomposition of the DCPD is instantaneous. The vapor-phase process has the disadvantage that C10 codimers presented in the DCPD also crack at the high temperatures, producing C5 diolefins such as isoprenes and piperylenes. The C5 diolefins make the purification of the CPD much more difficult. To minimize the cracking of C10 codimers, one needs to maintain the temperature below 250°C (43–45).

Because CPD reacts spontaneously with oxygen to form gummy peroxide-containing products, it must be protected from air if not being used immediately. To minimize dimerization, CPD should be stored at a temperature below −20°C.

Health and Safety Concerns

DCPD is a toxic substance. By oral administration in rats, the LD_{50} is 353 mg/kg of body weight, and by skin absorption in rabbits, the LD_{50} is 6.72 mL/kg. An atmospheric concentration of 2000 ppm causes death in rats exposed for a period of 4 h. Studies with rats indicate that DCPD has no deleterious effects on the blood and blood-forming organs. Toxicological effects are similar to terpenes rather than to benzene. The TLV and PEL for DCPD are both 5 ppm as established by ACGIH and OSHA. Chronic exposure causes damages to the liver, kidneys, and lungs.

Uses of Cyclopentadiene and Dicyclopentadiene

There are two general categories of industrial end uses of CPD and DCPD: (*1*) commodity resins and polymers, which include hydrocarbon resins, unsaturated

polyester resins, and ethylene–propylene–diene monomer (EPDM) rubbers and (*2*) specialty polymers and fine chemicals, which include cyclic olefin copolymers, flame retardants, agrochemicals, specialty norbornenes, flavor and fragrance intermediates. Over 90% of the U.S. consumption of CPD and DCPD is in the first category.

Hydrocarbon Resins. About 50% of the DCPD produced is used in hydrocarbon resins. Crude DCPD with 60–75% purity is typically used in this application. Other components in the feedstock may consist of codimers of CPD with isoprene, piperylene, and methylcyclopentadiene, and a small amount of the dimers of methylcyclopentadiene. Both DCPD and the codimers are incorporated into the hydrocarbon resins (46,47). Other C5 diolefins can also be added to the process.

The hydrocarbon resins can be produced by a simple thermal polymerization process (48–50) or by Lewis acid catalyzed reaction (51). The thermal process is carried out at a high temperature in the range of 200–280°C and a reactor pressure above 300 psig. At temperatures below 200°C, the Diels–Alder polymers are formed. They are not desirable in most resins because they are insoluble in aromatic solvents. If reaction temperature exceeds 280°C, decomposition of the resins would occur.

In the acid-catalyzed process, crude DCPD is mixed with a Lewis acid such as BF_3 in the presence of an alcohol or ether (52). An aromatic co-solvent may also be used. Temperature control is critical for producing the resin. After reaction, the Lewis acid is removed by a caustic solution and the resin is further washed with water to remove any caustic and catalyst residues. Unreacted DCPD and the co-solvent are removed by steam stripping.

The DCPD concentration and reaction temperatures have strong influence on the properties of the final resins such as the softening point, color, unsaturation, and reactivity. The resin may be hydro-treated to improve the color and thermal stability. The resins are sold in the solid form as flakes or pellets. The main applications of the resins are in adhesives, tackifiers in tires and floor tiles, surface coating and varnishes, and ink. Water-white resins produced by the hydrogenation process are used in road-marking paint, hot melt adhesives with thermoplastic rubber which can be found in diapers and feminine hygiene products.

Unsaturated Polyester Resins. Unsaturated polyester resins based on DCPD are produced by reacting glycols, maleic anhydride, and DCPD (12). There are at least four different methods (12,53) in making the DCPD-based polyesters. They are usually two-step batch processes. In one commonly used method, the glycol and maleic anhydride are first allowed to react at a temperature below 150°C, typically around 130°C. Then DCPD is added to the mixture and the reactor temperature is gradually raised to 200°C. After an acid number between 30 and 40 is obtained, the polyester is allowed to cool and is diluted with a mixture of styrene and inhibitors.

Dicyclopentadiene-based polyester resins have several advantages over the conventional polyester resins based on phthalic anhydride. Besides the lower cost of the DCPD, low cost glycols like ethylene glycol can be used instead of the more expensive propylene glycol. Since the DCPD-based resins require less styrene than the phthalic anhydride based resin, there is less styrene emission in the production and processing of the DCPD-based resins.

The resins are used primarily in the fiber-reinforced form as laminates, castings, and coatings (54,55). Glass fiber is one of the common fillers for the reinforcement. Because of the low viscosity of the resin, the DCPD-based sheet molding compounds can incorporate a greater amount of the low cost fillers. The low print-through of the fillers makes the DCPD-based resins ideal for applications in which aesthetic effects are important. These include marine applications (recreation boats, jet ski), automotive parts, safety helmets, bathroom counter tops, shower stalls, and tubs. In the nonreinforced form, the resins have been used as insulation coating for electrical coils (56,57).

Elastomers. Ethylene–propylene–diene monomer (EPDM) rubbers is a terpolymer of ethylene, propylene, and a nonconjugated diene. The diene provides the double bonds in the polymer for the cross-linking, thus increasing the flexibility of the polymer. Dicyclopentadiene and ethylidene norbornene (ENB), a CPD derivative, are among the most important dienes. Typically, high purity DCPD in the >94% range is used. High purity DCPD is also preferred in the synthesis of ENB, which is a two-step process. EPDM rubber has a wide variety of applications, particularly in the automotive industry. It is used in side walls of tires, door and window weatherstripping, cable insulation, radiator and heater hose, and belting (see ETHYLENE–PROPYLENE ELASTOMERS).

In the ENB production, DCPD is thermally cracked to CPD, which subsequently reacts, via the Diels–Alder mechanism, with butadiene to form 5-vinylbicyclo[2.2.1]-hept-2-ene [3048-64-4] (VNB) (**7**) (58,59). The vinyl double bond is then isomerized in the presence of a selective super-base catalyst such as NaK amide to yield 5-ethylidenebicyclo[2.2.1]-hept-2-ene [16219-75-3] (ENB) (**8**) (60–62).

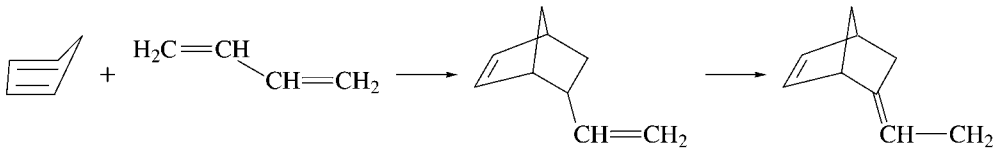

1 **7** **8**

Cyclic Olefin Copolymers. Cyclic olefin copolymers (COC) are produced by copolymerization of ethylene with a cyclic olefin monomer such as norbornene, dihydro DCPD, phenylnorbornene, and tetracyclododecene. Ziegler–Natta and metallocene catalysts are used in the polymerization processes. COC resins have excellent transparency, near zero birefringence, low density, low water uptake, and good chemical resistance. The target markets for the polymers are in high density electronic storage media such as optical disks, high quality lenses, medical labware, high performance films, and pharmaceutical blister packaging (63).

Cyclic olefin monomers are derivatives of CPD or DCPD. Norbornene derivatives are produced by the Diels–Alder condensation of an olefin and CPD. For instance, 2-norbornene (**9**) is obtained by reacting excess ethylene with DCPD at a high temperature (>200°C) and pressure (>2900 psia), the condition in which the DCPD is cracked to CPD (64). Reactions of CPD or DCPD at high temperatures with styrene and norbornene yield, respectively, the phenylnorbornene (**10**) and tetracyclododecene (**11**) (see ETHYLENE–NORBORNENE COPOLYMERS).

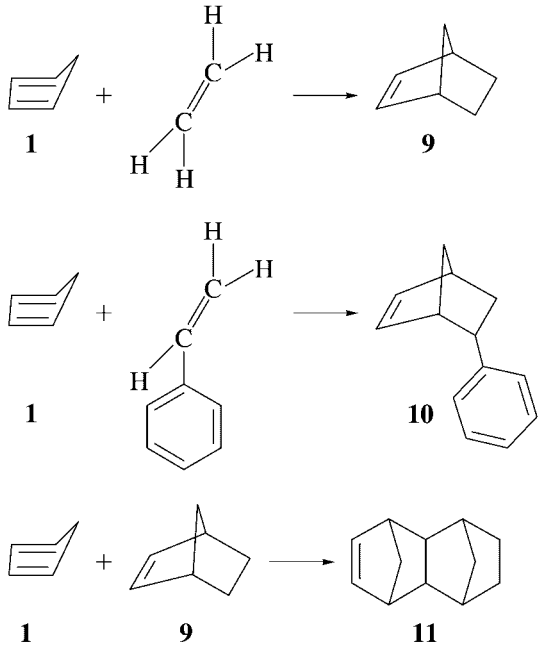

Polydicyclopentadiene. Ultrapure (>98%) DCPD can be polymerized catalytically to form polydicyclopentadiene [25038-78-2], a low viscosity gel which is dark in color and flows like water. Very intricate moldings with good impact resistance can be obtained after curing the polyDCPD. In reaction injection molding, polyDCPD is formed by injecting into a mold two equal amounts of DCPD, one part containing a metal catalyst and the other part containing aluminum alkyl activators (65,66). Upon mixing, the catalyst is activated and initiates the metathesis polymerization. The whole process lasts for 30 s to a few minutes. Reviews of the chemistry and properties of polyDCPD have been published (67,68). Companies like Hercules, B. F. Goodrich, Orkem, Shell, Nippon Zeon, and Teijin hold many patents on the polyDCPD synthesis, catalysts, modifiers, and applications. The major industrial uses of polyDCPD are in moldings for golf carts, automobile bumpers, housing for the hull and body of recreation water vehicles, and body panels for automobiles.

Cyclopentene. High purity cyclopentene is produced from CPD by selective hydrogenation. The process involves the cracking of DCPD to high purity CPD, followed by the selective saturation of one of the two double bonds of CPD in a fixed bed reactor containing a palladium-based catalyst. Cyclopentene is used as an intermediate in the production of many specialty chemicals.

Pesticides. Hexachlorocyclopentadiene, produced by reacting CPD with chlorine, is the starting material for a host of insecticides, including aldrin, chlordane, dieldrin, and heptachlor. Because of environmental regulation, most of the DCPD-based insecticides are no longer produced and used in the United States.

Flame Retardants. Chlorendic anhydride [115-27-5] (**12**), produced by the Diels–Alder condensation of hexachlorocyclopentadiene and maleic anhydride, is

used as a flame retardant for unsaturated polyester resins. The anhydride is incorporated in the resins by the esterification reaction with glycols.

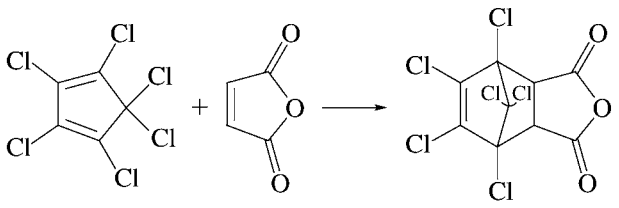

12

Flame retarded polyester formulation may contain 10–50% of the anhydride, with 30% being typical. They are used primarily in construction including shower systems, lavatories, panels in exterior sidings of office buildings, roof lights, glazing, and door panels. The chlorendic anhydride based resins tend to demand high prices because of their translucency and increased corrosion resistance.

Specialty Uses and Applications. Numerous reactions of DCPD and higher oligomers have been described in the patent literature. These involve the addition of the reacting chemical at the double bond of the bicycloheptene ring of the DCPD molecule to give such products as secondary alcohols (**13**), ethers, esters, and halides. When the reaction is acid-catalyzed at elevated temperatures, the resulting products have the exo configuration even though endo DCPD is used as the starting material. For example, in the presence of sulfuric acid, water adds to DCPD to form the exo secondary alcohol. Dicyclopentadiene alcohol can be used as a component of unsaturated polyester resins, perfumes, and plasticizers. Some DCPD esters are also used as perfume components (69). Dicyclopentadiene alcohol, a number of esters, ethers, and glycol adducts have been claimed as coal and ore flotation aids.

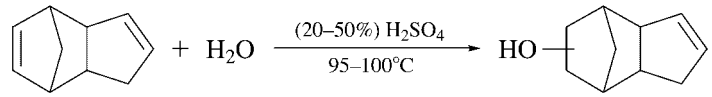

2 **13**

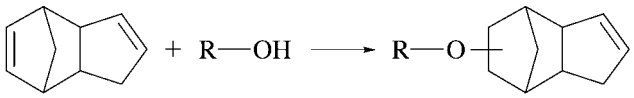

2

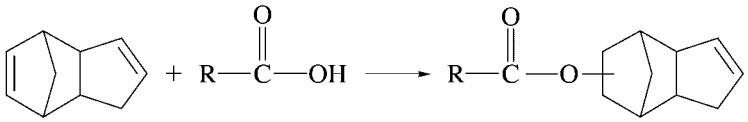

2

Cyclopentadiene oligomers have been formed by vapor deposition of CPD on kaolin to afford a sorbent for removal of oil from water (70). They are also employed as coatings for controlling release rates of fertilizers (71). Thermal addition

of sulfur to a mixture of DCPD and CPD oligomers has led to a number of beneficial applications such as wastewater oil adsorbent powdery foam (72), plasticized backing for carpets and artificial turfs (73), and in modified sulfur cements for encapsulating low level radioactive wastes (74).

Cyclopentadiene itself has been used as a feedstock for carbon fiber manufacture (75). It is also a component of supported metallocene–alumoxane polymerization catalysts in the synthesis of polyethylene and polypropylene polymers (76), as a nickel or iron complex in the production of methanol and ethanol from synthesis gas (77), and as Group VIII metal complexes for the production of acetaldehyde from methanol and synthesis gas (78).

Adamantane, tricyclo[3.3.1.1]decane [281-23-2] (**14**), can be produced by heating tetrahydrodicyclopentadiene [6004-38-2] (**15**) in the presence of aluminum trichloride (79). It is the base for drugs that control German measles and influenza (79,80).

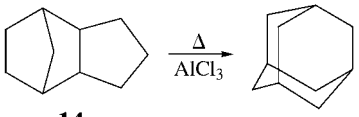

14 **15**

Other specialty applications of DCPD and CPD derivatives include dicyclopentadiene dioxide, dicyclopentadiene diepoxide, and dicyclopentadiene dicarboxylic acid in surface coatings, and the tetrahydrogenated DCPD and CPD as high energy fuels for racing cars, missiles, and jet (81,82).

BIBLIOGRAPHY

"Cyclopentadiene Polymers" in 1st ed., Vol. 4, pp. 563–568, by I. Kuntz, Esso Research and Engineering Co.; in *EPST* 2nd ed., Vol. 4, pp. 537–542, by I. Kuntz, Exxon Chemical Co.

1. A. F. Pame and J. M. Terent'eva, *Usp. Khim.* **20**, 560 (1951).
2. J. H. Walls and P. J. Wilson, *Chem. Rev.* **34**, 1 (1944).
3. M. Moulin, *Bull. Assoc. Fr. Tech. Pet.* **135**, 563 (1959).
4. A. S. Onishchenko, *Diene Synthesis*, Old Bourne Press, London, 1964, pp. 274–320.
5. Y. Ishii, *Sekiyu Gakkaishi* **32**, 229–236 (1989).
6. Y. Ishii, *Petrotech (Tokyo)* **11**, 785–787 (1988).
7. G. Xu, Y. Ye, and S. Xu, *Shiyou Huagong* **14**, 175–185 (1985).
8. V. N. Vostrikova and A. A. Grigor'ev, *Khim. Prom-st (Moscow)* (3), 134–138 (1985).
9. V. N. Vostrikova and T. S. Volkova, *Neftepererab. Neftekhim. (Moscow)* (7), 26–28 (1983).
10. C. Lou, *Huaxue Tongbao* (7), 415–421 (1982).
11. H. Komai and A. Ishikawa, *Petrotech (Tokyo)* **3**, 422–437.
12. W. Meyer, *Hydrocarbon Process.* (Sept. 1976).
13. C5 Olefins and Dienes, Report No. 75-6, Chem Systems Inc., New York, June 1976.
14. E. Samuel and M. D. Rausch, *J. Am. Chem. Soc.* **95**, 6263 (1973).
15. A. H. Wright, *Organomet. Chem.* **16**, 351–384 (1987).
16. W. E. Watts, *Organomet. Chem.* **14**, 342–372 (1986).
17. P. M. Maitlis, *Chem. Soc. Rev.* **10**, 1–48 (1981).
18. K. G. Caulton, *Coord. Chem. Rev.* **38**, 1–43 (1981).

19. B. Kanellakoupulos, *Nato Adv. Study. Inst. Ser., Ser. C* **44** (1978) (*Organomet. f-Elem.*), 1–35 (1979).
20. *NIST Mass Spec. Data Center*, S. E. Stein, Director.
21. K. C. Ramey and D. C. Lini, *J. Magn. Reson.* **3**, 94 (1970).
22. J. G. Martin and R. K. Hill, *Chem. Rev.* **61**, 537 (1961).
23. D. R. Eckroth, *J. Org. Chem.* **41**, 394 (1976).
24. U.S. Pat. 4,138,419 (Feb. 6, 1979), M. Arakawa and co-workers, (to Japan Synthetic Rubber Co.).
25. A. Taketa, *Chem. Econ. Eng. Rev.* **8**, 26–30 (1976).
26. E. D. Bergmann, *Chem. Rev.* **68**, 41–84 (1968).
27. U.S. Pat. 5,659,107 (Aug. 19, 1997), T. T. P. Cheung and M. M. Johnson (to Phillips Petroleum Co.).
28. G. B. Kistiakowsky and co-workers, *J. Am. Chem. Soc.* **58**, 146 (1936).
29. J. Pirsch, *Ber.* **67B**, 1115 (1934).
30. K. Alder and G. Stein, *Ber.* **67B**, 613 (1934).
31. K. Alder and co-workers, *Ann.* **496**, 204 (1932).
32. G. Becker and W. A. Roth, *Ber.* **67B**, 627 (1934).
33. U.S. Pat. 5,866,735 (Feb. 2, 1999), T. T. P. Cheung and M. M. Johnson (to Phillips Petroleum Co.).
34. N. A. Milas and L. S. Maloney, *J. Am. Chem. Soc.* **62**, 1841 (1940).
35. R. Criegee, *Ann. Chem.* **481**, 263 (1940).
36. P. Sequin, *Compt. Rend.* **216**, 667 (1943).
37. G. O. Schenk and D. E. Dunlap, *Angew. Chem.* **68**, 248 (1956).
38. E. T. McBee and H. E. Ungnade, *Chem. Rev.* **58**, 249 (1958).
39. C. G. Venier and E. W. Casserly, *Am. Chem. Soc. Div. Petr. Chem.* **35**, 260–264 (1990).
40. E. W. Casserly and C. G. Venier, *Am. Chem. Soc. Div. Petr. Chem.* **35**, 265–271 (1990).
41. U.S. Pat. 2,831,904 (Apr. 22, 1958), R. W. R. Krept (to Shell Development Co.).
42. *Estimates from data in Process Evaluation/Research Planning Dicyclopentadiene and Derivatives 97/98S7*, Chem Systems Inc., Tarrytown, New York, 1998.
43. U.S. Pat. 3,719,718 (Mar. 6, 1973), F. Grude and co-workers, (to Farbenfab Bayer AG).
44. Jpn. Pat. 61,227,537 (Oct. 9, 1986), M. Usui and co-workers, (to Sumitomo Chemical Industries K.K.).
45. Jpn. Pat. 60,116,634 (June 24, 1985), E. Kudo and S. Minegishi (to Hitachi Chemical K.K.).
46. Jpn. Kokai 51-83688 (July 22, 1976), K. Kudo and co-workers, (to Sumitomo Chemical Industries K.K.).
47. French Pat. 1,500,162 (Nov. 3, 1967), J. Broca and co-workers, (to Esso Research & Engineering Co.).
48. U.S. Pat. 3,084,147 (Apr. 2, 1963), L. P. Wilks (to Velsicol Chem. Corp.).
49. Eur. Pat. 149,909 (July 31, 1985), B. Bossaert and co-workers, (to Exxon Research & Engineering Co.).
50. Jpn. Pat. 63,260,913 (Oct. 27, 1988), S. Hayashida, K. Kimura, Y. Shimada, and E. Takahashi (to Maruzen Petrochemical K.K.)
51. U.S. Pat. 3,023,200 (Feb. 27, 1962), M. E. Epstein and N. C. Gangemi (to Pennsylvania Industrial Chemical Corp.).
52. Belgian Pat. 841,705 (Nov. 16, 1976) (to ICI.).
53. P. L. Smith, C. W. McGary Jr., and L. R. Comstock, *Proc. Annual Tech. Conf. SPI, Reinf. Plast. Div. 22nd Annual Meeting*, Washington, D.C., Jan. 31–Feb. 3, 1967, pp. 1–12.
54. U.S. Pat. 4,532,297 (July 30, 1985), H. C. Gardner (to Union Carbide Corp.).
55. U.S. Pat. 4,522,977 (June 11, 1985), H. C. Gardner (to Union Carbide Corp.).
56. U.S. Pat. 4,623,696 (Nov. 18, 1986), D. W. Mabrey and J. M. Dye (to P. D. George Co.).
57. U.S. Pat. 4,535,146 (Aug. 13, 1985), A. Mekjian (to U.S. Steel Corp.).

58. Jpn. Pat. 49-36713 (Apr. 26, 1971) (to Japan Oil).
59. Jpn. Kokai 48-92353 (Mar. 15, 1972) (to Asahi Chemical.).
60. U.S. Pat. 3,347,944 (Oct. 17, 1967), H. E. Fritz, K. E. Atkins, and G. L. O'Connor (to Union Carbide Corp.).
61. Jpn. Kokai 53-121753 (Mar. 31, 1977) (to Japan Synthetic Rubber).
62. Jpn. Kokai 49-11868 (May 17, 1972) (to Mitsui Petrochemical).
63. *Chem. Mark. Rep.* (Apr. 19, 1999).
64. Can. Pat. 1,215,399 (Dec. 16, 1986), M. G. Dokurno (to Dupont Canada).
65. U.S. Pat. 4,426,502 (Jan. 17, 1984), R. J. Minchak (to B. F. Goodrich Co.).
66. U.S. Pat. 4,400,340 (Aug. 3, 1983), D. W. Klosiewicz (to Hercules Inc.).
67. R. P. Geer, *Plast. Eng.* **41**(11), 41–49 (1985).
68. D. S. Breslow, *CHEMTECH* **20**, 540–544 (Sept. 1990).
69. Eur. Pat. 249,005 (Dec. 16, 1987), W. Kleinehama (to Huls A. G.).
70. USSR Pat. 1,344,401 (Oct. 15, 1987), V. A. Diner, V. N. Cheshchevo, and V. A. Polushkin.
71. U.S. Pat. 4,678,710 (July 7, 1987), S. Sakimoto and co-workers, (to Showa Denko K.K.).
72. Jpn. Pat. 49,060,323 (June 12, 1974), M. Chono and co-workers, (to Asahi Chemical Industries K.K.)
73. U.S. Pat. 4,012,545 (Mar. 15, 1973), W. G. Toland (to Chevron Research Co.).
74. P. D. Kalb, J. H. Heiser III, and P. Columbo, *Summary and Proceedings of The Twelfth Annual U.S. DOE Low-Level Waste Management Conference*, Chicago, Ill., Aug. 28–29, 1990, pp. 113–125.
75. Jpn. Pat. 61,282,426 (Dec. 12, 1986), K. Nakamura (to Asahi Chemical Industries K.K.).
76. U.S. Pat. 4,892,851 (Jan. 9, 1990), J. A. Ewen and A. Razavi (to Fina Technology Inc.).
77. U.S. Pat. 4,434,248 (May 4, 1982), M. T. Barlow (to British Petroleum Ltd.).
78. P. von R. Schleyer, *J. Am. Chem. Soc.* **79**, 3292 (1957).
79. *Chem. Week* **94**, 119 (Apr. 25, 1964).
80. R. C. Fort Jr. and P. von R. Schleyer, *Chem. Rev.* **64**, 277 (1964).
81. U.S. Pat. 3,381,046 (Apr. 30, 1968), C. A. Cohen and C. W. Muessig (to Esso Research & Engineering Co.).
82. U.S. Pat. 3,002,829 (Oct. 3, 1961), J. J. Kolfenbach and H. K. Wiese (to Esso Research & Engineering Co.).

T. T. PETER CHEUNG
Phillips Petroleum Company

DEGRADATION

Introduction

Most common polymers are organic materials, with chains mainly of carbon, hydrogen, oxygen, and nitrogen. Their chemical bonds are the same as those in small molecules, as are the intermolecular forces. Polymers derive their useful properties from their long, entangled chains, not from any special properties of the atoms and bonds making up those chains.

The energies of the chemical bonds and the intermolecular forces in polymers are typical of organic molecules. They are in the range that allows both chemical reactions and molecular motions at the temperatures at which polymers are used. Thus polymer properties are typically more sensitive to both temperature and time than are those of other materials, such as metals and ceramics. One consequence of the weak intermolecular forces that hold together thermoplastic polymers is that both chemical changes and molecular rearrangements can take place in time scales which are shorter than the expected lifetime and polymers may lose their desirable properties by both chemical and physical changes.

A molded thermoplastic polymer typically has been heated to 20–100°C above its melting point or glass transition, forced at very high pressure through a small hole into a mold and cooled in a minute or less. Many of the chains, especially those close to the outer surface, cool into the extended state that was induced during flow. As it cools in the mold, the outer sections of the part harden first. Later cooling of the core causes shrinkage stresses which compress the surface and put the core into tension. The thermal expansion coefficient of a polymer is also sensitive to orientation, with more expansion and contraction occurring across the chain axis than parallel to it. Hence large shrinkage stresses can be set up around regions where the polymer was extended during flow. In semicrystalline polymers (qv) the shrinkage on cooling through the melting point can be more

Encyclopedia of Polymer Science and Technology. Copyright John Wiley & Sons, Inc. All rights reserved.

than 10%, and this makes the problems much more significant. This means that the properties of a plastic article may change with time, as a result of annealing or creep, even without any chemical reaction. If the part is reheated above the glass transition, molecular relaxation leads to shrinkage. However, even below the glass transition, polymers can show physical aging (1), the initial non equilibrium state slowly becoming more dense as a result of continuing crystallization or molecular rearrangement in the glassy state, so that the polymer can slowly distort during use (see AGING, PHYSICAL; GLASS TRANSITION).

Stresses can also arise from differential expansion where polymer is attached to metal or wood. A typical thermal expansion coefficient for a plastic is about $1 \times 10^{-4}/^{\circ}$C; for a metal it is $2 \times 10^{-5}/^{\circ}$C; and for glasses it is lower still. This means that a 150°C temperature change on cooling from the solidification temperature can result in a strain large enough to cause eventual fracture (qv) if the plastic does not creep to relieve it (see VISCOELASTICITY).

Commercial polymer production is dominated by the cheap and simple carbon-chain polymers, especially polyolefins, their substituted derivatives, and hydrocarbon elastomers. Their value is that they can be fabricated very easily and cheaply, by high temperature processing of the molten polymer. The price is that chemical degradation during processing may be significant and much effort is put into developing methods of preventing processing degradation. One problem is that the chemical changes induced by processing may have a determining effect on the lifetime of the polymer in subsequent use.

In use, plastics usually fail because of localized stresses in combination with some weakening of the material. Embrittlement is the most important practical consequence of any reaction of the polymer that reduces its molecular weight and/or cross-links the chains. A second common consequence of degradation is yellowing. Polyolefins are especially vulnerable to oxidation. If they are not stabilized in some way, they may have a lifetime of only a few days in bright sunlight before they become weakened and useless.

Very little chemistry may be needed to destroy the mechanical properties of a polymer. If 1% of the C—C bonds in a hydrocarbon fluid are broken, the effect is to form a small fraction of impurities, usually of little significance. The same fraction of breaks in a polyolefin will reduce it from a high molecular weight polymer to an oligomeric wax. Thus in polymers a very low level of chain breaks will cause failure, and polymers may lose their mechanical properties rather easily with negligible changes in mass. Some other properties, for example the dielectric constant, may be even more sensitive to formation of polar groups by oxidation.

Although academic studies of polymer degradation usually involve a single, pure polymer, the physical properties of commercial polymers are almost invariably modified by additives (qv). These may be low molecular weight substances, such as plasticizers (qv), pigments, stabilizers, fire retardants, antistatic agents (qv), and antiblocking agents, among many others (see RELEASE AGENTS). They also include particulate materials such as pigments and fillers. Physical loss, or chemical degradation, of these agents can lead to changes in properties over time. Contact with other materials can also cause changes in properties, owing to migration of additives from one material to another. Thus, the properties of an object may change with time, even without any chemical reactions of the polymer from which it is made.

Thus, polymers are not simple materials and articles fabricated from them are often complex formulations. The base polymer may vary in microstructure, molecular weight, molecular weight distribution, and structural defects and impurities. It usually forms one part of a complex product, containing many different types of additive, which may be there to improve the product, to provide color, to aid in its manufacture, to prolong its life, or to protect it from extremes, such as fire. In use or storage, the formulation will be exposed to oxygen and may be exposed to elevated temperatures, to contacting liquids, to sunlight, and to atmospheric pollutants, including very reactive compounds, such as ozone. All of this means that polymers are subject to a wide range of degradative influences, both physical and chemical. Physical degradation effects, especially aging, physical (qv) and environmental stress cracking are discussed elsewhere; in the following sections chemical degradation mechanisms are discussed in more detail.

Thermal Degradation, Mechanistic Studies

Thermal degradation of polymers is the collection of chemical reactions that result in deterioration of properties in the absence of air or radiation. Purely thermal degradation, in inert atmosphere or vacuum (pyrolysis), defines the ultimate stability of a polymer in the absence of other degradative influences. It represents the point where the chemical bonds of the polymer acquire enough thermal energy to break or rearrange spontaneously at significant rates.

Pure thermal degradation is rarely significant in long-term use of polymers, because applications usually involve air contact and oxidative reactions dominate. However, it plays an important part in determining processibility. It can also introduce functional groups into the polymer, which produce color or influence long-term oxidative stability. Although pure thermal degradation is largely irrelevant to service use of polymers, there is continuing interest in its study, partly because of its role in the important areas of flammability and fire retardance, partly because of increased interest in the incineration of polymeric wastes, and partly because of increased interest in the possibility of recovering useful materials from waste plastics by inert-atmosphere pyrolysis.

Thermal degradation involves reactions at high temperatures in a solid or a very viscous liquid and loss of volatile products tends to be diffusion controlled, except in extremely thin films. Because the primary reaction products are trapped in the polymer at high temperatures, secondary reactions are common. None of this is of concern in pragmatic studies of industrial pyrolysis, except in the sense that laboratory studies need to be carried out under conditions matching the practical ones as closely as possible. In the academic sense however, thermal degradation is very difficult to study well and the literature contains much indifferent research and "paper chemistry." Model compound studies, although widely used, are often unreliable, either because the polymer decomposes through pathways different from those of the model compound or because polymers contain weak links arising from impurities or structural defects. For example, polyethylene (PE) decomposes rapidly enough to be measured easily at 300°C, whereas pure linear hydrocarbons are stable to over 400°C.

Thermal degradation reactions of polymers can be divided into two broad groups: molecular rearrangement reactions and reactions which involve homolytic scission of bonds to produce free radicals. In both cases the chemistry is typically complicated by the fact that primary products may be very reactive at the high temperatures involved in thermolysis, leading to rapid secondary chemistry. For example, the primary thermal degradation reaction in poly(ethylene terephthalate) (PET) is ester elimination at between 250 and 300°C to give carboxylic acid and vinyl ester groups:

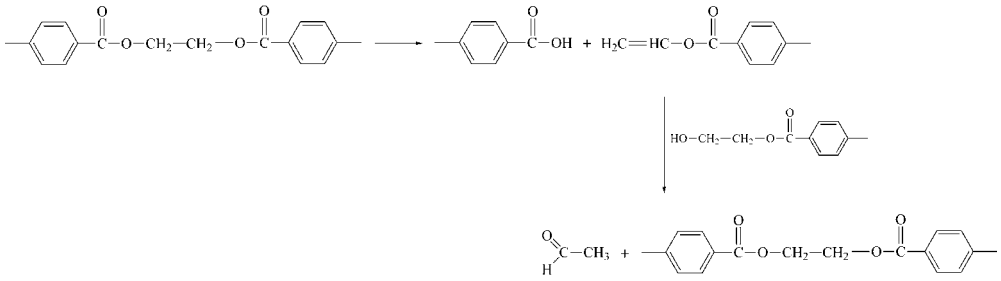

(**1**)

At degradation temperatures the vinyl ester groups are not stable and rapidly form the first major volatile degradation product, acetaldehyde (**1**) (the keto tautomer of vinyl alcohol), possibly by transesterification with hydroxy ester end groups (2). Acetaldehyde formation is of some concern in the use of PET for manufacture of beverage bottles.

Most studies of thermal degradation of polymers are carried out under conditions where the rate is fast enough to give measurable reaction in times from seconds to hours. Whatever the mechanism, the rate constant for any elementary reaction can be expressed as a function of temperature in terms of the Arrhenius relation:

$$k = A \exp\left(- \frac{E_a}{RT} \right) \tag{1}$$

where k is the rate constant at temperature T, and E_a and A are the activation energy and preexponential factor. Equation 1 is soundly based in statistical mechanics only for elementary reactions in the gas phase. For reactions in liquid or solid phases, E_a is rarely a constant over a wide temperature range. This may be because the reaction is a complex process, but even elementary reactions in liquids and solids often have variable activation energies (3).

It is also important to remember that if parallel reactions have comparable rates at a given temperature, the one with the highest activation energy will increase in rate more rapidly with increasing temperature and slow down more rapidly with decreasing temperature. Thus, degradation at high temperatures may be dominated by high activation energy reactions which are relatively unimportant at lower temperatures.

It is now fairly clear that there can be substantial distinctions between addition and step-reaction (condensation) polymers. Addition polymers typically have C—C bonds along the chain and large numbers of aliphatic hydrogen atoms. The

dominant mechanisms of degradation typically involve the breaking of C—C bonds to form free radicals. At the temperatures of rapid decomposition of carbon-chain polymers (typically in the range 300–500°C), the resulting radicals are highly reactive and can readily undergo a range of reactions, including recombination and chain transfer, leading to complex mixtures of products, often with a great deal of uncertainty as to the exact mechanism of formation of any particular product.

In contrast, typical step-reaction polymers have polar functional groups at regular intervals along the chain. Although, like carbon-chain polymers, they can decompose by homolytic scission at high enough temperatures, they can also decompose by molecular rearrangement reactions, which are often highly selective for the particular functional groups in the chain and can occur at lower temperatures than do radical processes.

After many years of study, three distinct mechanisms of thermal degradation can be identified, although they are not mutually exclusive, and most polymers degrade by more than one mechanism, depending on the temperature. Detailed mechanisms of degradation of a wide range of carbon-chain polymers have been reviewed (4); degradation of step-reaction polymers has also been reviewed (5).

Chain Scission with Depropagation. Many carbon-chain polymers and other simple chains, such as acetal resins (polyethers), are produced by chain reaction polymerization, either via double bonds or by ring opening. Such polymerizations involve repeated addition of a monomer molecule to an active center, which may be a radical, an ion, or a coordination complex.

In principle, any such reaction is an equilibrium and can be written in the form

$$P_n^* + M \rightleftharpoons P_{n+1}^* \tag{2}$$

where P^*_n and P^*_{n+1} represent propagating chains with n and $n+1$ monomer units respectively. For large values of n (typically $n > 3$–4), it is well established that the rates of propagation and depropagation are independent of n, so that the two species P^*_n and P^*_{n+1} are not distinguishable. Thus, the equilibrium constant K_e is simply 1/[M], where [M] is the monomer concentration, and K_e can be written in the form

$$\Delta G^\circ = \Delta H^\circ - T\Delta S^\circ = -RT \ \ln K_e = RT \ln[M] \tag{3}$$

where ΔG°, ΔH° and ΔS° are the standard free energy, enthalpy, and entropy of polymerization respectively (6,7).

Thus, any concentration of monomer is in equilibrium with the corresponding propagating, or depropagating, chains at a temperature given by

$$T_c = \Delta H^\circ / (\Delta S^\circ + R \ \ln[M]) \tag{4}$$

Note that ΔH° and ΔS° depend upon the state of the polymer and the monomer. If [M] is set equal to the bulk concentration, T_c is the so-called *ceiling temperature* and is the upper limit at which propagating chains and monomer can coexist in equilibrium. Another approach is to recognize that polymerization requires

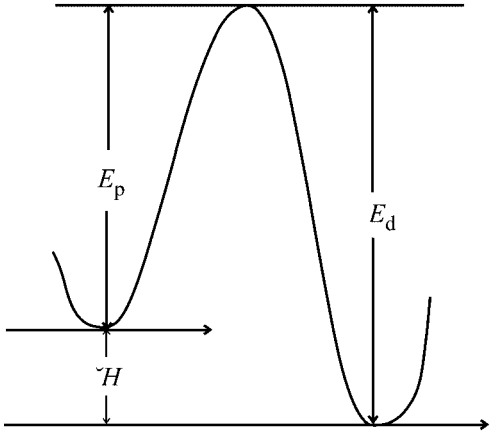

Fig. 1. Change in energy of a polymerization/depolymerization equilibrium along the reaction coordinate, showing the relation of the activation energies of propagation and depropagation and the heat of polymerization.

ordering of monomer units into regular chains and must have negative entropy change. The requirement for a negative free-energy change for spontaneous polymerization implies exothermic polymerization. This in turn means that the activation energy for depropagation must be higher than that for propagation by an amount equal to the heat of polymerization (Fig. 1). Thus as the temperature is raised, depropagation increases in rate faster than does propagation; for a given monomer concentration, the ceiling temperature is then the point at which the two rates become equal.

If a polymer is heated to the point where chemical bonds begin to break, radicals will normally be formed, rather than ions. Thus if chain scission takes place to produce free radicals at temperatures above T_c, rapid radical depolymerization, with production of monomer, is expected. This rapid depropagation is often termed *unzipping*. Table 1 shows some typical values for T_c for common polymers. They range widely from quite close to room temperature for polyacetal to close to 600°C for polytetrafluoroethylene. In reality, side reactions, which are discussed

Table 1. Ceiling Temperatures of Common Monomers

Monomer	State[a]	T_c, °C
Trioxane	lc	36
α-Methylstyrene	lc	45
α-Methylstyrene	ls	61
Formaldehyde	gc	118
Methyl methacrylate	lc	197
Propylene	gc	271
Propylene	lc	384
Styrene	lc	451
Tetrafluoroethylene	gc	600

[a] lc: liquid monomer with solid polymer; ls: liquid monomer with dissolved polymer; gc: gaseous monomer with solid polymer.

later, mean that rather few polymers actually decompose smoothly to monomer by depropagation, the most well-studied example being poly(methyl methacrylate) (PMMA).

Most polymers are actually stable at temperatures above T_c because the activation energy for chain scission is high enough that radicals can only be formed by thermal scission at higher temperatures. This, however, has its own dangers. If radicals are induced in a polymer at temperatures above T_c then depolymerization may be very rapid. For example, it is common to mold PMMA at temperatures above T_c. Under these conditions chain scission induced by mechanochemical damage to the polymer in the high shear fields of the extrusion or molding operation results in the near instantaneous conversion of that chain into gaseous monomer, which can lead to bubbles or surface imperfections in the molding. Similarly, exposure of PMMA to uv, electron beam, or γ-irradiation above T_c will lead to very rapid degradation; degradation reactions of this type are the basis of some photoresist technologies.

In principle, depropagation is initiated by the thermal scission of a main-chain backbone bond to produce a pair of depropagating radicals. If the depropagation is a simple chain reaction, the effective activation energy E_{ef} should be given by

$$E_{ef} = E_d + \frac{1}{2} E_i - \frac{1}{2} E_t \tag{5}$$

where E_d, E_i, and E_t are the activation energies for depropagation, initiation, and termination respectively. If E_i corresponds to the dissociation energy for the weakest bonds in the backbone, then E_{ef} should be an inherent property of the polymer. In practice it is sometimes found that the activation energy rises with temperature or degree of degradation, to reach a limiting value only at high temperatures or high conversions. It is also found that the rate of thermal degradation of, eg, PMMA is dependent on the initial degree of polymerization of the polymer. This behavior is associated with the presence of bonds that are weaker than average and can initiate production of depropagating radicals at lower temperatures. An important feature of the design of polymers is control of these thermally sensitive groups.

The presence and nature of "weak links" in polymer chains has been hotly debated over many years. The most important, and the most firmly established, example of such links is the end groups, associated with the initiator, with chain transfer, or with termination. Others include copolymerized oxygen, oxidation of the polymer in storage, and wrongly inserted monomer units. Control of polymerization conditions or post-polymerization modification of polymer structures can reduce the significance of such reactions and give polymers of greater thermal stability, and end-group control can be important in industrial processes. It has been shown (8) that the degradation of PMMA prepared by conventional radical polymerization occurs in at least three steps, which are associate with scissions of head-to-head linkages, with decomposition of vinylidene end groups, and with random main-chain scissions in order of increasing thermal stability. No difference between polymers produced with azo or peroxy initiators was detected (8).

An example of the importance of end-group control is in acetal resin or polyoxymethylene (POM). As normally prepared from cationic polymerization of sym-trioxane, this polymer has —OH end groups, which readily initiate depropagation to formaldehyde (**2**) by a molecular mechanism (9):

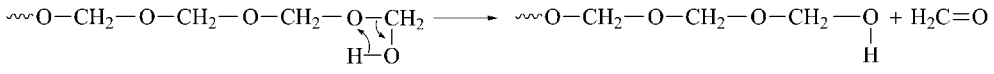

2

This reaction can be blocked by acetylation of the chain ends, leading to a polymer which can survive above T_c because there is no mechanism of chain scission with a low enough activation energy to initiate depropagation. Another approach is to copolymerize a small amount of a second monomer, such as styrene. The polymer is heated to initiate depropagation, which occurs until it encounters the first comonomer unit, at which point further depropagation is blocked. The evolved monomer is recycled.

Even where a polymer decomposes by simple depropagation reactions the kinetics of degradation are complex. The complexity is shown by the dependence of degradation rate on subtle changes in polymer structure, as discussed earlier (8), and by variations of the activation energy with conversion as chains of different stability are destroyed (10).

The kinetics of degradation of polymers which depropagate have been discussed in detail, especially for PMMA (see eg, Refs. 11–13). The analysis is complicated because the reaction volume changes with conversion as volatiles are evolved and because the *kinetic chain length* (the average number of depropagation events for each initial chain scission) may be controlled by the molecular weight of the chain. Termination may be by the bimolecular interaction of pairs of radicals or by radicals evaporating from the polymer.

Exactly what happens depends on the details of the reaction, but two extremes can be considered. If the reaction is initiated at the chain ends and the depropagation has a long kinetic chain length, all molecules have an equal probability of being initiated and each initiation results in the corresponding chain being completely removed as monomer. In this case the mass of the polymer decreases with degradation but there is no change in average molecular weight or in the distribution. In contrast, if the reaction is initiated by random scission and the kinetic chain length is long, long chains have a greater probability of scission and are removed completely as monomer. In this case, the mass of polymer falls, and the average molecular weight decreases with degradation.

In the ideal case, where only depropagation occurs, the mechanism can be deduced from the dependence of the observed first-order rate constant for weight loss on the initial degree of polymerization of the polymer. If depolymerization is both chain-end and chain-scission initiated and termination is first-order then application of the steady-state assumption to the concentration of depolymerizing radicals leads to the following relation (14,15):

$$k_{\mathrm{obs}} = \left(\frac{k_{\mathrm{i}}}{P_n} + 2k_{\mathrm{i}}'\right)\frac{k_{\mathrm{d}}}{k_{\mathrm{t}}'} \tag{6}$$

where P_n is the initial degree of polymerization, k_{obs} is the observed first-order rate constant for mass loss, and k_d is the rate constant for depropagation, k_i and k'_i are the rate constants for chain end and random scission initiation respectively, and k'_t is the rate constant for first-order termination. Thus the relative contributions of end initiation and main-chain scission can be deduced from the linear plot of k_{obs} against $1/P_n$.

Conversely, if termination is bimolecular, then it can be shown (14,15) that

$$k_{obs}^2 = \left(\frac{k_i}{P_n} + 2k_i'\right)\frac{k_d^2 u}{2k_t \rho} \tag{7}$$

where k_t is the rate constant for bimolecular termination, u is the molecular weight of the polymer repeat unit, and ρ is the density of the polymer. Here the relative contributions of end initiation and main-chain scission can be deduced from the linear plot of $k^2{}_{obs}$ against $1/P_n$.

In a study of degradation of PMMA with end groups derived from chain transfer to lauryl mercaptan (11), it was shown that degradation at low (<340°C) temperatures was by end initiation with unimolecular termination. As the temperature was increased there was an increasing contribution from chain-scission initiation and at temperatures above 450°C it became the dominant initiation mechanism. At the highest temperatures low molecular weight polymers showed complete depropagation but the higher molecular weight ($D > 1500$) chains showed termination during unzip.

Random Scission without Depropagation. In radical polymerization, the simple chain-growth mechanism is complicated by side reactions of the propagating free radicals, which may undergo chain-transfer reactions in which the radical activity is transferred from one center to another, typically by hydrogen atom abstraction.

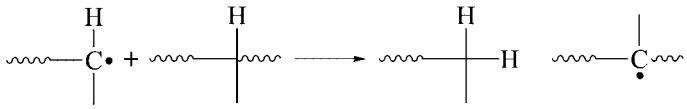

The hydrogen atom may come from any species in the mixture. Chain-transfer agents, often thiols, are often used to control molecular weight and end-group structure in polymerization chemistry.

Because the activation energy for chain propagation is much lower than that for chain transfer, transfer is usually a minor process in polymerization, although it can have important effects on both polymerization rate and polymer structure. The same is not true of depropagation. Although the activation energy for depropagation is higher than that for propagation, the high temperatures involved mean that rates of depropagation and chain transfer are comparable for most polymers at the temperatures involved in thermal degradation. Because of this, rather few polymers depropagate cleanly to high yields of monomer, because, as soon as a radical is produced, it undergoes chain transfer.

The relative frequency of chain transfer compared to depropagation is determined by the stability of the chain-end radical and by the availability of

Table 2. Some Typical Monomer Yields in Polymer Pyrolysis

Polymer	Monomer, %
Poly(methyl methacrylate)	100
Polystyrene	42
Poly(α-deuterostyrene)	70
Poly(α-methylstyrene)	100
Polyacrylonitrile	<5
Polymethacrylonitrile	100
Polytetrafluoroethylene	100
Poly(methyl acrylate)	0
Polyethylene	<1
Polypropylene	2
Polyisobutene	32
Polybutadiene	1.5
Polyisoprene	12

readily abstracted hydrogen atoms; only the very few polymers where a relatively stable radical is formed and chain transfer is restricted by the absence of easily abstractable hydrogen atoms depropagate cleanly. For example, while PMMA depolymerizes virtually completely, poly(methyl acrylate) with its readily abstractable α-hydrogen atom gives less than 1% monomer on pyrolysis, degrading instead to a complex mixture of low molecular weight fragments and char. Chain depropagation may also be inhibited by the presence of even very small fractions of comonomer units in the polymer chain acting as blocking groups for the unzip process. The resulting chain-end radicals often undergo transfer reactions.

Table 2 shows the typical monomer yields for thermolysis of common polymers. Essentially PMMA is the only polymer in common use which depropagates totally to monomer, although poly(α-methyl styrene) and poly(tetrafluoroethylene) also give close to 100% yields of monomer. For other polymers, the monomer yield ranges from zero to a significant fraction of the total volatile products.

The effect of chain transfer depends upon its frequency and the location of the abstractable hydrogens, but is typically the production of a complex mixture of low molecular weight volatile products.

Transfer may be intramolecular ("backbiting"), in which case it yields oligomeric fragments such as dimer and trimer by a process which is sometimes referred to as "unbuttoning." It has been suggested that products arising from six-membered backbite rings are at least an order of magnitude more probable than those from any other intramolecular process (16).

In contrast, if transfer occurs intermolecularly, then the new radical center is not at the chain end. Its scission results in rapid drop in molecular weight, initially without significant production of volatiles and the polymer undergoes random scission. As an example, pyrolysis–gas chromatography was used (17) to show that high molecular weight polyisobutene can degrade thermally to give more than 60 volatile products. A statistical analysis of the distribution of pyrolysis products,

grouped into general oligomeric types up to nonamer, suggested that random scission is the predominant mechanism leading to the wide range of oligomeric products. The observed monomer, dimer, and trimer yields were found to exceed the predictions of a statistical model, and these products were deduced to be due to depropagation plus backbiting transfer.

A problem arises when oligomers are observed as the principal products of thermal decomposition. They may arise from a high degree of random scission, intramolecular transfer during unzip, and/or secondary reactions of the primary products. These mechanisms can be differentiated by appropriate statistical plots of the yields of the products, quantitative measurements of rate constants for the evolution of the volatiles, and measurements of product yields and ratios as a function of sample size (18).

Where a polymer has functional groups in the main chain, typical of polymerization by step-reaction chemistry or chain polymerization of heterocyclic monomers, the functional groups in the chain are often the weakest and may undergo reactions which do not produce radicals. Thermal degradation by random scission, without significant yield of volatiles is typical of polymers such as polyesters, polyamides, and polyurethanes, all of which undergo thermolysis by reaction at the functional groups (5).

Examples of random scission reactions in step-reaction polymers include the decomposition of polyurethanes, which produces cleavage of the urethane groups via the facile transfer of the N—H hydrogen atom to the neighboring oxygen:

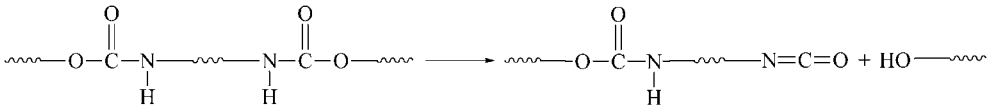

This reaction may give random scission or stepwise depolymerization, depending upon whether it occurs preferentially at the chain ends. Nylon-6 also degrades by formation of ε-caprolactam by random scission or stepwise depolymerization.

Aliphatic polyesters and polyesters formed from aromatic diacids and aliphatic diols eg, poly(ethylene terephthalate) and poly(butylene terephthalate) (**3**) cannot decompose by reversion of the polymerization, because the water, or alcohol, eliminated in the synthesis is no longer available. They initially decompose by β-C—H transfer reactions via a six-membered transition state:

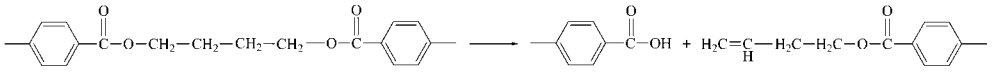

(**3**)

Nylon 6,6 (**4**) initially decomposes by an α-C—H shift to yield amine and cyclopentanone end groups. At the temperature of thermolysis, the cyclopentanone end groups decompose further to produce cyclopentanone and isocyanate end groups.

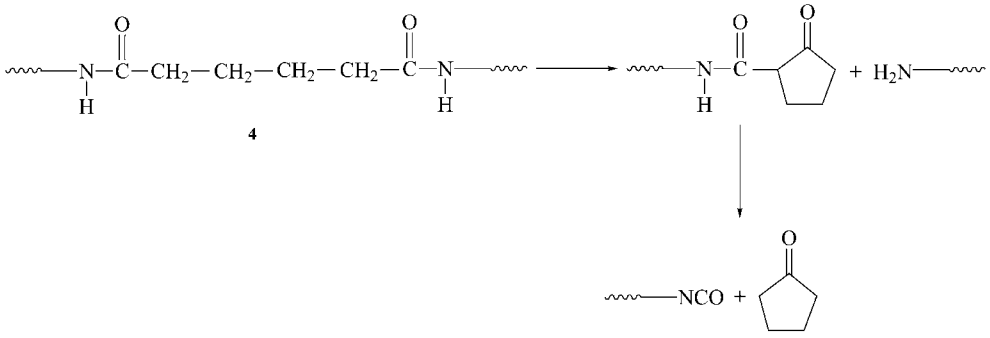

4

At typical pyrolysis temperatures the isocyanate groups produced in pyrolysis of polyamides and polyurethanes are not stable and readily decompose to yield nitrile groups.

Random scission is also typical of the degradation of many polymers by reaction of chain bonds with other reagents. Hydrolytic and other chemical reactions and biological attack frequently show purely random scission, provided that the accessibility of the chain to the degrading agent is not limited by, eg, crystallinity or water permeability.

If the average chain lengths at time zero and time t are P_0 and P_t respectively and the average number of scissions per initial chain at time t is s then, if scission is purely statistical,

$$P_t = \frac{P_0}{s+1} \tag{8}$$

For random scission, the fraction of bonds broken at time t, α, is then given by

$$\alpha = \frac{1}{P_n} - \frac{1}{P_n^0} = kt \tag{9}$$

where k is the rate constant for the scission reaction. Thus a plot of α against time will be linear. For example, the natural bacterial polyester poly(hydroxybutyrate) (PHB) degrades thermally at temperatures just above its crystal melting point by the ester rearrangement to yield carboxylic acid and olefin end groups. A study of the degradation of this polymer under melt extrusion conditions (19) showed that equation 9 is followed well, although the gradient depended on the origin and degree of purity of the polymer, suggesting some catalysis of the scission by impurities.

A more severe test for random scission is the recognition that, whatever the initial distribution of molecular weights, random scission should lead to the "(Flory) most probable" distribution with a polydispersity index ($\bar{M}_w/\bar{M}_n$) equal to 2.0.

If α is the fraction of bonds which have undergone scission then the weight distribution function for the molecular weight in the case of random scission becomes (20):

$$w_x = x\alpha^2(1-\alpha)^{x-1} \tag{10}$$

where w_x is the weight fraction of chains with degree of polymerization x. Taking logarithms of both sides of equation 11

$$\ln(w_x/x) = 2\ \ln\alpha + (x+1)\ln(1-\alpha) \tag{11}$$

is obtained.

Equation 11 is the equation to a straight line whose slope and intercept are both determined by α. The assessment of random scission can thus be based on the extent to which molecular weight data fit a plot of equation 11, and (more particularly) the correspondence of values of α calculated from both the intercept and the slope of the plot (20,21).

This method can be more sensitive to small deviations from random scission. For example, the number and weight distributions of the oligomeric products observed on degradation of PHB have been compared with those predicted statistically (21). The results show that total thermolysis can be interpreted exclusively in terms of a random scission mechanism. However, the partial pyrolysis results are not consistent with random scission statistics; these results imply that there are some kinetically favored scissions occurring near the ends of the molecules. The product distributions from methanolysis were also slightly inconsistent with those expected on the basis of random scission and it was suggested that dimers hydrolyze more readily than do higher molecular weight species.

Although equation 9 implies a linear plot of α against time, such plots frequently show intercepts on the α-axis, which can be explained by the presence of small fractions of weak links which degrade preferentially at the beginning of the reaction. Such links are common in polymers synthesized by radical mechanisms, and are most likely due to small contents of copolymerized oxygen.

Thermal Reaction without Chain Scission. In any polymer, the chemical changes that occur at the highest rate at any given temperature will be the most significant causes of changes in properties. Often these are reactions that involve chain scission, either via radical intermediates or in molecular rearrangements which lead to scission. However, there are many other examples where reactions of substituent groups take place before scission, or may compete with it. In these cases the degree of polymerization remains the same but new structures are formed along the polymer chain.

Perhaps the most common such reaction in carbon-chain polymers is elimination of the substituent, with the formation of a double bond. The classic, and most important, example is the dehydrochlorination of poly(vinyl chloride)(PVC), which can be written formally as

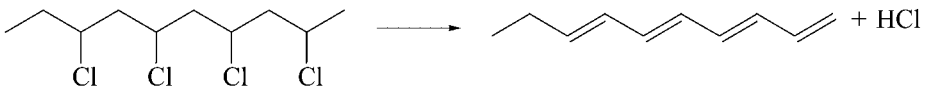

The important feature is the formation of polyene sequences by successive eliminations. These absorb visible light, causing the polymer initially to become yellow and eventually black. Similar reactions can occur with many polymers,

eg, poly(vinyl alcohol), poly(vinyl acetate), and cellulose and its esters. If the elimination reactions are allowed to go to high conversions, the polymer is typically transformed into a carbonaceous char, which may be quite thermally stable. Much of fire-retardant chemistry is aimed at increasing char yields in polymer thermolysis.

The reaction of PVC is important because it is the major pathway for degradation of this high tonnage polymer at relatively low temperatures. At high temperatures elimination and chain scission are competitive. PVC degradation has been extensively reviewed (see eg, Refs. 22–25). Despite a huge literature, even the most basic features remain contentious, and it is clear that the process has a much more complex mechanism than is implied by the equation above. It is initiated at reactive defect sites in the chain and catalyzed by the eliminated hydrochloric acid. Reactive sites include those which are part of the virgin polymer, such as allylic or tertiary chlorine atoms, produced in chain-transfer or termination reactions during polymerization; and hydroperoxy groups, introduced by thermal oxidation during processing. Although a wide variety of such sites has been identified in laboratory samples of PVC, it is probable that the hydroperoxides are dominant in processed commercial PVC materials.

Since many PVC formulations also contain pigments, plasticizers, and impact modifiers, this can be one of the most complex of plastics. Simple elimination is not the only reaction possible. Indeed, in pyrolysis conditions PVC containing plasticizer or impact modifier produces a very wide range of products, some from each component and others from cross-reactions (26,27). There has been considerable concern about the possibility of forming polychlorinated dibenzodioxins (PCDD) and dibenzofurans (PCDF) in PVC pyrolysis, related to the increased presence of PVC in input streams to commercial waste incinerators and the toxicity of PCDDs and PCDFs. Tars produced by PVC pyrolysis under different conditions of temperature and oxygen concentration have been analyzed (28). The tar collected after low temperature pyrolysis (500°C) in reduced oxygen atmosphere (12% O_2) had the highest toxicity, mainly owing to a high PCDF concentration. Pyrolysis at higher temperatures and higher oxygen pressures essentially eliminated the toxic products.

Another important example of a polymer which gives coloration due to side-group elimination is polyacrylonitrile (**5**), which colors slowly when heated and very rapidly on exposure to alkalis. This is usually attributed to the formation of conjugated, cyclic structures by reactions of the form

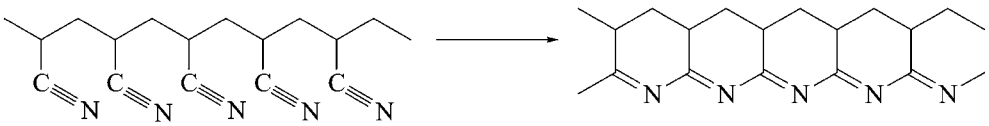

5

Although elimination reactions are clearly degradation, leading to color and char formation, they can have advantages. Conjugated sequences and ladder structures confer thermal stability on the polymers, forming stable chars. This is the basis of the preparation of carbon fibers by pyrolysis of polyacrylonitrile. It is also one reason for the use of plasticized PVC in electrical insulation; in a

fire, the char acts as a protective coating and maintains the electrical insulation properties of the cable.

Although elimination is a common and important nonscission reaction in degradation, it is not the only such reaction. For example, polymers which contain carboxylic acid groups undergo coupling reactions to form anhydride groups at relatively low temperatures. Anhydride formation may be intramolecular or intermolecular; in the latter case it produces cross-links.

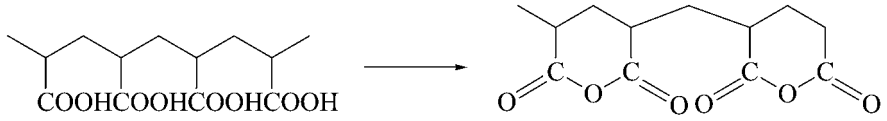

The carboxyl groups may be present in the original polymer, but can also be formed by elimination reactions. Again, the product balance depends upon the relative rates of the possible reactions. For example, ester elimination in PMMA is impossible because of the absence of β-hydrogen atoms. In poly(*t*-butyl methacrylate) (**6**) there are nine β-hydrogens and thermolysis leads to virtually no monomer; elimination followed by cyclization is the dominant mechanism.

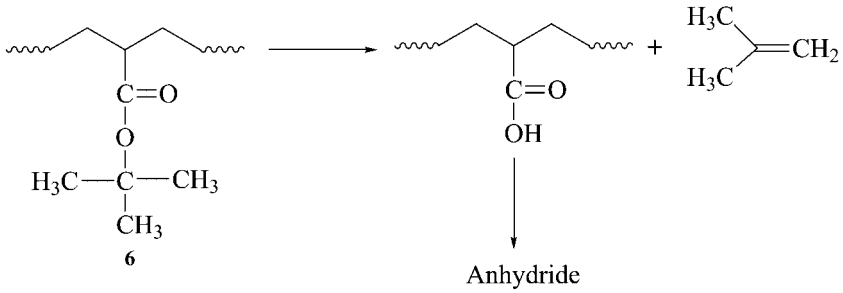

Other poly(*n*-alkyl methacrylate)s give a mixture of depolymerization and side-group rearrangement, depending on the number of β-hydrogens and the temperature.

Thermal Degradation, Analytical Methods

As outlined above, thermal degradation of polymers is complex and can be broadly divided between studies aimed at elucidating the fundamental mechanisms of reactions of the polymer, typically using tiny amounts of very pure polymer, and more pragmatic studies under conditions more representative of degradation of bulk material in fire or in industrial processing conditions.

Depending on the mechanism of degradation, a polymer may undergo chemical changes with virtually no loss of mass, or it may be converted almost entirely into volatile products. The latter may have a wide range of molecular weights, from easily condensable oils to very low boiling gases. The condensable oils are often referred to as the "cold-ring" fraction, because they are found as a condensate at the exit of the pyrolysis chamber. Both the solid residue and the gaseous products may

be quite simple, or they may be highly complex mixtures. Many normal chemical analytical techniques are routinely applied to study thermal degradation. They include ir and nmr spectroscopies of residues and cold-ring fractions, gas chromatography to separate gaseous products, and mass spectroscopy for their analysis and identification. However, the field has also developed a number of more specialized techniques.

Thermogravimetric Analysis. Thermogravimetric analysis (tga) is a deceptively simple technique, which has been very widely used in degradation studies because of the ready availability of commercial instruments at reasonable prices. Its use has been widely reviewed (29).

In its simplest form, a tga instrument consists of a small crucible holding a few milligrams of sample and attached to a recording microbalance. The crucible is positioned in a small furnace in which the atmosphere can be controlled, both inert and oxidizing conditions being possible. In a typical experiment the sample is heated at a programmed rate (typically 1–20°C/min) from ambient temperature to 800°C and the changes in mass with temperature are recorded. There are a number of critical features in the design of a good tga instrument to ensure that the sample temperature is known and controlled and that exothermic and endothermic reactions in the polymer do not lead to errors in measuring the sample temperature. These were problematic in early tga instruments, which used large samples. Modern instruments are usually exemplary in furnace and microbalance design. In most modern tga instruments, software provided by the manufacturer also allows differentiation of the weight-loss curve to produce a differential thermogravimetric (dtg) curve which has peaks corresponding to maxima or rate of weight loss. Figure 2 shows typical tga and dtg curves.

A recent development in tga is the so-called "high resolution" tga. In a conventional tga the heating rate is constant. In a high resolution instrument the heating rate is automatically varied with the rate of weight loss. If the sample is stable and not losing weight, the heating rate is kept high; if the sample begins to lose weight then the heating rate is automatically reduced. It is claimed that high resolution tga can help to separate thermal processes in similar temperature ranges.

The major information provided by a tga is the number of distinguishable stages of breakdown, the temperatures of onset and maximum rate of weight loss, and the amount of material lost at each temperature. In addition to giving information on degradation, tga can also be used in favorable cases to determine the content of inorganic fillers or carbon black by degrading away all of the polymer to leave the filler.

The major weakness of classical tga is that it gives information on weight loss but no chemical information. To overcome this problem, some modern tga instruments have been designed to be interfaced to chemical analysis instruments, the most popular being mass spectroscopy and Fourier transform infrared (ftir) spectroscopy. Both can give extremely useful information but care is needed to avoid problems from secondary reactions of volatile products and from loss of volatile products by condensation in transfer lines. The use of these so-called hyphenated techniques has been reviewed (30).

Although the thermal degradation of a polymer is complex and may involve successive and/or parallel steps, kinetic analysis of thermogravimetric data is

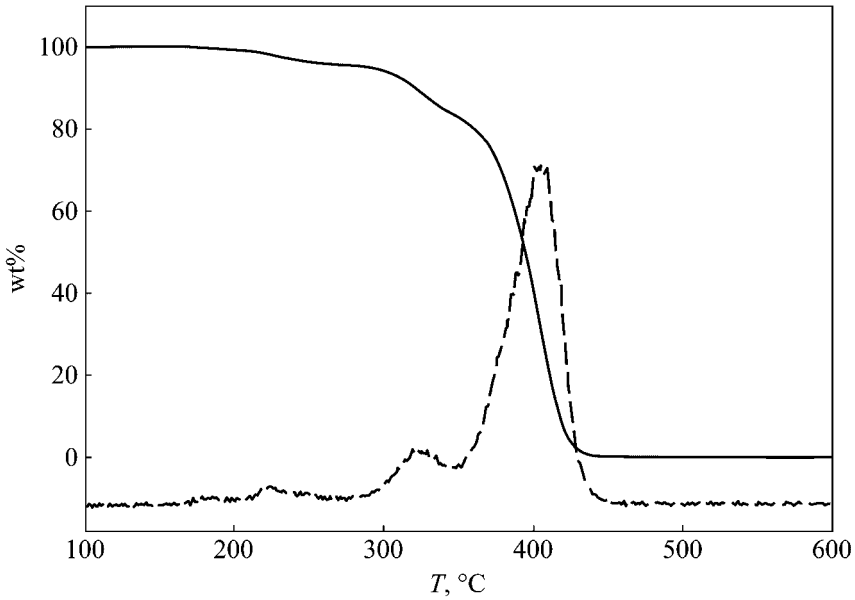

Fig. 2. Typical TG (solid line) and DTG (dotted line) curves. The example is for poly(methyl methacrylate) produced by free-radical polymerization. The major weight loss is due to depolymerization of chains with saturated ends. The peaks at lower temperatures are due to depolymerization of chains with weak links (copolymerized oxygen or unsaturated ends, produced by disproportionation termination).

often performed by using a single-step kinetic equation:

$$\beta \frac{\mathrm{d}\alpha}{\mathrm{d}T} = Af(\alpha) \exp\left(-\frac{E}{RT}\right) \tag{12}$$

where α is the fractional conversion at temperature T, β is the heating rate, $f(\alpha)$ is the differential form of the reaction model, relating the rate of reaction to α, and E_a and A are an activation energy and preexponential factor respectively. The three parameters E_a, A, and $f(\alpha)$ are often called the kinetic triplet. It might be easy to believe that appropriate mathematical manipulation of equation 12 should allow the kinetic parameters $f(\alpha)$, E_a and A to be determined from one or more tga experiments. Unfortunately, equation 12 is deceptively simple and a very wide range of approximate solutions has been proposed, leading to different methods for evaluation of the kinetic parameters by using a single tga curve recorded at a certain heating rate. The application of these methods typically consists in plotting a characteristic straight line. It is assumed that the true activation parameters correspond to the kinetic model for which the best linearization of the characteristic straight line is obtained. However, because of statistical variations it is often possible to fit the same tga curve equally well with more than one kinetic model and activation energies may vary by more than an order of magnitude, with equally good correlation coefficients, by simply choosing different reaction models (31). The fact that different models often fit the same data equally well suggests that these methods should be used more cautiously than is common.

There are two groups of approaches to the use of equation 12. In the first, the degradation is treated as a chemical process subject to the simple laws of homogeneous kinetics. The function $f(\alpha)$ is taken as

$$f(\alpha) = (1 - \alpha)^n \tag{13}$$

where n is the reaction order, and attempts are made to determine the appropriate kinetic parameters and relate them to a reaction mechanism. Other authors have suggested that the use of equation 13 is inappropriate to describe complex reactions and choose instead to use arbitrary versions of $f(\alpha)$ and fit the data with "apparent" kinetic parameters. Although this approach can give good fits to the data, the assumption that the parameters so derived will have value for different degradation conditions or for temperatures outside the measurement range is to say the least questionable. It is important to recognize that the use of a single tga curve for evaluation of the kinetic parameters of thermal and thermo-oxidative degradation is one of the main causes of much controversial kinetic data reported in the literature and that kinetic parameters evaluated using a single tgs curve cannot be used for prediction of the polymer degradation in conditions other than those corresponding to the tga curve used (32,33). Overinterpretation of tga data is facilitated by modern high performance computing and interpretation of tgs curves in terms of kinetic models should be undertaken only with extreme caution.

A much more reliable approach to tga data, which has developed rapidly in recent years, again because of advances in computation, is the use of model-free isoconversional methods. Such methods have been reviewed and compared with model-fitting approaches for thermal degradation of nitrate explosives (31). The basic assumption in these studies is that $f(\alpha)$ is independent of both temperature and heating rate and can be eliminated by using data measured at a series of heating rates, or a series of isothermal data, to calculate E_a as a function of α. Such models give internally consistent results from isothermal and nonisothermal data. In addition, since they do not force fit the data to a single activation energy, they can reveal kinetic complexity by showing variations of E_a as a function of α.

Analysis of tga data for thermal decomposition reactions has been the subject of a major comparative review (the ITACT project) of the application of various methods to both experimental and simulated data (34–37). The final conclusion is that isoconversional analyses tend to work fairly well and that "kinetic analysis using single heating rate methods should no longer be considered acceptable" (37).

Thermal Volatilization Analysis. While tga has been one of the most popular techniques for studying kinetics of polymer thermolysis, thermal volatilization analysis (tva) has been a popular method of studying product distribution (see eg, Ref. 38). Despite its utility no commercial tva instrument has been produced.

The basic approach of tva is to record (as a function of temperature or time) the pressure of volatile material produced when a small sample of polymer is heated in a continuously pumped vacuum chamber. Since the pressure developed is proportional to the rate of degradation, the tva curve is analogous to a dtg curve. A more advanced version of the tva instrument interposes a series of cold traps between the reaction chamber and the pumping system at temperatures in the range −196 to 0°C, with pressure sensing (Pirani) gauges between the traps.

Thus the output of the instrument consists of a series of tva curves for products fractionated according to their volatility and a considerable amount of data can be obtained from a single experiment. In the hands of its protagonists tva has been a powerful method of study, especially of complex polymers and formulations.

An advantage of tva over many other methods is that the volatile products are not destroyed by the pressure analysis but are trapped in their respective cold traps from which they can be recovered for analysis by conventional spectroscopic methods. At the same time, both residue and cold-ring fractions can be collected for analysis.

Coupled Pyrolysis Techniques. Perhaps the most powerful techniques currently available are those in which the polymer is pyrolyzed for a short time in a pyrolysis system directly coupled to a modern analytical instrument capable of analysis of the volatile products. Although direct pyrolysis coupled with ftir is available, the most common techniques have been gas chromatography, mass spectroscopy, and combinations of the two. In contrast to tga, these techniques provide no real information on the onset temperature of degradation or on the number of distinct stages, but they can give very detailed information about the products of reaction.

Pyrolysis–gas chromatography (Py-gc) takes advantage of the ability of gas chromatography to separate volatile species rapidly and efficiently. Since gc analysis of a mixture requires the near-instantaneous injection of a small sample of mixture into the flowing carrier gas, the technique requires very rapid degradation of the sample. This is achieved by mounting the sample directly in the inlet of the gc instrument and subjecting it to a brief pulse of heating to a temperature high enough to pyrolyze enough of the sample to give a measurable signal. Py-gc has been reviewed (12).

A close relative of Py-gc is direct pyrolysis mass spectroscopy (Py-ms or DPy-ms). In this technique a polymer sample is pyrolyzed directly in the inlet of the mass spectrometer and the products of degradation analyzed. The most sophisticated version is the use of tandem mass spectroscopy. The initial pyrolysis fragments are subjected to soft ionization in the first ms stage so as to determine their masses and to separate the individual fragments. The ions are then transferred to a second ms stage where they are fragmented by electron impact and the fragmentation pattern used to give structural information. This is an extremely expensive method of study but capable of enormous amounts of information. A more recent development is the use of laser radiation to pyrolyze a polymer at the inlet of the mass spectrometer. DPy-ms methods have been reviewed (39).

A third approach is pyrolysis gas chromatography–mass spectroscopy (Py-gcms). This is a hybrid of the two previous methods, in which the pyrolysis products are separated by gc and then injected directly into an on-line MS, often a small quadrupole instrument. The gc serves to give rapid separation of the products where the MS acts both as a gc detector (in total ion current mode) and as an analytical tool.

Pyrolyzer designs for Py-gc have been reviewed (40). Although many different designs have been published, most modern instruments use either filament or Curie point methods. In a filament pyrolyzer the sample is heated by passing a current through a resistive filament in the gc inlet. In many designs the electronics are arranged to give an initial high pulse of current to heat the filament very

rapidly to the pyrolysis temperature. The most sophisticated version (41) of this approach uses a thermocouple welded to the filament to provide feedback control of the temperature.

In an alternative approach (42) the sample is coated on a ferromagnetic wire in the inlet of the gc machine, surrounded by a coil connected to a radio frequency generator. A short pulse of radio frequency power causes the temperature of the wire to rise rapidly to its Curie point, where it remains until the power is switched off. In theory the great advantages of this approach are its self-thermostat action and the absence of direct contact between the power unit and the pyrolysis wire and this has made Curie point pyrolysis popular, with commercial units available. However, it has been pointed out (12) that neither the speed of temperature rise nor the self-thermostat action is as reliable as is often claimed.

Coupled pyrolysis techniques find three distinct areas of application. Polymers which degrade cleanly to relatively few volatile products, such as PMMA, polyisobutene, and many step-reaction polymers, are often amenable to detailed product analysis and to kinetic analysis of the formation of individual products (12,43).

In more complex cases it may not be possible to analyze the mechanisms in detail but identification of the fragments can be used as a method for analyzing microstructure of the original polymer or copolymer. This application is analogous to the classical methods of organic chemistry, in which an unknown compound is degraded by chemical reactions of predictable mechanism to give recognizable fragments, and the structure of the original molecule is deduced. In the hands of experts this approach to pyrolysis of polymers has given a great deal of information about sequence distribution in copolymers and similar problems (see eg, Refs. 44–50). It has also been used to characterize highly intractable cross-linked polymers, including lignins (51–53) (see LIGNIN).

Finally, in many cases the pyrolysis product distribution is so complex that it is not possible to separate and identify all of the components. In such cases a chemometric method, simply treating the pyrogram as a pattern, can be used to compare one sample with another. This approach has found many applications in forensic analysis, for example, of paints and in analysis of authenticity of art works (54). It has even been used to type bacteria (55–57). These applications often take advantage of the fact that the high sensitivity of the analytical method allows minute samples to be analyzed; they depend upon a database of pyrograms obtained under well-controlled conditions and analysis involves a statistical pattern-matching approach.

Direct Mass Spectroscopy. Although mass spectrometry (qv) has been used in studies of natural and synthetic polymers for many years, the applications have been mainly limited to polymers which have been chemically or thermally degraded to fragments small enough for conventional mass spectrometry. In recent years, the introduction of matrix-assisted laser desorption/ionization (MALDI) and electrospray ionization (ESI) combined with the use of time-of-flight (TOF) and Fourier transform ion cyclotron resonance (FTICR) spectrometers has revolutionized the applicability of MS to polymers, by extending the accessible mass range to 500,000 and beyond and providing means of getting polymers into the mass spectrometer and ionized without fragmentation (58). Applications of MS to polymers have recently been reviewed (59). These applications are beginning to

influence degradation studies, because they allow structural analysis of polymers at low levels of degradation.

In ESI, a solution of the polymer is injected into the MS through a very fine needle so as to produce an aerosol. If the solution is very dilute, no droplet contains more than one polymer molecule, and evaporation of the solvent leaves the isolated polymer molecules in the gas phase. Ionization occurs as a result of a potential applied to the needle tip. Although ESI has had a major impact on studies of biopolymers, its use for synthetic polymers has been more limited, mainly because of the formation of multiply charged species (58).

The MALDI approach involves homogeneous dispersion of the polymer in a large excess of the "matrix," which is a small organic molecule. With high laser power and at the wavelength absorbed by the polymer it is possible to degrade the polymer but in MALDI the matrix and the laser wavelength are chosen so that the energy is absorbed by the supporting matrix. The high energy density causes evaporation of a small volume of the substrate and a mixture of ionized matrix and polymer molecules is released without damage to the polymer. MALDI of polymers has been reviewed (39,60).

In principle, MALDI is capable of measuring the molecular weight distribution (MWD) of a polymer, and hence all of the average molecular weights. However, even its most ardent early advocates have now recognized that the results are only reliable for polymers of relatively low polydispersity. Many of the problems have been reviewed (39). Most are a function of instrument design. For a mass spectrum to reflect the MWD over a wide range of molecular weights, both the ionization yield of the spectrometer and the detector response must be independent of chain length and neither of these conditions is fully met in current spectrometers. Additionally there can be mass discrimination in the laser desorption process and some care is needed to avoid degradation in MALDI experiments (61). Even if these problems can be overcome, it is important to recognize that MS is a number technique—the ideal detector response is proportional to the mole fraction of species of a given chain length, so that MWD data are biased toward low molecular weights.

Many of the problems of MALDI of polydisperse polymers can be overcome by using a combination of an initial fractionation by size exclusion chromatography (sec) followed by MALDI, taking advantage of the enormous sensitivity of MALDI to analyze the minute amounts of polymer eluted from the sec. This is probably now the best available method for getting MWD information but is complex.

Despite the problems of analyzing MWD information from MALDI, it remains an extremely powerful technique for getting information about structure in degraded polymers because the precise resolution allows chains of the same length with different end-groups to be separated. The method is being increasingly applied to polymer degradation. MALDI has been used to examine pyrolysis residues from many step-reaction polymers (39,62–64). Other examples include MALDI-TOF characterization of highly cross-linked, degradable polymer networks (65) and studies of poly(ethylene glycol) (66,67) and of poly(tetrahydrofuran) (68). The method is also finding applications to oxidation reactions. For example it has recently been applied to oxidation of nylon-6 (69) and of ethylene oxide–propylene oxide–ethylene oxide triblock copolymers (70).

Oxidative Degradation, Chemistry

Although pure thermal degradation is an important limiting factor in the processing of polymers and in their use at high temperatures, it has little relevance to applications at room temperature, especially when the polymer is in contact with air. For almost all polymers, the long-term stability is determined by resistance to oxidation.

Oxidation can be defined as the reaction of a polymer with oxygen at temperatures where thermal degradation is negligible. Thus it can be distinguished from *combustion*, which is the reaction between oxygen and the volatile products of thermal decomposition of the polymer. In fire situations the *degradation* is typically a complex mixture of oxidation and combustion, depending on the polymer and the conditions of degradation.

Studies of simple hydrocarbon models suggest that polymers should not oxidize significantly at service temperatures and this led to a widespread belief that polymers do not degrade in normal use. In fact, oxidation is a major technological problem and rather few polymers can be processed or used without stabilization. The reason is the presence of impurities and structural defects in polymers, especially after processing.

Oxidation is typically a very slow reaction between a solid, possibly semicrystalline, polymer and a gas. It is kinetically very complex, in the sense that the apparently simple overall behavior can be fitted by a very wide range of models, and the literature is characterized by a good deal of "paper chemistry". The main differences from thermal degradation are that the reactions are slow, over weeks or years, the production of volatiles may be almost negligible, and diffusion of oxygen into the polymer is required.

The conditions under which oxidation takes place vary widely, but there are two main cases. The first is during processing, where the temperature is high and there may be local "hot-spots" due to shear. The polymer is molten, the oxygen concentration is very low, and the high level of shear leads to the possibility of radical formation by mechanochemical scission of polymer chains. The second is normal use, where the polymer is solid, reactions are very slow, there is oxygen saturation, and there may be exposure to uv light, atmospheric pollutants, etc.

Oxidation of solid polymers in service use may lead to loss of mechanical properties—toughness, impact strength, elongation to break, flexural strength, etc, and the polymer typically embrittles at quite low levels of oxidation. It may also lead to marked changes in appearance—chalking, cracking, loss of gloss, and yellowing are all common.

Our understanding of the basic chemistry of oxidation is based on the classic work of Bolland and Gee (71–73) on natural rubber, and on earlier work on hydrocarbon oxidation. These studies showed that oxidation involves the chain reaction cycle of initiation, propagation, and termination. In the following, X is a primary radical, the origin of which is discussed later (Fig. 3).

(1) *Initiation*

$$RH + X \longrightarrow R\bullet + XH$$

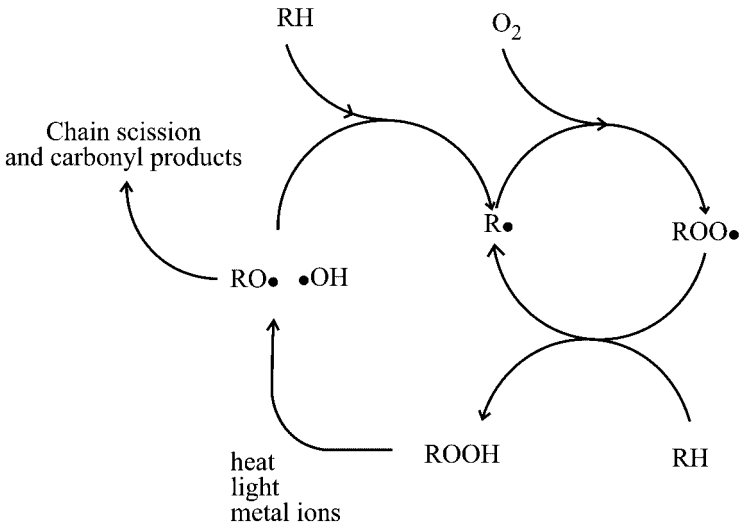

Fig. 3. The important reactions in polymer oxidation expressed as the interlocking cycles which eventually destroy the polymer through the scission reactions of alkoxy radicals.

(2) *Propagation*

$$R\bullet + O_2 \longrightarrow RO_2\bullet$$
$$RO_2\bullet + RH \longrightarrow ROOH + R\bullet$$

(3) *Termination*

$$RO_2\bullet(R\bullet) + RO_2\bullet(R\bullet) \longrightarrow \text{Inert products}$$

The product of this primary cycle is the polymer hydroperoxide ROOH. Under use conditions, these are unstable and decompose to yield new radicals, which initiate new chains. Thus, a chain reaction that regenerates its own initiator is started and the result is autoacceleration. Typically, there is an induction period of slow reaction, followed by rapid oxidation, as illustrated in Figure 4, which shows some data for accelerated aging of polypropylene (PP). In some cases, eg, PP, the formation of peroxides may be faster than their decomposition (depending on the temperature), so that they accumulate in the polymer. In other cases the peroxides are so unstable that they decompose as soon as they are formed.

Many initiation reactions have been proposed in the literature, eg,

$$RH \longrightarrow R\bullet + H\bullet$$
$$RH + O_2 \longrightarrow R\bullet + HO_2\bullet$$

All such direct reactions of the polymer by itself or with oxygen are thermodynamically unlikely at normal use and processing temperatures (which is why pure model compounds do not oxidize readily). The exact origin of initiation is still

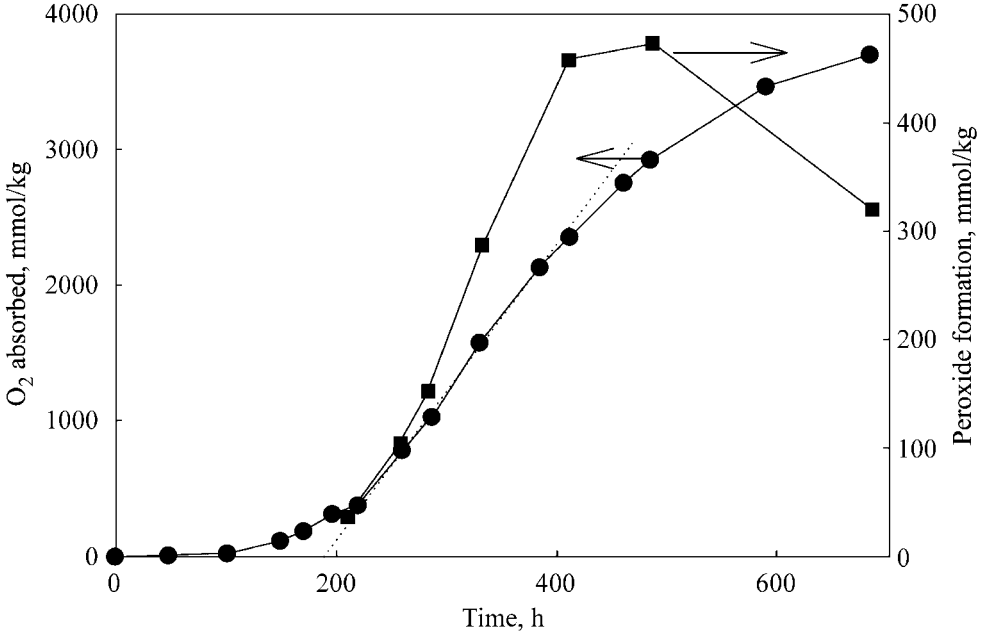

Fig. 4. Typical curves for oxygen uptake and formation of titratable peroxides in an unstabilized sample of PP at 70°C. The reaction is autoaccelerating. Extrapolation of the approximately linear part of the oxygen uptake curve, as indicated by the dotted line, gives the *induction period* where the polymer loses its useful mechanical properties. The amount of oxygen absorbed is low, corresponding to less than one molecule for every 100–150 polymer repeat units. Adapted from Ref. 74.

somewhat uncertain. The production of polymers totally free of impurities is not possible and small amounts of catalyst residues and other contaminants are always present and may react with the polymer, especially at the high temperatures of processing. Peroxides may also be formed in processing simply due to the effects of heat and mechanical shear in the presence of trace oxygen. It is now generally believed that most initiation is by the decomposition of traces of hydroperoxide, created by mechanochemically induced oxidation during processing.

Hydroperoxides are thermally unstable because of the weak O—O bond. The simplest decomposition is the unimolecular scission of the O—O bond to yield two radicals

$$\mathrm{ROOH} \longrightarrow \mathrm{RO\bullet} + \bullet\mathrm{OH}$$

Both alkoxy and hydroxy radicals are very reactive and HO• rapidly abstracts H from the polymer to form water:

$$\mathrm{HO\bullet} + \mathrm{RH} \longrightarrow \mathrm{R\bullet} + \mathrm{H_2O}$$

The RO• radical may react the same way to give ROH. In polymers it also leads to chain scission as discussed below.

In fact the situation is much more complex. In hydrocarbon media, hydrogen bonding of the polar hydroperoxides causes them to dimerize, leading to bimolecular decomposition:

$$2\ ROOH \longrightarrow RO\bullet + RO_2\bullet + H_2O$$

Again, RO• and RO_2• radicals produce R• by abstraction or scission reactions.

Hydroperoxides are also very sensitive to traces of metal ions with multiple oxidation states (eg Fe, Ti, Co, Mn, Cu, Cr). These are always present from catalysts or processing equipment and can catalyze rapid decomposition of peroxides:

$$ROOH + M^+ \longrightarrow RO\bullet + {}^-OH + M^{2+}$$

$$ROOH + M^{2+} \longrightarrow RO_2\bullet + H^+ + M^+$$

This catalysis is normally a disadvantage but can be used to accelerate degradation. Further, hydroperoxides are very sensitive to photolysis at solar wavelengths. The extinction coefficients are very low, but the quantum efficiency for scission is close to 1. Hydroperoxide photolysis can be sensitized by pigments.

Of the two reactions that form the propagation cycle, the first, reaction of the alkyl radical with oxygen, is very much the faster. For almost all radicals involved in common polymers, it is encounter-controlled, with zero activation energy (75), so that alkyl radicals have very short lifetimes if there is oxygen in the polymer. The second stage, abstraction of a hydrogen atom from the polymer to form a new alkyl radical and a hydroperoxide, is much slower. Its activation energy depends upon the dissociation energy of the C—H bond being broken. Thus, in polymers like PP, which have several different RH bonds, the location of oxidation will depend on the reactivity of the RH bonds. In PP, most oxidation takes place at the tertiary C—H bonds. Similarly, in natural rubber, most oxidation is at the α-methylene groups and in nylons it is at the methylene groups α to nitrogen.

In oxidation of liquids, propagation is expected to be statistically random. In the solid phase the mobility of radicals can be limited, so that propagation takes place in a "zone" of local oxidation; eg, in PP there is evidence of intramolecular propagation:

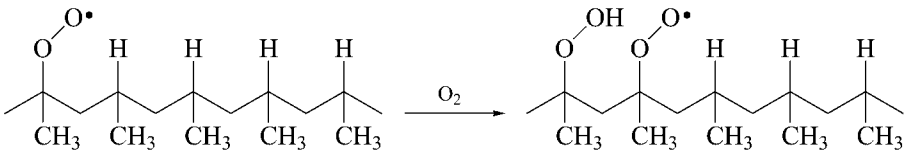

This gives short sequences of hydroperoxides. In polyethylene and rubbers, where mobility is higher, sequences are less common but hydroperoxidation may still be nonuniform.

Note also that the relative concentration of R• and RO_2• radicals depends upon the relative rates of the two propagation steps and therefore on the

concentration of oxygen. Under oxygen saturation conditions, the radical population is expected to be dominated by $RO_2\bullet$ radicals, but R• radicals may be much more important in processing, where the oxygen concentration is much lower; this has important implications for the choice of stabilizers (see eg, Ref. 76).

The chain termination reaction by bimolecular interaction of radicals may be more important in polymers than in liquids, because the kinetic chain length of solid-phase oxidation may be short. In oxygen-deficient conditions, coupling reactions of carbon-centered radicals can lead to cross-linking, and formation of gel particles can be a problem in film blowing of polyethylene. Under more normal conditions, the reactivity of carbon-centered radicals with oxygen means that only coupling of alkyl-peroxy radicals is significant.

Bimolecular interaction of alkyl-peroxy radicals must initially produce a highly unstable linear tetroxide. Where one of the radicals is secondary, this species rapidly reacts via the so-called Russell mechanism (77) to give a carbonyl and a hydroxy group:

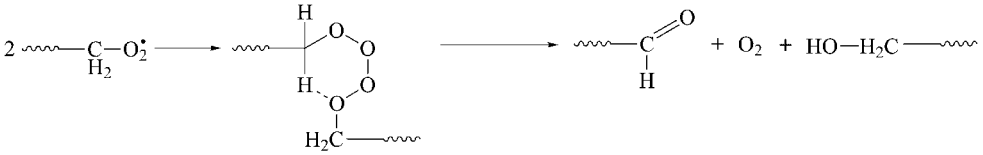

This reaction is of some interest because it is implicated in the ultraweak chemiluminescence emitted by oxidizing polymers (78–82).

In the case of PP, where the terminating radicals are both expected to be tertiary, the Russell reaction is not possible and bimolecular interaction of radicals is believed to follow the path

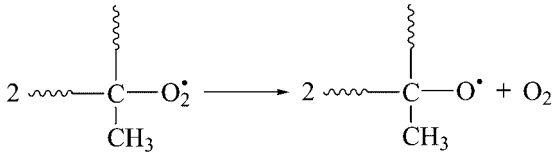

The existence of this reaction has been elegantly confirmed (83) by the unambiguous demonstration that the photochemical oxidation of PP in an atmosphere containing both $^{32}O_2$ and $^{36}O_2$ generates $^{34}O_2$.

The reaction cycle discussed so far consumes oxygen and converts it to hydroperoxides on the polymer chain. If this were the only set of reactions, it would not cause much trouble, except in applications involving high frequency electrical fields, where the introduction of polar groups has deleterious effects on dielectric losses. The real problem is that side reactions of radicals can cause chain scission and cross-linking.

In general, alkyl-peroxy radicals are rather stable and do not undergo side reactions. In an oxygen-saturated polymer, alkyl radicals are rapidly converted to alkyl-peroxy radicals by reaction with oxygen, so that their other reactions are not important. The most important side reaction is that of the alkoxy radical. In liquid hydrocarbons, the main reaction of alkoxy radicals is hydrogen abstraction to give

an alcohol. In contrast, in polymers β-scission can compete, to give a carbonyl group and an alkyl radical:

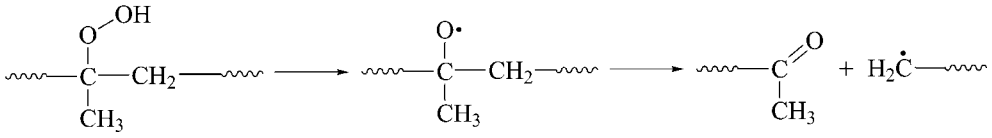

This is a key reaction because it leads to chain scission. The aldehyde or ketone formed is more reactive to oxidation than is the polymer. In the early stages of oxidation, the side products are mainly aldehydes and ketones but carboxylic acids, esters, and cyclic lactones become increasingly important with conversion.

Note that carbonyl groups are good photoinitiators for oxidation, so that increasing oxidation leads to increasing photosensitivity. Production of acids may also be important if the polymer has acid-sensitive groups, eg, polyacetals. Scission can be measured by following changes in molecular weight. It typically follows oxygen uptake, as is illustrated in Figure 5. Scission is inefficient, about 10 molecules of O_2 being absorbed for each scission.

In principle, termination of two alkoxy radicals would give a peroxide cross-link, where as termination of an alkoxy radical with an alkyl radical would give an ether cross-link. It is very difficult to get direct experimental evidence for either of these reactions, since both dialkyl peroxides and ethers are difficult to detect; however, there is no doubt that chain scission is dominant in saturated hydrocarbon polymers.

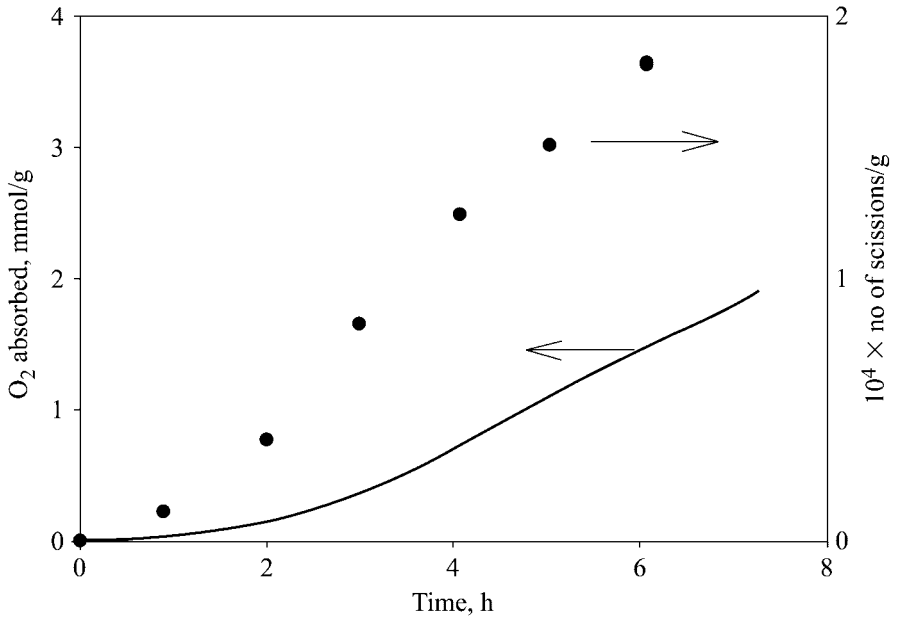

Fig. 5. Chain scission and oxygen absorption during oxidation of unstabilized PP at 120°C. The amount of scission is proportional to the amount of oxygen absorbed, although typically around 20 molecules of oxygen are taken up for each scission.

The alkoxy radical is most important because its high reactivity and ability to survive in the presence of oxygen mean that its reactions are responsible for chain scission and for most of the stable products of oxidation. Thus, the oxidation of saturated polymers under conditions of oxygen saturation leads to scission. In contrast, in unsaturated rubbers, the high concentration of C=C bonds means that attack on the C=C bond can compete with propagation and scission.

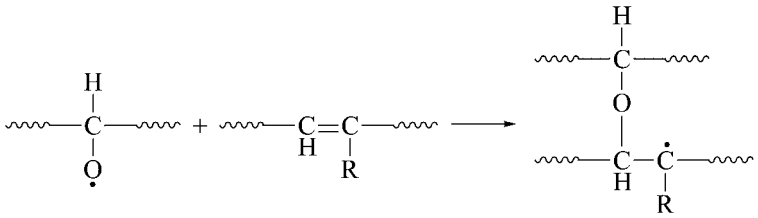

The result is that cross-linking, epoxidation, and formation of cyclic peroxides all occur in unsaturated rubbers. The increasing cross-link density leads to hardening of rubbers on oxidation.

If the oxygen concentration is low, as in processing, R• radicals are stable enough to react independently. There is a competition between recombination cross-linking and β-scission. The relative importance depends on the polymer: eg, polypropylene (**7**) undergoes scission in processing, but polyethylene (**8**) cross-links.

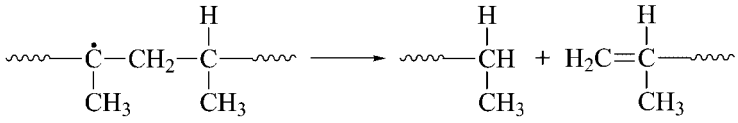

7

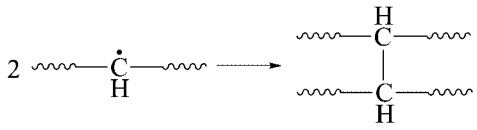

8

An extreme case of polymer oxidation is the involvement of polymers in fires, where the reactions may be a mixture of oxidation of the molten polymer, pyrolysis of the polymer, and oxidative combustion of volatile products. These reactions are discussed in more detail elsewhere, in the context of fire retardants. They have attracted the attention of the thermal analysis community and a number of quite elegant tga studies of polymer degradation in air have appeared. In general, the effect of changing the atmosphere in a tga experiment from nitrogen to air is to destabilize the polymer, causing a large downward shift in the temperature of rapid weight loss, and isoconversional methods of data analysis often show activation energies which vary with conversion (84). A notable exception is PMMA, whose initial pyrolysis temperature is increased by as much as 70°C in the presence of air or nitric oxide (85). This effect has been interpreted as due

to the trapping of radicals by oxygen or nitric oxide, leading to blocking of the depropagation reaction (10).

Although tga studies of oxidation are relevant to combustion, it must be emphasized that studying degradation under conditions of rapid weight loss from liquid samples at over 200°C has no relevance for degradation of solid polymers in service use. Furthermore, unless exceedingly thin sample are used, such studies are almost certainly influenced by oxygen diffusion effects discussed below.

Heterogeneous Oxidation. Oxidation of a polymer in service is a reaction between the solid polymer and a reactive gas, oxygen. In polyolefins the situation is complicated by the semicrystalline morphology. It is important to ask whether oxidation can be treated as effectively homogeneous and subject to the normal rules of liquid-phase kinetics, or whether the oxidation is more heterogeneous.

Although there is a massive literature on the kinetics of polymer oxidation, based on homogeneous models, the possibility that the reactions are actually locally heterogeneous has been considered seriously. It has been suggested (86,87) that the uneven distribution of catalyst residues and other impurities in PP can lead to oxidation in localized zones of a few micrometers in size, which spread through the matrix. More recently, chemiluminescence imaging studies (88,89) have supported this view.

Raman microscopy has been used to probe photo-oxidation of unstabilized PP (90). It was concluded that the catalyst residues, for the type of PP studied, tend to stabilize the polymer in the immediate vicinity, but also form reactive species that diffuse away from the catalyst to initiate oxidation. Localized oxidation was also confirmed by examining the distribution of polystyrene grafted onto the hydroperoxide sites in photo-oxidized PP (91).

It has been suggested (92–94) that oxidation of PP can be modeled as a process of "infectious spreading," analogous to the spread of infectious disease. However, these kinetic arguments must be interpreted with caution. It has been shown (95–99) that kinetic models of PP oxidation based on both homogeneous and heterogeneous models can give equally good fits to data for functional group formation in oxidation of PP. It seems that in most cases sufficient data of enough precision are not available to distinguish complex models.

Whatever the situation at the micrometer level, there is no doubt that oxidation of bulk polymer samples may be heterogeneous in the sense that oxygen may be consumed at the surface of the sample, leading to a profile of oxidation across the sample thickness. Such surface limited degradation has been demonstrated in many ways (100), including density profiling (101), modulus profiling (102), and ftir, using both microscopy and photoacoustic techniques (103). The thickness of the oxidized layer depends on the relative rates of oxygen diffusion and consumption, and theoretical models have been reviewed (104–106).

A rigorous test of theoretical treatments for diffusion-limited oxidation has been reported (107); an extensive series of radiation-initiated oxidation experiments was conducted on a commercial rubber. Oxidation profiles were monitored from density changes; the resulting profile shapes and magnitudes could be quantitatively fitted, and the theoretical parameters derived from fitting allowed quantitative confirmation of a governing theoretical expression relating them to independently measured values for the oxygen consumption and permeation rates.

Mechanical Effects of Oxidation

Whatever the chemical reactions, the ultimate problem of oxidation is that it leads to failure of the polymer. Whether the initial material is a rubber or a tough plastic, failure will usually take one of two forms. Either the product loses its surface appearance by discoloration, loss of gloss, or appearance of white deposits (chalking) or it cracks and breaks. The relation between chemical change and mechanical failure is quite complex.

Fracture (qv) is the result of the stress on the object, locally exceeding the breaking strength. If the polymer is an intrinsically tough material, such as PE, it normally yields and deforms under excess load, rather than fracturing. One common consequence of degradation is a progressive loss of toughness, until the polymer becomes brittle and fails by cracking. The stress that causes the failure may be externally imposed in use, or internal stress resulting from differential shrinkage or expansion of different sections of the piece. In some cases the loss of tensile elongation is gradual; in other cases, especially where effective stabilizers are used, failure can be very rapid at the end of a long induction period in which the properties are stable.

In unsaturated rubbers, the dominant chemical process in oxidation is cross-linking, owing to radical formation in the presence of high concentrations of double bonds. Increased cross-link density reduces the average molecular weight between cross-links and causes an increase in modulus until the glass-transition temperature rises sufficiently above the use temperature that the polymer becomes brittle. If the sample is thin enough, crack propagation under load then causes mechanical failure. Embrittlement failure of this type is typical of rubbers in film or sheet form. In extreme cases, the rubber may deteriorate to a friable powder.

In contrast, in thick samples oxygen diffusion restrictions may limit the initial oxidation to the surface of the polymer. The effect of surface cross-linking may be to further restrict diffusion of oxygen into the bulk, giving a hardened surface layer which protects the bulk polymer from further oxidation. The effect is analogous to passivation of aluminum by formation of an oxide layer. It is this which allows the successful use of a highly oxygen-sensitive material like natural rubber in large slabs for a variety of engineering and building applications, where very long lifetimes are expected. Many of the newer rubbers formed by ring-opening metathesis chemistry also fall into the category of self-protecting polymers.

In semicrystalline polyolefins, failure is also often by embrittlement, but for different reasons. The main mechanism is chain scission, with lowering of molecular weight and of T_g. Failure occurs at very low levels of oxidation; the molecular weight typically falls by less than a factor of 2 and there is less than one O_2 molecule per 100 carbon atoms. The reason for this sensitivity lies in the complex morphology of many polymers.

Many of the most oxidation-sensitive polymers, especially polyolefins, are semicrystalline, their morphology depending on the conditions of crystallization. Slow crystallization at low undercooling gives spherulites. Rapid crystallization at high undercooling gives much less organization, although often similar overall crystallinity is measured by, eg, x ray or dsc. In PE, where T_g is -100°C, crystallization is easy. In PP, T_g is much closer to room temperature and very rapid

cooling during molding may lead to a highly disordered smectic crystal structure. Diffusion of oxygen is restricted to the amorphous component of semicrystalline polymers and oxidation is restricted to the amorphous phase. This is fortunate because stabilizers also cannot get into the crystalline regions.

The useful mechanical properties of polyolefins arise from this semicrystalline morphology. For normal use temperatures ($T_g < T < T_m$) these polymers are effectively "composites" of rigid crystalline units in a soft, rubbery matrix. In slow loading, the ability of the chains to slip through crystals gives great toughness. At lower temperatures or higher strain rates (impact), failure becomes brittle, although the frequencies required for embrittlement of undegraded materials may be close to ballistic.

Chain scission changes the balance between plastic flow and brittle fracture, toward brittle fracture. Scission is confined to the amorphous regions between crystallites, so that it removes the ability to transfer load to the crystallite, decreasing plastic flow. Also, scission increases the freedom of the chains, especially at the surface. It allows recrystallization at the surface to relieve stress. The result is increased surface density and crystallinity, together with formation of surface cracks.

The final result depends on the point where crack propagation becomes favored over plastic flow. In a thick molding this may only happen at the surface, so that changes in surface appearance occur with little loss in bulk strength. In marginally tough materials, a crack started by surface embrittlement can propagate across the remaining tough plastic. In films, where great toughness is needed, small amounts of degradation can cause rapid embrittlement.

In contrast to semicrystalline polymers (qv), amorphous polymers (qv), such as PVC, typically discolor and chalk with less loss of strength. Amorphous, glassy polymers such as polystyrene are typically quite resistant to loss of mechanical properties by oxidation, but are prone to discoloration. Oxidation of polymers which have aromatic rings can lead to hydroxylation of the ring, followed by oxidative coupling of the phenolic products. The coupling products may show intense absorption of visible light, so that polymers such as polystyrene, poly(ethylene terephthalate), and aromatic polyurethanes often show major yellowing without much loss of tensile strength.

The extensive use of polymers in engineering applications has led to the development of many biphasic polymer blends, in which a small fraction of rubber particles is dispersed in a matrix of the host polymer. Such particles act to improve impact strength by dissipating energy at the tip of a propagating crack. Examples where the matrix is amorphous include high impact polystyrene (HIPS) and acrylonitrile–butadiene–styrene (ABS) copolymers. These are typically made by polymerizing styrene or styrene–acrylonitrile mixtures in the presence of a polybutadiene latex. Another very important group is the rubber-toughened polyolefins. These may be produced by mechanical blending of, eg, ethylene–propylene (EP) rubber or natural rubber into PP. Alternatively they can be made by feeding ethylene into a PP synthesis at the end of the reaction so as to form the so-called reactor "block copolymers." PP toughened with EP rubber is a major engineering plastic, with many applications in motor vehicles, eg, as bumpers.

In such materials the effects of degradation are complex and depend upon the chemistry and relative extent of degradation of the two phases. For materials

toughened with diene polymers, oxidative cross-linking and hardening of the rubber causes rapid loss of impact strength, while oxidation of the styrenic component in HIPS or ABS causes simultaneous yellowing. In contrast, in toughened PP the rubber is usually the more stable phase and degradation of thick sections such as bumper moldings most often involves surface deterioration through microcracking, with loss of color and gloss.

Photodegradation and Photo-oxidation

Many polymers are sensitive to light and photodegradation has been extensively studied. For any chemical reaction to be photoinitiated, several conditions have to be satisfied. First, the light must be absorbed by the reacting molecule or an impurity; second, the absorbed photon must have sufficient energy to break the appropriate bonds; and third, the excited molecule must photoreact rather than losing its energy in other ways.

For polymers in normal use, the usual source of light is solar radiation. Although the sun emits light from the infrared to the high energy ultraviolet, the combined effects of atmospheric oxygen and ozone cut off all radiation below around 300 nm. The exact range depends on latitude and atmospheric conditions (108,109).

There is a very large literature on the effects of ultraviolet radiation, typically at 254 nm, on polymers in inert atmospheres or vacuum (see eg Refs. 110 and 111). Most of this is irrelevant to polymers in normal use, although there are a few exceptions, for example the use of polycarbonate as impact-resistant lenses for mercury-vapor lamps in street lighting.

Because polymers in normal use are likely to be exposed to light only above 290–300 nm, they can be divided into two groups: those which have structural features (chromophores) that are able to absorb wavelengths in this range, and those which do not. In the former group, photochemistry is an inherent property of the polymer while in the second it is associated with impurities. A second important factor is the presence of oxygen. Since photodegradation involves chain scission, radicals are formed and their reactions in the presence and absence of oxygen may be quite different. Photodegradation of polymers has been very extensively reviewed (112).

Polymers with Intrinsic Chromophores. The most important intrinsic chromophore for solar radiation in many commercial polymers is the carbonyl group, in the form of ester, amide, and carbonate groups. These typically have weak absorbance above 290 nm, offset partially by the high concentration of chromophore groups. Fortunately, the quantum efficiencies for chain scission in rigid polymers are usually very low and materials such as polycarbonate, aromatic polyesters, and PMMA are regarded as reasonably stable. However, they will suffer loss of mechanical properties over long periods of solar exposure. Polycarbonate and polyesters also slowly yellow. PMMA degrades by unzipping and does not discolor.

Studies of the photolysis of carbonyl-containing polymers (see eg Ref. 113) have revealed two main mechanisms of degradation. The first, the Norrish

Type I cleavage, involves direct scission of the bond α to the excited carbonyl, with the production of two radicals.

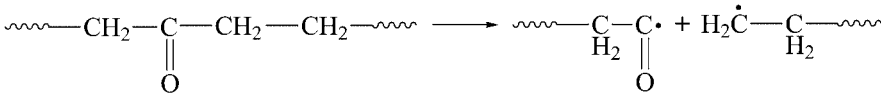

Although this reaction dominates gas- and liquid-phase photolysis of ketones, the quantum efficiency in polymers is usually low (0.001), because the formation of two radicals in close proximity in a rigid matrix often leads to recombination. The overall effect of Norrish I cleavage depends upon temperature and the presence of oxygen. At high enough temperatures, in inert atmospheres, it can initiate depolymerization. At temperatures well below the ceiling temperature the effects may be scission or cross-linking, depending upon the structure and reactions of the radicals. In the presence of oxygen, the quantum efficiency for scission can be high because reaction of the radicals with oxygen competes with their recombination and may initiate photo-oxidation. However, the most important point is that the polymer can undergo continuing radical photochemistry even in the absence of oxygen. For example PET and aromatic polyurethanes undergo photoinduced cross-linking and darken in color even if they are irradiated in inert atmosphere. Indeed the darkened polymer may photobleach if irradiated in air, because the products of inert atmosphere photolysis are themselves sensitive to photo-oxidation. This is a familiar problem with many modern white paints.

Competition between photolysis and photo-oxidation can also occur when thick sections of materials such as PET are irradiated. Here, the low permeability of the polymer to oxygen can mean that the surface layers undergo photo-oxidation, while the deeper layers photolyze. It is fortunate for many applications that the quantum efficiencies of all of these processes are low.

An alternative to photochemical radical generation is the Norrish Type II reaction, which is effectively a hydrogen abstraction by the excited carbonyl.

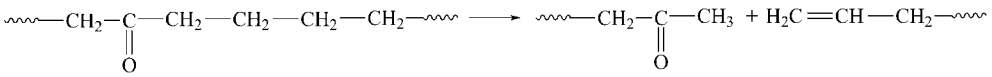

This leads to a chain scission without producing radicals. The quantum efficiency is much higher than for the Type I reaction (typically around 0.02) but is still low in polymers because of the constraints on formation of the six-membered transition state. It has been shown that ketone groups in polymers are photolyzed almost exclusively by the Norrish II mechanism, whereas aldehydes photolyze almost completely by the Norrish I mechanism (114). Since aldehydes do not normally survive in oxidative conditions, being rapidly oxidized to acid, the Norrish II mechanism is more important.

The deliberate introduction of carbonyl groups into polymers, either in the main chain by copolymerization with carbon monoxide or in the side chains by copolymerization with vinyl ketones, is the basis of at least one type of plastic designed to photodegrade rapidly in outdoor exposure (115). These copolymers are widely used in the United States for the six-pack ring packaging of soft drinks, whose damaging effect on marine life has been of great concern.

Aliphatic esters absorb light at rather shorter wavelengths than the ketone copolymers and, like PMMA, are regarded as having good photostability. Aliphatic polyamides are much less photostable and nylons degrade in outdoor exposure by a combination of photocleavage and photo-oxidation (116–118).

The introduction of aromatic groups increases extinction coefficients and shifts the maximum absorption to longer wavelengths. The ability of aromatic groups to dissipate excitation energy reduces the quantum efficiency for photo-reactions relative to other deactivation processes. It also allows the formation of conjugated aromatic structures, which can lead to yellowing. Although the wide range of aromatic polymers are regarded as stable, high performance materials, most suffer from yellowing, cross-linking, scission, and deterioration of properties on solar exposure over long periods.

Polystyrene absorbs solar uv, because of the aromatic group. It degrades slowly via a mixture of scission and oxidation reactions (119–121). The polymer yellows even on irradiation in vacuum, due to formation of conjugated sequences of double bonds.

It has been shown (122) that aromatic polyesters degrade by a combination of Norrish I and Norrish II photolyses, with photo-oxidation playing an important part. Aromatic esters may also undergo an important photochemical reaction, known as the photo-Fries rearrangement (123).

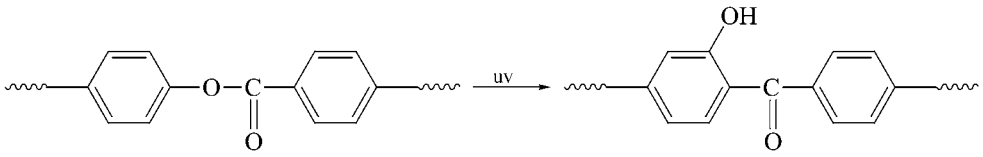

This reaction is important in polymer photochemistry, because it can occur with significant efficiency even in glassy, solid polymers. It has been suggested to contribute significantly to photoinduced yellowing in aromatic polymers, particularly polycarbonates (124). The photo-Fries rearrangement has also been identified as a source of photo-yellowing in aromatic polyamides (125). However, more recently, it has been suggested (126–128) that the photo-Fries reaction is more important for wavelengths below 300 nm, and that photo-oxidation reactions may be more important in yellowing of aromatic polymers at solar wavelengths. In a review (129) of degradation of polycarbonate by sunlight in Florida exposure it was shown that the observed products originate in a combination of Fries reactions and photo-oxidation of both the ring and the aliphatic components.

The combination of photoscission, photo-oxidation, and photorearrangement means that even very high performance polymers, such as epoxy resins, aromatic polyethers polyketones, and polysulfones, and the aromatic polyamides poly(1,3-phenylene isophthalamide) and poly(1,4-phenylene terephthalamide) (Nomex and Kevlar respectively) will degrade significantly on solar exposure. For example, it has been shown (108) that poly(phenylene oxide) and polysulfone both lose about 50% of their initial tensile strength after 2 years of outdoor exposure in Queensland.

Polymers with Impurity Chromophores. Although all the polymers with intrinsic chromophores are inherently sensitive to degradation, at least some are regarded as relatively stable materials, able to resist solar exposure for long

periods. In contrast, polymers such as the polyolefins and the hydrocarbon rubbers have remarkably poor lifetimes when exposed to solar light. Unstabilized PP film, for example, has a lifetime of only a few weeks in outdoor exposure.

At first sight, this observation is strange, because simple hydrocarbon analogues of these polymers have absorption spectra which have no overlap with the solar radiation spectrum at the earth's surface. The implication is that the effective chromophore for uv light is an impurity.

There have been many candidates for the chromophoric impurity in polymers. They include oxygen–polymer charge-transfer complexes; carbonyl and hydroperoxide groups, introduced by mechanochemical oxidation in processing; catalyst residues; pigments; and polynuclear aromatic hydrocarbons deriving from atmospheric pollution. The potential significance of these species has been discussed at length in the literature (see eg, Refs. 112,130, and 131).

Although there is little doubt that all can be important in particular circumstances, it is generally agreed that hydroperoxides are normally the key to the initial photoinstability in hydrocarbon polymers. Hydroperoxides are present in commercial PP at levels of around 10^{-3} – 10^{-4} mol/kg and have molar extinction coefficients at 310 nm of around 0.4 l/(mol·cm). Carbonyl groups are typically present at around 10^{-3} mol/kg and have molar extinction coefficients at 310 nm of around 10 l/(mol·cm) (112). However, the quantum efficiency for radical generation in hydroperoxide photolysis is 1, whereas it is of the order of 0.05 for carbonyl groups, partly because radicals formed by Norrish I reaction recombine rather easily and partly because of the preference for Norrish II chemistry, which does not give radicals.

There have been major improvements in recent years in reducing the initial concentration of oxidation products in processed polymers. Better process stabilization, lower catalyst residues, and better extruder materials have all contributed to cleaner polymers. However, even these materials photo-oxidize readily if unstabilized. There is some evidence that oxygen charge-transfer complexes may play a role in polymers which have very low hydroperoxide content (132), although this is still controversial (133,134). It has been demonstrated (135) that lifetimes of PP in accelerated photoaging are influenced by atmospheric ozone levels and suggested that radical generation by photolysis of ozone may contribute to initiation; nitrogen and sulfur oxides from atmospheric pollution may have a similar role. However, others were unable to reproduce the ozone effect in laboratory conditions (136).

Apart from the photochemical initiation, the photo-oxidation of polymers follows the same mechanism as thermal oxidation, although there may be kinetic differences arising from the different temperatures. This is true at least up to the point where the buildup of carbonyl groups is large enough to allow their photolysis to become significant. The key reaction is the chain scission, by decomposition of the polymeric alkoxy radical, produced in photoscission of the hydroperoxides. This reaction occurs solely in the oxygen-permeable amorphous phase of polyolefins. It leads to restructuring and recrystallization of amorphous material, producing microcracks in the polymer surface and a consequent dramatic loss in tensile properties.

An important point in photo-oxidation is that it is a chain reaction. The accumulation of reaction products and hence of chain scissions is a function of

both the total amount of light absorbed and the rate of its absorption. Low light intensities are expected to give longer kinetic chains than do high intensities. Thus for the same total dose, more mechanical damage is expected from low intensities of light over long periods than from the same dose absorbed rapidly. This is an important concept for comparison of natural and accelerated aging data.

Methods of Study of Oxidation and Lifetime Prediction

Studies of oxidation of polymers are divided into two main groups. In academic laboratories the concern is usually to establish oxidation conditions which do not lead to diffusion control and then to measure the kinetics of oxygen absorption and the formation of intermediate and final products, with the aim of elucidating detailed mechanisms of oxidation. In industrial laboratories, where the need is to try to predict service life of formulated products, the approach is typically more pragmatic and involves exposure of the polymer to high temperatures and/or artificial sunlight and measurement of loss of significant properties, typically embrittlement or loss of surface appearance.

It might be thought that measurement of oxygen absorption would be the most straightforward method of following oxidation, and methods of measurement have been reviewed (137). They typically involve monitoring the pressure change in a closed system resulting from oxygen uptake. In principle modern pressure transducers allow virtually limitless sensitivity. However, the sensitivity is limited by the problem of temperature control, even where a reference volume is used in the same thermostat. There are also problems associated with the emission of volatile materials from the polymer, particularly at higher degrees of oxidation. For these reasons, oxygen uptake has never enjoyed real popularity.

The primary product of oxidation is the hydroperoxide group and analysis of peroxide formation is an important feature of many studies. The most commonly used methods take advantage of the ability of hydroperoxides to oxidize either iron (II) or iodide ions in acidic solutions (138,139). They can be extremely sensitive but are time consuming and require very careful control to avoid problems from adventitious oxidation of solvents. In principle, hydroperoxides are detectable by ir spectroscopy, but their characterization is complicated by the broad absorption due to hydrogen bonding interaction with other hydroperoxides and with —OH groups, and the overlap with —OH vibrations. Studies of hydroperoxides in PP using CPMAS nmr spectroscopy on ^{13}C-enriched polymer have been reported (140).

Undoubtedly the most powerful method of study in academic laboratories has been ir spectroscopy, advanced rapidly in recent years by the development of FTIR and microspectroscopy and by rapid improvement in sampling methods. Infrared spectroscopy can easily detect the formation of hydroxyl and carbonyl species, and a common technique is to monitor the time dependence of the so-called *carbonyl index*, the ratio of the intensity of the carbonyl absorption envelope to that of a chosen reference band.

A problem with FTIR studies is that —OH, —C=O, and —OOH groups are all formed simultaneously, often in many different forms and with overlapping and interacting bands. The major advance in the last few years, which has transformed the understanding of polymer oxidation mechanisms, has been the development

of gas-phase reagents which react with specific functional groups in the polymer to give products with high extinction coefficients and absorptions in otherwise clear regions of the ir spectrum. This approach has been reviewed (141). It has proved to be an extremely powerful tool for study of degradation mechanisms (see eg, Refs. 142 and 143).

One example is the reaction of nitric oxide with oxidized polymers, which converts —OH to alkyl nitrite groups and —OOH to alkyl nitrate groups. Since these groups are not H bonded, they have sharp, intense bands and it is possible not only to distinguish —OH and —OOH groups but to identify primary, secondary, and tertiary groups (144). Another example is the reaction of SF_4 with oxidized polymers, which converts all C—OH species to C—F. This has proved to be a particularly valuable reagent, since it converts —COOH groups to —COF, allowing quantitative discrimination of —COOH groups from other carbonyls; since —COOH groups are produced by chain scission, they are one of the best groups to monitor in predicting loss of mechanical properties.

A recent approach to analysis of the multicomponent mixtures produced by polymer oxidation has been reported (145) in a study of the oxidation of polyisoprene in ^{17}O-labeled oxygen. It was shown that it is easily possible to identify nonvolatile degradation products by ^{17}O nmr spectroscopy, even at relatively low concentrations; the very high cost of ^{17}O-labeled oxygen means that this approach is unlikely to become very popular.

Prediction of service lifetimes is a continuing major challenge for the polymer industry, especially for materials expected to perform reliably for many decades. It is also critical in guiding the comparative evaluation of new materials in the development stages. In view of the importance of degradation to commercial users, there are many pragmatic methods that attempt to predict the lifetime of a sample of polymer under ambient conditions from accelerated measurements, without specific chemical analysis. Manufacturers wish to be able to guarantee a lifetime for a particular formulation of polymer and stabilizers without having to test samples for five or more years. The usual method is to adopt some regime of accelerated aging at high levels of illumination or high temperatures. These results are extrapolated to give expected lifetimes under normal conditions.

If thermal degradation is considered, it is reasonable to measure a time to failure at a series of temperatures and extrapolate to room temperature. Failure may be defined in terms of an extent of discoloration, a degree of oxygen absorption, fracture under a fixed load or other convenient test. Since oxidation processes show an induction time followed by accelerating reaction, most measurements will yield reasonably consistent data if they detect the end of the induction time.

The obvious method of extrapolation is to assume that the rate-determining step is characterized by a single activation energy and the Arrhenius equation can be applied (146). The applicability of this method has been analyzed critically and it has also been suggested that it is normally invalid except for extrapolation over a short range of temperature (147). Failure models have also been described based on the concept that material damage is cumulative (148). For the case where degradation data can be rigorously time–temperature superposed over a given temperature range, the researchers (148) show that the remaining lifetime at a second, higher temperature should be linearly related to the aging time prior to the step. This implies that it should be possible to estimate the remaining and

therefore the service lifetime of polymers by completing the aging at an accelerated temperature. They refer to this method as the "wear-out" approach.

As outlined above, degradation can occur through various pathways and the relative importance of these is likely to change with temperature. Thus, as was pointed out earlier, degradation at high temperatures may be dominated by high activation energy reactions which are relatively unimportant at lower temperatures. It is this feature that makes predicting polymer lifetimes by extrapolation to lower temperatures of data obtained at the high temperatures of typical experiments extremely hazardous. This is particularly true of oxidation reactions where both the chemistry and the physical properties of stabilizing additives contribute to lifetime. For example, it has been shown (149) that the Arrhenius plot for times to embrittlement of PP samples stabilized with a phenolic antioxidant is downwardly and upwardly curved at higher and lower temperatures, respectively, thus having a sigmoidal shape. The reasons for these complexities are not always clear and there may be more than one contributory factor. For instance, an antioxidant which is effective at scavenging radicals at high temperatures where it is mobile, may be less effective at low temperatures where rates could be dominated by diffusion of oxygen molecules to radicals. Similarly antioxidant loss may be diffusion limited at high temperatures but limited by evaporation rate at low temperatures. It has been suggested (150) that curvature in the Arrhenius plot for lifetimes of PP is due to the catalytic effect of catalyst residues on hydroperoxide decomposition at low temperatures being swamped by the much higher activation energy noncatalyzed decomposition at high temperatures. Multicomponent materials are even more likely to show complex, non-Arrhenius responses to aging temperature.

Similar points can be made in relation to photo-oxidative degradation where it is normal to test lifetimes using artificial irradiation with a solar distribution of wavelengths but very high intensity (for example the Xenotest). If care is taken to keep the sample at 20°C, it is natural to extrapolate the expected lifetime by multiplying by a factor which is the ratio of test intensity to normal averaged solar intensity. However, the higher rate of radical generation can be expected to change the relative importance of radical recombination processes and so change the overall kinetics. One compromise is to expose samples under natural sunlight in regions where most days are sunny. The two conditions usually considered are hot and dry (Arizona or Israel) and hot and humid (Florida or Queensland). Atmospheric acid pollution might also be added as a further factor by choosing a city environment.

Although all extrapolations are unsatisfactory, there is little choice since actual lifetime testing is impracticable. Accelerated tests are widely used to compare different stabilizer formulations. Interpretation must be coupled with some understanding of underlying mechanisms based on a range of complementary methods for monitoring degradation. A wide range of methods has been critically reviewed (151).

Degradation by High Energy Radiation

The degradation of polymers resulting from exposure to high energy radiation is an important subject for many reasons. In a negative sense, polymers are increasingly

exposed to radiation in their applications in eg, insulation of cables used in nuclear installations, where any degradation is critical (152). Radiation is also increasingly used for sterilization of medical plastics and degradation during storage or use can be important (153–155). In a more positive sense, the degradation of polymers by radiation forms the basis of most of the modern lithographic techniques used in forming electronic devices. Radiation-induced degradation has been well reviewed (156–159).

High energy radiation is defined as all forms of radiation with energies much higher than those of chemical bonds. It includes both electromagnetic radiation (x-rays, γ-rays, etc) and particulate beams (α- and β-particles, electrons, neutrons, etc). The range of energies is very wide but much higher than chemical bond energies. Unlike the absorption of visible and near-uv light, discussed earlier, high energy radiation is absorbed nonspecifically; ie, it does not require a chromophore. Radiation is absorbed by interaction with either the atomic nuclei or the electron clouds; for the light atoms typical of polymers, absorption by the electron clouds is usually more important. The efficiency of absorption varies widely. α-particles are stopped by condensed matter in very short (mm) distances, whereas γ-radiation can penetrate large (>cm) distances.

Whatever the nature of the radiation, interaction with the electron clouds of molecules initially results in the transfer of energy to the molecules to form ions, with the ejection of a secondary electron (160,161). These secondary electrons usually have enough kinetic energy to cause further ionization and excitation of nearby molecules. In the case of highly penetrating radiation, interaction between the primary photon and the substrate electrons may be relatively rare, whereas secondary electrons lose their energy in the region of their formation. Thus energy absorption occurs in a heterogeneous manner along "tracks," each consisting of a series of "spurs."

The immediate consequence of absorption of high energy radiation is thus the formation of a range of energetic species, including trapped electrons, ions, and radical ions. These are usually highly transient species at room temperature, although they can have long lifetimes in glassy materials at low temperatures. The decay of the excited species usually results in fragmentation to give free radicals. In many polymers, scission of main-chain C-C bonds gives radical pairs which recombine rather rapidly because of the close proximity of two macroradicals. In contrast, scission of C—H bonds leads to relatively stable radicals and formation of molecular hydrogen. Thus, the overall effect of radiation at room temperature is typically to produce polymer-derived free radicals. Radicals formed by radiation are easily detected by esr spectroscopy and there is a very large literature on the subject. The primary radical formed by irradiation may not be stable. For example, irradiation of PE with γ-radiation at 77 K produces the secondary radical, which is stable more or less indefinitely at this temperature. However, if the sample is allowed to warm up, the first process is the elimination of hydrogen and formation of the allyl radical (**9**):

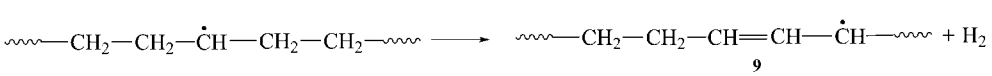

9

Color change is an important problem in commercial applications involving the radiation-processing of polymers, or their use in optical devices in radiation

environments. Discoloration arises due to formation of two different types of color centers: "permanent" and "annealable" (162,163). Annealable color centers are associated with radical or ionic species trapped in the polymer matrix. They disappear with time through recombination reactions and reaction with oxygen diffusing from the surrounding atmosphere. The ratio of permanent and annealable color centers and the rate of post-irradiation annealing vary greatly in different polymer types. The ability of a polymer to form conjugated structures, under the influence of the free-radical chemistry induced by irradiation, is an important factor in the extent to which the material discolors.

It is important to bear in mind that a free radical, once formed, has no "memory" of its origins and its reactions will be exactly the same as a radical produced by any other means. In the absence of oxygen, carbon-centered radicals may undergo cross-linking, by recombination, or chain scission, by β-elimination, or both, depending on the radical structure. This is the same chemistry as described earlier for alkyl radicals in the absence of oxygen, although the balance of the two reactions may be different in irradiation conditions at room temperature and in high temperature processing conditions.

Polymers can thus be divided into two main groups, those which respond to radiation in inert conditions by cross-linking, with a concomitant increase in molecular weight, and those which lose molecular weight by chain scission, although both can occur in many polymers. The ability of radiation to induce cross-linking or scission is usually expressed as the corresponding G value, G_X or G_S, where G is the number of bonds formed or broken for each 100 eV of absorbed energy.

Table 3 shows some typical values of G_X and G_S for common polymers. In general, an increase in the degree of substitution of the carbon backbone increases the contribution of chain scission.

Table 3. Radiation Chemical Yields of Chain Scission and Cross-linking in Polymers Irradiated in Inert Atmosphere[a]

Polymer	G_S[b]	G_X[b]	Dominant process
Polyethylene		2.0	Cross-linking
Polypropylene	0.6	0.9	Cross-linking
Polyisobutene	4.0	<0.05	Scission
Polystyrene	0.02	0.03	Cross-linking
Poly(α-methylstyrene)	0.25		Scission
Poly(methyl methacrylate)	1.8		Scission
Poly(vinyl chloride)	2.2		Scission
Poly(tetrafluoroethylene)	0.1–0.2		Scission
Poly(ethylene oxide)	2.0	1.8	Cross-linking
Poly(dimethylsiloxane)	0.07	2.3	Cross-linking
Poly(butene-1-sulfone)	10.7		Scission
Nylon-6,6	2.4	0.7	Scission
Poly(ethylene terephthalate)	0.07	2.3	Cross-linking
Cellulose	3.3–6.8		Scission
DNA	0.8		Scission

[a] Adapted from Ref. 157 with additions.
[b] G = number of bonds formed (G_X) or broken (G_S) for each 100 eV of absorbed energy.

The sensitivity of PE to cross-linking by radiation is the basis of commercial processes for producing cross-linked polymers by, eg, electron-beam irradiation. Conversely the easy scission of polysulfones, with elimination of SO_2, is the basis of some photoresists.

Because of the involvement of free radicals, and their reactivity with oxygen, radiation-induced degradation is highly sensitive to oxygen. Indeed, high energy irradiation is an excellent means of initiating oxidation. Once carbon radicals are formed, their reactions with oxygen are identical to those of any other radical and the chemistry is the same as that of thermal or photo-oxidation. However, the accelerating effect of radiation means that the combination of radiation and oxygen can be extremely destructive. Since oxidation can lead to both cross-linking and chain scission, depending on the polymer, the effects are quite complex. They are further complicated by the fact that the high rate of initiation induced by radiation can result in oxygen being depleted in the polymer faster than it can be replaced by diffusion. This leads to dose-rate-dependent behavior. Thus a polymer which cross-links on irradiation but scissions on oxidation may show softening of the surface layers and hardening of the bulk, to a degree dependent on dose rate, and the converse may also occur (164). Oxidation under the influence of irradiation is a key problem in many applications of polymers, especially the increasingly popular use of γ-radiation or electron beams to sterilize medical prosthetic devices and instruments (154,165).

Hydrolytic and Biological Degradation

Hydrolytic Degradation. Many applications of polymers involve contact with water, either in weathering by rain or in their use as containers and pipes. Contact with liquids can have deleterious effects due to stress cracking or due to leaching of antioxidants (qv) or plasticizers (qv). However, direct chemical reaction between the polymer and water is also a possible route to degradation.

Hydrolysis can occur only if the polymer has functional groups capable of reaction with water and if the water can gain access. Hydrocarbon polymers are very resistant to hydrolysis because they are not wetted by water and contain no hydrolyzable groups. In the polyolefins, water access is also restricted by the semicrystalline nature of the polymers. In complete contrast, many natural polymers, especially the polysaccharides (cellulose, starch, etc), are quite readily hydrolyzed at appropriate pH, because they are water absorbing and contain readily hydrolyzable links.

Most synthetic polymers lie between these two extremes. Typical step-reaction polymers, such as polyesters, polyamides, polycarbonates, polyurethanes, and cellulose esters, all contain hydrolyzable groups in the main chain. On the other hand, many chain reaction polymers, such as polyacrylonitrile, PMMA, and PVC, contain substituent groups which may hydrolyze at appropriate pH.

Most of these polymers are regarded as highly stable in water because they are insoluble, often semicrystalline, and absorb only very low levels of water. However, most of them will undergo surface attack in acids or alkalis and are generally unsatisfactory for long-term use in these media. The same is true of

most cross-linked materials; epoxy resins, formaldehyde resins, and unsaturated polyesters all suffer hydrolytic scission over long periods, especially at extremes of pH.

Another problem can arise when some of these thermosetting resins are used as the matrix in fiber-reinforced composites. In such materials there is a high area of fiber-matrix interface and hydrolysis in the interfacial zones is a common source of failure. Interfacial degradation is a common problem in the use of glass-reinforced polyester in marine applications.

Water-soluble or -swellable synthetic polymers, such as poly(vinyl alcohol), polyacetals, poly(acrylic acid), and polyacrylamide, are all relatively stable at neutral pH, but undergo quite rapid chain scission under acidic or basic conditions. Typical commercial polymers can be classified according to their resistance to hydrolysis (158) as follows.

Polymers resistant to hydrolysis in all media include polyolefins, hydrocarbon rubbers, polystyrene, polytetrafluoroethylene, and unplasticized poly(vinyl chloride). Polymers sensitive to hydrolysis in both alkaline and acidic media are, eg, cellulose esters, plasticized poly(vinyl chloride), poly(methyl methacrylate), polyacrylonitrile, polyoxymethylene, polyamides, polyesters, polycarbonates, and polysulfones. Polymers sensitive to alkalis but not acids are unsaturated polyester resins and phenol-formaldehyde resins.

Hydro-biodegradation. Most organic polymers are much more hydrophobic than those found in nature, and living organisms have not evolved enzymes which can effectively penetrate and cleave them. Polymers which resist hydrolysis are also resistant to biodegradation, since enzymes operate in aqueous media. Thus synthetic polymers are typically much more resistant to biological attack than are the natural polymers, such as proteins and polysaccharides. Biodegradability of polymers has been well reviewed (see eg, Refs. 166–169) (see BIODEGRADABLE POLYMERS, MEDICAL APPLICATIONS).

Water-swellable or -soluble polymers may be biodegraded by microorganisms if they contain functional groups that are susceptible to enzymatic cleavage. There is considerable evidence that biodegradation is synergistic with hydrolysis, which may be chemical or enzymatic and is required to reduce the molecular weight to the point where bioassimilation is possible.

Much of the discussion of biodegradability is bedeviled by problems of definition. Under appropriate conditions pure cellulose can be biodegraded completely to carbon dioxide and water in a few weeks. In contrast, lignin, although undoubtedly biodegradable, may survive for centuries, as is shown by the very long lifetimes of some tree species after falling. Many synthetic polymers can support growth of microorganisms to a degree wholly unacceptable in biomedical applications, yet are highly resistant to complete bioassimilation.

Nature has evolved enzymes that can cleave the links in natural polymers, so that proteins, nucleic acids, and polysaccharides are highly biodegradable. Synthetic polymers are much more resistant since they usually contain functional groupings resistant to enzymatic cleavage, often have surface energies that resist wetting, and are resistant to water permeation. Further, even when an enzymatic cleavage is available, it frequently results in attack from the chain ends, with only a very slow reduction in molecular weight, and little effect on mechanical properties.

Intrinsically biodegradable polymers have clear advantages in some applications, notably in medicine and agriculture. Unfortunately, most of the readily degradable natural polymers are not amenable to fabrication by the usual methods of the polymer engineer, because they undergo thermal degradation at temperatures well below those at which they become thermoplastic. The major group of processible synthetic polymers susceptible to biodegradation is the aliphatic polyesters, which are found as components of several commercial polymer systems, notably some block copolymer elastomers. Some examples are poly(ε-caprolactone), poly(lactic acid), and poly(2-hydroxybutyrate).

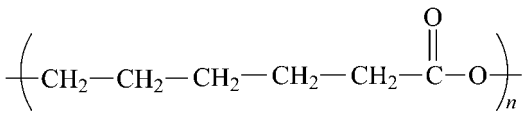

10

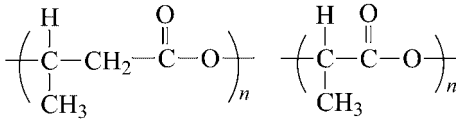

11 **12**

Poly(ε-caprolactone) (**10**) has been used as a biodegradable polymer in agricultural applications and other aliphatic polyesters find applications in medicine, as biodegradable sutures.

The natural polyester, poly(2-hydroxybutyrate) (**11**), is prepared commercially by bacterial fermentation (170) and finds limited markets where its biodegradation is an asset. Poly(lactic acid) (**12**) is another thermoplastic polyester with good biodegradability (171). It finds applications in sutures and is being developed as a "green" packaging material. Other biodegradable polymers include poly(vinyl alcohol) and its copolymers, and some aliphatic polyurethanes and poly(ester-amides), again often as segments of copolymer elastomers.

Although native starch is not thermoplastic, it can be gelatinized by cooking in an extruder to produce a processable material which is biodegradable (172). However, the high moisture sensitivity makes it of limited application. Thermoplastic biodegradable polymers can also be formed by blending of starch with synthetic polymers. Novamont (Italy) has pioneered starch-based biodegradable materials, and now has several classes of materials, sold under the trademark Mater-Bi, all containing starch and different synthetic components (172–175). Some grades contain ethylene-vinyl alcohol copolymers and are classified as biodegradable but not compostable. Other grades contain aliphatic polyesters and are classified as both biodegradable and compostable.

Another approach to biodegradability is to blend a biodegradable natural polymer with a thermoplastic synthetic polymer. Blends of starch with PE or with poly(vinyl alcohol) have been commercialized as packaging materials (176), although they have mainly been used in niche markets. Early materials were rather poor because the encapsulating effect of the PE on the starch protected it from water access, and, even if the starch was biodegraded, the PE was left

behind as a mechanically weak but nonbiodegradable residue. In an only partially successful effort to overcome these problems a wide range of pro-oxidant additives, typically mixtures of fatty acids and transition metal salts, has been added to the PE used in these formulations.

Oxo-biodegradation. Synthetic polymers are very resistant to biodegradation. However, there is very strong synergism between thermal or photochemical oxidation and subsequent biodegradation (see eg, Refs. 177–180). Although it is widely believed that synthetic polymers are biologically inert, there is now ample evidence that they will become completely biodegradable if they are initially heavily enough oxidized to reduce the molecular weight and introduce enough polarity to allow the polymer to be wetted (166,168,181–184).

This is an important feature of the so-called oxo-biodegradable polymers, which have applications in agriculture as mulch films, and are increasingly of interest for applications in packaging and landfill cover. A typical example is the Scott–Gilead process (185). PE film is doped with a mixture of iron and nickel salts which provide stability during processing but initiate photochemical formation of radicals in sunlight, causing the polymer to photodegrade at a rate controlled by the iron/nickel ratio. More recently, similar materials based on thermal activation rather than photoactivation have been commercialized (186–189).

BIBLIOGRAPHY

"Chemical Degradation" in *EPST* 1st ed., Vol. 4, pp. 647–716, by N. Grassie, The University of Glasgow; "Degradation" in *EPSE* 2nd ed., Vol. 4, pp. 630–696, by D. J. Carlsson and D. M. Wiles, National Research Council of Canada.

1. L. C. E. Struik, *Physical Aging in Amorphous Polymers and Other Materials*, Elsevier, Amsterdam, 1978.
2. H. Zimmermann, *Dev. Polym. Degrad.* **5**, 79–119 (1984).
3. S. Vyazovkin, *New J. Chem.* **24**, 913–917 (2000).
4. I. McNeill, in G. C. Eastmond, A. Ledwith, P. Russo, and P. Sigwalt, eds., *Comprehensive Polymer Science*, Vol. **6**, Pergamon, Oxford, 1989, pp. 451–500.
5. G. Montaudo and C. Puglisi, in S. L. Aggarwal and S. Russo, eds., *Comprehensive Polymer Science, Supplement 1*, Pergamon, Oxford, 1992, pp. 227–251.
6. H. Sawada and K. F. O'Driscoll, *Thermodynamics of Polymerization*, Vol. **1**, Marcel Dekker, Inc., New York, 1976.
7. K. J. Ivin, *J. Polym. Sci., Chem.* **38**, 2137–2146 (2000).
8. T. Kashiwagi and co-workers, *Macromolecules* **19**, 2160–2168 (1986).
9. N. Grassie and M. Roche, *Die Makromol. Chem.* **112**, 16–33 (1968).
10. J. D. Peterson, S. Vyazovkin, and C. A. Wight, *J. Phys. Chem. B* **103**, 8087–8092 (1999).
11. G. Bagby, R. S. Lehrle, and J. C. Robb, *Polymer* **10**, 683–689 (1969).
12. J. Hammond and R. S. Lehrle, in C. Booth and C. Price, eds., *Comprehensive Polymer Science*, Vol. **1**, Pergamon, Oxford, 1988, pp. 589–612.
13. D. M. Bate and co-workers, *Polym. Degrad. Stab.* **62**, 73–83 (1998).
14. R. S. Lehrle, R. E. Peakman, and J. C. Robb, *Eur. Polym. J.* **18**, 517–529 (1982).
15. R. Lehrle and co-workers, *Polym. Degrad. Stab.* **42**, 281–291 (1993).
16. R. S. Lehrle and C. S. Pattenden, *Polym. Degrad. Stab.* **63**, 153–158 (1999).
17. R. S. Lehrle and C. S. Pattenden, *Polym. Degrad. Stab.* **63**, 321–340 (1999).
18. R. S. Lehrle and co-workers, *Polym. Degrad. Stab.* **52**, 183–196 (1996).
19. N. C. Billingham, T. J. H. Henman, and P. A. Holmes, *Dev. Polym. Degrad.* **7**, 81–121 (1987).

20. R. Lehrle and co-workers, *Macromolecules* **28**, 4408–4414 (1995).
21. R. S. Lehrle and C. S. Pattenden, *Polym. Degrad. Stab.* **61**, 309–318 (1998).
22. W. H. Starnes, *Am. Chem. Soc. Adv. Chem. Ser.* **169**, 309 (1977).
23. E. Owen, *Degradation and Stabilisation of PVC*, Elsevier Applied Science, London, 1984.
24. D. Braun and E. Bezdadea, in L. I. Nass and C. A. E. Heiberger, eds., *Encyclopaedia of PVC*, 2nd ed., Vol. **1**, Marcel Dekker, Inc., New York, 1986, pp. 397–434.
25. W. H. Starnes and S. Girois, in R. A. Pethrick, ed., *Polymer Yearbook*, Vol. **12**, Harwood, London, 1995, pp. 105–131.
26. I. C. McNeill and L. Memetea, *Polym. Degrad. Stab.* **43**, 9–25 (1994).
27. I. C. McNeill, L. Memetea, and W. J. Cole, *Polym. Degrad. Stab.* **49**, 181–191 (1995).
28. I. C. McNeill and co-workers, *Polym. Degrad Stab.* **62**, 145–155 (1998).
29. P. K. Gallagher, in E. A. Turi, ed., *Thermal Characterization of Polymeric Materials*, Vol. **1**, Academic Press, New York, 1997.
30. T. Provder, M. Urban, and H. Barth, eds., *Hyphenated Techniques in Polymer Characterisation: Thermal, Spectroscopic and Other Methods* (ACS Symposium Series, Vol. **581**), American Chemical Society, Washington, D.C., 1994.
31. S. Vyazovkin and C. A. Wight, *Thermochim. Acta* **341**, 53–68 (1999).
32. M. E. Brown, *J. Therm. Anal.* **49**, 17–32 (1997).
33. P. Budrugeac, *Polym. Degrad. Stab.* **71**, 185–187 (2000).
34. M. E. Brown and co-workers, *Thermochim. Acta* **355**, 125–143 (2000).
35. M. Maciejewski, *Thermochim. Acta* **355**, 145–154 (2000).
36. S. Vyazovkin, *Thermochim. Acta* **355**, 155–163 (2000).
37. A. K. Burnham, *Thermochim. Acta* **355**, 165–170 (2000).
38. I. McNeill, *Dev. Polym. Degrad.* **1**, 43–86 (1977).
39. G. Montaudo, M. S. Montaudo, and F. Samperi, in Ref. 59, pp. 419–521.
40. T. Hammond, R. S. Lehrle, and A. Shortland, *Polym. Degrad. Stab.* **50**, 169–173 (1995).
41. R. S. Lehrle, J. C. Robb, and J. R. Suggate, *Eur. Polym. J.* **18**, 443–461 (1982).
42. J. Schmidt, P. Schmidt, and W. Simon, *Chromatographia* **9**, 597 (1976).
43. R. S. Lehrle, *J. Anal. Appl. Pyrolysis* **11**, 55–64 (1987).
44. A. Ballistreri and co-workers, *Macromolecules* **22**, 2107–2111 (1989).
45. A. Ballistreri and co-workers, *Macromolecules* **23**, 5059–5064 (1990).
46. G. Montaudo, *Rapid Commun. Mass Spectrom.* **5**, 95–100 (1991).
47. M. S. Montaudo, A. Ballistreri, and G. Montaudo, *Macromolecules* **24**, 5051–5057 (1991).
48. M. S. Montaudo and G. Montaudo, *Die Makromol. Chem., Macromol. Symp.* **65**, 269–278 (1993).
49. G. Montaudo and M. S. Montaudo, *J. Macromol. Sci., A: Pure Appl. Chem.* **31**, 1053–1059 (1994).
50. M. S. Montaudo, *Macromol. Symp.* **141**, 95–101 (1999).
51. E. R. E. VanderHage, M. M. Mulder, and J. J. Boon, *J. Anal. Appl. Pyrolysis* **25**, 149–183 (1993).
52. E. R. E. VanderHage and J. J. Boon, *J. Chromatogr., A* **736**, 61–75 (1996).
53. V. A. Klap and co-workers, *Org. Geochem.* **28**, 707–727 (1998).
54. R. S. Lehrle, *J. Anal. Appl. Pyrolysis* 40–41, 3–19 (1997).
55. E. M. Timmins and R. Goodacre, *J. Appl. Microbiol.* **83**, 208–218 (1997).
56. R. Goodacre, P. J. Rooney, and D. B. Kell, *J. Antimicrob. Chemother.* **41**, 27–34 (1998).
57. E. M. Timmins and co-workers, *J. Clin. Microbiol.* **36**, 367–374 (1998).
58. J. H. Scrivens and A. T. Anthony, *Int. J. Mass Spectrom.* **200**, 261–276 (2000).
59. G. Montaudo and R. P. Lattimer, eds., *Mass Spectrometry of Polymers*, CRC Press, Inc., Boca Raton, Fla., (2002).
60. G. Montaudo, *Trends Polym. Sci.* **4**, 81–86 (1996).
61. R. S. Lehrle and D. S. Sarson, *Polym. Degrad. Stab.* **51**, 197–204 (1996).

62. R. P. Lattimer, M. J. Polce, and C. Wesdemiotis, *J. Anal. Appl. Pyrolysis* **48**, 1–15 (1998).
63. C. Puglisi and co-workers, *Macromolecules* **32**, 8821–8828 (1999).
64. G. Montaudo and C. Puglisi, in Ref. 59, pp. 181–235.
65. A. K. Burkoth and K. S. Anseth, *Macromolecules* **32**, 1438–1444 (1999).
66. T. J. Kemp and co-workers, *Polym. Degrad. Stab.* **64**, 329–338 (1999).
67. R. P. Lattimer, *J. Anal. Appl. Pyrolysis* **56**, 61–78 (2000).
68. R. P. Lattimer, *J. Anal. Appl. Pyrolysis* **57**, 57–76 (2001).
69. D. Chionna and co-workers, *Macromol. Rapid Commun.* **22**, 524–529 (2001).
70. G. Gallet and co-workers, *Polymer* **43**, 1081–1094 (2002).
71. J. Bolland and G. Gee, *Trans. Faraday Soc.* **42**, 236–243 (1946).
72. J. Bolland and G. Gee, *Trans. Faraday Soc.* **42**, 244–252 (1946).
73. J. Bolland and G. Gee, *Proc. R. Soc. London, Ser. A* **186**, 218–236 (1946).
74. P. Gijsman, J. Hennekens, and J. Vincent, *Polym. Degrad. Stab.* **42**, 95–105 (1993).
75. K. U. Ingold, *Acc. Chem. Res.* **2**, 1–9 (1969).
76. H. Zweifel, *Stabilization of Polymeric Materials*, 1st ed., Springer-Verlag, Berlin, 1998.
77. G. A. Russell, *J. Am. Chem. Soc.* **79**, 3871–3877 (1957).
78. R. Kellogg, *J. Am. Chem. Soc.* **91**, 5433–5435 (1969).
79. R. Vassil'ev, *Die Makromol. Chem.* **126**, 231–238 (1969).
80. N. C. Billingham and E. S. O'Keefe, in A. V. Patsis, ed., *Advances in the Stabilization and Controlled Degradation of Polymers*, Vol. **1**, Technomic, Basel, 1989, pp. 1–8.
81. G. A. George, *Dev. Polym. Degrad.* **3**, 173–171, 206 (1981).
82. G. A. George, G. T. Egglestone, and S. Z. Riddell, *Polym. Eng. Sci.* **23**, 412–418 (1983).
83. J. L. Philippart and J. L. Gardette, *Polym. Degrad. Stab.* **71**, 189–194 (2000).
84. J. D. Peterson, S. Vyazovkin, and C. A. Wight, *Macromol. Chem. Phys.* **202**, 775–784 (2001).
85. J. D. Peterson, S. Vyazovkin, and C. A. Wight, *Macromol. Rapid Commun.* **20**, 480–483 (1999).
86. J. B. Knight, P. D. Calvert, and N. C. Billingham, *Polymer* **26**, 1713–1718 (1985).
87. N. C. Billingham, *Die Makromol. Chem., Macromol. Symp.* **28**, 145–163 (1989).
88. M. Celina, G. A. George, and N. C. Billingham, *Polym. Degrad. Stab.* **42**, 335–344 (1993).
89. M. Celina and co-workers, *Polym. Degrad. Stab.* **47**, 311–317 (1995).
90. I. Blakey and G. A. George, *Polym. Degrad. Stab.* **70**, 269–275 (2000).
91. H. Liu and co-workers, *Polym. Degrad. Stab.* **72**, 543–550 (2001).
92. G. George and M. Celina, in M. Hamid, ed., *Handbook of Polymer Degradation*, 2nd ed., Vol. **1**, Marcel Dekker, Inc., New York, 2000, pp. 273–309.
93. B. G. S. Goss and co-workers, *Polym. Degrad. Stab.* **74**, 523–532 (2001).
94. B. G. S. Goss and co-workers, *Polym. Degrad. Stab.* **74**, 271–282 (2001).
95. F. Gugumus, *Polym. Degrad. Stab.* **55**, 21–43 (1997).
96. F. Gugumus, *Polym. Degrad. Stab.* **52**, 131–144 (1996).
97. F. Gugumus, *Polym. Degrad. Stab.* **52**, 145–157 (1996).
98. F. Gugumus, *Polym. Degrad. Stab.* **52**, 159–170 (1996).
99. F. Gugumus, *Polym. Degrad. Stab.* **53**, 161–187 (1996).
100. R. L. Clough and K. T. Gillen, *Am. Chem. Soc. Symp. Ser.* **280**, 411–422 (1985).
101. K. T. Gillen, R. L. Clough, and N. J. Dhooge, *Polymer* **27**, 225–232 (1986).
102. K. T. Gillen, R. L. Clough, and C. A. Quintana, *Polym. Degrad. Stab.* **17**, 31–47 (1987).
103. L. Gonon, O. J. Vasseur, and J. L. Gardette, *Appl. Spectrosc.* **53**, 157–163 (1999).
104. N. C. Billingham, in P. P. Klemchuk and J. Pospisil, eds., *Oxidation Inhibition in Organic Materials*, Vol. **1**, CRC Press, Inc., Boca Raton, Fla. 1989, p. 269.
105. N. C. Billingham, in G. Scott, ed., *Atmospheric Oxidation and Antioxidants*, Vol. **II**, Elsevier, London, 1993, pp. 219–244.

106. K. T. Gillen and R. L. Clough, in N. P. Cheremisinoff, ed., *Handbook of Polymer Science and Technology*, Vol. **2**, Marcel Dekker, Inc., New York, 1989, pp. 167–202.
107. K. T. Gillen and R. L. Clough, *Polymer* **33**, 4358–4365 (1992).
108. A. Davis, *Dev. Polym. Degrad* **1**, 249–278 (1977).
109. J. E. Pickett, *Chem. Eng. News* **71**, 5 (1993).
110. R. B. Fox, *Prog. Polym. Sci.* **1**, 45–90 (1967).
111. G. Geuskens, in C. Bamford and C. Tipper, eds., *Comprehensive Chemical Kinetics*, Vol. **14**, Elsevier, Amsterdam, 1975, pp. 333–420.
112. F. Gugumus, in H. Zweifel, ed., *Plastics Additives Handbook*, 5th ed., Hanser, Munich, 2000, pp. 141–424.
113. J. Guillet, *Polymer Photophysics and Photochemistry*, Cambridge University Press, Cambridge, 1985.
114. F. Gugumus, *Polym. Degrad. Stab.* **65**, 259–269 (1999).
115. J. E. Guillet, in G. Scott and D. Gilead, eds., *Degradable Polymers, Principles and Applications*, Chapman and Hall, London, 1995, pp. 216–246.
116. A. Roger, D. Sallet, and J. Lemaire, *Macromolecules* **18**, 1771–1775 (1985).
117. A. Roger, D. Sallet, and J. Lemaire, *Macromolecules* **19**, 579–584 (1986).
118. D. Fromageot, A. Roger, and J. Lemaire, *Angew. Makromol. Chem.* **170**, 71–85 (1989).
119. Z. Khalil, S. Michaille, and J. Lemaire, *Die Makromol. Chem.* **188**, 1743–1756 (1987).
120. R. P. Singh and co-workers, *Polym. Int.* **36**, 309–313 (1995).
121. J. L. Gardette, B. Mailhot, and J. Lemaire, *Polym. Degrad. Stab.* **48**, 457–470 (1995).
122. D. M. Wiles, *Polym. Eng. Sci.* **13**, 74–77 (1973).
123. H. Kobsa, *J. Org. Chem.* **27**, 2293–2298 (1962).
124. S. K. L. Li and J. E. Guillet, *Macromolecules* **10**, 840–844 (1977).
125. D. M. Wiles and D. J. Carlsson, *Polym. Degrad. Stab.* **3**, 61 (1980).
126. A. Rivaton, D. Sallet, and J. Lemaire, *Polym. Photochem.* **3**, 463–481 (1983).
127. A. Rivaton, D. Sallet, and J. Lemaire, *Polym. Degrad. Stab.* **14**, 23–40 (1986).
128. A. Rivaton, D. Sallet, and J. Lemaire, *Polym. Degrad. Stab.* **14**, 1–22 (1986).
129. A. Factor, *Adv. Chem. Ser.* **249**, 59–76 (1996).
130. D. J. Carlsson and D. M. Wiles, *J. Macromol. Sci., C: Rev. Macromol. Chem.* **14**, 155 (1976).
131. F. Gugumus, *Dev. Polym. Stab.* **1**, 261–308 (1979).
132. P. Gijsman, *Angew. Makromol. Chem.* **252**, 45–54 (1997).
133. G. Scott, *Polym. Degrad. Stab.* **60**, 215–216 (1998).
134. P. Gijsman, *Polym. Degrad. Stab.* **60**, 217–219 (1998).
135. F. Gugumus, *Polym. Degrad. Stab.* **62**, 403–406 (1998).
136. G. Meijers and P. Gijsman, *Polym. Degrad. Stab.* **74**, 387–391 (2001).
137. J. Scheirs, S. W. Bigger, and N. C. Billingham, *Polym. Test* **14**, 211–241 (1995).
138. J. L. Gardette and J. Lemaire, *Polym. Photochem.* **7**, 409–416 (1986).
139. J. Scheirs, D. J. Carlsson, and S. W. Bigger, *Polym.-Plast. Technol. Eng.* **34**, 97–116 (1995).
140. R. A. Assink and co-workers, *Macromolecules* **33**, 4023–4029 (2000).
141. D. J. Carlsson and co-workers, *Am. Chem. Soc. Symp. Ser.* **364**, 376–389 (1988).
142. J. Lacoste and co-workers, *Polym. Degrad. Stab.* **34**, 309–323 (1991).
143. C. Wilhelm and J. L. Gardette, *Polymer* **39**, 5973–5980 (1998).
144. D. J. Carlsson and co-workers, *Polym. Degrad. Stab.* **17**, 303–318 (1987).
145. T. M. Alam and co-workers, *Macromolecules* **33**, 1181–1190 (2000).
146. J. M. Cardamone and P. Brown, *Adv. Chem. Ser.* **212**, 43–75 (1986).
147. K. T. Gillen and co-workers, *Trends Polym. Sci.* **5**, 250–257 (1997).
148. K. T. Gillen and M. Celina, *Polym. Degrad. Stab.* **71**, 15–30 (2000).
149. F. Gugumus, *Polym. Degrad. Stab.* **63**, 41–52 (1999).
150. P. Gijsman, J. Hennekens, and J. Vincent, *Polym. Degrad. Stab.* **39**, 271–277 (1993).

151. F. Gugumus, *Dev. Polym. Stab.* **8**, 239–289 (1987).
152. R. L. Clough and K. T. Gillen, *Nuc. Techno.* **59**, 344–354 (1982).
153. L. Costa and co-workers, *Biomaterials* **19**, 1371–1385 (1998).
154. L. Costa and co-workers, *Biomaterials* **19**, 659–668 (1998).
155. E. B. delPrever and co-workers, *Biomaterials* **17**, 873–878 (1996).
156. C. David, in Ref. 111, pp. 175–332.
157. W. S. Schnabel, in H. H. G. Jellinek, ed., *Aspects of Degradation and Stabilization of Polymers*, Elsevier, Amsterdam, 1978, pp. 149–193.
158. W. S. Schnabel, *Polymer Degradation. Principles and Practical Applications*, Hanser, Munich, 1981.
159. V. S. Ivanov, *Radiation Chemistry of Polymers*, VSP, Amsterdam, 1992.
160. A. Swallow, *Radiation Chemistry*, Longman, London, 1973.
161. J. W. T. Spinks and R. J. Woods, *An Introduction to Radiation Chemistry*, John Wiley & Sons, Inc., New York, 1976.
162. R. L. Clough and co-workers, *Polym. Degrad. Stab.* **49**, 305–313 (1995).
163. R. L. Clough and co-workers, *Radiat. Phys. Chem.* **48**, 583–594 (1996).
164. J. Wise, K. T. Gillen, and R. L. Clough, *Radiat. Phys. Chem.* **49**, 565–573 (1997).
165. D. J. Carlsson and co-workers, *Am. Chem. Soc. Symp. Ser.* **280**, 359–371 (1985).
166. C. David and co-workers, *Angew. Makromol. Chem.* **216**, 21–35 (1994).
167. A. C. Albertsson and S. Karlsson, in S. L. Aggarwal and S. Russo, eds., *Comprehensive Chemical Kinetics, Supplement 1*, Pergamon, Oxford, 1992, pp. 285–297.
168. S. Karlsson and A. C. Albertsson, *Polym. Eng. Sci.* **38**, 1251–1253 (1998).
169. S. J. Huang, in G. C. Eastmond, A. Ledwith, S. Russo, and P. Sigwalt, eds., *Comprehensive Chemical Kinetics*, Vol. **6**, Pergamon, Oxford, 1989, pp. 597–606.
170. D. Byrom, in D. P. Mobley, ed., *Plastics from Microbes*, Hanser, Munich, 1994, pp. 5–33.
171. G. B. Kharas, F. Sanchez-Riera, and D. K. Severson, in Ref. 170, pp. 93–137.
172. C. Bastioli, in Ref. 115, pp. 112–138.
173. C. vonProschek and C. Bastioli, *Agro Food Ind. Hi-Tech* **7**, 4–6 (1996).
174. C. Bastioli, *Macromol. Symp.* **135**, 193–204 (1998).
175. C. Bastioli, *Polym. Degrad. Stab.* **59**, 263–272 (1998).
176. G. J. L. Griffin, *Chemistry and Technology of Biodegradable Polymers*, Blackie, London, 1994.
177. R. Arnaud and co-workers, *Polym. Degrad. Stab.* **46**, 211–224 (1994).
178. G. Scott, in Y. Doi and K. Fukuda, eds., *Biodegradable Plastics and Polymers*, Elsevier, Amsterdam, 1994, pp. 79–91.
179. G. Scott, *Trends Polym. Sci.* **5**, 361–368 (1997).
180. G. Scott, *Polymers in the Environment*, Royal Society of Chemistry, London, 1999.
181. A. C. Albertsson, S. O. Andersson, and S. Karlsson, *Polym. Degrad. Stab.* **18**, 73–87 (1987).
182. M. Weiland, A. Daro, and C. David, *Polym. Degrad. Stab.* **48**, 275–289 (1995).
183. J. Lemaire and co-workers, *J. Macromol. Sci., A: Pure Appl. Chem.* **32**, 731–741 (1995).
184. F. Khabbaz, A. C. Albertsson, and S. Karlsson, *Polym. Degrad. Stab.* **63**, 127–138 (1999).
185. D. Giliad, in Ref. 115, pp. 186–199.
186. D. M. Wiles, B. E. Cermak, J. G. Gho, and C. W. J. Hare, in Addcon World '98, RAPRA Technology, Shawbury, U.K., 1998, p. 14.
187. J. F. Tung, D. M. Wiles, B. E. Cermak, J. G. Gho, and C. W. J. Hare, in Addcon world, RAPRA Technology, Shawbury, U.K., 1999, p. 17.
188. D. M. Wiles, B. E. Cermak, J. G. Gho, C. W. J. Hare, and J. F. Tung, in W. Bidlingmaier ed., *Organic Recovery and Biological Treatment*, Rhombos, Weimar, Germany, 1999, pp. 547–552.

189. N. C. Billingham and co-workers, in Addcon World, DO, RAPRA Technology, Shawbury, U.K., 2000, p. 6.

N. C. BILLINGHAM
University of Sussex

DENDRONIZED POLYMERS.

See Volume 2.

DENTAL APPLICATIONS.

See Volume 2.

DIACETYLENE AND TRIACETYLENE POLYMERS.

See Volume 2.

DIELECTRIC RELAXATION

Introduction

The control of dielectric permittivity and loss of solid polymers, through an understanding of the origins of their dipole relaxation and ionic conduction processes, is essential for their use in electrical insulation, in electrical/electronic circuits, and devices operated over wide power ranges. This article discusses dielectric properties and behavior of polymers and briefly describes measurement techniques and applications.

Dielectric Properties

The dielectric properties of polymer materials are usually expressed in terms of the complex dielectric permittivity $\varepsilon(\omega)$ relative to vacuum, defined as $\varepsilon(\omega) = \varepsilon'(\omega) - i\varepsilon''(\omega)$, where $i = \sqrt{-1}$, $\omega = 2\pi f$, and f is the measurement frequency. The real permittivity ε' and loss factor ε'' for polymers depend on frequency due to (*1*) electric polarization arising from the tumbling motions of electric dipoles in the polymer chains and (*2*) conduction due to the translational motions of electric charges (intrinsic or extrinsic ions and electrons) (1–4). For essentially nonpolar polymers such as polyethylene, polypropylene, polystyrene, and polytetrafluoroethylene in their pure state, the absence of dipoles and ions results in (*1*) low values of ε' (in the range 2–3 since here $\varepsilon' \sim n^2$, where n is the optical refractive index), and (*2*) very small values of loss ($\varepsilon'' < 10^{-3}$) across the entire frequency range from 10^{-6} to 10^{12} Hz. These low permittivity, low loss materials are dielectric insulators and so find wide applications in electrical cables and capacitors and in electrical and electronic circuits. Polar polymers contain dipolar groups, such as

Encyclopedia of Polymer Science and Technology. Copyright John Wiley & Sons, Inc. All rights reserved.

ether, ester, halide, and amide groups, repeated regularly along the chains. Those polar polymers that are glasses (eg, poly(vinyl chloride), poly(methyl methacrylate), aliphatic and aromatic polyesters, and polycarbonates at room temperature) or are highly crystalline (eg, polyoxymethylene and polyoxyethylene at room temperature) also exhibit low values of ε' and ε'' since the dipoles and the extraneous ions present are immobilized. Polar polymers that are liquid or elastomeric (eg, polar polymers above their glass-transition temperature T_g) exhibit frequency-dependent ε' values (typically in the range 3–20) together with complementary losses because above T_g the dipolar groups are mobile, allowing the dipole polarization to contribute to $\varepsilon(\omega)$. If such polymers also contain ions, as in polymer electrolytes, then ionic conduction and electrode polarization effects contribute to ε' and ε'' at low frequencies ($<10^5$ Hz), leading to large values ($>10^2$) of both ε' and ε''. The dielectric properties of polymers, as observed in plots of ε' and ε'' against log f/Hz, reflect contributions due to the reorientational motions of dipoles and the translational motions of ions and from the effects of interfacial and electrode polarizations (1–4).

When an electric field E is applied as a step at $t = 0$ to a slab of dielectric material the electric charge passing through the material has two components $q_P(t)$ and $q_i(t)$ due to electric polarization and ion conduction, respectively. For $q_P(t)$ the initial response q_∞ is rapid ($<10^{-12}$ s) and is due to both electronic polarization (arising from the displacement of electron charge clouds in the molecules) and atomic polarization (arising from the relative displacement of atomic positions in the molecules). There is a delayed response that takes q_P up to a steady value q_0 because the field perturbs the spatial distribution of dipole directions, giving a macroscopic dipole polarization P in line with the field. The timescale for this response is determined by the rate of the reorientational motions of the chain dipoles in the absence of the field, which will depend on the chemical structure of the polymer and its temperature. Below T_g the response time becomes very large and so there is little or no dipole polarization. The material appears to be nonpolar [except from a minor contribution to $q_P(t)$ from small-amplitude motions of dipoles in the glassy state (see below)]. On removal of the field the process is reversed; the fast decay of $q_P(t)$ is followed by the delayed response. The normalized rise and decay functions for dipole relaxation $\Phi(t) = [q_P(t) - q_\infty]/(q_0 - q_\infty)$ are equivalent; this is one condition for a linear dielectric material, the other being that $\varepsilon(\omega)$ is independent of the field strength. An *average relaxation time* $\langle\tau\rangle$ is defined as the time taken for the decay function to fall to $1/e$ of its original value at $t = 0$. For liquid water, $\langle\tau\rangle \sim 10^{-11}$ s. For polymers temperature has a large effect on the rate of molecular motions, eg, $\langle\tau\rangle$ for poly(vinyl acetate) increases from about 10^{-11} to 10^2s as the temperature is reduced toward T_g.

In addition, ionic conduction causes a charge $q_i(t)$ to pass through the material, which rises from zero and then becomes linearly dependent on time to give a constant current $I(t) = dq_i/dt$. In contrast to $q_P(t)$, which becomes constant at long times (since the dipolar system reaches thermodynamic equilibrium in the presence of the steady field), $q_i(t)$ increases without limit in the absence of interfacial and electrode polarization effects, giving a continual dissipation of energy via the conduction process. The fact that the steady conduction current takes time to get established means that the ac real conductivity $\sigma'(\omega)$ is constant at low frequencies and becomes f-dependent at high frequencies.

Although the nature of dipole polarization and ionic conduction are readily understood in the time domain, dielectric measurements for polymers are normally made in the frequency domain. The range 10^{-6}–10^{12} Hz can be covered using a combination of techniques, but the working range for most studies in the older literature was from about 1 to 10^7 Hz (1–5). Below 1 MHz the dielectric may be regarded as an electrical equivalent circuit comprising a capacitor C_p in parallel with a resistor R_p measured at a frequency $f = \omega/2\pi$ (1). Measurements made using an impedance analyzer allow the complex electrical admittance $Y(\omega)$ or its reciprocal—the impedance $Z(\omega)$—to be determined where

$$Y(\omega) = G_P(\omega) + i\omega C_P(\omega) \tag{1}$$

Here $G_p(\omega) = [R_p(\omega)]^{-1}$ is the electrical conductance. The complex permittivity ε, complex conductivity $\sigma = \sigma' + i\sigma''$, and complex electrical modulus $M = M' + M''$ are determined from Y, using the relations

$$\varepsilon(\omega) = \frac{Y(\omega)}{i\omega C_0} = \frac{\sigma(\omega)}{i\omega\varepsilon_v} = \frac{1}{M(\omega)} \tag{2}$$

Here ε_v is the permittivity of vacuum ($= 8.854 \times 10^{-12}$ F·m^{-1}) and C_0 is the geometrical capacitance of the sample. The dielectric properties of polymers are variously reported in terms of Z, Y, ε, M, σ and its reciprocal, the resistivity ρ. This is a source of confusion and makes it difficult to compare literature data for different polymer materials. The preferred representations of data when dipole polarization and ion conductivity are present will be indicated below.

At microwave frequencies ($f > 10^8$ Hz) a polymer material is regarded as a distributed circuit having a complex propagation coefficient $\gamma = \alpha + i\beta$, where α and β are the electrical attenuation and phase factors of the material. These are measured using microwave techniques and ε' and ε'' follow as

$$\varepsilon'(\omega) = [n(\omega)]^2\{1 - [\alpha(\omega)/\beta(\omega)]^2\}; \qquad \varepsilon''(\omega) = 2[n(\omega)]^2\alpha(\omega)/\beta(\omega) \tag{3}$$

where $n(\omega) = c\beta(\omega)/\omega$ is the refractive index at ω and c is the velocity of light.

As an example of dielectric relaxation behavior, Figure 1 shows plots of ε' and ε'' against log f/Hz for glycerol, a polyhydroxyl liquid, studied over a wide temperature range. At each temperature, ε' at low frequencies is constant (at ε_0) and then falls with increasing frequency to values typical of a nonpolar material. Dispersion of ε' is accompanied by a loss peak whose frequency of maximum loss (f_{max}) determines the average relaxation time $\langle\tau\rangle = [2\pi f_{max}]^{-1}$. For glycerol $\langle\tau\rangle$ increases by 10 orders of magnitude as the temperature is reduced toward T_g. In addition, ionic conduction gives the increasing loss at low frequencies. The dielectric behavior of glycerol is representative of all amorphous polymers and glass-forming liquids that contain dipolar molecules (1–5).

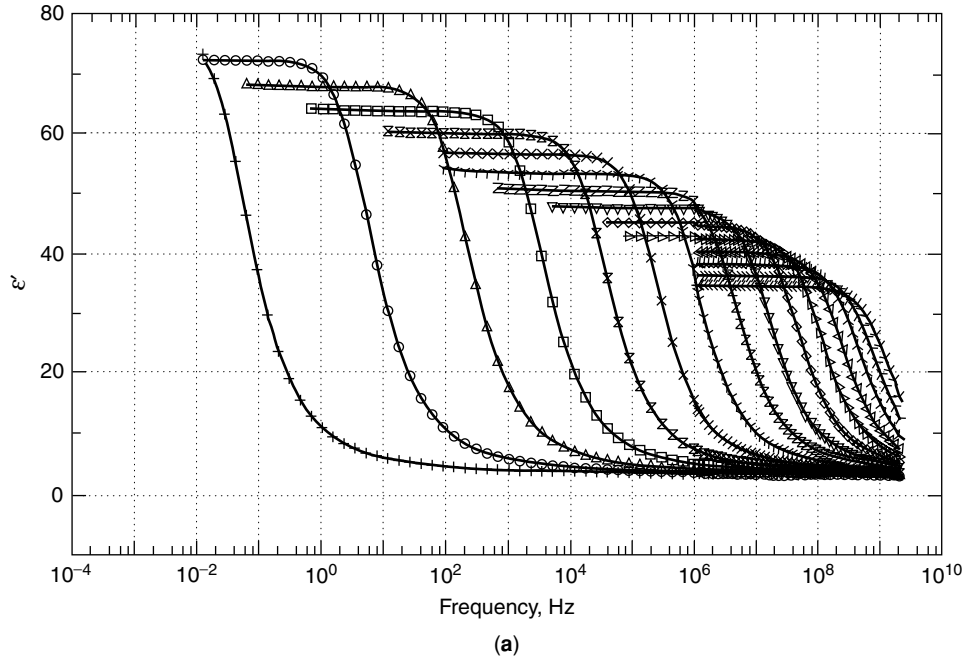

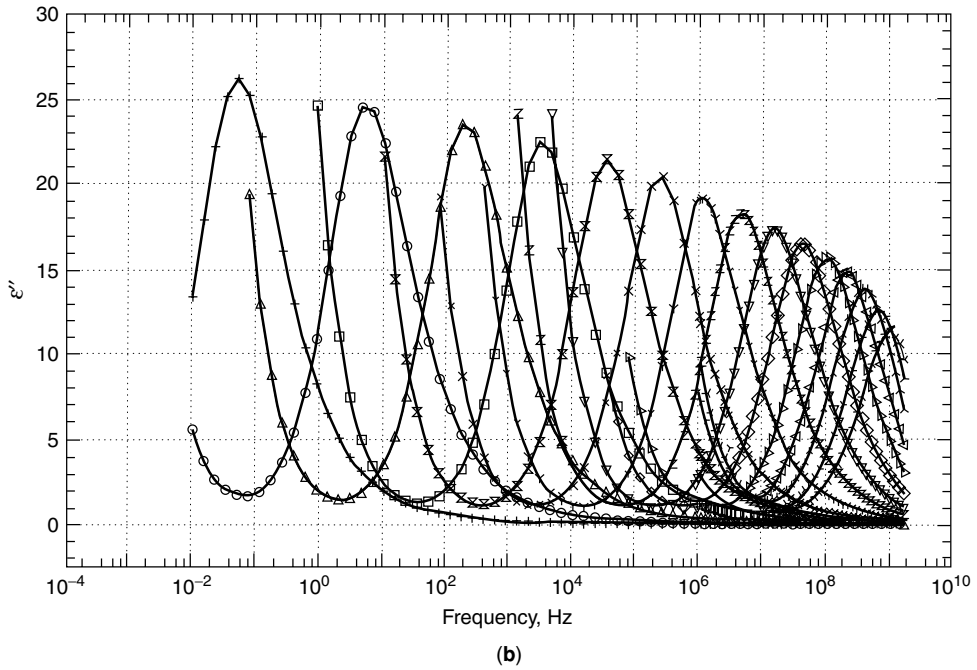

Fig. 1. Plots of (**a**) ε' and (**b**) ε'' against frequency (Hz) for glycerol at 10 K intervals from 193.15 K (+) to 333.15 K (◊). Data provided by Dr G. Schaumburg, Novocontrol GmbH.

Theory

The normalized decay function $\Phi(t)$ of the dipole polarization is related to $\varepsilon(\omega)$ according to (1,5)

$$\frac{\varepsilon(\omega)-\varepsilon_\infty}{\varepsilon_0-\varepsilon_\infty}=1-i\omega\Im[\Phi(t)] \tag{4}$$

Where ε_0 and ε_∞ are the limiting low and high frequency real permittivities, and $\Im$ indicates a one-sided Fourier transformation. A simple form for $\Phi(t)$ is the single exponential decay function

$$\Phi(t)=\exp(-t/\tau) \tag{5}$$

Insertion into equation 4 gives the paired relations

$$\frac{\varepsilon'(\omega)-\varepsilon_\infty}{\varepsilon_0-\varepsilon_\infty}=\frac{1}{1+\omega^2\tau^2} \tag{6}$$

$$\frac{\varepsilon''(\omega)}{\varepsilon_0-\varepsilon_\infty}=\frac{\omega\tau}{1+\omega^2\tau^2} \tag{7}$$

Here $\varepsilon_0-\varepsilon_\infty$ ($=\Delta\varepsilon$, say) is the relaxation strength. Figure 2 shows plots of ε' and ε'' against log $\omega\tau$ for $\varepsilon_0=13$, $\varepsilon_\infty=3$ for equations 6,7 [the single relaxation time (SRT) function]. $\omega_{\max}\tau=1$ at the loss peak. Thus dielectric relaxation is characterized by $\Delta\varepsilon$ and τ for this function. The steady ionic conductivity σ_0 contributes an additional, rising loss at low frequencies given by $\varepsilon_i''=\sigma_0/\omega\varepsilon_v$, but this process makes no contribution to $\varepsilon'(\omega)$ in this case.

In practice dielectric relaxation curves for polymers (1–5) and glass-forming liquids (eg, Fig. 1) are far broader than that for an SRT process. Numerous empirical relaxation functions have been proposed for this behavior (1,2,5). One function is the stretched exponential function of Kohlrausch, Williams, and Watts (KWW) (4–6), that is widely applied to dielectric and other relaxation data for amorphous polymers:

$$\Phi(t)=\exp[-(t/\tau)^{\bar\beta}] \tag{8}$$

$0<\bar\beta\leq 1$. Figure 2 includes curves for ε' and ε'' calculated using equation 4 and the KWW function for $\bar\beta=0.50$. The loss curve is broad and nonsymmetrical, with a total half-width $\Delta_{1/2}\sim 2.2$ (cf 1.14 for the SRT process). The dielectric data for glycerol conform approximately to the KWW function ($\bar\beta$ increases from about 0.6 to 0.95 as temperature is increased). Thus dielectric relaxation in polymers and other materials is characterized by the *shapes* of the ε' and ε'' curves in addition to $\Delta\varepsilon$ and $\langle\tau\rangle$.

Molecular theories for the static permittivity ε_0 of dipolar liquids developed originally by Onsager, Kirkwood, and Fröhlich were adapted for linear bulk

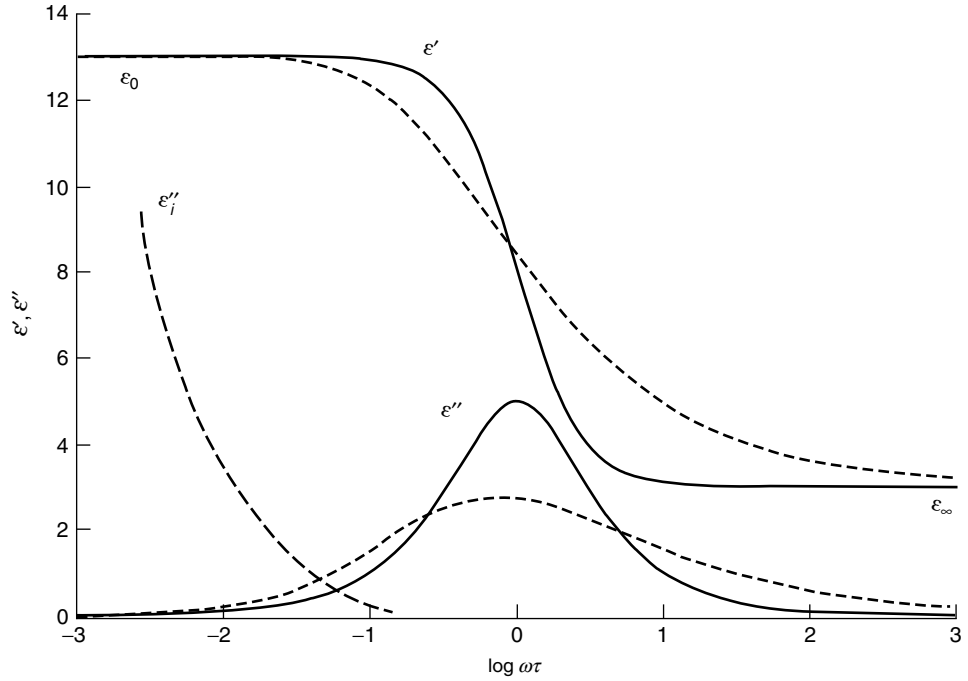

Fig. 2. Plots of ε' and ε'' against $\log_{10}\omega\tau$ for the SRT function (——) $\beta = 1.0$ and the KWW function (- - - -) for $\bar{\beta} = 0.50$. The increasing loss ε_i'' at low frequencies (– – –) is due to the steady conductivity σ_0.

polymers by Williams and co-workers (1,7) giving

$$\varepsilon_0 - \varepsilon_\infty = \frac{4\pi}{3kT}\left(\frac{3\varepsilon_0}{2\varepsilon_0 + \varepsilon_\infty}\right)\left(\frac{\varepsilon_\infty + 2}{3}\right)^2 c_r g \mu^2 \tag{9}$$

Where c_r is the concentration of the dipolar repeat units, each of dipole moment μ, and g is the Kirkwood–Fröhlich factor for orientational correlations of dipoles along and between chains.

$$g = 1 + \sum_{ij} \langle \cos \theta_{ij} \rangle \tag{10}$$

where $\langle \cos \theta_{ij} \rangle$ is the equilibrium average projection of dipole j on a reference dipole i, which can be calculated using statistical mechanics (4,5,8). Parallel or antiparallel alignment of dipoles leads to $g > 1$ and $g < 1$, respectively. The large values of ε_0 for glycerol (Fig. 1) arise since intermolecular H-bonding leads to $g > 1$. In liquid water, H-bonding gives $g \sim 2.5$, which raises ε_0 to ~80 at room temperature.

Dipole relaxation in polymers is conveniently considered in terms of the normalized dipole correlation function $\Phi_\mu(t)$ for the reorientational motions of dipolar groups.

$$\Phi_\mu(\mathrm{t}) = \frac{\langle \mu_i(0)\mu_i(\mathrm{t})\rangle + \sum_j \langle \mu_i(0)\mu_j(\mathrm{t})\rangle}{\langle \mu_i^2\rangle + \sum_j \langle \mu_i(0)\mu_j(0)\rangle} \tag{11}$$

where $\langle \mu_i(0)\mu_i(\mathrm{t})\rangle$ and $\langle \mu_i(0)\mu_j(\mathrm{t})\rangle$ are the autocorrelation function (ACF) and cross-correlation function (CCF) for dipole motions of a reference dipole i and further dipoles j along and between chains. The ACF is readily understood. At time $t = 0$ the dipole i has a particular value $\mu_i(0)$. The normalized ACF $\langle \mu_i(0)\mu_i(t)\rangle / \langle \mu_i^2\rangle = \langle \cos\theta_{ii}(t)\rangle$ is the average projection of $\mu_i(t)$ at time t on $\mu_i(0)$ at $t = 0$. This decays to zero with time. The CCFs in equation 11 account for the dynamic cross-correlations between dipole i and the neighboring dipoles j. It is found (5) that $\Phi_\mu(t) \approx \Phi(t)$, the macroscopic relaxation function, and so $\varepsilon(\omega)$ can be determined using equation 4. $\Phi_\mu(t)$ may decay as a SRT function, a broadened function (eg, the KWW function), a weighted sum of SRT functions (known as a "distribution of relaxation processes"), or decay in several discrete stages—which leads to discrete multiple loss peaks in the f-domain (1,3,5). The overall loss curve gives information on the mechanism(s) of the dipole relaxation process(es) in the polymer material (1–5).

For ionic conduction the complex conductivity is given by (9,10)

$$\sigma(\omega) = \sum_i a_i \Im\langle v_i(0)v_i(t)\rangle = \omega^2 \sum_i a_i \Im\left[\left\langle \Delta R_i^2(t)\right\rangle\right] \tag{12}$$

Here $a_i = [c_i q_i^2 / kT]$, c_i and q_i are, respectively, the concentration and charge of species i (anions and cations). $\langle v_i(0)v_i(t)\rangle$ and $\langle \Delta R_i^2(t)\rangle$ are, respectively, the velocity correlation function (VCF) and mean-squared displacement in time of species i. The steady current behavior at long times in the step-on experiment (see above) means that $\langle \Delta R_i^2(t)\rangle$ becomes linearly dependent on time, giving the Nernst–Einstein equation that connects the low-f conductivity $\sigma'(0)$ $(=\sigma_0)$ to the diffusion coefficients D_i for the translational motions of the ions (9,10):

$$\sigma_0 = \sum_i a_i D_i \tag{13}$$

$$D_i = \frac{1}{3}\int_0^\infty \langle v_i(0)v_i(t)\rangle \mathrm{d}t \tag{14}$$

$$D_i = \frac{1}{6}\frac{\left\langle \Delta R_i^2(t)\right\rangle}{t} \tag{15}$$

Hopping motions of ions at short times are influenced by the surrounding molecules, leading to a "bounce-back mechanism" that causes $\langle \Delta R_i^2(t)\rangle$ to be lower at short times than it would be if the long time behavior was extrapolated to zero (9,10). As a result the real conductivity $\sigma'(\omega)$ for polymers and most amorphous disordered solids is a constant (σ_0) at low frequencies but obeys a power law $(\omega^m, 0 < m \leq 1.0)$ at high frequencies (9,10).

In view of the above we note that plots of $\varepsilon''(\omega)$ against log f/Hz give information on the *reorientational motions* of chain dipoles through $\Phi_\mu(t)$ (eqs. 4, 6,7 and 11) while plots of $\sigma'(\omega)$ against log f/Hz give information on the *translational motions* of ions through $\langle v_i(0)v_i(t)\rangle$ and $\langle \Delta R_i^2(t)\rangle$ (eqs. 12 and 14,15).

The other representations Z, Y, M, and ρ refer indirectly to these molecular dynamic properties (see eq. 2).

Dielectric Behavior of Polymers

Dielectric spectroscopy (DS) provides a means of studying chain dynamics of amorphous, crystalline, and liquid crystalline (LC) polymers (1,3–5,11). As one example Figure 3 shows plots of ε'' against $\log f$/Hz for the amorphous polymer poly(vinyl acetate) at different temperatures. The α loss peak (Fig. 3a) is due to the large-scale motions of chain dipoles and moves to ultralow frequencies as T_g is approached. $\langle\tau_\alpha(T)\rangle$ obeys the Vogel–Fulcher–Tammann equation

$$\langle\tau_\alpha(T)\rangle = A\exp[B/(T - T_\infty)] \tag{16}$$

where A, B, and T_∞ are material constants. T_g is often defined operationally as the temperature at which $\langle\tau_\alpha\rangle = 10^2$ s. The loss curves for poly(vinyl acetate) may be fitted approximately using the KWW function ($\bar{\beta}$ increases from 0.6 to 0.8 in this T-range). Below T_g a small secondary loss process (β process) is observed (Fig. 3b) because of limited motions of chain backbones and side chains. $\langle\tau_\beta(T)\rangle$ obeys the Arrhenius equation with activation energy $Q_\beta \sim 40$ kJ·mol^{-1}. All dipolar amorphous polymers (and small-molecule glass-forming liquids) give dielectric behavior similar to poly(vinyl acetate) (1–5) [ie, they exhibit an α process (lower-f process with large $\Delta\varepsilon_\alpha$) and a β process (higher-f process with small $\Delta\varepsilon_\beta$)]. Syndiotactic poly(methyl methacrylate) is an exception, having $\Delta\varepsilon_\beta > \Delta\varepsilon_\alpha$ (1,3). Static permittivities $\varepsilon_0(T)$ have been reported for numerous amorphous polymers and (using eq. 9) have enabled $g\mu^2$ to be determined in several cases (1,5,8).

Dielectric relaxation data for individual polymers are frequently compared with complementary data obtained from NMR, dynamic mechanical, quasi-elastic light/neutron scattering, and time-resolved fluorescence depolarization experiments (12). Many studies show (1–5,12) that the β process is due to spatially limited motions of chain segments or side chains occurring in a range of local environments, leading to a dielectric relaxation strength $\Delta\varepsilon_\beta \propto\langle\mu^2\rangle - \langle\mu\rangle^2]$, where $\langle\mu\rangle$ is the mean dipole moment that remains after the local motions (β process) have taken place. The α-process is due to the large-scale motions (micro-Brownian motions) of chains and has a relaxation strength $\Delta\varepsilon_\alpha \propto\langle\mu\rangle^2$. If pressure is applied in order to reduce $\Delta\varepsilon_\beta$, there is a complementary increase in $\Delta\varepsilon_\alpha$ [as demonstrated for poly(alkyl methacrylates) (3–5)]. For polymers with rotatable side groups [eg, poly(alkyl methacrylates)] the dielectric α and β processes merge in the MHz region to form the $\alpha\beta$ process (1–5,13). For polymers without rotatable side groups, eg, poly(ethylene terephthalate), polyesters and polycarbonates, the α and β processes merge only at very high frequencies ($>10^9$ Hz) (1–5,13). The origins of α,β and $\alpha\beta$ relaxations, their relaxation functions, and their T-dependencies for amorphous polymers and glass-forming liquids have received much attention (1–5,11–13). Models for chain dynamics based on mode-coupling theories, transient energy landscapes, and local "dynamic heterogeneities", together with large-scale molecular dynamics/Monte Carlo simulations of assemblies of polymer chains, have been developed and applied to relaxation, spectroscopic, and scattering data

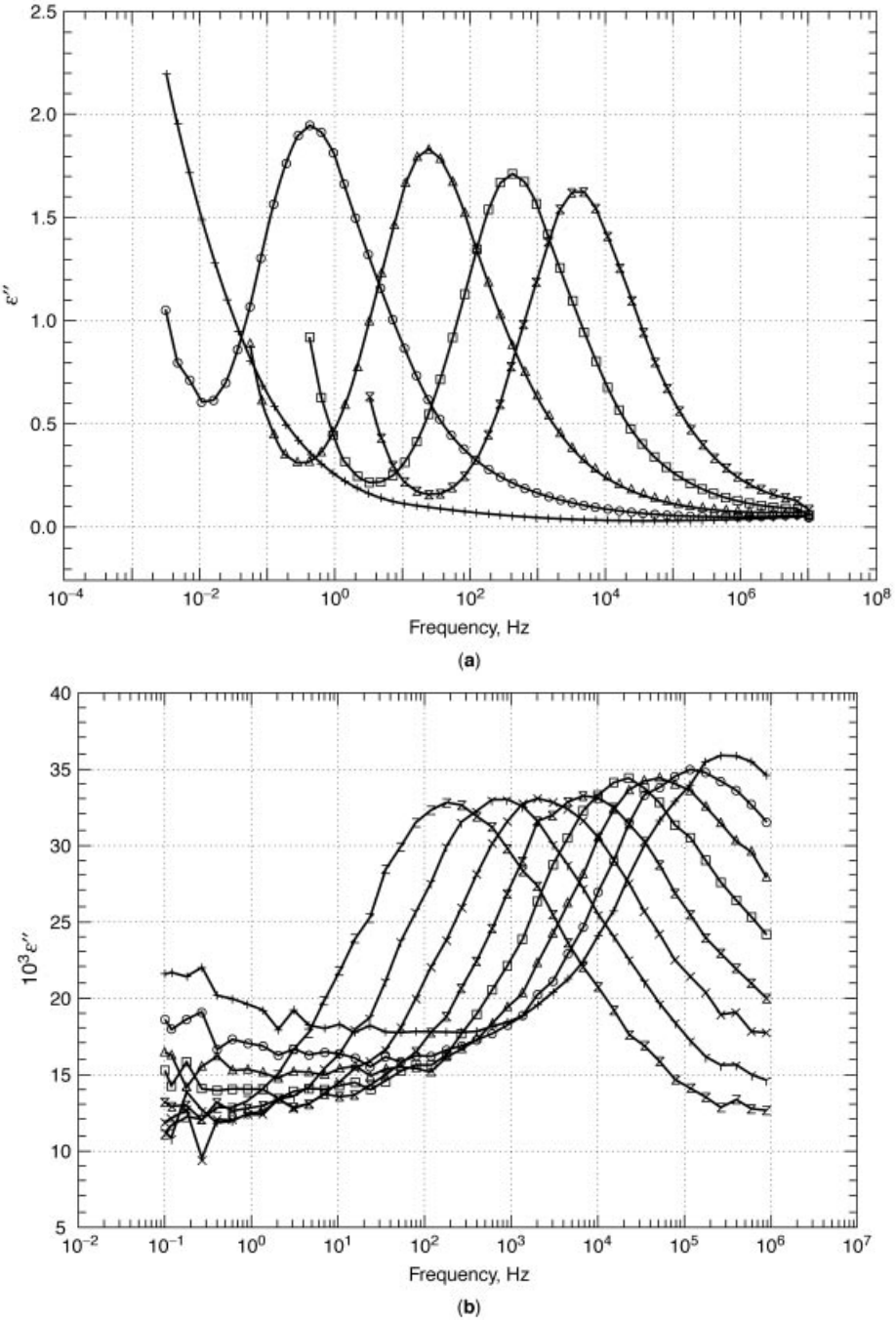

Fig. 3. Plots of ε'' against frequency (Hz) for poly(vinyl acetate): (**a**) the α-relaxation region from 293.15 K (+) to 333.15 K (Δ) in intervals of 10 K and (**b**) the β-relaxation region from 183 K (z) to 253 K (+) in intervals of 10 K. Data provided by Dr G. Schaumburg, Novocontrol GmbH.

(see, eg, Ref. 12). At a more practical level, DS is used to study the structure and dynamics of complex amorphous polymer systems. For example local inhomogeneity in polymer blends and random copolymers that exhibit a single T_g was revealed for blends of poly(*o*-chlorostyrene)/polystyrene and their random copolymers using broadband DS (see Ref. 14 and references therein). The width $\Delta_{1/2}$ of the α-peak was far broader than those for the pure homopolymers and broadened further as temperature was reduced, showing the presence of microphase separation and allowing the distribution of local concentrations to be determined (14). In certain polymers (eg, polypropylene oxide and polyisoprene) there is a small cumulative dipole moment along the chain contour and so for these materials DS can monitor the long-range motions (Rouse modes) of linear chains and multi-armed stars (11,15,16). The dependence of dielectric relaxation time $\langle\tau\rangle$ on molecular weight M is of interest; eg, for linear *cis*-polyisoprenes, $\langle\tau\rangle \sim M^2$ for $M < M_c$ and $\langle\tau\rangle \sim M^{3.7}$ for $M > M_c$, where M_c is the critical value for chain entanglements (15). The dielectric and dynamic mechanical relaxation data for the normal-mode relaxations in such polymers may be compared.

The dielectric behavior of crystalline polymers is more complex (1,2,4,17). For most materials (eg, the nylons, polyesters) motions of dipoles in the crystalline regions are totally suppressed. Polyethylene is an exception since chain rotation accompanied by translation of whole chains occurs within the lamellar crystals (17). Chain motions are possible in disordered regions on the surfaces of the lamellae (as occur in linear polyethylenes) or in the abnormal amorphous regions between the lamellar (as in the nylons). For polyethylene, which is nonpolar, motions occurring within the lamellae (α_c and γ_c processes) and the amorphous regions (β_a and γ_a processes) are activated for dielectric studies by incorporating carbonyl or C—Cl dipoles into the chains (1,3,17). Melt-crystallized polyamides (nylons) and polyesters are 100% spherulitic (by optical microscopy) but may be only ~50% crystalline. The motions of the amorphous phase within spherulites are severely influenced by the crystals, giving an α' process that is far broader and slower than the normal α process for the amorphous form of the polymer. Real-time dielectric studies of such polymers [eg, poly(ethylene terephthalate)] made during crystallization monitor the disappearance of the α process and the appearance of the α' process (18), thus providing a novel means of studying both the kinetics of crystallization and the dynamics of chains in the abnormal amorphous regions within spherulites.

Dielectric studies have been made for thermotropic LC polymers having mesogenic (LC-forming) dipolar groups in the side chains. These are a rare example of *dielectrically variable materials*, ie materials whose dielectric properties can be changed *in situ* using applied electric or magnetic fields. Motions of the mesogenic groups give four active dielectric relaxation modes (00, 01, 10, and 11) while motions of the chain backbone contribute to an α process (3,4,19,20). Aligned LC polymer films are made using strong ac electric fields of high and low frequencies ("two-frequency addressing principle"), yielding samples having homeotropic (H), planar (P), or intermediate (I) alignment of the LC director (n) with respect to the measuring field direction (the z-axis normal to the the plane of the film) (19,20). H samples ($n \| E$) and P samples ($n \perp E$) exhibit [00, 01] and [10,11] modes, respectively, and so have very different dielectric properties. The δ process (00 mode) is dominant for the H material but is absent for the P material. In general

$$\varepsilon(\omega) = (1 + 2S_d)\varepsilon_{\parallel}(\omega)/3 + 2(1 - S_d)\varepsilon_{\perp}(\omega)/3 \quad (17)$$

S_d is the "director order parameter" and is 1, 0, −1/2 for H-unaligned and P-aligned materials, respectively. $\varepsilon_{\parallel}(\omega)$ and $\varepsilon_{\perp}(\omega)$ are the principal permittivities of the LC phase and are related to dipole moment components $\mu_{\parallel}$ and $\mu_{\perp}$ of the side groups and the local order parameter S_l of the phase. Ferroelectric polymers, made by introducing chiral polar groups as mesogenic groups in side-chain LC polymers (21), exhibit two low frequency dielectric processes, (*1*) the Goldstone mode and (*2*) the soft mode, both having large relaxation strengths. The soft mode occurs only in the chiral S^*_c phase and is suppressed by application of a biasing electric field (21).

Solid polymer electrolytes are of interest for battery applications, and are either homogeneous polymers having electrically charged chains with labile counterions or blends of neutral polymers with inorganic salts. A practical aim is to prepare stable films having dc conductivities $\sigma_0 > 10^{-5}$ S·cm^{-1} at room temperature. Many materials have been investigated (22). In all cases σ_0 decreases by up to 8 orders of magnitude as temperature is reduced toward T_g(polymer) as a result of two effects: (*1*) reduced ion mobility, due to the slowing down of molecular motions, and (*2*) increasing ion-association, which removes ions and creates dipolar aggregates that exhibit dielectric relaxation. Plots of $\sigma'(\omega)$ against log f/Hz feature (*1*) a plateau over a wide intermediate f-range that provides $\sigma_0(T)$ values, (*2*) a decrease in σ' at low frequencies as a result of electrode polarization, and (*3*) a power-law increase of σ' at high frequencies (see, eg, Refs. 22 and 23) as a result of the short-time "backlash effect" mentioned above. Such data for a polymer electrolyte at different temperatures or applied pressures (23) are used to construct a master curve of log $\sigma'(\gamma\omega)/\sigma_0$ against log $\gamma\omega$, where log γ is a horizontal shift factor (9,10). Near-universal behavior for these master plots is obtained for polymer electrolytes and many other disordered amorphous materials (9,10). Models proposed to account for this behavior include those for the hopping of charge carriers over local barriers between temporary sites in the solid (9,10). In general, polymer electrolytes contain dipolar species in addition to the ions, and so give dipole relaxation processes in addition to ionic conduction. Insufficient attention has been given in the literature to the separation of dipole relaxation and conduction processes in the plots of $\sigma'(\omega)$ and $\varepsilon''(\omega)$ against log f/Hz for polymer electrolytes.

Real-time dielectric studies of polymerizing systems give information on the changes in molecular dynamics that occur during reaction. Condensation (step) and radical-chain (addition) reactions yielding glassy or elastomeric products, initiated thermally or photochemically, have been studied in this way (see Refs. 24–26 and references therein). Figure 4 shows 3D plots of ε' and ε'' against {log f/Hz, time/s} for the reaction of an equimolar mixture of a diepoxide DGEBA (diglycidyl ether of bisphenol A) with an alicyclic diamine at 60°C (27). ε' values (Fig. 4a) decrease from those of a liquid at $t = 0$ to a glass at long times. The ε'' curves (Fig. 4b) exhibit (*1*) losses at low frequencies/short times due to ionic conduction, that decrease rapidly as the viscosity of the reaction mixture increases, and (*2*) the α-relaxation process, which moves to ultralow frequencies with time as the glass is formed. These data, taken together with those for the extent of reaction with time, show that decreasing molecular mobility (as monitored by the location of the α-process) causes the reaction to become diffusion-controlled, leading to a

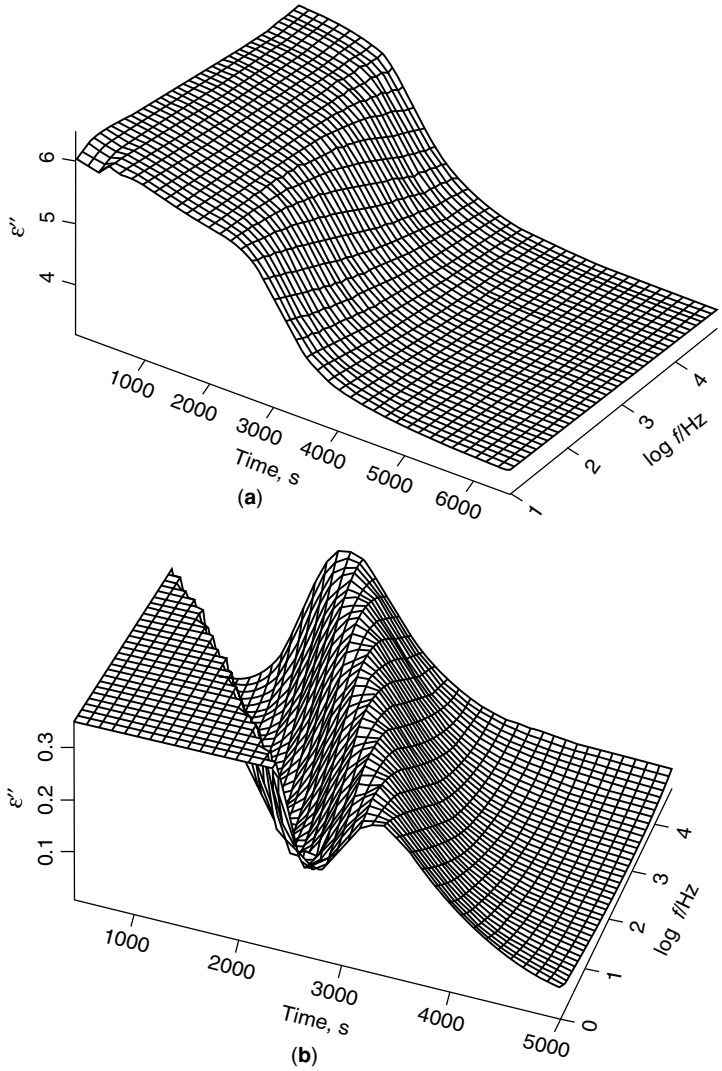

Fig. 4. Plots of (**a**) ε' and (**b**) ε'' against $\{\log_{10} f/\text{Hz}, \text{time/s}\}$ for an epoxide/amine thermosetting reaction at 60°C. Data provided by Dr I.K. Smith (27).

chemically unstable glass at long times. In other cases reaction is completed before diffusion-control sets in, and so a chemically stable elastomer is formed (25,26). The "floor temperature" T_f, below which the product is a glass and above which the product is an elastomer, can be determined using DS for thermopolymerization reactions (25,26).

Measurement Techniques and Applications

Measurements of $\varepsilon(\omega)$ and $\sigma(\omega)$ are made using commercial frequency-reponse analyzers (10^{-5} – 10^6 Hz), impedance analyzers (10^2 – 10^6 Hz), time-domain

reflectometers ($10^6 - 10^9$ Hz), and network analyzers ($10^7 - 10^{12}$ Hz) (28). At very high frequencies (GHz to THz) special quasi-optical and far-infrared spectrometers have been developed (28,29). At ultralow frequencies ($10^{-5} - 1$ Hz) transient charge/current methods provide an alternative (and faster) method to ac methods (1,28). Thermally stimulated current methods (30) provide a very useful way of observing multiple relaxation peaks for polymers at low effective frequencies ($<10^{-2}$ Hz).

The control of dielectric permittivity and loss of solid polymers, through an understanding of the origins of their dipole relaxation and ionic conduction processes, is essential for their use in electrical insulation, in electrical/electronic circuits, and devices operated over wide power ranges. DS provides information on chain dynamics and charge transport in amorphous, crystalline, LC polymers, and polymer electrolytes. It is ideally suited to the study of polymers in confined environments (eg, in sol–gel–glass) and thin films [since capacitance $\propto$ 1/(film thickness)]. Real-time DS can be applied inter alia to polymer systems undergoing crystallization and polymerization; the switching behavior of LC polymers and polymer-dispersed liquid crystals; phase separation in polymer mixtures/blends induced by chemical reaction or heating [that gives an additional loss process in the product due to interfacial (Maxwell–Wagner) polarization (1,25,31)].

BIBLIOGRAPHY

"Dielectric Relaxation" in *EPSE* 2nd ed., Vol. 5, pp. 23–36, by S. Matsuoka, AT&T Bell Laboratories.

1. N. G. McCrum, B. E. Read, and G. Williams, *Anelastic and Dielectric Effects in Polymeric Solids*, Dover, New York, 1991.
2. J. P. Runt and J. J. Fitzgerald, eds., *Dielectric Spectroscopy of Polymeric Materials*, American Chemical Society, Washington, D.C., 1997.
3. G. Williams, *Adv. Polym. Sci.* **33**, 60 (1979).
4. G. Williams, in E. L. Thomas, ed., *Structure and Properties of Polymers* (Materials Science and Technology Series, Vol. **12**) VCH, Weinheim, 1992, pp. 472–523.
5. G. Williams, in Ref. 2, p. 3.
6. G. Williams and D. C. Watts, *Trans. Faraday Soc.* **66**, 80 (1970).
7. M. Cook, D. C. Watts, and G. Williams, *Trans. Faraday Soc.* **66**, 2503 (1970).
8. R. Diaz-Calleja and E. Riande, in Ref. 2, p. 139.
9. J. C. Dyre, *J. Appl. Phys.* **64**, 2456 (1988).
10. J. C. Dyre and T. B. Schroeder, *Rev. Mod. Phys.* **72**, 873 (2000).
11. A. Schönhals, in Ref. 2, p. 81.
12. See special issues of *J. Non-Cryst. Solids* "Relaxations in Complex Systems", (a) **131–133** (1991), (b) **172–174** (1994), (c) **235–237** (1998).
13. M. Beiner, *Macromol. Rapid Commun.* **22**, 868 (2001).
14. N. Miura, W. J. MacKnight, S. Matsuoka, and F. E. Karasz, *Polymer* **42**, 6129 (2001).
15. K. Adachi and T. Kotaka, *Macromolecules* **18**, 466 (1985).
16. F. Kremer, D. Boese, and L. Fetters, *J. Non-Cryst. Solids* **131–133**, 728 (1991).
17. C. R. Ashcraft and R. H. Boyd, *J. Polym. Sci., Polym. Phys. Ed.* **14**, 2153 (1976).
18. T. A. Ezquerra and F. J. Balta-Calleja, in M. Vazquez and A. Hernando, Eds., *Nanostructured and Non-Crystalline Materials*, World Scientific, Singapore, 1995, pp. 186–196.
19. G. S. Attard, K. Araki, J. J. Moura-Ramos, and G. Williams, *Liq. Cryst.* **3**, 861 (1988).
20. G. P. Simon, in Ref. 2, p. 329.

21. F. Kremer, in Ref. 2, p. 423.
22. W. H. Meyer, *Adv. Mater.* **10**, 439 (1998).
23. H. Pu, W. H. Meyer, and G. Wegner, *Solid State Ionics* **140**, 233 (2001).
24. D. E. Kranbuehl, in Ref. 2, p. 303.
25. G. Williams, I. K. Smith, P. A. Holmes, and S. Varma, *J. Phys.: Condens. Matter* **11** A57 (1999);
26. G. Williams, I. K. Smith, G. A. Aldridge, P. Holmes, and S. Varma, *Polymer* **42**, 3533 (2001).
27. I. K. Smith, Ph. D. dissertation, University of Wales, 1997.
28. F. Kremer and M. Arndt, in Ref. 2, p. 67.
29. P. Lunkenheimer, U. Schneider, R. Brand, and A. Loidl, *Contemporary Phys.* **41**, 15 (2000).
30. G. Teyssedre, S. Mezghani, A. Bernes, and C. Lacabanne, in Ref. 2, p. 227.
31. I. K. Partridge and G. M. Maistros, *High Perform. Polym.* **8**, 1 (1996).

GRAHAM WILLIAMS
University of Wales

DNA. See POLYNUCLEOTIDES.

ELASTOMERS, THERMOPLASTIC

Introduction

Thermoplastic elastomers were introduced in the 1960s. They have shown rapid growth since then and have been the subject of many conferences, symposia, etc. In particular, the developments in this field have been covered fairly recently in two books: one being a comprehensive survey of the subject (1) and the other being a general introduction (2). Thermoplastic elastomers have many of the physical properties of rubbers, ie, softness, flexibility, and resilience; but in contrast to conventional rubbers, they are processed as thermoplastics. Rubbers must be cross-linked to give useful properties. In the terminology of the plastics industry, vulcanization is a thermosetting process. Like other thermosetting processes, it is slow and irreversible and takes place upon heating. With thermoplastic elastomers, on the other hand, the transition from a processible melt to a solid, rubber-like object is rapid and reversible and takes place upon cooling. Thermoplastic elastomers can be processed using conventional plastics techniques, such as injection molding and extrusion; scrap is usually recycled.

Because of increased production and the lower cost of raw material, thermoplastic elastomeric materials are a significant and growing part of the total polymers market. World consumption in 2000 was estimated to be about 1,300,000 t (3). However, because the melt to solid transition is reversible, some properties of thermoplastic elastomers, eg, compression set, solvent resistance, and resistance to deformation at high temperatures, are usually not as good as those of the conventional vulcanized rubbers. Applications of thermoplastic elastomers are, therefore, in areas where these properties are less important, eg, footwear, wire insulation, adhesives, polymer blending, and not in areas such as automobile tires.

Encyclopedia of Polymer Science and Technology. Copyright John Wiley & Sons, Inc. All rights reserved.

Table 1. Comparison of Thermoplastic Elastomers with Conventional Plastics and Rubbers

	Processing method	
Property	Thermosetting	Thermoplastic
Rigid	Epoxies, phenol–formaldehyde, urea–formaldehyde	Polystyrene, polypropylene, PVC, high density polyethylene
Flexible	Highly filled and/or highly vulcanized rubbers	Low density polyethylene, EVA, plasticized PVC
Rubbery	Vulcanized rubbers (NR, SBR, IR, etc)	Thermoplastic elastomers

The classification given in Table 1 is based on the process, ie, thermosetting or thermoplastic, by which polymers in general are formed into useful articles and on the mechanical properties, ie, rigid, flexible, or rubbery, of the final product. All commercial polymers used for molding, extrusion, etc, fit into one of these six classifications; the thermoplastic elastomers are the newest.

Structure

Most thermoplastic elastomers are multiphase compositions in which the phases are intimately dispersed. In many cases, the phases are chemically bonded by block or graft copolymerization. In others, a fine dispersion is apparently sufficient. In these multiphase systems, at least one phase consists of a material that is hard at room temperature but becomes fluid upon heating. Another phase consists of a softer material that is rubber-like at room temperature. A simple structure is an A–B–A block copolymer, where A is a hard phase and B an elastomer, eg, poly(styrene-*b*-elastomer-*b*-styrene) (see BLOCK COPOLYMERS).

Most polymer pairs are thermodynamically incompatible and mixtures separate into two phases. This is true even when the polymeric species are part of the same molecule, as in these block copolymers. Poly(styrene-*b*-elastomer-*b*-styrene) copolymers, in which the elastomer is the main constituent, should have a structure similar to that shown in Figure 1. Here, the polystyrene end segments form separate spherical regions, ie, domains, dispersed in a continuous elastomer phase. Most of the polymer molecules have end polystyrene segments in different domains. At room temperature, these polystyrene domains are hard and act as physical cross-links, tying the elastomer chains together in a three-dimensional network. In some ways, this is similar to the network formed by vulcanizing conventional rubbers using sulfur cross-links. The main difference is that in thermoplastic elastomers the domains lose their strength when the material is heated or dissolved in solvents. This allows the polymer or its solution to flow. When the material is cooled down or the solvent is evaporated, the domains harden and the network regains its original integrity. This explanation of the properties of thermoplastic elastomers has been given in terms of a poly(styrene-*b*-elastomer-*b*-styrene) block copolymer, but it would apply to any block copolymer with the multiblock structure A–B–A–B····, as well as to branched block copolymers $(A–B)_n x$ (where x represents an n functional junction point). In principle, A can be any polymer normally regarded as a hard

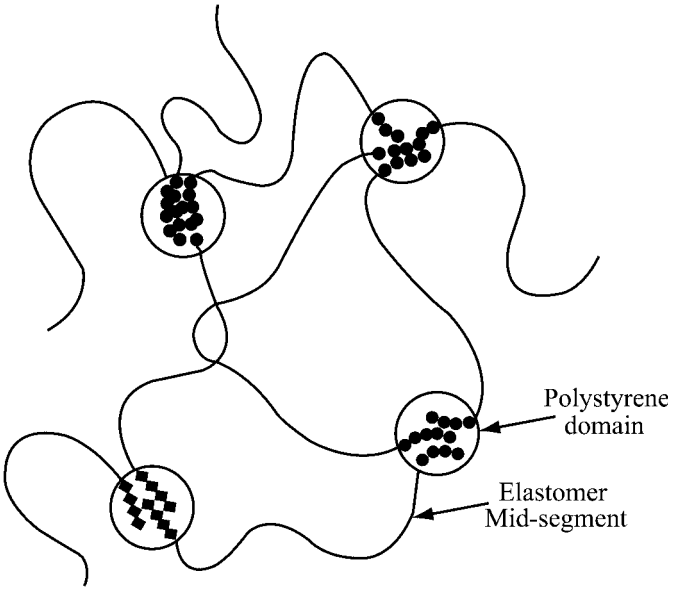

Fig. 1. Phase arrangement in styrenic block copolymers.

thermoplastic, eg, polystyrene, polyethylene, or polypropylene, and B can be any polymer normally regarded as elastomeric, eg, polyisoprene, polybutadiene, poly(ethylene-propylene), or polydimethylsiloxane (Table 2).

Block copolymers with structures such as A–B or B–A–B are not thermoplastic elastomers, because for a continuous network to exist, both ends of the elastomer segment must be immobilized in the hard domains. Instead, they are much weaker materials resembling conventional unvulcanized synthetic rubbers (4).

Besides the thermoplastic elastomers based on poly(styrene-*b*-elastomer-*b*-styrene) block copolymers, five others are of commercial importance: polyurethane/elastomer block copolymers, polyester/elastomer block copolymers, polyamide/elastomer block copolymers, polyolefin block copolymers, and polyetherimide/polysiloxane block copolymers. All five have the multiblock A–B–A–B····· structure. The morphology of the polyurethane, polyester, polyamide, and polyolefin block copolymers is shown diagrammatically in Figure 2. It has some similarities to that of poly(styrene-*b*-elastomer-*b*-styrene) equivalents (Fig. 1) and also some important differences: (*1*) the hard domains are more interconnected; (*2*) they are crystalline; and (*3*) these long A–B–A–B····· molecules may run through several hard and soft phases. The polyetherimide–polysiloxane block copolymers share some features of both types. As in the poly(styrene-*b*-elastomer-*b*-styrene) analogues, their hard domains are amorphous. However, these polymers have multiblock A–B–A–B····· structure rather than A–B–A, and so again, each molecule may run through several hard and soft phases.

Not all thermoplastic elastomers are block copolymers. Those that are not are usually combinations of a hard thermoplastic with a softer, more rubber-like polymer (Table 3) (see POLYMER BLENDS).

Table 2. Thermoplastic Elastomers Based on Block Copolymers

Hard segment, A	Soft or elastomeric segment, B	Structure[a]	References
Polystyrene	Polybutadiene and polyisoprene	T, B	4–6
Polystyrene	Poly(ethylene-*co*-butylene) and poly(ethylene-*co*-propylene)	T	5
Polystyrene and substituted polystyrenes	Polyisobutylene	T, B	7
Poly(α-methylstyrene)	Polybutadiene, polyisoprene	T	6
Poly(α-methylstyrene)	Poly(propylene sulfide)	T	6
Polystyrene	Polydimethylsiloxane	T, M	8
Poly(α-methylstyrene)	Polydimethylsiloxane	T	6,8
Polysulfone	Polydimethylsiloxane	M	9
Poly(silphenylene siloxane)	Polydimethylsiloxane	M	10
Polyurethane	Polyester and polyether	M	11,12
Polyester	Polyether	M	13
Poly(β-hydroxyalkanoates)	Poly(β-hydroxyalkanoates)	M	14
Polyamide	Polyester and polyether	M	15
Polycarbonate	Polydimethylsiloxane	M	16–18
Polycarbonate	Polyether	M	19,20
Polyetherimide	Polydimethylsiloxane	M	21
Polymethyl methacrylate	Poly(alkyl acrylates)	T, B	22
Polyurethane	Poly(diacetylenes)	M	23
Polyethylene	Poly(α-olefins)	M	24,25
Polyethylene	Poly(ethylene-*co*-butylene) and Poly(ethylene-*co*-propylene)	T	6,24
Polypropylene (isotactic)	Poly(α-olefins)	X	24
Polypropylene (isotactic)	Polypropylene (atactic)	X	24,25

[a]T: Triblock, A–B–A; B: branched, $(A–B)_n x$; M: multiblock, A–B–A–B···; X: mixed structures, including multiblock.

Table 3. Thermoplastic Elastomers Based on Hard Polymer/Elastomer Combinations

Hard polymer	Soft or elastomeric polymer	Structure[a]	References
Polypropylene	EPR or EPDM	B	24,25
Polypropylene	EPDM	DV	24–27
Polypropylene	Poly(propylene/1-hexene)	B	25
Polypropylene	Poly(ethylene/vinyl acetate)	B	25
Polypropylene	Butyl rubber	DV	28
Polypropylene	Natural rubber	DV	29
Nylon	Nitrile rubber	DV	26
Polypropylene	Nitrile rubber	DV	26
PVC	Nitrile rubber + DOP[b]	B, DV	30–32
Halogenated polyolefin	Ethylene interpolymer	B	30
Polyester	EPDM	B, DV	25
Polystyrene	S–B–S + Oil	B	33,34
Polypropylene	S–EB–S + Oil	B	33,34

[a]B: Simple blend; DV: dynamic vulcanizate.
[b]DOP: Dioctyl phthalate; other plasticizers can also be used.

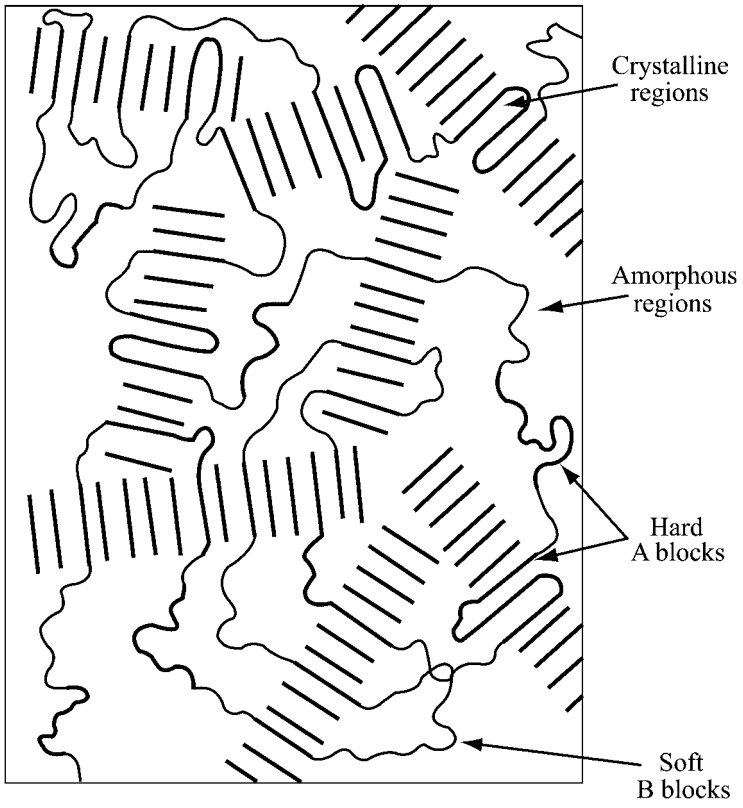

Fig. 2. Phase arrangement in crystalline block copolymers.

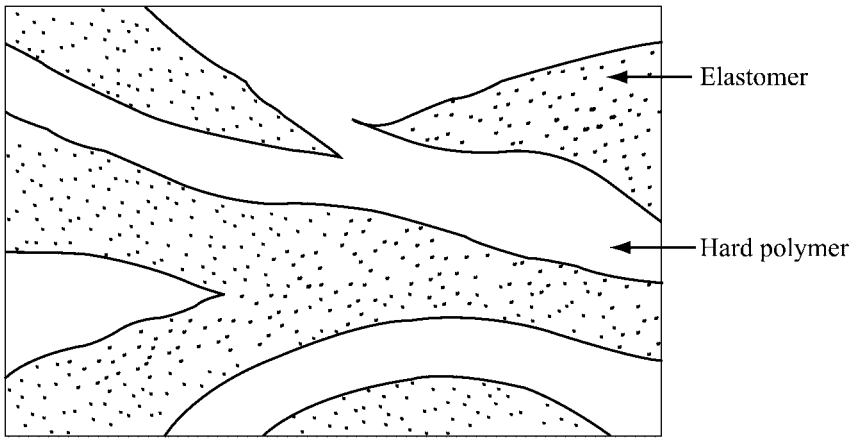

Fig. 3. Phase arrangement in hard polymer/elastomer blends.

Usually, the components are mechanically mixed together (24,25), although it is sometimes possible to produce the rubber component *in situ* during polymerization. Typically, the two components form interdispersed multiphase systems and a diagrammatic structure for blends of this type is shown in Figure 3. Blends

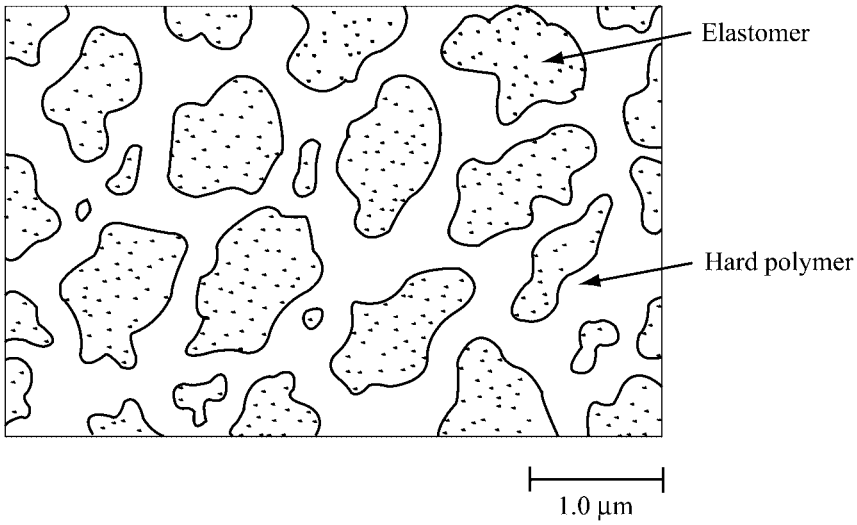

Fig. 4. Phase arrangement in hard polymer/elastomer combinations in which the elastomer phase has been dynamically vulcanized.

of polypropylene with ethylene–propylene–diene monomer (EPDM) were the first materials of this type (24,25). Blends with ethylene–propylene copolymer (EPR) are now more important commercially, and propylene copolymers often replace polypropylene homopolymer as the hard phase. However, some combinations of a hard thermoplastic with a rubber-like polymer are claimed to be single-phase systems (30). In some cases, the elastomer phase is cross-linked while the mixture is being highly sheared (24–26). This process is often referred to as "dynamic vulcanization" (27) and gives a finely dispersed and cross-linked elastomer phase (Fig. 4.).

Other thermoplastic elastomer combinations, in which the elastomer phase may or may not be cross-linked, include blends of polypropylene with nitrile (26), butyl (28), and natural (29) rubbers, blends of PVC with nitrile rubber and plasticizers (30–32), and blends of halogenated polyolefins with ethylene interpolymers (30). Commercially important products (33,34) based on blends of polystyrene with S–B–S and oil and also on blends of polypropylene with S–EB–S and oil are described later in this article. They are also considered as thermoplastic elastomer combinations. The oils used in these products are usually hydrocarbons but blends with silicone oils have also been described (35). Collectively, all thermoplastic elastomers of this type (both bends and dynamic vulcanizates) are referred to herein as hard polymer/elastomer combinations.

Thermoplastic elastomers based on blends of a silicone rubber (cross-linked during processing) with block copolymer thermoplastic elastomers have also been produced (36,37). Other types that have been studied (38) include graft copolymers and elastomeric ionomers, but these have not become commercially important.

Property–Structure Relationships

With such a variety of materials, it is to be expected that the properties of thermoplastic elastomers cover an exceptionally wide range. Some are very soft and

rubbery where others are hard and tough, and in fact approach the ill-defined interface between elastomers and flexible thermoplastics.

Since most thermoplastic elastomers are phase-separated systems, they show many of the characteristics of the individual polymers that constitute the phases. For example, each phase has its own glass-transition temperature (T_g) (or crystal melting point T_m if it is crystalline). These, in turn, determine the temperatures at which a particular thermoplastic elastomer goes through transitions in its physical properties. Thus, when the modulus of a thermoplastic elastomer is measured over a range of temperatures, there are three distinct regions (see Fig. 5).

At very low temperatures, both phases are hard and so the material is stiff and brittle. At a somewhat higher temperature the elastomer phase becomes soft and the thermoplastic elastomer now resembles a conventional vulcanizate. As the temperature is further increased, the modulus stays relatively constant (a region

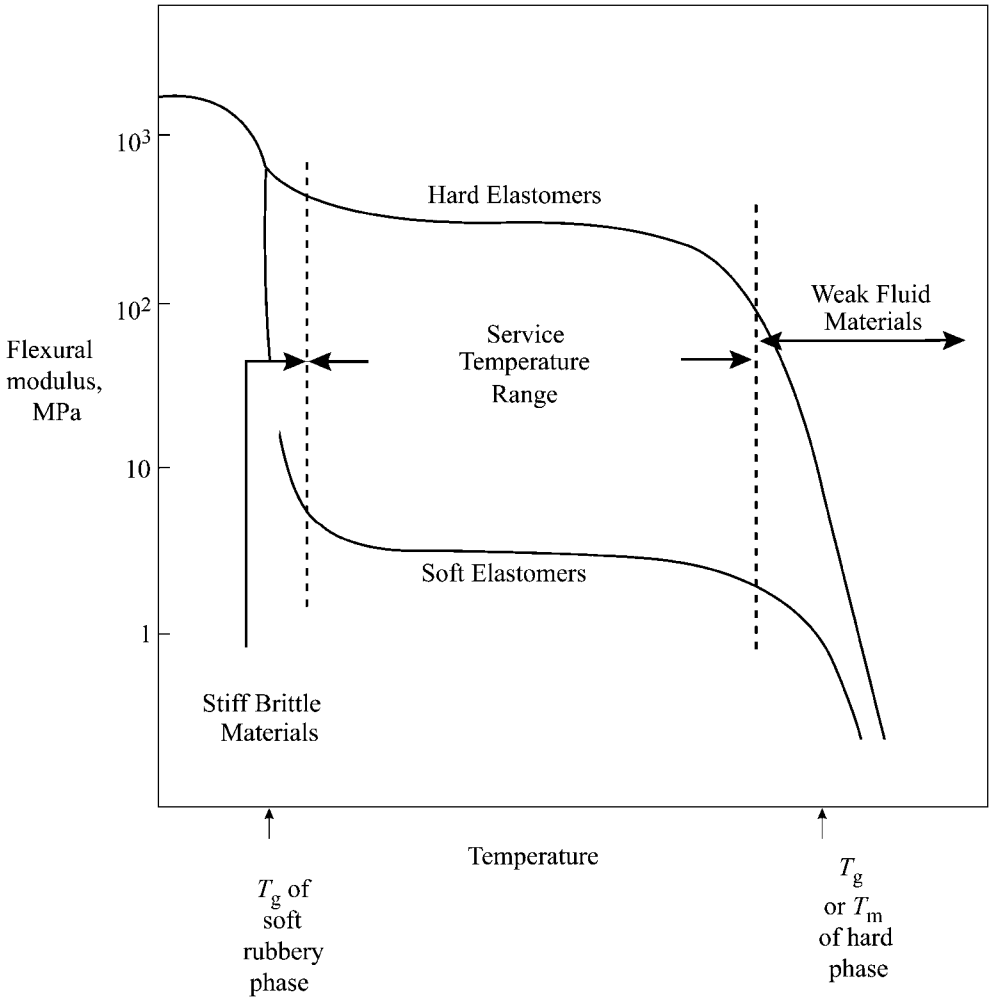

Fig. 5. Stiffnes of typical thermoplastic elastomers at various temperatures.

Table 4. Glass Transition and Crystal Melting Temperatures

Thermoplastic elastomer type	Soft, rubbery phase T_g, °C	Hard phase T_g or T_m, °C
Polystyrene/elastomer block copolymers		
S–B–S	−90	95 (T_g)
S–I–S	−60	95 (T_g)
S–EB–S and S–EP–S	−60	95 (T_g) and 165 (T_m)[a]
Multiblock copolymers		
Polyurethane/elastomer block copolymers	−40 to −60[b]	190 (T_m)
Polyester/elastomer block copolymers	−40	185 to 220 (T_m)
Polyamide/elastomer block copolymers	−40 to −60[b]	220 to 275 (T_m)
Polyethylene/poly(α-olefin) block copolymers	−50	70 (T_m)[c]
Polyetherimide/polysiloxane block colymers	−60	225 (T_g)
Hard Polymer/elastomer combinations		
Polypropylene/EPDM or EPR combinations	−50	165 (T_m)
Polypropylene/butyl rubber combinations	−60	165 (T_m)
Polypropylene/natural rubber combinations	−60	165 (T_m)
Polypropylene/nitrile rubber combinations	−40	165 (T_m)
PVC/nitrile rubber/DOP combinations	−30	80 (T_m)

[a] In compounds containing polypropylene.
[b] The values are for polyethers and polyesters respectively.
[c] This low value for T_m is presumably the result of the short length of the polyethylene segments.

often described as the "rubbery plateau") until finally the hard phase softens. At this point, the thermoplastic elastomer becomes fluid.

Thus, thermoplastic elastomers have two service temperatures. The lower service temperature depends on the T_g of the elastomer phase while the upper service temperature depends on the T_g or T_m of the hard phase. Values of T_g and T_m for the various phases in some commercially important thermoplastic elastomers are given in Table 4.

Some of the parameters that can be varied in order to change the properies of thermoplastic elastomers include the following:

Molecular Weight. Compared with homopolymers of similar molecular weight, styrenic block copolymers have very high melt viscosities which increase with increasing molecular weight. These effects are attributed to the persistence of the two-phase domain structure in the melt and the extra energy required to disrupt this structure during flow (4,5). If the styrene content is held constant, the total molecular weight has little or no effect on the modulus of the material at

ambient temperatures. This is attributed to the modulus of the elastomer phase being inversely proportional to the molecular weight between entanglements in the elastomer chains and the fact that this quantity is not affected by the total molecular weight.

Proportion of Hard Phase. The tensile behavior of otherwise similar block copolymers with differing hard segment contents shows a family of stress–strain curves (4,6,7,24). As the hard segment content is increased, the products change from very weak, soft, rubber-like materials to strong elastomers, then to leathery materials, and finally to hard flexible thermoplastics. The latter have been commercialized as clear, high impact polystyrenes under the trade name K-Resin (39) (Phillips Petroleum Co.). Thermoplastic elastomers in general show similar behavior; that is, as the ratio of the hard to soft phase is increased, the product in turn becomes harder.

Elastomer Phase. The choice of elastomer segment has a profound effect on the properties of block copolymers. In the styrenic block copolymers, four elastomers are commercially important: polybutadiene [9003-17-2], polyisoprene [9003-31-0], poly(ethylene-*co*-butylene) [9019-29-8], and poly(ethylene-*co*-propylene) [9010-79-1]. Polyisobutylene has also been extensively investigated (7,40) but the products have not been produced commercially. The corresponding styrenic triblock copolymers are referred to as S–B–S, S–I–S, S–EB–S,S–EP–S, and S–iB–S, respectively. Polybutadiene and polyisoprene both have one double bond per monomer unit. These double bonds are an obvious source of instability and limit the thermal and oxidative stability of the S–I–S and S–B–S block copolymers. In contrast, poly(ethylene-*co*-butylene) and poly(ethylene-*co*-propylene) are completely saturated, and so S–EB–S and S–EP–S block copolymers are much more stable. Another important aspect is the modulus of the materials. It is postulated that the modulus of styrenic block copolymers is inversely proportional to the molecular weight between chain entanglements (M_e), as well as to the effects of the polystyrene domains acting as reinforcing filler particles (4,40). Values of M_e are as follows (3,40): polyisobutylene, 8900; polyisoprene (natural rubber), 6100; polybutadiene, 1700; and poly(ethylene-*co*-propylene), 1660. The M_e for poly(ethylene-*co*-butylene) is similar to that of poly(ethylene-*co*-propylene). Because of these differences in M_e, S–iB–S block copolymers are the softest of all, S–I–S block copolymers are softer than the S–B–S analogues, and the S–EB–S and S–EP–S analogues are the hardest (40).

All these elastomers, especially poly(ethylene-*co*-butylene) and poly (ethylene-*co*-propylene), are nonpolar. The corresponding block copolymers can thus be compounded with hydrocarbon-based extending oils, but do not have much oil resistance. Conversely, block copolymers with polar polyester or polyether elastomer segments have little affinity for such hydrocarbon oils and so have better oil resistance.

Among the polyurethane, polyester, and polyamide thermoplastic elastomers, those with polyether-based elastomer segments have better hydrolytic stability and low temperature flexibility, whereas polyester-based analogues are tougher and have the best oil resistance (12). Polycaprolactones and aliphatic polycarbonates, two special types of polyesters, are used to produce premium-grade polyurethanes (12).

In the polyolefin-based block copolymers, the elastomeric segment is typically a copolymer of ethylene and 1-octene. It is nonpolar and very stable, as is the polysiloxane elastomer segment in the polyetherimide/polysiloxane block copolymers.

In the hard polymer/elastomer combinations, the elastomer is most often a stable nonpolar rubber such as EPR or EPDM. As noted above, substitution of a polar rubber (such as nitrile rubber) and/or cross-linking improves the resistance to oils and solvents.

Hard Phase. The choice of the hard phase determines the upper service temperature and also influences the solvent resistance. In styrenic block copolymers, those based on poly(α-methylstyrene) [25014-31-7] have higher upper service temperature and tensile strength than analogues based on polystyrene [9003-53-6] (6); both are soluble in common solvents. Replacing the polystyrene end segments in S–EB–S by polyethylene (giving E–EB–E block copolymer) improves solvent resistance; the phases are not separated in the melt (6).

In polyurethane/elastomer, polyester/elastomer, and polyamide block copolymers, the crystalline end segments, together with the polar center segments, impart good oil resistance and high upper service temperatures. In the polyolefin block copolymers, polyethylene is the hard phase. The polyethylene in this phase has a relativly low T_m (about 70°C) (24) and so these thermoplastic elastomers should have a low upper service temperature. The hard segment in the polyetherimide/polysiloxane block copolymers has a very high T_g (about 225°C) and so these thermoplastic elastomers have a very high upper service temperature.

Polypropylene is used as the hard phase in many hard polymer/elastomer combinations. It is low in cost and density and its T_m is quite high (about 165°C). This crystalline polypropylene phase imparts resistance to solvents and oils, as well as providing the products based on it with relatively high upper service temperatures.

Synthesis. Block copolymers are synthesized by a variety of methods; most important are sequential (41–46) and step-growth polymerization (47). In sequential polymerization, a polymer $(A)_n$ is first synthesized in such a way that it contains at least one group per molecule that can initiate polymerization of another monomer B.

$$A + A + A + \cdots \rightarrow A_n$$
$$A_n + B + B + B + \cdots \rightarrow A_n\text{–}B_m$$

The product can be converted to a triblock copolymer by further addition of A:

$$A_n\text{–}B_m + A + A + A + \cdots \rightarrow A_n\text{–}B_m\text{–}A_n$$

In a variation of this process, polymerization can start in the center (B_m) segment, and A_n segments can then be polymerized onto each end. Alternatively, A_n–B_m can be joined together by a coupling agent:

$$2A_n\text{–}B_m + X \rightarrow A_n\text{–}B_m\text{–}X\text{–}B_m\text{–}A_n$$

In this example, X is difunctional and the product is linear. If the functionality of X is higher, the product is a branched $(A–B)_nX$ polymer.

In step-growth polymerization, one or both segments can be produced separately as difunctional prepolymers. The products can then be linked together:

$$A_n + B_m + A_n + B_m + \cdots \rightarrow A_n–B_m–A_n–B_m\cdots$$

or react with more difunctional monomer:

$$A_n + mB + mC \rightarrow A_n–(BC)_m–A_n–(BC)_m\cdots$$

Thermoplastic elastomers that are hard polymer/elastomer combinations are usually not synthesized directly. Instead, the two polymers that form the hard and soft phases are intimately mixed on high shear equipment.

Commercial Production

The commercially available poly(styrene-*b*-elastomer-*b*-styrene) materials are made by anionic polymerization (5,6,40–42). An alkyllithium initiator (R^+Li^-) first reacts with styrene [100-42-5] monomer:

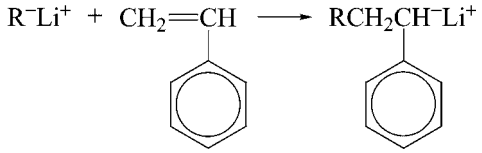

This product acts as an initiator for further polymerization:

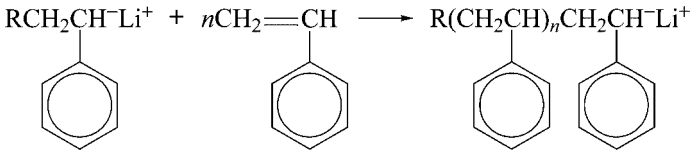

The product, referred to here as S^-Li^+, is able to initiate further polymerization. Similar products have been termed living polymers (45). Addition of a second monomer, such as butadiene [106-99-0], gives

$$S^-Li^+ + nCH_2{=}CH{-}CH{=}CH_2 \rightarrow S{-}(CH_2CH{=}CHCH_2)_{(n-1)}CH_2CH{=}CH{-}CH_2^-Li^+$$

The product of this reaction ($S–B^-Li^+$) may initiate a further reaction with styrene monomer to give $S–B–S^-Li^+$. This, in turn, can react with an alcohol, ROH, to give S–B–SH + LiOR. Alternatively, $S–B^-Li^+$ may react with a coupling agent such as an organohalogen (46):

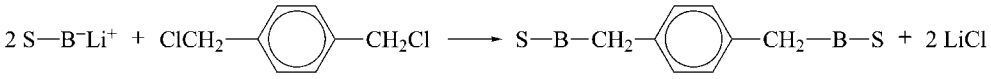

Other coupling agents include esters (46), chlorosilanes (41,46), and divinylbenzene (41). The last gives highly branched materials, whereas the others can give branched or linear products, depending on the functionality of the coupling agent. Another variation of anionic polymerization uses multifunctional initiators (5,6,40,41,45,46), in which the polymer chains grow outward from the center of the molecule. In the case considered here, a difunctional initiator ($Li^{+-}R^{-}Li^{+}$) first reacts with butadiene monomer:

$$Li^{+-}R^{-}Li^{+} + CH_2{=}CH{-}CH{=}CH_2 \rightarrow Li^{+-}B{-}R{-}B^{-}Li^{+}$$

This product is a difunctional initiator and can polymerize styrene monomer:

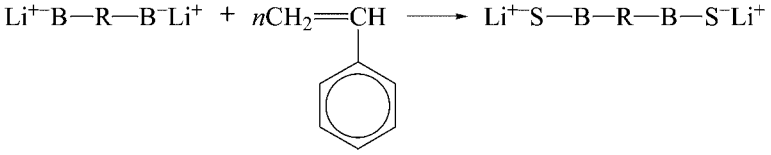

and the final product can again react with an alcohol to give S–B–S, ignoring the minor amount of the R radical that is left at the center of the polymer.

All these polymerizations proceed only in the absence of oxygen or water, which react with the highly reactive propagating species. Polymerization is usually carried out in an inert, hydrocarbon solvent and under a nitrogen blanket. Under these conditions, polymers with narrow molecular-weight distributions and precise molecular weights can be produced in stoichiometric amounts.

Only three common monomers, styrene, butadiene, and isoprene [78-79-5] are easy to polymerize anionically; therefore only two useful A–B–A block copolymers, S–B–S and S–I–S, can be produced directly. In both cases, the elastomer segments contain double bonds which are reactive and limit the stability of the product. To improve stability, the polybutadiene mid-segment can be polymerized as a random mixture of two structural forms, the 1,4 and 1,2 isomers, by addition of an inert polar material to the polymerization solvent; ethers and amines have been suggested for this purpose (41). Upon hydrogenation, these isomers give a copolymer of ethylene and butylene.

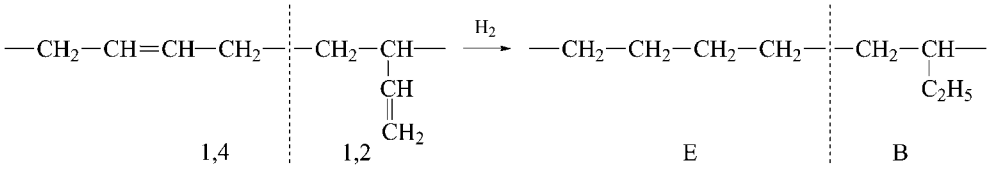

The S–EB–S block copolymers produced in this way have excellent resistance to degradation. Similarly, S–I–S block copolymers can be hydrogenated to give the more stable S–EP–S equivalents.

S–iB–S block copolymers are made by cationic polymerization (7,40,43). So far, they have not been produced commercially.

Polyurethane block copolymers are produced from prepolymers by polycondensation (12,48). A relatively *high* molecular weight polyester or polyether with terminal hydroxy groups (a polyglycol) first reacts with an excess of a diisocyanate.

$$HOR_1OH + 2OC\ NR_2NCO \rightarrow OCNR_2NHCOOR_1OOCNHR_2NCO$$

This reaction continues to give a prepolymer in which the segments originally derived from the polyglycol and the diisocyanate alternate, and which is terminated by isocyanate groups. This prepolymer, designated $OCNR_3NCO$, cannot crystallize because it has an irregular structure (polyglycols are not a single species but have a broad range of molecular weights). It becomes the elastomeric or soft segment in the final polymer. It, in turn, reacts with a *low* molecular weight glycol such as 1,4-butanediol and with more diisocyanate.

$$OCNR_3NCO + HO(CH_2)_4OH + OCNR_2NCO \longrightarrow$$

prepolymer

$$+OOCNHR_3NHCOO(CH_2)_4OOCNHR_2NHCOO(CH_2)_4+_n$$

soft rubbery segment — hard crystalline segment

The segments derived from the condensation reaction of the *low* molecular weight glycol with the diisocyanate have a regular structure and so can crystallize. They agglomerate into separate hard domains. The elastomeric chains are thus cross-linked to form a network similar in many ways to that given by the simple poly(styrene-*b*-elastomer-*b*-styrene) polymer described previously (4,5,11). However, the polymer is a multiblock A–B–A–B····· rather than a simple A–B–A triblock, and the molecular weights and molecular weight distributions of the segments are not as well controlled. 4,4′-Diphenylmethane diisocyanate is the most common diisocyanate used in this application (12,48) but toluene and hexamethylene diisocyanates are alternatives.

Commercial polyester block copolymers are synthesized in a similar way (13,48) by the reaction of a relatively high molecular weight polyether glycol with terephthalic acid (or its dimethyl ester) to give a prepolymer. This then reacts with a low molecular weight glycol (usually 1,4-butanediol) and more terephthalic acid. The segments derived from the polyether-based prepolymer become the soft segments in the final product, whereas the terephthalic acid–1,4-butanediol copolymer forms the hard crystalline domains. Because the soft segments are derived from polyethers, these polymers are often known as polyether ester elastomers.

There are several types of polyamide block copolymers (15,48). Their synthesis is similar to that of the polyurethane and polyester equivalents. In some cases, only the soft segments are prepolymers; whereas in others, prepolymers are used to give both segmental types. Both polyesters and polyethers are used for the soft segments, and this choice affects the final properties of the product. Various

polyamides, including those based on aromatic groups, may be used for the hard segments. These all have different melting points and degrees of crystallinity and so give products with a wide range of properties.

The polyolefin thermoplastic elastomers are produced using metallocene catalysts (44). These are typically based on cyclopentadienyl groups linked to a halide of a transition metal (eg, Ti, Zr, Hf). Under the right conditions, these polymerize mixtures of ethylene and α-olefin monomers (usually 1-octene) into polymers with long repeating polyethylene segments, rather than into random copolymers. These polyethylene segments form the hard phase in the polymer. There are also copolymer segments with pendant groups, usually arranged atactically. Because of their random atactic structures, these segments cannot crystallize. Instead, they are amorphous materials with low glass-transition temperatures and so are soft and rubber-like at room temperature. They form the soft phase in the polymer.

The polyetherimide/polysiloxane block copolymers are synthesized by step-growth polymerization (47). Many other synthetic methods for preparing block copolymers have been described (14,16–20,22–25) but are currently not believed to be commercially important.

The production of the hard polymer/elastomer combinations is more simple. The two components are mixed together under conditions of intensive shear. To achieve a satisfactory dispersion, both the viscosities (at the mixing conditions) and the solubility parameters of the polymers must be carefully matched (49). In some cases, grafting may occur. In a variation of this technique, the elastomer can be cross-linked while the mixing is taking place and the products are described as dynamic vulcanizates (26,27,49).

Many dynamically vulcanized compositions have been investigated (26). In some cases, the components are technologically compatibilized by use of a grafting reaction, but usually a fine dispersion of the two phases is formed that is sufficient to give the product the properties of a thermoplastic elastomer.

Economic Aspects

Global consumption of thermoplastic rubbers of all types is estimated at about 1,300,000 tons/year (3). Of this, the market is estimated to be divided as follows: styrenic block copolymers, 50%; blends and thermoplastic vulcanizates based on polyolefins, 29%; polyurethane block copolymers and polyester block copolymers, 16%; and others, 6%. Annual growth rate during the period 1990–2000 was estimated to be 7%. The ranges of the hardness values, prices, and specific gravities of commercially available materials are given in Table 5.

Applications

The applications of these thermoplastic elastomers are described in detail in References 33 and 34. Trade names and suppliers of commercial thermoplastic elastomers of all types are given in Tables 6–8.

Table 5. Price and Property Ranges for Thermoplastic Elastomers[a]

Elastomer	Price range, $/kg	Specific gravity	Hardness (Shore A or D)
Polystyrene/elastomer block copolymers			
S–B–S (pure)	1.9–2.9	0.94	65A–75A
S–I–S (pure)	2.2–2.9	0.92	32A–37A
S–EB–S (pure)	4.1–6.2	0.91	65A–75A
S–B–S (compounds)	2.0–3.3	0.9–1.1	40A–45D
S–EB–S (compounds)	2.8–5.0	0.9–1.2	5A–60D
Multiblock Copolymers			
Polyurethane/elastomer block copolymers	5.0–8.3	1.05–1.25	70A–75D[b]
Polyester/elastomer block copolymers	6.1–8.3	1.15–1.40	35D–80D
Polyamide/elastomer block copolymers	9.9–12	1.0–1.15	60A–65D
Polyethylene/poly(α-olefin) block copolymers	1.8–2.4	0.85–0.90	65A–85A
Polyethimide/polysiloxane block copolymers	44	1.2	70D
Hard polymer/elastomer combinations			
Polypropylene/EPDM or EPR blends	1.8–2.7	0.9–1.0	60A–65D
Polypropylene/EPDM dynamic vulcanizates	3.6–6.6	0.95–1.0	35A–50D
Polypropylene/butyl rubber dynamic vulcanizates	4.6–7.9	0.95–1.0	50A–80D
Polypropylene/natural rubber dynamic vulcanizates	3.1–3.5	1.0–1.05	60A–45D
Polypropylene/nitrile rubber dynamic vulcanizates	4.4–5.5	1.0–1.1	70A–50D
PVC/nitrile rubber/DOP blends	2.9–3.3	1.20–1.33	50A–90A
Halogenated polyolefin/ethylene interpolymer blends	4.9–6.1	1.10–1.25	50A–80A

[a]These price and property ranges do not include fire-retardant grades or highly filled materials for sound deadening.
[b]As low as 60A when plasticized.

Styrenic Block Copolymers. In all their commercial application, the styrenic block copolymers are never used as pure materials. Instead, they are compounded with other polymers, oils, fillers, resins, etc, to give materials designed for the specific end use.

Substitute for Conventional Vulcanized Rubbers. For this application, the products are processed by techniques and equipment developed for conventional thermoplastics, ie, injection molding, extrusion, etc. The S–B–S and S–EB–S polymers are preferred (small amounts of S–EP–S are also used). To obtain a satisfactory balance of properties, they must be compounded with oils, fillers, or other polymers; compounding reduces costs. Compounding ingredients and their effects on properties are given in Table 9. Oils with high aromatic content should be avoided because they plasticize the polystyrene domains. Polystyrene is often used as an ingredient in S–B–S-based compounds; it makes the products harder and improves their processibility. In S–EB–S-based compounds, crystalline polyolefins such as polypropylene are preferred. Some work has been reported on blends of

Table 6. Some Trade Names of Thermoplastic Elastomers Based on Styrenic Block Copolymers

Trade name (Manufacturer)	Type	Elastomer segment	Notes
KRATON D (Kraton Polymers)[a]	Linear and branched	B or I	General purpose, soluble. Also compounded products
VECTOR (Dexco)[b]	Linear and branched	B or I	
SOLPRENE[c] (Phillips)	Branched	B or I	
TAIPOL (Taiwan Synthetic Rubber Company)	Linear and branched	B or I	
QUINTAC (Nippon Zeon)	Linear and branched	I	
FINAPRENE (Fina)	Linear	B	General purpose, soluble.
COPERBO (Petroflex)	Linear	B	Not available as compounded
TUFPRENE & ASAPRENE (Asahi)	Linear	B	products
CALPRENE (Dynasol)	Linear and branched	B	
KIBITON (Chi Mei)	Branched	B	
EUROPRENE SOL T (Enichem)	Linear and branched	B or I	
STEREON (Firestone)	Linear	B	High polystyrene content
K-RESIN (Phillips)	Branched	B	Very high polystyrene content. Hard and rigid
KRATON G (Kraton Polymers)[a]	Linear	EB or EP	
SEPTON (Kuraray)	Linear	EB or EP	Improved stability. Soluble
TUFTEC (Asahi)	Linear	EB	when uncompounded
CALPRENE H (Dynasol)	Linear	EB	
DYNAFLEX (GLS)	Linear	B or EB	
MULTI-FLEX (Multibase)	Linear	EB	
HERCUPRENE[d] (J-VON)	Linear	B or EB	Only compounded products
FLEXPRENE (Teknor Apex)	Linear	B	
TEKRON (Teknor Apex)	Linear	EB	
ELEXAR (Teknor Apex)[a]	Linear	EB	Wire and cable compounds
C-FLEX (Concept)[e]	Linear	EB	Medical applications. Contains silicon oil

[a] Formerly produced by Shell.
[b] Joint venture of Dow and Exxon.
[c] No longer made in the United States. Similar products are produced by Taiwan Synthetic Rubber and Enichem.
[d] Formerly produced by J-PLAST.
[e] Now Consolidated Polymer Technologies Inc.

liquid polysiloxanes (silicone oils) with S–EB–S block copolymers (35). The products are primarily intended for medical and pharmaceutical-type applications. Compounds based on S–EB–S with hardnesses as low as 5 on the Shore A scale have been reported (50).

Table 7. Some Trade Names of Thermoplastic Elastomers Based on Multiblock Copolymers

Trade name (Manufacturer)	Hard segment	Elastomer segment	Notes
ESTANE (B.F. Goodrich) MORTHANE[a] (Morton International) PELLETHANE[a] (Dow) ELASTOLLAN (BASF) DESMOPAN and TEXIN (Bayer)[b]	Polyurethane	Polyether or amorphous polyester	Hard and Tough. Abrasion and oil resistant. Good tear strength
HYTREL (DuPont) LOMOD (DSM)[c] URAFIL (Akzo) RITEFLEX (Hoechst) ECDEL (Eastman) ARNITEL (DSM)	Polyester	Polyether	Similar to polyurethanes but more expensive. Better low temperature flexibility. Low hysteresis. Fairly high cost
PEBAX (Elf Atochem) VESTAMIDE (Huls) GRILAMID and GRILON (EMS America)	Polyamide	Polyether or amorphous Polyester	Similar to polyurethanes but can be softer. Good low temperature flexibility Expensive
ENGAGE & AFFINITY(Dow) EXACT (Exxon) FLEXOMER (Union Carbide)	Polyethylene	Poly(α-olefins)	Flexible and low cost. Good low temperature flexibility. Limited at higher temperatures
SILTEM (GE)	Poly(etherimide)	Polysilicone	Fire resistant. Very high cost

[a]Including some with polycarprolactone segments.
[b]Formerly marketed by Mobay and Miles.
[c]Formerly GE.

Large amounts of inert fillers, such as whiting, talc, and clays, can be added. Very dense fillers, such as barium or strontium sulfates, are used to make compounds intended for sound-deadening applications. In contrast, high levels of reinforcing fillers, such as carbon black, produce undesirable properties in the final product.

A large volume usage of S–B–S-based compounds is in footwear. Canvas footwear, such as sneakers and unit soles, can be made by injection molding. Frictional properties resemble those of conventionally vulcanized rubbers and are superior to those of the flexible thermoplastics, such as plasticized poly(vinyl chloride). The products remain flexible under cold conditions because of the good low temperature properties of the polybutadiene segment.

Table 8. Some Trade Names of Thermoplastic Elastomers Based on Hard Polymer/Elastomer Combinations

Trade name (Manufacturer)	Type	Hard polymer	Elastomer	Notes
REN-FLEX (D&S)[a] HIFAX (Himont) POLYTROPE (Schulmam) TELCAR (Teknor Apex) FERROFLEX (Ferro) FLEXOTHENE (Equistar)[b]	Blend	Polypropylene	EPDM or EPR	Relatively hard, low density, not highly filled
SANTOPRENE (AES)[c] SARLINK 3000 & 4000 (Novacor)[d] NIPRENE (Teknor Apex) HIFAX MXL (Himont)	DV[e]	Polypropylene	EPDM	Better oil resistace, low compression set, softer
TREFSIN (AES) and SARLINK 2000 (Novacor)[d]	DV	Polypropylene	Butyl Rubber	Low permeability, high damping
VYRAM (AES)	DV	Polypropylene	Natural Rubber	Low cost
GEOLAST (AES)	DV	Polypropylene	Nitrile Rubber	Oil resistant
ALCRYN (Advanced Polymer Alloys)[f]	Blend	Halogenated Polyolefin	Ethylene Interpolymer	Single phase, oil resistant
SARLINK 1000 (Novacor)[d]	DV	PVC	Nitrile Rubber	Oil Resistant
CHEMIGUM (Goodyear	Blend			
APEX N(Teknor Apex)	Blend			
RIMPLAST (Petrarch Systems)	Blends of TPEs with Silicone Rubbers			Medical applications

[a] A joint venture between Dexter and Solvay.
[b] Formerly Quantum. Product is a blend of PP and EPR produced in the polymerization reactor.
[c] Advanced Elastomer Sytems—a joint venture between Solutia (formerly Monsanto) and Exxon Chemical.
[d] Now a part of DSM.
[e] Dynamic Vulcanizate—a composition in which the soft phase has been dynamically vulcanized, i.e., cross-linked during mixing.
[f] Formerly DuPont.

Compounds based on S–EB–S usually contain polypropylene, which improves solvent resistance and processibility and raises upper service temperatures. Compounds intended for use in the automotive industry are able to survive 1000 h of air exposure at temperatures of 125°C with only minor changes in properties (51). Very soft compounds have been developed to replace foam rubber for interior trim parts. In this and similar applications, these soft compounds are usually insert-molded over polypropylene or metal and then coated with flexible polyurethane paint (52). Other automotive applications include products intended

Table 9. Compounding Styrenic Block Copolymers

	Component				
Properties	Oils	Polystyrene	Polyethylene	Polypropylene	Fillers
Hardness	Decreases	Increases	Increases	Increases	Small increase
Processibility	Improves	Improves	Improves	Improves, especially with S–EB–S	Improves
Effect on oil resistance	None	None	Improves	Improves	None
Cost	Decreases	Decreases	Decreases	Decreases	Decreases
Other	Decreases uv resistance		Often gives satin finish	Improves high temperature properties	Often improves surface appearance

Table 10. Resins Used to Formulate Adhesives, Sealants, etc from Styrenic Block Copolymers

Resin type	Segment compatibility[a]
Polymerized C_5 resins (synthetic polyterpenes)	I
Hydrogenated rosin esters	B
Saturated hydrocarbon resins	EB
Naphthenic oils	I, B
Paraffinic oils	EB
Low molecular weight polybutenes	EB
Aromatic resins	S

[a] I indicates compatible with polyisoprene segments; B, compatible with polybutadiene segments; EB, compatible with poly(ethylene–butylene) segments; and S, compatible with polystyrene segments.

for sound deadening, flexible air ducts, and gear shifter boots, as well as improving the properties of sheet molding compounds.

Other uses for which special compounds have been developed include materials intended for food contact, wire insulation, and pharmaceutical applications.

Commercial products have hardnesses from 5 on the Shore A scale (which is extremely soft) to 45 on the Shore D scale (almost leathery). Specific gravities usually range from 0.9 to 1.20; some products intended for soundproofing have specific gravities as high as 1.95. Processing is relatively easy. In general, products based on S–B–S are processed under conditions appropriate for polystyrene, whereas products based on S–EB–S are processed under conditions appropriate for polypropylene. Predrying is usually not needed and scrap is recycled.

Adhesives, Coatings, and Sealants. For these applications, styrenic block copolymers must be compounded with resins and oils (Table 10) to obtain the desired properties (53–56). Materials compatible with the elastomer segments

soften the final product and give tack, whereas materials compatible with the polystyrene segments impart hardness. The latter are usually styrenic resins with relatively high softening points. Materials with low softening points are to be avoided, as are aromatic oils, since they plasticize the polystyrene domains and reduce the upper service temperature of the final products.

These resins and oils have low molecular weights, ie, typically below 1000. This, combined with the relatively low molecular weights of the styrenic block copolymers, typically 40,000–150,000, allows solutions in common solvents to be formulated at high solids levels. Alternatively, the products can be applied as hot melts, with considerable advantages in terms of safety, production rates, energy consumption, and air pollution.

Blends with Other Polymeric Materials. Styrenic block copolymers are technologically compatible with a surprisingly wide range of materials and can be blended to give useful products (57,58). Blending can often be carried out on the equipment producing the final article. Blends of S–B–S with polystyrene, polyethylene, or polypropylene show improved impact and tear resistance. Both S–B–S and S–EB–S can be blended with poly(phenylene oxide) to improve impact resistance (59). S–EB–S can also be blended with the less polar engineering thermoplastics such as polycarbonates. An unusual feature of these block copolymers is their ability to enable useful blends to be made from incompatible polymers, eg, polystyrene or poly(butylene terephthalate) with polyethylene (60). Another development is the use of functionalized S–EB–S block copolymers as impact modifiers for more polar engineering thermoplastics such as polyesters and polyamides (58). The functionality is given by maleic acid/anhydride groups grafted to the S–EB–S polymer chain. These functionalized S–EB–S block copolymers have also been found useful in the compatibilization of polyolefins with polyamides (61) and with poly(phenylene oxide) (62).

Special grades of styrenic block copolymers are useful modifiers for sheet molding compounds based on thermoset polyesters. They improve surface appearance, impact resistance, and hot strength.

Blends with Asphalts. Blends with styrenic block copolymers improve the flexibility of bitumens and asphalts. The block copolymer content of these blends is usually less than 20%; even as little as 3% can make significant differences to the properties of asphalt. The block copolymers make the products more flexible, especially at low temperatures, and increase their softening point. They generally decrease the penetration and reduce the tendency to flow at high service temperatures; and they also increase the stiffness, tensile strength, ductility, and elastic recovery of the final products. Melt viscosities at processing temperatures remain relatively low so the materials are still easy to apply. As the polymer concentration is increased to about 5%, an interconnected polymer network is formed. At this point the nature of the mixture changes from an asphalt modified by a polymer to a polymer extended with an asphalt.

It is important to choose the correct grade of asphalt; those with a low asphaltene content and/or high aromaticity in the maltene fraction usually give the best results (63,64). Applications include road surface dressings such as chip seals (applied to hold the aggregate in place when a road is resurfaced); slurry seals; hot-mix asphalt concrete (a mixture of asphalt and aggregate used in road surfaces); road crack sealants; roofing; and other waterproofing and adhesive

applications (64–66). Because of their lower cost, S–B–S block copolymers are usually chosen for this application; but in roofing and paving applications, the S–EB–S block copolymers are also used because of better long-term aging resistance.

Oil Gels. As noted previously, the styrenic block copolymers are very compatible with mineral oils. Blends with as little as 5% of an S–EB–S block copolymer (the remainder being 90% mineral oil and 5% wax) have been described for use as cable filling compounds (67,68). These fill the voids in "bundled" telephone cables and prevent water seepage. Another potential application is toys, hand exercising grips, etc (69).

Multiblock Copolymers. Replacement of conventional vulcanized rubber is the main application for the polar polyurethane, polyester, and polyamide block copolymers. Like styrenic block copolymers, they can be molded or extruded using equipment designed for processing thermoplastics. Melt temperatures during processing are between 175 and 225°C, and predrying is essential; scrap is reusable. These polymers are mostly used as essentially pure materials, although some work on blends with various thermoplastics (12,13,15,33,34,70–72) such as plasticized and unplasticized PVC and also ABS and polycarbonate has been reported. Plasticizers intended for use with PVC have also been blended with polyester block copolymers (70).

All three types of these block copolymers are relatively hard (from 70 on the Shore A scale to 70 on the Shore D scale) with specific gravities of 1.00–1.25. Applications (12,13,15,33,34) taking advantage of toughness, abrasion resistance, flexibility, and resistance to oils and solvents include belting, hydraulic hose, tires, shoe soles, wire coatings, and automobile parts. The surface of these molded parts can be easily painted or metallized. Medical uses, such as implants, are a significant application for the polyurethane block copolymers with polyether elastomer segments (73). Blends with silicone rubbers have been described for these applications (36,37). Another application is the use of a clear polyester thermoplastic elastomer as a replacement for glass bottles in medical applications.

Some grades of polyurethane and polyester copolymers are used as hot-melt adhesives. Applications include shoe manufacture and as an adhesive interlayer in coextrusion.

The polyolefin block copolymers are lower in cost. Their suggested applications (74) include wire and cable insulation, replacements for PVC and styrenic block copolymers, and blends with polypropylene, either to improve impact resistance or as the soft phase in a hard polymer/elastomer combination. Processing conditions are similar to those for polyethylene, and thermal stability is excellent.

The polyetherimide–polysiloxane multiblock copolymers are relatively hard (about 70 on the Shore D scale). Their main application is flame-resistant wire and cable covering (21,47), where they combine very low flammability with a low level of toxic products in the smoke. This unusual and vital combination of properties justifies their relatively high price, about $44/kg, at a specific gravity of about 1.2.

Hard Polymer/Elastomer Combinations. Substitution of conventional vulcanized rubbers is the main application for these materials (24–26,33,34).

The first ones to be developed were simple blends of polypropylene and EPDM, made by conventional mixing of the two components (24,25,49). EPR has largly replaced EPDM in this application because of its lower cost. These simple blends had some limitation, because unvulcanized EPDM or EPR has almost no tensile strength or oil resistance. Thus only fairly hard products, ie, those containing small amounts of these elastomers, had satisfactory properties and so the first products of this type had hardness values in the Shore D range (although somewhat softer versions are now available). In later work, products based on dynamic vulcanization (26) were produced. In this process, the elastomer, typically EPDM, is simultaneously cross-linked and mixed into the hard polymer, typically polypropylene. The result is a very fine dispersion of vulcanized elastomer particles in a hard polymer matrix. The improved properties of the elastomer phase allow much higher levels to be used, giving quite soft products (as low as about 35 on the Shore A scale). Compared to the mixtures of EPDM or EPR with polypropylene, the corresponding dynamic vulcanizates have lower compression set and better oil resistance. Natural (29) and butyl rubbers (28) have been used to replace EPDM in similar dynamically vulcanized products. Those based on natural rubber are low in cost and have properties intermediate between the EPDM-based dynamic vulcanizates and the simple EPDM-based mixtures. Those based on butyl rubber have low gas permeability and high damping, thus they can be used as vapor barriers or vibration isolators. An unexpected property advantage with those based on butyl rubber is that some grades show excellent adhesion when insert-molded against such polar engineering thermoplastics as poly(butylene terephthalate) and polyamides (75). Specific gravities of these various combinations of polypropylene with EPDM, EPR, butyl, and natural rubbers are between about 0.9 and 1.05. Molding and extrusion conditions are similar to those used for polypropylene, and the scrap is reusable. Important applications are wire insulation, appliance parts, and automobile exterior and interior parts (both painted and unpainted).

Even though vulcanized EPDM has some oil resistance, in contrast to unvulcanized EPDM which has virtually none, a rubber with inherent oil resistance should be even better. For this reason, more polar rubbers have replaced EPDM in applications where oil resistance is critical. Dynamic vulcanizates of nitrile rubber with polypropylene are the most important example. Commercial grades are somewhat harder than EPDM equivalents (between 70 on the Shore A scale to 40 on the Shore D scale) and are also more dense (about 1.0–1.1 specific gravity) (26,49).

PVC/nitrile rubber blends usually contain plasticizers such as dioctyl phthalate (30). Similar dynamic vulcanizates appear to be less important commercially. These blends have excellent oil resistance as well as resistance to flex cracking and abrasion (31–34). Hardness ranges from about 50 to 90 on the Shore A scale and specific gravity from about 1.2 to 1.3. Processing is basically similar to that of plasticized PVC. Blends of halogenated polyolefins with ethylene interpolymers are claimed to give single-phase systems (30). They have a very rubber-like feel and are similar to the PVC/nitrile rubber combinations as far as processing, hardness, and specific gravity are concerned. Like them, they have good oil resistance. All these products based on the more polar rubbers are often used in

molded appliance, automotive, and similar rubber-like parts where oil resistance is needed at a reasonable cost.

Health and Safety

Most thermoplastic elastomers are stable materials and decompose only slowly under normal processing conditions. If decomposition does occur, the products are usually not particularly hazardous and should not present a problem if good ventilation is provided. Products based on PVC and halogenated polyolefins are exceptions, and care should be taken to avoid overheating these materials. Extra caution should also be exercised when processing polyurethanes, especially those containing polycaprolactone segments. In these cases the decomposition products may include isocyanates and caprolactam, both of which are potential carcinogens.

Of course, all materials that are processed in the molten state can cause burns if the hot material comes in contact with the skin. Care must be taken to avoid this, and it should be noted that molten material left in the barrel of an extruder or injection-molding machine can "spit" unexpectedly. In all cases, it is recommended that the manufacturer's Material Safety Data Sheet be consulted before working with any of these materials.

Reprocessing

Easy reprocessing is one of the great advantages that thermoplastic elastomers have over conventional vulcanized rubbers. The scrap can be reground and is usually blended with virgin material before being reworked. Regrinding is not difficult if it is remembered that rubber must be cut rather than shattered. This means that the cutter blades must be sharp and clearances minimized. Immediately after regrinding, softer products should be dusted with an antiblocking agent. It is usually best to dry the ground scrap before reworking it, and for the polyurethanes, polyesters, and polyamides, drying is a necessity. Thermoplastic elastomers can also be used to "sweeten" regrind; that is, they can be blended with reground scrap from conventional thermoplastics to restore impact strength and reduce brittleness. Many applications, eg, coextrusion, generate mixed scrap, which usually has very poor properties. Thermoplastic elastomers can often convert this into useful material (60–62).

BIBLIOGRAPHY

"Elastomers, Thermoplastic" in *EPSE* 2nd ed., Vol. 5, pp. 416–430, by G. Holden, Shell Development Co.

1. G. Holden, N. R. Legge, R. P. Quirk, and H. E. Schroeder, eds., *Thermoplastic Elastomers*, 2nd ed., Hanser & Hanser/Gardner, Munich 1996.

2. G. Holden, *Understanding Thermoplastic Elastomers*, Hanser & Hanser/Gardner, Munich, 2000.
3. Ref. 2, Chapt. 8.
4. G. Holden, E. T. Bishop, and N. R. Legge, *J. Polym. Sci., Part C* **26**, 37 (1969).
5. G. Holden and N. R. Legge, in Ref. 1, Chapt. 3.
6. R. P. Quirk and M. Morton, in Ref. 1, Chapt. 4.
7. J. P. Kennedy, in Ref. 1, Chapt. 13.
8. J. C. Saam, A. Howard, and F. W. G. Fearon, *J. Inst. Rubber Ind.* **7**, 69 (1973).
9. A. Noshay, M. Matzner, and C. N. Merriam, *J. Polym. Sci., Part A-1*, 3147 (1971).
10. R. L. Merker, M. J. Scott, and G. G. Haberland, *J. Polym. Sci., Part A-2*, 31 (1964).
11. S. L. Cooper and A. V. Tobolsky, *Tex. Res. J.* **36**, 800 (1966).
12. W. Mekel, W. Goyert, and W. Wieder, in Ref. 1, Chapt. 2.
13. R. K. Adams, G. K. Hoeschele, and W. K. Wisiepe, in Ref. 1, Chapt. 8.
14. K. D. Gagnon, in Ref. 1, Chapt. 15B.
15. R. G. Nelb and A. T. Chen, in Ref. 1, Chapt. 9.
16. H. A. Vaughn, *J. Polym. Sci., Part B-7* 569 (1969).
17. P. Kambour, *J. Polym. Sci., Part B-7* 573 (1969).
18. D. G. LeGrand, *J. Polym. Sci., Part B-7* 579 (1969).
19. E. P. Goldberg, *J. Polym. Sci., Part B-7* 707 (1963).
20. K. P. Perry, W. J. Jackson Jr., and J. R. Caldwell, *J. Appl. Polym. Sci.* **9**, 3451 (1965).
21. J. Mihalich, Paper presented at the 2nd International Conference on Thermoplastic Elastomer Markets and Products, Schotland Business Research, Orlando, Fla., Mar. 15–17, 1989.
22. R. Jerome, P. Boyard, R. Fayt, C. Jacobs, S. K. Vashney, and P. Teyssie, in Ref. 1, Chapt. 15D.
23. P. T. Hammond and M. F. Rubner, in Ref. 1, Chapt. 15E.
24. E. N. Kresge, in Ref. 1, Chapt. 5.
25. E. N. Kresge, *Rubber World* **217**(1), 30 (1997).
26. A. Y. Coran and R. P. Patel, in Ref. 1, Chapt. 7.
27. U.S. Pat. 3,037,954 (June 5, 1962), A. M. Gessler (to Esso Research & Engineering Co.).
28. R. C. Puydak, Paper presented at the 2nd International Conference on Thermoplastic Elastomer Markets and Products, Schotland Business Research, Orlando, Fla., Mar. 15–17, 1989.
29. A. J. Tinker, Paper presented at the Symposium on Thermoplastic Elastomers Sponsored by the ACS Rubber Division, Cincinnati, Ohio, Oct. 18–21, 1988.
30. G. H. Hoffman, in Ref. 1, Chapt. 6
31. M. Stockdale, Paper presented at the Symposium on Thermoplastic Elastomers, ACS Rubber Division, Cincinnati, Ohio, Oct. 18–21, 1988.
32. P. Tandon and M. Stockdale, Paper presented at the 4th International Conference on Thermoplastic Elastomer Markets and Products, Schotland Business Research, Orlando, Fla., Feb. 13–15, 1991.
33. G. Holden, in Ref. 1, Chapt. 16.
34. Ref. 2, Chapt. 7.
35. *Mod. Plast.* **60**(12), 42 (1983).
36. B. C. Arkles, *Med. Dev. Diagnost. Ind.* **5**(11), 66 (1983).
37. U.S. Pat. 4,500,688 (Feb. 19, 1985), B. C. Arkles (to Petrarch Systems).
38. Ref. 2, Chapt. 6.

39. Technical Bulletin, TIB 200, Phillips 66 Co., 1991.
40. Ref. 2, Chapt. 3.
41. P. Dreyfuss, L. J. Fetters, and D. R. Hansen, *Rubber Chem. Technol.* **53**, 738 (1980).
42. H. L. Hsieh and R. P. Quirk, *Anionic Polymerization: Principles and Practical Applications*, Marcel Deker, Inc., New York, 1993.
43. K. Matyjaszewski, *Cationic Polymerizations: Mechanisms, Synthesis and Applications*, Marcel Deker, Inc., New York, 1996.
44. J. L. Laird, M. S. Edmonson, and J. A. Riedel, *Rubber World* **217**(1) 42 (1997).
45. M. Szwarc, M. Levy, and R. Milkovich, *J. Am. Chem. Soc.* **78**, 2656 (1956).
46. N. R. Legge, S. Davison, H. E. DeLaMare, G. Holden, and M. K. Martin, in R. W. Tess and G. W. Poehlein, eds., *Applied Polymer Science*, 2nd ed. (ACS Symposium Series No. 285), American Chemical Society, Washington, D.C., 1985, chapt. "9".
47. T. E. Long and S. R. Turner, in C. Carraher and C. Craver, eds., *Applied Polymer Science—21st Century*, Elsevier Science Ltd., Amsterdam, 2000, chapt. "45".
48. Ref. 2, Chapt. 4.
49. Ref. 2, Chapt. 5.
50. R. J. Deisler, Paper presented at the 4th International Conference on Thermoplastic Elastomer Markets and Products, Schotland Business Research, Orlando, Fla., Feb. 13–15, 1991.
51. G. Holden and K. H. Speer, *Autom. Polym. Des.* **8**(3), 15 (1988).
52. G. Holden and X.-Y. Sun, Paper presented at the 4th International Conference on Thermoplastic Elastomer Markets and Products, Schotland Business Research, Orlando, Fla., Feb. 13–15, 1991.
53. D. J. St. Clair, *Rubber Chem. Technol.* **54**, 208 (1982).
54. S. G. Chu and J. Class, *J. Appl. Polym. Sci.* **30**, 805 (1985).
55. G. Kraus, K. W. Rollman, and R. A. Gray, *J. Adhesion* **10**, 221 (1979).
56. Shell Chemical Co., Bulletin SC:198–92, Houston, Tex., 1992.
57. A. L. Bull and G. Holden, *J. Elastom. Plast.* **9**, 281 (1977).
58. Shell Chemical Co., Bulletin SC:165–93, Houston, Tex., 1993.
59. U.S. Pat. 4,167,507 (1990), W. R. Haaf (to General Electric Co.).
60. D. R. Paul, in Ref. 1, Chapt. 15C.
61. M. J. Modic and L. A. Pottick, *Plast. Eng.* **47**(7), 37 (1991).
62. U.S. Pat 4,795,782 (Jan. 3, 1989), R. G. Lutz, R. Gelles, and W. P. Gergen (to ShellOil).
63. E. J. van Beem and P. Brasser, *J. Inst. Petrol.* **59**, 91 (1973).
64. Piazza, A. Acrozzi, and C. Verga, *Rubber Chem. Technol.* **53**, 994 (1980).
65. J. L. Goodrich, Asphalt and Polymer-Modified Asphalt Properties Related to the Performance of Asphalt Concrete Mixes, Asphalt Paving Technologist Proceedings, AAPT, Vol. 57, 1988.
66. M. G. Bouldin, J. H. Collins, and A. Berker, *Rubber Chem. Technol.* **64**, 577 (1991).
67. D. M. Mitchel and R. Sabia, Proceeding of the 29th International Wire and Cable Symposium, Nov. 1980, p. 15.
68. Technical Bulletin SC:1102-89, Shell Chemical Co., Houston, Tex., 1989.
69. U.S. Pats. 4,369,284 (1983), 5,262,468 (1993), and 5,508,344 (1996), J. Y. Chen (to Applied Elastomerics, Inc.),
70. E. I. du Pont de Nemours & Co., Inc., Hytrel Bulletin HYT-302R(1), 1981.
71. E. I. du Pont de Nemours & Co., Inc., Hytrel Bulletin IF-HYT-370.025, 1976; U.S. Pat. 3,718,715 (Feb. 27, 1973), R. W. Crawford and W. J. Witsiepe (to Du Pont).
72. A. T. Chen, Paper presented at the 3rd International Conference on Thermoplastic Elastomer Markets and Products, Schotland Business Research, Dearborn, Mich., Mar. 28–30, 1990.

73. M. Szycher, V. L. Poirier, and D. Demsey, *Elastomerics* **115**(3), 11 (1983).
74. Technical Bulletin H-69216, DuPont-Dow Elastomers, Wilmington, Del., 1996.
75. S. Abdou-Sabet, Paper presented at the 4th International Conference on Thermoplastic Elastomer Markets and Products, Schotland Business Research, Orlando, Fla., Mar. 15–17, 1989.

GEOFFREY HOLDEN
Holden Polymer Consulting, Inc.

ELECTRICALLY ACTIVE POLYMERS

Introduction

The discovery that polyacetylene doped with iodine exhibited electrical conductivity many orders of magnitude higher than neutral polyacetylene was made in 1976 by Hideki Shirakawa, Alan MacDiarmid, and Alan Heeger; they received the 2000 Nobel Prize in Chemistry (1,2) for their work in this area. This discovery triggered the development of a new multidisciplinary field known as "synthetic metals" (3). The field of synthetic metals is at the crossroads of chemistry, physics, materials science and engineering, and biomedical engineering. This discovery marked what has been described as the "fourth generation of polymeric materials" (4). Since the early pioneering work of Shirakawa, MacDiarmid, and Heeger, numerous additional developments and discoveries in conductive polymers have occurred. As a result, the field of plastic electronics and photonics has matured to offer the promise of a wide range of novel applications exploiting the unique chemical, physical, and electrical properties of conductive polymers.

In order to begin describing electrically conductive polymers, several definitions of conductive polymers must be presented. There are four major classes of conducting polymers: filled polymers, ionically conducting polymers, charge-transfer polymers, and electrically conducting polymers (ECPs).

Filled polymers are intrinsically nonconductive polymers loaded with conductive fillers such as carbon black, graphite fiber, metal particles, or metal oxide particles (5–9). Filled polymers have the longest history and broadest application in electronic devices. These materials have been used since the 1930s in the prevention of corona discharge and later in advanced printed circuitries. The extensive use of these materials lies in their ease of processing, wide range of electrical properties, and relatively low cost. However, these materials are inhomogeneous,

Encyclopedia of Polymer Science and Technology. Copyright John Wiley & Sons, Inc. All rights reserved.

containing three distinct phases: polymer, filler, and interface. This inhomogeneity results in a lack of reproducibility, a heavy process dependency, and a steep percolation threshold in conductivity (see CONDUCTIVE POLYMER COMPOSITES).

Ionically conducting polymers, also called ionomers (qv) or polyelectrolytes (qv), have been known for more than 30 years; several excellent reviews are available (10–13). These materials have found a wide range of potential commercial applications including rechargeable batteries (14,15), fuel cells (16,17), and polymer light-emitting devices (18). Ionic polymers are highly processable and can be synthesized using a wide variety of approaches. The major drawback to these materials is their sensitivity to moisture and humidity.

Charge-transfer materials were first investigated during the 1950s with the discovery of electrical conductivity on the order of 10^3 S/cm (19) in molecular charge-transfer complexes. In the 1960s a similar observation was made with iodine-doped poly(vinyl carbazole) (PVK) (20,21). The addition of an oxidant such as $SbCl_5$ and/or tri-(*p*-bromophenyl)ammonium hexachloroantimonate) to a charge-transport polymer (PVK) has produced materials that are known as semiconducting charge-transfer polymers (22). By varying the oxidant and charge-transport polymer combinations, various semiconducting polymers have been produced (23,24). The conductivity of these materials can be readily tuned by adjusting the concentrations of the charge transport group and oxidant. These materials offer many advantages as a result of their wide range of conductivities, high stability, excellent wear resistance, and high dielectric strength. However, the major drawback to these materials has been their low conductivities. The highest conductivities of polymeric charge-transfer materials have been only on the order of 10^{-5} S/cm (25).

The final materials to be discussed are intrinsically conducting/electrically conducting polymers (ICPs/ECPs) and/or electrically active polymers, which will be the focus of this review. While these terms have been used interchangeably, ICPs/ECPs are by definition conductive; electrically active polymers include ICPs/ECPs as well as conjugated but poorly conductive polymers. Throughout this article, the term electrically active polymers (EAPs) will be used to describe conjugated polymers, regardless of conductivity. EAPs are composed of conjugated polymer chains with delocalized π-electrons along the polymer backbone.

EAPs are either insulating or semiconducting in the undoped or neutral form. These neutral polymers are converted to the electrically conductive or doped forms by oxidation or reduction reactions, which form delocalized charge carriers. To maintain charge balance in such systems, an oppositely charged counterion is required. The conductivity of these materials is electronic in nature; there is no concurrent ion migration occurring in the polymer solid state, and the doping processes are reversible. These redox doping processes can be achieved by chemical and/or electrochemical methods. Thus, the conductivities of EAPs range from those of insulators ($<10^{-10}$ S/cm), to semiconductors like silicon ($\sim 10^{-5}$ S/cm), and as high as metals such as copper ($>10^4$ S/cm) (Table 1) (26,27).

There are many excellent reviews of EAPs that the reader is encouraged to examine that chronicle the historical achievements in this field of chemistry since 1976 (17,28–42). This article will review the synthesis, properties, and applications of redox-dopable electrically conducting polymers. Several specific examples will be used to illustrate general concepts and principles.

Table 1. Comparison of Electrical Conductivities of Insulators, Semiconductors, Metals, and EAPs[a]

Materials	Conductivity ($\log\sigma$), S/cm	EAPs	Classification
Ag, Cu, Pt	6		Metal
Fe	5	*d*-Polypyrrole,[b] *d*-polythiophene,[b] m*d*-poly(*para*-phenylene),[b] and *d*-polyacetylene	Metal
Bismuth	4	*d*-Polyaniline	Metal
InSb	1	*d*-Poly(phenylene sulfide)[b]	Semiconductor
Germanium	−2	trans-Polyacetylene	Semiconductor
Silicon	−5	trans-Polyacetylene	Semiconductor
Silicon bromide	−8	cis-Polyacetylene	Insulator
Glass	−10	Polyaniline	Insulator
DNA	−12		Insulator
Diamond	−14	Polythiophene, polypyrrole	Insulator
Nylon	−14		Insulator
Sulfur	−16		Insulator
Teflon/quartz	−18	Polystyrene	Insulator

[a]Refs. 26–28.
[b]Doped material.

Synthesis of Electrically Active Polymers

The number of new conducting polymer structures that are reported in the open literature continues to grow at nearly 500 articles per month. This incredible amount of research devoted to the study of EAPs attests to their unique scientific properties and their potential widespread use in commercial applications. In order to fully exploit their potential applications one must begin with their synthesis and properties.

The synthetic routes that have been developed for the preparation of conjugated polymers are diverse. This diversity is driven in part by the desire to develop substitutes for metallic conductors and semiconductors, but other properties unique to EAPs have also attracted intense interest. The effort to synthesize materials with tailor-made properties has been and continues to be pursued by hundreds of research groups. These researchers are seeking to develop EAP materials and improve their electrical, mechanical, optical, processing, and thermal properties. New EAP device concepts are being used to incorporate the most promising EAP material solutions.

Currently, there are several classes of EAPs that have been shown to exhibit conductivities of metals and semiconductors in the doped state. They are the polyacetylenes, poly(para-phenylene)s, polyheterocycles, poly(phenylene vinylene)s, polyanilines, and conjugated ladder polymers. Conducting polymers are made by both chemical and electrochemical polymerization. In the neutral (uncharged) state, EAPs are insulators or semiconductors. Oxidized (p-doped) EAPs have had electrons removed from the backbone, resulting in delocalized polymer cation formation. Reduced (n-doped) EAPs have had electrons added to the backbone, resulting in polymer anion formation.

The most stable (and therefore the most intensely studied) EAPs are the oxidized, cationic salts of highly conjugated polymers, although stability varies widely with chemical composition. Some cationic salts are quite stable in air (40), while others are highly reactive. The cationic salts (or p-doped polymers) are obtained by oxidation (chemical or electrochemical) of neutral polymers or of monomers. Chemical oxidation in this context refers to the removal of electrons using a chemical oxidant such as ferric chloride (43), whereas electrochemical oxidation occurs under an applied potential in the presence of an electrolyte (44). Anionic salts (n-doped polymers) can also be prepared from highly conjugated polymers by electrochemical reduction or treatment with reagents such as sodium naphthalide. However, the anionic salts, while conducting, are typically less stable than their cationic counterparts because they can react with air and water (45). Stability of both cationic and anionic salts of EAPs varies significantly with chemical composition.

Electropolymerization offers several advantageous features. Simple monomer oxidation (or more rarely, reduction) results in rapid synthesis of the doped, conducting form of the polymer adhered to the electrode surface, thus simplifying isolation and purification. Film thickness is easy to control, and patterned electrodes can be used for precise placement of the polymer. No catalyst is necessary, and aqueous polymerization is possible with a wide variety of monomers, so electropolymerization can be an environmentally friendly process. Disadvantages of electropolymerization include the relatively small scale of the reactions and the need for expensive equipment; additionally, some monomers do not polymerize electrochemically.

Polyacetylenes. Polyacetylene, one of the most studied of the EAPs, possesses the simplest EAP structure, consisting of alternating single and double carbon–carbon bonds, in either a cisoid or transoid configuration. (Fig. 1). The transoid configuration is thermodynamically favored, but cis–trans isomerization is a reversible process.

The first reported synthesis of polyacetylene was by Natta and co-workers in 1958 (46). For many years this polymer remained a material of limited interest to organic/polymer chemists and theoreticians because of its poor processability (47,48). However, Ito and co-workers discovered a synthetic route for making high quality flexible films of polyacetylene in 1974 (49). This discovery and the subsequent discovery that the electrical conductivity of doped polyacetylene could

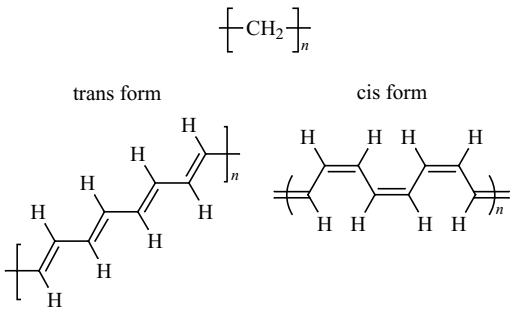

Fig. 1. Structure of polyacetylene.

be increased from the semiconductor form to the metallic form ushered in the current field of EAPs (1,50,51). This synthetic process is known as the Shirakawa technique. The technique involves the polymerization of acetylene on a thin-film coating of a heterogeneous Ziegler–Natta initiator system (eq. 1), which consists of a combination of $Ti(O\text{-}n\text{-}C_4H_9)_4$ and $(C_2H_5)_3Al$. The initiator is soluble in organic solvents and is highly active for acetylene. The process produces mechanically strong, free-standing films of polyacetylene. The reagents are commercially available, allowing for low cost production.

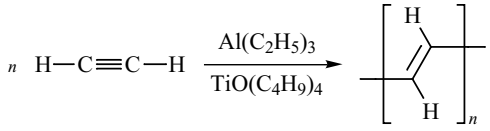

(1)

The films obtained from these early studies were insoluble in all solvents and infusible, so structural characterization was not possible. The films had conductivities about 0.5 and 38 S/cm when doped with bromine and iodine, respectively (1,2,51), and 560 S/cm when doped with AsF_5 (52). Both the conducting and the insulating forms of these films are unstable in air. There have been numerous attempts to improve the conductivities of doped polyacetylene films and the synthetic methods leading to higher quality films. There are now several routes by which high quality polyacetylene can be prepared. Shirakawa has recently published an excellent review of synthetic approaches to polyacetylene (53).

There are a wide variety of Ziegler–Natta, Luttenger, and metathesis catalysts that are very effective in the polymerization of acetylene; however, some of these catalysts produce undesireable by-products during the polymerization. Careful selection of the catalyst is important to produce good yields of high quality polyacetylene. Heterogenous catalysts are almost always employed to allow easy removal of the residual catalyst from the polymer.

The polymerization of acetylene with Luttinger catalysts was first carried out in the 1960s (47,54). The Luttinger catalyst consists of a hydridic reducing agent such as sodium borohydride and a salt or complex of a group VIII metal such as nickel chloride. This synthetic technique produces high molecular weight polyacetylene with no byproduct formation. It is easier to handle experimentally than the Ziegler–Natta or metathesis processes; hydrophilic solvents can be employed. In contrast, the Ziegler–Natta and metathesis processes require vigorously dehydrated hydrocarbon reagents and the rigorous exclusion of air and moisture. The catalytic activity of the Luttinger catalysts is much lower than that of the Ziegler–Natta catalysts, and high quality films of polyacetylene are typically difficult to obtain. However, Lieser and co-workers prepared high quality thin films of cis-rich polyacetylenes that showed no difference in morphology from those obtained using a Ziegler–Natta catalyst (55).

The polymerization of acetylene using metathesis catalysts was carried out by Aldissi and co-workers (56). Uniform films were prepared using a concentrated solution of a soluble catalyst in toluene. Polyacetylene has also been produced using Rh and Re catalysts (57,58). The chlorine-bridged Rh(I) complexes such as $[Rh(COD)Cl]_2$ and $Rh(NBD)Cl]_2$ where COD is cycloocta-1,5-diene and NBD

is bicyclo[2.2.1]hepta-2,5-diene with sodium ethoxide as cocatalyst produce polyacetylene as solid flakes. These catalysts are similar to the Luttinger catalyst in that they are stable in air and their catalytic ability is not inhibited by the presence of oxygen or moisture. Acetylene has also been polymerized by electrochemical methods (59), on the surface of metal oxides such as rutile (TiO_2) (60) and γ-alumina (γ-Al_2O_3) (61), and in the presence of a catalytic amount of AsF_5 at -75 to -198°C (62). Several miscellanous techniques have also been employed to polymerize acetylene, such as irradiation with γ-rays from a ^{60}Co source (63) and high pressure (64).

Each of the above techniques has resulted in high quality polyacetylene films. The major drawback for these techniques has been the intractable nature of polyacetylene, resulting in difficulties in purification, characterization, and processing. To eliminate these processability problems, it is necessary to employ a precursor route such as the widely studied Durham method to polyacetylene (65,66). In this process, an acetone-soluble precursor polymer is formed; processing occurs in this phase of the synthesis before conversion to the intractable polyacetylene. This approach is shown in equation 2.

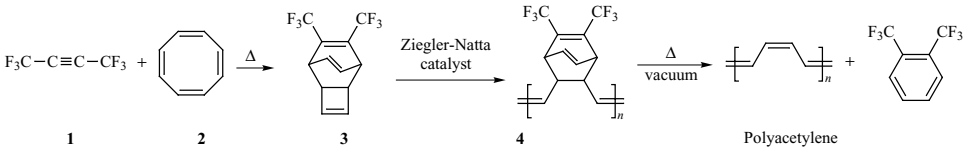

(2)

Monomer synthesis is first accomplished by the thermal reaction of hexafluorobut-2-yne (**1**) with 1,3,5,7-cyclooctatetraene (COT) (**2**) to yield 7,8-bis(trifluoromethyl)tricyclo-[4.2.2.$0^{2,5}$]deca-3,7,9-triene (**3**). Ring-opening metathesis polymerization of **3** using a catalyst such as WCl_6–$(C_2H_5)_4Sn$ (W/Sn = 1:2) gives a cis/trans mixture of polyacetylene after thermal treatment of (**4**). The classical Ziegler–Natta catalyst such as $TiCl_4$-$(C_2H_5)_3Al$(Ti/Al = 1:2) gives the precursor polymer (**1**). Low temperature (ca 60°C) thermal elimination gives predominantly *cis*-polyacetylene, while higher temperatures yield the predominantly trans polymer. The major problem with the Durham method and other precursor routes is the neccessity of eliminating a large molecule during the thermal process. An alternative precursor method developed to eliminate this problem is the ring-opening metathesis polymerization (ROMP) of the highly reactive and commercially available monomer benzvalene (**5**) (67). The reaction is shown in equation 3.

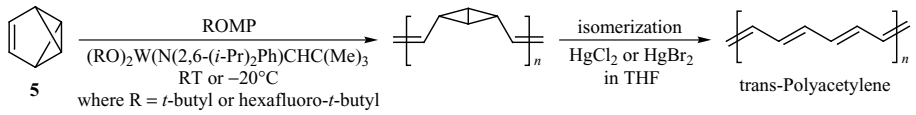

(3)

A method has been developed recently to eliminate the thermal process for producing polyacetylene films. This technique is a liquid-crystal polymerization

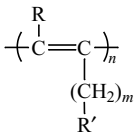

Fig. 2. Functional modifications of polyacetylene. Where R = H, alkyl, aryl; R′ = alkyl, aryl, ester, ether, amine, thienyl, cyano, vinyl, ethynyl, alkyl ammonium; $m = 0, 2$.

method, which allows oriented films to be prepared directly through an anisotropic reaction field (68–70). The field is produced by macroscopically orientated nematic liquid crystals, which are used as the polymerization solvent for a Ziegler–Natta catalyst. This technique yields highly oriented films in the trans configuration. This process produces polyacetylene with good conductivity (10^4 s/cm) without the need for thermal treatment and stretching, which causes defects and breaks fibrils in films.

Although most of the previous approaches have been directed at the synthesis of polyacetylene, much additional work has gone into the synthesis of derivatized polyacetylene (see ACETYLENIC POLYMERS, SUBSTITUTED). Incorporation of side groups, either before or after polymerization, is commonly used to improve solubility (71) and impart functionality. Functional groups such as ester, ether, amine, thienyl, cyano, vinyl, ethynyl (72,73), aryl (74), and ionic substituents such as pyridinium (75), alkyl sulfonates (76), and alkyl ammoniums (76) also yield soluble polymers (Fig. 2). In most cases, solubility increases are accompanied by decreases in conductivity due to loss of conjugation resulting from unfavorable steric interactions (75). Liquid crystalline groups are incorporated to increase order in the polymer, with alignment resulting in improved conductivity, reduced band gaps, and interesting photoresponsive properties (77,78).

Poly(*para*-phenylene). Poly(*para*-phenylene) (PPP) can be synthesized by both direct (79) and indirect methods (80). A comprehensive review of these synthetic routes has been presented by Schluter (81).

The direct approach consists of using monomers that contain a phenylene group that becomes the repeat unit of the final polymer. In the indirect approach, a precursor polymer is synthesized first, and the PPP is obtained after thermal treatment. Both approaches have serious drawbacks. In the direct approach, regioirregularities often result from the coupling reactions, as do low molecular weights, cross-linking, and other side reactions. In the indirect approach, structural irregularities contained in the precursor polymer are transplanted into the final product, and there are very few suitable precursor polymers available for PPP synthesis.

The direct approach has been demonstrated by Yamamoto (82,83); *p*-dibromobenzene was combined in a Grignard-type coupling reaction with one equivalent of magnesium in the presence of a transition-metal catalyst in THF to give a para-linked low molecular weight PPP (eq. 4). Linear poly(*p*-phenylene) and poly(*m*-phenylene) have also been obtained through a reductive coupling of *p*-dihalobenzene by electrolysis or with chemical reductants, although these materials remained insoluble and could not be completely characterized (84,85).

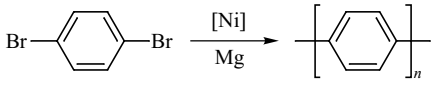

(4)

Several alternative direct methods have been employed to increase the molecular weight and processability of PPP. The key is the incorporation of solublizing substituents, such as long alkyl or alkoxy chains. Mullen reported the synthesis of relatively high molecular weight PPP derivatives by preparing alkylated polytetrahydropyrenes from the corresponding dibromo monomers using Ni/Mg catalysts (86). Highly soluble PPP derivatives have been obtained by oxidative copolymerization of alkoxy-substituted benzenes (87) and by polymerization of a charge-transfer (CT) complex between the monomer *N*,*N*-dimethylaniline and tetrachloro-*p*-quinone (88).

Perhaps the most successful direct approach to soluble PPPs is that pioneered by Rehahn and co-workers, first published in 1988 (89). In this method, aryl bromides are coupled with aryl boronic acids (or boronic esters) with palladium catalysts under Suzuki cross-coupling conditions (eq. 5). When the bromo and boronic acid groups are both on the same phenylene ring (**6**), the result is a homopolymer as shown in equation 5; copolymers can be prepared through reactions of dibromophenylenes with bisboronic acid substituted phenylenes. Boronic acids are typically much more stable than the corresponding Grignard compounds, allowing for purification of the intermediates and resulting in higher molecular weight polymers. This approach is now commonly used for the synthesis of soluble PPPs; an excellent review of the Suzuki polycondensation has recently been published (90).

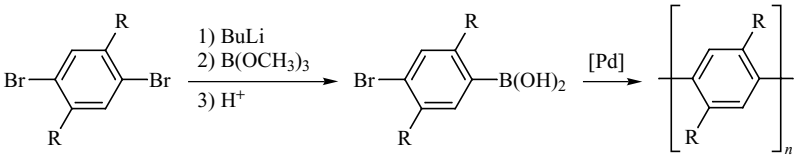

6

(5)

The indirect or precursor method for the preparation of PPPs was poineered by Marvel in the 1950s (91,92). Although Marvel's pioneering work produced low molecular weight precursor polymer, ICI researcher Ballard was successful in developing a monomer based on cyclohexadiene (93). The reaction sequence is shown in equation 6. The reaction starts with monomer **7**, which is a derivative of 5,6-dihydroxycyclohexa-1,3-diene and is polymerized using radical initiators to high molecular weight polymer precursors (**8**). The precursors are soluble in common organic solvents, and films and spun fibers can be produced. Thermal treatment results in elimination of the side groups to yield fully aromatic PPP, which is insoluble and intractible. An industrial process based on this chemistry was found to be impratical because the synthesis was unscaleable.

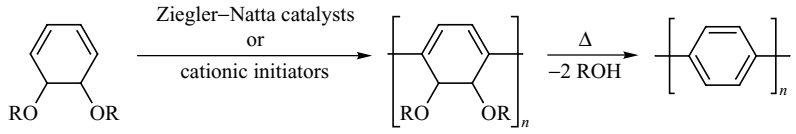

7 8 (6)

However, Ballard used a biomediated synthesis to circumvent these obstacles. The microorganism *Pseudomonous putida* 11767 oxidizes benzene within the bacterial cell (79). The dioxygenase E1 with the assistance of the protonated cocatalyst nicotinamide adenine dinucleotide (NADH) reacts with oxygen to give 5,6-dihydroxycyclohexa-1,3-diene. The organism was genetically modified in order to eliminate the aromatization step of 5,6-dihydroxycyclohexa-1,3-diene. The mild conditions of this process were found to be scaleable and are used in an industrial process. The resultant PPP has limited regio and stereospecific control during polymerization and is therefore not entirely composed of 1,4-linkages; approximately 15% 1,2-linkages result from this process.

Polyheterocycles. Heterocyclic monomers constitute a third class of monomers that can be polymerized to form fully conjugated polymers; the most common of these monomers, shown in equation 7, are pyrrole (X = NH), thiophene (X = S), and furan (X = O). They can be doped to give electrical conductivity when polymerization occurs in the 2,5-positions. These monomers can be polymerized both by electrochemical and chemical methods. The polyheterocycles have received considerable attention for their electron-rich nature, which leads to materials that are easily oxidized and therefore more stable in the oxidized state. Additionally, the increased structural complexity of polyheterocycles relative to polyacetylenes makes structural modifications possible for improved processability.

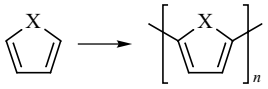

where X = O, NH, S (7)

By far the most commonly exploited polymerization of heterocycles is the oxidative polymerization, which can be carried out using chemical or electrochemical oxidation conditions. Chemical oxidative polymerization is advantageous in that the reactions are fast and simple, using relatively mild conditions (94), and polymers could presumably be mass-produced at a reasonable cost (95). Oxidation potentials depend upon the electron density of the monomers; the more electron-rich a monomer is, the easier it is to oxidize. The oxidative polymerization of thiophene is shown in Figure 3; this mechanism is equally applicable to other heterocycles. The mechanism is thought to involve a one-electron oxidation of the monomer to form a resonance-stabilized radical cation. This can couple with a molecule of starting material to form a radical cation dimer, which loses another electron to form the dicationic dimer, or the radical cation can couple with another radical cation to form a dicationic dimer. The dicationic dimer then loses two protons to form the neutral dimer, and the entire process is repeated to form polymer. The fundamental polymerization mechanism is the same for both chemical and

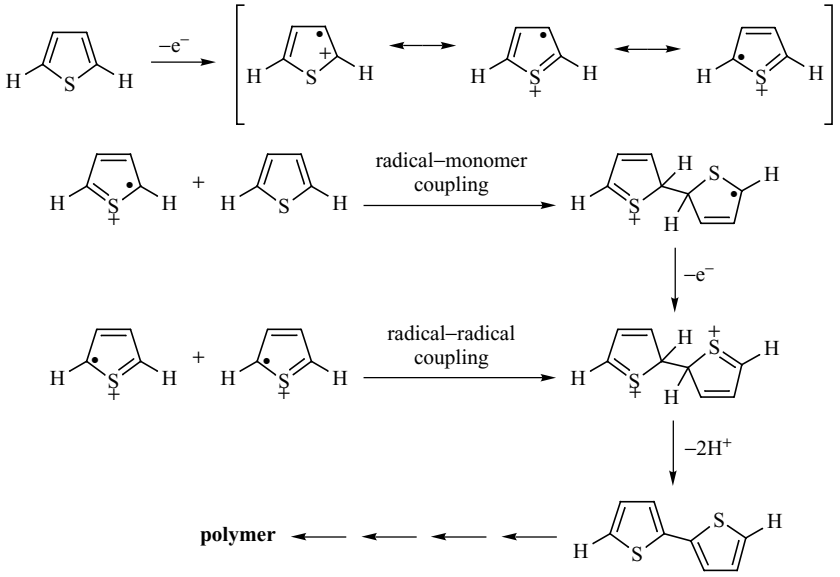

Fig. 3. Mechanism of oxidative polymerization of thiophene.

electrochemical polymerization, although there are additional factors (diffusion, scan rate, electrode characteristics, etc) that must be considered for electrochemical polymerization.

Among the problems associated with oxidative polymerization is the abundance of possible side reactions. Oxidation of the simple, unsubstituted heterocycles results in poorly soluble, poorly processable materials, so structural modifications are typically used to improve polymer properties. Often, the strong oxidation conditions required to effect polymerization cause overoxidation and decomposition. While coupling at a carbon adjacent to the heteroatom is favored, as it is the most electron-rich site, coupling is also possible at other unsubstituted carbons, and irregular polymer backbones can be formed as shown in Figure 4 for oxidative polymerization of thiophene. Coupling of heterocycles occurs predominantly through the 2- and 5-positions (α,α-coupling), but some coupling also occurs at the 3- and 4-positions to give a small amount of α,β and β,β-couplings. The mixture of couplings induces larger twist angles, reducing conjugation and yielding poor electronic properties (96). Multiple couplings on the same heterocyclic molecule can also occur, resulting in cross-linked polymers.

Coupling at β-positions during polymerization can be avoided by blocking the 3- and 4-positions of the heterocycle. If symmetrical substitution is used, problems associated with regioirregularity (see below) can be avoided. For instance, in the polymerization of 3,4-ethylenedioxythiophene (EDOT) shown below (Fig. 5), the ethylenedioxy bridge effectively prevents β-coupling, thereby yielding a linear polymer.

Polypyrroles. The first reported polymerization of pyrrole was in 1916 (97). Polypyrrole was prepared by the chemical oxidation of pyrrole using hydrogen peroxide. An amorphous black powder known as “pyrrole black” was obtained, which

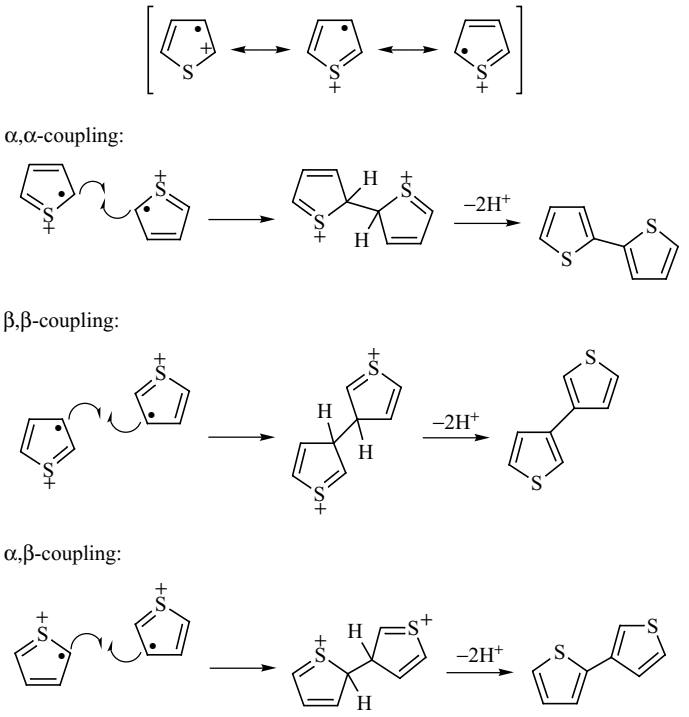

Fig. 4. Coupling pathways during oxidative polymerization of thiophene.

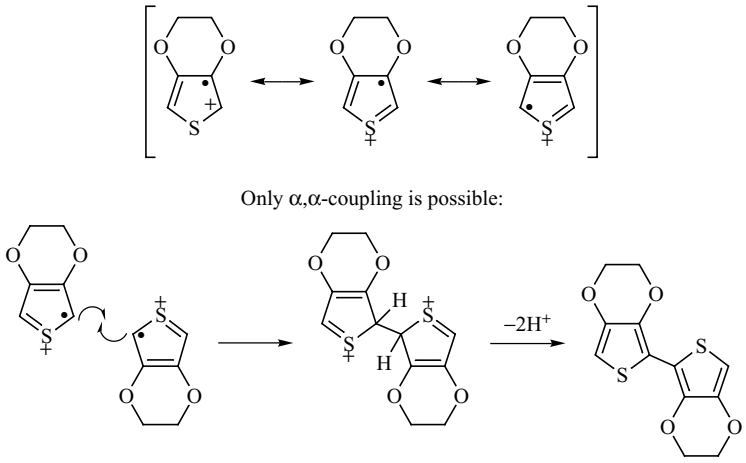

Fig. 5. Coupling pathways during oxidative polymerization of EDOT.

was insoluble in common organic solvents. One of the advantages of polypyrrole (PPy) is the low oxidation potential of pyrrole relative to other EAP precursors, facilitating oxidative polymerization; the half-wave oxidation potentials (in acetonitrile/0.5 M $NaClO_4$) of benzene, thiophene, and pyrrole are 2.08, 1.60, and

0.76 V vs Ag/Ag^+, respectively (44,98). Numerous oxidizing reagents have been used to polymerize pyrrole, including hydrogen peroxide in acetic acid, lead dioxide, ferric chloride, nitrous acid, and ozone (99,100).

The chemical oxidative polymerization of pyrrole results in low conductivities in the range of 10^{-10} to 10^{-11} S/cm, although conductivities of 10^{-5} S/cm have been reported with iodine doping (101). The low conductivities obtained from acid and peroxide initiators have been attributed (102) to the high degree of saturation of the pyrrole ring due to either oxygen incorporation and/or hydrogen saturation. The use of oxidative transition-metal ions such as ferric salts (eg $FeCl_3$, $Fe(NO_3)_3$, $Fe(ClO_4)_3$, $FeBr_3$) at low temperatures in both aqueous and organic solvents has improved the conductivities of PPy from 10^{-5} to 200 S/cm (103–106). The polymers that were obtained are infusible and insoluble powders. Approaches to produce processable PPy materials include the synthesis and polymerization of pyrrole compounds containing solubilizing groups in the 3-position (107) or attached to the nitrogen (108) as well as the use of soluble precursor molecules (109,110). Although these efforts result in improved processability of the polypyrroles, there is a concurrent loss of conductivity.

The chemical polymerization of pyrrole remains the simplest route to PPy, but electrochemical polymerization is the most important and versatile method for producing PPy films of high conductivity (111). There are numerous examples of PPy doped with a wide variety of anions that can be electrochemically polymerized on a variety of electrode materials in both aqueous and organic solvents (112–114).

Polythiophenes. Preparations of polythiophene (PT) include chemical oxidative couplings of thiophene (95), the cross-coupling of Grignard reagents of dihalothiophenes (96,115), and electrochemical polymerization (95,116). The PT powders and films that are produced either chemically or electrochemically are insoluble and infusible. In order to better characterize and process PTs, synthetic methods were developed to incorporate functional groups (such as *n*-alkyl groups) on the 3-position to improve processibility without significantly sacrificing conductivity. The synthesis of poly(3-alkylthiophene)s (P3ATs) that are chemically stable, soluble, processable, and moderately to highly conductive has been achieved by several research groups. Early work on the synthesis of P3ATs utilized the Kumada cross-coupling reaction (115), oxidative polymerization using $FeCl_3$ (116) or Cu powder with a catalytic amount of $PdCl_2$ in pyridine (118). These methods produce irregular homopolymers and copolymers of P3ATs with reasonable molecular weights and low to moderate conductivities.

Unsymmetrical monomers such as 3-alkylthiophenes are said to have a "head" (ie the 2-position of the thiophene ring) and a "tail" (ie the 5-position of the thiophene ring). Standard homopolymerization of 3-alkylthiophenes yields P3ATs that have "head-to-head" (2,2′, or H-H), "head-to-tail" (2,5′, or H-T), and "tail-to-tail" (5,5′, or T-T) bonds. Polymers having this type of bonding are said to be regioirregular, while polymers possessing purely H-T bonds are regioregular (Fig. 6). Regioirregular P3ATs are poorly conjugated, because the mixture of linkages leads to unfavorable interaction of side chains, resulting in a sterically driven twist of the polymer backbone (118). Polymer morphology is also affected by regiochemistry; regioregular polymers are typically crystalline, while regioirregular polymers are amorphous (119,120). Regioregularity problems can also be

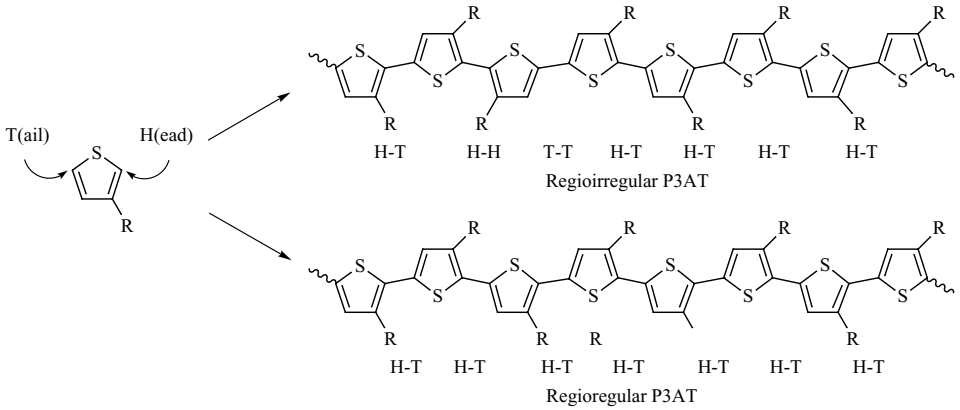

Fig. 6. Regiochemistry in poly(3-alkylthiophene).

avoided by using symmetrical monomers; extended conjugation monomers such as alkyl-substituted terthiophenes (121) and mixed heterocycle extended conjugation monomers (122,123) have become commonplace (124). These extended conjugation monomers also exhibit lower oxidation potentials, and they can be designed to tailor properties for specific applications.

Several groups have demonstrated regiospecific synthetic processes for obtaining regioregular P3ATs. In the now-standard method pioneered by McCullough and Lowe (125), a monomer (2,5-dibromo-3-alkylthiophene) is reacted with lithium diisopropylamide at cryogenic temperatures, followed by transmetallation with $MgBr_2 \cdot Et_2O$. Polymerization is then accomplished using Kumada cross-coupling methods with catalytic amounts of $NiCl_2$(dppp) to give P3ATs with 98–100% H-T coupling in moderate to high yields (eq. 8) (126–128).

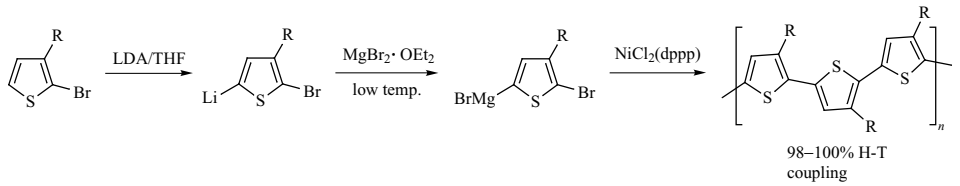

(8)

Since this early work by McCullough and others, improvements have been made in the synthesis of analytically pure highly regioregular H-T P3ATs without cryogenic temperatures. The Grignard metathasis (GRIM) polymerization (eq. 9) (129,130) is quick, easy, and cost-effective. The synthesis is as follows: a 2,5-dibromo-3-alkylthiophene is treated with one equivalent of an alkyl or vinyl Grignard reagent, followed by polymerization at room temperature with a catalytic amount of $NiCl_2$(dppp).

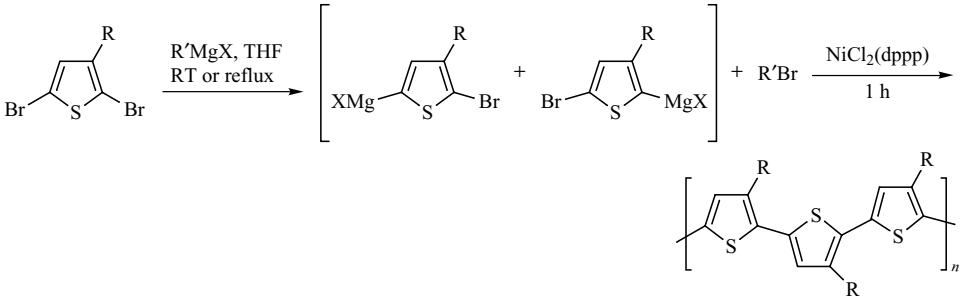

(9)

An alternative synthetic approach to the preparation of regioregular P3ATs was demonstrated by Chen and Rieke (131,132). Their method utilizes the highly reactive "Rieke zinc" (Zn∗), which is added to a solution of 2,5-dibromo-3-alkylthiophene at cryogenic temperatures. The metal reacts quantitatively to form a mixture of isomers: 2-bromo-3-alkyl-5-(bromozincio)thiophene and 2-(bromozincio)-3-alkyl-5-bromo-thiophene. The ratio between these two isomers depends on reaction temperature and the steric influence of the alkyl groups. The addition of a nickel cross-coupling catalyst leads to the formation of regioregular P3ATs (regardless of the isomer ratio), and regiorandom P3ATs are formed with the addition of a palladium cross-coupling catalyst (133).

Several additional homo-, co-, and terpolymers based on P3ATs have been synthesized recently. Monomers that incorporate two or three thiophenes such as the 4,4-dialkyl-2,2′-bithiophenes or 3,3-dialkyl-2,2′-bithiophenes with various substituent groups such as alkyl, oxyalkyl, β-aryl have been prepared by chemical and electrochemical methods (134–137).

The introduction of electron-donating substituents such as ether moieties lowers the *polymer band gap* (the energy difference between the valence and conduction bands of the polymer; for a more thorough discussion on band gap, please see under Transport Theory) by raising the energy of the valence electrons (HOMO destabilization) along the conjugated chain (138,139). These alkoxy substituents also decrease the oxidation potential of both the monomers and their polymers, allowing milder oxidative polymerization conditions, which results in fewer side reactions. Polymers based on 3,4-disubstituted thiophene derivatives such as EDOT (Fig. 5) have recently been synthesized by chemical and electrochemical methods. Poly(3,4-ethylenedioxythiophene) (PEDOT) (140–142) has a band gap of 1.5–1.6 eV as compared to thiophene (2.0–2.1 eV); poly(3,4-dimethoxythiophene) has an electrochemical band gap of 1.37 eV (143,144).

Polyfurans. Relative to polythiophenes and polypyrroles, little has been reported on polyfurans (PFu); this is likely a result of the high oxidation potential of furan ($\geq$1.7 V vs Ag/Ag$^+$), which results in side reactions during polymerization (145). While chemical polymerization of furan has been reported (146), the majority of PFu publications focus on electrochemically prepared PFu.

PFu was first reported by Tourillon and Garner (147), who used an electrochemical technique similar to that used by Diaz and co-workers to polymerize pyrrole (148). This PFu had reported conductivities from 10^{-5} to 10^{-3} S/cm. However, these early reports on the synthesis of PFu were incorrect because of inconsistent chemical and spectroscopic properties of the polymer obtained (149).

The high voltages required for electropolymerization (1.8–2.5 V vs SCE) of furan result in irreversible oxidation of the polymer, and the polymer contains significant hydrogenated units (150). A polyfuran structure was reported by Zotti and co-workers (151) by the cathodic reduction of 2,5-dibromofuran in acetonitrile using a Ni^{2+} catalyst. The PFu was obtained in trace amounts, with a significant content of the undoped, insulating form, which resulted in incomplete characterization of the material. Polyfuran films doped with ClO_4^- were obtained potentiostatically at several deposition potentials (152) and characterized by cyclic voltammetry, which showed highly complex voltammograms, indicative of a poorly defined polymer system. Free-standing films of PFu were obtained by the electrochemical polymerization of furan at 1.2 V vs Ag/AgCl in a binary solvent system (153); the resultant PFu showed well-defined cyclic voltammetry, moderate conductivity when doped with I_2 (10^{-2} S/cm), and good mechanical properties.

Regioregular and regiorandom poly-3-alkylfurans have also been reported (154). Conductivity was found to be highly dependent on degree of regioregularity, reaching 10^{-2} S/cm in the 95% head-to-tail (H-T) polymer but only 10^{-7} S/cm in the 75% H-T polymer.

To avoid the problems associated with furan's high oxidation potential, extended conjugation monomers incorporating furan have been prepared (145,155). A PFu prepared from terfuran showed a conductivity of 10^{-3} S/cm when doped with $CF_3SO_3^-$ (155). The PFu was highly susceptible to acid/base effects, which led to ring opening and a decrease in the conjugation length.

Poly(phenylene vinylene)s. The earliest reported synthesis of a Poly(p-phenylenevinylene) (qv) was accomplished by McDonald and Campbell in 1960 (156). They produced a PPV oligomer by a repetitive Wittig-type coupling of an aromatic bisphosphonium salt and a bisaldehyde. Several routes have been investigated for producing PPVs, such as coupling reactions of dichlorobenzene in liquid ammonia (157), reactions of tetrabromo-*p*-xylene with two equivalents of methylithium (158), and McMurray deoxygenative coupling of an aromatic dialdehyde (159). In all these cases PPVs were produced that were either insoluble or sparingly soluble and poorly processable.

Precursor routes to PPVs can be easy and efficient, and they produce soluble and processable high molecular weight PPVs The most widely used soluble precursor method is the Wessling and Zimmerman route eq. 10. This process involves the synthesis of the bis-sulfonium salt of 1,4-bis(chloromethyl)benzene, followed by sodium hydroxide elimination and polymerization at 0°C to give an aqueous solution of a precursor polymer. The soluble precursor is processed into films, foams, and/or fibers and converted to PPV by thermal elimination (160–163). The heating occurs under vacuum at temperatures ranging from 120°C for bromide salts to 200°C for chloride and fluoride salts to 300°C for acetate salts (164). Normally, a large variety of substituents can be tolerated on the aromatic ring, such as aromatic (165), alkoxy (166), silyl (167), halogen (168), sulfur (169), and amino groups (170), but electron-poor substitutents such as nitro or cyano groups polymerize with extreme difficulty (171). The major disadvantages of this method are the instability of the intermediate polymers and the stench of the sulfonium salts.

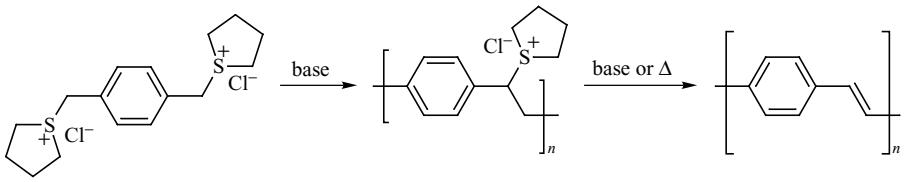

poly(phenylene vinylene)
(PPV)

(10)

There are several alternate routes for preparing PPV from soluble precursors. The Gilch route (172) uses a dichloro-*p*-xylene that is polymerized with potassium *tert*-butoxide in organic solvents. The alkoxy route (173) uses a methoxy-substituted polymer that is soluble in common organic solvents and is more stable than the sulfonium precursor. Polymerization is accomplished by removal of the alkoxy group by acid catalysis, followed by heating to produce PPV derivatives. A third route utilizes the Heck coupling reaction, which is compatible with a wide variety of functional groups (174,175), allows regiospecific synthesis (176), and yields polymers with molecular weights ca 10^4 g/mol (174,177). The Heck polymerization involves coupling of vinyl groups with bromides or iodides, either in an AA/BB copolymerization (as in the reaction of ethylene or a divinylbenzene with a dibromobenzene) or in an AB homopolymerization (typically the reaction of a 1-bromo-4-vinylbenzene), in the presence of a palladium catalyst (174).

All of these alternate routes allow a large range of substituted organic-soluble PPV derivatives to be synthesized, but none of the methods has a distinct advantage over Wessling and Zimmerman's sulfonium precursor method. The most studied solution-processable PPV is poly(1-methoxy-4-(2-ethylhexyloxy)-*p*-phenylene vinylene (MEH-PPV), commonly prepared via the Gilch method (178). Careful choice of PPV substitutents allows for tuning of the optical band gap, enabling the use of these polymers in electrooptical applications.

Several heteroaromatic ring structures have also been incorporated into poly(arylene vinylene) structures using the same soluble-precursor polymer methods used for PPV. Poly(thienylene vinylene) (179) and poly(furylene vinylene) (180) have been prepared. Metalloporphyrins have also been incorporated into poly(arylene vinylene)s (175) to investigate photorefractive properties. Aromatic poly(azomethines) have also been prepared from a solution condensation of an aromatic diamine with aromatic dialdehydes (181), but these materials are less conjugated than their PPV counterparts. Various copolymers of phenylene vinylenes with phenylene, thienylene, and furylene moieties have also been studied (182).

Polyanilines. Polyaniline was made nearly 140 years ago in 1862 by H. Letheby (183). At that time, polyaniline was known as "aniline black." This material was prepared by the oxidation of aniline under mild conditions. The material found use in dyes and printing. Initial preparations of polyaniline (PANI) led to insoluble materials that had poor thermal processability and solvent solubility. Only recently has the structure of PANI been fully determined. This was accomplished by using model compounds and polymers for definitive structural analysis. Poly(*p*-phenylene amineimine) (PPAI) was synthesized directly to demonstrate that PANI is purely para-linked (184–186).

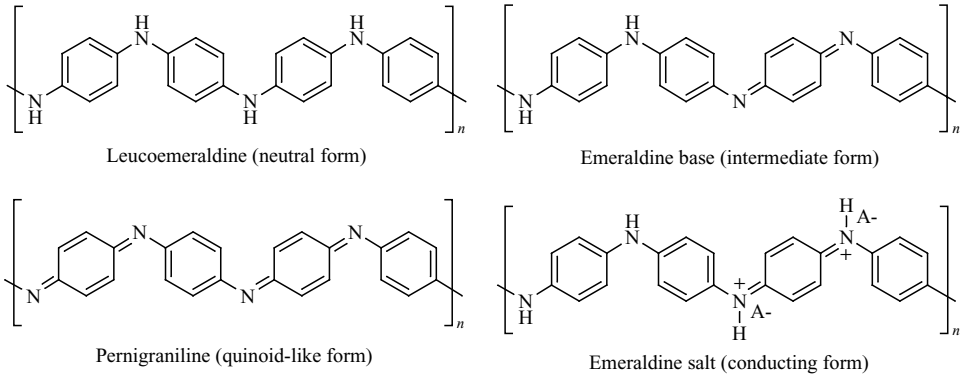

Fig. 7. Oxidation states of polyaniline.

PANI is commonly prepared by chemical polymerization of aniline using $(NH_4)_2S_2O_8$ in hydrogen chloride solution (187) and/or by electrochemical polymerization (188). PANI can exist in four different oxidation states: leucoemeraldine (neutral form), pernigraniline (quinoid-like form), emeraldine base (intermediate form), and emeraldine salt (conductive form), as shown in Figure 7. PANI is prepared as the emeraldine salt and then treated with base to yield the emeraldine base form, which is soluble in common organic solvents. After film casting or other processing, the emeraldine base can be treated with HCl to regenerate the conductive emeraldine salt form of PANI.

Methods have been developed to improve solubility and processability by introducing various alkyl, alkoxy, aryl, sulfonyl, and amino groups onto the PANI backbone (189). However, the presence of these substituents dramatically reduces yields of polymer, polymer molecular weight, and conductivity. Novel water-soluble PANI has been recently synthesized using horseradish peroxidase catalyzed by oxidative free-radical coupling of 2,5-diaminobenzenesulfonate (190). Unlike standard PANI preparations, the resultant polymer is fully sulfonated upon treatment with fuming sulfuric acid, and it shows strong pH dependance of absorption and other physical properties.

Conjugated Ladder Polymers. Since the 1930s double-stranded, ladder-type polymers have been prepared in a multistep process with limited success of cyclization (191,192). Other routes have also been explored such as those for poly(acrylonitrile) (193,194), poly(1,2-butadiene), poly(3,4-isoprene) (195), or poly(butadiyne)s (196). These materials were found to be poorly soluble and unworkable, with a considerable number of defects in the structure (incomplete cyclization, cross-linking, radical sites). The first successful synthesis of a ladder polymer with a completely defined structure was accomplished in 1991 by Sherf and Mullen (197). The first step was the AA/BB-type polycondensation of an aromatic diboronic acid with a substituted 2,5-dibromo-1,4-dibenzoylbenzene to give a single-stranded precursor PPP-type polymer, followed by cyclization to the ladder structure (Fig. 8). Several other examples exist that have resulted in ladder-type structures. These include angular polyacene (198,199), Diels–Alder polyaddition of AB-type diene–dienophiles (200), AA/BB-type Diels–Alder polyaddition of a bisdiene and a bisdienophile (201), thienylene units (202),

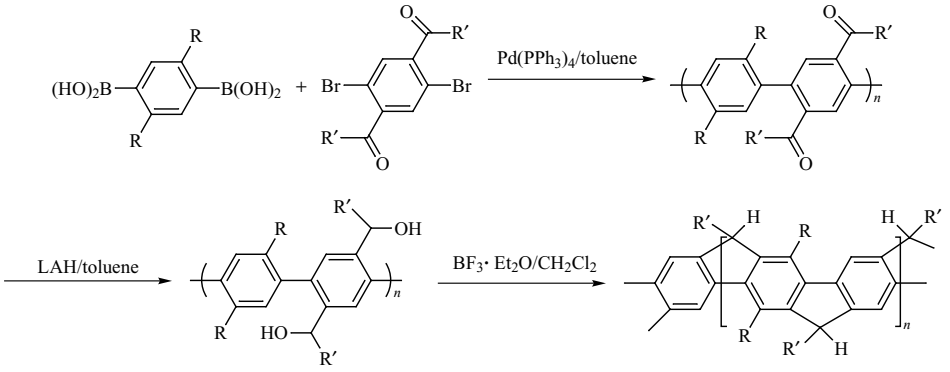

Fig. 8. Formation of ladder structures. Where R = n-C_6H_{13}; R′ = −1,4-C_6H_4-n-$C_{10}H_{21}$.

and polybenzimidazobenzophenanthroline (BBL) (203). All of these materials are structurally defined materials, but their drawbacks include poor solubility, poor thermal processability, and generally lack of workability.

Alternative Synthetic Approaches. Most EAPs are prepared via chemical or electrochemical oxidative polymerization, precursor routes, or coupling chemistry. However, several alternative approaches have recently been gaining attention.

Template-assisted polymerization is used to prepare specific conducting polymer architectures for use in a variety of applications (204). Polyacetylene has been prepared in the presence of liquid crystalline solvents for subsequent alignment (68–70). Polyaniline has been synthesized in the presence of DNA (205) to form helical PANI with interesting electrochemistry that is useful as a biosensor. Fibrillar morphologies can be produced by polymerization in channelized templates (such as microfiltration membranes); the resulting polymers show improved conductivity over analogous polymer films and were suggested for use in polymer light-emitting diodes (206,207). A variety of polymers have been grown around self-assembled colloidal templates (see Photonics section, below); the template can subsequently be dissolved away from the conducting polymers, producing opal-like EAP structures with the aim of improved charge transport for battery and capacitor applications. (208,209) While not strictly a template method, EAPs have also been prepared on the surface of a wide variety of particles and fibers (210,211), typically via chemical oxidative polymerization; the resulting composites/nanocomposites have found commercial application in static-dissipating paints, cloths, and carpets.

One synthetic approach gaining popularity for its ecologically friendly nature and its potential biological applications is that of biomediated polymerization. Enzymatic oxidants, such as horseradish peroxidase (212,213), are commonly used for chemical oxidative polymerization. Additionally, bacteria can be used to effect chemical reactions, as in the Ballard route to PPP described above (79).

Plasma polymerization is a solvent-free process that can be used to rapidly deposit thin polymer films onto a wide variety of substrates at room temperature (214,215). Monomer vapor is exposed to an electric field, and the resultant reactive fragments recombine to form polymer films. This technique is used for a wide

variety of polymer types including EAPs, and properties of the resultant polymers are often quite different from those prepared using more traditional techniques. Reaction conditions, including monomer flow rate, plasma power, reactor pressure, deposition time, and gas-phase composition, can be varied to tailor the properties of the resultant polymer. Other benefits of this technique include the environmentally friendly aspect of the solvent-free process, the ease of controlling film thickness, and the pinhole-free nature of the films. Plasma polymerization has been used to prepare polythiophene (216), polypyrrole (217), and polyaniline (218,219). While mechanical properties are typically better than those of traditionally prepared polymers (219), relatively poor conductivities are common in plasma-polymerized EAPs, possibly as a result of structural defects.

Conducting Polymer Blends, Composites, and Colloids. EAPs are in most cases prepared in the form of intractable films, gels, or powders that are insoluble in common organic solvents. Incorporation of solubilizing functional groups is but one technique available for chemists, materials scientists, and engineers to improve the processability of conductive polymers. Over the past decade research has focused on improving the processing characteristics of EAPs through the use of polymer blends, composites, and colloids (220).

Blends and composites of polymers offer certain combinations of desired properties that cannot be obtained from the individual components. EAP blends and composites offer a unique combination of good mechanical properties of an insulating host combined with the electrical conductivity of the guest. The conductive component's concentration threshold for the onset of electrical conductivity can be reduced to volume fractions well below that required for classical percolation (221). The critical factor in these formulations is the amount of EAP used; it must be enough to give a continuous conductive network (222). Blends and composites of EAPs are formed via simple, electrochemical, or diffusive mixing, by chemical treatment, by light-induced conversion and by counterion-induced processability. Numerous examples exist that describe the various methods used to form blends and composites using conductive polymers (221,223).

EAP colloids typically consist of a colloidal suspension of EAP particles or EAP-coated particles (latex, metal, silica, etc) in an aqueous medium; the dimensions of the dispersed particles are in the 1–1000-nm range. These materials are normally prepared via dispersion polymerization (224,225). While colloidal dispersions of EAPs are more processable than their noncolloidal EAP counterparts, the dispersions do not readily form films because of the high glass-transition temperatures (T_gs) of the EAPs, and applications are limited (226). A more promising approach involves coating particles (polystyrene, polyurethane, etc) with EAPs to form colloidal composites and nanocomposites. Much lower concentrations (ca 5–20%) of EAPs are used, so that the majority of the material is composed of low T_g, film-forming material. Conductivities of EAP-coated particles range from 10^{-5} to 10^{1} S/cm (227–229), and these materials are currently being marketed as water-borne anticorrosion and antistatic coatings.

Transport Theory

Conjugation and Conduction. As conjugation length increases, as with the progression from ethylene to 1,3-butadiene to 1,3,5,7,9,11-dodecahexane to

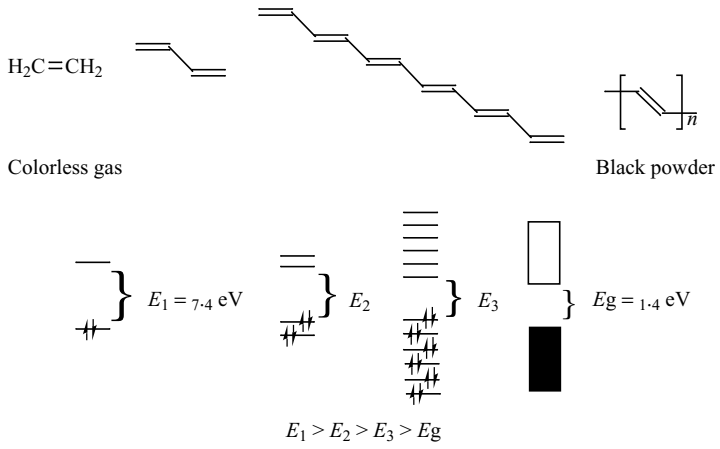

Fig. 9. Effect of conjugation on molecular energetics.

polyacetylene (Fig. 9), the degenerate orbitals spread to form nondegenerate energy bands, and the energy difference between the highest occupied molecular orbital (HOMO) and the lowest unoccupied molecular orbital (LUMO) decreases. This energy difference is a simple π to $\pi*$ transition in simple molecules and a band gap (E_g) in case of polymers (44). It can be determined for a neutral species from the onset of absorption in the UV–vis spectrum. Much research has focused on the development of low E_g materials for electrochromics applications (230). E_g can be lowered by functional group modification to raise the energy of the HOMO, but as a result the neutral polymers are very easily oxidized, and stability can be an issue.

Just as increasing conjugation length from ethylene to polyacetylene decreases the π to $\pi*$ transition, it also lowers oxidation potential. This is due to the high HOMO and increased resonance stabilization of the radical formed in the process. Similarly, other EAPs have lower oxidation potentials than their monomeric counterparts. Increasing conjugation in monomers also lowers oxidation potentials (124); the oxidation potential of thiophene (2.07 V vs SCE) is much higher than that of terthiophene (1.05 V vs SCE), which is higher than that of polythiophene (0.7 V vs SCE) (231). Extended conjugation monomers have therefore received considerable interest, because lower oxidation potentials lead to fewer side reactions and fewer defects (232,233). Among the defects minimized through the use of extended conjugation monomers are those caused by α,β-coupling, since several α,α-linkages are predetermined in these materials.

The conjugated nature of neutral EAPs allows them to have two electronically extreme states (eqs. 11 and 12). Unlike all other EAPs, the two resonance forms in *trans*-polyacetylene are degenerate, ie their ground states are thermodynamically equivalent (234). Other organic electroactive polymers possess nondegenerate ground states (235); for example, poly(*p*-phenylene) has both benzenoid and quinoid configurations (eqs. 11 and 12), of which the latter is the higher energy configuration (44), and so makes less of a contribution. Addition of either donors or acceptors in the process known as doping results in charge transfer and

the formation of charge carriers along the polymer chain, yielding the conductive form of EAPs (235). Several comprehensive treatments of charge carriers in EAPs can be found in the literature (38,236–238).

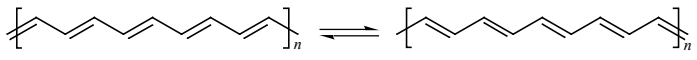

(11)

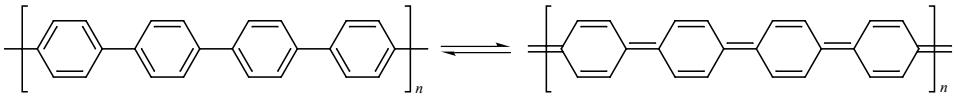

(12)

As a result of the degenerate ground states of *trans*-polyacetylene, charges formed during doping readily separate (because there is no increase in distortion energy.) The charge carrier, called a soliton, is relatively stable as a result of the degeneracy, and the energy required to create and move such a defect is relatively small (235). Calculations suggest that solitons are delocalized over 15 carbon atoms (239).

The most widely accepted mechanism of conduction in nondegenerate EAPs, illustrated in Figure 10 for polythiophene, was proposed simultaneously by Bredas and co-workers (240) and Bishop and co-workers (241) in 1981. This mechanism involves a one-electron oxidation to form a radical cation, which is called a polaron. This radical cation is resonance-stabilized over several rings. Removal of a second electron gives a dicationic species with no unpaired electrons, called a bipolaron. The two ions in a bipolaron need to be isolated from each other to minimize unfavorable interactions; recent work suggests that at least five rings are needed to stabilize a dicationic species (242,243). The conversion between neutral, polaronic, and bipolaronic species is reversible, using either chemical or electrochemical means to oxidize or reduce the polymer.

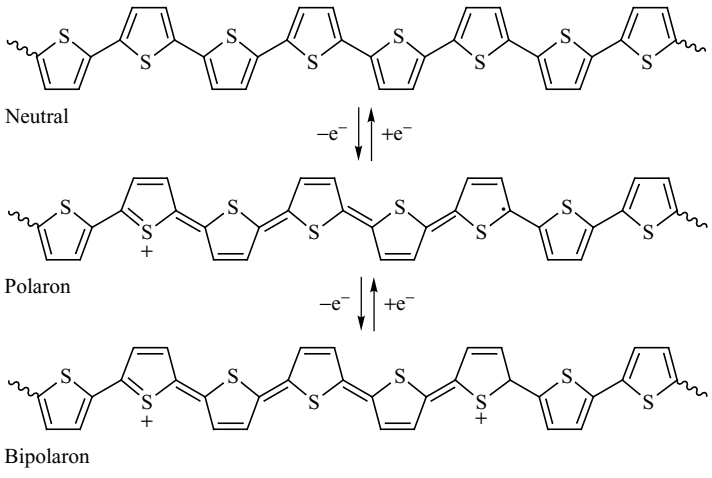

Fig. 10. Mechanism of conduction in nondegenerate EAPs.

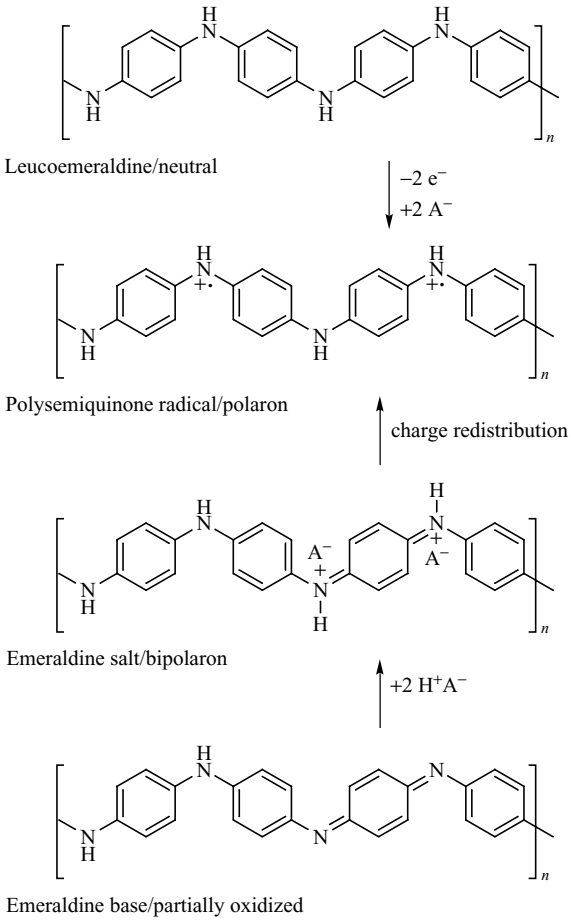

Fig. 11. Chemical doping of polyaniline.

PANI and other ECPs possessing strongly basic functionalities undergo a more complex chemical doping mechanism (187,188) (Fig. 11). While the leucoemeraldine form can undergo oxidative doping, leading to radical cation (polaron) formation, the emeraldine base form of PANI can also undergo protonation by acid–base chemistry to yield the emeraldine salt (bipolaron) form. Internal charge redistribution in the emeraldine salt also yields the polaron form.

Doping Processes. Reversible doping can be achieved by both chemical and electrochemical methods. The control of electrical conductivity of a conductive polymer from insulator to metal can be accomplished through the doping process; conductivity increases with an increase in the doping level (194–196). Several techniques exist for doping conjugated polymers (38). These techniques are as follows: (*1*) chemical doping by charge transfer, (*2*) electrochemical doping, (*3*) doping of PANI by acid–base chemistry (discussed above), (*4*) photodoping, and (*5*) charge injection at the metal–semiconducting polymer interface.

Chemical doping involves charge-transfer redox chemistry. Oxidative doping (p-type, electron accepting) with dopants such as I_2, AsF_5, O_2, and $FeCl_3$ is

commonly used, while reductive doping (n-type, electron donating) using dopants such as sodium naphthalide (244) or alkali metal vapors (245) is less common because of the reactivity of n-doped materials. This technique is simple and efficient, but control of the degree of doping is limited. High levels are easily achieved, whereas intermediate levels are not usually obtained.

Electrochemical doping refers to the supply by an electrode of the necessary redox potential to the conducting polymer (197). Ions diffuse in and out of the polymer structure from the nearby electrolyte, compensating for electronic charge formation along the polymer backbone. The doping level is controlled by the voltage between the conducting polymer and the counterelectrode. Thus, precise control of doping levels can be achieved.

Photodoping is a rapid process in which light is used to generate ions in solid polymer films (38). When an appropriate wavelength of light is absorbed to create an excited state, a close contact ion pair can be formed. No external counterions are present to stabilize these two mobile charge carriers. A transient change in the optical properties of the polymer occurs upon charge separation; resultant applications may include nonlinear optics and waveguides. In the absence of an electric field, the charges recombine in either a radiative (ie photoluminescence) or nonradiative process. In an electric field, these charges migrate to opposite electrodes, generating current; applications include solid-state photovoltaic cells.

Doping can also be accomplished by charge injection at a metal–semiconducting polymer interface. This type of doping, found in light-emitting diodes, occurs when electrons and holes are injected into the π and $\pi*$ bands of an EAP. In this method, the polymer is not doped in the chemical or electrochemical sense, because there are no counterions present.

Properties

While many properties of EAPs are also found in other materials, EAPs exhibit unique combinations of properties that have led to use in a variety of applications. Perhaps the most promising feature of EAPs is the switchable nature of many of the properties. The ability to reversibly switch EAPs between insulating and conducting, opaque and transparent, absorptive and emissive, or expanded and contracted drives much of the current EAP research.

Stability. In most cases, stability of EAPs is gauged in terms of changes in electrical conductivity. Thus, doped polyacetylene, while highly conductive in an inert environment, loses conductivity when exposed to air and is therefore considered unstable (51). Polypyrroles and polyanilines, on the other hand, are counted among the most stable EAPs, while polythiophenes exhibit intermediate stabilities. Environmental and thermal effects on polypyrrole and poly(3-alkylthiophene)s have been studied extensively (246,247); increased oxygen exposure and increased temperature frequently have detrimental effects on conductivity.

Mechanical Properties. Normally the mechanical properties of conductive polymers are very poor (211) because of the inherent nature of EAPs, which are normally intractable and poorly processable. Poor mechanical properties result from a lack of flexible linkages in the polymer backbone as well as from

low molecular weights. PANI is one exception that can be prepared as highly oriented crystalline fibers (248). The incorporation of EAPs into non-conductive polymer matrixes such as poly(vinyl chloride) (PVC) or poly(vinyl alcohol) (PVA) yields blend, composite, or laminate EAPs with unique combinations of electrical conductivity and processability (249). Such materials are discussed in detail elsewhere in this chapter. Processability is also improved by incorporating solublizing moieties pendant to the conjugated polymer chain as discussed previously; this often results in improved molecular weights, because polymer molecular weight is frequently solubility-limited.

Optical Properties. The optical properties of EAPs are a direct consequence of the electronic structure, which is determined by the chemical structure of the polymer. The optical properties of EAPs result from the energy difference between the valence and conduction bands in the conjugated polymer; this energy difference is called the band gap (E_g). EAP band gaps range from 0.5 to 3.0 eV (230,250), and typical absorption coefficients are on the order of 10^5 cm^{-1} (251).

The absorption characteristics of EAPs can be controlled by tailoring molecular structure; common methods include incorporation of electron-donating and electron-withdrawing groups (138,252–254) as well as alterations in conjugation length (usually by introduction of steric constraints). Because conjugation in neutral and doped EAPs is very different, changes in optical properties commonly occur during the redox process, leading to a variety of applications. These properties are exploited in the development of electrochromic and light-emitting devices, where materials have been produced spanning the entire spectrum.

Electrical Properties/Electrical Conductivities of EAPs. While conductivity in EAPs is typically at least one order of magnitude lower than that of the best metals, the ability to switch EAPs from conducting to insulating and the ease of processability of many EAPs have led to some unique applications.

The electrical conductivity, σ, of a conjugated polymer is equal to the inverse of its specific resistivity, ρ, which is a measure of the ability of the conjugated polymer to conduct an electrical charge. Electrical conductivity is determined by measuring the resistance, R, to charge transport through a known volume, where L is the length over which resistance is being measured and A is the cross-sectional area through which the current passes:

$$\sigma = 1/\rho = L/(R \cdot A)$$

Typically, electrical conductivity of EAPs is measured in units of S/cm. Both two- and four-point probe techniques are used to measure σ in films and pressed pellets (255). Conductivities as high as 10^5 S/cm have been reported for several EAPs. Values vary depending on synthetic procedures, fabrication techniques, and measurement methods. EAPs are typically only partially crystalline (256–258); amorphous EAPs have been reported (259–261). Therefore, disorder plays a significant role in their electrical conductivities, and the conductivity arises from the metal–insulator transition (262). As an example, PA with the highest conductivity reported so far shows temperature dependence of conductivity (263). Thus, electrical conductivity is limited by the disorder-induced localization of the electrons rather than by the intrinsic conductivity of the delocalized charges on the polymer backbone. Table 2 shows conductivities for several well-known EAPs (26–28).

Table 2. Electrical Conductivities of EAPs

EAP	Conductivity, S/cm
Poly(acetylene) (PA)	10^3–10^5
Poly(pyrrole) (PPy)	10^2–10^3
Poly(thiophene) (PT)	10^2
Poly(aniline) (PANI)	10–10^2
Poly(*p*-phenylene) (PPP)	10^2–10^3
Poly(phenylene vinylene) (PPV)	10^3–10^4

Applications

Light-Emitting Diodes (LEDs)/Light-Emitting Electrochemical Cells (LECs). *Electroluminescence* (EL) is the emission of light from a material when it is excited by an electric current. The discovery of EL in neutral (undoped, nonconductive) conjugated polymers, specifically PPVs, by Burroughs and co-workers in 1990 (264) led to extensive research into materials development and polymer light-emitting diode (PLED) research. EAPs compete with and may eventually replace current display technologies such as those based on inorganic materials and liquid crystalline displays (LCDs). Inorganic EL materials have been used in display applications for years; light-emitting diodes (qv) based on these materials have been commercially available since the 1960s (265).

PPV is a yellow fluorescent EAP with emission maxima at 551 nm (2.25 eV) and 520 nm (2.4 eV), in the yellow–green region of the visible spectrum (266). Soluble PPVs have been prepared by the precursor method, allowing for solution processing by spin coating onto a substrate (267).

PPVs and other EAPs offer unique advantages over their inorganic LED counterparts. Advantages include ease of processing on large-area substrates, good tensile properties of the chain-extended polymer (allowing the polymer to survive harsh conditions during device operation), and the ability to fine-tune the electronic and optical properties of EAPs through functionalization. The simplest PLED is a thin film of PPV sandwiched between two electrodes. The anode (hole-injecting electrode) is a semitransparent, high work-function material such as indium tin oxide (ITO), whereas the cathode (electron-injecting electrode) is a low work-function metal such as Al, Ca, or Mg (Fig. 12).

Under an applied voltage in an LED, oppositely charged carriers (electron and holes) are injected into the emissive layers from the opposing contacts and are swept through the device by the high electric field. The efficiency for EL devices is measured by the number of photons emitted per electron injected. This number is called the internal efficiency and is based on the assumption that all light generated is received by the viewer. The external efficiency is a factor of $2n^2$ smaller than the internal efficiency (where n is the refractive index). Typical external efficiencies for LED devices are between 0.1 and 5% (268); normal luminous efficiencies for LEDs range from 1 to 10 lm/W (269,270), and quantum efficiencies are now greater than 10% (269). Such a single-layer device is called an EL diode because it shows nonlinear I–V characteristics typical of diodes.

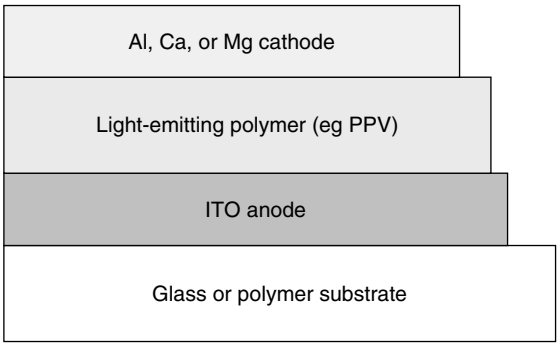

Fig. 12. Polymer LED.

The most studied of the PPV compounds are those containing at least one solubilizing alkoxy group (271–273); poly[(2-methoxy-5-(2-ethylhexyl)oxy-1,4-phenylene]vinylene (MEH-PPV) is most commonly used (274). The ability to fine-tune the color to produce red, green, and blue PLEDs has been demonstrated by appropriate functionalization of polymers (275–279), copolymerization (280–282), and blending (283–285). Several representative electroluminescent polymers covering the visible spectrum are shown in Table 3 (286–290).

In single-layer PLED devices the EL occurs mainly in the vicinity of the cathode because of the better mobility of the positive charges in conjugated polymers. The major drawback is the negative impact on luminance efficiency. To overcome this problem, two-layer devices have been investigated (291,292) in which the cathode and the EL polymer are separated by an electron-conducting/hole-blocking layer such as a polyoxadiazole (293). Multilayer devices made from several EL polymers have also been developed to emit white light (294,295). The enormous progress in developing materials with high purity, processibility (ink-jet techniques), and good thermal and oxidative stability has allowed commercialization of such devices by Epson, Philips, Toshiba, and UNIAX (296). Highly pure, undoped materials have been the primary focus for LEDs; doped polymers in such devices lead to a dramatic decrease in luminescence and device performance (297).

Light-emitting electrochemical cells (LECs) have received considerable interest because of the involvement of ionic species in the luminescent layer. LECs exhibit many unique features different from conventional LEDs (298). The principal idea behind the operation of an LEC is electrochemical doping to combine

Table 3. Light-Emitting Polymers Covering the Visible Spectrum

Polymer	Color (λ_{max}), nm
MEH-PPV	Red–orange (610)
CN-PPV	Red (710)
PT	Red (662)
PPV	Green (550)
PPP	Blue (459)

electrons and holes (forming a pn junction) *in situ*. An electrolyte provides the necessary ionic conductivity, allowing dopant ions to mix with the EAP. Under an applied electric field the electrons and holes interact to form excited species, which undergo radiative decay to emit light (299). Numerous examples of LECs are found in the literature (300,301), but slow response times (normally a second or longer) have limited the ability of LECs to compete with their LED counterparts (302–304).

Electrochromism. One of the most promising applications for EAPs is in electrochromic devices. Electrochromism, a reversible, reproducible spectral change that is produced electrochemically, results from changes in conjugation during the redox process. Until recently, the majority of research in this area has focused on inorganics, organometallics, and molecular organics (305–309), but developments in the area of EAPs have shifted the focus in recent years (310–313). EAPs are desirable substitutes for other types of electrochromic materials because EAPs typically switch much faster, they make good films, and their structures can be tailored to provide the desired color changes. Most work in electrochromics has focused on the ultraviolet and visible spectra; IR and RF electrochromics have also received attention.

Visible Electrochromics. Most EAPs exhibit UV–vis electrochromism, but not all exhibit significant optical contrast or switching stability for use in electrochromic devices. Polypyrrole switches reversibly between yellow in the neutral state and blue–black in the oxidized state, but contrast is poor in all but the thinnest films, and practical applications are limited (311). Polythiophene switches reversibly between red (neutral) and blue (oxidized), (313) while polyaniline switches very rapidly between four color states (yellow/green/blue/black). PANI switching stability is very good ($>10^6$ cycles) when switching is limited to the yellow–green transition, although this somewhat limits its potential applications (311).

With goals of additional color states, increased optical contrast, faster switching, and higher stability, recent research has looked at modifications of basic EAP structures. Incorporation of electron-donating substituents as in the PEDOT-based systems mentioned earlier lowers oxidation potentials and decreases band gaps while increasing the stability of oxidized polymers (314), and further incorporation of alkyl substituents tunes color and improves contrast without (in some cases) detracting from switching speeds (315). Carbazoles have been incorporated, providing multiple color transitions, fast switching, reasonable contrast, and high switching stability (316,317). Visible electrochromic applications for EAPs include smart windows, displays, automatically dimming rearview car mirrors (already commercially available), protective eyewear, and optical storage.

Infrared Electrochromics. While applications for visible electrochromics are widespread with many commercial possibilities, infrared (3–17 μm) electrochromics applications are limited. Disordered transition-metal oxides have been pursued because of their broad polaron absorption (318), but slow response times and processing difficulties have limited applications. As with most electrochromics applications, EAPs are attractive for IR electrochromics because of their rapid response times and ease of processing. Research to date in EAPs for IR electrochromics has focused on polyaniline-based (319–321) and poly(3,4-alkylenedioxythiophene)-based (322,323) systems. The

poly(3,4-alkylenedioxythiophene)-based devices exhibit improved contrast ratios over the PANI-based devices and good switching stability.

Microwave/Radio Frequency Electrochromics. In radio direction and ranging (radar) systems, electromagnetic waves are bounced off a target and collected by a receiver. The receiver analyzes the signal and determines the range, direction, and speed of the target. RF electrochromics function by absorbing the electromagnetic waves rather than reflecting them back to the receiver. RF electrochromics find use in commercial electromagnetic interference (EMI) shielding, and in law enforcement and military radar systems. EMI shielding materials (addressed below) are typically used in the conductive state only.

A number of studies on the microwave properties of EAPs have been published (324–328). EAP-coated textiles (329–331) and devices (332,333) have been explored for use in radio frequency applications.

Photovoltaics. The use of EAPs in the construction of plastic photovoltaic cells is another example of the versatility of these materials (334–336). Photovoltaic cells are constructed in a similar manner to single-layer PLEDs, but the photovoltaic cell transforms radiant energy into electricity (337,338). The most basic device construction consists of a conjugated polymer sandwiched between two working electrodes, usually Al and ITO. In devices this simple, the photoinduced charge generation is inefficient (339).

To improve these devices it is necessary to have an electron-accepting molecule in close proximity to the undoped conjugated polymer, which acts as an electron donor upon photoexcitation; a charge separation takes place because of photoinduced electron transfer. This process produces a stable charge storage configuration in which the polaron produced is highly delocalized and mobile. One of the best electron-accepting materials for this process is the fullerene molecule (C_{60}). The construction of photovoltaic cells using a combination of semiconducting polymer as the donor and molecular electron acceptor such as fullerene has been studied (340–344). Devices based on fullerenes and composite films of semiconducting polymer are known as "bulk-heterojunction" polymer photovoltaic cells. These devices have shown fast photoinduced charge transfer at the donor–acceptor interface. This results in a metastable charge-separated state. The interpenetrating network of both components consists of a large interfacial area and results in efficient charge generation. Photovoltaic power conversion efficiencies (η_e) of 2.5% under AM 1.5 illumination have been reported (345).

Organic Field Effect Transistors/Molecular Electronics. Organic field effect transistors (OFETS) and molecular electronics are two areas of intensive research for both academic and industrial institutions (346). The extensive research on these devices stems from their ability to be processed at low temperatures and from their compatibility with plastic substrates. Several applications of OFETs have been proposed, including smart cards (347), active matrix displays (348), and logic circuits (349). Both polymeric and oligomeric materials have been studied for use in OFETs because the properties can be tailored to vary the HOMO–LUMO gap; physical characteristics such as mechanical flexibility and processability are also advantageous (350).

Typical OFET construction is similar to that of inorganic FETs, which are a critical component of computer chips. The OFET device consists of electrodes (drain, gate, and source), a dielectric layer, and a semiconducting layer (Fig. 13).

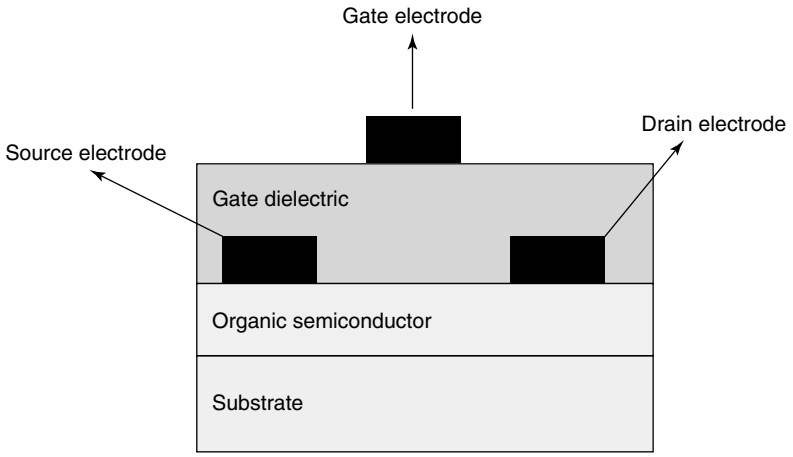

Fig. 13. OFET device.

The current flow between the drain and source electrodes is modulated by the applied gate voltage. When there is no voltage between the source and gate electrodes, the FET is in an insulating state. The device is activated by application of an electric field, resulting in charge carrier formation. These charge carriers can then move between source and drain; the charge carrier concentration can be controlled by small variations in the gate voltage. A crucial parameter in OFETs is the On/Off ratio, which is the ratio of conductivities with the gate voltage switched on and off (351). Highly purified and ordered layers of oligomers typically have charge carrier mobilities of between 0.1 and 0.2 $cm^2/(V \cdot s)$ (352), sufficient for most commercial applications.

Molecular electronics is an emerging field that proposes to replace wire, transistor, and other solid-state silicon components with conjugated, organic-based molecules of precise length and constitution (353). The main disadvantage of these systems is the difficulty of inducing three-dimensional order to allow for rapid charge transport (354,355). This fact currently limits their use as replacements in logic circuits and computing systems.

Nonlinear Optical Applications. Second-order nonlinear (NLO) materials based on EAPs have shown promise for use in the photonics industry; extensive research has been conducted in this area over the past several decades (356,357). Devices based on poly(diacetylene) have been used to demonstrate all-optical switching at 1.6 μm (358). The NLO process occurs when an electromagnetic field interacts with a medium. When the medium is subjected to an electric field $E(0)$ and an optical field $E(\omega)$, the nonlinear effect arises from field-induced modulation of the refractive index. This is known as the second-order NLO effect or the linear electrooptic (Pockels) effect. An NLO chromophore acts as the active molecular component that gives rise to the NLO property in π-conjugated polymers. These polymers typically consist of donor–acceptor (D-A) groups attached to a conjugated polymer backbone for increased charge transfer through π-electron

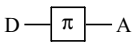

Fig. 14. Donor–acceptor groups attached to a conjugated polymer backbone.

delocalization (Fig. 14). The π-bridge system is very important in construction of the dye molecule; acetylenic and vinylic groups have been used extensively to construct such molecules (359,360).

Nonlinear optical materials are recognized as the key element for future photonic applications. Photonics, a technology that uses photons rather than electrons to carry information, offers several advantages over electronics. Advantages include larger bandwidths, faster response times, and less noise from extrinsic electromagnetic fields (361). Several approaches using EAPs for photonics applications have been reported (362).

Biomedical Applications. Electronic properties of EAPs are often very sensitive to small perturbations caused by exposure to chemical/biochemical analytes. This high degree of sensitivity and the variety of properties that are affected result in systems far superior to the conventional small molecule devices known as chemosensors (363). Surface charge characteristics are fundamental to cellular–biomaterial interactions (364); thus, the ability to control charge density in EAPs has led to promising biomedical applications in the areas of chemical/biological sensors, drug delivery, and for monitoring dynamic cell behavior. Applications of EAPs in tissue engineering and nerve regeneration are also promising, although little work has been published to date (365). Most of the biomedical applications of EAPs have focused on polypyrrole because of its proven stability in biological systems.

Chemical/Biological Sensors. EAPs are unique materials for coupling analyte–receptor interactions and nonspecific interactions into an observable response (366). Several EAP properties, including absorption and emission spectra as well as redox activity, are exploited for use in chemical and biological sensors. The band gap of EAPs yields efficient absorption or emission at the band edge, giving rise to a strong luminescence of the EAP. Fluorescence is widely used because of its high sensitivity (367), and because this method offers diverse transduction schemes based on changes in intensity, energy transfer, wavelength, and lifetime (368,369). Many sensors rely on the redox activity of EAPs; exposure to many analytes results in oxidation-state changes. These changes are manifested as changes in conductivity, which can easily be monitored. For a review of polymer-based chemical sensors, see reference 370.

Numerous examples are found in the literature of analyte detection using EAP systems. Arrays of EAPs are used in biomolecular recognition schemes, resulting in devices known as “electronic noses” and “electronic tongues” (371–373) that mimic the mammalian sensor receptors. EAPs functionalized to contain polyalkyl ether and crown ether moieties (374–378) or polymerized in the presence of polyelectrolyte dopants (379) have been used to detect a variety of ions (Li^+, Na^+, K^+, Ba^{2+}, Mg^{2+}, Cs^+, Zn^{2+}, Cu^+, $NR_4{}^+$) (see Fig. 15). EAPs have also been prepared with enantioselectivity toward chiral dopant ions (380,381) and functionalized for molecular recognition (382).

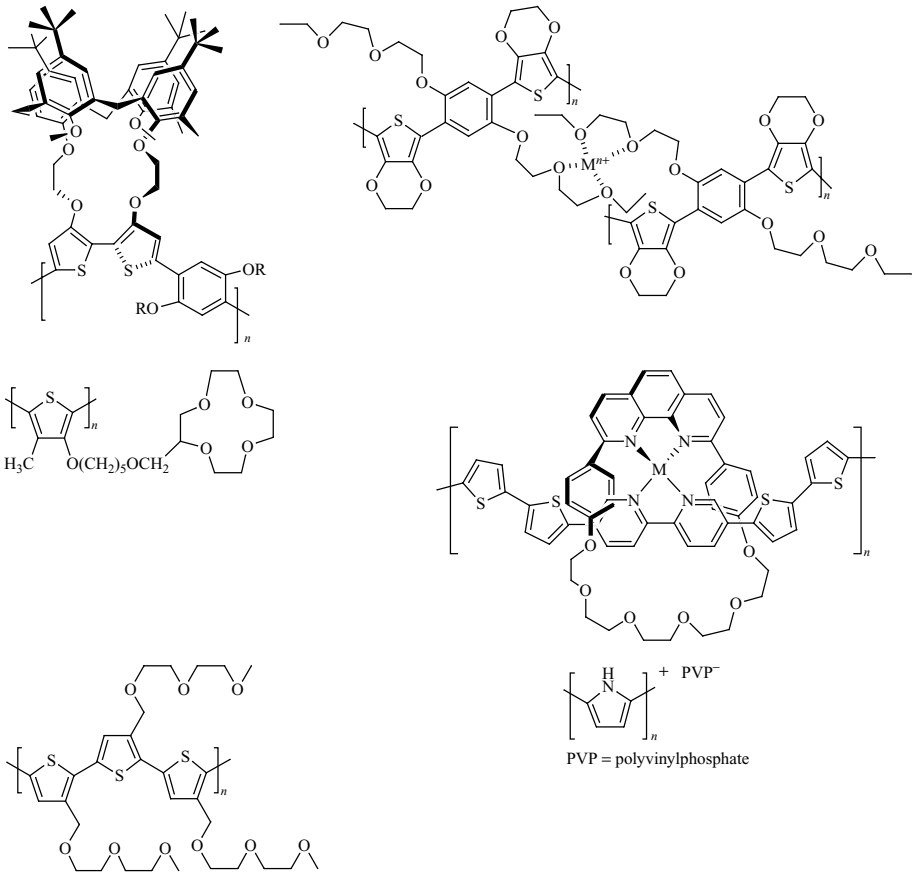

Fig. 15. EAPs functionalized with polyalkyl ether and crown ether moieties.

EAPs have proved to be effective at detection of small quantities of biomolecules, specifically in cancer detection and real-time monitoring of blood-borne analytes such as glucose and nucleic acids (383–389). These sensors employ EAPs containing natural biomolecular recognition units sometimes referred to as "biosensors." These biosensor moieties can be ligands, single strands of DNA, enzymes, antibodies, or synthetic proteins that can detect whole cells or individual proteins (390–392).

Drug Delivery. One very promising application for EAPs is in the area of drug delivery. This method takes advantage of the swelling and deswelling that occur in EAPs during the redox process. Bioactive molecules such as dopamine (393–395) and ATP (396–398) can be reversibly trapped in the polymer during polymerization or polymer oxidation and then released during reduction of the polymer. Such systems could conceivably be used in conjunction with biosensors as electroresponsive membranes, delivering small quantities of medicines as needed.

Dynamic Cell Behavior. While not as well-explored as sensors and drug delivery systems, dynamic cell behavior can also be investigated using EAPs.

Cell motility, motion, and proliferation can be monitored. For example, DNA-functionalized EAPs can be used to monitor genetic mutations (399). Direct detection of DNA hybridization has been accomplished with a functionalized polypyrrole (400).

Membranes for Gas Separation and Ion Exchange. As a result of the volume changes that occur as part of the redox process, EAPs undergo reversible changes in porosity. This interesting effect has led to studies of EAP membranes for separation of gases and liquids. Water permeability of PANI and PPy is much higher in the doped state than in the neutral state (401). Gas separation has been demonstrated with EAPs (402–404), and ion permselectivity has also been observed (405).

Batteries/Supercapacitors. Electrochemical charge storage systems (batteries and supercapacitors) are currently employed in a wide variety of applications (14); there is a constant demand for performance improvements and reduced environmental impact. Redox-active polymers are promising materials for use in batteries and supercapacitors because of their high gravimetric and volumetric charge capacities, fast charge/discharge rates, robustness, environmentally friendly nature, and lower costs relative to noble metal oxides (406–408).

Battery designs using electroactive polymers feature the EAP as the cathode, which is separated from an anode (such as Li, Na, Mg, and Zn) by an electrolyte. Normally, high specific energies of up to 3.5 V can be obtained (409). EAPs that have been used in rechargeable batteries include polyacetylene-, PANI-, PPy-, PT-, and PPP-based materials (410). The current drawback to full utilization of EAPs for rechargeable batteries is the rate limitations associated with low ionic mobilities of the polymers as well as the electrolytes (14).

Electroactive polymers have also been investigated for use in supercapacitors. These devices provide a higher power density than batteries at a lower operating voltage. Supercapacitors have a higher energy density than traditional capacitors because of the high capacitance of the electrode materials (411). Target applications are as computer memory backup, peak power for electric vehicles, and burst power for military platforms. Ruthenium oxide, the most promising inorganic supercapacitor material, exhibits capacitance values up to 720 F/g (412). EAP-based supercapacitors, which are expected to be less expensive than those based on metal oxides, exhibit capacitance values up to 350 F/g (413); further research is expected to increase this value considerably. Most EAP-based supercapacitors combine one or two p-dopable polymers (type I and type II supercapacitors, respectively); devices based on polypyrrole (414), polythiophenes (413,415), polyaniline (416), and poly(3,4-ethylenedioxythiophene) (417,418) have been investigated. Type III supercapacitors, those combining a p-dopable and an n-dopable polymer, could theoretically yield higher energy and power densities and operate at higher voltages than type I or type II supercapacitors (419). However, type III supercapacitors are currently plagued with long-term stability issues related to instability of the n-doped polymers.

Conductive Coatings for Electromagnetic Shielding and Static-Dissipating Applications. In addition to the RF electrochromics research discussed above, EAPs are also used as conductive coatings on textiles for radar-absorbing materials (RAMs) (420). Polypyrrole and PANI are both examples of EAPs used in composite formulations as RAMs (420,422).

Electromagnetic interference (EMI) shielding has become increasingly important because of the combination of increasing number of electrical systems (vehicles, computers, etc) and the increasing use of microwaves in advanced navigation and domestic appliances. Traditional EMI shielding has involved incorporation of conductive fillers (metal particles, conducting carbon black, or graphite fibers) into plastic housing materials (423,424); poor mechanical properties (328) and poor reproducibility of performance characteristics are the major drawbacks of these composite systems (324). EAPs do not necessarily suffer from these problems and have therefore been investigated as replacements for these filled materials (326), although mechanical instability of many EAPs of interest has led to the use of EAPs blended with non-conductive polymers (324,328,425).

The need for improved static control or electrostatic discharge materials poses a challenge for materials scientists and engineers (426). The protection of sensitive electronic devices requires an environment in which unwanted electrical charges, voltages, and electric fields are dissipated. The bulk of electronic packaging requires an insulating material that is clear, durable, and inexpensive. Insulating plastics are widely used as structural materials for the packaging industry, and static charge often builds up; the accumulated charge must be dissipated as rapidly as it is formed, and so conductive additives are required. Static-dissipating materials should have resistivities between 10^6 and 10^9 Ω/sq, and they should be transparent and durable even under extreme conditions (427).

The cheapest and most-often-employed materials have been polymer blends or composites containing carbon black as filler (428,429). However, high loading levels of conductive fillers are often required, leading to significant decreases in durability and transparency. In these cases, the use of EAPs, either as coatings or as fillers, is becoming more common (426).

EAPs are currently used as additives and melt processed with conventional resins such as polyethylene to form static-control articles such as films and trays (430). EAP coatings are also used in the production of static-dissipating carpets (431) and fabrics (432). Recently, EAP coatings have been shown to dissipate static in energetic materials more effectively than carbon black additives, providing a much-needed safety feature for the handling and storage of energetic materials (433).

Actuators. Inorganic piezoelectric and electrostrictive materials have shown a major technological role in converting electrical energy to mechanical energy in actuators. However, electroactive polymers offer several unique advantages over inorganic materials, including large dimensional changes, high stress generation, high work capacity per cycle, ease of fabrication, and low cost (434).

Numerous electroactive polymers, including polythiophenes, polypyrrole, poly(*p*-phenylene vinylene)s, poly(*p*-phenylene)s, and polyaniline, have shown significant dimensional changes upon doping and dedoping (435–440). These dimensional changes result from changes in the volume required to accommodate anions, cations, and/or cointercalating solvent species. Volume changes ranging from 0.1 to 10% are normally observed with doping (441).

This unique behavior has been exploited for applications including controlled release (discussed above) and electrochemically driven actuators.

EAP-based actuators have been explored for use in artificial muscle fibers (AMFs) (442–444) and microelectromechanical systems (MEMS) (437). Non-conductive polymeric gel systems have been used for several decades as actuator devices (445–447); but with low elastic modulus and low yield strength, applications of gel-based actuators are very limited. Gel-based actuators offer one significant advantage over EAPs in that their volume changes can exceed a factor of a thousand (448).

Corrosion Inhibition. EAPs have been investigated over the past decade as corrosion-inhibiting materials (449). The most extensively studied of the EAPs for corrosion prevention has been PANI (450–452). Researchers at Los Alamos National Laboratory (LANL) and the NASA Kennedy Space Center demonstrated that doped PANI coatings inhibited corrosion of carbon steel (451). Their tests were conducted in a 3.5 wt% NaCl/0.1 *M* HCl environment using ca 0.005-cm-thick films of PANI doped with *p*-toluenesulfonic acid on carbon steel; the PANI was covered with an epoxy topcoat. The PANI/epoxy coating performed significantly better than the epoxy topcoat alone. These initial results were used by researchers at LANL–NASA to develop EAP coatings to resist the corrosive effects of acid vapor generated during space shuttle launches. Their approach was based on earlier work suggesting that the interfacial contact between the metal and a doped EAP would generate an electric field that would restrict the flow of electrons from the metal to an outside oxidizing species, thus preventing and/or reducing corrosion (453).

There have been numerous reports in the literature regarding the use of EAPs in retarding corrosion on steel alloys (454,455). There is still debate on whether the doped or undoped form of PANI provides the best corrosion protection; several reports have shown that the undoped form of PANI can perform as well as or better than the doped form of PANI (456,457).

While there is general agreement that PANI performs well in retarding corrosion on carbon steel, the mechanism for this process is still under investigation. Several hypotheses are suggested for corrosion protection using EAPs: (*1*) PANI contributes to the formation of an electric field at the metal surface, restricting the flow of electrons from metal to oxidant; (*2*) PANI forms a dense, strongly adhering, low porosity film similar to a barrier coating; and (*3*) PANI causes the formation of protective layers of metal oxides on a metal surface.

While PANI has been extensively studied for corrosion control, its major drawback is its pH dependence. It works very well in acidic environments because of the formation of the conductive emeraldine salt, but at higher pH (>7) the non-conductive emeraldine base is formed, and the material no longer provides adequate protection against corrosion. Thus, use in a marine environment (pH $\sim$ 8) is not possible.

For marine applications, pH-stable EAPs have been investigated. Double-stranded PANI has been coated onto Al alloys (458); immersion tests in simulated seawater showed improved corrosion resistance as compared to control samples (epoxy coating) (459). Recently, poly(bis-dialkylamino)phenylene vinylene) (BAM-PPV) was shown to adhere to Al alloy in an immersion test using simulated seawater (pH $\sim$ 8) to retard corrosion (460,461). Quantitative evidence was obtained to show corrosion inhibition as compared to noncoated Al alloys.

Summary

The reversible addition or removal of electrons from the backbones of electrically active polymers is accompanied by significant changes in their physical and chemical properties. The ability to reversibly switch EAPs between insulating and conducting, opaque and transparent, absorptive and emissive, and expanded and contracted drives much of the current research. EAP properties are strongly dependent on polymer structure; the ability to tailor these properties through thoughtful synthetic methods facilitates the development of new devices to meet the increasing demands of today's society. Industry has already achieved success with commercial devices that utilize EAPs. Attempts to increase stability and to better understand structure–property relationships are crucial to the development of materials for new and improved applications.

BIBLIOGRAPHY

"Electrically Conductive Polymers" in *EPSE* 2nd ed., Vol. 5, pp. 462–507, by Jane E. Frommer and Ronald R. Chance, Allied-Signal Corporation.

1. H. Shirakawa, E. Louis, A. MacDiarmid, and A. Heeger, *Chem. Commun.* 578 (1977).
2. A. G. MacDiarmid and A. J. Heeger, *Synth. Met.* **1**, 1013 (1978).
3. J. L. Bredas, S. R. Marder, and W. R. Salaneck, *Macromolecules* **35**(4), 1 (2002).
4. B. Ranby, in W. R. Salaneck, I. Lundstrom, and B. Ranby, eds., *Conjugated Polymers and Related Materials: The Interconnection of Chemical and Electronic Structures*, Oxford University Press, Oxford, 1993, Chapt. "3".
5. R. H. Norman, *Conductive Rubbers and Plastics*, Elsevier, Amsterdam, 1970.
6. E. K. Sichel, ed., *Carbon Black Polymer Composites*, Marcel Dekker, Inc., New York, 1982.
7. S. K. Bhattacharya, *Metal-Filled Polymers: Properties and Applications*, Marcel Dekker, Inc., New York, 1986.
8. W. M. Wright and G. W. Woodham, in J. M. Margolis, ed., *Conductive Polymers and Plastics*, Chapman and Hall, New York, 1989.
9. K.-M. Jager, D. H. McQueen, I. A. Tchmutin, N. G. Ryvkina, and M. Kluppel, *J. Phys. D: Appl. Phys.* **34**, 2699 (2001).
10. A. Eisenberg, *Ion-Conducting Polymers*, Academic Press, Inc., New York, 1977.
11. A. Eisenberg and J.-S. Kim, *Introduction to Ionomers*, John Wiley & Sons, Inc., New York, 1998.
12. J. R. MacCallum and C. A. Vincents, eds., *Polyelectrolytes*, Elsevier, New York, 1989.
13. J. Owen, in C. Booth and C. Price, eds., *Comprehensive Polymer Science: The Synthesis, Characterization, Reactions, and Applications of Polymers*, Vol. **2**, Pergamon Press, Oxford, 1989, Chapt. "21".
14. P. Novak, K. Muller, K. S. V. Santhanam, and O. Haas, *Chem. Rev.* **97**, 207 (1997).
15. F. B. Dias, L. Plomp, and J. B. J. Veldhuis, *J. Power Sources* **88**, 169 (2000).
16. C. Heitner-Wirguin, *J. Membr. Sci.* **120**, 1 (1996).
17. G. Inzelt, M. Pineri, J. W. Schultze, and M. A. Vorotyntsev, *Electrochim. Acta* **45**, 2403 (2000).
18. A. J. Heeger and J. Long Jr. *Opt. Phot. News* p. 24, August 1996.
19. D. O. Cowan and F. M. Wiygul, *Chem. Eng. News*, **28**, July 21, 1986.
20. H. Akamatu, H. Inokutchi, and Y. Matsunaga, *Nature* **173**, 168 (1954).
21. A. H. Hermann and A. Rembaum, *J. Polym. Sci., C* 109 (1967).

22. H. Block, S. M. Bowker, and S. M. Walker, *Polymer* **19**, 531 (1978).
23. J. Mort, S. Grammatica, D. J. Sandman, and A. Troup, *J. Electron. Mater.* **9**, 411 (1980).
24. U.S. Pat. 5,549,851 (1996), M. Fukushima, M. Aramata, and S. Mori (to Shin-Etsu Chemical Co. Ltd.).
25. B. R. Hsieh and Y. Wei, in B. R. Hsieh and Y. Wei, eds., *Semiconducting Polymers: Aplications, Properties and Synthesis* (ACS Symposium Series 735) American Chemical Siciety, Washington, D.C., 1999, Chapt. "1".
26. R. S. Kohlman, J. Joo, and A. J. Epstein, in J. E. Mark, ed., *Physical Properties of Polymers Handbook*, API Press, Woodbury, N.Y., 1996, p. 453.
27. A. J. Epstein, *MRS Bull.* **22**(6), 16 (1997).
28. G. Wegner, *Angew. Chem., Int. Ed. Engl.* **20**, 361 (1981).
29. K. J. Wynne and G. B. Street, *I&EC Prod. Res. Dev.* **21**, 23 (1982).
30. R. L. Greene and G. B. Street, *Science* **226**, 651 (1984).
31. J. R. Reynolds, *J. Mol. Elec.* **2**, 1 (1986).
32. A. J. Epstein, in T. A. Skotheim, ed., *Handbook of Conducting Polymers*, Vol. **2**, Marcel Dekker, Inc., New York, 1986, p. 1041.
33. J. R. Reynolds, *CHEMTECH* **18**, 440 (1988).
34. J. R. Reynolds and M. Pomerantz, in T. A. Skotheim, ed., *Electroresponsive Molecular and Polymeric Materials*, Marcel Dekker, Inc., New York, 1991.
35. J. Heinze, *Top. Curr. Chem.* **152**, 1 (1990).
36. J. D. Stenger-Smith, *Prog. Polym. Sci.* **23**, 57 (1998).
37. D. Kumar and R. C. Sharma, *Eur. Polym. J.* **34**, 1053 (1998).
38. A. J. Heeger, *J. Phys. Chem. B.* **105**, 8475 (2001).
39. B. Wessling, *Chem. Innov.* **31**(1), 34 (2001).
40. A. Pron and P. Rannou, *Prog. Polym. Sci.* **27**, 135 (2002).
41. R. A. Pethrick, in R. Arshady, ed., *Desk Reference of Functional Polymers*, American Chemical Society, Washington, D.C., 1997, Chapt. "3.4".
42. T. A. Skotheim, R. L. Elsenbaumer, and J. R. Reynolds, eds., *Handbook of Conducting Polymers*, 2nd ed., Marcel Dekker, Inc., New York, 1998.
43. P. C. Searson and T. P. Moffit, *Crit. Rev. Surf. Chem.* **3**(3/4), 171 (1994).
44. G. P. Evans, in H. Gerischer and C. W. Tobias, eds., *Advances in Electrochemical Science and Engineering*, Vol. **1**, VCH Publishers, New York, 1990, Chapt. "1".
45. D. Chen, M. J. Winokur, Y. Chao, A. J. Heeger, and F. E. Karasz, *Phys. Rev. B: Condens Metter.* **45**, 2035 (1992).
46. G. Natta, G. Mazzanti, and P. Corradini, *Atti. Acad. Naz. Lincei, Cl. Sci. Fis. Mat. Nat. Rend.* **25**(8), 3 (1958).
47. L. B. Luttinger, *J. Org. Chem.* **27**, 1591 (1962).
48. A. A. Ovchinnikov, I. I. Ukrainskii, and G. V. Kventsel, *Sov. Phys. Usp.* **15**, 575 (1973).
49. T. Ito, H. Shirakawa, and S. Ikeda, *J. Polym. Sci., Polym. Chem. Ed.* **12**, 11 (1974).
50. C. K. Chiang, C. R. Fincher Jr., Y. W. Park, A. J. Heeger, H. Shirakawa, E. J. Louis, S. C. Gau, and A. G. MacDiarmid, *Phys. Rev. Lett.* **39**, 1098 (1977).
51. J. W. Chien, *Polyacetylene: Chemistry, Physics, and Materials Science*, Academic Press, Inc., Orlando, Fla., 1984.
52. H. G. Kiess, ed., *Conjugated Polymers*, Kluwer Academic Publishers, Dordrecht, 1991.
53. H. Shirakawa, in Ref. 42, Chapt. 7.
54. H. Shirakawa and S. Ikeda, *J. Polym. Chem. Chem. Ed.* **12**, 929 (1974).
55. G. Lieser, G. Wegner, W. Muller, and V. Enkelmann, *Makromol. Chem., Rapid Commun.* **1**, 621 (1980).
56. M. Aldissi, C. Linaya, J. Sledz, F. Schue, L. Giral, J. M. Fabre, and M. Rolland, *Polymer* **23**, 243 (1982).
57. V. M. Kobryanskii, *Synth. Met.* **46**, 251 (1992).
58. F. Cataldo, *Polym. Commun.* **33**, 3073 (1992).

59. S.-A. Chen and H.-J. Shy, *J. Polym. Sci., Polym. Chem. Ed.* **23**, 2441 (1985).
60. V. Rives-Arnau and N. Sheppard, *J. Chem. Soc., Faraday Trans. 1* **76**, 394 (1980).
61. N. Kurokawa, M. Tabata, and J. Sohma, *J. Polym. Sci., Polym. Lett. Ed.* **19**, 355 (1985).
62. K. Soga, Y. Kobayashi, S. Ikeda, and K. Kawakami, *J. Chem. Soc., Chem. Commun.* 931 (1980).
63. Y. Tabata, B. Saito, H. Shibano, H. Sobue, and K. Oshima, *Makromol. Chem.* **76**, 89 (1964).
64. K. Aoki, Y. Kakudate, S. Usuba, M. Yoshida, K. Tanaka, and S. Fujiwara, *Solid State Commun.* **64**, 1329 (1987).
65. J. H. Edwards and W. J. Feast, *Polym. Commun.* **21**, 595 (1980).
66. J. H. Edwards, W. J. Feast, and D. C. Bott, *Polymer* **25**, 395 (1984).
67. T. M. Swager, D. A. Dougherty, and R. H. Grubbs, *J. Am. Chem. Soc.* **110**, 2973 (1988).
68. S. Shibahara, M. Yamane, K. Ishikawa, and H. Takezoe, *Macromolecules* **31**, 3756 (1998).
69. N. Coustel, N. Foxonet, J. L. Ribet, P. Bernier, and J. E. Fischer, *Macromolecules* **24**, 5867 (1991).
70. H. Shirakawa, T. Otaka, G. Piao, K. Akagi, and M. Kyotani, *Synth. Met.* **117**, 1 (2001).
71. S. M. Karim, R. Nomura, and T. Masuda, *J. Polym. Sci., Part A : Polym. Chem.* **39**, 3130 (2001).
72. J. W. Y. Lam, J. Luo, Y. Dong, K. K. L. Cheuk, and B. Z. Tang, *Macromolecules* **35**, 8288 (2002).
73. H. Z. Chen, R. S. Xu, Q. Sun, J. W. Y. Lam, M. Wang, and B. Z. Tang, *Polym. Adv. Technol.* **11**, 442 (2000).
74. K. Kanki, Y. Misumi, and T. Masuda, *J. Polym. Sci., Polym. Chem. Ed.* **40**, 1075 (2002).
75. S. Subramanyam, M. S. Chetan, and A. Blumstein, *Macromolecules* **26**, 3212 (1993).
76. M. Lonergan, C. H. Cheng, B. L. Langsdorf, and X. Zhou, *J. Am. Chem. Soc.* **124**, 690 (2002).
77. K. Lino, H. Goto, K. Akagi, H. Shirakawa, and A. Kawaguchi, *Synth. Met.* **84**, 967 (1997).
78. S. Koltzenburg, F. Stelzer, and O. Nuyken, *Macromol. Chem. Phys.* **200**, 821 (1999).
79. D. G. H. Ballard, A. Courtis, I. M. Shirley, and S. C. Taylor, *Macromolecules* **21**, 294 (1988).
80. P. Kovacic and M. B. Jones, *Chem. Rev.* **87**, 357 (1987).
81. A. D. Schluter, in Ref. 42, p. 209.
82. T. Yamamoto, Y. Hayashi, and A. Yamamoto, *Bull. Chem. Soc. Jpn.* **51**, 2091 (1978).
83. T. Yamamoto, A. Morita, Y. Miyazaki, T. Maruyama, H. Wakayama, Z. Zhou, Y. Nakamura, T. Kanbara, S. Sasaki, and K. Kubota, *Macromolecules* **25**, 1214 (1992).
84. J.-F. Fauvarque, M.-A. Petit, and A. Digua, *Makromol. Chem.* **188**, 1833 (1987).
85. M. Rehahn, A. D. Schluter, and G. Wegner, *Makromol. Chem.* **191**, 1991 (1990).
86. M. Kreyenschmidt, R. Uckert, and K. Mullen, *Macromolecules* **28**, 4577 (1995).
87. M. Ueda, T. Abe, and H. Awano, *Macromolecules* **25**, 5125 (1992).
88. R. Zhang, H. Zheng, and J. Shen, *Macromolecules* **29**, 7627 (1996).
89. M. Rehahn, A. D. Schluter, and W. J. Feast, *Synthesis* 386 (1988).
90. A. D. Schluter, *J. Polym. Sci., Part A: Polym. Chem.* **39**, 1533 (2001).
91. C. S. Marvel and G. E. Hartzell, *J. Am. Chem. Soc.* **81**, 448 (1959).
92. P. E. Cassidy, C. S. Marvel, and S. Ray, *J. Polym. Sci., Part A: Polym. Chem.* **3**, 1553 (1965).
93. D. G. H. Ballard, A. Courtis, I. M. Shirley, and S. C. Taylor, *J. Chem. Soc., Chem. Commun.* 954 (1983).
94. T. Okada, T. Ogata, and M. Ueda, *Macromolecules* **29**, 7645 (1996).
95. N. Toshima and S. Hara, *Prog. Polym. Sci.* **20**, 155 (1995).
96. R. D. McCullough and P. C. Ewbank, in Ref. 42, Chapt. 9.

97. A. Angeli, *Gazz. Chim. Ital.* **46**, 279 (1916).
98. A. Deronzier and J.-C. Moutet, *Acc. Chem. Res.* **22**, 249 (1989).
99. H. S. Nalwa, J. G. Rabe, W. F. Schmidt, and L. R. Dalton, *Makromol. Chem., Rapid Commun.* **7**, 533 (1986).
100. H. S. Nalwa, *Mater. Sci.* **27**, 210 (1992).
101. M. Salmon, K. K. Kanazawa, A. F. Diaz, and M. Kournbi, *J. Polym. Sci., Polym. Lett. Ed.* **20**, 187 (1982).
102. J. W. Loveland and G. R. Dimeler, *Anal. Chem.* **33**, 1196 (1961).
103. S. Rapi, V. Bochi, and G. P. Gardini, *Synth. Met.* **24**, 217 (1988).
104. Y. A. Bubitsky, B. A. Zhubanov, and G. G. Maresch, *Synth. Met.* **41–43**, 373 (1991).
105. V. Bocchi and G. P. Gardini, *J. Chem. Soc. Chem. Commun.* 148 (1986).
106. S. Machida and S. Miyata, *Polym. Prepr. Jpn.* **36**, 1886 (1987).
107. N. Ono, H. Hironaga, K. Simizu, K. Ono, K. Kuwano, and T. Ogawa, *J. Chem. Soc., Chem. Commun.* 1019 (1994).
108. A. Deronzier, and J.-C. Moutet, *Acc. Chem. Res.* **22**, 249 (1989).
109. N. Ono, C. Tsukamara, Y. Nomura, H. Hironaga, T. Murashima, and T. Ogawa, *Adv. Mater.* **9**(2), 149 (1997).
110. K. E. Geckeler, N. Arsalani, and B. L. Rivas, *Macromol. Rapid Commun.* **18**, 503 (1997).
111. J. Rodriguez, H.-J. Grande, and T. F. Otero, in H. S. Nalwa, ed., *Handbook of Organic Conducting Molecules and Polymers*, Vol. **2**, John Wiley & Sons, Inc., New York, 1997, Chapt. "10".
112. M. Zhou and J. Heinze, *J. Phys. Chem. B* **103**, 8443 (1999).
113. K. M. Cheung, D. Bloor, and G. C. Stevens, *Polymer* **29**, 1709 (1988).
114. J. Joo, J. K. Lee, S. K. Lee, K. S. Jang, E. J. Oh, and A. J. Epstein, *Macromolecules* **33**, 5131 (2000).
115. F. Wudl, M. Kobayashi, and A. J. Heeger, *ACS Polym. Prepr.* **25**(2), 257 (1984).
116. M. Pomerantz, J. J. Tseng, H. Zhu, S. J. Sproull, J. M. Reynolds, R. Uitz, and H. J. Arnott, *Synth. Met.* **41–43**, 825 (1991).
117. M. D. McClain, D. A. Whittington, D. J. Mitchell, and M. D. Curtis, *J. Am. Chem. Soc.* **117**, 3887 (1995).
118. R. D. McCullough, *Adv. Mater.* **10**, 93 (1998).
119. R. D. McCullough, S. Tristam-Nagle, S. P. Williams, R. D. Lowe, and M. Jayaraman, *J. Am. Chem. Soc.* **115**, 4910 (1993).
120. T.-A. Chen, X. Wu, and R. D. Rieke, *J. Am. Chem. Soc.* **117**, 233 (1995).
121. E. E. Havinga and L. W. van Horssen, *Makromol. Chem., Makromol. Symp.* **24**, 67–76 (1989).
122. R. Danieli, P. Ostoja, M. Tiecco, R. Zamboni, and C. Taliani, *J. Chem. Soc., Chem. Commun.* 1473 (1986).
123. J. A. Irvin and J. R. Reynolds, *Polymer* **39**, 2339 (1998).
124. J. P. Ferraris and D. J. Guerrero, in Ref. 42 Chap 10.
125. R. D. McCullough and R. D. Lowe, *J. Chem. Soc., Chem. Commun.* 70 (1992).
126. R. D. McCullough, R. D. Lowe, M. Jayaraman, and D. L. Anderson, *J. Org. Chem.* **58**, 904 (1993).
127. R. D. McCullough, R. D. Lowe, M. Jayaraman, P. C. Ewbank, D. L. Anderson, and S. Tristam-Nagle, *Synth. Met.* **55**, 1198 (1993).
128. R. D. McCullough, S. P. Williams, S. Tristram-Nagle, M. Jayaraman, P. C. Ewbank, and L. Miller, *Synth. Met.* **67**, 279 (1995).
129. R. S. Loewe, P. C. Ewbank, J. Liu, L. Zhai, and R. D. McCullough, *Marcomolecules* **34**, 4324 (2001).
130. R. S. Loewe, S. K. Khersonsky, and R. D. McCullough, *Adv. Mater.* **3**, 250 (1999).
131. X. Wu, T.-A. Chen, and R. D. Reike, *Macromoleclues* **28**, 2101 (1995).

132. T.-A. Chen, R. A. O'Brian, and R. D. Rieke, *Macromolecules* **26**, 3462 (1993).
133. V. N. Kalinin, *Synthesis* 413 (1992).
134. J. P. Ferraris and M. D. Newton, *Polymer* **33**, 391 (1992).
135. G. Zotti, M. C. Gallazi, G. Zerbil, and S. V. Meille, *Synth. Met.* **73**, 217 (1995).
136. M. Berggren, O. Inganas, G. Gustafsson, J. Rasmusson, M. R. Anderson, T. Hjertberg, and O. Wennerstrom, *Nature* **372**, 444 (1994).
137. M. Zagorska and B. Krische, *Polymer* **31**, 1379 (1990).
138. J. R. Reynolds, J. P. Ruiz, A. D. Child, K. Nayak, and D. S. Marynick, *Macromolecules* **24**, 678 (1991).
139. M. Leclerc and D. Daost, *Synth. Met.* **41**, 529 (1991).
140. L. Groenendaal, F. Jonas, D. Freitag, H. Pielartzik, and J. R. Reynolds, *Adv. Mater.* **12**, 481 (2000).
141. G. A. Sotzing, J. R. Reynolds, A. R. Katritzky, J. Soloducho, and R. Musgrave, *Polym. Mater. Sci. Eng.* **72**, 317 (1995).
142. G. Sotzing and J. R. Reynolds, *J. Chem. Soc., Chem. Commun.*, 703 (1995).
143. M. Leclerc and G. Daoust, *Chem. Commun.* 273 (1990).
144. D. Fichou, ed., *Handbook of Oligo- and Polythiophenes*, Wiley-VCH, Weinheim, Germany, 1999.
145. J. R. Reynolds, A. D. Child, J. P. Ruiz, S. Y. Hong, and D. S. Marynick, *Macromolecules* **26**, 2095 (1993).
146. K. Yoshino, K. Tanaka, and T. Yamabe, *Jpn. J. Appl. Phys.* **23**, L899 (1984).
147. G. Tourillon and F. Garnier, *J. Electroanal. Chem.* **135**, 173 (1982).
148. K. K. Kanazawa, A. F. Diaz, G. P. Gardini, W. D. Gill, P. M. Grant, J. F. Kwak, and G. B. Street, *Synth. Met.* **1**, 329 (1980).
149. E. T. Kang and K. G. Neoh, *Eur. Polym. J.* **23**, 719 (1987).
150. F. Tedjar, *Eur. Polym. J.* **21**, 317 (1985).
151. G. Zotti, G. Schiavon, N. Comisso, A. Berlin, and G. Pagani, *Synth. Met.* **36**, 337 (1990).
152. M. J. Gonzalez-Tejera, I. Carrillo, and I. Hernandez-Fuentes, *Synth. Met.* **73**, 135 (1995).
153. X. Wan, F. Yan, S. Jun, X. Liu, and G. Xue, *Chem. Mater.* **11**, 2400 (1999).
154. J. K. Politis, J. C. Nemes, and M. D. Curtis, *J. Am. Chem. Soc.* **123**, 2537 (2001).
155. S. Glenis, M. Benz, E. Legoff, J. L. Schindler, C. R. Kannewurf, and M. G. Kanatzidis, *J. Am. Chem. Soc.* **115**, 12519 (1993).
156. R. N. McDonald and T. W. Campbell, *J. Am. Chem. Soc.* **82**, 4669 (1960).
157. D. F. Hoeg, D. I. Lusk, and E. P. Goldberg, *J. Polym. Sci., Part B: Polym. Lett.* **2**, 687 (1964).
158. I. Moritani, T. Nagai, and Y. Shirota, *Kogyo Kagaku Zasshi* **68**, 296 (1965).
159. M. Rehahn and A. D. Schulter, *Macromol. Chem Rapid Commun.* **11**, 375 (1990).
160. U.S. Pat. 3,404,132 (1968), R. A. Wessling and R. G. Zimmerman (to The Dow Chemical Company).
161. U.S. Pat. 3,532,643 (1970), R. A. Wessling and R. G. Zimmerman (to The Dow Chemical Company).
162. R. A. Wessling, *J. Polym. Sci., Polym. Symp.* **72**, 55 (1985).
163. D. R. Gagnon, J. D. Capistran, F. E. Karasz, and R. W. Lenz, *Polymer* **28**, 567 (1987).
164. J. B. Schlenoff and L.-J. Wang, *Macromolecules* **24**, 6653 (1991).
165. R. O. Garay, F. E. Karasz, and R. W. Lenz, *J. Macromol. Sci., Pure Appl. Chem., A* **32**, 905 (1995).
166. K.-J. Moon, K.-S. Lee, and H.-K. Shim, *Synth. Met.* **71**, 1719 (1995).
167. S. Hoger, J. J. McNamara, S. Schricter, and F. Wudl, *Chem. Mater.* **6**, 171 (1994).
168. I.-N. Kang, G-J. Lee, D.-H. Kim, and H.-S. Kim, *Polym. Bull.* **33**, 89 (1994).
169. J.-I. Kim, C.-K. Park, and H.-K. Shim, *J. Polym. Sci., Part A: Polym. Chem.* **29**, 93 (1991).

170. J. D. Stenger-Smith, A. P. Chafin, and W. P. Norris, *J. Org. Chem.* **59**, 6107 (1994).
171. I. D. Parker and H. H. Kim, *Appl. Phys. Lett.* **64**, 1774 (1994).
172. H. G. Gilch and W. L. Wheelwright, *J. Polym. Sci., Part A: Polym. Chem.* **4**, 1337 (1966).
173. P. L. Burn, D. D. C. Bradley, A. R. Brown, R. H. Friend, and A. B. Holmes, *Synth. Met.* **41–43**, 261 (1991).
174. M. Pan, A. Bao, and L. Yu, *Macromolecules* **28**, 5151 (1995).
175. Z. Bao, Y. Chen, and L. Yu, *Macromolecules* **27**, 4629 (1994).
176. Y. Liu, P. M. Lahti, and F. La, *Polymer* **39**, 5241 (1998).
177. I. K. Spiliopoulos and J. A. Mikroyannidis, *Macromolecules* **35**, 2149 (2002).
178. F. Wudl, P.-M. Allemand, G. Srdanov, Z. Ni, and D. McBranch, in S. R. Marder, J. E. Sohn, and G. D. Stucky, eds., *Materials for Nonlinear Optics: Chemical Perspectives*, American Chemical Society, Washington, D.C., 1991, p. 683.
179. K.-Y. Jen, M. Maxfield, L. W. Shacklette, and R. L. Elsenbaumer, *J. Chem. Soc., Chem. Commun.* 309 (1987).
180. S. Yamada, S. Tokito, T. Tsutsui, and S. Saito, *J. Chem. Soc., Chem. Commun.* 1448 (1987).
181. C. J. Yang and S. A. Jenekhe, *Macromolecules* **28**, 1180 (1995).
182. H.-K. Shim, R. W. Lenz, and J.-I. Jin, *Makromol. Chem.* **190**, 389 (1989).
183. H. Letheby, *J. Chem. Soc.* **15**, 161 (1862).
184. F-L. Lu, F. Wudl, M. Nowak, and A. J. Heeger, *J. Am. Chem. Soc.* **108**, 8311 (1988).
185. L. W. Shacklette, J. F. Wolf, S. Gould, and R. H. Baughman, *J. Chem. Phys.* **88**, 3955 (1988).
186. A. J. Epstein, W. S. Huang, and A. G. MacDiarmid, *Synth. Met.* **18**, 303 (1987).
187. A. G. MacDiarmid, J.-C. Chiang, A. E. Richter, N. L. D. Somaisiri, and A. J. Epstein, in L. Alcacer, ed., *Conducting Polymers*, Reidel, Dordrecht, Holland, 1987, p. 105.
188. J. O. Iroh and R. R. Rajagopalan, *J. Appl. Polym. Sci.* **76**, 1503 (2000).
189. J. A. Conklin, S. C. Huang, S. M. Huang, T. Wen, and R. B. Kanar, *Macromolecules* **28**, 6522 (1995).
190. K. S. Alva, J. Kumar, K. A. Marx, and S. K. Tripathy, *Marcomolecules* **30**, 4024 (1997).
191. C. S. Marvel and C. L. Levesque, *J. Am. Chem. Soc.* **60**, 280 (1938).
192. C. S. Marvel, J. O. Cormer, and E. H. Riddle, *J. Am. Chem. Soc.* **64**, 92 (1942).
193. N. Grassie and R. McGuchan, *Eur. Polym. J.* **7**, 1357 (1970).
194. J. E. Bailey and A. J. Clarke, *Nature* **234**, 529 (1971).
195. R. J. Angelo, M. L. Wallach, and R. M. Ikeda, *Polym. Prepr.* **8**, 221 (1967).
196. A. W. Snow, *Nature* **292**, 40 (1982).
197. U. Scherf and K. Mullen, *Makromol. Chem., Rapid Commun.* **12**, 489 (1991).
198. N. Saito, T. Kanbara, T. Saito, and T. Yamamoto, *Polym. Bull.* **30**, 285 (1993).
199. T. Yamamoto, *Prog. Polym. Sci.* **17**, 1153 (1992).
200. A. D. Schluter, *Adv. Mater.* **3**, 282 (1991).
201. S. Wegener and K. Mullen, *Chem. Ber.* **124**, 2101 (1991).
202. M. Forster, K. O. Annan, and U. Scherf, *Macromolecules* **32**, 3159 (1999).
203. T. Yohannes, H. Neugebauer, S. Luzzati, M. Catellani, S. A. Jenekhe, and N. S. Sariciftci, *J. Phys. Chem B.* **104**, 9430 (2000).
204. C. R. Martin, in Ref. 42, Chapt. 16.
205. R. Nagarajan, W. Liu, J. Kumar, S. K. Tripathy, F. F. Bruno, and L. A. Samuelson, *Macromolecules* **34**, 3921 (2001).
206. C. R. Martin, *Science* **266**, 1961 (1994).
207. M. Granstrom, M. Berggren, and O. Inganas, *Science* **267**, 1479 (1995).
208. P. N. Bartlett, P. R. Birkin, M. A. Ghanem, and C.-S. Toh, *J. Mater. Chem.* **11**, 849 (2001).
209. T. Sumida, Y. Wada, T. Kitamura, and S. Yanagida, *Chem. Commun.* 613 (2000).
210. A. Malinauskas, *Polymer* **42**, 3957 (2001).

211. H. H. Kuhn and A. D. Child, in Ref. 42, Chapt. 35.
212. W. Liu, J. Kumar, S. Tripathy, K. J. Senecal, and L. Samuelson, *J. Am. Chem. Soc.* **121**, 71 (1999).
213. J. Shan and S. Cao, *Polym. Adv. Tech.* **11**, 288 (2000).
214. H. Yasuda, *Plasma Polymerization*, Academic Press, Inc., New York, 1985.
215. N. Morosoff, in R. d'Agostino, ed., *Plasma Deposition, Treatment, and Etching of Polymers*, Academic Press, Inc., New York, 1990.
216. M. S. Silverstein and I. Visoly-Fisher, *Polymer* **43**, 11 (2002).
217. G. J. Cruz, J. Morales, and R. Olayo, *Thin Solid Films* **342**, 119 (1999).
218. H. Hernandez, A. F. Diaz, R. Waltman, and J. Bargon, *J. Phys. Chem.* **88**, 3333 (1984).
219. X. Gong, L. Dai, A. W. H. Mau, and H. J. Griesser, *J. Polym. Sci., Polym. Chem. Ed.* **36**, 633 (1998).
220. L. A. Utracki, *Polymer Alloys and Blends*, Hanser Publishers, Munich, 1990.
221. J. Anad, S. Palaniappan, and D. N. Sathyanarayana, *Prog. Polym. Sci.* **23**, 993 (1998).
222. D. Stauffer and A. Aharony, *Introduction to Percolation Theory*, 2nd ed., Taylor and Francis, London, 1992.
223. R. Gangopadhyay and A. De, *Chem. Mater.* **12**, 608 (2000).
224. S. P. Armes, in Ref. 42, Chapt. 17.
225. H. Eisazadeh, G. Spinks, and G. G. Wallace, *Polymer* **35**, 3801 (1994).
226. M. Akif Khan and S. P. Armes, *Adv. Mater.* **12**, 671 (2000).
227. A. E. Wiersma, L. M. A. vd Steeg, and T. J. M. Jongeling, *Synth. Met.* **71**, 2269 (1995).
228. Eur. Pat. 589,529 (1993), A. E. Wiersma and L. M. A. vd Steeg.
229. L. G. B. Bremer, M. W. C. G. Verbong, M. A. M. Webers, and M. A. M. M. van Doorn, *Synth. Met.* **84**, 355 (1997).
230. M. Pomerantz, in Ref. 42, Chapt. 11.
231. A. F. Diaz, J. Crowley, J. Bargon, G. P. Gardini, and J. B. Torrance, *J. Electroanal. Chem.* **121**, 355 (1981).
232. P. Marque, J. Roncali, and F. Garnier, *J. Electroanal. Chem.* **218**, 107 (1987).
233. J. Roncali in Ref. 42, Chapt. 12.
234. W.-P. Su, J. R. Schrieffer, and A. J. Heeger, *J. Phys. Rev. B* **28**, 1138 (1980).
235. D. Bloor in G. Allen, and J. Bevington, eds., *Comprehensive Polymer Science*, vol. **2**, Pergamon Press, Elmsford, N.Y., 1989, Chapt. "22".
236. J. L. Bredas, K. Cornil, F. Meyers, and D. Beljonne, in Ref. 42, Chapt. 1.
237. J. L. Bredas and G. B. Street, *Acc. Chem. Res.* **18**, 309 (1985).
238. C. Kuhn, in Ref. 42, Chapt. 4.
239. J. L. Bredas, R. R. Chance, and R. Silbey, *Phys. Rev. B* **26**, 5843 (1982).
240. J. L. Bredas, R. R. Chance, and R. Silbey, *Mol. Cryst. Liq. Cryst.* **77**, 319 (1981).
241. A. R. Bishop, D. K. Campbell, and K. Fesser, *Mol. Cryst. Liq. Cryst.* **77**, 253 (1981).
242. D. J. Irvin, D. S. Dudis, and J. R. Reynolds, *Polym. Prepr.* **38**, 318 (1997).
243. D. J. Irvin, *Modification of the Electronic Properties of Conjugated Polymers*, PhD dissertation, University of Florida, 1998.
244. D. C. Trivedi, *Bull. Electrochem.* **8**, 94 (1993).
245. R. H. Baughman, N. S. Murthy, and G. G. Miller, *J. Chem. Phys.* **79**, 515 (1983).
246. Y. Wang and M. F. Rubner, *Synth. Met.* **39**, 153 (1990).
247. Y. Wang, M. F. Rubner, and L. J. Buckley, *Synth. Met.* **41/43**, 1103 (1991).
248. B. Wessling, R. Hiesgen, and D. Meissner, *Acta Polym.* **44**, 132 (1993).
249. N. V. Bhat, A. P. Gadre, and V. A. Bambole, *J. Appl. Polym. Sci.* **80**, 2511 (2001).
250. E. M. Conwell and H. A. Mizes, in T. S. Moss, ed., *Handbook of Semiconductors*, Elsevier, Switzerland, 1992, p. 583.
251. M. Sinclair, C. H. Seager, D. McBranch, A. J. Heeger, and G. L. Baker, in C. Warde, J. Stamatoff, and W. I. Wang, eds., *Materials for Optical Information Processing* (MRS Symposium Series, 228m), Materials Research Society, Pittsburg, 1992, p. 79.

252. R. J. Waltman, J. Bargon, and A. F. Diaz, *J. Phys. Chem.* **87**, 1459 (1983).
253. H. S. Li, J. Roncali, and F. Garnier, *J. Electroanal. Chem.* **263**, 155 (1989).
254. A. Pelter, I. Jenkins, and D. E. Jones, *Tetrahedron* **53**, 10357 (1997).
255. C. L. Wang and F. Martino, *Phys. Rev. B* **34**, 5540 (1986).
256. M. J. Winokur, D. Spiegel, Y. Kim, S. Hotta, and A. J. Heeger, *Synth. Met.* **28**, C419 (1989).
257. S.-A. Chen and J.-M. Ni, *Macromolecules* **25**, 6081 (1992).
258. M. D. Curtis, *Macromolecules* **34**, 7905 (2001).
259. J. P. Ruiz, J. R. Dharia, and J. R. Reynolds, *Macromolecules* **25**, 849 (1992).
260. C. Nicolini, E. Maccioni, and M. K. Ram, *Thin Solid Films* **303**, 27 (1997).
261. S. Nishio, A. Matsuzaki, and H. Sato, *Synth. Met.* **84**, 367 (1997).
262. M. Reghu, Y. Cao, D. Moses, and A. J. Heeger, *Phys. Rev. B* **47**, 1758 (1993).
263. Y. W. Park, E. S. Choi, and D. S. Suh, *Synth. Met.* **96**, 81 (1998).
264. J. H. Burroughs, D. D. C. Bradley, A. R. Brown, R. N. Marks, K. MacKay, R. H. Friend, P. L. Burn, and A. B. Holmes, *Nature* **347**, 539 (1990).
265. E. W. Williams and R. Hall, *Luminescence and the Light Emitting Diode*, Pergamon, Oxford, 1987.
266. A. Kraft, A. C. Grimsdale, and A. B. Holmes, *Angew. Chem., Int. Ed. Engl.* **37**, 402 (1998).
267. P. L. Burn, D. D. C. Bradley, R. H. Friend, D. A. Halliday, A. B. Holmes, R. W. Jackson, and A. Kraft, *J. Chem. Soc., Perkin. Trans. 1* 3225 (1992).
268. N. C. Greenham, R. H. Friend, and D. D. C. Bradley, *Adv. Mater.* **6**, 491 (1994).
269. B. G. Levi, *Phys. Today* **53**(12), 19 (2000).
270. H. Becker, S. E. Burns, and R. H. Friend, *Phys. Rev. B.* **56**, 1893 (1997).
271. G. Gustafsson, Y. Cao, G. M. Treacy, F. Klavetter, N. Colaneri, and A. J. Heeger, *Nature* **357**, 477 (1992).
272. G. J. Sarnecki, P. L. Burn, A. Kraft, R. H. Friend, and A. B. Holmes, *Synth. Met.* **55**, 914 (1993).
273. D. Baum, E. G. J. Staring, R. C. J. E. Demandt, G. L. J. Rikken, Y. A. R. R. Kessener, and A. H. J. Venhuizen, *Synth. Met.* **66**, 75 (1994).
274. I. D. Parker, *J. Appl. Phys.* **75**, 1656 (1994).
275. S. Hoger, J. J. McNamara, S. Schricker, and F. Wudl, *Chem. Mater.* **6**, 171 (1994).
276. S. T. Kim, D.-H. Hwang, X.-C. Li, J. Gruner, R. H. Friend, A. B. Holmes, and H.-K. Shim, *Adv. Mater.* **8**, 979 (1996).
277. J. D. Stenger-Smith, P. Zarras, L. H. Merwin, S. E. Shaheen, B. Kippelen, and N. Peyghambarian, *Macromolecules* **31**, 7566 (1998).
278. P. Barta, F. Cacialli, R. H. Friend, and M. Zagorska, *J. Appl. Phys.* **84**, 6279 (1998).
279. M. J. Marsella, D.-K. Fu, and T. M. Swager, *Adv. Mater.* **7**(2), 145 (1995).
280. E. G. J. Staring, R. C. J. E. Demandt, D. Braum, G. L. J. Rikken, Y. A. R. R. Kessener, A. H. J. Venhuizen, M. M. F. van Knippenberg, and M. Bouwmanns, *Synth. Met.* **71**, 2179 (1995).
281. E. Z. Faraggi, H. Chayet, G. Cohen, R. Neumann, Y. Anvy, and D. Davidov, *Adv. Mater.* **7**, 742 (1995).
282. A. Donat-Bouillud, I. Levesque, Y. Tao, M. D'Iorio, S. Beaupre, P. Blondin, M. Ranger, J. Bouchard, and M. Leclerc, *Chem. Mater.* **12**, 1931 (2000).
283. G. Yu, N. Nishino, A. J. Heeger, T.-A. Chen, and R. D. Rieke, *Synth. Met.* **72**, 249 (1995).
284. H. N. Cho, D. Y. Kim, Y. C. Kim, J. Y. Lee, and C. Y. Kim, *Adv. Mater.* **9**, 326 (1997).
285. H. N. Cho, D. Y. Kim, Y. C. Kim, J. Y. Lee, and C. Y. Kim, *Proc. SPIE Int. Soc. Opt. Eng.* **3418**, 151 (1997).
286. J. R. Sgeats, H. Antoniadis, M. Hueschen, W. Leonard, J. Miller, R. Moon, D. Roitman, and A. Stocking, *Science* **273**, 884 (1996).

287. N. C. Geenham, S. C. Moratti, D. D. C. Bradley, R. H. Friend, and A. B. Holmes, *Nature* **365**, 628 (1993).
288. F. Chen, P. G. Mehta, L. Takiff, and R. D. McCullough, *J. Mater. Chem.* **6**, 1763 (1996).
289. J. C. Carter, I. Grizzi, S. K. Heeks, D. J. Lacey, S. G. Latham, P. J. May, O. R. de los Panos, K. Pichler, C. R. Towns, and H. F. Wittmann, *Appl. Phys. Lett.* **71**, 34 (1997).
290. G. Grem, G. Leditzky, B. Ullrich, and G. Leising, *Synth. Met.* **51**, 383 (1992).
291. Y. Yang and Q. Pei, *J. Appl. Phys.* **77**, 4807 (1995).
292. M. Yoshida, H. Kawahara, A. Fujii, Y. Ohmori, and K. Oshino, *Jpn. J. Appl. Phys.* **34**, L1237 (1995).
293. T. Tsutsui, E.-I. Aminaka, Y. Fujita, Y. Hamada, and S. Saito, *Synth. Met.* **57**, 4157 (1993).
294. A. R. Brown, N. C. Greenham, J. H. Borroughs, D. D. C. Bradley, R. H. Friend, P. L. Burn, A. Kraft, and A. B. Holmes, *Chem. Phys. Lett.* **200**, 46 (1992).
295. M. Hamaguchi and K. Yoshino, *Appl. Phys. Lett.* **69**, 143 (1996).
296. M. T. Bernius, M. Inbasekaran, *J. O'Brien, and W. Wu, Adv. Mater.* **12**, 1737 (2000).
297. Q. Pei, G. Yu, C. Zhang, Y. Yang, and A. J. Heeger, *Science* **269**, 1086 (1995).
298. I. H. Campbell and D. L. Smith, *Appl. Phys. Lett.* **72**, 2565 (1998).
299. Q. Pei, Y. Yang, G. Yu, Y. Cao, and A. J. Heeger, *Synth. Met.* **85**, 1229 (1997).
300. F. Hide, M. A. Diaz-Garcia, B. J. Schwartz, and A. J. Heeger, *Acc. Chem. Res.* **30**, 430 (1997).
301. L. Dai, B. Winkler, L. Dong, L. Tong, and A. W. H. Mau, *Adv. Mater.* **13**, 915 (2001).
302. Q. Pei and Y. Yang, *J. Am. Chem. Soc.* **118**, 7416 (1996).
303. C. Yin, Y.-Z. Zhao, C.-Z. Yang, and S.-Y. Zhang, *Chem. Mater.* **12**, 1853 (2000).
304. T. Johansson, W. Mammo, M. R. Andersson, and O. Inganas, *Chem. Mater.* **11**, 3133 (1999).
305. W. C. Dautremont-Smith, *Displays* 3 (1982).
306. W. C. Dautremont-Smith, *Displays* 67 (1982).
307. P. M. S. Monk, R. J. Mortimer, and D. R. Rosseinsky, *Electrochromism*, VCH Publishers, New York, 1995.
308. A. J. Bard, A. Ledwith, and H. J. Shine, *Adv. Phys. Org. Chem.* **13**, 155 (1976).
309. R. J. Mortimer, *Chem. Soc. Rev.* **26**, 146 (1997).
310. A. Panero, S. Passerini, and B. Scrosati, *Mol. Cryst. Liq. Cryst.* **229**, 97 (1993).
311. K. Hyodo, *Electrochim. Acta* **39**, 265 (1994).
312. D. M. Welsh, A. Kumar, M. C. Morvant, and J. R. Reynolds, *Synth. Met.* **102**, 967 (1999).
313. D. R. Rosseinsky and R. J. Mortimer, *Adv. Mater.* **13**, 783 (2001).
314. G. Heywang and F. Jonas, *Adv. Mater.* **4**, 116 (1992).
315. A. Kumar, D. M. Welsh, M. C. Morvant, F. Piroux, K. A. Abboud, and J. R. Reynolds, *Chem. Mater.* **10**, 896 (1998).
316. J. L. Reddinger, G. A. Sotzing, and J. R. Reynolds, *Chem. Commun.* 1777 (1996).
317. G. Zotti, G. Schiavon, S. Zecchin, J.-F. Morin, and M. Leclerc, *Macromolecules* **35**, 2122 (2002).
318. C. Trimble, M. DeVries, J. S. Hale, D. W. Thompson, T. E. Tiwald, and J. A. Woollam, *Thin Solid Films* **355/356**, 26 (1999).
319. P. Topart and P. Hourquebie, *Thin Solid Films* **352**, 243 (1999).
320. P. Chandrasekhar, G. C. Birur, P. Stevens, S. Rawal, E. A. Puerson, and K. L. Miller, *Synth. Met.* **119**, 293 (2001).
321. P. Chandrasekhar, B. J. Zay, G. C. Birur, S. Rawal, E. A. Pierson, L. Kauder, and T. Swanson, *Adv. Funct. Mater.* **12**, 95 (2002).
322. I. Schwendeman, J. Hwang, D. M. Welsh, D. B. Tanner, and J. R. Reynolds, *Adv. Mater.* **13**, 634 (2001).

323. H. Pages, P. Topart, and D. Lemordant, *Electrochim. Acta* **46**, 2137 (2001).
324. L. Olmedo, P. Hourquebie, and F. Jousse, *Adv. Mater.* **5**, 373 (1993).
325. P. V. Wright, T. C. P. Wong, B. Chambers, and A. P. Anderson, *Adv. Mater. Opt. Electron.* **4**, 253 (1994).
326. P. Hourquebie and L. Olmedo, *Synth. Met.* **65**, 19 (1994).
327. L. Olmedo, P. Hourquebie, and F. Jousse, *Synth. Met.* **69**, 205 (1995).
328. I. K. Varma, G. Gupta, and C. S. Sidhu, *Macromol. Symp.* **164**, 401 (2001).
329. R. V. Gregory, W. C. Kimbrell, and H. H. Kuhn, *Synth. Met.*, **28**, C823 (1989).
330. R. V. Gregory, W. C. Kimbrell, and H. H. Kuhn, J. Coated, *Fabrics* **20**, 1 (1991).
331. A. D. Child and H. H. Kuhn, *Polym. Prepr.* **35**, 249 (1994).
332. T. L. Rose, S. D'Antonio, M. H. Jillson, A. B. Kon, R. Suresh, and F. Wang, *Synth. Met.* **85**, 1439 (1997).
333. B. Chambers, *Electron. Lett.* **30**, 1626 (1994).
334. T. Yohannes and O. Inganas, *Sol. Energy Mater. Sol. Cells* **51**, 193 (1996).
335. L. S. Roman, M. R. Andersson, T. Yohannes, and O. Inganas, *Adv. Mater.* **9**, 1164 (1997).
336. G. Yu and A. J. Heeger, *Synth. Met.* **85**, 1183 (1997).
337. C. J. Brabec, N. S. Sariciftci, and J. C. Hummelen, *Adv. Funct. Mater.* **11**, 15 (2001).
338. G. Jorgensen, J. Pern, S. Kelley, A. Czanderna, and P. Schissel, in R. Arshady, ed., *Desk Reference of Functional Polymers; Syntheses and Applications*, American Chemical Society, Washington, D.C., 1997, Chapt. "4.2".
339. H. Antoniadis, B. R. Hsieh, M. A. Abkowitz, and S. A. Jenekhe, *Synth. Met.* **62**, 265 (1994).
340. D. L. Vangeneugden, D. J. Vanderzande, J. Salbeck, P. A. van Hal, R. A. J. Janssen, J. C. Hummelen, C. J. Brabec, S. E. Shaheen, and N. S. Sariciftci, *J. Phys. Chem. B* **105**, 11106 (2001).
341. N. S. Sariciftci, L. Smilowitz, A. J. Heeger, and F. Wudl, *Science* **258**, 1474 (1992).
342. K. Tada, M. Onoda, A. A. Zakhidov, and K. Yoshino, *Jpn. J. Appl. Phys.* **36**, L306 (1997).
343. A. C. Arias, M. Granstrom, D. S. Thomas, K. Petritsch, and R. H. Friend, *Phys. Rev. B* **60**, 1854 (1999).
344. J. S. Kim, M. Granstrom, R. H. Friend, N. Johansson, W. R. Salaneck, R. Daik, W. J. Feast, and F. C. Cavcialli, *J. Appl. Phys.* **84**, 6859 (1998).
345. S. E. Shaheen, J. C. Brabec, F. Padinger, T. Fromherz, J. C. Hummelen, and N. S. Sariciftci, *Appl. Phys. Lett.* **78**, 841 (2001).
346. G. Horowitz, *Adv. Mater.* **10**, 365 (1998).
347. H. Sirringhaus, N. Tessler, and R. H. Friend, *Science* 1741 (1998).
348. A. Dodabalapur, Z. Bao, A. Makhuja, J. G. Lanquindanum, R. Raju, Y. Feng, H. E. Katz, and J. Rogers, *Appl. Phys. Lett.* **73**, 142 (1998).
349. A. R. Brown, A. Pomp, C. M. Hart, and D. M. de Leeuw, *Science* **270**, 972 (1995).
350. J. J. Morrison, M. M. Murray, X. C. Li, A. B. Holmes, S. C. Morratti, R. H. Friend, and H. Sirringhaus, *Synth. Met.* **102**, 987 (1999).
351. H. E. Katz and Z. Bao, *J. Phys. Chem.* **104**, 671 (2000).
352. H. Fuchigami, A. Tsumura, and H. Koezuka, *Appl. Phys. Lett.* **63**, 1372 (1993).
353. J. M. Tour, *Acc. Chem. Res.* **33**, 791 (2000).
354. J. M. Tour, *Chem. Rev.* **96**, 537 (1996).
355. D. L. Pearson and J. M. Tour, *J. Org. Chem.* **62**, 1376 (1997).
356. P. N. Prasad and D. J. Williams, *Introduction to Nonlinear Optical Effects in Molecules and Polymers*, John Wiley & Sons, Inc., New York, 1991.
357. L. R. Dalton, W. H. Steier, B. H. Robinson, C. Zhang, A. Ren, S. Garner, A. Chen, T. Londergan, L. Irwin, B. Carlson, L. Fifield, G. Phelan, C. Kincaid, J. Amend, and A. Jen, *J. Mater. Chem.* **9**, 1905 (1999).

358. B. L. Lawrence, W. E. Torruellas, and G. Baker, *Phys. Rev. Lett.* **73**, 597 (1994).
359. L. T. Cheng, W. Tam, S. H. Stevenson, G. R. Meredith, G. Rikken, and S. R. Marder, *J. Phys. Chem.* **95**, 10631 (1991).
360. L. T. Cheng, W. Tam, S. R. Marder, A. E. Stiegman, A. E. Rikken, and C. W. Spangler, *J. Phys. Chem.* **95**, 10643 (1991).
361. J. I. Chen, S. Marturunkakul, J. Kumar, and S. K. Tripathy, in Ref. 42, Chapt. 26.
362. H. S. Nalwa, T. Watanabe, and S. Miyata, in H. S. Nalwa and S. Miyata, eds., *Nonlinear Optics for Organic Molecules and Polymers*, CRC Press, New York, 1997, Chapt. "4".
363. T. M. Swager, *Acc. Chem. Rev.* **31**, 201 (1998).
364. N. G. Maroudas, *J. Theor. Biol.* **49**, 417 (1975).
365. V. R. Shastri and M. V. Pishko, in D. L. Wise, G. E. Wnek, D. J. Trantolo, T. M. Cooper, and J. D. Gresser, eds., *Electrical and Optical Polymer Systems: Fundamentals, Methods, and Applications*, Marcel Dekker, Inc., New York, 1998, Chapt. "30".
366. D. T. McQuade, A. E. Pullen, and T. M. Swager, *Chem. Rev.* **100**, 2537 (2000).
367. J.-S. Yang and T. M. Swager, *J. Am. Chem. Soc.* **120**, 11864 (1998).
368. O. S. Wolfbeis, *Anal. Chem.* **72**, 81R (2000).
369. S. Yamakawa, *Sens. Mater.* **9**, 187 (1997).
370. R. Zhou, K. E. Geckeler, and W. Gopel, in R. Arshady, ed., *Desk Reference of Functional Polymers: Synthesis and Applications*, American. Chemical Society, Washington, D.C., 1997, Chapt. "4.4".
371. L. M. Goldenberg, M. R. Bryce, and M. C. Petty, *J. Mater. Chem.* **9**, 1957 (1999).
372. K. J. Albert, N. S. Lewis, C. L. Schauer, G. A. Sotzing, S. A. Stitzel, T. P. Vaid, and D. R. Walt, *Chem. Mater.* **100**, 2595 (2000).
373. G. A. Sotzing, S. M. Briglin, R. H. Grubbs, and N. S. Lewis, *Anal. Chem.* **72**, 3181 (2000).
374. K. B. Crawford, M. B. Goldfinger, and T. M. Swager, *J. Am. Chem. Soc.* **120**, 5187 (1998).
375. J. A. Irvin, I. Schwendeman, Y. Lee, K. A. Abboud, and J. R. Reynolds, *J. Polym. Sci., Polym. Chem.* **39**, 2164 (2001).
376. R. D. McCullough and S. P. Williams, *J. Am. Chem. Soc.* **115**, 11608 (1993).
377. B. A. Boldea, I. Levesque, and M. Leclerc, *J. Mater. Chem.* **9**, 2133 (1999).
378. S. S. Zhu and T. M. Swager, *J. Am. Chem. Soc.* **119**, 12568 (1997).
379. J. M. Davey, S. F. Ralph, C. O. Too, and G. G. Wallace, *Synth. Met.* **99**, 191 (1999).
380. P. A. Bross, U. Schoberl, and J. Daub, *Adv. Mater.* **3**, 198 (1991).
381. R. Fiesel, D. Neher, and U. Sherf, *Synth. Met.* **102**, 1457 (1999).
382. J.-C. Lepretre, E. Saint-Aman, and J. P. Utille, *J. Electroanal. Chem.* **347**, 465 (1993).
383. E. A. H. Hall, *ACS Symp. Ser.* **487**, 1 (1992).
384. A. Kros, S. W. F. M. van Hovell, N. A. J. M. Sommerdijk, and R. J. M. Nolte, *Adv. Mater.* **13**, 1555 (2001).
385. C. A. Thomas, K. Zong, P. Schottland, and J. R. Reynolds, *Adv. Mater.* **12**, 222 (2000).
386. L. Kumpumbu-Kalemba and M. Leclerc, *Chem. Commun.* 1847 (2000).
387. W. J. Sung and Y. H. Lee, *Anal. Chem.* **72**, 2177 (2000).
388. S. Cosniew, M. Stoytcheva, A. Senillou, H. Perrot, R. P. M. Furriel, and F. A. Leone, *Anal. Chem.* **71**, 3692 (1999).
389. J. Wang, M. Jiang, and B. Mukherjee, *Anal. Chem.* **71**, 4095 (1999).
390. W. Spevak, J. O. Nagy, and D. H. Charych, *Adv. Mater.* **7**, 85 (1995).
391. D. Charych and J. O. Nagy, *CHEMTECH* 24 (1996).
392. K. Faid and M. Leclerc, *J. Am. Chem. Soc.* **120**, 5274 (1998).
393. L. L. Miller and Q.-X. Zhou, *Macromolecules* **20**, 1594 (1987).
394. Q.-X. Zhou, L. L. Miller, and J. R. Valentine, *J. Electroanal. Chem.* **261**, 147 (1989).

395. J. R. Reynolds, H. Ly, F. Selampinar, and P. J. Kinlen, *Polym. Prepr.* **40**, 307 (1999).
396. M. Pyo, G. Maeder, R. T. Kennedy, and J. R. Reynolds, *J. Electroanal. Chem.* **368**, 329 (1994).
397. M. Pyo and J. R. Reynolds, *Chem. Mater.* **8**, 128 (1996).
398. J.-M. Pernaut and J. R. Reynolds, *J. Phys. Chem. B* **104**, 4080 (2000).
399. T. Livache, A. Roget, E. Dejean, C. Barthet, G. Bidan, and R. Teoule, *Synth. Met.* **71**, 2143 (1995).
400. T.-Y. Lee and Y.-Y. Lee, *Anal. Chem.* **73**, 5629 (2001).
401. V. M. Schmidt, D. Tegtmeyer, and J. Heitbaum, *J. Electroanal. Chem.* **385**, 149 (1995).
402. W. Liang and C. R. Martin, *Chem. Mater.* **3**, 390 (1991).
403. M. R. Anderson, B. R. Mattes, H. Reiss, and R. B. Kaner, *Science* **252**, 1412 (1991).
404. B. D. Reid, V. H. M. Ebron, I. H. Musselman, J. P. Ferraris, and J. Balkus Jr., *J. Membr. Sci.* **195**, 181 (2002).
405. C. Ehrenbeck and K. Juttner, *Electrochim. Acta* **41**, 1815 (1996).
406. J. P. Ferraris, M. M. Eissa, J. D. Brotherston, D. C. Loveday, and A. A. Moxey, *J. Electroanal. Chem.* **459**, 57 (1998).
407. S. Ghosh and O. Inganas, *Adv. Mater.* **11**, 1214 (1999).
408. F. Fusalba, H. A. Ho, L. Breau, and D. Belanger, *Chem. Mater.* **12**, 2581 (2000).
409. R. B. Kaner, A. G. MacDiarmid, and R. J. Mammone, *ACS Symp. Ser.* **242**, 575 (1984).
410. P. Passiniemi and J.-E. Osterholm, *Synth. Met.* **18**, 637 (1987).
411. C. Arbizzani, M. Mastragostino, and B. Scrosati, in H. S. Nalwa, ed., *Handbook of Organic Conductive Molecules and Polymers: Vol. 4. Conductive Polymers: Transport, Photophysics, and Applications*, John Wiley & Sons, Inc., New York, 1997, Chapt. "11".
412. J. P. Zheng, P. G. Cygan, and T. R. Low, *J. Electrochem. Soc.* **142**, 2699 (1995).
413. A. Laforgue, P. Simon, C. Sarrazin, and J.-F. Fauvarque, *J. Power Sources* **80**, 142 (1999).
414. C. Arbizzani, M. Mastragostino, and L. Meneghello, *Electrochim. Acta* **41**, 21 (1996).
415. J. P. Ferraris, M. M. Eissa, I. D. Brotherston, and D. C. Loveday, *Chem. Mater.* **10**, 3528 (1998).
416. F. Fusalba, P. Gouerec, D. Villers, and D. Belanger, *J. Electrochem. Soc.* **148**, A1 (2001).
417. J. C. Carlberg and O. Inganas, *J. Electrochem. Soc.* **144**, L61 (1997).
418. J. D. Stenger-Smith, C. K. Webber, N. Anderson, A. P. Chafin, K. Zong, and J. R. Reynolds, *J. Electrochem. Soc.* **149**, A973 (2002).
419. A. Rudge, J. Davey, I. Raistrick, S. Gottesfeld, and J. P. Ferraris, *J. Power Sources* **47**, 89 (1994).
420. W.-P. Liao and F.-L. Chu, *IEEE Trans. Microwave Theor. Techn.* **44**, 1188 (1996).
421. T. C. P. Wong, B. Chambers, A. P. Anderson, and P. V. Wright, *Electron. Lett.* **28**, 1651 (1992).
422. T. C. P. Wong, B. Chambers, A. P. Anderson, and P. V. Wright, *Anten. Propag.* **4/7**, 441 (1995).
423. M. E. Achour, M. El Malhi, J. L. Miane, and F. Carmona, *J. Appl. Polym. Sci.* **61**, 2009 (1996).
424. P. Annadurai, A. K. Mallick, and D. K. Tripathy, *J. Appl. Polym. Sci.* **83**, 145 (2002).
425. A. Bel Hadj Mohamed, J. L. Miane, and H. Zangar, *Polym. Int.* **50**, 773 (2001).
426. R. B. Rosner, *IEEE Trans. Device Mater. Reliab.* **1**, 9 (2001).
427. V. G. Kulkarni, in Ref. 42, p. 1068.
428. K. Miyasaka, K. Wanante, E. Jojima, H. Aida, M. Sumita, and K. Ishikawa, *J. Mater. Sci.* **17**, 1610 (1982).
429. M. Narkis, G. Lidor, A. Vaxman, and L. Zuri, *IEEE Trans. Electron. Pack. Manufact.* **23**, 239 (2000).
430. J. Avlyanov, M. Cooper, and S. Dahman, *Proc. EOS/ESD Symp.* 269 (1999).

431. U.S. Pat. 4,981,718 (1991), H. H. Kuhn, and W. C. Kimbrell (to Milliken Research Corp.).
432. U.S. Pat. 5,624,736 (1997), A. R. DeAngelis, A. D. Child, and D. E. Green (to Milliken Research Corp.).
433. J. A. Irvin, S. Fallis, D. Stasko, A. J. Guenthner, K. R. Davis, D. Kline, and A. Paiz, *Polym. Mater. Sci. Eng.* **86**(1), 11 (2002).
434. R. H. Baughman, L. W. Shacklette, R. L. Elsenbaumer, E. Plichta, and C. Becht, in J. L. Bredas and R. R. Chance, eds., *Opportunities in Electronics, Optoelectronics and Molecular Electronics*, Kluwer, Dordrecht, 1990, p. 559.
435. M. R. Gandhi, P. Murray, G. M. Spinks, and G. G. Wallace, *Synth. Met.* **73**, 247 (1995).
436. Q. Pei and O. Inganas, *J. Phys. Chem.* **97**, 6034 (1993); M. Kaneko and K. Kaneto, *Synth. Met.* **102**, 1350 (1999).
437. D. J. Irvin, S. H. Goods, and L. L. Whinnery, *Chem. Mater.* **13**, 1143 (2001).
438. S. Maw, E. Smela, K. Yoshida, P. Sommer-Larsen, and R. B. Stein, *Sens Actuators, A* **89**, 175 (2001).
439. J. Plocharski, M. Rozanski, and H. Wycislik, *Synth. Met.* **102**, 1354 (1999).
440. M. Kaneko and K. Kaneto, *Synth. Met.* **102**, 1350 (1999).
441. R. H. Baughman, N. S. Murthy, H. Eckhardt, and M. Kertesz, *Phys. Rev. B* **46**, 10515 (1992).
442. T. F. Otero, H. Grande, and J. Rodriguez, *J. Phys. Org. Chem.* **9**, 381 (1996).
443. R. H. Baughman, *Synth. Met.* **78**, 339 (1996).
444. T. F. Otero and H.-J. Grande, in Ref. 42, Chapt. 36.
445. W. Kuhn, B. Hargaitay, A. Katchalsky and H. Eisenberg, *Nature* **165**, 514 (1950).
446. I. Z. Steinberg, A. Oplatka, and A. Katchalsky, *Nature* **210**, 568 (1966).
447. Y. Osada, *Adv. Polym. Sci.* **82**, 1 (1987).
448. D. DeRossi, M. Suzuki, Y. Osada, and P. Morasso, *J. Intell. Mater. Syst. Struct.* **3**, 75 (1992).
449. T. P. McAndrew, *TRIP* **5**(1), 7 (1997).
450. K. G. Thompson, C. J. Bryan, B. C. Benicewicz, and D. A. Wrobleski, *Los Alamos Natl. Lab. Rep.* LA-UR-92-360 (1991).
451. D. A. Wrobleski, B. C. Benicewicz, K. G. Thompson, and B. J. Bryan, *Polym. Prepr.* **35**, 265 (1994).
452. M. A. Phillips, *New Sci.* **144**, 24 (1994).
453. F. C. Jain, J. J. Rosato, K. S. Laonia, and V. S. Agarwala, *Corrosion* **42**, 700 (1986).
454. M. M. Musiana, G. Mengoli, and F. Furlanetto, *J. Appl. Polym. Sci.* **29**, 4433 (1984).
455. I. Sekine, K. Kohara, T. Sugiyama, and M. Yuasa, *J. Electrochem. Soc.* **22**, 756 (1992).
456. S. Jasty and A. J. Epstein, *ACS PSME Prepr.* **72**, 565 (1995).
457. Y. Wei, J. Wang, X. Jia, J. M. Yeh, and P. Spellane, *Polymer* **36**, 4535 (1995).
458. L. Sun, H. Liu, R. Clark, and S. C. Yang, *Synth. Met.* **85**, 67 (1997).
459. S. C. Yang, R. Brown, R. Racicot, Y. Lin, and F. McClaraon, *ACS Polym. Prepr.* **41**, 1776 (2000).
460. P. Zarras, J. D. Stenger-Smith, G. S. Ostrom, and M. H. Miles, in B. R. Hsieh and Y. Wei, eds., *Semiconducting Polymers: Applications, Properties and Synthesis*, (ACS Symposium Series 735), American Chemical Society, Washington, D.C., 1999, p. 280.
461. N. Anderson, D. J. Irvin, C. Webber, J. D. Stenger-Smith, and P. Zarras, *Polym. Mater., Sci. Eng.* **86**, 6 (2002).

PETER ZARRAS
JENNIFER IRVIN
Naval Air Warfare Center Weapons Division (NAWCWD)

ELECTRONIC PACKAGING. See Volume 2.

ELECTROOPTICAL APPLICATIONS. See Volume 2.

EMULSION POLYMERIZATION. See HETEROPHASE POLYMERIZATION.

ENGINEERING THERMOPLASTICS, OVERVIEW.
See Volume 2.

ENVIRONMENTALLY DEGRADABLE PLASTICS

Introduction

Environmentally degradable plastics are sometimes referred to as "green plastics" where the word "green" is used in an ecological sense. The impact of plastics on the environment is hardly a new theme, but with increased interest in "green chemistry" and the broader "green revolution," the relationship between plastics and the environment is a topic of current interest.

Overviews on environmentally degradable plastics have recently appeared for the nonspecialist (1–4) as well as more technical symposia proceedings (5–13). Several extensive Web sites are maintained (14,15) and a commercial market report has been available (16) (see BIODEGRADABLE POLYMERS, MEDICAL APPLICATIONS).

Throughout the 1990s the two major issues relevant to a plastic's "greenness" were feedstock renewability and alternative late-stage disposal options based on degradability, biodegradability, and compostability. These issues are related to 2 of the 12 "principles of green chemistry" elucidated by Anastas and co-workers (17,18): (*1*) a feedstock should be renewable wherever technically and economically practicable and (*2*) products, at the end of their function, should break down into innocuous degradation products (17, p. 30).

Political considerations not particularly connected with the environment have also played a role in focusing attention on the production of plastics, including growing concern over dependence on foreign sources of crude oil, the desire to find additional markets for agricultural products, and the increasing costs and other difficulties of waste management (particularly strong in Europe and Japan) (3).

Since 1993, the International Standards Organization (ISO), through its Technical Committee 207, has been developing the 14000 series,

Encyclopedia of Polymer Science and Technology. Copyright John Wiley & Sons, Inc. All rights reserved.

"Standardizations in the Field of Environmental Management." The long-term goal of this effort is to formulate life-cycle assessment (LCA) programs, environmental auditing procedures, product standards, and product-labeling programs that incorporate environmental aspects (14). In particular, LCA would provide the analytical tools and protocols for producing an inventory analysis of the material and energy inputs and outputs for a product system, and an environmental impact assessment that includes the inventory analysis and a product's complete environmental profile (19). One central concern in LCA is the origin and fate of the carbon contained in or released as carbon dioxide in the production, use, and disposal of the product. ISO 14040 describes the uses and limitations of LCA methodology.

LCA of plastic products is still in the early stages of development. While future reports on "green plastics" may have the benefit of well-documented LCAs containing quantitative results obtained with consensus analytical tools, the present report is limited to the two factors originally motivating attention to the environmental impact of plastics—the origin of the plastics feedstocks (renewable vs nonrenewable) and the ultimate environmental fate of discarded plastics (degradable/biodegradable/compostable vs recalcitrant).

Greenness and price are two separate issues. Even green plastics will have to have favorable price–performance ratios in order to compete in the marketplace, but complicating the issue of price is the reality that no accepted method for determining total cost exists that would account for such factors as the depletion of natural resources, the costs of guaranteeing the supply of raw materials, or the environmental burden of waste management.

Definitions. Standardization of definitions, test methods, and performance criteria are required for degradable, biodegradable, and compostable plastics (as for other plastics), to allow product stewardship, to enable regulatory programs, and to support consumer confidence. In the United States these responsibilities lie with the American Society for Testing and Materials (ASTM).

ASTM definitions of technical terms used in the plastics industry are the responsibility of ASTM Committee D20 on Plastics. Its Subcommittee D20.92 on Terminology originated, for example, ASTM document D883-00, "Standard Terminology Relating to Plastics." Several of the most important ASTM definitions from that standard related to the degradation of plastics are reproduced here:

Degradation: A deleterious change in the chemical structure, physical properties, or appearance of a plastic (see DEGRADATION).

Degradable plastic: A plastic designed to undergo a significant change in its chemical structure under specific environmental conditions, resulting in a loss of some properties that may vary as measured by standard test methods appropriate to the plastic and the application in a period of time that determines its classification.

Hydrolytically degradable plastic: A degradable plastic in which the degradation results from hydrolysis.

Oxidatively degradable plastic: A degradable plastic in which the degradation results from oxidation.

Photodegradable plastic: A degradable plastic in which the degradation results from the action of natural daylight.

Biodegradable plastic: A degradable plastic in which the degradation results from the action of naturally occurring microorganisms such as bacteria, fungi, and algae.

Compostable plastic: A plastic that undergoes degradation by biological processes during composting to yield carbon dioxide, water, inorganic compounds, and biomass at a rate consistent with other known compostable materials and leaves no visually distinguishable or toxic residues.

A plastic can be degradable but not necessarily biodegradable; it can be biodegradable without being compostable (ie, the rate of degradation is part of the definition of compostable); and it can be compostable without being biodegradable (ie, the degradation may be abiotic). Also notice that the definition of biodegradable plastic refers only to degradation by microorganisms, not macroorganisms.

Test Methods. Industry standard test methods for determining the environmental degradability, biodegradability, and compostability are the responsibility, in the United States, of ASTM's Subcommittee D20.96 on Environmentally Degradable Plastics. Standard ASTM test methods used to assess biodegradability include measurements of carbon dioxide production (eg, Sturm test and soil test), weight loss, extent of fragmentation, tensile properties, molecular weight and molecular weight distribution, enzyme assays, biochemical oxygen demand (BOD), and ecotoxicity (eg, cress seed test and earthworm test).

Multiple test procedures are necessary in evaluating a material because some tests are subject to false-positive interpretations. Examples are (*1*) an observed weight loss may result from the leaching of additives rather than polymer degradation; (*2*) carbon dioxide production might result from the degradation only of a low molecular weight polymer fraction; and (*3*) a large loss of material strength might come from a very small change in chemical makeup. To illustrate the application of such test procedures it can be said, for example, that poly(ε-caprolactone), by its disappearance in a soil burial test, is potentially biodegradable in soil, whereas unmodified polyolefins like polyethylene, polypropylene, and polystyrene are recalcitrant.

A distinction is necessary between evaluations of a polymer and a plastic made from that polymer because Additives (qv) (Plasticizers (qv), stabilizers, etc), processing, and fabrication may all have effects on environmental behavior. For example, a polymer or blend may be biodegradable and compostable as film, fibers, or foam, whereas injection-molded products may be inherently biodegradable but not environmentally compostable.

ASTM D6400. In 1999 ASTM announced its "Standard Specification for Compostable Plastics" (D6400-99). The standard establishes criteria to be met before a product can be labeled compostable. Briefly, a product must, at minimum, satisfy ASTM tests showing conversion to carbon dioxide at 60% for a homopolymer or a statistical random copolymer and 90% for other types of copolymers and blends in 180 days or less, and leave no more than 10% of the original weight on a 2-mm screen. If carbon-14 tests are used a test period of 365 days is allowable. Environmental toxicity issues are also addressed, including limits for heavy metals. The ASTM standard has counterparts in German (DIN 54900), European (EN 13432), and international (ISO 14855) documents.

The relatively short time scale of 6 months in ASTM D6400 identifies plastics that compost quickly, completely, and safely, and serves well the purpose

of diverting waste from landfills and incinerators to composting facilities. Some common and inherently compostable biomaterials, however, including wood and leaves, do not satisfy the D6400 specification. Discussion continues as to whether complete biodegradability is required for compostability. A longer time scale for compostability, with less rapid carbon dioxide evolution, may be suitable for purposes of providing long-term soil enhancers, and it may turn out that ASTM will develop a second standard of compostability aimed at plastics that degrade more slowly. But the potential impact of the accumulation of undegraded plastic residues on long-term agricultural productivity is an important issue that has not yet been resolved either by long-term scientific measurements or by consensus.

Products that comply with the ASTM specification, as confirmed by independent testing, can bear a logo developed jointly by the international Biodegradable Products Institute (BPI) and the United States Composting Council (USCC). Certified products are listed on the BPI Web site at www.bpiworld.org.

Markets. Green plastics typically can be produced in various forms (pellets, film, and fibers) and are compatible with a variety of processing methods (Extrusion (qv) and molding). Markets for green plastics are, therefore, potentially the same as those for conventional plastics. In order to be successful in those markets, green plastics will have to possess the physical properties required for the intended application and be cost-competitive; that is, regardless of the intended market, success will be determined by the cost–performance ratio in comparison to the conventional plastics targeting the same market.

Beyond that, however, markets for green plastics can be distinguished according to how biodegradability and compostability are related to the application. In some applications, biodegradability and compostability serve intrinsic functional purposes and give the product a performance capability that often cannot be matched by alternative products. For example, agricultural mulching films control soil temperature and moisture, reduce leaching of nutrients, and prevent weed growth, increasing productivity for vegetable and fruit crops (eg, tomatoes, peppers, melons, and sweet corn) by 50–350% (2). Compostable agricultural mulching film that can be plowed under after use eliminates the costs of collecting and disposing of nondegradable polyethylene covers. Similar advantages accrue with other compostable agricultural and horticultural products, such as planting pots, baling rope and twine, string, clips and hooks, labels, seed mats, time-released fertilizers (greensticks), and others.

Biodegradability and compostability are also central to the function of collection bags for compostable materials (like yard waste and food waste) and of trash bin liners. Approximately 10% of the 1.5 billion pounds of trash bags produced in the United States are used for lawn and leaf bags. Nondegradable bags and liners add to the costs of composting: (*1*) they have to be separated from the waste to avoid contamination of the compost, (*2*) imperfect separation degrades compost quality, and (*3*) nondegradable bags require disposal. Compostable waste bags and trash bin liners avoid these problems. Biodegradability is an intrinsic feature of some other applications, such as the institutional use of laundry bags that dissolve during the washing and then biodegrade after disposal into sewage.

In other applications the product's compostability, rather than serving a functional requirement of the application, provides an alternative waste-disposal method. Composting diverts waste from landfills and incinerators and contributes

to the sustainability of agriculture. Composting is especially important in Europe and Japan, where land is scarce and high landfill fees are common. In Japan, land is so scarce that over 90% of the solid-waste stream is incinerated, but concern has grown over the observed increasing levels of environmental dioxins. In the United States, many states are developing their composting infrastructures, especially for commercial and institutional sources, in order to increase their overall recycling rates.

Plastic packaging is an increasing component of municipal solid waste, and markets for compostable plastics are potentially large in the area of packaging—for industrial, commercial, and household use. Examples include single-use and limited-use disposable materials such as packaging film for food and nonfood items, bottles, jars, loose-fill packaging, and rigid foam packaging.

Food-service items constitute another significant end use, including cutlery, plates, cups, trays, and plastic coatings for paper products like plates and cups. Markets include institutions (hospitals, schools, prisons, and the military), the fast-food industry, and the general public. Another end use category is consumer products, including such products as diapers, personal care and hygiene articles, sports and recreation items, and others.

Some manufacturers emphasize the physical properties of their products, with little or no emphasis on biodegradability except as a corollary benefit.

Green plastics comprise only a very small part (less than 1%) of today's plastics. They do, however, make up a significant part of some specialty, niche markets: starch-based loose-fill packaging now constitutes 30% of the loose-fill packaging market. The plastics described here are those currently commercially available, and are limited mainly to those available in the United States. Manufacturers are named only for illustrative purposes; the list is not intended to be comprehensive. The plastics materials are described generically, with respect to the major polymer constituent(s); for each generic type there are likely to be many specific formulations. Brief mention is made, at the end, of some materials that have been studied in the laboratory. Biomedical applications are described separately (see BIODEGRADABLE POLYMERS, MEDICAL APPLICATIONS).

Many of the polymers mentioned below have separate entries in the encyclopedia. Here the focus is on their specialized use in the production of environmentally degradable plastics.

Petroleum-Based Polymers

Activated Polyolefins. Polyolefins degrade by oxidation (eq. 1) (2) but the rate in the environment is extremely slow; polyolefins are environmentally recalcitrant. In "activated polyolefins" the environmental degradation is enhanced. An early example was the photodegradable plastic produced when an olefin is copolymerized with carbon monoxide (CO) (2,20) (see POLYKETONES). A copolymer of ethylene and (∼1%) CO, on exposure to outdoor sunlight for approximately 3 weeks, becomes embrittled and fragments to a friable powder. A major application is the manufacture of plastic six-pack holders for beverage containers, which became important after 1990 when the United States Congress, in response to public concern over litter, passed Public Law 100-556 requiring that plastic ring carriers be made of degradable material. Manufacturers include Dow and DuPont.

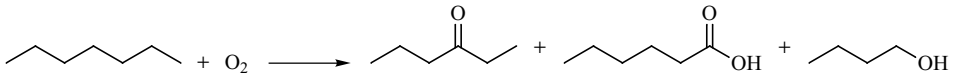

(1)

Various conventional ketone monomers can also be used in copolymerizations with olefins to introduce groups that promote oxidation. Transition-metal complexes (iron, nickel, cobalt) introduced after polymerization act as antioxidant stabilizers during processing but, following an induction period (the length of which depends on concentration), the complexes convert to products that are oxidation activators. Through formulation variations, the length of the induction period and the rate of degradation that follows can be controlled.

For applications where the expected disposal environment is earth burial, commercially available additive packages can be incorporated (~3% by weight) into polyethylene or polypropylene during processing to induce accelerated oxidative degradation initiated by natural daylight, heat, and/or mechanical stress. Applications include agricultural mulching film, compost bags, shopping and grocery bags, baling twine, and packaging film.

Activated polyolefins do not meet the requirements of compostability specified in ASTM D6400. They have market acceptance where cost is of paramount importance and adherence to the ASTM D6400 specification is not mandated.

Poly(vinyl alcohol), Poly(glycolic acid), and Poly(ε-caprolactone). Poly(vinyl alcohol) (**1**) (see VINYL ALCOHOL POLYMERS) is the most-produced water-soluble polymer in the world. It is prepared by free-radical polymerization of vinyl acetate followed by alcoholysis. It environmentally degrades (21,22) by oxidation to form carbonyl groups along the chain, and subsequent hydrolysis. Poly(vinyl alcohol) is an exception to the general rule that chains of carbon–carbon single bonds (as in polyolefins) are recalcitrant. Although considered to be a biodegradable synthetic polymer (the oxidation can be both enzymatic and nonenzymatic), the extent of degrading microorganisms appears to be limited. Poly(vinyl alcohol) has applications in hospital laundry bags, water-soluble packaging, agricultural products, and other film products. Poly(vinyl alcohol) is also used in blends (see below).

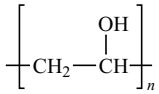

1

Poly(glycolic acid) (**2**) (23) is synthesized from condensation polymerization of glycolic acid or catalytic-ring-opening polymerization of the glycolide. (Although glycolic acid is found in nature it is commercially produced mainly through synthesis.) Poly(glycolic acid) is not only biodegradable, it is biocompatible—nontoxic and not rejected by the intended organism. It is therefore used in various biomedical applications (see BIODEGRADABLE POLYMERS, MEDICAL APPLICATIONS). In applications intended for large-scale use, glycolic acid is widely used in combination with either petroleum-based or renewable components (see below).

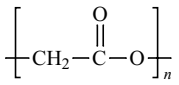

2

Poly(ε-caprolactone) (**3**) (23) is synthesized by ring-opening polymerization of ε-caprolactone using tin-octanoate as a catalyst (24). It is used, for example, as blown film for compost bags or in materials where it serves as a matrix for the controlled release of pesticides, herbicides, and fertilizers. The low melting point of poly(ε-caprolactone) (60°C) (Table 1) limits applications, but it has good mechanical properties and is more hydrophobic than—and compatible with—many biopolymers. It is therefore widely used to modify the properties of other degradable plastics in blends (see below).

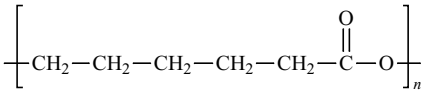

3

Aliphatic polyesters like poly(glycolic acid) and poly(ε-caprolactone) are biodegradable through the action of nonspecific enzymes including the esterases found abundantly in soil (23,33–36).

Copolyesters and Poly(ester amides). Many biodegradable thermoplastic copolyesters (aliphatic and aliphatic–aromatic) and poly(ester amides) are manufactured from conventional petroleum-based monomers (23). (see POLYESTERS, THERMOPLASTIC). The process often involves diols (eg, ethylene glycol, 1,4-butanediol, 1,6-hexanediol) and dicarboxylic acids (eg, adipic, succinic, sebacic). Terephthalic acid is sometimes a component; the aromatic diacid increases chain rigidity. These copolyesters biodegrade in a composting environment by surface growth of bacteria and fungi, and the action of hydrolytic enzymes. Degradation rates in compost depend on composition.

They are typically available as resins, films, or fibers; are usually extrusion-processed; and are characteristically strong, elastic, and waterproof. Applications variously include agricultural mulching film, compost bags, shopping bags that can later be used as compostable garbage bags, transparent film packaging, film coatings for paper and paperboard containers (eg, drinking cups), coatings for starch film, disposable diapers, nonwoven and fiber applications, and others.

EastarBio copolyester (**4**), (Table 1), manufactured by Eastman Chemical, is a random poly(butylene adipate-*co*-terephthalate) containing 50% terephthalate; film is prepared by solvent casting (Fig. 1). EastarBio copolyester biodegrades to the extent of 80% in 150 days in a compost environment.

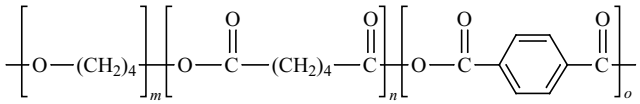

4

Ecoflex, manufactured by BASF, is a random copolyester based on terephthalic acid (40–45%), adipic acid (55%), and 1,4-butanediol, plus chain-extending additives (Table 1). A modified poly(ethylene terephthalate) copolyester is manufactured by DuPont as Biomax (Table 1).

A fraction of the ester linkages can be substituted with amide linkages, which modifies interchain hydrogen bonding. Examples are the BAK poly(ester amides) previously manufactured by Bayer.

Table 1. Selected Properties: Typical Values for Film Products or Product Families

	Manufacturer	Trade name	Product	Density, g/cc	T_g,°C	Melting temperature, °C	Tensile strength, MPa	Elongation, %	Tensile modulus, MPa	Reference
Low density polyethylene[a]				0.921	−35	—	10.3	620	165.5	25
Polypropylene[a]				0.903	−20	164	35.5	—	1380	25
Poly(ε-caprolactone)	Dow	TONE	P-767	1.145		60	24.8	800	435	26
			P-787	1.145		60	41.4	900	386	26
Copolyester	Eastman	EastarBio	GP	1.22	−30	108	22	700	107	27
			Ultra	1.22	−33	102–115	30	>600	113	27
Copolyester	BASF	Ecoflex	F BX 701.1	1.25–1.27	—	110–115	32/36	580/820	—	28
Copolyester	Dupont	Biomax		1.35	—	200	14–48	40–500	60–2100	29
Poly(lactic acid)	Cargill Dow	Natureworks	4042D[b]	1.25	52	135	110/145	160/100	3310/3860	30
Poly(hydroxybutyrate-*co*-hydroxyvalerate)	Metabolix	Biopol		1.25	−25 to 6	90–178	18–43	10–1000	100–3600	31
Starch/poly(ε-caprolactone)	Novamont	MaterBi	Z-class	1.23	—	—	25–45	250–886	100–450	32

[a]LDPE and PP included for comparison.
[b]Biaxially oriented film.

Fig. 1. A compostable garbage bag made from EastarBio™ copolyester. Courtesy of Eastman Chemical Co.

Polymers from Renewable Sources

Cellulose. Cellulose (qv), $\beta[1\rightarrow4]$-linked D-glucose (**5**) (37), is the most abundant biopolymer on earth and accounts for 40% of all organic matter. It is the main component of plant structural fiber that keeps the plant cell wall intact and gives it strength. Oven-dried cotton (qv) contains about 90% cellulose. An average wood (q.v.) has about 50% cellulose, the remaining components being lignin (qv) and hemicellulose. Well over 68 million metric tons of cellulose are produced commercially each year, mainly from wood.

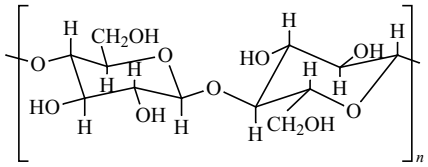

5

Cellophane is an example of "regenerated cellulose." In the viscose process (38,39), shredded wood pulp is treated with caustic soda, producing alkali cellulose. After aging to produce the desired extent of cellulose degradation, the cellulose is treated with carbon disulfide to form a thick solution of xanthated cellulose, called viscose. The viscose is "ripened," and extruded into a bath of sulfuric

acid and sodium sulphite, generating a coagulated gel. The transluscent gel is washed, purified, and bleached. Softening agents—often either glycerol or ethylene glycol—and other chemicals are then added, and the resulting material is cast into a sheet consisting of an amorphous felt. The sheet has high water-vapor permeability, but good resistance to oils and greases. Coatings of nitrocellulose-wax or poly(vinylidene chloride) provide barriers to moisture and gases, solvent sealability, and heat sealability. Cellophane has a water-vapor permeability comparable to high density polyethylene.

Newer technology, based on the use of *N*-methylmorpholine-*N*-oxide as a cellulose solvent (40), has been developed with the aim of reducing hazardous by-products and producing a more environmentally friendly process. The viscose technology, however, still dominates (see CELLULOSE FIBERS, REGENERATED).

Production of cellophane peaked in the 1960s at about 340,000 t a year in the United States, but since then has largely been replaced by synthetic plastics such as polypropylene. Cellophane is still used in food packaging for such items as potato chips, candies, and baked goods; its stiffness allows bags to stand upright on shelves. Nonfood applications include cigarette packages, cigar wrappings, and others; it tears well when notched and has excellent printability.

Uncoated cellophane film readily biodegrades beginning with a hydrolysis reaction catalyzed by the extracellular enzyme cellulase. It disintegrates in 10–14 days and totally biodegrades in 1–2 months. Nitrocellulose–wax coatings also totally biodegrade, in 6 months or so. Coatings of poly(vinylidene chloride) do not biodegrade; they disintegrate to a friable powder.

Cellulose is not thermoplastic but can be chemically modified to produce a wide variety of cellulosic plastics—some of which are thermoplastic—and fibers. Before 1950 cellulosics were the most important group of thermoplastics; today, cellulosic fibers still make up about 8% of the fiber market. Some chemically modified celluloses do not have the biodegradability of cellulose.

Cellulose acetate, one of the most important cellulosics, is produced by the reaction of cotton fiber with acetic acid and acetic anhydride using sulfuric acid as a catalyst. It is thermoplastic, and films can be obtained by extrusion as well as by casting from acetone solution. The film is clear and strong, and has high oxygen and water-vapor permeability. It "breathes" and does not fog, making it useful as packaging film for fresh produce and baked goods. It is also resistant to oils and greases. Cellulose acetate can also be molded (see CELLULOSE ESTERS).

The degradation of cellulose acetate begins with abiotic hydrolysis and oxidation, followed by complete biodegradation, but acetylation decreases the biodegradation rate relative to cellulose. For example, increasing the degree of substitution from an average of 1.7 of the three hydroxyl groups per monomer (**5**) to 2.5 significantly reduces the rate of biodegradation.

Starch. Starch, thermoplastic? (qv) (41,42) is a major agricultural commodity and, by far, the most inexpensive commercial biopolymer; it is the only biopolymer that is competitive with polyethylene in price. Annual world production, over 32 million metric tons, is from corn (maize), potatoes, rice, tapioca (cassava), barley, wheat, and other crops. Approximately 16 million metric tons are produced in the United States each year, mainly by extraction from corn but also from potatoes, wheat, and other sources.

Well over half the starch produced is partially hydrolyzed to manufacture corn syrup, dextrose (glucose), and other hydrolysis products that are used as sweeteners or as feedstocks for various manufacturing processes in the chemical, pharmaceutical, and brewing industries. Approximately 75% of the remaining starch, either in native form or modified, is used for nonfood industrial purposes in the manufacture of paper and cardboard, paper coatings and sizings, textile and carpet sizing, and adhesives. Food uses include baby foods, bread batter, cake mixes, confectioneries, puddings, pie fillings, glazes, and sauces.

Starch serves an energy storage function in plants; when starch is metabolized by plants, energy is released and used for plant growth. The major polymer components of starch are amylose and amylopectin. Amylose (**6**) is $\alpha[1 \rightarrow 4]$-linked D-glucose; its molecular weight ranges from 2×10^5 to 2×10^6. Amylopectin has a backbone of $\alpha[1 \rightarrow 4]$-linked D-glucose with $\alpha[1 \rightarrow 6]$-linked D-glucose at branch points; it has molecular weights up to 4×10^8. The relative amounts of amylose and amylopectin vary with the source plant. Cornstarch is typically 28% amylose and 72% amylopectin, but it can be genetically modified to have as much as 85% amylose or, for all practical purposes, 100% amylopectin (waxy maize starch). The physical properties of starch depend on the amylose/amylopectin ratio.

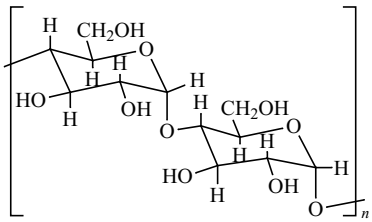

6

Natural starch occurs in the cell in the form of granules. The starch granules are gelatinized upon heating, whereupon the starch molecules become more disordered; the gelatinization temperature ranges from about 70°C in excess water to above 200°C at low moisture content. Depending upon treatment conditions, the starch granules and their crystalline structure may be completely destroyed. In time the starch may retrograde; that is, it reassociates into aggregates and precipitates at low concentrations or sets to a gel at higher concentrations, eventually becoming cloudy, releasing water, and shrinking into a rubbery consistency.

Under proper conditions of temperature, pressure, water content, and shear, the starch granular structure is totally disrupted (43). The starch exists as a continuous phase and in this state is called thermoplastic starch (TPS). TPS can be extruded, injection-molded, or formed into foams (44–48).

The major limitation in developing applications, representing an obstacle to be overcome, is the hydrophilicity of starch, which leads to water sensitivity in physical properties. Strategies for decreasing sensitivity to water include derivitization. For example, acetylation at a degree of substitution greater than 1.5 of the three hydroxyl groups per monomer (**6**) leads to water-resistant "hydrophobic" starch. Chemical modifications often increase water resistance without

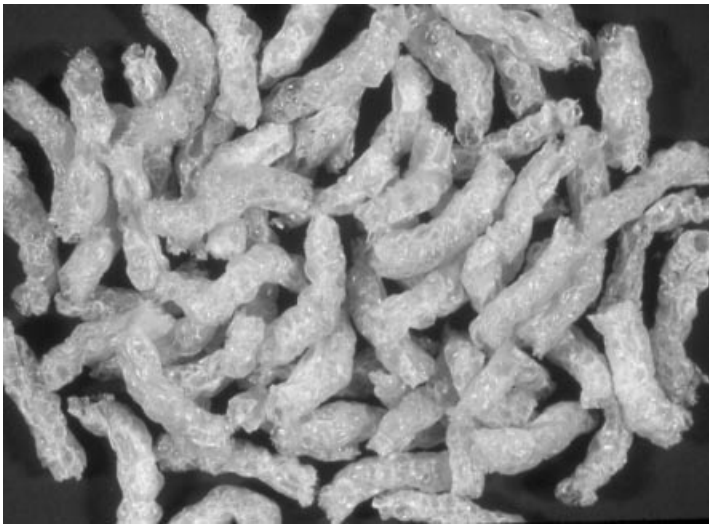

Fig. 2. Water-resistant foam packaging "peanuts" made by extruding starch acetate and water. Courtesy of R. Shogren, U. S. D. A.

significantly decreasing biodegradability. Plasticizers (qv) like glycerol acetate and diethyl succinate can be used to improve processability.

Extruded starch foam is produced by the flash generation of steam as the starch leaves the die (49,50). Foam packaging "peanuts," as a replacement for polystyrene, can be made by extruding starch acetate or hydroxypropylated starch and water (Fig. 2). A commercial example is EcoFoam, a water-soluble extruded hydroxypropylated starch foam manufactured by National Starch and Chemical Co.

Other strategies for overcoming the water sensitivity of starch include blending with other polymers and forming composites by the addition of polymeric or mineral fillers (see below).

Poly(lactic acid). Lactic acid, $CH_3CHOHCOOH$, occurs naturally in animals and in microorganisms. It can be produced commercially by chemical synthesis, but in the United States fermentation is the major route. In *bioreactors*, microorganisms are fed a carbon source substrate, such as dextrose, with yields of lactic acid greater than 90%. The lactic acid is recovered from the fermentation broth and purified in a multistep process that represents a major part of production costs. Eighty percent of the world's production of lactic acid is from corn sugar.

Poly(lactic acid) (PLA) (**7**) (Table 1) is the polyester synthesized from lactic acid (51–54). Condensation polymerization produces a low molecular weight prepolymer ($M_n \sim 5000$) that is treated with chain extenders to yield high molecular weight PLA. Condensation polymerization yields high molecular weight PLA directly when carried out in a high boiling point azeotropic solvent with removal of water by distillation at reduced pressure. Alternatively, the prepolymer is depolymerized in the melt under reduced pressure to produce lactide, the cyclic dimer of lactic acid (a dilactone). Metal-catalyzed ring-opening polymerization of lactide

produces a high molecular weight polymer ($M_n = 60{,}000–150{,}000$) PLAs are also called Polylactide (qv).

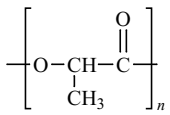

7

PLA from L- or D-monomers is semicrystalline, with a melting transition near 180°C and glass temperature around 67°C. In contrast, a racemic mixture of L- and D-lactic acid produces amorphous polymers with glass temperatures near room temperature. During the depolymerization of the prepolymer the stereoisomers are separated. The L-lactide is the primary component of the high molecular weight PLA; varying the amount of D-lactide allows a variation in physical properties (Table 1).

PLA is thermoplastic and can be processed by extrusion, injection molding, blow molding, and thermoforming. It is unstable in acid and alkaline solution, but is insoluble in water and has good moisture and grease resistance. Its mechanical properties depend on molecular weight and crystallinity. Properties can be varied so as to display, for example, the clarity of polystyrene, the stiffness and tensile strength of poly(ethylene terephthalate), and the twist-retention of cellophane. Other features include favorable flavor and aroma barrier properties, low temperature heat-sealing, and printability. Lactic acid can be copolymerized with glycolic acid or ε-caprolactone to extend the range of properties further.

Major current applications of PLA include clear packaging film and thermoformed articles for disposable food service items and other containers (Fig. 3). PLA can also be spun, and other current major applications are as fibers used in bedding products, clothing, carpets, sheets and towels, and wall coverings (Fig. 4). In addition, PLA can be used for agricultural mulching film and other compostable agricultural and horticultural products, compost bags, trash bin liners, sporting items such as golf tees, coatings for paper and cardboard, and other products. An example is NatureWorks manufactured by Cargill Dow (Figs. 3 and 4).

PLA degrades by hydrolysis, even in the absence of enzymes, and can be recycled back to the monomer. It is compostable, but the rate of biodegradability in a composting environment depends strongly on conditions of temperature, crystallinity, and size and shape of the article (23,34,55–58). The resistance of PLA to degradation by microorganisms plays a role in food packaging applications. PLA is also biocompatible (see BIODEGRADABLE POLYMERS, MEDICAL APPLICATIONS).

As new markets develop for the monomer, lactic acid, through, for example, its conversion to ethyl lactate for use as a biobased solvent, the cost of PLA may be reduced.

Microbial Polyhydroxyalkanoates. Some microorganisms produce polyesters as energy and carbon storage materials, metabolizing them when no external carbon source is available (59,60). Microbial polyesters are now produced commercially through large-scale fermentation processes carried out in bioreactors. Microorganisms (eg, *Ralstonia eutropha*) are fed carbon source substrates, promoting cell growth followed by polymer accumulation, which can result in as

Fig. 3. Sealed packaging tray made from NatureWorks™ PLA. Courtesy of Cargill Dow Co.

much as 80–95% of the cell's dry weight. The bacteria are collected and washed, and the cells ruptured. The polymer is extracted with a solvent, precipitated from water as a white powder, and converted to pellets (61).

The major commercial microial polyesters are polyhydroxyalkanoates (PHAs) (see POLY(3-HYDROXYALKANOATES)) Poly(3-hydroxybutyrate) (PHB) (**8**) is brittle, but as the number of carbon atoms in the side chains of PHAs increases, eg, poly(3-hydroxyvalerate) (PHV) (**9**), the properties tend from polypropylene-like to elastomeric. Copolymers, poly(3-hydroxybutyrate-*co*-3-hydroxyvalerate) (PHBV), have a range of properties depending on composition (Table 1).

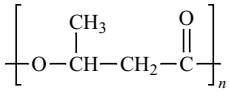

8

Fig. 4. Bedding products made from NatureWorks™ PLA. Courtesy of Cargill Dow Co.

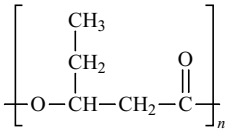

9

The composition of the copolymer is controlled through the ratio of feedstocks used: glucose or sucrose (from sugar cane, sugar beets, or starch hydrolysates) can be used as substrates for butyrate; propionic acid (eg, from the fermentation of wood pulp waste) can be used for valerate.

PHBV is thermoplastic and can be processed by injection molding, extrusion, blow molding, film and fiber forming, and lamination techniques. Significantly, PHBV is stable in humid air and its barrier properties are not humidity-dependent.

Commercial PHBV can be processed into packaging materials such as bottles, jars, and films; food service products such as eating utensils, cups, and plates; toiletry articles such as combs and razor handles; and other products including credit cards, golf tees, and plant pots. An example is Biopol and other PHAs manufactured by Metabolix (Table 1).

Just as there is a wide range of microorganisms that can synthesize PHAs, there are a large number of microorganisms that can degrade PHAs. PHA biodegradation (23,62,63) begins with bacterial or fungal surface colonization. An extracellular PHA depolymerase degrades and solubilizes the polymer into

fragments that are then absorbed by the cell, resulting in complete biodegradation. PHAs biodegrade at a rate that depends on copolymer composition, molecular weight, degree of crystallinity, and the size and shape of the article. PHBV is also recyclable.

PHAs are biocompatible as well as biodegradable and PHBV is used in biomedical applications (see BIODEGRADABLE POLYMERS, MEDICAL APPLICATIONS). One of its degradation products, butyric acid, is a mammalian metabolite found in low concentrations in humans.

Blends and Composites

Starch-Based. Granular starch was used early on as a particulate filler of conventional polymers (eg, polyethylene and polypropylene) in films (64–66). The starch granules are surface-treated to increase compatibility with the hydrophobic matrix: poly(ethylene-*co*-acrylic acid) or poly(ethylene-*co*-vinyl alcohol) plasticizers may be used to reduce brittleness. At starch levels of less than 10%, intended applications were degradable agricultural mulching film and compost bags. The polyethylene encapsulates the starch granules and biodegradation of the starch granules leads to fragmentation of the film. Photocatalytic additives (transition-metal compounds, unsaturated polymers, oils, fats) aim to enhance degradation of the polyethylene. Compost bags, of 23–25% starch, have "curb sturdiness." Starch–polyethylene formulations of 20–80% starch have also been commercialized. Issues connected with the environmental fate and impact of the polyethylene residues remain, and are the subject of current research.

TPS (see above) interacts with hydrophilic and hydrophobic polymers, and can be blended with petroleum-based polymers that are biodegradable. By varying the composition and processing of the blends it is possible to manipulate blend properties to produce plastics that resist property changes at high relative humidity but are nevertheless compostable. Starch–poly(vinyl alcohol) blends, for example, are thermoplastic and can be processed by extrusion (qv), injection molding (qv), blow molding (qv), film blowing, and thermoforming (qv) (67). Their properties depend on composition and processing. In films there is some sensitivity to humidity, and in water they swell but do not dissolve. With one formulation, the mechanical properties at 55% relative humidity are similar to those of polyethylene. The degree of crystallinity of the poly(vinyl alcohol) component varies according to the level of residual acetate groups that remains following the preparation of the poly(vinyl alcohol) by alcoholysis of poly(vinyl acetate). A range of water-soluble blends can thereby be produced by varying the amount of poly(vinyl alcohol), its molecular weight, and its crystallinity. One application is water-soluble laundry bags (68). Starch–poly(vinyl alcohol) films degrade hydrolytically at a rate that depends on composition and crystallinity. In sludge, carbon dioxide measurements indicate greater than 90% degradation in 10 months.

Starch–poly(vinyl alcohol) blends can also be extruded as foams. The poly(vinyl alcohol) increases water resistance relative to foam made from starch alone, allowing shaped applications such as foamed cups and plates.

Fig. 5. Agricultural products (mulch film, planting pots, clips) made from MaterBi™. Courtesy of Novamont S. P. A.

Starch–poly(ε-caprolactone) blends (69) are also water-resistant and totally biodegradable. Their strength and water resistance depend on composition, and film properties can be varied from those resembling low density to high density polyethylene. Applications include agricultural mulching film (12–15 μm) that biodegrades over a controlled period of time to allow cultivation periods from 1 to 5 months. Other applications are trash bin liners, compostable yard waste bags, plant pots, shopping bags, packaging film, cutlery and food service ware, diaper backings, and consumer items. An example of starch-based blends is MaterBi manufactured by Novamont S.P.A. (Italy) (Fig. 5) (Table 1).

Minerals—silicates (clay) or carbonates—increase the stiffness and toughness of starch. Earthshell Packaging manufactured by Earthshell Corp. is a starch–calcium carbonate fiber composite made for a variety of applications including the hinged-lid "clamshell" sandwich containers used in the fast-food industry (Fig. 6). Potato starch and limestone make up about 80% of the composite. They are mixed with water and fiber (eg, cellulose from recycled paper) to form a batter. Thickeners and release agents are added and the batter is placed between two heated mold plates. The water is converted to steam, expanding the batter. The product is finished with protective and water-proofing coatings.

Others. Triacylglycerols (triglycerides) (**10**) (70–72) make up a large part of the storage lipids in animal and plant cells. They are now receiving renewed attention as a candidate feedstock for the production of polymer resins. When liquid at room temperature they are called oils. Commercially important oils are produced from the seeds of soybeans, corn (maize), cotton, sunflowers, flax (linseed), rape, castor beans, tung, palms, peanuts, olives, almonds, coconuts, and canola. Over 7.3 million metric tons of vegetable oils are produced in the United States each year, mainly from soybean, flax, and rapeseed. Soy oil alone accounts for 80% of the seed oils produced in the United States. Soy oil contains about 55% linoleic acid (**11**), 22% oleic acid (**12**) and 10% palmitic acid (**13**).

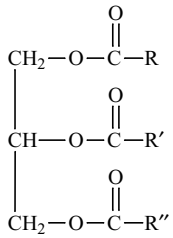

10

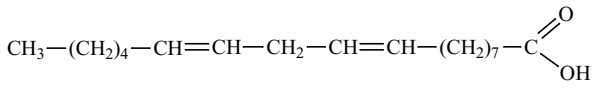

11

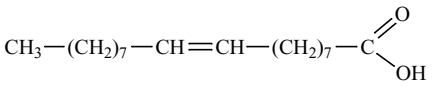

12

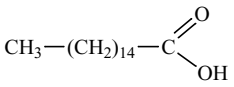

13

Vegetable and animal oils can be made more chemically reactive (eg, by epoxidation), and then cross-linked to form sturdy thermosets. Reinforced with glass fiber the composites have applications in the areas of agricultural equipment and the automotive industry. Plant fiber reinforcement, eg, from jute, hemp, flax, sisal, keraf, wood, straw, or hay, provides a biodegradable option (73).

A triglyceride-based thermoset has been developed from soybean and corn polymers as a sheet-metal alternative for side panels in agricultural equipment, replacing the conventional petroleum-based options (Fig. 7). Initial testing in 1997 involved the University of Delaware's ACRES (Affordable Composites from Renewable Resources) Program and the United Soybean Board. The vegetable-oil composite is strong and weighs 25% less than steel—and less than the petroleum-based products typically used to make panels. It also accepts paint. In 1999, a soy-based polymer was tested in the rear panel of John Deere combines, and beginning

Fig. 6. Earthshell® Packaging disposable food service ware. Courtesy of Earthshell Corp.

Fig. 7. Prototype John Deere side panel for a hay baler (8′ × 3′, 25 lb.). A foam core is enclosed on both sides with a thermoset composite made from soybean oil resin reinforced with glass fiber. Courtesy of University of Delaware Center for Composite Materials.

with the 2002 model year, John Deere Harvester Works' line of combines has included panels made from the material HarvestForm.

Polyurethanes (qv) are now being made from polyols derived from soybean oil, eg, SoyOyl manufactured by Urethane Soy Systems Co. (USSC). Applications include carpet backing and padding, furniture and automobile seating foam, foam insulation, and others.

Laboratory Studies

Many other compositions and processes have been studied in the laboratory; some are in the development stage on their way to commercial production. A few illustrative examples are given here.

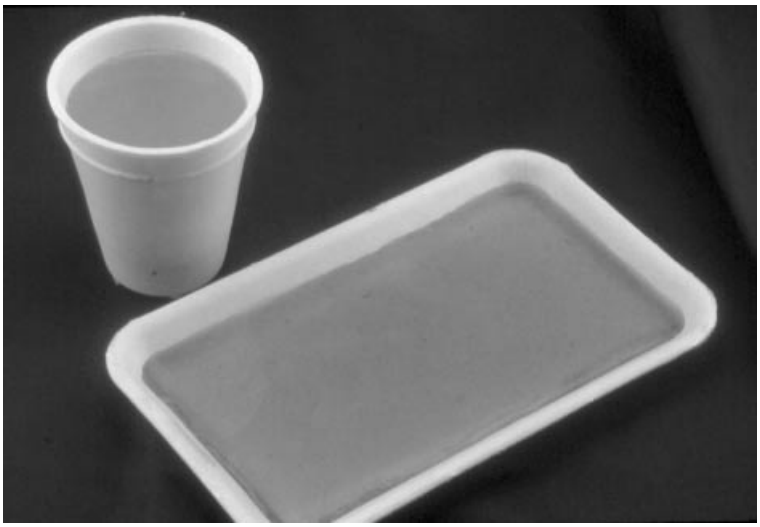

Fig. 8. Starch foam cup and tray coated with water-resistant PHBV. An adhesive layer of shellac, a natural resin, prevents delamination of PHBV from the starch. Courtesy of R. Shogren, U. S. D. A.

Nodax, under development by Proctor & Gamble, is made from renewable sources. It consists of a family of copolymers of 3-hydroxybutyrate and one or more 3-hydroxyalkanoates having a longer side chain, where the side chain has anywhere from 3 to 20 carbon atoms. The structures thereby resemble linear low density polyethylene, with the 3-hydroxybutyrate units providing a basis for crystallinity and the other units introducing structural irregularity and reduced crystallinity. Nodax can be converted into sheets, molded articles, foams, films, fibers, and nonwoven fabrics, and is both biodegradable and compostable.

Modifying the hydrophilicity of starch has been the goal of many strategies, so as to improve the resistance of starch to water. Starch has been chemically modified by reaction with caprolactone, producing a thermoplastic that needs no plasticizer (74). Coatings can also be used, as when starch films are coated with an waterproofing layer of a nitrocellulose–wax blend, as is done with cellophane. Or, starch sheeting can be laminated with a water-resistant layer of poly(ε-caprolactone) by coextrusion (75).

Starch-based foams can provide compostable packaging for the fast-food industry. The extruded starch foam can be coated with a outer layer of acetylated starch to provide water resistance, or a foamed starch-acetylated starch blend can be so coated (76,77). Starch has also been coated with the microbial polyester PHBV to provide resistance to hot and cold water; a natural resin, shellac, prevents delamination (78) (Fig. 8).

Starch can be blended with biodegradable polyesters from renewable sources, such as PLA or PHBV, or with biodegradable petroleum-based copolyesters or poly(ester amides). In these cases, the aim is to combine low cost starch with higher cost polymers having greater hydrophobicity and better physical properties. For example, biodegradable and compostable plastic eating utensils can be made using 55% cornstarch and 45% PLA (Fig. 9).

Fig. 9. Plastic eating utensils. The utensils on the left are made of 55% cornstarch and 45% poly(lactic acid). They are biodegradable and compostable. For comparison, nondegradable polystyrene utensils are shown on the right. Courtesy of R. Shogren, U. S. D. A.

Starch is also compatible with other biopolymers, including polysaccharides such as pectin (79) and agarose (80), and proteins such as casein (81) and gelatin (82).

Chitin (qv), a polysaccharide produced from shellfish waste, and chitosan (deacetylated chitin) are not thermoplastic, but films and fibers prepared by evaporation of solvent have good mechanical properties and low oxygen permeability (83). They mainly have pharmaceutical and biomedical applications, such as contact lenses and wound-healing treatments. Pullulan, a polysaccharide, is prepared commercially through yeast fermentation. It can be processed into a bioplastic that is hard, strong, tough, and elastic. Pullulan has good oxygen barrier properties and has been developed for food-packaging applications. Fibers have been drawn from concentrated solutions.

Commercial proteins (84) include zein—a water-insoluble protein from corn (maize). Zein is thermoplastic and can be processed with extrusion and injection-molding techniques. It forms strong, grease-resistant, and dyeable fibers. Starch has been blended with zein to increase water resistance; natural fibers were added for increased modulus (85). Other commercial proteins include wheat protein, soy protein, and casein.

Epoxidized soybean oil has been polymerized with citric acid and used to coat kraft paper for biodegradable agricultural mulching covers (86); the coating extends the lifetime of the paper mulch to a practical length (Figa. 10). Other plant oils that are being studied include castor seed oil, sunflower seed oil, corn (maize) oil, and rapeseed oil.

Lignin (qv) is an abundant renewable natural resource; it accounts for over 20% of all organic matter and is second in abundance only to cellulose. Approximately 46 million metric tons are isolated in the United States each year as a by-product of wood pulp processing. Its underutilization has often been described,

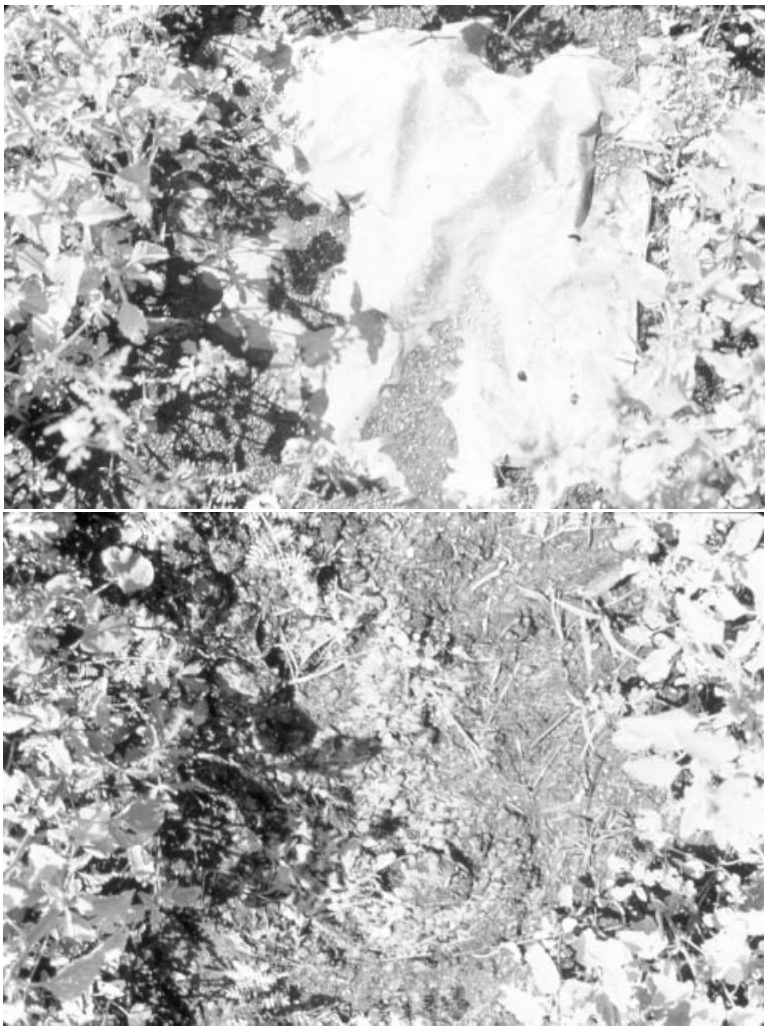

Fig. 10. Biodegradable mulch—kraft paper coated with a polyester made from a reaction product of epoxidized soybean oil and citric acid. The coating reduces the degradation rate and increases wet strength so the mulch can inhibit weed growth for more than 10 weeks. Courtesy of R. Shogren, U. S. D. A.

and the significance of its large-scale potential use in thermoplastics or thermosets has been noted (87). The development of lignin-containing plastics is a compelling objective because it would raise lignin to the status of a high value commodity material. Lignin bioproducts could also provide a stabilizing component to composts: lignin degrades at a slower rate than most other biopolymers, and in composts it would provide an important soil stabilizer, helping to maintain organic content and moisture level.

Lignin has been studied as a component in many nonbiodegradable thermoplastics materials: as a filler in lowdensity polyethylene and polypropylene

(88,89), in compression-molded unplasticized poly(vinyl chloride)–lignin blends (90), in blends of organosolv lignin and poly(vinyl chloride-*co*-vinyl acetate) (91), and in solvent-cast films of hydroxypropyl lignin–caprolactone copolymers blended with poly(vinyl chloride) (92).

Lignin and lignin esters have also been blended with various biodegradable thermoplastics: poly(ε-caprolactone)–lignin blends prepared by solvent casting (93), kraft lignin–poly(vinyl alcohol) blends (94), lignin–poly(ethylene oxide) blends (95), methylated lignin–poly(ethylene oxide) blends (95), and lignin and lignin esters blended with cellulose acetate butyrate, with poly(hydroxybutyrate), and with a starch-poly(ε-caprolactone) copolymer blend (96,97).

Derivatized kraft lignin has been incorporated at a level of 85% into poly(vinyl acetate) to produce a thermoplastic material that can be extrusion-molded (98). Alkylated 100% kraft lignin has been shown to give thermoplastic material that possesses tensile properties similar to polystyrene; pyrrolidinone was used as a solvent, diethyleneglycol dibenzoate and indene were used as plasticizers (99).

Lignin has also been used in thermosetting resins as additions to polyurethanes, epoxy resins, acrylic resins, and phenol resins. For example, IBM has explored the use of epoxidized lignin in producing thermosetting resins for circuit board applications (100).

How Green are Green Plastics?

There is a hope that LCA (8) of plastics will be developed to the point that meaningful product environmental profiles can be produced, whereby the environmental impacts of various plastics can be compared with one another. Initial LCA development has focused, in particular, on energy consumption and carbon dioxide release, but even then the dependence of carbon dioxide release on disposal method, for example, is not treated uniformly. In the coming years LCA methodologies are likely to be improved.

Certain trends, however, are beginning to emerge. A review of 20 LCA studies of biodegradable polymers (101,102) indicates that thermoplastic starch, the major component of approximately 75% of green plastics production, offers important environmental benefits compared to conventional polymers. Compared to starch, the environmental benefits of poly(lactic acid), currently accounting for 10–15% of production, and of biodegradable polymers made from nonrenewable resources, eg, poly(vinyl alcohol) and poly(ε-caprolactone), accounting for approximately 10% of production, seem to be smaller, but still greater than that of conventional polymers. For microbial polyhydroxyalkanoates, which currently make up a very small part of total green plastics production, the environmental advantage seems to be small (or perhaps nonexistent), but the fermentation technologies for producing microbial polyhydroxyalkanoates are among the most recently developed, and both the production method and the scale of production can influence evaluations of the overall environmental balance. One LCA that was published in the popular literature and received much attention (103) was limited to poly(lactic acid) and microbial polyhydroxyalkanoates; thermoplastic starch was not considered.

Future Prospects

The future of green plastics will be determined by the cost–performance ratio, where performance will include environmental attributes as well as physical properties. More than 90% of current conventional plastics are environmentally nondegradable, but at the present time they have a significant cost advantage. Within the group of degradable/biodegradable/compostable plastics, activated polyolefins, on account of the cost advantage they now enjoy and in spite of remaining questions related to their environmental fate and impact, will likely find continued market acceptance, especially in third-world countries where environmental considerations are perforce relegated to secondary status, and where interim solutions are being sought pending optimization of the bioplastics industry.

Hybrid materials, containing biodegradable, but nonrenewable, petroleum-based polymers combined with renewable biopolymers (mainly starch), constitute an environmental compromise, but hybrids provide improved physical properties relative to the biopolymers alone; they are biodegradable; and, in many cases, they are compostable. Hybrids satisfy many of the growing environmental concerns of the major industrialized regions of North America, Europe, and Asia.

Developing bioplastics, ie, biodegradable and compostable plastics that are derived entirely or almost entirely from renewable raw materials, faces the greatest technological challenge. Reducing cost will be a critical factor. Most surveys indicate that for green plastics consumers might be willing to pay a premium of 10–20% above the cost of conventional plastics. The cost of green plastics now exceeds that amount, partly because of unoptimized technologies and limited production.

One can envision two, not mutually exclusive, directions for the future. The usefulness of biomass polymers (starch, cellulose, and others) will continue to be extended through chemical modification, novel formulations, and processing innovations to produce an increasing number and variety of materials and applications. Concurrently, biomass polymers will be transformed into an increasing array of polymerizable monomers, using enzymatic and conventional means, followed by polymerization, also using both enzymatic and conventional means, to produce polymer materials having sequences and molecular weights required for the targeted applications.

As the "green chemistry" movement presses the polymer industry toward sustainability and low environmental impact, technologies that produce shifts in those directions will continue to emerge and develop. Significantly, the new technologies are being aided with help from governments that are impelled by environmental concern, need for reduced dependence on foreign crude oil, and desire for increased agricultural markets. The allure of a sustainable industry producing commodity plastics for an increasing world population will no doubt persist. It remains to be seen at what rate the required technologies will develop.

BIBLIOGRAPHY

1. E. S. Stevens, *Green Plastics. An Introduction to the New Science of Biodegradable Plastics*, Princeton University Press, Princeton, 2002.

2. G. Scott, *Polymers and the Environment*, Royal Society of Chemistry, Cambridge, UK, 1999.
3. National Research Council, Committee on Biobased Industrial Products, *Biobased Industrial Products: Priorities for Research and Commercialization*, National Academy Press, Washington, D. C., 2000.
4. R. A. Gross and B. Kalra, *Science* **297**, 803–807 (2002).
5. G. Scott and D. Gilead, eds., *Degradable Polymers: Principles and Applications*, Chapman and Hall, London, 1995.
6. R. M. Ottenbrite, S. J. Huang, and K. Park, eds., *Hydrogels and Biodegradable Polymers for Bioapplications* (American Chemical Society Symposium Series 627), American Chemical Society, Washington, D. C., 1996.
7. G. Fuller, T. A. McKeon, and D. D. Bills, eds., *Agricultural Materials as Renewable Resources: Nonfood and Industrial Applications* (American Chemical Society Symposium Series 647), American Chemical Society, Washington, D. C., 1996.
8. J. D. Hamilton and R. Sutcliffe, eds., *Ecological Assessment of Polymers. Strategies for Product Stewardship and Regulatory Programs*, Van Nostrand Reinhold Co., Inc., New York, 1997.
9. D. L. Kaplan, ed., *Biopolymers from Renewable Resources*, Springer-Verlag, Berlin, 1998.
10. L. A. Kleintjens, ed., *"Petro" Polymers vs. "Green" Polymers* (Macromolecular Symposia 127), Hüthig & WepfVerlag, Zug, Switzerland, 1998.
11. S. H. Imam, R. V. Greene, and B. R. Zaidi, eds., *Biopolymers: Utilizing Nature's Advanced Materials* (American Chemical Society Symposium Series 723), American Chemical Society, Washington, D. C., 1999.
12. C. Scholz and R. A. Gross, eds., *Polymers from Renewable Resources: Biopolyesters and Biocatalysis* (American Chemical Society Symposium Series 764), American Chemical Society, Washington, D. C., 2000.
13. R. A. Gross and C. Scholz, eds., *Biopolymers from Polysaccharides and Agroproteins* (American Chemical Society Symposium Series 786), American Chemical Society, Washington, D. C., 2001.
14. International Center for Science and High Technology (ICS), United Nations Industrial Development Organization (UNIDO) Web site: www.ics.trieste.it (pure and applied chemistry/ environmentally degradable plastics). Accessed February 7, 2003.
15. http://www.biopolymer.net, a general informational Web site. Accessed February 7, 2003.
16. Biodegradable Polymers, www.buscom.com/plastics/P175.html. Accessed February 7, 2003
17. P. T. Anastas and J. C. Warner, *Green Chemistry. Theory and Practice*, Oxford University Press, Oxford, 1998.
18. P. T. Anastas, P. H. Bickart, and M. M. Kirchhoff, *Designing Safer Polymers*, John Wiley & Sons, Inc., New York, 2000.
19. B. W. Vigon, B. A. Tolle, and V. McGinnis, in Ref. 8, pp. 307–335.
20. G. Harlan and C. Kmiec, in Ref. 5, pp. 153–168.
21. T. Suzuki, Y. Ichihara, M. Yamada, and K. Tonomura, *Agric. Biol. Chem.* **37**, 747 (1973).
22. S. Matsumara and K. Toshima, in Ref. 6, pp. 137–148.
23. C. Scholz and R. A. Gross, in Ref. 12, pp. 1–11.
24. A. Duda and S. Penczek, in Ref. 12, pp. 160–198.
25. P. T. DeLassus and N. F. Whiteman, in J. Brandrup and co-workers, eds., *Polymer Handbook*, 4th ed., John Wiley & Sons, Inc., New York, 1999, pp. V164–V165.
26. http://www.dow.com. Accessed February 7, 2003.
27. http://www.eastman.com. Accessed February 7, 2003.

28. http://www.basf.com. Accessed February 7, 2003.
29. http://www.dupont.com. Accessed February 7, 2003.
30. http://www.cargilldow.com. Accessed February 7, 2003.
31. Personal communication, Metabolix Inc., Cambridge, Mass., December 13, 2002.
32. Personal communication, Novamont S. P. A., Italy, January 10, 2003.
33. Y. Tokiwa, T. Ando, and T. Suzuki, *J. Ferment. Technol.* **54**, 603 (1976).
34. Y. Tokiwa, T. Ando, T. Suzuki, and K. Takeda, in J. E. Glass and G. Swift, eds., *Agricultural and Synthetic Polymers. Biodegradability and Utilization* (American Chemical Society Symposium Series 433), American Chemical Society, Washington, D. C., 1990, pp. 136–148.
35. G. L. Siparsky, in Ref. 12, pp. 230–251.
36. P. Jarrett, C. Benedict, J. P. Bell, J. A. Cameron, and S. J. Huang, in S. W. Shalaby and co-workers, eds., *Polymers as Biomaterials*, Plenum Press, New York, 1984, pp. 181–192.
37. R. D. Gilbert and J. F. Kadla, in Ref. 9, pp. 47–95.
38. J. M. Krotchta and C. L. C. De Mulder-Johnson, in Ref. 7, pp. 120–140.
39. J. Brydson, *Plastics Materials*, 7th ed., Butterworth Heinemann, Oxford, 1999, pp. 632–634.
40. H. P. Fink, P. Weigel, H. J. Purz, and J. Ganster, *Prog. Polym. Sci.* **26**, 1473–1524 (2001).
41. R. L. Shogren, in Ref. 9, pp. 30–46.
42. P. J. Frazier, P. Richmond, and A. M. Donald, eds., *Starch: Structure and Functionality*, Royal Society of Chemistry, Cambridge, 1997.
43. U.S. Pat. 4,133,784 (Jan. 9, 1979), F. H. Otey and R. P. Westhoff (to U.S.D.A.).
44. R. L. Shogren, G. F. Fanta, and W. M. Doane, *Starch/Stärke* **45**, 276–280 (1993).
45. S. Simmons, C. E. Weigand, R. J. Albalak, R. C. Armstrong, and E. L. Thomas, in C. Ching, D. L. Kaplan, and E. L. Thomas, eds., *Biodegradable Polymers and Packaging, Technomic*, Publishing Co., Inc., Lancaster, Pa., 1993, pp. 171–207.
46. U.S. Pat. 5,362,777 (Nov. 8, 1994), I. Tomka.
47. C. Bastioli, in Ref. 5, pp. 112–137.
48. W. J. Bergthaller, U. Funke, M. G. Lindhauer, S. Radosta, F. Meister, and E. Taeger, in Ref. 11, pp. 14–38.
49. G. M. Glenn, R. E. Miller, and D. W. Irving, in Ref. 7, pp. 88–106.
50. G. M. Glenn, W. J. Orts, R. Buttery, and D. Stern, in Ref. 13, pp. 42–60.
51. J. W. Leenslag and H. J. Pennings, *Macromol. Chem.* **188**, 1809–1814 (1987).
52. H. R. Kricheldorf, I. Kreiser-Saunders, and C. Boettcer, *Polymer* **36**, 1253–1259 (1995).
53. M. H. Hartmann, in Ref. 9, pp. 367–411.
54. J. Lunt, *Polym. Degrad. Stab.* **59**, 145 (1998).
55. M. Vert, G. Schwarch, and J. Coudane, *J. Macromol. Sci., Pure Appl. Chem. A* **32**, 787–796 (1995).
56. S. Jacobsen, Ph. Degée, H. G. Fritz, Ph. Dubois, and R. Jérôme, *Polym. Eng. Sci.* **39**, 1311–1319 (1999).
57. S. Karlsson and A.-C. Albertsson, in Ref. 10, pp. 219–225.
58. J. Tuominen, J. Kylmä, A. Kapanen, O. Venelampi, M. Itävaara, and J. Seppälä, *Biomacromolecules* **3**, 445–455 (2002).
59. Y. Doi, *Microbial Polyesters*, John Wiley & Sons, Inc., New York, 1990.
60. L. J. R. Foster, in Ref. 12, pp. 42–60.
61. D. Kemmish, in C. Ching, D. L. Kaplan, and E. L. Thomas, eds., *Biodegradable Polymers and Packaging*, Technomic Publishing Co., Inc., Lancaster, Pa., 1993, pp. 225–232.
62. L. J. R. Foster, R. C. Fuller, and R. W. Lenz, in Ref. 6, pp. 68–92.
63. T. M. Scherer, M. M. Rothermich, R. Quinteros, M. T. Poch, R. W. Lenz, and S. Goodwin, in Ref. 12, pp. 254–280.

64. G. J. L. Griffin, *Am. Chem. Soc. Div. Org. Coat. Plast. Chem.* **33**, 88 (1973).
65. U.S. Pat. 4,016,117 (Apr. 5, 1977), G. J. L. Griffin (to Coloroll Ltd.).
66. U.S. Pat. 4,519,161 (May 28, 1985), D. Gilead and G. Scott.
67. C. Bastioli, V. Bellotti, L. Del Giudice, and G. Gilli, in M. Vert, J. Feijen, A.-C. Albertsson, G. Scott, and E. Chiellini, eds., *Biodegradable Polymers and Plastics*, Royal Society of Chemistry, Cambridge, UK, 1992, pp. 101–111.
68. W. M. Doane, C. L. Swanson, and G. F. Fanta, in R. M. Rowell, T. P. Schultz, and R. Narayan, eds., *Emerging Technologies for Materials and Chemicals from Biomass* (American Chemical Society Symposium Series 476), American Chemical Society, Washington, D. C., 1992, pp. 206–230.
69. L. Avérous, L. Moro, P. Dole, and C. Fringant, *Polymer* **41**, 4157–4167 (2000).
70. T. A. McKeon, J.-T. Lin, M. Goodrich-Tanrikulu, and A. Stafford, in Ref. 7, pp. 158–178.
71. M. O. Bagby, in Ref. 7, pp. 248–257.
72. S. F. Thames, M. D. Blanton, S. Mendon, R. Subramanian, and H. Yu, in Ref. 9, pp. 249–280.
73. R. P. Wool, *CHEMTECH* 44–48 (June 1999).
74. C. Pellegrini and I. Tomka, in Ref. 10, pp. 31–35.
75. L. Wang, R. L. Shogren, and C. Carriere, *Polym. Eng. Sci.* **40**, 499–506 (2000).
76. R. Shogren, *Carbohydr. Polym.* **29**, 57–62 (1995).
77. G. M. Glenn, W. J. Orts, R. Buttery, and D. Stern, in Ref. 13, pp. 42–60.
78. U.S. Pat. 5,756,194 (May 26, 1998), R. L. Shogren and J. W. Lawton (to U. S. D. A.).
79. P. D. Hoagland, in N. Parris, A. Katon, L. K. Cramer, and J. Pearce, eds., *Macromolecular Interactions in Food Technology* (American Chemical Society Symposium Series 650), American Chemical Society, Washington, D. C., 1996, pp. 145–154.
80. A. H. Mohammed, M. W. N. Hember, R. K. Richardson, and E. R. Morris, *Carbohydr. Polym.* **36**, 27–36 (1998).
81. I. Arvanitoyannis, E. Psomaidou, and A. Nakayama, *Carbohydr. Polym.* **34**, 179–192 (1997).
82. N. A. Abdulmola, M. W. N. Hember, R. K. Richardson, and E. R. Morris, *Carbohydr. Polym.* **31**, 53–63 (1996).
83. Reports Group—Technical Insights, *Chitin and Chitosan: An Expanding Range of Markets Awaits Exploitation*, 3rd ed., John Wiley & Sons, Inc., New York, 1998.
84. K. P. McGrath and D. L. Kaplan, *Protein-Based Materials*, Birkhäuser, Boston, 1997.
85. S. T. Lim and J.-L. Jane, in M. Yalpani, ed., *Carbohydrates and Carbohydrate Polymers*, ATL Press, Mount Prospect, Ill., 1993, pp. 288–297.
86. R. L. Shogren, *J. Sustainable Agric.* **16**, 33–47 (2000).
87. W. G. Glasser, R. A. Northey, and T. P. Schultz, eds., *Lignin: Historical, Biological, and Materials Perpectives* (American Chemical Society Symposium Series 742), American Chemical Society, Washington, D. C., 2000.
88. P. Alexy, B. Kosikova, and G. Podstranska, *Polymer* **41**, 4901–4908 (2000).
89. C. G. Sanchez and L. A. E. Alvarez, *Angew. Makromol. Chem.* **272**, 65–70 (1999).
90. S. El Raghi, R. R. Zahran, and B. E. Gebril, *Mater. Lett.* **46**, 332–342 (2000).
91. D. Feldman, D. Banu, J. Campanelli, and H. Zhu, *J. Appl. Polym. Sci.* **81**, 861–874 (2001).
92. W. DeOliviera and W. G. Glasser, *J. Appl. Polym. Sci.* **51**, 563–571 (1994).
93. J. C. Li, Y. He, and Y. Inoue, *Polym. J.* **33**, 336–343 (2001).
94. E. Corradini, E. A. G. Pineda, and A. A. W. Hechenleitner, *Polym. Degrad. Stab.* **66**, 199–208 (1999).
95. S. Kubo, J. F. Kadla, and R. S. Gilbert, *Polym. Mater. Sci. Eng.* **86**, 374–375 (2002).
96. I. Ghosh, *Blends of Biodegradable Thermoplastics with Lignin Esters*, MS thesis, Virginia Polytechnic Institute and State University, Va., 1998.
97. I. Ghosh, R. K. Jain, and W. G. Glasser, in Ref. 87, pp. 331–350.

98. Y. Li, J. Mlynar, and S. Sarkanen, *J. Polym. Sci., Part B: Polym. Phys.* **35**, 1899–1910 (1997).
99. Y. Li and S. Sarkanen, in Ref. 87, pp. 331–366.
100. L. Kosbar, J. Gelome, R. Japp, and W. Fotorny, *J. Industrial Ecol.* **4**, 93–105 (2000).
101. M. Patel, Paper presented at the 7th World Conference on Biodegradable Polymers and Plastics, Pisa, Italy, June 2002.
102. M. Patel, C. Bastioli, L. Marini, E. Würdinger, http://www.chem.uu.nl/nws/www/general/personal/Biopoly.pdf. Accessed February 7, 2003.
103. T. U. Gerngross and S. C. Slater, *Sci. Am.* 37–41 (Aug. 2000).

E. S. STEVENS
Binghamton University

ENZYMATIC POLYMERIZATION. See Volume 2.

ETHYLENE COPOLYMERS

Introduction

Polyethylene and polystyrene are two high volume commodity polymers, widely studied in materials research, exemplifying the classes of semicrystalline polymers (qv) and amorphous polymers (qv) respectively (see ETHYLENE POLYMERS, HDPE; STYRENE POLYMERS). There has been considerable interest to produce copolymers from ethylene (E) and styrene (S). The incorporation of aromatic groups in polyethylene has been associated, for example, with enhanced radiation resistance (1) or electrical-breakdown resistance by enabling space charge dissipation (2). A variety of different copolymer molecular architectures can potentially be produced. In addition to the different comonomer distributions (random, alternating, or blocky nature), there are possibilities for chain branching and stereoregularity in the copolymer chain microstructure.

Various references describe efforts to copolymerize ethylene and styrene. The production of copolymers has been attempted by using conventional polymerization routes for either polyethylene or polystyrene with introduction of the alternate comonomer into the process. Many reported copolymerizations produce heterogeneous polymers consisting of mixtures of copolymers and homopolymers (3), for example U.S. patent number 3,117,945 describes the production of a "gross" copolymer, composed of various fractions that could be separated on the basis of their solubility parameter. Copolymers containing low levels ($<$4 mol%) of styrene incorporation have been prepared by both conventional Ziegler-Natta Catalysts (qv) (4–6) and free-radical processes (7). U.S. patent number 4,076,698 allegedly has examples of copolymers of ethylene with styrene and α-methylstyrene produced by coordination catalysts at low temperature (8), but does not give any significant characterization data for the polymers. These early synthetic routes

Encyclopedia of Polymer Science and Technology. Copyright John Wiley & Sons, Inc. All rights reserved.

that were investigated do not provide commercially viable routes for the production of copolymers.

Developments published in the early 1990s demonstrated the ability of specific classes of metallocene catalysts (see METALLOCENES) to efficiently copolymerize ethylene and vinyl aromatic monomers, such as styrene. In particular, INSITE Technology (The Dow Chemical Co.), including developments of single-site, constrained-geometry, addition polymerization catalysts (9–11) has provided an efficient route to produce essentially random copolymers based on ethylene and styrene (see SINGLE-SITE CATALYSTS). The primary focus of subsequent sections is the preparation, characterization, and utility of poly(ethylene-*co*-styrene); "ethylene-*co*-styrene polymer" is also used as an alternate terminology throughout this chapter for coherence. It is pertinent to mention that INDEX Interpolymers (The Dow Chemical Co.) is the descriptive term for the family of products, including poly(ethylene-*co*-styrene), produced by INSITE technology, and many references have used the terminology "ethylene/styrene interpolymers," abbreviated to ESI, as a descriptor for the copolymers.

Metallocene-Catalyzed Polymerizations

Many studies have focused on catalysts that could potentially copolymerize ethylene and vinyl aromatic monomers, together with the associated polymerization chemistry and chemical analyses of the produced polymers. It is evident from a number of references (eg 12–14) that the catalyst structure and polymerization conditions, such as temperature and monomer feed ratios, have major influences on the reaction product in terms of production efficiency, product composition (copolymer, homopolymer contents), and copolymer microstructure, including stereoregularity.

Popular catalysts investigated for the preparation of copolymers have been single-site, constrained-geometry, addition polymerization catalysts based on titanocene complexes, exemplified by dimethylsilyl(tetramethylcyclopentadienyl)-(*t*-butylamido) titanium dichloride [$(CH_3)_2Si(CH_3)_4Cp$)(*N*-*t*-Butyl)$TiCl_2$]. Other catalysts of significant interest have been based on fluorenyl and indenyl ligand structures, such as those described by Mitsui Toatsu (15). A short overview of technology (16) has included identification of the most widely investigated catalysts cited in basic patents. Studies of catalyst systems that produce syndiotactic polystyrene provided the starting point for research at the University of Salerno (17). Some of their subsequent work on the production and characterization of copolymers, including aspects related to stereoregularity and crystallinity of copolymers, has been referred to in a review article by Pellecchia and Oliva (18).

Many copolymers that have been produced to date have contained less than 50 mol% styrene, in large part because the catalysts typically utilized for copolymerization have not allowed the incorporation of adjacent styrene units into the growing polymer chains. This structural feature is discussed further under Properties. Limited literature (19,20) has described the production of copolymers in which the catalyst selection and polymerization conditions employed have resulted in the incorporation of adjacent styrene units in the polymer chain. Hou and

co-workers (21) have recently reported on catalyst systems that can copolymerize the monomers into block styrene–ethylene copolymers, although the reaction products were mixtures of block copolymer with homopolymers.

A research program conducted in the group of Mulhaupt (University of Freiburg, Germany) included copolymerization of ethylene with styrene using methaluminoxane-activated half-sandwich complexes (22) and methaluminoxane-activated bis(phenolate) complexes (23). The influence of polymerization conditions on the copolymerization of styrene with ethylene using $(CH_3)_2Si((CH_3)_4Cp)(N\text{-}t\text{-butyl})TiCl_2$/methylaluminoxane (MAO) catalyst/cocatalyst system was studied (14). The fractionation and comprehensive characterization of a poly(ethylene-*co*-styrene) having 13.8 mol% styrene provided (24) strong evidence of a single-site mechanism for the copolymerization.

Alternating ethylene–styrene (ES) copolymers, or copolymers that contain alternating $(ES)_n$ sequences, have been synthesized. Suzuki and co-workers (25) described the preparation of alternating atactic $(ES)_n$ copolymers via hydrogenation of poly(phenylbutadienes), produced by anionic polymerization. Miyatake and co-workers (26) have disclosed the production of copolymers having a high degree of alternating isotactic polymer chain sequences. They further reported (27) that the alternating isotactic copolymer had a crystalline melting point of 116°C. Later references (eg 12,13,28) provide more details regarding catalysts, reaction mechanisms, and characterization of produced copolymers having stereoregular, alternating ES chain sequences. For example, Venditto and co-workers (28) described the composition, stereoregularity, and crystallinity of copolymers produced by ansa–zirconocene and half-titanocene based catalysts, with copolymers reported as having melting points in the range of 100–145°C, attributed to crystallization of alternating stereoregular $(ES)_n$ sequences. Izzo and co-workers (29) have produced low molecular weight model compounds of alternating ES copolymers with a range of catalysts, and characterization was considered to confirm the isotactic structure of copolymers.

Arai and co-workers (30) have shown that a copolymer having alternating polymer chain sequences that are isotactic and crystallizable can be produced when copolymerization is carried out at temperatures of 50°C or below, using, for example, *rac*-[isopropylidenebis(1-indenyl)]zirconium dichloride. Although the presence of crystallizable $(ES)_n$ polymer chain sequences could contribute to properties such as mechanical strength, it appears (31) that annealing or exposure to solvent is required to develop a significant level of crystallinity. This observation is analogous to the behavior of isotactic polystyrene; the latter polymer also has a slow rate of crystallization that has hindered its commercialization, because of the restricted ability to develop crystallinity under common melt-fabrication conditions (32).

Terpolymerizations. A number of references, mainly patents, teach the metallocene-catalyzed polymerization of ethylene and styrene with a range of additional monomers, providing potential manufacturing routes to materials with modified properties and functionality relative to ethylene-*co*-styrene polymers. Dienes such as ethylidene norbornene, 1,3-butadiene, and 1,5-hexadiene (33) introduce vinyl unsaturation into the copolymers, enabling more facile cross-linking of the copolymers. Other monomers of interest include propylene, higher α-olefins, and norbornene (34,35).

Propylene (P) is a termonomer that has received the most attention. Structure–property relationships of terpolymers based on ethylene, styrene, and propylene, have been published (36). The terpolymers are most differentiated from ethylene-*co*-styrene polymers when there is measurable crystallinity in the solid-state microstructure, because the introduction of methyl groups on the polymer chain modifies both the crystalline and amorphous phases of the solid-state microstructure. In another aspect of terpolymerization, ethylene has been investigated as a catalyst reactivator in propylene–styrene copolymerization by Caporaso and co-workers (37), with the research directed at introducing styrene units into isotactic polypropylene.

Chung and co-workers (38) have reported the synthesis of copolymers of ethylene and paramethylstyrene and has extended these studies to produce and characterize elastomeric terpolymers that further include propylene and 1-octene as the additional monomers (39,40).

Copolymer Manufacture: Solution Polymerization

The two monomers of major interest, styrene and ethylene, are well known and details can be found on all aspects of their technology elsewhere. Poly(ethylene-*co*-styrene) is primarily produced via solution polymerization techniques using metallocene catalyst/co-catalyst systems, analogous to the production of copolymers of ethylene with α-olefin monomers. Solvents that can be employed include ethyl-benzene, toluene, cyclohexane, and mixed alkanes (such as ISOPAR E, available from Exxon). The thermodynamic properties of poly(ethylene-*co*-styrene), including solvent interactions and solubility parameter assessments, are important factors in relation to polymer manufacture and processing, and have been reported by Hamedi and co-workers (41).

Key factors in the copolymer manufacture are

(1) Purity and cleanup of the solvent and monomers, especially styrene. Metallocene catalysts are noted for their susceptibility to polar molecules, and effective removal of species such as stabilizers, water, and oxygen is required to achieve high efficiencies.

(2) Polymer recovery via separation from unreacted monomers, especially styrene, and the process solvent. Typically carried out by devolatilization, as in the manufacture of polystyrene, the conditions (such as temperature and residence time) employed determine the amount, if any, of atactic polystyrene in the final product resulting from free-radical polymerization of styrene.

(3) Recovery and handling of the final product. A range of copolymers are either amorphous or have low levels of crystallinity and further have glass-transition temperatures (T_g's) close to or below 25°C, as discussed under Properties. These are soft tacky materials under typical ambient conditions. If produced in pellet form, these copolymers can require some form of antiblocking technology, such as the development of novel pellet coatings (42), to allow effective material handling.

Although classic analytical techniques can be employed, specific procedures such as Fourier transform infrared spectroscopy for analysis of polystyrene and copolymerized styrene (43) have contributed to the characterization and quality assurance of copolymer products.

Properties of Poly(ethylene-*co*-styrene)

Poly(ethylene-*co*-styrene) constitutes a broad family of materials. Although copolymers with stereoregular chain sequences could be produced, the catalyst and process conditions most often employed for production to date give copolymers that are atactic, and contain typically up to about 50 mol% (~ 80 wt%) styrene content. These copolymers have been described (10) as "pseudorandom," since successive head-to-tail styrene chain insertions have been shown to be absent, even at high levels of styrene incorporation. This structural feature, represented schematically in Figure 1, is important; each aromatic group is typically separated from its near neighbor by at least three methylene units, in contrast to polystyrene. Much of the research and technology developments are reported for copolymers with this chain microstructure. These copolymers have a continuum of solid-state microstructures ranging from highly crystalline to essentially amorphous, dependent primarily upon comonomer composition ratio.

A review (44) has provided more details on the structure, properties, and applications of the copolymers. Researchers at Case Western Reserve University, Cleveland, Ohio, have contributed significantly to the understanding of viscoelastic behavior and mechanical properties of these copolymers (45,46).

Thermal Properties, Crystallinity, and Density. Figure 2 correlates crystallization (T_c), melting (T_m), and glass-transition (T_g) temperatures measured by differential scanning calorimetry (DSC) with copolymer styrene content, and Figure 3 correlates the degree of crystallinity and density with copolymer styrene content.

Crystalline melting temperatures and crystallinity decrease with increasing copolymer styrene content. Copolymers with styrene contents of less than 40 wt% (~15 mol%) generally exhibit a well-defined melting process. Copolymers with styrene contents above 45 wt% (~18 mol%) are essentially amorphous. A critical sequence length of $(CH_2)_n$ units is required to enable crystallization of chain segments. Thus, introduction of pendent phenyl groups by copolymerization suppresses the crystallinity resulting from $(CH_2)_n$ polymer chain sequences because the phenyl groups are excluded from crystalline domains. It is pertinent to comment here that subtle differences may be found in the copolymer monomer sequence distributions as a consequence of catalyst selection and polymerization

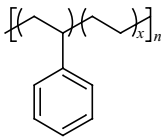

Fig. 1. Schematic representation of so-called pseudorandom copolymer structure.

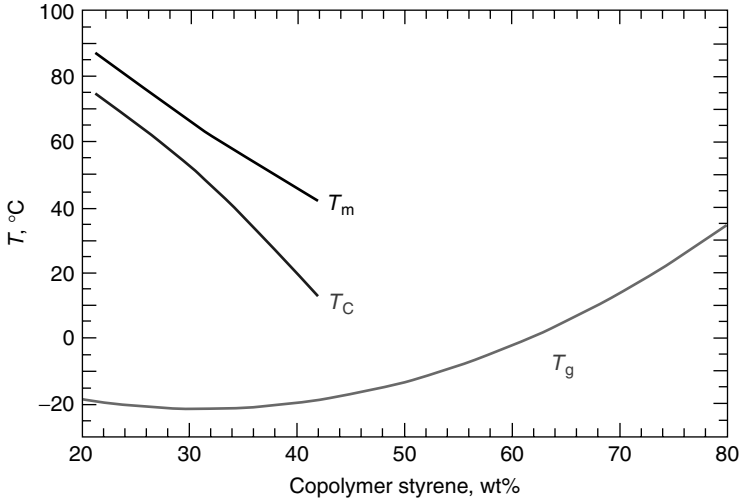

Fig. 2. Thermal transitions of poly(ethylene-*co*-styrene) (DSC data; 10°C/min heating, cooling rates).

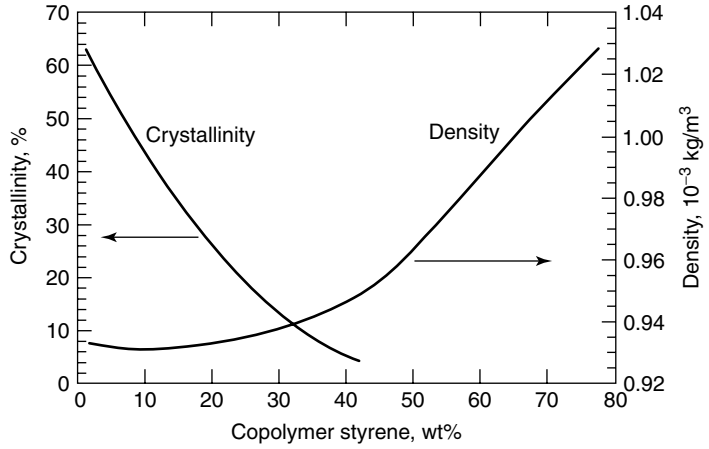

Fig. 3. Density and crystallinity of poly(ethylene-*co*-styrene).

conditions employed. As a result of this, copolymers with nominally the same comonomer content can exhibit some differences in structure-property relationships.

The copolymers have glass-transition temperatures in the range −20 to +30°C. Above about 45 wt% (18 mol%) styrene content, the copolymer T_g increases with increasing styrene content. Satisfactory correlation between copolymer composition and T_g has been found by considering them either as random copolymers of ethylene and styrene or as random copolymers of ethylene and ES dyads. Thus, T_g data were shown by Chen and co-workers (46) to satisfactorily fit

the Fox equation in the form

$$\frac{1}{T_g} = \frac{(1 - 1.27w_s)}{T_{g,e}} + \frac{1.27w_s}{T_{g,es}}$$

where $T_{g,e}$ is the glass-transition temperature of polyethylene, $T_{g,es}$ is the glass-transition temperature of the alternating ethylene–styrene copolymer, and w_s is the weight fraction of styrene incorporated into the copolymer. Extrapolation gave a glass-transition temperature of -66°C for amorphous polyethylene and 44°C for an alternating ES copolymer.

Thermogravimetric analyses (TGA) in both air and nitrogen show weight loss occurs at temperatures above 220°C for the copolymers, reflecting random chain scission as a predominant degradation mechanism.

Viscoelastic Properties: Dynamic Mechanical Spectroscopy (DMS). The viscoelastic properties and time–temperature–rate dependency of properties are key elements of the materials science of ethylene-*co*-styrene polymers. Dynamic mechanical loss spectra are presented in Figures 4a and 4b for selected semicrystalline copolymers, and low crystallinity and amorphous copolymers, respectively.

For the essentially amorphous copolymers, T_g increases with increasing styrene content. The mechanical loss processes associated with the amorphous-phase T_g have peak widths comparable to the T_g process for atactic polystyrene, and this provides strong evidence that the glass-transition process is characteristic of a homogeneous amorphous material. Of further note in Figure 4 is the so-called γ-transition. This low temperature mechanical loss process can be associated with local chain motions, analogous to polyethylenes (47).

For the semicrystalline copolymers, the loss peak in the temperature range -50 to $+50^\circ$C shows increasing breadth of the relaxation process as the copolymer styrene content decreases. The relaxation processes associated with this loss peak are complex in nature. The long-range chain segmental motions associated with the T_g process become hindered because of the restrictions imposed by the crystallites. The copolymers with less than about 25 wt% (8 mol%) comonomer styrene exhibit complex thermal transition behavior as a result of the increasing influence of the crystalline domains, restricting molecular mobility in the amorphous region, similar to the behavior of high density polyethylene (HDPE) (48).

Further detailed aspects of the viscoelastic behavior of amorphous copolymers that have been reported includes linear stress-relaxation behavior (49) and creep properties in the glass-transition region (50). Chen and co-workers (51) have also reported the large strain–stress relaxation and strain recovery of copolymers at temperatures above T_g, and found that the observed behavior could be rationalized in terms of various network models.

Mechanical Properties. The tensile stress–strain behavior of ethylene-*co*-styrene polymers, including the effects of crystallinity and molecular weight, has been extensively reported and analyzed. Figure 5 presents tensile stress–strain data for a series of copolymers differing primarily in styrene content. The copolymers generally exhibit large strain at rupture, and have been found to show uniform deformation behavior (46).

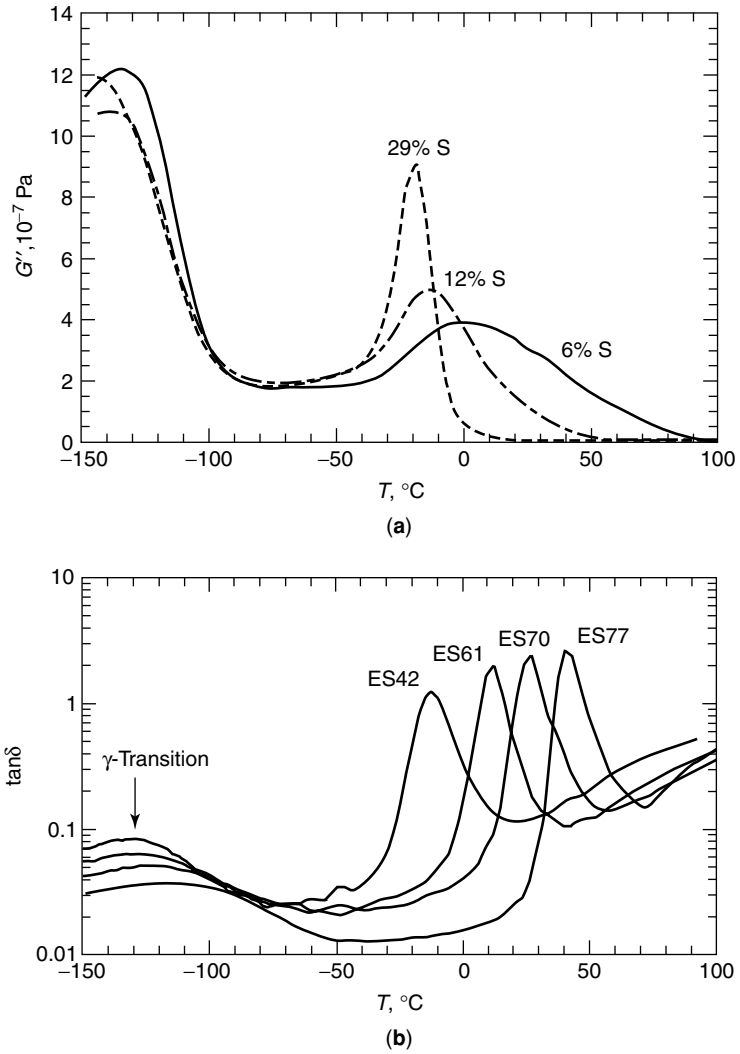

Fig. 4. Dynamic mechanical loss spectra of (**a**) Three semicrystalline ethylene-*co*-styrene polymers having different wt% comonomer compositions. (**b**) Amorphous or low crystallinity ethylene-*co*-styrene polymers. (The label ES## refers to a copolymer having ## wt% copolymerized styrene comonomer content.)

Chang and co-workers (52,53) studied the large-scale deformation behavior and recovery behavior of semicrystalline ethylene-*co*-styrene polymers as a function of temperature, comonomer content, and crystallinity and compared them to the behavior of metallocene-produced ethylene/1-octene copolymers. Chen and co-workers (54) have provided an in-depth comparison of the morphological structure and properties of copolymers and confirmed that aspects of deformation that depended on crystallinity, such as yielding and cold drawing, were determined primarily by comonomer content for both sets of copolymers.

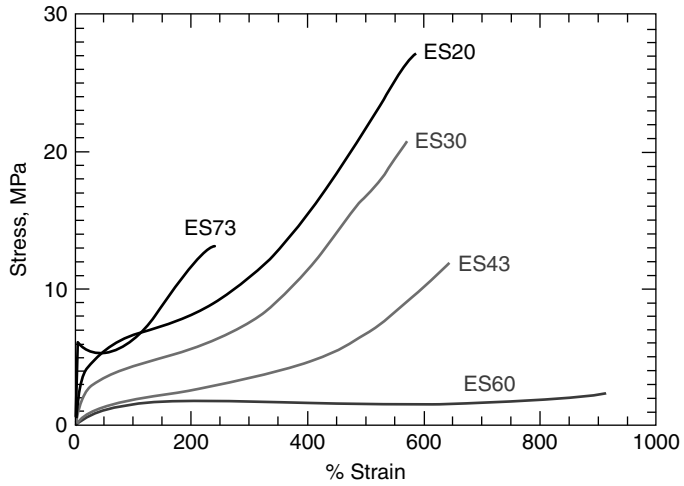

Fig. 5. Engineering stress–strain data (23°C, 5.7 min^{-1}) for ethylene-*co*-styrene polymers.

The copolymers with 40–60 wt% (about 15–30 mol%) styrene comonomer are characterized by low modulus and they show some elastomeric behavior. D'Aniello and co-workers (55) reported the physical properties for a poly(ethylene-*co*-styrene) having 20 mol% copolymer styrene, showing that the copolymer showed good elastic properties. Information on the deformation and recovery behavior of selected copolymers was reported by Mudrich and co-workers (56), with a copolymer having 45 wt% styrene of particular note in terms of strain recovery after deformation.

The effects of styrene become dominant in the high styrene region where the modulus and yield stress are seen to increase. Copolymers with T_g above ambient temperature are amorphous glasses, and these copolymers are reported (57) as exhibiting interesting shape/reshape functionality.

Good low temperature toughness of copolymers has been found in impact testing and low temperature tensile testing. Chen and co-workers (49) provided estimates of the copolymer entanglement molecular weights (M_e). The low M_e values found suggest high entanglement density in these copolymers, and was considered to contribute to the ability of the copolymers to shear yield at temperatures below T_g rather than undergo brittle fracture.

Melt Rheology and Processability. The melt rheological properties of a series of copolymers having up to 20.5 mol% styrene content were reported by Lobbrecht and co-workers (58). DMS data were generated for temperatures ranging from 120 to 200°C. Master curves were generated, and data analysis was considered to show that there was a difference in rheological behavior for those copolymers having greater than 16.5 mol% styrene.

The rheological properties and associated melt-processing characteristics of ethylene-*co*-styrene polymers, including solid-state DMS, melt strength, and pressure–volume–temperature (PVT) data, have been reported by Karjala and co-workers (59,60). Rheological master curves were generated via time–temperature

superposition, and viscosity–shear rate dependence were analyzed with a Cross model as a function of both styrene content and molecular weight.

The melt processability of copolymers is considered as favorable toward most fabrication techniques. Copolymers have been reported to show good thermal stability at melt-processing temperatures, viscosities that are a strong function of styrene content, in addition to molecular weight, shear thinning behavior at high shear rates, and good melt strength. These characteristics have allowed the fabrication of articles by a wide range of standard melt-processing techniques, including injection molding, film fabrication, blow-molding, and melt extrusion. The potential utility in calendering operations has been described by Karjala and coworkers (61). Selected copolymers were found to demonstrate the requisite rheological properties and thermal stability to be successfully calendered, and this was supported by commercial-scale validation. Where required, the standard thermal-stabilizer packages used in polyolefin formulations to improve processibility can also be employed in ethylene-*co*-styrene polymers.

Copolymer Utility: Materials Engineering Aspects

For many applications, the use of poly(ethylene-*co*-styrene) in preference to other ethylene homopolymers and copolymers will be determined by specific attributes that the aromatic functionality imparts. In one aspect, the aromatic ring can be chemically modified by sulfonation (62), and by a variety of electrophilic and nucleophilic reagents (63) to produce polymers with specific functionality.

In addition to showing good compatibility with a wide range of materials, other key characteristics, including the glass-transition temperature (T_g), viscoelastic properties, and excellent processability, further suggest that copolymers will find applications as components in formulated systems. The copolymers have shown inherent compatibility with low molecular weight materials, including bitumens (64), plasticizers (65), and tackifiers (66), in addition to a wide range of other polymers and fillers. The technology of blend systems, which includes copolymers as components and filler composites, is considered of particular relevance, and is discussed in more detail below.

Poly(ethylene-*co*-styrene) as a Polymer Blend Component. Diehl and co-workers (67) have reported that the copolymers are compatible with many other polymer families. The controllable combination of olefinic and aromatic functionality contributes to the compatibility of blends containing ethylene-*co*-styrene polymers. Significant toughening of atactic polystyrene (68) and syndiotactic polystyrene (69) can be achieved with selected copolymers. The olefinic functionality helps provide compatibility with olefin homopolymers and copolymers, including both polyethylenes and polypropylenes (70). Polymer families that have been blended with ethylene-*co*-styrene polymers include styrene block copolymers (71), poly(vinyl chloride) (PVC) based polymers (72), and polyphenylene ethers (73). Specific copolymers have also been demonstrated as effective blend compatibilizers, for example in polystyrene/polyethylene blends (74,75).

Blends of Poly(ethylene-*co*-styrene): Miscibility. Blends of two random copolymers are often immiscible when the difference in comonomer content between the copolymers is above a certain critical value. A study of

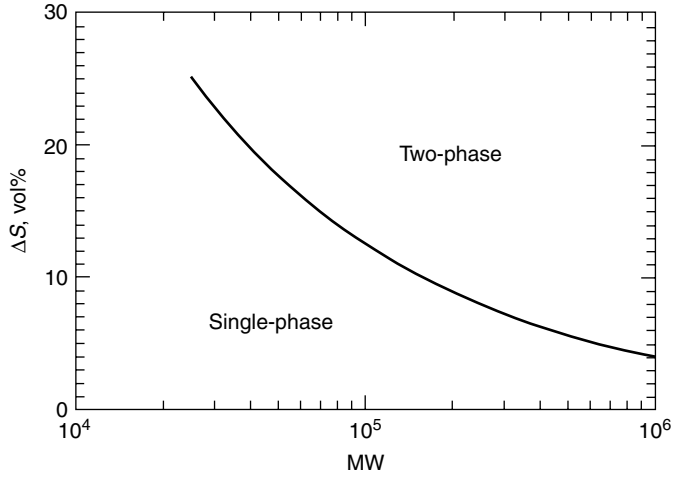

Fig. 6. Miscibility map for copolymer blends: the critical styrene content difference (ΔS in vol%) between two copolymers versus molecular weight (MW) of blend components for the onset of phase separation.

poly(ethylene-*co*-styrene) blends has combined predictions of miscibility with experimental observations (76). Critical composition differences for miscibility between ethylene-*co*-styrene polymers as a function of molecular weight are presented in Figure 6. Blends are predicted to be immiscible when the composition difference exceeds about 10 vol% (∼10 wt%) styrene between copolymers having molecular weights around 10^5 (note: vol%, the model parameter used, approximates to wt% in this case). This miscibility criteria was shown to be valid for copolymer blends from analysis of the thermal transitions of the blends and blend components.

The above rationale regarding miscibility extends to copolymer blends with polystyrene and polyethylene. Copolymers having less than about 90 wt% styrene comonomer content will be immiscible with polystyrene, unless the molecular weights of the respective polymers are very low. Similarly, copolymers with more than about 10 wt% styrene comonomer content will be immiscible with polyethylene.

Chen and co-workers (77) studied binary blends of copolymers over the full range of copolymer styrene contents for both amorphous and semicrystalline blend components. The transition from miscible to immiscible blend behavior, and the determination of upper critical solution temperature (UCST) for blends were uniquely evaluated by atomic force microscopy (AFM) techniques via the small, but significant, modulus differences between the respective copolymers used as blend components (78).

Blends of two or more copolymers differing in comonomer composition and/or molecular weight characteristics of the individual blend components find potential use in a range of applications. Thus, applications such as flooring systems, artificial leather and foams can utilize materials that have combinations of two or more interpolymers differing in styrene content to engineer, for example,

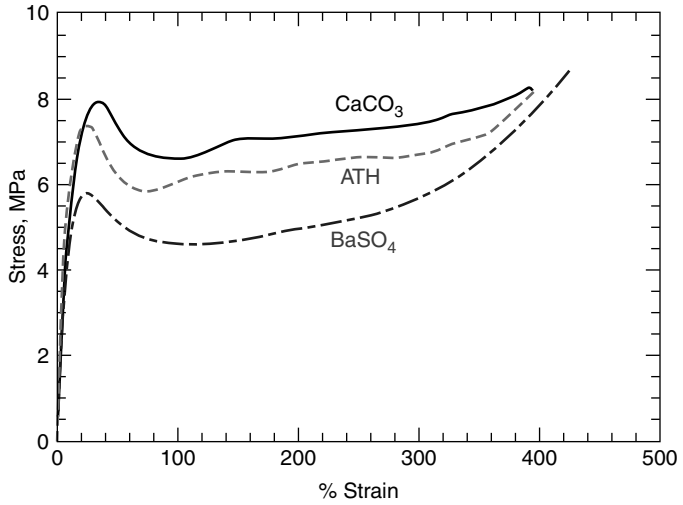

Fig. 7. Engineering stress–strain data (23°C, 5.7 min^{-1}) for an ethylene-*co*-styrene polymer (30 wt% styrene) containing 40 vol% filler.

the modulus–temperature relationship, glass-transition behavior, and damping characteristics.

Filler Composites. It is well known that the addition of fillers to polymers can enhance the stiffness, dimensional stability, upper service temperature, tensile strength, damping characteristics, and ignition resistance, as well as lower the cost of fabricated parts. The performance requirements for many applications that utilize poly(ethylene-*co*-styrene) can be met by modifying the balance of properties through the addition of fillers. The copolymers show good filler acceptance with a broad range of inorganic fillers, including calcium carbonate, barium sulfate, alumina trihydrate (ATH) and magnesium hydroxide ($Mg(OH)_2$) (79,80). Figure 7 presents tensile stress–strain data for a poly(ethylene-*co*-styrene) filled with 40 vol% of three different fillers. The resulting composite materials generally exhibit very good mechanical properties, even for relatively high loadings of fillers.

The filled copolymers have shown rheological characteristics which suggest that the compositions can be easily fabricated into final parts. Filled compositions are expected to find broad utility in applications, including, for example, wire and cable (81), flooring systems (82), injection-molded articles, film and sheet structures, and profile extrusions.

Applications

Potential markets/applications for poly(ethylene-*co*-styrene) can be discerned from various references and patent literature. In addition to the applications identified in the preceding sections, important applications discussed or identified include adhesives (66), paintable injection-molded toys (83), footwear,

Fig. 8. Examples of foam applications utilizing ethylene-*co*-styrene polymers.

automobile parts, bitumen modification, packaging, and blow-molded articles. Although intermaterial substitutions in existing applications based on thermoplastic elastomers such as styrene–butadiene block copolymers, flexible PVC, and polyethylene homopolymers and copolymers are potential application areas for copolymers, the novel combination of material attributes suggests that new application areas will emerge.

Developments using copolymer-based materials in foam applications are of particular note. Novel foam structures offer attractive properties and characteristics, including softness, aesthetics, and drape, for a wide range of thermoplastic and cross-linked foam applications. Other product technologies of interest are as injection-molded structural foams, as foamed layers in multilayer structures and as foamed blends of interpolymers with styrenic and olefinic polymers (Fig. 8) (84–86). Interpolymers also have potential for coextruded film and sheet applications.

Summary. Copolymers based on ethylene and styrene are a novel class of polymers exhibiting unique combinations of material attributes that are not found in polyethylenes, polystyrenes, or their blends. These copolymers offer unique opportunities for innovative developments in basic polymer chemistry, catalyst and process development, materials science and engineering, and application technology.

The effective production of these novel copolymers has been enabled by INSITE Technology. A product development plant to produce Interpolymers (Sarnia, Canada) had a successful start-up in September 1999. This plant, having a nameplate production capacity of around 22,500 metric tons per annum, has enabled further product and process developments, and application validation.

BIBLIOGRAPHY

1. R. A. Terteryan and co-workers, *Plast. Massy* **7**, 3–5 (1973).
2. Y. Tanaka, Y. Ohki, and M. Ikeda, *IEEE Trans. Electr. Insul.* **27**, 432–439 (1992).
3. U.S. Pat. 3,117,945 (Jan. 14, 1964), W. F. Gorham and A. G. Farnham (to Union Carbide Corp.).
4. S. Kobayashi and A. Nishioka, *J. Polym. Sci., Part A: Polym. Chem.* **2**, 3009 (1964).
5. Y. Kawai and S. Katsuta, *J. Polym. Sci., Part A: Polym. Chem.* **8**, 2421 (1970).
6. K. Soga, D. H. Lee, and H. Yanagihara, *Polym. Bull.* **20**, 237–241 (1988).
7. U.S. Pat. 4,748,209 (May 31, 1988), Y. Orikasa, S. Kojima, T. Inoue, K. Yamamoto, A. Sato, and S. Kawakami (to Nippon Petrochemicals Co. Ltd.).
8. U.S. Pat. 4,076,698 (Feb. 28, 1978), W. A. Anderson and G. S. Stamatoff (to E. I. Du Pont de Nemours and Co.).
9. Eur. Pat. EP 416,815 B1 (Aug. 30, 1997), J. C. Stevens, F. J. Timmers, D. R. Wilson, G. F. Schmidt, P. N. Nickias, R. K. Rosen, G. W. Knight, and S. Lai (to The Dow Chemical Co.).
10. U.S. Pat. 5,703,187 (Dec. 30, 1997), F. J. Timmers (to The Dow Chemical Co.).
11. P. S. Chum, W. J. Kruper, and M. J. Guest, *Adv. Mater.* **12**, 1759–1767 (2000).
12. L. Oliva, P. Longo, L. Izzo, and M. Di Serio, *Macromolecules* **30**, 5616–5619 (1997).
13. G. Xu, *Macromolecules* **31**, 2995–2402 (1998).
14. F. G. Sernetz and R. Mulhaupt, *Macromol. Chem. Phys.* **197**, 1071–1083 (1996).
15. U.S. Pat. 5,652,315 (July 29, 1997), N. Inoue, S. Tetsunosuke, and K. Masahiro (to Mitsui Toatsu Chemicals, Inc.).
16. *Ethylene–Styrene Interpolymers: Technologies, Products and Markets, The Metallocene and Single Site Catalyst Monitor*, Dec. 2000, Special Feature I.
17. P. Longo, A. Grassi, and L. Oliva, *Makromol. Chem.* **191**, 2387–2396 (1990).
18. C. Pellechia and L. Oliva, *Rubber Chem. Technol.* **72**, 553–558 (1999).
19. T. Arai, T. Ohtsu, and S. Suzuki, *Macromol. Rapid Commun.* **19**, 327–331 (1998).
20. U.S. Pat. 6,191,245 (Feb. 20, 2001), R. E. Campbell, M. H. McAdon, P. N. Nickias, J. T. Patton, O. D. Redwine, and F. J. Timmers (to The Dow Chemical Co.).
21. Z. Hou, Y. Zhang, H. Terzuka, P. Xie, O. Tardif, T. Koizumi, H. Yamazaki, and Y. Watasuki, *J. Am. Chem. Soc.* **122**, 10533–10543 (2000).
22. F. G. Sernetz, R. Mulhaupt, F. Amor, T. Eberle, and J. Okuda, *J. Polym. Sci., Part A: Polym. Chem.* **35**, 1571–1578 (1997).
23. F. G. Sernetz, R. Mulhaupt, S. Fokken, and J. Okuda, *Macromolecules* **30**, 1562–1569 (1997).
24. Y. Thomann, F. G. Sernetz, R. Thomann, J. Kressler, and R. Mulhaupt, *Macromol. Chem. Phys.* **198**, 739–748 (1997).
25. T. Suzuki, Y. Tsuji, Y. Watanabe, and Y. Takegami, *Macromolecules* **13**, 849–852 (1980).
26. U.S. Pat. 5,043,408 (Aug. 27, 1991), M. Kakugo, T. Miyatake, and K. Mizunuma (to The Sumitomo Chemical Co.).
27. T. Miyatake, K. Mizunuma, and M. Kakugo, *Makromol. Chem., Macromol. Symp.* **66**, 203–214 (1993).
28. V. Venditto, G. De Tullio, L. Izzo, and L. Oliva, *Macromolecules* **31**, 4027–4029 (1998).
29. L. Izzo, L. Oliva, A. Proto, and M. Trofa, *Macromol. Chem. Phys.* **200**, 1086–1088 (1999).
30. T. Arai, T. Ohtsu, and S. Suzuki, *Polym. Prepr. (Am. Chem. Soc., Div. Polym. Chem.)* **38**, 349–350 (1997).
31. U.S. Pat. 5,883,213 (Mar. 16, 1999), T. Arai, A. Nakamura, S. Suzuki, T. Otsu, and A. Okamoto, (to Denki Kagaku K. K.).

32. A. J. Pasztor, *Encyclopedia of Polymer Science*, Vol. **16**, 2nd ed., John Wiley & Sons, Inc., New York, 1989, pp. 114–117.
33. F. G. Sernetz, R. Mulhaupt, and R. M. Waymouth, *Polym. Bull.* **38**, 141–148 (1997).
34. U.S. Pat. 5,872,201 (Feb. 16, 1999), Y. W. Cheung, M. J. Guest, F. J. Timmers, and S. F. Hahn (to The Dow Chemical Co.).
35. F. G. Sernetz and R. Mulhaupt, *J. Polym. Sci.* **35**, 2549–2560 (1997).
36. M. J. Guest, Y. W. Cheung, T. P. Karjala, J. M. Ruiz, and B. W. S. Kolthammer, Proc. SPE ANTEC 59th Annu. Conf., 1709–1713 (2001).
37. L. Caporaso, L. Izzo, and L. Oliva, *Macromolecules* **32**, 7329–7331 (1999).
38. T. C. Chung and H. L. Lu, *J. Polym. Sci. Part A: Polym. Chem.* **35**, 575–579 (1997).
39. H. L. Lu, S. Hong, and T. C. Chung, *Macromolecules* **31**, 2028–2034 (1998).
40. T. C. Chung, H. L. Lu, and S. Hong, *Rubber Chem. Technol.* **72**, 283–298 (1999).
41. M. Hamedi, N. Lützow, H. S. Betz, J. L. Duda, and R. P. Danner, *Ind. Eng. Chem. Res.* **40**, 3002–3008 (2001).
42. PCT Pat. WO 01/12716 (Feb. 22, 2001), J. W. McMichael, J. R. Montanye, F. Bunge, and S. V. Dhodapkar (to The Dow Chemical Co.).
43. D. Qin, *Appl. Spectrosc.* **55**, 871–876 (2001).
44. M. J. Guest, Y. W. Cheung, C. F. Diehl, and S. M. Hoenig, in J. Scheirs and W. Kaminski, eds. *Metallocene-Based Polyolefins: Preparation, Properties and Technology*, Vol. **2**, John Wiley & Sons, Inc., New York, 1999, Chapt. "12", pp. 271–292.
45. H. Chen, PhD thesis, *Department of Macromolecular Science*, Case Western Reserve University, Cleveland, Ohio, 2000.
46. H. Chen, M. J. Guest, P. S. Chum, A. Hiltner, and E. Baer, *J. Appl. Polym. Sci.* **70**, 109–119 (1999).
47. N. G. McCrum, B. E. Read, and G. Williams, *Anelastic and Dielectric Effects in Polymeric Solids*, John Wiley & Sons, Inc., New York, 1967.
48. H. A. Flocke, *Kolloid-Z.* **180**, 118 (1962).
49. H. Y. Chen, E. V. Stepanov, S. P. Chum, A. Hiltner, and E. Baer, *Macromolecules* **33**, 8870–8877 (2000).
50. H. Y. Chen, E. V. Stepanov, S. P. Chum, A. Hiltner, and E. Baer, *J. Polym. Sci., Part B: Polym. Phys.* **37**, 2373–2382 (1999).
51. H. Y. Chen, E. V. Stepanov, S. P. Chum, A. Hiltner, and E. Baer, *Macromolecules* **32**, 7587–7593 (1999).
52. A. Chang, E. V. Stepanov, M. Guest, S. Chum, A. Hiltner, and E. Baer, Proc. SPE ANTEC 56th Annu. Conf., 1803–1807 (1998).
53. A. Chang, Y. W. Cheung, A. Hiltner, and E. Baer, *J. Polym. Sci., Part B: Polym. Phys.* **40**, 142–152 (2002).
54. H. Y. Chen, S. P. Chum, A. Hiltner, and E. Baer, *J. Polym. Sci., Part B: Polym. Phys.* **39**, 1578–1593 (2001).
55. C. D'Aniello, F. de Candia, L. Oliva, and V. Vittoria, *J. Appl. Polym. Sci.* **58**, 1701–1706 (1995).
56. S. F. Mudrich, Y. W. Cheung, and M. J. Guest, Proc. SPE ANTEC 55th Annu. Conf., 1783–1787 (1997).
57. U.S. Pat. 6,156,842 (Dec. 5, 2000), S. M. Hoenig, R. R. Turley, Y. W. Cheung, M. J. Guest, C. F. Diehl, K. B. Stewart, and J. Sneddon, (to The Dow Chemical Co.).
58. A. Lobbrecht, C. Friedrich, F. G. Sernetz, and R. Mulhaupt, *J. Appl. Polym. Sci.* **65**, 209–215 (1997).
59. T. P. Karjala, Y. W. Cheung, and M. J. Guest, Proc. SPE ANTEC 55th Annu. Conf., 1086–1090 (1997).
60. T. P. Karjala, Y. W. Cheung, and M. J. Guest, Proc. SPE ANTEC 57th Annu. Conf., 2127–2131 (1999).

61. T. P. Karjala, B. W. Walther, A. S. Hill, and R. Wevers, Proc. SPE ANTEC 57th Annu. Conf., 2139–2143 (1999).
62. PCT Pat. WO 99/20691 (Apr. 29 1999), Y. W. Cheung, S. F. Hahn, J. C. Stevens, F. J. Timmers, G. F. Schmidt, T. H. Ho, and R. H. Terbrueggen (to The Dow Chemical Co.).
63. U.S. Pat. 6,313,252 (Nov. 6, 2001), R. E. Drumright, R. H. Terbrueggen, K. A. Burdett, F. J. Timmers, and S. F. Hahn (to The Dow Chemical Co.).
64. U.S. Pat. 6,107,374 (Aug. 22, 2000), J. C. Stevens, F. J. Timmers, A. L. Gatzke, C. J. Bredeweg, K. W. McKay, W. A. Gros, and C. F. Diehl (to The Dow Chemical Co.).
65. U.S. Pat. 5,739,200 (Apr. 14, 1998), Y. W. Cheung, J. J. Gathers, M. J. Guest, and J. R. Bethea (to The Dow Chemical Co.).
66. U.S. Pat. 6,344,515 B1 (Feb. 5, 2002), D. Parikh, M. J. Guest, and D. R. Speth (to The Dow Chemical Co).
67. C. F. Diehl, M. J. Guest, B. I. Chaudhary, Y. W. Cheung, W. R. Van Volkenburgh, and B. W. Walther, Proc. SPE ANTEC 57th Annu. Conf., 2149–2153 (1999).
68. C. P. Park, Proc. SPE ANTEC 57th Annu. Conf., 2134–2138 (1999).
69. U.S. Pat. 6,063,872 (May 16, 2000), K. L. Nichols, J. M. Warakomski, D. H. Bank, and C. F. Diehl (to The Dow Chemical Co.).
70. U.S. Pat. 6,184,294 B1 (Feb. 6, 2001), C. P. Park, J. Thoen, R. Broos, M. J. Guest, Y. W. Cheung, B. I. Chaudhary, J. J. Gathers, and L. S. Hood (to The Dow Chemical Co.).
71. U.S. Pat. 5,741,857 (Apr. 28, 1998), C. P. Esnault and M. S. Edmonson (to The Dow Chemical Co.).
72. U.S. Pat. 6,136,923 (Oct. 24, 2000), Y. W. Cheung and M. J. Guest (to The Dow Chemical Co.).
73. U.S. Pat. 6,201,067 B1 (Mar. 13, 2001), Y. W. Cheung, M. J. Guest, P. S. Chum, and C. Kao (to The Dow Chemical Co.).
74. U.S. Pat. 5,460,818 (Oct. 24, 1995), C. P. Park, G. P. Clingerman, F. J. Timmers, J. C. Stevens, and D. E. Henton (to The Dow Chemical Co.).
75. C. P. Park and G. P. Clingerman, Proc. SPE ANTEC 54th Annu. Conf., 1887–1891 (1996).
76. Y. W. Cheung and M. J. Guest, *J. Polym. Sci., Part B: Polym. Phys.* **38**, 2976–2987 (2000).
77. H. Y. Chen, Y. W. Cheung, A. Hiltner, and E. Baer, *Polymer* **42**, 7819–7830 (2001).
78. H. Y. Chen, S. P. Chum, A. Hiltner, and E. Baer, *Macromolecules* **34**, 4033–4042 (2001).
79. M. J. Guest, Y. W. Cheung, S. R. Betso, and T. P. Karjala, Proc. SPE ANTEC 58th Annu. Conf., 2116–2120 (1999).
80. U.S. Pat. 5,973,049 (Oct. 26, 1999), J. O. Bieser, Y. W. Cheung, M. J. Guest, J. A. Thoen, and J. J. Gathers (to The Dow Chemical Co.).
81. S. R. Betso, M. J. Guest, R. M. Remenar, A. W. Field, and F. E. Keen, Proc. SPE ANTEC 58th Annu. Conf., 3012–3016 (2000).
82. U.S. Pat. 6,245,956 B1 (July 3, 2001), J. B. I. Kjellqvist, S. R. Betso, R. Wevers, J. A. Thoen, and J. O. Bieser (to The Dow Chemical Co.).
83. D. Chang and Y. W. Cheung, Proc. SPE ANTEC 59th Annu. Conf., 1704–1708 (2001).
84. U.S. Pat. 6,048,909 (Apr. 11, 2000), B. I. Chaudhary, R. P. Barry, and S. C. Cirihal (to The Dow Chemical Co.).
85. U.S. Pat. 5,993,707 (Nov. 30, 1999), B. I. Chaudhary, L. S. Hood, R. P. Barry, and C. P. Park (to The Dow Chemical Co.).
86. B. I. Chaudhary, R. P. Barry, and M. H. Tusim, *J. Cell. Plast.* **36**, 397–421 (2000).

MARTIN J. GUEST
Y. WILSON CHEUNG
Polyolefins R&D, The Dow Chemical Company

ETHYLENE POLYMERS, CHLOROSULFONATED.
See Volume 2.

ETHYLENE POLYMERS, HDPE. See Volume 2.

ETHYLENE POLYMERS, LDPE. See Volume 2.

ETHYLENE POLYMERS, LLDPE. See Volume 2.

ETHYLENE–ACRYLIC ELASTOMERS. See Volume 2.

ETHYLENE–NORBORNENE COPOLYMERS. See Volume 2.

ETHYLENE–PROPYLENE ELASTOMERS

Introduction

Copolymers of ethylene and propylene (EPM) and terpolymers of ethylene, propylene, and a diene (EPDM) as manufactured today are rubbers based on the early work of Natta and co-workers (1). A generic formula for EPM and EPDM may be given as follows, where $m = \sim 1500$ ($\sim$60 mol%), $n = \sim 975$ ($\sim$39 mol%), o = $\sim$25 for EPDM ($\sim$1 mol%) and 0 for EPM in an average amorphous molecule, and the comonomers are preferably statistically distributed along the molecular chain.

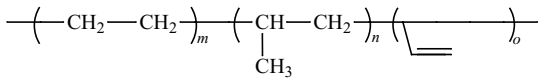

1

EPM can be vulcanized radically by means of peroxides. A small amount of built-in third nonconjugated diene monomer in EPDM permits conventional vulcanization with sulfur at the allylic carbon atoms relative to the pendent sites of carbon–carbon unsaturation.

Among the variety of synthetic rubbers, EPM and EPDM are particularly known for their excellent ozone resistance in comparison with natural rubber (*cis*-1,4-polyisoprene) and its synthetic counterparts IR (isoprene rubber), SBR (styrene–butadiene rubber), and BR (butadiene rubber). Secondly, EPDM rubber can be extended with fillers and plasticizers to a very high level in comparison with the other elastomers mentioned, and still give good processability and properties in end articles. This leads to an attractive price/performance ratio for these polymers.

Encyclopedia of Polymer Science and Technology. Copyright John Wiley & Sons, Inc. All rights reserved.

Even though EPM and EPDM rubbers have been commercially available for more than 40 years, the technology concerning these products, both their production and their applications, is still very much under development.

Polymer Properties

The properties of EPM copolymers are dependent on a number of structural parameters of the copolymer chains: the relative content of comonomer units in the copolymer chain, the way the comonomers are distributed in the chain (more or less randomly), the variation in the comonomer composition of different chains, average molecular weight, and molecular weight distribution. In the case of EPDM terpolymers there are additional structural features to be considered: amount and type of unsaturation introduced by the third monomer, the way the third monomer is distributed (more or less randomly) along the chain, and long-chain branching. These structural parameters can be regulated via the operating conditions during polymerization and the chemical composition of the catalyst.

Although the rubbery properties of ethylene–propylene copolymers are exhibited over a broad range of compositions, weight percentages of commercial products generally range from 45:55 to 80:20 wt% ethylene/propylene. On the high propylene side the polymer fails on thermal and ozone stability, because of the lower oxidative stability of the propylene units relative to ethylene units; on the high ethylene side the polymer is too highly crystalline and looses its rubbery character. Depending on the catalyst system and polymerization conditions used, the ethylene units may tend to group together to form blocky or sequential structures. The higher the ethylene/propylene ratio, the more pronounced is this tendency. These ethylene sequences impart a level of crystallinity to the EP(D)M rubbers of less than 1% at room temperature for 50:50 ethylene/propylene ratio—also designated as amorphous EP(D)M rubber—till above 10% for the high ethylene/propylene ratio—also called semicrystalline or sequential EP(D)M. Crystallinity renders the EP(D)M rubber a certain green strength: tensile strength in the unvulcanized state, making the polymer easier to handle and to store. Moreover, it adds to the strength of EP(D)M vulcanizates in those cases where carbon blacks cannot be used as reinforcing fillers and only less reinforcing light colored fillers can be applied. On the other side, these blocky structures or crystallinity have a detrimental effect on the rubbery properties of the polymer, particularly at subambient temperatures. They enhance the thermoplastic nature of the polymer.

In addition to the ethylene/propylene ratio, the average molecular weight of the rubber is controlled by polymerization variables. While the polymer chemist generally measures the average molecular weight by gel permeation chromatography or intrinsic viscosity, the rubber compounder uses Mooney viscosity for practical purposes. The ethylene–propylene rubbers are controlled within a range of raw polymer Mooney viscosities that has been found to fit the various processing and applications requirements of the rubber industry and includes most other commercial synthetic rubbers. Mooney viscosity of EPM and EPDM is preferably measured 4 min after a 1-min warm-up at 125°C (2,3). The measurement is expressed as ML $(1+4)$ at 125°C and ranges between ca 10 and 90. Grades with higher molecular weight are also produced, but are generally extended with

either paraffinic or sometimes naphthenic oil to reduce the Mooney viscosity for processing purposes.

The structure of EPM shows it to be a saturated synthetic rubber. There are no double bonds in the polymer chain as there are in the case of natural rubber and most of the common commercial synthetic rubbers. The main-chain unsaturation in these latter materials introduces points of weakness. When exposed to the degrading influences of light, heat, oxygen, and ozone, the unsaturated rubbers tend to degrade through mechanisms of chain scission and cross-linking at the points of carbon–carbon unsaturation. Since EPM does not contain any carbon–carbon unsaturation, it demonstrates an inherently higher resistance to degradation by heat, light, oxygen, and, in particular, ozone.

The double bonds in natural rubber and the common polydiene synthetic rubbers are essential to their curing, or also commonly called vulcanization into useful rubber products using conventional chemical accelerators and sulfur. As a saturated elastomer, EPM cannot be cured or cross-linked using these chemicals pertinent to the unsaturated rubbers. It can be vulcanized using peroxides. EPDM is a more commercially attractive product that retains the outstanding performance features, ie, heat, oxygen, and ozone resistance. It includes some carbon–carbon unsaturation—pendent to the main chain—from a small amount of an appropriate nonconjugated diene monomer to accommodate it to conventional sulfur vulcanization chemistry. A great variety of dienes were investigated in the past as third monomers (4), of which only two are used commercially at present in significant quantities. A characteristic of the structure of commercially used third monomers is that the two double bonds are nonconjugated. They are cyclic and bicyclic dienes with a bridged ring system.

The most commonly used third monomer is 5-ethylidene-2-norbornene [16219-75-3] (**2**), or ENB:

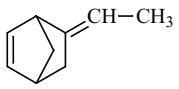

2

which is polymerized into the ethylene–propylene chain to give poly(ethylene-*co*-propylene-*co*-ENB) [25038-36-2] (**3**). The norbornene double bond in the bridged, or strained, ring is the more active with respect to polymerization and the five-membered ring with its double bond is left as a pendent substituent to the main polymer chain.

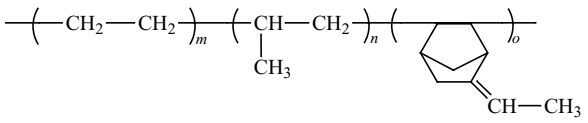

3

Less commonly used as third monomer is dicyclopentadiene [77-73-6] (**4**), or DCPD, for which, because of its symmetrical shape, the tendency of the second

double bond to take part in the polymerization process is more pronounced than for ENB. This is one of the reasons for the formation of long-chain branches. The resulting product is poly(ethylene-*co*-propylene-*co*-DCPD) [25034-71-3].

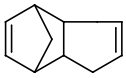

4

Formerly, one manufacturer of EPDM used a noncyclic diene: 1,4-hexadiene [592-45-0], but this was displaced by ENB because of the latter's superior performance both in incorporation during polymerization and in vulcanization. EPDM containing hexadiene is not commercially available anymore.

Recently, the development of commercial EPDMs with 5-vinyl-2-norbornene [3048-64-4] (**5**), a precursor in the synthesis of ENB, as third monomers has been reported, aiming at a higher vulcanization yield with peroxide curatives, relative to ENB- or DCPD-containing EPDMs (5):

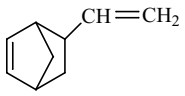

5

Also other third monomers are being proposed for better or faster vulcanization with sulfur or peroxide curatives, but have not reached commercial status yet (6).

Combinations of more than 1 third monomer are also applied. The amount of third monomer in general-purpose grades is about 1 mol% or ca 4 wt%. For faster curing grades this amount may be as high as 2 mol% or ca 8 wt% and there is a tendency to go to even higher amounts. At equal amounts of a third monomer (in mol%), DCPD as a third monomer leads to polymers which require about twice as long a curing time for sulfur vulcanization than ENB (7). Because of the consequent economic benefits in processing, ENB is mostly preferred as the third monomer.

Both EPDM and EPM show outstanding resistance to heat, light, oxygen, and ozone because one double bond is lost when the diene enters the polymer and the remaining double bond is not in the polymer backbone but external to it. Properties of typical EPDM rubbers are shown in Table 1.

Manufacture

The two principal raw materials for EPM and EPDM, ethylene [74-85-1] and propylene [115-07-1], both gases, are available in abundance at high purity. Propylene is commonly stored and transported as a liquid under pressure. Although ethylene can also be handled as a liquid, usually at cryogenic temperatures, it is generally transported in pipelines as a gas. Of the third monomers, DCPD is

Table 1. Properties of Raw Ethylene–Propylene–Diene Co- and Terpolymers

Property	Value
Specific gravity	0.86–0.87
Appearance	Glassy–white
Ethylene/propylene ratio by wt	
Amorphous types	50/50
Crystalline or sequential types	75/25
Onset of crystallinity, °C	
Amorphous types	Below −50
Crystalline types	Below ca 30
Glass-transition temperature,[a] °C	−45 to −60
Heat capacity, kJ/(kg·K)	2.18
Thermal conductivity, W/(m·K)	0.335
Thermal diffusivity, m/s	1.9×10^{-5}
Thermal coefficient of linear expansion per °C	1.8×10^{-4}
Mooney viscosity, ML (1 + 4) 125°C[b]	10–90

[a] Dependent on third monomer content.
[b] Oil extended grades, when viscosity > 100 for the raw polymer.

also available in large quantities. ENB is produced in a two-step process: a Diels–Alder reaction of cyclopentadiene (in equilibrium with DCPD) and butadiene; the resulting product vinyl-norbornene (VNB) is rearranged to ethylidene norbornene via proprietary processes.

EPM and EPDM rubbers are produced in continuous processes. All EPDM manufacturing processes are highly proprietary and differ greatly between various suppliers. A great series of patents covers the many details of various processes.

Solution Process. Most widely used are solution processes, in which the polymer produced is in the dissolved state in a hydrocarbon solvent (eg hexane). The choice of catalyst system is determined, among other things, by the nature of the third monomer and factors such as the width of the molecular weight distribution to be realized in the product. A number of articles review the influence of catalyst systems on the structural features of the products obtained (4,8–10). The catalyst comprises two main components: first, a transition metal halide, such as $TiCl_4$, VCl_4, $VOCl_3$, of which $VOCl_3$ is the most widely used; second, a metal alkyl component such as diethylaluminum chloride, $(C_2H_5)_2AlCl$, or monoethylaluminum dichloride, $(C_2H_5)AlCl_2$, or most commonly a mixture of the two, ie, ethylaluminum sesquichloride, $(C_2H_5)_3Al_2Cl_3$.

Under polymerization conditions, the active center of the transition-metal halide is progressively reduced to a lower valance state, ultimately to V^{2+}, which is unable to polymerize monomers other than ethylene. The ratio V^{3+}/V^{2+}, in particular, under reactor conditions is a measure for catalyst activity to produce EPM and EPDM species. This ratio V^{3+}/V^{2+} can be upgraded by adding to the reaction mixture a promoter, which causes oxidation of V^{2+} to V^{3+}. Examples of promoters in the earlier literature were carbon tetrachloride, hexachlorocyclopentadiene, trichloroacetic ester, and benzotrichloride (11). Later, butyl perchlorocrotonate and other proprietary compounds were introduced (12–14).

For EPDM, long-chain branching and gel can be introduced during the polymerization. This may happen by at least two mechanisms: by Ziegler polymerization through both double bonds of the diene third monomer or through cationic coupling of pendent double bonds (15,16). For Ziegler polymerization to occur through both double bonds, both must be accessible to the polymerization catalyst. The strained five-member ring in the norbornene structures is highly reactive and is rapidly incorporated in the polymer chain. Reaction of the second double bond results in a tetrafunctional branch point in the EPDM backbone. The ethylidene double bond in ENB is so sterically hindered that Ziegler polymerization of the second double bond is not possible under the production conditions for EPDM. Conversely, the use of a diene, such as VNB and to a lesser extent DCPD, can result in substantial amounts of branching because of the accessibility of the vinyl group in VNB to the polymerization catalyst and the second five-member ring in DCPD (see ZIEGLER–NATTA CATALYSTS).

During Ziegler polymerization it is also possible to couple the chains cationically through pendent olefinic groups (15). The extent of this reaction strongly depends on the Lewis acidity of the catalyst components. In general, the amount of cationic coupling decreases as the aluminum alkyl cocatalyst is varied from $(C_2H_5)AlCl_2$ through $(C_2H_5)_2AlCl$ to triethyl aluminum. Particularly ENB tends to cationically couple with another ENB molecule built into another polymer chain, thereby creating another form of long-chain branches. In the presence of Lewis bases this amount of branching is markedly reduced. By the same mechanism, the coordination Ziegler–Natta catalysts are extremely sensitive to water and other polar materials, as they decompose the catalyst to Lewis acids. Only a few parts per million of water are allowed in any of the feed streams. Extended forms of long-chain branching finally lead to gel formation, which damage the processability of the products in the final application.

In the solution process making use of Ziegler–Natta catalysis, dry solvent, ethylene, propylene, diene, and catalyst and cocatalyst solutions are continuously and proportionately fed to one or a series of polymerization vessels. Polymerization of individual molecules, or chains, is extremely fast, and a few seconds at most is the average life of a single growing polymer molecule from initiation to termination. The polymerization is highly exothermic. The heat must be removed, since the polymerization temperature (ca 35°C) has to be kept within narrow limits to ensure a product with the desired average molecular weight and molecular weight distribution. Therefore, these processes can be grouped into those in which the reactor is completely filled with the liquid phase, and those in which the reactor contents consist partly of gas and partly of a liquid phase. In the first case the heat of reaction (ca 2500 kJ/kg EPDM) is removed by means of cooling systems, either external cooling of the reactor wall or deep cooling of the reactor feed, or combinations. In the second case the evaporation heat from unreacted monomers also removes most of the heat of reaction. Most commonly hydrogen is used as chain transfer agent to regulate the average molecular weight.

As the polymer molecules form and dissociate from the catalyst, they remain in solution. The viscosity of the solution increases with increasing polymer concentration. As the EPDM polymerization is a continuous process run in stirred reactor(s) at high conversion and rubber solids concentration, the practical upper limit of solution viscosity is dictated by considerations of heat transfer, mass

transfer, and fluid flow. At a rubber solids concentration of 5–10%, depending on the molecular weight of the polymer produced a further increase in the solution viscosity becomes impractical, and the polymerization is stopped by killing the catalyst. This is usually done by vigorously stirring the solution with water. If this is not done quickly, the unkilled catalyst continues to react, leading to above described uncontrolled side reactions, resulting in an increase in Mooney viscosity called Mooney jumping.

The reactivity of ethylene is high, whereas that of propylene is low, and the various dienes have different polymerization reactivities. The viscous rubber solution contains some unpolymerized ethylene, propylene, unpolymerized diene, and about 5–10% EPDM, all in homogeneous solution. This solution is passed continuously into a flash tank, where reduced pressure causes most of the unpolymerized monomers to escape as gases, which are collected and recycled.

Catalyst residues, particularly vanadium and aluminum and chlorine, have to be removed as soluble salts in a water-washing and decanting operation. Vanadium residues, and to a lesser extent chlorine residues, in the finished products are kept to a few parts per million, because these may have a strong negative influence on the ageing characteristics of the EPDM. If oil-extended EPDM is the product, a metered flow of oil is added at this point. In addition, antioxidant, typically of the hindered phenol type, is added at this point.

The rubber is then separated from its solvent by steam stripping. The viscous cement is pumped into a violently agitated vessel partly full of boiling water. The hexane flashes off and, together with water vapor, passes overhead to a condenser and to a decanter for recovery and reuse after drying. Residual unpolymerized ethylene and propylene appear at the hexane condenser as noncondensibles, and are recovered for reuse after drying. Unreacted diene may be recovered with the solvent and further fractionated for purification and recycling. The polymer, freed from its carrier solvent, falls into the water in the form of crumb.

The rubber crumb, now a slurry in hot water, is pumped over a shaker screen to remove excess water. The dewatered crumb is fed to the first stage of a mechanical-screw dewatering and drying press. Here, in an action similar to a rubber extruder, all but 3–6% of the water is expressed as the rubber is pushed through a perforated plate by the action of the screw. The cohesive, essentially dry rubber then passes into the second-stage press. This is similar to the first-stage dewatering machine, except that the mechanical action of the screw causes the rubber in the barrel to heat up to temperatures as high as 150°C. This rubber is extruded through a perforated die plate at the end of the machine, the small amount of remaining water is flashed off as a vapor, and the nearly dry rubber crumb is finally subjected to air-drying in a fluid bed or tunnel drier at temperatures of ca 110°C to reduce the level of remaining volatile matter to <0.7, preferably <0.3 wt%. This EPDM crumb is then continuously weighed, pressed into bales, and packaged for storage and shipment. Highly crystalline or sequential types are sufficiently form-stable to be produced in the form of pellets by a direct extruder operation, if necessary with application of a small amount of a separating or partitioning agent.

Slurry Process. In this process a nonsolvent diluent and an operating temperature are used so that the monomers are soluble, but not the polymer. The diluent must also be inert with respect to the catalyst components.

As diluent the monomer propylene is used. It is of course not an inert substance, but its conversion level is low enough to allow for its use as a nonsolvent diluent.

The advantages of this process reside in the low viscosity of the dispersion of precipitated crumby EPDM particles in the low viscosity propylene medium. This bears on heat transfer, solvent recycle capacity, and slurry transport problems. For example, temperature control of the reactor can more readily be effected by controlled evaporation of the propylene and to a lesser extent ethylene. Another advantage lies in much higher production rates due to higher slurry concentrations (20–40%) compared to the solution process. The slurry process also allows for higher molecular weight EPDMs, because a viscosity rise of the solution does not apply in this case. Another advantage is the lower catalyst levels needed in comparison with the solution process, because the great abundance of propylene as monomer being diluent at the same time.

The disadvantage of the slurry process lies in the problems related to the removal of catalyst residues. Catalyst tends to become occluded in the precipitated EPDM. Although the slurry process has lower catalyst consumption, the problem with removing catalyst residues leads to higher catalyst residues in the final polymer. These catalyst residues then have the tendency to become involved in intermolecular branching reactions of the type described above, which increases the probability of premature cross-linking reactions (=gelation) during the killing step and during storage. Further, these catalyst residues contribute significantly to the degradation of rubber vulcanizates properties upon heat ageing.

The greatest benefit of this technology is achieved if the steam-stripping operation is replaced by a progressive series of degassing operations, vessels and extruders, for cost reasons and to do away with water in the whole operation (17).

Gas-Phase Process. Another noteworthy development in the field of EPDM manufacture is the so-called gas-phase process, as an extension of the well-known gas-phase processes for polyethylene and polypropylene (18). The process uses a fluid-bed reaction vessel to which gaseous ethylene, propylene, and third monomer ENB are fed. The reaction heat is removed through circulation of the gas, which serves to fluidize the polymer bed as well as to act as the raw material for the polymerization. In fact, this process can be pictured as a continuous percolating fountain of small EPDM granules, coated *in situ* with a steady stream of fluidization aid in order to prevent sticking together of the granules. As fluidization aid finely ground furnace carbon black is being used up till quantities of about 16 wt% or 20 phr (parts per hundred rubber) (19). This carbon black remains in the EPDM. The gas-phase technology is solvent- or diluent-free, and so no stripping is required. The nonconverted monomers are recovered by purging and are recycled. Drying and finishing is therefore not applicable to gas-phase produced EPDM as no water is involved in the process. The product is delivered in granular form, as directly recovered from the reactor.

Also this process offers the possibility of greatly reduced finishing operations and consequent cost savings. The gas-phase process does not permit catalyst removal. This is both an advantage in cost and a disadvantage in terms of catalyst residue. These polymers will have a high catalyst residue as long as conventional Ziegler–Natta catalysts are used. It may be possible to lower catalyst residue if

metallocene catalysts can be adapted for this process (see next section). It should also be noted that removal of unreacted ENB from the gas-phase product is not a trivial matter. An additional purging step is needed to remove the third monomer (20). The question applies, whether this technology will offer a comparable flexibility in due course to make the wide variety of EPDM molecular structures, which have been designed over the years to comply with market requirements for the various applications of EPDM rubber.

New Catalysis Technologies Using Metallocenes. Through the last years a very rapid development of single-site metallocene catalysts has taken place, primarily for polyethylene and polypropylene, but with spin-offs to EPDM manufacture (21–24). In combination with methylaluminoxane as the cocatalyst, these metallocene catalysts show an enormous increase in activity relative to the traditional Ziegler–Natta catalysts. They show a greatly increased catalyst activity for higher alpha-olefins, like the third monomers. In addition, they keep their activity at higher polymerization temperatures than commonly employed for Ziegler–Natta catalysts. Metallocene catalysts (qv) usually give a different comonomer distribution than traditional Ziegler–Natta catalysts (qv).

Various advantages are claimed for metallocene catalyst technology: such a low catalyst consumption that catalyst residues do not need to be removed from the polymer after deactivation. Further, the higher operating temperature of the catalyst allows for a higher temperature regime of the total process, resulting in a reduction of cooling operations. It also allows for higher solution concentrations with consequent lower stripping energies involved, particularly if this technology is combined with an older technology where the steam-stripping operation is replaced by the water-free finishing mentioned before (17).

In spite of the many advantages claimed for this technology, it has to be noted that many of these are offset by various countereffects: the need for higher pressure operations and consequent additional investments if the increased temperature regime of this technology is to be exploited; the need for highly purified raw materials, because these catalysts are much more sensitive to poisoning by adverse compounds than the traditional Ziegler–Natta catalysts; the question whether this technology will have a comparable flexibility in order to make the wide variety of EPDM molecular structures, which have been designed over the years as dictated by the market requirements.

Production Capacities. Production capacities of EPM/EPDM of the largest manufacturers are listed in Table 2 (25).

Compounding

EPM/EPDM grades have to be compounded with reinforcing fillers if high levels of mechanical properties are required. EPM/EPDM grades with a high Mooney viscosity and a high ethylene content are particularly capable of accepting high loadings of filler (eg, 200–400 phr) and plasticizer (eg, 100–200 phr) and still giving useful vulcanizates.

Carbon blacks are usually used as fillers. The semireinforcing types, such as FEF (fast extrusion furnace) and SRF (semireinforcing furnace), give the best performance. To lower the cost and improve the processability of light colored

Table 2. EPM/EPDM Rubber Production Capacities[a]

Manufacturer	Country	Capacity, t/year
Bayer/Polysar	United States and Germany	110,000
DSM Elastomers	United States, the Netherlands, and Brasil, Japan	216,000
DuPont Dow	United States	90,000
EniChem Elastomeri	Italy	85,000
ExxonMobil Chemical	United States and France	174,000
Herdilia	India	10,000
Japan Synthetic Rubber	Japan	65,000
Korea Polychem	South Korea	40,000
Mitsui Petrochemical	Japan	60,000
Sumitomo Chemical	Japan	35,000
Union Carbide	United States	90,000
Uniroyal Chemical Co.	United States	93,000
Others		30,000

[a] Ref. 20.

compounds, or to reduce the cost of black compounds, calcined clay or fine-particle-size calcium carbonates are used.

The most widely used plasticizers are paraffinic oils. For applications that specify high use temperatures, or for peroxide cures, paraffinic oils of low volatility are definitely recommended. Because paraffinic oils may tend to exudation at low temperatures from EPDM vulcanizates, or from high ethylene EPDMs, they are sometimes blended with naphthenic oils. On the other hand, naphthenic oils interfere with peroxide cures. Aromatic oils reduce the mechanical properties of vulcanizates, and they also interfere with peroxide cures. Therefore, they are generally not recommended for EPM/EPDM.

Although EPM can only be cross-linked with peroxides, peroxide or sulfur plus accelerators or even other vulcanization systems like resol resins can be used for EPDM. The choice of chemicals used in an EPDM vulcanizate depends on many factors, such as mixing equipment, mechanical properties, cost, safety, and compatibility. In sulfur vulcanization, ENB-containing EPDM is about twice as fast as DCPD-containing EPDM. If peroxide cures are required for better heat stability, DCPD-containing EPDM gives higher cure states than EPM. The reactivity of ENB–EPDM is a little lower in peroxide cures. For peroxide cures of EPM and to a lesser degree of DCPD–EPDM, activators such as small amounts of sulfur, acrylates, or maleimides are also needed. The chemistry involved in sulfur and resol resin curing of ENB-containing EPDM has been investigated in detail by several authors (26–29).

Because of the low level of C=C unsaturation in the polymer compared to, eg, natural rubber (NR) and SBR, EPDM needs significant amounts of highly active accelerators for sulfur vulcanization. Usually, combinations of benzothiazole derivatives or sulfenamides with so-called ultra-accelerators like thiuram compounds or dithiocarbamates are used. Because of the limited solubility of these various accelerators in EPDM versus the large quantities needed to obtain a sufficient level of vulcanization, an EPDM compound often contains four or more

accelerators next to elemental sulfur; every accelerator obeys its own maximum dosage related to its solubility limit.

Modern legislation puts much emphasis on the prevention of the formation of carcinogenic secondary *N*-nitrosamines as by-products of sulfur vulcanization (30). This limits the choice of possible accelerators to those which have no secondary amine groups embedded in their chemical structure or may contain residual secondary amines dating back to their synthesis: usually the ultra-accelerators mentioned above. In such cases it is extra difficult to develop a proper vulcanization system. New ultra-accelerator systems like dibenzyl dithiocarbamate or tetrabenzyl thiuramdisulfide may be used in such cases, where the dibenzylamine embedded in these compounds is an exception in that it does not generate *N*-nitrosamines carcinogenic to human beings (31).

In Table 3 a few examples are given of typical EPDM recipes with pertinent cured properties.

Processing

The larger part of EPM and EPDM rubber finds applications in continuous extruded profiles or calendered sheets for automotive and building sealing applications. A smaller part is being used for a diversity of applications, from molded goods till viscosity modifiers for lubricant oils. The processing of EPM and EPDM rubbers must be viewed in relationship to the sort of application envisaged.

Mixing. Compounds of low Mooney EPM or EPDM grades can be mixed on open mills. For most applications EPM and EPDM compounds are almost exclusively mixed in internal mixers. The mechanisms involved in the mixing of EPM/EPDM as a function of molecular structural parameters, in particular molecular weight, molecular weight distribution (32–34), and long-chain branching (35,36), have been studied in great detail. It turns out that the speed of carbon black dispersion is greatly dependent on these parameters for practical mixing cycles. The molecular weight distribution and level of long-chain branching of the EPM/EPDM rubber should be suitably chosen, depending on the desired degree of carbon black dispersion in the application concerned: a narrow distribution for average carbon black dispersions, and a broad distribution for applications requiring excellent carbon black dispersions. A pronounced high molecular weight fraction within the molecular weight distribution—often called *bimodality* or *tailored molecular weight*—has a beneficial effect on mixing behavior by raising the shear toughness of the EPDM: it allows for higher shear forces exerted by the mixer and consequently a better dispersion of the reinforcing filler: the better dispersed filler is somewhat less reinforcing, which generally results in a lower viscosity of the mixed compound (32–34). On the other hand, a more pronounced fraction of low molecular weight material acts like a plasticizer and also has a decreasing effect on the viscosity of the mixed compound. The concept of controlled long-chain branching, combining a narrow molecular weight distribution with a high level of long-chain branching, has proven to be particularly beneficial for ease of processing and good mechanical properties as a result of this (36).

For EPM/EPDM grades with high ethylene contents, the disintegration of the bales is a dominating factor. If the polymer is in the form of a compact

Table 3. Typical EPM/EPDM Compounding Recipes for a 60° IRHD Hardness Solid Application

	Sulfur cure[a]	Low nitrosamine sulfur cure[a]	Peroxide[b] cure[b]
Components			
EPDM, 4 wt% ENB, Keltan[c] 4802	100	100	—
EPDM, 4 wt% DCPD, Keltan[c] 720	—	—	100
Zinc oxide	5	5	—
Stearic acid	1	2	0.5
Carbon black, N 683	105	—	—
Carbon black, N 765	—	95	—
Carbon black, N 550	—	—	110
$CaCO_3$ whiting	50	—	80
Oil, Sunpar[d] 2280	70	50	—
Oil, Sunpar[d] 150	—	—	75
CaO, 75% paste	8	6	6
Poly(ethylene glycol) 4000	—	—	2
N-Cyclohexylbenzothiazole-2-sulfenamide, 70%	2.1	—	—
Zinc dibutyldithiocarbamate, 80%	2.5	—	—
Ethylthiurea	1.0	—	—
Tellurium diethyl dithiocarbamate, 75%	0.63	—	—
Tetramethylthiuram disulfide, 50%	1.0	—	—
Zinc dialkyl dithiophosphate, 67%	—	2.5	—
Dithiodiacaprolactam, 80%	—	1.0	—
Zinc dibenzyldithiocarbamate, 70%	—	1.0	—
2-Mercaptobenzothiazole, 80%	—	1.9	—
Sulfur	1.5	1.5	—
1,3-Bis(*t*-butylperoxy-isopropyl)benzene, 40%	—	—	6
1,1-Di-*t*-butylperoxy-3,3,5-trimethylcyclohexane, 40%	—	—	3
Trimethylolpropane trimethacrylate	—	—	1
Properties			
Compound Mooney[e] ML (1 + 4) 100°C	83	92	44
Profile vulcanization	UHF/hot air	UHF/hot air	LCM
Temperature, °C (time, s)	250 (160)	250 (215)	240 (60)
Hardness[f] IRHD	64	60	61
Tensile strength,[g] N/mm^2	10.0	13.7	7.7
Elongation at break,[g] %	400	460	330
Compression set,[h] 22 h/70°C, %	13	19	—
Compression set,[h] 22 h/100°C, %	—	—	16

[a] Automotive profile, phr.
[b] Building profile, phr.
[c] Keltan is a registered trademark of DSM Elastomers.
[d] Sunpar is a registered trademark of Sun-Oil Co.
[e] ISO 289.
[f] ISO 48.
[g] ISO 37.
[h] ISO 815.

bale, it is difficult to disintegrate the rubber sufficiently to form a fine dispersion with the other compounding ingredients, so that the shearing action of the mixer can disperse the ingredients evenly. In such cases particulate forms of the rubber such as crumbs, pellets, and friable bales may shorten the mixing cycle considerably.

Extrusion. For automotive and building sealing profiles, extrusion is the common shaping technology. In general, EPM/EPDM compounds can be extruded on all commercial rubber extruders. The extrusion behavior of EPM and EPDM compounds must be seen in relation to the compound quality, as achieved during mixing and influenced by the same molecular structural parameters as quoted above (34,37–40).

Also for extrusion purposes long-chain branching has a particularly positive effect (40): it increases extrusion speed and the resistance against collapse: the tendency of extruded profiles of complicated shapes to deform under the influence of gravity between the extruder and the vulcanization line.

Curing. EPM/EPDM compounds are cured on all of the common rubber-factory equipment: press cure, transfer molding, steam cure, hot-air cure, and injection molding are all practical. Where profile extrusion is the shaping technique, hot-air tunnel curing and ultrahigh frequency (UHF) electromagnetic heating followed by a hot-air tunnel or molten-salt bath (LCM) cure are the most common vulcanization techniques (41).

Many hot-air lines are homemade and differ substantially in quality and efficiency. It is a cheap curing technique and therefore often favored. A wide variety of air temperatures and tunnel lengths are directly related to the production speed, which can be achieved with a particular line. Air speed is another important factor. The heat transfer from the hot air to the EPDM rubber profile is poor compared to the other techniques, dictating much longer hot-air lines than, eg, LCM or UHF lines to achieve the same states of cure.

UHF heating is the continuous curing technique most commonly applied. The purpose of the UHF unit is a fast and homogeneous heating of even very complex shaped profiles, within a short distance. The following hot-air tunnel then serves to keep the profile at the curing temperature. Much milder hot-air conditions and shorter lines can be used than for hot air alone.

In spite of the somewhat old-fashioned nature and environmental problems of this curing technique, LCM curing is still the second most important continuous curing technique for EPDM sealing profiles. A major reason why this technique still survives or rather revives relative to the others is that this is the only continuous curing technique which allows for peroxide vulcanization. Peroxide vulcanization with free access of oxygen from the air—like in hot-air curing—leads to an intricate interaction between the oxygen molecules and peroxy radicals, which results in surface degradation instead of vulcanization and a consequent stickiness of the profile surface. This is an intrinsic problem of curing with peroxides, occurring with all other rubbers as well. The molten salt effectively shields the profile surface from this free oxygen. Another reason for the LCM revival is that this curing technique in general leads to the smoothest surface finish of extruded EPDM sponge profiles (see below).

Sponge Processing. Extrusion sponge represents a part of EPDM application technology, which requires the highest level of know-how, and consequently

includes all aspects of EPDM-compounding and EPDM-processing technology (42). In line with major automotive requirements calling for improved comfort and luxury, automotive body seals and profiles are becoming increasingly complex and numerous. Sponge plays a major role in this context. On a weight basis it represents a minor part of the profile technology, but because of the fact that sponge in most cases is coextruded with solid/dense profiles it represents about 50% of the sealing profiles on a volume basis. This combination with solid/dense extrusions calls for an integrated approach (43).

In summary the requirements on sponge converge on finding a good compromise between what could be called "the Magic Triangle" in EPDM-sponge technology:

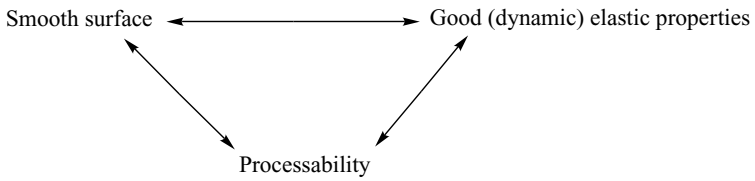

Many, if not all, of these performance aspects can directly or indirectly be influenced by

(1) the seal cross-sectional design and dimensions;
(2) the sponge density, which must be adjusted by a proper balance between the amount of blowing agent and the curing accelerator package: to vary between 0.2 g/cm^3 till completely solid;
(3) closed vs open cell structure: a phenomenon difficult to quantify or adjust, but of major influence on the closed surface skin and the tendency of the sponge profile to absorb water.

With the great variety of curing techniques as described previously, it is not possible to come forward with "general" compounding rules for sponge. Every curing technique in combination with the vulcanization system requires its own set of compounding rules to obtain the best results. In summary a series of requirements can be formulated which generally apply:

(1) The Mooney viscosity of the sponge compound is generally adjusted to such a level, that the blowing agent can expand the compound to the required density, before being arrested by the curing: compound Mooney ML$(1+4)$ 100°C typically between 30 and 45 (but not limiting).
(2) Compound viscosity variations should be kept to a minimum to guarantee a reproducible and constant amount of blowing and curing from batch to batch: compound Mooney typically ± 2 Mooney units.
(3) A homogeneous and very fine dispersion of ingredients to guarantee a homogeneous blowing.

(4) Blowing agents are most often used in combinations and occasionally with activators. The selection and use of a proper blowing agent depends on many factors and is a difficult matter. They are activated by numerous compounding ingredients, generally reducing the decomposition temperature of the blowing agents. The reader is referred to the pertinent literature (44,45) for details.

(5) Carbon black loading alone tends to create a coarse cell structure and irregular sponge surface. Hence sponge compounds are often modified by the addition of mineral fillers such as whiting, calcined clay, and platy talcum: they serve as nucleating agents for the blowing agents, resulting in a fine and homogeneous cell structure and smooth surface finish.

(6) The choice of the vulcanization system in combination with the blowing agent(s) to produce smooth weatherstrip sponge is another difficult aspect. Commonly, highly active cure systems are applied with a variety of vulcanization accelerators added to their maximum solubility level in the compound, in order to raise the vulcanization speed and reduce scorch time. To achieve the right dimensions of the sponge profile at the right density, the expanding foam needs to be arrested by scorch just at the right moment. Many attempts were made to simulate this mutual interaction of blowing and curing in laboratory simulations (46–48), but it still is the experience and craftsmanship of the compounder which determines the chance of a quick success: the result of many iterative trials.

Properties of EPM and EPDM Vulcanizates

Mechanical properties depend considerably on the structural characteristics of the EPM/EPDM and the type and amount of fillers in the compound. A wide range of hardnesses can be obtained with EPM/EPDM vulcanizates. The elastic properties are superior to those of many other synthetic rubber vulcanizates, particularly of butyl rubber, but they do not reach the level obtained with NR of SBR vulcanizates. The resistance to compression set is surprisingly good, in particular for EPDM with a high ENB content or when cured with peroxide.

The resistance to heat and ageing of optimized EPM/EPDM vulcanizates is better than that of SBR and NR. Peroxide-cured EPM can, for instance, be exposed to 150°C for 1000 h without significant hardening. Particularly noteworthy is the ozone resistance of EPM/EPDM vulcanizates. Even after exposure for many months to ozone-rich air of 100 pphm, the vulcanizates will not be seriously harmed. EPM/EPDM vulcanizates have an excellent resistance to chemicals, such as dilute acids, alkalis, and alcohol. This is in contrast to the resistance to aliphatic, aromatic, or chlorinated hydrocarbons. EPM/EPDM vulcanizates swell considerably in these nonpolar media.

The electrical-insulating and dielectric properties of the pure EPM/EPDM are excellent, but in compounds they are also strongly dependent on the proper choice of fillers. The electrical properties of vulcanizates are also good at high temperatures and after heat-ageing. Because EPM/EPDM vulcanizates absorb little moisture, their good electrical properties suffer minimally when they are submerged in water.

Health and Safety Factors

EP(D)M is not classified as a hazardous material. It is not considered carcinogenic according to OSHA Hazard Communications Standard and IARC Monographs. Commonly used paraffinic extender oils contain less than 0.1 wt% polynuclear aromatic compounds PNAs.

In handling EPM/EPDM, normal industrial hygienic procedures should be followed. It is advisable to minimize skin contact. The use of EPM/EPDM is permitted for food contact under the conditions given in the respective FDA paragraphs: § 177.1520 for olefin polymers, and § 177.2600 for rubber articles intended for repeated contact with food.

Uses

Expressed as percentages of total annual synthetic rubber consumption worldwide, EPM and EPDM have increased from 0% in 1964 to 8.9% in 2000, as shown in Table 4. EPM and EPDM still show a steady growth over the years.

The main uses of EPM and EPDM are in automotive applications as weatherstrip profiles, automotive coolant hoses, air-conditioning and brake hoses, and seals. In building and construction EPDM is used in sealing profiles, roofing foil, and seals; in cable and wire as cable insulation and jacketing; and in appliances in a wide variety of mostly molded articles.

With respect to automotive coolant hoses, the ever-increasing temperatures under the hood, combined with a performance requirement of 10 years or 200,000 km, have led to significantly more stringent testing conditions. Temperatures commonly occurring under the hood in the area of the radiator hose are 110–125°C, with peak temperatures as high as 140°C locally. Sulfur-cured EPDM has established itself as the most preferred elastomer for radiator coolant hoses under these conditions. The newer automotive standards request for higher temperature resistance: typical operating temperatures between 125 and 150°C continuous use, with peaks as high as 175°C. Further, new metal alloys containing aluminum and magnesium are used for the car engines. These new metals as well as the higher temperatures dictate appropriate changes in the compositions of the cooling liquids, in particular the stabilization packages against metal corrosion. These lead to an increased tendency to form deposits with zinc and accelerator-remnants leached out of sulfur-cured EPDM. The deposits tend to block the cooling capillaries in the engine and the radiator, reducing heat transfer and eventually

Table 4. Worldwide EPM and EPDM Consumption as Percentage of Total Rubber Consumption[a]

Year	EPM/EPDM, t/year	EPM/EPDM consumption, %[b]
1964		0.0
1970	89,000	
1980	328,000	
1990	609,000	
2000	919,000	8.9

[a] Ref. 20.
[b] Of total synthetic rubber consumption.

leading to engine break down. In these cases, where zinc is not acceptable in EPDM compounds, as well as for those cases where the temperature requirements surpass the ageing performance commonly achieved with sulfur cure, the alternative of peroxide curing of EPDM is the preferred method (49,50).

For the same reason of increased temperatures under the hood, the use of EPDM for dynamic applications is gaining importance as a replacement of NR, the natural choice for such applications because of its excellent fatigue resistance and low hysteresis. Applications envisaged are automotive engine mounts, vibration mountings, and muffler mounts. By a proper selection of EPDM characteristics—very high molecular weight, narrow molecular weight distribution, in combination with a relatively low amount of fillers added during compounding, EPDM practically matches the dynamic performance of NR in these applications. Its temperature resistance can even be improved by choosing peroxide rather than sulfur for the vulcanization, although the dynamic properties of peroxide cured compounds are generally somewhat reduced in comparison with sulfur cures (51).

The use of EPDM in low and medium voltage wire and cable applications has made steady progress, as a result of its superior electrical treeing retardancy. EPDM rubber insulated cables are more stable under wet conditions than crosslinked polyethylene insulation. The choice among various EPDM grades in designing insulation compounds is governed by the service requirements such as low electric loss, extrudates free of surface defects, high extrusion output, and good heat ageing properties (52). Also for this application long-chain branching has shown to be particularly beneficial for overall optimum performance (53).

Another application for EPDM is in blends with general-purpose rubbers. Ozone resistance is thus provided with the host rubber comprising the principal portion of the blend. This technique has been applied in enhancing the ozone and weathering resistance of tire sidewalls and cover strips. This use accounts for essentially all EPDM consumption in tires, as the dynamic and wear properties of EPDM do not favor its use for the carcass and tread parts of the tire. EPDM compounds are, moreover, nontacky, whereas tackiness is a prerequisite for building tires. Although this can be solved to some extent, there are no all-EPDM tires currently being produced. Economic factors favor the use of natural and general-purpose synthetic rubbers in tires.

Considerable amounts of EPM and EPDM are also used in blends with thermoplastics, eg, as impact modifier in quantities up to about 25 wt% for polyamides, polystyrenes, and particularly polypropylene. The latter products are used in many exterior automotive applications such as bumpers and body panels. In blends with polypropylene, wherein the EPDM component may be increased to become the larger portion, a thermoplastic elastomer is obtained. Provided the EPDM phase is vulcanized during the mixing with polypropylene (dynamic vulcanization) to suppress the flow of the EPDM phase, it gives the end product good set properties (54).

Substantial amounts of EPM are also used as viscosity modifiers in lubrication oils. Molecular weight, molecular weight distribution, ethylene propylene ratio and in particular sequence distribution are important parameters to meet the desired performance. They markedly influence the thickening efficiency, low temperature properties, temporary and permanent viscosity loss due to shear, and engine performance as a whole. Much work aims at modification of the EPM

backbone as a post-polymerization step with polar groupings: eg, by grafting maleic anhydride onto the EPM chain, followed by a reaction with a variety of polar groupings such as amines (55,56).

BIBLIOGRAPHY

"Ethylene-Propylene Elastomers" in *EPSE*, 2nd ed., Vol. 6, pp. 522–564, by G. Ver Strate, Exxon Chemical Co.

1. G. Natta, *Chim. Ind.* **39**, 733–743 (1957).
2. Evaluation procedures, *ISO 4097 Rubber, Ethylene–Propylene–Diene (EPDM)*, Non-oil extended raw general-purpose types.
3. J. W. M. Noordermeer, *Kautsuh. Gummi Kunstst.* **49**, 521–531 (1996); *Rubber World* 18–22 (May 1997) and 16–26 (July 1997).
4. S. Cesca, *Macromol. Rev.* **10**, 1–230 (1975).
5. F. P. Baldwin and G. VerStrate, *Rubber Chem. Technol.* **45**, 709–881 (1972).
6. EP Pat. 691 354 (1996) and WO Pat. 9 620 150 (1996), T. Ishida, M. Yasuda, H. Onishi, N. Kihara, T. Tsutsui, T. Sagano, M. Kawasaki, K. Takahashi, and H. Nakahama (both to Mitsui Petrochemical Industries Ltd.).
7. C. A. van Gunst, J. W. F. van 't Wout, and H. J. G. Paulen, *Gummi Asbest Kunstst.* **29**, 184–189 (1976).
8. J. Boor, *Ziegler Natta Catalysts and Polymerizations*, Academic Press, New York, 1979, p. 563.
9. C. Cozewith and G. VerStrate, *Macromolecules* **4**, 482 (1971).
10. G. Natta, A. Valvasori, and G. Satori, in J. P. Kennedy and E. G. M. Törnquist, eds., *Polymer Chemistry of Synthetic Elastomers*, John Wiley & Sons, Inc., New York, 1969, p. 687.
11. D. L. Christman, *J. Polym. Sci., Part A-1* **10**, 471 (1972).
12. H. Emde, *Angew. Makromol. Chem.* **60/61**, 1–20 (1977).
13. U. S. Pats. 4,420,595 (1983) and 4,435,552 (1984), G. Evens (both to Stamicarbon).
14. U. S. Pats. 6,147,251 (2000) and 6,310,237 (2001), X. W. Feng and W. Nudenberg (both to Uniroyal Chemical Co.).
15. E. N. Kresge, C. Cozewith, and G. Ver Strate, in *ACS Rubber Division Meeting*, Indianapolis, May 8, 1984.
16. C. Cozewith, W. W. Graessley, and G. Ver Strate, *Chem. Eng. Sci.* **34**, 245–248 (1979); *J. Appl. Polym. Sci.* **25**, 59–62 (1980).
17. U. S. Pat. 3,726,843 (1973), C. Anolick and E. W. Slocum (to E. I. du Pont de Nemours & Co., Inc.).
18. U. S. Pat. 4,710,538 (1987), R. J. Jorgensen (to Union Carbide Chemicals & Plastics Technology Corp.).
19. EP Pat. 0 570 966 (1993), R. J. Boysen, C. R. Mure, L. S. Scarola, and A. S.-J. Rhee (to Union Carbide Chemicals & Plastics Technology Corp.).
20. U. S. Pat. 5,191,062 (1993), R. J. Bernier and D.-F. Wang (to Union Carbide Chemicals & Plastics Technology Corp.).
21. EP Pat. 416 815 (1991) and WO Pat. 9 308 221 (1993), G. W. Knight, S. Lai, J. C. Stevens, and J. R. Wilson (both to the Dow Chemical Co.).
22. EP Pat. 129 368 (1984), J. A. Ewen and H. C. Welborn (to Exxon Research & Engineering Co.).
23. A. Malmberg and B. Lofgren, *J. Appl. Polym. Sci.* **66**, 35–44 (1997).
24. W.-J. Wang, S. Zhu, and S.-J. Park, *Macromolecules* **33**, 5770–5776 (2000).
25. *World Rubber Statistics 2000*, International Institute of Synthetic Rubber Producers Inc., Houston, Tex.

26. E. F. J. Duynstee, *Kautsch. Gummi Kunstst.* **40**, 205–209 (1987).
27. M. van Duin, *Rubber Chem. Technol.* **74**, 138 (2001).
28. M. van Duin, *Kautsch. Gummi Kunstst.* **55**, 150 (2002).
29. M. van Duin and A. Souphanthong, *Rubber Chem.Technol.* **68**, 717 (1996); *Rubber Chem. Technol.* **73**, 706 (2000).
30. TRGS 552 Technical Rules for Dangerous Substances, Bundesarbeitsblatt, Germany, Sept. 1988.
31. D. Seeberger and G. Raabe, *Kautsch. Gummi Kunstst.* **48**, 364 (1995).
32. J. W. M. Noordermeer and M. Wilms, *Kautsch. Gummi Kunstst.* **41**, 558–563 (1988); *Kautsch. Gummi Kunstst.* **44**, 679–683 (1991).
33. J. W. M. Noordermeer and M. Wilms, in P. N. Cheremisinoff, ed., *Handbook of Applied Polymer Processing Technology*, Marcel Dekker, Inc., New York, 1996, p. 549.
34. G. Stella and J. R. Schauder, in *Rubbercon '95*, Gothenburg, Sweden, May 9–12, 1995.
35. K. P. Beardsley and R. W. Tomlinson, in *ACS Rubber Division Meeting*, Detroit, Oct. 17–20, 1989.
36. H. J. H. Beelen, *Kautsch. Gummi Kunstst.* **52**, 406–412 (1999).
37. N. P. Cheremisinoff, *Polym.-Plast. Technol. Eng.* **27**(1), 93–126 (1988).
38. G. Stella and N. P. Cheremisinoff, *Polym.-Plast. Technol. Eng.* **28**, 185–1999 (1989).
39. H. J. H. Beelen, L. R. Maag, and J. W. M. Noordermeer, *Rubber World* 18–26 (July 1998).
40. J. W. M. Noordermeer and H. J. H. Beelen, in *ACS Rubber Division Meeting*, Dallas, Tex., Apr. 4–6, 2000.
41. A. Hill, *Die kontinuierliche Vulkanisation von Elastomerdichtprofilen: Stand der Technik und Neuentwicklungen, in: Spritzgiessen und Extrudieren von Elastomeren*, VDI-Verlag GmbH, Düsseldorf, Germany, 1996 (German).
42. J. W. M. Noordermeer, *Cell. Polym.* **16**, 331–348 (1997).
43. J. R. Schauder and G. Stella, *Kautsch. Gummi Kunstst.* **12**, 1055–1059 (1992).
44. D. G. Rowland, *Rubber Chem. Technol.* **66**, 463–475 (1993).
45. D. G. Rowland, *Rubber Plast. News* (21), 14 (1987).
46. R. Franko, *Elastomerics* 30–32 (Jan. 1989).
47. W. R. Randall and J. A. Riedel, *Rubber World* 23–31 (Jan. 1993).
48. G. Stella and N. P. Cheremisinoff, in International Rubber Conference, Paris, France, June 12–14, 1990, pp. 43–67.
49. G. Vroomen, J. Noordermeer, and M. Wilms, in ACS Rubber Division Meeting, Nashville, Tenn., Sept. 29 – Oct. 2, 1998.
50. J. R. Schauder, T. A. Mills, and G. Stella, Europlast '94, Paris, France, Oct. 6, 1994.
51. P. M. van de Ven and M. Koch, *Elastomerverarbeitung: vom Konzept zur Serie*, VDI-Verlag GmbH, Düsseldorf, Germany, 1999 (English).
52. R. B. Blodgett, *Rubber Chem. Technol.* **52**, 410–424 (1979).
53. P. S. Ravishankar and N. R. Dharmarajan, in ACS Rubber Division Meeting, Cleveland, Ohio, Oct. 21–24, 1997.
54. A. Y. Coran and R. P. Patel, in ACS Rubber Division Meeting, Nashville, Tenn., Nov. 4, 1992.
55. K. Marsden, *Lub. Sci.* **1**, 265–280 (1989).
56. M. K. Mishra and R. G. Saxton, *CHEMTECH* 35–41 (Apr. 1995).

JACOBUS W. M. NOORDERMEER
DSM Elastomers, R&D

EXTRUSION. See Volume 2.

FATIGUE

Introduction

Polymers and polymer-based composites are increasingly displacing more traditional materials in a wide variety of engineering applications, and estimates by the National Institute of Standards and Technology place the total annual loss of engineering components due to fracture at more than $110 billion. Failure may occur for a variety of reasons. Most notably, failure can occur if the applied stress exceeds the strength limits of the material. Failure may also be attributed to material property deficiencies resulting from improper processing conditions that lead to defects (eg, gas or shrinkage pores, inclusions, and weld-and-flow-line defects). Surface defects can result from mechanical processing or handling. These include scratches, gouges, and other markings that introduce stress concentrations. Finally, defects can nucleate and grow in a material during service as a result of repeated loading at stress levels below the nominal yield strength, even when the material has satisfactory properties and contains no adventitious defects. When these failures occur as a consequence of a hygrothermal or mechanically induced cyclic loading condition, they are referred to as fatigue failures.

In general, a variety of mechanisms may contribute to the failure of actual components in service. These may include chemical degradation or oxidation: a chemical mechanism that may induce cross-linking and chain-scission. Alternately, other physical processes may alter the state of the polymer (eg, surface active agents in the presence of stress may induce crazes due to local diffusion of the agents near defects). These aspects are not discussed in this article.

Failure of a component due to fatigue generally occurs through a two-step process. The first step involves the initiation of microcracks or other damage at inhomogeneities or defects in the material. This damage can initiate and evolve

Encyclopedia of Polymer Science and Technology. Copyright John Wiley & Sons, Inc. All rights reserved.

at nominal stress levels far below the yield or tensile strength of the material. This step is commonly referred to at the initiation stage. The second step involves the growth of damage through the coalescence of microcracks and the subcritical propagation of these small cracks to form large cracks and ultimately cause component failure. This step in the failure process is referred to as the propagation stage. For most polymeric materials, the initiation time can be orders of magnitude greater than the propagation time. The initiation of such microcracks and their subsequent propagation form the subject of this article. This article places emphasis on the fatigue behavior, and not necessarily on aspects of fatigue crack propagation (FCP), which is considered to be a topical subset of the fracture behavior of polymers and is out of the scope of this article (see FRACTURE). Nevertheless, some aspects of FCP and fracture are discussed as they relate to specific cumulative damage theories and lifetime prediction methods. Earlier reviews in polymer fatigue and FCP have appeared (1–7).

General Terminology

A common aspect to all fatigue failures is that they occur as a consequence of an imposed cyclic hygrothermal and/or mechanical loading process. In general, any cyclic loading condition can be imposed on any specimen geometry. However, the most common loading conditions for mechanically induced fatigue involve uniaxial (tension and/or compression) or flexural loading conditions. Although the stress state changes with specimen geometry and loading condition, the common approach is to describe the fatigue behavior in terms of the magnitude of some imposed cyclic stress. Two common specimen geometries used for fatigue studies include the *dogbone*-shaped tensile bars (ASTM D638) (8) for tension–tension fatigue experiments or flexure specimens (ASTM D671-71) (9) for tension–compression fatigue studies. These two specimen geometries are schematically shown in Figure 1. The flexural fatigue specimen in Figure 1 is tapered along its gage length to produce a nominal stress distribution that is constant along the gage length of the specimen. The flexure geometry is tested in a cantilever beam configuration. This configuration produces a bending moment across the specimen thickness that is linearly distributed along the beam length. By linearly altering the beam bending moment of inertia (via the tapered width), the stresses along the specimen gage length become constant. For polymer-based composites, flexural fatigue using the geometries illustrated in Figure 1, are quite common. Thus, both the tensile and flexure fatigue geometries produce stress distributions that are nominally constant along their gage lengths and are below those imposed at the grips. These attributes are critical for accurate measures of fatigue resistance of a material to ensure that specimen geometry does not alter the result by promoting premature failure at the grip locations.

It should be noted that there are subtle differences when comparing data generated in uniaxial tension and flexural fatigue tests. A uniaxially applied load nominally imposes a uniform normal stress throughout the cross section of the specimen, with a plane strain condition occurring at the specimen's center. In contrast, the normal stresses in a flexure test are linearly distributed across the specimen, with the maximum occurring at the outer surfaces of the specimen, and

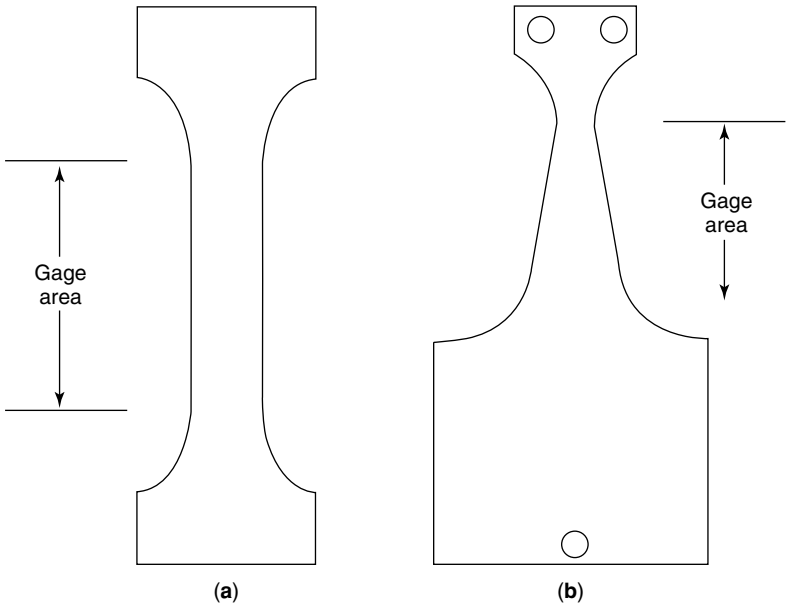

Fig. 1. Schematic of common specimen geometries used in fatigue testing of polymeric materials. (**a**) Tensile test specimen. (**b**) Flexural test specimen.

are zero at specimen's neutral axis (typically at the center for most specimens). Consequently, flexural fatigue tests are more affected by surface flaws while uniaxial tests are more affected by flaws within the specimen's interior. Also, because of the high internal damping and low thermal conductivity characteristic of most polymers, hysteretic heating and the associated effects are more prevalent in uniaxial tests than in flexure tests.

In mechanically induced fatigue tests, the stress or strain is oscillated about some mean stress (strain). If the peak or maximum stress is defined by σ_0 and the minimum stress by σ_u, then the stress ratio is often defined by R where

$$R = \frac{\sigma_0}{\sigma_u} \tag{1}$$

The type of cyclic is typically a sinusoidal, triangular, or square wave with the amplitude, mean stress, and frequency all adjustable parameters to consider. Some of these parameters are shown in Figure 2.

Numerous studies have shown that the cyclic lifetime of a test bar or component varies inversely with the magnitude of the applied cyclic stress, strain, or deflection. As a consequence, various test procedures have been developed to obtain mechanical property information useful in fatigue design analysis. Long ago, Wöhler (10) developed a procedure wherein a notched or unnotched specimen is subjected to a cyclic stress (σ) and the number of loading cycles (N) to cause failure is recorded. This procedure is repeated for a range of stress levels, and the data are presented in the form of a σ–N curve (11,12). Examples of σ–N fatigue curves are shown in Figure 3 (12).

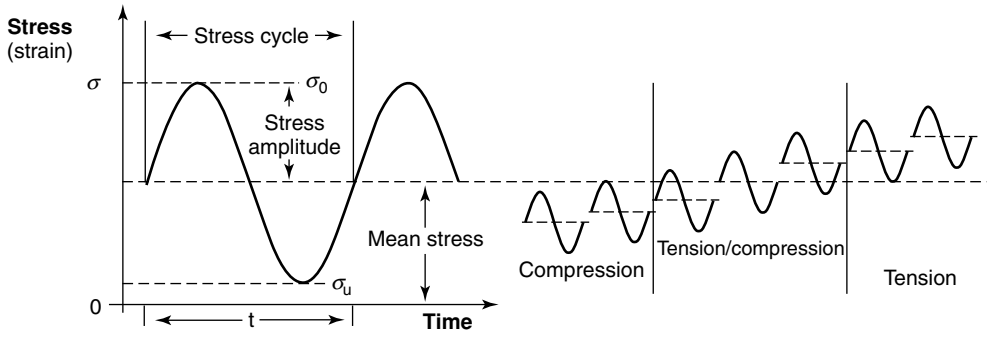

Fig. 2. Important parameters for fatigue experiments.

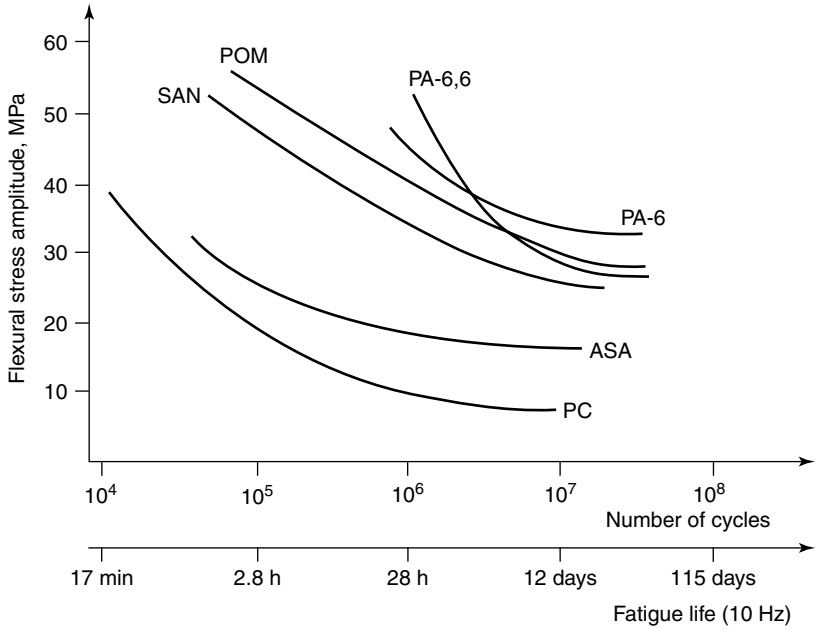

Fig. 3. Wöhler curves for different thermoplastics, generated via flexural fatigue loading at 10 Hz (12). To convert MPa to psi, multiply by 145.

The cyclic lifetime of a given polymer decreases with increasing applied stress consistent with greater damage accumulation per cycle at higher stress. Some of the plots in Figure 3 exhibit a relatively well-defined plateau, suggesting an endurance limit for a particular polymer below which fatigue damage does not significantly accumulate. By contrast, other engineering plastics reveal a steadily decreasing allowable cyclic stress with increasing number of loading cycles. Stress cyclic lifetime curves are used to define the permissible operating stress (or strain) in order to preclude fatigue failure for an anticipated number of cyclic excursions. For example, if it is desired that a component withstand at least N_1 loading cycles in a given lifetime, the part should be designed so that the applied cyclic stress is less than σ_1.

Fatigue tests are both costly and time consuming because of the number of samples that must be tested in an expensive test machine for days or weeks until fracture. Also, since fracture is a stochastic process by nature, repeated tests should be conducted at each stress level considered. Finally, the number of cycles to failure, N_I, gives no clear indication of the fatigue limits for a given application of a polymeric material because in many cases, the definition of failure is ambiguous. For example, failure may be defined as a decrease in specimen stiffness or other irreversible changes rather than actual specimen fracture.

Fatigue Behavior

In general, fatigue failure occurs by one of two possible modes: a mechanically dominated mechanism or a thermally dominated mechanism. A mechanically dominated process involves the nucleation of damage and its subsequent growth in the form of crazes, microcracks, and ultimately large cracks that are responsible for specimen failure. This process occurs at relatively lower stresses and frequencies and results in a higher fatigue life. This regime is commonly referred to as the high cycle regime and the failure mode of the polymeric material is quite often brittle in nature (13–16). This regime is also referred to as the *true* fatigue response of the material.

At relatively higher stresses and frequencies, hysteretic heating affects the physical and mechanical properties of the polymer. This effect is a combined consequence of the fact that most polymers demonstrate high internal damping and low thermal conductivity. In this process, heat generated from mechanical fatigue cannot be dissipated to the surroundings and the polymer temperature rises throughout the test. Failures usually occur rather quickly and the failure mode is usually ductile (13–16). This regime is referred to as the low cycle regime and is not considered to be an intrinsic response of the material to fatigue loading conditions. If one polymer exhibits a greater tendency than another for hysteretic heating under cyclic loading conditions, the relative ranking of the two polymers may differ greatly when the tests are conducted at both high and low cyclic frequencies.

Identifying whether a particular set of fatigue conditions is mechanically or thermally dominated can be observed in the evolution of the hysteresis loops. This is shown characteristically for the case of polyacetal in Figure 4 (13). In the low cycle region, hysteresis loops show a progressive increase in compliance and irreversible work as the material is fatigued. In contrast, the high cycle hysteresis loops show that the material initially becomes slightly stiffer and less viscoelastic (as evidenced by the decrease in irreversible work) as the cycles increase. This is fatigue-induced embrittlement and occurs prior to craze initiation and subsequent crack growth. A Wöhler plot of polyacetal showing the thermally and mechanically dominated regions is shown in Figure 5 (13). Note that a discontinuity occurs in the σ–N at the stress level where the transition occurs. This is critically important to recognize since data in the thermally dominated regime suggest that an endurance limit has been reached. However, as the stress level is reduced, a transition in the failure mode occurs from ductile to brittle, and failure is measured at a finite cycle number below the apparent endurance limit. Hence, extreme care should

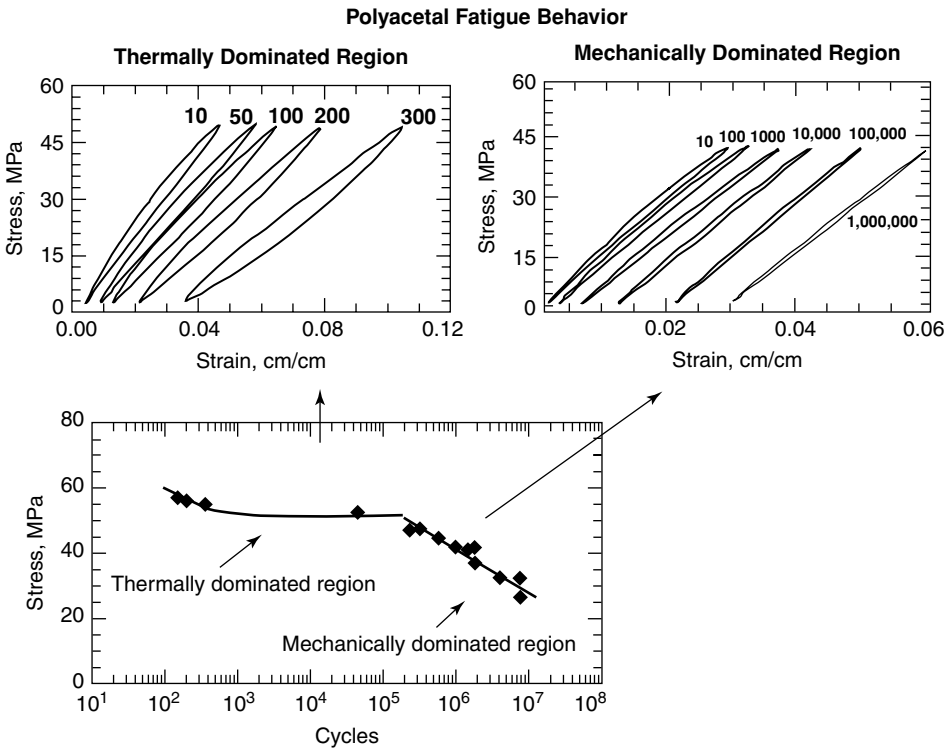

Fig. 4. Plots of hysteresis loops for polyacetal fatigued in the low cycle (thermally dominated) and high cycle (mechanically dominated) regions. The numbers located by each hysteresis loop indicate the cycle number (13). To convert MPa to psi, multiply by 145.

be exercised when using fatigue data for design considerations to ensure that the proper failure mode is observed from the accelerated tests.

Hysteretic Heating and the Low Cycle Regime. At relatively high frequencies and stress levels, many polymers may become overheated as a result of the accumulation of hysteretic energy generated during the loading cycles. Such energy dissipation produces a significant temperature rise within the specimen, which, in turn, causes the elastic modulus of the material to decrease. As a result, large specimen deflections contribute to even greater hysteretic energy losses with further cycling. In the limit, an autoaccelerating tendency for rapid specimen heating and increased compliance is experienced. Such thermal failure corresponds to the number of loading cycles at a given applied stress range that bring about an apparent modulus decay to 70% of the original modulus of the specimen (10–13). Extreme care should be taken in ranking the fatigue resistance of polymeric materials since the test conditions may effect the measurement of the true or the intrinsic fatigue resistance of the material. In general, results like those presented in Figure 3 should only be used to rank materials once it is assured that the tests are run properly to ensure the appropriate failure mechanisms. These test results can be applied in design only when all design factors including magnitude and state of the stress, part size and shape, temperature, heat transfer

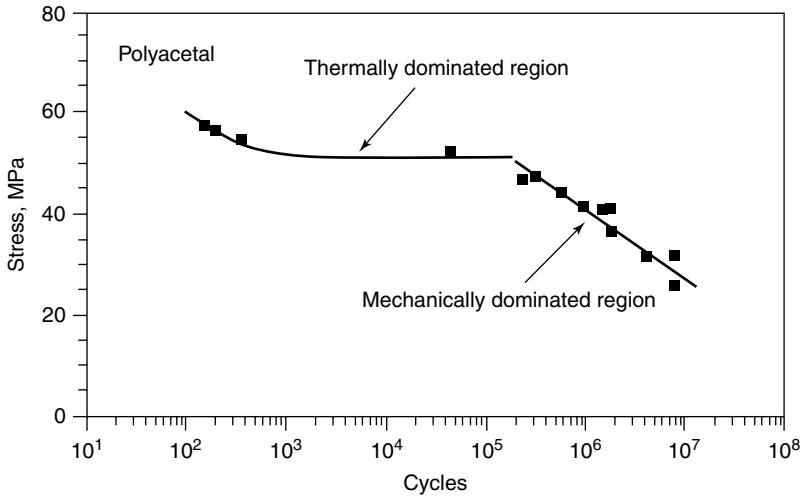

Fig. 5. Plot of fatigue σ–N curve for polyacetal resin, illustrating both thermally dominated and mechanically dominated regions. Note in the thermally dominated region an apparent endurance limit appears (13). To convert MPa to psi, multiply by 145.

conditions, cyclic frequency, and environmental conditions are comparable to the test conditions.

Studies (17–19) have shown that the energy dissipation rate under cyclic loading conditions varies directly with the test frequency, the loss compliance of the material, and the square of the applied stress. Neglecting heat losses to surrounding environment the temperature rise in the sample per unit time can be calculated as

$$\Delta\dot{T} = \frac{\pi f J''(f,T)\sigma^2}{\rho_{\mathrm{p}}^c} \tag{2}$$

where $\Delta\dot{T}$ is the temperature change/unit time, f the frequency, J'' the loss compliance, σ the peak stress, ρ the density, and c_{p} the specific heat. Previous studies (15,16,20) have shown that for all stress levels above the endurance limit, the polymer heats to the point of melting at failure. The temperature rise is stabilized at a maximum below the point of thermal failure. It should be noted that for conditions associated with thermal failure, cyclic lives can be enhanced by intermittent rest periods during the cyclic history of the sample (20–22). Temperature rise resulting from adiabatic heating can thus be dissipated periodically. Therefore, component life can be enhanced via cooling in thermally dominated fatigue applications (23).

The transition from thermal to mechanical failure has been described in terms of a changeover stress level, which depends on test frequency, mean stress, cyclic waveform, and specimen surface area-to-volume ratio (24). An empirical relationship between the uniaxial changeover stress and test frequency is shown in Figure 6 (24) and is given by

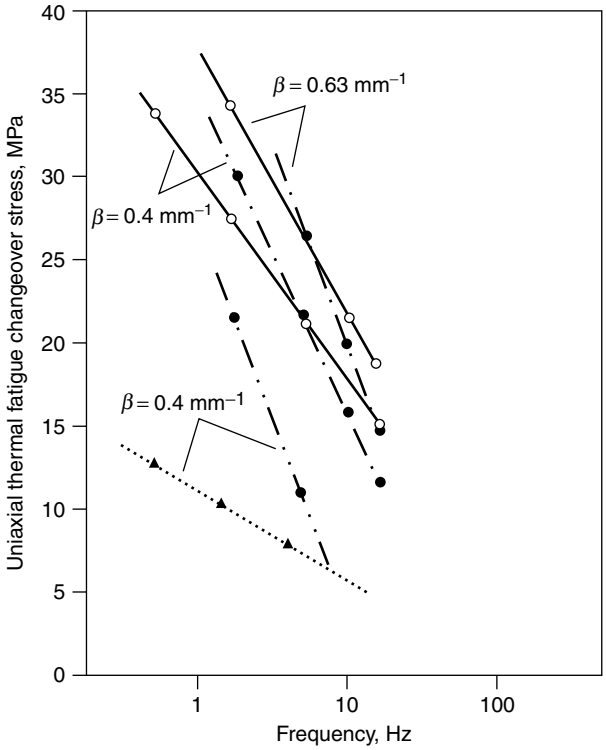

Fig. 6. Changeover stress from mechanical to thermal failure as a function of specimen surface area-to-volume ratio β and test frequency (24). To convert MPa to psi, multiply by 145.

$$\sigma_c = \sqrt{A/V}(C_1 - C_2 \log_{10} f) \tag{3}$$

where σ_c is the changeover stress, A the specimen surface area, V the specimen volume, and f the cyclic frequency. C_1 and C_2 are empirical constants and related to the heat capacity of the polymer and properties of the environment that the polymer is fatigued in. A similar methodology is also presented in Reference 16.

High Cycle Fatigue and Polymer Embrittlement. In the high cycle region (ie, at stress levels and frequencies low enough such that hysteretic heating is stabilized), failure of the material occurs through the nucleation of damage and subsequent propagation of cracks. In general, the total fatigue life of a specimen is a combination of an initiation (N_i) and a propagation (N_p) stage. The initiation stage is associated with the cycles required to initiate damage and develop a defect (crack) of a size such that the threshold stress intensity is reached. The propagation stage is associated with the number of cycles required to propagate the crack under subcritical conditions from the threshold size to the critical size (such that failure is imminent). Thus far, all discussions have associated with the total cycles (N) and

$$N = N_i + N_p \tag{4}$$

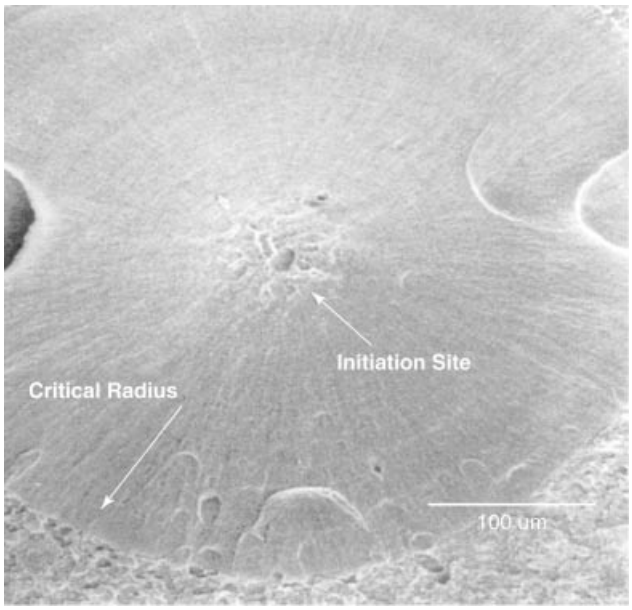

Fig. 7. Fracture surface in polyacetal resin specimen subjected to tensile fatigue. The penny-shaped crack initiated at a void or other inhomogeniety at its center (25).

If a defect is present in a component at the outset of its service life, N corresponds largely to the propagation stage of crack extension. Depending on the size and shape of the defect, N_i represents either a small or a large fraction of N. Depending on the polymer and processing conditions, damage may nucleate relatively early and the total life is dominated by the subcritical fracture resistance of the polymer. Figure 7 (12) illustrates such a case for poly(methyl methacrylate) (PMMA), where the time for craze initiation is relatively short compared to the total life of the specimen. In other cases (more typical of engineering thermoplastics with controlled processing conditions), the initiation stage governs the total fatigue life. Table 1 (13) shows a comparison between the initiation and propagation life for two engineering thermoplastics: polyacetal and nylon-6,6 exposed to a sinusoidally applied maximum cyclic stress of 30 MPa at 2 Hz. When comparing the cycles for initiation and propagation in Table 1, it is clear that the early stages of damage development involve mechanisms and kinetics not well described by processes that govern the subcritical fatigue crack growth (discussed in a later section).

Table 1. Comparison between Fatigue Initiation and Propagation Lifetimes for Polyacetal and Nylon-6,6[a]

Material	K_{th}, MPa·m$^{1/2}$	K_{Ic}, MPa·m$^{1/2}$	A	m	N_p	N_f	N_i
Nylon-6,6	2.0	6.0	5.4×10^{-9}	6.8	9000	2×10^7	$\sim 2 \times 10^7$
Polyacetal	2.5	3.1	1.3×10^{-17}	20.0	186000	5×10^6	$\sim 4.8 \times 10^6$

[a]Ref. 13.

It is generally well accepted that damage initiates at preexisting defects or other inhomogeneities within the material. This is typically illustrated in Figure 7 for a polyacetel resin specimen (25). Figure 7 shows the fracture surface from an injection molded ASTM D638 tensile bar subjected to a tensile cyclic fatigue. The initiation of the penny-shaped crack occurred at a void or other inhomogeniety and propagated subcritically under cyclic fatigue to a critical length prior to sudden failure. The specimen was subjected to approximately 5×10^6 cycles to cause failure and the number of cycles required to propagate the penny-shaped crack to the critical size is of the order of 2×10^5 cycles. Thus, the initiation of the penny-shaped crack at the defect site governed the total life of the polymer.

If the preexisting defects in the material are well below the threshold size of the polymer, the initiation process may involve a variety of morphological and microstructural changes. One phenomenon observed in some polymers involves the process of mechanically induced embrittlement. In this process, the polymer becomes slightly stiffer and less viscoelastic as evidenced by the hysteretic response of the material (13). This is illustrated for the case of polyacetal in Figure 4. Notice that the hysteresis loops in the high cycle region become slightly stiffer and the corresponding irreversible work decreases as the material is continually fatigues. This occurs while damage in the form of crazes, cavitation, and microcracks would all decrease the stiffness of the material. This suggests that additional morphological changes may occur during the fatigue of a polymer. Potential mechanisms of this process are discussed in a later section.

Classical Modeling Studies

Wöhler (10) curves are commonly used to rank polymers and identify endurance limits (see Fig. 3) for particular applications. However, they are of little use beyond this without the implementation of a theory that allows for the prediction of fatigue life under more arbitrary loading histories. Predictive methodologies that allow for lifetime estimates have been developed to address this issue. These theories are generally referred to as cumulative damage theories and may or may not incorporate aspects from fracture mechanics or physical characteristics of the materials. Some early theories developed originally for metals (26,27) recognize that total fatigue life is dominated by the initiation stage (see eq. 4) and therefore do not consider the propagation stage in lifetime estimates.

One of the earliest, and most popular, cumulative damage theory was introduced by Minor (26), and is now referred to as *Minor's Law*. Minor proposed that if a material would last a 100 cycles at a particular stress level, then 1/100 of its life is consumed in every cycle at that stress level. This basic postulate provides a framework whereby the σ–N curve (eg, Figs. 3 and 5) can be used to estimate the fatigue life of a material subjected to an arbitrary loading history. Consider that an arbitrary loading history can be fractionated into m blocks of cycles, each under constant fatigue conditions. Then, Minor's law can be written as

$$\sum_{j=1}^{m} \frac{n_j}{N_j} = 1 \tag{5}$$

In equation 5, n_j is the number of cycles within a block applied at stress level σ_j and N_j is the total number of cycles to failure at that stress level (obtained from the σ–N curve). If validated for a particular material, equation 5 can be used for any arbitrary loading condition. In this way, the fatigue data generated in the laboratory is referred to as an accelerated test and equation 5 is used much in the same way that time–temperature superposition is used to predict the viscoelastic deformation of a material. Note, however, that any predictive methodology like that presented in equation 5 must be validated before it is employed for lifetime estimates. In the case of Minor's law, the sequence of the loading history should have no effect on the total lifetime. That is, if one specimen is loaded for a selected portion of its life at stress level σ_1 and the remaining part of its life at σ_2, then the same total life would be achieved if the specimen is first loaded at stress level σ_2 followed by σ_1.

Another common theory was proposed by Manson (27) and is referred to as the *universal slopes equation*. In this model, the plastic strain or permanent deformation, is considered as a measure of the damage imposed in the material. On this basis, the true plastic strain amplitude can be used as a measure of the fatigue behavior. Moreover, the fatigue curve can be predicted in terms of the monotonic stress–strain curve. This empirical approach was initially statistically correlated with many metals and takes the following form:

$$\Delta\varepsilon = \left(\frac{N}{D}\right)^{-0.6} + 3.5\left(\frac{\sigma_u}{E}\right)N^{-0.12} \tag{6}$$

where $\Delta\varepsilon$ is the total strain, D is the ductility, E is the elastic modulus, and σ_u is the ultimate tensile strength. The ductility term D is calculated by

$$D = \ln\left(\frac{A_0}{A}\right) \tag{7}$$

In equation 7, A_0 is the original cross-sectional area and A is the final cross-sectional area at specimen failure. The coefficients 3.5, -0.6, and -0.12 in equation 6 are based on a statistical fit of over 29 metals. In that sense equation 6 universally predicts the fatigue behavior of a wide range of metals by using data obtained from a monotonic tensile test.

Opp and co-workers (14) attempted to extend the universal slopes equation to predict the behavior of polymer fatigue. However, in their attempts they showed that a form of equation 6 was not useful for predicting polymer behavior and instead developed a model to predict the low cycle fatigue behavior based on hysteretic heating. And in this sense is consistent with those presented in equation 3 and References 15–17.

Other classical methods to predict the fatigue behavior in complex or random load patterns involve the so-called rainflow and Markov methods (28). These methods utilize any form of a cumulative damage theory to predict the lifetime in random loading situations.

McKenna and Penn (29) developed a model for predicting the fatigue life of polymers and applied it to an amorphous glass, PMMA, and polyethylene. The model is characterized within the framework of a cumulative damage model. They

show that the mean failure times in constant rate of stress experiments can be successfully predicted from a model using a time to fail function obtained from constant stress experiments. In this manner they were able to bridge the gap between creep and fatigue loading conditions. In their model, the time to fail, t_b, is related to the stress history $\sigma(\xi)$ by the following equation:

$$\int_0^{t_b} \frac{d\xi}{\tau_b[(\xi)]} = 1 \tag{8}$$

where $\tau_b(\sigma)$ is the mean time to failure in constant stress experiments. Thus, each increment of time $d\xi$, during which the load is $\sigma(\xi)$, is weighted inversely as the lifetime $\tau_b(\sigma)$, which the specimen would have had under a constant stress σ.

Once $\tau_b(\sigma)$ is determined from creep (constant load experiments), equation 8 can be used to predict the failure under any stress history. The form of $\tau_b(\sigma)$ that was found to describe the data in Reference 29 is

$$\tau_b(\sigma) = Ae^{-B\sigma} \tag{9}$$

where A and B are constants. Equation 9 uses the form that is derived from molecular considerations by Tobolsky and Eyring (30), Coleman (31,32), and Zhurkov (33). Given the form for time to failure under constant stress in Equation 9, an explicit expression for a constant rate of stress can be explicitly obtained by integrating equation 8. The final expression takes the following form:

$$t_b = \frac{\ln(AB\,\dot{\sigma} + 1)}{B\,\dot{\sigma}} \tag{10}$$

In equation 10, t_b becomes the time to failure at a constant stress rate $\dot{\sigma}$. Similarly, for a sinusoidal stress history

$$\sigma(t) = p + q\sin(\omega t) \tag{11}$$

the time to failure becomes

$$t_b = \frac{\hat{t}_b(p)}{I_0(Bq)} \tag{12}$$

In equation 12, I_0 is the zero-order Bessel function, B is the constant from equation 9, and $\hat{t}_b(p)$ is the time to fail at a constant stress p.

Using equation 12, data from creep tests can be used to predict the failure in sample subjected to a sinusoidal load history. Figure 8 presents a comparison between experimental results and theoretical predictions (29) for PMMA by using equation 12. In this case the prediction underestimates the lifetime in some cases by nearly an order of magnitude but is generally very good. In the case of polyethylene (not shown) the model overestimates the experimentally observed fatigue life. Another practical limitation to the methodology presented in equations 8, 9, 10, 11, 12 is that creep failure data is needed to predict the fatigue

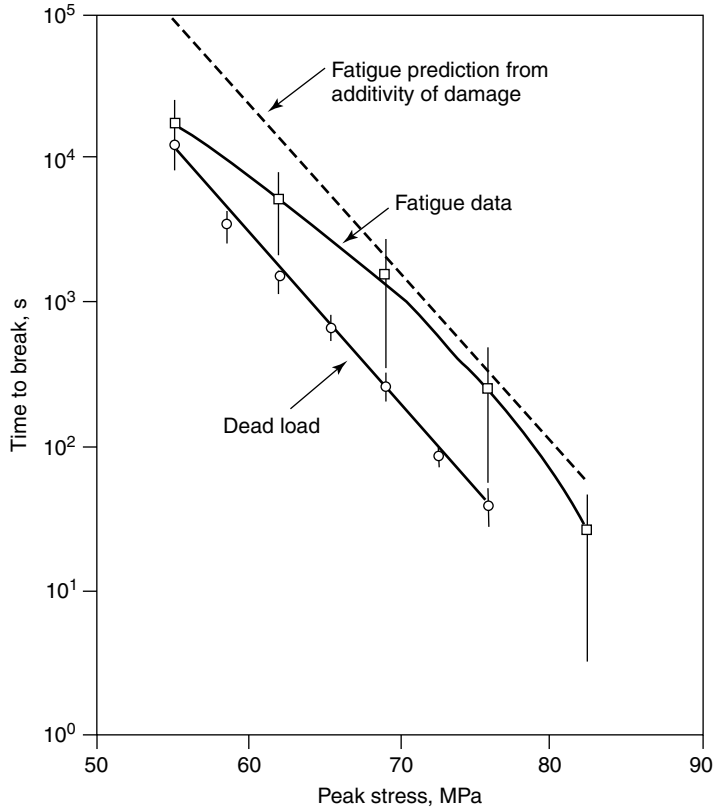

Fig. 8. Comparison of failure times obtained in zero-tension sinusoidal fatigue experiments with those predicted by equation 9 for PMMA at 0.164 Hz, $T = 297$ K (29). To convert MPa to psi, multiply by 145.

lifetime. Experimentally, creep experiments take considerably longer to conduct than fatigue experiments to failure.

Other approaches have been suggested to more formally define the form of damage that occurs during fatigue (34–37). These methods model damage as an array of microcracks (34,35) that inevitably require a tensoral definition of damage (36,37). These methodologies allow for multiaxial stress states to be considered. Thus far, these theories have had only limited applications in polymeric materials. One difficulty that arises from such a framework is the necessity to sum over an array of damage using Green's functions and hence linearity in the constitutive behavior of the material is required. Nonetheless, these approaches may be useful in applications where the nonlinearity imposed from the damage array dominates the material response.

Fatigue Damage Initiation

Physical and Morphological Changes. Some studies have discussed the microstructural and morphological changes that occur in polymers as a consequence of fatigue loads. These effects may occur before the formation of noticeable

damage in the form of voids or microcracks occur. These changes may be critical to understanding the nucleation of damage as well as its growth kinetics. Bouda (38) found that the effects of fatigue on glassy polymers can manifest either as a strain hardening or softening, depending, among other things, on the particular material being investigated. Changes in the dynamic viscoelastic behavior were also reported as well. Similarly, Takahara and co-workers in numerous investigations (39–41) measured changes in the viscoelastic response of a variety of different polymer systems. Both changes in the storage and loss moduli were observed during fatigue. More recently, Sakurai and co-workers (42) conducted a comprehensive investigation of changes induced in polyurethanes subjected to fatigue. They presented dramatic evidence of microstructural changes occurring after a fatigue load was applied. These changes were attributed to changes in crystallinity in addition to dissociation of the hard-segment microdomains.

A recent paper (13) presents results from *in situ* measurements of both the dynamic viscoelastic properties and energetics (ie, potential energy, strain energy, and irreversible work) of nylon-6,6 and polyacetal specimens subjected to fatigue. The measurements of dynamic viscoelastic behavior illustrate how the bulk material properties may be changing during fatigue. Measurements of the strain energy, potential energy, and irreversible work also indicate material changes but can also be more directly used in calculating energy release rates for crack growth. Thus, the evolution of energy release rates may also be an indicator of when crack (damage) growth occurs in the specimen. A plot of the dynamic viscoelastic behavior is shown in Figure 9 and the corresponding evolution of the energetics is given in Figure 10.

The transition from the low cycle to high cycle fatigue occurs between 48 and 50 MPa at a frequency of 2 Hz for polyacetal and this transition is clearly evident in both graphs. In the low cycle regime, the materials become softer and more viscoelastic as evidenced by the dramatic drop in storage modulus and corresponding increase in tan δ. Also, both the potential energy and irreversible work increase considerably in the low cycle regime. All of these results are consistent with the softening of the material due to hysteretic heating.

In the high cycle regime, the polyacetal becomes more compliant (see Figs. 9 and 10) as well, but the amount is more subtle than in the low cycle regime. More interesting, the material also becomes less viscoelastic as evidenced by the drop in tan δ and irreversible work. This is in contrast to low cycle regime and suggests that other morphological changes are occurring in addition to damage. Subsequent studies (13) also showed that the crystallinity increased slightly in both nylon-6,6 and polyacetal.

A similar study on polycarbonate showed that cyclic stress induced physical aging on polycarbonate (43). In this work it was noted that both the Young's moduli increases while the loss modulus decreases. This related phenomenon is referred to as fatigue aging. In contrast, thermophysical aging is the process of the spontaneous approach of the glassy state toward thermodynamic equilibrium. This phenomenon has been reviewed extensively by Struik (44) (see AGING PHYSICAL). This spontaneous change is accelerated perceptibly when the temperature of the glass is increased toward the glass transition. Physical aging causes an increase in density, relaxation modulus, and other properties. Physical aging alters the relative kinetics of crazing and shear banding processes, so that a normally tough

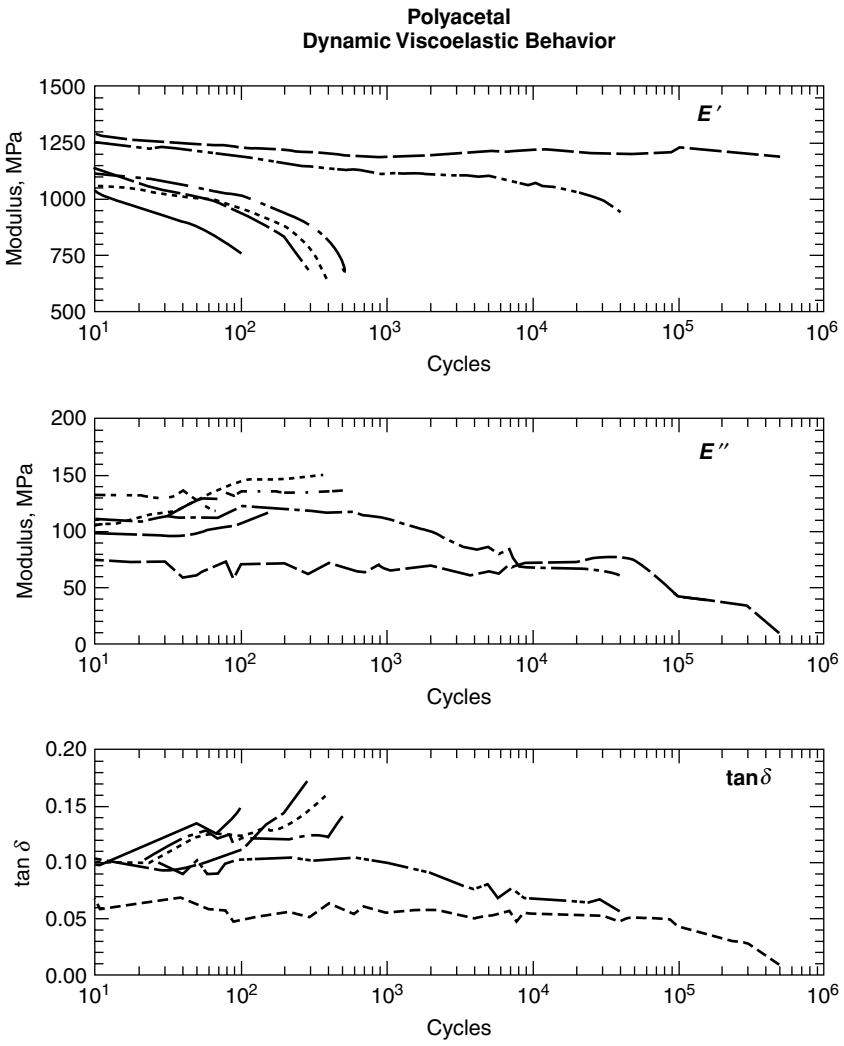

Fig. 9. Plots of dynamic viscoelastic response during fatigue of polyacetal over a range of maximum stress levels. All tests were conducted at a frequency of 2 Hz at room temperature (13). ——— 56 MPa; —— 54 MPa; - - - - - 52 MPa;— - 50 MPa; — - - 48 MPa; — – 45 MPa. To convert MPa to psi, multiply by 145.

polymer becomes very brittle upon aging (45,46) apparently because the shear yielding process becomes retarded.

A common method employed to detect physical aging in glassy polymers involves the use of differential scanning calorimetry. Careful studies of the thermograms show an enthalpic overshoot as the polymer is heated through the glass-transition region. This overshoot occurs both with thermophysical aging and fatigue aging but the peak temperature of the endotherm is slightly increased for the fatigue aged samples (43). Figure 11 shows how the endothermic overshoots are affected by the stress amplitude for polycarbonate samples exposed to different

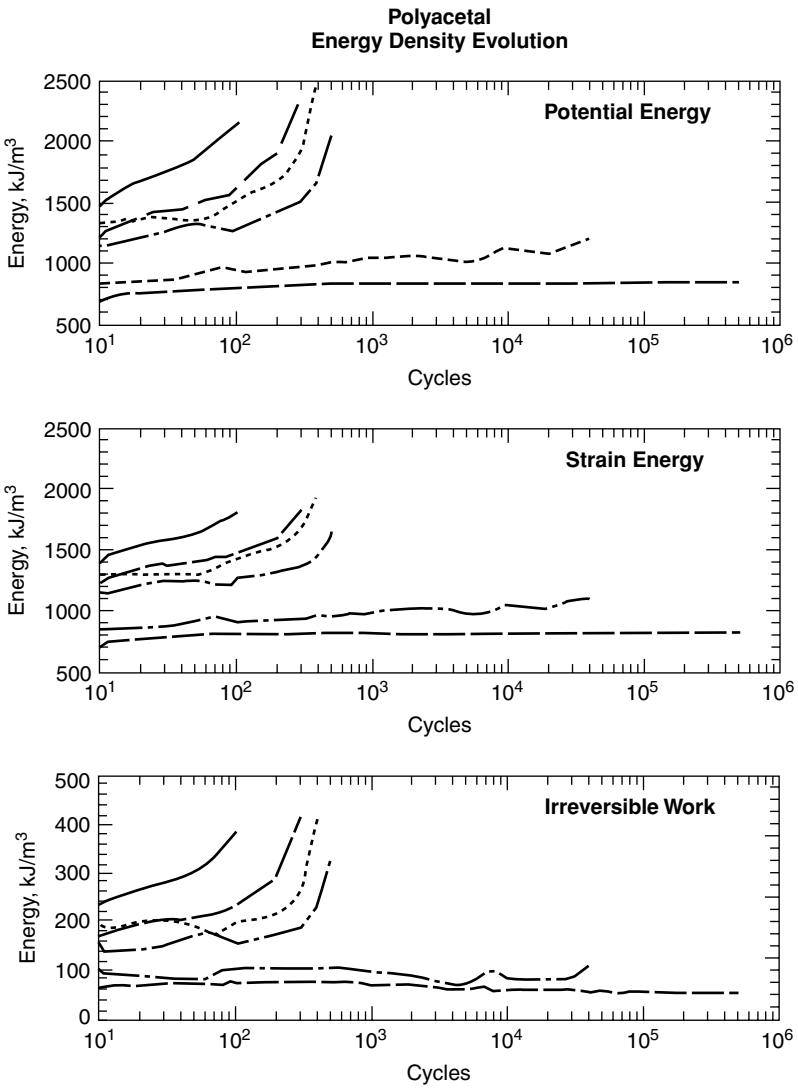

Fig. 10. Plots presenting the energy density evolution for polyacetal over a range of stress levels. All tests were conducted at a frequency of 2 Hz at room temperature (13). ——— 56 MPa; —— 54 MPa; - - - - - 52 MPa; —- 50 MPa; —·- 48 MPa; —– 45 MPa. To convert MPa to psi, multiply by 145.

thermal histories before loading. In all cases, the fatigue tests were stopped after 8000 cycles. For samples exposed to low or moderate annealing prior to fatiguing, an increase in the enthalpic overshoot appeared and was relatively insensitive to the amplitude of stress. For the highly annealed material, the fatigue actually reduced the endothermic overshoot (ie, reversed the physical aging). Similarly Figure 12 shows how the enthalpic overshoot evolves during the early stages of fatigue.

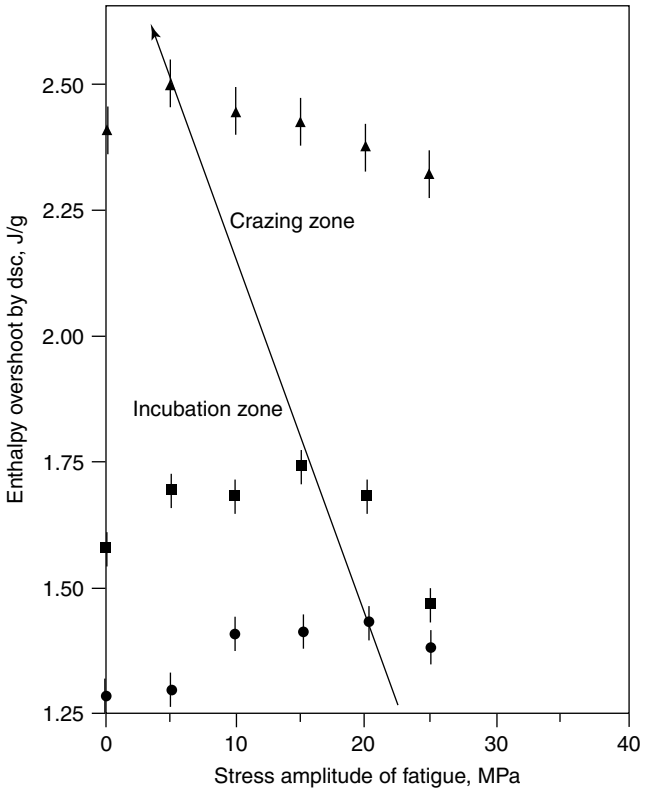

Fig. 11. Differential Scanning Calorimetry enthalpy overshoot of samples of different previous physical aging histories plotted as a function of cyclic stress amplitude for a fixed 8000 cycles (43). ▲ aged at 130°C for 24 h; ■ aged at 130°C for 12 h; ● aged at 130°C for 6 h. To convert MPa to psi, multiply by 145.

Early Stages of Damage Formation. A variety of studies have indicated that void formation, cavitation, or incipient nano-sized cracks occur in the polymer during the early stages of fatigue. The nucleated voids then continue to grow and coalesce while the fatigue process continues. The subcritical crack growth kinetics has been measured over a wide range of polymers (discussed in the next section). Once the flaws reach a threshold flaw size (of the order of 10^{-3} m for many polymers), the subcritical crack growth kinetics are generally well described for many polymers. However, the sizes of these flaws that nucleate and grow during a large portion of the fatigue life are quite often below the threshold flaw size for subcritical crack growth kinetics to govern. This section discusses research devoted to damage at this length scale.

Studies by Zhurkov (33,47) introduced the idea that breakage of primary chemical bonds plays a major role in the fracture of polymers. He found that the time to failure under a resistant uniaxial stress of PMMA and polystyrene below their glass-transition temperature could be expressed in terms of a thermally activated process involving three kinetic parameters:

$$t_b = t_0 e(U_0 - \gamma\sigma_0)/RT \tag{13}$$

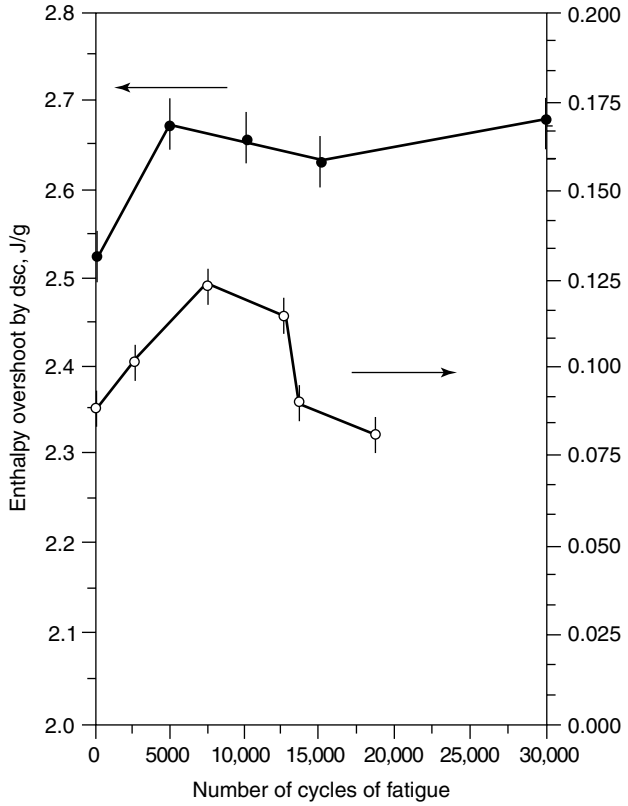

Fig. 12. Differential Scanning Calorimetry enthalpy overshoot as a function of cycle number at a given stress amplitude. Note the different scales in the data (43). ● aged at 130°C for 40 h and fatigued at 20 MPa; ○ quenched from 165°C and fatigued at 31 MPa. To convert MPa to psi, multiply by 145.

In equation 13, t_b is the time to failure, U_0 is interpreted as the activation energy for chain scission, t_0 is interpreted as the inverse of the molecular oscillation frequency, and γ is a structure-sensitive parameter. Experimentally he (47) observed the formation of platelet-shaped nanoscopic voids, which he referred to as incipient cracks, that form very early in the polymer once a tensile load is applied. Both the incipient cracks and their number density were measured from small-angle x-ray scattering studies on samples that had tensile loads applied to them. The characteristic sizes and number densities of the incipient cracks are included in Table 2. Zhurkov showed that the incipient cracks formed at the very early stages and the remaining life was associated with the coalescence of these incipient cracks to ultimately cause failure.

LeGrand and co-workers (48) conducted positional small-angle x-ray scattering studies on high impact polystyrene exposed to fatigue loading conditions. Their results clearly indicated that flaws of some type are nucleated and grow as a result of increasing fatigue. They also suggested that the nucleation and growth of flaws appears to follow a simple exponential law. However, the results regarding

Table 2. Characteristics of Incipient Cracks in Polymers[a]

Polymer	Microcrack longitudinal, nm	Diameter transverse, nm	N_{cr}, cm^{-3}	Density calculated	$\Delta p/p$ measured
Polyethylene	15	17	6×10^{15}	—	—
Polypropylene	20	32–35	7×10^{14}	—	—
Poly(vinyl chloride)	—	60	8×10^{14}	—	—
Poly(vinyl butyral)	—	50	3×10^{14}	—	—
Poly(methyl methacrylate)	80	170	4×10^{12}	0.4×10^{-2}	0.3×10^{-2}
Polycaproamide	5	9–25	5×10^{16}	1.8×10^{-2}	2.0×10^{-2}

[a]Ref. 47.

how material properties or loading conditions affect the growth rates were clearly inconclusive in this study.

Positron annihilation lifetime spectroscopy studies (49) polycarbonate samples subjected to fatigue. Positron annihilation lifetime spectroscopy was used to probe structural changes in terms of the hole volume and number density of fatigued samples. The *ortho*-positronium (o-Ps) pickoff annihilation lifetime τ_3, as well as intensity I_3, were measured as a function of cyclic stress. It was found that τ_3, the longest of the three lifetime components, increases with fatigue cycles. The *holes* where the o-Ps can localize become larger upon fatigue aging. Commensurate with increasing hole size was an indication of hole coalescence from the o-Ps annihilation intensity. It was suggested that this process was the precursor to crazing. Complimentary transmission electron microscopy indicated that isolated voids of the order of 100 nm could be seen (50).

Tensile dilatometry (51–54), which is commonly used to monitor cavitation in rubber-modified glassy polymers, was extended to fatigue application to monitor the volume changes that occur during fatigue loading conditions (55). In this method, axial and transverse strain gages are attached to the sample during a uniaxial fatigue test. From the axial and transverse strain measurements the total volume change $(\frac{\Delta V}{V})_T$ can be calculated from

$$\left(\frac{\Delta V}{V}\right)_T = (1+\varepsilon_a)(1+\varepsilon_t)^2 - 1 \tag{14}$$

where ε_a is the axial strain and ε_t is the transverse strain. The volume change can then be further decomposed into an elastic part and an irreversible part denoted by the subscripts e and i respectively in equation 15 below:

$$\left(\frac{\Delta V}{V}\right)_T = \left(\frac{\Delta V}{V}\right)_e + \left(\frac{\Delta V}{V}\right)_i \tag{15}$$

The total volume change can be measured at the peak load during the fatigue test and the irreversible part can be measured at the unloaded portion of the cycle. In this way the evolution of both the elastic and inelastic volume change can be monitored during a fatigue test. Figure 13 shows how the irreversible

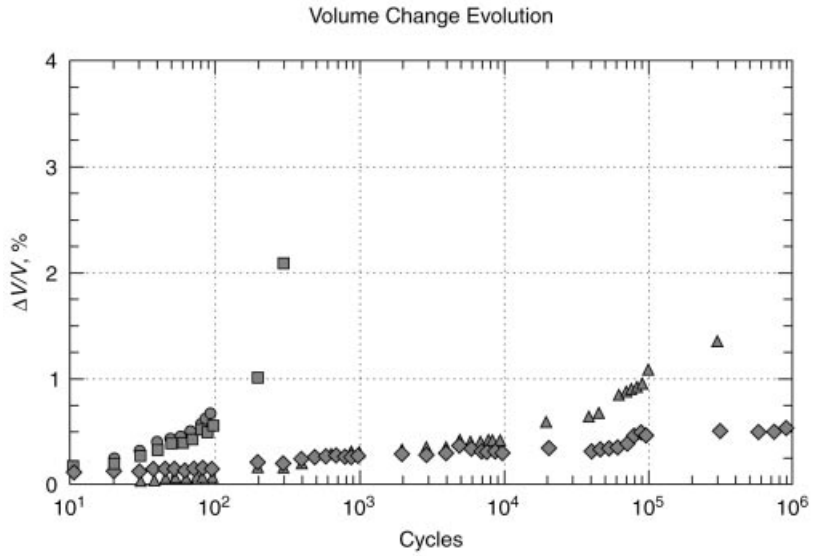

Fig. 13. Irreversible volume change evolution for polyacetal samples fatigued over a range of stress levels (55). ● $\sigma = 56$ MPa, $N_f = 10^2$ cycles; ■ $\sigma = 54$ MPa, $N_f = 3 \times 10^2$ cycles; ▲ $\sigma = 48$ MPa, $N_f = 3 \times 10^5$ cycles; ◆ $\sigma = 45$ MPa, $N_f = 10^6$ cycles. To convert MPa to psi, multiply by 145.

volume change evolves as a polyacetal specimen is fatigued over a range of stress levels. The results show that the irreversible volume increased as the sample was fatigued over a broad range of stress levels. Further, the Poisson's ratio (see Fig. 14) increases in the low cycle regime but decreases in the high cycle regime. The decrease in Poisson's ratio is characteristic of an increase in porosity in the material.

Recent studies on PMMA have shown that craze initiation appears at a relatively early stage in the fatigue life of the material (12). The total fatigue life is compared to the onset of craze initiation in Figure 15. In this particular case the lifetime is governed primarily by the growth of crazes until a defect (crack) approaches the threshold size.

More direct morphological studies were conducted on isotactic polypropylene (iPP) to isolate the mechanisms of fatigue damage and their kinetics (56). The damage imposed to samples fatigued in the high cycle regime occurs in the form of crazes. These are shown typically in Figure 16 for the case of iPP subjected to 6×10^6 cycles.

Figure 17 shows a sequence of optical micrographs illustrating the evolution of damage. During fatigue, small crazes initiate and grow homogenously through the material. However, as the fatigue test continues, small crazes coalesce and the arrangement of crazes becomes neither even nor randomly distributed. This becomes especially evident in the samples with a high level of fatigue damage. Clear patterns arise in the form of cascades of crazes (see high magnification in Fig. 17) that are clear evidence of craze–craze interactions where the stress intensity at one craze tip is shielded by the formation of another craze. Also, careful

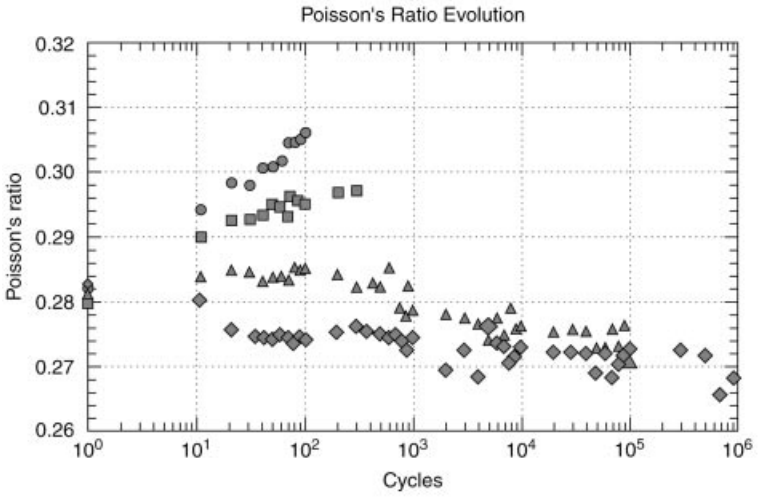

Fig. 14. Poisson's ratio evolution for polyacetal samples fatigued over a range of stress levels (55). ● $\sigma = 56$ MPa, $N_f = 10^2$ cycles; ■ $\sigma = 54$ MPa, $N_f = 3 \times 10^2$ cycles; ▲ $\sigma = 48$ MPa, $N_f = 3 \times 10^5$ cycles; ◆ $\sigma = 45$ MPa, $N_f = 10^6$ cycles. To convert MPa to psi, multiply by 145.

inspection of mature crazes indicates that as the crazes mature, much smaller crazes initiate and grow around each main craze in the form of a process zone, much like that which has been observed in crack propagation in polymers. Ultimately the sample becomes saturated with crazes that resemble a planar array of damage that is evidently completely dominated by the craze–craze interactions.

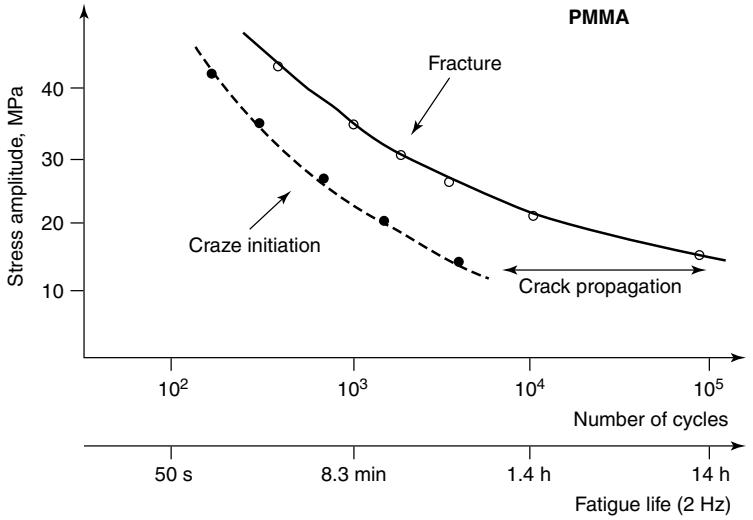

Fig. 15. Plot comparing total fatigue life and time for craze initiation for PMMA (12). To convert MPa to psi, multiply by 145.

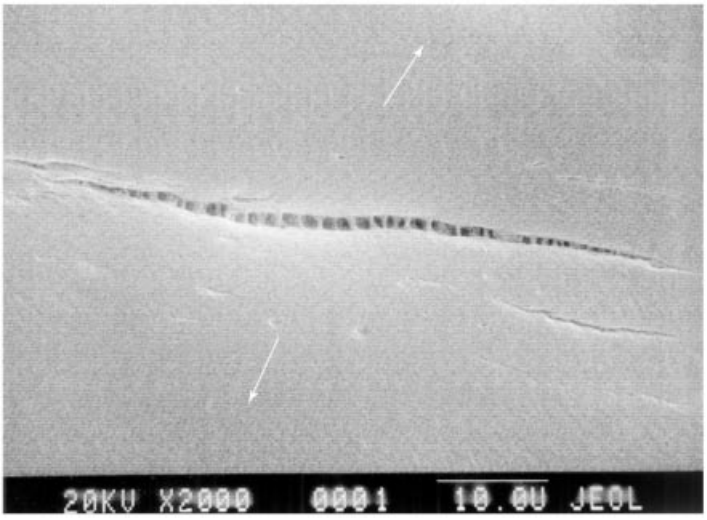

Fig. 16. Scanning electron micrograph of fatigue-damaged iPP. The arrows denote the direction of applied load (56).

Eventually, of the crazes approaches the threshold size and subcritical crack propagation ensues until failure.

The fatigue damage described in Figure 16 has also been quantitatively described and the energetics of craze growth has been evaluated (56). This analysis involved first approximating the stress intensity of a single craze by treating the craze as a microcrack of equivalent size with the craze fibrils replaced by a closure stress (traction) across the microcrack face. If a single craze is considered in an infinite plate, the stress intensity factor K_{tot} for the craze can be written as (56)

$$K_{\mathrm{tot}} = K_{\sigma_\infty} + K_{\sigma_c} = (\sigma_\infty - \sigma_c)\sqrt{\pi \ell} \tag{16}$$

where σ_∞ is the remotely applied stress, σ_c is the closure traction produced by the craze fibrils, and ℓ is the craze radius. By substituting an expression for the effective stress across the craze face as $\sigma = \sigma_\infty - \sigma_c$, the stress intensity due to a single craze takes the same form as that of a single crack. Hence, the potential energy change of a body containing a single craze would be given by

$$\frac{\Delta\Pi}{b} = 2\int_0^\ell G\,\mathrm{d}\ell = \frac{2}{E_0}\int_0^\ell K_{\mathrm{tot}}^2\,\mathrm{d}\ell = \frac{\pi\sigma^2\ell^2}{E_0} \tag{17}$$

In equation 17, $\Delta\Pi$ denotes the potential energy change in the specimen, b is the specimen thickness, G is the energy release rate, and E_0 is the storage modulus of the undamaged iPP.

In accordance with a Griffith-type criterion for the growth of a craze ($G - 2\gamma = 0$ for the necessary condition for craze growth), the following expression for the specific energy γ to form a craze is given by

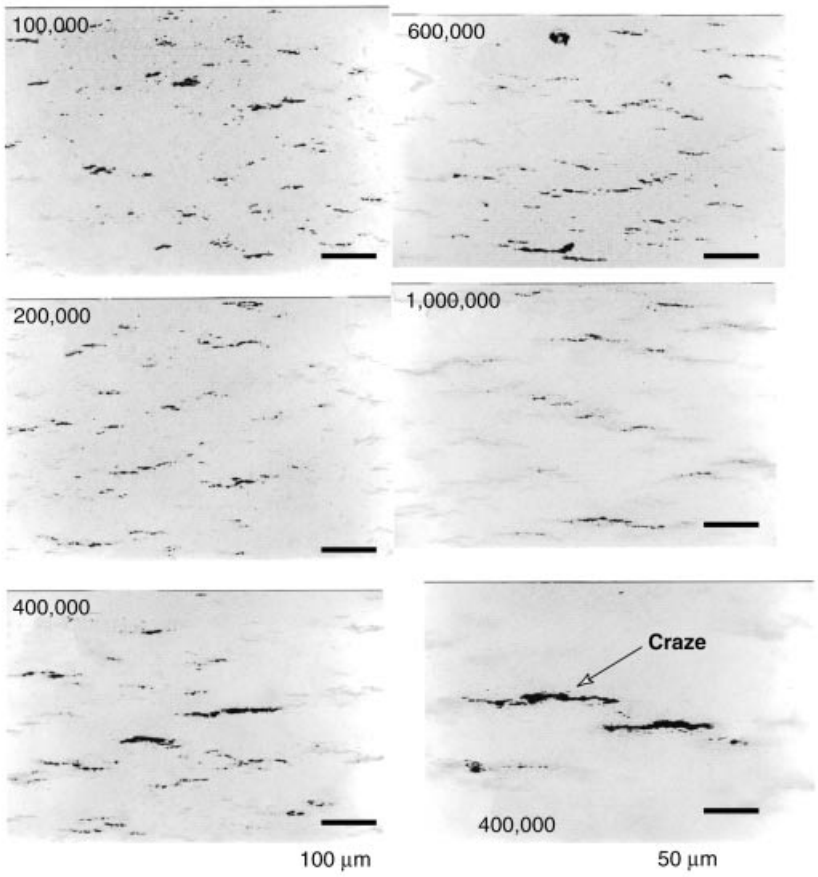

Fig. 17. Optical micrographs of fatigue damage in iPP tensile base, showing the progression of damage with increasing cycle number (56).

$$G = 2\gamma$$
$$\frac{K_{\text{tot}}^2}{E_0} = \frac{\sigma^2 \pi \ell}{E_0} = 2\gamma \tag{18}$$

Rearranging terms in equations 18 yields the following relationship:

$$\frac{\sigma^2}{E_0} = \frac{2\gamma}{\ell} \tag{19}$$

Thus far, the relationships apply to an isolated craze embedded in a specimen. To evaluate the energy release associated with an ensemble of crazes, the interaction of the crazes must be considered. In Reference 56, a damage parameter, similar in fashion to that introduced by Bristow (57), for a two-dimensional case was considered:

$$\rho = \frac{1}{A}\sum_{i=1}^{n} \ell_i^2 \approx n\ell^2 \tag{20}$$

In equation 20, A is some representative area and n becomes the number density of crazes of radius ℓ. The representative area A is related to the representative volume V by $V = bA$. Figure 18a describes how the number density of crazes and mean craze radii (from Fig. 17) change with fatigue life, while Figure 18b shows how the damage density ρ, as defined by equation 20, evolves. Note from the graphs in Figure 18 that the number density of crazes decreases with increasing

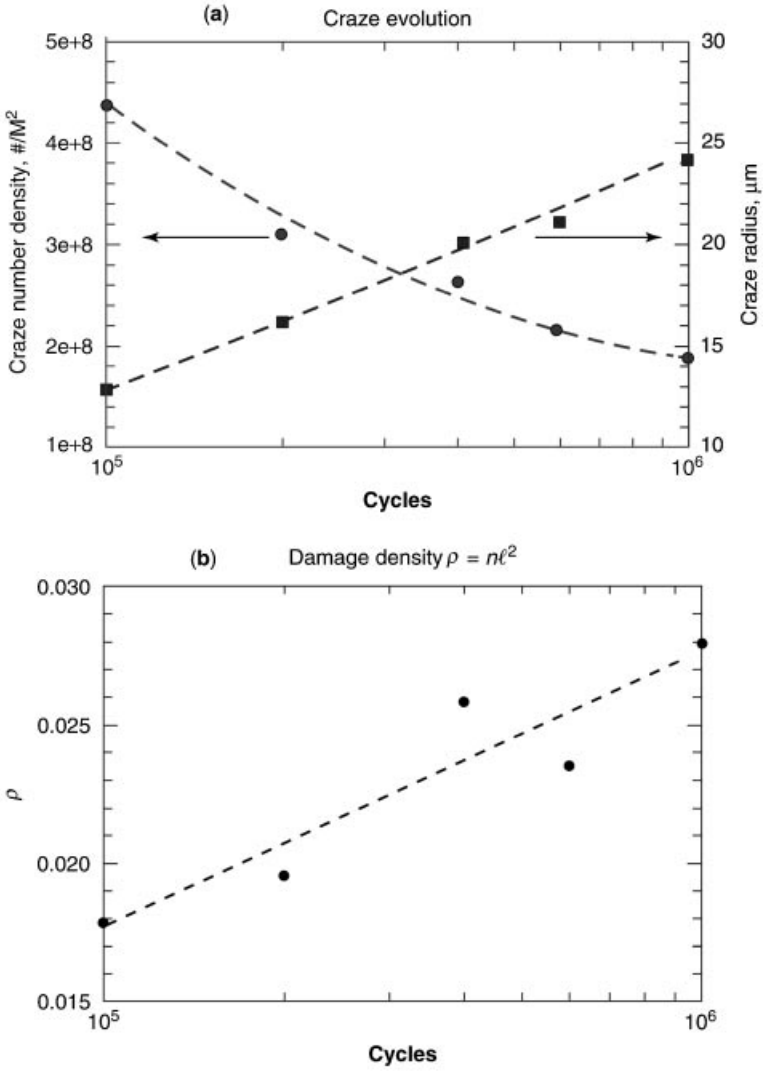

Fig. 18. Graphs describing the evolution of damage between 10^5 and 10^6 cycles. (**a**) Craze number density (circles and short dashes) and average craze radius (squares and long dashes) vs cycle number. (**b**) Damage density (eq. 20) vs number of cycles (56).

cycle number while the craze length continually increases. This indicates that coalescence is a dominating process during the stage of the fatigue process. Also, the damage density ρ continually increases as the fatigue process continues.

For a dilute suspension of cracks (crazes), Bristow (57) showed that the effective modulus E is linearly affected by the damage density in accordance with the following relationship:

$$\frac{E}{E_0} = 1 - \pi\rho = 1 - n\pi\ell^2 \tag{21}$$

In 1993, Kachanov (58) showed that the following nonlinear approximation (eq. 22) actually remains highly accurate at high crack (craze) densities, provided the crazes are homogeneously distributed.

$$\frac{E}{E_0} = \frac{1}{1+\pi\rho} = \frac{1}{1+n\pi\ell^2} \tag{22}$$

Kachanov showed that equation 22 holds at high crack (craze) densities since the competing interactions of shielding and amplification result in the following expression. In Reference 56, an expression for the change in the potential energy density (potential energy change per representative volume) associated with craze growth can be derived by combining equations 16, 17, 18, 19, 20, 21, 22:

$$\begin{aligned} \frac{\Delta\Pi}{V} &= n\left(2\int_0^{\ell} G\,\mathrm{d}\ell\right) = n\left(2\int_0^{\ell} \frac{K_{\mathrm{tot}}^2}{E}\,\mathrm{d}\ell\right) \\ \frac{\Delta\Pi}{V} &= \frac{\sigma^2\pi}{E_0}\left(n\ell^2 + \frac{1}{2}\pi n^2\ell^4\right) \\ \frac{\Delta\Pi}{V} &= \gamma(2n\ell + \pi n^2\ell^3) \end{aligned} \tag{23}$$

The latter expression in equations 23 describes the specific energy for craze growth in terms of changes in the potential energy density during the fatigue test. Using equations 23 along with measured information regarding the number density of crazes and craze radii (Fig. 17), the specific energy for craze growth, γ, was evaluated for iPP. The results indicated that the energy required to grow a craze is of the order of 13 J/m^2 and was generally constant over the decade of cycles measured.

Fatigue Crack Propagation

Background and Overall Considerations. Many aspects of FCP including both experimental approach and theory evolve from concepts well established in the area of fracture mechanics. Many treatments dealing with both the theory (59–63) as well as associated treatments to polymeric materials (2,5,64,65) have been published. The basic tenent of fracture mechanics is that the strength of most real solids is governed by the presence of flaws. Many theories have been

developed mathematically to describe the stresses in the presence of a crack as well as the energy released during crack propagation. Griffith (59) introduced a criterion based on an energy principle and argued that when the change in the elastic potential of a brittle glass equals or exceeds the energy required to create new crack surface area, the crack will propagate uncontrollably. It has been shown (60–63) that the Griffith criterion can be related to the elastic energy release rate and stress intensity factor for an elastic body. Thus, two parallel criteria arose to describe the critical conditions for the failure of a body containing a crack (defect). These criteria are written as follows:

$$\begin{aligned} G_{\mathrm{I}} &\geq G_{\mathrm{Ic}} \\ K_{\mathrm{I}} &\geq K_{\mathrm{Ic}} \end{aligned} \tag{24}$$

In equations 24, whenever the energy release rate G_{I} becomes greater than or equal to the critical energy release rate G_{Ic}, the fracture (failure) occurs. Similarly, when the stress intensity factor K_{I} exceeds the fracture toughness K_{Ic}, the fracture occurs. It should be noted that the subscript I in equations 24 refer to mode I failure (opening mode), and similar criteria can be written for modes II (shearing mode) and III (tearing mode). The criteria in equations 24 are conceptually different but are mathematically identical for a linear elastic body since the energy release rate and stress intensity factor are related by

$$G_{\mathrm{I}} = \frac{K_{\mathrm{I}}^2}{E'} \tag{25}$$

where $E' = E$ under plane stress conditions and $E' = E/(1 - \nu^2)$ under plane strain conditions. Both the energy release rate and stress intensity factor are a function of the specimen global geometry, applied stress level, and crack length. Consequently, the stress intensity (and/or energy release rate) will increase even if the stress level remains constant when the crack length increases. Thus, specimens with larger flaws have a lower nominal strength than specimens in which the flaw sizes are smaller. This type of approach is commonplace in many engineering applications today and has proven successful to describe the fracture behavior of a wide range of materials.

For a given stress level, if the flaw (crack) size is large enough such that the critical condition(s) expressed in equation(s) 24 is reached, then immediate failure is expected. If however, the stress level or flaw size is reduced, then immediate failure is postponed but subcritical crack growth may occur. Subcritical crack growth refers to the slow progressive growth of a crack prior to reaching a critical condition. One of the most common processes to accelerate this process is to apply a fatigue load to the body. Consequently, the associated study of subcritical crack growth under fatigue load is referred to as fatigue crack propagation (FCP). Many studies and texts have been devoted to measuring FCP kinetics of polymers and an excellent summary is provided in Reference 2.

One of the earliest attempts to describe the fatigue behavior of materials in general is referred to as the Paris Law (66–68). The Paris Law is an empirical relationship that exists between the crack growth rate $\mathrm{d}\ell/\mathrm{d}N$ and the change

in stress intensity factor by

$$\frac{d\ell}{dN} = A(\Delta K_I)^m \tag{26}$$

In equation 26, $\Delta K_I = K_{Imax} - K_{Imin}$, and K_{Imax} relates to the stress intensity factor associated with the maximum stress level in a given cycle and K_{Imin} is the corresponding stress intensity factor associated with the minimum stress in a given cycle. The coefficients A and m in equation 26 are considered material constants. Paris Law (eq. 26) and variations therein have been widely used to describe the crack growth kinetics of a broad range of materials (eg, Ref. 1). However, the application of equation 26 has shown to be applicable only over a certain range of stress intensities (which relates to a certain range of crack sizes).

Many studies have verified the log–log linear relationship between $d\ell/dN$ and ΔK, as predicted by equation 26, but others have shown sigmoidally shaped FCP plots. Crack growth rates almost always decrease to vanishingly low values as ΔK approaches a limiting threshold value ΔK_{th} and increase markedly at very high ΔK when K_{Imax} approaches K_{Ic}. The asymptote at low ΔK conditions describes FCP rates that diminish rapidly. As such, a limiting stress intensity factor range ΔK_{th} is defined and represents a service operating limit below which fatigue damage does not obey the Paris Law.

Figure 19 illustrates a typical sigmoidal-shaped crack growth behavior as illustrated by regions I, II, and III. In region I, a crack is below the threshold size and thus does not follow the growth kinetics as described by equation 26. Thus, region I is many times referred to as the nucleation stage. In region II, equation 26 applies. Region II is associated with subcritical crack growth and equation 26

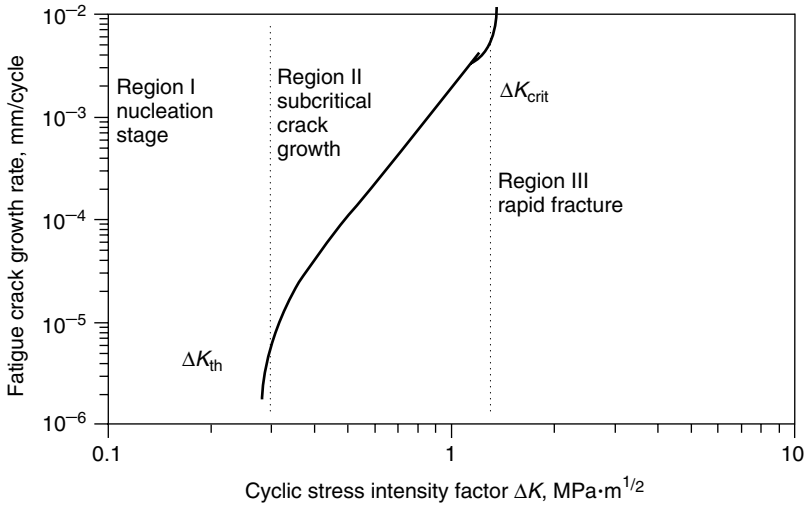

Fig. 19. Illustration of typical sigmoidal curve in $d\ell/dN$ vs ΔK plot of FCP data. Three regions are identified: region I associated with damage nucleation; region II associated with subcritical crack growth; and region III associated with unstable, rapid failure.

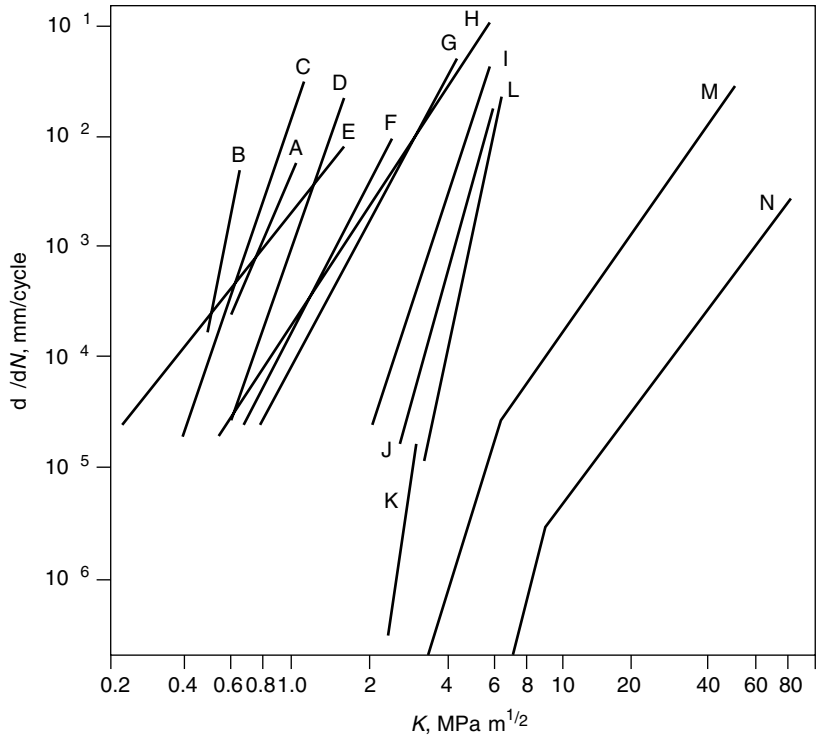

Fig. 20. FCP rates vs ΔK for several engineering plastics and metal alloys (39). A, LDPE; B, epoxy; C, PMMA; D, polysulfone; E, polystyrene; F, PVC; G, poly(phenylene oxide); H, polycarbonate; I, nylon-6,6; J, HI-nylon-6,6; K, poly(vinylidene fluoride); L, acetal resins; M, 2219-T851 aluminum alloy; N, 300M steel alloy.

can be integrated to predict remaining life of a body containing a crack in this region. Region III is associated with unstable, rapid fracture once the flaw has grown to a critical size.

Characteristic plots of the FCP data are shown in Figure 20 for several engineering plastics and metal alloys (69). The samples A–L are polymeric materials (both amorphous and semicrystalline) while M and N are metal alloys. Figure 20 demonstrates the universality of equation 26 to describe the subcritical crack growth kinetics of a wide range of materials. The data also generally suggest values for the threshold flaw size and critical stress intensity factor for each material. Notice that some semicrystalline materials show resistance to crack growth approaching that of metals.

Several studies have determined the threshold stress intensity for engineering plastics, eg, polycarbonate (5). The $d\ell/dN$ values are in excellent agreement for growth rates $> 10^{-5}$ mm/cycle but differ significantly for lower values. Additional threshold data have been reported for PMMA as a function of stress ratio R, where $R = K_{min}/K_{max}$ (70). Other studies have been conducted to characterize the near threshold crack propagation behavior (12,71). Figure 21 (12) shows a σ–N curve for polyethersulfone, including data at the near threshold level. Similarly

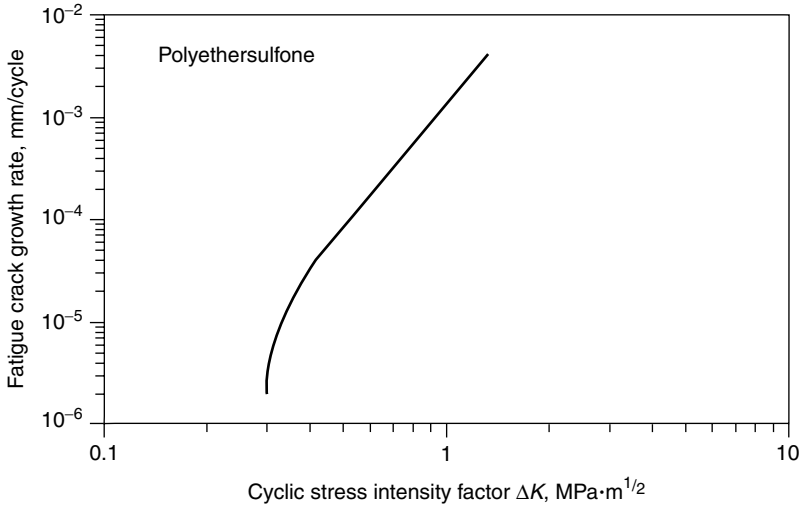

Fig. 21. Fatigue crack growth data for polyethersulfone, including data in the near threshold regime (12).

Table 3 (71) defines the threshold stress intensity and the range over which the Paris equation is valid for ultrahigh molecular weight polyethylene (UHMWPE) subjected to different processing conditions. From Table 3, it is clear that subtle processing conditions can alter the threshold level and the onset of FCP.

Unusual crack growth behavior has been reported in some semicrystalline polymers with FCP rates decreasing with increasing ΔK at intermediate levels (72–76). This transient response has been related in low density polyethylene (LDPE) to a change in the scale of the fracture micromechanism (72), whereas others attribute this kinetic transient to localized crack-tip heating, reasoning that such heating would reduce the yield strength and result in a large increase in the depth of the crack-tip damage layer (74). Chudnovsky and Moet (75,76) developed another theory to accommodate for this behavior changes. This theory, referred to as the *crack layer theory*, is formulated within the framework of thermodynamics of irreversible processes. The crack layer theory treats the crack and surrounding damage as a single entity. The rate of crack propagation becomes a thermodynamic

Table 3. Fatigue Threshold Stress Intensity Factor and Paris Regime or UHMWPE Subjected to Different Processing Conditions[a]

GUR 415	ΔK_{th} (threshold), MPa·m	Paris regime, MPa·m
Compression molded	1.8	1.80–2.8
Compression molded γ-air	1.2	1.20–1.8
Extruded 90° orientation	1.7	1.70–2.3
Extruded 0° orientation	1.3	1.30–1.9
Extruded 0° γ-air	1.01	1.01–1.7
Extruded 0° γ-peroxide	1.12	1.12–1.3

[a]Ref. 71.

flux within the theory, with complimentary thermodynamic forces being described through the energy release rate. This theory is capable of predicting the *stick-slip* character observed in some growth rates.

In the crack layer theory (75,76) the movement of the crack and surrounding damage is decomposed into elementary movements: translation, rotation, isotropic expansion, and distortion. In this way, the damage surrounding the tip can evolve in a general sense. These elementary movements become thermodynamic fluxes. The reciprocal forces contain an active part (energy release rates associated with each movement) A_i, and a resistive part (an energy barrier) R_i. Within the context of classical irreversible thermodynamics, the entropy of the system, S_i, can be expressed in terms of a bilinear form of forces and fluxes shown in equation 27.

$$T\dot{S} = \sum_{i=1}^{n} (A_i - \gamma R_i)\, \dot{\nu}_i \tag{27}$$

In equation 27, $(A_i - \gamma R_i)$ represent the thermodynamic forces for each elementary movement and ν_i are the corresponding reciprocal fluxes. The active parts correspond to the energy release associated with each movement. The resistive parts constitute the materials resistance to these movements and contain the *intrinsic material property*, γ, the specific enthalpy of damage (eg, crazing). The ability of this formalism to account for size and shape changes in the process zone during crack propagation produces changes in the translational crack propagation rate. Thus, non-Paris FCP can be modeled using this approach.

Effect of Test and Process Conditions. Many studies have evaluated the effects of test frequency on the FCP rates in polymers. Although hysteretic heating explains a decrease in fatigue resistance with increasing cyclic frequency in unnotched polymer test samples (eg, eq. 3, Fig. 6, Ref. 24), the fatigue resistance of notched polymers is exceedingly complex. FCP rates can decrease, remain unchanged, or increase with increasing test frequency (77–79). Figure 22 illustrates the effect that cyclic frequency has on the FCP rate of poly(vinyl chloride) (PVC). In the case of PVC, the crack speed decreases with increasing frequency, but the threshold stress intensity K_{th} and the fracture toughness K_{Ic} remain unchanged. Also notice from the similarity of slopes in the FCP data in Figure 22 that the material coefficient m as defined in the Paris equation (Eq. 26) is insensitive to test frequency. Similar studies (78,79) on polycarbonate showed that cyclic frequency had virtually no effect on its FCP kinetics. In contrast, the FCP kinetics in nylon-6,6 over a range of frequencies shows that higher crack speeds occur at higher frequencies. Consequently, no universal behavior is evident.

As expected, test temperature will have a dramatic effect on the FCP kinetics of polymers owing considerably to their temperature-dependent viscoelastic nature. Indeed, studies of polystyrene and acrylonitrile–butadiene–styrene (ABS) have shown that FCP rates for given ΔK level generally decrease with decreasing test temperature (80). By contrast, a minimum FCP resistance was noted in polycarbonate and polysulfone at intermediate test temperatures (81,82). A complex test-temperature response was also noted in studies on the influence

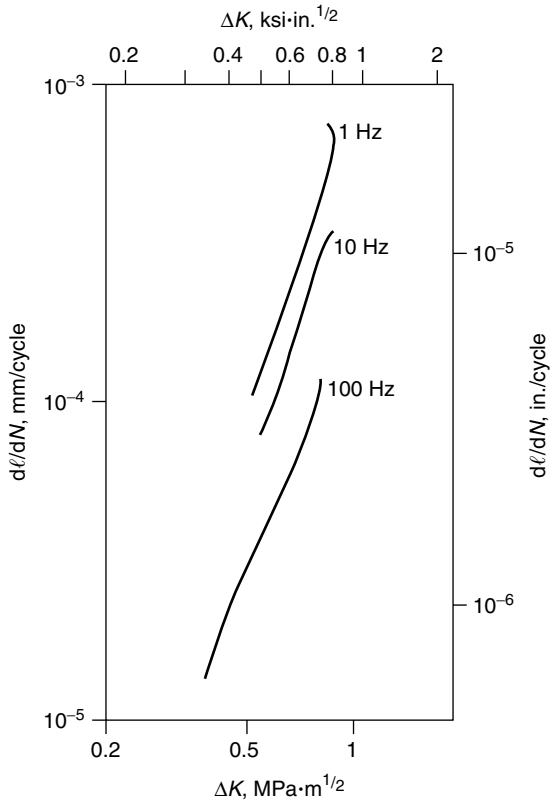

Fig. 22. Effect of cyclic frequency on the FCP rate in PVC (77–79).

of test temperature and absorbed water on FCP in nylon-6,6 (83). Of particular interest was the possibility to normalize the data (83) through empirical use of time–temperature superposition principles.

The effect of thermal history and process conditions can affect both the unnotched fatigue behavior (43) through physical aging (44) or through changes in the crystal morphology. Similarly the FCP behavior of semicrystalline polymers can also be affected through differences in thermal history (84–88). Some studies suggest that resistance to crack propagation increases with decreasing spherulite size (84,85), while others claim spherulite size has no effect (86,87). A recent report (88) showed that annealed specimens to have a lower resistance to crack initiation and subsequent propagation. Although the same fracture mechanism, in which the brittle crack gradually becomes more ductile, prevailed in both cases, the annealed material proved to be weaker. This was attributed to differences in the failure mechanisms at the root of the crack. The annealed sample showed a voided and fibrillated crack tip while the quenched sample showed a nonfibrillated structure.

Effect of Molecular Architecture, Morphology, and Microstructure. Striking effects of molecular weight on FCP rates in notched PMMA (89) and PVC (90) have been noted (91,92), and similar strong effects have been reported for

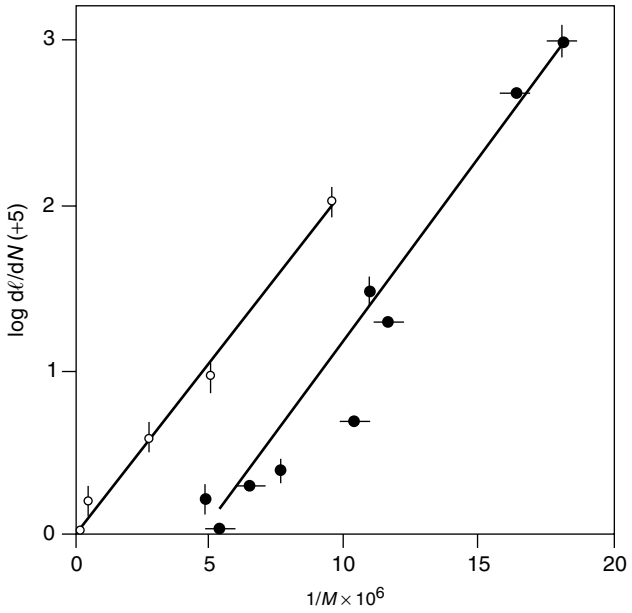

Fig. 23. Functional relationship between FCP rates in PMMA and PVC and reciprocal of molecular weight at 10 Hz for $\Delta K = 0.6$ MPa·m$^{1/2}$ (89). Data for PVC displaced to the right by a factor of 2.

polycarbonate (93) and polystyrene (94). In general, the Paris law is followed over a wide range of ΔK. It was found (94,95) that this data followed the following empirical relationship:

$$\frac{d\ell}{dN} = A' e^{B'/M_w} (\Delta K)^n \tag{28}$$

where A', B', and n are constants depending on the material and test conditions. Thus, even though values of static toughness may change relatively little over a given range of molecular weight, small increases in the molecular weight M_w may result in up to several orders of magnitude decrease in crack growth rate. Also, the effect is greater at lower molecular weights. This is shown for the case of PMMA and PVC in Figure 23 (89).

It has also been found (92) that the addition of small amounts of high or medium molecular weight to PMMA results in greater resistance to both fatigue and static loading, whereas the addition of low molecular weight has a deleterious effect. Since the FCP response can be correlated semiquantitatively with the proportion of high M_w species estimated by gel-permeation chromatography (96), it has been suggested that resistance to cyclic disentanglement is favored by high M_w species. While the short time scale of static fracture tests permits relatively little disentanglement, the longer time scale involved in fatigue allows the fracture process to reflect more strongly the energy dissipation concerned in breakdown of the entanglement network (2). In this sense, the fatigue process resembles the

longtime relaxation processes in time-to-failure tests (97,98) in which strong effects of molecular weight are also seen. Hence it is likely that during cycling, the entanglements in craze fibrils involving low M_w species are progressively broken down, but the longer molecules permit considerable strain hardening to occur in the fibrils (2,4,99). This conclusion is supported by fractographic evidence obtained for specimens of PMMA containing high and low molecular weights (100).

The FCP resistance in semicrystalline polymers is typically higher at higher molecular weight. Examples include high density and ultrahigh molecular weight polyethylene (101–103), acetal resin (104,105), nylon-6,6 (104), and polypropylene (103). The effect of molecular weight on the FCP rates for these polymers is shown in a comparative plot in Figure 24. In general, however, the sensitivity of the crack

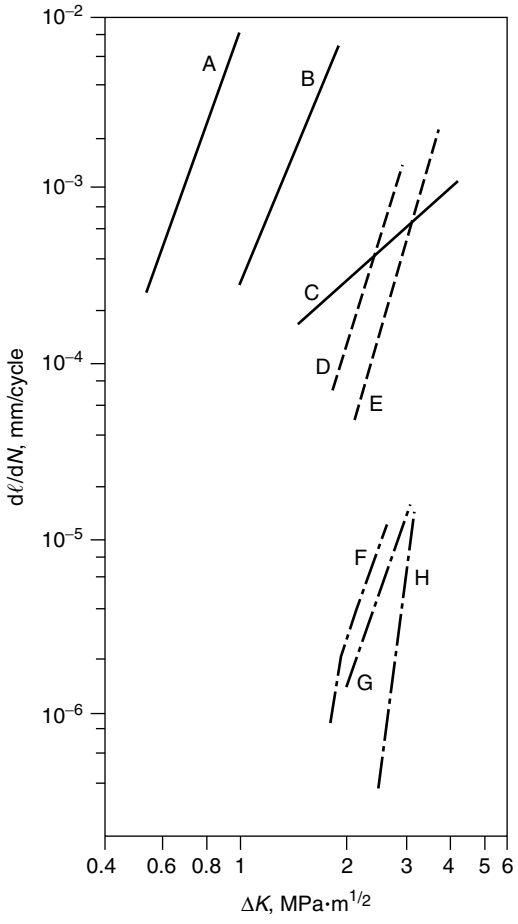

Fig. 24. Effect of molecular weight on fatigue crack growth rates in high density polyethylene (solid line): $M_w = 45{,}000$ (**A**), 70,000 (**B**), 200,000 (**C**) (101,102); nylon-6,6 (dashed line): $M_n = 17{,}000$ (**D**), 34,000 (**E**) (104); and acetal resins (dotted-dashed line): $M_n = 30{,}000$ (**F**), 40,000 (**G**), 70,000 (**H**) (105).

growth rate to molecular weight is less than that in amorphous polymers. This may be due to the effect of the crystal structure stabilizing the polymer through tie chains and the like.

Some attempts have been made to develop quantitative theories to rationalize the effects of molecular weight and have met with some success, at least with PMMA, PVC, and polystyrene (94,95,106). Thus it has been proposed that the FCP rate can be expressed as the product of two functions, one involving ΔK and the other characteristic of the relaxation process in the plastic zone (95):

$$\frac{\mathrm{d}\ell}{\mathrm{d}N} = f(\Delta K) \times \frac{1}{\tau_\mathrm{f}} \tag{29}$$

where $f(\Delta K)$ reflects the effect of applied stress and τ_f, the relaxation time, reflects the resistance to chain disentanglement. Increased FCP resistance has been correlated with increased characteristic stress-relaxation times in PVC (107) and a rubber–polystyrene interpenetrating polymer network (108). Considering that the relaxation time follows a Zhurkov-type rate process (33), the following may be expected:

$$\tau_\mathrm{f} = A' \exp\left(\frac{-V\sigma}{RT}\right) \tag{30}$$

where A' is a constant and V is the activation volume. Assuming that the stress involved is a localized average mean stress in the plastic zone, the following equation can be derived:

$$\frac{\mathrm{d}\ell}{\mathrm{d}N} = f(\Delta K) \exp\left(\frac{\sigma_{\mathrm{m,y}} V_\infty}{RT} \Psi(M)\right) \tag{31}$$

In equation 31, $\sigma_{\mathrm{m,y}} = \sigma_\mathrm{y}\ (1 + R)/2$, where σ_y is the yield stress and R is the load ratio. V_∞ is the activation volume for infinite molecular weight M, and $\psi(M)$ reflects the fraction of molecules that can form a mechanically effective entanglement network. In terms of molecular weight, $\psi(M)$ is defined as $\psi(M) = (V_\infty/V) = (W - W*)/(1 - W*)$, where W is the weight fraction of molecules when $M > M_0$; M_0 is the minimum value of M required for a stable network; and $W*$ is the minimum weight fraction of those molecules required to form a stable craze. The value of $(1 - W*)$ is consistent with the void volume of mature crazes in PMMA and PVC (95).

The model applies to PMMA and PVC and gives values of V that agree fairly well with values for static fracture. Thus a combination of rate process theory with fracture mechanics can usefully relate molecular and continuum ideas in rationalizing fatigue fracture. Vertical shifting of FCP curves gives master curves relative to a very high molecular weight specimen ($\psi \cong 1$) as long as ΔK_th is independent of M, ie, when M is greater than some limiting value. This is shown in Figure 25 for the case of polystyrene (94). The shift factor a_v is related to V and $\psi(M)$:

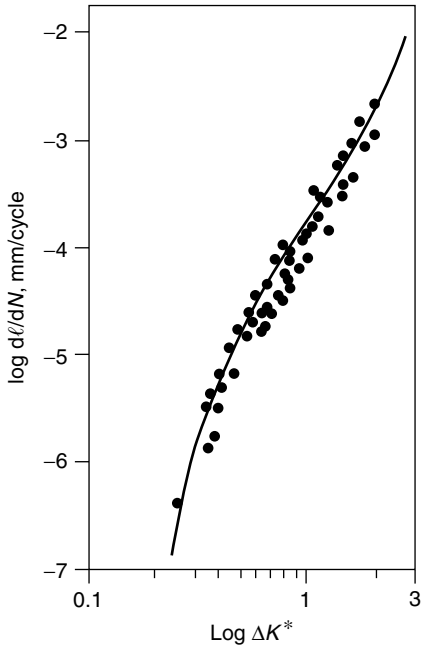

Fig. 25. Master curve for FCP in polystyrene (10 Hz, sine wave) as a function of stress intensity factor (94). Curve includes data for 12 specimens varying greatly in molecular weight and its distribution, and encompasses both the threshold of crack growth and the approach to catastrophic fracture.

$$a_v = \frac{\exp(V\sigma_{m,y})}{\exp(V_\infty \sigma_{m,y})} \tag{32}$$

An alternative, simpler approach has been proposed in which crack growth is essentially considered the reverse of crack healing (105). In effect, disentanglement is taken to be the reverse of interdiffusion of molecules at the surfaces of two planes in close contact. Thus, assuming scaling laws for characterizing molecular reptation hold, it has been suggested that $d\ell/dN$ is proportional to the quotient of the distance of interpenetration x to t_∞, the time required for complete molecular diffusion and interpenetration. Since $x \propto M^{1/2}$ and $t_\infty \propto M^3$, then

$$\frac{d\ell}{dN} \propto M^{-2.5} \tag{33}$$

Both equations 32 and 33 give a good agreement when applied to data in Reference 105.

A few controlled studies on the effects that cross-linking has on the FCP resistance have been done. When irradiation was used to increase M_w in polystyrene, keeping M_n constant, the fatigue life was affected very little by the total dose applied. In fact, the FCP behavior did not alter significantly even up to the gel point and beyond. The FCP resistance of cross-linked polystyrene is lower than

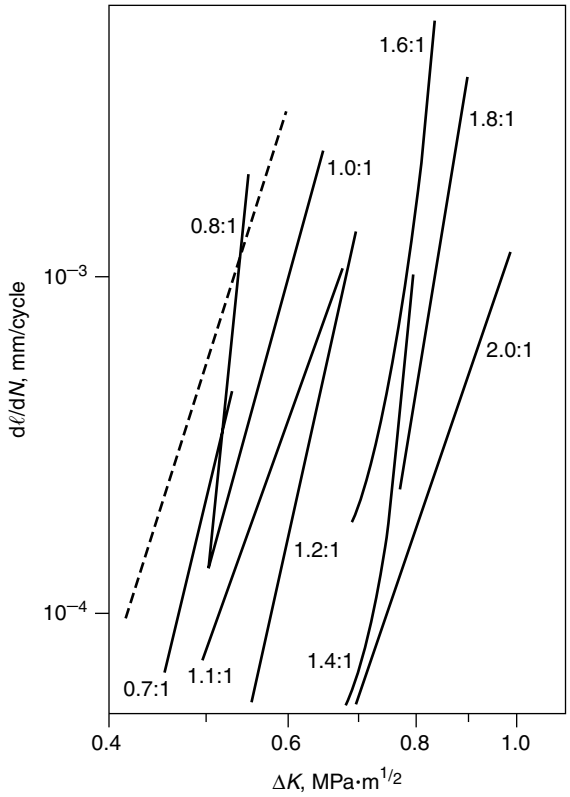

Fig. 26. FCP behavior in Epon 828/MDA epoxy as a function of amine/epoxy ratio (numbers labeling curves) at 10 Hz (113). Dotted line represents other data (110).

that of polystyrene or rubber-modified polystyrene (109). A typical epoxy resin is much less resistant to FCP than thermoplastic polymers (2,110). This observation is generally consistent with the ability of cross-linking to inhibit segmental mobility, crazing, and consequent energy dissipation.

Most systematic studies of cross-linked polymers confirm the above hypothesis, but one study reveals an interesting exception. As the percentage of a multifunctional acrylate cross-linking agent in PMMA increased from 0 to 11, the FCP rates increased by over 2 orders of magnitude (at $\Delta K = 0.5$ MPa·m$^{1/2}$); the slopes of the $d\ell/dN$ curves also increased (111). Similar deleterious effects of cross-linking are described in a study of static and fatigue performance in bisphenol A epoxies cured with methylenedianiline (112). These results are presented in Figure 26. Note that as the amine/epoxy ratio decreased from 2:1 to 1:1 (i.e., from a nearly linear to a densely cross-linked resin) K_{Ic} decreased and FCP rates increased by over an order of magnitude at a given ΔK. While an excess of amine increased FCP resistance, an excess of epoxy had the opposite effect. This difference can be explained by considering that the epoxy is difunctional and the curing agent is tetrafunctional. When an excess of di-epoxy exists, the resulting network has an effective increase in molecular weight between cross-links, approaching that of a rubbery network. However, when an excess of curing agent exists, the

molecular weight between cross-links is not necessarily increased and many terminal uncross-linked ends are produced. Thus, the results reflect this difference in network architecture. Note, however, that it would be interesting to compare fatigue results at similar temperatures relative to their glass transition rather than at one temperature since the glass transition is inversely related to the molecular weight between cross-links.

Fractography. The fatigue-fracture-surface micromorphology of engineering plastics is complex. In general, the surface may reveal a range of roughness, and this roughness is usually associated with either a change in stress intensity factor or stress states. In the interior of a specimen, the stress state is more confining than near the edges, and careful inspection of fracture surfaces usually reveals this effect. For example, the surface shown in Figure 7 (25) illustrates greater texture near the initiation site where the nucleation and growth process below the threshold level occurs. Once subcritical crack growth is established, the fracture surface produces a smoother and uniform texture. At the critical size, rapid fracture occurs and the crack speed approaches the stress wave speed in the material. A clear distinction appears at the critical radius in Figure 7, denoting this sudden change in crack speed. Note in this case, that the surface beyond the critical size is notably rougher than the other part of the surface (see also FRACTOGRAPHY).

Figure 27 illustrates a fracture surface on another semicrystalline polymer, an aliphatic polyketone terpolymer (114). When comparing Figure 7 with Figure 27, some generic features are noticed, but there are also some contrasting differences. Much like that observed in Figure 7, Figure 27 contains a clear penny-shaped crack whose center locates the nucleation site. However, in stark contrast to that observed in Figure 7, Figure 27 shows a distinctly more textured fracture surface up to the critical radius (see **A** in Fig. 27). Just at the regime where the crack reached a critical size, the fracture surface becomes remarkably smoother, followed by a more textured region, and ultimately a very textured region near the edge (**C** in Fig. 27). The region near the edge (Fig. 27C) illustrates how the boundary condition near the free edge affects the texture and indicated a *tearing* of the last ligaments during the last stage of failure.

In many polymers, fatigue striations can be observed at relatively high ΔK levels. These striations correspond to the successive location of the advancing crack front after each loading cycle or local crack jump. There is a clear distinction between macroscopically observed clamshell markings, which represent periods of

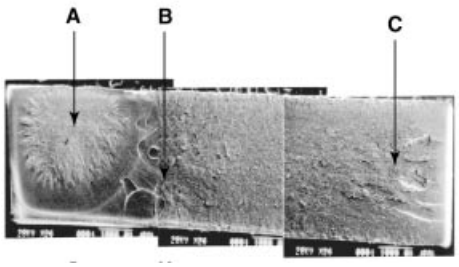

Fig. 27. Scanning electron composite micrograph of fatigue-induced fracture surface in aliphatic polyketone terpolymer: (**A**) initiation site and subcritical crack growth, (**B**) critical radius, and (**C**) texture associated with remaining ligaments (114).

growth during which hundreds or thousands of loading cycles may have occurred, and fatigue striations, which represent the extent of crack-front advance during one load excursion. Each fatigue clamshell marking may, therefore, represent the extent of crack advance corresponding to thousands or tens of thousands of individual load or strain excursions. The microscopic measurement of the FCP rate, ie, striation width, is in excellent agreement with macroscopically determined crack growth rates (115). This strong correlation between macroscopic and microscopic growth rates in polymeric solids reflects the fact that 100% of the fracture surface in this ΔK regime is striated—an observation not typically found in metal alloy systems. In the latter instance, other fracture mechanisms such as cleavage, microvoid coalescence, and intergranular failure are observed in various locations on the fracture surface.

It is common for significant damage to evolve under the crack surface as well. This occurs because the high stress in the vicinity of the crack tip promotes the formation of damage. This damage consumes significant energy and is largely responsible for the high apparent toughness that many polymers exhibit. The damage in the vicinity of the tip can take many different forms and is largely associated with the polymer. Common features include crazing in most semicrystalline polymers and some glassy polymers (eg, polystyrene). Glassy polymers with higher cohesive energy densities promote shear banding. Stress state will also play a role in this process. An excellent treatise describing these morphological features can be found in Reference 65. The damage that occurred below the surface shown in Figure 27 is illustrated in Figure 28 (114). The damage in this polymer occurs as an array of crazes, with the highest density near the surface of the main craze. As the distance from the fracture surface is increased, the size and density of crazes reduce. Earlier stages of this same process are illustrated for iPP in close-up micrograph in Figure 17 (56).

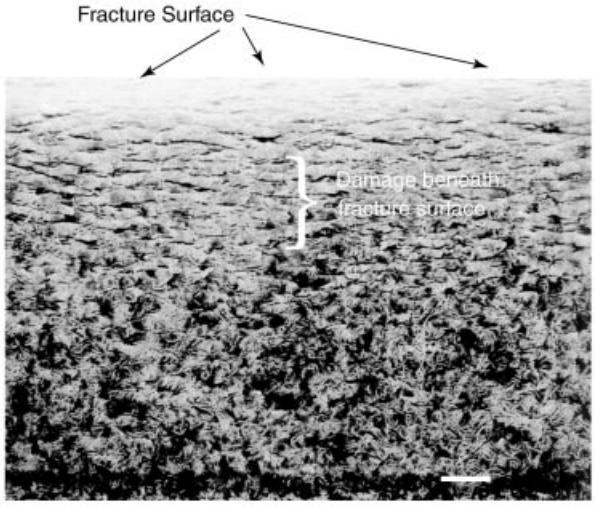

Fig. 28. Scanning electron micrograph of damage occurring below crack surface in an aliphatic polyketone polymer (Ref. 114). Note that the highest density of crazes occurs near the crack surface.

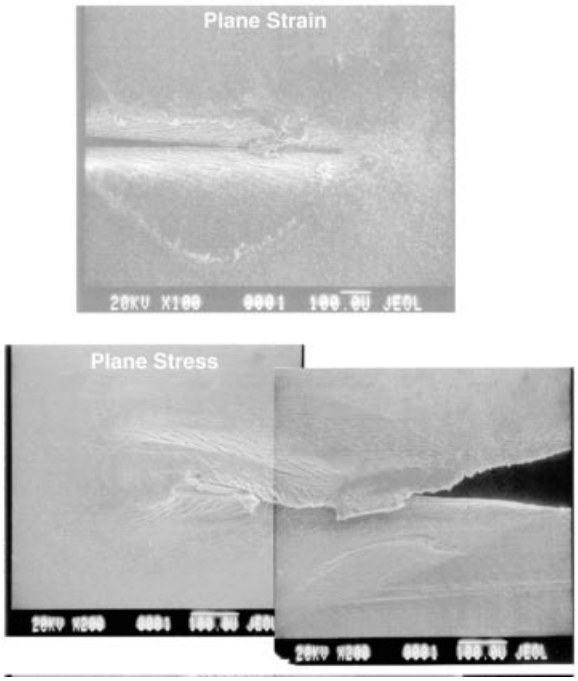

Fig. 29. Scanning electron micrographs of crack tip in plane strain (above) and plane stress (below) conditions for an aliphatic polyketone terpolymer (114).

The damage mechanisms produced in unnotched fatigue specimens can be compared to those where a controlled defect (razor sharp notch) is introduced into fatigue specimens. Figure 29 (13) illustrates the damage that surrounds the crack tip both in the interior of the specimen (plane strain condition) and at the outer surface (plane stress condition). In the plane strain condition, a high concentration of collinear crazes is apparent and is consistent with the damage produced at a natural defect (Fig. 28). Note that in both the plane strain and plane stress conditions, the damage surrounds the crack. This damage is referred to as a process zone since it is closely associated with the fracture process. In the case of plane stress (Fig. 29), the damage is inclined with respect to the fracture surface. These inclined features are shear bands and occur in the constraint-free regime near the surface.

Other factors can affect the type of fatigue damage, thereby changing the FCP and fracture toughness of the material. This is illustrated for the case of β-phase nucleated iPP (25) (see Fig. 30). When comparing the differences between beta phase (Fig. 30) and α-phase (Fig. 6), a clear difference in the fatigue damage is noticed. In the α-nucleated polymer (Fig. 6), highly fibrillated crazes evolve orthogonal to the loading condition and are not altered by the spherulitic morphology. In contrast, in the β-nucleated polymer (Fig. 30), the crazes show no fibrillation and appear to follow the lamellar direction of the spherulite.

The state of stress can dramatically affect the failure mode and strength of polymers. This effect alters the fracture surface characteristics when different modes of fracture are applied. Figure 31 shows comparative micrographs of

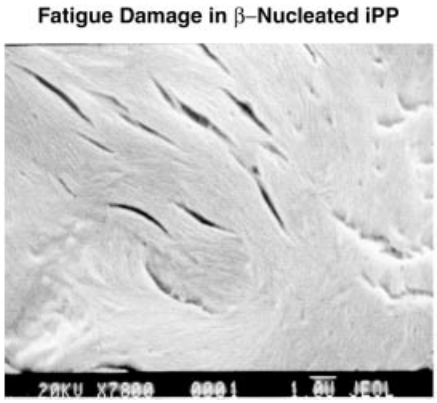

Fig. 30. Scanning electron micrograph of β-nucleated iPP subjected to 10^6 cycles (25).

fracture surfaces in carbon fiber epoxy resin composites tested in mode I (opening mode) and mode II (shear mode) loading conditions. Notice that the mode I fracture surface appears relatively smooth while the mode II surface has a characteristic hackled surface. Also, the fracture energy for the mode II sample is greater than that of the mode I sample.

Other Factors Affecting Total Fatigue Life

Effects of Chemistry in Homogeneous Polymers. Without knowing the relative importance of initiation and propagation stages of fatigue damage accumulation, it is many times difficult to identify the role of material characteristics such as molecular weight and impact modifier content on these two stages of fatigue damage process. Some preliminary experiments have been reported to identify the extent of the fatigue crack initiation process as influenced by molecular weight, impact modifier level (116), and stress level (6,117). Figure 32 shows a three-dimensional plot illustrating the interactive effects of M_w and rubber content (%) on fatigue crack initiation (FCI) lifetime (N_i) in impact-modified PVC. The rubber phase is methacrylate–butadiene–styrene (MBS) polymer. N_i is defined as the number of loading cycles necessary to nucleate a crack 0.25 in length from a semicircular surface notch with a radius of 1.59 mm. FCI lifetimes increase with increasing molecular weight for all rubbery phase contents. Conversely, in high M_w PVC blends, rubber modification lowers FCI resistance although the addition of MBS in low M_w PVC slightly improves FCI resistance. The addition of a rubbery phase to epoxy resin and nylon-6,6 also reduces FCI lifetimes and hastens thermal fatigue, respectively.

In addition to the FCP behavior, the molecular weight and distribution profoundly affect both thermal and mechanical properties of polymers (118–120). Thus tensile strength of many polymers is very low or negligible when the average M is low ($<10^4$ to 10^5), but increases rapidly above M_0, a characteristic value of molecular weight, and then levels off (119–124). When $M > M_0$, the relationship between strength and molecular weight may often be expressed by an empirical equation of the form

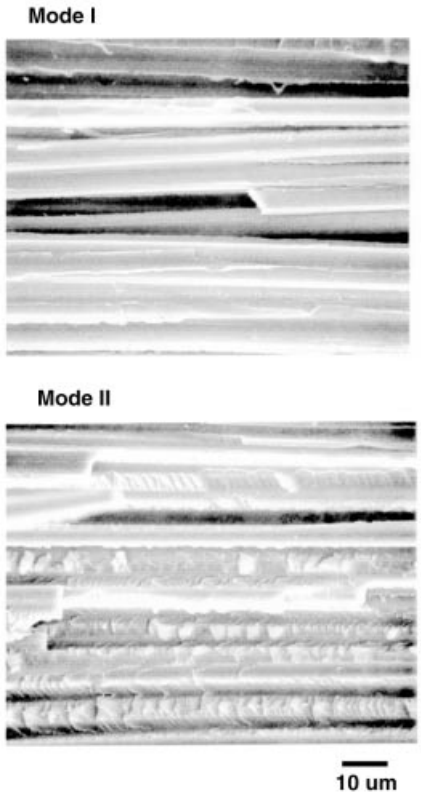

Fig. 31. Scanning electron micrographs of unidirectional carbon fiber epoxy resin composites tested in modes I and II test conditions (25).

$$\sigma_B = A - B/M_x \tag{34}$$

where σ_B is tensile strength, A and B are constants, and M_x is an average molecular weight. Often the number-average molecular weight M_n, which strongly reflects the presence of chain ends as defects, is appropriate (121,122). Other physical properties vary in a similar fashion (125–128); a sigmoidal shape over the whole range of M may sometimes be discerned on a log–log plot. The initiation and propagation of fatigue damage also depends strongly on molecular weight. Indeed both static and fatigue fracture are controlled by similar viscoelastic processes, although the balance of processes and intensity of expression in failure rates differ significantly (2). Energies and volumes of activation tend to be similar for molecular flow and fatigue processes (108,109), and the fatigue resistance of many polymers correlates well with fracture toughness (2). Thus an earlier proposal (124) that the nature of entanglement networks controls M_0 and fracture generally has been confirmed and amplified. Much evidence suggests that only molecules longer than the average length spanning a craze can form a ductile network that can effectively resist crack propagation (113,125,126,129–132). Equation 34 has been derived on this basis, with $A = \sigma_B$ for infinite M (132), and the role of l_c, the contour length between entanglements, has been shown to control

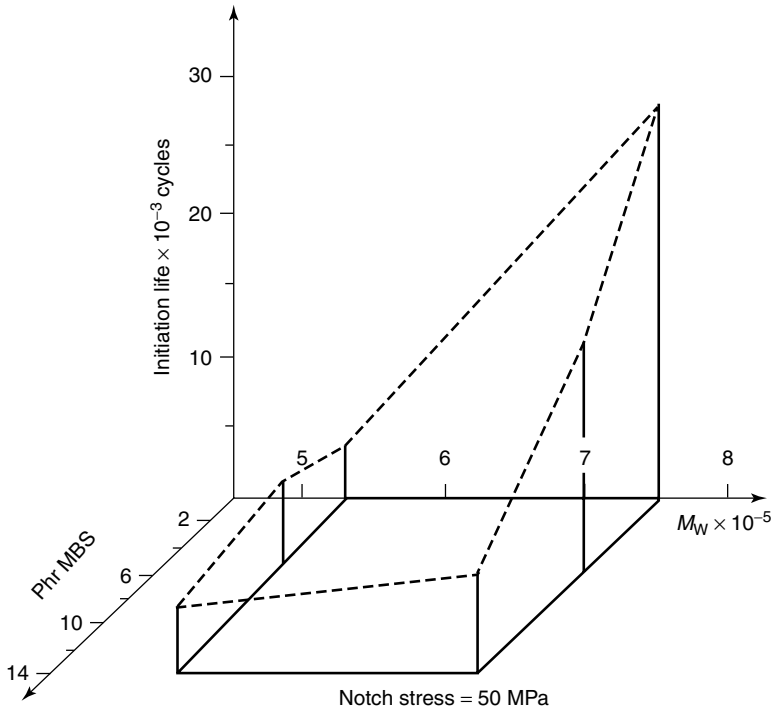

Fig. 32. Three-dimensional plot revealing interactive effects of M_w and rubber content (MBS) % on FCI lifetime in PVC (116).

the maximum elongation possible for a polymer (133,134). In addition, high and low values of the ratio of l_c to the rms end-to-end distance between entanglements tend to be associated with crazing and shear yielding, respectively. Experimental evidence clearly shows that dense, stable crazes can develop only when $M > M_0$ (113,135). Although molecular weight may or may not affect the crazing stress (135–137), a direct correlation exists between higher M values and greater ability to resist propagation of a crack through a craze.

The fatigue resistance depends strongly, and often dramatically, on molecular weight and its distribution (2,4). As M_w increases from 1.6×10^5 to 2×10^6 in three polystyrenes with narrow molecular weight distributions, the S–N (stress–fatigue life) curves (obtained under conditions yielding negligible hysteretic heating) shift upwards and to the right, and the fatigue endurance limit increases from ∼1/14 to 1/2 of the breaking stress (4,138) (see Fig. 33). Similar improvements in fatigue life with increasing molecular weight have also been noted in pulsed compression tests on polystyrene (104). Tensile strength increases by 25% over the range of molecular weight, whereas fatigue strength increases by 100% (4,138–140). Equation 34 holds for tensile strength, but a different dependence is seen for fatigue strength; the ratio of the former to the latter varies from 0.1 to 0.3. The σ–N curve for a polydisperse polystyrene ($M_w = 2.7 \times 10^5$) was not parallel to the others in Figure 33, and yielded an endurance limit higher than predicted on the basis of the other specimens (4,138,140). This finding is similar to that in which the addition of only 1% of high molecular weight species ($M_w = 7 \times 10^5$)

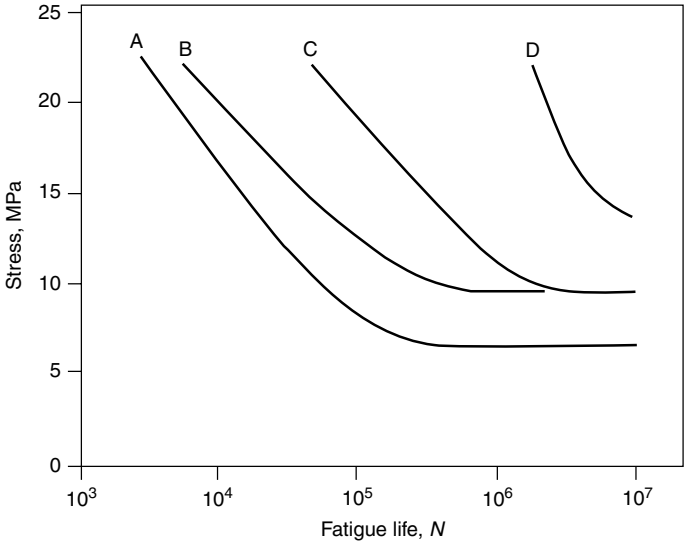

Fig. 33. Effect of molecular weight on fatigue life in polystyrene. $M_w = 1.6 \times 10^5$ (**A**), 3.3×10^5 (**B**), 8.6×10^5 (**C**), 2.0×10^6 (**D**). Specimen B has a broader distribution of molecular weight than the others (4). To convert MPa to psi, multiply by 145.

was able to induce craze stability in a brittle, low molecular weight polystyrene ($M_w = 10^4$) (113). These results have been attributed to increased entanglement density, and hence, orientation hardening of crazed fibrils, and decreased concentration of defects in the form of chain ends in long molecules (4,122). At the same time, increases in fatigue life are not noted when molecular weight is increased by irradiation, so that polydispersity is essentially constant (140). Under such conditions, even below the gel point, the benefits of increased molecular weight are clearly overwhelmed by the flaws introduced by chain ends.

Effect of Diluents and Plasticizers. Diluents, plasticizers (qv), residual solvents or monomers, or absorbed environmental agents greatly affect the viscoelastic response of a polymer and related properties such as damping, modulus, glass-transition temperature T_g, and yield strength. This resultant changes in properties can therefore affect fatigue behavior whether the diluents are dispersed uniformly in the bulk or only at the surface. The effects of lower stiffness differ depending on whether testing is conducted under constant stress or constant deflection conditions. In the first case, fatigue behavior may deteriorate because of the increase in strain experienced by more compliant specimen. In the latter case, the more compliant specimens (which experience lower stresses) may exhibit superior performance. The increase in compliance may also increase the fatigue life of a specimen by plasticizing the crack tip and blunting an otherwise brittle failure. Conversely, it may reduce the fatigue life by reducing the strength of the material in the presence of the crack or craze tip.

The σ–N behavior in tension–compression at 7 Hz of plasticized PVC containing 10 phr of dioctyl adipate exhibits several features characteristic of other polymers (141). Under conditions of high strain amplitude, high ambient temperature, and specimen cooling by natural convection, thermal failures are observed:

a steady increase in damping (tan δ) and a decrease in modulus was observed as failure was approached. In contrast, brittle failure along with crack temperatures, and an increase in storage modulus and a decrease in tan δ prior to failure. However, when thermal failure conditions are coupled with forced-air cooling, brittle fracture is also typical. Also, the criterion (142) for thermal failure is valid (141).

In PVC plasticized with dioctyl phthalate (DOP), FCP rates reportedly increased as the DOP concentration increased from 0 to 10–20% (143), suggesting that lower yield stress and modulus, and resultant tendency toward creep, may play an important role. Quite different results were obtained in a later study at a higher frequency, which may have hindered such creep (90). In this case, FCP rates were relatively unchanged by the presence of DOP, although K_{Ic} values were somewhat reduced, especially at the lowest concentration, 6%. Evidently the antiplasticizing embrittling effect of DOP at low concentrations was manifested more in the static than in the fatigue response. It is believed that PVC can form an effective entanglement network and stable crazes in the presence of much DOP, and the long time scale loading characteristic of fatigue may permit extensive cyclic disentanglement.

With internally plasticized PMMA, i.e., a copolymer with butyl acrylate, still other effects have been seen (89). As the concentration of butyl acrylate increases to mole fractions of 0.1 and then 0.2, FCP rates increase dramatically and K_{Ic} values decrease, presumably because increased ductility is associated with lower strength and modulus. However, with a mole fraction of 0.3 butyl acrylate, localized crack-tip heating and blunting develop from an increase in damping, and FCP rates decrease, so that the overall behavior, with respect to FCP only, resembles that of a commercial PMMA. Hence it appears that a plasticizing comonomer in a chain significantly facilitates the detailed local viscoelastic response and weakens craze fibrils, whereas a semimiscible external plasticizer may not necessarily inhibit the ability to form strong craze fibrils.

The plasticizing influence of absorbed water on the FCP response of polyamides has also been studied (144–150). Earlier data were difficult to interpret because various experiments employed different test frequencies, mean stress levels, amounts of imbibed water (0–8.5%), and different specimen configurations. According to the principles of linear elastic fracture mechanics, specimen configuration should have no bearing on material fatigue response, since the propagation of fatigue crack is assumed to be controlled entirely by the stress field near the crack tip and therefore to be a function of ΔK only. However, for the case of engineering plastics that exhibit significant viscoelastic heating at the prevailing test conditions, variations in specimen configuration have been shown to alter FCP resistance as a result of changes in overall stress range ($\Delta\sigma$) acting on the specimen (150,151). For example, crack growth rates determined with the center-cracked (CCT) specimens exceed those using wedge-opening load (WOL) samples (151). In addition, greater hysteretic heating occurs in the CCT samples when compared with those measured in WOL samples. These results are readily understood in terms of the expression for the stress intensity factor range, which takes into account the different geometries.

$$\Delta K = Y(\Delta\sigma)\sqrt{\ell} \tag{35}$$

In equation 35, the function Y accounts for the different specimen geometries (64). Since Y is much smaller for the CCT specimen than for the WOL specimen (64), it follows that $\Delta\sigma_{CCT}$ is much larger than $\Delta\sigma_{WOL}$; the latter difference in far-field stress distribution alters the hysteretic heat generation capability and the relative stiffness of these samples. Simply stated, the far-field stresses must be increased in the CCT specimen to achieve the same change in stress intensity as the WOL specimen. These higher far-field stresses, in turn, produce more hysteretic heating.

Nylon–water interactions and their associated influence on mechanical response are of considerable engineering importance since the absorption of moisture occurs readily when the nylon component is in service. Roughly 2.5 wt% water is imbibed after equilibration at 50% rh. Depending on the property and the amount of water absorbed, effects may be beneficial or deleterious. For example, RT modulus increases marginally with the addition of 2.2% water in nylon-6,6 but is significantly reduced with 8.5% water (152). Such differences in elastic modulus have been traced to the manner by which the water molecules are incorporated in the nylon. At low absorbed moisture, the polar H_2O molecules interrupt the hydrogen bonds between amide groups in neighboring chain segments and create water bridges between these groups. This tightly bound state is believed to persist until all of the hydrogen atoms bond in the amorphous fraction group ratio of 1/2 (153,154). At higher concentrations, weakly bound water is imbibed and essentially serves as a diluent.

Fatigue tests on unnotched samples have demonstrated that the fatigue strength (the stress corresponding to failure at a given number of cycles) is reduced by as much as 30% when nylon-6,6 is equilibrated at 50% rh (152) (see Fig. 34). In marked contrast, it has been found that fatigue growth rates in nylon-6,6 exhibit a pronounced minimum at an absorbed moisture content of 2.6 wt% water, and

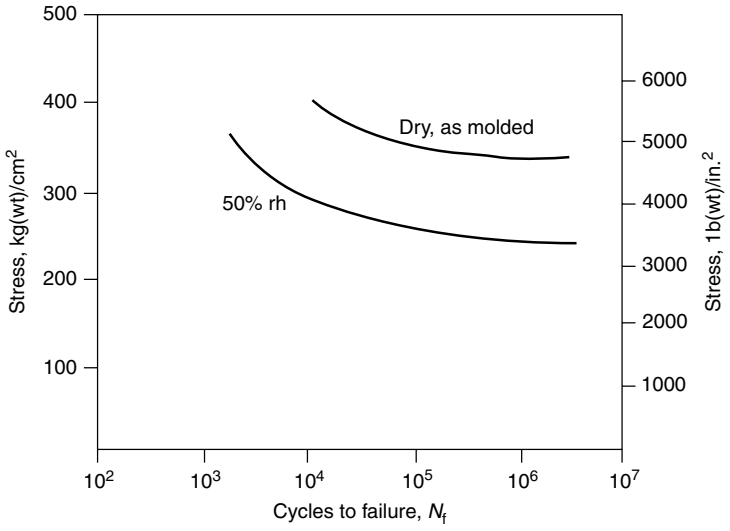

Fig. 34. Unnotched fatigue life in nylon-6,6 as a molded and equilibrated at 50% rh (155). The test specimen is 0.775 cm thick.

crack growth rates are higher in saturated material (8.5 wt% water) than in the dry polymer (149,156). The decrease in crack growth rates with increasing water content at low moisture can be attributed to enhanced chain mobility and an attendant increase in crack-tip blunting associated with localized crack-tip heating. In addition, fatigue resistance is believed to increase with the slight increase in elastic modulus that accompanies the addition of up to 2.5 wt% water. Conversely, the marked increase in crack growth rates at moisture >2.5 wt% is believed to result from the pronounced reduction of elastic modulus which accompanies high amounts of loosely bound absorbed water (152,154).

The complex influence of absorbed water on FCP resistance in nylon-6,6 and in nylon-6 (149) reflects a competition between the beneficial influence of crack-tip blunting and the deleterious effect of modulus degradation. This competitive interaction is reflected in the fatigue-mechanism transition discussed below. The blunting mechanism dominates the fatigue response at low moisture levels and the decrease in modulus overshadows crack blunting at higher water contents. The same deformation processes occur in fatigue tests on unnotched samples; however, overall global stress levels in these samples are much larger than for the case of precracked specimens. As a result, the greater amount of hysteretic heating in nylon-6,6 samples equilibrated at 50% rh reduces specimen stiffness resulting in more damage per cycle than that experienced inferior fatigue properties in the σ–N test.

The influence of absorbed water on FCP resistance is expected to be more significant for high impact nylon-6,6 (HI-N66) since this blend exhibits greater amounts of hysteretic heating than neat nylon-6,6 (157). In general, the effect of water content on relative ranking in FCP resistance for various nylon-6,6 blends is related to specimen temperature. At low water contents and low values of ΔK, heating is beneficial, and blends with more rubber show the best FCP resistance. For these conditions, heating is localized and contributes to crack-tip blunting, which lowers the effective ΔK. With increasing water content, and/or ΔK, greater specimen heating occurs which is detrimental to fatigue resistance. Since rubbery additions and extensive hysteretic heating bring about a substantial reduction in E', the principal cause for reduced FCP resistance in the rich blends containing water, it is interesting to note that when ΔK is normalized with respect to the elastic modulus, the richer blends exhibit greater resistance to cyclic strain (157). In general, variations in FCP behavior of HI-N66 depend strongly on changes in the dynamic storage and loss moduli resulting from hysteretic heating. Heat-induced changes in modulus are more important than the absolute temperature increase of the sample.

The absorption of water by PMMA also influences fatigue resistance in this amorphous polymer (158). There is significant reduction in fatigue lifetime with up to 1% water content for extruded PMMA ($M_w = 79{,}300$) tested at 27.6 MPa and 2 Hz (see Fig. 35). This is related to plasticization and reduction in resistance to craze initiation and subsequent breakdown. At higher water content, no further deterioration takes place even though the water molecules tend to cluster and aggregate.

Surface Finish and Modification. Previous examples involve essentially homogeneous polymer–diluent systems. Interesting effects with practical consequences also occur when unnotched samples are exposed to various environmental

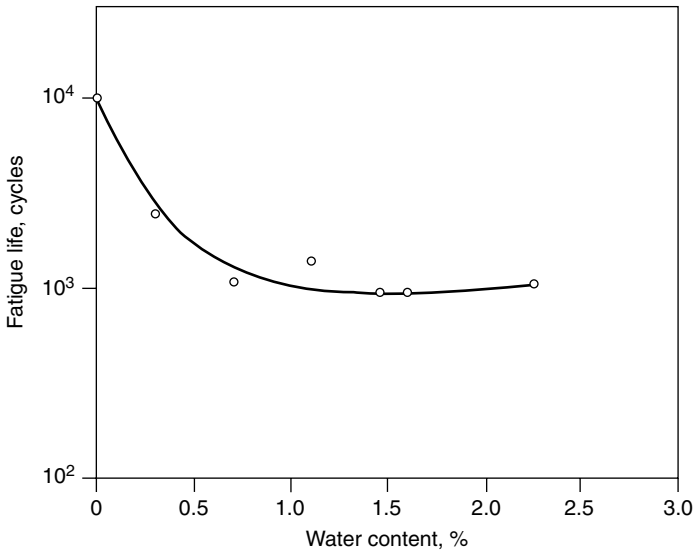

Fig. 35. Fatigue life vs water content in extruded PMMA (M_w = 79,300) tested at 27.6 MPa and 2 Hz (158).

media (4,159). Because fatigue failure in many cases usually involves initiation at the surface, such effects are to be expected.

Deleterious effects of atmospheric exposure on mechanical properties are well known. Surface oxidation in rubbers results in embrittlement, surface cracking, enhanced fatigue propagation, and reduced fatigue life. Even in a ductile plastic, the formation of brittle surface layers and cracks invariably facilitates the onset of crack propagation under static (51,160) or fatigue loading. For example, when exposed to natural weathering (qv), the fatigue strengths of polystyrene, ABS and acetal resin decrease both in an absolute sense and in a relative sense with respect to tensile and blending strength.

The role of surface oxidation in the fatigue of polystyrene has been clearly demonstrated (159). While control samples exhibit an average fatigue life of 25,000 cycles in air, lifetimes increase ~90% by coating with a ductile metal (aluminum or gold, 200 nm thick), and ~100% by testing in nitrogen. Coating with flexible, rubber polymers or with a low molecular weight oligomer of polystyrene also increases fatigue life in polystyrene (159,161). The relative effect is greater for unpolished specimens; interestingly, the coatings themselves are more effective than polishing. It seems likely that these coatings reduce stress concentrations at surface flaws. Even though the natural rubbers used are susceptible to oxidation, the polishing effect is dominant. On the other hand, coating high molecular weight brittle polystyrene layer results in a decrease in fatigue life (4); the propensity for facile initiation of craze cracks evidently overcomes any protective effect. Of course, oxidation is favored by stress.

Although liquid environments often induce environmental-stress crazing or crazing in glassy plastics, not all liquids are deleterious to fatigue performance, and some are beneficial. Typical liquids, eg, heptanes, esters, and alcohols,

decrease the fatigue life of polystyrene (162); the decrease is greater when solubility parameter is closer to that of polystyrene. The increased solubility and plasticization lowers the crazing stress and hence facilitates crack development. In contrast, with liquids known to increase crazing stresses in polystyrene, eg, water, ethylene glycol, or glycerol, fatigue lifetimes increase ~3×, 4×, and 9×, respectively. This effect is attributed to enhanced hydrogen bonding, to filling of surface voids and flaws, or to surface tension changes.

Increase in fatigue life for nylon-6,6 exposed to petroleum ether, water, and alcohols has been reported (163), and the effects of various liquids on fatigue of polycarbonate have been described (164). Various vapors can be beneficial to fatigue life in polystyrene (4,44).

Thermal History. This is an important parameter in determining viscoelastic and mechanical behavior (165). For example, in amorphous polymers, quenching from temperature above T_g increases the free volume and enthalpy, increases yield stress, and decreases fracture toughness (see also AGING). With crystalline polymers, the morphology (qv) depends very much on the balance between nucleation and growth corresponding to the rate and pattern of cooling from melt.

Although the fatigue behavior of semicrystalline polymers can be significantly altered by varying the thermal history, effects of such history on fatigue in amorphous polymers are not well documented. Even though sub-T_g annealing of polycarbonate reduces the static fracture toughness, relatively little effect on FCP response is noted (165). Similarly, only modest and difficult-to-reproduce FCP effects of quenching and annealing on FCP behavior have been reported for PVC (166,167). Although repetitive cycling can condition the state of a polymer, at least under some conditions (168), the fact that yielding occurs within the plastic zone implies the attainment of a state of mobility equivalent to a temperature high enough to erase some or all of the effects of the applied history.

Semicrystalline Polymers. As a class, semicrystalline polymers (qv) tend to exhibit superior fatigue resistance, relative to that of amorphous polymers (qv), both in terms of σ–N behavior and FCP rates (2,4,169), as long as tests are conducted at frequencies low enough to minimize excessive hysteretic heating. This is so, even allowing for variations, due to molecular weight. Indeed even though performance in a standard S–N test at 30 Hz may be relatively poor, many such polymers behave very well under service conditions involving lower frequencies and strains. Thus polypropylene is an excellent material for integral hinges.

Such inherently superior fatigue resistance is not fortuitous. Semicrystalline polymers having adequate intercrystalline linkages can not only dissipate considerable energy when the crystallites are deformed but also form a new and strong crystalline morphology (170,171). Crystallization developed during straining of amorphous polymers is responsible for the superior fatigue resistance of strain-crystallizing rubbers (172,173).

Confirmation of the general fatigue superiority of semicrystalline polymers is implicit in studies of σ–N behavior at frequencies low enough to minimize temperature rises (169). While the ratios of the endurance limit to tensile strength for typical amorphous polymers (polystyrene, PMMA, and cellulose acetate) are approximately 0.2, values for nylon-6,6, acetal resin, and polyterafluoroethylene are 0.3, 0.5, and 0.5, respectively. At a low frequency, polyethylene ($M_w > 50{,}000$) exhibits no failure after 5×10^6 cycles, even at the relatively high alternating stress

of 21 MPa (300 psi) (169). Curves for polymers such as nylon-6,6, poly(vinylidene fluoride), and acetal resin appear to the right of the curve and data for nylon-12 also fall in this region.

Polymer Alloys, Blends, and Composites. The fatigue behavior of multicomponent polymers can be complex. On one hand, the addition of inhomogeneities produces stress concentrations that can reduce the fatigue life of a structure dramatically. On the other hand, the heterogeneities may provide mechanisms of reinforcement, enhanced energy dissipation, or other features that may dramatically improve the overall fatigue life of a material (see POLYMER BLENDS).

With regard to particulate-filled or rubber-modified systems, the polymer matrix must provide the load bearing capability. The geometry and elastic properties of the discrete phase, together with quality of the interface, can all affect the stress concentration developed by the introduction of the particle. One can consider that at nominally low cyclic stresses the matrix material in the vicinity of the particles may be effectively cycling at much higher stresses. This, in turn, may shift the apparent high cycle/low cycle fatigue transition (eg, see Figs. 4 and 5) to lower stress levels or cycles. Also, the initiation time for damage may be effectively reduced by the introduction of the stress concentration. However, once the damage initiates, these same mechanisms may reduce the subcritical crack growth kinetics significantly by dramatically increasing the size of the process zone and increasing the energy dissipated within the process zone. For example, cavitation of a rubber particle can change the failure mode of the matrix polymer from a brittle mechanism (crazing or microcracking) to a ductile mechanism (shear banding), thereby increasing the fracture toughness of the material by as much as an order of magnitude (51).

The effect of a rubbery phase on the fatigue behavior is an example of such complex behavior. As with an unmodified polymer, high stresses or frequencies may generate enough hysteretic heating to induce failure by softening the matrix while at lower stresses and/or frequencies a nominally brittle failure can occur. This is shown for the case of ABS in Figure 36 (174). Although hysteretic heating is common without the introduction of a second phase, the rubbery phase can cause several specific effects. First, a significant decrease in the yield stress and modulus are typical along with an increase in the creep response. Moreover, the reduction in ultimate elongation associated with cyclic softening may be greater in rubber-modified polymers (175).

In another more recent study (176), FCP studies were conducted on rubber-toughened polycarbonate. The results indicated that over all ranges of ΔK, the crack growth rate was roughly a factor of 20 lower than that for unmodified polycarbonate. This was found over a range of mean stress levels. However, the threshold stress intensity factor ΔK_{th} dropped significantly in the modified system as compared to the unmodified system, indicating that the rubber-toughened system may have a shorter initiation time since smaller defects may start to propagate as cracks.

The behavior of polymer alloys and immiscible blends have generally the same complex behavior as rubber-modified systems. In the case of polystyrene/polyethylene blends (177), the crack growth rates of the blends were as much as 20 times lower than that of unmodified polystyrene. However, like the results in Reference 176, the results in Reference 177 show that

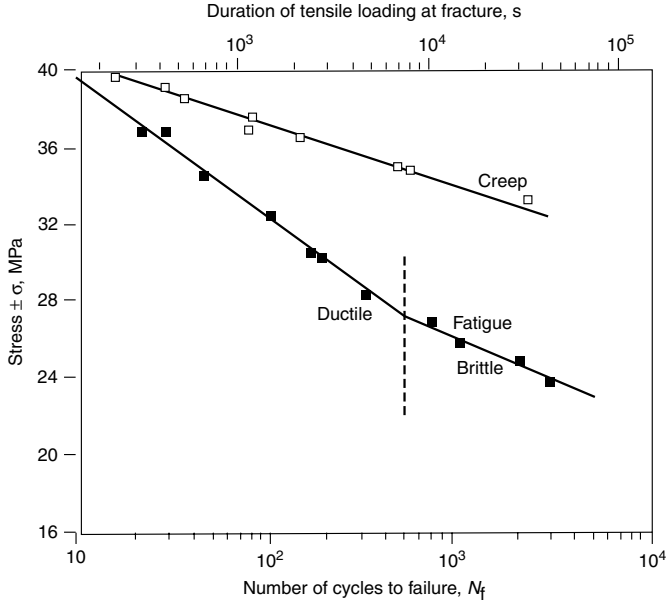

Fig. 36. Comparison of σ–N curve under a square-wave loading with creep-rupture data for a typical ABS polymer (175). Note that the creep-rupture time scale is equivalent to that of the fatigue cycle scale in terms of time under tensile load. To convert MPa to psi, multiply by 145.

the threshold stress intensity of the blend is lower than that of the modified system.

In some cases, the heterogeneity may provide an effective reinforcement for the matrix material (eg, chopped fiber composite). In this type of material, the load is transferred to the fiber from the matrix through shear and the mode II fracture strength of most polymers is much greater than the mode I strength (eg, Fig. 31). Thus, transmitting the load from the matrix to the reinforcement via shear is an efficient approach. Once the load is transferred, the fiber may provide the necessary strength and long-term durability. In order to realize this type of reinforcement, adequate fiber lengths and high interface strength are necessary.

BIBLIOGRAPHY

"Fatigue" in "Fracture and Fatigue" in *EPSE* 2nd ed., Vol. 7, pp. 378–453, by R. W. Hertzberg and J. A. Manson, Lehigh University.

1. J. A. Manson and R. W. Hertzberg, *Crit. Rev. Macromol. Sci.* **1**, 433 (1973).
2. R. W. Hertzberg and J. A. Manson, *Fatigue of Engineering Plastics*, Academic Press, Inc., Orlando, Fla., 1980.
3. J. C. Radon, *Int. J. Fract.* **16**, 533 (1980).
4. J. A. Sauer and G. C. Richardson, *Int. J. Fract.* **16**, 499 (1980).
5. M. T. Takemori, *Annu. Rev. Mater. Sci.* **14**, 171 (1984).
6. J. A. Sauer and C. C. Chen, *Adv. Polym. Sci.* **52/53**, 169 (1983).

7. J. M. Schultz, in J. M. Schultz, ed., *Treatise on Materials Science and Technology, Part B*, Academic Press, Inc., Orlando, Fla., 1977, p. 599.
8. *ASTM D638, Standard for Uniaxial Tensile Testing*, Vol. 08.01, American Society for Testing and Materials, Philadelphia, Pa., 1985, p. 277.
9. *ASTM D671, Standard for Metric Practice*, Vol. 08.01, American Society for Testing and Materials, Philadelphia, Pa., 1985, p. 277.
10. A. Wohler, *Engl. Abstr. Eng.* **2**, 199 (1971).
11. M. N. Riddell, *Plast. Eng.* **30**(4), 71 (1974).
12. J. Kallrath and co-workers, *Polym. Testing* **18**, 11 (1999).
13. A. J. Lesser, *J. Appl. Polym. Sci.* **58**, 869 (1995).
14. D. A. Opp, D. W. Skinner, and R. J. Wiktorek, *Polym. Eng. Sci.* **9**(2), 121 (1970).
15. I. Constable, L. E. Culver, and J. G. Williams, *Int. J. Fract. Mech.* **6**, 279 (1970).
16. J. L. Weaver and C. L. Beatty, *Polym. Eng. Sci.* **12**, 1117 (1978).
17. S. B. Ratner and V. I. Korobov, *Mekh. Polim.* **1**(3), 93 (1965).
18. A. X. Schmidt and C. A. Marlies, *Principles of High Polymer Theory and Practice*, McGraw-Hill Book Co., New York, 1948, p. 578.
19. J. D. Ferry, *Viscoelastic Properties of Polymers*, 3rd ed., John Wiley & Sons, Inc., New York, 1980.
20. M. N. Riddell, G. P. Koo, and J. L. O'Toole, *Polym. Eng. Sci.* **9**, 339 (1966).
21. L. J. Broutman and S. K. Gaggar, *Int. J. Polym. Mater.* **1**, 295 (1972).
22. K. Oberbach, *Kunstoffe* **55**, 356 (1965).
23. H. Hachmann and E. Strickle, in Soviet Plastics and Engineering Annual Technology Conference, Vol. 26, 1968, p. 512.
24. R. J. Crawford and P. P. Benham, *Polymer* **16**, 980 (1975).
25. A. J. Lesser, Unpublished results, 1998.
26. M. A. Minor, *J. Appl. Mech.* **67**, A159 (1945).
27. S. S. Manson, *Avoidance, Control, and Repair of Fatigue Damage, Metal Fatigue Damage-Mechanism Detection, Avoidance and Repair*, ASTM STP495, American Society for Testing and Materials, Philadelphia, Pa., 1970, p. 254.
28. M. Frendahl and I. Rychlik, *Int. J. Fatigue* **15**, 265–272 (1993).
29. G. B. McKenna and R. W. Penn, *Polymer* **21**, 213–220 (1980).
30. A. Tobolsky and H. J. Eyring, *Chem. Phys.* **11**, 125 (1943).
31. B. D. Coleman, *J. Polym. Sci.* **20**, 447 (1956).
32. B. D. Coleman, *J. Appl. Phys.* **29**, 527 (1958).
33. S. N. Zhurkov, *Int. J. Fract. Mech.* **1**, 311 (1965).
34. L. M. Kachanov, *Int. J. Sol. Struct.* **23**(1), 23 (1987).
35. A. I. Kunin, in E. Kroner, ed., *Mechanics of Generalized Continua*, Springer-Verlag, Heidelberg, Germany, 1968.
36. Z. P. Bazant, *J. Eng. Mech.* **117**, 1070 (1991).
37. C. L. Chow and Y. Wei, *Int. J. Fracture* **50**, 301 (1991).
38. V. Bouda, *J. Polym. Sci., Polym. Phys.* **14**, 2313 (1976).
39. A. Takahara and co-workers, *J. Appl. Polym. Sci.* **25**, 597 (1980).
40. N. Kaiya, A. Takahara, and T. Kajiyama, *Polymer* **22**, 859 (1990).
41. T. Kajiyama and A. Takahara, *Memoirs Fac. Eng.* **51**(3), 163 (1991).
42. S. Sakurai and co-workers, *Polymer* **35**, 532 (1994).
43. L. B. Liu, A. F. Yee, and D. W. Gidley, *J. Polym. Sci., Polym. Phys.* **30**, 221 (1992).
44. L. C. E. Struik, *Physical Aging in Amorphous Polymers and Other Materials*, Elsevier Science, New York, 1978.
45. D. G. LeGrand, *J. Appl. Polym. Sci.* **13**, 2129 (1969).
46. R. A. Bubeck, S. E. Bales, and H. D. Lee, *Polym. Eng. Sci.* **24**, 1142 (1984).
47. S. N. Zhurkov and co-workers, *J. Polym. Sci.* **10**, 1509 (1972).
48. D. E. LeGrand and co-workers, *Polym. Eng. Sci.* **22**, 929 (1982).

49. L. B. Liu, D. Gidley, and A. F. Yee, *J. Polym. Sci., Polym. Phys.* **30**, 231 (1992).
50. H. A. Hristov, A. F. Yee, and D. Gidley, *Polymer* **30**, 3604 (1994).
51. C. B. Bucknall, *Toughened Plastics*, Applied Science, Publishers, London, 1977.
52. H. J. Sue and A. F. Yee, *J. Mater Sci.* **24**, 1447 (1989).
53. U. Yilmazer and R. J. Farris, *J. Appl. Polym. Sci.* **28**, 3369 (1983).
54. M. L. Shiaao and co-workers, *Polymer* **35**, 306 (1994).
55. A. J. Lesser, *Polym. Eng. Sci.* **36**, 2366 (1996).
56. N. A. Jones and A. J. Lesser, *J. Polym. Sci., Polym. Phys.* **36**, 2751 (1998).
57. J. R. Bristow, *J. Appl. Phys.* **11**, 81 (1960).
58. M. Kachanov, in J. Hutchinson and T. Wu, eds., *Advances in Applied Mechanics*, Academic Press, Inc., New York, 1993, p. 259.
59. A. A. Griffith, *Trans. R. Soc. London A* **221**, 163 (1920).
60. H. M. Westergaard, *Trans. ASME J. Appl. Mech.* **61**, 49 (1939).
61. G. R. Irwin, *Trans. ASME J. Appl. Mech.* **24**, 361 (1957).
62. G. R. Irwin, *Handb. Phys.* **7**, 551 (1958).
63. G. R. Irwin, *Trans. ASME Ser. D* **82**, 417 (1960).
64. J. G. Williams, *Fracture Mechanics of Polymers*, Ellis Horwood Ltd., London, 1984.
65. A. J. Kinloch and R. J. Young, *Fracture Behavior of Polymers*, Elsevier Applied Science Publishers, Ltd., Barking, U.K., 1983.
66. P. C. Paris and F. Erdogan, *J. Basic Engg.* **85**, 528 (1963).
67. P. C. Paris, in Proceedings of the 10th Sagamore Army Materials Research Conference, Syracuse University Press, Syracuse, Italy, 1964, p. 107.
68. P. C. Paris, M. P. Gomez, and W. E. Anderson, *Trends Engg.* **13**, 9 (1961).
69. J. A. Manson, R. W. Hertzberg, and P. E. Bretz, in S. R. Valuri, D. M. R. Taplin, R. RamaRao, J. F. Knott, and R. Dubey, eds., *Advances in Fracture Research, Proceedings of the 5th International Conference on Fracture*, Vol. **1**, Pergamon Press, Oxford, U.K., 1982, p. 443.
70. L. Jilken and C. G. Gustsfson, in Backlund, A. Blom, and C. J. Beevers, eds., *Fatigue Thresholds, Fundamental and Engineering Applications*, EMAS, Warley, U.K., 1981, p. 715.
71. L. Pruitt and L. Bailey, *Polymer* **39**, 1545 (1998).
72. E. H. Andrews and B. J. Walker, *Proc. R. Soc. London, Ser. A* **325**, 57 (1971).
73. P. E. Bretz, R. W. Hertzberg, and J. A. Manson, *Polymer* **20**, 575 (1981).
74. T. A. Morelli and M. T. Takemori, *J. Mater. Sci.* **19**, 385 (1984).
75. A. Chudnovsky and A. Moet, *Org. Coat. Plast. Chem.* **45**, 607 (1981).
76. A. Chudnovsky and A. Moet, *Polym. Eng. Sci.* **22**, 922 (1982).
77. M. D. Skibo, *Ph.D. dissertation*, Lehigh University, 1977.
78. R. W. Hertzberg, J. A. Manson, and M. D. Skibo, *Polym. Eng. Sci.* **15**, 252 (1975).
79. R. W. Hertzberg, M. D. Skibo, and J. A. Manson, *ASTM STP700, Standard for Metric Practice*, American Society of Testing and Materials, Philadelphia, Pa., 1980, p. 490.
80. Y. W. Mai and J. G. Williams, *J. Mater. Sci.* **14**, 1933 (1979).
81. G. C. Martin and W. W. Gerberich, *J. Mater. Sci.* **11**, 231 (1976).
82. R. J. Wann, G. C. Martin, and W. W. Gerberich, *Polym. Eng. Sci.* **16**, 645 (1976).
83. M. T. Hahn and co-workers, *Polymer* **27**, 1017 (1986).
84. J. Runt and M. Jacq, *J. Mater. Sci.* **24**, 1421 (1989).
85. R. A. Bubeck and H. M. Baker, *Polymer* **23**, 1680 (1982).
86. J. T. Yeh and J. Runt, *J. Polym. Sci., Polym. Phys.* **29**, 371 (1991).
87. K. Karger-Kocsis, *Composites* **21**, 243 (1990).
88. J. J. Strebel and A. Moet, *J. Polym. Sci., Polym. Phys.* **33**, 1969 (1995).
89. S. L. Kim and co-workers, *Polym. Eng. Sci.* **17**, 194 (1977).
90. M. D. Skibo, J. A. Manson, and R. W. Hertzberg, *J. Macromol. Sci., Part B: Phys.* **14**, 525 (1977).

91. C. M. Rimnac and co-workers, *J. Macromol. Sci. Phys.* **19**, 351 (1981).
92. S. C. Kim and co-workers, *Polym. Eng. Sci.* **18**, 1093 (1978).
93. G. Pitman and I. M. Ward, *J. Mater. Sci.* **15**, 635 (1980).
94. J. C. Michel, J. A. Manson, and R. W. Hertzberg, *Polym. Prepr. (Am. Chem. Soc., Div. Polym. Chem.)* **26**(2), 141 (1985).
95. J. C. Michel, J. A. Manson, and R. W. Hertzberg, *Polymer* **25**, 1657 (1981).
96. R. E. Robertson, in R. D. Deanin and A. M. Crugnola, eds., *Toughness and Brittleness of Plastics* (Advances in Chemistry Series No. 154), American Chemical Society, Washington, D.C., 1976, p. 89.
97. J. F. Rudd, *Polym. Lett.* **1**, 1 (1963).
98. D. M. Bigg, R. T. Leininger, and C. S. Lee, *Polymer* **22**, 539 (1981).
99. R. W. Hertzberg, M. D. Skibo, and J. A. Manson, *ASTM STP675*, American Society for Testing and Materials, Philadelphia, Pa., 1979, p. 471.
100. J. Janiszewski, R. W. Hertzberg, and J. A. Manson, *ASTM STP743*, Standard for Metric Practice, American Society for Testing and Materials, Philadelphia, Pa., 1981, p. 125.
101. F. X. de Charentenay, F. Laghouati, and J. Dewas, *Deformation, Yield and Fracture of Polymers*, Plastics and Rubber Institute, London, 1979, p. 6.1.
102. G. M. Connelly and co-workers, *J. Orthoped. Res.* **2**, 119 (1984).
103. C. Sheu and R. D. Goolsby, *Org. Coat. Appl. Polym. Sci. Proc.* **48**, 833 (1983).
104. P. E. Bretz, J. A. Manson, and R. W. Hertzberg, *J. Appl. Polym. Sci.* **27**, 1707 (1982).
105. R. W. Hertzberg, M. D. Skibo, and J. A. Manson, *J. Mater. Sci.* **13**, 1038 (1978).
106. R. P. Wool, *Polym. Prepr. (Am. Chem. Soc., Div. Polym. Chem.)* **23**(2), 62 (1982).
107. C. Su, *M.S. Report*, Lehigh University, 1984.
108. S. Qureshi, J. A. Manson, J. C. Michel, R. W. Hertzberg, and L. H. Sperling, in S. S. Labana and R. A. Dickie, eds., *Characterization of Highly Cross-Linked Polymers* (ACS Symposium Series No. 243), American Chemical Society, Washington, D.C., 1984, p. 109.
109. R. W. Hertzberg, J. A. Manson, and W. C. Wu, *ASTM STP536*, American Society for Testing and Materials, Philadelphia, Pa., 1973, p. 391.
110. S. A. Sutton, *Eng. Fract. Mech.* **6**, 587 (1974).
111. S. Qureshi, in Ref. 2, p. 122.
112. S. L. Kim and co-workers, *Polym. Eng. Sci.* **18**, 1093 (1978).
113. S. Wellinghoff and E. Baer, *J. Macromol Sci., Part B: Phys.* **11**, 367 (1975).
114. N. A. Jones and A. J. Lesser, *J. Polym. Sci., Polym. Phys.* **37**, 3246 (1999).
115. P. B. Lindley and A. Stevenson, in F. Sherratt and J. B. Sturgeon, eds., *Materials, Experimentation and Design in Fatigue*, Westbury House Publishers, Ltd., Surrey, U.K., 1981, p. 181.
116. J. T. Turkanis (Brennock), R. W. Hertzberg, and J. A. Manson, *Deformation, Yield and Fracture of Polymers*, Plastics and Rubber Institute, London, U.K., 1985, Paper 54.
117. J. F. Mandell and J. P. F. Chevaillier, *Polym. Eng. Sci.* **25**, 170 (1985).
118. H. H. Kausch, *Polymers Properties and Applications*, Vol. **2**, Springer-Verlag, New York, 1978.
119. H. W. McCormick, F. M. Brower, and L. Kim, *J. Polym. Sci.* **39**, 87 (1959).
120. J. R. Marin, J. F. Johnson, and A. R. Cooper, *J. Macromol. Sci., Part C: Rev. Macromol. Chem.* **8**, 57 (1972).
121. P. I. Vincent, *Polymer* **1**, 425 (1960).
122. J. A. Sauer, *Polymer* **19**, 859 (1978).
123. J. H. Golden, B. L. Hammant, and E. A. Hazell, *J. Polym. Sci., Part A* **2**, 4787 (1964).
124. A. N. Gent and A. G. Thomas, *J. Polym. Sci., Part A-2* **10**, 571 (1972).

125. R. P. Kusy and D. T. Turner, *Polymer* **17**, 161 (1976).
126. R. P. Kusy and M. J. Katz, *J. Mater. Sci.* **19**, 1475 (1984).
127. J. P. Berry, *J. Polym. Sci., Part A* **2**, 4069 (1964).
128. G. L. Pitman and I. M. Ward, *Polymer* **20**, 895 (1979).
129. R. P. Kambour, *J. Polym. Sci., Macromol. Rev.* **7**, 1 (1973).
130. H. H. Kausch, *Kunstoffe* **65**, 1 (1976).
131. G. W. Weidmann and W. Doll, *Colloid Polym. Sci.* **254**, 205 (1976).
132. D. J. Turner, *Polymer* **23**, 626 (1982).
133. A. M. Donald and E. J. Kramer, *J. Polym. Sci., Polym. Phys. Ed.* **20**, 899 (1982).
134. A. M. Donald and E. J. Kramer, *Polymer* **23**, 457 (1982).
135. D. L. G. Lainchbury and M. Bevis, *J. Mater. Sci.* **19**, 2222 (1984).
136. J. F. Fellers and B. F. Kee, *J. Appl. Polym. Sci.* **18**, 2355 (1974).
137. J. A. Sauer and C. C. Chen, *Toughening of Plastics*, Plastics and Rubber Institute, London, 1985, Paper 26.
138. J. A. Sauer, E. Foden, and D. R. Morrow, *Polym. Eng. Sci.* **17**, 246 (1977).
139. C. L. Beatty and J. L. Weaver, *Bull. Am. Phys. Soc.* **24**, 378 (1979).
140. S. Warty, J. A. Sauer, and A. Charlesby, *Eur. Polym. J.* **15**, 445 (1979).
141. A. Takahara and co-workers, *J. Appl. Polym. Sci.* **25**, 597 (1980).
142. I. Constable, J. G. Williams, and D. J. Burns, *J. Mech. Eng. Sci.* **12**, 20 (1970).
143. K. Suzuki and co-workers, *Kobunshi Kagaku* **28**, 920 (1971).
144. P. E. Bretz, R. W. Hertzberg, J. A. Manson, and A. Ramirez, in S. P. Rowland, ed., *Water in Polymers* (ACS Symposium Series No. 127), American Chemical Society, Washington, D.C., 1980, p. 32.
145. S. Arad, J. C. Radon, and L. E. Culver, *J. Appl. Polym. Sci.* **17**, 1467 (1973).
146. S. Arad, J. C. Radon, and L. E. Culver, *Eng. Fract. Mech.* **4**, 511 (1972).
147. H. A. El-Hakeem and L. E. Culver, *Int. J. Fract.* **1**, 133 (1979).
148. R. W. Hertzberg and co-workers, *Polymer* **39**, 1754 (1998).
149. P. E. Bretz, R. W. Hertzberg, and J. A. Manson, *J. Mater. Sci.* **16**, 2061 (1981).
150. M. T. Hahn and co-workers, *Polymer* **23**, 1675 (1982).
151. R. W. Lang and co-workers, *J. Mater. Sci. Lett.* **3**, 224 (1924).
152. *Zytel Design Handbook*, E. I. du Pont de Nemours & Co., Wilmington, Del., 1972.
153. N. G. McCrum, B. F. Read, and G. Williams, *Anelastic and Dielectric Effects in Polymeric Solids*, John Wiley & Sons, Inc., New York, 1967.
154. R. Puffr and J. Sabeda, *J. Polym. Sci., Part C* **5**, 79 (1967).
155. M. I. Kohan, *Nylon Plastics*, John Wiley & Sons, Inc., New York, 1973.
156. P. E. Bretz, R. W. Hertzberg, and J. A. Manson, *Polymer* **39**, 2482 (1998).
157. M. T. Hahn, R. W. Hertzberg, and J. A. Manson, *J. Mater. Sci.* **21**, 31 (1986).
158. C. C. Chen, J. Shen, and J. A. Sauer, *Polymer* **26**, 89 (1985).
159. J. A. Sauer, S. Warty, and S. Kaka, in Ref. 137, Paper 28.
160. C. C. Chen, N. Chheda, and J. A. Sauer, in Ref. 102,109.
161. S. Warty, J. A. Sauer, and D. R. Morrow, *Polymer* **19** 1465 (1978).
162. S. B. Ratner and N. L. Barasch, *Mekh. Polim.* **1**(1), 124 (1965).
163. J. Miltz, A. T. DiBenedetto, and S. Petrie, *J. Appl. Polym. Sci.* **28**, 2037 (1983).
164. N. Chheda, C. Chen, and S. Kaka, cited in J. A. Sauer in Ref. 4.
165. J. A. Manson, R. W. Hertzberg, S. L. Kim, and W. C. Wu, in Ref. 96, p. 146.
166. S. Webler, *Ph.D. dissertation*, Lehigh University, 1983.
167. C. M. Rimnac, *Ph.D. dissertation*, Lehigh University, 1983.
168. T. C. Ho, *Ph.D. dissertation*, Rensslaer Polytechnic Institute, Troy, N.Y., 1973.
169. J. A. Sauer and K. D. Pae, in H. J. Kaufman and J. J. Falcetta, eds., *Introduction to Polymer Science*, John Wiley & Sons, Inc., New York, 1977, Chapt. "7".
170. G. P. Koo and L. G. Roldan, *J. Polym. Sci., Polym. Lett. Ed.* **10**, 1145 (1972).
171. G. Meinel and A. Peterlin, *J. Polym. Sci., Polym. Lett. Ed.* **9**, 67 (1971).

172. E. H. Andrews, *Fracture of Polymers*, Elsevier Science Publishing Co., New York, 1968.
173. E. H. Andrews, *J. Appl. Phys.* **32**, 542 (1961).
174. C. B. Bucknall and W. W. Stevens, *Toughening of Plastics*, Plastics and Rubber Institute, London, 1978, Paper 24.
175. G. Menges and E. Weigand, in Proceeding of the 21st Annual Technical Conference of the Society of Plastics Engineers, 1975, p. 465.
176. E. J. Moscala, *J. Appl. Polym. Sci.* **49**, 53 (1994).
177. M. N. Bureau, J. I. Dickson, and J. Denault, *J. Mater. Sci.* **33**, 1405 (1998).

ALAN J. LESSER
University of Massachusetts

FERROELECTRIC LIQUID CRYSTALLINE ELASTOMERS

Introduction

Ferroelectric materials are a subclass of pyro- and piezoelectric materials (Fig. 1) (see PIEZOELECTRIC POLYMERS). They are very rarely found in crystalline organic or polymeric materials because ferroelectric hysteresis requires enough molecular mobility to reorient molecular dipoles in space. So semicrystalline poly(vinylidene fluoride) (PVDF) is nearly the only known compound (1). On the contrary, ferroelectric behavior is very often observed in chiral liquid crystalline materials, both low molar mass and polymeric. For an overview of ferroelectric liquid crystals, see Reference 2. Tilted smectic liquid crystals that are made from chiral molecules lack the symmetry plane perpendicular to the smectic layer structure (Fig. 2). Therefore, they develop a spontaneous electric polarization, which is oriented perpendicular to the layer normal and perpendicular to the tilt direction. Because of the liquid-like structure inside the smectic layers, the direction of the tilt and thus the polar axis can be easily switched in external electric fields (see Figs. 2 and 3).

Here, we discuss materials (LC-elastomers) that combine a liquid crystalline phase and ferroelectric properties (preferably the chiral smectic C$*$ phase) in a polymer network structure (see Fig. 4). The coupling of the liquid crystalline director to the network or the softness of the network is chosen so that reorientation of the polar axis is still possible. Thus, densely cross-linked systems that possess a polar axis but cannot be switched (11) will be excluded. It is the role of the network (1) to form a rubbery matrix for the liquid crystalline phase and (2) to stabilize a director configuration. LC-materials that have these properties can be made either (see Fig. 4) by covalently linking the mesogenic groups to a slightly

Encyclopedia of Polymer Science and Technology. Copyright John Wiley & Sons, Inc. All rights reserved.

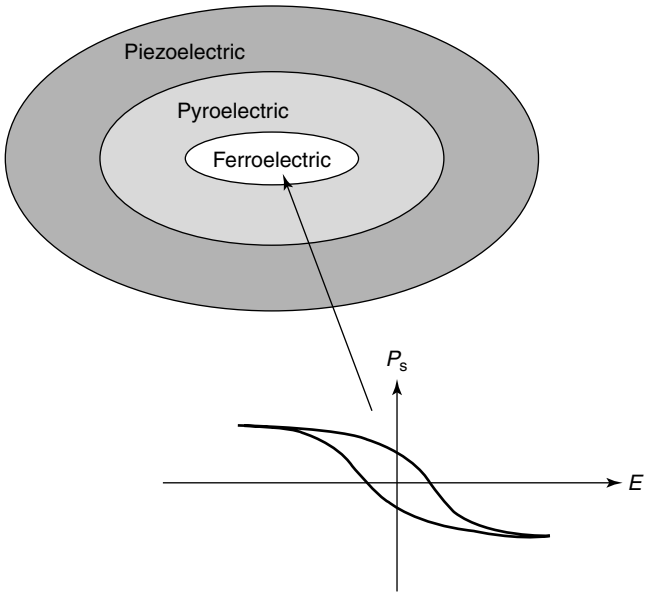

Fig. 1. Ferroelectric hysteresis that shows the spontaneous polarization P_S of a ferroelectric material reversed by an applied electric field E.

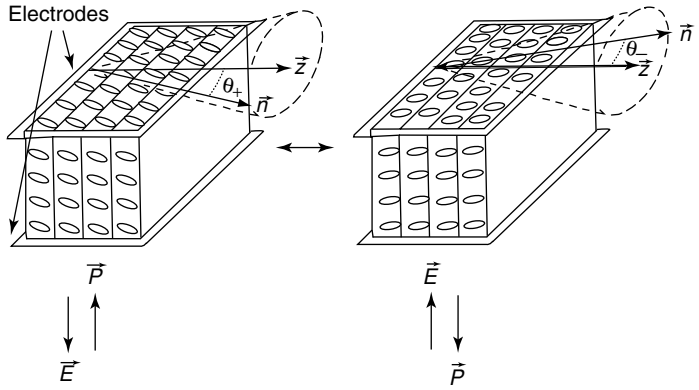

Fig. 2. Schematic drawing of the bistable switching of a ferroelectric liquid crystal in the "surface stabilized FLC" configuration.

cross-linked rubbery polymer network structure (see Fig. 4a) (4–6) or by dispersing a phase-separated polymer network structure within a low molar mass liquid crystal (see Fig. 4b) (9,12). Both systems possess locally a very different structure. They may show, however, macroscopically similar properties.

LC-elastomers (see Fig. 4a) have been investigated in detail (4–8). Although the liquid crystalline phase transitions are nearly unaffected by the network, the network retains the memory of the phase and director pattern during cross-linking

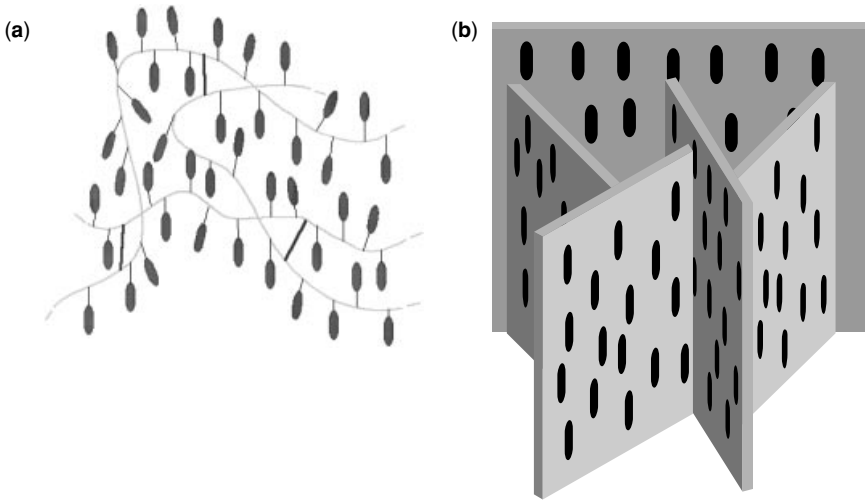

Fig. 3. Network: soft, can be transformed like rubber band, but retains its shape and couples to director orientation because (**a**) director is preferably parallel (or perpendicular) to polymer chains (LC-elastomer) (4–9); (**b**) director aligns (parallel) to chains in oriented phase-separated polymer network structure (low molar mass LC in LC-thermoset) (9,10).

(7,8). In addition, it freezes fluctuations of the smectic layers and leads to a real long range order in one dimension (13). An attempt to change the director pattern by electric or magnetic fields in LC-elastomers leads to a deformation of the network and to an elastic response (see Fig. 3). As a consequence of this, nematic LC-elastomers could never be switched in electric fields, if the shape of the elastomer was kept fixed. For freely suspended pieces of nematic LC-elastomers, shape variations in electric fields have been observed sometimes (14,15). In ferroelectric liquid crystals, the interaction with the electric field is, however, much larger. Thus, it has been possible to prepare real ferroelectric LC-elastomers (see Fig. 3) (3,16). In these systems, the polymer network stabilizes one switching state like a soft spring. It is, however, soft enough to allow ferroelectric switching. Therefore the ferroelectric hysteresis can therefore be measured in these systems. It is, however, shifted away from zero voltage (see Fig. 3).

Synthesis of Ferroelectric LC-Elastomers

The ferroelectric LC-elastomers described so far (3,16–21) are mostly prepared from cross-linkable ferroelectric polysiloxanes (see Fig. 5), which are prepared by hydrosilylation of precursor polysiloxanes (22) (see SILICONES). The cross-linking is finally initiated by irradiating a photoradical generator, which leads to oligomerization of acrylamide or acrylate groups (see Fig. 5). The functionality of the net points is thus high (equal to the degree of polymerization) and varies with the cross-linking conditions.

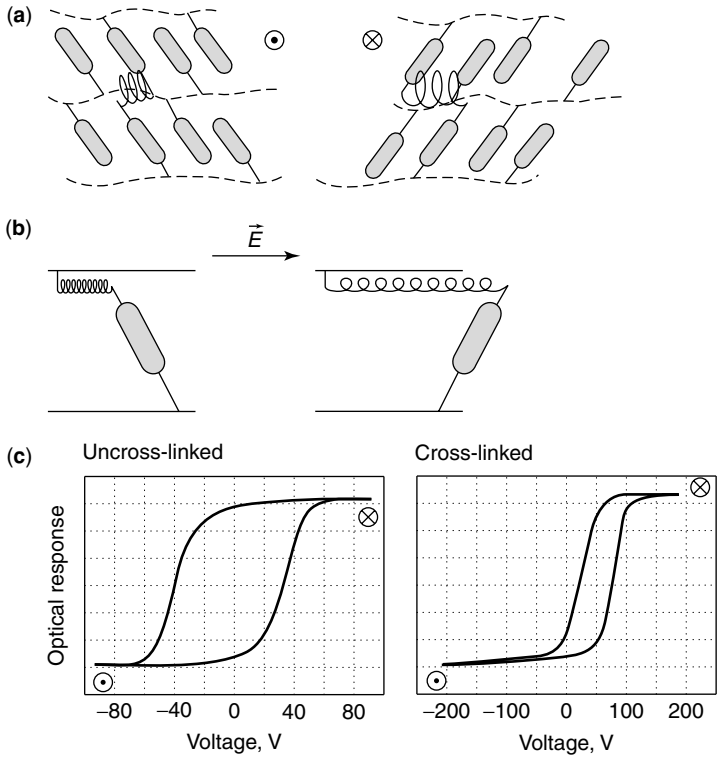

Fig. 4. Schematic drawing of the ferroelectric LC-elastomer and its two switching states (3): (**a**) A polymer chain acts as cross-linking point by connecting different mesogenic groups attached to the main polymer chains. A ferroelectric switching in this elastomer extends polymer chains. (**b**) The entropy elasticity arising from this acts like a spring that stabilizes one state. (**c**) For the uncross-linked system (left), the hysteresis is symmetrical to zero voltage and both states are equal. After cross-linking in one polar state (right), only that state is stable with no electric field, and the hysteresis is no longer symmetrical to zero voltage.

The advantage of this photochemical-initiated cross-linking is that the cross-linking can be started—at will after the liquid crystalline polymer is oriented and sufficiently characterized in the uncross-linked state (see Fig. 6). The advantage of using polymerizable groups (acrylates) for cross-linking is that small amounts of these groups are sufficient to transform a soluble polymer into a polymer gel and that the chemical reaction happens far away from the mesogen. Cinnamoyl moieties, on the other hand (23), require a high concentration of these groups for cross-linking. The dimers thus formed are, in addition, nonmesogenic. Figure 7 summarizes the ferroelectric LC-elastomers discussed in this article. Two different positions of cross-linkable groups are used. In polymer P1, the cross-linking group is close to the siloxane chains, which are known to microphase-separate from the mesogenic groups (22,23). Therefore, the cross-linking should proceed mostly within the siloxane sublayers. In polymers P2 and P3, the cross-linking group is located at the end of mesogens. Therefore, the cross-linking should proceed mostly

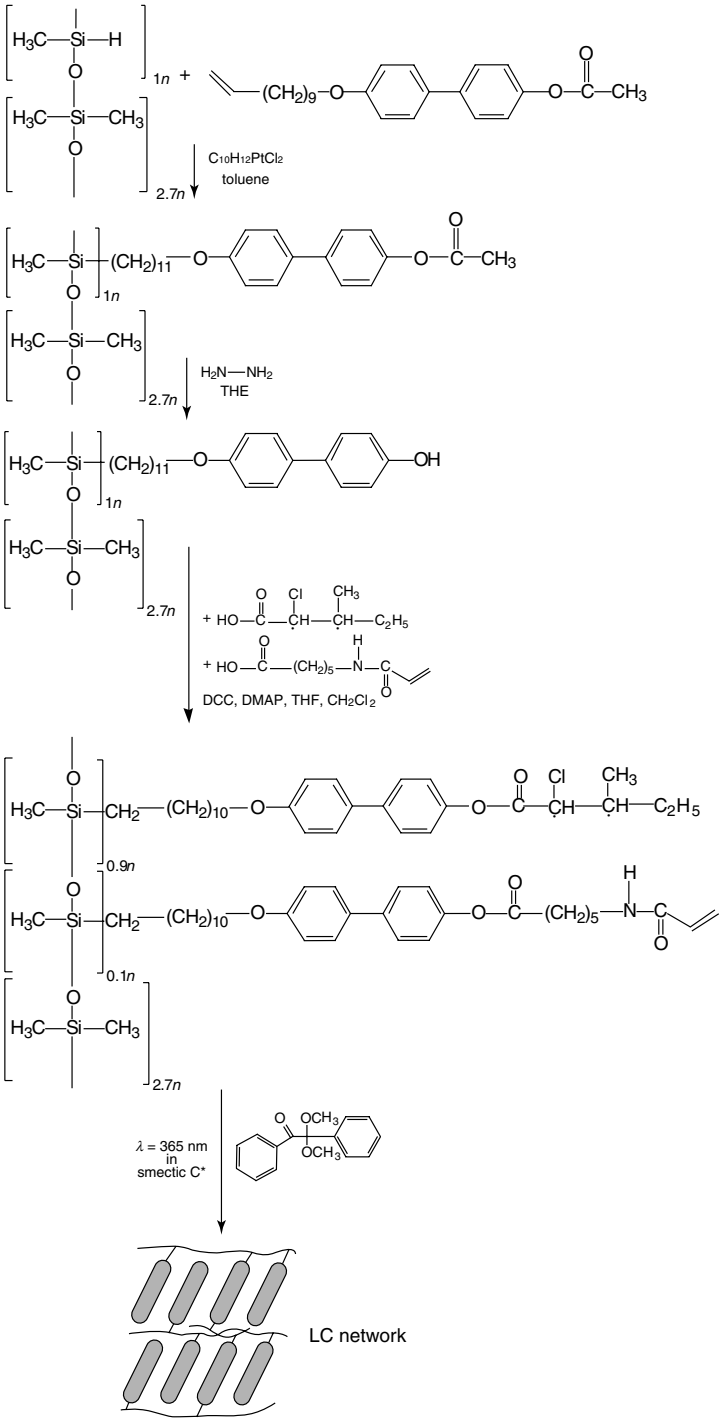

Fig. 5. Synthetic route to the cross-linkable polysiloxane P2 and the following preparation of the oriented smectic C∗ network using uv light in the presence of a photoinitiator (1,1-dimethoxy-1-phenyl-acetophenone) (3).

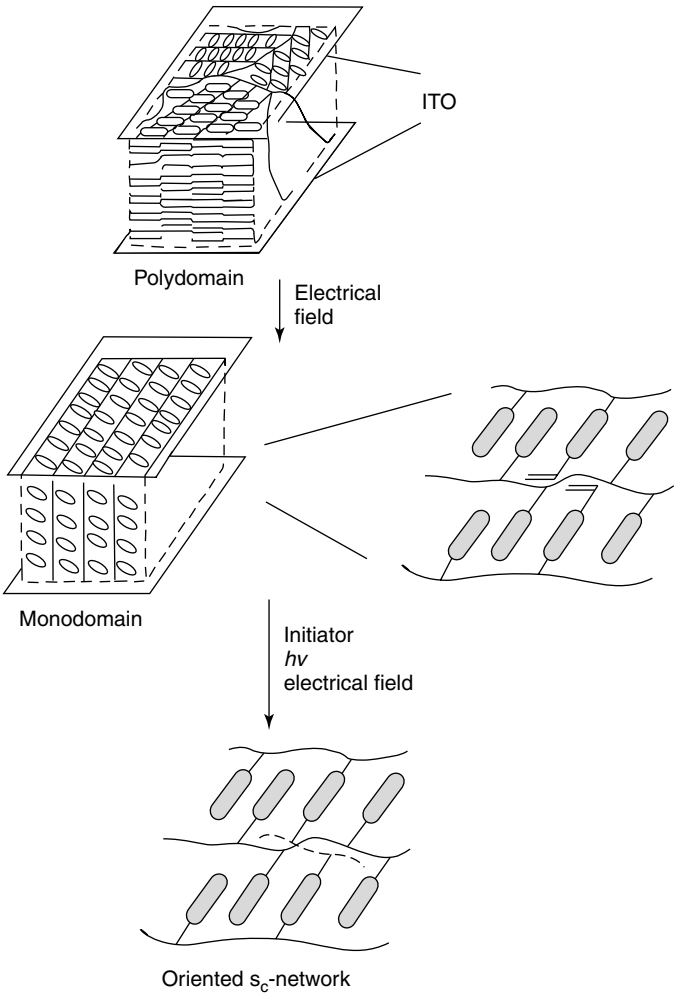

Fig. 6. Preparation of polar smectic C∗ monodomains (3,16) (ITO: indium tin oxide).

between different siloxane layers (see Fig. 7). A comparison of these elastomers allows evaluating structure–property relationships (18,24,25).

Properties and Characterization

Ferroelectric Characterization (Uncross-linked Systems). Before cross-linking, polarization, tilt angle, and switching times can be determined in the usual way (18,22,26). Figure 8 shows the temperature dependence of the spontaneous polarization for polymers P1–P3. For the homopolymer related to polymer P2, all relevant parameters were determined in a careful study (27). It seems that the electroclinic effect is especially strong in these polysiloxanes (16). This has implications for the freezing of a memory of the tilt angle present during

cross-linking. Therefore, ferroelectric elastomers, which have been crosslinked in the smectic A phase while applying an electric field, produce a stable macroscopic polarization (tilt) after cooling into the smectic C$*$ phase (18).

Mechanical Properties of Ferroelectric LC-Elastomers. The cross-linking reactions of a series of copolymers analogous to polymer P2, but differing in the amount of cross-linkable groups, were studied by ftir spectroscopy (17). These measurements show a decrease of the acrylamide double bond on irradiation. Conversions between 60 and 84% were observed. The uncertainty of the conversion, however, is high because only very few double bonds are present in polymer P2 and they are visible in the infrared spectrum at rather low intensity.

Mechanical measurements which show how this photo-chemical cross-linking (conversion of double bonds) leads to an elastic response of the network are, however, still at the beginning because photocross-linking can be performed only in thin layers of a few micrometers. It is best performed between two glass slides to exclude oxygen.

AFM measurements of photocross-linked free standing films show changes in topology during stretching (24). They, however, do not allow measuring elastic moduli.

The most promising approach to obtaining elastic data for these ferroelectric elastomers is investigation of LC-elastomer balloons (25,28). For this purpose, an experimental setup was developed on the basis of an apparatus designed to study smectic bubbles (28). Freely suspended films of the uncross-linked material behave like ordinary smectic films. They can be inflated to spherical bubbles several millimeters in diameter (the thickness of a smectic-layer skin is about 50 nm). These bubbles are stabilized by the smectic-layer structure and their inner pressure p is related to the surface tension and the bubble radius R by the Laplace–Young equation, $p \propto 1/R$. After exposure to uv light, the material is cross-linked, and an anisotropic elastomer is formed. When the cross-linked bubbles are inflated/deflated, the radius–pressure curve reverses its slope and gives direct access to the elastic moduli of the material (25). Because the deformation during inflation of the balloon is isotropic in the layer plane, the material should contract in the direction of the layer normal.

Mechanical measurements of chemically crosslinked LC-elastomers have been made extensively (4,5,29–34). For these systems, it can be shown that stretching allows orientation of the liquid crystalline phase. In ideal situations, it is thus possible to prepare a ferroelectric monodomain by stretching (30,31,35). This result can be rationalized as a two-stage deformation process (see Fig. 9) (31). This possibility of orienting or reorienting the polar axis mechanically is the basis for the piezoelectric properties to be discussed later. Ferroelectric switching could not be observed for any of the chemically crosslinked systems. This may occur because chemically cross-linked films are too thick (several 100 μm compared to about 10 μm for photochemically cross-linked systems) and the electric field applied is therefore too small. In addition, the cross-linking density in chemically cross-linked systems is presumably higher.

Ferroelectric Properties (Cross-linked Systems). The ferroelectric properties of the photochemically crosslinked elastomers E1–E3 differ significantly and depend on the topology of the network formed. For the systems that have interlayer cross-linking (see Fig. 7, E2 and E3), the switching time

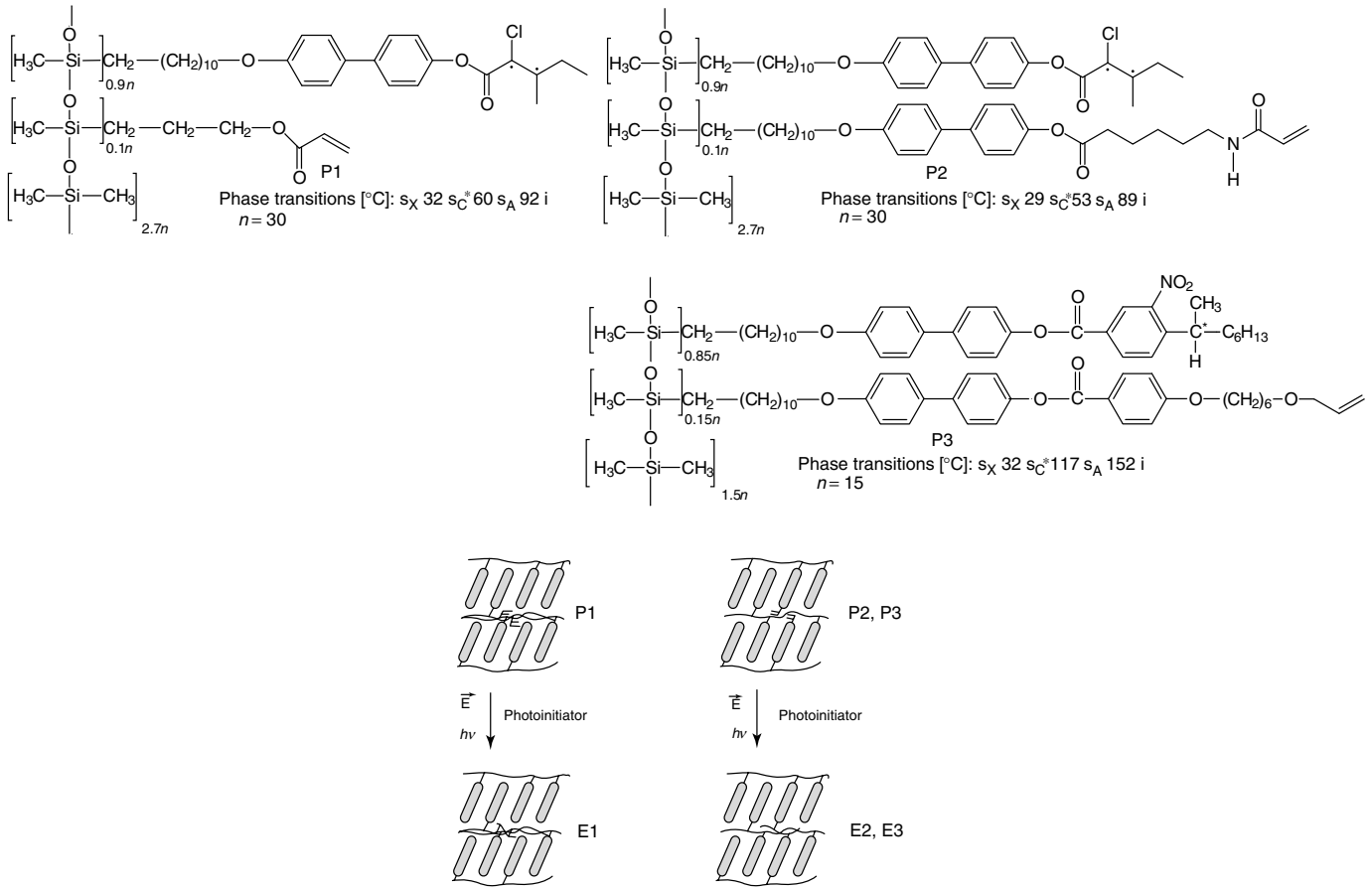

Fig. 7. Chemical structure and phase-transition temperatures of polymers P1–P3 (18). (**a**) P1 is designed to favor intralayer cross-linking; (**b**) P2 and P3 form an interlayer network.

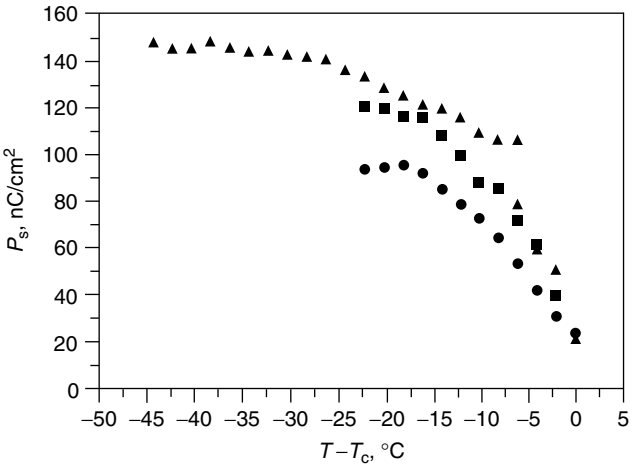

Fig. 8. Temperature dependence of the spontaneous polarization P_S for the polymers P1–P3 measured by the triangular wave method (18). p1 : ■, p2 : ●, p3 : ▲.

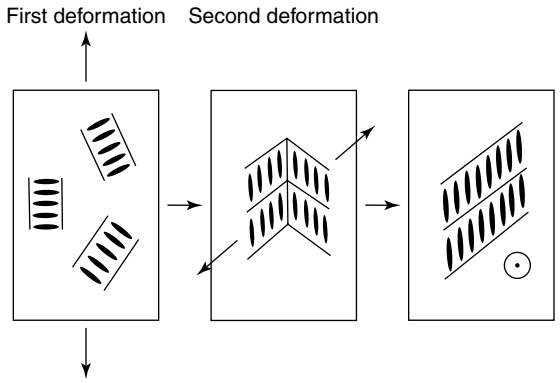

Fig. 9. Two-step deformation process of a chiral smectic C∗ elastomer that displays macroscopic polarization at the end (31).

is increased greatly. Therefore, spontaneous polarization can no longer be determined by the triangular wave method. Slow switching is, however, still possible and therefore ferroelectric hysteresis can be measured optically (see Figs. 3c and 10) (3,16). After photochemical cross-linking in a ferroelectric monodomain, the ferroelectric hysteresis shows stabilization of the orientation present during cross-linking. At zero external voltage, only this state is stable. The second switching state can, however, be reached. Therefore, the network acts like a spring that stabilized one state because switching to the other state leads to a deviation from the most probable conformation of the polymer chain (36) (see Fig. 10). Then, the shift of the center of the hysteretic loop away from zero voltage gives the magnitude of the electric field necessary to balance the mechanical field of the network. The asymmetry of the hysteresis increases with the cross-linking density (18). For

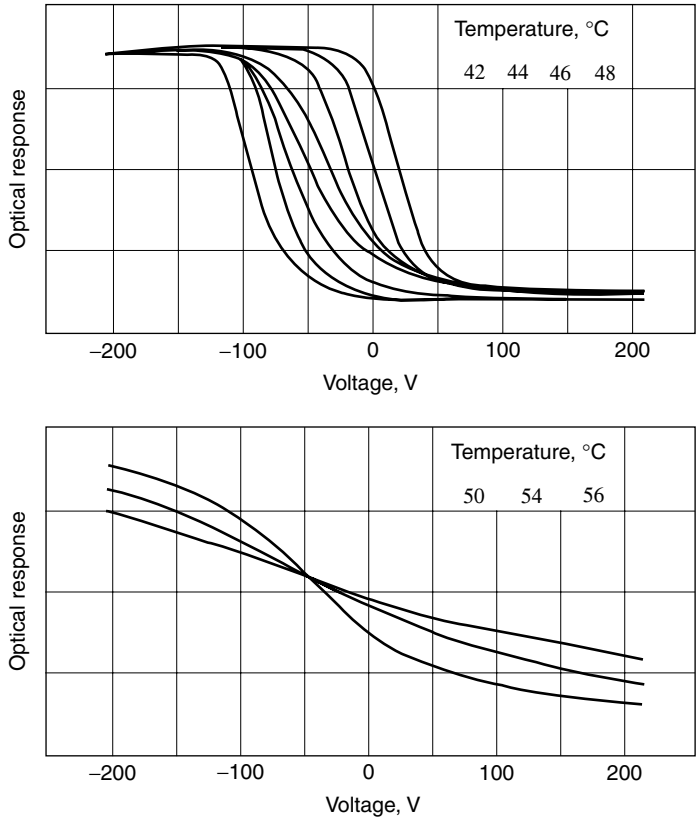

Fig. 10. Temperature dependence of the optical hysteresis of elastomer E2 (S_C* 49°C S_A) (15). (**a**) Ferroelectric behavior of the S_C* phase (42, 44, 46, and 48°C, respectively). (**b**) Electroclinic behavior of the S_A phase (50, 54, and 56°C, respectively).

high cross-linking densities, switching remains possible only if the spontaneous polarization is rather high (18). Otherwise, the network prohibits switching. The asymmetry of ferroelectric switching could also be proven by polarized ftir spectroscopy (37). Increasing the temperature of this ferroelectric elastomer leads to narrowing of the hysteretic loop, which is lost at the transition to the smectic A phase (see Fig. 10).

This behavior is best interpreted by plotting the liquid crystalline potential, the elastic potential of the network, and their superposition in one graph (16) (see Fig. 11). As the network is formed in the smectic C* phase, an internal elastic field is created, which has its minimum value for the tilt angle and tilt direction during cross-linking. Other tilt angles are destabilized.

The elastomer that has preferable intralayer cross-linking (E1, see Fig. 7) shows completely different behavior (see Fig. 12) (18,38). In this case, the switching time increases by less than a factor of 2, the polarization can still be determined, and measurement of the ferroelectric hysteresis shows no stabilization of the switching state present during cross-linking. Then, the coupling between the orientation of the mesogens and the network conformation is obviously very

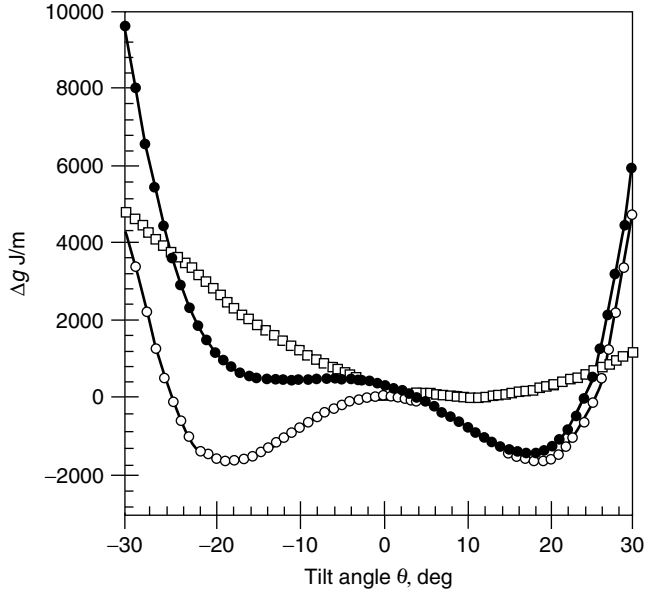

Fig. 11. Effect of network force on the free energy density (16) 2 K below the phase transition, S_C* phase: (○) calculated potential of the S_C*phase, (◇) force due to the network, and (●) superposition of both.

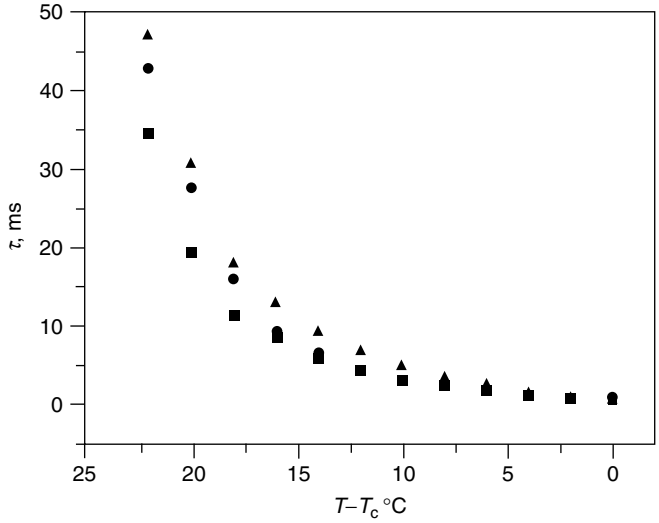

Fig. 12. Temperature dependence of the switching time τ (defined as 0–100% change in transmission) for P1 and E1 [see Ref. 18 for comparison].

weak. The network stabilizes the smectic layer structure, but it does not stabilize the tilt direction. Therefore, the polar axis can be switched easily. This is the result of the network topology (see Fig. 7) in which interlayer cross-linking is rare.

AFM Imaging of Thin Films. Freestanding films can be prepared from uncross-linked polymers (see also the smectic balloons in this context). They can be photocross-linked and transferred to a solid substrate. Thereafter, the topology of the films can be imaged by afm, which gives direct visualization of the smectic layer structure at low temperatures. The uncross-linked polymers can only be imaged at low temperatures, deep inside the smectic phase and in the tapping mode, which does not induce strong lateral forces. At higher temperatures, the sample is too soft and mobile to allow imaging. Cross-linked elastomers, on the other hand, are mechanically stable, and films sustain the tapping mode and also the contact mode of the atomic force microscope (39). This holds both for intra- and interlayer cross-linked systems. Because measurements can be done in all phases, it is also possible to determine the change of the smectic layer thickness at the phase transitions directly. For elastomer E1, for example, the smectic layer thickness is 4.2 nm in the smectic C$*$ phase (36°C, tilt angle about 30°). It increases to 4.4 nm at 50°C in the smectic A phase (39). This corresponds to x-ray measurements.

To analyze the impact of the molecular structure on network properties, elastomers are compared, which are identical except for the molecular position of the cross-linkable group: (*1*) elastomer E1 that has cross-linkable groups attached to the backbone via a short spacer (intralayer cross-linking) and (*2*) elastomer E2 where the cross-linkable group is in the terminal position of a mesogenic side group (interlayer cross-linking) (24,40). When mechanical stress (stretching) is imposed on thin films in homeotropic orientation, the two elastomers react differently to the deformation (24,40), as seen by afm imaging of the surface topology (see Fig. 13). For elastomer E1, "intralayer" cross-linking results in two-dimensional networks in the backbone layers, separated by liquid-like FLC side-group layers. Because there are practically no vertical connections in this intralayer network, no vertical distortions occur. Therefore, this elastomer can be stretched up to 100%, the surface remains smooth, and the layers deform affinely. In elastomer E2, a three-dimensional "interlayer" network is formed; the system reacts by distorting the smectic layering. Therefore, only smaller stretching ratios are accessible and the surface roughens and buckles during stretching. The distortion strength increases with a higher cross-linking density.

Piezoelectric Properties of Ferroelectric LC-Elastomers. Because a ferroelectric material has to be piezoelectric (see Fig. 1), observation of a piezoresponse is natural. It has been observed for ferroelectric LC-elastomers (3,16,19–21) and also for more densely cross-linked systems (10,31,41,42) for which no ferroelectric switching could be observed. For the elastomers described here it is, however, possible to change the piezoresponse (3) by reorienting the polar axis in an external field (see E2 in Fig. 14). For this experiment, the polar axis was kept in one orientation during cross-linking. This resulted in a positive piezoresponse (see Fig. 14). Thereafter, the direction of the polar axis was inverted by applying an external field of opposite direction. Then, the external field was removed and the piezocoefficient was measured. At first, a piezoresponse of opposite sign (negative) but identical value is determined (see Fig. 14). In the field-free state, this piezoresponse continuously decreases, it goes through zero, increases again, and finally reaches the original positive value. This experiment is comparable to the hysteresis measurements of Figs. 3 and 10 because it shows

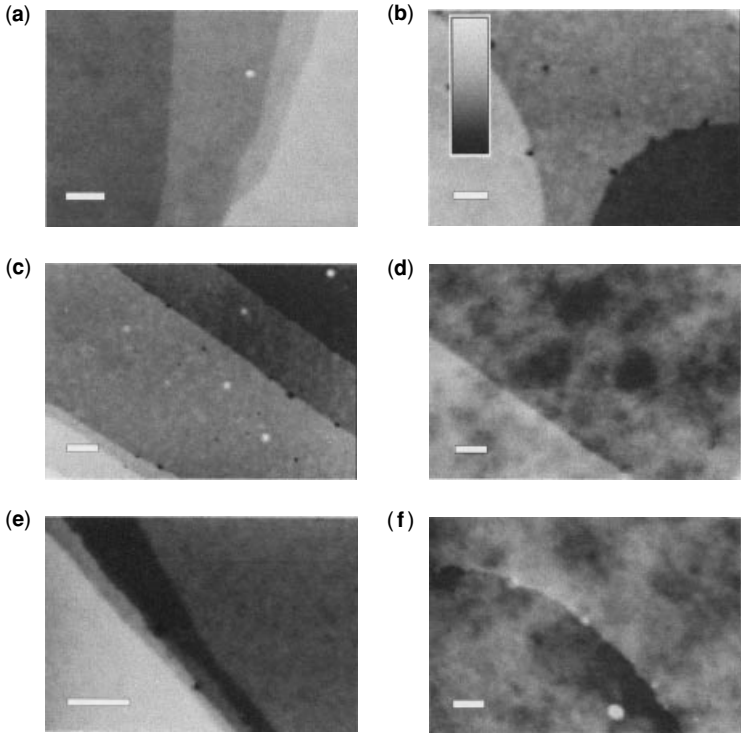

Fig. 13. Surface topography of prepared and stretched transferred films of elastomer $E1_{x=0.1}$ (**a**: $\lambda = 0$, **b**: $\lambda = 10\%$), $E2_{x=0.07}$ (**c**: $\lambda = 0$, **d**: $\lambda = 12\%$), and $E2_{x=0.25}$ (**e**: $\lambda = 0$, **f**: $\lambda = 2\%$,). Scale bars 1 μm, height scale 25 nm valid for all images. The surface of all polymers show plateau patterns. In the E2 samples, the lateral strain leads to surface deformation (40).

that two polar states are accessible, but the one present during cross-linking is stabilized.

The shape variation under application of an external electric field was most intensively studied for microtomized pieces of ferroelectric elastomers, which had been oriented by drawing (19–21). These experiments show only a small shape variation if the field is applied parallel to the polar axis of the monodomain. The effects become, on the other hand, rather large if the smectic layer structure (chevron texture) rearranges (19,21). To get a large electrostrictive response, which can be understood on a molecular level, the geometry presented in Fig. 15 was chosen (43). The application of an electric field parallel to a smectic layer leads to a tilt of the mesogens (electroclinic effect). Thereby, the thickness of the layer decreases. For a stack of layers, the effect sums up over all layers. As a result, the thickness perpendicular to the smectic layers decreases if a field is applied parallel to the layers (see Fig. 15). Because the electroclinic effect is relatively large in these polymers (16,37), a large variation in thickness is expected.

X-ray diffraction measurements prove the electrically induced shrinkage of single smectic layers. A freestanding ultrathin (75 nm) film of a ferroelectric liquid

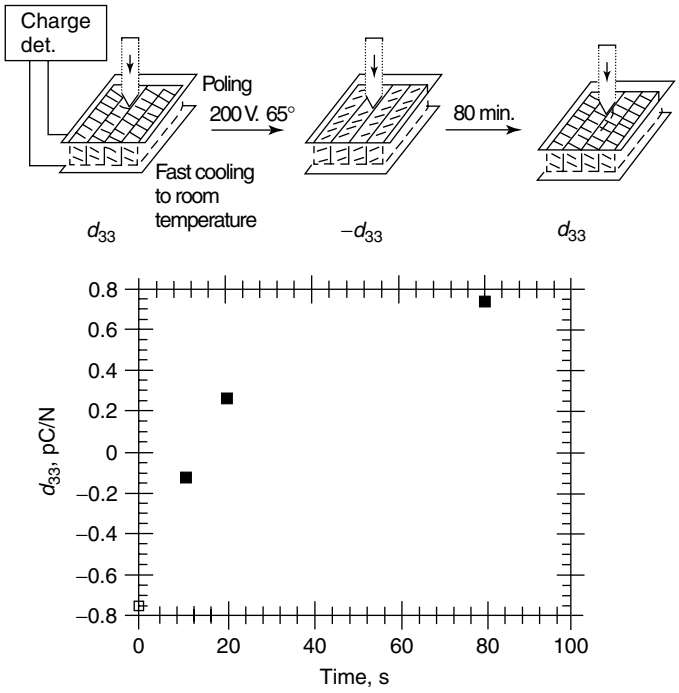

Fig. 14. Relaxation of the piezocoefficient d_{33} of elastomer E2 at room temperature after reversal poling at 65°C (S_A phase) (3).

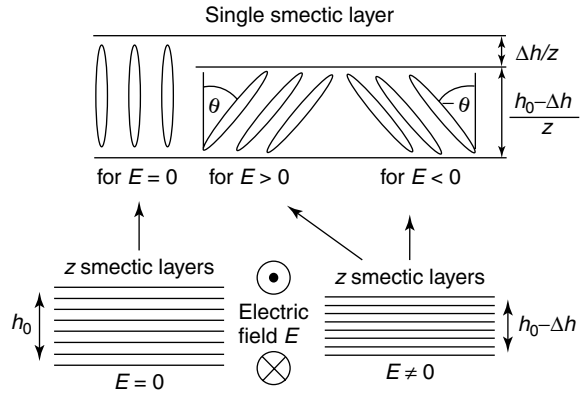

Fig. 15. In the S_A* phase, the mesogenic parts (depicted as ellipsoids) of the elastomeric macromolecule stand upright ($\theta = 0°$) inside the single smectic layers. By applying a lateral electric field (perpendicular to the plane of the paper), a tilt angle θ that is proportional to the electric field E can be induced (electroclinic effect). The sign of the tilt depends on the sign of the electric field E. Hence, each smectic layer shrinks by $\Delta h/z$ twice during one period of the electric field. The shrinkage Δh of the whole film is measured by the interferometer as an optical phase shift between the sample beam and the reference beam.

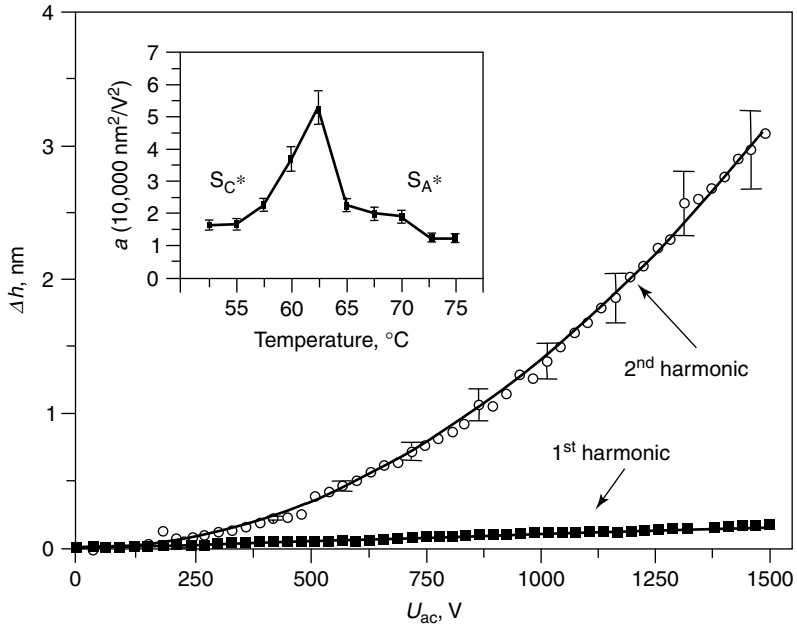

Fig. 16. Electrostriction of a ferroelectric LC-elastomer (43). Big diagram: Thickness variation Δh as a function of the applied ac voltage U_{ac}. Interferometric data were obtained at the fundamental frequency of the electric field (piezoelectricity, first harmonic: +) and at twice the frequency (electrostriction, second harmonic: ○). Sample temperature: 60°C. Inset: Electrostrictive coefficient a (+) versus temperature. At the temperature where the non-cross-linked polymer would have its phase transition S_C*–S_A* (about 62.5°C), the tilt angle of 0° is unstable. That is why the electroclinic effect is most effective at this temperature. An electric field of only 1.5 MV/m is sufficient to induce lateral strains of more than 4%.

crystalline elastomer (similiar to E2) was used to measure the shape variation (electrostrictive response) associated with this (43). It was measured by a high precision (±3 pm at 133 Hz) Michelson interferometer. The measurements (see Fig. 16) exhibit extremely high electrostrictive strains of 4% in an electric field of only 1.5 MV/m, which is, to our knowledge, a new world record for the corresponding electrostrictive coefficient a. The effect exhibits typical electroclinic behavior, which means that it is caused by an electrically induced tilt of the chiral LC molecules. As a consequence of chirality, the primary strain is perpendicular to the applied field. Hence, a new material that has a giant electrostriction effect is introduced, where the effect can be fully understood on a molecular level.

BIBLIOGRAPHY

1. M. G. Broadhurst and G. T. Davis, in P. M. Galetti, D. E. De Rossi, and A. S. De Reggi, eds., *Medical Applications of Piezoelectric Polymers*, Gordon and Breach, Amsterdam, 1988, pp. 3–14.

2. J. W. Goodby and co-workers, *Ferroelectric Liquid Crystals, Principles, Properties and Applications, Ferroelectricity and Related Phenomena*, Gordon and Breach, Philadelphia, 1991.
3. M. Brehmer and co-workers, *Macromol. Chem. Phys.* **195**, 1891–1904 (1994).
4. R. Zentel, *Angew. Chem.* **101**, 1437–1445 (1989).
5. M. Brehmer and R. Zentel, *Mol. Cryst. Liq. Cryst.* **243**, 353–376 (1994).
6. F. J. Davis, *J. Mater. Chem.* **3**, 551–562 (1993).
7. W. Gleim and H. Finkelmann, in C. B. McArdle, ed., *Side Chain Liquid Crystalline Polymers*, Blackie and Son, Glasgow, 1989.
8. H. Finkelmann, in A. Ciferri, ed., *Liquid Crystallinity in Polymers*, VCH, Weinheim, 1991.
9. R. A. M. Hikmet, H. M. Boots, and M. Michielsen, *Liq. Cryst.* **19**, 65–76 (1995).
10. R. A. M. Hikmet and J. Lub, *Prog. Polym. Sci.* **21**, 1165–1209 (1996).
11. A. Hult and co-workers, *Liq. Cryst.* **20**, 23–28 (1996).
12. R. A. M. Hikmet and H. Kempermann, *Nature* **392**, 476–478 (1998).
13. G. C. L. Wong and co-workers, *Nature* **389**, 576–579 (1997).
14. R. Zentel, *Liq. Cryst.* **1**, 589 (1986).
15. N. R. Barnes, F. J. Davis, and G. R. Mitchell, *Mol. Cryst. Liq. Cryst.* **13**, 168 (1989).
16. M. Brehmer and co-workers, *Liq. Cryst.* **21**, 589–596 (1996).
17. E. Gebhard and co-workers, in K. te Nijenhuis and W. J. Mijs, eds., The Wiley Polymer Networks Group Review Series, Vol. **1**, *Chemical and Physical Networks*, Wiley, Chichester, 1998, pp. 387–397.
18. E. Gebhard and R. Zentel, *Macromol. Chem. Phys.* **201**, 902–922 (2000).
19. F. Kremer and co-workers, *Polym. Adv. Technol.* **9**, 672–676 (1998).
20. W. Lehmann and co-workers, *Ferroelectrics* **208**, 373–383 (1998).
21. W. Lehmann and co-workers, *J. Appl. Phys.* **86**, 1647–1652 (1999).
22. H. Poths and R. Zentel, *Liq. Cryst.* **16**, 749–767 (1994).
23. L.-C. Chien and L. G. Cada, *Macromolecules* **27**, 3721 (1994).
24. H. M. Brodowsky and co-workers, *Langmuir* **15**, 274–278 (1999).
25. H. Schüring and co-workers, *Macromolecules* **34**, 3962–3972 (2001).
26. H. Poths and co-workers, *Liq. Cryst.* **18**, 811–818 (1995).
27. A. Kocot and co-workers, *Phys. Rev. B* **50**, 16346–16357 (1994).
28. R. Stannarius and C. Cramer, *Europhys. Lett.* **42**, 43 (1998).
29. J. Küpfer and H. Finkelmann, *Macromol. Chem. Phys.* **195**, 1353–1367 (1994).
30. K.-H. Hanus and co-workers, *Polym. Prepr.* **30**, 493 (1989).
31. I. Benné, K. Semmler, and H. Finkelmann, *Macromolecules* **28**, 1854–1858 (1995).
32. E. Nishikawa, H. Finkelmann, and H.-R. Brand, *Macromol. Rapid Commun.* **18**, 65 (1997).
33. J. Kundler and H. Finkelmann, *Macromol. Chem. Phys.* **199**, 677–686 (1998).
34. E. Nishikawa and H. Finkelmann, *Macromol. Chem. Phys.* **200**, 312–322 (1999).
35. R. Zentel and co-workers, *Makromol. Chem.* **190**, 2869 (1989).
36. L. R. G. Treloar, *The Physics of Rubber Elasticity*, Clarendon, Oxford, 1975.
37. S. Shilov and co-workers, *Macromolecules* **32**, 1570–1575 (1999).
38. M. Brehmer and R. Zentel, *Macromol. Chem., Rapid Commun.* **16**, 659–662 (1995).
39. H. M. Brodowsky and co-workers, *Langmuir* **13**, 5378–5382 (1997).
40. H. M. Brodowsky and co-workers, *Ferroelectrics* **243**, 115–123 (2000).

41. M. Mauzac and co-workers, *Chem. Phys. Lett.* **240**, 461 (1995).
42. S. U. Vallerien and co-workers, *Makromol. Chem., Rapid Commun.* **11**, 593 (1990).
43. W. Lehmann and co-workers, *Nature* **410**, 447–450 (2001).
44. J. Zhao and co-workers, *Jpn. J. Appl. Phys.* **34**, 5658 (1995).
45. T. Jaworek and co-workers, *Science* **279**, 57 (1998).

RUDOLF ZENTEL
University of Mainz

FIBERS, ELASTOMERIC

Introduction

Elastomeric fibers can be made from natural or synthetic polymeric materials that provide a product with high elongation, low modulus, and good recovery from stretching. Currently, these fibers are made primarily from polyisoprenes (natural rubber) or segmented polyurethanes, and to a lesser extent from segmented polyesters. In the United States the generic designation "spandex" has been given to a manufactured fiber in which the fiber-forming substance is a long-chain synthetic polymer consisting of at least 85% of a segmented polyurethane (1); in Europe the equivalent term "elastane" is commonly used.

The experimental production of elastomeric fibers based on segmented polyurethanes (qv) was first reported in the early 1950s by Farbenfabriken Bayer, a pioneer in urethane and diisocyanate chemistry (2,3). This was followed by semicommercial-scale production of polyurethane-based fibers by DuPont, in the late 1950s (4,5). Prior to development of the polyurethanes, most elastomeric fibers were made with natural rubber. Two processes were used: slitting rubber sheets to produce cut-rubber threads or extruding rubber latex into an acid coagulation bath, followed by washing, drying, and curing. Smaller amounts of cut-rubber threads have also been produced from synthetics such as neoprene and nitrile rubbers, especially where improved solvent resistance is required. Fiber cross sections are square or rectangular for cut rubbers and essentially round for extruded latex threads.

Thermoplastic, inelastic fibers, such as nylon and polyester, may be processed to provide spring-like, helical, or zigzag structures. These fibers can exhibit high elongations as the helical or zigzag structure is stretched, but the recovery force is very low. This apparent elasticity results from the geometric form of the filaments

Encyclopedia of Polymer Science and Technology. Copyright John Wiley & Sons, Inc. All rights reserved.

as opposed to elastomeric fibers whose elastic properties depend primarily on entropy changes inherent within their polymer structure. Thus processed inelastic fibers must comprise a significant portion of a stretch fabric whereas an elastomeric fiber provides the necessary stretch properties at 5–20% of fabric weight.

Other elastomeric-type fibers include the biconstituents, which usually combine a polyamide or polyester with a segmented polyurethane-based fiber. These two constituents are melt-extruded simultaneously through the same spinnerette hole and may be arranged either side by side or in an eccentric sheath–core configuration. As these fibers are drawn, a differential shrinkage of the two components develops to produce a helical fiber configuration with elastic properties. An applied tensile force pulls out the helix and is resisted by the elastomeric component. Kanebo Ltd. has introduced a nylon–spandex sheath–core biconstituent fiber for hosiery, with the trade name Sideria (6).

Nonspandex elastomeric fibers are based on segmented polyesters; the fibers produced can be melt-spun into threads (7). The generic name for these fibers has been designated as "elastoesters" by the Federal Trade Commission because even though they are similar to polyester fibers chemically, they are physically different enough to warrant a new name. Teijin Ltd. produces an elastomeric fiber of this type with the trade name Rexe (see also POLYESTERS, FIBERS).

Chemical Composition

Rubber. Natural rubber, *cis*-1,4-polyisoprene [104389-31-3], itself is not elastomeric, but is converted into an elastomer for elastomeric fibers by blending the polymer with sulfur, and curing the material at an elevated temperature to promote vulcanization (see RUBBERS NATURAL). Prior to heat treatment the polymer mixture is either cast into a film and the final product is slit into rectangular threads, or the polymer mixture is extruded through a capillary to form a round rubber fiber. The molecular weight of the polymer between cross-links is of the order of 3000–10,000. The *cis*-1,4-polyisoprene chains are flexible and highly mobile because of the ease of rotation of the four-carbon unit in the polymer molecules. The chains are randomly oriented in the relaxed state at room temperature. The force required to stretch the fiber initally is very low, but at higher extensions the chains begin to crystallize, increasing the modulus and breaking strength of the fiber. Stretch-induced crystallization is an important property for elastomeric materials so that they may survive textile processing and wear without breaking. If the material is stretched to an extension below its breaking point, elastomeric fibers have the ability to return to their original unstretched dimension. After the stretching force is removed the covalent cross-links in the rubber thread and the mobility of the polymer chains are responsible for returning the stretched fiber to its original dimension.

Rubber threads are susceptible to oxidative degradation, and high concentrations of antioxidants are added to the mixture to make the high surface area fibers more resistant. Pigments, such as titanium dioxide, are used as fillers or to impart whiteness to the thread. Carbon black reinforcement is used in colored rubber materials. Other agents include accelerators and activators to promote the vulcanization process. With all the additives, a typical high grade rubber thread contains less than 85% elastomer.

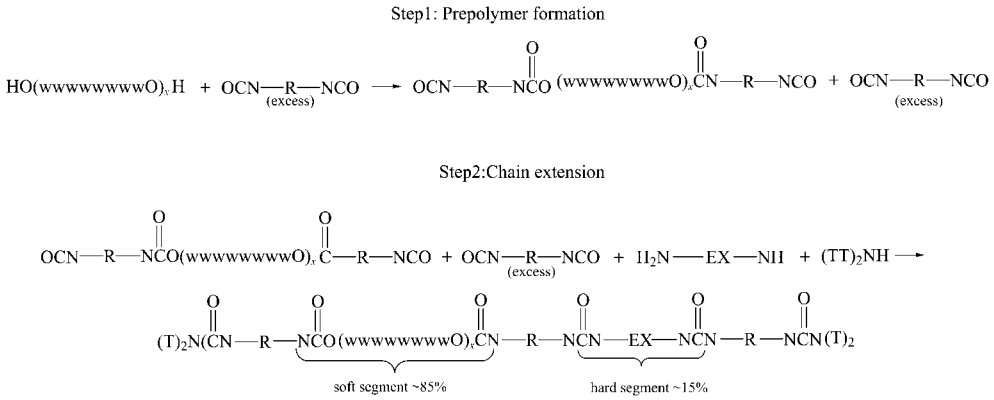

Fig. 1. Two-step synthesis of spandex polymer.

Synthetic rubber threads can also be produced, but do not have the same elastomeric properties as natural rubber because the polymer chains are less mobile and do not crystallize at high elongations. They are used in applications which require solvent resistance.

Spandex. Elastomers made for spandex fibers are segmented block copolymers that consist of a flexible "soft" segment made of long polyether or polyester sections that are liquid at the use temperature and therefore flow past each other and allow the fiber to stretch, and rigid "hard" segments that hydrogen bond between polymer chains to provide recovery after stretching back to the fiber's original dimension. The elastomer is made in a two-step reaction (Fig. 1), in which a prepolymer is made by reacting each end of the bifunctional macroglycol of 1000–4000 molecular weight with an excess of diisocyanate molecules to form an isocyanate-terminated prepolymer. The soft segment macroglycol can be either a polyether, a polyester, a polycarbonate, hydroxyl-terminated polycaprolactone, or a combination of these. Urethane groups are formed by the reaction of each end of the glycol polymers with one end of the diisocyante molecule. In the second step of polymerization, the rigid small diamine or diol molecules react both with the excess diisocyanate molecules and with the isocyanate ends of the prepolymer to extend the polymer chain into an elastomeric polymer. Urea groups are formed by the reaction of each isocyanate group and amine end. The molecular weight of the polymer is controlled by a monofunctional secondary amine molecule to give molecular weight of the order of 50,000–100,000. The general formula can be written as shown in Figure 1.

The long soft segment makes up between 80- and 85% of the polymer weight. For the fiber to be elastomeric the soft segment material must be a liquid at room temperature in order for these segments of the chain to be mobile and allow the yarn to be easily stretched. The other 15–20% of the polymer weight is made up of the rigid hard segment material. The urea groups in the hard segment can interact with one another by hydrogen bonding to form a psuedo crosslink. This is one of the most important characteristics of a spandex polymer for the balance of properties and processing advantages.

Because the polymer chains do not need to undergo a cross-linking step prior to spinning, the fibers can be made by economical solution or melt-spinning

methods. The cross-linking step required in conventional rubber processing is eliminated with a spandex polymer. The majority of the hydrogen bonding then occurs in the spinning cell. With fiber formation, hard segments from several chains associate into strongly bonded cluster domains which aggregate and convert the polymer to a phase-separated, three-dimensional network (8). Each phase has a different glass-transition temperature. The "tie points" allow the soft segments of the chains to slide past one another to a limit determined by the hard segment resistance. A liquid soft segment at the temperature the yarn will be used, and interacted/cross-linked chains are necessary characteristics of a synthetic spandex polymer.

Interchain bonding must be not only strong enough to prevent molecular slippage, but also concentrated so that the connecting soft segments can comprise a large fraction of the polymer chain. This result in high stretch along with low modulus. Urea hard segments that comprise less than 25% of polymer mass provide this needed concentrated bonding force. In contrast, the network structure in rubber depends on covalent bonds between chain molecules that result from vulcanization with sulfur. In both polyurethanes and rubber, modulus is directly related to tie-point density. Similarly, the relationship for maximum elongation is an inverse function of tie-point density. In rubber fibers, tie-point density is controlled by the amount of vulcanizing agent, accelerant, and reaction conditions. In polyurethanes, tie-point (hard segment) density is controlled by the soft segment molecular weight and the molar ratio used to prepare the glycol–diisocyanate prepolymer.

Mechanical Properties

In both rubber thread and spandex fibers, mechanical properties may be varied over a relatively broad range. In rubber, variations are made in the degree of cross-linking or vulcanization by changing the amount of vulcanizing agent, usually sulfur, and the accelerants used. In spandex fibers, many more possibilities for variation are available and there are a large number of polymers in the classification. Mechanical properties (qv) may be affected by changing the particular polyester or polyether glycol, diisocyanate, diamine(s), and monoamine used; they can be further modified by changing the molecular weight of the glycol and by changing the glycol–diisocyanate molar ratio (9,10).

The physical characteristics of current commercial rubber and spandex fibers are summarized in Table 1. Typical stress–strain curves for elastomeric fibers, hard fibers, and hard fibers with mechanical stretch properties are compared in Figure 2.

Manufacture

To produce cut-rubber thread, smoked rubber sheet or crepe rubber is milled with vulcanizing agents, stabilizers, and pigments. This milled stock is calendered into sheets of 0.3–1.3-mm thickness, depending on the final size of the rubber thread desired. Multiple sheets are layered, heat-treated to vulcanize, and then slit into

Table 1. Physical Properties of Elastomeric Fibers

Property	Spandex	Extruded rubber	Cut rubber
Sizes available[a]	1.1–250 tex[b]	16–610 tex[b]	2.5–21 μm dia[c]
Tenacity, N/tex[d]	0.05–0.13	0.02–0.03	0.01–0.02
Elongation, %	400–800	600–700	600–700
Modulus,[e] N/tex[d]	0.013–0.045	0.004–0.005	0.002–0.004
Stability[f]			
UV light	Good	Fair	Fair
Ozone	Good	Poor	Poor
NO_x	Fair, yellows	Poor	Poor
Active Cl	Fair, yellows	Poor	Poor
Body oils	Fair	Poor	Poor
Cosmetics	Good	Fair	Fair
Dyeability	Dyeable	Not dyeable	Not dyeable
Abrasion resistance	Very good	Poor	Poor

[a]Spandex size is usually expressed in denier which is weight in g/9000 m length. However, the SI unit is tex, the weight in g/1000 m. Rubber size is expressed as gauge, which is the reciprocal of diameter or size in inches.
[b]To convert tex to den, multiply by 9.09.
[c]1200–10,000 gauge.
[d]To convert N/tex to g·f/den, multiply by 11.33.
[e]First cycle stress at 300% elongation.
[f]Both spandex fibers and rubber threads normally contain antioxidants and other stabilizers.

threads for textile uses (Fig. 3). Individual threads have either square or rectangular cross sections.

In the manufacture of extruded latex thread, a concentrated (up to ca 50% solids) natural rubber latex is blended with aqueous dispersions of vulcanizing agents, stabilizers, and white pigments. This compounded latex is held under controlled temperature conditions until partial vulcanization occurs. This has the effect of increasing wet strength and thus the processibility of the extruded threads. The matured latex is extruded at constant pressure through precision-bore glass capillaries into a 15–55% acetic acid [64-19-7] bath where coagulation into thread form occurs. Threads are removed from the coagulation bath by transfer rollers, washed free of excess acid with water, and conducted through a dryer, after which a silicone oil-based finish is applied and the threads are formed into multiend ribbons. The ribbons are then vulcanized by multiple passes on a conveyer belt through an oven that can increase curing temperature in stages up to about 150°C. After vulcanization the multiend ribbons are packed without support in boxes for shipment to the customer. A typical extruded latex thread production line is shown in Figure 4. Latex thread production rates vary with thread size and equipment but, owing to hydrodynamic drag and the weak nature of the coagulating thread, maximum line take-up speeds are about 30 m/min.

Four different processes are currently used to produce spandex fibers commercially: melt extrusion, reaction spinning, solution dry spinning, and solution wet spinning. As shown in Figure 5, these processes involve different practical applications of basically similar chemistry. If the diol or diamine(s) reaction with the prepolymer is carried out in a solvent, the resulting block copolymer solution may

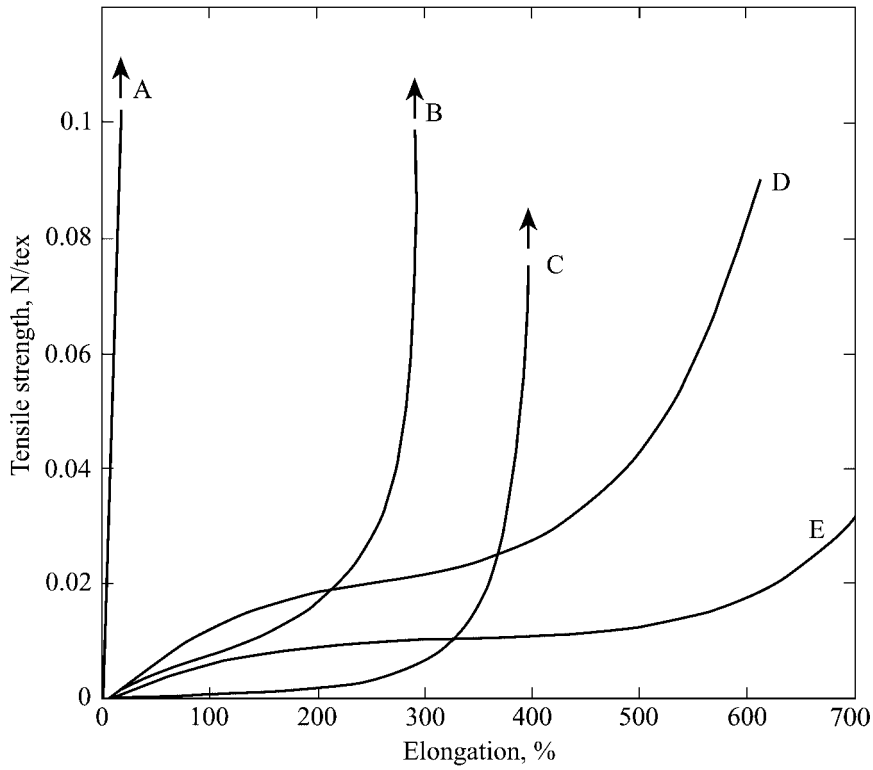

Fig. 2. Stress–strain curves: A, hard fiber, eg, nylon; B, biconstituent nylon–spandex fiber; C, mechanical stretch nylon; D, spandex fiber; E, extruded latex thread. To convert N/tex to g·f/den, multiply by 11.33.

be wet- or dry-spun into fiber. Alternatively, the prepolymer may be reaction-spun by extrusion into a bath containing diamine to form a fiber, or the prepolymer may be permitted to react in bulk with a diol and the resulting polymer melt-extruded in fiber form.

Currently, the principal producer of melt-spun spandex fibers is Far Eastern Textile, Ltd., in Taiwan. However, melt-spun spandex fibers are also produced by Nisshinbo Industries, Inc., and Kanebo Goshen, Ltd., both in Japan. Because of thermal stability constraints, only polymers that contain all urethane hard segments (glycol extended) can be melt-extruded. The intermolecular association between all urethane hard segments is inherently weaker compared with urea-based hard segments produced from diamine extenders; melt-spun fibers are normally made at higher diisocyanate–glycol ratios which in effect produce a relatively longer hard segment to compensate for the weaker intermolecular bonding forces.

More recently, melt-spun biconstituent sheath–core elastic fibers have been commercialized. They normally consist of a hard fiber sheath (polyamide or polyester) along with a segmented polyurethane core polymer (11,12). Kanebo Ltd. in Japan currently produces a biconstituent fiber for hosiery end uses, called Sideria.

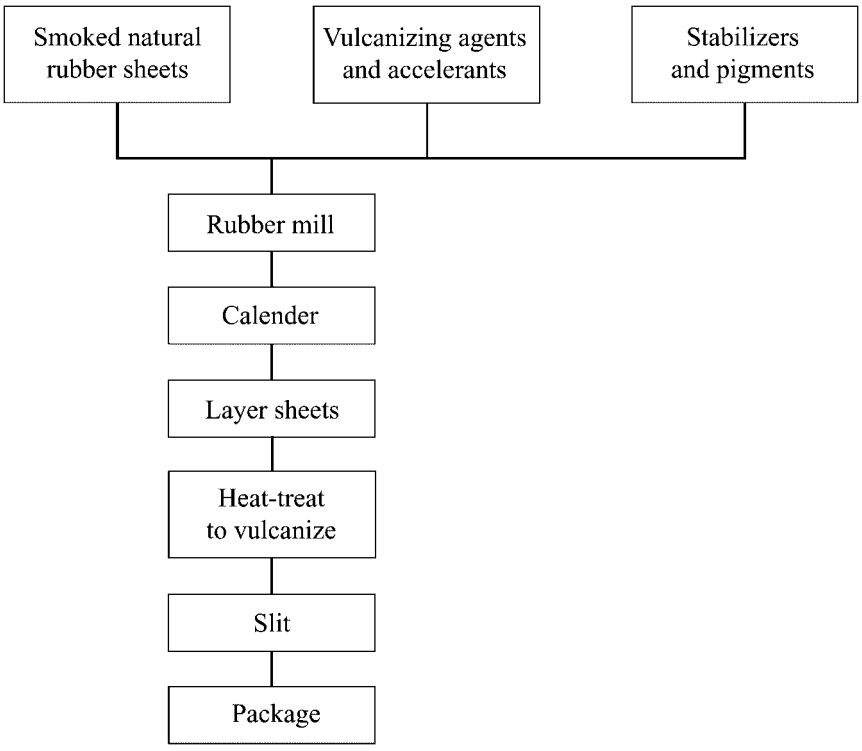

Fig. 3. Cut-rubber thread manufacture.

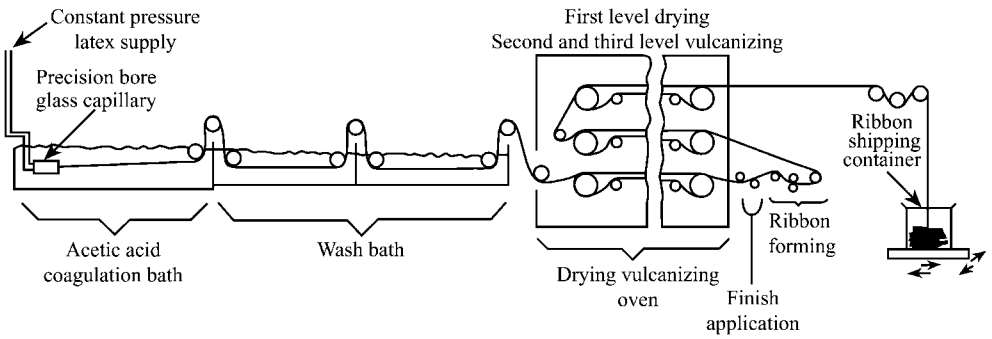

Fig. 4. Extruded latex thread production.

Several commercial spandex fibers were produced by reaction spinning in the 1950s by Globe Manufacturing Co. (13). This was the only producer of reaction-spun spandex fibers. Recently Radicci Spandex Corp. acquired Globe Manufacturing and its assests. Reaction-spun fibers include only products 7.7 tex (70 den) or higher; finer Radicci spandex fibers are dry-spun.

To produce a spandex fiber by reaction spinning, a 1000–3500 molecular weight polyester or polyether glycol reacts with a diisocyanate at a molar ratio of about 1:2. The viscosity of this isocyanate-terminated prepolymer may be adjusted

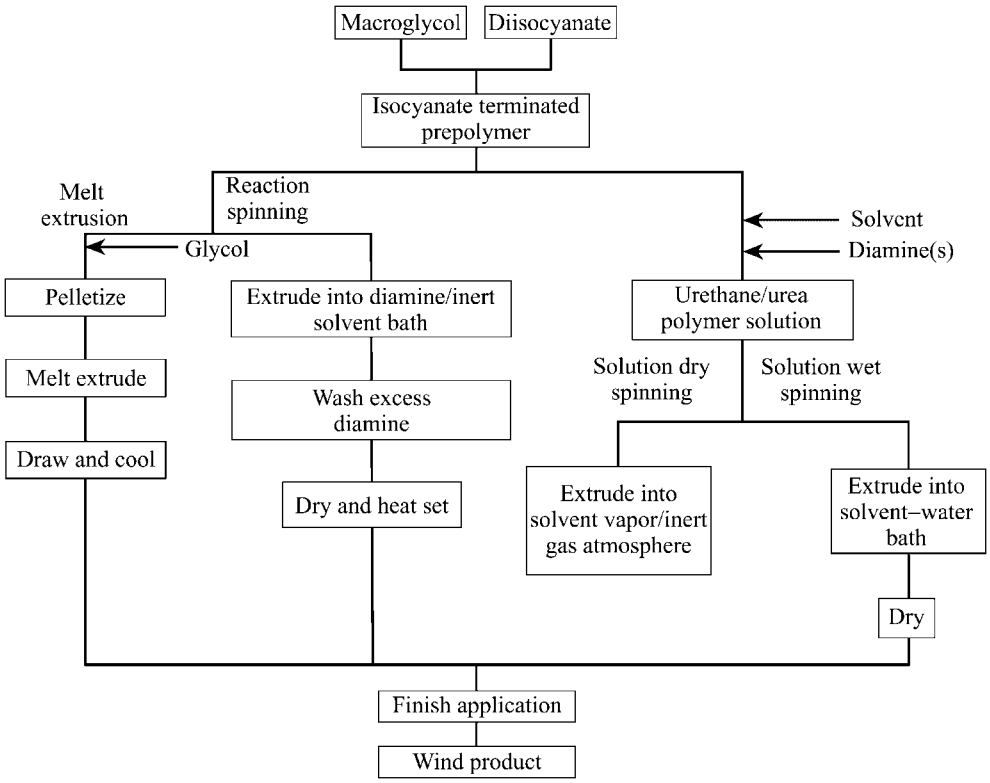

Fig. 5. Spandex fiber production methods.

by adding small amounts of an inert solvent, and then extruded into a coagulating bath that contains a diamine so that filament and polymer formation occurs simultaneously. Reactions are completed as the filaments are cured and solvent evaporated on a belt dryer. After application of a finish, the fibers are wound on tubes or bobbins and rewound if necessary to reduce interfiber cohesion.

Trifunctional hydroxy compounds, eg, glycerol [56-81-5] or 2-ethyl-2-(hydroxymethyl)-1,3-propanediol [787-99-6], may be added with the macroglycol to produce covalent cross-links in the reaction-spun spandex fiber. Also, covalent cross-links may result from allophanate and/or biuret formation during curing by reaction of free isocyanate end groups with urethane or urea —NH groups along the polymer chain. A multiplicity of filaments are normally extruded from each spinnerette of about 1.1–3.3 tex (10–30 den), and then collected in bundles of the desired tex at the exit of the reaction bath. This approach makes the surface area-to-mass ratio and diamine diffusion into the prepolymer cross section substantially constant irrespective of the final tex produced, thus minimizing condition changes required in changing tex. Because the individual filaments have reacted incompletely and are in a semiplastic state at the exit of the diamine bath, they interbond quite tightly into a fused multifilament. Production speeds in reaction spinning are limited by filament weakness in the bath along with hydrodynamic drag. Take-up speeds are limited to about 100 m/min.

Stabilizers and pigments are normally slurried with macroglycol and added to the polymeric glycol charge, prior to diisocyanate addition. Therefore, care must be taken to avoid additives that react significantly with diisocyanates or diamines under processing conditions. Also, stabilizers should be chosen that have no adverse catalytic effect on the prepolymer or chain-extension reactions.

Reaction-spinning equipment is quite similar to that of solution wet spinning. It differs principally in the use of fewer wash baths and in the use of belt-type dryers instead of heated cans.

The initial step to prepare polyurethane polymers for solution wet or dry spinning includes reaction of 1000–3500 molecular weight macroglycol with a diisocyanate at molar ratios of between about 1:1.4 and 1:2.0. Reaction conditions must be carefully selected and controlled to minimize side reactions, eg, allophanate and biuret formation, which can result in trifunctional branched chains and ultimately to insoluble cross-linked polymers. For the prepolymer reaction, poly(tetramethylene ether) glycol [25190-06-1] and bis(4-isocyanatophenyl) methane [101-68-8] are currently the most commonly used macroglycol and diisocyanate. Several types of polyester-based macroglycols are included in spandex producers product lines, but with the exception of Dorlastan, made by Bayer AG in Germany, the polyester-based products represent only a minor part of their spandex fiber production.

In the polymerization reaction, called chain extension, the prepolymer is dissolved in a solvent and reacts with diamine(s) to form a urethane–urea polymer in solution. In all commercial processes, the solvent used is either *N*,*N*-dimethylformamide [68-12-2] or *N*,*N*-dimethylacetamide [127-19-5]. Normally, one or two diamines are used as chain extenders. Because the reaction of diamine with diisocyanate is exceedingly rapid, prepolymer is normally diluted with solvent so that mixing in the polymer reactor is optimized. An improved mixing and chain-extension process has been described, whereby the solvent-diluted prepolymer is separated into two groups with chain extension being initiated by reaction of diamine solution with one of these groups, after which the prepolymer of the other group is mixed in and chain extension is completed (14). Molecular weights of polymers made in solution can be controlled by adding small amounts of a secondary monoamine to provide dialkylurea end groups. Branching reactions must be minimized in order to obtain a stable polymer solution for spinning. Stoichiometry of polymerization is normally adjusted to provide a urethane polymer solution of 20–40% solids and viscosity of 100–200 Pa·s (1000–2000 P). The viscosities and solids of solutions for dry spinning are generally higher than those used for wet spinning.

Stabilizers, pigments, and other additives (qv) are milled in spinning solvent, normally along with small amounts of the urethane polymer to improve dispersion stability; this dispersion is then blended to the desired concentration with polymer solution after chain extension. Most producers combine prepolymerization, chain extension, and additive addition and blending into a single integrated continuous production line.

On a worldwide basis, greater than 90% of all spandex fibers are produced by various adaptations of dry-spinning (15,16). The solution dry-spinning process is illustrated in Figure 6. The polymer spinning solution is metered at a constant

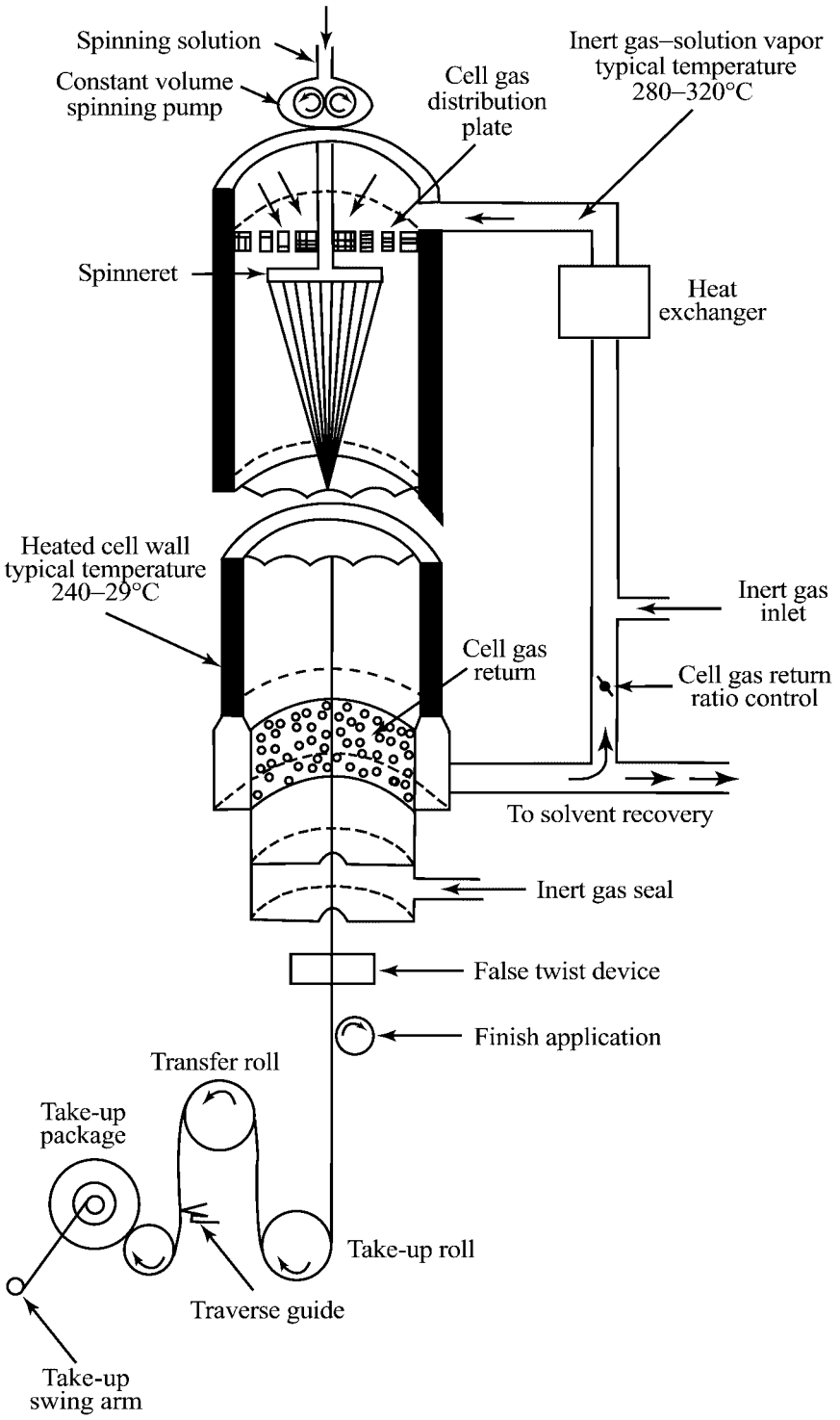

Fig. 6. Spandex production, solution dry-spinning process.

temperature by a precision gear pump through a spinnerette into a cylindrical spinning cell 3–8 m in length. Heated cell gas, made up of solvent vapor and an inert gas, normally nitrogen, is introduced at the top of the cell and passed through a distribution plate behind the spinnerette pack. Because both cell gas and cell walls are maintained at high temperatures, solvent evaporates rapidly from the filaments as they travel down the spinning cell. The spinning solvent is then condensed from the cell gases, purified by distillation, and returned for reuse. Individual filament size is normally maintained in the range of 0.6–1.7 tex (5–15 den) to maximize, within operable limits, surface area-to-mass ratio and solvent removal rate. Individual filaments are grouped into bundles of the desired final tex at the exit of the spinning cell by a coalescence guide. A commonly used guide employs compressed air to create a minivortex which imparts a false twist and rounded cross section to the filament bundle. Solution dry-spun spandex fibers are normally referred to as continuous multifilaments or coalesced multifilaments. However, the individual filaments do not coalesce into larger structures but remain discrete; they adhere to one another because of natural elastomer tack at their surface.

After coalescence, a finish is applied to the multifilament bundle before it is wound onto a tube. Commonly used finishing agents include polydimethylsiloxane [9016-00-6] (17) and magnesium stearate [557-04-0] (18) which provide lubrication for textile processing and prevent fibers from sticking together on the package. Windup speeds are in the range of 300–500 m/min, depending on tex and producer.

Any urethane–urea polymer that can be dry-spun may also be wet-spun; however, the productivity constraints of wet-spun processes have limited their utility. A typical wet-spinning process line is shown in Figure 7. Spinning solution is pumped by precision gear pumps through spinnerettes into a solvent–water coagulation bath. As with dry spinning, individual filament size is maintained at about 0.6–1.7 tex (5–15 den) in order to optimize solvent removal rates. At the exit of the coagulation bath, filaments are collected in bundles of the desired tex. A false twist may be imposed at the bath exit to give the multifilament bundles a more rounded cross section. After the coagulation bath, the multifilament bundles are countercurrently washed in successive extraction baths to remove residual solvent, then dried and heat-relaxed, generally on heated cans. Finally, as in dry

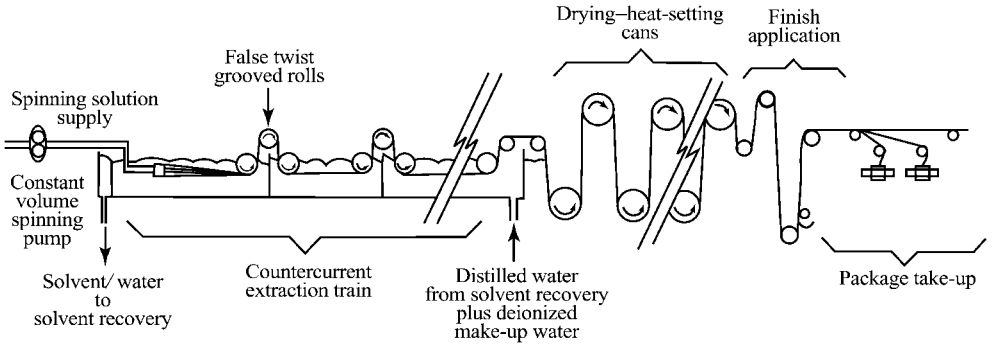

Fig. 7. Spandex production, solution wet-spinning process.

spinning, a finish is applied and the multifilaments wound on individual tubes. A typical spinning line may produce 100–300 multifilaments at side-by-side filament spacings of less than 5 mm.

Water is continuously added to the last extraction bath and flows countercurrently to filament from bath to bath. Maximum solvent concentration of 15–30% is reached in the coagulation bath and maintained constant by continuously removing the solvent–water mixture for solvent recovery. Spinning solvent is generally recovered by a two-stage process in which the excess water is initially removed by distillation followed by transfer of crude solvent to a second column where it is distilled and transferred for reuse in polymer manufacture.

In wet-spinning processes, spinning speeds are limited to about 100–150 m/min by hydrodynamic drag of the bath medium. It is this limitation that has apparently caused most spandex fiber producers to have chosen dry-spinning techniques. However, this limitation has been minimized by subjecting the spandex filament to drawing as much as three to four times after the spinning bath (19,20). Temperatures and residence times are selected so that the filaments are brought to temperatures above their second-order transition points, ie, the hard segment melting points. This allows the molecular chains to move freely to relieve stresses and results in filaments of fine tex but with similar mechanical properties as the heavier tex feed. Thus it is possible to windup fibers from a wet-spinning process at speeds in excess of 300 m/min by continuously drawing and heat-relaxing the filaments after drying.

Chemical Properties

Both rubber and spandex fibers are subject to oxidative attack by heat, light, atmospheric contaminants such as NO_x, and active chlorine. Rubber is especially subject to oxidative degradation from exposure to ozone whereas urethane polymers are relatively inert. Both rubber and spandex fibers are likely to contain antioxidants; the spandex fibers may also be stabilized to uv light and to atmospheric contaminants that cause discoloration. Spandex fibers use a variety of monomeric and polymeric hindered phenolic-type antioxidants (qv). Many spandex fibers also include uv screeners based on hydroxybenzotriazoles (see ANTIOXIDANTS; UV STABILIZERS). Several producers include the more recently developed hindered amine-type light stabilizers (21) that apparently act as radical scavengers and therefore also possess antioxidant activity. Compounds with tertiary amine functionality are commonly added to spandex fibers to inhibit discoloration from atmospheric pollutants such as oxides of nitrogen and chemicals that develop under smog-like conditions. Spandex producers have been designing stabilizers that are highly compatible with the segmented urethane polymer to enhance their effectiveness and durability (22–24). Spandex fibers based on polyester soft segments are susceptible to mildew attack in end uses such as swimwear; this type of degradation is minimized by either using antimildew additives or by soft segment structural modifications (25).

Elastomeric fibers tend to swell in certain organic solvents; rubber fibers swell in hydrocarbon solvents such as hexane. Spandex fibers become

highly swollen in chlorinated solvents such as tetrachloroethylene [127-18-4] (Perclene). Although the physical properties of spandex fibers return to normal after the solvent evaporates, considerable amounts of its stabilizers may have been extracted. Therefore, the development of stabilizers that are more resistant to solvent extraction has become important as solvent scouring during mill processing replaces aqueous scouring at many mills, especially in Europe (26).

Spandex fibers have an affinity for dispersed or acid dyes; rubber fibers normally cannot be dyed. Perfect dye matches between spandex and hard fibers are usually not necessary because the elastomer is well-hidden in the fabric. Clear spandex fibers can be left undyed when plied with dyed hard fiber yarns, thus avoiding loss of stretch properties from conditions of dyeing or bleaching. Nylon–spandex combinations are often dyed with disperse dyes, or, for better fastness, with acid dyes (27). Retarders may be needed to prevent the nylon from depleting the acid dye from the bath before the spandex fiber is dyed. With polyester–spandex fabrics, disperse dyes have been used with pressure dyeing or carriers to increase the dyeing rate for the hard fiber. However, spandex fibers exhibit relatively poor wetfastness to disperse dyes, and their retractive power can be reduced under pressure dyeing conditions needed for full shades on disperse dyed polyesters. For this reason, many polyester spandex fabrics now contain cationic dyeable polyester in combination with clear (transparent) spandex fiber. Since the spandex fibers have low affinity for cationic dyes, fastness is not a problem, and the fabrics can be dyed at lower temperatures to preserve spandex retractive power.

Economic Aspects

A worldwide list of spandex fiber and related elastomer producers is shown in Table 2. Most process developments have occurred in the United States, Germany, Japan, and Korea. A large proportion of worldwide capacity is controlled by DuPont, either directly or through subsidiaries and joint ventures. These include three plants in North America, two in South America, three in Europe, and three in Asia.

Commercially, elastomeric fibers are almost always used in combination with hard fibers such as nylon, polyester, or cotton. Use levels vary from a low of about 3% in some filling stretch cotton fabrics to a high of about 40% in some warp-knit tricot fabrics. Raschel fabrics used in foundation garments normally contain 10–20% spandex fiber.

Prices of spandex fibers are highly dependent on thread size; selling price generally increases as fiber tex decreases. Factors that contribute to the relatively high cost of spandex fibers include (*1*) the relatively high cost of raw materials, (*2*) the small size of the spandex market compared to that of hard fibers, which limits scale and thus efficiency of production units, and (*3*) the technical problems associated with stretch fibers, which limit productivity rates and conversion efficiencies. As an increasing number of companies have begun production of spandex fibers, the global market has become saturated in recent years. With a more competitive market, the price of spandex has drastically been reduced.

Table 2. Producers of Spandex and Related Fibers

Competitor	Country	Trade Name
Acelon Chemicals & Fiber Corp.	Taiwan	
Asahi Chemical Industry Co.	Japan	Roica
Baoding Swan Chemical Fiber Co. Ltd.	China	
Bayer AG	Germany	Dorlastan
Bayer Corp.	United States	Dorlastan
E.I. du Pont de Nemours & Co.	United States	Lycra
Far Eastern Textile Ltd.	Taiwan	
Fillattice, Inc.	Italy	Linel
Formosa Asahi Spandex Co.	Taiwan	
Fuji Spinning Co., Ltd.	Japan	Fujibo Spandex Soflas
Fujian Changle Urethane Fibre Co. Ltd.	China	
Haishan Urethane Elastic Fibre Industry Co., Ltd.	China	
Hua Feng Industry Co. Ltd.	China	QianXi
Hyosung Corporation	Korea	Creora Toplon
Israel Spandex Co., Ltd.	Israel	Filabell
JiangSu Changshu Sai Lenshi Fiber Co.	China	
JiangSu Nan Huanghai Co. Ltd	China	
Jilin Liaoyuan Deheng Fibre Co. Ltd.	China	
Kanebo Goshen, Ltd.	Japan	Lubell
Kolon Industries, Inc.	Korea	
Lianyungang Zhongshan Urethane Fiber Co. Ltd.	China	Aoshen
Nisshinbo Industries, Inc.	Japan	Mobilon
RadiciSpandex Corp.	United States	Glospan Clerspan
Saehan Industries	Korea	
Shandong Zibo Urethane Elastic Fibre Co., Ltd.	China	Wanli
Shaoxing Polyester	China	
Shei Heng Sheiflex Co.	Taiwan	Sheiflex
Sibur-Volzhsky	Russia	
Taekwang Ind. Co., Ltd.	Korea	Acelan
Teijin Ltd.	Japan	Rexe
Tong Hwa Synthetic Fiber Co., Ltd.	Taiwan	Townspun
Tongkook Synthetic Fibres Co., Ltd.	Korea	Texlon
Toyobo Co.	Japan	Espa
Unitika Ltd.	Japan	Success
Yantai Urethane Elastic Fibre Co. Ltd.	China	
Zhejiang NinBao Synthetic Fiber Manufactory	China	
Zhong Yuan Enterprise Group	China	Zylon

Uses

The manufacturing technology for cut and extruded rubber thread is much older and more widely known than that for spandex fibers. Because production facilities can be installed with relatively modest capital investment, manufacture of rubber thread is fragmented and more widely distributed with a few major and many minor producers. On a worldwide basis, Fillattice of Italy is the largest rubber thread producer with modern extruded latex plants in Italy, Spain, Malaysia, and the United States. They also produce spandex fibers.

Table 3. Spandex Fiber Uses

Fiber form	Fabric types	Uses
Bare	Warp knits, circular knits, narrow fabrics (woven, knits, and braids), and hosiery (knit)	Foundation garments, swimwear, control tops for pantyhose, brassieres, elastic gloves, waist and leg bands, sportswear, and upholstery
Covered	Warp knits, circular knits, hosiery (knit), and narrow fabrics	Hosiery, elastic bandages, sportswear, upholstery, and sock tops
Core-spun	Wovens, circular knits, and men's hosiery (knit)	Shirting, slacks, and sportswear
Core-plied	Wovens	Blouses and trousers

Most extruded latex fibers are double covered with hard yarns in order to overcome deficiencies of the bare threads, such as abrasiveness, color, low power, and lack of dyeability. During covering, the elastic thread is wrapped under stretch, which prevents its return to original length when the stretch force is removed; thus the fiber operates farther on the stress–strain curve to take advantage of its higher elastic power. Covered rubber fibers are commonly found in narrow fabrics, braids, surgical hosiery, and strip lace.

Spandex fibers are supplied for processing into fabrics in four basic forms as outlined in Table 3. Bare yarns are supplied by the manufacturer on tubes or beams and can be processed on conventional textile equipment with the aid of special feed and tension devices. In covered yarns, the spandex fibers are covered with one or two layers of an inelastic filament or staple yarn; the hard yarn provides strength and rigidity at full extension, which facilitates knitting and weaving.

With core-spun yarns, the spandex fibers are stretched and combined with a roving of inelastic cotton or cotton–polyester staple fibers; twisting action of the hard sheath fibers around the elastomeric fiber core produces a spun yarn that contracts when tension is relieved. Woven fabrics with core-spun yarns generally contain small amounts of spandex fibers; stretch characteristics are the result of the intrinsic properties of the spandex fibers in their final form and interactions with hard fibers, which take place during weaving and heat setting (28). These interactions provide a permanent weave crimp in the hard fiber, which, together with the spandex component, imparts stretch and recovery to the fabric. Core-plied yarns are formed when stretched spandex fibers are plied with extended textured continuous filament yarns on a twisting machine; these yarns are used in high stretch woven fabrics.

Spandex fibers are available as fine as 1.1 tex (10 den), and the finest extruded latex thread available is about 16 tex (140 den). The availability of spandex fibers in such fine sizes and their unique properties compared to rubber, eg, dyeability, high modulus, abrasion resistance, and whiteness, has allowed extensive penetration into hosiery and sportswear markets.

BIBLIOGRAPHY

"Fibers, Elastomeric" in *EPST* 1st ed., Vol. 6, pp. 573–593; by S. M. Ibrahim and A. J. Ultee, E. I. du Pont deNemours & Co.; "Fibers, Elastomeric" in *EPSE* 2nd ed., Vol. 6, pp. 733–755, by A. J. Ultee, E. I. du Pont de Nemours & Co., Inc.

1. *Textile Fibers Products Identification Act, U.S. Public Law 85–897*, U.S. Federal Trade Commission, Washington, D.C., effective Mar. 3, 1960.
2. Ger. Pat. 826,641 (1952), E. Windemuth (to Farbenfabriken Bayer).
3. Ger. Pat. 886,766 (1951), W. Brenschede (to Farbenfabriken Bayer).
4. U.S. Pat. 2,957,852 (Oct. 25, 1960), P. Frankenburg and A. Frazer (to E. I. du Pont de Nemours & Co., Inc.).
5. U.S. Pat, 2,929,804 (Mar. 22, 1960), W. Steuber (to E. I. du Pont de Nemours & Co., Inc.).
6. Jpn. Appl. 63 189132 (1988), I. Matsuya (to Kanebo Ltd.).
7. G. Richeson and J. Spruiell, *J. Appl. Polym. Sci.* **41**, 845 (1990).
8. H. Lee, Y. Wang, and S. Cooper, *Macromolecules* **20**, 2089 (1987)
9. D. Allport and A. Mohajer, in D. Allport and W. H. Janes, eds., *Block Copolymers*, John Wiley & Sons, Inc., New York, 1973, pp. 443–492.
10. R. Bonart, *Angew. Makromol. Chem.* **58/59**, 259 (1977).
11. Jpn. Pat. Appl. 138, 124 (1975), T. Hidaka, K. Ikawa, and S. Mizutani (to Toray Industries, Inc.).
12. Jpn. Pat. Appl. 63 256719 (1988), S. Tanaka, Y. Yamakawa, and K. Hirasa (to Kanebo Ltd.)
13. U.S. Pat. 3,387,071 (June 4, 1968), J. Cahill, J. Powell, and E. Gartner (to Globe Mfg. Co.).
14. Jpn. Appl. 63 231244 (1988), K. Tani, K. Katsuo, and H. Tagata (to Toyobo Co., Ltd.).
15. H. Ishihara and co-workers, *J. Polym. Eng.* **6**, 237 (1986).
16. T. Kotani and co-workers, *J. Macromol. Sci., Phys.* **831**, 65 (1992).
17. U.S. Pat. 3,296,063 (Jan. 3, 1967), C. Chandler (to E. I. du Pont de Nemours & Co., Inc.).
18. U.S. Pat 3,039,895 (June 19, 1962), J. Yuk (to E. I. du Pont de Nemours & Co., Inc.).
19. U.S. Pat 4,002,711 (Jan. 11, 1977), T. Peters.
20. Jpn. Pat. Appl. 76 04,313 (1976), Y. Ikeda, T. Hirukawa, and Y. Ishiki (to Fuji Spinning Co., Ltd.).
21. H. Miller, *Polym. Prep. (Am. Chem. Soc., Div. Polym. Chem.)* **25**(1), 21 (1984).
22. Jpn. Pat. Appl. 62 86,047 (1987), H. Hanabatake and A. Kitsuri (to Asahi Chemical Industries).
23. U.S. Pat. 5,028,642 (July 2, 1991), C. Goodrich and W. Evans (to E. I. du Pont de Nemours & Co., Inc.).
24. U.S. Pat. 4,824,929 (Apr. 25, 1989), G. Arimatsu and co-workers (to Toyobo Co., Ltd.).
25. Ger. Pat. 3,641,703 (1988), M. Kausch and co-workers (to Farbenfabriken Bayer).
26. Jpn. Pat. Appl. 61 218,659 (1986), Y. Fujimoto, S. Gotou, and Y. Fujita (to Asahi Chemical Industries).
27. C. Pernetti, *Tinctoria* **80**, 133 (1983).
28. S. Ibrahim, *Ph.D. dissertation*, University of Leeds, UK, 1969.

GENERAL REFERENCES

A. J. Ultee, in J. I. Kroschwitz, ed., *Fibers and Textiles, A compendium (Polymers)*, John Wiley & Sons, Inc., New York, 1990, pp. 305–327.

John E. Boliek, and Arnold W. Jensen in J. I. Kroschwitz, ed., *Encyclopedia of Chemical Technology*, 4th ed., Vol. **10**, John Wiley & Sons, Inc., New York, 1993, pp. 624–638.
M. Couper, in M. Lewin and J. Preston, eds., *High Technology Fibers*, Marcel Dekker, Inc., New York, 1985, pp. 51–85.
M. Joseph, *Essentials of Textiles*, 3rd ed., Holt, Rinehard and Wilson, New York, 1984.

JOHN E. BOLIEK
STACY A. DENNEY
E. I. du Pont de Nemours & Co., Inc.

FILMS, MANUFACTURE

Introduction

Virtually every polymer can be used in film form. Most thermoplastic polymer films are prepared by conventional extrusion techniques based on calendering, casting, and blown-film, or tenter-film systems. Other polymers, which cannot be easily melted, are formed into films by solvent casting. In the selection of a film for a particular application, the properties of the polymeric materials must be considered in view of the application. Thermal properties, molecular characteristics, and crystallinity of the polymer affect processing and film properties. Additives influence extrusion and orientation processes and improve film properties.

Polymer Properties

Molecular Weight and Molecular Weight Distribution. Molecular weight and molecular weight distribution affect extrusion and orientation processes and the physical properties of the film, eg, tensile strength, elongation, impact resistance, (qv) and optics (see MOLECULAR WEIGHT DETERMINATION).

Films prepared from high molecular weight materials exhibit excellent mechanical strength, impact strength, and orientability. As molecular weight increases, melt strength increases. Tubular orientation requires high molecular weight and a melt index (MI) of 0.1–3 (ASTM D1238E) to provide adequate melt strength during extrusion and orientation. However, high molecular weight impedes processing and results in a film with poor optical clarity, despite orientation. Films of lower molecular weight material are brittle, difficult to orient and have lower melt strength. Low molecular weight resins are characterized by good clarity and high extrusion or processing rates. Resins of low molecular weight

Encyclopedia of Polymer Science and Technology. Copyright John Wiley & Sons, Inc. All rights reserved.

with a melt flow (MF) of 6–12 (ASTM D1238E) are used for sheet casting because melt strength is not required but good clarity is of prime importance. For tenter-process extrusion, polymers of a middle range are employed, eg, as polypropylene (PP) with MF 1.5–7 (ASTM D1238L), because melt strength is less critical. This is also true of tubular film processes that employ an initial melt quenching step. At the same molecular weight, optics, draw down, and impact strength increase as molecular weight distribution narrows, whereas melt strength, die swell, shrinkage, and processibility decrease.

Catalyst systems used for polymerization have a large impact on the molecular weight distribution and have undergone tremendous changes in the last decade (1). As older catalysts systems are replaced by new catalysts, film manufacturing processes and material selection have become more critical to ensure maintenance or improvement in film properties without adversely impacting the manufacturing process.

Crystallinity. The properties of a material are determined by its molecular structure and bulk properties are controlled by the spatial arrangement of the molecules. Polycrystalline materials are best understood in terms of a two-phase model consisting of amorphous and crystalline domains (2). The properties of each phase differ (see AMORPHOUS POLYMERS; SEMICRYSTALLINE POLYMERS). The observed properties of a material depend on the component-phase properties and the interaction of the two phases. Structural parameters are determined by the ratio of the two phases and the average orientation of the molecules in each phase (3). For polyolefin materials, such as polypropylene and polyethylene, new catalyst systems based upon metallocene materials are dramatically changing the molecular structure of the polymer chain relative to existing catalysts. The new molecular structure results in new material properties because of better control of the polymerization process. These new materials exhibit differences in melting point, crystallinity, and molecular weight distribution, and have a dramatic impact on film processing conditions and final film properties (4).

Increasing crystallinity of a semicrystalline polymer is accompanied by increases in modulus, stiffness, density, yield stress, chemical resistance, melting point, glass-transition temperature, abrasion resistance, creep resistance, and dimensional stability, and by reduction in impact resistance, elongation, thermal expansion, permeability, and swelling.

Final film crystallinity and crystalline- and amorphous-phase orientation for a given polymer depend strongly upon film processing conditions.

Thermal Properties. The chemical nature of the polymer determines its stability to temperature, light, water, and solvents. Polymer chains form ordered structures, and the thermodynamics of this ordered state determines melting point T_m, the glass-transition temperature T_g, and mechanical and electrical properties. Thermal properties (qv) of film polymers are given in Table 1 (5–11). The polymers best suited for films have a glass-transition temperature below 0°C, a melting point above 100°C, and a decomposition temperature at least 50°C above the melting point. Such polymers, eg, polyethylene (PE), polypropylene (PP), and polystyrene (PS), can be extruded in conventional extruders. Semicrystalline polymers with T_g above room temperature, such as poly(ethylene terephthalate) (PET), are most suitable for films if oriented to improve room temperature physical properties but are prone to pin hole cracking if flexed excessively.

Table 1. Thermal Properties of Film Polymers[a]

Class	Polymer	Common symbol	Glass-transition temperature T_g, °C	Melting temperature T_m, °C	Decomposition temperature T_{dec}, °C
Polyolefin	High density polyethylene	HDPE	−120 to −140	130–137	335–450
	Low density polyethylene	LDPE	−95 to −130	106–110	335–450
	Polypropylene	PP	−10	170	328–410
	Ethylene–propylene copolymer	EP	−30	128–145	328–410
	Poly(1-butene)	PB	−24	126	288–425
	Poly(4-methyl-1-pentene)	TPX	30	235	335
	Polytetrafluoroethylene	PTFE	27	330	508–538
Vinyl polymers	polystyrene	PS	85–105	240	285–440
	Poly(vinyl acetate)	PVAC	75–105	240	213–325
	Poly(vinyl chloride)	PVC	75–105	212–310	200–300
	Poly(vinylidene chloride)	PVDC	−18	210	225–275
	Poly(vinyl fluoride)	PVF	40	200–235	372–480
	Polyacrylonitrile	PAN	97	320	250–280
	Poly(methyl methacrylate)	PMMA	65	160	170–300
Polyethers	Polyoxymethylene	POM	−85 to −110	181	100
	Poly(phenylene sulfone)		220	300	310
	Cellulose triacetate	LA	105	306	250–310
Polyesters	poly(ethylene terephthalate)	PET	81	265	283–306
	Polycarbonate	PC	147	225	420–620
Polyamides	Polycaprolactam	NYLON-6	40–87	220	310–380
	Polyhexamethyleneadipimide	NYLON-6,6	50	265	310–380
	Polyundecanoamide	NYLON-11	46	194	310–380
	Polyimide			310–365	310–380

[a]Temperature quoted represents values for specific grades of commercial materials and may not be representative of all materials of this classification.

When the polymers' melting temperature is too close to the decomposition temperature a film can be produced by solvent casting. Alternatively, a reduction of the melting point of the polymer by copolymerization (12) is possible. This reduces the crystalline order of the polymer and lowers the melting point by decreasing the energy required for melting. In addition, the decomposition rate can be controlled by adding stabilizers. Extruder and die are designed with streamlined flow lines to avoid melt stagnation and push the polymer through extruder and die as quickly as possible. A lubricating additive may also be added to minimize melt adhering to the metal surface, reducing residence time and degradation. Unplasticized poly(vinyl chloride) (PVC), polyamides, and polyesters are extruded in this way (13). When the melting temperature is above the decomposition temperature, as with cellulose, poly(vinyl alcohol), or polyacrylonitrile, solvent casting and coagulation are used.

When no solvent is convenient and the use temperature of the film is below the T_g of the polymer, a nonvolatile liquid is required, which acts as solvent at high temperatures and as plasticizer at room temperature; both the T_g and the processing temperature are reduced. PVC plasticized with phthalates up to half its weight (13) can be extruded, as can be vinylidene chloride–vinyl chloride copolymer.

Additives. Organic and inorganic additives or coatings impart functionality to the finished product as demanded by the customer (9,14–16) (see Table 2). Additives (qv) must conform to government regulations for material handling and health hazards for both workers and consumers.

Stabilizers reduce degradation during film processing to prevent formation of lower molecular weight polymers, which would result in poor film properties, gels, and discoloration. Hindered phenol antioxidants combined with phosphites reduce thermal degradation of polyolefins. Other stabilizers improve long-term stability to heat and light (see STABILIZATION).

Slip agents such as saturated and unsaturated fatty acid amides can overcome film surface friction. These agents migrate to the film surface during processing and upon aging at elevated temperatures (see RELEASE AGENTS).

Antiblock agents (qv) are typically used to prevent adherence, ie blocking, of two film surfaces. They are small particle-size fillers affecting surface smoothness, controlling film-to-film surface separation distances without greatly affecting clarity.

Antistatic agents (qv), typically amine derivatives of glycerol monostearate, are primarily used to reduce static generation in packaging equipment. These additives are particularly effective for films designed for packaging powders by minimizing dust pick up on seal areas and package surfaces.

Rheology. *Rheology* is the study of deformation and flow. For polymers the viscous and elastic behavior of melts determines the design of extruder screws, melt pipes, filters, and die configuration. The elastic nature of the melt at any temperature affects surface smoothness, layer thickness, and stability. Solid phase rheology influences stretching, such as that occurs in the stepwise or simultaneous biaxial orientation. The rheology of the finished product also determines film behavior on packaging machines, printing presses, or laminators where the film is both heated and loaded by tension changes (14,15) (see also RHEOLOGY).

Table 2. Film Additives

Additive function	Supplier	Trade name	Chemical name or class
Antioxidants	Goodrich	Goodrite 3114	Phenolic
	Goodrich	Goodrite 3140	Amine
	Uniroyal	BHT	Butylated hydroxytoluene
	Albright & Wilson	Albrite DLHP	Organic phosphite
	AKZO Nobel		Tributyl phosphite
	GE Specialty Chemicals		Dilauryl phosphite
	CIBA-GEIGY	Irgonox	High molecular weight hindered phenols
	Eastman	Poly TDP-2000	Thiodipropionate polyester
Antistatic agents	ICI Surfactants	Atmer	compound
			compound
	Rhone-Poulenc	Rhodafac RE-610	Anionic
	AKZO Nobel	Armostat	Amines
	ICI Surfactants	Atmer 122, 122K	Glycerol esters
Heat stabilizers	Cardinal	CC-7711	organotin
	American Cyanamide	Cyastab	Lead-based carbonates, sulfates, phthalates
	Ciba Specialty Chemicals	Irganox B-Blends	Phosphites
	Ferro	Synpron	Barium–cadmium powder
	Total Specialty	Cal-Z Series	Cadmiun–zinc liquids
	FERRO	Snypron	Antomony mercaptides
	Uniroyl Chemical	Naugard	Amines
UV stabilizers	Cytec	Cyasorb	Benzophenone
	Ciba Specialty Chemicals	Tinuvin	Benzotriazole
	Clariant	Sanduvor	Oxalanide
	Ciba Specialty Chemicals	Tinuvin	Hindered amine (HALS)[a]
Slip agents	Witco	Kenamide	Fatty acid amide
	Dow Corning	Dow 200 fluid	Polydimethylsiloxane
	Allied	A-C Polyethylene	PE wax
		Admer	Polyolefin
Fillers, antiblock agents	Georgia Marble Co., OMYA Inc.		Calcium carbonate
		DiCaperl Hp-510	Glass bubble
	North Georgia Minerals & Chemicals		Aluminum trihydrate
			Celstite
			Barites
			Talc
	James River	Solka-Floc	Cellulose
	Manville	Celite	Diatomaceous earth
	Manville	Micro-Cel	Hydrous calcium silicate
		Suzorite	Mica
		Wollastonite	Calcium-*m*-silicate
		Glomax	Calcined kaolin clay
		Kaopaque	Delaminated aluminum silicate

Table 2. (Continued)

Additive function	Supplier	Trade name	Chemical name or class
	3M	Zeeosphere	Ceramic spheres
Antimicrobial	Morton	Vinylzene	10,10-Oxybisphenoxarsine-2-n
	Ferro	Micro-Check	2-*n*-Octyl-4-isothiazolin-3-one
	Olin Corp.	Omacide	Zinc pyrithione

[a]HALS = hindered amine light stabilizer.

Extrusion-Based Manufacturing Processes

Extrusion. Extrusion (qv) is widely used for the manufacture of polymeric films because it permits the preparation of highly uniform polymer melts at high rates (17–20). An extruder (Fig. 1) consists of a hollow cylindrical barrel fitted with external heaters. The inner surface is coated with a hard metal liner such as Xaloy. A screw is fitted into this cylinder with a specific geometry determined by the polymer and the desired thermal condition of the melt. The screw is driven by an electric motor through a gear reducer sized for the speed and power requirements of the screw. The typical barrier screw shown in Figure 2 takes advantage of the melting mechanism in the extruder to increase efficiency. Most of the energy required to melt the polymer is supplied by the motor (21,22). Barrel temperature is maintained by electric heaters, which often contain channels for cooling water.

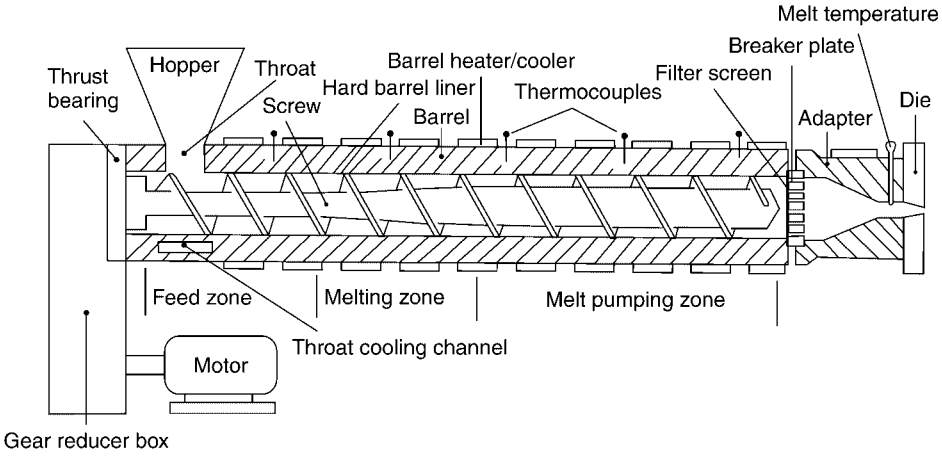

Fig. 1. Extruder.

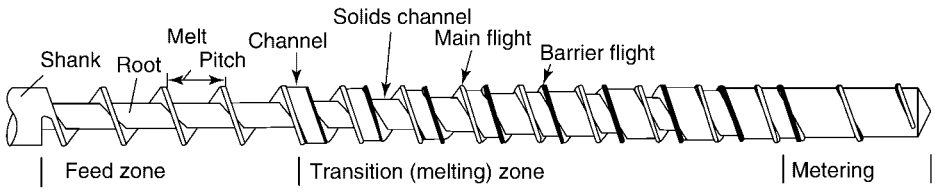

Fig. 2. Barrier flight screw.

The solid polymer is introduced into the feed throat of the extruder and conveyed into the screw by its turning motion (17). It is compacted into a solid plug, which is melted by contact with the hot barrel. Molten polymer is collected by the screw flights and pumped toward the end of the extruder. At the end of the screw, the polymer is completely melted. The melt is mixed by the screw rotation, which generates enough pressure to push the melt through a die and to the next step (23,24). The condition or quality of the melt is extremely important for film quality and process stability. The extrusion conditions affect crystallization behavior and molecular weight of the film.

The melt is produced by the viscous dissipation of mechanical energy into a very thin layer of molten polymer located between the compressed solid plug and the heated barrel surface (18) (Fig. 3). Owing to the high viscosity of the polymer melt, typically 50–1000 Pa·s (500–10,000 P), large amounts of energy are dissipated in the melt as the motor turns the screw. The energy is converted into heat, which is transferred to the solid polymer and the barrel, raising the temperature of the melt. Excessive temperatures or mechanical work can cause thermal, oxidative, or mechanical degradation of the polymer. A new generation of energy-efficient screw designs have been developed, which minimize the melt temperature by mixing the collected melt with the solid particles of the compacted bed (25,26). This is accomplished by purposely disrupting the melting mechanism of Figure 3 at some point, by changing the screw geometry to mix the solid with the melt.

The polymer melt flows through a die to the next process step; flat, circular, or slot dies are preferred. The flow through the die must be uniform across the exit plane. However, this is complicated by the nonlinear dependence of melt viscosity on both temperature and shear rate in the die (23,24). The suitability of a material is determined by measuring the flow properties with a capillary rheometer in the temperature and shear-rate range expected. Melt elasticity can cause flow instabilities, which affect haze and thickness (27,28) or the operation of downstream equipment. Exit melt velocity, flow characteristics, and quenching rate may impart significant orientation to the polymer. In some instances, melt orientation is reduced; in others, it is maintained by quenching.

In flat-die extruders, slot and coat hanger die geometries (Fig. 4) predominate, whereas in circular die extruders, spiral dies (Fig. 5) predominate. A die

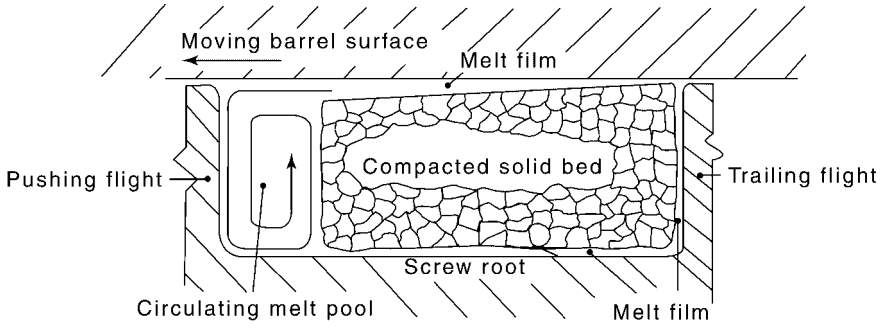

Fig. 3. Melting mechanism of single screw extruders.

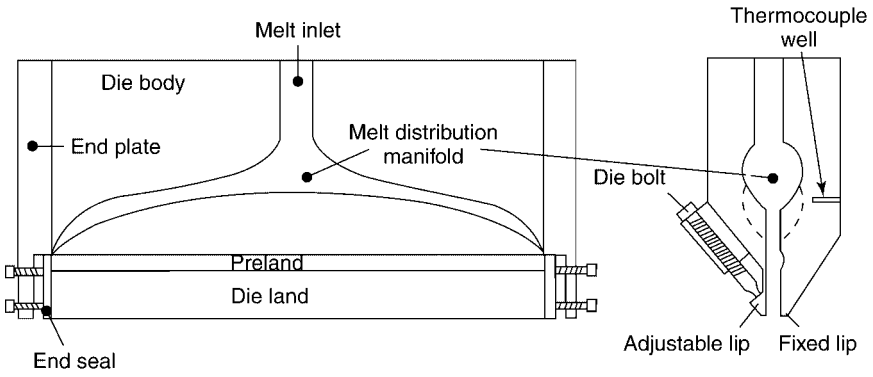

Fig. 4. Coat-hanger die.

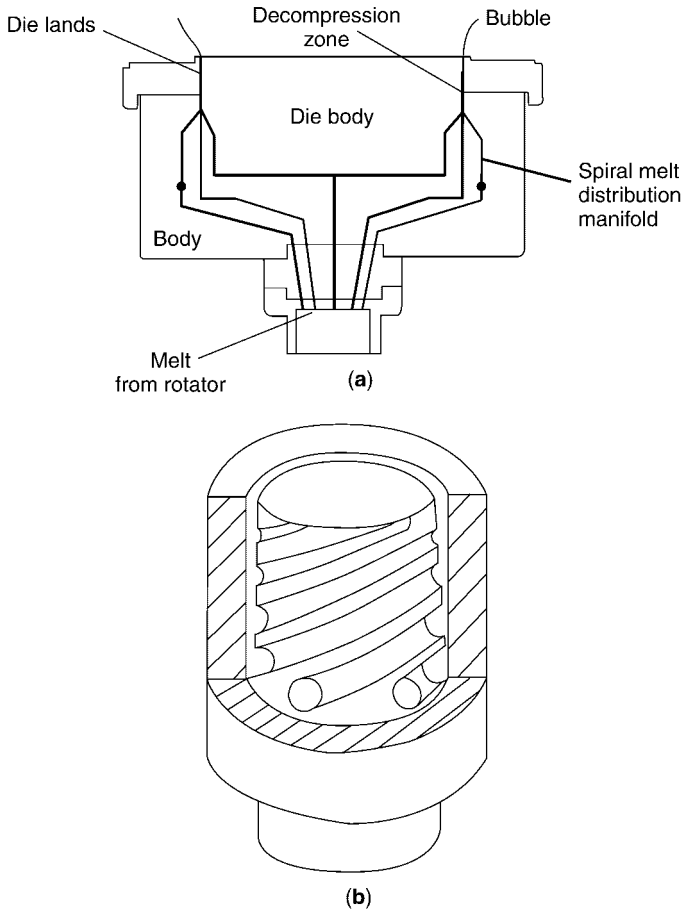

Fig. 5. (**a**) Tubular (three-layer) spiral die; (**b**) detail of spiral melt manifold.

is usually constructed of tool steel and heated to maintain the desired temperature for optimum flow. Temperature uniformity is very important. A uniform flow through the die is determined by the design of the internal distribution manifold. For good melt distribution, this section must be designed to maintain uniform flow rate, pressure drop, and shear (24). Independent flow adjustment is usually provided by an adjustable die lip or choker bar. These devices ensure a uniform flow by selectively changing the shear rate of the melt before it leaves the die. Multiple temperature zones, standard on most dies, permit the selective alteration of the temperature across the die face, ensuring production of a flat sheet. This is necessary to counteract gauge variations caused by possible nonhomogeneous melt from the extruder, inadequacies in the die design, and the physical limitations imposed in the machining of the internal configuration of the dies.

To ensure isothermal flow, die temperatures are maintained as close to the melt temperature as is practical. Die gaps vary, depending upon the speed with which material is removed from the die lips, as this determines the shear rate. This is important because of die swell and melt fracture. Die gap also determines the final film thickness. Die gaps are 0.25–2.5 mm (0.010–0.10 in.), which is small compared with the typical die width of 39–305 cm.

Coextrusion. Coextrusion technology has been developed in conjunction with new polymers, providing the film structures required for flexible packaging (see COEXTRUSION). Coextrusion is perhaps the most economical method of combining polymers into functional multilayer films.

Multiple melt streams from several extruders are combined either in a feed block (Fig. 6) or in a multiple cavity die (Fig. 7), resulting in a stratified flow from

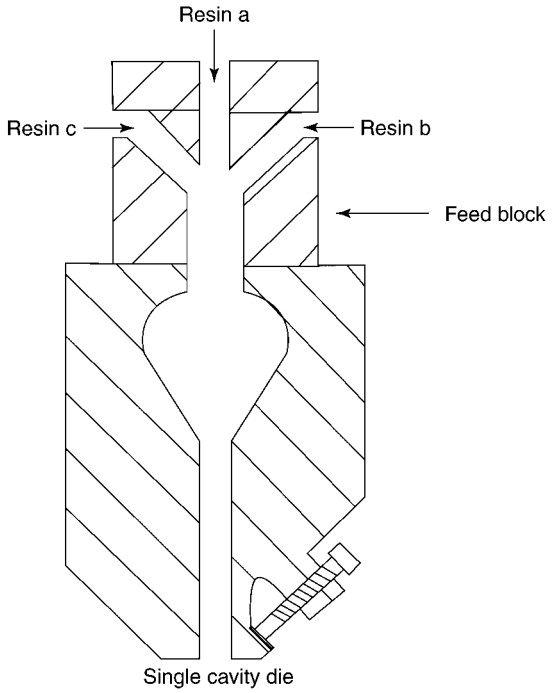

Fig. 6. Coextrusion system (single cavity die) using a feed block for three polymer streams.

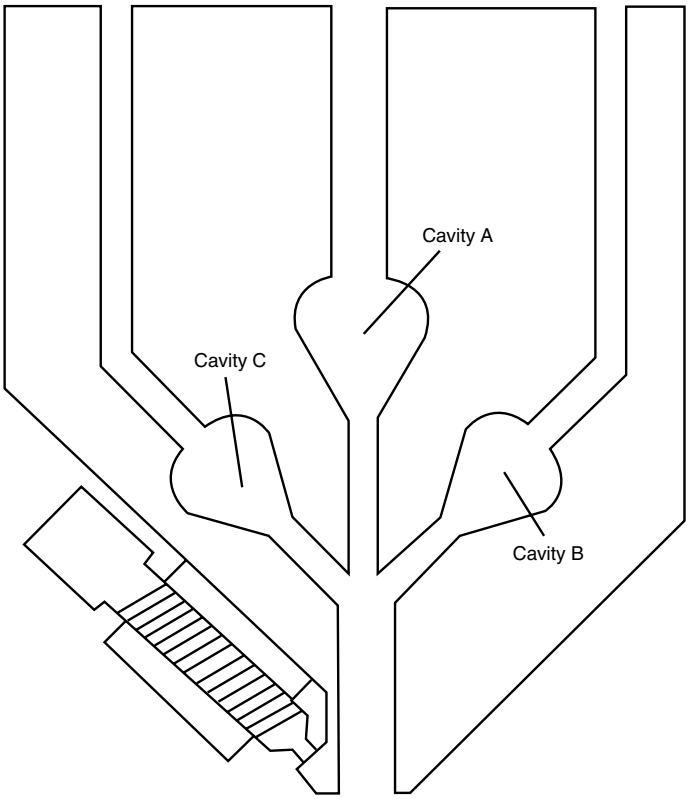

Fig. 7. Multiple cavity coextrusion die with multiple melt-distribution manifolds.

the die. A feed block may be used with a single cavity die or in conjunction with one cavity of a multiple cavity die to produce structures with many layers. Multiple cavity dies are used for films requiring several layers, which interact chemically to improve adhesion between the polymers but which may disturb the interface stability or noninteracting polymers, which must remain separate for as long as possible owing to poor rheological compatibility.

Coextrusion is promoted by the laminar flow of the melt in the feed block and die, which prevents the mixing of the various layers. The laminar flow is due to the low Reynolds numbers (low inertia between flow planes) that result from the high melt viscosities (23,24). However, the generation of interfaces between the flowing materials requires that melt viscosities and melt elasticity between the layers be sufficiently matched to prevent the formation of flow instabilities (29–32). Therefore, coextrusion requires superior equipment and process control throughout.

Multilayer spiral dies are becoming more common but are limited to rheological compatible polymers in the layers much as with the feed block method in flat dies. This is due to the long flow distances required for layer uniformity in the multilayer spiral dies, which makes them more prone to generate interfacial instabilities.

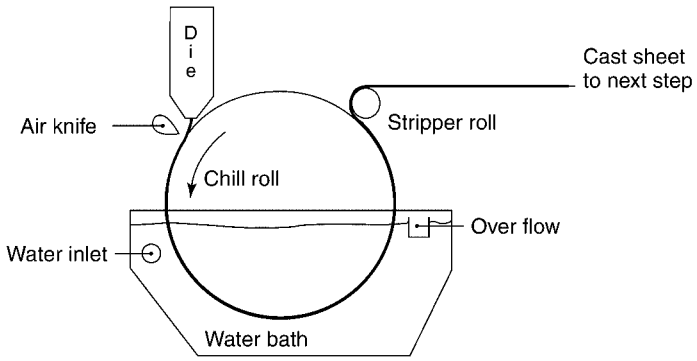

Fig. 8. Water bath–chill roll quenching system.

In another method, two or three melt streams from separate extruders can be combined and cast to form a multilayer structure. Alternatively, a melt stream and a quenched web or a quenched and uniaxially oriented web are combined on a chilled drum, providing the web with new surface functionality. This method is known as the extrusion coating process (14).

Casting. In casting, a self-supporting film or sheet is formed from a melt supplied by an extrusion system. Processing conditions have a profound effect on sheet properties and subsequent operations. Depending on the polymer, the rate of heat removal determines the extent and morphology of crystallinity of the sheet and the degree of residual orientation. Also important is the temperature at which the heat is removed from the sheet. Thus, heat-transfer analysis of casting processes is essential for the design of an efficient system.

Quenching is a continuous operation and must be regarded as an unsteady state. It can take place in water, on a continuous steel band, on a casting drum, or by a combination of these methods (see Fig. 8). The heat-transfer analyses for these systems are similar, differing primarily in the magnitude of heat-transfer coefficients. Heat-transfer rate, heat-transfer temperature, melt temperature, and crystallization kinetics determines the optimum quenching conditions. The cast sheet must be strong enough to be transported to the next stage of the manufacturing process.

If a high quality surface or a uniform heat-transfer rate is required, a pinning step may be needed. Pinning is defined as the forcible application of the molten film to the casting surface, it may be carried out by an air knife, a vacuum box, a nip roll, or a strong electrostatic field. Pinning is needed for high production rates while maintaining uniform properties across the quenched web. The pinning force prevents air from being trapped between the film and the casting surface. Choice of pinning method depends upon the speed of the operation and the quality of the sheet required for the particular product to ensure intimate contact with the surface against which the polymer is being solidified.

Examples of cast film are high clarity, low density polyethylene (LDPE) film for bread bags, pallet wraps, PVC sheets, and polycarbonate (PC) or acrylic sheets for glazing applications. Casting is the initial step in the production of biaxially oriented PP, PS, and PET films.

Uniaxial Orientation. Uniaxial orientation enhances the physical properties of sheets and films in one direction; properties in the perpendicular direction are usually far inferior (29). The orientation temperature, governed by the material, and the extent of orientation determines the final properties. Semicrystalline polymers (qv) are oriented between the glass-transition temperature T_g and the melting point T_m, whereas amorphous polymers (qv) are oriented above T_g. In general, rapid stretching in the temperature ranges described above, followed by rapid quenching, orients the polymer. Rapid quenching ensures that the orientation is not lost by molecular relaxation. The degree of orientation is determined by the extension rate and the degree of extension (3). A wide variety of commercial equipment is available for uniaxial orientation, as well as proprietary equipment developed for special processes or high production rates (see FILMS, ORIENTATION).

Orientation is a continuous operation and occurs in the direction of the film motion or the machine direction (MD). Usually, a cast sheet is transported on heated rollers (Fig. 9) to permit the sheet to reach a uniform temperature at which the polymer molecules are sufficiently mobile. Having reached this temperature, the sheet is abruptly accelerated between two rollers of different speeds. This point is defined as the draw point. In some instances, additional heat may be required to boost the temperature, or nip rolls are needed to regulate tension and to prevent film slippage (Fig. 9). Uniaxial film can be obtained by orienting perpendicular (transverse) to the MD using tenter frames or melt inflation, where the melt removal rate is equal to the melt velocity at the die. However, these two methods are seldom employed. The properties required by the user determine the orientation required to develop the desired physical properties.

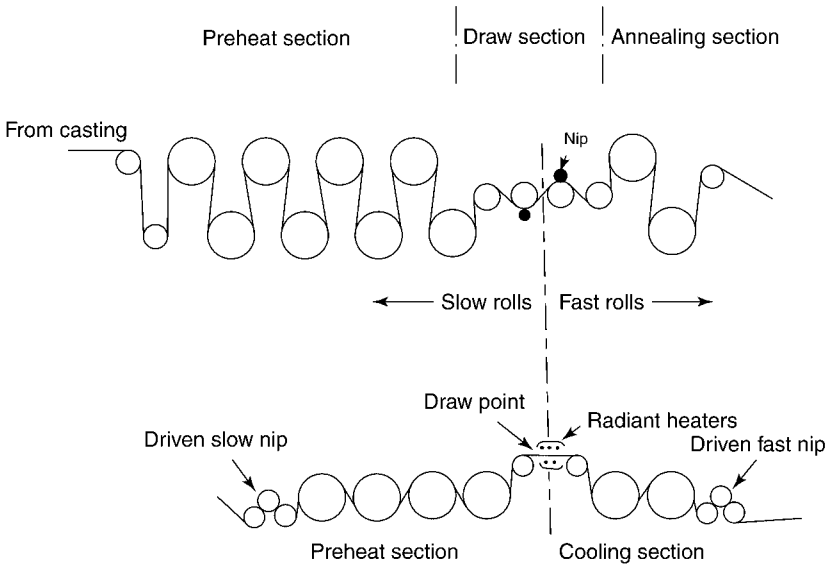

Fig. 9. Machine-direction (MD) orientation.

Amorphous and semicrystalline polymers behave very differently when subjected to uniaxial orientation. Amorphous polymers may be drawn to any extent or thickness if properly supported, whereas semicrystalline polymers show distinct and abrupt thickness changes, called necking, when drawn (3). Necking may limit the rate at which the polymer is drawn because of the heat generated in the neck region. The heat generated can be high enough to cause chain scission, resulting in breakage of the sheet at the draw point (33). Necking serves to define a minimum draw ratio for the material at the temperature and draw rate employed.

The relationships between physical properties and molecular orientation of uniaxial products are well understood for both amorphous and semicrystalline polymers (34). The principal change that occurs upon orientation is the preferential alignment of the *c*-axis of molecular chains in the direction of the orientation in the amorphous and crystalline phases of semicrystalline polymers (35,36). The preferred *c*-axis orientation allows the strong covalent bonds along the chain backbone to carry loads applied in the orientation direction. Perpendicular to the orientation direction, the weaker intermolecular van der Waals forces predominate between the molecular chains, giving a much lower load-carrying capability. For amorphous polymers, an average orientation function defines the only measure required to define the orientation state completely; it relates directly to the load-carrying amorphous phase. In semicrystalline polymers, the Hermans orientation function (3) describes the orientation contribution by the crystalline phase. This must be combined with the amorphous phase orientation to describe an average molecular orientation. Average orientation is more difficult to relate directly to physical properties because the crystalline phase does not contribute greatly to the load-bearing capabilities of the structure. Therefore, a more detailed analysis of the semicrystalline materials is required to determine the contributions from the amorphous and crystalline phases (34). Advanced analytical techniques are needed that are not readily available to many workers.

Biaxial Orientation. Biaxial orientation substantially improves the physical properties of the film and increases its commercial value. Biaxially oriented films are produced by stretching polymers in directions perpendicular to each other in the melt or rubbery state. The improvement over uniaxially oriented films is due to the redistribution of *c*-axis chain orientation (36). This results in a film with enhanced physical properties in both directions. The direction perpendicular to the MD is defined as the transverse direction (TD).

Commercial biaxially oriented films are produced by the tenter-frame (Fig. 10), double-bubble (Fig. 11), or blown-film process (Fig. 12). In the tenter-frame and double-bubble processes, the polymer is stretched in the solid state below the crystalline melting point. In the blown-film process, the polymer is oriented in the melt, followed by rapid quenching to immobilize the orientation.

The theoretical descriptions of biaxial orientation and the relationships to physical properties are not as well developed as those of uniaxial orientation. In amorphous polymers, birefringence can measure total molecular orientation and can be used to predict properties. For semicrystalline polymers, a more

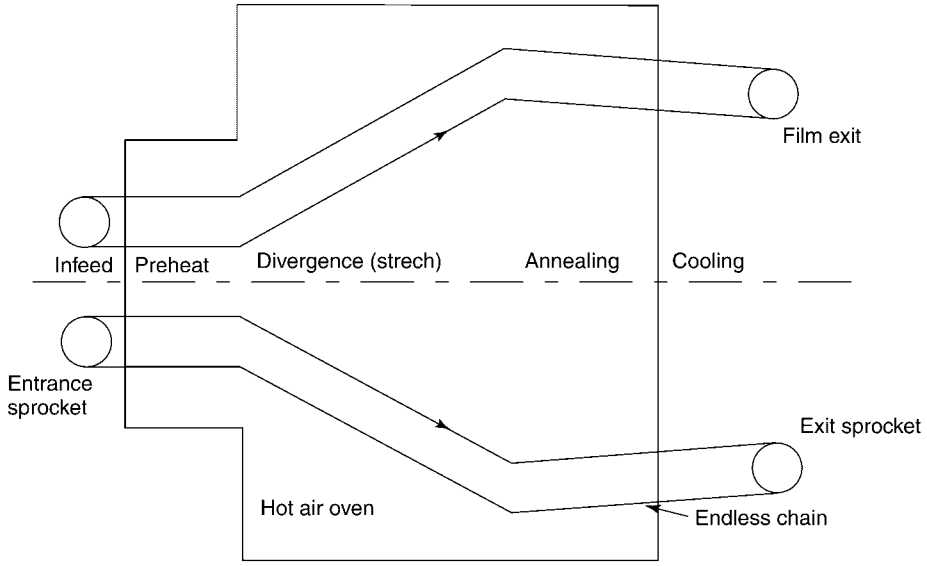

Fig. 10. Tenter orientation.

detailed description of the orientation is required before prediction of properties is possible.

Average-orientation, amorphous-orientation, and crystalline-orientation functions are required to describe the oriented state completely (3,36). This description permits the calculation of amorphous-phase orientation, which is required to relate and predict physical properties. The determination of crystalline orientation requires the more advanced analytical techniques of X-ray diffraction or dichroic ratios from polarized infrared spectroscopy. Average or total orientation functions are measured by birefringence. Amorphous and crystalline orientation functions are separated by measuring the sonic modulus and assuming a molecular model for the semicrystalline polymer (3).

Tenter-Frame Process. Tenter frames (Fig. 10) consist of two side-by-side endless chains that diverge at constant angle. The divergence of the chains forces the polymer to stretch as it is transported along the chain, and imparts the desired orientation. Stretch rate is determined by the chain speed, divergence angle, and extent of orientation. The extent of orientation is determined by the ratio of the width of the film entering to the width of the film leaving the system. Tenter systems have been developed primarily to impart TD orientation. Specialized systems allow simultaneous MD and TD stretching, but because of the mechanical complexity of these systems usually only TD orientation is carried out. The tenter frame, as part of a larger, sequential, biaxial-orientation system, can be located before or after MD orientation; it is usually located after MD orientation.

Depending upon polymer, the resin is extruded or coextruded as a flat sheet, approximately 0.75–2.5 mm thick, onto a large chill roll. For PP, the chill roll is in a water quench bath. The cast sheet is reheated and stretched in the longitudinal direction on a series of heated chrome rolls and fed into a tenter chain

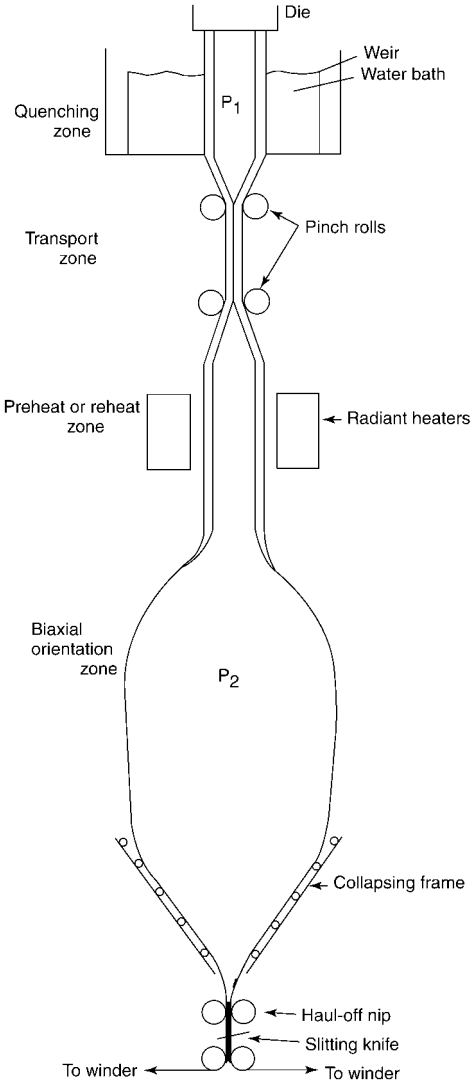

Fig. 11. Double-bubble orientation.

equipped with clips to grip the film. The chain system is located within a heat-transfer oven, where the sheet is heated to the temperature at which it is to be stretched. Heating is critical because the reliability of the stretching process and the film properties depend upon the temperature, stretch rate, and stretch ratio.

After preheating, the film is drawn in the transverse or cross direction by the divergence of the tenter chains, annealed, and released. The edges of the film are slit off, ground, and recycled, and the web may be wound full width or split into narrower webs, which are electric discharge or flame treated for enhancing printability and then wound onto rolls for further processing.

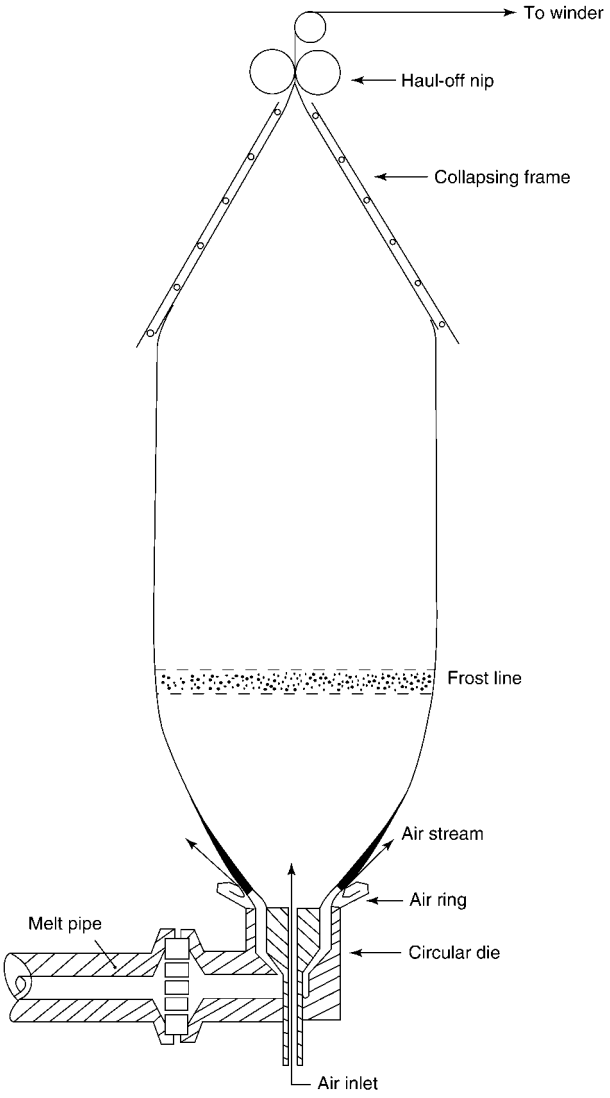

Fig. 12. Melt orientation.

In contrast to the double-bubble process, the tenter-frame process permits the direct manufacture of a film with improved dimensional stability because it is heat-set by adding a length of chain after the divergent section at the finished film width. This is very important for applications requiring good registration, as in printing or photographic applications. The film can be heated or cooled to a specific temperature while being restrained by the chain system. With line speeds in excess of 300 m/min possible and widths of 8–10 m common, oven heat transfer rates must also be high to control film annealing and crystallization.

Recently a new simultaneous biaxial orientation system has been developed using linear motors to drive the clips and impart MD stretch as the film travels

down the diverging tenter rails (37). This has replaced the mechanical complexity of the earlier simultaneous systems with electronic control complexity, which is readily handled by computer. This new tenter design has been implemented commercially and offers the potential to develop films with new orientation ratios and low melting surface polymers not possible with existing sequential stretching systems.

Blown-Film Processes. Bubble orientation technology permits simultaneous biaxial orientation directly from the melt (24) or by inflation of a quenched tube. With homogeneous films, the latter method may give films of slightly different properties than those of films produced on tenter frames. Melt orientation is less effective and properties are different because of lower orientation.

Double-Bubble Method. In the double-bubble method (Fig. 11), the resin is extruded as a tube that is quenched and gauged in cold water. The tube is then reheated and oriented by blowing it into a bubble. Simultaneously, the speed of the takeoff roll is increased for MD orientation; radiant electrical heaters control temperature. The bubble is collapsed, passed through nip rolls, reinflated, annealed in a controlled-temperature chamber, and collapsed again. After trimming the edges, it is separated into two webs, which are then treated by electric discharge for printability and wound onto rolls.

Melt Orientation. In melt orientation, the polymer melt is extruded from an annular die into a tube, which is simultaneously pulled away from the die as air is blown into the tube and around the outer surface (by an air ring attached to the die) to stabilize and quench the tube (24). This cools the melt as it accelerates in the machine and in the radial direction, thus conferring orientation. The action of the air solidifies the melt. The solidification point is called the frost line. The frost line height is important in determining the reliability of the process and the film properties. Above the frost line, the inflated tube is gradually collapsed and fed to the haul-off nip, which supplies the power to pull the melt from the die and prevents the bubble from collapsing by trapping air in the tube. The MD orientation is determined by the speed at which the melt is pulled away from the die (haul-off rate), the quenching rate (frost-line height), the die gap, and the melt properties. The TD orientation is determined by the final diameter of the inflated tube in relationship to the die diameter (*blow-up ratio*). The ratio of the die gap to the film thickness is called the *draw down ratio*. It affects the stability of the process and the orientation of the product. The tension pulling the melt away from the die (24) is called the *haul-off tension*. It cannot exceed the melt strength or the critical stress for melt fracture; the haul-off tension affects process stability and film properties.

Tensilizing. After biaxial orientation, film properties can be enhanced by additional MD orientation. This step is called tensilizing, and is performed by MD-drawing of the film after the initial biaxial MD and TD orientation, using sets of rollers, as previously discussed. Tensilized film can be produced with improved MD tensile strengths to permit use of thinner films as for magnetic recording tape or to increase the MD shrinkage of the film for use as a shrink label for complex packages such as cans and bottles.

A typical tensilized process consists of the casting step, the MD-orientation step, the TD-orientation step, and another MD-orientation or tensilizing step. This second MD orientation may be performed in-line as an additional step on the

orienter (38) or out-of-line as the film is slit for sale. It is also possible to add this second MD orientation to a tenter-frame or double-bubble process (39).

Solvent-Solution Casting

Films and sheets may be made from polymers that cannot be melt-extruded or that are extremely heat-sensitive by using polymer solutions. In this technology, a homogeneous polymer solution is filtered and degassed, followed by formation and drying of a gel film. The gel films are formed from the solutions by evaporation and coagulation. Drying of the gel films into self-supporting films is the rate-limiting step because it is diffusion-rate controlled. This also is of prime consideration in the formation of thick films, where drying times may be excessive. Consequently, these methods are generally limited to thin films. The characteristics of these films are low residual orientation, uniform properties in all directions, and excellent surface finishes (14,15).

Coagulation. Gel formation by coagulation depends upon the differential solubility of polymers in a blend of solvent, and nonsolvent, and solubility changes resulting from concentration changes of added chemicals. For example, solvents A and B are a good solvent and poor or nonsolvent, respectively, for polymer Y. A solution of Y is prepared in A and extruded into a bath of solvent mixture of A and B. The concentration difference causes diffusion of A out of the solution into the bath and the diffusion of B into the polymer solution. As the concentration of B increases and that of A decreases, the polymer becomes less soluble and eventually precipitates as insoluble gel; complete evaporation of A and B leaves the finished film. As an alternative, changes of pH by chemical additives may be sufficient to reverse the solubility or change the chemical nature of a polymer in solution, transforming it into an insoluble, stable gel. A good example of this technology is the casting of cellophane (15) (Fig. 13).

Evaporation. In this method (Fig. 14), the polymer solution is pumped through a die, cast upon a stainless-steel belt, and transferred to a drying chamber to evaporate. The solvent is recovered (15). As the solvent evaporates, a gel forms. Further drying gives a stable film. The film is stripped from the belt and rolled up.

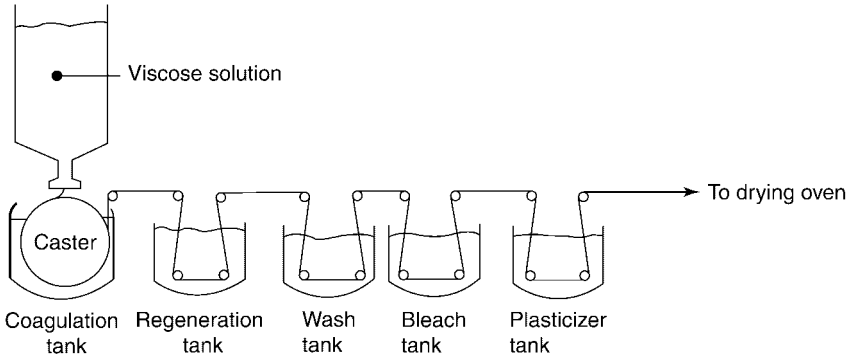

Fig. 13. Cellophane casting process.

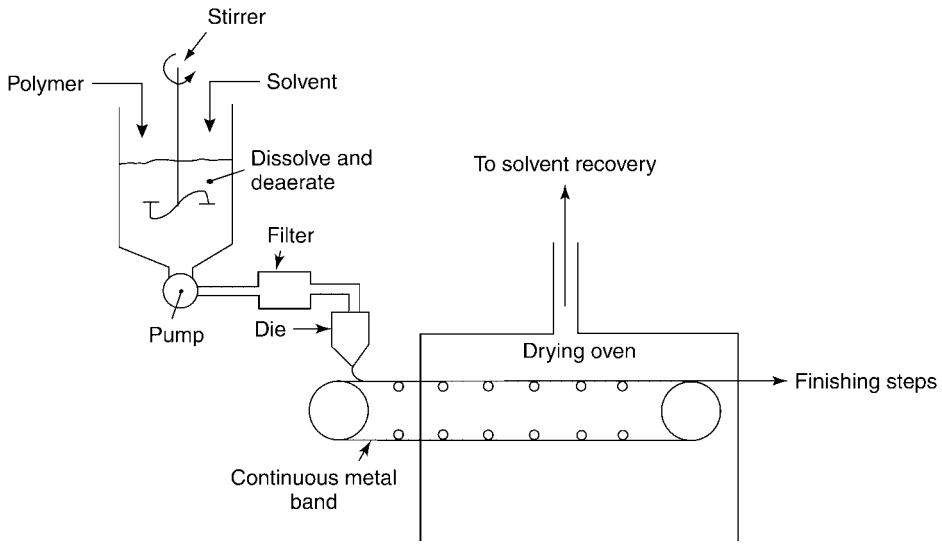

Fig. 14. Solvent casting process.

Rolling

Rolling produces a film with predominately MD orientation by accelerating the film from a nip point where the thickness is reduced. Large forces are found at the nip point, but overall orientation can be increased over other forms of MD orientation. Plastic strapping is oriented by this method (40).

Calendering

Calendering produces an unoriented cast sheet with uniform gauge at high throughput (41,42). The equipment (Fig. 15) is expensive and consists of a stack of especially hardened, driven rolls. The rolls are often supported in such a manner that they may be bent or skewed relative to one another during operation. This operation is required to maintain uniform thickness by overcoming the roll bending forces developed in the calender nip. The high separation forces, ie 180–1080 kg/cm of roll face, are generated by the melt (stock) viscosity and elasticity as the material passes through the nip point.

Calenders are usually composed of four rolls that form three nips: feed nip, metering nip, and finishing nip. The polymer is supplied to the feed nip from a compounding operation and further mixed and heated by the circulating melt bank formed at the feed nip. Alternatively, a melt of partially fluxed compound may be supplied to the calender from an extruder or Banbury. The sheet is reduced at the metering nip to the final desired thickness. The gauge uniformity is adjusted at the finishing nip by bending the last roll or skewing the middle or third roll.

Finishing Operations

Coating. Films are coated by metering a coating solution onto the surface and removing the excess solvent in an evaporation oven. Hundred percent solid

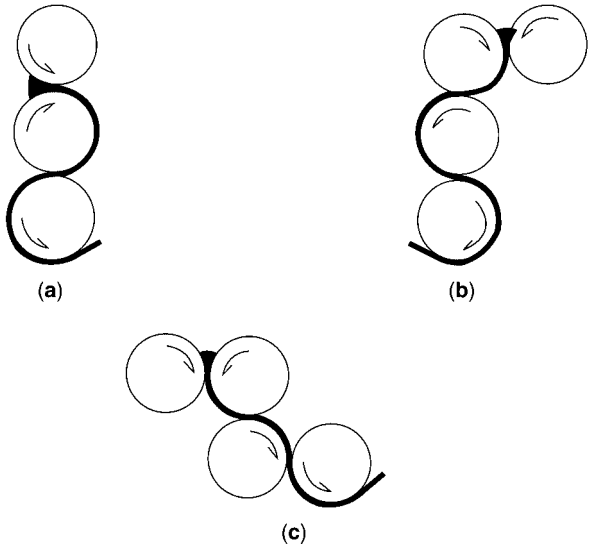

Fig. 15. Calendering-roll configurations: (**a**) three-roll superimposed type; (**b**) four-roll inverted-L type; (**c**) four-roll Z type.

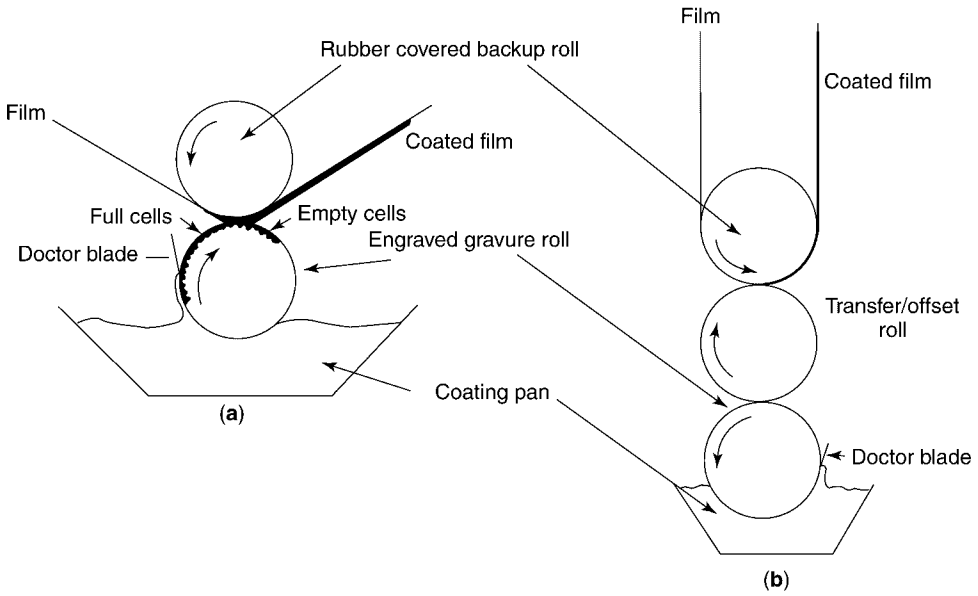

Fig. 16. (**a**) Direct and (**b**) indirect gravure systems.

(solvent-less) coatings are becoming more popular and may be heat or radiation cured. For metering, air knife-coaters, Meyer rod coaters, slot dies, and direct or indirect gravure coaters (Fig. 16) are used. The film is unwound onto the coater and may require surface treatment to ensure proper wet-out, especially with water-based coatings. The film is coated at the coating station and transferred to a drying oven. After drying, the film is rewound and ready for further processing (see also COATING METHODS).

Embossing. Embossing is used to modify the film texture or to decorate the film with a three-dimensional pattern (14). The film is heated to the softening point and distorted by passing it between a cooled roll with the three-dimensional pattern and a nip. This immobilizes the distorted pattern imposed by the embossing roll. The degree of distortion depends upon the film properties and the processing conditions. Microembossing may also be performed on coextruded or coated films to produce diffraction patterns and holographic images when metallized. In this process only the surface is embossed by first heating the film or just the film surface and then passing it through a nip between the etched embossing roll and a backing roll to force the polymer surface into the etched roll. This force is required to transfer the etched roll pattern to the film surface. The pattern is then enhanced by metallization of the film to cause light refraction from the patterned surface. This is a growing use for films in decorative and security applications.

Metallization. Film metallizing is a growing use for films for both decorative and the functional enhancement of light and gas barrier properties. A thin layer of aluminum metal coats film by a process of physical vapor deposition or sputtering. Rolls of film are mounted into a high vacuum chamber and evacuated to approximately 1×10^{-5} torr. Once this pressure level is reached aluminum metal is melted and flash evaporated on ceramic boats. The film is passed above the evaporation area at speeds approaching 500 m/min. This deposits a layer of aluminum approximately 100 nm thick. This layer thickness of aluminum reflects approximately 99% of the incident light and reduces the amount of moisture and oxygen permeation through the film to create an excellent packaging film for products subject to rancidity. Industrial uses for static dissipation, visible and IR radiation reflective window films, as well as clear IR radiation reflective films for glazing have also been widely used.

Surface Treatment. Most film surfaces require surface treatment for use in subsequent steps of coating, printing, lamination, or metallization. This treatment results in the chemical modification of the polymer at the surface. The most widely employed surface modification is oxidation of the polymer to create a polar surface (43). Processes that are widely employed are corona and flame treatment. Wet chemical oxidative treatments are seldom used and are restricted to low speed operations. A new surface oxidation technique has been recently developed which uses an atmospheric plasma generated in a hollow cathode with helium or helium gas blends (44).

BIBLIOGRAPHY

"Films and Sheeting" in *EPST* 1st ed., Vol. 6, pp. 764–794, by L.E. Wolinski, E. I. du pont de Nemours & Co., Inc.; "Films, Manufacture" in *EPST* 2nd ed, Vol. 7, pp. 88–106, by H. C. Park and E. M. Mount III, Mobil Chemical Co.

1. E. P. Moore, *The Rebirth of Polypropylene: Supported Catalysts*, Hanser/Gardner Publications, Inc., Cincinnati, 1998.
2. L. Mandelkern, *Polym. Eng. Sci.* **7**, 232 (Oct. 1967).
3. R. J. Samuels, *Structured Polymer Properties*, John Wiley & Sons, Inc., New York, 1974.
4. U.S. Pat. 6,090,325 (July 18, 2000), W. R. Wheat and A. Hanyu (to Fina Technology, Inc.).
5. L. Reich and S. S. Stivala, *Elements of Polymer Degradation*, McGraw-Hill, Inc., New York, 1971.

6. H. Swada, in K. F. O'Driscoll, ed., Thermodynamics of *Polymerization*, Marcel Dekker, Inc., New York, 1976, p. 317.
7. C. J. Hilado, *Flammability Handbook for Plastics*, 3rd ed., Technomic Publishing Co., Inc., Lancaster, Pa., 1982, pp. 28–30.
8. J. A. Brydson, *Plastics Materials*, 3rd ed., R. E. Krieger Publishing Co., Inc., Melbourne, Fla., 1975, pp. 60–61.
9. J. Agranoff, ed., Modern Plastics Encyclopedia, Vol. **60** (10A), McGraw-Hill, Inc., New York, 1983, pp. 470–501.
10. J. Brandrup and E. M. Immergut, *Polymer Handbook*, Wiley-Interscience, New York, 1967, Sects. III and V.
11. L. A. Wall, ed., *Fluoropolymers*, Wiley-Interscience, New York, 1972.
12. H. V. Boenig, *Polyolefins, Structure & Properties*, Elsevier, Amsterdam, 1966.
13. C. E. Schildknecht, *Vinyl and Related Polymers*, John Wiley & Sons, Inc., New York, 1952, pp. 425–441.
14. J. Briston, *Plastics Films*, 2nd ed., Longman, Inc., New York, 1983.
15. C. J. Benning, *Plastics Films for Packaging*, Technomic Publishing Co., Inc., Lancaster, Pa., 1983.
16. A. A. Schoengood, *SPE J.* **28**(6), 21 (1972).
17. Z. Tadmor and co-workers, *Polym. Eng Sci.* **7**(3), 198 (1967).
18. B. H. Maddox, *SPE J.* **15**, 383 (1959).
19. J. Shapiro and co-workers, *Polymer* **17**, 905 (1976).
20. E. M. Mount III, J. G. Watson, and C. I. Chung, *Polym. Eng. Sci.* **22**, 729 (1982).
21. C. I. Chung, *Extrusion of Polymers Theory and Practice*, Hanser Publishers, Munich, 2000.
22. C. Rauwendaal, *Polymer Extrusion*, Hanser Publishers, New York, 1986.
23. J. McKelvey, *Polymer Processing*, John Wiley & Sons, Inc., New York, 1962.
24. S. Middleman, *Fundamentals of Polymer Processing*, McGraw-Hill, Inc., New York, 1977.
25. U.S. Pat. 4,173,417 (Nov. 6, 1979), G. A. Kruder (to HPM Corp.).
26. U.S. Pat. 4,405,239 (Sept. 20, 1983), C. I. Chung and R. A. Barr.
27. H. Ashizawa, J. E. Spruiell, and J. L. White, *Polym. Eng. Sci.* **24**, 1035 (1984).
28. N. C. Huck and P. L. Clegg, *SPE Trans.* **1**, 121 (1961).
29. C. D. Han, *Rheology in Polymer Processing*, Academic Press, Inc., New York, 1976.
30. N. D. Waters and A. M. Keeley, *J. Non-Newtonian Fluid Mech.* **24** 161–181 (1987).
31. E. J. Hinch and co-workers, *J. Non-Newtonian Fluid Mech.* **43** 311–324 (1992).
32. G. M. Wilson and B. Khomami, *J. Rheol.* **37** 315–339 (1993).
33. V. A. Marikhin and L. P. Myasnikova, in G. Bodor, ed., *Orientation Effects in Solid Polymers*, John Wiley & Sons, Inc., New York, 1977, pp. 97–107.
34. J. C. Seferis and R. J. Samuels, *Polym. Eng. Sci.* **19**, 875 (1979).
35. S. Hoshino and co-workers, *J. Polym. Sci.* **58**, 185 (1962).
36. A. J. De Vries, C. Bonnebat, and J. Beautempts, *J. Polym. Sci. Symp. C.* **58**, 109 (1977).
37. U.S. Pat. 4,853,602 (Aug. 1, 1989), W. J. Hommes and J. J. Keegan, (to E. I. du pont de Nemours & Co.).
38. U.S. Pat. 5,691,043 (Nov. 25, 1997), L. E. Keller and M.-F. Nothnagle (to Mobil Oil Corp.).
39. U.S. Pat. 5,851,610 (Dec. 22, 1998), W. J. Ristey, G. A. Senich, W. J. Hill, and H. S. Anderson (to Applied Extrusion Technologies, Inc.).
40. U.S. Pat. 4,428,720 (Jan. 31, 1984), D. l. Van Erden, R. J. Gould, and Y. A. Matsunnaga, (to Signode Corp.).
41. G. W. Eighmy Jr., in Ref. 7, Vol. 59 (10A), 1982, pp. 220–222.
42. R. A. Elden and A. D. Swan, *Calendering of Plastics*, American Elsevier Co., Inc., New York, 1971.

43. C.-M. Chan, *Polymer Surface Modification and Characterization*, Hanser/Gardner, Cincinnati, 1994.
44. U.S. Pat. 6,118,218 (Sept. 12, 2000), A. Yializis, S. A. Prizada, and W. Decker (to Sigma Technologies International, Inc.).

ELDRIDGE M. MOUNT III
EMMOUNT Technologies

FILMS, MULTILAYER. See COEXTRUSION.

FILMS, ORIENTATION. See Volume 2.

FLASH DEVOLATILIZATION

Introduction

Flash devolatilization is a method for removing solvents and unreacted monomers from a polymer solution. The solution is heated and flashed into a chamber operated at reduced pressure. Boiling occurs by homogeneous nucleation and generates the surface area necessary for mass transfer of the volatile components from the liquid phase to the vapor phase. The overhead product is sent to a solvent recovery system. The bottom product, devolatilized polymer, is collected compressed, and pumped away. Figure 1 shows a typical process. Flash devolatilization is commonly used in vinyl polymerizations and in some condensation polymerizations. High volume, commercial examples include the removal of unreacted ethylene from low density, high pressure polyethylene (LDPE), the removal of hexane in the solution process for high density polyethylene (HDPE), and the removal of styrene and ethylbenzene in the bulk polymerization of polystyrene (see ETHYLENE POLYMERS, LDPE; ETHYLENE POLYMERS, HDPE; STYRENE POLYMERS; BULK AND SOLUTION POLYMERIZATIONS REACTORS.

Important process variables are the preflash temperature T_{in} and the post-flash pressure P_{out}. The flash illustrated in Figure 1 is rapid, adiabatic, and approaches thermodynamic equilibrium. The response variables are the outlet compositions of the vapor and polymer streams and their common outlet temperature T_{out}. The first step in analyzing this process is the estimation of thermodynamic equilibrium.

Equilibrium Calculations

A heat balance gives

$$T_{\text{out}} = T_{\text{in}} - \frac{\nu\lambda}{C_{\text{p}}} \tag{1}$$

Encyclopedia of Polymer Science and Technology. Copyright John Wiley & Sons, Inc. All rights reserved.

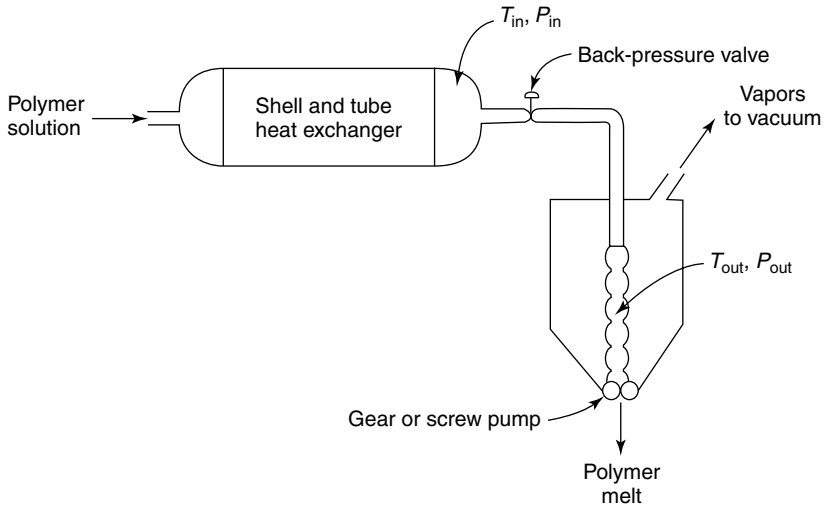

Fig. 1. Flash devolatilization process.

where ν is the weight fraction of the entering stream that is vaporized, λ is the heat of vaporization evaluated at T_{out}, and C_p is the specific heat of the polymer solution, prior to evaporation, evaluated as a mean value over the range from T_{in} to T_{out}. An overall material balance gives

$$w_{in} = \nu + (1 - \nu)_{out} \tag{2}$$

where w is the weight fraction of solvent. The volume fraction of solvent defined as

$$\phi = \rho_{mixture}/\rho_{solvent} \tag{3}$$

Assume that the partial pressure of the solvent equals the total pressure P_{out} in the flash chamber. Then

$$\frac{P_{out}}{P_{sat}} = \phi_{out} \exp\left[\left(1 - \frac{1}{m}\right)(1 - \phi_{out}) + \chi(1 - \phi_{out})^2\right] \tag{4}$$

where m is the degree of polymerization and χ is the FIory-Huggins interaction coefficient (typically 0.45 for a good solvent). The vapor pressure of the pure solvent P_{sat} is a function of T_{out} and is obtained from correlations such as the Antoine or Lee–Kesler equations. Equations 1–4 are solved simultaneously to determine the outlet temperature and solvent concentration.

The above treatment assumes there is only one volatile component, but the equations can be extended to multicomponent systems by writing a separate version of equation (4) for each component.

$$\frac{\text{Partial pressure of component } n}{\text{Vapor pressure of pure component } n} = (\phi_{out})_n \exp\left[\left(1 - \frac{1}{m}\right)(1 - \phi_{out}) + \chi(1 - \phi_{out})^2\right] \tag{5}$$

where $(\phi_{out})_n$ is the volume fraction of the nth component. The various partial pressures sum to P_{out}. The exponential term in equation 5 is the activity coefficient for that component. As indicated above, the same value is assumed for each solvent. It will have a value of about 4 for nearly complete devolatilization of a high molecular weight polymer. Special cases arise when the mixed solvents are highly nonideal or if the polymer crystallizes during the flash.

Many polymers degrade at the temperatures needed for devolatilization. Unzipping to monomer is typical of stryenics. The resulting volatiles are removed in the flash but will be regenerated if there is a substantial inventory of polymer in the process line after the flash. The degradation kinetics can be measured by isothermal weight loss in a thermal gravimetric analyzer. The degradation rates can be fit as a first-order reaction with Arrhenius temperature dependence. Unzipping to monomer imposes a practical limit of a few hundred ppm for polystyrene (see DEGRADATION).

Staged Flashes and Induced Foaming

A common application of flash devolatilization is the removal of 10–15% styrene-ethylbenzene from polystyrene. One commercial process uses $T_{in} = 240^{\circ}C$ and $P_{out} = 1.3$ kPa (10 torr). Equilibrium calculations for an adiabatic flash predict $T_{out} = 220^{\circ}C$ and $w_{out} = 500$ ppm; actual operation gives about 1200 ppm.

The secret to approaching equilibrium in a flash is the generation of surface area through foaming. Vapor bubbles nucleate, grow, and coalesce into an open-celled foam provided T_{out} exceeds the glass-transition temperature of the polymer. The small web thickness allows quick diffusion of the solvent from the polymer film, and the open-celled structure allows ready escape of the vapors. Thus equilibrium is approached; but as suggested by the polystyrene example, mass transfer limitations arise when w_{out} is low. Market demands for lower volatiles than achievable in a single flash prompted the use of a second flash. One process decreases the severity of the first flash so that 1–2% volatiles remain to cause natural foaming in the second flash. The partially devolatilized polymer is reheated and flashed a second time, again with $P_{out} = 1.3$ kPa (10 torr) but now with $T_{out} \cong 240^{\circ}C$ because the adiabatic temperature drop in the second flash is small. In practice, this process gives w_{out} 500–700 ppm. An alternative process retains the severe first flash but injects a foaming agent prior to the second flash. The foaming agent should be innocuous and highly volatile. It need not have significant solubility in the polymer, eg, water has been used for polystyrene. The primary purpose of the foaming agent is to generate an open-celled foam. A secondary benefit is the reduction in solvent partial pressure at a fixed total pressure in the flash chamber. The foaming agent can be mixed with the polymer using a short, melt-fed single-screw extruder. Pressure is applied so that the foaming agent remains a liquid. Static mixers have also been used.

A strictly adiabatic flash has disadvantages when polymerization or degradation reactions occur in the heat exchanger. Adiabatic operation forces high values of T_{in}, which can lead to by-products or undesired low molecular weight polymer. When the inlet viscosity is high, flashed polymer can be displaced from the heat exchanger by the incoming polymer solution. This allows boiling in the heat exchanger, giving higher heat transfer coefficients and a lower value for T_{in} because

some of the heat of vaporization is supplied directly rather than as sensible heat. In theory, the equilibrium flash calculations are easily modified to account for a partially vaporized feed. In practice, the extent of vaporization occurring within the tubes is difficult to calculate. A conservative approach to designing the heat exchanger is to assume that boiling does not occur. However, there is no need to apply back-pressure to the heat exchanger when the entering solution is highly viscous. For polystyrene, entering concentrations of 70% polymer are sufficient to allow boiling in the heat exchanger. Some designs install the heat exchanger directly above the flash chamber with no intermediate piping. Other designs use elaborate nozzles and foam distributors, but there is little evidence that these devices provide any practical advantage.

The generic process in Figure 1 can be applied to relatively dilute polymer solutions, although two- or three-staged flashes are needed for complete devolatilization. A process for recovering 10% polyethylene from a xylene solution employs a first flash with $w_{in} = 0.10$, $T_{in} = 280^{\circ}C$, and $P_{out} = 55$ kPa (8 psig). This gives a $T_{out} = 180^{\circ}C$ and $w_{out} = 0.85$. The P_{in} for this flash is set at 1896 kPa (275 psig) to avoid boiling and possible plugging of the heat exchanger. The second flash gives $w_{out} = 0.99$ and provides the fed to a rear-vented, single-screw extruder to complete the devolatilization.

Extruder and Wiped-Film Devolatilization

The surface area needed for mass transfer from the polymer phase to the vapor phase can be generated by mechanical devices such as single- and twin-screw extruders and wiped-film evaporators, but strictly mechanical generation of surface area scales up very poorly. The throughput of such devices scales as D^3, but the generation of surface area scales only as D^2 where D is the screw diameter. Surface area created by foaming scales as D^3 so that foaming is a highly desirable complement to the mechanical generation of surface area. Foaming occurs naturally in many extrusion processes so that some vendors suggest using $D^{2.5}$ as the scale-up factor where there is no explicit flash. Figure 2 shows a devolatilization scheme that has been employed in extruders to attain maximum removal of solvents.

The polymer solution is preheated and then flashed into the barrel of the extruder at a point downstream from the normal inlet. The polymer moves from left to right. Solvent vapors flow countercurrently and are removed at the rear end of the extruder. The partially devolatilized polymer is transported to the right. It is compressed, reheated, and pumped to a milling zone where additional devolatilization is caused by the mechanical generation of surface area. Figure 3 shows idealized results for devolatilization as a function of operating and scale-up variables. The y-axis indicates the extent of devolatilization, measured as $(w_{out} - w*)/(w_{in} - w*)$ where $w*$ is its equilibrium concentration of volatiles corresponding to the temperature and pressure in the extruder vent. The x-axis measures the collection of operating and scale-up variables that determine the extent of devolatilization according to a conventional model. These variables are the screw diameter D, the molecular diffusivity of the volatile component D the screw speed N, and the polymer flow rate Q (see EXTRUSION).

For the case of devolatilization extrusion with back-venting, Figure 2 shows a discontinuity at the origin that corresponds to a flash step at the inlet of the extruder. To a first approximation, the decrease in solvent concentration for this

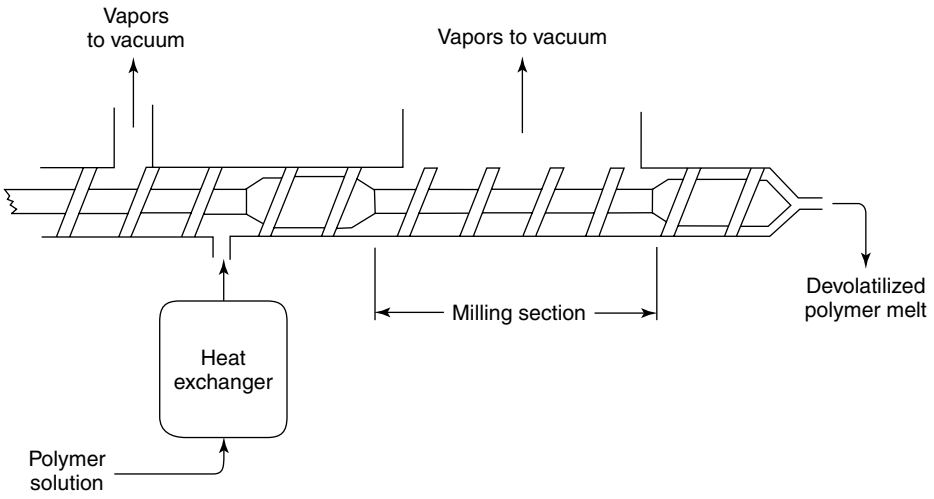

Fig. 2. Devolatilizing extruder with back-venting.

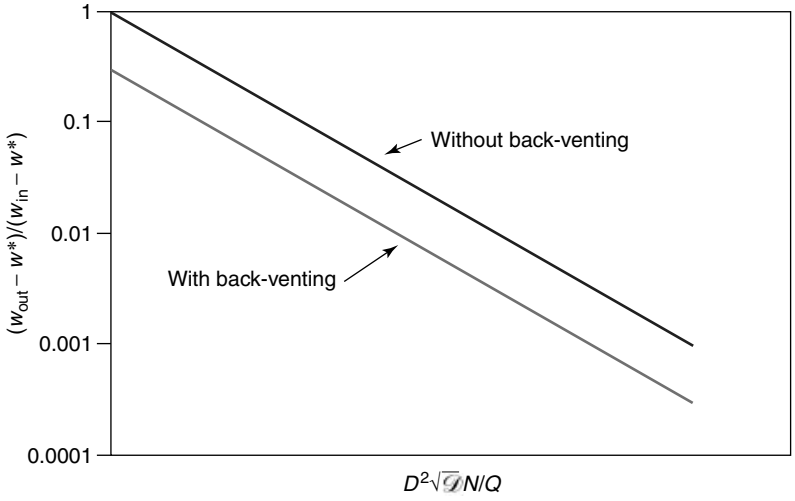

Fig. 3. Scale-up of devolatilizing extruders.

flash is independent of $D^2\sqrt{\mathcal{D}N}/Q$ and thus occurs to the same extent in any extruder, regardless of size. In the milling region, the solvent concentration decreases gradually, and the devolatilization capacity of this region scales rather uneconomically as $D^2\sqrt{\mathcal{D}N}/Q$. In practice, some foaming occurs in the milling section of extruders and in wiped-film evaporators. This foaming significantly improves devolatilization. Some extruder vendors suggest using a scale-up factor of $D^{2.5}\sqrt{\mathcal{D}N}/Q$ to account for foaming.

Equipment Considerations

Flash devolatilization is a relatively mature technology for the removal of volatile components from polymer melts and solutions. It was developed by major

companies during the 1960s and is now used in single-train units at rates exceeding 25 tons/h. The basic technology is applicable to a wide variety of systems. The capital cost is low compared to mechanical devolatilization, and the confidence in scaling up from pilot plant data is high. Despite these advantages, flash devolatilization is still confined to a relatively small number of companies that developed the technology originally or that acquired it from other companies. Dissemination of the technology has been inhibited by the lack of commercially available pilot-plant equipment. Individual units must be designed and fabricated from components. This is in sharp contrast to the situation with extruders and wiped-film devolatilizers, where many vendors supply pilot-scale units. The major equipment item for flash devolatilization is the pump used to extract the polymer from the flash chamber. Large capacity, jacketed gear pumps are available from several vendors. The inlet port to these pumps has been expanded to expose the gear teeth. These pumps work when the polymer foam falls on the gear teeth. There is no need for a suction head.

Conventional shell-and-tube heat exchangers are usually used to preheat the polymer solution prior to a flash, but flat-plate and spiral-wound heat-exchangers can be used for heat-sensitive materials.

BIBLIOGRAPHY

"Devolatilization" in *EPSE* 2nd ed., Vol. 4, pp. 745–751, by J. A. Biesenberger, Stevens Institute of Technology; "Flash Devolatilization" in *EPSE* 2nd ed., Suppl. Vol., pp. 317–323, by E. B. Nauman, Rensselaer Polytechnic Institute.

1. B. J. Meister and A. E. Platt, *Ind. Eng. Chem. Res.* **28**, 1659 (1989).
2. U.S. Pat. 3,668,161 (June 6, 1972), E. B. Nauman, T. T. Szabo, F. P. Kloser, and S. Kaufman (to Union Carbide Corp.).
3. U.S. Pat. 4,808,262 (Feb. 28, 1989), V. P. Aneja and J. P. Skilbeck (to General Electric Co.).

BRUCE NAUMAN
Rensselaer Polytechnic Institute

FLUOROCARBON ELASTOMERS. See Volume 2.

FOAMED PLASTICS. See CELLULAR MATERIALS.

FRACTOGRAPHY. See Volume 2.

FRACTURE. See Volume 2.

FREE RADICAL POLYMERIZATION. See RADICAL POLYMERIZATION.

FRP. See RADICAL POLYMERIZATION.

GELATIN

Introduction

Gelatin [9000-70-80] is a protein obtained by partial hydrolysis of collagen, the chief protein component in skin, bones, hides, and white connective tissues of the animal body (see COLLAGEN). Type A gelatin is produced by acid processing of collagenous raw material; type B is produced by alkaline or lime processing. Because it is obtained from collagen by a controlled partial hydrolysis and does not exist in nature, gelatin is classified as a derived protein. Animal glue and gelatin hydrolysate, sometimes referred to as liquid protein, are products obtained by a more complete hydrolysis of collagen and can thus be considered as containing lower molecular-weight fractions of gelatin.

Use of animal glues was first recorded ca 4000 BC in ancient Egypt (1). Throughout subsequent centuries, glue and crude gelatin extracts with poor organoleptic properties were prepared by boiling bone and hide pieces and allowing the solution to cool and gel. Late in the seventeenth century, the first commercial gelatin manufacturing began. At the beginning of the nineteenth century, commercial production methods gradually were improved to achieve the manufacture of high molecular weight collagen extracts with good quality that form characteristic gelatin gels (1–3).

Uses of gelatin are based on its combination of properties: reversible gel-to-sol transition of aqueous solution; viscosity of warm aqueous solutions; ability to act as a protective colloid; water permeability; and insolubility in cold water, but complete solubility in hot water. It is also nutritious. These properties are utilized in the food, pharmaceutical, and photographic industries. In addition, gelatin forms strong, uniform, clear, moderately flexible coatings which readily swell and absorb water and are ideal for the manufacture of photographic films and pharmaceutical capsules.

Encyclopedia of Polymer Science and Technology. Copyright John Wiley & Sons, Inc. All rights reserved.

Chemical Composition and Structure

Gelatin is not a single chemical substance. The main constituents of gelatin are large and complex polypeptide molecules of the same amino acid composition as the parent collagen, covering a broad molecular weight distribution range. In the parent collagen, the 18 different amino acids are arranged in ordered, long chains, each having ~95,000 mol wt. These chains are arranged in a rod-like, triple-helix structure consisting of two identical chains, called α_1, and one slightly different chain called α_2 (4–6). These chains are partially separated and broken, ie, hydrolyzed, in the gelatin manufacturing process. Different grades of gelatin have average molecular weight ranging from ~20,000 to 250,000 (7–18). Molecular weight distribution studies have been carried out by fractional precipitation with ethanol or 2-propanol and by complexing with anionic detergent molecules. The coacervates are isolated and recovered as gelatin fractions (19–22).

Analysis shows the presence of amino acids from 0.2% tyrosine to 30.5% glycine. The five most common amino acids are glycine [56-40-6], 26.4–30.5%; proline [147-85-3], 14.8(18%; hydroxyproline [51-35-4], 13.3–14.5%; glutamic acid [56-86-0], 11.1–11.7%; and alanine [56-41-7], 8.6–11.3%. The remaining amino acids in decreasing order are arginine [74-79-3], aspartic acid [56-84-8], lysine [56-87-1], serine [56-45-1], leucine [61-90-5], valine [72-18-4], phenylalanine [63-91-2], threonine [72-19-5], isoleucine [73-32-5], hydroxylysine [13204-98-3], histidine [71-00-1], methionine [63-68-3], and tyrosine [60-18-4] (18–25).

Warm gelatin solutions are more levorotatory than expected on the basis of the amino acid composition, indicating additional order in the molecule, which probably results from Gly-Pro-Pro and Gly-Pro-Hypro sequences (26). The α-chain form of gelatin behaves in solution like a random-coil polymer, whereas the gel form may contain as much as 70% helical conformation (27). The remaining molecules in nonhelical conformation link helical regions together to form the gel matrix. Helical regions are thought to contain both inter- and intramolecular associations of chain segments.

Gelatin structures have been studied with the aid of an electron microscope (28). The structure of the gel is a combination of fine and coarse interchain networks; the ratio depends on the temperature during the polymer–polymer and polymer–solvent interaction leading to bond formation. The rigidity of the gel is approximately proportional to the square of the gelatin concentration. Crystallites, indicated by X-ray diffraction pattern, are believed to be at the junctions of the polypeptide chains (29).

Homogeneous α-chain gelatin has been prepared by pretreating collagen with pronase in the presence of 0.4 M CaC_{l2} [10043-52-4], and extracting the gelatin with hot water at 80°C and pH 7.0 after inactivating the enzyme and removing the salts.

Stability. Dry gelatin stored in airtight containers at room temperature has a shelf life of many years. However, it decomposes above 100°C. For complete combustion, temperatures above 500°C are required. When dry gelatin is heated in air at relatively high humidity, < 60% rh, and at moderate temperatures, ie, above 45°C, it gradually loses its ability to swell and dissolve (25,26). Aqueous solutions or gels of gelatin are highly susceptible to microbial growth and breakdown by

proteolytic enzymes. Stability is a function of pH and electrolytes and decreases with increasing temperature because of hydrolysis.

Physical and Chemical Properties

Commercial gelatin is produced in mesh sizes ranging from coarse granules to fine powder. In Europe, gelatin is also produced in thin sheets for use in cooking. It is a vitreous, brittle solid, faintly yellow in color. Dry commercial gelatin contains about 9–13% moisture and is essentially tasteless and odorless with specific gravity between 1.3 and 1.4. Most physical and chemical properties of gelatin are measured on aqueous solutions and are functions of the source of collagen, method of manufacture, conditions during extraction and concentration, thermal history, pH, and chemical nature of impurities or additives.

Gelation. Perhaps the most useful property of gelatin solution is its capability to form heat reversible gel–sols. When an aqueous solution of gelatin with a concentration greater than about 0.5% is cooled to about 35–40°C, it first increases in viscosity, and then forms a gel. The gelation process is thought to proceed through three stages: (*1*) rearrangement of individual molecular chains into ordered, helical arrangement, or collagen fold (27–39); (*2*) association of two or three ordered segments to create crystallites (34,40,41); and (*3*) stabilization of the structure by lateral interchain hydrogen bonding within the helical regions. The rigidity or jelly strength of the gel depends on the concentration, the intrinsic strength of the gelatin sample, pH, temperature, and additives.

Because the economic value of gelatin is commonly determined by jelly strength, the test procedure for its determination is of great importance. Commercially, gelatin jelly strength is determined by standard tests which measure the force required to depress the surface of a carefully prepared gel by a distance of 4 mm using a flat-bottomed plunger 12.7 mm in diameter. The force applied may be measured in the form of the quantity of fine lead shot required to depress the plunger and is recorded in grams. The measurement is termed the Bloom strength after the inventor of the lead shot device (42,43). In the early 1990s, sophisticated testing equipment utilizing sensitive load cells for the measurement are commonly used.

The conversion temperature for gelatin is determined as setting point, ie, sol to gel, or melting point, ie, gel to sol. Commercial gelatins melt between 23 and 30°C, with the setting point being lower by 2–5°C. Melting point determination, described in Reference 44, utilizes test tubes filled with gelatin solution that are gently chilled to form a gel. The tubes are tilted and colored carbon tetrachloride solution is placed on the gelatin surface. The tube is gradually warmed and the end point is determined when the descent of the colored solution is observed. Several methods have been used to determine the setting point of gelatin (45).

Solubility. In most commercial applications, gelatin is used as a solution. Gelatin is soluble in water and in aqueous solutions of polyhydric alcohols such as glycerol [56-81-5] and propylene glycol [57-55-6]. Examples of highly polar, hydrogen-bonding organic solvents in which gelatin dissolves are acetic acid [64-19-7], trifluoroethanol [75-89-8], and formamide [75-12-7] (46). Gelatin is

practically insoluble in less polar organic solvents such as acetone, carbon tetrachloride, ethanol, ether, benzene, dimethylformamide, and most other nonpolar organic solvents. Many water-soluble organic solvents are compatible with gelatin, but interfere with gelling properties (47). Dry gelatin absorbs water exothermally. The rate and degree of swelling is a characteristic of the particular gelatin. Swelled gelatin granules dissolve rapidly in water above 35°C. The cross-linking of gelatin matrix by chemical means is used extensively in photographic products, and this so-called hardening permanently reduces the solubility of gelatin (33,48–54).

Amphoteric Character. The amphoteric character of gelatin is due to the functional groups of the amino acids and the terminal amino and carboxyl groups created during hydrolysis. In strongly acidic solution the gelatin is positively charged and migrates as a cation in an electric field. In strongly alkaline solution, it is negatively charged and migrates as an anion. The intermediate point, where net charge is zero and no migration occurs, is known as the isoelectric point and is designated in pH units (55,56). A related property, the isoionic point, can be determined by utilizing a mixed-bed ion-exchange resin to remove all nongelatin cations and anions. The resulting pH of the gelatin solution is the isoionic point and is expressed in pH units. The isoionic point is reproducible, whereas the isoelectric point depends on the salts present. Type A gelatin has a broad isoionic region between pH 7 and pH 10; type B is in a lower, more reproducible region, reaching an isoionic point of 5.2 after 4 weeks of liming, which drops to 4.8 after prolonged or more vigorous liming processes (57–60). The isoelectric point can also be estimated by determining a pH value at which a gelatin solution exhibits maximum turbidity (61). Many isoionic point references are recorded as isoelectric points even though the latter is defined as a pH at which gelatin has net charge of zero and thus shows no movement in the electric field (62).

Viscosity. The viscosity of gelatin solutions is affected by gelatin concentration, temperature, molecular weight of the gelatin sample, pH, additives, and impurities. In aqueous solution above 40°C, gelatin exhibits Newtonian behavior. Standard testing methods employ use of a capillary viscometer at 60°C and gelatin solutions at 6.67 or 12.5% solids (43,45). The viscosity of gelatin solutions increases with increasing gelatin concentration and with decreasing temperature. For a given gelatin, viscosity is at a minimum at the isoionic point and reaches maxima at pH values near 3 and 10.5 (63). At temperatures between 30 and 40°C, non-Newtonian behavior is observed, probably due to linking together of gelatin molecules to form aggregates (64,65). Addition of salts decreases the viscosity of gelatin solutions. This effect is most evident for concentrated gelatin solutions (66–68).

Colloid and Emulsifying Properties. Gelatin is an effective protective colloid that can prevent crystal, or particle, aggregation, thereby stabilizing a heterogeneous suspension. It acts as an emulsifying agent in cosmetics and pharmaceuticals involving oil-in-water dispersions. The anionic or cationic behavior of gelatin is important when used in conjunction with other ionic materials. The protective colloid property is important in photographic applications where it stabilizes and protects silver halide crystals while still allowing for their normal growth and sensitization during physical and chemical ripening processes.

Coacervation. A phenomenon associated with colloids wherein dispersed particles separate from solution to form a second liquid phase is termed

coacervation. Gelatin solutions form coacervates with the addition of salt such as sodium sulfate [7757-82-6], especially at pH below the isoionic point. In addition, gelatin solutions coacervate with solutions of oppositely charged polymers or macromolecules such as acacia. This property is useful for microencapsulation and photographic applications (69–74).

Swelling. The swelling property of gelatin is not only important in its solvation but also in photographic film processing and the dissolution of pharmaceutical capsules. That pH and electrolyte content affect swelling has been explained by the simple Donnan equilibrium theory, treating gelatin as a semipermeable membrane (75). This explains why gelatin exhibits the lowest swelling at its isoelectric pH. At pH below the isoelectric point, proper choice of anions can control swelling, whereas above the isoelectric point, cations primarily affect swelling. These effects probably involve breaking hydrogen bonds, resulting in increased swelling. The rate of swelling follows approximately a second-order equation (76,77). In photographic products, the swelling of the gelatin layer is controlled by coating conditions, drying conditions, chemical cross-linking, and the composition of the processing solutions (49–54). Conditioning at 90% rh and 20°C for 24 h greatly reduces swelling of hot dried film coatings (78–80). The ratio of lateral to vertical swelling is of great concern in the photographic industry since it can cause curling of photographic papers or films when changes in humidity or general moisture content take place.

Manufacture and Processing

Although new methods for processing gelatin, including ion exchange and cross-flow membrane filtration, have been introduced since 1960, the basic technology for modern gelatin manufacture was developed in the early 1920s. Acid and lime processes have separate facilities and are not interchangeable. In the past, bones and ossein, ie, decalcified bone, have been supplied by India and South America. In the 1990s, slaughterhouses and meat-packing houses are an important source of bones. The supply of bones has been greatly increased since the meat-packing industry introduced packaged and fabricated meats, assisted by the growth of fast-food restaurants. Dried and rendered bones yield about 14–18% gelatin, whereas pork skins yield about 18–22%.

Most type A gelatin is made from pork skins, yielding grease as a marketable by-product. The process includes macerating of skins, washing to remove extraneous matter, and swelling for 10–30 h in 1–5% hydrochloric acid [7647-01-0], phosphoric acid [7664-38-2], or sulfuric acid [7664-93-9]. Then four to five extractions are made at temperatures increasing from 55–65°C for the first extract to 95–100°C for the last extract. Each extraction lasts about 4–8 h. Grease is then removed, the gelatin solution filtered, and, for most applications, deionized. Concentration to 20–40% solids is carried out in several stages by continuous vacuum evaporation. The viscous solution is chilled, extruded into thin noodles, and dried at 30–60°C on a continuous wire-mesh belt. Drying is completed by passing the noodles through zones of successive temperature changes wherein conditioned air blows across the surface and through the noodle mass. The dry gelatin is then ground and blended to specification.

Type B gelatin is made mostly from bones, but also from bovine hides and pork skins. The bones for type B gelatin are crushed and degreased at the rendering facilities, which are usually located at a meat-packing plant. Rendered bone pieces, 0.5–4 cm, with less than 3% fat, are treated with cool, 4–7% hydrochloric acid from 4 to 14 days to remove the mineral content. An important by-product, dibasic calcium phosphate, is precipitated and recovered from the spent liquor. The demineralized bones, ie, ossein, are washed and transferred to large tanks where they are stored in a lime slurry with gentle daily agitation for 3–16 weeks. During the liming process, some deamination of the collagen occurs with evolution of ammonia. This is the primary process that results in low isoelectric ranges for type B gelatin. After washing for 15–30 h to remove the lime, the ossein is acidified to pH 5–7 with an appropriate acid. Then the extraction processing for type A gelatin is followed. Throughout the manufacturing process, cleanliness is important to avoid contamination by bacteria or proteolytic enzymes.

Bovine hides and skins are substantial sources of raw material for type B gelatin and are supplied in the form of splits, trimmings of dehaired hide, rawhide pieces, or salted hide pieces. Like pork skins, the hides are cut to smaller pieces before being processed. Sometimes the term calfskin gelatin is used to describe hide gelatin. The liming of hides usually takes a little longer than the liming of ossein from bone.

Most manufacturing equipment should be made of stainless steel. The liming tanks, however, can be either concrete or wood. Properly lined iron tanks are often used for the washing and acidification, ie, souring, operations. Most gelatin plants achieve efficient processes by operating around the clock. The product is tested in batches and again as blends to confirm conformance to customer specifications.

Economic Aspects

World gelatin production in 2000 was believed to be about 260,000 t. The United States produced about 45,000 t, followed by Germany, France, Brazil, Japan, and India. Of the gelatin produced in the United States, 59% is acid-processed, ie, type A. The U.S. food industry consumes about 25,000 t/year, with an annual growth rate of 0.5%; the pharmaceutical industry consumes about 20,000 t/year; and the photographic industry about 10,000 t/year. In the United States, the pharmaceutical gelatin market is expected to grow on the average of 2.5% per year. The photographic gelatin market has been stable or declining slightly.

Analytical Test Methods and Quality Standards. Gelatin is identified by a positive test for hydroxyproline [51-35-4], turbidity with tannic acid [1401-55-4], or a yellow precipitate with acidic potassium dichromate [7778-50-9] or trinitrophenol [88-89-1]. A 5% aqueous solution exhibits reversible gel-to-sol formation between 10 and 60°C. Gelatin gives a positive color test for aldehydes and sugars that are considered undesirable impurities in photographic gelatin; nucleic acids are considered restrainers in photographic gelatins and their concentration is monitored closely for this application (81). Elemental analysis of commercial gelatin is reported as carbon, 50.5%; hydrogen, 6.8%; nitrogen, 17%; and oxygen

25.2% (82); a purer sample analyzed for 18.2–18.4% nitrogen (23,25). Regulations for quality standards vary from country to country, but generally include specifications for ash content, SO_2, heavy metals, chromium, lead, fluoride, arsenic, odor, and for the color or clarity of solutions (83). In addition, certain bacteriological standards, including E. coli and Salmonella, are specified. Restrictions on certain additives and preservatives are also listed. In the United States, the *Food Chemicals Codex* published an updated specification for food-grade gelatin in 1996. Standard testing procedures for viscosity, pH, ash, moisture, heavy metals, arsenic, bacteria, and jelly strength are described (42,83–87). Additional test procedures have been published by the photographic and gelatin industries including the Japanese PAGI Method (88,89). Specific tests for photographic gelatin have been devised by the International Working Group for Photographic Gelatin (IAG) (90) in Fribourg, Switzerland, and by individual photographic companies and gelatin companies.

Uses

Food Products. Gelatin formulations in the food industry use almost exclusively water or aqueous polyhydric alcohols as solvents for candy, marshmallow, or dessert preparations. In dairy products and frozen foods, gelatin's protective colloid property prevents crystallization of ice and sugar. Gelatin products having a wide range of Bloom and viscosity values are utilized in the manufacture of food products, specific properties being selected depending on the needs of the application. For example, a 250-Bloom gelatin may be utilized at concentrations ranging from 0.25% in frozen pies to 0.5% in ice cream; the use of gelatin in ice cream has greatly diminished. In sour cream and cottage cheese, gelatin inhibits water separation, ie, syneresis. Marshmallows contain as much as 1.5% gelatin to restrain the crystallization of sugar, thereby keeping the marshmallows soft and plastic; gelatin also increases viscosity and stabilizes the foam in the manufacturing process. Many lozenges, wafers, and candy coatings contain up to 1% gelatin. In these instances, gelatin decreases the dissolution rate. In meat products, such as canned hams, various luncheon meats, corned beef, chicken rolls, jellied beef, and other similar products, gelatin in 1–5% concentration helps to retain the natural juices and enhance texture and flavor. Use of gelatin to form soft, chewy candies, so-called gummi candies, has increased worldwide gelatin demand significantly (ca 1992). Gelatin has also found new uses as an emulsifier and extender in the production of reduced-fat margarine products. The largest use of edible gelatin in the United States, however, is in the preparation of gelatin desserts in 1.5–2.5% concentrations. For this use, gelatin is sold either premixed with sugar and flavorings or as unflavored gelatin packets. Most edible gelatin is type A, but type B is also used.

Pharmaceutical Products. Gelatin is used in the pharmaceutical industry for the manufacture of soft and hard capsules. The formulations are made with water or aqueous polyhydric alcohols. Capsules are usually preferred over tablets in administering medicine (91). Elastic or soft capsules are made with a rotary die

from two plasticized gelatin sheets which form a sealed capsule around the material being encapsulated. Methods have been developed to encapsulate dry powders and water-soluble materials which may first be mixed with oil. The gelatin for soft capsules is low bloom type A, 170–180 g; type B, 150–175 g; or a mixture of type A and B. Hard capsules consisting of two parts are first formed and then filled. The manufacturing process is highly mechanized and sophisticated in order to produce capsules of uniform capacity and thickness. Medium-to-high bloom type A, 250–280 g; type B, 225–250 g; or the combination of type A and B gelatin are used for hard capsules. Usage of gelatin as a coating for tablets has increased dramatically. In a process similar to formation of gelatin capsules, tablets are coated by dipping in colored gelatin solutions, thereby giving the appearance and appeal of a capsule, but with some protection from adulteration of the medication. The use of glycerinated gelatin (83) as a base for suppositories offers advantages over carbowax or cocoa butter base (92). Coated or cross-linked gelatin is used for enteric capsules. Gelatin is used as a carrier or binder in tablets, pastilles, and troches.

For arresting hemorrhage during surgery, a special sterile gelatin sponge known as absorbable gelatin sponge (28) or Gelfoam is used. The gelatin is partially insolubilized by a cross-linking process. When moistened with a thrombin or sterile physiological salt solution, the gelatin sponge, left in place after bleeding stops, is slowly dissolved by tissue enzymes. Special fractionated and prepared type B gelatin can be used as a plasma expander.

Gelatin can be a source of essential amino acids when used as a diet supplement and therapeutic agent. As such, it has been widely used in muscular disorders, peptic ulcers, and infant feeding, and to spur nail growth. Gelatin is not a complete protein for mammalian nutrition, however, since it is lacking in the essential amino acid tryptophan [73-22-3] and is deficient in sulfur-containing amino acids.

Photographic Products. Gelatin has been used for over 100 years as a binder in light-sensitive products. The useful functions of gelatin in photographic film manufacture are a result of its protective colloidal properties during the precipitation and chemical ripening of silver halide crystals, setting and film-forming properties during coating, and swelling properties during processing of exposed film or paper. Quality requirements of photographic gelatin may be very elaborate and can include over 40 chemical and physical tests, in addition to photographic evaluation. Most chemical impurities are limited to less than 10 ppm. Aqueous solutions are employed for emulsions. Photographic gelatins are manufactured to standard specifications since the testing is time-consuming and costly. A new gelatin product may require 6–12 months of testing, including extensive field testing prior to commercialization. Photographic products may have up to 20 gelatin layers grouped into three categories: (*1*) light-sensitive silver halide-bearing layers of 2–10 μm thickness, referred to as emulsion layers; (*2*) surface, spacer, filter, or protective layers of 1–2 μm thickness; and (*3*) backing, antihalo, or noncurl layers coated on the opposite side of the film substrate from the emulsion layer. The quality and uniformity standards are highest for emulsion gelatin because it controls silver halide nucleation, crystal growth, chemical sensitization, latent image stability, and numerous other factors affecting the total photographic response. Since the early 1970s, the photographic industry has switched from so-called

active gelatins derived from hides to inert types derived from bones. The latter are very low or void of natural restrainers, reduction, and sulfur sensitizers. Other changes in techniques have been brought about by abandoning the lengthy noodle wash technique used to remove salts after silver halide precipitation in favor of precipitating, coagulating, or derivatizing gelatin and washing the precipitate by decanting or utilizing ultrafiltration techniques; by new coating techniques that allow simultaneous coating of several layers at one time at speeds 10 times as fast as before; and by short-time high temperature processing which may require new cross-linking agents unlike the aldehydes and metal salts previously used. Many new hardeners are extremely fast-acting and are metered into the solution during the coating operation. It is quite common to use a derivatized gelatin, such as phthalated gelatin, to precipitate silver halide (74). These materials with a low pH isoionic point form a coacervate at pH < 4.0. Precipitation in this case is accomplished by lowering the pH, washing at low pH, and then increasing pH to above 6.5 to dissolve and redisperse the emulsion before reconstituting it with gelatin. Gelatin used in the auxiliary layers must be able to withstand high temperature processing and allow high speed coating.

Gelatin is also used in so-called subbing formulations to prepare film bases such as polyester, cellulose acetate [9004-35-7], cellulose butyrate, and polyethylene-coated paper base for coating by aqueous formulations. Solvents such as methanol [67-56-1], acetone [67-64-1], or chlorinated solvents are used with small amounts of water. Gelatin containing low ash, low grease, and having good solubility in mixed solvents is required for these applications (see COATINGS). In certain lithographic printing, light-sensitive dichromated gelatin is used. Light causes permanent cross-linking of gelatin in the presence of the dichromate; this phenomenon is used to make relief images for printing. Dichromated gelatin coatings are commonly used in production of high quality holographic images. In this application, the light sensitivity of the image-receiving medium is less important than the image-resolving power (93,94). Gelatin coatings in photographic products are further tested for brittleness, scratch resistance, friction, swelling rate, drying rate, curling tendency, dry adhesion, wet adhesion, and pressure sensitivity. These properties are becoming more critical with the development of more sophisticated cameras and printing and processing equipment. Photographic technology offers a rapidly changing, highly sophisticated, very competitive market for photographic gelatin manufacturers.

Derivatized Gelatin. Chemically active groups in gelatin molecules are either the chain terminal groups or side-chain groups. In the process of modifying gelatin properties, some groups can be removed, eg, deamination of amino groups by nitrous acid [10024-97-2] (95), or removal of guanidine groups from arginine [74-79-3] by hypobromite oxidation (96); the latter destroys the protective colloid properties of gelatin. Commercially successful derivatized gelatins are made mostly for the photographic gelatin and microencapsulation markets. In both instances, the amino groups are acylated. Protein detergent is made by lauroylating gelatin. Phthalated gelatin is now widely used in the photographic industry (97). Arylsulfonylated gelatin has been patented for microencapsulation (qv) (98). Carbamoylated gelatin, made by treating gelatin with cyanate or nitrourea in neutral aqueous solution, is also used by the photographic industry (24,99–101). Active double bonds react with the amino groups in gelatin, and

acrylic polymers have been grafted to gelatin (102). Gelatin has been derivatized by epoxides (103), cyclic sulfones (104), and cyanamide [420-04-2] (105). Cross-linking or hardening of gelatin attacks the same active groups, but an agent with two active sites is needed, eg, divinylsulfone [77-77-0], bis(isomaleimide) [13676-54-5], aziridines, bisepoxides, epichlorohydrin [106-89-8], polyisocyanates, and dichlorotriazine. Aldehydes such as formaldehyde [50-00-0] and glyoxal [107-22-2] are still used and to a small extent even potassium chromium alum [7788-99-0], $Cr_2K_2(SO_4)_4 \cdot 24H_2O$, and potassium aluminum alum [7784-24-9], $Al_2K_2(SO_4)_4 \cdot 24H_2O$.

BIBLIOGRAPHY

"Gelatin" in *EPST* 1st ed., Vol. 7, pp. 446–460, by H. H. Young, Swift and Co.; "Gelatin" in *EPSE* 2nd ed., Vol. 7, pp. 488–513, by P. I. Rose, Eastman Kodak Co.

1. P. Koepff, in H. Ammann-Brass and J. Pouradier, eds., Photographic Gelatin, in Proceedings of the Fourth IAG Conference, 1983 Internationale Arbeitsgemeinschaft für Photogelatine, Fribourg, Switzerland, 1985, pp. 3–35.
2. R. H. Bogue, *The Chemistry and Technology of Gelatine and Glue*, McGraw-Hill Book Co., Inc., New York, 1922.
3. P. I. Smith, *Glue and Gelatine*, Pitman Press, London, 1929.
4. A. H. Kang, *Biochemistry* **5**, 509–515 (1966).
5. A. H. Kang, *Biochem. Biophys. Res. Commun.* **36**, 345–349 (1969).
6. K. A. Piez, *Brookhaven Symp. Biol.* **21**, 345–357 (1968).
7. A. Courts, *Biochem. J.* **58**, 70 (1954).
8. S. Aoyagi, in H. Ammann-Brass and J. Pouradier, eds., Photographic Gelatin, in Proceedings of the Fourth IAG Conference, 1983 Internationale Arbeitsgemeinschaft für Photogelatine, Fribourg, Switzerland, 1985, pp. 79–94.
9. D. Larry and M. Vedrines, in H. Ammann-Brass and J. Pouradier, eds., Photographic Gelatin, in Proceedings of the Fourth IAG Conference, 1983 Internationale Arbeitsgemeinschaft für Photogelatine, Fribourg, Switzerland, 1985, pp. 35–54.
10. C. Xiang-Fang and P. Bi-Xian, in H. Ammann-Brass and J. Pouradier, eds., Photographic Gelatin, in Proceedings of the Fourth IAG Conference, 1983 Internationale Arbeitsgemeinschaft für Photogelatine, Fribourg, Switzerland, 1985, pp. 55–64.
11. J. Butel, in H. Ammann-Brass and J. Pouradier, eds., Photographic Gelatin, in Proceedings of the Fourth IAG Conference, 1983 Internationale Arbeitsgemeinschaft für Photogelatine, Fribourg, Switzerland, 1985, pp. 65–78.
12. P. Koepff, in H. Ammann-Brass and J. Pouradier, eds., *Photographic Gelatin Reports 1970–1982*, The International Working Group for Photographic Gelatin, Fribourg, Switzerland, 1984, pp. 197–209.
13. I. Tomka, in H. Ammann-Brass and J. Pouradier, eds., *Photographic Gelatin Reports 1970–1982*, The International Working Group for Photographic Gelatin, Fribourg, Switzerland, 1984, p. 210.
14. J. Bohonek, A. Spühler, M. Ribeaud, and I. Tomka, in R. J. Cox, ed., *Photographic Gelatin II*, Academic Press, Inc., New York, 1976, pp. 37–55.
15. T. Ohno, Y. Okawa, M. Horiuchi, N. Fijita, N. Kobayashi, R. Muratubaki, N. Nishida, O. Hounokidani, and N. Nakagawa, in M. DeClercq, ed., Photographic Gelatin,

in Proceedings of the Seventh IAG Conference, Louvain-la-Neuve, 1999, The International Working Group for Photographic Gelatin, Fribourg, Switzerland, 1999, pp. 64–71.
16. Y. Okawa, H. Suzuki, J. Kobayashi, H. Kobayashi, and T. Ohno, in M. DeClercq, ed., Photographic Gelatin, in Proceedings of the Seventh IAG Conference, Louvain-la-Neuve, 1999, The International Working Group for Photographic Gelatin, Fribourg, Switzerland, 1999, pp. 72–78.
17. E. Quanten, M. DeClercq, ed., Photographic Gelatin, in Proceedings of the Seventh IAG Conference, Louvain-la-Neuve, 1999, The International Working Group for Photographic Gelatin, Fribourg, Switzerland, 1999, pp.79–95.
18. T. J. Sims, A. J. Bailey, and D. S. Field, *Imaging Sci. J.* **45**(3/4), 171–177 (1997).
19. J. Pouradier and A. M. Venet, *J. Chim. Phys.* **47**, 381 (1950).
20. G. Stainsby, P. R. Saunders, and A. G. Ward, *J. Polym. Sci.* **12**, 325 (1954).
21. L.-J. Chen and A. Shohei, *J. Photogr. Sci.* **40**, 159 (1992).
22. S. Aoyagi N. Ohkubo, and Y. Otsubo, *Imaging Sci. J.* **45**(3/4) 178–182 (1997).
23. J. E. Eastoe, in G. N. Ramachandran, ed., *Treatise on Collagen*, Vol. 1, Academic Press, Inc., New York, 1967, pp. 1–72.
24. P. Johns, in A. G. Ward and A. Courts, eds., *The Science and Technology of Gelatin*, Academic Press, Inc., New York, 1977, pp. 475–506.
25. J. E. Eastoe, *Biochem. J.* **61**, 589 (1955).
26. J. Josse and W. F. Harrington, *J. Mol. Biol.* **9**, 269 (1964).
27. G. Stainsby, *J. Chim. Phys.* **47**, 127 (1950).
28. I. Tomka, J. Bohonek, J. Spühler, and M. Ribeaud, *J. Photogr. Sci.* **23**, 97 (1975).
29. T. Fujii, *Bull. Soc. Sci. Photogr.* **16**, 274 (1966).
30. E. M. Marks, D. Tourtelotte, and A. Andux, *Food Technol.* **22**, 99 (1968).
31. R. T. Jones, in K. Ridgway, ed., *Hard Capsules Development and Technology*, The Pharmaceutical Press, London, 1987, pp. 41–42.
32. Standard Methods for Sampling and Testing Gelatins, Gelatin Manufacturers' Institute of America, Inc., New York, 1986.
33. P. H. von Hippel and W. F. Harrington, *Biochim. Biophys. Acta* **36**, 427 (1959).
34. P. H. von Hippel and W. F. Harrington, *Brookhaven Symp. Biol.* **13**, 213 (1960).
35. P. J. Florey and E. S. Weaver, *J. Am. Chem. Soc.* **82**, 4518 (1960).
36. S. Takahashi, T. Nakakima, K. Suzuki, Y. Okawa, H. Kobayashi, and T. Ohno, in M. DeClercq, ed., Photographic Gelatin, in Proceedings of the Seventh IAG Conference, Louvain-la-Neuve, 1999, The International Working Group for Photographic Gelatin, Fribourg, Switzerland, 1999, pp. 137–146.
37. D. P. Knight, *Imaging Sci. J.* **45**(3/4), 183–190 (1997).
38. A. Bot, R. H. W. Wienjes, and K. H. de Haas, *Imaging Sci. J.* **45**(3/4), 191–196 (1997).
39. T. Kobayashi, T. Ohno, H. Kobayashi, Y. Okawa, C. Endo, and T. Hongo, *Imaging Sci. J.* **45**(3/4), 210–214 (1997).
40. J. Engel, *J. Arch. Biochem.* **97**, 150 (1962).
41. H. Bredtker and P. Doty, *J. Phys. Chem., Ithica* **58**, 968 (1954).
42. A. Veis, in B. L. Horecker, N. D. Kaplan, and H. E. Sheraga, eds., *Molecular Biology*, Vol. **V**, Academic Press, Inc., New York, 1964, Chapt. "5".
43. E. Fuchs, *Adhesion* **5**, 225 (1961).

44. *Sampl. Test. Gelatins, Brit. Stand.* **6**, 757 (1975).
45. F. W. Wainwright, *GGRA Bull.* **17**(3), 10 (1966).
46. C. A. Finch and A. Jobling, in Ref. 24, pp. 271–272; A. R. Krough, in Ref. 24, pp. 439–475.
47. J. Q. Umberger, *Photogr. Sci. Eng.* **11**, 385 (1967).
48. K. M. Hornsby, *Br. J. Photogr.* **103**, 17, 28, (1956).
49. J. Janus, A. W. Kechington, and A. G. Ward, *Research* **4**, 247 (1951).
50. N. Itoh, *J. Photogr. Sci.* **40**, 200 (1992).
51. B. E. Tabor, R. Owers, and J. F. Janus, *J. Photogr. Sci.* **40**, 205 (1992).
52. T. Takahashi, *J. Photogr. Sci.* **40**, 212 (1992).
53. J. Rottman and H. Pietsch, *J. Photogr. Sci.* **40**, 217 (1992).
54. J. M. Dolphin, *The Imaging Sci. J.* **45**(3/4), 252–255 (1997).
55. T. D. Weatherill, R. W. Henning, and K. A. Smith, *J. Photogr. Sci.* **40**, 220 (1992).
56. S. Aoyagi, in M. DeClercq, ed., Photographic Gelatin, in Proceedings of the Seventh IAG Conference, Louvain-la-Neuve, 1999, The International Working Group for Photographic Gelatin, Fribourg, Switzerland, 1999, pp. 45–53.
57. C. R. Maxey and M. R. Palmer, in R. J. Cox, ed., *Photographic Gelatin II*, Academic Press, Inc., New York, 1976, pp. 27–36.
58. C. Li-juan, in H. Ammann-Brass and J. Pouradier, eds., Photographic Gelatin, in Proceedings of the Fourth IAG Conference, 1983 Internationale Arbeitsgemeinschaft für Photogelatine, Fribourg, Switzerland, 1985, pp. 136–144.
59. Y. Toda, in H. Ammann-Brass and J. Pouradier, eds., Photographic Gelatin, in Proceedings of the Fourth IAG Conference, 1983 Internationale Arbeitsgemeinschaft für Photogelatine, Fribourg, Switzerland, 1985, pp. 107–124.
60. Y. Toda, in S. J. Band, ed., Photographic Gelatin, in Proceedings of the Fifth RPS Symposium, Oxford, U.K., 1985 The Imaging Science and Technology Group of the Royal Photographic Society, 1987, pp. 28–37.
61. J. E. Eastoe and A. Courts, *Practical Analytical Methods for Connective Tissue Proteins*, Spon, London, 1963, Chapt. "6".
62. A. Veis, B. L. Horecker, N. D. Kaplan, and H. E. Sheraga, eds., *Molecular Biology*, Vol. **V**, Academic Press, Inc., New York, 1964, Chapt. "5", p. 112.
63. G. Stainsby, *Nature (London)* **169**, 662–663 (1952).
64. G. Stainsby, in H. Sauverer, ed., *Scientific Photography*, Pergamon Press, London, 1962, p. 253.
65. S. B. Ross-Murphy, *The Imaging Sci. J.* **45**(3/4), 205–209 (1997).
66. C. W. N. Crumper and A. E. Alexander, *Aust. J. Sci. Res. A* **5**, 146 (1952).
67. G. Stainsby, *J. Chim. Phys.* 109–136. (1950).
68. O. M. Simion, in M. DeClercq, ed., Photographic Gelatin, in Proceedings of the Seventh IAG Conference, Louvain-la-Neuve, 1999, The International Working Group for Photographic Gelatin, Fribourg, Switzerland, 1999, pp. 163–172.
69. V. Zitko and J. Rosik, *Chem. Zvesti* **17**, 109 (1963).
70. Br. Pat. 930,421 (1963) (to Upjohn Co.).
71. P. D. Wood, *J. Chim. Phys.* 419–422 (1950).
72. B. Kuznicka and J. Kuznicki, *Research* 206–212 (1951).
73. R. J. Croome, in H. Ammann-Brass and J. Pouradier, eds., Photographic Gelatin, in Proceedings of the Fourth IAG Conference, 1983, Internationale Arbeitsgemeinschaft für Photogelatine, Fribourg, Switzerland, 1985, pp. 267–282.
74. D. L. Kramer, *J. Photogr. Sci.* **40**, 152 (1992).
75. H. R. Proctor and J. A. Wilson, *J. Chem. Soc.* **109**, 307 (1916).
76. A. Libicky and D. I. Bermane, in R. J. Cox, ed., *Photographic Gelatin*, Academic Press, Inc., New York, 1972, pp. 29–48.

77. R. Poerschke, *Imaging Sci. J.* **45**(3/4), 215–216 (1997).
78. D. W. Jopling, *J. Appl. Chem.* **6**, 79 (1956).
79. R. F. Rainville, in M. DeClercq, ed., Photographic Gelatin, in Proceedings of the Seventh IAG Conference, Louvain-la-Neuve, 1999, The International Working Group for Photographic Gelatin, Fribourg, Switzerland, 1999, pp. 1–17.
80. Y. Toda, in M. DeClercq, ed., Photographic Gelatin, in Proceedings of the Seventh IAG Conference, Louvain-la-Neuve, 1999, The International Working Group for Photographic Gelatin, 1999, pp. 43–44.
81. J. Russell and D. L. Oliff, *J. Photogr. Sci.* **14**, 9 (1966).
82. C. R. Smith, *J. Am. Chem. Soc.* **43**, 1350 (1921).
83. The United States Pharmacopeia XXII (USP XXII–NFXVII), The United States Pharmacopeial Convention, Inc., Rockville, Md., 1989.
84. K. Helrich, ed., *AOAC, Official Methods of Analysis*, 15th ed., Association of Official Analytical Chemists, Arlington, Va., 1990.
85. G. C. Hider, in M. DeClercq, ed., Photographic Gelatin, in Proceedings of the Seventh IAG Conference, Louvain-la-Neuve, 1999, The International Working Group for Photographic Gelatin, Fribourg, Switzerland, 1999, p. 96.
86. A. Raab, and J. Dolphin, in M. DeClercq, ed., Photographic Gelatin, in Proceedings of the Seventh IAG Conference, Louvain-la-Neuve, 1999, The International Working Group for Photographic Gelatin, Fribourg, Switzerland, 1999, pp. 97–104.
87. S. Tani, and T. Tani, in M. DeClercq, ed., Photographic Gelatin, in Proceedings of the Seventh IAG Conference, Louvain-la-Neuve, 1999, The International Working Group for Photographic Gelatin, Fribourg, Switzerland, 1999, pp. 105–111.
88. PAGI Method, 8th ed., Photographic and Gelatin Industries, Japan, Tokyo, 1997.
89. S. Takahashi, in M. DeClercq, ed., Photographic Gelatin, in Proceedings of the Seventh IAG Conference, Louvain-la-Neuve, 1999, The International Working Group for Photographic Gelatin, 1999, pp. 195–202.
90. IAG Test, Gelatin Manufacturers Institute of America, New York; see also Ref. 1.
91. Consumer Survey, A. C. Nielsen Co., Northbrook, Ill., 1976.
92. L. F. Tice and R. E. Abrams, *J. Am. Pharm. Assoc.* **14**, 24 (1953).
93. *Sci. J.* **4**(10), 27 (1968).
94. A. P. Giraud, in M. DeClercq, ed., Photographic Gelatin, in Proceedings of the Seventh IAG Conference, Louvain-la-Neuve, 1999, The International Working Group for Photographic Gelatin, 1999, pp. 18–23.
95. A. W. Kenchington, *Biochem. J.* **68**, 458 (1958).
96. P. Davis, in G. Stainsby, ed., *Recent Advances in Gelatin and Glue Research*, Pergamon Press, London, 1958, p. 225.
97. U.S. Pat. 3,184,312 (May 18, 1965), J. W. Gates and E. Miller (to Eastman Kodak Co.).
98. Br. Pat. 1,075,952 (July 19, 1967), R. C. Clark and co-workers (to Gelatin and Glue Research Assoc.).
99. U.S. Pat. 2,525,753 (Oct. 10, 1950), H. C. Yutzky and G. F. Frame (to Eastman Kodak Co.).
100. U.S. Pat. 3,108,995 (Oct. 29, 1963), D. Tourtellotte and E. M. Marks (to Charles B. Knox Gelatin Co., Inc.).
101. U.S. Pat. 2,816,099 (Dec. 10, 1959), H. H. Young and E. F. Christophen (to Swift and Co.).
102. U.S. Pat. 3,291,611 (Dec. 13, 1966), J. J. Krajewski (to Swift and Co.).
103. Belg. Pat. 672,906 (Nov. 26, 1965), F. Dersch and S. L. Paniccia (to GAF Corp.).

104. Br. Pat. 1,033,189 (June 15, 1956), J. W. Gates Jr. and P. E. Miller (to Kodak Ltd.).
105. Br. Pat. 1,100,842 (Jan. 24, 1968), R. J. Chamberlain (to American Cyanamid Co.).

THOMAS R. KEENAN
Knox Gelatine, Inc.

GELS. See HYDROGELS.

GENE-DELIVERY POLYMERS

Introduction to Human Gene Therapy

Gene therapy may be defined as the treatment of human disease by the transfer of genetic material into specific cells of the patient (1). The advances in molecular biology and biotechnology of the last 30 years have greatly enhanced our understanding of the genetics of pathogenesis and have led to the identification of numerous disease-causing genes. With the impending completion of the Human Genome Project, the list of genetic disease targets is likely to grow tremendously. It is not difficult to envision treatment of genetic diseases such as hemophilia (2), muscular dystrophy (3–5), or cystic fibrosis (6) through replacement of errant genes within the affected cells. However, gene therapy approaches are also being developed for treatments of virtually all forms of cardiovascular diseases (7), neurological diseases (8–10), infectious diseases (11), wound healing (12), and cancer (13–15). In these instances, the delivered genes may be intended to augment naturally occurring proteins (eg growth factors or cytokines), to alter the expression of existing genes facilitating a desired cellular or tissue response, or to produce cytotoxic proteins or prodrug-activating enzymes, for example, to kill tumor cells in cancer treatment (13,15) or proliferating endothelial cells to inhibit restenosis following balloon angioplasty (7,16). Finally, it has been shown that expression of viral genes within certain tissues can result in an efficient immune response, leading to the development of DNA vaccines (17).

Because of the potential to revolutionize treatment of a broad range of human diseases, including some of mankind's most-hated and currently intractable afflictions, gene therapy has been heavily investigated over the past decade. More than 17,000 papers containing the keywords "gene therapy" have appeared in the MEDLINE database since 1990. The first gene therapy clinical trial, for

Encyclopedia of Polymer Science and Technology. Copyright John Wiley & Sons, Inc. All rights reserved.

severe combined immunodeficiency caused by a defect in the gene encoding the enzyme adenosine deaminase, was initiated in 1990 (18). However, it was not until April 2000 that Cavazzana-Calvo and co-workers (19) reported the first clinical success by treating two infants with γc-severe combined immunodeficiency. Also that year, Kay and co-workers (20) reported positive data in an early hemophilia clinical trial and Khuri and co-workers (21) reported the successful completion of a phase II clinical trial using a combination of a viral vector and traditional chemotherapy to treat recurrent squamous cell carcinoma of the head and neck. Considering that a total of 596 clinical trials have been completed, are ongoing, or are pending worldwide (22), the small number of successes has been disappointing.

A variety of factors is impacting the progress of human gene therapy. The first step is to identify the proper genes and target cells that will elicit the desired therapeutic effect. It is then necessary to transfer that gene, often specifically to the target cells only, with the highest possible efficiency. While short-term gene expression is sufficient for some applications, such as cancer therapies, long-term expression is needed for treatment of chronic conditions, including most genetic diseases. Unfortunately, however, maintenance of the expression has been difficult. Similarly, for many applications it will be critical to regulate the gene expression, keeping it at the required levels and also controlling when and how the gene expression is turned on and off. Finally, one must obviously accomplish each of these tasks in a way that is safe for the patient. Both toxicity/pathogenicity of the delivery vehicle and the patient's immune response to the treatment must be considered. The majority of these factors, with the exception of identifying a therapeutic gene, are primarily functions of gene delivery. Thus, the key limitation to development of human gene therapy remains the lack of a safe, efficient, and controllable methodology for gene delivery (23).

Methods of Gene Delivery

Gene delivery vehicles can be divided into essentially one of two categories: recombinant viruses and synthetic vectors. The majority of synthetic vectors, furthermore, can be divided into polymers (the subject of this review) and liposomes. Each type of material has important advantages and disadvantages. In order to best understand the problems facing polymer-based gene delivery vehicles and their current state of development, it is useful to briefly examine the alternate methodologies (Table 1).

Viral Vectors. The primary function of a virus is to efficiently carry its own genome from one host cell to another through (perhaps) "hostile" environments, enter the new target cell, navigate to the cell nucleus, and initiate expression of its genome—albeit for the purpose of self-replication. Viruses can be transformed into gene delivery vehicles by removing part of the virus' genome and replacing it with a therapeutic gene. If done carefully, the resulting recombinant virus will retain the functions essential for infection of specific target cells, but will be rendered incapable of replication and, hence, will be nonpathogenic. Because viruses evolved essentially as sophisticated gene delivery vehicles, such recombinant viral vectors are incredibly efficient. Viral vectors have been employed in the majority of gene

Table 1. Comparison of Three Classes of Gene Delivery Vectors

	Advantages	Disadvantages
Recombinant viruses 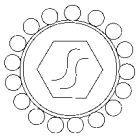	Highly efficient Can infect dividing cells Prolonged expression possible Used in most clinical trials to date	Lack of cell specificity Pathogenicity Immunogenicity Difficult and expensive production and purification
Liposomes 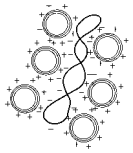	Relatively efficient Perform well *in vivo* Little immunogenicity Used in some clinical trials	Poorly stable Toxicity Lack of cell-specific targeting
Polyplexes 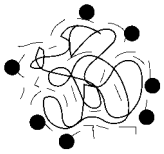	Simple Inexpensive Potential for cell-specific targeting Flexible chemistry Potentially biocompatible	Low efficiency Work poorly *in vivo* Not used in clinical trials to date

delivery studies reported in the literature and in nearly three quarters of gene therapy clinical trials (429 of 596 protocols approved as of September 2001) (22).

Viral gene delivery vectors have been based upon retrovirus, lentivirus (eg, HIV), adenovirus (AdV), adeno-associated virus (AAV), herpes simplex virus (HSV), and pox virus. There are several important properties that determine the suitability of a viral vector for a specific indication. The duration and regulation of gene expression are often critical factors. For example, retrovirus, lentivirus, and AAV integrate their genetic payload with the host genome, leading to the potential for prolonged transgene expression. The range of host cells that may be infected is also very important. Retrovirus, AdV, and AAV can infect a wide variety of cell types while (wild-type) lentivirus and HSV are limited to specific white blood cells and neurons, respectively. Furthermore, most retroviruses can infect only actively dividing cells, which greatly limits the host cell range, especially for *in vivo* gene transfer. In contrast, the closely related lentivirus, as well as AdV and AAV, can infect nondividing cells. For more information on recombinant viral gene delivery vectors, several excellent reviews have been published recently (24–28).

While viruses are extremely efficient gene delivery vehicles, they are not ideal vectors for human gene therapy. Safety concerns have been the primary bottleneck to clinical application of viral gene delivery vectors. While recombinant viral vectors have been rendered nonreplicative, and therefore nonpathogenic, there still exists the possibility for reverting to a wild-type virion or copurifying replication competent virions. Furthermore, viruses are inherently immunogenic, not only leading to difficulty with repeat administrations, but also the possibility

of dangerous immune reactions. In fact, the death of 18-year-old Jesse Gelsinger in a gene therapy clinical trial in September 1999 was ultimately caused by a severe immune response to the adenoviral gene delivery vector employed in the study. Viral vectors are also limited by their natural target-cell specificity. Some viruses will infect only a limited number of cell types, and their specificity seldom overlaps with the needs of human gene therapy. Further, some viruses (including AdV, AAV, and the pseudotyped retro- and lentiviruses) are quite nonspecific, but for *in vivo* applications, it is often necessary to target only one type of cell. Finally, because the viral vectors are complex biological agents, production and purification are difficult and expensive.

Synthetic Vectors. Although viruses are incredibly efficient gene delivery agents, synthetic vectors provide opportunities for improved safety, greater flexibility, and more facile manufacturing. In general, synthetic vectors are materials that bind electrostatically to DNA or RNA, condensing the genetic material into nanometer-scale complexes (a few tens to several hundred nanometers in diameter) that protect the genes and allow them to enter cells. Such materials have included cationic peptides, proteins, polymers, and liposomes. Various synthetic vectors, including (diethylamino)ether (DEAE)-dextran (29) and calcium phosphate (30), have been used extensively for *in vitro* gene transfer studies since the 1960s. However, development of nonviral vectors for *in vivo* gene delivery, especially clinical applications, has suffered from problems including toxicity, low gene transfer efficiency, and *in vivo* instability.

Cationic Lipids. Use of cationic lipids for gene delivery was first reported in 1987 (31). Since that time, many different lipid structures have been used. Indeed, greater than 30 products are currently available commercially for *in vitro* gene transfer (eg, Transfectam®, LipofectAMINE®, Lipofectin®, and Lipofectace®). These various lipids differ in terms of the nature of their cationic headgroup, their hydrophobic tails, and the spacers linking the two. Cationic headgroups displaying different numbers of charged groups comprising primary, secondary, tertiary, and quaternary amines have been reported. The lipid tails can be saturated or unsaturated and of varying length. Also, cholesterol-based structures have been reported (eg, DC-Chol (32)). The linker can vary in length and hydrophilicity, and some have been designed to incorporate degradable linkages to enhance biocompatibility. These structural properties affect not only the interactions of the lipids with the polyanionic genetic material, but also influence the membrane properties of liposomes formed from them, both of which have been found to have a strong influence on gene delivery efficiency (33). Furthermore, the cationic lipids typically require a helper lipid, commonly di-oleoyl phosphatidylethanolamine (DOPE), that provides the membrane fluidity required to mediate efficient endocytosis and liposome-cell membrane fusion (34).

The variety of lipids and lipid mixtures used in gene delivery has resulted in steadily improving gene transfer efficiencies. This progress has been documented in several excellent reviews (35–38). As a result of their relatively high efficiency, cationic lipids have been the most widely studied of the synthetic vectors. “Lipofection” has been routinely employed in both *in vitro* and *in vivo* gene delivery studies, and in several human gene therapy clinical trials (22). However, lipid-based gene delivery has several critical limitations including lack of cell-specific targeting capacity, difficulty in reproducibly fabricating liposomes and

DNA–liposome complexes, and toxicity, especially upon systemic administration (39).

Cationic Polymers. Cationic polymers have been used as gene carriers since the late 1980s (40). Like the cationic lipids, these polymers, including off-the-shelf materials and polymers specifically designed for gene delivery, have included a wide variety of chemistries. DNA-binding moieties include primary, secondary, tertiary, and quaternary amines, as well as other positively charged groups such as amidines. The charges may reside in the polymer backbone, in pendant groups, or in grafted oligomers. The polymers themselves comprise linear, branched, and dendrimeric structures. Because of this flexibility in polymer chemistries that are available, it may be possible to provide the multiple functions required for efficient gene delivery while maintaining biocompatibility, facile manufacturing, and robust and stable formulation of DNA–polymer complexes (polyplexes). As a result, cationic polymers have great potential for human gene therapy. However, the poor gene transfer efficiency achieved thus far has limited clinical application of these vectors. The specific advantages and disadvantages of several important classes of cationic polymers is described in more detail below.

Barriers to Gene Delivery. All gene delivery vectors, whether viral or synthetic, must perform the same task of escorting genes from solution (eg, in a vial) to the cell nucleus. In order to complete this task, a vector must navigate a series of obstacles, both extracellular and intracellular (41). Viruses have evolved a set of functions to address each challenge. As a result, recombinant viral vectors are highly efficient gene delivery vehicles. In contrast, synthetic vectors are generally unsatisfactory because they typically lack one, or several, of the necessary functions. Therefore, consideration of the important barriers to gene delivery in the next two sections is important in order to understand the limitations of currently available cationic polymers and is necessary for the rational design of new polymers.

Extracellular Barriers

Gene delivery vectors face a first set of barriers in transporting genes from the test tube to the outer membrane of a target cell. These include *in vitro* barriers, such as binding and condensing plasmid DNA and maintaining the complex in solution, as well as *in vivo* barriers, including stability and survival in the blood stream, penetrating the blood vessel wall and surrounding tissue, and specific binding to the target cells of interest. Several of these barriers are discussed in this section.

Gene Packaging. Plasmid DNA is a fragile macromolecule and must be protected from ubiquitous nucleases found both *in vivo* and *in vitro*. Binding of plasmids by cationic polymers provides the needed protection by sterically blocking access of enzymes to the DNA backbone. Further, the physical size of plasmid DNA (∼3–5,000,000 Da; radius of gyration of several hundred nanometers) prevents it from easily crossing the membrane of most cells. The vector material must, therefore, condense the DNA into a smaller, more compact structure. Binding and condensation of genes by the vector material is a necessary first step to efficient gene delivery.

Gene delivery vectors bind to DNA through charge–charge interactions between the negative phosphates along the DNA backbone and positive charges displayed on the vector material. The process of condensation is entropically driven; the free energy decrease resulting from the increased translational entropy of counterions and water molecules dominates the binding energy and loss of entropy in the DNA and polymer (42). Thus, polyplexes form spontaneously upon mixing of cationic polymers with plasmid DNA. The resulting particles are typically toroidal or spherical structures (43,44) with diameters ranging from a few tens of to several hundred nanometers. Each polyplex particle typically comprises several DNA molecules along with many polymer chains. The structure and morphology of polyplexes appears to be kinetically controlled (45) and often depends on the order of mixing (polymer to DNA solution or DNA to polymer solution). Efforts have been made to better understand condensation (42,45,46), but further improvements in the theoretical understanding of the process and better physicochemical characterization of the resulting complexes are needed.

The structure of the polymer can affect DNA binding and condensation. Linear, branched, and dendrimeric polymers all bind plasmid DNA with similar strengths, but complexes containing linear poly-L-lysine (PLL) or polyamidoamine (PAMAM) dendrimers tend to aggregate while branched polyethylenimine (PEI) and "fractured" PAMAM dendrimers (Fig. 1) do not (47). The aggregation apparently leads to decreased gene transfer efficiency. Not surprisingly, the number of cationic moieties has a strong effect on the polymer–DNA interaction. Several groups have reported that a minimum of six to eight charges are required for efficient DNA condensation (48–52). The same groups disagree, however, on the effect of the oligopeptide sequence. Wadhwa and co-workers reported that addition of a single tryptophan (Trp) residue into PLL oligomers increased DNA binding (48). In contrast, Plank and co-workers found that Trp residues had no major effect on DNA binding and, in fact, decreased the "DNA-compacting potency" of the peptides (50). Additionally, placing the cationic moiety nearer the polymer backbone and keeping the charges to a minimum separation along the polymer backbone correlated with increased binding (53).

It is important to note that strong binding and efficient DNA condensation do not correlate directly with gene delivery efficiency. In fact, in some cases the opposite is true. This is likely because too tight binding prevents transcription from those plasmids that do reach the nucleus. Thus, a polymer must balance sufficient binding strength to protect the plasmid during transit to the nucleus with the ability to release the plasmid, perhaps due to competitive binding of genomic DNA or anionic lipids (54), once in the nucleus (52).

Solution Stability. The solution stability of polyplexes depends on the polymer structure and on the DNA/polymer charge ratio. Neutral polyplexes quickly form large aggregates, which are generally ineffective gene delivery agents. In contrast, positively charged polyplexes, as evidenced by zeta potential measurements, typically remain in solution. However, new studies have shown that the solubility and aggregate size of even positive complexes is time-dependent (45).

The concentration ranges over which polyplexes are soluble and stable are limited. For example, PLL/DNA complexes precipitate above about 20 μg DNA/mL

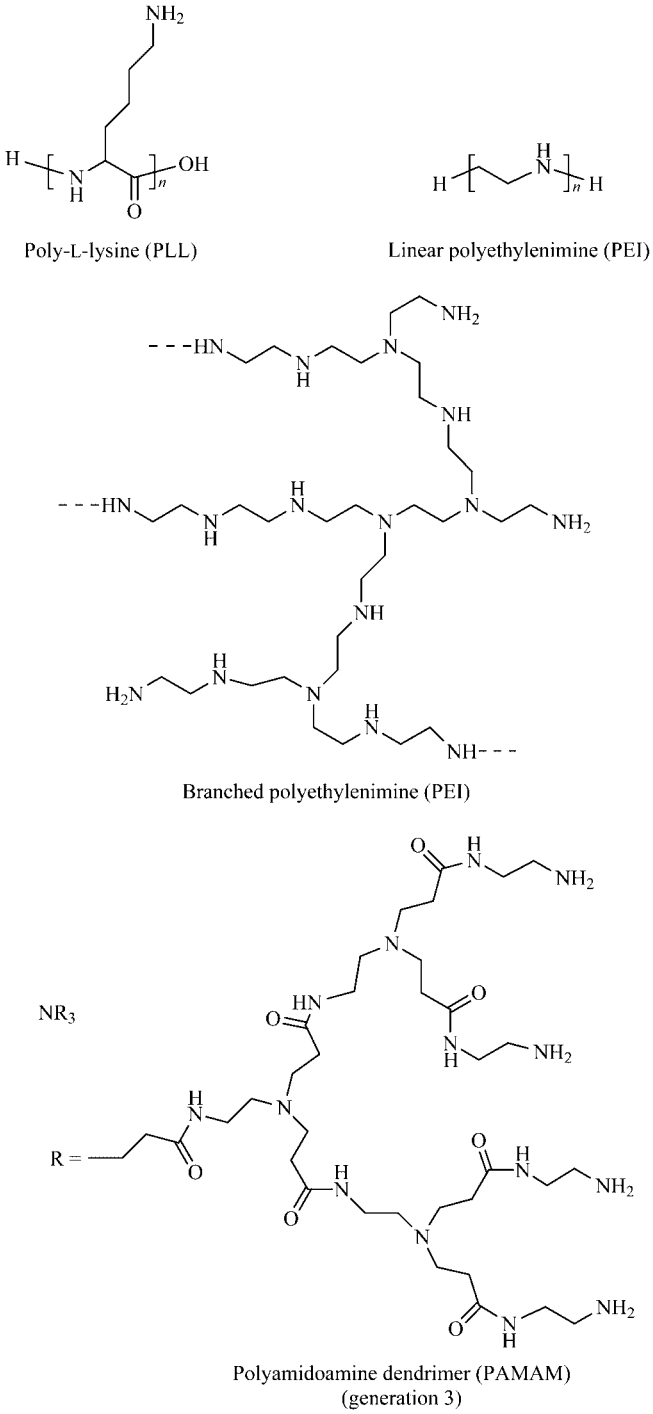

Fig. 1. Structures of several off-the-shelf gene delivery polymers.

(55). Other polymers show similar limits. The limited solubility imposes a maximum dose that can be administered in a reasonable injection volume.

Solution stability is further modified by the presence of salts and especially the protein milieu of the *in vivo* environment. In the presence of physiological salt concentrations, many polyplexes aggregate even at concentrations at which they are stable in water, which further limits the achievable dose and can even be toxic because of embolization of the particulates in the lung. Adsorption of serum albumin and other negatively charged proteins causes further aggregation and can lead to rapid clearance of the polyplexes by phagocytic cells and the reticuloendothelial system (56). Finally, polyplexes containing PLL, a fifth generation PAMAM dendrimer, and PEI, as well as some lipoplexes, have been shown to strongly activate the complement system upon intravenous administration (57).

Modification of polyplexes with poly(ethylene glycol) (PEG), typically grafted onto the polymer as a "brush," can stabilize polyplexes against salt-, protein-, and complement-induced inactivation (58,59). The increased stability due to PEGylation is presumed to result from steric effects leading to decreased particle–particle and particle–protein interactions. The effect depends on the PEG molecular weight, the grafting density, and the method of attachment of PEG to the polymer (58,60). Attachment of other hydrophilic polymers such as *N*-(2-hydroxypropyl)methacrylamide (HPMA) (59,61–64), oligosaccharides (59,65,66), sugars (67,68), and proteins (69) had similar effects.

Cell-Specific Targeting. The degree of target-cell specificity required for a given gene therapy varies widely. For some applications, such as hemophilia, the identity of the transduced cells is of little concern so long as sufficient levels of the therapeutic protein are produced. In other applications, such as cystic fibrosis, the transgene will act only in specific types of cells; expression in other cell types is largely benign. But in applications such as cancer therapies, wherein the goal is to kill the target cells, gene delivery to a very specific set of cells is required.

Polymers generally do not possess a capacity for cell-specific targeting. A typical polyplex, exhibiting an excess of positively charged groups over the negative phosphates, will bind to the negatively charged cell surface through nonspecific electrostatic interactions (70). However, polymers do provide flexible chemistry for modifying polyplexes with desired targeting moieties allowing both increased cell uptake and, often, cell specificity. Many membrane-bound receptor proteins can be used as targets. Derivatization of amino groups with glycosidic moieties, including galactose, glucose, mannose, and lactose (71–78), as well as other small molecules such as folate (79,80), provides selective targeting to cell types displaying the appropriate receptor protein. In two classic examples of protein-mediated targeting, asialoorosomucoid was attached to polylysine (40,81–83) in order to target the asialoglycoprotein receptor on hepatocytes, while Wagner and co-workers developed a method for targeting polyplexes to a variety of cell types, especially hematopoietic cells, through attachment of the iron-transport protein transferrin (43,84–87). Finally, certain other proteins may provide targeting to a more limited range of cells. Examples include epidermal growth factor (EGF) (88,89), antibodies or antibody fragments (90), and integrin-binding sequences (91).

The success of a targeting strategy, and the degree of specificity, will depend on the conjugation chemistry, the length of spacer between ligand and polyplex, the ligand–receptor binding strength, and the number of targeting ligands per polyplex. A variety of common cross-linking chemistries have been used to attach targeting ligands to the polymers including covalent bonds and biotin-streptavidin (88). However, care must be taken to ensure that the ligand-receptor interaction is not disrupted by the conjugation chemistry. Schaffer and co-workers found that for EGF-biotin/avidin-PLL conjugates, short cross-linkers between the EGF and biotin interfered with EGF/EGF-receptor binding, but a 30 Å spacer allowed nearly unhindered binding and resulted in significantly higher gene transfer efficiency. There also exists a balance between the specific targeting interactions and nonspecific electrostatic binding to the cell surface. Cell uptake and gene expression were found to be specific only within a narrow window of polymer/DNA ratios near electroneutrality (92). Finally, there is typically an optimum in ligand valency, because of saturation of both receptor binding and the cell's internalization machinery (92). Thus, efficient cell-specific targeting requires careful optimization of the various parameters that affect cell–surface binding.

Intracellular Barriers

Upon binding to the surface of a target cell and being internalized, gene delivery vehicles are challenged with a new set of intracellular obstacles. Several studies have shown that although >95% of cells in culture may internalize vectors rather efficiently (>100,000 copies per cell (93)), only a small fraction, typically <50%, express the transgene. Polyplexes are generally internalized by endocytosis, and once in the endocytic pathway, polyplexes may be trafficked to lysosomes, acidic vesicles filled with degradative enzymes (94). Gene delivery vectors must escape this pathway into the cytoplasm. Once in the cytoplasm, the vectors must be transported toward the nucleus and subsequently cross the nuclear membrane. Finally, at some point during this process, the polymer must release the genes so that the genes can be transcribed in the nucleus. The process is illustrated in Figure 2. Each step of this process represents a potential efficiency-limiting barrier, and a vector needs to provide functionality to overcome each one.

Endolysosomal Escape. Polyplexes bind to the surface of cells via nonspecific electrostatic interactions and are internalized via adsorptive pinocytosis. Alternatively, polyplexes derivatized with targeting ligands may bind to specific cell–surface receptors, in which case they are often internalized by receptor-mediated endocytosis. In either case, the polyplexes become localized within endocytic vesicles, which isolate the polyplex from the rest of the cell. The endocytic pathway represents a hostile environment for polyplexes. The first vesicle, termed the early endosome, fuses with sorting endosomes from which the internalized material may be transported back to the membrane and out of the cell by exocytosis. More generally, however, polyplexes are believed to be trafficked into late endosomes, vesicles that rapidly acidify to pH 5–6 because of the action of an ATPase proton-pump enzyme in the vesicle membrane. Polyplexes may subsequently be trafficked into lysosomes, which further acidify to

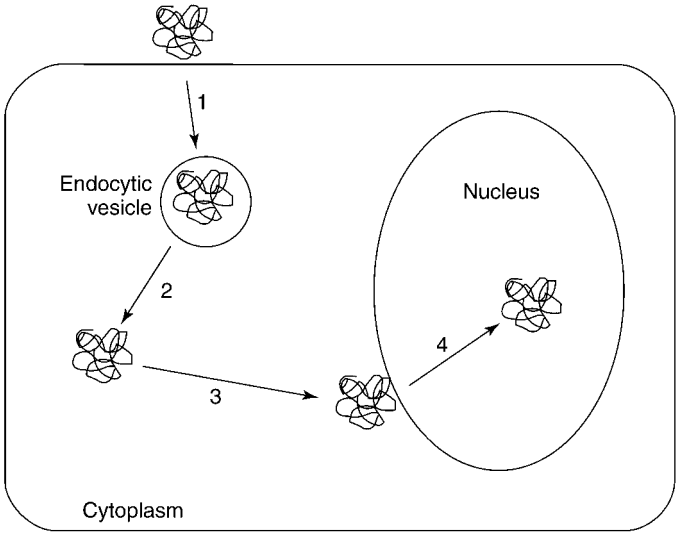

Fig. 2. Intracellular trafficking of polymer gene delivery vectors. 1, Internalization (often by adsorptive pinocytosis or receptor-mediated endocytosis); 2, escape from endocytic vesicles; 3, transport through the cytosol; 4, transport across the nuclear membrane. In addition, polyplexes must be unpackaged at some point in the process, although it is not known where in the process unpackaging occurs.

pH ~4.5 and contain various degradative nucleases, proteases, and lipases. It is believed that polyplexes will become trapped in these vesicles and be degraded. Only those vectors that escape into the cytoplasm can go on to reach the nucleus.

Several strategies have been employed to overcome this barrier. Concurrently, treating cells at the time of transfection with chloroquine, which is known to accumulate in the acidic vesicles and buffer their pH, results in improved gene delivery (95). While this approach has been commonly employed in *in vitro* studies with polymers such as PLL, it is impractical for *in vivo* gene delivery. Other researchers have tried to overcome this barrier by incorporating additional functional groups into polyplexes to provide for endosomal escape. For example, covalent attachment of whole, inactivated AdV particles to PLL was found to enhance gene transfer up to 2000-fold (96–99). It was proposed that this enhancement is due to more efficient endosomal escape, but the virion particle may also provide functionality for addressing subsequent barriers (see below). While successful, this approach is not practical because of the increased difficulty of preparing the vector and the safety concerns, especially immunogenicity, raised by the presence of the virus. Alternatively, fusogenic viral (100–103) or synthetic (104–108) peptides may also provide the endosomal escape function (109,110). These peptides are typically pH-sensitive amphiphiles that undergo a structural change, such as α-helix formation, at acidic pH and then insert into and disrupt the vesicle membrane. The peptides may be associated with polyplexes via electrostatic interactions or covalently attached to the polymer. Gene transfer is typically enhanced 1–3 orders of magnitude in this fashion.

Because of the versatile structures available in cationic polymer gene delivery vehicles, it is possible to build an endosomal escape function into the polymer itself. Polymers such as PEI and PAMAM dendrimers, which contain a large number of secondary and tertiary amines, can undergo large changes in protonation between physiological pH and lysosomal pH. It has been hypothesized that these polymers can, in fact, prevent acidification of endocytic vesicles. Furthermore, these polymers may act as "proton sponges" wherein their buffering capacity results in osmotic swelling and rupture of the endocytic vesicles (111–113). While it is not clear how these polymers function (whether simply by protecting the DNA from acidic pH and enzymatic degradation or by osmotic swelling of the vesicles), there is a clear relationship between polymer buffering capacity and gene delivery (47). Indeed, polymers designed specifically to provide such buffering capacity have proven to be highly successful (*vide infra*) (114–117).

Transport through the Cytoplasm. Once released from endosomal compartments, polyplexes must move through the cytoplasm to the nucleus. However, the cytoplasm is quite concentrated with protein, microtubules, and other organelles, all of which may hinder polyplex transport. In fact, previous studies have indicated that movement through the cytoplasm is size-dependent. Fluorescence recovery after photobleaching studies showed that dextran polymers with hydrodynamic radius more than 260 Å appear to be immobile (118). More recent studies of DNA mobility showed again that diffusion is size-dependent, with DNA larger than 3000 bp being essentially immobile (119). Given the large size of polyplexes, one might expect these vectors to be immobile as well. This fact, together with the known degradation of DNA in the cytosol as a result of the presence of cytosolic nucleases (120), presents an often-overlooked barrier to efficient gene delivery.

Viruses, in contrast, typically have evolved mechanisms for cytoplasmic transport. Subgroup C adenoviruses, including types 2 and 5 (Ad2 and Ad5) escape endosomes rapidly following endocytosis and, thus, are typically "far" from the nucleus. These virus particles have evolved mechanisms by which they then use cytoplasmic dynein motor proteins for active transport along microtubules (MT) toward the nucleus. In contrast, subgroup B Ad (eg, Ad7) lacks the ability to utilize dynein-mediated MT transport. Rather, Ad7 remains in endocytic vesicles and is transported toward the nucleus with their endocytic vesicles (as early endosomes mature into late endosomes and finally lysosomes, the vesicles are transported along MT toward the nuclear envelope). Ad7 then escapes from lysosomes (triggered by lower pH) near the nucleus, thereby mitigating the effects of low cytoplasmic motility (121). It may be possible that positively charged polyplexes use similar mechanisms by nonspecifically interacting with motor proteins, for example. Alternatively, polyplexes may be redistributed throughout the cell, with some ending up near the nucleus, becasue of the mixing that occurs during mitosis. The mechanisms of cytoplasmic polyplex transport need to be better characterized in order to facilitate design of improved polymeric vectors.

Nuclear Localization. Therapeutic genes must reach the cell nucleus to be expressed by the target cell. However, because the genome and nuclear machinery are vital to a cell's functions, nature has isolated the nucleus behind a

double-bilayer membrane with tightly regulated pores to allow import and export of a very specific set of biomolecules. The nuclear pore complex, a 10^7-kDa assembly of at least 30 distinct proteins, allows passage of small molecules, but proteins larger than 10–20 kDa require active transport via specific nuclear import proteins (eg, importins). Viruses have evolved mechanisms to utilize the cell's nuclear import machinery; polymers clearly do not have this capacity. Transfection immediately before cell division (and concomitant disruption of the nuclear membrane) is 30- to 500-fold more effective than transfection of cells at the beginning of their cell cycle (122). In contrast, nondividing cells are poorly transfected compared to dividing cells (122,124). Thus, transport across the nuclear membrane, especially for nondividing cells, appears to be a formidable obstacle to nonviral gene delivery vectors.

It may be possible to modify polyplex vectors to allow efficient nuclear import (125). For example, it is well known that many proteins are targeted to the nucleus by the presence of nuclear localization signals (NLS), short peptide sequences, typically highly cationic, that are recognized by importins. Because of their positive surface charge, it is possible that polyplexes could mimic NLS to a limited extent (126), but if so they are very inefficient as very few vectors typically reach the nucleus (127). However, there is some evidence that this is not a general phenomenon. Other polymers and cationic liposomes do not show an NLS effect (128,129). Several investigators have modified polyplexes by attachment of NLS with generally modest results (128–132). Further, nucleotide sequences on the genes themselves may provide some nuclear targeting (133–135), but this will not find general use as the nucleotide sequences are hidden by the polymer in most cases. In short, nuclear import of polyplex vectors is one of the most poorly characterized steps in the gene delivery process. A better understanding of nuclear transport mechanisms is needed.

Unpackaging. Just as incorporation into a polymer complex protects DNA from enzymatic degradation, so too will complexation prevent binding of the proteins required for initiation of gene expression. Thus, a gene delivery vector must release its DNA at some point in the delivery process. Indeed, efficient nuclear localization does not correlate with high gene expression. Several studies have found that reducing the polymer/DNA binding strength, by reducing the number of positive charges (136), conjugation of PEG chains (60), or decreasing the polymer molecular weight (52), leads to increased gene expression. Polymers must clearly be designed to incorporate a mechanism for nonspecific or environmentally responsive release of the genes, ideally in the nucleus.

"Off-the-Shelf" Polymers in Gene Delivery

Many of the early studies on polymer-mediated gene delivery employed commercially available polymers. As they were not designed for gene delivery, their efficacy as delivery vectors is somewhat serendipitous. Off-the-shelf polymers have nonetheless been very widely studied and form the basis for much of the gene delivery polymer literature. However, significant problems face these polymers, most

notably with cytotoxicity. Three of the major off-the-shelf polymers are described below.

Poly-L-lysine. Poly-L-lysine (PLL; Fig. 1) was one of the first cationic polymers used in the modern era of gene delivery research (40,55). It is commercially available in a range of sizes from oligomers to several hundred kilodaltons. For gene delivery, 20–50 kDa PLL is most commonly used. Polyplexes of DNA and PLL itself are poor gene delivery vectors, but addition of targeting ligands greatly enhances *in vitro* and *in vivo* gene delivery efficiency.

Some of the first reports of PLL-mediated gene delivery employed conjugation of the asialoorosomucoid glycoprotein to target the asialoglycoprotein receptor on mouse hepatocytes *in vitro* and *in vivo* (40,81,82). Shortly thereafter, a series of papers by Wagner and colleagues developed a process, termed transferrinfection, based on conjugation of the iron transport protein, transferrin, to PLL (reviewed in Refs. 87 and 137). These thorough studies provided a firm basis for much of the subsequent gene delivery literature, including some of the first studies of polyplex formation (43) and mechanisms of endolysosomal escape (86,99,100). PLL/DNA complexes have also been targeted to specific cells through conjugation of sugars (49,71–73,136,138), folate (79), RGD-displaying peptides (91,139), and antibodies (140).

Early studies on PLL were promising, but it now appears unlikely that PLL-based polyplexes will reach clinical application. Development has been limited by the relatively low efficiency. This is generally accepted to be the result of poor escape from the endocytic pathway. In recent years, PLL has been relegated to a role in basic mechanistic studies or as a point of comparison in studies of more promising polymers.

Polyethylenimine. PEI has been used as a gene delivery vector since 1995 (111). The polymer has been known for many years and has traditionally been used as a chelator, in water purification, and in shampoos. It is available in two main forms: linear and branched (Fig. 1). The branched polymer is synthesized via acid-catalyzed polymerization of aziridine, while the linear form is synthesized in a similar way but at reduced reaction temperatures (141). A range of molecular weights (eg, $<$1, 2, 22, 25, 50, 70, and 800 kDa) are commercially available from several manufacturers.

PEI is one of the most effective gene delivery polymers studied to date (142). Depending on the cell line, it is typically several orders of magnitude more efficient than PLL. Importantly, PEI mediates gene delivery efficiently in the absence of any exogenous endosomolytic agent such as chloroquine, inactivated viruses, or fusogenic peptides. PEI-containing polyplexes have been targeted to specific cell types by the conjugation of ligands including galactose (74,76), mannose (143), transferrin (90,144), and antibodies (145). Also, PEI has been highly successful for *in vivo* gene delivery to a variety of tissues including the central nervous system (146,147), kidney (148), lung (149,150), and tumor (151) (reviewed in Ref. 142).

The relatively high gene transfer efficiency mediated by PEI is believed to be due in large part to efficient escape from the endocytic pathway through a proposed mechanism known as the "proton-sponge" hypothesis (111,112) (Fig. 3). Endocytic vesicles are acidified by the action of an ATPase enzyme that actively transports protons from the cytosol into the vesicle. Because every third atom of the polymer

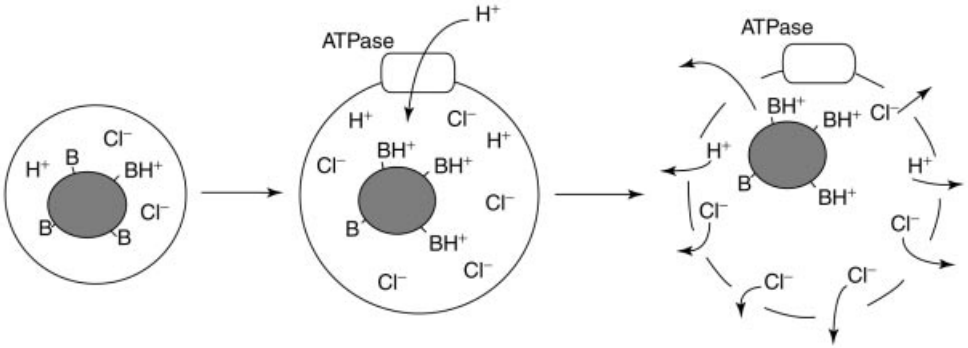

Fig. 3. Schematic of endocytic vesicle swelling and rupture as proposed by the "proton-sponge" hypothesis. The polymer, containing unprotonated basic moieties at neutral pH, buffers the pH within the vesicle and causes the ATPase to pump excess protons into the compartment. The concomitant influx of counterions increases the osmotic pressure across the membrane, causing the vesicle to swell and ultimately rupture.

is a nitrogen, PEI has a very high density of protonatable amines, only 15–20% of which are protonated at physiological pH (152). As a result, PEI will tend to buffer the endosomes causing the ATPase to transport many more protons to reach the desired pH. The accumulation of protons in the vesicle must be balanced by an influx of counterions, typically chloride. The increased ion concentration results in osmotic swelling of the vesicle and, eventually, in the rupture of the endosome membrane.

Despite its advantages, development of PEI gene delivery systems has been hindered by the polymer's relatively high cytotoxicity. Toxicity appears to be dependent on the polymer molecular weight. Recently, it has been shown that PEI as small as 10 kDa is a relatively successful vector with very low toxicity (153,154). Based on these findings, Gosselin and co-workers (155) generated a novel vector by cross-linking 800 Da PEI with disulfide linker groups. They hypothesized that the cross-links would be cleaved upon exposure to the reducing environment of the cytoplasm, presumably leading to lower toxicity. Gene expression mediated by these polymers was slightly reduced relative to 25 kDa PEI, but for some of the polymers cytotoxicity was virtually eliminated. Taking a different tack, Han and co-workers (156) synthesized a cholesterol-derivatized, low-molecular-weight PEI (termed water-soluble lipopolymer) that is less toxic than the standard 25-kDa PEI and mediates two- to threefold higher gene delivery efficiency, as well.

Polyamidoamine Dendrimers. Polyamidoamine ("Starburst") dendrimers are spheroidal, cascade polymers (Fig. 1) that can be synthesized from an ammonia or ethylenediamine core by successive addition of methyl acrylate and ethylenediamine (157). The size of the polymer, and importantly the surface charge, are controlled by varying the number of "generations" in the synthesis. Haensler and Szoka (113) originally reported the use of PAMAM dendrimers for gene delivery. They examined dendrimers of generations 1–10 and found that the sixth generation dendrimer was better than the others by ~10-fold. Because

of the large number of secondary and tertiary amines on the polymer, and its resulting buffering capacity, PAMAM dendrimers are thought to efficiently escape from the endocytic trafficking pathway by a mechanism similar to PEI. Indeed, gene delivery is unaffected by chloroquine, suggesting that endosomal escape is not limiting. Because of its relatively high gene delivery efficiency and good biocompatibility, PAMAM dendrimers have recently been employed in several *in vivo* gene delivery studies (158–161).

Interestingly, a partially degraded form of PAMAM dendrimer appears to be a more effective gene transfer agent than the intact polymer. Heat treatment of the polymer in various solvolytic solvents (eg, water or butanol) significantly degrades the polymer at the amide linkages, resulting in a heterodisperse population of compounds with molecular weight ranging from <1500 kDa to tens of kilodaltons. These "fractured" dendrimers show >50-fold enhanced transfection activity (162). The mechanism of the enhancement appears to be twofold. First, the fractured dendrimer exhibits greater flexibility, allowing a more beneficial interaction with the plasmid DNA (162). Second, polyplexes containing fractured PAMAM appear to have enhanced solution stability in comparison to polyplexes containing intact polymer, which tend to aggregate (47).

Polymers Designed for Gene Delivery

Many different types of polymers have been specifically designed for use as gene delivery vectors. In many cases, the polymers were designed to address one of the perceived gene delivery barriers; for example, DNA packaging and stability *in vivo*, biocompatibility, and endosomal escape have all been used as design criteria. The results of such studies have been mixed, with some polymers performing as well as, or even slightly better than, PEI and the PAMAM dendrimers. In the following, we cannot describe all of the polymers designed for gene delivery. Rather, we have chosen several new classes of polymers that appear to show promise.

Imidazole-Containing Polymers. "Proton-sponge" polymers are some of the best available off-the-shelf materials for gene delivery. However, they are limited by considerable cytotoxicity in some cell lines. It would be desirable to mimic the proton-sponge mechanism, which requires high buffering capacity between physiological and lysosomal pH, in a polymer that is more biocompatible. Several groups have recognized that imidazole exhibits the required protonation properties ($pK_a \sim 6$). Further, because imidazole is a component of several biological species (eg, the amino acid histidine), polymers incorporating imidazole may be expected to show increased biocompatibility.

One approach that has been reported was to use a homopolymer of histidine (pHis) (MW ~11,000) that was derivatized with gluconic acid to increase its solubility in aqueous solutions (G-pHis) (Fig. 4) (114). The polymer was shown to efficiently condense plasmid DNA into particles of ~100 nm diameter. Ternary complexes of DNA, G-pHis, and transferrin–polylysine conjugates (Tf-PLL) transfected COS-7 cells, in the absence of any exogenous endosomolytic agents, with efficiency similar to that of DNA/Tf-PLL complexes that required addition of

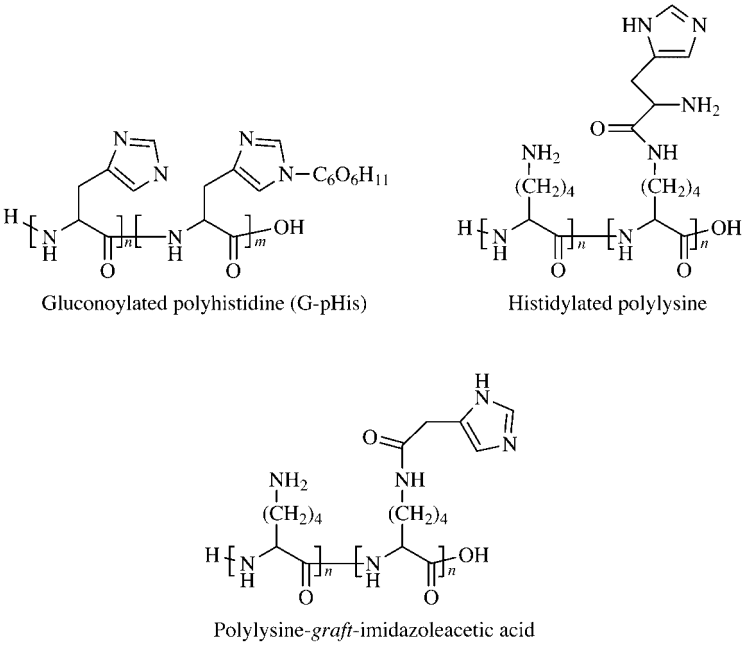

Fig. 4. Imidazole-containing, biocompatible "proton-sponge" polymers (114,115,117).

chloroquine. Further, the polymer showed negligible toxicity at concentrations employed in gene delivery studies.

A second approach is to derivatize PLL with imidazole-containing pendant groups (Fig. 4). Three chemistries have been reported. In the first, the $\bar{\varepsilon}$-amino groups of PLL or oligolysine were derivatized with (Boc-protected) histidine, resulting in an amide linkage with a primary amine (from the histidine) remaining (117,163). Thus, the imidazole group was introduced without reduction of the number of positive charges available for binding DNA. In the second, PLL was derivatized with imidazoleacetic acid yielding a similar amide linkage, but in the absence of the primary amine (115). Both polymers were found to efficiently transfect a variety of cell types in the absence of any exogenous endosomolytic agent, and gene expression levels increased with increasing imidazole content. Gene expression levels mediated by histidylated PLL were 3–4 orders of magnitude higher than with underivatized PLL (117). In fact, Putnam and co-workers reported gene expression levels comparable to those achieved with PEI polyplexes, yet in the absence of any cytotoxicity (under the same conditions, PEI reduced cell viability by ~80%). Finally, Benns and co-workers (164) reported a comb-type polymer of polyhistidine grafted onto the ε-amino groups of polylysine. This polymer was slight more efficient than PLL, but was still enhanced approximately two-fold by the addition of chloroquine.

Cyclodextrin-Containing Polymers. Cyclodextrins (CD) are cyclic oligomers of $\bar{\alpha}$-1,4-linked glucopyranose units that exhibit interesting guest–host properties. The cavity of the CD ring is relatively hydrophobic. Thus, CDs form inclusion complexes with many small hydrophobic molecules. This property has

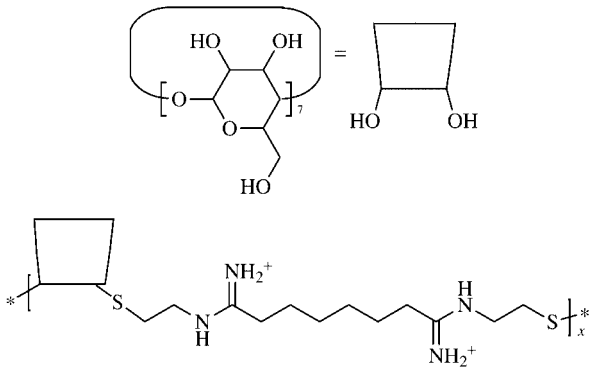

Fig. 5. Example of a cyclodextrin-containing polymer incorporating amidine linkages (166).

been exploited for drug delivery applications. An excellent review of CDs is available (165).

Linear CD-containing polymers for gene delivery have been synthesized by condensation of diamino-CD monomers with diimidate comonomers to yield a diamidine-containing polycation (Fig. 5) (166,167). The CDs were functionalized with amino groups of varying structure placed on opposite sides of the CD ring (166). Further, the length and chemistry of the spacer between the amidine moieties was systematically varied from 4 to 10 methylene units (167). Typically, the syntheses yielded highly water-soluble oligomers with degree of polymerization from 4 to 6 and molecular weights between 5800 and 8800. These polymers condensed plasmid DNA into particles of 100–150 nm in diameter at +/− charge ratios greater than 5, as measured by dynamic light scattering and transmission electron microscopy, and transfect cells at +/− ratios greater than 10. The best polymers of this class transfected cells in culture with efficiencies comparable to PEI and Lipofectamine. Transfection was enhanced 20-fold by the addition of chloroquine suggesting that, as for many other polymers, escape from the endocytic pathway is an efficiency-limiting barrier.

An important aspect of these polymers is their lack of cytotoxicity. The IC_{50} (polymer concentration at which cell viability is reduced by 50%) is in the millimolar range. Furthermore, the LD_{40} (dose of polymer in milligrams per kilogram that will cause death in 40% of the animals) in mice for the polymer shown in Figure 5 was found to be 200 mg/kg. These values are at least 10-fold higher than for other gene delivery polymers such as PEI. The low toxicity is clearly due to the presence of the CD (167).

Finally, it is interesting to note that the CD moieties provide an interesting opportunity for modification of the polyplexes with a variety of functionalities. For example, it may be possible to introduce receptor-targeting or nuclear-localization moieties with a bifunctional molecule containing the targeting moiety on one end and a CD-intercalating moiety (eg, adamantane) on the other end. Such a relatively simple route to introduce structural and functional diversity to the polyplexes may have many exciting applications.

Degradable Polycations. Two of the important barriers to polymeric gene delivery, unpackaging of the plasmid and cytotoxicity, have recently been addressed via synthesis of biodegradable polycations. For example, several cationic polyesters have been reported (168–171). One of these polymers, poly[$\bar{\alpha}$-(4-aminobutyl)-L-glycolic acid] (PAGA) was designed as a biodegradable mimic of PLL (170). PAGA (MW ~3300) degraded quickly in aqueous solution at pH 7.3 (37°C), but the degradation process was much slower for the polymer in polyplexes with plasmid DNA. PAGA showed no cytotoxicity under conditions where PLL reduced cell viability by 80%. In the presence of chloroquine, PAGA transfected cells threefold better than PLL at optimized conditions (170). Furthermore, PAGA has shown efficacy in delivering plasmid DNA *in vivo* by reducing the severity of autoimmune insulitis in nonobese diabetic mice (172,173) and in cytokine gene delivery for cancer treatment (174). Similarly, a hyperbranched poly(amino ester) was synthesized as a biodegradable mimic of PEI and/or PAMAM dendrimers (171). This polymer was minimally toxic in comparison to PEI and PAMAM dendrimers. Transfection efficiency was 1–2 orders of magnitude less efficient than PEI or PAMAM, but was 10-fold better than PAGA (without chloroquine).

Another class of polymers that has recently been developed for gene delivery are the poly($\bar{\beta}$-amino esters), synthesized by the addition of primary or secondary amines to diacrylates (175–177). Initially, a set of three poly(β-amino esters) (Fig. 6) was shown to be capable of binding and condensing plasmid DNA and exhibited negligible cytotoxicity to cells in culture (175). Subsequently, the authors employed a combinatorial approach to synthesis of a library of poly(β-amino esters) (177). Seven diacrylate monomers were reacted with 20 amine monomers to yield 140 structurally unique polymers (MW 2,000–50,000). The library was screened for solubility in aqueous buffer (pH 5) and DNA binding by gel electrophoresis. Fifty-six of the 70 water-soluble polymers interacted sufficiently with DNA to allow transfection studies. Six polymers were identified as "hits" worthy of further study, and two of the polymers mediated gene delivery similar to or exceeding that observed with PEI.

Another novel approach has been to employ disulfide-containing moieties that will be cleaved in a reducing medium such as the cytosol and nucleus. In one

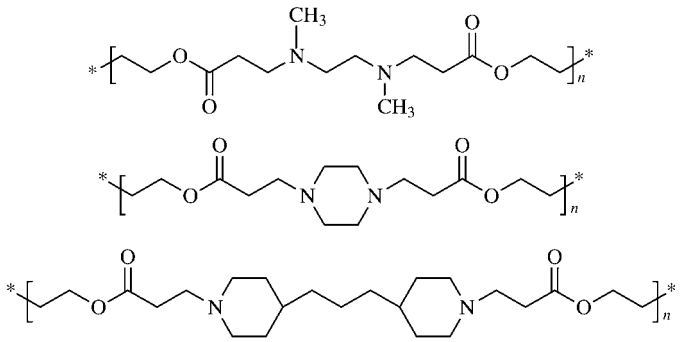

Fig. 6. Biodegradable poly(β-amino ester) polycations synthesized from the addition of diamine monomers to diacrylate comonomers (175).

such polymer, poly[Lys-(AEDTP)], the lysine ε-amino groups are substituted with 3-(2-aminoethyldithio)-propionyl residues such that the amino groups interacting with the DNA phosphates are linked to the polymer via a disulfide bond (178). Decondensation of polyplexes was observed in the presence of reducing agents including dithiothreitol and glutathione. Transfection of HepG2 cells was 50-fold more efficient with poly[Lys-(AEDTP)] compared to PLL polyplexes. PEI (800 Da) was reacted with two cross-linking reagents, dithiobis(succinimidylpropionate) and dimethyl-3,3′-dithiobispropionimidate, at two different amine cross-link ratios to generate a set of reducible conjugates (155). The gene transfer efficiency was found to be proportional to conjugate size. While none of the polymers was as effective as the commonly used 25-kDa PEI, they were all less toxic.

Conclusions

A variety of polymers has been employed in gene delivery studies to date, but their effectiveness as gene therapy vectors remains orders of magnitude poorer than viral vectors. As a result, polymers are generally considered unacceptable for clinical applications. The important extra- and intracellular barriers to efficient gene delivery are known. The lack of efficiency of polymer gene delivery vectors is due to a lack of functionality for overcoming one or several of these barriers. Based on the large number of studies of off-the-shelf gene delivery polymers, much has been learned about the structure–function relationships of polymer vectors. This knowledge has been applied to design and synthesis of new polymers, tailor-made for gene delivery, and a number of promising candidates have been reported in recent years. With our growing understanding of polymer gene delivery mechanisms and the continued efforts of creative and talented polymer chemists, it is likely that polymer-based gene delivery systems will become an important tool for human gene therapy.

BIBLIOGRAPHY

1. R. C. Mulligan, *Science* **260**, 926–932 (1993).
2. J. N. Lozier and K. M. Brinkhous, *J. Am. Med. Assoc.* **271**, 47–51 (1994).
3. K. Inuii, S. Okada, and G. Dickson, *Brain Dev.* **18**, 357–361 (1996).
4. D. Hartigan-O'Connor and J. S. Chamberlain, *Sem. Neurol.* **19**, 323–3332 (1999).
5. D. Hartigan-O'Connor and J. S. Chamberlain, *Microsc. Res. Tech.* **48**, 223–238 (2000).
6. E. W. F. W. Alton, D. M. Geddes, D. R. Gill, C. F. Higgins, S. C. Hyde, J. A. Innes, and D. J. Porteous, *Gene Ther.* **5**, 291–292 (1998).
7. E. G. Nabel, *J. Nucl. Cardiol.* **6**, 69–75 (1999).
8. S. B. Dunnett and A. Bjorklund, *Nature* **399**, A32–A39 (1999).
9. J. M. Alisky and B. L. Davidson, *Hum. Gene Ther.* **11**, 2315–2329 (2000).
10. M. Barkats, A. Bilangbleuel, M. H. Buccaron, M. N. Castelbarthe, O. Corti, F. Finiels, P. Horellou, F. Revah, O. Sabate, and J. Mallet, *Prog. Neuorbiol.* **55**, 333–341 (1998).
11. D. R. Chadwick and A. M. L. Lever, *Exp. Op. Ther. Patents* **8**, 983–990 (1998).
12. J. Bonadio, S. A. Goldstein, and R. J. Levy, *Adv. Drug Delivery Rev.* **33**, 53–69 (1998).
13. R. G. Vile, S. J. Russell, and N. R. Lemoine, *Gene Ther.* **7**, 2–8 (2000).

14. J. Folkman, *Proc. Natl. Acad. Sci. U.S.A.* **95**, 9064–9066 (1998).
15. J. A. Roth and R. J. Cristiano, *J. Natl. Cancer Inst.* **89**, 21–39 (1997).
16. E. G. Nabel, *Atherosclerosis* **118**(Suppl.), S51–S56 (1995).
17. J. J. Donnelly, J. B. Ulmer, J. W. Shiver, and M. A. Liu, *Annu. Rev. Immunol.* **15**, 617–648 (1997).
18. R. M. Blaese, K. W. Culver, A. D. Miller, C. S. Carter, T. Fleisher, M. Clerici, G. Shearer, L. Chang, Y. Chiang, P. Tolstoshev, J. J. Greenblatt, S. A. Rosenberg, H. Klein, M. Berger, C. A. Mullen, W. J. Ramsey, L. Muul, R. A. Morgan, and W. F. Anderson, *Science* **270**, 475–480 (1995).
19. M. Cavazzana-Calvo, S. Hacein-Bey, G. de Saint Basile, G. Gross, E. Yvon, P. Nusbaum, F. Selz, C. Hue, S. Certain, J.-L. Casanova, P. Bousso, F. Le Deist, and A. Fischer, *Science* **288**, 669–672 (2000).
20. M. A. Kay, C. S. Manno, M. V. Ragni, P. J. Larson, L. B. Couto, A. McClelland, B. Glader, A. J. Chew, S. J. Tai, R. W. Herzog, V. Arruda, F. Johnson, C. Scallan, E. Skarsgard, A. W. Flake, and K. A. High, *Nat. Genet.* **24**, 257–261 (2000).
21. F. R. Khuri, J. Nemunaitis, I. Ganly, J. Arseneau, I. F. Tannock, L. Romel, M. Gore, J. Ironside, R. H. MacDougall, C. Heise, B. Randlev, A. M. Gillenwater, P. Bruso, S. B. Kaye, W. K. Hong, and D. H. Kim, *Nat. Med.* **6**, 879–885 (2000).
22. *J. Gene Med., accessed Dec.* **6**, 2001 [http://www.wiley.co.uk/genetherapy/clinical/].
23. I. M. Verma and N. Somia, *Nature* **389**, 239–242 (1997).
24. H. Varmus, *Science* **240**, 1427–1435 (1988).
25. M. J. During, *Adv. Drug Delivery Rev.* **27**, 83–94 (1997).
26. T. R. Flotte and B. J. Carter, *Gene Ther.* **2**, 357–362 (1995).
27. H. Kotani, P. B. Newton, S. Zhang, Y. L. Chiang, E. Otto, L. Weaver, R. M. Blaese, W. F. Anderson, and G. J. McGarrity, *Hum. Gene Ther.* **5**, 19–28 (1994).
28. R. G. Vile, A. Tuszynski, and S. Castleden, *Mol. Biotechnol.* **5**, 139–158 (1996).
29. A. Vaheri and J. S. Pagano, *Virology* **27**, 434–436 (1965).
30. F. L. Graham and A. J. V. D. Eb, *Virology* **52**, 456–467 (1973).
31. P. L. Felgner, T. R. Gadek, M. Holm, R. Roman, H. W. Chan, M. Wenz, J. P. Northrop, G. M. Ringold, and M. Danielsen, *Proc. Natl. Acad. Sci. U.S.A.* **84**, 7413 (1987).
32. X. Gao and L. Huang, *Biochem. Biophys. Res. Commun.* **179**, 280–285 (1991).
33. I. Koltover, T. Salditt, J. O. Radler, and C. R. Safinya, *Science* **281**, 78–81 (1998).
34. S. W. Hui, M. Langner, Y.-L. Zhao, P. Ross, E. Hurley, and K. Chan, *Biophys. J.* **71**, 590–599 (1996).
35. A. Rolland and P. L. Felgner, *Adv. Drug Delivery Rev.* **30**, 1–3 (1998).
36. J. Smith, Y. Zhang, and R. Niven, *Adv. Drug Delivery Rev.* **26**, 135–150 (1997).
37. J. Zabner, *Adv. Drug Delivery Rev.* **27**, 17–28 (1997).
38. X. Gao and L. Huang, *Gene Ther.* **2**, 710–722 (1995).
39. M. C. Fillion and N. C. Phillips, *Int. J. Pharm.* **162**, 159–170 (1998).
40. G. Y. Wu and C. H. Wu, *J. Biol. Chem.* **262**, 4429–4432 (1987).
41. S. J. Hwang and M. E. Davis, *Curr. Opin. Mol. Ther.* **3**, 183–191 (2001).
42. V. A. Bloomfield, *Biopolymers* **44**, 269–282 (1997).
43. E. Wagner, M. Cotten, R. Foisner, and M. L. Birnstiel, *Proc. Natl. Acad. Sci. U.S.A.* **88**, 4255–4259 (1991).
44. H. G. Hansma, R. Golan, W. Hsieh, C. P. Lollo, P. Mullen-Ley, and D. Y. Kwoh, *Nucl. Acids Res.* **26**, 2481–2487 (1998).
45. E. Lai and J. H. van Zanten, *Biophys. J.* **80**, 864–873 (2001).
46. A. V. Kabanov, I. V. Astafyeva, M. L. Chikindas, G. F. Rosenblat, V. I. Kiselev, E. S. Severin, and V. A. Kabanov, *Biopolymers.* **31**, 1437–1443 (1991).
47. M. X. Tang and F. C. Szoka, *Gene Ther.* **4**, 823–832 (1997).
48. M. S. Wadhwa, W. T. Collard, R. C. Adami, D. L. McKenzie, and K. G. Rice, *Bioconjugate Chem.* **8**, 81–88 (1997).

49. M. S. Wadhwa, D. L. Knoell, A. P. Young, and K. G. Rice, *Bioconjugate Chem.* **6**, 283–291 (1995).
50. C. Plank, M. X. Tang, A. R. Wolfe, and F. C. Szoka, *Hum. Gene Ther.* **10**, 319–332 (1999).
51. S. Gottschalk, J. T. Sparrow, J. Hauer, M. P. Mims, F. E. Leland, S. L. C. Woo, and L. C. Smith, *Gene Ther.* **3**, 448–457 (1996).
52. D. V. Schaffer, N. A. Fidelman, N. Dan, and D. A. Lauffenburger, *Biotechnol. Bioeng.* **67**, 598–606 (2000).
53. M. A. Wolfert, P. R. Dash, O. Nazarova, D. Oupicky, L. W. Seymour, S. Smart, J. Strohalm, and K. Ulbrich, *Bioconjugate Chem.* **10**, 993–1004 (1999).
54. O. Zelphati and F. C. Szoka, *Proc. Natl. Acad. Sci. U.S.A.* **93**, 11493–11498 (1996).
55. W. Zauner, M. Ogris, and E. Wagner, *Adv. Drug Delivery Rev.* **30**, 97–113 (1998).
56. P. R. Dash, M. L. Read, L. B. Barrett, M. A. Wolfert, and L. W. Seymour, *Gene Ther.* **6**, 643–650 (1999).
57. C. Plank, K. Mechtler, F. C. Szoka, and E. Wagner, *Hum. Gene Ther.* **7**, 1437–1446 (1996).
58. M. Ogris, S. Brunner, S. Schuller, R. Kircheis, and E. Wagner, *Gene Ther.* **6**, 595–605 (1999).
59. V. Toncheva, M. A. Wolfert, P. R. Dash, D. Oupicky, K. Ulbrich, L. W. Seymour, and E. H. Schacht, *Biochim. Biophys. Acta* **1380**, 354–368 (1998).
60. M. G. Banaszczyk, C. P. Lollo, D. Y. Kwoh, A. T. Phillips, A. Amini, D. P. Wu, P. M. Mullen, C. C. Coffin, S. W. Brostoff, and D. J. Carlo, *J. Macromol. Sci. A* **36**, 1061–1084 (1999).
61. D. Oupicky, C. Konak, and K. Ulbrich, *J. Biomater. Sci.* **10**, 573–590 (1999).
62. D. Oupicky, K. A. Howard, C. Konak, P. R. Dash, K. Ulbrich, and L. W. Seymour, *Bioconjugate Chem.* **11**, 492–501 (2000).
63. P. R. Dash, M. L. Read, K. D. Fisher, K. A. Howard, M. Wolfert, D. Oupicky, V. Subr, J. Strohalm, K. Ulbrich, and L. W. Seymour, *J. Biol. Chem.* **275**, 3793–3802 (2000).
64. K. A. Howard, P. R. Dash, M. L. Read, K. Ward, L. M. Tomkins, O. Nazarova, K. Ulbrich, and L. W. Seymour, *Biochim. Biophys. Acta.* **1475**, 245–255 (2000).
65. P. Erbacher, T. Bettinger, P. Belguise-Valladier, S. M. Zou, J. L. Coll, J. P. Behr, and J. S. Remy, *J. Gene Med.* **1**, 210–222 (1999).
66. W. Wang, L. Tetley, and I. F. Uchegbu, *J. Colloid Int. Sci.* **237**, 200–207 (2001).
67. P. Erbacher, M. T. Bousser, J. Raimond, M. Monsigny, P. Midoux, and A. C. Roche, *Hum. Gene Ther.* **7**, 721–729 (1996).
68. M. Nishikawa, S. Takemura, Y. Takakura, and M. Hashida, *J. Pharm. Exp. Ther.* **287**, 408–415 (1998).
69. R. Kircheis, L. Wightman, A. Schreiber, B. Robitza, V. Roessler, M. Kursa, and E. Wagner, *Gene Ther.* **8**, 28–40 (2001).
70. K. A. Mislick and J. D. Baldeschwieler, *Proc. Natl. Acad. Sci. U.S.A.* **93**, 12349–12354 (1996).
71. J. C. Perales, T. Ferkol, H. Geegen, O. D. Ratnoff, and R. W. Hanson, *Proc. Natl. Acad. Sci. U.S.A.* **91**, 4086–4090 (1994).
72. P. Erbacher, A. C. Roche, M. Monsigny, and P. Midoux, *Bioconjugate Chem.* **6**, 401–410 (1995).
73. T. Ferkol, J. C. Perales, F. Mularo, and R. W. Hanson, *Proc. Natl. Acad. Sci. U.S.A.* **93**, 101–105 (1996).
74. M.-A. Zanta, O. Boussif, A. Adib, and J.-P. Behr, *Bioconjugate Chem.* **8**, 839–844 (1997).
75. T. Bettinger, J. S. Remy, and P. Erbacher, *Bioconjugate Chem.* **10**, 558–561 (1999).
76. K. Sagara and S. W. Kim, *J. Controlled Release* **79**, 271–281 (2002).
77. Y. H. Choi, F. Liu, J.-S. Park, and S. W. Kim, *Bioconjugate Chem.* **9**, 708–718 (1998).

78. Y. H. Choi, F. Liu, J.-S. Choi, S. W. Kim, and J.-S. Park, *Hum. Gene Ther.* **10**, 2657–2665 (1999).
79. C. P. Leamon, D. Weigl, and R. W. Hendren, *Bioconjugate Chem.* **10**, 947–957 (1999).
80. J. M. Benns, R. I. Mahato, and S.-W. Kim, *J. Controlled Release* **79**, 255–269 (2002).
81. G. Y. Wu and C. H. Wu, *J. Biol. Chem.* **263**, 14621–14624 (1988).
82. C. H. Wu, J. M. Wilson, and G. Y. Wu, *J. Biol. Chem.* **264**, 16985–16987 (1989).
83. G. Y. Wu, J. M. Wilson, F. Shalaby, M. Grossman, D. A. Shafritz, and C. H. Wu, *J. Biol. Chem.* **266**, 14338–14342 (1991).
84. M. Cotten, F. Längle-Rouault, H. Kirlappos, E. Wagner, K. Mechtler, M. Zenke, H. Beug, and M. L. Birnstiel, *Proc. Natl. Acad. Sci. U.S.A.* **87**, 4033–4037 (1990).
85. E. Wagner, M. Zenke, M. Cotten, H. Beug, and M. L. Birnstiel, *Proc. Natl. Acad. Sci. U.S.A.* **87**, 3410–3414 (1990).
86. M. Zenke, P. Steinlein, E. Wagner, M. Cotten, H. Beug, and M. L. Birnstiel, *Proc. Natl. Acad. Sci. U.S.A.* **87**, 3655–3659 (1990).
87. K. Zatloukal, E. Wagner, M. Cotten, S. Phillips, C. Plank, P. Steinlein, D. T. Curiel, and M. L. Birnstiel, *Ann. N.Y. Acad. Sci.* **660**, 136–153 (1992).
88. D. V. Schaffer, R. L. Neve, and D. A. Lauffenburger, *Tissue Eng.* **3**, 53–63 (1997).
89. D. V. Schaffer, Ph.D. dissertation, Massachusetts Institute of Technology, 1998.
90. R. Kircheis, A. Kichler, G. Wallner, M. Kursa, M. Ogris, T. Felzmann, M. Buchberger, and E. Wagner, *Gene Ther.* **4**, 409–418 (1997).
91. R. P. Harbottle, R. G. Cooper, S. L. Hart, A. Ladhoff, T. McKay, A. M. Knight, E. Wagner, A. D. Miller, and C. Coutelle, *Hum. Gene Ther.* **9**, 1037–1047 (1998).
92. D. V. Schaffer and D. A. Lauffenburger, *J. Biol. Chem.* **273**, 28004–28009 (1998).
93. W. C. Tseng, F. R. Haselton, and T. D. Giorgio, *J. Biol. Chem.* **272**, 25641–25647 (1997).
94. S. Mukherjee, R. N. Ghosh, and F. R. Maxfield, *Physiol. Rev.* **77**, 759–803 (1997).
95. P. Erbacher, A. C. Roche, M. Monsigny, and P. Midoux, *Exp. Cell Res.* **225**, 186–194 (1996).
96. D. T. Curiel, S. Agarwal, E. Wagner, and M. Cotten, *Proc. Natl. Acad. Sci. U.S.A.* **88**, 8850–8854 (1991).
97. R. J. Cristiano, L. C. Smith, and S. L. C. Woo, *Proc. Natl. Acad. Sci. U.S.A.* **90**, 2122–2126 (1993).
98. E. Wagner, K. Zatloukal, M. Cotten, H. Kirlappos, K. Mechtler, D. T. Curiel, and M. L. Birnstiel, *Proc. Natl. Acad. Sci. U.S.A.* **89**, 6099–6103 (1992).
99. M. Cotten, E. Wagner, K. Zatloukal, S. Phillips, D. T. Curiel, and M. L. Birnstiel, *Proc. Natl. Acad. Sci. U.S.A.* **89**, 6094–6098 (1992).
100. E. Wagner, C. Plank, K. Zatloukal, M. Cotten, and M. L. Birnstiel, *Proc. Natl. Acad. Sci. U.S.A.* **89**, 7934–7938 (1992).
101. C. Plank, K. Zatloukal, M. Cotten, K. Mechtler, and E. Wagner, *Bioconjugate Chem.* **3**, 533–539 (1992).
102. C. Plank, B. Oberhauser, K. Mechtler, C. Koch, and E. Wagner, *J. Biol. Chem.* **269**, 12918–12924 (1994).
103. P. Midoux, C. Mendes, A. Legrand, J. Raimond, R. Mayer, M. Monsigny, and A. C. Roche, *Nucl. Acids Res.* **21**, 871–878 (1993).
104. T. B. Wyman, F. Nicol, O. Zelphati, P. V. Scaria, C. Plank, and F. C. Szoka, *Biochemistry* **36**, 3008–3017 (1997).
105. H. Lee, J. H. Jeong, and T. G. Park, *J. Controlled Release* **76**, 183–192 (2001).
106. L. Vaysse, I. Burgelin, J. P. Merlio, and B. Arveiler, *Biochim. Biophys. Acta* **1475**, 369–376 (2000).
107. J. Han and Y. I. Yeom, *Int. J. Pharm.* **202**, 151–160 (2000).
108. A. Kichler, I. Freulon, V. Boutin, R. Mayer, M. Monsigny, and P. Midoux, *J. Gene Med.* **1**, 134–143 (1999).
109. C. Plank, W. Zauner, and E. Wagner, *Adv. Drug Delivery Rev.* **34**, 21–35 (1998).

110. E. Wagner, *J. Controlled Release* **53**, 155–158 (1998).
111. O. Boussif, G. Lezoualc'h, M. A. Zanta, M. D. Mergny, D. Scherman, B. Demeneix, and J.-P. Behr, *Proc. Natl. Acad. Sci. U.S.A.* **92**, 7297–7301 (1995).
112. J.-P. Behr, *Chimia* **51**, 34–36 (1997).
113. J. Haensler and F. C. Szoka, *Bioconjugate Chem.* **4**, 372–379 (1993).
114. D. W. Pack, D. Putnam, and R. Langer, *Biotechnol. Bioeng.* **67**, 217–223 (2000).
115. D. Putnam, C. A. Gentry, D. W. Pack, and R. Langer, *Proc. Natl. Acad. Sci. U.S.A.* **98**, 1200–1205 (2001).
116. P. Midoux, A. Kichler, V. Boutin, J.-C. Maurizot, and M. Monsigny, *Bioconjugate Chem.* **9**, 260–267 (1998).
117. P. Midoux and M. Monsigny, *Bioconjugate Chem.* **10**, 406–411 (1999).
118. K. Luby-Phelps, P. E. Castle, D. L. Taylor, and F. Lanni, *Proc. Natl. Acad. Sci. U.S.A.* **84**, 4910–4913 (1987).
119. G. L. Lukacs, P. Haggie, O. Seksek, D. Lechardeur, N. Freedman, and A. S. Verkman, *J. Biol. Chem.* **275**, 1625–1629 (2000).
120. D. Lechardaeur, K.-J. Sohn, M. Haardt, P. B. Joshi, M. Monck, R. W. Graham, B. Beatty, J. Squire, H. O'Brodovich, and G. L. Lukacs, *Gene Ther.* **6**, 482–497 (1999).
121. N. Miyazawa, R. G. Crystal, and P. L. Leopold, *J. Virol.* **75**, 1387–1400 (2001).
122. S. Brunner, T. Sauer, S. Carotta, M. Cotten, M. Saltik, and E. Wagner, *Gene Ther.* **7**, 401–407 (2000).
123. A. Subramanian, P. Ranganathan, and S. L. Diamond, *Nat. Biotechnol.* **17**, 873–877 (1999).
124. C. J. S. Edgell, D. T. Curiel, P. C. Hu, and H. S. Marr, *BioTechniques* **25**, 264ff (1998).
125. C. W. Pouton, *Adv. Drug Delivery Rev.* **34**, 51–64 (1998).
126. H. Pollard, J.-S. Remy, G. Loussouarn, S. Demolombe, J.-P. Behr, and D. Escande, *J. Biol. Chem.* **273**, 7507–7511 (1998).
127. W. T. Godbey, K. K. Wu, and A. G. Mikos, *Proc. Natl. Acad. Sci. U.S.A.* **96**, 5177–5181 (1999).
128. C. K. Chan and D. A. Jans, *Hum. Gene Ther.* **10**, 1695–1702 (1999).
129. C. K. Chan, T. Senden, and D. A. Jans, *Gene Ther.* **7**, 1690–1697 (2000).
130. M. G. Sebestyén, J. J. Ludtke, M. C. Bassik, G. Zhang, V. Budker, E. A. Lukhtanov, J. E. Hagstrom, and J. A. Wolff, *Nat. Biotechnol.* **16**, 80–85 (1998).
131. L. J. Brandén, A. J. Mohamed, and C. I. E. Smith, *Nat. Biotechnol.* **17**, 784–787 (1999).
132. C. Ciolina, G. Byk, F. Blanche, V. Thuillier, D. Scherman, and P. Wils, *Bioconjugate Chem.* **10**, 46–55 (1999).
133. F. Langle-Rouault, V. Patzel, A. Benavente, M. Taillez, N. Silvestre, A. Bompard, G. Sczakiel, E. Jacobs, and K. Rittner, *J. Virol.* **72**, 6181–6185 (1998).
134. D. A. Dean, *Exp. Cell Res.* **230**, 293–302 (1997).
135. G. L. Wilson, B. S. Dean, G. Wang, and D. A. Dean, *J. Biol. Chem.* **274**, 22025–22032 (1999).
136. P. Erbacher, A. C. Roche, M. Monsigny, and P. Midoux, *Biochim. Biophys. Acta* **1324**, 27–36 (1997).
137. M. Cotten, E. Wagner, and M. L. Birnstiel, *Methods Enzymol.* **217**, 618–644 (1993).
138. M. Hashida, S. Takemura, M. Nishikawa, and Y. Takakura, *Adv. Drug Delivery Rev.* **53**, 301–310 (1998).
139. M. Colin, M. Maurice, G. Trugnan, M. Kornprobst, R. P. Harbottle, A. Knight, R. G. Cooper, A. D. Miller, J. Capeau, and M. C. Brahimi-Horn, *Gene Ther.* **7**, 139–152 (2000).
140. W. Suh, J.-K. Chung, S.-H. Park, and S. W. Kim, *Controlled Release* **72**, 171–178 (2001).
141. C. R. Dick and G. E. Ham, *J. Macromol. Sci. A* **4**, 1301–1304 (1970).
142. G. F. Lemkine and B. A. Demeneix, *Curr. Opin. Mol. Ther.* **3**, 178–182 (2001).

143. S. S. Diebold, M. Kursa, E. Wagner, M. Cotten, and M. Zenke, *J. Biol. Chem.* **274**, 19087–19094 (1999).
144. R. Kircheis, R. Blessing, S. Brunner, L. Wightman, and E. Wagner, *J. Controlled Release* **72**, 165–170 (2001).
145. U. Wojda and J. L. Miller, *J. Pharm. Sci.* **89**, 674–681 (2000).
146. B. Abdallah, A. Hassan, C. Benoist, D. Goula, J.-P. Behr, and B. A. Demeneix, *Hum. Gene Ther.* **7**, 1947–1954 (1996).
147. D. Goula, J. S. Remy, P. Erbacher, M. Wasowicz, G. Levi, B. Abdallah, and B. A. Demeneix, *Gene Ther.* **5**, 712–717 (1998).
148. A. Boletta, A. Benigni, J. Lutz, G. Remuzzi, M. R. Soria, and L. Monaco, *Hum. Gene Ther.* **8**, 1243–1251 (1997).
149. D. Goula, C. Benoist, S. Mantero, G. Merlo, G. Levi, and B. A. Demeneix, *Gene Ther.* **5**, 1291–1295 (1998).
150. S. Ferrari, A. Pettenazzo, N. Garbati, F. Zacchello, J. P. Behr, and M. Scarpa, *Biochim. Biophys. Acta* **1447**, 219–225 (1999).
151. J. L. Coll, P. Chollet, E. Brambilla, D. Desplanques, J. P. Behr, and M. Favrot, *Hum. Gene Ther.* **10**, 1659–1666 (1999).
152. J. Suh, H. J. Paik, and B. K. Hwang, *Bioorg. Chem.* **22**, 318–327 (1994).
153. D. Fischer, T. Bieber, Y. X. Li, H. P. Elsasser, and T. Kissel, *Pharm. Res.* **16**, 1273–1279 (1999).
154. T. Bieber and H. P. Elsasser, *BioTechniques* **30**, 74ff (2001).
155. M. A. Gosselin, W. Guo, and R. J. Lee, *Bioconjugate Chem.* **12**, 989–994 (2001).
156. S.-O. Han, R. I. Mahato, and S. W. Kim, *Bioconjugate Chem.* **???**, ??? (2001).
157. D. A. Tomalia, A. M. Naylor, and W. A. Goddard, *Angew. Chem., Int. Ed. Engl.* **29**, 138–175 (1990).
158. S. Tanaka, M. Iwai, Y. Harada, T. Morikawa, A. Muramatsu, T. Mori, T. Okanoue, K. Kashima, H. Maruyama-Tabata, H. Hirai, E. Satoh, J. Imanishi, and O. Mazda, *Cancer Gene Ther.* **7**, 1241–1249 (2000).
159. C. Rudolph, J. Lausier, S. Naundorf, R. H. Muller, and J. Rosenecker, *J. Gene Med.* **2**, 269–278 (2000).
160. Y. Harada, M. Iwai, S. Tanaka, T. Okanoue, K. Kashima, H. Maruyama-Tabata, H. Hirai, E. Satoh, J. Imanishi, and O. Mazda, *Cancer Gene Ther.* **7**, 27–36 (2000).
161. H. Marayuma-Tabata, Y. Harada, T. Matsumura, E. Satoh, F. Cui, M. Iwai, M. Kita, S. Hibi, J. Imanishi, T. Sawada, and O. Mazda, *Gene Ther.* **7**, 53–60 (2000).
162. M. X. Tang, C. T. Redemann, and F. C. Szoka, *Bioconjugate Chem.* **7**, 703–714 (1996).
163. C. Pichon, M. B. Roufai, M. Monsigny, and P. Midoux, *Nucl. Acids Res.* **28**, 504–512 (2000).
164. J. M. Benns, J.-S. Choi, R. I. Mahato, J-S. Park, and S. W. Kim, *Bioconjugate Chem.* **11**, 637–645 (2000).
165. J. Szejtli and T. Osa, *Comprehensive Supramolecular Chemistry*, Vol. **3**: Cyclodextrins, Elsevier Science, New York, 1996.
166. H. Gonzalez, S. J. Hwang, and M. E. Davis, *Bioconjugate Chem.* **10**, 1068–1074 (1999).
167. S. J. Hwang, N. C. Bellocq, and M. E. Davis, *Bioconjugate Chem.* **12**, 280–290 (2001).
168. D. Putnam and R. Langer, *Macromolecules* **32**, 3568–3662 (1999).
169. Y.-B. Lim, Y. H. Choi, and J.-S. Park, *J. Am. Chem. Soc.* **121**, 5633–5639 (1999).
170. Y.-B. Lim, C.-H. Kim, K. Kim, S. W. Kim, and J.-S. Park, *J. Am. Chem. Soc.* **122**, 6524–6525 (2000).
171. Y.-B. Lim, S.-M. Kim, Y. Lee, W.-K. Lee, T.-G. Yang, M.-J. Lee, H. Suh, and J.-S. Park, *J. Am. Chem. Soc.* **123**, 2460–2461 (2001).
172. J. J. Koh, K. S. Ko, M. Lee, S. Han, J. S. Park, and S. W. Kim, *Gene Ther.* **7**, 2099–2104 (2000).
173. K. S. Ko, M. Lee, J. J. Koh, and S. W. Kim, *Mol. Ther.* **4**, 313–316 (2001).

174. A. Maheshwari, R. I. Mahato, J. McGregor, S.-O. Han, W. E. Samlowski, J.-S. Park, and S. W. Kim, *Mol. Ther.* **2**, 121–130 (2000).
175. D. M. Lynn and R. Langer, *J. Am. Chem. Soc.* **122**, 10761–10768 (2000).
176. D. M. Lynn, M. M. Amiji, and R. Langer, *Angew. Chem., Int. Ed. Engl.* **40**, 1707–1710 (2001).
177. D. M. Lynn, D. G. Anderson, D. Putnam, and R. Langer, *J. Am. Chem. Soc.* **123**, 8155–8156 (2001).
178. C. Pichon, E. LeCam, B. Guerin, D. Coulaud, E. Delain, and P. Midoux, *Bioconjugate Chem.* **13**, 76–82 (2002).

DANIEL W. PACK
University of Illinois at Urbana-Champaign

GLASS TRANSITION. See Volume 2.

GRAFT COPOLYMERS

Introduction

Graft copolymers are composed of a main polymer chain (the backbone) to which one or more side chains (the branches) are chemically connected through covalent bonds. A graft copolymer with one branch can be considered as a miktoarm star copolymer. The backbone and the branches may be homopolymers or copolymers but they differ in chemical nature or composition (1). The branches are usually equal in length and randomly distributed along the backbone because of the specific synthetic techniques used for their preparation. However, more elaborate recent methods have allowed the synthesis of regular graft copolymers with equally spaced and identical branches and of exact graft copolymers, where all the molecular and structural parameters can be accurately controlled (Fig. 1).

A simple graft copolymer can be represented as A_k-*graft*-B_m or polyA-*graft*-polyB or poly(A-*g*-B), where A_k or polyA is the backbone to which the B_m or polyB branches are grafted. The nomenclature of graft copolymers follows the rules recommended by the IUPAC Commission on Macromolecular Nomenclature (2).

Graft copolymers have been mainly used to modify polymer properties because of their unique mechanical, thermal, dilute solution, and melt properties (3–7). The availability of such materials has permitted the researchers to explore the correlation between the structure of the graft copolymers and their properties.

Synthesis of Graft Copolymers

Three general methods have been developed for the synthesis of randomly branched graft copolymers: (*1*) the "grafting onto", (*2*) the "grafting from", and (*3*) the macromonomer method (or "grafting through" method) (8) (Fig. 2).

Encyclopedia of Polymer Science and Technology. Copyright John Wiley & Sons, Inc. All rights reserved.

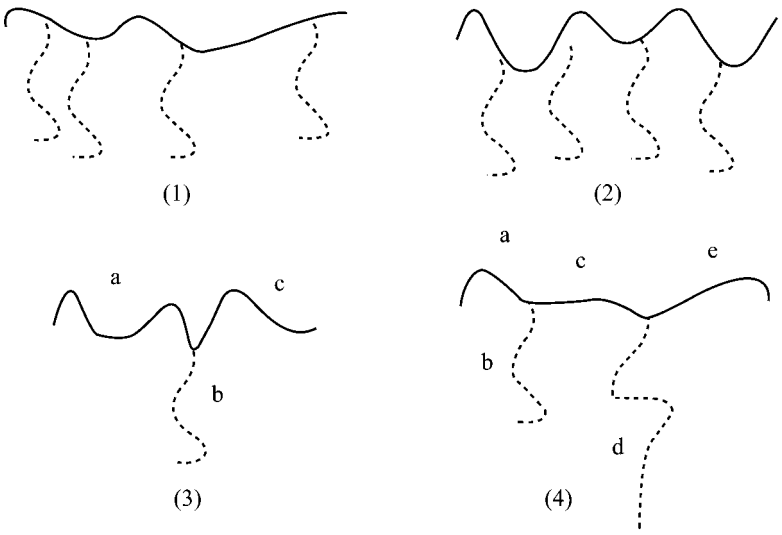

Fig. 1. Graft Copolymers (1) random graft copolymer (identical branches randomly distributed along the backbone); (2) regular graft copolymer (identical branches equally spaced along the backbone); (3) simple graft copolymer (3-miktoarm star copolymer); and (4) graft copolymer with two trifunctional branch points. Exact graft copolymers.

The "grafting onto" method involves the use of a backbone chain containing functional groups X randomly distributed along the chain and branches having reactive chain ends Y. The coupling reaction between the functional backbone and the end-reactive branches lead to the formation of graft copolymers.

In the "grafting from" method active sites are generated randomly along the backbone. These sites are capable of initiating the polymerization of a second monomer, leading to graft copolymers.

The most commonly used method for the synthesis of graft copolymers is the macromonomer method. Macromonomers are oligomeric or polymeric chains bearing a polymerizable end group. Macromonomers having two polymerizable end groups have also been reported (8). Copolymerization of preformed macromonomers with another monomer yields graft copolymers.

"Grafting onto" Methods. In the "grafting onto" method, reaction of preformed polymeric chains having functional groups, with other polymeric chains having active chain ends, takes place. In most cases the incorporation of functional groups is performed by chemical modification of the backbone (9–14). A common procedure is the chloro(bromo) methylation of polystyrene (eq. 1), and the subsequent reaction with living polymeric chains.

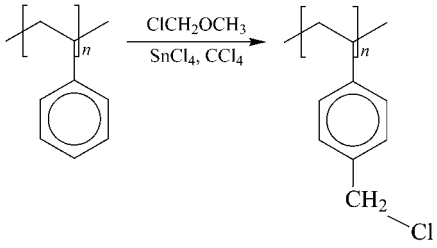

(1)

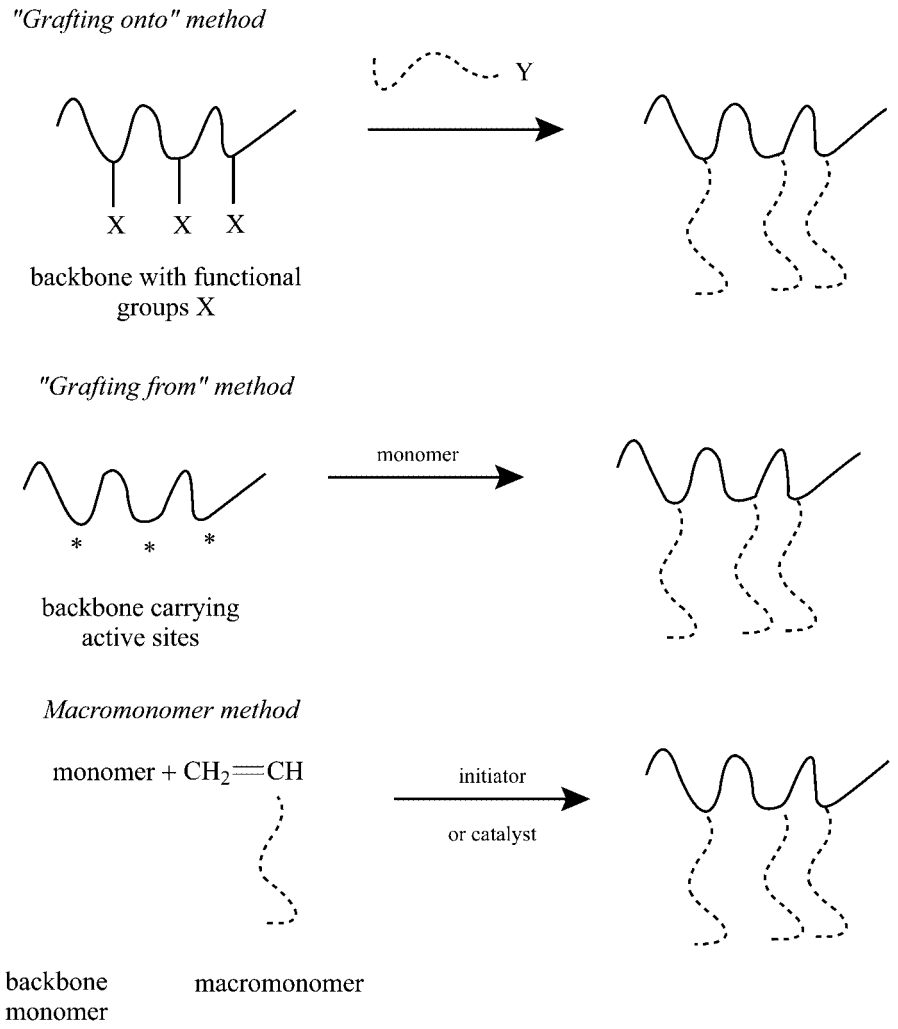

Fig. 2. Three general methods of synthesis of randomly branched graft copolymers.

Using this method polystyrene-*g*-poly(ethylene oxide) (PS-*g*-PEO) graft copolymers were prepared (9–12). The chloromethylation of PS was performed using a CCl_4 solution of PS with chloromethyl methyl ether, with $SnCl_4$ as the catalyst. The reaction conditions were controlled in such a way so as to give low chloromethyl content (<10 wt%). A similar synthetic approach was adopted for the synthesis of PS-*g*-polyisoprene (PS-*g*-PI) graft copolymers (10,11). In order to avoid the side reactions involving lithium–chlorine exchange, the $-CH_2Cl$ groups were transformed to the $-Si(CH_3)_2Cl$ group before reaction with the living polymers. PS-*g*-poly(2-vinylpyridine) (PS-*g*-P2VP) and PS-*g*-P4VP graft copolymers were prepared by partial chloromethylation of PS polymeric chains (13,14). Grafting efficiency, ie, the ratio of the number of $-CH_2Cl$ groups used for the grafting reaction and the number of the incorporated groups on the backbone, was as low as 40% in this case. Chloromethylation of poly(*N*-vinyl carbazole) (PVCz) was also

used in order to synthesize poly(*N*-vinyl carbazole)-*g*-PI graft copolymers (15). The chloromethyl ether method was used in the presence of $ZnCl_2$. The grafting efficiency of PI chains was also found to be limited. Bromomethylation of anionically prepared PS backbone was used for the synthesis of PS-*g*-poly(methyl methacrylate) (PS-*g*-PMMA) copolymers (16). The polydispersity index of the resulted grafts was higher than the polymeric precursors, indicating the presence of undesirable reactions.

By taking advantage of living PS and PI anions with the phenyl rings of P2VP, P2VP-*g*-PS and P2VP-*g*-PI graft copolymers were synthesized (17) (eq. 2)

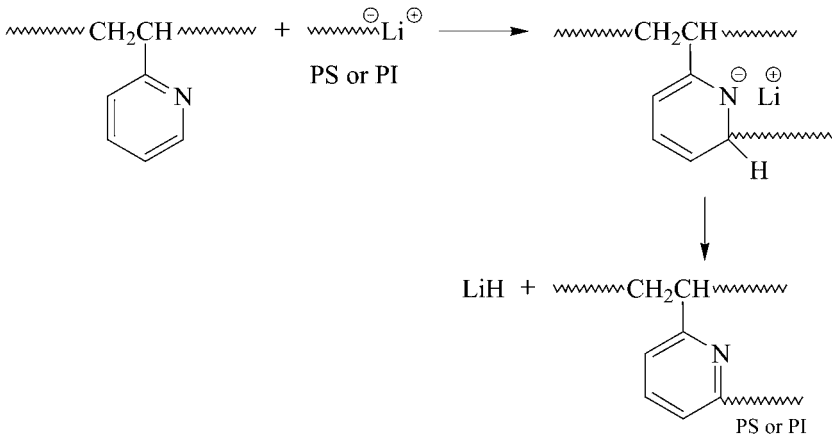

(2)

An excess of living chains compared to the 2VP groups were added. The polydispersity index of the final products was higher than the polydispersity of the backbone and the grafted chains, especially in the case of P2VP-*g*-PI samples. Graft copolymers having as backbone random terpolymers of styrene, maleic anhydride, and ethylhexyl methacrylate, or diethylfumarate, were synthesized by radical polymerization (18). In all cases, polyethylene oxides (PEO) were the grafted chains. Polyethylene glycol monomethyl ether was grafted to the backbones after reaction with the succinic anhydride groups. When the reaction was allowed to proceed to high conversions, gelation occurred. This was attributed to the presence of difunctional polyethylene glycol, which connects many backbones forming high molecular weight and cross-linked products.

The "grafting onto" methodology was followed also for the preparation of graft copolymers having poly(glycidyl methacrylate) as backbone and a mixture of PI and PS grafted chains (19). The epoxy groups were used as grafting sites for living PS and PI anionic chains. Graft terpolymers having poly[styrene-*co*-4-(vinylphenyl)-1-butene] as backbone and either PS, PI, or grafted chains were also prepared (20,21). The synthesis of the backbone involved the anionic copolymerization of styrene with 4-(vinylphenyl)-1-butene. The backbone was partly hydrosilylated, and the incorporated chlorodimethylbutylsilyl active groups were reacted with living PS or PI chains. The graft terpolymers exhibited low polydispersity

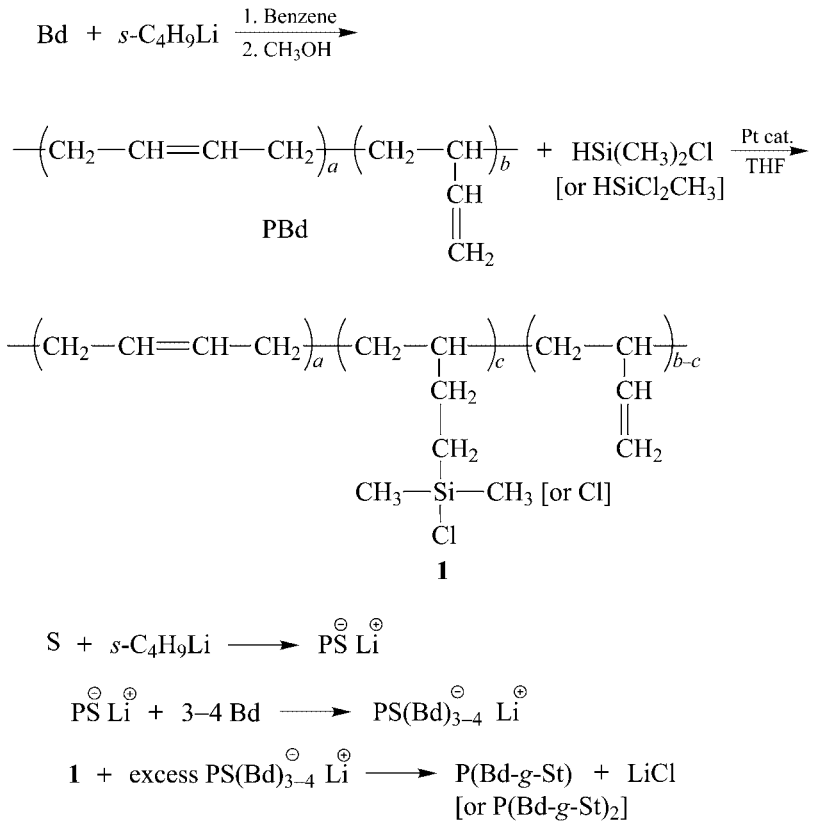

Fig. 3. Butadiene–styrene graft and double graft copolymers.

index comparable to the one of the precursors. Poly(carboxymethylcellulose)-*g*-poly(*N*-isopropylacrylamide) (CMC-*g*-PNIPAM) graft copolymers were synthesized (22) through formation of amide bonds. Amino-terminated NIPAM polymeric chains were obtained by radical polymerization in water. The coupling reaction between the carboxyl groups of the backbone and the terminal amine group of the grafts, performed in water, resulted in the formation of the desired products.

Well-defined butadiene–styrene graft copolymers (PBd-*g*-PS) were synthesized using hydrosilylation reactions (23). Catalytic hydrosilylation of the 1,2-Bd units (∼10%) of PBd introduced chlorosilane groups (Fig. 3). Linking reactions between living PS anions and the —Si—Cl groups of the backbone (**1**) gave PBd-*g*-PS graft copolymers with randomly placed single PS branches. When $HSiCl_2CH_3$ was used in the hydrosilylation step, difunctional branching sites were introduced in the backbone, resulting in the formation of P(Bd-*g*-S)$_2$ double grafts.

Block graft copolymers are copolymers having a backbone composed of a diblock copolymer. Grafted chains can be attached to one or both of the backbone blocks (Fig. 4). Block grafts with a triblock as the backbone are also possible (see BLOCK COPOLYMERS).

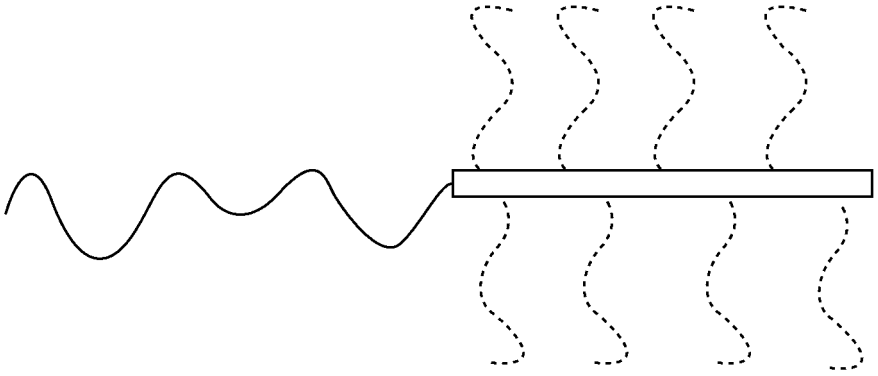

Fig. 4. Block-graft copolymer. In this case only one of the backbone blocks is grafted.

Using anionic polymerization techniques poly{styrene-*b*-[(4-vinylphenyl-dimethylsiloxane)-*g*-isoprene]}, P[S-*b*-(VS-*g*-I)], block graft copolymer was synthesized (24,25). The block copolymer P(S-*b*-VS) was prepared by the sequential addition of styrene and 4-vinyl phenyl dimethyl vinylsiloxane. Living PI chains were reacted with the vinylsilane groups of the block copolymer to form the block graft copolymers. In a similar fashion poly{4-methylstyrene-*b*-[(styrene-*co*-3- methylstyrene)-*g*-2-vinyl pyridine]} block graft terpolymers were synthesized (26). The backbone was prepared by coordination polymerization and sequential addition of 4-methylstyrene and a mixture of styrene and 3-methylstyrene. Chlorination of the methyl groups of the substituted styrenic monomeric units generated the grafting sites. The final coupling was accomplished by adding a THF solution of the chlorinated terpolymer to living P2VP chains at low temperature.

PS-*g*-PI, (PS-*g*-PI)-*b*-PS, and (PS-*g*-PS)-*b*-(PS-*g*-PI) copolymers have been synthesized by using a combination of TEMPO (2,2,6,6-tetramethylpiperidinyl-1-oxy) living free-radical and anionic polymerization (27) (Fig. 5).

The PS backbone of the PS-*g*-PI was synthesized by living free-radical batch copolymerization of styrene and *p*-chloromethylstyrene. PI living chains prepared by anionic polymerization, end capped with 1,1-diphenylethylene, reacted with the chloromethyl groups to give the grafts. In a similar way the synthesis of the (PS-*g*-PI)-*b*-PS block graft copolymers was performed. The synthetic approach of the (PS-*g*-PS)-*b*-(PS-*g*-PI) graft-block-graft copolymer involved first the preparation of the PS-*g*-PS grafts, followed by the copolymerization of styrene and *p*-chloromethyl styrene by living radical polymerization using the nitroxide end group of the PS backbone as the initiating site. Finally, living diphenylethylene-capped PI chains, prepared by anionic polymerization, were reacted with the chloromethyl groups of the extended PS backbone.

Model block-double graft copolymers and terpolymers of styrene, butadiene, and isoprene of the type poly[S-*b*-(PBd-1,2-*g*-X)] were recently synthesized (28), where X is either S, Bd, I, or S-*b*-I by a combination of anionic polymerization, hydrosilylation, and chlorosilane linking chemistry. The backbone P(S-*b*-1,2Bd) was synthesized by sequential addition of the monomers. The vinyl groups of the PBd-1,2 block were hydrosilylated with $HSiCH_3Cl_2$ and used for the attachment

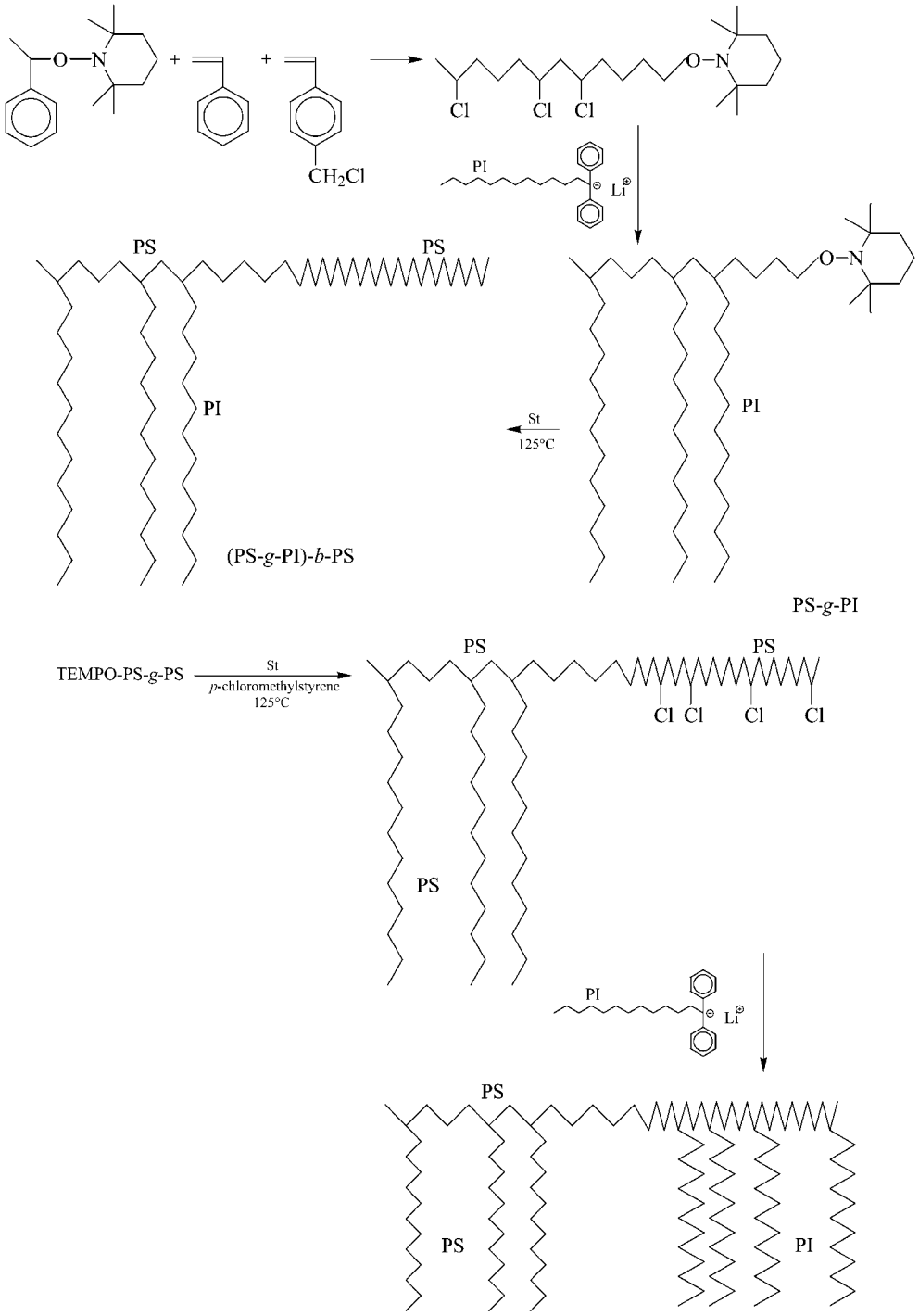

Fig. 5. Polystyrene–polyisoprene graft and block copolymers.

of living chains X, resulting in the formation of the corresponding block double graft copolymers.

"Grafting from" Methods. In the "grafting from" method, the backbone is chemically modified in order to introduce active sites capable of initiating the polymerization of a second monomer. The number of grafted chains can be controlled by the number of active sites generated along the backbone assuming that each one of them participate to the formation of one branch. However, mainly because of kinetic and steric hindrance effects there may be a difference in the lengths of the produced grafts.

Anionic grafting techniques were used for the synthesis of PI-*g*-PS and PBd-*g*-PS copolymers (29–33). The active sites were generated by metallation of the allylic double bonds of the polydiene backbone, by organometallic compounds such as n-C_4H_9Li, in the presence of strong chelating agents that facilitate the reaction (eq. 3). The most common metallation procedure involves the use of n-C_4H_9Li in the presence of *N*,*N*,*N*′,*N*′-tetramethylethylenediamine (TMEDA). The activated polydiene then reacts in the styrene. The graft copolymers exhibited well-defined molecular characteristics.

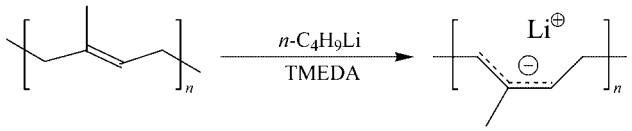

(3)

By using the "grafting from" technique, PMMA-*g*-(β-butyrolactone) (34) copolymers were synthesized. Anionically polymerized PMMA was treated with 18-crown-6 complex of potassium hydroxide resulting in a macromolecular initiator (**2**) (Fig. 6).

The carboxylate active groups were used as initiating sites of β-butyrolactone. It was found that the grafting efficiency was high, and the density

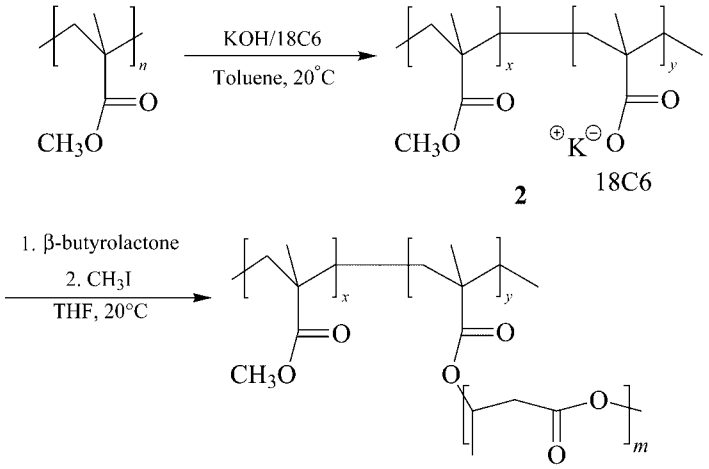

Fig. 6. PMMA backbone with β-butyrolactone grafts.

of grafting chains could be easily controlled. Poly(ethylene-*g*-styrene) copolymers were also prepared (35). The approach for the synthesis of the backbone involved the copolymerization of ethylene and *p*-methylstyrene by metallocene catalysts, such as $[C_5(CH_3)_4(Si(CH_3)_2N\text{-}t\text{-}C_4H_9)]TiCl_2/C_2H_5(Ind)_2ZrCl_2$. The methyl groups of the *p*-methylstyrene units were then metallated with $s\text{-}C_4H_9Li$/TMEDA complex. The active sites produced were used to initiate the anionic polymerization of styrene. The efficiency of the metallation was found to be 65%.

Cationic grafting techniques have been used for the synthesis on poly(ethyl vinyl ether-*g*-ethyloxazoline) graft copolymers (36). A random copolymer of ethyl vinyl ether with a small quantity of 2-chloroethyl vinyl ether was synthesized by cationic polymerization. The pendant alkyl groups were the initiating sites of the cationic polymerization of ethyloxazoline grafts. In a similar way, acid chloride groups were incorporated along the polymer chain by partial hydrolysis of poly(vinyl acetate) (**3**) and reaction of the produced hydroxyl groups with phosgene or diphosgene (37) (eq. 4). These groups were the initiating sites for the polymerization of 2-phenyl or 2-methyl oxazoline in the presence of potassium iodide (eq. 5).

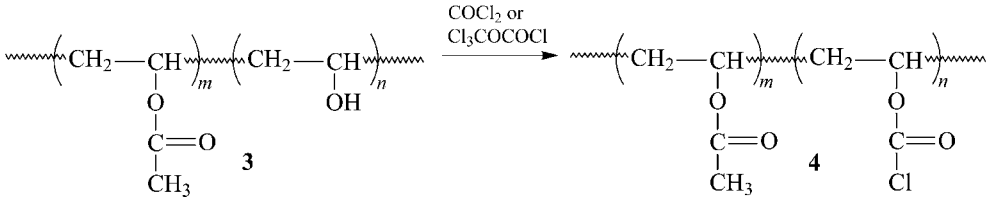

(4)

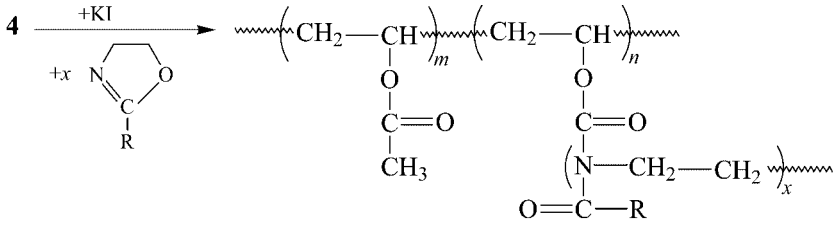

(5)

Poly(isobutylene-*g*-indene) and poly(isobutylene-*g*-styrene) copolymers were synthesized by cationic polymerization (38). The backbone was prepared by cationic copolymerization of isobutylene and *p*-chloromethylstyrene, using $TiCl_4/t\text{-}C_4H_9Cl$ as the initiator. The chloroalkyl groups were used, in the presence of $Al(C_2H_5)_2Cl$, as the initiation sites of the cationic polymerization of indene or styrene. The grafting efficiency was as low as 40–50 %. [MMA-*co*-(*p*-chloromethylstyrene)]-*g*-[2-methyl-2-oxazoline] amphiphilic copolymers were prepared by combining radical and cationic polymerization techniques (39). The synthesis of the backbone was performed by radical copolymerization of MMA and *p*-chloromethylstyrene in the bulk. The cationic macroinitiator was dissolved in benzonitrile along with 2-methyl-2-oxazoline (MeOXz) and the

production of PmeOXz grafts took place at 110°C. A convenient route for the preparation of poly(methylphenylsilane)-*g*-PS was presented (40). The synthetic approach involved the alkali metal mediated reductive-coupling reaction of dichloro methylphenylsilane with sodium in toluene at 100°C (eq. 6). The phenyl groups were then bromomethylated (eq. 7), and the incorporated bromomethyl groups were used as the initiators of the polymerization of styrene by atom transfer radical polymerization (ATRP) (eq. 8).

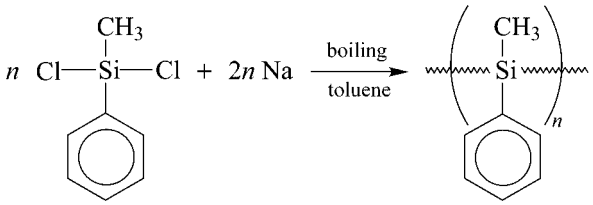

5 (6)

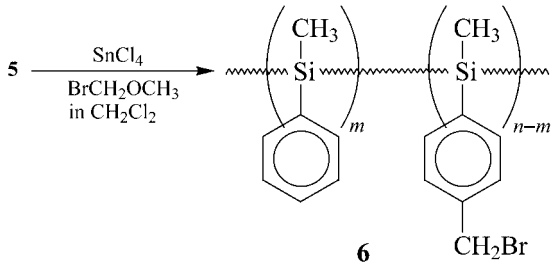

6 (7)

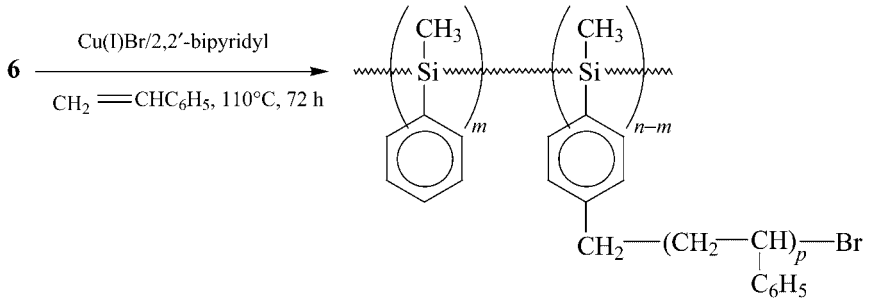

(8)

Polypropylene-*g*-PS copolymers were synthesized by combination of metallocene and TEMPO living free-radical polymerization techniques (41). The backbone was synthesized by copolymerization of propylene and a TEMPO-functionalized derivative containing a α-double bond. The TEMPO groups were then used for the polymerization of styrene by living free-radical polymerization (Fig. 7).

By using ATRP, poly(2-hydroxyethyl methacrylate)-*g*-PS (PHEMA-*g*-PS) and PHEMA-*g*-poly(*n*-butyl acrylate) (42) were synthesized. The backbone, comprised

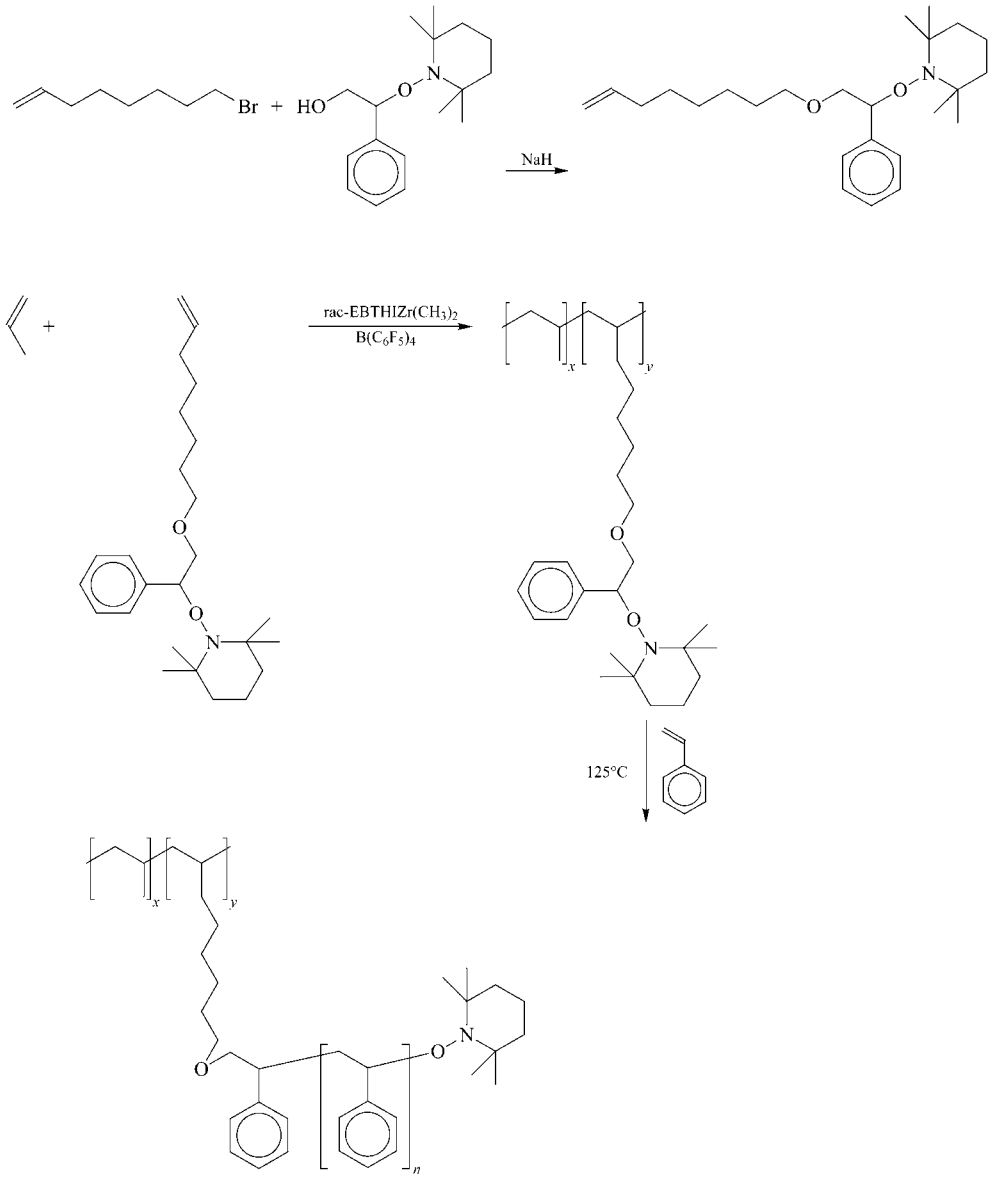

Fig. 7. Synthesis of Polypropylene-*g*-polystyrene.

of trimethylsilyl-protected 2-hydroxyethyl methacrylate, was synthesized by using ATRP methodology, followed by deprotection of the hydroxyl group. Subsequent esterification (eq. 9) with 2-bromoisobutyryl bromide resulted in poly[2-(2-bromoisobutyryloxy)ethyl methacrylate]. (**7**).

PS or poly(*n*-butyl methacrylate) were then grafted from the macromolecular initiator (eq. 10). Subsequent analysis revealed that all the initiation sites participated in the polymerization of the second monomer.

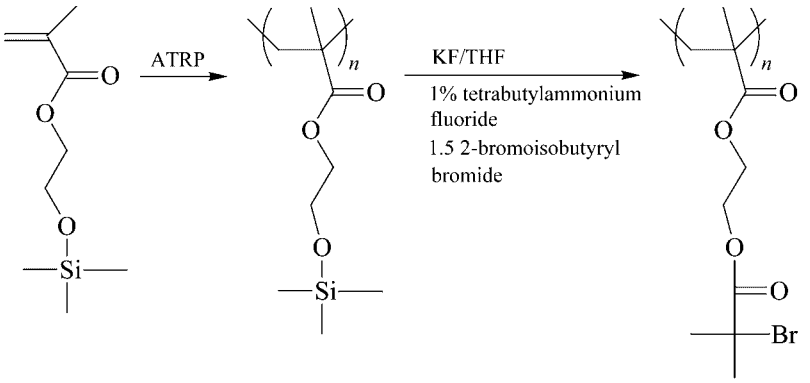

7 (9)

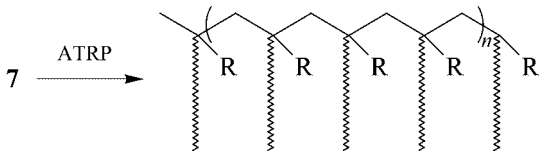

(10)

In a later work, copolymers of PVC with various grafted chains like poly(butyl acrylate), PMMA, PS, and poly(methyl acrylate) were synthesized (43). The backbone was a random copolymer of vinyl chloride and vinyl acetate. The carbonyl substituted alkyl halide groups were used as the initiator for the polymerization of these monomers by ATRP.

Metallocene and ATRP techniques were combined for the synthesis of graft ter- and quaterpolymers poly(ethylene-*co*-styrene) as backbone and one of PS, PMMA, PMMA-*b*-PS, PMMA-*b*-polymethylacrylate, and PMMA-*b*-PHEMA as grafted chain (44). The aromatic rings of styrene were partially brominated and the C–Br groups that were formed were subsequently used as initiating sites for ATRP polymerization.

Block-graft copolymers have also been prepared by the "grafting from" method. Reaction of the block copolymers P(S-*b*-V) (25) with n-C_4H_9Li in THF at -30°C for 1 h leads to metallation of the vinyl groups of the vinyl segments. Then D_3 was added for the formation of P[(S-*b*(VS-*g*-DMS)] block graft copolymers. The molecular characterization revealed that the number of the introduced PDMS branches was between 170 and 325.

The synthesis of the poly[styrene-*b*-(hydroxystyrene-*g*-ethylene oxide)-*b*-styrene] (25), P[S-*b*-(HS-*g*-EO)-*b*-PS], has been reported. The backbone was a triblock copolymer, poly(styrene-*b*-*t*-butoxystyrene-*b*-styrene) (**8**), prepared by anionic polymerization by sequential addition of monomers. The protected *t*-butyl group was removed by treatment with HBr leading to the formation of P(S-*b*-HS-*b*-S) triblocks (**9**) (eq. 11). The metallation of the hydroxyl groups was performed in THF using either cumyl potassium or diphenylethylene potassium (eq. 12). The addition of EO generated the block graft copolymers (eq. 13).

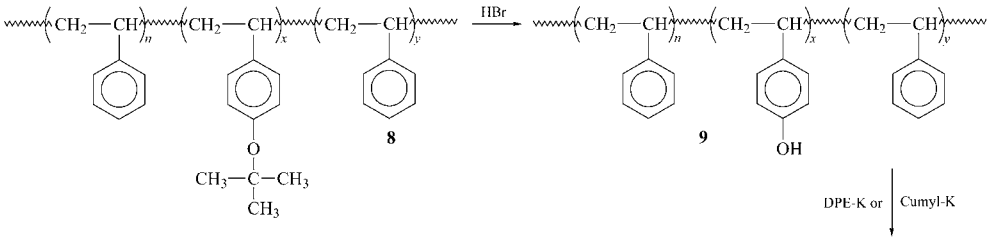

(11)

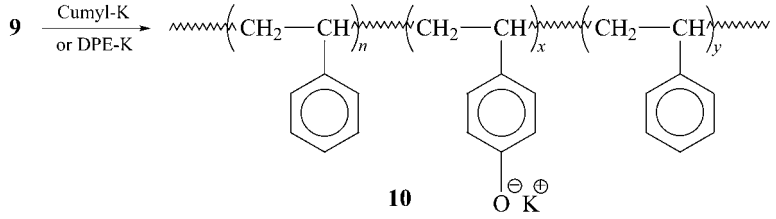

(12)

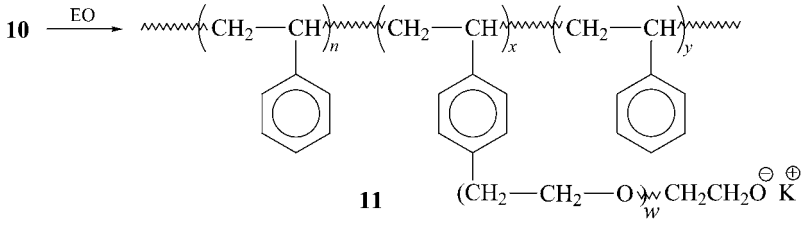

(13)

P(S-*g*-*t*-BMA) and PS-*b*-P(S-*g*-*t*-BMA) block graft copolymers were prepared using TEMPO living and atom transfer radical polymerization techniques (45). The backbone of the P(S-*g*-*t*-BMA) copolymer was synthesized by TEMPO living radical copolymerization of styrene and *p*-chloromethylstyrene. Subsequently, the chloromethyl groups in the presence of CuBr and bipyridine were used as initiation sites of ATRP of *t*-BMA. In the case of PS-*b*-P(S-*g*-*t*-BMA) copolymer, the synthesis was performed in a similar way.

Macromonomer Method. The synthesis of graft copolymers by the macromonomer method is characterized by its own specific features (46–49). The number of branches is determined by the ratio of the macromonomer and comonomer molar concentrations and their copolymerization behavior, described by the reactivity ratios r_1 and r_2. These parameters determine how random the placement of the branches along the backbone will be. It is evident that during the copolymerization the relative concentrations of the macromonomer and the comonomer change with time, leading to the formation of graft copolymers with subsequently different number of branches. In addition, the copolymerization is not homogeneous throughout the course of the reaction since phase separation may occur. For the above reasons it can be concluded that the graft copolymers prepared by this method are generally characterized by increased compositional and chemical heterogeneity.

The synthesis of macromonomers can be accomplished by almost all the available polymerization techniques. Among them, living polymerization methods offer unique control over the molecular weight, the molecular weight distribution, and chain-end functionalization.

Anionic polymerization is one of the best methods for the synthesis of well-defined macromonomers. Functional initiation or termination by a suitable electrophilic reagents are the best ways for the incorporation of the reactive end groups (50). According to this methodology living polystyryllithium initially reacts with ethylene oxide to form the less reactive alkoxide, followed by the reaction with methacryloyl chloride for the synthesis of the macromonomer (eq. 14) (51).

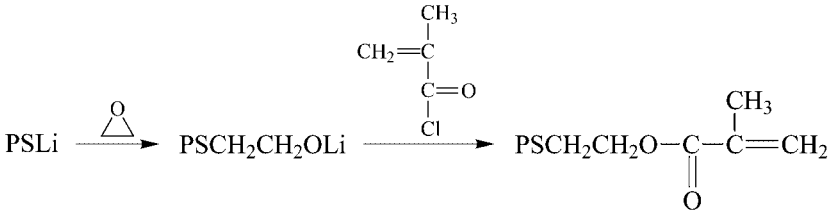

(14)

These macromonomers were then copolymerized with vinyl monomers mainly by free-radical techniques (52) and also other methods as by metallocene catalysts (53) to provide graft copolymers. The reaction of polystyryllithium with *p*-chlorovinylbenzene at low temperatures affords macromonomers with styryl end groups (eq. 15) (54).

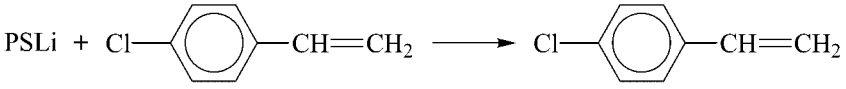

(15)

Allyllithium was used to polymerize hexamethylcyclotrisiloxane, D_3 (eq. 16). Subsequent termination (eq. 17) with chlorotrimethylsilane yielded polydimethylsiloxane (PDMS) macromonomers carrying allyl end groups (55).

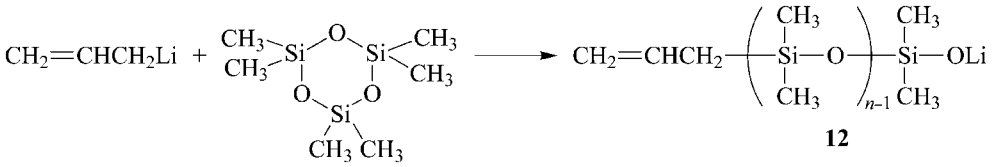

12

(16)

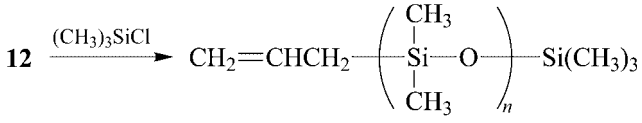

(17)

Examples of graft copolymers synthesized using anionically prepared macromonomers are given in Table 1.

Table 1. Graft Copolymers Prepared by Macromonomers Synthesized Anionically

Macromonomer	End group	Comonomer	Copolymerization	Reference
PS	Methacrylate	MMA	Radical	56,57
PS	*p*-Vinylbenzene	MMA	Radical	54
PS	Norbornene	Norbornene	ROMP	58
PS	*p*-Vinylbenzene	Butadiene	Anionic	59
PS	Methacrylate	Ethyl acrylate	Radical	60
PDMS	Methacrylate	MMA	GTP	61
PMMA	*p*-Vinylbenzene	Styrene	Radical	62
PI	Methacrylate	MMA	GTP	61
PS-*b*-PI	Methacrylate	Styrene	Radical	63
PDMS	Allyl	Ethylene	Ziegler–Natta	55
PDMS	Methacrylate	Styrene	Radical	64
PS-*b*-PDMS	Diol	Diphenylmethyl diisocyanate + butanediol	Polycondensation	65
$P_tC_4H_9$ Ma[a]	*p*-Vinylbenzene	4-Vinylpyridine	Radical	66
PI	*p*-Vinylbenzene	Styrene	Metallocenes	67
PBd	Norbornene	Norbornene	ROMP	68
PEO	Norbornene	Norbornene	ROMP	69
PS	Allyl	Propylene	Metallocene	70
PEO	Methacrylate	Styrene	ATRP	71
PDMS	Methacrylate	MMA	ATRP, radical	72
PS, PI, PDMS	Methacrylate	MMA	Metallocene	53

[a]Poly(*t*-butyl methacrylate).

Cationic polymerization has also been used for the synthesis of macromonomers, especially after the development of living cationic polymerization techniques (73). Macromonomers were prepared by the cationic ring-opening polymerization of tetrahydrofuran (THF) using methyltrifluoromethane sulfonate, followed by termination with 3-sodio-propyloxydimethylvinylsilane to give a macromonomer with vinyl silane end groups (74) (eq. 18).

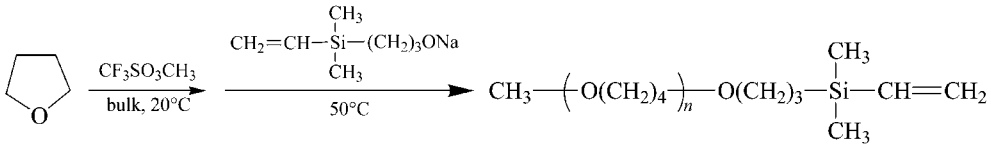

(18)

These macromonomers were copolymerized with vinyl acetate (Vac) using azobisisobutyronitrile (AIBN) as radical initiator to produce PVAc-*g*-PTHF graft copolymers. Subsequent saponification using NaOH provided poly(vinyl alcohol)-*g*-PTHF graft copolymers.

Termination of living PTHF (**13**) with 3-(dimethylamino propyl) isocyanide leads to the formation of macromonomers having end isocyanide groups (75) (eq. 19).

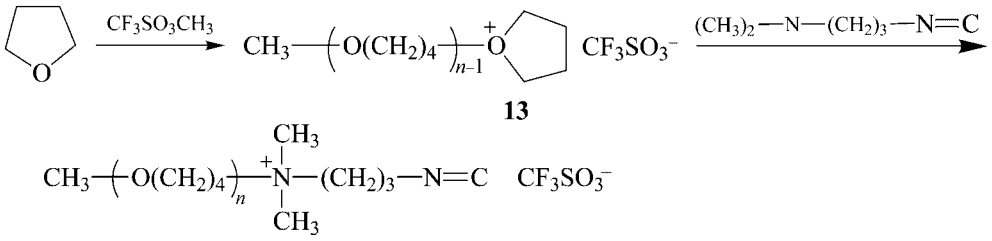

(19)

p-Iodomethylstyrene was used as a functional initiator to promote the polymerization of 2-phenyl-2-oxazoline leading to the formation of macromonomers having styryl end groups (76) (eq. 20).

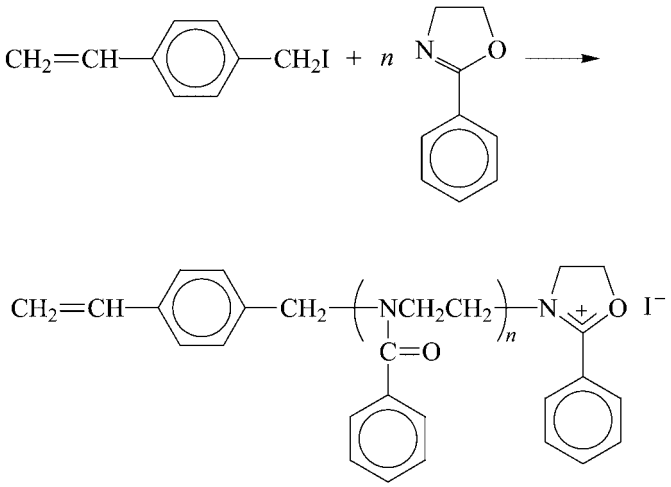

(20)

Radical copolymerization with styrene produced PS-*g*-poly(2-phenyl-2-oxazoline) graft copolymers. Other examples of graft copolymers prepared using macromonomers, which were synthesized by cationic polymerization, are given in Table 2.

Free-radical polymerization has been the most common technique for the synthesis of macromonomers because of its less demanding experimental conditions, the absence of special purification procedures of reagents used, and its

Table 2. Graft Copolymers Prepared by Macromonomers Synthesized by Cationic Polymerization

Macromonomer	End group	Comonomer	Copolymerization	Reference
Poly(2-alkyl-2-oxazoline)	Diethanolamine	ε-Caprolactone + 4,4′-methylene di(phenylisocyanate)	Polycondensation	77
Poly(2-alkyl-2-oxazoline)	(Meth)acrylate			78
PPO, poly (epichlorohydrin)	(Meth)acrylate	Styrene, MMA	Radical	79
Polyisobutylene	Methacrylate	MMA	GTP	80

applicability to a wide variety of monomers. However, the method suffers many disadvantages such as the poor control over the molecular weight, the molecular weight distribution, and the degree of functionalization. The basic method for the incorporation of the functional end groups involves the use of chain-transfer agents (81).

Poly(methyl methacrylate) (PMMA) macromonomers have been prepared using thioglycolic acid as a chain-transfer agent, followed by reaction with glycidyl methacrylate (82) (eq. 21).

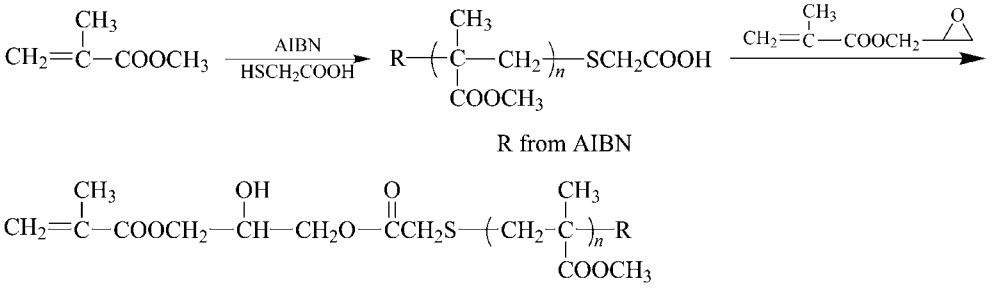

(21)

α-(Bromoethyl) acrylate has been also used as a chain-transfer agent for the synthesis of PMMA macromonomers carrying acrylic end groups (83) (eq. 22).

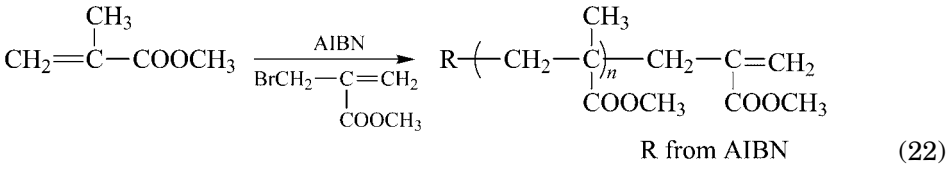

(22)

Table 3 summarizes examples of graft copolymers prepared by macromonomers that were synthesized by free-radical polymerization methods.

The evolution of the living free-radical polymerization techniques (mainly TEMPO (2,2,6,6-tetramethylpiperidinyl-1-oxy) and ATRP methods) very soon led to the synthesis of macromonomers. These methods combine the advantages of the free-radical polymerization with those of the living polymerization techniques, despite the fact that control over the functionalization reaction is not always comparable to the anionic polymerization methods (91,92).

A multifunctional reagent (**14**) containing reactive sites [TEMPO, oxazoline, and *t*-butyl dimethyl silyl protected hydroxyl (TBDMS) group] able to initiate anionic, cationic, and living free-radical polymerization was used to prepare a variety of macromonomers (93). Styrene was polymerized at high temperatures through the alkoxyamine functional group to produce macromonomers with oxazoline end groups (**15**) (eq. 23). Cationic copolymerization of these macromonomers with oxazoline using methyl triflate as initiator leads to the formation of polyoxazoline-*g*-PS graft copolymers.

Table 3. Graft Copolymers Prepared by Macromonomers Synthesized by Free-Radical Polymerization

Macromonomer	End group	Comonomer	Copolymerization	Reference
PMMA	Methacrylate	Acrylic acid	Radical	84
PMMA	Acrylate	Styrene, vinyl chloride, vinyl acetate	Radical	83
Polyvilylpyrrolidone	*p*-Vinylbenzene	Styrene	Radical	85
Poly(4-vinylpyridine)	*p*-Vinylbenzene	Styrene	Radical	85
PMMA	Aromatic dicarboxy	Terephthalic acid + bisphenol	Polycondensation	86
PS	Carboxyl	Ethyl cellulose	UV irradiation	87
PMMA	Dihydroxyl	ε-Caprolactone	Polycondensation	88
Poly(ethyl methacrylate), poly(*n*-butyl methacrylate)	Methacrylate	Methacrylic acid	Radical	89
PMMA	Acrylate	Styrene	ATRP	90

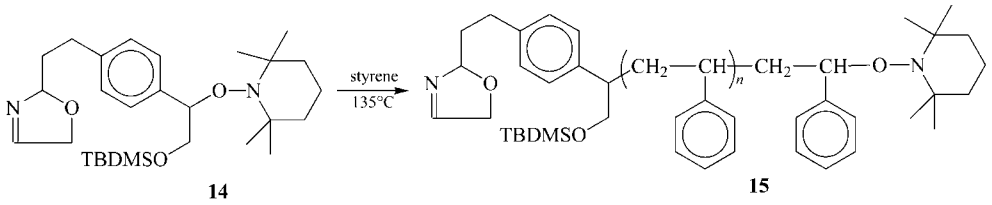

14 **15**

(23)

Poly(dimethylaminoethyl methacrylate) macromonomers were prepared by ATRP using allyl 2-bromoisobutyrate (ABIB, (**16**))/CuBr/tris[2-di(butyl acrylate) aminoethyl] amine, (BA6-TREN) or allyltrichloroacetamide/CuBr/BA6-TREN as the initiation systems (94) (eq. 24).

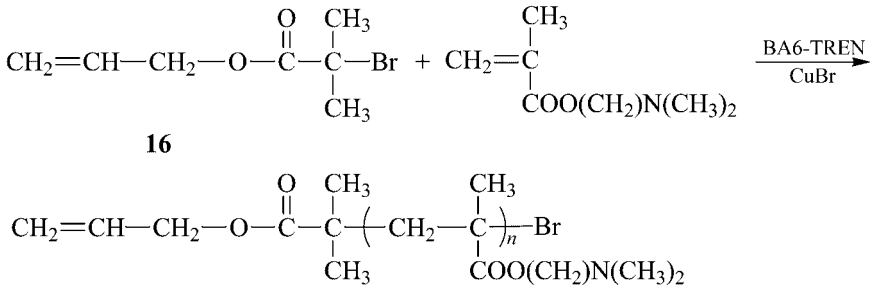

16

(24)

Group transfer polymerization has also been used for the synthesis of macromonomers. The functional end groups are incorporated mainly using the suitable initiation system (95). Trimethylsilyloxy ethyltrimethylsilyl dimethyl ketene was used as initiator for the synthesis of PMMA macromonomers (**17**)

in the presence of tetrabutylammonium benzoate as the catalyst (eq. 25). Treatment with dilute HCl (eq. 26) provided the —OH functional macromonomers (**18**), followed by the reaction with acryloyl chloride to give the final macromonomer structure (96) (eq. 27).

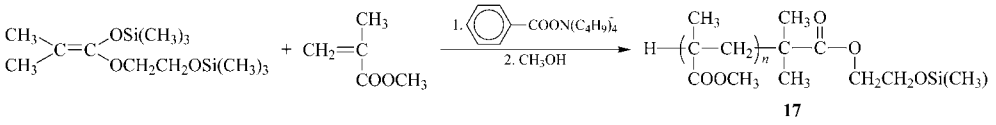

17

(25)

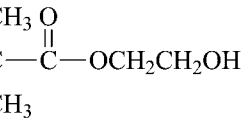

18 (26)

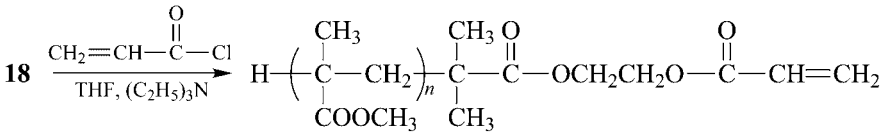

(27)

Polyacrylate macromonomers were prepared using triphenyl phosphine and trimethylchlorosilane in the presence of zinc halide as the catalyst (97) (eq. 28). The resulting polymers (**19**), having trimethylphosphinium end groups, were transformed to the corresponding macromolecular ylide (**20**) by reaction with sodium ethanolate (eq. 29). Subsequent Wittig reaction (eq. 30) of the ylide provides the macromonomer (**21**) where R = methyl, ethyl, or *n*-butyl.

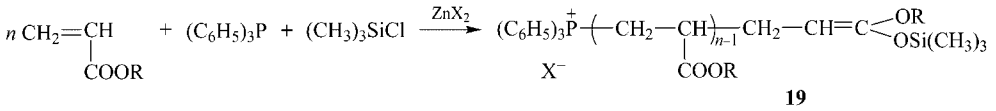

19

(28)

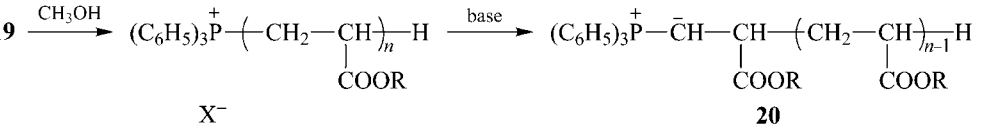

20

(29)

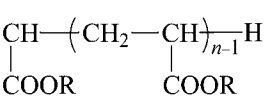

(30)

More examples concerning the synthesis of macromonomers by group transfer polymerization and the subsequent formation of graft copolymers are given in Table 4.

Table 4. Graft Copolymers Prepared by Macromonomers Synthesized by Group Transfer Polymerization

Macromonomer	End group	Comonomer	Copolymerization	Reference
Poly(vinyl alcohol)	*p*-Vinylbenzene	Styrene	Radical	98,99
Poly(2-phenyl-1,3,2-dioxaborole)	*p*-Vinylbenzene	Styrene	Radical	100
Methyl, hexyl, *n*-butyl acrylate	Vinyl	Styrene	Radical	97
PMMA	*p*-Vinylbenzene	Styrene	Radical	101
PMMA	Methacrylate	*n*-Butyl acrylate	ATRP, radical	102

Polycondensation techniques have been employed for the synthesis of macromonomers. Depending on the nature of the functional end group the copolymerization with comonomers can be performed with addition polymerization techniques, giving rise to very interesting graft copolymer structures.

Poly(γ-benzyl-L-glutamate) macromonomers were prepared by polymerization of benzyl(*S*)-3-(2,5-dioxo-1,3-oxazolidin-4-yl)propionate (**21**) (or γ-benzyl-L-glutamate-*N*-carboxyanhydride) using the primary amino group of the *N*-methyl-*N*-4-vinylphenethyl ethylene diamine (**22**)(103,104) (eq. 31).

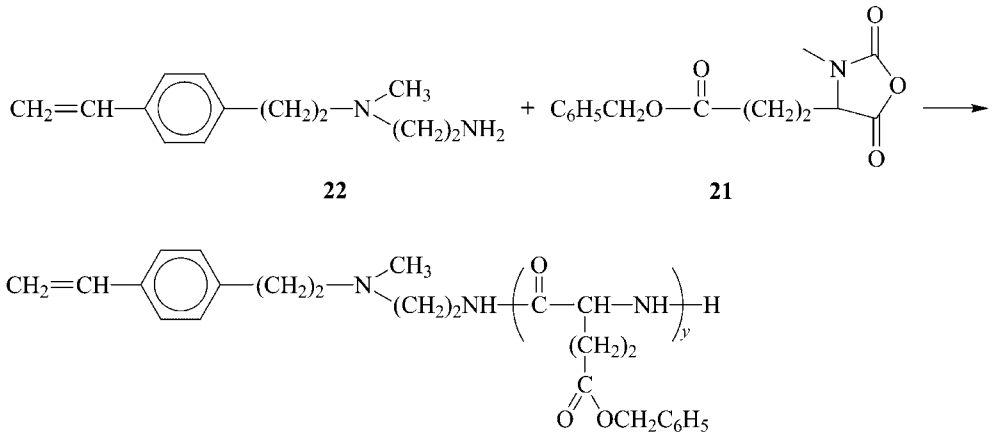

22 **21**

23

(31)

Subsequent reaction with aminoalcohols provides another type of macromonomer with side —OH groups (eq. 32).

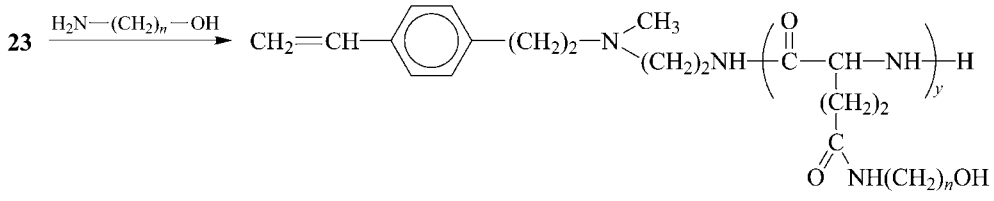

(32)

Table 5. Graft Copolymers Prepared by Macromonomers Synthesized by Polycondensation Methods

Macromonomer	End group	Comonomer	Copolymerization	Reference
Polyguanamine	Isopropenyl substituted triazine	Styrene, MMA	Radical	105
Polyurethane	Methacrylate	MMA	Radical	106,107
Polyamine	*p*-Vinylbenzene	2-Hydroxyethyl methacrylate	Radical	108

Characteristic examples concerning the synthesis of macromonomers prepared by polycondensation reactions and the subsequent formation of graft copolymers are given in Table 5.

Macromonomers have been also prepared by post-polymerization reactions. Poly(ethylene oxide) (PEO) or poly(propylene oxide) (PPO) has one or two —OH end groups depending on the method of their preparation. These —OH groups may react with (meth)acryloyl chloride, *p*-vinyl benzyl chloride, norbornenyl chloride, 4-vinyl benzoyl chloride, etc. for the synthesis of the corresponding macromonomers (109,110) (eq. 33).

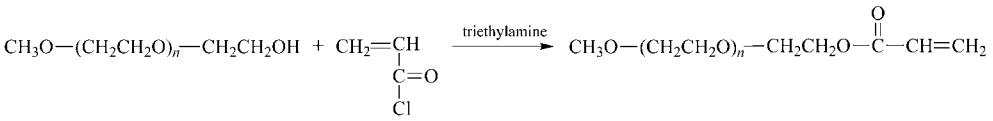

(33)

Hydrosilyl-terminated PDMS chains may undergo hydrosilylation reactions with comonomers having double bonds to produce macromonomers (111,112) (eq. 34).

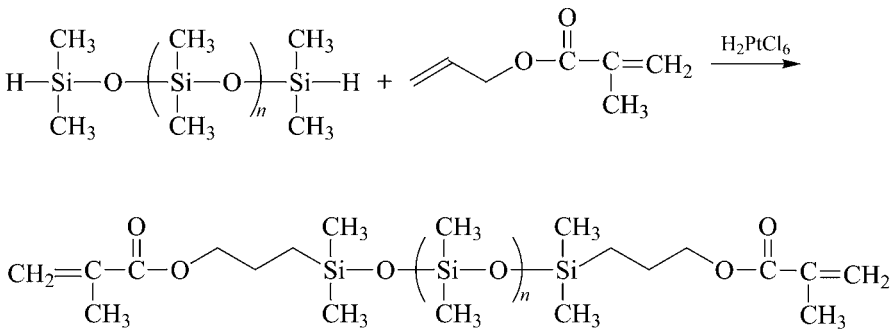

(34)

More examples of macromonomers prepared by post-polymerization reactions are provided in Table 6.

Other methods have also been employed for the synthesis of macromonomers. They do not have always general applicability but can be successfully used in specific cases. For example, polypropylene macromonomers with

Table 6. Graft Copolymers Prepared by Macromonomers Synthesized by Post-Polymerization Reactions

Macromonomer	End group	Comonomer	Copolymerization	Reference
PEO	Acrylate	Styrene	Radical	109
PDMS	Methacrylate	Styrene	Radical	112
PPO	Norbornene	Norbornene derivative	ROMP	113
PEO	*p*-Vinylbenzene	*n*-Butyl methacrylate	Radical	110
PEO	Methacrylate	Acrylamide	Radical	114
Oligo(α-hydroxyalkanoic acid)	Methacrylate	*t*-Butyl acrylate	Radical	115
PEO	Allenyloxy		Coordination polymerization	116

vinylidene end groups were prepared using metallocene-catalyzed polymerization. Bis(cyclopentadienyl)zirconium dichloride/methylaluminoxane (Cp_2ZrCl_2/MAO) and other catalytic systems were used. The olefinic end groups were obtained through the β-hydrogen elimination mechanism. These macromonomers were either used directly to produce graft copolymers after copolymerization with olefins using metallocene catalysts or were transformed to other structures by post-polymerization reactions. Addition of thioacetic acid introduced thiol functional groups, whereas hydroboration and subsequent reaction of the resulting hydroxyl group with methacrylic acid produced methacryloyl-terminated polypropylenes. Radical copolymerization with MMA provided PMMA-*g*-PP graft copolymers (117).

Styryl amylose amide (VAA) was prepared from maltopentose-substituted styrene (VM5A) by phosphorylase-catalyzed polymerization of glucose-1-phosphate (Glu-1P) (118) (Fig. 8). Subsequent radical copolymerization with acrylamide gave the corresponding graft copolymers..

Ring-opening metathesis polymerization was employed for the synthesis of polynorbornene macromonomers (**24**). A well-defined molybdenum initiator of the type $Mo(CHC(CH_3)_2C_6H_5)(N\text{-}2,6\text{-}(i\text{-}C_3H_7)_2C_6H_3)(OR)_2$ [R = $OC(CH_3)_3$, $OCCH_3(CF_3)_2$] was used. The polymers produced were cleaved from the initiator fragment in a Wittig-like reaction using *p*-$(CH_3)_3SiC_6H_4CHO$, according to a well-established method (eq. 35). Deprotection under basic conditions gave macromonomers having phenyl end groups (**25**) (eq. 36). Subsequent reaction with norbornene carboxylic acid chloride yields macromonomers with norbornene end groups (119) (eq. 37).

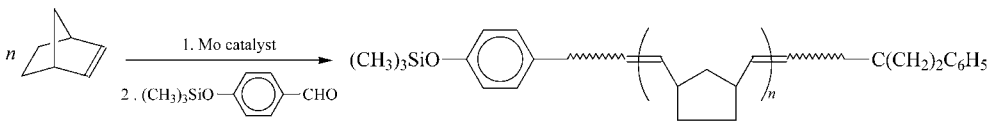

24

(35)

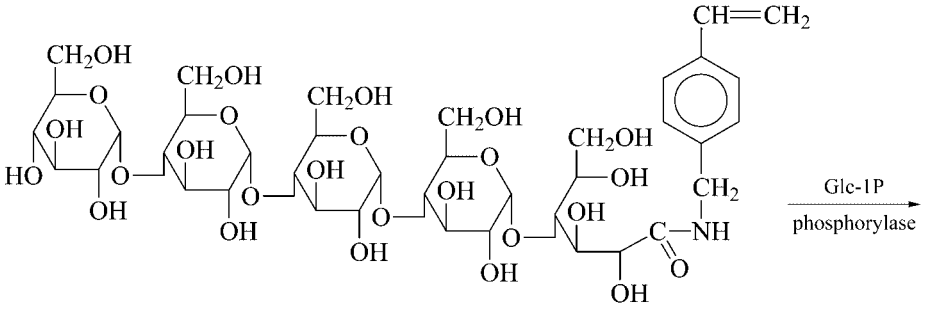

VM5A

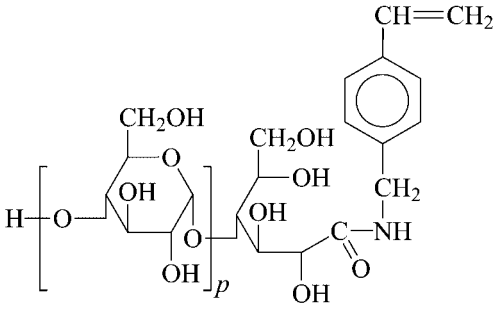

VAA, p = 24 and 158

Fig. 8. Preparation of the macromonomer VAA.

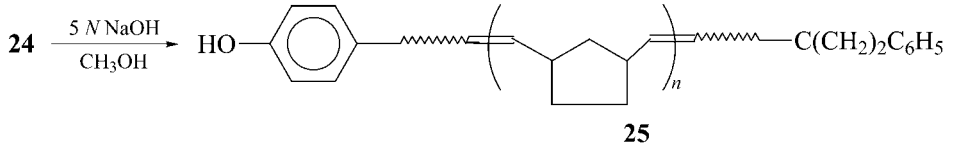

25

(36)

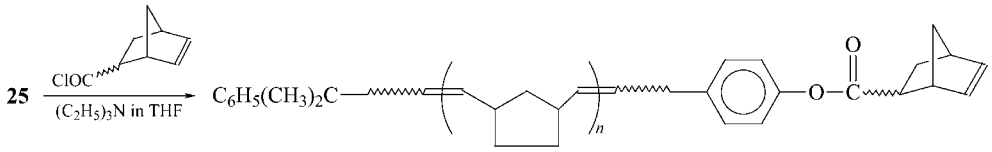

(37)

Regular Graft Copolymers. The term regular graft copolymers corresponds to graft copolymers with identical equally spaced branches along the backbone. Regular graft copolymers of PI-*g*-PS have been prepared. The synthetic approach involves the selective replacement of one chlorine atom of methyltrichlorosilane by PS followed by step-growth polymerization of the produced $(PS)Si(CH_3)Cl_2$ with α,ω-dilithium PI. The polydispersity of the reaction products

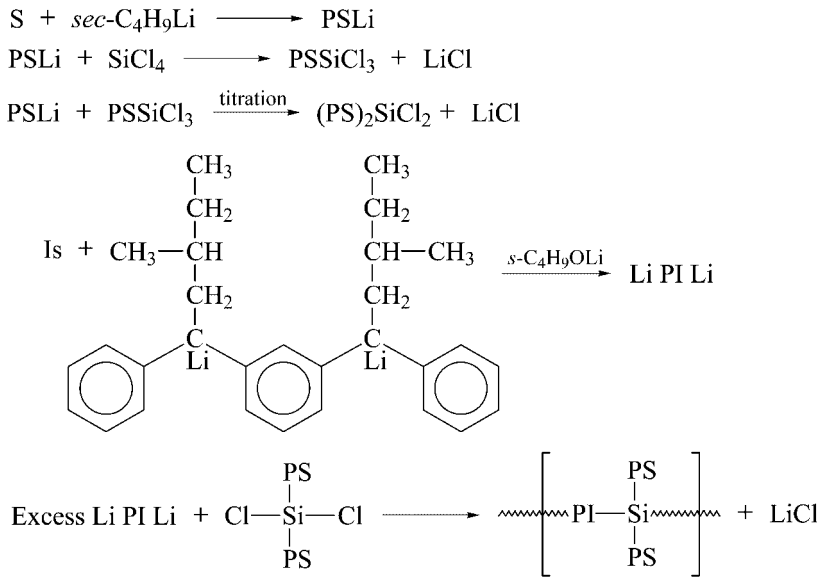

Fig. 9. Synthetic approach to regular PI–PS graft copolymers.

is high ($M_w/M_n = 2.0–3.0$) but it is reduced by fractionation ($M_w/M_n = 1.2–1.5$). By using $SiCl_4$ instead of $Si(CH_3)Cl_3$ and by the replacement of two chlorines by PS, graft copolymers with tetrafunctional branching points are synthesized (120) (Fig. 9).

Exact Graft Copolymers. The term exact graft copolymers refers to molecules where all the molecular and structural characteristics, such as the backbones' and branches' molecular weights and molecular weights distribution, the number of branches, and the specific grafting points on the backbone, can be controlled and varied at will. The parameters that are most difficult to control are the number and the spacing distribution of branches along the backbone chain.

Exact graft copolymers having rather simple structures, ie one or two branches, have been prepared so far. Among these are the A_2B and AA′B single graft copolymers (121–128) and the H- and π-shaped copolymers (129–131) (Fig. 10). Several techniques have been used for the synthesis of these structures and mainly anionic polymerization and controlled chlorosilane chemistry.

A new promising methodology was reported for the synthesis of exact graft copolymers with PI backbone and PS branches (132) (Fig. 11). The method is

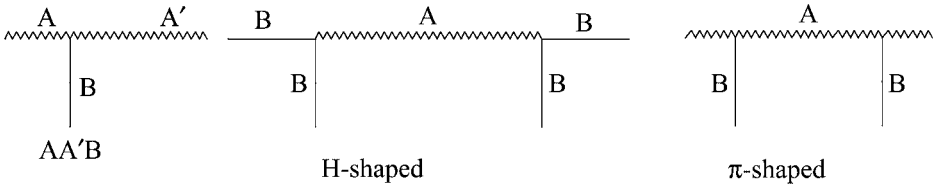

Fig. 10. Exact graft copolymers: AA′B, H-shaped, and π-shaped.

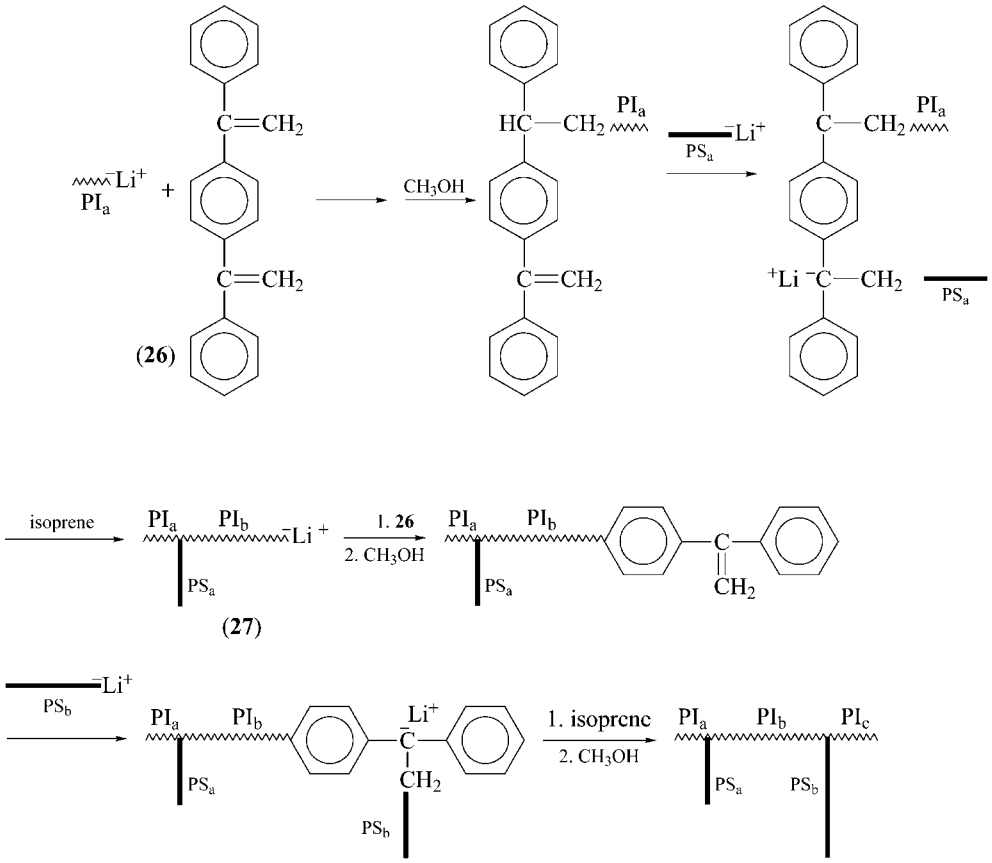

Fig. 11. Synthesis of exact graft copolymers of styrene and isoprene.

based on the use of 1,4-bis(1-phenylethenyl)benzene (**27**), which upon reaction with living polyisoprenyllithium leads to the formation of a PI macromonomer. This macromonomer is subsequently linked with polystyryllithium, followed by the anionic polymerization of isoprene. The living single graft copolymer (**27**) then reacts again with (**26**) and the same reaction sequence is repeated to produce the exact graft copolymer with two branches. In principle it is possible to continue the synthesis of graft copolymers with more branches, using the same reaction series.

Purification and Molecular Characterization of Graft Copolymers

Molecular characterization is an essential step in the study of graft copolymers since the knowledge that is gained is essential in deducing the structure–property relationships. Graft copolymers, like all copolymers, may present molecular weight, compositional, and architectural (distribution in the number of branches and the position of the branching points) heterogeneity (133–135). Following the synthesis of graft copolymers, the next step is to thoroughly characterize the

obtained samples in order to determine their average molecular weight, average composition, molecular and compositional homogeneity and obtain information on the architectural characteristics of the material. Additionally, information about the molecular size of the individual macromolecule may be desired. Because of the imperfections present in the synthetic methodology used for the preparation of nearly every synthetic macromolecule, the resulting material is a very complex system whose identity can only be revealed by the employment of a combination of analytical techniques (133,135).

Sometimes a number of purification procedures must be followed before the desired materials can be isolated and characterized. Graft copolymers may contain varying amounts of impurities, like homopolymers (ie, backbone or branches resulting from incomplete coupling) or copolymers of different architecture, as a result of the synthetic strategy followed for their preparation. These heterogeneities in all cases affect the final properties of the material. Fractionation is a powerful tool usually employed to separate heterogeneous mixtures of polymers before the final characterization of each fraction (134). Copolymers can be fractionated according to their molecular weight or chemical composition (135). The mostly used fractionation methods that result in the isolation of actual samples (fractions) are batch fractionation and column-elution fractionation. In some cases extraction with solvents selective for a specific impurity can be used, ie, in separating excess homopolymer branches.

Determination of Molecular Weight, Constitution, and Composition. Many analytical techniques are available for the determination of the primary molecular structure of a block copolymer and its average chemical composition. Among them spectroscopic techniques used for low molecular weight compounds are the most powerful and most widely employed. NMR can provide both qualitative and quantitative information with respect to comonomer composition and stereochemical configuration of polymeric molecules (136,137). The IR technique provides information on chemical, structural, and conformational aspects of polymeric chains (138). Because of the inherently high sensitivity of UV spectroscopy the technique is often utilized for the identification and quantitative determination of comonomers in block copolymers.

The average molecular weight of block copolymer is a very important parameter that characterizes a certain copolymer sample and it is strongly related with the properties of the polymeric material. Therefore, its determination and knowledge is imperative in the study of these materials. A variety of techniques are available for the determination of different average molecular weights of graft copolymers and polymers in general. These include membrane osmometry and light scattering for the determination of the absolute values of M_n and M_w respectively (133). In the case of light scattering it should be always kept in mind that the M_w obtained is apparent, unless the dn/dc is high for all parts of the graft copolymer (backbone and branches) and the material is characterized by high molecular weight and compositional homogeneity. Knowledge of the molecular weights of the individual components of the graft copolymer can be combined with the determination of the total molecular weight in order to determine the average number of branches per macromolecule. This determination can be aided by the selective sampling of individual parts of the graft copolymer during synthesis, when this is possible, or selective degradation of a part of the macromolecule

after isolation of the product. Size exclusion chromatography (sec) has emerged as a powerful analytical technique for the determination of molecular weight and molecular weight and composition distribution of block copolymers (139). A number of different types of mass/concentration and molecular mass detectors have been developed so far for simultaneous use in sec instruments, providing a large amount of information in a single run.

In cases where the molecular size of the graft copolymer must be known in solution, several methods can be applied. These include primarily static and dynamic light scattering, small-angle neutron and x-ray scattering, and viscometry. Static light, small-angle neutron (sans) and x-ray (saxs) scattering provide information for the radius of gyration of isolated chains (or parts of them using sans and contrast variation techniques) whereas dynamic light scattering and viscometry measure the hydrodynamic radius and properties of the molecules (133,140,141).

Properties and Uses

Solution Properties. Graft copolymer properties in solutions have been studied extensively for many decades. Because of the arrangement of branches along the backbone certain changes in its conformation and effective stiffness are observed. Studies on model graft copolymers have shown that the conformation of the whole molecule becomes more extended compared to linear chains (32,122,142). The phenomenon is more pronounced in the case of polymacromonomers (graft copolymers that are derived from the homopolymerization of macromonomers) where each repeating unit of the backbone carries a polymer chain (143–147). Crowding effects are maximal in this case, resulting in an increased induced stiffness on the backbone and a bottlebrush conformation. This specific conformation can impart interesting rheological properties in the corresponding solutions of polymacromonomers.

Detailed light scattering investigations were performed in the case of poly(isoprene-*g*-styrene) block copolymers in thermodynamically good solvents, isorefractive for different parts of the molecule (32). This technique enabled the determination of the size of the backbone and the branches independently, leading to the conclusion that segregation exists between the backbone and the grafts even in nonselective solvents and the molecule adopts a more or less core–shell structure.

In solvents selective for one of the parts of the molecule, graft copolymers show the ability for micelle formation (148–157). Micelles with cores comprised from the insoluble part and coronas comprised from the soluble one are formed. However, aggregation numbers and size of the micelles are lower than the corresponding ones for linear block copolymers. Critical micelle concentrations are also higher in the case of graft copolymers. This was attributed to the additional constraints imposed to micelle formation because of the presence of a large number of branching points along the backbone. Ideally these branching points should be situated at the micelle core–corona interface, a requirement that increases the free energy of the system as excluded volume effects between the branches and conformational entropy due to looping of backbone are increased. As a result of the molecular architecture, unimolecular micelles of graft copolymers are more easily

formed especially in the case where the solvent is selective for the branches (151–153). In this case the backbone can adopt a collapsed conformation protected from unfavorable interactions with the solvent molecules by the well-solvated branches forming the corona. The increased number of branches favors the stabilization of the structure in solution.

Morphology. The peculiar macromolecular architecture of graft copolymers also influences their bulk properties. The arrangement of a relatively large number of branching points along one of the constituent chains (the backbone) imparts some additional constraints in the formation of microphases and the geometry of the final microstructure. Macrophase separation cannot be excluded in graft copolymer systems where there is a large molecular, compositional, and architectural heterogeneity. Nevertheless, the bulk morphology of a graft copolymer substantially influences other properties of the material (mechanical, rheological, optical, etc). Therefore, elucidation of equilibrium morphology and factors affecting ordering are essential in the design of new materials for specific applications.

The effect of chain architecture on the phase separation, order–disorder transition, and final morphology of graft copolymer systems has been investigated both experimentally (123,127,129–131,158–161) and theoretically (162–164). Studies on model graft copolymers elucidated, using transmission electron microscopy (TEM) and saxs or sans, many aspects of microphase separation of these complex macromolecules. In general, microphase separation and long-range order decrease as the number of branches increases. The morphology of graft copolymers can be predicted from the four morphologies of the simple constituting units which is a miktoarm star copolymer. The same is valid in the case of π and H exact graft copolymers (Fig. 12).

This is attributed to the presence of the branching points. Each one of them can be considered as a point where interfacial curvature between the two phases changes, and this causes severe frustration during the organization of macromolecules within the microphases. Consequently, microdomain sizes and grain structure are altered.

Mechanical Properties. The viscoelastic and mechanical properties of bulk graft copolymers are directly connected to their morphology, which in turn depends on the molecular characteristics of the copolymer. Chemical nature of the backbone and grafts and their mutual solubility as well as the molecular weight and the degree of branching are the primary parameters affecting the mechanical properties of such systems (165–167). For example, Young's modulus, stress at break, toughness and yielding stress for poly(butyl acrylate-*g*-styrene) graft copolymers were found to increase, whereas yield elongation decreased as the number of branches increased (at the same branch molecular weight) (165) (Fig. 13).

This behavior was identified as a result of the increase in the hard phase (PS) content in the graft copolymer. Grafting of styrene and vinylacetate onto EPDM (ethylene–propylene–diene terpolymer) improved the tensile strength of the resulting material in comparison to ungrafted EPDM, whereas grafting of N-substituted acrylamides on EPDM gave copolymers with decreased tensile strength (166). Poly(isoprene-*g*-styrene) copolymers with tetrafunctional branch points were found to have increased strain at break (167) than the commercial thermoplastic elastomers (Fig. 14). The mechanical properties of polymeric blends

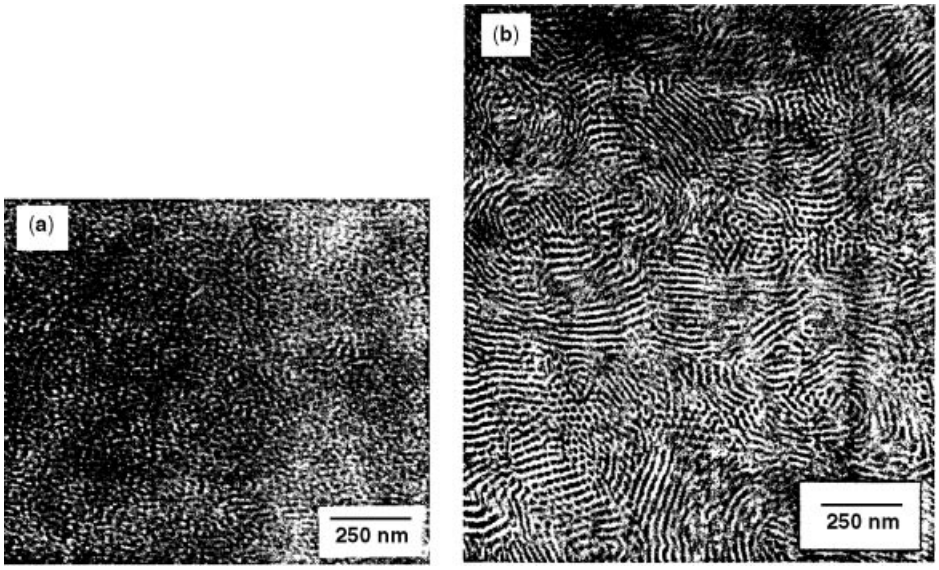

Fig. 12. (**a**) Transmission electron microscopy image of poly(butadiene-*g*-styrene) randomly branched graft copolymers with two PS branches on every grafting point. (**b**) Corresponding image for a poly(isoprene-*g*-styrene) regular graft copolymer with two PS branches on every grafting point. The copolymers contain approximately 61% and 67% by volume PS respectively. Notice the poor long-range order and the grain structure characteristics. From Refs. 158 and 159.

compatibilized with graft copolymers have received a relatively larger attention (168–171).

Compatibilization of Polymer Blends. Polymer blending is one of the most general, flexible, and efficient methods for generating new polymeric high performance materials (172). The resulting polymer mixture combines the properties of its components. These properties may in principle be varied by changing the blend composition according to the desired final performance of the material. However, because of entropic reasons, the majority of polymer pairs are incompatible. Graft copolymers are widely used as compatibilizing agents of immiscible blends (172–182). The different parts of a graft copolymer can be chosen and synthesized in such a way that interactions with the constituents of the blends are maximized. The constituents of the graft copolymer may have the same chemical structure with either the components of the blend or a chemical constitution (ie, complementary functional groups) that favors the interactions with the functional groups of the components. In this way graft copolymers are aiding in the adhesion of the different phases by forming a bicompatible interface. The interface reduces the interfacial energy between the phases in the blend and permits a more stable and finer dispersion of the components. The resulting mechanical properties of the formulation are improved since strong adhesion of phases helps in assimilating stresses and stains without disruption of the blend's morphology. The possibility of morphology changes during processing conditions is also minimized. A more recent compatibilization methodology, namely reactive blending, involves the formation of block or graft copolymers *in situ* (183–193). The method relies on the use

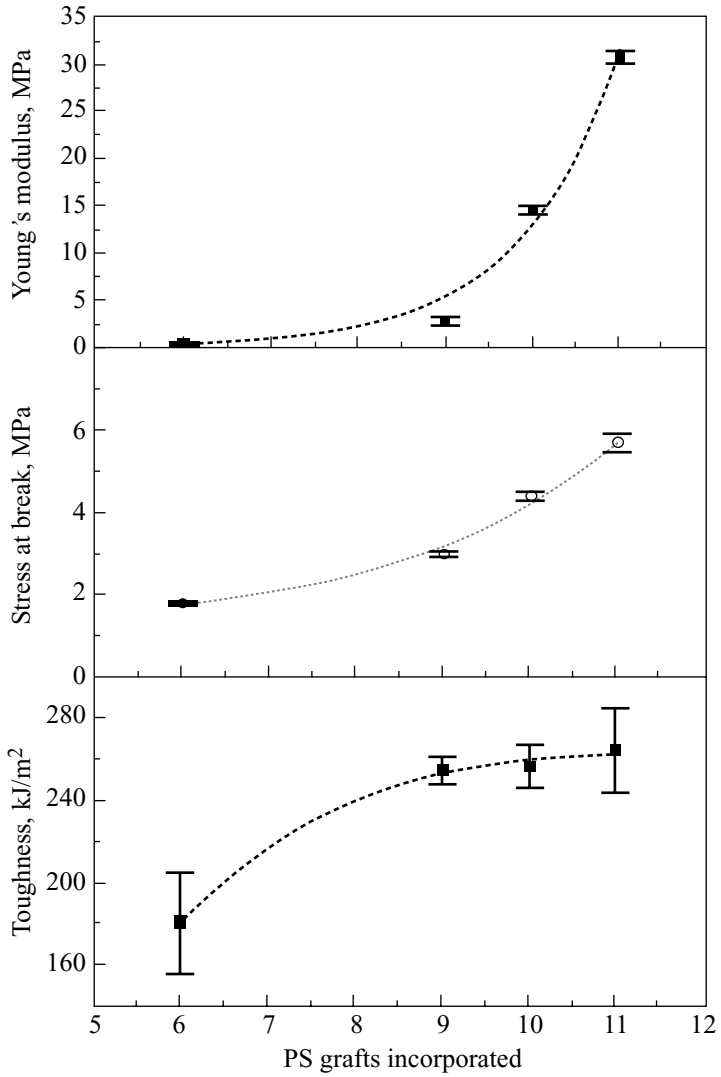

Fig. 13. Variation of the Young's modulus (E), tensile strength at break (σ_B), and toughness as a function of the number of PS grafts on the backbone for a poly(n-butyl methacrylate-g-styrene) graft copolymer prepared by the macromonomer technique. To convert MPa to psi, multiply by 145, to convert kJ/m^2 to ft·lbf/in.^{2}, divide by 2.10. From Ref. 165.

of reactive functionalities previously incorporated in one or more polymers of the blend for the production of block or graft copolymers after mixing the individual components and during melt-processing. This concept has been applied to a number of blend systems such as polyamide/polyolefins, polyamide/ABS, PS/olefins, polyester/polyamide using different types of reactions that can occur rapidly at elevated processing temperatures.

Other Present and Potential Applications. Graft copolymers are steadily assuming an increased importance because of their tremendous industrial

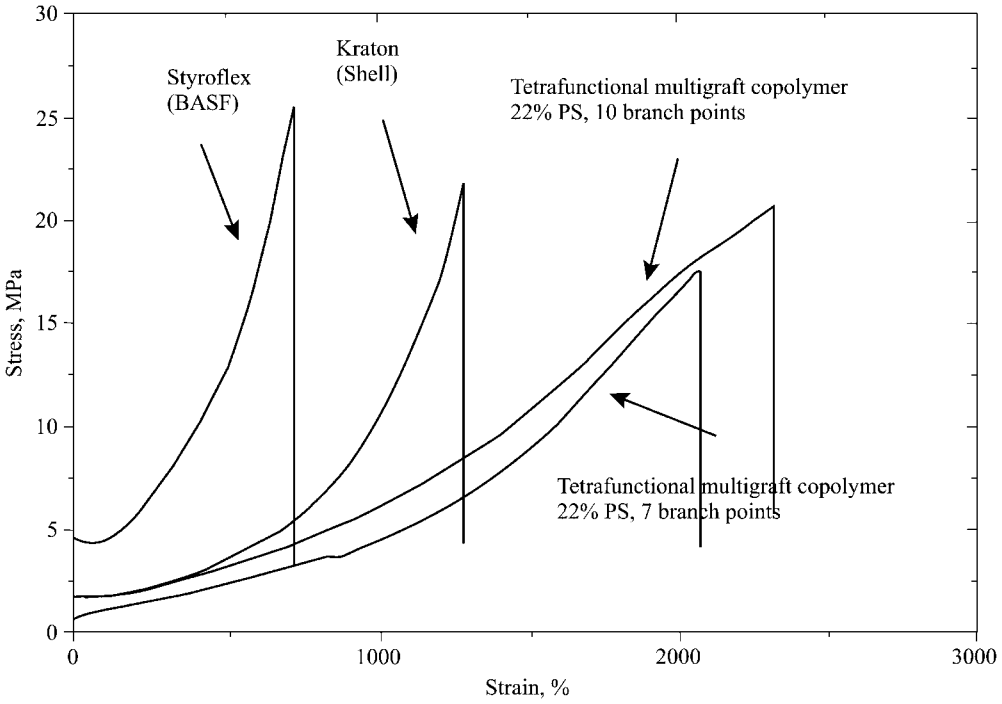

Fig. 14. Comparison of the mechanical properties of tetrafunctional multigraft poly(isoprene-*g*-styrene) copolymers with commercial Styroflex and Kraton copolymers. From Ref. 167.

application potential (194–205). Graft copolymers of commercial utility include ABS, obtained by grafting acrylonitrile and styrene monomers onto polybutadiene, high impact polystyrene, a family of poly(butadiene-*g*-styrene) materials, alkali-treated cellulose-*g*-acrylonitrile and starch-*g*-acrylonitrile which are used as "superabsorbent" components in diapers, sanitary napkins, and the like. Graft copolymers containing acrylic monomers are used as pressure-sensitive adhesives (197). Other graft copolymers are essential materials in oil recovery operations. A large number of commercial paint, printing, and coating formulations involve graft copolymers as dispersion stabilizers, rheology modifiers, and final coating properties improvers (eg, corrosion resistivity, environmental compatibility, etc.) (198–205).

The potential of using graft copolymer micelles and nanoparticles derived from graft copolymers as drug carriers for controlled drug delivery systems and for environmental purification methodologies is high (206–211). These applications rely on the ability of the micelles to solubilize low molecular weight compounds in their cores. By controlling the molecular characteristics of the copolymers and the chemical nature of the corona, drug containing vehicles of the desired size, loading capacity, release kinetics, targeting capabilities, biocompatibility and biodegradability can be produced. Formulations in the gel and bulk state are also candidates for this kind of application. Size and loading capabilities of the micellar microcontainers are also important in water treatment systems. The application of graft

copolymer membranes in separation processes, like removal of deleterious organic compounds from contaminated drinking water, is also of interest (212–214). With judicious choice of chemical components in conjunction with graft copolymer morphology design, perselectivity and permeability of the resulting membranes can be adjusted.

Graft Copolymer Production/Consumption

It is difficult to accurately measure the amount of graft copolymers produced commercially. Here we refer to those polymers made either by the reaction of two polymers with each or by the growth of a chain of one monomer from a polymer made of a different one. In each case one has a nonlinear structure where the various segments of the resultant polymer (ie, backbone, branches, etc.) are chemically different. The difficulty in determining how much of this kind of polymer is produced is that it is done in many ways, and it is not even clear whether the producers are always cognizant of what they have made. The grafting often occurs during a mixing process, and the graft polymer itself is not separated from the other components of the blend. However, it is clear that graft copolymer technology is crucial to the modern plastics industry and that graft copolymers are present in a large fraction of the plastic materials made today.

The largest portion of this can be found in the styrenic polymers. Impact polystyrene [often called high impact polystyrene (HIPS)] is produced by polymerizing styrene monomer in the presence of polybutadiene. This results in grafting of some of the growing PS chains to the PB ones, giving good impact strength to the final product. Of the 12.7 million tons (10^6 t) of PS made worldwide each year (215), perhaps a quarter to a third is HIPS (216–218). ABS is made in a similar fashion as HIPS, except that acrylonitrile is also added to the styrene as a polymerizing monomer (219–222). About 4.9×10^6 t of this polymer is made each year. The next most common use of grafting is probably in the "super-tough" polyamides, made by a grafting reaction between the polyamide and a functionalized ethylene–propylene rubber (223–227). Perhaps 10–20% of the 1.8×10^6 t of polyamide is made this way. There are many other uses of graft copolymers, mostly for compatibilizing various polymer blends (228). As stated above, it is difficult to capture the amount of these made. However, it is safe to say that between 5 and 10% of the 141×10^6 t of plastics made each year contain a significant fraction of graft copolymer.

BIBLIOGRAPHY

"Block and Graft Copolymers" in *EPST* 1st ed., Vol. 2, pp. 485–528, by R. J. Ceresa, W. R. Grace & Co.; Suppl. Vol. 2, pp. 129–158, by M. Matzner, L. M. Robeson, and A. Noshay, Union Carbide Corp., and J. E. McGrath, Virginia Polytechnic Institute and State University; "Graft Copolymers" in *EPSE* 2nd ed., Vol. 7, pp. 324–434, by P. Dreyfuss, Michigan Molecular Institute, and R. P. Quirk, University of Akron.

1. Basic Definitions of Terms Relating to Polymers, *Pure Appl. Chem.* **40**, 482 (1974).
2. W. Ring and co-workers, *Pure Appl. Chem.* **57**, 1427 (1985).

3. R. J. Ceresa, ed., *Block and Graft Copolymerization*, Vol. **1**, Wiley-Interscience, New York, 1973.
4. D. J. Meier, *J. Polym. Sci., Part C* **26**, 81 (1969).
5. E. Helfand, *Macromolecules* **8**, 552 (1975).
6. E. Helfand and Z. R. Wasserman, *Macromolecules* **9**, 879 (1976).
7. E. Helfand, *Acc. Chem. Res.* **8**, 295 (1975).
8. M. Pitsikalis and co-workers, *Adv. Polym. Sci.* **135**, 1 (1998).
9. F. Candau, F. Afchar-Taromi, and P. Rempp, *Polymer* **18**, 1253 (1977).
10. D. Rahlwes, J. Roovers, and S. Bywater, *Macromolecules* **10**, 604 (1977).
11. J. Roovers, P. Toporowski, and J. Martin, *Macromolecules* **22**, 1897 (1989).
12. M. George and co-workers, *Polymer* **28**, 1217 (1987).
13. J. Selb and Y. Gallot, *Polymer* **20**, 1259 (1979).
14. J. Selb and Y. Gallot, *Polymer* **20**, 1273 (1979).
15. S. Ishikawa, *Macromol. Chem. Phys.* **196**, 485 (1995).
16. Z. Yousi and co-workers, *Polymer* **39**, 2665 (1998).
17. H. Watanabe and co-workers, *Macromolecules* **27**, 2336 (1994).
18. H. Derand and B. Wesslen, *J. Polym. Sci., Polym. Chem. Ed.* **33**, 571 (1995).
19. H. Zhang and E. Ruckenstein, *Macromolecules* **31**, 4753 (1998).
20. E. Ruckenstein and H. Zhang, *Macromolecules* **32**, 6082 (1999).
21. H. Zhang and E. Ruckenstein, *Macromolecules* **32**, 5495 (1999).
22. G. Bokias and co-workers, *Macromolecules* **34**, 4958 (2001).
23. M. Xenidou and N. Hadjichristidis, *Macromolecules* **31**, 5690 (1998).
24. K. Se and co-workers, *Polym. Prepr.* **29**(2), 110 (1988).
25. K. Se and co-workers, *Polym. Prepr.* **29**(2), 112 (1988).
26. M. Kawabe and M. Murata, *Macromol. Chem. Phys.* **202**, 1799 (2001).
27. T. Tsoukatos, S. Pispas, and N. Hadjichristidis, *Macromolecules* **33**, 9504 (2000).
28. G. Velis and N. Hadjichristidis, *J. Polym. Sci., Polym. Chem. Ed.* **38**, 1136 (2000).
29. J. Falk, R. Schlott, and D. J. Hoeg, *Macromol. Sci. Chem.* **7**, 1647 (1973).
30. J. Falk and co-workers, *Macromol. Sci. Chem.* **7**, 1669 (1973).
31. J. Falk and co-workers, *Rubber Chem. Technol.* **46**, 1044 (1973).
32. N. Hadjichristidis and J. Roovers, *J. Polym. Sci., Part A: Polym. Chem.* **16**, 851 (1978).
33. M. M. F. Al-Jarrah, J. K. H. Al-Kafaji, and R. L. Apikian, *Brit. Polym. J.* **18**, 256 (1986).
34. M. Kowalczuk, G. Adamus, and Z. Jedlinski, *Macromolecules* **27**, 572 (1994).
35. T. Chung, H. Lu, and R. Ding, *Macromolecules* **30**, 1272 (1997).
36. G. Sinai-Zingde and co-workers, *Polym. Prepr.* **31**(1), 63 (1990).
37. C. Schulz and A. Dworak, *Macromol. Symp.* **85**, 203 (1994).
38. B. Pary and co-workers, *Eur. Polym. J.* **21**, 393 (1985).
39. J. Rueda-Sanchez and M. Galloso, *Macromol. Rapid Commun.* **22**, 859 (2001).
40. R. Jones and S. Holder, *Macromol. Chem. Phys.* **198**, 3571 (1997).
41. U. Stehling and co-workers, *Macromolecules* **31**, 4396 (1998).
42. K. Beers, S. Gaynor, and K. Matyjaszewski, *Macromolecules* **31**, 9413 (1998).
43. H. Paik, S. Gaynor, and K. Matyjaszewski, *Macromol. Rapid. Commun.* **19**, 47 (1998).
44. S. Liu and A. Sen, *Macromolecules* **34**, 1529 (2001).
45. P. Moschogianni, S. Pispas, and N. Hadjichristidis, *J. Polym. Sci., Polym. Chem. Ed.* **39**, 650 (2001).
46. P. Rempp and E. Franta, *Adv. Polym. Sci.* **58**, 1 (1984).
47. T. Corner, *Adv. Polym. Sci.* **62**, 95 (1984).
48. T. Saegusa, *Topics Curr. Chem.* **100**, 75 (1982).
49. P. Rempp and E. Franta, in T. E. Hogen-Esc and J. Smid, eds., *Recent Advances in Anionic Polymerization*, Elsevier, New York, 1987 p. 353.

50. H. L. Hsieh and R. P. Quirk, *Anionic Polymerization: Principles and Practical Applications*, Marcel Dekker Inc., New York, 1996.
51. G. O. Schulz and R. Milkovich, *J. Appl. Polym. Sci.* **27**, 4773 (1982).
52. G. O. Schulz and R. Milkovich, *J. Polym. Sci., Polym. Chem. Ed.* **22**, 1633 (1984).
53. C. Batis and co-workers, *Macromolecules* **25**, 8925 (2000).
54. S. Tanaka and co-workers, *Polymer* **36**, 2219 (1995).
55. W. Li and B. Huang, *Makromol. Chem.* **190**, 2373 (1898).
56. S. Teramachi and co-workers, *Macromolecules* **25**, 4025 (1992).
57. H.-Q. Xie and Y. Liu, *Eur. Polym. J.* **27**, 1339 (1991).
58. R. L. Norton and T. J. McCarthy, *Polym. Prepr.* **28**(1), 174 (1987).
59. M. Arnold, W. Frank, and G. Reinhold, *Polym. Bull.* **24**, 1 (1990).
60. D. G. Peiffer and M. Rabeony, *J. Appl. Polym. Sci.* **51**, 1283 (1994).
61. A. M. Hellstern, S. D. Smith, and J. E. McGrath, *Polym. Prepr.* **28**, 328 (1987).
62. K. Hatada and co-workers, *Polym. Bull.* **19**, 231 (1988).
63. G. O. Schulz and R. Milkovich, *Ind. Eng. Chem. Prod. Res. Dev.* **25**, 148 (1986).
64. G. G. Gordon and M. S. Chisholm, *Polymer* **26**, 437 (1985).
65. Y. Tezuka, S. Nobe, and T. Shiomi, *Macromolecules* **28**, 8251 (1995).
66. K. Ishizu and K. Mitsutani, *Makromol. Chem.* **189**, 2875 (1988).
67. K. Endo and K. Senoo, *Macromol. Rapid Commun.* **19**, 563 (1998).
68. V. Heroquez and co-workers, *Macromol. Chem. Phys.* **199**, 1405 (1998).
69. V. Heroquez and co-workers, *Macromolecules* **29**, 4459 (1996).
70. O. Henschke, A. Neubauer, and M. Arnold, *Macromolecules* **30**, 8097 (1997).
71. Y. Wang and J. Huang, *Macromolecules* **31**, 4057 (1998).
72. H. Shinoda, P. J. Miller, and K. Matyjaszewski, *Macromolecules* **34**, 3186 (2001).
73. M. Sawamoto and M. Kamagaito, in J. R. Ebdon and G. C. Eastmond, eds., *New Methods of Polymer Synthesis*, 1st ed., Vol. **2**, Chapman & Hall, London, 1995, p. 37.
74. Y. Tezuka, A. Okabayashi, and K. Imai, *Macromol. Chem.* **190**, 753 (1989).
75. B. Grassl, S. Rempp, and J. C. Galin, *Macromol. Chem. Phys.* **199**, 239 (1998).
76. R. C. Schulz and E. Schwarzenbach, *Makromol. Chem., Macromol. Symp.* **13/14**, 495 (1988).
77. S. Kobayashi, H. Uyama, and H. Shirasaka, *Makromol. Chem., Rapid Commun.* **11**, 11 (1990).
78. S. Kobayashi and co-workers, *Macromolecules* **22**, 2878 (1989).
79. T. Biendron and co-workers, *Polym. Int.* **36**, 73 (1995).
80. A. Tacacs and R. Faust, *J. Macromol. Sci., A: Pure Appl. Chem.* **33**(2), 117 (1996).
81. G. Odian, *Principles of Polymerization*, 2nd ed., Wiley-Interscience, New York, 1981.
82. Y. Yamashita and co-workers, *Polym. J.* **14**, 255 (1982).
83. B. Yamata and co-workers, *Polym. Bull.* **25**, 423 (1991).
84. H.-Q. Xie, G.-C. Xu, and J.-S. Guo, *J. Macromol. Sci., A: Pure Appl. Chem.* **29**, 263 (1992).
85. K. Yoshinaga, T. Yokoyama, and T. Kito, *Polym. Adv. Technol.* **4**, 38 (1993).
86. Y. Chujo, H. Kobayashi, and Y. Yamashita, *J. Polym. Sci., Polym. Chem. Ed.* **27**, 2007 (1989).
87. E. A. Abdel Razik, *J. Photochem. Photobiol., A* **73**, 53 (1993).
88. S. Rimmer and M. H. George, *Eur. Polym. J.* **29**, 205 (1993).
89. Y. Tsukahara and co-workers, *J. Polym. Sci., Polym. Chem. Ed.* **27**, 1099 (1989).
90. S. A. F. Bon and co-workers, *Macromolecules* **33**, 5819 (2000).
91. E. E. Malmstrom and C. J. Hawker, *Macromol. Chem. Phys.* **199**, 923 (1998).
92. K. Matyjaszewski, ed., *Controlled Radical Polymerization*, (ACS Symposium Series No. 685), American Chemical Society, Washington, D.C., 1997.

93. R. D. Puts and D. Y. Sogah, *Macromolecules* **30**, 7050 (1997).
94. F. Zeng and co-workers, *Macromolecules* **33**, 1628 (2000).
95. D. Y. Sogah and O. W. Webster, *Macromolecules* **19**, 1775 (1986).
96. M. S. Sheridan, A. Verma, and J. E. McGrath, *Polym. Prepr.* **33**, 904 (1992).
97. W.-P. Shen and H.-M. Jin, *Makromol. Chem.* **193**, 743 (1992).
98. B. Charleux, C. Pichot, and M. F. Llauro, *Polymer* **34**, 4352 (1993).
99. B. Charleux and C. Pichot, *Polymer* **34**, 195 (1993).
100. G. Wulff and P. Birnbrich, *Makromol. Chem.* **194**, 1569 (1993).
101. R. Asami, Y. Kondo, and M. Takaki, in T. E. Hogen-Esch and J. Smid, eds., *Recent Advances in Anionic Polymerization*, Elsevier, New York, 1987, p. 381.
102. S. G. Roos, A. H. E. Muller, and K. Matyjaszewski, *Macromolecules* **32**, 8331 (1999).
103. N. Niebner and W. Heitz, *Makromol. Chem.* **191**, 1463 (1990).
104. N. Ishiyama and co-workers, *Makromol. Chem.* **190**, 2417 (1989).
105. H. Kunisada and co-workers, *Polym. J.* **23**, 1455 (1991).
106. D. Wilson and M. H. George, *Polymer* **33**, 3723 (1992).
107. D. Wilson and M. H. George, *Polym. Commun.* **31**, 90 (1990).
108. A. Muruyama, E. Senda, and T. Tsuruta, *Makromol. Chem.* **187**, 1895 (1986).
109. B. Geetha, A. Baran Mandal, and T. Ramasami, *Macromolecules* **26**, 4083 (1993).
110. S. Kawaguchi, M. A. Winnik, and K. Ito, *Macromolecules* **28**, 1159 (1995).
111. E. Akiyama, Y. Takamura, and Y. Nagase, *Makromol. Chem.* **193**, 1509 (1992).
112. M. S. O'Shea and G. A. George, *Polymer* **35**, 4190 (1994).
113. S. Grutke, J. H. Hurley, and W. Risse, *Macromol. Chem. Phys.* **195**, 2875 (1994).
114. S. C. de Vos and M. Moller, *Makromol. Chem., Macromol. Symp.* **75**, 223 (1993).
115. C. Juin and co-workers, *Macromol. Chem., Rapid Commun.* **20**, 289 (1999).
116. M. Taguchi and co-workers, *Macromol. Chem. Phys.* **201**, 1025 (2000).
117. T. Duschek and R. Mulhaupt, *Polym. Prepr.* **33**(1), 170 (1992).
118. K. Kobayashi, S. Kamiya, and N. Enomoto, *Macromolecules* **29**, 8670 (1996).
119. K. Nomura, S. Takahashi, and Y. Imanishi, *Macromolecules* **34**, 4712 (2001).
120. H. Iatrou, J. W. Mays, and N. Hadjichristidis, *Macromolecules* **31**, 6697 (1998).
121. J. W. Mays, *Polym. Bull.* **23**, 247 (1990).
122. H. Iatrou and co-workers, *J. Polym. Sci., Polym. Phys. Ed.* **33**, 1925 (1995).
123. D. J. Pochan and co-workers, *Macromolecules* **29**, 5091 (1996).
124. I. M. Khan and co-workers, *Macromolecules* **25**, 3002 (1992).
125. H. Ba-Gia, T. Jerome, and P. Teyssie, *J. Polym. Sci., Polym. Chem. Ed.* **18**, 3483 (1980).
126. A. Avgeropoulos and N. Hadjichristidis, *J. Polym. Sci., Polym. Chem. Ed.* **35**, 813 (1997).
127. C. Lee and co-workers, *Macromolecules* **30**, 3738 (1997).
128. N. Hadjichristidis, *J. Polym. Sci., Polym. Chem. Ed.* **37**, 857 (1999).
129. S. P. Gido and co-workers, *Macromolecules* **29**, 7022 (1996).
130. C. Lee and co-workers, *J. Chem. Phys.* **107**, 6460 (1997).
131. C. Lee and co-workers, *Polymer* **39**, 4631 (1998).
132. S. Paraskewa and N. Hadjichristidis, *J. Polym. Sci., Polym. Chem. Ed.* **38**, 931 (2000).
133. H. G. Barth and J. W. Mays, eds., *Modern Methods of Polymer Characterization*, Wiley-Interscience, New York, 1991.
134. L. H. Tung, ed., *Fractionation of Synthetic Polymers: Principles and Practices*, Marcel Dekker, New York, 1977.
135. G. Riess and P. Callot, in Ref. 134, p. 445.
136. H. N. Cheng, in Ref. 133, Chapt. 11.
137. F. A. Bovey, *High Resolution NMR of Macromolecules*, Academic Press, New York, 1972.

138. K. Holland-Moritz and H. W. Siesler, *Appl. Spectrosc Rev.* **11**, 1 (1976).
139. H. Pasch and B. Trathnigs, *HPLC of Polymers*, Springer, Heidelberg, 1997.
140. B. J. Berne and R. Pecora, *Dynamic Light Scattering*, Wiley-Interscience, New York, 1976.
141. J. S. Higgins and H. C. Benoit, *Polymers and Neutron Scattering*, Clarendon Press, Oxford, 1994.
142. S. Pispas, N. Hadjichristidis, and J. W. Mays, *Macromolecules* **29**, 7378 (1996).
143. K. Ishizu, K. Tsubaki, and T. Ono, *Polymer* **39**, 2935 (1997).
144. S. Kawaguchi and co-workers, *Polym. J.* **30**, 1004 (1998).
145. M. Wintermantel and co-workers, *Macromol. Rapid Commun.* **15**, 279 (1994).
146. M. Wintermantel and co-workers, *Macromolecules* **29**, 978 (1996).
147. N. Nemoto and co-workers, *Macromolecules* **28**, 3854 (1995).
148. J. Selb and Y. Gallot, in I. Goodman, ed., *Developments in Block Copolymers*, Vol. **2**, Elsevier, London, 1985, p. 27.
149. J. Selb and Y. Gallot, *Mackromol. Chem.* **182**, 1513 (1981).
150. J. Selb and Y. Gallot, *Mackromol. Chem.* **182**, 1775 (1981).
151. C. Price and D. Woods, *Polymer* **15**, 389 (1974).
152. A. Kikuchi and T. Nose, *Polymer* **37**, 5889 (1996).
153. Y. Ma, T. Cao, and S. E. Webber, *Macromolecules* **31**, 1773 (1998).
154. S. Pispas and co-workers, *Macromolecules* **33**, 1741 (2000).
155. H. Iatrou and co-workers, *Macromolecules* **29**, 581 (1996).
156. M. Pitsikalis and co-workers, *Macromolecules* **30**, 5384 (1997).
157. U. Bayer and R. Stadler, *Makromol. Chem. Phys.* **195**, 2709 (1994).
158. M. Xenidou and co-workers, *Macromolecules* **31**, 7659 (1998).
159. F. L. Beyer and co-workers, *Macromolecules* **33**, 2039 (2000).
160. D. J. Pochan and co-workers, *Macromolecules* **29**, 5099 (1996).
161. N. Hadjichristidis and co-workers, *Macromolecules* **26**, 5812 (1993).
162. H. Benoit and G. Hadziioannou, *Macromolecules* **21**, 1449 (1988).
163. A. Shinozaki, D. Jasnow, and A. C. Balazs, *Macromolecules* **27**, 2496 (1994).
164. D. P. Foster, D. Jasnow, and A. C. Balazs, *Macromolecules* **28**, 3450 (1995).
165. M. L. Cerrada and co-workers, *Polymer* **42**, 4647 (2001).
166. K.-C. Park and co-workers, *J. Appl. Polym. Sci.* **74**, 3259 (1999); T. Hoang and co-workers, *J. Appl. Polym. Sci.* **77**, 2296 (2000).
167. R. Weidisch and co-workers, *Macromolecules* **34**, 6333 (2001).
168. P. Jannasch and B. Wesslen, *J. Appl. Polym. Sci.* **70**, 1887 (1998).
169. D. Bikiaris and C. Panagiotou, *J. Appl. Polym. Sci.* **70**, 1503 (1998).
170. W.-F. Lee and C.-C. Lai, *J. Appl. Polym. Sci.* **67**, 307 (1998).
171. Z. Oommen and S. Thomas, *J. Appl. Polym. Sci.* **65**, 1245 (1997).
172. C. Koning and co-workers, *Prog. Polym. Sci.* **23**, 707 (1998).
173. S. Subramanian and S. Lee, *Polym. Eng. Sci.* **39**, 2274 (1999).
174. Z. Yin and co-workers, *Polymer* **39**, 547 (1998).
175. J. D. Tucker, S. Lee, and R. L. Einsporn, *Polym. Eng. Sci.* **40**, 2577 (2000).
176. A. Hallden, B. Ohlsson, and B. Wesslen, *J. Appl. Polym. Sci.* **78**, 2416 (2000).
177. L. Krist, H. Bertilsson, and P. Menller, *Polym. Eng. Sci.* **38**, 1303 (1998).
178. H. Feng and co-workers, *Polymer* **39**, 1787 (1998).
179. B. G. Soares, R. V. Barbosa, and J. C. Coras, *J. Appl. Polym. Sci.* **65**, 2141 (1997).
180. P. Jannasch and B. Wesslen, *J. Appl. Polym. Sci.* **58**, 753 (1995).
181. T. Tang, X. Jing, and B. Huang, *J. Macromol. Sci., Phys.* **33**, 287 (1994).
182. D. G. Peiffer and M. Rabeony, *J. Appl. Polym. Sci.* **51**, 1283 (1994).
183. F. Ide and A. Hasegawa, *J. Appl. Polym. Sci.* **18**, 963 (1974).
184. W. E. Baker and M. Saleem, *Polymer* **28**, 2057 (1987).
185. R. Greco and co-workers, *Polymer* **28**, 115 (1987).

186. S. George and co-workers, *Polymer* **36**, 4405 (1995).
187. S. Fakirov, M. Evstatiev, and S. Petrovich, *Macromolecules* **26**, 5219 (1993).
188. K. L. L. Eersels, A. M. Aerdts, and G. Groeninckx, *Macromolecules* **29**, 1046 (1996).
189. M. Xanthos, *Polym. Eng. Sci.* **28**, 1392 (1988).
190. B. Majumdar, H. Keskkula, and D. R. Paul, *Polymer* **35**, 3164 (1994).
191. C.-T. Maa and F.-C. Chang, *J. Appl. Polym. Sci.* **49**, 913 (1993).
192. K. Dedecker and G. Groeninckx, *Polymer* **39**, 4985 (1998).
193. S. Thomas and G. Groeninckx, *Polymer* **40**, 5799 (1999).
194. G. W. Ehrenstein, *Polymeric Materials: Structure-Properties-Applications*, Hanser & Gardner Publ. Inc., New York, 2001.
195. D. Craver and C. E. Carraher Jr., *Applied Polymer Science in the 21st Century*, Elsevier Science Ltd., London, 2000.
196. G. Holden, *Handbook of Elastomers*, Hanser & Gardner Publ. Inc., New York, 2001.
197. D. Satas, ed., *Handbook of Pressure-Sensitive Adhesive Technology*, Van Nostrand Reinhold, New York, 1982.
198. M. Yoshinobu, M. Morita, and I. Sakata, *J. Appl. Polym. Sci.* **45**, 805 (1992).
199. J. A. Lewis and co-workers, *J. Am. Cer. Soc.* **83**, 1905 (2000).
200. W. Liang, G. Bognolo, and T. F. Tadros, *Langmuir* **16**, 1306 (2000).
201. M. Kamel, I. A. El-Thalouth, and S. H. Nassar, *J. Textile Assoc.* **61**, 78 (2000).
202. M. M. El-Molla and I. A. El-Thalouth, *Polym. Polym. Composites* **7** 501, (1999).
203. S. Huang and co-workers, *J. Appl. Polym. Sci.* **71**, 2209 (1999).
204. J. Huybrechts and co-workers, *Progr. Org. Coat.* **38**, 67 (2000).
205. S. Kumar, M. Alagar, and V. Mohan, *Eur. Coat. J.* 64 (1999).
206. K. Kataoka, A. Harada, and Y. Nagasaki, *Adv. Drug Deliv. Rev.* **47**, 113 (2001).
207. S. Sakuma, M. Hayashi, and M. Akashi, *Adv. Drug Deliv. Rev.* **47**, 21 (2001).
208. F. Madsen and N. A. Peppas, *Biomaterials* **20**, 1701 (1999).
209. Y. Volland, C. Li, and T. Kissel, *Polymer* **39**, 3087 (1998).
210. I. Castellano and co-workers, *Int. J. Pharmacol.* **146**, 71 (1997).
211. R. S. Harland and N. A. Peppas, *Eur. J. Pharmacol. Biopharm.* **39**, 229 (1993).
212. T. Uragami, H. Yamada, and T. Miyata, *J. Membr. Sci.* **187**, 255 (2001).
213. J. M. Yang and co-workers, *J. Membr. Sci.* **128**, 133 (1997).
214. K. Usha and V. N. S. Pillai, *Polym. Int.* **38**, 263 (1995).
215. W. Prätorius, *Kunststoffe* **90**(7), 22–25 (English version pp. 6–8) (2000).
216. U.S. Pat. 4,876,312 (1989), B. J. Meister, C. D. Dryzga, and L. C. Tien (to The Dow Chemical Company).
217. U.S. Pat. 3,213,159 (1965), D. Adomaitis (Amoco).
218. U.S. Pat. 4,427,826 (1984), A. Echte and co-workers (to BASF).
219. U.S. Pat. 3,538,191 (1970), C. L. Meredith, R. E. Barrett, and W. A. Bishop (to Copolymer Rubber and Chemical Corp.).
220. U.S. Pat. 3,509,237 (1970), N. E. Aubrey (to Monsanto).
221. U.S. Pat. 3,288,887 (1966), M. Yoshino and H. Morikawa (to Kanegafuchi).
222. U.S. Pat. 4,885,337 (1989), H. Eichenauer, A. Pischtschan, and K.-H. Ott (to Bayer).
223. U. S. Pats. 4,172,859 and 4,174,358 (1979), B. N. Epstein (to E.I. du Pont de Nemours & Co., Inc.).
224. U.S. Pat. 4,594,386 (1986), E. J. Olivier (to Copolymer Rubber and Chemical Corp.).
225. U.S. Pat. 4,757,112 (1988), S. V. Phadke (to Copolymer Rubber and Chemical Corp.).
226. U.S. Pat. 4,847,322 (1989), M. K. Akkapeddi, J. C. Haylock, and J. A. Gervasi (to Allied-Signal).

227. U.S. Pat. 4,339,555 (1982), Y. Ohmura, S. Maruyama, and H. Kawasaki (to Mitsubishi Chemical).
228. S. Datta and D. J. Lohse, *Polymeric Compatibilizers: Uses and Benefits in Polymers Blends*, Hanser Publishers, Munich, 1996.

N. HADJICHRISTIDIS
S. PISPAS
M. PITSIKALIS
H. IATROU
University of Athens
D. J. LOHSE
ExxonMobil Research and Engineering Company

HEAT STABILIZERS

Introduction

Heat stabilizers protect polymers from the chemical degrading effects of heat or uv irradiation. These additives include a wide variety of chemical substances, ranging from purely organic chemicals to metallic soaps to complex organometallic compounds. By far the most common polymer requiring the use of heat stabilizers is poly(vinyl chloride) (PVC). However, copolymers of PVC, chlorinated poly(vinyl chloride) (CPVC), poly(vinylidene chloride) (PVDC), and chlorinated polyethylene (CPE), also benefit from this technology. Without the use of heat stabilizers, PVC could not be the widely used polymer that it is, with worldwide production of over 20 million metric tons in 2000 (see VINYL CHLORIDE POLYMERS).

The discussion centers on heat stabilizers for PVC because this polymer is the most important class of halogenated polymers requiring these chemical additives. PVC of ideal chemical structure (**1**) should be a relatively stable compound as predicted from model studies using 2,4,6-trichloroheptane [13049-21-3] (**2**) (1).

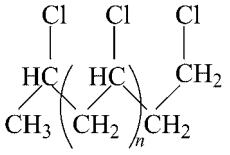

(**1**)

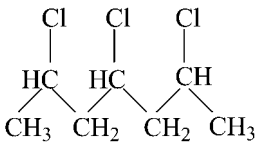

(**2**)

Encyclopedia of Polymer Science and Technology. Copyright John Wiley & Sons, Inc. All rights reserved.

During the polymerization process the normal head-to-tail free-radical reaction of vinyl chloride deviates from the normal path and results in sites of lower chemical stability or defect sites along some of the polymer chains. These defect sites are small in number and are formed by autoxidation, chain termination, or chain-branching reactions. Heat stabilizer technology has grown from efforts to either chemically prevent or repair these defect sites. Partial structures (**3**), (**4**), (**5**), (**6**) are typical of the defect sites found in PVC homopolymers (2–5).

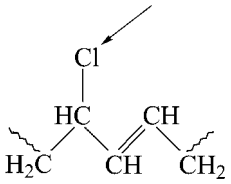

(**3**)

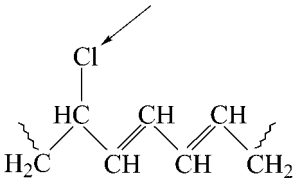

(**4**)

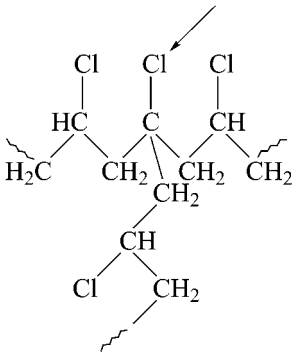

(**5**)

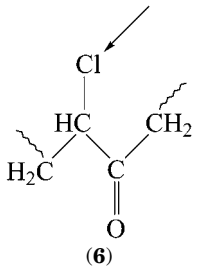

(**6**)

The dissociation energies for the highlighted (by pointing arrows) carbon–chloride bonds are significantly lower than that of a normal secondary C—Cl bond and can lead to thermal dehydrochlorination of the polymer backbone. In addition, the released HCl acts to catalyze further dehydrochlorination, indicating that both

homolytic and ionic processes are involved. As the conjugated polyene sequences grow in length, further weakening of the carbon–chlorine bond occurs, leading eventually to rapid, catastrophic dehydrochlorination, cross-linking, and chain scission resulting in loss of mechanical, electrical, and rheological properties in the final articles. A good indication of the onset of thermal degradation is the appearance of color in the polymer. When the conjugated polyenes reach a length of about seven double bonds, this chromophore begins to absorb visible light and appears yellow in color. Further degradation leads to brown and eventually black-colored products.

Some work has been conducted on the *in situ* or preventative stabilization of PVC, but these efforts have been largely unsuccessful, centering primarily on copolymerizing vinyl chloride with other vinyl monomers to block the conjugative ordering of the chlorine atoms in the polymer (6). The commercially important heat stabilizers are arrestive in nature. They chemically repair the defect sites or in some way reduce the deleterious nature of these sites during the processing and use of PVC articles. Just as important, most of the active heat stabilizers are also good HCl scavengers and reduce the catalytic effects of this deleterious by-product. PVC is so widely used because its properties are so easily manipulated by an inexhaustible variety of added components. Applications can range from rugged PVC pipes to crystal clear drinking water bottles to colorful toys to supple artificial leather, depending on the choice of additives in the formulation. The needs and choices of the heat stabilizer are dependent upon the final desired physical properties, compatibility with the other additives used, -and the processing methods used to form the articles. Figure 1 shows the complexity of PVC formulation alternatives. Only the heat stabilizers and, normally, lubricants are essential additives to process the polymer. All of the other classes of additives are

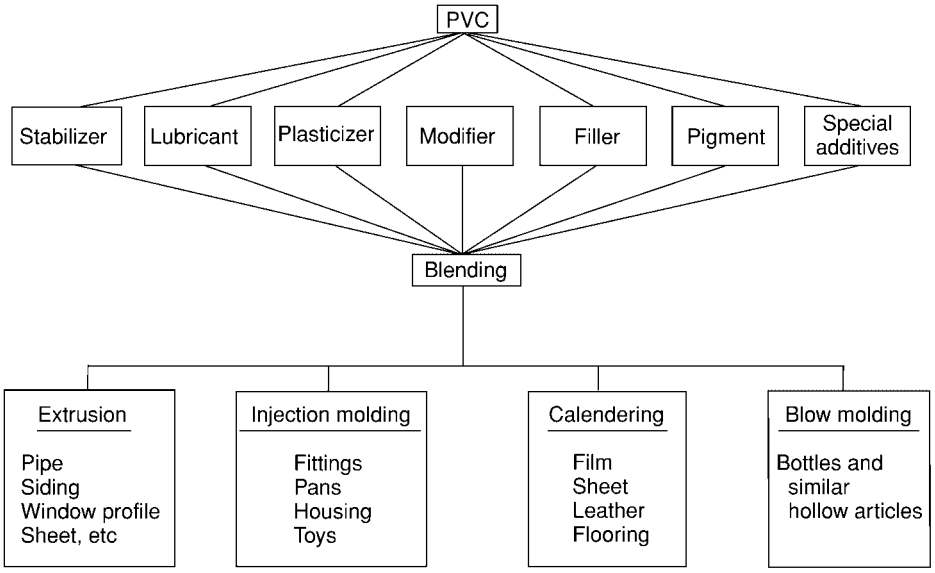

Fig. 1. PVC formulation alternatives.

discretionary, ie, they are present to change the physical properties of the final processed PVC articles.

In normal operations, PVC resin is intimately mixed with the desired ingredients under high intensity shear mixing conditions to produce a homogeneous dry powder compound. The heat stabilizers can be either liquids or powders and are added early in the blending cycle to afford stabilizing action during this operation. Preheating the resin to about the glass-transition temperature facilitates the adsorption of the liquid additives, giving the final compound better powder flow properties and decreasing the bulk density. Post-compounding operations, eg, extrusion pelletizing, can increase the overall heat history of the polymer, thus requiring slightly higher levels of heat stabilizers to compensate for this.

History of Stabilizer Development

Although PVC was discovered in the late nineteenth century in Germany, it was not until the discovery that certain lead soaps improved the thermal stability of the polymer in the early 1930s that commercialization of PVC began. Lead-based stabilizers have continually been used in certain applications, such as wire and cable coatings. Today, because of toxicity and ecotoxicity concerns, considerable efforts are being made to eliminate all uses of lead-based heat stabilizers, worldwide. In the mid-1930s, workers in the United States found that organotin carboxylates also provided good heat stability. The high activity, nonstaining, nondusting characteristics, and complete compatibility, allowing total transparency, made the organotin stabilizers good choices for rigid, flexible, and even plastisol end uses. During the 1940s, alkali and alkaline-earth metal soaps, especially those of cadmium, barium, zinc, and calcium, were discovered and commercialized as PVC heat stabilizers. By the 1950s combinations of these metal soaps with organic costabilizers, such as phosphites and epoxides, demonstrated great processing latitude and cost effectiveness, particularly in plasticized PVC. Some of these formulations remain state-of the-art technology for certain end uses. Just as in the case for lead, considerable pressure has been exerted on the plastics industry to discontinue uses of cadmium for both stabilizers and pigments because of its high toxicity. Organotin mercaptide chemistry was introduced as a new class of PVC heat stabilizers during the 1950s and played a significant role in the development of many rigid PVC applications. The efficiency per unit dose remains unsurpassed for the organotin mercaptide-stabilized formulations for food packaging (qv), water pipes, weatherable construction panels, and molded parts. Antimony mercaptides were also discovered in the 1950s and did complete with the organotin mercaptides in rigid PVC applications for several years, but again, toxicity concerns have nearly eliminated the use of this class of stabilizer.

Function of Stabilizers

Although great progress has been made since the 1960s to sort out the many reactions ongoing during the thermal degradation of PVC, much of the formulating and use of stabilizers remains an art in commercial practice. PVC degradation

proceeds by both free-radical and ionic reactions, although the latter appears to be the more important route. Lewis acid catalysts, such as zinc chloride or hydrogen chloride, can greatly accelerate the rate of dehydrochlorination of the polymer. Heat stabilizers serve several distinct functions during PVC processing: absorption of hydrogen chloride, replacement of labile chlorines, prevention of autoxidation, and disruption of polyunsaturated sequences. An ancillary function of many heat stabilizers is provision of uv stability, leading to good weathering properties for the final articles. Good uv stability depends on having adequate heat stability because partially degraded PVC is susceptible to uv degradation regardless of the choice of uv absorber additives used.

Absorption of Hydrogen Chloride. Effective heat stabilizers have the ability to bind hydrogen chloride. Most stabilizer systems contain one or more metallic soaps or salts which readily undergo a simple acid–base reaction with the by-product hydrogen chloride as the PVC degrades:

$$M(X)_n + HCl \rightarrow M(X)_{n-1}Cl + HX$$

$$M(X)_{n-1}Cl + HCl \rightarrow M(X)_{n-2}Cl_2 + HX$$

where M is a metal, usually Pb, Zn, Ca, Ba, or Cd, and X is a carboxylic acid, usually a weakly acidic fatty acid ligand. Typical examples of effective metal soaps and salts used as PVC stabilizers include lead stearate, dibasic lead phthalate, tribasic lead sulfate, zinc octanoate [557-09-5], barium tallate, cadmium 2-ethylhexanoate, calcium stearate, calcium nonylphenate [30977-64-1].

A new type of inorganic metal complex, called hydrotalcite, has appeared (ca 1990). These synthetic minerals, functionally akin to zeolites, have layered structures of Al and Mg and function to trap hydrogen chloride between these layers (7). The hydrotalcite minerals are generally used with other stabilizers as part of a stabilizer system. A typical hydrotalcite may be represented by a formula such as $Mg_4Al_2(OH)_{12}CO_3 \cdot 3H_2O$. Many modifications can be made by changing the Al-to-Mg ratio and by including other metal salts, such as zinc oxide. Unlike most metallic salts, the hydrotalcites are compatible with PVC and can provide completely transparent PVC articles.

Many PVC stabilizer formulations also contain one or more organic costabilizers that can also absorb hydrogen chloride. Typical of these additives are epoxidized fatty acid esters and organophosphites:

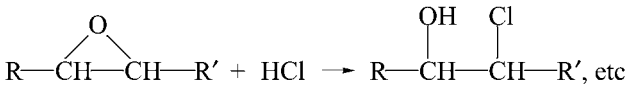

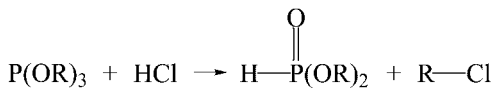

Organotin mercaptides can also absorb hydrogen chloride.

$$R{-}Sn(SR')_3 + HCl \rightarrow R{-}Sn(SR')_2Cl + HSR'$$

$$R{-}Sn(SR')_3Cl + HCl \rightarrow R{-}Sn(SR')\,Cl_2 + HSR', \text{ etc}$$

Some of these stabilizers are added specifically to react with evolved hydrogen chloride. When the primary function of the stabilizer is to repair defect sites or disrupt autoxidation reactions, the degree that these stabilizers react with hydrogen chloride can actually detract from their primary function, requiring the use of higher dosages of stabilizers in the PVC formulation.

Replacement of Labile Chlorines. When PVC is manufactured, reactions competing with the normal head-to-tail free-radical polymerization can sometimes take place. These side reactions are few in number yet their presence in the finished resin can be devastating. These abnormal structures have weakened carbon–chlorine bonds and are more susceptible to certain displacement reactions than are the normal PVC carbon–chlorine bonds. Carboxylate and mercaptide salts of certain metals, particularly organotin, zinc, cadmium, and antimony, attack these labile chlorine sites and replace them with a more thermally stable C—O or C—S bound ligand. These electrophilic metal centers can readily coordinate with the electronegative polarized chlorine atoms found at sites similar to structures (**3**), (**4**), (**5**), (**6**).

In the early 1960s, two different ^{14}C and one ^{113}Sn radio-labeled di-*n*-butyltin bis(isooctylthioglycolate) stabilizers were synthesized. Heat stability studies with these organotin compounds demonstrated the important replacement reactions, leading to the following proposed mechanism (8). It is believed that the salts of zinc, cadmium (9), and lead (10) also undergo these reactions resulting in their respective ligands substituting on the PVC chains.

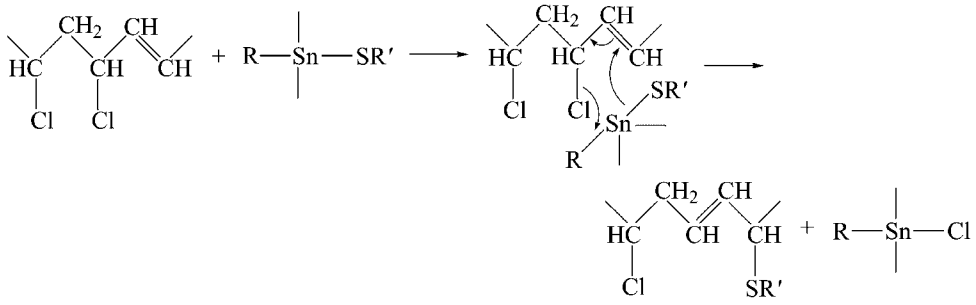

This mechanism not only accounts for the substitution of the more labile chlorine atom on the polymer chain, but also results in the elimination of a new potential initiation site by moving the double bond out of conjugation with any adjacent chlorine atoms. The newly formed C—O or C—S bonds, with $\Delta H > 484$ kJ/mol (100 kcal/mol), are significantly more thermally stable than even the normal C—Cl bonds in PVC at about 411 kJ/mol (85 kcal/mol) (11).

Ultimately, as the stabilization reactions continue, the metallic salts or soaps are depleted and the by-product metal chlorides result. These metal chlorides are potential Lewis acid catalysts and can greatly accelerate the undesired dehydrochlorination of PVC. Both zinc chloride and cadmium chloride are particularly strong Lewis acids compared to the weakly acidic organotin chlorides and lead chlorides. This significant complication is effectively dealt with in commercial practice by the coaddition of alkaline-earth soaps or salts, such as calcium stearate or barium stearate, ie, by the use of mixed metal stabilizers.

Displacement of activated chlorine atoms also proceeds with certain types of organic compounds, but only in the presence of Lewis acid catalysts. Particular examples include epoxides, polyhydric alcohols, trialkylphosphites (12), and β-aminocrotonates (13). These additives are commonly used in conjunction with metallic stabilizers to provide complete, high performance, commercial stabilizer packages.

Prevention of Autoxidation. The observation that PVC thermally degrades more rapidly in air than in a nitrogen atmosphere leads to the conclusion that the prevention of oxidative reactions can improve the thermal stability of PVC (14). When phenolic antioxidants are included in the formulation, the rate of hydrogen chloride evolution, at 180°C in air, is noticeably retarded. Therefore, good stabilizers must also provide antioxidant protection. Many of the additives previously discussed, which provide HCl scavenging and labile chlorine displacements, are also fairly good antioxidants as evidenced by their activity in other nonhalogenated polymers, particularly trialkyl- and triarylphosphites, β-aminocrotonates, and organotin mercaptides. The organotin mercaptides are particularly efficient in their reduction of hydroperoxides (15):

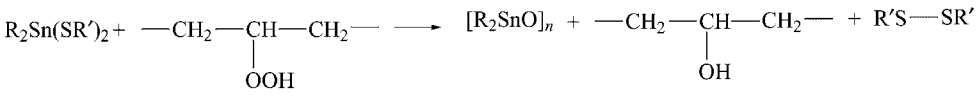

Disruption of Polyunsaturated Sequences. Sequential lengthening of the conjugated double bonds along a PVC molecule leads to the gradual development of color resulting from absorption of visible light (see COLOR). This lengthening conjugation further weakens the already weak allylic C—Cl bonds and leads to further loss of hydrogen chloride which, in turn, catalyzes further degradation. Left unchecked, the complete catastrophic degradation of the polymer is imminent.

Disruption of the conjugation of these long polyene groups can lead to color bleaching of the partially degraded PVC. Simple mercaptans effectively add to these highly reactive double bonds (16). Organotin mercaptides are also known to undergo this reaction, although it is likely that the actual reagent is the free mercaptan resulting from reaction with evolved HCl (17):

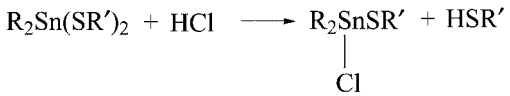

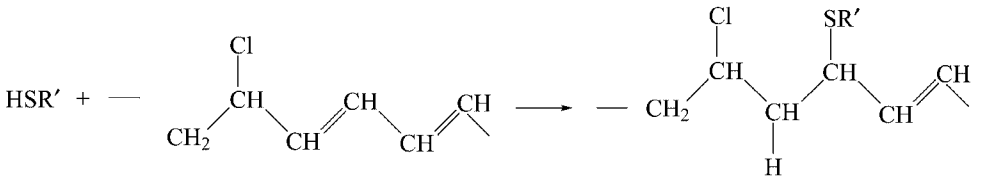

The organotin maleate and maleate half-ester derivatives also exhibit this bleaching effect reportedly by a Diels–Alder addition reaction (18). The reaction is specific to the organotin maleates; other organotin carboxylates containing normal dieneophiles fail to produce similar results (19).

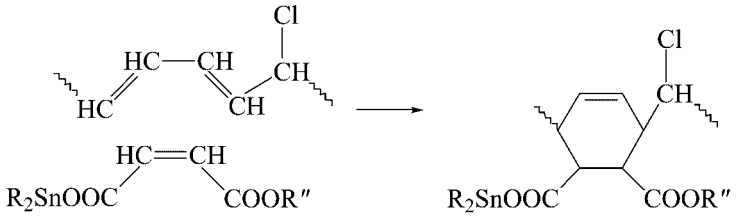

Stabilizer Test Methods

Heat stabilizers are tested in a variety of ways to simulate their performance during PVC processing, ie, calendering, extrusion, pressing, heat curing, and molding. Because of the wide number of these applications, it is impossible to provide one or two definitive laboratory tests for all stabilizer products. In general, heat stabilizers are tested as a component in a complete formulation where each ingredient has a measured effect on the overall performance. Stabilizer performance is generally evaluated by visually inspecting the color of the test pieces as a function of heating and processing time. Static oven aging, dynamic two-roll milling, and torque rheometry are three of the most common tests used to evaluate heat stabilizers. A whole host of tests are conducted on the final products of the various processes to make judgments as to the effectiveness of any particular PVC formulation. Standard tests for stabilizer evaluation include ASTM D2115, Oven Stability of PVC Compounds; ASTM D2538, Fusion of PVC Compounds Using a Torque Rheometer; ASTM D1499, Stability of PVC to Light Exposure; and DIN 53-381F, Heat Stability of PVC Compounds by Metrastat Oven.

Classes of Heat Stabilizers

Organotin Compounds. Organotin-based heat stabilizers are the most efficient and universally used PVC stabilizers. Nearly 40% of the 75,000 t of stabilizers used in the United States during 2000 were organotin-based products. These are all derivatives of tetravalent tin, and all have either one or two alkyl groups covalently bonded directly to the tin atom. The commercially important

alkyltins are the methyltin, *n*-butyltin, and *n*-octyltin species. For about 10 years between 1980 and 1990, estertin or β-carboalkoxyethyltin derivatives were produced commercially. Aryltin and branched alkyltin derivatives are relatively poor heat stabilizers (20). The class of tri-*n*-alkyltin compounds are known to be toxic, and because they are very poor stabilizers, they are completely avoided in PVC heat stabilizer applications. The anionic ligands can be chosen from a wide variety of groupings but are normally chosen from maleate, alkylmaleate, esters of thioglycolic acid, or esters of mercaptoethanol, depending on the end-use application and the processing conditions for the PVC compound. Almost all organotin stabilizer products are formulated with mixtures of monoalkyltin and dialkyltin species in a ratio so as to maximize the stability of the PVC, together with all of the other microingredients in a given PVC formulation for a given processing method.

Alkyltin Intermediates. For the most part, organotin stabilizers are produced commercially from the respective alkyltin chloride intermediates. There are several processes used to manufacture these intermediates. The desired ratio of monoalkyltin trichloride to dialkyltin dichloride is generally achieved by a redistribution reaction involving a second-step reaction with stannic chloride [tin(IV) chloride]. By far, the most easily synthesized alkyltin chloride intermediates are the methyltin chlorides because methyl chloride reacts directly with tin metal in the presence of a catalyst to form dimethyltin dichloride cleanly in high yields (21). Coaddition of stannic chloride to the reactor leads directly to almost any desired mixture of mono- and dimethyltin chloride intermediates:

$$Sn^{\circ} + 2\,Cl_2 \longrightarrow SnCl_4$$

$$Sn^{\circ} + 2\,CH_3Cl \longrightarrow (CH_3)_2SnCl_2$$

$$(y + x)\,(CH_3)_2SnCl_2 + x\,SnCl_4 \longrightarrow y\,(CH_3)_2SnCl_2 + 2x\,CH_3SnCl_3$$

The direct reaction of other alkyl chlorides, such as butyl chloride, results in unacceptably low overall product yields along with the by-product butene resulting from dehydrochlorination. All alkyl halides having a hydrogen atom in a β position to the chlorine atom are subject to this complication.

The other important direct alkylation processes involve reaction of electron-rich olefinic compounds with either tin metal or stannous chloride [tin(II) chloride] in the presence of stoichiometric amounts of hydrogen chloride (22). Butyl acrylate (R = C_4H_9) was used commercially in this process to prepare the estertin or β-carboalkoxyethyltin chlorides as illustrated in the following.

$$Sn^{\circ} + 2\,HCl + 2H_2C{=}CHCOOR \longrightarrow (ROOCCH_2CH_2)_2SnCl_2$$

$$Sn^{\circ}Cl_2 + HCl + H_2C{=}CHCOOR \longrightarrow ROOCCH_2CH_2SnCl_3$$

A number of activated olefinic compounds react very well in this scheme, including methacrylates, crotonates, acrylonitrile, and vinyl ketones. These reactions are typically run in an etherial solvent and can be run without the complications of undesirable side reactions leading to trialkylated tin species.

The other commercially important routes to alkyltin chloride intermediates utilize an indirect method having a tetraalkyltin intermediate. Tetraalkyltins are made by transmetallation of stannic chloride with a metal alkyl where the metal is typically magnesium or aluminum. Subsequent redistribution reactions with additional stannic chloride yield the desired mixture of monoalkyltin trichloride and dialkyltin dichloride. Both *n*-butyltin and *n*-octyltin intermediates are manufactured by one of these schemes.

$$2\ R_2Mg + SnCl_4 \rightarrow R_4Sn + 2\ MgCl_2$$

$$4\ R_3Al + 3\ SnCl_4 \rightarrow 3\ R_4Sn + 4\ AlCl_3$$

$$R_4Sn + 2\ SnCl_4 \rightarrow 2\ RSnCl_3 + R_2SnCl_2$$

Stabilizer Synthesis. The selected alkyltin chloride intermediate reacts with either a carboxylic acid or a mercaptan in the presence of an appropriate base, such as sodium hydroxide, to yield the alkyltin carboxylate or alkyltin mercaptide heat stabilizer. Alternatively, the alkyltin chloride can react with the base to yield the alkyltin oxide, which may or may not be isolated for subsequent condensation with the selected carboxylic acid or mercaptan.

$$R_2SnCl_2 + 2\ R'SH + 2\ NaOH \rightarrow R_2Sn(SR')_2 + 2\ NaCl + H_2O$$

$$R_2SnCl_2 + 2\ NaOH \rightarrow (R_2SnO)_n + 2\ NaCl + H_2O$$

$$(R_2SnO)_n + 2\ R'COOH \rightarrow R_2Sn(OOCR')_2 + H_2O$$

Typically, alkyltin carboxylates are prepared from isolated alkyltin oxides because this route leads to higher efficiency and purity for these products. In many of the modern alkyltin mercaptide stabilizers, sulfide sulfur ligands are also used in combination with mercaptide ligands. Usually the sulfide groups are introduced as sodium sulfide and added along with the mercaptan and base to the alkyltin chloride intermediate. The resulting stabilizer is a mixture of products having both sulfide and mercaptide groups bound to each of the alkyltin compounds.

Costabilizers. In most cases the alkyltin stabilizers are particularly efficient heat stabilizers for PVC without the addition of costabilizers. Many of the traditional coadditives, such as antioxidants, epoxy compounds, and phosphites, used with the mixed metal stabilizer systems, afford only minimal benefits when used with the alkyltin mercaptides. Mercaptans are quite effective costabilizers

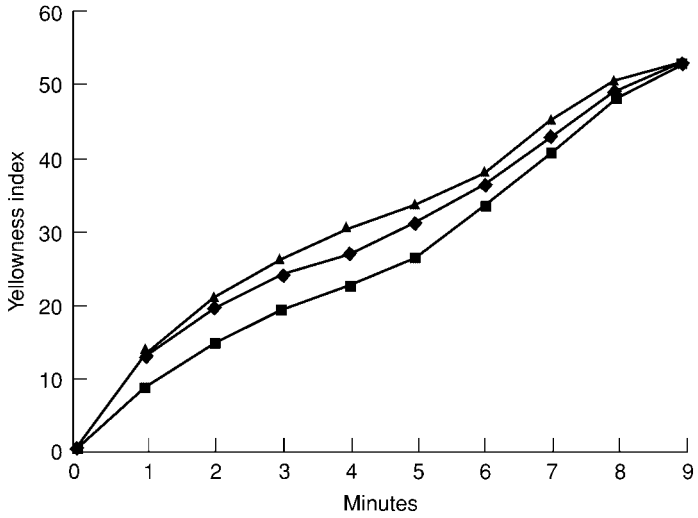

Fig. 2. Yellowness index vs two-roll mill heat stability, where the mercaptide ligands,—SCH_2COOR (▲), $–SCH_2CH_2\ COOR'$ (◆), and $–SCH_2CH_2\ COOR' + HSCH_2\ CH_2COOR'$ (■), are 17, 9, and 6% Sn, respectively. $R=C_8H_{17}$; $R' = C_{18}H_{33}$.

for some of the alkyltin mercaptides, particularly those based on mercaptoethyl ester technology (23). Combinations of mercaptan and alkyltin mercaptide are currently the most efficient stabilizers for PVC extrusion processes. The level of tin metal in the stabilizer composition can be reduced by up to 50% while maintaining equivalent performance. Figure 2 shows the two-roll mill performance of some methyltin stabilizers in a PVC pipe formulation as a function of the tin content and the mercaptide groups at 200°C. The test formulation contains 100 parts of PVC (Fikentscher K = 65), 1.2 parts of paraffin wax, 0.6 parts of calcium stearate, and 0.4 parts of methyltin-based stabilizers.

The various lubricants formulated into PVC to improve the processing can also enhance the performance of the stabilizer. In pigmented applications, calcium soaps, eg, calcium stearate, are commonly used as lubricants to promote PVC fusion and reduce melt viscosity. This additive is also a powerful costabilizer for the alkyltin mercaptide stabilizers at use levels of 0.2–0.7 phr. Calcium stearate can significantly improve the early color and increase the long-term stability at low levels; however, as the concentration increases, significant yellowing begins to occur particularly at low pigment dosages.

Commercial Stabilizers. A wide variety of alkyltin stabilizers have been used commercially since the 1960s, because no particular compound universally satisfies every requirement of PVC processing. In general, the alkyltin mercaptides exhibit the highest overall heat stability together with imparting excellent rheological properties to the polymer. The alkyltin carboxylates, on the other hand, are unsurpassed for imparting excellent weathering properties but generally give poor rheological characteristics. Table 1 lists the commercially important alkyltin stabilizer compounds. These compounds are typically formulated with several different adjuvants, both active and inert, to tailor their performance to given

Table 1. Commercially Important Alkyltin Compounds

Name	CAS registry number	Structure
Poly(dibutyltin maleate)	[32076-99-6]	$+(C_4H_9)_2SnOOCCH{=}CHCOO+_n$
Poly(dioctyltin maleate)	[32077-00-2]	$+(C_8H_{17})_2SnOOCCH{=}CHCOO+_n$
Dibutyltin bis(butyl maleate)	[17209-76-6]	$(C_4H_9)_2Sn(OOCCH{=}CHCOOC_4H_9)_2$
Dimethltin bis(2-ethylhexyl) thioglycolate)	[26636-01-1]	$(CH_3)_2Sn(SCH_2COOC_8H_{17})_2$
Dibutyltin bis(2-ethylhexyl) thioglycolate)	[25168-24-5]	$(C_4H_9)_2Sn(SCH_2COOC_8H_{17})_2$
Dioctyltin bis(2-ethylhexyl) thioglycolate)	[26401-97-8]	$(C_8H_{17})_2Sn(SCH_2COOC_8H_{17})_2$
Dibutyltin sulfide	[4253-22-9]	$[(C_4H_9)_2SnS]_3$
Methyltin tris(2-ethylhexyl) thioglycolate)	[54849-38-6]	$CH_3Sn(SCH_2COOC_8H_{17})_3$
Butyltin tris(2-ethylhexyl) thioglycolate)	[25852-70-4]	$C_4H_9Sn(SCH_2COOC_8H_{17})_3$
Octyltin tris(2-ethylhexyl) thioglycolate)	[26401-86-8]	$C_8H_{17}Sn(SCH_2COOC_8H_{17})_3$
Methyltin tris(2-mercaptoethyl) oleate)	[59118-9-5]	$CH_3Sn(SCH_2CH_2OCOC_{17}H_{33})_3$
Methyltin (2-mercaptoethyl oleate)sulfide	[68442-12-6]	$CH_3Sn(SCH_2CH_2OCOC_{17}H_{33})(S)$

Table 2. U.S. Producers and Trade Names of Alkyltin Stabilizers and Mixed Metal Stabilizers

	Trade name	
Producers	Alkyltin	Mixed metal
Akzo Chemicals, Inc., Dobbs Ferry, N.Y.	Stanclear	Interstab
Atofina, Inc., Philadephia, Pa.	Thermolite	
Crompton Corp., New York, N.Y.	Mark	Mark
Rohm and Haas Co., Philadephia, Pa.	Advastab	
Ferro Corp., Bedford, Ohio		Therm-Chek Synpro
M-R-S Chemicals, Inc., Maryland Hts, Mo.		MiRaStab

commercial applications. Table 2 lists the stabilizer manufacturers and the trade names associated with each.

Economics. The pricing of stabilizers is generally based on the PVC processing application, the type of PVC used, and the other microingredients present in the formulation. In facile extrusion operations, such as the manufacture of PVC pipes, stabilizer formulations usually contain relatively low levels of the alkyltin compounds; about 5–10% tin is usual. More difficult extrusion applications, such as window lineals, extruded sheets, and house siding, require significantly higher levels of more efficient stabilizers. Injection molding of pipe

Table 3. Typical Uses and Prices for Alkyltin Stabilizers

Application	Stabilizer type	Use level[a]	Tin (%)	Price,[b] $/kg
	Extrusion			
PVC pipe	Mercaptide/mercaptan	0.3–0.6	5–10	2.75–4.50
Window profile/siding	Mercaptide	1.3–1.7	14–19	7.00–10.00
Siding substrate	Mercaptide/mercaptan	0.7–1.2	9–14	4.00–8.50
Weatherable clear	Carboxylate	2.5–3.5	14–20	9.00–14.00
	Molding			
Pipe fittings	Mercaptide	1.3–2.0	16–19	8.00–10.00
	Mercaptide/mercaptan	1.3–2.0	11–16	4.5–8.50
Food bottles	Methyl/octyltin Mercaptides	0.8–1.4	16–19	8.00–11.00
	Calendered sheet			
Food packaging film	Methyl/octyl tin mercaptides	0.8–1.4	16–19	8.00–11.00
General-purpose film	Mercaptides	1.0–2.0	16–19	8.00–10.00

[a]Parts per hundred parts of PVC resin.
[b]2000.

fittings and accessories also requires more efficient stabilizers. Blow molding and calendered sheet applications, particularly where glass-like clarity is required, are the most demanding processing conditions. Stabilizers for these applications are typically the highest efficiency formulations in the marketplace. Table 3 summarizes the typical applications of the tin stabilizers and their current price range.

Health and Safety Aspects. Many of the alkyltin stabilizers are considered safe to use in almost every conceivable end use for PVC (24). Particularly, the U.S. FDA, German BGA, and Japanese JHPA have sanctioned the use of mixtures of dimethyltin and monomethyltin isooctyl thioglycolate (25), mixtures of di-*n*-octyltin and mono-*n*-octyltin isooctyl thioglycolate (26), and poly(di-*n*-octyltin maleate) as the primary heat stabilizers for PVC used for food-packaging purposes. This same group of products is also approved for use in pharmaceutical applications such as pill containers and PVC tubings (27). Since the migration into water of the alkyltin mercaptide-based products from PVC is found to be extremely low, most of these stabilizers are suitable for pipes carrying drinking water according to NSF International (28), a private industry supported regulatory agency complying with all current U.S. EPA guidelines. Tin-stabilized formulations for drinking water pipes have been in use since the late 1960s throughout North America. A risk analysis on the use of these stabilizers in PVC has been compiled (29), which emphasizes the low toxicity and ecotoxicity of this class of PVC stabilizers. The key to the safety and low toxicity for the alkyltin stabilizers lies in the fact that modern manufacturing practices eliminate the production of any significant amounts of the more toxic trialkyltin species from all stabilizers.

Several studies have chosen to focus on the volatility of the alkyltin stabilizers and their by-products of PVC stabilization, alkyltin chlorides, during the calendering operation because this process presents a worst case scenerio for PVC processing: relatively high stabilizer levels, very high exposed surface area of hot

PVC melt, and high processing temperatures. In two of these studies conducted by the NATEC Institute in Germany, extremely low levels of volatilized alkyltin compounds were observed (30). Similar studies conducted by Morton International (now Rohm and Haas Co.) confirmed these results (31). All of these studies demonstrate that the level of volatile tin compounds in the air during PVC processing operations are significantly below the TLV of 0.1 mg/m^3 for tin compounds established for the United States workplace.

Mixed Metal Stabilizers. The second most widely used class of stabilizers, with nearly 29,000 t sold in the United States in 2000, are the mixed metal combinations. These products predominate in the flexible PVC applications in the United States; however, they find competition from the lead-based products in Europe Mixed metal products are growing rapidly for electrical wire and cable coatings where the lead products have been the preferred stabilizers for many years. Alternative mixed metal stabilizers are continually being commercialized to replace the leads in this application, as well. In Europe, mixed metal stabilizers are preferred for the extruded rigid building profiles because they provide good weathering and physical properties to the PVC in this use.

The commercially important alkali and alkaline-earth metals used in these stabilizer systems are based on the salts and soaps of calcium, zinc, magnesium, barium, and cadmium. These metal salts and soaps are combined to make a stabilizer system; there is synergy between these compounds during PVC processing. Because the chloride salts of both zinc and cadmium are easily formed during PVC processing and are strong Lewis acids, it is not surprising that short stability times and catastrophic degradation are observed when either zinc or cadmium soaps are used alone. In fact, zinc carboxylates, by themselves, are worthless as PVC stabilizers. When zinc and cadmium salts are combined with other compounds, which prevent or delay the formation of the respective Lewis acids, good PVC stability can be obtained. Particularly, the salts of calcium and barium serve this purpose. Other organic compounds, such as phosphites, epoxides, polyols, and β-diketones, can also be added to enhance the performance further.

The most popular commercial products are combinations including calcium–zinc, barium–calcium–zinc, barium–zinc, and barium–cadmium. Barium–cadmium combinations were, at one time, the most widely used mixtures, but as of the early 1990s their use has decreased considerably because of toxicity and ecotoxicity concerns surrounding cadmium compounds. In fact, many Eurpoean countries have imposed bans on the uses of cadmium in all applications for plastics. Modern calcium–zinc, barium–zinc, and barium–calcium–zinc mixtures are touted as effective replacements for many of these barium–cadmium formulations. The safety of these newer products are unquestioned and certain calcium–zinc mixtures are widely used to stabilize PVC food packaging, mineral water bottles, and pharmaceutical containers throughout the world. In many applications, particularly in plasticized PVC, the mixed metal products effectively offer the right combination of processibility, heat and light stability, low odor, and nonsulfur staining characteristics to be the best choice of stabilizer.

Stabilization Mechanism. Zinc and cadmium salts react with defect sites on PVC to displace the labile chloride atoms (32). This reaction ultimately leads to the formation of the respective chloride salts, which can be very damaging to the polymer. The role of the calcium and/or barium carboxylate is to react with the newly formed zinc–chlorine or cadmium–chlorine bonds by exchanging ligands (33). In effect, this regenerates the active zinc or cadmium stabilizer and delays the formation of significant concentrations of strong Lewis acids.

Reaction with defect site

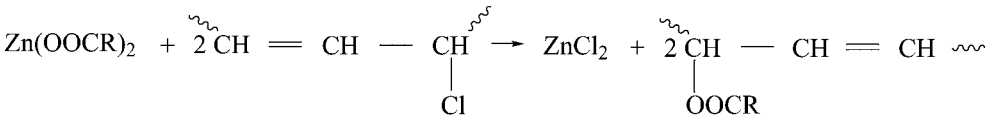

Regeneration of stabilizer

The chloride salts of calcium and barium are weak Lewis acids and do not tend to promote PVC degradation. By carefully choosing the ratio of zinc or cadmium salt to calcium and/or barium soap, the overall stabilizing effects can be tuned to an optimum level for a given application or process. The typical mixed metal products usually contain between a 2:1 and 1:2 ratio of the metal salts. Ultimately, though, these delaying tactics are spent and the zinc or cadmium chlorides form, resulting in rapid hydrogen chloride evolution and cross-linking reactions leading to a brittle, black, crumbling product of no value. Although it is not completely understood, the maximum level of stability for these mixtures is reached at a concentration of stabilizer of about 4–5% of the polymer. Adding higher amounts of stabilizer has little effect on the overall stability of the PVC; this same phenomenon is also observed for the alkyltin stabilizers.

Mixed Metal Stabilizer Synthesis. The mixed metal salts and soaps are generally prepared by reaction of commercially available metal oxides or hydroxides with the desired C_8–C_{18} carboxylic acids. The liquid stabilizer products sometimes employ metal alkylphenates and overbased metal alkylphenates, particularly calcium or barium alkylphenates, in place of the metal carboxylates. The desired ratio of metal salts can be achieved by coprecipitation from the appropriate ratio of metal oxides or, more often, from isolated metal salts by blending to give the correct ratios. During the blending process, a variety of other coadditives or secondary stabilizers, such as phosphites, polyols, epoxides, β-diketones, or antioxidants, can be added to complete the stabilizer package. Modern stabilizers are provided as either liquids or nondusting powders, which are easily handled in totally automated compounding operations.

Commercial Stabilizers. There is a great variety of commercial formulations utilizing the mixture of the alkali and alkaline-earth metal salts and soaps.

In many cases, products are custom formulated to meet the needs of a particular application or customer. The acidic ligands used in these products vary widely and have dramatic effects on the physical properties of the PVC formulations. The choice of ligands can affect the heat stability, rheology, lubricity, plate-out tendency, clarity, heat sealability, and electrical and mechanical properties of the final products. No single representative formulation can cover the variety of PVC applications where these stabilizers are used.

Typically, solid stabilizers utilize natural saturated fatty acid ligands with chain lengths of C_8–C_{18}. Zinc stearate [557-05-1], zinc neodecanoate [27253-29-8], calcium stearate [1592-23-0], barium stearate [6865-35-6], and cadmium laurate [2605-44-9] are some examples. To complete the package, the solid products also contain other solid additives such as polyols, antioxidants, and lubricants. Liquid stabilizers can make use of metal soaps of oleic acid, tall oil acids, 2-ethyl-hexanoic acid, octylphenol, and nonylphenol. Barium bis(nonylphenate) [41157-58-8], zinc 2-ethylhexanoate [136-53-8], cadmium 2-ethylhexanoate [2420-98-6], and overbased barium tallate [68855-79-8] are normally used in the liquid formulations along with solubilizers such as plasticizers, phosphites, and/or epoxidized oils. The majority of the liquid barium–cadmium formulations relies on barium nonylphenate as the source of that metal. There are even some mixed metal stabilizers supplied as pastes. The U.S. FDA approved that calcium–zinc stabilizers are good examples because they contain a mixture of calcium stearate and zinc stearate suspended in epoxidized soya oil. Table 4 shows examples of typical mixed metal stabilizers.

Costabilizers. The variety of known costabilizers for the mixed metal stabilizers is a very long listing. There are, however, a relatively small number of commercially used costabilizers. Some of these additives can also be added by the PVC compounder or processor in addition to the stabilizer package to further enhance the desired performance characteristics. The epoxy compounds and phenolic antioxidants are among the most commonly used costabilizers with the mixed metal stabilizers.

Epoxy Compounds. Epoxidized soya oil (ESO) is the most widely used epoxy-type additive and is found in most mixed metal stabilized PVC formulations at 1.0–3.0 phr because of its versatility and cost effectiveness. Other useful epoxy compounds are epoxidized glycerol monooleate, epoxidized linseed oil, and alkyl esters of epoxidized tall oil fatty acid.

Antioxidants. Phenolic antioxidants, added at about 0.1–0.5 phr, are usually chosen from among butylated hydroxytoluene [128-37-0], and *p*-nonylphenol [104-40-5] for liquid stabilizer formulations and bisphenol A [80-05-7]

Table 4. Formulations of Mixed Metal Stabilizers, %

Liquid formula	Solid formula	Paste formula
Barium tallate overbase, 30	Barium stearate, 25	Zinc stearate, 15
Barium bis(nonylphenate), 20	Cadmium laurate, 50	Calcium stearate, 15
Zinc 2-ethylhexanoate, 15	Bisphenol A, 5	Tris(nonylphenyl) phosphite, 30
Diphenyl decylphosphite, 30	Pentaerythritol, 20	
Dibenzoylmethane, 5		Epoxidized soya oil, 40

[2,2-bis-(*p*-hydroxyphenyl)propane] for the solid systems. Low melting thioesters, dilauryl thiodipropionate [123-28-4] or distearyl thiodipropionate [693-36-7], are commonly added along with the phenolics to enhance their antioxidant performance. Usually a 3:1 ratio of thiodipropionate to phenolic antioxidant provides the desired protection. Most mixed metal stabilizer products contain the antioxidant ingredient (see ANTIOXIDANTS).

Polyols. Polyols, such as pentaerythritol [115-77-5], dipentaerythritol [126-58-9], and sorbitol [50-70-4], most likely chelate the active metal centers to reduce their activity toward the undesired dehydrochlorination reaction. These additives are generally included in the stabilizer formulation, used in the range of 0.2–0.7 phr.

Phosphites. Tertiary phosphites are also commonly used and are particularly effective in most mixed metal stabilizers at a use level of 0.25–1.0 phr. They can take part in a number of different reactions during PVC processing: they can react with HCl, displace activated chlorine atoms on the polymer, provide antioxidant functionality, and coordinate with the metals to alter the Lewis acidity of the chloride salts. Typical examples of phosphites are triphenyl phosphite [101-02-0], diphenyl decyl phosphite [3287-06-7], tridecyl phosphite [2929-86-4], and polyphosphites made by reaction of PCl_3 with polyols and capping alcohols. The phosphites are often included in commercial stabilizer packages.

β-Diketones. A new class of costabilizer has emerged that is effective with the mixed metal systems. The β-diketones can significantly enhance the performance of the calcium–zinc and barium–calcium–zinc systems when used at 0.1 to about 0.7 phr. Although relatively expensive, the β-diketones greatly improve early color stability and rheological performance while benefitting the weatherability of the final PVC articles. Typical of these additives are dibenzoylmethane [2929-86-4] and stearoyl benzoyl methane [58446-52-9]. These additives are generally formulated as part of the mixed metal stabilizer package.

Specialty Amines. Some substituted nitrogenous compounds can provide similar benefits. Esters of 2-aminocrotonate and bis-2-aminocrotonate, and appropriately substituted dihydropyridines, eg, 3,5-bis-lauryloxycarboxy-2,6-dimethyl-1,4-dihydropyridine [37044-66-7] and 3,5-bis-ethoxycarboxy-2,6-dimethyl-1,4-dihydropyridine [1149-23-1], are examples of these costabilizers. These relatively expensive costabilizers are used at 0.1–0.7 phr and are particularly effective when added to the calcium–zinc stabilizers.

Hydrotalcite. Synthetic hydrotalcite minerals are gaining commercial acceptance for their ability to costabilize PVC in the presence of other primary stabilizers (see Table 2). The performance of the mixed metal stabilizers are particularly boosted when an equal part level, about 2–3 phr, of hydrotalcite is added to the PVC formulation. These minerals function by trapping HCl within the layered lattice arrangement of atoms. The formula, $Mg_4Al_2(OH)_{12}CO_3{\cdot}3H_2O$, is commonly written; however, these minerals are generally nonstoichiometric by nature and can include some amounts of alternative elements in their compositions. They function similarly to the zeolites but exist in layered structures and have a different trapping mechanism. In addition to their performance enhancement, the hydrotalcite minerals are compatible with PVC and can be

used effectively in clear PVC applications as well as the pigmented formulations.

Economics. As with the alkyltin stabilizers, the market pricing of the mixed metal stabilizers tend to be directed by the particular application. The calcium–zinc and barium–cadmium packages are typically used at 2.0–3.0 parts per hundred of PVC resin (phr) in the formulation. These completely formulated products are sold for $2.40–5.50/kg for the liquid products and $2.00–4.00/kg for the solids and pastes. The higher efficiency products aimed at rigid applications tend toward the higher end of the cost range.

The basic metal salts and soaps tend to be less costly than the alkyltin stabilizers; for example, in the United States, the market price in 2000 for calcium stearate was about $1.30–1.60/kg, zinc stearate was $1.70–2.00/kg, and barium stearate was $2.40–2.80/kg. Not all of the coadditives are necessary in every PVC compound. Typically, commercial mixed metal stabilizers contain most of the necessary coadditives and usually an epoxy compound and a phosphite are the only additional products that may be added by the processor. The required costabilizers, however, significantly add to the stabilization costs. Typical phosphites, used in most flexible PVC formulations, are sold for $3.00–4.50/kg. Typical antioxidants are bisphenol A, selling at $2.00/kg; *p*-nonylphenol at $1.25/kg; and BHT at $3.50/kg, respectively. Pricing for ESO is about $1.50–2.00/kg. Polyols, such as pentaerythritol, used with the barium–cadmium systems, sells at $2.00/kg, whereas the derivative dipentaerythritol costs over three times as much. The β-diketones and specialized dihydropyridines, which are powerful costabilizers for calcium–zinc and barium–zinc systems, are very costly. These additives are $10.00 and $20.00/kg, respectively, contributing significantly to the overall stabilizer costs. Hydrotalcites are sold for about $3.00–5.00/kg.

Health and Safety Aspects. Overall, the mixed metal stabilizer industry is undergoing significant change during the early 1990s because of the increasing restrictions on cadmium compounds. Most of the research effort has focused on new products to replace the traditional barium–cadmium formulations with technical and cost-effective products. In some regions, cadmium is allowed only in applications where there are no effective replacement technologies. The replacement products generally contain salts of barium, zinc, calcium, and/or potassium; all these compositions are considered safe in the many flexible PVC end uses.

Calcium–zinc soaps are used in many PVC food container applications because these heat stabilizers are universally accepted as safe by the U.S. FDA, German BGA, Japanese JHPA, and other government regulatory groups.

Organic Stabilizers. Since the early 1990s there has been a significant effort to reduce or eliminate most metals from PVC heat stabilizers. This crusade was launched in the name of improving both human health and environmental effects from metals that leach from PVC products. As a result, a totally new class of heat stabilizers was developed which relies on nonmetallic organic chemicals as the primary heat stabilizing components. The idea of these nonmetallic stabilizers is to make PVC products, particularly drinking water piping systems that have no metals to leach either into the water or into the environment. Significant interest in these new stabilizer types is strong in the Nordic countries, particularly Sweden

and Denmark, where both lead- and tin-based stabilizers have been targeted for elimination by environmental regulations.

The earlier entry into this new class of stabilizers was built upon a 6-aminouracil compound (**7**) formulated with some costabilizers, particularly the hydrotalcites (34,35) and lubricants. Shortly after this, another chemistry was introduced which relied on "protected" mercaptan compounds, called "latent mercaptans" of general structure (**8**). In this second type, a small amount of a metal "kicker" must be added to start the stabilizing activity of the latent mercaptan (36). The preferred metal kicker is reported to be zinc which could be used at as low as 0.04% in the PVC to be effective in the new stabilizer. Most of the stabilizer development has been for applications in soft PVC formulations; however, the more recent work has focused on efficient stabilizer one-packs for rigid extrusion compounds.

Both stabilizer systems reportedly provide sufficient heat stability for PVC pipe extrusion and provide excellent physical properties in the final pipes.

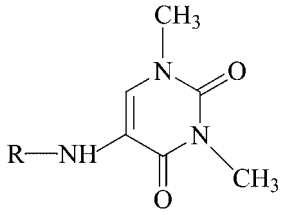

(**7**)

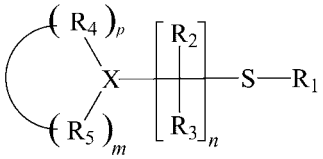

(**8**)

Significant efforts have been made to completely demonstrate the efficiencies of these emerging stabilizer chemistries, although they remain noncommercial because of their higher projected costs compared to the current lead-stabilizer systems and because the lead-based systems continue to be allowed until at least 2002.

Lead Stabilizers. In use since the 1940s, the lead-based stabilizers have played an extremely important role in the development of PVC as a high performance polymer. The myriad of toxicological and ecotoxicological problems surrounding the use of any lead chemicals has restricted lead stabilizers to uses in flexible PVC wire and cable coatings in the United States, with consumption in the mid-1990s estimated at 15,000 t, but it has leveled off during the past few years. In Europe and Asia, the lead stabilizers predominate for wire and cable uses and are also widely used to stabilize PVC pipe and weatherable building profiles. It is estimated that as much as 70% of all stabilizers sold in Europe and Asia are based on some type of lead compounds. These are solid products and are supplied as powders, flakes, or strands, usually in special packaging to control dusting.

The commonly used commercial lead-based PVC stabilizers rely on one or more lead(II) oxide groups bound to the primary bivalent lead salt. These overbased lead compounds have higher levels of lead and are more basic, thus reacting more readily with evolved hydrogen chloride during PVC processing. It is typical to find combinations of mono-, di-, and tribasic lead compounds as the primary heat stabilizers because these often work together to provide a good balance of both early and long-term stability. The choice of anion also effects the performance by reducing the reactivity of the lead oxide toward other ingredients in the formulation as well as the polymer. The stabilization by-product, lead dichloride, is nearly inert, ie, it is white in color, nonionic, insoluble in water, and has low Lewis acidity. It is these properties that give lead-stabilized PVC such a low conductivity in electrical applications. Commercially, most lead stabilizers are combinations containing lead stearates which also provide good lubrication to PVC compounds. Additional lubricants often are not necessary for thermally processing these PVC formulations.

Their high toxicity has greatly limited the applications for lead stabilizers in North America and is now spreading around the world. Environmental agencies such as WHO and U.S. EPA are continually lowering recommended human exposures to lead compounds. Another limitation is that lead products have a high refractive index and as a result can only be used in opaque applications. Overbased lead salts have a high degree of reactivity and tend to interact, many times disfavorably, with other ingredients in the formulation. Also, they have a very high specific gravity compared to other stabilizers, resulting in higher density PVC products. Lastly, the lead stabilizers can react with almost any source of sulfur to form black lead sulfide, the so-called *lead stain phenomenon*. Despite these drawbacks, they remain highly effective PVC heat stabilizers.

Stabilization Mechanism. Traditionally, lead salts were thought to perform only as acid scavengers during PVC stabilization; it is likely that this activity leads to good long-term stability. Bivalent lead compounds can readily form complexes, and recently workers have proposed that these products also displace labile chlorines on the polymer in a fashion similar to the mixed metal stabilizers. A free-radical mechanism is proposed for this displacement which improves the early color hold of the PVC (10). Because the lead chloride is such a weak Lewis acid, costabilizers used in the mixed metal systems are generally ineffective and unnecessary. Increasing stabilizer concentration in the polymer generally leads to increased stability times.

Lead Stabilizer Synthesis. Most commercial stabilizers are produced by reaction of a water slurry of lead oxide with the appropriate acid while heating, yielding a solid product with a particle size of about 1 μm. This condensation proceeds, leaving the desired level of overbasing in the final product. Most often, the lead product is treated with a coating agent to reduce dusting and improve dispersability in the PVC. The stabilizer is then filtered, dried, and packaged. During the drying and coating step, other coadditives such as pigments, lubricants, and fillers can be blended into the mixture to make a total package formulation.

Commercial Stabilizers. There are six lead salts and soaps that are typically used in the commercial PVC stabilizers. The lead stearate soaps are often combined with the lead salts to provide lubrication and added stabilizer activity.

Table 5. Principal Lead Stabilizers

Stabilizer	CAS registry number	Formula	PbO (%)	Specific gravity
Tribasic lead sulfate	[12202-17-4]	$PbSO_4 \cdot 3PbO \cdot H_2O$	89	6.9
Dibasic lead phosphite	[12141-20-7]	$PbHPO_3 \cdot 2PbO \cdot \frac{1}{2}H_2O$	90	6.1
Dibasic lead phthalate	[17976-43-1]	$C_4H_4(COO)_2Pb \cdot 2PbO$	80	4.2
Basic lead carbonate	[1319-46-6]	$2PbCO_3 \cdot Pb(OH)_2$	87	6.7
Dibasic lead stearate	[56189-09-4]	$Pb(OOCC_{17}H_{35})_2 \cdot 2PbO$	55	2.0
Lead stearate	[1092-35-7]	$Pb(OOCC_{17}H_{35})_2$	29	1.4

The key to the high activity of these stabilizers is the very high lead content. Table 5 describes six commonly used lead stabilizers.

By far the most common lead salt used for PVC stabilization is tribasic lead sulfate. It can be found either alone or combined with another lead salt in almost every lead-stabilized PVC formulation. Many of the combinations are actually coprecipitated hybrid products, ie, basic lead sulfophthalates. Dibasic lead stearate and lead stearate are generally used as costabilizers combined with other primary lead salts, particularly in rigid PVC formulations where they contribute lubrication properties; dibasic lead stearate provides internal lubrication and lead stearate is a good external lubricant.

Flexible Applications. The only remaining application of the lead stabilizers in the United States is in flexible wire and cable coating applications. The nonconductive nature of lead stabilizers is unsurpassed by other classes of stabilizers. Rather high levels of stabilizers are necessary for these uses because of the required high temperature aging specifications for most insulating materials. Typically 5–8 phr of lead stabilizer is needed in most insulation compounds. Careful consideration must be given to the choice of lead stabilizer because of the high reactivity of the basic lead oxide groups with other ingredients in the formulation. This is particularly true of the plasticizer choice. The more demanding, high temperature applications require stabilizers rich in dibasic lead phthalate to provide high levels of heat aging stability; the less demanding applications, jacketing and low temperature insulation, usually rely on tribasic lead sulfate as the primary stabilizer. Under high temperature aging conditions, tribasic lead sulfate tends to react with the ester-type plasticizers to increase volatility and reduce the resilience of the PVC insulation.

Rigid Applications. The use of the lead stabilizers is very limited in the United States; but, they are still used in several rigid PVC applications in Europe and Asia. The highest use of lead stabilizers in rigid PVC is for pipe and conduit applications. Tribasic lead sulfate is the primary heat stabilizer, with lead stearates included to provide lubrication. The lead products are typically fully formulated, usually including lubricants and pigments for pipe extrusion applications. These lead one-packs, when used at about 1.8–2.5 phr, provide all of the stabilizer and lubrication needed to process the polymer. A lead one-pack contains tribasic lead sulfate, dibasic lead stearate, calcium stearate, polyethylene wax, paraffin wax, ester wax, and pigments.

Dibasic lead phosphite is used in rigid building profile applications because the PVC weathering properties are found to be very good. Normally, the titanium dioxide pigment loading is increased to about 5 phr in these formulations. In less critical uses, ie, interior profiles, tribasic lead sulfate remains the standard. There remains only one U.S. producer of note for lead stabilizers: Hammond Lead Co., Halstab Div., (Hammond, Indiana) sells Halstab, Halbase, Halphal, Halphos, Tribase, Dythal Dyphos, and Leadstar.

Economics. The lead-based stabilizers tend to be priced relatively low, with 2000 prices ranging from $1.40 to $3.60/kg in the United States. The lead phthalates tend toward the higher end of this range, whereas the pipe one-pack products fall into the low end.

Health and Safety Aspects. Worldwide, there is continuing pressure by environmental and human toxicologists to reduce the use of heavy metals such as lead in every application. In the United States, the EPA and OSHA provide regulations over the producers and users of lead stabilizers. The permissible exposure level (PEL) of workers is regulated at 50 $\mu g/m^3$ of airborne lead per 8-h workday. Further, workers are not allowed to be exposed to greater than 30 $\mu g/m^3$ for more than 30 days/year (37). The state of California increased the safety factor further in 1990 by regulating exposure to less than 5 $\mu g/m^3$ for any exposure. Warning labels describing the toxic effects of lead compounds must be applied to all lead stabilizer packaging. In some states, ie, New Jersey and California, any product containing more than 0.1% lead must be labeled as containing lead.

Lead stabilizers have not been used to manufacture drinking water pipes in the United States since 1970 because of the migration levels of lead found in the water from the stabilizers. In 1991, U.S. EPA further reduced the allowable level of lead in drinking water to zero (action level of only 15 ppb lead). In 1993, WHO provided new guidelines targeting the level of lead in drinking water to less than 10 ppb. All uses of lead in PVC pipes are under scrutiny and the stabilizer industry is responding with nontoxic tin-based and calcium–zinc-based technologies. Significant efforts are underway to reduce the uses of lead stabilizers in flexible wire and cable applications as well. New mixed metal formulations are now being touted as providing the needed high levels of both heat stability and nonconducting electrical properties.

Antimony Mercaptide Stabilizers. In the mid-1950s antimony mercaptides were first proposed as PVC heat stabilizers (38). Antimony tris(laurylmercaptide) [6939-83-9] and antimony tris(isooctylthioglycolate) [27288-44-4] are typical of this class of heat stabilizers. These compounds were used mainly in rigid PVC applications, particularly pipes, competing with the alkyltin mercaptides. Their use has greatly diminished during the late 1980s and early 1990s for a variety of reasons. Particularly, questions raising doubts about the toxicological safety of antimony compounds have arisen. The performance of the antimony products has also reduced their uses in many processes. For example, they are less compatible with PVC, which leads to a cloudy appearance in clear applications; they react with sulfur sources to form Sb_2S_3, an orange-colored byproduct; and they detract from the weatherability of PVC formulations. Further, because the cost of tin metal decreased significantly during the 1980s, antimony pricing has continued to rise, making these products less economically attractive than they once had been.

The performance of the antimony stabilizers is significantly enhanced by adding polyhydroxybenzene compounds, eg, catechol, to the PVC (39). In commercial practice, about 5–10% catechol is formulated with the antimony mercaptide stabilizer products. The antimony mercaptides are normally prepared by heating antimony oxide with the appropriate mercaptan, normally isooctyl thioglycolate, under conditions to remove water.

$$Sb_2O_3 + 6\,HSCH_2COOR' \rightarrow 2\,Sb(SCH_2COOR')_3 + 3\,H_2O$$

Health and Safety Aspects. The U.S. EPA has significantly reduced the allowed levels of antimony compounds in drinking water, causing a toxicity cloud over the viability of this class of stabilizers. Presently, antimony products are no longer allowed for use as potable water pipe stabilizers under NSF International's current Standard 61(28). For these reasons, antimony stabilizer technology is no longer commercial in the United States.

BIBLIOGRAPHY

1. G. Ayrey, R. C. Poller, and I. H. Siddiqui, *J. Polym. Sci., Part B* **8**, 1 (1970).
2. D. Braun, in G. Geuskens, ed., *Degradation and Stabilization of Polymers*, John Wiley & Sons, Inc., New York, 1975, pp. 23–41.
3. W. H. Starnes Jr., *Am. Chem. Soc., Div. Polym. Chem. Polym. Prepr.* **18**, 493 (1977).
4. A. Guyot and co-workers, *J. Pure Appl. Chem.* **53**, 401 (1981).
5. G. Ayrey, B. C. Head, and R. C. Poller, *J. Polym. Sci. Macromol. Rev.* **8**, 1 (1974).
6. M. J. R. Cantow and co-workers, *Mod. Plast.* **46**(6), 126 (1969).
7. U.S. Pat. 4,963,608 (Oct. 16, 1990), M. Kunieda and H. Takida (to Kyowa Kagaku Kogin Kabushiki Kaisha).
8. A. H. Frye, R. W. Horst, and M. A. Paliobagis, *J. Polym. Sci.*, Part A-2 1765, 1785, 1801 (1964).
9. A. H. Frye and R. W. Horst, *J. Polym. Sci.* **40**, 419 (1959); *J. Polym. Sci.* **45**, 1 (1960).
10. E. W. Michell, *J. Vinyl Technol.* **8**, 55 (1986).
11. R. C. Weast, ed., *CRC Handbook of Chemistry and Physics*, 72nd ed., CRC Press, Inc., Boca Raton, Fla., 1991.
12. E. D. Owen, in E. D. Owen, ed., *Degradation and Stabilization of PVC*, Elsevier, London, 1984, pp. 223–236.
13. A. Michel, T. V. Hoang, and A. Guyot, *J. Macromol. Sci., Part A* **12**, 411 (1978).
14. D. Dresedow and C. F. Gibbs, *Nat. Bur. Stand. Circ.* **525**, 69 (1953).
15. D. E. Winkler, *J. Polym. Sci.* **35**, 3 (1959).
16. W. H. Starnes and co-workers, *Polym. Prep. (Am. Chem. Soc., Div. Polym. Chem.)* **19**, 623 (1978).
17. H. O. Wirth and H. Andreas, *Pure Appl. Chem.* **49**, 627 (1977).
18. L. S. Troitskaya and B. B. Troitski, *Plast. Massy* 12 (1968).
19. E. Parker, *Kunstoffe* **47**, 443 (1957).
20. G. Ayrey and R. C. Poller, in G. Scott, ed., *Developments in Polymer Stabilization-2*, Applied Science, London, 1980, p. 1.
21. U.S. Pat. 3,857,868 (Dec. 31, 1974), R. C. Witman and T. G. Kugele; 3,862,198 (Jan. 21, 1975), T. G. Kugele and D. H. Parker (both to Cincinnati Milacron, Inc.).

22. R. E. Hutton, J. W. Burley, and V. Oakes, *J. Organometal. Chem.* **156**, 369 (1978).
23. U.S. Pat. 4,701,486 (Oct. 20, 1987), R. E. Bresser and K. R. Wursthorn (to Morton International, Inc.).
24. K. Figge, *Pack. Technol. Sci.* **3**, 2 **7**, 41 (1990).
25. *U.S. Code Of Federal Regulations, Title 21: Food and Drugs*, 21 CFR 178.2010, Washington, D.C., 1992.
26. *U.S. Code Of Federal Regulations, Title 21: Food and Drugs*, 21 CFR 178.2650, Washington, D.C., 1992.
27. *U.S. Code Of Federal Regulations, Title 21: Food and Drugs*, 21 CFR 314.420, Washington, D.C., 1992.
28. *Drinking Water System Components—Health Effects*, ANSI/NSF Standard 61, NSF International, Ann Arbor, Mich., 1990.
29. K. A. Mesch and T. G. Kugele, *J. Vinyl Tech.* **14**, 131 (1992).
30. D. Van Battum, Report 06236/76 and 07822A.75, CIVO, Zeist, the Netherlands, 1976; A.-M. Dommröse, Report 88 9787, Natec Institut, Hamburg, Germany, 1988.
31. T. G. Kugele, *China Plast. Rubber J.* **20**, 40 (1989).
32. A. Guyot and A. Michel, in Ref. 20, p. 89.
33. P. P. Klemchuk, *Adv. Chem. Ser.* **85**, 1 (1968).
34. U.S. Pat. 5,859,100 (Jan. 12, 1999), W. Wehner and co-workers (to Ciba Specialty Chemicals).
35. U.S. Pat. 5,925,696 (Jul. 20, 1999), W. Wehner and co-workers (to Ciba Specialty Chemicals).
36. G. M. Conroy, K. A. Mesch, and T. C Duval, in *Proceedings PVC 99—From Strength to Strength*, Brighton, U.K., Apr. 20–22, 1999, Institute of Materials, London, pp. 377–387.
37. *OSHA Standard For Occupational Exposure To Lead (29 CFR 1910–1025) Washington*, D.C.; *Fed. Reg.* 43 52952 (Nov. 14, 1978).
38. U.S. Pats. 2,680,726 (June 8, 1954) and 2,684,956 (July 27, 1954), E. L. Weinberg and co-workers (both to M&T Chemicals).
39. U.S. Pat. 4,029,618 (June 14, 1977), D. Dieckmann (to Synthetic Products Co.).

GENERAL REFERENCES

L. I. Nass and C. A. Heilberger, eds., *Encyclopedia of PVC*, 2nd ed., Vol. **1**, Marcel Dekker, Inc., New York, 1985.
L. I. Nass and C. A. Heilberger, eds., *Encyclopedia of PVC*, 2nd ed., Vol. **2**, Marcel Dekker, Inc., New York, 1987.
E. D. Owen, in E. D. Owen, ed., *Degradation and Stabilization of PVC*, Elsevier, London, 1984, Chapt. "5".
J. Edenbaum, ed., *Plastics Additives and Modifiers Handbook*, Van Nostrand Reinhold Co., Inc., New York, 1992, Sect. II.
H. Andreas, in R. Gächter and H. Müller, eds., Plastics Additives Handbook, 3rd ed., Hanser, Munich, 1990, Chapt. "4".
G. Pritchard, ed., *Plastics Additives: An A–Z Reference*, Kluwer Academic Publishers Dordrecht, the Netherlands, 1998.
Proceedings SPE Vinyl RETEC, New Brunswick, N.J., Sept. 29–Oct. 1, 1992, Society of Plastics Engineers, Stamford, Conn., pp. 33–82.
Proceedings SPE Vinyl RETEC, Cincinnati, Ohio, Oct. 24–25, 1995, Society of Plastics

Engineers, Stamford, Conn., pp. 93–112.
Proceedings SPE Vinyl RETEC, Cincinnati, Ohio, Oct. 15–16, 1996, Society of Plastics Engineers, Stamford, Conn., pp. 157–174.
Proceedings PVC 96—New Perspectives, Brighton, U.K., Apr. 23–25, 1996, Institute of Materials, London, pp. 337–360.
Proceedings PVC 99—From Strength to Strength, Brighton, U.K., Apr. 20–22 1999, Institute of Materials, London, pp. 341–387.

KEITH A. MESCH
Rohm and Haas Company

HETEROPHASE POLYMERIZATION

Introduction

Heterophase polymerization is a generic term that describes polymerization reactions under nonhomogeneous conditions with respect to physical and chemical properties of the reaction mixture. This means the existence of gradients such as in density and chemical composition and consequently, the coexistence of different phases. Heterophase polymerizations are best defined in a very general way as processes resulting in polymer dispersions. *Polymer dispersion* is a state of matter where polymers are finely dispersed in a continuous phase. In this sense these polymerization processes are colloidal in nature and thus bridge two important scientific areas: polymer science and colloid science. Colloid science characterizes systems by two general features, heterogeneity and dispersity, which necessarily occur mutually. *Heterogeneity* means the coexistence of different phases and is a qualitative feature. It implies that phase boundaries, processes at phase boundaries, mixed interfaces, and in some cases phase formations also are of importance. *Dispersity* is a quantitative measure that characterizes the degree of division of the heterophase system. It is defined as the reciprocal average characteristic length scale. Besides dispersity the shape, the size, and the interface per mass of the dispersed phase are other characteristic features. In particular, dispersity is responsible for new properties of colloidal systems absent in homogeneous ones, because with increasing dispersity interfacial effects become more and more important. Furthermore, heterogeneity and dispersity together cause an energetic characterization of a dispersion, that is, the existence of an interfacial tension between coexisting phases and an interfacial free energy (interfacial tension times interfacial area). The interfacial free energy contributes substantially to the overall free energy of dispersions, and in many cases it governs the

Encyclopedia of Polymer Science and Technology. Copyright John Wiley & Sons, Inc. All rights reserved.

Table 1. Colloidal Dispersions Made of Various Combinations of States of Matter

Dispersed phase	Continuous phase	Examples	Technical term
Liquid	Gas	Clouds/sprays	Aerosol
Solid	Gas	Smog/dust	Aerosol
Gas	Liquid	Lather/meringue	Foam
Liquid	Liquid	Milk/creams	Emulsion
Solid	Liquid	Paint/blood	Suspension
Gas	Solid	Pumice/cork	Solid foam
Liquid	Solid	Oil shale/opals	Porous material
Solid	Solid	Bones/teeth	Solid suspension

behavior completely. Also, the interface is responsible for all peculiarities, for all pros and cons of heterophase polymerization techniques.

The context of heterogeneity and dispersity requires that the material forming the dispersed phase is insoluble/immiscible in the continuous phase. From that follows directly that the interfaces in dispersed systems can be made of all possible combinations of states of matter except the gas–gas combination. Examples of dispersed colloidal systems are given in Table 1. It is interesting to note that indeed all of these combinations can be used to carry out polymerizations. The various kinds of heterophase polymerization techniques are put together in Table 2 in the order of ascending number of components; the components are listed, except the initiating system.

In most polymerizations the kind of dispersed system changes in the course of the process owing the fact that a gaseous or liquid monomer is transformed into a solid polymer. Examples are catalytic gas-phase polymerizations on solid catalyst beads (1) or polymerizations in liquid continuous phases of gaseous monomers. Heterophase polymerization can also be carried out in pores of inorganic solid materials such as Zeolites (2–5), or mesoporous MCM-41 and similar silicates (6,7), or inside interlayers of montmorillonite (8). Other special types of heterophase polymerizations in a solid continuous phase are used to modify the pores in solid polymer monoliths (9) or pores in polymeric membranes (10).

Table 2. Overview of Heterophase Polymerization Techniques

Technique (common name)	Components
Bulk or mass polymerization[a]	Monomer, polymer
Gas-phase polymerization	Monomer, polymer
Precipitation polymerization	Dispersion medium, monomer, polymer
Suspension polymerization	Stabilizer, dispersion medium, monomer, polymer
Microsuspension polymerization	Stabilizer, dispersion medium, monomer, polymer
Dispersion polymerization	Stabilizer, dispersion medium, monomer, polymer
Emulsion polymerization	Stabilizer, dispersion medium, monomer, polymer
Miniemulsion polymerization	Stabilizer, dispersion medium, monomer, polymer
Microemulsion polymerization	Stabilizer, dispersion medium, monomer, polymer

[a]Only if the polymer is insoluble in its own monomer such as vinyl chloride/poly (vinyl chloride) or acrylonitrile/polyacrylonitrile.

The dramatic changes in the physico-chemical properties on the way from monomers to polymers leads to changes in the overall reaction conditions during any kind of polymerization. In the case of heterophase polymerizations these changes have a considerable influence on the colloidal properties as well, raising questions with respect to the existence of equilibrium situations of important colloid chemical properties. In this sense the final, stable polymer dispersion is a colloidal system in equilibrium and very well suited as models for colloid chemical investigations.

In practice, the term *polymer dispersion* is used almost exclusively for systems with a liquid continuous phase. In this sense and from the colloid chemical point of view, heterophase polymerizations deal with emulsions and suspensions. A polymer dispersion is nowadays frequently also called a latex, which in Latin means "liquid or "fluid," and goes back to the Greek word *látax*, which means "droplet". The word latex has become a generic term that comprises all kinds of polymer dispersions (11). In this article the terms *polymer dispersion, polymer suspension*, and *latex* are used interchangeably. Synonyms for the continuous phase are *dispersion medium, homogenous phase*, and *serum*. Any liquid can be a dispersion medium provided it is a nonsolvent for the dispersed material. But in fact, by far the most important industrial dispersion agent is water, for cost, safety, and environmental reasons. In this article, heterophase polymerization and polymer dispersion means an aqueous continuous phase whereas the term *inverse*, put in front, denotes systems with organic continuous phases. Furthermore, a chain-growth polymerization by a free-radical initiation mechanism is considered, if not otherwise stated. The aim of this article is to provide a condensed view of heterophase polymerizations in liquid media, ie to point out common features rather than to give comprehensive or detailed views on peculiarities of the different kinds of heterophase polymerizations. The list of references is intended to be useful as a starting point for further literature searches rather than an attempt to provide all references, which would be daunting to author and reader alike. After a brief look at the history and the actual meaning of polymer dispersions, general features will be considered, which thereafter will be applied to the variants of heterophase polymerizations.

History. It is historically proven that the Mayas already in 1600 BC were able to use the sap of certain trees to make out of it useful things such as rubber balls, glue, waterproofed clothes, medicine, and much more (12–14). They called this sap *caa o-chu* "crying wood," from which the French word for rubber, *caoutchouc*, was derived. A broader scientific interest in *caoutchouc* was initiated by the report of Charles de la Condamine and Francois Fresneau on their tour through South America in 1736 and their experiences with the milky white resin and the products thereof (15). There is no doubt that the development of polymer science has been strongly connected with polymer dispersions, ie the investigation of natural rubber (see RUBBER, NATURAL). Michael Faraday determined the exact composition of natural rubber as hydrocarbon in 1826 (16), and precisely described the separation of the rubber and its cleaning—basically with the same techniques that are applied still today. After the discovery of vulcanization by Charles Goodyear in 1839, natural rubber became a raw material of increasing importance. Thirty years later, C. Greville Williams isolated by destructive distillation *caoutchouc* decomposition products and named the lightest isoprene (17)

and concluded that the *caoutchouc* hydrocarbon is composed of isoprene polymers. Less than two decades later it was claimed that the reverse process was possible, ie, rubber could be synthesized by polymerizing isoprene (18). Note, the term *polymeric* was introduced 1832 by J. Berzelius from the Greek $\pi o\lambda\nu\zeta$, which means "several," to describe substances possessing the same composition but different properties (19).

In the first decade of the 20th century a team headed by F. Hofmann in Germany was successful in developing polymerization of isoprene either in bulk or in benzene solution. The polymerizations were initiated thermally and carried out in autoclaves at temperatures below 250°C for 10–150 h. (20). The idea of using an aqueous emulsion of a monomer to carry out polymerization dates back to 1912, when the first patent was filed (21). This patent represents the birth of what we call today heterophase polymerization, and Kurt Gottlob was the pioneer researcher (22,23). In order to copy the conditions employed by Nature during the synthesis of *caoutchouc*, Gottlob used viscous fluids such as egg albumin, starch, or gelatin as stabilizers. The addition of alkali or organic bases leads to an improvement of the latex stability, and coagulation was possible by decreasing the pH. Polymerization was started thermally with 7 g of egg albumin in 500 g of water and 300 mL of isoprene in an autoclave. The mixture was stirred for several weeks at 60°C. Significant progress in the development of heterophase polymerizations was made during the following decades, when typical surfactants such as oleates and alkyl aryl sulfonates were used together with water as well as monomer-soluble peroxides (24–26). An almost comprehensive overview of the development of synthetic rubber and products thereof until the early thirties can be found in References 27 and 28. A description of developments that took place on polymerizations of olefins and diolefins during the following period of time until the end of World War II can be found in References 29 and 30. The pace of development in these early days of heterophase polymerization was mainly determined in industrial research labs, with the benefit that the time span between first laboratory results and commercially available products was short. After World War II more and more research activities were started at universities and independent research institutes all over the world. Summaries of today's knowledge of heterophase polymerization techniques can be found in References 31–36. Whereas there were only a handful of polymeric products based on heterophase polymerizations during the 1930s in Germany (37), by 1951 there were nearly 200 synthetic latexes made of various polymers commercially available in the USA (38), and today products based on heterophase polymerization techniques determine in almost all fields our living standard, including construction and automobile industry, medical diagnostics, and paper making (39).

Economic Importance of Heterophase Polymerizations. Polymer dispersions are an important part of the worldwide polymer business, not only because of their outstanding role in the historic development of polymer chemistry but mainly because of their versatility with respect to both properties and applications. Figure 1 illustrates both the position of polymer dispersions in the hierarchy of science and shows the variety of applications in which they are found. These examples illustrate on the one hand the different branches of industry, that take advantage of polymer dispersions and on the other hand how the daily life is influenced. Heterophase polymerizations are important technologies that can

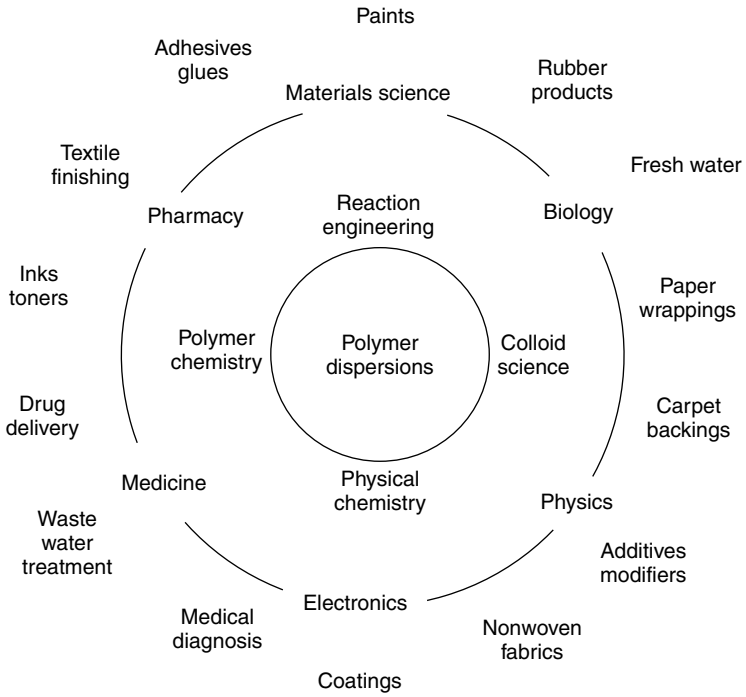

Fig. 1. Illustration of the importance and meaning of heterophase polymerizations/polymer dispersions. Polymer dispersions as the centerpiece belong to chemistry and have strong interrelations to disciplines of chemistry mentioned in the next level. Also, other scientific areas, which are listed in the third level, use polymer dispersions for research and development. Finally, the outer level contains important application fields of polymers, which were produced by heterophase polymerizations.

produce on a volume scale from only a few milliliters up to 200 m^3 high quality polymers with specifically tailored properties. Polymer dispersion is a description for a special state of matter and not connected to a special chemical composition of the polymeric material. Any kind of polymer can be transferred into the state of polymer dispersion. For instance, water-soluble polymers are prepared by inverse heterophase polymerization techniques in organic media. Poly(acrylic acid) or poly(methacrylic acid) polymers and copolymers, quaternary ammonium polymers and copolymers, and polyacrylamide polymers and copolymers belong to this class of important synthetic polymers. The main application areas of these polymers are water and wastewater treatment, detergents, papermaking, coatings, adhesives, textiles, and super-absorbent polymers. The generic term *polymer dispersion* can be illustrated by means of a "family tree," as depicted in Figure 2. Primary dispersions are the direct result of heterophase polymerizations and can be subdivided into naturally occurring latexes and synthetic latexes. Secondary dispersions comprise examples where polymers are transferred into polymer dispersions only after their preparation. Artificial latexes are obtained after dispersing solid polymer or emulsifying polymer solution in a proper dispersion medium. The emulsion can be transferred in a second step into a suspension by removing

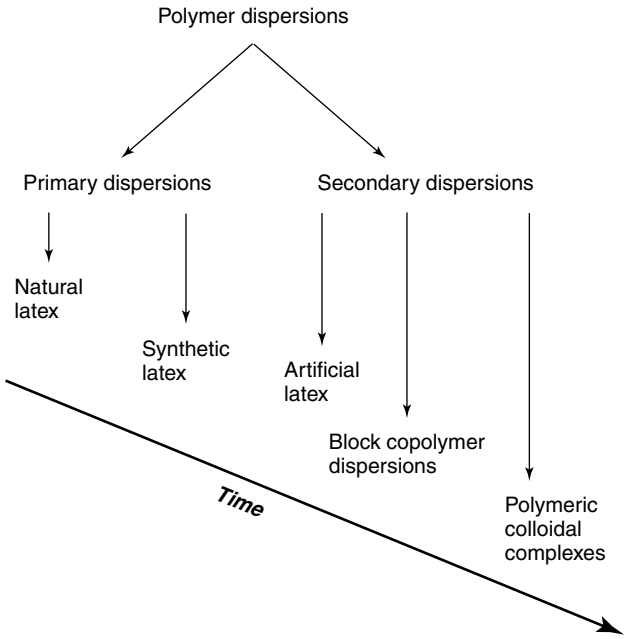

Fig. 2. Family tree of polymer dispersions. The time axis in this graph denotes the time when the different kinds of polymer dispersions came to awareness of mankind starting with natural latex and ending with recent developments in polymeric colloidal complexes. Some important historic milestones are the following: the biosynthesis of natural rubber in plants takes place on earth since millions of years, the first heterophase polymerization was mentioned in a patent filed in 1912 (21), the first process description to make an artificial latex was published in 1923 (40), and the first block copolymer dispersion made by heterophase polymerization was described in 1952 (41).

the solvent. Artificial latexes have until now never gained much industrial interest although several methods have been developed. There are basically three driving forces for the development of artificial latexes: The first is economic because it is more advantageous to transport polymers as dry solid material instead of as dispersions with about 50% by weight dispersion medium. The second reason has to do with the superior material properties of polymers that cannot be prepared by heterophase polymerization techniques—such as polyurethanes or chlorosulfonated polyolefins—but whose application as polymer dispersion is advantageous or desirable. Combinations of different materials such as mineral substances and polymers in the form of composite polymer dispersions for various potential applications are the third reason for an ongoing research on artificial latexes. Block copolymers in selective solvents for only one block form micelles, which are in fact sterically stabilized polymer particles and thus belong to the class of polymer dispersions (42–44). Moreover, heterophase polymerization techniques can be used to prepare bock copolymers in a very efficient way (45–48). One of the oldest attempts, if not the oldest, to prepare block copolymers by radical polymerization was undertaken via aqueous heterophase polymerization (41). Polymeric colloidal complexes are the result of manipulating polymer solutions

by inducing interactions that lead to dispersions. These interactions can be either hydrophobic or electrostatic in nature. Examples are the formation of hollow spheres via layer-by-layer assembly of oppositely charged polyelectrolytes onto various templates (49–52). But also a single kind of block copolymer can form polymeric colloidal complexes via self-assembly, such as poly(ethylene glycol)-b-poly(*N*-isopropyl acrylamide) copolymers, where the poly(*N*-isopropyl acrylamide) block becomes insoluble at temperatures above 32°C and particles are formed via hydrophobic interactions. These particles consist of a poly(*N*-isopropyl acrylamide) core and a stabilizing poly(ethylene glycol) shell. Such particles can easily be prepared by heterophase polymerization started with poly(ethylene glycol)–ceric ion redox system (53). Other examples of such dispersions are complexes between amphiphilic block copolymers with one polyelectrolyte block and either oppositely charged surfactants (48,54–56) or other amphiphilic block copolymers with oppositely charged polyelectrolyte block (48,57). Besides these recent developments in research on preparation of polymer dispersions, they also play an important role (*1*) as model systems for soft matter physics, especially in understanding interactions in colloids (58–60), (*2*) as materials to trigger new characterization methods (61), (*3*) as objects to observe directly nucleation and growth of crystals (62), (*4*) as components in advanced material science research (63), and (*5*) also as object of single particles' handling and modification (64). The economic importance of heterophase polymerization products is not easy to quantify. There is on the one hand the direct value of the polymer products and on the other hand the value added to products, which are made involving polymer dispersions or which are even made only on the base of very specialized polymer dispersions. Table 3 presents the breakdown of worldwide annually produced amounts of different kinds of polymers/polymer dispersions by aqueous heterophase polymerization techniques. According to these numbers about 25% of the total amount of synthetic polymers, that is at the moment some 2×10^8 t per annum worldwide (39), is prepared by heterophase polymerizations. Except some very minor amount of copolymers for paints, poly(vinyl chloride) is exclusively produced by heterophase polymerization techniques. About 80% is produced by suspension polymerization, followed with about 15% by emulsion and microsuspension polymerization, and the rest is by mass or bulk polymerization (65,66,70). Contrary to polystyrene, poly(vinyl chloride) is insoluble in its own monomer. But vinyl chloride still swells its polymer to about 35% at saturation [the Flory–Huggins interaction parameter is between 0.9 and 1.0 (71)] and hence, the vinyl chloride bulk polymerization is a precipitation polymerization where a swollen polymeric phase is formed after a

Table 3. Worldwide Aqueous Heterophase Polymerization Products (Solids)

Product	Amount, 10^6 t	Reference
Poly(vinyl chloride)	25	65,66
Synthetic rubber	10	67
Other latexes	8	68
Natural rubber	7	66
Polystyrene	2	69

few percents of conversion. The 2×10^8 t of polymers produced worldwide represent a financial value of more than euro 200 billion (39) and consequently, as a rough estimate, heterophase polymerization techniques contribute at least with one quarter. This is very likely a lower limit because the about 8×10^6 t of emulsion polymers represent a value of more than euro 20 billion (72). Inverse heterophase polymerization techniques are employed on an industrial scale to produce about 1.5×10^6 t of various synthetic water-soluble polymers. The global consumption of such polymers in the year 2000 was about 2.2×10^6 t representing a value of about euro 3.5 billion, where roughly two-thirds is estimated to be realized by polymers produced via inverse heterophase polymerization techniques (73).

Peculiarities of Heterophase Polymerization

The peculiarities of heterophase polymerizations are directly connected with the dispersed state. Figure 3 shows schematically the main difference between 1 g of polystyrene as bulk material and as a dispersion. The bulk material is a single particle with a diameter (D) of 1.22 cm and a total surface area (A_P) of 4.676 cm^2, whereas the same amount of material in the dispersed state with an average particle size of 50 nm is subdivided or compartmentalized into 1.455×10^{16} particles (N), with a total surface of 1.143×10^6 cm^2. This increase in both N and A_P causes both the advantages and problems of heterophase polymerizations and polymer dispersions compared to homogeneous counterparts. The prices mentioned in Figure 3 for that 1 g of polystyrene in different states show interestingly that the increase in the total surface area almost corresponds to the increase in the

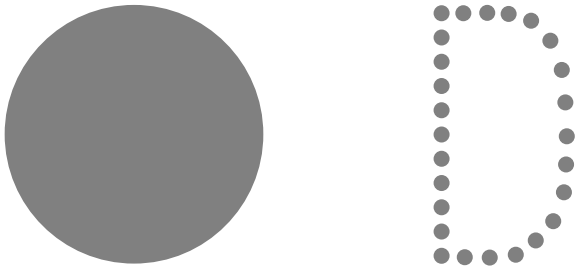

Macroscopic	Dispersed
$D = 1.22$ cm	$D = 50 \times 10^{-7}$ cm
$N = 1$	$N = 1.455 \times 10^{16}$
$A_P = 4.767$ cm^2	$A_P = 1.143 \times 10^6$ cm^2
Price: ~ € 1×10^{-3} g^{-1}	Price: ~ € 3.1×10^2 g^{-1}

Fig. 3. Illustration of the physical effect of dispersion (not to scale); 1 g of polystyrene with a volume V_p of 0.952 cm^3.

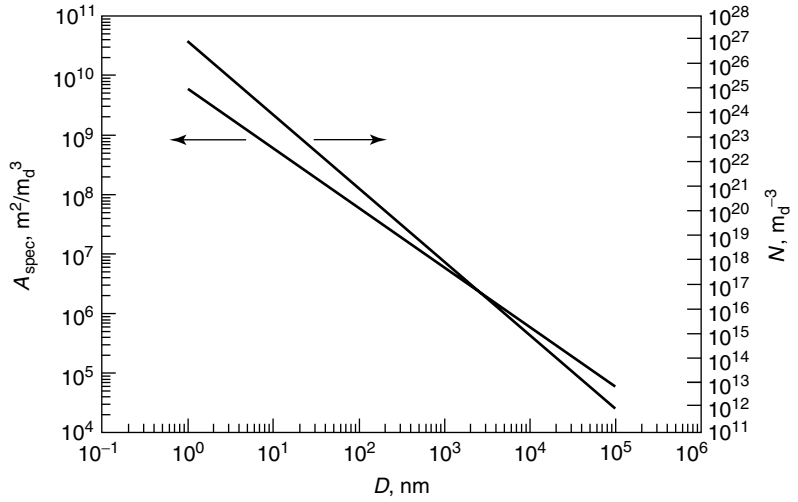

Fig. 4. Specific surface area and particle number for the model dispersion in dependence on the average particle size.

price. The price for the dispersion is that of carboxylated polystyrene spheres with a diameter of 50 nm, which are sold as size-calibration standards in 10-ml batches with a solids content of 2.5% (74). Some of the most important consequences of compartmentalization are illustrated by means of a model dispersion, which is composed of equal volumes of water and organic phase in dependence on average particle size (D in nm). These features are the specific surface area (A_{spec}) and the number of particles (N), both calculated per dispersion volume in $m_d{}^3$ (cf Fig. 4), the average distance between dispersed particles (d_{pp}) and the amount of surfactant relative to the mass of total organic phase ($W_{surf,t}$) (cf Fig. 5), the number

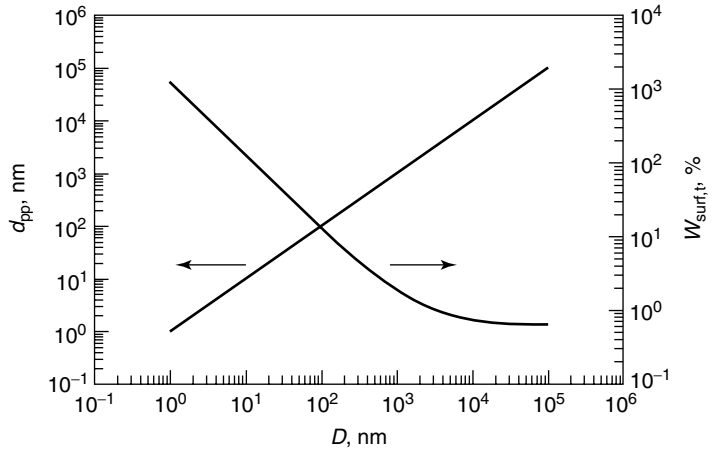

Fig. 5. Average distances between the particles and amount of surfactant to cover the whole interface with a saturated layer in dependence on average particle size for the model dispersion.

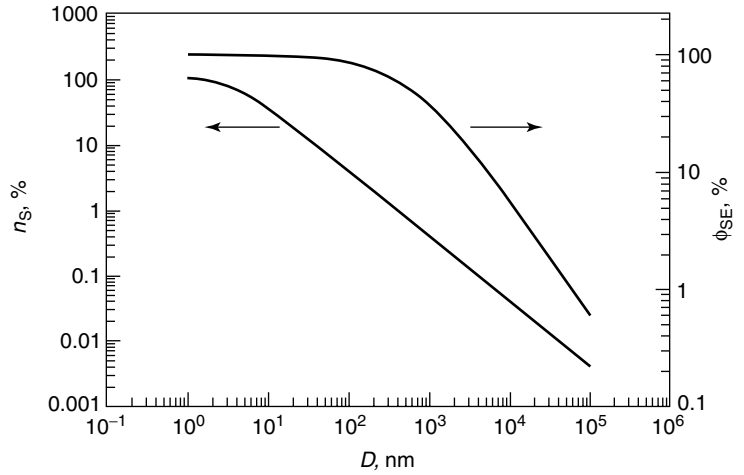

Fig. 6. Fraction of interface molecules per particle and fraction of interfacial free energy in dependence on average particle size for the model dispersion.

of molecules in the surface layer of the particle relative to the total number of molecules per particle (n_S) and the fraction of free surface energy relative to the total free energy of the droplet (ϕ_{SE}) (cf Fig. 6).

$$A_{spec} = \frac{6}{D} 10^9 \tag{1}$$

$$N = \frac{\varphi_{dp} 6}{\pi D^{-3}} 10^{27} \tag{2}$$

$$d_{pp} = \sqrt[-3]{N} \tag{3}$$

$$W_{surf,t} = \frac{10^2 M_S}{\varphi_{dp} \rho_{dp}} \left(cmc + \frac{A_{spec}}{N_A a_s} \right) \tag{4}$$

$$n_s = 10^2 \left(1 - \frac{(D - 2D_{dp})^3}{D^3} \right) \tag{5}$$

$$\phi_{SE} = \frac{\sigma A_{spec}}{\sigma A_{spec} + P_d v} \tag{6}$$

Figures 4–6 were generated by means of the following assumptions. The volume fraction φ_{dp} of the dispersed phase is 0.5, its density ρ_{dp} is 0.9 g/cm^3, the surfactant is sodium dodecylsulfate with a molecular weight $M_S = 288.4$ g/mol, a surface coberage $a_s = 0.50$ nm^2 per molecule, and a critical micelle concentration cmc $= 10^{-2}$ M, the volume of a single particle is v and the pressure inside is $P_d = 10^5$ N/m^2, the interfacial tension between dispersed phase and continuous

fluid phase is $\sigma = 10^{-2}$ N/m, and the size of a molecule of the dispersed phase is $D_{dp} = 0.7$ nm. Note that the terms *particle* and *droplet* are used interchangeably, to describe the dispersed phase without taking into account at the moment a particular state of matter of this phase. σA_{spec} corresponds to the amount of work required to expand the interfacial area or surface area. The data depicted in Figures 3–6 clearly reveal the colloidal nature of heterophase polymerization systems. In particular, model dispersions with an average particle size of 50 nm and 50 μm consist of 7.643×10^{21} m_d^{-3} and 7.643×10^{12} m_d^{-3} particles, have specific surfaces of 1.2×10^8 m^2/m_d^{-3} and 1.2×10^5 m^2/m_d^{-3}, an average distance between particle surfaces of 50.8 and 50,800 nm, an amount of 8.167% and 8.4×10^{-3}% of surface molecules, need 26.15% and 0.665% of sodium dodecylsulfate to cover the interface completely, and the surface free energy contributes with 92.3 and 1.18% to the overall free energy, respectively. Just for comparison, a soccer field is about 10^4 m^2 large and a ball for that game has a fraction of 8.75×10^{-7}% surface molecules, provided it consists of bulk rubber. The high surface free energy and hence the higher total free energy of a dispersion in comparison with a homogeneous system is the reason that permanently acting forces reduce the total free energy, ie they lower the interfacial area by coalescence or coagulation processes. Thus, working with heterophase polymerization techniques also means facing the problem of colloidal stability.

From a technical point of view there are three main advantages compared with homogeneous systems because of the compartmentalization. First, the viscosity of polymer dispersions is independent of the degree of polymerization and can be kept low up to high solids content. Second, the heat of polymerization caused by the enthalpy of the chain growth reaction, which for common monomers is between −50 and −100 kJ/mol is removed easily in tiny portions coming from the individual particles through the continuous phase. Third, the particle size in the micrometer and submicrometer range allows morphological variations on length scales, which are accessible with difficulty by means of other procedures.

Another important relation of these rather general considerations is with respect to the initiator concentration (C_I), which for radical polymerizations is typically in the order of 10^{-3} M. Interesting quantities are the (formal) number of initiator molecules per particle (n_I) and the number of radicals in the steady state ($n_{R,equ}$) per particle calculated according to equation 7 assuming a termination rate constant k_t of 10^8 L/(mol · s) and an initiator decomposition rate constant $2fk_d$ of 8.5×10^{-5} s^{-1}.

$$n_{R,equ} = \frac{1}{N}\left(\frac{2fk_dC_I}{k_t}\right)^{1/2} \tag{7}$$

Curves for n_I and $n_{R,equ}$ are plotted in Figure 7 for two initiator concentrations $C_I = 10^{-3}$ M (curves a_1, b_1) and $C_I = 1$ M (curves a_2, b_2). The horizontal gray line meets the curves at values for n_I and $n_{R,equ}$ equal to 1. The corresponding particle or droplet sizes represent limiting values above which enough initiator molecules are present and radicals are generated to have one initiator molecule per particle and to start polymerization in each compartment, respectively. Note that for both initiator concentrations, even for the unrealistically high value of

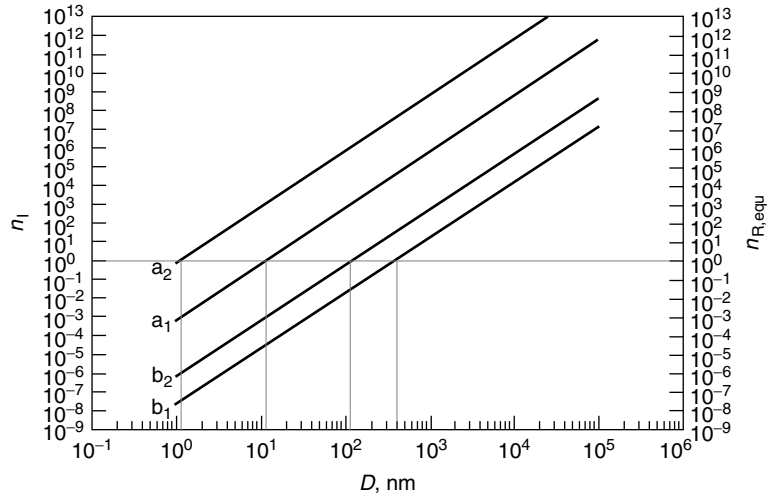

Fig. 7. Average number of initiator molecules per particle (a_1, a_2, left axis) and steady-state radical concentration per particle (b_1, b_2, right axis) in dependence on the average particle size for the model dispersion.

$C_I = 1\ M$, the necessary particle sizes to contain at least one growing radical per particle are above 100 nm. Even if this is a formal and crude appraisal, it leads to interesting consequences with respect to polymerizations in preformed monomer drops.

The various heterophase polymerization techniques mentioned in Table 2 can be distinguished with respect to the average particle sizes at the end of the polymerization. Figure 8 compares these values with characteristic length scales of other colloidal systems and the wavelength of electromagnetic radiations, which are frequently used to investigate polymer dispersions. This diagram clarifies that heterophase polymerization techniques cover the whole size range of colloidal systems. The larger the size of the final latex, the broader is the size range the particles pass through during their genesis and consequently, the larger is the changes in colloidal properties and effects influencing particle morphology. For instance, microemulsion polymerization, where the final particle size is clearly below 100 nm and in many cases even below 50 nm, the particles change their size only few tens of nanometers during the process. In contrast, during precipitation polymerization the average particle size changes over several orders of magnitude, say from less than 50 nm to more than 500 μm in some cases. Second, joint consideration of Figures 5 and 8 reveals that the amount of stabilizer necessary for a particular type of heterophase polymerization strongly depends on the average particle size. This is important with respect to end use properties of the polymeric product because stabilizers are auxiliary materials that may influence the desired polymer properties badly. Microemulsion polymerizations require amounts of stabilizers in the order of the monomer mass, whereas suspension polymerization at the other end of the size scale manage with stabilizer concentrations less than 0.1% relative to monomer mass.

The interrelation between polymer and colloid science in the case of heterophase polymerizations is nicely expressed by the following consideration.

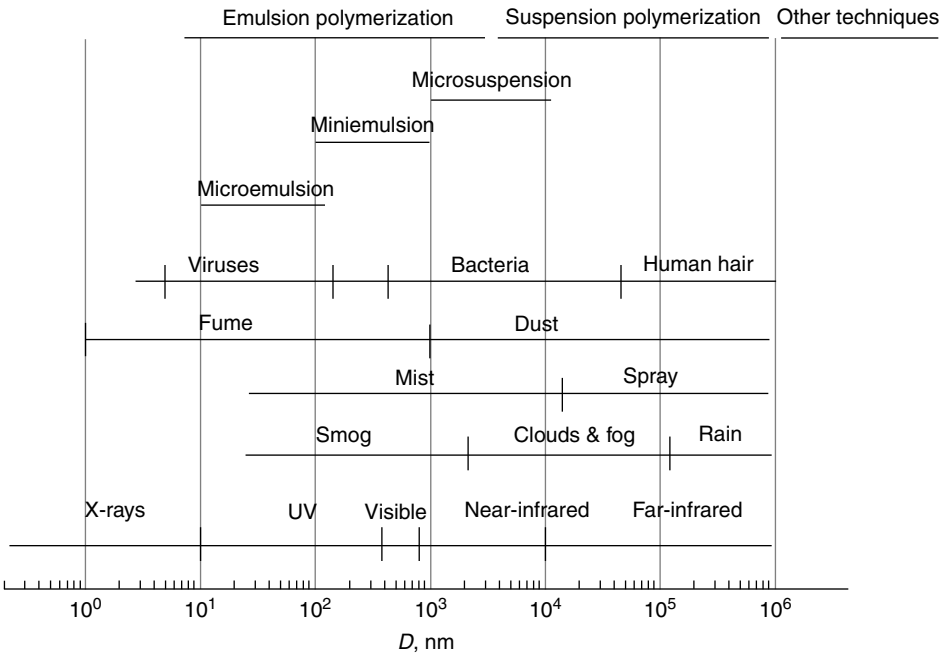

Fig. 8. Characterization of colloidal systems by characteristic length scales.

Heterophase polymerizations may be considered as compartmentalized homogeneous polymerizations, with a lot of interactions between the compartments (particles, drops) on the one hand and between compartments and the continuous phase on the other. In almost all cases, a polymer particle consists of more than one macromolecule. For instance, if the polystyrene of the example given in Figure 3 has a molecular weight of 6.022×10^5 g/mol (average degree of polymerization P_n of about 6000) the single bulk particle consists of 10^{18} macromolecules, whereas each of the colloidal particles is composed of 69 polymer molecules. Each polymer chain can be regarded as a permanent record of all the reactions by which it was produced. For a free-radical polymerization mechanism, which is by far the most important one for heterophase polymerizations, the duration of these reactions (τ_{pol}) can be estimated by means of equation 8 to be in the order of seconds or even less for the above polystyrene example, depending on the polymerization temperature (monomer concentration $C_{\mathrm{M}} \approx 6\,M$, propagation rate constant $k_{\mathrm{p}} =$ 237, 341, 480 L/(mol · s) for 50, 60, 70°C, respectively (75).

$$\tau_{\mathrm{pol}} = \frac{P_n}{k_{\mathrm{p}} C_{\mathrm{M}}} = \frac{2}{(2 f k_{\mathrm{d}} C_{\mathrm{I}} k_{\mathrm{t,d}})^{1/2}} \tag{8}$$

In contrast to single polymer molecules, the particles grow during the entire reaction and hence, they can be regarded as a permanent record of the overall polymerization reaction. The duration of heterophase polymerizations is typically in the order of hours. In this sense, recording molecular weight and particle size data should allow an almost perfect reaction control on different timescales.

Another peculiarity of heterophase polymerization is that almost all kinds of hydrophilic and hydrophobic monomers, stabilizers, initiators, chain-transfer agents, and other auxiliary materials can be applied together in one polymerization system. Of course, this can lead to a pretty muddled scenario where a variety of interactions and reactions between both phases have to be taken into account. Furthermore, a clear demarcation between the different kinds of heterophase polymerizations is often not possible. The particle size is not suited to classify heterophase polymerizations unambiguously, because between all techniques regions exist that more or less overlap, and the particle size at the end of the polymerization depends on particular conditions. Also the names of heterophase polymerizations appear somewhat illogical rather than rational. For example, according to the general definitions in Table 1, the names *emulsion* and *suspension* polymerization describe the situations at the beginning and at the end of the process, respectively, whereas the name dispersion polymerization is based on the generic term in colloid science. However, this situation points out the importance of whether a liquid (emulsion) or a solid (dispersion) forms the dispersed phase, which may change in the course of the polymerization. The main difference between a liquid and a solid interface with respect to the surface tension is given. In either case, the surface tension is a region where the stress differs from that in the bulk of the droplets. In case of a liquid, the surface tension is the same at all points and for all directions in the surface. It is a force that stretches the interface isotropically in all directions. But the surface tension of a solid surface need not be isotropic and hence, its value can be different for different directions in the surface. The impacts of this fundamental difference between an emulsion and a suspension on the mechanism of heterophase polymerizations are poorly understood.

Despite all the problems mentioned, an attempt at demarcation is made in Table 4 by means of the absolutely necessary prerequisites to carry out a particular type of heterophase polymerization. The minimum requirements for carrying out emulsion polymerization are a certain concentration of monomer dissolved in the continuous phase and an initiator. The concentration of the monomer must be high enough to ensure that both the chain length and the concentration of oligomers or polymers formed during the initial period in the continuous phase are high enough to form polymer particles. The same minimum requirements are

Table 4. Absolutely Necessary Prerequisites for Various Kinds of Heterophase Polymerizations in Liquid Dispersion Media

Polymerization	Stabilizer	Free or dispersed monomer phase	Solubility of initiator
Bulk	No	Yes	Monomer phase
Precipitation	No	No	Either phase
Dispersion	No	No	Either phase
Suspension	Yes	Yes	Monomer phase
Microsuspension	Yes	Yes	Monomer phase
Emulsion	No	No	Either phase
Miniemulsion	Yes	Yes	Either phase
Microemulsion	Yes	Yes	Either phase

necessary for bulk, precipitation, and dispersion polymerizations. Note that in a bulk polymerization the monomer also forms the continuous phase for its own insoluble polymer. With this it is possible to make a clear demarcation between suspension, microsuspension, miniemulsion, and microemulsion polymerizations, where the presence of a free, dispersed monomer phase (monomer droplets) is a prerequisite by definition. Another criterion to distinguish between bulk, suspension, and microsuspension polymerization and the different techniques is the initiator type: whereas the former techniques need an initiator that is soluble in the monomer phase, the initiator type plays practically no role for the other polymerization techniques listed in Table 4.

Kinetics of Heterophase Polymerizations

In general, all reactions according to the particular polymerization mechanism can take place in either phase of a two-phase system. For free-radical polymerization this means initiation, propagation, termination, and chain transfer can take place in both the continuous and the dispersed phase. The kinetics inside the dispersed phase is of special interest, as the goal of heterophase polymerization is to take advantage of the compartmentalized reaction system, which is only possible if the major part of the monomer conversion takes place inside the particles. If this condition is fulfilled, the overall polymerization rate (r_P) can be expressed by equation 9. The product $k_p C_M P$ is the expression for a homogeneous reaction system, where k_p, C_M, and P are the polymerization rate constant, the monomer concentration, and the radical concentration, respectively. The further equality on the right-hand side describes the overall rate of a compartmentalized polymerization, where $C_{M,p}$ is the monomer concentration inside the compartments and the radical concentration is expressed by means of the average number of radicals per particle ($\bar{n}$), the total number of particles (N), and Avogadro's number (N_A).

$$r_P = k_P C_M P = k_p C_{M,p} \frac{\bar{n}\, N}{N_A} \tag{9}$$

All of the four unknowns in equation 9 (k_p, $C_{M,p}$, $\bar{n}$, and N) can be determined experimentally. Values for k_p are nowadays also determined by pulse polymerization techniques in combination with size-exclusion chromatography under conditions of heterophase polymerizations. Briefly, high radiation pulses generate radicals, where a few of them terminate but most of them will start to propagate. After a distinct time interval a second pulse generates again a lot of small radicals, which terminate almost all of the growing radicals. If termination between two pulses is neglected, the propagation rate constant can now be estimated by $k_p = \mathrm{DP}/(C_M \Delta t)$. DP is the degree of polymerization determined by size-exclusion chromatography, Δt is the time between two pulses, and C_M is the monomer concentration, which in case of neat droplets is $C_M = 1/v_{mon}$ where v_{mon} is the molar volume of the monomer. N is calculated via the relation

$$N = \frac{6\mathrm{FG}}{\pi \left(100 - \mathrm{FG}\right) \rho_2 D^3}$$

where ρ_2 is the particle density. The calculation of N requires the determination of both solids content and average particle size. In contrast, the determination of $C_{M,p}$ is much more lavish because it requires the determination of the amount of unreacted monomer that can be present either in the form of neat monomer droplets or inside monomer-swollen polymer particles. For a monomer, which is liquid at room temperature, $C_{M,p}$ can be determined in the following way. A certain amount of latex with known solids content is centrifuged just with a speed that is high enough to separate the monomer, which is present in neat droplets. Then, to the latex, which still contains monomer-swollen particles, initiator is added and a polymerization is started. After determination of the solids content of the treated latex, the amount of monomer in the swollen particles can be calculated from the increase in solids content. Finally, $\bar{n}$ can be calculated from equation 9 and the heterophase polymerization is completely characterized by experimental means. From the viewpoint of the mechanism of heterophase polymerization both $\bar{n}$ and N have inspired researchers since the early days of heterophase polymerization research. N is strongly connected with the particle nucleation mechanism and $\bar{n}$ with the distribution of active centers among the phases and hence the overall kinetics.

The Formation of Polymer Particles

The common feature among heterophase polymerization techniques with respect to particle formation is the formation of a new phase, ie the polymeric phase. Besides phase formation the terms *generation* or *nucleation* of particles can be used synonymously to describe the process, which finally leads to the manifestation of the polymer as new phase. This phase formation may, in some cases where the reaction system is at the beginning a homogenous single phase, coincide with the development of the heterogeneous nature of the polymerizing system as it is, according to Table 4, the case for dispersion, precipitation, and heterogeneous bulk and emulsion polymerizations. In such cases the polymerization reaction starts in the homogeneous phase and the generation of the polymer phase exhibits all characteristics of a first-order phase transformation, ie thermodynamic functions and parameters such as molar volume and free energy show abrupt changes at the phase transition point. In contrast, if the reaction system is at the beginning heterogeneous, the polymerization reaction can start in either phase. If the polymerization happens predominantly inside the monomer droplets the kind of phase transformation depends on the Flory–Huggins interaction parameter ($\chi_{m,p}$).

The criteria for solubility or insolubility within the framework of the Flory–Huggins theory are for high molecular weight polymers over the whole composition range $\chi_{m,p} \leq 0.5$ and $\chi_{m,p} \geq 0.5$, respectively. The larger the $\chi_{m,p}$, above 0.5, the *more insoluble* is the polymer in its own monomer or the less favored is the interaction between monomer and polymer. For example, for the systems styrene/polystyrene, vinyl chloride/poly(vinyl chloride), and acrylonitrile/polyacrylonitrile, $\chi_{m,p}$ values are $\sim$0.5, > 0.9, and >1, respectively. These values suggest that polystyrene is completely soluble in styrene, and poly(vinyl chloride) is only swollen by its monomer, but polyacrylonitrile is insoluble in acrylonitrile. Hence, the consequences for formation of the polymer phase during polymerization

inside monomer droplets are as follows. For styrene/polystyrene, the transition from monomer droplets to polymer particles proceeds very smoothly via a polymer in monomer solution. The polymer concentration of this solution increases correspondingly to the overall conversion as long as at complete conversion solid polystyrene particles remain. Vinyl chloride is not a solvent for its polymer and hence, phase separation inside the monomer phase takes place at low conversion. But as the polymer is swollen by its monomer, the transition into the glassy (solid) state starts only at a conversion above 70%. The situation is still a little more different for acrylonitrile, which swells its polymer only to a negligible extent, as in that case $\chi_{m,p} \geq 1$ (76). Consequently, a sharp phase transition (first-order) takes place at very low conversion but in contrast to the other two systems the polymerization proceeds in an outer layer by precipitation of growing polymer chains onto existing polymer particles. Another consequence of the absence of an interaction between monomer and polymer is the formation of nonspherical particles, as the glass-transition temperature of polyacrylonitrile ($T_g \sim 100^\circ$C) is higher than polymerization temperature and hence the polymer inside the particles is almost immobile, and the spherical equilibrium shape, which is obtained if the particle is able to minimize its interfacial free energy, cannot be attained. Note that for a given interfacial tension the interfacial free energy is determined by the interfacial area, and the area per unit volume is the lowest for a sphere compared with any other body (eg the surface area per unit volume is 4.83 for sphere, 5.56 for a right cylinder, 6 for a cube or cuboid, and 6.83 for a cone). In summary, if formation of the polymer phase takes place inside the monomer droplets (a process that is sometimes referred to as droplet nucleation) the phase transformation itself is rather unspectacular. The transition from a solution to a solid is, if it ever will takes place during the polymerization under the particular conditions, finished only at high conversion, when the T_g of the polymer/monomer mixture in the particles is above the polymerization temperature. Thus, the more interesting case is the formation of polymer particles in the continuous phase, such as during dispersion and emulsion polymerization. Under these conditions, a clear first-order phase transition is observed because the system changes in a very short period of time from homogeneous to heterogeneous.

Nucleation in emulsion polymerization has been a matter of controversial discussion because for more than five decades no direct experimental data on the nucleation process were available. Discussions were mainly centered on the question of the role of emulsifying agents, in particular on the role of micelles as precursors of polymer particles. "Micellar nucleation theory," as it was expressed by Smith–Ewart (77) on the baseis of ideas developed by William Harkins (78–80), states:

> When a free radical from the surrounding water phase enters a micelle, it initiates polymerization of the monomer in the micelle. When this polymerization starts, monomer from the surrounding medium diffuses into the polymerizing region until shortly this region is no longer identified as a micelle, but is now considered a growing polymer particle. . . .

In other words, a polymer particle is formed ad hoc when a radical enters a micelle. That this is an oversimplification is revealed in Harkin's original papers.

He considered three possible loci for "the initiation of polymer particle nuclei" (79), based on his studies during 1942–1943 in connection with the Rubber Reserve Company (Synthetic Rubber Program of the United States Government) (*1*) the soap micelles, if present, (*2*) the aqueous phase, excluding soap micelles and polymer–monomer particles, and (*3*) the monomer droplets. He considered the monomer droplets as

> . . . relatively unimportant in initiating new polymer particles, since thus far no evidence has been obtained to show that a monomer droplet can do more than change into a polymer particle of smaller size.

With regard to the micelles as locus of polymer particle initiation, Harkins described very interesting results of X-ray scattering investigations (78,80,81). It was found that styrene at saturation concentration increases the diameter of fatty acid micelles by 1.2 nm (styrene is present only as dissolved in water and solubilized in micelles but not as droplets) but upon polymerization initiated with peroxodisulfate the size of the micelles decreased to its initial value. This process could be repeated several times by consecutive swelling and polymerization until the surface of the polymer particles was grown so large that the soap concentration decreased as a result of the adsorption on the particles below the cmc. These results led to the important conclusion that a growing polystyrene chain is incompatible with the alkyl chains in the interior of micelles and hence, polymer chains grow out of micelles. The incompatibility between polystyrene and alkyl chains was repeatedly proved more than 50 years later by attempts to polymerize the monomer inside double layers of dioctadecyldimethyl ammonium bromide vesicles. Transmission electron microscopy pictures reveal that phase separation takes place during the polymerization in a way that the polystyrene molecules gather at a particular place, whereas the monomer was uniformly distributed over the whole bilayer (82). A remaining question of importance is at which chain length of the growing polymer molecule the phase separation occurs. If the further fate of escaped radicals is considered, two other mechanisms of particle formation are possible. besides micellar nucleation. The first of these nonmicellar theories of particle formation is known as homogeneous nucleation and its development and quantification owes entirely to Robert Fitch (83–86). This theory, originally developed for more water-soluble monomers such as methyl methacrylate, considers initiation in the aqueous phase, capture of growing radicals by existing particles, and precipitation of a single chain if it becomes insoluble in water as individual steps. The second possibility is called aggregative nucleation, according to which nucleation occurs when a critical supersaturation of growing or dead oligomers in the continuous phase is reached and this solution becomes unstable and separates into a polymer phase and a less concentrated continuous phase (87,88). In contrast to so-called homogeneous nucleation the aggregative nucleation is a multichain process, which is governed by thermodynamic rules known from classical nucleation theory (89) or spinodal decomposition (90). It is interesting to note that Harkins came to a conclusion, which completely agrees with aggregative nucleation mechanism when he concluded (81), that in the absence of monomer droplets, "It is not improbable that several polymer molecules may meet each other and form a small aggregate as the source of a single particle." Experimental techniques have

been developed that allow a direct observation of the nucleation step in emulsion polymerization (88,91–93), The results obtained so far clearly support the aggregative nucleation mechanism. Moreover, the results confirm that nucleation in heterophase polymerization can be considered and treated within the framework of general nucleation theories as bubble formation, or condensation, or crystallization processes. According to these theories nucleation requires supersaturation of the nucleating species, which are oligomers born in the continuous phase. In this sense another nucleation criterion for heterophase polymerizations is to bring the system, which is in this situation a solution of oligomers in the continuous phase, into a thermodynamically unstable intermediate state.

Role of Emulsifiers. There is no doubt that all kinds of surface-active compounds have a strong influence on particle formation as they influence the interfacial tension of the nuclei, which is an essential parameter. On the other hand, emulsion polymerization can be carried out at emulsifier concentrations below the cmc or even in the absence of emulsifiers. In the latter case one has to take care that polymer end groups arising from primary radicals or water-soluble comonomers contribute to stability. However, as a general rule for all kinds of heterophase polymerizations, for a given recipe the particle number depends strongly on the stabilizer concentration as is shown in Figure 9. Similar curves were also obtained for styrene, with ammonium peroxodisulfate as initiator as well as for different acrylic and methacrylic acid ester monomers (94). The most striking feature of the curve in Figure 9 is the S shape, which suggests regions of different stabilizer efficiency with respect to particle concentration if it would be expressed as d log$N$/d logC_s (cf Fig. 10). Another measure for the efficiency of a surfactant is its surface tension–concentration plot. A comparison of both plots (as is also shown

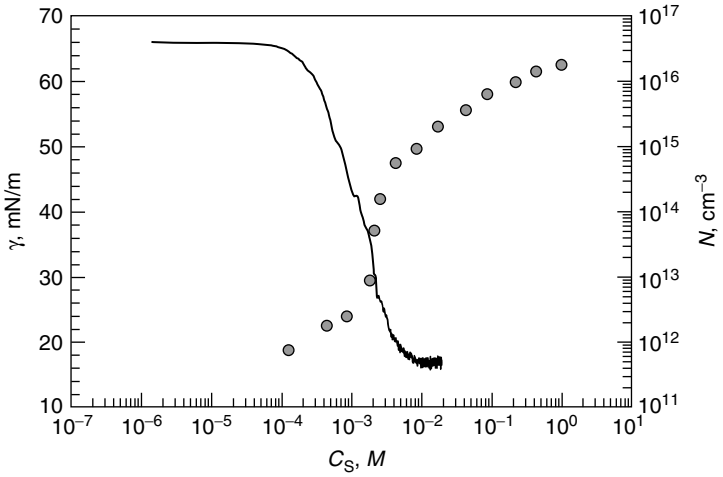

Fig. 9. Particle concentration in dependence on SDS concentration for batch emulsion polymerization of styrene (filled circles) and interfacial tension concentration plot for SDS (black line, further details see text). (Recipe: 40 g of water, 10 g of styrene, 0.32 g of potassium peroxodisulfate, variable amounts of SDS, temperature 80°C, particle concentration calculated from solids content and particle size at final conversion, particle size: intensity average from dynamic light scattering.)

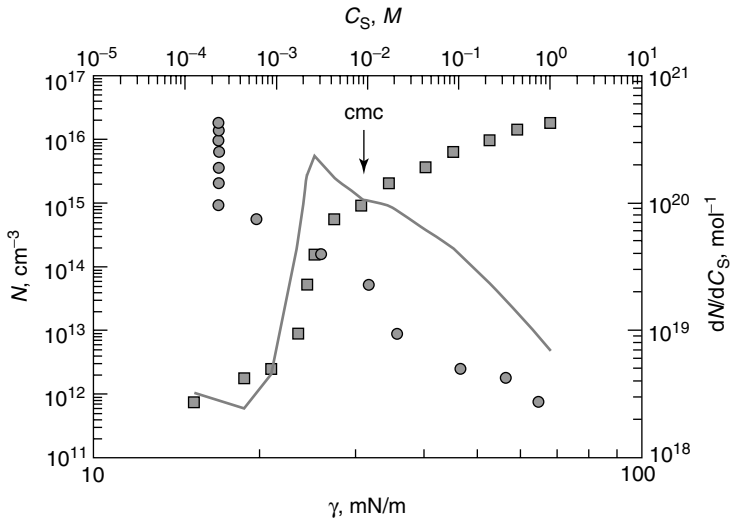

Fig. 10. Plots of the final particle number of styrene emulsion polymerization versus interfacial tension of a SDS solution with the same concentration (filled circles), final particle number versus SDS concentration (filled squares), and the efficiency of the surfactant with regard to the final particle number in a styrene emulsion polymerization (gray line) (recipe: cf. caption of Fig. 9).

in Figure 9) reveals that the regions with the steepest change in both curves coincide. The surface tension–concentration plot was measured with a bubble pressure tensiometer using the bubble pressure difference method as described in Reference 95. This method is especially designed not to measure exact surface tension values but rather changes under various conditions even inside stirred reactors at elevated temperatures. To draw conclusions regarding the role of emulsifiers in heterophase polymerizations the surface tension measurements should be conducted under conditions that correspond as closely as possible to those during the polymerizations. This is of special importance because it is known that the cmc of sodium dodecylsulfate increases with temperature but decreases with increasing ionic strength (96). The surface tension–concentration plot depicted in Figure 9 was obtained at polymerization temperature (80°C) in presence of potassium sulfate at a concentration corresponding to the potassium peroxodisulfate concentration employed for polymerization and the water was saturated with toluene to mimic the influence of styrene. Experimental conditions have been controlled so that the curves in Figure 9 can be directly compared. The steep decrease in γ and the steep increase in N originate from the effect of increasing surfactant adsorption at a given surface area. In the case of γ measurement this is the nitrogen bubble interface to water and during emulsion polymerization it is the particle water interface. The strong dependence between γ and N at surfactant concentrations below the cmc shows in the logN versus logγ plot in Figure 10. Furthermore, this plot proves that the S shape of the logN–logC_S curve is a consequence of surfactant adsorption. If this is true, then the good correlation between N and γ suggests that the interface area of the nuclei formed during the particle nucleation period does not depend on the surfactant concentration but is rather

constant for a given rate of initiation. Consequently, the surfactant concentration and the adsorption behavior of the surfactant determines the particle surface area, which can be stabilized and hence the number of final latex particles. This argument leads to the conclusion that it could happen that the number or the total surface area of nuclei formed at the end of the particle nucleation period is at low surfactant concentration larger than the amount that can be stabilized by the particular surfactant concentration. Consequently, the number of particles decreases by coagulation or coalescence processes until the particle area matches the area of surfactant necessary for stabilization, which is $a_s C_{S,C}$, where a_s is the area covered by 1 mol of surfactant and $C_{S,C}$ is the critical surfactant concentration necessary for stabilization of all nuclei formed during the nucleation period. Increasing the surfactant concentrations leads to a point where the surface area of the nuclei matches $a_s C_{S,C}$ and the number of particles remains constant after nucleation. The higher the surfactant concentration, the longer is the duration of the nucleation period. On the other hand, increasing surfactant concentration means that the period of time between the start of the polymerization and the appearance of the first particles (ie the duration of the prenucleation period) decreases, as it was concluded from model calculations (88). All these effects have also been observed experimentally (88,91,97). The data summarized in Figures 9 and 10 make clear that the cmc is no special point with regard to the final particle concentration as it falls in a region where the efficiency ($\mathrm{d}\log N/\mathrm{d}\log C_s$) decreases in dependence on the sodium dodecylsulfate concentration. The decreasing efficiency with increasing surfactant concentration can be explained with the increasing duration of the nucleation period. The longer the nucleation period, the larger the earlier-formed particles can grow and the more they compete with the newly formed ones for the surfactant. This interpretation of the role of emulsifier in emulsion polymerization agrees with experimental results, which were obtained in a series of very well designed experiments by Dunn and Al-Shahib (98–100). They used a series of sodium alkyl sulfate surfactants from C_8 to C_{18} at equal concentrations of 60 mM in styrene emulsion polymerization and were able to show that the number of micelles initially present does not govern the final particle number. A reexamination of these results as it was done in Reference 101 revealed that the number of particles correlates with the cmc (the lower the cmc, the higher is the number) and the adsorption energies of the surfactants (the higher the adsorption energy, the higher is the number). These results clearly support the idea that the stabilizing power or the adsorption strength of the surfactants, which are the stronger the larger the hydrophobic chains, determines the final particle number. This is the same effect as expressed in Figure 10 by the correlation between the surface tension and the particle number for a particular surfactant.

For heterophase polymerizations, which start in the continuous phase, such as emulsion polymerization (in the absence of monomer droplets) or dispersion polymerization (cf Table 4), a question of importance might be at which degree of conversion or, more general, at which solids content the first particles appear. This question can be answered by sensitive in-line or on-line characterization techniques such as conductivity and turbidity measurements or dynamic light scattering as described for emulsion polymerization in References 91 and 93 or dispersion polymerization in Reference 102. These results show that nucleation takes place after a distinct period of time where polymerization proceeds under

homogeneous conditions (the prenucleation period) at very low solids content. For instance, the duration of the prenucleation period for an emulsifier-free styrene emulsion polymerization started with potassium peroxodisulfate (2.5 mM) at 60°C was found to be 431 s. Within 1 s a huge number of particles is formed (1.76×10^{13} cm^{-3}), with an average diameter of 13 nm (92). From these numbers it can be concluded that each particle consists of about 7000 styrene units at maximum, and the minimum amount of polystyrene formed up to this moment is 2.13×10^{-5} g/cm^3. For dispersion polymerization of methyl methacrylate in methanol (5 wt%) at 55°C with poly(vinylpyrrolidone) as stabilizer and 2,2′-azobisisobutyronitrile as initiator, the first particles were detected with dynamic light scattering 3–4 min after starting the reaction (102). Both sets of experiments reveal another common feature, which is typical for phase transformation or nucleation processes (103). The experimental data are afflicted with large scatter and to get trustworthy results requires enormous experimental efforts and a large number of repeats. The reason for this is of general nature, ie, any first-order phase transition is characterized by the necessity to surmount an energy barrier via fluctuations. A free energy of activation for such processes exists, which strongly depends on all experimental conditions such as temperature, pressure, and composition. Even minor changes in the experimental conditions can cause huge effects, because the rate of the phase transition depends exponentially on the activation free energy. This strong influence on heterophase polymerizations means, for example, that the kind of reactor material or even the replacement of a stirrer can change reaction rate and product properties. In a comprehensive study it was shown that emulsion polymerization of methyl methacrylate is strongly influenced by the kind of reactor material (stainless steel, Teflon, glass) especially at low emulsifier concentrations (104).

In many technical emulsion polymerizations the problems connected with particle nucleation are avoided by using so-called seed latexes. In this case polymerization is started heterogeneously in presence of preformed polymer particles (seed particles). Polymerization recipe and procedure are adjusted (sometimes) carefully in such a way that a high radical absorption rate (cf eq. 12) is realized to capture all radicals from the continuous (aqueous) phase by seed particles in order to avoid both supersaturation of oligomers in the continuous phase and subsequently nucleation of new particles (105). Although the particular mechanism may differ, the common feature of particle nucleation in heterophase polymerizations is the formation of the polymeric phase. Furthermore, the final number of polymeric particles depends on the stabilization, which is employed in the particular heterophase polymerization process. Again, the larger the average particle size at a given solids content, the lower is the interfacial area, which has to be stabilized and hence, the lower the amount of stabilizing groups needed. In aqueous emulsion polymerization the micellar nucleation mechanism is very popular, although clear experimental evidence has not been found at any time. There might be mainly two reasons for this popularity. First, it is the simplicity of this approach together with the similarity to seed polymerization techniques where polymerization starts inside the seed particles by entry of radicals from the continuous phase. Although seed particles differ from micelles in many respects (dynamic behavior, size, and composition) a clear demarcation is complicated as several common features exist, such as swelling with monomer and ability of radical absorption

from the continuous phase. The situation is even more complicated in the case of micelles made of polymeric surfactant, where the gap to a seed particle is still narrower because dynamic behavior and composition can be almost identical to seed particles (106,107). Second, the lack of any direct experimental data on the nucleation step during aqueous heterophase polymerization may have hindered the acceptance of nucleation models based on general nucleation theories, although for dispersion polymerization in organic media the classical nucleation theory has been considered as a possible mechanism at least since the mid-1970s (108).

Compartmentalized Polymerization Kinetics

Average Number of Radicals per Particle. The centerpiece of equation 9 and of all heterophase polymerization kinetics is a formula to calculate the concentration of growing radicals inside each compartment. The situation sketched in Figure 11 can be used to derive a suitable general expression. If the number of radicals per particles is denoted with n the particles can be classified as N_n, which means the number of particles containing n radicals. The formation of radicals by initiator decomposition and subsequent initiation of the chain growth is allowed to take place in either phase ($r_{\mathrm{i,w}}$ and $r_{\mathrm{i,d}}$ is rate of initiation in continuous and dispersed phase, respectively). Furthermore, the number of radicals in the dispersed phase increases by absorption or entry (r_{abs} denotes the rate) and decreases by exit or desorption and termination. In these equations $k_{\mathrm{d,w}}$ and $k_{\mathrm{d,d}}$ are the rate constants of initiator decomposition in the continuous and in the dispersed phases, respectively, and f is the efficiency factor, $k_{\mathrm{abs,i}}$ is the rate constant of primary radical absorption by the droplets, $k_{\mathrm{abs}}^{\mathrm{j},e}$ is the absorption rate constant of propagating radicals ($P_{j,e,\mathrm{w}}$) in dependence on chain length (j) and kind of end group (e), $k_{\mathrm{t,d}}$ is the termination rate constant in the dispersed phase, and k_{des} is the desorption rate constant. If in steady-state the rate of formation of N_n particles

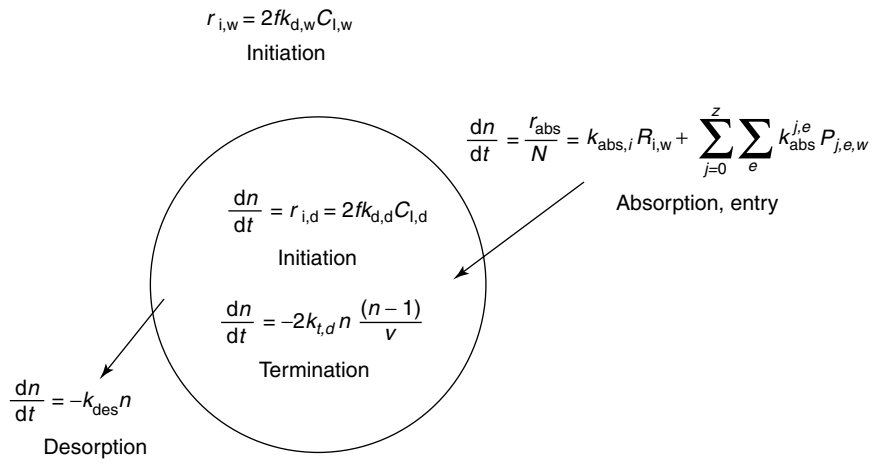

Fig. 11. Illustration of most important reactions in heterophase polymerization systems.

equals the rate of their disappearance the recursion formula given by equation 10 is obtained.

$$(n+2)(n+1)N_{n+2}+\delta(n+1)N_{n+1}+\alpha N_{n-1}+\beta_{\mathrm{d}}N_{n-2}=\ \mathrm{N}_n\left[n(n-1)+\delta n+\alpha\right]+\beta_{\mathrm{d}}N_n \tag{10}$$

A balance of the radicals in the continuous phase leads to equation 11, where $k_{\mathrm{t,w}}^{\mathrm{j},e}$ is the termination rate constant of propagating radicals ($P_{j,e,\mathrm{w}}$) in dependence on chain length (j) and kind of end group (e), termination rate constant of primary radicals and $R_{\mathrm{i,w}}$ is the concentration of primary radicals.

$$r_{\mathrm{abs}}=r_{\mathrm{i,w}}+k_{\mathrm{des}}\sum_{n=1}^{\infty}nN-2\sum_{j=0}^{z}\sum_{e}k_{\mathrm{t,w}}^{\mathrm{j},e}P_{\mathrm{j},e,\mathrm{w}}^{2}-2k_{\mathrm{t,w}}R_{\mathrm{i,w}}^{2} \tag{11}$$

Rearrangement, and defining, the coefficient by combination of rate constants into equations 12, lead to equation 13, which together with equation 10 can be used to calculate $\bar{n}$. The average number of radicals per particles is defined by equation 14.

$$\delta=\frac{k_{\mathrm{des}}\upsilon N_{\mathrm{A}}}{k_{\mathrm{t,d}}};\ \alpha=\frac{r_{\mathrm{abs}}\upsilon N_{\mathrm{A}}^{2}}{Nk_{\mathrm{t,d}}};\ \beta_{\mathrm{d}}=\frac{r_{\mathrm{i,d}}\upsilon N_{\mathrm{A}}^{2}}{k_{\mathrm{t,d}}N};\ \beta_{\mathrm{d}}=\frac{r_{\mathrm{i,d}}\upsilon N_{\mathrm{A}}^{2}}{k_{\mathrm{t,d}}N}$$

$$r_{\mathrm{abs}}=k_{\mathrm{abs,i}}R_{\mathrm{i,w}}+\sum_{j=0}^{z}\sum_{e}k_{\mathrm{abs}}^{\mathrm{j,e}}P_{\mathrm{j,e,w}}\cong k_{\mathrm{abs}}C_{\mathrm{rad,w}}\ Y=\frac{2Nk_{\mathrm{t,d}}k_{\mathrm{t,w}}}{k_{\mathrm{abs}}^{2}\upsilon N_{\mathrm{A}}^{2}} \tag{12}$$

$$\alpha=\beta_{\mathrm{w}}+\delta\ \bar{n}\ -Y\alpha^{2} \tag{13}$$

$$\bar{n}\ =\frac{\sum nN_{\mathrm{n}}}{N}\quad\text{with}\quad N=\sum N_{\mathrm{n}} \tag{14}$$

Various researches have contributed over decades to our present knowledge. Wendell Smith and Roswell Ewart started in 1948 (77) by writing down their famous recursion formula for emulsion polymerization, which takes into account absorption, desorption, and termination of radicals, where initiator decomposition is assumed to take place exclusively in the continuous phase. Two months after the Smith–Ewart paper appeared, anarticle—nowadays virtually forgotten—was submitted by Haward dealing with polymerization in a system of discrete particles (109). He took into account generation of either single radicals or two at once inside particles and termination. Either consideration (77,109) led to the identical recursion formula if the formation of single radicals inside the particles is considered to be equivalent to radical entry from the continuous phase. As an analytical solution of the recursion formula is impossible, approximations have to

be considered. Assuming that there is only radical entry or generation of single radicals inside particles, and termination equation 10 leads for $n = 0$, 1, and 2 to equations 15, 16, 18,

$$n = 0 \Rightarrow N_2 = \frac{\alpha}{2} N_0 \tag{15}$$

$$n = 1 \Rightarrow N_3 = \frac{\alpha}{6} (N_1 - N_0) \tag{16}$$

$$n = 2 \Rightarrow N_4 = \frac{\alpha}{12} \left[\frac{\alpha}{2} N_0 - (N_1 - N_0) \right] \tag{17}$$

Now Haward's argumentation was as follows. The higher the dispersity (ie smaller the v or larger the N), the smaller the α, and for $v \to 0$ or $N \to \infty$, this results in $N_2 = N_3 = N_4 = 0$. From equations 16 and 17, it follows that $N_1 = N_0$ and hence that $\bar{n} = \frac{1}{2}$, which is an important limiting case for small particles. This result is identical to the famous Smith–Ewart's case 2, where they argued that $\bar{n} = \frac{1}{2}$ when the particles are so small that entry of a radical into a particle N_1 results in immediate termination. Thus a particle contains either none or only one radical on average. The argumentation that $v \to 0$ or $N \to \infty$ is obviously more appropriate, as equations 10–14 suggest that $\bar{n}$ strongly depends on the degree of dispersity. However, the treatment of Smith–Ewart is more general than that of Haward as it allows radical exchange between both phases via radical absorption into the particles from the continuous phase and radical exit out of the particles into the continuous phase. This leads to an analogous form of equation 15 if radical exit, entry, and termination are considered:

$$n = 0 \Rightarrow N_1 = \frac{1}{\delta} \left(\alpha N_0 - 2N_2 \right) \text{ or } N_2 = \frac{1}{2} (\alpha N_0 - \delta N_1)$$

Following the arguments of Smith and Ewart (77), two more limiting cases with respect to $\bar{n}$ are possible. Case 1: if $\delta \gg \alpha$, it follows that $N_1 \to 0$ and $N \to N_0$, and hence $\bar{n} \ll 1$. Case 3: if radical absorption (or generation inside particles) is much larger than desorption ($\delta \ll \alpha$), it follows that $N_2 \Longrightarrow N_0$, which leads, only if the particle size is large enough, to $\bar{n} \gg \frac{1}{2}$ and hence to an approximation of bulk kinetics. In the next two decades, Stockmayer (110) and O'Toole (111) dealt with exact solutions of the recursion formula by means of modified Bessel functions. In particular, O'Toole presented explicit expressions for N_n and showed that the solution obtained by Stockmayer is physically questionable for small but finite rates of radical desorption. Although these contributions represent a crucial step in the direction of a better understanding of heterophase polymerization kinetics, they still leave important questions unanswered, especially regarding the interplay between kinetic events inside and outside the particles. John Ugelstad and his group in two benchmark papers in 1967 and 1976 have treated in particular the role of continuous phase kinetics (112,113). They introduced radical balances in the continuous phase as described by equations 11 and 13. They solved equation 13 taking the procedure described by O'Toole with Bessel functions. Employing continued fractions to describe the ratio of Bessel functions, they finally obtained

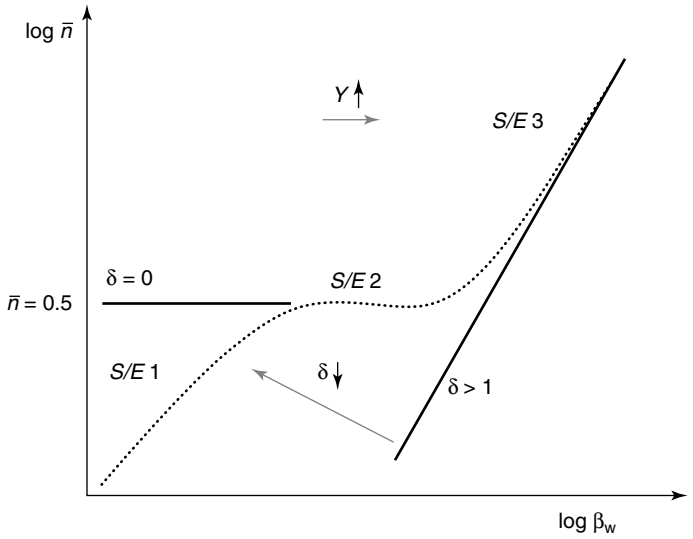

Fig. 12. Illustration of an Ugelstad plot.

a rather simple expression in form of a series:

$$\bar{n} = \frac{1}{2}\frac{2\alpha}{\delta} + \frac{2\alpha}{\delta+1} + \frac{2\alpha}{\delta+2} + \cdots$$

which converges fast for all $\alpha \geq 0$ and $\delta \geq 0$ (112). $\bar{n}$ is now computed in dependence on α for given values of δ, and finally equation 13 is solved with these values of $\bar{n}$ and appropriate values of Y to get corresponding values of β_w. The results of this procedure are the famous Ugelstad plots, where $\log \bar{n}$ is plotted versus $\log\beta_w$, with δ and Y as parameters. Such a plot is schematically shown in Figure 12. The three limiting cases of the Smith–Ewart theory can be clearly seen. The gray arrows indicate the shift of the solution behavior if one of the parameters δ or Y is changed. For instance, on the one hand decreasing δ values (which means decreasing desorption or increasing termination) lead to the appearance of a typical Smith–Ewart case 2 behavior characterized by $\bar{n} = 0.5$. On the other hand increasing Y from zero ($Y = 0$ means, according to equation 11, that no termination takes place in the continuous phase) leads to a spreading of the curves, with δ as the parameter along β_w-axis. This means that the linear relation $\log \bar{n}$ versus $\log\beta_w$, which is obtained for $\delta > 1$, is shifted to larger β_w values. Shinzu Omi has pointed out that a recursion formula, which considers only radical formation inside the particles and desorption (only β_d and δ are considered in eq. 10) could be used to describe polymerization in large monomer droplets (114). As α (ie the droplet size) increases, $\bar{n}$ converges to a straight line, which corresponds to the solution of bulk kinetics [$\bar{n} = (\beta_d)^{1/2}$].

The average number of radicals per compartment is indeed the centerpiece of heterophase polymerization kinetics. For theoretical descriptions of $\bar{n}$, detailed knowledge not only about kinetic events in either phase but also regarding exchange processes between particles and dispersion medium are required.

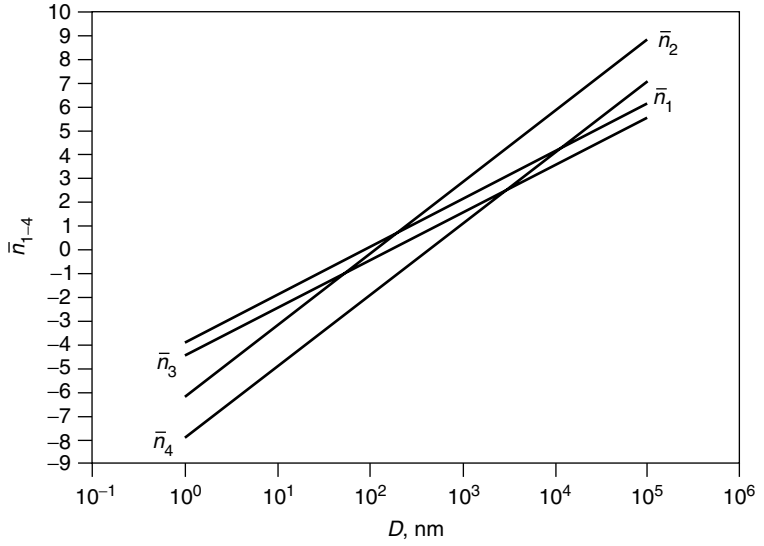

Fig. 13. Calculation of with various approximations of $\bar{n}$ the recursion formula equation 10 (cf text).

The Influence of Dispersity. For different types of heterophase polymerization and in context with dispersity as a characteristic feature, it is necessary to emphasize that $\bar{n}$ strongly depends on particle size. To describe this behavior, several approximations based on equation 10 can be found (113,114). In Figure 13, some $\bar{n}$ approximations are compared regarding their dependence on the particle size, which is given by the definitions in equations 12. The first approximation $\bar{n}_1 = (\alpha/2)^{1/2}$ is based on Stockmayer's solution for the Smith–Ewart case 3 ($\bar{n} \gg 1$). This can be directly compared with the approximation for bulk kinetics proposed by Omi (114), $\bar{n}_4 = (\beta_d)^{1/2}$, and also with the hypothetical number of radicals per particle in equilibrium ($n_{R,equ}$), as depicted in Figure 7. Another approximation derived by Ugelstad and Hansen for Smith–Ewart case 3 kinetics is $\bar{n}_3 = (\beta_w/4Y)^{1/2}$, with consideration of water phase termination ($Y \neq 0$). Finally an approximation for Smith–Ewart case 1 derived by Ugelstad and Hansen (113) is considered ($\bar{n}_2$), which however is valid for the whole range of $\bar{n}$ as long as the following relations are fulfilled: $\delta\,\bar{n} \gg \beta_w\, Y\alpha^2$ and $Y\alpha^2 \gg \alpha - \delta\bar{n}$. Equation 9 can be used to calculate $\bar{n}$ from experimental polymerization rate data provided $C_{M,p}$, k_p and N are known. To do so is really extensive and tedious work, as one has to determine solids content, particle size, and monomer concentration inside the particles in the course of the polymerization. Figure 14 shows an example of such investigations for a batch styrene emulsion polymerization in dependence on both conversion (X) and average particle size (115). The results of this procedure are influenced by some experimental problems such as the estimation of r_P by numerical differentiation of conversion–time curves, the experimental determination of $C_{M,p}$, and the proper choice of the particle size average value to calculate N. Despite all these problems the results depicted in Figure 14 lead to important conclusions. Batch emulsion polymerization of styrene, even if 2,2′-azobisisobutyronitrile is used as initiator,

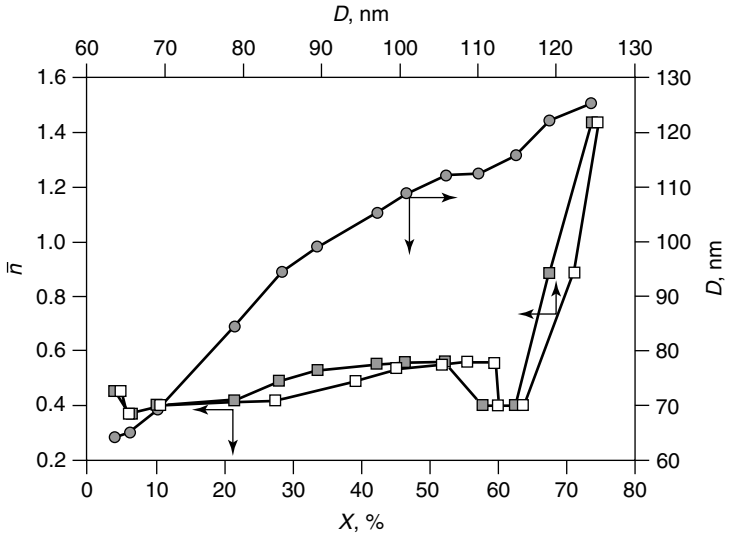

Fig. 14. Average number of radicals per particles in dependence on both conversion and particle size and particle size in dependence on conversion for a batch styrene emulsion polymerization; gray squares $\bar{n}$ versus conversion; open squares $\bar{n}$ versus particle size; gray circles' D versus conversion. (Recipe: 1000 g of water, 200 g of styrene, 4.268 g of SDS, and 1.74 g of 2,2′-azobisisobutyronitrile as initiator, temperature 60°C, for details see Ref. 115.

which is soluble in both phases [about 10% of AIBN is dissolved in water at 25°C (116)] obeys Smith–Ewart case 2 nicely as $\bar{n}$ is between 0.4 and 0.6, with a slight tendency to increase between 5 and 60% of conversion and to increase much steeply thereafter. This increase, even if only slight at conversions below 65%, indicates that there are still other conditions influencing $\bar{n}$. One of these possible influences is the change in the average particle size during polymerization, which may cause a change in $\bar{n}$ as discussed above. The particle size data depicted in Figure 14 (gray circles, bottom x-axis and right y-axis) show an almost linear increase with conversion over the whole range. Indeed, the change in D can explain the slight increase in $\bar{n}$ at low conversions. The steep increase in $\bar{n}$, however, cannot be explained with the increase in D, which is very smooth (cf data in Fig. 13). Another possible explanation of the increase in $\bar{n}$ is, according to equation 9, a change in $C_{\mathrm{M,p}}$. Figure 15 shows that $C_{\mathrm{M,p}}$ also changes over the whole conversion range (115,117,118). $C_{\mathrm{M,p}}$ is expressed as the volume fraction of monomer in the swollen particles ϕ_{M}, which relates to $C_{\mathrm{M,p}}$ with the following relation: $\phi_{\mathrm{M}} = C_{\mathrm{M,p}} \mathrm{v}\, V_{\mathrm{mon}}$. This experimental result contradicts an important assumption of emulsion polymerization theory, where constant $C_{\mathrm{M,p}}$ values are assumed as long as a free monomer phase is present. For styrene, this should be a conversion of up to about 50%. But the experimental results are trustworthy because they were obtained at different times, in different laboratories, and by different researchers. Consequently, the decrease in $C_{\mathrm{M,p}}$ may contribute over the whole conversion range to increasing $\bar{n}$ values. Waning monomer concentration inside the droplets V/particles leads to an increase in viscosity, which at the same time causes decreasing mobility and radical termination inside the droplets. This gel or Trommsdorff effect, although known

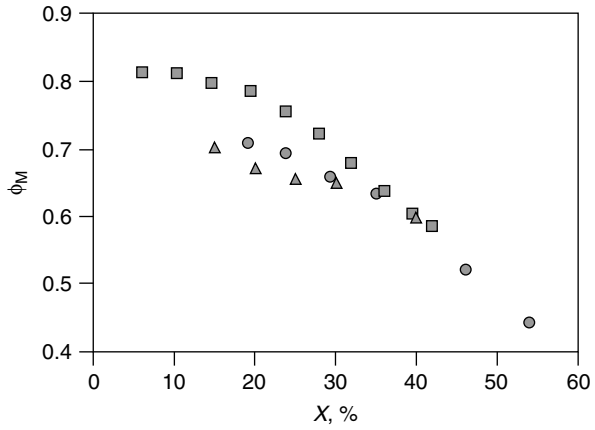

Fig. 15. Change of monomer volume fraction in latex particles during batch styrene emulsion polymerization with SDS as emulsifier. △ Initiator: potassium peroxodisulfate (117); □ Initiator: 2,2′-azobisisobutyronitrile (118); ○ Initiator: 2,2′-azobisisobutyronitrile (115).

to be not very pronounced in styrene emulsion polymerization (70), finds its expression under conditions of emulsion polymerization in a steep increase in $\bar{n}$. In contrast, a drastic increase in the number of radicals per particle by more than an order of magnitude was directly observed in emulsion polymerizations of methyl methacrylate (MMA) with electron spin resonance spectroscopy (119).

A Smith–Ewart case 1 behavior ($\bar{n} \ll 1$) can be observed during emulsion polymerization of monomers with a high chain-transfer rate constant such as vinyl chloride because the monomer radicals have a high tendency to escape from the particles. Especially for vinyl chloride emulsion polymerization, Ugelstad and Hansen (113) derived the following equation 18 to calculate $\bar{n}$, which predicts dependence, $\bar{n} \propto D^{3/2}$.

$$\bar{n} = N^{-1/2} \left(k_1 D^3 + k_2 D^2\right)^{1/2} \; k_1 = \left(6/\pi\right) \left(r_{\mathrm{i,w}}/2k_{\mathrm{t,w}}\right) \; k_2 = \left(6/\pi\right)^{2/3} \left(r_{\mathrm{i,w}}/2k_{\mathrm{des}}\right) \tag{18}$$

It was shown that $\bar{n}$ values calculated with this equation agree well with estimated ones by means of equation 9 up to a conversion of some 60% in batch emulsion polymerization of vinyl chloride, leading to particle sizes below 80 nm (120). Under these conditions the $\bar{n}$ values for vinyl chloride, are between 10^{-4} and 10^{-3}. However, for technically important continuous emulsion polymerizations of vinyl chloride, it was found that under steady-state conditions $\bar{n}$ depends on the square of D, as described by equation 19 (120).

$$\bar{n} = k'' D^2 \tag{19}$$

The data depicted in Figure 16 show that for a continuous emulsion polymerization of vinyl chloride leading to a very broad particle size distribution (10 nm $< D <$ 2000 nm) $\bar{n}$ changes over almost 5 orders of magnitude from 10^{-4} up to 10.

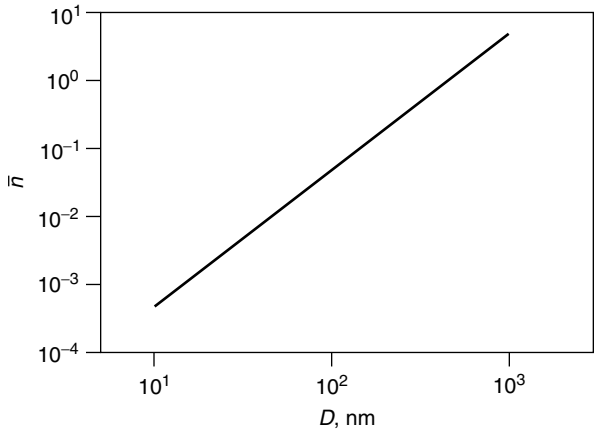

Fig. 16. Calculated average number of radicals per particle during a continuous emulsion polymerization of vinyl chloride (120).

This is a peculiar situation because at the same time particles do coexist, showing all features of compartmentalization effect ($\bar{n} < 1$) together with particles obeying bulk or solution kinetics ($\bar{n} > 1$).

In summary of this part, the average number of radicals per compartment is the centerpiece of heterophase polymerization kinetics. Its value depends mainly on the rate with which active, propagating centers appear inside the particles either by decomposition of monomer-soluble initiators or by entry from the continuous phase. Furthermore, particle size and overall concentration of compartments influence $\bar{n}$ in such a way that it increases with both increasing D and decreasing N. If the viscosity inside the particles is so high that termination by radical recombination is hindered, $\bar{n}$ increases as an expression of the gel effect in compartmentalized polymerization systems.

Competitive Growth of Particles with Different Size. Particle growth kinetics is an important aspect especially if at the end of polymerization a certain particle size or size distribution is required. In this context the relative growth of particles with different diameters is of importance (so-called competitive growth) and consequently, how a given particle size distribution changes during polymerization (if nucleation of new particles is excluded by taking appropriate action). The volume growth of a particle is given by equation 20, where K is assumed to be independent of particle size.

$$\frac{\mathrm{d}v}{\mathrm{d}t} = KD^{\mathrm{x}} \tag{20}$$

For the size growth follows equation 21, with volume $v = \frac{\pi}{6}D^3$, which leads under the assumption that both K and K' independent of time (ie K and K' only depend on polymerization conditions) after integration to equation 21. Note that the particle size is always the unswollen size; thus using equation 21 means the size dependence of the monomer concentration is neglected, which is reasonable for surfactant-stabilized particles with sizes larger than 50 nm (121). D and D_0

are the sizes at the beginning and the end of polymerization with duration Δt, respectively.

$$\frac{\mathrm{d}D}{\mathrm{d}t} = K' D^{x-2} \tag{21}$$

$$D^{3-x} - D_0^{3-x} = K'' \Delta t \tag{22}$$

A closer inspection of equations 21 and 22 reveals that if $x < 3$, smaller particles will grow faster and the particle size distribution is self-sharpening. On the contrary, if $x > 3$, the distribution becomes broader as larger particles grow faster than smaller ones. However, if $x = 3$, particle growth does not depend on particle size. There is experimental evidence that competitive growth during seeded emulsion polymerization slightly favors smaller particles (122). Other experimental and theoretical studies confirmed in the case of water-soluble peroxodisulfate initiator growth exponents of $x = 2.5$ for particle sizes larger than about 150 nm, which decreased toward zero when the particle size was decreased below 150 nm. However, for oil-soluble initiators, x was equal to 2.5 for a larger size range until the particles reached a critical size needed to sustain two growing radicals (123). This means that for larger particles, ie pseudo-bulk systems, particle growth does not depend on particle size and hence, the particle size distribution evolves uniformly in time. In a series of vinyl chloride emulsion polymerizations an exponent of x between 2 and 3 was determined, which slightly decreases with increasing initiator concentration (peroxodisulfate) as predicted by a theory considering desorption and reabsorption of radicals (124). Model calculations on the kinetics of competitive growth in aqueous polymerization of bidisperse seed systems with oil-soluble initiators showed that x is strongly dependent on rate of initiator decomposition, desorption rate, and the diameter ratio. If only 1% of the initiator is soluble in water, x approaches a value of 3 for low and high decomposition rates, independent of desorption rate. For intermediate values of initiator decomposition rate, $x < 3$ is obtained, indicating self-sharpening of the particle size distribution. In contrast, with a completely water-insoluble initiator the order is found to be constantly equal to 3, which indicates size-independent growth rate (125). Also, more sophisticated model considerations with regard to particle growth come to similar conclusions; for example, one author stated that as particle size distribution evolves it usually becomes narrower, and a more monodisperse distribution can be obtained provided formation of new particles can be avoided (126).

An essential advantage of heterophase polymerization, especially emulsion polymerization and related procedures, is that it allows simultaneously high polymerization rates and high molecular weights owing to its compartmentalized nature. In this context a question arises with regard to the relation between particle size and molecular weight. There are at least two contradictory effects necessary to consider: the dependence of the average number of radicals on the particle size (cf above) and the dependence of the monomer concentration inside the particles (cf below). As both values get larger with increasing particle size and on the one hand the molecular weight increases with increasing monomer concentration but decreases with higher $\bar{n}$, a theoretical prediction is very hard. Figure 17 shows for

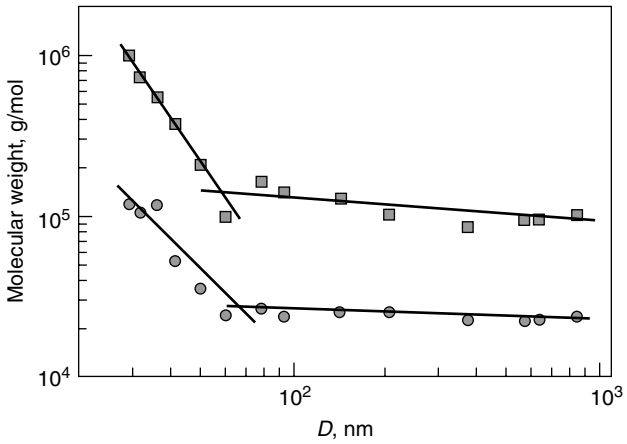

Fig. 17. Average molecular weights in dependence on average particle sizes for emulsion polymerizations of styrene, where changing emulsifier concentration varied the particle size (conditions cf. caption of Fig. 9); lines are for guiding the eye. □ M_w; ○ M_n.

the same polymerization as in Figures 9 and 10 the experimentally determined dependence of the weight- and number-average molecular weights on the average particle size for the final latexes. For this particular set of experiments the average molecular weight increases with decreasing average particle size. The slope in this log–log plot changes for particle sizes below 100 nm. For smaller particles the molecular weight increase is much steeper than for larger particles. The plots in Figure 18 reveal that in dependence on the emulsifier concentration

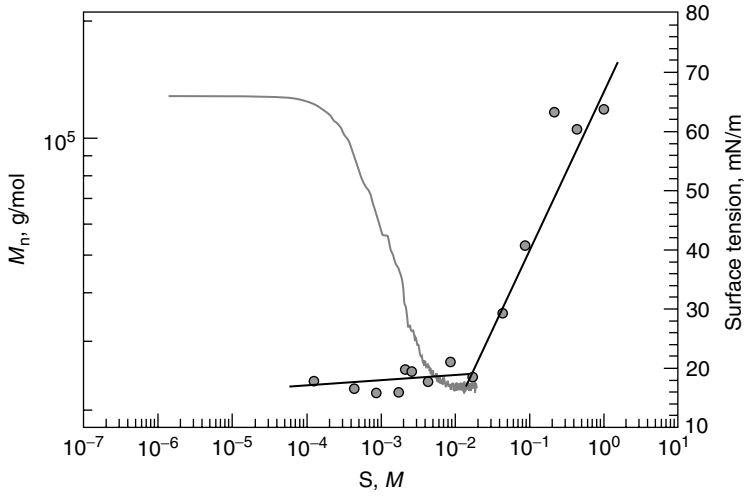

Fig. 18. Experimentally obtained relation between number-average molecular weight (M_n), left ordinate, and surface tension, right ordinate, and emulsifier concentration (for polymerization conditions, see caption of Fig. 9); lines are for guiding the eye. — surface tension; ○ M_n.

the increase in the molecular weight starts in the vicinity of the critical micelle concentration. At this point a large number of particles can be stabilized and the effect of compartmentalization really starts to act.

Technical Realizations

The easiest way to carry out heterophase polymerization is to mix water and a monomer, say styrene, which is able to undergo thermal polymerization, in a vessel at elevated temperatures. After a couple of hours. (the time depends on the temperature) the mixture becomes turbid because of the formation of polystyrene particles. Figure 19 shows a transmission electron microscopy picture of polystyrene particles obtained in this simple way. Although the amount of polystyrene formed was low and the reproducibility of this procedure very bad, a heterophase polymerization took place, and this offers a nice example of how easily heterophase polymerization can be carried out.

Recipes. The minimum number of chemically different components for heterophase polymerizations is two. This is the case if a monomer, which is a nonsolvent for its own polymer is polymerized in bulk. Light-induced bulk polymerization of acrylonitrile and vinyl chloride might be examples for this procedure. However, well-defined products especially with regard to colloidal properties, require more efforts. In order to carry out reproducible heterophase polymerization up to high conversions with highly controlled polymeric and colloidal properties, at

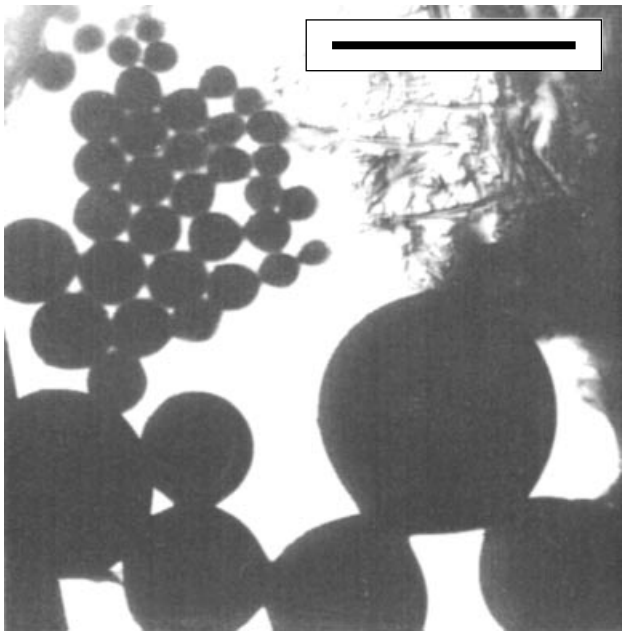

Fig. 19. Transmission electron microscopy pictures of polystyrene particles obtained by thermal polymerization at 90°C in an all-Teflon (DuPont) reactor after duration of 7 h; the bar indicates 3.5 μm.

least three more components may be necessary, that is, an initiator, a dispersion medium or continuous phase, and a stabilizer. The kind of chain-growth mechanism (condensation or addition) together with the desired polymeric product determines whether a catalyst or an initiator, and which kind, is employed. The thermal properties of the monomers and polymers determine the polymerization temperature and hence the properties of the initiating system.

The Continuous Phase. As a general rule any polymerization recipe that works well under homogeneous conditions can be transformed into a heterogeneous system by the choice of a corresponding continuous phase that should be liquid at least at polymerization temperature. The continuous phase has to fulfill three basic requirements: it should be chemically inert, a nonsolvent for the polymer, and possess good heat-transfer properties. If however, the continuous phase interferes with recipe components, the transfer from homogeneous to heterogeneous polymerization conditions requires additional efforts and if needed, changes of one or the other recipe component. Table 5 gives examples of the types of polymerization chemistry applied in heterogeneous polymerization with fluid continuous phases. A variety of different media have been used as continuous phases, for example, aqueous solutions with high ionic strength (130), polymeric melts (47), or supercritical CO_2 (132).

Other Components. The smaller the particle size, at a given phase ratio, the more difficult it is to ensure colloidal stability (cf Fig. 5). This means that for aqueous heterophase polymerizations in the order suspension < microsuspension < emulsion ≤ miniemulsion < microemulsion, the stabilizer concentration increases. Contrary to the simple polymerization of styrene in water, polymerization recipes for industrially important polymer dispersions comprise up to six monomers, frequently more than two emulsifiers, more than one initiating system, and a few other aids like biocides, defoaming agents, plasticizers for supporting film formation (39). The monomer-to-water ratio is adjusted in such a way that a solid content results typically between 40 and 60% or even higher. The amounts of surfactants and initiator (mainly peroxodisulfate) are typically between 0.5 and 2% (w/w) relative to the monomers and 0.5% (w/w) relative to water, respectively.

A peculiarity of suspension polymerization relates somewhat to recipes and more so to reactor operation. Industrial suspension polymerizations are carried out batchwise in reactors with a volume of up to 200 m^3. These reactors are designed with a maximum cooling capacity corresponding to the maximum heat release. However, the maximum heat release normally occurs only for a limited period of time (gel effect) and hence the average heat release during the entire polymerization is much lower. In order to increase the reactor output, so-called initiator cocktails are used that allow polymerization as long as possible at the maximum rate (148,149). Another possibility to avoid a substantial loss in reactor productivity at conversions where the maximum rate of polymerization is not attained is the use of temperature-programmed reaction. An example of such a procedure in order to increase the productivity of vinyl chloride suspension polymerization reactors is given in Reference 150.

Reactors and Operation Modes. A large variety of reactors and mixing systems can be used for heterophase polymerizations. The enzymatic biosynthesis of natural rubber in *Hevea brasiliensis* trees or of poly-3-(hyroxyalkylalkanoates) in bacteria cells takes place in living organisms. For instance, the enzymatic

Table 5. Types of Polymerization Chemistry Applied in Heterophase Polymerization

Polymerization chemistry	Example	Reference
Enzymatic biosynthesis	(*1*) Synthesis of *cis*-1,4-polyisoprene by enzymatic condensation of *iso*-pentenyl pyrophosphate in plants	127
	(*2*) Synthesis of poly-3-(hydroxyalkylalkanoates) in bacteria even an industrial scale	128
Condensation	(*1*) Preparation of polyurethanes via miniemulsion from isophorone diisocyanate and bisphenol A or dodecane diol in aqueous media	129
	(*2*) Tetraethyl silicate reaction in alcoholic solution in presence of water under alkaline conditions	130
Ring opening (pseudo-anionic)	(*1*) Polymerization of cyclic esters such as ε-caprolactone in 1,4-dioxane and heptane with diethyl aluminum ethoxide or sodium trimethyl silanoate as initiator	131
	(*2*) Copolymerization of D,L-lactide and glycolide in supercritical CO_2 with stannous octoate as catalyst	132
Ionic polymerization	(*1*) Cationic polymerization of permethyl cyclosiloxanes with tetraalkylammonium chloride surfactants in alkaline aqueous solutions	133
	(*2*) Anionic polymerization of permethyl cyclosiloxanes with dodecylbenzene sulfonic acid as both catalyst and surfactants in acid aqueous solutions	134
	(*3*) Styrene polymerization in hexane with *sec*-butyl lithium as initiator	135
Noble metal–olefin complexes	(*1*) Olefin complexes of rhodium(I) chloride for aqueous emulsion polymerization of 1,3-butadiene to get crystalline *trans*-1,4-polybutadiene	136
	(*2*) Binuclear nickel ylide catalysts to get high density polyethylene in aqueous emulsion or miniemulsion	137
	(*3*) Monocyclopentadienyl complex of trimethoxy titanium with a borate activator as metallocene catalyst to polymerize styrene in aqueous emulsions in presence of surfactants	138
Radical, conventional	Most prominent way to initiate heterophase polymerization in organic and aqueous continuous phases	36,139
Radical, controlled	Various controlled radical techniques: reversible addition fragmentation chain transfer	140–142,144
	Atom-transfer radical polymerization nitroxide mediated	145–147

condensation of dimethylallylpyrophosphate to *cis*-poly-1,4-isoprene takes place in tubular vessels in the tissues of the tree, which might be considered as a continuous tube reactor at least during the harvest. There are basically two different types of reactors for synthetic heterophase polymerization: the well-mixed stirred tank reactors or the tube flow reactors. The former may operate batchwise, semibatchwise, or continuously whereas the latter is restricted to continuous operations. Both types of reactors, that is a single continuous stirred-tank reactor and a tube flow reactor, differ significantly in their residence time distribution. This is of particular importance because the particle size distributions, provided particle growth processes mainly govern the size distribution, reflect the residence time distributions. Remember, particles grow during the entire reaction time in contrast to the case of polymer molecules in radical polymerizations.

Compared with homogeneous condensation or bulk polymerizations, the technical realization of emulsion polymerizations in both laboratory and on an industrial scale is easy. The minimum equipment needed is a container that can be closed and that is chemically resistant to water and the monomers. In the case of gaseous monomers, the container must additionally withstand the corresponding vapor pressure. This type of reactor, for instance beverage bottles of different styles with crown caps or caps with a septum to allow sampling, was employed for many investigations during the early days of emulsion polymerization (151). These so-called bottle reactors were fixed to a rotating shaft and immersed in a thermostated bath. Nowadays rotation thermostats with metal block heaters are available and frequently in use (152). With a large number of reaction vials it is possible to investigate many recipe variations simultaneously or to acquire conversion time data with sampling volumes large enough for the necessary latex and polymer characterizations. Moreover, for laboratory investigations, stirred vessels with heating and cooling jackets are widely used, although, especially if larger sampling volumes are desired, the bottle reactors still have some advantages.

In industrial processes stirred reactors with numerous technical variations are mainly employed. Besides jacket cooling, the heat of polymerization can be removed by various techniques as, for instance, hot cooling or internal fittings inside the reactor. Reactors for commercial processes have a size between 10 and 200 m^3 and are pressure-proof up to 200 MPa (2000 atm) if necessary (39). The vessels normally have a cylindrical shape with dished tops and bottoms. The mixing system depends on the particular heterophase polymerization technique, as it has to fulfill different requests. A detailed discussion is beyond the scope of this article and the reader is referred to chemical engineering text books or reviews dealing with special heterophase polymerization techniques such as for emulsion polymerization (153,154) and for bulk and suspension polymerization (155,156).

Currently, commercially pure batch processes play a major role for suspension and bulk polymerization but only a minor role for emulsion polymerizations. The most important procedure for effecting polymer dispersions by emulsion polymerization on a technical scale is semibatch or feed processes, which are very flexible regarding product properties. Depending on the required properties with respect to particle size distribution, molecular weight distribution, chemical composition in the case of copolymerization, and particle morphology, numerous feeding policies have been developed. Almost all kinds of consecutive

shell morphologies can be prepared nowadays by means of computer-controlled monomer feed streams. This is a tremendous improvement compared to the early attempts to prepare heterogeneous particle morphology by changing the monomer feed compositions with the aid of so–called near tanks and far tanks, as described in Reference 157. A variety of emulsion polymerizations [for example poly(vinyl chloride) and rubber production] are carried out continuously, mainly in continuous stirred-tank reactors (CSTRs) or in a series consisting of up to 8 CSTRs. In the latter case intermediate feed streams are frequently applied to control copolymer composition and particle morphology. A specific and very exciting feature of continuous processes in stirred tank reactors is the occurrence of damped or sustained oscillation of conversion and also of latex and polymer properties (particle size, molecular weight, and the corresponding distributions) even at the steady state for different monomers (158–163).

Although continuous emulsion polymerization technology is more than 60 years old it is still attracting researchers investigating the dynamic behavior in order to achieve control (164) and also developing procedures that allow transfer of products from batch or semibatch processes to continuous reactors in order to increase productivity (165).

In large-scale technical reactors, the hydrodynamic conditions are much more important than in laboratory-scale reactors. Sufficient emulsification is essential for a proper control of the polymerization process and product properties. If the stirring conditions are not optimized, problems can arise regarding the homogeneity of the reaction mixture as well as heat removal. In contrast, if the shear forces are too high the latex may become unstable to coagulation [cf below and (39)]. It is generally assumed that agitation has no effect on the kinetics and this topic is ignored in almost all textbooks. However, a few results have been published indicating an influence. For example, kinetics may be affected if the inert gas for purging contains traces of oxygen, if a chain-transfer agent has to diffuse out of the monomer droplets into the particles (166), if the monomer diffusion to the reaction loci is influenced (167), or if the emulsifier distribution between the interfaces is changed considerably (168). Nowadays, the influence of the stirrer speed receives more and more attention (169–172), and increasing the stirrer speed, starting from well-mixed conditions, has been carried out in all these investigations. A drastic change in both the kinetics and the polymer and particle properties has been reported if the stirrer speed is increased starting from values so low that a bulky free monomer phase on top of the reactor still exists (104). Increasing the stirrer speed leads to an increase in the polymerization rate, the particle size, and the molecular weight. Besides stirred tank reactors, in which the composition per volume unit is the same over the entire reactor volume, tubular reactors have aroused increasing interest over the last few years. The references in Table 6 seem to support this trend. Even for suspension polymerization, more and more continuous procedures based on tube reactors are being investigated. For instance, a 5-m^3 batch tank reactor can be replaced by a 0.05-m^3 continuous loop reactor (175).

In summary, many different technical realizations exist for preparing polymer dispersions, ranging from biosynthesis in many plants and bacteria over bottle reactors to high-tech and computer-controlled production systems. Emulsion polymerizations have even been carried out in space under the conditions

Table 6. Developments in Reactor Design for Heterophase Polymerizations

Reactor type	Design element	Reference
Tubular reactor	Development of a pulsation operation mode to eliminate reactor fouling and plugging; comparison between batch and continuous stirred-tank reactors; review on tubular reactors	173
Pulsed tubular reactor	Styrene emulsion polymerization	174
Loop process	Experimental investigations and modeling of emulsion copolymerization in continuous loop reactors	175
Tubular reactor	Suspension polymerization to prepare large porous polymer beads in a tubular reactor; less polydisperse particle size distribution than in batch stirred-tank reactor	176
Wicker tube reactor	Emulsion polymerization; 100-m-length tube, with an inner diameter of 1 cm; high cooling capacity; residence time distribution comparable with a cascade of 600–1500 continuous stirred-tank reactors	177
Tubular reactor	Inverse suspension polymerization of acrylamide in a batch oscillatory baffled reactor 1 m in length, with a diameter of 5 cm); up to 9 baffles oscillate with a frequency between 1 and 5 Hz	178
Couette–Taylor	Continuous emulsion polymerization of styrene in a Couette–Taylor vortex flow reactor; comprehensive kinetic study in dependence on reactor operation parameters	179
Taylor vortex flow	Continuous emulsion polymerization of Styrene, influence of flow conditions	180
Pulsed-packed column	Continuous seeded copolymerization of styrene and methyl methacrylate	181

of zero gravity (182) under the supervision of the Lehigh Emulsion Polymers Institute.

Procedures. From a technological point of view heterophase polymerizations can be carried out either batchwise, semicontinuous (or semibatch), or continuous. In the batchwise case the reactor is filled with all ingredients before the polymerization is started and the reactor content is removed at the end of the polymerization. In a semibatch procedure, at the start of the polymerization the reactor is filled only partially and a stream of either neat monomers or monomer emulsion with constant or deliberately changed composition is fed continuously until the reactor is filled. After a final post-feeding batch reaction period, the reactor is emptied. A continuous procedure means that all necessary ingredients are fed and final latex is removed continuously. In all three cases the polymerization can be carried out in the absence or presence of preformed particles (so-called seed particles). Reactions in the absence of seed particles are frequently called ab initio polymerizations and require that particle nucleation takes place. Table 7 is an

Table 7. Heterophase Polymerization Techniques with Continuous Fluid Phases

Common name	Initiator	Stabilizer	Procedures	Particle size	Reference
Precipitation	Lyophobic, Lyophilic	None	Batch	mm range	183–186
Suspension	Lyophobic	Polymeric or protective colloid	Mainly Batch	10–500 μm	155,187–191
Dispersion	Lyophilic	Polymeric	Batch	1–20 μm	192–196)
Microsuspension or minisuspension	Lyophobic	Polymeric plus surfactant	Batch; high shear	1–10 μm	197–199
Emulsion	Lyophobic, Lyophilic	All kinds or none	Batch; semi-batch; continuous; seed	5 nm–10 μm	101,153,200–204
Miniemulsion	Lyophilic, Lyophobic	All kinds	Batch, semibatch; continuous	50–500 nm	205–211
Microemulsion	Lyophilic, Lyophobic	All kinds	Batch, semibatch	10–100 nm	212–222

attempt at a condensed view of the great variety of procedures for carrying out heterophase polymerization. A few typical characteristics of various techniques are put together there. The references given in Table 7, except those for dispersion polymerization, refer mainly to water as continuous phase. As already pointed out, the corresponding processes with nonaqueous continuous phases are denoted with the prefix inverse (223). In inverse heterophase polymerization systems the dispersed phase is hydrophilic and in cases where the monomer is a solid and insoluble in the continuous phase, aqueous solutions of the monomers are used in order to support emulsification. In this sense all procedures except dispersion polymerization have inverse mirror images. The interested reader can find detailed information with regard to inverse precipitation and suspension polymerization in Reference 224, inverse emulsion and suspension polymerization in Reference 225, all types of inverse polymerization in Reference 139, and inverse emulsion and microemulsion polymerization in References 226 and 227.

On closer examination of this information, together with that in Tables 2 and 4, one may come to the conclusion that a classification with regard to the final particle size is much more meaningful than with regard to separate recipe components as is frequently done. The final polymer dispersion is the result of a complicated interplay between all recipe components and the polymerization temperature that governs thermodynamics. This is especially true for technical polymerizations owing to the increased number of components.

Initiators and Stabilizers. The combinations of initiator and stabilizer play a crucial role. Studies of the influence of the kind of initiator on heterophase polymerization and latex properties have been published. Some efforts have been made to investigate the influence of water-soluble and oil-soluble initiators on emulsion polymerization (213,228–230) and microemulsion polymerization (116,231). In systematic kinetic studies it turned out that the general behavior of emulsion polymerization is the same for water-soluble and oil-soluble initiators (232). The reason for the similar behavior is the desorption of initiator radicals from the polymer particles, which governed the kinetics under the particular conditions, rather than the contribution of the fraction of oil-soluble initiators dissolved in the dispersed phase. Note that this can only be valid for recipes containing surfactants because the polymerization of lyophobic monomers with lyophobic initiators in the absence of stabilizers is a precipitation polymerization without any control of colloidal stability. There are not only similarities but also differences between lyophobic and lyophilic initiators. For instance in Reference 229, the authors found that use of dibenzoyl peroxide leads to lower average molecular weight (about a factor of 5) of the polystyrene than use of potassium peroxodisulfate (emulsifier: hexadecanoic acid) because of chain transfer to the initiator. But for both initiators the authors claimed a rapid exchange of low molecular weight radicals between latex particles and water phase. The type of oil-soluble peroxide, especially its polarity, influenced the results (233). The authors found that higher the polarity, higher was the initiation rate in emulsion polymerization (emulsifier: Nekal, which is of the short-chain alkyl naphthalene sulfonate type) compared to bulk polymerization of styrene. Thus *sec*-butylhydroperoxide had a 14000 times higher initiation rate in emulsion polymerization whereas that of dibenzoyl peroxide was the same in both cases. The application of a mixture of potassium peroxodisulfate and dibenzoyl peroxide in emulsion polymerization styrene (emulsifier:

alkyl sulfonate, E30) is described in Reference 234. The authors found that the rate of polymerization depends on potassium peroxodisulfate concentration but not on dibenzoyl peroxide concentration. In contrast, the molecular weight depends on dibenzoyl peroxide concentration and not on peroxodisulfate concentration under the particular polymerization conditions. However, these results are contradictory to those of Reference 229 and reveal the necessity to compare experimental data obtained under almost identical conditions. Also, for heterophase polymerizations there is the sensitivity of radical polymerization kinetics to changes in colloidal conditions that must be considered. A systematic study of emulsion polymerization of styrene with different initiator–emulsifier systems (IES) at temperatures between ambient and 100°C was carried out (235). This study included sodium dodecylsulfate and sodium C_{15}-alkylsulfonate (E30, average carbon chain length of 15) as emulsifiers and potassium peroxodisulfate, 2,2′-azobisisobutyronitrile, and various symmetrical poly(ethylene glycol)–azo compounds as initiators (PEGA initiators where the added number denotes the molecular weight of the poly(ethylene glycol) chain). Note, PEGA200 is soluble in both phases owing to the bizarre solubility pattern of poly(ethylene glycol) (45,47 and references therein) and PEGAS200 (the sulfate of PEGA200) is a surface-active initiator mainly located at the interface. With this selection all possible loci of initiator decomposition were covered: the water phase, the oil phase, and the interface. The experiments were evaluated in the form of Arrhenius plots for the average degree of polymerization and the particle number. Both data sets revealed a strong influence of the IES on the experimentally observed dependencies in the case of styrene emulsion polymerization. For instance, the activation energy of the mean degree of polymerization mainly depends on the initiator decomposition and on the locus of radical formation. The activation energy changes in the following order: potassium peroxodisulfate ($E_A \sim -35$ kJ/mol), 2,2′-azobisisobutyronitrile and PEGA200 ($E_A \sim -50$ kJ/mol), and PEGAS200 ($E_A \sim -80$ kJ/mol), independent of the kind of emulsifier and its concentration. The foregoing results for a variety of lyophilic and lyophobic initiators were obtained with low molecular surfactants/emulsifiers as is typical of emulsion or microemulsion recipes. For suspension polymerizations polymeric stabilizers such poly(vinyl alcohol) are typically employed. In a study of suspension polymerization of vinyl chloride [stabilizer: poly(vinyl alcohol) having a degree of hydrolysis of 72.5%] it was shown that the locus of initiator decomposition has an influence on the final particle size distribution. This study is special in the sense that the oil-soluble initiator [bis(4-*t*-butylcyclohexyl)peroxodicarbonate] was either dispersed in the continuous phase or predissolved in the monomer (236). When the initiator was predissolved in the monomer, the polymerization occurred uniformly in all drops (ideal suspension polymerization behavior), whereas in the other case, additionally to suspension polymerization an emulsion polymerization took place leading to a fraction of smaller-sized particles. The following recipe was used to investigate the influence of the kind of initiator (water- or oil-soluble or both) on the suspension polymerization of styrene at 80°C: 40 g of water, 10 g of styrene, 10 mg of poly(vinyl alcohol) (type W25/140 from Wacker Polymer Systems with a degree of hydrolysis of 84–89%), 1.184×10^{-3} *M* initiator (ie 0.32 g of potassium peroxodisulfate or 0.2867 g of dibenzoyl peroxide or 0.673 g PEGA200). The final dispersions at complete conversion have a different appearance, as illustrated by the photograph in Figure 20. From potassium peroxodisulfate to

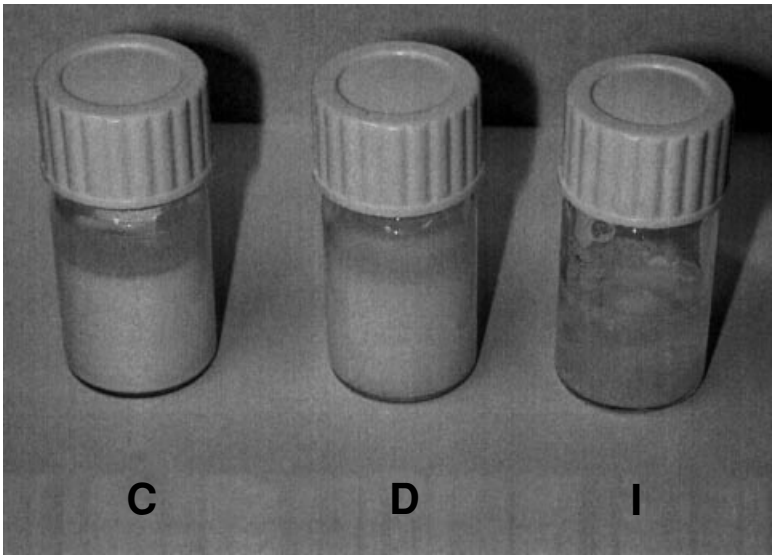

Fig. 20. Appearance of polystyrene dispersions stabilized with poly(vinyl alcohol) prepared with different initiators. *C*: initiator soluble in the continuous phase, potassium peroxodisulfate; *D*: initiator soluble in the disperse phase, dibenzoyl peroxide; *I*: initiator located mainly at the interface, PEGA200.

dibenzoyl peroxide to PEGA200, the main loci of initiator decomposition is shifted from the aqueous phase via the oil phase to the interface. The dispersion appears coarser and coarser. In case of PEGA complete phase separation occurred, with large aggregates floating around. The difference between dibenzoyl peroxide and potassium peroxodisulfate is less pronounced—but clearly revealed by the transmission electron microscopy pictures shown in Figure 21. The particles obtained in presence of potassium peroxodisulfate look like normal latex particles (spherical solid particles), whereas the particles prepared with the oil-soluble initiator resemble much softer or bleeded structures. However, the scanning electron microscopy pictures of the main fractions of both dispersions (cf Fig. 22) at a glance hardly show any difference. If there is a difference, then the particle size distribution of dispersion (*D* with dibenzoyl peroxide) appears to be a little broader. Furthermore, in case of initiation in the styrene phase with dibenzoyl peroxide, a few larger particles are also visible (cf Fig. 23), representing either polymerized single-monomer droplets or coalescence structures. These results on the one hand confirm the results of Brooks (236) and on the other reveal that the overall particle size distribution for poly(vinyl alcohol) as polymeric stabilizer depends strongly on the kind of initiator, in contradiction to the above results with low molecular weight emulsifiers. Besides the distinctions in morphology, differences with regard to the molecular properties also exist, as shown by means of molecular weight distributions (cf Fig. 24) and average molecular weights (cf Table 8). Looking at these data, one has to consider that, although the initiator concentration was the same on a molar basis, the decomposition rates, and hence the initiation rates, were different. The decomposition rate constants at 80°C for potassium peroxodisulfate,

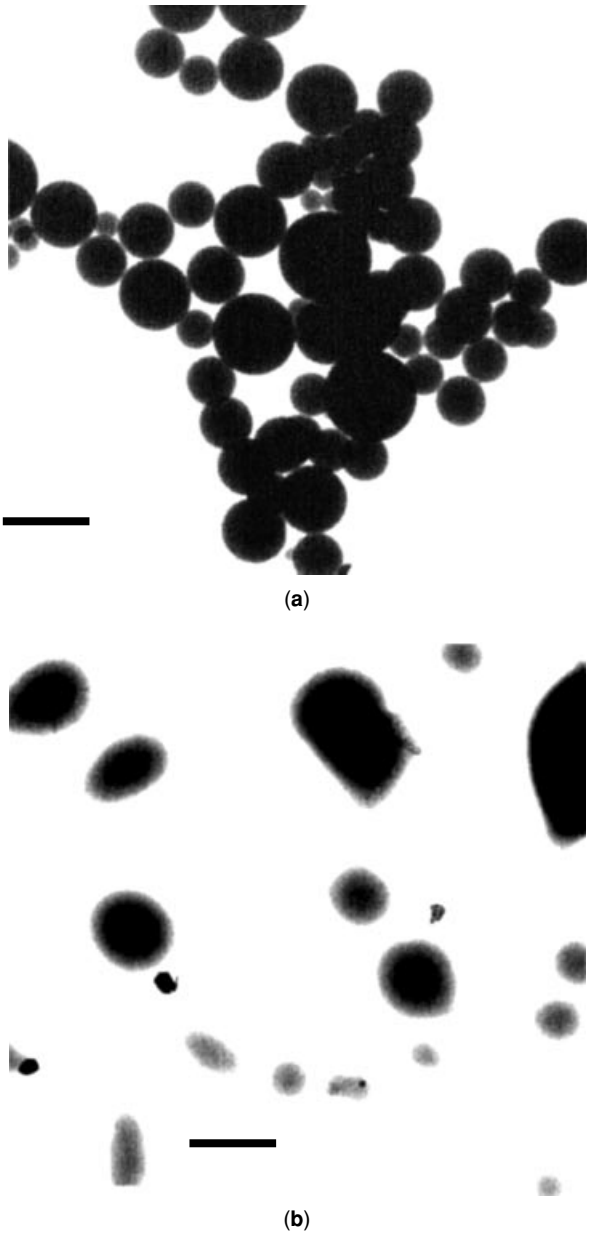

(**a**)

(**b**)

Fig. 21. Transmission electron microscopy pictures of the small particle size fraction of the dispersion shown in Figure 20a. Sample C (potassium peroxodisulfate); b Sample D (dibenzoyl peroxide); the bars indicate 1 μm.

dibenzoyl peroxide, and PEGA 200 are $3.5 \times 10^{-4}\,s^{-1}$ (237), $8.1 \times 10^{-4}\,s^{-1}$ (238), and $6.0 \times 10^{-4}\,s^{-1}$ (47), respectively. A comparison with the data in Table 8 shows, that obviously effects other than the initiator decomposition rate determine the molecular weight (potassium peroxodisulfate should lead to the lowest molecular

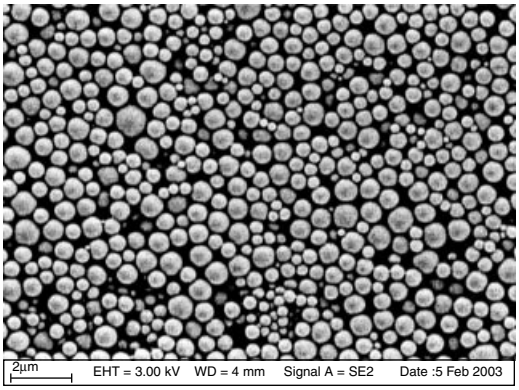

(**a**)

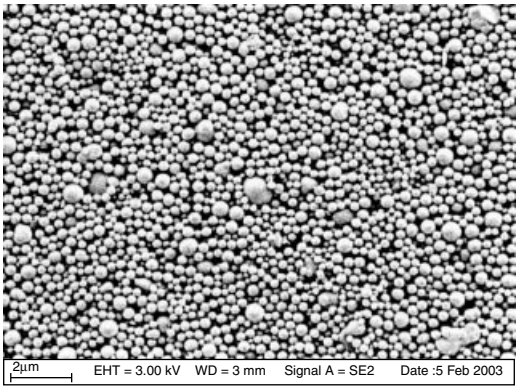

(**b**)

Fig. 22. Scanning electron microscopy pictures of the main fraction of polymer dispersions C and D of Figure 20a. Sample C (potassium peroxodisulfate); b. Sample D (dibenzoyl peroxide); the bars indicate 2 μm.

weight and dibenzoyl peroxide to the highest). One possibility to explain the low molecular weights in case of dibenzoyl peroxide is the chain-transfer reaction as mentioned in Reference 229. This effect might contribute but cannot explain the whole situation. Moreover, there are distinct differences not only in the average molecular weights but also in the shape of the molecular weight distribution. Polymerization I leads to the polymer with the highest molecular weight, followed by sample C and finally sample D. The molecular weight distribution in all three cases is characterized by shoulders or even separated peaks in a range between 2 and 3×10^4 g/mol and about 10^5 g/mol. Additionally the polymer obtained with PEGA200 has a shoulder at 10^6 g/mol, which is typical for this kind of initiator (152). The distributions of Figure 24 show that sample *D* covers the lower molecular weight range whereas sample I covers the higher molecular weight range and interestingly, sample C extends over the whole range. Note that all the molecular weight data are reproducible, as indicated by the average values given in Table 8. In the sense that the molecular weight distribution is a permanent record of the polymerization reaction, an explanation of these data (Fig. 24 and Table 8) might

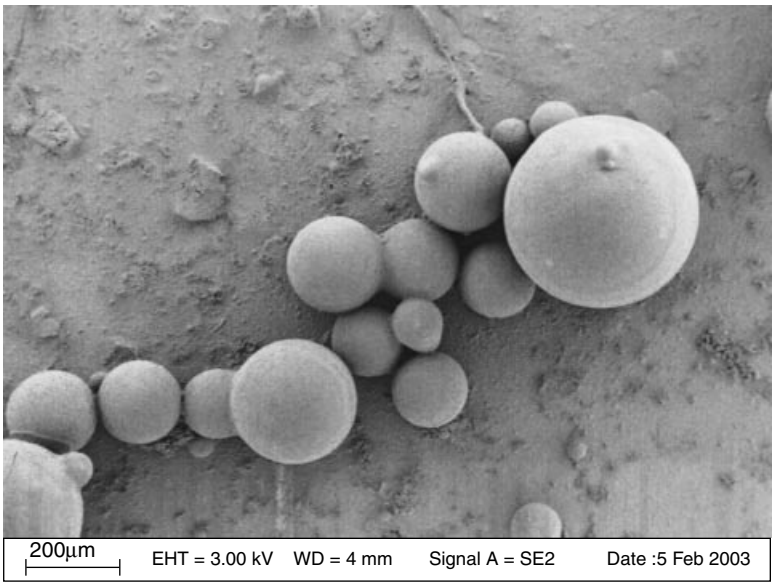

Fig. 23. Scanning electron microscopy picture of the large particle size fraction of the dispersion D of Figure 20 (dibenzoyl peroxide).

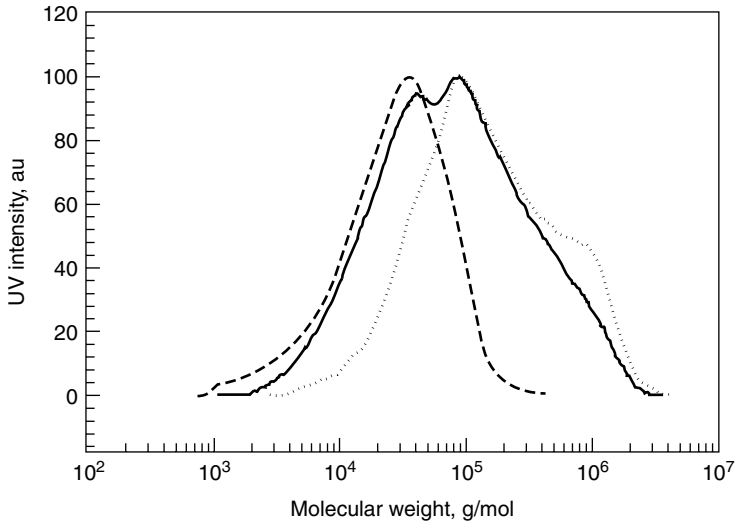

Fig. 24. Molecular weight distribution dependence on the locus of initiator decomposition (cf. Fig. 20). — C; - - - D; · · · · I.

be attributed to various reaction loci (continuous phase, dispersed phase, and interface), but a real proof needs further investigation. Consequently, an important point in heterophase polymerization is the control of the particle size or particle size distribution, especially in cases where the dispersed state, besides the polymer properties, is important for application.

Table 8. Weight- and Number-Average Molecular Weights (M_w, M_n) of the Polymers Prepared with Different Initiators[a]

Sample	M_w, g/mol	M_n, g/mol	M_w/M_n
C	2.13×10^5	3.13×10^4	6.87
	1.76×10^5	3.38×10^4	5.21
D	3.33×10^4	1.29×10^4	2.58
	3.97×10^4	1.57×10^4	2.52
I	2.73×10^5	6.42×10^4	4.25
	2.78×10^5	6.84×10^4	2.78

[a] cf Fig. 20 and text.

Control of Particle Size. In principle, particle size control requires the control of the formation of the dispersed phase either by control of the nucleation process or by restricting the polymerization to a preformed dispersed state. Because the control of nucleation is complicated, the second possibility is the method of choice for most of the industrial applications of heterophase polymerization. A more or less well-defined dispersed state as a starting point for polymerization is realized either by the application of seed particles or by emulsification processes. The former method means that preformed particles are used, which serve as reaction loci. The seed particles can either be swollen with the monomer mixture (seeded batch process) or the monomer mixture can be continuously fed into the reactor (so-called seed and feed procedures, or semibatch or semicontinuous process). The polymerization can be restricted to the seed particles by the application of proper means (33) such as the application of radical scavengers (which are soluble in the continuous phase) in the case of radical polymerizations. The second method requires the preparation of monomer droplets of average size a little larger than the desired final particle size because of the shrinkage taking place during polymerization. The two principal techniques for the preparation of emulsions are comminution and condensation (cf (239) and references therein). Comminution techniques require the input of mechanical energy to crush the bulk monomer phase into smaller drops, whereas condensation techniques are thermodynamically driven phase transitions leading to droplet formation. Four main groups of comminution techniques can be distinguished: rotor/stator systems (including all type of stirrers), high pressure homogenizers, ultrasound devices, and membranes. Except for membrane techniques these methods are based on the input of mechanical energy, in the course of which eddies are formed, transferring the mechanical energy to the droplets. The emulsification proceeds in such a way that as soon as the shear exerted by the turbulent microeddies on the droplet interface exceeds the cohesive forces of the liquids in the drops, they split up to smaller units. The cleavage occurs as long as a balance between the external stress and the internal stress is reached. At this steady state the droplet size distribution becomes time-independent. The final droplet size is influenced by various parameters such as the volume–phase ratio, the viscosity of both phases, the mutual solubility of both phases, the kind and concentration of surfactants, the power input, the stirrer as well as the vessel geometry, the diminution energy, and thermodynamic changes during the emulsification process (reactions, temperature). Contrary to

comminution techniques, the preparation of emulsions by condensation does not require mechanical energy, except gentle stirring sometimes to avoid creaming or settling as a result of density differences between both phases. Condensation processes are mainly determined by thermodynamic principles. There are basically two different types of condensation methods: droplet nucleation and swelling of dispersed phases; but the combination of both also has some meaning, especially for heterophase polymerizations (cf Swelling and Nucleation). Microemulsions are the most prominent example of purely thermodynamically driven emulsion formation, which can be considered as swelling of surfactant solutions. Preparation of emulsions and their use in various heterophase polymerization processes has been reviewed (239). An emulsion made by comminution techniques is thermodynamically not stable and hence it is exposed to degradation processes.

Degradation of Emulsions. Emulsions can degrade via different mechanisms: phase separation, Ostwald ripening, aggregation (as generic term for flocculation or coagulation and coalescence), and phase inversion. Additionally, changes in the thermodynamic conditions (composition and temperature) compared to the preparation conditions may have a devastating influence on emulsion stability. *Phase separation* means that an emulsion may separate into two phases: one phase enriched with the droplets and the other enriched with the continuous phase. Depending on the density difference between the continuous and dispersed phase these kinds of separation are called creaming or sedimentation depending on whether the upper or the lower phase is formed by the droplets, respectively. *Aggregation* processes (flocculation, coagulation, coalescence) can take place when the average distance between emulsion droplets is so close that attractive forces become dominant. The stability of emulsions can be controlled very effectively by the addition of proper stabilizers in sufficient concentrations so that generally in practice the aggregation of emulsions is not a serious problem. *Phase inversion* is a process where for a given stabilizer the continuous phase becomes the dispersed one and vice versa. This is mainly observed in the case of polymeric surfactants with a stabilizing moiety possessing a critical solution temperature. Prominent examples are surfactants with poly(ethylene glycol) units. Increasing the temperature leads to an increase in the hydrophobicity of the surfactant and it may subsequently promote the stabilization of water in oil instead of oil in water emulsion (cf Bancrofts's rule). Furthermore, whether phase inversion occurs or not depends on the polarity of the oil phase; the kind of electrolyte and its concentration; other additives as for example organic, water-soluble solvents increasing the oil solubility in water; and on the oil volume fraction. Ostwald *ripening* as a degradation mechanism is a direct consequence of the polydispersity of the droplet size distribution after comminution. Thermal fluctuation in the size or in the curvature may produce polydispersity as well. It is easy to show (cf for instance (239)) that the chemical potential of a dispersed phase compared to that of the same bulk material is increased by $4\sigma V_{\mathrm{mon}}/D_{\mathrm{d}}$. Consequently, for the concentration of the dispersed phase just at the interface $C(D)$ (where σ holds) follows equation 23, with C_0 being the solubility of the dispersed phase in the continuous medium.

$$k_{\mathrm{B}}T\,\ln C\,(D) = \frac{4\sigma v_{\mathrm{mon}}}{D_{\mathrm{d}}} + k_{\mathrm{B}}T\,\ln C_0 \tag{23}$$

From equation 23 it can be seen that smaller the objects, higher is the $C(D)$. As D_d goes to infinity $C(D)$ equals C_0. This means that smaller objects have a tendency to dissolve whereas larger objects grow by the uptake of matter that is released from the small ones. Two points are important for heterophase polymerization: (*1*) For Ostwald ripening to occur, a certain water solubility is required (this is given for many monomers in Table 9) and (*2*) a direct contact between the droplets is not necessary as molecular diffusion through the continuous phase is sufficient. On the basis of these considerations it was supposed that it might be possible to stabilize emulsions against Ostwald ripening by addition of small amounts of a lyophobic substance. This was done by Higuchi and Misra (240) and experimentally verified by stabilization of carbon tetrachloride droplets in water with hexadecane. Kabalnov investigated Ostwald ripening theoretically under such conditions (241). Two cases are of special interest for polymerization. First, that the solubility of the lyophob in the continuous phase is zero ($C_{LC0} = 0$), which means that the total number of particles remains constant. However, the distribution of the dispersed phase from small to large particles changes the composition of the particles. The volume fraction of the lyophob (ϕ_L) in the smaller particles increases and in the larger ones decreases. Indeed, investigations on Ostwald ripening with sedimentation field-flow fractionation in fluorocarbon emulsions confirmed this theoretical prediction (242). This redistribution of the dispersed phase comes to an end when the capillary and the concentration forces (Raoult's law) are in equilibrium. The equilibrium condition requires that the chemical potential of the monomer is the same in all particles. Equation 24 illustrates the situation at equilibrium (subscript e) regarding the lyophob for two particles [superscripts (1) and (2)] of different diameters, where v_m is the molar volume of the monomer.

$$\phi_{L,e}^{1} - \frac{4\sigma v_{mon}}{k_B T} \frac{1}{D_{d,e}^{(1)}} = \phi_{L,e}^{2} - \frac{4\sigma v_{mon}}{k_B T} \frac{1}{D_{d,e}^{(2)}} \tag{24}$$

Compensating for the Ostwald ripening requires ϕ_L values depending on the droplet size, in the sense that smaller drops require a higher ϕ_L and *vice versa*. However, this is practically impossible to control during the initial emulsification process and consequently, Ostwlad ripening inevitably takes place during and after any emulsification process and leads to a change in droplet size distribution during a certain maturation time. An equilibrium size distribution can be reached and Ostwald ripening will stop if between the average drop size ($\bar{D}_{d,i}$) and ϕ_L at the end of the comminution process (subscript i) the inequality given by equation 25 holds. A detailed discussion and derivation of the equations can be found in References 239 and 241.

$$\phi_{L,i} > \frac{4\sigma v_{mon}}{3k_B T\, \bar{D}_{d,i}} \tag{25}$$

If this condition is not met, Ostwald ripening will further increase the differences in the chemical potential for particles with different sizes. This means that

Table 9. Water Solubility of Monomers

Monomer	Solubility, *M*	Temperature	Source
n-Octyl acrylate	0.00034	25–50°C	253
Dimethylstyrene	0.00045	25–50°C	253
Vinyl neodecanoate	0.000504	20°C	254
2-Ethyl hexyl acrylate	0.0005389		255
2-Ethyl hexyl acrylate	0.000543	20°C	94
Vinyl neononanoate	0.000543	20°C	254
Vinyl 2-ethylhexanoate	0.000587	20°C	254
Vinyl toluene	0.001	25–50°C	253
n-Hexyl acrylate	0.0012	25–50°C	253
Styrene	0.00192		94
Styrene	0.002256	30°C	256
Styrene	0.00261	25°C	257
Styrene	0.002976	25°C	256
Styrene	0.003	20°C	255
Styrene	0.00308	40°C	257
Styrene	0.0035	25–50°C	353
Styrene	0.00368	50°C	257
n-Butyl methacrylate	0.00423		94
n-Butyl methacrylate	0.004389	20°C	255
Hydroxyoctyl methacrylate	0.005	50°C	259
Styrene	0.005568	30°C	256
Butadiene	0.00628	50°C, 760 mm Hg	257
Vinyl pivalate	0.0078	20°C	254
n-Butyl acrylate	0.0109		94
n-Butyl acrylate	0.011	20–50°C	253
Butadiene	0.011	30°C, 760 mm Hg	257
n-Butyl acrylate	0.0129		256
Chloroprene	0.013	25–50°C	253
Butadiene	0.015	25–50°C	253
Butadiene	0.0152	25°C, 760 mm Hg	257
n-Butyl acrylate	0.0161	20°C	254
n-butyl acrylate	0.0167	20°C	255
Butadiene	0.0229	15°C, 760 mm Hg	257
Butadiene	0.024	15°C, 798 mm Hg	256
Hydroxyhexyl methacrylate	0.037	50°C	258
Butadiene	0.0389	0°C, 760 mm Hg	257
Propyl methacrylate	0.0447		94
Ethyl methacrylate	0.0454		94
Propyl acrylate	0.05	20°C	255
Ethyl methacrylate	0.05	20°C	255
Vinylidene chloride	0.066	25–50°C	253
Methyl methacrylate	0.1498	30°C	256
Ethyl acrylate	0.15	25–50°C	253
Methyl methacrylate	0.15	25–50°C	253
Ethyl acrylate	0.1504	20°C	255
Methyl methacrylate	0.1504	20°C	255
Methyl methacrylate	0.159		94
Methyl methacrylate	0.1598	25°C	254
Vinyl chloride	0.1672	20°C	255

Table 9. (Continued)

Monomer	Solubility, M	Temperature	Source
Vinyl chloride	0.17	25 −50°C	253
Hydroxybutyl methacrylate	0.710	50°C	258
Ethyl acrylate	0.179		256
Ethyl acrylate	0.184		94
Vinyl acetate	0.232	20°C	254
Vinyl acetate	0.29	25–50°C	253
Vinyl acetate	0.29	28°C	256
Vinyl acetate	0.296	20°C	255
Hydroxypropyl methacrylate	0.382	50°C	258
Ethylene	0.4	25–50°C	253
Methyl acrylate	0.604		256
Methyl acrylate	0.616		94
Methyl acrylate	0.635	20°C	255
Methyl acrylate	0.65	25–50°C	253
Acrylonitrile	1.358	0°C	256
Acrylonitrile	1.376	20°C	256
Acrylonitrile	1.395	25°C	256
Acrylonitrile	1.6	25–50°C	253
Acrolein	3.1	25–50°C	253
Methacrylic acid	11.6	25°C	254
Hydroxyethyl methacrylate	∞	50°C	258

the addition of a completely water-insoluble hydrophobic compound during the emulsification also does not per se prevent Ostwald ripening. Ostwald ripening takes place in any case, except for an exactly monodisperse droplet size distribution, which is hard to realize in actual practice. Hexadecane, which is frequently used as lyophob in miniemulsion polymerization, has a water solubility of about $4 \times 10^{-11}\,M$ at room temperature (243), which is low but not zero. In this case the analysis of Ostwald ripening (241) shows that there exists a critical drop size ($D_{d,c}$) in the droplet size distribution for which the flux of the lyophob out of the drops is zero. The critical drop size is given by equation 26, where C_{LC} is the concentration of the lyophob in the continuous phase.

$$D_{d,c} = \frac{4v_{mon}\sigma}{k_B T \ln\left[C_{LC}/C_{LC0}\phi_L(D_{d,c})\right]} \tag{26}$$

Note that for $D_d > D_{d,c}$ and $D_d < D_{d,c}$, the flux is positive and negative, respectively. The characteristic time of the exchange of monomer from droplets during Ostwald ripening (τ_{ex}) is given by relation 27, where ϕ_{MC} is the dimensionless solubility of the monomer in the continuous phase ($\phi_{MC0} = C_{MC0}V_{mon}$) and D_{MC} is the monomer diffusion coefficient in the continuous phase.

$$\tau_{ex} \propto \frac{D_d^2}{\phi_{MC0} D_{MC}} \tag{27}$$

To preserve the droplets as reaction loci, the polymerization has to compete with the bleeding of the emulsion droplets (239). A consequence of these considerations is that the best lyophob for the preparation of emulsion droplets for subsequent polymerization are polymers in form of seed particles. Swelling is a thermodynamically controlled process and consequently, swollen seed particles are not subjected to degradation processes to the same extent as emulsion droplets made by comminution processes. Furthermore, in most cases the chemistry of the seed particles does not interfere with the final properties of the dispersion. For example a seed particle with a diameter of 20 nm represents in final particles of about 100 nm diameter only less than 1% of the total volume. However, seed processes with suppressed nucleation of new particles are not always the method of choice.

High Solids Polymer Dispersions. Polymer dispersions with higher solids content, clearly above 50 wt%, gain increasing interest for at least two reasons: increasing reactor capacity or productivity (cost reduction) and improved product properties (244–246). From the practical point of view the problem of high solids polymer dispersions is directly connected with rheology, as the viscosity of dispersions goes to infinity at certain solids content. The central problem is very general, that is, consideration of filling space with spheres goes back to Johannes Kepler. The stacking of cannon balls or oranges is intuitively done in a way that uses the available space in the most effective way. In two dimensions, exactly six spheres fit around a single sphere in the center, and six fit around each of the outer spheres. The next layer of spheres fits into the hollows of the first layer and again there is a hexagonal pattern. Kepler suspected that this filling pattern (about 75%) is the tightest way to pack spheres, but he was unable to prove it. This is known as Kepler's conjecture and is still today a matter of research (247). For latex spheres close packing depends on the potential that imparts stability to them. Soft potentials interact over long distances and prevent closer contacts between the particles (cf stabilization). In this sense it is not the mass fraction (solids content) but the effective volume fraction (including a hydrodynamic layer thickness) that determines viscosity. To get latexes with solids content of about 70% or even higher requires polymodal particle size distributions with larger and smaller spheres (the smaller spheres have to fit in the interstitial space between the larger ones). This principle was successfully applied to get high solids polymer latexes, with up to 70% solids content and low viscosity (245). It was found that there is a critical ratio between the larger and smaller sphere diameters, which should be above 10 in order to get both low viscosities and high solids content. The preparation of polymodal latexes requires the occurrence of multiple nucleation events in the course of the polymerization, which can be realized either by emulsifier feeding policies (244,246) and/or by proper choice of recipe components (comonomers) (245). In summary, the application of seed particles in heterophase polymerizations is very promising and indeed, for many industrial polymerizations state-of-the-art (39). Furthermore, particles with special properties such as particle size, monodispersity, functionality, and porosity are prepared by the application of seed particles and activated swelling procedures [cf below and (248–250,252)].

Solubility and Solubilization in the Continuous Phase

Monomers. One of the most important properties of a particular monomer or monomer mixture that is subjected to heterophase polymerization is its solubility in the continuous phase. Table 9 summarizes the water solubility of monomers, which are frequently used in heterophase polymerizations. Monomers with different water solubility of course behave differently during the polymerization process in several ways. Although the data in Table 9 for a particular monomer show some scatter they confirm that there is indeed no limit for monomers with regard to their water solubility to be applied in heterophase polymerization. Even if the monomers are so hydrophilic that their polymers are water-soluble they can be applied as comonomers together with more hydrophobic monomers. Of course, the water solubility of monomers depends on temperature, and for gaseous monomers also on pressure, as indicated in Table 9. However, the water-solubility is not always a linear function of temperature, as is demonstrated in Figure 25 for styrene and methyl methacrylate. Besides the range of the solubility, the shape of the curves is also distinctly different for both monomers. Whereas the water solubility for styrene increases over the entire temperature range, the curve for methyl methacrylate goes through a shallow minimum at about 45°C. At temperatures

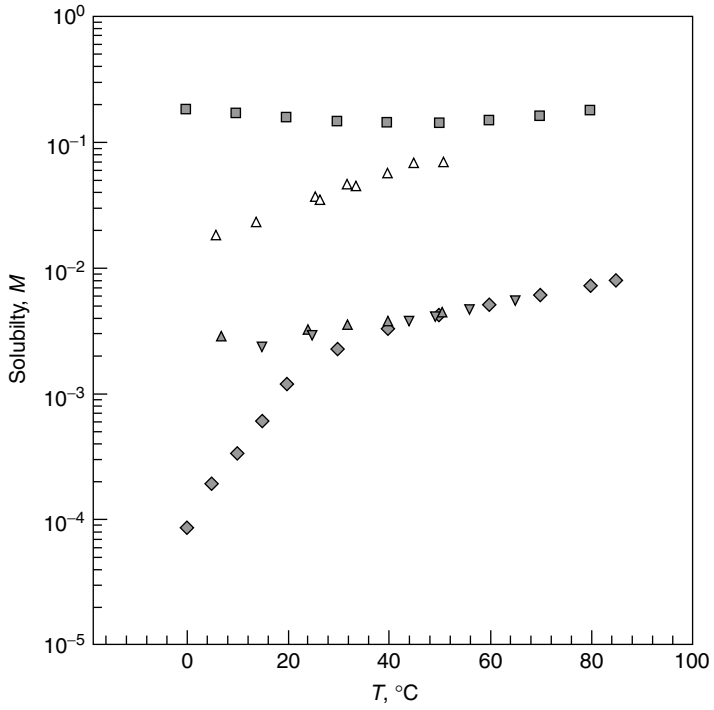

Fig. 25. Solubility values for styrene and methyl methacrylate in aqueous emulsions. △ water in styrene, determined with either Karl–Fischer titration or cloud point (261); ▲ strene in water, determined with formaldehyde–sulfuric acid reagent (261); ▽ styrene in water determined via cloud point (261); ◇ MMA in water (260); □ (262).

Table 10. Interfacial Tensions between Monomer Droplets ($\sigma_{m,w}$) and the Corresponding Polymer Particles ($\sigma_{p,w}$) and Water, and Surface Area of Sodium Dodecyl Sulfate Occupied at Saturation (a_S)

Monomer/polymer	$\sigma_{m,w}$, mN/m	$\sigma_{p,w}$, mN/m[a]	a_S[a] nm^2
Methyl acrylate	13–14[a]	1.75	
Vinyl acetate	18–19[a]	23.5	1.1
Ethyl acrylate	21–22[a]		0.90
Propyl acrylate	26–27[a]		0.69
n-Butyl acrylate	30–31[a]		0.60
Styrene	40–43[a]	32.7	0.50
Vinyl chloride	20.2[b]	37.8	0.40
Methyl methacrylate	20.8[b]	26.0	0.79
n-Butyl methacrylate	38.7[b]	36.7	0.54
n-Octyl methacrylate	51.6[b]		

[a]Values from Ref. 255.
[b]Values calculated from the regression $\sigma_{m,w} = -11.667 \times \log C_{m,w} + 11.179$, which was determined from data given in Ref. 255.

below 25°C the values for styrene obtained with different methods do not agree closely, but at temperatures above 40°C the agreement is almost perfect. Furthermore, Figure 25 reveals that it is always necessary to consider mutual solubilities for a particular monomer/water combination as not only monomers are soluble in water but water also is soluble in monomers. In the case of some hydrophobic monomers like styrene, the solubility of water in the organic phase is even higher than that of the monomer in water. This is the case for many alkanes and alcohols as well (259). The consequence of this fact is of some importance as together with water, hydrophilic radicals may enter the monomer phase and start polymerization. Moreover, as the forces between the molecules of the liquids forming an emulsion (the cohesive and adhesive forces) determine not only the interfacial tension but also the mutual solubilities there is a relation between the interfacial tension and the miscibility (the higher the miscibility, the lower is the interfacial tension). Table 10 summarizes values for the interfacial tension between monomer droplets and the corresponding polymer particles and water, respectively, which clearly show this effect. The interfacial tensions of polymer–water interfaces are not directly accessible, but have been calculated mainly on the basis of polymer polarity data (255). Furthermore, Table 10 shows that the sodium dodecylsulfate adsorption on the polymer particles is also influenced by the polarity of the polymer surface. There is a general rule: the higher the polarity of the interface, the larger is the area covered by one sodium dodecylsulfate molecule in a saturated adsorption layer. Consequently, the lower the number of stabilizing groups per unit area, the higher is the polarity of the interface. Thus, the hydrophilicity of a monomer and the polarity of a polymer have direct influence on all colloid chemical properties during heterophase polymerization, as the interfacial tension influences nucleation, swelling of the particles with monomer, surfactant adsorption, and stability of the droplets/particles. Also, the polymerization kinetics in both phases is influenced because the rate of polymerization is directly proportional to the monomer concentration (cf above)..

Table 11. Solubility and Solubilization of Organic Molecules (Monomers and *n*-Heptyl Mercaptan) in Water and Surfactant Solutions, Respectively[a]

Monomer	Surfactant	Solubility/solubilization, *M*
Butadiene	None	0.0351,50°C, saturation pressure
Butadiene	2.8% SF[b]	0.196,50°C, saturation pressure
Styrene	None	0.00308, 40°C
Styrene	0.093 *M* KP	0.096,40°C
Styrene	None	0.00368, 50°C
Styrene	0.093 *M* KP[c]	0.139,50°C
MMA	None	0.1598, 25°C[d]
MMA	1% CTAB[e]	0.2
MMA	3% CTAB	0.32
n-Hm[f]	None	0.00007
n-HM	0.3 *M* SDS	0.0925

[a]From Ref. 264.
[b]SF is a commercial fatty acid surfactant.
[c]KP is potassium palmitate.
[d]Value from Ref. 254.
[e]DCTAB is cetyl trimethyl ammonium bromide.
[f]*n*-HM is *n*-heptyl mercaptan.

In the context of solubility it is necessary to briefly mention the phenomena of solubilization. This *terminus technicus* was introduced by J. W. McBain for a particular process of increasing the solution concentration of substances in a given medium (263). Solubilization can be understood as a sorption phenomenon as it leads to a decrease in the number of molecules of a substance in a reservoir outside the solution but in equilibrium with the solution, by adding an adsorbent to the solution (see ADSORPTION). For heterophase polymerizations the adsorbents are surfactant molecules, which decrease the number of molecules outside the continuous phase (eg in monomer droplets). The amount of the adsorbed or solubilized material increases steeply with increasing stabilizer concentration and levels in the vicinity of the cmc. Solubilization has nothing to do with a true solution but is an effect connected with colloidal systems, which can be formed either by micelles or other particles able to interact with the adsorbate. For aqueous heterophase polymerizations this means that the solubilizing power of micelles, or in other words the solubility of a monomer in a surfactant solution is much greater than in water (cf selected data in Table 11). As solubilization is mediated by micelles and hence colloidal in nature, it depends on the ionic strength in aqueous solution and on temperature.

Dissolved Gases. Oxygen is known to interfere with radical polymerization in different ways. On the one hand its presence leads to detrimental effects such as induction periods, retardation, and side products via peroxide formation. On the other hand in vinyl chloride emulsion polymerization, a certain level of oxygen leads in the presence of basic buffers to an acceleration of the polymerization as a result of decomposition of *in situ*–formed peroxides (265). Either at higher concentrations of oxygen or in the absence of buffer, retardation of the polymerization and long inhibition periods are observed. Studies of the influence of oxygen have been carried out since the beginning of heterophase polymerization

research, when oxygen was, even if unintentionally, the sole initiator (21,24). Under conditions of heterophase polymerization, it is important to consider oxygen partition between all phases. In principle, there are three places where oxygen can be found: in the headspace, the continuous phase, and the dispersed phase. In aqueous emulsion polymerization, most of the oxygen is concentrated in the headspace and smaller amounts only in organic phases and water. However, it is necessary to consider that the solubility of oxygen is higher in many organic solvents than in water (266).

In a calorimetric study of both seeded styrene and seeded styrene/butyl acrylate emulsion polymerization, the presence of oxygen leads to an inhibition period and in due course the redistribution of oxygen from the headspace causes a retardation of the reaction (267). The action of oxygen as both a water–soluble and a monomer–soluble gas was proven in a series of styrene emulsion polymerizations at 60°C with sodium dodecyl sulfate as emulsifier and potassium peroxodisulfate as initiator (268). The authors determined the saturation concentration of oxygen in watery solutions of various compositions at polymerization temperature. The saturation value for pure water, water plus emulsifier, and water plus emulsifier plus styrene was found to be 5.40, 5.58, and 6.53 ppm, respectively. A saturated continuous phase under polymerization conditions (water plus emulsifier plus styrene) sparged with nitrogen of high purity would decrease in dissolved oxygen to a level lower than 0.05 ppm in about 10 min. The authors observed a significant inhibition period only if oxygen is present in concentrations higher than 50% of the saturation concentration. Furthermore, at the end of the inhibition period the oxygen level in the aqueous phase was found to be about 3 ppm independent of the starting values. This experimental finding suggests that high enough initiation rates can outweigh the inhibition action of dissolved oxygen. Another action of dissolved gas, not only oxygen but also nitrogen or other inert gases, is its interference with the nucleation process, as was shown in Reference 91. The reproducibility during the nucleation stage of an ab initio emulsion polymerization was drastically improved if the water and the monomer were carefully degassed instead of purged with nitrogen prior to polymerization and if the water was added to the reactor at a temperature higher than polymerization temperature in order to avoid bubble generation.

Swelling of Polymer Particles

Swelling means that polymer particles in a dispersed state even in the presence of an excess amount of solvent for the polymer do not dissolve but imbibe only a limited amount of that solvent. The importance of this phenomenon for heterophase polymerizations becomes clear by the fact that most of the monomers (acrylates, methacrylates, styrene) are good solvents note only for their own but also other polymers. Thus, during heterophase polymerization monomer droplets and polymer particles can coexist side by side. Swelling is of special practical importance because the colloidal particles consisting of both polymer and monomer are the main reaction loci. The monomer concentration in swollen polymer particles is governed by equilibrating the free energy of mixing between polymer and monomer with the interfacial free energy of the particles and the swelling

pressure (cf equation 28) (121). The term on the right-hand side of equation 28 is the free energy of mixing between polymer and monomer, where the Flory–Huggins–Rehner expression for cross-linked polymers is used. In equation 28, σ is the interfacial tension between the swollen particles and the continuous phase, P_{SW} is the swelling pressure, χ_{mp} is the polymer monomer interaction parameter, ϕ_2 is the polymer volume fraction in the swollen particle, RT is the thermal energy, j is the average degree of polymerization of the polymer molecules, ρ_2 is the polymer density, and $\bar{M}_c$ is the average molecular weight between two cross-links in the network. If the latex particles are not cross-linked ($\bar{M}_c \Longrightarrow \infty$) and if P_{SW} 0, equation 28 becomes identical with the Morton–Kaizerman–Altier equation (269) also (270). Between ϕ_1, the monomer volume fraction, and ϕ_2, the relation $\phi_1 + \phi_2 = 1$ exists. The swollen (r) and unswollen particle radii (r_0) are connected with ϕ_2 via $(r/r_0)^3 = 1/\phi_2$, whereas ϕ_1 is related to $C_{M,p}$ via $\varphi_1 = C_{M,p} V_{mon} = \frac{V_{m,p}}{V_{m,p} + V_{p,p}}$, with $V_{m,p}$ and $V_{p,p}$ being the monomer volume and the polymer volume inside the swollen particles, respectively.

$$\left(\frac{2\sigma}{r} + P_{SW}\right)\frac{v_{mon}}{RT} = -\left[\ln(1-\phi_2) + \left(1 - \frac{1}{j}\right)\phi_2 + \chi_{m,p}\phi_2^2 + \frac{v_{mon}\rho_2}{\bar{M}_C}(\phi_2^{1/3} - \phi_2/2)\right] \tag{28}$$

The right-hand side of equation 28, except the last term, for which one needs to consider only for cross-linked particles, promotes swelling whereas the terms on the left-hand side counteract swelling. The first term on the left-hand side is the interfacial free energy, which counteracts swelling as a result of an increase in the particle interface. The second term on the left-hand side originates from a volume work due to attractive forces between polymer chains in concentrated solutions, as it has been concluded from osmotic modulus measurements (271). The pressure in equation 28 can be considered as swelling pressure of colloidal particles, comparable to that known from the swelling of macroscopic gels, contributing together with the partial molar free interfacial energy to the equilibrium with the chemical potential of the swelling agent ($\Delta\mu_1$). It can be in the order of up to 10 MPa, depending on the decoration of the particle interface (272). An illustration of the dependence of the equilibrium monomer volume fraction (ϕ_1) on the particle size is shown in Figure 26. The higher the ϕ_1, the larger are the particles, the lower is the interfacial tension, and the higher is the temperature, but it decreases with increasing degree of cross-linking and with increasing Flory–Huggins interaction parameter. The two limiting cases of equation 28 for $r \Longrightarrow \infty$ and $\phi_2 \Longrightarrow$ o is of special meaning. In the case of a bulk polymer ($r \Longrightarrow \infty$) the resulting equation is the osmotic or swelling pressure relation given by the equation $\Delta\mu_1 = -\Pi_s V_{mon}$, with $P_{SW} = -\pi_s$. If the polymer concentration is vanishing ($\phi_2 \Longrightarrow 0$), the result is the Young–Laplace equation ($\Delta P_d = 2\sigma/r$) for a colloidal droplet or bubble embedded in a fluid phase. This behavior can be regarded as expression of the situation that the swollen latex particles represent a polymer gel or solution but with colloidal dimensions. Equation 28 considers the influence of surfactants on swelling only via the interfacial tension. But this may be insufficient as entropy effects are completely neglected. The above results

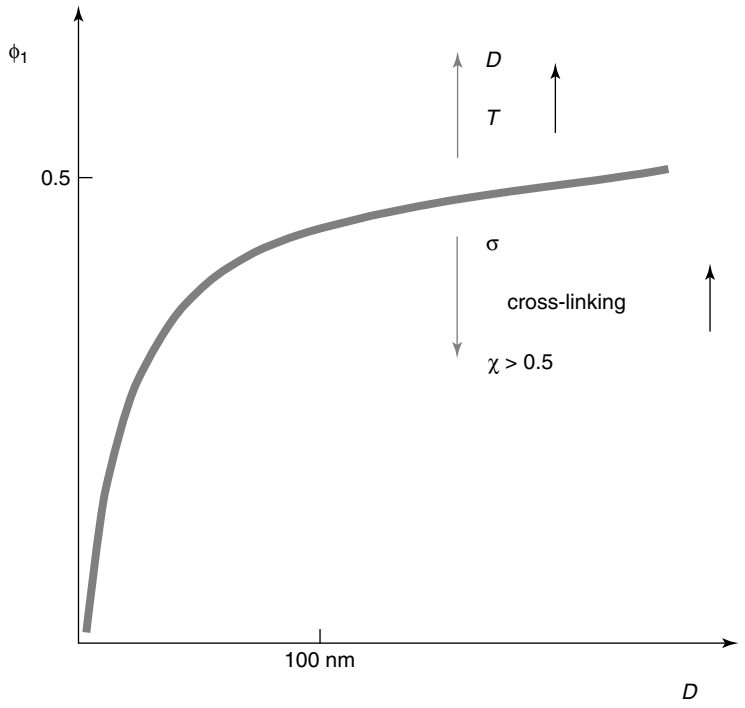

Fig. 26. Illustration of the dependence of ϕ_2 on polymer and particle parameters.

with regard to the behavior of swollen micelles, which are stable as long as the monomer is not polymerized and the surfactant tails can keep their mobility, demonstrate the influence of entropic effects on surfactant–monomer interaction. For monomer partition inside swollen latex particles, which are stabilized with adsorbed surfactants these effects favor the formation of a monomer rich shell rather than a uniform distribution throughout the whole particle volume. This effect is very similar to adsolubilization, which describes the solubilization of organic compounds inside adsorbed stabilizer layers on inorganic particles in order to modify them by admicellar polymerization (273). There is clear experimental evidence by small-angle X-ray scattering that in poly(methyl methacrylate) particles swollen with methyl methacrylate the monomer is concentrated inside an outer shell of approximately 2-nm thickness. The particles were stabilized with two kinds of surfactants: sodium dodecylsulfate, which was present already during the polymerization, and sodium dodecylbenzenesulfate, which was added during the swelling experiments to avoid coagulation (274). Swollen polymer particles are high concentration polymer solutions (about 50% by weight) and hence, the swelling pressure counteracts swelling due to attractive forces between entangled polymer chains and might contribute to formation of the monomer-rich shell. This gradient with regard to monomer concentration inside swollen particles should cause during polymerizations, especially in seeded polymerizations, a morphology gradient with regard to composition. In this sense, the morphology of polymer particles in heterophase polymerization, especially emulsion polymerization, has

been a matter of ongoing discussion for several decades (275–279). The monomer concentration inside the particles as main reaction loci (ie swelling of latex particles) determines rate of polymerization, particle morphology, molecular weight, and in copolymerizations the chemical composition also of the copolymers. Consequently, methods either to measure or to predict the monomer concentration inside particles are a key aspect in heterophase polymerization research and are of permanent importance (280–282).

John Ugelstad's theoretical and experimental work to development new methods of monomer emulsion preparation (283) makes good use of one of the pillars of colloid science, the Kelvin equation. The Kelvin equation says that larger objects, in coexistence with smaller ones, will grow in size at the expense of the smaller objects, which have a tendency to dissolve. This effect is known in colloid science as Ostwald ripening (discussed earlier). Equation 29 shows the Kelvin equation for liquid droplets surrounded by vapor where p' is the vapor pressure outside the drop, p_0 is the bulk vapor pressure, v″ is the molar volume of the liquid, and RT is the thermal energy (284). The smaller the radius of the drops (r), the larger is p' and hence, the higher the tendency to degrade.

$$\ln\frac{p'}{p_0} = \frac{2\sigma}{r}\frac{v''}{\mathrm{RT}} \tag{29}$$

However, as discussed above, the dissolution can be retarded or even prevented if the drops contain a substance that is insoluble in the continuous phase (compound 2 or lyophob). In this case the decrease in size increases the chemical potential of the lyophob inside the smaller drops and generates a force counteracting Ostwald ripening. A detailed discussion of emulsion stability with regard to subsequent polymerization can be found in Reference 239. In addition to the stabilizing effect of compound 2, Ugelstad was able to show that compound 2 has an additional effect on swelling, as the entropy term in the swelling equation (eq. 28), is $(1 - 1/j)\phi_2$, becomes more and more important as long as compound 2 has a low molecular weight (or suppose it is an oligomer where j is in the order of about 5). On the basis of these two effects, Ugelstad and co-workers developed an activated two-step swelling procedure, which enabled them to prepare and to commercialize large monodisperse particles for various applications as high value specialty polymer colloids (251,285). In brief, in the first step an emulsion of the low molecular and highly water-insoluble compound 2, which may contain a solvent that is water-soluble, is added to a suspension of polymer particles (seed). The solvent promotes the transport of compound 2 through the aqueous phase and allows swelling of the polymer particles, which is further facilitated if the emulsion droplets are smaller than the seed particles (action of the Kelvin equation). Then, in a second swelling step the monomer emulsion is added. Because of the high entropy gain caused by mixing of compound 2, with the monomer inside the particles the swelling ability of the seed is activated compared to particles without compound 2. For instance, using dioctyladipate as compound 2, it was possible to swell polystyrene particles with a diameter of 1.55 μm with chlorobenzene as model compound to a diameter of about 30 μm, ie the seed particles imbibed more than a 7000-fold amount of their own volume. During subsequent polymerization,

if instead of chlorobenzene a monomer is used in the second swelling step, precautions are necessary to avoid nucleation of new particles. The interaction between monomers and polymers during heterophase polymerizations is very complex and determines essential features of the particular heterophase polymerization technique such as polymerization rate and particle morphology. A control of swelling enables the preparation of polymer particles with specially tailored properties.

Shrinkage of Monomer-Swollen Polymer Particles

Any polymerization reaction causes a decrease in the average distance between the acting molecules, ie the average distance between individual monomer molecules is larger than that between the repeating units in the polymer. This causes an increase in density although the length of a carbon–carbon double bond is shorter than that of single bond. Table 12 summarizes densities of selected monomers and polymers, which play an important role in heterophase polymerization. The densities of the monomers depend much more on the temperature than those for the polymers, as shown in Figure 27. To illustrate the shrinkage, the volume per monomer molecule and per repeating unit $v_{\mathrm{mol}}^{\mathrm{mon}}$ and $v_{\mathrm{ru}}^{\mathrm{mol}}$, respectively, can be calculated by means of equation 30, where M_{mon} is the molecular weight of the monomer, N_{A} the Avogadro's number, and ρ_1 and ρ_2 are the monomer and polymer densities, respectively..

Table 12. Densities of Selected Monomers (ρ_{m}) and Corresponding Polymers (ρ_{p}) at Various Temperatures

	Monomer		Polymer	
	T°C	ρm[a] g/cm^3	$T^{\circ}C$	ρp,[b] g/cm^3
Methyl methacrylate	20	0.9428	0	1.195
	40	0.9203	20	1.190
	60	0.8971	25	1.180
	80	0.8730		
Styrene	20	0.9049		ρ_{p}- 1.04–1.065; Average $\rho_{\mathrm{p}} = 1.05$
	40	0.8869		
	60	0.8686		
	80	0.8498		
Vinyl chloride	20	0.9115		ρ_{p}- 1.391–1.431; depending on polymerization temperature, average ρ_{p}- 1.40
	40	0.8760		
	60	0.8375		
	80	0.7950		
Vinyl acetate	20	0.9323	20	1.191
	40	0.9075	25	1.190
	60	0.8816	50	1.17
	80	0.8544	1120	1.110

[a]Values taken from Ref. 286.
[b]Values taken from Ref. 287.

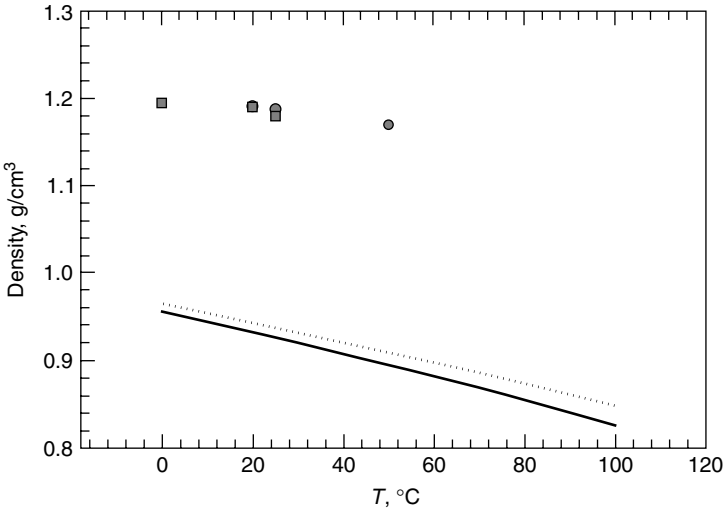

Fig. 27. The dependence of density of selected monomers and polymers on temperature (cf also Table 12). — Vinyl acetate; -●- poly(vinly acetate); ····· methyl methacrylate; -□- poly(metnyl methacrylate).

$$v_{\mathrm{mol}}^{\mathrm{mon}} = \frac{M_{\mathrm{mon}}}{N_{\mathrm{A}}\rho_1} \; v_{\mathrm{mol}}^{\mathrm{ru}} = \frac{M_{\mathrm{mon}}}{N_{\mathrm{A}}\rho_2} \tag{30}$$

With the data given in Table 12 the corresponding values for styrene are, at 80°C when the average polystyrene density of 1.05 g/cm^3 is used, $v_{\mathrm{mol}}^{\mathrm{mon}} = 2.04 \times 10^{-22}$ cm^3 and $v_{\mathrm{mol}}^{\mathrm{ru}} = 1.65 \times 10^{-22}$ cm^3. These values mean that styrene drops, under the assumption that there is no mass transfer, would shrink from the start until the end of the polymerization at 80°C by about 19.12%. This is an enormous number and has in the case of heterophase polymerizations much more important consequences than for homogeneous polymerizations, where the reaction volume shrinks evenly. The sketch in Figure 28 elucidates these consequences. Case A is the ideal behavior where a polymerization proceeds smoothly within a droplet beginning from the center and ending with an evenly shrunk particle with homogeneous density throughout the whole particle volume. Case B represents the other extreme where polymerization starts at the particle–water interface and thus, a shell is formed that might prevent shrinkage of the polymerizing drop (indicated by the stacking of the triangles). In that case, as polymerization proceeds, monomer moves from the center to the shell as a result of swelling and leaves just one big hole in the middle. Because the size of the final particle is that of the starting drop, this process is called constraint shrinkage. Case C is intended to illustrate the real situation where polymerization begins at many sites inside a drop. In that case shrinkage is in between both extremes, and a void structure on the nanometer-size scale characterizes the particle morphology. Equations 31 can be used to quantify the droplet shrinkage and to estimate the magnitude of the

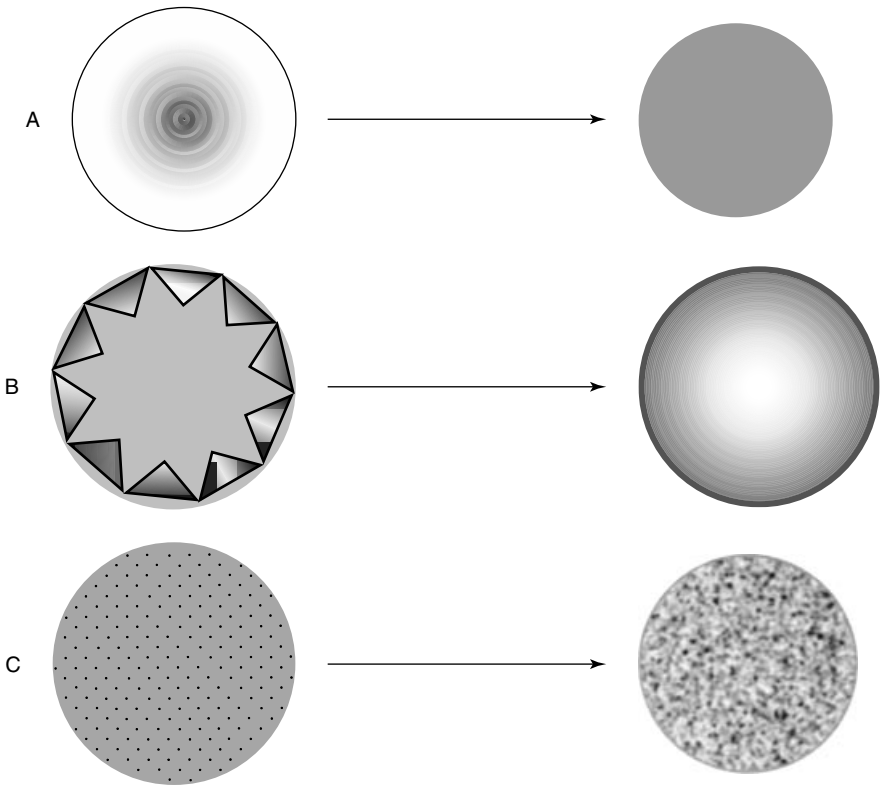

Fig. 28. Illustration of effects caused by volume shrinkage during polymerization in discrete particles.

effects. D_p and D_m denote the polymer particle and monomer droplet diameter, respectively, ΔD is the decrease in diameter due to shrinkage according to case A, and d_h is the size of the single hole formed as described in case B (cf Fig. 28).

$$D_p = D_m \left(\frac{\rho_m}{\rho_p}\right)^{1/3} \quad \Delta D = D_m \left[1 - \left(\frac{\rho_m}{\rho_p}\right)^{1/3}\right] \quad d_h = D_m \left(1 - \frac{\rho_m}{\rho_p}\right)^{1/3} \tag{31}$$

The data plotted in Figure 29 show the development of Δ_D and d_h for styrene and vinyl chloride polymerizations in dependence on temperature, where for the polymers the average density value as given in Table 8 were used. These model calculations show that shrinkage is an important factor during heterophase polymerization, which decisively influences particle morphology and should not be neglected, especially not in cases where the polymerization takes place mainly inside monomer-swollen droplets. Shrinkage may lead to porous particles and can also be utilized to prepare hollow particles.

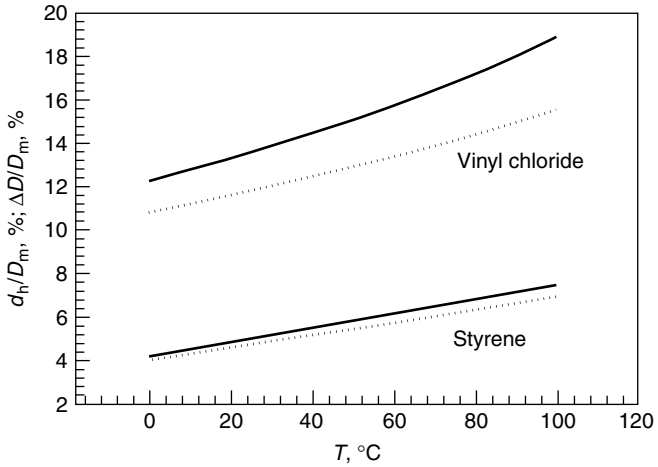

Fig. 29. Shrinkage and hole diameter with respect to the droplet size for polymerization of styrene and vinyl chloride in dependence on polymerization temperature (according to equations 31 and case A and B in Fig. 28). — ΔD; $\cdots\cdots$ d_h.

Stabilization and Stabilizers

The excess interfacial energy of polymer dispersions, compared with bulk or solution systems, is the driving force for an inherent tendency to decrease the interfacial area and hence, to instability. Stabilization of particles and droplets was recognized as a key issue in heterophase polymerization from the very beginning, when Kurt Gottlob described in the first patent (21) the utilization of natural polymers such as starch, egg albumin, or gelatin as stabilizers. Some excellent contributions placing special emphasis on colloidal stabilization in connection with heterophase polymerization can be found in References 288–291. The most important principle of stabilization is that the stabilizer or the stabilizing groups must be soluble in or strongly interacting with the continuous phase. This principle is known as Bancroft's rule and was formulated in 1912 by Wilder Bancroft in a paper on titled The Theory of Emulsification, when he generalized the results of emulsification experiments known at that time: "When water is the dispersing phase, the emulsifying agent should be a hydrophile colloid. . ., the emulsifying agent should be an oleophile colloid in case the emulsion is to contain water in drops" (292). The same principle is behind the empirical HLB (hydrophilic–lipophilic balance) concept, which was developed mid-20th century in order to make the choice of the most effective emulsifier for a desired emulsion easier (293). Hydrophilic emulsifiers, which favor the formation of oil-in-water emulsions have HLB numbers greater than 10, whereas emulsifiers that are more soluble in oil phases have lower HLB numbers and stabilize water–in–oil emulsions more easily. A scientific basis for the HLB concept can be found in the cohesive energy ratio of emulsions that was developed by Beerbower and Hill (294) and which was successfully applied to formulate for instance polymerizable microemulsions (295). Stability is achieved if the Gibbs free energy of mixing is negative. In this sense colloids can be of two basic types, lyophobic and lyophilic. Lyophilic colloids interact strongly

whereas lyophobic colloids have only a very restricted interaction with the continuous phase. Polymer dispersions can be of both types. Examples of lyophilic polymer dispersions, which can also be absolutely stable in a stricter thermodynamic sense are block copolymers in selected solvents or microgel particles such as cross-linked polystyrene in toluene or cross-linked poly(styrene sulfonate) particles in water. In contrast lyophobic polymer colloids in a bare state are thermodynamically unstable and need, in order to keep dispersed for a longer period of time, to be stabilized by third substances.

Attractive Forces. The origin of attractive forces, which are summarized as van der Waals forces, between adjacent particles is the interaction between the molecules and atoms of which the particles are made and is basically electromagnetic in nature. There are three sources of forces attracting uncharged molecules: First, forces produced by aligned permanent dipoles in separate molecules (Keesom forces). Second, forces between permanent dipoles and induced dipoles (Debye forces). Both forces account mainly for binary interactions, because two dipoles, which are in optimum alignment for attractive interaction, cannot be at the same time in the optimum position for attractive interaction with a third molecule. The third kind of forces are of quantum-mechanical nature (London forces) and caused by interaction due to the coupling of random fluctuations of the electrical fields of adjacent molecules, which reduces the free energy and hence are attractive. The London attractive forces are fundamentally different from Keesom or Debye forces, as a molecule can interact by means of London forces with all molecules in its neighborhood at the same time. The attractive potential energy (V_A) decreases with increasing separation distance (d_{pp}) according to equation 32, where k_L is the London interaction constant, Z is the number of electrons in the outer shell, ν_c is the frequency of the fluctuations, h is Planck's constant, and α_0 the static polarizability of the molecules.

$$V_A = -\frac{k_L}{d_{pp}^6}\; k_L = 0.75 Z^{0.5} h \nu_c \alpha_0^2 \tag{32}$$

The calculation of the attractive potential between condensed particles separated by vacuum goes back to Hamaker (296–298). He obtained, under the assumption that the pairwise interaction as used by London for gas molecules can be applied to condensed phases, from an integration over all possible interactions between attracting elements of two particles the following expression (eq. 33), where A is the Hamaker constant, which has the dimension of energy, q is the concentration of interacting centers per unit volume, and H a geometrical function of the particles. An approximate expression of H is given for two spheres of radius r at distance $d_{pp} \ll r$. Equation 33 shows that the energy of attraction varies with the reciprocal of the separation distance. Model calculations have shown that it might be of importance over a distance of tens of nanometers rather than within the close-contact region below 1 nm.

$$V_A = -AH\; A = \pi^2 q^2 k_L\; H = \frac{D}{2} \cdot \frac{1}{d_{pp \cdot 12}} \tag{33}$$

There are several possibilities to refine these calculations such as the consideration of correlation frequencies over the whole spectral range (London considered only ultraviolet frequencies) and the use of a continuum electrodynamic model rather than the assumption of pairwise interaction. Notwithstanding these problems, the Hamaker model can also be applied to the interaction of condensed particles in liquid media to gain knowledge of the basic principles. As the electromagnetic coupling of fluctuating dipoles needs a certain time the fluctuations can move out of phase in dependence on the distance of the interacting particles, which leads to decreasing attractive potential (retardation effect). The properties of the intervening medium between interacting bodies contribute in specific ways. The primary medium effect is due to the medium influence on the transmission of the electromagnetic field between interacting particles. The strength of the radiation of the electric field depends inversely on the dielectric constant, and the optical path length between interacting particles increases in proportional to the square root of the dielectric constant of the medium. The latter influences the retardation effect and reduces attraction. The secondary medium effect considers the finite attraction between particles and molecules of the continuous phase. Under such circumstances the attractive energy is smaller than that between the particles in vacuum, and for the energy balance one has to consider that particle–molecule contacts of the medium will be replaced by particle–particle contacts. This means that chemically identical or similar particles will attract each other, but that this must not necessarily be the case for chemically different particles, where under particular circumstances the dispersed state may be energetically favored. For attracting particles the secondary medium effect finds its expression in a so–called effective Hamaker constant, as defined by equation 34, where A_p is the Hamaker constant of the polymeric particles and A_m that of the medium in vacuum.

$$A_{eff} = \left(A_p^{1/2} - A_m^{1/2}\right)^2 \tag{34}$$

Some values of Hamaker constants for various polymers and liquids that can be applied as continuous phase in heterophase polymerizations are put together in Tables 13 and 14. These data reveal that effective Hamaker constants are clearly smaller than the values for the corresponding polymers and continuous phases. However, the data collected in Table 13 show that Hamaker constants of various polymers are not that much different but the values obtained with different methods for the same polymer differ much more. Consequently, before using values of Hamaker constants it is always necessary to check their origin in order to be sure to compare values obtained with same approximations. According to equation 34 it is possible that the effective Hamaker constant, and hence the London attraction forces also, can be zero. Such situations are virtually obtained in the case of lyophilic microgel particles, which are highly swollen with dispersion medium.

To counteract the attractive forces in lyophobic colloids repulsive forces must operate and consequently, the question regarding an overall interaction potential between colloidal particles arises. Equation 31 leads for separation distances close

Table 13. Hamaker Constants for Different Polymers (A in 10^{-20} J) Calculated with Different Approximate Procedures[a]

Polymer	1[b]	2[c]	3[d]	4[e]	5[f]	6[g]
Polystyrene	4.62	7.7	7.7	—	5.7	3.46
Poly(ethylene terephthalate)	3.94	8.4	6.4	4.0	5.2	3.05
Polyethylene	3.97	8.25	6.2	—	4.4	3.08
Polypropylene	3.87	8.25	6.2	—	3.6	3.06
Polyamide-6	3.33	8.1	6.1	4.3	4.7	2.59
Polyacrylonitrile	3.47	8.0	6.0	2.8	—	2.96
Regenerated cellulose	4.19	—	6.5	3.9	3.8	—

[a] From Ref. 299.
[b] From spectroscopic data with ionization energy I_E, $A = 27\, I_E(\epsilon-1)^2/[64(\epsilon + 2)^2]$
[c] Same equation in footnote b but from refractive index measurements.
[d] Approximate formula, $A = 4.02 \times 10^{-19}((\varepsilon - 1)/(\varepsilon + 1))^2$.
[e] Approximate formula, $A = 6\pi\, r^2\, \gamma_s{}^d$, where $\gamma_s{}^d$ is the surface tension dispersion part, and $6\pi r^2$ is the size of interacting surface volume element.
[f] Same approximate formula as in footnote e but different methods to determine $\gamma_s{}^d$.
[g] Approximate formula, $A_{11} = 0.75 h v_c\, \alpha_0^2\{1 - [3\pi q \alpha_0(\varepsilon - 1)/(\varepsilon + 1) - 1.5]\}$.

Table 14. Effective Hamaker Constants for Different Combinations of Materials

	$A_{eff} \times 10^{-20}$ J	
Material	Air	H_2O
Water[a]	3.7	0
Pentane	3.8	0.3
Hexane	4.1	0.4
Decane	4.8	0.5
Tetradecane	5.1	0.5
Hexadecane	5.2	0.5
Paraffin wax[b]		0.02
Poly(methyl methacrylate)[c]	7.11	1.05
Poly(vinyl chloride)[c]	7.78	1.30
Polystyrene[c]	6.58	0.95
Polystyrene[c]	6.37	0.911
Polyisoprene[c]	5.99	0.437
Polytetrafluoroethylene[c]	3.8	0.333

[a] Values taken from Ref. 300.
[b] Values taken from Ref. 301 (cf. footnote d in Table 13).
[c] Values taken From Ref. 302.

to zero to an infinite attraction. However, this result contradicts the practical experience that any material can be comminuted into colloidal objects.

Repulsive Forces. For an overall balance of interaction forces, one has to consider the repulsion that occurs if surfaces come as close as an atomic diameter together. This strong repulsion is known as Born repulsion ($V_{R,B}$) and changes in proportion to d_{pp}^{-x}, where x is a number of order larger than 10 (290). As the Born repulsive potential acts only at separation distances of atomic diameters, it does not contribute to the stability of colloidal polymer dispersions. There are

other forces counteracting already the inherent attraction at larger separation distances.

Charge Stabilization. The contact between materials with different dielectric constants leads according to Coehn's rule (303,304) to electric charges, as the material with the lower permittivity charges negatively. For water as continuous phase, with a permittivity of about 80, which is larger than that of polymers and many inorganic materials, this means that interfaces in contact will charge negatively. Coehn's rule means furthermore that charge stabilization is inherently present in colloidal systems.

For practical applications in polymer dispersions (ie also during heterophase polymerizations) the effect of charge stabilization due to permanent charges, either by ionic stabilizers, comonomers, or initiator fragments, is much more important. The repulsive potential between two equally charged particles ($V_{R,es}$) separated at a center-to-center distance of ($d_{pp} + D$) is given by equation 35, where Q is the charge on each particle and α is the permittivity of the continuous phase.

$$V_{R,es} = \frac{Q^2}{(d_{pp} + D)\varepsilon} \tag{35}$$

Equation 35 can be rewritten by using the capacitance of a conducting sphere ($CD\varepsilon/2$) and the surface potential ($\Psi = Q/C$) in the form of equation 36.

$$V_{R,es} = \frac{\Psi^2 \left(D/2\right)^2 \varepsilon}{\left(d_{pp} + D\right)} \tag{36}$$

A closer inspection of equation 36 reveals that (*1*) particles in water have both larger capacitance and repulsive potential than those in organic continuous media, (*2*) the repulsive potential falls with increasing separation between the particles, and (*3*) at separation distances much smaller than the particle size, larger particles are easier to stabilize than smaller ones because $V_{R,es} = (D/4)\varepsilon \times \zeta$ and the ratio $V_{R,es}\ V_A$ is independent of D. For electrostatically stabilized particles the interaction energy between two approaching particles can be calculated by means of a theory, which was developed independently during the 1940s by Derjagin and Landau in the former Soviet Union and by Verwey and Overbeek in the Netherlands. This so–called DLVO theory assumes that long-range interactions determine colloidal stability and hence, the interaction potential (V_{int}) is calculated as the sum of attractive van der Waals–London forces and repulsive electrostatic forces based on the Goy–Chapman theory of charge distribution near a surface (305). Equations 37a–c can be used to calculate V_{int} in dependence on the separation distance in order to get insight into the principles of the interaction between charge-stabilized colloids. In these equations A_{eff} is the effective Hamaker constant of particles interacting through the continuous phase, V_{salt} is the ionic strength, κ^{-1} is the Debye screening length, ε and ε_0 are the permittivities in the continuous phase and in vacuum, z is the stoichiometric valency of the electrolyte,

and Ψ is the surface potential of the particles.

$$V_{\text{int}}(d_{\text{PP}}) = \pi a\left[-\frac{A_{\text{eff}}}{12\pi}\frac{1}{d_{\text{PP}}} + \frac{64k_{\text{B}}TC_{\text{salt}}\Gamma_0^2}{\kappa^2}\exp(-\kappa d_{\text{PP}})\right] \tag{37a}$$

$$\kappa^{-1} = \left(\frac{\varepsilon\varepsilon_0 k_{\text{B}}T}{\sum_i (z_{\text{i}}e)^2 C_{\text{salt}}}\right)^{0.5} \tag{37b}$$

$$\Gamma_0 = \tanh\left(\frac{ze\Psi}{4k_{\text{B}}T}\right) \tag{37c}$$

Figures 30a and 30b illustrate the interaction between charged particles in dependence on particle size and ionic strength in the continuous phase. Both parameters (D and V_{salt}) have a strong influence on the interaction potential. The maximum at small separation distances (usually d_{pp} <10 nm) in the interaction potential, which is frequently called primary maximum, prevents the particles from coagulating irreversibly in the primary minimum, which is at still smaller separation distances and which has a depth of approximately twice the dispersive contribution to the surface energy of the particles. The primary maximum is larger, the larger the particles at a given ionic strength, and is smaller, the higher the ionic strength at a given particle size. Furthermore, the depth of the secondary minimum also depends on particle size and ionic strength and is responsible for much looser particle aggregation than in the primary minimum, where the colloidal system is completely unstable. At high ionic strength (Fig. 30b at $C_{\text{salt}} = 10^{-1}$ M) the primary maximum vanishes and the electrostatic system becomes unstable to coagulation. On the other hand at low ionic strength the repulsive forces are extended to pretty large distances. This is an effect that essentially contributes to the crystallization of monodisperse polymer colloids, which occurs at still lower ionic strength. The ionic strength has a strong influence on the Debye screening length (eq. 37b), which determines at which distance a particle recognizes a second particle in his neighborhood. For example, at ionic strengths of 1×10^{-3}, 1×10^{-2}, 1×10^{-1}, and 1 M, the Debye screening length κ^{-1} is 9.2, 2.9, 0.92, and 0.29 nm, respectively. For the sake of completeness, heterocoagulation is the *terminus technicus* for association of oppositely charged particles that are either of the same or different size and are composed either of the same or different materials. This technique can be utilized to prepare polymer particles with special architecture (290).

Perikinetic and Orthokinetic Flocculation. Particles in a dispersion are subjected under any circumstances to Brownian motion (the average velocity is distributed according to the Boltzmann exponential law) and hence, it is the absolute barrier height compared to the thermal energy ($k_{\text{B}}T$) that determines stability. This means that larger particles are more stable against thermal motion (perikinetic flocculation) than smaller particles. However, of practical importance during heterophase polymerization is the behavior of particles in dependence on the stirrer speed (orthokinetic flocculation), where their velocity depends on the

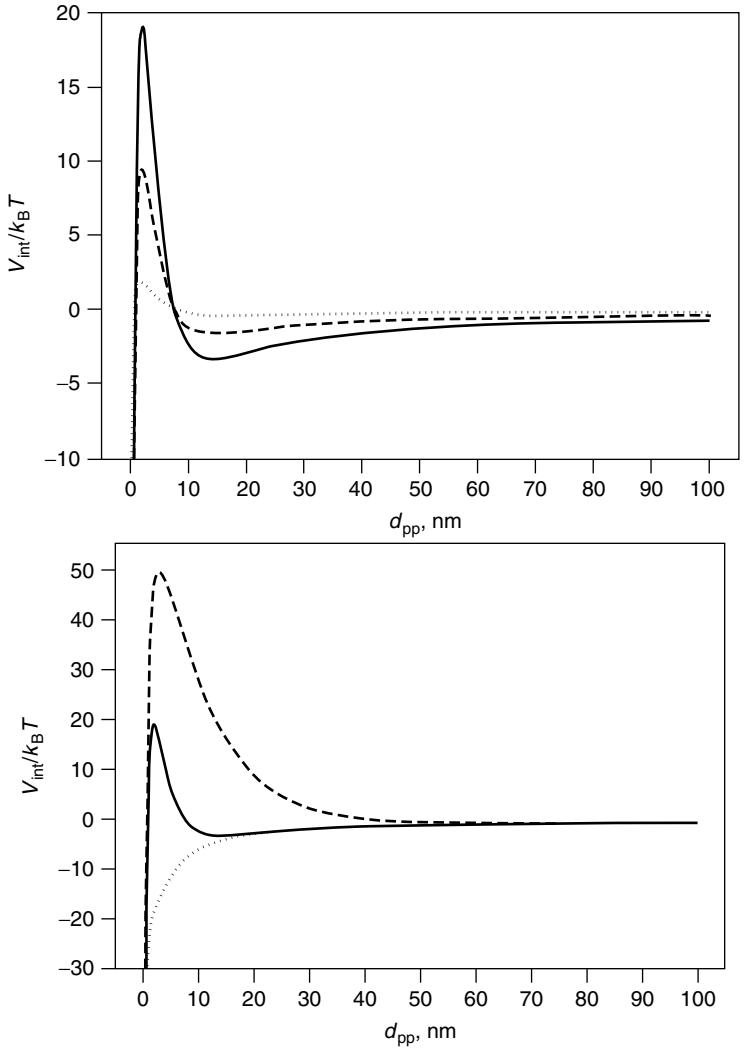

Fig. 30. (**a**) Interaction potential of charged stabilized particles calculated according to equations (37a–c) for particles of different size. Other parameters: $\Phi = -45$ mV, $C_{salt} = 1 \times 10^{-2}$ M, $A_{eff} = 6 \times 10^{-20}$ J. — $D = 100$ nm; --- $D = 50$ nm; (10) $D = 10$ nm. (**b**) Interaction potential of charged stabilized particles calculated according to equations (37a–c) for particles at various ionic strengths in the continuous phase. Other parameters: $\Phi = -45$ mV, $D = 100$ nm, $A_{eff} = 6 \times 10^{-20}$ J. — $C_{salt} = 10^{-2}$ M; $\cdots$ $C_{salt} = 10^{-1}$ M; --- $C_{salt} = 10^{-3}$ M;

local shear field. The kinetic energy of the particles can be approximated by equation 38, where ρ_{dp} is their density and v_{rel} is the relative velocity in collision, which is proportional to the shear gradient.

$$E_{kin} = \frac{1}{2} D^3 \rho_{dp} v_{rel}^2 \tag{38}$$

The important conclusion for heterophase polymerization where shear fields are applied is that in the case of electrostatically stabilized particles the tendency to coagulation increases with both increasing stirrer speed and particle size (particle mass). Furthermore, purely electrostatically stabilized particles are more stable in dispersion media of high permittivity (polar liquids or water) against orthokinetic flocculation.

Stabilization by Tethered Polymers. As discussed in the case of lyophilic colloids, interactions between the polymer forming the dispersed phase and the dispersion medium may contribute considerably to stability. This means that polymers that are able to interact with both the continuous phase and the particles can act as stabilizers as well. If the lyophilic groups are uncharged, it is called *steric stabilization* (288,290) and if these groups are charged it is called *electrosteric stabilization*. Polymer dispersions that are stabilized by either kind of polymers possess very special properties. Particles of this kind consist of a polymeric core surrounded by a stabilizer layer of the thickness ΔR. Inside this layer the concentration of lyophilic polymer per unit volume is $C_{S,L}$. The origin of the stability can be enthalpic or entropic or a combination of both and is theoretically treated within the framework of polymer solution theories. If the continuous phase is a nonpolar liquid and the interactions with the stabilizing polymer are only weak, stabilization is dominated by entropic effects (configurational entropy). In contrast, enthalpic effects are more important in polar continuous phases. A simplified discussion just to outline the principles is given below. It is based on a consideration of the change in the energy of mixing of the soluble polymer in the overlap region of approaching particles, where the concentration of lyophilic polymer is $2C_{S,L}$. This increase in concentration gives rise to an osmotic force, sucking in continuous phase liquid into the overlap region and pushing the particles away. A steric repulsion potential can be formulated as in equation 39, (290,305).

$$V_{st} \propto \frac{C_{S,L}^2}{v_{cp}\rho_{S,L}^2}\left(\Psi_1 - \chi_{S,cp}\right)\left[\left(\Delta R - \frac{d_{pp}}{2}\right)^2\left(3\frac{D}{2} + 2\Delta R + \frac{d_{pp}}{2}\right)\right] \tag{39}$$

In equation 39, v_{cp} is the molar volume of the continuous phase, $\rho_{S,L}$ is the density of the lyophilic polymer, Φ_1 is an entropy parameter for mixing of the overlap region, and $\chi_{S,cp}$ is the interaction parameter between the lyophilic polymer and the dispersion medium. The interaction of the stabilizer layers on approaching particles gives rise to large repulsive forces, which start to act suddenly. However, any change in the solution state of the lyophilic polymer leads to an influence on the stability of the dispersion. In this sense an important parameter for steric stabilization is the temperature. The stabilizing ability of lyophilic polymers can be lost if the temperature is close to their critical solution temperature where the molecules start to become lyophobic. A similar situation can occur in the case of aqueous dispersions upon the addition of electrolytes when the interaction between polymer and continuous phase molecules is decreased with increasing ionic strength. Donald Napper and co-workers have carried out an intense investigation of the thermodynamics of steric stabilization (304). Whether or not flocculation occurs upon changing the thermodynamic conditions of the stabilizing polymer

depends on the change in the free energy. ΔG_f, the free energy describing the flocculation process (cf eq. 40), must be positive to ensure stabilization (that is, flocculation is thermodynamically not favored), and if it becomes negative, the dispersion will flocculate.

$$\Delta G_f = \Delta H_f - T\Delta S_f \tag{40}$$

Equation 40 quantifies the above statement that both enthalpic and entropic effects contribute to steric stabilization, that is, one can easily find conditions when either ΔH_f or ΔS_f or both at a given T and pressure lead to $\Delta G_f > 0$. Flocculation is thermodynamically impossible if ΔH_f is positive and ΔS_f is negative. This is called combined enthalpic–entropic stabilization and is observed in dioxane–water and methanol–water mixtures as the continuous phase for dispersions stabilized with poly(vinyl alcohol) and poly(ethylene glycol), respectively. If the magnitude of $T\Delta S_f$ is larger than that of ΔH_f and both ΔS_f and ΔH_f are negative, it is called entropic stabilization because the large negative entropy causes stability. However, entropically stabilized systems may flocculate upon cooling as ΔG_f might become smaller than zero. In the case of an enthalpically stabilized system, which might become unstable upon heating, the magnitude of ΔH_f is larger than that of $T\Delta S$, and both ΔH_f and ΔS_f are greater than zero. The stabilization of dispersions in toluene or *n*-heptane with polystyrene and poly(12-hydroxy stearic acid), respectively, is entropic,. whereas poly(vinyl alcohol) in 2 *M* sodium chloride aqueous solution and polyisobutylene in 2-methylbutane act as enthalpic stabilizers. Note that poly(ethylene glycol) can act in entropic, enthalpic, and combined stabilization in methanol, 0.48 *M* aqueous magnesium sulfate solution, and methanol–water mixture, respectively.

Depletion Interactions. A polymer need not necessarily be adsorbed to impart stability to a colloidal dispersion. This kind of interaction, is described as depletion interaction, emphasizing the nonadsorbed (or the depleted particle–water interface) state of the lyophilic polymers. The interaction between dispersed particles and dissolved polymers can be described by means of phase diagrams showing regions of stability and instability depending on the concentration and size of both species. Again a simple but vivid picture can be used to explain the principle of this kind of interaction. The action of dissolved polymers on dispersed particles depends on two characteristic lengths: the size of the dissolved polymer (D_{ee}) and the average distance between the particles (d_{pp}, cf above). If $d_{pp} \gg D_{ee}$, that is a stable situation as the particle density is low and both particles and polymers move freely in the continuous phase. If the particle concentration increases and d_{pp} decreases such that $d_{pp} > D_{ee}$, a situation may possibly be reached where the local concentration of the polymer in the vicinity of two particles is higher than that in a region of lower particle density. Thus, an osmotic force arises, and in order to dilute this region, continuous phase fluid soaks in and pushes the particles apart. However, if $D_{ee} > d_{pp}$ and the concentration of dissolved polymer is larger outside an interstitial volume between particles, the flux of continuous phase fluid, which tries to dilute the local high polymer concentration, presses the particles together and hence, leads to coagulation of the dispersion. An analogous situation to depletion interaction, purely entropically driven, might also exist in neat colloidal suspensions of hard monodisperse spheres, that is, in good

approximation in purely nonionically stabilized particles possessing cutoff or hard repulsive potential. In the case of such particles, a higher degree of order must not necessarily mean a loss of entropy. In random close packing at space filling of 64%, direct contact between the particles occurs. In contrast, in a crystalline hexagonal arrangement at maximum space filling of about 75%, free volume exists between the particles and hence, each sphere has freedom of movement (mainly rotation). This entropy of the free volume outweighs the configurational entropy (with regard to the sphere center) at 54.5% space filling and crystallization starts purely driven by the gain of configurational entropy. In a mixture of a few large and many small spheres (a situation that is comparable with the above particle plus dissolved polymers) both entropy-driven attraction and repulsion can occur. Around each large sphere is an excluded volume for the smaller particles with a thickness of their size. If the distance between the larger spheres is below the size of the smaller spheres, the excluded volume regions can overlap and hence, the effective volume for the smaller spheres is increased by Δv_c, which causes an entropy gain $\Delta S_{sl} = k_B N_{ss} \ln[(v_c + \Delta v_c)/v_c]$, where v_c is the volume of continuous phase and N_{ss} the number of small particles. This entropy gain causes a decrease in the free energy and the existence of an attractive force for the larger particles. In the reverse case, if the distance between the larger drops is greater, then an entropic repulsive force exists. This is because before another particle fits in the gap the volume of continuous phase has to increase and then it might be larger per particle within the gap than outside. This again causes a gain in entropy and a loss in free energy (307). Obviously, dissolved polymers with large D_{ee} can lead to so–called bridging flocculation if they are able to strongly interact with colloidal particles. Such processes are carried out commercially in breweries or in wastewater treatment facilities with water-soluble polymers prepared by means of heterophase polymerization in organic media.

Combinations of Electrostatic and Steric Stabilization. From the application point of view in heterophase polymerizations, steric stabilization does not require the presence of high molecular weight polymers and can also be realized by low molecular weight nonionic stabilizer based on poly(ethylene glycol) as hydrophilic groups (low molecular weight means a molar mass below 10^3–10^4 g/mol). The simplest case, which indeed is frequently applied, is the joint application of ionic and nonionic low molecular weight surfactants. Advantage can be taken from the fact that the combination of electrostatic and steric stabilization gives on the one hand additional stability at low electrolyte concentrations and on the other hand the dispersion remains sterically stabilized at higher electrolyte concentrations (290). The effect of steric stabilization caused by adsorbed poly(ethylene glycol) chains has been clearly demonstrated by Napper and co-workers (308,309). The remarkable results of these studies are as follows: First, the critical coagulation concentration of sterically stabilized poly(vinyl acetate) dispersions against magnesium sulfate is increased by two orders of magnitude compared with purely electrostatic stabilized dispersions (3.9×10^{-1} versus 6.2×10^{-3} M $MgSO_4$ at 298 K). Second, for poly(vinyl acetate) latexes with diameters between 30 and 230 nm stabilized with poly(ethylene glycol) moieties (chain length of about 220), the point of incipient flocculation is independent of the particle size. Third, the electrolyte stability of particles stabilized jointly by electrostatic and steric components is governed by the steric contribution. Moreover, the flocculation conditions

are independent of the poly(ethylene glycol) chain length. Fourth, if once flocculated sterically stabilized particles can easily be redispersed if the conditions that have caused flocculation are removed, provided the stabilizer is strongly adsorbed. In other words, dispersions with only poorly anchored steric stabilizers may be flocculated more easily and may not be redispersed. Fifth, increasing the molecular weight of the steric stabilizer can kinetically retard the displacement of weakly anchored stabilizer. Sixth, both nonaqueous and aqueous dispersions stabilized with polymers require for stability that the continuous phase liquid is better than a Θ solvent for the stabilizing chains. This is the application of Bancroft's rule and later refinements (cf above) to polymeric stabilizers. Compared with low molecular weight surfactants, polymers possess more degrees of freedom regarding the modification of their properties. There are many possibilities, such as the molecular weight or molecular weight distribution and in the case of random copolymers their composition and the distribution of chemically different groups along the chain. Block copolymers can offer additional possibilities with regard to various architectures such as linear block copolymers, or star-shaped block copolymers, or graft block copolymers. Furthermore, polymers can stabilize dispersions via all stabilization mechanisms (electrostatic and steric stabilization) and offer additional possibilities by a combination of various mechanisms in a single molecule. In the sense of combined stabilization, block copolymers made of one polyelectrolyte and one strong anchor block offer another possibility of so–called electro–steric stabilization absent in the above simply joint application of both ionic and nonionic stabilizers. A great deal has been done during the last few years with regard to both theoretical and experimental investigations of the behavior of polyelectrolytes on surfaces in dependence on various parameters such as concentration, chain length, geometry of the surface, and the ionic strength (C_{salt}) in the continuous phase. The use of such block copolymers with strong acid groups (such as sulfonates) as stabilizers in aqueous heterophase polymerization has, compared with poly(carboxylic acid) blocks, the advantage that the stability is practically independent of the pH. Pincus derived, for strong polyelectrolyte tethered to spherical particles and forming a corona of thickness ΔR, a scaling relation that predicts a dependence of $\Delta R \propto C^{\alpha}{}_{\text{salt}}$, with $\alpha = -1/5$ (310). This relation predicts an extraordinary electrolyte stability compared with low molecular weight stabilizers, which show an exponential dependence on the ionic strength (cf equations 37a–37c). Indeed, the extraordinary stability against electrolytes was experimentally observed for various types of polyelectrolyte block copolymers such as poly(alkyl methacrylate-*b*-sulfonated glycidyl methacrylate) (311) but also for poly(ethyl ethylene-*b*-styrene sulfonate) (312) as stabilizers for polymer dispersions. Moreover, in the latter case a Pincus brush behavior ($\Delta R \propto C^{\alpha}{}_{\text{salt}}$) was observed but with clear experimental evidence that the exponent α depends on the ratio of corona thickness to particle size. If the ratio $2\Delta R/D$ is lower than 0.7, α is about -0.1, but at larger corona thickness in relation to particle size, the Pincus behavior ($\alpha = -0.2$) is observed (313). A shrinkage of the corona with over several orders of magnitude increase in ionic strength was also observed for triblock copolymer particles composed of poly(styrene sulfonate-*b*-*N*-isopropyl acrylamide-*b*-styrene), which were directly prepared by heterophase polymerization as described in Reference 48. Furthermore, experimental evidence is given that the shrinkage of the corona is directly related to the polyelectrolyte

behavior of the poly(styrene sulfonate) hairs because in case of nonionic sterically stabilized particles of poly(ethylene glycol-*b*-*N*-isopropyl acrylamide-*b*-methyl methacrylate), the corona thickness remains unchanged under the same conditions.

Optimum Stabilization and Heterophase Polymerization Technique. In summary, effective stabilization of particles during heterophase polymerization requires, besides some theoretical knowledge in physical and polymer chemistry, a lot of experience also and is always dependent on to the particular polymerization process. Aqueous and nonaqueous heterophase polymerizations require not only different stabilization mechanisms but also different stabilizers. Another expression of Bancroft's rule of thumb for emulsions that are for many heterophase polymerizations the starting point is that the liquid with the highest solubility for the stabilizer forms the continuous phase wherein the other liquid is dispersed. In principle, there are no limitations for the choice of a stabilizer for heterophase polymerizations if only the above general rules are complied—anionic, cationic, amphoteric, or nonionic, monomeric or polymeric, organic or inorganic, linear or branched, comb-like or star-like all, reactive or nonreactive, single or mixed systems, monofunctional or multifunctional, naturally occurring or synthetic—and even colloidal solid spheres have been applied as stabilizers. In the case of colloidal solid spheres, so–called Pickering stabilizers, which have practical meaning for suspension polymerizations, the starting emulsion is a three-phase rather than a two-phase system. The interaction between a Pickering stabilizer and the continuous phase is expressed by means of the contact angle. Droplets of a second liquid are stabilized in a continuous phase if the contact angle between the continuous phase and the sphere is below 90°, whereas if the contact angle is above 90° the inverse emulsion is preferably formed (314,315). During heterophase polymerizations, as well as during storage of the dispersions, stabilizers are needed to maintain the colloidal state and to guarantee the maximum possible benefit from that state. However, during the final application when the colloidal state is no longer needed, they may lead to problems as they are in general not compatible with the polymer produced. For example, in case of hydrophobic coatings made from aqueous polymer dispersions, low molecular weight stabilizers have a tendency to assemble in hydrophilic domains and finally can cause failure of the coating. One strategy to solve this problem is the use of stabilizers that are fixed in place. This is possible either by the use of polymeric or reactive surfactant that can participate in the polymerization reaction. A summary of recent developments in this field where a great deal has been done during the last decade can be found in Reference 316. Recently, the possibility of tailoring polymeric surfactants has been demonstrated as poly(ethylene glycol-*b*) (partly sulfonated olefin) have been synthesized and successfully applied as stabilizers in aqueous heterophase polymerization. These polymeric stabilizers combine all kinds of stabilization mechanisms in one molecule, that is, electrostatic, steric, and electrosteric stabilization together with reactivity in radical polymerization (152). The development of stabilizers for heterophase polymerization is an ongoing topic. But, for any new surfactant or stabilizer one faces with the problem that it is only an auxiliary material that has to meet strict cost requirements and has to improve existing solutions in two, frequently contradictory, fields, that is, during polymerization and during application of the solid products.

Copolymerization

The majority of polymers prepared by heterophase polymerizations are copolymers. Copolymerization is an effective way to tailor polymer properties for a variety of applications with only a limited construction set of monomers. The hierarchical or modular assembly of polymer dispersions, which goes in descending order with regard to size from dispersion via particles to polymer molecules and finally to monomer units offers almost unlimited possibilities to tailor required properties. For general considerations concerning copolymerization mechanism, the reader is referred to standard textbooks such as References 317–319 (see also BLOCK COPOLYMERS and GRAFT COPOLYMERS). In general, the composition of the copolymer chain is a function of the reactivity ratios and of the instantaneous concentrations of the monomers at the reaction loci. Considering a binary copolymerization, which means that there are two kinds of growing chains, one ended with a radical of monomer 1 (P_1) and the other ended with a radical of monomer 2 (P_2), equations 37b as defined below are frequently used. In these equations f_1 and f_2 are the mole fractions of monomers 1 and 2, respectively, at any time in the reaction loci ($f_1 + f_2 = 1$), F_1 and F_2 are the mole fractions of monomer 1 and 2, respectively, in the copolymer formed at that time ($F_1 + F_2 = 1$), M_1 and M_2 are the monomer concentrations of both monomers in the reaction loci at any time, r_1 and r_2 are the reactivity ratios, k_{11}, k_{22} , k_{12}, and k_{21} are the rate constants for the possible four propagation reactions $P_1 + M_1$, $P_2 + M_2$, $P_1 + M_2$, and $P_2 + M_1$, respectively.

$$F_1 = \frac{(r_1 - 1)\, f_1^2 + f_1}{(r_1 + r_2 - 2)\, f_1^2 + 2\,(1 - r_2)\, f_1 + r_2} \qquad r_1 = \frac{k_{11}}{k_{12}} \qquad r_2 = \frac{k_{22}}{k_{21}} \tag{41}$$

F_1 and F_2 are the instantaneous copolymer compositions and depend on the particular conditions at a given time in a given reaction loci in the heterogeneous reaction system. The overall or cumulative copolymer composition is the sum over all times and reaction loci, and may be different from that obtained in a homogeneous reaction system. The application of equations 41 for heterophase polymerization requires the knowledge of the relative concentrations of both monomers in the reaction loci or their partitioning behavior between the different phases. An additional complication arises from the fact that heterophase copolymerization is carried out with monomers that differ markedly in their solubility in the different phases. For instance, in many industrially important emulsion polymerizations, acrylic or methacrylic acid is used as comonomer to impart useful properties to latex particles during polymerization and application. This means that the composition of the monomer mixture in water and in the monomer-swollen polymer particles differs considerably. Thus, the composition of the copolymers formed in both phases differs as well. Wang and Poehlein investigated the composition of cooligomers formed during styrene–acrylic acid batch emulsion copolymerization (318). The cooligomers were isolated by precipitating a dioxane solution of dried latex samples in an excess of water (1/15 v/v). After separating the precipitated copolymer the water phase was dried and the residual solids (a mixture

Table 15. Characterization of Styrene–Acrylic Acid Oligomers Formed during a Batch Emulsion Polymerization[a]

Seed	$f1$	Conc., %	$F1$	MW	n_1	n_2
No	0.861	9.19%	0.235	599	2	6
No	0.861	16.99	0.372	511	2	4
No	0.725	16.33	0.063	1046	1	14
No	0.725	26.32	0.092	1000	1	13
Yes	0.861	7.00	0.334	787	3	9
Yes	0.861	21.16	0.341	767	3	9
Yes	0.725	9.11	0.086	1113	1	15
Yes	0.725	22.00	0.064	1175	1	16

[a]Polymerizations at 50°C with SDS as stabilizer and potassium peroxodisulfate as initiator 320; 1: styrene; 2: acrylic acid; MW: molecular weight without end groups, in g/mol; n_1, n_2: number of styrene and acrylic acid units per cooligomer.

of cooligomers, inorganic salts, and emulsifier) were dissolved in ethanol in order to isolate the cooligomers. They found that the composition of these products depends, besides on the starting monomer ratio, mainly on the presence or absence of seed particles. The data are summarized in Table 15 with the same abbreviations as used for equation 41. The values for f_1 and f_2 refer to the overall concentrations in the reactor and not to the reaction locus, which is the aqueous phase. These data confirm on the one hand the importance of identifying and characterizing the particular reaction loci in heterophase copolymerizations and on the other hand the necessity to carry out future work in order to understand the role of reactions in the continuous phase that are crucial although only a minor part of all monomers is converted there. Despite these problems, it is proved in many examples that the main reaction locus in heterophase polymerization is the monomer-swollen dispersed phase, and if the concentration of monomers in the whole reaction system is allowed to adjust according to the partition coefficients and f_1/f_2 can be estimated in the reaction locus, then there is good agreement between experimental and calculated compositions using equation 41 and r values derived from homogeneous kinetics. This is the case even for monomers with huge differences in their water solubility, such as styrene and acrylonitrile, as long as monomer droplets are present (321). For further information on emulsion copolymerization, the reader is referred to References 322–324. It is the general case for batch polymerizations that $F_1 \neq f_1$, that is, both monomers are not consumed with equal rates, which means that the less reactive monomer will be accumulated in the remaining monomer mixture as the reaction proceeds. In the case of an azeotropic point in the F_1–f_1 diagram, the mutual reactivity of both monomers changes, that is, if $F_1 > f_1$ the monomer 1 is more reactive, whereas if $F_1 < f_1$ the monomer 2 is more reactive. Thus, the composition of the copolymer is shifted, or a composition drift occurs, during copolymerization in accordance with equation 41. This composition drift cannot be avoided during batch or discontinuous heterophase copolymerizations where the monomers are fed into the reactor only at the beginning. However, the shift in the copolymer composition can be compensated if proper feeding strategies are applied. If the goal is constant copolymer composition throughout the whole reaction, the monomers have to feed into the reactor according to their consumption. In order to do so it is very

helpful to know the instantaneous copolymer composition or the f values in the reaction loci. For instance, the f values can be determined by gas chromatography (321), and the cumulative copolymer composition by nuclear magnetic resonance spectroscopy (325), from which the instantaneous copolymer composition can be deduced. Both methods need much longer times to deliver results than the characteristic growth time of a copolymer molecule, which is on the order of a minute (cf above). Notwithstanding these difficulties a lot of experimental data is a prerequisite for successful modeling. An example is the work of Jean Guillot on emulsion copolymerization (326). Starting from monomer-swollen particles as the main reaction loci he examined two possibilities to calculate f values. The first approach is based on experimental partition coefficients and the second on more general consideration with regard to thermodynamics of polymer solutions. Another way to control heterophase polymerization reactors is based on mathematical modeling in connection with reaction calorimetry, which means in the simplest case monitoring reactor temperature. To combine copolymer composition with reactor temperature control is of special benefit for large-scale, industrial reactors owing due to the exothermic polymerization reaction. A summary of possibilities to control emulsion polymerization reactors can be found in References 327–330. Composition control is by far more complicated in heterophase copolymerizations because of the more compartmentalized nature than in homogeneous copolymerizations. This situation may tempt researchers to the question whether it will ever be possible to model heterophase copolymerizations. Some of the problems toward satisfying models of emulsion copolymers, especially with respect to obtaining reliable kinetic constants and other model parameters, have been discussed in an overview paper by van Herk and German (331). As accurate, detailed models to solve the problem are not available today a possible way out is the use of hierarchical fuzzy-logic model based controllers as described for styrene–butadiene emulsion copolymerization in Reference 332 or neural networks as developed for a batch polymerization of methyl methacrylate (333). From the point of view of materials science, heterophase copolymerization is extremely important because it is the method of choice to tailor application properties of polymer dispersions and that of the products made thereof. Mechanical properties of the polymers such as glass-transition temperature or film formation temperature, elasticity, durability, tensile strength, water uptake, adhesion, light resistance, or solvent resistance, and also colloidal properties such as stability against electrolyte or temperature changes (freeze–thaw stability), surfactant adsorption, or interaction with pigments and other fillers are influenced by copolymer composition in the particle interior and on the surface, respectively. The diversity of monomers allows the preparation of polymers with desired glass-transition temperatures, somewhere in between 150 and -100°C by radical heterophase polymerization techniques (cf T_g values of homopolymers in Table Table 16). Provided the copolymerization behavior is known, the comonomer mixture to realize a particular glass-transition temperature can be approximated fairly well from the T_g's of the homopolymers according to equation 42, where the w's are weight fractions of the monomers in the random copolymer.

$$\frac{1}{T_g} = \sum_i \frac{w_i}{T_{g,i}} \tag{42}$$

Table 16. Glass-Transition Temperatures (T_g) for Some Homopolymers[a]

Homopolymer	T_g, °C
Acrylamide	153
Methacrylic acid	130
o-Vinyl toluene	115–125
Phenyl methacrylate	110
t-Butyl methacrylate	107
Acrylonitrile	96–106
Acrylic acid	106
Methyl methacrylate	105
Cyclohexyl methacrylate	104
p-Vinyl toluene	101
Styrene	100
i-Propyl methacrylate	81
Vinyl chloride	80
Vinyl pivalate[a]	70
m-Vinyl toluene	72–82
Ethyl methacrylate	65
sec-Butyl methacrylate	60
2-Hydroxyethyl methacrylate	55
t-Butyl acrylate	41
n-Propyl methacrylate	35
n-Hexadecyl acrylate	35
Vinyl acetate[b]	33
Vinyl acetate	32
2-Hydroxypropyl methacrylate	26
n-Butyl methacrylate	20
Tetradecyl acrylate	20
Cyclohexyl acrylate	16
Vinyl propionate	12
Vinyl propionate[b]	10
Methyl acrylate	5–8
Vinyl versatate	−3
Vinyl isopropylether	−3
n-Dodecyl acrylate[b]	−3
n-Hexyl methacrylate	−5
i-Propyl acrylate	−5
Tetradecyl methacrylate	−9
i-Butylvinyl ether	−19
n-Octyl methacrylate	−20
Ethyl acrylate	−20 to −27
Vinylidene chloride	−23
Vinyl 2-ethylhexanoate[b]	−36
n-Propyl acrylate[c]	−37
Ethyl vinyl ether	−42
n-Propyl acrylate	−52
n-Butyl acrylate	−52 to −57
Butyl vinyl ether	−55
n-Hexyl acrylate[b]	−57
Vinyl caproate	−60 to −85

Table 16. (Continued)

Homopolymer	T_g °C
2-ethylhexyl acrylate	−60 to −77
n-octyl acrylate[b]	−65
n-dodecyl methacrylate	−65
n-decyl methacrylate	−70
Ethylene	−70 to −77
Butadiene	−87
Octadecyl methacrylate	−100

[a]Data taken from Ref. 334, except those indicated otherwise.
[b]Ref. 254.
[c]Ref. 33.

Equation 42 is an empirical relation, which is based on the experimental observation that the T_g values of a binary copolymer ($i = 2$) vary monotonically with composition. T_g values are important because they determine many application properties of polymers and in relation to the application temperature whether it is rubbery or glassy. In case of film formation and coatings applications of polymer dispersions, the T_g values determine at which temperature interdiffusion of polymer molecules across particle boundaries can start. Besides this application as building blocks for the main polymer (which is a random copolymer) comonomers are also applied to act with the aim either to contribute to colloidal properties or to allow subsequent chemical reactions. Monomers frequently employed in radical heterophase polymerizations are put together in Table 17. The monomers listed in Tables 9, 10, 16, and 17 suggest that there is an almost infinite number of combinations that can be applied in radical heterophase copolymerizations.

The individual comonomers used in a particular comonomer mixture employed in commercial heterophase polymerization have to fulfill different tasks. The main monomers, ie the monomers of greater molar portion in the copolymers are responsible for the mechanical properties such as glass-transition temperature, film formation temperature, mechanical strength, elasticity, and so on. Functional monomers, which are only a minor part of the monomer mixture, have nevertheless to fulfill important tasks. They are in most cases more lyophilic than the main monomers and hence may contribute to latex stability. The most important examples in this sense, for aqueous continuous phases, are carboxylic acid monomers, with several benefits. These groups can exist in both ionized and un-ionized form; depending on pH, their copolymers contribute in ionized form to colloidal stabilization as electrosteric stabilizers; they can be used to adjust dispersion viscosity in dependence on pH; in case of latex paints they improve adhesion as well as incorporation of pigments; and finally carboxylic acid groups are available as reactive sites for further reactions. Possibilities to carry out reaction either between particles or polymer molecules are crucial for a variety of applications. One of the technically important fields for post-polymerization reactions is cross-linking of the polymer during film formation in order to increase the properties of coatings (259,332–336). With regard to chemical diversity there are virtually no limitations in heterophase polymerization for reactive groups.

Table 17. Classification of Monomers for Radical Heterophase Polymerizations

Acryl monomers
Ethyl acrylate
Butyl acrylate
2-Ethylhexyl acrylate
Methyl methacrylate
Butyl methacrylate
Diethyl amino ethyl methacrylate
Dimethyl amino ethyl methacrylate
Acrylonitrile
Acrylamide
Methacrylamide
Vinyl monomers
Ethylene
Styrene
Vinyl chloride
Vinyl acetate
Vinyl propionate
Vinyl 2-ethylhexanoate
Vinyl neononanoate
Vinyl neodecanoate
Vinyl sulfate
Diene monomers
Butadiene
Chloroprene
Isoprene
Monomers with multiple, nonconjugated double bonds
Diallyldimethyl ammonium chloride
Diisopropenyl benzene
Divinyl benzene
Ethyleneglycol dimethacrylate
Trimethylolpropane triacrylate
Penterythritol teraacrylate
Specialty monomers with reactive groups
Carboxyl acid
Acrylic acid
Methacrylic acid
Maleic acid
Itaconic acid
Hydroxyl
Hydroxyethyl acrylate
Hydroxyethyl methacrylate
Hydroxypropyl acrylate
Hydroxypropyl methacrylate
N-Methylol acrylamide
N-Methylol methacrylamide
Hydroxymethylated diacetone acrylamide
Epoxy
Glycidyl acrylate
Glycidyl methacrylate

Table 17. (Continued)

Aldehyde
Acrolein
Alkoxy
n-Isobutoxymethyl acrylamide
n-Butoxymethyl methacrylamide
n-Methoxymethyl acrylamide
Allyl *n*-Methylol carbamate
Hydroxymethylated *N*-formyl-*N*′-acryloylmethylenediamine
Peroxy
t-Butyl peroxoacrylate
2-*t*-Butylperoxyethyl acrylate
Silane
Vinyl trimethoxy silane
γ-Methacryloxypropyl trimethoxysilane
β-Methacryloxyethoxytrimethoxysilane

Some of the most important reactive groups used as cross-linking sites in latex paints are listed in Table 18, together with some additional information regarding reaction conditions (cf Table 17 also for functional comonomers).

Particle Morphology

The development of inhomogeneous particle morphology is certain to happen in all kinds of heterophase polymerizations, not only with regard to the molecular weight of the polymers formed at different times during the polymerization but also with regard to chemical composition. This radial distribution of properties from the core to the periphery of the particles is a direct consequence of the heterogeneous nature of the reaction system and cannot be avoided. Driving forces are differences in the compatibility caused by enthalpic or entropic effects of various species, which differ either with regard to size or composition. In this sense hydrophilic and hydrophobic groups tend to assemble at the particle water interphase and in the interior of the particles, respectively. Consequently, the question arises to what extent a particular particle morphology represents an equilibrium structure. This is mainly governed by the mobility of the chains and hence, on the particular polymerization conditions such as T_g of the polymer, polymerization temperature, degree of swelling, degree of polymerization, and whether cross-linking occurs or not. In other words, the particle morphology is basically determined by competition between thermodynamic and kinetic factors during the particular heterophase polymerization process. Modeling morphology development during particle growth is complicated mainly by difficulties in treating the mobility of the polymer chains inside the particles in a proper way. During homopolymerization the situation is comparatively easy, as on the one hand low molecular weight species try to stay in place in less dense parts of the particle where they can gain more configurational entropy, and on the other hand hydrophilic end groups try to reach the aqueous phase in order to minimize

Table 18. Combinations of Reactive Group for Cross-Linking Reactions in Latexes

Functional group	Examples	Partner	Catalyst
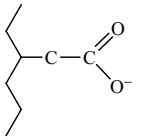	Acrylic acid Methacrylic acid	Polyvalent metal Polyhydric alcohols Methylol compounds Epoxides Amino groups Self-cross-linking	Heat Acidic Acidic Basic Acidic Heat
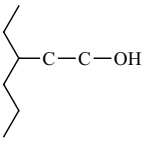	Hydroxyalkyl acrylates Hydroxyalkyl methacrylates Carboxylic acid	Other C-methylol Ester interchange Amino groups	Acidic Acidic Acidic
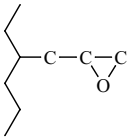	Glycidyl acrylate	Carboxylic acid	Acidic
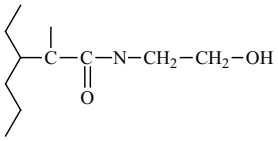	Glycidyl methacrylate *N*-Methylol acrylamide	Amino groups Self-cross-linking	Basic Acidic
	N-Methylol methacrylamide	Amino groups	Acidic
		Epoxides	Acidic
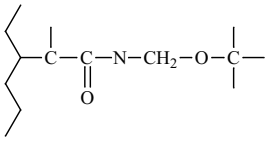	*i*-Butoxymethyl acrylamide	Self-cross-linking	Acidic
	i-Butoxymethyl methacrylamide	Amino groups	Acidic
		Alkyd resins	Acidic

interaction energy. The situation is different for composite particles, where the interaction energy must be additionally considered; this is mainly the interfacial energy between chemically different components. Torza and Mason (339) pioneered this type of investigation when they determined the final morphology of a three-component heterophase emulsion (three mutually immiscible liquids, where mobility effects play no major role) by minimizing the interfacial free energy given by equation 43.

$$\Delta G_{\mathrm{I}} = \sigma_{1,2}A_{1,2} + \sigma_{1,3}A_{1,3} + \sigma_{2,3}A_{2,3} \tag{43}$$

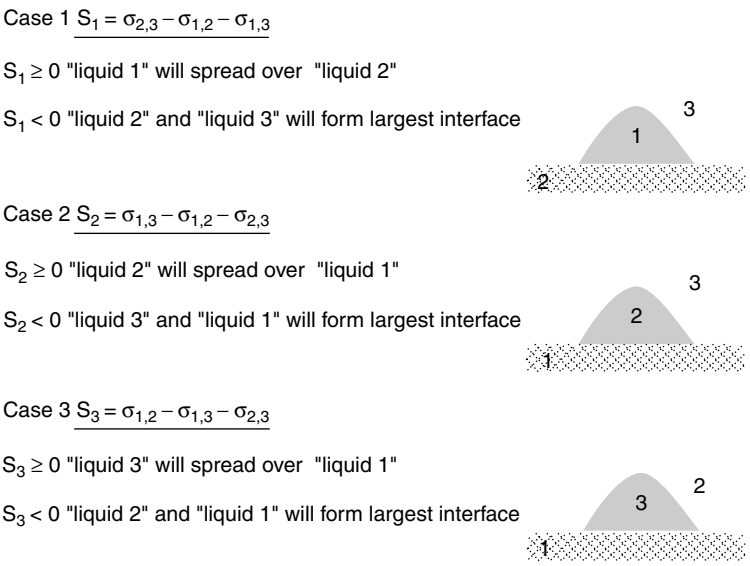

Fig. 31. Illustration of the spreading-coefficients approach to determine the thermodynamically favored morphology by means of the wetting picture, where a drop (gray) sits on a surface (patterned) both surrounded by a third component (white).

The σ's are the interfacial tension and the A's are the interfacial area between the liquids 1, 2, and 3. The conventions were made that phase 1 is chosen so that $\sigma_{1,2} > \sigma_{2,3}$ (which means that $S_1 < 0$), and that liquid 2 forms the continuous phase in which drops of both liquid 1 and liquid 3 are present. The analysis has been carried out by means of spreading coefficients for each liquid (S), which are defined by equation 44 and illustrated in Figure 31 by means of the well-known phenomenon of wetting. In this sense spreading coefficients greater than zero mean the drop wets the surface and forms a thin film, while for negative S's the liquid forms a lens, and interfacial contact between all three phases is thermodynamically favored. Spontaneous spreading or wetting means that the contact angle between the corresponding phases is zero and that the spreading molecules adhere to the substrate molecules more strongly than they cohere with one another.

$$S_1 = \sigma_{2,3} - \sigma_{1,2} - \sigma_{1,3} \quad S_2 = \sigma_{1,3} - \sigma_{1,2} - \sigma_{2,3} \quad S_3 = \sigma_{1,2} - \sigma_{1,3} - \sigma_{2,3} \tag{44}$$

Knowing the spreading coefficients it is now possible to predict thermodynamically favored morphologies. The predicted morphologies in Table 19 are easy to imagine with the information in Figure 31. According to the above convention that liquid 2 forms the continuous phase and $S_1 > 0$ is excluded, there are only three equilibrium morphologies possible, that is, core shell, single drops, and partial engulfing. This analysis revealed that the interfacial tensions between the phases are key factors that govern the final morphology. For practical applications, equilibrium interfacial tensions, for which one nneds to consider mutual

Table 19. Effect of Spreading Coefficients (Interfacial Tensions) on Mixed Particle Morphology[a]

Spreading coefficient	Largest interface between liquids	Spreading	Resulting morphology
S1 < 0	2 and 3	[b]	Core: liquid 1
S2 < 0	3 and 1	[b]	Shell: liquid 3
S3 > 0	[b]	3 over 1	Continuous phase: liquid 2
S1 < 0	2 and 3	[b]	No core shell
S2 < 0	3 and 1	[b]	All liquids to contact
S3 < 0	2 and 1	[b]	Partial engulfing
S1 < 0	2 and 3	[b]	No core shell
S2 > 0	[b]	2 over 1	No contact between 3/1
S3 < 0	2 and 1	[b]	Single drops in liquid 2
S1 < 0	2 and 3	[b]	Not realizable
S2 > 0	[b]	2 over 1	System cannot decide
S3 > 0	[b]	3 over 1	No equilibrium

[a]Spreading coefficients as defined by equation 42 and in Figure 31.
[b]Either no interface is formed or no spreading occurs.

solubilities and swellabilities of all components, must be used because initial spreading can be very different from equilibrium spreading. According to equation 43, it is necessary to also consider the interfacial areas with regard to minimizing the free energy. In other words, the final morphology also depends on the relative amounts of the components. Methods to estimate the morphology in dependence on both the interfacial tensions and the volume fractions of the dispersed phases were developed and applied by several groups such as Sundberg (340–344), Törnell (345,346), El-Aasser (347,348), and Waters (349) to tailor particle morphology. The results can be summarized as follows. In order to determine the thermodynamically favored morphology, which is that with the lowest free energy, it is necessary to compare ΔG_1 for as many as possible morphologies. To show the principle, two simple cases are considered in context with Figure 31. The continuous phase is formed by liquid 2; lyophobic liquid 3 is present in the form of seed particles, with size D_3; and lyophilic liquid 1 is added to form composed particles of size D_t as a result of interaction with the seed particles. First, the change in free interfacial energy for the formation of normal core shell particles ($\Delta {G_1}^{cs}$) with the lyophilic liquid 1 forming the shell is given by equation 45. This is the normal or expected core shell morphology because the lyophilic phase forms the shell. The reference or starting free energy state is that for the lyophobic seed particles, which also forms the core in the final particles.

$$\Delta G_I^{cs} = \sigma_{1,3}\pi D_3^2 + \sigma_{1,2}\pi D_t^2 - \sigma_{2,3}\pi D_3^2 \tag{45}$$

It is advantageous to reduce $\Delta {G_1}^{cs}$ by $\Pi \times {D_3}^2$ and to ascribe the change in the free energy per unit area of seed particles to interfacial tension. This leads to equation 46.

$$\frac{\Delta G_{\mathrm{I}}^{\mathrm{cs}}}{\pi D_3^2} = \Delta\sigma^{\mathrm{cs}} = \sigma_{1,3} + \sigma_{1,2}\frac{D_{\mathrm{t}}^2}{D_3^2} - \sigma_{2,3} \tag{46}$$

Second, the reduced free energy change for the formation of inverted core shell particles (α) with the lyophobic liquid 3 and the lyophilic liquid 1 in the shell and the core, respectively, leads to equation 47. Note that the same reference state is assumed as above.

$$\Delta\sigma^{\mathrm{ics}} = \sigma_{1,3}\frac{D_1^2}{D_3^2} + \sigma_{2,3}\frac{D_{\mathrm{t}}^2}{D_3^2} - \sigma_{2,3} \tag{47}$$

Equations 46 and 47 clearly show the influence of the amount of material forming a particular phase on the thermodynamically favored morphology. It is possible to consider simple morphologies other than these and examples can be found in References 340–349. The sizes of the phases can be expressed as volume fractions, leading to equations, that are independent of particle size. The crucial point to use this type of equations in predicting particle morphology is to get reliable data for the various surface tensions. In general, these results mean for aqueous two-stage heterophase polymerizations that the more hydrophilic polymer that has the lower interfacial tension to water tends to form the particle shell (normal core–shell structure). This is absolutely true from the thermodynamic point of view but the influence of the particular polymerization conditions can lead to a variety of morphologies in between such as raspberry-, sandwich-, or acorn-like structures, or occlusions ("salami"-like structures), and even inverted core-shell structures are possible.

The influence of the polymerization procedure was demonstrated impressively in a series of experiments carried out by Lee and Rudin (350). The authors showed that if styrene is polymerized onto poly(methyl methacrylate) seed particles under conditions maintaining a high core viscosity or low mobility, that is, with a redox initiator at low temperatures with a slow monomer feed (no swelling), composite particles with an inverted core-shell morphology are formed, as the more hydrophilic poly(methyl methacrylate) should, from a thermodynamic point of view, form the shell. In contrast, if the polymerization is conducted in a way that favors higher mobility in the seed particles (no monomer feed but batchwise monomer addition with swelling of the seed particles before initiation with potassium peroxodisulfate at 60°C), the result is a salami-like morphology showing occlusions of polystyrene subparticles and that large parts of the poly(methyl methacrylate) core have been moved at the water interface. The morphology formation in the course of heterophase polymerization in seed particles swollen with a second-stage monomer is extremely interesting, as phase separation and nucleation processes take place either consecutively or in parallel. These processes are influenced strongly by polymerization kinetics and thermodynamics of phase separation and hence, the final morphology is determined by the chain mobility inside the particles, which to some extent is the result of a competition between thermodynamics and polymerization kinetics. Note that, whereas the influence of polymerization kinetics ends sometime or other, thermodynamics acts as long as the particles exist. Indeed some authors describe change in particle morphology

during storage of polymer dispersions (344). An interesting approach to model this behavior is described by Gonzales-Ortiz and Asua in a series of papers (351–353). They treated the polymerization of monomer 1 in seed particles of polymer 2. Phase separation leads to the formation of clusters. The motion of the clusters inside the particles is determined by a balance between van der Waals and viscous forces. Furthermore, cluster coalescence is allowed and polymerization is assumed to take place in both domains inside the particles. The authors simulated methyl methacrylate polymerization in polystyrene seed particles and found that the final particle morphology depends strongly on the polymerization kinetics and that the slower the rate of polymerization, the closer the final morphology is to the equilibrium structure. The formation of particles with a particular morphology is not only impossible to avoid but is moreover an advantage of heterophase polymerization processes, because by means of controlling morphology formation application properties can be tailored to very specific needs.

The following examples of practical importance should illustrate these possibilities for aqueous heterophase polymerizations. In this case it is practically impossible to avoid the concentration of hydrophilic groups at the particle–water interface, which means that it is difficult not to build up particles with a core–shell structure. Hydrophilic groups can arise from initiators or comonomers, or sidereactions such as hydrolysis of ester groups in monomers [acrylic or methacrylic acid ester monomers or vinyl acetate cf (93)] or oxidation reaction in the aqueous phase in connection with initiator decomposition (92,237,354–356). The first example is comonomers with functional groups, which are mostly of polar, hydrophilic character (cf Table 18) and which are employed in concentrations of a few percent relative to the main monomers in order to prepare polymer molecules with reactive sides for post-polymerization modifications such as cross-linking to increase mechanical properties of coatings. It might be of interest to control the distribution of these comonomers over the entire particle volume rather than to have them accumulated at the particle–water interface. There are two general and one specific possibility to do so in dependence on the properties of the hydrophilic comonomer (cf (337,357,358). The first of the general possibilities is the use of main monomers with a higher solubility in water (ethyl acrylate, instead of butyl acrylate, for instance, cf Table 9) leads to the formation of more hydrophobic copolymer with these reactive comonomers and favors a more equal distribution in the particle volume. The second general possibility is the control of the hydrophilic comonomer content in the monomer mixture during feed procedures. The amount of hydrophilic comonomer units at the particle–water interface is the lowest if the whole amount of this comonomer is added at the beginning of the feed process; it is in a middle range if it is equally distributed over the entire feed duration; and it is highest if it is added only at the end of the monomer feed period. The third principle can be additionally applied if the hydrophilicity of the comonomers can be easily controlled, such as in case of carboxylic acid comonomers by changing the pH value. These comonomers are much more hydrophobic in the acid form than in the carboxylated form and hence, at high pH-values they will preferably be accumulated at the particle–water interface. Note that emulsifier adsorption depends strongly on the polarity of the particle-water interface and is the lower with regard to the adsorbed amount the higher the polarity (cf above, Solubility and Solubilization) (255,336,357).

Another example of desired core-shell morphologies are polymer particles composed of regions with different mechanical or optical properties. For instance, impact modifiers for hard and brittle plastic materials are core-shell latex particles with a cross-linked rubbery core and a hard shell. The shell polymer should be identical to the hard material and must be grafted to the rubber core in order to prevent phase separation. Only in this case the modifier particles can effectively absorb tensile stresses and impart additional impact strength. Impact modifiers are used to improve mechanical properties of various commodity polymers such as polystyrene, poly(vinyl chloride), and poly(methyl methacrylate). The problem of impact modification is more complex if the optical properties such as transparency, clarity, and glass-like appearance of the polymeric material should not be changed. This necessitates an adaptation of the refractive indices between the bulk material and the modifier particles. However, the problem is not that easy to solve, as the refractive index is strongly temperature-dependent, especially for particle sizes with good stress-absorbing properties. Making the particles smaller may solve the problem with regard to the temperature dependence of the refractive index but at the expense of a decrease in mechanical properties. The solution of this problem is multilayered particles, where the core and the outer shell are composed of the hard polymer and in between both is the cross-linked rubber layer, which is on the one hand thick enough to impart the required impact modification and on the other hand thin enough to retain unchanged the optical properties over a larger range of temperatures. The morphology can be specifically tailored by multiple arrangements of rubber layers followed by hard polymer layers, where it is unimportant what the core material consists of provided the thickness of the rubber layers is smaller than the wavelength of visible light to ensure only a slight dependence of the refractive index on temperature. However, this example elucidates that it is important to have strategies to prepare well-defined core–shell transitions. In extension of Sütterlin (237), the following conditions can be formulated in order to get well-defined or less-defined shells (Table 20). Note that the preparation of core-shell morphologies requires a heterophase polymerization technique that allows the application of consecutive monomer addition.

A specific core-shell morphology is given when the core is a void (hollow particles), that is, the particle is a porous material. In the dried state these particles

Table 20. Conditions to Prepare Polymer Particles with Shells of Different Properties

Sharp core shell transition	Diffuse core shell transition
Polymerization rate $\gg$ monomer feed rate	Monomer feed rate $\gg$ polymerization rate
Avoid swelling of core polymer	Allow swelling of core polymer
Cross-linked core	Non-cross-linked core
More lyophobic core on more lyophilic shell	More lyophilic core on more lyophobic shell
More incompatible core and shell	More compatible core ad shell
Lower stabilizer concentration	Higher stabilizer concentration
More lyophilic emulsifier	Less lyophilic emulsifier
Lower polymerization temperature	Higher polymerization temperature
More lyophilic initiator	Less lyophilic initiator
Higher initiator concentration	Lower initiator concentration

can be considered as polymer gas (mostly air) composites. From the synthetic point of view it is necessary to distinguish between particles with a single hole and really porous particles consisting of a network of pores and channels. Single hollow particles find for instance application as synthetic low density pigments (due to the large difference of refractive index between polymer and air) in the paint and paper industry or as UV protection filters in cosmetic industry, whereas porous particles find application as the stationary phase in separation processes (chromatography).

There are several ways to make hollow particles. The first way (cf 337,359) is a multistep process, which starts with the preparation of particles with a high content of carboxylic acid groups. These hydrophilic particles are used as seed in a subsequent polymerization and covered with a more hydrophobic shell made of polymer with T_g above the desired service temperature of the composite material. In a next step the pH is increased at a temperature above the T_g of the shell, which causes the particles to swell considerably and to fill with water. This structure can be frozen in by decreasing the temperature again and after drying and dewatering, the carboxylic acid rich polymer in the core collapses onto the shell and air diffuses into the particles. Another possibility of making hollow particles, which is interesting from the general viewpoint of the various possibilities offered by heterophase polymerization techniques, requires the exchange of the continuous phase. Core–shell particles composed of a low molecular weight polymer in the core and a slightly cross-linked shell are transferred from a continuous phase in which both the core polymer and the shell polymer are insoluble into a medium that is a good solvent for the core and a swelling agent for the shell. Under these conditions the core polymer diffuses into the continuous phase if the cross-link density of the shell is properly adjusted and by ultrafiltration the core can be drained (360,361). A summary of the work done over the last decades on preparation of voided particles by encapsulation of an organic liquid, which is a nonsolvent for the polymer, can be found in Reference 362. It is a two-stage process, where the first stage is a batch process leading to encapsulation of a mixed liquid drop with a polymer layer and the second stage is stabilization of the drops by further polymerization in the shell with a monomer feed process containing cross-linking monomers. The formation of the polymer shell surrounding the liquid drops requires low molecular weight polymers and hence the polymerization is carried out in the presence of mercaptans as chain-transfer agents. Shell formation takes place at a certain degree of conversion when the nonsolvent (isooctane) monomer (styrene) mixture becomes a progressively poorer solvent for the polymer (polystyrene). Phase separation takes place predominantly at the drop–water interphase owing to energetic reasons, as the polystyrene–water interfacial tension (32.7 mN/m, cf Table 10) is lower than that for isooctane–water [the value for *n*-octane–water is 51.5 mN/m (363)]. The authors performed some thermodynamic calculations (equilibrium model based on Flory–Huggins theory) that were successful in characterizing the initial and final stages of the process. The process conditions can be adjusted in a way that particles either with a single void or with diffusive microvoids are obtained. A procedure to prepare multihollow particles by a stepwise treatment of polymer particles consisting of carboxylic acid copolymers was developed by Okubo and co-workers. The process of hole formation is similar to the one above based on core-shell particles. Increasing the pH

at elevated temperatures leads to a swelling of the particles with water and the subsequent decrease in pH leads to a collapse of the chains, followed by void formation. Deceasing the temperature below T_g causes the structure to freeze, as explained in Reference 364. The authors showed that this principle is virtually universal as they were able to obtain similar morphologies also with copolymer particles containing dimethyl 2-amino ethyl methacrylate instead of methacrylic acid upon the reverse order of pH changes (365). Multihollow particles can also be prepared by so–called double emulsion, that is, an emulsion droplet is itself an emulsion and hence a host for smaller drops. In a water-in-oil-in-water emulsion (w/o/w), drops that are water-in-oil emulsions are dispersed in an aqueous continuous phase. This type of emulsion needs two sets of emulsifiers: hydrophobic ones (smaller HLB values) designed to stabilize the interface of the internal water-in-oil emulsion, and emulsifiers with a higher HLB value to stabilize the external interface of the oil-in-water emulsion. If the oil in the water-in-oil emulsion is a monomer, hollow particles should result after polymerization and drying where the water has acted practically as porogen. To control void concentration and droplet stability is not that easy because stability has to be controlled for both kinds of dispersed droplets. It was found that stability is improved if a urethane macromonomer as viscosity enhancer was incorporated in the monomer mixture (methyl methacrylate and ethylene glycol dimethacrylate as cross-linker). The results clearly show that increasing the amount of urethane macromonomer up to 15 W% relative to the monomer mixture increases both the yield of particles with holes and the number of holes per particle (366).

Another way of making porous particles is the application of so–called porogens, which are liquids that are essentially immiscible with the continuous phase and nonsolvent for the polymer but solvents for the monomers. This procedure leads exclusively to porous (multihollow) particles and requires, as in the case of encapsulation of liquid drops, the polymerization to start from an emulsion or highly swollen seed particles. This technique is the application of the principle of macroscopic gel formation to heterogeneous polymerization techniques. Porous polymeric materials, either macroscopic or beads, are prepared by copolymerization in the presence of a cross-linker such as radical polymerization of styrene in presence of divinylbenzene, which is the very “classical system.” Materials of this kind are porous only upon swelling. To control pore size and porosity an inert substance is added, which is only responsible for pore formation and which will be recovered before the material is used. The former procedure leads to materials that are porous only in the swollen state, whereas the latter results in permanent porosity (367). The inert component can either be a nonsolvent for the polymer or a linear polymer, preferably of the same kind as the network polymer but uncross-linked, where its molecular weight controls the pore properties. In general, the pore size is controlled by both the concentration of cross-linker and inert component. The larger the amount of inert component for a given amount of cross-linker, the larger is the pore size, whereas the pore size decreases with increasing cross-linker concentration at given ratio of inert component. Furthermore, the poorer the interaction between porogen and polymer, the easier the phase separation occurs and hence, the larger the pores. These principles are more than 50 years old, but remarkable developments have taken place during the 1990s. The “classical” poly(styrene-*co*-divinylbenzene) beads are very hydrophobic, but

as separation tasks are more and more shifted toward aqueous systems more hydrophilic beads are needed. One example is permanently porous hydrogel beads made of poly(vinylpyrrolidinone-*co*-ethylene dimethacrylate), which were prepared by aqueous suspension polymerization (vinyl pyrrolidinone/ethylene dimethacrylate = 1.5 w/w) with a mixture of cyclohexanol and dodecan-1-ol (4:l w/w) as inert diluent (150 w-% relative to the amount of monomers). In order to carry out the heterophase polymerization, the composition of the aqueous phase and the stabilizing system employed were rather unusual. The aqueous phase was a 20 w-% solution of sodium chloride containing 7 w-% magnesium chloride. This high ionic strength is needed to avoid polymerization in the continuous phase. At polymerization temperature, before inserting the organic phase, 1 *M* sodium hydroxide was added drop wise under stirring, thus forming the stabilizer, which is colloidal magnesium hydroxide. Then the organic phase, containing 2,2-azobisisobutyronitrile, was added and the polymerization allowed to proceed until final conversion. At the end of the polymerization the magnesium hydroxide stabilizer was dissolved by adding HCl (368).

Another modern development in the field of polymer beads as stationary phases for separation techniques is their equipment with chiral properties, thus enabling the separation of enantiomers. Examples are described in References 369 and 370 in which the authors do not use suspension polymerization, but rather highly swollen polymer particles, prepared via Ugelstad's activated swelling method. In brief, the process is as follows: A monodisperse polystyrene seed (prepared by emulsifier-free emulsion polymerization) was activated by swelling with dibutyl phthalate, which was added in the form of an aqueous emulsion stabilized with sodium dodecylsulfate. The monomer mixture containing the chiral monomer, initiator, cross-linker, and toluene was sonicated in an aqueous sodium dodecyl sulfate solution and added to the activated seed particles. After the emulsion drops were sucked up by the activated particles, poly(vinyl alcohol) was added as polymeric stabilizer and the polymerization started by heating. After washing and drying, the particles were treated with toluene to extract the linear polystyrene. The polystyrene acts in this case as both seed polymer and porogen.

Another new development during the last decade is the use of supercritical CO_2 as porogen, which has the advantage that macroporous polymer beads can be synthesized in aqueous suspension polymerization in the absence of any organic solvents. The results show that the pressure, which is applied to adjust the solvency of the supercritical CO_2 together with the stirring speed, controls the pore size (371). All these processes for hollow or porous particle preparation are multistep procedures, but there are also results indicating that hollow particles can be obtained in single-step polymerizations. An interesting possibility, which is also of general importance for heterophase polymerizations, is described in Reference 372. The authors investigated suspension polymerization of styrene in the presence of divinylbenzene as cross-linker, with gelatin and poly(diallyl dimethyl ammonium chloride) as stabilizer, and either 2,2′-azobisisobutyronitrile or dibenzoyl peroxide as initiator. The reaction was started after emulsification at 40°C by increasing the temperature to its final value (between 60 and 80°C). If the polymerization reaction takes place predominantly in the outer shell of the droplets, then porous particles with a single hole in the center are obtained. The copolymers produced early during the polymerization have a higher degree of cross-linking

due to the reactivity ratios and form a dense shell at the droplet water interface. For geometric reasons this cross-linked shell cannot shrink as much as required by the density change from monomer to polymer. As polymerization proceeds the swelling of the shell with monomer will change gradually in dependence on cross-linking (cf eq. 48) and consequently the core depletes in monomer until finally a hole is formed (cf Shrinkage and Fig. 28). Hole formation was observed at high polymerization rates, that is, at higher temperatures and higher initiator concentrations. Phase separation that takes place inside the confined space of latex particles can also cause the formation of hollow or voided particles. For instance, hollow particle formation, besides other morphologies, was observed in styrene emulsion polymerizations either initiated with poly(ethylene glycol)–azo initiators (312) or in the presence of poly(ethylene glycol) macromonomers (373). Also, ionic groups, if they are present at high concentrations, can cause phase separation and the formation of multihollow morphologies. Such behavior was observed in the case of low molecular weight polystyrene latex particles and is discussed in detail in References 92 and 374.

Also, for pure homopolymers particle morphology can be an issue, such as in the case of vinyl chloride polymerization. Poly(vinyl chloride) particles are by no means homogeneous, but rather possess a complicated morphology, which is determined by various parameters. The properties of poly(vinyl chloride) grains prepared by suspension polymerization such as size, density, and porosity are primarily determined by the nature and concentration of the stabilizer and initiator and by the hydrodynamic conditions in the reactor. These grains can have a size up to a few hundred micrometers and are in fact aggregates of a number of droplets with a size of some ten micrometers. Each of these particles is composed of smaller ones with a size of only a few micrometers, which are aggregated into a porous network. These smaller particles consist of still smaller domains (69,156). But these smaller particles also have an internal structure and so on. The smallest substructures have a size of about 10 nm and were identified by of electron microscopy of particles, which were etched with gas molecules (375–377). All investigations regarding the morphology of poly(vinyl chloride) particles, regardless of the polymerization procedure, are in conformity with a hierarchical structure composed of domains with various sizes. The morphology of poly(vinyl chloride) grains is not only determined by the polymerization process but for dispersions prepared by emulsion and microsuspension polymerization also by the conditions during spray-drying, which is used to isolate the polymer (69,156). Control of the grain morphology is very important as for many applications the grains are dispersed in plasticizers that, before further processing can occur, have to swell the grains.

Controlled Aggregation

Besides the methods of morphology formation during the polymerization process, the morphology of polymer colloids can also be changed after polymerization by controlled aggregation processes, as already briefly mentioned above. Such processes require close contact between latex particles and hence, they always face the problem of stability control because at the end there should still be a colloidal

polymer dispersion and not a completely coagulated system. From the thermodynamic stability point of view the process of decreasing the interfacial area is always favored. One possibility to carry out such processes is heterocoagulation in aqueous dispersions (water is phase 2 according to Fig. 31) of small particles (phase 3) on oppositely charged larger ones (phase 1) as described by Ottewill and Waters (378–380). Combined stability with ionic and nonionic stabilizers is advantageous in order to ensure stability during the whole process. The application of above principles of minimization of free energy (the reference state is characterized by both kinds of particles being separated) and introducing volume fractions (ϕ_1, ϕ_3) in equation 48 defines conditions for engulfment of smaller particles (phase 3) by larger particle (phase 1).

$$\frac{\sigma_{2,3} - \sigma_{1,3}}{\sigma_{1,2}} > \frac{1 - \phi_1^{2/3}}{\phi_3^{2/3}} \tag{48}$$

Equation 48 reveals the influence of several variables on the thermodynamics of the engulfment. The process is favored the more hydrophobic the smaller particles the more hydrophilic the larger particles, the less the interfacial tension between both polymers, and the larger the volume fraction of the smaller particles that are forming the core in the composite particles. The applicability of these kinds of predictions as well as of the whole process to prepare composite latex particles has been successfully demonstrated (290,378–380). In a comprehensive study the possibilities of controlled aggregation processes to enlarge the particle size of polymer dispersions were investigated (381–383). Such processes might also be of technical importance as it is possible to produce aggregates with a narrowly distributed size of a few micrometers (up to 15 μm). The aggregation process of negatively charged latexes was induced by the addition of a cationic surfactant under stirring. If the concentration of the cationic surfactant is in a proper range, which causes only partial charge neutralization, the final aggregates are stable and still possess a negative surface potential. This indicates that the surfactant binding to the primary particles is a cooperative process, and besides being controlled by electrostatic interaction is also controlled by hydrophobic interaction of the surfactant tails. The whole aggregation is a three-step process, starting with formation of a gel-like network, which is broken up by shear forces and finally leads to smaller but compacter primary aggregates. These can further agglomerate into larger, secondary aggregates. Their size is mainly determined by the stirring speed and the surface chemistry of the particles (stabilization). Narrow size distribution of the secondary aggregates was only observed for latexes prepared in the presence of acrylic acid, which causes additional stabilization because of the formation of an electrosteric layer. Another kind of controlled aggregation is described in Reference 384. The authors describe the pH-induced coagulation of two rubbery latexes, poly(butyl acrylate) and poly(styrene-co-butadiene), both stabilized by stearic acid. Controlling the decrease in the pH leads to coagulation of the poly(butyl acrylate) particles onto the more hydrophilic poly(styrene-*co*-butadiene) particles.

Particle Morphology and Application. The morphology of the particles is the main key controlling their properties and application fields. Although in many practical cases the particle morphology, which builds up during the polymerization process, is not known in detail, it is the specific particle morphology that makes a dispersion suited for a particular application. Table 21 gives a few general examples of how certain particle morphologies can contribute to solution of application problems.

Hybrid Polymer Dispersions. Particle morphology is not only an issue in the case of heterophase copolymerization or seeded polymerizations but also so–called hybrid systems are arousing increasing interest. *Hybrid systems* mean in the widest sense the combination of materials arising from different manufacturing processes, such as a combination of more than one generic class of polymers (polyurethanes–acrylics or epoxy–acrylics) or also a combination of heterophase polymerizations with inorganic materials. The former class of hybrid systems plays an important role in the preparation of paints (336). The most widely utilized technique is the application of seed polymers, which are not prepared by heterophase polymerizations but by other techniques, in aqueous emulsion polymerizations. The seed can be either directly water–dispersable owing to hydrophilic functional groups or can be emulsified in water using a combination of surfactants and high shear; if necessary or possible, it can also be dissolved in the monomer mixture prior to emulsification. This kind of sequential polymerization can lead to superior products because totally different properties can be combined on nanometer size scales first in the particles and after application in the final coating. An example of this kind of hybrid heterophase polymerization is given in Reference 385. The colloidal size scale makes heterophase polymerizations a promising tool to prepare hybrid materials with inorganic components. Table 22 lists some recently published examples prepared by polymerization of the particular monomer or monomer mixture in the presence of inorganic material. Composites offer unusual combinations of mechanical properties (stiffness, strength, weight and cost reduction) that are hard to attain from the individual components alone. Heterophase polymerization in this context means not only the encapsulation of inorganic material (as most of the examples given in Table 22) but also the polymerization inside layered structures in the inorganic material, such as silicates (montmorillonites). This so–called intercalation polymerization leads to modification on size scales of a few nanometers and to additional benefits compared to microcomposites or reinforced plastics on millimeter length scales (401). Preparation of nanocomposites also requires specific interactions between the polymers and the inorganic material in order to avoid phase separation (with regard to short–term and long–term storage or use) and to profit form modifications on nanometer length scales.

Nonclassical or Novel Developments

In the kind of heterophase polymerizations considered so far, except microemulsion polymerization, the stabilizers are used to impart colloidal stability to the disperse phases, which are either monomer droplets or polymer particles in spherical shape. In addition to these “classical” heterophase polymerizations there are also

Table 21. Selection of Core Shell Particle Morphologies for Particular Applications

Application	Monomers	Morphology	Benefit
Adhesive	Styrene/(meth)acrylates	Core: high T_g Shell: low T_g	Core: cohesion Shell: adhesion
Pressure-sensitive adhesives	(Meth)acrylates/styrene	Core: (meth)acrylates	Retention of adhesive strength; warp resistance
Thermoset coatings	Various plus reactive methylol groups	Core: $T_{pol} > 60^{\circ}C$ Shell: $T_{pol} < 60^{\circ}C$	Cross-linking
Paper coating	Styrene butadiene plus polar monomers	Core: styrene butadiene Shell: acrylic acid, acrylamide, acrylonitrile	Increased water resistance and higher gloss
Hydrophilic filler	Hydrophobic plus (meth)acrylic acid	Core: hydrophobic Shell: plus acrylic acid	Water retention in plastics
Galenical polymer	Methyl methacrylate plus (meth)acrylic acid	Core: methyl methacrylate; Shell: (meth)acrylic acid	Redispersable Powder
Diagnostic material	Hydrophobic monomer plus reactive monomer	Core: high; T_g Shell: reactive, activated	High stability coupling of proteins
White finish	Hard and soft monomers	Composite morphology, no statistical copolymer	High elasticity and low caking
Glue	Polyurethanes polyester polyols	Secondary dispersions in water	Crystalline parts give high strength
Mortar	Vinyl acetate plus various comonomers	Poly(vinyl alcohol) as protective colloid	Redispersable powder
Research products	Various amphiphilic block copolymers	Core: hydrophobic Shell: hydrophilic	Redispersable pure solids

Table 22. Polymeric–inorganic Hybrid Composites Prepared with Heterophase Polymerization Techniques

Inorganic material	Heterophase polymerization	Reference
Magnetite	Suspension, styrene/divinyl benzene	386
Pfizers magnetite	Suspension, monomer mixture	387
Na–montmorillonite	Emulsion, methyl methacrylate	388
$LiClO_4$, fumed silica	Poly(ethylene glycol)dimethacrylate	389
$CaCO_3$	Emulsion, styrene	390
$CaCO_3$	Miniemulsion, styrene	391
TiO_2	Miniemulsion, styrene	392
SiO_2, Al_2O_3, TiO_2	(Mini)emulsion, *n*-butyl acrylate	393,394
Carbon black	Miniemulsion, styrene	395
Magnetite	Inverse emulsion, hydroxyethyl methacrylate, methacrylic acid	396
Na–montmorillonite	Emulsion, aggregation, styrene	397
SiO_2	Emulsion, 4-vinyl pyridine plus *n*-butyl acrylate or *n*-butyl methacrylate	398
Montmorillonite	Emulsion, acrylonitrile plus butadiene plus styrene	399
Layered silicate	Emulsion or suspension, Methyl methacrylate	400

heterophase polymerizations where the stabilizer determines the morphology and the shape of the disperse phase. To illustrate this, Figures 32 and 33 show illustrations of binary and ternary surfactant phase diagrams, respectively (402). The surfactant concentrations for all the "classical" heterophase polymerizations is in the left part of both phase diagrams, that is, in regions where surfactants form

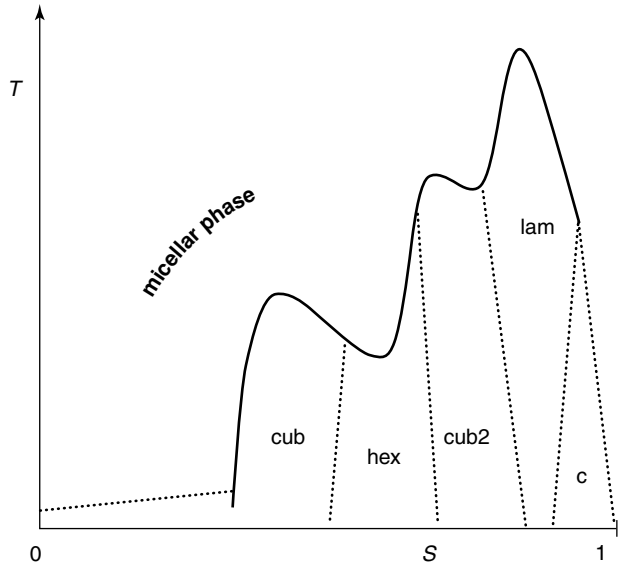

Fig. 32. Illustration of a binary phase diagram of a surfactant solution. *S*: weight fraction, surfactant; *T*: temperature; cub: cubic phase built up of discrete globular micelles; hex: hexagonal phase; cub2: bicontinuous cubic phase; lam: lamellar phase; c: crystalline phase.

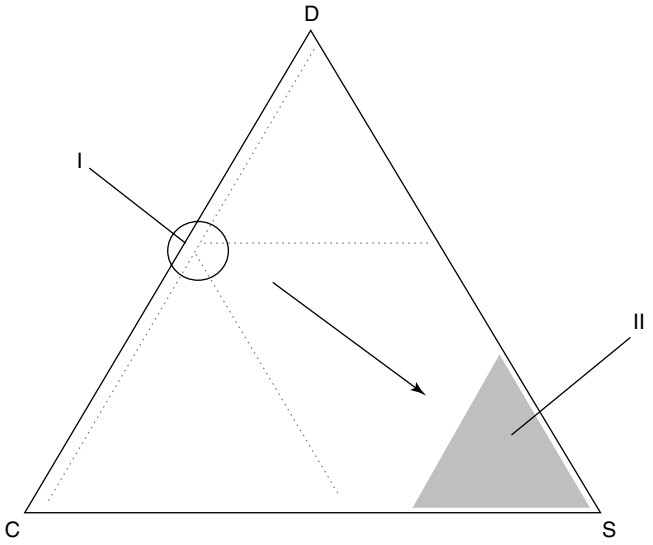

Fig. 33. Schematic drawing of a ternary phase diagram for heterophase polymerizations (part of the ternary phase prism at constant temperature). *I*: range for "normal" heterophase polymerizations; *II*: range for heterophase polymerizations in lyotropic phases.

only micelles. Searches have been inspired by the question as to what will happen if polymerizations are carried out in cubic, hexagonal, or lamellar phases, that is, at much higher surfactant concentrations. Basically, there are two possibilities: first, the use of normal monomers as third phase, which swell the surfactant phase (ternary case), and second, the use of reactive, that is polymerizable surfactants (binary case). In either case the interesting question is whether or not it will be possible to replicate the surfactant phase by polymerization. There is no general answer for either case. For the binary case, it was shown in a comprehensive study that for retention of surfactant lyotropic liquid crystalline phases during polymerization, the best position of the polymerizable group is neither at the end of the hydrophobic chain nor within the hydrophilic head group but rather a position where on the one hand chain mobility is reduced and on the other hand head group interactions are not able to prevent polymerization (403). The latter point means that in the case of ammonium surfactants, methacryloyloxyethyl groups attached to the nitrogen behave more readily than allyl groups. Similar results were obtained for (2-methacryloyloxyethyl)dodecyldimethyl ammonium bromide in comparison with 11-(methacryloylundecyl)trimethyl ammonium bromide. Whereas the former polymerizes readily in all phases (cubic, hexagonal, and lamellar) the polymerization of the latter one ceases in the hexagonal phase at about 60%. But both surfactants polymerize under retention of the macroscopic order (404). The situation for the ternary case is more complicated. Here the interesting question is whether or not it might be possible to use the swollen lyotropic phases as templates for the final polymer phase. It has been shown that the very first formed polymer changes the bicontinuous phase structure. Although a direct templating does not seem possible, the kind of lyotropic starting phase influences the final structure (405).

A review describing the state of the art using templates (including lyotropic surfactant phases) to prepare organic polymeric networks has recently been published (406).

The monomer solubility in the continuous phase plays in heterophase polymerization, a crucial role as long as diffusion processes through the continuous phase are necessary. This is for instance the case during emulsion polymerization. where the monomer has to diffuse from the reservoir (either droplets or tank in case of batch or feed procedures, respectively) to the particles. However, if the goal is to restrict the polymerization to droplets formed by diminution techniques (for instance suspension or miniemulsion polymerization) a zero solubility in the continuous phase is desirable because Ostwald ripening and bleeding of the drops is impossible (cf above). For some applications very hydrophobic polymers are needed. It is difficult to bring highly hydrophobic monomers such as lauryl methacrylate or stearyl acrylate through the aqueous phase into the particles as the main reaction loci during technically important emulsion polymerization. Recently it was found that β-cyclodextrins, which are cyclic oligosaccharides made up of seven glucopyranose units, can form inclusion complexes with hydrophobic substances. One example is the application of cyclodextrin instead of surfactants for emulsion polymerization of moderately hydrophobic monomers such as butyl methacrylate (407) or emulsion homopolymerization of very hydrophobic monomers such as dodecyl and octadecyl methacrylate, also in the absence of emulsifying agents (408). These hydrophobic monomers led to massive coagulation and incomplete conversion during emulsion polymerization in the presence of common sulfonate surfactants. Another example is the application of cyclodextrins as "transport shuttle" for hydrophobic monomers in emulsion copolymerization (409,410). This application is of interest also in order to increase the hydrophobicity of polymeric materials.

Process Models. The demands in industry on increasing product quality and constancy, on most efficient use of reaction space, and on cost reduction require increasing efforts with regard to process and product quality control. Much progress has been made in this field during the last decade. One way to meet industrial requirements is the development and application of process models, which are often applied together with on-line data acquisition systems. In order to completely master a polymerization process a multidisciplinary approach that considers kinetic and polymer property models (rate of polymerization, copolymer composition, particle size, and molecular weight distributions), hardware and software sensors, nonlinear observers for the data interpretation, and easily tuneable, robust controllers (411,412) are needed. The complexity of heterophase polymerization processes makes them difficult to model in detail, especially because the estimation of model parameters is the crucial point. There are basically two ways out of this dilemma in order to fulfill the demand of reactor and product control: First, the development of on-line techniques, that allow a fast determination of important product properties in time frames fast enough to allow remediation when problems occur during the polymerization. Second, the development of mathematical algorithms that provide accurate estimates of the properties of the reactor content. An example of the state of the art, and how to design such an observer, can be found in References 413. The authors developed a continuous–discrete observer that accurately estimates parameters for emulsion copolymerization and

that has been applied for batch copolymerization of styrene and butyl acrylate as well as for semibatch copolymerization of methyl methacrylate and butyl acrylate.

The control of batch heterophase polymerizations is a difficult task owing to the gel effect and the absence of lasting stable operation conditions. Frequently in these cases an adapting, self-tuning controller is applied. An example of this for a styrene batch suspension polymerization can be found in Reference 414. The application of a nonlinear predictive controller for a batch vinyl chloride suspension polymerization is given in Reference 415. All these controllers and software techniques require input data on the polymerization reactions. An important application property of a polymer is its molecular weight and hence, its control during polymerization is of special importance. Because of the lack of on-line methods (hardware sensors) a software sensor was developed that calculates the feed streams of monomer and chain-transfer agent required to get a desired molecular weight distribution (416). The control strategy uses a nonlinear-model–based controller and experimental data of both unreacted monomer and chain-transfer agent obtained with gas chromatography. Also, another strategy was developed, which is based on reaction calorimetry data (417). Recently it was shown that it is possible to carry out on-line monitoring of molecular masses during polymerization reactions. To perform this a diluted reactant stream from a polymerization reactor was made to flow through a series of detectors comprising refractive index, ultraviolet absorbance, and time-dependent static light scattering. This combination of detectors allows the determination of the absolute weight-averaged molecular weight of polymers (418). In order to get viscosity data it is also possible to include single-capillary viscometer in the series of detectors (419). The methodology was further improved to allow the finding of instantaneous weight-averaged molecular mass distributions during polymerization reactions and hence, it allows the on-line monitoring of polydispersity (420). Using this technique it was possible to analyze acrylamide polymerization in aqueous solution and to deduce from on-line data important kinetic parameters such as reaction orders and initiator decomposition rate constant (421). Reviews of on-line techniques to get required data can be found in References 422–424).

Reaction Calorimetry. The easiest way to follow a polymerization is to monitor the temperature of the reaction mixture or to use reaction calorimetry (cf above). Landau gives an excellent review on reaction calorimetry, its principles and application in chemical research in Reference 425. Table 23 summarizes papers dealing with reaction calorimetry of heterophase polymerizations. Reaction calorimetry gives on-line information with regard to the overall heat released during the reaction. This heat release is directly connected with the monomer conversion (eq. 49).

$$H_F \equiv r_p = -\frac{dM}{dt} = \frac{dV_P}{dt} \propto \left(D^3 \frac{dN}{dt} + ND^2 \frac{dD}{dt} \right) \tag{49}$$

Equation 49 can be considered as the basic relation in the case of on-line monitoring of compartmentalized polymerizations. H_F is the heat flow, r_p is the rate of polymerization, M is the overall monomer concentration, t is the time, V_P is the total polymer volume, D is the average particle diameter, and N is the particle

Table 23. Reaction Calorimetry in Heterophase Polymerizations

Characteristics	Reference
Feed policies to maximize productivity, principles, modeling semi-batch emulsion polymerization	426
Adiabatic calorimetry, radical heterophase polymerization, data acquisition, mass balances, parameter estimation	427
Kinetics styrene emulsion polymerization, varying emulsifier and initiator concentration (sodium dodecyl sulfate and potassium peroxodisulfate)	428–431
Suspension polymerization of styrene, thermokinetic parameters for scale-up	432
Heterophase polymerization, different monomers, initiators and emulsifiers, reaction rate profiles	433
Semi-batch acrylate emulsion polymerization, isoperibolic calorimetry, increase reactor performance	434
Isoperibolic calorimetric investigation of styrene heterophase polymerization with polyurethane emulsifiers	435

concentration. Equation 49 leads immediately to two important conclusions: First, the heat flow practically contains all information about the polymerization process. Second, for a compartmentalized polymerization this information can be extracted only if an additional on-line method is applied. The second method should preferably be a method for the analysis of the particle size or better yet the particle size distribution (PSD). Such a combination is described in References 436 and 437. A small aliquot of dispersion was withdrawn from the reactor with a sampling loop and passed through an on-line density meter (to determine the monomer conversion) and capillary hydrodynamic fractionation apparatus (to measure the PSD). The methods described so far with the *terminus technicus* "on-line" require the removal of an aliquot of the reaction to carry out the analysis. The only exception is reaction calorimetry, where the temperature is measured either inside the reactor or through its walls.

There is another group of techniques available, so–called in-line techniques, which neither require the removal of reaction mixture nor its destruction or dilution. The majority of these techniques is based on various kinds of radiation and hence mainly comprise spectroscopic methods. Owing to the rapid progress in the recent years with regard to optical fiber techniques, and computer techniques these techniques are ready to use inside closed reactors. A summary of papers dealing with in-line techniques to investigate heterophase polymerizations is given in Table 24. These selections suggest that there are a variety of in-line techniques under development or already available to monitor almost all characteristic quantities of heterophase polymerizations. Most of the techniques are only useful to investigate special features in laboratory experiments at low solids content (high dilution) such as transmission measurements, fluorescence spectroscopy, or surface tension. For some others the equipment is very expensive and the gain of additional information frequently does not justify the enormous price and running costs of these methods such as nuclear magnetic resonance or electron spin resonance spectroscopy. In contrast, other methods such as infrared and Raman spectroscopy or ultrasound are very promising.

Table 24. Selection of In-Line Methods to Analyze Heterophase Polymerizations

Method	Application	Reference
Near-infrared spectroscopy (short wavelength 700–1100 nm)	Styrene emulsion polymerization conversion monitoring	438,439
Near-infrared spectroscopy (wave-length 1500–1800)	suspension polymerization evaluation of average particle size	440,441
Near-infrared spectroscopy	Emulsion polymerization, detection of monomer droplets upon addition of butyl acrylate and methyl methacrylate individually and in mixtures	442
Raman spectroscopy	Emulsion polymerization of methyl methacrylate and copolymerization of styrene/butyl acrylate	443
Raman spectroscopy	Styrene suspension polymerization (signal evaluation)	444
Raman spectroscopy	Emulsion copolymerization of styrene and butadiene, determination of styrene monomer in the reactor	445
Ultrasound	Emulsion homo- and copolymerization principles of applications, conversion	446,447
Ultrasound	Conversion (from velocity) and particle size distribution (from attenuation) for poly(vinyl chloride) and polyterafluoroethylene dispersions	448
Ultrasound velocity and attenuation	All kinds of dispersions, to determine particle size distribution and zeta potential	449–453
Electron spin resonance (ESR)	Radical concentrations during emulsion polymerization, lifetime of radicals in reaction compartments	454–456
Time–resolved fluorescence	Emulsion polymerization of styrene spectroscopy pyrene–labeled macroinitiators; dynamics in polymerizing particles	457,458
Solid–state nuclear magnetic resonance spectroscopy	Emulsion polymerization of butyl acrylate in D_2O, conversion	459
Surface tension	Emulsion polymerization of styrene and methyl methacrylate, emulsifier-free	93,95
Combination of turbidity and conductivity, surface tension, Fourier-transformed infrared spectroscopy	Nucleation during emulsion polymerization of styrene, vinyl acetate, and methyl methacrylate; continuous emulsion polymerization of methyl methacrylate, phase transition of polystyrene oligomers with Fourier-transformed infrared spectroscopy	93

From Batch to Continuous Operation. A last point to mention here is that over the last few years technological developments took place in order to transfer classical batch heterophase polymerization processes such as suspension, miniemulsion, and microemulsion polymerization into semibatch or even continuous operation. In the case of suspension (cf Table 6) and miniemulsion polymerization (460,461) this is done in order to increase reactor productivity. The polymerization inside preformed drops requires for continuous operation more than one continuous stirred-tank reactor or plug flow reactors in order to realize residence time distributions, which are as much as possible similar to that of batch reactors. This is necessary in order to achieve an almost equal conversion in all droplets. Continuous stirred-tank reactors possess an exponential residence time distribution whereas the residence time distribution in batch reactors is an orthogonal function. For microemulsion polymerization the goal to develop semibatch procedures is primarily to improve the yield with regard to emulsifier usage as at the end of batch operations polymer particles coexist with empty micelles. The high emulsifier concentration at the start, which was necessary to form the microemulsion, is at the end of the process much too high to ensure particle stability. It is now well established to start monomer feed and if necessary some initiator at the end of the batch period in order to increase the solids content and hence also the emulsifier yield (217,259,270,462). The average particle size stays small (a small increase in average particle is observed, because besides new nucleation and growth seed polymerization also takes place as a result of swelling of the first generation of particles), because there is enough emulsifier available to stabilize newly formed particles. If the fed monomer differs from the first-stage monomer, a special kind of composite particle is obtained that possesses interesting mechanical properties, compared with products from common emulsion polymerization (274) owing to the smaller particle sizes.

In final conclusion, heterophase polymerization is a generic term that describes a complex field of polymer science, that spans preparation of both organic and inorganic polymer and mixtures thereof and that is not restricted to a certain polymerization mechanism or technology. It is among the oldest areas in polymer chemistry but it is developing with ever-increasing speed and comprises nowadays more than "classical" emulsion and suspension polymerization techniques.

BIBLIOGRAPHY

"Emulsion Polymerization" in *EPST* 1st ed., Vol. 5, pp. 801–859, by Edward W. Duck, The International Synthetic Rubber Company; "Emulsion Polymerization" in *EPSE* 2nd ed., Vol. 6, pp. 1–51, by Gary W. Poehlein, Georgia Institute of Technology; "Suspension Polymerization" in *EPST* 1st ed., Vol. 13, pp. 552–571, by Elliot Farber, Tenneco Chemicals, Inc.; "Suspension Polymerization" in *EPSE* 2nd ed., Vol. 16, pp. 443–473, by Eric A. Grulke, Michigan State University.

1. J. Kosek, Z. Grof, A. Novák, F. Stepánek, and M. Marek, *Chem. Eng. Sci.* **56**, 3951–3977 (2001).
2. H. L. Frisch, *Br. Polym. J.* **17**, 149–153 (1985).
3. P. Enzel and T. Bein, *J. Phys. Chem.* **93**, 6270–6272 (1989).
4. C.-G. Wu and T. Bein, *Science* **264**, 1757–1759 (1994).
5. A. Matsumoto, T. Kitajima, and K. Tsutsumi, *Langmuir* **15**, 7626–7631 (1999).

6. Y. S. Ko and S. I. Woo, *Macromol. Chem. Phys.* **202**, 739–744 (2001).
7. S. Spange, A. Gräser, A. Huwe, F. Kremer, C. Tintemann, and P. Behrens, *Chem. Eur. J.* **7**, 3722–3728 (2001).
8. M. Biswas and S. S. Ray, *Polymer* **39**, 6423–6428 (1998).
9. U. Meyer, F. Svec, J. M. J. Frechet, C. J. Hawker, and K. Irgum, *Macromolecules* **33**, 7769–7775 (2000).
10. T. Yamaguchi, T. Suzuki, T. Kai, and S.-I. Nakao, *J. Membr. Sci.* **194**, 217–228 (2001).
11. D. C. Blackley, *Polymer Lattices*, Vol. **1**, 2nd ed., Chapman & Hall, London, 1997, pp. 1–2.
12. D. Hosler, S. L. Burkett, and M. J. Tarkanian, *Science* **284**, 1988–1991 (1999).
13. J. Falbe and M. Regitz, eds., *Römpps Chemie Lexikon*, 9th ed., Georg Thieme Verlag Stuttgart, New York, 1993, p. 2945.
14. H.-G. Elias, *Große Moleküle*, Springer Verlag, Berlin, 1986, pp. 5–7.
15. C. de la Condamine and F. Fresneau, *Mem. Acad. R. Sci.* 488–510 (1751).
16. M. Faraday, *Q. J. Sci. Liter. Art* **21**, 19–28 (1826).
17. C. G. Williams, *Philos. Trans. R. Soc. London* **150**, 241–255 (1860).
18. M. G. Bouchardat, *Compt. Rend.* **89**, 1117–1120 (1879).
19. J. Berzelius, *Jahresbericht Physische Wissenschaften* **12**, 64 (1833).
20. Ger. Pat. DRP 250,690 (Sep. 6, 1909) (to Farbenfabriken, former F. Bayer & Co.).
21. Ger. Pat. DRP 254,672 (Dec. 12, 1912) (to Farbenfabriken, former F. Bayer & Co.).
22. K. Gottlob, *Gummi-Ztg.* **33**, 508–509 (1919).
23. K. Gottlob, *Gummi-Ztg.* **33**, 534–535 (1919).
24. Ger. Pat. DRP 558,890 (Jan. 9, 1927) (to I. G. Farbenindustrie Akt.-Ges.).
25. U.S. Pat. 1,732,795 (Oct. 22, 1929), R. P. Dinsmore (to Goodyear title a rubber company of Aleion, Ohio).
26. H. Fikentscher, H. Gerrens, and H. Schuller, *Angew. Chem.* **72**, 856–867 (1960).
27. G. S. Whitby and M. Katz, *Ind. Eng. Chem.* **25**, 1204–1211 (1933).
28. G. S. Whitby and M. Katz, *Ind. Eng. Chem.* **25**, 1338–1348 (1933).
29. W. P. Hohenstein and H. Mark, *J. Polym. Sci.* **1**, 127–145 (1946).
30. W. P. Hohenstein and H. Mark, *J. Polym. Sci.* **1**, 549–580 (1946).
31. F. A. Bovey, I. M. Kolthoff, A. I. Medalia, and E. J. Meehan, *Emulsion Polymerization*, Wiley-Interscience, New York, 1955.
32. D. C. Blackley, *Emulsion Polymerisation Theory and Practice*, Applied Science Publishers Ltd., London, 1975.
33. R. G. Gilbert, *Emulsion Polymerization, A Mechanistic Approach*, Academic Press, Inc., London, 1995.
34. R. M. Fitch, *Polymer Colloids: A Comprehensive Introduction*, Academic Press, Inc., San Diego, 1997.
35. J. M. Asua, ed., *Polymeric Dispersions: Principles and Applications*, Kluwer Academic Publishers, Dordrecht, 1997.
36. P. A. Lovell, M. S. El-Aasser, eds., *Emulsion Polymerization and Emulsion Polymers*, John Wiley & Sons, Inc., Chichester, 1997.
37. H. Fikentscher, *Angew. Chem.* **51**, 433 (1938).
38. F. A. Bovey, I. M. Kolthoff, A. I. Medalia, and E. J. Meehan, *Emulsion Polymerization*, Wiley-Interscience, New York, 1955, pp. 1–25.
39. D. Distler, *Wäßrige Polymerdispersionen: Synthese, Eigenschaften, Anwendungen*, Wiley-VCH, Weinheim, 1999.
40. J. B. Tuttle, *India Rubber World*, 488–490 (1923).
41. A. S. Dunn and H. W. Melville, *Nature* **169**, 699–700 (1952).
42. S. Förster and M. Antonietti, *Adv. Mater.* **10**, 195–217 (1998).
43. K. Mortensen, *Polym. Adv. Technol.* **12**, 2–22 (2001).
44. A. Milchev, A. Bhattacharya, and K. Binder, *Macromolecules* **34**, 1881–1893 (2001).

45. K. Tauer, *Polym. Adv. Technol.* **6**, 435–440 (1995).
46. L. Rosengarten and K. Tauer, *Ber. Bunsen-Ges. Phys. Chem.* **100**, 734–737 (1996).
47. K. Tauer, M. Antonietti, L. Rosengarten, and H. Müller, *Macromol. Chem. Phys.* **199**, 897–908 (1998).
48. K. Tauer and V. Khrenov, *Macromol. Symp.* **179**, 27–52 (2002).
49. F. Caruso, R. A. Caruso, and H. Möhwald, *Science* **282**, 1111–1114 (1998).
50. E. Donath, G. B. Sukhorukov, F. Carauso, S. A. Davis, and H. Möhwald, *Angew. Chem, Int. Ed.* **37**, 2201–2205 (1998).
51. F. Caruso and H. Möhwald, *J. Am. Chem. Soc.* **121**, 6039–6046 (1999).
52. F. Caruso, *Chem. Eur. J.* **6**, 413–419 (2000).
53. M. D. C. Topp, I. H. Leunen, P. J. Dijkstra, K. Tauer, C. Schellenberg, and J. Feijen, *Macromolecules* **33**, 4986–4988 (2000).
54. T. K. Bronich, A. V. Kabanov, V. A. Kabanov, K. Yu, and A. Eisenberg, *Macromolecules* **30**, 3519–3525 (1997).
55. E. A. Lysenko, T. K. Bronich, A. Eisenberg, V. A. Kabanov, and A. V. Kabanov, *Macromolecules* **31**, 4511–4515 (1998).
56. E. A. Lysenko, T. K. Bronich, A. Eisenberg, V. A. Kabanov, and A. V. Kabanov, *Macromolecules* **31**, 4516–4519 (1998).
57. A. Zintchenko, H. Dautzenberg, K. Tauer, and V. Khrenov, *Langmuir* **18**, 1386–1393 (2002).
58. R. Klein and G. Nägele, *Curr. Opin. Colloid Interface Sci.* **1**, 4–10 (1996).
59. T. Okubo and K. Kiriyama, *Ber. Bunsen-Ges. Phys. Chem.* **100**, 849–856 (1996).
60. T. Palberg, *J. Phys.: Condens. Matter* **11**, R323–R360 (1999).
61. C. Sinn, R. Niehuser, E. Overbeck, and T. Palberg, *Particle Particle Syst. Charact.* **16**, 95–101 (1999).
62. U. Gasser, E. R. Weeks, A. Schofield, P. N. Pusey, and D. A. Weitz, *Science* **292**, 258–262 (2001).
63. Y. Xia, B. Gates, Y. Yin, and Y. Lu, *Adv. Mater.* **12**, 693–713 (2000).
64. H. Misawa and S. Juodkazis, *Prog. Polym. Sci.* **24**, 665–697 (1999).
65. M. Engelmann, Klassische Polymere im Aufwind, in (Gendorf) Meeting of the GDCh Fachgruppe Makromolekulare Chemie, TU Dresden, Germany, Mar. 25–26, 1996.
66. D. R. Bassett, in Polymeric Dispersions: Principles and Applications, Elizondo, Spain, June 23–July 5, 1996, NATO Advanced Study Institute.
67. H. Mooibroek, K. Cornish, *Appl. Microbiol. Biotechnol.* **53**, 355–365 (2000).
68. D. Urban, K. Takamura, eds., *Polymer Dispersions and Their Industrial Applications*, Wiley-VCH, New York, 2002.
69. J. M. Sosa and K. P. Blackmon, in J. C. Salamone, ed., *Polymeric Materials Encyclopedia*, CRC Press, Inc., Boca Raton, 1996, pp. 8032–8042.
70. P. V. Smallwood, in J. I. Kroschwitz, ed., *Encyclopedia Polymer Science and Engineering*, Vol. **17**, 2nd ed., John Wiley & Sons, Inc., New York, 1989, pp. 295–297.
71. H. Gerrens, *Dechema Monographien* **49**, 53–73 (1964).
72. Freedonia, Study 1457, Sept. 2001.
73. Hewin International, Inc., in "Water-Soluble Polymers: Potential Applications and Markets", Trends, Developments, and Forecasts into the 21st Century, Amsterdam, the Netherlands, 1996.
74. Polyscience, Inc., Monomers and Polymers Catalog 2000, p. 70.
75. A. M. van Herk, in J. M. Asua, ed., *Polymeric Dispersions: Principles and Apllications*, Kluwer Academic Publishers, Dordrecht, 1997, pp. 17–30.
76. C. Hagiopol, *Copolymerization: Toward a Systematic Approach*, Kluwer Academic/Plenum Publishers, New York, 1999, p. 201.
77. W. V. Smith and R. H. Ewart, *J. Chem Phys.* **16**, 592–599 (1948).
78. W. D. Harkins, *J. Chem. Phys.* **13**, 381–382 (1945).

79. W. D. Harkins, *J. Chem. Phys.* **14**, 47–48 (1946).
80. W. D. Harkins, *J. Am. Chem. Soc.* **69**, 1428–1444 (1947).
81. W. D. Harkins, *J. Polym. Sci. V* 217–251 (1950).
82. M. Jung, I. van Casteren, M. J. Monteiro, A. M. van Herk, and A. L. German, *Macromolecules* **33**, 2320–3629 (2000).
83. R. M. Fitch, C. H. Tsai, *Polym. Lett.* **8**, 703–710 (1970).
84. R. M. Fitch, C. H. Tsai, in R. M. Fitch, ed., *Polymer Colloids*, Plenum Press, New York, 1971, pp. 73–102.
85. R. M. Fitch, *Br. Polym. J.* **5**, 467–483 (1973).
86. R. M. Fitch, *Off. Dig., J. Paint Technol. Eng.* **37**, 32–48 (1965).
87. K. Tauer and I. Kühn, *Macromolecules* **28**, 2236–2239 (1995).
88. K. Tauer, I. Kühn, in J. M. Asua, ed, *Polymeric Dispersions: Principles and Apllications*, Kluwer Academic Publishers, Dordrecht, 1997, pp. 49–65.
89. D. Kashiev, *Nucleation: Basic Theory with Applications*, Butterworth-Heinemann, Oxford, 2000.
90. K. Binder, in P. Haasen, ed., *Material Science and Technology, Vol. 5: Phase Transformations in Materials*, VCH, Weinheim, 1991, pp. 405–471.
91. I. Kühn and K. Tauer, *Macromolecules* **28**, 8122–8128 (1995).
92. K. Tauer, R. Deckwer, I. Kühn, and C. Schellenberg, *Colloid Polym. Sci.* **277**, 607–626 (1999).
93. K. Tauer, K. Padtberg, and C. Dessy, in E. S. Daniels, E. D. Sudol, and M. S. El Aasser, eds., *Polymer Colloids, Science and Technology of Latex Systems* (American Chemical Society Symposium Series 801), American Chemical Society, Washington, D.C., 2001, pp. 93–112.
94. N. Sütterlin, in R. M. Fitch, ed., *Polymer Colloids II*, Plenum Press, New York, 1980, pp. 583–597.
95. K. Tauer, C. Dessy, S. Corkery, and K.-D. Bures, *Colloid Polym. Sci.* **277**, 805–811 (1999).
96. P. Mukerjee and K. J. Mysels, *Critical Micelle Concentrations of Aqueous Surfactant Systems*, Nat. Stand. Ref. Data Ser., (Nat. Bur. Stand. (U.S.), NSRDS-NBS 36) Washington, D.C., 1971, pp. 51–52.
97. K. Tauer, I. Kühn, and H. Kaspar, *Prog. Colloid Polym. Sci.* **101**, 30–37 (1996).
98. W. A. G. R. Al-Shahib, and A. S. Dunn, *J. Polym. Sci., Polym. Chem. Ed.* **16**, 677–684 (1978).
99. A. S. Dunn and W. A. Al-Shahib, in R. M. Fitch, ed., *Polymer Colloids*, Plenum Press, New York, 1971, pp. 619–628.
100. A. S. Dunn, in I. Piirma, ed., *Emulsion Polymerization*, Academic Press, Inc., New York, 1982, pp. 221–245.
101. K. Tauer, in J. Texter, ed., *Reactions and Synthesis in Surfactant Systems*, Marcel Dekker, Inc., New York, 2001, pp. 429–453.
102. S. Shen, E. D. Sudol, and M. S. El-Aasser, *J. Polym. Sci., Part A: Polym. Chem.* **32**, 1087–1100 (1994).
103. A. Laaksonen, V. Talanquer, and D. W. Oxtoby, *Annu. Rev. Phys. Chem.* **46**, 489–524 (1995).
104. K. Tauer, C. Schellenberg, and A. Zimmermann, *Macromol. Symp.* **150**, 1–12 (2000).
105. D. Distler, *Wäßrige Polymerdispersionen: Synthese, Eigenschaften, Anwendungen*, Wiley-VCH, Weinheim, 1999, pp. 16–19.
106. T. Rager, W. H. Meyer, G. Wegner, K. Mathauer, W. Mächtle, W. Schrof, and D. Urban, *Macromol. Chem. Phys.* **200**, 1681–1691 (1999).
107. M. Gerst, H. Schuch, and D. Urban, in J. E. Glass, ed., *Associative Polymers in Aquepus Media* (ACS Symposium Seres 765), American Chemical Society, Washington, D.C., 2000, pp. 37–51.

108. K. E. J. Barrett, H. R. Thomas, in K. E. J. Barrett, ed., *Dispersion Polymerization in Organic Media*, John Wiley & Sons, Inc., New York, 1975, pp. 151–108.
109. R. N. Haward, *J. Polym. Sci.* **4**, 273–287 (1949).
110. W. H. Stockmayer, *J. Polym. Sci.* **XXIV**, 314–317 (1957).
111. J. T. O'Toole, *J. Appl. Polym. Sci.* **9**, 1291–1297 (1965).
112. J. Ugelstad, P. C. Mork, and J. O. Aasen, *J. Polym. Sci., Part A1* **5**, 2381–2388 (1967).
113. J. Ugelstad and F. K. Hansen, *Rubber Chem. Technol.* **49**, 536–609 (1976).
114. S. Omi, H. Yuyama, and G.-H Ma, *J. Polym. Sci., Part A: Polym. Chem.* **36**, 367–369 (1998).
115. K. Stähler, Ph.D. dissertation, Max Planck Institute of Colloids and Interfaces, Gohn, and University of Potsdam, Germany, 1994.
116. K. Suzuki and M. Nomura, *Macromol. Symp.* **179**, 1–12 (2002).
117. B. M. E. van der Hoff, *Adv. Chem. Ser.* **34**, 6–31 (1962).
118. M. S. Ryabova, S. M. Sautin, and N. I. Smirnov, *Zh. Prikl. Khim.* **48**, 1577–1582 (1975).
119. H.-Y. Parker, D. G. Westmoreland, and H.-R. Chang, *Macromolecules* **29**, 5119–5127 (1996).
120. K. Tauer, G. Reinisch, H. Gajewski, and I. Müller, *J. Macromol. Sci. Chem. A* **28**, 431–460 (1991).
121. K. Tauer, H. Kaspar, and M. Antonietti, *Colloid Polym. Sci.* **278**, 814–820 (2000).
122. J. W. Vanderhoff, J. F. Vitkuske, E. B. Bradford, and T. Alfrey Jr., *J. Polym. Sci.* **XX**, 225–234 (1956).
123. G. W. Poehlein and J. W. Vanderhoff, *J. Polym. Sci., Polym. Chem. Ed.* **11**, 447–452 (1973).
124. J. Ugelstad, H. Flogstad, F. K. Hansen, and T. Ellingsen, *J. Polym. Sci., Polym. Symp.* **42**, 473–485 (1973).
125. P. C. Mork, *J. Polym. Sci. Part A: Polym. Chem.* **33**, 2305–2316 (1995).
126. Ref. 33, pp. 236–244.
127. R. A. Backhaus, *Isr. J. Botany* **34**, 283–293 (1985).
128. G. Q. Chen, G. Zhang, S. J. Park, and S. Y. Lee, *Appl. Microbiol. Biotechnol.* **57**, 50–55 (2001).
129. F. Tiarks, K. Landfester, and M. Antonietti, *J. Polym. Sci., Part A: Polym. Chem.* **39**, 2510–2524 (2001).
130. W. Stöber, A. Fink, and E. Bohn, *J. Colloid Interface Sci.* **26**, 62–69 (1968).
131. S. Slomkowski, S. Sosnowski, and M. Gadzinowski, *Colloid Surf., A* **153**, 111–118 (1999).
132. D. D. Hile and M. V. Pishko, *J. Polym. Sci., Part A: Polym. Chem.* **39**, 562–570 (2001).
133. U. S. Pat. 2,891,920 (1959), J. F. Hyde, and J. R. Wehrly (to Dow Corning Corp.).
134. D. R. Weyenberg, D. E. Findlay, J. Cekada Jr., and A. E. Bey, *J. Polym. Sci., Part C* **27**, 27–34 (1969).
135. M. A. Awan, V. L. Dimonie, and M. S. El-Aasser, *J. Polym. Sci., Part A: Polym. Chem.* **34**, 2633–2649 (1996).
136. R. E. Rinehart, *J. Polym. Sci., Part C* **27**, 7–25 (1969).
137. A. Tomov, J.-P. Broyer, and R. Spitz, *Macromol. Symp.* **150**, 53–58 (2000).
138. B. Manders, L. Sciandrone, G. Hauck, and M. O. Kristen, *Angew. Chem. Int. Ed.* **40**, 4006–4007 (2001).
139. K. Landfester and H.-P. Hentze, in J. Texter, ed., *Reactions and Synthesis in Surfactant Systems*, Marcel Dekker, Inc., New York, 2001, pp. 471–499.
140. J. Qiu, B. Charleux, and K. Matyjaszewski, *Prog. Polym. Sci.* **26**, 2083–2134 (2001).
141. M. F. Cunningham, *Prog. Polym. Sci.* **27**, 1039–1067 (2002).
142. A. Butte, G. Storti, and M. Morbidelli, *Macromolecules* **34**, 5885–5896 (2001).
143. J. G. Tsavalas, F. J. Schork, H. de Brouwer, and M. J. Monteiro, *Macromolecules* **34**, 3938–3946 (2001).

144. G. Moad, J. Chiefari, Y. K. Chomg, J. Krstina, R. T. A. Mayadunne, A. Postma, E. Rizzardo, and S. H. Thang, *Polym. Int.* **49**, 993–1001 (2000).
145. S. Jousset, J. Qiu, and K. Matyjaszewski, *Macromolecules* **34**, 6641–6648 (2001).
146. J. Qiu, T. Pintauer, S. G. Gaynor, K. Matyjaszewski, B. Charleux, and J. P. Vairon, *Macromolecules* **33**, 7310–7320 (2000).
147. G. Scmidt-Naake, M. Drache, and C. Taube, *Angew. Makromol. Chem.* **265**, 62–68 (1999).
148. A. E. Kanakov, A. G. Kronman, Yu. D. Semchikov, G. L. Groshev, E. F. Sitnikova, and T. V. Vodop'yanova, *Russ. J. Appl. Chem.* **70**, 1308–1312 (1997).
149. J. M. Pinto and R. Giudici, *Chem. Eng. Sci.* **56**, 1021–1028 (2001).
150. G. D. Longeway and D. E. Witenhafer, *J. Vinyl Additive Techn.* **6**, 100–103 (2000).
151. Ref. 31, pp. 271–324.
152. K. Tauer, A. Zimmermann, and H. Schlaad, *Macromol. Chem. Phys.* **203**, 319–327 (2002).
153. G. W. Poehlein, in J. I. Kroschwitz, ed., *Encyclopedia Polymer Science and Engineering*, Vol. **6**, 2nd ed., John Wiley & Sons, Inc., New York, 1986, pp. 1–51.
154. G. W. Poehlein, in J. M. Asua, ed., *Polymeric Dispersions: Principles and Apllications*, Kluwer Academic Publishers, Dordrecht, 1997, pp. 305–331.
155. E. A. Grulke, in J. I. Kroschwitz, ed., *Encyclopedia Polymer Science and Engineering*, Vol. **16**, 2nd ed., John Wiley & Sons, Inc., New York, 1989, pp. 443–473.
156. P. V. Smallwood and M. J. Bunten, in J. I. Kroschwitz, ed., *Encyclopedia Polymer Science and Engineering*, Vol. **17** 2nd ed., John Wiley & Sons, Inc., New York, 1989, pp. 295–376.
157. D. R. Bassett and K. L. Hoy, in D. R. Bassett, and A. E. Hamielec, eds., *Emulsion Polymers and Emulsion Polymerization* (ACS Symposium Series 165), American Chemical Society, Washington D.C., 1981, pp. 371–387.
158. B. Jacobi, *Angew. Chem.* **64**, 539–543 (1952).
159. G. W. Poehlein and D. J. Dougherty, *Rubber Chem. Technol.* **50**, 601–638 (1977).
160. C. Kiparissides, J. F. McGregor, and A. E. Hamielec, *Can. J. Chem. Eng.* **58**, 48–55 (1980).
161. A. W. DeGraff and G. W. Poehlein, *J. Polym. Sci., Part A-2* **9**, 1955–1976 (1971).
162. G. W. Poehlein, *Polym. Intern.* **30**, 243–251 (1993).
163. F. J. Schork, in C. McGreavy, ed., *Polymer Reactor Engineering*, Chapman and Hall, London, 1994, pp. 148–202.
164. N. Ohmura, K. Kitamoto, T. Yano, and K. Kataoka, *Ind. Eng. Res.* **40**, 5177–5183 (2001).
165. H. N. Hipps, G. W. Poehlein, and F. J. Schork, *Polym. React. Eng.* **9**, 135–160 (2001).
166. H. Gerrens, *Fortschr. Hochpol. Forsch.* **1**, 234–328 (1959).
167. K. Arai, M. Arai, S. Iwasaki, and S. Saito, *J. Polym. Sci., Polym. Chem. Ed.* **19**, 1203–1215 (1981).
168. M. Nomura, M. Harada, W. Eguchi, and S. Nagata, *J. Appl. Polym. Sci.* **16**, 835–84 (1972).
169. M. F. Kemmere, J. Meuldijk, A. A. Drinkenburg, and A. L. German, *J. Appl. Polym. Sci.* **74**, 3225–3241 (1999).
170. M. Zubitur and J. M. Asua, *J. Appl. Polym. Sci.* **80**, 841–851 (2001).
171. M. F. Kemmere, J. Meuldijk, A. A. Drinkenburg, and A. L. German, *J. Appl. Polym. Sci.* **79**, 944–957 (2001).
172. S. Oprea and T. Dodita, *Prog. Org. Coat.* **42**, 192–201 (2001).
173. D. A. Paquet Jr. and W. H. Ray, *AIChE J.* **40**, 73–87 (1994).
174. C. Sayer and R. Giudici, *Braz. J. Chem. Eng.* **19**, 89–103 (2002).
175. C. Abad, J. C. de la Cal, and J. M. Asua, in J. M. Asua, ed., *Polymeric Dispersions: Principles and Applications*, Kluwer Academic Publishers, Dordrecht, 1997, pp. 333–347.

176. P. J. Dowding, J. W. Goodwin, and B. Vincent, *Colloid Polym. Sci.* **278**, 346–351 (2000).
177. M. Apostel, W. Pauer, H.-U. Moritz, J. Kermeskötter, and K.-D. Hungenberg, *Chimia* **55**, 229–230 (2001).
178. X. Ni, D. C. Bennett, K. C. Symes, and B. D. Grey, *J. Appl. Polym. Sci.* **76**, 1669–1676 (2000).
179. X. Wei, H. Takahashi, S. Sato, and M. Nomura, *J. Appl. Polym. Sci.* **80**, 1931–1942 (2001).
180. K. Kataoka, N. Ohmura, M. Kouzu, Y. Simamura, and M. Okubo, *Chem. Eng. Sci.* **50**, 1409–1416 (1995).
181. F. H. A. M. van den Bommen, J. Meuldijk, and D. Thoenes, *Chem. Eng. Sci.* **54**, 3283–3290 (1999).
182. J. W. Vanderhoff, M. S. El-Aasser, F. J. Micale, E. D. Sudol, C. M. Tseng, A. Silwanowizc, D. M. Kornfeld, and F. A. Vicente, *J. Dispersion Sci., Technol.* **5**, 231–246 (1984).
183. G. Vidotto, A. Crosato-Arnaldi, and G. Talamini, *Makromol. Chem.* **122**, 91–104 (1969).
184. M. Carenza and G. Palma, *Eur. Polym. J.* **21**, 41–47 (1985).
185. A. Guyot, in J. C. Salamone, ed., *Polymeric Materials Encyclopedia*, Vol. **9**, CRC Press, Boca Raton, 1996, pp. 7228–7237.
186. H. D. H. Stöver, in J. C. Salamone, ed., *Polymeric Materials Encyclopedia*, Vol. **9**, CRC Press, Boca Raton, 1996, pp. 7237–7238.
187. H. Bieringer, K. Flatau, and D. Reese, *Angew. Makromol. Chem.* **123/124**, 307–334 (1984).
188. H. G. Yuan, G. Kalfas, and W. H. Ray, *J. Macromol. Sci.—Rev. Macromol. Chem. Phys. C* **31**, 215–299 (1991).
189. J. E. Puig and E. Mendizabal, in J. C. Salamone, ed., *Polymeric Materials Encyclopedia*, Vol. **10**, CRC Press, Boca Raton, 1996, pp. 8215–8220.
190. E. Vivaldo-Lima, P. E. Wood, A. E. Hamielec, and A. Penlidis, *Ind. Eng. Chem.* **36**, 939–965 (1997).
191. P. J. Dowding and B. Vincent, *Colloids Surf., A* **161**, 259–269 (2000).
192. D. J. Walbridge, in G. C. Eastmond, A. Ledwith, S. Russo and P. Sigwalt, eds., *Chain Polymerization II*, Vol. **4**, Pergamon Press, Oxford, 1989, Chapt. "15", pp. 243–260.
193. H. D. H. Stöver, in J. C. Salamone, ed., *Polymeric Materials Encyclopedia*, Vol. **3**, CRC Press, Boca Raton, 1996, pp. 1900–1905.
194. J. L. Cawse, in P. A. Lovell, and M. S. El-Aasser eds., *Emulsion Polymerization and Emulsion Polymers*, John Wiley & Sons, Inc., Chichester, 1997, pp. 743–761.
195. W.-H. Li, K. Li, and H. D. H. Stöver, *J. Polym. Sci., Part A: Polym. Chem.* **37**, 2295–2303 (1999).
196. K. E. J. Barrett, ed., *Dispersion Polymerization in Organic Media*, John Wiley & Sons, Inc., London, 1975.
197. M. F. Cunningham, *Polym. React. Eng.* **7**, 231–257 (1999).
198. P. C. Mork, B. Saethre, and J. Ugelstad, in J. C. Salamone, ed., *Polymeric Materials Encyclopedia*, Vol. **10**, CRC Press, Boca Raton, 1996, pp. 8559–8566.
199. M. J. Bunten, in J. I. Kroschwitz, ed., *Encyclopedia Polymer Science and Engineering*, Vol. **17**, 2nd ed., John Wiley & Sons, Inc., New York, 1989, pp. 329–376.
200. G. Markert, *Angew. Makromol. Chem.* **123/124**, 285–306 (1998).
201. Q. Wang, S. Fu, and T. Yu, *Prog. Polym. Sci.* **19**, 703–753 (1994).
202. M. S. El-Aasser, E. D. Sudol, in P. A. Lovell and M. S. El-Aasser, eds., *Emulsion Polymerization and Emulsion Polymers*, John Wiley & Sons, Inc., Chichester, 1997, pp. 37–58.
203. S. Sajjadi and B. W. Brooks, *Chem. Eng. Sci.* **55**, 4757–4781 (2000).
204. H. Kawaguchi, in T. Sugimoto, ed., *Fine Particles: Synthesis, Characterization and Mechanism of Growth*, Marcel Dekker Inc., New York, 2000, pp. 592–608.
205. B. Saethre, P. C. Mork, and J. Ugelstad, *J. Polym. Sci., Part A: Polym. Chem.* **33**, 2951–2959 (1995).

206. I. Aizpurua, J. Amalvy, M. J. Barandiaran, J. C. de La Cal, and J. M. Asua, *Macromol. Symp.* **111**, 121–131 (1996).
207. E. D. Sudol, M. S. El-Aasser, in P. A. Lovell, and M. S. El-Aasser, eds., *Emulsion Polymerization and Emulsion Polymers*, John Wiley & Sons, Inc., Chichester, 1997, pp. 699–722.
208. Y. Luo, J. Tsavala, and F. J. Schork, *Macromolecules* **34**, 5501–5507 (2001).
209. I. Capek and C. S. Chevn, *Adv. Polym. Sci.* **155**, 101–165 (2001).
210. M. Antonietti and K. Landfester *Prog. Polym. Sci.* **27**, 689–757 (2002).
211. J. M. Asua *Prog. Polym. Sci.* **27**, 1283–1346 (2002).
212. F. Candau, in J. I. Kroschwitz, ed., *Encyclopedia Polymer Science and Engineering*, Vol. **9**, 2nd ed., John Wiley & Sons, Inc., New York, 1989, pp. 718–724.
213. I. Capek and P. Potisk, *Eur. Polym. J.* **31**, 1269–1277 (1995).
214. J. Santhanalakshmi, and K. Anandhi, *J. Appl. Polym. Sci.* **60**, 293–304 (1996).
215. L. M. Gan and C. H. Chew, in J. C. Salamone, ed., *Polymeric Materials Encyclopedia*, Vol. **10**, CRC Press, Boca Raton, 1996, pp. 4321–4331.
216. M. Antonietti, in J. C. Salamone, ed., *Polymeric Materials Encyclopedia*, Vol. **10**, CRC Press, Boca Raton, 1996, pp. 4331–4333.
217. M. Rabelero, M. Zacarias, E. Mendizabal, J. E. Puig, J. M. Dominguez, and I. Katime, *Polym. Bull.* **38**, 695–700 (1997).
218. N. Girard, Th. F. Tadros, and A. I. Bailey, *Colloid Polym. Sci.* **276**, 999–1009 (1998).
219. F. Candau, M. Pabon, and J.-Y. Anquetil, *Colloids Surf., A* **153**, 47–59 (1999).
220. N. Sosa, R. D. Peralta, R. G. Lopez, L. F. Ramos, I. Katime, C. Cesteros, E. Mendizabal, and J. E. Puig, *Polymer* **42**, 6923–6928 (2001).
221. C. C. Co, P. Cotts, S. Burauner, R. de Vries, and E. W. Kaler, *Macromolecules* **34**, 3245–3254 (2001).
222. F. Reynolds, K. Jun, and Y. Li, *Macromolecules* **34**, 165–170 (2001).
223. D. Hunkeler, F. Candau, C. Pichot, A. E. Hamielec, T. Y. Xie, J. Barton, V. Vaskova, J. Guillot, M. V. Dimonie, and K.-H. Reichert, *Adv. Polym. Sci.* **112**, 115–133 (1994).
224. V. F. Kurenkover and V. A. Myagchenkov, in J. C. Salamone, ed., *Polymeric Materials Encyclopedia*, Vol. **10**, CRC Press, Boca Raton, 1996, pp. 47–54.
225. D. J. Hunkeler and J. Hernandez-Barajas, in J. C. Salamone, ed., *Polymeric Materials Encyclopedia*, Vol. **10**, CRC Press, Boca Raton, 1996, pp. 3322–3333.
226. F. Candau, in P. A. Lovell and M. S. El-Aasser, eds., *Emulsion Polymerization and Emulsion Polymers*, John Wiley & Sons, Inc., Chichester, 1997, pp. 723–741.
227. Ref. 34, pp. 64–68.
228. H. Edelhauser and J. W. Breitenbach, *J. Polym. Sci.* **XXXV**, 423–428 (1959).
229. J. W. Breitenbach and H. Edelhauser, *Makromol. Chem.* **44–46**, 196–211 (1961).
230. I. Capek, *Adv. Colloid Interface Sci.* **91**, 295–334 (2001).
231. J. E. Puig, V. H. Pérez-Luna, M. Pérez-González, E. R. Macíac, B. E. Rodríguez, and E. W. Kaler, *Colloid Polym. Sci.* **271**, 114–123 (1993).
232. J. M. Asua, V. S. Rodriguez, and E. D. Sudol, M. S. El-Aasser, *J. Polym. Sci., Part A: Polym. Chem.* **27**, 3569–3587 (1989).
233. S. S. Ivanchev, N. I. Solomko, V. V. Konovalnko, and V. A. Jurshenko, *Dokl. Akad. Nauk SSSR* **191**, 593–595 (1970).
234. V. N. Pavljuchenko, N. N. Lesnikova, N. A. Birdina, G. A. Otradina, and A. P. Agapitov, *Vysokomol. Soedin.* **35**, 240–243 (1993).
235. K. Tauer and S. Kosmella, *Polym. Int.* **30**, 253–258 (1993).
236. M. Zerfa and B. W. Brooks, *DECHEMA Monogr.* **131**, 249–257 (1995).
237. I. M. Kolthoff and I. K. Miller, *J. Am. Chem. Soc.* **73**, 3055–3059 (1951).
238. G. Odian, *Principles of Polymerization*, Wiley-Interscience, New York, 1991, p. 215.
239. K. Tauer, in K. Holmberg, ed., *Handbook of Applied Surface and Colloid Chemistry*, John Wiley & Sons, Inc., New York, 2001, pp. 8175–200.

240. W. I. Higuchi and J. Misra, *J. Pharm. Sci.* **51**, 459–466 (1962).
241. A. S. Kabalnov, A. V. Pertzov, and E. D. Shchukin, *Colloids Surf.* **24**, 19–32 (1987).
242. J. G. Weers, and R. A. Arlauskas, *Langmuir* **11**, 474–477 (1995).
243. K. S. Birdi, in K. S. Birdi, ed., *Handbook of Surface and Colloid Chemistry*, CRC Press, Boca Raton, 1997, p. 100.
244. F. Chu, C. Graillat, and A. Guyot, *J. Appl. Polym. Sci.* **70**, 2667–2677 (1998).
245. R. Becker, A. Hashemzadeh, and H. Zecha, *Macromol. Symp.* **151**, 567–573 (2000).
246. C. Tang and F. Chu, *J. Appl. Polym. Sci.* **82**, 2352–2356 (2001).
247. J. C. Lagarias, *Discrete Comput. Geom.* **27**, 165–193 (2002).
248. D. Horak, *Acta Polym.* **47**, 20–28 (1996).
249. M. Okubo, M. Shiozaki, M. Tsujihiro, and Y. Tsukuda, *Colloid Polym. Sci.* **269**, 222–226 (1991).
250. M. Okubo and T. Nakagawa, *Colloid Polym. Sci.* **270**, 853–858 (1992).
251. J. Ugelstad, Mfutakamba, P. C. Mork, T. Ellingsen, A. Berge, R. Schmid, L. Holm, A. Jorgendahl, F. K. Hansen, and K. Nustad, *J. Polym. Sci., Polym. Symp.* **72**, 225–240 (1985).
252. J. Ugelstad, P. Stenstad, L. Kilaas, W. S. Prestvik, A. Rian, K. Nustad, R. Herje, and A. Berge, *Macromol. Symp.* **101**, 491–500 (1996).
253. J. W. Vanderhoff, *Chem. Eng. Sci.* **48**, 203–217 (1993).
254. G. A. Vandezande, O. W. Smith, and D. R. Bassett, in P. A. Lovell and M. S. El-Aasser, eds., *Emulsion Polymerization and Emulsion Polymers*, John Wiley & Sons, Inc., Chichester, 1997, pp. 563–587.
255. B. R. Vijayendran, in R. M. Fitch, ed., *Polymer Colloids II*, Plenum Press, New York, 1980, pp. 209–224.
256. E. R. Blout and H. Mark, *Monomers*, Interscience Publishers, Inc., New York, 1951.
257. Ref. 31, pp. 156–158.
258. J. J. G. S. van Es, J. M. Geurts, J. M. Verstegen, and A. L. German, in J. M. Asua, ed., *Polymeric Dispersions: Principles and Applications*, Kluwer Academic Publishers, Dordrecht, 1997, pp. 451–462.
259. A. S. de Buruaga, J. C. de la Cal, and J. M. Asua, *Polymer* **41**, 1269–1276 (2000).
260. A. L. Warg, W. J. Roberts, in E. R. Blout, and H. Mark, eds., *Monomers*, Interscience Publishers, Inc., New York, 1951, p. 51.
261. W. H. Lane, *Ind. Eng. Chem.* **18**, 295–296 (1946).
262. F. Wenzel and K. Lehmann, *Lexikon der technischen Chemie*, Vol. **16**, 4th ed., VCH, Weinheim, 1978, p. 610.
263. M. E. L. McBain and E. Hutchinson, *Solubilization and Related Phenomena*, Academic Press, Inc., New York, 1955.
264. Ref. 31, pp. 114–163.
265. P. C. Mork and J. Ugelstad, *Eur. Polym. J.* **5**, 483–492 (1969).
266. *Tabellenbuch Chemie*, 7th ed., VEB Deutscher Verlag für Grundstoffindustrie, Leipzig, 1975, p. 298.
267. L. Lopez de Arbina, L. M. Gugliotta, M. J. Barandiaran, and J. M. Asua, *Polymer* **39**, 4047–4055 (1998).
268. M. F. Cunningham, K. Geramita, and J. W. Ma, *Polymer* **41**, 5385–5392 (2000).
269. M. Morton, S. Kaizerman, and M. W. Altier, *J. Colloid Sci.* **9**, 300–312 (1954).
270. O. Braun, J. Selband, and F. Candau, *Polymer* **42**, 8499–8510 (2001).
271. W. Burchard, *Prog. Colloid Polym. Sci.* **78**, 63–67 (1988).
272. M. Antonietti, H. Kaspar and K. Tauer, *Langmuir* **12**, 6211–6217 (1999).
273. J. O'Haver, B. Grady, J. H. Harvell, and E. A. O'Rear, in J. Texter, ed., *Reactions and Synthesis in Surfactant Systems*, Marcel Dekker, Inc., New York, 2001, pp. 537–545.
274. A. Aguiar, S. Gonzalez-Villegas, M. Rabelero, E. Mendizabal, J. E. Puig, J. M. Dominguez and I. Katime, *Macromolecules* **32**, 6767–6771 (1999).

275. S. S. Medvedev, in IUPAC International Symposium on Macromolecular Chemistry "Kinetics and Mechanism of Polyreactions," Budapest, Hungary, 1969, Akadémiai Kiadó, Budapest 1971, pp. 39–63.
276. M. R. Grancio and D. J. Williams, *J. Polym. Sci., Part A1* **8**, 2617–2629 (1970).
277. D. H. Napper, *J. Polym. Sci., Part A1* **9**, 2089–2091 (1971).
278. P. Keusch and D. J. Williams, *J. Polym. Sci., Polym. Chem. Ed.* **11**, 143–162 (1973).
279. J. L. Gardon, *J. Polym. Sci., Polym. Chem. Ed.* **11**, 241–251 (1973).
280. R. Tognacci, G. Storti, and A. Bertucco, *J. Appl. Polym. Sci.* **62**, 2341–2349 (1996).
281. A. L. German, B. G. Manders, H. F. Zirkzee, B. Klumperman, and A. M. van Herk, *Macromol. Symp.* **111**, 107–120 (1996).
282. H. Bodugöz and O. Güven, *J. Appl. Polym. Sci.* **83**, 349–356 (2002).
283. J. Ugelstad, P. C. Mork, K. H. Kaggerud, T. Ellingsenand, and A. Berge, *Adv. Colloid Interface Sci.* **13**, 101–140 (1980).
284. R. Defay, I. Prigogine, A. Bellemans, and D. H. Everett, *Surface Tension and Adsorption*, Longmans, Green & Co. Ltd., London, 1966, 217–222.
285. J. Ugelstad, P. Stenstad, L. Kilaas, W. S. Prestvik, A. Rian, K. Nustad, R. Herje, and A. Berge, *Macromol. Symp.* **101**, 491–500 (1996).
286. T. E. Daubert, R. P. Danner, H. M. Sibul, and C. C. Stebbins, *Physical and Thermodynamic Properties of Pure Chemicals Data Compilation, Part 1-5*, Taylor and Francis, Washington, D.C., 1998.
287. J. Brandrup and E. H. Immergut, *Polymer Handbook*, 3rd ed., John Wiley & Sons, Inc., New York, 1989, Section V.
288. D. H. Napper, *Polymeric Stabilization of Colloidal Dispersions*, Academic Press, Inc., London, 1983.
289. D. W. J. Osmond, F. A. Waite, in K. E. J. Barrett, ed., *Dispersion Polymerization in Organic Media*, John Wiley & Sons, Inc., London, 1975, pp. 9–44.
290. R. H. Ottewill, in P. A. Lovell, and M. S. El-Aasser, eds., *Emulsion Polymerization and Emulsion Polymers*, John Wiley & Sons, Inc., New York, 1997, pp. 59–121.
291. I. Piirma, *Polymeric Surfactants* (Surfactant Science Series 42), Marcel Dekker, Inc., New York, pp. 1–16.
292. W. Bancroft, *J. Phys. Chem.* **16**, 177–233 (1912).
293. W. C. Griffin, *J. Soc. Cosmetic Chemists* **1**, 311–326 (1949).
294. A. Beerbower and M. W. Hill, *Detergents & Emulsifiers* 1971 Annual, pp. 223–236.
295. C. Holtzscherer and F. Candau, *Colloid Surf.* **29**, 411–423 (1988).
296. H. C. Hamaker, *Rec. Trav. Chim.* **55**, 1015–1026 (1936).
297. H. C. Hamaker, *Rec. Trav. Chim.* **56**, 3–25 (1937).
298. H. C. Hamaker, *Rec. Trav. Chim.* **56**, 727–748 (1937).
299. H.-J. Jacobasch and K.-H. Freitag, *Acta Polym.* **30**, 453–469 (1979).
300. D. F. Evans and H. Wennerström, *The Colloidal Domain*, VCH, Weinheim, 1994, p. 221.
301. F. W. Fowkes, *Ind. Eng. Chem.* **56**, 40–52 (1964).
302. D. B. Hough and L. R. White, *Adv. Colloid Interface Sci.* **14**, 3–41 (1980).
303. G. Jung, *Z. Elektrochem. Angew. Phys. Chem.* **35**, 1–2 (1929).
304. A. Kuhn, *Wörterbuch der Kolloidchemie*, Verlag von Theodor Steinkopff, Dresden, 1932, pp. 25–26, 100.
305. D. F. Evans and H. Wennerström, *The Colloidal Domain*, VCH, Weinheim, 1994, pp. 110–127, and pp. 333–338.
306. D. H. Napper, *Polymeric Stabilization of Colloidal Dispersions*, Academic Press, Inc., London, 1983, pp. 144–159.
307. C. Bechinger, H.-H. von Grünberg, and P. Leiderer, *Phys. Bl.* **55**, 53–56 (1999).
308. D. H. Napper and A. Netschey, *J. Colloid Interface Sci.* **37**, 528–535 (1971).

309. D. H. Napper, *J. Colloid Interface Sci.* **32**, 106–114 (1970).
310. P. Pincus, *Macromolecules* **24**, 2912–2919 (1991).
311. L. Leemans, R. Fayt, Ph. Teyssie, and N. C. de Jaeger, *Macromolecules* **24**, 5922–5925 (1991).
312. K. Tauer, H. Müller, L. Rosengarten, and K. Riedelsberger, *Colloids Surf., A* **153**, 75–88 (1999).
313. H. Müller, PhD thesis, Max Planck Institute of Colloids and Interfaces, Golm, and University of Potsdam, Germany, Cuvillier Verlag Göttingen, 1997, pp. 82–85.
314. G. Lagaly, O. Schulz, and R. Ziemehl, *Dispersionen und Emulsionen: eine Einführung in die Kolloidik feinverteilter Stoffe einschließlich der Tonminerale*, Dr. Dietrich Steinkopff Verlag, Darmstadt, 1997, pp. 254–262.
315. S. Abend, N. Bonnke, U. Gutschner, and G. Lagaly, *Colloid Polym. Sci.* **276**, 730–737 (1998).
316. A. Guyot and K. Tauer, in J. Texter, ed., *Reactions and Synthesis in Surfactant Systems*, Marcel Dekker, Inc., New York, 2001, pp. 547–575.
317. G. Odian, *Principles of Polymerization*, 3rd ed., John Wiley & Sons, Inc., New York, 1991.
318. S. L. Rosen, *Fundamental Principles of Polymeric Materials*, 2nd ed., John Wiley & Sons, Inc., New York, 1993, 200–213.
319. C. Hagiopol, *Copolymerization: Toward a Systematic Approach*, Kluwer Academic/Plenum Publishers, New York, 1999.
320. S.-T. Wang and G. W. Poehlein, *J. Appl. Polym. Sci.* **50**, 2173–2183 (1993).
321. A. Guyot, J. Guillot, C. Pichot, and L. Rios Guerrero, in D. R. Bassett, and A. E. Hamielec, eds., *Emulsion Polymers and Emulsion Polymerization* (ACS, Symposium Series 165), American Chemical Society, Washington, D.C., 1981, pp. 415–436.
322. J. Guillot and C. Pichot, eds., *Emulsion Copolymerization*, Hüthig & Wepf, Basel, 1985; Reprinted from *Makromol. Chem., Suppl.* **10/11**, 1–536 (1985).
323. D. C. Blackley, *Polymer Lattices Science and Technology Vol. 2: Types of Lattices*, Chapman & Hall, London, 1997, pp. 206–232.
324. Ref. 319, pp. 192–206.
325. F. A. Bovey and P. A. Mirau, *NMR of Polymers*, Academic Press, Inc., San Diego, 1996, pp. 212–220.
326. J. Guillot, *Makromol. Chem. Suppl.* **10/11**, 235–264 (1985).
327. J. Dimitratos, G. Elicabe, and C. Georgakis, *AICheE J.* **40**, 1993–2021 (1994).
328. M. Embirucu, E. L. Lima, and J. C. Pinto, *Polym. Eng. Sci.* **36**, 433–447 (1996).
329. R. Giudici, *Latin Am. Appl. Res.* **30**, 351–356 (2000).
330. C. Kiparissides, *Chem. Eng. Sci.* **51**, 1637–1659 (1996).
331. A. M. van Herk and A. L. German, *Macromol. Theory Simul.* **7**, 537–565 (1998).
332. J. M. Asua, *Polym. React. Eng.* **9**, 37–67 (2001).
333. J. Zhang, A. J. Morris, E. B. Martin, and C. Kiparissides, *Chem. Eng. J.* **69**, 135–143 (1998).
334. J. Snuparek, *Prog. Org. Coat.* **29**, 225–233 (1996).
335. Ref. 323, pp. 355.
336. J. C. Padget, *J. Coat. Technol.* **66**, 89–105 (1994).
337. N. Sütterlin, *Makromol. Chem. Suppl.* **10/11**, 403–418 (1985).
338. Ref. 323, pp. 358–368.
339. S. Torza and S. G. Mason, *J. Colloid Interface Sci.* **33**, 67–83 (1970).
340. D. C. Sundberg, A. P. Casassa, J. Pantazopoulos, and M. R. Muscato, *J. Appl. Polym. Sci.* **41**, 1425–1442 (1990).
341. C. L. Winzor and D. C. Sundberg, *Polymer* **33**, 4269–2279 (1992).
342. E. J. Sundberg and D. C. Sundberg, *J. Appl. Polym. Sci.* **47**, 1277–1294 (1993).

343. Y. G. Durant and D. C. Sundberg, *J. Appl. Polym. Sci.* **58**, 1607–1618 (1995).
344. D. C. Sundberg and Y. G. Durant, in J. M. asua, ed., *Polymeric Dispersions: Principles and Applications*, Kluwer Academic Publishers, Dordrecht, 1997, pp. 177–188.
345. J.-E. L. Jönsson, H. Hassander, L. H. Jansson, and B. Törnell, *Macromolecules* **24**, 126–131 (1991).
346. J.-E. L. Jönsson, H. Hassander, and B. Törnell, *Macromolecules* **27**, 1932–1937 (1994).
347. Y.-C. Chen, V. L. Dimonie, and M. S. El-Aasser, *Macromolecules* **24**, 3779–3787 (1991).
348. V. L. Dimonie, E. S. Daniels, O. L. Shaffer, and M. S. El-Aasser, in P. A. Lovell, and M. S. El-Aasser, eds., *Emulsion Polymerization and Emulsion Polymers*, J. Wiley & Sons, Inc., New York, 1997, pp. 293–326.
349. J. A. Waters, *Colloids Surf., A* **83**, 167–174 (1994).
350. S. Lee and A. Rudin, *J. Polym. Sci., Part A: Polym. Chem.* **30**, 2211–2216 (1992).
351. L. J. Gonzales-Ortiz and J. M. Asua, *Macromolecules* **28**, 3135–3145 (1995).
352. L. J. Gonzales-Ortiz and J. M. Asua, *Macromolecules* **29**, 383–389 (1996).
353. L. J. Gonzales-Ortiz and J. M. Asua, *Macromolecules* **29**, 4520–4527 (1996).
354. D. A. House, *Chem. Rev.* **62**, 185–203 (1962).
355. E. J. Behrman and J. O. Edwards, *Rev. Inorg. Chem.* **2**, 179–206 (1980).
356. K. Tauer and R. Deckwer, *Acta Polymerica* **49**, 411–416 (1998).
357. B. R. Vijayendran, *Makromol. Chem. Suppl.* **10/11**, 271–295 (1985).
358. D. I. Lee, *Makromol. Chem., Macromol. Suppl.* **33**, 117–131 (1990).
359. V. N. Pavlyuchenko, O. V. Sorochinskaya, S. S. Ivanchev, V. V. Klubin, G. S. Kreichman, V. P. Budtov, M. Skrifvars, E. Halme, and J. Koskinen, *J. Polym. Sci., Part A: Polym. Chem.* **39**, 1435–1449 (2001).
360. C. Schellenberg, S. Akari, M. Regenbrecht, K. Tauer, F. M. Petrat, and M. Antonietti, *Langmuir* **15**, 1283–1290 (1999).
361. C. Schellenberg Ph.D. thesis, Max Planck Institute of Colloids and Interfaces, Golm, Germany and University of Potsdam, Germany, Shaker Verlag, Germany 2000.
362. C. J. McDonald, K. J. Bouck, A. B. Chaput, and C. J. Stevens, *Macromolecules* **33**, 1593–1605 (2000).
363. K. S. Birdi, in K. S. Birdi, ed., *Handbook of Surface and Colloid Chemistry*, CRC Press, Boca Raton, 1997, pp. 71–118.
364. M. Okubo, K. Ichikawa and M. Fujimura, *Colloid Polym. Sci.* **269**, 1257–1262 (1991).
365. M. Okubo and H. Mori, *Colloid Polym. Sci.* **275**, 634–639 (1997).
366. J.-W. Kim, Y.-G. Joe, and K.-D. Suh, *Colloid Polym. Sci.* **277**, 252–256 (1999).
367. J. Seidl, J. Malinsky, K. Dusek, and W. Heitz, *Adv. Polym. Sci.* **5**, 113–213 (1967).
368. D. Horak and M. J. Benes, *React. Function. Poly.* **45**, 189–195 (2000).
369. K. Lewandowski, F. Svec, and J. M. J. Frechet, *Chem., Mater.* **10**, 385–391 (1998).
370. M. Xu, E. Brahmachary, M. Janco, F. H. Ling, F. Svec, and J. M. J. Frechet, *J. Chromatogr. A* **928**, 25–40 (2001).
371. C. D. Wood and A. I. Cooper, *Macromolecules* **34**, 5–8 (2001).
372. Y.-D. Jo, K.-S. Park, J.-H. Ahn, and S.-I. Ihm, *Eur. Polym. J.* **32**, 967–972 (1996).
373. S. Kawaguchi, K. Tano, M. Maniruzzman, and K. Ito, *Macromol. Symp.* **150**, 101–108 (2000).
374. K. Tauer, K. Riedelsberger, R. Deckwer, A. Zimmermann, H. Dautzenberg, and J. Thieme, *Macromol. Symp.* **155**, 95–104 (2000).
375. H. Zecha, I. Zenke, H. J. Purz, and C. Bischof, *Angew. Makromol. Chem.* **104**, 169–188 (1982).
376. A. Büchtemann, E. Schulz, and K. Tauer, *Acta Polym.* **36**, 654–657 (1985).
377. K. Tauer, E. Schulz, A. Büchtemann, G. Kurjakova, and W. Jaeger, *Plaste Kautschuk* **33**, 51–53 (1986).
378. R. H. Ottewil, A. B. Schofield, and J. A. Waters, *Colloid Polym. Sci.* **274**, 763–771 (1996).

379. R. H. Ottewill, A. B. Schofield, J. A. Waters, and N. St. J. Williams, *Colloid Polym. Sci.* **275**, 274–283 (1997).
380. R. H. Ottewill, A. B. Schofield, and J. A. Waters, *J. Dispersion Sci., Technol.* **19**, 1151–1162 (1998).
381. L. Lazar, S. A. M. Hesp, and G. E. Kmiecik-Lawrynowicz, *Part. Sci., Technol.* **18**, 103–120 (2000).
382. L. Lazar and S. A. M. Hesp, *Part. Sci., Technol.* **18**, 121–142 (2000).
383. L. Lazar and S. A. M. Hesp, *Part. Sci., Technol.* **18**, 143–162 (2000).
384. K. Maruyama, M. Kawaguchi, and T. Kato, *Colloids Surf., A* **189**, 211–223 (2001).
385. F. J. Schork, G. W. Poehlein, S. Wang, J. Reimers, J. Rodrigues, and C. Samer, *Colloid Surf., A* **153**, 39–45 (1999).
386. M. Ochiai, M. Masui, M. Asanae, M. Tokunaga, and T. Iimura, *J. Imag. Sci., Technol.* **38**, 415–420 (1994).
387. H. K. Mahabadi, T. H. Ng, and H. S. Tan, *J. Microencaps.* **13**, 559–573 (1996).
388. D. C. Lee and L. W. Jang, *J. Appl. Polym. Sci.* **61**, 1117–1122 (1996).
389. J. Hou and G. L. Baker, *Chem. Mater.* **10**, 3311–3318 (1998).
390. J. Yu, J. Yu, Z.-X. Guo, and Y.-F. Gao, *Macromol. Rapid Commun.* **22**, 1261–1264 (2001).
391. N. Bechthold, F. Tiarks, M. Willert, K. Landfester, and M. Antonietti, *Macromol. Symp.* **151**, 549–555 (2000).
392. B. Erdem, E. D. Sudol, V. L. Dimonie, and M. S. El-Aasser, *Macromol. Symp.* **155**, 181–198 (2000).
393. Q. Wang, H. Xia, and C. Zhang, *J. Appl, Polym. Sci.* **80**, 1478–1488 (2001).
394. H. Xia, C. Zhang and Q. Wang, *J. Appl. Polym. Sci.* **80**, 1130–1139 (2001).
395. F. Tiarks, K. Landfester, and M. Antonietti, *Macromol. Chem., Phys.* **202**, 51–60 (2001).
396. K. Wormuth, *J. Colloid Interface Sci.* **241**, 366–377 (2002).
397. M. B. Ko and J. Y. Jho, *Polym. Bull.* **46**, 315–322 (2001).
398. J. I. Amalvy, M. J. Percy, and S. P. Armes, *Langmuir* **17**, 4770–4778 (2001).
399. L. W. Jang, C. M. Kang, and D. C. Lee, *J. Polym. Sci., B: Polym. Phys.* **39**, 719–727 (2001).
400. X. Huang and W. J. Brittain, *Macromolecules* **34**, 3255–3260 (2001).
401. E. P. Giannelis, *Adv. Mater.* **8**, 29–35 (1996).
402. B. Jönsson, B. Lindman, K. Holmberg, and B. Kronberg, *Surfactants and Polymers in Aqueous Solutions*, John Wiley & Sons, Inc., Chichester 1998, pp. 74–82.
403. K. M. McGrath and C. J. Drummond, *Colloid Polym. Sci.* **274**, 612–621 (1996).
404. D. Pawlowski, A. Haibel, and B. Tieke, *Ber. Bunsen-Ges. Phys. Chem.* **102**, 1865–1869 (1998).
405. M. Antonietti and H.-P. Hentze, *Colloid Polym. Sci.* **274**, 696–702 (1996).
406. H.-P. Hentze and M. Antonietti, *Curr. Opin. Sol. State Mat. Sci.* **5**, 343–353 (2001).
407. S. Rimmer and P. I. Tattersall, *Polymer* **40**, 6673–6677 (1999).
408. S. Rimmer and P. I. Tattersall, *Polymer* **40**, 5729–5731 (1999).
409. E. E. Meyer, M. F. Islam, W. Lau, and H. D. Qu-Yang, *Langmuir* **16**, 5519–5522 (2000).
410. R. J. Leyrer and W. Mächtle, *Macromol. Chem., Phys.* **201**, 1235–1243 (2000).
411. T. F. McKenna, S. Othman, G. Fevotte, A. M. Santos, and H. Hammouri, *Polym. React. Eng.* **8**, 1–38 (2000).
412. P. Guinot, N. Othman, G. Fevotte, and T. F. McKenna, *Polym. React. Eng.* **8**, 115–134 (2000).
413. C.-M. Astorga, N. Othman, H. Hammouri, and T. McKenna, *Contr. Eng. Practice* **10**, 3–13 (2002).
414. R. F. Machado and A. Bolzan, *Chem., Eng. J.* **70**, 1–8 (1998).
415. Z. Nagy and S. Agachi, *Comp. Chem., Eng.* **21**, 571–591 (1997).

416. A. Echevarria, J. R. Leiza, J. C. de la Cal, and J. M. Asua, *AIChE J.* **44**, 1667–1679 (1998).
417. M. Vicente, S. BenAmor, L. M. Gugliotta, J. R. Leiza, and J. M. Asua, *Ind. Eng. Chem.* **40**, 218–227 (2001).
418. F. H. Florenzano, R. Strelitzki and W. F. Reed, *Macromolecules* **31**, 7226–7238 (1998).
419. R. Strelitzki, W. F. Reed, *J. Appl. Polym. Sci.* **73**, 2359–2368 (1999).
420. W. F. Reed, *Macromoelcules* **33**, 7165–7172 (2000).
421. A. Giz, H. Catalgil-Giz, A. Alb, J.-L. Brousseau, and W. F. Reed, *Macromoelcules* **34**, 1180–1191 (2001).
422. W.-D. Hergeth, in J. M. Asua, ed., *Polymeric Dispersions: Principles and Apllications*, Kluwer Academic Publishers, Dordrecht, 1997, pp. 267–288.
423. W.-D. Hergeth, in J. M. Asua, ed., *Polymeric Dispersions: Principles and Apllications*, Kluwer Academic Publishers, Dordrecht, 1997, pp. 243–256.
424. O. Kammona, E. G. Chatzi, and C. Kiparissides, *J. Macrmol. Sci., Rev.—Macromol. Chem., Phys. C* **39**, 57–134 (1999).
425. R. N. Landau, *Thermochim. Acta* **289**, 101–126 (1996).
426. P. E. Gloor, R. J. Warner, *Thermochim. Acta* **289**, 243–265 (1996).
427. M. Mosebach and K.-H. Reichert, *J. Appl. Polym. Sci.* **66**, 673–681 (1997).
428. L. Varela de la Rosa, E. D. Sudol, M. S. El-Aasser, and A. Klein, *J. Polym. Sci., Part A: Polym. Chem.* **34**, 461–473 (1996).
429. L. Varela de la Rosa, E. D. Sudol, M. S. El-Aasser, and A. Klein, *J. Polym. Sci., Part A: Polym. Chem.* **37**, 4054–4065 (1999).
430. L. Varela de la Rosa, E. D. Sudol, M. S. El-Aasser, and A. Klein, *J. Polym. Sci., Part A: Polym. Chem.* **37**, 4066–4072 (1999).
431. L. Varela de la Rosa, E. D. Sudol, M. S. El-Aasser, and A. Klein, *J. Polym. Sci., Part A: Polym. Chem.* **37**, 4073–4089 (1999).
432. G. Maschio, I. Ferrara, C. Bassani, and H. Nieman, *Chem., Eng. Sci.* **54**, 3273–3282 (1999).
433. K. Tauer, H. Müller, C. Schellenberg, and L. Rosengarten, *Colloid Surf. A.* **153**, 143–151 (1999).
434. S. Erwin, K. Schulz, H.-U. Moritz, C. Schwede, and H. Kerber, *Chem., Eng. Technol.* **24**, 305–311 (2001).
435. K. Jahny, H.-J. P. Adler, and H.-U. Moritz, *Macromol. Chem. Phys.* **202**, 2915–2920 (2001).
436. V. Liotta, C. Georgakis, E. D. Sudol, and M. S. El-Aasser, *Ind. Eng. Chem., Res.* **36**, 3252–3263 (1997).
437. V. Liotta, E. D. Sudol, M. S. El-Aasser, and C. Georgakis, *J. Polym. Sci., Polym. Chem.* **36**, 1553–1571 (1998).
438. C. Wu, J. D. S. Danielson, J. B. Callis, M. Eaton, and N. L. Ricker, *Prog. Control Qual.* **8**, 1–23 (1996).
439. C. Wu, J. D. S. Danielson, J. B. Callis, M. Eaton, and N. L. Ricker, *Prog. Control Qual.* **8**, 25–40 (1996).
440. A. F. Santos, E. L. Lima, and J. C. Pinto, *J. Appl. Polym. Sci.* **70**, 1737–1745 (1998).
441. A. F. Santos, E. L. Lima, and J. C. Pinto, *J. Appl. Polym. Sci.* **77**, 453–462 (2000).
442. R. A. M. Viera, C. Sayer, E. L. Lima, and J. C. Pinto, *Polymer* **42**, 8901–8906 (2001).
443. A. Al-Khanbashi, M. Dhamdhere, and M. Hansen, *Appl. Spectr. Rev.* **33**, 115–131 (1998).
444. T. J. Vickers, D. R. Lombardi, B. Sun, H. Wang, and C. K. Mann, *Appl. Spectr.* **51**, 1251–1253 (1997).
445. C. Bauer, B. Amram, M. Agnely, D. Charmot, J. Sawatzki, N. Dupuy, and J.-P. Huvenne, *Appl. Spectr.* **54**, 528–535 (2000).

446. M. Morbidell, G. Storti and A. Siani, in J. M. Asua, ed., *Polymeric Dispersions: Principles and Apllications*, Kluwer Academic Publishers, Dordrecht, 1997, pp. 257–266.
447. A. Siani, G. Storti, and M. Morbidelli, *J. Appl. Polym. Sci.* **72**, 1451–1477 (1999).
448. G. Storti, A. K. Hipp, and M. Morbidelli, *Polym. React. Eng.* **8**, 77–94 (2000).
449. A. S. Dukhin, P. J. Goetz, and V. Hackley, *Colloid, Surf., A* **138**, 1–9 (1998).
450. T. H. Wines, A. S. Dukhin, and P. Somasundaran, *J. Colloid Interface Sci.* **216**, 303–308 (1999).
451. A. S. Dukhin, P. J. Goetz, T. H. Wines, and P. Somasundaran, *Colloid, Surf., A* **173**, 127–158 (2000).
452. A. S. Dukhin and P. J. Goetz, *Colloid Surf. A. Physicochem. Eng. Asp.* **192**, 267–306 (2001).
453. A. S. Dukhin and P. J. Goetz, *Adv. Colloid Interface Sci.* **92**, 73–132 (2001).
454. S. S. Kim and D. G. Westmoreland, *J. Polym. Sci., Part A: Polym. Chem.* **32**, 3031–3037 (1994).
455. H.-Y. Parker, D. G. Westmoreland, and H.-R. Chang, *Macromolecules* **29**, 5119–5127 (1996).
456. H. R. Chang, W. Lau, H.-Y. Parker, and D. G. Westmoreland, *Macromol. Symp.* **111**, 253–263 (1996).
457. S. Rudschuk, J. Adams, and J. Fuhrmann, *Macromol. Chem., Phys.* **199**, 771–776 (1998).
458. S. Rudschuk, J. Adams, and J. Fuhrmann, *Nucl. Instrum Methods Phys. Res., Sect. B* **151**, 341–345 (1999).
459. K. Landfester, S. Spiegel, R. Born, and H. W. Spiess, *Colloid Polym. Sci.* **276**, 356–361 (1998).
460. C. J. Samer and F. J. Schork, *Polym. React. Eng.* **5**, 85–124 (1997).
461. G. W. Poehlein and J. Schork *TRIP* **1**, 298–302 (1998).
462. S. Roy and S. Devi, *Polymer* **38**, 3325–3331 (1997).

KLAUS TAUER
Max Planck Institute of Colloids and Interfaces

Abbreviations

A: Hamaker constant (general)
$A_{1,2}$, $A_{1,3}$, $A_{2,3}$: interfacial areas between phases 1–2, 1–3, and 2–3, respectively
A_{eff}: effective Hamaker constant of interacting particles
A_m: Hamaker constant of the medium between interacting particles
A_p: total surface/interface of dispersed phase material
A_p: Hamaker constant of interacting particles
a_s: area covered by a surfactant molecule
A_{spec}: specific surface/interface of dispersed phase either per unit mass or volume of either dispersed phase or water (eq. 1)
C: capacity of a conducting sphere
C_0: solubility of the dispersed phase material in the continuous phase
C_I: initiator concentration
C_{LC}: concentration of the lyophob in the continuous phase
C_{LC0}: solubility of the lyophob in the continuous phase
C_M: monomer concentration

$C_{M,p}$: monomer concentration inside dispersed phase particles
cmc: critical micelle concentration of surfactant/stabilizer
C_{MC0}: solubility of the monomer in the continuous phase
C_S: surfactant/stabilizer concentration
$C_{S,C}$: critical surfactant concentration for stabilization of particles after nucleation
$C_{S,L}$: concentration of stabilizing polymer (lyophilic polymer) in the volume of the hydrodynamic layer
C_{salt}: ionic strength in the continuous phase
D: diameter of dispersed phase material
D_0: diameter of seed particles
D_d: droplet diameter
$D_{d,c}$: critical droplet diameter for which Ostwald ripening stops (eq. 25)
$D_{d,e}$: droplet diameter at equilibrium
D_{dp}: size of dispersed phase molecule
D_{ee}: characteristic length of a dissolved polymer molecule
d_h: diameter of a single hole
D_m: monomer droplet diameter
D_{MC}: diffusion coefficient of monomer in the continuous phase
D_p: monomer particle diameter
d_{pp}: interparticle distance (eq. 3)
D_t: diameter of final composite particles
e: type of end group
E_{kin}: kinetic energy of particles in a shear field (approximation)
f: radical efficiency for starting polymerization
f_1, f_2: mole fractions of monomer 1and 2 in a comonomer mixture
F_1, F_2: mole fractions of monomer 1 and 2 build in the copolymer
FG: solids content in parts per 100 parts dispersion
h: Planck's constant
H: geometrical function of interacting particles
j: chain length
$k_{11}, k_{22}, k_{21}, k_{12}$: propagation rate constants of M_1 with P_1, M_2 with P_2, M_1 with P_2, and M_2 with P_1, respectively
$k_{abs,i}$: rate constant of primary radical absorption by particles of dispersed phase
k_B: Boltzman's constant
$k_{d,d}$: rate constant of initiator decomposition in the dispersed phase
$k_{d,w}$: rate constant of initiator decomposition in the continuous phase
k_{des}: rate constant of radical desorption
k_L: London interaction constant
k_p: propagation rate constant
$k_{t,d}$: termination rate constant in dispersed phase
$k_{t,w}$: rate constant of radical termination in the continuous phase
M_1, M_2: concentration of both comonomers
M_{mon}: molecular weight of the monomer
M_S: molecular weight of surfactant/stabilizer
N: number of particles of dispersed phase material (eq. 2)
n: number of growing centers per particle of dispersed phase
N_A: Avogadro's number

n_I: number of initiator molecules per particle of dispersed phase
N_n: number of particles of dispersed phase with n growing centers
$n_{R,equ}$: number of radicals per particle of dispersed phase at steady state (eq. 7)
n_S: number of molecule of disperse phase at the surface/interface (eq. 5)
N_{ss}: number of small spheres in the mixture with large spheres
P: concentration of propagating radicals
p': vapor pressure outside the drop (eq. 29)
p_0: bulk vapor pressure of the liquid forming a drop (eq. 29)
P_1, P_2: growing chain ended with a radical of monomer 1 and growing chain ended with a radical of monomer 2, respectively
P_d: pressure inside dispersed phase particle
$P_{j,e,w}$: concentration of radicals of chain length j and end group e in the continuous phase
P_n: average degree of polymerization
P_{SW}: swelling pressure
Q: concentration of interacting centers per unit volume
R: gas constant
r: radius of swollen particles
r_0: radius of unswollen particles
r_1, r_2 reactivity ratios (eq. 41)
r_{abs}: absorption rate of radicals from the continuous phase into particles
$r_{i,d}$: rate of initiation in the dispersed phase
$r_{i,w}$: rate of initiation in the continuous phase
r_p: overall rate of polymerization (eq. 9)
S_1, S_2, S_3: spreading coefficients of phase 1, 2, and 3, respectively (eq. 44)
T_g: glass-transition temperature
$T_{g,i}$: glass-transition temperature of a homopolymer of monomer i
v: particle volume
v'': molar volume of the liquid forming a drop (eq. 29)
V_A: attractive potential (eq. 32)
v_c: volume of continuous phase
$v_{c,p}$: molar volume of the molecules forming the continuous phase
V_{int}: interaction potential between charge–stabilized spheres (eq. 37a)
$v_{m,p}$: monomer volume in swollen particles
v_{mon}: molar volume of the monomer
$v_{p,p}$: polymer volume in swollen particles
$V_{R,B}$: Born's repulsion potential
$V_{R,es}$: repulsion potential between equally charged spheres
v_{rel}: relative velocity of two approaching particles in a shear field
V_{st}: steric repulsion potential
w_i: weight fraction of monomer i in a copolymer
$W_{surf,t}$: amount of surfactant relative to the total mass of organic phase (or dispersed phase) (eq. 4)
Z: number of electrons in the outer shell of a molecule
z: stoichiometric valency of the electrolyte dissolved in the continuous phase
ΔD: decrease in diameter caused by shrinkage during polymerization
ΔG_f: free energy of the flocculation process
ΔG_I: interfacial free energy (eq. 43)

ΔH_f: change in enthalpy during flocculation
ΔP_d: Young–Laplace pressure
ΔR: hydrodynamic stabilizer layer thickness
ΔS_f: change in entropy during flocculation
ΔS_{sl}: entropy gain between interacting small and large hard spheres
Δv_c: increase in the effective volume for the smaller spheres due to overlap of the excluded volume regions of the larger spheres
$\Delta \mu_1$: chemical potential of swelling agent (monomer)
Θ: theta condition of a dilute polymer solution (in the limit of infinite molecular weight, the situation where $\Delta \mathrm{H} = T\Delta S$)
Ψ: surface potential
α: exponent in the scaling relation between the hydrodynamic layer thickness (ΔR) and the ionic strength (C_{salt})
α_0: static polarizability of molecules
$\chi_{m,p}$: Flory–Huggins interaction parameter between monomer and polymer
$\chi_{S,cp}$: Flory–Huggins interaction parameter between the stabilizing polymer and the continuous phase
ε: permittivity
ϕ_1: monomer volume fraction inside swollen particles.
ϕ_1, ϕ_3: volume fractions of phase 1 and 3, respectively (eq. 48)
ϕ_2: polymer volume fraction inside swollen particles
ϕ_L: volume fraction of the lyophob inside dispersed phase droplets
$\phi_{L,e}$: volume fraction of the lyophob inside dispersed phase droplets in equilibrium
$\phi_{L,i}$: volume fraction of the lyophob inside dispersed phase droplets just after comminution
ϕ_{MC0}: molar solubility fraction of monomer in the continuous phase
ϕ_{SE}: fraction of free surface energy relative to total free energy of a particle of dispersed phase (eq. 6)
γ: interfacial tension liquid vapor
ψ_{dp}: volume fraction of dispersed phase
κ^{-1}: Debye's screening length (eq. 37b)
ν_c: frequency of fluctuations
π_s: osmotic pressure of a bulk gel
ρ_{dp}: density dispersed phase
ρ_{m1}: monomer density
ρ_{p1}: polymer density
σ: interfacial tension dispersed fluid continuous fluid phase
$\sigma_{1,2}$, $\sigma_{1,3}$ $\sigma_{2,3}$: interfacial tension between phases 1–2, 1–13, and 2–3, respectively
τ_{ex}: exchange time of a droplet during Ostwald ripening
τ_{pol}: duration to form an average polymer molecule (eq. 8)
$\bar{n}$: average number of radicals per particle
$k_{abs}^{j,e}$: rate constant of absorption of propagating radicals with chain length j and end group e
$k_{abs}^{t,e}$: rate constant of radical termination in the continuous phase with chain length j and end group e
$\bar{D}_{d,i}$: average droplet diameter just after comminution

$\bar{M}_C$: average molecular weight between two cross-links
v_{mol}^{mon}: volume per monomer molecule
v_{mol}^{ru}: volume per repeating unit of the monomer in the polymer
ΔG_{cs}^{I}: change in interfacial free energy for the formation of core–shell particles (eq. 45)
$\Delta\sigma^{cs}i$: change in reduced interfacial free energy for the formation of core–shell particles or inserted core-shell particles (eqs. 46 and 47)
$2fk_d$: initiator decomposition rate constant, including efficiency for initiating polymerization (f)

HIGH DENSITY POLYETHYLENE.

See ETHYLENE POLYMERS, HDPE.

HYDROGELS.

See Volume 2.

β-HYDROXYALKANOATES.

See POLY3-(HYDROXYALKANOATES).

HYPERBRANCHED POLYMERS.

See Volume 2.

IMPACT RESISTANCE

Introduction

Impact resistance is a measure of the ability of a material, specimen, or structure to withstand a sudden load without failure. The impact resistance of a specimen or structure is therefore a complex function not only of intrinsic factors such as the mechanical properties of the material but also of extrinsic factors such as geometry, mode of loading, load application rate, environment, and, quite importantly, the definition of failure.

The issue of stress geometry or mode of loading is all-important: a material highly resistant to failure in one mode of loading can fail catastrophically in another. Therefore, the impact resistance of a structure is relevant only with respect to a particular mode of loading. A soundly designed structure can fail unexpectedly if the geometry of a structural component is altered by the gradual change of shape, material wear, or crack growth, or if the mode of loading is changed, as when a force is applied in an unforeseen manner. Thus, it is often necessary to test the material or structure under conditions more severe than those of actual use. It is also prudent to follow certain well-established design guidelines. Last but not least, the use of damage tolerant materials may contribute to the avoidance of catastrophic failure.

Impact often implies a high loading rate, but the type of failure usually associated with impact can also occur under apparently innocuous conditions, even at low rates of loading. In addition to high strain rates, low temperatures and sharp notches tend to reduce fracture resistance. When the rate of strain energy accumulation is higher than can be contained in or dissipated by the material in the vicinity of a crack or a flaw, sudden and unstable fracture can occur, often entailing crack speeds of hundreds of meters per second. Higher

Encyclopedia of Polymer Science and Technology. Copyright John Wiley & Sons, Inc. All rights reserved.

speeds are more likely to cause unstable fracture, other conditions being equal, for then even small flaws, less severe geometries, or milder temperatures can become critical. This is partly due to the viscoelastic nature of polymers. Under truly high speed conditions, ie, when inertial effects are involved, the deformation and fracture behavior are complicated by wave propagation and constraint effects (1–4).

In contrast to impact resistance, the fracture toughness of a solid polymer is much better defined for a given set of quasi-static low strain rate testing conditions (see also FRACTURE; FATIGUE and ASTM D5045-99). Toughness can often be improved by the incorporation of a soft, elastomeric phase into the rigid polymer matrix. The art and science of material modification for the purpose of toughening is extremely complex (5). Enhancement of toughness improves impact resistance.

The performance of a material or a structure also depends on local variations due to processing conditions, such as cooling rate, shear stress, and melt-flow paths, which result in orientation and residual stress. Multiphase materials can exhibit even greater local variations in material properties than those observed in single phase polymers. A structure produced by a given process may possess significant morphological differences from test specimens. Ultimately, it may be necessary to test the impact resistance of components.

Since the impact toughness of a material, as it is commonly called, depends on the technique of measurement, the testing instruments and the technique must be considered first.

Testing Machines and Techniques

Several types of machines are in use for different types of tests, offering advantages and disadvantages as well as different information. Impact strength is measured by many different empirical methods, some of which may not be appropriate for the performance evaluation of finished products. More sophisticated and meaningful testing devices are under development but remain mostly in research laboratories. The following is a description of the machines and techniques that have gained wide currency. However the foregoing should serve to warn the reader to be cautious about the validity of the results for applications. For this and other reasons a number of standardized test methods are used to approximate actual use conditions.

Standard Test Methods. Many impact tests are sufficiently standardized to have ASTM designations (see Table 1).

Pendulum-Type Instruments. Pendulum-type machines are used for notched or unnotched specimens that may be of different sizes and supported as a cantilever (Izod) or as a bar supported at its ends (Charpy). These tests are also referred to as flexed-beam impact tests.

The Izod impact test is based on an old, established test originally designed for metals in which a notched-bar specimen is tested in cantilever fashion with an excess energy pendulum machine. Izod (ASTM D256), Charpy (ASTM D6110 and Research Report D20-1034, to become a new standard), and the tensile-impact (ASTM D1822) tests can be performed with pendulum machines.

Table 1. Standard Tests for Impact Resistance[a]

Test	Designation	Description
Brittleness temperature	ASTM D746	The temperature is determined at which plastics and elastomers exhibit brittle failure under impact.
Falling weight	ASTM D3029	Impact resistance indicated by energy to break or crack rigid plastics by means of a falling weight (tup); constant drop height and variable weight (tup)[b] are recommended.
Falling weight	ASTM D1709	Similar to D3029 but for measuring impact resistance of polyethylene film by free-falling round-headed dart.
Falling weight	ASTM D2444	For impact resistance of thermoplastic pipe and fittings by falling weight (tup).[b]
Fracture toughness	ASTM D5045	For plane-strain fracture toughness.
High rate stress/ strain (tension)	ASTM D2289	Area under stress–strain curve measures impact resistance at testing speeds up to 254 m/min.
Izod impact	ASTM D256[c]	Energy to break a notched cantilever beam specimen upon impact by a pendulum. Notch tends to promote brittle failure. Unnotched impact strength is obtained by reversing the notched specimen in the vise. Notch sensitivity can be determined by using Method D.
Charpy impact	ASTM D6110 (also, Research Report D20-1034)	Similar to Izod impact test. Notched specimen is supported on two ends and struck by a pendulum in the middle, a three-point-bend setting.
Tensile impact	ASTM D1822	Recommended for plastic materials too flexible, too thin, or too rigid to be tested by ASTM D256. Measures energy to break by "shock in tension" imparted by a swinging pendulum.

[a] Ref. 6.
[b] Designation of the weight.
[c] Includes Charpy impact testing.

In these machines a mass is attached to the end of an arm that rotates about a pivot point; a striker is attached to a mass. The arm is raised to a predetermined position. When the arm is released, it swings downward and strikes the specimen, which is mounted rigidly in a vise or a fixture. The precise mounting position and the type of fixture depends on the test. The mass, length of the arm, and angle at the raised position determine the amount of available energy. The total energy must be high enough to give a complete break. Typical pendulum machines of the Izod and Charpy types are depicted in Figures 1 and 2, respectively; specimen geometries are shown in Figure 3. After the striker breaks the specimen at the bottom of its swing, it continues to swing upward until all the kinetic energy is

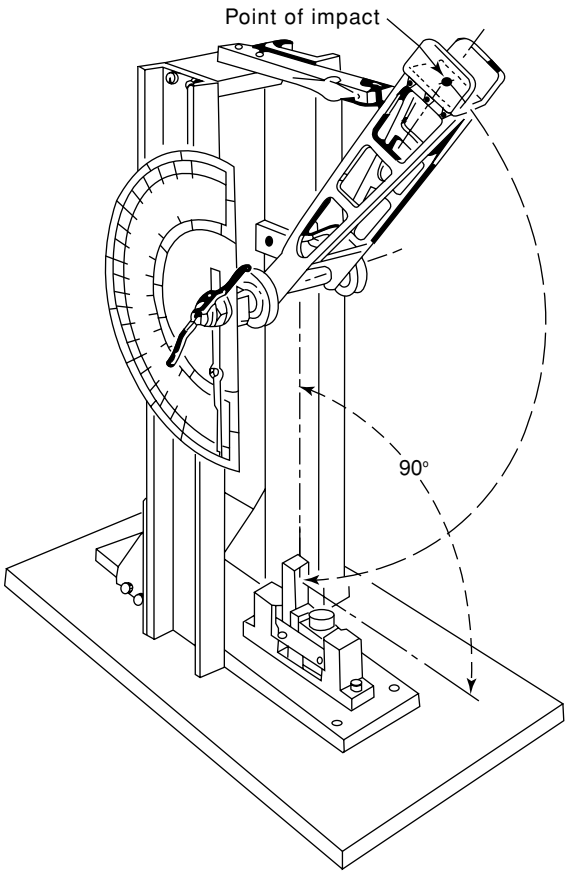

Fig. 1. Izod-type pendulum impact machine, ASTM D256.

converted to potential energy. The energy absorbed by the specimen, E_s, is found by

$$E_{\mathrm{S}} = E_I - E_{\mathrm{R}} - E_{\mathrm{F}} - E_{\mathrm{w}}$$

where E_{I} is the initial energy available, E_{R} the energy at the maximum angular travel, E_{F} the energy dissipated by friction, and E_{w} the kinetic energy to remove the broken, detached half-specimen as it is thrown forward by the pendulum. The last one is usually small; E_{F} can be found by performing the test without a specimen in place. Machines are usually equipped with a dial with calibration marks mounted in the plane of rotation in such a way that E_{I} and E_{R} can be read directly. An "instrumented" pendulum machine is equipped with a load cell, usually a piezoelectric quartz device for high frequency response, mounted on the striker or on the mounting block to which the specimen vise is attached. The electric signal from the load cell is amplified, digitized, and recorded by electronic memory. The energy is calculated from the load–time relationship by a computer connected to the instrument. The total energy can be displayed by a digital readout, or the

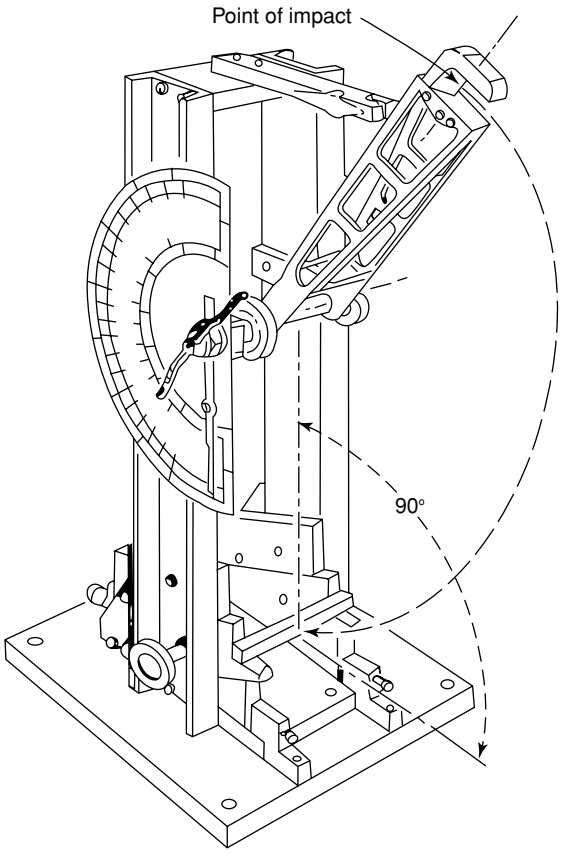

Fig. 2. Charpy-type pendulum impact machine, ASTM D256.

entire load–time trace can be displayed on a cathode-ray tube screen. In the latter instance, a microcomputer is attached and the information can be processed as desired.

The Izod test is used mostly in the United States and the United Kingdom [British Standard (BS) 2782, Method 306A]. The notched specimen is firmly clamped in a vertical position in a vise fixed in the base of the apparatus (Fig. 1). A pendulum fitted with a striker head of 3.2-mm radius, falling from a height of 0.61 m (ASTM) or 0.31 m (BS), hits the specimen horizontally at a point above the notch. At least 10 samples are required to obtain a satisfactory assessment of impact strength.

The U.S. test method has now been accepted as an International Standardization Recommendation ISO/R180, 2000. The material from which the test pieces are cut must be prepared under carefully controlled conditions to ensure development of full strength and freedom from strain caused by uneven heating or rapid cooling. The cutting of the notch requires special care, particularly with notch-sensitive materials. Small variations in the notch can give wide variations in impact values. The notch should be cut with a tool in good condition and shaped smoothly and accurately to the dimension called for in the test specification. Errors are caused

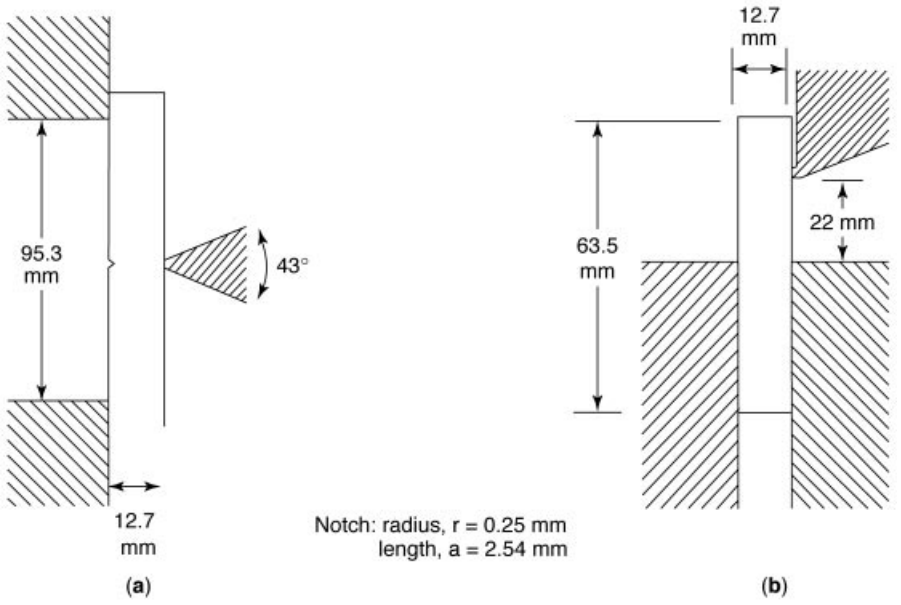

Fig. 3. Geometry of testing and specimen support arrangement for (**a**) Charpy and (**b**) Izod tests specified in ASTM D256 (7). Courtesy of Applied Science Publishers Ltd.

by variations in clamping pressure, failure to strike the specimens squarely, and the condition of the cutter and the cutting techniques for machining notches (8,9). Impact strength decreases linearly with increasing clamping pressure. A taper of 13 min of an arc on the specimen induces errors up to 25% of the expected impact strength of a perfectly parallel specimen. Variations in excess of 10% in expected impact strength were observed from differences in the notch cutter. Torsional stresses caused in the Izod specimen by skewness between the pendulum striker head and the surface of the specimen increase impact strengths even for small angles of skewness (Table 2).

Table 2. Effect of Skew Striking on Impact Strength of Poly(methyl methacrylate) Sheet[a,b]

Angle of skewness	Impact strength, J/m[c] of notch[d] at clamping pressure	
	16.5 MPa[e]	49.6 MPa[e]
10′	26.05	22.42
50′	27.75	25.78
1°10′	28.02	26.95
4°50′	29.78	29.36
5°10′	29.78	29.52

[a]Ref. 8.
[b]Perspex, Imperial Chemical Industries.
[c]To convert J/m to ft·lbf/in., divide by 53.38.
[d]British standard.
[e]To convert MPa to psi, multiply by 145.

Table 3. Energy for Crack Initiation and Propagation for Standard Cast PMMA[a,b]

	Notched impact strength, J/m[c]	Energy, %		Energy ratio[d]
		Crack propagation	Crack initiation	
ASTM	17.08	69	31	2.22
BS	24.02	49	51	0.96

[a]Ref. 8.
[b]Perspex, Imperial Chemical Industries.
[c]To convert J/m to ft·lbf/in., divide by 53.38.
[d]Crack propagation to crack initiation.

The total breaking energy as measured by the Izod test comprises the following: energy to initiate fracture; energy to propagate fracture across the specimen; energy for plastic deformation; energy to throw the broken fragment away from the test piece; and energy lost through friction and vibration (9).

The energy to initiate and propagate fracture depends largely on the notch geometry. The energy for plastic deformation is important in materials that, even when notched, break by ductile failure. The energy to separate the broken fragments is important in materials of low impact strength and high density, eg, mineral filled phenolic resin. The effect is corrected by placing the fragment on the striker head of the machine, striking it again, and subtracting the energy absorbed from the original apparent impact strength. However, in being thrown forward the fragment may adopt different modes of movement, and may rotate only under the first strike. For high impact, low density materials, this source of error is less important. Points of increased stress or of stress concentration can be introduced during machining; their effect is less for the ASTM specimen than for the BS specimen (8).

As can be seen in Table 3, in the ASTM test the energy required for crack propagation in PMMA is more than twice of that required for crack initiation; in the BS test they are about equal. Therefore the ASTM test results are much less likely to be affected by the specimen preparation than are BS test results. The BS specimens are more susceptible to imperfections in the notch surface and to the direction of machine marks (ie, stress-concentrating imperfections). Moreover, since a machined surface is never as smooth as a molded surface, molded (notched) specimens are expected to give higher values. This has been confirmed with specimens prepared from PMMA moldings where molded notch values are higher than machined notch values by a factor of 1.8. In addition, specimens with molded notches, especially those from crystalline polymers, exhibit higher impact strength than those with machined notches because of the difference in morphology or thermal stresses due to rapid cooling near the surface and slower cooling in the interior.

In the Charpy impact tester the specimen is mounted on a span support and struck centrally with a swinging pendulum (see Fig. 2). The results are expressed in terms of breaking energy per unit of cross-sectional area.

The Charpy pendulum impact test is most commonly employed in the European continent. Both the standard test bar and the small standard test bar are specified in the German Standard DIN 53453. The sample is notched and is

supported horizontally against the stops at either end. The pendulum striker hits the sample centrally behind the notch and the excess energy of the pendulum is measured by the angle of the subsequent swing. A large number of tests is necessary to give an average value. The Charpy-type test used in the United States is ASTM D6110 (Research Report D20-1034); in the United Kingdom, it is BS 2782, Methods 306 D and E.

Although the Charpy impact test is accurate and reproducible, significant errors may occur (10). Testing and machine variables tend to produce abnormally high values, since they retard the pendulum swing or otherwise cause excess energy losses. The recorded energy may be in error by as much as 100–200% at low energy and 15–20% at high energy levels. Differences are usually caused by the condition of the test machines; methods of machining and finishing the specimens; and cooling and testing (5). With strict controls and carefully prepared specimens, an average impact value should be accurate to within 5% for values up to 27.1 J (20 ft·lbf).

Pendulum-type machines are inexpensive and simple to use and maintain. Data can be produced from which fracture toughness G_{Ic} (more correctly known as the critical strain-energy release rate in Mode I) can be calculated (see FRACTURE and ASTM D5045-99 and later in this article). However, these machines are limited in the range of impact speeds, with a maximum of 3.4 m/s. Furthermore, the common practice of reporting only the total energy does not allow easy interpretation of the data, which can be overcome by using the instrumentation described previously. The use of instrumentation as described previously is often helpful for this purpose.

Falling-Weight Impact Instruments. Falling-weight methods are usually employed for sheet specimens. The weight may be gradually increased in mass, or dropped from increasing heights on the same specimen or onto a series of specimens. Like the pendulum tester, the machine is driven by gravity. The specimen, ordinarily in the form of sheet, is subjected to a direct blow from a falling weight. The weight is raised to a known height and is allowed to fall almost freely inside a guide tube or along a set of guide rails (see Fig. 4). A striker is mounted beneath the weight or in a guide resting on top of the specimen; the Gardner impact tester, usually preferred, is of the latter type. In recent years drop towers of considerable height have become commercially available. However, as the terminal velocity depends on the square root of the drop height, the maximum velocity that can be conveniently obtained is limited. In the case of the drop tower an arrangement similar to that described for the instrumented pendulum impact tester is necessary to determine the load applied to the specimen and the terminal velocity. Since the maximum velocity achieved with this type of machine is considerably higher than that available from the pendulum-type machine, vibration and inertial effects can interfere with the recording of the load signal. Therefore all supporting components must be as rigid as possible, and the piezoelectric load cell assembly must be of low mass and high rigidity to produce a high natural frequency. In addition to the load, the velocity of the falling weight must be determined. Frictional effects can result in significant errors when calculating the velocity by assuming free fall. The velocity must therefore be measured directly by a linear array of, for example, photoelectric sensors positioned near the end of the fall, just above where the specimen is struck. An accelerometer attached to the falling weight

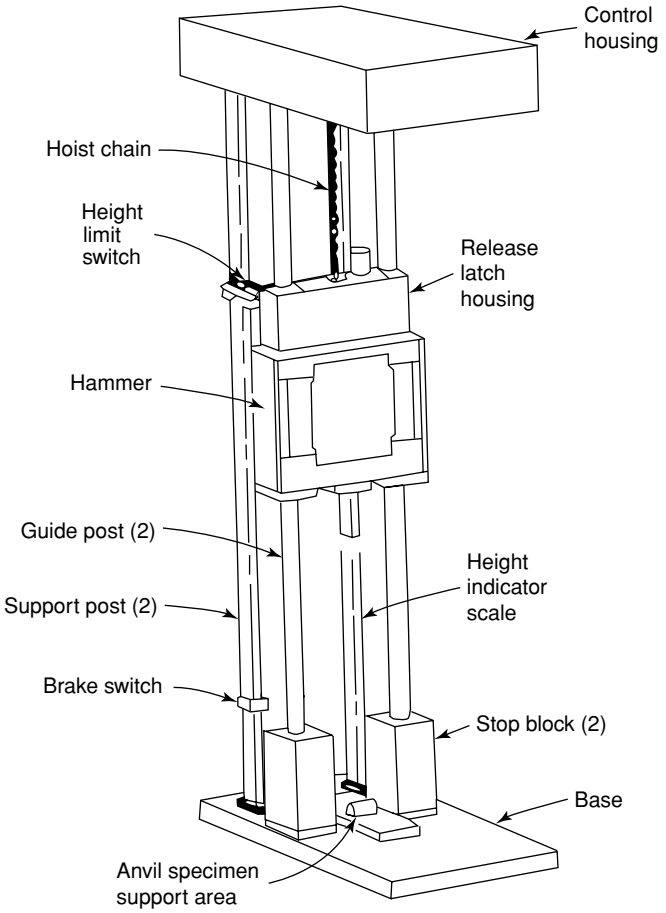

Fig. 4. Typical drop-weight testing machine (11). Courtesy of ASTM.

measures load and velocity separately. The electric signal from the accelerometer is recorded digitally as before. The absorbed energy and the force are calculated from the change in velocity caused by the impact. The results are obtained by processing the acceleration signal in the computer. The accelerometer must be mounted near the tip of the striker to minimize interference from reflected shock waves. An accelerometer is preferred over a load cell at high test velocities.

In the falling-weight test (BS 2782, Method 306B) also known as a dart-drop test or Gardner impact test, a spherical ball striker, 12.7 mm in diameter, is fastened to a load-carrying device to which weights can be attached. The striker assembly slides freely in vertical guides and is released from a predetermined height to strike centrally on a specimen, which is supported on the base of the equipment. In the so-called staircase method the load is increased by fixed increments on successive specimens, each struck once, until a specimen fails. The weight is then reduced by fixed increments until a specimen withstands the impact, after which it is increased again by fixed increments until a specimen fails again. This procedure is repeated on at least 20 samples to determine the energy

Drop height t, m	Impact, J	F_{50} = 268 J	Failure	No failure
2.74	366			
2.64	352			
2.54	339			
2.44	325			
2.34	312			
2.24	298			
2.13	285	o o o o o o o o o	9	0
2.03	271	x o o x x o o o x x o o o x x o o o o o	14	9
1.93	258	x x o x x x x x x x	2	14
1.83	244	x x	0	2
1.73	230			
1.63	217			

Fig. 5. Typical results of a dart-drop test using the "staircase" method of analysis (12). To convert J to ft·lbf, divide by 1.35. Courtesy of the Society of Plastics Engineers.

level at which 50% of the specimens break; the result is quoted as the impact strength for 50% failure (F_{50}) (see Fig. 5). An important source of uncertainty in this test is the criterion used to determine failure. Sometimes failure is obvious, as when the specimen shatters; other times failure is indicated by a small crack. As this is usually a visual test, whether or not failure has occurred depends on the judgment of the testing technician.

In the Probit method (13), a set of energy levels for the falling weight is selected. A series of specimens is tested at each level, and the failure–impact energy relation determined. With the help of a detailed failure–impact energy curve a simple control test can be carried out by testing a small number of specimens at a single fixed energy level. This procedure is far more reliable and economical than the F_{50} values.

In the common drop-weight test, force and displacement are not recorded by electronic instruments. On the other hand, in fully instrumented procedures a weight–height combination at which the specimen is consistently broken is found by trial and error, or by choosing a height that produces a desired terminal velocity and adjusting the weight to break the specimen consistently. A number of drop tests are then performed under identical conditions. Each test is recorded by an electronic instrument. The exact number of tests required depends on the divergence of the data and the confidence limit desired. This method requires fewer specimens. The velocity can be varied as desired (within the limits of the tester), and an entire set of data can be obtained at the same velocity. The deformation behavior, including the point of crack initiation, can in many cases be deduced from the load–deflection curve, reducing operator errors. Furthermore, the ability of a material to decelerate a moving mass can be assessed.

Many materials that give low Izod impact values on notched specimens fail in a ductile manner when tested in sheet form. Notched impact strength and the impact properties of sheet are not correlated because the stress states and the material responses differ.

The cause of failure of sheet material in practice is more likely to be revealed by a falling-weight impact test than by an Izod test (14). Falling-weight tests thus

give a better guide to practical behavior unless the molded article contains ribs, sharp corners, and similar geometry. Any anisotropy present, such as excessive orientation leading to weakness in a given direction, is revealed in the test. For example, an oriented injection-molded specimen may fail with a single straight crack at a low energy, whereas a substantially unoriented compression molded specimen of the same material would fail with cracks in several directions after having withstood much higher impact energies.

In falling-dart testers impact is produced by means of a pointed weight or dart. This method assesses the toughness of plastic film under certain specified conditions, such as sample geometry, dimensions of the dart head, and velocity. In one such apparatus, a perfectly flat specimen is clamped by a vacuum and held in uniform tension. The flat test film is placed over the specimen holder and kept wrinkle-free by the vacuum. The dart is automatically released from an electromagnet as soon as the correct pressure differential is reached. Darts of various weights are dropped, and the percent failure is plotted against dart weight on probability graph paper. A straight line is drawn through the plot. The intersection of the line with 50% failure is the weight in grams for F_{50} impact failure. ASTM D1709 gives a formula for the calculation of impact strength without a graph. In the examination of tubular film the edge fold as well as the face of the film may be tested. The U.S. specification for the falling-dart method (ASTM D1709-01) refers specifically to polyethylene film, whereas the U.K. standard (BS 2782, Method 306F) covers all flexible plastic film. In an equipment modification two electromagnetic counters are provided: one records the number of specimens tested and the other, which is operated by a push switch, the number of breaks. For tests of thick film, a clamping ring is provided in addition to the vacuum clamping to prevent film slippage, which is especially important in this case. In both specifications the dart, which has a 38-mm-diameter hemispherical head, falls freely 0.66 m to strike the specimen. The weight of the dart is adjusted with loose weights to determine the limit required to fracture 50% of the specimens. Other more recent versions are commercially available, usually equipped with digital recording devices and computer analysis of the results.

Tensile-Impact Instruments. A standard Izod impact-testing machine, a variation of the swinging pendulum, is easily adapted at little cost to tensile impact testing. The conventional Izod vise is replaced by one capable of holding the fixed end of a tensile specimen and a metal crosshead is secured to the other end of the specimen (see Fig. 6). The swinging pendulum strikes the crosshead removing both the crosshead and half of the specimen. Development of this instrument led to the specification ASTM D1822-99 (tensile impact energy to break plastics and electrical insulating material). This method can be used to measure the impact resistance of test pieces cut from actual moldings, and help to assess directional differences in stress that arise from flow-induced molecular orientation produced during mold filling. It is also very useful for the evaluation of very small samples. The energy required to produce failure can be obtained by varying the height of fall or the mass of the falling weight or by measuring the excess swing of the pendulum. Transducers and electronic instruments can provide load–deflection curves. The results show reasonable correlation with the falling-weight test of film and with the performance of moldings and sheet. Tensile impact instruments require less material than the usual falling-weight impact test. At relatively low

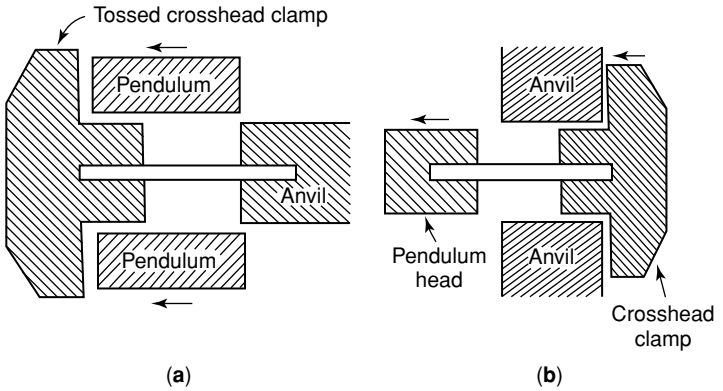

Fig. 6. Tensile impact machines. (**a**) Specimen in base; (**b**) specimen in head.

speeds they often give good correlation with falling-weight tests. This correlation is due to the fact that in both tests the tensile mode of stress is generated by the testing geometry. The falling-weight test, however, generates a biaxial tensile stress that can more easily give rise to failure. This is a consequence of the higher component of hydrostatic tensile stress in the biaxial tensile test, which favors the cohesive mode of failure.

Special Test Machines. Hydraulically and pneumatically driven machines have found increasing use in research and quality control laboratories; ASTM standards have not yet been established. These machines require higher operator skills and are more expensive, but offer better control and produce more information.

Hydraulic and pneumatic impact testing machines differ in the way in which the impact energy is derived, in the amount of energy and maximum velocity that can be developed, and in the amount of deceleration suffered by the striker. A hydraulic fluid or a gas under high pressure is stored in an accumulator. Upon receiving an electrical signal, a valve is opened, and the fluid or gas is transferred to a cylinder, wherein a low friction piston is connected to the load application device. The pressure difference between the two sides of the piston causes acceleration to a high velocity. Different designs in the valve and pressure return arrangement, and, increasingly, high speed digital electronics and signal processors allow the velocity to be controlled to varying degrees of success. The maximum load capacity of the testing machine depends on the pressure of the fluid, piston area, and pressure drop in the valve and upon expansion. The maximum velocity depends on the pressure, the flow rate allowed by the valve, the size of the accumulator, the inertia of the moving mass, and the distance allowed for acceleration. Commercial hydraulically driven impact testers are now capable of generating a maximum speed of 22 m/s at a maximum load of 900 kg (see Fig. 7); different designs are available including computers for control and data acquisition and analysis. Possible tests include tensile impact, puncture (flexed-plate) impact, and flexed-beam impact. A pneumatic machine is shown in Figure 8; anvils for various types of impact tests are shown in Figure 9. The high compressibility of gases means that the striker could decelerate significantly if the force required to deform the test specimen is high.

Fig. 7. Hydraulic high speed impact tester. (**a**) Specimen enclosed in environmental chamber; (**b**) hydraulic drive unit at the end of the rails for component testing. Courtesy of Instron Corp., Canton, Mass.

A principal advantage of hydraulic pneumatic machines employing feedback control is that a higher fixed velocity can be maintained. Much depends, of course, on the specifics of the design.

In pendulum machines the velocity upon striking the specimen is initially constant at 2.4 m/s in the Izod test, and 3.4 m/s in the Charpy test. After the specimen is struck the velocity decreases, depending on the amount of energy absorbed. This problem is more serious in tough specimens. In drop-weight tests, the velocity upon impact depends on the drop height, and yet the test results often report only the product of weight and drop height, ignoring the impact velocity. Since polymeric materials are rate sensitive in their mechanical behavior, tests using gravity-driven machines could produce misleading results because the terminal velocity just prior to striker contact with the specimen could vary widely. The use

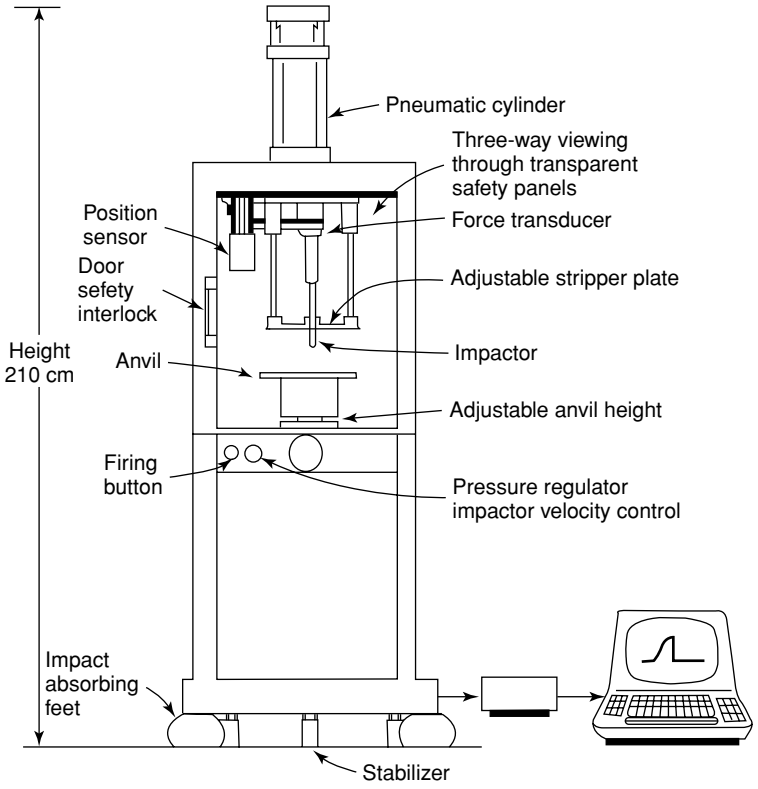

Fig. 8. Pneumatic impact tester. Various types of impactors, anvils, and force transducers are available for different applications. Courtesy of ICI Australia Operations Pty Ltd., Dingley, Victoria, Australia.

of the special machines described here avoids such problems. (This test standard has been discountinued in 1992.)

Product Testing. Standardized specimens are specially prepared for falling weight tests, swinging-pendulum tests, tensile impact tests, and others. However, frequently results from such tests fail to predict the performance of actual fabricated components in service. For this reason, the conventional forms of impact testing are more useful as control or material comparison tests. This limitation has become more serious in recent years with the rapid introduction of many new polymers and their blends. One reason for the difference in performance is the fact that the fabricating process can influence impact strength. A typical example is the effect of flow-induced orientation in thin-walled moldings. The flow behavior of the material during the filling of the mold may be more important than the basic impact properties of the unoriented material in governing the impact behavior of the thin-wall moldings. Specimen geometry is also important because the stress state and rate of stress buildup are governed by the size and shape of the article. Therefore the impact strength of the finished product may need to be tested under appropriate conditions in addition to the usual control and quality tests.

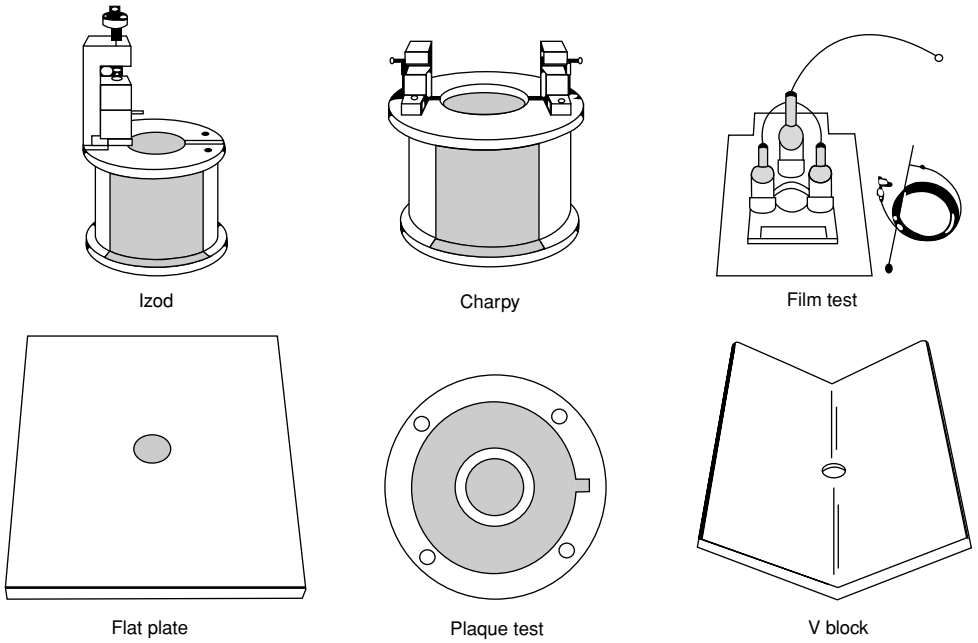

Fig. 9. Accessory anvils for gravity, hydraulic, and pneumatic testers. Courtesy of ICI Australia Operations Pty Ltd., Dingley, Victoria, Australia.

Mechanical Behavior

Tensile Impact. The tensile impact test subjects a specimen to uniaxial tension at a strain rate of approximately $10^2 s^{-1}$. This strain rate is 3–6 orders of magnitude higher than that encountered in conventional uniaxial tension testing (7,15,16). The effect of strain rate on uniaxial tensile behavior depends on the scale of deformation and the temperature range. At small strains the tensile modulus E increases with strain rate, but the magnitude of change depends on the temperature range. If the relaxation process is significant, eg, the glass transition or a strong secondary relaxation occurs near the test temperature, the modulus would also be rate dependent. The change can be about a factor of 2 for a secondary relaxation, and an order of magnitude or more for a temperature somewhat below T_g. If no significant relaxation occurs near the test temperature, E can be unaffected by the strain rate. At room termperature, PMMA has a strain-rate senstitive modulus whereas PC has not, although at sufficiently high rates strain-rate sensitivity develops. At strains beyond 1–2%, some materials become brittle even at low strain rates. An example is commercial PS, which typically contains small amounts of foreign material that serves as nucleation centers for craze initiation. Pure PS without surface flaws may be susceptible to shear yielding; increasing strain rate reduces flaw tolerance. If the material is not brittle enough to fracture, it eventually reaches a yield point defined as the maximum in the load–elongation curve. This yield point is not necessarily due to shear yielding. Impact-modified polystyrene, for example, exhibits a yield point independent

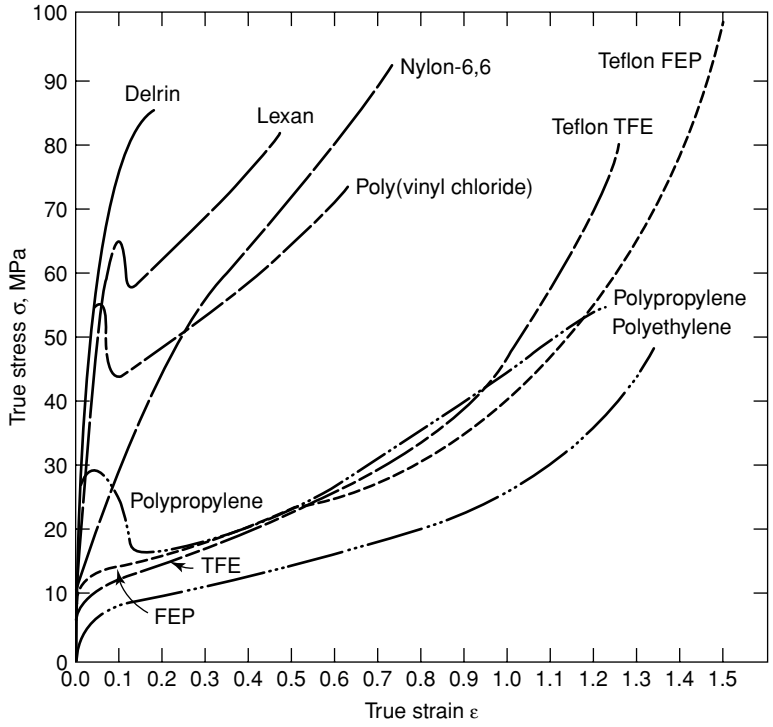

Fig. 10. True stress–true strain behavior of polymers. Delrin is an acetal resin; Lexan, a polycarbonate; Teflon TFE designates the tetrafluoroethylene homopolymer; Teflon FEP is a copolymer of tetrafluoroethylene and hexafluoropropylene (17). To convert MPa to psi, multiply by 145. Courtesy of Polymer Engineering and Science.

of shear yielding. If the load maximum is due to shear yielding, further straining results in a neck because of strain softening (16). Some crystalline polymers do not exhibit a maximum in the load–elongation curve but merely a knee because of the strengthening effect of the spherulites. Yield strength usually increases with strain rate (15,16). The strain-rate sensitivity of the shear yield stress behaves in much the same fashion as the modulus; it also depends on a significant relaxation process near the test temperature. After neck formation the strain-rate sensitivity stabilizes and neck extension occurs (16). On the other hand, thinning of the neck results in ductile fracture, which can also be due to high strain rates.

Examples of uniaxial tensile true stress–true strain behavior of polymers deformed at low strain rates are shown in Figure 10. Common engineering stress–strain curves cannot be used to determine the elongational strain because the shape for a given set of testing conditions depends on the specimen geometry. Some polymers show ductile deformation after yield by a process of necking and cold drawing. The apparent neck extension depends on the length of the specimen gauge section if the conventional method of calculating engineering strain $\varepsilon = \Delta l/l_0$ is used, where Δ_1 is the elongation and l_0 the original gauge length. The true value of the extensional strain can be ascertained only by direct measurement of the strain in the necked section. If the specimen dimensions are identical and

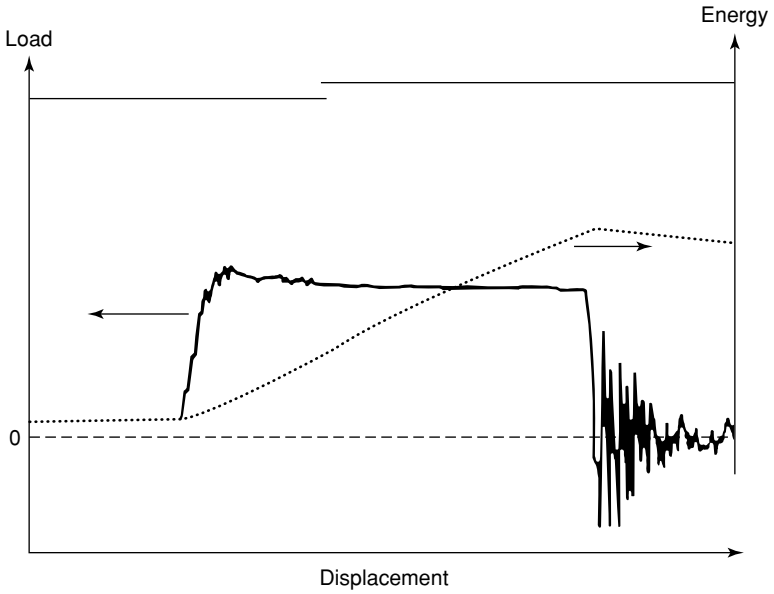

Fig. 11. Typical load and energy data from tensile impact test on polypropylene using an instrumented pendulum tester. The dotted line shows the accumulated energy as the deformation increases. Courtesy CEAST SpA, Torino, Italy.

the extents of necking comparable, the apparent maximum engineering strain can be used as a relative ductility index. Ductility usually decreases with strain rate or decreasing temperature. At a given strain rate and temperature, ductility depends on molecular weight and amount of filler or impurity in the material. Stresses applied orthogonal to the principal stress direction can also affect ductility. *Tensile impact toughness*, a measure of the total energy absorbed by a dog-bone-shaped specimen in uniaxial tension, is the integrated value of the typical force–elongation curve. It is highly sensitive to the ductility of the material at the testing rate. The tensile impact behavior of polypropylene is shown in Figure 11. The curve is typical of a pendulum impact tester equipped with transducers and digital storage instruments. The strain-softening behavior is clearly discernible even at such a high strain rate. The advantage of electronic instrumentation can be seen immediately.

Flexed-Plate Impact. In flexed-plate impact, a ball, dart, or striker is driven by gravity or pressure into a thin plate supported by or clamped over an annular area. The nose of the dart is usually hemispherical, though sometimes square. A flex-plate impact test corresponds closely to conditions of actual use. However, geometric factors, such as specimen thickness and dart-to-annular opening ratio, cannot be readily standardized, and furthermore, the geometry itself can cause a change in the deformation mode (14). The progression of deformation processes associated with the load–deflection curve can be seen in Figure 12. In Figure 12A the specimen failed in a ductile manner and the plastic deformed extensively around the dart nose. The remaining unsupported material was cold drawn. Partially deformed specimens and finite-elements analysis reveal yielding

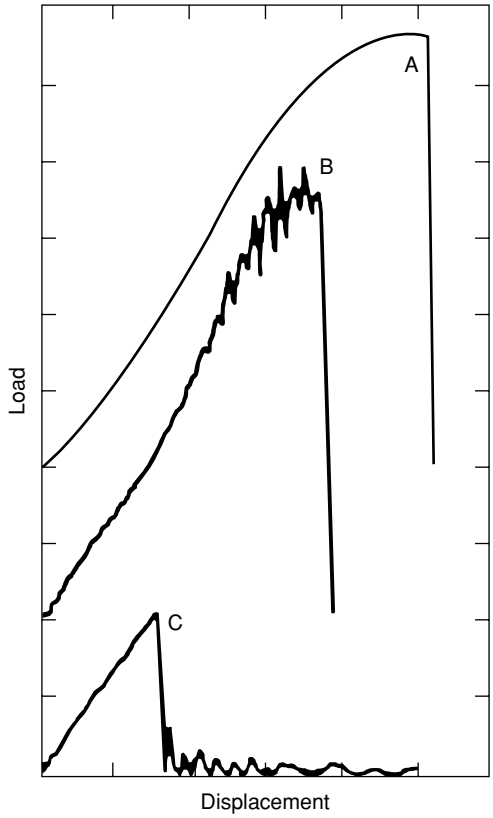

Fig. 12. Typical load–deflection data from puncture impact tests. (A) ductile failure; (B) cracking started at about 50% of the maximum load; (C) brittle failure (18).

under the dart early in the deformation process, at about 25% of the maximum load. This initial yielding is marked by a slight decrease in the slope. Subsequently a yielded zone in the shape of a hemispherical dome develops around the dart nose. As deflection continues, the net area undergoing yielding also increases, which results in geometric hardening, ie, the load increase is due to the change in specimen geometry as described above. The processes of material softening and geometric hardening eventually combine to result in a slight increase in slope. At this stage of the deformation the unsupported area of the specimen is akin to that of a membrane rather than a plate. The stress in the membrane is essentially uniaxial tension in the radial direction. Finally, excessive thinning takes place somewhere in the specimen, the exact location being dependent on the geometry, and rupture causes the load to drop precipitously (18,19). Thus, the total energy absorbed, which is the area under the load–deflection curve, depends in a very complex manner on both the testing geometry and the yield and deformation behavior of the material. The curve of Figure 12B is obtained when the specimen develops a crack during the membrane-stretching process. The sudden release of elastic energy upon cracking causes the load-cell assembly to vibrate at its natural frequency and results in the "ringing" signal. The crack is stabilized by the

specimen geometry and does not propagate. Consequently the specimen is able to carry an increasing load even though, by some definitions, the specimen would be considered to have failed (18). The curve in Figure 12C is obtained when the specimen fails in a totally brittle manner; no decrease in the slope of the load–deflection curve is discerned. Cracking occurs on the tension side opposite the area where the dart or striker contacts the plate. Little or no plastic deformation occurs anywhere on the specimen. Brittle fracture of this type occurs more readily in thick plates even for materials normally considered to be ductile. This observation serves to warn against treating such test results as material properties. Clearly, the test specimen and specimen holding fixture contribute importantly to the test results.

In addition to plate thickness, decreasing temperature, increasing deformation rate, or environmental aging can transform ductile-type failure (Fig. 12A) to brittle-type failure. In the case of a ball or a hemispherical dart impact test, it is commonly assumed that the resultant stress state at the center of the plate is biaxial tension. This assumption is erroneous because the normal force on the plate is significant and could lead to over optimistic values on ductile-to-brittle transition conditions, whether expressed as a critical temperature or aging time. This behavior is caused by normal stress suppressing brittle failure (15,18,20).

Flexed-Beam Impact. Flexed-beam impact tests are sometimes carried out on unnotched specimens, though notched specimens are preferred. The Izod and Charpy tests are examples of flexed beam tests. These two testing geometries are different, but both types of notches create a severe stress concentration. Many materials that are tough in the tensile and flexed-plate impact tests become brittle in notched flexed-beam tests because the stress state near the base of the notch favors a brittle response due to the high component of hydrostatic tensile stress mentioned above. For a given specimen thickness, the impact toughness depends on the notch tip radius (see Fig. 13). Subjecting a thin, notched specimen to bending creates a tensile stress concentration along two orthogonal directions: the main one along the specimen length, the other parallel to the notch or crack direction. The magnitude of the former depends on the notch sharpness. The minor stress is due to constraints created by notch-free sections of the specimen, which are at a lower stress. Because the specimen is thin, it contracts freely in the thickness direction; a state of plane stress is said to exist in this instance. The biaxial tension state is more favorable than the uniaxial tension state for craze or crack formation because of the larger hydrostatic or dilatational stress component in the former case. Many polymers that are ductile in uniaxial tension exhibit brittle behavior in this stress state; other polymers are able to shear-yield. Shear yielding creates a large plastic zone at the notch tip, and subsequent failure is due to ductile tearing of the material. This mode of failure usually absorbs a large amount of energy. Some impact-modified materials are able to form a plastic zone ahead of the notch containing of a high density of crazes. Considerable energy can be absorbed by this mechanism. The load–deflection behavior of tough plastics is illustrated in Figure 14.

Subjecting a thick notched, notch-sensitive specimen to bending creates a tensile stress component that is perpendicular to the specimen faces. This third stress is due to constraint in the thickness direction because the material ahead of

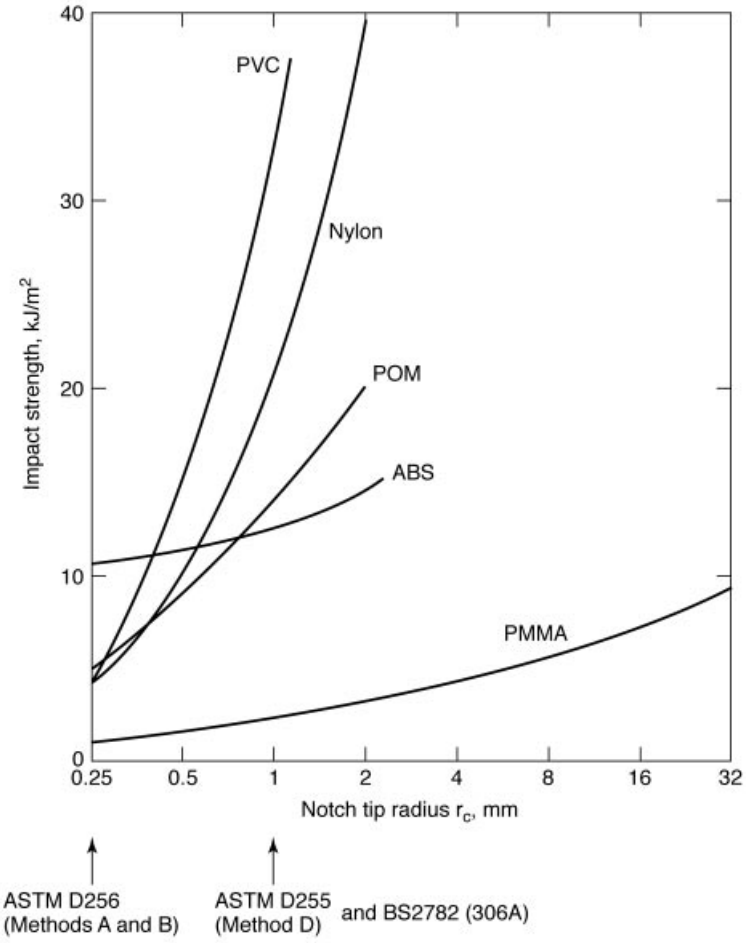

Fig. 13. Impact strength as a function of notch tip radius for different polymers (21). To convert kJ/m^2 to $ft{\cdot}lbf/in.^2$, divide by 2.10. POM = polyoxymethylene. Courtesy of The Plastics and Rubber Institute.

the notch is unable to contract freely in this direction; the constraint effect is said to be due to plane strain. The triaxial tension state is even more favorable than the biaxial tension state for the formation of crazes, again because of the larger dilatational stress component in the former. With sufficiently large thickness and sharp cracks few unmodified polymers are able to deform in a completely ductile manner owing to the intrinsically low cohesive strength of polymers relative to their yield strengths. The fracture is due to craze formation and rapid crack propagation. At intermediate thicknesses or notch radii the specimen can deform in mixed mode: plane-strain in the specimen center and plane-stress near the surfaces. In the plane-stress region, plastic deformation zones are often found. Their size determines the amount of energy absorbed by the specimen; the plane-strain zone, by contrast, absorbs little energy.

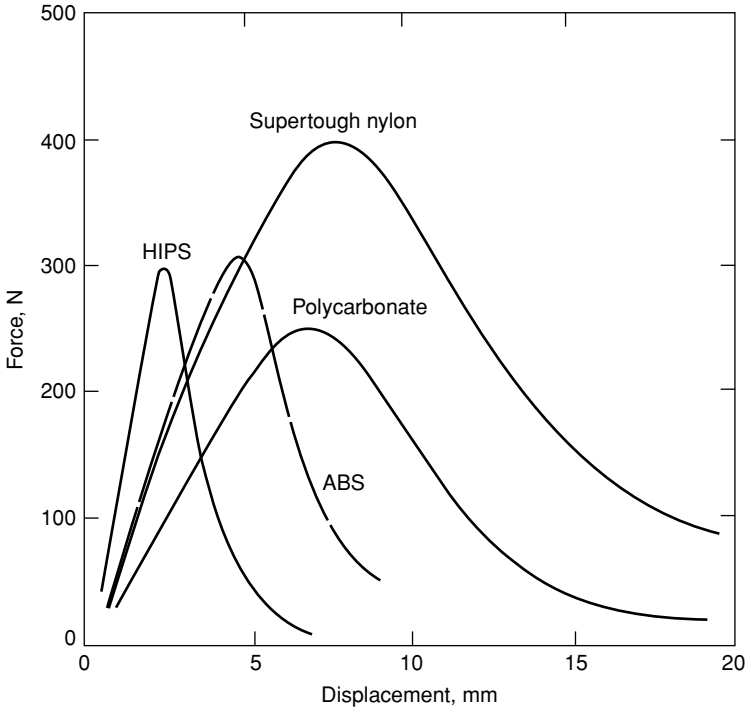

Fig. 14. Load–deflection behavior of a number of tough polymers tested in the notched Charpy geometry at low rates (22). To convert N to kgf, multiply by 0.102. Courtesy of the Society of Plastics Engineers.

The impact toughness of a material, as measured by a flexed-beam test on a notched specimen, depends on the thickness of the specimen and the radius of the notch, and therefore cannot be considered a material property. Furthermore, the transition from predominantly plane-stress to predominantly plane-strain is unpredictable when complex geometries are encountered in structural components. Because this transition can create unexpected and catastrophic failures, some polymers normally considered to be very tough and ductile may benefit from impact modification. The modified versions are less sensitive to geometric variations.

The transition from plane-stress to plane-strain can also be brought about by impact rate (23), temperature (Fig. 15), molecular weight, and thermal history (24). The effects of thickness and rate are shown by an example in Figure 16. In this example notched polycarbonate (PC) specimens are tested at various bending speeds. The thick (6.4 mm) specimens are uniformly brittle, whereas the thin (3.2 mm) specimens are uniformly ductile. The intermediate thickness (4.4 mm) specimens exhibit a ductile-to-brittle transition at about 0.3 cm/s. In toughened PC even the 6.4-mm-thick specimens are tough up to about 40 cm/s (see Fig. 17).

Fracture Toughness from Flexed-Beam Impact Tests. As stated above, the so-called impact toughness values obtained from Izod and Charpy tests are not material properties because they depend on specimen thickness, notch depth, notch radius, and other factors unrelated to material properties. These

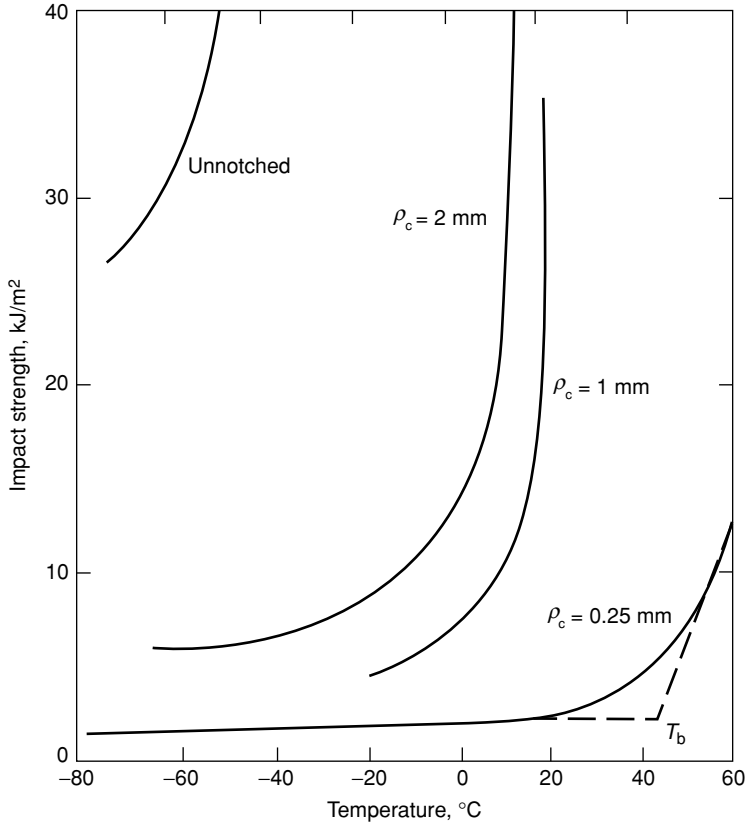

Fig. 15. Effect of test temperature on the impact strength of PVC specimens containing various notch radii (21). T_b = brittle temperature. To convert kJ/m^2 to ft·lbf/in.^{2}, divide by 2.10. Courtesy of The Plastics and Rubber Institute.

values are therefore useful only for the comparison of different materials, and are useless for design calculations. By contrast, fracture toughness (ASTM D5045-99), which is a material property, is useful in design calculations. Consequently it is desirable to have fracture toughness values that are taken under impact conditions, and especially if they could be obtained from the Izod or Charpy test machines.

The fracture toughness G_{Ic} can be determined from the impact energy U if the geometry of the specimen is known (25) and if the specimen fails in plane-strain. To determine if the latter condition is satisfied one could examine the fracture surface. If the top edges of the fracture surface remain in the planes of the sides of the specimen and no sign of large-scale plastic drawing in front of the notch tip is observed then this condition is probably satisfied. Another signature for plane-strain fracture is the load–deflection curve, which would have the shape of a right triangle. This points out the desirability of using an instrumented tester.

In this analysis it is assumed that linear elastic fracture mechanics (LEFM) applies. When a specimen containing a sharp notch of depth a is subjected to

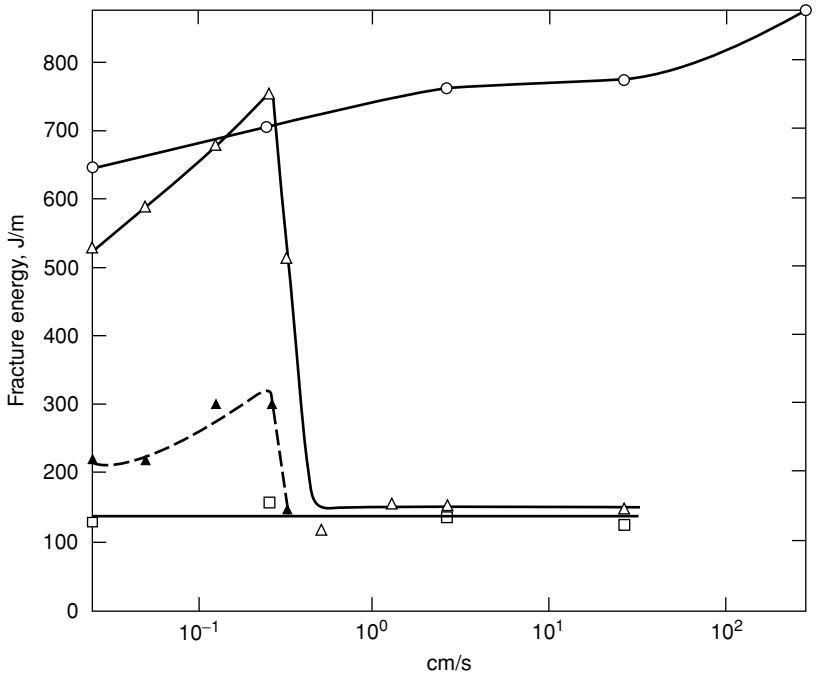

Fig. 16. Effect of test speed on the fracture energy of polycarbonate specimens of various thicknesses tested in the notched Charpy geometry. ○, 3.2 mm; △, 4.4 mm; ▲, energy up to load maxima for 4.3 mm; □, 6.4 mm (22). To convert J/m to ft·lbf/in., divide by 53.38.

bending with a load P, a deflection x results. The energy U stored is given by

$$U = Px/2 \tag{1}$$

When the crack grows, compliance $C = x/P$ increases as the stored energy is released. Thus, if it is known how C changes with a the strain-energy release rate G can be calculated from equation 1

$$U = P^2C/2 \tag{2}$$

For a specimen of uniform thickness B,

$$G = \frac{1}{B}\frac{\mathrm{d}U}{\mathrm{d}a} = \frac{1}{B}\frac{\mathrm{d}U}{\mathrm{d}C}\frac{\mathrm{d}C}{\mathrm{d}a} \tag{3}$$

When fracture occurs, the critical strain-energy release rate G_c is calculated:

$$G_c = \frac{P^2}{2B}\frac{\mathrm{d}C}{\mathrm{d}a} \tag{4}$$

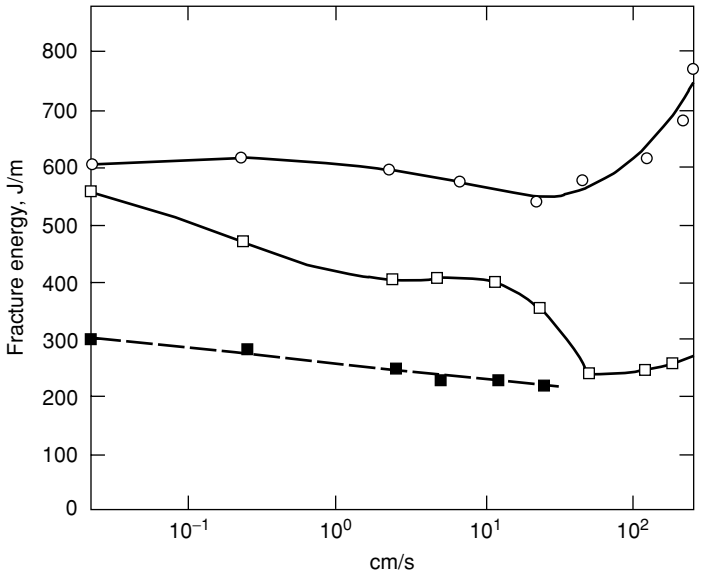

Fig. 17. Effect of test speed on the fracture energy of an impact-modified PC as in Figure 16. ○, 3.2 mm; □, 4.4 mm; ■, energy up to load maxima for 6.4 mm (22). To convert J/m to ft·lbf/in., divide by 53.38.

In an impact test, usually only the energy U is determined. Combining equations 2 and 4 gives

$$U = G_c B \frac{C}{\mathrm{d}C/\mathrm{d}a} \tag{5}$$

In practice, U is determined for a series of specimens with various notch depths a. It is therefore more convenient to express equation 5 in terms of

$$G_c = \frac{U}{BDC} \frac{\mathrm{d}C}{\mathrm{d}(a/D)} \tag{6}$$

where D is the specimen width. The dimensionless compliance function

$$\phi = \frac{C}{\mathrm{d}C/\mathrm{d}(a/\mathrm{D})}$$

can be determined experimentally from quasi-static bending tests, and has been calculated analytically for this geometry (26). Equation 6 can then be rewritten as

$$U = G_c B \mathrm{D} \phi \tag{7}$$

predicting that a linear relationship should exist between the impact energy U and $BD\phi$, the slope of which should be equal to G_c. G can then be obtained by

Table 4. Strain-Energy Release Rates[a]

	G_c, J/m^{2b}	
Material	Charpy	Izod
Polystyrene		
General purpose	0.83×10^3	0.83×10^3
HIPS	15.8×10^{3c}	14.0×10^{3c}
PVC		
Darvic 110	1.42×10^3	1.38×10^3
Modified	10.05×10^3	10.00×10^3
PMMA	1.28×10^3	1.38×10^3
Nylon-6,6	5.30×10^3	5.00×10^3
Polycarbonate[d]	4.85×10^3	4.83×10^3
PE		
Medium density[e]	8.10×10^3	8.40×10^3
High density[f]	3.40×10^3	3.10×10^3
Low density	34.7×10^3	34.4×10^3
ABS		
Lustran 244	49.0×10^{3c}	47.0×10^{3c}

[a] Ref. 25. *Courtesy of Polymer Science and Engineering*.
[b] To convert J/m^2 to ft·lbf/in.^{2}, divide by 2.10×10^{-3}.
[c] J_c as defined in Ref. 1.
[d] Specimens cut in the extrusion direction.
[e] Density = 0.940; MI = 0.2.
[f] Density = 0.960; MI = 7.5.

determining U for a series of specimens with various notch depths if the relationship is indeed linear. If the impact tester is instrumented, a further criterion would be a rapid drop in load P after reaching a peak, ie, the load–deflection curve should have the shape of a right triangle. If the notch is too blunt and a significant amount of plastic flow occurs, which would cause the top of the load–deflection curve to round off, a correction factor may be needed, ie, the crack length a is increased by the plastic zone size r_P (25,27):

$$a_f = a + r_P$$

The plastic zone size can usually be determined from the appearance of the fracture surface and is distinguished by a whitened or very rough area directly ahead of the original notch tip. The G_c, values for some plastics for both the Izod and Charpy geometries (25) are in Table 4. With the same method, the G_{Ic} of a number of polymers was determined (3) at different rates (Fig. 18).

The procedure outlined above can be useful if the specimens are prepared carefully to ensure that LEFM applies. The specimen should be as thick as is practicable, and the notches should be very sharp. If a razor blade is used for cutting, a compressive plastic zone must be avoided at the notch tip. This can be accomplished by slicing the notch tip rather than by pressing the blade into the notch. If the fracture surface contains plastic flow, the crack size most likely has

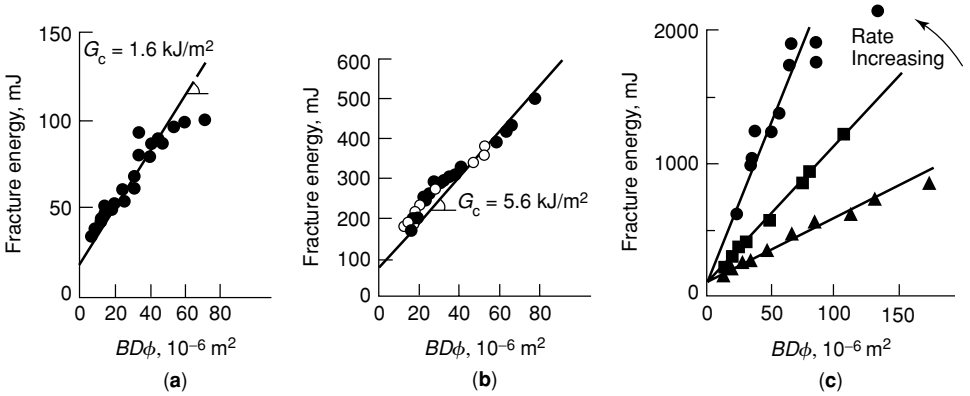

Fig. 18. Fracture energy as a function of $BD\phi$ for (**a**) PMMA at 20°C; (**b**) PTFE at 25°C (○, Charpy; ●, Izod); (**c**) HDPE at 20°C and several rates (▲, 26 s^{-1}; ■, 122 s^{-1}; ●, 620 s^{-1}) (3). To convert J to ft·blf, divide by 1.355. To convert kJ/m^2 to ft·lbf/in.^{2}, divide by 2.10. Courtesy of The Institute of Physics, Great Britain.

to be corrected. The method for determining fracture toughness can be extended to tensile impact of a notched specimen (28).

Improving the Impact-Resistance of Materials

Impact resistance is not an absolute term. It depends on the design of the structure as much as it does on the intrinsic material toughness. Nevertheless the impact resistance of a material can be increased by modifying it with toughening. This increase is sometimes at the cost of reduced modulus and strength, and perhaps fatigue resistance. The impact toughness of commercial plastics is shown in Table 5.

High Impact Polystyrene (HIPS), Acrylonitrile–Butadiene–Styrene Copolymer (ABS), and Modified Poly(xylenol ether) (PXE). Polystyrene is a transparent, rigid, easily processable, inexpensive material. Its chief disadvantages are extreme brittleness and high susceptibility to crazing by organic liquids. It was also among the first materials to be produced in a toughened form, commonly known as HIPS, in order to allow the material to be used in applications with moderate loadings such as electrical applicances.

In the most common production method rubbery polybutadiene (PBD) is precipitated from a styrene–polybutadiene solution in styrene during the polymerization of styrene. The precipitated phase itself typically contains 2–10-μm particles consisting of a rubbery sphere containing spheroidal polystyrene inclusions that are separated by thin membranes of PBD rubber (see Fig. 19). It is believed that this type of composite particle has an advantage over solid rubber spheres because for a given weight fraction, it maximizes the effective volume fraction of the rubbery phase, thus enhancing the impact toughness without causing undue reduction in modulus. The rubbery phase can also be introduced by blending PS with

Table 5. Typical Notched Izod Impact and Drop-Weight Impact Toughness[a]

	Notched Izod, J/m[b]		Falling dart,[c] N·m[d]	
Thermoplastic	22°C	−40°C[e]	22°C	−40°C[e]
Acetal	53–53			
Nylon, amorphous	587–1121	213–480[f]		
Nylon-6[g]	53–81			
Impact modified nylon[g]	961	294[f]	65	57[f]
Nylon-6,6[g]	27–64			
Toughened nylon-6,6[g]	907–1174			
33% glass[g]	219			
Nylon/ABS	998	96[f]	73	35[f]
Nylon/PPO	213	133[f]	51	40
Polyarylate	294	213		
Polycarbonate	641–854	133–598		
Polycarbonate/ABS	454–641	267–614[f]	38–61	30–46[f]
Polycarbonate/PBT[g,h]	694–854	160–641	56–57	49[f]
Polycarbonate/PET	907	694[f]		50[f]
Polyester, aromatic (LCP)[i]	53–534			
Thermoplastic polyester, PBT[h]	43–53			
Impact modified PBT[h]	801–854	747–801[f]	43–54	43[f]
Impact modified PBT/PET	801–854		54	
30% glass-reinforced PET, thermoplastic polyester	101	96		
Toughened 30% glass PET	139–235	123–160		
Polyetheretherketone	59–81			
Polyetherimide	32–53		34–36	
Polyethersulfone	53–81			
Poly(phenylene oxide) modified	267–534	133–187	15–34	3–11
Poly(phenylene sulfide)	27–75			
Poly(phthalate carbonate)	534			
Polysulfone	69	64		
Polyurethane, engineering thermoplastic	53–213			

[a] Ref. 6.
[b] To convert J/m to ft·lb$_f$/in., divide by 53.38.
[c] Gardner or falling dart.
[d] To convert N·m (J) to in.·lb, divide by 0.113.
[e] Unless otherwise stated
[f] At −29°C
[g] Dry as molded.
[h] Poly(butylene terephthalate).
[i] LCP indicates liquid crystalline polymer.

a triblock copolymer such as poly(styrene–butadiene–styrene) (SBS). The toughening is believed to be due to the nucleation and controlled growth of extensive crazing at the rubber–PS interface (29). The appearance of stress-whitening is due to the high density of crazes generated by deformation. The stress–strain behavior of ABS, PS, and a typical HIPS are shown in Figure 20. It is readily apparent that HIPS has much lower modulus and tensile strength, but much higher elongation

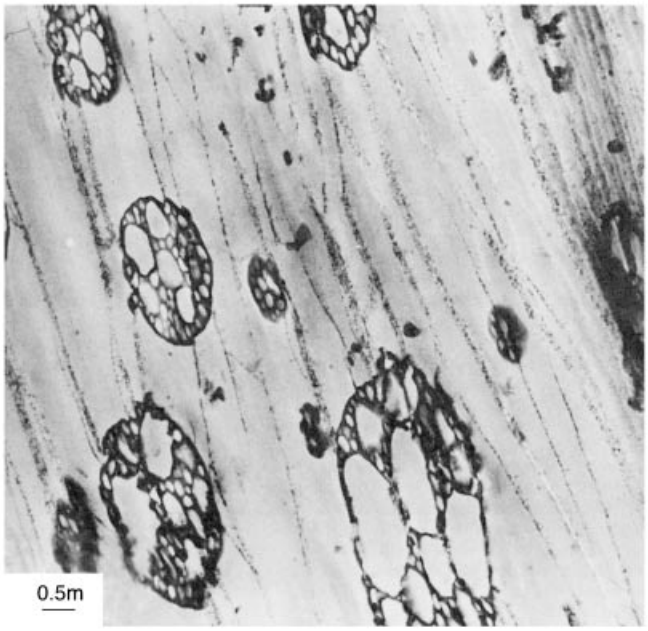

Fig. 19. Electron micrograph of an osmium tetroxide stained ultrathin section of HIPS. This micrograph shows the typical morphology of the dispersed rubber particles. The thin lines connecting the particles are crazes formed after the material has undergone deformation.

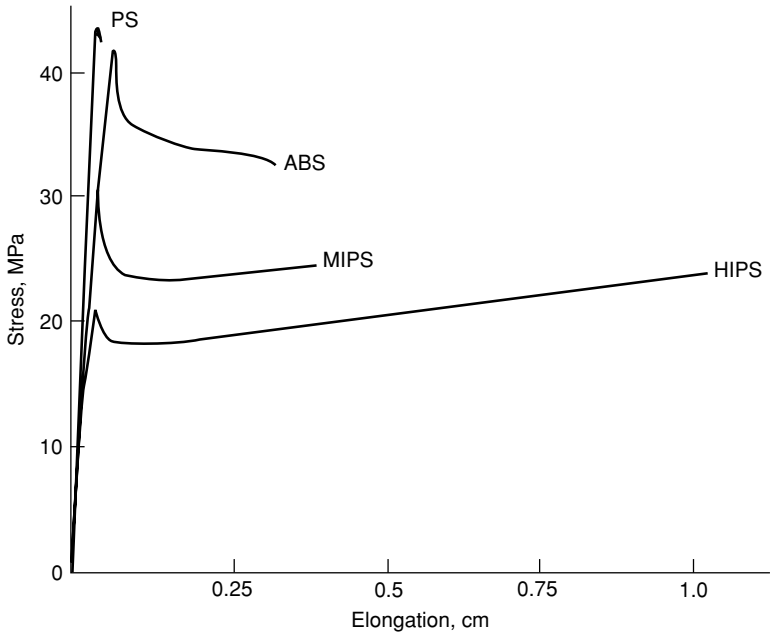

Fig. 20. Typical uniaxial tensile stress–strain behavior of PS, medium-impact PS (MIPS), high-impact PS (HIPS), and ABS (30). To convert MPa to psi, multiply by 145. Courtesy of Springer-Verlag.

than PS. At the cost of a decrease in modulus and strength, ductility and impact toughness are greatly enhanced because of the higher volume fractions of rubber particles in the tougher materials.

Acrylonitrile–butadiene–styrene polymers (qv), the impact-modified version of SAN (styrene–acrylonitrile copolymer), are produced in the same manner as HIPS. Block copolymers such as SBS may also be used as the second phase. The morphologies of ABS and HIPS are very similar except that for optimal impact toughness the rubber particles in ABS are smaller than those in HIPS, ca 1–5 μm in diameter. The difference between ABS and HIPS, as far as mechanical behavior is concerned, is due to the fact that SAN is more ductile than PS. Consequently, the impact toughness of ABS is higher than that of HIPS. Because of compositional and morphological differences, these materials exhibit a range of mechanical properties. For a given volume fraction of rubber particles in ABS, higher AN (acrylonitrile) content enhances toughness. The toughening mechanism is believed to consist of the formation of numerous shear bands in addition to massive crazing (29); both are due to the presence of the rubber particles. In certain ABS grades deformation in tension causes the formation of cavities inside the rubber particles, leading to the formation of shear bands from these cavitated particles (31).

The toughest member in this category of plastic materials is a blend of poly(xylenol ether) [PXE, poly(2,6-dimethylphenylene oxide)] and PS and a rubbery impact modifier; PXE is also known as PPO [poly(phenylene oxide)] (Table 6). However, PPO, a registered trademark, can be confused with poly(propylene oxide), and therefore PXE is the preferred abbreviation. PXE is completely miscible with PS and forms a true solid solution (32); T_g is high and the material is ductile. Melt viscosity is also very high. Processability is improved by blending with PS; the viscosity of the mixture is approximately the weighted average of the two components, whereas T_g varies with the composition (32). Compared with the weighted average, moduli and yield strengths are higher but the fracture toughness is lower (32,33). Commercial grades are usually impact-modified by a dispersion of rubbery particles, which are sometimes obtained by directly blending PXE with HIPS instead of PS. The stress–strain behavior of HIPS/PS/PXE blends is shown in Figure 21. The PXE/HIPS blends exhibit a good overall combination of mechanical properties. The toughening mechanism is believed to be a combination of shear banding and massive crazing (29). The PXE/HIPS blends are much more expensive than HIPS or ABS. Furthermore, they require precise

Table 6. Composition of HIPS/PS/PXE Blends (wt%) Investigated

Blend	HIPS	PS	PXE
A	50	50	0
B	50	37.5	12.5
C	50	25	25
D	50	12.5	37.5
E	50	0	50

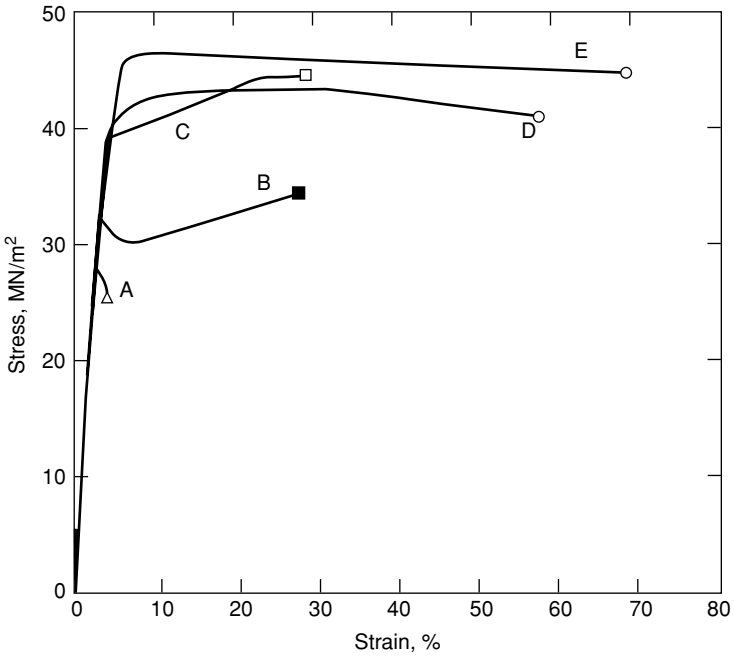

Fig. 21. Uniaxial tensile stress–strain behavior of HIPS/PS/PXE blends at 20°C showing the effects of matrix composition. Strain rate 4×10^{-4} s^{-1} (29). To convert MN/m^2 to psi, multiply by 145. Courtesy of Applied Science Publisher Ltd.

processing control in injection molding because of the relatively high melt viscosity of commercial PXE.

The terms HIPS, ABS, and PXE refer to families of polymers, within which there are variations in composition, morphology, and properties. This is especially true of PXE blends, which exhibit behaviors in between those of HIPS and PXE. Processing and applications must be specific to each grade. As in other materials, pigments, flame retardants, and especially reinforcing fillers can have significant effects on impact toughness. The relevant properties must be determined for each composition.

Since the toughness of these materials depends on the presence of rubber particles, the destruction or oxidation of these particles reduces impact toughness. Excessively high temperatures or shear rate during processing and prolonged exposure to oxidative environments destroy or cross-link the rubber and must be avoided. Prolonged exposure to ultraviolet radiation degrades these materials because of the decomposition of the PBD rubber and sometimes PXE. Saturated elastomers resist oxidative degradation better than unsaturated PBD. In such instances, the low temperature impact toughness of the material might be impaired because the T_g of the saturated rubber is usually higher than that of PBD. UV stabilizers may improve the resistance of PXE to sunlight. The rubber particles act as effective sites for the nucleation of crazes in cyclic fatigue.

Therefore fatigue initiation occurs more readily in the impact-modified versions than in the unmodified versions; crack propagation is slower in the former (30).

Polycarbonates, Other Ductile Glassy Polymers, and Their Impact-Modified Versions. A number of glassy polymers possess some degree of ductility at or near room temperature at moderate rates of strain ($<100\%\ s^{-1}$). Ductility is defined here as the percentage of permanent elongation after yield in a uniaxial tension test. These polymers include polycarbonate (PC), polysulfone (PSU), polyethersulfone (PES), some polyesters, and others as well as copolymers derived therefrom. Some low T_g difunctional epoxies also belong in this category. Poly(vinyl chloride) (PVC), which may possess a low degree of crystallinity, and which loses its ductility more readily under adverse external conditions such as low temperatures and impact rates than other members in this category, may be included here. The class of materials discussed here, whether impact-modified or not, generally exhibits high values of tensile-impact toughness compared with the styrenic materials discussed previously. Drop-weight impact toughness may also be high. However, a flexed-beam impact test (ie, Izod or Charpy) performed on notched specimens of these materials may produce brittle behavior. Using typical notched Izod impact geometries (notch depth of 2.5 mm, notch tip radius of 0.25 mm) and a specimen thickness of 3.2 mm, some of these materials fail in a brittle mode and exhibit impact toughness values that are surprisingly low, given the fact that these same materials are ductile in uniaxial tension. Other materials, PC for example, fail in a ductile mode and absorb large amounts of energy when the specimen thickness is 3.2 mm or less, but dramatically change to the brittle fracture mode when the specimen thickness is increased or the temperature lowered. The specimen thickness effect is due to the difference in constraints at the surfaces and in the interior of the specimen. The temperature effect is not well understood, but is undoubtedly due to the different temperature dependencies of the shear yield stress and crazing stress. These dependencies may be correlatable to molecular relaxations.

The need for impact modification of this type of materials is not based on brittleness but on notch sensitivity. Impact modification does not necessarily enhance toughness when tensile impact and drop-weight impact tests are the criteria. Impact modification is achieved by melt blending a second soft, usually elastomeric, phase, which may be in the form of a dispersion of spherical particles or a network-like structure. To aid the dispersion of the second phase, compatibilization is usually required; that is, the elastomer is copolymerized or altered chemically to reduce the interfacial energy between the two polymer phases. Inadequate compatibilization can lead to unstable morphologies after melt processing, which can in turn produce weak knit lines in injection-molded articles, or skin and core morphologies that interfere with the proper functioning of the processed article and reduce the impact resistance of the molded articles.

It appears that the toughening effect near a crack tip occurs as follows: after initial deformation, cavitation occurs within or around the soft phase in a zone surrounding the crack tip. This zone is known as the process zone. The newly created surface around these cavities in the process zone allows the latter to grow plastically, thus absorbing some energy. Localized shear deformations, often referred to as shear bands, may also grow from these cavities. If the volume fraction

of the soft phase is sufficiently large, these shear bands may merge or coalesce. Since the localized deformation in shear bands cannot be recovered, it is known as plastic deformation. If the plastically deforming material is adjacent to a surface, eg, a crack, then the unloading that occurs there absorbs additional energy (34). The latter may be a significant mechanism of energy absorption in materials that exhibit this mechanism. However it may not occur if the crack growth is terminated by unstable fracture, which often occurs, due to the geometry of crack growth or to very high rate of deformation.

Cavitation in or around the soft phase causes stress-whitening, which is often observed at and near the fracture surface of broken specimens. Stress-whitening is sometimes mistakenly attributed to crazing. While profuse crazing could certainly give rise to intense whitening, the latter could also be due to the occurrence of numerous cavities associated with the rubber phase. Cavitation (including crazing) is an essential step in the toughening process because it relieves the triaxial tension around each cavity initially built up at the crack tips. After the triaxial tension is relieved by cavitation, the stress that remains is more favorable for shear yielding. Since these materials are more prone to shear yielding than to crazing, ductile fracture is restored.

Evidence for the initial deformation process described above can be seen in the three micrographs of an epoxy toughened with elastomer, shown in Figure 22. In Figure 22a, cavitated rubber particles can be seen in a scanning electron micrograph of the fracture surface. In Figure 22b, the cavitated rubber particles can be clearly discerned beneath the fracture surface. The shear bands between the rubber particle cavities are revealed by viewing the specimen between crossed-polarizers in Figure 22c.

Semicrystalline Polymers and Their Toughened Versions. Semicrystalline polymers are different in mechanical behavior from glassy polymers. Conventional melt processing techniques may produce semicrystalline morphologies in many polymers. The polymers in this category include high density polyethylene (HDPE), polypropylene (PP), polyacetals (POM), polyamides (PA, or nylons), poly(ethylene terephthalate) (PET), poly(butylene terephthalate) (PBT), and more recent materials such as poly(phenylene sulfide) (PPS), and polyetheretherketone (PEEK). Low modulus polymers such as low density polyethylene (LDPE) and certain thermoplastic elastomers can be included. Crystallinity is typically between 30 and 40%, though it can be as low as a few percent and as high as 80% in HDPE. Mechanical behavior of semicrystalline polymers depends strongly on the degree and distribution of crystallinity and the differential cooling rates between the surface and the interiors of the specimens. In molded articles, the interior of a thick section contains many large spherulites. Since, in the presence of a notch, the interior is in plane-strain, resulting in triaxial tension, large spherulites invariably cause brittleness, apparently due to weak interspherulitic boundaries. In very thick sections voiding can also occur during the crystallization process. Sometimes, in the mistaken belief that larger cross-sections provide greater strength and a more gentle radius reduces stress concentration, a designer specifies very thick sections at the junction between two surfaces. This causes the growth of very large spherulites and voids, resulting in brittleness. Brittleness in this circumstance may be avoided by using thin sections. Stiffness can be overcome by the proper choice of cross-sectional geometries.

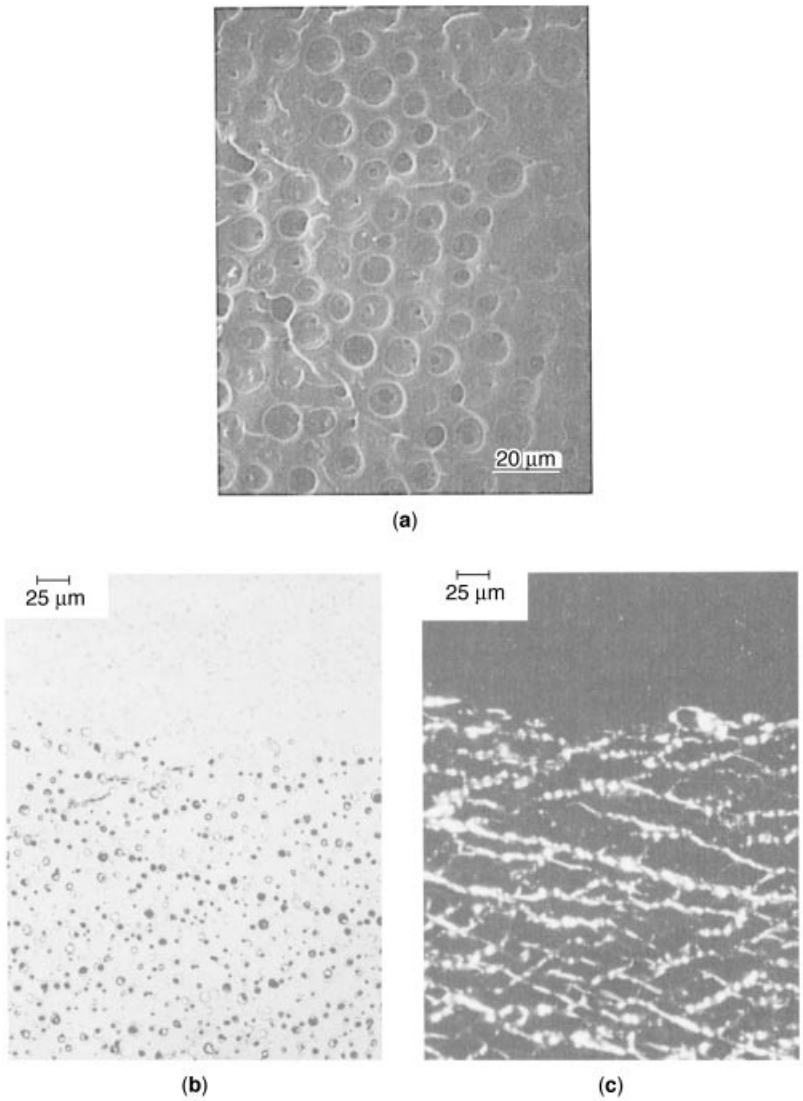

Fig. 22. (**a**) Scanning electron micrograph of the fracture surface of an elastomer-modified epoxy. (**b**) Optical micrograph of a thin section of the same epoxy. (**c**) The same optical micrograph viewed between crossed-polarizres.

Enhancement of impact toughness in some semicrystalline polymers is similar to techniques used for some glassy polymers. Usually an elastomeric phase is melt-blended into the host polymer, resulting in a dispersion of spheroidal elastomeric particles or a network. Compatibilization is obtained by copolymerization or chemical reaction at the interface. The toughening mechanisms may include both massive crazing and cavitation-plastic deformation, depending on the polymer blend, morphology, and degree of adhesion. The elastomeric phase may alter

the morphology of the semicrystalline phase, for example, by nucleating additional spherulites, perhaps of a different crystalline structure, thus improving the inherent toughness of the crystalline phase by reducing the spherulitic size. If toughening is caused by the formation of shear bands, deformation of spherulites contributes to energy absorption.

Incompatible Blends of Rigid Polymers. Some blends are composed of rigid polymers, one or both of which may be rubber-modified. Examples of these materials include PC/ABS, PVC/ABS, PC/PBT, and nylon/PXE. Other combinations are also possible. An important difference between these materials and the PS/PXE blend described above is that the latter is thermodynamically compatible, and behaves as a homogeneous material, whereas the former are thermodynamically incompatible. The incompatibility causes the components, though intimately mixed, to form a continuous-dispersed phase morphology, or a cocontinuous morphology; in the latter neither component can be considered a dispersion. The ABS blends are tough, presumably because the ABS component is already toughened. The commercial versions of the other two examples contain an elastomeric impact modifier. The morphologies and mechanical behaviors of these materials have not yet been studied in detail. However, because of the potential for being able to combine the desirable properties of each of the components, this type of material will undoubtedly become increasingly important.

BIBLIOGRAPHY

"Impact Resistance" in *EPST* 1st ed., Vol. 17, pp. 574–629, by C. A. Brighton and D. A. Lannon, British Geon Ltd; "Impact Resistance" in *EPST* 2nd ed., Vol. 8, pp. 36–68, by Albert F. Yee, University of Michigan.

1. J. G. Williams, *Fracture Mechanics of Polymers*, Halsted Press, New York, 1984, p. 237ff.
2. P. E. Read, in E. H. Andrews, ed., *Developments in PolymerFracture-1*, Applied Science Publishers, London, 1979, Chapt. "4".
3. J. M. Hodgkinson and J. G. Williams, *Phys. Technol.* **13**, 152 (1982).
4. S. N. Kukureka and I. M. Hutchings, in Proceedings of the Conference on High Energy Rate Fabrication, Leeds, U.K., 1981, p. 29.
5. C. B. Bucknall, *Toughened Plastics*, Applied Science Publishers Ltd., London, 1977.
6. *Guide to Engineered Materials*, American Society for Metals, Metals Park, Ohio, 1986.
7. A. J. Kinloch and R. J. Young, *Fracture Behavior of Polymers*, Applied Science Publishers, London, 1983, p. 107.
8. C. E. Stephenson, *Brit. Plastics* **30**, 99 (1957).
9. C. E. Stephenson, *Brit. Plastics* **34**, 543 (1961).
10. N. H. Fahey, *Mater. Res. Std.* **1**, 871 (1961).
11. J. K. Rieke, in R. E. Evans, ed., *Physical Testing of Plastics, Correlations with End-Use Performance (ASTM STP 736)*, American Society For Testing and Materials, Philadelphia, Pa., 1981, pp. 59–76.
12. W. J. Moritz, in Proceedings of the Society of Plastics Engineers, 33rd ANTEC, 1975, p. 540.

13. S. Turner, *Mechanical Testing of Plastics*, 2nd ed., The Plastics and Rubber Institute, London, 1983, p. 199ff.
14. S. Turner, *Mechanical Testing of Plastics*, 2nd ed., The Plastics and Rubber Institute, London, 1983, p. 139ff.
15. I. M. Ward, *Mechanical Properties of Solid Polymers*, 2nd ed., John Wiley & Sons, Inc., Chichester, U.K., 1983, p. 329ff.
16. P. B. Bowden, in R. N. Haward, ed., *Physics of Glassy Polymers*, Halsted Press, New York, 1973, Chapt. "5", p. 287ff.
17. S. Bahadur, *Polym. Eng. Sci.* **13**, 266 (1973).
18. L. M. Carapellucci, A. F. Yee, and R. P. Nimmer, in Proceedings of the Society of Plastics Engineers, 44th ANTEC, 1986, p. 622.
19. R. P. Nimmer, *Polym. Eng. Sci.* **23**, 155 (1983).
20. P. B. Bowden and J. A. Jukes, *J. Mater. Sci.* **3**, 183 (1968).
21. P. I. Vincent, *Impact Tests and Service Performance of Thermoplastics*, Plastics Institute, London, 1971.
22. A. F. Yee, *J. Mater. Sci.* **12**, 757 (1977).
23. G. C. Adams and T. K. Wu, in Proceedings of the Society of Plastics Engineers, 39th ANTEC, 1981, p. 185.
24. J. T. Ryan, *Polym. Eng. Sci.* **18**, 264 (1978).
25. E. Plati and J. G. Williams, *Polym. Eng. Sci.* **15**, 470 (1975).
26. W. F. Brown Jr. and J. F. Srawley, *ASTM Special Technical Publication*, ASTM, Philadelphia, Pa., 1966, p. 12.
27. J. G. Williams and M. W. Birch, in Proceedings of the 4th International Conference on Fracture (ICF4), Vol. 1, Part IV, 1977, p. 501.
28. L. V. Newman and J. G. Williams, *Polym. Eng. Sci.* **20**, 572 (1980).
29. Ref. 5, p. 182ff.
30. J. A. Saver and C. C. Chen, in H. H. Kausch, ed., *Crazing in Polymers* (Advances in Polymer Science, Vol. **52/53**), Springer-Verlag, New York, 1983.
31. H. Breuer, F. Haaf, and J. Stabenow, *J. Macromol. Sci., B: Phys.* **14**, 387 (1977).
32. A. F. Yee, *Polym. Eng. Sci.* **17**, 213 (1977).
33. A. F. Yee and M. A. Maxwell, *J. Macromol. Sci., B: Phys.* **17**, 543 (1980).
34. A. F. Yee, in Proceedings of the International Conference on Toughening of Plastics II, London, 1985, p. 19.1.

GENERAL REFERENCES

A. J. Kinloch and R. J. Young, *Fracture Behavior of Polymers*, Applied Science Publishers, London, 1983. This is a particularly comprehensive treatise and contains much up-to-date (early 1980s) information.

I. M. Ward, *Mechanical Properties of Solid Polymers*, 2nd ed., John Wiley & Sons, Inc., Chichester, U.K., 1983. Provides many of the background concepts, mostly from a polymer physics point of view.

J. G. Williams, *Stress Analysis of Polymers*, 2nd ed., Halsted Press, Chichester, 1980. Presents fundamental mechanics using relatively simple mathematics. The last chapter is particularly relevant.

C. B. Bucknall, *Toughened Plastics*, Applied Science Publishers, London, 1977. Contains mid-1970s state-of-the-art information on the science and technology of impact-modified plastics.

ASTM Standards, Philadelphia, Pa. The current edition of this series contains detailed information on testing techniques and data analysis.
D. R. Paul and C. B. Bucknall, *Polymer Blends*, John Wiley & Sons, Inc., New York, 2000.

ALBERT F. YEE
University of Michigan
HUNG-JUE SUE
Texas A&M University

INFRARED SPECTROSCOPY. See VIBRATIONAL SPECTROSCOPY.

INITIATORS, FREE-RADICAL

Introduction

Free-radical initiators are chemical substances that, under certain conditions, initiate chemical reactions by producing free radicals:

$$\underset{\text{Initiator}}{\text{I}} \longrightarrow \underset{\text{Radical}}{\text{I}\cdot} \qquad (1)$$

Initiators contain one or more labile bonds that cleave homolytically when sufficient energy is supplied to the molecule. The energy must be greater than the bond dissociation energy (BDE) of the labile bond. Radicals are reactive chemical species possessing a free (unbonded or unpaired) electron. Radicals may also be positively or negatively charged species carrying a free electron (ion radicals). Initiator-derived radicals are very reactive chemical intermediates and generally have short lifetimes, ie, half-life times less than 10^{-3} (1).

The principal commercial initiators used to generate radicals are peroxides and azo compounds. Lesser amounts of carbon–carbon initiators and photoinitiators, and high energy ionizing radiation are also employed commercially to generate radicals. Emerging technologies use *N*-alkoxyamines as free-radical initiators or employ atom or group transfer facilitated by transition metals.

Free-Radical Formation and Use

There are three general processes for supplying the energy necessary to generate radicals from initiators: thermal processes, microwave or ultraviolet (uv) radiation

Encyclopedia of Polymer Science and Technology. Copyright John Wiley & Sons, Inc. All rights reserved.

processes, and electron transfer (redox) processes. Radicals can also be produced in high energy radiation processes. Initiators are sometimes called radical catalysts. However, initiators are not true catalysts because they are consumed in amounts ranging from substoichiometric up to stoichiometric or greater when they are employed as initiators in chemical reactions. True catalysts such as enzymes are not consumed in the chemical reaction they catalyze.

Once formed, radicals undergo two basic types of reactions: propagation reactions and termination reactions. In a propagation reaction, a radical reacts to form a covalent bond and to generate a new radical. The three most common propagating reactions are atom abstraction, β-scission, and addition to carbon–carbon double bonds or aromatic rings. In a termination reaction, two radicals interact in a mutually destructive reaction in which both radicals form covalent bonds and reaction ceases. The two most common termination reactions are coupling and disproportionation. Because the propagation reaction is a chain reaction, it has become the most significant aspect of commercial free-radical chemistry. Radical chain reactions are involved in many commercial processes.

Radicals are employed widely in the polymer industry, where their chain-propagating behavior transforms vinyl monomers into polymers and copolymers (see RADICAL POLYMERIZATION). The mechanism of addition polymerization involves all three types of reactions discussed above, ie, initiation, propagation by addition to carbon–carbon double bonds, and termination: Initiation

$$\mathrm{I} \longrightarrow \mathrm{I}\cdot \tag{2}$$

$$\mathrm{I}\cdot + \mathrm{M} \longrightarrow \mathrm{I{-}M}\cdot \tag{3}$$

Propagation

$$\mathrm{I{-}M}\cdot + n\mathrm{M} \longrightarrow \mathrm{I{-}M_{\mathit{n}}{-}M}\cdot \tag{4}$$

Termination

$$2\ \mathrm{I{-}M_{\mathit{n}}{-}M}\cdot \longrightarrow \mathrm{I{-}M_{\mathit{n}}{-}M{-}M{-}M_{\mathit{n}}{-}I} \tag{5}$$

$$2\ \mathrm{I{-}M_{\mathit{n}}{-}M}\cdot \longrightarrow \mathrm{I{-}M_{\mathit{n}}{-}M'} + \mathrm{I{-}M_{\mathit{n}}{-}M''} \tag{6}$$

In these equations, I is the initiator and I· is the radical intermediate, M is a vinyl monomer, I–M· is an initial monomer radical, I–M_nM· is a propagating polymer radical, and M′ and M″ are polymer end groups that result from termination by disproportionation. Common vinyl monomers that can be homo- or copolymerized by radical initiation include ethylene, butadiene, styrene, vinyl chloride,

vinyl acetate, acrylic and methacrylic acid esters, acrylonitrile, *N*-vinylimidazole, *N*-vinyl-2-pyrrolidinone, and others (2).

Two other important commercial uses of initiators are in polymer cross-linking and polymer degradation. In a cross-linking reaction, atom abstraction, usually a hydrogen abstraction, occurs, followed by termination by coupling of two polymer radicals to form a covalent cross-link:

$$\mathrm{P{-}H + I\cdot \longrightarrow I{-}H + P\cdot} \tag{7}$$

$$\mathrm{2\,P\cdot \longrightarrow P{-}P} \tag{8}$$

P—H is a polymer with covalently attached hydrogen, I· is the initiating radical, and P—P is a cross-linked polymer. Cross-linking is a commercially important reaction of thermoplastics (such as polyethylene) and elastomers. In polymer degradation, hydrogen abstraction is followed by β-scission that results in breakage of the polymer chain:

$$\mathrm{P{-}\underset{\displaystyle R}{\overset{|}{C}}H{-}CH_2{-}P' + I\cdot \longrightarrow I{-}H + P{-}\underset{\displaystyle CH_2{-}P'}{\overset{\displaystyle R}{\overset{|}{\underset{|}{C}}}}\cdot} \tag{9}$$

$$\mathrm{P{-}\underset{\displaystyle CH_2{-}P'}{\overset{\displaystyle R}{\overset{|}{\underset{|}{C}}}}\cdot \xrightarrow{\beta\text{-scission}} P{-}\underset{\displaystyle R}{\overset{|}{C}}{=}CH_2 + P'\cdot \longrightarrow P'H} \tag{10}$$

I· is the initiating radical, P′· is the chain-propagating polymer radical that subsequently abstracts a hydrogen atom from another polymer molecule, P—CHR—CH_2—P′ is the polymer before, and P—CR=CH_2 and P′—H are polymer chains after degradation. Polymer degradation is important in facilitating the commercial processing (molding and extruding) of polypropylene (the degradation is more commonly called controlled rheology or vis-breaking). In the β-scission reaction the first-formed radical cleaves to a polymer radical and to an electronically neutral molecule (polymer with an unsaturated end group) by scission of a carbon–carbon bond β to the atom bearing the initial radical center.

Other common radical-initiated polymer processes include curing of resins, eg, unsaturated polyester–styrene blends; curing of rubber; grafting of vinyl monomers onto polymer backbones; and telomerizations.

A typical example of a nonpolymeric chain-propagating radical reaction is the anti-Markovnikov addition of hydrogen sulfide to a terminal olefin. The mechanism involves alternating abstraction and addition reactions in the propagating steps:

Initiation

$$\mathrm{I} \longrightarrow \mathrm{I}\cdot \tag{11}$$

$$\mathrm{I}\cdot + (\text{excess})\ \mathrm{H_2S} \longrightarrow \mathrm{I{-}H} + \mathrm{HS}\cdot \tag{12}$$

Propagation

$$\mathrm{HS}\cdot + \mathrm{CH_2{=}CH{-}R} \longrightarrow \mathrm{HSCH_2{-}\overset{\displaystyle H}{\underset{\displaystyle R}{\overset{|}{\underset{|}{C}}}}\cdot} \tag{13}$$

$$\mathrm{HSCH_2{-}\overset{\displaystyle H}{\underset{\displaystyle R}{\overset{|}{\underset{|}{C}}}}\cdot} + \mathrm{H_2S} \longrightarrow \mathrm{HSCH_2CH_2R} + \mathrm{HS}\cdot \tag{14}$$

Termination

$$\mathrm{HS}\cdot \longrightarrow \text{Nonradical sulfur compounds} \tag{15}$$

Other nonpolymeric radical-initiated processes include oxidation, autoxidation of hydrocarbons, chlorination, bromination, and other additions to double bonds. The same types of initiators are generally used for initiating polymerization and nonpolymerization reactions. Radical reactions are extensively discussed in the chemical literature (3–20).

Structure–Reactivity Relationships. Much has been written about the structure reactivity of radicals. No single unifying concept has satisfactorily explained all radical reactions reported in the literature. A long standing correlation of structure and reactivity involves comparisons of the energies required to homolytically break covalent bonds to hydrogen. It is assumed that this energy, the hydrogen BDE, reflects the stability and the reactivity of the radical coproduced with the hydrogen atom (21–24). However, this assumption should really be limited to radical reactivity and selectivity in hydrogen atom abstraction reactions, and can be particularly misleading for reactions with polar transition states, in which radicals can behave either as nucleophiles or electrophiles (25). Solvent interactions with transition-state species can also influence the reactivity (26–30). Nevertheless, the correlation of radical reactivity with BDE is quite useful. Table 1 shows some general BDE values for the formation of various carbon and oxygen radicals from various precursors. According to the theory, the higher the BDE, the higher the reactivity and the lower the stability of the radical formed

Table 1. Bond Dissociation Energies

Precursor	BDE, kJ/mol[a]
$(R)_3C—H$	381
$(R)_2CH—H$	406
$RCH_2—H$	418
$CH_3—H$	439
RO—H	439
RCOO—H	444
$C_6H_5—H$	469
HO—H	498

[a]To convert kJ/mol to kcal/mol, divide by 4.184.

by removal of a hydrogen atom. Thus bulky *tert*-alkyl radicals are more stable and less reactive than less bulky secondary alkyl radicals that in turn are more stable and less reactive than primary alkyl radicals. Hydroxyl radicals are the most reactive radicals listed. Methyl radicals are more reactive than other primary alkyl radicals and are about as reactive as alkoxy radicals. Lower stability and increased reactivity correspond to less discriminating radical behavior, resulting in faster and less-selective radical reactions with other molecules. In organic systems, this reaction is usually hydrogen atom abstraction. Consequently, methyl radicals and oxy radicals (carboxy, alkoxy, hydroxy) are considered good hydrogen-atom-abstracting radicals, and are suitable for cross-linking, grafting, and degradation reactions. Enhanced stability and reduced reactivity correspond to more discriminating radical behavior, resulting in slower and more selective subsequent reactions. Therefore, reactions other than hydrogen abstraction are favored. Substituted carbon radicals, such as the ethyl radical, are ineffective hydrogen-abstracting radicals; thus these radicals are more likely to react with carbon–carbon double bonds. Initiators that generate these types of radicals are suitable for vinyl monomer polymerizations that avoid undesirable side reactions (cross-linking, grafting, etc).

The BDE theory does not explain all observed experimental results. Addition reactions are not adequately handled at all, mostly owing to steric and electronic effects in the transition state. Thus it is important to consider both the reactivities of the radical and the intended coreactant or environment in any attempt to predict the course of a radical reaction (31). Application of frontier molecular orbital theory may be more appropriate to explain certain reactions (32,33). Radical reactivities have been studied by esr spectroscopy (34–36) and modeling based on general reactivity and radical polarity (37). Recent radical trapping studies have provided considerable insight into the course of free-radical reactions, particularly addition polymerizations, using radical traps such as 2,4-diphenyl-4-methyl-1-pentene (α-methylstyrene dimer, MSD) (38–44) and 1,1,3,3-tetramethyl-2,3-dihydro-1*H*-isoindol-2-yloxyl (45–49).

The choice of an initiator for a given radical process depends on the reaction conditions and the reactivity of the initiator. These two factors must be balanced so that the reaction is successful. Knowing the decomposition behavior of initiators is important to ensure proper selection. The stabilities or reactivities of initiators

such as organic peroxides and aliphatic azo compounds are significantly affected by structural variations close to the labile bond or bonds, ie, the oxygen–oxygen bond in peroxides and the carbon–nitrogen bonds in aliphatic azo compounds. The reactivity differences, resulting from structural differences between initiators, are due to several electronic and steric factors. Alkyl and aryl substituents stabilize carbon radicals through resonance and field effects. These substituent effects on radical stability are reversed for initiator stability. Initiators that decompose to produce highly alkylated or arylated carbon radicals are less stable (more reactive) than those that decompose to less alkylated or arylated carbon radicals. Electronic factors introduced by electron-donating or electron-withdrawing substituents can also affect initiator stability–reactivity; electron-donating substituents stabilize, whereas electron-withdrawing groups destabilize incipient carbon radicals. Initiators with bulky groups on either side of the labile, radical-forming bonds are less stable (more reactive) than initiators with less bulky groups since decomposition to radicals relieves ground-state steric strain (50).

Activation Parameters. Thermal processes are commonly used to break labile initiator bonds in order to form radicals. The amount of thermal energy necessary varies with the environment, but absolute temperature T is usually the dominant factor. The energy barrier, the minimum amount of energy that must be supplied, is called the activation energy E_a. A third important factor, known as the frequency factor A_3 is a measure of bond motion freedom (translational, rotational, and vibrational) in the activated complex or transition state. The relationships of A, E_a, and T to the initiator decomposition rate k_d are expressed by the Arrhenius first-order rate equation (eq. 16), where R is the gas constant, and A and E_a are known as the activation parameters.

$$k_d = A\, e^{(-E_a/RT)} \quad \text{or} \quad \ln k_d = \ln A - E_a/RT \tag{16}$$

Increasing temperature increases initiator decomposition rate. When a single labile bond is broken in the rate-determining step, the frequency factor is high. When multiple bonds are broken, the activated complex is restricted, the frequency factor is low, and the rate of decomposition is reduced (assuming no change in activation energy). Generally, slower rates of decomposition of the initiator mean higher activation energy values. Steric and electronic factors affect the activation energy of the initiator. Factors that enhance the stabilities of the incipient radicals reduce the activation energy and thus increase the decomposition rate.

The activation parameters for an initiator can be determined at normal atmospheric pressure by plotting $\ln k_d$ vs $1/T$ using initiator decomposition rates obtained in dilute solution (0.2 M or lower) at several temperatures. Rate data from dilute solutions are required in order to avoid higher order reactions such as induced decompositions. The intercept for the resulting straight line is $\ln A$ and the slope of the line is $-E_a/R$; therefore both A and E_a can be calculated. Activation parameters can also be determined by differential scanning calorimetry (51), although consideration must be given to the influence of decomposition products on the values obtained.

Initiator Half-Life. Once these activation parameters have been determined for an initiator, *half-life times at a given temperature*, ie, the time required

for 50% decomposition at a selected temperature, and *half-life temperatures for a given period*, ie, the temperature required for 50% decomposition of an initiator over a given time, can be calculated. In selecting appropriate initiators for radical applications such as vinyl monomer polymerizations and polyolefin cross-linking, care must be exercised in the use of calculated half-life data for temperatures, pressures, and solvents different than those used in determining the activation parameters. Half-life data are useful for comparing the activity of one initiator with another when the half-life data are determined in the same solvent and at the same concentration and, preferably, when the initiators are of the same class. Because producers of initiators and their customers roughly correlate the thermal stability of initiators with temperature, it is useful to express this stability in terms of 1- and 10-h half-life temperatures, ie, the temperatures at which 50% of the initiator has decomposed in 1 and 10 h, respectively. An extensive compilation of rate data for initiators is available (52). Half-life temperatures are usually provided in manufacturers' product catalogs (53,54). Rate data for commercial organic peroxide initiators are often available from special manufacturers' half-life bulletins (55).

Although a variety of methods for generating radicals by one or more of these three methods are reported in the literature, commercial initiators are primarily organic and inorganic peroxides, aliphatic azo compounds, certain organic compounds with labile carbon–carbon bonds, and photoinitiators.

Peroxides

Organic Peroxides. Organic peroxides are compounds possessing one or more oxygen–oxygen bonds. They have the general structure ROOR′ or ROOH, and decompose thermally by the initial cleavage of the oxygen–oxygen bond to produce two radicals:

$$\mathrm{ROOR'} \longrightarrow \mathrm{RO\cdot} + \mathrm{\cdot OR'} \tag{17}$$

Depending on the peroxide class, the rates of decompositions of organic peroxides can be enhanced by specific promoters or activators, which significantly decrease the energy necessary to break the oxygen–oxygen bond. Such accelerated decompositions occur well below a peroxide's normal application temperatures and usually result in generation of only one useful radical, instead of two. An example is the decomposition of hydroperoxides with multivalent metals (M), commonly iron, cobalt, or vanadium:

$$\mathrm{ROOH} + \mathrm{M^{n+}} \longrightarrow \mathrm{RO\cdot} + \mathrm{HO^-} + \mathrm{M^{(n+1)+}} \tag{18}$$

Solvent polarity also affects the rate of peroxide decomposition (56). Most peroxides decompose faster in more polar or polarizable solvents. This is true even if the peroxide is not generally susceptible to higher order decomposition reactions. This phenomenon is illustrated by various half-life data for *tert*-butyl peroxypivalate [927-07-1]. The 10-h half-life temperature for *tert*-butyl peroxypivalate varies from 62°C in decane (nonpolar) to 55°C in benzene (polarizable) and 53°C in methanol (polar).

Following radical generation, the radicals produced (RO· and R′·) can initiate the desired reaction. However, when the radicals are generated in commercial applications, they are surrounded by a solvent, monomer, or polymer "cage." When the cage is solvent, the radical must diffuse out of this cage to react with the desired substrate. When the cage is monomer, the radical can react with the cage wall or diffuse out of the cage. When the cage is polymer, reaction with the polymer can occur in the cage. Unfortunately, other reactions can occur within the cage and can adversely affect efficiency of radical generation and radical reactivity. If the solvent reacts with the initiator radical, then solvent radicals may participate in the desired reaction.

Two secondary propagating reactions often accompany the initial peroxide decomposition: radical-induced decompositions and β-scission reactions. These intermolecular and intramolecular radical reactions compete kinetically with the desired reaction. Both reactions affect the reactivity and efficiency of the initiation process. Peroxydicarbonates and hydroperoxides are particularly susceptible to radical-induced decompositions. In radical-induced decomposition, a radical in the system reacts with undecomposed peroxide, eg:

$$R^{\cdot} + ROOR \longrightarrow ROR' + RO\cdot \tag{19}$$

Radical-induced decomposition is an inefficient method of generating radicals, since the peroxide is induced to decompose without adding radicals to the system. Such decompositions are suppressed in vinyl monomer polymerizations, since the vinyl monomers quickly and efficiently scavenge radicals. In nonscavenging environments, eg, in nonolefinic solvents, induced decompositions occur with those peroxides that are susceptible, and they become more pronounced as the peroxide concentration increases. Although the homolysis of organic peroxides is a first-order reaction, the radical-induced decomposition is generally a higher-order reaction. Therefore, in those peroxide systems where induced decomposition is occurring, decomposition rates are significantly higher than the true first-order decomposition rates.

The other secondary propagation reaction that occurs during initiation is β-scission, as shown in equations 20 and 21:

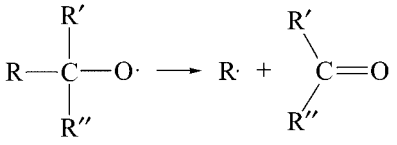

(20)

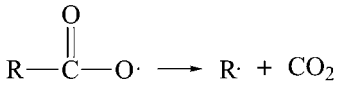

(21)

Although reaction 21 is a β-scission reaction, it is more commonly termed decarboxylation. In both reactions, the energetics and other properties of the radicals are changed. The initially formed oxygen radicals become carbon radicals. The earlier discussion of relative BDEs for the two types of radicals is applicable here.

Steric and temperature effects are also important in β-scission. In equation 20, the newly formed alkyl radical R· is generally derived from the bulkiest alkyl group of the alkoxy radical, and it is usually the most stable radical. An exception here is the phenyl radical, which does not form upon β-scission of α-cumyloxy radicals, owing to its high energy. Instead, β-scission of the α-cumyloxy radical gives methyl radical and acetophenone. For *tert*-alkoxy radicals, the difference in generation of a *tert*-butoxy radical or a *tert*-amyloxy radical from a *tert*-alkyl peroxide can make a significant difference in the course of the resulting radical reaction. β-Scission of the *tert*-butoxy radical produces a methyl radical having about the same energy (as indicated by BDE) and reactivity as a *tert*-butoxy radical. β-Scission of the *tert*-amyloxy radical produces an ethyl radical having significantly lower energy and reactivity than the *tert*-amyloxy radical.

In equation 21, only one alkyl radical is possible; however, the rate of β-scission is greatly influenced by the bulk of the R group. As with β-scission of α-cumyloxy radicals, benzoyloxy radicals do not decarboxylate as readily as other acyloxy radicals, owing to formation of high energy phenyl radicals. If the R group is sufficiently bulky, decarboxylation occurs simultaneously with scission of the oxygen–oxygen bond. Increased temperatures enhance β-scission. For more thermally stable peroxides, the higher decomposition temperatures result in increased β-scission. Solvent interaction with the transition state for β-scission also facilitates the reaction (26–30).

Approximately 100 different organic peroxide initiators, in well over 300 formulations (liquid, solid, paste, powder, solution, dispersion), are commercially produced throughout the world, primarily for the polymer and resin industries. Considerable published literature exists that describes the synthesis, chemical properties, and utility of organic peroxides (57–68). A multiclient study covers the commercial producers and users of organic peroxides as well as other initiators, and their commercial markets and applications (69).

The eight classes of organic peroxides that are produced commercially for use as initiators are listed in Table 2. Included are the 10-h half-life temperature ranges (nonpromoted) for the members of each peroxide class.

Peroxide half-life data provide useful guidance for comparing the activity of one peroxide with another in a given application, if the previously discussed limitations of half-life data are considered. Several producers of organic peroxides provide customers with extensive half-life data on commercial and developmental organic peroxides (56,70). In addition, customer guidance is provided for selection of organic peroxides for various commercial applications, eg, vinyl monomer polymerizations, curing of unsaturated polyester resins, cross-linking of elastomers and polyolefins, and reactive extrusion, based on peroxide type and half-life criteria. This information is available in a manufacturer's half-life bulletin and associated personal computer interactive software (56), and in many available application-focused brochures (71–77).

Table 2 shows that commercial organic peroxides are available with 10-h half-life temperature activity varying from about room temperature to about 130°C. Organic peroxide classes such as diacyl peroxides and peroxyesters show a strong correlation between structural variation and 10-h half-life temperature activity. Other organic peroxide classes, eg, peroxydicarbonates and monoperoxycarbonates, show very little change in activity with structural variation. The

Table 2. Commercial Organic Peroxide Classes[a]

Organic peroxide class	Structure	10-h $t_{1/2}$, °C[b,c]
Diacyl peroxides	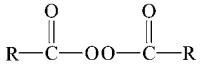	21–75
Dialkyl peroxydicarbonates	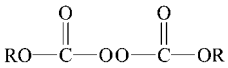	49–51[d]
tert-Alkyl peroxyesters	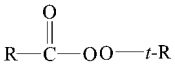	38–107
OO-tert-Alkyl *O*-alkyl monoperoxycarbonates	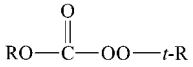	99–100
Di(*tert*-alkylperoxy)ketals	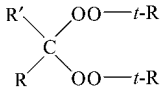	92–110
Di-*tert*-alkyl peroxides	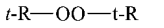	115–128
tert-Alkyl hydroperoxides	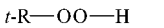	—[e]
tert-Alkyl hydroperoxides	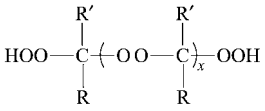 + other structures	—[e]

[a] $x = 0$ or 1.
[b] Temperature at which $t_{1/2} = 10$ h.
[c] In benzene, unless otherwise noted.
[d] In trichloroethylene (TCE).
[e] Not applicable.

diperoxyketals and dialkyl peroxides show a moderate change in activity with variation in peroxide structures. In the cases of hydroperoxides and ketone peroxides, precise half-life data are difficult to obtain owing to the susceptibilities of these thermally stable peroxide classes to induced decompositions and transition-metal catalysis. Furthermore, radicals are usually generated from these two classes of peroxides at lower temperatures using activators (or promoters), and first-order decomposition rates have no significance. Although the low temperature acyl sulfonyl peroxide, acetyl cyclohexanesulfonyl peroxide (ACSP) [3179-56-4] (with a 10-h half-life temperature of 42°C), is still used to some extent commercially, it is only produced captively; hence its peroxide class was not included in Table 2.

Diacyl Peroxides. Table 3 lists several commercial diacyl peroxides and their corresponding 10-h half-life temperatures, determined in benzene and other solvents (78). Although diacyl peroxides cleave at the oxygen–oxygen bond, decarboxylation can occur, either simultaneously or subsequently (eq. 22):

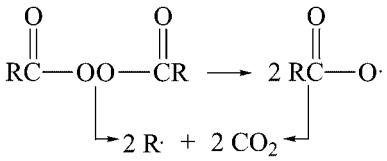

(22)

Table 3. Commercial Diacyl Peroxides

Name	CAS registry number	Structure	10-h $t_{1/2}$, °C[a]	Solvent
Dibenzoyl peroxide	[94-36-0]	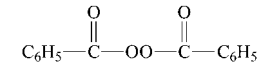	73	Benzene
			72	TCE[b]
Dilauroyl peroxide	[105-74-8]	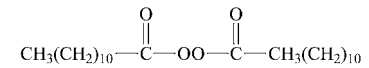	62	Benzene
			64	TCE
Succinic acid peroxide	[123-23-9]	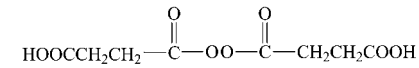	66	Acetone
Diisononanoyl peroxide	[58499-37-9]	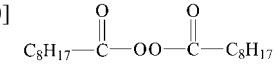	61	TCE

[a]Temperature at which $t_{1/2} = 10$ h.
[b]TCE is trichloroethylene.

The extent of decarboxylation primarily depends on temperature, pressure, and the stability of the incipient R· radical. The more stable the R· radical, the faster and more extensive the decarboxylation. With many diacyl peroxides, decarboxylation and oxygen–oxygen bond scission occur simultaneously in the transition state. Acyloxy radicals are known to form initially only from diacetyl peroxide [110-22-5] and from dibenzoyl peroxides (because of the relative instabilities of the corresponding methyl and phenyl radicals formed upon decarboxylation). Diacyl peroxides derived from non-α-branched carboxylic acids, eg, dilauroyl peroxide, may also initially form acyloxy radical pairs; however, these acyloxy radicals decarboxylate very rapidly and the initiating radicals are expected to be alkyl radicals. Diacyl peroxides are also susceptible to induced decompositions:

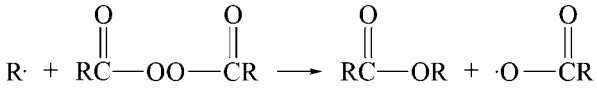

(23)

Diacyl peroxides are used in a broad spectrum of applications, including curing of unsaturated polyester resin compositions, cross-linking of elastomers, production of poly(vinyl chloride), polystyrene, and polyacrylates, and in many nonpolymeric addition reactions. The activities of acyloxy radicals in vinyl monomer polymerization (79,80) and under high-pressure conditions (81,82) have been investigated.

Aromatic diacyl peroxides such as dibenzoyl peroxide (BPO) [94-36-0] may be used with promoters to lower the useful decomposition temperatures of the peroxides, although usually with some sacrifice of radical generation efficiency. The most widely used promoter is dimethylaniline (DMA). The BPO–DMA combination is used for hardening (curing) of unsaturated polyester resin compositions, eg, body putty in auto repair kits. Here, the aromatic *tert*-amine promoter reacts with the BPO to initially form *N*-benzoyloxydimethylanilinium benzoate (ion pair), which

subsequently decomposes at room temperature to form a benzoate ion, a dimethylaniline radical cation, and a benzoyloxy radical that, in turn, initiates the curing reaction (83):

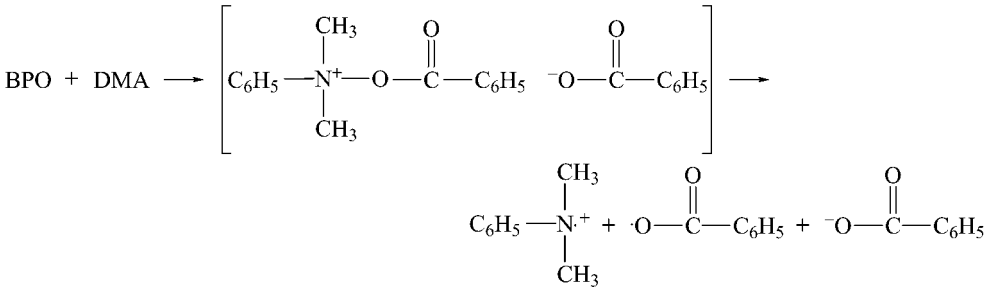

(24)

Although the BPO–DMA redox system works well for curing of unsaturated polyester blends, it is not a very effective system for initiating vinyl monomer polymerizations, and therefore it generally is not used in such applications (83). However, combinations of amines (eg, DMA) and acyl sulfonyl peroxides (eg, ACSP) are very effective initiator systems at 0°C for high conversion suspension polymerizations of vinyl chloride (84). BPO has also been used in combination with ferrous ammonium sulfate to initiate emulsion polymerizations of vinyl monomers via a redox reaction (85). Decompositions of BPO using other promoters have been reported, including organoaluminum compounds (86), chromium(II) acetate (87), nitroxyl radicals (88), tin(II) chloride with *o*-sulfonic benzoylimide (89), benzoyl thiourea [614-23-3] (90), and other reducing agents (91).

***tert*-Alkyl Peroxyesters.** Table 4 lists several commercial *tert*-alkyl peroxyesters and their corresponding 10-h half-life temperatures (determined in dodecane and other solvents) (92). Only *tert*-alkyl peroxyesters are commercially available. As illustrated in Table 2, the peroxyester class offers the broadest range of temperature activity of any of the peroxide classes.

Peroxyesters undergo single- or multiple-bond scission to generate acyloxy and alkoxy radicals, or alkyl and alkoxy radicals and carbon dioxide:

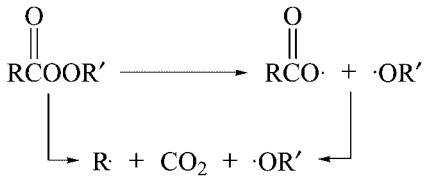

(25)

Acyloxy radicals can decarboxylate, as noted above for the diacyl peroxides. The alkoxy radicals (R′·) can undergo the β-scission reaction, leading to greater radical reaction selectivity. Variation of the R group or the R′ group provides a convenient means of altering the relative activity of peroxyesters. For example, increasing the steric bulk of either or both of R and R′ generally lowers the thermal stability of a peroxyester. Thermal stability decreases as follows: for R,

Table 4. Commercial *tert*-Alkyl Peroxyesters

Name	CAS registry number	Structure	10-h $t_{1/2}$, °C[a,b]
tert-Butyl peroxybenzoate	[614-45-9]	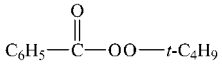	104
tert-Butyl peroxyacetate	[107-71-1]	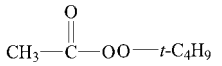	102
tert-Butyl peroxymaleate	[1931-62-0]	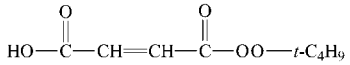	87[c]
tert-Butyl 2-ethylperoxyhexanoate	[3006-82-4]	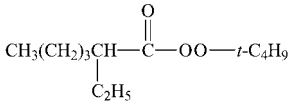	77
tert-Amyl 2-ethylperoxyhexanoate	[686-31-7]	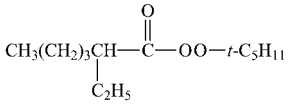	75
2,5-Di(2-ethylhexanoylperoxy)-2,5-dimethylhexane	[13052-09-0]	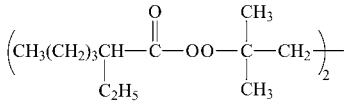	73
tert-Butyl peroxypivalate	[927-07-1]	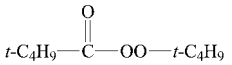	62
α-Cumyl peroxyneoheptanoate	[104852-44-0]	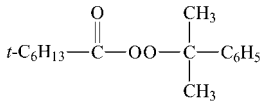	43[d]
3-Hydroxy-1,1-dimethylbutyl peroxyneodecanoate	[95718-78-8]	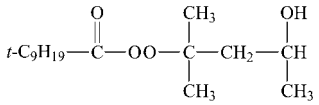	37[d]
OO-tert-Butyl *O*-(isopropyl) monoperoxycarbonate	[2372-21-6]	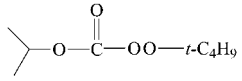	100
OO-tert-Amyl *O*-(2-ethylhexyl) monoperoxycarbonate	[70833-40-8]	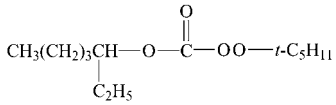	98
Polyether poly(*OO-tert*-butyl monoperoxycarbonate)		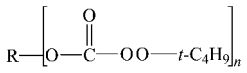	100[e]

[a] Temperature at which $t_{1/2} = 10$ h.
[b] In dodecane, unless otherwise noted.
[c] In acetone.
[d] In trichloroethylene (TCE).
[e] In ethylbenzene.

$CH_3 > RCH_2 > R_2CH > R_3C$; for R′, *tert*-butyl > *tert*-amyl > *tert*-octyl > α-cumyl > 3-hydroxy-1,1-dimethylbutyl. By way of example, *tert*-butyl peroxyacetate [107-71-1] is more thermally stable than 3-hydroxy-1,1-dimethylbutyl peroxyneodecanoate [95718-78-8]. Although other factors affect thermal stability, the trends shown can be used to qualitatively predict peroxyester reactivity trends. The order of activity of the R′ group in peroxyesters is also observed in other *tert*-alkyl peroxy-containing compounds. The mechanism of decomposition of *tert*-alkyl peroxypivalates has been studied by use of a nitroxyl compound to trap the radicals formed (93). The behavior of peroxyesters under pressure has been investigated (94–98).

Peroxyesters, particularly those with α-hydrogens or conjugated double bonds, are susceptible to induced decomposition under certain conditions, but they are generally less susceptible than diacyl peroxides. Lower molecular weight peroxyesters that have some water solubility can be hydrolyzed.

The more selective nature of the radicals produced by *tert*-amyl peroxyesters and other *tert*-amyl peroxides has led to their use in commercial polymer applications requiring discriminating radicals, such as polyol grafting and high solids acrylic resin production (99,100). *tert*-Amyl peroxides have been replacing aliphatic α-cyanoazo initiators in these applications. Owing to their diverse structures and associated reactivities, peroxyesters are also used in many other applications, including polymerization of ethylene, vinyl chloride, styrene and acrylate esters, and curing of unsaturated polyester resins.

Monoperoxycarbonates. Some commercially available *OO-tert*-alkyl *O*-alkyl monoperoxycarbonates and their corresponding 10-h half-life temperature (determined in dodecane) are listed in Table 2 (92). Monoperoxycarbonates are related to peroxyesters and also generate alkoxy radicals, ·OR′, which again as above can undergo β-scission.

$$RO-\overset{\overset{O}{\|}}{C}-OOR' \longrightarrow RO-\overset{\overset{O}{\|}}{C}-O\cdot + \cdot OR' \qquad (26)$$

Changing the structure of R′ affects the activity of monoperoxycarbonates as previously discussed for peroxyesters. The other cogenerated radical is an alkoxycarbonyloxy radical. The nature of the R group has practically no effect on the reactivity of monoperoxycarbonates having the same *OO-tert*-alkyl group. The 10-h half-life temperature remains at 100°C for almost all *OO-tert*-butyl *O*-alkyl monoperoxycarbonates.

Monoperoxycarbonates are similar in thermal stability to *t*-alkyl peroxybenzoates and can be used in applications where there is concern that benzene will be formed as a by-product of peroxybenzoate initiation. For example, *OO-tert*-butyl *O*-(2-ethylhexyl) monoperoxycarbonate [34443-12-4], with a 10-h half-life temperature of 99°C, can be used in place of *tert*-butyl peroxybenzoate, with a 10-h half-life temperature of 104°C, for the polymerization of styrene with only slight changes in reaction conditions.

Recently, poly(monoperoxycarbonates) have been introduced for the commercial polymerization of vinyl monomers (101). They provide improved productivity in existing polymerization processes. Perhaps more interesting are possibilities of

Table 5. Commercial Diperoxyketals

Name	CAS registry number	Structure	10-h $t_{1/2}$, °C[a,b]
Ethyl 3,3-di(*tert*-amylperoxy)butyrate	[67567-23-1]	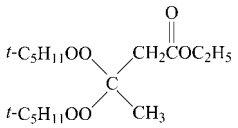	112
n-Butyl 4,4-di(*tert*-butylperoxy)valerate	[995-33-5]	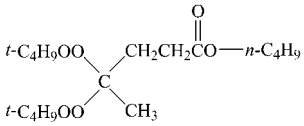	109
1,1-Di(*tert*-butylperoxy)cyclohexane	[3006-86-8]	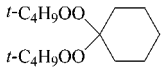	97
1,1-Di(*tert*-amylperoxy)cyclohexane	[15667-10-4]	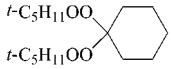	93

[a]Temperature at which $t_{1/2} = 10$ h.
[b]In dodecane.

forming polymers with enhanced molecular weight and enhanced properties due to the formation of polyradical initiating species.

Diperoxyketals. Some commercially available di(*tert*-alkylperoxy)ketals and their corresponding 10-h half-life temperatures (determined in dodecane) are listed in Table 5 (102). Diperoxyketals thermally decompose by cleavage of only one oxygen–oxygen bond initially, usually followed by β-scission of the resulting alkoxy radicals (103–107). For acyclic diperoxyketals, β-scission produces an alkyl radical and a peroxyester.

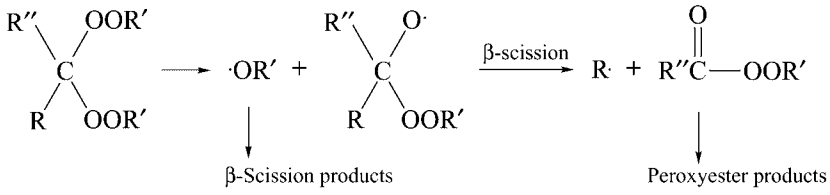

(27)

Owing to similarity of thermal stability, the peroxyester decomposes, as discussed previously. Cyclic diperoxyketals such as 1,1-di(*tert*-butylperoxy)cyclohexane cleave the cycloalkyl ring during β-scission to give an alkyl radical with an attached peroxyester group. The effect, after peroxyester decomposition, is the production of two monoradicals (·OR′), a diradical (·R′—R·), and carbon dioxide. Because of the generation of diradicals, cyclic diperoxyketals such as 1,1-di(*tert*-butylperoxy)cyclohexane are effective in enhancing polymer molecular weight or increasing polymer productivity when employed as initiators in commercial vinyl monomer polymerizations (108,109). Diperoxyketals are used commercially in styrene polymerizations, curing of elastomers, and in elevated

Table 6. Commercial Dialkyl Peroxides

Name	CAS registry number	Structure	10-h $t_{1/2}$, °C[a,b]
2,5-Di(*tert*-butylperoxy)-2,5-dimethyl-3-hexyne	[1068-27-5]	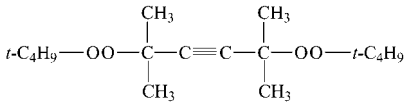	131
2,5-Di(*tert*-butylperoxy)-2,5-dimethylhexane	[78-63-7]	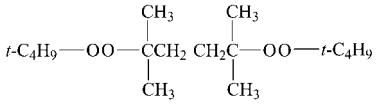	120
1,3(4)-Bis(2-(*tert*-butylperoxy)-1-methylethyl)benzene	[25155-25-3]	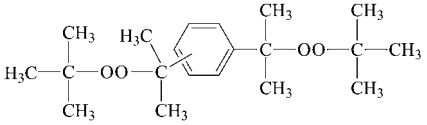	119
Di(*tert*-butyl) peroxide	[110-54-4]	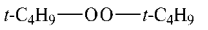	129
Di(*tert*-amyl) peroxide	[10508-09-5]	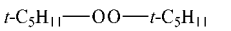	123
Dicumyl peroxide	[80-43-3]	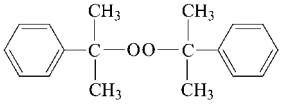	117

[a] Temperature at which $t_{1/2} = 10$ h.
[b] In dodecane.

temperature curing of unsaturated polyester resin compositions. *tert*-Amyl diperoxyketals are good initiators for acrylics, especially in the preparation of high solids coatings resins (110).

Di(*tert*-alkyl) Peroxides. Some commercially available dialkyl peroxides and their corresponding 10-h half-life temperatures in dodecane are listed in Table 6 (111). Dialkyl peroxides initially cleave at the oxygen–oxygen bond to generate alkoxy radical pairs:

$$R_3C{-}OO{-}CR_3 \longrightarrow 2\ R_3C{-}O\cdot \xrightarrow{\beta\text{-scission}} 2\ R\cdot + 2\ R_2C{=}O \qquad (28)$$

Because high temperatures are required to decompose dialkyl peroxides at useful rates, β-scission of the resulting alkoxy radicals is more rapid and more extensive than for most other peroxide types. When methyl radicals are produced from alkoxy radicals, the dialkyl peroxide precursors are very good initiators for cross-linking, grafting, and degradation reactions. When higher alkyl radicals such as ethyl radicals are produced, the dialkyl peroxides are useful in vinyl monomer polymerizations. The behavior of di(*tert*-butyl) peroxide [110-54-4] under high pressure has been investigated (112,113).

Dialkyl Peroxydicarbonates. Some commercially available dialkyl peroxydicarbonates and their corresponding 10-h half-life temperatures (determined in trichloroethylene solutions) are listed in Table 7 (114). These peroxides are active at low temperatures and initially undergo homolytic cleavage to produce

Table 7. Commercial Dialkyl Peroxydicarbonates

Name	CAS registry number	Structure	10-h $t_{1/2}$, °C[a,b]
Di(*n*-propyl) peroxydicarbonate	[16066-38-9]	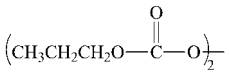	50
Di(*sec*-butyl) peroxydicarbonate	[19910-65-7]	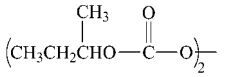	50
Di(2-ethylhexyl) peroxydicarbonate	[16111-62-9]	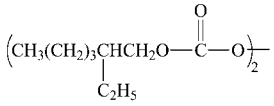	49
Di(*n*-hexadecyl) peroxydicarbonate	[26322-14-5]	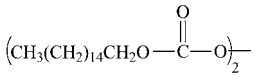	50
Di(4-*tert*-butylcyclohexyl) peroxydicarbonate	[15520-11-3]	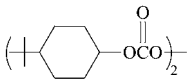	48

[a] Temperature at which $t_{1/2} = 10$ h.
[b] In trichloroethylene (TCE).

alkoxycarbonyloxy radical pairs that may subsequently decarboxylate to produce alkoxy radicals:

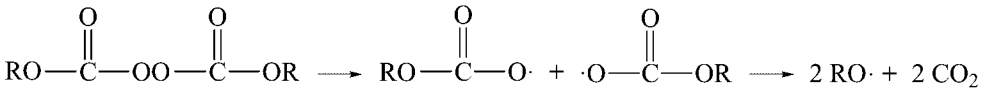

(29)

Table 7 shows that the nature of the alkyl group, whether primary alkyl, secondary alkyl, or cycloalkyl, does not affect the 10-h half-life temperatures of dialkyl peroxydicarbonates in trichloroethylene (TCE) [79-01-6]. All peroxydicarbonates have about the same 10-h half-life temperature in TCE (48–50°C).

As a peroxide class, dialkyl peroxydicarbonates are very susceptible to radical-induced decompositions:

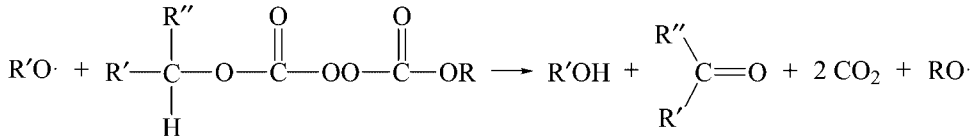

(30)

Decomposition rate studies on dialkyl peroxydicarbonates in various solvents reveal dramatic solvent effects that primarily result from the susceptibility of peroxydicarbonates to induced decompositions. These studies show a decreasing order of stability of peroxydicarbonates in solvents as follows: TCE > saturated hydrocarbons > aromatic hydrocarbons > ketones (69). Decomposition rates are lowest

Table 8. Commercial *tert*-Alkyl Hydroperoxides

Name	CAS registry number	Structure
tert-Butyl hydroperoxide	[75-91-2]	t-C_4H_9OOH
tert-Amyl hydroperoxide	[3425-61-4]	t-$C_5H_{11}OOH$
α-Cumyl hydroperoxide	[80-15-9]	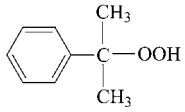
2,5-Dihydroperoxy-2,5-dimethylhexane	[3025-88-5]	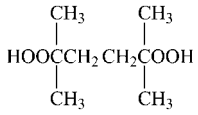
para-Menthane hydroperoxide[a]	[26762-92-5]	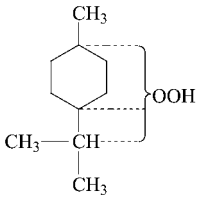
m/*p*-Isopropyl-α-cumyl hydroperoxide	[98-49-7]	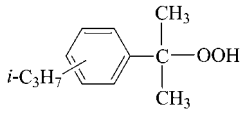

[a]The —OOH group may be attached to any of the three positions indicated.

in TCE where radicals are scavenged before they can induce the decomposition of peroxydicarbonate molecules.

Peroxydicarbonates are efficient polymerization initiators for most vinyl monomer polymerizations, especially for monomers such as acrylates, ethylene, and vinyl chloride. They are particularly good initiators for less reactive monomers such as those containing allyl groups. They are also effective for curing of unsaturated polyester molding resins. In order to increase the shipping and handling safety of peroxydicarbonates, stabilized formulations have been developed and commercialized (115–120).

***tert*-Alkyl Hydroperoxides.** Some commercially available *tert*-alkyl hydroperoxides (121) are listed in Table 8. Hydroperoxides can decompose thermally to initially form alkoxy and hydroxy radicals:

$$\mathrm{ROOH} \longrightarrow \mathrm{RO}\cdot + \cdot\mathrm{OH} \qquad (31)$$

However, because of the high temperature nature of this class of peroxides (10-h half-life temperatures of 133–172°C) and their extreme sensitivities to radical-induced decompositions and transition-metal activation, hydroperoxides have very limited utility as thermal initiators. The acid-promoted decomposition to produce radicals has been reported (122). The oxygen–hydrogen bond in

hydroperoxides is weak [368–377 kJ/mol (88.0–90.1 kcal/mol) BDE] and is susceptible to attack by higher energy radicals:

$$\mathrm{ROOH} + \mathrm{R'}\cdot \longrightarrow \mathrm{R'{-}H} + \mathrm{ROO}\cdot \tag{32}$$

Further reactions of the alkylperoxy radical (ROO·) depend on the environment but generally cause generation of other radicals that can attack undecomposed hydroperoxide, thus perpetuating the induced decomposition chain. Radicals also can attack undecomposed peroxide by radical displacement on the oxygen–oxygen bond:

$$\mathrm{R'}\cdot + \mathrm{ROOH} \longrightarrow \mathrm{R'OH} + \cdot\mathrm{OH} \text{ or } \mathrm{R'OH} + \mathrm{RO}\cdot \tag{33}$$

This is basically the same type of induced decomposition that occurs with other peroxide classes, eg, the dialkyl peroxydicarbonates and diacyl peroxides.

Hydroperoxides are more widely used as initiators in low temperature applications (at or below room temperature) where transition-metal (M) salts are employed as activators. The activation reaction involves electron-transfer (redox) mechanisms:

$$\mathrm{ROOH} + \mathrm{M}^{n+} \longrightarrow \mathrm{RO}\cdot + \mathrm{OH}^{-} + \mathrm{M}^{(n+1)+} \tag{34}$$

$$\mathrm{ROOH} + \mathrm{M}^{(n+1)+} \longrightarrow \mathrm{ROO}\cdot + \mathrm{H}^{+} + \mathrm{M}^{n+} \tag{35}$$

Either oxidation state of a transition metal (Fe, Mn, V, Cu, Co, etc) can activate decomposition of the hydroperoxide. Thus a small amount of transition-metal ion can decompose a large amount of hydroperoxide. Trace transition-metal contamination of hydroperoxides is known to cause violent decompositions. Because of this fact, transition-metal promoters should never be premixed with the hydroperoxide. Trace contamination of hydroperoxides (and ketone peroxides) with transition metals or their salts must be avoided.

Transition-metal ions also react with the generated radicals to convert the radicals to ions:

$$\mathrm{RO}\cdot + \mathrm{M}^{n+} \longrightarrow \mathrm{RO}^{-} + \mathrm{M}^{(n+1)+} \tag{36}$$

This reaction is one example of several possible radical–transition-metal ion interactions. The significance of this and similar reactions is that radicals are destroyed and are no longer available for initiation of useful radical reactions. Consequently, the optimum use levels of transition metals are very low. Although the hydroperoxide decomposes quickly when excess transition metal is employed, the efficiency of radical generation is poor.

Ketone Peroxides. These materials are mixtures of compounds with hydroperoxy groups and are composed primarily of the two structures shown in Table 2. Ketone peroxides are marketed as solutions in inert solvents such as nonvolatile esters. They are primarily employed in room-temperature-initiated curing of unsaturated polyester resin compositions (usually containing styrene

monomer) using transition-metal promoters such as cobalt naphthenate. Ketone peroxides contain the hydroperoxy (—OOH) group and thus are susceptible to the same hazards as hydroperoxides. By far the most popular commercial ketone peroxide is methyl ethyl ketone peroxide [1338-23-4]. Smaller quantities of ketone peroxides such as methyl isobutyl ketone peroxide [28056-59-9], cyclohexanone peroxide [12262-58-7], and 2,4-pentanedione peroxide [37187-22-7] are used commercially (123).

The cyclic trimer ketone peroxides (eg, methyl ethyl ketone peroxide cyclic trimer [24748-23-0]) have been selectively prepared in dilute solution (in a safety solvent due to the shock sensitivity of the pure peroxide) for use as unpromoted, thermal initiators (124,125). They have been shown to effectively modify polyolefins under certain conditions in a manner similar to dialkyl peroxides.

Selection of organic peroxides for various commercial applications has been reviewed (55,126,127), particularly for vinyl chloride polymerizations (72). Recent innovations in peroxide technology include new promoted systems (128,129), peroxide-containing surfactants (130–133), and peroxides bonded to inorganic fillers (134).

Inorganic Peroxides

Inorganic peroxide–redox systems have been employed for initiating emulsion homo- and copolymerizations of vinyl monomers. These systems include hydrogen peroxide–ferrous sulfate, hydrogen peroxide–dodecyl mercaptan, potassium peroxydisulfate–sodium bisulfite, and potassium peroxydisulfate–dodecyl mercaptan (85,135). Potassium peroxydisulfate [7727-21-2], $K_2S_2O_8$, (or the corresponding sodium or ammonium salt), is an inorganic peroxide that is used widely in emulsion polymerization (eg, latexes and rubbers), usually in combination with a reducing agent. Without reducing agents, the peroxydisulfate ion decomposes to give sulfate ion radicals:

$$S_2O_8^{2-} \longrightarrow 2\,{\cdot}SO_4^- \tag{37}$$

With transition-metal activators, the initiation process is postulated as

$$S_2O_8^{2-} + Fe^{2+} \longrightarrow Fe^{3+} + {\cdot}SO_4^- + SO_4^{2-} \tag{38}$$

The reaction with mercaptans is believed to generate initiating sulfur radicals:

$$K_2S_2O_8 + 2\,RSH \longrightarrow 2\,KHSO_4 + 2\,RS{\cdot} \tag{39}$$

Hydrogen peroxide, in combination with reducing agents (transition metals), also is used in those applications where its high water and low oil solubility is not a problem or is easily overcome.

Peroxide Safety. When handling and using peroxide initiators, care should be exercised since they are thermally sensitive and decompose (sometimes

violently) when exposed to excessive temperatures, especially when they are in their pure or highly concentrated states. However, they are useful as initiators because of their thermal instability. What may be a safe temperature for one peroxide can be an unsafe temperature for another, since peroxide initiators encompass a wide activity range. Because some peroxides are shock or friction sensitive in the pure state, they are generally desensitized by formulating them into solutions, pastes, or powders with inert diluents and dispersions or emulsions with aqueous diluent. All manufacturers' literature should be carefully scrutinized and the peroxide safety literature should be reviewed before handling and using specific peroxide initiator compositions (71–78,92,102,111,114,121,123,127,136–140).

Azo Compounds

Generally, the commercially available azo initiators are of the symmetrical azonitrile type:

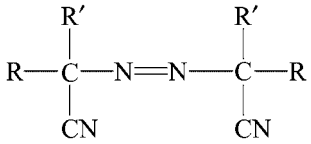

The symmetrical azonitriles are solids with limited solubilities in common solvents (141,142). Some commercial aliphatic azo compounds and their 10-h half-life temperatures are listed in Table 9.

Azo initiators decompose thermally by cleavage of the two carbon–nitrogen bonds, either stepwise or simultaneously, to form two alkyl radicals and a nitrogen molecule:

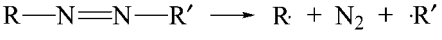

(40)

In commercial azo initiators, *tert*-alkyl-type radicals are generated, which are generally more stable than most of the radicals generated from peroxide initiators. Thus when azonitriles are used as initiators for vinyl monomer polymerizations, the primary initiator radicals generally do not abstract hydrogens from polymer backbones as can sometimes occur when peroxide initiators are employed. Therefore branch grafting is suppressed and linear polymers having reduced long-chain branching are obtained.

Azonitriles are not susceptible to radical-induced decompositions (142) and their decomposition rates are not usually affected by other components of the environment. Cage recombination of the alkyl radicals occurs when azo initiators are used, and results in the formation of toxic tetrasubstituted succinonitrile derivatives (142). This can be a significant drawback to the use of azo initiators. In contrast to some organic peroxides, azonitrile decomposition rates show only minor solvent effects (141,142) and are not affected by transition metals, acids, bases, and many other contaminants. Thus azonitrile decomposition rates are predictable. Azonitriles can be used as thermal initiators for curing resins that

Table 9. Commercial Azo Initiators

Name	CAS registry number	Structure	10-h $t_{1/2}$, °C[a]	Solvent
2,2′-Azobis(4-methoxy-2,4-dimethylpentanenitrile)	[15545-97-8]	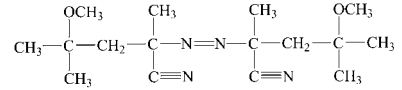	33	toluene
2,2′-Azobis(2,4-dimethylpentanenitrile)	[4419-11-8]	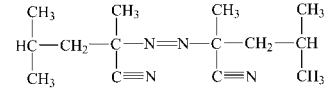	52	toluene
2,2′-Azobis(isobutyronitrile)	[78-67-1]	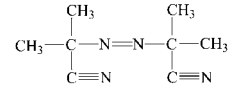	64	toluene
2,2′-Azobis(2-methylbutyronitrile)	[13472-08-7]	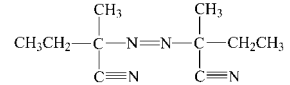	67	trimethylbenzene
1,1′-Azobis(cyclohexanecarbonitrile)	[2094-98-6]	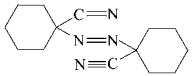	88	toluene
4,4′-Azobis(4-cyanovaleric acid)	[2638-94-0]	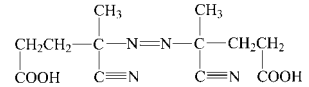	66	water
Dimethyl 2,2′-azobis(2-methylpropionate)	[2589-57-3]	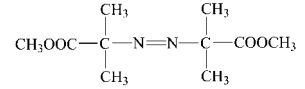	66	toluene
Azobis(2-acetoxy-2-propane)	[40888-97-9]	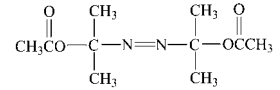	189	benzene
2,2′-Azobis(2-amidinopropane) dihydrochloride	[2997-92-4]	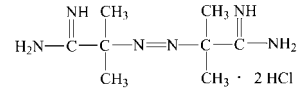	56	toluene

[a]Temperature at which $t_{1/2} = 10$ h.

contain a variety of extraneous materials since cure rates are not affected. In addition to curing of resins, azonitriles are used for polymerization of commercial vinyl monomers.

tert-Amyl peroxides are viable commercial alternatives to azo initiators and can produce low energy ethyl radicals that are similar in initiating and hydrogen-abstracting properties to those produced by aliphatic azo compounds. *tert*-Amyl peroxides have been replacing aliphatic azo compounds in many commercial polymer applications, eg, production of high solids acrylic resins (99,100).

Care should be exercised in handling and using azo initiators in their pure and highly concentrated states because they are thermally sensitive and can decompose rapidly when overheated. Although azonitriles are generally less sensitive to contaminants, the same cautions that apply to peroxides should also be applied to handling and using azo initiators. The manufacturers' safety literature should be read carefully (141). The potential toxicity hazards of decomposition products must be considered when using azonitriles. Such hazards are present primarily when pure or highly concentrated azonitrile solutions are decomposed in poorly ventilated areas. The chemistry of aliphatic azo compounds has been reviewed (15,143–146).

Carbon–Carbon Initiators

Carbon–carbon initiators are hexasubstituted ethanes that undergo carbon–carbon bond scission when heated to produce radicals. The thermal stabilities of the hexasubstituted ethanes decrease rapidly with increasing size of the alkyl groups (147). The 10-h half-life temperature range of this class of initiators is very broad, extending from about 100°C to well above 600°C. An extensive compilation of half-life data on carbon–carbon initiators has been published (147). The commercially available carbon–carbon initiators are tetrasubstituted 1,2-diphenylethanes that undergo homolyses to generate low energy, *tert*-aralkyl radical pairs:

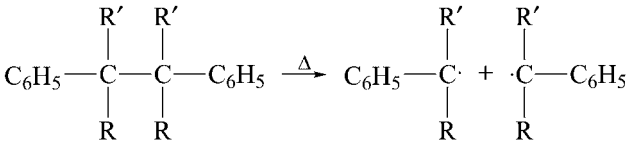

(41)

Three carbon–carbon initiators are currently available commercially: 2,3-dimethyl-2,3-diphenylbutane [1889-67-4] (**1**), 3,4-dimethyl-3,4-diphenylhexane [10192-93-5] (**2**), and poly(1,4-diisopropylbenzene) [25822-43-9] (**3**).

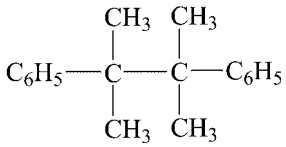

(**1**)

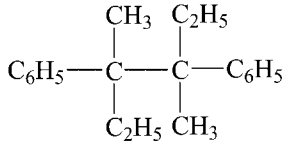

(**2**)

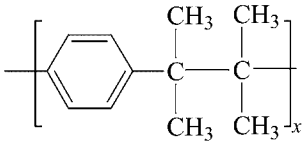

(**3**)

Initiators (**1**) and (**2**) have 10-h half-life temperatures of 237 and 201°C, respectively. It has been reported that, unlike organic peroxides and aliphatic azo compounds, carbon–carbon initiators (**1**) and (**2**) undergo endothermic decompositions (54). These carbon–carbon initiators are useful commercially as fire-retardant synergists in fire-resistant expandable polystyrenes (148). Accelerators for the thermal decomposition of diphenylethane initiators have been reported (149).

Initiators for Mediated Radical Reactions

Recently, there has been considerable interest in controlling the generation of free radicals in polymerization reactions both initially and throughout the course of the reaction (150). There are many reasons for this: controlling the polydispersity of the polymer formed ($M_n/M_w < 1.5$), control of polymer end groups, prevention of side reactions, preparation of block copolymers, chemical control of the reaction kinetics, design of new polymer architectures, and controlled graft modification of polyolefins (151,152).

Early work to control radical polymerization involved initiators that generated one radical capable of initiating a polymer-forming chain reaction and one radical that reversibly reacted with the propagating polymer radical. This reversible termination established an equilibrium between propagating and dormant polymer chains, and retarded irreversible termination reactions such as coupling and disproportionation. An initiator that provided mediated polymerization was called an *iniferter*, a combination of *ini*tiator, trans*fer* agent, and *ter*minator. Known photochemical iniferters are sulfides and disulfides (particularly thiuram disulfides, eg, tetraethylthiuram disulfide [97-77-8]). Thermal iniferters can be carbon–carbon initiators (eg, tetraphenylethanes, *vide supra*) and certain azo compounds (eg, phenylazotriphenylmethane [981-18-0]). Using iniferters, telomers, block copolymers, and other polymer architectures have been prepared using free-radical reactions (153,154).

More recently, refinements and new approaches for controlling radical polymerization have been described (155). Two of the most studied methods feature either stable counter-radicals, eg, nitroxyl-mediated polymerization (NMP), or reversible activation of carbon–halogen bonds by transition-metal species in a

process called atom-transfer radical polymerization (ATRP) (see LIVING RADICAL POLYMERIZATION).

In NMP, the nitroxyl radicals, either alone or in the presence of additional modifiers, react reversibly with the propagating polymer radical to establish an equilibrium between active and dormant propagating radicals present in the system (156):

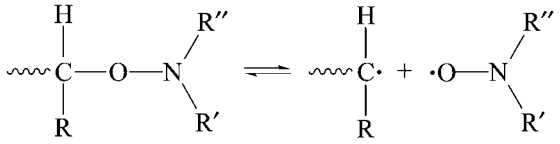

(42)

New monomer units are thus added to the active radicals of the growing chain in a controlled manner, and when the monomer is completely consumed the usual termination reactions (coupling and disproportionation) are prevented by the presence of the nitroxyl, allowing the polymer chain to continue "living." Thus, in effect, each growing polymer chain becomes a polymerization initiator for continued reaction according to the equilibrium between dormant and active species, which is controlled by the structures of the polymer and nitroxyl radicals, the solvent, and the temperature (157–164). The resulting product from nitroxyl-mediated polymerization of a single monomer can be used as a macroinitiator for copolymerizing one or more new monomers, resulting in block copolymers or other designed molecular architectures.

NMP can be achieved in either of two ways: (*1*) by adding a stable nitroxyl radical to the polymerization reaction initiated by traditional initiators (peroxides or azo compounds) to generate an alkoxyamine *in situ*, or (*2*) by preparing an alkoxyamine to be used as the initiator. Two widely studied examples of stable nitroxyl radicals are 2,2,6,6-tetramethylpiperidinyl-1-oxyl [2564-83-2] (**4**, TEMPO) or 4-substituted derivatives thereof and *N*-*tert*-butyl-*N*-[1-(diethylphosphono)-2,2-dimethylpropyl]nitroxide [188526-94-5] (**5**) (165–172).

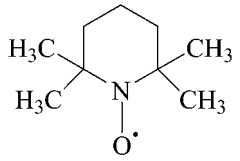

(**4**)

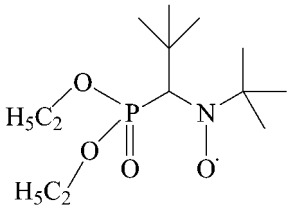

(**5**)

Many mono- and poly(*N*-alkoxyamines) have been synthesized and investigated in NMP reactions (161,173–185). Halogen-terminated polymers have been converted into alkoxyamine macroinitiators (186).

NMP has been studied mostly for polymerization of styrene and acrylates. It is limited in its application because of the equilibrium conditions, particularly high temperature, required to achieve a reasonable polymerization rate. A variation of this system does not use conventional free-radical initiators, using instead only the nitroxyl compound, an alkyl or aryl metal compound (such as an alkyl aluminum), and an appropriate strongly binding ligand (187). Nitroxyl-mediated polymerizations can be promoted by organic acids (188,189), organic salts (190), and acylating agents (191).

In ATRP, the growing polymer radical is deactivated to prevent termination reactions by reversible transfer of an atom or group (eg, halogen) between the propagating polymer radical and a transition-metal compound, thus providing controlled, equilibrium concentrations of growing polymer chains and dormant chains:

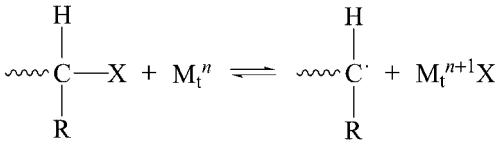

(43)

In this equation M_t^n represents a transition metal of valence n and X represents a halogen atom. The most studied system of this type involves three components: an alkyl or aryl halide, a metal catalyst, and specific ligands (192–195), eg, 1-phenylethyl chloride [672-65-1], copper(I) chloride, and 2,2′-bipyridine [366-18-7]. In these systems, concentrations of propagating and dormant species must be carefully controlled for successful polymerization and narrow polydispersity to be achieved. The concept of "reverse" ATRP, involving conventional peroxide and azo initiators and the oxidized form of the metal catalyst [eg, copper(II) chloride], has also been reported (196). Like NMP, ATRP has been studied mostly for the polymerization of styrene and acrylic monomers, although other monomers have been polymerized successfully, eg, vinylidene difluoride (197). Other metal catalysts have been reported, such as bis(ortho-chelated) arylnickel(II) complexes (198) and porphyrin cobalt(III) organometallic complexes (199).

Various other approaches to mediated radical polymerization have been investigated. A living system has been reported, wherein borinate radicals react reversibly with the growing chain and are generated by autoxidation of trialkylboranes through an alkylperoxyborane intermediate (200). Organochromium–macrocyclic polyamine systems and peroxide–trialkylphosphite systems (201) have also been investigated. Photochemical-mediated systems involving polymerization of acrylate monomer using alkyl cobaloximes as photoinitiators have been reported (202).

Other Radical Generating Systems

There are many chemical methods for generating radicals reported in the literature, that involve unconventional initiators (91,203–224). Most of these radical-generating systems cannot broadly compete with the use of conventional initiators

in industrial polymer applications owing to cost or efficiency considerations. However, some systems may be well-suited for initiating specific radical reactions or polymerizations, eg, grafting of monomers to cellulose using ceric ion (225).

Initiation through Radiation and Photoinitiators

High energy ionizing radiation sources (eg, x-rays, γ-rays, α-particles, β-particles, fast neutrons, and accelerator-generated electrons) can generate radical sites on organic substrates (226). If the substrate is a vinyl monomer, radical polymerization can occur (227). If the substrate consists of a polymer and a vinyl monomer, then polymer cross-linking, degradation, grafting of the monomer to the polymer, and polymerization of the monomer can all occur (228). Radical polymerizations of vinyl monomers with ionized plasma gases have been reviewed (229). Ultrasonic polymerization of vinyl monomers using special initiators (eg, dodecanethiol) has been described (230).

Initiation of radical reactions with uv radiation is widely used in industrial processes (231). In contrast to high energy radiation processes where the energy of the radiation alone is sufficient to initiate reactions, initiation by uv irradiation usually requires the presence of a photoinitiator, ie, a chemical compound or compounds that generate initiating radicals when subjected to uv radiation. There are two types of photoinitiator systems: those that produce initiator radicals by intermolecular hydrogen abstraction and those that produce initiator radicals by photocleavage (232–239).

In the case of intermolecular hydrogen abstraction, a hydrogen (H) atom donor is required. Typical donors have an active H atom positioned alpha to an oxygen or nitrogen, eg, alcohols (R_2CHOH), ethers (R_2CHOR), and *tert*-amines (R_2CHNR_2), or an active H atom directly attached to sulfur, eg, thiols (RSH). Some of the commercial photoinitiators that undergo intermolecular H abstraction from the H atom donor upon excitation by uv radiation are listed in Table 10. A reaction illustrating this photoinitiation process is given below for benzophenone (photoinitiator) and an alcohol (H atom donor):

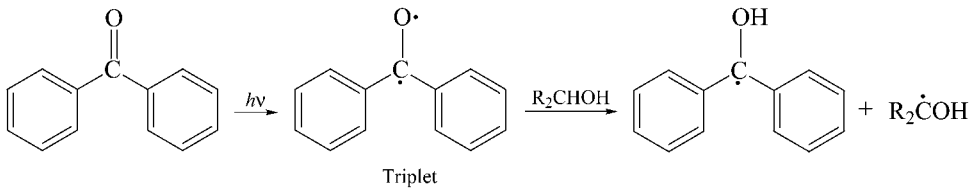

(44)

Upon exposure to uv light, ground-state benzophenone is excited to the triplet state (a diradical), which abstracts an alpha H atom from the alcohol, resulting in the formation of two separate initiating radicals. With amine H atom donors, an electron transfer may precede the H transfer, as in triplet exciplex formation between benzophenone and amine (eq. 46):

Table 10. Photoinitiators That Abstract Hydrogen

Name	CAS registry number	Structure
Benzophenone	[119-61-9]	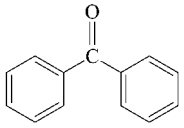
4-Phenylbenzophenone	[2128-93-0]	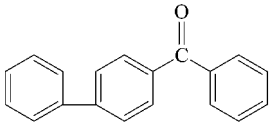
Xanthone	[90-47-1]	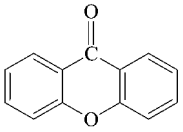
Thioxanthone	[492-22-8]	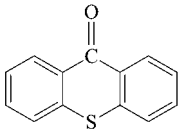
2-Chlorothioxanthone	[86-39-5]	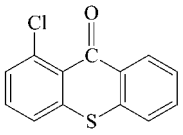
4,4′-Bis(*N*,*N*′-dimethylamino) benzophenone (Michler's ketone)	[90-94-8]	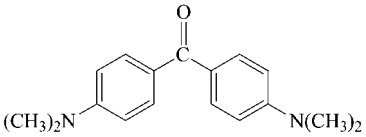
Benzil	[134-81-6]	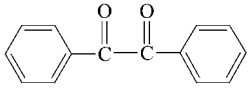
9,10-Phenanthraquinone	[84-11-7]	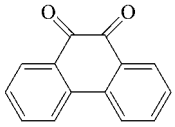
9,10-Anthraquinone	[84-65-1]	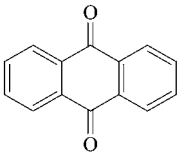

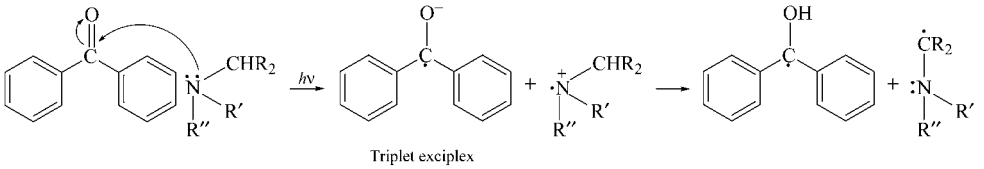

(45)

Some commercial photoinitiators (Table 11) undergo a photocleavage to form two initiating radical fragments directly, eg, benzoin ethers:

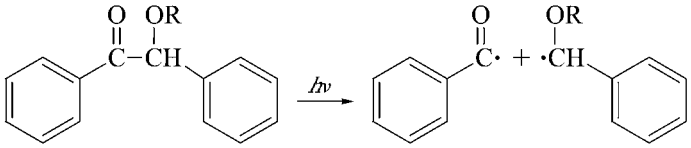

(46)

In many photoinitiated processes, a photosensitizer may be used. A photosensitizer absorbs light and subsequently transfers the absorbed energy to an energy acceptor, which then can produce initiator radicals by H abstraction or by photocleavage. The energy-transfer agent (photosensitizer) usually undergoes no net change. A variety of photosensitizers have been used such as eosin, chlorophyll, methylene blue, and thioxanthone. In photosensitized processes, the energy acceptor often is referred to as a co-initiator. These co-initiators do not absorb light but accept energy from the excited photosensitizer, which distinguishes them from the photoinitiators listed in Tables 10 and 11. Typical co-initiators that undergo H abstraction are the H donors mentioned above. An example of a co-initiator undergoing photocleavage is quinoline-8-sulfonyl chloride [18704-37-5] photosensitized by thioxanthone (233).

The peroxide and azo thermal initiators also are photochemically unstable and have been used as radical sources at well below their normal thermal decomposition temperatures. However, their industrial use as photoinitiators has been limited because their light-absorption characteristics frequently are unsuitable and because of the obvious potential complication owing to their slow thermal decomposition, which leads to poor shelf life and nonreproducible photoactivity in given formulations (237).

Economic Aspects

The principal worldwide producers of organic peroxide initiators (trade names and available Internet addresses) are Atofina Chemicals, Inc. (Lupersol, Luperox, http://www.luperox.com); Akzo Nobel (Trigonox, Perkadox, Cadox, Cadet, Laurox, Liladox, Kenodox, Lucidol, Butanox, Cyclonox, http://www.polymerchemicals.com); Degussa-Hüls AG (formerly LaPorte companies), which includes Aztec Peroxides, Inc. (in the United States) (Aztec) and Peroxid-Chemie GmbH (in Europe) (Interox) (http://www.degussa-initiators.com, http://www.laporteplc.com); Crompton Corp. (formerly Witco Corp.) (Esperox, Esperal, USP, Quickset, Hi Point, http://www.cromptoncorp.com); Nippon Oil & Fats Co.

Table 11. Photoinitiators That Undergo Photocleavage

Name	CAS registry number	Structure
α,α-Dimethyl-α-hydroxyacetophenone	[7473-98-5]	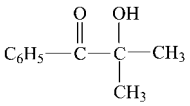
1-(1-Hydroxycyclohexyl)phenylmethanone	[947-19-3]	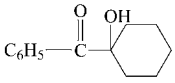
Benzoin methyl ether	[3524-62-7]	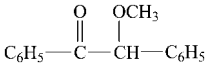
Benzoin ethyl ether	[574-09-4]	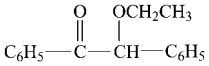
Benzoin isobutyl ether	[22499-12-3]	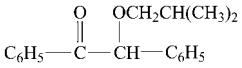
α,α-Dimethoxy-α-phenylacetophenone	[24650-42-8]	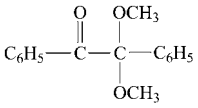
α,α-Diethoxyacetophenone	[6175-45-7]	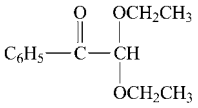
1-Phenyl-1,2-propanedione, 2-(*O*-benzoyl)oxime	[17292-57-8]	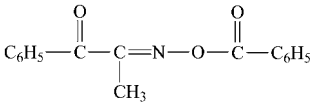
Diphenyl(2,4,6-trimethylbenzoyl) phosphine oxide	[75980-60-8]	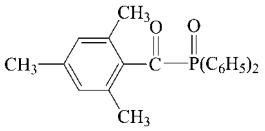
α-Dimethylamino-α-ethyl-α-benzyl-3,5-dimethyl-4-morpholinoacetophenone	[119313-12-1]	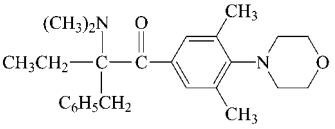

(Nyper, Perbutyl, Percumyl, Perhexa, Permek, Peroyl, http://www.nof.co.jp); The Norac Company, Inc. (Benox, Norox, http://www.norac.com); and GEO Specialty Chemicals (formerly Hercules Inc.). (DiCup, VulCup, http://www.geosc.com). Worldwide the three leading producers of organic peroxides are Akzo Nobel, Atofina Chemicals Inc., and Degussa-Hüls (formerly LaPorte). Sales volumes and value are difficult to estimate because of the many initiator formulations and dilutions that are available. Particularly for dialkyl peroxides, there are many small formulators and distributors that purchase a peroxide from a primary

manufacturer and formulate it for a particular end-use application. Approximate North American sales of organic peroxide initiators in 2000 were valued at $\sim\$300 \times 10^6$; worldwide sales were valued at $\sim\$800 \times 10^6$.

The principal worldwide producers of organic azo initiators (trade names, Internet address) are DuPont (Vazo, http://www.dupont.com/vazo/), Atofina Chemical Inc. (AZDN, http://www.atofinachemicals.com), and Wako Pure Chemical Industries, Ltd. (Wako, http://www.wako-chem.co.jp/egaiyo/). The worldwide market for organic azo initiators is small, being only about 10% of the market for organic peroxide initiators.

Ciba Speciality Chemicals, Inc. (Darocur, Irgacure, http://www.cibasc.com) and Sartomer (distributor of Lamberti S.p.A. Esacure photoinitiators, http://www.sartomer.com, http://www.esacure.com) are significant suppliers of photoinitiators. Ciba Specialty Chemicals supplies alkoxyamines (Chimassorb). Nitroxyl radicals are available from Aldrich and Degussa-Hüls. Sales figures on photoinitiators are not readily available. The market for these initiators has been reviewed (240). Because most of the consumption of organic peroxides and azo initiators is in the developed countries, market growth in 2000 and beyond is expected to be modest, ie, 2–3% annually.

BIBLIOGRAPHY

1. D. Griller and K. U. Ingold, *Acc. Chem. Res.* **9**(1), 13 (1976).
2. C. H. Bamford, in H. F. Mark, N. M. Bikales, C. G. Overberger, G. Menges, J. I. Kroschwitz, eds., Encyclopedia of Polymer Science and Engineering, 2nd ed., Vol. **13**, Wiley-Interscience, New York, 1988, pp. 708–867.
3. W. A. Pryor, ed., *Organic Free Radicals* (ACS Symposium Series, Vol. **69**), American Chemical Society, Washington, D.C., 1978.
4. J. M. Hay, *Reactive Free Radicals*, Academic Press, Inc., New York, 1974.
5. J. K. Kochi, ed., *Free Radicals*, Vol. **I**, John Wiley & Sons, Inc., New York, 1973.
6. J. K. Kochi, ed., *Free Radicals*, Vol. **II**, John Wiley & Sons, Inc., New York, 1973.
7. C. Walling, *Free Radicals in Solution*, John Wiley & Sons, Inc., New York, 1957.
8. W. G. Lloyd, *CHEMTECH* 176 (Mar. 1971); *CHEMTECH* 371 (June 1971); *CHEMTECH* 687 (Nov. 1971); *CHEMTECH* 182 (Mar. 1972).
9. J. M. Tedder and J. C. Walton, *Acc. Chem. Res.* **9**, 183 (1976).
10. W. A. Pryor, *Chem. Eng. News* 70 (Jan. 15, 1968).
11. I. P. Gragerov, *Russ. Chem. Rev.* **38**, 626 (1969).
12. K. U. Ingold, *Free Radical Substitution Reactions*, Wiley-Interscience, New York, 1971.
13. E. S. Huyser, *Free Radical Chain Reactions*, Wiley-Interscience, New York, 1970.
14. G. Sosnovsky, *Free Radical Reactions in Preparative Organic Chemistry*, Macmillan, New York, 1964.
15. C. Walling, in N. H. Jaffrey, ed., *Energetics of Organic Free Radicals, (Struct. Energ. React. Chem. Ser.*, Vol. **4**), Chapman & Hall, New York, 1996, p. 1.
16. G. Moad and D. H. Solomon, *The Chemistry of Free Radical Polymerization*, Pergamon Press, London, 1995, pp. 7–41.
17. R. P. T. Chung and D. H. Solomon, *Prog. Org. Coat.* **21**, 227 (1992).
18. J. Fossey, D. Lefort, and J. Sorba, *Free Radicals in Organic Chemistry*, John Wiley & Sons, Inc., New York, 1995.

19. D. P. Curran, in B. M. Trost and I. Fleming, eds., *Comprehensive Organic Synthesis*, Pergamon Press, New York, 1991, Vol. **4**, Chapt. "4.2.6".
20. J. C. Bevington, *Makromol. Chem., Macromol. Symp.* **10/11**, 89 (1987).
21. A. A. Zavitsas, *J. Am. Chem. Soc.* **94**, 2779–2788 (1972).
22. R. T. Sanderson, *J. Am. Chem. Soc.* **97**, 1367 (1975).
23. D. M. Golden and S. W. Benson, *Chem. Rev.* **69**, 125 (1969).
24. P. Gray, A. A. Herod, and A. Jones, *Chem. Rev.* **71**, 247 (1971).
25. J. M. Tedder, *Tetrahedron* **38**, 313 (1982).
26. Y. P. Tsentalovich and co-workers, *J. Phys. Chem., Part A* **102**, 7975 (1998).
27. C. Walling and P. J. Wagner, *J. Amer. Chem. Soc.* **86**, 3368 (1964).
28. C. Walling and P. J. Wagner, *J. Amer. Chem. Soc.* **85**, 2333 (1963).
29. J. D. Bacha and J. K. Kochi, *J. Org. Chem.* **30**, 3272 (1965).
30. D. V. Avila and co-workers, *J. Amer. Chem. Soc.* **115**, 466 (1993).
31. J. M. Tedder and J. C. Walton, *Tetrahedron* **36**, 701 (1980).
32. D. Lefort, *New J. Chem.* **16**, 219 (1992).
33. C. Rüchardt, *Free Rad. Res. Comms.* **2**(4–6), 197 (1987).
34. P. G. Mekarbane and B. J. Tabner, *Magn. Reson. Chem.* **36**, 826 (1998).
35. P. G. Mekarbane and B. J. Tabner, *Macromolecules* **32**, 3620 (1999).
36. P. G. Mekarbane and B. J. Tabner, *Magn. Reson. Chem.* **38**(3), 183 (2000).
37. A. D. Jenkins, *Polymer* **40**, 7045 (1999).
38. Y. Watanabe and co-workers, *Polym. J.* **29**, 940 (1997).
39. Y. Watanabe and co-workers, *Chem. Lett.* 1993, 1089.
40. Y. Watanabe and co-workers, *Polym. J.* **29**, 366 (1997).
41. Y. Watanabe and co-workers, *Polym. J.* **29**, 192 (1998).
42. Y. Watanabe and co-workers, *Polym. J.* **29**, 693 (1997).
43. Y. Watanabe and co-workers, *Polym. J.* **29**, 733 (1997).
44. Y. Watanabe and co-workers, *Polym. J.* **29**, 603 (1997).
45. W. K. Busfield and co-workers, *Poly. Adv. Technol.* **9**, 94 (1998).
46. T. Nakamura and co-workers, *Polymer* **40**, 1395 (1999).
47. T. Nakamura and co-workers, *J. Org. Chem.* **62**, 5578 (1997).
48. W. K. Busfield, I. D. Grice, and I. D. Jenkins, *Polym. Int.* **27**, 119 (1992).
49. P. G. Griffiths, E. Rizzardo, and D. H. Solomon, *J. Macromol. Sci., A: Chem.* **17**(1), 45 (1982).
50. C. Rüchardt, *Top. Curr. Chem.* **88**, 1 (1980).
51. K. E. J. Barrett, *J. Appl. Polym. Sci.* **11**, 1617 (1967).
52. J. C. Masson, in J. Brandrup and E. H. Immergut, eds., *Polymer Handbook*, 3rd ed., John Wiley & Sons, Inc., New York, 1989.
53. *Organic Peroxides & Specialty Chemicals*, General Catalog, Atofina Chemical, Inc., Philadelphia, Pa., Apr. 1997. Internet URL: http://www.atofinachemicals.com/orgper/Products.cfm.
54. *Initiators for Polymer Production—Product Catalog*, Akzo Chemicals, Inc., Chicago, Ill. Internet URL: http://www.polymerchemicals.com.
55. Technical Publication, *HALFLIFE—Peroxide Selection Based on Half—Life*, 2nd ed., and Copyrighted Software, Elf Atochem North America, Inc., Philadelphia, Pa. Internet URL: http://www.atofinachemicals.com/orgper/software.cfm.
56. J. M. Tanko and N. Kamrudin Suleman, in Ref. 15, p. 224.
57. S. Patai, ed., *The Chemistry of Peroxides*, John Wiley & Sons, Inc., New York, 1983.
58. S. Patai, ed., *Supplement E2: The Chemistry of Hydroxyl, Ether and Peroxide Groups*, John Wiley & Sons, Inc., New York, 1993.
59. W. Ando, ed., *Organic Peroxides*, John Wiley & Sons, Inc., New York, 1992.
60. A. G. Davies, *Organic Peroxides*, Butterworths, London, 1961.

61. E. G. E. Hawkins, *Organic Peroxides*, E. and F. F. Spon Ltd., London, 1961.
62. A. V. Tobolsky and R. B. Mesrobian, *Organic Peroxides*, Interscience Publishers, New York, 1954.
63. D. Swern, ed., *Organic Peroxides*, Vol. **I**, Wiley-Interscience, New York, 1970.
64. D. Swern, ed., *Organic Peroxides*, Vol. **II**, Wiley-Interscience, New York, 1971.
65. D. Swern, ed., *Organic Peroxides*, Vol. **III**, Wiley-Interscience, New York, 1972.
66. H. Klenk, P. H. Götz, R. Seigmeier, and W. Mayr, in B. Elvers, S. Hawkins, and G. Schultz, eds., Ullmann's Encyclopedia of Industrial Chemistry, Vol. **A19**, VCH Verlagsgellschaft GmbH, Weinheim, Germany, 1991, pp. 199–233.
67. G. Moad and D. H. Solomon, in G. Allen and co-workers, eds., *Comprehensive Polymer Science*, Vol. **3**, Pergamon Press, Elmsford, N.Y., 1989, pp. 97–121.
68. J. Sanchez and T. N. Myers, in J. I. Kroschwitz, ed., *Encyclopedia of Chemical Technology*, 4th ed., Vol. **18**, John Wiley & Sons, Inc., New York, 1996, pp. 230–310.
69. *Current Polymerization Catalysts—Peroxide, Azo and Other Initiators*, Multiclient Study, Catalyst Consultants, Inc., Spring House, Pa., Nov. 1991.
70. P. Callais and co-workers, *Plast. Compound.* **15**(1), 49 (1992).
71. *Meeting Customer Needs for Organic Peroxides*, Organic Peroxides, Atofina Chemicals, Inc., Philadelphia, Pa.
72. *Selection Guide for PVC*, Organic Peroxides, Atofina Chemicals, Inc., Philadelphia, Pa.
73. *Peroxide Selection Guide for Molding Unsaturated Polyester Resins at Elevated Temperatures*, Organic Peroxides, Atofina Chemicals, Inc., Philadelphia, Pa.
74. *Recent Research and Development in the Field of Reactive Processing*, Organic Peroxides, Atofina Chemicals, Inc., Philadelphia, Pa.
75. *Lower Temperature Organic Peroxide Crosslinking Agents*, Organic Peroxides, Atofina Chemicals, Inc., Philadelphia, Pa.
76. *Chemical Curing of Elastomers and Crossing of Thermoplastics*, Organic Peroxides, Atofina Chemicals, Inc., Philadelphia, Pa.
77. *Crosslinking Elastomers with Improved Productivity Using Novel Scorch Resistant Peroxide Formulations*, Organic Peroxides, Atofina Chemicals, Inc., Philadelphia, Pa.
78. *Diacyl Peroxides*, Product Bulletin, Organic Peroxide, Atofina Chemical, Inc., Philadelphia, Pa. Internet URL: http://www.atofinachemicals.com/orgper/diacyl.cfm.
79. G. Moad, E. Rizzardo, and D. H. Solomon, *Makromol. Chem., Rapid Commun.* **3**, 533 (1982).
80. C. Hinton, *Chem. N. Z.* **62**(6), 12 (1998).
81. M. Buback and C. Hinton, *Z. Phys. Chem.* **199**, 229 (1997).
82. M. Buback and C. Hinton, *Z. Phys. Chem.* **193**(1/2), 61 (1996).
83. Ref. 2, pp. 766–767.
84. U.S. Pat. 3,629,220 (Dec. 21, 1971), J. Sanchez (to Atofina Chemicals, Inc., formerly Pennwalt Corp.).
85. H. F. Mark, in N. M. Bikales, ed., Encyclopedia of Polymer Science and Technology, Vol. **3**, Wiley-Interscience, New York, 1965, pp. 26–34.
86. Z. Florjanczyk and M. Siudakiewicz, *J. Polym. Sci., Part A: Polym. Chem.* **24**, 1849 (1986).
87. M. Lee and Y. Minoura, *J. Chem. Soc., Faraday Trans. I* **74**, 1726 (1978).
88. G. Moad, E. Rizzardo, and D. H. Solomon, *Tetrahedron Lett.* **22**, 1165 (1981).
89. W. Zhang, B. Dong, and J. Zhou, *Reguxing Shuzhi* **14**(3), 14 (1999).
90. Jpn. Pat. Appl. 02/279759 (Nov. 15, 1990), S. Furusawa and co-workers, (to Mitsui Chemicals, Inc.).
91. C. H. Bamford, in Ref. 67, pp. 123–139.
92. *Peroxyesters*, Product Bulletin, Organic Peroxides, Atofina Chemicals, Inc., Philadelphia, Pa. Internet URL: http://www.atofinachemicals.com/orgper/esters.cfm.

93. T. Nakamura and co-workers, *J. Org. Chem.* **65**, 16 (2000).
94. M. Buback and J. Sandmann, *Z. Phys. Chem.* **214**, 583 (2000).
95. M. Buback and co-workers, *Z. Phys. Chem.* **210**(2), 199 (1999).
96. J. Aschenbruecker and co-workers, *Z. Phys. Chem. B* **120**, 5552 (1998).
97. M. Buback and H. Lendle, *Z. Naturforsch., A: Phys. Sci.* **36A**, 1371 (1981).
98. P. Mehrling and co-workers, *Chem. Ber.* **118**, 240 (1985).
99. U.S. Pat. 4,777,230 (Oct. 11, 1988), V. R. Kamath (to Pennwalt Corp.).
100. P. Callais, in D. Satas, ed., *Coatings Technology Handbook*, Marcel Dekker, Inc., New York, 1991, pp. 521–527.
101. U.S. Pat. 5,760,149 (June 2, 1998), J. Sanchez and co-workers (to Atofina Chemicals, Inc., formerly Elf Atochem North America, Inc.).
102. *Peroxyketals*, Product Bulletin, Organic Peroxides, Atofina Chemicals, Inc., Philadelphia, Pa. Internet URL: http://www.atofinachemicals.com/orgper/ketals.cfm
103. Y. Sugihara and co-workers, *Bull. Chem. Soc. Jpn.* **65**, 664 (1992).
104. Y. Watanabe, K. Ohta, and S. Suyama, *Bull. Chem. Soc. Jpn.* **65**, 2063 (1992).
105. Y. Watanabe, H. Ishigaki, and S. Suyama, *Polym. J.* **24**, 257 (1992).
106. Y. Watanabe and co-workers, *Polym. J.* **24**, 971 (1992).
107. K. Matsuyama and H. Kumura, *J. Org. Chem.* **58**, 1766 (1993).
108. V. R. Kamath, *Mod. Plast.* **58**, 106, 108, 110 (Sept. 1981).
109. U.S. Pat. 4,125,695 (Nov. 14, 1978), V. R. Kamath (to Atofina Chemicals, Inc., formerly Pennwalt Corp.).
110. P. A. Callais, V. R. Kamath, and M. G. Moskal, in Proc. Water-Borne, Higher-Solids, Powder Coat. Symp., Vol. 19, (1992), p. 156.
111. *Dialkyl Peroxides*, Product Bulletin, Organic Peroxides, Atofina Chemicals, Inc., Philadelphia, Pa. Internet URL: http://www.atofinachemicals.com/orgper/dialkyl.cfm.
112. M. Buback and L. Wittkowski, *Z. Phys. Chem.* **210**(1), 61 (1999).
113. M. Buback and H. Lendle, *Z. Naturforsch., A: Phys. Sci.* **34A**, 1482 (1979).
114. *Peroxydicarbonates*, Product Bulletin, Organic Peroxides, Atofina Chemicals, Inc., Philadelphia, Pa. Internet URL: http://www.atofinachemicals.com/orgper/dicarbonates.cfm.
115. U.S. Pat. 5,548,046 (Aug. 20, 1996), J. Sanchez (to Atofina Chemicals, Inc., formerly Elf Atochem North America, Inc.).
116. U.S. Pat. 5,155,192 (Oct. 13, 1992), E. Boelema, M. C. Tammer, and J. Nuysink (to Akzo Nobel N.V.).
117. U.S. Pat. 5,714,626 (Feb. 3, 1998), C. Abma and co-workers (to Crompton Corp., formerly Witco Corp.).
118. U.S. Pat. 5,719,304 (Feb. 17, 1998), P. Frenkel and C. Abma (to Crompton Corp., formerly Witco Corp.).
119. U.S. Pat. 5,654,463 (Aug. 5, 1997), C. Abma and P. Frenkel (to Crompton Corp., formerly Witco Corp.).
120. U.S. Pat. 5,654,464 (Aug. 5, 1997), C. Abma, P. Frenkel, and L. Bock (to Crompton Corp., formerly Witco Corp.).
121. *Tertiary Alkyl Hydroperoxides*, Product Bulletin, Atofina Chemicals, Inc., Philadelphia, Pa. Internet URL: http://www.atofinachemicals.com/orgper/hydro.cfm.
122. E. Rizzardo and D. H. Solomon, *J. Macromol. Sci., A: Chem.* **11**, 1697 (1977).
123. *Ketone Peroxides*, Product Bulletin, Organic Peroxides, Atofina Chemicals, Inc., Philadelphia, Pa. Internet URL: http://www.atofinachemicals.com/orgper/ketone.cfm.
124. U.S. Pat. 5,808,110 (Sept. 15, 1998), R. Torenbeek and co-workers (to Akzo Nobel N.V.).
125. U.S. Pat. 5,907,022 (May 25, 1999), L. A. Stigter, J. Meijer, and A. P. van Swieten (to Akzo Nobel N.V.).
126. C. S. Sheppard and V. R. Kamath, *Polym. Eng. Sci.* **19**, 597 (1979).

127. C. S. Sheppard, in J. I. Kroschwitz, ed., Encyclopedia of Polymer Science and Engineering, 2nd ed., Vol. **11**, Wiley-Interscience, New York, 1988, p. 1.
128. PCT Appl. WO 99/06144 (filed Aug. 4, 1997), P. Frenkel and T. M. Pettijohn (to Crompton Corp., formerly Witco Corp.).
129. Jpn. Pat. Appl. 2000/186169 (July 4, 2000), S. Kawachi (to Kayaku Akzo Corp.).
130. U.S. Pat. 5,312,997 (May 17, 1994), M. Bohnenpoll, A. Schmidt, and H. Alberts (to Bayer Aktiengesellschaft).
131. L. Wang and X. Liu, *Macromolecules* **31**, 3446 (1998).
132. L. Wang and X. Liu, *Langmiur* **14**, 6879 (1998).
133. R. A. Moss and K. W. Alwis, *Tetrahedron Lett.* **21**, 1303 (1980).
134. U. Velten and co-workers, *Macromolecules* **32**, 3590 (1999).
135. D. C. Blackley, *Emulsion Polymerization—Theory and Practice*, John Wiley & Sons, Inc., New York, 1975, Chapt. "6", pp. 155–250.
136. *Organic Peroxides: Their Safe Handling and Use*, Atofina Chemicals, Inc., Philadelphia, Pa. Internet URL: http://www.atofinachemicals.com/orgper/safety.cfm.
137. *Safety and Handling of Organic Peroxides: A Guide*, The Organic Peroxide Producers Safety Division, The Society of the Plastics Industry, Inc., Publication # AS-109. Internet URL: http://www.plasticsindustry.org/about/organicperoxide.htm.
138. *Organic Peroxides General Information Safe Handling*, Aztec Peroxide, Inc., Publication, P3.3.1e, Sept. 1999.
139. *Suggested Relative Hazard Classification of Organic Peroxides*, Technical Publication, Organic Peroxide Producers Safety Division, The Society of the Plastics Industry, Inc., New York, 1992.
140. *The Storage and Handling of Organic Peroxides in the Reinforced Polyester Fabricating Plant*, Technical Bulletin No. 19, Organic Peroxide Producers Safety Division, The Society of the Plastics Industry, Inc., New York, 1978 revision.
141. *Du Pont Vazo Polymerization Initiators—Properties, Uses, Storage and Handling*, Product Information Bulletin, Du Pont Chemicals, Wilmington, Del., July 1984. Internet URL: http://www.dupont.com/vazo/.
142. C. S. Sheppard, in J. I. Kroschwitz, ed., Encyclopedia of Polymer Science and Engineering, 2nd ed., Vol. **2**, Wiley-Interscience, New York, 1985, pp. 143–157.
143. H. Zollinger, *Azo and Diazo Chemistry, Aliphatic and Aromatic Compounds*, Wiley-Interscience, New York, 1961, Chapts. "9" and "12".
144. S. Patai, ed., *The Chemistry of the Hydrazo, Azo, and Azoxy Groups*, John Wiley & Sons, Inc., New York, 1975.
145. C. G. Overberger, J.-P. Anselme, and J. G. Lombardino, *Organic Compounds with Nitrogen–Nitrogen Bonds*, The Ronald Press Co., New York, 1966, Chapt. "4".
146. P. A. S. Smith, *The Chemistry of Open-Chain Organic Nitrogen Compounds*, Vol. **II**, W. A. Benjamin, Inc., New York, 1966, Chapt. "11".
147. C. Rüchardt and H. Beckhaus, *Angew. Chem., Int. Ed. Engl.* **19**, 429 (1980).
148. *Polystyrene: Initiators for Styrene Polymerization*, Technical Information, Akzo Nobel N.V., Deventer, the Netherlands, Nov. 1985.
149. U.S. Pat. 4,219,626 (Aug. 26, 1980), H. Wolfers and H. J. Rosenkrantz (to Bayer Aktiengesellschaft).
150. G. Moad and D. H. Solomon, *Aust. J. Chem.* **43**, 215 (1990).
151. C. J. Hawker, *Acc. Chem. Res.* **30**, 373 (1997).
152. E. E. Malmström and C. J. Hawker, *Macromol. Chem. Phys.* **199**, 923 (1998).
153. T. Otsu, *J. Polym. Sci., Part A: Polym. Sci.* **38**, 2121 (2000).
154. A. ebenik, *Prog. Polym. Sci.* **23**, 875 (1998).
155. K. Matyjaszewski, in K. Matyjaszewski, ed., ACS Symposium Series, Vol. **768**, American Chemical Society, Washington, D.C., 2000, p. 2.
156. D. Bertin, M. Destarac, and B. Boutevin, *Polym. Surf.* 47 (1998).

157. C. J. Hawker, *Trends Polym. Sci.* **4**(6), 183 1996.
158. M. K. Georges and co-workers, *Trends Polym. Sci.* **2**(2), 66 (1994).
159. M. Husseman and co-workers, *Macromolecules* **32**, 1424 (1999).
160. C. J. Hawker and co-workers, *Macromolecules* **29**, 5245 (1996).
161. P. J. MacLeod and co-workers, *Macromolecules* **30**, 2207 (1997).
162. C. Detrembleur and co-workers, *Macromolecules* **31**, 7115 (1998).
163. EPC Appl. EP 906,937 (Oct. 1, 1998), D. Bertin, B. Boutevin, and J.-J. Robin (to Atofina Chemicals, Inc., formerly Elf Atochem S.A.).
164. EPC Appl. EP 911,350 (Oct. 22, 1998), D. Bertin, M. Destarac, and B. Boutevin (to Atofina Chemicals, Inc., formerly Elf Atochem S.A.).
165. D. Benoti and co-workers, in K. Matyjaszewski, ed., *ACS Symposium Series*, Vol. **685**, American Chemical Society, Washington, D.C., (1998), p. 225.
166. S. Grimaldi and co-workers, *Acta Crystallogr., Sect. C: Cryst. Struct. Commun.* **54**, 1712 (1998).
167. S. Grimaldi and co-workers, *Macromolecules* **33**, 1141 (2000).
168. D. Benoit and co-workers, *J. Am. Chem. Soc.* **122**, 5929 (2000).
169. PCT Appl. WO 96/24620 (Aug. 15, 1996), S. Grimaldi and co-workers (to Atofina Chemicals, Inc., formerly Elf Atochem S.A.).
170. C. LeMercier and co-workers, in Ref. 155, p. 108.
171. PCT Appl. WO 00/40526 (July 13, 2000), J.-P. Gillet, O. Guerret, and P. Tordo (to Atofina Chemicals, Inc., formerly Elf Atochem S.A.).
172. PCT Appl. WO 00/40550 (July 13, 2000), J.-P. Gillet, O. Guerret, and J.-P. Lascombe (to Atofina Chemicals, Inc., formerly Elf Atochem S.A.).
173. U.S. Pat. 4,581,429 (Apr. 8, 1986), D. H. Solomon, E. Rizzardo, and P. Cacioli (to Commonwealth Scientific and Industrial Research Organization).
174. D. Benoit and co-workers, *J. Am. Chem. Soc.* **121**, 3904 (1999).
175. D. Benoit and co-workers, in Ref. 155, p. 123.
176. B. A. Howell, B. Pan, and D. B. Priddy, *Polym. Mater. Sci. Eng.* **76**, 387 (1997).
177. D. Wang and Z. Wu, *Macromolecules* **31**, 6727 (1998).
178. I. Q. Li and co-workers, *Macromolecules* **29**, 8554 (1996).
179. D. Benoit and co-workers, *Macromolecules* **33**, 363 (2000).
180. J. Dao, D. Benoit, and C. J. Hawker, *J. Polym. Sci., Part A: Polym. Chem.* **36**, 2161 (1998).
181. B. A. Howell and co-workers, *Thermochim. Acta* **340/341**, 279 (1999).
182. C. J. Hawker and co-workers, *Polym. Mater. Sci. Eng.* **80**, 90 (1999).
183. PCT Appl. WO 98/13392 (Apr. 2, 1998), L. Vertommen and co-workers (to Akzo Nobel N.V.).
184. G. Moad and E. Rizzardo, *Macromolecules* **28**, 8722 (1995).
185. PCT Appl. WO 00/49027 (Aug. 24, 2000), J.-L. Couturier and co-workers, (to Atofina Chemicals, Inc., formerly Elf Atochem S.A.).
186. M. Sawamoto and M. Kamigaito, in Ref. 165, p. 296.
187. U.S. Pat. 5,312,871 (May 17, 1994), D. Mardare and K. A. Matyjaszewski (to Carnegie Mellon University).
188. M. K. Georges and co-workers, *Macromolecules* **27**, 7228 (1994).
189. R. P. N. Veregin and co-workers, *Macromolecules* **29**, 4161 (1996).
190. P. G. Odell and co-workers, *Macromolecules* **28**, 8453 (1995).
191. E. Malmström, R. D. Miller, and C. J. Hawker, *Tetrahedron* **53**, 15225 (1997).
192. U.S. Pat. 5,807,937 (Sept. 15, 1998), K. Matyjaszewski and co-workers (to Carnegie Mellon University).
193. U.S. Pat. 5,763,548 (Jun. 9, 1998), K. Matyjaszewski and J.-S. Wang (to Carnegie Mellon University).
194. K. Matyjaszewski and co-workers, *Macromolecules* **31**, 1527 (1998).

195. J.-S. Wang and K. Matyjaszewski, *Macromolecules* **28**, 7901 (1995).
196. W. Wang and co-workers, *Hecheng Xiangjiao Gongye* **22**(1), 47 (1999).
197. M. Destarac and co-workers, *Macromolecules* **33**, 4613–4615 (2000).
198. C. Granel and co-workers, *Macromolecules* **29**, 8576–8582 (1996).
199. B. B. Wayland and co-workers, *J. Am. Chem. Soc.* **116**, 7943 (1994).
200. T. C. Chung, H. L. Lu, and W. Janvikul, *Polym. Prepr.* **36**, 241 (1995).
201. S. Gaynor and co-workers, *J. Macromol. Sci, A: Pure Appl. Chem.* **31**, 1561 (1994).
202. U.S. Pat. 5,468,785 (Nov. 21, 1995), M. P. Greuel, L. D. Arvanitopoulos, and H. J. Harwood (to the University of Akron).
203. C. I. Hill and G. M. Whitesides, *J. Am. Chem. Soc.* **96**, 870 (1974).
204. W. Kawai, M. Ogawa, and T. Ichihashi, *J. Polym. Sci., Part A-1* **9**, 1599 (1971).
205. C. W. Brown and H. M. Longbottom, *J. Appl. Polym. Sci.* **14**, 2927 (1970).
206. J. Bond and P. I. Lee, *J. Polym. Sci., Part A-1* **6**, 2621 (1968).
207. N. H. Anderson and R. O. C. Norman, *J. Chem. Soc. B* 993 (1971).
208. M. Imoto, K. Ueda, and K. Takemoto, *Makromol. Chem.* **138**, 11 (1970).
209. J. Barton, V. Durdovic, and V. Horanska, *Makromol. Chem.* **133**, 205 (1970).
210. C. M. M. da Silva Correa and W. A. Waters, *J. Chem. Soc. C* 1880 (1968).
211. T. Otsu and S. Kubota, *Polym. Rep.* **147**, 18 (1970).
212. S. C. Dickerman and co-workers, *J. Org. Chem.* **34**, 714 (1969).
213. M. Kinoshita, N. Yoshizumi, and M. Imoto, *Makromol. Chem.* **127**, 185 (1969).
214. M. Ya. Turkina and I. P. Gragerov, *J. Org. Chem. USSR* **5**, 575 (1969).
215. S. V. Kulkarni, A. E. Fiebig, and R. Filler, *Chem. Ind.* **11**, 364 (1970).
216. E. I. Heiba, R. M. Dessau, and W. J. Koehl Jr., *J. Am. Chem. Soc.* **91**, 138 (1969).
217. T. Koenig and J. M. Owens, *J. Am. Chem. Soc.* **96**, 4052 (1974).
218. T. Koenig and W. R. Mabey, *J. Am. Chem. Soc.* **92**, 3804 (1970).
219. L. Benati, A. Tundo, and G. Zanardi, *J. Chem. Soc., Chem. Commun.* 590 (1972).
220. P. Spagnolo and co-workers, *J. Chem. Soc. Perkin I* 93 (1972).
221. U.S. Pat. 5,405,913 (Apr. 11, 1995), H. J. Harwood and S. D. Goodrich (to The University of Akron).
222. U.S. Pat. 5,470,928 (Nov. 28, 1995), H. J. Harwood and S. D. Goodrich (to The University of Akron).
223. U.S. Pat. 4,330,638 (May 18, 1982), H. Wolfers and co-workers (to Bayer Aktiengesellschaft).
224. U.S. Pat. 4,369,329 (Jan. 18, 1983), H. Wolfers and co-workers (to Bayer Aktiengesellschaft).
225. J. C. Arthur Jr., in J. I. Kroschwitz, ed., Encyclopedia of Polymer Science and Engineering, 2nd ed., Vol. **3**, Wiley-Interscience, New York, 1985, pp. 68–86.
226. V. T. Stannett, J. Silverman, and J. L. Garnett, in G. Allen and co-workers, eds., *Comprehensive Polymer Science*, Vol. **4**, Pergamon Press, Elmsford, N.Y., 1989, pp. 317–336.
227. H. Yasuda and Y. Iriyama, in Ref. 226, pp. 319–323.
228. Ref. 227, pp. 327–329.
229. Ref. 227, pp. 357–375.
230. U.S. Pat. 5,466,722 (Nov. 14, 1995), J. O. Stoffer and O. C. Sitton.
231. J. Hutchison, *Photoinitiated Free Radical Chain Reaction*, Vol. **11** (*Energy Research Abstracts*, Abstract No. 51555), Electricity Council Research Centre, 1986.
232. S. P. Pappas, ed., *UV Curing: Science and Technology*, Technology Marketing Corp., Stamford, Conn., 1978, Chapt. "1".
233. S. P. Pappas, in Ref. 127, pp. 186–212.
234. S. P. Pappas, in Ref. 226, pp. 337–355.
235. H. J. Hageman, *Progr. Org. Coatings* **13**, 123 (1985).
236. A. Ledwith, *Pure Appl. Chem.* **49**, 431 (1977).

237. A. Ledwith, *J. Oil Colour Chem. Assoc.* **59**(5), 157 (1976).
238. A. Pryce, *J. Oil Colour Chem. Assoc.* **59**(5), 166 (1976).
239. B. M. Monroe and G. C. Weed, *Chem. Rev.* **93**, 435–448 (1993).
240. C. Verbanic, *Chem. Bus.* **15**(3), 13–18 (1993).

TERRY N. MYERS
Atofina Chemicals, Inc.

INJECTION MOLDING. See Volume 3.

INORGANIC POLYMERS. See Volume 3.

INTERFACIAL PROPERTIES. See SURFACE PROPERTIES.

IONOMERS

Introduction

In the 1950s it was already known that the presence of carboxylate ionic groups had a strong influence on the properties of elastomers; the early work on the carboxylic elastomers has been documented in a review (1). Since then, it has been recognized that the ionic interaction is one of the very important factors in modifying polymer properties, giving to the polymers many of the properties of vulcanized and filled systems.

The origin of the word *ionomer* dates back to 1965 (2), when it was used for the first time to describe a class of thermoplastics (Surlyn, E. I. du Pont de Nemours & Co., Inc.) consisting of ethylene and partly neutralized methacrylic acid. Historically, the definition of the ionomer referred to thermoplastic polymers of low dielectric constant, containing a relatively small amount of ionic groups (<15 mol%). Later, however, Eisenberg and Rinaudo, who noticed that ionomers in solution sometimes showed polyelectrolyte behavior, proposed another definition; (3) *ionomers* are polymers whose bulk properties are governed by ionic interactions in discrete regions of the material (ionic aggregates). Typical examples of the structures of random ionomers [ie, poly(styrene-*co*-sodium methacrylate), P(S-*co*-MANa) (**1**) and poly(styrene-*co*-sodium styrenesulfonate), P(S-*co*-SSNa) (**2**)] are depicted below.

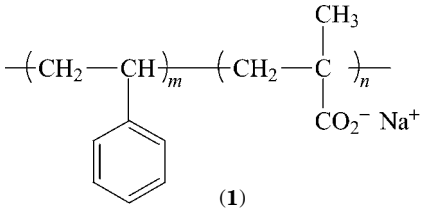

(**1**)

Encyclopedia of Polymer Science and Technology. Copyright John Wiley & Sons, Inc. All rights reserved.

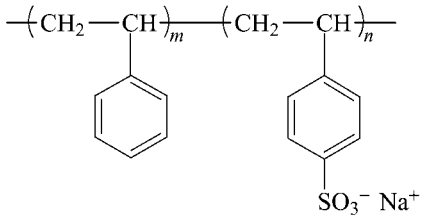

(**2**)

There are several ways of expressing ion concentration in ionomers. In the case of vinyl polymers, the easiest way of expressing ion content is mole percent (mol%), which means the ratio of the number of repeat units containing ionic groups to the total number of repeat units (multiplied by 100). For example, in the case of the P(S-*co*-MANa) and P(S-*co*-SSNa) ionomers, chemical structures **1** and **2**, the ion content is $[100 \times n/(n + m)]$ mol%. However, in the case of highly aromatic or rigid chain systems, for example, milliequivalent per unit weight or moles per liter might be more convenient. In this article mol% is generally used for expressing ion content.

The following four cases are probably useful to illustrate the effect of ionic interactions on the properties of ionomers; they involve the glass-transition temperature, mechanical properties, transport, and melt viscosity. The first case is the glass transitions of inorganic polymers. In 1965, it was found that the glass-transition temperature (T_g) of poly(phosphoric acid), $(HPO_3)_x$, was $-10°C$, but that neutralization of the polymer with Na^+ increased the T_g to 280°C (4). In the case of the ionomer neutralized with Ca^{2+}, the T_g increased further to 520°C. Thus, it was concluded that the increase in the T_g was strictly ascribed to the neutralization of the acid groups (ie, ionization) and to the ionic interaction between anions and cations. The T_g can be related to the strength of the ionic interaction through a q/a effect, where q is the cation charge and a is the distance between the centers of an anion and a cation. The q/a value suggests that the T_g is proportional to the electrostatic work needed to separate the anion from the cation (5). The magnitude of the change in the T_g values (from -10 to 520°C) indicates the importance of ionic interactions on the T_g of polymers. A similar relation was observed for the 100% ionized silicates (6), acrylates (7), and ionenes (8). A number of theories of the T_g and q/a effect in ionomers have been developed (9–11).

The second case is the mechanical properties as a function of temperature for P(S-*co*-MANa) ionomers. Shown in Figure 1 are the storage modulus (E') and loss tangent (tan δ) for P(S-*co*-MANa) ionomers (12,13). The behavior of the P(S-*co*-MANa) ionomer containing 5.4 mol% of ions resembles that of a phase-separated blend or a block copolymer in which the volume fraction of a high T_g (ca 200°C) phase is ca 50%. The volume fraction of the phase can be calculated from the relative area under two loss tangent peaks. In addition, the calculated activation energies for the glass transitions are characteristics of those for glass transitions of nonionic polymers. In the case of the ionomer containing 9.6 mol% of ionic groups, the low T_g phase becomes a minor component, while the high T_g phase becomes dominant. The low and high T_g's of the 9.6 mol% ionomer are ca 150 and 230°C, respectively. It should also be noted that in the 9.6 mol% ionomer, ca 90% of the material is still styrene. Finally, for the 21.6 mol% ionomer, the loss tangent peak at low temperatures disappears, while the

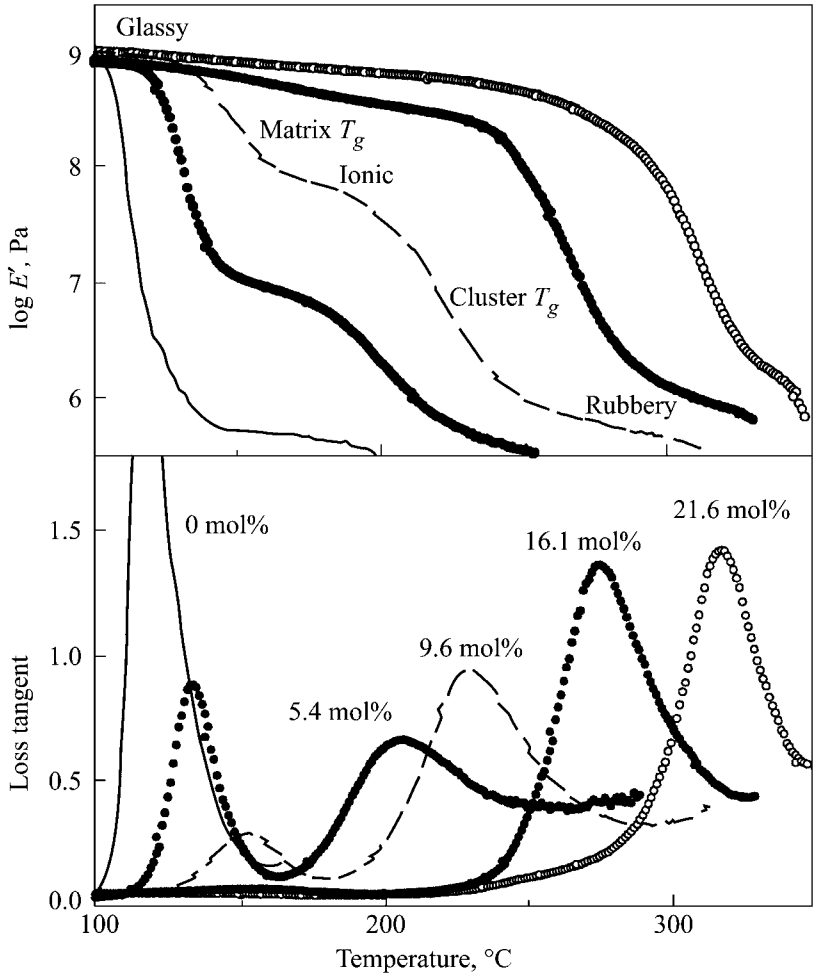

Fig. 1. Storage moduli (E') and loss tangent measured at 1 Hz as a function of temperature for P(S-*co*-MANa) ionomers with ion contents marked near each plot (data were obtained from Refs. 12 and 13).

peak at high temperatures shows its maximum at ca 320°C. At this point it should be mentioned that the estimated T_g of poly(sodium methacrylate) is ca 310°C (14), and thus it is clear that the 21.6 mol% ionomer possesses a T_g very close to that of the poly(sodium methacrylate). This result implies that unusual copolymerization effects must be taken into account. The presence of ions also affects ionomer modulus significantly. For example, at 200°C polystyrene is a viscous material. However, the modulus of the 5.4 mol% ionomer is ca $10^{6.3}$ Pa, and that of the material containing 21.6 mol% of ions is ca $10^{8.8}$ Pa. This behavior is partly due to an increase in the T_g of the ionomer. It should also be noted that for the ionomers of intermediate ion contents, the modulus value changes from the glassy modulus, through the glass transition of the matrix phase, through the "ionic" modulus, through the glass transition of the ion-rich phase, through the rubbery modulus, to modulus for flow behavior.

The third case demonstrates the effect of ions on the transport properties of polymers, especially conductivity. Since their first appearance, the perfluorosulfonate (eg, Nafion, E. I. du Pont de Nemours & Co., Inc.) (15) and perfluorocarboxylate ionomers (eg, Flemion, Asahi Glass Inc.) (16) have been recognized as becoming conductive in the presence of water. The high conductivity has been attributed to the hydration of ionic aggregates, resulting in the formation of percolative ionic domains containing water that allow the ionomers' high conductance. Similar results were also obtained in methyl methacrylate-based (17) and styrene-based ionomers (18) in the presence of water. For example, in the case of poly(methyl methacrylate-*co*-sodium methacrylate) ionomers, conductivity percolation, ie, abrupt insulator–conductor transition, was achieved at the ion content of 5 mol% (17). Above that ion content the ionomer exhibited a conductivity of ca $10^{-2}\ \Omega^{-1}\cdot cm^{-1}$, which was comparable to that of semiconductors.

The last case illustrates the melt viscosity of ionomers. The melt viscosity of polystyrene homopolymer was found to be 400 Pa·s (4×10^3 P) at 220°C (19). However, the melt viscosity of identical molecular weight polystyrene containing 3 mol% of carboxylate ionic groups increased to 7×10^4 Pa·s (7×10^5 P). In the case of a sulfonated sample, the melt viscosity increased further to 9×10^7 Pa·s (9×10^8 P), ie, an increase of over 5 orders of magnitude. As expected, the melt viscosity also increased with increasing ion content. These four cases mentioned above are typical significant effects encountered whenever ionic interactions are introduced into polymers. Ionic interaction and ion aggregation, being responsible for all of the effects mentioned above, have received considerable attention from industrial and academic arenas.

Ionomer Models

In 1970, it was suggested that ions in media of low dielectric constants form aggregates (20). This ion aggregation is one of the major features in the study of ionomers, and is the fundamental basis of the discussion of morphology. The ionic aggregates, termed *multiplets* (20), frequently give rise to a pronounced peak in the small-angle region of the x-ray scattering profile (see Fig. 2). The ionic species has a high atomic number, which gives the scattering centers a high electron density (21). Since the appearance of the first article, published in 1968 (21), dealing with this "ionomer" peak of the ethylene ionomer, a very wide range of morphology studies has confirmed the existence of the ionomer peak in most ionomers, at least under some conditions. However, the interpretation of this ionomer peak is not straightforward and has been a theoretical challenge; as a result, different models have been proposed. Among them, two models based on ionomer morphologies and the so-called Eisenberg–Hird–Moore (EHM) model will be discussed below.

Hard-Sphere Model. In 1973, it was suggested that the ionomer peak is ascribed to the distance between ionic aggregates, with the contrast provided by the difference in the electron density between the ionic aggregates and the hydrocarbon phase (22). The scattering centers are considered to be points on a paracrystalline lattice. In 1983, a refined model was proposed (23); in this hard-sphere model, the multiplets have liquid-like order and the distance of closest approach

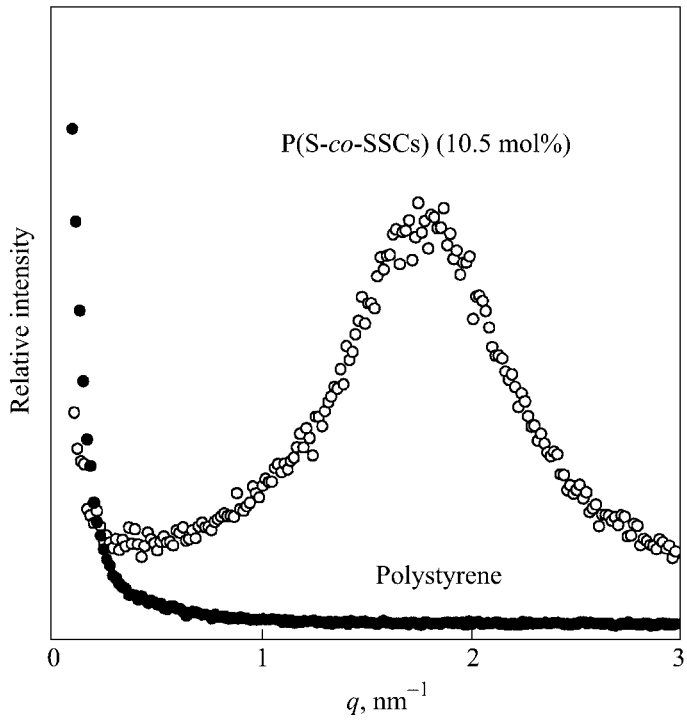

Fig. 2. Small-angle x-ray scattering data as a function of q ($=4\pi \sin\theta/\lambda$, θ is half the scattering angle and λ is the x-ray wavelength) for polystyrene and poly(styrene-*co*-cesium styrenesulfonate) ionomer containing 10.5 mol% of ions.

is governed by the thickness of a layer containing polymer chains on the surface of each multiplet.

Core–Shell Model. In 1974, the observed small-angle x-ray scattering (saxs) peak was interpreted (24) as resulting from the characteristic intraparticle distances. In that model, called core–shell model, an ionic core of ca 1 nm radius is surrounded by a shell of hydrocarbon material containing no ionic groups, and is, in turn, surrounded by a shell of polymeric materials of somewhat higher ion content. In contrast to the hard-sphere model, the core–shell model suggests that the distance between the two ion-rich regions, ie, the core and the outer shell, gives rise to the ionomer peak. This model was elaborated in 1980. It was found that the saxs profiles of the ethylene ionomers depended on sample elongation, and thus it was postulated that the ionic core might not be spherical but lamellar (25).

EHM Model. The Eisenberg–Hird–Moore (EHM) model or multiplet/cluster model, incorporating both morphological and mechanical features, is also based on the existence of ionic aggregates, ie, multiplets (26). In the EHM model, it is assumed that the saxs peak is a result of interparticle scattering along the line suggested in References 22 and 23.

The primary ionic aggregates consist of several ion pairs, and the size of a multiplet is limited by a number of factors (20). The most important factor is a

steric effect of the polymer chain segments adjoining the ion pair, which cannot get out of the way when the aggregates are formed. This effect, which leads to an upper limit on the size, arises from the fact that each ion pair is attached through primary bonds to a polymer chain or to a spacer, and that all the ionic groups must be inside a multiplet, while the organic polymer segments must be outside the multiplet.

Naturally, a number of other factors also influence the size of multiplets, such as the size of ion pairs (27), the dielectric constant of polymers (4), the distance between an ionic group and a polymer backbone (28), and an ion content (28,29). For example, small ion pairs attached to a relatively bulky chain backbone would lead to small multiplets, while large ion pairs attached to a very flexible backbone are expected to form large multiplets. If the dielectric constant of the polymer were high enough, as is the case of the polyphosphates, the ions would be solvated, and thus no multiplet would be found.

In the case of polystyrene ionomers, in which an ionic group is attached to the para position of benzene ring through a flexible alkyl side chain, the effect of the distance between the pendant ion and the backbone on the multiplet size was studied by using a saxs technique (28). Shown in Figure 3 are the relationships

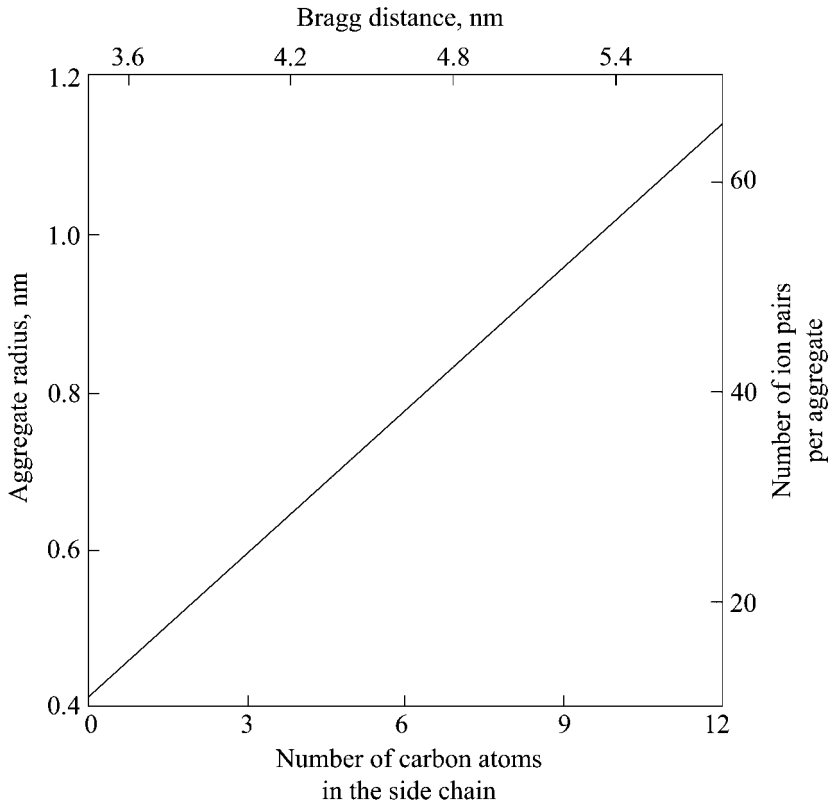

Fig. 3. Aggregate radius–number of carbon atoms in the side chain–number of ion pairs per aggregate–Bragg distance relationships in alkyl side-chain ionomers (data were obtained from Ref. 28).

between the aggregate radius of the alkyl side-chain ionomers containing 7.5 mol% of ions, the number of carbon atoms in the side chain, the number of ion pairs per aggregate, and the Bragg distance. It is shown that the Bragg distance (the distance between aggregates) is a linear function of the number of carbon atoms. The number of ion pairs per aggregate could be calculated for ionomers containing side chains of 2 carbons, 6 carbons, and 11 carbons; they are 21, 37, and 60 ion pairs, respectively. In the figure, it is also shown that the radius of the aggregate increases linearly with increasing the side-chain length, extrapolating to a value of ca 0.4 nm for the cesium–methacrylate system. In the case of the ionomer containing the alkyl chain of 11 carbons, the radius of the aggregate is ca 1.1 nm.

In the case of P(S-*co*-MANa) and P(S-*co*-SSNa) ionomers, every ion pair in the multiplet has two chains emanating from it. Thus, the spherical multiplets, consisting of a few of ionic groups, resemble physical cross-links. A novel feature of the EHM model is a reduced mobility of the polymer chains in the immediate vicinity of the multiplets (26). The chains emanating from the multiplet will be restricted in their mobility, with the restriction decreasing as the distance between the polymer chain segments and the multiplet increases (30,31). Because the chains are anchored rigidly to the multiplets, the mobility of polymer chains surrounding the multiplets is believed to be considerably lower than that of the chains in nonionic polymers. Other mechanisms leading to a reduction of chain mobility were also proposed. Bridging between neighboring multiplets through polymer chains is expected to put the polymer chains under tension, causing a decrease in the chain mobility. The crowding of polymer chains would also affect the mobility; it has been suggested that crowding may possibly be the dominant factor in the reduction of chain mobility (32). Thus, with considerations of the three mechanisms mentioned above, one would expect that the chains in the vicinity of the multiplets do not move as easily as the chains in nonionic bulk polymers. Regarding the restricted mobility of polymer chains, a considerable amount of supportive evidence has been collected by using nuclear magnetic resonance, dynamic mechanical techniques, and other methods (30,31,33–37).

The EHM model postulates that the thickness of the layer of reduced mobility is of the order of the persistence length of the polymer chain (eg, ca 1 nm for polystyrene). Thus, the size of the reduced mobility region of a material including the multiplet is of the order of 3 nm or less (see Fig. 4). However, a certain critical dimension, probably in the range of 5–10 nm, must be exceeded for a polymer to have its own glass transition, and thus the size of the reduced mobility region of ca 3 nm is too small to show its own glass transition.

As the ion content increases, the number of multiplets also increases, and regions of restricted mobility start overlapping. As a result, the sizes of these regions become large enough to exceed a threshold value for independent phase behavior. These large regions of reduced mobility are called *clusters* (26). This overlapping of reduced mobility regions results in the appearance of a second T_g at a temperature higher than that of the normal T_g. As the ion content increases further, the clustered regions become dominant and even continuous.

Apart from the three models described in this section, many other models and morphologies have been proposed; other attempts have also been made to describe the morphologies of ionomers. Interested readers are referred to the original literature (38–73).

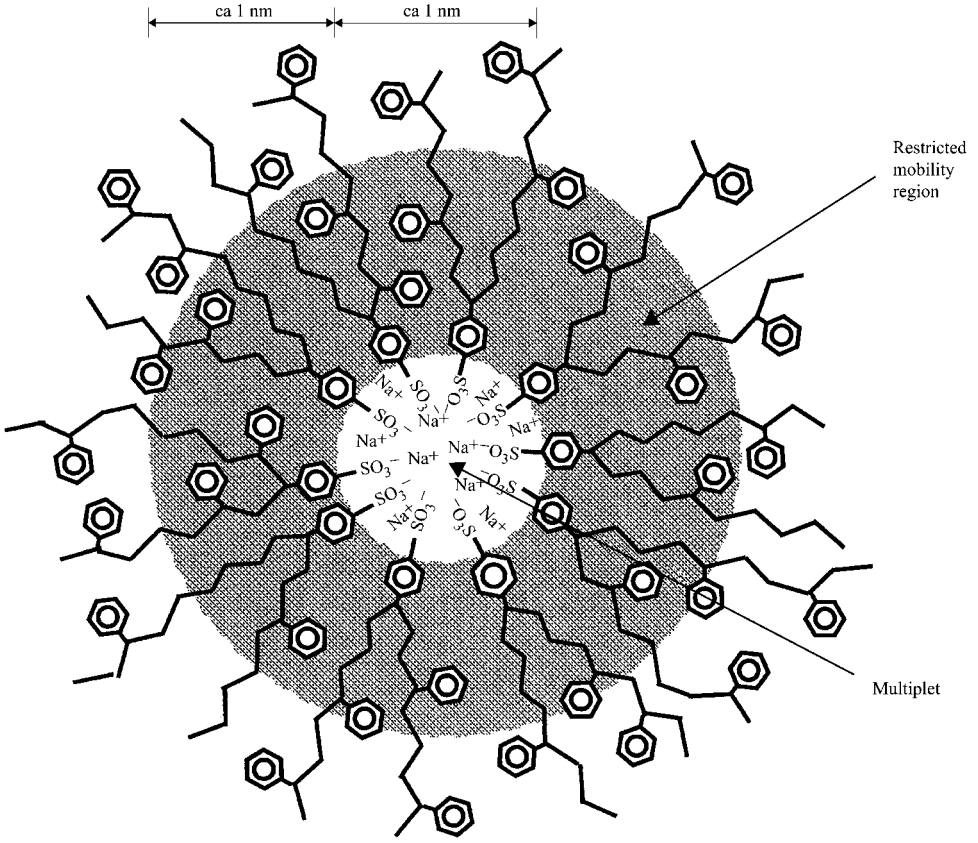

Fig. 4. Representative scheme of a multiplet and of the region of restricted mobility surrounding it in a P(S-*co*-SSNa) ionomer.

It should also be mentioned that the ionomer morphologies were investigated by other techniques rather than saxs, which include transmission electron microscopy (tem) (74–77) and scanning transmission electron microscopy (stem) (78–80). It is worth noting that different sample preparation methods can lead to different morphologies. For example, spherical aggregates were found in the polystyrene-based ionomers by using a tem technique (76), but in some cases, vesicular aggregates were observed by using stem technique (80). In addition to the tem and stem methods, a small-angle neutron scattering technique was also used to study the interphase morphology of ionomers as well as chain conformation (81–90). It should also be mentioned that an extended x-ray absorption fine structure technique was employed to determine the structure around the neutralizing cations in multiplets (91–98).

Recently, the multiple morphologies of block ionomers in solution have been investigated extensively (99–101). The equilibrium, near-equilibrium, and nonequilibrium morphologies observed to date are spheres, rods, bicontinuous rods, bilayers, lamellae, vesicles, inverse bicontinuous rods, large compound micelles, aggregates of spheres, large rod-shaped compound micelles, large compound vesicles, and many others (101).

Glass-Transition Temperatures

In polystyrene-based ionomers, two glass transitions (T_g's) are observed, especially by dynamic mechanical techniques. In the plots of modulus vs. temperature for pure polystyrene and the P(S-*co*-MANa) ionomer containing 21.6 mol% of ions (see Fig. 1), it is shown that the two polymers have only one loss tangent peak at 120°C and at 320°C, respectively. The activation energies obtained from Arrhenius plots of a maximum of the peak at different frequencies are 520 kJ/mol for the polystyrene and 640 kJ/mol for the 21.6 mol% ionomer (13). These values imply that these two peaks indeed represent glass transitions. The ionomers of intermediate ion contents show two drops in the modulus curves as a function of temperature and two loss tangent peaks. The positions of the peaks as a function of ion content for the P(S-*co*-MANa) system are shown in Figure 5 along with those obtained from P(S-*co*-SSNa) ionomers (13,102,103). It is clear that there are two groups of lines; the lower and higher T_g's are referred to as the matrix and the cluster T_g's, respectively. Several other investigations have been performed to bear on the duality of the glass transitions in polystyrene ionomers by using a differential scanning calorimeter (13,102,104–107) and by measuring the volume of ionomers as a function of temperature (108) (see GLASS TRANSITION).

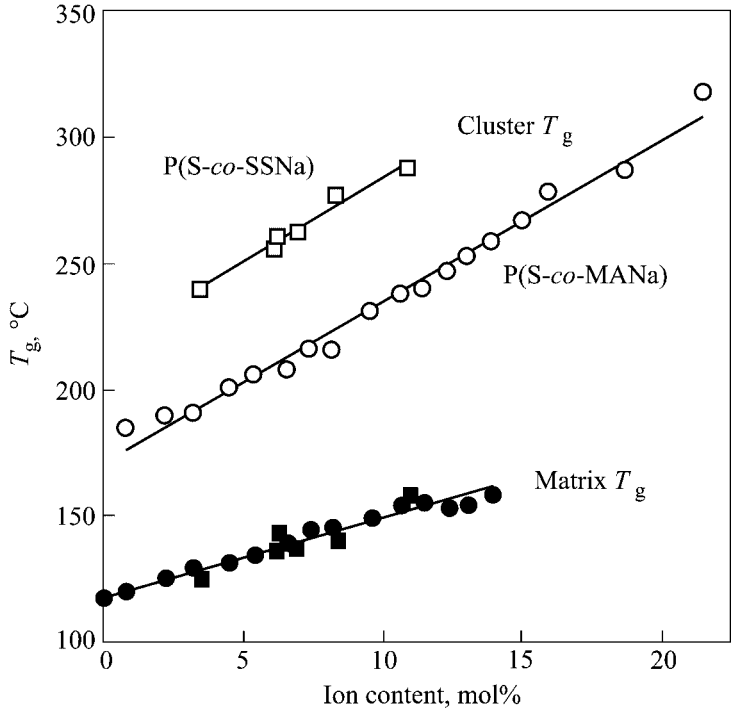

Fig. 5. Glass-transition temperatures of matrix and clustered regions vs ion content for P(S-*co*-MANa) and P(S-*co*-SSNa) ionomers (some of data were obtained from Refs. 13,102, and 103).

Glass-Transition Temperature of Unclustered Regions. A study (109) of the effect of the degree of neutralization on the T_g of poly(ethylene-*co*-sodium methacrylate) ionomers suggested that the loss tangent peak at ca 0°C was due to a β relaxation occurring in the amorphous branched polyethylene phase from which most of the ions had been depleted. The peak position was found to shift to lower temperatures with the increasing degree of neutralization. It was found that the T_g of the poly(ethylene-*co*-sodium acrylate) ionomers increased with increasing ion content (110).

In the case of the P(S-*co*-MANa) ionomers, it was reported that the T_g increased slowly up to ca 6 mol% of ions, but took a sharp turn above that ion content (111). According to the EHM model, the reason for the increase in the matrix T_g is following: in polystyrene ionomers, isolated multiplets and the surfaces of clusters would act as cross-links, and thus the matrix T_g naturally increases with increasing ion content (26).

At this point, it should be noted that the T_g does not always increase with ion content. When poly(styrene-*co*-styrenesulfonic acid) copolymers are quaternized with various amines, in which at least one of the substituents on the nitrogen is an alkyl chain, the T_g decreases with increasing ion content if the alkyl chain is long enough (112). As can be expected, in that system the long alkyl chain acts as an internal plasticizer.

An investigation (113) of the T_g of the poly(styrene-*co*-vinylpyridine) copolymers quaternized with iodoalkane found that the T_g increased with increasing ion content, but that the increasing rate of the T_g with ion contents (dT_g/dc) depended on the length of an alkyl chain. For example, dT_g/dc for the ionomer quaternized with iodomethane was ca 3.2°C/mol%, while for the ionomer quaternized with iododecane it was only ca 1.1°C/mol%.

Glass-Transition Temperature of Clustered Regions. Regarding the cluster T_g, the most extensively investigated system is the P(S-*co*-MANa) ionomers (13). At low ion contents, the cluster T_g increases almost in parallel with the matrix T_g, but only along the temperatures ca 60°C higher than the latter (see Fig. 5). However, with increasing ion contents, the cluster T_g increases more sharply so that for the ionomer containing 15 mol% of ions the difference between the two T_g's now widens to ca 110°C. It is also found that the type of ionic groups changes the temperature difference between the two T_g's. For example, the cluster T_g of the P(S-*co*-SSNa) ionomers is much higher than that of the P(S-*co*-MANa) ionomers (see Fig. 5) (102,103,114,115). In the case of the sulfonated ionomer containing 3.5 mol% of ions, the difference between the matrix and cluster T_g's is ca 115°C, but for the 11 mol% ionomer it widens to ca 130°C. It has been suggested that the ionic interaction of a sodium sulfonate ion pair is much stronger than that of a sodium carboxylate ion pair owing to the difference in the three-dimensional arrangement of the cation and the anion (115).

In terms of the cluster T_g, one very interesting system is the poly(styrene-*co*-*N*-methyl-4-vinylpyridinium iodide) copolymers (27,116). Although the matrix T_g increases with increasing ion content in exactly the same way as it does for other polystyrene-based ionomers, the loss tangent peak for the cluster T_g is not observed. This implies that this system is unclustered. The reason for the absence of clustering in vinylpyridinium ionomers is that the *N*-methyl vinylpyridinium cation and the iodide anion are too large for strong

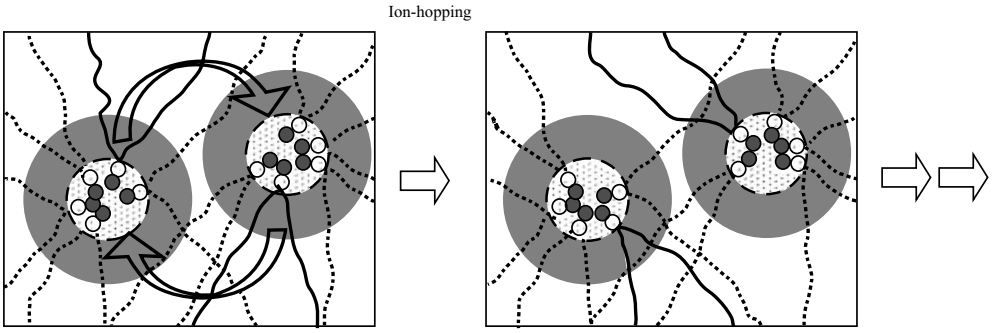

Fig. 6. Schematic drawing of the "ion-hopping" mechanism. Inner circles represent multiplets containing several ion pairs, indicated by smaller black and white circles. The shaded area represents restricted mobility regions. The thicker curved lines are polymer chain segments, which are subjected to move from one multiplet to the other.

ionic interactions. In addition, the T_g of the polymer matrix is too high for those ionic groups to form a sufficient number of multiplets. Therefore, no clustering is observed. Above the matrix T_g, only the chain entanglement governs the ionomer properties. However, when the ionomer is plasticized, which lowers the T_g of the polymer (leading to a decrease in the thermal energy kT_g of polymer chains), clustering is induced in this system (27), and thus, two loss tangent peaks are now observed.

While the mechanism of the matrix glass transition is the same as that of nonionic polymer, the mechanism of the cluster glass transition is still rather ambiguous. An *ion-hopping mechanism* (the actual removal of ion pairs with sufficient thermal energy from multiplets; see Fig. 6) was proposed to occur at and above the cluster T_g (103,117). According to this possibility, the glass transition can only be encountered when ion pairs can move out of the multiplets at a fast rate. Furthermore, the activation energies for ion hopping in the P(S-*co*-MANa) system are generally higher than those in the P(S-*co*-SSNa) system despite the opposite trend in the strength of ionic interaction (13,103). Thus, the strength of the ionic interaction influences the cluster T_g, but is not directly related to the activation energies for ion hopping (13).

As was mentioned before, the polyphosphates show only one glass-transition behavior. In that system, based on electrostatic considerations the T_g should be determined by the strength of ionic interactions, since the polymers have a high dielectric constant and a high T_g. Thus, the separation of ionic species, ie, ion hopping, determines the mobility of polymer chains, and a q/a dependence should be expected.

Properties of Styrene Ionomers

Stress Relaxation. In a study (111) of stress relaxation behavior of P(S-*co*-MANa) ionomers, it was found that below ca 6 mol% of ions, time–temperature superposition was applicable. However, above that ion content,

time–temperature superposition broke down. This could be understood: Below the percolation threshold (ca 5.4 mol% for this system) (13) for the connectivity of clustered regions, the matrix phase was responsible for the behavior. Above the percolation threshold, however, both the clustered and unclustered regions caused the results, and thus time–temperature superposition failed.

Dynamic Mechanical Properties and Filler/Percolation Concepts. One of the detailed dynamic mechanical studies of the P(S-*co*-MANa) ionomers in terms of storage modulus and loss tangent as a function of temperature has already been discussed (see Fig. 1). In the plot of modulus as a function of temperature, the ionomers of intermediate ion content showed two inflection points. The modulus values at a higher inflection point, called the "ionic" modulus, were in the range of ca $10^{6.5}$ to $10^{8.5}$ Pa, depending on the ion content, and the modulus value at a lower inflection point was ca $10^{5.5}$ Pa, which was independent of the ion content. Since the modulus–temperature curves of the ionomers resembled those of the filled materials, the ionic modulus might be interpreted as due to a filler effect. With the volume fraction of a clustered regions obtained from the areas under the loss tangent curves, the value of ionic modulus was calculated by the Guth equation [$E^* = E(1 + 2.5V_f + 14.1V_f^2)$, where E^* was the Young's modulus of the filled regions, E was that of the unfilled regions, and V_f was the volume fraction of filler] (118), assuming that the filler effect was operative here. Then, one could find that the calculated ionic modulus values were close to the experimental points, up to ca 3 mol% of ions (ca 45 vol% of a clustered phase) (13). This implied that clusters acted as fillers in the temperature range between the two T_g's of the ionomers, when the ion content was below the percolation threshold.

When one looks at the morphological picture given in the EHM model, one might suggest that the percolation concept is applicable to the clustering in ionomers (13). Thus, the ionic modulus of the P(S-*co*-MANa) system was attempted to be fitted with percolation theory. It was found that the log(ionic modulus) yielded a straight line when it was plotted against log $(f - f_c)^n$, where f was the volume fraction of clustered regions, f_c was the critical volume fraction at the percolation threshold, and n was the critical exponent (13). The slope of the plot, ie, critical exponent n, was found to be ca 1.3. This value is very close to the universal value for conductivity percolation (ca 1.5), which means that the percolation concept is indeed applicable.

Sulfonate vs Methacrylate vs Carboxylate. A comparison study (19) of the melt viscosity values of polystyrene ionomers, either randomly carboxylated or sulfonated in the para position of a benzene ring, showed that the melt viscosity values at 220°C of the two ionomers were significantly different. For example, at 2 mol% of ions, the melt viscosity of sodium sulfonated polystyrene ionomer was more than 2 orders of magnitude higher than that of the sodium carboxylated polystyrene ionomer.

The storage moduli against temperature for the P(S-*co*-SSNa) and P(S-*co*-MANa) ionomers containing ca 6 mol% of ions are shown in Figure 7. One can find two differences. First, the "ionic plateau" extends to higher temperatures for the P(S-*co*-SSNa) ionomer. Since the ionic interaction between the sodim sulfonate ionic groups is stronger than that between sodium methacrylate, it is expected that the ionic plateau of the sulfonate ionomer persists to higher temperatures. Second, the height of the ionic plateau is lower for the P(S-*co*-SSNa)

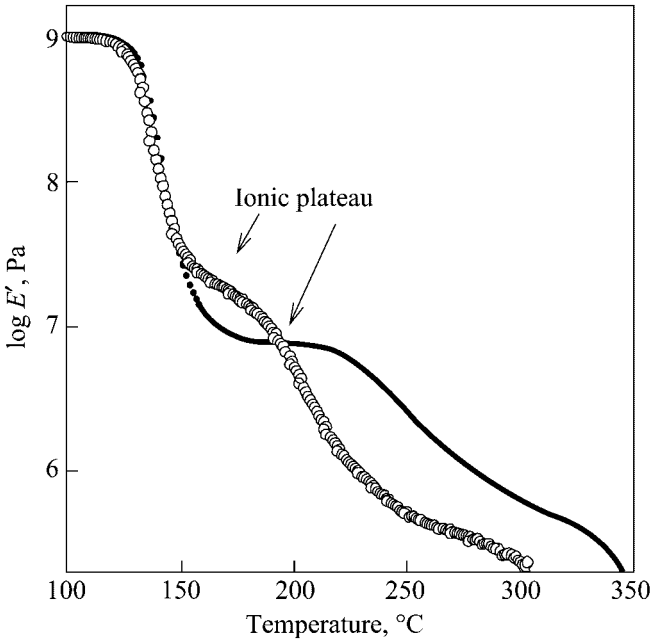

Fig. 7. Storage moduli (E') measured at 1 Hz as a function of temperature for P(S-*co*-MANa) (○) and P(S-*co*-SSNa) (●) ionomers containing 6.5 and 6.3 mol% of ions, respectively.

ionomer than for the P(S-*co*-MANa) ionomer. This can be understood: The ionic groups in the sulfonated ionomer are located in the para position of the benzene ring, while in the methacrylate ionomer they are directly attached to the main chain (103). Thus, larger multiplets form in the sulfonated systems because the distance between the ionic group and the main chain is longer, leading to less steric hindrance for the ionic groups to form multiplets. Since the multiplets are larger, there are fewer multiplets; since the thickness of the restricted mobility layer is presumably the same in the two systems, the total volume of restricted mobility regions is lower in the sulfonates (see Fig. 8). At this point, it is worth recalling that the strength of the ionic interaction also changes the multiplet size; that is, the stronger ionic interaction is, the more ion pairs in the multiplets are. This also enlarges the multiplet size of the P(S-*co*-SSNa) ionomer, compared to that of the P(S-*co*-MANa) ionomer (103).

Comparison of the dynamic mechanical properties of the *p*-carboxylated polystyrene ionomers and those of the P(S-*co*-MANa) ionomers shows a more subtle difference. For the *p*-carboxylate ionomers the ion pairs are farther from the polymer backbone than for the P(S-*co*-MANa), and thus form larger multiplets (102,103). Again, since the size of multiplets is smaller for the P(S-*co*-MANa), the total number of multiplets is larger, which results in the smaller amount of reduced mobility regions for the carboxylated polystyrene system, at a comparable ion content. As a result, the ionic modulus should be lower in the *p*-carboxylate system than in the methacrylate system.

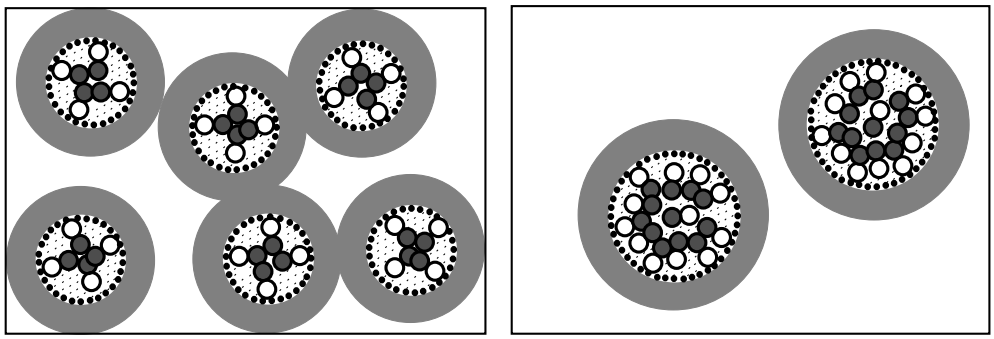

(a) (b)

Fig. 8. Schematic diagrams of restricted mobility regions (shaded area) in ionomers containing multiplets that are smaller in their size but larger in their number (**a**), and that are larger in their size but smaller in their number (**b**). The thickness of the restricted mobility layer was assumed to be the same. The white and black circles represent ionic groups.

In the case of the *p*-sulfonated polystyrene ionomer, the ion pairs are at the same distance from the backbone as in the *p*-carboxylated polystyrene ionomer. As was mentioned above, however, the ionic interaction in the sulfonated ionomer is stronger than that in the carboxylated ionomer. Thus, at the identical ion content, the modulus–temperature curves show longer ionic plateau, and the volume fraction of reduced mobility regions for the *p*-sulfonated ionomer is smaller than for the *p*-carboxylated ionomer (103), leading to less clustering for the *p*-sulfonated ionomers.

Physical Properties of Other Ionomers

A wide range of ionomers based on other polymer backbones has also been studied. Even though an extensive discussion of properties of partly crystalline ionomers as well as the other ionomer families is beyond the scope of the present review, it will be useful to discuss very briefly the properties of some of them. In partly crystalline polyethylene-based and perfluorinated ionomers the degree of crystallinity makes the interpretation of experimental results difficult.

Polyethylene-Based Ionomers. Since their appearance in 1965 under the trade name Surlyn, ethylene ionomers have been studied extensively (2,21,24,38–40,109,110,119–123), and are well known for their flexibility, transparence, toughness, and melt processibility. An example of stress relaxation behavior of an ethylene-based ionomer is shown in Figure 9 (38). It is shown that the rate of stress relaxation is very slow, and a sharp glass-transition region is not observed. The shapes of the curves are different from those obtained from amorphous styrene ionomers. However, the results are very similar to those of some amorphous ionomers of very high ion content or highly crystalline nonionic polymers. When superposition of the individual curves is carried out, it is found that the shift factors are not the WLF (Williams–Landel–Ferry) type, and that master curves cannot be constructed since more than one mechanism may be involved in the relaxation of the material.

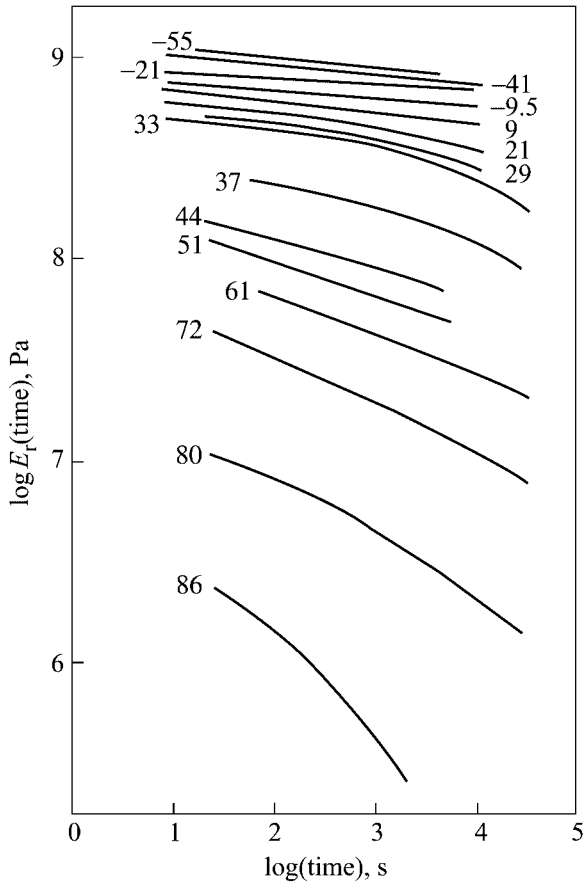

Fig. 9. Stress relaxation curves for an annealed poly(ethylene-*co*-methacrylate) ionomer containing 8 mol% of acid groups, 47% of which were neutralized with NaOH (modified from Ref. 38).

One experiment provides another case in point in the relaxation behavior of polyethylene ionomers (109). In the plots of decrement against temperature, four peaks were observed. The first peak (γ) at ca -120°C was assigned to the crankshaft motion of short hydrocarbon segments in the amorphous phase. The second peak (β) was shown in the temperature range of -20 to 0°C. The peak height increased slightly, but its position remained at a constant temperature in spite of the increasing degree of neutralization. Similar results were also found in the ethylene ionomers of various ion contents (120). Thus, the peak was ascribed to a relaxation in the amorphous branched polyethylene phase having no ionic group. In the case of the third peak (β') (0–50°C), with increasing degree of neutralization, its intensity decreased; however, the peak position remained at a constant temperature. This peak was assigned to micro-Brownian motion of polymer chains, occurring in the amorphous polymer having hydrogen bonds. The fourth peak (α) at high temperatures ($>50^{\circ}$C) shifted to even higher temperatures with increasing degree of neutralization, which was attributed to micro-Brownian

motions of relatively large segments of polymer backbone. This peak was also assumed to reflect the dissociation of the ionic aggregates. At a relatively high degree of neutralization, an additional relaxation, the α' relaxation peak at ca 50°C, was identified (121). Since the peak was not sensitive to frequency, it was assigned to an order–disorder transition of ionic clusters.

Polytetrafluoroethylene-Based Ionomers. Studies on the properties of perfluorosulfonate ionomers have been carried out extensively (124–128). In one of the studies, the nonionic precursor containing $-SO_2F$ groups at the end of the side chain, was compared with the ionomer of an equivalent weight of 1155 (125). It was found that if the degree of crystallinity in both the precursor and the acid-type polymers were low, time–temperature superposition of stress relaxation curves, measured over 4 orders of magnitude of time, could be applicable. In the case of a potassium-neutralized ionomer, time–temperature superposition broke down up to ca 180°C, but above that temperature it became applicable again (124). In the plots of the 10 second tensile modulus values of the precursor, the acid form, and the potassium-neutralized ionomer as a function of temperature, it was found that the two step drop in the modulus was not observed (125). This was probably due to the crystallinity and the different morphology in the tetrafluoroethylene ionomers, compared to styrene ionomers.

The loss tangent curves of the acid form of Nafion and the completely neutralized Cs ionomer are shown in Figure 10 as a function of temperature (124). Three peaks are shown. The peak at highest temperature (α) is ascribed to the glass transition in ionic cluster regions, the β peak at intermediate temperature is attributed to the glass transition in the matrix regions, and the peak at lowest temperature (γ) is due to local motions of CF_2 groups of the polymer main chains

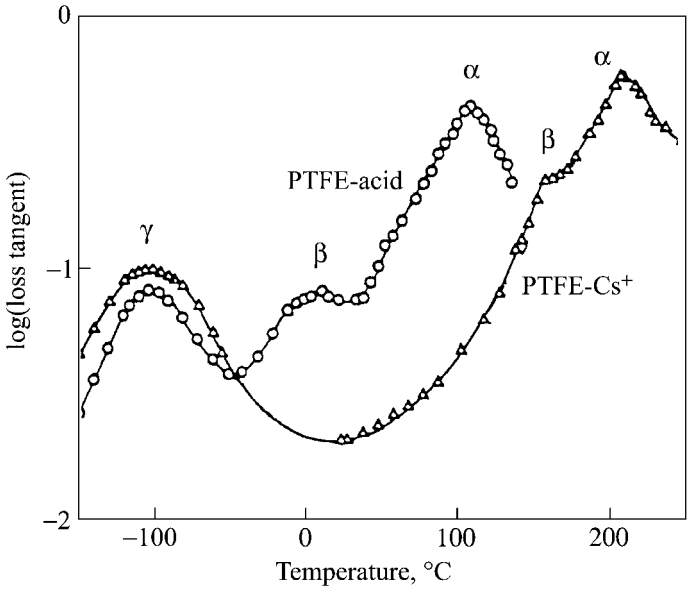

Fig. 10. Loss tangent vs temperature for Nafions (PTFE) in the acid and Cs^+ ionomer form (modified from Ref. 124).

in noncrystalline regions of polytetrafluoroethylene. Also the α peak was found to shift to higher temperature with the increasing degree of neutralization (126).

In the study of the effect of crystallinity on the 10 second tensile modulus, it was found that the modulus curve of the amorphous Nafion (prepared by melting Nafion by heating and subsequently quenching it) was essentially parallel to that of the crystalline Nafion, but only moved along the temperatures ca 40°C lower than the latter (126,128). Thus, it was concluded that the small degree of crystallinity, ie, ca 7%, in perfluoroethylene ionomers shifted the modulus–temperature curve to ca 40°C higher.

In the case of the perfluorocarboxylate ionomers (129), in addition to the three main peaks, a β' peak was also identified, but the mechanism for the relaxation was not identified. A γ' peak between temperatures for the β and γ relaxation was assigned to local motions of the polar side groups in the matrix.

Block Ionomers. The block ionomers to be discussed are of AB or ABA type, in which one of the blocks is ionic (eg, sodium methacrylate) and the other consists of nonionic units (eg, polystyrene). While ionic block copolymers in a micelle form in both aqueous and nonaqueous solutions have been studied extensively (99–101,130,131), the viscoelastic properties of block ionomers in bulk have not received much attention (132–137). If the short ionic blocks formed micelle-like aggregates, which were surrounded by nonionic blocks, the viscoelastic properties of the diblock ionomers would be very similar to those of stars or polymers of low molecular weight (136). Thus, above the T_g of the nonionic blocks, as the temperature increased the modulus dropped rapidly with a very short rubbery plateau. For example, in a dynamic mechanical study, it was found that a homopolymer containing 490 styrene units showed a T_g at ca 115°C, and started to flow at ca 150°C. However, in the case of a diblock ionomer containing 490 styrene units and 40 sodium methacrylate ionic units showed a T_g at ca 116°C, and flow behavior was observed above ca 165°C, which was only 15°C higher than that of nonionic polystyrene (135).

Triblock polystyrene ionomers exhibited an extended rubbery plateau, and the height of the rubbery plateau increased with increasing the length of the ionic block (135). For the triblock ionomer with ionic endblocks of 22 units and a polystyrene midblock of 490 units, the rubbery modulus was ca 10^6 Pa, while for the triblock ionomer with ionic endblocks of 44 units and a midblock of an identical block length, the rubbery modulus increased by approximately 1 order of magnitude; it was suggested that trapped entanglements of chains influenced the modulus more significantly for the longer ionic block ionomer than for the shorter ionic block ionomer. It was also observed that the onset of flow occurred at ca 250°C for the ionic block of 8 units and at ca 290°C for the ionic block of 22 units. For the ionomer of a block length of 44 units, the significant flow behavior was not observed below the decomposition temperature. As expected, however, in the case of the acid triblock ionomers the second drop in the modulus was seen at ca 200°C, at which the acid polymer began to flow (135).

Triblock ionomers consisting of lightly sulfonated styrene endblocks connected by hydrogenated butadiene (ie, ethylene/butylene) midblock have also been investigated (134). It was found that the ion association increased the T_g of polystyrene phase, and that a new modulus plateau region appeared above the T_g. It was also observed that the modulus values between the T_g's of the

ethylene/butylene-rich and polystyrene-rich phases decreased with the increasing level of sulfonation.

Telechelic Ionomers. Telechelic ionomers are polymers containing ionic groups placed at both ends of the polymer chain. Telechelics have been actively studied (49,138–143); even though those studies have mainly been devoted to solution properties, in some cases bulk properties have also been investigated (138,139,142,143). The findings to this date show that the viscosities of the telechelics are higher than those of the nonionic polymers because of the presence of aggregation of ionic groups at the ends of polymer chain (138). Naturally, the type of cation affects viscoelastic properties appreciably, since it changes the degree of association of ionic groups. In addition, a study of molecular weight effect demonstrates that the lowest molecular weight yields a well-developed rubbery plateau, supporting the importance of ionic interactions for the behavior (139).

Star Ionomers. The star ionomers have mainly been studied by a few research groups (144–151). One example of the star ionomers consisted of a central benzene ring, from which three polyisobutylene chains containing a terminal sulfonate ionic group emanated. In the penetration depth–temperature plots of the unfunctionalized tri-arm star of 14,000 molecular weight, a sharp drop in the modulus, that was characteristically found in the modulus of polymers of very low molecular weight, was observed (148). However, when the ends of tri-arm star were terminated with a sulfonic acid group, a rubbery inflection point at a relatively low level was observed. Furthermore, if the acid groups were neutralized with potassium, a modulus increased to a much higher value. It was also found that the modulus increased by decreasing the polydispersity of molecular weight but that the elongation at break decreased (150). Recently, star block ionomers were also prepared and investigated (151).

Since it is not possible to describe all the ionomer families in this article, we will just name a few more extensively studied ionomers here; polyurethane ionomers (152–155), polypentenamers (156,157), ionenes (158–160), polysiloxane dizwitterionomers (161,162), ethyl (or butyl) acrylate zwitterionomers (163,164), ethyl acrylate ionomers (165–167), methyl methacrylate ionomers (168–171), and liquid crystalline ionomers (172–179). An area which has been a subject of considerable investigation but not discussed here is ionomer blends. Some reviews summarize this subject, and thus interested readers are referred to those review articles (180–183). It should also be mentioned that even though the solution properties of ionomers are of great importance, the discussion on the topic is omitted; readers who are interested in the topic can look up other review articles (184–187).

Plasticization

Since ionomers have the amphiphilic nature, it should be possible to plasticize independently the ionic regions and the regions of low polarity, ie, the hydrocarbon-rich regions, in ionomers by using plasticizers of high or low polarity, respectively. An early example of such a study on dual plasticization is Reference 188. It was found that the ion-rich regions in the sulfonated polystyrene ionomers containing 1–5 mol% of ions could be plasticized by using a polar

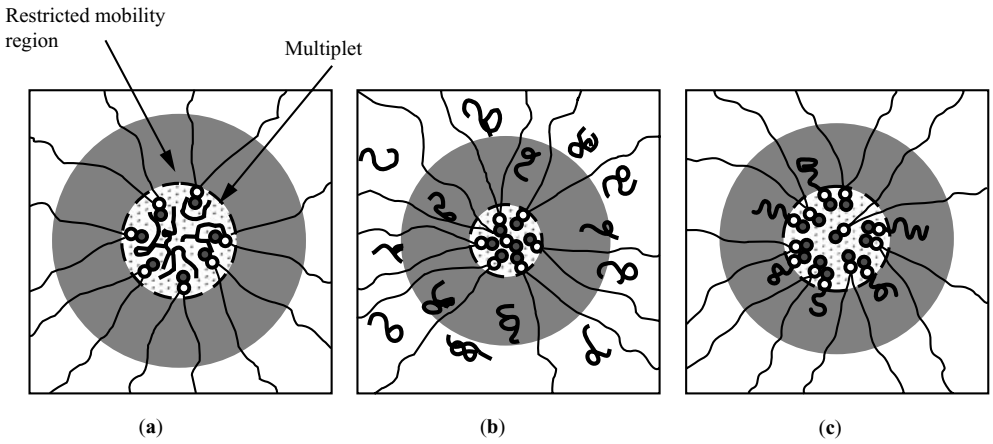

Fig. 11. Schematic diagrams of a multiplet and restricted mobility region surrounding it for plasticized ionomers: (**a**) polar plasticization, (**b**) nonpolar plasticization, and (**c**) amphiphilic plasticization. The thicker curved lines represent plasticizer molecules.

plasticizer such as glycerol. The polar plasticizer weakens the ionic interactions, leading to the fast rate of ion hopping, which decreases the cluster T_g (see Fig. 11). As a result, the bulk viscosity of the ionomer decreases substantially. A nonpolar plasticizer such as dioctylphthalate is, however, probably distributed quite evenly throughout both the matrix and cluster regions, interacts with the nonpolar hydrocarbon regions of ionomers, and thus lowers both the matrix and cluster T_g's. Because of the importance of plasticizers in ionomers for processing, this section is devoted to this topic. The section is divided into three parts dealing, respectively, with polar, nonpolar, and amphiphilic plasticizers.

Polar Plasticizers. At low concentrations, polar plasticizers enter ionic aggregates, shield ionic groups, which decreases the strength of ionic interactions to the point where the ionic core becomes mobile, and thus reduces the energy for ion hopping (see Fig. 11a). As a consequence, ions can be removed at a fast rate. Therefore, the cluster T_g shifts to lower temperature, and the melt viscosity decreases. At sufficiently high concentration, the multiplets may even be disrupted completely. However, the polar plasticization has little effect on the matrix T_g (188).

It was found that the addition of methanol to sulfonated polystyrene ionomers lowered the saxs intensity and shifted the saxs peak to a lower angle at low plasticizer contents; at somewhat high plasticizer contents (ca 10 wt%), the addition of methanol depleted the saxs peak completely (189). Thus, it was suggested that the addition of polar plasticizer increased the size of the ionic core, leading to the reduction of the electron density difference between the ionic core and the hydrocarbon-rich phase. However, in the case of the Zn-sulfonated polystyrene ionomer plasticized with water, it was found that with the increasing amount of water, the x-ray peak shifted to a lower angle, but its intensity increased (190). It was suggested that the water swelled the ionic core and induced a morphological

rearrangement, leading to the change in the fraction of ionic groups that formed ionic aggregates and in the number of the multiplets in the ionomer.

Nonpolar Plasticizers. Plasticizers of low polarity, such as diethylbenzene or dioctylphthalate, are miscible with polymers of low polarity, such as polystyrene. Since both cluster and unclustered regions of the polystyrene ionomer are primarily polystyrene, a nonpolar plasticizer should exist almost evenly in the cluster and matrix regions (see Fig. 11b). For example, it was found that both loss tangent peaks for the matrix and cluster T_g's shifted to lower temperatures as the amount of diethylbenzene increased; in some concentration range, the two T_g's were depressed in parallel (191). In the morphology study of plasticized ionomers, it was found that the saxs peaks did not change much with the different amounts of plasticizer (192). As was mentioned before, in ionomer systems while a polar plasticizer lowered the melt viscosity strongly, but had little effect on the matrix T_g, nonpolar plasticizer lowered the melt viscosity slightly, but lowered the matrix T_g substantially.

Amphiphilic Plasticizers. In one study (193) when ethylene–propylene terpolymer containing Zn-sulfonate (Zn-EPDM) (0.6–1.4 mol% of ions) was mixed with Zn-stearate, clustering was not observed because of the very low ion content. However, as the amount of the plasticizer increased, the matrix T_g and rubbery modulus of the polymer increased slightly. In addition, the temperature at which the modulus started to decrease, which accompanied the flow and was presumably associated with the onset of ion hopping, descended with the increasing amount of plasticizer. Above 120°C, a dramatic decrease in the modulus occurred over a narrow temperature range, which might be associated with the melting of the Zn-stearate. Some of the Zn-stearate could be present in microphase-separated forms as micelles or highly crystalline regions, possibly acting as fillers below their melting temperature. Thus, the matrix T_g increased slightly with increasing the amount of Zn-stearate. Subsequently, it was confirmed that the excess Zn-stearate formed small crystalline regions, with a size of less than ca 0.5 μm (194). On the other hand, the rest of Zn-stearate partitioned into the multiplets, in which the ionic groups of the Zn-stearate presumably aggregated directly with the multiplet, and the stearate hydrocarbon chains resided in the matrix phase. It should be noted that the ionic group attached to the stearate was a carboxylate group, while the ionic group of the ionomer was a sulfonate group. Thus, the carboxylate head group, which was incorporated into the sulfonate aggregate, would plasticize the multiplet to some extent, and thus decreased the modulus even further. Recently, it was found that the saxs peak at $q = 1.6\ \text{nm}^{-1}$ ($d_{\text{Bragg}} = 3.9$ nm) due to the presence of crystalline Zn-stearate disappeared at temperatures between 115 and 130°C, depending on the amount of the Zn-stearate (195). It was proposed that the saxs peak corresponded to the long period of a bilayer crystal of Zn-stearate chains tilted ca 27°.

When the P(S-*co*-SSNa) ionomer was plasticized with a surfactant, sodium dodecylbenzenesulfonate, the hydrophilic head group of which was the same as that of the pendant ionic group of the ionomer (196), the matrix T_g decreased only slightly, whereas the cluster T_g decreased significantly. It was suggested that the head ionic group of the surfactant was incorporated into the multiplet without disrupting or plasticizing it, since the ionic groups of the surfactant and the ionomer

were identical, and that the hydrocarbon tail of the surfactant resided in the restricted mobility regions surrounding the multiplets (see Fig. 11c). Therefore, the main effect of the addition of the surfactant was an increase in the mobility of the chains in the immediate vicinity of the multiplets.

A styrene oligomer (molecular weight = ca 800), one end of which contained Cs- and Ba-neutralized *p*-carboxylate unit, could be used to plasticize the ionic domains of *p*-carboxylated polystyrene (69). The short carboxylated styrene oligomer, again, plasticized the restricted mobility regions surrounding the multiplet, and thus eliminated or suppressed the reduced mobility layer, resulting in a reduction of clustering.

Applications of Ionomers

At present, ionomers are used in a broad range of applications, and the aim of this section is to describe some of the more interesting applications. The particular examples are selected mostly for illustrative purposes to suggest the scope of the applications. Regarding applications of ionomers, extended abstracts appeared in 1988 (197), and several review articles deal with, sometimes in part, the ionomer applications (198–210); interested readers are referred to the original articles.

Membranes. One of the most useful applications of ionomers is their use as a membrane of superpermselectivity (206,211) (see MEMBRANE TECHNOLOGY). The most important ionomer in this category is the perfluorinated ionomers, eg, Nafion, which are copolymers of tetrafluoroethylene and a perfluorinated monomer containing a sulfonate group at the end of a long side chain. The perfluorinated ionomers can allow water transport and the diffusion of cations at a fast rate. Because the cation is in an environment of pendant anions, the pendant sulfonate groups directly attached to the polymer backbone limit the diffusion of anions through the membrane. Since polytetrafluoroethylene is well known for its high dimensional and thermal stability, the perfluorinated ionomers also show high stability. Thus, these ionomers find extensive applications in the chlor-alkali industry, in which the ionomer membranes are used to separate the cathode and anode compartments for the electrolysis process of NaOH. The use of these membranes saves the cost of electricity considerably, and produces pure NaOH.

The perfluorinated ionomers can also be used in fuel cells (206,207). In the fuel cells, the energy generated from chemical reactions can be converted into electrical energy, and thus the fuel cells can be used as electric power sources for transportation. The fuel cell employing the H_2/O_2 (a fuel/an oxidant) reaction consists of anode and cathode compartments, which are separated by an electrolyte; the electrochemical reactions between H_2 and O_2, producing water and electricity, take place at the electrodes. The stationary electrolyte for fuel cells should not contain corrosive liquids and have high energy efficiency per unit mass and long-term stability, eg, ca 1×10^4 h at ca 90°C. For such cells, ionomers as cation-exchange resins can be used as membrane electrolytes. The perfluorosulfonate ionomers such as Nafion are promising candidates for the cell membranes because of their thermal and dimensional stability. However, Nafions are too expensive to be used in fuel cells, and thus extensive researches have been going on to understand why the Nafions are excellent as the membrane and to find the ways to produce other membranes that are less expensive.

Plastics. Ionomers have found extensive applications as plastics, which include golf ball covers, bowling pin covers, bumper guards and body side molding strips of automobiles, shoe parts, bottle stoppers, and ski boot shells. Among them, perhaps the most well-known application is golf ball covers (206,212). In general, two properties are required as ionomer plastics: toughness and moldability. The blend of partly Zn-neutralized and partly Na-neutralized ethylene-based ionomers satisfies these two requirements. The injection molding can be used for the blend to make golf ball covers. In addition, by blending both Zn-neutralized and Na-neutralized ionomers, problems encountered in ionomers containing single cation, eg, the cold crack problem in Na-ionomers and the low rebound problem in Zn ionomers, can be solved effectively. Other examples of applications of the ethylene-based ionomers include packaging materials, impact modifiers, rheology modifiers, modifiers for glass-reinforced thermoplastics, and ionomer foams.

Elastomers. The Zn-EPDM can be used as a self-vulcanizing rubber. The ion aggregation in these ionomers makes it unnecessary to vulcanize the polymer chemically, in contrast to normal elastomers. These ionomers can be used as roofing materials (206,213). Since the material is thermoreversibly cross-linked, a certain degree of creep is inevitable while the ionomer is being used; however, the problem of rupture can be avoided. This type of materials assures advantages for the sealing of rubber sheets through thermal treatment and for the reprocessing of ionomers by simply heating and subsequently molding them.

Catalysis or Catalytic Supports. Ionomers have been used as catalysts. Perfluorosulfonated ionomers have been used as superacid catalysts in various reactions (214–216). In addition, the ionic aggregates can serve as microreactors, implying a wide range of potential applications in this area. Thus, active ions or metals in the phase-separated regions of the ionomer can be used as catalysts (206). For example, when various gases are catalyzed by cations in the multiplets, amines, hydrides, and carbonyls are formed (206,217,218). The cations in the multiplets can also be reduced, and converted to metallic particles which can also act as catalysts (219–225).

Drilling Fluids. Sulfonated polystyrene and sulfo-EPDM have been used as drilling fluid (226–228). The purpose of the ionomer in this application is to improve the suspension property of various agents. It should be remembered that in the drilling operation, the drilling fluids are exposed to very severe shear conditions at high temperatures. Thus, the ionomers are expected to keep the drilling products as well as elements necessary to assist the drilling under the harsh conditions. In addition, the ionomers have advantages for extending an applicable temperature of drilling fluids to much higher temperatures than nonionic polymers.

Coating for Fertilizers. The application of ionomers as a coating for agricultural fertilizers enhances the effectiveness, for example, by improving release properties. A case in point is the Zn sulfo-EPDM ionomers which are used as a coating material for slow release of fertilizers (229). The volatile polar solvent plasticizes multiplets, causing a significant decrease in the solution viscosity, which, in turn, allows easy spraying of ionomer solutions on the urea fertilizers. As the polar solvent evaporates very rapidly, the aggregation of the ionic groups yields a strong film with uniform thickness and high melt strength. Using this idea, various release patterns can be obtained, depending on the size of fertilizer particles and

film thickness. When the urea fertilizers are exposed to water, the water molecules diffuse through the coating layer, and dissolve the urea particles, resulting in a sharp increase in the osmotic pressure of water inside the coating layer. As the amount of water increases, and the pressure on the coating layer increases to a point where damage to the coating layer occurs, then the urea solution is released through the crack of the coating layer. Because of the variation in the average thickness of the coating layers, the release of the urea solution occurs over long time. Thus, ionomeric-coating technique on the fertilizer particles allows that the appropriate amount of fertilizers can be released on the time when they are most needed.

BIBLIOGRAPHY

"Ionic Polymers" in *EPSE* 2nd ed., Vol. 8, pp. 393–423, by R. D. Lundberg, Exxon Chemical Co.

1. H. P. Brown, *Rubber Chem. Technol.* **30**, 1347 (1957).
2. R. W. Rees and D. J. Vaughan, *Polym. Prepr. (Am. Chem. Soc., Div. Polym. Chem.)* **6**, 287 (1965).
3. A. Eisenberg and M. Rinaudo, *Polym. Bull.* **24**, 671 (1990).
4. A. Eisenberg, H. Farb, and L. G. Cool, *J. Polym. Sci., Part A-2* **4**, 855 (1966).
5. A. Eisenberg, in J. E. Mark and co-workers, eds., *Physical Properties of Polymers*, ACS Professional Reference Book, American Chemical Society, Washington, D.C., 1993, Chapt. "2".
6. A. Eisenberg and K. Takahashi, *J. Non-Cryst. Solids* **3**, 279 (1970).
7. A. Eisenberg, H. Matsura, and T. Yokoyama, *J. Polym. Sci., Part A-2* **9**, 2131 (1971).
8. A. Eisenberg, H. Matsuura, and T. Yokoyama, *Polymer J.* **2**, 117 (1971).
9. R. Becker, *Z. Phys. Chemie, Lipzig* **4**, S667 (1976).
10. T. Tsutsui and T. Tanaka, *Polymer* **18**, 817 (1977).
11. D. G. Peiffer, *Polymer* **21**, 1135 (1980).
12. J.-S. Kim, *Ph.D. dissertation, Department of Chemistry*, McGill University, Montreal, 1994.
13. J.-S. Kim, R. J. Jackman, and A. Eisenberg, *Macromolecules* **27**, 2789 (1994).
14. R. J. Andrews and E. A. Grulke, in J. Brandrup and co-workers, eds., *Polymer Handbook*, 4th ed., John Wiley & Sons, Inc., New York, 1999, p. VI 205.
15. W. Y. Hsu, J. R. Barkley, and P. Meakin, *Macromoleules* **13**, 198 (1980).
16. H. Ukihashi and M. Yamabe, in Ref. 211, Chapt. 17.
17. A. A. Gronowski and co-workers, *J. Membr. Sci.* **82**, 83 (1993).
18. M. Jiang and co-workers, *Macromolecules* **27**, 6541 (1994).
19. R. D. Lundberg and H. S. Markowski, in A. Eisenberg, ed., *Ions in Polymers*, (Advances in Chemistry Series 187), American Chemical Society, Washington, D.C., 1980, Chapt. "2".
20. A. Eisenberg, *Macromolecules* **3**, 147 (1970).
21. F. C. Wilson, R. Longworth, and D. J. Vaughan, *Polym. Prepr. (Am. Chem. Soc., Div. Polym. Chem.)* **9**, 505 (1968).
22. C. L. Marx, D. F. Caulfield, and S. L. Cooper, *Macromolecules* **6**, 344 (1973).
23. D. J. Yarusso and S. L. Cooper, *Macromolecules* **16**, 1871 (1983).
24. W. J. MacKnight, W. P. Taggart, and R. S. Stein, *J. Polym. Sci., Polym. Symp.* **45**, 113 (1974).
25. E. J. Roche and co-workers, *J. Polym. Sci., Polym. Phys. Ed.* **18**, 1497 (1980).
26. A. Eisenberg, B. Hird, and R. B. Moore, *Macromolecules* **23**, 4098 (1990).

27. D. Wollmann, C. E. Williams, and A. Eisenberg, *Macromolecules* **25**, 6775 (1992).
28. R. B. Moore and co-workers, *Macromolecules* **24**, 1376 (1991).
29. H. Tomita and R. A. Register, *Macromolecules* **26**, 2791 (1993).
30. Z. Gao, X.-F. Zhong, and A. Eisenberg, *Macromolecules* **27**, 794 (1994).
31. P. Vanhoorne and co-workers, *Macromolecules* **27**, 2548 (1994).
32. I. A. Nyrkova, A. R. Khokhlov, and M. Doi, *Macromolecules* **26**, 3601 (1993).
33. S. Yano, K. Tadano, and R. Jérôme, *Macromolecules* **24**, 6439 (1991).
34. G. Tsagaropoulos and A. Eisenberg, *Macromolecules* **28**, 6067 (1995).
35. G. Tsagaropoulos, J.-S. Kim, and A. Eisenberg, *Macromolecules* **29**, 2222 (1996).
36. B. Grassl and co-workers, *Macromolecules* **30**, 236 (1997).
37. S. Kutsumizu and S. Schlick, *Macromolecules* **30**, 2329 (1997).
38. T. C. Ward and A. V. Tobolsky, *J. Appl. Polym. Sci.* **11**, 2403 (1967).
39. R. Longworth and D. J. Vaughan, *Nature (London)* **218**, 85 (1968).
40. S. Bonotto and E. F. Bonner, *Macromolecules* **1**, 510 (1968).
41. F. L. Binsbergen and G. F. Kroon, *Macromolecules* **6**, 344 (1973).
42. A. Moudden, A. M. Levelut, and M. Pineri, *J. Polym. Sci., Polym. Phys. Ed.* **15**, 1707 (1977).
43. D. Graiver, M. Litt, and E. Baer, *J. Polym. Sci.: Polym. Chem. Ed.* **17**, 3573 (1979).
44. K. A. Mauritz, C. J. Hora, and A. J. Hopfinger, in Ref. 19, p. 123.
45. S. R. Lowry and K. A. Mauritz, *J. Am. Chem. Soc.* **102**, 4665 (1980).
46. H. L. Yeager and A. Steck, *J. Electrochem. Soc.* **128**, 1880 (1981).
47. M. Fujimura, T. Hashimoto, and H. Kawai, *Macromolecules* **14**, 1309 (1981).
48. W. Y. Hsu and T. D. Gierke, *Macromolecules* **15**, 101 (1981).
49. G. Broze, R. Jérôme, and Ph. Teyssié, *J. Polym. Sci., Polym. Lett. Ed.* **19**, 415 (1981).
50. T. D. Gierke, G. E. Munn, and F. C. Wilson, *J. Polym. Sci., Polym. Phys. Ed.* **19**, 1687 (1981).
51. M. Fujimura, T. Hashimoto, and H. Kawai, *Macromolecules* **15**, 136 (1982).
52. W. C. Forsman, *Macromolecules* **15**, 1032 (1982).
53. V. K. Datye, P. L. Taylor, and A. J. Hopfinger, *Macromolecules* **17**, 1704 (1984).
54. K. A. Mauritz and C. E. Rogers, *Macromolecules* **18**, 483 (1985).
55. B. Dreyfus, *Macromolecules* **18**, 284 (1985).
56. C. E. Williams and co-workers, *Macromolecules* **19**, 2877 (1986).
57. P. Aldebert, B. Dreyfus, and M. Pineri, *Macromolecules* **19**, 2651 (1986).
58. P. Aldebert and co-workers, *J. Phys. (France)* **49**, 2101 (1988).
59. Y. S. Ding and co-workers, *Macromolecules* **21**, 1698 (1988).
60. D.-C. Lee and co-workers, *Macromolecules* **21**, 998 (1988).
61. J. P. Gouin, C. E. Williams, and A. Eisenberg, *Macromolecules* **22**, 4573 (1989).
62. D. Feng and co-workers, *J. Macromol. Sci., A: Chem.* **26**, 1151 (1989).
63. K. Tadano, E. Hirasawa, H. Yamamoto, and S. Yano, *Macromolecules* **22**, 226 (1989)
64. D. Feng and co-workers, *J. Appl. Polym. Sci.* **37**, 1549 (1989).
65. B. Dreyfus and co-workers, *J. Phys. (France)* **51**, 1341 (1990).
66. L. N. Venkateshwaran and co-workers, *Polymer* **33**, 2277 (1992).
67. T. Hashimoto and co-workers, *Polymer* **35**, 2672 (1994).
68. D. Nguyen and co-workers, *Macromolecules* **27**, 5086 (1994).
69. M. Plante, C. G. Bazuin, and R. Jérôme, *Macromolecules* **28**, 1567 (1995).
70. R. Sobry and co-workers, *Macromolecules* **31**, 4240 (1998).
71. P. Y. Vuillaume, C. G. Bazuin, and J.-C. Galin, *Macromolecules* **33**, 781 (2000).
72. R. F. Storey and D. W. Baugh III, *Polymer* **41**, 3205 (2000).
73. P. Y. Vuillaume, J.-C. Galin, and C. G. Bazuin, *Macromolecules* **34**, 859 (2001).
74. D. L. Handlin, W. J. MacKnight, and E. L. Thomas, *Macromolecules* **14**, 795 (1981).

75. P. K. Agarwal and E. B. Prestridge, *Polymer* **24**, 487 (1983).
76. C. Li, R. A. Register, and S. L. Cooper, *Polymer* **30**, 1227 (1989).
77. C. E. Williams, C. Colliex, J. Horrion, and R. Jérôme, in L. A. Utracki and R. A. Weiss, eds., *Multiphase Polymers: Blends and Ionomers* (American Chemistry Society Symposium Series 395), American Chemical Society, Washington, D.C., 1989, pp. 439–443.
78. J. H. Laurer and K. I. Winey, *Macromolecules* **31**, 9106 (1998).
79. K. I. Winey, J. H. Laurer, and B. P. Kirkmeyer, *Macromolecules* **33**, 507 (2000).
80. B. P. Kirkmeyer, R. A. Weiss, and K. I. Winey, *J. Polym. Sci., Part B: Polym. Phys.* **39**, 477 (2001).
81. C. T. Meyer and M. Pineri, *J. Polym. Sci., Polym. Phys. Ed.* **16**, 569 (1978).
82. E. J. Roche, R. S. Stein, and W. J. MacKnight, *J. Polym. Sci. Polym. Phys. Ed.* **18**, 1035 (1980).
83. E. J. Roche and co-workers, *J. Polym. Sci., Polym. Phys. Ed.* **19**, 1 (1981).
84. T. R. Earnest and co-workers, *Macromolecules* **14**, 192 (1981).
85. R. A. Register, G. Pruckmayr, and S. L. Cooper, *Macromolecules* **23**, 3023 (1990)
86. S. A. Visser and S. L. Cooper, *Macromolecules* **24**, 6769 (1991).
87. J.-P. Gouin, A. Eisenberg, and C. E. Williams, *Macromolecules* **25**, 1368 (1992).
88. G. Gebel and J. Lambard, *Macromolecules* **30**, 7914 (1997).
89. G. Gebel, *Polymer* **41**, 5829 (2000).
90. G. Gebel and R. B. Moore, *Macromolecules* **33**, 4850 (2000).
91. Y. S. Ding and co-workers, *J. Appl. Phys.* **56**, 2396 (1984).
92. D. J. Yarusso and co-workers, *J. Polym. Sci., Polym. Phys. Ed.* **22**, 2073 (1984).
93. A. Meagher and co-workers, *Polymer* **27**, 979 (1986).
94. G. Vlaic and co-workers, *Polymer* **29**, 173 (1988).
95. B. P. Grady, *Macromolecules* **32**, 2983 (1999).
96. A. Welty, S. Ooi, and B. P. Grady, *Macromolecules* **32**, 2989 (1999).
97. B. P. Grady, *Polymer* **41**, 2325 (2000).
98. K. V. Farrell and B. P. Grady, *Macromolecules* **34**, 7198 (2001).
99. M. Moffitt, K. Khougaz, and A. Eisenberg, *Acc. Chem. Res.* **29**, 95 (1996).
100. S. E. Webber, P. Munk, and Z. Tuzar, eds., *Solvents and Self-Organization of Polymers*, Kluwer Academic Publishers, Dordrecht, the Netherlands, 1996.
101. N. S. Cameron, M. K. Corierre, and A. Eisenberg, *Can. J. Chem.* **77**, 1311 (1999).
102. J.-S. Kim, G. Wu, and A. Eisenberg, *Macromolecules* **27**, 814 (1994).
103. B. Hird and A. Eisenberg, *Macromolecules* **25**, 6466 (1992).
104. T. Kanamoto and co-workers, *Makromol. Chem.* **176**, 3497 (1975).
105. J. J. Maurer, in B. Miller, ed., *Thermal Analysis: Proceedings of the Seventh International Conference on Thermal Analysis*, Vol. **2**, John Wiley & Sons, Inc., New York, 1982, pp. 1040–1049.
106. X. Tong and C. G. Bazuin, *Chem. Mater.* **4**, 370 (1992).
107. M. Ehmann and co-workers, *Macromolecules* **26**, 4910 (1993).
108. T. Takamatsu and A. Eisenberg, *J. Appl. Polym. Sci.* **24**, 2221 (1979).
109. W. J. MacKnight, L. W. McKenna, and B. E. Read, *J. Appl. Phys.* **38**, 4208 (1967).
110. E. P. Otocka and T. K. Kwei, *Macromolecules* **1**, 401 (1968).
111. A. Eisenberg and M. Navratil, *Macromolecules* **6**, 604 (1973).
112. R. A. Weiss, P. K. Agarwal, and R. D. Lundberg, *J. Appl. Polym. Sci.* **29**, 2719 (1984).
113. D. Wollman, S. Gauthier, and A. Eisenberg, *Polym. Eng. Sci.* **26**, 1451 (1986).
114. M. Rigdahl and A. Eisenberg, *J. Polym. Sci., Polym. Phys. Ed.* **19**, 1641 (1981).
115. J. A. Lefelar and R. A. Weiss, *Macromolecules* **17**, 1145 (1984).
116. S. Gauthier, D. Duchesne, and A. Eisenberg, *Macromolecules* **20**, 753 (1987).
117. P. Vanhoorne and R. A. Register, *Macromolecules* **29**, 598 (1996).

118. E. Guth, *J. Appl. Phys.* **16**, 20 (1945).
119. R. Longworth and D. J. Vaughan, *Polym. Prepr. (Am. Chem. Soc., Polym. Chem. Div.)* **9**, 525 (1968).
120. K. Tadano and co-workers, *Macromolecules* **22**, 226 (1989).
121. H. Tachino and co-workers, *Macromolecules* **26**, 752 (1993).
122. H. Tachino and co-workers, *Macromolecules* **27**, 372 (1994).
123. H. Hashimoto and co-workers, *Macromolecules* **34**, 1515 (2001).
124. S. C. Yeo and A. Eisenberg, *J. Appl. Polym. Sci.* **21**, 875 (1977).
125. I. M. Hodge and A. Eisenberg, *Macromolecules* **11**, 289 (1978).
126. T. Kyu and A. Eisenberg, in Ref. 16, Chapt. 6.
127. T. Kyu, M. Hashiyama, and A. Eisenberg, *Can. J. Chem.* **61**, 680 (1983).
128. T. Kyu and A. Eisenberg, *J. Polym. Sci., Polym. Symp.* **71**, 203 (1984).
129. Y. Nakano and W. J. MacKnight, *Macromolecules* **17**, 1585 (1984).
130. J. Selb and Y. Gallot, in E. J. Goethals, ed., *Polymeric Amines and Ammonium Salts*, Pergamon Press, New York, 1980, pp. 205–218.
131. J. Selb and Y. Gallot, in I. Goodman, ed., *Development in Block Copolymers*, Vol. **2**, Elsevier Applied Science, London, 1985, pp. 27–96.
132. S. Gauthier and A. Eisenberg, *Macromolecules* **20**, 760 (1987).
133. T. E. Long, R. D. Allen, and J. E. McGrath, in J. L. Benham and J. F. Kinstel, eds., *Chemical Reaction on Polymers*, (ACS Symposium Series 364), American Chemical Society, Washington, D.C., 1988, Chapt. "19".
134. R. A. Weiss and co-workers, *Polymer* **32**, 2785 (1991).
135. A. Desjardins and A. Eisenberg, *Plast. Rubber Compos. Process. Appl.* **18**, 161 (1992).
136. L. N. Venkateshwaran and co-workers, *Polymer* **33**, 2277 (1992).
137. K. Yoshikawa and co-workers, *Macromolecules* **29**, 1235 (1996).
138. G. Broze and co-workers, *J. Polym. Sci., Polym. Phys. Ed.* **21**, 2205 (1983).
139. R. Jérôme and G. Broze, *Rubber Chem. and Technol.* **58**, 223 (1984).
140. G. Broze, R. Jérôme, and Ph. Teyssié, in P. Dubin, ed., *Polymer Science and Technology*, Vol. **30**, Plenum Press, New York, 1985.
141. R. Jérôme, in E. Goethals, ed., *Telechelic Polymers: Synthesis and Applications*, CRC Press, Inc., Boca Raton, Fla., 1989, Chapt. "11".
142. P. Charlier and co-workers, *Macromolecules* **25**, 617 (1992).
143. P. Vanhoorne and R. Jérôme, in S. Schlick, ed., *Ionomers: Characterization, Theory, and Applications*, CRC Press, Inc., Boca Raton, Fla., 1996, Chapt. "9".
144. Y. Mohajer and co-workers, *Polym. Bull.* **8**, 47 (1982).
145. S. Bagrodia and co-workers, *Polym. Bull.* **9**, 174 (1983).
146. Y. Mohajer and co-workers, *J. Appl. Polym. Sci.* **29**, 1943 (1984).
147. S. R. Bagrodia, G. L. Wilkes, and J. P. Kennedy, *J. Appl. Polym. Sci.* **30**, 2179 (1985).
148. S. Bagrodia and co-workers, *Polymer* **28**, 2207 (1987).
149. R. F. Storey, S. E. George, and M. E. Nelson, *Macromolecules* **24**, 2920 (1991).
150. D. Loveday and co-workers, *J. Appl. Polym. Sci.* **63**, 507 (1997).
151. R. F. Storey, B. J. Chisholm, and Y. Lee, *Polym. Eng. Sci.* **37**, 73 (1997).
152. D. Dieterich, W. Keberle, and H. Witt, *Angew. Chem. Int. Ed.* **9**, 40 (1970).
153. M. Rutkowska and R. Zielinski, in M. Pineri and A. Eisenberg, eds., *Structure and Properties of Ionomers* (NATO ASI Series C: Mathematical and Physical Sciences, Vol. 198), D. Reidel Publishing Co., Dordrecht, the Netherlands, 1987, pp. 469–479.
154. S. A. Visser and S. L. Cooper, *Macromolecules* **24**, 2576 (1991).
155. H. X. Xiao and K. C. Frisch, eds., *Advances in Urethane Ionomers*, Technomic Publishing Company, Inc., Lancaster, Pa., 1995.
156. W. J. MacKnight, in Ref. 153, pp. 269–297.

157. D. Rahrig and W. J. MacKnight, in Ref. 19, Chapts. 6 and 7.
158. A. Eisenberg, H. Matsuura, and T. Yokoyama, *Polymer J.* **2**, 117 (1971).
159. D. Feng and co-workers, *Polymer* **33**, 526 (1992).
160. T. Tsutsui, in A. D. Wilson, ed., *Development in Ionic Polymers-2*, Elsevier, New York, 1980, Chapt. "4".
161. D. Graiver, M. Litt, and E. Baer, *J. Polym. Sci., Polym. Chem. Ed.* **17**, 3607 (1979).
162. D. Graiver, M. Litt, and E. Baer, *J. Polym. Sci., Polym. Chem. Ed.* **17**, 3625 (1979).
163. C. G. Bazuin and co-workers, *Polymer* **30**, 654 (1989).
164. M. Ehrmann and co-workers, *Macromolecules* **26**, 4910 (1993).
165. H. Matuura and A. Eisenberg, *J. Polym. Sci., Polym. Phys. Ed.* **14**, 1201 (1976).
166. X. Tong and C. G. Bazuin, *Chem. Mater.* **4**, 370 (1992).
167. J.-S. Kim, Y. H. Nah, and S. S. Jahng, *Polymer* **42**, 5567 (2001).
168. A. A. Gronowski and co-workers, *J. Membr. Sci.* **82**, 83 (1993).
169. X. Ma, J. A. Sauer, and M. Hara, *Macromolecules* **28**, 3953 (1995).
170. X. Ma, J. A. Sauer, and M. Hara, *Polymer* **38**, 4425 (1997).
171. J.-S. Kim, H.-S. Kim, and A. Eisenberg, *Bull. Korean Chem. Soc.* **19**, 625 (1998).
172. B. Zhang and R. A. Weiss, *J. Polym. Sci., Part A: Polym. Chem.* **30**, 91 (1992).
173. A. Wiesemann, R. Zentel, and T. Pakula, *Polymer* **33**, 5315 (1992).
174. Y. Zhao and H. Lei, *Macromolecules* **27**, 4525 (1994).
175. C. G. Bazuin and A. Tork, *Macromolecules* **28**, 8877 (1995).
176. Y. Xue and M. Hara, *Macromolecules* **30**, 3803 (1997).
177. C. Chovino and co-workers, *J. Polym. Sci., Part A: Polym. Chem.* **35**, 2569 (1997).
178. J.-F. Gohy and co-workers, *Macromol. Chem. Phys.* **199**, 1791 (1998).
179. E. Barmatov and co-workers, *Macromol. Rapid Commun.* **21**, 281 (2000)
180. P. Smith, M. Hara, and A. Eisenberg, in R. M. Ottenbrite, L. A. Utracki, and S. Inoue, eds., *Current Topics in Polymer Science*, Vol. **2**, Hanser Publisher, New York, 1987, pp. 256–283.
181. A. Natansohn, R. Murali, and A. Eisenberg, *Makromol. Chem. Macromol. Symp.* **16**, 175 (1988).
182. Z. Gao, A. Molnár, and A. Eisenberg, in M. R. Tant, K. A. Mauritz, and G. L. Wilkes, eds., *Ionomers: Synthesis, Structure, Properties and Applications*, Blackie Academic & Professional, London, 1996, Chapt. "10".
183. C. G. Bazuin, in J. C. Salamone, ed., *Polymeric Materials Encyclopedia*, Vol. **5**, CRC Press, Inc., Boca Raton, Fla., 1996, pp. 3454–3460.
184. R. D. Lundberg, in Ref. 153, pp. 387–397.
185. C. W. Lantman, W. J. MacKnight, and R. D. Lundberg, *Annu. Rev. Mater. Sci.* **295**, 19 (1989).
186. M. Hara, in M. Hara, ed., *Polyelectrolytes: Science and Technology*, Marcel Dekker, Inc., New York, 1993, Chapt. "4".
187. M. Hara, in Ref. 183, pp. 3473–3481.
188. R. D. Lundberg, H. S. Makowski, and L. Westerman, in Ref. 19, Chapt. 3.
189. J. J. Fitzgerald and R. A. Weiss, *J. Polym. Sci., Part B: Polym. Phys.* **28**, 1719 (1990).
190. D. J. Yarusso and S. L. Cooper, *Polymer* **26**, 371 (1985).
191. C. G. Bazuin and A. Eisenberg, *J. Polym. Sci., Part B: Polym. Phys.* **24**, 1137 (1986).
192. R. A. Weiss, J. J. Fitzgerald, and D. Kim, *Macromolecules* **24**, 1064 (1991).
193. P. K. Agarwal, H. S. Makowski, and R. D. Lundberg, *Macromolecules* **13**, 1679 (1980).
194. I. Duvdevani and co-workers, in A. Eisenberg and F. E. Bailey, eds., *Coulombic Interactions in Macromolecular Systems* (ACS Symposium Series 302), American Chemical Society: Washington, D.C., 1986, Chapt. "15".

195. D. A. Jackson, J. T. Koberstein, and R. A. Weiss, *J. Polym. Sci., Part B: Polym. Phys.* **37**, 3141 (1999).
196. J.-S. Kim and co-workers, *Macromolecules* **26**, 5256 (1993).
197. Extended abstracts in *Polym. Prepr. (Am. Chem. Soc., Div. Polym. Chem.)* **29**, 429–445 (1988).
198. R. H. Kinsey, *Appl. Polym. Symp.* **11**, 77 (1969).
199. R. A. Weiss and co-workers, in Ref. 194, Chapt. 1.
200. W. J. MacKnight, in Ref. 153, p. 1.
201. R. D. Lundberg, in Ref. 153, p. 279.
202. R. D. Lundberg, in Ref. 153, p. 429.
203. J. S. Tan, in Ref. 153, p. 439.
204. R. D. Lundberg, in J. I. Kroschwitz, ed., Encyclopedia of Polymer Science and Engineering, Vol. **8**, John Wiley & Sons, Inc., New York, 1987, pp. 393–423.
205. R. D. Lundberg and P. K. Agarwal, *Indian J. Technol.* **31**, 400 (1993).
206. W. M. Risen Jr., in Ref. 143, Chapt. 12.
207. H. L. Yeager and A. A. Gronowski, in Ref. 182, Chapt. 8.
208. R. Longworth and H. Nagel, in Ref. 182, Chapt. 9.
209. H. Reiff and D. Dieterich, in Ref. 182, Chapt. 11.
210. R. D. Lundberg, in Ref. 182, Chapt. 12.
211. A. Eisenberg and H. L. Yeager, eds., *Perfluorinated Ionomer Membranes* (ACS Symposium Series 180), American Chemical Society, Washington, D.C., 1982.
212. R. J. Statz, *Polym. Prepr. (Am. Chem. Soc., Div. Polym. Chem.)* **29**, 435 (1988).
213. A. U. Paeglis and F. X. O'Shea, *Rubber Chem. Technol.* **61**, 223 (1988).
214. G. A. Olah, J. Kaspi, and J. Bukala, *J. Org. Chem.* **42**, 4187 (1977).
215. G. A. Olah, K. Laali, and A. K. Mehrotra, *J. Org. Chem.* **48**, 3360 (1983).
216. G. A. Olah and D. Meidar, *Synthesis* 358 (1978).
217. D. M. Barnes and co-workers, in Ref. 194, Chapt. 5.
218. W. M. Risen Jr., in Ref. 153, p. 87.
219. M. Möller, *Synth. Met.* **41**, 1159 (1991).
220. C. C. Cummins, R. R. Schrock, and R. E. Cohen, *Chem. Mater.* **4**, 27 (1992).
221. Y. Ng Cheong Chan, R. R. Schrock, and R. E. Cohen, *J. Am. Chem. Soc.* **114**, 7295 (1992).
222. M. Antonietti and co-workers, *Adv. Mater.* **7**, 1000 (1995).
223. J. Spatz, A. Roescher, and M. Möller, *Adv. Mater.* **8**, 337 (1996).
224. M. Moffitt and A. Eisenberg, *Chem. Mater.* **7**, 1178 (1995).
225. M. Moffitt and co-workers, *Chem. Mater.* **7**, 1185 (1995).
226. U.S. Pat. 4,425,455 (1984), S. Turner and co-workers. (to Exxon Research and Engineering Co.)
227. U.S. Pat. 4,425,461 (1984), R. S. Turner and co-workers. (to Exxon Research and Engineering Co.)
228. R. C. Portnoy, R. D. Lundberg, and E. R. Welein, in *IADC/SPE*, Drilling Conference, Dallas, Tex., Feb. 10–12, 1986, Paper 14795.
229. E. N. Drake, *Polym. Mater. Sci. Eng.* **71**, 14 (1994).

GENERAL REFERENCES

L. Holliday, ed., *Ionic Polymers*, Applied Science Publishers, London, 1975.
A. Eisenberg and M. King, *Ion-Containing Polymers, Physical Properties and Structure*, Academic Press, Inc., New York, 1977.

A. D. Wilson and H. J. Prosser, eds., *Developments in Ionic Polymers*, Applied Science Publishers, London, 1983.
S. Schlick, ed., *Ionomers: Characterization, Theory, and Applications*, CRC Press, Inc., Boca Raton, Fla., 1996.
M. R. Tant, K. A. Mauritz, and G. L. Wilkes, eds., *Ionomers: Synthesis, Structure, Properties and Applications*, Blackie Academic Professional, New York, 1996.
A. Eisenberg and J.-S. Kim, *Introduction to Ionomers*, John Wiley & Sons, Inc., New York, 1998.

JOON-SEOP KIM
Chosun University

ISOCYANATE-DERIVED POLYMERS

Introduction

Organic diisocyanates and polymeric diisocyanates are widely used as monomers in reaction polymerization reactions (1,2). By far their widest use is in the manufacture of polyurethanes produced by an addition reaction from macroglycols and isocyanates. Modification of polyurethanes (qv) by partial trimerization of the isocyanate group is used in the manufacture of rigid cellular plastics (polyurethane isocyanurate foams), and in the molding of solid cross-linked elastomers, using the RIM (reaction injection molding) process. Also, poly(urethane ureas) are produced by using a diamine extender or a macrodiamine as one of the comonomers. An example is the use of diethyltoluenediamine as an extender in the RIM of automotive parts. The use of amine monomers, which react very rapidly with isocyanates, increases the reaction rates in the corresponding molding processes. Also, diamine extender or macrodiamines are used in spray applications and in the manufacture of elastic Spandex fibers. Poly(urethane isocyanurates) and poly(urethane ureas) are treated adequately under polyurethanes (qv), and they are not included in this article (see POLYURETHANES).

The homopolymerization of diisocyanates is only useful for specialty diisocyanates, such as aliphatic 1,2- or 1,3-diisocyanates (3) and aromatic *o*-diisocyanates (4), which polymerize via cycloaddition processes. Anionic homopolymerization of monoisocyanates takes place by addition across the C=N bond to form nylon-1 polymers. Polyamides are also obtained from diisocyanates and enamines or ketenaminals. This reaction proceeds by a $[2+2]$ cycloaddition reaction with subsequent ring opening to form polyamides. $[2+4]$ cycloaddition polymerization to form heterocyclic polymers is observed with carbonyl diisocyanate (5). Ring-opening polymerization occurs in the reaction of bis-epoxides

Encyclopedia of Polymer Science and Technology. Copyright John Wiley & Sons, Inc. All rights reserved.

with aromatic diisocyanates to give poly(2-oxazolidinones). Vinyl isocyanates undergo addition polymerization across their vinyl group to give polyisocyanates with a very high isocyanate content, which are difficult to handle. Copolymerization of vinyl isocyanate with other vinyl monomers allows the synthesis of useful polyisocyanates. Other difunctional nucleophiles, such as bis-mercaptans, hydrazine, dihydrazides, or dioximes, are also used as comonomers in polyaddition processes.

Reaction polymerization reactions of isocyanates with suitable monomers can be performed in an extruder or in a RIM machine. In the latter reaction thermosets (cross-linked polymers) are produced. In an extruder usually linear polymers are manufactured. For example from methylene di-*p*-phenylene isocyanate (MDI), with some macroglycols and 1,4-butanediol as extenders, segmented polyurethane elastomers are produced in an extruder (6). However, linear condensation polymers are also produced in a vented extruder. For example from MDI, with macrodicarboxylic acids and dicarboxylic acids as extenders thermoplastic block copolyamide elastomers are produced. The by-product of the condensation reaction, carbon dioxide, is removed in the vented extruder. The polycondensation process can also be performed in solution. For example, MDI can be added to a solution of dicarboxylic acids in tetramethylene sulfone, with simultaneous removal of the carbon dioxide. Tetramethylene sulfone is the solvent of choice for solution polymerization of isocyanates (7). In addition to dicarboxylic acids trimellitic acid anhydride and benzophenonetetracarboxylic acid dianhydride (BTDA) are utilized as monomers for condensation polymers. With these monomers poly(amide imides) and poly(imides) are produced. The diisocyanate-derived commercial polycondensation products are listed in Table 1.

Often it becomes necessary to lower the melting points of the derived polymers to allow processability. This is best achieved by using mixtures of the diisocyanates. For example, high temperature fibers (PI 2080) are produced using 80% 2,4-TDI and 20% MDI and BTDA. Also, poly(amide imides) are modified with 20% isophthalic acid, and azelaic acid is often used as comonomer to reduce the crystallinity of the derived polymers. The utilization of comonomers

Table 1. Condensation Polymers Derived from Diisocyanates and Suitable Monomers

Isocyanate	Comonomers	Polymers
MDI	Polyester dicarboxylic acids, azelaic acid	Segmented poly(amide) elastomers
MDI	Isophthalic acid, azelaic acid	Engineering thermoplastic poly(amides)
MDI	Azelaic acid	Semicrystalline engineering plastic poly(amide)
MDI, TDI	Trimellitic acid anhydride, isophthalic acid	Copoly(amide imide) films
MDI, TDI	Benzophenonetetracarboxylic acid dianhydride	Poly(imide) fibers and films
MDI, TDI	—[a]	Poly(carbodiimide)

[a]A phospholene oxide catalyst is used in this polycondensation reaction.

allows the manufacture of numerous condensation polymers from diisocyanates. Segmented thermoplastic polyamide elastomers and some engineering thermoplastic polyamides are available from Dow, and Lenzing AG in Austria has produced PI 2080 fibers. Oligomeric carbodiimides obtained from sterically hindered aromatic diisocyanates are used as stabilizers for polyesters, polyester-based polyurethanes, and polyether-based poly(urethane ureas) (8). The mechanism of stabilization of polyesters with oligomeric carbodiimides is based on the rapid reaction of carbodiimides with carboxylic acids generated in the hydrolysis of a polyester. Oligomeric carbodiimides can also function as chain-mending agents, preventing loss of molecular weight. The carbodiimide oligomers derived from sterically hindered aromatic diisocyanates are commercially available under the trade name Stabaxol from Rhein Chemie, a subsidiary of Bayer.

Diisocyanates have also been used as monomers in the manufacture of thermally stable addition/condensation heterocyclic polymers. For example, reaction of dihydroxyaryl-dicarboxylic acid esters with diisocyanates produce poly(benzoxazindiones), which are useful as high performance wire coatings (9). The addition/condensation procedure was also used in the manufacture of poly(parabanic acid) from MDI and hydrogen cyanide (10). The use of the toxic hydrogen cyanide as monomer has prevented the commercialization of this useful polymer.

Monomers

Diisocyanates are usually synthesized by phosgenation of the corresponding diamines. A tabulation of diisocyanates synthesized up to 1972 with pertinent methods of synthesis is available (11). Instead of the toxic phosgene gas, the liquid trichloromethyl chloroformate (diphosgene) (12) or the solid bistrichloromethyl carbonate (triphosgene) (13) can be used in the laboratory (see PHOSGENE). Also, oligomeric *t*-butylcarbonates are used to convert diamines into diisocyanates (14).

The principal commercial aromatic isocyanates are toluene diisocyanate (TDI), polymeric isocyanate (PMDI), and its coproduct (MDI), but some specialty aromatic isocyanates and some aliphatic diisocyanates are also available. The latter are used in the manufacture of color stable polyurethanes. TDI is mainly produced as a 80:20 mixture of the 2,4- and the 2,6-isomers, but a 65:35 mixture of the same isomers, pure 2,4-TDI and a crude partially trimerized product, are also available. PMDI is a mixture of the MDI isomers and their higher oligomers, and MDI is mainly the 4,4′-diisocyanate. The principal commercially available isocyanates are listed in Table 2.

Sulfonyl diisocyanates, such as *m*-phenylenedisulfonyl diisocyanate, are used as monomers for base-soluble polymers (15). 4-Isocyanatobenzenesulfonyl isocyanate can also be used as a monomer for base-soluble polymers. Reaction of *p*-toluenesulfonyl isocyanate with polymers having amide units in the backbone structure affords sulfonyl urea derivatives, which on hydrolysis with 1 *N* NaOH degrade the polymer to carboxylic acids (16). Likewise, polymerization of the monomer derived from acrylamide and *p*-toluenesulfonyl isocyanate affords a homopolymer, which on hydrolysis with 1 *N* NaOH affords poly(acrylic acid) (17).

Table 2. Major Aromatic Isocyanates

Name	Boiling point, °C/kPa[a]	Melting point, °C	Structure	Producer
PPDI	110–112/90	94–96	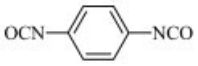	Akzo
TDI	120/75	14	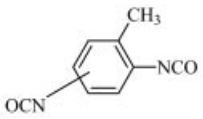	BASF, Bayer, Dow, Lyondell
MDI	171/7.5	37	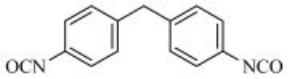	BASF, Bayer, Dow
PMDI		— [b]	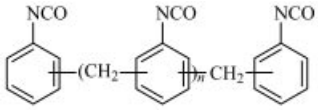	BASF, Bayer, Dow
NDI	244/0.98	130–132	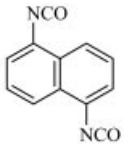	Bayer
TODI	160–170/3.75	71–72	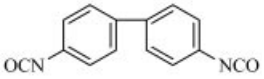	Nippon Soda

[a] To convert kPa to mm Hg, divide by 7.5.
[b] Light to dark brown liquid.

Some aliphatic diisocyanates are also commercially available and they are listed in Table 3.

Because of its relatively low boiling point HDI is currently only supplied in the form of derivatives (trimer, allophanate, biuret, etc) (18). Polymeric aliphatic isocyanates are obtained by copolymerization of 2-isocyanatoethyl methacrylate and styrene (19). Hydroxyalkyl acrylates and methacrylates are used as monomers to form hydroxyl group containing polymers, which are cross-linked with diisocyanates or blocked diisocyanates (20). The elusive parent diisocyanate, O=C=N–N=C=O, is only stable at −75°C, and therefore it is not suitable as a monomer or comonomer in polymerization reactions (21).

The market for polyurethanes in 2000 was of the order of 8 million tons per year. Therefore, diisocyanates and polymeric isocyanates are readily available at reasonable cost, and their use as monomers for other addition and condensation polymers is indicated.

Blocked isocyanates can be used in the cross-linking of hydroxyl group containing polymers in the formulation of powder coatings. Blocking agents include phenol, caprolactam, ketoximes, and 3,5-dimethylpyrazole. The latter has the lowest dissociation temperature (22). Currently, virtually all automobiles produced use a blocked isocyanate in the formulation of cationic electrodeposition coatings (23). The [2 + 2] cycloadduct derived from MDI and diarylketenes is used as an initiator in the nylon RIM process (24).

Table 3. Major Aliphatic Isocyanates

Name	Boiling point, °C/kPa[a]	Structure	Producer
HDI	130/98	$OCN(CH_2)_6NCO$	Bayer
TMHDI	149/75	$OCNCH_2C(Me)_2CH_2CH(Me)CH_2CH_2NCO$ $OCNCH_2CH(Me)CH_2C(Me)_2CH_2CH_2NCO$	Huels
CHDI	122–124/90		Akzo
H_6XDI	110/7.5	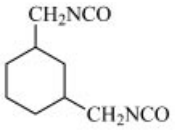	Takeda
m-TMXDI	150/23	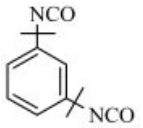	American Cyanamid
IPDI	153/75	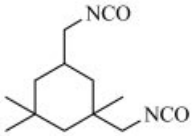	Bayer, Huels
$H_{12}MDI$[b]	179/6.75	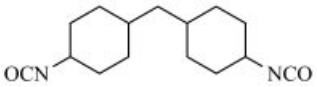	Bayer

[a] To convert kPa to mm Hg, divide by 7.5.
[b] Mixture of stereoisomers.

Also, isocyanates are used in the formulation of interpenetrating polymer networks (IPNs) (25). A polyester–polyurethane IPN with a ratio typical for sheet molding compound (SMC) is obtained from MDI, poly(caprolactone triol), an unsaturated polyester resin, and styrene monomer (26). IPNs are also reviewed under polyurethanes.

Isocyanates in general are toxic chemicals and require great care in handling. Oral ingestion of substantial quantities of isocyanates can be tolerated by the human body, but acute symptoms may develop from inhalation of much smaller amounts. The suppliers Material Safety Data Sheets (MSDS) have to be consulted for the most current information on the safe handling of isocyanates.

Homopolymerization

The anionic homopolymerization of monoisocyanates proceeds by addition across their C=N double bond to give nylon-1 polymers (27). The reaction is generally conducted in dimethyl formamide (DMF) at −50°C, using sodium cyanide as the initiator. The infrared spectra of the nylon-1 homopolymers show a strong absorption band at 1700 cm^{-1} (C=O) and a band from 1280 to 1390 cm^{-1}, indicating a disubstituted amide structure. The nylon-1 polymers obtained in the anionic polymerization reaction are listed in Table 4.

Table 4. Nylon-1 Polymers Obtained by Anionic Polymerization of Monoisocyanates

Isocyanate	Yield, %	Softening temp., [a] °C	Melt temp., °C
Vinyl			300
Ethyl	48		250
Allyl	10	180	260–290
n-Propyl	70	180	250
n-Butyl	75	180	209
Isobutyl	18	173	210–220
n-Amyl	67	145	209
n-Hexyl	85	120	195
n-Nonyl	100		
n-Undecyl	70	45	155
n-Octadecyl	2	40	94
9-*n*-Decenyl	75	75	180–240
Benzyl	50		250
Phenyl	28		197
m-Tolyl	60		200
p-Tolyl	25		
p-Methoxyphenyl	35		212–214
m-Dimethylaminophenyl			315

[a]Temperature at which the polymer first become plastic without sticking on a metal temperature-gradient bar.

The melt temperature of nylon-1 polymers depends on the legth of the side chain. The longer the side chain, the lower the melting point of the polymer. Steric requirements for the homopolymerization of monoisocyanates are severe. No homopolymers are obtained from isopropyl, cyclohexyl, *o*-methoxyphenyl, and α-naphthyl isocyanate. All alkyl nylon-1 polymers, with the exception of poly(allyl isocyanate), have a low order of crystallinity as shown by X-ray diffraction. However, the polymerization of *n*-butyl isocyanate and phenyl isocyanate in various solvents at -78°C, initiated by lithium or sodium alkyls, produces crystalline polymers (28). The mechanism of the sodium cyanide catalyzed polymerization in DMF involves intermediates having a spiro structure (29).

The solution properties of alkyl poly(isocyanates) in a variety of solvents indicate an unusual chain stiffness similar to the α-helical poly(α-amino acids) (30). Optically active poly(isocyanates) are obtained by anionic polymerization of the optically active monomers (31). The temperature-dependent optical activity and circular dichroism suggest a large preference of one of the helical senses (32).

Vinyl isocyanate is polymerized across the isocyanato group to give the nylon-1 polymer **1**. Treatment of **1** with azoisobutyronitrile and UV light at room temperature produces the ladder polymer **2** (33).

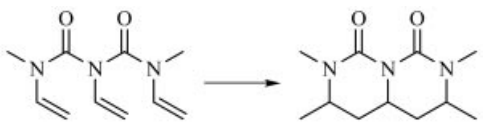

1 **2**

The double bond also survives in the homopolymerization of 2-isocyanatoethyl methacrylate (34).

The nylon-1 polymers are thermally not stable because unzipping occurs on heating, giving rise to the formation of monomers and cyclic trimers. The decomposition temperature of poly(alkyl isocyanates) is about 140°C. The main fragmentation products from alkyl nylon-1 polymers are the cyclic trimers, while aryl nylon-1 polymers afford mainly the monomers. The unzipping of the homopolymers can be prevented by using $Cl_3TiOCH_2CF_3$ to stabilize the living ends of the homopolymer. When the homopolymers contain functional groups, $CpTi(OCH_2CF_3)Cl_2$ can be used for this purpose (35). Poly(isocyanatocarboxylic acid esters) are obtained by conducting the polymerization at −40°C in toluene in the presence of *n*-butyllithium (36). Silylated isocyanato carboxylic acids are likewise polymerized, and the protecting group is removed using HF in ethanol (37). The rapid degradation of the nylon-1 polymers has been used to create raster images upon treatment with electron beams (38). Poly(isocyanates) with chiral azo chromophores can undergo photoisomerization of the chiral side chain. This reaction can be used as a switch, whose effect is amplified in the polymer backbone (39). A review article on nylon-1 polymers appeared in 1976 (40).

The homopolymerization of aliphatic diisocyanates across their C=N bond is limited to aliphatic 1,2- and 1,3-diisocyanates and cyclohexane-1,2 and 1,3-diisocyanate (3). These diisocyanates are cyclopolymerized by an alternating, intermolecular–intramolecular propagation mechanism, using sodium cyanide as the catalyst. The cyclopolymers obtained in this manner are listed in Table 5.

The cyclopolymerization of 1,2-diisocyanatodecane (**3**) in the presence of $CpTiClN(CH_3)_2$ affords the cyclopolymer **4**, which is soluble in many organic solvents (41).

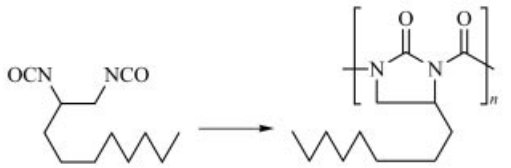

3 **4**

Aromatic *o*-diisocyanates, such as 2,3-TDI, are also homopolymerized via a cycloaddition mechanism (4). The anionic homopolymerization of 2,4-TDI in DMF, using sodium cyanide as the initiator, occurs only through the nonhindered isocyanato group to give linear polymers containing free isocyanato groups (42). Homopolymers are also obtained by coupling polymerization of MDI, using samarium iodide to induce the electron transfer necessary to achieve the polymerization (43). Condensation homopolymerization of PMDI affords low density poly(carbodiimide) foams (see later under Condensation Polymers).

4-Vinylphenyl isocyanate also undergoes homopolymerization across the C=C double bond. This reaction is conducted in toluene at 60°C, using 3 mol% of AIBN as the catalyst (44). Ruthenium catalysts are used to convert *p*-nitropolystyrene in the presence of methanol into the corresponding methyl carbamate, which is a masked polyisocyanate (45).

Table 5. Cyclopolymers Derived from 1,2- and 1,3-Diisocyanatoalkanes

Monomer	Polymer structure	Mp, °C	Inherent viscosity,[a] dL/g
1,2-Diisocyanatoethane	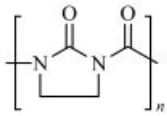	365	0.85
1,2-Diisocyanatopropane	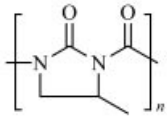	287	1.35
1,2-Diisocyanatocyclohexane	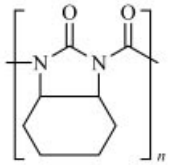	303	0.38
1,2,3-Triisocyanatopropane	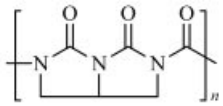	365–400	0.28[b]
1,3-Diisocyanatopropane	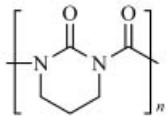	420–425	—
1,3-Diisocyanatocyclohexane	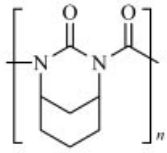	224–265	0.1

[a]Concentration 0.5% w/v in tetrachloroethane/phenol (40/60).
[b]In conc. sulfuric acid.

When a group reactive with the isocyanate group is attached to an aryl isocyanate A–B homopolymers are obtained. For example, from isocyanatophenols, polyurethanes are obtained. Substituents next to the isocyanate or hydroxyl group increase the stability of isocyanatophenols (46). Polyurethanes are also obtained from α,γ-aminoalcohols and di-*t*-butyldicarbonate, and the intermediate α,γ-hydroxyalkyl isocyanates are polymerized using $Zr(acac)_4$ as catalyst (47). Polyamides are obtained from sterically hindered aliphatic aminoisocyanates (48) and poly(imides) are obtained from 4-isocyanatophthalic anhydride (49). Polyamides are also obtained by interfacial polymerization of 4-isocyanatobenzoyl chloride. Reaction of isocyanatocarboxylic acid chlorides with glycols gives poly(ester urethanes) (50). Similarly, reaction of 4-isocyanatobenzenesulfonyl chloride with diamines affords poly(sulfonamide ureas) (51).

When two reactive groups are attached to the aryl isocyanate, hyperbranched homopolymers are obtained. For example, 3,5-dihydroxyphenyl isocyanate,

generated from 3,5-dihydroxybenzoyl azide, undergoes polymerization with network formation (52). Hyperbranched polyurethanes are also constructed using phenol blocked 1,3-diisocyanatobenzene with a CH_2OH group in the 5-position in combination with 4-methylbenzyl alcohol for end capping. Homopolymerization proceeds by thermally unblocking the isocyanato groups (53).

Copolymers

Copolymerization of 4-vinylphenyl isocyanate and styrene at 60°C in toluene in the presence of AIBN affords the expected copolymers (44). Also, 1:1 copolymers from vinyl isocyanate and maleic anhydride are known (54). The copolymeriation of *n*-butyl isocyanate with a variety of olefins is conducted in toluene/THF at −80°C, using sodium biphenyl as initiator (55). Anionic copolymerization of styrene and hexyl isocyanate affords rod–coil block copolymers. The styrene polymer forms the coil block, while the polyisocyanate block assumes the rod shape (56). Vinyl-, 9-decenyl-, or β-allyloxyethyl isocyanate undergoes copolymerization reactions with styrene or methyl methacrylate (57).

The anionic copolymerization of isocyanates and ketenes is conducted in DMF at −60°C, using sodium cyanide as initiator. This method gives copolymers of dimethylketene and isocyanates (58) and diphenylketene and phenyl isocyanate (59). The structure of the copolymers **5** was elucidated by spectral and degradative studies (60).

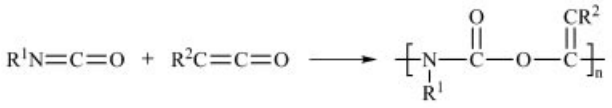

5

The sterically hindered *o*-methoxyphenyl isocyanate does not copolymerize with ketenes. Copolymers derived from isocyanates and ketenes are listed in Table 6.

Alkoxyallenes **6** and aryl isocyanates undergo copolymerization at 80°C to give alternating polyamide copolymers **7** (61).

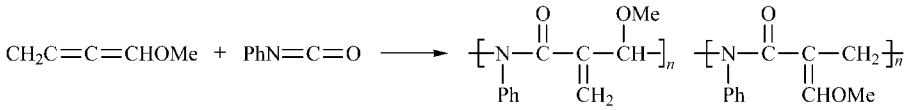

6 **7**

The same alternating copolymers are obtained from methoxyallene and *p*-chlorophenyl isocyanate. Initiators are not required in this copolymerization reaction (62).

Copolymers of diynes **8** with phenyl isocyanate afford poly(2-pyridones) **9**. This copolymerization reaction uses nickel(0) complexes as initiators (63).

Table 6. Copolymers from Isocyanates and Ketenes

Ketene	Isocyanate	Ratio	Yield, %	Melt temp., °C
Diphenyl	Phenyl		70	179–186
Phenylmethyl	Phenyl		30	200–204
Phenylethyl	Phenyl	0.84:1	4	170–179
Phenylethyl	Phenyl	1.3:1	12	186–197
Phenylethyl	Phenyl	2:1	40	189–199
Phenylethyl	Phenyl	3.2:1	51	201–220
Phenylethyl	*p*-Chlorophenyl	1:1	45	152–167
Phenylethyl	*m*-Chlorophenyl	1:1	18	148–156
Phenylethyl	*p*-Methoxyphenyl	3:1	22	174–185
Phenylethyl	*p*-Methoxyphenyl	4:1	35	178–192
Phenylethyl	*p*-Methoxyphenyl	6.5:1	63	203–209
Phenylethyl	*m*-Methoxyphenyl	1:1	7	167–175
Phenylethyl	*m*-Methoxyphenyl	1.5:1	29	180–192
Phenylethyl	*m*-Methoxyphenyl	2:1	46	167–182

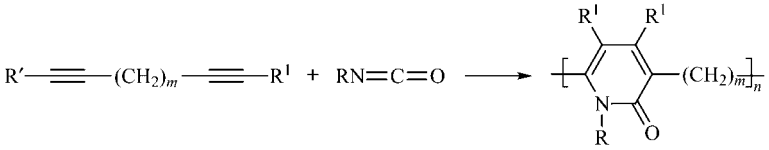

8 **9**

From diethynylbenzene and aromatic or aliphatic isocyanates also copolymers are obtained. Aryl isocyanates produce 1:1 copolymers using equimolar amounts of the monomers. An excess of aliphatic isocyanates is necessary to give the 1:1 copolymers (64). Similarly, from 1,4-bis(phenylethynyl)benzene and alkyl- or aryl isocyanates rigid poly(2-pyridones) are obtained (65). Soluble ladder poly(2-pyridones) are obtained from macrocyclic diynes and aryl- or alkyl isocyanates (66).

Anionic copolymerization of isocyanates with chloral (67), cyanopropionaldehyde (68), and acrolein dimer (69) is also known. For example, reaction of phenyl isocyanate with chloral in DMF at −68°C, using potassium cyanide as initiator, affords chloroform-soluble copolymers **10**, which melt at about 230°C (67).

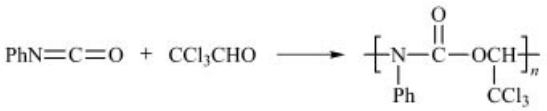

10

Copolymers produced in diethyl ether with *n*-butyllithium as initiator are insoluble and melt as high as 329°C. The infrared and melting point data indicate a marked difference in crystallinity of the differently initiated copolymers.

The reaction of cyanopropionaldehyde with methyl isocyanate, initiated with the benzophenone dilithium complex at −78°C affords a 1:1 copolymer (68). Also,

copolymerization of acrolein dimer with methyl-, ethyl-, or phenyl isocyanate at 15°C in toluene affords 1:1 copolymers (69). The copolymerization of ethylene oxide with aromatic isocyanates is conducted in toluene at −78°C, using triethylaluminum as initiator.The shown acetal structure **11** is proposed for the copolymer (70).

11

Alkyl isocyanates do not copolymerize with ethylene oxide.

Block copolymers are obtained from aromatic diisocyanates and vinyl monomers, such as styrene, isoprene, and methyl methacrylate via anionic polymerization, using *n*-butyllithium as initiator (71). Since TDI undergoes selective reaction through the nonhindered isocyanato group poly(butadiene-*block*-imide) block copolymers are obtained (72).

Addition Polymers

The reaction of MDI with enamines produces polyamides by a [2+2] cycloaddition reaction across the C=C bond. Ring opening in the initial reaction forms an amide bond and regenerates the double bond, which undergoes the same reactions again (73). With formic acid in DMF the enamine polymer hydrolyzes to give the corresponding keto polymer (74). From MDI **12** and ketene aminals **13**, polyamides **14** are formed in a similar manner (75). These reactions can be performed in a RIM machine.

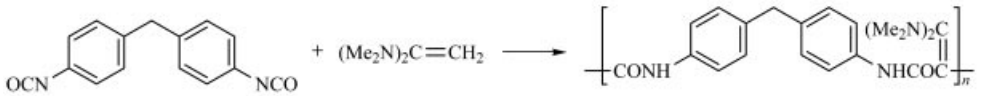

12 **13** **14**

Glycidyl ethers derived from bisphenol A (**15**) or diglycidyl tetrephthalate can also be used as monomers in diisocyanate reactions. The reaction of 2,4-TDI with **15** proceeds by ring-opening [2+3] cycloaddition polymerization across the 1,3-dipol generated from the bis-epoxides to form a linear poly(2-oxazolidinone) (**16**) (76).

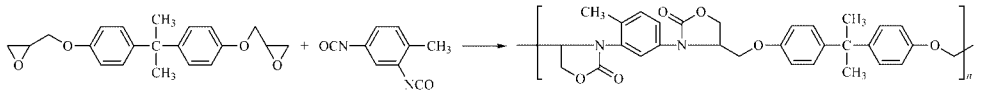

15 **16**

The reaction of bis-epoxides with aromatic diisocyanates can also be conducted in DMF in the presence of lithium chloride (77).

Diisocyanates also react with other difunctional nucleophiles to give addition polymers. The use of hydrazine as extender in the manufacture of Spandex fibers

is discussed under polyurethanes. Reaction of MDI with isophthalic dihydrazides **17** in DMSO affords poly(semicarbazides) **18** (78). Dioximes and diisocyanates react in a similar manner to give polyaddition products (79).

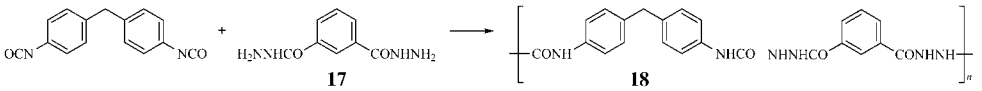

The polyaddition reaction of MDI with benzyloxamine in dimethylacetamide (DMAc) in the presence of 1,8-diazabicyclo [5-3-0] undec-7-ene (DBU) affords a poly(biuret) (80).

Condensation Polymers

Polycarbodiimides **19** are obtained from diisocyanates by the phospholene oxide catalyzed condensation–elimination sequence (81).

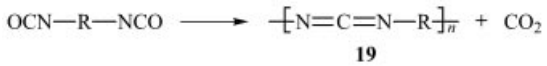

The reaction proceeds at room temperature at a sufficiently fast rate to allow fabrication of polymers from liquid monomers. However, only thermosets are produced because of cross-linking of the linear poly(carbodiimides). The generated carbon dioxide can be utilized as a blowing agent and low density cellular products are readily obtained from PMDI (82). Copolymerization of diisocyanates and monoisocyanates, the latter as chain stoppers, affords processable oligomeric carbodiimides. For example, polymerization of MDI with controlled amounts of phenyl isocyanate in xylene at 120°C, using 1-phenyl-3-methyl-2-phospholene oxide as the catalyst, affords low molecular weight linear carbodiimides (83). The reaction of HDI with a phospholene oxide catalyst affords low molecular weight trifunctional oligomers, in which the isocyanate and the carbodiimide groups are cotrimerized with the generated carbon dioxide (84).

Carbodiimide groups undergo a [2+2] cycloaddition reaction with isocyanates to form four-membered ring cycloadducts. This reaction is used to convert the low melting MDI into a liquid commercial product (Isonate 143-L) (85) The liquid MDI is used in RIM applications.

The manufacture of polyamides by reaction polymerization of MDI with macrodicarboxylic acids, dicarboxylic acids, and trimellitic acid anhydride was pioneered in the 1970s at the D.S. Gilmore Research Labs of the Upjohn Co (86). Some of these products are commercially available from Dow. For example, segmented polyamide elastomers are obtained in the reaction of MDI with dicarboxylic acids and a carboxylic acid terminated aliphatic polyester, polycarbonate, or polyether prepolymer with an average molecular weight of M_n 500–5000 (87). The dicarboxylic acid serves as the hard segment chain extender and the macrodicarboxylic acid forms the soft-segment matrix for the polyamide elastomers. The reaction is conducted in a polar solvent, using a phospholene oxide catalyst. Preferrably, a

continuous reaction in a vented extruder is used. The polyamide elastomers produced in this manner have light yellow to brown color and they are soluble in polar solvents. Molecular weights in inherent viscosity terms range between 0.8 and 1.1 dL/g measured as 0.5 wt% solution in *N*-methylpyrrolidinone (NMP). Polyamide elastomers retain useful tensil properties where most other thermoplastic elastomers cannot even be tested. Polyesteramide elastomers are also resistant to dry heat aging at 150°C. Alloys of poly(ethylene adipate) (PEAs) with nylon-66 and poly(butylene terephthalate) (PBT) display useful high temperature properties and improved impact properties, respectively.

Homopolymers derived from MDI and azelaic acid are semicrystalline engineering plastics with a T_g of 135°C and a T_m of 290°C (88). Copolymers of MDI with azelaic acid, containing 20–30 mol% of adipic acid show a eutectic T_m of approximately 240°C. These amorphous or slightly crystalline copolymers have mechanical properties comparable to transparent nylons or polycarbonates. Although injection molded samples are transparent, they will crystallize and turn opaque. Copolyamides derived from MDI and aromatic dicarboxylic acids are more difficult to prepare. Because of the very high T_m (420°C) of the isophthalic acid/MDI block it was necessary to prevent the formation of any appreciable crystalline blocks, which was accomplished by prereacting a portion of the isophthalic acid (15–20 mol%) with 2,4-TDI. In this manner crystallization of the isophthalic acid/MDI blocks was surpressed (89). Thus, copolyamides containing IPA/azelaic acid (50:50) are obtained with thermal and mechanical properties similar to polysulfone.

The preparation of poly(amide imides) from isocyanates was explored by Rhone Poulenc, Amoco, and Upjohn (now Dow). For example, MDI was reacted with trimellitic acid anhydride in NMP and the solutions were directly converted into films (Rhodeftal) or fibers (Kermel). When the polymer is isolated it crosslinks, and it can no longer be redissolved. Upjohn produced poly(amide imides) from MDI and trimellitic acid anhydride or from MDI, trimellitic acid anhydride, and various dicarboxylic acid as comonomers in tetramethylene sulfone (90). In this manner high molecular weight polymers are obtained, which can be redissolved in polar solvents, such as DMF or NMP after isolation. As an example, PAI 8020 was made by reacting a 80:20 mol% mixture trimellitic acid anhydride/isophthalic acid with MDI. PAI 8020 would not injection mold by itself unless modified by copolymerization or alloying with other thermoplastics. Its high temperature properties can be further enhanced by blending with polyimide 2080 (see below). Films of PAI 8020 are useful as cable and wire wrap and in other high temperature applications. Poly(amide imide) foams have also been prepared from PMDI and trimellitic acid anhydride (91,92).

Polyimides are also obtained in one step in the reaction of diisocyanates with tetracarboxylic acid dianhydrides. As an example, BTDA is reacted with a mixture of 2,4-TDI and MDI in DMF (93). This copolyimide, PI 2080, is used as a high temperature fiber and it is also sinter molded into solid shapes with exceptional mechanical properties. From PMDI and benzophenone-tetracarboxylic acid dianhydride polyimide foams with outstanding thermal properties and flame resistance are produced (94). Polyimides derived from *p*-phenylene diisocyanate (PPDI) or naphthalene diisocyanate (NDI) and pyromellitic dianhydride or BTDA are also synthesized using DMAc as solvent (95).

An A–B polyimide is also obtained from 4-isocyanatophthalic anhydride (49). Processable polyimides **21** are obtained from the diisocyanate **20** and pyromellitic dianhydride (96).

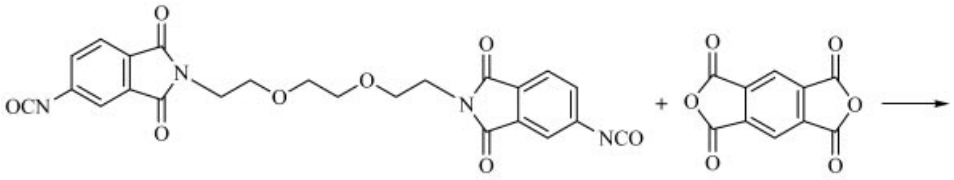

20

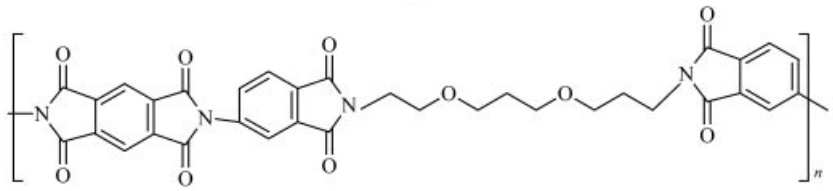

21

Poly(arylene ethers) are obtained from *n*-propyl isocyanate blocked highly aromatic bisphenols and difluoroarenes. In this manner polymers containing hole (electron) transport moieties are obtained (97).

Addition/Condensation Polymers

High temperature resistant heterocyclic polymers are obtained from diisocyanates and suitable monomers containing groups which undergo addition polymerization, followed by condensation polymerization reactions with neighboring groups. For example, dihydroxydicarboxylic esters **22** react with MDI in DMSO, in the presence of a tertiary amine catalyst, to form linear addition polymers, which undergo subsequent cyclization to produce poly(benzoxazindiones) **23** (9).

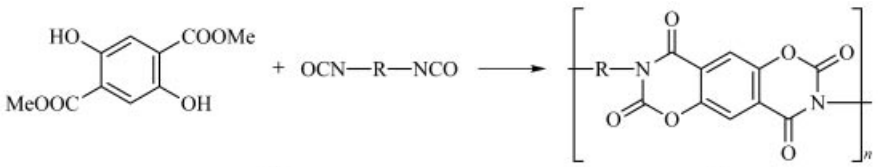

22 **23**

The addition/condensation polymers derived from dihydroxybiphenyl dicarboxylate and diphenylether-4,4-diisocyanate have outstanding thermal stability (−180 to 300°C). The hydrolytic stability of poly(benzoxazinedione) films to concentrated acids and dilute bases is excellent.

Similarly, 4,4′-diaminobiphenyl-3,3′-dicarboxylic acid (**24**) reacts with diisocyanates to produce linear polyureas **25**, which on dehydration at 160–180°C give the condensation polymers **26**. Further heating of **26** to 230–250°C causes

rearrangement to give poly(quinazolinediones) **27**, a polymer exhibiting outstanding thermal stability (98). The polymerization can also be conducted in polyphosphoric acid.

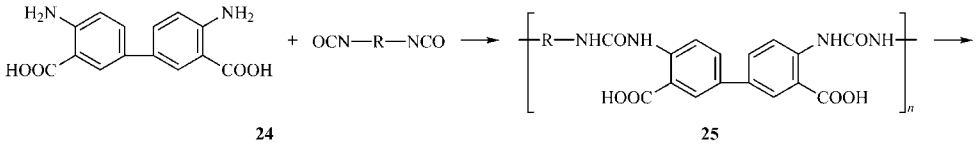

24 **25**

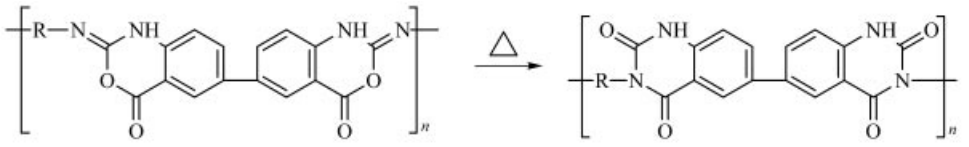

26 **27**

Reaction of MDI with hydrogen cyanide gives linear cyanoformamidines **28**, which cyclize to give poly(iminoimidazolidinones) **29**. The latter are hydrolyzed to poly(parabanic acids) **30** (10).

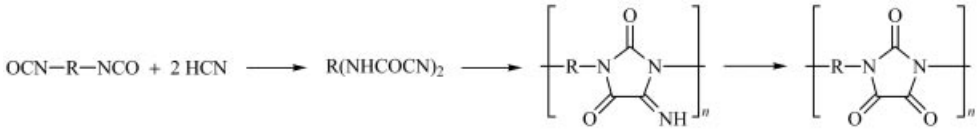

28 **29** **30**

The reaction of diisocyanates with difunctional glycinates **31** affords linear polymers **32**, which cyclize to form poly(hydantoins) **33**. Phenol and cresol are the preferred solvents, and the cresol solutions of **33** can be used directly for wire coating and other applications (99).

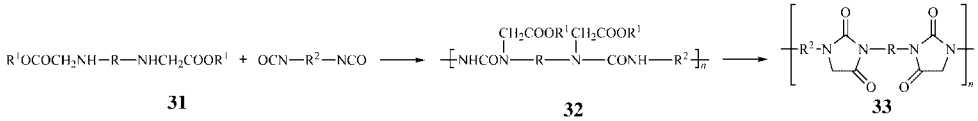

31 **32** **33**

Another approach to poly(hydantoins) involves cyclization of α-cyanoalkyl substituted polyureas, obtained from aromatic diisocyanates and the corresponding nitriles. Hydrolysis of the resultant poly(iminoimidazolidinones) affords poly(hydantoins) (100).

The reaction of aromatic diisocyanates with *N*,*N*-arylenedioxamide acid esters **34** affords poly(2,4,5-trioxoimidazolidines) **35** (101).

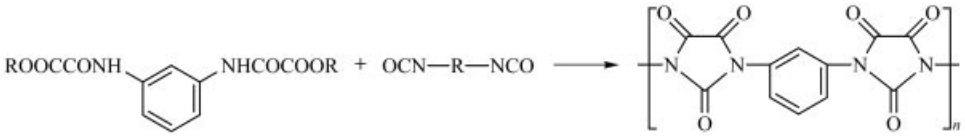

34 **35**

Poly(oxazolininediones) **36** are obtained from α-hydroxy acid esters and aromatic diisocyanates (99).

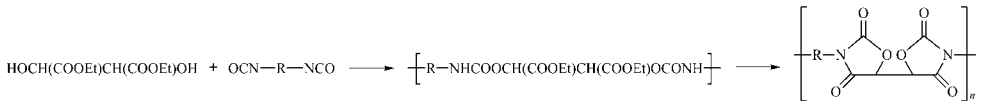

36

In the reaction of *N*,*N*′-bis(2-carbomethoxyethyl)-1,6-hexanediamine (**37**) with aromatic diisocyanates poly(hydrouracils) **38** are formed. The intermediate linear poly(ureas) are cyclized in polyphosphoric acid (100).

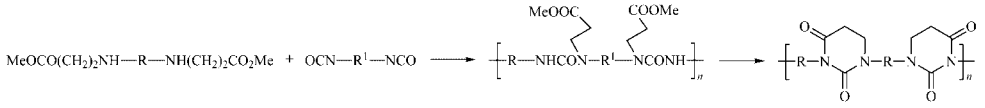

37 **38**

BIBLIOGRAPHY

"Isocyanate Polymers" in *EPST* 1st ed., Vol. 7, pp. 743–754, by C. G. Overberger, The University of Michigan and J. A. Moore, Polytechnic Institute of Brooklyn; "Isocyanate-Derived Polymers" in *EPSE* 2nd ed., Vol. 8, pp. 448–462, by Henri Ulrich, The Dow Chemical Company.

1. W. F. Gum, W. Riese, and H. Ulrich, *Reaction Polymers*, Hanser Publishers, Munich, 1992.
2. H. Ulrich, "Isocyanates Organic" in *Encyclopedia of Chemical Technology*, 4th ed., Vol. **14**, 1995, John Wiley & Sons, Inc., New York, 1995, pp. 982–934.
3. Y. Iwakura, K. Uno, and K. Ichikawa, *J. Polym. Sci., Part A* **2**, 3387 (1964).
4. W. J. Schnabel and E. Kober, *J. Org. Chem.* **34**, 1162 (1969).
5. E. Nachbaur, *Monatsh. Chem.* **97**, 361 (1966).
6. H. W. Bonk, A. A. Sardanopoli, H. Ulrich, and A. A. R. Sayigh, *J. Elastoplast.* **3**, 157 (1971).
7. H. Ulrich, *J. Polym. Sci., Macromol. Rev.* **11**, 93 (1976).
8. W. Neumann and P. Fischer, *Angew. Chem., Int. Ed.* **1**, 621 (1962).
9. L. Bottenbruch, *Angew. Macromol. Chem.* **13**, 109 (1970).
10. T. L. Patton, *Polym. Prepr.* **12**, 162 (1971).
11. A. A. R. Sayigh, H. Ulrich, and W. J. Farrissey Jr., in J. K. Stille and T. W. Campbell, eds., *Condensation Monomers*, John Wiley & Sons, Inc., New York, 1972, pp. 369–476.

12. K. Kurita, T. Matsumura, and Y. Iwakura, *J. Org. Chem.* **41**, 2070 (1976).
13. H. Eckert and B. Forster, *Angew. Chem.* **99**, 922 (1987).
14. H. W. Peerlings and E. W. Meijer, *Tetrahedron Lett.* **40**, 1021 (1999).
15. H. Ulrich, B. Tucker, and A. R. R. Sayigh, *J. Polym. Sci., Polym. Chem. Ed.* **13**, 267 (1975).
16. T. Iwamura, I. Tomita, M. Suzuki, and T. Endo, *J. Polym. Sci., Part A* **38**, 3440 (2000).
17. T. Iwamura, I. Tomita, M. Suzuki, and T. Endo, *J. Polym. Sci., Part A* **36**, 1515 (1998).
18. H. J. Laas, R. Halpaap, and J. Pedain, *J. Prakt. Chem.* **336**, 185 (1994).
19. M. R. Thomas, Preprints of papers presented by the Division of Organic Coatings and Plastic Chemistry at the 183rd National ACS Meeting, Las Vegas, 1982, p. 506.
20. D. H. Klein and W. J. Elms, *J. Paint Tech.* **43**, 68 (1971).
21. G. Maier, M. Naumann, H. P. Reisenauer, and J. Eckert, *Angew. Chem., Int. Ed.* **35**, 1696 (1996).
22. U.S. Pat. 5,246,557 (1993), A. H. Hughes and A. Topham (to The Baxenden Chemical Co.).
23. U.S. Pat. 4,134,816 (1979), J. F. Bosso and L. C. Sturni (to PPG Industries).
24. U.S. Pat. 4,604,450 (1986), S. A. Dai, S. J. Grossman, and K. Onder (to Upjohn).
25. L. H. Sperling, D. Klempner, and L. A. Utracki, *Interpenetrating Polymer Networks* (Advances in Chemistry Series No. 239), American Chemical Society, Washington, D.C., 1994.
26. Y. S. Yang and L. J. Lee, *Macromolecules* **20**, 1490 (1987).
27. V. E. Shashoua, W. Sweeny, and R. F. Tietz, *J. Am. Chem. Soc.* **82**, 866 (1959).
28. G. Natta, J. DiPietro, and M. Cambini, *Makromol. Chem.* **56**, 200 (1962).
29. Y. Okamoto, Y. Nagamura, K. Hatada, C. Kathri, and M. M. Green, *Macromolecules* **25**, 5536 (1992).
30. J. Pierre and E. Marshal, *J. Polym. Sci., Part B* **13**, 11 (1975).
31. M. Goodman and S. C. Chen, *Macromolecules* **4**, 625 (1971).
32. S. Lifson, C. Andreola, N. O. Peterson, and M. M. Green, *J. Am. Chem. Soc.* **111**, 8850 (1989).
33. C. G. Overberger, S. Ozaki, and H. Mukamal, *J. Polym. Sci., Part B* **2**, 627 (1964).
34. T. E. Patten and B. M. Novak, *Macromolecules* **26**, 436 (1993).
35. T. E. Patten and B. M. Novak, *Polym. Prepr. (Am. Chem. Soc., Polym. Div.)* **33**, 172 (1992).
36. W. Mormann, *Makromol. Chem., Macromol. Symp.* **25**, 117 (1989).
37. W. Mormann, A. Schwabe, and R. Sikora, *Makromol. Chem.* **187**, 133 (1986).
38. A. W. Levine, M. Kaplan, and J. Fech Jr., *J. Polym. Sci., Part A-1* **11**, 311 (1973).
39. M. Müller and R. Zentel, *Macromolecules* **27**, 4404 (1994).
40. A. J. Bur and L. J. Fetters, *Chem. Rev.* **76**, 727 (1976).
41. B. M. Novak, T. E. Patten, and S. M. Hoff, *J. Macromol. Sci., A: Pure Appl. Chem.* **31**, 1619 (1994).
42. M. Morton and L. J. Fetter, *Macromol. Rev.* **2**, 101 (1967).
43. J. Wang, R. Nomura, and T. Endo, *J. Polym. Sci., Part A* **33**, 869 (1995).
44. A. Suda, K. Nishimura, Y. Nakamura, and T. Endo, *J. Polym. Sci., Part A* **37**, 4483 (1999).
45. S. R. Gaonkar, N. Y. Sapre, S. Bhaduri, and G. Sudesh, *Macromolecules* **23**, 3533 (1990).
46. H. Ulrich, R. Richter, and B. Tucker, *Synthesis* 277 (1979).
47. R. M. Versteegen, R. P. Sijbesma, and E. W. Meijer, *Angew. Chem., Int. Ed.* **38**, 2917 (1999).
48. DE Pat. 3,135,489 (1983), J. Disteldorf, W. Huebel, and R. Reiffer (to Huels).
49. H. Ulrich and R. H. Richter, *J. Org. Chem.* **38**, 2557 (1973).
50. Y. Iwakura, K. Hayashi, S. Kang, and K. Inagaki, *Makromol. Chem.* **95**, 205 (1966).

51. L. M. Alberino, H. Ulrich, and A. A. R. Sayigh, *J. Polym. Sci., Part A* **5**, 3212 (1967).
52. A. Kumar and S. Ramakrishnan, *J. Chem. Soc., Chem. Commun.* 1453 (1993).
53. R. Spindler and J. M. J. Frechet, *Macromolecules* **26**, 4809 (1993).
54. W. Mormann and K. Schmalz, *Macromol. Rapid Commun.* **13**, 377 (1992).
55. J. J. Fetters, *J. Res. Natl. Bur. Stand. A* **70**, 421 (1966).
56. J. T. Chen, E. L. Thomas, C. K. Ober, and C. S. Wang, *Macromolecules* **28**, 1688 (1995).
57. G. B. Butler and S. B. Monroe, *J. Macromol. Sci., Part A: Chem.* **5**, 1057 (1971).
58. Y. Yamashita, S. Nunomoto, and S. Miura, *Kogyo Kagaku Zasshi* **69**, 317 (1966).
59. S. Nunomoto and Y. Yamashita, *Kogyo Kagaku Zasshi* **71**, 2067 (1968).
60. E. Dyer and E. Sineich, *J. Polym. Sci., Part A-1* **11**, 1249 (1973).
61. J. Mizuja, T. Yokozawa, and T. Endo, *Macromolecules* **24**, 2299 (1991).
62. J. Mizuja, T. Yokozawa, and T. Endo, *Chem. Lett.* 479 (1989).
63. T. Tsuda and H. Hokazono, *Macromolecules* **26**, 1796 (1993).
64. T. Tsuda and A. Tobisawa, *Macromolecules* **28**, 1360 (1995).
65. T. Tsuda and A. Tobisawa, *Macromolecules* **27**, 5943 (1994).
66. T. Tsuda and H. Hokazono, *Macromolecules* **26**, 5528 (1993).
67. G. Odian and L. S. Hiraoka, *J. Polym. Sci., Part A-1* **8**, 1309 (1970).
68. K. Hashimoto and H. Sumitomo, *J. Polym. Sci., Part A-1* **9**, 107 (1971).
69. Y. Kitahana, H. Ohama, and H. Kobayashi, *J. Polym. Sci., Part A-1* **7**, 935 (1969).
70. K. Harada, A. Deguchi, J. Furukawa, and S. Yamashita, *Macromol. Chem.* **132**, 281, 295 (1970).
71. R. A. Godfrey and G. W. Miller, *J. Polym. Sci., Part A-1* **7**, 2387 (1969).
72. W. L. Hergenrother and R. J. Ambrose, *J. Polym. Sci., Polym. Lett.* **12**, 343 (1974).
73. D. F. Regelman and L. M. Alberino, *Org. Coatings* **44**, 151, 157 (1981).
74. W. H. Daly, Polymer Preprints of the 152nd Meeting of the ACS, New York 1966, p. 569.
75. D. F. Regelman, L. M. Alberino, and R. J. Lockwood, *ACS Symp. Ser.* **270**, 125 (1985); see also N. Kihara, Y. Sugimoto, and T. Endo, *J. Polym. Sci., Part A* **37**, 3079 (1999).
76. S. R. Sandler, F. Berg, and G. Kitazawa, *J. Appl. Polym. Sci.* **9**, 1994 (1965).
77. J. E. Herweh and W. Y. Whimore, *J. Polym. Sci., Part A-1* **8**, 2759 (1970).
78. E. A. Tomic, T. W. Campbell, and V. S. Foldi, *J. Polym. Sci.* **62**, 387 (1962).
79. T. W. Campbell, V. S. Foldi, and R. G. Parrish, *J. Appl. Polym. Sci.* **2**, 81 (1959).
80. S. Ishii, S. Watanabe, S. Nishimura, and K. Kurita, *J. Polym. Sci., Part A* **32**, 575 (1994).
81. T. W. Campbell and V. S. Foldi, *Macromol. Synthesis* **3**, 109 (1968).
82. H. Ulrich and H. E. Raymore, *J. Cell. Plast.* **21**, 350 (1985).
83. L. M. Alberino, W. J. Farrisseey Jr., and A. A. R. Sayigh, *J. Appl. Polym. Sci.* **21**, 999 (1977).
84. K. Wagner, K. Findeisen, W. Schaefer, and W. Dietrich, *Angew. Chem.* **93**, 855 (1981).
85. U.S. Pat. 3,384,653 (1968), W. E. Erner and A. Odinak (to Upjohn).
86. K. Onder, in Ref. 1, pp. 405–452.
87. U.S. Pat. 4,649,180 (1987), K. Onder and A. T. Chen (to Upjohn).
88. K. Onder and A. T. Chen, *Polym. Eng. Sci.* **25**, 942 (1985).
89. K. Onder, P. S. Andrews, W. J. Farrissey Jr., and J. N. Tilley, *Polym. Prepr.* **21**(2), 130 (1980).
90. U.S. Pat. 4,225,686 (1980), K. Onder and F. R. Recchia (to Upjohn).
91. S. Terney, J. Keating, J. Zielinski, J. Hakala, and H. Scheffer, *J. Polym. Sci., Part A-1* **8**, 683 (1970).
92. U.S. Pat. 4,738,990 (1988), G. R. Nelb and K. G. Saunders (to the Dow Chemical Company).
93. U.S. Pat. 3,787,367 (1974), W. J. Farrissey Jr. and P. S. Andrews (to Upjohn).
94. W. J. Farrissey Jr., J. S. Rose, and P. S. Carleton, *J. Appl. Polym. Sci.* **14**, 1093 (1970).

95. M. Barikani and S. Medipour Ataei, *J. Polym. Sci. Part A* **37**, 2245 (1999).
96. H. Yeganeh and S. Medipour Ataei, *J. Polym. Sci., Part A* **38**, 1528 (2000).
97. J. Lu, A. R. Hill, A. S. Hay, T. Maindron, J. Dodelet, J. Lam, and M. D'iorio, *J. Polym. Sci., Part A* **38**, 2740 (2000).
98. N. Yoda, R. Nakanishi, M. Kurihara, Y. Bamba, S. Tohyama, and K. Ikeda, *Polym. Lett.* **4**, 11 (1966).
99. R. Mertin, *Angew. Chem.* **83**, 339 (1971).
100. E. Dyer and J. Hartzler, *J. Polym. Sci., Part A* **17**, 833 (1969).
101. E. Kraft and J. Reese, *Angew. Chem.* **85**, 982 (1973).

HENRI ULRICH
Consultant

LANGMUIR–BLODGETT FILMS

Introduction

Langmuir–Blodgett (LB) films, one of the earliest examples of smart materials, provide the opportunity to control the structure of thin films at the molecular level. In this method, a single layer of molecules is first organized on a liquid surface, usually water, before being transferred onto a solid support to form a thin film whose thickness is a constituent molecule. If the process is repeated, multilayered films can be prepared. The layer of molecules on a liquid surface is termed a *Langmuir monolayer*, and after transfer it is called a *Langmuir–Blodgett film*. The ability to control the thickness of an organic film at the molecular level and to control the placement of molecules in multilayer assemblies forms the basis of many "smart" applications of LB films. Applications include electronics, optics, microlithography, and chemical sensors, as well as biosensors and biochemical probes. Many comprehensive review articles and books exist on the subject of LB films (1–4).

History

The technique is named after Irving Langmuir and Katharine Blodgett, researchers at the General Electric Co. in the first half of the twentieth century. Langmuir, who was awarded the Nobel prize for chemistry in 1932 for his studies of surface chemistry, used floating monolayers to learn about the nature of intermolecular forces. In the course of his studies, Langmuir developed several new techniques that are still used today in studying monomolecular films. Together with Langmuir, Katharine Blodgett refined the method of transferring the floating monolayer onto solid supports. In addition to treating many practical details of LB

Encyclopedia of Polymer Science and Technology. Copyright John Wiley & Sons, Inc. All rights reserved.

methods, publications and patents by Langmuir and Blodgett cover a number of potential applications, including controlling the reflectivity of glass, a step gauge for optically measuring the thickness of thin films, submicrometer mechanical filters, and biosensing.

Although the methods are commonly named after Langmuir and Blodgett, numerous observations and experiments on floating organic films predate them (1,5,6). The practice of pouring oil on water to calm choppy seas has been known for centuries. Benjamin Franklin, however, who was aware of the effect, is credited with the earliest scientific account of spreading oil on water, which he reported in a paper presented to the Royal Society and published in 1774. An extract from that paper reads as follows (1):

> At length being at Clapham where there is, on the common, a large pond, which I observed to be one day very rough with the wind, I fetched out a cruet of oil, and dropped a little of it on the water. I saw it spread itself with surprising swiftness upon the surface. . .
> In these experiments, one circumstance struck me with particular surprise. This was the sudden, wide and forcible spreading of a drop of oil on the face of water. . . it spreads instantly, many feet around, becoming so thin as to produce the prismatic colors, for a considerable space, and beyond them so much thinner as to be invisible, except in its effect of smoothing the waves at a much greater distance. It seems as if a mutual repulsion between its particles took place as soon as it touched the water. . .

In the late 1800s, Lord Rayleigh became interested in surface layers on water. When Langmuir determined that certain films on water indeed had the thickness of only one molecule, it confirmed an earlier suggestion by Rayleigh. After publishing on the way overlayers on water influenced surface tension, he received a communication from Agnes Pockels who had quantified that the surface tension of water depended on the surface coverage of "contaminant." Building on Pockels's method of measurement, Rayleigh went on to estimate the size of an olive oil "molecule."

Modern studies of floating monolayers and LB films fall largely into two areas. The first area includes detailed fundamental studies of the physical nature and structure of Langmuir monolayers and LB films. The second involves applications that take advantage of thin films that have controlled thickness and composition. Much of the current work on applications derives inspiration from the pioneering work of Hans Kuhn in the 1960s (7). Kuhn used LB methods to control the position and orientation of functional molecules within complex assemblies, an elegant early example of what is currently being called "supramolecular assembly." To acknowledge Kuhn's contributions, some authors now use the term Langmuir–Blodgett–Kuhn (LBK) films for transferred films of functional molecules.

Equipment

References 1 and 2 both discuss common equipment. Essentially, all LB film work begins with the Langmuir–Blodgett trough (alternatively called Langmuir trough

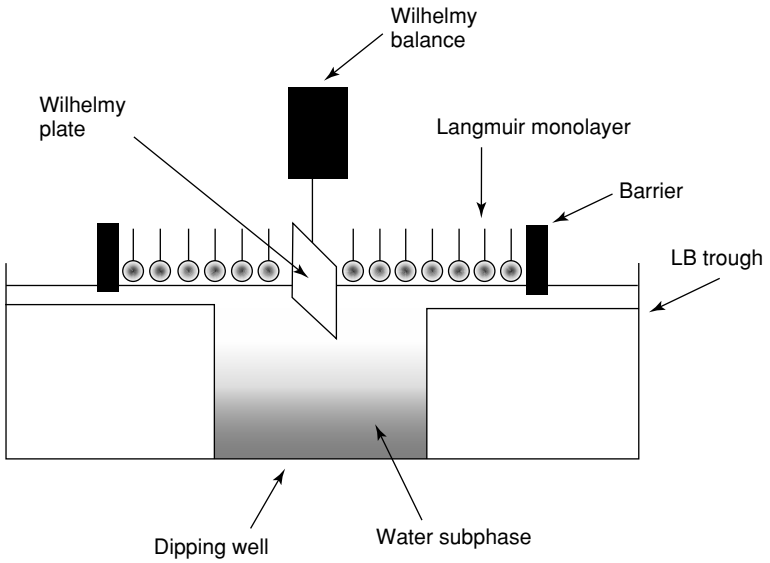

Fig. 1. Schematic of a Langmuir trough and its components.

or Langmuir film balance), which, save for modern materials and electronics, is similar in design and function to the early apparatuses of Pockels and of Langmuir. The trough that contains the subphase is normally about 1 cm deep. The surface area can range from about 100 cm^2 for smaller troughs to more than 1 m^2 for larger systems, designed primarily for transferring large amounts of material. Modern troughs are generally inert and hydrophobic, for example, made from or coated with Teflon or a similar polymer. Moveable barriers that can skim the surface of the subphase permit controlling the surface area available to the floating monolayer. The simplest approach is a bar that moves across the top of a rectangular trough, as shown in Figure 1. For transfer onto solid supports, troughs contain a dipping well—a section that is deep enough to allow immersing the substrate into the subphase—and a sample holder that can vertically displace the substrate. A photo of a complete LB film system is shown in Figure 2.

The rectangular trough that has a moveable barrier is the most common design, but other systems are also widely used. Some variations include circular troughs, systems that use a continuous flexible belt for compression, moving-wall troughs, and troughs designed for continuous deposition or alternate layer deposition. All systems are equipped with a mechanism for monitoring the state of the monolayer on the water surface during the course of experiments, usually, by measuring the surface pressure using either a Wilhelmy plate or Langmuir balance.

Film-Forming Molecules and Polymers

The classic "LB active" molecules are fatty acids such as stearic acid (**1**). The long-chain examples, *n*-octadecanoic (stearic), *n*-eicosanoic (arachidic), and *n*-docosanoic (behenic) acids constitute the best-studied class of Langmuir monolayers and LB films; work dates back to the original papers by Langmuir and

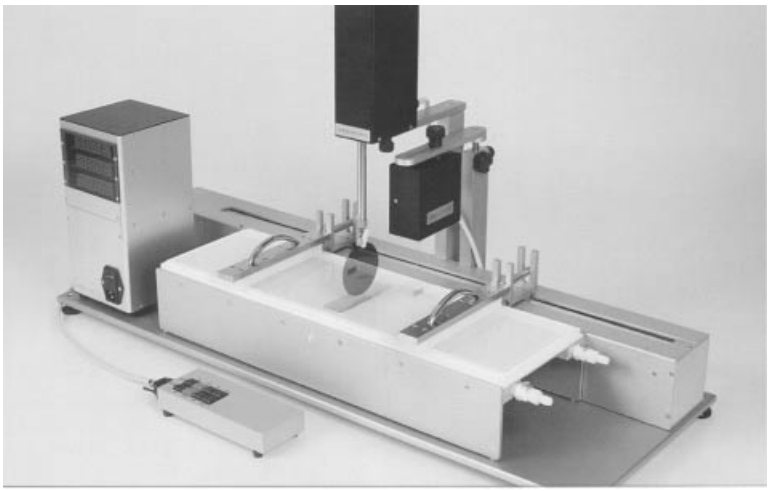

Fig. 2. Photograph of a modern Langmuir–Blodgett system. Courtesy of KSV Instruments.

Blodgett. These molecules can be used to demonstrate most of the principles involved in floating monolayers. However, Langmuir monolayers can be prepared from many variations of straight-chain molecules, polymerizable molecules, polymers, and conductive materials (1,2,4,8).

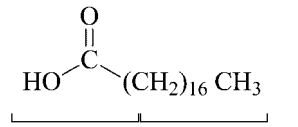

Hydrophilic head group — Hydrophobic chain

1

Fatty Acids. Fatty acids possess clearly defined hydrophilic (carboxylic acid) head groups and hydrophobic (linear alkane) tails. The amphiphilic nature of these molecules leads to a preferred orientation at the air–water interface, where the hydrophobic tails extend from the water surface. Other film-forming molecules normally possess similar hydrophobic and hydrophilic parts. For example, replacing the carboxylic acid by other functional head groups leads to alkylamines, amides, nitriles, esters, alcohols, and phosphonic acids, all of which form Langmuir monolayers. In addition to the head groups, the hydrophobic tail can be modified. Double bonds, triple bonds, and aromatic groups can normally be incorporated into the hydrophobic tail, and the film-forming properties are retained. In addition to hydrocarbon amphiphiles, molecules that have fluorocarbon tails also form Langmuir monolayers.

Phospholipids and Related Biomolecules. The structural features of phospholipids that lead to naturally occurring bilayer structures, such as those found in biological membranes, also make them good film-forming amphiphiles.

The double hydrocarbon chains can be saturated, or they can contain double bonds. The state of the monolayer, whether it is expanded or condensed, at a given temperature depends on the length and nature of the hydrocarbon chains. The polar head groups vary, but all contain phosphate groups that are anionic at neutral pH. Phosphatidic acids, phosphatidylethanolamines (cephalins), phosphatidylcholines (lecithins), and phosphatidylserines are some of the many types of phospholipids studied as Langmuir monolayers. Other components of biological membranes also form Langmuir monolayers. Derivatives of sterols (such as cholesterol), naturally occurring pigments (porphyrins and carotenes) (9), cellulose (10), vitamin B_{12} (11), and proteins have been incorporated into monolayers as single-component films or as mixtures. Commonly, fatty acid molecules are employed in mixtures to stabilize monolayers of compounds that may not form stable monolayers alone.

Polymers. Polymeric monolayers are formed either by spreading preformed polymers or by polymerizing reactive monomers on the water surface. A large variety of preformed polymers has been studied, including polyacrylates and polymethacrylates, poly(vinyl butyral), poly(vinyl methyl ether), poly(vinyl acetate), poly(vinyl fluoride), poly(vinylidene fluoride), (12), silicone copolymers, maleic anhydride copolymers, and polypeptides (1). Monomers that have been successfully polymerized at the air–water interface include derivatives of aniline (13), vinyl alcohol (14), and styrene (15). In addition to the interesting chemistry and the two-dimensional structural control, polymer LB films are much more robust than films formed from straight-chain amphiphiles.

Langmuir Monolayer Formation

To form a Langmuir monolayer, the molecule of interest is dissolved in a volatile organic solvent (frequently chloroform or hexane) that will not react with or dissolve in the subphase (1,2,4). A quantity of this solution is placed on the surface of the subphase, and as the solvent evaporates, the surfactant molecules spread and alter the surface pressure of the water surface. A barrier designed to measure this surface pressure (Π), relative to that of the pure subphase, is the principle behind the Langmuir balance. Alternatively, the surface pressure is measured as the difference between the surface tension (γ) of the monolayer and that of the pure subphase (γ_0), $\Pi = \gamma_0 - \gamma$. A common method for measuring surface tension involves using a Wilhelmy plate, usually a piece of platinum or paper that is wetted by the subphase, suspended from a balance. As the monolayer is compressed by using the moveable barrier to reduce the surface area, the surface pressure increases. A plot of the surface pressure versus surface area is called a pressure versus area isotherm (or Π–A isotherm). Isotherms are normally plotted in terms of area/molecule, and the units of surface pressure are mN/m.

A representative pressure versus area isotherm is shown in Figure 3. As the pressure increases, the two-dimensional monolayer goes through different phases that have some analogy to three-dimensional gas, liquid, and solid states. If the area/molecule is sufficiently high, the floating film is in a two-dimensional gas phase where the surfactant molecules are not interacting. As the monolayer is compressed, the pressure rises, signaling a change in phase. The molecules begin

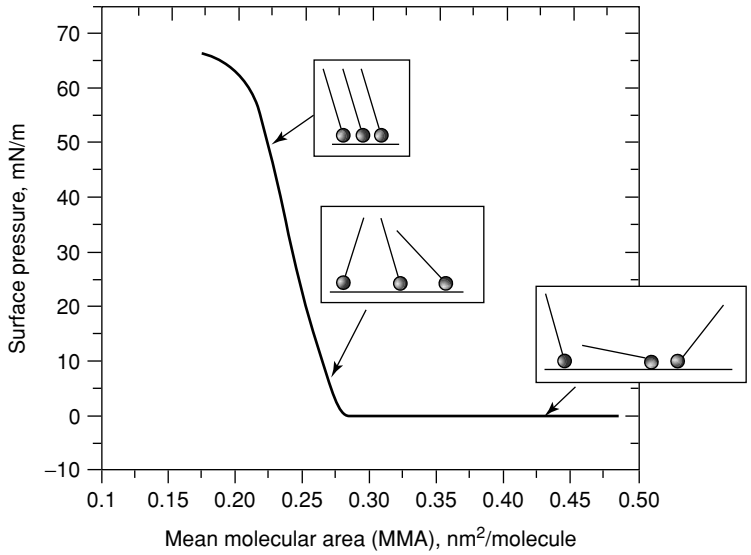

Fig. 3. A representative pressure vs. area isotherm. The cartoons represent idealized gas-analogous, liquid-expanded, and liquid-condensed phases of the monolayer. Two phases often coexist at a given temperature and surface pressure.

to interact, forming a two-dimensional phase, called a liquid-expanded (LE) phase, which is analogous to a three-dimensional liquid. Upon further compression, the pressure begins to rise more steeply, as the liquid-expanded phase gives way to a condensed phase (or a series of condensed phases). This transition, analogous to a liquid–solid transition in three dimensions, does not normally result in a true two-dimensional solid. Rather, condensed phases tend to be liquid crystalline in nature and are called liquid-condensed (LC) phases. Condensed phases have low compressibility, so the slope of the Π–A curve becomes quite steep. As the pressure is increased further, the monolayer eventually collapses under the pressure and either slides over upon itself or folds under into the subphase. When two phases such as gas and LE or LE and LC phases are in equilibrium, the surface pressure plateaus across a range of mean molecular areas. An image of two phases in equilibrium is shown in Figure 4.

The mean molecular area of an amphiphile is determined foremost by the size of the hydrophilic head group and its interactions with counterions in the subphase and with other head groups within the plane. Once these interactions are at an energetic minimum, the alkyl chains pack to maximize both van der Waals interactions and alkane density. By extrapolating the steepest part of the curve before the collapse at zero pressure, a minimum cross-sectional area per molecule can be found. This approach was one of the original methods used in attempts to measure the size of a molecule.

Isotherms differ from one molecule to another, and they also differ as a function of temperature. Monolayers, like three-dimensional substances, undergo temperature-dependent phase transitions. At any given temperature, the monolayer may pass through several phases during compression, or only a couple. The various states of monolayers can be detected in a number of ways, including surface potential measurements, optical spectroscopy, and optical imaging. One imaging

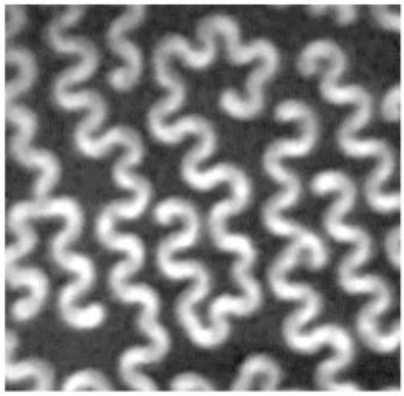

Fig. 4. Brewster angle micrograph of stearylamine on a water/glycerol subphase, showing contrast between liquid-expanded (darker regions) and liquid-compressed (lighter regions) phases. Photo courtesy of C. Mingotaud.

method is fluorescence microscopy, which involves adding to the subphase a fluorescent probe molecule that will be either included or excluded from the surface layer, depending on the state of the monolayer. Imaging the surface yields the structure of domains of phases in equilibrium. Brewster angle microscopy (BAM) is an imaging technique that does not depend on a probe molecule. Laser light is reflected from the subphase surface and is detected by a CCD camera. The light is reflected at the *Brewster angle* of water, the minimum angle where light is totally internally reflected. As the monolayer is compressed, its refractive index changes, leading to reflection of the laser light. Different phases will have different optical properties, leading to clear images of the state of the monolayer (Fig. 4). Grazing incidence x-ray diffraction (gixd) has been used to identify the structures of condensed phases. Highly collimated x-rays from a synchrotron source sample the monolayer at a low angle of incidence. The in-plane packing and tilt angles of the alkyl tails of many fatty acid phases have been determined in this way.

Langmuir–Blodgett Films

According to one reference (16), the "resulting degree of control over film thickness and molecular architecture (using LB deposition) is unsurpassed by any other deposition technique." The term Langmuir–Blodgett film traditionally refers to Langmuir monolayers that have been vertically transferred from the water subphase onto a solid support such as glass, silicon, mica, or quartz. Vertical deposition is the most common method of LB transfer; however, horizontal lifting of Langmuir monolayers onto solid supports is also possible through the Langmuir–Blodgett–Schaefer method.

Monolayer or Multilayer Transfer. Highly hydrophilic or highly hydrophobic substrates are desirable for preparing LB films. Rigid Langmuir monolayers are difficult to transfer, so some flexibility in the monolayer is necessary. When hydrophobic, the substrate originates above the water surface. After the monolayer has been spread and compressed to the desired transfer pressure, the substrate is dipped vertically through the monolayer; transfer is by hydrophobic

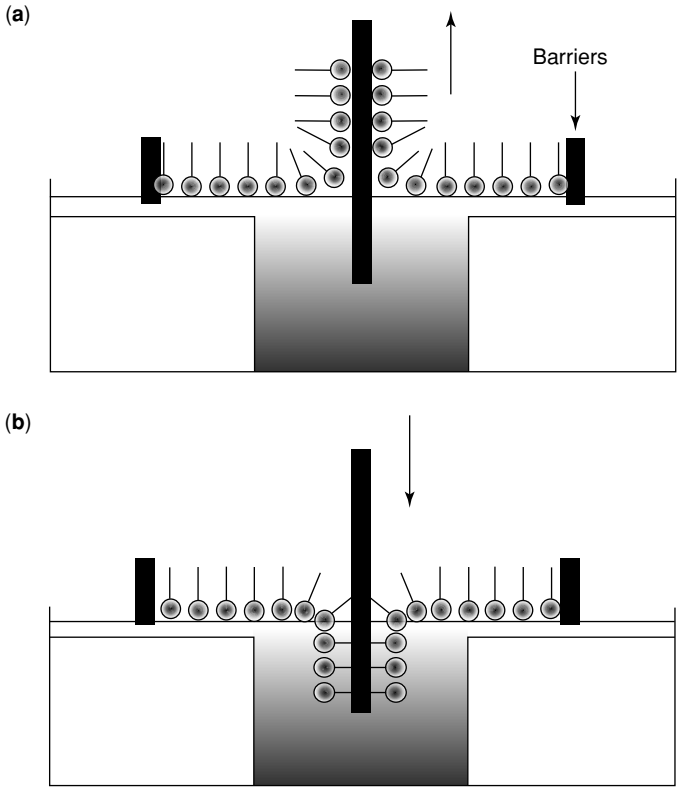

Fig. 5. Schematic of Langmuir–Blodgett transfers. The gray circles represent the hydrophilic head groups, and the thin black lines represent the alkyl chains. The molecules have been spread on an aqueous subphase. (**a**) A hydrophilic substrate is being withdrawn from the dipping well and is attracting the hydrophilic head groups that drive the film transfer. (**b**) A hydrophobic substrate is being pushed down through the monolayer. The alkyl chains are transferred, and the monolayer is pulled off the surface by hydrophobic interactions.

interactions between the alkyl chains and the surface. A hydrophilic substrate is submerged in the aqueous subphase before spreading and compressing the monolayer film. After the monolayer is stabilized, the substrate is withdrawn from the subphase, and the hydrophilic interactions drive the transfer (Fig. 5).

Three common film architectures can result from vertical deposition (Fig. 6). In X-type LB films, a Langmuir monolayer is consistently transferred onto a hydrophobic substrate so that it maintains head–tail interactions. In Z-type LB films, the monolayer is transferred onto a hydrophilic substrate that also forms head–tail interactions. X- and Z-type films are not common but can be prepared on a specially designed trough. However, some amphiphiles prefer this type of interaction, and upon regular dipping these structures form spontaneously. Y-type multilayers are most common, can be prepared on either hydrophilic or hydrophobic substrates, and are typically the most stable due to the strength of the head–head and tail–tail interactions. Even when films of some amphiphiles have been deliberately transferred by an X or Z method, the spacing between the hydrophilic

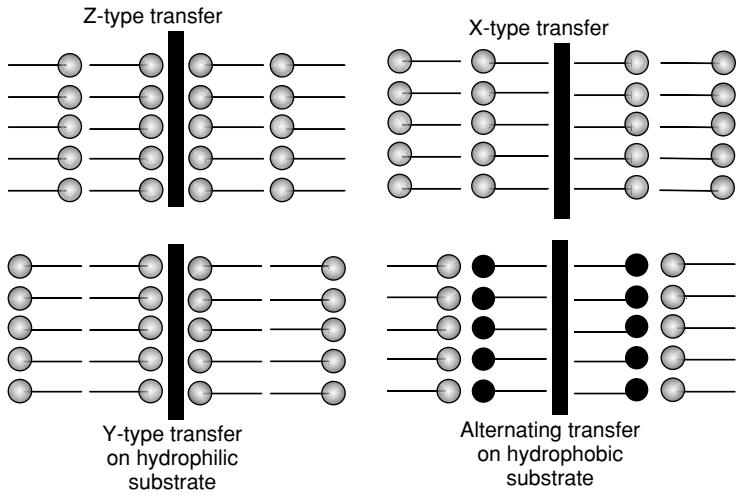

Fig. 6. Representations of X-, Y-, and Z-type LB films. Z-type LB films have head–tail interactions between layers and are transferred onto hydrophilic substrates. X-type LB films also have head–tail interactions but are transferred onto hydrophobic substrates. Y-type films can be transferred onto either hydrophilic or hydrophobic substrates but involve head–head and tail–tail interactions between layers. Alternating films can be transferred by using specially designed "double troughs."

head groups shows packing similar to Y-type films, implying that some molecular rearrangement occurs during or shortly after deposition. Ultimately, the molecular structure of the amphiphile determines the preferred method of dipping; multilayers can be built by repeating the vertical deposition procedure.

The quality of the transferred film is first indicated by the transfer ratio (τ), which is a measure of the change in the area of the floating monolayer versus the area of the substrate coated by the transferred monolayer. A transfer ratio of unity indicates that the monolayer transferred has the same area per molecule as it occupied on the water surface. Assuming that the monolayer on the water surface was stable and the monolayer was not reorganizing significantly during transfer, τ should be between 0.95 and 1.05 to be considered a successful transfer. A consistent deviation from unity could imply a change in organization upon transfer, but if the transfer ratio is irregular or significantly different from unity, the transferred film is most likely of poor quality.

Characterization of Transferred Films. Many analytical techniques are used to study transferred films. The film characteristics typically of interest are thickness, interlayer spacing, molecular orientation and packing, film coverage, surface topology, chemical composition, and optical and magnetic properties. The techniques used to study these parameters are well described in the literature (1,2,4).

Film Thickness and Layered Structure. X-ray diffraction is a reliable technique for probing interlayer spacing, and film thickness can be inferred from interlayer spacing. This technique is very sensitive to long-range periodicity. Many orders of 00l Bragg peaks, indicative of a well-defined layered architecture, are often observed for LB films. Neutron diffraction is similar to x-ray diffraction in

that both result in interference effects that can lead to an understanding of film organization. Film thickness can be determined by ellipsometry, which compares the amplitude and phase of s- and p-polarized light reflected from a film. Differences in amplitude and phase of the reflected light between the coated surface and the untouched substrate can be related to the film thickness.

Molecular Orientation and Molecular Packing. Grazing incidence x-ray diffraction was mentioned earlier as a method for determining the arrangement of molecules within a floating Langmuir monolayer. The same methods can be applied to transferred films. Transmission electron diffraction has also been observed in LB films and used to determine molecular packing, although the organic films are mostly unstable to the electron beam. Atomic force microscopy (qv) (afm) at molecular scale resolution has also been used to observe the arrangement of molecules in transferred monolayer and multilayer films (17).

Chemical Composition. Standard spectroscopic methods, including ftir, Raman scattering, and uv–visible absorption can be used to study the chemical makeup of films vibrational spectroscopy. These methods are often sensitive enough to be applied even to monolayer films. In the Raman scattering, the signal can be enhanced by preparing the LB film on a noble metal substrate, such as Au or Ag, or by interacting the film with surface plasmons. For each of these techniques, polarization studies can be used to determine the orientation of chromophores within the transferred films. Solid-state nmr has also been applied to LB films. Studies have included ^{1}H, ^{13}C, and ^{31}P magic-angle spinning experiments (18). NMR is complicated by the small amount of materials available, so these studies are not routine. The elemental composition, and possibly atomic proportions, within a film can be determined by x-ray photoelectron spectroscopy (xps), which measures the energy of an expelled electron as the surface is bombarded by a monochromatic x-radiation source. Binding energies are unique to each element in the film, as well as to that element's chemical environment and oxidation state. The intensities of the xps peaks can be used to determine the relative ratios of the elements present and can indicate the type of crystalline lattice formed. However, the intensities of the xps peaks are sensitive to many parameters, such as the element's electron escape depth, which can complicate determination of the elemental ratios (19).

Imaging. Imaging of the film is sometimes possible by using a transmission electron microscope (tem). Films are either transferred directly onto a tem-appropriate surface, such as a Cu grid, or are removed from the original substrate by, for example, submerging the film in highly diluted hydrofluoric acid and lifting it onto a grid surface for imaging by tem. Scanning probe microscopy, including atomic force microscopy (afm) and scanning tunneling microscopy (stm), can be used to obtain direct nanometer-scale images of surfaces without significant film degradation, which plagues some other imaging techniques (17) (see MICROSCOPY).

Applications

A wide range of potential applications exists for materials formed by the LB technique. A few examples include coatings, chemical or gas sensors, conducting LB films, NLO and SHG materials, and magnetic films.

LB coatings have been used as photoresists. In the area of ultrathin (single molecule) photoresists, spin-coated polymers tend to lack the consistency in structure and thickness necessary for these applications. However, preformed polymer LB films or polymerized monomeric LB films are extremely uniform, and can be used in these applications. Photo-cross-linking of poly(*p*-phenylene) and photopolymerization of ω-tricosenoic acid and methacrylic acid LB films have been investigated (20,21). Etching resulted in patterns that had resolutions of ca 60 nm. (see LITHOGRAPHIC RESISTS)

Chemical or gas sensors have been prepared by the LB technique. Sensing LB films often comprise chromionophores that have two functionally different groups on the same molecule. The ionophore component senses the presence of specific ions, and the chromophore component translates information from the ionophore into an optical signal. Gas sensors can translate oxidation or reduction by an atmospheric gas into an optical signal. Porphyrin, porphine, and phthalocyanine LB films have been studied for gas sensing of NH_3, I_2, O_2, CO, and NO_x (22–25). However, chemical sensing does not have to trigger an optical change. LB films of redox materials such as polythiophene and polypyrrole, ferrocene, TTF, and metallo porphyrins, as well as fullerenes and Schiff bases, have been used to modify electrodes for electrochemical sensing of a guest molecule or ion (26).

Conductivity has been studied in organic LB films based on porphyrins, phthalocyanines, and charge transfer complexes of derivatives of the electron donor, tetrathiafulvalene (TTF), and electron acceptor, TCNQ (2). Partially filled conduction bands can be achieved by forming films of nonstoichiometric mixtures of the donors and acceptors or by using donors and acceptors that have incomplete electron transfer, and electrical conduction is possible. Because LB films are not completely crystalline in the plane of the film, electrical conductivities are averages across crystalline domains (2). Films of TTF derivatives have been successfully prepared whose in-plane dc conductivities ranged from 10^{-3} to 10^{1} S cm^{-1} (27). LB films of conducting polymers, such as poly- and oligo(arylarenes) have also been fabricated (see ELECTRICALLY ACTIVE POLYMERS). LB films have been used as active and inactive layers in heterostructured electronic devices, including diodes and field effect transistors (28–30). Fullerene LB films have been investigated for their photovoltaic and charge transfer properties (31).

A material that can interact with electromagnetic radiation to generate new waves that have a different phase, frequency, or other propagative characteristics is called a nonlinear optical (NLO) material. Some NLO materials react in second-order processes that lead, for example, to frequency-doubling of laser radiation and electro-optic modulation of light (see ELECTROOPTICAL APPLICATIONS). Materials with such NLO behavior are called second-harmonic-generation (SHG) materials. To be suitable for NLO applications, the material should be typically highly conjugated and have an asymmetrical charge distribution along the primary molecular axis. The solid-state structure must also be noncentrosymmetric. The LB technique can enable the control of molecular architecture to build noncentrosymmetric crystalline environments. Nonlinear optical materials are prepared by either LB transfer of asymmetrical molecules, noncentrosymmetric transfers, such as X- or Z-type transfers, or by transfer of alternating films of NLO active and passive amphiphiles (1,2,4). Additionally, diluting an NLO active molecule in a fatty acid matrix can lead to noncentrosymmetric aggregation that can enhance

NLO or SHG effects. In a related application, LB films have been used as thin film optical waveguides (2).

Some derivatives of poly(*p*-phenylenevinylene) (qv) coupled with poly(pyridine) derivatives behave as a light-emitting layer and an electron-transport layer, respectively, (see LIGHT EMITTING DIODES) (32). Dye molecules are pervasive in the LB literature. Azobenzenes have been studied in LB films along with their trans–cis isomerization properties (33). Anthracene, pyrene, and numerous heterocyclic long-chain derivatives have been studied in LB films. Kuhn studied cyanine dyes as one of his original examples of energy transfer molecules incorporated into multilayer films, and hemicyanine dyes are studied for photoelectric conversion (34). Porphyrins and phthalocyanines, which are important in biological energy transport systems, have been extensively studied in LB films for their in-plane electrical conductivity and interplane charge transfer properties (35,36). Quinolinium salts, which are electron acceptors, can be bridged to electron donors (such as naphthalene), and it has been observed that they operate as multifunctional dyes that exhibit SHG and photoelectric conversion behavior (37). Electroluminescent devices have also been prepared using LB films of quinolinium salts (38).

By incorporating functional inorganic layers into the polar part of LB bilayers, phenomena typical of an inorganic solid state have been engineered into these normally organic assemblies (39). For example, LB films can be formed from organophosphonic acids, and if metal ions are bound to the head groups, a continuous inorganic lattice is formed in the polar part of the film. The inorganic lattice energy greatly stabilizes the films. Although LB films are often unstable to heat and solvents, mixed organic/inorganic metal phosphonate films can be thermally cycled to more than 100°C and are stable to both organic and aqueous conditions (40,41). When the inorganic ions are Mn^{2+} or Cu^{2+}, these films—it has also been shown—order magnetically. Another example of a magnetic LB film is a mixed organic–inorganic film that incorporates a Prussian blue lattice.

Some LB films exhibit a temperature-dependent pyroelectric coefficient that makes them candidates for thermal imaging applications (1). Both X- and Z-type films and alternating Y-type films (Fig. 6) can be built with permanent polarization, whose magnitude is often temperature-dependent. Their pyroelectric coefficient p is small relative to standard semiconducting and ceramic materials, but so is their permittivity ε; this makes their ratio p/ε, the figure of merit, comparable to that as for currently employed inorganic materials. The advantage of LB methods is that they can be used to prepare very thin, very uniform films.

BIBLIOGRAPHY

1. G. G. Roberts, ed., *Langmuir–Blodgett Films*, Plenum Press, New York, 1990.
2. M. C. Petty, *Langmuir–Blodgett Films: An Introduction*, Cambridge University Press, New York, 1996.
3. G. J. Gaines, *Insoluble Monolayers at Liquid–Gas Interfaces*, Wiley-Interscience, New York, 1966.
4. A. Ulman, *An Introduction to Ultrathin Organic Films: From Langmuir–Blodgett to Self-Assembly*, Academic Press, Boston, 1991.
5. C. H. Giles, S. D. Forrester, and G. G. Roberts, *Langmuir–Blodgett Films*, Plenum Press, New York, 1990, Chapt. "1".

6. C. H. Giles, *Chem. Ind. (London)* **45**, 1616 (1969).
7. H. Kuhn, D. Möbius, and H. Bücher, in A. Weissberger and B. W. Rossiter, eds., *Techniques of Chemistry* Vol. **1**, Part IIIB, John Wiley & Sons, Inc., New York, 1972, pp. 577–702.
8. A.-F. Mingotaud, C. Mingotaud, and L. K. Patterson, *Handbook of Monolayers*, Academic Press, San Diego, 1993.
9. T. Matsuura, A. Nishimura, and Y. Shimoyama, *Jpn. J. Appl. Phys.* **39**, 3557–3561 (2000).
10. N. Ranieri and G. Wegner, *Colloids Surf., A* **171**, 65–73 (2000).
11. K. Ariga and co-workers, *Colloids Surf., A* **169**, 47–58 (2000).
12. O. A. Aktsipetrov and co-workers, *Surf. Sci.* **454**, 1016–1020 (2000).
13. L. J. Kloeppner and R. S. Duran, *Langmuir* **14**, 6734–6742 (1998).
14. J. H. Batten and R. S. Duran, *Macromolecules* **31**, 3148–3150 (1998).
15. R. Rolandi and co-workers, *Langmuir* **11**, 3119–3129 (1995).
16. T. Richardson, *Langmuir–Blodgett Films* (Chemistry in Britain), 1989, pp. 1218–1222.
17. D. K. Schwartz and co-workers, *Science* **257**, 508–511 (1992).
18. G. E. Fanucci, C. R. Bowers, and D. R. Talham, *J. Am. Chem. Soc.* **121**, 1088–1089 (1999).
19. H. Byrd and co-workers, *J. Am. Chem. Soc.* **116**, 295–301 (1994).
20. M. Remmers, D. Neher, and G. Wegner, *Macromol. Chem. Phys.* **198**, 2551–2561 (1997).
21. H. Takano and M. Fujihara, *Thin Solid Films* **273**, 312–316 (1996).
22. D. Manno and co-workers, *Sen. Actuators, B* **57**(1–3), 179–182 (1999).
23. D. P. Jiang and co-workers, *Sens. Actuators, B* **66**, 207–209 (2000).
24. C. DiNatale and co-workers, *Anal. Chim. Acta* **384**, 249–259 (1999).
25. D. B. Papkovsky, *Sens. Actuators, B: Chem.* **29**, 213–218 (1995).
26. L. M. Goldenberg, M. R. Bryce, and M. C. Petty, *J. Mater. Chem.* **9**, 1957–1974 (1999).
27. W. Czerwinski, L. A. Linden, and J. F. Rabek, *J. Mater. Sci.* **35**, 455–463 (2000).
28. W. Czerwinski, L. A. Linden, and J. F. Rabek, *J. Mater. Sci.* **35**, 455–463 (2000).
29. G. Appel and co-workers, *Chem. Phys. Lett.* **313**, 411–415 (1999).
30. T. Bjornholm, T. Hassenkam, and N. Reitzel, *J. Mater. Chem.* **9**, 1975–1990 (1999).
31. J. Jin and co-workers, *Langmuir* **15**, 4565–4569 (1999).
32. G. Y. Jung and co-workers, *J. Mater. Chem.* **10**(1), 163–167 (2000).
33. H. Tachibana and co-workers, *Chem. Mater.* **12**, 854–856 (2000).
34. J. Zhai and co-workers, *J. Mater. Chem.* **10**, 625–630 (2000).
35. H. L. Anderson, *Chem. Commun.* **23**, 2323–2330 (1999).
36. E. Itoh and M. Iwamoto, *Jpn. J. Appl. Phys., Part 1* **38**, 5945–5948 (1999).
37. G. J. Ashwell, D. Zhou, and K. Skjonnemand, *IEICE Trans. Electron.* **E83-C**(7), 1057–1061 (2000).
38. J.-M. Ouyang and co-workers, *Thin Solid Films* **363**, 130–133 (2000).
39. C. T. Seip and co-workers, *J. Am. Chem. Soc.* **119**, 7084–7094 (1997).
40. M. A. Petruska and D. R. Talham, *Chem. Mater.* **10**, 3672–3682 (1998).
41. C. M. Nixon and co-workers, *Chem. Mater.* **11**, 965–976 (1999).

CHRISTINE M. LEE
Unilever Research US
DANIEL R. TALHAM
University of Florida

LASER LIGHT SCATTERING. See Volume 3.

LDPE. See ETHYLENE POLYMERS, LDPE.

LIGHT-EMITTING DIODES. See Volume 3.

LIGNIN. See Volume 3.

LINEAR LOW DENSITY POLYETHYLENE. See ETHYLENE POLYMERS, LLDPE.

LIQUID CRYSTALLINE POLYMERS, MAIN-CHAIN. See Volume 3.

LIQUID CRYSTALLINE THERMOSETS. See Volume 3.

LITERATURE OF POLYMERS. See INFORMATION RETRIEVAL.

LITHOGRAPHIC RESISTS

Introduction

Lithography in its original meaning describes a method of printing where a master pattern or design is first formed on a stone or metal surface using a hydrophobic material, the pattern is wetted with a hydrophobic ink, and finally the inked pattern is transferred to paper to produce copies of the master. Today, the meaning of the term has broadened to include a number of methods for replicating a predetermined pattern on a substrate, for an increasing variety of purposes. In most cases, replication is effected by first coating the substrate with a photosensitive polymer film termed a *lithographic resist*, and then exposing the film to a pattern of light (1–3). Photochemically induced changes in areas of the film exposed to light alter solubility to such an extent that either exposed or unexposed areas can be selectively dissolved to reveal portions of the substrate surface. If the exposed areas of resist become insoluble, then the resist is termed negative-acting; if solubility of the exposed regions increases, then the resist is termed positive-acting.

In certain applications, the resist film becomes a permanent, functional component of the device being constructed, typically serving as an electrical insulator or protective encapsulant. In such cases the patterned film often will be treated to enhance chemical resistance and mechanical properties (4). Most commonly, however, the resist pattern is a temporary template, and is removed or stripped after the image has been transferred to the substrate. Numerous methods of image transfer have been practiced, including plating and deposition (*additive* processing), chemical etching or physical milling to erode the exposed substrate (*subtractive* processing) or bombardment with energetic ions that become implanted in the substrate surface. Figure 1 summarizes the steps comprising the lithographic process.

Encyclopedia of Polymer Science and Technology. Copyright John Wiley & Sons, Inc. All rights reserved.

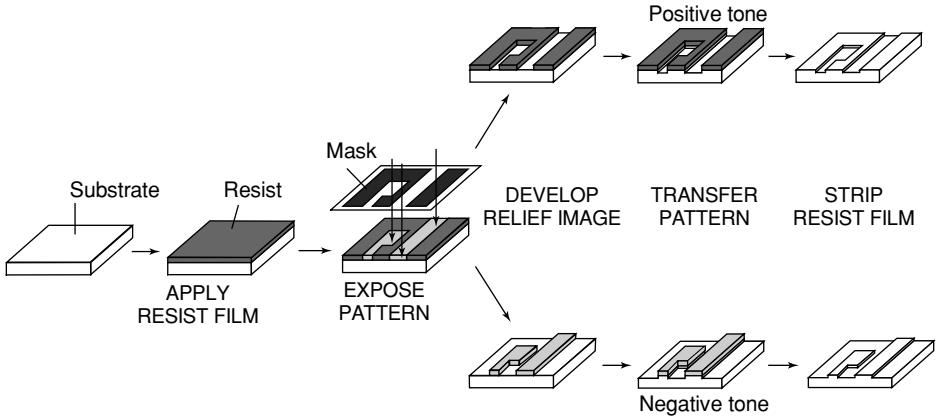

Fig. 1. The lithographic process. A substrate is coated with a photosensitive polymer film called a resist. A mask with transparent and opaque areas directs radiation to predetermined regions of the resist film. Depending on resist characteristics, exposed or unexposed portions of the film are removed using a developer solvent. The resulting pattern is then transferred to the substrate surface and the resist is stripped.

Lithographic resists enable a host of technological advances that have had far-ranging impact. For example, the rapid progress in microelectronics technology in large part stems from refinement of the lithographic techniques used to fabricate computer integrated circuits. The ability to pack ever-increasing numbers of discrete electronic components in a given area of an integrated circuit, when coupled with the economies of scale that result from high volume manufacturing, has led to both improved performance and lower cost with each succeeding device generation (5). In calendar year 2000, the annual global market for semiconductors exceeded US$200 billion.

The advantages of miniaturization are now being exploited in areas beyond microelectronics. Adaptation of materials and processes originally devised for semiconductor manufacture has allowed fabrication of sensors (for example, pressure meters and accelerometers used in the automotive industry) (6,7), complex optical (8) and micromechanical (6,7,9) assemblies, and devices for medical diagnostics (6,7,10), all using lithographic resists.

Essential Attributes of Lithographic Resists. Regardless of the specific application, all resists must display certain fundamental functional properties:

(1) The resist composition must form *uniform, defect-free films* on the substrate of interest. To achieve this, the resist components must be soluble in and inert toward the selected coating solvent or medium, the formulation must form glassy films without component precipitation, separation or dewetting, and must be stable during post-application heating steps. A variety of different coating techniques have been applied, including spray coating, curtain coating, spin coating or whirling, dip coating, dry-film lamination, and most recently, electrodeposition onto a conducting substrate from an aqueous emulsion of resist components.

(2) The coated film must display *adequate* adhesion to the substrate after coating, and through the develop and image transfer steps. Adherence is influenced by resist composition, substrate surface composition, preparation and cleanliness, coating conditions, develop and etch process details, and, with negative cross-linking resists, by the exposure dose. Adhesion loss in mild cases is manifested by the lifting of a resist pattern at its perimeter (often visible under microscopic examination as a contrasting band or color at the edge of the image) and in extreme cases by complete detachment of the resist pattern.

(3) The resist must have suitable *radiation sensitivity*. Today's exposure tools are so costly that tool throughput is a key measure of performance. The overall time to expose a resist film is the sum of the times to load and position the substrate in the exposure tool, to align the substrate and the mask, to irradiate the film, and to unload the completed part. In the optimum case the resist exhibits sufficient radiation sensitivity so that the fraction of the overall cycle apportioned to irradiate the film does not limit the overall throughput.

(4) The resist must provide *high fidelity reproduction* of the mask image on the substrate. This attribute is generally quantified as the resist's *resolution*, that is, the smallest feature that can be consistently printed, and its *contrast*, which is a fundamental measure of how the resist response changes with increasing radiation dose. In high resolution lithography, diffraction and imperfections in the optical system cause stray radiation to be scattered into regions of the resist pattern that nominally are unexposed. A resist with high contrast can effectively reject the stray radiation and yield a more accurate replica of the original mask. Resist contrast is fundamentally related to the dissolution properties of the polymer matrix and is influenced by resist composition, and by process conditions and exposure tool characteristics.

(5) The patterned resist must provide an effective *protective barrier* during image transfer. The image transfer step frequently includes harsh chemical or physical treatments that erode or otherwise degrade the resist pattern. A resist's capacity to withstand the more vigorous image transfer processes (for example plasma etching) can vary widely with its composition.

(6) After image transfer, the patterned resist must be readily and completely *removable* without substrate damage. The pattern often can be stripped from the substrate with a mild organic solvent. Proprietary stripper formulations or plasma oxidation treatments are utilized when the imaging chemistry or image transfer process has insolubilized the pattern.

Physics of Image Formation. Spatially directed radiation chemistry is the basis of all modern lithographic processes. While numerous approaches for the localized activation of chemical processes have been pursued, by far the predominant means for fabricating microdevices today employs optical *projection photolithography* to bring about photochemical reactions in the resist film in an imagewise fashion (11). In this technique, a light image of the desired pattern, transmitted through a mask, is reduced in size and precisely focused onto a resist-coated wafer using a system of lenses (Fig. 2). Because of diffraction and

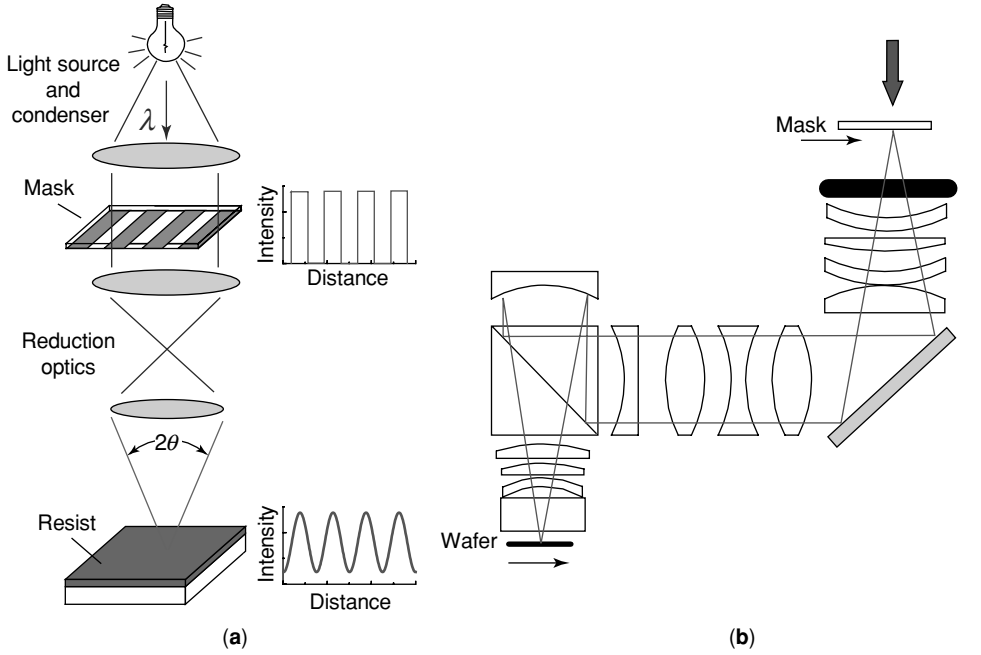

Fig. 2. Projection lithography. (**a**) Schematic diagram illustrating the essential components in a projection exposure tool. (**b**) Optical elements in a modern projection exposure tool used for device manufacturing. The additional components enhance the precision of the projected light image by correcting for optical aberrations and distortions (12).

slight imperfections in the optical components, a nominally square wave pattern of light intensity is presented as a sinusoidal pattern of light at the wafer plane. The ratio of light intensity in the nominally bright and dark regions, a measure of the *aerial image contrast*, varies with the wavelength and optical characteristics of the exposure tool. Since this ratio determines how the extent of photochemical reaction of the nominally exposed and unexposed areas of the resist film differs, it controls the ability to selectively dissolve one of these areas during the develop step. As the aerial image contrast decreases, differentiation during development between exposed and unexposed regions grows increasingly difficult and ultimately determines the limits of spatial resolution.

The minimum resolution R achievable with projection lithography is governed by the relation

$$R = k_1 \lambda / \mathrm{NA} \tag{1}$$

where λ is the wavelength of exposing radiation, k_1 is a process- and material-dependent parameter in the range of 0.4–1, and NA is the numerical aperture, equal to the refractive index of the surrounding medium ($\sim$1 for air) times the sine of the angle θ subtended by the objective lens of the system (13).

The depth of focus (DOF) for the same tool is given by the equation

$$\mathrm{DOF} = k_2 \lambda / (\mathrm{NA})^2 \tag{2}$$

where k_2 is a process-dependent parameter of the order of 0.5–1, and λ and NA are defined as before. A large value for DOF is desired as it increases the tolerance of the process to deviation of the substrate surface from perfect planarity.

The evolutionary refinement of projection optical lithography since its introduction can be understood by consideration of these equations. The overall goal is improved resolution while maintaining a maximum DOF. Resolution improvements may be realized by increasing the NA, by reducing the exposure wavelength λ, or by process and tool refinements that reduce the value of k_1. There are practical limits to each of these approaches, however.

To improve resolution by increasing the NA of the lens system, either the diameter of the lens must be increased or the focal length reduced. The net overall result is a lens system of increased size, mass, complexity, and cost. Since the NA appears as a squared term in the equation for DOF, a resolution improvement achieved via increased NA is accompanied by a proportionately larger decrease in DOF. Moreover, complex polarization effects arise as the angle θ exceeds $\sim 45^\circ$ (an NA of ~ 0.7) (14).

According to equations 1 and 2, improving resolution by reducing the exposing wavelength does not incur as great a penalty in DOF, but brings the requirement that a suitable photoresist, light source, and selection of optical lens materials be available for the decreased wavelength. The development of new generations of photoresists for leading-edge microlithographic applications has been driven in large part by the need for imaging materials optimized for a specific exposure wavelength.

The first projection exposure tools, introduced in the mid-1970s, were designed to print features at the >2000-nm scale, using light of 400–450-nm wavelength (15). Improvements in optical fabrication and design allowed the use of the resist systems designed for this wavelength range for an extended period, with increases in the NA as the primary means for realizing improved resolution. In the mid-1980s, as feature dimensions decreased below 1000 nm, a shift to exposure tooling based on an illumination wavelength of 365 nm signaled the start of the now-familiar trend where improved resolution derives in large part from reduction of exposure wavelength. This was soon followed by the development of exposure tools based on ultraviolet (uv) excimer lasers operating at 248-nm (KrF) and later at 193-nm (ArF) wavelengths. Current research and development activities are exploring the issues that accompany the use of 157-nm illumination from a F_2 excimer laser as a source in projection lithography.

Several less evolutionary routes to achieving improved resolution through wavelength reduction are also being pursued, including x-ray proximity lithography ($\lambda \sim 1$ nm) (16), extreme-uv lithography ($\lambda \sim 13$ nm) (17), and lithography using charged-particle beams of electrons (18) or positive ions (19). In the latter two technologies the particle deBroglie wavelengths are so small that resolution is limited by aberrations in the ion optics and ion–ion repulsion rather than diffraction. Each of these approaches brings with it unique requirements for optical components, masks, and resists; intensive research and engineering activities have been pursued for a number of years in the attempt to bring each of these approaches to practical implementation.

Modern Resists for Microlithography

Most modern lithographic resists are evolved from materials first developed for the printing industry (20). Increasingly specialized resists and processing techniques have been introduced as applications of lithographic technology have grown in scope and sophistication. Today the market for photoresists used in the manufacture of integrated circuits is estimated to be US$1.4 billion annually, with diazonaphthoquinone–cresol novolac (DNQ-novolac) resist products accounting for about two-thirds of this. Commercial resist systems designed for deep-ultraviolet applications are now being used to build the critical levels of most leading-edge semiconductor products, however, and use of such advanced materials is expected to grow at the expense of the older DNQ-novolac systems.

DNQ-Novolac Photoresists. The bulk of the world's semiconductor processing is carried out using DNQ-novolac resin based photoresists and exposure tools equipped with mercury arc lamp illumination sources (producing uv wavelengths of 365 or 436 nm) (21). These photoresists consist of a photoactive DNQ dispersed in a phenolic matrix resin (a low molecular weight condensation product of formaldehyde and cresol isomers known as *novolac*) (Fig. 3). The phenolic structure renders the novolac polymer weakly acidic, and readily soluble in aqueous alkaline solutions. In admixture with an appropriate DNQ the polymer's dissolution rate is sharply decreased, typically by 2–3 orders of magnitude. Photolysis causes the DNQ to undergo a multistep reaction sequence (a photochemical Wolff

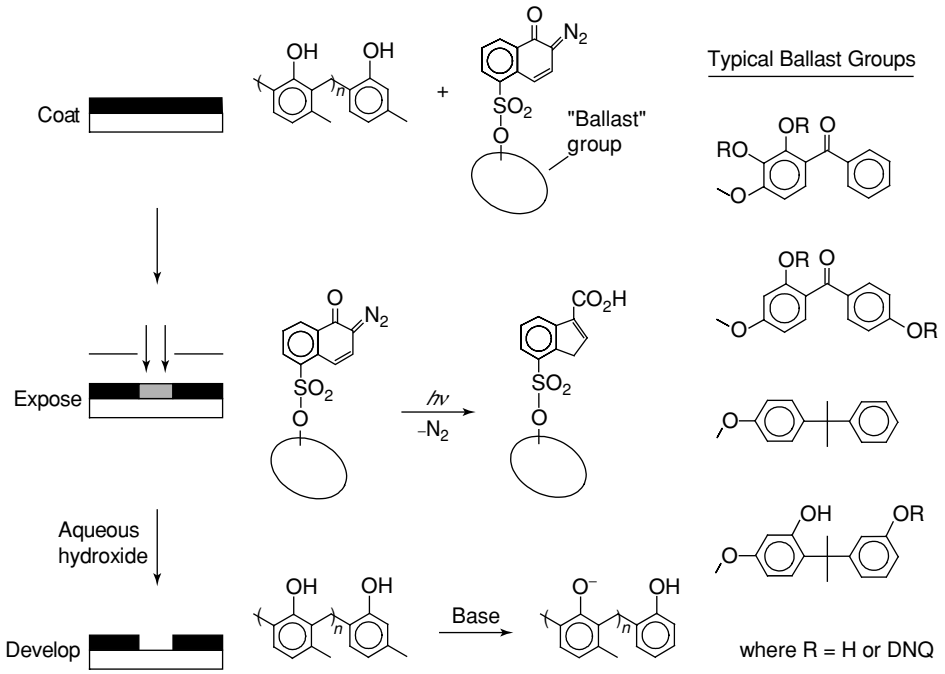

Fig. 3. Chemistry of diazonaphthoquinone–cresol novolac positive-acting resist. During patternwise exposure, the DNQ undergoes photolysis that destroys its inhibitory effect on film dissolution.

rearrangement), ultimately forming a base-soluble carboxylic acid that does not inhibit film dissolution. Immersion of a patternwise-exposed film of the resist in an aqueous solution of hydroxide ion (typically containing 0.2–0.3 *N* tetramethylammonium hydroxide) leads to rapid dissolution of the exposed areas and only very slow dissolution of unexposed regions. Since the polymer itself undergoes no reaction during the image formation process, the film solubility is controlled by *chemical* and *polarity* differences rather than molecular size.

DNQ-novolac resist chemistry has proved to have remarkable flexibility and extendibility. First used in electronic manufacturing applications in the 1960s, the performance of these materials has been continually improved by careful optimization of the polymer and DNQ dissolution inhibitor. Today, highly optimized DNQ-novolac resists are used to manufacture integrated circuits with device geometries on the 350-nm scale.

Deep-Ultraviolet Chemically Amplified Resists Based on Acid Catalysis. Unfortunately DNQ-novolac resists are not suitable for use at deep-ultraviolet (DUV) wavelengths ($\lambda \sim 250$ nm), the succeeding evolutionary step in the progression of optical lithography tools to higher resolution. There are two principal reasons for this. The first can best be understood by consideration of

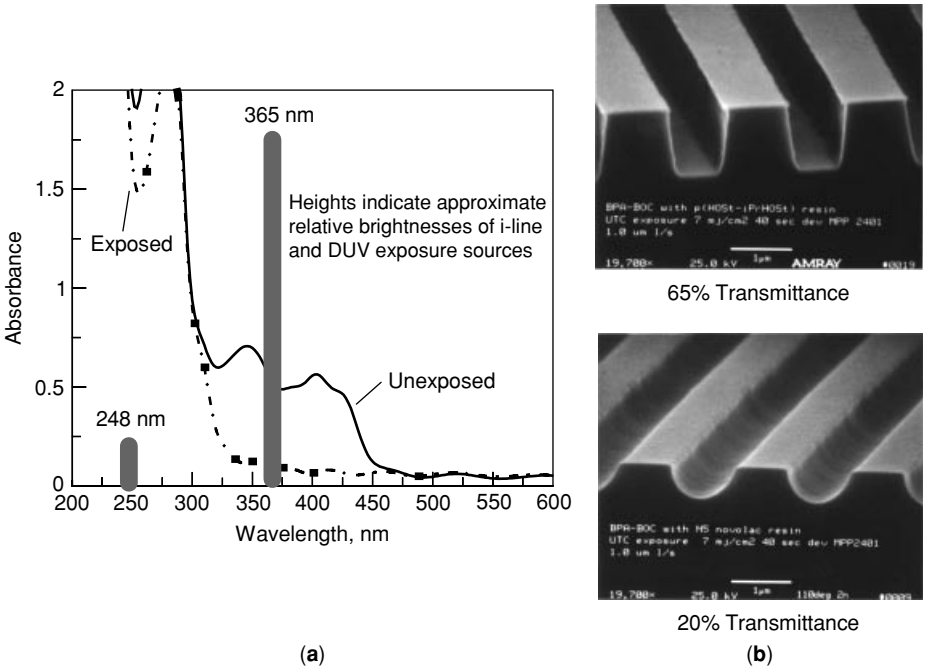

Fig. 4. Impact of optical absorption on resist performance. (**a**) optical absorption spectrum of a typical DNQ-novolac resist before and after exposure. (**b**) Impact of optical absorbance on photoresist imaging properties. Shown are scanning electron micrographs of relief images obtained using two different photoresist formulations, processed under identical conditions. The formulations are functionally identical but differ in the transparency of the film at the exposing wavelength (22). (top) image obtained when the film is weakly absorbing; (bottom) image obtained when the film absorbs strongly at the exposing wavelength. Note the incomplete development to substrate and the sloping sidewalls.

resist optical properties. Figure 4a shows the optical absorption spectrum of a typical DNQ-novolac photoresist film before and after exposure with 365-nm light. The absorption band at long wavelengths (300–450 nm) is that of the DNQ sensitizer. As the DNQ is photolyzed this characteristic absorption decreases. The increased transparency facilitates efficient photolytic conversion of the sensitizer throughout the depth of the film. If such a film is exposed at 248 nm, however, the strong nonbleaching absorbance at that wavelength (due in part to the novolac matrix polymer, and in part to the DNQ and its photoproduct) sharply attenuates the beam as it passes through the film. The result is highly nonuniform photolysis of photosensitizer in the resist film, with insufficient conversion near the substrate interface to effect solubilization. Figure 4b illustrates the damaging effect of this on resist imaging properties. As will be seen in later sections, the need to circumvent excessive resist absorbance is a repeating theme in the evolution of resist materials.

Second, the overall brightness of light sources available for DUV exposure is much less than that of mercury arc lamps used for 365-nm imaging. Although KrF excimer lasers are generally regarded as powerful sources of uv light, the spectral output line is relatively broad. Limitations of available lens materials make correction for chromatic aberration difficult, and so the source output beam must span only a very narrow wavelength range. Introduction of optical line narrowing elements into the beam leads to a large overall attenuation. Figure 4a illustrates the relative intensities at the wafer plane for typical 365- and 248-nm exposure tools. Roughly speaking, a photoresist designed for use with current DUV exposure tooling must be at least 10 times more efficient in its utilization of absorbed photons than a DNQ-novolac resist. Since the quantum yield for DNQ-novolac systems is of the order of $\sim$0.3, a 10-fold improvement in efficiency is a considerable challenge, and obviously calls for a different approach.

One means of attaining this increased efficiency is by the photochemical generation of an initiating species or catalyst that is active in a subsequent thermal reaction. A familiar example of this is found in photoinitiated free-radical polymerizations, and this approach has seen extensive application in photoresists intended for use in the production of printed circuit boards (23). Each single photochemical event (formation of a free radical) can result in the polymerization of a large number of olefin monomers, giving an effective quantum yield for bond formation that is much higher than that of the initiating photochemical reaction and which can exceed unity. Such photopolymerization resists are not well-suited for use in microlithographic applications because of their limited resolution, a consequence of excessive solvent swelling during the develop step.

This "chemical amplification" (CA) concept can be extended to catalytic reactions. In 1982, it was recognized that if a photosensitizer producing an acidic product is photolyzed in a polymer matrix containing acid-labile groups, the acid could serve as a spatially localized catalyst for the formation or the cleavage of chemical bonds (24). An early practical example of this concept is shown in Figure 5. The acid-generating sensitizer is an onium salt, a class of compounds that efficiently generate a Brönsted acid upon photolysis. The polymer is poly(*tert*-butoxyoxycarbonylstyrene) (PTBOCST). Photolysis forms a small quantity of acid in those areas exposed to radiation. During a later heating step the acid catalyzes thermolysis of pendant *tert*-butoxyoxycarbonyl (TBOC) groups, largely

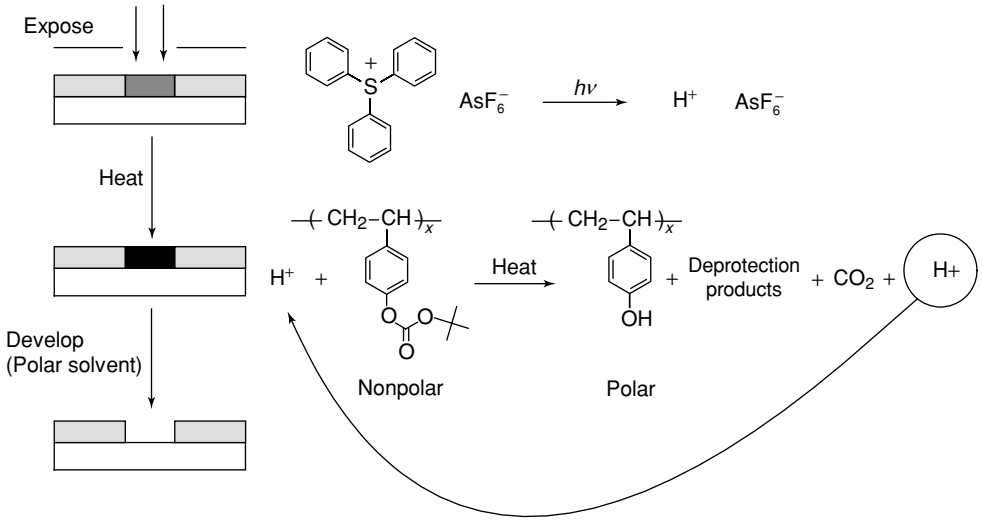

Fig. 5. Chemistry of PTBOCST chemically amplified resist. In the first step, patternwise exposure creates small quantities of acid. In a second heating step, pendant TBOC groups are cleaved under acid catalysis. The exposed and deprotected areas can be selectively dissolved in a polar solvent.

converting the nonpolar PTBOCST into the polar poly(hydroxystyrene) (PHOST) and gaseous products, while regenerating the initial acid. The converted latent image can be developed either in positive tone by selecting a polar solvent or in negative tone by selecting a nonpolar solvent as the developer. The catalytic chain length for this system, that is, the average number of TBOC groups fragmented by each acid molecule, has been measured to be in the range 800–1100 (25). Therefore an extremely low exposure dose (in the range of 1–5 mJ/cm^2) is needed to image this system, roughly 2 orders of magnitude more photosensitive than typical DNQ-novolac resists.

Since the original proof of concept, and a later demonstration of its practical use in semiconductor manufacturing (26), applications and extensions of this concept have proliferated. CA resists now find use in virtually all leading-edge photolithographic manufacturing processes, and it is anticipated that this dominance will continue into the foreseeable future regardless of the specific exposure technologies. In the following sections the general characteristics of CA resists are discussed using as examples those targeted for 248-nm exposure. Following that, the key factors that ultimately limit extendibility of lithographic resists are enumerated. Finally, examples are provided of how CA resists are being tailored to suit the requirements of specific future exposure technologies. Throughout the discussion that follows, the relation between functional properties and resist composition is emphasized.

Characteristics of CA Photoresists for 248-nm Exposure. CA DUV photoresists differ from DNQ-based resists in a fundamental way. In the latter, the dissolution inhibitor component (the DNQ) is itself photoactive (Fig. 3). Typically in a CA resist the photoactivity and solubilization functions are separate. The photolysis of the photo-acid generator (PAG) does not of itself significantly promote dissolution [although exceptions to this have been noted (27)]. Reaction of the acid

with the protected phenols bound to the polymer backbone must take place to achieve a significant change in polymer solubility. The nature and the efficiency of the imaging chemistry are dictated by the reactivity of the acid-labile functional groups, the properties of the polymer and PAG, and by lithographic processing conditions. We detail here how these factors shape the imaging characteristics of CA resists.

Acid-Catalyzed Chemistry. Acid-catalyzed reactions form the basis for essentially all CA resist systems for microlithographic applications. These reactions can be generally classified as either cross-linking/photopolymerization or deprotection/rearrangement reactions. Polymer cross-linking and photopolymerization reactions lead to increases in molecular weight. Since this causes a reduction in the film solubility, these find application in negative-tone resist systems. Deprotection and rearrangement reactions are typically used to unmask acidic functionality such as pendant phenolic or carboxylic acid groups. These impart solubility in aqueous alkaline solution and therefore such reactions are used in positive-tone resists. Representative examples of each type of chemistry are described below.

Positive-Tone Imaging Chemistry. The ester, carbonate, and ketal acidolysis reactions that form the basis of most positive tone CA resists are thought to proceed by specific acid catalysis (28). In this mechanism (type AAL1), illustrated here for the hydrolysis of *tert*-butyl acetate (29), the first step is a rapid equilibrium where the proton is transferred between the photogenerated acid and the ester:

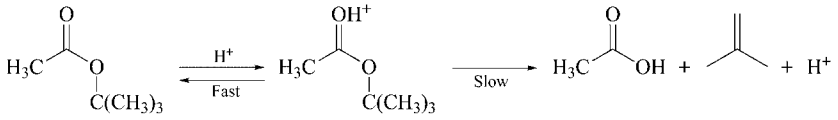

The rate of the reaction in such case is $R = k[PH^+]$, where PH^+ is the protonated *tert*-butyl ester. In the corresponding polymeric resist system, PH^+ is the repeat unit bearing the acid-labile protecting group.

In formulated resist systems the situation is more complex. The photogenerated acid can be so strongly acidic that it dissociates completely upon formation. In such a case, the proton will reside on other basic components of the resist film, which can include polymer functionality (ie, pendant ester or ether groups), and adventitious impurities such as water or residual casting solvents, as well as additives such as coating aids. The reactant PH^+ will be in equilibrium with all other protonated species in the resist film. The concentration of each protonated species is then determined by the basicity of its unprotonated conjugate. As deprotection proceeds, the concentrations of the basic resist components will change, shifting the equilibria and influencing the overall kinetics. Substitution of an acid of different strength, or introduction of a basic impurity or additive, will perturb the concentration of PH^+ and thereby the imaging behavior of the resist.

Figure 6 lists representative acid-labile protecting groups that have been incorporated in positive-tone CA resist systems. These groups can be pendant to the matrix polymer chain, can be attached to a monomeric or polymeric additive that acts as a dissolution inhibitor (30–32), or even can be appended to the PAG structure (33).

Negative-Tone Imaging Chemistry. In many negative-tone CA resists cross-linking is employed to effect insolubilization of the exposed pattern. In the

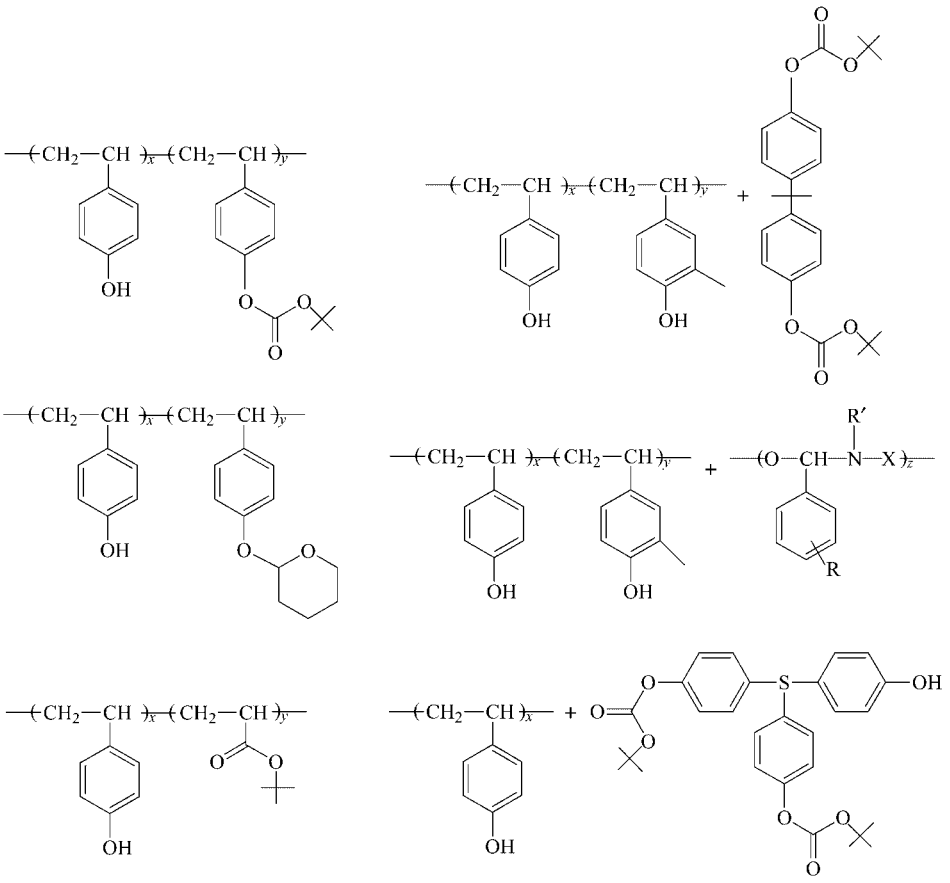

Fig. 6. Representative polymers and protecting groups used in positive-tone CA resists. On the left are shown three examples where the acid-labile protecting groups are pendant to the polymer chain; the right column provides three examples where the acid-labile groups are found on small molecules added to the polymer film.

limiting case, an acid-catalyzed bond-forming reaction can convert the polymer film from a glassy matrix of individual polymer strands into a three-dimensional network that is effectively a single molecule bound to the substrate surface. Full cross-linking is not always required, however. A small increase in molecular weight due to partial cross-linking, or simply a change in polarity stemming from grafting of the cross-linking agent to the polymer chain, can cause a change in dissolution properties that is adequate for imaging.

One of the first CA resist systems described in the chemical literature is based on the acid-catalyzed cross-linking of epoxy groups (top reaction of Fig. 7) (34). While such resists display excellent photospeed, they suffer from solvent-induced image distortion during development, the result of swelling of the cross-linked polymer during development. Careful attention to formulation and process conditions is required to achieve high resolution imaging. This difficulty, coupled with the practical problems associated with the use of organic solvents in a manufacturing setting, has limited the acceptance of such resists.

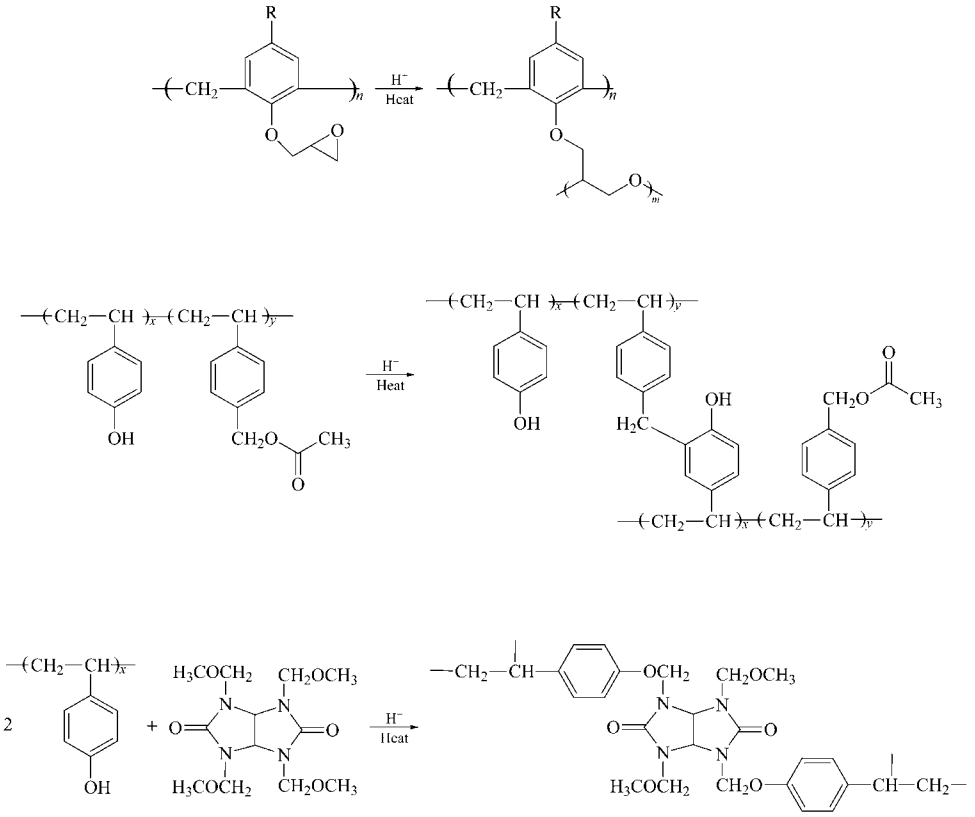

Fig. 7. Representative imaging chemistry employed in negative-tone CA resists: (top) epoxy polymers requiring organic solvent development; (center) PHOST-based cross-linking systems requiring aqueous development; and (bottom) monomeric cross-linking agents used in PHOST matrix polymers.

Several CA negative-tone photoresists exploit the high reactivity of aromatic structures toward electrophilic substitution by incorporating the cross-linking chemistries shown as the middle and bottom reactions of Figure 7. In these examples the phenolic structure renders these systems developable in aqueous alkaline solution. Since the dissolution properties for such polymers closely resemble the surface-limited etching found in DNQ-novolac positive resists, image distortion due to solvent swelling is not observed. Systems have been described where the active cross-linking group is covalently bound to the polymer (35,36), or is incorporated as a nonpolymeric additive (37). Bond formation can take place at the hydroxyl site or on the ring (36).

While cross-linking systems have been most widely studied, negative-tone patterning can be achieved by exploiting the polarity change that accompanies deprotection. The PTBOCST resist (Fig. 5) is a familiar example, since use of a nonpolar developer solvent produces negative-tone images. In a second example, a pinacol rearrangement changes a polar diol into a less polar carbonyl group, allowing negative-tone imaging when developed in an appropriate organic solvent (38).

Polymers for 248-nm CA Resists.

Optical Properties. It was noted earlier that novolac-based resists absorb too strongly in the 248-nm spectral region to be used for exposure at that wavelength. Experience has shown that the optimum optical absorbance for a nonbleaching photoresist is about 0.3–0.4 absorbance units at the required film thickness (typically 600–1000 nm for 248-nm resists), representing a balance between conflicting requirements for high transparency to provide uniform illumination through the depth of the film, and high absorption to suppress thin-film optical reflectivity effects that reduce process latitude (39,40). To maximize light absorption by the photosensitizer, the polymer should be as transparent as possible at the exposure wavelength. A rule of thumb is that polymeric component's contribution to the absorbance should not exceed 0.2 at the required film thickness. A number of different polymer families are transparent at this wavelength; Figure 8 compares the optical absorption characteristics of an acrylic polymer and PHOST to that of a *meta*-cresol novolac resin. The acrylic polymer in particular appears well-suited for 248-nm exposure, and early work in DUV resists took advantage

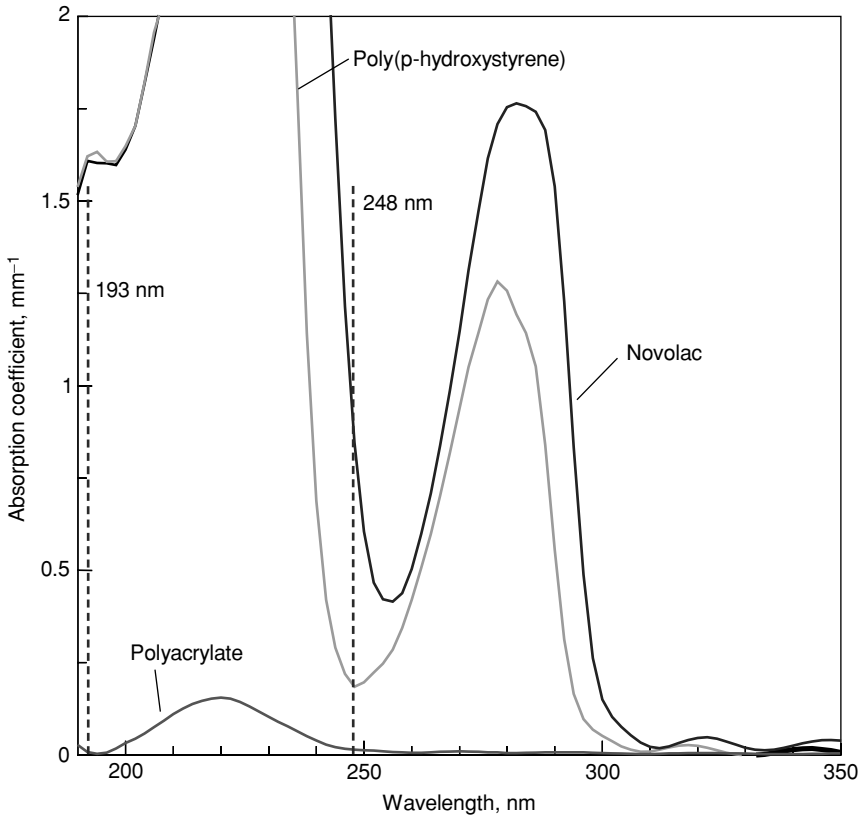

Fig. 8. Optical absorption spectra of thin, 1000-nm-thick films of novolac, poly(hydroxystyrene), and poly(acrylate) polymers. The novolac resin is transparent only above 300 nm. While poly(hydroxystyrene) also absorbs strongly below 300 nm, it exhibits a region of adequate transparency centered near 248 nm. The acrylate polymer is quite transparent over the uv range.

of that characteristic (41). While suitable for wet-etch image transfer processes, acrylic-based polymers have such poor resistance to the plasma etch image transfer processes now commonly used in semiconductor fabrication that their use is impractical (42). Materials based on the PHOST structure are far more robust toward plasma etching, and many derivatives of PHOST are sufficiently transparent at 248 nm to provide a useful polymer platform for resist design.

Polymer Synthesis. Typically the resists used in 248-nm DUV lithography are based on copolymers of hydroxystyrene and an acid-labile comonomer as depicted in the examples of Figures 6 and 7. These polymers are almost always produced by free-radical solution polymerization of a derivative of 4-hydroxystyrene (HOST), and thus are usually medium molecular weight (5000–100,000) polymers with relatively narrow polydispersities (between 1.5 and 2.5) (43). Although structurally similar, the functional properties of phenolic resins based on HOST bear little resemblance to those of novolac, whose unique properties stem in part from the unusual step-growth polymerization mechanism (44), which produces substantial quantities of oligomeric products and high molecular weight branched polymer.

Poly(hydroxystyrene) (PHOST) is often prepared by polymerization of 4-acetoxystyrene, followed by base-catalyzed hydrolysis (Fig. 9a). The acetoxystyrene monomer's stability and polymerization kinetics allow production of PHOST of higher quality than is easily obtained via direct radical polymerization of HOST. The PHOST homopolymer formed thereby is then partially or fully derivatized with an acid-cleavable functionality to produce the final resist component. In some instances the resist polymer can be prepared in a single step by direct polymerization of the protected monomer(s) (23,45), entirely avoiding the intermediate PHOST. HOST-containing resist polymers have also been prepared by free-radical copolymerization of a latent HOST and a stable, acid-labile monomer, for example, the copolymerization of acetoxystyrene with *tert*-butyl acrylate, followed by selective removal of the acetoxy group (46) (Fig. 9b).

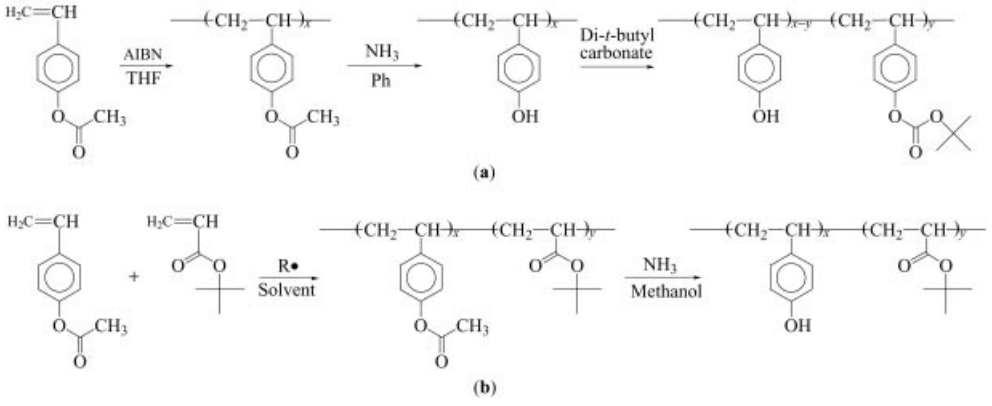

Fig. 9. Examples of synthetic methods for the preparation of polymers for 248-nm CA resists. (**a**) Synthesis of PHOST from acetoxystyrene monomer, followed by partial protection with an acid-labile pendant group to form poly(*tert*-BOCstyrene-*co*-hydroxystyrene); (**b**) synthesis of the acid-labile copolymer poly(hydroxystyrene-*co*-*tert*-butylacrylate) by radical copolymerization using a latent HOST, followed by selective deprotection.

Relating Polymer Properties and Lithographic Properties. While the nature of the imaging chemistry is a central element determining the functional characteristics of a CA resist composition, the impact of other polymer properties must also be considered in resist design. Polymer molecular weight (47,48) and molecular weight distribution (49,50) exert a strong influence on the solubilization properties of phenolic polymers in aqueous base, and therefore must be carefully controlled to ensure a reproducible and optimum dissolution response to the imaging chemistry. There is evidence that the polymer molecular weight can also impact the fine-scale definition of the final developed resist image (51,52) (the line-edge roughness, discussed later in greater depth). The dissolution of base-soluble copolymers is influenced both by the relative amounts of each monomer incorporated in the polymer and by how the different monomers are distributed along the chains (53,54).

Free-radical polymerization chemistry, and the transition metal catalysis chemistry used to make some 193-nm resist polymers (discussed later in this article), places fragments of the initiating species at the terminuses of the polymer chains. Although their effective concentration in a resist film is low relative to the polymer repeat unit, these end groups can have a discernible impact on its functional lithographic properties. End groups can have several independent effects (55,56). First, if the initiator fragment absorbs uv light, an undesirable decrease in the transparency of the polymer can occur. The efficiency of acid-catalyzed deprotection is influenced by the choice of initiator, presumably a consequence of an acid–base interaction of the initiator residue with the photogenerated acid. In some instances, eg, with polymers prepared by cationic polymerization, the end groups can render the chains susceptible to acid-catalyzed depolymerization. Finally, properties of the end group can influence dissolution behavior of the final polymer; nonpolar groups can suppress aqueous base dissolution compared to the same polymer prepared with a polar initiator. Since the concentration of the end groups is directly related to the number of polymer chains in a given volume or mass, their effects are accentuated as polymer molecular weight is decreased and their effective concentration is increased.

Photoacid Generators. The chemical and physical properties of the PAG component play an important role in determining the functional behavior of a CA resist. A variety of PAG compounds (both ionic and nonionic structures) have been developed as researchers have sought to optimize the photochemical properties of the initial PAG (quantum yield of acid generation, wavelength response) and the properties of the photogenerated acid (pK_a, volatility, mobility), while maintaining acceptable solubility, thermal stability, low manufacturing cost, and low toxicity.

Ionic Photoacid Generators. The application of onium salts as photochemical sources of catalyst for acid-catalyzed polymerization was first reported in the 1970s (57). Sulfonium and iodonium salts have become the most widely used members of this group because of ease of synthesis, high thermal stability, and high quantum yield. Representative examples are depicted in structures **a–d** in Figure 10 (58–61).

The properties of the photoacid can be readily modified by varying the counterion in these salts, generally accomplished through a metathesis reaction. This exchange usually has no significant impact on the photochemical reactivity of the

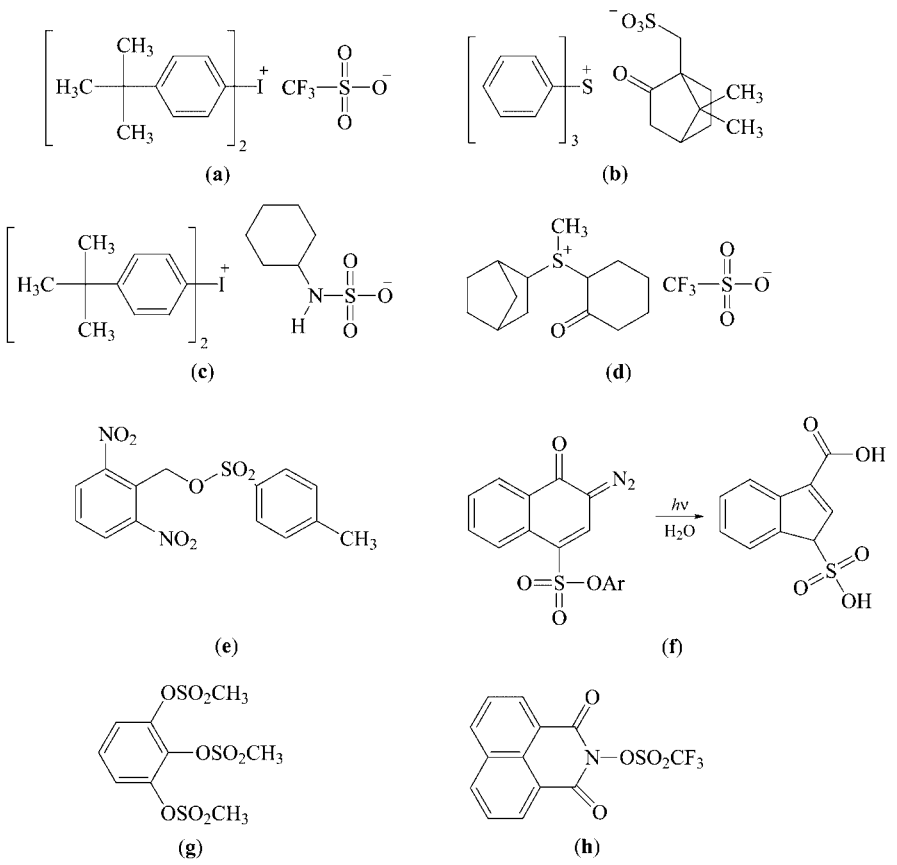

Fig. 10. Typical examples of the photoacid generators used in CA resist formulations; **(a)–(d)** are examples of onium salts; **(e)–(h)** are nonionic PAGs.

cation. In this way the acid strength of the photogenerated acid can readily be adjusted from that of so-called *super acids* to the comparatively weak organic acids (62). Modifying the acid strength can shift acid–base equilibria within the film. Since the catalyzed deprotection occurs via a protonated intermediate species, its concentration will be affected by this shift and thereby the concentration of that intermediate and the rate of deprotection can be manipulated.

The solubility of the PAG in the solid polymeric matrix can influence CA resist performance (63). This is a particular issue for the ionic onium salts; if the polarities of polymer and PAG are sufficiently different, phase segregation will occur, and the poor mixing of photoacid and polymer effectively reduces the efficiency of catalyzed deprotection. Additionally, resist contrast can be affected when the solubility of the photoproducts differs from that of the original onium salt. In fact onium salts can serve as dissolution inhibitors in novolac polymers, analogous to diazonaphthoquinones, even in the absence of any acid-sensitive chemical function on the polymer (27).

Simple aryl onium salts (structures **a–c** in Fig. 10) absorb in the wavelength range of 200–330 nm, making them well-suited for applications requiring DUV

exposure. Spectral response can be shifted to longer wavelengths either by varying substituents or by sensitization. The absorption properties also can be shifted to shorter wavelengths by replacing the aromatic groups in the onium cation with aliphatic groups (e.g., structure **d** in Fig. 10). These latter materials have been used in resists designed for exposure with 193-nm light, where aryl-substituted onium salts are claimed to increase absorption of the formulated resists to unacceptably high values (59).

There is evidence for several mechanistic pathways leading to formation of acid products from photolysis of onium salts: a direct irradiation route and two photosensitization routes proceeding either through a triplet intermediate or an electron-transfer mechanism. In the direct route, radicals, cations, and radical cations all have been proposed as reactive intermediates. The latter two species are believed to be immediate precursors of the photogenerated acid (top reaction of Fig. 11) (64). In the case of electron-transfer photosensitization (bottom reaction of Fig. 11), aromatic radical cations (generated from the photosensitizer) are believed to be a proton source as well (65). The electron-transfer route provides a convenient means to shift an onium salt's wavelength response and to tune its photospeed at the shifted wavelength without the need for chemical synthesis. By careful selection of aromatic hydrocarbon sensitizers with low oxidation potentials, the activity of triaryliodonium salts can be shifted to wavelengths >500 nm via electron-transfer sensitization (66).

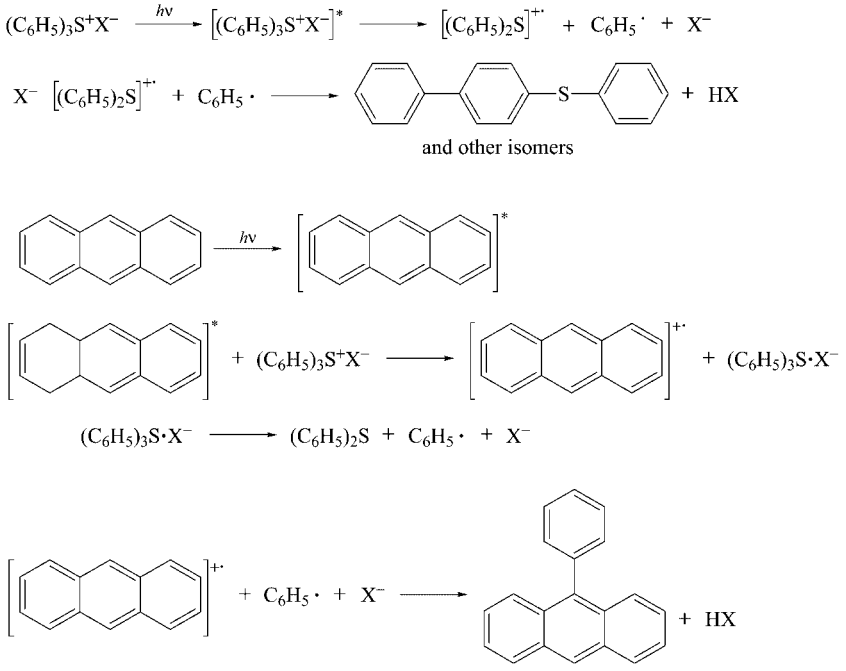

Fig. 11. Proposed photochemical mechanisms for the generation of acid from sulfonium salt photolysis. The top scheme illustrates photon absorption by the onium salt (direct irradiation) and the bottom scheme is an example of electron-transfer sensitization, initiated by irradiation of an aromatic hydrocarbon.

Nonionic Photoacid Generators. A number of nonionic compounds have been demonstrated to produce a Brönsted acid upon irradiation. Some examples are depicted by structures **e–h** in Figure 10 (67–70). The photochemical rearrangements leading to acid production vary. As one example, irradiation of the 2,6-dinitrobenzyl ester (structure **e** in Fig. 10) induces an intramolecular rearrangement [the well-known *ortho*-nitrobenzyl rearrangement (71)], ultimately producing toluenesulfonic acid (62). Unlike onium salts, in this case no radical flux is produced upon photolysis, minimizing the potential for cross-linking side reactions that can cause resist scumming or even negative-tone behavior in positive resist systems. 4-Sulfonyl DNQ sulfonic acid generators, shown in structure **f** of Figure 10, have been used as PAGs in CA resists, most effectively at exposure wavelengths longer than 300 nm (70).

In another example of photosensitization, electron-transfer from a photoexcited phenolic moiety of the polymer matrix to a PAG such as structure **g** in Figure 10 leads to the formation of methanesulfonic acid (68). Sulfonic acids can also be produced from *N*-hydroxyimide derivatives (such as structure **h** in Fig. 10) (69) by such an electron-transfer route, or by direct excitation.

Processing Characteristics of CA Resists. While the increased radiation sensitivity afforded by CA resists offers enormous practical advantages, it brings the need for far more stringent control of the lithographic process. Any factor that influences the course of the catalytic reaction will have an effect that is amplified by a factor equal to the catalytic chain length.

Post-Exposure Boke (PEB) Temperature Control. Experience has shown that precise temperature control is required to achieve reproducible high resolution imaging with CA resists. A typical PEB process calls for heating the exposed film coated on a silicon wafer substrate with a hot plate at a specified temperature in the range of 90–140°C for a 60-s period. To achieve acceptable dimensional control in the final resist images, the temperature across the entire wafer (which in today's manufacturing processes can be up to 300 mm in diameter) must be uniform, varying not more than 0.5°C, during PEB. The sensitivity of a CA resist's PEB process to small changes in temperature has been assessed by measuring the shift in the width of a printed image with temperature (72–74). Such image blur or spreading is the result of a complex interplay between the initial acid profile, the acid mobility, and the chemical kinetics of the acid-catalyzed reaction. The activation energy (E_a) for deprotection, which characterizes how its rate changes with temperature, has a large impact on CA resist processing characteristics. Correlations between the E_a of the deprotection reaction and the magnitude of the image dimensional shift with temperature have been noted. The image shift in PTBOCST resist (E_a for deprotection ~28 kcal/mol) has been measured to be 40 nm/°C (72), while the image shift for a CA resist based on acid-catalyzed acetal deprotection ($E_a \sim 15$ kcal/mol) shows essentially no dimensional shift with temperature (74). These "low activation energy" systems typically undergo deprotection at room temperature upon exposure, and so another of their potential advantages is a reduced dependence on the precise timing of process steps (75,76) since there is in effect no delay between the exposure and postbake steps. Deprotection at room temperature is not always desirable, however (see later under Outgassing of Resist Components), and the intrinsically higher reactivity can reduce the stability of the formulated resist solutions during storage (ie, its shelf life). As with

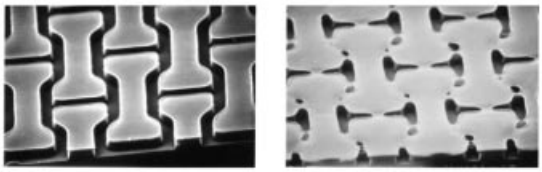

Fig. 12. Scanning electron micrographs illustrating the effects of airborne basic chemical contamination. The image on the left was formed when a positive-tone CA resist was processed without any delay after coating. The image on the right was formed when an identical film was stored after coating for 15 min in an atmosphere containing 10 ppb of *N*-methylpyrrolidone, and then processed identically to the first.

PAGs, the choice of the best protecting group for a specific system calls for a balancing of functional properties to optimize overall resist performance.

Processing Delay Time Effects. A critical and at-first puzzling problem was encountered during early manufacturing trials of CA resists. Sporadically, severely distorted resist profiles would be formed in positive-tone CA resists, displaying what seemed to be a cap on the upper surface of the resist image (Fig. 12). In severe cases this cap or "T-top" would appear as a skin or crust over the entire wafer surface that prevented development of the pattern. The magnitude of the effect varied dramatically between laboratories and appeared to grow more severe as the time interval between exposure and postexposure bake was increased.

Ultimately, it was demonstrated that contamination of the resist surface by airborne basic impurities present at parts-per-billion levels caused neutralization of the photogenerated acid near the resist–air interface, locally suppressing the acid-catalyzed chemistry and producing the observed effects. *N*-methylpyrrolidone (NMP), a common solvent used in semiconductor manufacturing as a stripping and coating solvent, was the first basic contaminant to be identified in laboratory air (77,78). Even though an amide like NMP is generally considered to be a weak base (the pK_a of protonated NMP is ~ -1.0), when compared to the basicity of the polymer matrix (the pK_a of most protonated esters, ethers, and phenols is in the range of -6 to -7) NMP is sufficiently basic to effectively compete for the proton catalyst, slowing the rate of the deprotection reaction (and the overall extent of conversion) in the contaminated region of the resist film. Other sources of airborne clean-room contaminants now have been identified (77). These include paints, adhesives, and sealants, materials that, like NMP, cannot be readily eliminated from the semiconductor manufacturing process.

The impact on negative CA resists of airborne base contamination differs qualitatively from their positive-tone counterparts. Suppression of acid-catalyzed chemistry at the surface of a negative resist results in some film erosion at the top of the exposed fields and in some cases an apparent loss of photosensitivity, but in general the relief images formed exhibit the expected cross-sectional profile. This is in sharp contrast with the typical behavior seen with positive-tone CA resists, where suppression of acid-catalyzed chemistry at the surface causes an insoluble surface skin.

Much attention has been given to means of reducing susceptibility of CA resists to airborne contamination. Process engineering changes such as the addition of special activated carbon filters to the environmental chambers surrounding

the exposure tools (77,79), overcoating the resist with a soluble protective film to isolate the resist from the environment (78,80,81), or modifications of the process flow to minimize the time interval between exposure and postexposure bake have been shown to improve CA resist processability. Resist materials modifications have also been pursued. For example, researchers have purposely introduced basic additives into the resist formulation (82,83) with the notion that a resist already containing added base should be less affected by the absorption of further small amounts of basic contaminants. A side benefit of this approach is improved resolution through a reduction in image blur (see under Limits of Extendibility for Lithographic Resists).

Resist process stability in the presence of airborne bases has also been improved by carefully tuning the polymer characteristics to reduce the rate of contaminant absorption. For example, the rate of NMP uptake was found to vary by almost a factor of 50 depending on the polymer structure in a study using radiotracers to quantify the kinetics and extent of contaminant absorption (84). The contaminant uptake of each polymer could be related to its solubility parameter (which characterizes contaminant solubility in the film) and the T_g of the polymer. Films with T_g values below the post-apply bake temperature undergo polymer film annealing during post-apply baking, leading to a reduction in free volume (present as a consequence of the nonequilibrium nature of the spin coating process), which reduces diffusant mobility. The practical conclusion that can be drawn from this result is that susceptibility to airborne chemical contaminants can be minimized if a CA resist film is baked after coating at a temperature at or above its T_g. By deliberately selecting polymers, protecting groups, and PAGs with thermal properties and stability in mind, CA resists have been designed that can be heated without thermolysis at or above T_g (85,86). Such resists display sharply improved environmental stability compared to analogous systems processed below T_g.

Outgassing of Resist Components. The evolution of reactive volatile organic material from CA resists during exposure has been recognized to be a significant issue. Deposition of volatilized substances on optical surfaces degrades the projected image, and if the deposited material undergoes radiation chemistry during exposure then permanent damage can result (87). Mass spectral analysis of the material evolved upon exposure (88) provides evidence that the contaminants originate from both PAG and polymer: the PAG radiation chemistry (Fig. 11) generates volatile, low molecular weight, reactive products, and a small degree of polymer deprotection and/or chain fragmentation takes place on the timescale of the exposure. The degree of outgassing is strongly tied to the polymer and PAG structures.

Limits of Extendibility for Lithographic Resists

Image Blur in CA Resists. The mobility of the acid catalyst in the film influences CA resist performance. At the molecular level, the proton must move from site to site to effect acid-catalyzed reactions in the resist film. If the mobility is too great, however, the initial spatial profile of photogenerated acid will be blurred and the final developed resist image will appear distorted. The problem becomes more acute at finer resolution. In those situations where diffusion of the

positively charged proton causes a net displacement of positive charge, as is the case for diffusion in a concentration gradient, it must be accompanied by diffusion of the anion so as to maintain overall charge neutrality. In such cases the proton movement is coupled to that of the anion, and those properties of the anion that affect its mobility, for example its volumetric size, will influence the overall acid transport. The use of onium salts bearing sterically bulky counterions [eg, where camphorsulfonate anion (Fig. 10**d**) is used rather than methanesulfonate] has been examined as a means for reducing acid mobility (89).

While excessive acid diffusion leads to image blur, even in cases where diffusion has been suppressed to an insignificant level (e.g., by means of an immobile anion), significant image spreading will still occur during PEB (90). When imaging at dimensions near the resolution limit of a projection exposure tool, diffraction leads to partial illumination, and therefore generation of some amount of acid, in areas of the resist that nominally are unexposed. Because of this, the deprotection reaction proceeds rapidly at the center of the exposed image but also at a significant, although slower, rate in the nominally unexposed regions. This causes the width of the deprotected region—which ultimately defines the shape of the developed image—to spread beyond the desired boundaries. This can be suppressed by purposely adding to the resist formulation a small amount of a basic substance such as an amine or an organic hydroxide (82,83,91). The amount of base is calculated to slightly exceed the amount of acid formed in the dark areas of the pattern, suppressing image spreading there with minimal impact on the chemistry in the exposed areas.

Line-Edge Roughness. Random fluctuation in the width of a resist feature, termed line-edge roughness or LER, is anticipated to be a significant source of line-width variations that could ultimately limit the extendibility of conventional lithographic resists to nanoscale fabrication. Analyses of imaged resists have revealed LER values that vary over a wide range (51,52,92–94). Potential sources of LER include the molecular weight and molecular weight distribution of the resist polymer (51), the molecular structure of resist components (94), inhomogeneity in the distribution of resist components within the film (63), statistical effects influencing film dissolution (95), and intrinsic properties of the imaging chemistry (96).

The standard dimensional tolerance used in semiconductor fabrication is $\pm 10\%$ of the minimum feature size; for example, a minimum dimension of 50 nm will require dimensional control of the order of 5 nm. In resist patterns prepared under optimal imaging conditions, for a wide range of resist chemistries the minimum LER was found to be in the range of 2–7 nm (52). This minimum roughness is of the order of the molecular size of polymers typically used in resist formulations, as estimated by the radius of gyration for polymers with molecular weights in the range of 5000–100,000. One factor that strongly influences the degree of LER is the sharpness of the aerial image (Fig. 13); the more blurred the light image, the greater is the LER of the final resist image. This correlation is taken as evidence that nanoscale inhomogeneity in solubility properties is present at the intermediate dose range of the resist line-edge and is replicated in the developed image.

Characterization of the origins of LER and the design of strategies to minimize LER are today active areas of research. In recent work, experimental electron beam resist formulations comprising nonpolymeric materials (eg, liquid crystals

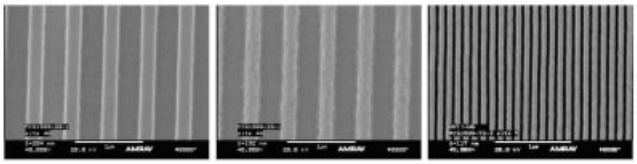

Fig. 13. Top-down scanning electron micrographs of developed resist images depicting line-edge roughness; (left) low LER obtained when printing 250-nm lines and spaces with a sharply defined aerial image in a commercial CA photoresist; (center) increased LER obtained with the same resist when exposed with a degraded aerial image; (right) LER obtained on the same resist when printing 50-nm lines/spaces with a sharply defined aerial image.

or fullerene derivatives) (97,98) have displayed very high resolution (10-nm feature sizes) accompanied by very low LER (∼1 nm or less).

Image Collapse. Although resist feature dimensions have undergone continuing reductions in line width, image thickness has not scaled proportionately. This is because significant erosion of the resist occurs during image transfer. While refinement of plasma etch processes has significantly reduced resist erosion, the improvements have not kept pace with the line-width shrinkage. As a result the *aspect ratio* required of resist features, that is, the ratio of its height to its width, has increased with time as line widths have grown smaller. The extent to which the aspect ratio can increase ultimately is limited by mechanical failure of the images during processing, typically manifested as image collapse. Figure 14 shows a typical example of this.

Studies of this problem have shown that the image collapse occurs following post-develop rinsing of the nascent resist images (99,100). During the post-rinse drying step, unequal surface tension forces from the rinse liquid trapped between

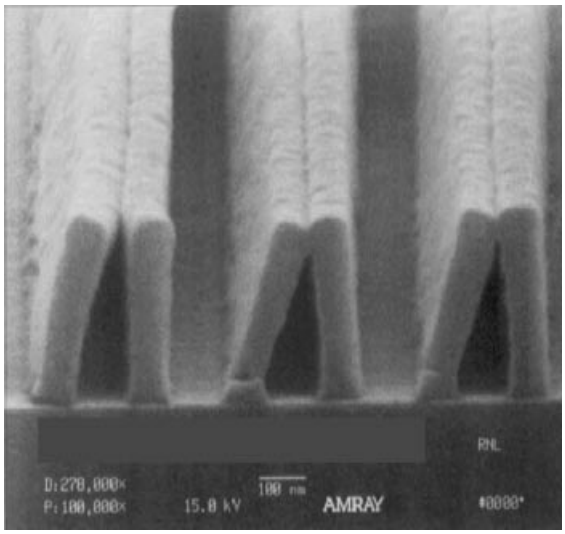

Fig. 14. Scanning electron micrograph of a CA resist pattern illustrating image collapse during postdevelop drying. Note the fracture of the resist structure near its base. Courtesy of D. Medeiros of IBM.

features distort and then fracture the fragile structures. Isolated lines, which are not subjected to unsymmetrical forces, do not show image collapse.

The propensity for image collapse depends on the width and proximity of the features, its aspect ratio, the substrate surface, and the mechanical properties of the imaged resist. Two characteristic failure modes have been identified: deformation, where fracture occurs within the resist structure, and adhesion loss, where the resist feature separates from the substrate at their interface. Low surface-tension rinse liquids [in the extreme, supercritical fluids (101)] and the use of rigid and highly adhesive resists reduce the frequency of image collapse.

Resists for Emerging Exposure Technologies

Photolithography at 193-nm Wavelength. Projection photolithography using 193-nm light is anticipated to find initial implementation in semiconductor manufacturing processes in the year 2002. The design of resists for this exposure technology has proved to be a significant challenge. Existing resist materials developed for use at longer wavelengths were found to be too opaque for exposure at 193 nm, a circumstance reminiscent of the earlier shift from 365- to 248-nm exposure tools. This triggered a decade-long large-scale development effort to devise suitable 193-nm resist materials. A particularly demanding aspect of this undertaking is that the first use of 193-nm resists will be to fabricate device levels whose minimum feature sizes are 130 nm, a dimension substantially smaller than the exposure wavelength. The first large-scale use of 248-nm resists was with the 500-nm device generation, that is, at a feature size of twice the exposure wavelength. With evolutionary materials and optical improvements, 248-nm resists have been applied to devices with increasingly smaller features, now reaching dimensions below 150 nm through the use of complex (and costly) optical resolution enhancement techniques that sharpen the projected light image (102). One implication of this is that a first-generation 193-nm resist must be at a level of refinement equivalent to a fourth-generation 248-nm resist.

Phenolic polymers in many respects are ideal for microlithographic resists as they provide predictable, well-controlled dissolution behavior, excellent adhesion properties, and acceptable plasma etch resistance. But the strong absorption of phenolic polymers at 193 nm (illustrated in Fig. 8) precludes their use at that wavelength, and 193-nm resist efforts can be characterized as the pursuit of new transparent polymer systems that combine these three functional attributes as effectively as do their phenolic counterparts.

193-nm Resist Design Strategies. For a typical target thickness of ~400 nm, the optical density of the formulated resist should be of the order of 0.2–0.3. This transparency requirement precludes the use of unsaturated functionality such as aromatics and vinylics, but aliphatic, cycloaliphatic, carboxylic ester and acid, ether, nitrile, and sulfone groups exhibit acceptable optical properties. Using such building blocks, resist chemists have worked to achieve both good plasma etch resistance and good lithographic performance. Experience has shown that this calls for a balancing of the at-times-conflicting properties of the building blocks through copolymerization and blending.

Analyses of the relation between polymer structure and plasma etch resistance have led to a set of guidelines applicable to resist design (103–105). Polymer materials with "cyclic carbon," ie, those having a significant mass of carbon in the repeat unit incorporated as ring structures with high C—C connectivity, exhibit improved etch resistance (103). In 193-nm resist materials, the restriction against incorporating aromatic structures reduces this to a simple rule: maximize the alicyclic groups (aliphatic rings) in the polymer to maximize etch resistance. The alicylic structure can be integrated into the polymer chain, or can be incorporated as inert or acid-labile pendant groups (105).

Perhaps the most significant challenge in the design of 193-nm resists is the control of dissolution properties in 0.26 N aqueous tetramethylammonium hydroxide, the industry-standard developer solution. Transparent, base-labile functional groups such as carboxylic acids and anhydrides and lactones have emerged as functional substitutes for phenols. The dissolution behavior of carboxylic acids differs markedly from that of phenols, presumably because of the much stronger acidity of the former, which affects the extent of ionization and therefore the polarity of the ionized chains when contacted by developer. While the inclusion of a large proportion of alicyclic groups improves polymer etch resistance, the added hydrophobic character further complicates its dissolution behavior. By reaching the proper hydrophilic/hydrophobic balance it is possible to achieve a large difference in solubility between exposed (deprotected) and unexposed resist, at useful dissolution rates and without swelling. To further tune solubility properties, low molecular weight aliphatic dissolution inhibitors (often cholate esters) frequently are added to 193-nm resist formulations (106). The inclusion of such compounds allows more flexible control of dissolution properties and acts to plasticize the film, a benefit at times since several of the polymer systems under study for 193-nm resists have very high glass-transition temperatures (200°C or more) (Table 1).

Research efforts in 193-nm resists in large part have focused on three polymer families: poly(acrylates), poly(cycloolefins), and cyclic olefin–maleic anhydride (COMA) copolymers. The main characteristics of each of these are detailed below.

Photoresists Based on Acrylic Polymers. Acrylate and methacrylate polymers as a class are quite transparent in the 193-nm spectral range (Fig. 8). Positive-tone CA resists based on acrylic polymers, although first designed for printed circuit fabrication where minimum dimensions are 50 μm or more, have been demonstrated to produce high resolution images using 193-nm exposure tooling (107).

The methacrylate terpolymer shown in Figure 15a typifies this class of material. In the terpolymer, each monomer type imparts specific characteristics to the polymer, providing a mechanism for precise balancing of functional properties. The polymer contains a protecting group (acid labile), a more polar group that improves adhesion and solubility of the PAG in the film, and a smaller amount of a carboxylic acid to modify film polarity and dissolution. Such polymers are prepared by simple free-radical solution polymerizations that are readily scalable to manufacturing levels. The copolymerization properties of methacrylate monomers, where the ester groups exert little influence on reactivity toward polymerization, make it straightforward to optimize resist properties by synthesizing ter- or tetrapolymers.

Table 1. Generalized Strategy for 193-nm Resist Design

Polymer	Protecting group	Photo-acid generator	Additives
FUNCTIONAL PROPERTIES			
Film forming	Polarity switch	Efficiency	T_g modifier
Etch resistance	Shrinkage	Acidity	Dissolution modifier
Optical transparency	Thermal stability	Volatility	Resolution enhancement
Adhesion	Outgassing	Size	Coating aid
Thermal stability		Interfacial distribution	
MATERIALS SET			
Acrylate	Acetal/ketal	Aryl sulfonium salts	Additive material chemical classes
Methacrylate	*tert*-Butyl ester	Aryl iodonium salts	Amines
Cyclic olefin	Alicyclic ester	Alkyl sulfonium salts	Organic ionic hydroxides
Alternating copolymer	Inert modifiers	Nonionic PAGs	Surfactants
Cyclopolymer			Cholate esters
Hybrid (eg, acrylic/alternating)			

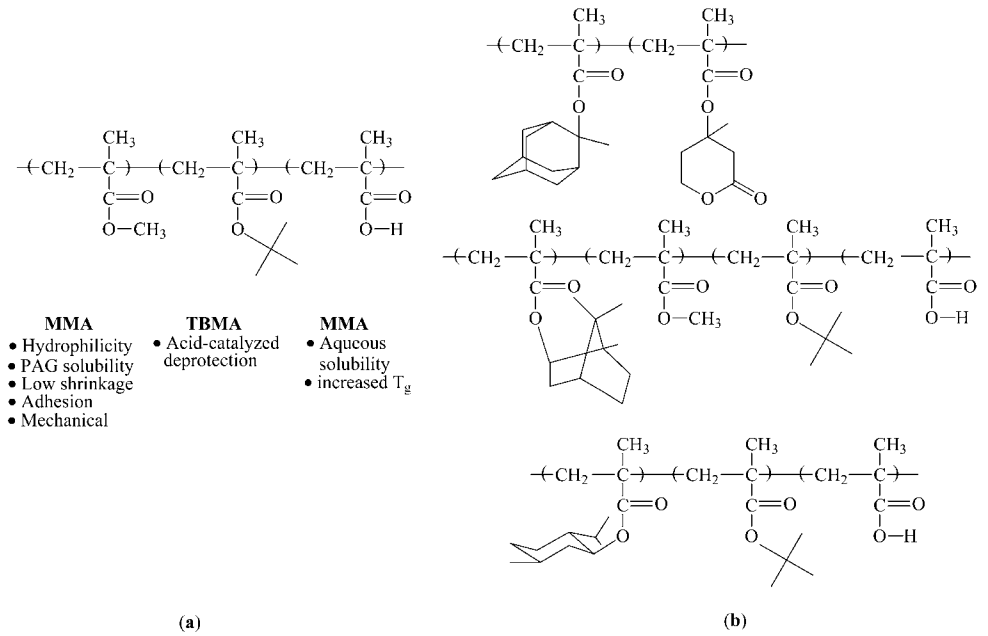

Fig. 15. Candidate polymers for 193-nm resists. (**a**) An acrylic terpolymer designed for chemically amplified resist applications. The properties each monomer contributes to the final polymeric structure are enumerated. (**b**) Examples of acrylic copolymer structures that have been applied in 193-nm CA photoresists.

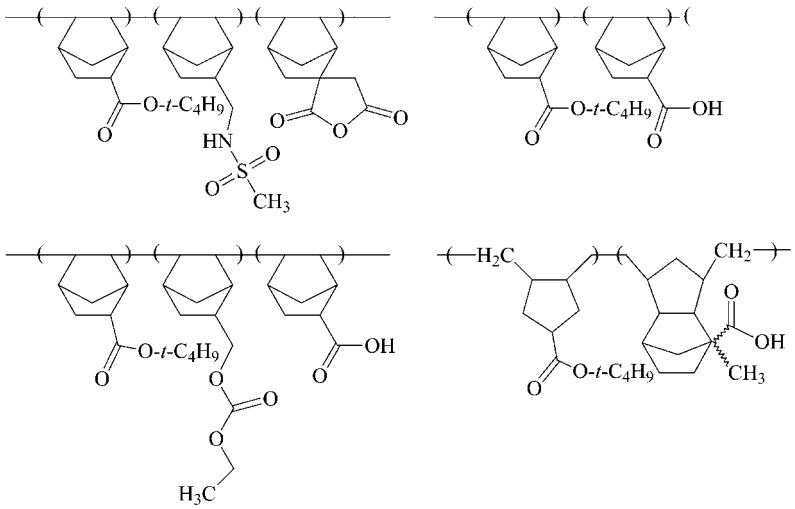

Fig. 16. Cyclic olefin copolymers evaluated for 193-nm resist applications.

The etch resistance of common acrylic polymers is poor but can be improved without reducing 193-nm optical transparency by the attachment of alicyclic pendant groups to the backbone. For example, a 1:1 copolymer of *tert*-butyl methacrylate and adamantyl methacrylate (108) exhibits a nearly twofold reduction in plasma etch rate compared to the *tert*-butyl methacrylate homopolymer. Figure 15b provides examples of alicyclic ester groups that have been assessed (109–111).

Acrylate polymers slowly undergo chain scission upon irradiation with uv light and electron beams. While this property has been used to advantage [acrylic polymers such as poly(methyl methacrylate) have seen use as high resolution but low sensitivity electron beam and DUV resists], in this instance it is undesirable as it compromises plasma etch resistance, and complicates the metrology of acrylate resist patterns when using scanning electron microscopy (112).

Photoresists Based on Cyclic Olefins. These resists have received significant attention, as the base polymers are extremely robust in plasma etch processes (113). Figure 16 depicts illustrative examples of this class of polymer that have been examined for 193-nm lithographic applications (114–116). The polymers typically are prepared by means of a metal-catalyzed addition or ring-opening metathesis polymerization process using substituted norbornene monomers. Polymers prepared by the metal-catalyzed addition have relatively low molecular weight (3000–10,000), polydispersities of ∼1.5, and very high glass-transition temperatures (>250°C). In the ring-opening process, product molecular weight can be controlled over a wide range by the addition of α-olefins to the polymerization mix. Cyclic-olefin-based resists have been notable for their atypical development properties in aqueous base (a tendency toward significant swelling), but nonetheless have been used to formulate resists capable of high resolution imaging properties.

Photoresists Based on COMA Copolymers. Introduction of an anhydride linkage into the cyclic olefin polymer structure leads to a significant and useful improvement in dissolution properties: COMA copolymers require a much lower

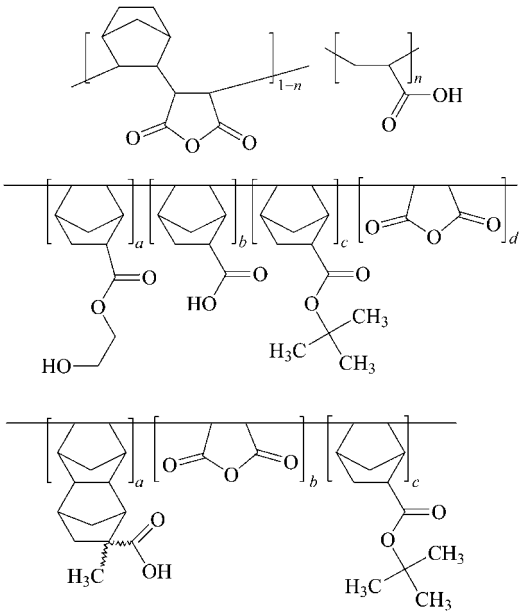

Fig. 17. Cyclic olefin–maleic anhydride copolymers for 193-nm lithographic applications.

proportion of carboxylic acid to achieve aqueous dissolution, and that dissolution proceeds without the substantial swelling that is characteristic of cyclic olefin polymers (116). Hydrolytic ring opening of the anhydride during development, producing a hydroxyl group and a carboxylate anion in the alkaline developer medium, occurs synchronously with development. Presumably the additional ionization of the backbone increases its rate of dissolution such that swelling is minimized.

COMA polymers (Fig. 17), synthesized by conventional radical polymerization, have a 1:1 alternating structure, a consequence of the preference for each radical to react exclusively with the other monomer. As a rule, the products are high T_g materials; for example poly(norbornene-*co*-maleic anhydride) has a $T_g > 300^\circ$C. The polymerization allows the incorporation of small amounts of other vinyl monomers (e.g. acrylic acid) without disruption of the alternating structure (117). Substituted norbornenes can be included in the polymerization mixture to incorporate acid-labile functionality, to modify polymer polarity, and to improve film adhesion (118). Cholate dissolution inhibitors can be added in the formulated resist to further modify functional properties (119).

Vinyl ether monomers also have been combined with maleic anhydride to prepare alternating copolymers. Conceptually similar to COMA systems, these polymers have lower glass-transition temperatures and possibly improved imaging properties (120).

Photolithography at 157-nm Wavelength. As recently as 1997, 157-nm lithography was not regarded as a viable manufacturing technology, primarily because of concern about the availability of suitable materials for optical components and masks (121). Because of that view, no significant resist R&D efforts had been undertaken up to that time. Recent improvements and innovation in optical materials (122) and increasing concern about the timing of availability of complex new nonoptical lithographic technologies (see below) have fostered an intense interest

in 157-nm technology as the immediate successor to 193-nm lithography (123). At this time (early 2001) technical solutions to the issues of laser sources, optical design, and contamination control are considered to be well in hand, and the primary challenge is regarded to be the design of polymers for the new resists this exposure technology will require.

Like their 193-nm counterparts, 157-nm resists will be first used for printing feature sizes (100–70 nm) well below the exposure wavelength. The requirement for very high resolution coupled with the intrinsically low transparency of organic polymers makes the design of these resist systems particularly challenging. Consideration of the factors that dictate resist thickness, such as focus latitude, etch resistance, and mechanical stability of the features, suggests a target thickness of ~200 nm for a 157-nm single layer resist used to print 70-nm features. Using the optical absorbance of current 248-nm resists (of the order of 0.30, or 50% transmission) as a guide, a resist for 157-nm exposure must therefore have an optical density of no greater than 1.5/μm. As a rule, 248- and 193-nm resist polymers have optical densities at 157 nm in the range of 6–8/μm, much too high for lithographic applications (124). This stringent requirement has dictated the direction of materials R&D for 157-nm lithography.

Molecular Absorption at 157 nm. This wavelength (63,700 cm^{-1}, 7.89 eV) falls in the middle of the vacuum ultraviolet (VUV) region of the electromagnetic spectrum. At such energies the electronic transitions of organic molecules include excitations into Rydberg orbitals along with the familiar valence shell transitions (ie, the π–$\pi*$ transitions of aromatic molecules) found at longer wavelengths (125). Molecular Rydberg transitions, in which the excited electron occupies a diffuse orbital large compared to the size of molecule, can have easily identifiable sharp atomic-like features but can also appear as broader transitions difficult to distinguish from valence shell excitations. While a significant body of work (both experimental and theoretical) has been compiled on the VUV spectroscopy of organic molecules in the gas phase (126) there is less data on the absorbance properties in solution or solid phase. Simple extrapolations from absorption spectra of small molecules in the gas phase to polymeric systems are complicated by the fact that Rydberg transitions are usually shifted or absent in condensed media.

Some generalizations are possible, however. It is well known that replacement of hydrogen with the highly electronegative fluorine atom can cause spectral shifts to shorter wavelength (higher energy) through perturbation of the sigma-bonded framework (126). This effect can influence adjacent atomic centers in the framework, leading, for example, to a decrease in the oxygen atom's contribution to 157-nm absorption in fluorinated alcohols and esters. A survey of polymers of different structural types does show that fluorinated resins as a class exhibit suitable transparency (124). A second polymer class identified as potential 157-nm resins in this survey was the silsesquioxanes with minimal hydrocarbon content (127). At present these two material families serve as the basis for 157-nm resist development.

Single-Layer 157-nm Resists. As with other CA resists, the design of a 157-nm photoresist material must include functionality that confers aqueous base solubility, plasma etch resistance, and efficient imaging based on acid catalysis. Although the phenolic and carboxylate groups that provide these functions in 248- and 193-nm CA resists are not well-suited for 157-nm lithography, fluorinated variants that offer improved optical transparency show promise.

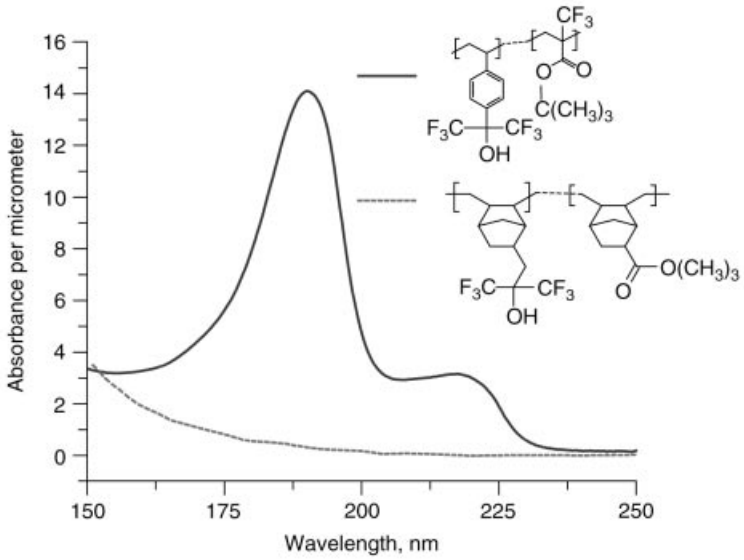

Fig. 18. Polymers for 157-nm resists containing HFIPA units. The structures and VUV absorption properties are shown for two copolymers that typify the materials now under investigation.

Fluorinated alcohols such as hexafluoroisopropyl alcohol (HFIPA) have good transparency at 157 nm [and in fact have been used as solvents for VUV spectroscopy (128)]. Their acidity ($pK_a \sim 11$) is roughly equal to that of the phenolic groups upon which most 248-nm resists are based, and they exhibit similar solubility behavior in aqueous base (52). Like phenols, fluoroalcohols can be coupled to acid-labile protecting groups such as carbonates or ketals. Some recent examples of candidate polymers for 157-nm resists can be viewed as fluorinated analogues of 248-nm CA resists, for example, copolymers of HFIPA–styrene, either with its protected form poly(TBOC–HFIPA–styrene-*co*-HFIPA–styrene) or with α-trifluoro-*tert*-butylmethacrylate (129,130). Figure 18 shows the structure of this last polymer (upper structure) and its VUV absorption spectra.

Other experimental 157-nm resists can be considered to be derived from 193-nm CA resists. The homopolymer poly(HFIPA–norbornene) has an optical density of 1.8/μm (130). First used in 193-nm resist polymers (131), HFIPA–norbornene monomer can be incorporated into cyclic olefin polymers prepared via organometallic catalysis, and can be copolymerized with vinyl monomers such as acrylates or fluorinated acrylates using standard free-radical polymerization to give products with optical densities of less than 3/μm (Fig. 18, lower structure) (132,133). Still other fluorinated monomers can be employed in 157-nm resists, and resist systems based on polymers of fluorinated olefins and vinyl alcohols have been described (134,135). In general, it appears that incorporation of fluorine compromises the etch resistance of resists when compared with their hydrocarbon analogues (136).

The development of practical 157-nm resists brings its share of challenges. Achieving the proper dissolution characteristics in polymer systems containing

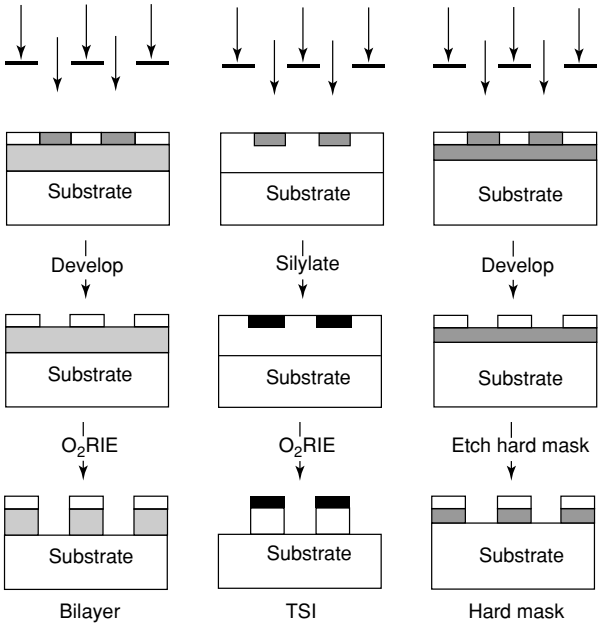

Fig. 19. Schematic diagram of three approaches to multilayer resist imaging.

a high proportion of fluorine can be difficult, a problem analogous to that encountered with 193-nm resists. Because of the high photon energies at 157 nm (183 kcal/mol, which far exceeds C—C single bond strengths) there is the potential for significant photochemical degradation of the polymer (ie, backbone scission or side-chain cleavage), with the attendant problems due to resist outgassing.

Multilevel 157-nm Systems. One flexible approach that allows optimization of optical absorbance without compromising etch resistance is to decouple the two properties into separate thin-film layers. This *multilevel resist* or *thin-film imaging* approach was first introduced in the 1970s (137) and many variants on the concept have since been described (138). Examples of current interest include silicon-based *bilayer* resists (139), *top surface imaging* (TSI) processes (140), and the combination of *ultrathin resists* (UTR) with inorganic *hard masks* (141) (Fig. 19). In each of these approaches the lithographically formed image is confined to a thin film, or a thin layer within a film, and is then transferred into a second nonimaging layer that serves as the etch-resistant mask for final substrate etching. The initially formed image typically is replicated into the underlayer using a selective anisotropic etch step. By careful selection of etch chemistries and materials design, the final relief image can provide a robust barrier for the final image transfer. The added complexity of multilevel resist approaches compared with a single-layer resist process is a drawback but is offset by the advantages that accrue from (*1*) imaging very thin films, which eases the requirements for high transparency and reduces the impact on image quality of drifts in focus; and (*2*) forming thicker, high aspect ratio films, which improves the integrity of the protecting pattern while circumventing the problem of image collapse. Until now, the added complexity has generally outweighed the intrinsic benefits, and

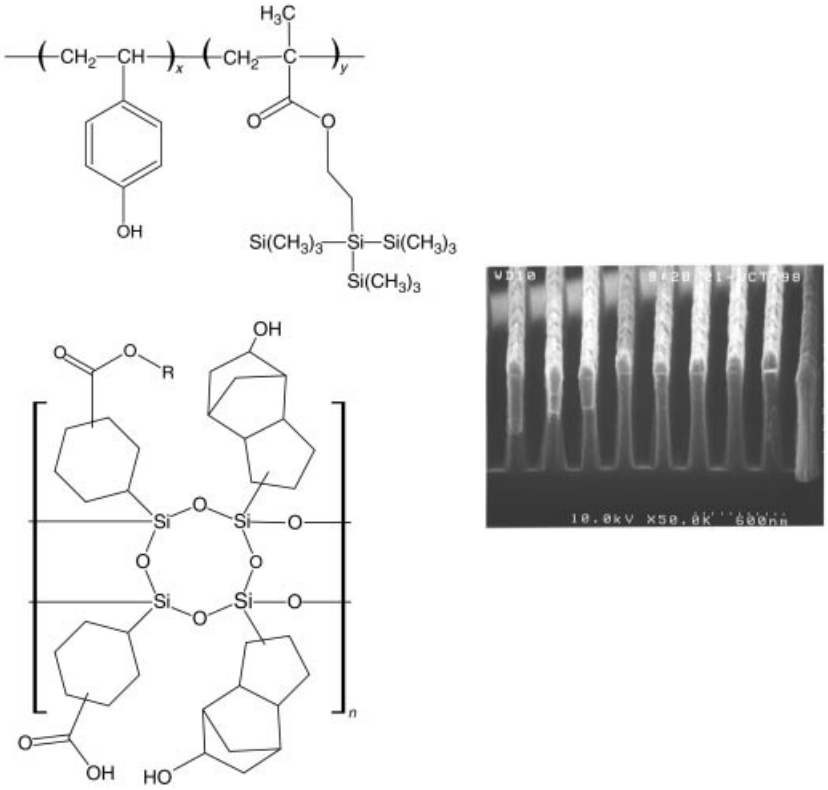

Fig. 20. Examples of silicon-containing polymers for use in bilayer resist formulations. The top structure is used in a 248-nm bilayer CA resist. The scanning electron micrograph shows the high aspect ratio images that can be obtained using 248-nm projection lithography with a bilayer resist based on this polymer. The bottom structure shows an example of a silicon-containing polymer designed for use in 193-nm lithography.

so multilevel resists have not yet seen widespread manufacturing use. The limited selection of polymeric materials suitable for 157-nm resist formulation has brought renewed interest in multilevel systems.

Figure 20 provides examples of silicon-containing polymers specifically designed for use in CA bilayer resists. Silsesquioxane polymers (eg, the lower structure in Fig. 20) have seen extensive use in bilayer resists developed for both 248- and 193-nm applications (142–144). Fluorocarbinol derivatives of silsesquioxanes have particularly good transparency at 157-nm wavelengths. Positive-tone resists can be prepared from such polymers by protecting the hydroxyl group with an acid-labile group such as *tert*-butoxycarbonate. Negative-tone silsesquioxane resists have been formulated by incorporating the acid-catalyzed cross-linking chemistry described earlier.

A high silicon content in the resin is advantageous as it provides the basis for etch selectivity in an oxygen plasma. When a thin film of a resist containing silicon is patterned atop a polymer underlayer containing no silicon, and then immersed in an oxygen plasma, the imaged film immediately forms a highly etch-resistant layer of SiO_2 while the unprotected underlayer rapidly erodes. In general, the greater the silicon content, the more effectively this silicon oxide barrier resists the

plasma. Using a specialized variant of plasma etching, termed reactive ion etching, the underlayer etch can be performed anisotropically, transferring the pattern of the top film vertically into the thick underlayer. The final etched bilayer pattern serves as a resist relief image useful for pattern transfer to substrate. Figure 20 provides an example of the high aspect ratio features that can be formed using bilayer imaging, in this instance using 248-nm lithography.

The TSI scheme shown in Figure 19 exploits the high optical absorption of the polymer to confine the imaging chemistry, and a subsequent reactive silylation step, to a thin layer at the top of the film. Since an oxygen plasma etching step is used to form the relief image, TSI offers benefits similar to the bilayer resist approach. In the past, pronounced line-edge roughness has restricted practical implementation of the TSI technique (145). Recent modifications to the reactive ion etch procedure and the transparency of the polymers employed in 193-nm imaging systems have been reported to minimize LER (146,147) and these efforts are being extended to the more challenging 157-nm TSI systems (148).

Resists for "Next-Generation Lithography" Applications. As recently as 1999, five different technologies were being evaluated as possible successors to optical lithography (149). Because of the economics and infrastructure of the semiconductor industry it is likely that only one or at most two different lithographic technologies can be fully developed and supported by the worldwide manufacturing community. The current consensus, based on a collection of factors including evaluations of the extensibility of each approach, is that extreme ultraviolet (EUV) lithography (17) will be the successor to 157-nm lithography for high volume manufacturing, and that electron projection lithography (EPL) (150,151) may be used in certain other types of manufacturing applications. On the basis of the projected brightness of the radiation sources, it is anticipated that CA resists will be a requirement for both exposure technologies.

Photolithography at EUV Wavelengths. EUV projection lithography uses light of wavelengths in the range of 10–14 nm (the soft x-ray region), produced by a plasma source. Since no materials have significant transmission at such wavelengths, EUV technology uses a series of curved mirrors and a reflective mask to project the light image. In this wavelength range the absorption coefficient of any material depends on the atomic weight percent and the density of each element in the absorbing material, and can be calculated from the mass absorption coefficients of the individual elements (17). Phenolic and acrylate-based resists absorb strongly at this wavelength (although less so than at 157 nm), and there is little likelihood that polymer structural modifications will lead to a significant increase in transparency at EUV wavelengths (152). As a consequence, current development is focused on developing hard mask processes (Fig. 19) that use 248 nm resists modified for higher EUV sensitivity, at thicknesses of 100–120 nm where transparency is adequate (141).

Resists for Electron-Beam Lithography. In *direct-write* electron-beam lithography a finely focused beam of high energy (1–100 keV) electrons is scanned in a pattern across a resist-coated substrate. This technique, used extensively in the manufacture of photomasks, is capable of exquisite resolution (~10 nm or less), but the serial nature of the exposure limits its throughput. A variant on this technique, termed *electron projection lithography* (EPL) (15,150), employs a thin membrane or stencil mask, patterned with a material that strongly scatters electrons, to project a high contrast image through an aperture onto the

resist-coated substrate. The inherent parallelism of this approach provides much higher throughput while maintaining some of the resolution capabilities of the direct write systems. EPL technology is now being refined for use in future semiconductor manufacturing.

At the high accelerating voltages commonly used, the exposing beam readily penetrates through the depth of a resist film, and so resist "transparency" is not considered an issue. Because the source current must be limited to suppress beam blur due to electron–electron repulsions, electron-beam lithographies targeted for high throughput (such as EPL) require very sensitive (CA) resists. To date, development activities for EPL resists have focused on the modification of existing 248-nm resist chemistries to enhance electron-beam sensitivity (153–155). On the basis of pulse radiolysis studies, it has been proposed that electron-beam irradiation of a CA electron-beam resist produces a polymer-based radical cation that undergoes an electron-transfer reaction with the PAG to produce an acidic product, akin to the electron-transfer sensitization mechanism proposed for dye sensitization in CA photoresists (156).

BIBLIOGRAPHY

"Photoresists" in *EPST* 1st ed., Suppl Vol. 1, pp. 401–443, by G. A. Delzenne, Photochemical Research Laboratory, Agfa-Gevaert; "Lithographic Resists" in *EPSE* 2nd ed., Vol. 9, pp. 97–138, by R. W. Blevins, R. C. Daly, and S. R. Turner, Eastman Kodak Company.

1. G. Willson, L. Thompson, and M. Bowden, eds., *Introduction to Microlithography*, 2nd ed., American Chemical Society, Washington, D.C., 1994.
2. W. Moreau, *Semiconductor Lithography*, Plenum Press, New York, 1988.
3. E. Reichmanis and A. Novembre, *Annu. Rev. Mater. Sci.* **23**, 11 (1993).
4. J. Shaw and co-workers, *J. Vac. Sci. Technol., B* **7**, 1709 (1989).
5. G. Moore, *Proc. Soc. Photo-Opt. Instr. Eng.* **2438**, 2 (1995).
6. J. Bryzek, K. Pedersen, and W. McCulley, *IEEE Spectrum* **31**(5), 20 (1994).
7. G. Kovacs, K. Petersen, and M. Albin, *Anal. Chem.* **68**, 407A (1996).
8. L. Lin and co-workers, *IEEE Photon. Technol. Lett.* **6**, 1445 (1994), and references therein.
9. D. Cho and co-workers, eds., *Micromechanical Sensors, Actuators and Systems*, American Society of Mechanical Engineers, New York, 1991.
10. M. Eggers and D. Ehrlich, *Hematol. Pathol.* **9**(1), 1 (1995).
11. M. King, in N. Einspruch, ed., *VLSI Electronics: Microstructure Science*, Vol. **1**, Academic Press, New York, 1981, Chapt. "2".
12. S. Holmes, P. Mitchell, and M. Hakey, *IBM J. Res. Dev.* **41**, 7 (1997).
13. M. Born and E. Wolf, *Principles of Optics*, 6th ed., Pergamon Press, Oxford, 1983, pp. 415, 441.
14. D. Flagello and T. Milster, *Appl. Opt.* **36**, 8944 (1997).
15. J. Bruning, *Proc. Soc. Photo-Opt. Instr. Eng.* **3049**, 14 (1997).
16. J. Silverman, *J. Vac. Sci. Technol., B* **16**, 3137 (1998).
17. C. Gwyn and co-workers, *J. Vac. Sci. Technol., B* **16**, 3142 (1998).
18. M. McCord and M. Rooks, in P. Rai-Choudhury, ed., *Handbook of Microlithography, Micromachining and Microfabrication*, Vol. **1**, SPIE Press, Bellingham, Wash., 1997, Chapt. "2".
19. I. Berry, *J. Vac. Sci. Technol., B* **16**, 2444 (1998).
20. P. Hartsuch, *Chemistry of Lithography*, Lithographic Technical Foundation, New York, 1961.

21. R. Dammel, *Diazonapthoquinone-Based Resists*, Tutorial Texts in Optical Engineering, Vol. **TT 11**, SPIE Optical Engineering Press, Bellingham, Wash., 1993.
22. G. Pawlowski and co-workers, *Proc. Soc. Photo-Opt. Instr. Eng.* **1262**, 391 (1990).
23. W. DeForest, *Photoresist: Materials and Processes*, McGraw-Hill, New York, 1975.
24. H. Ito, *IBM J. Res. Dev.* **41**, 69 (1997).
25. D. McKean, U. Schaedeli, and S. MacDonald, in E. Reichmanis, S. MacDonald, and T. Iwayanagi, eds., *Polymers in Microlithography* (ACS Symposium Series 412), American Chemical Society, Washington, D.C., 1989, p. 27.
26. J. Maltabes and co-workers, *Proc. Soc. Photo-Opt. Instr. Eng.* **1262**, 2 (1990).
27. H. Ito and E. Flores, *J. Electrochem. Soc.* **135**, 2322 (1998).
28. T. Lowery and K. Richardson, *Mechanism and Theory in Organic Chemistry*, 3rd ed., Harper and Row, New York, 1987, Chapt. "7".
29. J. March, *Advanced Organic Chemistry*, 4th ed., Wiley-Interscience, New York, 1992, p. 380.
30. D. McKean and co-workers, *Proc. Soc. Photo-Opt. Instr. Eng.* **920**, 60 (1988).
31. R. Allen and co-workers, *Proc. Soc. Photo-Opt. Instr. Eng.* **1925**, 246 (1993).
32. H. Ito, M. Ueda, and R. Schwalm, *J. Vac. Sci. Technol., B* **6**, 2259 (1988).
33. D. Funhoff, H. Binder, and R. Schwalm, *Proc. Soc. Photo-Opt. Instr. Eng.* **1672**, 46 (1992).
34. H. Ito and G. Willson, in T. Davidson, ed., *Polymers in Electronics* (ACS Symposium Series 242), American Chemical Society, Washington, D.C., 1984, p. 11.
35. R. Allen, W. Conley, and J. Gelorme, *Proc. Soc. Photo-Opt. Instr. Eng.* **1672**, 513 (1992).
36. B. Reck and co-workers, *Polym. Eng. Sci* **29**, 960 (1989).
37. W. Feely, J. Imhof, and C. Stein, *Polym. Eng. Sci.* **26**, 1101 (1986).
38. H. Ito, Y. Maekawa, R. Sooriyakumaran, and E. Mash, in L. Thompson, G. Willson, and S. Tagawa, eds., *Polymers for Microelectronics* (ACS Symposium Series 537), American Chemical Society, Washington, D.C., 1994, p. 64.
39. T. Ohfuji, O. Nalamasu, and D. Stone, *J. Vac. Sci. Technol., B* **11**, 2714 (1993).
40. W. Conley, *Proc. Soc. Photo-Opt. Instr. Eng.* **2438**, 41 (1995).
41. E. Reichmanis, C. Wilkins, and E. Chandross, *J. Vac. Sci. Technol.* **19**, 1338 (1981).
42. L. Pederson, *J. Electrochem. Soc.* **129**, 205 (1982).
43. J. McGrath, *J. Chem. Educ.* **58**, 844 (1981).
44. J. Stille, *J. Chem. Educ.* **58**, 862 (1981).
45. O. Nalamasu and co-workers, *Proc. Soc. Photo-Opt. Instr. Eng.* **1925**, 155 (1993).
46. H. Ito and co-workers, *J. Photopolym. Sci. Technol.* **7**, 433 (1994).
47. R. Allen, K. Chen, and P. Gallagher-Wetmore, *Proc. Soc. Photo-Opt. Instr. Eng.* **2438**, 250 (1995).
48. T. Long and F. Rodriguez, *Proc. Soc. Photo-Opt. Instr. Eng.* **1466**, 188 (1991).
49. M. Hanabata, F. Oi, and A. Furuta, *Proc. Soc. Photo-Opt. Instr. Eng.* **1466**, 132 (1991).
50. G. Barclay and co-workers, *Proc. Soc. Photo-Opt. Instr. Eng.* **2724**, 249 (1996).
51. T. Yoshimura and co-workers, *Jpn. J. Appl. Phys.* **32**, 6065 (1993).
52. M. Sanchez and co-workers, *Proc. Soc. Photo-Opt. Instr. Eng.* **3678**, 160 (1999).
53. H. Ito, *J. Photopolym. Sci. Technol.* **11**, 379 (1998).
54. G. Wallraff and co-workers, *J. Imaging Sci. Technol.* **36**, 468 (1992).
55. H. Ito, W. England, and S. Lundmark, *Proc. Soc. Photo-Opt. Instr. Eng.* **1672**, 2 (1992).
56. H. Momose and co-workers, *Proc. Soc. Photo-Opt. Instr. Eng.* **4345**, 695 (2001).
57. J. Crivello, in J. P. Fouiassier and J. F. Rabek, eds., *Radiation Curing in Polymer Science and Technology, Vol. II: Photoinitiating Systems*, Elsevier, New York, 1993, Chapt. "8".
58. R. Allen, G. Wallraff, W. Hinsberg, L. Simpson, and R. Kunz, in L. Thompson, G. Willson, and S. Tagawa, eds., *Polymers for Microelectronics* (ACS Symposium Series 537), American Chemical Society, Washington, D.C., 1994, Chapt. "11", p. 165.

59. K. Nakano and co-workers, *Proc. Soc. Photo-Opt. Instr. Eng.* **2438**, 433 (1995).
60. F. Houlihan and co-workers, *Proc. Soc. Photo-Opt. Instr. Eng.* **3333**, 73 (1998).
61. M. Cronin and co-workers, *Proc. Soc. Photo-Opt. Instr. Eng.* **2195**, 214 (1994).
62. Ref. 29, p. 250.
63. D. McKean and co-workers, *Proc. Soc. Photo-Opt. Instr. Eng.* **1672**, 94 (1992).
64. N. Hacker, in J. P. Fouiassier and J. F. Rabek, eds., *Radiation Curing in Polymer Science and Technology, Vol. II: Photoinitiating Systems*, Elsevier, New York, 1993, Chapt. "9".
65. R. DeVoe, M. Sahyun, and E. Schmidt, *Can. J. Chem.* **66**, 319 (1988).
66. G. Wallraff and co-workers, *CHEMTECH* **23**(4), 22 (1993).
67. T. Neenan and co-workers, *Macromolecules* **23**, 145 (1990).
68. N. Hayashi and co-workers, *Proc. Soc. Photo-Opt. Instr. Eng.* **1466**, 377 (1991).
69. H. Ito and co-workers, *Proc. Soc. Photo-Opt. Instr. Eng.* **2438**, 53 (1995).
70. G. Buhr, H. Lenz, and S. Scheler, *Proc. Soc. Photo-Opt. Instr. Eng.* **1086**, 117 (1989).
71. R. Binkley and T. Flechtner, in W. Horspool, ed., *Synthetic Organic Photochemistry*, Plenum Press, New York, 1984, Chapt. "7".
72. S. Holmes and J. Sturtevant, *Microlithogr. World* **2**, 17 (1993).
73. W. Conley and co-workers, *Proc. Soc. Photo-Opt. Instr. Eng.* **3049**, 282 (1997).
74. U. Kumar and co-workers, *Proc. Soc. Photo-Opt. Instr. Eng.* **3049**, 135 (1997).
75. K. Przybilla and co-workers, *Proc. Soc. Photo-Opt. Instr. Eng.* **1925**, 76 (1993).
76. T. Hattori and co-workers, *J. Photopolym. Sci. Technol.* **9**, 611 (1996).
77. S. MacDonald and co-workers, *Proc. Soc. Photo-Opt. Instr. Eng.* **1466**, 1 (1991).
78. O. Nalamasu and co-workers, *Proc. Soc. Photo-Opt. Instr. Eng.* **1466**, 13 (1991).
79. A. Oikawa and co-workers, *Proc. Soc. Photo-Opt. Instr. Eng.* **2438**, 599 (1995).
80. T. Kumeda and co-workers, *Proc. Soc. Photo-Opt. Instr. Eng.* **1925**, 31 (1993).
81. A. Oikawa and co-workers, *Proc. Soc. Photo-Opt. Instr. Eng.* **1925**, 92 (1993).
82. K. Asakawa, T. Ushirogouchi, and M. Nakase, *Proc. Soc. Photo-Opt. Instr. Eng.* **2438**, 563 (1995).
83. S. Saito and co-workers, *J. Photopolym. Sci. Technol.* **9**, 677 (1996).
84. W. Hinsberg and co-workers, *Proc. Soc. Photo-Opt. Instr. Eng.* **1925**, 43 (1993).
85. H. Ito and co-workers, *Proc. Soc. Photo-Opt. Instr. Eng.* **1925**, 65 (1993).
86. G. Breyta and co-workers, *J. Photopolym. Sci. Technol* **7**, 449 (1994).
87. R. Kunz, V. Liberman, and D. Downs, *J. Vac. Sci. Technol., B* **18**, 1306 (2000).
88. R. Kunz and D. Downs, *J. Vac. Sci. Technol., B* **17**, 3330 (1999).
89. M. Cronin and co-workers, *Proc. Soc. Photo-Opt. Instr. Eng.* **2195**, 214 (1994).
90. F. Houle and co-workers, *J. Vac. Sci. Technol B* **18**, 1874 (2000).
91. W. Hinsberg and co-workers, *Proc. Soc. Photo-Opt. Instr. Eng.* **3999**, 148 (2000).
92. J. Hutchinson and co-workers, *Proc. Soc. Photo-Opt. Instr. Eng.* **3333**, 165 (1998).
93. E. Shiobara and co-workers, *Proc. Soc. Photo-Opt. Instr. Eng.* **3333**, 313 (1998).
94. J. Yamamoto and co-workers, *Jpn. J. Appl. Phys.* **35**, 6511 (1996).
95. L. Flanagin, V. Singh, and G. Willson, *J. Vac. Sci Technol. B* **17**, 1371 (1999).
96. T. Ushirogouchi and co-workers, *Proc. Soc. Photo-Opt. Instr. Eng.* **2438**, 609 (1995).
97. M. Rooks and A. Aviram, *J. Vac. Sci. Technol., B* **17**, 3394 (1999).
98. A. Robinson and co-workers, *J. Phys. D: Appl. Phys.* **32**, L75 (1999).
99. T. Tanaka, M. Morigumi, and N. Atoda, *Jpn. J. Appl. Phys.*, Part 1 **32**, 6059 (1993).
100. H. Cao, P. Nealey, and W. Domke, *J. Vac. Sci. Technol., B* **18**, 3303 (2000).
101. H. Namatsu, K. Yamazaki, and K. Kurihara, *Microelectron. Eng.* **46**, 129 (1999).
102. M. Levenson, *Proc. Soc. Photo-Opt. Instr. Eng.* **3049**, 2 (1997).
103. H. Gokan, S. Esho, and Y. Ohnishi, *J. Electrochem. Soc.* **130**, 143 (1983).
104. R. Kunz and co-workers, *Proc. Soc. Photo-Opt. Instr. Eng.* **2724**, 365 (1996).
105. T. Wallow and co-workers, *Proc. Soc. Photo-Opt. Instr. Eng.* **3333**, 92 (1998).
106. R. Allen and co-workers, *Proc. Soc. Photo-Opt. Instr. Eng.* **2438**, 474 (1995).

107. R. Kunz and co-workers, *Proc. Soc. Photo-Opt. Instr. Eng.* **1925**, 167 (1993).
108. Y. Kaimoto and co-workers, *Proc. Soc. Photo-Opt. Instr. Eng.* **1672**, 66 (1992).
109. M. Takahashi and co-workers, *Proc. Soc. Photo-Opt. Instr. Eng.* **2438**, 422 (1995).
110. K. Nozaki and co-workers, *J. Photopolym. Sci. Technol.* **9**, 509 (1996).
111. N. Shida and co-workers, *J. Photopolym. Sci. Technol.* **9**, 457 (1996).
112. M. Padmanaban and co-workers, *J. Photopolym. Sci. Technol.* **13**, 607 (2000).
113. R. Allen and co-workers, *Proc. Soc. Photo-Opt. Instr. Eng.* **2724**, 334 (1996).
114. U. Okoroanyanwu and co-workers, *Chem. Mater.* **10**, 3328 (1998).
115. U. Okoroanyanwu and co-workers, *Chem. Mater.* **10**, 3319 (1998).
116. H. Ito and co-workers, *Proc. Soc. Photo-Opt. Instr. Eng.* **3999**, 2 (2000).
117. T. Wallow and co-workers, *Proc. Soc. Photo-Opt. Instr. Eng.* **2724**, 355 (1996).
118. J. Jung, C. Bok, and K. Baik, *Proc. Soc. Photo-Opt. Instr. Eng.* **3333**, 11 (1998).
119. F. Houlihan and co-workers, *Proc. Soc. Photo-Opt. Instr. Eng.* **3049**, 84 (1997).
120. S. Choi and co-workers, *Proc. Soc. Photo-Opt. Instr. Eng.* **3999**, 54 (2000).
121. J. Canning, *J. Vac. Sci. Technol., B* **15**, 2109 (1997).
122. M. Rothschild and co-workers, *J. Vac. Sci. Technol. B* **17**, 3262 (1999).
123. International Technology Roadmap for Semiconductors, The Semiconductor Industry Association, San Jose, Calif., 2000 update.
124. R. Kunz and co-workers, *Proc. Soc. Photo-Opt. Instr. Eng.* **3678**, 16 (1999).
125. C. Sandorfy and L. Lussier, in S. McGlynn, G. Findley, and R. Huebner, eds., *Photophysics and Photochemistry in the Vacuum Ultraviolet*, D. Reidel Publishing, Dordrecht, Holland, 1985, p. 819.
126. M. Robin, *Higher Excited States of Organic Molecules*, Vol. **I–III**, Academic Press, New York, 1974.
127. R. Kunz and co-workers, *J. Vac. Sci. Technol., B* **17**, 3267 (1999).
128. J. Gandler and W. Jencks, *J. Am. Chem. Soc.* **104**, 1937–1951 (1982).
129. T. Fedynysyhn and co-workers, *Proc. Soc. Photo-Opt. Instr. Eng.* **4345**, 296 (2001).
130. T. Chiba and co-workers, *J. Photopolym. Sci. Technol.* **13**, 657 (2000).
131. H. Ito, N. Seehof, R. Sato, T. Nakayama, and M. Ueda, in H. Ito, E. Reichmanis, O. Nalamasu, and T. Ueno, eds., *Micro-and Nano-Patterning Polymers* (ACS Symposium Series 706), American Chemical Society, Washington, D.C., 1998, Chapt. "16".
132. H. Ito and co-workers, *Proc. Soc. Photo-Opt. Instr. Eng.* **4345**, 273 (2001).
133. R. Dammel and co-workers, *Proc. Soc. Photo-Opt. Instr. Eng.* **4345**, 350 (2001).
134. D. Schmaljohann and co-workers, in Proceedings of 12th International Conference on Photopolymers, Society of Plastics Engineers, Brookfield, Conn, 2000, p. 81.
135. R. Hung and co-workers, *Proc. Soc. Photo-Opt. Instr. Eng.* **4345**, 385 (2001).
136. N. Fender and co-workers, *Proc. Soc. Photo-Opt. Instr. Eng.* **4345**, 417 (2001).
137. U.S. Pat. 3,873,361 (1973) J. Franco, J. Havas, and H. Levine (IBM Corp.).
138. B. Lin, in L. Thompson, G. Willson, and M. Bowden, eds., *Introduction to Microlithography* (ACS Symposium Series 219), American Chemical Society, Washington, D.C., 1983, Chapt. "6".
139. R. Miller and G. Wallraff, *Adv. Mater. Opt. Electron.* **4**, 95 (1994).
140. S. MacDonald, H. Ito, H. Hiraoka, and G. Willson, in Proc. Reg. Tech. Conf on Photopolymers, Processes and Materials, Mid-Hudson Section, Society of Plastics Engineers, Ellenville, N.Y., 1985, p. 177.
141. C. Pike and co-workers, *J. Vac. Sci. Technol., B* **18**, 3360 (2000).
142. J. Hatakeyama and co-workers, *Proc. Soc. Photo-Opt. Instr. Eng.* **3333**, 62 (1998).
143. R. Sooriyakamaran and co-workers, *Proc. Soc. Photo-Opt. Instr. Eng.* **4345**, 319 (2001).
144. T. Fujigaya and co-workers, in Proceedings of 12th International Conference on Photopolymers, Society of Plastics Engineers, Brookfield, Conn., 2000, p. 219.
145. S. Palmateer and co-workers, *Proc. Soc. Photo-Opt. Instr. Eng.* **3333**, 634 (1998).
146. M. Somervell and co-workers, *J. Vac. Sci. Technol., B* **18**, 2551 (2000).

147. S. Mori and co-workers, *J. Vac. Sci. Technol., B* **16**, 3739 (1998).
148. A. Jamieson and co-workers, *Proc. Soc. Photo-Opt. Instr. Eng.* **4345**, 406 (2001).
149. G. Wallraff and W. Hinsberg, *Chem. Rev.* **99**, 1801 (1999).
150. L. Harriott, *J. Vac. Sci. Technol., B* **15**, 2130 (1997).
151. H. Pfeiffer, *Proc. Soc. Photo-Opt. Instr. Eng.* **3997**, 206 (2000).
152. N. Matsuzawa and co-workers, *J. Photopolym. Sci. Technol.* **12**, 571 (1999).
153. R. Tarascon and co-workers, *J. Vac. Sci. Technol., B* **13**, 2975 (1995).
154. K. Lee and W. Huang, *J. Vac. Sci. Technol., B* **11**, 2807 (1993).
155. M. Sato and co-workers, *J. Vac. Sci. Technol., B* **17**, 2873 (1999).
156. T. Kozawa and co-workers, *J. Vac. Sci. Technol., B* **15**, 2582 (1997).

W. D. HINSBERG
G. M. WALLRAFF
R. D. ALLEN
Almaden Research Center

LIVING POLYMERIZATION, ANIONIC.

See ANIONIC POLYMERIZATION.

LIVING POLYMERIZATION, CATIONIC.

See CARBOCATIONIC POLYMERIZATION.

LIVING RADICAL POLYMERIZATION

Introduction

Conventional free-radical polymerization (FRP) is characterized by the continuous formation of radicals (initiation) and continuous disappearance of radicals (termination) (see RADICAL POLYMERIZATION). The statistical nature of the FRP process leads to relatively polydisperse polymers, with a typical instantaneous polydispersity index (PDI) of 1.5 or 2, depending on the mode of termination (1). The complete growth of an individual chain in FRP takes typically in the order of seconds. The molar mass distribution (MMD) of an FRP product consists of an accumulation of instantaneous MMDs formed over the course of the reaction. Hence the final PDI may have a value significantly larger than 1.5 or 2. FRP is a versatile technique that allows the polymerization of monomers with various functional groups. Furthermore, the polymerization can be carried out in a variety of reaction media, ranging from bulk monomer, via solution polymerization, to heterogeneous media, eg emulsion and suspension polymerization, and polymerization in supercritical carbon dioxide. One of the main disadvantages of FRP is the poor control over the microstructure of the synthesized macromolecules. This includes the relatively high PDI, and also the practical impossibility to synthesize block copolymers, and other advanced structures.

Advanced structures can be synthesized via living polymerization techniques. Notable example of these techniques is anionic polymerization (2), which is known to allow the synthesis of low PDI materials as well as block copolymers. The

Encyclopedia of Polymer Science and Technology. Copyright John Wiley & Sons, Inc. All rights reserved.

main disadvantages of anionic polymerization are the limited choice of monomers, and the extremely demanding reaction conditions.

In order to overcome the disadvantages of FRP without sacrificing the above-mentioned advantages, it was recognized that a living character had to be realized in conjunction with the free-radical mechanism. At present three main mechanisms exist that ensure this living character by establishing an equilibrium between active (radical) and dormant chains. In a typical living radical polymerization (LRP), all chains are started early in the reaction, and are allowed to grow throughout the reaction. How this is achieved for individual LRPs will be detailed below. In general, the result of a successful LRP will be a polymer with low PDI, and predetermined (number-average) molar mass.

In this overview, the historical development of techniques will be summarized. In addition, the mechanisms and kinetics of the main three techniques will be highlighted. Finally, scope and limitations of the three techniques will be discussed on the basis of a number of examples.

Historical Overview

Probably the first publication that dealt with LRP already appeared in the late 1960s (3). In the 1970s and 1980s it was realized that the main drawback in FRP, ie, the broad polydispersities, and the inability to form block copolymers could be overcome by the introduction of reversible deactivation of the active radical. Otsu reported on several attempts to introduce this reversibility (4,5). The iniferter technique was developed, which comprises a UV-labile or thermally labile link that can be reversibly cleaved, and used for monomer insertion (6,7). Otsu showed that the technique allowed the synthesis of block copolymers, albeit with a PDI around 2. Currently it turns out that the iniferter technique may still have advantages over the more recent developments, eg when the synthesis of multiblock copolymers is aimed for (8).

In the mid-1980s, the first technique that relies on the reversible termination of radicals with a stable free radical was developed in the group of E. Rizzardo at CSIRO in Australia. Rizzardo and co-workers found that nitroxide-stable free radicals were able to add to carbon-centered radicals to form alkoxy amines (9). In certain cases these alkoxy amines are thermally unstable, so that they enter into an equilibrium between (transient) carbon-centered radical and (persistent) nitroxide radical on one side, and alkoxy amine on the other side. TEMPO was initially the most frequently used nitroxide in conjunction with the polymerization of styrene and its derivatives. The TEMPO–polystyrene adduct requires temperatures of 120°C or above in order to establish an equilibrium at which polymerization takes place. Around the mid-1990s Georges and co-workers focused on the TEMPO-mediated polymerization of styrene (10), and developed various strategies to overcome intrinsic weaknesses of the system. They used camphor sulfonic acid to enhance the rate of polymerization (11). This rate enhancement was later elucidated to be due to the destruction of excess nitroxide that builds up during the polymerization.

By the end of the 1990s, Hawker and Tordo independently developed alternative nitroxides that allowed polymerization at temperatures below 100°C, and also allowed the polymerization of acrylates (12,13).

A parallel development was initiated by the first publications from Sawamoto and Matyjaszweski. They reported independently on the transition-metal–catalyzed polymerization of various vinyl monomers (14,15). The technique, which was termed atom transfer radical polymerization (ATRP), uses an activated alkyl halide as initiator, and a transition-metal complex in its lower oxidation state as the catalyst. Similar to the nitroxide-mediated polymerization, ATRP is based on the reversible termination of growing radicals. ATRP was developed as an extension of atom transfer radical addition (ATRA), the so-called Kharasch reaction (16). ATRP turned out to be a versatile technique for the controlled polymerization of styrene derivatives, acrylates, methacrylates, etc. Because of the use of activated alkyl halides as initiators, the introduction of functional endgroups in the polymer chain turned out to be easy (17–22). Although many different transition metals have been used in ATRP, by far the most frequently used metal is copper. Nitrogen-based ligands, eg substituted bipyridines (14), alkyl pyridinimine (Schiff's base) (23), and multidentate tertiary alkyl amines (24), are used to solubilize the metal salt and to adjust its redox potential in order to match the requirements for an ATRP catalyst. In conjunction with copper, the most powerful ligand at present is probably tris[2-(dimethylamino)ethyl)]amine (Me_6-TREN) (25).

Many different polymer architectures have been synthesized via ATRP. These architectures include block copolymers (14), graft copolymers (26–29), star-branched polymers, etc. Some work was devoted to the reduction of the amount of catalyst used, or to the efficient removal of catalyst from the resulting polymer (30–33).

The third large development is, unlike nitroxide-mediated polymerization and ATRP, based on reversible chain transfer. Reversible degenerative chain transfer is a reaction in which chain-transfer activity is passed on from chain to chain. Although there are a number of examples of techniques that rely on this principle (34–37), the most noteworthy undoubtedly is reversible addition–fragmentation chain transfer (RAFT) (38,39). RAFT was developed by Rizzardo and co-workers in the late 1990s. Its most popular form makes use of thiocarbonylthio compounds that, depending on the activating substituent, can have very high chain-transfer values. Also, dependent on the activating substituent, the whole gamut of vinyl monomers can be polymerized in a controlled fashion, leading to low PDI materials. In contrast to NMP and ATRP, RAFT requires the continuous production of radicals to keep the polymerization going. Despite this continuous production of new chains, and the concomitant termination of growing chains, polymers with PDIs below 1.1 are readily achieved. Also, in this case, a wide range of polymer architectures has been synthesized.

Simultaneous with the first introduction of RAFT a similar development was introduced where specifically xanthates were employed as the reversible chain-transfer agent (40). The technique, called MADIX (macromolecular design via interchange of xanthates), can be seen as a special case of RAFT polymerization. Xanthates can be regarded as RAFT agents where the activating substituent is an alkoxy fragment. For most vinyl monomers, xanthates exhibit a low chain-transfer constant compared to some of the dithioesters. This leads to broader molar mass distributions, with PDIs around 2. A notable exception is the combination of vinyl esters with xanthates. Where it has proven very difficult to perform living polymerization of vinyl esters (eg vinyl acetate), the use of xanthates as RAFT agents

leads to poly(vinyl acetate) of predetermined molar mass, and low polydispersity (40).

The latest development in living radical polymerization at this stage is the use of diphenylethylene (DPE) (41). In the continuous search for systems that lead to living polymerization in combination with a minimal disturbance of the conventional free-radical process, DPE could be an interesting alternative (42). There are specific difficulties associated with LRP in emulsion (see RADICAL POLYMERIZATION) (43). DPE, although not fully investigated yet, may prove to be a valuable addition to the existing LRP techniques.

Nitroxide-Mediated Polymerization (NMP)

Nitroxides have been investigated extensively to control the homo- and copolymerization of styrene. NMP proceeds via the reversible trapping of carbon-centered radicals as indicated in equation 1. The two most commonly used ways to start the polymerization are

(1) Generation of free radicals from a conventional free-radical initiator (eg, azo compound or peroxide), addition of one or a few monomer units, followed by trapping of the carbon-centered radical by the nitroxide compound (**1**). The trapping reaction produces an alkoxy amine, which contains a thermally labile C—O bond (44).

(2) Thermal decomposition of an alkoxy amine (**2**), which was synthesized in a separate reaction (45).

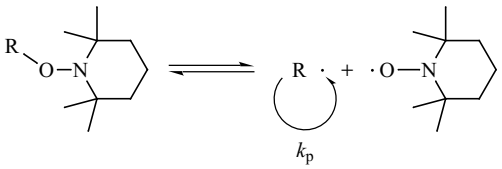

2 **1** (1)

Since the propagating species in LRP is a free radical, it may undergo the known reactions, including chain transfer and bimolecular termination. If bimolecular termination occurs, the equilibrium will gradually shift in the direction of the alkoxyamine. This is due to the gradual buildup of nitroxide. This process slows down the polymerization, and may lead to unacceptably long reaction times. Several approaches have been developed to overcome this phenomenon. In the early days of NMP, TEMPO was by far the most frequently used nitroxide. Because of the small equilibrium constant, the polymerization needed to be carried out at temperatures above 100°C. Under these conditions, styrene shows significant thermal (self)initiation. The presence of this additional radical source counterbalances the buildup of excess free nitroxide. Fukuda and co-workers measured the rate of TEMPO-mediated styrene polymerization, and found it to be identical to the conventional thermal polymerization of styrene (46). Workers at Xerox developed a method to increase the rate of polymerization by the addition

of camphor sulfonic acid (CSA) (11). Several explanations have been put forward for the mechanism of rate enhancement by CSA. Most likely the CSA degrades the excess free nitroxide, thus shifting the equilibrium more to the active species. An even more effective way to accelerate NMP consists of the addition of a slowly decomposing free-radical initiator (47,48).

Great improvements in NMP were brought about by the development of new nitroxides. Two independent groups worked on this topic. Tordo and co-workers developed β-phosponylated nitroxides, eg *N*-*tert*-butyl-*N*-(1-diethylphosphono-2,2-dimethylpropyl)nitroxide, which is commonly known as SG1 (13). Simultaneously, Hawker and co-workers synthesized a library of nitroxides and investigated their effectiveness in NMP (12). It turned out that the presence of a β-hydrogen greatly improves the performance of the nitroxide. *N*-*tert*-butyl-*N*-(1-diethylphosphono-2,2-dimethylpropyl)nitroxide and α-hydrido derivatives based on a 2,2,5-trimethyl-4-phenyl-3-azahexane-3-oxy skeleton, eg *N*-*tert*-butyl-*N*-(2-methyl-1-phenyl-propyl)nitroxide, both allow the NMP of acrylates. Furthermore, polymerization temperatures below 100°C are feasible, which greatly facilitates the use of NMP in emulsion polymerization. This will be discussed later.

In an NMP initiated by preformed alkoxyamines, the number-average degree of polymerization will be $\bar{P}_n = \Delta[M]/\left([R{-}T]_0 + 2\Delta[I]_0\right)$, where $[R{-}T]_0$ is the alkoxyamine at the start of the reaction, $\Delta[I]_0$ is the amount of (slowly decomposing) initiator converted (dissociated) and $\Delta[M]$ is the amount of monomer converted. The factor 2 associated with the amount of converted initiator accounts for the fact that one initiator molecule produces two radicals. This equation assumes the absence of chain-transfer reactions. Note that the occurrence of termination by disproportionation will not influence the number-average degree of polymerization, whereas termination by combination will lead to a (usually small) deviation from the predicted value. The PDI of the resulting polymer will obviously be influenced by the occurrence of any chain-breaking reaction (chain transfer or termination). Details on the prediction of the PDI will be given below.

In the group of Fischer, a considerable amount of work was dedicated to the kinetic description of NMP. They introduced the concept of the so-called persistent radical effect (PRE) (49,50). The PRE relies on the limited buildup of the concentration of deactivator, which in the case of NMP is the nitroxide, the persistent radical. On the basis of the PRE, it can be predicted which conditions will lead to narrow MMDs, and to a small fraction of irreversibly terminated "dead" chains.

Although many authors present linear relationships between $\ln([M]_0/[M])$ and time as one of the proofs that a polymerization is living, Fischer and co-workers show that $\ln([M]_0/[M])$ in many cases should scale with $t^{2/3}$, and that the persistent radical concentration increases with $t^{1/3}$.

In Figure 1 an experimental example from the work of Fischer's group is shown that obeys the kinetic relationship they introduced (51). If the kinetic model is accepted, the implication is a proper prediction of the PDI and the fraction of dead (irreversibly terminated) chains, etc. In other words, on the basis of kinetic parameters and relevant concentrations, a system can be optimized in terms of degree of livingness (low PDI and small fraction of dead chains).

For an overview of rate constants in NMP, the reader is referred to a review on the persistent radical effect by Fischer (52).

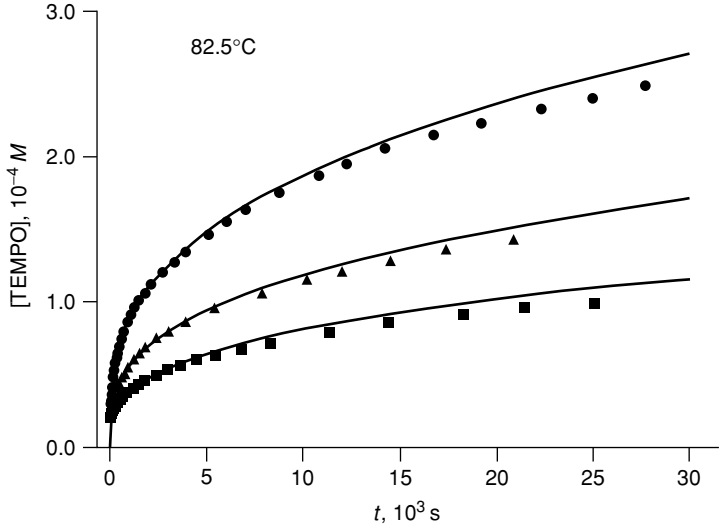

Fig. 1. Time dependence of the TEMPO concentration during thermolysis of cumyl–TEMPO: ● 1.16×10^{-2} M; ▲ 5.10×10^{-3} M; ■ 2.52×10^{-3} M.

Atom Transfer Radical Polymerization (ATRP)

ATRP is a more versatile technique than NMP, ie except for a few exceptions all vinyl monomers are susceptible to ATRP. Notable exceptions are unprotected acids (eg (meth)acrylic acid). Some other monomers may be difficult to polymerize since they exhibit side reactions, which may be affected by the choice of reaction conditions, nature of the catalyst, etc. An example of such a monomer is 4-vinyl pyridine (4-VP), which can undergo quaternization by the (alkyl halide) initiator (53). Nevertheless, successful polymerization of 4-VP has been reported.

In ATRP a transition-metal catalyst is used to reversibly activate halide-terminated dormant chains. The principal mechanism is outlined in equation 2.

$$\mathrm{R{-}X} + \mathrm{Cu^{(I)}X/ligand} \underset{+\mathrm{M}\ (k_p)}{\rightleftharpoons} \mathrm{R\cdot} + \mathrm{Cu^{(II)}X_2/ligand} \qquad (2)$$

The kinetic description of ATRP has received considerable attention. There is a similarity between the descriptions of NMP and of ATRP. Both rely on reversible activation of dormant chains, albeit the activation in the case of NMP is a unimolecular reaction whereas in the case of ATRP it is a bimolecular reaction. If the reaction medium is homogeneous, ie activator and deactivator are soluble in the reaction mixture, the monomer consumption as a function of time can be described as follows.

$$\ln\left(\frac{[\mathrm{M}]_0}{[\mathrm{M}]_t}\right) = \frac{k_\mathrm{p}k_\mathrm{a}[\mathrm{RX}]_0[\mathrm{Cu^I}]_0}{k_\mathrm{d}[\mathrm{Cu^{II}}]_0}t \tag{3}$$

$$\ln\left(\frac{[\mathrm{M}]_0}{[\mathrm{M}]_t}\right) = \frac{3}{2}k_p\left(\frac{k_\mathrm{a}[\mathrm{RX}]_0[\mathrm{Cu^I}]_0}{3\mathrm{k_d}\times 2k_\mathrm{t}}\right)^{1/3} t^{2/3} \tag{4}$$

Where $[\mathrm{M}]_0$ and $[\mathrm{M}]_t$ are the monomer concentrations at time zero and time t respectively. $[\mathrm{RX}]_0$ is the alkyl halide initiator concentration at time zero. $[\mathrm{Cu^I}]_0$ and $[\mathrm{Cu^{II}}]_0$ are the activator and deactivator concentrations, respectively, at time zero. $\mathrm{k_p}$ is the propagation rate constant, $\mathrm{k_a}$ is the activation rate constant, $\mathrm{k_d}$ is the deactivation rate constant, and $\mathrm{k_t}$ is the rate coefficient for bimolecular termination. Equation 3 applies to the situation where a pseudoequilibrium concentration of deactivator [Cu(II) in this case] is built up. In the case of many ATRP reactions where no deliberate addition of Cu(II) has taken place, equation 4 will provide a better match with experimental data. Fischer and co-workers have derived an expression for the concentration of deactivator necessary to switch from equation 4 to equation 3. The equation derived by Fischer reads (for ATRP):

$$[\mathrm{Cu^{(II)}}]_{0,t} = \sqrt{3K_\mathrm{eq}[\mathrm{RX}]_0[\mathrm{Cu^{(I)}}]_0\frac{k_\mathrm{t}}{k_\mathrm{p}}} \tag{5}$$

This theoretically derived concentration was experimentally confirmed in a study by Zhang and co-workers (54). In Figure 2, the experimental data as well as the theoretical fits to the data are shown from the study by Zhang. It is clear that the crossover from a $t^{2/3}$ to a linear dependence on time exactly coincides with the theoretical prediction. In the figure it is obvious that an inhibition period is observed, which increases with increasing concentration of Cu(II). The origin of the inhibition period is not completely clear.

In many cases the catalyst complex consists of a Cu(I) halide with multidentate aliphatic tertiary amines as ligands (eg *N*,*N*,*N*′,*N*″,*N*″-pentamethyl diethylene triamine, PMDETA). This ligand is cheap and provides relatively high rates of polymerization with still a reasonable degree of control. One of the peculiarities of this ligand is the fact that the Cu(II) complex has very limited solubility. In a study by Snijder and co-workers it is shown by ESR that a ceiling Cu(II) concentration is reached early in the polymerization of MMA. When this happens, the equations 1 and 2 no longer describe the monomer conversion versus time properly. On the basis of the experimental observation of constant deactivator concentration, Snijder derived a new expression that adequately describes monomer conversion versus time (55).

$$\ln\left(\frac{[\mathrm{M}]_0}{[\mathrm{M}]}\right) = \frac{k_\mathrm{p}[\mathrm{Cu^{II}X_2}]_c}{2k_\mathrm{tD}k_\mathrm{eq}}[3\xi t + [\mathrm{PX}]_0^{-3}]^{1/3} - \frac{k_\mathrm{p}[\mathrm{Cu^{II}X_2}]_c}{2k_\mathrm{tD}k_\mathrm{eq}[\mathrm{PX}]_0} \quad \text{with} \quad \xi = 2k_\mathrm{tD}\left(k_\mathrm{eq}/[\mathrm{Cu^{II}X_2}]_c\right)^2. \tag{6}$$

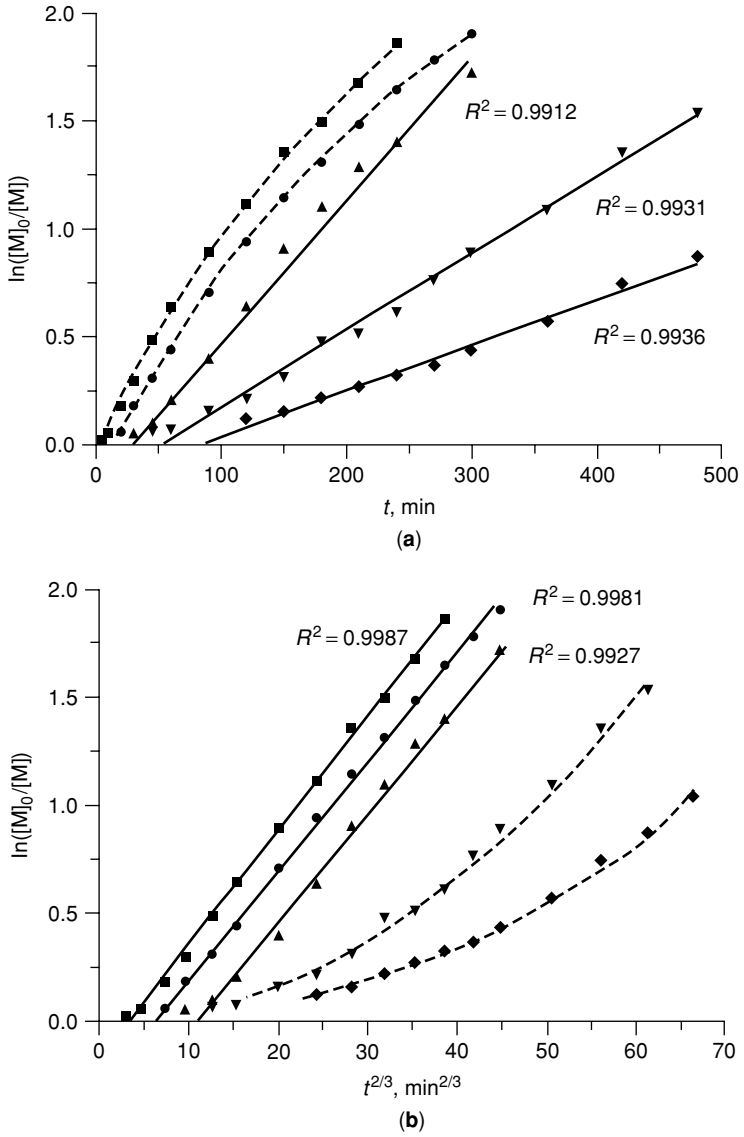

Fig. 2. Plots of $\ln([M]_0/[M])$ versus reaction time (t and $t^{2/3}$) for the ATRP of MMA in toluene at 90°C using different amounts of initially added $CuBr_2$. $[MMA]_0 = 2.8879\ M$, $[HEBIB]_0 = 0.0959\ M$, $[CuBr]_0 = [NHPMI]_0/3 = 0.0969\ M$. $[CuBr_2]_0/[CuBr]_0$: ■ 0; ● 0.05; ▲ 0.1; ▼, 0.2; ◆ 0.3.

As indicated above, the majority of work on ATRP has been conducted using copper as the transition metal. An enormous variety of nitrogen-based ligands have been used in conjunction with Cu(I) halide. The most popular ligands are

(1) Multidentate aliphatic tertiary amines (PMDETA, Me_6-TREN).
(2) Substituted bipyridines.
(3) Alkyl pyridylmethanimine.

The initial work by Matyjaszewski and co-workers largely concentrated on the use of substituted bipyridines (14). Although this ligand provides good living character to the polymerization, the rates of polymerization are quite low. In more recent work by Matyjaszewski and co-workers as well as in the research of other groups, more emphasis is placed on the use of multidentate aliphatic tertiary amines (24). The higher rates of polymerization, and to some extent the heterogeneous character of the polymerization, have certain advantages, which will be detailed under Scope and Limitations. The alkyl pyridylmethanimines were introduced by Haddleton and co-workers (23) and are mainly used for the polymerization of methacrylates.

Apart from copper-based complexes several other metals have been used as well. Fe (56–59), Ni (60), Ru (15), etc have been used to some extent. Especially noteworthy here is the work by Sawamoto and co-workers. As indicated in the Introduction, Sawamoto and Matyjaszewski simultaneously pioneered ATRP. Matyjaszewski started off with the use of copper, whereas Sawamoto spent most of his efforts on ruthenium-based catalysts. Recent work from Sawamoto and co-workers shows that the Ru-based complexes can compete with the Cu-based systems on many fronts. Although not yet perfect it seems that a specific Fe-based catalyst is the first to polymerize vinyl acetate via an ATRP mechanism (61).

The initiation in ATRP may occur in one of two different ways. The common way to initiate is via the reaction of an activated (alkyl) halide with the transition-metal complex in its lower oxidation state. Typical examples would be the use of ethyl 2-bromoisobutyrate and a Cu(I) complex for the initiation of a methacrylate polymerization (62), or 1-phenylethyl chloride for the initiation of a styrene polymerization (14). In addition, there are initiators like 2,2,2-trichloro-ethanol (63) that appear to be very efficient, and that result in hydroxy-functional polymer chains. Percec and co-workers reported on the use of sulfonyl chlorides as universal initiators in ATRP (64). Also the use of di-, tri-, or multifunctional initiators is possible, which will result in polymers growing in two, three, or more directions. All these variations open up possibilities to well-defined architectures.

The alternative way to initiate ATRP is via a conventional free-radical initiator, which is used in conjunction with a transition-metal complex in its higher oxidation state. Typically one would use AIBN in conjunction with a Cu(II) complex. Upon formation of the primary radicals and/or their adducts with a monomer unit, the Cu(II) complex very efficiently transfers a halogen to this newly formed chain. In doing so the copper complex is reduced, and the active chain is deactivated. It is easily envisaged that the system will arrive at the same equilibrium as depicted in equation 2, but now approaching it from the right-hand side. This alternative way of initiation was termed “reverse ATRP” (65,66).

Reversible Addition–Fragmentation Chain Transfer (RAFT)

In terms of polymerizable monomers, RAFT is at present the most versatile technique for conducting LRP. In contrast to the previously described NMP and ATRP, this system relies on chain transfer for the exchange between active and dormant chains. The chain end of a dormant chain carries a thiocarbonylthio moiety, which is chain-transfer–active. Upon chain transfer, the thiocarbonylthio

moiety is transferred to the previously active chain, which now becomes dormant, and the previously dormant chain carries the radical activity and is able to propagate. In equation 7, the basic mechanism of this exchange reaction via chain transfer is depicted. As can be seen in equation 7, in between the two states of dormant and active chains there is an intermediate radical, which will undergo the subsequent fragmentation reaction (67). In the present literature there is some controversy about the possible fates of this intermediate radical. Starting point of the controversy is an observed retardation in some examples of RAFT polymerization compared to the equivalent free-radical polymerization in the absence of the RAFT agent. Davis and co-workers explain the retardation by a slow rate of fragmentation, which leads to the buildup of a relatively large concentration of (intermediate) radicals (68,69). On the other hand, Monteiro and co-workers explain the retardation by irreversible termination of the intermediate radical (70). The remarkable point about this controversy is that the difference in the rate constants of fragmentation between Davis' and Monteiro's approaches is some 7 orders of magnitude. Fukuda and co-workers carried out independent rate measurements, which seem to support Monteiro's view (71). However, at present nobody has ever been able to detect the presence of three- or four-armed stars, which should result from the intermediate radical termination.

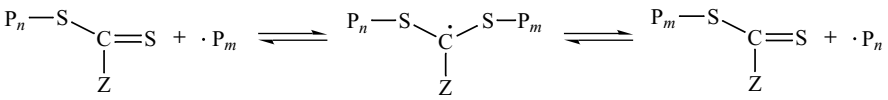

(7)

A whole variety of thiocarbonylthio compounds have been synthesized and used in RAFT polymerization. The initial work was focused to some extent on the use of dithioesters. More recently the range of RAFT agents is expanded to trithiocarbonates, dithiocarbamates, and xanthates.

To some extent the choice of RAFT agent determines the degree of control obtained. The general structure of a RAFT agent can be depicted as in structure (**3**), where the Z group is the activating group, and R is the homolytically leaving group.

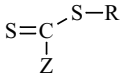

To a large extent the Z group determines the rate of addition, and the R group determines the rate of fragmentation. The choice of Z and R groups is dependent on the nature of the monomer to be polymerized. In Figure 3 an overview is given of different Z and R groups and the monomers that can be polymerized in a controlled fashion using these Z and R groups (72).

Although already in the initial patent from CSIRO the application of RAFT in emulsion is reported (38), it appeared to be quite troublesome to carry out a well-controlled reaction in emulsion.

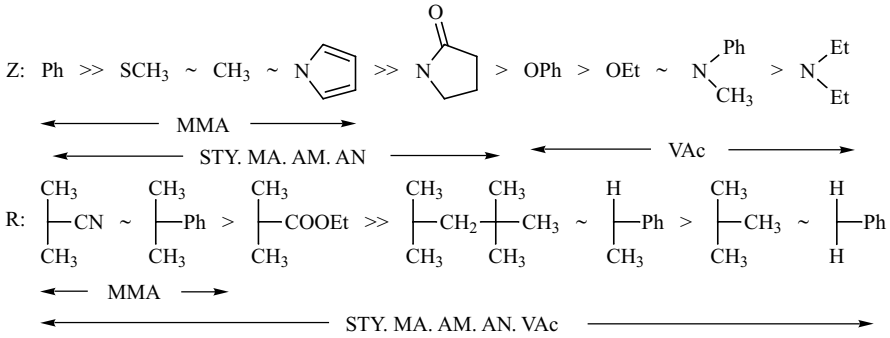

Fig. 3. Requirements for Z and R groups of RAFT agent for the controlled polymerization of styrene (STY), methyl methacrylate (MMA), methyl acrylate (MA), acrylamide (AM), acrylonitrile (AN), and vinyl acetate (VAc).

Scope and Limitations

Living radical polymerization (LRP) is developed on the basis of conventional free-radical polymerization (FRP). The main idea behind this development is to overcome intrinsic shortcomings of FRP without sacrificing any of its strengths. These strengths are

(1) Wide range of monomers, including functional ones (hydroxyl, epoxy, carboxylic acid, etc.).
(2) Nondemanding in terms of reaction conditions.
(3) Widely applied in academia as well as in industry for (co)polymer synthesis.

The intrinsic shortcomings are

(1) Poor control over chain length (distribution).
(2) Poor control over chain topology (block copolymers and more advanced topologies are virtually impossible to synthesize efficiently).
(3) No, or hardly any, control over tacticity.

To what extent did the efforts in LRP up till now lead to success in overcoming the shortcomings of FRP? The one shortcoming that has only been solved very recently is the control over tacticity. Matyjaszewski and co-workers have recently shown that the addition of lanthanides to an ATRP results in control over tacticity (73).

Various classes of monomers have been polymerized via LRP. Styrene and its derivatives can be polymerized using any of the three main techniques. Under the appropriate conditions NMP, ATRP, and RAFT all lead to polymers with a predetermined molar mass, and a low PDI. Also the synthesis of block copolymers where one of the blocks is poly(STY) has successfully been accomplished. Styrene is the monomer that poses the smallest demands on the choice of nitroxide in NMP. TEMPO has been used frequently, but

one requires relatively high reaction temperatures (125–140°C). When *N-tert*-butyl-*N*-(1-diethylphosphono-2,2-dimethylpropyl)nitroxide or *N-tert*-butyl-*N*-(2-methyl-1-phenyl-propyl)nitroxide is used, the reaction temperature can be lowered to 80–90°C. Similarly, in ATRP a wide variety of transition-metal complexes can be used in combination with a large selection of initiators. Styrene appears to posses an equilibrium constant for the activation–deactivation equilibrium, which is quite favorable for conducting these reactions. Finally, for RAFT also, the choice of RAFT agent is not very critical in the degree of success obtained. Usually, large chain-transfer rate constants are obtained, which results in polymers with low PDIs.

Methacrylates form an important class of monomers. They are available with a large number of different ester side groups. NMP is not capable of polymerizing methacrylates in a controlled fashion. Most frequently the nitroxide will undergo a disproportionation reaction, with the propagating radical leading to a dead polymer chain with an unsaturated chain end and a hydroxylamine.

ATRP can in general be carried out on methacrylates. The initial work on MMA polymerization was reported by the group of Matyjaszewski (62), including work on high molar mass polymer (74), detailed kinetics (75), and on substituted methacrylates (76–78). Haddleton and co-workers focused largely on the polymerization of methacrylates, and used most frequently alkyl pyridylmethanimine ligands with copper halide as the catalyst. The only occasion where ATRP on methacrylates leads to difficulties is when the ester side chain contains functional groups that interfere with the copper complex. Many other groups have investigated the polymerization of methacrylates. A variety of transition-metal complexes have been utilized for this purpose. The parent compound of methacrylates (methacrylic acid) cannot be polymerized as such via ATRP. Armes and coworkers showed that the sodium salt of methacrylic acid can be polymerized in aqueous media (79). Other groups used approaches where the acid functionality is protected via various methodologies, eg via *tert*-butyl ester, via trimethylsilyl ester, or via the tetrahydropyranyl ester (80).

RAFT is probably the most versatile technique to polymerize methacrylates. Regardless of the nature of the ester side group, RAFT can be employed for the LRP of methacrylates. Also, methacrylic acid can be polymerized without protecting group chemistry. There are some requirements in terms of activating Z group and homolytically leaving R group of the RAFT agent that have to be met in order to have a successful polymerization.

Acrylates can be polymerized using NMP when the proper nitroxide is employed. *N-tert*-butyl-*N*-(1-diethylphosphono-2,2-dimethylpropyl)nitroxide and *N-tert*-butyl-*N*-(2-methyl-1-phenyl-propyl)nitroxide were proven to be capable of controlling the polymerization of butylacrylate.

ATRP of acrylates is easily achieved. The equilibrium between active and dormant chains is much more to the dormant side. This results in relatively low rates of polymerization even though the propagation rate constant of acrylates is quite large. Methacrylate polymerizations, although having a much smaller propagation rate constant, proceed faster in ATRP than do acrylate polymerizations under identical conditions. In general, polyacrylates will posses a somewhat larger PDI than polymethacrylates synthesized via ATRP, especially at low molar mass. The main reason of this phenomenon is that during an activation–deactivation

cycle acrylates will undergo multiple monomer additions, whereas methacrylates will only undergo single monomer addition. In the long chain limit this effect will diminish. Also, in the case of acrylates, acrylic acid can only be polymerized in the nonprotonated form (sodium salt or protected as indicated above).

Similar to the polymerization of methacrylates, acrylates can easily be polymerized using RAFT. In this case the choice of RAFT agent is less critical, and functional groups (including acid) are not known or expected to result in any problems. The only point of caution is that depending on the choice of the RAFT agent significant retardation or inhibition may occur.

Butadiene and isoprene have to date only been polymerized in a living radical fashion via NMP (81). The group of Hawker has shown that nitroxides with an alpha C—H bond to the nitrogen can successfully be applied in the polymerization of dienes. The result is a linear increase of molar mass with conversion, and a PDI below 1.1.

Vinyl acetate is the monomer that has required significant efforts in order to achieve LRP. The first successful attempt was using RAFT with xanthates as a RAFT agent (also known as MADIX). At a later stage it turned out that certain dithiocarbamates also were able to induce LRP of vinyl acetate. Of all the attempts to polymerize VAc using ATRP, only specific iron complexes used by Sawamoto and co-workers were claimed to be successful (61). However, the PDIs they claimed were relatively large compared to other monomer/catalyst combinations.

Although the synthesis of polymers with narrow molar mass distributions is interesting from an academic point of view, the potential applications are more likely to be found in polymers with specific topologies. The most basic topology in reach of LRP is the block copolymer. Although it may occur as a trivial exercise to synthesize an A–B block copolymer, there are some precautions that need to be taken into account. The trivial one is that a maximum degree of livingness should be obtained for the first block. In general this requires some limitations to the maximum conversion in the synthesis of the first block. The probability of bimolecular termination significantly increases if the polymerization would be carried out to (almost) complete monomer conversion. The other important precaution concerns the sequence of block copolymer synthesis. Whether A–B or B–A is the preferred sequence mainly depends on the rate of initiation of the second monomer by the first block macroinitiator. As an example, when poly(STY-*b*-MMA) is the target structure, it is either the initiation of STY polymerization by the poly(MMA) macroinitiator or the initiation of MMA polymerization by the poly(STY) macroinitiator. In the case of ATRP as the LRP technique of choice, and without the use of any advanced techniques (which will be outlined below) initiation versus propagation needs to be studied. For the proper synthesis of a block copolymer a clean transition is required. Hence, initiation should be fast compared to propagation. When poly(STY) is used to initiate MMA this requirement is not met. Initiation is relatively slow, since for poly(STY) the activation–deactivation equilibrium lies strongly to the dormant side. To some extent this means that each chain that has undergone the transition to block copolymer is more reactive than the poly(STY) macroinitiator. The former chains will start to grow with a relatively high rate whereas the remaining macroinitiators still wait to be activated. The result is a broad molar mass distribution, or in the case of a low molar mass poly(MMA) block, a large fraction of unreacted poly(STY) macroinitiator.

Conversely, when poly(MMA) is used as a macroinitiator, initiation is relatively fast since the equilibrium between active and dormant chains lies more to the active side. The chains that get converted into block copolymer are less reactive in this case. In the limit it can be explained as a situation in which all the macroinitiators get converted into block copolymer before the chain growth of the second block [poly(STY)] commences.

As indicated above, this scenario holds for ATRP when no special techniques are invoked. There is one relatively straightforward technique to circumvent this forced order of block copolymer synthesis. This technique is called halogen-exchange (83). It relies on the difference in bond strength between an alkyl chloride and an alkyl bromide. The carbon–bromine bond is weaker than the carbon–chlorine bond. The result of this in a so-called mixed halogen system is that carbon–chlorine bonds are preferentially formed. In halogen exchange experiments, this phenomenon is used to slow down propagation relative to initiation. In practice this would mean that poly(STY) is synthesized from a bromine functional initiator using copper(I) bromide as the catalyst. In the second step, where MMA is polymerized, the bromine functional poly(STY) macroinitiator is used in conjunction with copper(I) chloride. The macroinitiator chain gets activated and adds an MMA unit. Subsequently, it is deactivated by $CuCl_2$ (or CuClBr), which results in the formation of a carbon - chlorine bond, and thus a chlorine functional dormant block copolymer chain. Because of the difference in bond strength, the poly(STY)—Br is now more reactive than the poly(STY-*b*-MMA)—Cl. Hence, all the macroinitiator gets converted into dormant block copolymer chains, followed by propagation of the MMA block. Initially, the work by Matyjaszewski and co-workers on halogen exchange strongly emphasized the negative effect on propagation rate. This obviously leads to an increased ratio of initiation rate to propagation rate. At a later stage it was shown by Klumperman and co-workers that, apart from the effect on propagation rate, the use of copper chloride also leads to an increased rate of initiation (larger value of the activation rate constant of a bromine functional macroinitiator).

In Figure 4 it is shown how halogen exchange in block copolymer synthesis influences the resulting molar mass distributions (82).

Advanced Architectures

As indicated above, conventional free-radical polymerization is not very well suited for the synthesis of advanced polymer architectures. Even the synthesis of di- or triblock copolymers is hardly possible using this technique. The main reason is the continuous initiation and termination of chains. This results in the early generation of dead polymer chains that no longer participate in the polymerization process. The consecutive addition of monomers as employed in living anionic polymerization for the synthesis of eg poly(styrene-*block*-butadiene) will only lead to the synthesis of a mixture of two homopolymers.

Advanced architectures are possible via LRP. A large fraction of the chains in an LRP will grow throughout the polymerization process. The subsequent addition of a second monomer will lead to the formation of a block copolymer. Various examples of this process can be found in recent literature employing any of the

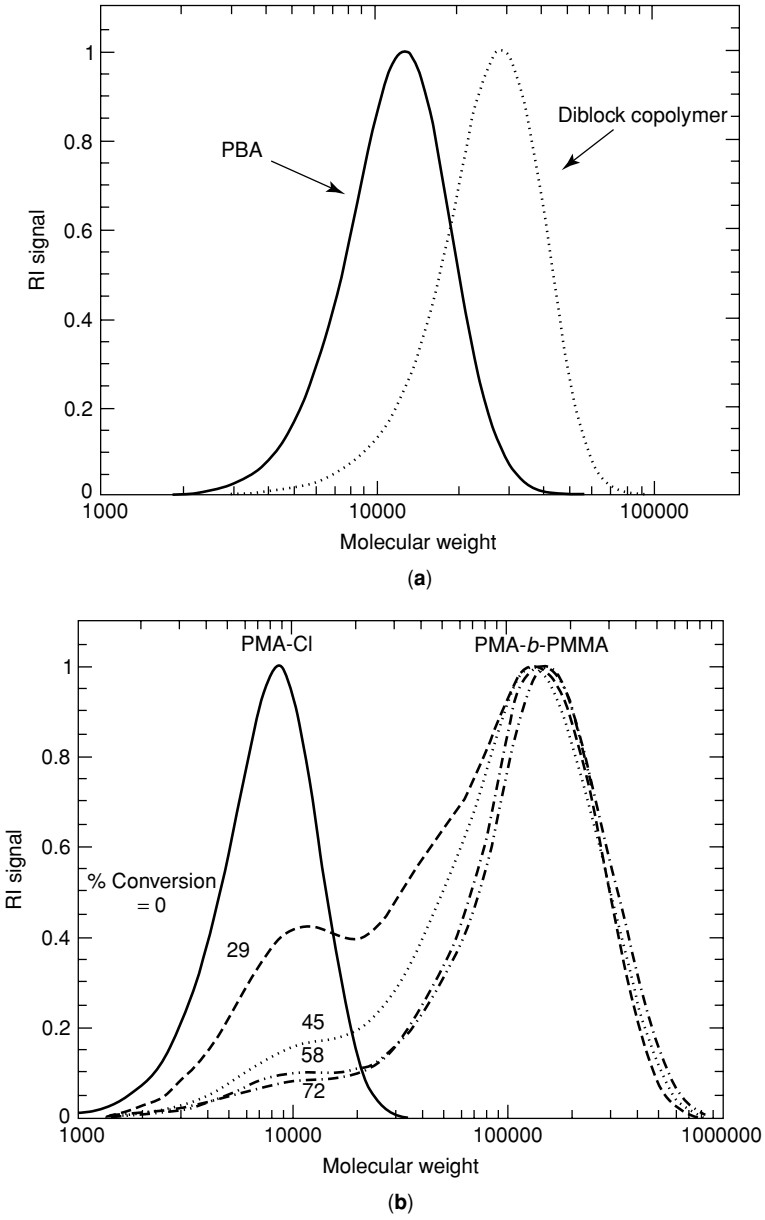

Fig. 4. Effect of halogen exchange on the molar mass distribution of an acrylate–methacrylate diblock copolymer. (**a**) Poly(BA-*b*-MMA) with halogen exchange; (**b**). Poly(MA-*b*-MMA) without halogen exchange (82).

known techniques ATRP, NMP, or RAFT (84,85). As indicated above, the sequence of the synthesis of a block copolymer may have a large influence on the degree of control.

The synthesis of an A—B—C triblock copolymer can be realized using an analogous procedure (86). Also, in this case the sequence of the comonomer additions

will influence the final result. However, in this case monomer B needs to be incorporated as the second block. Smart strategies, which include the proper choice of comonomer sequence and the possibility to employ halogen exchange in ATRP, are needed to optimize the resulting block copolymer. If the triblock copolymer is a symmetrical A–B–A copolymer, the most commonly employed synthetic strategy is the use of a difunctional initiator (NMP or ATRP) or transfer agent (RAFT). This allows the growth of the central B-block in two directions, and the subsequent addition of monomer A to synthesize the outer blocks. Here obviously the same precautions and limitations apply as in the synthesis of A–B diblock copolymers.

One of the more or less unique features of LRP in the synthesis of block copolymers is the possibility to incorporate a statistical copolymer as one of the blocks. Because of the very favorable reactivity ratios in radical polymerization compared to ionic polymerizations this is more easily achieved in LRP than in eg anionic polymerization. If the statistical copolymer is synthesized at its azeotropic conditions, there is little difference with the synthesis of a homopolymer block. If polymerization would take place under nonazeotropic conditions, the usual precautions need to be taken to avoid composition drift.

On the other hand, composition drift can be employed in LRP to synthesize gradient (or tapered) copolymers (87). The prediction of the composition drift can be carried out in exact analogy with composition drift in conventional free-radical copolymerization. The only, but important, difference is that in the case of LRP, the composition drift is superimposed on the growth of each individual chain. This then automatically leads to the formation of a gradient copolymer. In extraordinary cases the composition drift is such that a spontaneous block copolymerization will take place. One example that has been published in this regard is the synthesis of a poly(styrene-*block*-(styrene-*alt*-maleic anydride)). When a polymerization is started at a STY to MAnh molar ratio of 75:25, a copolymer with close to alternating monomer sequence is formed. This leads to a relatively fast depletion of MAnh, with the excess STY forming a homopolymer block. For the synthesis of alternating copolymers it turns out that the commonly used strategy in FRP of adding a Lewis acid to the copolymerization of styrene and acrylates can also be employed in ATRP (88)

Another class of architectures in reach of LRP are the so-called hyperbranched structures (see HYPERBRANCHED POLYMERS). The well known limit of these hyperbranched structures are dendrimers, where the consecutive growth of the polymer leads to (nearly) perfect globular macromolecules. The synthesis of dendrimers usually is a tedious multistep organic reaction. In the case of LRP, where monomers are polymerized that carry an initiator functionality as well, the synthetic procedure is quite straightforward. Examples have been reported on the basis of NMP (89) as well as on the basis of ATRP (90,91). It is very important to tailor the reactivities of initiator and monomer in this application. Two limiting cases can be recognized in that sense. If initiation is slow compared to propagation, linear chains will be formed that carry the initiator functionalities as pendent groups. In principle these polymers could be used for the synthesis of densely grafted polymers as described below. On the other hand, if initiation is very fast compared to propagation, monomers will be enchained in linear chains as well, but the polymer backbone now has a completely different architecture. In Figure 5, the two modes of polymerization are illustrated using *para*-vinylbenzylchloride.

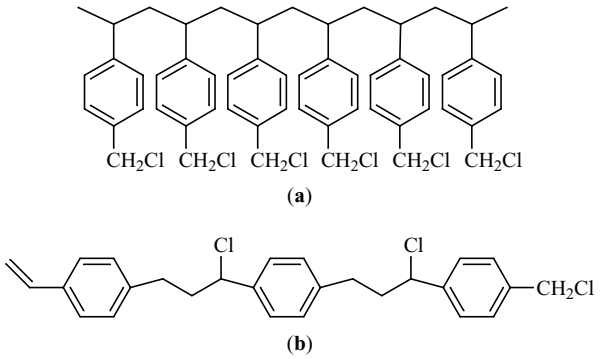

Fig. 5. Two modes of polymerization of *para*-vinylbenzylchloride, resulting from (**a**) fast propagation compared to initiation, and from (**b**) fast initiation compared to propagation.

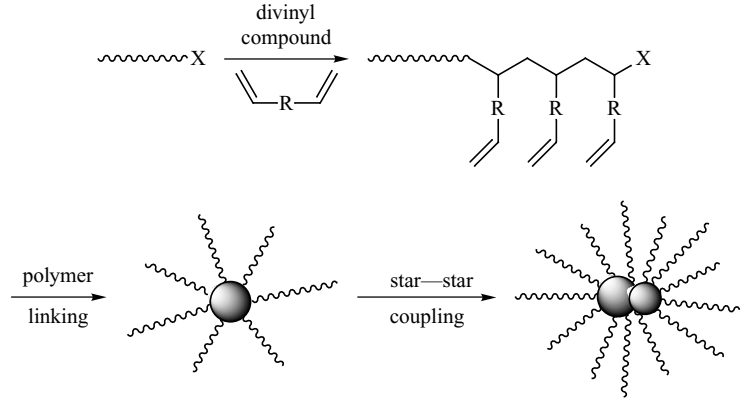

Fig. 6. Synthesis of star polymers via the "arm first" strategy (94).

It needs to be stressed that Figure 5 shows the hypothetical two extreme cases outlined above.

The first examples of star polymers synthesized via LRP were reported by Matyjaszewski and co-workers (92,93). At a later stage they reported on the synthesis of star polymers via the so-called arm first procedure (94). In this approach polymer chains are synthesized with a reactive chain end that allows coupling to the core of the star (Fig. 6).

The statistical nature of the growth process of the hyperbranched structures will inevitably lead to a relatively large variation in degree of branching. The closest one could get to a dendritic structure is by carefully matching the initiation and propagation rates. Here it needs to be taken into account that in the example shown in Figure 5, the initial primary halide will be turned into a secondary halide after the first monomer addition. This will greatly affect its activation–deactivation equilibrium. Alternatives to true hyperbranched structures in some applications are star-branched structures with a fixed and known number of arms. In LRP these structures are readily accessible via multifunctional

initiators or transfer agents. Examples have been published using NMP, but more notably using ATRP. In the work of Matyjaszewski it has been shown that any hydroxy functionality can be turned into an ATRP initiator via esterification using 2-bromo-2-methyl-propionyl bromide, as indicated in equation 8 (95).

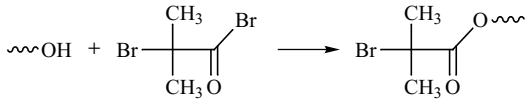

(8)

This approach was used by Haddleton and co-workers to synthesize multifunctional initiators and subsequently multiarm stars by using various sugars (96), and cyclodextrin (21-arm star) (97). The general advantages of LRP techniques also apply to the synthesis of the multiarm stars. This includes the possibility to synthesize block copolymer arms, gradient polymer arms, etc. One of the potential drawbacks is the enhanced tendency toward bimolecular termination, which in the case of termination by coupling leads to star–star coupling. It will be evident that the step from star–star coupling to network formation or cross-linking (gelation) is only a relatively minor one.

The final architecture that will be discussed here is that of densely grafted polymer chains. If the process described for the formation of hyperbranched structures is turned into a two-step process, it is possible to synthesize chains that contain a branch on each repeat unit of the polymer backbone. Because of the great steric congestion, these structures will behave like a rigid rod. The first example of a densely grafted polymer chain completely via LRP (ATRP) is based on the polymerization of trimethylsilyl-protected 2-hydroxyethyl methacrylate (HEMA-TMS) (77). In a post-polymerization reaction the trimethylsilyl groups are removed and the resulting hydroxy functionalities are turned into ATRP initiators by reaction with 2-bromoisobutyryl bromide to yield poly-(2-(2-bromoisobutyryloxy)ethyl methacrylate) (pBIEM). Subsequently, the densely grafted structure was obtained by polymerizing styrene or butyl acrylate as side chains from the initial backbone (pBIEM). In Figure 7 typical examples of these rigid rod structures are shown as observed by Atomic Force Microscopy (qv) (AFM).

Combined Mechanisms

LRP is a powerful tool for the synthesis of complex polymer architectures as was shown above. However, in some cases it is desirable to combine structures that are hardly or not at all accessible via radical polymerization techniques. In such cases it may be beneficial to combine LRP with another polymerization mechanism. Many examples have been reported so far. A few examples will be listed here. Polystyrene-*b*-polyisobutylene-*b*-polystyrene was synthesized via a combination of living cationic polymerization and ATRP (98). Polyolefin Graft Copolymers (qv) were synthesized by first polymerizing alkoxyamine-substituted olefins via metallocene catalysis, and subsequent polymerization of vinyl monomers via

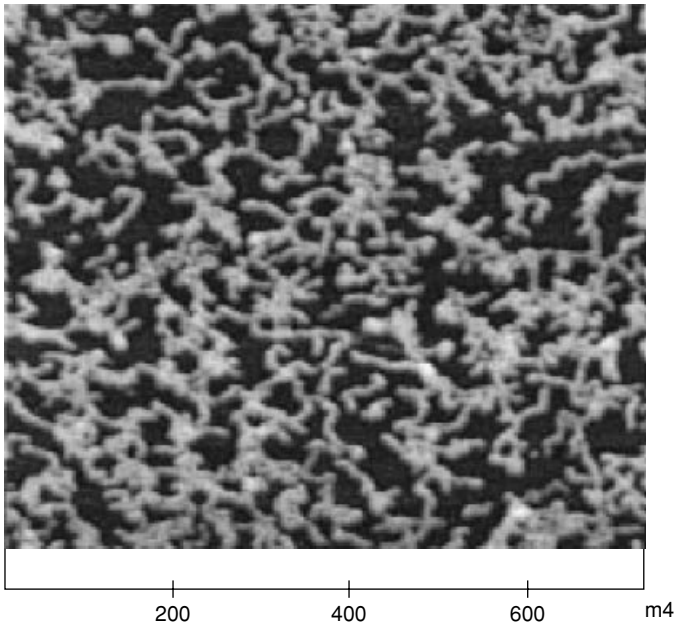

Fig. 7. AFM image of a densely grafted copolymer. Polystyrene grafted from pBIEM ($M_n = 55{,}500$; $M_w/M_n = 1.3$).

NMP (99). Living ring-opening polymerization of ε-caprolactone and lactides was combined with various LRP techniques (100). An approach to synthesize vinyl polymers with poly(vinyl ether) grafts is to make use of macromonomers. Cationic polymerization is used to synthesize the macromonomers with a methacryloyl pendent group. The macromonomers are then copolymerized via ATRP (101). Poly(ε-caprolactone)-graft-poly(methyl methacrylate) copolymers are prepared by the (co)polymerization of a cyclic ester containing an activated bromide functional group [γ-(2-bromo-2-methylpropionyloxy)-ε-caprolactone]. The activated bromide functionality is subsequently used to introduce the PMMA side chains via ATRP (102). Anionic Polymerization (qv) and ATRP are combined to synthesize eg A–B–C triblock copolymers (103). The same group demonstrated the versatility of end-group modification of various polymers into ATRP initiators (104,105). It needs to be stressed that this approach has been adopted by many research groups, and that probably the first attempts were published by Matyjaszewski and co-workers (18). Polyisoprene-*b*-polystyrene with a single fluorescent label at the junction between the two blocks is reported by Winnik and co-workers (106). They also use a combination of anionic polymerization and ATRP. Finally, LRP can be combined with enzymatic polymerization as shown by Meyer and co-workers (107). They use a bifunctional initiator (benzyl-3-(2-bromo-2-methylpropionyloxy)-2-hydroxymethyl-2-methylpropionate) with a primary hydroxy functionality to initiate the enzymatic ring-opening polymerization of ε-caprolactone, and an activated bromide functionality to initiate ATRP.

LRP in Emulsion

One of the great advantages of conventional FRP is the fact that the polymerization can be conducted in aqueous environment, viz suspension polymerization, emulsion polymerization (see HETEROPHASE POLYMERIZATION). Soon after LRP was first published, investigations were started to allow LRP to be carried out in aqueous media as well. This turned out to be far from trivial. Recently, the efforts to conduct LRP in emulsion were reviewed (108).

Bon and co-workers were the first to publish a successful attempt toward TEMPO-mediated LRP in emulsion (109). This first work was far from optimal, since it only worked in seeded emulsion polymerization, and temperatures above 100°C were required to obtain a dynamic equilibrium between dormant and active species. NMP improved quite significantly with respect to its applicability in emulsion polymerization when the above-mentioned developments led to polymerization temperatures below 100°C. Notable in this respect was the work by Charleux and co-workers, who employed *N*-*tert*-butyl-*N*-(1-diethylphosphono-2,2-dimethylpropyl)nitroxide as the mediating nitroxide for the LRP of styrene and butyl acrylate in emulsion (110,111).

ATRP in emulsion (112–116) and miniemulsion (117) was mainly investigated by Matyjaszewski and co-workers. The difficulties to remove the copper catalyst from the latex, and the low stability of the obtained latex were among the structural difficulties to develop an attractive alternative to the NMP-based systems.

RAFT polymerization in emulsion (118–121) and miniemulsion (122–125) received considerable attention. The initial results were not very promising. In many instances the stability of the emulsion during polymerization was very poor. Phase separation was often observed where the typical red color of the RAFT agent would disappear from the emulsion and form a sticky red layer on top of the emulsion. One of the alternatives to overcome this problem was the application of miniemulsion polymerization. In this technique, micron-size monomer droplets are absent. All the monomer is dispersed in submicron droplets, which are transformed into latex particles during the polymerization process. Stable latexes were obtained in a number of cases, where the polymers possess a reasonably narrow molar mass distribution. The disadvantage of miniemulsion polymerization is that relatively high surfactant concentrations and the use of a so-called cosurfactant or hydrophobe is required. It is therefore that further research was conducted to develop a strategy that allows LRP in conventional emulsion. At present the most successful attempt seems to be a two-stage process (126) in which a water-soluble monomer, eg acrylic acid, is polymerized in the presence of a RAFT agent in aqueous media. This polymerization is only conducted up to low molar mass. Subsequently, a monomer with low water solubility is dispersed in the reaction mixture, and further polymerization is carried out to yield a stable latex. Formally the polymer is a diblock copolymer, albeit with a short hydrophilic block. The polymer has a relatively low PDI.

The use of RAFT agents with a low activity (120,121) ie a low chain-transfer constant is another option that provides useful results. Xanthates represent a class of RAFT agents that are useful in this respect. The majority of polymer chains in such a system carry the xanthate as an end group. However, because of the

low chain-transfer constant the PDI of the polymer is around 2. In principle, the polymers can be used for chain extension, and for the synthesis of block copolymers (qv).

The final system that is worth mentioning in this chapter on LRP in emulsion is the use of 1,1-diphenylethylene (DPE) (127). DPE adds to a growing radical and forms a radical with a reactivity too low for propagation. The exact mechanism is not elucidated, but the incorporation of DPE leads to a chain that allows chain extension or block copolymer formation. More or less similar to what was described about the xanthates in RAFT polymerization, here also the molar mass distributions are relatively broad. The greatest advantage of DPE-mediated polymerization is the fact that it results in minimal disturbance of the polymerization process. The product latex does not contain any unusual extractable material (like the catalyst in ATRP), or polymer-bound colored moieties (like the thiocarbonylthio compound in RAFT). The obvious drawback is the limited control over chain architecture, and the limited understanding of the mechanistic details.

Future Directions

Presently, significant work has been done to develop and optimize various LRP techniques. Commercial applications are still scarce. The general expectation is that the products of LRP will mainly be employed in high-value-added products. These may include specialty coatings, adhesives, personal care products, biomedical applications, and optoelectronical applications. Examples of biomedical applications can be found in the work of eg, Müller (128), Haddleton (129), and Wooley (130,131). For materials in optoelectronical applications it is of great importance that many of the techniques from FRP can be adopted to LRP. An example is surface grafting from or onto various substrates, like silica (132) and gold (133). Much of the work of Hawker and co-workers is dedicated to the application of LRP in electronical applications (134).

BIBLIOGRAPHY

"Living Polymer Systems, Radical Polymerization" in *EPSE* 2nd ed., Suppl. Vol., pp. 429–436, by H. J. Harwood, University of Akron.

1. G. Odian, *Principles of Polymerization*, 3rd ed., John Wiley & Sons, Inc., New York, 1991.
2. M. Swarc, *Adv. Polym. Sci.* **2**, 275 (1960).
3. E. Borsig, M. Lazar, M. Capla, and S. Florian, *Angew. Makromol. Chem.* **9**, 89 (1969).
4. T. Otsu, M. Yoshida, and T. Tazaki, *Makromol. Chem., Rapid Commun.* **3**, 133–140 (1982).
5. T. Otsu and T. Tazaki, *Polym. Bull.* **16**, 277–84 (1986).
6. T. Otsu, K. Yamashita, and K. Tsuda, *Macromolecules* **19**, 287–290 (1986).
7. T. Otsu and M. Yoshida, *Polym. Bull.* **7**, 197–203 (1982).
8. D. R. Suwier, M. N. Teerenstra, B. Vanhaecht, and C. E. J. Koning, *Polym. Sci., Part A: Polym. Chem.* **38**, 3558–3568 (2000).
9. Eur. Pat. EP 135280 A2 (1985), D. H. Solomon, E. Rizzardo, and P. Cacioli (Commonwealth Scientific and Industrial Research Organization).

10. M. K. Georges, R. P. N. Veregin, G. K. Hamer, and P. M. Kazmaier, *Macromol. Symp.* **88**, 89–103 (1994).
11. M. K. Georges, R. A. Kee, R. P. N. Veregin, G. K. Hamer, and P. M. Kazmaier, *J. Phys. Org. Chem.* **8**, 301–305 (1995).
12. D. Benoit, V. Chaplinski, R. Braslau, and C. J. Hawker, *J. Am. Chem. Soc.* **121**, 3904–3920 (1999).
13. D. Benoit, S. Grimaldi, S. Robin, J.-P. Finet, P. Tordo, and Y. Gnanou, *J. Am. Chem. Soc.* **122**, 5929–5939 (2000).
14. J.-S. Wang and K. Matyjaszewski, *J. Am. Chem. Soc.* **117**, 5614–5615 (1995).
15. M. Kato, M. Kamigaito, M. Sawamoto, and T. Higashimura, *Macromolecules* **28**, 1721–1723 (1995).
16. D. P. Curran, in B. M. Trost and I. Fleming, eds., *Comprehensive Organic Synthesis*, Vol. **4**, Pergamon, Oxford, UK, 1991, p. 715.
17. V. Coessens, T. Pintauer, and K. Matyjaszewski, *Prog. Polym. Sci.* **26**, 337 (2001).
18. J.-S. Wang, D. Geszta, and K. Matyjaszewski, *Polym. Mater. Sci. Eng.* **73**, 416 (1995).
19. K. Matyjaszewski, S. Coca, and Y. Nakagawa, *J. Xia Polym. Mater. Sci. Eng.* **76**, 147 (1997)
20. C. Waterson and D. M. Haddleton, *Polym. Prepr.* **40**, 1045–1046 (1999).
21. D. M. Haddleton, D. Kukulj, E. J. Kelly, and C. Waterson, *Polym. Mater. Sci. Eng.* **80**, 145–146 (1999).
22. S. A. F. Bon, A. G. Steward, and D. M. Haddleton, *J. Polym. Sci., Part A: Polym. Chem.* **38**, 2678–2686 (2000).
23. D. M. Haddleton, M. C. Crossman, B. H. Dana, D. J. Duncalf, A. M. Heming, D. Kukulj, and A. J. Shooter, *Macromolecules* **32**, 2110–2119 (1999).
24. J. Xia and K. Matyjaszewski, *Macromolecules* **30**, 7697–7700 (1997).
25. J. Xia, S. G. Gaynor, and K. Matyjaszewski, *Macromolecules* **31**, 5958–5959 (1998).
26. H. J. Paik, S. G. Gaynor, and K. Matyjaszewski, *Macromol. Rapid Commun.* **19**, 47–52 (1998).
27. D. Mecerreyes, G. Moineau, P. Dubois, R. Jerome, J. L. Hedrick, C. J. Hawker, E. E. Malmstrom, and M. Trollsas, *Angew. Chem., Int. Ed.* **37**, 1274–1276 (1998).
28. T. Fonagy, B. Ivan, and M. Szesztay, *Polym. Mater. Sci. Eng.* **79**, 3–4 (1998).
29. K. L. Beers, S. G. Gaynor, K. Matyjaszewski, S. S. Sheiko, and M. Moeller, *Macromolecules* **31**, 9413–9415 (1998).
30. S. C. Hong and K. Matyjaszewski, *Macromolecules* **35**, 7592–7605 (2002).
31. S. Angot, N. Ayres, S. A. F. Bon, and D. M. Haddleton, *Macromolecules* **34**, 768–774 (2001).
32. A. J. Carmichael, D. M. Haddleton, S. A. F. Bon, and K. R. Seddon, *Chem. Commun.* 1237–1238 (2000).
33. D. M. Haddleton, S. G. Jackson, and S. A. F. Bon, *J. Am. Chem. Soc.* **122**, 1542–1543 (2000).
34. K. Matyjaszewski, S. G. Gaynor, and J.-S. Wang, *Macromolecules* **28**, 2093 (1995).
35. D. M. Haddleton, C. Topping, D. Kukulj, and D. Irvine, *Polymer* **39**, 3119–3128 (1998).
36. C. L. Moad, G. Moad, E. Rizzardo, and S. H. Thang, *Macromolecules* **29**, 7717–7726 (1996).
37. S. Jiang, H. G. Viehe, N. Oger, and D. Charmot, *Macromol. Chem. Phys.* **196**, 2349–2360 (1995).
38. PCT Int. Appl. WO 9801478 A1 (1998), T. P. Le, G. Moad, E. Rizzardo, and S. H. Thang (Commonwealth Scientific and Industrial Research Organization).
39. J. Chiefari, Y. K. Chong, F. Ercole, J. Krstina, J. Jeffery, T. P. T. Le, R. T. A. Mayadunne, G. F. Meijs, C. L. Moad, G. Moad, E. Rizzardo, and S. H. Thang, *Macromolecules* **31**, 5559–5562 (1998).

40. PCT Int. Appl. WO 9858974 A1 (1998), P. Corpart, D. Charmot, T. Biadatti, S. Zard, and D. Michelet (Rhodia).
41. P. C. Wieland, B. Raether, and O. Nuyken, *Macromol. Rapid Commun.* **22**, 700–703 (2001).
42. S. Viala, K. Tauer, M. Antonietti, R.-P. Kruger, and W. Bremser, *Polymer* **43**, 7231–7241 (2002).
43. J. Qiu, B. Charleux, and K. Matyjaszewski, *Prog. Polym. Sci.* **26**, 2083 (2001).
44. C. J. Hawker, G. G. Barclay, A. Orellana, J. Dao, and W. Devonport, *Macromolecules* **29**, 5245–5254 (1996).
45. G. Moad and E. Rizzardo, *Macromolecules* **28**, 8722–8788 (1995).
46. T. Fukuda, T. Terauchi, A. Goto, K. Ohno, Y. Tsujii, T. Miyamoto, S. Kobatake, and B. Yamada, *Macromolecules* **29**, 6393–6398 (1996).
47. A. Goto and T. Fukuda, *Macromolecules* **30**, 4272 (1997).
48. D. Greszta and K. J. Matyjaszewski, *Polym. Sci., Part A: Polym. Chem.* **35**, 1857 (1997).
49. H. Fischer, *J. Polym. Sci., Part A: Polym. Chem.* **37**, 1885–1901 (1999).
50. H. Fischer, *Macromolecules* **30**, 5666–5672 (1997).
51. T. Kothe, S. Marque, R. Martschke, M. Popov, and H. Fischer, *J. Chem. Soc., Perkin Trans.* **2**, 1553–1559 (1998).
52. H. Fischer, *Chem. Rev.* **101**, 3581–3610 (2001).
53. H. B. Sonmez and N. Bicak, *React. Funct. Polym.* **51**, 55–60 (2002).
54. H. Zhang, B. Klumperman, W. Ming, H. Fischer, and R. van der Linde, *Macromolecules* **34**, 6169–6172 (2001).
55. A. Snijder, B. Klumperman, and R. van der Linde, *Macromolecules* **35**, 4785–4790 (2002).
56. G. Moineau, Ph. Dubois, R. Jerome, T. Senninger, and Ph. Teyssie, *Macromolecules* **31**, 545–547 (1998).
57. S. Zhu, D. Yan, and G. Zhang, *Polym. Bull.* **45**, 457–464 (2001).
58. K. Matyjaszewski, M. Wei, J. Xia, and N. E. McDermott, *Macromolecules* **30**, 8161 (1997).
59. M. Teodorescu, S. G. Gaynor, and K. Matyjaszewski, *Macromolecules* **33**, 2335 (2000).
60. G. Moineau, M. Minet, P. Teyssie, and R. Jerome, *Macromol. Chem. Phys.* **201**, 1108–1114 (2000).
61. M. Wakioka, K.-Y. Baek, T. Ando, M. Kamigaito, and M. Sawamoto, *Macromolecules* **35**, 330–333 (2002).
62. M. Destarac, K. Matyjaszewski, and B. Boutevin, *Macromol. Chem. Phys.* **201**, 265–272 (2000).
63. V. Percec, H.-J. Kim, and B. Barboiu, *Macromolecules* **30**, 8526–8528 (1997).
64. J. S. Wang and K. Matyjaszewski, *Macromolecules* **28**, 7572 (1995).
65. J. Xia and K. Matyjaszewski, *Macromolecules* **30**, 7692 (1997).
66. A. Goto, K. Sato, Y. Tsujii, T. Fukuda, G. Moad, E. Rizzardo, and S. H. Thang, *Macromolecules* **34**, 402–408 (2001).
67. S. Perrier, C. Barner-Kowollik, J. F. Quinn, P. Vana, and T. P. Davis, *Macromolecules* **35**, 8300–8306 (2002).
68. P. Vana, T. P. Davis, and C. Barner-Kowollik, *Macromol. Theory Simul.* **11**, 823–835 (2002).
69. M. J. Monteiro and H. de Brouwer, *Macromolecules* **34**, 349–352 (2001).
70. A. Goto, K. Sato, Y. Tsujii, T. Fukuda, G. Moad, E. Rizzardo, and S. H. Thang, *Macromolecules* **34**, 402–408 (2001).
71. S. H. Thang, personal communication, 2001.
72. J. F. Lutz, D. Neugebauer, and K. Matyjaszewski, *J. Am. Chem. Soc.* (submitted).
73. J.-S. Wang and K. Matyjaszewski, *Macromolecules* **28**, 7901 (1995).
74. T. Grimaud and K. Matyjaszewski, *Macromolecules* **30**, 2216 (1997).

75. J.-L. Wang, T. Grimaud and K. Matyjaszewski, *Macromolecules* **30**, 6507 (1997).
76. X. Zhang, J. Xia, and K. Matyjaszewski, *Macromolecules* **31**, 5167 (1998).
77. K. L. Beers, S. G. Gaynor, K. Matyjaszewski, S. S. Sheiko, and M. Moeller, *Macromolecules* **31**, 9413 (1998).
78. K. L. Beers, S. Boo, S. G. Gaynor, and K. Matyjaszewski, *Macromolecules* **32**, 5772 (1999).
79. X.-S. Wang, R. A. Jackson, and S. P. Armes, *Macromolecules* **33**, 255–257 (2000).
80. X. Zhang, J. Xia, and K. Matyjaszewski, *Macromolecules* **32**, 7349 (1999).
81. D. Benoit, E. Harth, P. Fox, R. M. Waymouth, and C. J. Hawker, *Macromolecules* **33**, 363–370 (2000).
82. K. Matyjaszewski, D. A. Shipp, G. P. McMurthy, S. G. Gaynor, and T. Pakula, *J. Polym. Sci., Polym. Chem. Ed.* **38**, 2023 (2000).
83. K. Matyjaszewski, D. A. Shipp, J.-L. Wang, T. Grimaud, and T. E. Patten, *Macromolecules* **31**, 6836 1998.
84. K. A. Davis and K. Matyjaszewski, *Adv. Polym. Sci.* **159**, 2 (2002).
85. T. E. Patten and K. Matyjaszewski, *Adv. Mater.* **10**, 901 (1998).
86. K. A. Davis and K. Matyjaszewski, *Macromolecules* **34**, 2101 (2001).
87. K. Matyjaszewski, M. J. Ziegler, S. V. Arehart, D. Greszta and T. Pakula, *J. Phys. Org. Chem.* **13**, 775 (2000).
88. B. Kirci, J. F. Lutz and K. Matyjaszewski, *Macromolecules* **35**, 2448 (2002).
89. C. J. Hawker, J. M. J. Frechet, R. B. Grubbs and J. Dao, *J. Am. Chem. Soc.* **117**, 10763 (1995).
90. S. G. Gaynor, S. Edelman and K. Matyjaszewski, *Macromolecules* **29**, 1079 (1996).
91. K. Matyjaszewski, S. G. Gaynor, and A. Kulfan, *Macromolecules* **30**, 5192 (1997).
92. J.-S. Wang, D. Greszta and K. Matyjaszewski, *Polym. Mater. Sci. Eng.* **73**, 416 (1995).
93. K. Matyjaszewski, P. J. Miller, E. Fossum and Y. Nakagawa, *Appl. Organomet. Chem.* **12**, 667 (1998).
94. J. Xia, X. Zhang, and K. Matyjaszewski, *Macromolecules* **32**, 4482 (1999).
95. S. G. Gaynor and K. Matyjaszewski, *Macromolecules* **30**, 4241 (1997).
96. D. M. Haddleton, A. M. Heming, A. P. Jarvis, A. Khan, A. Marsh, S. Perrier, S. A. F. Bon, S. G. Jackson, R. Edmonds, E. Kelly, D. Kukuli, and C. Waterson, *Macromol. Symp.* **157**, 201–208 (2000).
97. K. Ohno, B. Wong, and D. M. Haddleton, *J. Polym. Sci., Part A: Polym. Chem.* **39**, 2206–2214 (2001).
98. X. Chen, B. Ivan, J. Kops, and W. Batsberg, *Macromol. Rapid Commun.* **19**, 585–589 (1998).
99. U. M. Stehling, E. E. Malmstroem, R. M. Waymouth, and C. J. Hawker, *Macromolecules* **31**, 4396–4398 (1998).
100. R. Jerome, D. Mecerreyes, D. Tian, P. Dubois, C. J. Hawker, M. Trollsas, and J. L. Hedrick, *Macromol. Symp.* **132**, 385–403 (1998).
101. K. Yamada, M. Miyazaki, K. Ohno, T. Fukuda, and M. Minoda, *Macromolecules* **32**, 290–293 (1999).
102. D. Mecerreyes, B. Atthoff, K. A. Boduch, M. Trollsaas, and J. L. Hedrick, *Macromolecules* **32**, 5175–5182 (1999).
103. F. Liu, S. Ying, N. Luo, B. Liu, Q. Liu, and *Polym. Prepr.* **40**, 1032–1033 (1999).
104. X.-S. Wang, N. Luo, S.-K. Ying, and Q. Liu, *Eur. Polym. J.* **36**, 149–156 (1999).
105. B. Liu, F. Liu, N. Luo, S.-K. Ying, and Q. Liu, *Chin. J. Polym. Sci.* **18**, 39–43 (2000).
106. J.-D. Tong, S. Ni, and M. A. Winnik, *Macromolecules* **33**, 1482–1486 (2000).
107. U. Meyer, A. R. A. Palmans, T. Loontjens, and A. Heise, *Macromolecules* **35**, 2873–2875 (2002).
108. J. Qiu, B. Charleux, and K. Matyjaszewski, *Prog. Polym. Sci.* **26**, 2083 (2001).

109. S. A. F. Bon, M. Bosveld, B. Klumperman, and A. L. German, *Macromolecules* **30**, 324–326 (1997).
110. C. Farcet, B. Charleux, and R. Pirri, *Macromol. Symp.* **182**, 249 (2002).
111. C. Farcet, J. Nicolas, and B. Charleux, *J. Polym. Sci., Part A: Polym. Chem.* **40**, 4410–4420 (2002).
112. S. Gaynor, J. Qiu, and K. Matyjaszewski, *Macromolecules* **31**, 5951 (1998).
113. J. Qiu, S. Gaynor, and K. Matyjaszewski, *Macromolecules* **32**, 2872 (1999).
114. K. Matyjaszewski, D. A. Shipp, J. Qiu, and S. G. Gaynor, *Macromolecules* **33**, 2296 (2000).
115. J. Qiu, T. Pintauer, S. G. Gaynor, K. Matyjaszewski, B. Charleux, and J.-P. Vairon, *Macromolecules* **33**, 7310 (2000).
116. S. Jousset, J. Qiu, K. Matyjaszewski, and C. Granel, *Macromolecules* **34**, 6641 (2001).
117. K. Matyjaszewski, J. Qiu, N. V. Tsarevsky, and B. Charleux, *J. Polym. Sci., Part A: Polym. Chem.* **38**, 4724 (2000).
118. I. Uzulina, S. Kanagasabapathy, and J. Claverie, *Macromol. Symp.* **150**, 33–38 (2000).
119. M. J. Monteiro, M. Hodgson, and H. De Brouwer, *J. Polym. Sci., Part A: Polym. Chem.* **38**, 3864–3874 (2000).
120. M. J. Monteiro, M. Sjoberg, J. Van der Vlist, and C. M. Gottgens, *J. Polym. Sci., Part A: Polym. Chem.* **38**, 4206–4217 (2000).
121. M. J. de Monteiro and J. Barbeyrac, *Macromolecules* **34**, 4416–4423 (2001).
122. A. Butte, G. Storti, and M. Morbidelli, *Macromolecules* **33**, 3485–3487 (2000).
123. J. G. Tsavalas, F. J. Schork, H. de Brouwer, and M. J. Monteiro, *Macromolecules* **34**, 3938–3946 (2001).
124. A. Butte, G. Storti, and M. Morbidelli, *Macromolecules* **34**, 5885–5896 (2001).
125. J. J. Vosloo, D. De Wet-Roos, M. P. Tonge, and R. D. Sanderson, *Macromolecules* **35**, 4894–4902 (2002).
126. C. J. Ferguson, R. J. Hughes, B. T. T. Pham, B. S. Hawkett, R. G. Gilbert, A. K. Serelis, and C. H. Such, *Macromolecules* **35**, 9243–9245 (2002).
127. S. Viala, K. Tauer, M. Antonietti, R.-P. Kruger, and W. Bremser, *Polymer* **43**, 7231–7241 (2002).
128. C. Schilli, A. H. E. Mueller, E. Rizzardo, S. H. Thang, and B. Y. K. Chong, *Polym. Prepr.* **43**, 687–688 (2002).
129. S. Monge and D. M. Haddleton, *Polym. Prepr.* **43**, 793–794 (2002).
130. K. S. Murthy, Q. Ma, C. G. Clark Jr., E. E. Remsen, and K. L. Wooley, *Chem. Commun.* 773–774 (2001).
131. J. Liu, Q. Zhang, E. E. Remsen, and K. L. Wooley, *Biomacromolecules* **2**, 362–368 (2001).
132. T. von Werne and T. E. Patten, *J. Am. Chem. Soc.* **123**, 7497–7505.
133. K. Ohno, K.-M. Koh, Y. Tsujii, and T. Fukuda, *Macromolecules* **35**, 8989–8993 (2002).
134. S. Blomberg, S. Ostberg, E. Harth, A. W. Bosman, B. Van Horn, and C. J. Hawker, *J. Polym. Sci, Part A: Polym. Chem.* **40**, 1309–1320 (2002).

BERT KLUMPERMAN
Eindhoven University

LLDPE. See ETHYLENE POLYMERS, LLDPE.

LOW DENSITY POLYETHYLENE. See ETHYLENE POLYMERS, LDPE.

MAGNETIC POLYMERS

Introduction

Typical behavior of small molecules or metal ions with unpaired electrons is that of a paramagnet, ie, magnetic interactions within the large ensemble of electron spins are negligible and a large external magnetic field is required to even partially align the electron spins. For ferromagnetism and other technologically useful types of magnetism, the quantum mechanical exchange interaction between electron spins is a prerequisite (1). In a ferromagnet, the exchange interactions within a three-dimensional structure align the spins in one direction, producing a large magnetic moment in magnetic domains of more than 10^4 electron spins, even in the absence of external magnetic field. The strength of this exchange interaction determines the *Curie temperature* (T_C), that is, the temperature above which the magnetic ordering is destroyed and the material becomes paramagnetic (1). (Analogously, T_C is referred to as ferrimagnetic Curie temperature in ferrimagnets).

Traditional magnetic materials are based upon metals (and metal ions) with partially filled *d*- and *f*-shells, ie, selected metals, metal alloys, and ceramics. Composite materials such as organic polymers filled with small metallic or inorganic magnetic particles fall into similar category (2).

The relatively recent magnetic materials, in which organic radicals function as the source of electron spin, are organometallic magnets and organic magnets. In organometallic magnets, the exchange interaction occurs between organic radicals or radical anions and metal ions. Many of such materials may be viewed as one-, two-, or three-dimensional coordination polymers (3–5). In organic magnets, based upon molecular solids of organic radicals (or radical ions), exchange interactions occur between molecules with unpaired electrons. Because

Encyclopedia of Polymer Science and Technology. Copyright John Wiley & Sons, Inc. All rights reserved.

such through-space interactions are inherently weak, the T_C's for organic ferromagnets are typically below 2 K, with the exception of the C_{60}-TDAE [TDAE = tetrakis(dimethylamine)ethylene] radical ion salt which has $T_C = 16$ K (6–8).

Organic polymers, in which exchange interactions between radicals are mediated by π-conjugated system, provide an alternative approach to organic magnets. As early as 1968, Mataga proposed few structures for plausible one- and two-dimensional "ferromagnetic" polymers, based upon cross-conjugated diphenylcarbenes and triphenylmethyls (9). Studies of numerous model diradicals (and dicarbenes) established the importance of connectivity of π-system mediating exchange interaction between the radicals. For two radicals linked through *m*-phenylene, triplet (spin multiplicity, $2S + 1 = 3$, for $S = 1$, where S is the total spin quantum number) ground state is found, as long as the π-system is approximately planar. The energy gap (ΔE_{ST}), between the singlet excited state and the triplet ground state, exceeds RT at room temperature in several diradicals. The analogous p- or o-connectivity leads to the singlet ground state, ie, pairing of two spins-1/2 (10,11). Such pairwise exchange interactions leading to the triplet and singlet ground states are referred to as ferromagnetic coupling and antiferromagnetic coupling, respectively. Strong ferromagnetic couplings ($\Delta E_{ST} > RT$), when extended in a three-dimensional network, could lead to ferromagnetism at room temperature (10). This goal was recently brought a step closer by discovery of magnetic ordering in a highly cross-linked conjugated organic polymer (12), which is described in the next section.

One of the measures of progress toward magnetic polymers is the average value of S in the ground state of the paramagnetic macromolecule. (For n ferromagnetically coupled spin-1/2, $S = n/2$). Several problems need to be addressed in synthesis of such conjugated polymers. Connectivity between the radicals within the π-system of the macromolecule must be strictly controlled; typically, the head-to-tail polymerization provides adequate connectivity for ferromagnetic coupling. However, even a single head-to-head (or tail-to-tail) connection may result in spin pairing (or interruption of exchange interaction) and, consequently, low value of average S will be obtained. Analogously, a severe out-of-plane twist of the π-system may interrupt exchange coupling or change ferromagnetic coupling to antiferromagnetic coupling. This particular problem is amplified by the need for sterically hindered groups in the macromolecule to prevent radicals from dimerization or other chemical decomposition pathways of radicals. The placement of sterically bulky groups and overall connectivity of the π-system should allow for significant delocalization of spin density from radicals to the linking π-system; this is a prequisite for a significant through-bond exchange interactions, including ferromagnetic coupling between the neighboring radicals. The chemical yield for generation of radicals must be near quantitative or, if radical monomers are used for polymerization, the radicals should survive polymerization conditions intact.

It is clear that the synthesis of magnetic polymers poses an extreme challenge for polymer science and organic chemistry, especially in view of the fact that the ultimate goal is a macromolecule with large number (10^4 or more) of interacting radicals (12). Not surprisingly, until late 1990s, the highest values of S in organic molecules and polymers were attained for strictly monodisperse organic molecules, eg, polyarylmethyl **1** with $S = 10$, prepared by laborious multistep syntheses (13–15) (Fig. 1). Even though stable triplet ground state ($S = 1$) diradicals

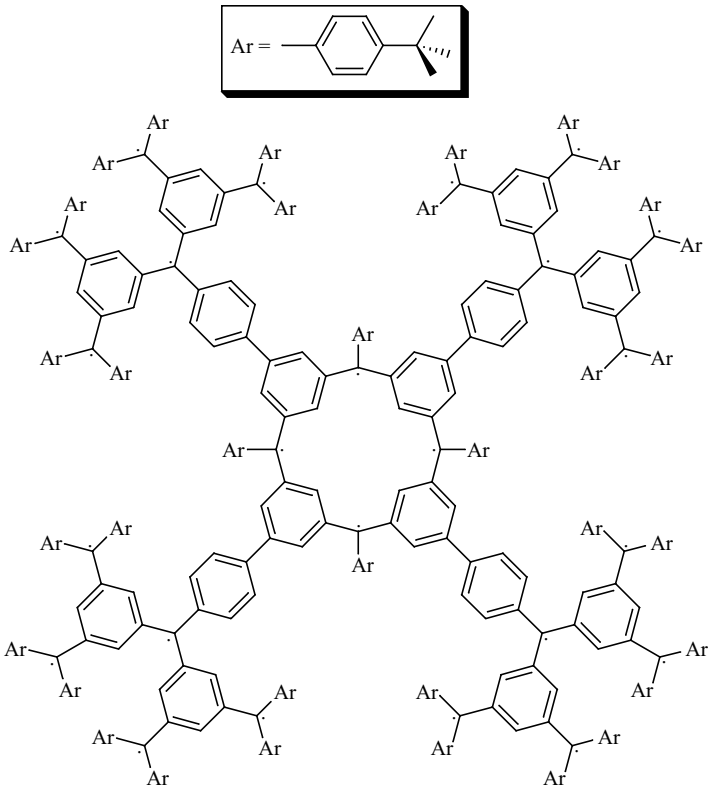

(**1**)

Fig. 1. Dendritic-macrocyclic polyradical **1**.

are well known, most of the reported "magnetic" polymers did not even reach $S \approx 1$, ie, a ferromagnetic coupling of two spin-1/2 radicals on average. Spurious reports of "ferromagnets" showing hystereses at room temperature in organic polymers with radical concentration on the order of 1% radical/unit or less are ignored in this review; magnetic behavior of such "magnetic" polymers has been shown to be associated with metal purities (16).

Two limiting approaches have been developed for connectivity between the radicals within conjugated polymers: Class I polyradicals, in which the radicals are within the π-system mediating exchange interactions, and Class II polyradicals, in which radicals are pendant groups attached to the conjugated polymer backbone.

Class I Polyradicals

The discussion of Class I polyradicals is focused on conjugated polymers **2** in which *m*-phenylene groups are employed to attain through-bond ferromagnetic coupling (Fig. 2). They are by far the most important of all organic polymers studied for their magnetic properties.

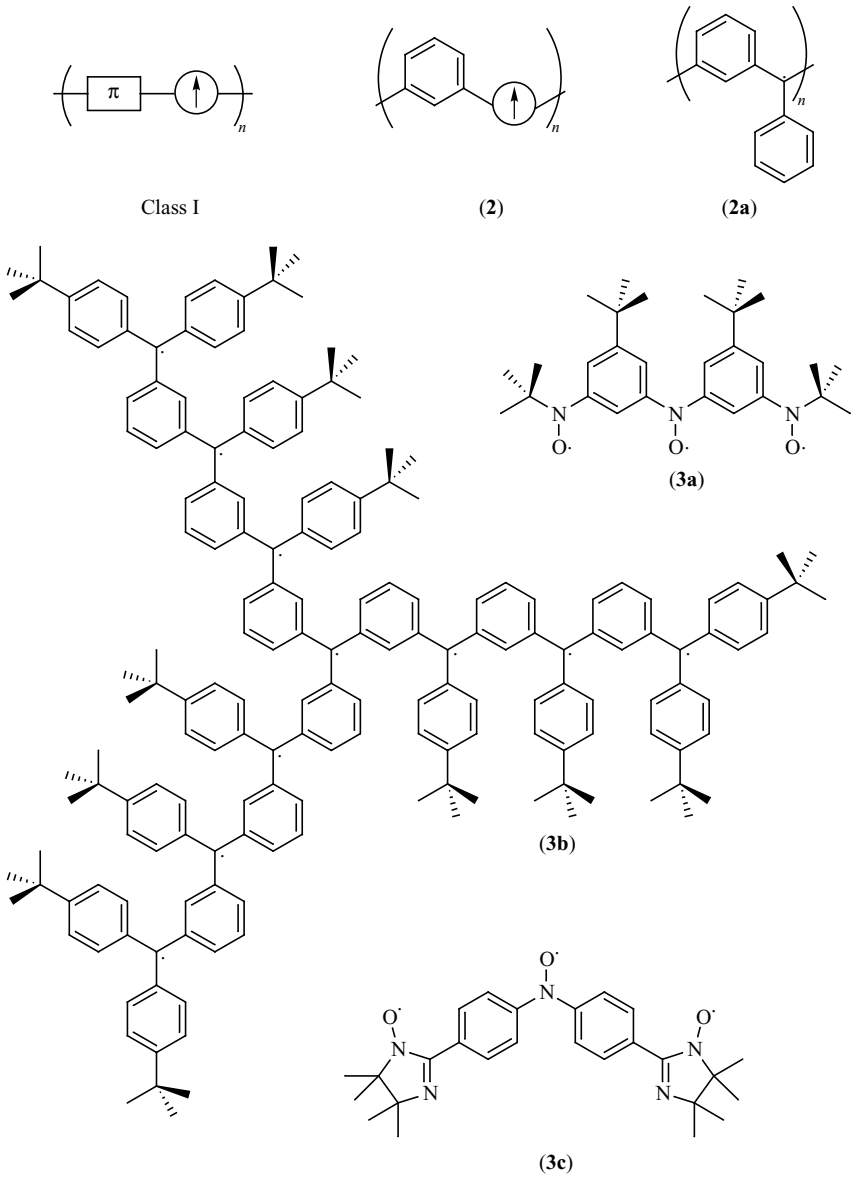

Fig. 2. Selected linear and branched neutral polyradicals with *m*-phenylene-like connectivities.

Linear polyarylmethyl polymer **2a** was prepared from the corresponding hydrocarbon with degree of polymerization (DP) of about 30. Magnetic studies showed an average value of $S \approx 2$; the radical concentration was not determined (17). The star-shaped model molecules had much higher values of S, eg, $S = 5$ for **3b**; oligoradicals **3** could be much better characterized compared to polymers **2** (Fig. 2) (18). Extension of star-shaped connectivity to dendrimers was not successful in improving the values of S (19).

While moderately sterically hindered polyarylmethyls can be handled in solution at low temperatures, the isoelectronic aminium radical cations and boride radical anions may offer stability at room temperature. However, such highly charged species may exist as complicated, medium-dependent oligomeric aggregates in solution. It is not uncommon that such intermolecular dimers and oligomers are diamagnetic, leading to overall very low radical concentrations. Nevertheless, the general idea of generating spin carrying polyradical polyions connected via *m*-phenylenes (or other ferromagnetic couplers) has attracted considerable interest ("polaronic ferromagnet") (20) (Fig. 3).

Electron spin resonance (ESR) spectra for disodium diboride (**4**) suggest triplet ($S = 1$) ground state or near degeneracy between the singlet and the triplet states; however, the resonance positions are highly solvent and counterion dependent (21). Such a complicated behavior for a simple diradical suggests that this system is not a promising candidate for magnetic polymers.

Bushby reported several aminium-based polymers (22). Polyamine **5a** ($M_w > 10^4$, GPC) was prepared by Suzuki reaction based polymerization, and then p-doped with antimony pentachloride. The resultant polyaminium polymer **5b** had radical concentration of ~0.5 radical/unit and an average value of $S \approx 4$ (22). The ferromagnetic coupling was rather weak, as expected for extended exchange pathway of *m*-phenylene with two *p*-phenylene spacers (Fig. 3).

ESR studies of numerous model aminium-based small monodisperse oligomers, eg, **6** and **7**, were reported in the past few years (Fig. 3) (23,24). For dications and trications, $S = 1$ and $S = 3/2$ states were detected (25–32). The $S = 3/2$ and $S = 1$ ground states for **6a** and **7b** were determined via spin nutation spectroscopy and magnetization study, respectively (Fig. 3) (24,32). For selected di- and trications bearing *p*-phenylenediamino-based radical cations, preliminary measurements of magnetic susceptibility using Evans NMR method suggested the low spin ground states ($S = 0$ and $S = 1/2$), though detailed studies with respect to medium and concentration effects for these highly charged species are needed (25–28). The $S = 1$ and $S = 3/2$ states were also detected for di- and trications derived from ylids **8a** and **8b**, respectively (Fig. 3) (33). There were reports of functionalized poly(*m*-aniline)s oxidized to the corresponding polyaminiums and polynitroxides; however, only values of $S \leq 1$ were obtained and, typically, radical concentrations were poor (34,35).

The radical cation based polymers and oligomers described in the previous section may be viewed as possessing very compact radical ions, centered on boron or nitrogen. An alternative approach is to use short, readily dopable fragments of π-system, which are linked together with *m*-phenylene couplers into a conjugated polymer. The representative examples of such polymers and oligomers, reported by Dougherty and co-workers, are p-doped polyacetylene-based **9**, p-doped heterocyclic-based **10**, and electrochemically n-doped fuchsone-based **11** (36,37) (Fig. 4). Polymers **9** and **10** (DP = 15–30) and polydisperse oligomer **11** (DP ≈ 7) were obtained using polymerizations based upon Suzuki coupling or Wittig reaction. For **9** and **10**, chemical p-doping (I_2 or AsF_5) gave polyradicals with very low radical concentrations (0.002–0.18 radical/unit) and an average value of $S = 1/2$ to 3, at low temperatures. Studies of model oligomers, *m*-phenylene connected bithiophenes and bipyrroles, revealed that radical cations form diamagnetic dimers, as expected from previous reports on conducting polymers and oligomers by Miller

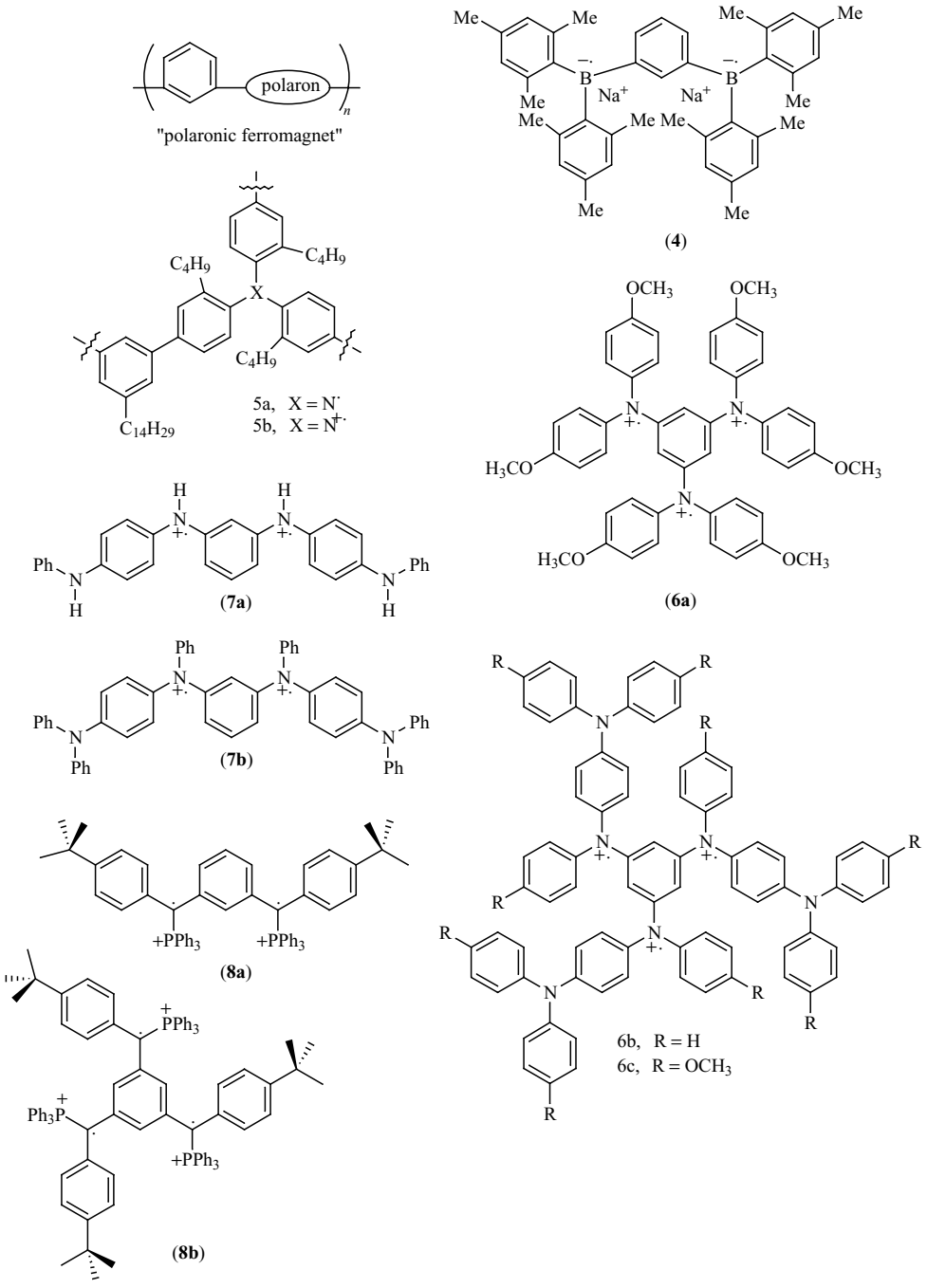

Fig. 3. Selected boron- and nitrogen-centered polaronic polyradicals.

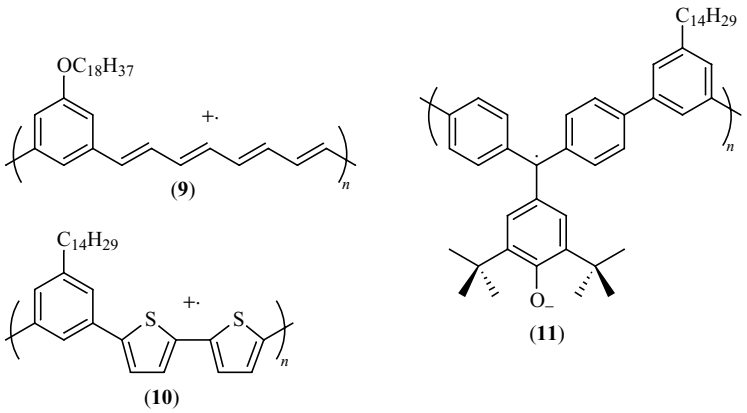

Fig. 4. Selected polaronic polyradicals with delocalized polarons.

and co-workers (38); this behavior is detrimental to attaining high concentration of radicals or large values of S in p-doped polymers (39). For oligomer **11**, better-controlled electrochemical n-doping is allowed to reach radical concentrations of 0.5 radical/unit. Average values of $S \approx 2$ are reasonable in view of DP and radical concentration for **11**; the temperature dependence of magnetic moment vs temperature is also consistent with the expected strength of ferromagnetic coupling in this oligomer. Overall, oligomer **11** and Bushby's polymer **5b** are perhaps the most promising systems for "polaronic ferromagnet."

Considering difficulties involved in efficient generation and characterization of polyradicals based upon radical ions, neutral radicals remain the most appealing source of spin. Further improvements in through-bond ferromagnetic coupling in polymers were guided by the studies on model monodisperse polyarylmethyls (40). In polymers **12** and **13**, calix[4]arene macrocycles are linked with bis(biphenylene)methyls (Fig. 5). Polymer **12**, which was obtained from the corresponding poly(arylmethylether) with $M_w = 30$ kDa (MALS), had radical concentration of 0.4–0.6 radical/triarylmethyl and an average $S \approx 18$. The branching and/or cross-linking of calix[4]arene macrocycles lead to further improvements in value of S. Polymers **13**, which were obtained from the benzene soluble fractions of the corresponding poly(arylmethylether)s with $M_w = 300$–500 kDa, had an average $S > 40$ (41). Magnetic properties of polymers **13**, which were prepared from benzene insoluble fractions of the poly(arylmethylether)s, depended on polymerization time beyond the gel point. When polymerization is stopped near the gel point, polymer **13** had $S = 600$–1500; for longer polymerization time $S = 3000$–7000 was obtained. The radical concentrations for polymers **13** were approximately 0.5 radical/triarylmethyl (12).

For the first time in a conjugated organic polymer, magnetic properties beyond simple paramagnetism were observed in polymer **13**. The onset of magnetic ordering is observed near the temperature of 10 K for a typical sample with $S \approx 5000$. Overall, the magnetic properties of polymer **13** are between insulating spin glasses and blocked superparamagnets, but closer to spin glasses. The soft magnetic behavior in polymer **13** is similar to the known small molecule based organic magnets, though the ordering temperature in polymer **13** is relatively high (6–8).

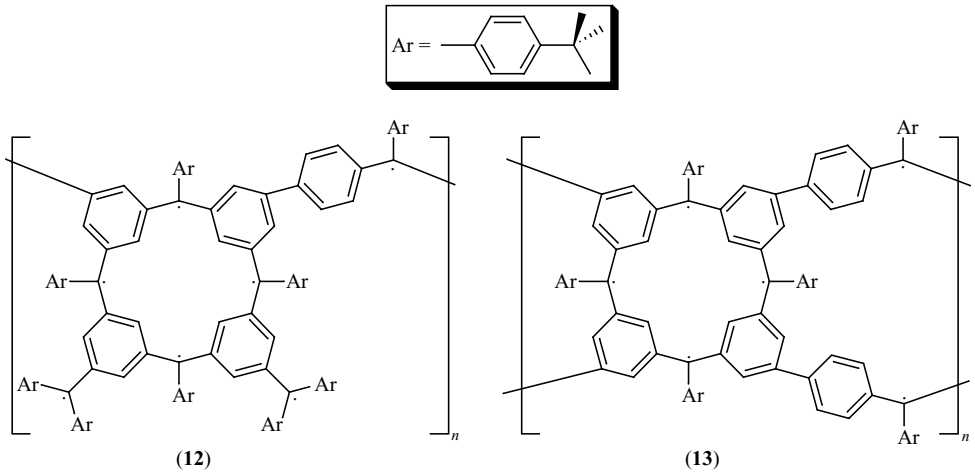

(**12**) (**13**)

Fig. 5. Calix[4]arene-based polyarylmethyl polymers.

Class II Polyradicals

Conjugated linear polymers, bearing multiple radicals as pendant groups, include several common π-systems as their conjugated backbones. Polyacetylene **14**, polydiacetylene **15**, various poly(arylene)s **16**, poly(aryleneethynylene)s **17**, and poly(arylvinylene)s **18** are among the leading examples (Fig. 6). Neutral stable radicals, such as phenoxyl, nitroxide, and nitronyl(nitroxide), are the most common pendant groups. Regioselective, typically head-to-tail, polymerizations are employed to attain the connectivity of the π-system, which is compatible with the ferromagnetic coupling. One of the advantages of pendant polymers is relatively straightforward synthesis.

Polyacetylene-based pendant polyradicals **14** were reported in late 1980s and early 1990s, as summarized in a recent review by Nishide and Kaneko (42). In

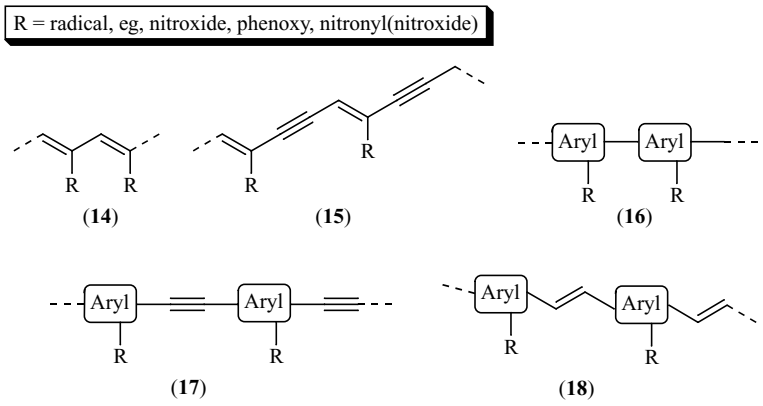

(**14**) (**15**) (**16**)

(**17**) (**18**)

Fig. 6. Polymers bearing radical pendants.

polyacetylenes, connectivity of non-Kekule π-system compatible with ferromagnetic coupling may be obtained by the attachment of conjugated pendant radical at the every other carbon of the polyene backbone (Fig. 6). Molecular weights (reported as either M_n or M_w) for many of such polymers were in the 10–100 kDa range, even for relatively bulky pendant groups, eg, galvinoxyl and diarylnitroxide. Although the radical concentrations were above 0.5 radical/unit in selected polymers, no ferromagnetic coupling was observed in any of the polyacetylene-based polymers (42). Most likely, severe out-of-plane twisting of the polyacetylene backbone, caused by the bulky radical pendants, prevents any significant exchange interactions (42). The magnetic properties of polymers **14** were compatible with $S = 1/2$ paramagnets (ie, independent, noninteracting spins-1/2).

Poly(diacetylene)-based polymers **15** (Fig. 6) were also studied but even for well-designed examples, such as polymers of 2-chloro-5-butadiynylphenyl *tert*-butylnitroxide, only low concentration of intact radicals were obtained, resulting in predominantly $S = 1/2$ paramagnetic behavior (43).

Availability of regioselective methods for polymerization of 3-substituted thiophenes and the efficient π-conjugation in the resultant polymers suggest that polythiophenes with radical pendant groups at 3-position are especially promising candidates for attaining polyradicals with $S > 1/2$ (44). Recently, three syntheses of poly[3-(3′,5′-di-*tert*-butyl-4′-oxyphenyl)thiophene] (**16a**) were reported (45–47) (Fig. 7). The $FeCl_3$-mediated and the Ni-catalyzed polymerizations of 3-(3′,5′-di-*tert*-butyl-4′-trimethysiloxyphenyl)thiophene and 2,5-dibromo-3-(3′,5′-di-*tert*-butyl-4′-trimethysiloxyphenyl)thiophene as monomers, respectively, gave polymers with M_w of 13 kDa (light scattering). However, the resultant polythiophenes lacked regioregularity and the magnetic characterization of corresponding polyradicals was lacking (45). Analogous $FeCl_3$-mediated polymerizations of 3-(3′,5′-di-*tert*-butyl-4′-methoxyphenyl)thiophene and 3-(3′,5′-di-*tert*-butyl-4′-methyloxymethoxyphenyl)thiophene gave only short oligomers (DP ≈ 6). Although the regioregularity was attained, the magnetic characterization of the corresponding polyradical (value of S, exchange interactions, yield of radicals) was not reported (46). Most recent $FeCl_3$-mediated polymerizations of 3-(3′,5′-di-*tert*-butyl-4′-acetoxyphenyl)thiophene gave polythiophenes with $M_n \approx 10$ kDa (GPC) and regioregularity reaching 96%. Although the radical concentration of 0.3 radical/unit was rather low, the average value of $S \approx 1$ was determined at cryogenic temperatures. Numerical fitting of the magnetic susceptibility data indicated a modest ferromagnetic coupling, which is comparable to that in a triplet ground state diradical with $\Delta E_{ST}/R \approx 100$ K (47). Similarly prepared poly(3-phenylgalvinoxylthiophene) (**16b**) had $M_n > 10$ kDa (GPC) and head-to-tail content of about 90% (Fig. 7). An excellent radical concentration of 0.9 radical/unit was attained but only $S = 1/2$ paramagnetic behavior was found (48). This is compatible with almost complete localization of spin density on the galvinoxyl moiety in the model monoradical **19** (48) (Fig. 7). Polythiophenes **16a** and **16b** doped with iodine showed a modest electrical conductivity (10^{-5} S·cm^{-1}) (47,48).

Another recent example of pendant poly(arylene) is poly(1,3-phenylene) (**16c**) (Fig. 7) (49). The Pd-catalyzed polymerization of *N*-*tert*-butyl-2,4-dibromoaniline and 1,3-phenylenebis(trimethylene boronate) gave poly(1,3-phenylene) with the DP of about 18 (GPC); oxidation of pendant secondary *tert*-butyl amine groups to the corresponding nitroxides yielded polymer **16c** with the radical concentration of

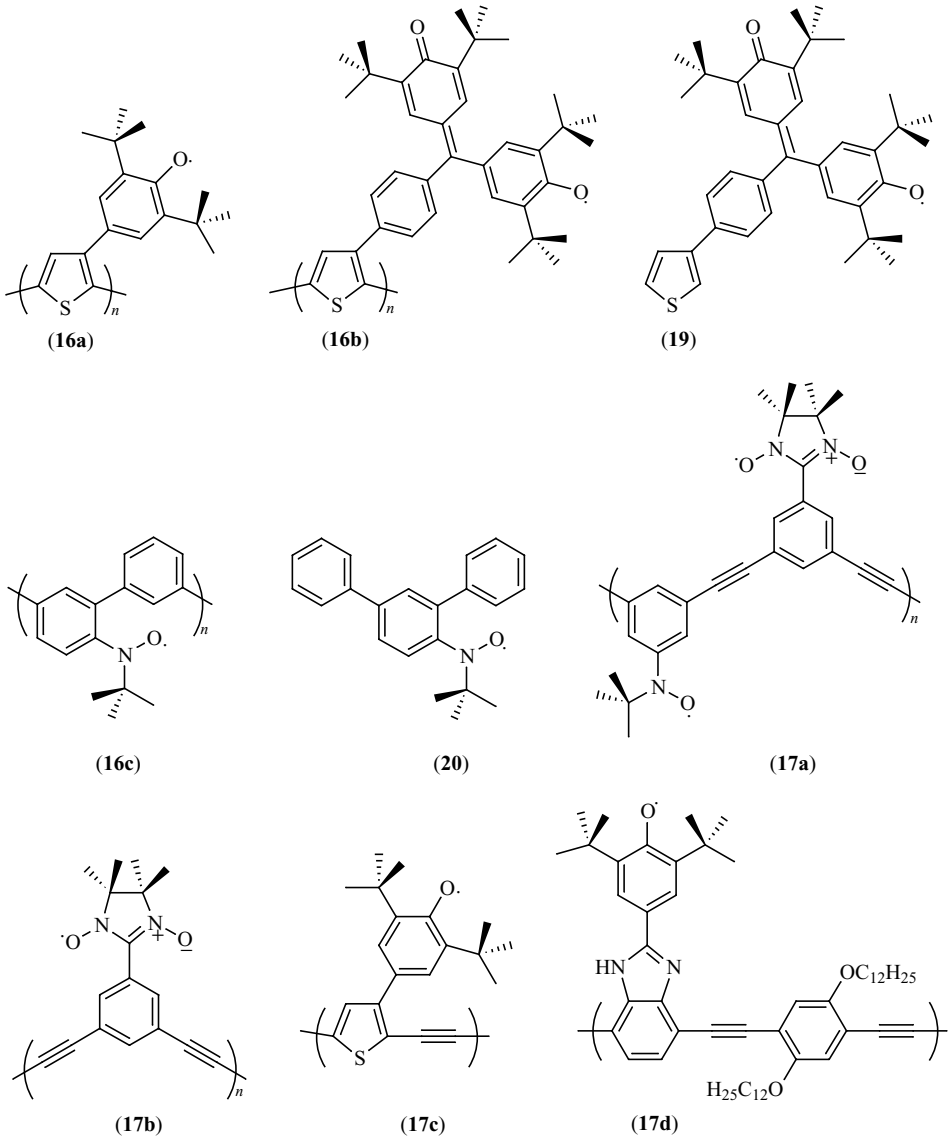

Fig. 7. Selected poly(arylene)s and poly(aryleneethynylene)s bearing radical pendants.

0.8 radical/unit. The X-ray crystallographic analysis of the model monoradical, *N*-*tert*-butyl-*N*-(2,4-diphenylphenyl)nitroxide (**20**) (Fig. 7), showed that the dihedral angle between the nitroxide moiety and the adjacent benzene ring is about 70°. This suggested that out-of-plane twisting of the pendant group might explain the failure to detect ferromagnetic coupling in polymer **16c** (49).

Various poly(aryleneethynylene)s **17** were recently reviewed by Miura (34). Because of mild reaction conditions for Pd-catalyzed C(sp)—C(sp^2) couplings, the polymerizations leading to poly(1,3-phenyleneethynylene)s **17a** may be carried

out with selected radical monomers, based upon stable radicals such as nitroxides and nitronyl(nitroxides) (Fig. 7). Even with the M_n values of 1–10 kDa and radical concentrations of about 0.8 radical/unit, no ferromagnetic coupling was detected (34). Similarly, the oxidative C(*sp*)—C(*sp*) couplings can be carried out on nitronyl(nitroxide) monomers, leading to poly(phenylenediethynylene)s with nitronyl(nitroxide) pendants **17b** (Fig. 7) (34,50). Poly(aryleneethynylene)s with phenoxyl-based pendant radicals **17c** and **17d** were prepared by polymerization of the corresponding phenol-based monomers, followed by oxidation of pendant phenols to phenoxyls (Fig. 7) (51,52). The M_n values of 1–10 kDa (GPC) were reported for the pendant-phenol polymers; however, no meaningful magnetic characterization was described for the corresponding polyradicals **17c** and **17d** (51,52).

Nishide and Kaneko reviewed numerous linear head-to-tail linked poly(1,4-phenylenevinylene)s and poly(1,2-phenylvinylene)s with pendant phenoxyls, nitroxides, galvinoxyls, and nitronyl(nitroxides) (42). For most of their polymers, molecular weights were in the 1–10 kDa range, radical concentrations were at about 0.5+ radical/unit level, and, most importantly, magnetic susceptibility measurements on neat powders revealed ferromagnetic couplings (42). The best example of such polymer was phenoxyl-based poly(1,2-phenylvinylene) (1,2-PPV) (**18a**) reported by Nishide and Lahti (53) (Fig. 8). Polymer **18a** had DP $\approx$ 17, radical concentration of $\sim$0.7 radical/unit, and an average value of $S \approx 2$ (53). For both polymer (**18b**) and the corresponding model triplet ground state diradicals (**21** and **22**), ferromagnetic couplings were measured; eg, $\Delta E_{ST}/R \approx 70$ K in **21** became only about 9 K in **22** (Fig. 8) (53). This suggested that polymer **18a** is very sensitive to defects, ie, pendant groups missing phenoxyl radical are likely to interrupt the through-bond ferromagnetic coupling.

In an attempt to increase the strength of ferromagnetic coupling, 1,2-PPV with 3,5-bearing phenoxyl radical pendants **18b** was prepared (Fig. 8). However, only oligomers with DP $\approx$ 4 and radical concentration of 0.5 radical/unit were obtained; their average value of $S \approx 1$ was disappointingly low (54). Although *m*-phenylene adequately mediates ferromagnetic coupling between phenoxyls (55), the model tetraradical **23** with the $S = 2$ ground state could not be prepared; magnetic studies of **23** revealed the radical concentration and an average value that are both similar to that of polymer **18b** (Fig. 8) (55).

Branched topologies of PPV backbone provide increased values of DP and S, compared to their linear chain counterparts. Branched polymer **24** had DP $\approx$ 70, radical concentration of 0.6 radical/unit, and an average value of $S \approx 7/2$ (Fig. 8) (56). Polymer **25** had $M_w \approx 32$ kDa (LS, 90 phenolic units), radical concentration of 0.4 radical/unit, and an average value of $S \approx 5$ (Fig. 8) (57).

Phenoxyl-based 1,2-PPVs, such as **18a**, **24**, **25**, are the most effective in mediating ferromagnetic coupling among all pendant polymers. Although the values of S for the best Class II polyradicals are still rather modest, their cross-linking via controlled incorporation of macrocycles should provide a very promising approach toward magnetic polymers (12,41,58). Another interesting course of study involves polaronic pendant polymers, as illustrated by model compounds **26** and **27**. Sugawara and co-workers prepared numerous model di- and triradicals that consist of a neutral radical(s) attached to a radical cation π-system (59–61). For example, in triradical **26**, the neutral nitronyl(nitroxide) pendants are connected

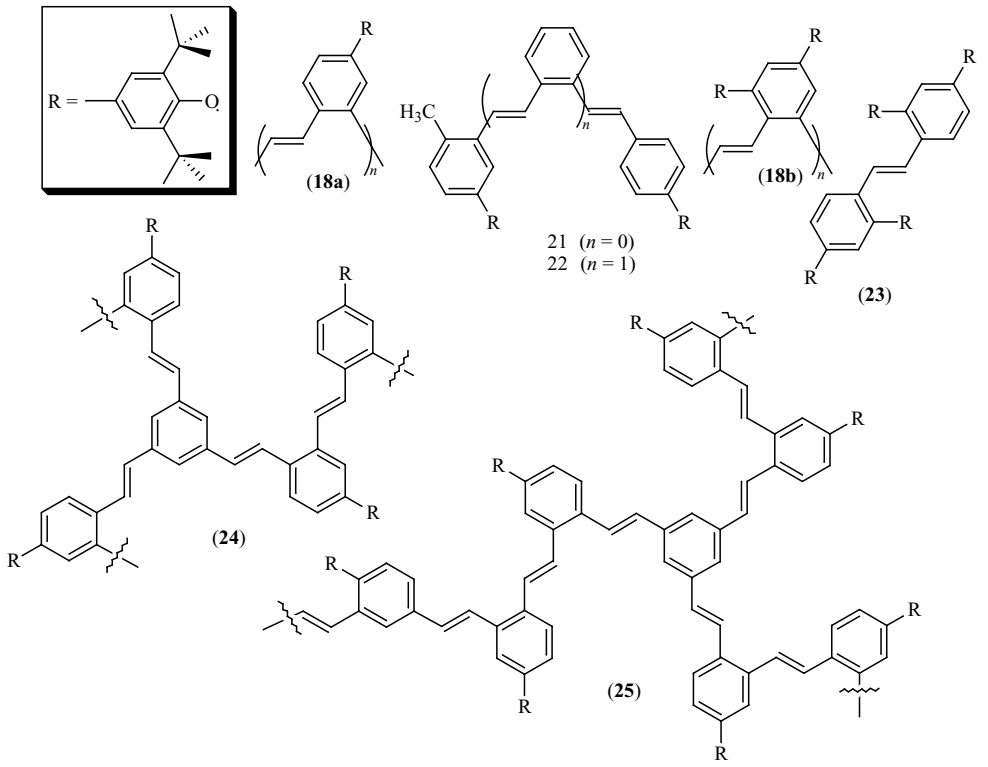

Fig. 8. Selected poly(1,2-phenylenevinylene)s bearing phenoxyl pendants.

to the polaronic (radical cation) thianthrene backbone (59). An alternative design was illustrated by van Meurs and Janssen; eg, in diradical **27**, the polaronic (radical cation) pendants are attached to the neutral 1,4-PPV backbone (62) (Fig. 9).

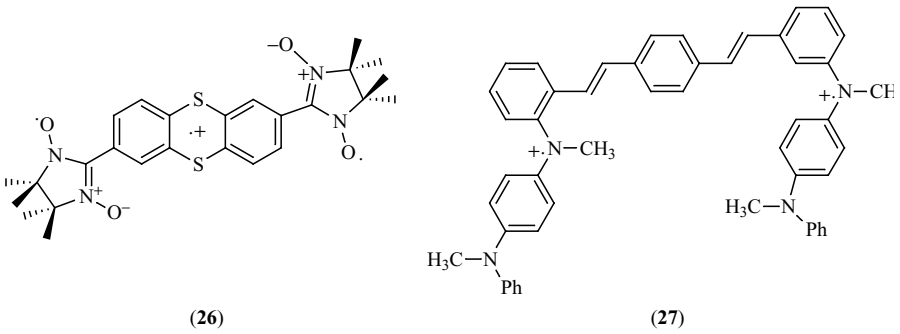

Fig. 9. Model triradical and diradical for polaronic pendant polymers.

Outlook

Among numerous designs for magnetic polymers explored so far, only a recently prepared highly cross-linked polyarylmethyls **13** showed magnetic ordering. The temperature of about 10 K, below which magnetic ordering was found, is relatively high among organic magnets. This suggests that the polymer approach to organic magnetism is very promising.

For a practical organic polymer magnet, both chemical stability and magnetic ordering at ambient conditions are important. However, polyarylmethyl-based polymer **13** has to be handled below 170 K and under oxygen-free atmosphere. Analogues of polymer **13**, where arylmethyls are replaced with ambient stable radicals, may provide the desired stability. Increase in temperature for magnetic ordering by more than an order of magnitude will require novel designs for magnetic polymers.

BIBLIOGRAPHY

"Magnetic Polymers" in *EPSE* 2nd ed., Suppl. Vol., pp. 446–455, by H. Ishida, Case Western Reserve University.

1. A. Aharoni, *Introduction to the Theory of Ferromagnetism*, 2nd ed., Oxford, Oxford, 2000.
2. B. Z. Tang, Y. Geng, Q. Sun, X. X. Zhang, and X. Jing, *Pure Appl. Chem.* **72**, 157–162 (2000).
3. A. Caneshi, D. Gatteschi, and P. Rey, *Progr. Inorg. Chem.* **39**, 331–429 (1991).
4. H. Iwamura, K. Inoue, and N. Koga, *New J. Chem.* 201–210 (1998).
5. J. S. Miller and A. J. Epstein, *Angew. Chem., Int. Ed.* **33**, 385–415 (1994).
6. M. Kinoshita, in H. S. Nalva, ed., *Handbook of Organic Conductive Molecules and Polymers*, Vol. **1**, John Wiley & Sons, Inc., New York, 1997, Chapt. "15", pp. 781–800.
7. P.-M. Allemand, K. C. Khemani, A. Koch, F. Wudl, K. Holczer, S. Donovan, G. Gruner, and J. D. Thompson, *Science* **253**, 301–303 (1991).
8. B. Narymbetov, A. Omerzu, V. V. Kabanov, M. Tokumoto, H. Kobayashi, and D. Mihailovic, *Nature* **407**, 883–885 (2000).
9. N. Mataga, *Theor. Chim. Acta* **10**, 372–376 (1968).
10. A. Rajca, *Chem. Rev.* **94**, 871–893 (1994).
11. P. M. Lahti, ed., *Magnetic Properties of Organic Materials*, Marcel Dekker, New York, 1999.
12. A. Rajca, J. Wongsriratanakul, and S. Rajca, *Science* **294**, 1503–1505 (2001).
13. A. Rajca, J. Wongsriratanakul, S. Rajca, and R. Cerny, *Angew. Chem., Int. Ed.* **37**, 1229–1232 (1998).
14. H. Iwamura and N. Koga, *Acc. Chem. Res.* **26**, 346–351 (1993).
15. A. Rajca, J. Wongsriratanakul, and S. Rajca, *J. Am. Chem. Soc.* **119**, 11674–11686 (1997).
16. J. S. Miller, *Adv. Mater.* **4**, 298, 435 (1992).
17. S. Utamapanya, H. Kakegawa, L. Bryant, and A. Rajca, *Chem. Mater.* **5**, 1053–1055 (1993).
18. A. Rajca, S. Utamapanya, and S. Thayumanavan, *J. Am. Chem. Soc.* **114**, 1884–1885 (1992); M. Tanaka, K. Matsuda, T. Itoh, and H. Iwamura, *J. Am. Chem. Soc.* **120**, 7168–7173 (1998); T. Ishida and H. Iwamura, *J. Am. Chem. Soc.* **113**, 4238–4241 (1991).

19. A. Rajca and S. Utamapanya, *J. Am. Chem. Soc.* **115**, 10688–10694 (1993).
20. H. Fukutome, I. Takahashi, and M. Ozaki, *Chem. Phys. Lett.* **133**, 34–38 (1987).
21. A. Rajca, S. Rajca, and S. R. Desai, *Chem. Commun.* 1957–1958 (1995).
22. R. J. Bushby and D. Gooding, *J. Chem. Soc., Perkin II* 1069–1075 (1998); R. J. Bushby, D. R. McGill, K. M. Ng, and N. Taylor, *J. Chem. Soc. Perkin Trans II* **7**, 1405–1414 (1997).
23. S. C. Blackstock and T. D. Selby, in Ref. 11, Chapt. 9, pp. 165–178.
24. M. M. Wienk, Ph.D. dissertation, Technische Universiteit Eindhoven, 1997.
25. K. R. Stickley, T. D. Selby, and S. C. Blackstock, *J. Org. Chem.* **62**, 448–449 (1997).
26. T. D. Selby, K. R. Stickley, and S. C. Blackstock, *Org. Lett.* **2**, 171–174 (1999).
27. T. D. Selby and S. C. Blackstock, *Org. Lett.* **2**, 2053–2055 (1999).
28. T. D. Selby and S. C. Blackstock, *J. Am. Chem. Soc.* **121**, 7152–7153 (1999).
29. S. I. Hauck, K. V. Lakshmi, and J. F. Hartwig, *Org. Lett.* **2**, 2057–2060 (1999); A. Ito, Y. Ono, and K. Tanaka, *Angew. Chem., Int. Ed.* **38**, 1072–1075 (1999); A. Ito, A. Taniguchi, T. Yamabe, and K. Tanaka, *Org. Lett.* **2**, 741–743 (1999).
30. M. M. Wienk and R. A. J. Janssen, *Chem. Commun.* 267–268 (1996).
31. M. M. Wienk and R. A. J. Janssen, *J. Am. Chem. Soc.* **118**, 10626–10628 (1996).
32. K. Sato, M. Yano, M. Furuichi, D. Shiomi, T. Takui, K. Abe, K. Itoh, A. Higuchi, K. Katsuma, and Y. Shirota, *J. Am. Chem. Soc.* **119**, 6607–6613 (1997).
33. M. M. Wienk and R. A. J. Janssen, *J. Am. Chem. Soc.* **119**, 5398–5403 (1997).
34. Y. Miura, in Ref. 11, Chapt. 13, pp. 267–284.
35. A. Ito, H. Ino, K. Tanaka, K. Kanemoto, and T. Kato, *J. Org. Chem.* **67**, 491–498 (2002).
36. M. M. Murray, P. Kaszynski, D. A. Kaisaki, W. Chang, and D. A. Dougherty, *J. Am. Chem. Soc.* **116**, 8152–8161 (1994).
37. K. K. Anderson and D. A. Dougherty, *Adv. Mater.* **10**, 688–692 (1998).
38. L. L. Miller and K. R. Mann, *Acc. Chem. Res.* **29**, 417–423 (1996).
39. J. A. E. H. van Haare, M. van Boxtel and R. A. J. Janssen, *Chem. Mater.* **10**, 1166–1175 (1998).
40. A. Rajca, *Chem. Eur. J.*, in press.
41. A. Rajca, S. Rajca, and J. Wongsriratanakul, *J. Am. Chem. Soc.* **121**, 6308–6309 (1999).
42. H. Nishide and T. Kaneko, in Ref. 11, Chapt. 14, pp. 285–303.
43. K. Inoue, N. Koga, and H. Iwamura, *J. Am. Chem. Soc.* **113**, 9803–9810 (1991).
44. R. D. McCullough and R. D. Lowe, *Chem. Commun.* 70–72 (1992); T. A. Chen, X. Wu, and R. D. Rieke, *J. Am. Chem. Soc.* **117**, 233–244 (1995).
45. T. Yamamoto and H. Hayashi, *J. Polym. Sci., Part A* **35**, 463–474 (1997).
46. C. Xie and P. M. Lahti, *J. Polym. Sci., Part A* **37**, 779–788 (1999).
47. M. Miyasaka, T. Yamazaki, E. Tsuchida, and H. Nishide, *Macromolecules* **33**, 8211–8217 (2000).
48. M. Miyasaka, T. Yamazaki, and H. Nishide, *Polym. J.* **33**, 849–856 (2001).
49. H. Oka, T. Tamura, Y. Miura, and Y. Teki, *J. Mater. Chem.* **9**, 1227–1232 (1999).
50. P. Swoboda, R. Saf, K. Hummel, F. Hofer, and R. Czaputa, *Macromolecules* **28**, 4255–4259 (1995).
51. H. Hayashi and T. Yamamoto, *Macromolecules* **30**, 330–332 (1997).
52. H. Hayashi and T. Yamamoto, *Macromolecules* **31**, 6063–6070 (1998).
53. H. Nishide, T. Kaneko, T. Nii, K. Katoh, E. Tsuchida, and P. M. Lahti, *J. Am. Chem. Soc.* **118**, 9695–9704 (1996).
54. H. Nishide, M. Miyasaka, R. Doi, and T. Araki, *Macromolecules* **35**, 690–698 (2002).
55. H. Nishide, R. Doi, K. Oyaizu, and E. Tsuchida, *J. Org. Chem.* **66**, 1680–1685 (2001).
56. H. Nishide, M. Miyasaka, and E. Tsuchida, *Angew. Chem. Int., Ed.* **37**, 2400–2402 (1998).
57. H. Nishide, T. Ozawa, M. Miyasaka, and E. Tsuchida, *J. Am. Chem. Soc.* **123**, 5942–5946 (2001).

58. H. Nishide, M. Takahashi, J. Takashima, Y.-J. Pu, and E. Tsuchida, *J. Org. Chem.* **64**, 7375–7380 (1999).
59. A. Izuoka, M. Hiraishi, T. Abe, T. Sugawara, K. Sato, and T. Takui, *J. Am. Chem. Soc.* **122**, 3234–3235 (2000).
60. J. Nakazaki, Y. Ishikawa, A. Izuoka, T. Sugawara, and Y. Kawada, *Chem. Phys. Lett.* **319**, 385–390 (2000).
61. H. Sakurai, A. Izuoka, and T. Sugawara, *J. Am. Chem. Soc.* **122**, 9723–9734 (2000).
62. P. J. van Meurs and R. A. Janssen, *J. Org. Chem.* **65**, 5712–5719 (2000).

ANDRZEJ RAJCA
University of Nebraska

MASS SPECTROMETRY. See Volume 3.

MECHANICAL TESTING. See MECHANICAL PERFORMANCE.

MELAMINE RESINS. See AMINO RESINS AND PLASTICS.

MEMBRANE TECHNOLOGY. See Volume 3.

METAL-CONTAINING POLYMERS

Introduction

The development of organometallic chemistry in the 1950s has played an important role in the redefinition of polymer chemistry. While organic and inorganic polymers (qv) were previously the only two classes of macromolecules, the introduction of metals into polymers marked the beginning of a new field of research (see INORGANIC POLYMERS). The combination of polymeric and metallic properties has caused a surging interest in the development of metal-containing polymers over the past few decades (1–5). It is well known that depending on the elements and the types of bonding present, the properties of these polymers differ dramatically. The degree of polymerization and the nature of the metal also have strong influences on the properties of polymeric materials. It is the diverse array of electrical, electrochemical, magnetic, optical, and catalytic properties that define the applications of metal-containing polymers.

In recent years, many reviews have been dedicated to advances in the field of metal-containing polymers (6–14). Although this article classifies these polymers according to their structures, many of these polymers could have been included in more than one section. The aim of this work is to give an overview of the synthesis, properties, and applications of metal-containing polymers, with a focus on the developments that have taken place over the past two decades.

Metals in Polymer Backbones, σ-Bonded Systems

Polymers with metals σ-bonded to organic spacers in their backbones have been studied in recent years because of their electrical and optical properties (14,15). This class of organometallic polymers can be prepared via reactions occurring

Encyclopedia of Polymer Science and Technology. Copyright John Wiley & Sons, Inc. All rights reserved.

at the metal center or at the ligand sites. Nickel complexes with bromo substituents (**2**) react with lithiated aromatic compounds (**1**) to yield the corresponding organonickel polymers (**3**) (eq. 1). The solubility of these polymers is low, and analysis of 3 indicates that their degree of polymerization is between 8 and 13 (16).

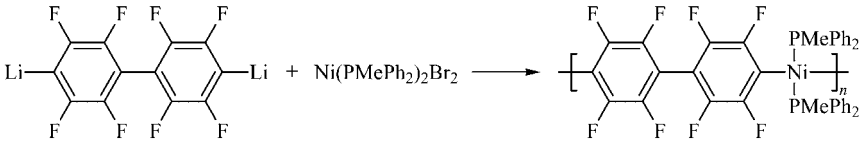

1 **2** **3** (1)

Many different transition metals have been incorporated into polymers containing C—C triple bonds in order to enhance metal $d\pi$–$p\pi^*$ back bonding, which is expected to contribute to π-electron delocalization (17–30). Although much of the research on organometallic acetylide polymers has dealt with Group 10 transition metals, the synthesis of acetylide polymers containing Ni (17), Pd (17–19), Pt (17,20–23), Fe (24,25), Ru (25,26), Os (25), Rh (23,27), Au (28,29), and Zr (30) has been reported. The incorporation of metals into polyynes generally results in materials with band gaps ranging from 2.4 to 3.2 eV, which is higher than that of many organic materials (<1 eV) (20). Lewis and co-workers demonstrated that incorporating alternating electron donor and acceptor groups into platinum acetylide polymers resulted in materials with band gaps below 2 eV (20). Equation 3 shows the synthesis of a rigid-rod iron acetylide polymer prepared via the reaction of a dichloro complex of iron (**4**) with a bistrimethylstannyl acetylide monomer (**5**), resulting in the formation of a conjugated polymer (**6**) with a weight average molecular weight of 173,000 (25).

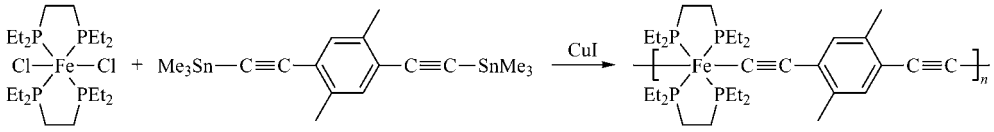

4 **5** **6** (2)

Reaction of terminal al kynes (**7**) with transition metal halides (**8**) in the presence of KOH has been used in the synthesis of gold-containing polymers (**9**) (28,29). It was found that the solubility of these polymers could be controlled through the choice of phosphine ligands at the gold centers.

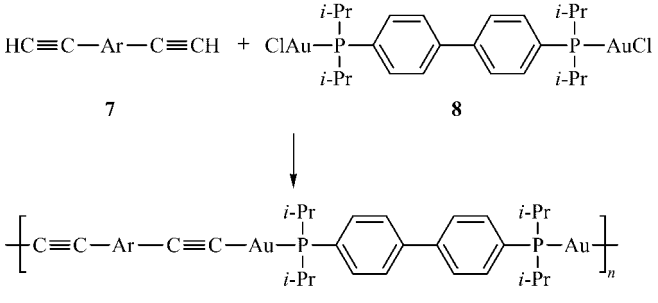

7 **8** **9** (3)

Oligomeric complexes containing metals σ-bonded and π-coordinated to organic groups have been prepared via palladium-catalyzed coupling reactions (24). The synthesis of zirconocene acetylene polymers (**12**) has been reported via the reaction (eq. 4) of bis(pentamethylcyclopentadienyl) zirconium(IV) dichloride (**10**) with dilithioacetylene or dilithiodiacetylene (**11**) R = C≡C or C≡C–C≡C (30). These polymers displayed poor solubility in organic solvents other than *n*-hexane, and their weight average molecular weights ranged from 55,000 to 68,000.

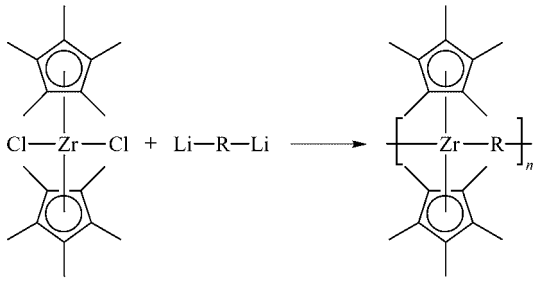

10 **11** **12** (4)

In 1973, the synthesis of titanium, zirconium, and hafnium polyesters via reaction of the dicyclopentadienylmetal dichloride complexes with disodium dicarboxylates in either aqueous or organic solvents was reported (31). Around the same time the synthesis of polyethers and amines of titanocene and polythioethers of zirconocene was also reported using similar methodologies (32,33).

Tilley and co-workers have reported the synthesis of polymers containing zirconacyclopentadiene rings in their backbones (34,35) (eq. 5). The zirconacyclopentadiene units were subsequently converted into organic functionalities while maintaining the integrity of the polymers. The synthesis of polymers containing cobaltacyclopentadiene groups within their backbones has also been investigated (36–39).

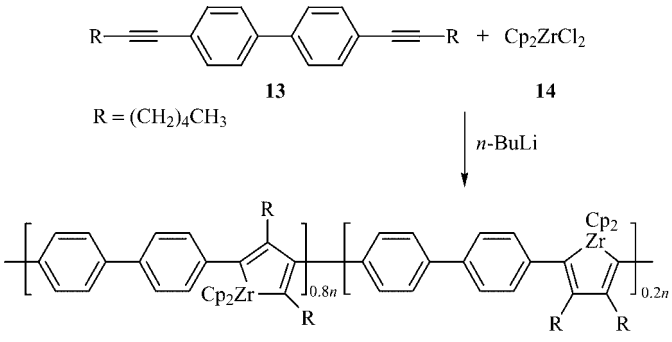

15 (5)

Polymers with Metal–Metal Bonds

Polymers with M—M bonds represent a relatively unexplored area of organometallic polymer chemistry. This is in part due to the instability of M—M bonds; however, such classes of photoreactive polymers are important in the design of degradable plastics and medical supplies as well as lithographic materials. Tyler and

co-workers have developed photochemically reactive polymers (**18**) via condensation reactions of monomers containing Fe—Fe or Mo—Mo bonds (**16**) with organic monomers such as diisocyanates (**17**) (40–43) (eq. 6). The resulting polymers could be photolyzed, resulting in cleavage of the metal–metal bonds.

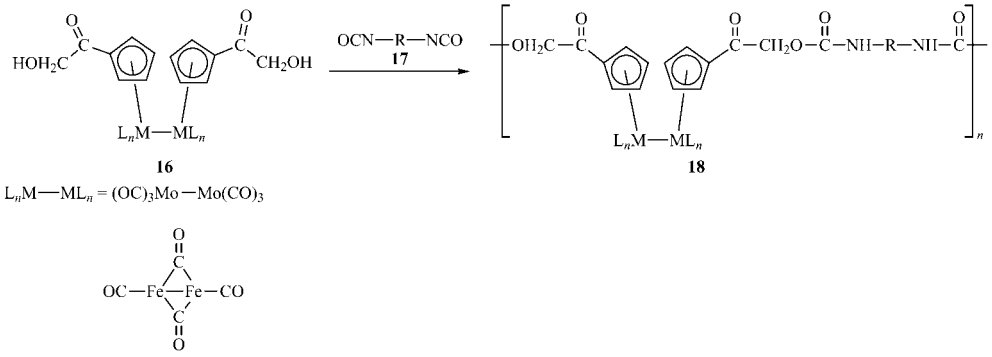

(6)

Cuadrado and co-workers have prepared a polymer with Fe—Fe bonds in its structure (**19**) via reaction of a polysiloxane with $Fe(CO)_5$ (44). The insoluble nature of this polymer indicated that cross-linking between polysiloxane chains occurred upon formation of the organoiron polymer. Silicon polymers containing Co—Co bonds (**20**) have been prepared via the reaction of $Co_2(CO)_8$ with the triple bonds of a silicon based polymer (45). Mixed metal systems were also described in which complexes containing arenes coordinated to chromium tricarbonyl were reacted with $Mo_2Cp_2(CO)_6$ or $Co_2(CO)_8$.

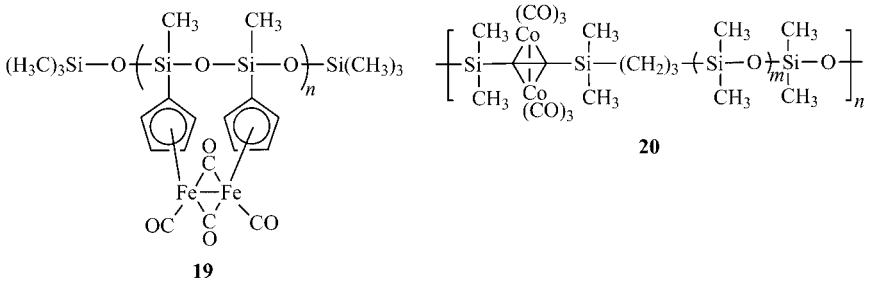

Polymeric materials containing Pt—Pt bonds in their backbones have been examined (46). The formation of platinum polymers (**23**) was achieved via reaction of the platinum complex (**21**) with diacetylides, diphosphines, or diisocyanides (**22**) (eq. 7).

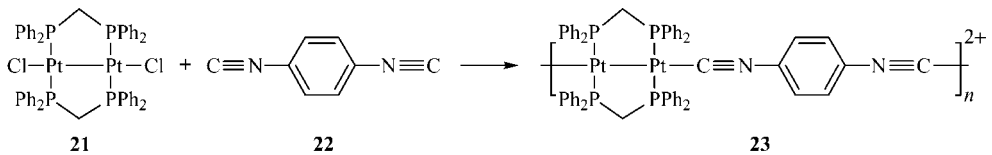

(7)

Polymers whose backbones consisted solely of metal–metal bonds have been synthesized by electrochemical reduction of ruthenium and osmium complexes (47,48). Reduction of $[M^{II}(trans\text{-}Cl_2)(bipy)(CO)_2]$ (M = Ru, Os) (**24**) to M^0 complexes generated a polymeric film (**25**) following loss of the *trans* chloride ligands (48) (eq. 8). Both the ruthenium- and osmium-based coordination polymers were selective for the reduction of carbon dioxide.

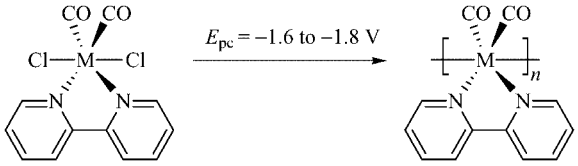

24 **25** (8)

Polymers containing metal–metal single (**26**) and multiple bonds (**27**) have also been prepared via reaction of bimetallic carboxylates with coordinating ligands (49–53). It has been found that polymeric materials containing Mo—Mo triple bonds crystallize from solutions of $Mo_2(O_2CCH_3)_4$ in bidentate ligands such as 1,2-bis(dimethylphosphino)ethane or tetramethylenediamine (53).

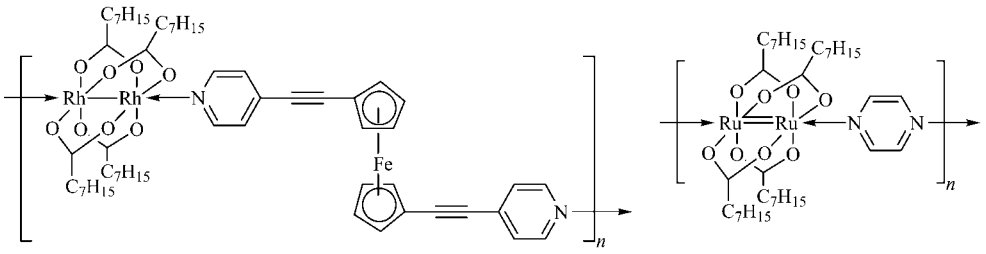

26 **27**

π-Coordinated Systems, Metallocene-Based Systems

Polymerization of ferrocene derivatives marked the beginning of a new era in polymer chemistry (54). In the early 1960s, Korshak and Nesmeyanov reported the synthesis of ferrocene-based polymers by reacting ferrocene with *tert*-butyl hydroperoxide (55,56). Neuse later reported that these polymers consisted of homoannular and heteroannular aliphatic ether-substituted units with number-average molecular weights less than 7000 (57). Methodologies using metal salts have also been implemented in the synthesis of polyferrocenylenes; however, these polymers had ambiguous structures and low molecular weights (58,59). The reaction of dihaloferrocenes with magnesium resulted in polyferrocenylenes with conductivities ranging from 10^{-2} to 10^{-4} S/cm (60–62). The conductivity of this crystalline polymer was higher than the conductivity of amorphous polyferrocenylene. In 1996, Nishihara and co-workers synthesized a soluble 1,1′-dihexylferrocene-based polymer and its electrochemical properties and photoconductivity were examined (63).

The synthesis and polymerization of a mercuriferrocene complex was reported in 1963 (64). Decomposition of this polymer gave 1,1′-diiodoferrocene or 1,1′-ferrocenedicarboxylic acid along with other products. It was later reported that poly(mercuriferrocenylene) could be converted to polyferrocenylene by reacting the poly(mercuriferrocenylene) with ferrocene at 245–260°C (65). Polymers prepared via reaction of ferrocenes functionalized with carboxylic acids, acid chlorides, alcohols, and amines have been utilized to synthesize condensation polymers containing ferrocenyl units in their backbones (54,66–69). In 1984, Rausch and co-workers reported the synthesis of polyamides and polyureas from the reaction of 1,1′-bis(β-aminoethyl)ferrocene (**28**) with diisocyanates (**29**) or diacid chlorides (**30**) (66) (eq. 9).

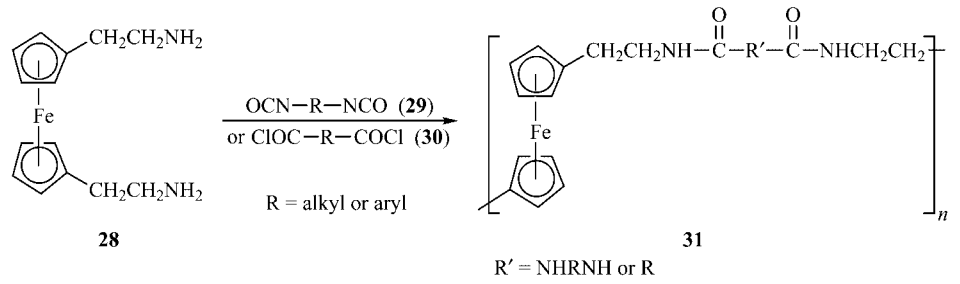

28 **31**

R′ = NHRNH or R

(9)

More recently, a soluble polymer (**32**) was prepared via reaction of 1,1′-ferrocenedimethanol with 4,4′-biphenyltetraamine in the presence of $[RuCl_2(P(C_6H_5)_3)_3]$ (70). Approximately 20% of the iron centers were found to be in the Fe(III) state as a result of oxidation by ruthenium complexes formed during the polycondensation reaction. Wright and co-workers have reported the synthesis of ferrocene-based polymers possessing nonlinear optical properties (**33**) (71–73). These polymers were formed by polycondensation of a difunctionalized ferrocene monomer (71).

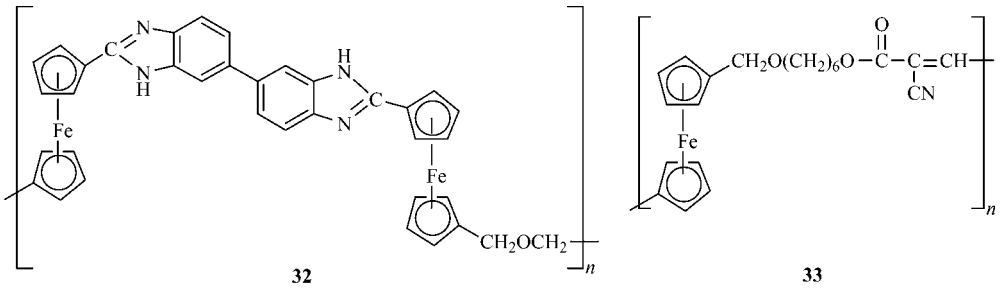

32 **33**

Like their isoelectronic ferrocene counterparts, cobaltocenium units are resistant to strong oxidizing agents and possess interesting electrochemical behavior. The synthesis of polyesters and polyamides containing cationic cobalt units in the main chain has been reported (32,74–76). Sheats and Carraher reported the synthesis of cobaltocenium polymers containing tin, antimony, titanium, and zirconium atoms in their backbone via the reaction of the dicarboxylic

acid complex of cobaltocenium with the corresponding organometallic monomers (32,75). Cuadrado and co-workers prepared polyamides containing siloxane bridges (**36**) via condensation of 1,1′-bis(chlorocarbonyl)cobaltocenium hexafluorophosphate (**34**) with a siloxane-based diamine (**35**) (76) (eq. 10). This polymer displayed very limited solubility in polar organic solvents; however, the analogous ferrocene-based polymer had an M_n value of 10,600 (77). These ferrocene-based polymers were utilized in the production of chemically modified electrodes.

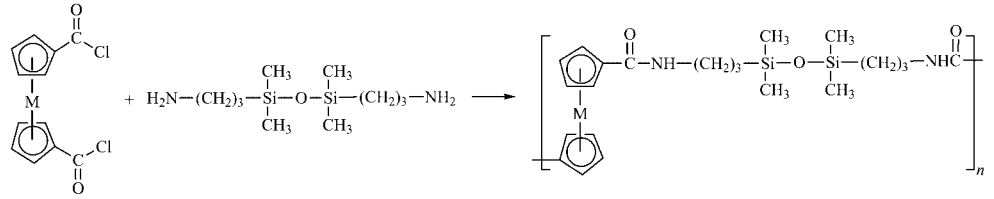

34 **35** **36**

M = Fe, $Co^+ PF_6^-$

(10)

The synthesis of conjugated polymers containing ferrocene units in their backbones has received much attention in recent years (78–81). Bochmann and co-workers have described the synthesis of ferrocene-based polymers via palladium-catalyzed coupling reactions of dihalide or divinyl functionalized ferrocene monomers with aromatic spacers (**37**) (78).

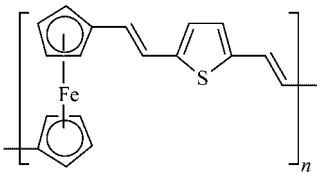

37

Conjugated polymers have also been prepared via reaction of dilithio bis(3-hexyl-4-methylcyclopentadienide)arylenes (**38**) with ferrous iodide (82). Using a similar strategy, poly(ferrocenylsilane) was prepared by reaction of the dilithium salt of dicyclopentadienyldimethylsilane (**38**, R = $Si(CH_3)_2$, R′, R″ = H) with ferrous chloride (83) (eq. 11).

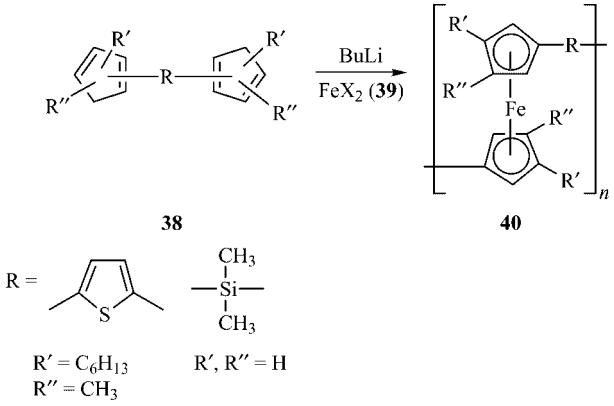

38 **40**

$R' = C_6H_{13}$, $R'' = CH_3$ R′, R″ = H

(11)

Reaction of 1,1′-ferrocenedithiol with diarylsilanes resulted in the formation of polymers containing sulfur–silicon bonds between the ferrocenyl units (84). These organometallic polymers exhibited good air and moisture stability. Ferrocene polymers containing disulfide linkages (**42**) have been synthesized by ring-opening polymerization (ROP) and desulfurization of [3]-trithiaferrocenenes (**41**) (85–87) (eq. 12). High molecular weight linear and network poly(ferrocene persulfides) were produced by reaction of the trithiaferrocenenes with $P(C_4H_9)_3$.

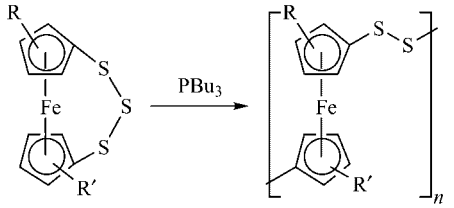

41 **42**

R, R′ = H, *n*-C_4H_9, *t*-C_4H_9 (12)

The ROP of [1]thia- and [1]selenaferrocenophanes has been accomplished thermally and in the presence of anionic initiators; however, the resulting polymers were insoluble (88). Methylation of the cyclopentadienyl rings of the [1]thiaferrocenophane, followed by ROP, allowed for the isolation of soluble poly(ferrocenyl sulfide). The cyclic voltammograms of these materials indicated the presence of two reversible oxidation processes, and it was found that these polymers possessed stronger Fe—Fe interactions than the analogous silicon-bridged materials (88). Polyferrocenes containing sulfide linkages were also prepared via thermal and cationic ROP of [2]carbathioferrocenophane (89).

Metallocenophanes containing hydrocarbon bridges have been polymerized thermally to give polymers containing insulating bridges between the cyclopentadienyl ligands (90–92) (eq. 13). It was found that if the R group in **43** was hydrogen, the resulting polymers were insoluble, whereas isomeric mixtures of **43** (R = CH_3) resulted in soluble polymetallocenes (**44**). Cyclic voltammetry of the poly(ruthenocenylethylenes) showed irreversible oxidation processes at 0.60 V, while poly(ferrocenylethylenes) underwent reversible oxidation processes at −0.27 V (92).

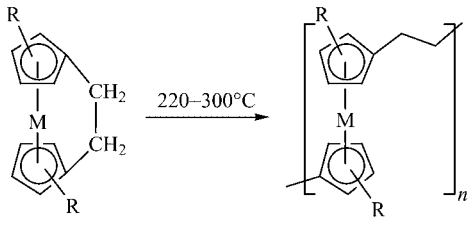

43 **44**

M = Fe, Ru
R = H, Me (13)

Ring-opening metathesis polymerization (ROMP) of ferrocenophanes containing bridging olefinic groups (**45**, **46** **48**) has been examined in order to synthesize conjugated ferrocene-based polymers (93–95). The polymers synthesized

from ROMP of **45–47** were all found to be insoluble; however, copolymerization of **45** with norbornene enhanced the solubility of this polymer and its M_w and M_n were 21,000 and 11,000, respectively (94). The polymer synthesized from ROMP of the alkyl functionalized monomer (**48**) had a weight-average molecular weight in excess of 300,000 (95). Cyclic voltammetry of poly(ferrocenylvinylene) formed from **45** showed two reversible redox waves ($\Delta E = 0.25$ V), indicating interactions between the iron centers. The homopolymer formed from ROMP of **45** was more conductive than polymers of **46** and **47** (93).

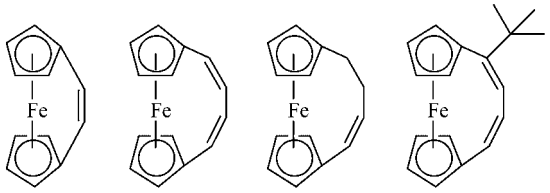

45 **46** **47** **48**

The synthesis and properties of poly(ferrocenylsilanes) have been extensively reviewed (7,11,96). Thermal, anionic, and transition-metal-catalyzed ROP of [1]silaferrocenophanes has led to the production of polymers containing a variety of functional groups attached to the silicon atoms (96–102). The structures and morphologies of this class of polymer have been examined using X-ray diffraction, optical, atomic force, and scanning electron microscopy as well as other techniques (103–107). Pannell and co-workers have recently tested these materials as coatings for tapered optical-fiber gas sensors (108).

Anionic polymerization of a silicon-bridged [1]ferrocenophane using C_4H_9Li allowed for the preparation of living polymers which could be copolymerized with a number of different monomers (109) (eq. 14). The number-average molecular weights of polymer **50** ranged from 7700 to 21,000. Block copolymers containing dimethylsiloxane, ferrocenyldimethylsilane, and styrene groups with M_n values as high as 60,000 (PDI = 1.28) were also synthesized. All of the homo- and copolymers had two redox couples in their cyclic voltammograms, which were separated by 0.27–0.29 V. Thermogravimetric analysis of these materials showed weight losses beginning around 310°C, while differential scanning calorimetry showed that their glass-transition temperatures ranged from 103 to −127°C (109). Ferrocenophanes containing phosphorus (110–115), tin (116,117), germanium (118), and boron (119) bridges have also been polymerized.

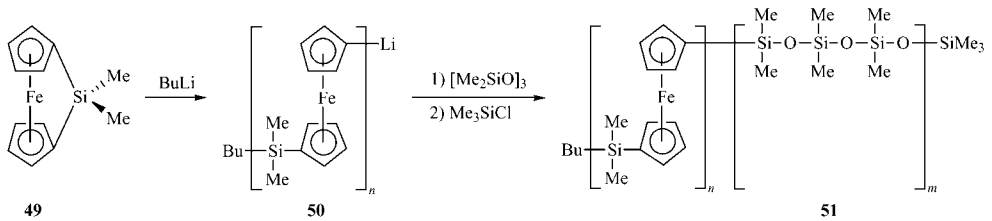

49 **50** **51**

(14)

Thermal ROP of the [1]chromarenophane (**52**) with the [1]ferrocenophane (**53**) led to the formation of copolymer **54** (eq. 15); however, ROP of **52** alone did

not allow for the isolation of the corresponding chromium polymer even though this monomer had significant ring strain (120).

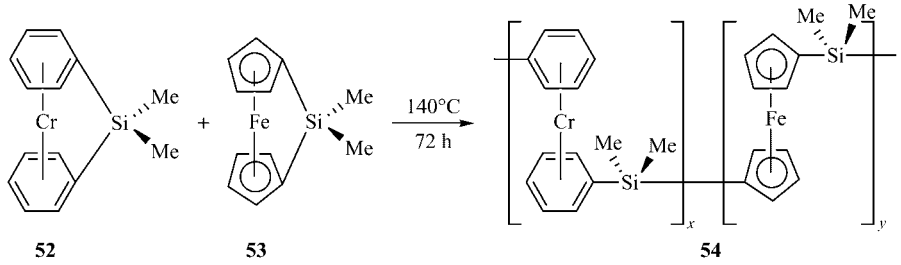

52 53 54

(15)

Multidecker transition metal complexes have been the focus of many investigations in light of their electrical and magnetic properties (121–126). Optically active cobalt-based systems have also been prepared by Katz and co-workers (126). Rosenblum and co-workers have described a number of different routes allowing for the generation of face-to-face polymetallocenes (121–123). One methodology involved the palladium-catalyzed cross-coupling reaction of 1,8-diiodonaphthalene with metallocenylzinc chloride (M = Fe, Ru) (122). High molecular weight, soluble face-to-face polymetallocenes were isolated by incorporating alkyl groups on the cyclopentadienyl rings (121–123). The face-to-face polyferrocene had a molecular weight in the range of 18,000 when R = H, R′ = 2-octyl, while the molecular weight of **55** when R = R′ = 2-octyl was 139,000 (121). The conductivity of polymer **55** (R = H, R′ = 2-octyl) upon doping with I_2 was 6.7×10^{-3} S/cm (122). Polymers incorporating nickelocene and cobaltocene units were also synthesized; however, the solubilities of these materials were quite low. The magnetic susceptibilities of the Ni \Fe and Co \Fe oligomers were $3.51\mu_B$ and $5.2\mu_B$, respectively, while a nickelocene-based polymer had a magnetic moment of $5.3\mu_B$. In all cases, the values obtained for the polymetallocenes were greater than those of either nickelocene or cobaltocene.

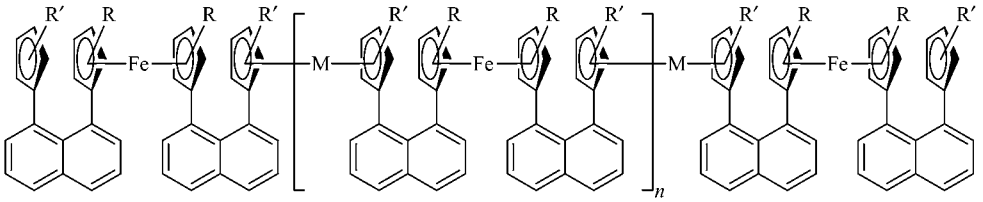

M = Fe, Ni, Co
R, R′ = H, alkyl, aryl group

55

Grimes and co-workers have reported the synthesis of polymetallacarborane staircase oligomers containing cobalt, nickel, and ruthenium (124,125). Oligomers with up to 17 metal atoms were prepared, and electrochemical analysis of these materials indicated that although there was evidence for electron delocalization within the tetradecker stacks, there was very little intersandwich electronic communication (124).

Coordination Polymers

Conjugated polymers containing metal porphyrins in their structures have potential use in optical and electronic devices, solar energy conversion, and as enzyme mimics (127–131). High molecular weight polymetalloporphyrins are often difficult to isolate because of the poor solubility of these rigid materials. As well, the bulkiness of metalloporphyrins can inhibit the formation of an extended π-conjugated system. Many researchers are working on the synthesis of high molecular weight, soluble metalloporphyrin polymers that have good film-forming properties (127–130).

Yamamoto and co-workers have studied the synthesis of zinc porphyrin polymers (**57**) by polycondensation of **56** using Ni and Pd catalysts (128) (eq. 16). Functionalizing the zinc porphyrins and aromatic spacers with alkyl groups enhanced the solubility of these polymers. In addition, various aromatic spacers were studied in order to decrease the steric crowding surrounding the porphyrins. The molecular weights of these polymers were between 4600 and 37,900 (PDI = 1.3–1.8), and thin films of these polymers were electrochemically active and exhibited electrochromism.

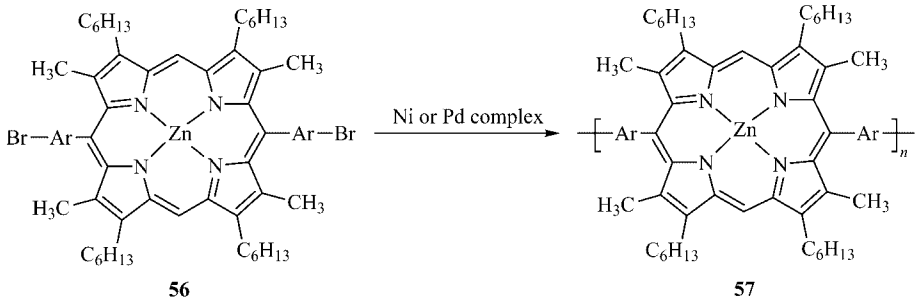

56 **57**

(16)

Anderson and co-workers found that the microscopic polarizability of porphyrins within polymers was 3 orders of magnitude greater than those of monomeric porphyrins (129). This was the largest one-photon-off-resonance third-order optical susceptibility reported for an organic substance, and was indicative of inter-porphyrin conjugation. Soluble zinc polymers were synthesized by incorporating bulky groups on the meso positions of porphyrin rings (130). The solubility of these polymers was very good in the presence of a small amount of a coordinating ligand such as pyridine.

The synthesis and properties of polymetallophthalocyanines have been reviewed (132,133). Although they are structurally similar to polymetalloporphyrins, the presence of an additional four arenes and four nitrogen atoms in their structures has a strong influence on the UV–vis spectra of metallophthalocyanine polymers. These polymers can be synthesized through the metal atoms (**58**) (131–135), through two or more of the aromatic rings of the macrocyclic structure (**59**) (131–133,136), or with the phthalocyanine ring as part of a polymer side chain (**60**) (132,136–138). Cofacial phthalocyanine polymers are materials in which the macrocyclic rings are stacked in a "shish kebab" manner with the metals as part of the polymeric chain (**58**). These polymers often display excellent thermal and

chemical stability and are conducting, sometimes even in the absence of a doping agent.

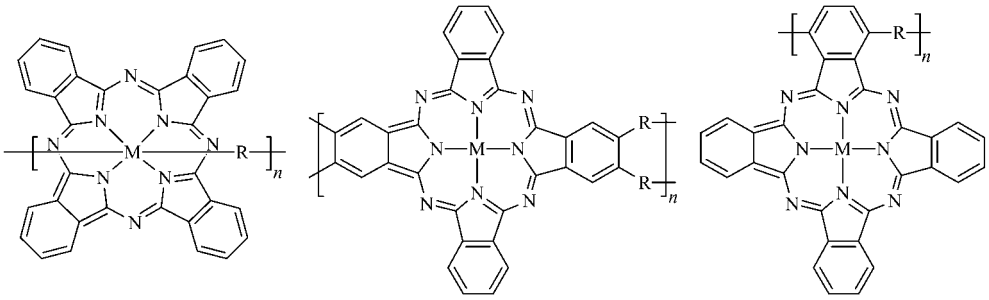

58 59 60

A recent report by Kimura and co-workers described the synthesis of copper and zinc phthalocyanine monomers substituted with either two (**61**) or eight (**62**) olefinic groups (136). Olefin metathesis of these monomers yielded a linear polymer and a three-dimensional network, respectively.

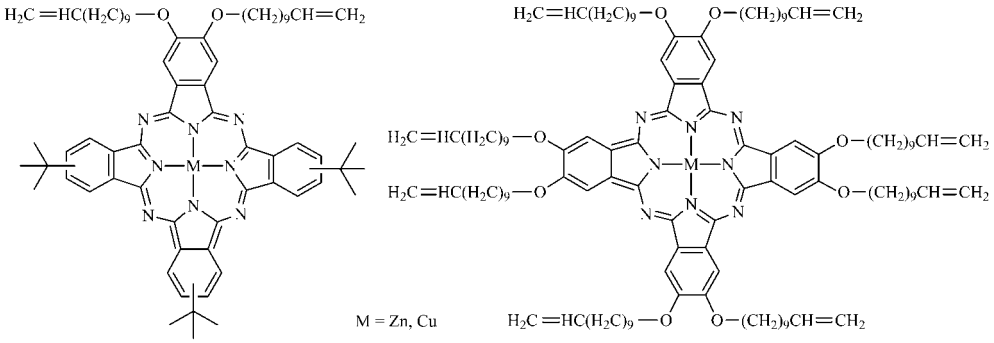

61 62

Since the late 1950s, polymers containing metals coordinated to Schiff base ligands have been reported (139). In 1961, Goodwin and Bailar prepared Schiff base polymers coordinated to Cu, Ni, Co, Fe, Cr, and Al ions (140). Since that time, many more metals have been incorporated into coordination polymers prepared using Schiff base ligands (141–146). Archer and co-workers have studied the effects of different spacers on the solubility of lanthanide coordination polymers (142–144). The incorporation of lanthanides into polymers is important since these metals introduce luminescence into materials. The use of tetradentate Schiff base ligands should shield the lanthanide ions from solvent molecules, thus decreasing the possibility of quenching the polymers' luminescent properties (143). These polymers (**65**) could be prepared via reaction of cerium ions (**64**) with ligands containing imine and phenolic groups (**63**) (142) (eq. 17). Analogous polymers containing europium and yttrium ions coordinated to bis(tetradentate) Schiff base ligands were also synthesized (143).

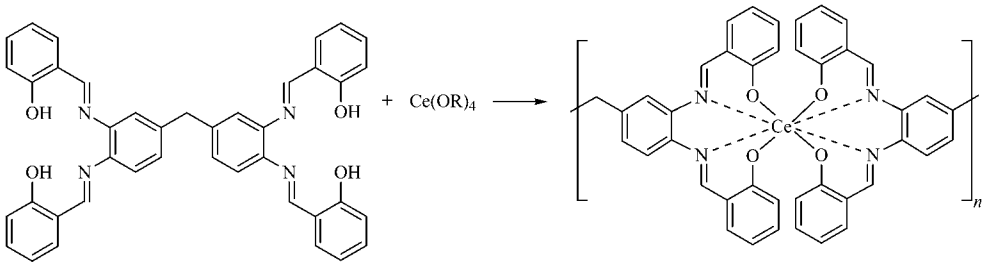

63 64 65

(17)

Polymeric systems containing interlocking rings (catenanes) and threaded rings (rotaxanes) containing metals coordinated to their structures have been studied over the past few years because of their electro- and photoactivity (147–149). A polymer containing copper ions coordinated within its structure was synthesized via polycondensation of a dicarboxylic acid with a dialcohol derivatized copper(I) catenate (147). The M_w and M_n of this polymer were determined to be 4,200,000 and 600,000, respectively. Swager and co-workers have reported the synthesis of conducting polymetallorotaxanes coordinated to zinc and copper ions (148,149).

There are many examples of polymers containing transition metals coordinated to bipyridine and related ligands (150–164). The luminescent properties of tris(bipyridine)ruthenium(II) complexes have generated a great deal of interest in these materials (152–158). Polymers containing metal ions coordinated to three bipyridine or substituted pyridines can contain the metal as an integral part of the polymer skeleton (**66**) (165–168), pendent to the polymer backbone (**67**) (154–156), or in a group pendent to the polymer backbone (**68**) (157,158).

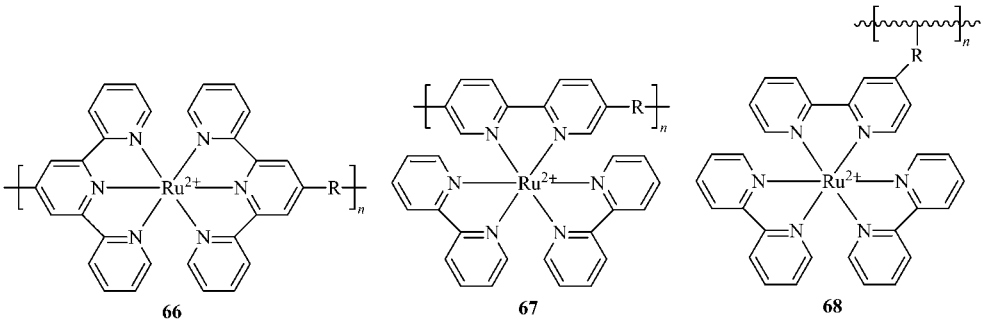

66 67 68

Rehahn and co-workers have described the synthesis of soluble ruthenium(II) coordination polymers by utilizing ligands that allow for the formation of unbranched polymers (150,151). The molecular weights of these polymers were in the range of 45,000, and they could be solubilized in organic or aqueous solutions depending on their counterion. This class of polymer could be prepared either via complexation of pyridine ligands to ruthenium or via polycondensation of metal-containing monomers, as shown in equation 18 (151). Petzold and Harruna have reported the synthesis of three-dimensional high performance

coordination polymers (152,153). A number of these thermally stable, soluble ruthenium-coordinated polymers were examined using optical spectroscopy.

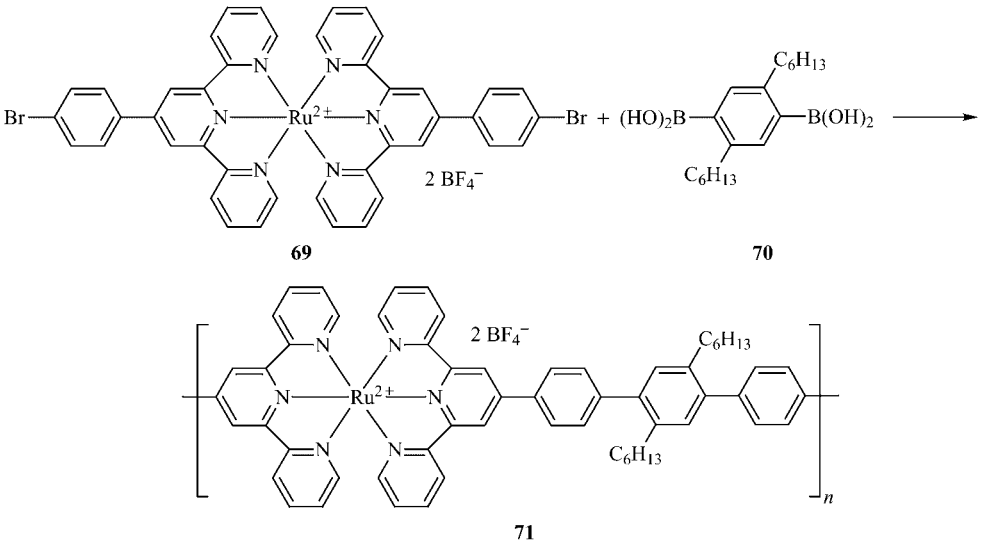

(18)

Polymers containing benzimidazole units in their backbones have also been used in the synthesis of coordination metallopolymers (159–162). Osmium and ruthenium coordinated polymers with bipyridine ligands have been prepared (159,160). These polymers (**72, 73**) possessed metal–metal interactions through their conjugated backbones. Communication between the ruthenium centers of **72** increased by deprotonating the imidazole protons (160). The osmium coordinated polymer (**73**) showed two reduction waves separated by 0.32 V, indicative of strong communication between the Os centers (159).

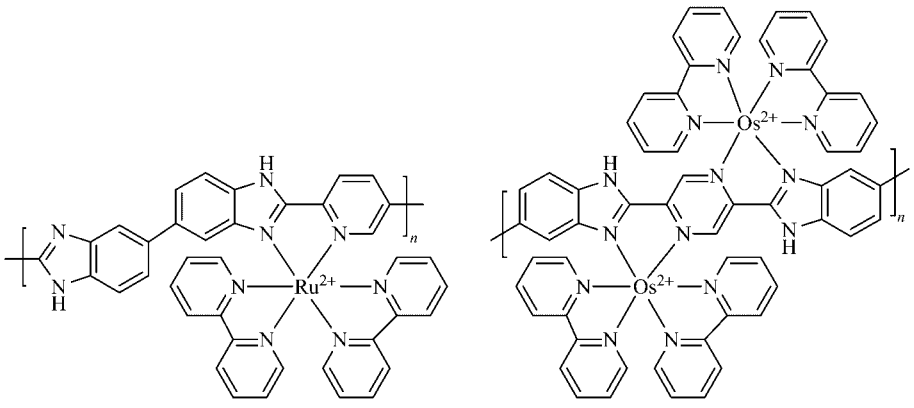

Metals Coordinated to the Polymer Backbone

The synthesis of polymers containing metallic moieties π-coordinated to four-, five-, and six-membered rings in their backbones has been studied. Polymers containing pendent cyclopentadienylcobalt moieties (**76**) have been prepared via direct reaction of monomers containing cyclopentadienylcobalt moieties coordinated to cyclobutadiene rings (**74**), or via rearrangement of cobaltacyclopentadiene units present in polymeric materials (**75**) (36–39,169–172) (eq. 19). Polymers containing aromatic spacers and long chain alkyl groups pendent to the cyclobutadiene rings demonstrated thermotropic liquid crystalline behavior (170,171). Bunz and co-workers have also described the synthesis of conjugated polymers containing cyclopentadienyl rings coordinated to manganese tricarbonyl units (173).

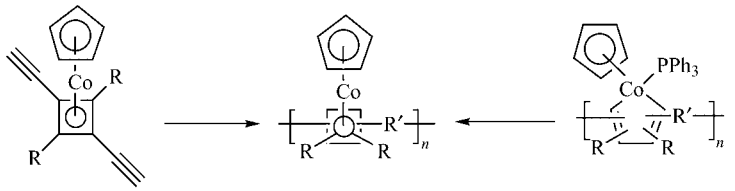

74 **76** **75**

R′ = or aryl

(19)

Organometallic polymers containing arenes coordinated to metallic moieties in their backbones have also been produced via metal complexation to organic polymers (174–179). Poly(9-hexylfluorene) and poly(1-hexylindene) were complexed to manganese tricarbonyl, pentamethylcyclopentadienylcobalt, and pentamethylcyclopentadienylrhodium moieties via η^4-, η^5-, and η^6-coordination (174,175). The photoluminescence of the organometallic poly(9-hexylfluorene) had a decreased intensity relative to its organic analogue (173).

Eyring and co-workers have reported the synthesis of organometallic poly(*p*-phenylene) (PPP) via reaction of the organic polymer with $M(CO)_3(CH_3CN)_3$ or $M(CO)_6$ (M = Cr, Mo) (176). It was determined that molybdenum tricarbonyl was complexed to about 25% of the aromatic rings of this polymer. The chromium and molybdenum functionalized polymers demonstrated increased conductivity relative to organic PPP. Nishihara and co-workers subjected poly(*n*-hexylphenylene) (PHP) to ligand exchange reactions to give molybdenum tricarbonyl and cyclopentadienyliron coordinated polymers (177–179) (eq. 20). These hexyl-substituted polymers displayed better solubility than metallated PPP in organic solvents as a result of the flexible alkyl chains on its backbone. Elemental analysis of the $Mo(CO)_3$-functionalized polymer showed that 1 in every 4.8 aromatic rings was coordinated to a metallic moiety (177,178). A $Cr(CO)_3$ coordinated poly(*n*-butylphenylene) (PBP) was also synthesized; however, this ligand exchange reaction was less efficient than when $Mo(CO)_3$ was used (177). In the case of the organoiron polymer, it was found that 1 in every 1.6 aromatic rings of the complexed PHP was coordinated to a cyclopentadienyliron moiety (179). Spectroelectrochemical measurements of this organoiron polymer indicated the formation

of a network between aromatic rings of neighboring polymer chains following reduction of the cationic iron centers to neutral radicals. Electrochemical and spectroscopic analysis of the organic and organometallic polymers showed that their conductivity increased upon metal coordination (2).

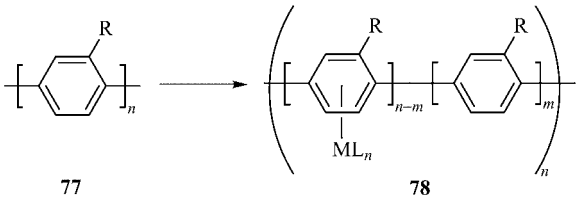

77 **78**

$ML_n = Mo(CO)_3$, $Cr(CO)_3$, $CpFe^+$
R = H, C_4H_9, C_6H_{13} (20)

Polymeric materials coordinated to $Cr(CO)_3$, $CpFe^+$, $CpRu^+$, and Cp^*Ru^+ moieties have been produced via condensation, coupling, and nucleophilic aromatic substitution reactions. In 1987, Jin and Kim reported the synthesis of polyamides coordinated to chromium tricarbonyl moieties (**81**) via condensation reactions of phenylenediamine $Cr(CO)_3$ (**79**) with various diacid chlorides (**80**) (180) (eq. 21). An enhancement of this polymer's solubility was achieved via the incorporation of chromium tricarbonyl moieties pendent to its backbone. The viscosities of these polymers were determined in concentrated sulfuric acid and it was found that the organometallic polymers had higher viscosities than their corresponding organic polymers. Dembek reported that high molecular weight polyamides coordinated to $Cr(CO)_3$ displayed nematic liquid crystalline texture, indicating that their rigid rod nature was retained upon metal coordination even though their solubilities were enhanced significantly (165).

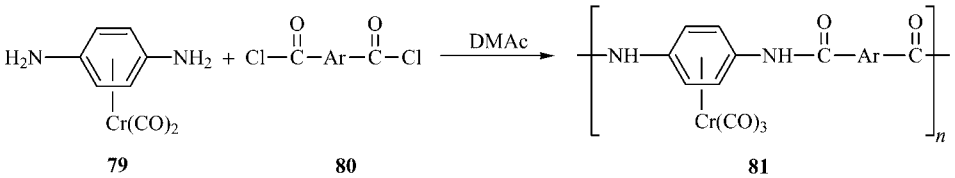

79 **80** **81**

(21)

A polyimine containing chromium tricarbonyl moieties pendent to aromatic rings in its backbone was prepared via reaction of η^6-terephthaldialdehyde–$Cr(CO)_3$ with 1,3-phenylenediamine (166). The resulting conjugated polyimine was insoluble in common organic solvents because of the rigidity of its backbone. The synthesis of polyether/imines coordinated to cyclopentadienyliron moieties (**84**) has also been reported (167) (eq. 22). These polymers were prepared by reaction of a dialdehyde complex of cyclopentadienyliron (**82**) with a number of aliphatic and aromatic diamines (**83**). These polymers were soluble in polar organic solvents such as DMF and DMSO.

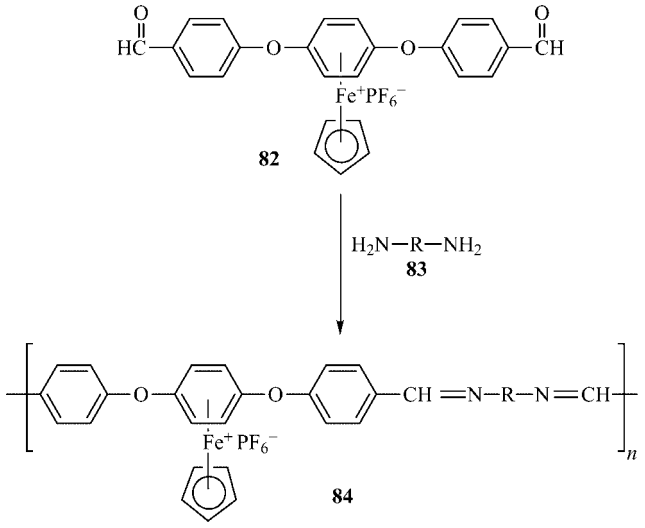

(22)

Poly(phenyl ethynyls) coordinated to chromium tricarbonyl moieties (**85**) were synthesized via palladium-catalyzed cross-coupling of η^6-1,3- and 1,4-dichloroarene chromium tricarbonyl complexes with organostannane reagents (168). Combustion analysis of these polymers indicated that their degree of polymerization was about 18, corresponding to molecular weights of about 7800. Combustion and IR analysis of polymers heated past 200°C indicated that cross-linking reactions occurred following loss of carbon monoxide from the $Cr(CO)_3$ moieties. Polymers with pendent metallic moieties as well as metals in their backbone (**86**) were also prepared (181).

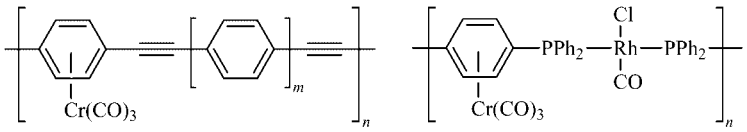

The π-coordination of transition metals to haloarenes activates the aromatic ring toward nucleophilic aromatic substitution reactions (182–189). In 1985, Segal reported the synthesis of soluble polyaromatic ethers coordinated to $CpRu^+$ moieties (182). Dembek and co-workers later prepared a number of polyaromatic ethers and thioethers coordinated to Cp^*Ru^+ moieties (183,184). The synthesis of soluble polyaromatic ethers, thioethers, and amines via S_NAr reactions of dichloroarene complexes of cyclopentadienyliron with oxygen, sulfur, and nitrogen based dinucleophiles has been reported (185–188) (eq. 23). Thermogravimetric analysis of these polymers showed two distinct weight loss steps; the first one corresponded to loss of the cyclopentadienyliron moieties while the second resulted from degradation of the polymer backbones (187). These polymers displayed very good thermal stability following loss of the metallic moieties around 220°C. The synthesis of polymers coordinated to $CpFe^+$ and Cp^*Ru^+ has also been reported (188).

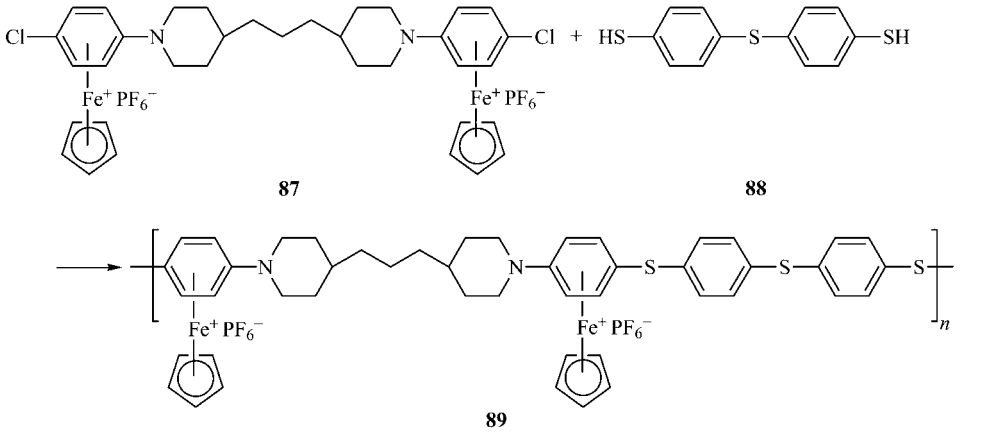

(23)

Polyaromatic ethers coordinated to $CpFe^+$ moieties have also been prepared via sequential S_NAr reactions of chloroarene complexes with hydroquinone (189). The electrochemical behavior of cationic aromatic ether, thioether, and sulfone complexes of cyclopentadienyliron has been studied using cyclic voltammetry and coulometry (190). Reaction of the aromatic ether complexes with sodium cyanide resulted in the formation of neutral adducts which underwent oxidative demetallation to give the corresponding organic aromatic nitriles (191).

Brammer and co-workers have reported the use of arene chromium tricarbonyl complexes as building blocks in supramolecular assembly (192,193). Polypyrrole containing an organoiron group bonded to nitrogen has been prepared via chemical and electrochemical oxidation (194,195). When dicarbonyl(η^5-cyclopentadienyl)(η^1-pyrrolyl)iron(II) (**90**) was subjected to chemical oxidation, the conductivity of the resulting organometallic polypyrrole was 0.25 S/cm (194), while oxidation with ferric chloride resulted in a polymer with a conductivity of 5.2×10^{-5} S/cm, and electrochemical polymerization resulted in polymers with very poor electroactivity. It was found that when the polypyrrole (**91**) was refluxed in either 1,2-dichloroethane or toluene, an azoferrocene-based polymer (**92**) was formed (195) (eq. 24).

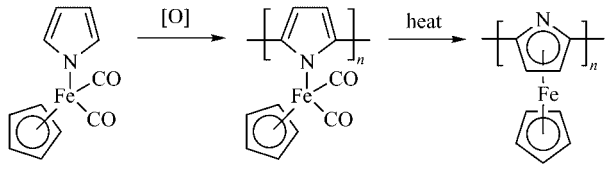

(24)

It has been reported that polymers with silole units in their backbones became coordinated to iron tricarbonyl when they were irradiated with UV light in

the presence of $Fe(CO)_5$ (196). This polymer was redshifted relative to its organic analogue, and was conducting upon doping.

Metallic Moieties in the Polymer Side Chains

As early as 1955, the synthesis of poly(ferrocenylethylene) was reported (197), and interest in this class of polymer is still increasing (1,3–6). Pittman and co-workers described the synthesis and polymerization of a number of ferrocene-based monomers containing acrylate and methacrylate functionalities (**93**) (198). The polymerization of vinylferrocene and 3-vinylbisfulvalenediiron was also performed in order to study the electrical properties of these polymers (199). Upon oxidation of the polymer formed from the radical polymerization of 3-vinylbisfulvalenediiron, the conductivity of this mixed valence polymer was between 6×10^{-3} and $9 \times 10^{-3}\ \Omega^{-1}\cdot cm^{-1}$. Monomers of chromium and iron tricarbonyl (**94, 95**) were also homo- and copolymerization to give their corresponding organometallic polymers (200,201).

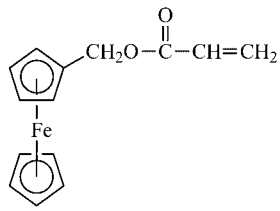

93

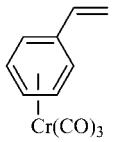

94

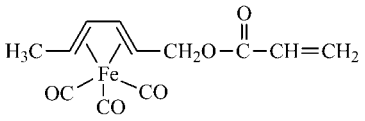

95

Functionalization of organometallic monomers containing olefinic groups has led to the production of organometallic polymers possessing interesting properties. Polymerization of organoiron monomers resulted in the production of liquid crystalline polymers containing ferrocene units in their side chains (**96**) (202–204). The nonlinear optical properties of polymers containing ferrocenyl groups in pendent groups have also been examined (205). The electrochemical behavior of ferrocenyl functionalized polymers has also been of interest (206). Neuse and co-workers have found that water-soluble ferrocene functionalized polymers possess interesting antiproliferative properties (**97**) (207–209). Coordination of Ru^+Cp^*, $Ru^+C_8H_{11}$, or $Ru^+H(PCy_3)_2$ to the aromatic rings of polystyrene has been reported (210). Depending on the bulkiness of the ligand attached to ruthenium, anywhere from 25 to 100% of the aromatic rings in the polymers became complexed to the ruthenium moieties. Recently, polymethacrylates with cationic cyclopentadienyliron moieties coordinated to their side chains (**98**) were prepared via radical polymerization of their corresponding organoiron monomers (211). Photolytic demetallation of the cyclopentadienyliron-coordinated polymethacrylates resulted in the isolation of the corresponding organic analogues, whose M_w's ranged from 48,000 to 68,000. Other examples of metal σ-bonded (**99**, **100**) and coordinated (**101**) monomers have also been examined (212–214).

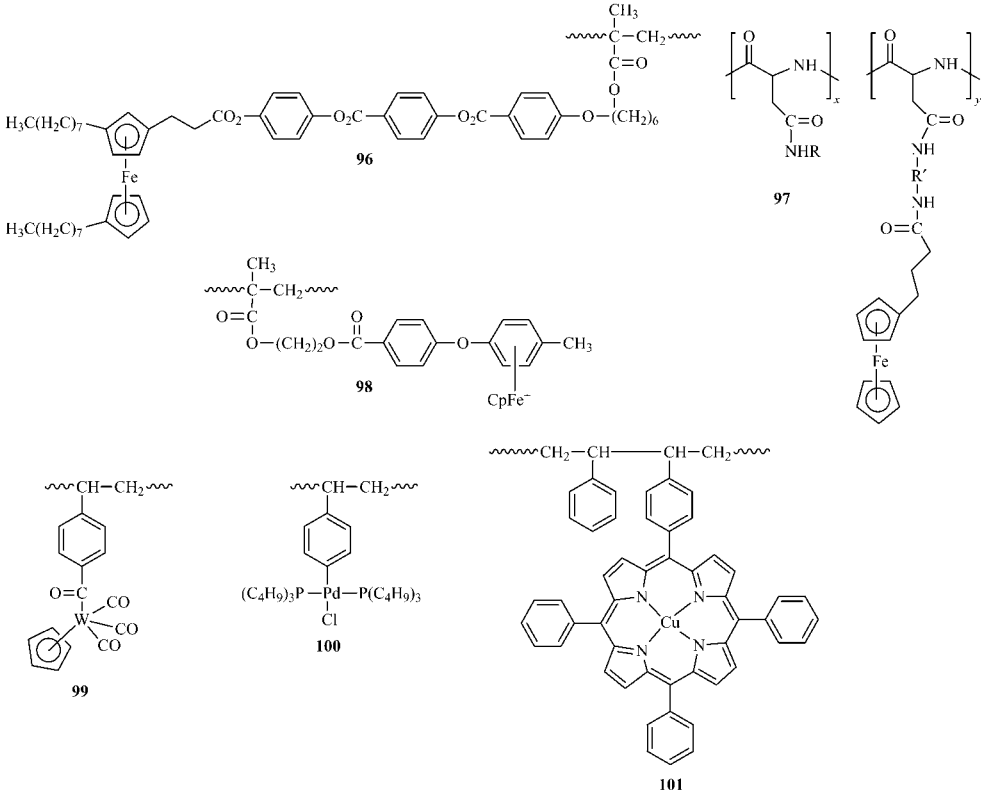

Allcock and co-workers have described the ROP of cyclic phosphazenes containing ferrocenyl units, resulting in the isolation of the corresponding organometallic polymers (**102**) (215). Polyphosphazenes containing chromium tricarbonyl units in their side chains were also isolated following ROP of an inorganic monomer, and subsequent functionalization of this polymer with chromium tricarbonyl (**103**) (216). Differential scanning calorimetry showed that the glass-transition temperatures of the $Cr(CO)_3$ functionalized polymers were higher than their organic analogues by approximately 50°C.

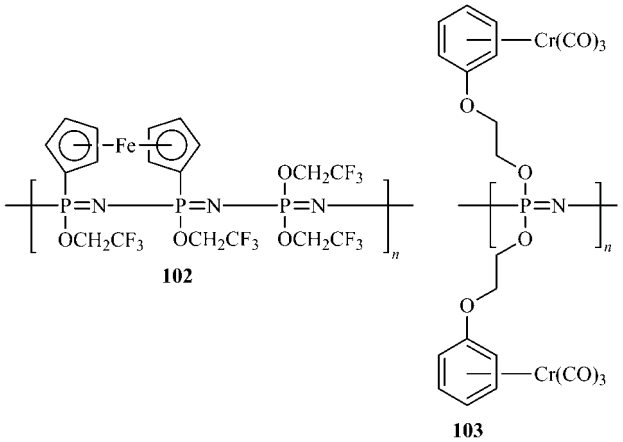

The ROP of *ansa*- and spirocyclic *ansa*-zirconocene complexes has been reported (217) (eq. 25). Polycarbosilane $[(CH_2)_3Si(\eta^5\text{-}C_5H_4)_2ZrCl_2]_n$ (**105**) was obtained from reaction of the spirocyclic silacyclobutane-bridged monomer $(CH_2)_3Si(\eta^5\text{-}C_5H_4)_2ZrCl_2$ (**104**) with Karstedt's catalyst. This polymer demonstrated moderate activity as a catalyst for ethylene polymerization.

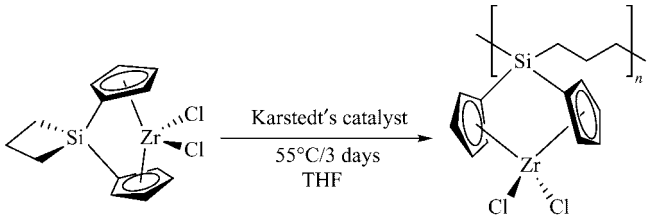

104 **105** (25)

The ROMP of norbornenes functionalized with neutral ferrocenyl moieties has been reported; the aim was to prepare redox-active polymers (218, 219) (eq. 26). The synthesis of polynorbornenes functionalized with cationic cyclopentadienyliron-coordinated aryl ethers has also been reported (220). Demetallation of metallated norbornenes and polynorbornenes led to the liberation of their organic analogues (221–223). Electrochemical analysis of the metallated polymers showed that the cationic iron centers were reduced between −1.2 and −1.4 V.

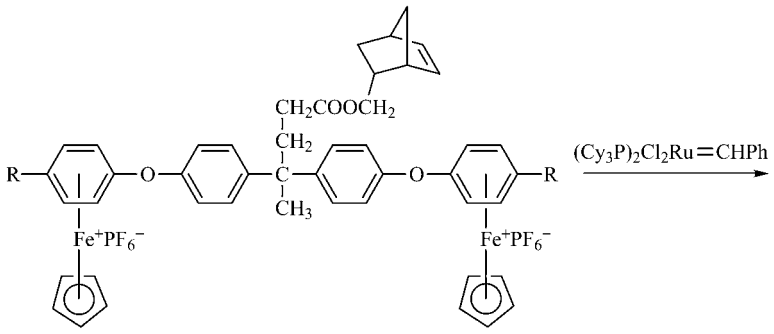

106

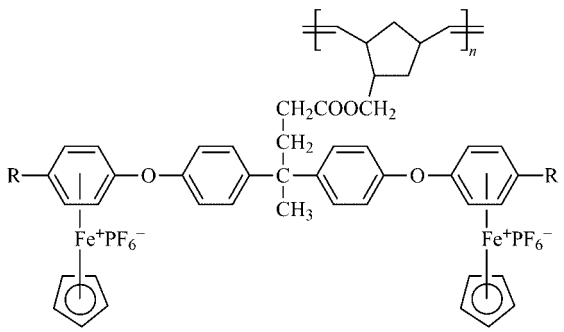

107 (26)

Dendrimers and Star Polymers

There has been considerable interest directed toward the synthesis of organometallic star polymers and dendrimers in recent years (see DENDRONIZED POLYMERS). The production of highly ordered, highly branched organometallic materials is of importance due to their electronic, optical, and biomedical applications (224–232).

Dendritic poly(aryl ethers) containing up to 24 peripheral ferrocenyl units have been synthesized using a stepwise convergent methodology (233). Cyclic voltammetry of these dendrimers showed that the iron centers were all reversibly oxidized around $E_{\frac{1}{2}} = 0.21$ V. Astruc and co-workers have explored the synthesis and properties of a number of different classes of ferrocene-based star polymers and dendrimers (234–238). A dendrimer containing 54 ferrocene units at its periphery was synthesized and reversible oxidation of all 54 iron centers was observed (234). Chemical oxidation of the neutral iron centers to cationic species could also be accomplished using $NOPF_6$. Dendrimers containing 243 ferrocenyl units at the periphery were also synthesized via ferrocenylsilation reactions of allyl terminated dendrimers (235). Nonametallic dendrimers containing ferrocenyl (237) or cobaltocenium (238) moieties (**108**) at their periphery were synthesized via reaction of amine functionalized dendrimers with the acid chlorides of ferrocene or cobaltocene. Deschenaux and co-workers have been investigating the synthesis of ferrocenyl-based polymers with liquid crystalline properties (239,240).

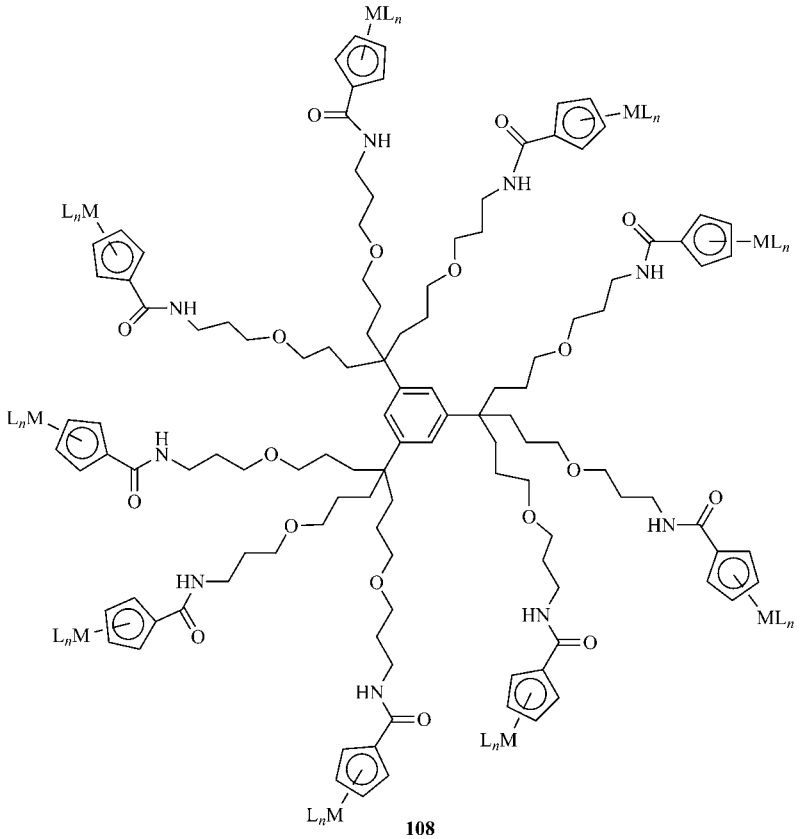

108

Cuadrado and co-workers have also been active in the synthesis of dendrimers containing ferrocene and cobaltocene moieties (241–244). The synthesis of propylenimine-based dendrimers with up to five generations and 64 peripheral ferrocenyl moieties underwent reversible oxidation processes at $E_{\frac{1}{2}} = 0.59$ V (241,242). The guest–host relationship of some low generation dendrimers with cyclodextrins was examined (241). Silicon-based ferrocenyl dendrimers possessing electrochemical communication between the iron centers were also synthesized (243).

Moss and co-workers have been synthesizing dendrimers containing Ru—C σ-bonds using a convergent approach (245). A fourth-generation dendrimer containing 48 organometallic moieties was prepared using complexes such as **109** as starting materials.

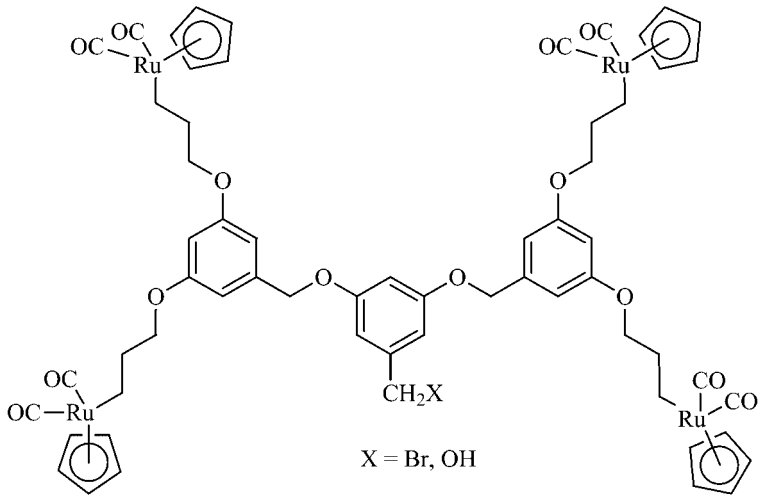

109

There has been a great deal of interest in the design of dendrimers using arene complexes of transition metals (246–252). Astruc has developed an efficient route to core molecules suitable for the synthesis of star and dendritic materials via peralkylation or allylation of methyl-substituted arene complexes of cyclopentadienyliron. The resulting branched polymers contained cationic cyclopentadienyliron moieties at the core and/or the periphery. Complexes containing aryl ethers coordinated to six $CpFe^+$ moieties (**110**) were synthesized via S_NAr reactions (248).

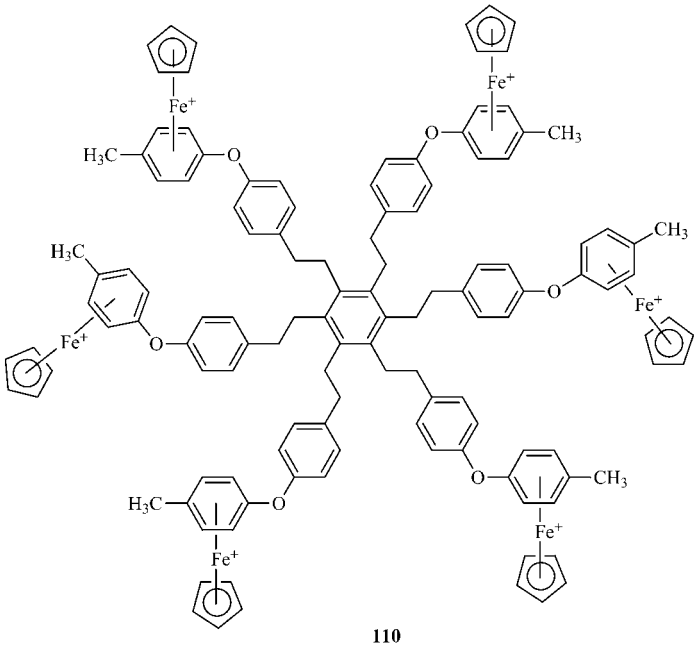

110

The synthesis of a water-soluble metallodendrimer containing six cationic cyclopentadienyliron moieties was also reported (249). This dendrimer was examined as a redox catalyst for the cathodic reduction of nitrates and nitrites to ammonia. Star-shaped polyaromatic ether complexes of cyclopentadienyliron were recently reported by Abd-El-Aziz and co-workers (250). These complexes contained up to 15 cationic cyclopentadienyliron moieties pendent to aromatic rings in the star branches (**111**). Electrochemical analysis of these star polymers showed that the iron centers underwent reversible reduction processes.

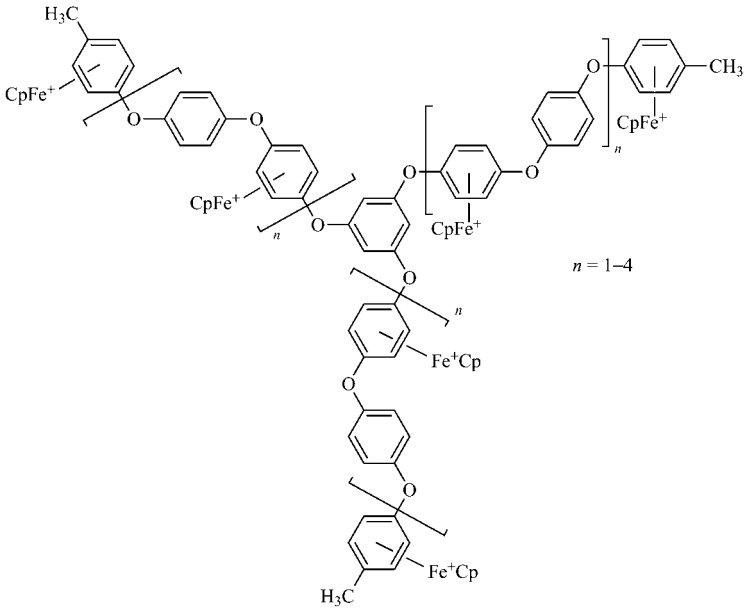

111

The synthesis of organosilane dendrimers coordinated to up to 72 Cp^*Ru^+ moieties has been reported by Tilley and co-workers (251). Mass spectrometry of the dendrimer coordinated to 72 positively charged ruthenium moieties (**112**) revealed that although the desired complex was present in the sample, complete coordination of the aromatic rings may have been hindered because of steric crowding. Organosilicon dendrimers containing chromium tricarbonyl moieties pendent to peripheral aromatic rings have also been synthesized (252). Cyclic voltammetry of these materials showed that oxidation of the chromium atoms occurred reversibly in the absence of nucleophilic species, and that the chromium tricarbonyl units behaved as isolated redox centers.

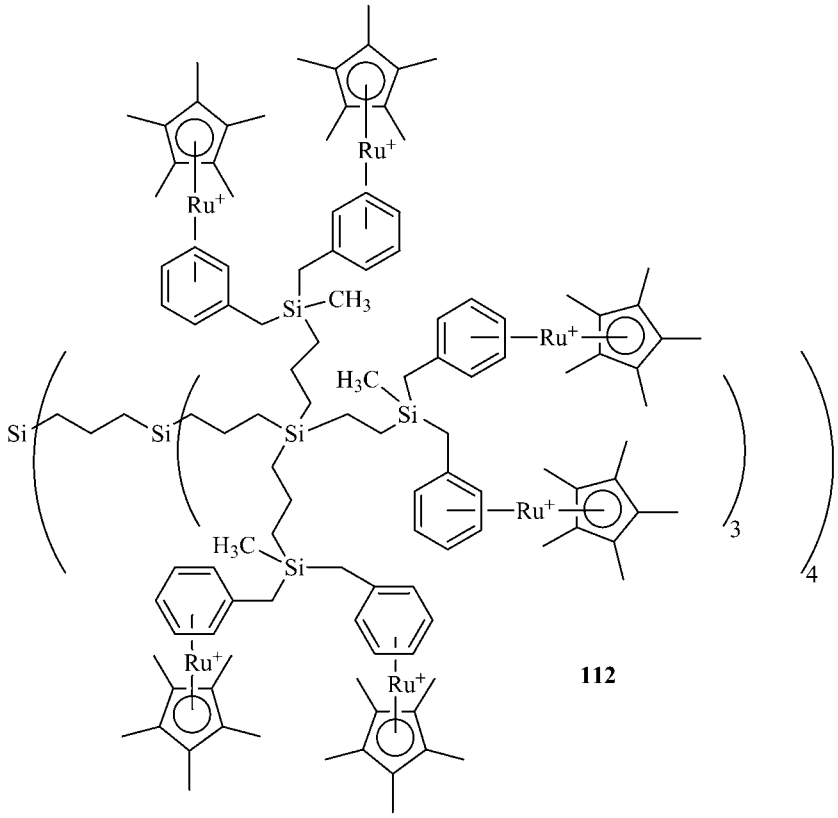

112

There are numerous examples of dendrimers and star polymers containing metal coordination complexes (253–259). The synthesis of polypyridine ruthenium coordination complexes incorporating Fe and Co (**113**) has been established (255). A ruthenium star-shaped complex with a $CpFe^+$-coordinated arene as the core has also been reported (254).

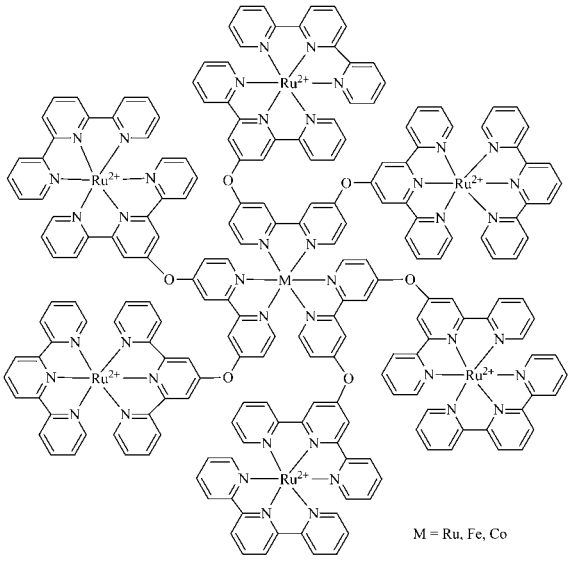

113

Platinum (260–262) and palladium (262,263) complexes have been incorporated into dendrimeric materials. Polymers incorporating both platinum and palladium units coordinated to bipyridine ligands have been reported by Puddephatt and co-workers (**114**) (262). These dendrimers were prepared via oxidative addition of a C—Br bond to a platinum complex, giving the core molecule. Further reaction with platinum or palladium complexes resulted in the homo- or heterometallic materials, respectively.

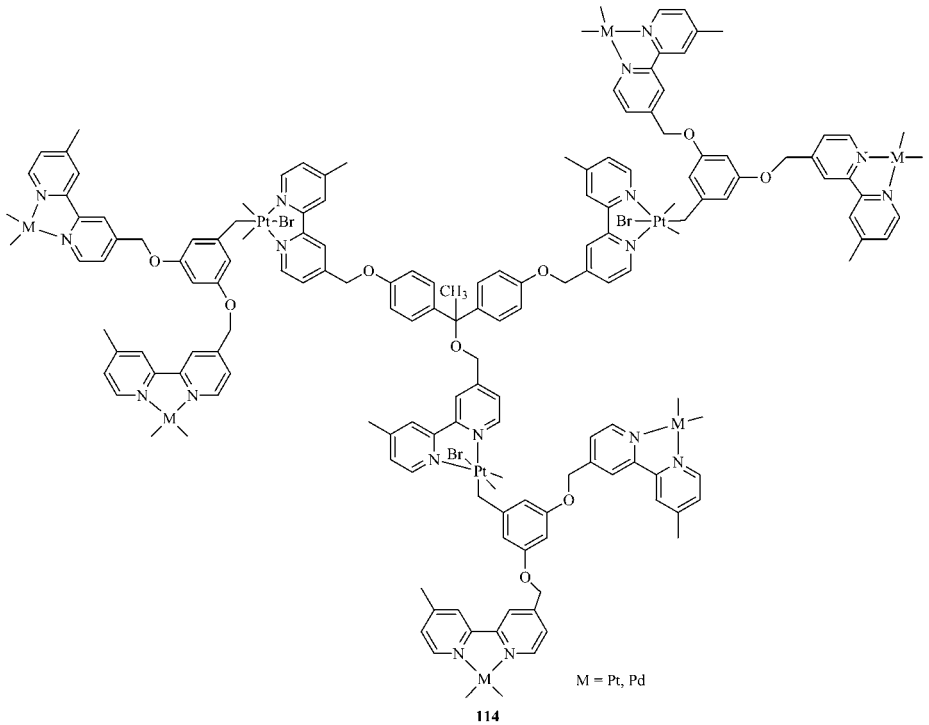

114

BIBLIOGRAPHY

"Organometallic Polymers" in *EPSE* 2nd ed., Vol. 10, pp. 541–594, by C. U. Pittman Jr., Mississippi State University, C. E. Carraher Jr., Florida Atlantic University, and J. R. Reynolds, University of Texas-Arlington.

1. R. D. Archer, *Inorganic and Organometallic Polymers*, Wiley-VCH, New York, 2001.
2. H. Nishihara, in H. S. Nalwa, ed., *Handbook of Organic Conductive Molecules and Polymers*, Vol. **2**, John Wiley & Sons, Inc., New York, 1997, p. 799.
3. C. U. Pittman Jr., C. E. Carraher Jr., M. Zeldin, J. E. Sheats, and B. M. Culbertson, eds., *Metal-Containing Polymeric Materials*, Plenum Press, New York, 1996.
4. A. D. Pomogailo and V. S. Savost'yanov, *Synthesis and Polymerization of Metal-Containing Monomers*, CRC Press, London, 1994.
5. J. E. Sheats, C. E. Carraher Jr., C. U. Pittman Jr., M. Zeldin, and B. Currell, eds., *Inorganic and Metal-Containing Polymeric Materials*, Plenum Press, New York, 1990.
6. A. S. Abd-El-Aziz, *Coord. Chem. Rev.*, in press.
7. K. Kulbaba and I. Manners, *Macromol. Rapid Commun.* **22**, 711 (2001).
8. D. Astruc and F. Chardac, *Chem. Rev.* **101**, 2991 (2001).
9. A. S. Abd-El-Aziz and E. K. Todd, *Polym. News* **5**, 26 (2001).
10. A. S. Abd-El-Aziz and S. Bernardin, *Coord. Chem. Rev.* **203**, 219 (2000).
11. P. Nguyen, P. Gomez-Elipe, and I. Manners, *Chem. Rev.* **99**, 1515 (1999).
12. P. G. Pickup, *J. Mater. Chem.* **9**, 1641 (1999).
13. M. Rehahn, *Acta Polym.* **49**, 201 (1998).
14. R. J. Puddephatt, *Chem. Commun.* 1055 (1998).
15. M. H. Chisolm, *Angew. Chem., Int. Ed. Engl.* **30**, 673 (1991).
16. K. G. Sturge, A. D. Hunter, R. McDonald, and B. D. Santarsiero, *Organometallics* **11**, 3056 (1992).
17. M. S. Khan, S. J. Davies, A. K. Kakkar, D. Schwartz, B. Lin, B. F. G. Johnson, and J. Lewis, *J. Organomet. Chem.* **424**, 87 (1992).
18. S. Takahashi, H. Morimoto, E. Murarta, S. Kataoka, K. Sonogashira, and H. Hagihara, *J. Polym. Sci., Polym. Chem. Ed.* **20**, 565 (1982).
19. P. Altamura, G. Giardina, C. Lo Sterzo, and M. V. Russo, *Organometallics* **20**, 4360 (2001).
20. M. Younus, A. Kohler, S. Cron, N. Chawdhury, M. R. A. Al-Mandhary, M. S. Khan, J. Lewis, N. J. Long, R. H. Friend, and P. R. Raithby, *Angew. Chem., Int. Ed.* **37**, 3036 (1998).
21. W.-Y. Wong, S.-M. Chan, K.-H. Choi, K.-W. Cheah, and W.-K. Chan, *Macromol. Rapid Commun.* **21**, 453 (2000).
22. R. D. Markwell, I. S. Butler, A. K. Kakkar, M. S. Khan, Z. H. Al-Zakwani, and J. Lewis, *Organometallics* **15**, 2331 (1996).
23. S. J. Davies, B. F. G. Johnson, M. S. Khan, and J. Lewis, *J. Chem. Soc., Chem. Commun.* 187 (1991).
24. A. Buttinelli, E. Viola, E. Antonelli, and C. Lo Sterzo, *Organometallics* **17**, 2574 (1998).
25. Z. Atherton, C. W. Faulkner, S. L. Ingham, A. A. Kakkar, M. S. Khan, J. Lewis, N. J. Long, and P. R. Raithby, *J. Organomet. Chem.* **462**, 265 (1993).
26. S. J. Davies, B. F. G. Johnson, J. Lewis, and P. R. Raithby, *J. Organomet. Chem.* **414**, C51 (1991).
27. H. B. Fyfe, M. Mlekuz, D. Zargarian, N. J. Taylor, and T. B. Marder, *J. Chem. Soc., Chem. Commun.* 188 (1991).

28. G. Jia, R. J. Puddephatt, J. D. Scott, and J. J. Vittal, *Organometallics* **12**, 3565 (1993).
29. G. Jia, N. C. Payne, J. J. Vittal, and R. J. Puddephatt, *Organometallics* **12**, 4771 (1993).
30. P. K. Sahoo, and S. K. Swain, *J. Polym. Sci., Part A: Polym. Chem.* **37**, 3899 (1999).
31. C. E. Carraher Jr., *Makromol. Chem.* **166**, 31 (1973).
32. C. E. Carraher Jr. and J. E. Sheats, *Makromol. Chem.* **166**, 23 (1973).
33. C. E. Carraher Jr. and R. J. Nordin, *J. Appl. Polym. Sci.* **18**, 53 (1974).
34. S. S. H. Mao and T. D. Tilley, *Macromolecules* **30**, 5566 (1997).
35. B. L. Lucht, S. S. H. Mao, and T. D. Tilley, *J. Am. Chem. Soc.* **120**, 4354 (1998).
36. T. Shimura, A. Ohkubo, N. Matsuda, I. Matsuoka, K. Aramaki, and H. Nishihara, *Chem. Mater.* **8**, 1307 (1996).
37. I. Matsuoka, K. Aramaki, and H. Nishihara, *J. Chem. Soc., Dalton Trans.* 147 (1998).
38. M. Murata, T. Hoshi, I. Matsuoka, T. Nankawa, M. Kurihara, and H. Nishihara, *J. Inorg. Organomet. Polym.* **10**, 209 (2000).
39. J.-C. Lee, A. Nishio, I. Tomita, and T. Endo, *Macromolecules* **30**, 5205 (1997).
40. S. C. Tenhaeff and D. R. Tyler, *Organometallics* **10**, 473 (1991).
41. S. C. Tenhaeff and D. R. Tyler, *Organometallics* **10**, 1116 (1991).
42. S. C. Tenhaeff and D. R. Tyler, *Organometallics* **11**, 1466 (1992).
43. J. L. Male, M. Yoon, A. G. Glenn, T. J. R. Weakley, and D. R. Tyler, *Macromolecules* **32**, 3898 (1999).
44. M. Moran, M. C. Pascual, I. Cuadrado, and J. Losada, *Organometallics* **12**, 811 (1993).
45. T. Kuhnen, M. Stradiotto, R. Ruffolo, D. Ulbrich, M. J. McGlinchey, and M. A. Brook, *Organometallics* **16**, 5048 (1997).
46. M. J. Irwin, G. Jia, J. J. Vittal, and R. J. Puddephatt, *Organometallics* **15**, 5321 (1996).
47. S. Chardon-Noblat, A. Deronzier, D. Zsoldos, R. Ziessel, M. Haukka, T. Pakkanen, and T. Venalainen, *J. Chem. Soc., Dalton Trans.* 2581 (1996).
48. S. Chardon-Noblat, A. Deronzier, F. Hartl, J. van Slageren, and T. Mahabiersing, *Eur. J. Inorg. Chem.* 613 (2001).
49. W.-M. Xue, F. E. Kuhn, E. Herdtweck, and Q. Li, *Eur. J. Inorg. Chem.* 213 (2001).
50. W.-M. Xue and F. E. Kuhn, *Eur. J. Inorg. Chem.* 2041 (2001).
51. M. H. Chisholm, *Acc. Chem. Res.* **33**, 53 (2000).
52. J. L. Wesemann and M. H. Chisolm, *Inorg. Chem.* **36**, 3258 (1997).
53. M. C. Kerby, B. W. Eichhorn, J. A. Creighton, and K. P. C. Vollhardt, *Inorg. Chem.* **29**, 1319 (1990).
54. E. W. Neuse and H. J. Rosenberg, *Macromol. Sci., C: Revs. Macromol. Chem.* **4**(1), 1 (1970).
55. V. V. Korshak, S. L. Sosin, and V. P. Alekseeva, *Dokl. Akad. Nauk SSSR* **132**, 360 (1960).
56. A. N. Nesmeyanov, V. V. Korshak, N. S. Voevodskii, S. L. Kochetkova, S. L. Sosin, R. B. Materikova, T. N. Bolotnikova, V. M. Chibrikin, and N. M. Bazhin, *Dokl. Akad. Nauk SSSR* **137**, 1370 (1961).
57. H. Rosenberg and E. W. Neuse, *J. Organomet. Chem.* **6**, 76 (1966).
58. H. Watanabe, I. Motoyama, and K. Hata, *Bull. Chem. Soc. Jpn.* **39**, 790 (1966).
59. I. J. Spilners and J. P. Pellegrini Jr., *J. Org. Chem.* **30**, 3800 (1965).
60. K. Sanechika, T. Yamamoto, and A. Yamamoto, *Polym. J.* **13**, 255 (1981).
61. T. Yamamoto, K. Sanechika, A. Yamamoto, M. Katada, I. Motoyama, and H. Sano, *Inorg. Chim. Acta* **73**, 75 (1983).

62. C. U. Pittman Jr. and Y. Sasaki, *Chem. Lett.* 383 (1975).
63. T. Hirao, M. Kurashina, K. Aramaki, and H. Nishihara, *J. Chem. Soc., Dalton Trans.* 2929 (1996).
64. M. D. Rausch, *J. Org. Chem.* **28**, 3337 (1963).
65. E. W. Neuse and R. K. Crossland, *J. Organomet. Chem.* **7**, 344 (1967).
66. K. Gonslaves, L. Zhan-ru, and M. D. Rausch, *J. Am. Chem. Soc.* **106**, 3862 (1984).
67. C. U. Pittman Jr., and M. D. Rausch, *Pure Appl. Chem.* **58**, 617 (1986).
68. M. M. Abd-Alla, M. F. El-Zohry, K. I. Aly, and M. M. M. Abd-El-Wahab, *J. Appl. Polym. Sci.* **47**, 323 (1993).
69. G. Wilbert, A. Wiesemann, and R. Zentel, *Macromol. Chem. Phys.*, **196**, 3771 (1995).
70. I. Yamaguchi, K. Osakada, T. Yamamoto, and M. Katada, *Bull. Chem. Soc. Jpn.* **72**, 2557 (1999).
71. M. E. Wright and E. G. Toplikar, *Macromolecules* **25**, 6050 (1992).
72. M. E. Wright and M. S. Sigman, *Macromolecules* **25**, 6055 (1992).
73. M. E. Wright, E. G. Toplikar, H. S. Lackrita, and J. Y. Kerney, *Macromolecules* **27**, 3016 (1994).
74. C. U. Pittman Jr., O. E. Ayers, B. Suryanarayanan, S. P. McManus, and J. E. Sheats, *Makromol. Chem.* **175**, 1427 (1974).
75. J. E. Sheats, in C. E. Carraher Jr., J. E. Sheats, and C. U. Pittman Jr., eds., *Organometallic Polymers*, Academic Press, New York, 1978, p. 87.
76. I. Cuadrado, C. M. Casado, F. Lobete, B. Alonso, B. Gonzalez, J. Losada, and U. Amador, *Organometallics* **18**, 4960 (1999).
77. C. M. Casado, M. Moran, J. Losada, and I. Cuadrado, *Inorg. Chem.* **34**, 1668 (1995).
78. M. Bochmann, J. Lu, and R. D. Cannon, *J. Organomet. Chem.* **518**, 97 (1996).
79. T. Yamamoto, T. Morikita, T. Maruyama, K. Kubota, and M. Katada, *Macromolecules* **30**, 5390 (1997).
80. S. L. Ingham, M. S. Khan, J. Lewis, N. J. Long, and P. R. Raithby, *J. Organomet. Chem.* **470**, 153 (1994).
81. R. Knapp, U. Velten, and M. Rehahn, *Polymer* **39**, 5827 (1998).
82. G. E. Southard and M. D. Curtis, *Organometallics* **16**, 5618 (1997).
83. J. Park, Y. Seo, S. Cho, D. Whang, K. Kim, and T. Chang, *J. Organomet. Chem.* **489**, 23 (1995).
84. I. Yamaguchi, H. Ishii, T. Sakano, K. Osakada, and T. Yamamoto, *Appl. Organomet. Chem.* **15**, 197 (2001).
85. C. P. Galloway and T. B. Rauchfuss, *Angew. Chem., Int. Ed. Engl.* **32**, 1319 (1993).
86. D. L. Compton and T. B. Rauchfuss, *Organometallics* **13**, 4367 (1994).
87. D. L. Compton, P. F. Brandt, T. B. Rauchfuss, D. F. Rosenbaum, and C. F. Zukoski, *Chem. Mater.* **7**, 2342 (1995).
88. R. Rulkens, D. P. Gates, D. Balaishis, J. K. Pudelski, D. F. McIntosh, A. J. Lough, and I. Manners, *J. Am. Chem. Soc.* **119**, 10976 (1997).
89. R. Resendes, P. Nguyen, A. J. Lough, and I. Manners, *Chem. Commun.* 1001 (1998).
90. J. M. Nelson, P. Nguyen, R. Petersen, H. Rengel, P. M. Macdonald, A. J. Lough, I. Manners, N. P. Raju, J. E. Greedan, S. Barlow, and D. O'Hare, *Chem. Eur. J.* **3**, 573 (1997).
91. J. M. Nelson, H. Rengel, and I. Manners, *J. Am. Chem. Soc.* **115**, 7035 (1993).
92. J. M. Nelson, A. J. Lough, and I. Manners, *Angew. Chem., Int. Ed. Engl.* **33**, 989 (1994).
93. C. E. Stanton, T. R. Lee, H. R. Grubbs, N. S. Lewis, J. K. Pudelski, M. R. Callstrom, M. S. Erickson, and M. L. McLaughlin, *Macromolecules* **28**, 8713 (1995).

94. M. A. Buretea and T. D. Tilley, *Organometallics* **16**, 1507 (1997).
95. R. W. Heo, F. B. Somoza, and T. R. Lee, *J. Am. Chem. Soc.* **120**, 1621 (1998).
96. I. Manners, *Chem. Commun.* 857 (1999).
97. X.-H. Liu, D. W. Bruce, and I. Manners, *Chem. Commun.* 289 (1997).
98. J. Rasburn, D. A. Foucher, W. F. Reynolds, I. Manners, and G. J. Vansco, *Chem. Commun.* 843 (1998).
99. P. Nguyen, G. Stojcevic, K. Kulbaba, M. J. MacLachlan, X.-H. Liu, A. J. Lough, and I. Manners, *Macromolecules* **31**, 5977 (1998).
100. K. N. Power-Billard and I. Manners, *Macromolecules* **33**, 26 (2000).
101. K. N. Power-Billard, T. J. Peckham, A. Butt, F. Jakle, and I. Manners, *J. Inorg. Organomet. Polym.* **10**, 159 (2000).
102. F. Jakle, Z. Wang, and I. Manners, *Macromol. Rapid. Commun.* **21**, 1291 (2000).
103. R. G. H. Lammertink, M. A. Hempenius, G. J. Vancso, K. Shin, M. H. Rafailovich, and J. Sokolov, *Macromolecules* **34**, 942 (2001).
104. V. S. Papkov, M. V. Gerasimov, I. I. Dubovik, S. Sharma, V. V. Dementiev, and K. H. Pannell, *Macromolecules* **33**, 7107 (2000).
105. Z. Chen, M. D. Foster, W. Zhou, H. Fong, D. H. Reneker, R. Resendes, and I. Manners, *Macromolecules* **34**, 6156 (2001).
106. J. Rasburn, F. Seker, K. Kulbaba, P. G. Klein, I. Manners, G. J. Vancso, and P. M. Macdonald, *Macromolecules* **34**, 2884 (2001).
107. M. J. MacLachlan, M. Ginzburg, N. Coombs, N. P. Raju, J. E. Greedan, G. A. Ozin, and I. Manners, *J. Am. Chem. Soc.* **122**, 3878 (2000).
108. L. I. Espada, M. Shadaram, J. Robillard, and K. Pannell, *J. Inorg. Organomet. Polym.* **10**, 169 (2000).
109. Y. Ni, R. Rulkens, and I. Manners, *J. Am. Chem. Soc.* **118**, 4102 (1996).
110. H. P. Withers Jr., D. Seyferth, J. D. Fellmann, P. E. Garrou, and S. Martin, *Organometallics* **1**, 1283 (1982).
111. T. J. Peckham, A. J. Lough, and I. Manners, *Organometallics* **18**, 1030 (1999).
112. T. J. Peckham, J. A. Massey, C. H. Honeyman, and I. Manners, *Macromolecules* **32**, 2830 (1999).
113. C. E. B. Evans, A. J. Lough, H. Grondey, and I. Manners, *New J. Chem.* **24**, 447 (2000).
114. L. Cao, I. Manners, and M. A. Winnik, *Macromolecules* **34**, 3353 (2001).
115. T. Mizuta, M. Onishi, and K. Miyoshi, *Organometallics* **19**, 5005 (2000).
116. F. Jakle, R. Rulkens, G. Zech, J. A. Massey, and I. Manners, *J. Am. Chem. Soc.* **122**, 4231 (2000).
117. H. K. Sharma, F. Cervantes-Lee, J. S. Mahmoud, and K. H. Pannell, *Organometallics* **18**, 399 (1999).
118. T. J. Peckham, J. A. Massey, M. Edwards, I. Manners, and D. A. Foucher, *Macromolecules* **29**, 2396 (1996).
119. A. Berenbaum, H. Braunschweig, R. Dirk, U. Englert, J. C. Green, F. Jakle, A. J. Lough, and I. Manners, *J. Am. Chem. Soc.* **122**, 5765 (2000).
120. K. C. Hultzsch, J. M. Nelson, A. J. Lough, and I. Manners, *Organometallics* **14**, 5496 (1995).
121. H. M. Nugent, M. Rosenblum, and P. Klemarczky, *J. Am. Chem. Soc.* **115**, 3848 (1993).
122. M. Rosenblum, H. M. Nugent, K.-S. Jang, M. M. Labes, W. Cahalane, P. Klemarczyk, and W. M. Reiff, *Macromolecules* **28**, 6330 (1995).
123. R. D. A. Hudson, B. M. Foxman, and M. Rosenblum, *Organometallics* **18**, 4098 (1999).
124. X. Meng, M. Sabat, and R. N. Grimes, *J. Am. Chem. Soc.* **115**, 6143 (1993).
125. X. Wang, M. Sabat, and R. N. Grimes, *J. Am. Chem. Soc.* **117**, 12227 (1995).

126. T. J. Katz, A. Sudhakar, M. F. Teasley, A. M. Gilbert, W. E. Geiger, M. P. Robben, M. Wuensch, and M. D. Ward, *J. Am. Chem. Soc.* **115**, 3182 (1993).
127. H. L. Anderson, *Chem. Commun.* 2323 (1999).
128. T. Yamamoto, N. Fukushima, H. Nakajima, T. Maruyama, and I. Yamaguchi, *Macromolecules* **33**, 5988 (2000).
129. S. M. Kuebler, R. G. Denning, and H. L. Anderson, *J. Am. Chem. Soc.* **122**, 339 (2000).
130. T. E. O. Screen, K. B. Lawton, G. S. Wilson, N. Dolney, R. Ispasoiu, T. Goodson III, S. J. Martin, D. D. C. Bradley, and H. L. Anderson, *J. Mater. Chem.* **11**, 312 (2001).
131. B. Jiang, S.-W. Yang, D. C. Barbini, and W. E. Jones Jr., *Chem. Commun.* 213 (1998).
132. N. B. McKeown, *J. Mater. Chem.* **10**, 1979 (2000).
133. S. Venkatachalam, in H. S. Nalwa, ed., *Handbook of Organic Conductive Molecules and Polymers*, Vol. **2**, John Wiley & Sons, Inc., New York, 1997, p. 741.
134. B. N. Diel, T. Inabe, N. K. Jaggi, J. W. Lyding, O. Schneider, M. Hanack, C. R. Kannewurf, T. J. Marks, and L. H. Schwartz, *J. Am. Chem. Soc.* **106**, 3207 (1984).
135. T. Inabe, J. G. Gaudiello, M. K. Moguel, J. W. Lyding, R. L. Burton, W. J. McCarthy, C. R. Kannewurf, and T. J. Marks, *J. Am. Chem. Soc.* **108**, 7595 (1986).
136. M. Kimura, K. Wada, K. Ohta, K. Hanabusa, H. Shirai, and N. Kobayashi, *Macromolecules* **34**, 4706 (2001).
137. S. Makhseed, A. Cook, and N. B. McKeown, *Chem. Commun.* 419 (1999).
138. Y. Meng, I. A. Abu-Yousef, A. R. Hlil, and A. S. Hay, *Macromolecules* **33**, 9185 (2000).
139. C. S. Marvel and N. Tarkoy, *J. Am. Chem. Soc.* **79**, 6000 (1957).
140. H. A. Goodwin and J. C. Bailar Jr., *J. Am. Chem. Soc.* **83**, 2467 (1961).
141. Y.-B. Dong, M. D. Smith, and H.-C. zur Loye, *Inorg. Chem.* **39**, 4927 (2000).
142. H. Chen, J. A. Cronin, and R. D. Archer, *Inorg. Chem.* **34**, 2306 (1995).
143. H. Chen and R. D. Archer, *Macromolecules* **29**, 1957 (1996).
144. R. D. Archer, H. Chen, J. A. Cronin, and S. M. Palmer, in Ref. 3, p. 81.
145. N. Chantarasiri, N. Sutivisedsak, and C. Pouyuan, *Eur. Polym. J.* **37**, 2031 (2001).
146. J. L. Reddinger and J. R. Reynolds, *Chem. Mater.* **10**, 1236 (1998).
147. J.-L. Weidmann, J.-M. Kern, J.-P. Sauvage, D. Muscat, and K. Mullen, *Chem. Commun.* 1243 (1996).
148. S. S. Zhu, P. J. Carroll, and T. M. Swager, *J. Am. Chem. Soc.* **118**, 8713 (1996).
149. S. S. Zhu and T. M. Swager, *J. Am. Chem. Soc.* **119**, 12568 (1997).
150. S. Kelch and M. Rehahn, *Macromolecules* **31**, 4102 (1998).
151. S. Kelch and M. Rehahn, *Macromolecules* **32**, 5818 (1999).
152. O. N. Petzold and I. I. Harruna, *J. Inorg. Organomet. Polym.* **10**, 231 (2000).
153. O. N. Petzold and I. I. Harruna, *J. Inorg. Organomet. Polym.* **10**, 249 (2000).
154. S. C. Yu, S. Hou, and W. K. Chan, *Macromolecules* **33**, 3259 (2000).
155. Q. Wang, L. Wang, and L. Yu, *J. Am. Chem. Soc.* **120**, 12860 (1998).
156. S. C. Yu, X. Gong, and W. K. Chan, *Macromolecules* **31**, 5639 (1998).
157. L. A. Worl, W. E. Jones Jr., G. F. Strouse, J. N. Younathan, E. Danielson, K. A. Maxwell, M. Sykora, and T. J. Meyer, *Inorg. Chem.* **38**, 2705 (1999).
158. C. N. Fleming, K. A. Maxwell, J. M. DeSimone, T. J. Meyer, and J. M. Papanikolas, *J. Am. Chem. Soc.* **123**, 10336 (2001).
159. C. G. Cameron and P. G. Pickup, *J. Am. Chem. Soc.* **121**, 7710 (1999).
160. C. G. Cameron and P. G. Pickup, *Chem. Commun.* 303 (1997).
161. S. C. Yu, S. Hou, and W. K. Chan, *Macromolecules* **32**, 5251 (1999).
162. K. D. Ley, C. E. Whittle, M. D. Bartberger, and K. S. Schanze, *J. Am. Chem. Soc.* **119**, 3423 (1997).

163. M. Kimura, M. Sano, T. Muto, K. Hanabusa, H. Shirai, and N. Kobayashi, *Macromolecules* **32**, 7951 (1999).
164. M. A. Camacho, A. K. Kar, W. E. Lindsell, C. Murray, P. N. Preston, and B. S. Wherrett, *J. Mater. Chem.* **9**, 1251 (1999).
165. A. A. Dembek, R. R. Burch, and A. E. Feiring, *J. Am. Chem. Soc.* **115**, 2087 (1993).
166. M. E. Wright and C. K. Lowe-Ma, *Inorg. Chim. Acta.* **232**, 223 (1995).
167. A. S. Abd-El-Aziz, T. H. Afifi, E. K. Todd, and G. Z. Ma, *Polym. Prepr.* **42**, 450 (2001).
168. M. E. Wright, *Macromolecules* **22**, 3256 (1989).
169. W. Steffen and U. H. F. Bunz, *Macromolecules* **33**, 9518 (2000).
170. Y. Sawada, I. Tomita, I. L. Rozhanskii, and T. Endo, *J. Inorg. Organomet. Polym.* **10**, 221 (2000).
171. M. Altmann and U. H. F. Bunz, *Angew. Chem., Int. Ed. Engl.* **34**, 569 (1995).
172. W. Steffen, B. Kohler, M. Altmann, U. Scherf, K. Stitzer, H.-C. zur Loye, and U. H. F. Bunz, *Chem. Eur. J.* **7**, 117 (2001).
173. U. H. F. Bunz, V. Enkelmann, and F. Beer, *Organometallics* **14**, 2490 (1995).
174. J. Matsuda, K. Aramaki, and H. Nishihara, *J. Chem. Soc., Faraday Trans.* **91**, 1477 (1995).
175. H. Nishihara, J. Matsuda, T. Hirao, and K. Aramaki, *Synth. Met.* **69**, 551 (1995).
176. S. I. Yaniger, D. J. Rose, W. P. McKenna, and E. M. Eyring, *Macromolecules* **17**, 2579 (1984).
177. H. Nishihara, H. Funaki, T. Shimura, and K. Aramaki, *Synth. Met.*, **55–57**, 942 (1993).
178. H. Funaki, K. Aramaki, and H. Nishihara, *Chem. Lett.* 2065 (1992).
179. H. Funaki, K. Aramaki, and H. Nishihara, *Synth. Met.* **74**, 59 (1995).
180. J.-I. Jin, and R. Kim, *Polym. J.* **19**, 977 (1987).
181. M. E. Wright, L. Lawson, R. T. Baker, and D. C. Roe, *Polyhedron* **11**, 323 (1992).
182. J. A. Segal, *J. Chem. Soc., Chem. Commun.* 1338 (1985).
183. A. A. Dembek, P. J. Fagan, and M. Marsi, *Macromolecules* **26**, 2292 (1993).
184. A. A. Dembek, P. J. Fagan, and M. Marsi, *Polym. Mater. Sci. Eng.* **71**, 158 (1994).
185. A. S. Abd-El-Aziz, E. K. Todd, and K. M. Epp, *Polym. Prepr. (Am. Chem. Soc. Dic. Polym. Chem.)* **39**, 300 (1998).
186. A. S. Abd-El-Aziz, E. K. Todd, and K. M. Epp, *J. Inorg. Organomet. Polym.* **8**, 127 (1998).
187. A. S. Abd-El-Aziz, E. K. Todd, and G. Z. Ma, *J. Polym. Sci., Part A: Polym. Chem.* **39**, 1216 (2001).
188. C. R. de Denus, L. M. Hoffa, E. K. Todd, and A. S. Abd-El-Aziz, *J. Inorg. Organomet. Polym.* **10**, 189 (2000).
189. A. S. Abd-El-Aziz, C. R. de Denus, M. J. Zaworotko, and L. R. MacGillivray, *J. Chem. Soc. Dalton Trans.* 3375 (1995).
190. A. S. Abd-El-Aziz, C. R. de Denus, K. M. Epp, S. Smith, R. J. Jaeger, and D. T. Pierce, *Can. J. Chem.* **74**, 650 (1996).
191. A. S. Abd-El-Aziz, D. A. Armstrong, S. Bernardin, and H. M. Hutton, *Can. J. Chem.* **74**, 2073 (1996).
192. R. Atencio, L. Brammer, S. Fang, and F. C. Pigge, *New J. Chem.* **23**, 461 (1999).
193. L. Brammer, J. C. Mareque Rivas, R. Atencio, S. Fang, and F. C. Pigge, *J. Chem. Soc., Dalton Trans.* 3855 (2000).
194. K. Martin, M. Dotson, M. Litterer, T. W. Hanks, and C. Veas, *Synth. Met.* **78**, 161 (1996).
195. K. F. Martin and T. W. Hanks, *Organometallics* **16**, 4857 (1997).
196. J. Ohshita, T. Hamaguchi, E. Toyoda, A. Kunai, K. Komaguchi, M. Shiotani, M. Ishikawa, and A. Naka, *Organometallics* **18**, 1717 (1999).

197. F. S. Arimoto and A. C. Haven Jr., *J. Am. Chem. Soc.* **77**, 6295 (1955).
198. C. U. Pittman Jr., R. L. Voges, and W. R. Jones, *Macromolecules* **4**, 298 (1971).
199. C. U. Pittman Jr. and B. Surynarayanan, *J. Am. Chem. Soc.* **96**, 7916 (1974).
200. C. U. Pittman Jr., *Macromolecules* **7**, 396 (1974).
201. C. U. Pittman Jr., P. L. Grube, O. E. Ayers, S. P. McManus, M. D. Rausch, and G. A. Moser, *J. Poly. Sci., Part A-1* **10**, 379 (1972).
202. R. Deschenaux, F. Turpin, and D. Guillon, *Macromolecules* **30**, 3759 (1997).
203. R. Deschenaux, I. Jauslin, U. Scholten, F. Turpin, D. Guillon, and B. Heinrich, *Macromolecules* **31**, 5647 (1998).
204. G. Wilbert and R. Zentel, *Macromol. Chem. Phys.* **197**, 3259 (1996).
205. M. E. Wright, E. G. Toplikar, R. F. Kubin, and M. D. Seltzer, *Macromolecules* **25**, 1838 (1992).
206. N. Kuramoto, Y. Shishido, and K. Nagai, *J. Polym. Sci., Part A: Polym. Chem.* **35**, 1967 (1997).
207. E. W. Neuse, M. C. Meirim, D. D. N"Da, and G. Caldwell, *J. Inorg. Organomet. Polym.* **9**, 221 (1999).
208. B. Schechter, G. Caldwell, and E. W. Neuse, *J. Inorg. Organomet. Polym.* **10**, 177 (2000).
209. E. W. Neuse, *Macromol. Symp.* **172**, 127 (2001).
210. B. Chaudret, G. Chung, and Y.-S. Huang, *J. Chem. Soc., Chem. Commun.* 749 (1990).
211. A. S. Abd-El-Aziz, E. K. Todd, G. Z. Ma, and J. Di Martino, *J. Inorg. Organomet. Polym.* **10**, 265 (2000).
212. S. F. Mapolie, J. R. Moss, and G. S. Smith, *J. Inorg. Organomet. Polym.* **7**, 233 (1997).
213. N. Fujita and K. Sonogashira, *J. Polym. Sci.* **12**, 2845 (1974).
214. A. D. Pomogailo, N. M. Bravaya, V. F. Razumov, I. S. Voloshanovskii, N. A. Kitsenko, V. V. Berezovskii, A. I. Kuzaev, and A. G. Ivanchenko, *Russ. Chem. Bull.* **45**, 2773 (1996).
215. I. Manners, G. H. Riding, J. A. Dodge, and H. R. Allcock, *J. Am. Chem. Soc.* **111**, 3067 (1989).
216. H. R. Allcock, A. A. Dembek, and E. H. Klingenberg, *Macromolecules* **24**, 5208 (1991).
217. T. Peckham, P. Nguyen, S. C. Bourke, Q. Wang, D. G. Harrison, P. Zoricak, C. Russell, L. M. Liable-Sands, A. L. Rheingold, A. J. Lough, and I. Manners, *Organometallics* **20**, 3035 (2001).
218. D. Albagli, G. Bazan, M. S. Wrighton, and R. R. Schrock, *J. Am. Chem. Soc.* **114**, 4150 (1992).
219. D. Albagli, G. Bazan, R. R. Schrock, and M. S. Wrighton, *J. Am. Chem. Soc.* **115**, 7328 (1993).
220. A. S. Abd-El-Aziz, L. J. May, J. A. Hurd, and R. M. Okasha, *J. Polym. Sci., Part A: Polym. Chem.* **39**, 2716 (2001).
221. A. S. Abd-El-Aziz, L. J. May, and A. L. Edel, *Macromol. Rapid Commun.* **21**, 598 (2000).
222. A. S. Abd-El-Aziz, A. L. Edel, K. M. Epp, and H. M. Hutton, *New J. Chem.* **23**, 569 (1999).
223. A. S. Abd-El-Aziz, A. L. Edel, L. J. May, K. M. Epp, and H. M. Hutton, *Can. J. Chem.* **77**, 1797 (1999).
224. I. Cuadrado, M. Moran, C. M. Casado, B. Alonso, and J. Losada, *Coord. Chem. Rev.* **193–195**, 395 (1999).
225. M. A. Hearshaw, A. T. Hutton, J. R. Moss, and K. J. Naidoo, in G. R. Newkome, ed., *Advances in Dendritic Macromolecules*, Vol. **4**, JAI Press, Greenwhich, Conn., 1999, p. 1.

226. F. J. Stoddart and T. Welton, *Polyhedron* **18**, 3575 (1999).
227. M. A. Hearshaw and J. R. Moss, *Chem. Commun.* 1 (1998).
228. N. Ardoin and D. Astruc, *Bull. Soc. Chem. Fr.* **132**, 875 (1995).
229. C. Valerio, S. Rigaut, J. Ruiz, J.-L. Fillaut, M.-H. Delville, and D. Astruc, *Bull. Pol. Acad. Sci.* **46**, 309 (1998).
230. P. Lange, A. Schier, and H. Schmidbaur, *Inorg. Chem.* **35**, 637 (1996).
231. S. Takahashi, K. Onitsuka, and F. Takei, *Macromol. Symp.* **156**, 69 (2000).
232. A. M. McDonagh, M. G. Humphrey, M. Samoc, and B. Luther-Davies, *Organometallics* **18**, 5195 (1999).
233. C.-F. Shu. and H.-M. Shen, *J. Mater. Chem.* **7**, 47 (1997).
234. S. Nlate, J. Ruiz, J.-C. Blais, and D. Astruc, *Chem. Commun.* 417 (2000).
235. S. Nlate, J. Ruiz, V. Sartor, R. Navarro, J.-C. Blais, and D. Astruc, *Chem. Eur. J.* **6**, 2544 (2000).
236. J.-L. Fillaut, J. Linares, and D. Astruc, *Angew. Chem., Int. Ed. Engl.* **33**, 2460 (1994).
237. C. Valerio, J.-L. Fillaut, J. Ruiz, J. Guittard, J.-C. Blais, and D. Astruc, *J. Am. Chem. Soc.* **119**, 2588 (1997).
238. E. Alonso, C. Valerio, J. Ruiz, and D. Astruc, *New J. Chem.* **21**, 1139 (1997).
239. R. Deschenaux, E. Serrano, and A.-M. Levelut, *Chem. Commun.* 1577 (1997).
240. B. Dardel, R. Deschenaux, M. Even, and E. Serrano, *Macromolecules* **32**, 5193 (1999).
241. R. Castro, I. Cuadrado, B. Alonso, C. M. Casado, M. Moran, and A. E. Kaifer, *J. Am. Chem. Soc.* **119**, 5760 (1997).
242. K. Takada, D. J. Diaz, H. D. Abruna, I. Cuadrado, C. M. Casado, B. Alonso, M. Moran, and J. Losada, *J. Am. Chem. Soc.* **119**, 10763 (1997).
243. I. Cuadrado, C. M. Casado, B. Alonso, M. Moran, J. Losada, and V. Belsky, *J. Am. Chem. Soc.* **119**, 7613 (1997).
244. C. M. Casado, B. Gonzalez, I. Cuadrado, B. Alonso, M. Moran, and J. Losada, *Angew. Chem., Int. Ed.* **39**, 2135 (2000).
245. Y.-H. Liao and J. R. Moss, *Organometallics* **15**, 4307 (1996).
246. F. Moulines and D. Astruc, *J. Chem. Soc., Chem. Commun.* 614 (1989).
247. F. Moulines, L. Djakovitch, R. Boese, B. Gloaguen, W. Thiel, J.-L. Fillaut, M.-H. Delville, and D. Astruc, *Angew. Chem., Int. Ed. Engl.* **32**, 1075 (1993).
248. J.-L. Fillaut and D. Astruc, *New J. Chem.* **20**, 945 (1996).
249. S. Rigaut, M.-H. Delville, and D. Astruc, *J. Am. Chem. Soc.* **119**, 11132 (1997).
250. A. S. Abd-El-Aziz, E. K. Todd, and T. H. Afifi, *Macromol. Rapid Commun.* **23**, 113 (2002).
251. J. W. Kriesel, S. Konig, M. A. Freitas, A. G. Marshall, J. A. Leary, and T. D. Tilley, *J. Am. Chem. Soc.* **120**, 12207 (1998).
252. F. Lobete, I. Cuadrado, C. M. Casado, B. Alonso, M. Moran, and J. Losada, *J. Organomet. Chem.* **509**, 109 (1996).
253. D. Armspach, M. Cattalini, E. C. Constable, C. E. Housecroft, and D. Phillips, *Chem. Commun.* 1823 (1996).
254. V. Marvaud and D. Astruc, *Chem. Commun.* 773 (1997).
255. E. C. Constable, *Chem. Commun.* 1073 (1997).
256. S. Achar, C. E. Immoos, M. G. Hill, and V. J. Catalano, *Inorg. Chem.* **36**, 2314 (1997).
257. G. R. Newkome and E. He, *J. Mater. Chem.* **7**, 1237 (1997).
258. G. R. Newkome, E. He, and L. A. Godinez, *Macromolecules* **31**, 4382 (1998).
259. M. Osawa, M. Hoshino, S. Horiuchi, and Y. Wakatsuki, *Organometallics* **18**, 112 (1999).
260. S. Achar and R. J. Puddephatt, *Angew. Chem., Int. Ed. Engl.* **33**, 847 (1994).

261. S. Achar, J. J. Vittal, and R. J. Puddephatt, *Organometallics* **15**, 43 (1996).
262. G.-X. Liu and R. J. Puddephatt, *Organometallics* **15**, 5257 (1996).
263. N. J. Hovestad, J. L. Hoare, J. T. B. H. Jastrzebski, A. J. Canty, W. J. J. Smeets, A. L. Spek, and G. van Koten, *Organometallics* **18**, 2970 (1999).

ALAA S. ABD-EL-AZIZ
The University of Winnipeg

METALLOCENE CATALYSTS.

See SINGLE-SITE CATALYSTS

METALLOCENES

Scope

Although the traditional usage of the term *metallocene* has encompassed sandwich structures containing two rings of five carbons each bound through all atoms to a central metal atom, common parlance in the field of olefin polymerization has expanded this definition to include structures having only one C_5 ring or none. The term is now applied to all single-site catalysts (qv) (ie, all catalysts having a single, well-defined active-center structure), in some cases restricted to complexes of the early- and middle-transition metals and lanthanides, to distinguish the catalysts from the recent families discovered by Brookhart and others based on late-transition metals. For the purposes of this publication, we equate the word *metallocene* with the family of compounds containing at least one C_5 ring (or analogous heterocycle) bound to an early-transition-metal or f-block atom that, in the presence of a cocatalyst if required, effect the polymerization of ethylene and other α-olefins. We will concentrate on those complexes, predominantly bis(cyclopentadienyl)zirconium(IV) compounds, that polymerize ethylene and propylene with high efficiency.

Historical Background

Although the discovery of $(C_5H_5)_2Fe$ (ferrocene), first reported by Kealy and Paulson in 1951 (1) but recognized as a sandwich compound by Wilkinson and co-workers (2), brought into being a new family of complexes that contain the Cp_2M ($Cp = C_5H_5$) fragment, it was not until the discoveries of Sinn and Kaminsky in the late 1970s that metallocenes, and specifically zirconocenes, were recognized

Encyclopedia of Polymer Science and Technology. Copyright John Wiley & Sons, Inc. All rights reserved.

as powerful olefin polymerization catalyst precursors. (For a good discussion of the succession of discoveries leading to the Kaminsky system, see Refs. 3) This work brought together two strands of research: (*1*) the investigation of the alkylation and polymerization chemistry of Cp_2MX_2 (M = Ti, Zr) (4,5), which had begun soon after the first reports of titanocene dichloride; and (*2*) the observation that small amounts of water added to the medium of certain Ziegler–Natta ethylene polymerizations caused marked increases in the rate of enchainment. It was the finding (by many accounts serendipitous) that large amounts of moisture, when added to the conventional Ziegler–Natta cocatalyst trimethylaluminum, dramatically improved the activity of mixtures of the aluminum alkyl with metallocenes, that set into motion the wave of industrial and academic research in this area.

Although the activities of the new metallocene catalysts were quite remarkable ($>1 \times 10^6$ g(PE)/mmol(Zr)), they would have probably remained a laboratory curiosity had they not exhibited a crucial characteristic: they were homogeneous. (Here we understand homogeneous to mean soluble and also having a single active-site structure.) Single-site catalysts were known, of course, for olefin polymerization. Catalysts based on vanadium had produced polymers with molecular weight distributions (M_w/M_n) of about 2, the value expected for ideal single-site behavior in polymerization and chain transfer. However, the vanadium family of single-site catalysts had aspects of its chemistry that made it less attractive to academic work and also to commercialization. First, these catalysts are generally mixtures of vanadium complexes of hard inorganic ligands such as halides, oxides, or acetylacetonate groups, most if not all of which would be expected to be lost upon reaction with a large excess of trialkylaluminum or chlorinated aluminum alkyl compound. Because of this, the precursor to the active catalyst generally lacks modifiable substituents that persist in the active complex, making group substitution and structure–property trend analysis futile. The paramagnetism of vanadium catalysts also precludes NMR spectroscopy, a key tool for characterization. Also, because of the generally low activity and temperature sensitivity of the vanadium-based single-site catalysts, use of these catalysts in modern large-scale industrial settings has been difficult, because such important processes as Union Carbide's UNIPOL or the slurry process of Phillips Petroleum have eliminated ash removal, and also require fairly high reaction temperatures (40–110°C) for a commercially acceptable operation, as dictated by the economics of heat transfer from the reactor. The early non–aluminoxane-based titanium catalysts (such as $Cp_2TiCl_2/(C_2H_5)_2AlCl$ (4)) were homogeneous, but not extremely active.

In one stroke, the discovery of methylaluminoxane (the product of the partial hydrolysis of trimethylaluminum) gave to researchers a system of interest to both the synthetic chemist and the reaction engineer. Thus we have seen a flowering of chemical discovery and innovation in open and patent literatures alike, as investigators have taken advantage of the stability of the Cp—M linkage during polymerization and have introduced substituents that change the active-site behavior in myriad ways. Driven as much by the desire for a degree of novelty that would confer patent protection as by the thirst for knowledge, researchers have extended the range of single-site catalysts far beyond those having Cp groups. The rise of metallocenes has in large part legitimized the study of olefin polymerization among "serious" organometallic chemists, and in turn, has forced captains of industry to become more fluent with the fundamentals of synthetic and mechanistic

chemistry than seemed possible only decades ago. One suspects that the ramifications of both changes will be felt for years to come, regardless of the ultimate commercial acceptance of metallocene polymerization technology.

Properties of Metallocenes

Structure and Bonding. Both bis- and mono-Cp complexes of early transition metals are marked by a pseudo-octahedral environment, which is evident from the bond angle between the halide atoms of zirconocene dichloride, for example, of 90°. The angle formed from the metal atom and the two centroids of the Cp rings in bis-Cp complexes is generally about 120°, although this can be raised or lowered, with the latter effect being more common, through the addition of bridging groups between the rings. Metallocenes useful for polymerization generally have d^0 electronic configurations, and are thus diamagnetic. Complexes containing Cp rings alone are usually weakly colored, often yellow–gold, but the fusion of an aromatic ring to the Cp ring results in a much stronger coloration, presumably because of L–M (π–d^*) transitions.

The molecular orbitals involved in bonds between the Cp_2M fragment and the remaining, nonring ligands are shown in Figure 1, adapted from Lauher and Hoffmann (6). In d^0 systems such as Cp_2ZrCl_2, the electrons filling these orbitals are derived solely from the non-Cp ligands. Alteration of the metallocene geometry, or in the electronic properties of any of the ligands will obviously change the energies of the molecular orbitals, with consequences for metal–alkyl reactivity. Because of the lack of metal-based electron density, however, Group IVB metallocenes are not strongly influenced by acceptor orbitals on non-Cp ligands such as the π^* orbitals of ethylene or CO.

Chemical Reactivity. Group IVB metallocenes are moderately air-stable compounds unless (*1*) there is a highly basic carbanion attached, either in the form of a highly alkylated Cp ring or a polycyclic C_5-containing ligand, or (*2*) there is an alkyl group attached directly to the metal; in the latter case the compound is extremely water- and oxygen-sensitive, and often decomposes upon heating or exposure to strong light. The hydrolysis products of Group IVB metallocene dichlorides are generally HCl and zirconia, as well as a mixture of organic compounds.

Preparation. Group IVB metallocenes and Lanthanocenes are conventionally prepared by ligand exchange between lithium or Grignard reagents and metal chlorides (eqs. 1a and 1b). Often the metal chlorides are present as etherate complexes; such complexes need to be prepared carefully, as the reaction is unusually exothermic.

$$m\ \mathrm{Cp'Li} + \mathrm{MX}_n \longrightarrow \mathrm{Cp'}_m\mathrm{MX}_{(n-m)} + m\ \mathrm{LiX} \tag{1a}$$

$$m\ \mathrm{Cp'MgX} + \mathrm{MX'}_n \longrightarrow \mathrm{Cp'}_m\mathrm{MX'}_{(n-m)} + m\ \mathrm{MgXX'}$$

[X,X′ = halide; M = transition metal; Cp′ = (substituted) cyclopentadienyl] (1b)

Milder preparatory schemes include the reaction of silyl or stannyl cyclopentadienides with metal halides, as shown in equation 2. (For the application of this

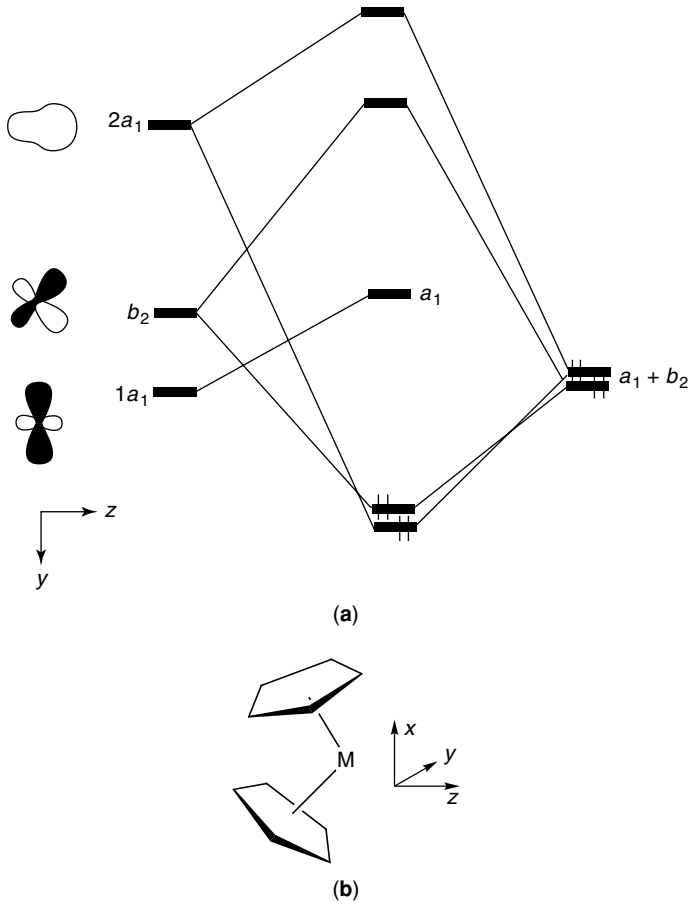

Fig. 1. (**a**) Orbitals responsible for metal–hydride bonding in Cp_2TiH_2. Left-hand orbitals derive from Cp_2Ti^{2+}, while the in-phase and out-of-phase combinations of the two H^- 1*s* orbitals are on the right. Coordinates defined in (**b**). Reprinted with permission from Ref. 6. Copyright (1976) American Chemical Society.

reaction to bridging ligands, see Ref. 7.) This method is especially well suited to the preparation of titanocenes, as the use of a strongly reducing metal alkyl such as LiCp is avoided. Another route to metallocenes involves the reaction of the neutral mono- or bis-Cp ligand with a metal tetraamide (eq. 3). This pathway has been demonstrated by Jordan (8) to allow the preparation of racemic bis(indenyl) zirconium compounds in high selectivity. Aluminum complexes of bis(indene) ligands will also undergo transmetallation reactions with zirconium tetraamides in high yield (9).

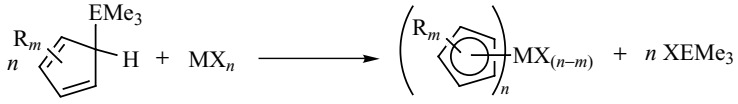

(2)

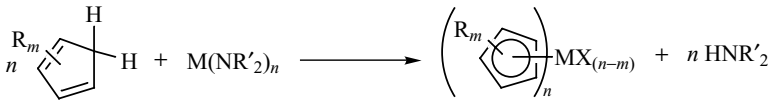

[X = halide; M = transition metal; E = Si, Ge, Sn] (3)

Toxicity. There is little known of the effects on living organisms of metallocene precursors beyond those of the parent compounds Cp_2MCl_2 (M = Ti, Zr). Titanocene dichloride has been reported (10) to be a potentially useful anticancer agent, while the zirconium analogue has been identified as a mutagen in at least one toxicological report (11). Prudence dictates that extreme care should be exercised with metallocenes, particularly those with polycyclic aromatic groups.

Cocatalysts for Polymerization

Aluminoxanes.

Health and Safety Considerations. Solutions of MAO are generally nonpyrophoric because of the low volatility of toluene. However, if toluene is removed, a finely divided white powder remains that is extremely air- and water-reactive, and will often spontaneously burst into flame. Contact of MAO or its solutions with water usually results in an immediate explosion, but caution must be maintained even after the initial reaction, because, similar to other aluminum alkyl reagents, MAO often forms a crust of alumina when hydrolyzed quickly. This crust tends to protect the remaining alkyl, and disturbing it without care may cause a second violent reaction.

Similar safety considerations apply to modified MAO, although when solvent has been removed these materials are often glasses or viscous oils. Modified MAO solutions in light alkanes such as isopentane may form dangerous mixtures with air because of the volatility of the solvent and the presence of an intrinsic source of ignition.

Methylaluminoxane. Methylaluminoxane (MAO) is prepared from the controlled hydrolysis (eq. 4) of trimethylaluminum (TMA), usually in toluene.

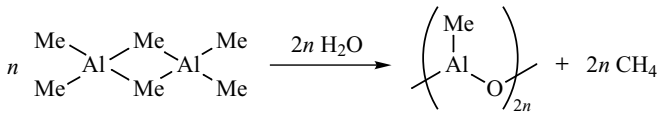

(4)

This is an extremely exothermic reaction and poses great hazards, as large amounts of heat and gas must be safely removed. Early workers employed hydrated inorganic salts as a controllable method for addition of water, but it appears that this procedure is not practiced commercially. The patent literature suggests that the main suppliers of MAO (Albemarle, Akzo Nobel, and Witco) add water directly, either by use of moist nitrogen or a marginally wet aromatic solvent. The precautions necessary for the synthesis of MAO add to the cost of this material, which suffers as well from the expense of TMA, which cannot be made by the normal routes available for the higher trialkylaluminum compounds, such as the

addition of olefin to AlH_3. MAO solutions normally have methyl/Al ratios greater than 1, reflecting the fact that some TMA (about 30 mol% on an Al basis) must be present for the solution to be stable. NMR analysis suggests that much of the excess methyl content, at least, is present as TMA [as opposed to $((CH_3)_2Al)_2O$), although it may be complexed to the MAO.

The function of the excess TMA is the focus of considerable controversy. To it have been ascribed the roles of alkylating agent, ionizing agent, chain-transfer agent, and deactivator. TMA can be removed, at least partially, by vacuum distillation, leaving a toluene-soluble material, which remains a competent activator for metallocene polymerization.

As noted above, the initial high activity metallocene catalysts involved zirconocenes and titanocenes mixed with methylaluminoxane. MAO is a poorly understood mixture of oligomers (generally with degree of polymerization of about 20), despite years of study. It can accurately be characterized by its proton NMR spectra, its methyl content, and its average molecular weight, but proposed structures for specific MAO oligomers or subunits remain highly speculative. As will be discussed in greater detail, the two actions of MAO are alkylation and activation by Lewis acid methyl anion abstraction. The key to the activity of MAO-activated metallocenes is the degree to which the anion formed from this process is relatively inert and well separated from the metallocene cation, which has only 14 valence electrons and tends to form bridging complexes such as shown in equation 5 and 1a with ordinary aluminum alkyls.

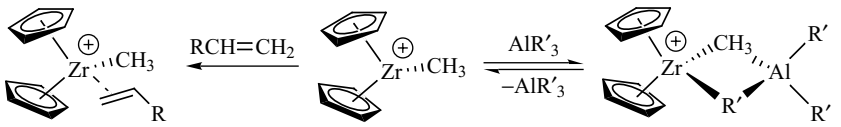

(5)

While the origin of the ability of MAO to effectively abstract methide and remain loosely associated with the metallocene is not well understood, the most convincing proposal comes from the work of Barron, in which structural studies of analogous oligomeric *t*-butylaluminoxanes (12) and their exchange reactions with $Cp_2Zr(CH_3)_2$ have led to the concept of "latent Lewis acidity," which can be paraphrased as a potential for the drum-like subunit of the structure of the aluminoxane to reversibly open up a highly electrophilic tricoordinate aluminum atom for methide abstraction, resulting in an anion of high stability and bulk, factors that militate for a weak ion–pair interaction (eq. 6).

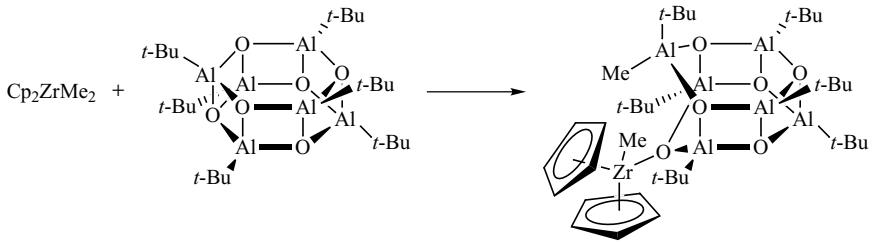

(6)

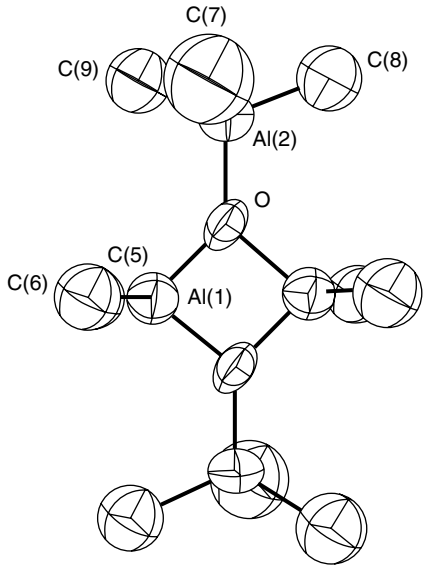

Fig. 2. Structure of $[Me_3)Al(OAlMe_2)]_2$ dianion. Reproduced from Ref. 13 by permission of The Royal Society of Chemistry.

The two crystal structures that come closest to shedding light on the actual form of MAO are shown in Figures 2 and 3, structures for a dianion of a MAO oligomer (13) and of a *t*-butylaluminoxane hexamer (14).

In practice, it has been found that MAO must be used at fairly high atomic ratio of Al to transition metal, conventionally between 300 and 10,000, although this is not necessarily the case when immobilized systems are used. For example,

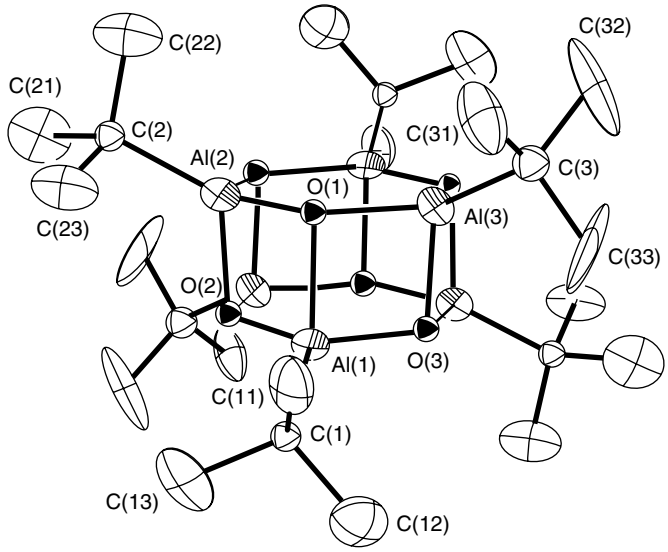

Fig. 3. Crystal structure of $(Al(t\text{-}Bu)O)_6$. Reprinted with permission from Ref. 14. Copyright (1993) American Chemical Society.

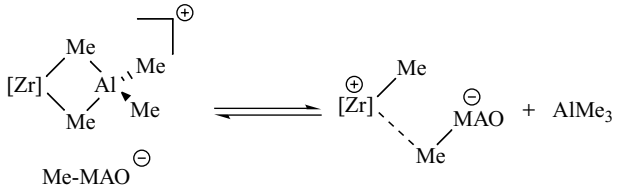

Scheme 1.

most of the silica-supported metallocene/MAO catalysts reported in the patent literature employ Al/Zr ratios of between 100 and 300. The high ratios required have led to speculation that there exists a particular oligomer or family of oligomers that perform the bulk of the activation. Experiments done by Sishta and co-workers have shown (15) that a very low Al/Zr ratio—perhaps representing the reaction of one molecule of MAO per metallocene—is sufficient to produce NMR spectra similar to those for much higher ratios. This result hints that the additional MAO is required either for scavenging of poisons, reactivation of metallocene in a dormant state, or agglomeration of MAO oligomers following activation of the metallocene, leading to larger anions and hence looser ion pairs. Recent NMR experiments led by Brintzinger have suggested that the large MAO counterion contains 150–200 aluminum atoms, and have given weight to the theory that the main effect of increasing Al/Zr ratio is to shift the equilibrium between coordinatively saturated zirconocene–trimethylaluminum dimers and ion pairs with more accessible open sites (Scheme 1) in favor of the latter (16).

Modified Methylaluminoxane. The fact that MAO is only soluble in aromatic solvents can present problems in handling; often a highly pyrophoric solid precipitates when these solutions are mixed with other reagents. For this reason, as well as to limit the consumption of expensive TMA, much effort was expended in making MAO soluble in aliphatic solvents, principally by replacing some of the methyl groups with higher alkyl substituents. The most commercially successful reagents, known as modified methylaluminoxanes, contain up to 30 mol% of isobutyl substitution. These complexes are made either by direct hydrolysis of a mixture of TMA and higher aluminum alkyl compound, or by a number of more exotic processes, and are extremely soluble in hexane or isopentane. Catalysts prepared from modified MAO are of comparable activity to those activated by MAO.

A nonhydrolytic method of making MAO has been described (17); it apparently results in an aluminoxane much reduced in residual TMA, which harms certain catalysts, yet of similar shelf life to conventional MAO. The procedure uses a carbonyl compound as the initial oxygen source (eq. 7a, 7b 7c), then calls for alkoxide ligand fragmentation and secondary hydrolysis to make the final product.

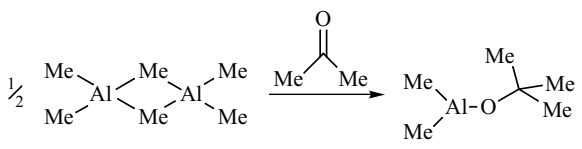

(7a)

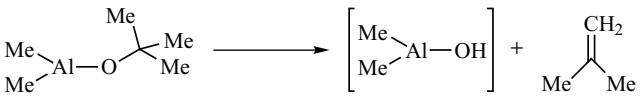

(7b)

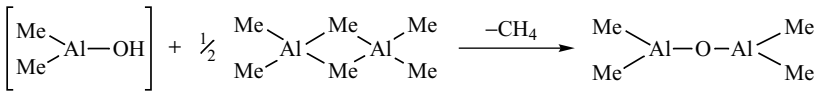

(7c)

Discrete Activators. MAO is a troublesome activator for several reasons. More expensive on a molar basis than cocatalysts such as $Al(C_2H_5)_3$ used by Ziegler–Natta catalysts, MAO seemed until recently to require a very large molar ratio to transition metal, preventing metallocenes from competing with conventional catalysts on a cost basis. From an academic perspective, MAO, an ill-defined mixture, hinders the detailed analysis of active-site structure. Not surprisingly, many attempts have been made over the years to replace MAO, the most successful of which have given us discrete activators based on perfluorinated aryl groups.

There are three popular modes by which these cocatalysts ionize the metallocene (which must be alkylated by a different agent such as triisobutylaluminum): Lewis acid extraction of the alkylide group by a neutral Lewis acid (eq. 8) or by a carbocation (eq. 9) and protonolysis of the alkylide group (eq. 10). (Ionization may also occur through direct reaction of the alkylated metallocene by a strong oxidant such as $[Cp_2Fe^+][B(C_6F_5)_4^-]$ (18).)

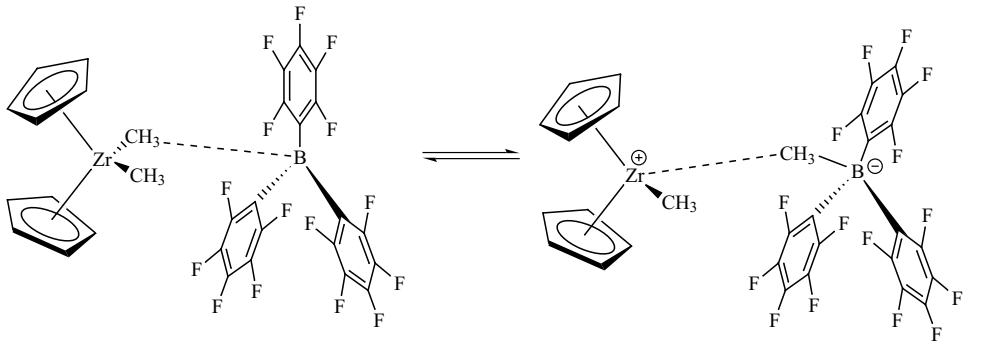
F
F
F
F
F
CH3
Zr
CH3
B
F
F
F
F

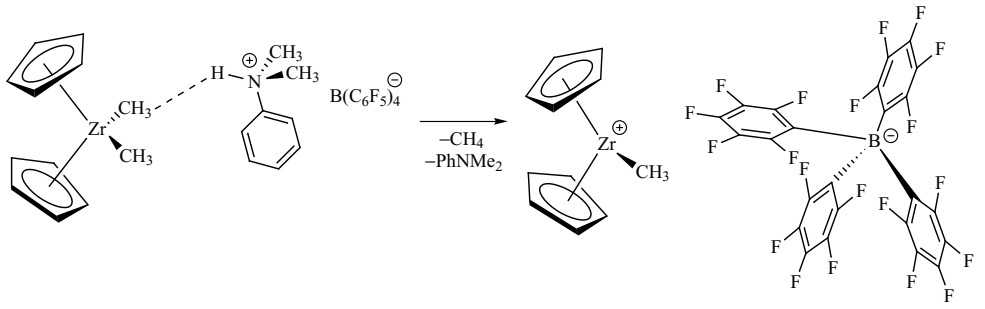

(10)

The first pathway, extensively studied by Marks and co-workers, is a rapidly reversible ionization (19). The second two routes, actually discovered prior to reaction 8 by scientists at Exxon and Fina, are technically irreversible, as one of the by-products is a kinetically unreactive alkane. (For protonation, see Ref. 20 and for methyl transfer, see Ref. 21.) In practice, more than one equivalent of discrete activator is usually employed. While the source of this requirement is still unknown, candidates include reactions with the trialkylaluminum species (present in excess as alkylating agents) that destroy the special activating power of the borane in equation 8 or the inertness of the anions in equations 9 and 10. Another possible culprit is the formation of dormant alkyl-bridged metallocene dimers (22). In equation 10, one of the by-products is a trisubstituted amine that might be expected to trap the coordinatively unsaturated cation formed in this reaction. (*N*,*N*-Dimethylaniline is shown, but is not exclusively used; tri-*n*-butylamine is another common component of the activator.) However, it does not appear to diminish catalytic activity. Variations on the structure of $B(C_6F_5)_n^-$ have been explored, including aluminum substitution for boron (23), silylation of the arene (24), and the use of larger perfluoroaryl substitutuents (24,25). Not surprisingly, activity rises with the size of the counterion. Use of the nonperfluorinated aryl groups phenyl (26), *p*-fluorophenyl (27), and 3,5-bis(trifluoromethyl)phenyl gives a zwitterionic catalyst (eq. 11), a fluorine-bridged ion pair (eq. 12), and a weakly active titanocene catalyst at low temperature (28), respectively. (This counterion has been used extensively by Brookhart and co-workers, especially for the activation of single-site cyclopentadienylcobalt polymerization catalysts; see Ref. 29.) In equation 12, activity appears to be high only for the metallocene $(C_5(CH_3)_5)_2Zr(CH_3)_2$, whose steric congestion is probably responsible for preventing decomposition.

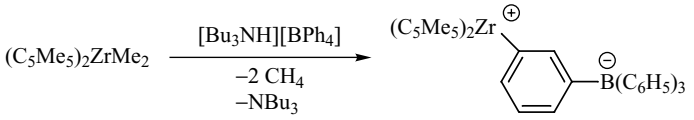

(11)

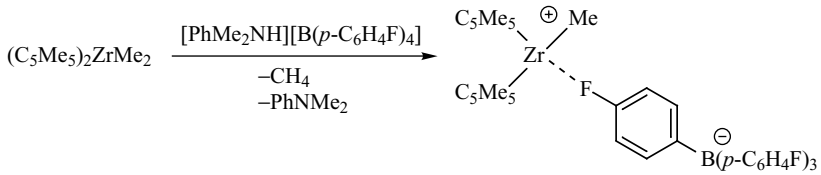

(12)

Other noncoordinating anions have been discovered that enable high activity polymerization. Among these are the metallacarboranes $[(C_2B_9H_{11})_2M]^-$ (M = Fe, Co, Ni), where catalyst ionization is by protic abstraction by an ammonium ion (30).

Commercially, Dow appears to have implemented activation by well-defined cocatalyst for its Insite solution-phase metallocene process. Aside from historical priority, one reason for the persistent use of MAO is that the perfluorinated boron compounds are difficult to prepare, thus raising their expense. (One of the intermediates, $(C_6F_5)Li$, must be handled at very low temperature to prevent violent decomposition.) Another is that, unlike the MAO systems, catalysts activated by discrete activators have no large excess of alkylaluminum to scavenge poisons from the reaction medium, while common scavengers may hinder activity by consuming the expensive activator.

Other Methods of Activation. Despite some early claims (31), the evidence for metallocene activation by simple trialkylaluminum compounds has not accumulated. Activation by alternate aluminoxanes such as isobutylaluminoxane (IBAO) has also been attested (32). The fact that these much cheaper methods have not consigned MAO to the ash-heap of history speaks, perhaps, of some limitations in these alternatives.

Some support materials can be rendered Lewis acidic enough to ionize dialkyl metallocenes. Marks and co-workers have reported (33) that alumina dried at very high temperatures can react at least to some small degree with both thorium- and zirconium-based metallocene dimethyl species to yield active catalysts for polyethylene. The resulting cationic metal center is believed to remain coordinated to the surface through an Al–O–M Lewis acid/base linkage, at least prior to exposure to ethylene. Hybrid surface/cocatalyst systems based on aluminum alkyl-treated clays have been developed (34) in which the solid substrate appears to play some role in promoting polymerization activity far beyond that expected for non–methyl aluminoxane- or trialkylaluminum-activated catalysts.

Forms of Catalyst Delivery

Porous Silica Supports. While single-site catalysts continue to be studied in solution polymerizations, especially in academic laboratories, the adaptation of metallocene technology to existing industrial processes has generally entailed the immobilization of the homogeneous catalyst on a solid surface of well-controlled morphology and porosity. Generally speaking, the support favored is amorphous silica containing fairly high pore volume (>1 cm^3/g) and average particle diameter of about 50 μm. Early on it was discovered that the extremely high atomic ratios of MAO to zirconium that had been needed to obtain high activity in solution polymerization were unnecessary when the catalyst was supported. (Excellent activities based on supported metallocene/MAO catalysts with Al/Zr <100 are reported in Ref. 35.) This has greatly facilitated the commercialization of metallocenes. Supporting the catalyst can have consequences for the reactivity pattern of the metallocene (36), indicating that the aluminoxane, when covalently bound to the silica surface through one or more Si–O–Al groups (each formed from the silanolysis of an Al—Me bond), displays different ion–pairing dynamics with

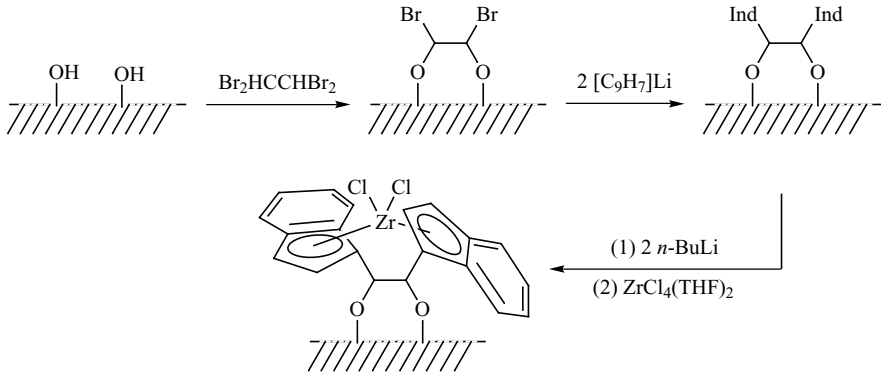

Fig. 4. Overview of bridge-anchored ansa-metallocene synthesis (Ref. 43).

the metallocene relative to the solution cocatalyst. Industrial research has yielded numerous examples of polymerization supports beyond silica, including alumina, zeolites, clays, and organic polymers. Metallocene catalysts have been covalently bound to polymer either through prior attachment of part of the ligand to a polymeric substrate (37), or through the incorporation of a pendent unsaturated group on the ligand itself into the growing polymer (38). In both cases, excellent particle morphology was claimed.

Alternate Modes of Catalyst Physisorption. Other forms of catalyst delivery to the reactor have been implemented. Catalyst solution has been injected directly into fluidized-bed gas-phase reactors (39), evidently creating a mist of *in situ* spray-dried catalyst. Spray-dried catalyst has been prepared *ex situ* as well, in an attempt to better control the morphology of the particles (40). Solid catalytically active materials have also resulted from precipitation of MAO by aliphatic solvent (41) and through a low conversion polymerization (prepolymerization) prior to introduction to the large-scale polymerization medium (42).

Supports as Part of Ligand Set. Solid supports bear functional groups that have been utilized as part of the ligand framework of metallocenes. Soga and co-workers covalently bound bridged metallocenes to silica through reaction of the surface silanols with reactive carbon halide or silicon halide bonds on the ligand bridge. The overview of the synthesis for one catalyst precursor is shown in Figure 4, with the indenyl rings in pseudo-racemic orientation because the high isotacticity of the polypropylene produced suggests a structural analogy to *rac*-Et$(Ind)_2ZrCl_2$. Activities were reported to be greatly superior to the homogeneous analogues (43).

Families of Metallocene Catalysts

In this section, we will briefly examine the salient features of the basic classes of metallocene catalysts. Polymerization activity comparisons and the mechanisms that govern polymerization will be treated in subsequent sections.

Group IVB Metallocenes.

Bis(cyclopentadienyl) Complexes. Representatives of the three most-intensively studied subfamilies of bis(Cp) metallocenes are **1**, **2**, and **3**. The parent

zirconocene (**1**) was the first to be exploited, and soon substitution of the Cp rings with alkyl groups and replacement of the Cp rings with indenyl and fluorenyl ligands was undertaken. Unbridged metallocenes of this sort exhibit a suite of characteristics that have caused their application in the commercial arena to be intense, but limited in scope. High activities are common to this family, and because of the relative ease of precatalyst synthesis, they are well suited to large-scale production of commodity grades of polyethylene. Facile chain transfer in the presence of α-olefin, however, renders these metallocenes nearly useless for making very low density copolymers of ethylene. With rare exception (covered in section Mixed Tacticity Polyolefins), they cannot polymerize α-olefins such as propylene with any degree of stereospecificity.

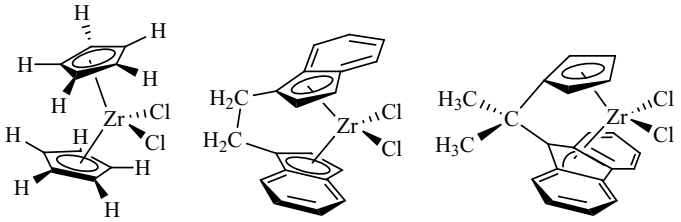

1 **2** **3**

Comparative studies of unbridged metallocene catalysts have indicated that, in general, alkylation of the Cp ring(s) causes an increase in polymerization activity, although substitution of all five carbons can lead to very low activities, as steric congestion prevents monomer approach. Bis(indenyl) and bis(fluorenyl)zirconium complexes have received far less attention, and in the latter case, this is almost certainly due to the greater lability of the fluorenyl–metal interaction.

Aside from the ubiquitous *n*-alkyl, halide, and alkoxide groups, metallocenes also bear carboxylate, trifluoromethanesulfonate (44), thiolate (45), and other more exotic moieties in addition to the Cp groups. It is commonly believed that these ligands are completely exchanged for alkyl groups originating on the aluminoxane in the case of MAO activation; however, this supposition does not imply that the groups have no effect on olefin polymerization as part of the counterion complex.

Monoanionic analogues of the cyclopentadienyl group have been explored. The bis(boratabenzene) complexes of Zr(IV) as in **4** have been shown by Bazan (46) to be catalysts for the oligomerization of ethylene to olefins, with the groups attached to boron influencing selectivity to α-olefin. Tethering the two C_5B rings (see structure **5**) tends to give polymer (47).

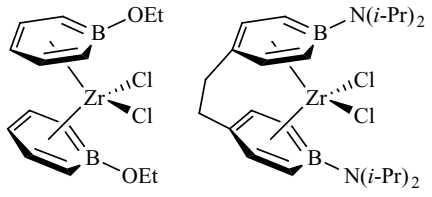

4 **5**

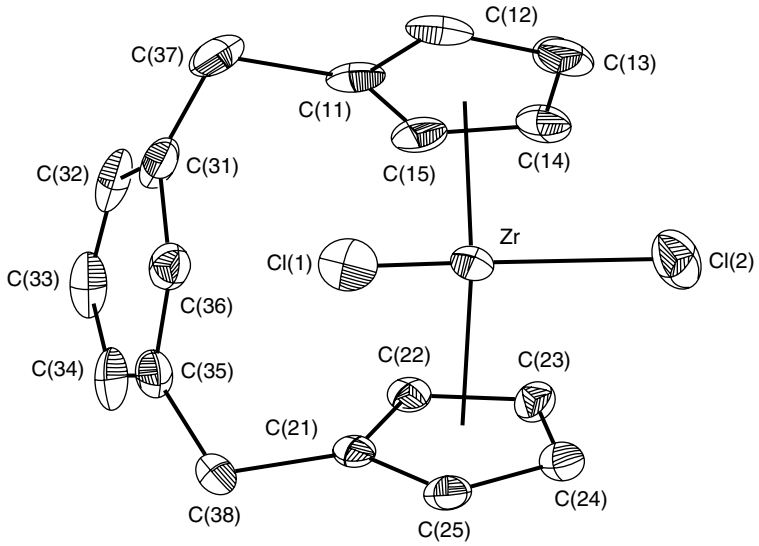

Fig. 5. Crystal structure of 1,3-bis(cyclopentadienylmethyl)benzenezirconium dichloride. Reproduced from Ref. 50 by permission of The Royal Society of Chemistry.

Bridged Metallocenes. The addition of a linkage between the two Cp rings has enabled the precise manipulation of the steric environment encountered by reactive molecules such as α-olefins, and the development of metallocenes for stereoregular olefin polymerization has proceeded from this advance (*vide infra*). The first and most widely employed bridges are $-[CR_2]_n-$ ($n = 1, 2$) and $-SiR_2-$ (R = methyl, phenyl), which are easily incorporated into ligands by reaction of two equivalents of Cp^- with α,ω-dibromoalkanes and dichlorosilanes, respectively. Increasing the bridge length generally increases the centroid–metal–centroid (Cp—M—Cp) angle, which can change polymerization characteristics. For example, the Cp—M—Cp angle rises in the series $(CH_2)_n(C_5H_4)_2TiCl_2$: 121° ($n = 1$); 128° ($n = 2$); 133° ($n = 3$) (48). The $-CH_2CH_2-$ and $-Si(CH_3)_2-$ bridges, by far the most popular bridging moieties, give rise to similar Cp—M—Cp angles, but the ethylene bridge allows a wide range of relative motion between the two halves of the ligand (49), which may lead to decreased molecular weight and stereocontrol in olefin polymerization relative to the more rigid silylene-bridged analogues. Increases in bridge length beyond that of 1,3-propanediyl generally lead to severe distortion, in which the bridge is rotated toward the wedge containing the nonchelating ligands, as in Figure 5 (50).

Bridging linkers also include R_2E (E = Ge, Sn) (51), as well as RB (52).

The Buchwald and Bercaw groups have reported (53,54) complexes in which two bridges tie the Cp rings together. The substituents on the Cp rings change the selectivity of olefin polymerization, as discussed in under Mixed Tacticity Polyobefins.

The bridging linkage need not be strictly covalent. In **6**, a bridged bis(cyclopentadienyl)zirconocene is depicted in which the two Cp's are connected via a Lewis acid–Lewis base interaction between P and B atoms attached to the

rings. A racemoid bis(indenyl) version gives highly isotactic PP at low temperatures, indicating the bridge is quite robust under polymerization conditions (55).

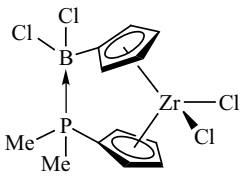

6

Bridges containing heteroatoms such as nitrogen that can bind directly to the transition metal have also been explored (56).

Siloxide (57) and amide (58) groups have been appended to Cp rings. Lewis acids such as Al atoms in MAO may reversibly coordinate to the heteroatom in these systems, leading to two distinct types of catalyst site and a bimodal distribution of polymer MW (59).

One of the perceived deficiencies of the early ethylene-bridged metallocenes in propylene polymerization was the relative lack of rigidity of the bridge. Several attempts have been made in recent years to make highly rigid bridged metallocenes, for example by use of cyclic groups in the bridge, as in **7** (60). Other uses of bulky bridges are to provide chiral centers, as in **8** (61), or to prevent the formation of mesoid isomers during synthesis due to bridge–ring repulsions, as in **9** (62).

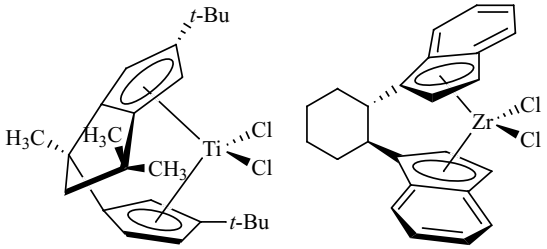

7

8

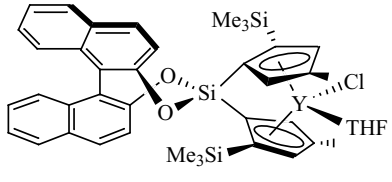

9

Polynuclear metallocene complexes may be produced through linking groups in which the alkyl group provides the bridge **10** (63). Other links may be through the Cp ring substituents, either indirectly, with a ferrocenyl bridge (64), or more directly through hydrocarbon-only linkages as in **11** (65).

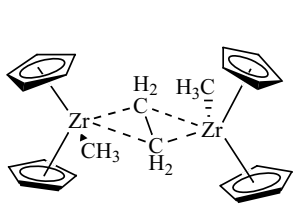

10

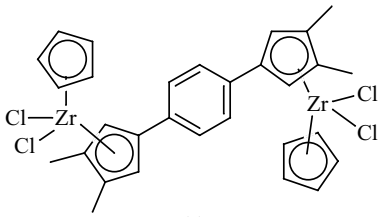

11

The aim of many of these investigations has been to facilitate cooperative behavior among the two or more catalytically active centers by forcing them to remain in proximity to each other. In some cases, positive enhancements in copolymerization have been observed (66).

Mono(cyclopentadienyl) Complexes. Metallocenes bearing a single cyclopentadienyl ring are not as widely used in polymerization as their bis-Cp cousins, but they display a distinct reactivity that makes them particularly suited to certain polymerizations. As with the bis-Cp metallocenes, they appear as both bridged and unbridged varieties, with structures **12** and **13** portraying the most prominent members of these respective families. The most successful of the mono-Cp catalyst precursors are titanocenes, which are distinguished from zirconocenes in having stable Ti(III) structures, such as **14**.

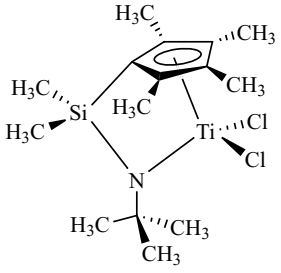

12

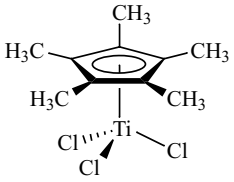

13

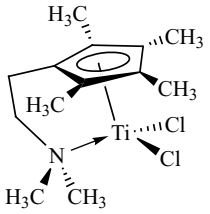

14

Mono-Cp complexes are generally prepared by the same routes as are the bis-Cp versions (see under preparation), but in addition they may be synthesized via comproportionation ($Cp'_2MX_2 + MX_4 = 2\ Cp'MX_3$; X = halide) (67) or by reaction of Cp salts with titanium compounds having only one substituent that is readily exchanged (68), such as $ClTi(OR)_3$.

Unbridged Complexes. Unbridged mono-Cp titanium complexes have been explored for polyethylene, but have found more consistent application in the area of polystyrene. In the latter case, reduction to Ti(III) appears to be necessary prior to entry into the polymerization cycle (69). Unbridged mono-Cp zirconocenes have been much scarcer in the polymerization literature. In many instances, the remaining substituents on the zirconium atom are divided into those ligands that are believed to exchange with aluminum alkyl groups and those assumed not to do so. The sole Cp ligand is thereby combined with a Cp analogue in a pseudo–bis-Cp metallocene–type active site arrangement, with catalytic performance typically intermediate between bis-Cp and bis-pseudo-Cp analogues. Cp

analogues include benzamidinate (70), tris(pyrazolyl)borate (71), and the chelating alkoxide (2-pyridyl)dimethylmethoxide (72). In the case of titanocenes, the strategy of mixing one Cp with a pseudo–Cp analogue has often led to the discovery of systems that far outperform typical bis- or mono-Cp catalysts, especially in the polymerization of ethylene and other α-olefins. These complexes are generally distinguished by significant steric bulk and a heteroatom with the potential for binding to titanium through multiple bonds. Two interesting examples from thisr subfamily are the phosphinimide complex **15** reported by Stefan and co-workers (73) and the phenoxide complex **16** described by researchers Sumitomo at (74). In both cases, activities are fairly good for ethylene/α-olefin copolymerization, and the levels of incorporated comonomer are high as well.

Recently, Baird and co-workers have reported (75) examples of polymerizations by a simple mono-Cp titanium complex, $(C_5(CH_3)_5)Ti(CH_3)_3$ activated with a Lewis acid ($B(C_6F_5)_3$) that not only copolymerizes ethylene and α-olefins but also induces polymerization of monomers normally associated with cationic polymerization such as isobutylene and vinyl ethers. Shaffer and Ashbaugh found (76) that for isobutylene and α-methylstyrene, the metal complex is an initiator rather than a catalyst (if it even participates at all), but that a transition from cationic to coordination polymerization occurs in styrene polymerization as temperature is raised. Even if it merely functions as an initiator, however, these investigations have revealed new polymerization systems based on anions such as $[RB(C_6F_5)_3]^-$ (R = alkyl, C_6F_5) that are less prone to side reactions tending to limit the MW and degree of polymerization of monomers like isobutylene at moderate temperatures ($T > -80^\circ C$).

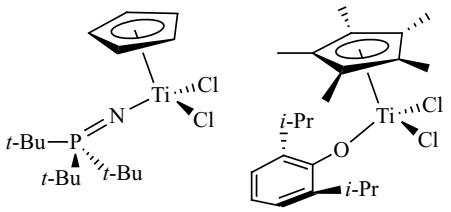

15 **16**

Bridged Complexes. The best-known bridged mono-Cp metallocene is the so-called constrained-geometry catalyst precursor **12**, a titanocene with a fairly bulky $C_5(CH_3)_4$ moiety on one side and a large amido group on the other. Despite this bulk, the short bridging unit, which enforces a Cp-centroid—Ti—N bite angle of 107.6° (77) (hence the sobriquet "constrained geometry"), ensures easy access of monomers to the active center. The ligand was first disclosed by Bercaw and co-workers in its complex with scandium (data published in—not first discloure—Ref. 78), a molecule with limited ethylene polymerization activity. Soon thereafter, patent applications from workers at Dow Chemical (79) and Exxon Chemical (80) appeared, claiming high activities for olefin polymerization using **12**. A heteroatomic analogue of **12** and **17** has also been found (81) to have good polymerization behavior.

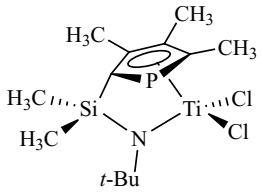

17

The bridged amido–Cp titanocenes such as **12** have risen to prominence presumably for the following features: (*1*) polymerization kinetics well suited to solution-phase reaction at high temperatures ($T > 120^{\circ}C$), the environment of Dow's commercial reactor; (*2*) high comonomer-incorporation ability, which makes production of amorphous polyethylenes practical; and (*3*) ability to generate long-chain branches that result in superior melt processability for LLDPE (see under Long-Chain Branching). Analogous complexes feature substituted indenyl or fluorenyl groups in place of the $C_5(CH_3)_4$ unit, as well as bulky alkyl or cycloalkyl substituents besides t-butyl on the nitrogen atom; any advantages in activity or performance appear to be offset by the complexity and expense of catalyst synthesis. A marked exception to this general trend is the heteroatom-substituted complex **18**, which shows (82) activities for ethylene–1-octene copolymerization far greater than those of complex **12**. The zirconium analogue of **12** and its relatives do not seem to share the high comonomer response of their titanium versions and are consequently much less widely employed. Also, titanium- and zirconium-based compounds with a single carbon atom bridging group show lower activity than does **12** (83).

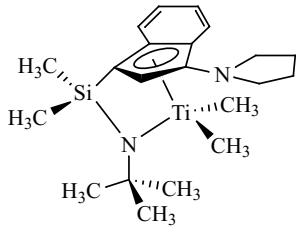

18

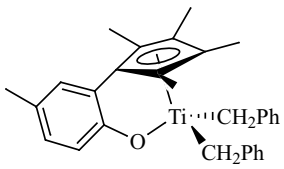

19

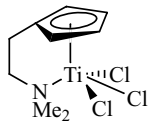

20

Other bridged metallocenes bearing one Cp ring have been described recently. One structure, **19**, reported by Marks and co-workers (84), has a direct Cp—phenoxide linkage. A series of Ti(IV) complexes, of which **20** (85) is an example, were developed by Chien and co-workers, bearing donor atoms that, based on NMR spectroscopic and polymerization data, coordinate to titanium prior to and upon activation by MAO. Compound **14** shown above also includes a Lewis basic

nitrogen bound to titanium, but in this case the bond appears in the precursor and the oxidation state of titanium is +3. Precursor **14**, developed by DSM under the name Lovacat (86), also produces rubbery ethylene–propylene copolymers, indicating that the reactivity of higher α-olefins in titanium-based copolymerizations with ethylene is similar in catalysts derived from Ti(III) and Ti(IV) precursors. Whether the oxidation state of complexes like **12** as well as **14** is also less than +4 in the active state has not been resolved.

Complexes with Open Pentadienyl Ligands. Open-chain analogues of the Cp ligand have only received limited attention. Compounds **21** (87) and **22** (88) have been featured in patent examples as moderately active polyethylene catalysts after activation by $[Cp_2Fe][B(C_6F_5)_4]$ and MAO, respectively.

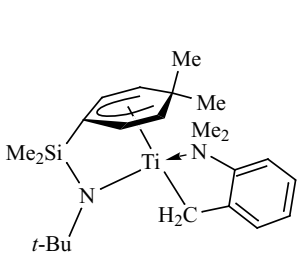

21

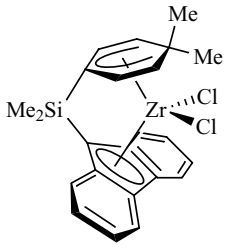

22

Complexes with Dianionic Ligands. In the search for metallocenes that do not require ionization, several workers have targeted the synthesis of Group IV complexes in which a dianionic ligand replaces a monoanionic Cp′ of bis-Cp′ metallocenes. Bazan has found good activity for TMM **23** (trimethylenemethane dianion) and TBM **24**, (tribenzylidenemethane dianion) complexes of zirconium (89).

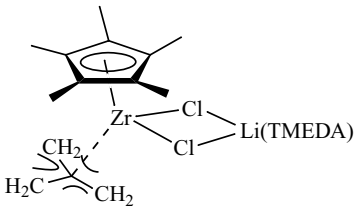

23

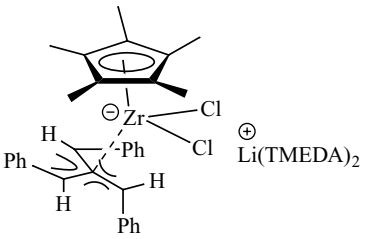

24

(The degree of association of Li with the Zr–Cl functionality appears to be dictated by the size of the dianionic substituent.) Although MAO is required for high productivity, similar activity from an unstable solution of the prealkylated neutral complex $(C_5(CH_3)_5)$(TBM)$ZrCH_3$ led the authors to propose that a similar neutral species is indeed the propagating site.

Carboranes were some of the first dianionic ligands to replace Cp in metallocenes. The unstable monomeric complexes **25a–c** were examined by Jordan and co-workers for ethylene activity. While **25b** and **25c** have fair activity for ethylene polymerization (~7 g/mmol(Zr)/h/atm for **25b**) (90), the titanium

analogue only dimerizes ethylene to 1-butene (91). The dianionic carborane (2,3-$(Si(CH_3)_3)_2$-2,3-$C_2B_4H_4$) has been used opposite Cp in complex **26** (92).

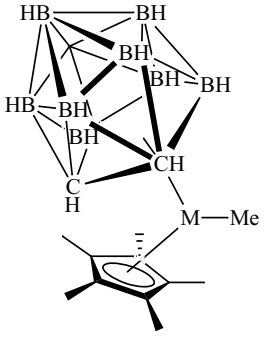

a: M = Ti
b: M = Zr
c: M = Hf

25

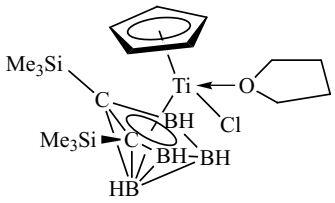

26

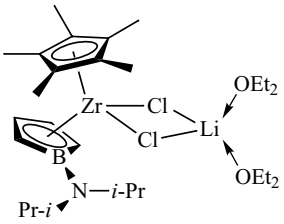

27

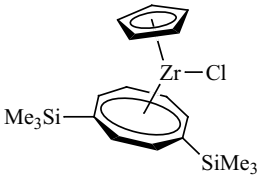

28

Quan and co-workers (93) have synthesized the aminoborollide complex **27**, bearing yet another dianionic Cp analogue. The cyclooctatetraene dianion complex **28** has shown fair polymerization activity with MAO (94).

Group IIIB and f-Block Metallocenes. The need for expensive cocatalysts has always hampered the development of metallocene catalysts for olefin polymerization. It was recognized early on that substitution of the Group IVB metal with a lanthanide or Group IIIB element in the +3, d^0 state would represent a cocatalyst-free analogue of the Kaminsky system. Active catalysts are indeed obtained from bis-Cp lanthanocenes and yttrium- and scandium-based congeners. The lutetium dimer **29** has an activity of >7 kg/mmol(Lu)/h/atm for ethylene polymerization in cyclohexane (95). (This remarkable compound can also break the C–H bonds of alkanes.)

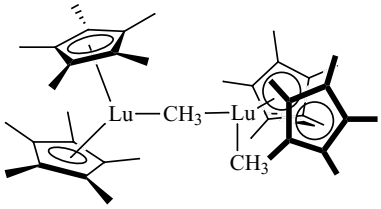

29

Because of their larger ionic radii, lanthanide (hereafter taken to include Y and Sc) atoms are usually bound to heavily substituted cyclopentadienyl groups such as $C_5(CH_3)_5$. Although ionization of the lanthanocene is unnecessary, preparation of the appropriate metal hydride or metal alkyl that can initiate polymerization is a matter of considerable art. Lanthanide alkyl complexes with β-hydrogens tend to decompose, while hydride and chloride species readily dimerize or form "-ate" complexes with lithium salts. In fact, not only the Cp-ligands but also the metal-bound alkyl substituent are often required to be large (such as $-CH(Si(CH_3)_3)_2$) (96), or the complex is further coordinated by a Lewis base molecule such as THF.

Lanthanocenes are even more reactive toward polar impurities than are Group IVB metallocene catalysts, which makes commercial use an even more daunting prospect. Another feature that limits the applicability of lanthanocenes is that the catalysts generally show high selectivity for ethylene insertion over larger olefins. Polyethylene produced by these catalysts generally is of very high density and MW. Larger olefins can be homooligomerized, but at rather low rates.

The scandium complex **30** disclosed by Shapiro and co-workers (97), which represents the first application of the bridging amido–Cp ligand in metallocene chemistry, is unusual in its moderate ability to polymerize larger olefins such as 1-pentene. A yttrium analogue initiates polymerization of *t*-butyl acrylate and acrylonitrile at room temperature and below (98). In the bis-Cp systems, a bridging group seems to improve reactivity toward α-olefins (99). The yttrocene dimer **31** produces highly isotactic polypropylene ($P_{mmmm} = 97\%$) (100).

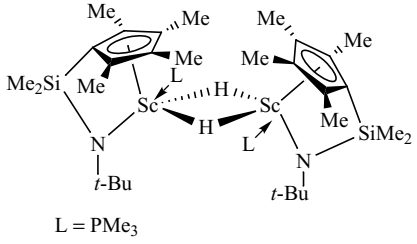

30

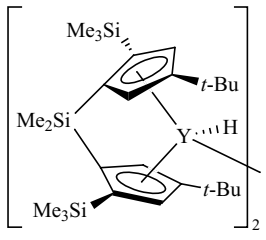

31

Although actinide complexes usually disqualify themselves from industrial utility by their radioactivity, the thorocene $(C_5(CH_3)_5)_2Th(CH_3)_2$ displays high activity for ethylene polymerization after activation (101). Like zirconocenes, this family of metallocenes tends to remain on the +4 manifold, and thus requires ionization by an appropriate cocatalyst (in this case, a highly Lewis acidic surface such as dehydroxylated alumina or $MgCl_2$) before it is active.

By their highly Lewis acidic nature, lanthanocenes are particularly suited to the polymerization of polar monomers such as acrylates and lactones (for a review, see Ref. 102). The lack of significant chain-transfer and -termination paths allows the production of block copolymers, including the case in which acrylate polymerization follows that of ethylene (103).

Group VB and VIB Metallocenes. Cyclopentadienylniobium and -tantalum compounds bearing amidinate ligands as in **32** (104) and **33** (105) have been occasionally used as ethylene polymerization precursors, usually with

MAO as activator. Generally, the turnover rates for these systems are only moderate, with that for **33** being on the high side at 470 g(PE)/mmol(Ta)/h/atm. Activities for **34** and the vanadium complex CpV(*N*-*p*-tolyl)Cl_2 were 0.2 and 8.3 g(PE)/mmol(M)/h/atm, respectively (106). Molybdenum- and tungsten-based systems are similarly mediocre catalysts (106).

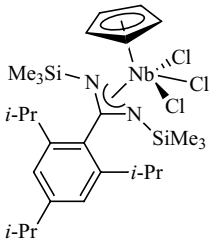

32

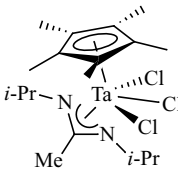

33

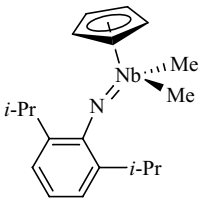

34

The mono-Cp butadiene complexes **35** and **36** have been found to polymerize ethylene at moderate rates as well (35.23 and 5.69 g/mmol(M)/h/atm, respectively, at 20°C, with 500 eq. MAO) (107). At low temperatures, the polymerizations appear to be living in nature (see under Living Polymerization).

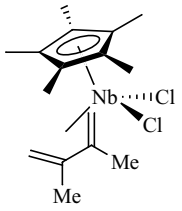

35

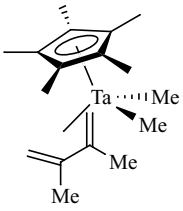

36

Cyclopentadienylchromium Compounds. Chromocene, a paramagnetic and somewhat labile metallocene, forms a polyethylene catalyst after chemisorption on silica (108). The reaction generates an equivalent of C_5H_6, and the propagating site has been proposed (109) to be as shown in equation 13. The characteristics of this ill-characterized catalyst are facile chain transfer to H_2, poor comonomer incorporation, and fairly broad molecular weight distribution (MWD). This catalyst is still in commercial use.

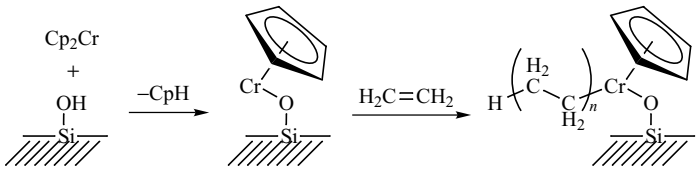

(13)

Theopold and co-workers have prepared unsupported mono-Cp ethylene polymerization catalysts by use of very bulky cyclopentadienyl and alkyl ligands on chromium; these catalysts do not require an activator. Precursors having both

unbridged **37** (110) and bridged **38** (111) ligand sets yield polyethylene with broad MWDs, indicating a considerable breadth in active-site structures.

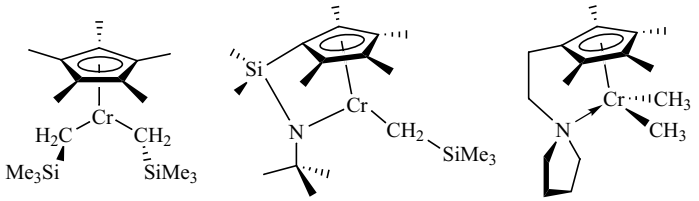

37 **38** **39**

Poor propylene incorporation by **38** is reported, although dimerization to 2-methyl-1-pentene was observed. Complexes such as **39** bearing electron-pair donor atoms, described by Döhring and co-workers (112), are active catalysts for ethylene polymerization (activity for **39**: 10.5 kg(PE)/mmol(Cr); conditions: 21°C, 2 atm ethylene, 100 eq. MAO); polymerization of propylene and higher olefins is approximately two orders of magnitude slower. Activities of up to 15 kg(PE)/mmol(Cr)/h/100 psi(C_2H_4) have been recorded for analogous unbridged mono-Cp chromium compounds such as $(C_5(CH_3)_5)Cr(CH_3)_2$(pyridine) supported on metal oxides and activated by isobutylaluminoxane (113). A noteworthy aspect of this system is that the MWD of the polymer produced is relatively narrow (2) $< M_w/M_n < 3$).

Another interesting catalyst system is the boratabenzene complex **40** from the Bazan group (114). This precursor, after activation by MAO, $B(C_6F_5)_3$, or $[(C_6H_5)_3C][B(C_6F_5)_4]$, polymerizes ethylene with activities comparable to Cp_2ZrCl_2.

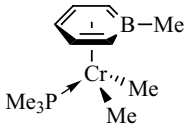

40

General Trends in Metallocene Polymerization

Although activity comparisons are fraught with perils, as the conditions of polymerization, including catalyst concentration, purity of monomers, reaction time, etc., greatly influence the lifetime and polymerization rates of catalysts, a few conclusions may be drawn from selected surveys. In Table 1, Kaminsky and co-workers compare (115) the activities of metallocenes with different metals and cocatalysts.

Under identical conditions, metallocenes based on Hf are approximately an order of magnitude less active than their zirconocene analogues, and titanocenes are likewise of low activity. (There are inportant exceptions to this rule: *rac*-$C_2H_5(Ind)_2$ $HfCl_2$ has been shown to have activity comparable to *rac*-$C_2H_5(Ind)_2ZrCl_2$; see Ref. (116).) Of the aluminoxanes, MAO is by far the

Table 1. Ethylene Polymerization Activities for Aluminoxane-Activated Unsubstituted Metallocenes 115

Catalyst	M, μmol	T, °C	Activity[a]	MW/1000	Cocatalyst
Cp_2TiCl_2	3	20	90	430	MAO
Cp_2ZrCl_2	0.01	90	5000	122	MAO
Cp_2ZrCl_2	1.5	70	23	>500	EAO
Cp_2ZrMe_2	3	70	175	>500	$(i\text{Bu}_2\text{Al})_2\text{O}$
Cp_2HfCl_2	0.03	70	65	490	MAO

[a]Units: g(PE)/g(M)/h/bar.

best activator. On the basis of periodic trends, the metal–carbon bond strength for the L_nM(polymer) cation should be greater for M = Hf, and this may explain the sluggishness of the third-row systems. A similar argument could be used to account for the much lower rates of chain transfer (in the absence of added H_2) in hafnocenes. In comparing the behavior of hafnocenes and zirconocenes, it is important to determine the level of Zr impurity in the Hf starting material (about 1 mol% in unenriched samples). This is normally carried through the synthesis and can lead to non–single-site behavior because of the much higher activity of the zirconium analogue (117).

Bridged metallocenes tend to incorporate larger olefins more readily than their unbridged counterparts. This probably has less to do with accessibility of the monomer than with electronic effects, although the fact that large-amplitude motions are restrained in the ansa-metallocenes cannot be ignored.

Electron-withdrawing substituents seem to cause polymerization activity to diminish, if steric effects are accounted for (118,119).

Effects of Additives on Polymerization

Compared with the effort spent in optimizing metallocene catalyst performance through modification of the ligand framework, tuning catalyst properties through the addition of catalyst modifiers has been far less popular. However, catalyst behavior is strongly influenced by the presence of certain agents, either directly (at the transition metal) or indirectly (by modifying the cocatalyst/anion). There are some reports of synergistic effects from mixed MAO/discrete activator cocatalyst systems (120). Modification of the MAO cocatalyst with Lewis bases such as $Si(OC_2H_5)_4$, hindered phenols, and bulky amines is described in an Exxon patent application (121), in which the catalyst derived from $(CH_3)(C_6H_5)Si(C_5(CH_3)_4)(N\text{-}t\text{-}C_4H_9)TiCl_2$ + MAO shows enhanced comonomer incorporation and altered chain-transfer rates in the presence of these agents. The seemingly simple catalysts based on Cp_2ZrCl_2 seem to show distinct two-site behavior depending on the cocatalyst, in which the degree of association between the ions apparently dictates fundamental kinetic parameters such as monomer selectivity (122).

In commercial reactor operation, one would like the ability to either reversibly or irreversibly deactivate the catalyst, depending on the type of reactor

upset. Benzyl chloride and CO_2 have been claimed to be useful for the reversible deactivation of metallocenes, with MAO added to reactivate the catalyst (123). Mobil workers have discovered that CO_2, among other agents, can change the MW-response of MAO-activated metallocenes (124).

Polymerization Using Metallocenes

Most of the experimental and computational work on metallocene polymerization has dealt with the classic bis-Cp zirconocene family, and therefore this section will focus on this area. However, many of the reactions delineated here can be expected to occur in polymerizations involving other early transition metal (early-TM) based catalysts.

Activation. The paths shown in equation 14 are generally accepted to be that by which a metallocene precursor is transformed into a catalytic site in aluminoxane-cocatalyzed polymerization, while equations 8–10 portray the three mechanisms for activation using Lewis and Brønsted acids.

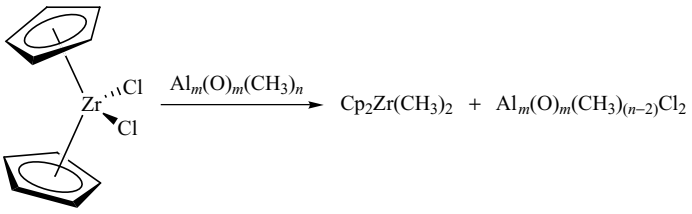

$$Cp_2Zr(CH_3)_2 + Al_m(O)_m(CH_3)_{(n-2)}Cl_2 \longrightarrow Cp_2Zr(CH_3)^+ + Al_m(O)_m(CH_3)_{(n-1)}Cl_2^- \quad (14)$$

The first step in equation 14 involves the exchange of the halide groups attached to the metal atom with the alkyl groups bound to one or more aluminum atoms. In equations 8–10, it is assumed that the metallocene is introduced into the reactor as a dialkyl complex, or that it has been converted into such form by a halide-exchange process involving an alkylating agent in the polymerization environment.

The next step in both MAO-activated and MAO-free systems is believed to involve the transfer of an alkylide group to a Lewis acid (eqs. 8 and 9) or a proton (eq. 10), which creates an electron-deficient (14 e^-) metal center with a site for the potential coordination of an olefin. The nature of the counterion strongly affects the ability of the site to polymerize olefins, and indeed may change the active-site geometry enough to drastically change the selectivity of polymerization as well as the chain-transfer rate. Cation–anion interactions have been reviewed by Bochmann (125). The reactivity of anion-free cationic metallocenes has been probed by ion-cyclotron resonance (ICR) spectroscopy (126).

One variation on the ionization of dialkyl metallocenes is shown in equation 15, in which a butadiene complex, which may be predominantly M(IV) or M(II) in nature, reacts with a Lewis acid to form a Zwitterion that is able to further polymerize olefins, as shown by Erker and co-workers (127).

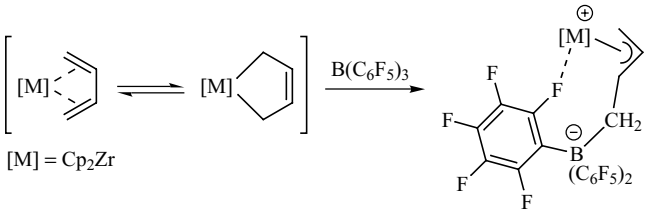

(15)

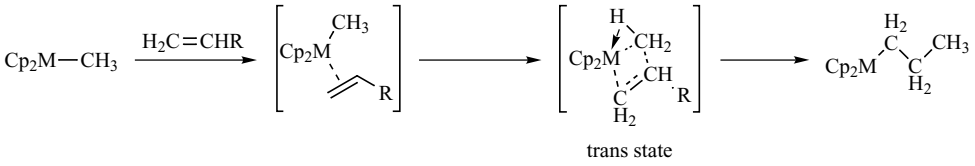

(16)

The approach and insertion of an olefin molecule may or may not pass through a local minimum or coordination complex (first in brackets in eq. 16); recent theoretical work (128) indicates that the well, if it indeed exists, is very shallow. The insertion of the new molecule into the growing chain is represented in equation 13 as a structure intermediate between reactants and products. The mechanism for this apparently concerted reaction does not involve the participation of metal-based electrons, and can be considered to be a Lewis acid–assisted anionic attack of the zirconium alkyl (ie, the polymer chain) upon one end of a carbon–carbon double bond. The concept of this reaction pre-dates metallocene study, and is merely a variant of the Cossee–Arlman mechanism (129) routinely invoked in Ziegler–Natta polymerization. Computational studies indicate (130) that an α-agostic interaction (131) provides much needed stabilization during the process of insertion.

A major consequence of this pathway, also known as migratory insertion, is that the growing chain sweeps from one side to another with every addition of monomer. This is a generalization, for some authors have explained the loss of stereoselection in metallocene polymerizations of propylene, for example, at low monomer concentrations to the action of a "windshield wiper" isomerization, in which the polymer chain and open coordination site switch places without the benefit of monomer insertion. At low insertion rates, this site inversion phenomenon may become competitive with insertion and thus render ineffective any substituent influences which differ between the two faces of the catalyst site. With appropriate ligand design, different or enantiomeric steric environments may be created for the two sides of the active site. This makes possible stereoselective polymerization of propylene and higher α-olefins, as will be seen below.

The use of discrete activators was instrumental in elucidating the structure and electronic nature of the active site for Group IVB metallocenes. A number of Lewis base–stabilized metallocene cations such as **41** (132), **42** (133), and **43** (134) were studied, chiefly by the Jordan group at the University of Iowa. Reactivity is not completely shut down by the base, although polymerizations are sluggish. Remarkably, agostic species such as **42** and **43**, which are believed to be important in chain transfer and propagation, respectively, can be characterized in such systems.

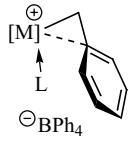

[M] = CP_2Zr; L = MeCN

41

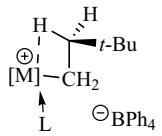

[M] = $(MeCP)_2Zr$; L = PMe_3

42

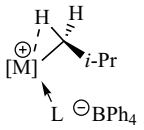

[M] = $(C_5Me_5)_2Hf$; L = PMe_3

43

Deactivation. One of the factors that complicates the quantification of active-site concentration (135) is the fact that metallocene cations are subject to equilibria between catalytically active and inactive forms. In situations in which intramolecular coordination of an arene group can occur, this process competes with monomer coordination in styrene (136) and possibly olefin polymerization. Another dormant state invoked to explain catalyst decay is the dimeric structure $[Cp_2Zr(CH_3)(\mu\text{-}CH_3)Zr(CH_3)Cp_2]^+$ in which a methyl group bridges two metallocene fragments. This has been characterized by NMR for the reaction of $Cp_2Zr(^{13}CH_3)_2$ with MAO and other cocatalysts (136).

Ethylene–α-Olefin Copolymerization. Linear low density polyethylene (LLDPE), engineered to match the flexibility of polyethylene made by free-radical processes (LDPE), contains short-chain branches, which reduce the crystallinity of the resin. The short-chain branches result from incorporation of α-olefins such as 1-butene, 1-hexene, or 1-octene (known collectively as *comonomers*) when added to the reactive mixture. Traditional catalysts such as $MgCl_2/TiCl_3/AlR_3$ incorporate these comonomers in a manner that is very inhomogeneous, that is, there is considerable breadth in the distribution of comonomer content both within individual chains and from chain to chain. The first form of inhomogeneity is often referred to as *blockiness*, and is best estimated by examination of the monomer sequence distribution as determined by ^{13}C NMR spectroscopy. The second, intermolecular type of inhomogeneity shows up in extraction experiments, and is particularly well suited to TREF chromatography (temperature rising elution fractionation chromatography, which separates polymer fractions on the basis of solubility as solvent temperature rises.) The single-site nature of metallocenes gives rise to extremely narrow intra- and intermolecular distributions of short-chain branching.

Figures 6 and 7 compare the sequence distributions and TREF chromatograms respectively for Ziegler–Natta- and metallocene-catalyzed ethylene–1-hexene copolymerizations. The lack of blockiness in the metallocene resin in Figure 6 is demonstrated by the low levels of homopolymer triads, whereas intermolecular compositional homogeneity is shown by the narrow peak for the metallocene resin in Figure 7. It should be noted that while the narrow intermolecular distribution of comonomer content is a direct consequence of the single-site nature of the catalyst, the absence of blockiness is a reflection of the relative magnitudes of the rate constants for insertion for the two monomers and does not speak to catalyst site diversity. The kinetics of insertion will be treated in the following section.

Exceptions to the rule of narrow intermolecular distribution of comonomer can and do occur. These often result from the activity of catalytic sites of different structure (ie, loss of single-site nature) or, less often, from mass-transfer

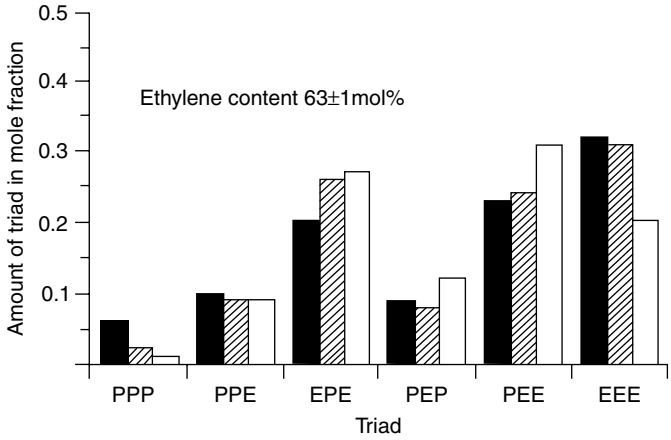

Fig. 6. A comparison of the triad distributions for three ethylene-propylene copolymers of similar propylene contents made by three different catalysts: $MgCl_2/TiCl_4/AlEt_3$ (black); $VOCl_3/Et_2AlCl$ (hatched); and Cp_2ZrCl_2 (white). Reprinted with permission from Ref. 138.

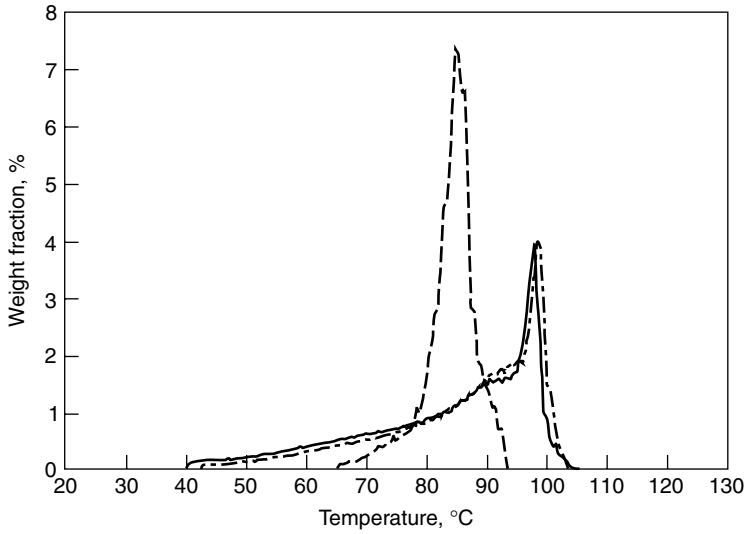

Fig. 7. TREF chromatograms for metallocene (dashed line; density = 0.922 g/mL) and Ziegler–Natta (solid and dot-dashed lines; densities = 0.921 and 0.930 g/mL, resp.) catalyzed ethylene-1-hexene copolymers. Reprinted from Ref. 139. Copyright (1994), with permission from Elsevier Science.

limitations that may occur between gas and catalyst solution, between gas and growing polymer particle, or between solution and polymer particle, depending on the process employed. Diffusional limitations only effect the distribution of comonomer content if there is a considerable gradient in the relative or absolute concentration of monomer(s) across a nonnegligible fraction of the diameter of the growing particle or volume of solution. Other potential sources of heterogeneity

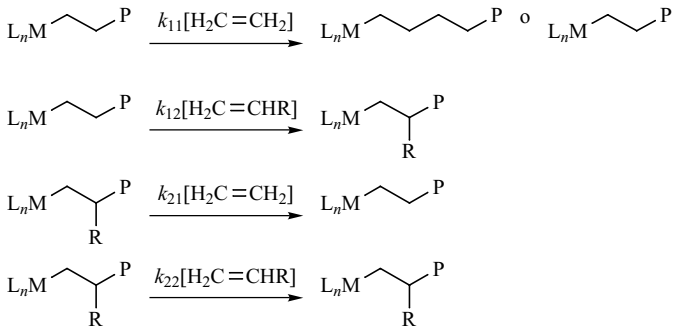

Scheme 2.

include distributions of reactor residence time and heat history, imposed either by the reactor design or by a wide range of catalyst particle sizes. Reports on the control of comonomer content heterogeneity have been few.

The relative rates of olefin insertion reactions lead to models for the reactivity of the catalyst site, and the complexity of any chosen model arises principally from the degree to which the last monomers to be inserted affect the rate of subsequent insertion. If the last inserted monomer is assumed to have no effect, then one obtains two rate constants for insertion: one for reaction with ethylene and one for reaction with α-olefin. The next level of discrimination, also called First-Order Markov theory, posits that the last-inserted monomer influences the rate of insertion of the next unit, yielding four rate constants (Scheme 2). Higher-level treatments lead to many more rate constants in obvious extension. Metallocene copolymerizations display the tell-tale signs of First-Order (or higher) Markov behavior. This is necessary, for example, to explain the tendency for ethylene–α-olefin copolymerizations to alternate between ethylene and comonomer insertions beyond the proportion predicted by a random distribution. While First-Order copolymerization has been the basis of many studies of metallocene-based copolymerization, some researchers, most notably Fink (140), have argued for Second-Order Markov kinetics. A persuasive and statistically meaningful fit of copolymer unit sequence data to a model with eight parameters is difficult to achieve, however; so this level of treatment is unlikely to be generally applied.

At the first-order level, the preference of the metallocene for one monomer over the other is quantified by the two reactivity ratios, r_1 ($= k_{11}/k_{12}$) and r_2 ($= k_{22}/k_{21}$). Since ethylene is invariably more reactive than any other monomer, $r_1 > 1$ and $r_2 < 1$. Study of the First-Order Markov constants (Table 2) reveals important correlations with metallocene and comonomer structure. As is to be expected, the larger the comonomer, the higher the r_1 value, indicating a steric hindrance to its insertion. Bridged metallocenes, such as structure **2**, give catalysts with much lower r_1 values than do unbridged metallocenes. In general, metallocenes copolymerize monomers with a tendency toward alternation of monomers, as indicated by a value for $r_1 r_2$ less than 1.

Herfert and co-workers resolved the copolymerization reactivity ratios for two bridged metallocenes at the second-Order Markov level (140), as shown in Table 3. The data demonstrate bridged metallocenes are somewhat sensitive to

Table 2. Reactivity Ratios for Ethylene/Propylene Copolymerization by Various Metallocenes

Catalyst	Temp, °C	r_1	r_2	r_1r_2	Reference
$(C_5Me_5)_2ZrCl_2$	50	250	0.002	0.5	141
$(MeCp)_2ZrCl_2$	50	60	—		141
Cp_2ZrCl_2	50	48	0.015	0.72	141
Cp_2ZrCl_2	50	16.1	0.025	0.40	142
rac-Me_2(3-*t*-BuCp)$_2ZrCl_2$	50	25.6	0.110	2.8	143
$(Me_3SiCp)_2ZrCl_2$	50	24	0.029	0.70	141
Cp_2HfCl_2	50	20.6	0.074	1.52	142
(n-BuCp)$_2ZrCl_2$	80	19	0.005	0.095	144
(n-BuCp)$_2ZrCl_2$	40	2.7	—	—	145
Cp_2TiCl_2	50	15.7	0.009	0.14	142
Ind_2ZrCl_2	40	13.75	0.182	2.45	146
rac-$C_2H_4(Ind)_2ZrCl_2$	50	6.61	0.06	0.40	147
rac-Me_2Si(2-Me-4-Ph-Ind)$_2ZrCl_2$	50	2.84	0.74	2.10	148
$Me_2C(Cp)(Flu)ZrCl_2$	25	1.3	0.2	0.26	149
$Me_2Si(Me_4Cp)$(N-*t*-Bu)$TiCl_2$	50	1.35	0.82	1.10	148

Table 3. Effect of Comonomer Size on Copolymerization Parameters for Two Bridged Metallocenes at 25°C (141)

Metallocene[a]	Comonomer	r_{11}	r_{21}	r_{12}	r_{22}
A	Propylene	4.1	3.9	0.153	0.065
A	1-Butene	7.9	6.8	0.085	0.017
A	1-Hexene	10.3	6.4	0.111	0.022
B	Propylene	3.4	2.2	0.270	0.153
B	1-Butene	3.6	2.9	0.210	0.041
B	1-Hexene	3.2	2.6	0.150	0.065

[a] (A = $Me_2Si(Ind)_2ZrCl_2$; B = $Me_2C(Cp)(Flu)ZrCl_2$)

the size of the comonomer, but that this effect is ligand-dependent. There is also a trend toward a greater degree of alternation of monomers as comonomer size rises, probably due to increased steric repulsion preventing consecutive α-olefin insertion.

In the case of terpolymerization of ethylene with two dissimilar α-olefins, an apparent competition between the larger monomers causes the increase in monomer concentration of one to cause a reduction in the incorporation of the other (150).

Within the best-described family of catalysts, the bis-Cp zirconocenes, steric congestion tends to reduce the ability to insert the bulkier α-olefin, as might be expected. Burger and co-workers have proposed (151) a two-parameter methodology for quantifying the steric resistance to monomer coordination. These parameters, denoted the coordination gap *aperture angle* and the coordination gap *obliquity angle* are demonstrated in Figure 8 for the bridged metallocene *rac*-$(CH_3)_2Si(3\text{-}C_6H_5Cp)_2ZrCl_2$. Electronic effects often dominate over steric effects, especially when polycyclic aromatic groups such as fluorenyl

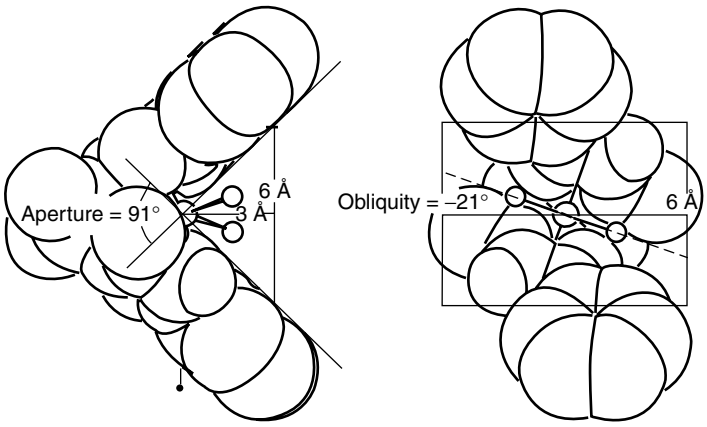

Fig. 8. Aperture and obliquity angles as defined in Ref. 151. Reprinted with permission of Wiley-VCH and the authors.

and benz[*e*]indenyl groups are considered. For example, in ethylene–1-octene copolymerization, *rac*-$(CH_3)_2$Si(benz[*e*]indenyl)$_2ZrCl_2$/MAO incorporates more comonomer than does *rac*-$(CH_3)_2$Si(Ind)$_2ZrCl_2$/MAO, despite the greater bulk of the benzannelated ligand (152).

The reader will note that the regiochemistry for the insertion of olefins in Scheme 2 and elsewhere is presumed to be that which causes carbon 1 of the α-olefin to be bound to the metal; this is denoted 1,2-insertion, while the case in which the monomer inserts with opposite arrangement is known as 2,1-insertion or regioerror. While chain-end studies have shown 1,2-insertion to be the dominant regiochemistry, misinsertion may exert an influence upon the rates of chain transfer or ultimate polymer properties out of proportion to its frequency. Regiochemical inversion seems to be rather prevalent in polypropylene produced by mono-Cp titanocene catalysts (153).

As is often the case with polyethylene catalysts, both single-site and otherwise, polymerization rates rise rapidly as the level of comonomer rises. This phenomenon, often called the comonomer boost, has generated some contention among researchers, as it is unclear whether the effect represents a rate enhancement for insertion based on the donor effect of comonomer, or whether it derives from a physical effect, such as a lowering of the mass-transport barrier between the reservoir of monomer and the catalyst site. The two causes are difficult to separate, but at least part of the effect is diffusional: transport of small molecules through polyethylene is believed to occur solely through amorphous regions, and so any reduction in bulk crystallinity, such as through the inclusion of short-chain branching, should dramatically increase the diffusion rate.

Chain Termination. In this section, we will cover how polymer chain growth ends and a new chain begins. This process, alternately called chain transfer or chain termination, leads to a distribution of molecular weights. These two terms, often used interchangeably in olefin polymerization, mean rather different things in other areas of polymerization, in which the reactivity of a polymer chain

end (eg, a radical) can either be transferred (eg by hydrogen atom migration) to a new monomer or be quenched or terminated by reaction with a sacrificial agent (eg, a radical trap). An ideal single-site catalyst will produce a distribution of chain lengths conforming to the Schulz–Flory model and this leads to the ratio between weight-averaged and number-averaged molecular weights, or polydispersity index (PDI), being equal to two. The PDI tends to the limiting value of 2.0 so long as (*1*) the rate of chain transfer is sufficiently large relative to the rate of initiation (activation), and (*2*) there are no reactions that lead to branched polymer, eg, diolefins or reactive polymer chain ends. In practice, the distribution in MW is also subject to complications similar to those that affect the comonomer distribution (see above), inevitably resulting in larger values for the PDI. Now we will take a closer look at the processes involved in chain transfer, and will divide them into two categories: those that are induced by the action of chain-transfer agents and those that occur in their absence.

Endogenous Chain Termination. Two processes are now claimed to represent the vast majority of chain-transfer events that happen without the intervention of chain-transfer agents. The first, known as β-hydride elimination and shown in equation 17, is a mechanism of considerable lineage in organometallic chemistry.

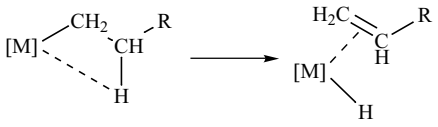

(17)

Here, the extrusion of a growing polymer chain is effected by the transfer to the metal atom of an equivalent of H^- from the carbon atom β to this metal. Theoreticians lean toward the existence of a discrete intermediate along this reaction coordinate, often designated the *agostic* complex, in which electron density is donated by the C—H bond undergoing the process of breaking. Agostic-type nonclassical bonding arrangements have been observed experimentally in special cases, but have been invoked for many aspects of early-TM polymerization, including the process of monomer insertion. The strength, estimated to lie in the range of 8–15 kcal/mol, of the agostic interaction is a testament to the electrophilicity of this electron-poor, cationic metal center. The reaction is completed by the dissociation of a polymer chain with an unsaturated chain end.

In copolymerizations, the double bond formed by β-hydride elimination may signify the nature of the last-inserted monomer. As shown in Scheme 3, the type of unsaturated group reflects whether the monomer was ethylene or comonomer (in this case, 1-hexene). In fact, the regiochemistry of the last insertion may also be given by the placement of the double bond. In normal insertion, followed by elimination, a pendent methylene group is observed, while regiomisinsertion will generate an internal olefinic group, whose regiochemistry is dictated by whether the hydrogen that is transferred to metal originates on C_1 or C_3 of the original α-olefin (This generalized discussion ignores isomerization reactions which may occur prior to chain release, and also does not treat the formation of trisubstituted olefinic chain ends, which have been reported.)

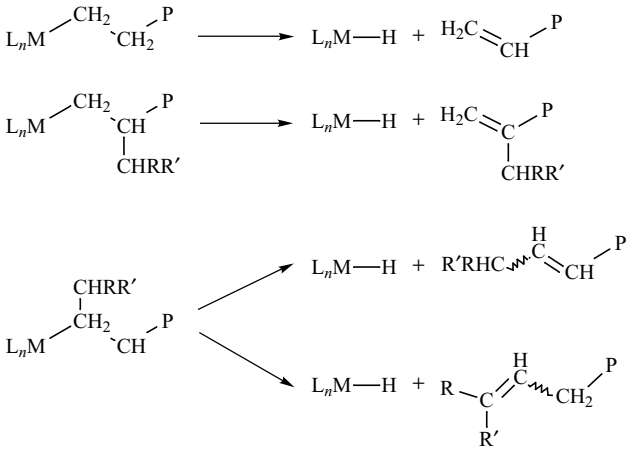

Scheme 3.

(In this Scheme, wavy lines indicate both E and Z isomers are possible, but in practice, only the trans isomer derived from path (a) is observed.) The correspondence between unsaturation structure and last-inserted monomer does break down: in certain documented cases (154), chain-end isomerization leads to a preponderance of *trans*-CH_3—CH=CH—CH_2P chain-termini from ethylene homopolymerization.

Another type of chain-transfer reaction that has gained believers in recent years is the reaction that we will call chain transfer to monomer (in this case, ethylene) (155) (eq. 18). Chain transfer here superficially resembles β-hydride elimination, in that the same olefinically terminated chains are formed from the same monomers, but in this case the β-hydride is transferred directly from the chain to another monomer molecule. The reader will note that this process is the conflation of β-hydride elimination followed by insertion of monomer into the new M—H bond, and indeed it is difficult to distinguish between these mechanisms by labelling studies, for example. Unlike β-hydride elimination, however, chain transfer to monomer is a first-order process in monomer concentration, and if one assumes a rate for monomer insertion that is also first order in monomer concentration, then the number-average MW should be unaffected by monomer concentration in the case of chain transfer to monomer, while it should rise in proportion to monomer concertration in the case of β-hydride elimination.

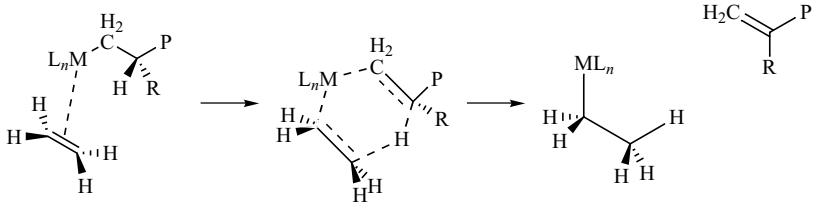

(18)

Some new work on ethylene homopolymerization indicates that this mechanism may dominate, at least under certain conditions (156). In fact, in the case

of "certain meso-bridged zirconocenes," ethyl branching occurs, and it is believed to derive from the reinsertion of a vinyl-terminated polymer chain after chain transfer to ethylene (157). However, it appears certain that β-hydride elimination is a large component of chain transfer in the presence of comonomer. Generally, the MW of metallocene copolymers falls sharply as comonomer content rises. This is attributed to the higher reactivity of the β-hydride group attached to a tertiary as opposed to a secondary carbon atom. There is ample evidence that the MW of copolymers rises as the overall monomer concentrations rise, even with the ratio of monomer concentrations held fixed and the comonomer content of the polymer remaining nearly constant. The most parsimonious explanation for this phenomenon is the existence of a unimolecular chain transfer process involving loss of a chain containing comonomer as the last inserted unit.

A process that has been noted in lanthanide metallocene polymerizations of α-olefins as well as in the polymerization of propylene by the highly sterically congested metallocene $(C_5(CH_3)_5)ZrCl_2$/MAO (158) is that shown below (eq. 19), in which an alkyl group attached to the β-carbon of the polymer chain is transferred to metal, resulting in the loss of a vinyl-terminated chain.

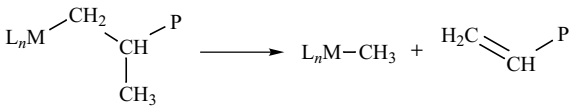

(19)

Transfer of side-chain substituents larger than methyl is unknown.

Endogenous chain-transfer rates commonly increase with temperature. The empirical activation energy found for H-transfer termination is about 34 kcal/mol estimated from relative barrier to *trans*-vinylene termination over propagation in Ref. 159.

Exogenous Chain Termination. Industrial Ziegler–Natta processes routinely use chain-transfer agents, predominantly hydrogen, for MW control. This reaction (eq. 17), as well as others, such as chain transfer to a metal alkyl compound such as diethylzinc or triisobutylaluminum, works well for metallocenes also. This type of chain transfer liberates a molecule with a saturated chain end. Hydrogen has also been reported to alter overall metallocene activity, either upwards or downwards. The phenomenon of rate acceleration by H_2 may be related to the reactivation of dormant catalyst sites that contain sterically demanding metal–polymer environments, eg following 2,1-insertion of propylene (160).

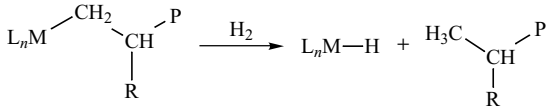

(20)

Other chain-transfer processes that have been observed are chain transfer to aluminum (eq. 21) and to silicon (eq. 22).

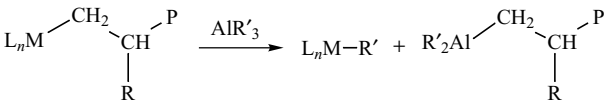

(21)

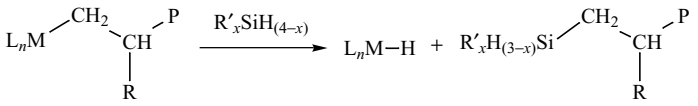

(22)

In an elegant adaptation of the latter reaction, Koo and Marks found (161) that 1,3,5-trisilylbenzene can lead to long-chain–branched copolymers through successive chain-transfer events (eq. 23).

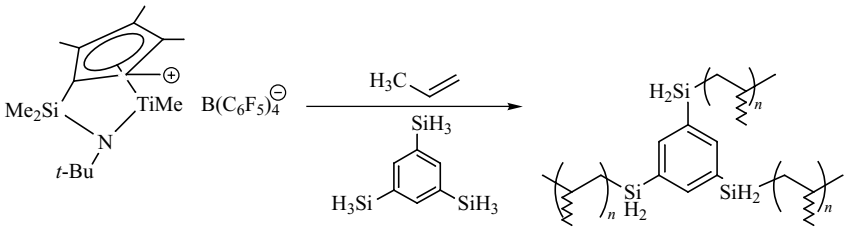

(23)

This technique was also applied to the production of block copolymers of dissimilar subunits, using silyl-capped polymer chains as chain-transfer agents. Both mechanisms for chain extension using silanes could in principle be mirrored in similar reactions with polyfunctional alkylaluminum or boron compounds, but the ensuing C—(Al/B) linkages would be vulnerable to hydrolysis, although oxidation of a borane-terminated polyethylene sample can lead to a growth point for methacrylate polymerization, yielding a diblock copolymer (162).

Living Polymerization. Polymerization in the absence of both chain transfer and termination, or living polymerization, has value to the study of metallocene reactivity, but little potential beyond very specialized applications. If initiation of polymerization is rapid on the timescale of the polymerization run, PDIs will approach 1.0, the limiting value representing monodispersity. Several examples of metallocene-based living olefin polymerization catalysts have appeared in the literature (105,163).

Long-Chain Branching. Processing metallocene polyethylene can be difficult, especially if extrusion equipment optimized for high pressure–low density LDPE is used. Not only is the polymer melt of relatively high viscosity for a desired application because of the narrow molecular weight distribution, it does not undergo shear thinning to the same extent as LDPE because of the lack of long-chain branches, which tend to reduce a polymer's radius of gyration. During the investigation of metallocene polymerization using catalysts with very low r_1 values for copolymerization, generally bridged bis(indenyl)zirconocenes, researchers noted rheological behavior indicative of long-chain branching (LCB) in polymer melts

and solutions. The mechanism for LCB formation in metallocene systems has been postulated as in equation 24, where reincorporation of a vinyl-terminated chain end from a dissociated polymer molecule, followed by further monomer insertion and finally chain loss, yields a polymer with three branches radiating from a methine carbon. (For the branches to have rheological impact, it is believed that they should be about the entanglement length of linear polyethylene, or about 3 kD.)

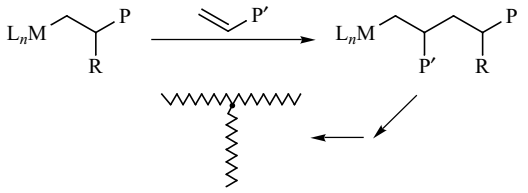

(24)

Reinking and co-workers have raised the possibility that at least some of the LCB seen in metallocene-based polymers may arise from an unusual aliphatic C—H activation of dissociated ("dead") polymer molecules (eq. 25) (As part of a study of non-metallocene vanadium catalysts, see Ref. 164). In this study, a bridged bis(indenyl) zirconocene was found to incorporate ethylene units into the heptane solvent, while an unbridged version, $(n\text{-}C_4H_9Cp)_2ZrCl_2$, did not.

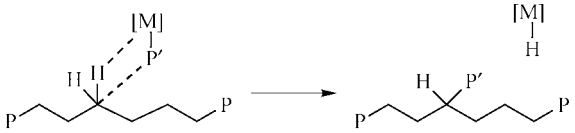

[M] = *rac*-$Me_2Si(Ind)_2Zr^+$ (25)

The reactions in both (equations 24 and 25 lead to long-chain branches of the Y-type, with three arms of appreciable length. The higher the level of LCB by these routes, the more one obtains polymer molecules of a bushy or dendritic structure (Fig. 9**a**). Cyclic structures cannot result from equation 24, a fact that reduces significantly the danger of passing into a cross-linked or gelled condition. Cross-linking is much more difficult to avoid when LCB is engendered by the copolymerization of an α,ω-diene such as 1,9-decadiene with ethylene (eq. 26),

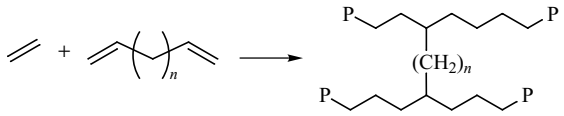

(26)

which results in an H-type or four-armed polymer node (Fig. 9**b**).

Because gelled or networked polyolefins are almost completely infusible and insoluble, even small amounts can adversely affect the appearance and mechanical performance of a fabricated article.

Side Reactions. Many of the reactions of metallocenes that occur as minor pathways during polymerization demonstrate the extreme electrophilicity of the metal cation, in that fairly unreactive bonds may be broken. Generally, the

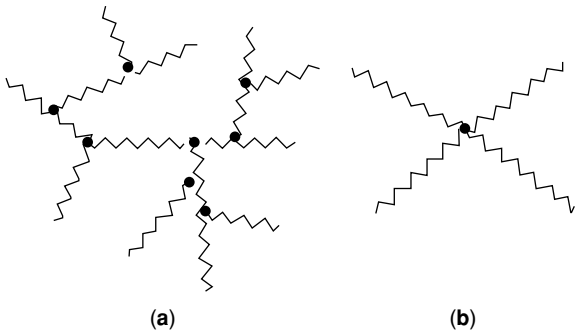

Fig. 9. Schematics of (**a**) a dendritic polymer (left) and (**b**) a four-armed star polymer.

occasion for such a process is the formation of a species that has a low rate of monomer insertion, thus increasing the likelihood of lower-probability reactions. One interesting reaction that may influence the rate of chain transfer in batch polymerizations is shown in equation 27). In the first step of this process, detected by NMR (165) and by ion-cyclotron resonance (166), activation of one of the allylic C—H bonds causes the extrusion of one molecule of H_2 and the formation of an allyl–Zr cation. This structure has been considered inactive for further propagation, yet there is evidence (167) that return to the polymerization cycle can occur, either through the reverse of the allylic-activation process or through the direct insertion of ethylene into the Zr–allyl bond, leading to unsaturation in the polymer backbone.

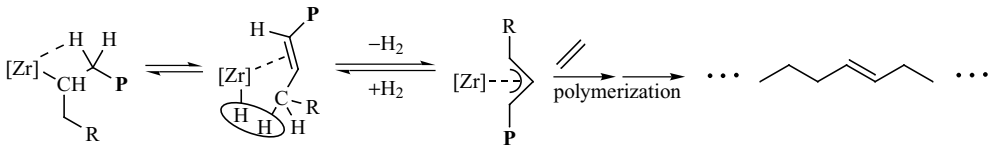

$[Zr] \equiv Ph_2C(Cp)(Flu)Zr^+$

(27)

Researchers have also noted that metallocene catalysts can exchange Zr—C and C—H bonds during propagation, leading to 1,3-enchainment of propylene, for example, following regiomisinsertion (eq. 28) (168).

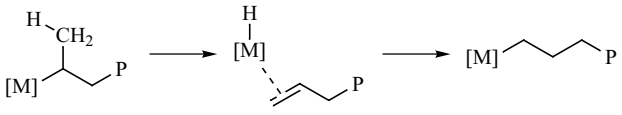

(28)

A number of very similar paths have been proposed (169) for the rearrangement of polyethylene chains attached to $(C_5(CH_3)_5)_2Zr^+$, another system in which propagation is sterically hindered (albeit by the ligand in this case). Interestingly,

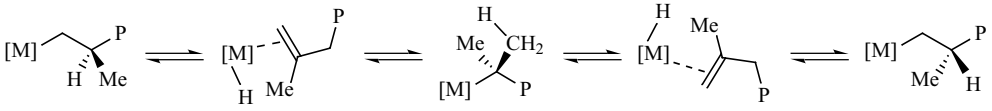

Scheme 4.

both of the previous two mechanisms require the existence, though transient, of a metal–olefin complex.

In the isotactic polymerization of propylene mediated by bridged metallocenes, certain errors in polymer microstructure have been conclusively found (170) to result from an elimination–reincorporation mechanism involving insertion of a 1,2-disubstituted unsaturated polymer chain end as in Scheme 4.

Although the metal–Cp linkage is usually assumed to be inviolable in most mechanistic treatments of metallocene polymerization, there is evidence that this assumption is flawed. The rac/meso ratios of certain bridged bis(indenyl) metallocenes have been shown to equilibrate in the presence of light (171), LiCl, or MeLi (172). These processes require the rupture of the M–Cp bond to one half of the ligand, the rotation of the dissociated C_5 ring, and its reassociation with the metal. Titanocenes and Group III metals appear to be more susceptible than zirconocenes to this process (although it is claimed to occur for the latter as well). Whether this reaction is important to polymerization has not been investigated, but it could affect catalyst quality, especially in isotactic polypropylene production.

Stereoselective Polymerization. In the early 1980s, Ewen (173) and Kaminsky (174,175) independently examined the polymerization behavior of metallocenes *rac*-Et(Ind)$_2$TiCl$_2$ and *rac*-Et(4,5,6,7-IndH$_4$)$_2$ZrCl$_2$ (**44**) each with two indenyl fragments linked by a dimethylene bridge.

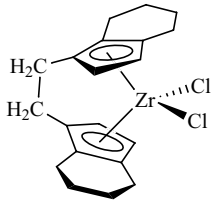

44

It was found that polypropylene made by such complexes (cocatalyzed by MAO) tended to be isotactic, as opposed to the atactic polypropylene that had been hitherto made by metallocenes such as Cp_2ZrCl_2. The strong relationship between ligand structure and polymer tacticity is considered to be the most secure proof of the migratory insertion mechanism for polymerization. The lure of homogeneous stereoselective olefin polymerization is responsible for much of the diversity of ligand structures within the bis(Cp) family.

Since metallocenes with ligands that protrude into the coordination zone in a fashion represented in Scheme 5 by complex A give rise to isospecific polymerization and those of structure B lead to syndiospecific polymerization, researchers generally assumed that the interactions causing stereoselection were

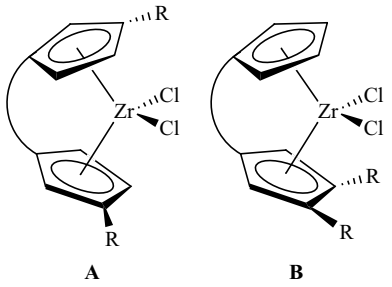

Scheme 5.

those directly between ligand and incoming monomer. Catalyst sites, therefore, of approximately C_2 symmetry (A) would then choose the same face of the prochiral monomer regardless of which side of the catalytic site the monomer approached. Sites with approximate C_s symmetry (B) would cause a selection of alternately re or si faces of the incoming monomer as the polymer chain switcheds sides. Bercaw has recently produced evidence (54) that the steric interactions that favor monomer face alternation in complexes of type B are those between the growing chain and the incoming monomer. (A similar mechanism for stereoregulation had earlier been proposed by Guerra and co-workers (176) for complexes of C_2 symmetry on the basis of molecular mechanics models.)

In this mechanism (Scheme 6), the directing effect of the ligand structure is upon the orientation of the polymer chain (lower dotted curve in Scheme), which then in turn dictates the preferred orientation of the incoming olefin. This leads to the somewhat counterintuitive conclusion that the methyl group in propylene is actually positioned toward the large fluorenyl side of the ligand in all insertions for Cp–fluorenyl complexes. While polymer–monomer interactions were advanced by Brintzinger and co-workers (177) as factors partially responsible for stereoselection in isospecific polymerization some years earlier, it is only in the case of syndiospecific polymerization that the hypotheses predict different monomer orientations with respect to the ligand. Combined *ab initio* and molecular mechanics calculations (178) had also led to the conclusion that the polymer chain controls the orientation of monomer in isospecific polymerization by $(CH_3)_2Si(1,3\text{-}(CH_3)_2Cp)Zr(P)^+$.

Isotactic Polypropylene. The bis(indenyl) metallocenes that are most often associated with isotactic polypropylene (iPP) and other isotactic polyolefins are shown in structures **45**–**49**.

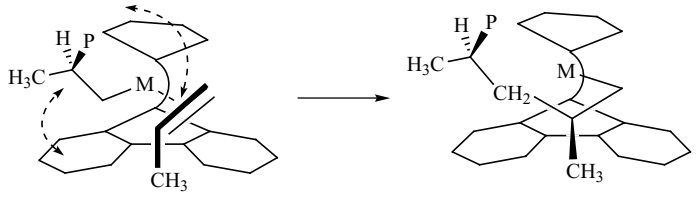

Scheme 6.

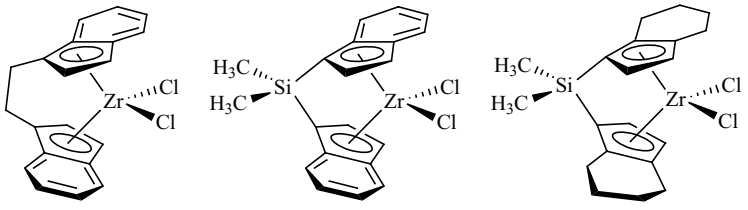

45

46

47

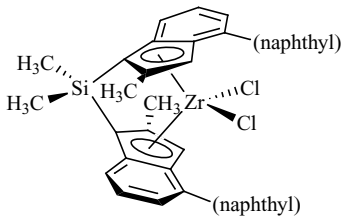

48

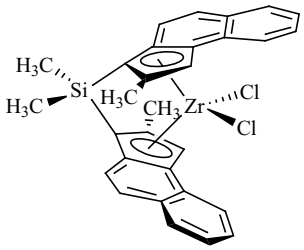

49

Synthesis of the complexes usually requires the separation (normally by fractional crystallization) of the racemic isomer pair from the meso isomer, since the latter leads only to atactic polymerization of propylene. The syntheses explored by Jordan, described above in the section Preparation, tend to raise the overall yield of racemic metallocene.

The resolution of the enantiomers of bridged bis(indenyl) metallocene dichlorides has been accomplished by the replacement of both halides by one enantiomer of binaphthol, followed by chromatography (179). Direct synthesis of enantiomerically pure precursors via chiral epoxides has been reported (180). Polymerization of α-olefins using such precursors does not lead to the production of appreciably chiral polymer due to the *de facto* mirror plane which exists in an isotactic poly(α-olefin) of reasonably high degree of polymerization (Fig. 10).

The quest for iPP of commercially acceptable melting point (MP) has led to preparation of bis(indene) ligands with increasingly elaborate substitution patterns. MP appears to correlate positively with the run length of isotactic dyads (stereoselective enchainment) as well as negatively with the level of regiomisinsertions. Substitution with small alkyl groups at the 2-position of the indene causes the iPP to be much reduced in regioerrors, while increasing bulk at the

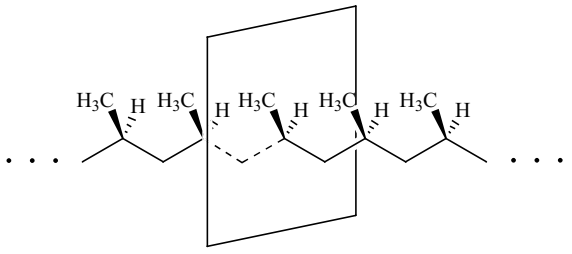

Fig. 10.

Table 4. Bridged Bis(indenyl) Zirconocenes as Polypropylene Catalysts Ligand Effects[a,b]

Catalyst	Zr, μmol	Activity[c]	M_w/1000	T_m, °C	P_{mmmm}[d]
rac-$Me_2Si(Ind)_2ZrCl_2$	5	190	36	138	81.7
rac-Me_2Si(2-Me-4-iPrInd)$_2ZrCl_2$	5	245	213	150	88.6
rac-Me_2Si(4,5-benzoindenyl)$_2ZrCl_2$	5	274	27	138	80.5
rac-Me_2Si(2-Me-4,5-benzoindenyl)$_2ZrCl_2$	5	403	330	146	88.7
rac-Me_2Si(2-Me-4-PhInd)$_2ZrCl_2$	3	755	729	157	95.2
rac-(Ph)(Me)Si(2-Me-4-PhInd)$_2ZrCl_2$	3	553	778	157	95.1
rac-Me_2Si(2-Me-5-PhInd)$_2ZrCl_2$	5	63	188	139	78.1
rac-Me_2Si(4-PhInd)$_2ZrCl_2$	5	48	42	148	86.5
rac-Me_2Si(2-Me-4-naphthylindenyl)$_2ZrCl_2$	3	875	920	161	99.1

[a]Reprinted with permission from Ref. 182. Copyright (1994) American Chemical Society.
[b]Conditions: 70°C, run time 1 h, liquid propylene, Al/Zr = 15,000.
[c]Units: kg(PP)/mmol(Zr)/h.
[d]Percentage of sequences of 5 propylene units that are perfectly isotactic.

4-position has the effect of suppressing stereoerrors. Table 4 details the effects of alkyl placement on indenyl ligands upon polypropylene properties, while Mise and co-workers (181) have collected data on a large number of bis(Cp) complexes.

Recent work in the area of isospecific olefin polymerization has challenged the mindset that C_2-symmetry is necessary for high isotacticity. For example, compound **50** gives P_{mmmm} between 80 and 91% (183). Another assumption which has been overturned is that, in the bridged indenyl systems, substitution at the 3-position defeats the stereocontrol enforced by the fused benzene ring. Complexes **51** (184) and **52** (185) give some of the highest-melting iPP produced by metallocenes (up to 162°C; R = H).

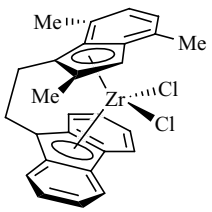

50

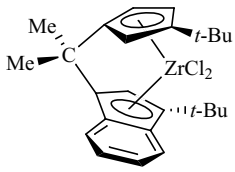

51

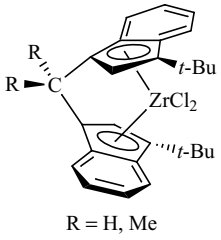

52

Regioerrors have also been linked to elevated chain-transfer rates (186). Ligand modification with the objective of altering the *electronic* environment of the propagating center has not been pursued systematically, although the inductive effects of substituents may influence the stereoselectivity: Lee and co-workers have shown electron-withdrawing groups to suppress stereoerrors in propylene polymerization by *rac*-$C_2H_4(Ind')_2ZrCl_2$/MAO (Ind′ = substituted indenyl) (119).

Isotactic polymers of 1-olefins higher/larger than propylene has been accomplished with metallocenes, as would be expected from the enhanced ability of these catalysts to incorporate large comonomers in ethylene–olefin copolymerization.

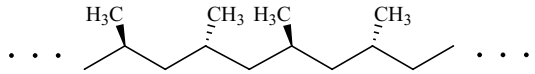

Fig. 11. Syndiotactic polypropylene.

Syndiotactic Polypropylene. Syndiotactic polypropylene (sPP) is a crystalline homopolymer with alternating stereochemistry at each successive methine carbon in the chain (Fig. 11).

Compared with iPP, sPP has lower modulus and melting point, making it less useful for applications demanding strength. It does, however, appear to be superior to iPP in such properties as clarity and flexibility (187,188). Although catalysts such as VCl_4 had been shown to produce sPP at low temperature, metallocenes with C_s symmetry such as **3** were the first catalysts to make sPP under practical conditions with high activity (189). The performance of some complexes in this family is shown in Table 5. Note the effects of bridge substituents on polymer MW (190).

Mixed Tacticity Polyolefins. The Waymouth group at Stanford has recently unveiled (193) a catalyst family for the production of elastomeric polypropylene, in which blocks of isotactic polymer are linked by segments of essentially atactic material, resulting in a product with geographically separate crystalline and amorphous domains, which is imbued with high flexibility and recovery. The underlying mechanism has been said to be as shown in Scheme 7, where an unbridged complex oscillates between racemoid and mesoid conformers on a timescale intermediate between that for monomer insertion and that for production of a single polymer molecule.

However, recent microstructural investigations have led Busico and others to advance an alternate mechanism (194), in which two enantiomeric racemoid catalysts interconvert (Scheme 8) at a rate nearly equal to monomer insertion.

In any case, the relative amounts of isotactic and atactic sequences depend on temperature, monomer concentration, transition-metal identity (Zr or Hf) as well as upon the size of the 2-indenyl substituent. Chien (195) and Collins (196) have also described metallocenes **53** and **54**, respectively) which produce elastomeric polypropylene.

Table 5. Comparison of Bridged Cp–Fluorenyl Metallocenes as Syndiotactic Polypropylene Catalysts

Catalyst	Al/M	Act.[a]	M_w/1000	T_m, °C	P_{rrrr}[b]	SI[c]	Reference
$Me_2C(Cp)(Flu)ZrCl_2$[d]	13,000	117	69	134, 140	82.7	—	191
$Me_2C(Cp)(Flu)HfCl_2$[d]	940	1.4	777	114	75.7	—	191
$(Ph)(Me)C(Cp)(Flu)ZrCl_2$[e]	2,700	93	435	—	—	96.1	192
$Ph_2C(Cp)(Flu)ZrCl_2$[e]	2,700	98	519	—	—	95.9	192

[a] Units of kg(PP)/mmol(M)/h.
[b] Percentage of sequences of 5 propylene units which are perfectly syndiotactic.
[c] Syndiotactic Index, as determined by 13C NMR.
[d] Conditions: 50°C, liquid propylene.
[e] Conditions: 70°C, liquid propylene.

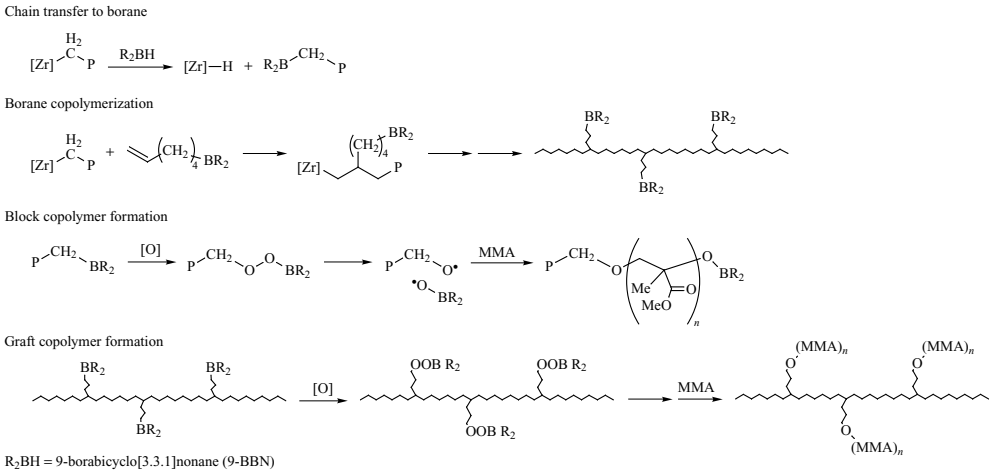

Scheme 7.

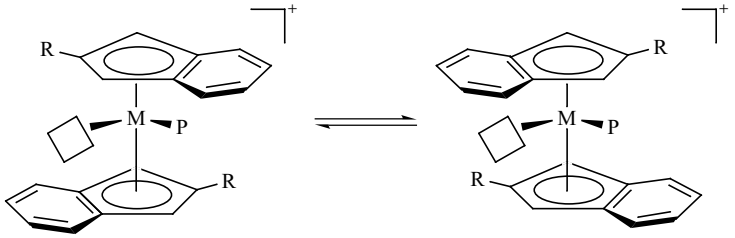

Scheme 8.

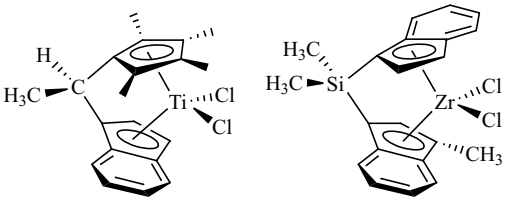

53 **54**

In both of these cases the metallocenes have a highly asymmetric character. The authors postulate a different kind of oscillation for the origin of the blockiness: a competition between migratory insertion and polymer chain migration without insertion. This is shown graphically for Collins' system in Scheme 9.

Isotactic sequences are here due to successive insertions upon the same side of the catalyst (rather than from alternate sides as is believed to occur in C_2-symmetric systems), which are made possible by "windshield-wiper" motions of the chain relative to the catalyst. The dibridged catalyst **55** switches from being predominantly syndiospecific to being moderately isospecific as temperature is raised and propylene concentration is lowered, probably due to a similar phenomenon (54). The fact that the catalyst with the chiral substituent projecting

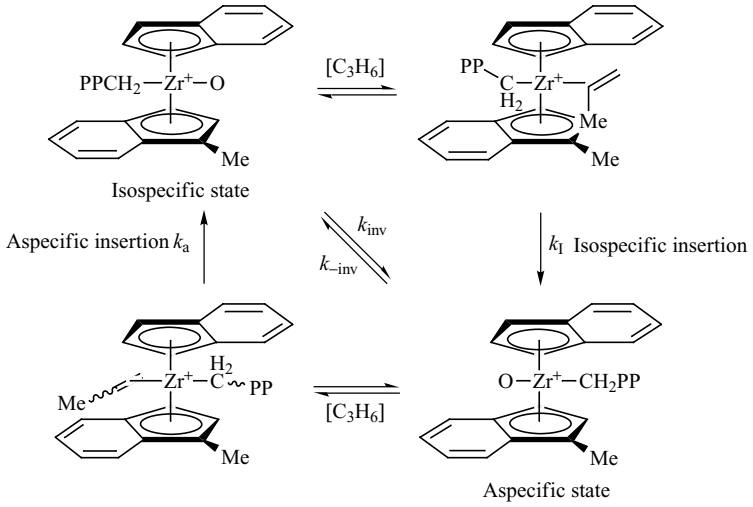

Scheme 9. (Reprinted with permission from Ref. 196. Copyright 1998 American Chemical Society.)

into the wedge (as shown in **55**) suppresses the strong syndiospecificity evident in the system with this substituent replaced by H is further evidence of a missed-insertion mechanism, since one side becomes significantly more crowded than the other.

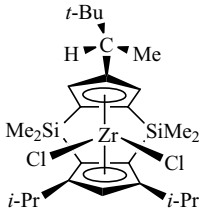

55

A subtle modification of the ligand sphere in Cp–fluorenyl complexes, as in structure **56**, changes the stereospecificity of the catalyst enough so that hemiisotactic polypropylene, rather than sPP, is produced (197). Apparently, the added substituent on the Cp ring is enough to remove any enantiofacial selectivity from one side of the site, but not enough to completely suppress monomer coordination to one side, as in Scheme 9. This material, shown in Figure 12, can be thought of as a syndio-isotactic stereoblock polymer.

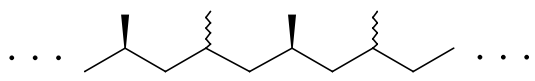

Fig. 12. Hemiisotactic polypropylene. (Wavy lines indicate methine units of indeterminate chirality.)

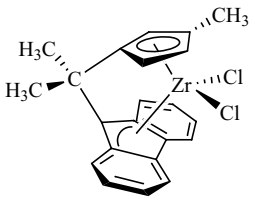

56

Catalysts such as **56** also lead to alternating isotactic ethylene–propylene copolymers through a similar mechanism (198), since conditions can be arranged such that ethylene incorporates predominantly on the more hindered catalyst side.

Other Monomers.

Dienes. Dienes tend to reduce the polymerization activity of metallocenes, and it is generally difficult to incorporate more than a few mole pernts into polyethylene. Monomers having two C=C bonds can be incorporated into one or two chains depending on the reactivity of the two unsaturated fragments. If conjugated, the diene can be incorporated via 1,2- or 1,4-insertion, leaving one double bond either in the polymer backbone or on a side chain. Conjugated dienes are particularly potent catalyst poisons for bis-Cp metallocenes, although there are occasional reports (199,200) of copolymerization with ethylene. Mono-Cp titanium complexes, by contrast, are fairly competent for the homopolymerization of 1,3-butadiene or isoprene (201). Incorporation of butadiene leads in some cases to the presence of *trans*-vinylidene groups and *trans*-1,2-cyclohexanediyl structures (202) and in others to *trans*-1,2-cyclopentanediyl and 1,2-cyclopropanediyl groups. (203). The oxidation state of titanium in the catalyst is (again) not known, but the ability of the $[C(C_6H_5)_3][B(C_6F_5)_4]$ activator to give high activity for polybutadiene (1240 g(BR)/mmol(Ti)/h at 30°C, giving about 80% cis and 15% vinyl microstructure) is suggestive of Ti(IV) character (204).

As mentioned in the section Long-Chain Branching, the presence of low levels of α,ω-dienes in the reaction mixture for ethylene polymerization can lead to polyethylene with LCB or cross-linked PE.

An interesting type of polymerization—cyclopolymerization—occurs with certain bridged metallocenes exposed to short α,ω-dienes such as 1,5-hexadiene (205,206). The homopolymerization, shown by (equation 29, involves the initial 1,2-insertion of the first vinylic group followed by the 1,2-insertion of the second, leading to cyclic groups.

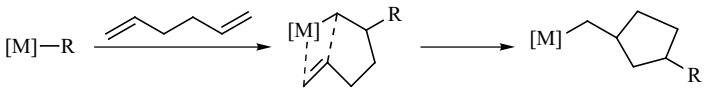

(29)

The microstructure, shown in Figure 13 for the *trans*-isotactic polymer, is defined by two types of stereoselection, intra- and inter-ring, since the two types of insertions in equation 29 differ chemically.

The structure of the metallocene influences the stereochemistry of acyclic insertion, with isospecific metallocenes tending to select the same enantioface for the

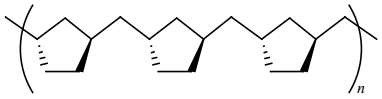

Fig. 13. Trans-isotactic poly(methylene-1,3-cyclopentylene).

nonring insertion; aspecific and isospecific catalysts both favor trans insertion for the ring-closing step. One intriguing property of polymer with a structure such as shown in Figure 13 is that the polymer has no mirror plane (unlike poly(α-olefins) as discussed in section Isotactic Polypsopylene), and hence can be optically active even at high MW. This was demonstrated by using a single enantiomer of the bridged racemic metallocene ethylenebis(η^5-4,5,6,7-tetrahydroindenyl)zirconium dichloride, itself selected by reaction with a single enantiomer of 1,1-bi-2-naphthol.

The most industrially relevant family of dienes used in metallocene polymerizations is represented by **57**, **58**, and **59** (ethylidene norbornene, 1,4-hexadiene, and dicyclopentadiene, respectively).

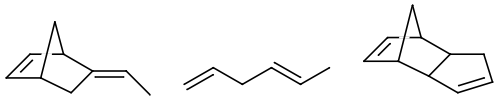

57 **58** **59**

These dienes, along with ethylene and propylene, are used to make EPDM, a sulfur-vulcanizable elastomer. Generally, EPDM contains 25–60 wt% propylene and 1–5 wt% diene, and is completely amorphous. Metallocene catalysts have inherent advantages in EPDM polymerization, the most important of which are the ability to incorporate large amounts of α-olefin with ease and the avoidance of long ethylene sequences that lead to crystallinity. Catalysts that appear to have found commercial application in EPDM include mono-Cp catalysts such **12** (207) and **14** (208).

Cycloolefins. The ability of metallocenes to controllably insert previously recalcitrant monomers is further evidenced by the homo- and copolymerization of cycloolefins such as cyclopentene. Initially, enchainment of cyclopentene was assumed (209) to proceed in normal 1,2-fashion, as shown in Figure 14**a**, and indeed this appears to hold true in copolymerizations with ethylene. However, later work (210) on homopolymers showed that isomerization following 1,2-incorporation is obligatory, presumably due to steric considerations, yielding 1,3-inserted units (Fig. 14**b**)

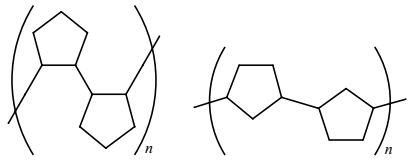

(**a**) (**b**)

Fig. 14. Polycyclopentene regiochemistries.

Polar Comonomers. Heteroatom-containing monomers have the potential to allow polyolefins to ameliorate deficiencies in key product areas such as printability and water permeability. Despite the well-deserved reputation of metallocenes for sensitivity to polar functional groups, Waymouth and co-workers have polymerized α-olefins bearing protected hydroxyl or dialkylamino groups on the terminal carbon, albeit at fairly low rates (211). The very bulky metallocene $(C_5(CH_3)_2)_2Zr(CH_3)_2$ combined with the discrete activator $[C_6H_5(CH_3)_2NH][B(C_6F_5)_4]$ displayed the highest activities for poly (5-(*N*,*N*-diisopropylamino)-1-pentene), apparently due to the inability of the nitrogen atom to coordinate to either transition metal or cocatalyst (212). Copolymerization of ethylene and 4-allylanisole followed by deprotection led to the preparation of polyethylene-bearing phenol groups (213). Incorporation of polymer stabilizers such as vinylic hindered amines (214) via copolymerization could potentially defeat the phase separation and blooming, which often compromise the activity of blended-in stabilizers.

Isobutylene. Unlike conventional Ziegler–Natta and most metallocene catalysts, the compound $(CH_3)_2Si(C_5(CH_3)_4)(NR)Ti(CH_3)_2$ (R = cyclododecyl; activators = MAO or discrete ion pair) can copolymerize isobutene with ethylene, as has been shown by an Exxon group (215). The isobutene units tend to be isolated, eliminating a carbocationic addition mechanism.

Methylenecycloalkanes. Strained cycloalkanes with exo-methylene groups have been homopolymerized as well as copolymerized with ethylene by catalysts such as $[(C_5(CH_3)_5)_2Zr(CH_3)]^+[(CH_3)B(C_6F_5)_3]^-$ and analogous Group IIIB and lanthanide metallocenes via the C—C bond migration mechanism shown in equation 30 (216).

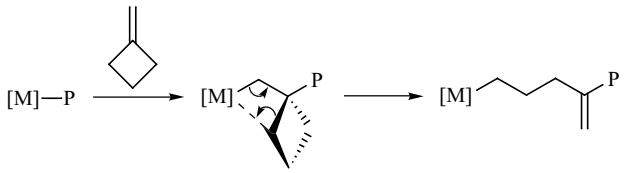

(30)

Styrene (as Random Comonomer with Ethylene). Both bis- and mono-Cp Group IVB metallocenes copolymerize ethylene and styrene (217). The catalysts are believed to be M(IV) in nature. The sequential enchainment of two styrene units is generally disfavored (an exception being the isopropyl-bridged metallocenes, as reported in Ref. 218, even at styrene levels approaching 50 mol% in the polymer, leading to nearly alternating ES copolymers. These copolymers have properties that vary from thermoplastics to elastomers to crystalline or glassy solids, depending on the level of styrene incorporation (218) (see Fig. 15).

Although the alternating ES copolymers are generally atactic, crystalline ($T_m = 145^\circ C$) isotactic *alt*-ES (Fig. 16) results from copolymerization at $-25^\circ C$ in the presence of *rac*-$Et(Ind)_2ZrCl_2$ (**2**) activated by MAO.

Mixed Metallocene Catalysts. By combining two or more metallocenes in the (co)polymerization of olefins, polymers of broadened MW distribution or comonomer distribution may be obtained. In certain cases, it seems the polymer

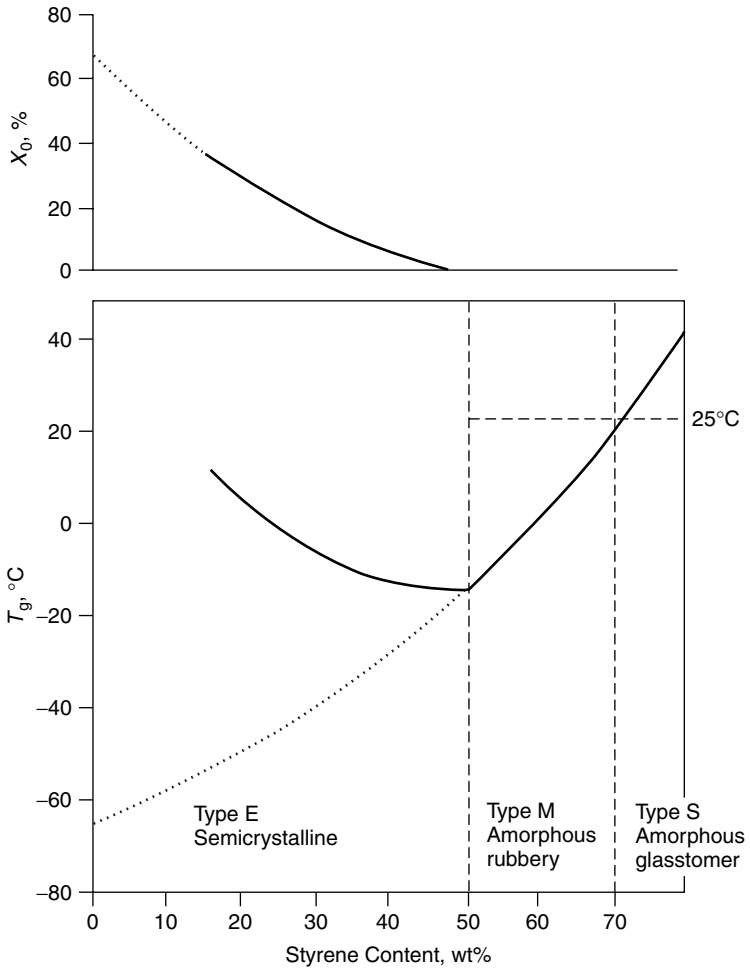

Fig. 15. Characteristics of ethylene–styrene copolymers made by INSITE technology. From 218. Copyright © (1998). This material is used by permission of Wiley-Liss, Inc., a subsidiary of John Wiley & Sons, Inc.

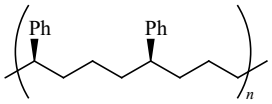

Fig. 16. Isotactic alternating ethylene–styrene copolymer.

chains produced by one metallocene can serve as a comonomer for a second, thus making LCB-containing polymer possible in cases where the two catalysts may not be competent to produce it by themselves.

In a variation of this concept, metallocene catalysts can function in the presence of olefin oligomerization catalysts, whether the latter be metallocenes

themselves, as in the case of Bazan's bis(boratabenzene)zirconium catalyst (219), or entirely different types of catalyst, as with the nickel-based single-component catalyst **60** (220).

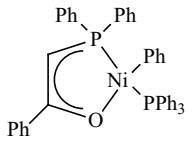

60

Polymerization of Monomers Other Than Alkenes

In this section we survey the use of metallocenes as catalyst precursors for polymerizations in which the predominant monomer is not ethylene or any α-olefin. The subject of metallocenes as initiators for the cationic polymerization of vinyl monomers is dealt with elsewhere. Except for styrene, true random copolymers of the monomers in this section with alkenes are not produced because the mechanisms for polymerization of the non-olefins differ greatly from that operating in Sinn–Kaminsky catalysis.

Styrene. Mono-Cp complexes of titanium are especially useful in the syndiotactic polymerization of styrene (first reported in Ref. 221, a material with high melting point ($\sim$278°C) and other useful features such as a rapid crystallization rate (222). The catalysts are believed (223) to be cationic Ti(III) monoalkyl species, which then undergo predominantly 2,1-insertions (Scheme 10). This is true even in the case of systems in which the activator is the fluorinated borane $B(C_6F_5)_3$. The mechanism of reduction is unclear, but appears to be accelerated in the presence of styrene.

Catalyst activities can be as high as 38 kg(PS)/mmol(Ti)/mol(styrene)/h in laboratory polymerizations, with syndiospecificities close to 99% (for the system

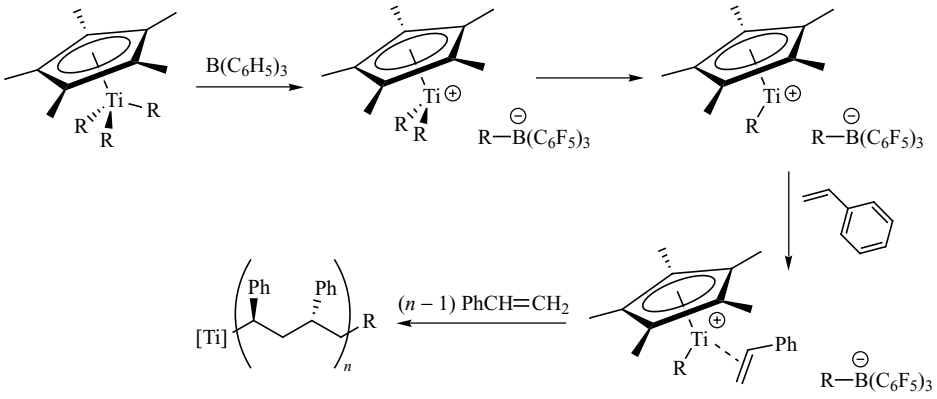

R = Me, CH_2SiMe_3; [Ti] = $(C_5Me_5)Ti^+$

Scheme 10.

$C_5(CH_3)_5Ti(OCH_2CH_2)_3N$, see Ref. 224). Solvent effects indicate that competition of aromatic solvent with monomer for the open coordination site affects activity (225).

Methyl Methacrylate. The quasi–living polymerization of methyl methacrylate can be achieved using lanthanide (226) and Group IVB metallocene complexes, with the latter requiring organozinc, organoaluminum, or borate salt activators. At the heart of the chemistry is a metal-assisted Michael addition, which can occur either through intra- (eq. 31) or intermolecular (eq. 32) C—C bond formation, the latter being more properly described as group-transfer polymerization.

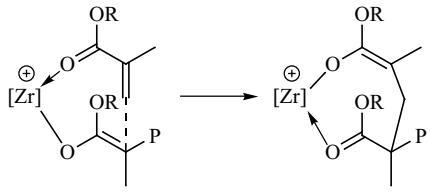

(31)

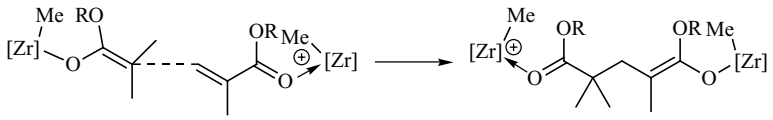

[Zr] = Cp_2Zr; R = Me, *t*-Bu.

(32)

In both cases, propagation requires the facile decomplexation of the polymer chain carboxylate and its replacement by that of the monomer. Isotactic PMMA results when a racemic bridged bis(indenyl) (227) or amidocyclopentadienyl half-sandwich complex is employed (228); enantiomorphic site control indicates that path (eq. 31) dominates in that case.

Lactones. Esters *cyclo*-$(CH_2)_nCO_2$ (n = 4, 5) have been shown by Yamashita and co-workers to be efficiently polymerized by the lanthanocenes $(C_5(CH_3)_5)_2Sm((CH_3))(THF)$ and $[Cp_2Yb(CH_3)]_2$ (229). Recent work of Evans and co-workers has revealed that the highly reactive, divalent pentamethylsamarocene, optionally solvated by THF, which can effectively polymerize ε-caprolactone by ring-opening (230), also copolymerizes ethylene carbonate and ε-caprolactone (eq. 33) (231). Even when present at levels up to 23 mol% in the copolymer, the carbonate units appear to be isolated, indicating a low level of blockiness.

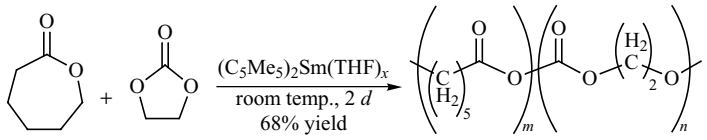

1 : 1 $m/(m + n) = 0.8$

(33)

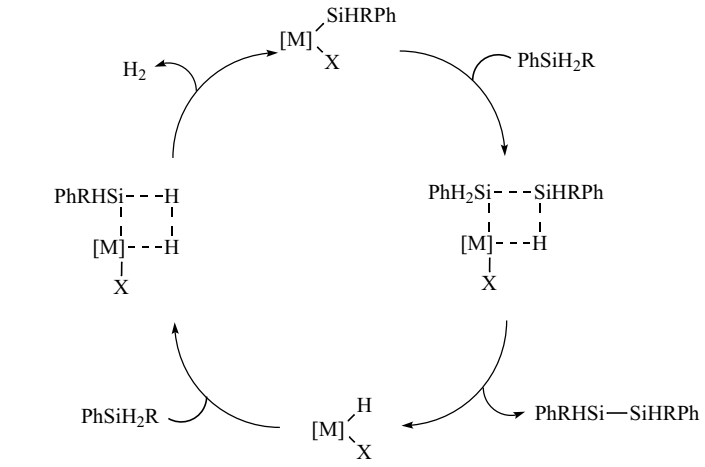

[M] = (Cp)(C_5Me_5)Hf; X = Cl; R = H or polymer chain.

Scheme 11.

Silanes. Group IVB metallocenes catalyze the stepwise polymerization (dehydrocoupling) of primary silanes, yielding H—(SiHR)$_n$—H and n H_2 (232). The mechanism appears to be strictly metathetical for such molecules as (Cp)($C_5(CH_3)_5$)Hf(X) (R = H, alkyl; X = H, alkyl, chloride), wherein the entire process takes place on the neutral manifold (Scheme 11) (233).

A different pathway, probably involving the coupling of free silyl radicals, appears to operate in polymerizations catalyzed by Group IVB complexes (eg, Cp_2ZrCl_2) activated by noncoordinating ionizing agents such as $[(C_6H_5)_3C][B(C_6F_5)_{4-n}(n\text{-}C_4H_9)_n]$ ($n = 0$–2) following pretreatment with n-C_4H_9Li (234).

Graft and Block Copolymerization of Olefins with Non-Olefins. The compositional homogeneity and relatively narrow molecular weight distribution that are typical for metallocene copolymers present an opportunity for the functionalization of the majority of polyolefin chains with chains composed of non-olefinic units. In these cases, the secondary polymerizations are mediated by catalysts or initiators that are unrelated to the polyolefin catalyst. The reactive groups at which anionic or free-radical polymerization can begin are either derived from chain-transfer events during metallocene polymerization or from olefinic comonomers. It is often necessary to chemically transform the end groups or side chains prior to the polymerization of the non-olefin. The potential advantages of this strategy, which has been thoroughly reviewed by Chung (235), lie in the compatibilization of polyolefins and other polymers (ie, homopolymers of the non-olefin blocks). Both graft and block copolymers of ethylene with methyl methacrylate can be made through the oxidation of borane side-chain or terminal groups, respectively, as shown in Scheme 12.

Miscellaneous. Patten and Novak have described (236) the polymerization of isocyanates using $CpTiCl_2(OCH_2CF_3)$ as a single-component catalyst. Unlike non-metallocene titanium catalysts, this species is active for the

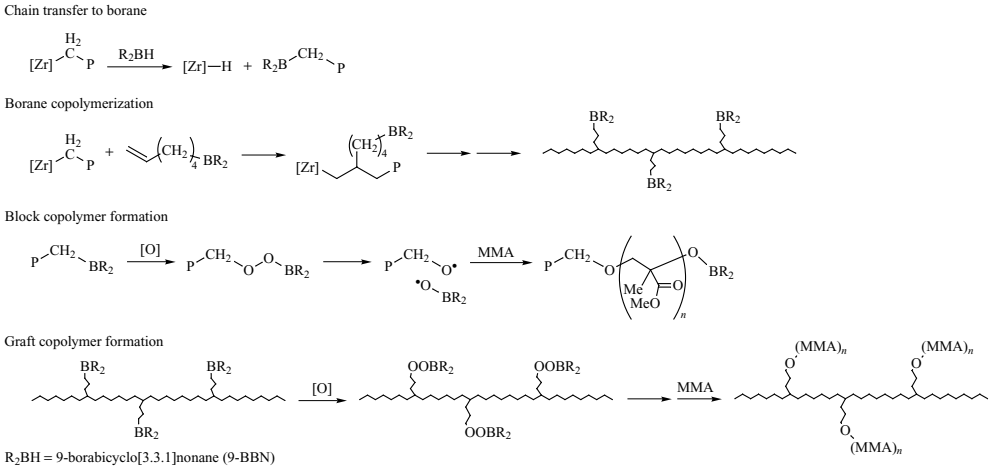

Scheme 12.

polymerization of isocyanates with functional side chains such as **61**. Acrylonitrile (237) has been polymerized by lanthanocenes.

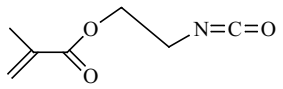

61

Reactions of Metallocenes Not Involving Polymerization

Transformations of small molecules using Group IVB metallocenes are important in organic chemistry, and it is impossible to give more than the most superficial treatment here. Noncatalytic chemistry will be covered only briefly.

A common theme in many reactions is the generation of an equivalent of Cp_2M through the reduction of a tetravalent precursor metallocene with a metal alkyl such as *n*-butyllithium. The chemistry of olefin complexes of Cp_2M is characterized by a facile interconversion between formally M(II) and M(IV) manifolds, as shown in equation 34. Another central motif of metallocene chemistry, especially that of titanocenes, is the accessibility of pathways connecting metallacycles and metal alkylidene complexes, eg in alkene metathesis (eq. 35).

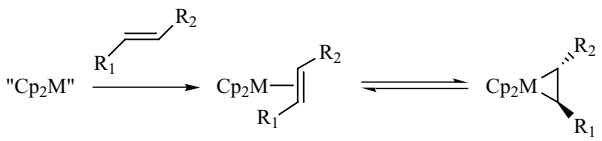

(34)

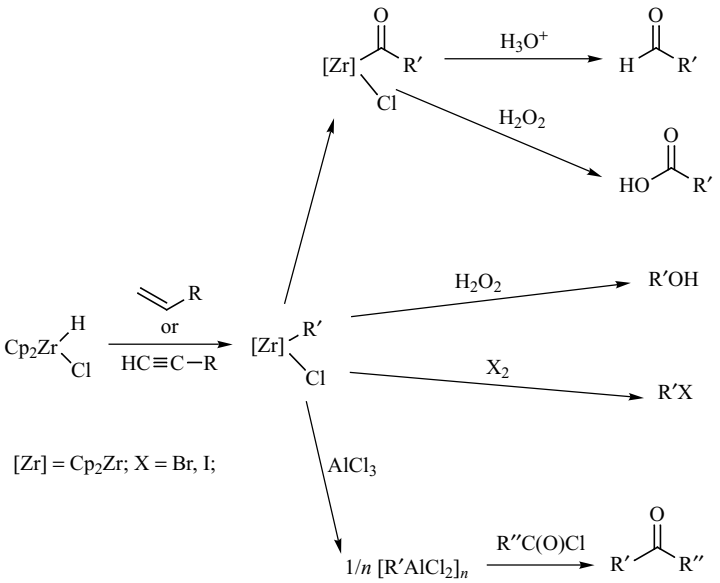

Scheme 13.

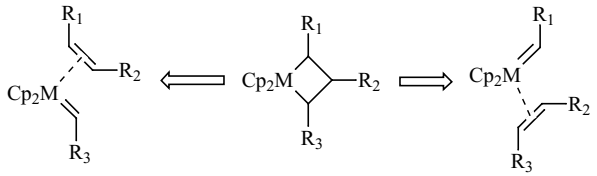

(35)

Stoichiometric Reactions.

Hydrozirconation. Of great use in preparative organic chemistry is the addition of the zirconium–hydride bond to alkenes and alkynes. Not only are the alkylzirconium species thus formed useful in themselves, giving rise to a diverse set of organic compounds depending on reagent used to destroy the Zr—C bond (238), they can undergo transmetallation reactions with chloroaluminum compounds with retention of stereochemistry to yield more reactive alkylaluminum moieties (239) (Scheme 13).

Coupling of Alkenes and Alkynes. The highly reactive [Cp_2Zr] fragment, generated through trapping of an alkyne complex with Lewis base (240), forms metallacycles with alkenes, alkynes, ketones, aldehydes, and nitriles (selected reactions shown in Scheme 14).

Another means of generating zirconocene, via the decomposition of dialkyl zirconocenes (241) can be used to produce bicyclic organic compounds from the cyclization reaction followed by carbonylation (Scheme 15).

In both cases, acyclic final products can be obtained through quenching reactions such as aqueous workup or addition of elemental halogen. Alkene

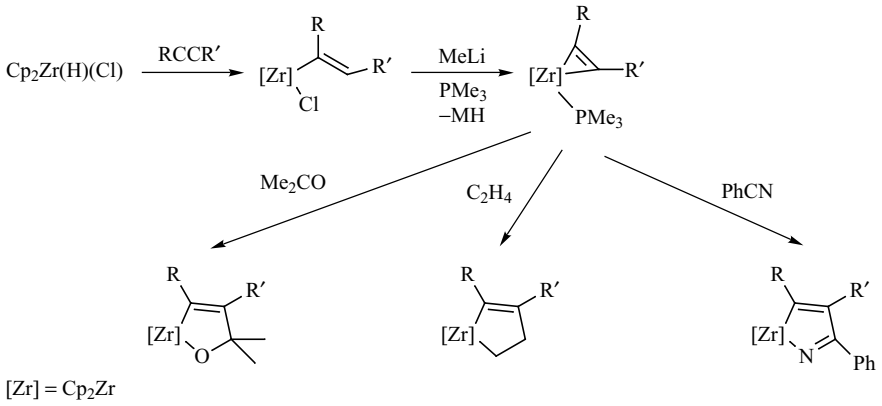

Scheme 14.

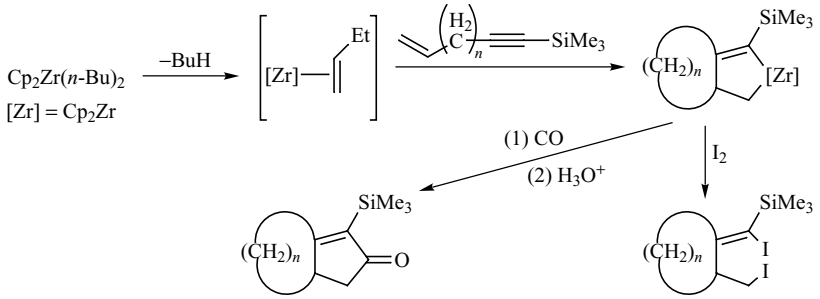

Scheme 15.

complexes of zirconocene will also form carbon–carbon bonds with alkenes to give *trans*-3,4-dialkylzirconacyclopentanes (eq. 36) with selectivity >98%; these can be reacted further, eg with CO or HCl to give cyclic and acyclic products, respectively (242).

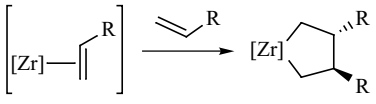

(36)

Metallocene complexes of *o*-benzyne will also add to alkenes or alkynes, yielding 1-metallaindans and 1-metallaindenes, respectively (243). The zirconacyclopentadienes formed from the dimerization of alkynes are convenient synthons for phospholes, siloles, and germoles (244).

Addition of styrenes to olefins leads to 2-aryl-4-alkylzirconacyclopentanes.

Reductions. Bromo- or chlorohydrocarbons may be efficiently dehalogenated by titanocene dichloride in the presence of metallic magnesium (eq. 37) (245). The source of the hydrogen for the reaction appears to be the

Cp rings of the titanocene, by way of the titanocene dimer, which has the structure **62**.

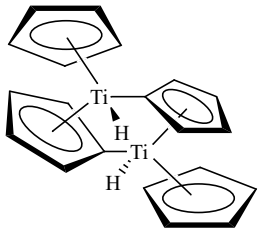

62

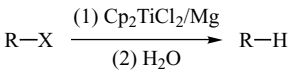

(37)

Noncatalytic metathesis of the carbenoid group of $Cp_2Ti{=}CH_2$ with organic carbonyl oxygen atoms leads to formation of the corresponding exo-methylene organic molecule. In this way, cyclohexanone is transformed into methylenecyclohexane and benzaldehyde into styrene (246). The oxophilicity of titanium is again called into service in the conversion of oxiranes, aldehydes, and esters (eq. 38) into the corresponding alkanes by sodium-reduced titanocene dichloride (247).

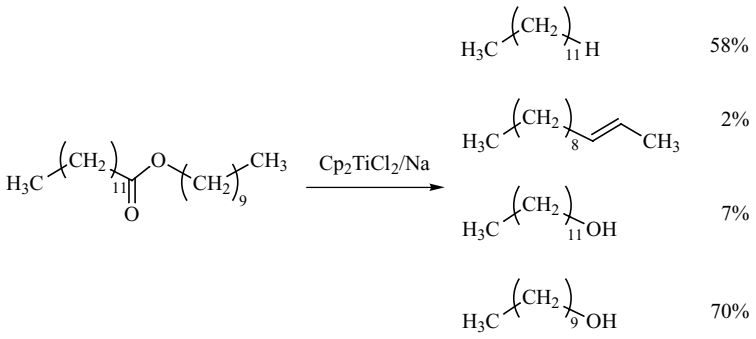

(38)

Titanocene has also been reported to reduce alkyl nitriles to alkanes (248).

Catalytic Reactions.

Hydrogenations. Olefins can be reduced to alkanes with good enantioselectivity with either neutral Ti(III) (249) (eq. 39) or cationic Zr(IV) (250) metallocenes bearing chiral bis(indenyl) ligands. Unbridged titanocenes and zirconocenes with bulky chiral substituents attached to the Cp rings asymmetrically hydrogenate 1,1-disubstituted olefins, though with somewhat lower e.e.'s (251).

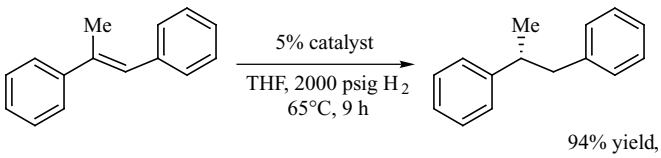

(39)

Assisted Metallations of Unsaturated Hydrocarbons. Titanocenes and zirconocenes catalyze the addition of M—R (M = B, Mg, Al; R = H, alkyl) bonds across C=C double bonds. The hydroboration of olefins (eq. 40) is believed to involve the species $Cp_2Ti(BH_4)_2$ (252).

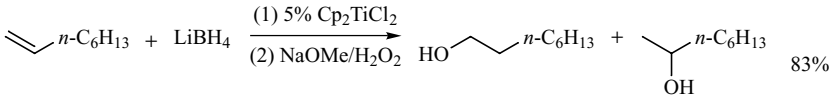

(40)

The carbomagnesation of olefins (eq. 41) is selective for terminal vinyl double bonds (253).

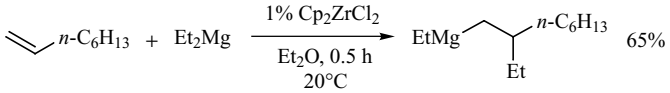

(41)

Alkynes may be converted to the corresponding substituted vinylalanes by the action of zirconocene dichloride and trimethylaluminum (Eq. 42) (254). The regioselectivity for Z-addition of the Al—R bond is generally >95%, but drops significantly if R is larger than the methyl group.

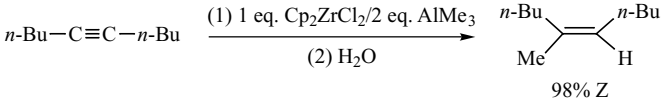

(42)

Titanocene difluorides also catalyze the hydrosilation of imines, presumably through the formation of the trivalent titanocene hydride $Cp'_2Ti—H$. This reaction can be made enantioselective, as shown in (equation 43) (255).

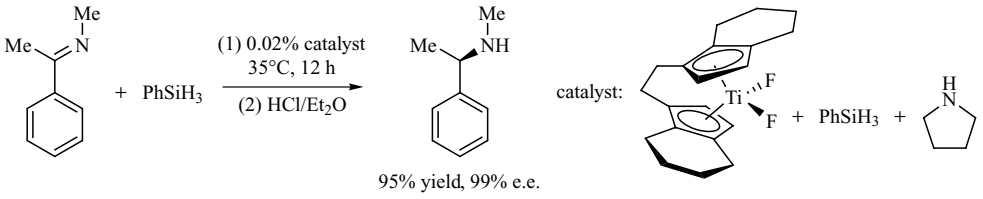

(43)

Alkene and Alkyne Dimerization and Trimerization. The low-valent mono-Cp zirconium compound $CpZrMe(DMPE)_2$ (DMPE = 1,2-bis(dimethylphosphino)ethane) catalyzes the dimerization of ethylene to 1-butene at low frequency (3 t.o./d), a process wherein the 1,3-butadiene complex **64** is presumed to be the catalyst (256). The clean dimerization of olefins using the Cp_2ZrCl_2/MAO (Al/Zr = 1) catalyst has recently been reported (257). Recently,

the monocyclopentadienyl titanium compound $[(\eta^5\text{-}C_5H_4C(CH_3)_2C_6H_5]TiCl_3$ has been shown to generate 1-hexene from ethylene with fairly high selectivity (258).

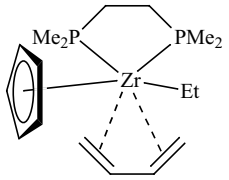

63

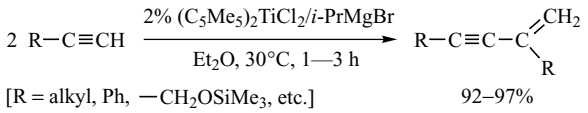

(44)

The highly regioselective head–tail dimerization of alkynes has been accomplished using a Grignard-reduced titanocene dichloride (eq. 45) (259).

Metatheses. Alkene metathesis can be catalyzed by the dinuclear metallacycle $Cp_2Ti(\mu\text{-}CH_2)(\mu\text{-}Cl)AlR_2$ (Tebbe's reagent) (260). Grubbs and co-workers have postulated (261) that the reaction proceeds first by the formation of a metallacyclobutane, followed by C—C bond cleavage to give a carbene–olefin complex that can exchange olefin through a dissociative process (Eq. 45).

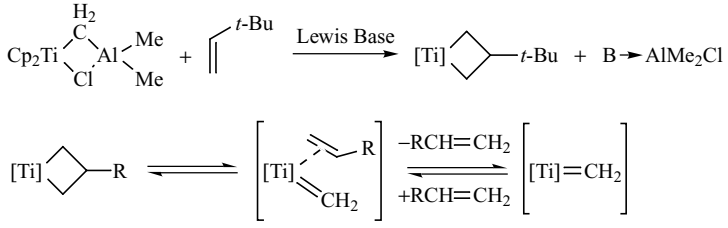

(45)

Titanacyclobutanes can serve as catalysts for the living ring-opening metathesis polymerization (ROMP) of cycloolefins through analogous metathesis chemistry (262) (Eq. 46). The driving force for polymerization is relief of ring strain.

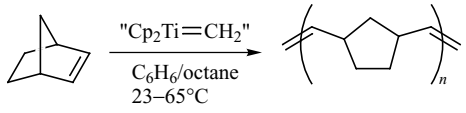

(46)

Olefin metathesis reactions involving Groups V and VIB metallocenes have also been thoroughly examined (263).

Allyl Coupling Reactions. Zirconocenes assist in the attack of allylmagnesium species on allyl alkyl ethers (eq. 44) and other activated allylic compounds (264).

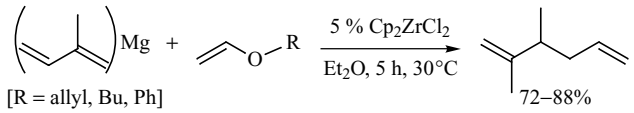

(47)

Alkylation. Use of the chiral metallocene *rac*-Et(Ind)$_2$Zr(CH$_3$)$_5$, activated with the protic salt [HN(C$_9$H$_5$)$_3$][B(C$_6$H$_5$)$_4$], couples 1-hexene and 2-picoline with some enantioselectivity (eq. 48), but at about one-tenth the turnover frequency of the analogous Cp$_2$Zr(CH$_3$)$_5$-derived catalyst (265).

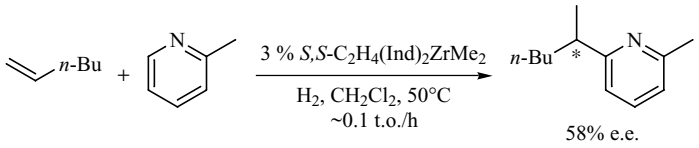

(48)

Commercial Overview

Patenting Activity. A large volume of patents has resulted from the globally intensive search for profitable application of metallocenes. Starting modestly in the mid-1980s, the rate of patenting activity rose rapidly through the early 1990s and has only recently begun to stabilize.

Four companies have historically led in the number of awarded patents, Exxon Chemical, Hoechst Aktiengesellschaft and its successors (Targor, Elenac), Mitsui Petrochemical, and Dow Chemical, as evinced by Figure 17. Other companies have tried to stake out smaller, more focused domains of intellectual property, with Fina (syndiotactic polypropylene), Idemitsu Kosan (syndiotactic polystyrene), and Ticona (cycloolefin copolymers) being notable examples. The vicissitudes of the struggles over patent rights are such that nothing can be said regarding the ultimate strength of any particular portfolio. However, the search for freedom to operate in the field of metallocenes has been a large factor in determining the direction and emphasis of research at many companies. The effects of mergers and patent litigation on the climate for metallocene implementation has been recently summarized (266).

Polyethylene. The polyethylene market is rather conservative and price-sensitive, especially in the commodity grades, so it is not surprising that metallocene resins, which are more expensive than the Ziegler–Natta materials they aim to replace, have made only small inroads here. The most promising area of market penetration is in specialty grades, especially in the very low density regime ($d < 0.910$ g/cc), where the absence of oligomers and high-melting crystallinity make for a clear, flexible product with low tackiness and odor. These products are well-suited for food packaging and cable insulation, and are beginning to find their way into markets hitherto dominated by plasticized PVC. Much of the emphasis in metallocene research for polyethylene applications has been directed toward adapting the polymer architecture so that the user may process the molten resin in existing equipment. This is facilitated by use of catalysts that

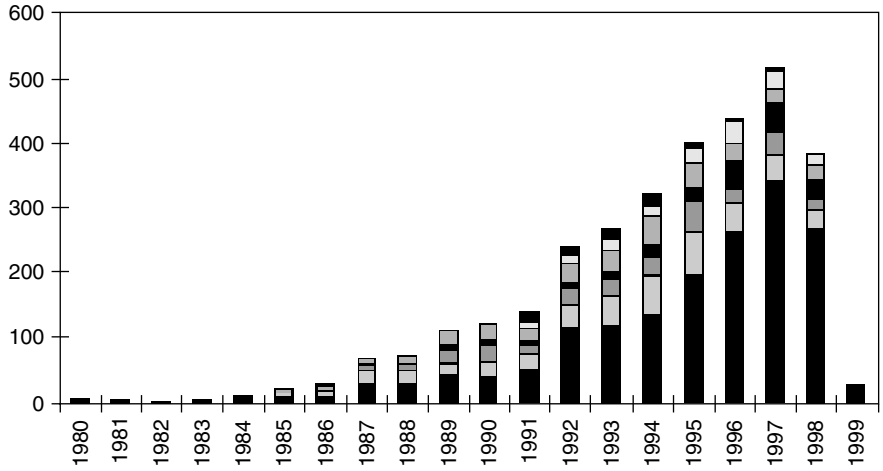

Fig. 17. Patenting activity by company in metallocene-based olefin polymerization (approximately all unique published applications by priority date as of May 2000). ■ Phillips, ■ BASF, ■ Hoechst, ■ Dow, ■ Mitsui, ■ Exxon, ■ Others.

give long-chain branched PE or by use of mixed catalyst systems to yield a polymer with broadened MW distribution.

Metallocene catalysts have been successfully adapted to all commercial polyethylene processes. Recently, companies have begun to join forces to avoid patent disputes as well as to accelerate the pace of commercialization. Joint ventures between Exxon and Union Carbide (Univation Technologies) and between Dow and BP were formed to leverage popular process technologies (variants of fluidized-bed gas-phase reactor systems) to expand the market for metallocene catalysts and products. The Dow–Union Carbide merger of 2001 could greatly influence the rate of technology dissemination.

Polypropylene. Metallocene iPP, as with metallocene PE, has made the least headway in the commodity resin market, where the catalyst technology based on $Mg_xTi_yCl_z$ and selectivity control agents already achieves the high isotacticity (>98%) and activity (<2 ppm Ti) metallocene catalysts have struggled to attain. The areas in which metallocene catalysts have inherent advantages are in (*1*) nonwoven fiber applications, because of the low melt-viscosity associated with narrow MW distribution resins, and (*2*) random copolymers with ethylene or butene, because of the low tendency to form long ethylene blocks. Metallocene iPP is also beginning to displace polystyrene in injection-molding applications.

Fina and Mitsui Toatsu have combined development efforts in syndiotactic polypropylene, but it is not clear where this material will have the greatest impact.

Elastomers. Ethylene–propylene elastomers (EPR) as well as ethylene–styrene elastomers (Index) have been commercialized using Dow's constrained-geometry technology, with the former material being produced and marketed out of the joint venture DuPont–Dow Elastomers. The low levels of crystallinity possible with single-site catalysts make the advantages of metallocenes over Ziegler catalysts much more apparent than in crystalline resins. Market acceptance of these rubbers, along with the very low-density ethylene–1-octene

copolymers made by Dex Plastomers (Exxon/DSM joint venture) and by Dow (Affinity grades), has been swift.

Cycloolefin (co)Polymers. Many metallocenes can incorporate bulky cycloolefins into polyethylene, but only a few companies, notably Hoechst and its successor Ticona, have attempted to sell the resulting materials. These glassy, amorphous copolymers have high rigidity, chemical resistance, and clarity, which predisposes them to be useful in optical applications and in pharmaceutical containers.

Polystyrene. Dow and Idemitsu have worked together to bring syndiotactic polystyrene (Questra) to market, where it has certain advantages over existing PS products, chiefly due to its crystallinity, such as high heat-distortion temperature.

Because of its popularity among both industrial and academic chemists, metallocene technology has been the subject of numerous reviews, some of which have been cited in earlier sections. An excellent listing of metallocene catalyst activities sorted by monomer system and catalyst structure has been collected by Gupta and co-workers (267); the review of Möhring and Coville (268) also stands out for its comparison of metallocene activities, and also thoroughly covers non-ethylene polymerizations. Reddy and Sivaram have produced an overview (269) that is especially strong in the area of aluminoxane structure and function. The constrained-geometry catalyst family has been reviewed by McKnight and Waymouth (270). A fine overview of the state of metallocenes in industry has been put together by Maier (271). A very good general reference for metallocene chemistry including stoichiometric reactions and Cp-equivalents has recently issued (272). Useful collections of articles on the subject of metallocene polymerization occasionally appear in review journals (273).

BIBLIOGRAPHY

1. T. J. Kealy and P. L. Paulson, *Nature* **168**, 1039–1040 (1951).
2. G. Wilkinson, M. Rosenblum, M. C. Whiting, and R. B. Woodward, *J. Am. Chem. Soc.* **74**, 2125–2126 (1952).
3. H. Sinn and W. Kaminsky, *Adv. Organomet. Chem.* **18**, 99–149 (1980).
4. U.S. Pat. 2,827,446 (priority date Sept. 27, 1955), D. S. Breslow (to Hercules Powder).
5. G. Natta, P. Pino, G. Mazzanti, U. Giannini, E. Mantica, and M. Peraldo, *Chim. Ind.* **39**, 19–20 (1957).
6. J. W. Lauher and R. Hoffmann, *J. Am. Chem. Soc.* **98**, 1729–1742 (1976).
7. I. E. Nifant'ev and P. V. Ivchenko, *Organometallics* **16**, 713–715 (1997).
8. G. M. Diamond, S. Rodewald, and R. F. Jordan, *Organometallics* **14**, 5–7 (1995).
9. B. Thiyagarajan and R. F. Jordan, *Organometallics* **18**, 5347–5359 (1999).
10. P. Koepf-Maier, *Eur. J. Clin. Pharmacol.* **47**, 1–16 (1994).
11. E. Zeiger, B. Anderson, S. Haworth, T. Lawlor, and K. Mortelmans, *Env. Mol. Mutagen.* **11**(12), 1–157 (1988).
12. C. J. Harlan, M. R. Mason, and A. R. Barron, *Organometallics* **13**, 2957–2969 (1994); C. J. Harlan, S. G. Bott, and A. R. Barron, *J. Am. Chem. Soc.* **117**, 6465–6474 (1995).
13. J. L. Atwood and M. J. Zaworotko, *J. Chem. Soc., Chem. Commun.* 302–303 (1983).
14. M. R. Mason, J. M. Smith, S. G. Bott, and A. R. Barron, *J. Am. Chem. Soc.* **115**, 4971–4984 (1993).
15. C. Sishta, R. M. Hathorn, and T. J. Marks, *J. Am. Chem. Soc.* **114**, 1112–1114 (1992).

16. D. E. Babushkin and H.-H. Brintzinger, *J. Am. Chem. Soc.* **124**, 12869–12873 (2002); and references therein.
17. U.S. Pat. 5,728,855 (priority date Oct. 19, 1995), G. M. Smith and D. B. Malpass (to Akzo Nobel NV).
18. Eur. Pat. Appl. 0 468 651 A1 (priority date July 3, 1990), R. E. LaPointe (to Dow).
19. X. Yang, C. L. Stern, and T. J. Marks, *J. Am. Chem. Soc.* **113**, 3623–3625 (1991); X. Yang, C. L. Stern, and T. J. Marks, *J. Am. Chem. Soc.* **116**, 10015–10031 (1994).
20. Eur. Pat. Appl. 0 277 004 A1 (priority date Jan. 30, 1987), H. W. Turner (to Exxon).
21. U.S. Pat. 5,155,080 (filed Oct. 10, 1989), M. J. Elder, A. Razavi, and J. A. Ewen (to Fina Technology).
22. M. Bochmann and S. J. Lancaster, *J. Organomet. Chem* **497**, 55–59 (1995).
23. Y.-X. Chen, C. L. Stern, and T. J. Marks *J. Am. Chem. Soc.* **119**, 2582–2583 (1997).
24. L. Jia, X. Yang, C. L. Stern, and T. J. Marks, *Organometallics* **16**, 842–857 (1997).
25. L. Li and T. J. Marks, *Organometallics* **17**, 3996–4003 (1998).
26. G. G. Hlatky, H. W. Turner and R. R. Eckman, *J. Am. Chem. Soc.* **111**, 2729–2731 (1989).
27. A. D. Horton and A. G. Orpen, *Organometallics* **10**, 3910–3918 (1991).
28. M. Bochmann and A. J. Jaggar, *J. Organomet. Chem.* **424**, C5–C7 (1992).
29. M. Brookhart, B. Grant, and A. F. Volpe Jr., *Organometallics* **11**, 3920–3922 (1992).
30. G. G. Haltky, R. R. Eckman, and H. W. Turner, *Organometallics* **11**, 1413–1416 (1992).
31. L. Resconi, S. Bossi, and L. Abis, *Macromolecules* **23**, 4490–4491 (1990); M. Kaminaka and K. Soga, *Polymer* **33**, 1105–1107 (1992).
32. Eur. Pat. Appl. 0 643 079 A2 (priority date Sept. 13, 1993), M. Galimberti and E. Albizzati (to Spherilene); World Pat. Appl. 95/27717 A1 (priority date Apr. 6, 1994), C. E. Bishop, R. L. Jones, K. Raman, V. A. Dang, L. Resconi, T. Dall'Occo, and M. Galimberti (to Spherilene).
33. T. J. Marks, *Acc. Chem. Res.* **25**, 57–65 (1992).
34. EP 0 683 180 A2 (priority date May 18, 1994), Y. Suga, Y. Maruyama, E. Isobe, Y. Uehara, Y. Ishihama, and T. Sagae (to Mitsubishi Chemical); EP 0 849 288 A1 (priority date Dec. 20, 1996), S. Hamura, H. Yasuda, T. Yoshida, and M. Sato (to Tosoh).
35. U.S. Pat. 4,752,597 (priority date Feb. 19, 1987), H. W. Turner (to Exxon).
36. U.S. Pat. 5,756,416 (priority date Feb. 25, 1998), E. P. Wasserman, S. C. Kao, and F. J. Karol (to Union Carbide).
37. M. Stork, M. Koch, M. Klapper, K. Müllen, H. Gregorius, and U. Rief, *Macromol. Rapid Commun.* **20**, 210–213 (1999).
38. U.S. Pat. 5,854,363 (priority date Jan. 8, 1997), M. Jung, H. G. Alt, and B. M. Welch (to Phillips Petroleum).
39. U.S. Pat. 5,317,036 (priority date Oct. 16, 1992), R. C. Brady, III, F. J. Karol, T. R. Lynn, R. J. Jorgensen, S.-C. Kao, and E. P. Wasserman (to Union Carbide).
40. U.S. Pat. 5,648,310 (priority date Dec. 23, 1993), E. P. Wasserman, M. W. Smale, T. R. Lynn, R. C. Brady III, and F. J. Karol (to Union Carbide).
41. U.S. Pat. 4,923,833 (priority date Dec. 27, 1986), M. Kioka, and N. Kashiwa (to Mitsui Petrochemical).
42. EP 0 447 071 A1 (priority date Mar. 12, 1990), J.-C. A. Bailly, and C. J. Chabrand (to BP Chemicals).
43. K. Soga, H. J. Kim, and T. Shiono, *Macromol. Chem. Phys.* **195**, 3347–3360 (1994).
44. G. A. Luinstra, *J. Organomet. Chem.* **517**, 209–215 (1996).
45. R. Fandos, M. Lanfranchi, A. Otero, M. A. Pellinghelli, M. J. Ruiz, and P. Terreros, *Organometallics* **15**, 4725–4730 (1996).
46. J. S. Rogers, G. C. Bazan, and C. K. Sperry, *J. Am. Chem. Soc.* **119**, 9305–9306 (1997).
47. A. J. Ashe III, S. Al-Ahmad, X. Fang, and J. W. Kampf, *Organometallics* **17**, 3883–3888 (1998).

48. J. A. Smith, J. von Seyerl, G. Huttner, and H. H. Brintzinger, *J. Organomet. Chem.* **173**, 175–185 (1979); and Refs. 7 and 8 within.
49. F. Piemontesi, I. Camurati, L. Resconi, D. Balboni, A. Sironi, M. Moret, R. Zeigler, and N. Piccolrovazzi, *Organometallics* **14**, 1256–1266 (1995).
50. C. Qian, J. Guo, C. Ye, J. Sun, and P. Zheng, *J. Chem. Soc., Dalton Trans.* 3441–3446 (1993).
51. W. A. Herrmann, M. J. A. Morawietz, and H.-F. Herrmann, *F. Küber, J. Organomet. Chem.* **509**, 115–117 (1996).
52. A. J. Ashe III, X. Fang, and J. W. Kampf, *Organometallics* **18**, 2288–2290 (1999); and references therein.
53. R. B. Grossman, J.-C. Tsai, W. M. Davis, A. Gutiérrez, and S. L. Buchwald, *Organometallics* **13**, 3892–3896 (1994).
54. T. A. Herzog, D. L. Zubris, and J. E. Bercaw, *J. Am. Chem. Soc.* **118**, 11988–11989 (1996).
55. K. A. O. Starzewski, W. M. Kelly, A. Stumpf, and D. Freitag, *Angew. Chem. Int. Ed.* **38**, 2439–2443 (1999).
56. C. Qian, Z. Xie, and Y. Huang, *J. Organomet. Chem.* **323**, 285–294 (1987).
57. R. Leino, H. Luttikhedde, C.-E. Wilén, R. Sillanpää, and J. H. Näsman, *Organometallics* **15**, 2450–2453 (1996).
58. H. Plenio and D. Burth, *J. Organomet. Chem.* **519**, 269–272 (1996); H. J. G. Luttikhedde, R. P. Leino, C.-E. Wilén, J. H. Näsman, M. J. Ahlgrén, and T. A. Pakkanen, *Organometallics* **15**, 3092–3094 (1996).
59. C. Müller, D. Lilge, M. O. Kristen, and P. Jutzi, *Angew. Chem. Int. Ed.* **39**, 789 (2000).
60. L. Atovmyan, S. Mkoyan, I. Urazowski, R. Broussier, S. Ninoreille, P. Perron, and B. Gautheron, *Organometallics* **14**, 2601–2604 (1995).
61. B. Rieger, *J. Organomet. Chem.* **428**, C33–C36 (1992).
62. J. P. Mitchell, S. Hajela, S. K. Brookhart, K. I. Hardcastle, L. M. Henling, and J. E. Bercaw, *J. Am. Chem. Soc.* **118**, 1045–1053 (1996).
63. T. Takahashi, K. Kasai, N. Suzuki, K. Nakajima, and E. Negishi, *Organometallics* **13**, 3413–3414 (1994).
64. M. Mitani, K. Oouchi, M. Hayakawa, T. Yamada, and T. Mukaiyama, *Macromol. Chem. Phys.* **197**, 1815–1822 (1996).
65. S. Jüngling, R. Mülhaupt, and H. Plenio, *J. Organomet. Chem.* **460**, 191–195 (1993).
66. L. Li, M. V. Metz, H. Li, M.-C. Chen, T. J. Marks, L. Liable-Sands, and A. L. Rheingold, *J. Am. Chem. Soc.* **124**, 12725–12741 (2002).
67. K. Mach, V. Varga, and H. Antropiusová, *J. Organomet. Chem.* **333**, 205–215 (1987).
68. A. Kucht, H. Kucht, S. Barry, J. C. W. Chien, and M. D. Rausch, *Organometallics* **12**, 3075–3078 (1993).
69. G. Xu and S. Lin, *Macromolecules* **30**, 685–693 (1997).
70. L. R. Sita and J. R. Babcock, *Organometallics* **17**, 5228–5230 (1998); and references therein.
71. U.S. Pat. 4,870,042 (priority date Oct. 8, 1987), T. Kohara, and S. Ueki (to Toa Nenryo K.K).
72. S. Doherty, R. J. Errington, A. P. Jarvis, S. Collins, W. Clegg, and M. R. J. Elsegood, *Organometallics* **17**, 3408–3410 (1998).
73. D. W. Stephan, J. C. Stewart, F. Guérin, R. E. v. H. Spence, W. Xu, and D. G. Harrison, *Organometallics* **18**, 1116–1118 (1999).
74. K. Nomura, N. Naga, M. Miki, K. Yanagi, and A. Imai, *Organometallics* **17**, 2152–2154 (1998).
75. Q. Wang, R. Quoyum, D. J. Gillis, M.-J. Tudoret, D. Jeremic, B. K. Hunter, and M. C. Baird, *Organometallics* **15**, 693–703 (1996).

76. T. D. Shaffer and J. R. Ashbaugh, *J. Polym. Sci, Part A: Polym. Chem.* **35**, 329–344 (1997).
77. J. L. Petersen, private communication, 1999.
78. P. J. Shapiro, E. Bunel, W. P. Schaefer, and J. E. Bercaw, *Organometallics* **9**, 867–869 (1990).
79. Eur. Pat. Appl. 0 416 815 A (priority date Aug. 31, 1989), J. C. Stevens, G. F. Schmidt, P. N. Nickias, R. K. Rosen, G. W. Knight, and S. Lai (to Dow Chemical).
80. Eur. Pat. Appl. 0 420 436 A (priority date Sept. 13, 1989), J. A. M. Canich (to Exxon Chemical).
81. World Pat. Appl. 98/41529 (priority date Mar. 19, 1997), R. E. Spence, X. Gao, L. Koch, S. J. Brown, and D. G. Harrison (to Nova Chemicals).
82. J. Klosin, W. J. Kruper Jr., P. N. Nickias, G. R. Roof, P. De Waele, and K. A. Abboud, *Organometallics* **20**, 2663–2665 (2001).
83. K. Kunz, G. Erker, S. Döring, S. Bredeau, G. Kehr, R. Fröhlich, *Organometallics* **21**, 1031–1041 (2002).
84. Y.-X. Chen, P.-F. Fu, C. L. Stern, and T. J. Marks, *Organometallics* **16**, 5958–5963 (1997).
85. J. C. Flores, J. C. W. Chien, and M. D. Rausch, *Organometallics* **13**, 4140–4142 (1994).
86. World Pat. Appl. WO96/13529 (priority date Oct. 31, 1994), J. A. M. van Beek, G. H. J. van Doremaele, G. J. M. Gruter, H. J. Arts, and G. H. M. R. Eggels (to DSM).
87. World Pat. Appl. 96/08497 A1 (priority date Sept. 12, 1994), D. R. Wilson, D. R. Neithamer, P. N. Nickias, and W. J. Kruper Jr. (to Dow Chemical).
88. World Pat. Appl. 97/10248 A1 (priority date Sept. 11, 1995), J. A. Ewen, R. W. Strozier, R. L. Jones Jr., and M. J. Elder (to Montell).
89. G. Rodriguez and G. Bazan, *J. Am. Chem. Soc.* **119**, 343–352 (1997).
90. D. J. Crowther, N. C. Baenziger, and R. F. Jordan, *J. Am. Chem. Soc.* **113**, 1455–1457 (1991).
91. C. Kreuder, R. F. Jordan, and H. Zhang, *Organometallics* **14**, 2993–3001 (1995).
92. N. S. Hosmane, Y. Wang, H. Zhang, J. A. Maguire, E. Waldhör, W. Kaim, H. Binder, and R. K. Kremer, *Organometallics* **13**, 4156–4158 (1994).
93. R. W. Quan, G. C. Bazan, A. F. Kiely, W. P. Schaefer, and J. E. Bercaw, *J. Am. Chem. Soc.* **116**, 4489–90 (1994).
94. Eur. Pat. Appl. 0 672 676 A2 (priority date Mar. 15, 1994), F. G. Cloke (to BP Chemicals).
95. P. L. Watson and G. W. Parshall, *Acc. Chem. Res.* **18**, 51–56 (1985).
96. G. Jeske, H. Lauke, H. Mauermann, P. N. Swepston, H. Schumann, and T. J. Marks, *J. Am. Chem. Soc.* **107**, 8091–8103 (1985).
97. P. J. Shapiro, E. Bunel, W. P. Schaefer, and J. E. Bercaw, *Organometallics* **9**, 867–869 (1990).
98. K. C. Hultzch, T. P. Spaniol, and J. Okuda, *Angew. Chem. Int. Ed.* **38**, 227–230 (1999).
99. G. Jeske, L. E. Schock, P. N. Swepston, H. Schumann, and T. J. Marks, *J. Am. Chem. Soc.* **107**, 8103–8110 (1985).
100. E. B. Coughlin and J. E. Bercaw, *J. Am. Chem. Soc.* **114**, 7606–7607 (1992).
101. P. J. Toscano and T. J. Marks, *J. Am. Chem. Soc.* **107**, 653–659 (1985); D. Hedden and T. J. Marks, *J. Am. Chem. Soc.* **110**, 1647–1649 (1988).
102. H. Yasuda and E. Ihara, *Bull. Chem. Soc. Jpn.* **70**, 1745–1767 (1997).
103. H. Yasuda, M. Furo, H. Yamamoto, A. Nakamura, S. Miyake, and N. Kibino, *Macromolecules* **25**, 5115–5116 (1992).
104. C.-T. Chen, L. H. Doerrer, V. C. Williams, and M. L. H. Green, *J. Chem. Soc., Dalton Trans.* 967–974 (2000).
105. J. M. Decker, S. J. Geib, and T. Y. Meyer, *Organometallics* **18**, 4417–4420 (1999).

106. WO94/01471 (priority date July 1, 1992), D. J. Crowther, R. A. Fisher, J. A. M. Canich, G. G. Hlatky, and H. W. Turner (to Exxon).
107. K. Mashima, S. Fujikawa, Y. Tanaka, H. Urata, T. Oshiki, E. Tanaka, and A. Nakamura, *Organometallics* **14**, 2633–2640 (1995).
108. U.S. Pat. 3,709,853 (priority date Apr. 29, 1971), G. L. Karapinka (to Union Carbide).
109. F. J. Karol, G. L. Karapinka, C. Wu, A. W. Dow, R. N. Johnson, and W. L. Carrick, *J. Polym. Sci., Part A-1* **10**, 2621–2637 (1972).
110. R. A. Heintz, S. Leelasubcharoen, L. M. Liable-Sands, A. L. Rheingold, and K. H. Theopold, *Organometallics* **17**, 5477–5485 (1998).
111. Y. Liang, G. P. A. Yap, A. L. Rheingold, and K. H. Theopold, *Organometallics* **15**, 5284–5286 (1996).
112. A. Döhring, J. Göhre, P. W. Jolly, B. Kryger, J. Rust, and G. P. J. Verhovnik, *Organometallics* **19**, 388–402 (2000).
113. U.S. Pat. 5,418,200 (priority date Mar. 29, 1991), M. J. Carney and D. L. Beach (to Chevron).
114. J. S. Rogers, X. Bu, and G. C. Bazan, *J. Am. Chem. Soc.* **122**, 730–731 (2000).
115. W. Kaminsky and H. Hahnsen, *Adv. Polyolefins (Proc. Amer. Chem. Soc. Intl. Symp. 1985)* 361–371 (1987).
116. K. Heiland and W. Kaminsky, *Makromol. Chem.* **193**, 601–610 (1992).
117. A. Toyota, T. Tsutsui, and N. Kashiwa, *J. Mol. Catal.* **56**, 237–247 (1989).
118. N. Piccolrovazzi, P. Pino, G. Consiglio, A. Sironi, and M. Moret, *Organometallics* **9**, 3098–3105 (1990).
119. I.-M. Lee, W. J. Gauthier, J. M. Ball, B. Iyengar, and S. Collins, *Organometallics* **11**, 2115–2122 (1992).
120. W. Michiels, *A. Muñoz-Escalona, Macromol. Symp.* **97**, 171–183 (1995).
121. World Pat. Appl. 93/13140 (priority date Dec. 23, 1991), J. A. M. Canich (to Exxon).
122. H. Katayama, H. Shiraishi, T. Hino, T. Ogane, and A. Imai, *Macromol. Symp.* **97**, 109–118 (1995).
123. U.S. Pat. 5,474,961 (priority date Sept. 12, 1991), R. Schlund, M. Kersting, and K.-D. Hungenberg (to BASF).
124. World Pat. Appl. 95/13385 (priority date Nov. 8, 1993), S. Cheruvu, F. Y.-K. Lo and S. C. Ong (to Mobil).
125. M. Bochmann, *J. Chem. Soc., Dalton Trans.* 255–270 (1996).
126. D. E. Richardson, N. G. Alameddin, M. F. Ryan, T. Hayes, J. R. Eyler, and A. R. Siedle, *J. Am. Chem. Soc.* **118**, 11244–11253 (1996).
127. J. Karl, G. Erker, and R. Fröhlich, *J. Organomet. Chem.* **535**, 59–62 (1997).
128. T. K. Woo, L. Fan, and T. Ziegler, *Organometallics* **13**, 432–433 (1994).
129. E. J. Arlman and P. Cossee, *J. Catal.* **3**, 99–104 (1964).
130. C. Janiak, *J. Organomet. Chem.* **452**, 63–73 (1993).
131. M. Brookhart, M. L. H. Green, and L.-L. Wong, *Prog. Inorg. Chem.* **36**, 1–124 (1988). W. Piers and J. E. Bercaw, *J. Am. Chem. Soc.* **112**, 9406–9407 (1990).
132. S. L. Borkowsky, N. C. Baenziger, and R. F. Jordan, *Organometallics* **12**, 486–495 (1993).
133. Y. W. Alelyunas, Z. Guo, R. E. LaPointe, and R. F. Jordan, *Organometallics* **12**, 544–553 (1993).
134. Z. Guo, D. C. Swenson, and R. F. Jordan, *Organometallics* **13**, 142–1432 (1994).
135. T. K. Han, Y. S. Ko, J. W. Park, and S. I. Woo, *Macromolecules* **29**, 7305–7309.
136. J. C. Flores, J. S. Wood, J. C. W. Chien, and M. D. Rausch, *Organometallics* **15**, 4944–4950 (1996).
137. I. Tritto, R. Donetti, M. C. Sacchi, P. Locatelli, and G. Zannoni, *Macromolecules* **30**, 1247–1252 (1997).
138. J. Koivumäki, *Acta Polytechn. Scand.* **227**, 1–50 (1995).

139. J. A. Parker, D. C. Bassett, R. H. Olley, and P. Jaaskelainen, *Polymer* **35**, 4140–4145 (1994).
140. N. Herfert, P. Montag, and G. Fink, *Makromol. Chem.* **194**, 3167–3182 (1993).
141. J. A. Ewen, in T. Keii, K. Soga, eds., *Catalytic Polymerization of Olefins*, Kodansha, Tokyo, 1986, p. 271.
142. J. C. W. Chien and D. He, *J. Polym. Sci., Part A: Polym. Chem.* **29**, 1585–1593 (1991).
143. M. Galimberti, F. Piemontesi, O. Fusco, and I. Camurati, *Macromolecules* **31**, 3409–3416 (1998).
144. F. J. Karol, S.-C. Kao, E. P. Wasserman, and R. C. Brady, *New J. Chem.* **21**, 797–805 (1997).
145. C. Lehtinen, P. Stark, and B. Löfgren, *J. Polym. Sci, Part A: Polym. Chem.* **35**, 307–318 (1997).
146. C. Lehtinen and B. Löfgren, *Eur. Polym. J.* **33**, 115–120 (1997).
147. H. Drögemüller, K. Heiland, and W. Kaminsky, in W. Kaminsky and H. Sinn, eds., *Transition Metals and Organometallics as Catalysts for Olefin Polymerization*, Springer-Verlag, Berlin, 1998, p. 303.
148. M. Galimberti, N. Mascellani, and F. Piemontesi, *I Camurati, Macromol. Rapid Commun.* **20**, 214–218 (1999).
149. A. Zambelli, A. Grassi, M. Galimberti, R. Mazzocchi, and F. Piemontesi, *Makromol. Chem., Rapid Commun.* **12**, 523–528 (1991).
150. J. V. Seppälä, J. Koivumäki, and X. Liu, *J. Polym. Sci., Part A, Polym. Chem.* **31**, 3447–3452 (1993).
151. P. Burger, K. Hortmann, and H.-H. Brintzinger, *Makromol. Chem., Macromol. Symp.* **66**, 127–140 (1993).
152. M. J. Schneider, J. Suhm, R. Mülhaupt, M.-H. Prosenc, and H.-H. Brintzinger, *Macromolecules* **30**, 3164–3168 (1997).
153. K. Soga and D. H. Lee, *Makromol. Chem.* **193**, 1687–1694 (1992).
154. R. Blom and I. M. Dahl, *Macromol. Chem. Phys.* **200**, 442–449 (1999).
155. T. K. Woo, P. M. Margl, T. Ziegler, and P. E. Blöchl, *Organometallics* **16**, 3454–3468 (1997).
156. J. B. P. Soares, J. D. Kim, and G. L. Rempel, *Ind. Eng. Chem. Res.* **36**, 1144–1150 (1997).
157. L. Izzo, L. Caporaso, G. Senatore, and L. Oliva, *Macromolecules* **32**, 6913–6916 (1999).
158. L. Resconi, F. Piemontesi, G. Franciscono, L. Abis, and T. Fiorani, *J. Am. Chem. Soc.* **114**, 1025–1032 (1992); see also refs. in footnotes 13–16 of this citation.
159. K. Thorshaug, J. A. Støvneng, E. Rytter, and M. Ystenes, *Macromolecules* **31**, 7149–7165 (1998).
160. A. Carvill, I. Tritto, P. Locatelli, and M. C. Sacchi, *Macromolecules* **30**, 7056–7062 (1997).
161. K. Koo, and T. J. Marks, *J. Am. Chem. Soc.* **121**, 8791–8802 (1999).
162. G. Xu, and T. C. Chung, *J. Am. Chem. Soc.* **121**, 6763–6764 (1999).
163. H. Hagihara, T. Shiono, and T. Ikeda, *Macromolecules* **31**, 3184–3188 (1998); Y. Fukui, M. Murata, and K. Soga, *Macromol. Rapid Commun.* **20**, 637–640 (1999).
164. M. K. Reinking, G. Orf, and D. McFaddin, *J. Polym. Sci., Part A: Polym. Chem.* **36**, 2889–2898 (1998).
165. A. D. Horton, *Organometallics* **15**, 2675–2677 (1996).
166. C. S. Christ Jr., J. R. Eyler, and D. E. Richardson, *J. Am. Chem. Soc.* **112**, 596–607 (1990).
167. E. P. Wasserman, E. Hsi, and W.-T. Young, *ACS Div. Polym. Chem., Polym. Prepr* **39**(2), 425–426 (1998); S. Lieber, M.-H. Prosenc, and H.-H. Brintzinger, *Organometallics* **19**, 377–387 (2000).

168. V. Busico, R. Cipullo, J. C. Chadwick, J. F. Modder, and O. Sudmeijer, *Macromolecules* **27**, 7538–7543 (1994).
169. K. Thorshaug, J. A. Støvneng, E. Rytter, and M. Ystenes, *Macromolecules* **31**, 7149–7165 (1998).
170. V. Busico, and R. Cipullo, *J. Am. Chem. Soc.* **116**, 9329–9330 (1994); J. C. Yoder, and J. E. Bercaw, *J. Am. Chem. Soc.* **124**, 2548–2555.
171. F. R. W. P. Wild, L. Zsolnai, G. Huttner, and H. H. Brintzinger, *J. Organomet. Chem.* **232**, 233–247 (1982); W. Kaminsky, A.-M. Schauwienold, and F. Freidanck, *J. Mol. Catal. A: Chem.* **112**, 37–42 (1996).
172. J. C. Yoder, M. W. Day, and J. E. Bercaw, *Organometallics* **17**, 4946–4958 (1998).
173. J. A. Ewen, *J. Am. Chem. Soc.* **106**, 6355–6364 (1984).
174. U.S. Pat. 4,769,510 (priority date Nov. 27, 1984), W. Kaminsky, K. Külper, M. Buschermöhle, and H. Lüker (to Hoechst)
175. W. Kaminsky, *Angew. Makromol. Chem.* **145/146**, 149–160 (1986).
176. G. Guerra, L. Cavallo, G. Moscardi, M. Vacatello, and P. Corradini, *J. Am. Chem. Soc.* **116**, 2988–2995 (1994).
177. W. Röll, H.-H. Brintzinger, B. Rieger, and R. Zolk, *Angew. Chem., Int. Ed. Engl.* **29**, 279–280 (1990).
178. H. Kawamura-Kuribayashi, N. Koga, and K. Morokuma, *J. Am. Chem. Soc.* **114**, 8687–8694.
179. F. R. W. P. Wild, J. Zsolnai, G. Huttner, and H.-H. Brintzinger, *J. Organomet. Chem.* **232**, 233–247 (1982); S. Collins, B. A. Kuntz, and Y. Hong, *J. Org. Chem.* **54**, 4154–4158 (1989); B. Chin, and S. L. Buchwald, *J. Org. Chem.* **61**, 5650–5651 (1996).
180. G. Jany, R. Fawzi, M. Steimann, and B. Rieger, *Organometallics* **16**, 544–550 (1997).
181. T. Mise, S. Miya, and H. Yamazaki, *Chem. Lett.* 1853–1856 (1989).
182. W. Spaleck, F. Küber, A. Winter, J. Rohrmann, B. Bachmann, M. Antberg, V. Dolle, and E. F. Paulus, *Organometallics* **13**, 954–963 (1994).
183. Eur. Pat. Appl. 0 962 462 A2 (priority date June 1, 1998), M. D. Rausch, E. J. Thomas, S. Bettonville, and D. Grandfils (to Solvay).
184. S. Miyake, Y. Okumura, and S. Inazawa, *Macromolecules* **28**, 3074–3079 (1995).
185. L. Resconi, D. Balboni, G. Baruzzi, C. Fiori, S. Guidotti, P. Mercandelli, and A. Sironi, *Organometallics* **19**, 420–429 (2000).
186. L. Resconi, F. Piemontesi, I. Camurati, D. Balboni, A. Sirone, M. Moret, H. Rychlicki, and R. Zeigler, *Organometallics* **15**, 5046–5059 (1996).
187. E. Shamshoum and D. Rauscher, *MetCon '93, Proceedings of meeting*, May 26–28 1993, Houston, Texas (Catalyst Consultants), 173–187;
188. T. Shiomura, *SPO '96, Proceedings of Sixth Intl. Bus. Forum on Specialty Polyolefins*, Sept. 25–27 1996, Houston, Texas (Schotland), 53–67.
189. J. A. Ewen, R. L. Jones, A. Razavi, and J. D. Ferrara, *J. Am. Chem. Soc.* **110**, 6255–6256 (1988).
190. A. Razavi, L. Peters, and L. Nafpliotis, *J. Mol. Catal. A: Chem.* **115**, 129–154 (1997).
191. U.S. Pat. 4,892,851 (priority date July 15, 1988), J. A. Ewen and A. Razavi (to Fina Technology).
192. Eur. Pat. 0 387 690 B1 (priority date Mar 11, 1989), A. Winter, J. Rohrmann, M. Antberg, V. Dolle, and W. Spaleck (to Hoechst).
193. G. W. Coates and R. M. Waymouth, *Science (Washington, D.C.)* **267**, 217–219 (1995).
194. V. Busico, R. Cipullo, W. Kretschmer, G. Talarico, M. Vacatello, and V. V. A. Castelli, *Macromol. Symp.* **189**, 127–141 (2002).
195. D. T. Mallin, M. D. Rausch, Y.-G. Lin, S. Dong, and J. C. W. Chien, *J. Am. Chem. Soc.* **112**, 2030–2031 (1990).
196. A. M. Bravakis, L. E. Bailey, M. Pigeon, and S. Collins, *Macromolecules* **31**, 1000–1009 (1998).

197. U.S. Pat. 5,036,034 (priority date Oct. 10, 1989), J. A. Ewen (to Fina Technology).
198. W. Fan, M. K. Leclerc and R. M. Waymouth, *J. Am. Chem. Soc.* **123**, 9555–9563 (2001).
199. World Pat. Appl. 88/04672 (priority date Dec. 19, 1986), H. C. Welborn Jr. (to Exxon).
200. W. Kaminsky and M. Schlobohm, *Makromol. Chem., Macromol. Symp.* **4**, 103–118 (1986).
201. C. Pellecchia, *Metallocenes '95, Proceedings of Intl. Congress on Metallocene Polymers*, Apr. 26–27 1995, Brussels, Belgium (Schotland), 75–85; and references therein.
202. M. F. Llauro, C. Monnet, F. Barbotin, V. Monteil, R. Spitz, and C. Boisson, *Macromolecules 34* **2001**, 6304–6311.
203. S. Pragliola, G. Milano, G. Guerra, and P. Longo, *J. Am. Chem. Soc.* **124**, 3502–3503 (2002).
204. S. Ikai, J. Yamashita, Y. Kai, M. Murakami, T. Yano, Y. Qian, and J. Huang, *J. Mol. Catal. A: Chem.* **140**, 115–119 (1999).
205. World Pat. Appl. 88/04673 (priority date Dec. 19, 1986), R. G. Austin and H. C. Welborn Jr., (to Exxon).
206. G. W. Coates and R. M. Waymouth, *J. Am. Chem. Soc.* **115**, 91–98 (1993).
207. *Chem. Week* **159**(19), 15 (1997).
208. *Chem. Market. Rep.* **249**(26), 3, 10 (1996).
209. W. Kaminsky and R. Spiehl, *Makromol. Chem.* **190**, 515–526 (1989).
210. S. Collins and W. M. Kelly, *Macromolecules* **25**, 233–237 (1992).
211. M. R. Kesti, G. W. Coates, and R. M. Waymouth, *J. Am. Chem. Soc.* **114**, 9679–9680 (1992).
212. U. M. Stehling, K. M. Stein, M. R. Kesti, and R. M. Waymouth, *Macromolecules* **31**, 2019–2027 (1998).
213. D.-J. Byun, K.-Y. Choi, and S. Y. Kim, *Macromol. Chem. Phys.* **202**, 992–997 (2001).
214. C.-E. Wilén, M. Auer, J. Strandén, J. H. Näsman, B. Rotzinger, A. Steinmann, R. E. King III, H. Zweifel, and R. Drewes, *Macromolecules* **33**, 5011–5026 (2000).
215. T. D. Shaffer, J.-A. M. Canich, and K. R. Squire, *Macromolecules* **31**, 5145–5147 (1998).
216. L. Jia, X. Yang, A. M. Seyam, I. D. L. Albert, P.-F. Fu, S. Yang, and T. J. Marks, *J. Am. Chem. Soc.* **118**, 7900–7913 (1996).
217. C. Pellecchia and L. Oliva, *Rubber Chem. Technol.* **72**, 553–558 (1999).
218. H. Chen, M. J. Guest, S. Chum, A. Hiltner, and E. Baer, *J. Appl. Polym. Sci.* **70**, 109–119 (1998).
219. R. W. Barnhart and G. C. Bazan, *J. Am. Chem. Soc.* **120**, 1082–1083 (1998).
220. C. Denger, U. Haase, and G. Fink, *Makromol. Chem., Rapid Commun.* **12**, 697–701 (1991).
221. N. Ishihara, T. Seimiya, M. Kuramoto, and M. Uoi, *Macromolecules* **19**, 2465–2466 (1986).
222. N. Tomotsu, N. Ishihara, T. H. Mewman, and M. T. Malanga, *J. Mol. Catal. A: Chem.* **128**, 167–190 (1998).
223. A. Grassi, A. Zambelli, and F. Laschi, *Organometallics* **15**, 480–482 (1996); T. H. Newman and M. T. Malanga, *J. Macromol. Sci., A: Pure Appl. Chem.* **34**, 1921–1927 (1997).
224. Y. Kim, E. Hong, M. H. Lee, J. Kim, Y. Han, and Y. Do, *Organometallics* **18**, 36–39 (1999).
225. G. Xu, *Macromolecules* **31**, 586–591 (1998).
226. H. Yasuda, H. Yamamoto, K. Yokota, S. Miyake and A. Nakamura, *J. Am. Chem. Soc.* **114**, 4908–4910 (1992).
227. H. Deng, T. Shiono, and K. Soga, *Macromolecules* **28**, 3067–3073 (1995); S. Collins, D. G. Ward, and K. H. Suddaby, *Macromolecules* **27**, 7222–7224 (1994).
228. H. Nguyen, A. P. Jarvis, M. J. G. Lesley, W. M. Kelly, S. S. Reddy, N. J. Taylor, and S. Collins, *Macromolecules* **33**, 1508–1510 (2000).

229. M. Yamashita, Y. Takemoto, E. Ihara, and H. Yasuda, *Macromolecules* **29**, 1798–1806 (1996).
230. W. J. Evans and H. Katsumata, *Macromolecules* **27**, 2330–2332 (1994).
231. W. J. Evans and H. Katsumata, *Macromolecules* **27**, 4011–4013 (1994).
232. C. Aitken, J. F. Harrod, and E. Samuel, *J. Organomet. Chem.* **279**, C11–C13 (1985).
233. H.-G. Woo, J. F. Walzer, and T. D. Tilley, *J. Am. Chem. Soc.* **114**, 7047–7055 (1992).
234. V. K. Dioumaev and J. F. Harrod, *Organometallics* **16**, 2798–2807 (1997).
235. T. C. Chung, *Prog. Polym. Sci.* **27**, 39–85 (2002).
236. T. E. Patten and B. M. Novak, *Makromol. Chem., Macromol. Symp.* **67**, 203–211 (1993).
237. J. Ren, J. Hu, and Q. Shen, *Yingyong Huaxue (Chin. J. Appl. Chem.)* **12**, 105–106 (1995). [Chem. Abs. 123:170382].
238. J. Schwartz and J. A. Labinger, *Angew. Chem. Int. Ed. Engl.* **15**, 333–340 (1976).
239. D. B. Carr and J. Schwartz, *J. Am. Chem. Soc.* **101**, 3521–3531 (1979).
240. S. L. Buchwald, B. T. Watson, and J. C. Huffman, *J. Am. Chem. Soc.* **109**, 2544–2546 (1987).
241. D. R. Swanson, C. J. Rousset, and E. Negishi, *J. Org. Chem.* **54**, 3521–3523 (1989).
242. D. R. Swanson, C. J. Rousset, E. Negishi, T. Takahashi, T. Seki, M. Saburi, and Y. Uchida, *J. Org. Chem.* **54**, 3521–3523 (1989).
243. S. L. Buchwald and R. B. Nielsen, *Chem. Rev.* **88**, 1047–1058 (1988).
244. P. J. Fagan, W. A. Nugent, and J. C. Calabrese, *J. Am. Chem. Soc.* **116**, 1880–1889 (1994).
245. T. R. Nelsen, and J. J. Tufariello, *J. Org. Chem.* **40**, 3159–3160 (1975).
246. F. N. Tebbe, G. W. Parshall, and G. S. Reddy, *J. Am. Chem. Soc.* **100**, 3611–3613 (1978).
247. E. E. van Tamelen, and J. A. Gladysz, *J. Am. Chem. Soc.* **96**, 5290–5291 (1974).
248. E. E. van Tamelen, H. Rudler, and C. Bjorklund, *J. Am. Chem. Soc.* **93**, 7113–7114 (1971).
249. R. D. Broene, and S. L. Buchwald, *J. Am. Chem. Soc.* **115**, 12569–12570 (1993). [Erratum: *J. Am. Chem. Soc.* **118**, 9458 (1996)].
250. M. V. Troutman, D. H. Appella, and S. L. Buchwald, *J. Am. Chem. Soc.* **121**, 4916–4917 (1999).
251. L. A. Paquette, M. R. Sivik, E. I. Bzowej, and K. J. Stanton, *Organometallics* **14**, 4865–4878 (1985).
252. K. Isagawa, H. Sano, M. Hattori, and Y. Otsuji, *Chem. Lett*, 1069 (1979).
253. U. M. Dzhemilev, and O. S. Vostrikova, *J. Organomet. Chem.* **285**, 43–51 (1985).
254. D. E. van Horn, and E. Negishi, *J. Am. Chem. Soc.* **100**, 2252–2254 (1978).
255. X. Verdaguer, U. E. W. Lange, M. T. Reding, and S. L. Buchwald, *J. Am. Chem. Soc.* **118**, 6784–6785 (1996).
256. Y. Wielstra, S. Gambarotta, and M. Y. Chiang, *Organometallics* **7**, 1866–1867 (1988).
257. J. Christoffers and R. G. Bergman, *Inorg. Chim. Acta* **270**, 20–27 (1998).
258. P. J. W. Deckers, B. Hessen, and J. H. Teuben, *Angew. Chem. Int. Ed.* **40**, 2516–2519 (2001).
259. M. Akita, H. Yasuda, and A. Nakamura, *Bull. Chem. Soc. Jpn.* **57**, 480–487 (1984).
260. F. N. Tebbe, G. W. Parshall, and D. W. Ovenall, *J. Am. Chem. Soc.* **101**, 5074–5075 (1979).
261. J. B. Lee, K. C. Ott, and R. H. Grubbs, *J. Am. Chem. Soc.* **104**, 7491–7496 (1982).
262. L. R. Gilliom and R. H. Grubbs, *J. Am. Chem. Soc.* **108**, 733–742 (1986).
263. R. H. Grubbs, in G. Wilkinson, F. G. A. Stone, E. W. Abel, eds., *Comprehensive Organometallic Chemistry*, Vol. **8**, Pergamon Press, Oxford, 1982, pp. 499–551.
264. A. G. Ibragimov, E. V. Gribanova, L. M. Khalilov, L. M. Zelenova, and U. M. Dzhemilev, *Zh. Org. Khim.* **21**, 259–265 (1985).
265. S. Rodewald and R. F. Jordan, *J. Am. Chem. Soc.* **116**, 4491–4492 (1994).
266. *Chem. Week* **162**(6), 35–37 (2000).

267. V. K. Gupta, S. Satish, and I. S. Bhardwaj, *J. Macromol. Sci., Rev. Macromol. Chem. Phys.* **C34**, 439–514 (1994).
268. P. C. Möhring and N. J. Coville, *J. Organomet. Chem.* **479**, 1–29 (1994).
269. S. S. Reddy and S. Sivaram, *Prog. Polym. Sci.* **20**, 309–367 (1995).
270. A. L. McKnight and R. M. Waymouth, *Chem. Rev.* **98**, 2587–2598 (1998).
271. R.-D. Maier, *Kunststoffe* **89**, 120–132 (Eng. transl. 45–52) (1999).
272. A. Togni and R. L. Halterman, eds., *Metallocenes: Synthesis Reactivity Applications*, Wiley-VCH, Weinheim, 1998.
273. J. A. Gladysz, ed., *Chem. Rev.* **100**, 1164–1682 (200).

ERIC PAUL WASSERMAN
Dow Chemical Company

METHACRYLIC ESTER POLYMERS.

See Volume 3.

MICROCELLULAR PLASTICS

Introduction

Microcellular plastics (MCPs), which were first invented at the Massachusetts Institute of Technology in 1979, refer to any polymeric materials that have closed cells of very small diameters, typically smaller than 50 μm. The cell density can be made to vary a great deal depending on the final application of a given MCP. MCPs can have as many as 10^{15} bubbles/cm^3 when the bubble diameter is 0.1 μm, 10^{12} bubbles/cm^3 for 1-μ- and 10^9 for 10-μ- diameter cells. They can be created in thermoplastics, thermosetting plastics, and elastomers. Figure 1 shows the microstructure of a typical MCP. See Reference 1 for a detailed historical account as well as a detailed review of MCPs.

The original impetus for the invention of MCPs was to create a plastic consuming less material without sacrificing mechanical properties, especially toughness. The saving of material was achieved by creating voids, and toughness was a result of making the diameter of the bubble smaller than a critical size. The central idea was to replace some of the polymers with a large number of very small bubbles that are smaller than the preexisting flaws in polymers. Small bubbles can blunt the crack tips and act as crazing—initiation sites, thus making the material tougher.

The basic processing method for all MCPs is the use of thermodynamic instability phenomena. A large amount of gas, typically CO_2 or N_2, is dissolved in the plastics under high pressure at the processing temperature so as to create a driving force for phase separation when the pressure is suddenly lowered.

Depending on the magnitude of the driving force, various nucleation sites are activated. The number of nucleation sites increases nearly exponentially with the amount of gas dissolved, when the polymer is supersaturated with the dissolved

Encyclopedia of Polymer Science and Technology. Copyright John Wiley & Sons, Inc. All rights reserved.

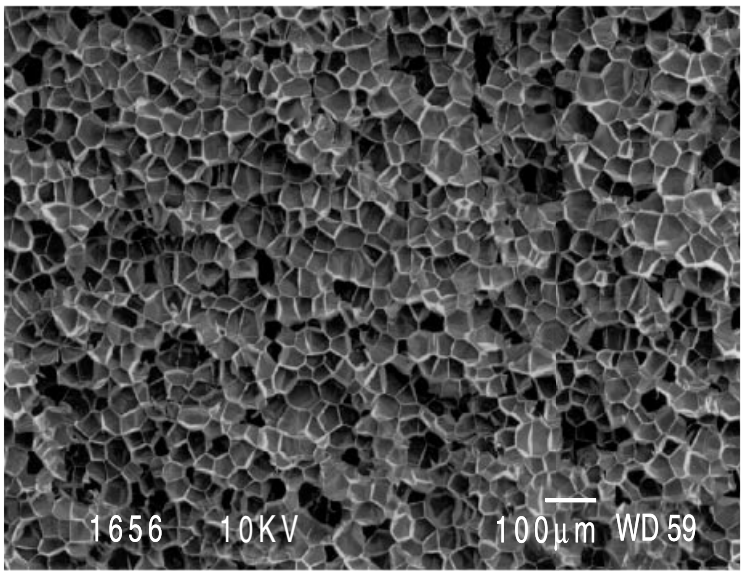

Fig. 1. Microstructure of microcellular plastics. This particular micrograph shows an average cell size of about 30 μm.

gas—relative to its equilibrium concentration at the pressure of 0.1 MPa (1 bar) and the operating temperature. Microcells form for the following reasons: the amount of gas dissolved must be shared equally by an extremely large number of nucleated sites, since the cells nucleate nearly simultaneously, preventing the preferential diffusion of the gas to the sites that have nucleated first. Because the driving force is so large, homogeneous nucleation dominates even when there are second-phase particles that would be the preferred heterogeneous nucleation sites because of its low activation energy.

MCPs have unique processing characteristics. The processing temperature is substantially less than the conventional processes because the viscosity of plastics is substantially reduced owing to the presence of gas between polymeric molecules. The throughput rate of a given extruder can also be greater because of the low viscosity. The cycle time of injection-molding machines is also reduced because the processing temperature is lower and the phase separation of gas from polymer instantaneously increases the rigidity of plastics. Furthermore, there is no shrinkage of the injection-molded part because it (shrinkage) is compensated by the internal expansion in the microcells, creating parts with minimal residual stress and warpage. Sometimes, depending on the color of the plastic and the smoothness of the molded surface, swirl marks may appear, which can be hidden through painting or texturing.

Certain properties of MCPs, such as modulus and strength, follow the rule of mixture, whereas such properties as toughness and coefficient of thermal expansion do not. When the cell size is less than a few micrometers, the toughness of certain MCPs should be equal to or better than the plastic without the cells. Small cells also lower the thermal conductivity when they are smaller than a critical size.

Many industrial firms worldwide are now making microcellular products through extrusion and injection molding (under license from Trexel, Inc.). Trexel, as the sole licensee of MITs has developed the MIT technology further for commercial applications. The trade name is MuCell. It is very likely that the number of new applications that use the microcellular technology will continue to increase at a rapid rate in the years to come.

MCP technology is in some ways in the early stages of research and development, notwithstanding its relatively long history. It has raised many interesting scientific and technological issues that can be the basis for thought-provoking ideas and research. Many academic institutions worldwide are conducting their research in the field of MCPs, which should further generate new ideas and applications. Many industrial firms are developing new applications for injection—molding and extrusion processes.

Design of MCPs

MCPs were designed to satisfy the following three functional requirements (FRs) based on axiomatic design (1,2):

(1) FR1 = Reduce plastics consumption
(2) FR2 = Maintain the toughness of plastics
(3) FR3 = Make 3-D parts

To satisfy these FRs, the concept of MCP was created by envisioning plastics with tiny bubbles (see Reference 1 for an historical account). Then the design parameters (DPs) of MCPs are the following:

(1) DP1 = Total volume of cells (ie, bubbles), V
(2) DP2 = Diameter of cells, d
(3) DP3 = Die or mold

The design equation that relates the FRs to the DPs of microcellular plastics may be written as

$$\begin{Bmatrix} FR1 \\ FR2 \\ FR3 \end{Bmatrix} = \begin{bmatrix} X & X & 0 \\ 0 & X & 0 \\ 0 & 0 & X \end{bmatrix} \begin{Bmatrix} DP1 \\ DP2 \\ DP3 \end{Bmatrix} \quad (1)$$

Equation 1 indicates that the design of an MCP is a decoupled one. It indicates that the bubble size must be determined first before setting the total volume of the bubbles.

In an ideal MCP, where spherical bubbles are packed in a body-centered cubic structure, the bubble size can be directly related to the bubble density. In a 1-cm cube of foamed material, the number of cells is inversely proportional to the cube of the bubble diameter. Therefore, an MCP with 10-μm bubbles has approximately 10^9 bubbles/cm^3 of unfoamed material, whereas MCPs with 1-μm

and 0.1-μm bubbles have approximately 10^{12} and 10^{15} bubbles/cm^3 of unfoamed material, respectively.

Since the volume taken by spherical bubbles in an ideal, closely packed hexagonal or cubic structure is approximately 74%, the plastic occupying the interstitial space takes up 26% of the volume. Therefore, the cell density of an ideal closely packed spherical MCP is equal to (1/cell size)^3 times 1/0.26. For an MCP with 1-μm cell diameter, the bubble density is 3.85×10^{12} cells/cm^3 of the solid plastic. The overall density of foam can decrease further when these cells expand, thinning the wall diameter and reducing the interstitial materials between the cells.

Design of MCP-Processing Techniques

Dissolution of Gases in Polymers. The basic physics of gas dissolution in polymers is as follows (3):

(1) The plastic must be supersaturated with sufficient gas (such as N_2 and CO_2) to nucleate simultaneously a large number of cells.
(2) The temperature of the plastic must be set so as to control the flow of plastics during processing.
(3) A gas with a suitable solubility and diffusivity for the plastic must be selected.
(4) Homogeneous nucleation must dominate the nucleation process to create a large number of microcells even when heterogeneous nucleation sites are available by providing sufficient driving force with a sufficient amount of dissolved gas.

The processing technique consists of forming a polymer/gas solution and then suddenly inducing a thermodynamic instability by either lowering the pressure or raising the temperature to change the solubility S. The solubility is a function of two thermodynamic properties such as temperature and pressure:

$$S = S(p, T) = H(p, T) \tag{2}$$

where H is known as Henry's law constant. At low pressures and low concentrations, H is constant. At high pressures, H depends on both pressure and temperature. The temperature dependence follows the Arrhenius-type rate equation. At low pressures, the gas solubility is low but Henry's constant is high. At higher pressures, the gas solubility is high, but the rate of the weight increase with pressure decreases with pressure.

The solubility of gas in polymers decreases with an increase in temperature. The solubility of N_2 is considerably less than that of CO_2. Since the amount of gas that can be dissolved is a function of the saturation pressure and since the gas diffusion rate is the rate-limiting process, we can use supercritical CO_2 to enhance the solubility and diffusion rate. CO_2 is supercritical at pressures and temperatures greater than 7.4 MPa and 31.1°C.

With dissolution of a large number of gas molecules in polymers, the glass-transition temperature and viscosity decrease with the increase in gas concentration. The change in the glass-transition temperature is quite substantial at high gas concentrations. These changes affect the processibility of polymers.

The change in the solubility can be expressed as

$$\Delta S = \frac{\partial S}{\partial p}\,\Delta p + \frac{\partial S}{\partial T}\,\Delta T \tag{3}$$

The $\P S/\P p$ term of equation 3 is positive, whereas the $\P S/\P T$ term is negative. Therefore, to decrease the solubility and to induce the thermodynamic instability, either the pressure must be decreased (ie, $\Delta p < 0$) or the temperature must be increased (ie, $\Delta T > 0$). Furthermore, regardless of whether the process is continuous or batch-type, the thermodynamic instability must be induced quickly so that the cells will nucleate simultaneously before significant diffusion of gas has taken place. Therefore, the higher the temperature of the polymer, the quicker the nucleation has to occur since the diffusion of the gas occurs faster at higher temperatures. Such simultaneous cell nucleation will assure a uniform cell-size distribution. The following two dimensionless numbers must be less than 1 for this to happen:

$$\frac{\text{Characteristic nucleation time}}{\text{Characteristic diffusion time}} \ll 1$$

$$\frac{\alpha}{\frac{dN}{dt}\mathrm{d}_c} \ll 1 \tag{4}$$

$$\frac{\text{Characteristic gas diffusion distance}}{\text{Characteristic spacing between stable nuclei}} \ll 1$$

$$2\rho_c^{1/3}(\alpha t_D)^{1/2} \ll 1 \tag{5}$$

The number of cells nucleated is a function of the supersaturation level relative to the equilibrium concentration at ambient pressure at the processing temperature. The higher the supersaturation level, the greater is the number of cells nucleated. Furthermore, since the amount of dissolved gas that fills the nucleated cells is finite, and since all the cells are nucleated almost simultaneously, the gas distributes more or less evenly among all these cells—a condition for making MCPs. The final bubble size is then determined by the total amount of gas per bubble, and by the flow characteristics of the polymer at the nucleation temperature.

To create a continuous process, processes and associated equipment to perform the following functions in extrusion and injection molding have been designed.

(1) Rapid dissolution of gas into molten flowing polymer to form a polymer/gas solution
(2) Nucleation of a large number of cells

(3) Control of the cell size
(4) Control of the geometry of the final product

To produce the MCP at an acceptable production rate through a continuous process, we must dissolve the gas in polymers quickly despite the slow diffusion rate. The diffusivity increases with temperature by an Arrhenius relationship:

$$\Delta = \Delta_0 \exp(-\Delta G/kT) \tag{6}$$

where δG is the activation energy, k is the Boltzmann's constant, and T is the absolute temperature. The time for gas diffusion is proportional to the thickness of the plastic ℓ as

$$t \propto \frac{\ell^2}{\alpha} \tag{7}$$

The diffusivity of CO_2 and N_2 are nearly the same and it takes a long time to diffuse gas into a polymer at room temperature. For example, the diffusivity of CO_2 in most thermoplastics at room temperature is in the range of 5×10^{-8} cm^2/s and the diffusion time is approximately 14 h when ℓ is 0.5 mm. The diffusivity at 200°C is 3–4 orders of magnitude greater than that at room temperature. Even at high temperatures, the diffusion rate is still the rate-limiting step in continuous processes.

To accelerate the diffusion rate and shorten the time for the formation of gas/polymer solutions, we must raise the temperature and shorten the diffusion distance. This is done by deforming the two-phase mixture of polymer and gas through shear distortion to decrease the diffusion path. This type of deformation occurs in an extruder under laminar-flow conditions. The bubbles are stretched by the shear field of the two-phase mixture and eventually break up to minimize the surface energy when a critical Weber number is reached (4). The disintegrated bubble size is calculated to be about 1 mm and the initial striation thickness after bubble disintegration is calculated to be about twice the bubble diameter (5). This striation thickness decreases with further shear, and the gas diffusion occurs faster as a result of the increase in the surface area and the decrease in striation thickness. The striation thickness in an extruder is estimated to decrease to about 100 μm. At this thickness, the diffusion time is about 1 min in PET, from 10 to 20 s in polystyrene (PS), poly(vinyl chloride) (PVC), and high density polyethylene (HDPE), and in the range of a few seconds in low density polyethylene (LDPE).

Nucleation. The key idea in the formation of an MCP is the nucleation of an extremely large number of bubbles (cells). Although cells can nucleate either homogeneously or heterogeneously, the driving force is so high owing to such a large amount of supersaturation of the gas in the polymer that both the homogeneous and the heterogeneous nucleation sites are expected to be nucleated. This can be seen from micrographs, which show that cells are nucleated both at and away from the heterogeneous sites.

For nucleation to occur, a finite energy barrier has to be overcome. The energy barrier depends on two competing factors: (*1*) the energy available in the gas diffused into the embryo of the cell and (*2*) the surface energy that must be supplied

Table 1. Potential Activation Sites for Cells and Rough Estimates of Potential Cell Density

Activation Sites	Cell density, cells/cm^3
Solid–polymer interface	10^5 to 10^6
Nonpolar polymer–polar polymer interface	—
High strain region	10^9
Free volume	10^9
Crystalline–amorphous interface in a polymer	10^{12}
Interface between crystallites	10^{18}
Morphological defects in a polymer	—
Polar groups of polymers	10^{22}

to form the surface of the cell. There is a critical cell size beyond which the cell becomes stable and grows, and below which the cell embryo collapses. Typically the cell nucleation rate is expressed as

$$\frac{dN}{dt} = N_0 f \, e^{\frac{-\Delta G}{kT}} \tag{8}$$

where N is the number of cells, N_0 is the number of available sites for nucleation, f is the frequency of atomic or molecular lattice vibration, ΔG is the activation energy barrier, k is the Boltzmann constant, T is the absolute temperature.

A variety of different nucleation sites may be nucleated when the driving force is very large, the most prominent of which are the free-volume sites. Also, in the case of semicrystalline polymers, the interfaces between the amorphous region and the crystalline region could be the nucleation sites. Depending on the gas supersaturation level, all or part of these nucleation sites will be activated. Table 1 shows the potential activation sites and the expected cell density when these sites become activated.

The activation energy associated with each one of these potential activation sites is expected to be substantially different, probably increasing with the available sites. The activation energy may be represented in terms of its probability density function as shown in Figure 2.

The activation energy also changes when the gas is dissolved. As a result, the change in the probability density of activation energy due to the dissolved gas may be schematically represented as shown in Figure 3 at a specific gas concentration.

The number of the available sites, N_0, is also affected by the gas dissolved since the gas changes the intermolecular forces, as indirectly evidenced by the change in the viscosity and melting point of the polymer/gas solution (see Fig. 4). N_0 is a function of both the original activation energy ΔG and the amount of the gas dissolved. Although there is no definite data available, the N_0 is expected to increase with higher activation energy since it appears that there are more activation sites at these higher level activation energies. This change in the available sites may be represented schematically as shown in Figure 5.

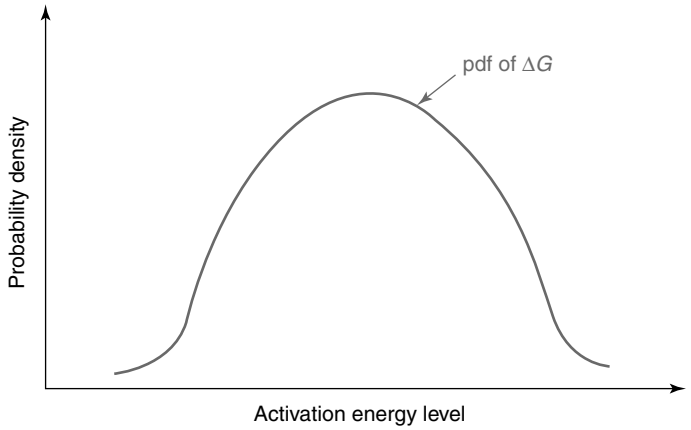

Fig. 2. Probability distribution of ΔG. Note that as the amount of dissolved gas increases, the sites with high activation energy is expected to be activated.

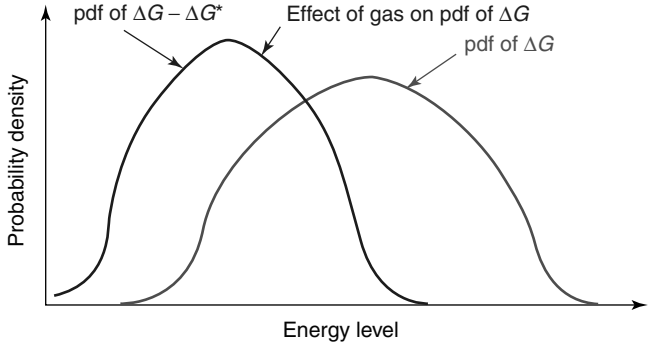

Fig. 3. Schematic representation of the effect of the dissolved gas on the probability density of activation energy.

Cell Growth. Immediately after the cells are nucleated, the pressure in the bubble is equal to the saturation pressure. Therefore, the cells expand if the polymer matrix is soft enough to undergo viscoelastic–plastic deformation. A cell expands until the final pressure inside the cell is equal to the pressure required to be in equilibrium with the surface forces and the stress in the viscoelastic cell wall.

Unlike in conventional foaming, in the case of MCPs, there are so many cells nucleated and the diffusion length is so short that the diffusion of the gas to the cell growth stops relatively quickly.

In practice, the temperature of the surface of the extrudate changes as a result of heat transfer, and thus, the expansion of the cells is constrained by the outer stiff layer. Also some of the gases from the cells near the surface escape, reducing the cells tendency to expand.

Cell Density and Cell Size. The cell density is a function of both the pressure drop and the pressure drop rate. During the cell nucleation stage, there

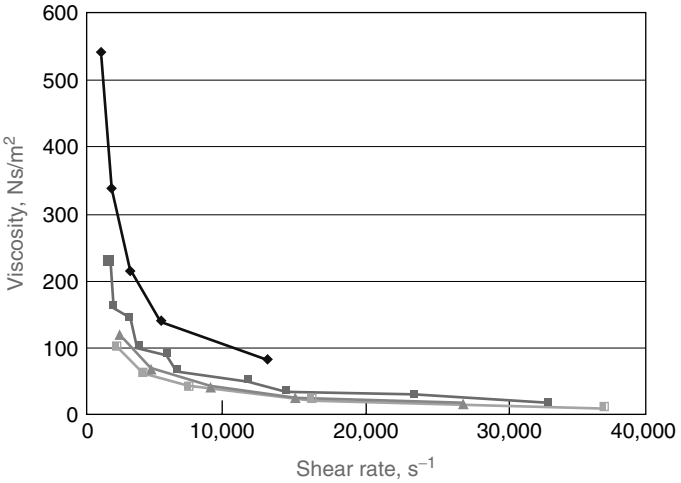

Fig. 4. Viscosity of ABS as a function of CO_2 concentration and shear rate at 370 F (Courtesy of Trexel, Inc.). Note that the relative viscosity change is most pronounced at low shear rates.

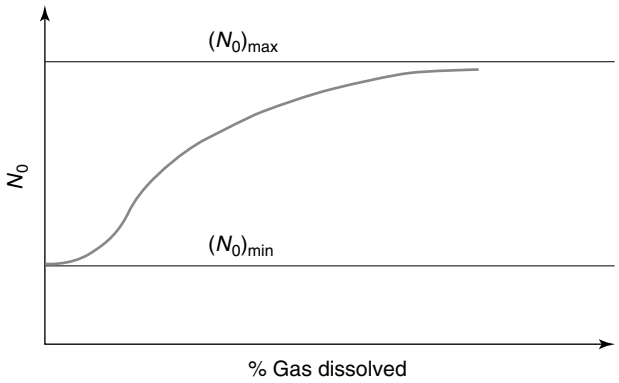

Fig. 5. Number of available sites for cell nucleation as a function of the gas dissolved. It is conjectured that $(N_0)_{max}$ is greater as the activation energy increases.

is a competition for gas between cell nucleation and cell growth if the cells do not nucleate simultaneously. When some cells nucleate before others, the gas in the solution will preferentially diffuse to the nucleated cells to lower the free energy of the system. As the gas diffuses to these cells, low gas concentration regions where nucleation cannot occur are generated adjacent to the stable nuclei. As the solution pressure drops further, the system will either both nucleate additional microcells and expand the existing cells by gas diffusion or only expand the existing cells. Therefore, when the pressure drop occurs rapidly, the gas-depleted region where nucleation cannot occur will be smaller and a more uniform cell distribution will result. It has been determined experimentally that a drop rate of 2 GPa/s is the minimum pressure drop rate required for MCP processing. Two dimensionless groups given in equations 4 and 5 give the condition for simultaneous nucleation

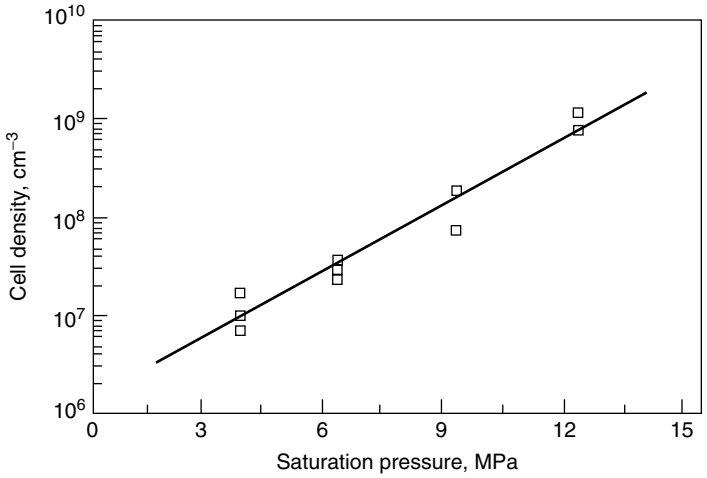

Fig. 6. Cell nucleation density as a function of N_2 pressure in polystyrene (6). To convert MPa to psi multiply by 145.

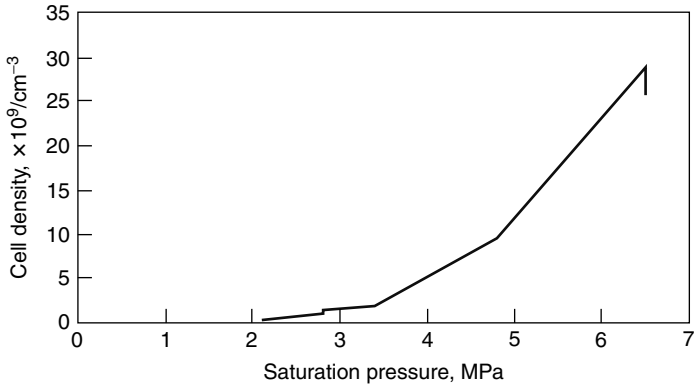

Fig. 7. Cell density as a function of N_2 pressure in polycarbonate (7).

of cells. Figures 6 and 7 show examples of the cell nucleation density as a function of the gas pressure.

Equipment and Die Design

The role of the extruder (or the plasticating unit of an injection-molding machine) is to melt the plastic, create a single-phase polymer/gas solution, and pump the solution through a die or inject it into a mold. To achieve these functions, high pressure CO_2 or N_2 gas is introduced into the extruder barrel by metering the exact amount of CO_2 or N_2 at pressures greater than 2000 psi. The flow rate of CO_2 into the extruder can be controlled using a special metering pump. The gas forms a large bubble in the extruder since the flow of the gas is briefly interrupted whenever the screw-flight wipes over the barrel.

Then to diffuse the gas in the bubble quickly in the molten plastic, the polymer–gas interfacial area is increased and the striation thickness of polymers between the gas bubbles is decreased. This is done by elongating the bubble in the barrel through the shear deformation of the two-phase mixture of the polymer and gas.

The approximate residency time required for diffusion and solution formation in the extruder is estimated to be as follows: <100 s for PET and <10 s for polystyrene at typical operating temperatures.

To design the process, the FRs and DPs are selected as

(1) FR1 = Reduce the amount of plastic used
(2) FR2 = Increase the toughness of the plastic product
(3) FR3 = Make 3-D geometrical shape
(4) DP1 = Microcellular plastics (uniform cell distribution in large numbers)
(5) DP2 = Diameter of microcells
(6) DP3 = Die shape

The process variables (PVs) for the process described that can satisfy the DPs given are

(1) PV1 = Supersaturation of the plastic with a large amount of gas and sudden pressure change (dp/dt)
(2) PV2 = Temperature of the molten polymer to control the expansion of cells at the die
(3) PV3 = Cross-sectional dimensions

The design equation for the extrusion process may be written as

$$\begin{Bmatrix} DP1 \\ DP2 \\ DP3 \end{Bmatrix} = \begin{bmatrix} X & 0 & 0 \\ X & X & 0 \\ 0 & 0 & X \end{bmatrix} \begin{Bmatrix} PV1 \\ PV2 \\ PV3 \end{Bmatrix} \tag{9}$$

Equation 9 shows that the process design is also a decoupled design. Therefore, each design satisfies the Independence Axiom. However, for concurrent engineering to be possible, the product of the product and process design matrices must also be diagonal or triangular. Because FRi = Aij DPj and DPj = Bjk PVk, FRi = Cjk PVk, where Cjk = Aij Bjk. However, the process design matrix with elements given by Cjk is neither diagonal nor triangular. This means that the foam density and toughness of the plastic part cannot be independently controlled by means of the PVs chosen unless the tolerances on the density variation or the toughness variation are large enough to change one of the two design matrices. Experiments support this conclusion.

DP1 and PV1 can be further decomposed as

(1) DP11 = Large number of nucleated cells
(2) DP12 = Uniform-sized cells

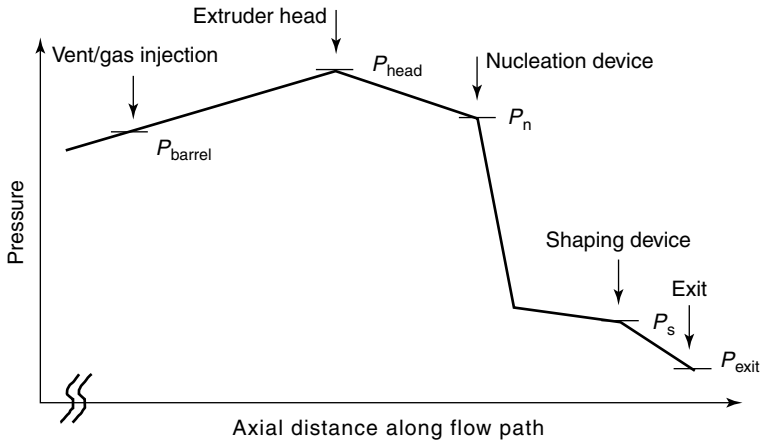

Fig. 8. Representative pressure profile along the polymer flow field in the extruder and die (8).

(3) PV11 = The level of supersaturation of CO_2
(4) PV12 = Rapid pressure drop dp/dt

The design matrix for this design may be represented as

$$\begin{Bmatrix} DP11 \\ DP12 \end{Bmatrix} = \begin{bmatrix} X & x \\ X & X \end{bmatrix} = \begin{Bmatrix} PV11 \\ PV12 \end{Bmatrix} \tag{10}$$

Equation 10 states that DP11 and DP12 are coupled slightly in that if the pressure drop rate is really slow, we cannot get a large number of cells and uniform-sized cells. In most cases, the effect of dp/dt on the number of cells is negligible. A typical pressure profile in a single-screw extruder is shown in Figure 8.

The role of the plasticating section of the injection-molding machine or the extruder is to melt the plastic and dissolve the gas in the polymer. The extruder must be under high pressure to maintain a single-phase solution. The cell density is primarily controlled by the amount of the dissolved gas and also partly by the pressure drop rate.

The die must be designed to control the pressure drop rate, which controls the uniformity of cell size. The desired pressure drop rate is greater than 1 GP/s. It also removes the thermal energy from the molded part. The die also creates 3-D shapes in the case of injection molding or the profile in the case of extrusion. It can be seen that the die design is as important as the extruder or the injection-molding design.

The highest-level FRs and DPs are given as

(1) FR1 = Control cell size
(2) FR2 = Control the number of cells
(3) FR3 = Control the geometry of the extrudate
(4) DP1 = P_i^*

(5) DP2 = dp/dt
(6) DP3 = Die shape & Accessories (Die & Acc.)

The design equation is given by

$$\begin{Bmatrix} \text{Cellsize} \\ \text{Celldensity} \\ \text{Geometry} \end{Bmatrix} = \begin{bmatrix} X & x & 0 \\ X & X & 0 \\ x & 0 & X \end{bmatrix} \begin{Bmatrix} P_i \\ dp/dt \\ \text{Die \&Acc.} \end{Bmatrix} \tag{11}$$

The corresponding PVs are chosen as

(1) PV1 = Extruder RPM
(2) PV2 = Die lip length
(3) PV3 = Means of controlling the profile

The design equation for the process is given by

$$\begin{Bmatrix} P_i \\ dp/dt \\ \text{Die \&Acc.} \end{Bmatrix} = \begin{bmatrix} X & x & 0 \\ X & X & 0 \\ 0 & 0 & X \end{bmatrix} \begin{Bmatrix} \Omega \\ L \\ \text{Profile} \end{Bmatrix} \tag{12}$$

The die design is illustrated in Figure 9. Cell nucleation and cell growth in a parallel die have been simulated (9). The results show that most of the cell nucleation occurs near the middle of the die lip and cell growth occurs within 2/4 die length once the cell nucleation begins.

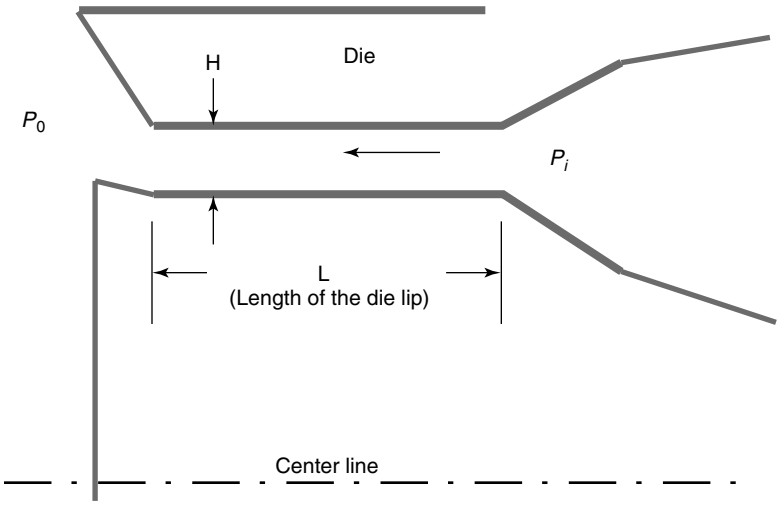

Fig. 9. Design of a tubular extrusion die.

Table 2. Comparison of Injection-Molding Process for Various Products with and without Microcellular Structure[a]

	Conventional	MCP	%
Air bag canister made of 33% glass-filled Nylon			
Part weight	365 g	252 g	30.9
Cycle time	45 s	35 s	22.2
Clamp. tonnage	150 ton	15 ton	90
Connector made of polycarbonate			
Part weight	48.8 g	42.9 g	10.6
Cycle time	17.5 s	15.9 s	9.1
Clamp. tonnage	140 ton	20 ton	85.7
Battery cover made of poypropylene			
Part weight	201 g	159 g	20.8
Cycle time	60 s	37 s	38.3
Clamp. tonnage	200 ton	15 ton	92.5

[a]Courtesy of Mar Lee Companies.

Advantages of Injection Molding with MCPs

The injection pressure of injection-molding process decreases substantially because of the presence of dissolved gas, which lowers the viscosity. The cycle time is also substantially reduced because of the elimination of the "hold and pack" time and also because of about 25% reduction in cooling time. Table 2 presents a comparison of the injection-molding process with and without the dissolved gas (see INJECTION MOLDING).

Figure 10 shows an extruded MCP part made of PVC and Figure 11 shows an injection-molded printer chassis for inkjet printers made of glass-filled

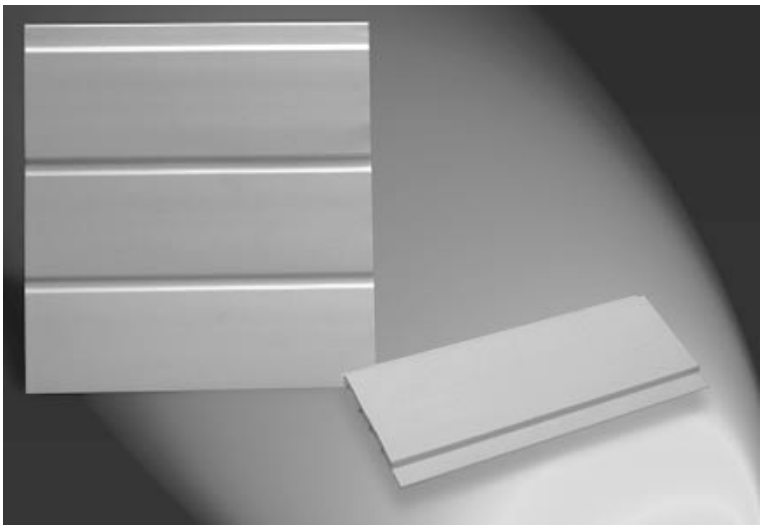

Fig. 10. Extruded commercial product of microcellular plastics (Courtesy of Trexel, Inc.).

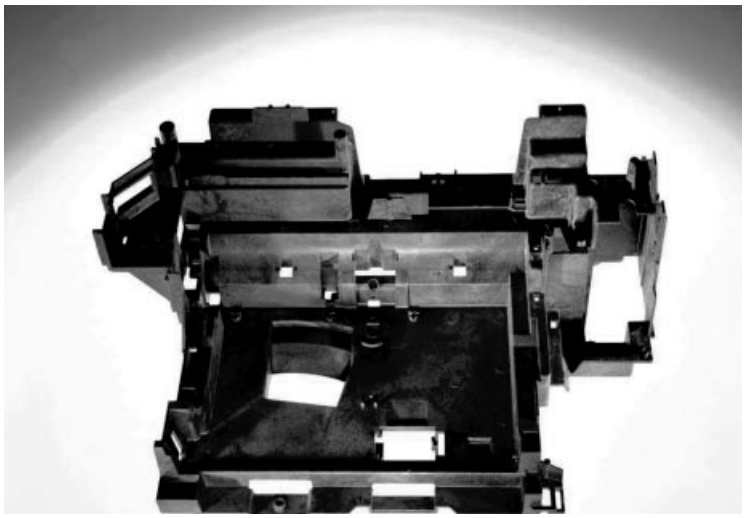

Fig. 11. Injection-molded printer chassis made of microcellular plastics (Courtesy of Trexel, Inc.).

engineering plastic (PPO/HIPS). The chassis made of MCPs has 50 % less warpage, 25% reduction in cycle time, and 8% weight reduction. The microcellular plastic also had higher toughness: 9.0 ft lb vs 6.7 ft lb by drop weight test, and 9.7 kJ/m^2 vs 7.3 kJ/m^2 by notched Izod impact test.

There are a large number of advantages of using MCPs:

(1) Reduction of material consumption (between 5 and 30%)
(2) Faster cycle time
(3) Higher productivity
(4) Greater toughness in some plastics
(5) Low residual stress
(6) Dimensional accuracy
(7) Dimensional stability
(8) Reduction in warping of injection-molded parts
(9) Appearance (no visible cells)
(10) Thin sections
(11) No sink marks
(12) Low temperature process
(13) Low pressure process
(14) Large number of cavities or smaller machines
(15) Most polymers
(16) Use of non-hydrocarbon solvents (CO_2 and N_2)
(17) No additives for nucleation
(18) No reactive components such as viscosity modifiers
(19) No special equipment other than gas supply system

Performance and Applications of MCPs

Some MCPs also exhibit better physical properties. Many MCPs are tougher and have a longer fatigue life. Also the specific mechanical strength is much better than conventional large-cell foamed plastics. MCPs can have densities as low as 0.03 g/cm^3. At such low densities, the thermal insulation properties of MCPs are excellent because of the small cell size.

Since the cell size is extremely small, the cells cannot be seen by the naked eye. Therefore, the foamed plastic resembles a solid plastic, having a good physical appearance. At conventional cell sizes, they are opaque, without the need to introduce pigments such as titanium dioxide.

MCPs save money for manufacturers owing to the use of less material and faster cycle time. Since about 70% of the cost of foamed plastic goods is the material cost and since up to 50% weight reduction is possible for some applications, the cost of plastic parts can be reduced by as much as 35%.

MCPs are environmentally acceptable since they are processed using CO_2 or N_2 instead of hydrocarbons or fluorinated materials. Since smaller amounts of plastics are used in a given product, there is less material to recycle or dispose. Furthermore, less raw material and energy are used to make the same plastic article.

MCPs find many applications in housing and construction, sporting goods, vehicles, electrical and electronic products, chemical and biochemical applications, and the textile and apparel industry. They can be used in siding, pipes, electrical wire, automotive seats and other parts, airplane parts, filters, shoe soles, office equipment housing, artificial paper, food containers, polishing cloth, thermal insulation around pipes, and other uses as well.

MCPs are processed at lower processing temperatures, since the glass-transition and melting temperatures and the viscosity of plastics decrease with increase in dissolved gas. As the gas is formed in the bubble during the nucleation and cell-growth phase, the viscosity and the melting temperature of plastics increases, reverting back to the original state. Therefore, MCPs "solidify" much more quickly—by almost a factor of two—and therefore, injection-molded MCP parts can be taken out of the mold quickly.

Process Research Issues

There are many research issues generated by MCPs. The following is a partial list:

(1) Molecular mechanism of the role of dissolved gas in affecting viscosity
(2) Crystallization process
(3) Solidification process during the phase separation of a gas/polymer solution
(4) Two-phase flow of a gas bubble/polymer mixture at the solid surface–polymer interface
(5) Modeling of the cell nucleation and growth in a die or a mold

Materials Research Issues

There are many research issues related to materials that can advance the field further as briefly listed below:

(1) Mechanical behavior of MCP parts and materials
(2) Effect of gas on morphology
(3) Fracture behavior of MCPs
(4) Fatigue behavior of MCPs

Conclusions

Because of their advantages in performance, cost, and processing MCP show great promise in changing the polymer-processing industry. A great deal is known about MCPs and their processing techniques, but the field is still full of research and development opportunities to satisfy the diverse requirements of the polymer-processing field.

BIBLIOGRAPHY

1. N. P. Suh, in J. Stevenson, ed., *Innovation in Polymer Processing: Molding*, SPE Books, Hanser Publishers, New York, 1996.
2. N. P. Suh, *The Principles of Design* Oxford University Press, New York, 1990.
3. U.S. Pat. 4,473,665 (Sept. 25, 1984), J. Martini-Vvedensky, F. A. Waldman, and N. P. Suh.
4. G. I. Taylor, *Proc. Royal Soc. (London), Series A* **146**, 501 (1934).
5. C. B. Park, Ph.D. dissertation Massachusetts Institute of Technology, Cambridge, Mass., May 1993.
6. V. Kumar, Ph.D. dissertation, Department of Mechanical Engineering, Massachusetts Institute of Technology, Cambridge, Mass., 1988.
7. V. Kumar, private communication, 2000.
8. D. F. Baldwin, C. B. Park, and N. P. Suh, *J. Design Manuf.* (1997).
9. Y. Sanyal, Ph.D. dissertation, Massachusetts Institute of Technology, Cambridge, Mass., June 1998.

GENERAL REFERENCES

D. F. Baldwin, Ph.D. dissertation, Massachusetts Institute of Technology, Cambridge, Mass., Jan. 1994.
D. F. Baldwin, C. B. Park, and N. P. Suh, *Polym. Eng. Sci.* (1996).
U.S. Pat. 5,334,356 (1994), D. F. Baldwin, N. P. Suh, C. B. Park, and S. W. Cha.
D. F. Baldwin, D. E. Tate, C. B. Park, S. W. Cha, and N. P. Suh, *J. Jpn. Soc. Polym. Process.* **6**, 187–194, 245–256, (1994).
U.S. Pat. 5,158,986 (Oct. 27, 1992), S. W. Cha, N. P. Suh, D. F. Baldwin, and C. B. Park.
S. W. Cha, Ph.D. dissertation, Massachusetts Institute of Technology, Cambridge, Mass., 1994.
U.S. Pat. 5,160,674 (Nov. 3, 1992), J. S. Colton and N. P. Suh.

S. W. Cha and Yoon, private communication, 2001.
J. S. Colton, Ph.D. dissertation, Massachusetts Institute of Technology, Cambridge, Mass., 1985.
J. S. Colton and N. P. Suh, *Polym. Eng. Sci.* **27**, 493–499 (1987).
J. S. Colton and N. P. Suh, *Polym. Eng. Sci.* **27**, 500–503 (1987).
U.S. Pat. 4,922,082 (Apr. 1990), J. S. Colton and N. P. Suh.
P. L. Durril and R. G. Griskey, *AIChE J.* **12**, 1147 (1960); *AIChE J.* **15**, 106 (1969).
J. Martini, S.M. dissertation, Massachusetts Institute of Technology, Cambridge, Mass., Jan. 1981.
J. Martini, F. A. Waldman, and N. P. Suh, *Soc. Plast. Eng. Techn. Pap.* **28**, 674–676 (1982).
C. B. Park, D. F. Baldwin, and N. P. Suh, *Polym. Eng. Sci.* **35**, 432–440 1995.
C. B. Park, D. F. Baldwin, and N. P. Suh, *Res. Eng. Design* (1995).
K. A. Seeler and V. Kumar, *J. Reinf. Plast. Compos.* **12**, 359–376 (1992).
M. Shimbo, D. F. Baldwin, and N. P. Suh, *Polym. Eng. Sci.* (1995).
U.S. Pat. 4,278,622 (July 14, 1981) N. P. Suh.
N. P. Suh, *J. Eng. Ind. Trans. ASME* **104**, 327–331 1981.
N. P. Suh, N. Tsuda, M. G. Moon, and N. Saka, *J. Eng. Ind., Trans. ASME* **104**, 332–338 1982.
N. P. Suh, *Axiomatic Design: Advances and Applications* Oxford University Press, New York, 2001.
N. P. Suh, D. F. Baldwin, S. W. Cha, C. B. Park, T. Ota, J. Yang, and M. Shimbo, Proceedings of the 1993 NSF Design and Manufacturing Systems Grantees Conference, Charlotte, N.C., Jan. 1993, pp. 315–326.
N. P. Suh and A. P. L. Turner, *Elements of the Mechanical Behavior of Solids* McGraw-Hill, New York, 1975.
J. R. Youn and N. P. Suh, *Polym. Compos.* **6**, 175–180 (1985).

NAM P. SUH
Massachusetts Institute of Technology

MICROEMULSION POLYMERIZATION

Introduction

The pioneering work on microemulsions was established in the late 1940s (1,2). Extensive studies on this unique colloidal system were carried out after the 1974 oil crisis. This then led to great interest in free-radical polymerization in vinyl monomer containing microemulsion. Microemulsion polymerization involves the propagation reaction of free radicals with vinyl monomer in very fine oil (or water) droplets dispersed in the continuous aqueous (or oily) phase. Unlike the classical emulsion, the transparent or translucent reaction system comprising microemulsion droplets is thermodynamically stable in nature and these tiny droplets (1–10 nm in diameter) exhibit an extremely large oil–water interfacial area ($\sim 10^5$ m^2/dm^3). Relatively stable polymer particles ($\sim$10 nm in diameter)

Encyclopedia of Polymer Science and Technology. Copyright John Wiley & Sons, Inc. All rights reserved.

consisting of only a few polymer chains per particle are produced and, therefore, the resultant polymer molecular weight is very high ($10^6 - 10^7$ g/mol) (3–7). This cannot be achieved readily by conventional emulsion polymerization (8,9) or miniemulsion polymerization (10). In addition, the particle nucleation and growth mechanisms and kinetics associated with microemulsion polymerization are quite different from those of emulsion and miniemulsion polymerization systems (see HETEROPHASE POLYMERIZATION). Research interests in microemulsion polymerization techniques have grown rapidly since the 1980s because of their potential applications in the preparation of fine latex particles, ultrahigh molecular weight water-soluble polymers (flocculants), novel porous materials, polymeric supports for binding metal ions, conducting polymers, colloidal particles containing various functional groups for the biomedical field, and transparent colloidal systems for photochemical and other chemical reactions (5).

Formation and Microstructure of Microemulsion

Considering a colloidal system at constant temperature, volume, and composition, the change of Helmholtz free energy (dF) for any process undergoing the expansion of the oil–water interfacial area ($dA > 0$) can be expressed as

$$\mathrm{d}F/\mathrm{d}A = \sigma - W_{\mathrm{des}} \tag{1}$$

where σ is the oil–water interfacial tension and W_{des} is the work of desorption of surfactant per unit interfacial area. W_{des} is the resultant of various components such as changes of entropy and surface charge density and molecular interactions between constituents of the interfacial film. When W_{des} is sufficiently large and σ is extremely small ($\sim 10^{-3}$ mN/m or lower), dF/dA becomes negative and, therefore, dF is smaller than zero. Under the circumstances, a spontaneous reduction in the average droplet size down to $10^0 - 10^1$ nm is achieved, thereby leading to a thermodynamically stable colloidal system (microemulsion). For example, a gradual transition from the milky oil-in-water (O/W) emulsion to the transparent microemulsion and then to the lamellar gel phase can be observed visually when 1-pentanol (C_5OH, approx. 0.4 g each time) is added successively to the mixture comprising 100 g of water, 11 g of sodium dodecyl sulfate (SDS), and 5.92 g of styrene (ST) only with mild mixing at room temperature. Incorporation of amphipathic cosurfactant (C_5OH) into the adsorbed layer of anionic surfactant (SDS) around oil (ST) droplets greatly decreases the electrostatic repulsion force between two surfactant molecules, minimizes σ, and reduces the persistence length of the interfacial film (ie, enhances the flexibility of the interfacial membrane). All these synergistic factors promote the spontaneous formation of a transparent one-phase microemulsion product that exhibits excellent fluidity. It should be noted that cosurfactant is not a must in the preparation of microemulsion.

Figure 1 shows a schematic representation of the pseudo three-component phase diagram of a surfactant/cosurfactant–oil–water system. Depending on formulas, fine oil droplets dispersed in the continuous aqueous phase [O/W (or direct) microemulsion] or fine water droplets dispersed in the continuous oily

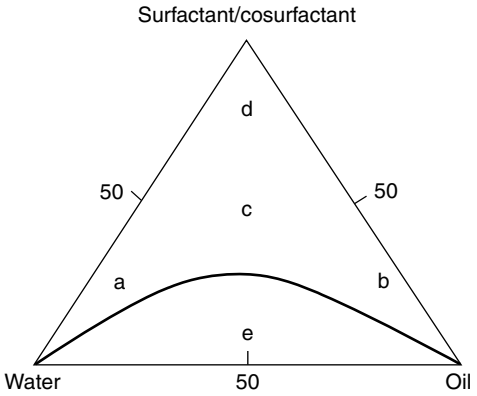

Fig. 1. A schematic representation of the pseudo three-phase diagram of surfactant/cosurfactant–oil–water systems: (**a**) oil-in-water microemulsion; (**b**) water-in-oil microemulsion; (**c**) bicontinuous structure; (**d**) lamellar structure; and (**e**) conventional two-phase emulsion.

phase [W/O (or inverse) microemulsion] are obtained. The intermediate region between the O/W microemulsion phase and W/O microemulsion phase is characterized by a bicontinuous structure in which the aqueous and oily microdomains are interconnected with each other (11,12). Such a middle phase was verified by the literature data (13). It was shown that the oil–water interfacial layer in the bicontinuous structure has a zero-mean curvature (ie, it is flat on the average) and this sponge-like structure is completely disordered. Such a structural aspect of microemulsion allows the monomer to be incorporated into different phases in the polymerization system [eg, the dispersed phase (microemulsion droplets), the continuous phase, or the bicontinuous phase]. This then makes it practical to design and prepare versatile microemulsion polymers for a variety of applications. The information on the initial condition of the reaction system (eg, the type of microemulsion, the dimension of microemulsion droplets, the physical properties of the oil–water interfacial film, the distance between two droplets, and the viscosity of microemulsion) is required in order to gain a better understanding of the subsequent polymerization kinetics and mechanisms. For more detailed information on this subject, please refer to References 3–5,14, and 15.

Microemulsion Polymerization Mechanisms and Kinetics

Significant research efforts have been devoted to the free-radical polymerization of hydrophobic monomers [eg, ST, methyl methacrylate (MMA), and butyl acrylate (BA)] in O/W microemulsions. The anionic surfactant SDS in combination with a short-chain alcohol (eg, C_5OH) as the cosurfactant is the most popular stabilization package. However, as more polymer forms with the progress of polymerization, the increase of free energy as a result of the conformational limitation and/or incompatibility between polymer and cosurfactant results in the instability or turbidity of microemulsion polymer (16). When a cationic surfactant,

dodecyltrimethylammonium bromide (DTAB), was used to stabilize the ST microemulsion polymerization, eventually no cosurfactant was required to form a satisfactory microemulsion product (17). It should be noted that the amount of monomer that can be solubilized within microemulsion droplets is generally quite low, whereas the levels of surfactant and cosurfactant required to stabilize the colloidal system are very high in O/W microemulsion products. For example, the weight percentage of ST does not exceed a few percent, which is much smaller than that of surfactant/cosurfactant (approx. 15% total) used in microemulsion polymerization. The acrylic monomer BA can partition into the oil–water interfacial layer to some extent. Therefore, it promotes the formation of microemulsion in the absence of a typical cosurfactant such as C_5OH (18).

The most widely investigated hydrophilic monomer in the W/O microemulsion polymerization is acrylamide (AM). In this case, AM is usually dissolved in water [50/50 (w/w)] immediately before the preparation of microemulsion because AM is in powder form. Thus, the resultant polymer particles are swollen with water and dispersed in the continuous organic medium. These polymer products are widely used for the flocculation of colloidal dispersions, sewage treatment, coatings, adhesives, and enhanced oil recovery (see ACRYLAMIDE POLYMERS). Just like the hydrophobic monomer BA, AM also tends to migrate toward the oil–water interfacial layer and it acts as a reactive cosurfactant in the formation of the W/O microemulsion using toluene as the continuous medium (19,20). Sodium bis(2-ethylhexyl) sulfosuccinate (AOT) is the anionic surfactant of choice. The polymerization can be initiated by thermal initiators, photochemical initiators, or γ-radiolysis. The W/O microemulsion polymerization system also suffers from the drawback that a very high ratio of surfactant to monomer (the ratio of surfactant to monomer = 2.5–25) is generally required to stabilize this colloidal system. The basic formulas, characteristics, and kinetic parameters of some representative O/W and W/O microemulsion polymerization systems can be found in References 3–7 and 4 and 5, respectively.

Candau and co-workers (19,21) proposed a mechanistic model for particle nucleation and growth in the W/O microemulsion polymerization system comprising AOT, AM/water, and toluene. They observed that the diameter of the resultant latex particles (d_p = 20–40 nm) is much larger than that of initial microemulsion droplets (d_m = 6 nm), that is, the final number of latex particles (N_p) is approximately two to three orders of magnitude smaller than the number of microemulsion droplets initially present in the polymerization system (N_m). Furthermore, on the average, only one polymer chain per particle was obtained. Based on these results, it was postulated that latex particles are nucleated continuously throughout the polymerization. This is not the case for the conventional emulsion polymerization in which the nucleation of latex particles stops at about 10–20% conversion (9). The growth of latex particles was attributed to the very limited fraction of initial microemulsion droplets that can be transformed successfully into latex particles. The remaining droplets only serve as a reservoir to supply particle nuclei with monomer and surfactant during the polymerization. The transport of monomer molecules from microemulsion droplets to latex particles can be achieved either by molecular diffusion through the continuous organic phase or by the mutual collision between one droplet and one latex particle. Monomer-swollen micelles (ie, microemulsion droplets) are present throughout the polymerization because of the

very high level of surfactant used to stabilize the colloidal system. The probability for primary radicals generated in the continuous organic phase to enter these micelles with a very large oil–water interfacial area is much higher in comparison with latex particles. Thus, the nucleation of latex particles is carried into the latter stage of polymerization and each latex particle is capable of capturing only one free radical during its lifetime on the average. This particle nucleation mechanism was verified experimentally (20). It was shown that N_p increases linearly with monomer conversion. On the other hand, d_p remains relatively constant with the progress of polymerization. Such reaction mechanisms with some minor modifications may also be adequate for the qualitative description of the nucleation and growth of latex particles in the O/W microemulsion polymerization.

The O/W microemulsion polymerization system such as SDS/C_5OH–ST/water has been investigated extensively in the last decade. Representative studies conducted by Guo and co-workers (22–25) are chosen for discussion hereinafter. Sodium persulfate (SPS) and 2,2′-azobis(2-methyl butyronitrile) (AMBN) were used as the water-soluble and oil-soluble initiators, respectively, in their experiments. The rate of polymerization (R_p) first increases to a maximum with the progress of the reaction (Region I, ranging from 0 to 20–25% conversion for polymerizations initiated by SPS and ranging from 0 to 10–15% conversion for polymerizations initiated by AMBN) and then decreases toward the end of the reaction (Region II). A schematic representation of R_p versus conversion (X) profile for the O/W microemulsion polymerization is shown in Figure 2a. For comparison, a typical R_p versus X profile for the conventional emulsion polymerization is also included in Figure 2b. It should be noted that the constant R_p period, often observed in conventional emulsion polymerization, is absent from microemulsion polymerization (Fig. 2). Furthermore, the gel effect [ie, the rapidly increased X with time (t) owing to the greatly retarded bimolecular termination reaction] is not experienced in the latter stage of microemulsion polymerization. This is simply because the resultant latex particles are not large enough (d_p = 20–30 nm) to accommodate more than one free radical therein.

Guo and co-workers (22–25) also showed that the nucleation of latex particles occurs throughout the polymerization. Microemulsion droplets (ie, monomer-swollen micelles, d_m = 4 nm) are primary loci for the nucleation of latex particles. However, the nucleation of particle nuclei in the continuous aqueous phase [homogeneous nucleation (8,9)] and limited flocculation of these particle nuclei cannot be completely ruled out. The molecular weight of polymer obtained is very large ($1 \times 10^6 - 2 \times 10^6$ g/mol) because of the predominant chain transfer of polymeric radicals to monomer inside the growing latex particles. The resultant monomeric radicals may desorb out of the very small latex particles, thereby leading to a value of the average number of free radicals per particle (n) smaller than 0.5. These monomeric radicals in the continuous aqueous phase may also be reabsorbed by latex particles. A mechanistic model was developed to simulate the reaction kinetics of the ST microemulsion polymerization. The entry rate coefficient of free radicals into microemulsion droplets estimated by this model is 7×10^5 cm^3/(mol · s), which is several orders of magnitude smaller than that of radicals into the monomer-swollen polymer particles. This is most likely due to the condensed interfacial layer of SDS and C_5OH on the microemulsion droplet surface, which acts as a physical barrier to the incoming radicals. As a

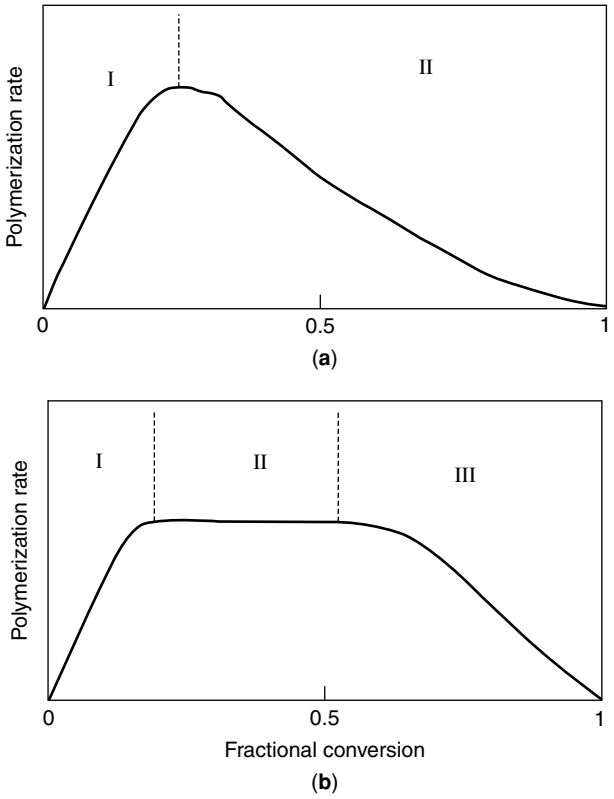

Fig. 2. A schematic representation of the rate of polymerization versus conversion profile: (**a**) oil-in-water microemulsion polymerization and (**b**) conventional emulsion polymerization.

result, only a small fraction ($\sim 10^{-3}$) of microemulsion droplets initially present in the reaction system can be successfully converted into latex particles. A satisfactory agreement between the experimental data and model predictions was achieved. However, the extremely small entry rate coefficient of free radicals into microemulsion droplets was thought to be physically unreasonable because this would lead to the greatly enhanced bimolecular termination rate in Guo's model (26).

Morgan and co-workers (26) derived the following compact equation for predicting microemulsion polymerization kinetics.

$$\ln(1 - X) = -fk_d[\mathrm{SPS}]_0 k_p[\mathrm{ST}]_{d,0} t^2 / [\mathrm{ST}]_0 \qquad (2)$$

The parameter f is the initiator efficiency factor, k_d is the initiator decomposition rate constant, k_p is the propagation reaction rate constant, and $[\mathrm{ST}]_{d,0}$ and $[\mathrm{ST}]_0$ are the initial monomer concentrations in microemulsion droplets and in the polymerization system, respectively. This kinetic model was based on the assumption that (*1*) all the free radicals generated in the continuous aqueous

phase enter microemulsion droplets (ie, particle nucleation loci) and initiate the polymerization therein, (*2*) the bimolecular termination reaction in the aqueous phase is negligible, (*3*) the entry of radicals into latex particles is insignificant, and (*4*) the growing polymeric radical in a latex particle is primarily terminated by the chain-transfer reaction. According to equation 2, plotting the $\ln(1 - X)$ versus t^2 data should result in a straight line with a slope of $(-fk_d[SPS]_0k_p[ST]_{d,0}/[ST]_0)$. This simple model predicts the behavior of the *n*-hexyl methacrylate (C_6MA) microemulsion polymerization reasonably well. In fact, it is the only existing model that can predict the course of microemulsion polymerization depicted schematically in Figure 2a. The general validity of this kinetic model was assessed by several sets of experimental data obtained from the ST microemulsion polymerization, and the poor performance of equation 2 in the high conversion region was often observed (27–30). Such a discrepancy between the experimental data and model predictions was attributed to the bimolecular termination and diffusion-controlled propagation reactions (28).

The technique of pyrene fluorescence intensity measurements was proposed to study the particle nucleation mechanisms involved in the O/W microemulsion polymerization (31). The experimental data showed that microemulsion droplets are the major particle nucleation loci for the polymerization system with the more hydrophobic ST as the monomer. This is followed by the flocculation of latex particles with the remaining droplets. In contrast, the polymer reactions taking place initially in the continuous aqueous phase (homogeneous nucleation) plays an important role in the MMA microemulsion polymerization.

The feasibility of using a water-insoluble dye to investigate the particle nucleation mechanisms in the ST microemulsion polymerization has been evaluated (30). The parameters chosen for this study include the cosurfactant type (C_iOH, $i = 4, 5, 6$), the SPS concentration, and the initiator type [the oil-soluble 2,2′-azobisisobutyronitrile (AIBN) versus water-soluble SPS]. Most of the dye molecules are solubilized within microemulsion droplets immediately before the start of polymerization. Dye molecules can be incorporated into latex particles only when free radicals enter these droplets and successfully convert them into particle nuclei. Primary particles nucleated in the continuous aqueous phase (homogeneous nucleation) should not contain any dye because the transport of dye molecules from droplets or latex particles, across the continuous aqueous phase, and then into latex particles originating from homogeneous nucleation is prohibited because of the very low water solubility of dye. Thus, the weight percentage of dye ultimately incorporated into final latex particles (P_{dye}) serves as an indicator for the extent of nucleation in microemulsion droplets. The dye content (P_{dye}) increases with increasing alkyl chain length of alcohols. Based on these experimental data, it was postulated that the importance of homogeneous nucleation in decreasing order is $C_4OH > C_5OH > C_6OH$. Guo and co-workers (22) showed that N_p increases with an increase in the persulfate initiator concentration. This trend was attributed to the enhanced flux of free radicals into microemulsion droplets. It was suggested in Reference 30 that the increase of the SPS concentration not only promotes the capture of radicals by microemulsion droplets but also increases the probability for oligomeric radicals to precipitate out of the aqueous phase and then form particle nuclei. The latter effect may override the former, thereby leading to the decreased P_{dye} with the SPS concentration.

Chern and Wu (30) also investigated the influence of the oil-soluble initiator AIBN on the particle nucleation and growth mechanisms in the ST microemulsion polymerization. Considering the limiting case that the particle nucleation process is controlled predominantly by the formation of AIBN radicals in the monomer phase, the value of P_{dye} should be much larger compared to the ST microemulsion polymerization initiated by SPS. However, this is not the case because the bimolecular termination reaction between two neighboring AIBN radicals produced in pair in the very small microemulsion droplets is significant. It was then postulated that the particle nucleation process involves (*1*) the desorption of one radical out of the microemulsion droplet containing two AIBN radicals, followed by the propagation reaction between the remaining AIBN radical and monomer, (*2*) the entry of one radical into the microemulsion droplet containing two AIBN radicals, followed by the bimolecular termination reaction and the subsequent propagation reaction between the survivor and monomer, or (*3*) the entry of one radical into the microemulsion droplet containing no radicals, followed by the propagation reaction between this radical and monomer therein. For the microemulsion polymerization initiated by AIBN, the particle nucleation process is characterized by a very low efficiency for the initiation reaction. Under the circumstances, a much higher AIBN concentration is required to give a value of P_{dye} comparable to that of the SPS-initiated polymerization.

Kaler and co-workers (26,28,32–36) have contributed a series of papers dealing with the effects of a number of kinetic parameters (eg, the monomer partitioning, bimolecular termination reaction, and diffusion limitation to the propagation reaction) on the reaction kinetics, latex particle size distribution, and polymer molecular weight distribution in various O/W microemulsion polymerization systems. Analytical expressions based on a mechanistic model were developed to predict the polymer particle size and molecular weight distributions (32). These computer simulations were verified by the experimental data obtained from quasielastic light scattering (QLS) and gel-permeation chromatography (GPC) (32) and online small-angle neutron scattering (SANS) (33). The results obtained from SANS also showed that the C_6MA monomer does not swell polymer particles during microemulsion polymerization (33). Mixed cationic surfactants of dodecyltrimethylammonium bromide and didodecyldimethylammonium bromide were used to stabilize this colloidal system. A model based on the latex particle comprising a polymer core surrounded by a monomer-rich shell is consistent with the kinetic data, and SANS measurements provided that the concentration of monomer in the shell is equal to that in the core of the C_6MA-swollen micelles.

The SANS technique was further adopted to study the partitioning of monomer between microemulsion droplets and polymer particles for various monomers (ST, *n*-butyl methacrylate, *t*-butyl methacrylate, and C_6MA) (34). It was found that, during microemulsion polymerization, the partitioning of monomer is strongly dependent on the composition of microemulsion, especially on the distance to the phase boundary in the pseudo three-phase diagram of the surfactant/cosurfactant–oil–water system. For example, the monomer partitioning is linear in nature and the concentration of monomer in polymer particles is quite low if the initial microemulsion composition is far away from the phase boundary. In contrast, the monomer partitioning is essentially nonlinear and the

concentration of monomer in polymer particles is much higher if the initial microemulsion composition is quite close to the phase boundary. The experimental data could be interpreted reasonably well by modeling the monomer partitioning behavior as a competition between the Flory-Huggins bulk polymer free energy and the Helfrich curvature elastic energy of the surfactant monolayer. The failure of equation 2 was then attributed to a combined effect of the nonlinear monomer partitioning, bimolecular termination reaction, and, in some cases, diffusion limitation to the propagation reaction (35). It is also very interesting to note that the weight-average molecular weight of polystyrene close to 1.5×10^7 g/mol, about one order of magnitude greater than that controlled by chain transfer to monomer ($\sim 2 \times 10^6$ g/mol), was obtained by the technique of GPC coupled with a multiangle laser light scattering detector and a differential refractive index detector (36). This was attributed to the diffusion-controlled desorption of monomeric radicals out of latex particles in combination with chain transfer to polymer. Although the results obtained from these studies made significant progress in this field, further research is still required to gain a better understanding of microemulsion polymerization mechanisms and kinetics.

In addition to the commercially available water-soluble polymers for the treatment of wastewater (37,38), the incorporation of various functional groups (eg, —OH, —COOH, and $-SO_3H$) onto microemulsion polymer particle surfaces for biomedical applications certainly deserves more attention (39). These functionalized latex particles with a diameter of 20–30 nm exhibit an extremely large particle surface area and they are especially effective for the adsorption of proteins, immobilization of enzymes and antibodies, and controlled drug delivery.

Polymerization in the Continuous or Bicontinuous Phases of Microemulsion. In an attempt to prepare hydrophobic polymers used to encapsulate water-soluble materials, W/O microemulsion polymerization systems were evaluated in the 1980s. For example, the influence of polymerization within the continuous organic phase (ST and acrylic monomers such as methyl methacrylate and methyl acrylate) on the regions of stable W/O microemulsion systems was investigated (16,40–42). It was observed that the formation of polymer results in serious phase separation during the reaction. Therefore, a much smaller region of stable microemulsion can be obtained in comparison with the counterpart in the absence of polymer. These results imply that a recipe adequate to the preparation of satisfactory microemulsion does not guarantee the successful transformation of this microemulsion into a unique polymer product. The factors responsible for this instability problem include changes in the molecular conformation (the entropy effect) and interactions among constituents (eg, monomer, polymer, and cosurfactant).

Porous polymeric materials can be prepared by the polymerization of ST in Winsor I, II, and III microemulsions (43,44). It was found that the porosity of polymer achieved by polymerization in the bicontinuous phase is higher than that in the continuous phase of the O/W or W/O microemulsion. This was attributed to the interconnected microdomains in the bicontinuous phase. In fact, the microstructure of polymer achieved is closely related to the nature of microemulsion (45–49). For example, porous polymer with a closed-cell structure (ie, the discrete

water pores are distributed throughout the polymer matrix) is produced when the polymerization of the W/O microemulsion takes place. In contrast, polymerization in the bicontinuous phase results in porous polymer with an open-cell structure in which water channels are interconnected throughout the polymer matrix. These results strongly indicate that the morphology of the resultant porous polymer retains the initial structure of microemulsion to some extent. Nevertheless, the dimension of the resultant porous microdomains ($\sim 10^3$ nm) is much larger than that of the initial structure of microemulsion ($<10^2$ nm) as a consequence of phase separation with the progress of polymerization. A recent breakthrough showed that it is possible to produce polymer with a pore size of 50–70 nm, which is on the order of that of the precursor microemulsion (50). The potential applications of such a polymerization technique for preparing novel polymeric materials include microfiltration, separation membranes, polymer blends with a unique microstructural morphology, and porous microcarriers for the culture of living cells and enzymes (5). Some other interesting ideas about the preparation of novel materials include the conductive composite film (51) and microporous silica gel (52).

BIBLIOGRAPHY

"Microemulsion Polymerization" in *EPSE* 2nd ed., Vol. 9, pp. 718–724, by F. Candau, Institut Charles Sadron.

1. J. H. Schulman and D. P. Riley, *J. Colloid Sci.* **3**, 383 (1948).
2. J. H. Schulman and J. A. Friend, *J. Colloid Sci.* **4**, 497 (1949).
3. F. Candau, in H. F. Mark, N. M. Bikales, C. G. Overberger, and G. Mengers, eds., *Encyclopedia of Polymer Science and Engineering*, Wiley-Interscience, New York, 1987, p. 718.
4. F. Candau, in C. M. Paleos, ed., *Polymerization in Organized Media*, Gordon & Breach, New York, 1992, Chapt. "4", p. 215.
5. F. Candau, in P. Kumar and K. L. Mittal, eds., *Handbook of Microemulsion Science and Technology*, Marcel Dekker, Inc., New York, 1999, p. 679.
6. I. Capek, *Adv. Colloid Interface Sci.* **80**, 85 (1999).
7. I. Capek, *Adv. Colloid Interface Sci.* **82**, 253 (1999).
8. R. G. Gilbert, *Emulsion Polymerization: A Mechanistic Approach*, Academic Press, Inc., New York, 1995.
9. C. S. Chern, in A. Hubbard, ed., *Encyclopedia of Surface and Colloid Science*, Marcel Dekker, Inc., New York, 2002, pp. 4220–4241.
10. I. Capek and C. S. Chern, *Adv. Polym. Sci.* **155**, 101 (2001).
11. L. E. Scriven, *Nature (London)* **263**, 123 (1976).
12. S. Friberg, I. Lapczynska, and G. Gillberg, *J. Colloid Interface Sci.* **56**, 19 (1976).
13. L. Auvray, J. P. Cotton, R. Ober, and C. Taupin, *J. Phys. Chem.* **88**, 4586 (1984).
14. K. Shinoda and S. Friberg, *Adv. Colloid Interface Sci.* **4**, 281 (1975).
15. L. M. Prince, *Microemulsions: Theory and Practice*, Academic Press, Inc., New York, 1977.
16. L. M. Gan, C. H. Chew, and S. E. Friberg, *J. Macromol. Sci. Chem. A* **19**, 739 (1983).

17. V. H. Perez-Puna, J. E. Puig, V. M. Castano, B. E. Rodriguez, A. K. Murthy, and E. Kaler, *Langmuir* **6**, 1040 (1990).
18. I. Capek, V. Juranicova, J. Barton, J. M. Asua, and K. Ito, *Polym. Int.* **43**, 1 (1997).
19. F. Candau, Y. S. Leong, G. Pouyet, and S. J. Candau, *J. Colloid Interface Sci.* **101**, 167 (1984).
20. M. T. Carver, E. Hirsch, J. C. Wittmann, R. M. Fitch, and F. Candau, *J. Phys. Chem.* **93**, 4867 (1989).
21. F. Candau, Y. S. Leong, and R. M. Fitch, *J. Polym. Sci., Polym. Chem. Ed.* **23**, 193 (1985).
22. J. S. Guo, M. S. El-Aasser, and J. W. Vanderhoff, *J. Polym. Sci., Polym. Chem. Ed.* **27**, 691 (1989).
23. J. S. Guo, E. D. Sudol, J. W. Vanderhoff, and M. S. El-Aasser, *J. Polym. Sci., Polym. Chem. Ed.* **30**, 691 (1992).
24. J. S. Guo, E. D. Sudol, J. W. Vanderhoff, and M. S. El-Aasser, *J. Polym. Sci., Polym. Chem. Ed.* **30**, 703 (1992).
25. J. S. Guo, E. D. Sudol, J. W. Vanderhoff, H. J. Yue, and M. S. El-Aasser, *J. Colloid Interface Sci.* **149**, 184 (1992).
26. J. D. Morgan, K. M. Lusvardi, and E. W. Kaler, *Macromolecules* **30**, 1897 (1997).
27. M. Nomura and K. Suzuki, *Macromol. Chem. Phys.* **198**, 3025 (1997).
28. R. de Vries, C. C. Co, and E. W. Kaler, *Macromolecules* **34**, 3233 (2001).
29. C. S. Chern and L. J. Wu, *J. Polym. Sci., Part A: Polym. Chem.* **39**, 898 (2001).
30. C. S. Chern and L. J. Wu, *J. Polym. Sci., Part A: Polym. Chem.* **39**, 3199 (2001).
31. D. R. Kim and D. H. Napper, *Macromol. Rapid Commun.* **17**, 845 (1996).
32. J. D. Morgan and E. W. Kaler, *Macromolecules* **31**, 3197 (1998).
33. C. C. Co and E. W. Kaler, *Macromolecules* **31**, 3203 (1998).
34. C. C. Co, R. de Vries, and E. W. Kaler, *Macromolecules* **34**, 3224 (2001).
35. R. de Vries, C. C. Co, and E. W. Kaler, *Macromolecules* **34**, 3233 (2001).
36. C. C. Co, P. Cotts, S. Burauer, R. de Vries, and E. W. Kaler, *Macromolecules* **34**, 3245 (2001).
37. U.S. Pat. 4,956,399 (1990), J. J. Kozakiewicz and S. Y. Huang (to American Cyanamid).
38. U.S. Pat. 5,132,023 (1992), J. J. Kozakiewicz and S. Y. Huang (to American Cyanamid).
39. Fr. Pat. 9,206,759 (1992), C. Larpent, J. Richard, and S. Vaslin (to Prolabo).
40. J. O. Stoffer and T. Bone, *J. Polym. Sci., Polym. Chem. Ed.* **18**, 2641 (1980).
41. J. O. Stoffer and T. Bone, *J. Dispersion Sci. Technol.* **1**, 37 (1980).
42. J. O. Stoffer and T. Bone, *J. Dispersion Sci. Technol.* **4**, 393 (1980).
43. E. Haque and S. Qutubuddin, *J. Polym. Sci., Polym. Lett. Ed.* **26**, 429 (1988).
44. S. Qutubuddin, E. Haque, W. J. Benton, and E. J. Fendler, in M. El-Nokaly, ed., *Polymer Association Structures: Microemulsions and Liquid Crystals* (ACS Symposium Series No. 384), American Chemical Society, Washington, D.C., 1989, p. 65.
45. M. Sasthav and H. M. Cheung, *Langmuir* **7**, 1378 (1991).
46. W. R. P. Raj, M. Sasthav, and H. M. Cheung, *Langmuir* **7**, 2586 (1991).
47. M. Sasthav, W. R. P. Raj, and H. M. Cheung, *J. Colloid Interface Sci.* **152**, 376 (1992).
48. W. R. P. Raj, M. Sasthav, and H. M. Cheung, *Langmuir* **8**, 1931 (1992).
49. W. R. P. Raj, M. Sasthav, and H. M. Cheung, *J. Appl. Polym. Sci.* **47**, 499 (1993).

50. L. M. Gan, T. D. Li, C. H. Chew, W. K. Teo, and L. H. Gan, *Langmuir* **11**, 3316 (1995).
51. D. A. Kaplin and S. Qutubuddin, *Synth. Met.* **63**(3), 187 (1994).
52. J. H. Burban, H. E. Mengtao, and E. L. Cussler, *AIChE J.* **41**(1), 159 (1995).

CHORNG-SHYAN CHERN
National Taiwan University of Science and Technology

MICROGELS. See SMART MATERIALS, MICROGELS.

MICROMECHANICAL PROPERTIES. See Volume 3.

MISCIBILITY

Introduction

The phase behavior of polymers, whether in solution or in mixtures with other polymeric components, differs considerably from that of small molecules. This difference is a direct consequence of the large size of polymer molecules. For mixtures of small molecules the driving force for miscibility is a result of the large gain in entropy that takes place on mixing, but this is not the case for polymers. The entropy of mixing is particularly small for polymer/polymer mixtures and, as a result, one-phase systems are obtained only in a limited number of cases.

Here, the term miscibility is used to describe a mixture containing two or more components that form a one-phase (solid or liquid) system. Whereas this definition is unequivocal as it corresponds to a precise thermodynamic description of the system, in practice for polymers the experimental determination of miscibility may be rather ambiguous. This is because the latter depends on the specific experimental technique adopted and, for example, while a system may appear one-phase if examined at sufficiently large length scales, it may not correspond to true miscibility at the molecular level.

One of the primary tasks in the past few decades in polymer science has been to control the structure and properties of multicomponent systems. Since the properties of multicomponent systems depend on their structure, the control and design of these structures is fundamental to produce novel properties. Phase separation and spinodal decomposition are used to design multiphase structures. To understand the fundamentals of these phenomena it is necessary to understand thermodynamics, phase transitions, (qv) and critical phenomena in polymer blends (qv) and be able to evaluate quantitatively the degree of miscibility between the polymeric blend components.

Encyclopedia of Polymer Science and Technology. Copyright John Wiley & Sons, Inc. All rights reserved.

Thermodynamics of Solutions of Small Molecules

The necessary condition for two substances to mix is that the Gibbs free energy of the solution, G_{12}, is lower than the sum of the Gibbs free energies of the separate constituents, G_1 and G_2. In other words, for a homogeneous solution to form, the Gibbs free energy of mixing, $\Delta G_m = G_{12} - (G_1 + G_2)$, should be less than 0. Therefore miscibility is governed by the Gibbs free energy of mixing ΔG_m, which is related to enthalpic ΔH_m and entropic ΔS_m components through the relationship

$$\Delta G_m = \Delta H_m - T\Delta S_m \quad (1)$$

It follows that the necessary condition for a mixture of two components to be miscible at a temperature T is that ($G_m < 0$ (it will be noted later that this is a necessary though not sufficient condition for thermodynamic miscibility).

Since ΔS_m is related to the number of "distinguishable" arrangements available to a system, it is a positive quantity; mixing always increases the disorder of the system. This is particularly evident for low molecular weight materials, where the large entropic change occurring on mixing provides the driving force to miscibility. For such systems, ΔG_m becomes more negative with increasing temperature and this favors miscibility.

The first term on the right-hand side of equation 1, ΔH_m, provides a measure of the extent of interactions between molecules. ΔH_m is negative if there are attractive interactions between the components, as this decreases ΔG_m. Obviously, ΔG_m increases if ΔH_m is positive (repulsive interactions). For an ideal solution $\Delta H_m = 0$ and this condition is satisfied when the intermolecular forces between both like and unlike molecules (ie the two components) are similar.

For an ideal mixture of small molecules, consisting of n_1 moles of component 1 and n_2 moles of component 2, the lattice model (Fig. 1a) can be used to determine the entropy of mixing. This is based on various assumptions: (*1*) solvent and solute molecules are identical in size and shape and each occupies a lattice site; (*2*) mixing is a random process since all possible arrangements are equi-energetic (ie $\Delta H_m = 0$); (*3*) no volume changes take place on mixing. By using this simplified model, it is possible to determine the number of possible "distinguishable" arrangements and therefore the entropy change for an ideal solution

$$\frac{\Delta S_m}{nR} = -[x_1 \ln x_1 + x_2 \ln x_2] \quad (2)$$

where x_1 and x_2 are the mole fractions of the two components, n is the total number of moles ($n = n_1 + n_2$), and R is the gas constant. Since the model assumes that the heat of mixing is zero (*athermal mixing*), the free energy of mixing of an ideal solution is simply

$$\frac{\Delta G_m}{nRT} = [x_1 \ln x_1 + x_2 \ln x_2] \quad (3)$$

For the ideal solution, mixing is a spontaneous process that is entropically driven.

Real solutions may deviate from ideality, particularly since the condition of athermal mixing is not usually encountered. The model can be modified to

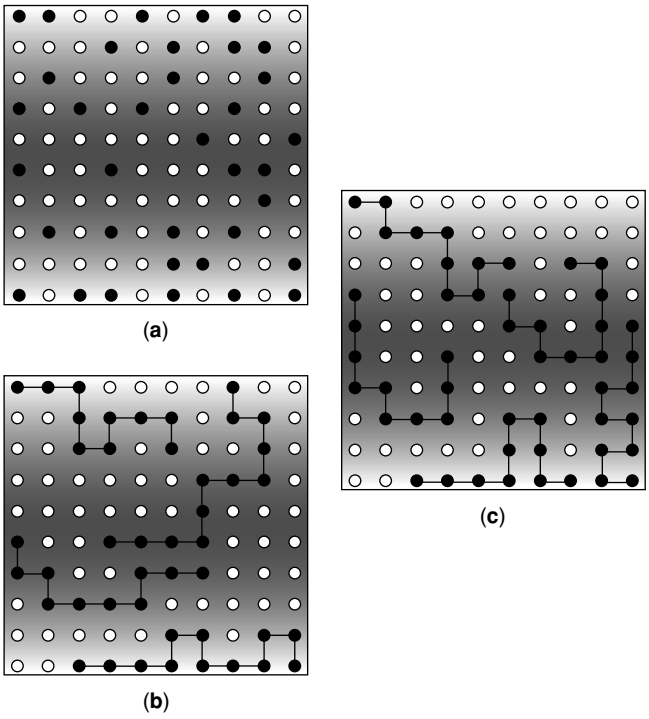

Fig. 1. Schematic representation of the lattice model for the determination of the combinatorial entropy of mixing: (**a**) mixture of small molecules; (**b**) polymer chain in a solvent; and (**c**) polymer/polymer mixture.

account for intermolecular interactions, which, within the lattice model, are of the first-neighbour-type. For a binary system, three kinds of interactions need to be considered: [1, 1], [2, 2], and [1, 2] contacts; and so the process of dissolution is given by

$$\frac{1}{2}[1,1]+\frac{1}{2}[2,2]\rightarrow[1,2] \tag{4}$$

A contact exchange energy, ΔW, can be defined as

$$\Delta W_{12}=\varepsilon_{12}-\frac{\varepsilon_{11}}{2}-\frac{\varepsilon_{22}}{2} \tag{5}$$

from the pair interaction energies ε.

In absence of special attractive forces such as those due to hydrogen bonding and complex formation, and assuming random mixing, the enthalpic term can be expressed as the product between the number of [1, 2] contacts in solution and ΔW_{12}

$$\Delta H_{\mathrm{m}}=nzN_{\mathrm{A}}\Delta W_{12}x_1x_2 \tag{6}$$

where z is the lattice coordination number and N_{A} is Avogadro's number. Equation 6 is often written in terms of the van Laar dimensionless segment–segment

interaction parameter χ_{12}:

$$\chi_{12} = \frac{z\,\Delta W_{12}}{kT} \tag{7}$$

and so

$$\Delta H_m = RT\,\chi_{12} x_1 x_2 \tag{8}$$

The modification introduced above leads to the free energy of mixing of a *regular solution*

$$\frac{\Delta G_m}{nRT} = [x_1 \ln x_1 + x_2 \ln x_2] + \chi_{12} x_1 x_2 \tag{9}$$

This equation, ie the van Laar model of solvent mixtures, can be considered the predecessor of the Flory–Huggins theory but, as explained later, it can be applied only to mixtures of small molecules.

As the temperature is decreased the interaction parameter becomes larger. This affects the free energy of mixing (ΔG_m) versus composition curves as shown in Figure 2. For χ_{12} values less than 2, ΔG_m is negative and the composition dependence is negative, while for $\chi_{12} > 2.0$ the curve changes shape. In this case, for compositions between the two points A and D, the system can lower the free energy by separating into two phases. As the temperature decreases, the interaction parameter becomes increasingly positive and this leads to positive ΔG_m values, which make the system immiscible.

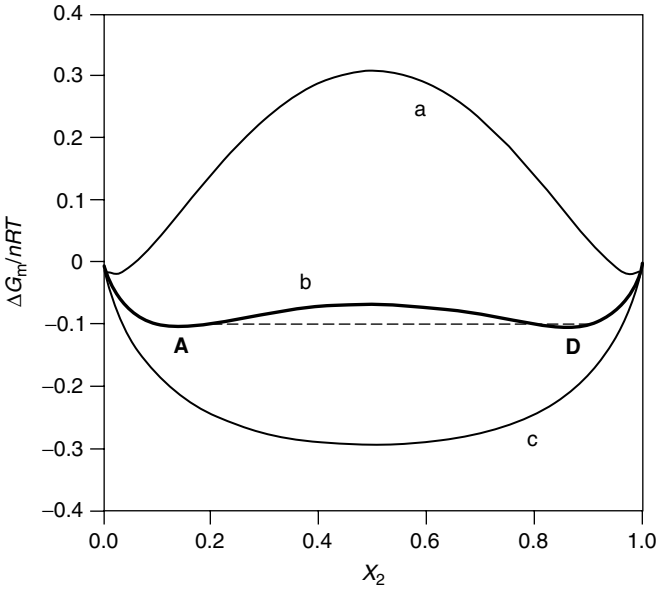

Fig. 2. Composition dependence of the free energy of mixing calculated for a regular solution. Different values of the interaction parameter χ_{12} have been used to generate the curves a ($\chi_{12} = 4$), b ($\chi_{12} = 2.3$), and c ($\chi_{12} = 1.6$).

The interaction parameter χ_{12} is often associated with *Hildebrand's solubility parameter* δ_i, which is in turn related to the *cohesive energy density (CED)* through the relationship (1)

$$\delta_i = \sqrt{CED_i} = \sqrt{\frac{\Delta E_i^{\text{vap}}}{V_i^{\text{o}}}} \tag{10}$$

where $\Delta E_i{}^{\text{vap}}$ is the energy of vaporization of component i. The relationship between χ_{12} and δ_i is given by

$$\chi_{12} = V_{\text{m}}(\delta_1 - \delta_2)^2 / RT \tag{11}$$

V_{m} being the molar volume. As expressed in terms of the solubility parameter, the interaction parameter χ_{12} is necessarily a positive quantity. In practice, negative χ_{12} can be obtained when, because of specific interaction, [1, 2] contacts are favored compared to contacts between like molecules. Thus the solubility parameter concept is only applicable to systems involving dispersive interactions and fails for those involving hydrogen bonds, donor–acceptor interactions, etc.

Thermodynamics of Polymer Solutions

Polymer solutions show deviations from the ideal behavior described in the previous section. In addition to intermolecular polymer–solvent interactions that make $\Delta H_{\text{m}} \neq 0$, chain connectivity causes ΔS_{m} to deviate from the ideal case (eq. 3). When dealing with polymer solutions where one of the components is much larger than the other, significant changes need to be introduced in the treatment of binary liquid–liquid mixtures (2).

The lattice model is still applicable and so are some of the assumptions made for simple liquids. As shown in Figure 1b, in order to position a polymer chain in the lattice, it can be divided into a number of segments, each equal in size to a solvent molecule and therefore each occupying a lattice site. Positioning of these subunits cannot be considered a random event; because of chain connectivity, two consecutive segments in the chain have to be placed in adjacent sites. The schematic diagram of Figure 1b clearly indicates that, for polymer solutions, one expects a reduction of the entropy of mixing compared to solutions of small molecules.

The calculation of the entropy of mixing, ΔS_{m}, of polymers in solution was carried out by Flory (3) and Huggins (4) in 1942. The Flory–Huggins (FH) theory, based on the rigid lattice model developed for solutions of small molecules, leads to the following expression for the free energy of mixing:

$$\frac{\Delta G_{\text{m}}}{RT} = [n_1 \ln \varphi_1 + n_2 \ln \varphi_2] + n_1 \varphi_2 \chi_{12} \tag{12}$$

where n_i represents the number of moles of component i. The FH equation can be written in alternative forms, and, particularly useful, is the expression in terms

of φ_1 and φ_2, the volume fractions of solvent and polymer:

$$\frac{\Delta G_m}{RT} = \frac{V}{V_R}\left[\varphi_1 \ln \varphi_1 + \frac{\varphi_2}{r_2} \ln \varphi_2 + \varphi_1\varphi_2\chi_{12}\right] \quad (13)$$

where $r_2(=V_2/V_1)$ are the number of segments per chain molecule, that is, the degree of polymerization of the polymer, V is the total molar volume of the two components, and V_R is a reference segment volume.

The above equation is similar to that derived in the previous section, the only difference being the replacement of mole fractions with volume fractions. This substitution makes it possible to account for the larger volume occupied by a polymer chain compared to a solvent molecule, while the use of mole fraction rests on the assumption that solute and solvent molecules have equal size.

It follows from equation 13 that, for polymer solutions, the entropy of mixing does not only depend on composition but also on the degree of polymerization of the chains, and it decreases as r_2 (the number of interconnected units) increases. Since r_2 is large, this reflects the reduction of the combinatorial entropy of mixing that arises from the constraints imposed by chain connectivity.

As shown in Figure 3, the free energy versus composition curve becomes highly asymmetric and gets skewed toward the dilute solution end of the composition range. Similar to the case of the regular solution, the temperature dependence of the interaction parameter causes changes in the free energy versus composition curves.

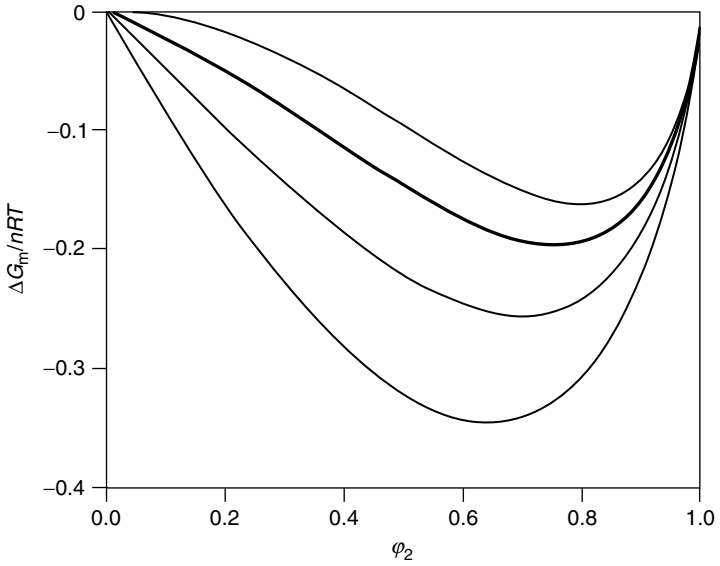

Fig. 3. Composition dependence of the free energy of mixing determined for a polymer ($r = 10^3$) in solution. The different curves have been generated using different values of the interaction parameter (in order of decreasing ΔG_m: $\chi_{12} = 1, 0.8, 0.5, 0.1$).

Phase Equilibria

It has been noted that as temperature decreases the interaction parameter increases; the interactions between molecules are increasingly less favorable to mixing and, at a given stage, a situation will be reached where the system will tend to phase separate into two different phases. Phase separation and limited solubility play a crucial role in situations of practical interest and therefore it is of great importance to establish the phase behavior of a mixture. For this purpose it is instructive to analze the free energy versus composition curves shown in Figure 2. For curve c, ΔG_m is always negative and the mixture cannot separate into two phases since this would lead to an increase in ΔG_m: the system is completely miscible in the whole composition range. On the contrary, for curve a, ΔG_m is always positive and the system is completely immiscible.

The situation represented by curve b is more complex. In this case, ΔG_m is always negative but there is a change of curvature in the middle of the composition range (between A and D). For clarity, this situation is reproduced in Figure 4, where a series of free energy versus composition curves are plotted, which correspond to different temperatures and therefore different values of the interaction parameter. With decreasing temperature, ΔG_m shows a local negative curvature between points A and D. Thus, for compositions between points A and D, the system can lower its free energy by separating into two phases of compositions φ_A and

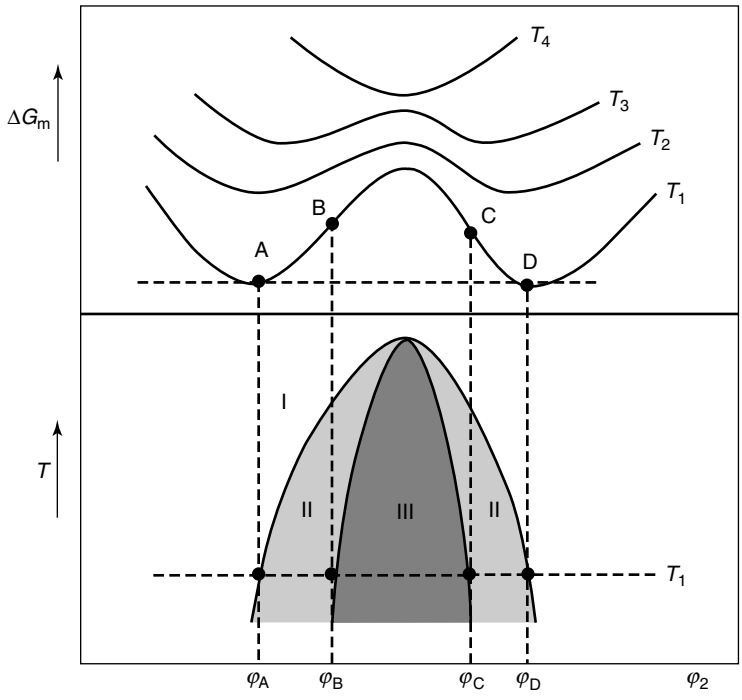

Fig. 4. Schematic representation of free energy of mixing versus composition curves at different temperatures $T_1 < T_2 < T_3 < T_4$ and corresponding phase diagram. In the lower section, I refers to the one-phase region while II and III are the metastable and unstable regions of the phase diagram, respectively.

φ_D that correspond to free energy minima. This implies that there is a miscibility gap between these two compositions. As shown in Figure 4, for $T = T_1$, a common line can be drawn to the free energy curve that is tangent to two points, called *binodal points*, A and D. In the region between points A and D, the free energy along the tangent line, ie the free energy of the two separate phases, lies below the curve that represents the free energy of the single-phase system. It follows that the phase-separated system is more stable, at this temperature and within this composition range, compared to the homogeneous phase. For this condition to be achieved, the ΔG_m versus composition curve needs to show two inflexion points, here indicated as φ_B and φ_C, where the curvature changes sign.

The conditions for miscibility can be found by differentiating the FH equation and by defining the minima and inflexion points. The first derivative, with respect to the number of solvent molecules, leads to the change in chemical potential:

$$\frac{\partial \Delta G_m}{\partial n_1} = RT\left[\ln(1-\varphi_2) + \left(1-\frac{1}{r_2}\right)\varphi_2 + \chi_{12}\varphi_2^2\right] \tag{14}$$

Maxima and minima can be derived by setting the above equation equal to zero. The binodal curve coincides with the set of points where the first derivative of the Gibbs free energy with respect to composition is zero.

The spinodal curve corresponds to the inflection points φ_B and φ_C where the relationship $\partial^2 \Delta G_m / \partial \varphi^2 = 0$ holds. From equation 14, this corresponds to

$$\frac{\partial^2 \Delta G_m}{\partial n_1^2} = \frac{-1}{(1-\varphi_2)} + \left(1-\frac{1}{r_2}\right) + 2\chi_{12}\varphi_2 \tag{15}$$

The binodal and spinodal points can be defined from the conditions above for different temperatures and this leads to the determination of the binodal and spinodal curves plotted in Figure 4. At the critical point, the two curves coincide; this condition is met when the following relationship is satisfied:

$$\frac{\partial^3 \Delta G_m}{\partial n_1^3} = \frac{1}{(1-\varphi_{2c})^2} + 2\chi_{12c} \tag{16}$$

Using equations 15 and 16, the following relationships are obtained:

$$\varphi_{2c} = \frac{1}{1+\sqrt{r}} \tag{17}$$

$$\chi_{12c} = 0.5 + r^{-1/2} + 0.5r^{-1} \tag{18}$$

A phase diagram relative to a polymer solution that phase separates on heating is shown in Figure 4. The solid line in this figure is called the *binodal* and it separates the stable from the metastable regions of the phase diagram. The dashed line is the *spinodal* curve, which separates the metastable and unstable regions. The spinodal touches the binodal at the critical point, T_C, which for a polymer solution is defined by equations 17 and 18.

For compositions between φ_B and φ_C, we have $\partial^2 \Delta G_m / \partial \varphi^2 < 0$, and because any small concentration fluctuations lower the free energy, the system tends to phase separate into two phases of compositions φ_A and φ_D. In this case, phase separation takes place spontaneously by a process called spinodal decomposition. Between φ_A and φ_B and φ_C and φ_D phase separation proceeds by nucleation and growth if there is a fluctuation in concentration large enough to overcome the potential barrier to demixing.

It follows from all the above considerations that for miscibility to be achieved, the following thermodynamic condition needs to be satisfied:

$$\left[\frac{\partial^2 \Delta G_m}{\partial \varphi_2^2}\right]_{T,p} > 0 \tag{19}$$

The temperature marking the upper limit of phase separation, defined by equations 17 and 18, is the so-called upper critical solution temperature (UCST). The UCST represents the maximum temperature (and composition) at which a system exists as two-phase. The phase diagram for polymer solution is molecular-weight–dependent and it becomes increasingly asymmetric with increasing molecular weight. The effect of chain length on the coexistence curve is illustrated in Figure 5. The critical point moves towards more dilute polymer solutions with increasing molecular weight. In the limit of infinite molecular weight, ie for $r \to 8$, the interaction parameter approaches 0.5 and $\varphi_{2c} \to 0$. On the contrary, for

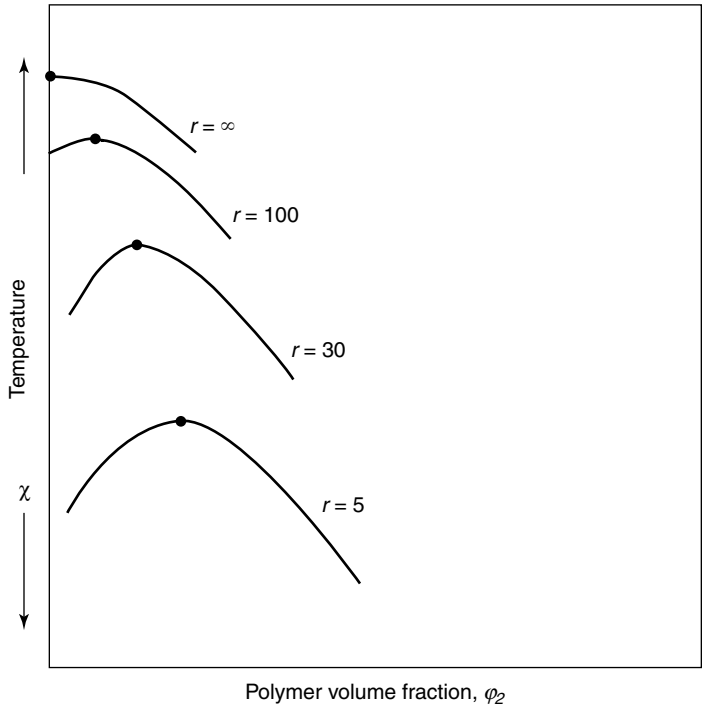

Fig. 5. Schematic diagram illustrating changes in the location of the coexistence curve as a function of molecular weight: with increasing r, and therefore M, the critical points move toward more dilute solutions, and it is located at higher temperatures.

$r = 1$, $\chi_{12c} = 2$ and $\varphi_{2c} = 0.5$ (result for regular solution). These results indicate that a high molecular weight polymer is less soluble than a low molecular weight sample, and this observation forms the basis for the fractionation of a polymer sample, by lowering the temperature of a thetsolution or by lowering the thermodynamic quality of the solvent, progressively.

Comparison between experimental results and theory has indicated that the experimental coexistence curve is always wider than the one predicted on the basis of the FH theory. This discrepancy between theory and experiment is a result of neglecting the composition dependence of the interaction parameter. When the latter is taken into account, accurate predictions of the coexistence curves can be made.

Phase Diagrams. The phase diagrams reported so far in Figures 2, 3, and 5 refer to UCS behavior. These types of phase equilibria are those predicted on the basis of the Flory–Huggins theory and are observed experimentally for solutions of small molecules as well as polymer solutions. This situation implies that mixing is favored by heating and that it is accompanied by a decrease of the interaction parameter, while cooling may lead to a two-phase system.

Experimentally, polymer solutions as well as mixtures of small molecules may show a wide range of phase behavior. A schematic representation of possible phase diagrams for binary mixtures of small molecules and polymers in solution is given in Figure 6. For some systems, eg water/triethylamine solutions, miscibility decreases with increasing temperature, phase separation taking place above a

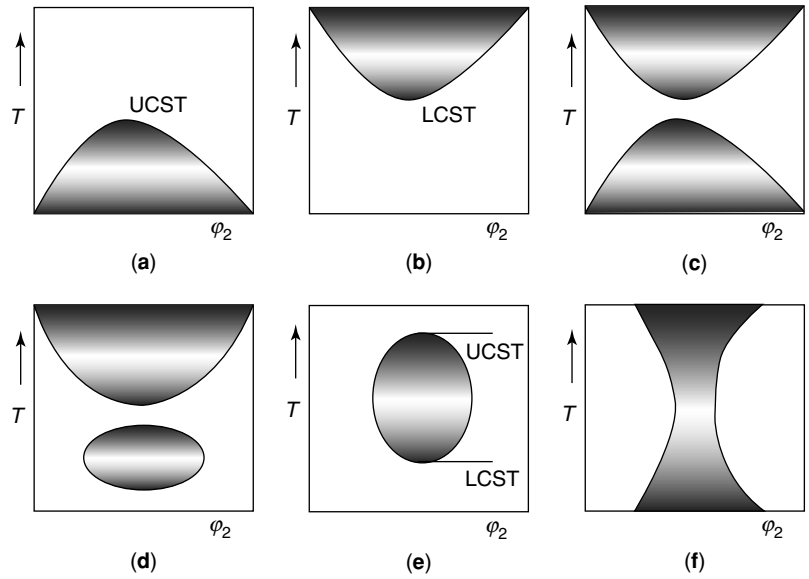

Fig. 6. Schematic representation of possible phase diagrams for binary mixtures; the shaded areas indicate two phase regions: (**a**) upper critical solution temperature behavior (UCST); (**b**) lower critical solution temperature behavior (LCST); (**c**) combination of LCST and UCST, mostly observed in nonpolar polymer solutions; (**d**) phase diagram showing upper, lower, and quasilower critical phase boundaries; (**e**) immiscibility loop; and (**f**) hourglass-shaped phase boundary obtained by convergence of upper and lower critical boundaries.

given temperature. This behavior is schematically shown in Figure 6b; it is referred to as lower critical solution (LCS) behavior and it is characterized by a corresponding lower critical solution temperature (LCST). Other systems, such as nicotine in water, exhibit both UCST and LCST, forming closed loops of miscibility as schematically shown in Figure 6e. An interesting behavior was observed for mixtures of poly(ethylene oxide)/water as this system exhibits both LCST and closed loops. Polymer solutions can show coexisting LCST and UCST as indicated in Figure 6c; the range of temperature separating UCST and LCST is a measure of solvent quality. As the solvent becomes poorer, the gap between the two phase boundaries becomes smaller, until these coalesce leading to the phase diagram of Figure 6f.

The separation of polymer/polymer or polymer/solvent systems into two phases as temperature increases is an established characteristic feature of polymeric systems that is not predicted by the Flory–Huggins theory. LCS phase diagrams are typical of polymer/solvent and polymer/polymer systems that involve specific interactions among the constituents. However, LCST behavior can also be observed in nonpolar systems.

As originally defined by the Flory–Huggins theory, the interaction parameter is independent of concentration and inversely dependent on temperature. This feature reproduces the UCS behavior experimentally observed in some systems. To account for the existence of a LCST, it is necessary to introduce a free-volume component (5–7) that accounts for the difference in size between polymer and solvent molecules. In this approach, a flexible expandable lattice is introduced, which can be envisaged to arise from the different rates of expansion of the polymer and the solvent, with increasing temperature.

Thermodynamics of Polymer Blends

The mixing together of two or more polymers is an established method used to arrive at new property combinations without having to synthesize new structures with the desired characteristics (8–10). The Flory–Huggins (FH) model originally developed for polymer solutions can be extended to polymer/polymer mixtures by introducing the concept of a reference segment volume V_R that is approximated to the smallest polymer repeat unit. For a binary polymer mixture, the combinatorial entropy of mixing ΔS_m can be expressed as (2)

$$\frac{\Delta S_m}{R} = -\left(\frac{V}{V_R}\right)\left[\frac{\varphi_1}{r_1}\ln\varphi_1 + \frac{\varphi_2}{r_2}\ln\varphi_2\right] \tag{20}$$

where r_i represents the number of segments per chain molecule (ie the degree of polymerization) of component i relative to the reference volume V_R, φ_i is the corresponding volume fraction, and V is the total molar volume of the two components.

For a binary mixture of two polymers, the Gibbs free energy of mixing can be obtained from equation 20, leading to an expression similar to equation 13

$$\frac{\Delta G_m}{RT} = \left(\frac{V}{V_R}\right)\left[\frac{\varphi_1}{r_1}\ln\varphi_1 + \frac{\varphi_2}{r_2}\ln\varphi_2 + \varphi_1\varphi_2\chi_{12}\right] \tag{21}$$

Equation 21 shows that the combinatorial entropy of mixing, which is usually the driving force for miscibility in mixtures of small molecules, is very small when r_i is large, ie for high molecular weight polymers. This situation is also schematically shown in Figure 1c where, because of requirements of chain connectivity, the number of possible arrangements are greatly reduced for a binary polymer mixture compared to a mixture of small molecules and polymer solutions. The large size of polymer molecules affects dramatically their thermodynamic behavior; when two high molar mass polymers are mixed, the entropic contribution ΔS_m is very small and any small interaction between the components that is unfavorable to mixing makes ΔG_m positive. In the early days of polymer blending, this observation together with the fact that the van Laar enthalpy of mixing (the third term in eq. 21) is usually endothermic or positive led to the pessimistic view that polymer materials should be largely immiscible.

This has been partly disproved by experiments and, despite the unfavorable entropic term, a number of polymer pairs were found to be miscible. Miscibility is achieved if $\Delta H_m \approx 0$, ie for systems with very similar chemical structures or when specific interactions such as dipole–dipole or hydrogen bonding are introduced among the blend components. In the latter case, $\Delta H_m \leq 0$ and ΔG_m is also negative.

The dependence of ΔG_m on composition φ_i and χ_{12} for a binary blend consisting of two polymers of equal molar mass can be determined from equation 21, and it is similar to that reported for polymer solutions. As temperature increases, the specific interactions between the two components weaken owing to molecular motion and the mixture phase separates. A large number of polymer blends show LCS behavior represented in Figure 6b. However, a UCST may still be observed in some polymeric binary systems, particularly low molecular weight nonpolar mixtures. In this case, even if the entropic term is small it is still larger than ΔH_m, and ΔS_m governs the miscibility.

The critical value of the interaction parameter can be estimated from equation 21, by differentiation:

$$\chi_{12} = 0.5\left[\frac{1}{\sqrt{r_1}} + \frac{1}{\sqrt{r_1}}\right]^2 \tag{22}$$

The critical value above which the two polymers phase separate can be determined from equation 22 for various mixtures with $r_1 = r_2$, and χ_{12} can be compared to the corresponding difference in solubility parameters, as shown in Table 1. The tolerated difference between the solubility parameters for miscibility to be achieved decreases with r_1 and, for high molecular weight polymers to mix, the solubility parameter must be very close. For example, polystyrene ($[\delta = 18.4$ $(J/cm^3)^{0.5}]$ and poly(α-methyl styrene) $[\delta = 18.1$ $(J/cm^3)^{0.5}]$ are predicted to be miscible up to $M_n \sim 60000$ while for miscibility to be achieved between poly(methyl methacrylate) $[\delta = 19.0$ $(J/cm^3)^{0.5}]$ and poly(methyl acrylate) $[\delta = 19.6$ $(J/cm^3)^{0.5}]$ M_n needs to be lower than 13000. Miscibility is expected to be strongly molecular/weight–dependent, as illustrated for polystyrene/poly(α-methyl styrene) blends in References 11 and 12.

Specific Interactions. In order to enhance miscibility between two polymers, the enthalpic term has to be made negative by introducing specific interactions between the two components. A wide range of miscible polymer pairs

Table 1. Critical Values of the interaction Parameter χ_{12c} as a Function of Molecular Weight and Comparison to the Required Difference between the Polymer Solubility Parameters, $(\delta_1 - \delta_2)_{critical}$

$m_1 = m_2$	χ_{12c}	$(\delta_1 - \delta_2)_{critical}$ $(J/cm^2)^{1/2}$
50	0.04	1.00
500	0.004	0.31
5000	0.0004	0.10

have been reported in the literature in which favorable intermolecular interactions such as hydrogen bonds, dipole–dipole, and ion–dipole interactions or charge-transfer complexation exist among the components (13). These interactions may either exist because of the presence of specific chemical groups in the polymer chain or may be introduced by design through copolymerization or other appropriate chemical reactions. For example, it has been demonstrated that when hexafluoro dimethyl carbinol groups are introduced into the phenyl rings of polystyrene (14), miscible blends can be obtained with a number of polymers containing proton acceptor groups, eg poly(vinyl acetate), poly(alkyl methacrylate)s, which are immiscible with polystyrene.

Examples of chemical groups that may lead to miscible polymer pairs are given in Tables 2 and 3. A polymer containing groups listed in column 1 may be miscible with a polymer containing groups listed in Table 2. For example, polystyrene forms miscible blends with poly(vinyl methylether) and this is attributed to interaction between the π-electrons of the phenyl rings and the lone pairs of the ether oxygens (15,16). Similarly, it is believed that a hydrogen bonding interaction exists between the carbonyl units of poly(methyl methacrylate) or poly(ε-caprolactone) and the α-hydrogen of poly(vinyl chloride) (C—O. . . . . H—C—Cl) (17,18).

In addition, it has been shown that by introducing groups capable of ion–ion, ion–dipole, and dipole–dipole interactions, it is possible to achieve miscibility between otherwise immiscible polymer pairs. For example, although polystyrene and poly(ethyl acrylate) are immiscible polymers, miscibility can be achieved by

Table 2. Examples of Interacting Groups Capable of Enhancing Blend Miscibility

Interacting Groups			
Polymer 1	Polymer 2	Strength	Examples
		Weak	PVC/polycaprolactone
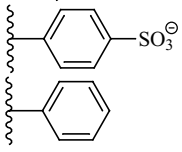	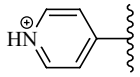	Moderate	Poly(styrene sulphonate)/poly(vinyl pyridine)
	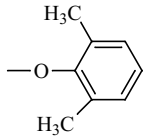	Weak	Polystyrene/poly(2,6-dimethyl phenylene oxide)
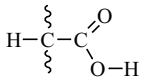	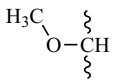	Strong	Poly(acrylic acid)/poly(vinyl methyl ether) or poly(ethylene oxide)

Table 3. Examples of Groups Used of Modify Polymers to Introduce Specific Intermolecular Interactions

Donor group	Acceptor group	Interaction
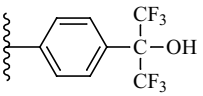	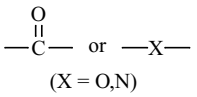	H-bonding
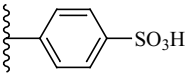	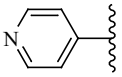	Ion–ion
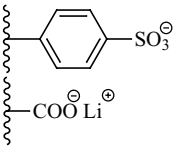	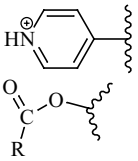	Ion–dipole
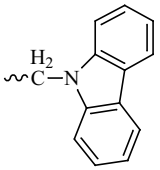	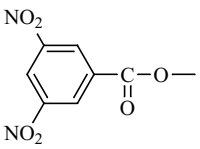	Charge-Transfer complex

introducing styrene sulphonic acid units in the PS chains and ethylacrylate can be copolymerized with small quantities of 4-vinyl pyridine (19). This system is now one-phase through the effect of coulombic attractions between the two copolymers (20–22).

Ion–dipole interactions are also exploited to achieve miscibility; the immiscibility between poly(ethylene oxide) and PS can be overcome by incorporating up to 10 mol% of the lithium salt of methacrylic acid into the PS chain. Weaker interactions arise from the use of donor–acceptor groups to form intermolecular charge-transfer complexes (23–25), and examples of groups that have been used for this purpose are given in Table 3.

Intramolecular Repulsive Interactions. Miscible blends can also be achieved in absence of specific interactions, by exploiting the so-called intramolecular repulsive effect. This is observed in mixtures where at least one of the components is a statistical copolymer; miscibility is restricted to a "miscibility window," that is, it takes place within a well-defined range of copolymer composition. For example, poly(styrene-*co*-acrylonitrile) (SAN) and poly(methyl methacrylate) form miscible blends for copolymer compositions in the range 9–39% acrylonitrile (26,27). Miscibility in these systems is not a result of specific interactions but it is due to the intramolecular repulsive effect (28) between the two monomer units in the copolymer such that, by mixing with a third component, these unfavorable contacts are minimized. The same situation is encountered in binary mixtures of two copolymers (29).

In general, for a binary mixture of two statistical copolymers poly(A-*co*-B) and poly(C-*co*-D), the interaction parameter is (30):

$$\chi_{\text{blend}} = xy\chi_{AC} + y(1-x)\chi_{BC} + x(1-y)\chi_{AD} + (1-x)(1-y)\chi_{BD} - x(1-x)\chi_{AB} - y(1-y)\chi_{CD} \quad (23)$$

where x is the volume fraction of monomer A in poly(A-*co*-B) and y is the volume fraction of monomer C in poly(C-*co*-D), and χ_{ij} are the interaction parameters for each of the segment–segment interactions in the mixture.

For the case of a copolymer A poly(C-*co*-D) and a homopolymer A, equation 23 simplifies to

$$\chi_{\text{blend}} = y\chi_{\text{AC}} + y(1-y)\chi_{\text{AD}} - y(1-y)\chi_{\text{CD}} \tag{24}$$

Equation 24 indicates that miscibility can be obtained by a suitable combination of χ_{ij} values that are unfavorable to mixing; in particular a large positive χ_{CD} value leads to a negative χ_{blend}, which favors the appearance of a "miscibility window."

By using experimental values of the binary interaction parameters it is possible to calculate miscibility maps and therefore predict the phase behavior of polymer/copolymer, copolymer/copolymer, and more complex blends. A list of segment–segment interaction parameters and corresponding interaction energy densities, B_{ij}, where

$$B_{ij} = \frac{\chi_{ij}RT}{V_{\text{R}}} \tag{25}$$

is given in Table 4. These were all determined experimentally or calculated with respect to one initial reference value for the styrene–methyl methacrylate interaction parameter of $\chi = 0.03$, obtained from the light-scattering results of Fukuda and co-workers (31). These consequently comprise a self-consistent set and while they may differ from values quoted in the literature by other workers, they predict phase behavior quite accurately. The other literature values may have been established using different reference points and should not be used in conjunction with this set.

Shortcomings and Extensions of the Flory–Huggins Theory

One of the limitations of the Flory–Huggins theory is that it assumes that all segments have the same size and shape and no volume change takes place on mixing. The theory is therefore unsuccessful in describing the phase behavior of high molecular weight polymer mixtures since it cannot reproduce the LCST that is experimentally observed for many polymer/polymer and polymer/solvent systems. Various factors have been suggested as giving rise to an LCST: (*1*) free-volume dissimilarities between the components that may become unfavorable to mixing at high temperature, (*2*) nonrandom mixing; and (*3*) a temperature-dependent heat of mixing due to the dissociation, upon heating, of the specific intermolecular interactions. Models have been formulated that account for volume changes upon mixing, and the equation-of-state approach has proved to successfully reproduce the LCST behavior.

In addition, in its original formulation, the interaction parameter was assumed to be independent of composition and inversely temperature-dependent. Experimental investigations using small-angle neutron scattering (SANS) (32) have shown that χ is not only temperature-dependent but it also varies with blend

Table 4. Segment–Segment Interaction Parameters Determined Experimentally from Polymer Blends[a]

Segments			
i	J	B_{ij}[b] (J/cm^3)	χ_{ij}
p-Nitrostyrene	Phenylene Oxide	6.2	0.25
Methyl methacrylate	Methyl acrylate	1.1	0.04
Methyl methacrylate	Ethyl acrylate	0.85	0.03
Methyl methacrylate	Itaconic anhydride	8.5	0.34
Methyl methacrylate	Acrylonitrile (Inter)	13.3	0.54
Methyl methacrylate	Acrylonitrile (Inter)	9.3	0.38
Methyl methacrylate	Methacrylonitrile	2.9	0.12
Methyl methacrylate	Phenyl itaconimide	1.2	0.05
Ethyl methacrylate	Ethyl acrylate	0.8	0.03
Butadiene	Choroethylene	1.4	0.06
Butadiene	Acrylonitrile	38	1.53
Butadiene	Vinyl chloride	1.0	0.04
Butadiene	Ethylene	4.8	0.19
Acrylonitrile	Ethylene	20.9	0.84
Acrylonitrile	Chloroethylene	17	0.69
Acrylonitrile	Methyl acrylate	1.0	0.04
Acrylonitrile	Itaconic anhydride	6.5	0.26
Acrylonitrile	Phenyl itaconimide	3.0	0.12
Styrene	Methyl methacrylate	0.71	0.03
Styrene	Acrylonitrile	22.8	0.92
Styrene	Butadiene	2.7	0.11
Styrene	Methacrylonitrile	6.6	0.27
Styrene	Vinyl methyl ether	0.14	0.006
Styrene	α-Methylstyrene	0.09	0.004
Styrene	m-Nitrostyrene	3.6	0.15
Styrene	p-Nitriostyrene	4.2	0.17
Styrene	Phenyl itaconimide	4.0	0.16
Styrene	Itaconic anhydride	12	0.48
Styrene	Phenylene oxide	−1.6	−0.06
Styrene	Maleic anhydride	40.0	1.61
α-Methylstyrene	Methyl methacrylate	0.44	0.02
α-Methylstyrene	Acrylonitrile	22.3	0.90
α-Methylstyrene	Ethylene	5.0	0.20
α-Methylstyrene	Chloroethylene	1.1	0.04
m-Nitrostyrene	Vinyl methyl ether	2.8	0.11
Acrylonitrile	Vinyl chloride	12.2	0.49
Vinyl chloride	Ethylene	3.3	0.13
Vinyl chloride	Chloroethylene	1.0	0.04
Ethylene	Chloroethylene	9.6	0.39

[a]All values are scaled to the original reference point "styrene-methyl methacrylate".

[b]All χ_{ij} values have been determined considering $V_R = 100$ cm^3/mol. In addition, since all χ_{ij} and B_{ij} values were derived from miscibility maps expressed in volume fractions, they should be used to predict phase diagrams in the same units.

composition, molecular weight, and chain architecture. Moreover, the temperature dependence may differ from that predicted by the FH model. Usually, χ_{12} values experimentally measured are complex functions of various parameters, and in this respect they differ considerably from the original Flory–Huggins parameter.

Recent studies have shown that structural differences among components, eg differences in tacticity, affect phase behavior (33–35). The inability of the Flory–Huggins theory to account for these experimental observations is mainly a result of neglecting the particular molecular structure of the polymer chains. Extensive studies have been undertaken in order to be able to link polymer phase behavior to molecular structure (36). The polymer reference interaction site model (PRISM) represents one of the successful approaches in understanding the relationship between molecular structure, local packing and thermodynamics.

BIBLIOGRAPHY

"Miscibility" in *EPSE* 2nd ed., Suppl. Vol., pp. 455–480, by J. M. G. Cowie, Heriot-Watt University, Edinburgh, UK.

1. J. H. Hildebrand and R. L. Scott, *Regular Solutions*, Prentice-Hall, Inc., Englewood Cliffs, N.J., 1962.
2. P. J. Flory, *Principles of Polymer Chemistry*, Cornell University Press, New York, 1953, Chapts. 12 and 13.
3. P. J. Flory, *J. Chem. Phys.* **10**, 51 (1942).
4. M. L. Huggins, *Ann. N.Y. Acad. Sci.* **43**, 1 (1942).
5. I. Prigogine, *The Molecular Theory of Solutions*, North Holland Publishing Co., Amsterdam, 1957.
6. D. Patterson, *Rubber Chem. Technol.* **40**, 1 (1967).
7. P. J. Flory, *Discuss. Faraday Soc.* **49**, 7 (1970).
8. D. R. Paul and S. Newman, eds., *Polymer Blends*, Academic Press, Inc., New York, 1978.
9. O. Olabisi, L. M. Robeson, and M. T. Shaw, *Polymer–Polymer Miscibility*, Academic Press, Inc., New York, 1969.
10. L. A. Utracki, *Polymer Alloys and Blends*, Hanser Publishers, Munich, 1989.
11. S. Saeki, J. M. G. Cowie, and I. J. McEwen, *Polymer* **24**, 60 (1983).
12. J. M. G. Cowie and I. J. McEwen, *Polymer* **26**, 1662 (1985).
13. M. H. Coleman, J. E. Graf and P. C. Painter, *Specific Interactions and the Miscibility of Polymer Blends*, Technomic Publishing Co., Inc., Lancaster, Pa., 1991.
14. E. M. Pearce, T. K. Kwei and B. Y. Min, *J. Macromol. Sci. A: Chem.* **21**, 1181 (1984).
15. D. Garcia, *J. Polym. Sci., Polym. Phys. Ed.* **22**, 107 (1984).
16. B. C. F. Larbi, S. Leloup, J. L. Halary and L. Monnerie, *Polym. Commun.* **27**, 23 (1986).
17. E. J. Vorenkamp and G. Challa, *Polymer* **29**, 86 (1988).
18. M. M. Coleman and J. Zarian, *J. Polym. Sci., Polym. Phys. Ed.* **17**, 837 (1979).
19. A. Eisenberg, P. Smith and Z. L. Zhou, *Polym. Eng. Sci.* **22**, 1117 (1982).
20. A. S. Michaels and R. G. Miekka, *J. Phys. Chem.* **65**, 1765 (1961).
21. P. Smith and A. Eisenberg, *J. Polym. Sci., Polym. Lett. Ed.* **21**, 223 (1983).
22. S. D. Clas and A. Eisenberg, *J. Polym. Sci., Polym. Phys. Ed.* **22**, 1529 (1984).
23. T. Sulzberg and R. J. Cotter, *J. Polym. Sci., Part A1* **8**, 2747 (1970).
24. N. Ohno and J. Kumanotani, *Polym. J.* **11**, 947 (1979).
25. H. A. Schneider, H. J. Cantow and V. Percec, *Polym. Bull.* **6**, 617 (1982).
26. M. Suess, J. Kressler and H. W. Kammer, *Polymer* **28**, 957 (1987).
27. D. J. Stein, R. H. Jung, K. H. Illers and H. Hendus, *Angew. Makromol. Chem.* **36**, 89 (1974).
28. G. ten Brinke and F. E. Karasz, *Macromolecules* **17**, 815 (1984).
29. J. M. G. Cowie and D. Lath, *Polym. Commun.* **28**, 300 (1987).
30. J. M. G. Cowie, *Macromol. Symp.* **78**, 15 (1994).
31. T. Fukuda, M. Nagata and H. Inagaki, *Macromolecules* **19**, 1411 (1986).

32. V. Arrighi and J. S. Higgins, in B. J. Gabrys, ed., *Application of Neutron Scattering to Soft Condensed Matter*, Gordon and Breach Science Publishers, Amsterdam, 2000, Chapt. 8.
33. R. Thomann, J. Kressler, S. Setz, C. Wang, and R. Mülhaupt, *Polymer* **37**, 2627 (1996).
34. Ref. 33, p. 2635.
35. R.-D. Maier, R. Thomann, J. Kressler, R. Mülhaupt, and B. Rudolf, *J. Polym. Sci., Polym. Phys. Ed.* **35**, 1135 (1997).
36. F. H. Case and J. D. Honeycutt, *Trends Polym. Sci.* **2**, 259 (1994).

V. ARRIGHI
J. M. G. COWIE
School of Engineering and Physical Sciences,
Heriot-Watt University

MODELING OF POLYMER PROCESSING AND PROPERTIES.

See Volume 3.

MOLECULAR MODELING

Introduction

Computational chemistry has been practiced since the earliest days of digital computing. Initially restricted to a small class of problems in the hands of a few specialists, the methods are now widely adopted by every type of scientist and engineer. Because the field is so broad, only a portion of it can be covered in this article. But before restricting the scope, it is essential to define our subject in comprehensive terms. We take computational science to be the application of a machine executable algorithm to the solution of either a single or a coupled set of equations that are devised to provide a description of matter. At one extreme of description are the elementary particles—electrons and nuclei—that require the methods of quantum mechanics. At the other limit, there are continuum models that generally assert the piecewise continuity of materials and which usually rely upon "engineering" or constituitive equations, quantified with material parameters frequently determined by experiment. Molecular modeling is everything in between, ie, from atoms up to coarse-grained collections of atoms that can be treated as discrete entities.

The earliest models of molecules were constructed of wire, wood, or plastic. The most famous of these, the Corey–Pauling–Koltun (CPK) models, were commercially available in plastic and consisted of a large variety of atom types representative of average atoms with, say, sp, sp^2, and sp^3 hybridization. The models were helpful because they enabled one to see the three-dimensional relations between atoms more accurately than could be portrayed on the printed page. The extent of the utility of the models was just that they helped to convey molecular architecture. With the advent of high speed graphical computing, physical models have been replaced with computerized pictures that enable one to visualize and move molecules in many different ways.

Encyclopedia of Polymer Science and Technology. Copyright John Wiley & Sons, Inc. All rights reserved.

Many of the earliest uses of computational graphics were in biochemistry. The ability to visualize large enzyme molecules was a boon to both structural biochemistry and the pharmaceutical industry, and the applications of computational chemistry to drug discovery led to the formation of several successful commercial ventures into scientific software. Molecular modeling continues to flourish in the life sciences, where the broader use of computers is developing in ways that are pertinent to current problems in drug design, genetics, proteomics, and other newly emerging disciplines. However, our purpose here is not to discuss the life sciences—we are focussed on the material properties of polymers.

For polymers, the advantage of a digital display over unwieldy physical models is that one may both view the model and simultaneously measure distances, bond angles, and dihedral (torsion) angles, for example, from the atomic coordinates that are stored in the machine, regardless of the size of the model. Furthermore, the types of information that can be displayed graphically, quantities such as quantum mechanical wave functions for molecules of all kinds, and the agility with which these can be manipulated make the computer displays tremendously more powerful than tangible models.

However, molecular modeling is much more than pictures. In defining modeling as the use of a computer to solve complicated theoretical models, we access methods that are capable of providing useful information related to the observable properties of materials, and not just the individual molecules that comprise them. While graphics provides valuable insights into chemical behavior that informs "chemical intuition," this aspect of modeling is now being supplemented by extremely potent quantitative information, of immediate engineering utility, that can be extracted from the mathematical models.

The boundary between theory and modeling can be sharply drawn: a theorist creates a mathematical description, whereas the modeler solves it numerically. A single individual may do both things, but they are different activities. The distinction between experiment and modeling is likewise sharply drawn: an experiment involves real materials, whereas modeling only requires an algorithmic reduction of a mathematical description.

Modeling is the third leg of the scientific tripod, the other two legs being experiment and theory. A theory that cannot be evaluated may be beautiful to contemplate, but it will likely not have very much practical value. Similarly, an experiment that simply generates data in the absence of some understanding of the meaning of the data is not apt to be very useful. In many respects, modeling is the bridge between data and theory, in that it provides a means to analyze data in terms of theory, thereby helping one to understand the data, and it renders the complexities of theory into simply comprehensible quantities that can be related to observations.

When applied to polymers, molecular modeling has to grapple with complexities that go beyond experiences with small molecules. The notion of a pure chemical substance is usually not applicable to polymers. The high molecular compounds that might be interesting for applications may have a distribution of molecular weights, tacticity, sequence, and may contain residual catalysts. They may be partially crystalline, glassy, or a cross-linked melt. In practice, polymers may be formulated with fillers, colorants, stabilizers, or plasticizers, and may be used as films, foams, adhesives, structural materials, fibers, gels, or elastomers.

Thus, the problems of interest to the polymer scientist or engineer involve much more than the behavior of individual molecules, or even of a single, "pure" material. Furthermore, there is a vast range of dynamical and mechanical behavior that is very challenging to describe by any method.

Many properties of interest will succumb to brute-force theoretical and modeling methods. For example, a molecular dynamics method that utilizes an accurate description of the potential energies of molecules and their interactions and which is executed within an appropriate statistical mechanical ensemble is capable, in principle, of solving for any "classical" (as opposed to quantum) problem. However, the computer resources necessary to get to the size and/or time domain where the property of interest manifests itself with this level of description might not yet exist. The certitude of this claim throughout the history of computational chemistry has generated a consistent and substantial effort to utilize the fastest and largest computers available for the problems of molecular modeling.

Fortunately, computers have advanced at an astounding rate since the invention of the integrated circuit. Moore's law, which states that the density of logic elements on chips doubles every 18 months, is expected to hold until about 2012. This leads to the prediction that laptop machines with CPU speeds operating in the range of 10–20 GHz will be available at that time. With the general reduction in the prices of integrated circuits, we expect that inexpensive teraflop personal computers, built with 50 processors operating at 20 GHz each, will be commonplace when silicon-based machines reach their asymptotic chip density. Beyond this, even greater computational power will be available for research problems, and so we are assured that the hardware will continue to add to our capacity to make discoveries and gain new insights. Yet even today, research is underway on the next generation of computers that will employ altogether different technology—perhaps utilizing photons that are switched with polymers!

However, rather than waiting for future developments, scientists and engineers have applied themselves to inventing a multitude of clever ways to negotiate the many different length and timescales that are manifest in the properties of polymers. This article is an attempt to portray a cross section of the methods that have been developed for this multitude of purposes, as well as to describe some of the outstanding results that have been obtained to date.

We have chosen to structure this article primarily around computational methods, as the type of problem that can be solved generally depends on the simulation tool that is available. Before addressing these methods, it is necessary to agree on the types of properties that are accessible to calculation. As alluded above, a complete description of typical polymer is beyond us, so modelers are usually working with the same sorts of idealizations as might apply to a small molecule system. In fact, modeling begins with small molecules, as it is necessary to build up a description of the forces between molecules by first investigating the more tractable systems, for which quantum methods can be conjoined to other simulation methods to provide a detailed description. These are our first concerns, before elaborating the methods. Finally, a selection of representative results that have been obtained is presented.

In preparing this article we have relied upon a great deal of original scientific literature, and our numerous citations will make clear which journals have been

receptive to modeling research. A few general interest journals have a relatively high concentration of polymer modeling papers:

(1) *Journal of Chemical Physics* (Americal Institute of Physics)
(2) *Macromolecules* (American Chemical Society)
(3) *Journal of Physical Chemistry B* (American Chemical Society)

Several journals specialize in the publication of molecular modeling papers:

(1) *Journal of Computational Chemistry* (Wiley), started in 1980
(2) *Molecular Simulation* (Gordon and Breach), started in 1987
(3) *Journal of Molecular Modeling* (electronic, Springer), started in 1995
(4) *Computational and Theoretical Polymer Science* (Elsevier), started in 1991 (discontinued in late 2001 by Elsevier; the journal *Polymer* has accepted responsibility for coverage previously provided by *CTPS*)
(5) *Macromolecular Theory and Simulation* (Wiley-VCH), started in 1992

As is clear from the titles, the latter two are dedicated to polymers. Monographs on modeling, many devoted to polymers, have also been published:

(1) *Statistical Mechanics of Chain Molecules* (1)
(2) *Computer Simulation of Liquids* (2)
(3) *Molecular Modeling of Polymer Structures and Properties* (3)
(4) *Monte Carlo and Molecular Dynamics Simulations in Polymer Science* (4)
(5) *Atomistic Modeling of Physical Properties* (5)
(6) *Computational Modeling of Polymers* (6)
(7) *Conformational Theory of Large Molecules: The Rotational Isomeric State Model in Macromolecular Systems* (7)
(8) *Rotational Isomeric State Models in Macromolecular Systems* (8)
(9) *Computer Simulation of Polymers* (9)
(10) *Interdisciplinary Workshop on Molecular Modeling of Polymers: Wild Dunes*, Isle of Palms, South Carolina (10)

Undoubtedly, the reader will find topics of interest in all of these resources, despite the fact that we are unable to adequately cover many of them owing to the limited scope of this article. We have not taken it upon ourselves to review every significant paper on polymer modeling that has been published. To do so would have been a very much larger task than could be managed within the scope of this Encyclopedia article. Instead, we have attempted to present a balanced view of the major trends in this enterprise, and by so doing we have found it necessary to omit some work. We have undoubtedly overlooked others. However, we are assured that the significance of our omissions will become apparent to the diligent researcher who traces the literature back through the references that we have provided. We apologize in advance to those whose contributions we have been unable to represent in this survey.

Objectives of Modeling

The point at which we start this discussion is somewhat arbitrary, but for our purposes the start of molecular modeling for polymer applications began with the the work of Flory's group at Stanford in the 1960s (1). The rotational isomeric state (RIS) models that were developed at that time were built on the theory invented by Volkenstein (11) and Birshtein and Ptitsyn (12), but it was Flory who polished up the theory and made it systematic and generally accessible. There were certainly very notable efforts to model the properties of single molecules prior to that time, exemplified in the work of Wall and co-workers (13), Teramoto and co-workers (14), and Verdier and Stockmayer (15). (This history is briefly reviewed in Section 17 of the monograph by Yamakawa (16).) These pioneering efforts utilized generic lattice models of chains; there was no systematic application of a theory to a wide range of different "real" molecular architectures preceding RIS theory. Flory's efforts were the first to use experimental data on small molecules to come to an understanding of rotational potentials in polymers and to assess the interplay between molecular structure, force fields, and chain configuration statistics.

As an end in itself, the configuration statistics of a molecule tells one relatively little about the material properties of the polymer. (However, it is precisely those properties of individual molecules that are of unquestioned historical significance in the characterization of polymers by investigation and interpretation of their dilute solution properties.) Most importantly, the methods that were developed within the RIS setting presaged more direct attacks on property prediction methods, as will be seen as our story unfolds.

The *elementary* properties that one would like to be able to calculate or predict with computations include the equation of state, $V(T, P)$, where V is the volume, T the absolute temperature, and the pressure. (For present purposes, the extensive thermodynamic variables are understood to be for any quantity of substance under consideration, and so apply equally well to small molecules as to polymers.) The temperature and volume dependence of energy, $E(V, T)$, are also of interest. While one would like to determine the free energy of a pure substance, $G(P, T)$, this is usually not possible because of the difficulties that will be addressed later.

The *next level* of problems of equilibrium thermodynamics involve more complex properties, such as the tensorial mechanical properties described by compliance and stiffness tensors, as well as those entailing interactions between two or more phases. The latter properties include surface tension as well as phase separation and equilibria. There is great interest in using simulations to probe polymer behavior and properties in environments that are not readily accessible to measurement, such as those encountered in the confined spaces between filler particles.

Several transport properties can be evaluated from equilibrium simulations with use of linear response theory, which relates correlation functions of spontaneously fluctuating molecular properties to phenomenological transport coefficients. These relations can be used to evaluate diffusion coefficients, thermal conductivities, viscosities, IR spectra, and so on. However, most of these properties are evaluated more directly using appropriately devised techniques of nonequilibrium molecular dynamics. Particularly challenging for polymers is the direct

calculation of the viscoelastic properties (the storage and loss moduli), simply because the usual time or frequency span of interest is so large. However, even these problems, at least in narrow time windows, are being effectively investigated today.

Finally, there are the problems related to the ultimate properties of polymers. These include environmental degradation (such as oxidation and photolysis), fracture, and other phenomena that involve bond breakage. All of these phenomena ultimately require a quantum mechanical description of transition states, which places the larger portion of this literature outside the scope of this review. However, there are some semiclassical descriptions that are being employed for these problems, and they are discussed here.

Models and Force Fields

The ability of a simulation to yield specific, rather than generic, information about a system is highly dependent on the quality of the potential energy function that is used to describe the interactions between the smallest entities in the simulation. These smallest units may be atoms, united atoms, beads, or other coarse-grained objects depending on the nature of the simulation. Most modelers who use coarser descriptions than united atoms are primarily interested in generic or global properties, and fairly crude estimates of the potentials suffice for these studies. Models in this category include the finitely extendable nonlinear elastic (FENE) descriptions of bond stretching (17), simple harmonic springs (18,19), square-well potentials for nonbond interactions (20), hard-core repulsions (18,21), and similar model parameterizations. Our primary focus in this section is on atomic and united atom descriptions; other methods are discussed in other sections. A general review with an extensive bibliography, encompassing a wide range of different materials and associated potentials, has appeared recently (22).

It is clear that a coarse-grained model for a polymer requires a compatible force field. As noted above, many of the potentials developed for this purpose have been intended for use in simulating generic properties, eg, the MW dependence of center of mass diffusion, and so have not been used for more detailed work. Efforts to generate more accurate force fields for calculation of thermodynamic properties with these types of models include the work of Boyd and co-workers (23,24) as well as that of Reith and co-workers (25).

General-purpose united atom force fields have also been developed, and one of the most widely cited of these is the OPLS force field of Jorgensen (26). The primary parameterization done in this work was on alkanes, including branched species; the nonbond parameters were fixed with Monte Carlo simulations on liquids. One advantage of a united atom model is that heat capacities for systems containing hydrogen can be computed with some reliability, at least at modest temperatures because the hydrogens are absent and cannot contribute to the equipartition of energy in the simulation (cf. seq.). It is of interest that the well depths for the dispersion interaction term for branched carbon atoms in the alkanes (26) are considerably shallower than for methyl and methylene carbons. This is also seen in the NERD force field (27), and has recently become apparent in an all-atom force field (28).

Just as there is a range of detail that can be invested in a computational model, there is a range of accuracy that is expected from potential energy functions (force fields). One of the more extensively used modeling packages is CHARMM, which comes equipped with a force field that has been developed largely for biological molecules (29). The aim of a general-purpose force field, such as the DREIDING force field of Goddard and co-workers (30) or the universal force field (UFF) of Rappé and co-workers (31–33) is to cover as much of the Periodic Table as possible. This wide scope is accomplished with use of general rules, such as average bond lengths for compounds containing X—Y bonds, or average angles for X—Y—Z bond angles, etc, where X, Y, and Z are any atoms. Data of all kinds have been used for these parameterizations, including quantum-calculated equilibrium structures as well as experimental diffraction studies of crystals and gases. These types of force fields are routinely used to get rapid estimates of structures, for which they are admirably suited. The geometry of an exotic molecule that has never before been synthesized might be amenable to description with DREIDING or UFF when other classes of force fields might not be able to give results, simply because the exotic has not been parameterized.

The disadvantage of these generic force fields is that they are usually not sufficiently accurate to predict condensed phase properties reliably. For example, "fair agreement" between experiment and UFF is a prediction of a bond length within 0.008 nm (33). (The accuracy for main groups elements with UFF is usually better than this.) This is a 4% error for a bond length of 0.2 nm, which translates into ca. 12% error in the density! The point is that a 4% error in the structure of an isolated molecule is barely perceptible to the eye, yet when physical properties of condensed phases are predicted for this structure, unfortunately large errors may be encountered.

The functions that are used for the broad coverage force fields are usually simple quadratic functions in the deviations from equilibrium bond lengths and bond angles. The higher accuracy force fields, such as MM3 (34) or CFF (35), make use of more complicated functions. The function used in CFF is

$$
\begin{aligned}
E_{\text{pot}} = {} & \sum_{\text{bonds}\, j} \sum_{s=2}^{nb} k_{js}\left(b_j - b_j^0\right)^s + \sum_{\text{angles}\, l} \sum_{t=2}^{n\alpha} h_{lt}\left(\theta_l - \theta_l^0\right)^t \\
& + \sum_{\text{dihedrals}\, k} \sum_{r=1}^{nt} V_r\left[1 - \cos\left(r\phi - \phi_r^0\right)\right] + \sum_{oop\, i} K_i \chi_i^2 + \sum_{\text{bond pairs}} F_{jk}^b\left(b_j - b_j^0\right)\left(b_k - b_k^0\right) \\
& + \sum_{\text{angle pairs}} F_{mn}^{\theta}\left(\theta_m - \theta_m^0\right)\left(\theta_n - \theta_n^0\right) + \sum_{\substack{\text{bond + angle} \\ \text{pairs}\langle i,l\rangle}} F_{il}^{b\theta}\left(b_i - b_i^0\right)\left(\theta_l - \theta_l^0\right) \\
& + \sum_{\substack{\text{bond + dihedral} \\ \text{pairs}\langle j,l\rangle}} \left(b_j - b_j^0\right) \sum_{k=1}^{m} V_k \cos(k\phi_l) + \sum_{\substack{\text{angle + dihedral} \\ \text{pairs}\langle j,l\rangle}} \left(\theta_j - \theta_j^0\right) \sum_{k=1}^{m} V_k \cos(k\phi_l) \\
& + \sum\sum\sum K_{lkk'} \cos(\phi_l)\left(\theta_k - \theta_k^0\right)\left(\theta_{k'} - \theta_{k'}^0\right) + \sum_{i>j} \frac{q_i q_j}{r_{ij}} + \sum_{i>j} \left(\frac{A_{ij}}{r_{ij}^n} - \frac{B_{ij}}{r_{ij}^6}\right)
\end{aligned}
\tag{1}
$$

Values with the superscript zero are reference values. The sums in each of the bonded terms (first four lines of the equation) run over all bonds, angles, etc,

in the molecules of the simulation, while the nonbond terms in the last line run over all pairs of atoms, both intermolecular and intramolecular. The nonbonded interactions within a molecule are usually included only for atoms separated by three or more bonds. In these types of force fields, a truncated Taylor's series approximation is used to describe the "real" function for the various atomic displacements, with the number of retained terms (usually no more than three or four) being determined by the required accuracy of the representation.

The first four terms of the above equation are "diagonal" in the sense that they do not cross-couple different displacements as do the next six terms. Terms of the latter category are required to describe the perturbation of one displacement by a neighbor. The force constants that appear as the coefficients of the displacement terms are carefully chosen to give good frequencies, and the cross-terms are added to give even better IR frequencies. The fourth term describes an out-of-plane (oop) bending degree of freedom (χ).

The nonbond interactions are summed over all partial atomic charges in pairs (separated by three or more bonds) taken as point monopoles in the Coulombic term. The dipole-induced dipole (London dispersion) interaction between polarizable atoms is contained in the last term, with the atomic overlap repulsion being included here (for algebraic convenience) as the 9th or 12th power. (CFF uses the 9th power, whereas the traditional Lennard–Jones choice is the 12th.)

The parameterization of a molecule with a function such as equation 1 usually proceeds in stages. First of all, it is assumed that the mathematical description of a chemical functional group is transferable from one molecule to another. In this approximation, there is only one ester group with aliphatic substituents, for example, but this group *may be different* from an ester with aromatic substituents. Any distinction that might be drawn between these two types of ester groups is decided on consideration of the desired level of accuracy. Each group consists of a number of *atom-types*. In principle, every symmetry-unique atom in a molecule is a different type of atom, requiring a unique set of parameters. However, at the level of accuracy that can be achieved today, it is not necessary to tune the force field to the level of individual atoms in each unique molecule. Functional groups, defined at the level that they are understood in organic chemistry, are sufficiently fine units for virtually all force field parameterizations. This is essential for polymers, as a parameterization of the repeat unit in a chain will suffice to describe the entire chain, with the exception of end groups. And they can be handled with similar methods even though they are different from the mid-chain units.

Even with atom typing and group parameterizations, a high accuracy potential energy function for even a relatively small molecule (say a typical solvent molecule) may require hundreds of parameters. The labor involved in generating these parameters is enormous if done by hand, which is what Allinger and co-workers have done in parameterizing MM3 and its predecessors (34,36–49). The labor can be automated to a considerable extent by making use of quantum mechanical (QM) calculations, in which the energies, gradients, and hessians of molecules containing a given functional group are calculated (35,50–61). This gives equilibrium values of bond lengths, bond angles, etc, as well as force constants. The plentiful QM data is parameterized by least-squares methods with a function such as equation 1, with the parameters being generated more or less automatically. Partial atomic charges are usually found by fitting the electrostatic

potential derived from QM to a point charge model, from which bond dipole parameters are constructed.

The QM calculations at any selected level of approximation are generally susceptible to systematic errors, but empirical corrections for these inaccuracies can be applied. Finally, the London dispersion interaction term is fit by performing simulations on a condensed phase to get the correct crystal structure, or in the case of liquids, the correct mass and cohesive energy densities. The dihedral terms in equation 1 are of considerable importance for polymer conformations and their transitions, and require careful treatment because of the coupling between nonbond and torsion terms (59). Even with some automation, the construction of a widely representative force field is a major undertaking.

The all-atom version of OPLS (62) is a diagonal force field, with parameters adapted largely from AMBER (63). Heats of vaporization for a range of organic liquids from alkanes to amides are predicted within about 2% with this force field, and densities are given to within 3%. The pressure dependence has apparently not been thoroughly investigated, but heat capacities are in good agreement with experiment. The latter are calculated from fluctuations in the energy during MC simulations of the condensed phase, which gives the intermolecular contribution. The intramolecular term, which might entail the hydrogen equipartition problem, is taken from experiment or a quantum statistics calculation. This is a practical solution to the heat capacity problem for small molecules, but it is not applicable to polymers. The quality of several different potentials for water, undoubtedly the most difficult small molecule to model correctly, was reviewed many years ago by Jorgensen and co-workers (64). This work is essential reading for anyone wanting to perform simulations on aqueous polymer solutions.

The GROMOS and GROMACS packages (65–67) from The Netherlands contains an MD engine that is supported by the GROMOS force field developed largely by van Gunsteren and Berendsen. This is best described as a diagonal force field with a 6–12 Lennard–Jones term. The GROMOS force field has been extended to a variety of molecules, such as cyclodextrins (68).

A force field that focusses on intramolecular interactions, and particularly on the force constants that determine vibrational frequencies, is the spectroscopically determined force field of Krimm and co-workers (50–52). They advocate very high level quantum calculations to fix the geometries, force constants, and electrostatic terms while using OPLS nonbond Lennard–Jones parameters. The recent focus of this work has been on highly polar molecules, as are discussed later. While this force field reproduces gas-phase IR data very accurately, it does not appear to have been tested on condensed phases.

A number of researches have developed special purpose force fields to enable simulations on specific polymers. Representative examples of both united-atom and all-atom parameterizations are:

(1) alkanes by Rigby and Roe (69)
(2) polymethylene by Boyd (23,70)
(3) polyisobutylene by Boyd and Pant (24)
(4) poly(ethylene oxide) and monatomic ions by Jaffe, Smith, and Yoon (71–73)
(5) poly(propylene oxide) by Ahlström, and co-workers (74)

(6) 1,4-polybutadiene by Smith and Paul (75)
(7) polytetrafluoroethylene by Holt and Farmer (60) and Chang and co-workers (76)
(8) poly(vinylidene fluoride) and trifluoroethylene by Abe and co-workers (77)
(9) poly(ethylene terephthalate) and related esters by Hedenqvist, Bharadwaj, and Boyd (78,79)
(10) polyimides by Young and co-workers (80)

In work of this type there is no implication that the "boutique" force field has applicability beyond its intended purpose, although there are clearly opportunities for transferring parameters for groups developed for one system to another molecule having the same or similar group (78,79). A closely related category of special purpose force fields is those derived from commercial or broad-coverage force fields by modification. The work by Ennari and co-workers (81) is illustrative of this method to develop new functionality from a springboard of established results.

The next phase in the development of high accuracy force fields will likely involve a treatment of polarizability. It is well documented that molecular polarization, as evidenced in depolarized scattering, strain birefringence, or the Kerr effect (1), is highly dependent on the molecular environment (82). The shell model (22), a highly successful potential function for the treatment of inorganic solids and used for poly(vinylidene fluoride) by Karawawa and Goddard (83) and Carbeck and co-workers (84), has polarizability as its primary focus. In this model, atoms are represented with positive cores and negative shell charges (or with positive shell charges for highly polarizable cations) with harmonic springs holding the shell charge to the center. An alternative to the shell model is provided by bond polarizibility tensors (85). This approach hews closely to the principles of the RIS model (1), but has not achieved widespread popularity.

Polarization of the kind envisioned here results when the dipolar molecules surrounding a given molecule, group, or atom induce a dipole moment in the object, the magnitude of which depends on magnitude of the electric field generated by the neighbors. The induced moment then reacts back on the neighbors, resulting in a self-consistent readjustment of the orientations and magnitudes of all the dipoles in the system. Obviously, this effect is more important the larger are the permanent dipoles and the atomic numbers, ie, polarizabilities, of the elements involved. Unfortunately, the parameterization of atomic and molecular polarizability is apt to be a substantial undertaking, as current methods are not highly accurate (86). The recent promising work of Krimm and co-workers (52) utilized very high level quantum calculations to determine the electrostatic potential of water and formaldehyde, which provided the data required to fit a variable atomic charges/atomic dipole model for the molecules, including bimolecular clusters. However, as this study shows, very extensive calculations are required to generate data of sufficient quality to enable accurate fitting of model parameters. That is, the more deeply one delves into refinements in force fields, the greater are the demands on the theoretical methods and the more difficult it is to find pertinent and accurate experimental data. There is a need to come to a better

understanding of many-body effects in general, and this will require a significant basic research program.

There is a pressing need for reactive force fields (87–90) that are capable of modeling both simple polymerizations and degradation reactions. Ab initio quantum methods can be coupled with dynamics to study chemical reactions, as they are in the Car–Parinello method (91), but the overhead of the QM calculation restricts these types of simulations to relatively short timescales. The use of semiempirical QM methods with MD has also been advocated (92), and this technique has spanned up to 200 ps with C_{60}. However, to induce chemistry on this timescale requires the use of very energetic initial states. There is a great need to develop less rigorous, but nonetheless useful and generally correct, descriptions of slow reactions for use in polymer lifetime simulations. Descriptions of this kind must get the chemistry right, but at a faster than natural rate that can be subsequently scaled to physical time.

Construction Methods

Placing Molecules in Containers. The construction of individual polymer molecules with use of graphical software is simply done by linking together specified number of atoms or groups by applying appropriate operations to the fundamental coordinate data structures of the units. Chemical bonding rules, with average bond lengths and bond angles selected from a general-purpose table of values for representative atoms, atom pairs, and atom triplets, are used together with elementary translations and rotations of coordinates so as to place atoms in more or less correct chemical relation to one another. On assignment of a potential energy to the molecule, an energy minimization may be performed using standard techniques to adjust the geometry of the molecule to adopt a low energy conformation if that is desired.

The construction of a condensed phase that is representative of a bulk amorphous material consisting of one or more molecules that have been built as described above requires that the molecules be packed in a container so as to enforce a predetermined density on the system. If the system is monoatomic, ie, is a nobel gas, the atoms are inserted one at a time in the box with evaluation of the energy at each attempted insertion. Those trials with too great an energy according to some criterion, most preferably the Metropolis Monte Carlo criterion (93) to be discussed, are discarded. Successive attempts to place atoms in the box are continued until the required density has been achieved. Of course, in this simple case it may be preferable to start with an easily constructed crystalline array and then randomize it by the molecular dynamics or Monte Carlo techniques to be described.

For molecular modeling of condensed polymeric phases (polymer melts and glasses), an important consideration is the generation of a well-relaxed molecular model at the density and temperature of interest. Unlike simple molecules whose structure can be prepared by simply starting from a known crystal structure and melting it, chain connectivity (ie, various intrachain constraints such as bond lengths, bond angles, and chain conformations) makes generation of well relaxed structures of condensed polymeric phases a nontrivial problem. Over the

last two decades of the twentieth century, several approaches were presented in the literature to tackle this problem; a brief summary of these methods along with the key results obtained in each study is presented in this section.

The early studies of molecular modeling of polymers attempted to generate structures of condensed polymeric phases in a manner analogous to that used for preparing structures of simple liquids, ie, starting from a regular, ordered (crystalline) structure and then melting this structure using either molecular dynamics or Monte Carlo methods to obtain a structure of polymer melt. This was the approach followed by Boyd (23) in the simulation of liquid *n*-tetracosane. However, such an approach encounters major difficulties when applied to polymers with larger monomeric units or for chains having complicated architecture, as mentioned above.

Another class of methods for generating structures of condensed polymeric phases consists of methods that grow the polymer chains in a bond-by-bond fashion in the simulation box. This approach was followed in one of the first molecular modeling studies of alkanes (which provided an initial approximation to polymers) at realistic experimental density reported by Vacatello and co-workers (94). In that work, an initial configuration of the chains was generated by starting with just one methylene group for each of the *n*-tricosane (C_{30}) chains. In the initial stages of the simulation, the chains were grown to their full length by a modification of the slithering snake move: upon addition of a new methylene group to one end of the chain, a methylene group from the other end was not removed if the chain was shorter than the required length. Another variant of the chain growth method, called the "Phantom Chain Growth" method, was presented by McKechnie and co-workers (95). In this method, an initial configuration of chains is produced without accounting for the excluded volume effects (long-range nonbond interactions). Such a procedure generates the correct conformational statistics of the chains but leads to severe interatomic overlaps, which are removed in the subsequent relaxation stage using molecular dynamics simulations (to be described) in which the short-range nonbonded interactions were modified. The method was successfully applied to polyethylene by these authors.

In general, because of their higher density and very long relaxation times, direct generation of structures of glassy polymers is a more difficult task than generating structures of polymer melts above T_g. Several approaches have been presented for generating structures of these materials. Theodorou and Suter (96) presented the first application of molecular modeling to a polymer glass—atactic polypropylene. For the generation of these models, a two-step approach was employed: Generation of a "reasonable" initial guess structure by growing the polymer chain bond-by-bond in the simulation box followed by minimization of the energy of the structure. An important consideration in generating an atomistically detailed model of this system at the experimental density and temperature of interest was that the conformational statistics of the chains in the bulk model should be similar to those for unperturbed chains. This was achieved by selecting the location of the new bond during the chain growth process from candidate positions determined by the rotational isomeric states of the chain as given by the RIS model. The energy minimization strategy involved a gradual increase in the magnitude of the nonbonded interactions between various atoms. This construction procedure was repeated several times to generate a small but

representative sample of structures drawn from the ensemble of amorphous glassy structures.

Suter and co-workers have also applied this technique for generating structures to glassy poly(vinyl chloride) (97), polycarbonate (98,99) and polystyrene (100). It was found, however, that when this technique was applied to polycarbonate and polystyrene, the initial structures generated had severe interatomic overlaps, and required tedious relaxation strategies involving 25 and 41 minimization stages respectively, in which the nonbonded interactions were gradually increased from their initial weakened values to full strength.

As described above, when the technique developed by Theodorou and Suter (96) is applied to polymers containing large or rigid monomer units, the resulting guess structures are highly strained and have large interatomic overlaps that require cumbersome relaxation strategies involving several stages of energy minimization. These problems can be removed to a large extent by combining this technique with the ideas of a "scanning method" as described by Meirovitch (101,102). In this approach, rather than considering the energy change associated with the addition of just one new bond at a time as in the original Theodorou and Suter method, the state of the current bond is selected by considering energies associated with several possible continuations of the chain over a specified number of future bonds. This technique facilitates the construction of amorphous and liquid crystalline phases of polymers containing large and/or rigid monomer units, and can also handle constructions of films confined by surfaces. Such an implementation of bond "look-ahead" (ie, accounting for several future extensions of the chain) is available in the Amorphous Cell package commercially distributed by Accelrys (103) (see Fig. 1).

Another class of methods for generating structures of condensed polymeric phases involves "polymerization" of the required number of monomers that are already placed in the simulation box. Rigby and Roe (69) used this approach in their study of polyethylene in the liquid and glassy state. They first placed centers of the required number of methylene groups randomly in the simulation box. Spatially close groups were then bonded to each other to form the initial configurations of the chains. The structure thus generated was relaxed using molecular dynamics with weakened potentials for all of the intrachain, bonded interactions, and full strength Lennard–Jones interactions for all of the nonbonded interactions. As the system relaxed, the force constants for the intrachain interactions were gradually increased toward their actual values. The approach used by Rigby and Roe (69) for generating configurations of condensed polymeric phases was extended by Khare and co-workers (104) to generate structures of glassy atactic polystyrene at realistic density. In that work, polystyrene chains were generated by "polymerization" of the required number of styrene monomers that were randomly distributed in the simulation box. The initial configuration thus obtained was relaxed using a combination of molecular mechanics and molecular dynamics simulations.

Kotelyanskii and co-workers (105) have presented an alternate approach for efficient building of large amorphous polymer structures. In this approach, a coarse-grained representation of the polymer structure is first created by generating trajectories for self-avoiding walks on a fully occupied lattice. The atomically detailed chains are then generated by placing the chain backbones along these trajectories and adding other atoms required to account for the specific chemical

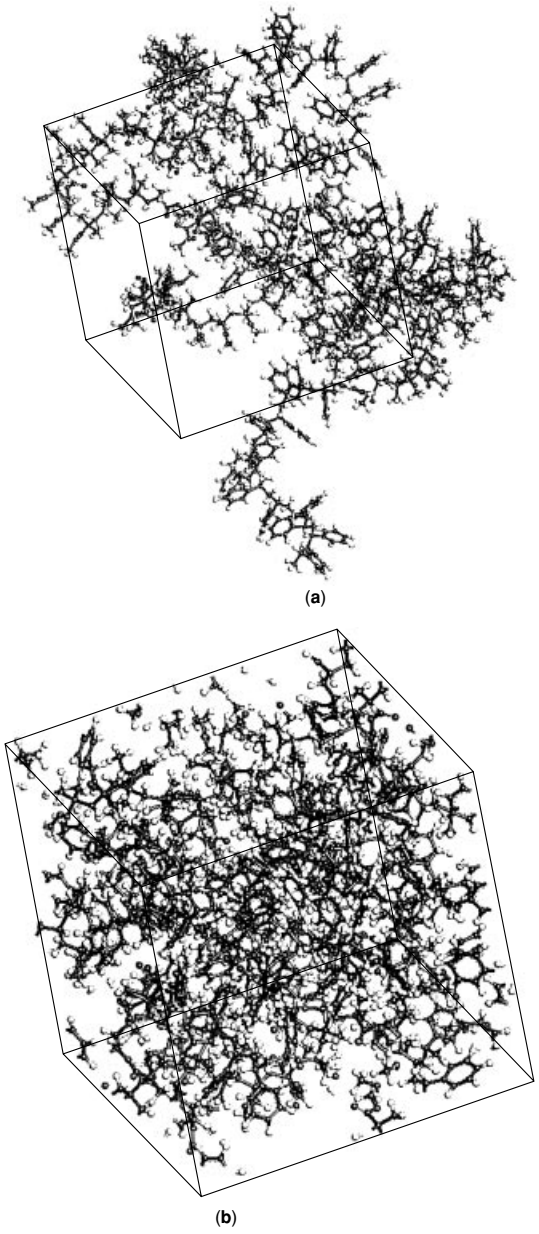

Fig. 1. A molecular model of a condensed phase polymer blend. The example shown is used to study a mixture containing atactic polystyrene 40-mer (2 chains) and atactic poly(methyl methacrylate) 40-mer (2 chains). Figure 1a shows the cell with the molecules configured as they are in space; the parts of the molecules lying outside the cell occupy adjacent cells in the periodic structure. To convey the space filling nature of the construction, Figure 1b shows the same molecules packed in the cell. The model system was constructed using the Amorphous Cell module in the *Materials Studio* software package distributed by Accelrys (103). The amorphous cell system was constructed at a density of 1.12 g/cm^3 at 300 K and the subsequent 80 ps of *NPT* dynamics at the same temperature and zero pressure equilibrated the system to a density of 1.057 g/cm^3.

structure of the polymer of interest. By proper choice of the two parameters (mapping between physical length and bond length on the lattice, and the number of atomistic monomers assigned to one lattice site) involved in this procedure, chain configurations obeying Gaussian statistics can be generated. Unlike other methods that require multistage energy minimization of the initial structures, the structure generated using this approach could be relaxed in a single minimization stage. The authors demonstrated the validity of this technique by applying it to atactic polystyrene to generate structures containing chain lengths of up to 364 repeat units. The X-ray scattering intensities calculated from these structures compared favorably with experimental data. A closely similar method of mapping chains onto lattices so as to make use of rapid Monte Carlo methods for equilibration has been developed by Mattice and co-workers (106,107).

Suter and co-workers (108,109) have more recently developed a slightly different technique for efficient generation of condensed polymer phases. In this method (108), the task of packing the required number of polymer chains at a given density in the simulation box is treated as a geometrical optimization problem. Using a "cost function" that accounts for interatomic overlaps, the geometrical packing problem is solved by approximating the nonbonded interactions between atoms with hard sphere potentials and accounting for the distribution of the torsional angle values given by the RIS model. The initial guess structures thus obtained are then relaxed using a combination of energy minimization and molecular dynamics and a "full" force field. Chain conformations (torsional angle distributions) in structures of glassy polystyrene obtained by this method (109) were found to be in much better agreement with the RIS model predictions than those obtained in the structures generated by Rapold and co-workers (100) using the traditional method.

Periodic Boundary Conditions. The representation of a condensed phase with a computer model requires careful attention to the boundary conditions. Obviously, any simulation is done with a relatively small number of particles (atoms, united atoms, beads, blobs, etc), and falls far short of a macroscopic amount of material. If one were to simply treat this collection of, say, a few thousand atoms as an isolated system, the surface/volume ratio would be quite large, and the properties that were determined would not be representative of the bulk material. The way around this problem is to use periodic boundary conditions, which is tantamount to making an infinite crystal of the model, regardless of whether the "unit cell" has symmetry or not.

In one of the earliest published studies of molecular modeling of condensed polymeric materials, Weber and Helfand (110) used molecular dynamics to simulate a polyethylene melt comprised of infinite length polyethylene chains. In this work, an infinitely long polyethylene chain was simulated by imposing an extra condition on the usual periodic boundary conditions: a random walk polyethylene chain containing appropriate fractions of the trans and gauche states was generated and it was required that the 200th carbon center be bonded to the periodic image of the first carbon center. This technique has not been used subsequently because of other limitations it imposes.

In implementing the boundary conditions for a periodic system, a distinction is made between a "parent" molecule and an "image." A parent molecule belongs to the parent cell if the first atom of the molecule was placed in the cell, regardless

of what happens to the molecule subsequently. For example, during a molecular dynamics simulation, a parent molecule may wander outside the parent cell. Also, this distinction is necessary because it is quite probable that a growing polymer will meander outside the parent cell as it is constructed. This is owing to the fact that the mean-squared diameter of a random coil exceeds the diameter of the domain having the same mass as the chain but the density of the bulk.

The parent cell and its contents are imagined to extend to infinity in all directions. The additional cells and molecules are "images" of the parent. The intramolecular energy of the cell consists of the energy of the parent molecules alone, whereas the intermolecular energy of the cell is calculated for all of the parent molecules interacting with all of the molecules, both parents and images, in the simulation (2). A more complete description of how this is done brings us to the next topic.

Simulation Methods

Molecular Dynamics. The technique of molecular dynamics (MD) is perhaps the most commonly used technique for classical simulations of polymeric materials. MD involves propagating the time evolution of a system of atoms using Newton's equations of motion. The force field for the system, $V(\{\mathbf{x}\})$, constructed using one of the force fields described above, is a function of the $3N$ coordinates, the set $\{\mathbf{x}\}$, of the particles (atoms, united atoms, beads, blobs, etc) in the system. The force f_j on the jth particle is given by the derivative $f_j = -\partial V(\{\mathbf{x}\})/\partial x_j$, and Newton's equation of motion for this degree of freedom is

$$m_j\left(d^2x_j/dt^2\right) = f \tag{2}$$

where m_j is the mass of the jth particle and, of course, t is the time. The forces exerted by the interacting atoms on each other are evaluated from the potential energy at each step in the numerical integration of this set of coupled equations. Given the right-hand side of equation 2, the differential on the left is approximated by a finite difference, and the state of the system is advanced by incrementing the time by an amount Δt, the magnitude of which is at the discretion of the modeler. After each integration step (also known as a "time step"), a new set of spatial positions and velocities is obtained for the particles, and by repeating this process several hundreds, thousands, or even millions of steps, the spatial and time evolution of the system is generated.

A number of different numerical integration methods have been proposed for solving the equations of motion [Verlet (111), leap-frog, Gear predictor-corrector, etc (2)]. Most atomistic simulators prefer the velocity Verlet algorithm, as this integrator preserves the volume element in phase space (112). The solution of a set of differential equations depends on initial conditions, and possibly also on boundary conditions. The method that is chosen for this part of the problem is usually couched in terms of the statistical mechanical ensemble that is used. The microcanonical ensemble holds constant the number of particles, N, the volume of the container, V, and the energy, E, written in shorthand notation as NVE. Of course, integration of the equation of motion within the NVE ensemble requires

specifying the initial state and energy of the system, which includes both potential and kinetic contributions. The kinetic component might be constructed by assigning velocities to the particles of the system with random numbers drawn from a Maxwell distribution defined at a temperature T. Since the total energy is an integration constant of Newton's equations of motion, an accurate integrator will hold the energy constant. Therefore, by monitoring the energy during the simulation, one can determine whether or not the integrator is performing properly.

Other ensembles, notably *NVT* (canonical), *NPE*, and *NPT*, are also used routinely. Since energy is constantly flowing back and forth from potential to kinetic terms in any MD simulation, it is necessary to regularly readjust the kinetic energy in the ensembles that hold the temperature constant. This is required because the temperature is defined by the classical statistical mechanical equation

$$kT = \langle m_i (\mathrm{d}x_i/\mathrm{d}t)^2 \rangle_i \tag{3}$$

where the average, indicated by the angle brackets, is taken over all the particles in the system, and where k is Boltzmann's constant. Thus, to hold the temperature constant, it is necessary to hold the kinetic energy constant. A number of algorithms have been described in the literature for simulations at constant *NVT* (113–116). Somewhat more elaborate techniques are required to hold the pressure constant. In the latter, the pressure of the system is calculated from the virial theorem

$$PV = NkT + \frac{1}{3}\sum_{j=1}^{3N} x_j f_j \tag{4}$$

The *NPT* algorithms of Andersen (113) and Berendsen and co-workers (116) are popular for simulations in this ensemble.

For reasons of numerical stability, the time step used for the numerical integration is determined by the frequency of the fastest oscillating mode in the system, and must be made even shorter for some applications, eg, close to the critical point of a fluid. Most often, the fastest mode is the vibration of hydrogen atoms in the system, and to handle these degrees of freedom requires using a time step of 1 fs or smaller. Clearly, such a small time step places severe restrictions on the total time duration that can be simulated and hence the timescales of the processes that can be investigated using MD. With this in mind, algorithms have been developed for performing MD with bond and angle constraints, eg, SHAKE (117,118) and RATTLE (119), constructed so as to suppress vibrations of the fastest modes in the system. These algorithms permit the use of a much larger time step, but we hasten to point out that in condensed phase simulations the intermolecular collisions ultimately control the size of the time step. The techniques of multiple time steps also offer an alternative for speeding up the simulations by separating out the motion of the faster modes in the system from the slower modes (120). However, this method has not achieved widespread popularity.

Brownian Dynamics. The technique of molecular dynamics simulations described above explicitly accounts for the motion of all of the atoms contained in the system and thus provides a detailed description of the dynamics of the

entire system. For some applications, there exists a large separation in length and timescales of motion of the different components of the system. Furthermore, detailed knowledge of dynamics of only a part of the system is of interest, the case in point being the dynamics of a long-chain polymer immersed in a solvent. The technique of Brownian dynamics (or Langevin dynamics) provides an efficient simulation approach in such a case (2). In a Brownian dynamics simulation, only some of the molecules in the system are treated explicitly, and the remaining components, most often just the solvent, are treated as a continuum. Typically, the polymer chain is modeled explicitly, whereas the effects of the motion of the solvent molecules are accounted for in an average fashion via a combination of frictional and random forces. The basic equation of motion in a Brownian dynamics simulation is

$$m_i \mathrm{d}^2 x_i / \mathrm{d}t^2 = -m\zeta \, \mathrm{d}x_i/\mathrm{d}t + f_i(t) + R_i(t) \tag{5}$$

where the first term on the right represents the frictional force, with ζ being the friction coefficient, the second term represents intermolecular forces between the particles that are being treated explicitly, and the third term represents the random forces. The random forces are chosen from a Gaussian distribution with variance related to the friction coefficient by

$$\langle R_i(t) R_i(t') \rangle = 2m_i kT\zeta \delta(t - t') \tag{6}$$

where $\delta(t)$ is the Dirac delta function. Because the solvent is treated as a continuum, fast modes of motion associated with solvent degrees of freedom are suppressed. This enables larger time steps to be used, which proves most useful for the investigation of long timescale, diffusive processes. Brownian dynamics was one of the very first dynamical methods to be applied to polymer problems, and it continues to find prominent applications that are appropriate for its range of validity.

Nonbond Energy Evaluation. The evaluation of the intramolecular energy of a system from the potential energy is a straightforward sum over all the molecules in the simulation, taken one at a time. The intermolecular energy requires more thought.

The trusted technique for determining the total energy of a crystal is Ewald summation (2). This method is used for amorphous systems as well, except that it is very slow. The boxes used for simulating amorphous systems usually contain thousands of atoms rather than the handful of atoms in the unit cell of a crystal, and this slows down the method tremendously. The routine application of Ewald summation to determine the energies of these large systems is very wasteful of computer time, and many modelers prefer to use faster methods of provable accuracy for amorphous phases.

The pair correlation function $g(r)$ in a monoatomic fluid is different from unity only within a range of about five atomic diameters from an atom at the origin. Roughly the same statement applies to the atom–atom pair correlation functions in polyatomic systems. This observation is put to use in simulations by algorithms that perform discrete sums over atom pairs out to a cutoff distance r_0 from a given atom and replace the remainder of the interactions out to infinity

by an integral with $g(r) = 1$ for $r > r_0$. The latter contribution generates the so-called tail correction. The Lennard–Jones term is the only one to survive this surgery in either an amorphous system or one with high symmetry. This happens for a nonelectrolyte, even if there are dipoles in the system, because the dipolar interactions are generally so weak that orientational correlations are lost very quickly with increasing distance of separation. The result is that the long-range electrostatic contribution averages to zero in either an amorphous system or in a crystal with high symmetry. The prudent modeler will verify that these conditions apply to the system of interest, and will demonstrate that various cutoff distances or Ewald summations give consistent results.

The treatment of charges with cutoffs has to be handled with care also. This is generally done with use of charge groups, which are neutral collections of atoms that travel together. Each charge group has an identified switching atom, usually selected to be near the center of the group. If the switching atom is inside the cutoff, all atoms in the charge group are included in the discrete sum, whereas if the switching atom is outside, all atoms in the group are excluded from the sum. This procedure avoids splitting dipoles, which could create a spurious electrostatic component to the interaction energy of the system.

Clearly, the considerations that need to be applied to electrolytes are somewhat different. However, Debye–Hückel screening for all except the most dilute electrolytes helps to limit the range over which discrete sums of Coulomb terms have to be carried out for amorphous systems, and the cell multipole method can be used to compute the longer range contributions (121). Sometimes it is useful to use cutoffs to propagate the MD simulation, and then use Ewald summations to intermittently evaluate the energy to test that the cutoff procedure is sufficiently accurate.

In general, a great deal of careful thought goes into the calculation of the nonbond interaction energy in molecular modeling, as this step, requiring as many as $O(N^2)$ operations, is the most costly of computer time. The tricks just discussed change one of the factors of N in this order of magnitude estimate to just the number of atoms that are near neighbors to a given atom, which speeds up calculations considerably. However, there is still a necessity to periodically perform the $O(N^2)$ steps that are required to build the neighbor lists for each of the atoms in the cell.

Classical Mechanics vs. Quantum Mechanics. The problems to MD that are posed by the equipartition theorem of classical statistical mechanics are best described in the context of the crystalline phase; polymer crystals have been of interest to modelers as a route to an understanding of the relations between phonon spectra, quantum corrections, and related issues. The vibrational modes of models of united atom polyethylene (PE) particles and crystals have been examined from time-averaged Hessian matrices, using eigenvalue methods to extract the phonon spectra (122). More conventional approaches to the study of PE crystals have been reviewed by Rutledge and co-workers (123), who show that quantum corrections to vibrational modes are very important. When doing a classical simulation with an all-atom force field, the equipartition of energy results in too much energy going into high frequency motions of hydrogen atoms. The result is that MD simulations on explicit atom systems containing light elements give too large heat capacities.

Methods to apply quantum corrections for this inadequacy of classical mechanics when applied to crystals, as well as other phases, have been explored (124–127), but there is not yet general agreement on how best to calculate thermodynamic properties for these types of systems. The practical solution of Berens and co-workers (124) entails "... calculating the velocity spectrum $S(\nu)$ from molecular dynamics and then integrating $S(\nu)$ over all frequencies with a weighting function which is the difference between the quantum and classical harmonic weighting functions for the thermodynamic variable of interest." However, as the statement avers, anharmonic contributions to the vibrational modes will not be captured correctly; this relatively minor shortcoming was addressed by Hardy and co-workers (128).

Molecular Mechanics. The term molecular mechanics (mm) refers to subjecting a model structure to energy minimization. If this is done for a crystal, the structure that is obtained is uniquely defined by the symmetry group. Such is not the case for an amorphous system. Instead, when the energy of a random system is minimized, the system falls into the nearest local energy minimum, and the structure that is obtained is but one member of an ensemble of a large number of similar structures. In a typical application of molecular mechanics to amorphous polymers, a molecular model of an amorphous phase of the polymer of interest is prepared at the experimental density and temperature of interest. The model is then minimized with respect to potential energy using a force field while holding the volume constant. In this minimized structure, the thermal motion of atoms is accounted for only in an average fashion via the volume available to atoms at the specified density. The minimized structure thus provides a 0 K representation of the polymer of interest at the experimental density—a state of suspended animation. One application of such a model to an amorphous system was the calculation of the vibrational spectrum of bulk isotactic poly(methyl methacrylate)(PMMA) from the Hessian matrix for the minimized system (129).

Another use of a calculation of this kind is to perform averages over configurations when the property of interest is primarily determined by energetic, rather than entropic, terms. A collection of several structures is built and minimized, and calculation of the property of interest is obtained as a simple arithmetic average of the value of the property for the individual structures. More sophisticated averages can also be constructed (130).

As discussed in the earlier section on Construction Methods, the technique of molecular mechanics has been used for investigating structural properties of glassy states of various polymers (70,96–100,131). In spite of the approximations mentioned above, ie, the absence of thermal motion of the atoms, these studies showed that the structural properties, such as X-ray scattering structure factors, radial distribution functions, etc, of the glasses can be very well represented by the simulated structures.

In addition to these methods, Boyd and Pant (70,131) presented a molecular mechanics method for generation of polymer glasses starting from a well-equilibrated polymer melt structure. Recognizing that densification is a key feature during vitrification of a polymer melt, they developed an energy minimization method in which periodic box dimensions were treated as variables, thus allowing the system density to change during the process of glass formation. Using this technique, the authors subjected a well-equilibrated PE (*n*-tetracosane) melt

configuration to energy minimization to generate the desired polyethylene glass structures. It was found that the specific volume of the system decreased by about 10% in going from the melt to the glassy state. The structures thus generated were considered to be polymer glasses at 0 K temperature. The calculated mechanical properties, eg, shear modulus, of these glasses showed reasonable agreement with the experimental values.

In addition to the investigation of static, equilibrium properties, the techniques of molecular mechanics have also been used for the investigation of dynamic properties of the polymeric materials. A number of dynamical processes, such as conformational transitions and penetrant molecule diffusion in a glassy polymer, occur on longer timescales than can be readily accessed with MD. Some of these processes can be studied using transition state theory with the help of molecular mechanics techniques (132). An intrinsic assumption in transition state theory is that the process of interest occurs on a much longer timescale than other processes in the system (typically those associated with random thermal motion or vibrations). In other words, the process of interest should have activation energy that is much larger than the thermal energy kT. In this approach, a reaction coordinate (a reaction path connecting the transition state with the stable configurations on either side) is first defined on the potential energy surface for the process of interest. Evaluation of the energy of interaction of, say, a diffusing molecule with the stationary polymer at grid points serves to identify energetically favorable neighborhoods where the diffusant is mechanically stable as well as the lowest energy paths that can be traversed in traveling from one neighborhood to the next. The point of highest energy on the path determines the transition state, which suffices to estimate the diffusion coefficient.

Monte Carlo. The method of MD simulations described above is a general, deterministic technique for the investigation of material properties. However, when applied to polymeric systems, MD simulations can probe only limited volume of the accessible phase space for these systems because of the long relaxation times involved. As a result of this, MD is generally restricted to relatively short timescale behavior, and is not a very efficient method for sampling configuration space. The technique of Monte Carlo (MC) simulations provides a solution to this problem; if cleverly designed, these can be used for efficiently sampling the phase space accessible to the material of interest. The disadvantage of MC is that it is not a true dynamical method, and so cannot directly provide time-dependent phenomena.

MC simulation is a stochastic simulation technique. The basis of the method lies in the evaluation of integrals by stochastic methods (2). A typical ensemble average in statistical mechanics involves a multidimensional integral over the configuration space. It is not possible to evaluate such an integral numerically by the traditional methods of numerical quadrature, but Monte Carlo methods provide an efficient approach for calculating these quantities. A typical MC simulation proceeds as follows: starting with an initial configuration of the system, the configuration is changed by applying a perturbation to the system (known as a "Monte Carlo move"). This "move" or the new configuration is then either accepted or rejected according to a probability chosen from a prescription. The key to devising an efficient MC algorithm resides in developing a prescription such that the sampling of the quantity of interest (the integrand) is concentrated in the region of phase space that makes important contributions to the integral.

The fundamental idea of the MC method was clearly described in the seminal paper by Metropolis and co-workers (93). In this method, static structures are evolved from one to another by moving one or more atoms to new locations. A move is accepted unconditionally if the new configuration, the nth, has a lower energy (E_n) than its predecessor (E_{n-1}), and is accepted with probability if $\sigma = \exp[-\beta(E_n - E_{n-1})]$ if $E_n - E_{n-1} \geq 0$. This condition is enforced by comparing the Boltzmann factor σ with a random number x lying in [0,1]. If $\sigma \leq x$ the new configuration is accepted; if it is rejected the preceding configuration is counted again before generating another move. A sequence of moves will thus generate a family of configurations that occur with probability equivalent to a canonical ensemble for the family. If information is available on the number of states of equal energy, these entropic factors are included in the acceptance criterion (133).

A well-constructed MC method is generally more efficient for equilibrating systems than is MD. However, there is no temporal causality in MC simulations, so they cannot be used directly for dynamical (transport) properties. Nonetheless, several authors map properties between MC and MD, and thereby establish an equivalent time step corresponding to an MC step (134,135). It will usually be the case that the equivalent time step will be system and property dependent, and may be different for different properties depending on the nature of the allowed moves. Furthermore, a wide variety of MC methods abounds. One of these mixes large MC steps with MD to alleviate the bad overlaps (136,137). The types of moves that one chooses, and the number of atoms to be moved in each step is arbitrary; there are no general rules that guide the choice of these parameters. MC moves are not difficult to construct and implement for simple models, for example, moving beads between neighboring 2-D lattice sites for isolated chains (138). Another example of a model allowing simple moves is the RMMC method of Honeycutt (139). Since the model that is being solved satisfies essentially the same conditions as RIS, a move in the algorithm makes a large change of a single torsion angle selected at random along the backbone of the chain. (This is a "pivot algorithm" (140), which was invented by Lal (141) for the excluded volume problem.) Even though the ends of chains swing through wide arcs when this is done, the absence of interactions between topologically remote neighbors permits a substantial acceptance of moves, so that the method is very effective in generating allowable configurations for chains *in vacuo* (or without explicit solvent). Other types of moves in torsion space have been developed (142), but the applications have been largely restricted to isolated molecule simulations. MC studies of the limited extensibility of isolated polyethylene chains have been used to infer important limitations to the enhancement of physical properties from processing (143), showing that very important conclusions can be drawn from more facile simulations than are required for a complete description of the condensed phase.

For simple fluids, eg, water, the MC moves consist of translation or rotation of individual molecules. These types of MC models are doomed to fail for a condensed phase, as the large motions almost certainly lead to unacceptably large overlap energies. For more realistic models of condensed phases, a considerable research effort may be required to determine the moves that yield an acceptable acceptance ratio (relative number of successful to unsuccessful moves). For polymer melts the moves have to be cautiously constructed, and may involve small atomic displacements (126,127,134), concerted (crankshaft) rotations (15,135,144), or cutting and

gluing (145,146), of which the so-called slithering snake moves (23,24,133,147,148) are an example.

In some of the early MC work on polymers, the move termed "reptation" (now preferably called "slithering snake" so as to avoid confusion with the de Gennes/Edward reptation concept) was widely used. A typical slithering snake move involves deleting a backbone atom (together with attached atoms) from one end of a polymeric chain and adding it to the other end of the chain. The move thus results in a serpent-like motion of the chain where the chain appears to move along its contour. Such a cut/splice move was used by Vacatello and co-workers (94) and by Boyd (23) in their MC simulations of polyethylene. The slithering snake move works well for short chains (containing up to about 20–30 carbon atoms), but for long-chain polymers it alone is inefficient in relaxing the internal parts of the chain and hence new moves need to be devised for such systems.

Continuum Configuration Bias. A major breakthrough in this regard was made by the development of the Continuum Configuration Bias (CCB) move (149–151). The CCB move consists of cutting a segment of any length from one end of a chain and regrowing it to yield a different configuration. During this regrowth process, several potential positions for each bond that is being added are considered and one of these is chosen using a prescription that favors (or biases) the lower energy configurations. The bias thus introduced in the process is removed subsequently in the probability that is used for accepting or rejecting this new configuration (or the MC move). Using such CCB moves, de Pablo and co-workers (151) simulated a system containing polyethylene chains consisting of 60 segments each. These authors showed that the simulated density–temperature behavior of this system was in reasonable agreement with the experimental data.

Monte Carlo Moves for Long-Chain Polymers. The CCB move, though efficient, also operates on one end of the chain. For systems containing very long chain polymers, the CCB move is not very efficient in relaxing the internal parts of the chain. Motivated by this, several new MC moves have been proposed in recent years for efficient relaxation of the condensed phase consisting of long-chain polymers in an MC simulation. Prominent amongst these are the "end-bridging" and the "concerted rotation" moves devised by Theodorou and co-workers (145, 152). The end-bridging move involves attaching a chain end to an internal segment of another chain by a trimer bridge, and in the process creating a new chain end on the second chain by removing a trimer segment adjacent to the newly formed bridge (145). The move thus alters the chain connectivity and leads to large jumps in the configurational space of the bulk polymer. The "concerted rotation" or the "intramolecular rebridging" moves involve selecting an internal part of the chain (consisting of five segments) and changing its internal conformation while leaving the rest of the chain unchanged (145,153). Recent work carried out by Mavrantzas and co-workers (152) has demonstrated that a combination of these moves can be used to efficiently equilibrate a polyethylene melt consisting of chains of lengths up to 500 methylene units, modeled in atomic detail, which is a feat not possible with any other MC or MD simulation. Recently, a few additional methods have been developed for enabling efficient equilibration of internal parts of the chain (and also simulation of cyclic molecules). Some examples include the "Self-Adapting Fixed-End-Point Configurational-Bias Monte Carlo" method developed by Wick

and Siepmann (154) and the "Rebridging Configurational-Bias" method developed by Chen and Escobedo (155).

Sadanobu and Goddard (156) have used a Continuous Configuration Boltzmann Biased Monte Carlo calculation of the free energy of two "independent" united atom C_{100} chains from very dilute vapor up to about 70% of physical density. While these are longer chains than are typically attainable with CCB methods, the densities of the Sadanobu and Goddard systems are generally lower.

Jorgensen and Tirado-Rives (157) have also used a united atom model for hexane to compare the rates of convergence to equilibrium of MC and MD methods. They conclude that the two methods give the same results, but that the MD is some 1.6–3.8 times slower than the MC. This result is consistent with the widespread use of MC to equilibrate polymer systems; if MC were not more efficient there would be little reason to use it. Of course, the disadvantage of MC is that dynamical processes such as diffusion cannot be evaluated without calibration relative to an absolute method such as MD. And this only for the case of "dynamical MC." For other types of MC algorithms, especially those in which cutting and splicing moves are invoked, the possibility of calibrating dynamical properties seems to be forfeited altogether.

Gibbs Ensemble Methods. The investigation of phase equilibria of polymeric systems by molecular simulation was made possible by the development of the technique of Gibbs ensemble simulation by Panagiotopoulos (158,159). In the Gibbs ensemble simulation method, the two coexisting phases are simulated simultaneously in separate simulation boxes. An *NVT* Gibbs ensemble simulation is carried out as follows: The phases in the individual boxes are equilibrated in a fashion analogous to the usual MC simulation by carrying out several types of equilibration moves (molecule translation, rotation, hybrid MC move, etc) and accepting or rejecting these according to a Metropolis criterion. In addition, mechanical equilibrium, ie, constant pressure, is maintained between the two boxes by implementing a volume swap move in which the volume of one of the boxes is changed by a certain amount accompanied by an equal and opposite change in the volume of the other box. Finally, various molecular species in the two simulation boxes are maintained at the same chemical potential by implementing a particle swap move, ie, a randomly chosen molecule is removed from one of the boxes and is inserted at a random location in the other box. Thus, the coexisting phases will be at the same temperature, pressure and all of the molecular species will have equal chemical potential in both of the boxes.

Such an *NVT* Gibbs ensemble method has become a popular tool for investigating the pure component vapor–liquid equilibrium of simple molecules and polymeric species. The technique has been used for simulating the vapor–liquid equilibria of simple gases such as nitrogen (160). The *NPT* variant of this technique has been widely used for the simulation of vapor–liquid and liquid–liquid mixture equilibria. The applications of this technique can be found in studies of the vapor–liquid mixture equilibria of methane, ethane, and carbon dioxide (161) as well as of nitrogen and butane mixtures (160).

As usual, a problem arises when the Gibbs ensemble technique is applied to a system consisting of polymeric molecules. In particular, when a chain molecule is removed from one box and an attempt is made to insert it into the other box (the "particle swap" move described above), the new configuration almost always

precipitates large interatomic overlaps, and the move will almost never get accepted. The problem can be overcome by combining Gibbs ensemble simulations with the CCB Monte Carlo method described above (162). Thus, instead of selecting a random conformation for the chain molecule being inserted in the other box, its internal conformation is chosen using the prescription given by the CCB method which favors low energy conformations, which in turn, increases the probability of acceptance of such a move. Such an approach has been widely used in the literature in recent years and has proved to be successful in predicting the phase equilibria of a wide array of low to medium molecular weight chemical species.

Histogram Reweighting. A conventional simulation yields values of various properties at the thermodynamic state at which the simulation was carried out. The technique of histogram reweighting (163,164) provides a methodology for extrapolating these results to other thermodynamic states that are in the vicinity of the state point at which the original simulation was run. In this method, the data, eg, distribution of values of various properties such as energy, obtained from a simulation are stored in histograms, and statistical mechanical relations are used to extrapolate these results to other thermodynamic states. The actual procedure involves reweighting of the stored histograms. Thus, by carrying out a selected number of simulations, thermodynamic properties over a range of state parameters can be obtained. This approach has been used by Panagiotopoulos and co-workers (165) to simulate the phase equilibria of lattice polymers and by Conrad and de Pablo (166) for simulating the phase equilibria of water. Histogram reweighting grand canonical MC simulations were used by Errington and Panagiotopoulos (167,168) for developing model parameters in their potential model for *n*-alkanes, benzene, and cyclohexane. It is to be expected that the technique of histogram reweighting, in combination with other simulation methods, will be used widely in future applications of molecular modeling to polymeric materials.

Parallel Tempering. As has been emphasized repeatedly, polymers present two problems to a molecular modeler: the long timescales associated with various relaxation processes and the algorithmic difficulties in efficiently carrying out configurational changes. Efficient sampling of the configuration space is thus always one of the main obstacles in the molecular modeling of polymeric materials. The technique of "parallel tempering" (169,170) provides a way for overcoming some of these sampling problems. In this method, several replicas of the system that do not interact with each other are simulated simultaneously by either MD or MC at different state points, eg, at different temperatures. The key step in this approach consists of an MC move where an attempt is made to swap the replicas at two different state points. Such an attempt is then either accepted or rejected using a criterion analogous to that used for accepting or rejecting a move in a conventional MC simulation. Bedrov and Smith (171) have demonstrated that parallel tempering provides a huge speedup over conventional MD simulations for the conformational relaxation of polymer melts. The reasons for this fast relaxation are twofold: each replica relaxes at a faster rate by virtue of having visited a state point where relaxation is fast (typically, a high temperature), and secondly, the calculated averages at each state point converge faster by having received contributions from several uncorrelated replicas of the system (171). Yan and de Pablo (172,173) have further extended this approach by combining the expanded

ensemble simulations with multidimensional parallel tempering, which they call "hyperparallel tempering." These authors showed that the hyperparallel tempering method provides a large speedup for the determination of the phase equilibria of very long chains modeled on a lattice (173). It is expected that these methods will also be used increasingly in the coming years for tackling problems in polymer science and engineering.

Bond Fluctuation and Other Lattice Methods. The bond fluctuation method (BFM) (174) and related lattice methods (175) have enjoyed considerable popularity because they are quite effective for equilibrating polymers. It is often the case that polymers, just as with small molecule systems, come to a state during an MD run in which the energy and volume appear to be relatively constant (within the usual fluctuations), but yet the chain configuration distribution function has not reached equilibrium. The only way to determine whether the latter condition is satisfied is to perform a sufficiently large simulation so that the population of chain configurations yields mean square values, eg, radius of gyration or end-to-end distance, that are consistent with either experimental values ("unperturbed" dimensions from neutron scattering, for example) or an RIS/RMMC calculation. The primary advantage of the BFM is that equilibration in this sense is relatively easy to achieve. However, the price that one pays for global equilibration of the chain configurations is essential loss of chemical information. As a result, the method has been primarily used for problems involving the generic physics of polymers. The several different MC techniques have been reviewed by Leontidis and co-workers (134).

A simple cubic lattice is used in BFM simulations, with statistical segments of the polymer occupying 2^d lattice sites in a d-dimensional simulation. The chains have great flexibility, in that the bonds that connect neighboring segments are allowed considerable bending and stretching freedom. However, the bond lengths are limited so as to prevent crossings. This is economically achieved by the multiple contiguous site occupancy for the elementary units of the chain and by limiting the length of bonds: Chains are prevented from crossing one another because the bonds restrict the spacings between the occupied sites so that neighboring sites cannot pass. As is usual in any lattice method, a significant fraction of unoccupied sites (approximately 50%) is required to allow movement.

The Binder group especially has treated a number of physical properties with the BFM method (4,176–178). It is not uncommon for these simulations to cover seven decades in "time," which enables one to explore slow relaxation processes such as those encountered in polymers close to the glass temperature. Here, as in all MC methods, an equivalence between MC moves and a time interval is either assumed or established by comparison with MD or experiment. Several different types of MC moves can be used with the BFM model, including both slithering snake and random hopping. Scaling laws, glass transitions, molecular diffusion, and entanglements are susceptible to investigation with the model.

Other Generic Models. The lattice methods that have been briefly considered are but one example of what we are calling "generic methods." These methods lose atomic detail through a coarse-graining procedure or ad hoc parameterization. The traditional Rouse spring-bead model is an example of this type of model. Clearly, a description of this kind is useful only to the extent that the properties one seeks to describe are generic. Thus, the Rouse model has been extremely

useful in understanding the universal aspects of the dilute solution viscoelastic behavior of flexible polymers (179).

Another model of wide applicability is the Ising lattice model. The RIS theory is an Ising model in one dimension; the model has been applied to other types of problems in spaces of two and higher dimensions. A recent 2-D model was developed to gain an understanding of the distribution of surfactant molecules in immiscible fluid systems (180).

One of the most successful recent applications of a generic model to a complex polymer problem is in the area of the microphase separation behavior of block copolymers. A highly successful self-consistent field theory describing the equilibrium phases and phase diagram of diblock copolymers was devised by Matsen and Schick (181), and this was extended to ABA triblocks by Matsen (182). Drolet and Fredrickson (183,184) have devised a modeling method to generate phase-separated patterns from a self-consistent field theory that does not require the assumption of a space group as required in the Matsen–Schick method. While the published work (183,184) reports two-dimensional (2-D) simulations only, the method shows promise of being very powerful in designing block copolymer architectures.

Many mean field or self-consistent field theories that use the computer for evaluation of functions fall outside our definition of modeling. The Drolet–Fredrickson method is at the borderline of our definition of a simulation method: it qualifies as a modeling method because it uses a random starting point based on underlying coupled fields (playing the role of concatenated particles) and evolves into a regular structure whose pattern may (conceivably) depend on the initial stucture in a way that cannot be anticipated from the initial data of the problem. Having said that, a dynamics method is required for these systems if one wants to study the time-evolution of the structures from, say, the homogeneous melt to the phase separated state.

Mesoscopic methods that link together a dynamical method, such as Langevin or Brownian dynamics, with the mean-field description of the free energy have been developed for this purpose. The sizes of the domains that are formed in microphase-separated block copolymers are comparable to the lengths of the homopolymer blocks, which implies that any finer detail than is contained in a coarse-grained or mean-field model will be computationally impossible if an attempt is made to model more than a few separate domains. A desire for detail notwithstanding, if the domains are amorphous, a description of their properties at the level of a coarse-grained model is sufficient with respect to the phase separation problem. Techniques that operate at this level of description include MesoDyn (185–187), Langevin methods (188–190), dissipative particle dynamics (DPD) (191–194), and a variety of coarse-grained MD and lattice methods (20, 144,148,195–197). The power of these methods resides in their ability to handle length and timescales that are appropriate to the problems that they are designed to address. In making this observation, it should also be clear that coarse-grained models will not necessarily yield all thermodynamic and/or transport properties with equal fidelity (198). The same is true of atomistic force fields, which reaffirms the wisdom of checking the results of any modeling study with many different properties if accuracy of quantitative predictions is an issue. General approaches to multiple length and timescale problems have been reviewed (199).

The study of the block copolymer morphologies has been intense, and highly sophisticated models have been developed to describe their large-scale structure. In particular, domain distortions have been treated with higher order Ginzburg–Landau models (200). Furthermore, MesoDyn (186) and DPD (192,201) can be used to study these systems under shear flows; different morphologies have very different viscosities, and can be interconverted under shear. The development of structure in block copolymer systems is paralleled by phase separation in binary mixtures with chemical reactions (202), which exemplifies the universality of phase ordering. However, the reacting systems apparently do not order to the extent that polymeric systems do.

A problem area that is not so amenable to mesoscale methods is polymer crystallization. This has proven to be one of the most difficult computational challenges in all of polymer science because the pertinent phenomena operate simultaneously over a wide range of length scales. The polymer crystallizes into a particular space group because of atomic detail, and the mechanical properties of the crystallites are determined by, and can only be calculated reliably with, atomic force fields with all atoms represented (126,127). Yet the size of the crystallites or spherulites is so large as to require mesoscopic methods for comprehension. But a crystalline polymer is almost never 100% crystalline. The interphases between crystalline and amorphous domains, with the possibilities for adjacent or nonadjacent reentry and tie-chain distributions, are critical to the properties of semicrystalline polymers. Only recently have models been developed (203) to rigorously address this problem area.

The crystallization of isolated polyethylene chains was first reported by Kavassalis and Sundararajan (204) using MD with the Nosé–Hoover thermostat. More recently, single polyethylene chains driven by Langevin dynamics have been used by Muthukumar and co-workers (205,206) to model the early stages of nucleation and growth of crystals in solution. But even simpler models of chains will form ordered domains, and hence they have been explored as a means to understand some of the aspects of crystallization (122,138). A lattice model has been used in conjunction with an MC technique to model crystallization in short polyethylene-like chains (207). The crystallite–amorphous interface is found to be rough, and to have a relatively low concentration of regular folds for even this lattice model.

An interesting block stacking algorithm based on the Sadler–Gilmer model of crystallization was developed by Goldbeck-Wood (208,209), with a variation on the algorithm being described by Doye and Frenkel (210,211). One starts with a uniform wall of blocks from which blocks are removed and restacked one at a time by kinetic MC moves with free energy terms that are determined by the number of contacts with neighbors. Chain connectivity is emulated by restricting the location of movable blocks to terminal stems or to "sliding diffusion" (209) in the interior of the crystallite model. Good agreement with experiment is claimed for a number of polymers (208).

The aggregation of polymers and surfactants has been studied with DPD (212). This algorithm provides an alternative to Langevin or Brownian dynamics, and can even be used with Widom insertion (212). The ad hoc potential that is used in DPD is not unlike a soft ellipsoidal model for polymer molecules (213,214), which suggests that DPD could be extended to polymer melts. Along these lines a

"blob" model that incorporates an algorithm to check for and manipulate uncrossability has been developed very recently (215). It is shown that the incorporation of entanglements by means of the algorithm has a significant effect on the dynamics of the system.

A method that has some similarity to DPD has been developed by Yuan and Doi (216). While restricted to two dimensions in the published work, the extension to three dimensions should be relatively straightforward if computationally demanding. They model a two-phase viscous fluid by means of a Voronoi tesselation, with discretized versions of continuum hydrodynamics serving as the equations of motion that motivate the centers and vertices of the tesselation polygons. Simulations under shear show that the dispersed phase elongates under flow, with the deformation of droplet size equilibrating at strains (not strain rates) of between 5 and 10. A refinement of this model was presented by Okuzono and co-workers (217), in which the continuum hydrodynamic equations are augmented with a Cahn–Hilliard theory for the interfacial structure. Two-dimensional simulations showed the coalescence and break-up of droplets. These simulations have not been extended to polymeric fluids, except insofar as they can be modeled as high viscosity Newtonian fluids.

Orientational orderings of liquid crystal domains, including dislocations and grain boundaries, are most often modeled on a lattice where a simple potential depending only on the mutual orientations of site vectors (218,219) is needed to generate interesting structures.

Theories for polymer networks have their basis in treatments of gelation and rubber elasticity (220). Cross-linked systems can be investigated with coarse-grained and atomistic MD methods (221–225). However, these methods cannot capture the effects of long-range connectivity, which are better analyzed with very coarse-grained MC methods (226–234). There are theoretical methods that compete with simulations (235–237), but these methods are usually not concerned with spatial correlations to the same extent as simulation methods. The Grest–Kremer group (225) has devoted considerable effort to understanding the role of entanglements, constraints, and cross-links on the mechanical properties of model elastomers. In these simulations, FENE chains interacting with a purely repulsive potential were subjected to step strains, following which the stress relaxation was monitored. The results were analyzed with theory to separate the entanglement and cross-link contributions to the stress. An even coarser ad hoc model was used by Masubuchi and co-workers (238) to model reptation in an entangled melt. Mechanical models of elastomers are also subject to investigations with modeling (239). The review by Burkhart (240) contains an extensive survey of modeling results on rubbery polymers.

A dynamical cross-linking simulation using the bond fluctuation model has been developed by Gilra and co-workers (241,242). They find a strong dependence of network properties on equilibration times, leading them to conclude that a 20% excess of cross-linker results in optimum properties. This conclusion is different from the assertion that balanced stoichiometry yields the best networks, as obtained both with statistical methods as well as the static MC method (226). As the authors point out, this may reflect slow relaxation of network systems beyond the gel point. The more "perfect" the network, the slower it will appear to relax because there are fewer fast-moving defect structures.

Group Additivity Methods. It is frequently desirable to rapidly explore or estimate the properties of materials in advance of more elaborate experimental or modeling studies. Group additivity, or QSPR (quantitative structure property relation), methods are widely used for this purpose. The standard reference for this material is the book of van Krevelen (243), which makes use of common atomic groups, eg, esters, aldehydes, methylenes, etc, and tabulated properties assigned to each. A related treatment is the "group interaction model" of Porter (244). The comprehensive method advocated by Bicerano (245) utilizes connectivity indices (derived from graph theoretical concepts) rather than atomic groups to encode structural information. The advantage of this method is that predictions can be made for molecules having novel structures that have not been synthesized, making it particularly useful for estimating the properties of polymers falling outside the norm.

More recent extensions of QSPR methods to more complex phenomena, such as the viscosity of dispersions (246) or diffusion of gases through polymers (247), have been developed. These works should be consulted for more penetrating bibliographies of literature in this field.

Applications

Modeling in the Service of Theory. There are many examples of recent "analytical" theories that have been developed, tested, or validated with MD or MC simulations. If simulations are used to validate theory, one might ask why make theories at all? The reasons are that (*1*) a good theory implies a level of understanding of the problem that the scientist or engineer aspires to, (*2*) evaluation of a theoretical equation, even if done with a computer, usually gives answers faster than a simulation, but most importantly (*3*) there are length and timescale problems that cannot be reached with straightforward MD or MC, and which require fresh theoretical approaches for their solution. The use of simulations to test and develop theories is especially helpful in those cases where the theory is difficult to compare with experiment or when the theory requires mathematical approximations whose validity is difficult to assess by other methods.

Baschnagel and co-workers (176,248) have emphasized this aspect of modeling in their study of the Gibbs–Di Marzio (249,250) and other theories of the glass transition. Simulations led to the resolution of the negative entropy anomaly in this theory by showing that a higher order approximation to the configurational entropy of the chains is needed.

Theories of the excluded volume expansion factor for polymers have a long history, and as discussed elsewhere, this problem led to some of the earliest applications of computer models to polymers. More recently, Krishnaswamy and Fixman have used simulations to verify a theoretical treatment of the expansion factor for polyelectrolytes (251).

The structure of a diblock copolymer confined between surfaces has important consequences for the properties of filled block copolymer systems. Because filled polymers are very complex heterogeneous materials (perhaps anisotropic as well), it is desirable to have a theoretical description of the properties of the

separate phases to put into higher level theories. The behavior of the polymer in this kind of environment is difficult to determine by experiment, but is quite amenable to lattice simulations (252–254) which are used to validate both density functional theories as well as simpler phenomenological theories.

Polymer miscibility—with solvents, other polymers, or in block copolymers—can be treated with integral equation methods such as PRISM (255–257) or density functional theory (252,258). Theories of this kind inevitably required approximations that are difficult to assess by independent methods, with the variety of closure relations having been developed in integral equation theories (259) illustrating the case in point. Molecular modeling can provide the detailed molecular-level information, such as pair correlation functions, that is needed to assess the validity of these types of theories (260,261).

A MC study (262) of two different types of relatively short chains on a lattice, with solvent molecules represented as vacancies, was used to explore phase separation of the UCST type; the conclusion was that the Freed–Dudowicz lattice theory (263,264) gives good agreement with simulations. A similar lattice model was used to investigate the behavior of chains tethered to a surface, with the MC results being compared with numerical self-consistent field theory (135). The essential identity of density profiles obtained by the two methods was taken to validate the self-consistent field theory.

The role of positional fluctuations in polymer networks is central to some theories of elasticity, and has been investigated with an MC method based on a modified bond-fluctuation model (265). The simple model used in the simulations gave results close to those calculated from theory for a Bethe lattice (also known as a Cayley tree). More extensive results bearing on the role of fluctuations in polymer networks have been reported by Grest and co-workers (225). They find that entanglements limit fluctuations, giving behavior similar to the description provided by the tube model.

Filled Polymers. Filled polymers are difficult to model directly for much the same reasons as semicrystalline polymers. The behavior of these systems develops over a wide range of length scales, which generally requires the modeler to select a scale that is believed to be the most appropriate for the phenomena of interest, and this scale determines the nature of the model. The influence of filler particles on chain configuration statistics has an impact on rubber elasticity, and so an MC calculation with the RIS model is appropriate for these investigations (266). Some MD work with a model of large spherical particles together with 1,4-*cis*-polybutadiene has been reported (267), but the simulations were done without periodic boundary conditions, resulting in the collapse of the chains.

Nanoscopic particles, dispersed in a block copolymer, have dimensions that are appropriate for Brownian dynamics simulations (268). Clay composites have a range of length scales, but if the gallery spacing between the layers is not large, MD methods can be used (269) with periodicity in the directions parallel to the clay platelets. However, continuum mechanical models need to be invoked for the description of exfoliated clay systems (270). These materials have so much interfacial area that adhesion properties are very important (271). Traditional continuum bounds methods (130) usually ignore the interphases on the grounds that they comprise a very small volume fraction of the total material, and so are not expected to be very accurate for exfoliated clay systems.

In the work of Wang and Teraoka (272), a lattice model was used to determine the partitioning of chains between bulk solution and a confined slit. They found that a "blob" description fit the simulation data well as the concentration of chains in the slit increased. For dilute chains, the end-to-end distance is the right correlation length to use in determining the partitioning of chains into a slit, but as the concentration increases the interaction between backbone segments is screened, and the configurational entropy becomes sensitive to more localized length scales. Block copolymer morphology in confined geometries was investigated by Wang and co-workers (273).

Fiber-reinforced systems have been modeled with use of an MC method to place parallel fibers into a polymer matrix, with a finite element algorithm (FEA) then being used to compute elastic properties (274). A generic meshing algorithm for use in FEA studies of nanoparticle reinforcement of polymers has been developed (275) and applied to the calculation of mechanical properties of whisker and platelet filled systems. The method should be applicable to void-containing low dielectric materials of such great utility in the semiconductor industry.

Disordered systems of rods have also been modeled with MC (276), and the Onsager–Flory transition to an anisotropic phase was observed. Chain configurations and surface energies of individual polymeric nanofibers have been investigated with Mattice's 2nnd lattice method (277). In short, methods exist to treat, say, cord-reinforced tires from atoms up to FEA on the whole tire.

An exception to difficult-to-model filled systems is provided by the norbornene-POSS polymers studied by Bharadwaj and co-workers (278). POSS is polyhedral oligomeric silsequioxane—groups that are pendant from the poly(norbornene) chains of the model. This can be viewed as a filled system, but one in which the filler is nanoscopic and chemically bonded to the chains. The simulations were done to determine T_g, density, thermal expansion, solubility parameter, POSS mobilities, and elastic moduli in a wide-ranging study. They conclude that the "ponderous nature of the POSS moieties" is largely responsible for the reinforcing effect.

Chemical Reactivity. An adequate coverage of molecular modeling applied to the chemical reactivity of polymers, which includes polymerization, chemical modification, and degradation (qv), could only be achieved in a separate article. For present purposes, it suffices to recommend a few recent studies that will provide gateways to the larger literature on these important topics. This excursion will not lead us to stray from molecular modeling for very long, because a thorough treatment of chemical reactivity requires primary attention to QM methods, and that would indeed divert us.

Zirconocene catalysts provide an unprecedented level of control over polyolefin structure, and this suffices to generate a high level of commercial interest in the substances. The structural variation within this group of catalysts is very wide, which has made them an attractive target for modeling. From the early work of Castonguay and Rappé (279) to more recent studies (280,281) the mechanism for the stereochemical control of the reaction has been thoroughly investigated with quantum chemical methods. Complementary theoretical work to determine rates of polymerization with use of transition state theory has also been presented (282). Zeigler–Natta catalysts also continue to be of interest (283).

One important class of modification reactions on polymers is those that induce cross-linking. Studies of the kinetics of end-linking reactions with a generic polymer model using proximity bonding have been conducted by Grest and co-workers (284) with the aim of relating stoichiometry to the relative rates of formation of network defects. A proximity bonding algorithm was also exploited by Doherty and co-workers (285) to study the structure of methacrylate networks. Jones and co-workers (286) have investigated cross-linking reactions, but with a greater emphasis on an atomistic understanding of radical stability and bonding probabilities for various groups. An interesting study of the technologically important imidization reaction of polyamic acids that combined quantum chemical calculations with MD was carried out by Young and co-workers (287). The further development of a general-purpose reactive force field, such as that initiated by Rappé and co-workers (87), would be a welcome addition to studies in these important areas of polymer science and engineering.

Information at the atomistic level of detail is required to understand the mechanisms of degradation of polymers. The work of Nyden (89,90) on thermal degradation aims at this level of detail. Statistical models, using more abstract representations of elementary reactions, have also been developed (288). In general, relatively little attention has been given to degradation reactions—they are difficult to study because they are slow and often nonspecific, requiring open-ended exploration of possibilities. At the very least, methods to sort through a manifold of potential reactions and identify the most probable under a given set of conditions would be a boon. Work in this direction for surface, catalyzed reactions (289) is well advanced.

Bond-Fluctuation Model Results. The BFM model has been applied to 2-D single-chain thermodynamics, appropriate for the description of strongly adsorbed polymer on a surface (19). Here it is claimed that formation of a 2-D glass depends on the choice of bond vectors. This is reminiscent of a phenomenon seen in the collapse transition of a single short chain (290), where fine details of the model cause "freezing out" of geometrical isomers. Perhaps these differences in the "effective" models are a reflection of the subtleties of molecular motions that determine the onset of the glass transition.

The disadvantage of the BFM is that very little chemical detail can be invested in it. Having extracted all the information that can be gleaned from a BFM simulation, there is nothing to be gained from its repetition. Other lattice methods promise more in this regard, one of which is the mapping/reverse mapping protocol of Mattice (106,107,175). Here a chemically detailed model is mapped onto a "2nnd" lattice formed by omitting every second site from a diamond lattice. Chains with relatively simple backbones can be coarse-grained and placed on this lattice with fidelity, meaning that the RIS-generated configurations of both the atomistic chain and the lattice chain can be made to coincide. Even when applied at physical densities, the coarse-grained lattice is only sparsely occupied, which facilitates the single-bead moves that are used to evolve the system. Finally, the atomistic chain can be recovered by reversing the mapping, thus allowing MD simulations to be run on the equilibrated systems to recover properties that depend on both global structure and local atomic detail. A similar lattice is used by Pakula and co-workers (291) in their cooperative motion algorithm. This algorithm has been used to simulate quite complex structures, including catenanes.

Isolated Chains and Chain Collapse. The RIS model continues to be of considerable utility in modeling, both because single-chain behavior is of interest for a number of applications, and because the unperturbed chain dimensions that one computes with RIS are needed to assess the approach to equilibrium in condensed phase simulations. It is therefore important to appreciate some of the underlying physics of RIS theory.

A practical measure of the difference between RIS weights, which are properly viewed as Boltzmann factors for potentials of mean force (PMF), and explicit potentials is contained in the work of Smith and co-workers (292). They reproduce local torsional populations obtained from direct MD of poly(ethylene oxide) chains in water by means of a standard RIS model (which can be described as a single gas-phase phantom chain) by adjustment of the RIS weights. Their results indicate that the PMFs are highly dependent on composition for some bonds and not for others, thus indicating subtleties in the influence of environment on the apparent potentials. This example shows why it is necessary to parameterize an RIS model with real data; we are still far from being able to quantify the perturbation of intramolecular potentials by neighboring molecules. However, MD simulation in the condensed phase gives these effects directly without additional effort, provided one can equilibrate the chain configurations (which is all-important for the attempted analysis) in a reasonable amount of computer time.

Isolated chain RIS calculations have been used to interpret the high strain behavior of elastomer (293), and they are reported to resolve discrepancies between Gaussian chain statistics and experiment stress-optical coefficients (294) for PE networks. RIS chains show larger correlations between bond vectors and the principal strain axis than do random Gaussian chains. Results such as this suggest that isolated chain simulations still have a role to play in the analysis of polymer properties, even though they do not convey the complexity of intermolecular interactions that are revealed condensed phase simulations, as mentioned above. In cases where rapid and comprehensive averages over configurations are desirable, and when care is taken in interpreting the results, single-chain vacuum calculations are appropriate.

Another example of single-chain dynamics is contained in the work of Srinivas and co-workers (295) who used Brownian dynamics with a spring-bead model to investigate the rate of collapse of a linear chain to a compact globular configuration. Their particular interest was in using simulations to gain an understanding of appropriate rate constants for Forster energy transfer between dye molecule donors and acceptors attached to linear chains. Dye-modified polymers are of considerable interest for experimentally probing configuration statistics and conformational transitions.

A clever method to equilibrate a model of a collapsed chain has been advocated by Paul and Müller (296). They allow the chain segments of their BFM to move in four dimensions. Any configuration in which all "atoms" of the model lie on a single three-dimensional (3-D) plane constitutes an allowable configuration of the 3-D system. As the authors describe, this is akin to allowing adsorption–desorption moves in the equilibration of molecules on a 2-D surface. The only disadvantage of an algorithm such as this is that it is restricted to simplified models, such as lattice models, for otherwise one gets involved in very

difficult questions as to the meaning of, say, quantum-derived force fields for four-dimensional space.

Interfaces. The study of polymer interfaces, including models of surface-adsorbed or bonded molecules, is of interest in problems of barrier diffusion, coatings (qv), adhesion (qv), and patterning. MC methods, both on-lattice (107,144,297,298) and off-lattice (299–301), have been utilized for these applications. Mattice and co-workers (106,302) have used the 2nnd lattice to study diffusion of centers of mass of C_{44} and C_{100} alkanes. They have also shown that chain ends will migrate to the surface of a free-standing film if the end group interaction with the mid-chain segments is not favorable. This suggests that there may be situations involving the adhesion of two polymer surfaces in which the properties of one or more of the surfaces has unanticipated properties owing to the segregation of minority constituents. Similar results have been obtained for free space simulations using both explicit atom and united atom models of C_{13} by Chang and co-workers (303).

Torres and co-workers (304) studied the dependence of T_g on film thickness, and found both increases and decreases in the apparent T_g of thin films, depending on whether the film is free or deposited on an attractive substrate. Kranbuehl and co-workers (305) found that T_g decreases with confinement by noninteracting surfaces consisting of planes (one dimensional, 1-D), tubes (2-D), and spheres (3-D). Perhaps the surface-to volume ratio, and the influence of free volume at the constraint surface, creates additional freedom of motion for the chains in these types of confinement. Consistent with this view is the observation that when chains are attracted to a surface, and thereby immobilized, the T_g increases (304). Similar conclusions were reached by Aoyagi and co-workers (306) in a spring-bead model simulation of confined chains.

The adsorption of FENE-model chains on a structureless surface was studied by Milchev and Binder (307). The energetics was such that the polymer segments preferred to interact with themselves rather than with the surface, resulting in polymer droplet formation. By careful analysis of the fluctuations in the position of the free surface of the droplets, the authors were able to evaluate the polymer–vacuum interfacial tension. It would be of considerable interest to extend this method to more accurate force field descriptions of a variety of polymers.

Diffusion. Diffusion processes in polymers have been extensively studied by simulation since about 1990. Not only is diffusion one of the more accessible transport properties to compute, it is also a property of considerable practical importance for barrier polymers and separation membranes.

Statistical mechanics provides two routes for evaluating diffusion coefficients using MD. The first approach involves monitoring the mean-squared displacement $\langle r^2 \rangle$ of the diffusing species as a function of time. More precisely stated, the Einstein relation

$$D = \lim_{t \to \infty} \left\langle (\mathrm{r}_t - \mathrm{r}_0)^2 \right\rangle / 6t \tag{7}$$

holds in the diffusive regime. Here $\mathbf{r}_t$ is the position of the diffusing particle at time t, and D is the diffusion coefficient. The angle brackets denote an average over an ensemble of systems. If the slope of a plot of $\langle r^2 \rangle = \langle (\mathbf{r}_t - \mathbf{r}_0)^2 \rangle$ with time is constant, the Einstein formula gives the diffusion coefficient of interest.

The second approach consists of monitoring the velocity autocorrelation function of the diffusing species and then using the Green–Kubo formula to evaluate the diffusion coefficient (259). This method is not as direct as monitoring the displacement directly. Furthermore, it is generally observed that correlation function methods are subject to uncertainty arising from statistical noise and slow convergence. Because of this, almost all of the MD simulation studies of penetrant diffusion in polymers have calculated diffusion coefficients by the evaluation of $\langle r^2 \rangle$ for the diffusing species.

As we have seen, computational resources currently available enable routine MD simulations of amorphous polymers to be carried out up to times of the order of a few nanoseconds. This short timescale places restrictions on the properties of polymeric materials that can be studied using direct MD simulation. The process of diffusion of small penetrants (eg, gases such as oxygen, nitrogen, methane etc) in amorphous polymers above T_g frequently has timescales shorter than the simulation timescales and is amenable to investigation by molecular dynamics simulation. Slower diffusion, as occurs in glasses, requires techniques such as transition state theory. A review of the simulation of diffusion in polymers using the methods of molecular dynamics and Transition State Theory (described in the section on molecular mechanics) has been presented by Gusev and co-workers (308).

Most of the simulations of diffusion in amorphous polymers have been carried out with systems containing up to several hundred heavy (nonhydrogen) atoms which translates to systems containing a few hundred monomer units for the hydrocarbon polymers typically studied. When the mean-squared displacement of the penetrant is monitored as a function of time for these systems, three distinct regimes can be identified. These are the initial, short-time ballistic regime, followed by a regime (referred to as anomalous diffusion) in which $\langle r^2 \rangle$ is proportional to t^n where $n < 1$. Finally, at long times, a regime of "true" diffusion can be identified where $\langle r^2 \rangle$ is proportional to t. Furthermore, it is observed that for most systems, the onset of the "true" diffusion regime is found to occur when $\langle r^2 \rangle$ is roughly equal to the square of the simulation box length. These observations motivated Cuthbert and co-workers (309) to investigate the system size dependence of the diffusion coefficient calculated by molecular simulations. Diffusivities of gases (of different sizes corresponding to helium, argon, and carbon dioxide) in amorphous polypropylene structures containing 125, 729, and 2197 monomers each were calculated in this work using MD simulation. The main conclusion of the study was that for the simulation system sizes investigated, the calculated diffusion coefficients were independent of the system size. This observation was rationalized based on the dynamics of the polymer matrix. It was shown that in the time required for the penetrant molecule to travel a distance corresponding to the box dimension, which is approximately the time required for the $\langle r^2 \rangle$ vs. time plot to show "true" diffusive behavior, the polymer matrix itself undergoes structural changes significant enough such that the local environment in the current position of the penetrant is quite different from what it was when the penetrant was in the vicinity of the periodic image of the current location.

The early MD simulations of penetrant diffusion in polymers focussed on diffusion of simple gases, eg, oxygen, through polyethylene-like polymers (24,310–316). These early studies showed that the simulated values of diffusion coefficients

were about an order of magnitude higher than the corresponding experimental values. Rather than achieving a quantitative prediction of the diffusion coefficients, the focus of these studies was on the investigation of the mechanism of diffusion and the effects of a number of factors such as the chain length (312) and free volume distribution (313).

The early work of Trohalaki and co-workers (317) on the diffusion of CO_2 in PE showed that both chain segment and gas molecule diffusion could be followed, and the activation energy for diffusion determined. Similar studies were conducted by Boyd and Pant on united atom models of PE and polyisobutylene (PIB) (24,131). They showed that the too-rapid diffusion predicted by the earlier simulations was a result of unsatisfactory force field parameters. Most importantly, they showed that the polymer density is the critical factor in determining the diffusion coefficient of small molecules. They found that the activation energy for diffusion of methane through PIB is about 20% larger than is that for PE over the temperature range from 250 to 600 K. In addition to PE and PIB, Boyd and co-workers have also studied the diffusion coefficients of methane in amorphous atactic polypropylene (318) and atactic polystyrene (319) using MD. The work was later extended to polyesters (79) at high temperatures (from ca. 425 to 625 K) by Bharadwaj and Boyd, who provide a good discussion of the cage effect and its disappearance with increasing temperature. Thus, free volume plays a very important role in diffusion, even though the diffusion process appears to have an Arrhenius temperature dependence. Much the same conclusion was reached by von Meerwall and co-workers (320,321) in an experimental study of alkane diffusion.

MD study of diffusion of simple gases (hydrogen, oxygen and methane) in amorphous polypropylene carried out by Müller-Plathe (322) also confirmed the hopping motion to be the primary mechanism of penetrant diffusion. However, the simulated diffusivities were found to be about an order of magnitude higher than the experimental values, in accord with other studies reported at the time. Later work carried out by Müller-Plathe and co-workers (323) also demonstrated (as was found by Pant and Boyd) that the over-prediction of the experimental diffusion coefficients by simulations was a result of the united atom force field used in the earlier simulations. Using an all-atom force field, these authors showed that the diffusivity of oxygen in polyisobutylene can be predicted to within a factor 2 using MD simulation. In a subsequent contribution (324) these authors investigated the diffusion coefficients of three gases (helium, hydrogen, and oxygen) in amorphous PIB using an all-atom force field. In this work, both equilibrium and nonequilibrium MD simulation methods were used for the purposes of evaluating the diffusion coefficient. The diffusivities calculated using the equilibrium MD simulations by monitoring the mean-squared displacements and using the Einstein relation were found to be larger than the experimental values by factors of 2–5. The diffusion coefficients obtained by nonequilibrium MD (where a constant external force was imposed on each of the penetrant molecules to encourage diffusion) were found to be even larger than the equilibrium MD values by a factor of about 2. The study concluded that there was little advantage in using nonequilibrium MD, as implemented in that work, instead of usual equilibrium MD for the evaluation of the diffusion coefficients.

Although most of the penetrant diffusion studies in polymers have been carried out on hydrocarbon polymers (polyethylene, polypropylene, and

polyisobutylene), diffusion of penetrants in polydimethylsiloxane (PDMS) has also received some attention in the literature. In an early investigation carried out by Sok and co-workers (325), diffusion of helium and methane in PDMS was studied using MD. Diffusion was found to occur by the mechanism of hopping between the holes, with the calculated diffusion coefficient of helium being about twice the experimental value. The calculated diffusion coefficient of methane showed excellent agreement with the experimental value. Tamai and co-workers (326) also reported an investigation of diffusion of methane, water, and ethanol in PDMS using MD. The calculated diffusion coefficient was smaller than the experimental value by a factor of about 4. [These authors showed that if the diffusivity was calculated based on a short MD run as was the case in the work reported by Sok and co-workers (325), the value so obtained, though derived from the anomalous diffusion regime, showed very good agreement with the experimental data.] Both water and ethanol were shown to form aggregates in the polymer matrix, which lowered the diffusivity by a factor of 50 compared with the values calculated in the absence of aggregation (by using only one penetrant molecule in the system). The calculated diffusivity under nonaggregating conditions was shown to agree quite well with the experimental data that was obtained in the presence of penetrant clusters. This observation led the authors to hypothesize that when a large amount of penetrant is used in the experiments, the penetrant first clusters in available holes in the polymer matrix and remains virtually immobile there, while the remaining molecules diffuse through the matrix as nonaggregated, isolated molecules.

Diffusion coefficients of a variety of penetrants (such as methane, methanol, ethanol, benzaldehyde, acetophenone, benzoic acid, fluocinolone acetonide, etc) in PE, PDMS, poly(methyl methacrylate-*co*-hydroxyethyl methacrylate), and ethyl and benzyl esters of hyaluronic acid were calculated by Li and co-workers (327) using molecular dynamics. The main conclusions of their study were that the values of the diffusion coefficient predicted by the simulations showed reasonable agreement with the experimental data for systems containing hydrophobic penetrants and hydrophobic polymers. However, these numbers showed large disagreement when either the penetrant or the polymer was hydrophilic. This might be ascribed to force field inadequacies. The diffusion of both O_2 and H_2O in aqueous solutions of polyvinylpyrrolidinone at a variety of concentrations was studied by Eichinger and co-workers (328).

Because of the long timescales associated with the diffusion of medium to large molecular weight species (molecular weight > 100) in amorphous polymers, investigations of diffusion of these molecules in polymers are scarce. An investigation of the diffusion of benzene molecules in a benzene–polystyrene system containing up to 84 wt% polystyrene was presented by Müller-Plathe (329). The problem of slower diffusion of these larger molecules (compared with the timescales of typical MD simulations) can be alleviated to some extent by carrying out the simulations at relatively high temperatures (higher than 450 K). Such an approach was used by Nath and co-workers (330) in their study of diffusion of hindered amine light stabilizer molecules in amorphous polyethylene. By fitting their high temperature diffusion data with the Williams–Landel–Ferry (WLF) equation (331), they showed that their simulation results were consistent with experimental data obtained at a lower temperature. Hahn and co-workers (332) investigated diffusion

of phenol in bisphenol-A–polycarbonate at temperatures in the range 500 to 640 K. These authors found that the diffusion coefficient showed Arrhenius behavior with the mechanism changing from a hopping diffusion at lower temperatures to continuous diffusion at higher temperatures.

The diffusion of polymer chains across an interface, as will occur in the welding of polymers, has been investigated by a variety of techniques as discussed above (see Ref. 333, for example). Jang and Mattice (334) have used the mapping/reverse-mapping technique with the dynamics being driven by the "dynamic MC" method executed on the 2nnd lattice to study the healing of an interface between films of melt PE (actually $C_{99}H_{200}$). They find three regimes following initial contact of relaxed films: (*1*) density repair at the interface, (*2*) redistribution of chain ends, and (*3*) intermixing of molecules from the two sides. The chain end redistribution is an interesting aspect of this simulation. It occurs because the initial polymer–vacuum interfaces are relatively rich in chain ends, as noted above. During equilibration, the ends will diffuse to locations that eliminate this initial bias. It is not clear that this is describable as reptation.

Although most of the work on diffusion through polymers has focussed on diffusion through amorphous polymer structures containing linear chains, some studies of diffusion in other types of polymer matrices have also appeared in the literature. An example is an investigation of gas diffusion through polymer networks reported by Sonnenburg and co-workers (335). These authors employed an idealized model of the polymer network made up of freely jointed chains joined with each other by tetravalent junctions and whose beads interacted with each other by a purely repulsive Lennard–Jones potential. The dependence of the diffusion coefficient of a simple penetrant on the temperature, the network packing fraction, and on the penetrant size was determined in this MD work.

The process of penetrant diffusion in rubbery and glassy polymers can be studied using the transition state theory. Initial attempts in this direction were made by Suter and co-workers (132,336). In the first instance (132), the motion of the penetrant molecules was considered to be completely uncoupled from that of the atoms of the polymer matrix. Values of diffusion coefficient thus calculated showed reasonable agreement with experiment only for the smallest penetrant (He) studied, while for all other penetrants considered (H_2, Ar, O_2, and N_2), the calculated diffusivity values were at least 3–4 orders of magnitude lower than the experimental values. In subsequent work (336), the approach was improved by assuming that the penetrant motion is coupled with the thermal or vibrational motion of the polymer atoms (but not with structural relaxations of the polymer). The thermal motion of the polymer matrix was accounted for by using a "smearing parameter" which could be calculated based on displacements of the host atoms evaluated from a MD simulation. The values of diffusion coefficients calculated for penetrants of various sizes such as Ar, N_2, O_2, H_2, and He agreed within an order of magnitude with the experimental data for diffusion in both rubbery and glassy polymers.

This approach proposed by Gusev and Suter (336) was further improved upon by Theodorou and co-workers (337,338), who explicitly accounted for the motion of the polymer atoms during the penetrant diffusion process. In this work, a geometric analysis of the glassy polypropylene structures was first carried out to obtain initial estimates of the local minima where penetrant molecules will

reside most of the time; transition states for the motion of the penetrant molecules between adjacent minima were also located. These guesses for transition states were then refined using a rigorous calculation on a multidimensional potential energy surface of the system. In addition to the penetrant molecule, the atoms of the polymer matrix in the vicinity of the penetrant were also considered to be mobile (or considered to constitute "flexible" degrees of freedom in the transition state formalism) in this procedure. It was found that in all about 350 atoms of the glassy polypropylene matrix moved cooperatively with the diffusing methane molecule. Such explicit incorporation of polymer degrees of freedom during the calculation led to much lower, and more realistic, energy barriers for the transition state than those found in the work of Gusev and Suter described above. Once the transition state was located, the reaction path connecting it with the local minima on either side was determined. Finally, a harmonic approximation to the potential energy surface at the minima and transition state was used to calculate the rate constant for the transition of the penetrant molecule from one energy minimum to another by means of the standard transition state theory formula.

Gray-Weale and co-workers (339) used the geometric data collected by Greenfield and Theodorou (337) to develop a somewhat approximate treatment of the diffusion in polymers in the spirit of transition state theory. In that work, rather than considering the motion of the penetrant molecule in a sea of polymer atoms, the polymer matrix was treated as a continuum. The activation energy for the transition state was then calculated by considering the energy required for deforming the polymer matrix to open up the channels for penetrant motion from one minimum to another. The predictions of this model were in semiquantitative agreement with experimental data.

Diffusion of O_2 through a thin film of PE was simulated by the Doi group (340) using a single configuration of 60 PE molecules of 100 united atoms. The Rigby-Roe potential for PE induced crystalline order at 300 K, which melted out at 500 K. The trajectories of individual O_2 molecules were followed in the simulation, which enabled the authors to conclude that the apparent increase in O_2 concentration as the temperature was lowered to 180 K was due to surface adsorption. (The obvious warning is that when performing simulations on small systems, do not be misled by a large surface-to-volume ratio.) By simulating the surface directly, the authors were able to follow all events of the encounter between gas-phase molecules and a polymer surface, with subsequent diffusion into the surface. Such studies should be quite useful in the analysis of barrier properties of films.

The influence of the glass transition on diffusion has been considered by several groups (319,341). Paul and co-workers (341) focus on anomalous diffusion, and show that this short-time behavior is related to the freezing-in of isolated packets of free volume. Their BFM included a preference for chain stiffness, and they showed that diffusing molecules tend to move parallel to the director of the nematic phase; that is, diffusants find it easier to move in the direction of the chain backbone (within the tube!) than perpendicular to it.

Fried and Goyal (342) studied the permeability of poly[1-(trimethylsilyl)-1-propyne] to several gases, and found good agreement with experiment. An insertion method was used to determine the solubility of He, O_2, N_2, CH_4, and CO_2 in the polymer, and diffusion coefficients were obtained from the Einstein relation. The DREIDING force field was used for the simulations. This polymer is

interesting in that it is highly permeable, which facilitates the thorough study carried out by Fried and Goyal.

Park and co-workers (343) used MD with a simple Lennard–Jones model of alkanes hosting a large spherical particle to show that this system could mimic the MW behavior of measured diffusion coefficients of methyl yellow in a range of *n*-alkanes and *n*-alcohols. In these simulations, no effort was made to analyze the results in terms of changes in the melting temperatures of the model alkanes. (The MW dependencies of the experimental diffusion coefficients extrapolated to 45°C have breaks at *n*-docosane and *n*-hexadecan-1-ol, both of which have melting temperatures at about 45°C! This work may be a new method to measure melting temperatures, which is not trivial owing to the dependence of phase transitions on the force field.)

It will be interesting to see how the interplay between Vogel–Fulcher behavior, free volume "adjustments," and Arrhenius activation resolve themselves as MD simulations extend to longer times and to more accurate descriptions of potentials. It seems to be a general rule that "stationary" random systems, of which a glassy polymer is an example, have frozen-in heterogeneities that are all important in determining properties. While intuition suggests that random systems should be "uniform," this seems not to be the case.

Ionic diffusion is important in battery and fuel cell applications as well as other areas, and it too has been the subject of simulation studies. Ennari and co-workers (81,344,345) produced a clever means to model proton diffusion in aqueous systems containing poly(ethylene oxide) (PEO) with sulfonic acid groups, and found the results to be in reasonable agreement with experiment. The diffusion of Li^+ in dry PEO melts has been simulated by Borodin and Smith (346). They find that the system slows down because of complexation of the cation by the O atoms of the PEO chains. The lifetimes of the complexes are relatively short, between 100 and 200 ps. At the concentrations of ions used in the simulations, the Li^+ and I^- form fairly tight ion pairs, which causes the two to diffuse at about the same rate.

Viscoelasticity. Direct MD simulations of the long-time dynamics of models of polyethylene using both united atom and explicit atom potentials were reported by Paul and co-workers (347) and Harmandaris and co-workers (348). In this work, relatively long (C_{100} in the former and C_{24}–C_{156} in the latter) alkanes were simulated for several nanoseconds with MD. It was shown that the chain dynamics, including the monomer friction coefficient, autocorrelation function of the end-to-end vector, and several other properties are well described by the Rouse model. These chain lengths are below the entanglement molecular weight, so that reptation was not expected. Importantly, the Rouse modes were shown to depart from simulations as the wavelength of the excitation decreased, ie, when atomic detail begans to invalidate the Rouse model.

An understanding of the influence of polydispersity on chain dynamics in the melt was achieved by Baschnagel and co-workers (177) in a simulation using BFM. These "dynamic Monte Carlo" simulations showed that long chains move more rapidly in the presence of short chains, and the short ones move more slowly in the presence of the long ones. The net effect is that the dynamics of a polydisperse melt is close to Rouse theory predictions, ie, the chains act as if they are not entangled! An indirect approach to reptation dynamics was described by Byutner

and Smith (349). They used direct MD simulations on relatively short polybutadiene with random microstructure (350) to evaluate a few molecular parameters (Rouse relaxation time, chain dimensions, and bulk density), which were then fed into various theories of viscoelasticity (qv) to estimate the storage and loss moduli of high polymer (see VISCOELASTICITY). Good agreement with experiment was obtained with the parameter set from simulations when used with Milner–McLeish theory (351). This hybrid approach to viscoelasticity is apt to be the only practical method to get to the very broad timescales typical of bulk polymer dynamics. However, as a comparison of these two results suggests, there are details that need to be considered very carefully. In particular, departures from Rouse dynamics have been seen in the same polybutadiene system (352), which is taken as a signal of the importance of intermolecular correlations. Smith and co-workers (350) have shown that it is important to get good representations for rotational potentials and chain microstructure for this polymer when attempting quantitative comparisons with NMR relaxation time experimental data. United atom potentials seem to make the torsional modes too "slippery" relative to all-atom potentials. That is, torsional motions of the backbone are subject to forces similar to those that create the ratcheted motion of methyl groups (see below), and explicit hydrogens are responsible for each.

Brownian dynamics has been used to study the behavior of dilute solutions of dendrimers in shear flow by Lyulin and co-workers (353). In this work they showed that the onset of shear-thinning depends on the number of generations, the details of the structure of the rod-bead model, and the strength of the hydrodynamic interaction. The SHAKE algorithm was used to impose the constraint of fixed bond lengths. Bond and torsion angles were free of constraints. One of the most interesting aspects of this work is the different shear behavior shown by dendrimers and linear chains—linear chains first expand, ie, the radius of gyration increases, and then contract with increasing shear rate, whereas dendrimers expand monotonically. This interplay between segment density, topology, and shear rate should provide fertile ground for both future simulations and practical applications.

Local Chain Motions. Continuing in the dynamical vein, high frequency methyl group librations in glassy polymers can be directly studied with MD (354). The distribution of potential barriers to rotation seen in simulations on polyisoprene at 150 K is very nicely correlated with inelastic neutron scattering. Methyl rotations in poly(vinyl methyl ether) and PMMA have also been studied by the Davies group (355,356) which has enabled them to conclude that packing effects are just as important, if not more so, than monomer structure in determining the barriers to rotation.

Short-range conformational transitions, such as backbone torsional motion or side-chain rotations as mentioned above, are often considered to play a major role in a number of subglass relaxations exhibited by polymeric materials as well as for diffusion of penetrants. As might be expected, these conformational transitions, especially of groups larger than the methyl group, usually occur on timescales too long to be captured by conventional MD in the glass, but they can be studied using molecular mechanics with the help of transition state theory. Suter and co-workers have applied this technique to the investigation of the phenyl ring flip motions in polycarbonate (99) and polystyrene glasses (100). In this study of the ring rotation process, the reaction coordinate in the transition state theory

formalism was defined simply to consist of only the ring torsion angle. The torsion angle of interest was "driven" through 180 degrees in steps of 5–10 degrees, and after each such change the energy of the system was minimized. The energy profiles obtained using this approach were used in conjunction with the transition state theory rate expression to determine the rate of the process of interest (the entropic contributions to the free energy barrier were assumed to be negligible).

It is to be expected that in a condensed polymeric phase such as a glassy polymer, even a local conformational change of a chain requires the cooperative motion of the neighboring chains. The approach followed by Suter and co-workers, as described above, focusses only on the change in the torsional angle of interest, and consequently ignores the cooperative nature of the motion between the ring torsion angle and the neighboring torsion angles. Khare and Paulaitis (357) explicitly accounted for this cooperative motion by considering a multidimensional reaction coordinate that included the two neighboring backbone torsion angles in addition to the phenyl ring torsion angle in their investigation of the phenyl ring flip motion in glassy polystyrene. Their work clearly demonstrated the cooperative nature of the process. The cooperativity of these local motions was also found for phenyl group ring flips in a polyimide (358).

The approach proposed by Khare and Paulaitis (357) seeks a middle ground between the extremes of considering only one dihedral angle as the reaction coordinate and considering a reaction coordinate made up of all of the degrees of freedom (all of the atoms or internal coordinates) in the system. It is to be noted that a priori selection of the degrees of freedom that are to be included in the multidimensional reaction coordinate is a difficult task and a judicious choice of these requires a detailed knowledge of the physics of the process being studied.

The dynamics of polymers depends on more than these selected examples of rotations/librations. Simulations to detect backbone rotations in polyisoprene, both above and below T_g, have been reported (359–361); similar results were found for 1,4-polybutadiene by Furuya and co-workers (362). It is found that backbone rotations are correlated, with neighboring bonds undergoing rotations of contrary handedness, thereby preserving the overall contours of the chains. Similar behavior is observed in amorphous PE below the glass temperature (363). [Obviously, the nature of the cooperativity of rotations is highly dependent on monomer architecture as well as temperature and density. Zuiniga and co-workers (364) did not find as many correlated rotations in PE, but their simulations were done *in vacuo*, for which the rotational transition behavior is very different from the bulk.] Below T_g, the bonds that have some rotational/librational freedom are localized in "hot-spots" (361), while other bonds do not experience any significant torsional motion on a 20-ns timescale. Similar results, indicating increasing heterogeneity of local motions with decreasing temperature, have also been obtained by Smith and co-workers (365) on 1,4-polybutadiene. This is an aspect of the heterogeneity of systems with frozen-in disorder, and is probably not an artifact of the algorithmic construction of cells. Another interesting aspect of polymer dynamics is emphasized in the work of Fukuda and Kikuchi (361). Their correlation functions are very slowly decaying unless the temperature is well above T_g. This phenomenon, ie, the further slowing of already slow motions as temperature is reduced, is typical for polymeric simulations, and is a major obstruction to the analysis of polymer dynamics. However, it is a problem that yields up more information the faster

is the computer that can be applied to it. For this reason, extension of existing methods to slower mode problems will continue to be of interest for many years to come.

The density dependence of backbone torsions in a united atom model of PE in the melt at 400 K has been investigated by Karatasos and co-workers (366–368). They found that second-neighbor torsional coupling (with relaxation times around 10 ps) increases with density, as the above results suggest. But most importantly, there appears to be a second reorientation process with much longer relaxation times that appears with increasing density and which is seen most clearly with longer chains. This motion "... can be thought to originate from an effective "*pipe*" formed from the surrounding chains constraining the relaxation of the chain axis, even after the correlation of the torsional angles is lost. This effect is not to be confused with the "*tube*" model associated with chain reptation" (367). It will be interesting to see if this is just the next slower process in a long sequence of different types of motion in polymeric systems [which is implied by the general viscoelastic behavior of bulk polymers (331)]. Longer simulations will determine if yet slower processes will be found.

The density and temperature dependence of some of the slow relaxations in PE were studied by Bharadwaj and Boyd (369) using *NVT* simulations with a relatively simple united atom model of the polymer. Runs of six nanoseconds for each of several conditions were performed, resulting in a comprehensive view of how relaxation processes depend on ρ and T. One insight provided by this work is that reorientation motion of the chains seems to require barrier crossings rather than free-volume "adjustments." This result suggests that there is a need for analysis tools that are capable of cross-correlating different types of motions with structural or packing aspects of amorphous polymers so as to unravel the complex interplay of phenomena that determine the dominant motions in these systems.

These results reinforce once again the need to go to longer and longer timescales to capture slowly relaxing modes of motion in polymeric systems. Depending on the property of interest, failure to account for the slow relaxation can sometimes bedevil the analysis of properties.

Glasses and Glass Transitions. One of the earliest investigations of polymer glasses, which utilized alkane models of polyethylene in both liquid and glassy states, was presented by Rigby and Roe (69,370–372) (see AMORPHOUS POLYMERS). By carrying out MD simulations over a range of temperatures, these authors showed that the simulated system behaved like the experimentally observed polymeric systems in the vicinity of the glass transition (qv). The authors presented a detailed investigation of various conformational (eg, distribution of torsional angles), structural (eg, radial distribution function, orientation correlation function, free-volume distribution), and dynamic (eg, conformational transitions, segmental self-diffusion coefficients) properties of polyethylene chains containing up to 50 monomeric units in both liquid and glassy states.

Simulating the kinetic transition of a polymeric system from the melt to the glass has been a modeling target for many years (69,131,176,248,370–379). Any of the techniques that have been discussed for performing either "dynamic MC" or MD is capable of yielding densities that exhibit the characteristic knee at T_g. Simulations, just as in the real world, give T_g's that depend on the rate of

cooling (248,380), molecular weight (69,248), and pressure (376). Obviously, the value that is obtained for T_g is very much dependent on the force field that is used, as switching off the torsion potential in a simple united atom model reduces the apparent T_g significantly (69,378). Results of the Mainz group (248) show that the Vogel–Fulcher law is well obeyed by diffusion coefficients obtained from "dynamic MC", but caution that interpretation of the apparent reference temperature resulting from the fit is subject to considerable uncertainty given the limited scope of the modeling data. This statement is generally true—the correspondence between simulated T_g's and experiments is open for discussion. The proper equilibration of polymer models, especially if one is interested in the MW dependence of T_g, is very important. Given the slow relaxation of large random coils, determination of the temperature dependence of density should be systematically explored for a variety of MWs, but this is rarely done. Given the sensitivity of the apparent T_g to the factors mentioned, especially the force field, agreement between simulations and experiment may at times be fortuitous.

The FENE model with short chains of ten beads interacting with a truncated Lennard–Jones potential has been used for an MD investigation (381,382) of mode coupling theory just above the predicted critical temperature, which in turn is above the T_g. It is too early to say whether this theory will prove to be of practical use for polymer science, but simulations of this kind are probing deeply into the nature of the glass transition, which can only help to illuminate the physics of this important transition.

A generic FENE model has also been used to study crazing in glassy polymers (383), with the resulting pictures looking very much like what one sees in micrographs. Earlier work with a 2-D lattice model of a cross-linked system exhibited much the same phenomena (384).

The influence of surface bonding on the glass transition has been studied with BFM (385). The adhesive strength of thermosetting resins is especially challenging to model, but progress is being made in this area by Stevens (386,387). A modified Grest–Kremer model with multifunctional units and breakable bonds has been used to construct a densely cross-linked system confined between parallel planes of atoms. The model was subjected to both normal and shear stresses by moving the surfaces, with strains up to the point of fracture. Both yield and plastic behavior as well as fracture are seen in the simulations. The pull-off from a bonded surface is dependent on the fraction of bonds to the surface, and the overall yield strain is determined by the minimum path from surface to surface. Viscoelastic contributions, as might become apparent upon varying strain rates, have not yet been extensively considered.

Crystalline Polymers. The thermodynamic properties of perfect crystals treated in the harmonic approximation constitute an important textbook example of the success of quantum statistical mechanics. Early examples of applications to polymers are found in the work of Tadakoro and colleagues (388–391). (see SEMICRYSTALLINE POLYMERS). This theory and elaborations thereof continue to be of considerable interest, especially because the free energy can today be calculated as a function of strain from first principles with the use of a high quality force field. Lacks and Rutledge (392) have described a method in which the Gibbs free energy is minimized as a function of applied strain. They perform molecular mechanics (MM) with fixed stress and cell parameters to locate the local energy minimum

while preserving the space group; this is repeated for a variety of different cell parameters. For each of these, the Hessian matrix for the unit cell is computed either analytically or numerically to obtain the harmonic force constants, and from these the phonon frequencies are obtained. Standard Debye theory gives the free energy, which is then minimized with respect to the cell parameters so as to obtain the strain, while the temperature dependence of the cell parameters yields the thermal expansion coefficient. (The reader will recall that thermal expansion is a manifestation of anharmonicity. The method of Lacks and Rutledge neatly solves this problem while retaining the simplicity of the harmonic approximation for the calculation of other thermodynamic properties.) This theory has been used successfully for several polymers.

Modeling is also useful for the determination of crystal structures, as the inversion of an X-ray diffraction pattern generally requires the construction of an atomic model of the system. This has been true since the earliest days of crystallography, when it was seen that a forward Fourier synthesis of the diffraction pattern was required to determine the phases of scattered rays (393,394). The prodigious calculations required for this analysis were a natural for computers, and some of the earliest chemical uses of computers were for this purpose. Continuing in this vein, molecular models and simulation have vastly improved the ability to solve very difficult structures. The work on poly(vinyl alcohol) (PVOH) (395–397) is illustrative of what can be done. Two competing structures for PVOH, one due to Bunn and the other to Sakaruda (see references in Ref. 397) were resolved in favor of the Bunn model. Assender and Windle (396) showed that a model incorporating water into the PVOH crystal reproduced the changes in relative intensities of two peaks seen in the experimental data. The Blackwell group (397) emphasized the importance of using MD, rather than simple MM, to understand subtle relations between cell dimensions and hydrogen bonding, thereby accounting for changes seen in the diffraction patterns for different tacticities.

A somewhat different situation is encountered in the structure of random copolymers of *p*-hydroxybenzoic acid and 2-hydroxy-6-naphthoic acid. These polymers do not crystallize in the traditional sense, yet they exhibit diffraction patterns that mimic those of partially crystalline polymers. Modeling (398,399) has been a crucial aid to understanding the relation between the conformational and translational disorder in these liquid crystalline polymers, despite some differences in the types of modeling done and interpretation thereof. Similar types of polyesters were investigated both experimentally and with modeling by Oda and Rutledge (400). Their interest was in understanding the influence of processing conditions on the molecular orientation, and MC modeling was used to produce a molecular level understanding of the noncrystalline domains.

Polyesters containing ethylene moities, namely polyethylene-biphenylate (PEBB) and naphthalate (EN) copolymers, were analyzed by Wendling and co-workers (401) in an effort to comprehend their crystal/amorphous structures. They found that minority repeat units were excluded from the crystalline phase of the majority comonomer when the concentrations of the two are very dissimilar, whereas the two comonomers are able to cocrystallize by segregation when their compositions are more nearly equal.

Techniques to determine the interplay between random copolymer statistics and crystallite stability in a situation where two comonomers (hydroxybutyrate

and hydroxyvalerate) can co-crystallize have been described by Wendling and Suter (402). The thermodynamic integration method was used for these simulations. The technique utilizes a mapping, $H(\lambda) = (1-\lambda)H_A + \lambda H_B$, between two Hamiltonians for species A, H_A, and B, H_B. If the two species are sufficiently close to one another in structure, the transformation of the system from A to B can be performed by gradually changing λ, allowing for equilibration of the hybrid system at each increment in the coupling parameter. While this thermodynamic integration method is fraught with hazards when applied carelessly, it is extremely potent when used judiciously, as it provides a means to evaluate the free energy change that accompanies the transformation of the system. [Two other methods are capable of yielding the free energy for a crystalline material such as this: normal mode analysis (123) and the Gibbs ensemble method (159).]

Phase transitions between crystalline polymorphs can also be approached with modeling. Sorensen and co-workers (403) calculated energies and free energies of PE as well as the hexagonal and orthorhombic forms of poly(oxymethylene) using their ab initio method (404) for predicting crystal structures of helical polymers. Good agreement with experimental structures was obtained with use of a "boutique" force field. Free energies were calculated from phonon dispersion curves with use of statistical mechanics in the usual way, and they found the energies of the two polymorphs to be equal within the uncertainty of the calculation. This work was one of the first to show how a phase transition could be calculated from first principles.

The use of modeling to estimate the elastic constants for the crystalline phases of semicrystalline polymers is becoming a reliable strategy to determine properties that are very difficult to estimate directly from experiment. A representative example of these types of simulations is the study of silk by Sinsawat and co-workers (405), who find reasonable agreement between the Young's modulus in the chain direction with the values determined experimentally. Earlier work by Klunzinger and Eby (406) showed that one could obtain reasonable values for the anisotropy of the thermal expansion coefficient of PE represented with the DREIDING force field by direct determination of the temperature dependence of cell dimensions obtained from MD simulations using the Parinello–Rahman algorithm (407).

The topic of chain folds at lamella surfaces has been controversial for decades. Very recently, molecular modeling has become sufficiently versatile to aid in understanding the complex interplay between crystal and amorphous densities, chain stiffness, and crystallite proximity effects. The simulations of Rutledge and co-workers (203,408,409) on a freely rotating united atom PE model with truncated Lennard–Jones interactions demonstrate that the lowest energy crystal face in a semicrystalline PE is the {201} face, in excellent agreement with experiment. (These authors review the extensive older literature on this problem as well as some of the controversies.) The most striking feature of this result is that this face has very few adjacent reentrant folds, in contrast to the {001} face. The method used to equilibrate these systems included four different types of MC moves: end-rotation, slithering snake, intrachain concerted rotations, and end-bridging. Further studies of this kind, with different polymers, would be welcome.

MC methods can be used with full atomistic descriptions, and these have been particularly useful for crystalline (127) and liquid crystalline (410) polymers. The

MC moves that can be made in these types of systems include rigid body rotations and translations besides the local displacements of atoms, and these larger moves greatly facilitate the exploration of the anisotropic domains in phase space. Moves of this type cannot be used for the amorphous phase, as rigid body rotations, for example, will most likely precipitate very energetic overlaps with neighboring molecules as has been discussed above.

Equation of State. A number of modeling studies of amorphous polymers have included *PVT* behavior, either as an end in itself, as a means to validate the potential functions, or to investigate other aspects of polymer behavior (411). Polymer melts and glasses that have been studied in some detail include polyethylene (23,370,412), poly(dimethylsiloxane) (413), poly(ethylene oxide) (414), and poly(ethylene terephthalate) (78). Dendrimers having a variety of generations have been compared with linear chains in the respect of their equation of state by means of a tangent hard sphere model by Lue (415).

Electrical Properties. The piezoelectricity of the technologically important polymer of vinylidene fluoride (PVDF) has been the subject of modeling for several decades (see PIEZOELECTRIC POLYMERS). An early example of the use of molecular mechanics to aid in the calculation of the mechanical and electrical properties of this polymer is found in the work of Tadokoro and co-workers (390,391). Subsequent investigation of PVDF by Karasawa and Goddard (83) focussed on the prediction of alternative crystal structures with use of the shell model to capture polarization effects. The latter phenomenon was further explored by Carbeck and co-workers (84), who used the shell model to show that the induced moment because of neighboring dipoles in the crystal increases the dipole per repeat unit by about 50% over its value in the isolated molecule.

Young and co-workers (80) studied the poling of a model polyimide film by using the "amorphous cell" technique, with the electric field being generated by an array of fixed charges. They relaxed the system at 2000 K under a poling field of 700 MV/m—harsh conditions that are feasible in the computer but physically unrealistic. However, this treatment enabled them to relax a very stiff polymer in a reasonable length of time (ca. 200 ps) and examine its polarization. They claim excellent agreement with experiment.

The calculation of dielectric permittivity is of considerable interest for a variety of reasons, most especially for electronic applications. Heinz and co-workers (416) tested several different techniques for determining the dielectric constant of liquid water, and determined that none is clearly better than the simplest route of evaluating the dipole moment autocorrelation function. The relations $\mathbf{P} = \chi_e \mathbf{E}$ and $\varepsilon = 1 + 4\pi\chi_e$ between the induced polarization $\mathbf{P}$, electric field strength $\mathbf{E}$, electric susceptibility χ_e, and dielectric constant ε, for an isotropic medium (417) can also be employed to determine the dielectric constant by application of an external field. An external field may be readily incorporated into an MD engine by adding a force term of the form $\mathbf{F} = q\mathbf{E}$, where q is the partial atomic charge on an atom, and by monitoring the induced polarization.

The use of quantum methods for large crystalline systems (418) may have appeal for the analysis of conductive polymers.

Polyelectrolytes. Multiple chain polyelectrolytes (qv) have been simulated by Limbach and Holm (419). They used a FENE model having beads that interact with both a truncated LJ potential and an electrostatic potential. Counte-

rions were observed to condense on the chains, but such that the segments in the center of the chain are more highly screened than are those at the chain ends. The mutual repulsion of backbone segments causes the chains to extend themselves, but if the solvent quality is poor, they collapse locally into a pearl necklace configuration. A range of polyelectrolyte properties has been studied by a combination of theory and simulation by Shew and Yethiraj (420–422).

Nanoscopic Systems. The considerable current interest in nanoscale particles and devices will appear to be familiar territory to polymer scientists and engineers, as this domain entails length scales that are commonly encountered with polymeric systems. United atom models for up to 60,000 atom models of PE droplets have been simulated with MD methods (423). The design of purposeful devices, eg, motors, at this length scale has been initiated (424). Furthermore, as semiconductor devices shrink in size, it is foreseen that the ultimate length scales will be in the nanometer range. The modeling territory that has been explored in working on polymer problems will be of considerable importance as these fields advance.

Mechanical Properties. In addition to structural properties, mechanical properties of glassy polymers can also be studied using the methods of molecular mechanics (131,425). In this application, a glass structure at a local energy minimum (and also mechanical equilibrium) is subjected to small deformations. The first and second derivatives (slopes and curvatures) of the potential energy can be evaluated numerically and related to the elastic constants of the polymer. Note that this approach assumes that the entropic contributions to the elastic response are negligible, an assumption shown to be valid for typical polymer glasses by Theodorou and Suter (425). The elastic constants of glassy atactic polypropylene calculated (425) using this approach showed very good agreement with experimental values. Subsequent to this work, Matheson (426,427) mustered more extensive experimental data on the pressure and temperature dependence of the bulk modulus to show that the entropic contribution is not always negligible for glassy polymers, and is certainly not negligible in the melt.

Pervaporation. In addition to the simulation of the penetrant diffusion in the polymeric matrices, the technique of molecular dynamics has also been applied for investigating the process of pervaporation separation using polymeric membranes (428). In this study, the process of separation of a 90:10 wt% water–ethanol mixture by a PDMS membrane and separation of a 90:10 wt% ethanol–water mixture by a PVA membrane was investigated by simulating systems containing the respective polymer matrices in direct contact with the respective liquid mixtures. The authors showed that within one nanosecond of MD simulation the liquid molecules were found to be absorbed in the polymer matrices. Furthermore, consistent with the experimental observations, an enrichment of ethanol in the PDMS matrix and an enrichment of water in the PVA matrix were observed.

Viscosity. The molecular modeling techniques used for determining the other transport coefficients, viscosity and thermal conductivity, in addition to diffusivity that was discussed above, fall into two categories. In the first category, the coefficients are calculated from Green–Kubo relations, with the required correlation functions being evaluated with equilibrium simulations at the desired state point. Indeed, this was the approach followed traditionally. However, the calculation of correlation functions is known to yield large statistical uncertainties. This

has led to the development of alternate techniques for evaluation of the transport coefficients. There is now a preference for using direct simulations of the phenomena that define the quantities. Perhaps the most popular of these is the "homogeneous shear" (often described as nonequilibrium molecular dynamics or NEMD in short) technique used for the calculation of viscosity (429). In a homogeneous shear simulation, a velocity gradient is set up in the simulated system by modifying the equations of motion and using "sliding brick" periodic boundary conditions. The viscosity of the fluid is then determined by measuring the appropriate component of the stress tensor, ie, the momentum flux. The results of homogeneous shear simulations are generally extrapolated to low shear rates to obtain the zero shear rheological properties, eg, zero shear viscosity. The technique has been applied to study the rheology of low to medium molecular weight *n*-alkanes (430–437) and branched alkanes (434–437). In addition, it was shown that the performance of the simulations for predicting the temperature and pressure dependence of viscosity for *n*-alkanes was comparable to that of empirical correlations based on experimental data (434). In addition to hydrocarbons, the technique has also been applied for investigating the viscosity of other small organic molecules such as *iso*-amyl alcohol and *n*-butyl acetate (438).

Shear Flow of Confined Fluids. The homogeneous shear simulation technique described above employs periodic boundary conditions in all three dimensions thus effectively simulating a small region in the bulk fluid. For many applications (eg, investigation of wall-slip behavior in polymer processing or understanding the results obtained by the Surface Forces Apparatus experiments), interfacial rheology plays an important role in the phenomena of interest and thus the surfaces confining the sheared fluid need to be considered explicitly in the simulation (see RHEOLOGY). Such processes can be studied using a simulation technique that closely mimics the setup of an experimental rheometer (or the Surface Forces Apparatus): the fluid of interest is confined to a film between two surfaces, and shear is imparted on the fluid by actual motion of these confining surfaces. Such an approach has been used to investigate the steady shear rheological behavior of molecularly thin films of simple fluids (439,440) as well as polymers that were modeled using both coarse grained bead-spring models (441–445) and more realistic united atom models (446–449). Recently, viscoelastic properties of thin films of simple and polymeric fluids were investigated by extending this approach to study oscillatory shear flow of the confined fluids (450,451).

Phase Transitions.

Traditional Methods. The Flory–Huggins χ parameter, in combination with the combinatorial entropy of mixing, controls liquid–liquid phase separation in polymer solutions and blends. Owing to the technical importance of polymer solutions for analytical work and the commercial importance of blend compatibility, there is considerable interest in finding methods to evaluate the χ parameter with theory or simulations. The initial view of the interactions between the components of a mixture led to the formulation of the interaction parameter χ as the energy change on forming unlike pair contacts (220). This led to the early development of algorithms that would report energies of interaction between molecules as the molecules were brought from "infinity" to a random configuration of minimum energy. With sampling of the contact configurations with an MC procedure, the energy change on forming unlike contacts could be evaluated (452).

On the next simplest level, solubility is predicted with use of regular solution theory. The computation of solubility parameters, δ, can be done reliably for small molecules, oligomers, and polymers, and the heat of mixing ΔE_M, estimated from (453)

$$\Delta E_M = \varphi_1 \varphi_2 V(\delta_1 - \delta_2)^2 \tag{8}$$

where the ϕ_i are the volume fractions of the two components and V is the mixture volume. This is the approach taken by Patnaik and Pachter (454) in one part of their study of the miscibility and properties of several different liquid crystal formers in poly(methyl methacrylate).

Perhaps the simplest phase transition for a polymeric system is the collapse of a single chain. There is much current interest in collapse transitions in relation to the protein folding problem (455). These simulations are often done with Brownian dynamics, and may include electrolyte effects. Low dimensional simulations (456) are of use in helping to understand this problem, particularly because theories of 1-D systems, which can be compared with simulations, are much easier to construct than for 2-D and 3-D.

Balazs and co-workers (17), in a study of comb polymers having hydrophobic and hydrophilic groups, observed the collapse of single chains in simple models of oil/water mixtures. The comb-like chains were modeled with FENE springs and a simple LJ potential with cutoff; combs with hydrophobic backbones and hydrophilic teeth as well as the converse were investigated. Surfactant behavior could be ascribed to the polymer by investigation of the spatial correlations between oil and chain segments. These early calculations presaged the results that would be obtained with DPD.

Honeycutt (457) showed that PRISM is capable of correctly predicting the influence of tacticity on phase separation in blend of poly(vinyl chloride) and poly(methyl methacrylate). In this work, the potentials for united atoms were taken to be independent of tacticity, but the chain statistics conveyed in the RIS models were tacticity dependent. This is not always the case. Direct simulations to obtain pair correlation functions that are pertinent to a phase separating system were performed with the 2nnd-lattice mapping/reverse-mapping technique by Akten and Mattice (458), who showed that the positive heat of mixing in polyethylene–polypropylene blends was the result of intermolecular potentials, and not chain statistics. It has long been theorized that these two polymers are incompatible (459), in agreement with experiment.

In the early work of Rigby and Roe (370) it was shown that a united atom model of PE would spontaneously pass from an isotropic to a nematic phase on lowering the temperature. More recently, the same model potential has been applied by Koyama and co-workers (460), who found a T_g at about 230 K, with significant ordering of the chains occurring between 300 and 330 K. The latter is taken to indicate incipient crystallization. The work on a polymer film by Ito and co-workers (340) used the same model, and found a crystalline structure below and at 300 K. Thus, if the simulation times are sufficiently long relative to the relaxation time of the modeled chains, it is possible to observe at least the onset of crystallization in a condensed phase. The timescale for crystallization in thin films may be shorter than in the bulk; Ito and co-workers (340) have shown that their PE film forms

crystallites with a grain boundary within a reasonable simulation time. Perhaps the tendency of chains to run parallel to the surfaces induces increased order, thereby enhancing the rate of nucleation. MC simulations on a lattice model of a thin film are reported to show similar behavior, (461), but here the speed advantage of MC allows greater exploration of the configuration space of the system.

Holt and Farmer studied the helix reversals in polytetrafluoroethylene crystals that are imputed in the "very rich phase behavior" of the polymer (462). They find that diffusive pairs of reversals that bracket relatively short-chain segments are readily formed, and increase in occurrence with increasing temperature. Another fluoropolymer of perennial interest is polyvinylidene fluoride. The ferroelectric phase transition of copolymers of vinylidene fluoride (VDF) and trifluorethylene (TrFE) was studied by Abe and Tashiro (463), who found that the introduction of TrFE leads to a decrease in the transition temperature. The transition is brought about by a disordering of the rotational states that is promoted by a density reduction that accompanies an increase in the TrFE content. This despite the fact that the TrFE monomer has higher rotational barriers than does the VDF repeat unit. This is an interesting example, but not an isolated one, where modeling correctly senses and balances some apparently contradictory trends in behavior.

Gibbs Ensemble Methods. As has become increasingly apparent with newer modeling techniques, especially those based on the Gibbs ensemble method, the entropic contributions to χ are often of considerable importance for quantitative work (464–467). While noncombinatorial contributions to χ have long been observed in experiments and with equation of state theories, it is only very recently that modeling methods have been able to discern this part of the interaction parameter. The Gibbs ensemble method has been used by de Pablo and co-workers (468) to investigate the pure component vapor–liquid equilibria of n-alkanes (469), branched alkanes (27), α-olefins (470), and mixture equilibria of alkanes (27,471) and alkenes (470). Siepmann and co-workers have used this methodology to investigate the pure component vapor–liquid equilibria of linear alkanes (472–474), branched alkanes (475), alkenes and alkylbenzenes (476), and alcohols (477) and the mixture equilibria of alkanes (474), alkenes and alkanes (154), and alcohols and alkanes (477). Fuchs and co-workers have investigated the pure component vapor–liquid equilibria of linear alkanes (478), cyclic alkanes (479), and sulfides and thiols (480) and mixture equilibria of linear alkanes (478). The approach has also been used to study the vapor–liquid phase equilibria of mixtures of alkanes and perfluoroalkanes with carbon dioxide (481).

In the Gibbs ensemble–CCB method used in most of the simulations reported above, the particle swap move still consists of inserting the entire chain into the other phase. Although the selection of a favorable chain conformation by the CCB method does help, the approach still becomes inefficient for chains longer than about 20 united atoms or for dense systems. This difficulty has led to the development of the expanded Gibbs ensemble, which enables simulation of phase equilibria of very long-chain molecules. In the Expanded Gibbs ensemble simulation technique as developed by Escobedo and de Pablo (482), instead of transferring an entire chain molecule from one box to another, the chain molecule is transferred in parts. Thus, during the course of the simulation, a chain molecule is chosen at random, and a part of it, made up of one or more united atoms, is removed from one box and added to the other box. Thus, parts of the selected chain

molecule exist simultaneously in both simulation boxes. In subsequent simulation steps, attempts are made to transfer the remainder of the molecule a part at a time, and this process is continued until the chain molecule as a whole occupies either of the boxes. After this, another chain molecule in the system is selected at random, and once again is subjected to the same procedure of transferring it in parts. The approach has been used by de Pablo and co-workers to investigate the pure component vapor–liquid equilibria of n-alkanes (469)and α-olefins (470), and the mixture equilibria of the two (470).

Widom's Test Particle Insertion Method. The solubility of small molecules at infinite dilution can be estimated based on the knowledge of the chemical potential of these molecules. Widom's test particle insertion method (483) provides a technique for calculating this quantity. The residual chemical potential (the difference between the chemical potentials of the fluid and the ideal gas at the same temperature and density) of a fluid is given by

$$\mu^r = -kT \ln\langle \exp(-U/kT)\rangle \tag{9}$$

where U is the energy of interaction between the test particle or molecule and the host matrix, and kT is Boltzmann's constant times the absolute temperature, as usual. The brackets denote an average over the fluidic host matrix containing N particles in a canonical ensemble. In application, a set of configurations of the host matrix is first generated from a simulation in a canonical ensemble using either MD or MC methods. The host matrix configurations are then frozen and the test molecule is inserted at a random location, and its interaction energy with the matrix is evaluated. The average in the above expression is calculated by repeating this process many times over (ie, by inserting the test molecule in several randomly chosen locations in the host matrix). The efficiency of the procedure can be improved by combining it with the "excluded volume map sampling" technique (484), which biases the insertion process such that the locations in the system where host matrix atoms are present are avoided. This approach has been used for obtaining the excess chemical potentials of methane, water, and ethanol in PE and PDMS (485) and for obtaining the chemical potentials of a series of penetrants (water, methane, argon, oxygen, etc) in amorphous PE (486).

As is to be expected with long chains, an insertion of a polymeric test molecule into a condensed phase will almost always result in interatomic overlaps with the host matrix atoms. Such an insertion will be rejected and will not contribute to the average denoted in the above expression. A modification of the technique thus has been proposed for polymers, where instead of inserting the entire polymer chain in the host matrix, only one segment is added to a preexisting chain (487). Kumar and co-workers (487) showed that this procedure yields the incremental residual chemical potential between a chain of length and $n+1$. The total chemical potential of a chain of length N can then be obtained by a simple, sequential sum of the incremental segmental potentials of all chains of lengths 1 through N. Furthermore, these authors also demonstrated that for simple bead-spring model chains, the incremental segmental chemical potential becomes independent of the chain length for chains longer than 5–10 beads, thus reducing the need for the number of simulations required for evaluating the sum of the incremental segmental chemical potentials for all of the longer chain lengths. This approach was used by Sheng and co-workers (488) to evaluate the chemical potentials of

bead-spring model chains of lengths up to 100. The vapor–liquid coexistence curves for these model systems were evaluated by devising an iterative procedure where coexisting vapor and liquid densities were found by requiring that the pressure and chemical potentials of the coexisting phases be equal.

Another approach for alleviating the problems encountered with polymer chain insertion in a condensed phase involves combining the Widom insertion process with the CCB chain growth method described earlier (489). Thus, instead of choosing a random conformation for the chain that is being inserted in the host matrix, positions of the first two segments of the chain are chosen at random, and then the rest of the chain is grown using the CCB method. This approach was used for evaluating the chemical potentials of alkanes as long as *n*-decane up to densities of 0.6 g/cc, using united atom models for these systems (489).

Even when the "test particle" being inserted is a small molecule, the straightforward Widom insertion process becomes impractical if the host matrix has a high density or if the chemical species in the system exhibit strong or long-range interactions. For studying such systems, Knopp and co-workers (490) proposed a modification that combines the Widom test particle insertion process with the technique of "thermodynamic integration." Suter and co-workers demonstrated the validity of such an approach by applying it to study the sorption behavior of water in polyamides (490,491), polycarbonate, and poly(vinyl alcohol) (492).

Outlook

Two major themes weave through the application of simulations to polymers. On the one hand there are efforts to extend the range of phenomena, as well as the time and length scales that are comprehensible, so as to gain an understanding of the universal phenomena that make polymers behave as they do. The other trend focusses on improvement in the accuracy of the description of the molecular structure and intermolecular interactions, so as to provide ever more accurate material properties predictions. We anticipate that both approaches will continue to be practiced side-by-side. The range of phenomena, relaxation times, and length scales is far from being exhausted. Simultaneously, there is a need to continue to improve accuracy so as to augment or even replace experiments where appropriate. Computer simulation is now firmly planted in the research enterprise as indispensably as are theory and experiment, and with each new and faster computer chip, we will see new polymer problems being solved.

BIBLIOGRAPHY

"Polymer Modeling" in *EPSE* 2nd ed., Vol. 12, pp. 605–617, by R. Potenzone Jr., Polygen Corp.

1. P. J. Flory, *Statistical Mechanics of Chain Molecules*, Wiley-Interscience, New York, 1969.
2. M. P. Allen and D. J. Tildesley, *Computer Simulation of Liquids*, Oxford University Press, Oxford, U.K., 1987.
3. B. R. Gelin, *Molecular Modeling of Polymer Structures and Properties*, Hanser Publishers, Munich, 1994.

4. K. Binder, ed., *Monte Carlo and Molecular Dynamics Simulations in Polymer Science*, Oxford University Press, Oxford, 1995.
5. L. Monnerie and U. W. Suter, ed., *Atomistic Modeling of Physical Properties*, Springer-Verlag, Berlin, 1994.
6. J. Bicerano, ed., *Computational Modeling of Polymers*, Marcel Dekker, Inc., New York, 1992.
7. W. L. Mattice and U. W. Suter, *Conformational Theory of Large Molecules: The Rotational Isomeric State Model in Macromolecular Systems*, Wiley-Interscience, New York, 1994.
8. M. Rehahn, W. L. Mattice, and U. W. Suter, *Adv. Polym. Sci.* **131/132**, 1-N157 (1997).
9. E. A. Colbourn, ed., *Computer Simulation of Polymers*, Longman Scientific and Technical, Essex, England, 1994.
10. G. C. Rutledge and D. N. Theodorou, ed., *Interdisciplinary Workshop on Molecular Modeling of Polymers: Wild Dunes*, Isle of Palms, South Carolina, Mar. 1–4, 1998, Wiley-VCH, Weinheim, Germany, 1998.
11. M. V. Volkenstein, *Configurational Statistics of Polymeric Chains*, Wiley-Interscience, New York, 1963.
12. T. M. Birshtein and O. B. Ptitsyn, *Conformations of Macromolecules*, Wiley-Interscience, New York, 1966.
13. F. T. Wall, L. A. Hiller, and D. J. Wheeler, *J. Chem. Phys.* **22**, 1036–1041 (1954).
14. E. Teramoto, M. Kurata, R. Chujo, C. Suzuki, K. Tani, and T. Kajikawa, *J. Phys. Soc. Jpn.* **10**, 953–959 (1955).
15. P. H. Verdier and W. H. Stockmayer, *J. Chem. Phys.* **36**, 227–235 (1962).
16. H. Yamakawa, *Modern Theory of Polymer Solutions*, Harper & Row, New York, 1971.
17. A. C. Balazs, Z. Zhou, and C. Yeung, *Langmuir* **15**, 2295–2300 (1992).
18. A. Broukhno, B. Jonsson, T. Akesson, and P. N. Vorontsov-Velyaminov, *J. Chem. Phys.* **113**, 5493–5501 (2000).
19. J. P. Downey, *Macromolecules* **27**, 2929–2932 (1994).
20. M. Muller and M. Schick, *J. Chem. Phys.* **105**, 8885–8901 (1996).
21. M. E. Starkweather, M. Muthukumar, and D. A. Hoagland, *Macromolecules* **32**, 6837–6840 (1999).
22. J. R. Hill, C. M. Freeman, and L. Subramanian, in K. B. Lipkowitz and D. B. Boyd, eds., *Review in Computational Chemistry*, Wiley-VCH, New York, 2000.
23. R. H. Boyd, *Macromolecules* **22**, 2477–2481 (1989).
24. R. H. Boyd and P. V. K. Pant, *Macromolecules* **24**, 6325–6331 (1991).
25. D. Reith, H. Meyer, and F. Muller-Plathe, *Macromolecules* **34**, 2335–2345 (2001).
26. W. L. Jorgensen, J. D. Madura, and C. J. Swenson, *J. Am. Chem. Soc.* **106**, 6638–6646 (1984).
27. S. K. Nath and J. J. de Pablo, *Mol. phys.* **98**, 231–238 (2000).
28. D. Rigby, private communication, 2000.
29. B. R. Brooks, R. E. Bruccoleri, B. D. Olafson, D. J. States, D. J. Swaminathan, and M. Karplus, *J. Comp. Chem.* **4**, 187–217 (1983).
30. S. L. Mayo, B. D. Olafson, and W. A. Goddard III, *J. Phys. Chem.* **94**, 8897–8909 (1990).
31. A. K. Rappe, C. J. Casewit, K. S. Colwell, W. A. Goddard III, and M. A. Skiff, *J. Am. Chem. Soc.* **114**, 10024–10035 (1992).
32. C. J. Casewit, K. S. Colwell, and A. K. Rappe, *J. Am. Chem. Soc.* **114**, 10035–10046 (1992).
33. C. J. Casewit, K. S. Colwell, and A. K. Rappe, *J. Am. Chem. Soc.* **114**, 10046–10053 (1992).
34. N. L. Allinger, Y. H. Yuh, and J. H. Lii, *J. Am. Chem. Soc.* **111**, 8551–8566 (1989).
35. J. R. Maple, M.-J. Hwang, T. P. Stockfisch, U. Dinur, M. Waldman, C. S. Ewig, and A. T. Hagler, *J. Comput. Chem.* **15**, 162–182 (1994).

36. J.-H. Lii and N. L. Allinger, *J. Comput. Chem.* **13**, 1138–1141 (1992).
37. J. H. Lii and N. L. Allinger, *J. Am. Chem. Soc.* **111**, 8566–8575 (1989).
38. J. H. Lii and N. L. Allinger, *J. Am. Chem. Soc.* **111**, 8576–8582 (1989).
39. N. L. Allinger, M. Rahman, and J. H. Lii, *J. Am. Chem. Soc.* **112**, 8293–8307 (1990).
40. N. L. Allinger, F. Li, and L. Yan, *J. Comput. Chem.* **11**, 848–867 (1990).
41. L. R. Schmitz and N. L. Allinger, *J. Am. Chem. Soc.* **112**, 8307–8315 (1990).
42. N. L. Allinger, M. Quinn, M. Rahman, and K. Chen, *J. Phys. Org. Chem.* **4**, 647–658 (1991).
43. N. L. Allinger, K. S. Chen, M. Rahman, and A. Pathiaseril, *J. Am. Chem. Soc.* **113**, 4505–4517 (1991).
44. K. Chen and N. L. Allinger, *J. Phys. Org. Chem.* **4**, 659–666 (1991).
45. N. L. Allinger, S. Rodrigues, and K. Chen, *J. Mol. Struct. (Theochem.)* **260**, 161–178 (1992).
46. N. L. Allinger, Z. Q. S. Zhu, and K. Chen, *J. Am. Chem. Soc.* **114**, 6120–6133 (1992).
47. N. L. Allinger and Y. Fan, *J. Comput. Chem.* **14**, 655–666 (1993).
48. N. L. Allinger, Y. Fan, and T. Varnali, *J. Phys. Org. Chem.* **9**, 159–167 (1996).
49. N. L. Allinger and Y. Fan, *J. Comput. Chem.* **15**, 251–268 (1994).
50. K. Palmo, L.-O. Pietila, and S. Krimm, *J. Comput. Chem.* **12**, 385–390 (1991).
51. W. Qian, N. G. Mirkin, and S. Krimm, *Chem. Phys. Lett.* **315**, 125–129 (1999).
52. B. Mannfors, K. Palmo, and S. Krimm, *J. Mol. Struct.* **556**, 1–21 (2000).
53. J. R. Maple, M. J. Hwang, T. P. Stockfisch, and A. T. Hagler, *Isr. J. Chem.* **34**, 195–231 (1994).
54. A. T. Hagler, R. Sharon, and M.-J. Hwang, *J. Am. Chem. Soc.* **118**, 3759–3760 (1996).
55. Z. Peng, C. S. Ewig, M.-J. Hwang, M. Waldman, and A. T. Hagler, *J. Phys. Chem. A* **101**, 7243–7252 (1997).
56. M.-J. Hwang, X. Ni, M. Waldman, C. S. Ewig, and A. T. Hagler, *Biopolymers* **45**, 435–468 (1998).
57. C. S. Ewig, T. S. Thacher, and A. T. Hagler, *J. Phys. Chem. B* **103**, 6998–7014 (1999).
58. W. L. Jorgensen and N. A. McDonald, *J. Mol. Struct. (Theochem.)* **424**, 145–155 (1998).
59. H. Sun, *J. Phys. Chem. B* **102**, 7338–7364 (1998).
60. D. B. Holt and B. L. Farmer, *Polymer* **40**, 4667–4672 (1999).
61. S. Ahmed, S. A. Bidstrup, P. A. Kohl, and P. J. Ludovice, *J. Phys. Chem. B* **102**, 9783–9790 (1998).
62. W. L. Jorgensen, D. S. Maxwell, and J. Tirado-Rives, *J. Am. Chem. Soc.* **118**, 11225–11236 (1996).
63. P. A. Kollman, D. A. Case, D. A. Pearlman, J. W. Caldwell, T. E. Cheatham III, J. Wang, W. S. Ross, C. Simmerling, T. Darden, K. M. Merz, R. V. Stanton, A. Cheng, J. J. Vincent, M. Crowley, V. Tsui, H. Gohlke, R. Radmer, Y. Duan, J. Pitera, I. Massova, G. L. Seibel, U. C. Singh, and P. Weiner, Amber web site: <http://www.amber.ucsf.edu/amber/>, 2000.
64. W. L. Jorgensen, J. Chandrasekhar, J. D. Madura, R. W. Impey, and M. L. Klein, *J. Chem. Phys.* **79**, 926–935 (1983).
65. W. F. van Gunsteren and H. J. C. Berendsen, *Gromos Manual*, <http://www.igc.ethz.ch/gromos/>, 2001.
66. *Gromacs User Manual, Version 3.0*, Bioson Research Institute, <http://www.gromacs.org/>, 1999.
67. A. R. van Buuren, S. J. Marrink, and H. J. C. Berendsen, *J. Phys. Chem.* **97**, 9206–9212 (1993).
68. A. E. Mark, S. P. van Helden, P. E. Smith, L. H. M. Janssen, and W. F. van Gunsteren, *J. Am. Chem. Soc.* **116**, 6293–6302 (1994).
69. D. Rigby and R. J. Roe, *J. Chem. Phys.* **87**, 7285–7292 (1987).
70. R. H. Boyd and P. V. K. Pant, *Macromolecules* **24**, 4073–4077 (1991).

71. R. L. Jaffe, G. D. Smith, and D. Y. Yoon, *J. Phys. Chem.* **97**, 12745–12751 (1993).
72. G. D. Smith, R. L. Jaffe, and D. Y. Yoon, *J. Phys. Chem.* **97**, 12752–12759 (1993).
73. G. D. Smith, R. L. Jaffe, and H. Partridge, *J. Phys. Chem. A* **101**, 1705–1715 (1997).
74. P. Ahlstrom, O. Borodin, G. Wahnstrom, E. J. W. Wensink, P. Carlsson, and G. D. Smith, *J. Chem. Phys.* **112**, 10669–10679 (2000).
75. G. D. Smith and W. Paul, *J. Phys. Chem. A* **102**, 1200–1208 (1998).
76. J. Chang, R. L. Jaffe, L. Yang, and D. Y. Yoon, *Polym. Mater. Sci. Eng.* **85**, 236–237 (2001).
77. Y. Abe, K. Tashiro and M. Kobayashi, *Comp. Theor. Polym. Sci.* **10**, 323–333 (2000).
78. M. S. Hedenqvist, R. Bharadwaj, and R. H. Boyd, *Macromolecules* **31**, 1556–1564 (1998).
79. R. K. Bharadwaj and R. H. Boyd, *Polymer* **40**, 4229–4236 (1999).
80. J. A. Young, B. L. Farmer, and J. A. Hinkley, *Polymer* **40**, 2787–2795 (1999).
81. J. Ennari, M. Elomaa, and F. Sundholm, *Polymer* **40**, 5035–5041 (1999).
82. B. J. Sherman, S. Sen, and V. Galiatsatos, *Polymer* **37**, 1759–1764 (1996).
83. N. Karasawa and W. A. Goddard III, *Macromolecules* **25**, 7268–7281 (1992).
84. J. D. Carbeck, D. J. Lacks, and G. C. Rutledge, *J. Chem. Phys.* **103**, 10347–10355 (1995).
85. R. H. Boyd and L. Kesner, *J. Chem Phys.* **72**, 2179–2190 (1980).
86. B. Ma, J. H. Lii, and N. L. Allinger, *J. Comput. Chem.* **21**, 813–825 (2000).
87. A. K. Rappe, M. A. Pietsch, D. C. Wiser, J. R. Hart, L. M. Bormann-Rochotte, and M. A. Skiff, *Mol. Eng.* **7**, 385–400 (1997).
88. J. Che, T. Cagin, and W. A. Goddard III, *Theor. Chem. Acc.* **102**, 346–354 (1999).
89. M. R. Nyden and J. W. Gilman, *Comp. Theor. Polym. Sci.* **7**, 191–198 (1997).
90. M. R. Nyden, T. R. Coley, and S. Mumby, *Polym. Eng. Sci.* **37**, 1496–1500 (1997).
91. R. Car and M. Parrinello, *Phys. Rev. Lett.* **55**, 2471–2474 (1985).
92. Y. W. Hsiao, K. Runge, M. G. Cory, and R. J. Bartlett, *J. Phys. Chem. A* **105**, 7004–7010 (2001).
93. N. Metropolis, A. W. Rosenbluth, M. N. Rosenbluth, A. H. Teller, and E. Teller, *J. Chem. Phys.* **21**, 1087–1092 (1953).
94. M. Vacatello, G. Avitabile, P. Corradini, and A. Tuzi, *J. Chem. Phys.* **73**, 548–552 (1980).
95. J. I. McKechnie, D. Brown, and J. H. R. Clarke, *Macromolecules* **25**, 1562–1567 (1992).
96. D. N. Theodorou and U. W. Suter, *Macromolecules* **18**, 1467–1478 (1985).
97. P. J. Ludovice and U. W. Suter, in Ref. 6, pp. 401–435.
98. M. Hutnik, F. T. Gentile, P. J. Ludovice, U. W. Suter, and A. S. Argon, *Macromolecules* **24**, 5962–5969 (1991).
99. M. Hutnik, A. S. Argon, and U. W. Suter, *Macromolecules* **24**, 5970–5979 (1991).
100. R. F. Rapold, U. W. Suter, and D. N. Theodorou, *Macromol. Theory Simul.* **3**, 19–43 (1994).
101. H. Meirovitch, *J. Chem. Phys.* **79**, 502–508 (1983).
102. H. Meirovitch, *J. Chem. Phys.* **114**, 3859–3867 (2001).
103. Amorphous Cell On-line Help, Materials Studio, Version 2.0, Accelrys Inc., San Diego, Calif., 2001.
104. R. Khare, M. E. Paulaitis, and S. R. Lustig, *Macromolecules* **26**, 7203–7209 (1993).
105. M. Kotelyanskii, N. J. Wagner, and M. E. Paulaitis, *Macromolecules* **29**, 8497–8506 (1996).
106. P. Doruker and W. L. Mattice, *Macromol. Symp.* **133**, 47–70 (1998).
107. J. H. Jang and W. L. Mattice, *Polymer* **40**, 4685–4694 (1999).
108. M. Muller, J. Nievergelt, S. Santos, and U. W. Suter, *J. Chem. Phys.* **114**, 9764–9771 (2001).
109. P. Robyr, M. Muller, and U. W. Suter, *Macromolecules* **32**, 8681–8684 (1999).
110. T. Weber and E. Helfand, *J. Chem. Phys.* **71**, 4760–4762 (1979).

111. L. Verlet, *Phys. Rev.* **159**, 98–103 (1967).
112. U. W. Suter, private communication, 2001.
113. H. C. Andersen, *J. Chem. Phys.* **72**, 2384–2393 (1980).
114. S. Nose, *Mol. Phys.* **52**, 255–268 (1984).
115. S. Nose, *J. Chem. Phys.* **81**, 511–519 (1984).
116. H. J. C. Berendsen, J. P. M. Postma, W. F. van Gunsteren, A. DiNola, and J. R. Haak, *J. Chem. Phys.* **81**, 3684–3690 (1984).
117. J. P. Ryckaert, G. Ciccotti, and H. J. C. Berendsen, *J. Comput. Phys.* **23**, 327–341 (1977).
118. W. F. van Gunsteren and H. J. C. Berendsen, *Mol. Phys.* **34**, 1311–1327 (1977).
119. H. C. Andersen, *J. Comput. Phys.* **52**, 24–34 (1983).
120. M. Tuckerman, B. J. Berne, and G. J. Martyna, *J. Chem Phys.* **97**, 1990–2001 (1992).
121. H. Q. Ding, N. Karasawa, and W. A. Goddard III, *J. Chem Phys.* **97**, 4309–4315 (1992).
122. D. W. Noid, K. Fukui, B. G. Sumpter, C. Yang, and R. E. Tuzun, *Chem. Phys. Lett.* **316**, 285–296 (2000).
123. G. C. Rutledge, D. J. Lacks, R. Martonak, and K. Binder, *J. Chem. Phys.* **108**, 10274–10280 (1998).
124. P. H. Berens, D. H. J. Mackay, G. M. White, and K. R. Wilson, *J. Chem. Phys.* **79**, 2375–2390 (1983).
125. R. E. Tuzun, B. G. Sumpter, and D. W. Noid, *Macromol. Theory Simul.* **7**, 203–209 (1998).
126. R. Martonak, W. Paul, and K. Binder, *Phys. Rev. E* **57**, 2425–2437 (1998).
127. R. Martonak, W. Paul, and K. Binder, *J. Chem. Phys.* **106**, 8918–8930 (1997).
128. R. J. Hardy, D. J. Lacks, and R. C. Shukla, *Phys. Rev. B* **57**, 833–838 (1998).
129. A. Soldera and J.-P. Dognon, *Macromol. Symp.* **119**, 157–164 (1997).
130. U. W. Suter and B. E. Eichinger, *Polymer* **43**, 575–582 (2002).
131. R. H. Boyd and P. V. K. Pant, *Macromolecules* **24**, 4078–4083 (1991).
132. A. A. Gusev, S. Arizzi, U. W. Suter, and D. J. Moll, *J. Chem. Phys.* **99**, 2221–2227 (1993).
133. A. Poncela, A. M. Rubio, and J. J. Freire, *J. Chem. Phys.* **114**, 8174–8180 (2001).
134. E. Leontidis, B. M. Forrest, A. H. Widmann, and U. W. Suter, *J. Chem. Soc., Faraday Trans.* **91**, 2355–2368 (1995).
135. M. P. Pepin and M. D. Whitmore, *J. Chem. Phys.* **114**, 8181–8195 (2001).
136. B. M. Forrest and U. W. Suter, *J. Chem. Phys.* **101**, 2616–2629 (1994).
137. B. M. Forrest and U. W. Suter, *Mol. Phys.* **82**, 393–410 (1994).
138. L. Toma, S. Toma, and J. A. Subirana, *Macromolecules* **31**, 2328–2334 (1998).
139. J. D. Honeycutt, *Comp. Theor. Polym. Sci.* **8**, 1–8 (1998).
140. N. Madras and A. D. Sokal, *J. Stat. Phys.* **50**, 109–186 (1988).
141. M. Lal, *Mol. Phys.* **17**, 57–64 (1969).
142. G. Favrin, A. Irback, and F. Sjunnesson, *J. Chem. Phys.* **114**, 8154–8158 (2001).
143. D. J. R. Taylor, R. F. T. Stepto, R. A. Jones, and I. M. Ward, *Macromolecules* **32**, 1978–1989 (1999).
144. A. C. Balazs, K. Huang, and C. W. Lantman, *Macromolecules* **23**, 4641–4647 (1990).
145. P. V. K. Pant and D. N. Theodorou, *Macromolecules* **28**, 7224–7234 (1995).
146. A. Uhlherr, *Macromolecules* **33**, 2351–2360 (2000).
147. S. Balijepalli and G. C. Rutledge, *J. Chem. Phys.* **109**, 6523–6526 (1998).
148. J. Huh, V. V. Ginzburg, and A. C. Balazs, *Macromolecules* **33**, 8085–8096 (2000).
149. D. Frenkel, G. C. A. M. Mooij, and B. Smit, *J. Phys.: Condens. Matter* **3**, 3053–3076 (1991).
150. J. I. Siepmann and D. Frenkel, *Mol. Phys.* **75**, 59–70 (1992).
151. J. J. de Pablo, M. Laso, and U. W. Suter, *J. Chem. Phys.* **96**, 2395–2403 (1992).
152. V. G. Mavrantzas, T. D. Boone, E. Zervopoulou, and D. N. Theodorou, *Macromolecules* **32**, 5072–5096 (1999).

153. L. Dodd, T. D. Boone, and D. N. Theodorou, *Mol. Phys.* **78**, 961–996 (1993).
154. C. D. Wick and J. I. Siepmann, *Macromolecules* **33**, 7207–7218 (2000).
155. Z. Chen and F. A. Escobedo, *J. Chem. Phys.* **113**, 11382–11392 (2000).
156. J. Sadanobu and W. A. Goddard III, *Fluid Phase Equilib.* **144**, 415, (1998).
157. W. L. Jorgensen and J. Tirado-Rives, *J. Phys. Chem.* **100**, 14508–14513 (1996).
158. A. Z. Panagiotopoulos, *Mol. Phys.* **61**, 813 (1987).
159. A. Z. Panagiotopoulos, N. Quirke, M. Stapleton, and D. J. Tildesley, *Mol. Phys.* **63**, 527–545 (1988).
160. J. L. Rivera, J. Alejandre, S. K. Nath, and J. J. de Pablo, *Mol. Phys.* **98**, 43–55 (2000).
161. A. Liu and T. Beck, *J. Phys. Chem. B* **102**, 7627–7631 (1998).
162. J. J. de Pablo, M. Laso, and U. W. Suter, *J. Chem. Phys.* **97**, 2817–2819 (1992).
163. A. M. Ferrenberg and R. H. Swendsen, *Phys. Rev. Lett.* **61**, 2635–2638 (1988).
164. A. M. Ferrenberg and R. H. Swendsen, *Phys. Rev. Lett.* **63**, 1195–1198 (1989).
165. A. Z. Panagiotopoulos, V. Wong, and M. A. Floriano, *Macromolecules* **31**, 912–918 (1998).
166. P. B. Conrad and J. J. de Pablo, *Fluid Phase Equilib.* **150/151**, 51–61 (1998).
167. J. R. Errington and A. Z. Panagiotopoulos, *J. Phys. Chem. B* **103**, 6314–6322 (1999).
168. J. R. Errington and A. Z. Panagiotopoulos, *J. Chem. Phys.* **111**, 9731–9738 (1999).
169. M. C. Tesi, E. J. J. van Rensburg, E. Orlandini, and S. G. Whittington, *J. Stat. Phys.* **82**, 155–180 (1996).
170. U. H. E. Hansmann, *Chem. Phys. Lett.* **281**, 140–150 (1997).
171. D. Bedrov and G. D. Smith, *J. Chem. Phys.* **115**, 1121–1124 (2001).
172. Q. Yan and J. J. de Pablo, *J. Chem. Phys.* **111**, 9509–9516 (1999).
173. Q. Yan and J. J. de Pablo, *J. Chem. Phys.* **113**, 1276–1282 (2000).
174. I. Carmesin and K. Kremer, *Macromolecules* **21**, 2819–2823 (1988).
175. P. Doruker and W. L. Mattice, *Macromol. Theory Simul.* **8**, 463–478 (1999).
176. K. Binder, J. Baschnagel, C. Bennemann, and W. Paul, *J. Phys.: Condens. Matter* **11**, A47–A55 (1999).
177. J. Baschnagel, W. Paul, V. Tries, and K. Binder, *Macromolecules* **31**, 3856–3867 (1998).
178. K. Okun, M. Wolfgardt, J. Baschnagel, and K. Binder, *Macromolecules* **30**, 3075–3085 (1997).
179. B. Zimm, *J. Chem. Phys.* **24**, 269–278 (1956).
180. J.-W. Liu and Y.-Q. Ma, *J. Chem. Phys.* **113**, 6398–6403 (2000).
181. M. W. Matsen and M. Schick, *Phys. Rev. Lett.* **72**, 2660–2663 (1994).
182. M. W. Matsen, *J. Chem. Phys.* **113**, 5539–5544 (2000).
183. F. Drolet and G. H. Fredrickson, *Phys. Rev. Lett.* **83**, 4317–4320 (1999).
184. F. Drolet and G. H. Fredrickson, *Macromolecules* **34**, 5317–5324 (2001).
185. J. G. E. M. Fraaije, B. A. C. van Vlimmeren, N. M. Maurits, M. Postma, O. A. Evers, C. Hoffman, P. Altevogt, and G. Goldbeck-Wood, *J. Chem. Phys.* **106**, 4260–4289 (1997).
186. D. Nicolaides, *Mol. Simul.* **26**, 51–72 (2001).
187. T. Spyriouni and C. Vergelati, *Macromolecules* **34**, 5306–5316 (2001).
188. H. Yokoyama, E. J. Kramer, and G. H. Fredrickson, *Macromolecules* **33**, 2249–2257 (2000).
189. V. V. Ginzburg, F. Qiu, M. Paniconi, G. Peng, D. Jasnow, and A. C. Balazs, *Phys. Rev. Lett.* **82**, 4026–4029 (1999).
190. F. Qiu, V. V. Ginzburg, M. Paniconi, G. Peng, D. Jasnow, and A. C. Balazs, *Langmuir* **15**, 4952–4956 (1999).
191. P. J. Hoogerbrugge and J. M. V. A. Koelman, *Europhys. Lett.* **19**, 155–160 (1992).
192. R. D. Groot, T. J. Madden, and D. J. Tildesley, *J. Chem. Phys.* **110**, 9739–9749 (1999).
193. A. G. Schlijper, P. J. Hoogerbrugge, and C. W. Manke, *J. Rheol.* **39**, 567–579 (1995).
194. P. Espanol and P. B. Warren, *Europhys. Lett.* **30**, 191–196 (1995).

195. R. L. C. Akkermans and W. J. Briels, *J. Chem. Phys.* **113**, 6409–6422 (2000).
196. V. V. Ginzburg, C. Gibbons, F. Qiu, G. Peng, and A. C. Balazs, *Macromolecules* **33**, 6140–6147 (2000).
197. T. Pakula, K. Karatasos, S. H. Anastasiadis, and G. Fytas, *Macromolecules* **30**, 8463–8472 (1997).
198. R. L. C. Akkermans and W. J. Briels, *J. Chem. Phys.* **114**, 1020–1031 (2001).
199. K. Kremer and F. Muller-Plathe, *MRS Bull.* **26**, 205–210 (2001).
200. Y. Tsori, D. Andelman, and M. Schick, *Phys. Rev. E* **61**, 2848 (2000).
201. R. D. Groot and P. B. Warren, *J. Chem. Phys.* **107**, 4423–4435 (1997).
202. S. Puri and H. L. Frisch, *Int. J. Mod. Phys. B* **12**, 1623–1641 (1998).
203. S. Balijepalli and G. C. Rutledge, *Comp. Theor. Polym. Sci.* **10**, 103–113 (2000).
204. T. A. Kavassalis and P. R. Sundararajan, *Macromolecules* **26**, 4144–4150 (1993).
205. C. Liu and M. Muthukumar, *J. Chem. Phys.* **109**, 2536–2542 (1998).
206. M. Muthukumar and P. Welch, *Polymer* **41**, 8833–8837 (2000).
207. W. Hu, *J. Chem. Phys.* **115**, 4395–4401 (2001).
208. G. Goldbeck-Wood, *Macromol. Symp.* **81**, 221–234 (1994).
209. K. L. Anderson and G. Goldbeck-Wood, *Polymer* **41**, 8849–8855 (2000).
210. J. P. K. Doye and D. Frenkel, *Polymer* **41**, 1519–1528 (2000).
211. J. P. K. Doye, *Polymer* **41**, 8857–8867 (2000).
212. R. D. Groot, *Langmuir* 7493–7502 (2000).
213. P. G. Bolhuis, A. A. Louis, J. P. Hansen, and E. J. Meijer, *J. Chem. Phys.* **114**, 4296–4311 (2001).
214. F. Eurich and P. Maass, *J. Chem. Phys.* **114**, 7655–7668 (2001).
215. J. T. Padding and W. J. Briels, *J. Chem. Phys.* **115**, 2846–2859 (2001).
216. X.-F. Yuan, and M. Doi, *Colloids Surf. A: Physicochem. Eng. Aspects* **144**, 305–318 (1998).
217. T. Okuzono, H. Shibuya, and M. Doi, *Phys. Rev. E* **61**, 4100–4106 (2000).
218. R. K. Bharadwaj, T. J. Bunning, and B. L. Farmer, *Liq. Cryst.* **27**, 591–603 (2000).
219. H. E. Assender and A. H. Windle, *Macromolecules* **27**, 3439–3441 (1994).
220. P. J. Flory, *Principles of Polymer Chemistry*, Cornell University Press, Ithaca, N.Y., 1953.
221. E. R. Duering, K. Kremer, and G. S. Grest, *Macromolecules* **26**, 3241–3244 (1993).
222. G. S. Grest, K. Kremer, and E. R. Duering, *Physica A* **194**, 330–337 (1993).
223. F. Muller-Plathe, *Ber. Bunsenges. Phys. Chem.* **102**, 1679 (1998).
224. R. A. Jones, J. I. Cail, R. F. T. Stepto, and I. M. Ward, *Macromolecules* **33**, 7337–7344 (2000).
225. G. S. Grest, M. Putz, R. Everaers, and K. Kremer, *J. Non-Cryst. Solids* **274**, 139–146 (2000).
226. Y.-K. Leung and B. E. Eichinger, in S. S. Labana and R. A. Dickie, eds., *Characterization of Highly Cross-Linked Polymers*, American Chemical Society, Washington, D.C., 1984.
227. L. Y. Shy and B. E. Eichinger, *Macromolecules* **19**, 2787–2793 (1986).
228. V. Galiatsatos and B. E. Eichinger, *J. Polym. Sci., B: Polym. Phys.* **26**, 595–602 (1988).
229. H. Tobita, *J. Polym. Sci., B: Polym. Phys.* **39**, 391–403 (2001).
230. H. Tobita, *J. Polym. Sci., B: Polym. Phys.* **39**, 404–414 (2001).
231. J. Somvarsky and K. Dusek, *Polym. Bull.* **33**, 369–376 (1994).
232. J. Somvarsky and K. Dusek, *Polym. Bull.* **33**, 377–384 (1994).
233. K. Dusek and J. Somvarsky, *Macromol. Symp.* **106**, 119–136 (1996).
234. J. Somvarsky, K. Dusek, and M. Smrckova, *Comp. Theor. Polym. Sci.* **8**, 201–208 (1998).
235. H. Rolfes and R. F. T. Stepto, *Comp. Theor. Polym. Sci.* **1**, 100–106 (1990).
236. H. Rolfes and R. F. T. Stepto, *Makromol. Chem. Theory Simul.* **1**, 245–260 (1992).

237. D. R. Miller and C. W. Macosko, *J. Polym. Sci., B: Polym. Phys.* **26**, 1–54 (1987).
238. Y. Masubuchi, J. I. Takimoto, K. Koyama, G. Ianniruberto, G. Marrucci, and F. Greco, *J. Chem. Phys.* **115**, 4387–4394 (2001).
239. G. Heinrich and M. Kaliske, *Comp. Theor. Polym. Sci.* **7**, 227–241 (1997).
240. C. W. Burkhart, *Rubber Chem. Tech.* **71**, 342–406 (1998).
241. N. Gilra, C. Cohen, and A. Z. Panagiotopoulos, *J. Chem. Phys.* **112**, 6910–6916 (2000).
242. N. Gilra, A. Z. Panagiotopoulos, and C. Cohen, *J. Chem. Phys.* **115**, 1100–1104 (2001).
243. D. W. Van Krevelen, *Properties of Polymers: Their Estimation and Correlation with Chemical Structure*, 2nd ed., Elsevier, Amsterdam, 1976.
244. D. Porter, *Group Interaction Modelling of Polymer Properties*, Marcel Dekker, Inc., New York, 1995.
245. J. Bicerano, *Prediction of Polymer Properties*, Marcel Dekker Inc., New York, (1993).
246. J. Bicerano, J. F. Douglas, and D. A. Brune, *J. Macromol. Sci.-Rev. Macromol. Chem. Phys., C* **39**, 561–642 (1999).
247. J. S. Todarski, A. J. Hopfinger, J. D. Hobbs, D. M. Ford, and J.-L. M. Faulon, *Comp. Theor. Polym. Sci.* **7**, 199–214 (1997).
248. J. Baschnagel, M. Wolfgardt, W. Paul, and K. Binder, *J. Res. Natl. Inst. Stand. Technol.* **102**, 159–170 (1997).
249. J. H. Gibbs and E. A. Di Marzio, *J. Chem. Phys.* **28**, 373–383 (1958).
250. E. A. Di Marzio and J. H. Gibbs, *J. Chem. Phys.* **28**, 807–813 (1958).
251. K. Krishnaswamy and M. Fixman, *J. Mol. Liq.* **61**, 209–220 (1994).
252. S. K. Nath, P. F. Nealey, and J. J. de Pablo, *J. Chem. Phys.* **110**, 7483–7490 (1999).
253. Q. Wang, S. K. Nath, M. D. Graham, P. F. Nealey, and J. J. de Pablo, *J. Chem. Phys.* **112**, 9996–10010 (2000).
254. Q. Wang, P. F. Nealey, and J. J. de Pablo, *Macromolecules* **34**, 3458–3470 (2001).
255. D. G. Gromov and J. J. de Pablo, *J. Chem. Phys.* **109**, 10042–10052 (1998).
256. C. S. Patrickios and L. Lue, *J. Chem. Phys.* **113**, 5485–5492 (2000).
257. J. G. Curro, K. G. Honnell, and J. D. McCoy, *Macromolecules* **30**, 145–152 (1997).
258. A. Yethiraj, H. Fynewever, and C.-Y. Shew, *J. Chem. Phys.* **114**, 4323–4330 (2001).
259. D. A. McQuarrie, *Statistical Mechanics*, Harper & Row, New York, 1976.
260. J. G. Curro, J. D. Weinhold, J. J. Rajasekaran, A. Habenschuss, J. D. Londono, and J. D. Honeycutt, *Macromolecules* **30**, 6264–6273 (1997).
261. L. G. MacDowell, M. Muller, C. Vega, and K. Binder, *J. Chem. Phys.* **113**, 419–433 (2000).
262. J. Jiang, Q. Yan, H. Liu, and Y. Hu, *Macromolecules* **30**, 8459–8462 (1997).
263. J. Dudowicz and K. F. Freed, *Macromolecules* **31**, 5094–5104 (1998).
264. K. F. Freed and J. Dudowicz, *Macromolecules* **31**, 6681–6690 (1998).
265. L. Zhang, Y. Xu and D. Zhao, *Eur. Polym. J.* **36**, 1607–1611 (2000).
266. M. A. Sharaf, A. Kloczkowski, and J. E. Mark, *Comp. Theor. Polym. Sci.* **11**, 251–262 (2001).
267. R. H. Gee, D. Henderson, and D. T. Wasan, *J. Colloid. Interface Sci.* **232**, 39–44 (2000).
268. A. C. Balazs, V. V. Ginzburg, F. Qiu, G. Peng, and D. Jasnow, *J. Phys. Chem. B* **104**, 3411–3422 (2000).
269. E. Hackett, E. Manias, and E. P. Giannelis, *J. Chem. Phys.* **108**, 7410–7415 (1998).
270. D. Shia, C. Y. Hui, S. D. Burnside, and E. P. Giannelis, *Polym. Compos.* **19**, 608–617 (1998).
271. A. C. Balazs, C. Singh, and E. B. Zhulina, *Macromolecules* **31**, 8370–8381 (1998).
272. Y. Wang and I. Teraoka, *Macromolecules* **30**, 8473–8477 (1997).
273. Q. Wang, Q. Yan, P. F. Nealey, and J. J. de Pablo, *J. Chem. Phys.* **112**, 450–464 (2000).
274. A. A. Gusev, P. J. Hine, and I. M. Ward, *Compos. Sci. Technol.* **60**, 535–541 (2000).
275. A. A. Gusev, *Macromolecules* **34**, 3081–3093 (2001).
276. G. Tanaka and W. L. Mattice, *Macromol. Theory Simul.* 1119–1137 (1997).

277. V. Vao-soongnern, P. Doruker, and W. L. Mattice, *Macromol. Theory Simul.* **9**, 1–13 (2000).
278. R. K. Bharadwaj, R. J. Berry, and B. L. Farmer, *Polymer* **41**, 7209–7221 (2000).
279. L. A. Castonguay and A. K. Rappe, *J. Am. Chem. Soc.* **114**, 5832–5842 (1992).
280. K. Thorshaug, J. A. Stovneng, E. Rytter, and M. Ystenes, *Macromolecules* **31**, 7149–7165 (1998).
281. A. K. Rappe, M. A. Skiff, and C. J. Casewit, *Chem. Rev.* **100**, 1435–1456 (2000).
282. J. P. A. Heuts, R. G. Gilbert, and L. Radom, *Macromolecules* **28**, 8771–8781 (1995).
283. M. Boero, M. Parrinello, H. Weiss, and S. Huffer, *J. Phys. Chem. A* **105**, 5096–5105 (2001).
284. G. S. Grest, K. Kremer, and E. R. Duering, *Europhys. Lett.* **19**, 195–200 (1992).
285. D. C. Doherty, B. N. Holmes, P. Leung, and R. B. Ross, *Comp. Theor. Polym. Sci.* **8**, 169–178 (1998).
286. R. A. Jones, D. J. R. Taylor, J. I. Cail, R. F. T. Stepto, and I. M. Ward, *Macromolecules* **32**, 8350–8355 (1999).
287. J. A. Young, J. A. Hinkley, and B. L. Farmer, *Macromolecules* **33**, 4936–4944 (2000).
288. T. Nemoto, S. Yonezawa, T. Soda, and K. Takeda, *Poly. Degrad. Stab.* **69**, 191–196 (2000).
289. D. J. Dooling and L. Broadbelt, *Ind. Eng. Chem. Res.* **40**, 522–529 (2001).
290. M. P. Taylor, *J. Chem. Phys.* **114**, 6472–6484 (2001).
291. T. Pakula and K. Jeszka, *Macromolecules* **32**, 6821–6830 (1999).
292. G. D. Smith, D. Bedrov, and O. Borodin, *J. Am. Chem. Soc.* **122**, 9548–9549 (2000).
293. J. E. Mark and J. G. Curro, *J. Chem. Phys.* **79**, 5705–5709 (1983).
294. J. I. Cail, D. J. R. Taylor, R. F. T. Stepto, M. G. Brereton, R. A. Jones, M. E. Ries, and I. M. Ward, *Macromolecules* **33**, 4966–4971 (2000).
295. G. Srinivas, A. Yethiraj, and B. Bagchi, *J. Phys. Chem. B* **105**, 2475–2478 (2001).
296. W. Paul and M. Muller, *J. Chem. Phys.* **115**, 630–635 (2001).
297. T. Haliloglu and W. L. Mattice, *Macromol. Theory Simul.* **6**, 667 (1997).
298. A. C. Balazs and C. P. Siemasko, *J. Chem. Phys.* **95**, 3798–3803 (1991).
299. C. Y. Kong and M. Muthukumar, *J. Chem. Phys.* **109**, 1522–1527 (1998).
300. J. C. Meredith, I. C. Sanchez, K. P. Johnston, and J. J. de Pablo, *J. Chem. Phys.* **109**, 6424–6434 (1998).
301. E. Lindberg and C. Elvingson, *J. Chem. Phys.* **114**, 6343–6352 (2001).
302. J. H. Jang, R. Ozisik, and W. L. Mattice, *Macromolecules* **33**, 7663–7671 (2000).
303. J. Chang, J. Han, L. Yang, R. L. Jaffe, and D. Y. Yoon, *J. Chem. Phys.* **115**, 2831–2840 (2001).
304. J. A. Torres, P. F. Nealey, and J. J. de Pablo, *Phys. Rev. Lett.* **85**, 3221–3224 (2000).
305. D. E. Kranbuehl, R. R. Knowles, A. M. Hossain, and A. M. Gilchriest, *Polym. Mater. Sci. Eng.* **85**, 239 (2001).
306. T. Aoyagi, J.-I. Takimota, and M. Doi, *J. Chem. Phys.* **115**, 552–559 (2001).
307. A. Milchev and K. Binder, *J. Chem. Phys.* **114**, 8610–8618 (2001).
308. A. A. Gusev, F. Muller-Plathe, W. F. van Gunsteren, and U. W. Suter, *Adv. Polym. Sci.* **116**, 207–247 (1994).
309. T. R. Cuthbert, N. J. Wagner, M. E. Paulaitis, G. Murgia, and B. D'Aguanno, *Macromolecules* **32**, 5017–5028 (1999).
310. H. Takeuchi and K. Okazaki, *J. Chem. Phys.* **92**, 5643–5652 (1990).
311. H. Takeuchi, *J. Chem. Phys.* **93**, 2062–2067 (1990).
312. H. Takeuchi, *J. Chem. Phys.* **93**, 4490–4491 (1990).
313. H. Takeuchi, *J. Chem. Phys.* **93**, 9042–9048 (1990).
314. P. V. K. Pant and R. H. Boyd, *Macromolecules* **25**, 494–495 (1992).
315. P. V. K. Pant and R. H. Boyd, *Macromolecules* **26**, 679–686 (1993).
316. S. Trohalaki, A. Kloczkowski, J. E. Mark, R. J. Roe, and D. Rigby, *Comput. Polym. Sci.* **2**, 147–151 (1992).

317. S. Trohalaki, D. Rigby, A. Kloczkowski, J. E. Mark, and R. J. Roe, *Polym. Prepr.* **30**, 23–24 (1989).
318. J. Han and R. H. Boyd, *Macromolecules* **27**, 5365–5370 (1994).
319. J. Han and R. H. Boyd, *Polymer* **37**, 1797–1804 (1996).
320. E. von Meerwall, S. Beckman, J. Jang, and W. L. Mattice, *J. Chem. Phys.* **108**, 4299–4304 (1998).
321. E. von Meerwall, E. J. Feick, R. Ozisik, and M. L., *J. Chem. Phys.* **111**, 750–757 (1999).
322. F. Muller-Plathe, *J. Chem. Phys.* **96**, 3200–3205 (1992).
323. F. Muller-Plathe, S. C. Rogers, and W. F. van Gunsteren, *Macromolecules* **25**, 6722–6724 (1992).
324. F. Muller-Plathe, S. C. Rogers, and W. F. van Gunsteren, *J. Chem. Phys.* **98**, 9895–9904 (1993).
325. R. M. Sok, H. J. C. Berendsen, and W. F. van Gunsteren, *J. Chem. Phys.* **96**, 4699–4704 (1992).
326. Y. Tamai, H. Tanaka, and K. Nakanishi, *Macromolecules* **27**, 4498–4508 (1992).
327. T. Li, D. O. Kildsig, and K. Park, J. Controlled, *Release* **48**, 57–66 (1997).
328. B. E. Eichinger, D. Rigby, and M. H. Muir, *Comp. Polym. Sci.* **5**, 147–1995 (1995).
329. F. Muller-Plathe, *Macromolecules* **29**, 4782–4791 (1996).
330. S. K. Nath, J. J. de Pablo, and A. D. De Bellis, *J. Am. Chem. Soc.* **121**, 4252–4261 (1999).
331. J. D. Ferry, *Viscoelastic Properties of Polymers*, 3rd ed., John Wiley & Sons, Inc., New York, 1980.
332. O. Hahn, D. A. Mooney, F. Muller-Plathe, and K. Kremer, *J. Chem. Phys.* **111**, 6061–6068 (1999).
333. C. Singh and A. C. Balazs, *Macromolecules* **29**, 8904–8911 (1996).
334. J. H. Jang and W. L. Mattice, *Polymer* **40**, 1911–1914 (1999).
335. J. Sonnenburg, J. Gao, and J. H. Weiner, *Macromolecules* **23**, 4653–4657 (1990).
336. A. A. Gusev and U. W. Suter, *J. Chem. Phys.* **99**, 2228–2234 (1993).
337. M. L. Greenfield and D. N. Theodorou, *Macromolecules* **26**, 5461–5472 (1993).
338. M. L. Greenfield and D. N. Theodorou, *Macromolecules* **31**, 7068–7090 (1998).
339. A. A. Gray-Weale, R. H. Henchman, R. G. Gilbert, M. L. Greenfield, and D. N. Theodorou, *Macromolecules* **30**, 7296–7306 (1997).
340. M. Ito, M. Matsumoto, and M. Doi, *Fluid Phase Equilib.* **144**, 395–401 (1998).
341. W. Paul, H. Weber, and K. Binder, *Ann. Phys. (Leipzig)* **7**, 554–563 (1998).
342. J. R. Fried and D. K. Goyal, *J. Polym. Sci., B: Polym. Phys.* **36**, 519–536 (1998).
343. H. S. Park, T. Chang, and S. H. Lee, *J. Chem. Phys.* **113**, 5502–5510 (2000).
344. J. Ennari, M. Elomaa, and F. Sundholm, *Polymer* **41**, 985–990 (2000).
345. J. Ennari, I. Neelov, and F. Sundholm, *Polymer* **41**, 4057–4063 (2000).
346. O. Borodin and G. D. Smith, *Macromolecules* **33**, 2273–2283 (2000).
347. W. Paul, G. D. Smith, and D. Y. Yoon, *Macromolecules* **30**, 7772–7780 (1997).
348. V. A. Harmandaris, V. G. Mavrantzas, and D. N. Theodorou, *Macromolecules* **31**, 7934–7943 (1998).
349. O. Byutner and G. D. Smith, *Macromolecules* **34**, 134–139 (2001).
350. G. D. Smith, W. Paul, M. Monkenbusch, L. Willner, D. Richter, X. H. Qiu, and M. D. Ediger, *Macromolecules* **32**, 8857–8865 (1999).
351. S. T. Milner and T. C. B. McLeish, *Phys. Rev. Lett.* **81**, 725–728 (1998).
352. G. D. Smith, W. Paul, M. Monkenbusch, and D. Richter, *J. Chem. Phys.*, 4285–4288 (2001).
353. A. V. Lyulin, G. R. Davies, and D. B. Adolf, *Macromolecules* **33**, 3294–3304 (2000).
354. F. Alvarez, A. Alegria, J. Colmeneor, T. M. Nicholson, and G. R. Davies, *Macromolecules* **33**, 8077–8084 (2000).

355. C. Saelee, T. M. Nicholson, and G. R. Davies, *Macromolecules* **33**, 2258–2265 (2000).
356. T. M. Nicholson, and G. R. Davies, *Macromolecules* **30**, 5501–5505 (1997).
357. R. Khare and M. E. Paulaitis, *Macromolecules* **28**, 4495–4504 (1995).
358. U. Natarajan and W. L. Mattice, *Macromol. Theory Simul.* **6**, 949–963 (1997).
359. N. E. Moe and M. D. Ediger, *Polymer* **37**, 1787–1795 (1996).
360. N. E. Moe and M. D. Ediger, *Macromolecules* **29**, 5484–5492 (1996).
361. M. Fukuda and H. Kikuchi, *J. Chem. Phys.* **113**, 4433–4443 (2000).
362. H. Furuya, O. Okada, K. Takemura, and T. Kanaya, *Polym. Mater. Sci. Eng.* **85**, 238 (2001).
363. R. H. Boyd and W. Jin, *Polym. Mater. Sci. Eng.* **85**, 234 (2001).
364. I. Zuniga, I. Bahar, R. Dodge, and W. L. Mattice, *J. Chem. Phys.* **95**, 5348–5354 (1991).
365. G. D. Smith, O. Borodin, D. Bedrov, W. Paul, X. H. Qiu, and M. D. Ediger, *Macromolecules* **34**, 5192–5199 (2001).
366. K. Karatasos and D. B. Adolf, *J. Chem. Phys.* **112**, 8225–8228 (2000).
367. K. Karatasos, D. B. Adolf, and S. Hotston, *J. Chem. Phys.* **112**, 8695–8706 (2000).
368. S. D. Hotston, D. B. Adolf, and K. Karatasos, *J. Chem Phys.* **115**, 2359–2368 (2001).
369. R. K. Bharadwaj and R. H. Boyd, *J. Chem. Phys.* **114**, 5061–5068 (2001).
370. D. Rigby and R. J. Roe, *J. Chem. Phys.* **89**, 5280–5290 (1988).
371. D. Rigby and R. J. Roe, *Macromolecules* **22**, 2259–2264 (1989).
372. D. Rigby and R. J. Roe, *Macromolecules* **23**, 5312–5319 (1990).
373. R. J. Roe, *J. Non-Cryst. Solids* **235/237**, 308–313 (1998).
374. T. Pakula, *J. Mol. Liq.* **86**, 109–121 (2000).
375. N. T. Huff, E. Demiralp, T. Cagin, and W. A. Goddard III, *J. Non-Cryst. Solids* **253**, 133–142 (1999).
376. J. R. Fried and B. Li, *Comp. Theor. Polym. Sci.* **11**, 273–281 (2001).
377. H. P. Wittmann, K. Kremer, and K. Binder, *J. Chem. Phys.* **96**, 6291 (1992).
378. R. J. Roe, *Adv. Polym. Sci.* **116**, 111–144 (1994).
379. P. Gestoso and J. Brisson, *Comput. Theor. Polym. Sci.* **11**, 263–271 (2001).
380. W. Paul and J. Baschnagel, in Ref. 4, pp. 307–355.
381. M. Aichele and J. Baschnagel, *Eur. Polym. J. E* **5**, 229–243 (2001).
382. M. Aichele and J. Baschnagel, *Eur. Polym. J. E* **5**, 245–2256 (2001).
383. A. R. C. Baljon and M. O. Robbins, *Macromolecules* **34**, 4200–4209 (2001).
384. Y. Termonia, *Macromolecules* **23**, 1976–1979 (1990).
385. P.-Y. Lai, *Macromol. Theory Simul.* **5**, 255–268 (1996).
386. M. J. Stevens, *Macromolecules* **34**, 1411–1415 (2001).
387. M. J. Stevens, *Macromolecules* **34**, 2710–2718 (2001).
388. K. Tashiro, M. Kobayashi, and H. Tadokoro, *Macromolecules* **11**, 908–913 (1978).
389. K. Tashiro, M. Kobayashi, and H. Tadokoro, *Macromolecules* **11**, 914–918 (1978).
390. K. Tashiro, M. Kobayashi, H. Tadokoro, and E. Fukada, *Macromolecules* **13**, 691–698 (1980).
391. K. Tashiro, H. Tadokoro, and M. Kobayashi, *Ferroelectrics* **32**, 167–175 (1981).
392. D. J. Lacks and G. C. Rutledge, *J. Phys. Chem.* **98**, 1222–1231 (1994).
393. M. F. Perutz, *R. Inst. Proc.* **62**, 183–198 (1990).
394. C. R. A. Catlow, J. M. Thomas, C. M. Freeman, P. A. Wright, and R. G. Bell, *Proc. R. Soc. Lond. A* **442**, 85–96 (1993).
395. H. E. Assender and A. H. Windle, *Polymer* **39**, 4295–4302 (1998).
396. H. E. Assender and A. H. Windle, *Polymer* **39**, 4303–4312 (1998).
397. J. D. Cho, W. S. Lyoo, S. N. Chvalum, and J. Blackwell, *Macromolecules* **32**, 6236–6241 (1999).
398. D. Hofmann, A. I. Schneider, and J. Blackwell, *Polymer* **35**, 5603–5610 (1994).
399. R. K. Bharadwaj and R. H. Boyd, *Macromolecules* **31**, 7682–7690 (1998).
400. D. C. Oda and G. C. Rutledge, *Polymer* **40**, 4647–4657 (1999).

401. J. Wendling, A. A. Gusev, U. W. Suter, A. Braam, L. Leemans, R. J. Meier, J. Aerts, J. V. D. Heuvel, and M. Hottenhuis, *Macromolecules* **32**, 7866–7878 (1999).
402. J. Wendling and U. W. Suter, *Macromol. Theory Simul.* **8**, 110–118 (1999).
403. R. A. Sorensen, W. B. Liau, L. Kesner, and R. H. Boyd, *Macromolecules* **21**, 200–208 (1988).
404. R. A. Sorensen, W. B. Liau, and R. H. Boyd, *Macromolecules* **21**, 194–199 (1988).
405. A. Sinsawat, S. Putthanarat, S. Zarkoob, Y. Magoshi, J. Magoshi, R. Pachter, M. Stone, and R. K. Eby, *Polym. Prepr.* **42**, 290–291 (2001).
406. P. E. Klunzinger and R. K. Eby, *Polymer* **38**, 4769–4772 (1997).
407. M. Parrinello and A. Rahman, *J. Appl. Phys.* **52**, 7182–7190 (1981).
408. S. Balijepalli and G. C. Rutledge, *Macromol. Symp.* **133**, 71–99 (1998).
409. S. Gautam, S. Baligepalli, and G. C. Rutledge, *Macromolecules* **33**, 9136–9145 (2000).
410. S. H. Foulger and G. C. Rutledge, *J. Polym. Sci., B: Polym. Phys.* **36**, 727–741 (1998).
411. A. Abe, T. Takeda, T. Hiejima, and H. Furuya, *Macromolecules*, **34**, 6450–6455 (2001).
412. C. Vega, L. G. MacDowell, and P. Padilla, *J. Chem. Phys.* **104**, 701–713 (1996).
413. H. Sun and D. Rigby, *Spectrochim. Acta A* **53**, 1301–1323 (1997).
414. D. Rigby, H. Sun, and B. E. Eichinger, *Polym. Int.* **44**, 311–330 (1997).
415. L. Lue, *Macromolecules* **33**, 2266–2272 (2000).
416. T. N. Heinz, W. F. van Gunsteren, and P. H. Hunenberger, *J. Chem. Phys.* **115**, 1125–1136 (2001).
417. J. D. Jackson, *Classical Electrodynamics*, 2nd ed., John Wiley & Sons, Inc., New York, (1975).
418. A. Canning, L. W. Wang, A. Williamson, and A. Zunger, *J. Comput. Phys.* **160**, 29–41 2000.
419. H. J. Limbach and C. Holm, *J. Chem. Phys.* **114**, 9674–9682 (2001).
420. C.-Y. Shew and A. Yethiraj, *J. Chem. Phys.* **110**, 676–681 (1999).
421. C.-Y. Shew and A. Yethiraj, *J. Chem Phys.* **110**, 5437–5443 (1999).
422. C.-Y. Shew and A. Yethiraj, *J. Chem. Phys.* **110**, 11599–11607 (1999).
423. K. Fukui, B. G. Sumpter, and D. W. Noid, *Polym. J.* **31**, 664–671 (1999).
424. T. Cagin, A. Jaramillo-Botero, G. Gao, and W. A. Goddard III, *Nanotechnology* **9**, 143 (1998).
425. D. N. Theodorou and U. W. Suter, *Macromolecules* **19**, 139–154 (1986).
426. R. R. Matheson Jr., *Macromolecules* **20**, 1847–1851 (1987).
427. R. R. Matheson Jr., *Macromolecules* **20**, 1851–1855 (1987).
428. D. Hofmann, L. Fritz, and D. Paul, *J. Membr. Sci.* **144**, 145–159 (1998).
429. D. J. Evans and G. P. Morriss, *Statistical Mechanics of Nonequilibrium Liquids*, Academic Press, New York, 1990.
430. G. P. Morriss, P. J. Daivis, and D. J. Evans, *J. Chem. Phys.* **94**, 7420–7433 (1991).
431. A. Berker, S. Chynoweth, U. C. Klomp, and Y. Michopoulos, *J. Chem. Soc., Faraday Trans.* **88**, 1719–1725 (1992).
432. C. J. Mundy, J. I. Siepmann, and M. L. Klein, *J. Chem. Phys.* **103**, 10192–10200 (1995).
433. S. T. Cui, S. A. Gupta, P. T. Cummings, and H. D. Cochran, *J. Chem. Phys.* **105**, 1214–1220 (1996).
434. R. Khare, J. J. de Pablo, and A. Yethiraj, *J. Chem. Phys.* **107**, 6956–6964 (1997).
435. M. Lahtela, M. Linnolahti, T. A. Pakkanen, and R. L. Rowley, *J. Chem. Phys.* **108**, 2626–2630 (1998).
436. L. I. Kioupis and E. J. Maginn, *J. Phys. Chem. B* **104**, 7774–7783 (2000).
437. J. D. Moore, S. T. Cui, H. D. Cochran, and P. T. Cummings, *J. Chem. Phys.* **113**, 8833–8840 (2000).
438. Y. Yang, T. A. Pakkanen, and R. L. Rowley, *Intl. J. Thermophys.* **21**, 703–717 (2000).
439. P. A. Thompson and M. O. Robbins, *Science* **250**, 792–794 (1990).
440. P. A. Thompson and M. O. Robbins, *Phys. Rev. A* **41**, 6830–6837 (1990).
441. P. A. Thompson, G. S. Grest, and M. O. Robbins, *Phys. Rev. Lett.* **68**, 3448–3451 (1992).

442. P. A. Thompson, M. O. Robbins, and G. S. Grest, *Isr. J. Chem.* **35**, 93–106 (1995).
443. E. Manias, G. Hadziioannou, I. Bitsanis, and G. ten Brinke, *Europhys. Lett.* **24**, 99–104 (1993).
444. E. Manias, G. Hadziioannou, and G. ten Brinke, *J. Chem. Phys.* **101**, 1721–1724 (1994).
445. R. Khare, J. J. de Pablo, and A. Yethiraj, *Macromolecules* **29**, 7910–7918 (1996).
446. S. A. Gupta, H. D. Cochran, and P. T. Cummings, *J. Chem. Phys.* **107**, 10316–10326 (1997).
447. S. A. Gupta, H. D. Cochran, and P. T. Cummings, *J. Chem. Phys.* **107**, 10327–10334 (1997).
448. S. A. Gupta, H. D. Cochran, and P. T. Cummings, *J. Chem. Phys.* **107**, 10335–10343 (1997).
449. A. Koike and M. Yoneya, *J. Phys. Chem. B* **102**, 3669–3675 (1998).
450. A. Koike, *Macromolecules* **31**, 4605–4613 (1998).
451. R. Khare, J. J. de Pablo, and A. Yethiraj, *J. Chem. Phys.* **114**, 7593–7601 (2001).
452. S. H. Jacobson, D. J. Gordon, G. V. Nelson, and A. C. Balazs, *Adv. Mater.* **4**, 198–205 (1992).
453. J. H. Hildebrand and R. L. Scott, *Regular Solutions*, Prentice-Hall, Inc., Englewood Cliffs, N.J., 1962.
454. S. S. Patnaik and R. Pachter, *Polymer* **40**, 6507–6519 (1999).
455. N. Lee and D. Thirumalai, *Macromolecules* **34**, 3446–3457 (2001).
456. E. Pitard and J.-P. Bouchaud, *Eur. Polym. J. E* **5**, 133–148 (2001).
457. J. D. Honeycutt, *Macromolecules* **27**, 5377–5381 (1994).
458. E. D. Akten and W. L. Mattice, *Macromolecules* **34**, 3389–3395 (2001).
459. P. J. Flory, B. E. Eichinger, and R. A. Orwoll, *Macromolecules* **1**, 287–288 (1968).
460. A. Koyama, T. Yamamoto, K. Fukao, and Y. Miyamoto, *J. Chem. Phys.* **115**, 560–566 (2001).
461. G. Xu and W. L. Mattice, *J. Chem. Phys.* **116**, 2277–2283 (2002).
462. D. B. Holt and B. L. Farmer, *Polymer* **40**, 4673–4684 (1999).
463. Y. Abe and K. Tashiro, *J. Polym. Sci., B: Polym. Phys.* **39**, 689–702 (2001).
464. S. K. Kumar, *Macromolecules* **27**, 260–271 (1994).
465. S. K. Kumar, I. Szleifer, C. K. Hall, and J. M. Wichert, *J. Chem. Phys.* **104**, 9100–9110 (1996).
466. S. K. Kumar, *Macromolecules* **30**, 5085–5095 (1997).
467. D. G. Gromov, J. J. de Pablo, G. Luna-Barcenas, I. C. Sanchez, and K. P. Johnston, *J. Chem. Phys.* **108**, 4647–4653 (1998).
468. J. J. de Pablo, Q. Yan, and F. A. Escobedo, *Ann. Rev. Phys. Chem.* **50**, 377–411 (1999).
469. S. K. Nath, F. A. Escobedo, and J. J. de Pablo, *J. Chem Phys.* **108**, 9905–9911 (1998).
470. S. K. Nath, B. J. Banaszak, and J. J. de Pablo, *J. Chem. Phys.* **114**, 3612–3616 (2001).
471. S. K. Nath, F. A. Escobedo, J. J. de Pablo, and I. Patramai, *Ind. Eng. Chem. Res.* **37**, 3195–3202 (1998).
472. B. Smit, S. Karaborni, and J. I. Siepmann, *J. Phys. Chem. B* **102**, 2126–2140 (1995).
473. M. G. Martin and J. I. Siepmann, *J. Phys. Chem. B* **102**, 2569–2577 (1998).
474. B. Chen and J. I. Siepmann, *J. Phys. Chem. B* **103**, 5370–5379 (1999).
475. M. G. Martin and J. I. Siepmann, *J. Phys. Chem. B* **103**, 4508–4517 (1999).
476. C. D. Wick, M. G. Martin, and J. I. Siepmann, *J. Phys. Chem. B* **104**, 8008–8016 (2000).
477. B. Chen, J. J. Potoff, and J. I. Siepmann, *J. Phys. Chem. B* **105**, 3093–3104 (2001).
478. J. Delhommelle, A. Boutin, B. Tavitian, A. D. Mackie, and A. H. Fuchs, *Mol. Phys.* **96**, 1517–1524 (1999).
479. B. Neubauer, A. Boutin, B. Tavitian, and A. H. Fuchs, *Mol. Phys.* **97**, 769–776 (1999).
480. J. Delhommelle, C. Tschirwitz, P. Ungerer, G. Granucci, P. Millie, D. Pattou, and A. H. Fuchs, *J. Phys. Chem. B* **104**, 4745–4753 (2000).
481. S. T. Cui, H. D. Cochran, and P. T. Cummings, *J. Phys. Chem. B* **103**, 4485–4491 (1999).
482. F. A. Escobedo and J. J. de Pablo, *J. Chem. Phys.* **105**, 4391–4394 (1996).

483. B. Widom, *J. Chem. Phys.* **39**, 2808–2812 (1963).
484. G. L. Deitrick, L. E. Scriven, and H. T. Davis, *J. Chem. Phys.* **90**, 2370–2385 (1989).
485. Y. Tamai, H. Tanaka, and K. Nakanishi, *Macromolecules* **28**, 2544–2554 (1995).
486. M. Fukuda, *J. Chem. Phys.* **112**, 478–486 (2000).
487. S. K. Kumar, I. Szleifer, and A. Z. Panagiotopoulos, *Phys. Rev. Lett.* **66**, 2935–2938 (1991).
488. Y.-J. Sheng, A. Z. Panagiotopoulos, S. K. Kumar, and I. Szleifer, *Macromolecules* **27**, 400–406 (1994).
489. J. J. de Pablo, M. Laso, and U. W. Suter, *J. Chem. Phys.* **96**, 6157–6162 (1992).
490. B. Knopp, U. W. Suter, and A. A. Gusev, *Macromolecules* **30**, 6107–6113 (1997).
491. B. Knopp and U. W. Suter, *Macromolecules* **30**, 6114–6119 (1997).
492. B. Nick and U. W. Suter, *Comp. Theor. Polym. Sci.* **11**, 49–55 (2001).

B. E. EICHINGER
RAJESH KHARE
Accelrys, Inc.

MORPHOLOGY

Introduction

Polymer morphology, literally the study of organization within solid polymers, seeks to read the messages from the specimen's history contained in its physical form and hence gain understanding of the physical processes involved in its creation. In crystalline polymers the morphological record is not only extremely rich, because long molecules are largely immobile and remain where they were placed, but it has also provided the most effective means of establishing the fundamental patterns of behavior of long molecules and the increasingly important materials they compose, paving the way for quantification by appropriate techniques.

Historically, synthetic polymers are essentially twentieth-century materials, coming into prominent use in the second half with the introduction of polyethylene and polypropylene. The earliest textural model, the fringed-micelle, was an interpretation of wide-angle X-ray scattering (WAXS) patterns containing evidence of both small crystalline and disordered (amorphous) regions (1). According to this, long molecules were partly entangled and meandered from one kind of region to the other with mechanical and other properties dependent on the *degree of crystallinity*, ie the proportion of crystalline phase. The scale of the fringed micelle was believed, on the basis of the small widths of WAXS reflections, to be of the order of 10 nm, a dimension well below what it was then possible to see. Only with the advent of the transmission electron microscope (TEM) did such resolution become feasible but then it became clear that organic materials were vulnerable to damage by the imaging electrons, which mostly destroyed crystals, thereby tending to distort the physical record and adding little to knowledge until the discovery of polymer single crystals in 1957.

Encyclopedia of Polymer Science and Technology. Copyright John Wiley & Sons, Inc. All rights reserved.

Single lamellar crystals were the second element of polymer texture to be identified, the first being spherulites, whose presence in polyethylene was reported in 1945 (2). Study with the polarizing microscope established that molecules lay tangentially to polyethylene spherulites and nearly so to those of polyamides and polyesters, systems with hydrogen bonding. Spherulites and their presumed substructure of fringed micelles were hard to reconcile (3), a difficulty that disappeared with the discovery of polyethylene single crystals and the inference of their internal molecular chainfolding. This is where modern polymer morphology started and much that was new and important was achieved within a few years. At the same time, the problem of radiation damage remained a serious obstacle to the study of melt-crystallized polymers for 20 years more and, until it was resolved, textural models were adopted from the limited information available and, unfortunately, have not always been substantiated, requiring radical revision when actual textures were eventually made visible.

Nowadays, polymer morphologies can be observed routinely, at least in the major polymers, to lamellar levels and, in combination with the complementary techniques of small-angle X-ray scattering (SAXS), WAXS, differential scanning calorimetry (DSC), ^{13}C nuclear magnetic resonance (NMR), neutron and Raman scattering among others, have served to lay firm foundations for the understanding of crystallization and texture-dependent properties not just in the materials studied but across all polymers. The central, but not the only, element in this understanding is the lamella.

Polymer Lamellae

The Inference of Chainfolding. The introduction of linear polyethylene in the late 1950s led quickly to the discovery that it could crystallize with a lamellar habit, visible in the optical microscope. First, surface steps were seen (4), then three individuals, Till (5), Fischer (6), and Keller (7) found that on cooling dilute solutions ($\sim$0.01%) in xylene, separate lamellar crystals precipitated. Their appearance closely matched that of *n*-alkane lamellae in which molecules are transverse to lamellae. Electron diffraction showed that this was also true of polyethylene lamellae that, given that molecular lengths were not significantly reduced by crystallization, led Keller to propose that molecules were chainfolded within lamellae (7). This inference has proved correct and chainfolded lamellae have now been shown to be a general feature of synthetic crystalline polymers including those grown from the melt.

The inference says nothing, however, about surface condition, whether folding is tight, occurring within four or so main-chain carbon atoms in polyethylene, or loose, extending over many more. Although there may be complete folding in isolated lamellae, in bulk material a proportion of molecules in adjacent lamellae must pass from one lamella to the next—*tie molecules*—and not fold back at a lamellar surface; otherwise mechanical integrity would be lost and eg the toughness associated with long polyethylene molecules be replaced by the waxy behavior of solid paraffins. Knowledge of the precise nature of fold surfaces still continues to be refined as more techniques are introduced and experiments performed and is currently a central theme of research. This reflects the fact that fold surfaces

are a major manifestation of the long molecular nature of polymeric solids in contrast to lamellar interiors whose crystal structures follow the same principles as in nonpolymeric materials.

Chainfolded Lamellae from Solution. Much of our basic knowledge of polymer lamellae and their properties was established relatively early from the study of monolayer or bilayer crystals grown from solution and examined on a supporting carbon substrate (8). It is possible to study these systems with diffraction imaging in a TEM for a short while until crystallinity is lost, then subsequently as residual amorphous pseudomorphs, which, when on a carbon substrate, retain the shapes of the original although they distort when embedded in a soft matrix such as gelatine. It was some 20 years before melt-crystallized textures could be examined in similar detail and, at the time, they were either assumed by some (9) to be basically similar although less well organized than lamellae grown from dilute solution or, by others (10), to be intrinsically different because the conditions for ordering from the melt were not present. In fact, most of the essential features shown by solution-grown lamellae do carry over at least in some degree to those grown from the melt although these are generally more disordered.

Crystal Habits. The habits of solution-grown polymer crystals are many and varied, with slow growth from the most dilute solutions giving the simplest objects. As usual, much is known about linear polyethylene (11) not only because this was the first system to be investigated and shows a profusion of informative detail but also because this is the closest approach to the ideal linear chain whose properties underlie those of all linear polymers. The basic habit of polyethylene lamellae is the lozenge, bounded by four {110} faces. At higher temperatures, $>$ $\sim$80°C from 0.01% solution in xylene, these are truncated by two {100} faces whose relative size increases with temperature. For crystallization from other solvents at higher temperatures, the truncating faces become the largest and may become slightly curved (12). Curved faces are not uncommon in other systems, but planar facets are the norm for most polyolefines. They even persist, albeit with very narrow widths $\sim$0.1 μm, for very rapid growth when dendrites form because diffusion limits the supply of material to the growth front (11,13).

The lozenge habit characteristic of orthorhombic polyethylene is paralleled by hexagons of polyoxymethylene (14) and i-polystyrene (15), squares of i-poly(4-methylpentene-1) (16), and, very unusually, triangles of poly(L-hydroxyproline) (17), in each case corresponding to the symmetry of the chain packing or subcell.

Twins occur, especially for lower molecular masses. For example, objects with six arms are common for {110} twinning in low mass polyethylene because (110) and $(1\bar{1}0)$ faces are inclined at 67.5°, close to 60° (18). Moreover, laths are prone to develop with such a twin boundary along its center line (11,19) because of the accelerated growth provided by the notch at its tip, which aids molecular attachment. More exotic, three-dimensional twins are shown by α-polypropylene in "quadrites" (20) and by interpenetrating layers in polyethylene (21).

Sectorization. The long lengths of polymer chains and chainfolding in particular are not directly reflected in the lateral habits of polymer lamellae. The first feature that does show their influence is sectorization, revealed by diffraction contrast, internal microstructure, or surface texture, possibly augmented by decoration with gold (22) or evaporated polyethylene (23). This is the division of a lamella into discrete regions bounded by a growth face, a phenomenon that is both

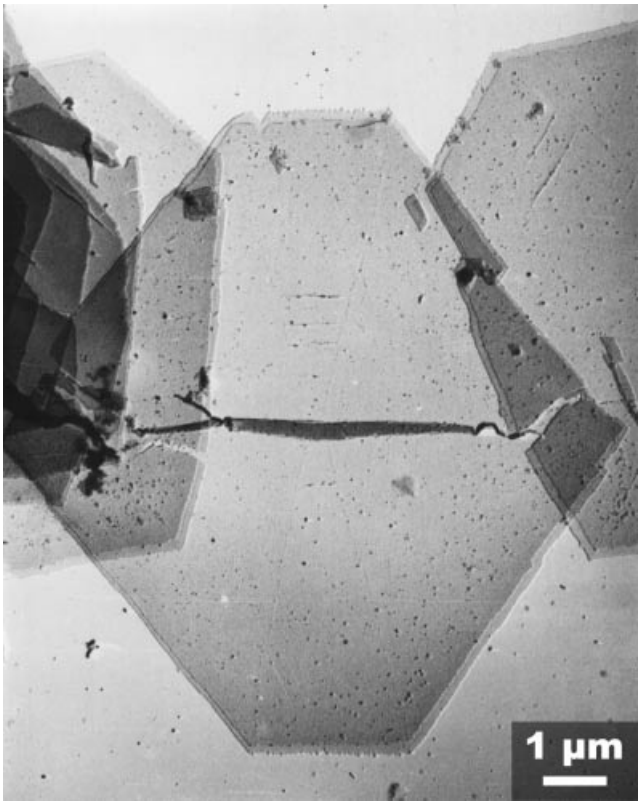

Fig. 1. A truncated lozenge of linear polyethylene, crystallized from 0.01% solution in xylene, with boundaries delineating its six sectors and a step at the outer edge where the crystallization temperature was reduced from 90 to 76°C. From Ref. 18.

a consequence and confirmation of chainfolding along the growth face; it would not occur if, for example, molecules prefolded into blocks before adding to a lamella.

Sectorization arises because such folding transforms a long molecule into a pleated sheet, which can extend across several successive lattice planes (24), but essentially lies along the relevant growth surface, denoted the *fold plane*. In so doing it breaks the symmetry of, and slightly distorts, the subcell lattice, ie the repetitive unit of chain packing within the lamella, excluding the surfaces. The fold plane in a given sector differs from nominally equivalent ones along which there is no folding and so transforms a single lamella into a multiple twin according to the respective fold planes. A four-sided polyethylene lozenge bounded by four {110} growth surfaces is, accordingly, a fourfold twin with four equivalent sectors in each of which one of the two nominally equivalent {110} surfaces will be parallel to the fold plane, the other not. When, at higher growth temperatures, lozenges become six-sided with truncating {100} surfaces, then there are six corresponding sectors (Fig. 1). The two new ones, denoted {100} sectors, are twinned with respect to each other but different in character to the four twinned {110} sectors because of the different fold plane with, for example, a lower melting point (25).

The size of a sector is governed by that of its growth face and can be very small, eg in dendritic growth, when individual facets, each of which has its own microsector attached, may be as little as 20 nm wide (13).

Nonplanar Geometries. One consequence of sectorization is to make lamellae nonplanar (18). This happens in two distinct ways, the first of which is a consequence of subcell distortion. Folding along the growth face makes nominally equivalent planes in the subcell become unequal, adopting slightly different spacings. For the three systems on which measurements have been made: polyoxymethylene, isotactic poly(4-methylpentene-1) (26), and low mass polyethylene (13), with, respectively, hexagonal, tetragonal, and orthorhombic subcells and all with chains normal to lamellae, the difference in spacing between otherwise equivalent planes only one of which is the fold plane is ~0.001 nm. In consequence, transverse axes of the subcell no longer meet precisely at 60° or 90°. Joining six or four such sectors, as appropriate, without dislocations (as is observed) gives, therefore, a lamella that is not strictly planar but slightly dished into a cone of semiangle ~89° rather than a planar sheet, as confirmed by direct observation (14). This deviation from planarity is sufficiently small to allow all sectors to be seen simultaneously in diffraction contrast from one principal reflection after a lamella has been flattened on a substrate prior to examination. In consequence, it is possible to make measurements of the small spacing difference of the same plane as it crosses a sector boundary, possible using bilayers and moiré patterns. Flattening also produces characteristic streaking normal to the growth face in each sector where slight local shearing in the fold plane has created the necessary additional surface (14).

Such small effects are probably universal in sectored polymer lamellae to which chains are normal. But they are overshadowed by much greater nonplanarity when chains are substantially inclined to lamellar normals, most notably in polyethylene of typical molecular weights. Then the diffraction pattern, eg for a single polyethylene lamella, is not generally single crystalline, as was initially assumed (7), but a composite with different reflections contributed by different sectors (27), according to the particular fold plane—showing that, in a flattened crystal, the molecular direction changes from sector to sector. In complementary dark-field images, only sectors with the same fold plane may appear in bright contrast.

These effects are a consequence of the collapse of what, in suspension, are highly nonplanar lamellae (27–29). The nonplanarity can take several forms but arises because molecular inclination to lamellar normals increases the surface area per end group or fold and so reduces surface congestion, as is common for the alkane subcell. The simplest polyethylene geometries are hollow pyramids that form, at higher temperatures, with {312} fold surfaces in {110} sectors and a common *c*-axis (30). The adoption of $\{31\ell\}$ planes is thought to reflect the asymmetric shape of sharp folds, both within and normal to the fold plane.

There are two other principal nonplanar habits of polyethylene lamellae: chair and ridged crystals. Chair crystals (30) form simultaneously with, and are related to, hollow pyramids; their shape may be described as resulting from a hollow pyramid divided in two along the short diagonal, the two halves rotated 180° around their long diagonal and then constrained to rejoin. The proportion of chair to hollow pyramidal crystals appears to vary with crystallization conditions.

It was first measured (30) to be equal, but later figures (31) have been as low as 10%; no more precise information is available.

At lower crystallization temperatures ($<\sim 80^{\circ}$C in xylene), hollow pyramidal crystals are replaced initially by ridged crystals, then by dendrites, which occur when growth is limited by diffusion, here of material to the growth interface (28). In the ridged crystals, each {110} sector contains alternating {314} facets that are in phase across the long but not the short diagonal. Intermediate forms such as half hollow pyramidal/half ridged or ridged lamellae with a central hollow pyramidal portion have also been found (30). As was suggested at the time, these changes in habit suggest that lamellae begin to form flat, with nonplanarity developing later. This has recently been demonstrated explicitly to be the case in melt-crystallized systems, for which it has major implications. New light has been shed on the significance of these various forms by recent work on melt crystallization (to be discussed later).

Although preparation for TEM involves drying lamellar suspensions when surface tension forces cause collapse on a rigid substrate, the nonplanar habits can be observed directly in the optical microscope, especially with dark-field imaging, while lamellae are floating in suspension or preserved, at least in part, if collapse can be limited, eg by sedimentation on glycerine or drying within gelatine (30).

Different nonplanar habits collapse in different ways. Hollow pyramids may occasionally fold in two along their short diagonal, revealing sectors in their original shape (11). More often they collapse by laying {110} sectors flat on the substrate, leaving a central triangular pleat of characteristic shape in which the excess material is located (27,32). In so doing, changes of slope at sector boundaries disappear, leaving a line along each visible boundary to outline the separate sectors (Fig. 1). In this collapsed form the two {200} sectors are thinner (33) than the other four and may show lines along the *b*-axis, suggesting that shear in {200} planes, parallel to *c*, may also have occurred. Ridged lamellae tend rather to collapse mostly by shear in {310} planes, parallel to *c*, creating a flat lamella, but this is often combined with some rotation of facets revealed by differential sector contrast in dark-field images.

Lamellar Thickness. The thinness of polymer lamellae is very important to crystalline polymers because of the many surfaces it creates that directly affect important properties such as melting point, chemical reactivity, and mechanical behavior among others. The actual thickness is primarily a physical property relating to crystallization rather than one depending on the chemistry of the molecular chain but is affected by chemistry, such as hydrogen bonding, in appropriate circumstances whose requirements limit the thickness to particular, rather than continuous, values. It increases with crystallization temperature (34) [sometimes, as in i-polystyrene, from a constant value at lower temperatures (35)] apparently without limit but as the crystallization rate slows at higher temperatures the higher thicknesses become increasingly unattainable in reasonable times.

Lamellae form because this is the fastest way for long molecules to crystallize. The actual thickness is determined at the growing edge, where a decrease of temperature will leave a sharp step for growth from solution (Fig. 1) but not from the melt (36), for which, with higher temperatures, there is subsequent thickening. This points to secondary nucleation at the growing edge as the determining process. If the lamellar thickness remains close to that of the secondary nucleus,

ℓ, then an expression for lamellar thickness as a function of temperature may be obtained as follows.

The fold surfaces add free energy to the system but crystallization is possible if this can be permanently offset by the free energy of crystallization of fold stems in lamellar interiors. The former quantity is $2\sigma_e/\ell$ per unit volume, where σ_e is the surface free energy per unit area, while the latter is per unit volume, $\Delta_g \approx \Delta h \Delta T/T_m{}^0$, with Δh, the enthalpy of fusion per unit volume; $\Delta T = T_m{}^0 - T_c$, the supercooling below $T_m{}^0$, the equilibrium melting temperature (of an infinitely thick crystal); and T_c, the crystallization temperature. The value of σ_e is $\sim$100 mJ·m^{-2}, an order of magnitude more than for side surfaces, and includes the work of chainfolding. Crystallization becomes possible once $\Delta g > 2\sigma_e/\ell$ requiring that

$$\ell > 2\sigma_e T_m^0 / \Delta h \Delta T$$

or, as usually expressed,

$$\ell = 2\sigma_e T_m^0 / \Delta h \Delta T + \delta\ell$$

with $\sigma\ell$ a small positive length. This expression identifies supercooling rather than temperature as the pertinent variable, which experiments using different solvents have confirmed to be the case (37).

Growth rates initially increase with supercooling when thermodynamics is the controlling factor—it is always faster for chains to fold at a shorter interval, provided they produce stable lamellae—but are liable to pass through a maximum and then decrease when transport becomes dominant (38).

Once formed, the presence of the extensive basal fold surfaces makes lamellae metastable with respect to an increase of thickness and a correspondingly lower melting point. It is readily shown (18) that the melting point, T_m, of a lamella, thickness ℓ, is given by

$$T_m = T_m^0[1 - 2\sigma_e/(\Delta h \cdot \ell)]$$

The second term in brackets gives the depression in melting point caused by lamellar thinness, which is considerable, amounting to $\sim$10–20 K in typical circumstances. The spread of melting points typical of a crystalline polymer is at least partly attributable to the spread of lamellar thicknesses it contains. It is also possible for the reduced melting point of a thin lamella to fall below the crystallization temperature of a thicker one. In this circumstance, gradual heating, such as happens in a DSC scan, is liable to transform the initial lamellar population into a thicker one during the course of the scan (39). Whether this is occurring can be checked by carrying out scan at different heating rates; a sufficiently fast one will record the original population while slower ones will allow a progressive transformation into a higher-melting population (40).

Because a thicker layer is more stable than a thinner one, it is always thermodynamically advantageous for a lamella to thicken irreversibly. If the lamellar thickness equals that of the secondary nucleus, ie $\delta\ell = 0$, then a lamella will melt at its crystallization temperature, as substitution into the two previous equations

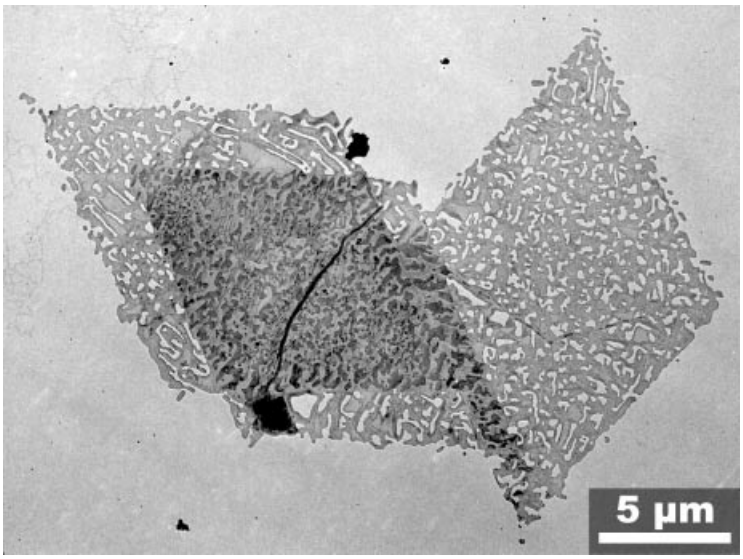

Fig. 2. Solution-grown lozenges of linear polyethylene heated, on a carbon substrate, until they had begun to thicken. Note that holes are confined to single layers; there are none where layers overlay. From Ref. 18.

verifies. That it does not, but at a greater figure, shows that the actual thickness exceeds that of the nucleus. In part this is required to obtain a positive crystallization flux but, in melt-crystallized materials, the discrepancy is so large as to indicate that a process of substantial isothermal lamellar thickening, ~3 for polyethylene (41), has occurred during crystallization. Two mechanisms are possible, partly melting then recrystallizing a sample as above (18) or solid-state thickening without melting (42); both have been identified unambiguously as cited.

Early experiments on solution-grown lamellae revealed not only the earlier melting of the {100} sectors in polyethylene lamellae (25) [which Atomic Force Microscopy (AFM) has confirmed (33) to be thinner than {110} sectors in collapsed, and presumably as-grown, crystals] but also the presence of holes (43) in lamellae that had been heated in contact with a carbon film (Fig. 2). While providing clear evidence of lamellar thickening, the presence of holes is a response to the carbon film, which restrains lateral contraction; holes do not appear on thickened upper layers of the same sample that are not so restrained.

These early and rapid successes in confirming the presence of chainfolding and demonstrating its consequences for solution-grown material brought much speculation as to the situation in melt-crystallized systems when molecules must compete to crystallize rather than add in the comparatively unrestricted circumstances of very dilute solutions. The presence of significant chainfolding in bulk melt-crystallized polyethylene was not finally confirmed until 1979 when analysis of neutron scattering data required that the probability of a molecule folding and reentering a polyethylene lamella at an adjacent lattice site was ≥ 0.67 (44). In the meantime, two morphological routes had been explored to shed light on systems that had still not been studied systematically by TEM.

One was study of polyethylene crystallized from increasingly concentrated solutions (45) to concentrations ~70%, whose principal demonstration was that the same, pseudospherulitic objects so formed had different appearances in different projections. What appeared as a well-faceted crystal in one projection appeared sheaf-like, as in an immature spherulite, in another at right angles while the view from the third Cartesian direction was of separated parallel multilamellar units. Such objects are termed axialites because, to a first approximation, they are formed of lamellae splaying about a common axis. The major difference from melt-grown spherulitic systems is that splaying, of the longer axis, makes *a* radial in solution-grown systems but *b* in melt-grown systems.

The second system was the crystallization of polyethylene under high pressures, ~0.5 GPa. The attraction of this system was that it gives exceptionally thick lamellae, sometimes exceeding 1 μm, which are readily observed in fracture surfaces (46). This behavior results from crystallization of a second polyethylene phase (47), which is hexagonally ordered normal to chains but disordered along them (48). The low heat of fusion brings, as with poly(tetrafluoroethylene) (PTFE), (49,50) a greater lamellar thickness, which then demonstrably increases isothermally. The precise thicknesses are lower in thinner samples (51) but increase with molecular length and crystallization time. They normally exceed 80 nm for polyethylene of 20,000 molecular mass while, for normal homopolymers—commonly attaining thicknesses visible in the optical microscope and sometimes much more—280 μm has been reported (52). Many of the features subsequently found for polymeric crystallization from the melt in general were first demonstrated in this system. They include fractional crystallization and kinetic competition between alternative modes of crystallization (53).

Melt-Crystallized Lamellae. Until the mid-to-late 1970s, radiation damage effectively restricted the examination of the internal lamellar organization of melt-crystallized polymers with TEM to the study of merely their fracture surfaces by replication. Although much was seen of interest in many systems (8), the method is open to criticism because it may not be representative of the material: the fracturing crack may select particular locations, such as concentrations of low mass polymer or follow particular paths through a sample in preference to others. The latter is the case for polyethylene for which {200} surfaces are fractured preferentially (36). These planes contain *b*, the growth direction, so that the view down *b* which is important and diagnostic, is rarely present.

This situation changed with the introduction of two new specimen preparation techniques, chlorosulfonation (54) and permanganic etching (55,56). The first is ostensibly a staining technique for polyethylene, that introduces electron-dense atoms at fold surfaces—chlorine, sulfur and, if uranyl acetate is added, uranium—producing strong contrast of black surfaces and white interiors when lamellae are viewed edge-on. Such images are remarkably stable in the electron beam but in the staining process samples lose much or all of their crystallinity (57) and give lower thicknesses than in fracture surfaces of the same sample (58). This is, nevertheless, a popular technique because it provides a clear measure of the lamellar thickness but it does not show other perspectives well, nor is it useful for other polymers.

Permanganic etching, on the other hand, is able to reveal lamellar textures well in all polyolefines plus a number of other polymers including aromatic

polyamides and poly(etheretherketone) (PEEK). Solutions of potassium permanganate in strong acids, sulfuric and/or phosphoric, selected according to the particular sample, will remove material preferentially from any surface—external, fracture, or cut—of these polymers by selective oxidation, leaving a topography of lamellar textures exposed, which may then be examined by TEM following replication or directly in the scanning electron microscope (SEM) at lower resolution.

The technique was first applied to polyethylene and i-polypropylene revealing itself to be sensitive to crystallinity, lamellar orientation, crystal structure, and crystal defects (55). Thus it penetrates between lamellae; attacks lamellar side surfaces more than their fold surfaces, α- more than β-i-polypropylene; and removes dislocation cores preferentially. As with chlorosulfonation, it allows systematic study of samples by cutting them open where desired. But it can also reveal the particular character of external or fracture surfaces, neither of which is usually random.

Both these two quite different preparative techniques gave the same new information for polyethylene, engendering confidence in its objectivity. Similar features have recurred as the use of permanganic etching has been extended to other polymers. The principal findings are, first, that high crystallinity polymers are full of lamellae; second, that lamellae are not all equivalent; and third, that in polyethylene, lamellae have different profiles, viewed down b, the growth axis, at low and high crystallization temperatures (59).

The first of these removed any lingering doubts that crystalline polymers are lamellar solids. The second lies at the heart of spherulitic growth, which is not only characteristic of melt-grown polymers but is responsible, in large measure, for their intrinsic spatial variation of properties. Inspection of quenched growth fronts shows that spherulites advance by the propagation of individual lead or *dominant* lamellae that branch and diverge. The space between dominant lamellae is, except in very low crystallinity materials, filled in later by *subsidiary* or *infilling* lamellae. This mode of growth tends to give dominant and subsidiary lamellae different properties for two reasons. On the one hand, fractional crystallization—which selective extraction (60) confirms to be widespread, especially at lower supercoolings—places shorter and/or more branched molecules in later-crystallizing polyethylene lamellae (61), with less tactic species similarly located in i-polypropylene. On the other hand, their different orientations, with dominant lamellae being essentially radial but subsidiary lamellae inclined to the radius at angles of 20° and more, makes their mechanical response differ as different deformation modes come into play. The dominant/subsidiary structure is characteristic of polymer spherulites throughout their temperature range of formation (62).

The conditions under which the different profiles of dominant lamellae occur are as follows (59). At crystallization temperatures $\geq\sim 127^\circ$C, melt-crystallized lamellae of linear polymer have {201} fold surfaces, the same basal surface typical of n-alkanes, allowing folds more surface area in a subcell with a comparatively small cross-sectional area per fold stem. Their profile viewed down b, the growth direction, has lamellar normals inclined at $\sim 35^\circ$ to c, indicating {201} surfaces. For higher mass materials, lamellae are planar, but for molecular masses of $\sim$30,000, {201} inclinations alternate in ridged lamellae (Fig. 3a). At immediately lower temperatures, the corresponding profile of dominant lamellae differs: it is then

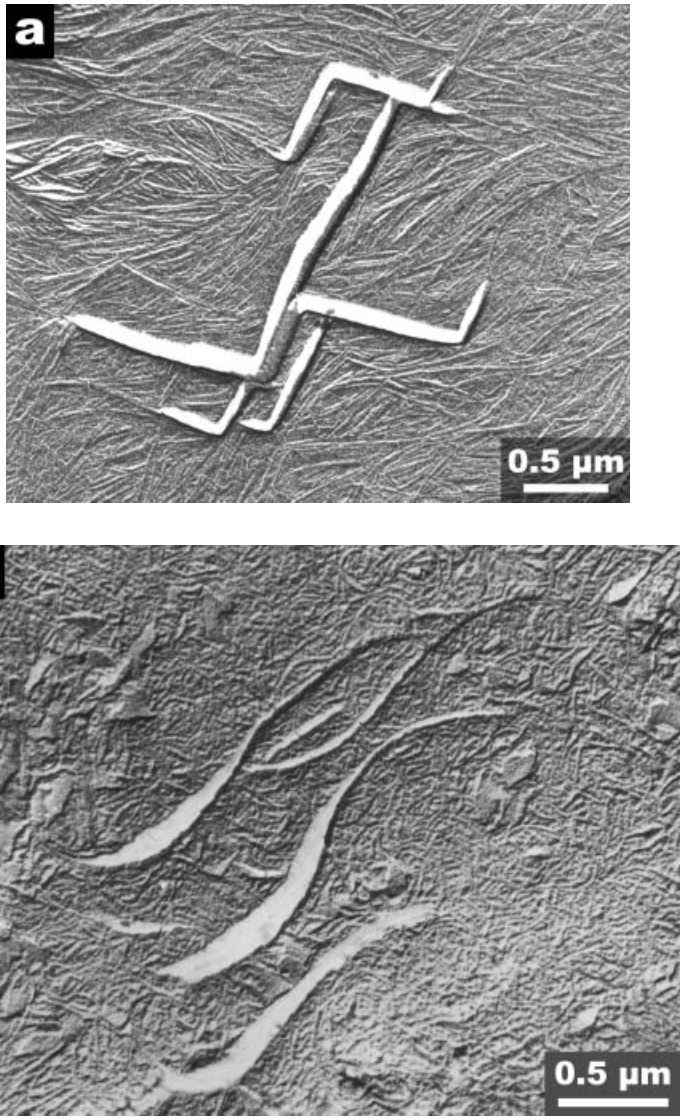

Fig. 3. Profiles of dominant lamellae of linear polyethylene viewed down the growth direction *b*. (**a**) For slower growth, at temperatures $\geq$127°C, lamellae grow with {201} facets. (**b**) For faster growth, at lower temperatures, dominant lamellae display S- or C-profiles. From Ref. 18.

S- or C-shaped (Fig. 3b), with the normal to the center of the S-profile also inclined at a maximum $\sim$35° to *c*, a figure that tends to reduce for lower temperatures and branched polymer. The change coincides with the onset of banding in spherulites, with a consistent orientation of the S-profile for a given sense of twist, an observation that is pertinent to the long-sought explanation of banding in spherulites (to be discussed later). It also coincides, more or less, with a discontinuity in kinetics interpreted as due to a change in growth regime (63). Accordingly, above $\sim$127°C,

depending slightly on molecular mass, regime I would correspond to a single nucleus per characteristic length of growth face while below this figure, regime II would have multiple nuclei active on the growth face.

The reason for the adoption of different profiles becomes clear when the chain inclination to the fold surface is monitored during growth. This is possible when a highly oriented (and so high melting) polyethylene fibre is used as a linear nucleus to form a row structure from a quiescent melt. By examining appropriate sections parallel to the fibre axis (exposed by suitable times of etching down from the outer surface) and looking down b, the inclination can be determined from the nucleus to the outer edge of the row. The change from {201}to S-profiled fold surfaces occurs at a critical growth rate that is characteristic of a given material and decreases for longer and/or more-branched molecules (64,65). The corresponding time to add a single 5-nm-thick molecular layer to the crystal is $\sim 10^{-1}$ s for linear polyethylene of 100,000 molecular mass. For slower growth, {201} surfaces occur and nucleate as such in contrast to faster growth, when lamellae nucleate with {001} surfaces and subsequently transform, behind the growth front, adopting S-profiles and thickening isothermally (65). For slower growth a molecule is able to achieve inclined fold packing as it adds to the crystal, but not for faster growth when improvements in fold packing must be accomplished within the constraints of a surrounding lamella. When a region of inclined packing is produced in the central, ie oldest portion of a lamella, this leads automatically to an S-profile in cross-section (66) (as discussed further below).

The lateral habits of melt-grown polyethylene lamellae are similar to those found for growth from solution at high temperatures in various solvents, ie becoming not only increasingly elongated along b for higher-temperature growth but also displaying increasingly curved side surfaces (67). The {110} surfaces remain planar but become progressively smaller until, for regime I at $\sim 130^{\circ}$C, they are barely detectable and are claimed to be only $\sim$100 nm wide (68). The lateral shape then has been described as elliptic (in the botanical sense) or lenticular, with macroscopically curved side surfaces (Fig. 4a). Theoretical analysis (69,70) explains the macroscopic curvature in terms of a succession of incomplete {200} surface growth strips according to the relative rates of lateral growth and strip completion.

Individual elliptic lamellae are often divided into two sectors along their major axes, especially for long crystallization times at the highest temperatures, corresponding to a single ridge in cross section (71). For lower masses ($\sim$30,000) the ridging becomes multiple (Fig. 4b), with alternate {201} facets extending along the crystal (61,66,71). The quite different habit of lamellae grown in regime II (Fig. 4c), in which no indications of sectorization have been reported, not only has the wider {110} facets expected of lower temperatures but also displays an S-profile, especially in its central, older regions.

The axis of the S-profile is not along b but inclined to it at $\sim 20^{\circ}$, thereby introducing an asymmetry pertinent to the propagation of banded growth that is achieved through isochiral arrays of screw dislocations systematically positioned to one side of the outward axis of the S-profile (66). It is to be expected that the axis of the S-profile will not be aligned along b because of the lack of crystallographic symmetry in fold placement; but to account for the large angle between them it has been suggested that the elastic energy of the nucleating S-profile needs to be

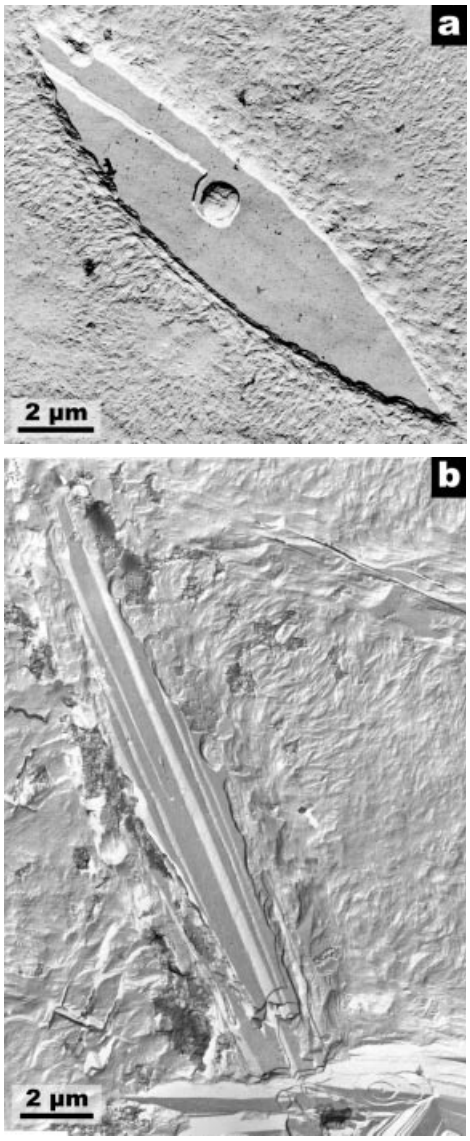

Fig. 4. Melt-crystallized polyethylene lamellae: (**a**) linear polymer crystallized at 130°C as a "planar" crystal in which successive layers spiraling around the central (etched-out) giant screw dislocation are not in contact; (**b**) ridging along *b* in a 17,000 mass fraction of linear polymer crystallized at 129°C; (**c**) an ethyl-branched copolymer crystallized at 123°C showing a central S-profile, asymmetrically placed screw dislocations and new layers diverging therefrom. From Ref. 66.

considered. Once the axis of the S-profile is so inclined then the associated shear stresses as the S-profile progresses lead naturally to the development of isochiral screw dislocations to one side, where the stress is highest.

As for solution growth, the lateral habits of melt-grown crystals reflect both the underlying crystal structure and the kinetics of growth. Thus i-polystyrene

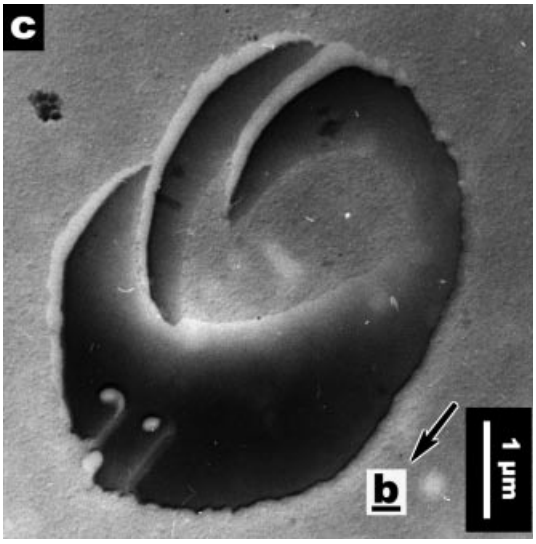

Fig. 4. (Continued)

forms hexagonal lamellae (72) [with sectors revealed by streaks normal to the surface (73) as for collapse of slightly nonplanar solution-grown crystals (14)]. Square lamellae occur for tetragonal i-poly(4-methylpentene-1) (62) and laths elongated along a^* for the monoclinic or α-form of i-polypropylene (74,75). Lamellae are circular for the high pressure hexagonal form of polyethylene when formed from the homopolymer but develop a modulated envelope when grown from a 5:95 blend with branched polymer, probably reflecting difficulties in transport of material as for dendritic growth (76).

Lamellar Surfaces

Polymer lamellae differ from those of oligomers and low mass materials primarily in their fold surfaces, which are a direct consequence of the long molecular length. Although at first, folds were treated as sharp and equivalent to end groups in oligomeric lamellae, with similar packing requirements leading to surfaces of low crystallographic index, the actual circumstances are more complicated. As melt-crystallized polyethylene shows clearly, surfaces form in two ways, depending on whether or not fold packing has time to order as molecules attach to the growing lamella. This is the case for slower growth at low supercoolings, but under normal conditions surfaces form as {001} and subsequently reorganize to inclined states (65). The implication is that surface packing requirements are overridden in rapid growth by the crystallization of fold stems, leaving the initial surfaces rather disorganized. This is true even for monodisperse n-alkanes in which rapid growth on quenching leaves methyl end groups in a disorganized surface (77). On the other hand, for slower growth, surface packing considerations may predominate over lattice distortion as has been explicitly demonstrated in monodisperse alkanes (78,79).

Once formed, polymer lamellae are metastable with respect to thickening and improved fold surface packing, both of which can be accomplished, at sufficiently high temperatures, using the strong longitudinal molecular vibrations. Thickening is accomplished both by an increased height of the growth edge and by incorporation of new material behind the growth front (64). But although the adoption of tighter folding should be relatively unhindered and fold placements should not be greatly altered in this process, the extent to which inclined fold packing can be adopted in an existing lamella is much constrained, hence the S-profiles (66).

The different nonplanar habits of solution-grown polyethylene lamellae (28) may well be open to a similar interpretation, given that the change from hollow pyramidal and chair crystals to ridged lamellae occurs at a similar critical growth rate to that for melt growth. The suggestion at the time (30) that inclined surfaces formed initially as {001} can refer only to the primary nucleus; the {312} inclination, once adopted, is then maintained in both hollow pyramidal and chair crystals. (This contrasts with melt-crystallized row structures for which only secondary nucleation is involved.) If the analogy applies, ridged lamellae with their {314} facets (30) would result from conversion from a rapidly grown lamella initially with {001} surfaces. There are known to be differences in the nature of the corresponding fold surfaces (11).

One of the consequences of surfaces transforming from an initially rough state is that the surface energies, σ_e, for crystallization will be higher than those measured subsequently in eg melting experiments. While fold adjustment at fixed inclination has long been recognized in principle (80), for which a 10% increase has been estimated, the change of inclination now observed is a more drastic change so that fold surface energies for crystallization may be considerably higher than this figure and so far appreciated. In consequence, claims made for the role of metastable phases in crystallization (81) may well be invalid.

Lamellar surfaces provide channels through which gases and liquids may penetrate; it has been shown that they are the preferential site of certain chemical reactions (82,83). Not only is the local density necessarily less at the surface, because of the van der Waals' force as opposed to covalent bonding, but this is supplemented by a degree of disorder, as SAXS data confirm (84). In part this will reflect loose and nonadjacent-reentry folding plus uncrystallized cilia. But the morphology of row structures suggests that there is also a finite separation, less than lamellar thicknesses, between lamellae growing in close-packed array (85). In terms of contemporary understanding, this is likely to be a consequence of cilia pressure during growth by which lamellae are kept apart, with the intervening space occupied by uncrystallized material. There is also evidence from swelling that solvent can penetrate fold surface regions reversibly (86). In sum the several strands of evidence support the concept of an "amorphous" region proximate to lamellar surfaces, which is the model used to interpret SAXS data (84).

Polymer Spherulites

Spherulites, literally little spheres, are a form of higher level ordering readily seen with a polarizing optical microscope (Fig. 5). They are characteristic of

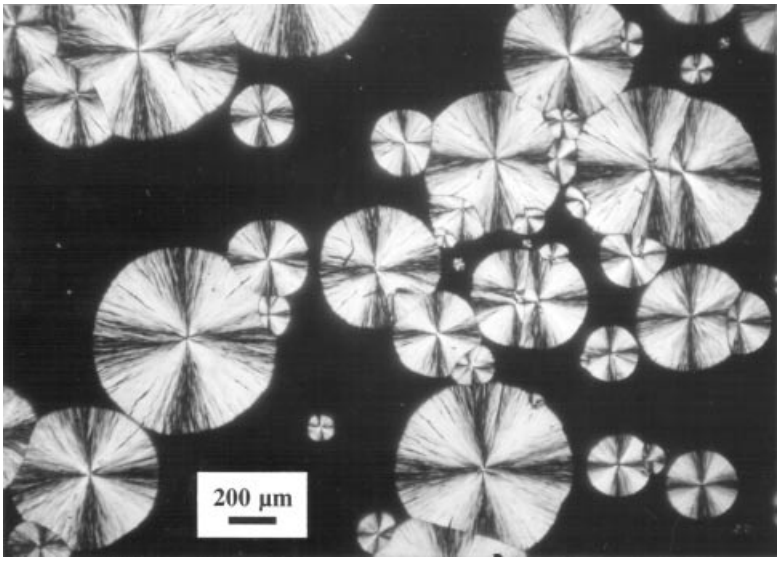

Fig. 5. Spherulites of the α-form of i-polypropylene viewed between crossed polars while crystallizing from the melt at 130°C. From Ref. 85.

melt-crystallized polymers, although their size and internal structure are highly variable depending upon primary nucleation, crystallization conditions, and the molecular constitution of the polymer, allowing the physical texture to be used by a skilled investigator to inform on these same factors. Primary nucleation controls the size and is almost always heterogeneous, ie of extraneous material such as catalyst particles. Homogeneous nucleation has only been demonstrated in systems subdivided into small spheres to isolate heterogeneous nuclei (88,89). Small spherulite size is often desired in commercial material to provide uniform properties but i-polypropylene in its normal α-form is difficult to nucleate and so often contains large spherulites. Most of the illustrations of spherulites in the literature tend to be of specially prepared specimens, often crystallized in thin films to accentuate relevant detail; sections cut from actual specimens may not be so clear or striking in appearance in part because the birefringence contrast of a section, particularly of banded spherulites, varies with distance from the spherulite center (90,91).

Figure 6 shows that the lamellar structure of polymer spherulites is built on a framework of individual dominant lamellae that branch repetitively and then diverge. The reasons for this are discussed below, but this construction leads, on a macroscopic level, to a typical succession of forms before the growing spherulite reaches maturity with a circular envelope and all radii crystallographically equivalent. Starting from an individual lamella, the progression is first to multilayer axialites in which the longest, ie fastest growing, lamellae splay most, presenting a sheaf-like appearance down the principal axis of splay, a lamellar habit at right angles to this and arrays of parallel but separate lamellae down the third Cartesian axis (45,93). When the diverging units eventually meet they enclose an inner area known as an eye or Popoff's leaves (94), which crystallizes separately, usually inward from its boundaries. How far development proceeds in an individual

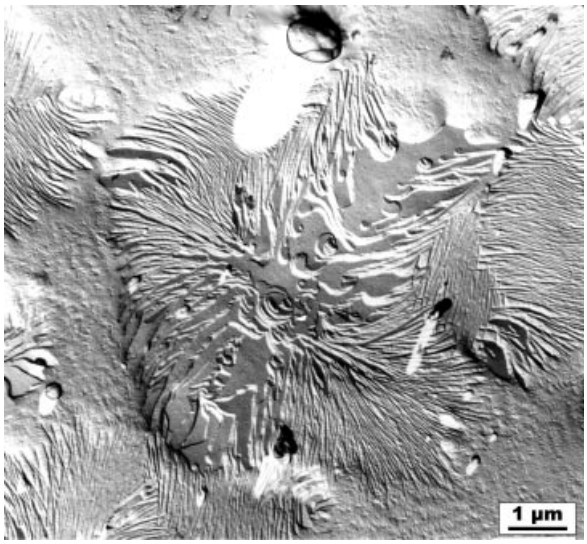

Fig. 6. Lamellar texture of a developing spherulite of linear low density polyethylene grown at 124°C. From Ref. 82.

case before impingement depends upon the nucleation density. The ideal spherical envelope may not have been attained before this occurs and, in particular cases, (95), may always preserve the legacy of its development to great distances. The boundaries between intersecting spheres are hyperboloids whose shape can be used to infer the respective times of nucleation; simultaneous nucleation gives a plane perpendicular to and bisecting the line of centers.

While spherulites grow from effectively point nuclei, other nucleation conditions are often encountered. Row structures result from linear nuclei, commonly fibres, on which growth is epitaxial, giving a cylinder whose radius is the same crystallographic axis as that of the spherulite. Transcrystallization is a consequence of nucleation on a surface to which this same direction is normal. In α-i-polypropylene the isothermal growth rates of all three have been measured to be the same (96). Once nucleated, similar growth processes ensue, unless segregation is significant when different diffusion conditions apply for the different geometries.

Spherulites and their formation are important because they are a major determinant of polymeric properties. Their size may cause significant light scattering, making products appear cloudy while interspherulitic boundaries may be weak, particularly in lower mass materials, and contribute to actual or potential brittleness. Moreover, spatial variability is inherent because diverging dominant lamellae are liable to behave differently from intervening regions. If these are crystalline, the infilling lamellae will probably be inclined to the dominants and contain later-crystallizing molecular species that, in the case of polyethylene, are liable to be shorter (61) and/or more branched (97), with intrinsically different behavior, including lower melting points.

Spherulitic Growth. The dominant/subsidiary lamellar organization within spherulites was not established until the early 1980s, notwithstanding

earlier results from fracture surfaces (8) and stained poly(isoprene) (98) showing that dominant lamellae advanced separately into the melt. There were claims to the contrary that this was restricted to higher growth temperatures (regime I) whereas lamellae were grouped into "fibres" at lower temperatures (99). This view derived in large measure from early attempts to open up the dense textures of spherulites for easier examination by blending, eg atactic with isotactic polypropylene (100). Although for high concentrations of the atactic component the isotactic material does then form multilamellar "fibres," systematic TEM shows that this is a consequence of blending and is not a typical behavior of homopolymer spherulites whose texture is established, over a wide temperature range, by individual dominant lamellae advancing into the melt (95).

The essential problem, concerning spherulitic growth, is to explain how and why a single lamellar precursor develops into a mature object whose radii are, to the resolution of the optical microscope, the same crystallographically, eg b in polyethylene and a^* in α i-polypropylene. The early proposal (101) that this was a problem of morphological instability and cellulation brought about by the segregation of species rejected at the growth front, has been shown not to be the case by the demonstration that, when cellulation does occur, in circumstances of high segregation of species that lower the local growth rate, this sets in only after spherulitic growth is well established (102,103). In other words it is a rather rare event, and an effect, not the cause, of spherulitic growth.

Although characteristic of melt-crystallized polymers, spherulitic growth is met with more widely, generally in viscous, often impure, inorganic systems for example (101,104). This has naturally led to the expectation that its explanation would not be specifically polymeric. What has now been shown in much detail is that there are specific features contributing to spherulitic growth in polymers, that are, however, of sufficient generality to be readily extended to apply to nonpolymeric systems. They are that lamellae diverge because they are pushed apart near their origins and/or that they form with rough surfaces, which do not pack parallel. The first of these was suggested initially from observations of the early stages of growth in which planar lamellae branch at rather regular angles (105–107) reinforced by the fact that successive layers of a spiral terrace (forming around a giant screw dislocation) are not in contact (71). Detailed confirmation, together with evidence for the second mechanism, has come from study of the monodisperse long n-alkanes discussed below.

The geometry of growth cited above, of what are very flexible lamellae, indicates that they grow undeformed after diverging near their origin. The angles of divergence are typically $\sim 20^\circ$ but increase with supercooling, ie for thinner lamellae (62). This requires a mesoscopically short-range repulsive force effective in the immediate neighborhood of a branch point. It was first suggested that, for polymers, this is due to the pressure of transient cilia, ie the uncrystallized portions of molecules partly attached to the growth face (105–107). They must (temporarily) occupy space adjacent to fold surfaces and will resist any competition for it with a rubbery modulus causing adjacent lamellae to diverge unless, exceptionally, they are incorporated within it (87). In another system with similar embryonic geometry, ice growing from a glycerine solution, the agent responsible for the force has been suggested to be osmotic pressure (108).

Monodisperse Long *n*-alkanes. The synthesis of monodisperse long *n*-alkanes, initially by Whiting (109) and then developed by Brooke and co-workers (110), has brought model materials, oligomeric to polyethylene, whose study has shed much light on how linear molecules crystallize. As expected, the methyl end groups tend to locate in basal surfaces giving lamellae of quantized thicknesses $\sim L \cos \theta/n$, where L is the molecular length; θ, the inclination of the c axis to lamellar normals ($\sim 35^\circ$); and n-1, the number of folds (111). This is not an invariable outcome, however, but merely the most ordered state. Unexpectedly the growth rate was found to pass through a minimum when the mode of crystallization changes from one quantized thickness to another, eg extended-chain to once-folded, attesting to the interference, at the growth surface, of one molecular conformer with the other (112).

In relation to spherulites, the first proposal tested was that, to the approximation that fold stems add as integral units, transient cilia and, therefore, spherulites would be present in once-folded growth when only one stem was attached to a lamella but not in extended-chain growth. This exactly matches the behavior of n-$C_{294}H_{590}$ in the region of the changeover between these two forms (113,114). On the other hand, lamellae do begin increasingly to diverge at higher supercoolings in this and other *n*-alkanes even when only extended-chain growth occurs, showing that a more detailed view of the attachment process is appropriate. The deviation of adjacent dominant lamellae is linear in supercooling over the narrow range possible to study, as will be cilium length, when taken to be the excess of molecular length over that of the secondary nucleus, but the plot of deviation against supercooling has a finite intercept at zero supercooling when, by this definition, cilium length must be zero (115). This points to a second factor contributing to lamellar divergence, which has been suggested to be (initially) rough surfaces, which do not pack parallel (116). This novel concept is supported both by SAXS on monodisperse *n*-alkanes and by contemporary work on the formation and reorganization of fold surfaces in polyethylene.

SAXS data show that the quantized thicknesses are not established immediately but that the long period passes through a nonintegrally folded (NIF) form, in which surfaces will not be well defined (77). There are also new infrared data showing that {001} surfaces of solution-crystallized deuterated *n*-alkanes are inherently disordered (117). Similarly, linear nucleation has shown that for most crystallization conditions, polyethylene fold surfaces form as {001} in a stressed condition from which they subsequently transform to S-profiles, with banding (65). Monodisperse n-$C_{294}H_{590}$ also forms banded spherulites of the once-folded form when quenched (113), signifying that, in this condition, its basal surfaces are stressed.

Banded Spherulites. Banded growth (Fig. 7a) is not a general feature of spherulites or rows but occurs in certain systems, seemingly those in which chains tend to be inclined to lamellar normals, these include various polyesters, poly(vinylidene fluoride) and polyethylene. Various strands of evidence on the last two systems have recently come together to provide a rudimentary account and an explanation of what has been a persistent puzzle. Although in some instances rhythmic growth patterns do occur (118), the concentric or spiraling extinction ring patterns are almost, if not always, due to a spiraling of the crystal axes around the maintained growth direction (90,91,118,120). Extinction

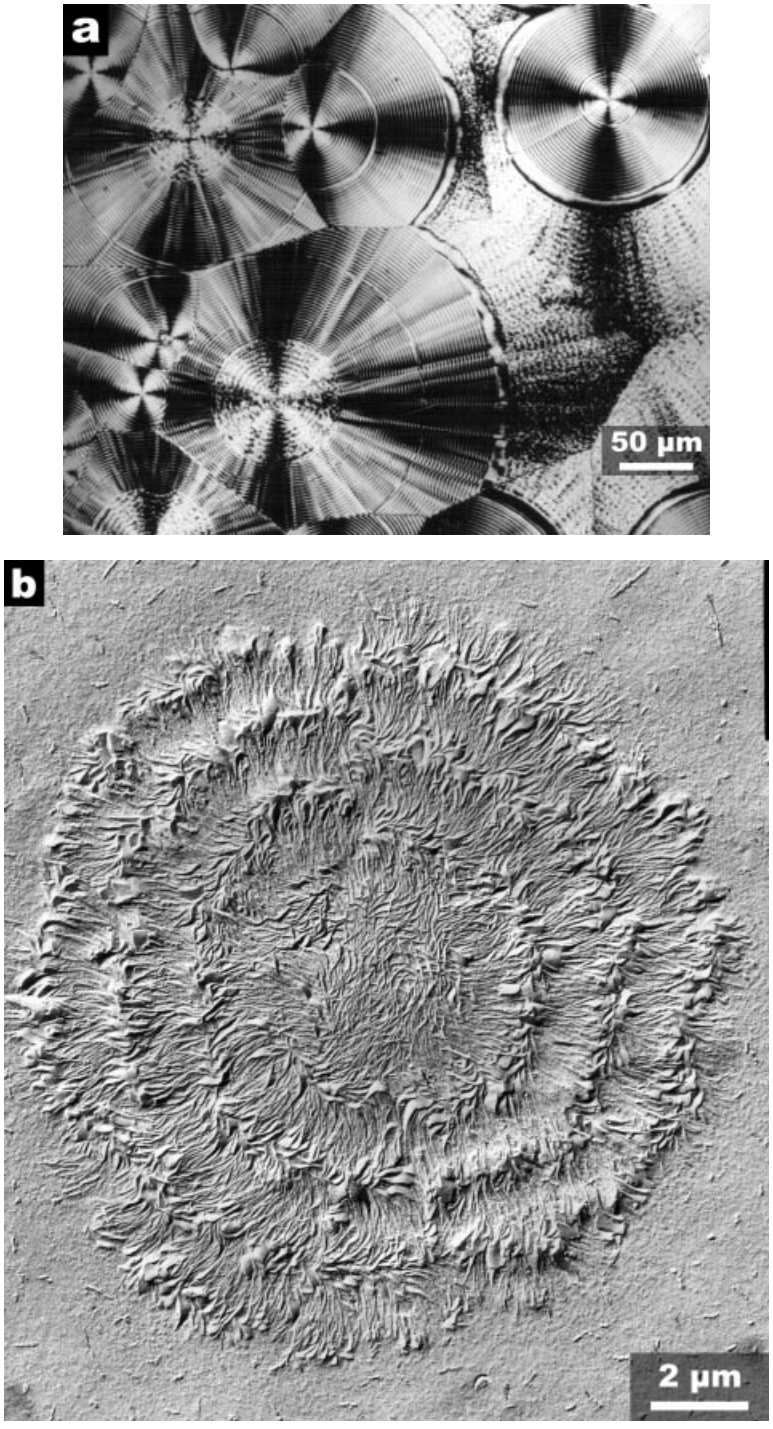

Fig. 7. (**a**) Banded spherulites of poly(trimethylene glutarate) viewed between crossed polars in a polarizing microscope. From Ref. 118.. (**b**) lamellar texture in a banded spherulite of butyl-branched linear low density polyethylene crystallized at 124°C. From Ref. 119.

(blackness) occurs whenever an optic axis is parallel to the viewing direction. For optic axes tangential to a spherulite, a uniaxial system will extinguish once per 180° turn but a biaxial system twice as each axis comes into position in turn.

The optical properties of banded spherulites were explained just as polymer single crystals were discovered but the relationship between the two has only recently been made clear. The average twist spirals uniformly around the spherulite radius, with an associated lamellar rotation (Fig. 7b) but packing considerations rule out uniformly twisted radial lamellae. The link between S-profiled dominant lamellae and twisting in polyethylene, with the concave surfaces advancing with increasing radius, came with the application of permanganic etching (121), but details of precise lamellar morphologies have only recently been published (66,122).

The unambiguous demonstration (6) that, in polyethylene, S-profiles develop after lamellae have formed with {001} surfaces and behind the growth front points to relief of (fold) surface stress as the driving force behind twisting. This will be greater in systems for which the preferred packing is inclined than for those where chains remain normal to lamellae. In polyethylene the asymmetry is introduced by the axis of the S-profile not being parallel to b, the growth axis. It is maintained via a series of isochiral giant screw dislocations positioned systematically to one side, created by the asymmetric shear stress generated by the change of fold surface inclination (66).

The fold surface stress thus described is built in during growth that occurs too rapidly for surfaces to have ordered. There is another situation in which initially ordered fold surfaces become stressed at a later stage when banded growth ensues. This occurs for slow growth of linear low density polyethylene once isothermal thickening brings initially excluded branches into surface regions (123).

Morphology and Mechanical Properties

Morphology affects mechanical properties in two ways. First, the macroscopic property falls below that of the crystal lattice, by some three orders of magnitude for Young's modulus, partly because of disorientation but more significantly because of the interruption of covalent bond sequences by fold surfaces. Second, boundaries and defects such as cracks, crazes, voids and dislocations can cause or influence yield, deformation, and fracture. A recent review of the effect of morphology on mechanical properties has been published recently (124).

Advanced Materials. The first major contributor to enhanced mechanical properties, orientation of chain axes and their covalent bonds, may be achieved by stretching or extrusion of the melt, from solution or gel states, or of solid polymer. But even in highly oriented fibres, the longitudinal Young's modulus is still well below the ideal value (of ∼300 GPa for polyethylene). To approach such figures, fold surfaces need to be reduced in number and/or strengthened with taut tie molecules. Some degree of folding is, however, helpful in retaining toughness, which would be absent for fully extended molecules (125). Various routes have been found to produce tough high modulus polyethylenes commercially, typically in the form of fibres some tens of nanometers in diameter (126–128). Different materials have different internal structures but all possess a transverse texture

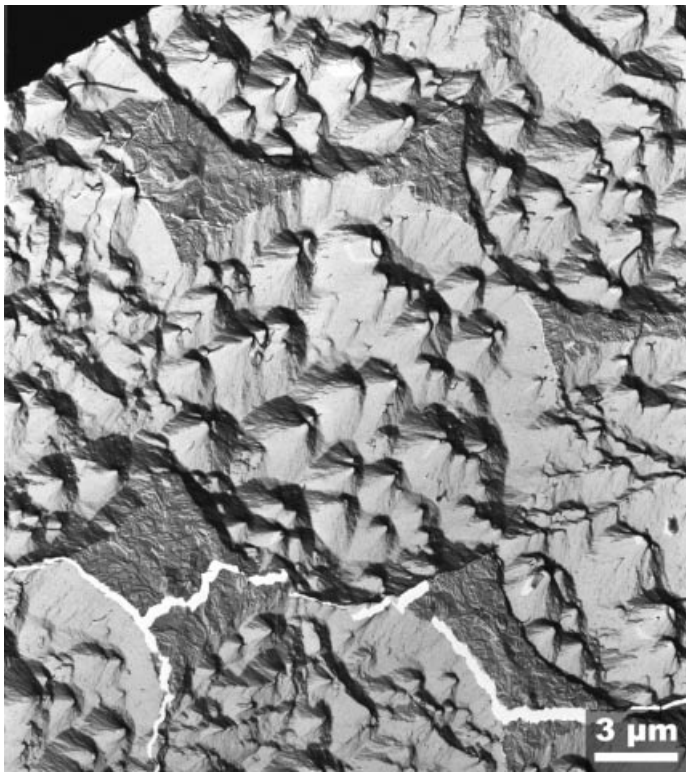

Fig. 8. A uniaxial compaction of high modulus, melt-spun polyethylene fibers seen in transverse section. The interstices between the individual fibres have been filled by material melting from the surfaces and then recrystallizing epitaxially thereon. Replica of etched surface viewed by TEM. From Ref. 132.

of higher melting internal walls from which lower melting lamellae have grown outwards as in transcrystalline growth (129). In longitudinal section, this can give the appearance of parallel shish-kebabs but there is no cylindrical symmetry (130).

Macroscopic samples with similarly good mechanical properties can be manufactured by hot compaction to make self-composites. For example (Fig. 8), an array of high modulus fibres held parallel in a matched mould and heated until just sufficient material melts from the surface to fill the gaps between fibres produces a uniaxial material retaining 90% of the fibre modulus but with good transverse strength, due to epitaxial bonding (131,132). Exceptional impact strengths are achieved by two-dimensional self-composites of polypropylene, made from compacted cloths (133).

Tensile Deformation. Following the discovery of polymer single crystals there was much interest in exploring their deformation behavior; for example, polyethylene monolayers stretched on an extensible substrate reveal a wide variety of transverse deformation modes (134). The influence of folds and the fold plane are evident in the different responses to cracks: those parallel to the fold plane are generally clean in contrast to those normal to it, which are bridged by

drawn threads (135). Detailed study (136) has widened this distinction and shown how local deformation modes of slip favor those in which slip occurs parallel to the fold plane. Such studies tend not to reveal deformation along the chain, whereas with melt-crystallized polyethylene chain slip has been identified as a major mode of lamellar deformation (137). By this, adjacent portions of a lamella can be displaced by shear in the chain direction until folds stop further slip unless covalent bonds are broken (124).

The deformation of spherulitic materials is considerably more complicated. Interspherulitic boundaries are a potential source of weakness, being liable to crack in lower mass material when there is insufficient crack blunting by tie molecules (138). Voids may form where three spherulites meet because of a dearth of material to compensate for the shrinkage in the final stages of crystallization (139,140) For spherulites themselves, there is an initial elastic response (to ∼30% strain) recoverable over many hours or a few days, followed by permanent, inhomogeneous changes with active modes involving various combinations of slip, twinning, and phase changes as identified for solution-grown lamellae (141). Which modes operate in given circumstances is strongly dependent on the orientation of lamellae and their chain axes to the applied stress. Figure 9 shows the different responses of lamellae in a polyethylene spherulite according to their inclination. Under tension or shear, lamellae rotate, disrupt, and/or fragment; under

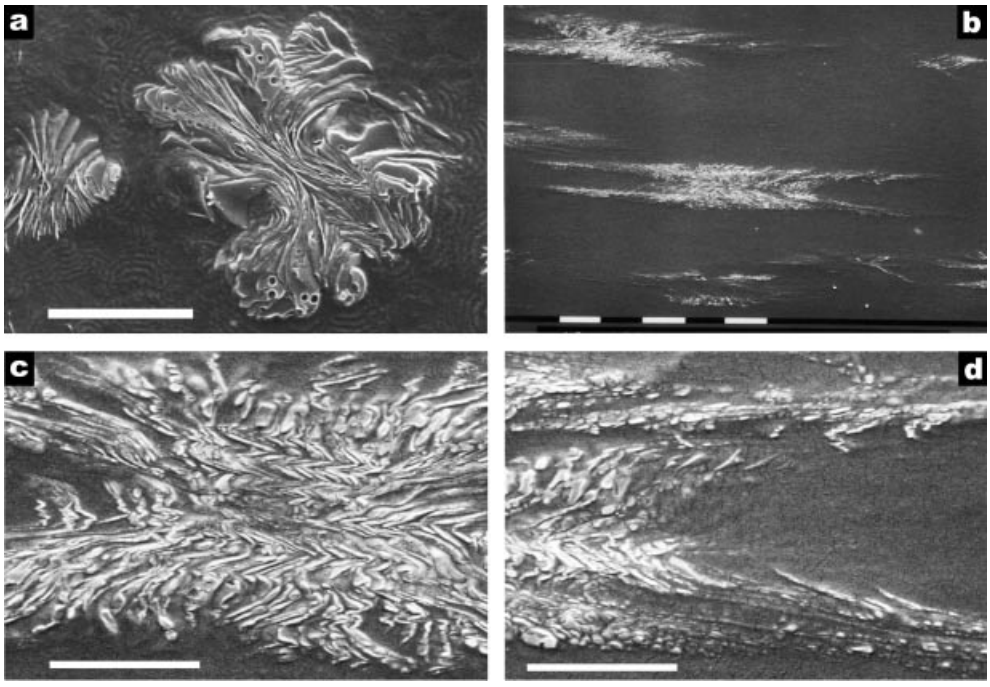

Fig. 9. Immature spherulites in a 5% blend of linear polyethylene in branched polymer: (**a**) undeformed; (**b**) drawn horizontally 4.5× at 75°C; (**c**) detail revealing zigzags of rotated lamellae in phase parallel to the draw direction; (**d**) detail of the extremity of an object as in (**b**), showing how individual lamellae have become disrupted giving an interrupted appearance. SEM images; bar = 10 μm. From Ref. 124.

compression they buckle and then kink cooperatively where the stress is highest (142).

Such situations are complex and it is rarely, if at all, possible to gain sufficient information for a thorough analysis. However, for long it was thought that no memory of the original morphologies remained in the fibrous structures produced at high draw ratios (143). Recent work has shown that this is not so. The earlier conclusion was reached from X-ray and microscopic examination perpendicular to the orientation axis, whereas it has now been shown, by looking down this direction, that traces of the original morphology do survive at high draw ratios ~50 (144,145).

Underlying all mechanical behavior is an important, central, aspect of morphology that lies beyond the scope of current capabilities to resolve. It is an entangled molecular network, transient in thermoplastic polymers, that sustains the applied stress and drives the slow elastic recovery of deformed spherulites, and without which materials would fail. Its extension leads to the extended nuclei for shish–kebabs and/or walls within fibres. One system in which it is suggested where entanglements are located is "overdrawn" fibres of polyethylene or i-polypropylene. These show a series morphology called Pisa structure with alternating draw ratios (146). Crazing and/or fibrillation occur for regions of higher draw ratio but where there is no discernible texture in the intervening regions, of lesser draw ratio, is the possible location of the entanglements.

In summary, polymer morphology in its twin aims of exposing and interpreting the nature of organization in macromolecular systems is essential to advance knowledge and understanding of these complex materials. It is a primary process to be followed, once the pattern of organization has been established, by complementary means to quantify and refine the underlying concepts.

BIBLIOGRAPHY

"Morphology" in *EPST* 1st ed., Vol. 9, pp. 204–274, by P. Ingram and A. Peterlin, Research Triangle Institute; "Morphology" in *EPSE* 2nd ed., Vol. 10, pp. 26–94, by Anton Peterlin, Consultant.

1. O. Gerngross, K. Herrmann, and W. Abitz, *Z. Physik. Chem. B* **10**, 371 (1930).
2. C. W. Bunn and T. C. Alcock, *Trans. Faraday Soc.* **41**, 317 (1945).
3. C. W. Bunn, in R. Hill, ed., *Fibres from Synthetic Polymers*, Elsevier, Amsterdam, 1953, p. 240.
4. R. Jaccodine, *Nature* **176**, 305 (1955).
5. P. H. Till, *J. Polym. Sci.* **17**, 447 (1957).
6. E. W. Fischer, *Z. Naturforsch* **12A**, 753 (1957).
7. A. Keller, *Philos Mag.* **2**, 21 (1957).
8. P. H. Geil, *Polymer Single Crystals*, Wiley-Interscence, New York, 1963.
9. H. D. Keith, in D. Fox, M. M. Labes, and A. Weissburger eds., *Physics and Chemistry of the Organic Solid State*, Wiley-Interscience, New York, 1963, p. 461.
10. P. J. Flory, *J. Am. Chem. Soc.* **84**, 2857 (1962).
11. D. C. Bassett and A. Keller, *Philos. Mag.* **7**, 1553 (1962).
12. S. J. Organ and A. Keller, *J. Mater. Sci.* **20**, 1571 (1985).
13. D. C. Bassett, *Philos. Mag.* **12**, 907 (1965).
14. D. C. Bassett, F. R. Dammont, and R. Salovey, *Polymer* **6**, 579 (1964).
15. H. D. Keith, R. G. Vadimsky, and F. J. Padden, *J. Polym. Sci., Part A-2* **8**, 1687 (1970).

16. F. C. Frank, A. Keller, and A. O'Connor, *Philos. Mag.* **3**, 64 (1958).
17. L. Cartier and B. Lotz, *Macromolecules* **31**, 3049 (1998).
18. D. C. Bassett, *Principles of Polymer Morphology*, Cambridge University Press, Cambridge, 1981.
19. F. Khoury and F. J. Padden, *J. Polym. Sci.* **47**, 455 (1960).
20. F. Khoury, *J. Res. Natl. Bur. Stand. A* **70A**, 29 (1966).
21. B. Lotz, A. J. Kovacs, and J. C. Wittman, *J. Polym. Sci., Polym. Phys. Ed.* **13**, 909 (1975).
22. G. A. Bassett, D. J. Blundell, and A. Keller, *J. Macromol. Sci., B* **1**, 161 (1967).
23. J. C. Wittman and B. Lotz, *J. Polym. Sci., Polym. Phys. Ed.* **23**, 205 (1985).
24. S. J. Spells, A. Keller, and D. M. Sadler, *Polymer* **25**, 749 (1984).
25. D. C. Bassett, F. C. Frank, and A. Keller, *Proc. Eur. Reg. Conf. Electron Micr.* **1**, 244. (1960).
26. D. C. Bassett, *Philos. Mag.* **10**, 595 (1964).
27. D. C. Bassett, F. C. Frank, and A. Keller, *Nature* **184**, 810 (1959).
28. D. C. Bassett, F. C. Frank, and A. Keller, *Philos. Mag.* **8**, 1739 (1963).
29. W. D. Niegisch and P. R. Swan, *J. Appl. Phys.* **31**, 1906 (1960).
30. D. C. Bassett, F. C. Frank, and A. Keller, *Philos. Mag.* **8**, 1753 (1963).
31. D. M. Sadler, Studies on the Surface of Solution Grown Polyethylene Crystals and Some Related Topics, PhD dissertation, University of Bristol, 1969.
32. D. H. Reneker and P. H. Geil, *J. Appl. Phys.* **31**, 1916 (1960).
33. Y. Nakagawa, H. Hayashi, T. Takahagi, F. Soeda, A. Ishitani, A. Toda, and H. Miyaji, *Jpn. J. Appl. Phys.* **33**, 3771 (1994).
34. A. Keller and A. O'Connor, *Discuss. Faraday Soc.* **25**, 114 (1958).
35. D. J. Jones, A. J. Latham, A. Keller, and M. Girolamo, *J. Polym. Sci., Polym. Phys. Ed.* **11**, 1759 (1973).
36. D. C. Bassett and A. M. Hodge, *Proc. R. Soc. London, Ser. A* **359**, 121 (1978).
37. P. J. Barham, R. A. Chivers, A. Keller, J. Martinez-Salazar, and S. J. Organ, *J. Mater. Sci.* **20**, 1625 (1985).
38. H. D. Keith and F. J. Padden, *J. Appl. Phys.* **35**, 1286 (1964).
39. H. E. Bair, R. Salovey, and T. W. Huseby, *Polymer* **8**, 9 (1967).
40. P. J. Holdsworth and A. Turner-Jones, *Polymer* **12**, 195 (1971).
41. J. D. Hoffman and J. J. Weeks, *J. Res. Natl. Bur. Stand., A* **66**, 13 (1962).
42. D. C. Bassett and D. Patel, *Polymer* **35**, 1855 (1994).
43. W. O. Statton and P. H. Geil, *J. Appl. Phys.* **3**, 357 (1960).
44. J. D. Hoffman, C. M. Guttman, and E. A. DiMarzio, *Discuss. Faraday Soc.* **68**, 394 (1979).
45. D. C. Bassett, A. Keller, and S. Mitsuhashi, *J. Polym. Sci., Part A: Polym. Chem.* **1**, 763 (1963).
46. P. H. Geil, F. R. Anderson, B. Wunderlich, and T. Arakawa, *J. Polym. Sci., Part A: Polym. Chem.* **2**, 3707 (1964).
47. D. C. Bassett and B. Turner, *Philos. Mag.* **29**, 925 (1974).
48. D. C. Bassett, S. Block, and G. J. Piermarini, *J. Appl. Phys.* **45**, 4146 (1974).
49. B. Wunderlich, *Pure Appl. Chem.* **31**, 49 (1972).
50. D. C. Bassett and R. Davitt, *Polymer* **15**, 721 (1974).
51. D. C. Bassett and B. A. Khalifa, *Polymer* **14**, 391 (1973).
52. T. Hatekayama, H. Kanetsuna, and T. Hashimoto, *J. Macromol. Sci., B* **7**, 411 (1973).
53. D. C. Bassett, in D. C. Bassett, ed., *Developments in Crystalline Polymers–1*, Applied Science, London, 1982, p. 115.
54. G. Kanig, *Kunstoffe* **64**, 470 (1974).
55. R. H. Olley, A. M. Hodge, and D. C. Bassett, *J. Polym. Sci., Polym. Phys. Ed.* **17**, 627 (1979).

56. R. H. Olley and D. C. Bassett, *Polymer* **23**, 1707 (1982).
57. A. M. Hodge and D. C. Bassett, *J. Mater. Sci.* **12**, 2065 (1977).
58. D. C. Bassett in D. C. Bassett, ed., *Developments in Crystalline Polymers–2*, Applied Science, London, 1988, p. 67.
59. D. C. Bassett and A. M. Hodge, *Proc. R. Soc. London, Ser. A* **377**, 25 (1981).
60. A. Mehta and B. Wunderlich, *Colloid Polym. Sci.* **253**, 193 (1975).
61. D. C. Bassett, A. M. Hodge, and R. H. Olley, *Proc. R. Soc. London, Ser. A* **377**, 39 (1981).
62. D. Patel and D. C. Bassett, *Proc. R. Soc. London, Ser. A* **445**, 577 (1988).
63. J. D. Hoffman, L. J. Frolen, G. S. Ross, and J. I. Lauritzen, *J. Res. Natl. Bur. Stand., A* **79**, 671 (1975).
64. M. I. Abo el Maaty and D. C. Bassett, *J. Macromol. Sci. Phys. B* **40**, 849 (2002).
65. M. I. Abo el Maaty and D. C. Bassett, *Polymer* **42**, 4957 (2001).
66. D. Patel and D. C. Bassett, *Polymer* **43**, 3795 (2002).
67. A. Toda and A. Keller, *Colloid Polym. Sci.* **271**, 328 (1993).
68. J. D. Hoffman and R. L. Miller, *Polymer* **38**, 3151 (1997).
69. M. L. Mansfield, *Polymer* **29**, 1755 (1988).
70. A. Toda, *Polymer* **32**, 771 (1991).
71. D. C. Bassett, R. H. Olley, and I. A. M. al Raheil, *Polymer* **29**, 1539 (1988).
72. H. D. Keith, *J. Polym. Sci., Part A: Polym. Chem.* **2**, 4339 (1964).
73. A. S. Vaughan, *Polymer* **33**, 2513 (1992).
74. F. J. Padden and H. D. Keith, *J. Appl. Phys.* **37**, 4014 (1963).
75. A. J. Lovinger, *J. Polym. Sci., Polym. Phys. Ed.* **21**, 97 (1983).
76. J. A. DiCorleto and D. C. Bassett, *Polymer* **31**, 1971 (1990).
77. G. Ungar and A. Keller, *Polymer* **27**, 1835 (1987).
78. H. M. White, I. L. Hosier, and D. C. Bassett, *Macromolecules* **35**, 6763 (2002).
79. I. L. Hosier and D. C. Bassett, *Polymer* **43**, 5959 (2002).
80. J. I. Lauritzen and E. Passaglia, *J. Res Natl. Bur. Stand., A* **71**, 261 (1967).
81. A. Keller and G. Goldbeck-Wood, in S. L. Aggarval, and S. Russo, eds., *Comprehensive Polymer Science, 2nd Suppl.*, Elsevier, Oxford, 1996, p. 241.
82. D. C. Bassett, *Polymer* **5**, 457 (1964).
83. I. R. Harrison and E. Baer, *J. Polym. Sci., Part A-2* **9**, 1305, 1971).
84. F. J. Baltà Calleja and C. G. Vonk, *X-Ray Scattering of Synthetic Polymers*, Elsevier, Amsterdam, 1989.
85. H. M. White and D. C. Bassett, *Polymer* **39**, 3211 (1998).
86. D. J. Blundell and A. Keller, *J. Macromol. Sci., B* **7**, 253 (1973).
87. D. C. Bassett, *Philos. Trans. R. Soc. London Ser. A* **348**, 29 (1994).
88. F. Gornick, G. S. Ross, and L. J. Frolen, *J. Polym. Sci. C* **18**, 79 (1967).
89. L. Dong, D. C. Bassett and R. H. Olley, *J. Macromol. Sci., B* **37**, 527 (1998).
90. H. D. Keith and F. J. Padden, *J. Polym. Sci.* **39**, 101 (1959).
91. H. D. Keith and F. J. Padden, *J. Polym. Sci.* **39**, 123 (1959).
92. D. C. Bassett, in M. Dosière, ed., *Crystallization of Polymers*, Kluwer, Dordrecht, 1993 p. 107.
93. P. H. Geil, in R. H. Doremus, B. W. Roberts, D. Turnbull, eds., *Growth and Perfection of Crystals*, John Wiley & Sons, Inc., New York, 1958, p. 579.
94. A. Keller, *Makromol. Chem.* **39**, 1 (1959).
95. R. H. Olley and D. C. Bassett, *Polymer* **30**, 399 (1989).
96. H. M. White and D. C. Bassett, *Polymer* **38**, 5515 (1997).
97. A. M. Freedman, D. C. Bassett, and R. H. Olley, *J. Macromol. Sci., Phys. B* **27**, 319 (1988).
98. P. J. Phillips, *J. Polym. Sci., Polym Phys. Ed.* **13**, 2117 (1975).
99. H. D. Keith and F. J. Padden, *Polymer* **27**, 1463 (1986).

100. H. D. Keith and F. J. Padden, *J. Appl. Phys.* **35**, 1270 (1964).
101. H. D. Keith and F. J. Padden, *J. Appl. Phys.* **34**, 2409 (1963).
102. M. I. Abo el Maaty, I. L. Hosier, and D. C. Bassett, *Macromolecules* **31**, 153 (1998).
103. M. I. Abo el Maaty, D. C. Bassett, R. H. Olley, and P. Jääskeläinen, *Macromolecules* **33**, 7800 (1998).
104. P. J. Phillips, in D. T. J. Hurle, ed., *Handbook of Crystal Growth*, Vol. **2**, Elsevier, Amsterdam, 1994, p. 1167.
105. D. C. Bassett and R. H. Olley, *Polymer* **25**, 935 (1984).
106. D. C. Bassett and A. S. Vaughan, *Polymer* **26**, 717 (1985).
107. D. C. Bassett, *CRC Crit. Rev.* **12**, 97 (1984).
108. G. T. Geering, PhD Thesis, Stanford (1968), cited in W. A. Tiller, *The Science of Crystallization: Macroscopic Phenomena and Defect Generation*, Cambridge University Press, Cambridge, 1991, p. 345.
109. O. I. Paynter, D. J. Simmonds, and M. C. Whiting, *J. Chem. Soc., Chem. Commun.* 1165 (1982).
110. G. M. Brooke, S. Burnett, S. Mohammed, D. Proctor, and M. C. Whiting, *Chem. Soc., Perkin Trans.* **1**, 1635 (1996).
111. G. Ungar, J. Stejny, A. Keller, and M. C. Whiting, *Science* **229**, 386 (1985).
112. G. Ungar and A. Keller, *Polymer* **27**, 1835 (1987).
113. D. C. Bassett, R. H. Olley, S. J. Sutton, and A. S. Vaughan, *Macromolecules* **29**, 1852 (1996).
114. D. C. Bassett, R. H. Olley, S. J. Sutton, and A. S. Vaughan, *Polymer* **37**, 4993 (1996).
115. I. L. Hosier and D. C. Bassett, *Polymer* **41**, 8801 (2000).
116. I. L. Hosier and D. C. Bassett, *Polymer* **43**, 307 (2002).
117. D. S. M. de Silva, X. Zeng, G. Ungar, and S. J. Spells, in *International Symposium on Polymer Crystallization*, Mishima, Japan, June 2002 p. 14.
118. A. Keller, *J. Polym. Sci.* **39**, 151 (1959).
119. D. C. Bassett, in C. Booth and C. Price, eds., *Comprehensive Polymer Science Vol. 1: Polymer Characterization*, Pergamon, Oxford, 1989, p. 841.
120. F. P. Price, *J. Polym. Sci.* **39**, 139 (1959).
121. D. C. Bassett and A. M. Hodge, *Proc. R. Soc. London, Ser. A* **377**, 61 (1981).
122. A. Toda, T. Arita, and M. Hikosaka, *Polymer* **42**, 2223 (2001).
123. M. I. Abo el Maaty and D. C. Bassett, *Polymer* **43**, 6541 (2002).
124. D. C. Bassett, in I. M. Ward, P. D. Coates, and M. M. Dumoulin, eds., *Solid Phase Processing of Polymers*, Hanser, Munich, 2000, p. 11.
125. F. C. Frank, *Proc. R. Soc. London Ser. A* **319**, 127 (1970).
126. G. Capaccio and I. M. Ward, *Polymer* **15**, 233 (1974).
127. P. Smith and P. J. Lemstra, *Colloid Polym. Sci.* **258**, 891 (1980).
128. D. C. Prevorsek, in M. Lewin and J. Preston, eds., *The Handbook of Fiber Science and Technology, Vol. 3: High Technology Fibers*, Marcel Dekker, Inc., New York, 1996, p. 1.
129. M. I. Abo el Maaty, R. H. Olley, and D. C. Bassett, *J. Mater. Sci.* **34**, 1975 (1999).
130. J. Teckoe, D. C. Bassett and R. H. Olley, *Polymer J.* **31**, 765 (1999).
131. P. J. Hine, I. M. Ward, R. H. Olley, and D. C. Bassett, *J. Mater. Sci.* **28**, 316 (1993).
132. R. H. Olley, D. C. Bassett, P. J. Hine, and I. M. Ward, *J. Mater. Sci.* **28**, 1107 (1993).
133. P. J. Hine, I. M. Ward and J. Teckoe, *J. Mater. Sci.* **33**, 2725 (1998).
134. P. H. Geil, *J. Polym. Sci., Part A: Polym. Chem.* **2**, 3813 (1964).
135. P. H. Lindenmeyer, *J. Polym. Sci., C* **1**, 5 (1963).
136. P. Allan, and M. Bevis, *Proc. R. Soc. London Ser. A* **341**, 75 (1975).
137. P. B. Bowden, R. J. Young, J. M. Ritchie, and J. G. Rider, *J. Mater. Sci.* **8**, 23 (1973).
138. F. C. Frank, *Proc. R. Soc. London Ser. A* **282**, 9 (1964).
139. Z. Bartczak and A. Galeski, *Polymer* **27**, 544 (1986).

140. R. H. Olley and D. C. Bassett, *J. Macromol. Sci., B* **33**, 209 (1994).
141. I. L. Hay and A. Keller, *Kolloid Z.* **201**, 43 (1965).
142. S. Y. Lee, R. H. Olley, and D. C. Bassett, *J. Mater. Sci.* **35**, 5101 (2000).
143. A. Peterlin, *J. Mater. Sci.* **6**, 490 (1971).
144. T. Amornsakchai, R. H. Olley, D. C. Bassett, M. O. M. Al-Hussein, A. P. Unwin, and I. M. Ward, *Polymer* **41**, 8291 (2000).
145. T. Amornsakchai, R. H. Olley, D. C. Bassett, A. P. Unwin, and I. M. Ward, *Polymer* **42**, 4117 (2001).
146. M. I. Abo el Maaty, D. C. Bassett, R. H. Olley, M. G. Dobb, J. G. Tomka, and I.-C. Wang, *Polymer* **37**, 213 (1996).

D. C. BASSETT
University of Reading

NOMENCLATURE

Overview

Nomenclature, as used in this article, refers to the naming of polymeric materials. The nomenclature of scientific communication is emphasized, although there is generally little reason for differences between scientific and other, eg, commercial, usages.

Since the publication of the first edition of this Encyclopedia, the International Union of Pure and Applied Chemistry (IUPAC) established the Commission on Macromolecular Nomenclature, which was, for the duration of its existence, the leading nomenclature body in the field of polymers. Between its inception in 1968 and the end of 2001, when the IUPAC underwent a major reorganization to a project-driven organization, the Commission promulgated a series of definitions and recommendations that established polymer nomenclature on a much more systematic basis than had previously been the case. The Commission developed a set of definitions for many of the basic terms dealing with polymer molecules, assemblies of polymer molecules, polymer solutions, polymer crystals, polymer melts and solids, polymerization reactions, etc. It also extended existing nomenclature to more complicated cases, such as double-strand (ladder and spiro) polymers. Completion of this work was accomplished by the early 1990s. Table 1 lists the Commission publications on polymer nomenclature.

Polymer naming and terminology became largely systematized and, following the IUPAC practice in other fields of chemistry, a compendium of polymer nomenclature recommendations was published in 1991 (30).

For 2002 and subsequent years, the IUPAC Macromolecular Division established the Subcommittee on Macromolecular Terminology, which has already embarked on the projects listed in Table 2.

Encyclopedia of Polymer Science and Technology. Copyright John Wiley & Sons, Inc. All rights reserved.

Table 1. Commission Publications on Polymer Nomenclature

Title	Comment	Ref.
Report on Nomenclature in the Field of Macromolecules (1952)	Obsolete	1
Report on Nomenclature Dealing with Steric Regularity in High Polymers (1962)	Superseded by Ref. 3	2
Report on Nomenclature Dealing with Steric Regularity in High Polymers (1966)	Superseded by Ref. 10	3
Report of the Committee on Nomenclature of the International Commission on Macromolecules (1968)	Obsolete	4
Basic Definitions of Terms Relating to Polymers (1974)	Superseded by Ref. 22	5
List of Standard Abbreviations (Symbols) for Synthetic Polymers and Polymer Materials (1974)	Superseded by Ref. 7	6
Use of Abbreviations for Names of Polymeric Substances (1986)		7
Nomenclature of Regular Single-Strand Organic Polymers (1975)	Superseded by Ref. 29	8
Stereochemical Definitions and Notations Relating to Polymers (1980)	Provisional Recommendations 1980	9 10
Nomenclature for Regular Single-Strand and Quasi-Single-Strand Inorganic and Coordination Polymers (1984)	Provisional Recommendations 1984	11 12
Note on the Terminology for Molar Masses in Polymer Science (1984)		13
Source-Based Nomenclature for Copolymers (1985)		14
Definitions of Terms Relating to Individual Macromolecules, Their Assemblies, and Dilute Polymer Solutions (1988)		15
Definitions of Terms Relating to Crystalline Polymers (1988)		16
A Classification of Linear Single-Strand Polymers (1988)		17
Nomenclature of Regular Double-Strand (Ladder and Spiro) Organic Polymers (1993)		18
Structure-Based Nomenclature for Irregular Single-Strand Organic Polymers (1994)		19
Graphic Representations (Chemical Formulae) of Macromolecules (1994)		20
Basic Classification and Definitions of Polymerization Reactions (1994)		21
Glossary of Basic Terms in Polymer Science (1996)		22

Table 1. (Continued)

Title	Comment	Ref.
Definitions of Terms Relating to Degradation, Aging, and Related Chemical Transformations of Polymers (1996)		23
Source-Based Nomenclature for Non-Linear Macromolecules and Macromolecular Assemblies (1997)		24
Definitions of Terms Relating to the Non-Ultimate Mechanical Properties of Polymers (1998)		25
Definitions of Basic Terms Relating to Low-Molar-Mass and Polymer Liquid Crystals (2001)		26
Generic Source-Based Nomenclature for Polymers (2001)		27
Definitions Relating to Stereochemically Asymmetric Polymerizations (2002)		28
Nomenclature of Regular Single-Strand Organic Polymers (2002)		29

The International Standardization Organization (ISO), primarily through its Technical Committee TC/61 Plastics, and various national nomenclature bodies (such as that of the American Chemical Society) are also helping to shape the field.

Chemical Abstracts Service (CAS) is also an authority on polymer nomenclature. CAS publishes *Chemical Abstracts*, which is available both in printed format and electronically via STN® International, Scientific and Technical Information Network. The *Chemical Abstracts* Registry file provides many examples of CAS polymer nomenclature principles, which are published as Section 222 of Appendix IV in every edition of the *CA Index Guide* (33).

Basic Definitions. No nomenclature document was more fundamental to polymer science than the one which set forth definitions of basic terms. First published by the IUPAC Commission in 1974 (5), this document defined 53 terms, including polymer, constitutional unit, monomer, polymerization, regular polymer, tactic polymer, block polymer, graft polymer, monomeric unit, degree of polymerization, addition polymerization, condensation polymerization, homopolymer, copolymer, bipolymer, terpolymer, copolymerization, and many others. Both structure-based and process-based definitions were given. In 1996, these recommendations were revised, enlarged, and updated (22). The new glossary, which provides a total of 135 terms, deals with three major groups of terms relating to molecules and molecular structure, substances, and reactions. These definitions are essential to any systematic polymer nomenclature and the reader is strongly encouraged to consult the full document.

The Principle of Source-Based Nomenclature. Traditionally, polymers have been named by attaching the prefix "poly" to the name of the real

Table 2. Subcommittee Projects on Polymer Nomenclature and Terminology[a]

Title	Anticipated Completion Date
Compendium of Macromolecular Terminology and Nomenclature (The Purple Book), 2nd Edition	2003
Definitions of Terms Relating to Reactions of Polymers and Functional Polymers	2003
Glossary of Class Names of Polymers Based on Their Chemical Structure and Molecular Architecture	2003
Guide to Macromolecular Terminology and Nomenclature	2003
Kinetics, Thermodynamics, and Mechanisms of Polymerizations	2003
Terminology and Nomenclature of Macromolecules with Cyclic Structures	2003
Terminology of Polymers with Ionizable Groups and Polymers Containing Ions	2003
Terminology Related to Multi-Phase Polymer Composites and Blends	2003
Terminology and Structure-Based Nomenclature of Dendritic and Hyperbranched Polymers	2003
Nomenclature for Chemically Modified Polymers	2004 or 2005
Nomenclature for Macromolecular Rotaxanes	2004 or 2005
Terminology Used in Sol–Gel Processing of Advanced Ceramics and Inorganic–Organic Polymeric Substances	2005

[a]An italicized title indicates a book; the other items listed will be published as recommendations in *Pure and Applied Chemistry*.

or assumed monomer (the "source") from which it is derived. Thus, polystyrene is the polymer made from styrene. When the name of the monomer comprises two or more words, parentheses should be used (7), as in poly(vinyl acetate), poly(methyl methacrylate), etc. Failure to use parentheses can lead to ambiguity: polychlorostyrene can be the name of either a polychlorinated (monomeric) styrene or of a polymer derived from chlorostyrene; polyethylene oxide can refer to either the polymer **1**, the polymer **2**, or the macrocycle **3**.

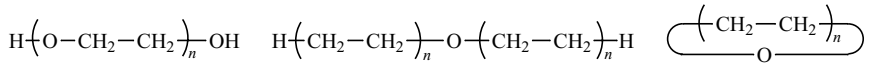

1 **2** **3**

These problems are easily overcome with parentheses: names such as poly(chloro)styrene, poly(chlorostyrene), and poly(ethylene oxide) clearly indicate the part of the name to which the prefix "poly" refers. The omission of parentheses is, unfortunately, still common in the literature.

The principal deficiency of source-based nomenclature is that the chemical structure of the monomeric unit in a polymer is not identical with that of the monomer (eg, —CHX—CH_2— versus CHX=CH_2); thus, a "polymonomer" name is actually a misnomer. The structure of the constitutional repeating unit may also not be implied in this scheme; for example, the name polyacrolein does not indicate whether the vinyl or the aldehyde group has polymerized.

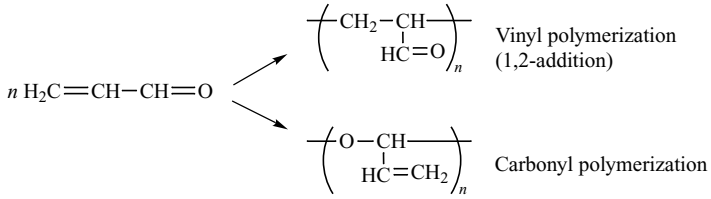

Depending on the polymerization conditions, different types of polymerization can take place with many other monomers. Furthermore, a name such as poly(vinyl alcohol) refers to a hypothetical source, since this polymer is obtained by hydrolysis of poly(vinyl acetate).

Despite these serious deficiencies, source-based nomenclature is still firmly entrenched in industrial literature and, to a lesser extent, in scientific communication. It originated at a time when polymer science was less developed and the structure of most polymers was ill-defined. The significant advances made during the last 50 years on the structure determination of polymers is gradually shifting the emphasis of polymer nomenclature away from starting materials and toward the structure of the macromolecules.

The Principle of Structure-Based Nomenclature. Structure-based nomenclature is based on a method of naming the sequence of constitutional or structural units that represent the ideal, and sometimes the actual, repeating pattern of the structure of a typical macromolecule in a polymer. The name has no direct relation to the structure of the (co)monomer(s) used to synthesize the polymer. Details are given below in both the IUPAC Nomenclature and Chemical Abstracts Nomenclature sections entitled "Structure-Based Nomenclature."

IUPAC Nomenclature

Source-Based Nomenclature.

Homopolymers. Although source-based names are usually simpler and less rigorous than structure-based names, historically the Commission has not systematically recommended source-based names for homopolymers because it considered that the more rigorous structure-based names were more appropriate for scientific communications (27). This rationale was based upon two specific points.

(1) A homopolymer that can be represented by a source-based name can usually be given a completely unambiguous structure-based representation, and such a representation should therefore be ideally accompanied by a structure-based name. A source-based name was therefore deemed redundant.

(2) There are cases in which the simplicity of source-based nomenclature leads to ambiguous names for homopolymers. Two examples illustrate this point.
   a. A source-based name such as poly(buta-1,3-diene) or polybutadiene does not indicate whether the structure is 1,2-, or 1,4-; its structure is a result of 1,2- or 1,4-polymerization.
   b. The polyacrylaldehyde example cited above.

Despite the Commission's long-standing position, the scientific community has continued to use source-based nomenclature for homopolymers such as polystyrene and poly(vinyl acetate) because of their simplicity, convenience, and obvious relationship with the monomers from which the homopolymers were prepared. The Commission therefore decided to recommend source-based nomenclature as an alternative official nomenclature for homopolymers in a 2001 publication (27). Consequently, both source-based and structure-based names are now available for most polymers. The names of monomers in the source-based names may be trivial or semi-systematic, if well established by usage, not necessarily only those retained in the 1993 *A Guide to IUPAC Nomenclature of Organic Compounds* (31).

The broad principle is to write the source-based name of a homopolymer by combining the prefix "poly" with the name of the monomer. When the latter consists of more than one word, or any ambiguity is anticipated, the name of the monomer is parenthesized.

The same publication (27) recommended generic source-based nomenclature, which comprises the optional addition of a polymer class name to the source-based name of the polymer. The addition is recommended only to avoid ambiguity or to add clarification.

Example: the source-based name poly(vinyloxirane) is ambiguous; ambiguity about the structure is removed by writing either polyalkylene:vinyloxirane to accompany the structure-based representation

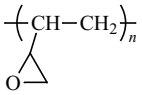

or polyether:vinyloxirane to accompany the structure-based representation

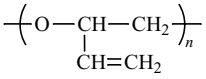

Copolymers. *Copolymers* are polymers that are derived from more than one species of monomer (22). Similarly to homopolymers, source-based nomenclature has been applied to copolymers (14). The principal problem in this scheme is to define the kind of arrangement in which various types of monomeric units are related to each other. Seven types of separate arrangements have been defined, which are shown in Table 3, where A, B, and C represent the names of monomers. The monomer names are linked through an italicized qualifier used as either a connective (infix), such as "*-co-*," to form the name of the copolymer, as in poly(styrene-*co*-acrylonitrile), or a prefix, such as "co". The order of citation of the monomers is arbitrary.

An equally acceptable alternative scheme, shown in the last column of Table 3, utilizes the prefix "copoly" followed by citation of the names of the monomers used, separated from each other by a solidus (oblique stroke). Parentheses are also needed. For example, copoly(styrene/butadiene) denotes an unspecified copolymer of styrene and butadiene. The other connectives of Table 3

Table 3. IUPAC Nomenclature of Copolymers[a]

Type	Arrangement of monomeric units	Representation	Connective	Example	
				Name	Alternative name
Unspecified	Unknown or unspecified	(A-*co*-B)	*-co-*	Poly[styrene-*co*-(methyl methacrylate)]	Copoly(styrene/methyl methacrylate)
Statistical	Obeys known statistical laws	(A-*stat*-B-*stat*-C)	*-stat-*	Poly(styrene-*stat*-acrylonitrile-*stat*-butadiene)	*stat*-Copoly(styrene/acrylonitrile/butadiene)
Random	Obeys Bernoullian statistics	(A-*ran*-B)	*-ran-*	Poly[ethylene-*ran*-(vinyl acetate)]	*ran*-Copoly(ethylene/vinyl acetate)
Alternating	Alternating sequence	$(AB)_n$	*-alt-*	Poly[(ethylene glycol)-*alt*-(terephthalic acid)]	*alt*-Copoly(ethylene glycol)/(terephthalic acid)
Periodic	Periodic with respect to at least three monomeric units	$(ABC)_n$ $(ABB)_n$ $(AABB)_n$ $(ABAC)_n$	*-per-*	Poly[formaldehyde-*per*-(ethylene oxide)-*per*-(ethylene oxide)]	*per*-Copoly(formaldehyde/ethylene oxide/ethylene oxide)
Block	Linear arrangement of blocks	—AAAAA—BBBBB—	*-block-*[b]	Polystyrene-*block*-polybutadiene	*block*-Copoly(styrene/butadiene)
Graft	Polymeric side chain different from main chain[c]	—AAAAAAAAAAAA— | B B B B B |	*-graft-*[d]	Polybutadiene-*graft*-polystyrene	*graft*-Copoly(butadiene/styrene)

[a] Main system described in IUPAC document 14; an alternative scheme is described in the text.
[b] The connective *-b-* has also been used.
[c] Main chain (or backbone) is specified first in the name.
[d] The connective *-g-* has also been used.

Table 4. Examples of the IUPAC Nomenclature Formats for Copolymers

Description	Nomenclature formats
A block copolymer containing 75 mass% of polybutadiene and 25 mass% of polystyrene	Polybutadiene-*block*-polystyrene (0.75:0.25 *w*) or *block*-copoly (butadiene/styrene) (75:25 mass%)
A graft copolymer, comprising a polyisoprene backbone grafted with isoprene and acrylonitrile units in an unspecified arrangement that contains 85 mol% of isoprene units and 15 mol% of acrylonitrile units	Polyisoprene-*graft*-poly(isoprene-*co*-acrylonitrile) (0.85:0.15 *x*) or *graft*-copoly[isoprene/(isoprene; acrylonitrile)] (85:15 mol%)
A graft copolymer comprising 75 mass% of polybutadiene with a relative molecular mass of 90 000 as the backbone, and 25 mass% of polystyrene in grafted chains with a relative molecular mass of 30 000	Polybutadiene-*graft*-polystyrene (75:25 mass%; 90 000:30 000 M_r)
A graft copolymer in which the polybutadiene backbone has a degree of polymerization (DP) of 1700 and the polystyrene grafts have an unknown DP	*graft*-Copoly(butadiene/styrene) (1700:*a* DP)

are placed *before* such names to provide additional structural information, as in *ran*-copoly(ethylene/vinyl acetate) or *alt*-copoly(styrene/maleic anhydride). It is unnecessary to use parentheses to enclose names of monomers comprising more than one word, eg, vinyl acetate, maleic anhydride, methyl acrylate; the names of the polymers, as written here, are unambiguous.

The names of copolymers, derived either from the main scheme or the alternative, can be further modified to indicate various structural features. For example, the chemical nature of end groups can be specified as α-X-ω-Y-poly(A-*alt*-B), as in α-butyl-ω-carboxy-*block*-copoly(styrene/butadiene).

Subscripts placed immediately after the formula of the monomeric unit or the block designate the degree of polymerization or repetition. On the other hand, mass and mole fractions and relative molecular masses, which in most cases are average quantities, are expressed by placing corresponding figures after the complete name of the copolymer. The order of citation is as for the monomeric species in the name. Unknown quantities are designated by *a*, *b*, etc. Table 4 gives some examples.

The complete document (14) should be consulted for names of more complex copolymers, eg, those having a multiplicity of grafts or having chains radiating from a central atom.

The utility of generic source-based nomenclature (27) can also be illustrated for source-based names of copolymers. As for homopolymers, the addition of a polymer class name is recommended only to avoid ambiguity or to add clarification.

Example: the source-based name poly[(benzene-1,2:4,5-tetracarboxylic dianhydride-*alt*-4,4′-oxydianiline] is ambiguous; ambiguity about the structure is removed by writing poly(amide-acid):[(benzene-1,2:4,5-tetracarboxylic

dianhydride)-*alt*-4,4′-oxydianiline] to accompany the structure-based representation

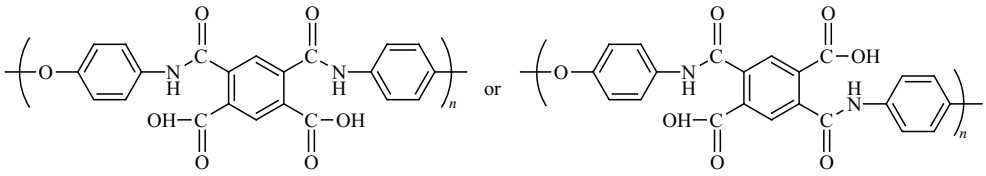

and polyimide:[(benzene-1,2:4,5-tetracarboxylic dianhydride)-*alt*-4,4′-oxydianiline] to accompany the structure-based representation

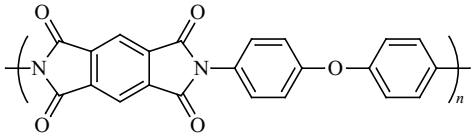

In 1997 the principles of source-based nomenclature for regular copolymers were extended to nonlinear macromolecules and macromolecular assemblies (24), which are classified according to the following terms: cyclic; branched (long- and short-branched); micronetwork; network; blend; semi-interpenetrating polymer network; interpenetrating polymer network; and polymer–polymer complex. The range of italicized qualifiers, listed as connectives in Table 3 for regular copolymers, was extended by addition of new qualifiers such as "blend," "comb," "star," or "net." Table 5 lists the new qualifiers, together with examples of their use. Quantitative characteristics of a macromolecule or an assembly of macromolecules, such as mass and mole fractions or percentages as well as the degrees of polymerization and molar masses, may be expressed by placing corresponding figures after the complete name. The complete document (24) should be consulted for details and more examples.

Structure-Based Nomenclature.

Regular Single-Strand Organic Polymers. For organic polymers that are regular (ie, have only one species of constitutional repeating unit in a single sequential arrangement) and comprise only single strands, the IUPAC has promulgated a structure-based system of naming polymers (29). Originally devised by the Nomenclature Committee of the American Chemical Society Polymer Division (34), the system consists of naming a polymer as "poly(constitutional repeating unit)," wherein the repeating unit is named as a bivalent organic group according to the usual nomenclature rules for organic chemistry. It is important to note that in structure-based nomenclature, the name of the constitutional repeating unit has no direct relationship to the source from which the unit was prepared. The name is simply that of the identifiable constitutional repeating unit in the polymer, and locants for unsaturation, substituents, etc, are dictated by the *structure* of the unit.

The steps involved in naming the constitutional repeating unit (CRU) are (*1*) identification of the unit (taking into account the kinds of atoms in the main chain and the location of substituents); (*2*) orientation of the unit; and (*3*) naming of the

Table 5. IUPAC Source-based Nomenclature for Non-linear Macromolecules and Macromolecular Assemblies

Macromolecule or assembly	Italicized qualifier	Examples	Comments
Cyclic	*cyclo*	*cyclo*-Poly(dimethylsiloxane)	
		cyclo-Poly(styrene-*stat*-α-methylstyrene)	
Branched, unspecified	*branch*	*branch*-Polystyrene-*v*-divinylbenzene	Polystyrene cross-linked with divinylbenzene, insufficient to cause a network to form
Short-chain-branched	*sh-branch*	*sh-branch*-Polyethylene	
Long-chain-branched	*l-branch*	*l-branch*-Poly(ethyl acrylate)-*v*-(ethylene dimethacrylate)	
Branched with branch points of functionality *f*	*f-branch* (*f* is given a numerical value)		
Comb(like)	*comb*	*comb*-Poly(styrene-*stat*-acrylonitrile)	Both the main chains and side chains are statistical copolymer chains of styrene and acrylonitrile
		Polystyrene-*comb*-polyacrylonitrile[a]	Main chains of styrene homopolymer; side chains of acrylonitrile homopolymer[b]
		Polystyrene-*comb*-[polyacrylonitrile; poly(methyl methacrylate)][a]	
Star	*star*	*star*-(polyA; polyB; polyC)	A variegated star copolymer molecule consisting of arm(s) of polyA, arm(s) of polyB, and arm(s) of polyC
		star-(polyA-*block*-polyB-*block*-polyC)	Star copolymer molecule, each arm of which consists of the same block copolymer chain
		star-[Polystyrene-*block*-poly(methyl methacrylate)]	Each arm of the star macromolecule is a block copolymer chain, with a polystyrene block attached to the central unit

Table 5. (Continued)

Macromolecule or assembly	Italicized qualifier	Examples	Comments
Star with f arms	f-star (f is given a numerical value)	4-*star*-Polystyrene	
		3-*star*-Polystyrene-*v*-methyltrichlorosilane	
		star-(Polyacrylonitrile; polystyrene) (M_r 100 000:20 000)	Star macromolecule consisting of arms of polyacrylonitrile of a total $M_r = 100\,000$ and arms of polystyrene of a total $M_r = 20\,000$
		6-*star*-(Polyacrylonitrile (f 3); polystyrene (f 3)) (M_r (arm) 50 000:10 000)	A six-armed star macromolecule consisting of three arms of polyacrylonitrile, each of $M_r = 50\,000$, and three arms of polystyrene, each of $M_r = 10\,000$
Network	*net*	*net*-Polybutadiene	
		net-Poly(phenol-*co*-formaldehyde)	
		net-Polybutadiene-*v*-sulfur	Polybutadiene vulcanized with sulfur
		net-Polystyrene-*v*-divinylbenzene	Polystyrene cross-linked with divinylbenzene to form a network
		net-Poly[(hexane-1,6-diyl diisocyanate)-*alt*-glycerol]	
		net-Poly[styrene-*alt*-(maleic anhydride)]-*v*-(ethylene glycol)	Alternating copolymer of styrene and maleic anhydride cross-linked with ethylene glycol to form a network
		Poly[(ethylene glycol)-*alt*-(maleic anhydride)]-*net*-oligostyrene	Unsaturated polyester cured with styrene
		Poly(methyl methacrylate)-*net*-poly(ethylene oxide)	
		[Poly(butyl vinyl ether)-*v*-(2-vinyloxyethyl methacrylate)]-*net*-[poly-(methyl methacrylate)-*v*-(2-vinyloxyethyl methacrylate)]	Poly(butyl vinyl ether) and poly(methyl methacrylate) chains cross-linked mutually with 2-vinyloxyethyl methacrylate to form a network

Micronetwork	μ-*net*	μ-*net*-Poly[styrene-*stat*-(vinyl cinnamate)]	Cross-linked copolymeric micronetwork
Polymer blend	*blend*	Polystyrene-*blend*-poly(2,6-dimethylphenol)	
		(*net*-Polystyrene)-*blend*-(*net*-polybutadiene)	Blend of two networks
Interpenetrating polymer network (IPN)	*ipn*	(*net*-Polybutadiene)-*ipn*-(*net*-polystyrene)	IPN of two networks
		[*net*-Poly(styrene-*stat*-butadiene)]-*ipn*-[*net*-poly(ethyl acrylate)]	IPN of two networks
Semi-interpenetrating polymer network (SIPN)	*sipn*	(*net*-Polystyrene)-*sipn*-poly(vinyl chloride)	SIPN of a polystyrene network and a linear poly(vinyl chloride)
Polymer–polymer complex	*compl*	Poly(acrylic acid)-*compl*-poly(4-vinylpyridine)	Complex of two species of linear macromolecules
		Poly[(methyl methacrylate)-*stat*-(methacrylic acid)]-*compl*-poly(*N*-vinyl-2-pyrrolidone)	Complex of statistical copolymer and homopolymer molecules

[a] In naming nonlinear copolymer molecules having linear subchains of two or more types, the italicized connective for the skeletal structure is placed between the source-based names of the types of constituent linear subchains. In the case of branched and comb-like macromolecules, the linear chain named before the connective is that which forms the main chain, whereas that (those) named after the connective forms (form) the side chain(s). The names of different species of side chain are separated by semicolons. In the case of variegated star macromolecules the prefix is placed before the name of the macromolecule with the different species of arms separated by semicolons.

[b] Equivalent to polystyrene-*graft*-polyacrylonitrile; *-graft-* is recommended for these cases. However, *comb* as a prefix cannot be replaced by *graft*.

unit. The CRUs are named systematically according to the IUPAC-recommended nomenclature of organic compounds (31). Examples of names for some common polymers are given in Table 6. Note that in this system, parentheses, brackets, braces, or a combination of these, are always used to enclose the CRU. For organic names, the IUPAC uses parentheses for the innermost set, then brackets, then braces, and thus {[(. . .)]}. If further nesting is required, this cycle is repeated: ({[(. . .)]}), [({[(. . .)]})], {[({[(. . .)]})]}, etc.

Structure-based nomenclature can be utilized to name polymers of great complexity, provided only that they be regular and single-stranded. Among these are polymers the constitutional repeating units of which consist, themselves, of a series of smaller subunits, polymers with hetero atoms or heterocyclic ring systems in the main chain, and polymers with substituents on acyclic or cyclic subunits of constitutional repeating units. It should be noted that structure-based nomenclature is also applicable to copolymers having a regular structure, regardless of the starting materials used, eg, poly(oxyethyleneoxyterephthaloyl) for poly(ethylene terephthalate) (14).

The basic principles of structure-based nomenclature have been extended beyond regular, single-strand organic polymers (29) to single-strand and quasi-single-strand inorganic and coordination polymers (12), double-strand (ladder and spiro) polymers (18), irregular single-strand organic polymers (19), and other complex systems. Work in this field is continuing.

Structure-based nomenclature has gained wide acceptance in the scientific literature, eg, in Chemical Abstracts, because it overcomes many of the deficiencies of source-based nomenclature.

Inorganic and Coordination Polymers. The nomenclature of regular single-strand inorganic and coordination polymers (12) is governed by the same fundamental principles as those for single-strand organic polymers. The name of such a polymer is that of the smallest constitutional repeating unit prefixed by the terms "poly," "*catena*" (for linear chains) or other structural indicator, and designations for end groups. The structural units are named by the nomenclature rules for inorganic and coordination chemistry. Table 7 lists some examples.

Stereochemical Definitions and Notations. Structure-based nomenclature of regular polymers (10) can denote stereochemical features if the repeating unit used is the configurational base unit, ie, a constitutional repeating unit having one or more sites of defined stereoisomerism in the main chain of a polymer molecule (22). Structure-based names are then derived in the usual fashion. The various stereochemical features that are possible in a polymer must be defined.

The pioneering work of Natta and co-workers introduced the concept of *tacticity*, ie, the orderliness of the succession of configurational repeating units in the main chain of a polymer. For example, in polypropene (polypropylene), possible steric arrangements are (shown in Fischer projections displayed horizontally) as follows:

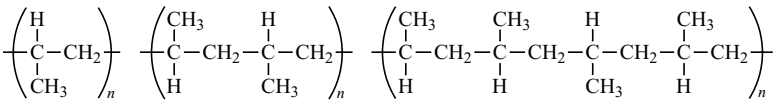

Isotactic Syndiotactic Atactic

Table 6. Examples of Structure-based and Source-based Names for some Common Polymers[a]

Structure	Structure-based name	Source-based or trivial name
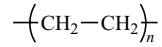	Poly(methylene)	Polyethylene
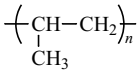	Poly(1-methylethylene)	Polypropene; polypropylene
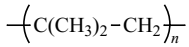	Poly(1,1-dimethylethylene)	Polyisobutylene
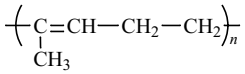	Poly(1-methylbut-1-ene-1,4-diyl)	Polyisoprene
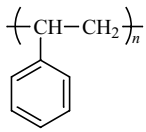	Poly(1-phenylethylene)	Polystyrene
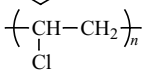	Poly(1-chloroethylene)	Poly(vinyl chloride)
	Poly(1-cyanoethylene)	Polyacrylonitrile
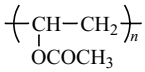	Poly(1-acetoxyethylene)	Poly(vinyl acetate)
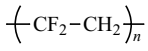	Poly(1,1-difluoroethylene)	Poly(vinylidene fluoride)
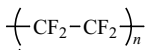	Poly(difluoromethylene)	Polytetrafluoroethylene
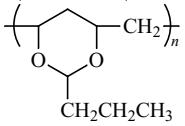	Poly[(2-propyl-1,3-dioxane-4,6-diyl)methylene]	Poly(vinyl butyral)
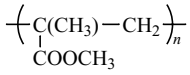	Poly[1-(methoxycarbonyl)-1-methylethylene]	Poly(methyl methacrylate)
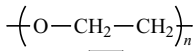	Poly(oxyethylene)	Poly(ethylene oxide)
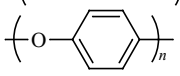	Poly(oxy-1,4-phenylene)	Poly(phenylene oxide)
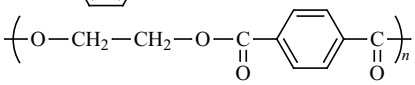	Poly(oxyethylene-oxyterephthaloyl)	Poly(ethylene terephthalate)
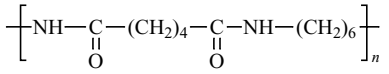	Poly(iminoadipoyliminohexane-1,6-diyl)	Poly[hexamethylenediamine-*alt*-(adipic acid)] or poly(hexamethylene adipamide)
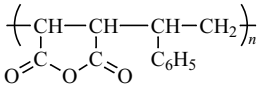	Poly[(2,5-dioxotetrahydrofuran-3,4-diyl)-(1-phenylethylene)]	Poly(maleic anhydride-*alt*-styrene)

[a]Ref. 29.

Table 7. Examples of Inorganic and Coordination Polymers[a]

Name	Structure
catena-Poly[dimethyltin]	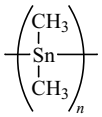
catena-Poly[titanium-tri-μ-chloro]	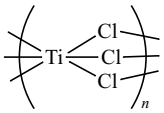
catena-Poly[nitrogen-μ-thio]	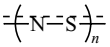
catena-Poly[silver-μ-(cyano-*N*:*C*)]	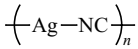
catena-Poly[(diphenylsilicon)-μ-oxo]	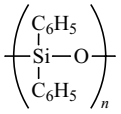
α-Ammine-ω-(amminedichlorozinc)-*catena*-poly[(amminechlorozinc)-μ-chloro]	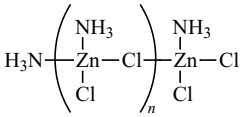

[a] If named according to the rules for linear organic polymers (29), the polymers on lines 1 and 5 would be oriented and named poly(dimethylstannanediyl) and poly[oxy(diphenylsilanediyl)] respectively.

An isotactic polymer has only one species of configurational base unit in a single sequential arrangement and a syndiotactic polymer shows an alternation of configurational base units that are enantiomeric, whereas in an atactic polymer the molecules have equal numbers of the possible configurational base units in a random sequence distribution. This can be generalized as follows:

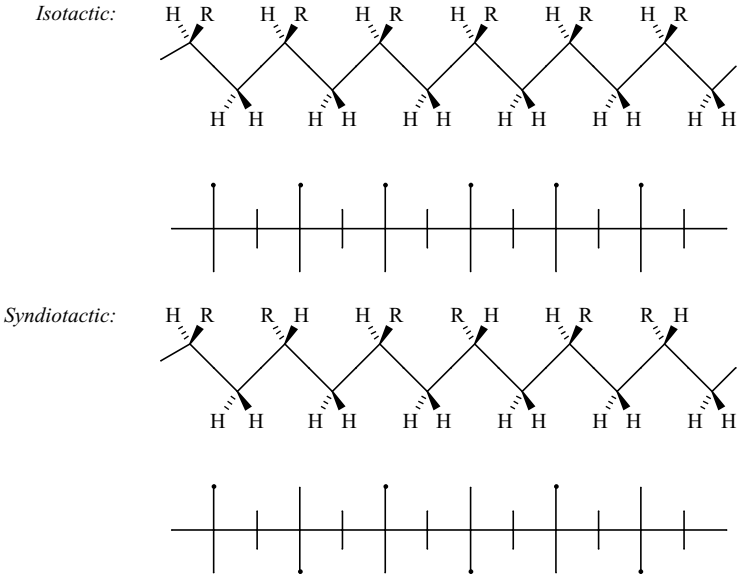

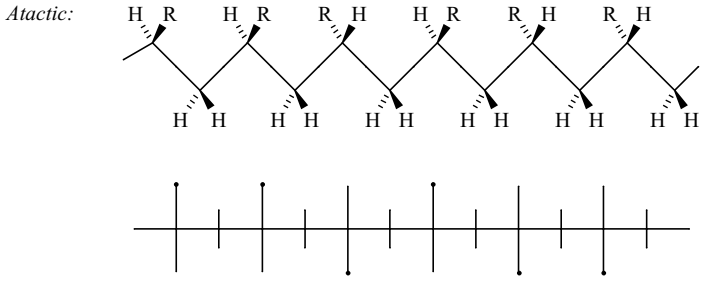

Further examples of tactic polymers are

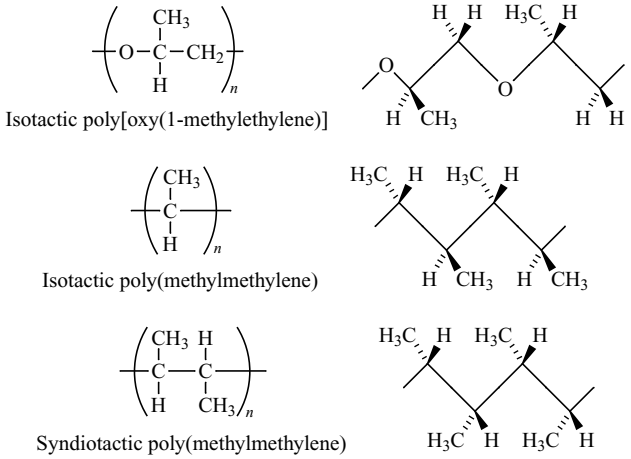

The published IUPAC document (10) should be consulted for more information.

Regular Double-Strand (Ladder and Spiro) Organic Polymers. Structure-based and source-based nomenclature rules have been extended to regular double-strand (ladder and spiro) organic polymers (18). A *double-strand polymer* is defined as a polymer, the molecules of which are formed by an uninterrupted sequence of rings with adjacent rings having one atom in common (spiro polymer) or two or more atoms in common (ladder polymer).

The structure-based nomenclature rests upon the selection of a preferred CRU (22,29) of which the polymer is a multiple; the name of the polymer is the name of this repeating unit prefixed by "poly." The unit itself is named wherever possible according to the established principles of organic nomenclature (31). For double-strand polymers, this unit usually is a tetravalent group denoting attachment to four atoms. Since some of these attachments may be double bonds, the unit may be hexavalent or octavalent. Table 8 lists some examples.

As in linear, single-strand polymers, substituents that are clearly part of the constitutional repeating unit are denoted by means of prefixes affixed to the name of the subunit to which they are bound.

End groups are specified by prefixes cited in front of the name of the polymer. The ends designated by α and α' are those attached to the left side of the

Table 8. Examples of Structure-Based Nomenclature for Regular Double-Strand (Ladder and Spiro) Organic Polymers

Name	Structure
Poly(buta-1,3-diene-1,4:3,2-tetrayl)	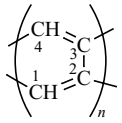
Poly(naphthalene-2,3:6,7-tetrayl-6,7-dimethylene)	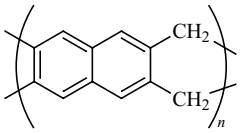
Poly[(7,12-dihydro-7,12-dioxobenzo[*a*]anthracene-3,4:9,10-tetrayl)-9,10-dicarbonyl]	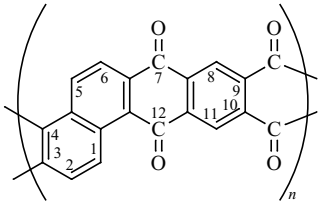
Poly(cyclohexane-1,1:4,4-tetrayl-4,4-dimethylene)	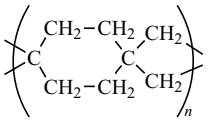

constitutional repeating unit as drawn; the end groups attached to the right side are designated by ω and ω′. End groups are named by the nomenclature rules for organic compounds (31). The designations and names of the end groups proceed in a clockwise direction starting from the lower left: α,α′,ω,ω′. Table 9 lists two examples with substituents (lines 1 and 2) and one with both substituents and end groups (line 3).

Source-based nomenclature identifies the starting monomer(s) from which the double-strand polymer is prepared with addition of an appropriate prefix "*ladder-*" or "*spiro.-*" Examples are

(1) *ladder*-poly(1,4-diphenyldiacetylene)
(2) *ladder*-poly(2,5-dichloro-3,6-dihydroxy-*p*-benzoquinone)
(3) *ladder*-poly[(pyromellitic dianhydride)-*alt*-(1,2,5,6-tetraaminoanthraquinone)]
(4) *spiro*-poly[dispiro[3.1.3.1]decane-2,8-bis(carbonyl chloride)]

The rules are complex, and the published IUPAC document (18) should be consulted for more information.

Irregular Single-Strand Organic Polymers. *Irregular single-strand organic polymers* are single-strand organic polymers that can be described by the repetition of more than one type of constitutional unit or that comprise

Table 9. Examples of Nomenclature for Regular Double-Strand (Ladder and Spiro) Organic Polymers with Substituents and End Groups

Name	Structure
Poly[(1,4-dimethyl-7-azabicyclo[2.2.1]heptane-2,3:5,6-tetrayl)-5,6-dicarbonyl]	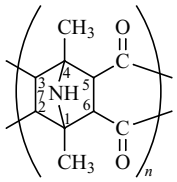
Poly(2,4-dimethyl-1,3,5-trioxa-2,4-disilapentane-1,5:4,2-tetrayl)[a]	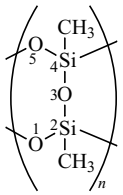
α,α′-dihydro-ω,ω′-dihydroxypoly(2,4-diphenyl-1,3,5-trioxa-2,4-disilapentane-1,5:4,2-tetrayl)[a]	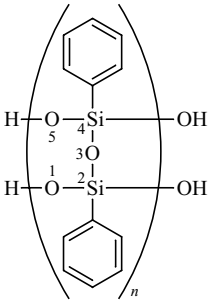

[a]The CRU is named using replacement nomenclature ('a' nomenclature) (18,31).

constitutional units not all connected identically with respect to directional sense. A new system (19) names irregular polymers for which the source-based system is inadequate, eg, polymers that have undergone partial chemical modification, homopolymers having both head-to-tail and head-to-head arrangements of monomeric units, and polymers derived from a single monomer that can provide more than one kind of monomeric unit.

The new system also provides a structure-based alternative to source-based nomenclature for copolymers. Irregular polymers, oligomers, or blocks are named by placing the prefix "poly" before the structure-based names of the constitutional units; the latter are collectively enclosed in parentheses, with the names of the component constitutional units separated by solidi (oblique strokes).

Block copolymers are named by using dashes (double-length hyphens) for the bonding of blocks with each other and with junction units. With graft and star polymers, the grafts or the arms, respectively, are considered to be substituents to the main chain, and the structure is named in the same way as a regular or irregular polymer. Table 10 lists some examples.

The published IUPAC document (19) should be consulted for more information.

Table 10. Examples of Nomenclature for Irregular Single-Strand Organic Polymers

Characteristics	Name	Structure[a]
A statistical copolymer comprising units derived from 1-phenylethene and l-chloroethene joined head-to-tail	Poly(l-chloroethylene/l-phenylethylene)	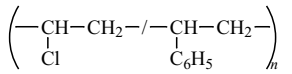
An irregular polymer derived from l-chloroethene, the units of which are linked both head-to-tail and head-to-head	Poly(l-chloroethylene/2-chloroethylene)	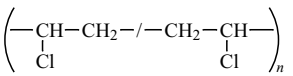
A modified (chlorinated) poly(methylene)	Poly(chloromethylene/dichloromethylene/methylene)	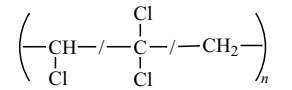
A modified (partially hydrolyzed) head-to-tail poly(1-acetoxyethylene)	Poly(1-acetoxyethylene/1-hydroxyethylene)	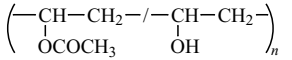
A triblock copolymer consisting of a sequence of three blocks joined directly or through unspecified junction units	Poly(oxy-1,4-phenylene)–poly(2-cyanoethylene)–poly(ethyleneoxy)	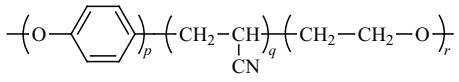
A diblock copolymer in which the blocks are joined by a specific junction unit	Poly(ethyleneoxy)–dimethylsilanediyl–poly(1-chloroethylene)	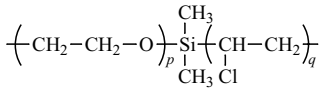
A graft copolymer with many of one type of graft unit	Poly[methylene/poly(2-phenylethylene)methylene]	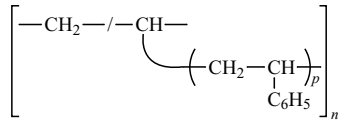
A poly(oxyphenylene) with a poly(2-chloroethylene) block grafted through a carbonyloxy group (a junction unit) to the 2-position in some of the rings	Poly{oxy-l,4-phenylene/oxy-2-[poly(2-chloroethylene)carbonyloxy]-l,4-phenylene}	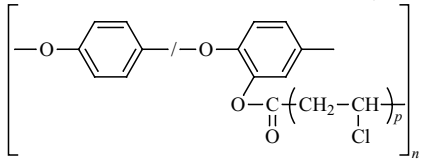
A four-armed star polymer comprising silane substituted with different polymer blocks	Bis[poly(but-2-ene-1,4-diyl)][poly(1-phenylethylene)][poly(2-phenylethylene)]silane	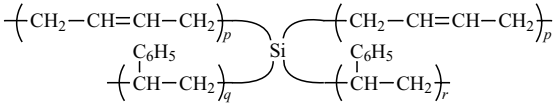

[a]The dashes at each end of the formulas on lines 1, 2, 3, 4, 7, and 8 are drawn fully inside the enclosing marks, because they do not necessarily denote terminal chemical bonds of the macromolecules.

Chemical Abstracts Nomenclature

Chemical Abstracts Service is the publisher of *Chemical Abstracts* and corresponding products and services, which are available in the following formats: printed, microform, online databases, CD-ROM, World Wide Web. Polymers selected for inclusion in the CAS Chemical Registry System and the *CA Chemical Substance Indexes* are indexed in two ways:

(1) in terms of the component monomer(s) from which they are prepared
(2) in terms of the structural representation of the polymer formed

CAS has published its own set of principles governing how each type of polymer is registered and named (33). Specific polymers are named on the basis of the monomers from which they are formed and/or on the basis of their structure, as represented by a structural repeating unit (SRU). Since original documents sometimes provide insufficient structural information to allow generation of the SRU name, the method most frequently used for describing polymeric substances is by citation of the component monomers. However, a few commercial polymers, including poly(ethylene terephthalate) (PET), nylon-6,6, and nylon-6, each of which has a large number of index entries, are exceptions; they are indexed *only* at the SRU-based systematic polymer name.

CAS chemical nomenclature is in general agreement with the IUPAC recommendations. However, there is one important difference. For any given chemical substance, the IUPAC nomenclature guidelines always lead to an unambiguous name, but not necessarily to only one name. In most communications about chemical substances, this approach causes few problems, but where a formal, rigidly controlled index is needed, such as the *CA Chemical Substance Indexes*, it is insufficiently rigorous. CA Index names must be unique, unambiguous, completely reproducible, and written in a way that brings together alphabetically all structurally related substances (33). CAS recognizes that a unique name is required for indexing purposes and for substance identification, but it is not expected that the highly structured CA Index names would be used in normal communications among authors or lecturers, or in industry and in the primary publications.

The more fully systematic IUPAC rules were adapted for the highly ordered alphabetical CA indexes. Most common names and special rules for some classes of substances were discontinued in 1972. Names used in the previous CA indexes as well as trivial names used in the literature have been retained as cross-references in the *CA Index Guide* and in the CAS database, and are available for polymer searching and retrieval. For each identifiable substance, a rigid order of precedence of chemical functions and compound classes is followed to determine first the preferred *index heading parent*, and then a single preferred name.

Systematic names of chemical substances in the indexes are arranged in inverted format as follows. The *index heading parent* (usually the basic skeleton name with a locant and suffix that denotes the principal function), a comma, any *substituents*, and any *modification* (derivative of the principal function). Table 11 lists some common monomers, with both common names and CA Index names.

Table 11. Examples of Common Monomers with Common Names and CA Index Names

Common name	CA Index name
Acrylamide	2-Propenamide
Acrylic acid	2-Propenoic acid
Acrylonitrile	2-Propenenitrile
Adipic acid	Hexanedioic acid
p-Aminobenzoic acid	Benzoic acid, 4-amino-
Bisphenol A	Phenol, 4,4′-(1-methylethylidene)bis-
Butadiene	1,3-Butadiene
Butylene glycol	1,4-Butanediol
ε-Caprolactam	2*H*-Azepine-2-one, hexahydro-
ε-Caprolactone	2-Oxepanone
Dimethyl terephthalate	1,4-Benzenedicarboxylic acid, dimethyl ester
Ethylene	Ethene
Ethylene glycol	1,2-Ethanediol
Ethylene oxide	Oxirane
Fumaric acid	2-Butenedioic acid (2*E*)-[a]
Glycolic acid	Acetic acid, hydroxy-
Hexafluoropropylene	1-Propene, 1,1,2,3,3,3-hexafluoro-
Hexamethylenediamine	1,6-Hexanediamine
Hydroquinone	1,4-Benzenediol
p-Hydroxybenzoic acid	Benzoic acid, 4-hydroxy-
Isobutylene	1-Propene, 2-methyl-
Isophthalic acid	1,3-Benzenedicarboxylic acid
Isoprene	1,3-Butadiene, 2-methyl-
Lactic acid	Propanoic acid, 2-hydroxy-
Maleic acid	2-Butenedioic acid (2*Z*)-[a]
Maleic anhydride	2,5-Furandione
Melamine	1,3,5-Triazine-2,4,6-triamine
Methacrylic acid	2-Propenoic acid, 2-methyl-
Methyl acrylate	2-Propenoic acid, methyl ester
Methyl methacrylate	2-Propenoic acid, 2-methyl-, methyl ester
4,4′-Methylenedianiline	Benzenamine, 4,4′-methylenebis-
Methylenedi-*p*-phenylene diisocyanate	Benzene, 1,1′-methylenebis[4-isocyanato-
4,4′-Oxydianiline	Benzenamine, 4,4′-oxybis-
m-Phenylenediamine	1,3-Benzenediamine
p-Phenylenediamine	1,4-Benzenediamine
Phthalic anhydride	1,3-Isobenzofurandione
Propylene	1-Propene
Propylene oxide	Oxirane, methyl-
Pyromellitic dianhydride	1*H*,3*H*-Benzo[1,2-*c*:4,5-*c*′]difuran-1,3,5,7-tetrone
Styrene	Benzene, ethenyl-
Terephthalic acid	1,4-Benzenedicarboxylic acid
2,4-Toluene diisocyanate	Benzene, 2,4-diisocyanato-1-methyl-
Vinyl acetate	Acetic acid ethenyl ester[a]
Vinyl alcohol	Ethenol
Vinyl chloride	Ethene, chloro-
Vinyl fluoride	Ethene, fluoro-
Vinylidene chloride	Ethene, 1,1-dichloro-
Vinylidene fluoride	Ethene, 1,1-difluoro-

[a]No typical comma between the parts of the name is present, because of a special formatting rule for large, subdivided index headings.

Table 12. Examples of Multiplying and Substituent Groups with Common Names and CA Equivalents

Common name	CA equivalent	Common name	CA equivalent
Adipoyl	1,6-Dioxo-1,6-hexanediyl	Allyl	2-Propenyl
sec-Butyl	1-Methylpropyl	*tert*-Butyl	1,1-Dimethylethyl
Ethylene	1,2-Ethanediyl	Hexamethylene	1,6-Hexanediyl
Isobutyl	2-Methylpropyl	Isophthaloyl	Carbonyl-1,3-phenylenecarbonyl
Isopropyl	1-Methylethyl	*p*-Phenylene	1,4-Phenylene
Succinyl	1,4-Dioxo-1,4-butanediyl	Terephthaloyl	Carbonyl-1,4-phenylenecarbonyl
Vinyl	Ethenyl	Vinylene	1,2-Ethenediyl

Table 13. Examples of Common Names and Their CA Index Name Equivalents

Common name	CA index name	Molecular formula
Poly(*p*-aminobenzoic acid)	Benzoic acid, 4-amino-, homopolymer	$(C_7H_7NO_2)_x$
Poly(methyl methacrylate)	2-Propenoic acid, 2-methyl-, methyl ester, homopolymer	$(C_5H_8O_2)_x$
Polystyrene	Benzene, ethenyl-, homopolymer	$(C_8H_8)_x$
Poly(vinylidene fluoride)	Ethene, 1,1-difluoro-, homopolymer	$(C_2H_2F_2)_x$

Similarly, many commonly named multiplying and substituent groups have their systematic equivalents in CA indexes. Table 12 lists some examples.

Source-Based Nomenclature.

Homopolymers. The CA Index name is written by citation of the name of the monomer, and the term *homopolymer* is cited in the *modification*. Table 13 lists some examples.

Copolymers. The CA Index name is written by citation of the name of the senior comonomer, in inverted format, followed by a comma. The modification contains the expression "polymer with B, C, D, . . . and Z", where B, C, D, . . . and Z are the names of the other comonomers, alphabetized, and in uninverted format, and also stereochemical and structural terms such as *isotactic, syndiotactic, alternating, block*, or *graft* whenever applicable. The senior comonomer is chosen by a set of principles that include a strict order of precedence of chemical functions and compound classes (33). The format is A, Polymer with B, C, D, . . . and Z in which A, B, C, D,. . . and Z are the comonomers.

Before 2002, for most records, in addition to the CA Index names, systematic Index names were generated for each comonomer. Thus, for a copolymer containing n comonomers, a total of $(n-1)$ additional Index names, each beginning with the name of a different comonomer in the copolymer, were created. This practice was discontinued in 2002. Examples are

(1) CA Index name: 1-Propene, polymer with ethene

(2) Other CA names: Ethene, polymer with 1-propene

Table 14. Examples of Post-Treated Polymers

Post-Treated polymer[a]	CA Index name
Acrylic acid–methyl methacrylate copolymer esterified to an unknown degree to methyl acrylate	2-Propenoic acid, 2-methyl-, methyl ester, polymer with 2-propenoic acid, methyl ester[b]
Acrylic acid–styrene copolymer esterified to an unknown degree to methyl acrylate	2-Propenoic acid, polymer with ethenylbenzene, methyl ester
Ethylene–methacrylic acid copolymer neutralized to an unknown degree to sodium methacrylate	2-Propenoic acid, 2-methyl-, polymer with ethene, sodium salt[c]
Isophthalic acid–ethylene glycol copolymer post-treated to form the diallyl ester	1,3-Benzenedicarboxylic acid, polymer with 1,2-ethanediol, di-2-propenyl ester

[a]The degree of modification (esterification for lines 1 and 2, neutralization for line 3) is not part of the chemical record.

[b]Notice the difference in word order between the CA Index name of this modified copolymer and that of the unmodified methyl acrylate–methyl methacrylate copolymer, in which the second comonomer name is written in uninverted format: 2-propenoic acid, 2-methyl-, methyl ester, polymer with methyl 2-propenoate.

[c]Notice the difference in word order between the CA Index name of this modified copolymer and that of the unmodified ethylene–sodium methacrylate copolymer: 2-propenoic acid, 2-methyl-, sodium salt, polymer with ethene.

(3) CA Index name: 2-Propenoic acid, 2-methyl-, polymer with ethene, 1-propene and 2-propenoic acid

(4) Other CA names: 1-Propene, polymer with ethene, 2-methyl-2-propenoic acid and 2-propenoic acid 2-Propenoic acid, polymer with ethene, 2-methyl-2-propenoic acid and 1-propene

(5) Ethene, polymer with 2-methyl-2-propenoic acid, 1-propene and 2-propenoic acid

The CA Index name of a post-treated (modified) polymer is written by citation of the name of the polymer, inverted as described above; the *modification* segment of the name indicates how the polymer was post-treated. Post-treated polymers fall into two subcategories.

For esters, ethers, and salts of homopolymers and copolymers, this information is associated with the CA Index name and is part of a unique CAS Registry record. Table 14 lists some examples.

For other types of post-treated homopolymers and copolymers, such as those that have been aminated, chlorinated, hydrolyzed, etc, this type of information is present in the Index entry only when associated with a specific document. CAS Registry numbers are not assigned to such post-treated polymers except for use in certain regulatory inventories, such as those mandated by the Toxic Substances Control Act. Table 15 lists some examples.

Telomers are named as copolymers with the term "telomer with" cited in the *modification* under either the monomer (taxogen) or the chain-transfer agent (telogen), depending on which is the senior component. Table 16 lists some examples.

There is no provision for structuring and naming end groups in source-based representations, except for ester-terminated polymers (see Table 14) and mixed polyalkylene glycols (see below).

Table 15. Examples of Post-Treated Polymers (Halogenated or Chlorosulfonated to an Unknown Degree)

Post-Treated polymer	CA Index entry
Post-brominated polystyrene	Benzene, ethenyl-, homopolymer, brominated
Post-chlorosulfonated polyethylene (chlorosulfonation introduces both —Cl and —SO_2Cl groups)	Ethene, homopolymer, chlorinated, chlorosulfonated

Table 16. Examples of Telomers

Telomer	CA index name	Molecular formula structure representation
Vinylpyrrolidone homopolymer terminated with 3-mercaptopropionic acid	Propanoic acid, 3-mercapto-, telomer with 1-ethenyl-2-pyrrolidinone	$(C_6H_9NO)_x \cdot C_3H_6O_2S$ 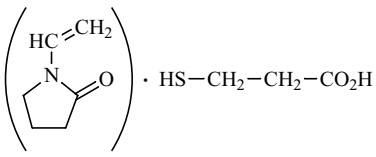
Acrylic acid–vinyl chloride copolymer terminated with carbon tetrachloride	2-Propenoic acid, telomer with chloroethene and tetrachloromethane	$(C_3H_4O_2 \cdot C_2H_3Cl)_x \cdot CCl_4$ $(H_2C{=}CH{-}CO_2H \cdot H_2C{=}CH{-}Cl)_x \cdot CCl_4$

Structure-Based Nomenclature. When the regular structure of a polymer is well documented, or can be confidently assumed, in addition to the main entry with a source-based name, a *supplementary* entry is made for the SRU and its accompanying systematic structure-based name.

Assumptions are made for

(1) polyamides formed from a diamine and a dibasic acid, ester, or dihalide; from an amino acid, ester, or halide; from a lactam;
(2) polycarbonates formed from a dihydric alcohol or phenol and carbonic acid, ester, or dihalide;
(3) polyesters formed from a dihydric alcohol or phenol and a dibasic acid, anhydride, ester, or dihalide; from a hydroxy acid, ester, or halide; from a lactone;
(4) polyurethanes formed from a diisocyanate and a dihydric alcohol or phenol.

The SRU is named by citation of one or more multivalent radicals of regular substitutive nomenclature. The CAS SRU is equivalent to the IUPAC CRU. CAS and the IUPAC are virtually in perfect agreement with regard to the guidelines for identification and orientation of repeating units; the guidelines are given above in the IUPAC section entitled “Structure-Based Nomenclature.”

Table 17. Examples of Structure-Based Representations

Common name	CA Index name	Molecular formula structure representation
Poly(ethylene terephthalate)	Poly(oxy-1,2-ethanediyloxycarbonyl-1,4-phenylenecarbonyl)	$(C_{10}H_8O_4)_n$ (see Table 6 for structure)
Nylon-6,6	Poly[imino(1,6-dioxo-1,6-hexanediyl)imino-1,6-hexanediyl]	$(C_{12}H_{22}N_2O_2)_n$ (see Table 6 for structure)
Nylon-6	Poly[imino(1-oxo-1,6-hexanediyl)]	$(C_6H_{11}NO)_n$ 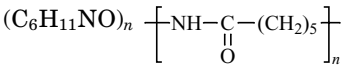
Poly(*p*-phenylene oxide)	Poly(oxy-1,4-phenylene)	$(C_6H_4O)_n$ 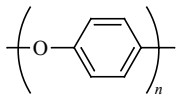
Poly(*p*-phenylene sulfone)	Poly(sulfonyl-1,4-phenylene)	$(C_6H_4O_2S)_n$ 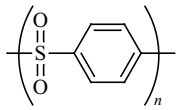

Table 18. Examples of Poly(alkylene glycols)

Common name	CA Index name[a]	Molecular formula structure representation
Polyethylene glycol	Poly(oxy-1,2-ethanediyl), (α-hydro-ω-hydroxy-	$(C_2H_4O)_nH_2O$ 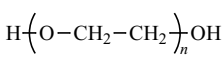
Polyethylene glycol monomethyl ether	Poly(oxy-1,2-ethanediyl), α-methyl-ω-hydroxy-	$(C_2H_4O)_nCH_4O$ 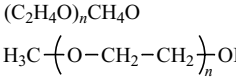
Polybutylene glycol diacetate	Poly(oxy-1,4-butanediyl), α-acetyl-ω-(acetyloxy)-	$(C_4H_8O)_nC4H_6O_3$ 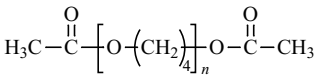

[a]End-group citation order is governed by a set of rules (33), not by alphabetization.

The CA Index name of a structure-based representation is written by citation of the name of the SRU, parenthesized, and preceded by the prefix "poly." Table 17 lists some examples.

Poly(alkylene glycols) and their ethers and esters are indexed as SRUs; end groups, when known, are added as *substituents* after the name of the repeating unit. Table 18 lists some examples.

Because the fragment sequences are unknown, mixed glycols such as polyethylene–polypropylene glycol or polyethylene–polytetramethylene glycol are

Table 19. List of Abbreviations and Acronyms for Polymers

Abbreviation	Polymer
ABS[a]	Poly(acrylonitrile/butadiene/styrene)
AEPDS[a]	Poly[acrylonitrile/(ethylene/propylene/diene)/styrene] (generic)
AMMA[a]	Poly[acrylonitrile/(methyl methacrylate)]
ASA[a]	Poly(acrylonitrile/styrene/acrylate)
CA[a]	Cellulose acetate
CAB[a]	Cellulose acetate butyrate
CAP[a]	Cellulose acetate propionate
CF[a]	Poly(cresol/formaldehyde)
CMC[a]	Carboxymethylcellulose
CN[a]	Cellulose nitrate
CP[a]	Cellulose propionate
CPE[b]	Chlorinated polyethylene
E/P[a]	Poly(ethylene/propene)
EC[a]	Ethylcellulose
EEAK[a]	Poly(ethylene/ethyl acrylate)
EP[a]	Epoxide resin; epoxy (generic)
EVAC[a]	Poly(ethylene/vinyl acetate)
FEP[a]	Poly[perfluoro(ethylene/propene)]; poly(tetrafluoroethylene/hexafluoropropene)
MF[a]	Melamine/formaldehyde resin
MP[a]	Melamine/phenol resin
PA[a]	Polyamide (generic)
PAC[b]	Polyacrylonitrile
PAN[a, c]	Polyacrylonitrile
PAPI; PMPPI[b]	Polymethylenepolyphenylene isocyanate
PBAK[a]	Poly(butyl acrylate)
PB[a]	Poly(1-butene)
PBI[b]	Polybenzimidazole (generic)
PBT[a]	Poly(butylene terephthalate)
PC[b]	Polyacrylonitrile
PC[a, b, c]	Polycarbonate
PCF[b]	Poly(chlorotrifluoroethylene)
PCO[b]	Polycarbonate
PCTFE[a, c]	Poly(chlorotrifluoroethylene)
PDAP[a]	Poly(diallyl phthalate)
PDMS[b]	Poly(dimethylsiloxane)
PE[a, b, c]	Polyethylene
PE[b]	Polyester (generic)
PEA[b]	Poly(ethyl acrylate)
PEC[b]	Chlorinated polyethylene
PE-C[b]	Chlorinated polyethylene
PEEK[a, b, e]	Polyetheretherketone
PEG[b]	Poly(ethylene glycol)
PEKK[b, f]	Polyetherketoneketone
PEO[b, c]	Poly(ethylene oxide)
PEOX[a, b]	Poly(ethylene oxide)
PET[a, b]	Poly(ethylene terephthalate)

Table 19. (Continued)

Abbreviation	Polymer
PETP[b, c]	Poly(ethylene terephthalate)
PF[a]	Phenol/formaldehyde resin
PFA[a, b]	Perfluoroalkoxy resins[g] (generic)
PIB[a, b, c]	Polyisobutene; polyisobutylene
PMMA[a, b, c]	Poly(methyl methacrylate)
PMP[a, b]	Poly(4-methyl-1-pentene)
POM[a, b, c]	Poly(oxymethylene); polyformaldehyde; polyacetal
POP[b]	Poly(oxy-1,4-phenylene); poly(1,4-phenylene oxide)
PP[a, b, c]	Polypropene; polypropylene
PPO®[b]	Poly(oxy-1,4-phenylene); poly(1,4-phenylene oxide)
PPS[a, b]	Poly(sulfanediyl-1,4-phenylene); poly(thio-1,4-phenylene); poly(1,4-phenylene sulfide)
PS[a, b, c]	Polystyrene
PTFE[a, b, c]	Poly(tetrafluoroethylene)
PTMEG[b]	Poly(tetramethylene ether glycol); poly(tetrahydrofuran)
PU[b]	Polyurethane (generic)
PUA[a]	Polyurea (generic)
PUR[a, b]	Polyurethane (generic)
PVA[b]	Poly(vinyl acetate)
PVA[b]	Poly(vinyl alcohol)
PVAC[a, b, c]	Poly(vinyl acetate)
PVAL[a, b, c]	Poly(vinyl alcohol)
PVB[a]	Poly(vinyl butyral)[h]
PVC[a, b, c]	Poly(vinyl chloride)
PVDC[a, b, c]	Poly(vinylidene dichloride)
PVDF[a, b, c]	Poly(vinylidene difluoride)
PVF[a, b, c]	Poly(vinyl fluoride)
PVFM[a]	Poly(vinyl formal)[i]
PVK[a]	Poly(vinylcarbazole); poly(*N*-vinylcarbazole)
PVME[b]	Poly(vinyl methyl ether)
PVOH[b]	Poly(vinyl alcohol)
PVP[a, b]	Poly(vinylpyrrolidinone); poly(*N*-vinylpyrrolidone)
SB[a]	Poly(styrene/butadiene)
SMS[a, b]	Poly(styrene/α-methylstyrene)
SI[a]	Silicone (generic)
SIS[b]	Poly(styrene/isoprene/styrene)
UF[a]	Urea/formaldehyde resin
UP[a]	Unsaturated polyester (generic)
VC/E[b]	Poly[(vinyl chloride)/ethylene]
VCE[a]	Poly[(vinyl chloride)/ethylene]
VC/E/VAC[b]	Poly[(vinyl chloride)/ethylene/(vinyl acetate)]
VCEVAC[a]	Poly[(vinyl chloride)/ethylene/(vinyl acetate)]
VC/E/MA[b]	Poly[(vinyl chloride)/ethylene/(methyl acrylate)]
VCEMAK[a]	Poly[(vinyl chloride)/ethylene/(methyl acrylate)]
VC/MA[b]	Poly[(vinyl chloride)/(methyl acrylate)]
VCMAK[a]	Poly[(vinyl chloride)/(methyl acrylate)]
VC/MMA[b]	Poly[(vinyl chloride)/(methyl methacrylate)]
VCMMA[a]	Poly[(vinyl chloride)/(methyl methacrylate)]

Table 19. (Continued)

Abbreviation	Polymer
VC/VAC[b]	Poly[(vinyl chloride)/(vinyl acetate)]
VCVAC[a]	Poly[(vinyl chloride)/(vinyl acetate)]
VCVDC[a]	Poly[(vinyl chloride)/(vinylidene chloride)]

[a]Ref. 44.
[b]Ref. 46.
[c]Ref. 7.
[d]"PC" usually means poly[oxycarbonyloxy-1,4-phenylene(dimethylmethylene)-1,4-phenylene], but it can also mean "polycarbonates" in a generic sense.
[e]Structure-based name poly(oxy-1,4-phenyleneoxy-1,4-phenylenecarbonyl-1,4-phenylene).
[f]Structure-based name poly(oxy-1,4-phenylenecarbonyl-1,4-phenylenecarbonyl-1,4-phenylene).
[g]Copolymers of tetrafluoroethylene with perfluorinated alkyl vinyl ethers.
[h]Predominantly poly(vinyl acetate) hydrolyzed to poly(vinyl alcohol) and then cyclized by reaction with butanal (butyraldehyde). Depending upon the degree of hydrolysis, some residual monomeric units of vinyl acetate may be present. See Table 6 for idealized, completely cyclized polymer.
[i]Predominantly poly(vinyl acetate) hydrolyzed to poly(vinyl alcohol) and then cyclized by reaction with formaldehyde. Depending upon the degree of hydrolysis, some residual monomeric units of vinyl acetate may be present.

structured and named as copolymers of the respective monomers:

(1) CA Index name: Oxirane, methyl-, polymer with oxirane
(2) CA Index name: Furan, tetrahydro-, polymer with oxirane

Ethers (end-groups) of such mixed polyalkylene glycols are named analogously to the post-treated (modified) polymers:

(1) CA Index name: Oxetane, polymer with methyloxirane, dipropyl ether

Wiley's *Polymer Handbook* (4th ed.) contains a comprehensive chapter on "Chemical Abstracts Registry Numbers and Online Dabase Searching for Polymer Literature" (35), which contains examples of CA Index names for over 500 homopolymers and copolymers.

Trade Names and Abbreviations

Because the systematic names of polymers can be cumbersome, trade names and abbreviations are frequently used as a shortcut in industrial literature and oral communication. For example, the simple generic name nylon-6,6, in which the first number refers to the number of carbon atoms of the diamine component and the second number to that of the diacid component used to form the polyamide, appears often in the literature in lieu of systematic names such as poly(iminoadipoyliminohexane-1,6-diyl) (structure-based name) or poly[hexamethylenediamine-*alt*-(adipic acid)] (source-based name). Useful compilations of trade names for polymers can be found in references (36–43) and (47–53).

Perhaps the most widely used shortcut is the use of abbreviations for common industrial polymeric materials. The IUPAC recognizes that there may be

advantages in some cases to the use of abbreviations, but urges that each abbreviation be fully defined the first time it appears in the text and that no abbreviation be used in titles of publications. Because of the inherent difficulties in assigning systematic and unique abbreviations to polymeric structures, only a short list has the IUPAC's official sanction (7). This list, published in 1987, will be updated in 2003. ISO published a more extensive list in 2001 (44), and in the mid-1980s the American Chemical Society's Polymer Nomenclature Committee compiled a master-list of all known abbreviations in the polymer field (45). The *Polymer Handbook* (46) contains an extensive list. A selection of abbreviations and acronyms from these sources is reproduced in Table 19.

BIBLIOGRAPHY

"Nomenclature" in *EPST* 1st ed., Vol. 9, pp. 336–344, by R. B. Fox, U.S. Naval Research Laboratory, and Chairman (1963–1967), Polymer Nomenclature Committee of the American Chemical Society.

"Nomenclature" in *EPSE* 2nd ed., Vol. 10, pp. 191–204, by N. M. Bikales, National Science Foundation, and Secretary (1978–1987), IUPAC Commission on Macromolecular Nomenclature.

1. Report on Nomenclature in the Field of Macromolecules. *J. Polym. Sci.* 8, 257–277 (1952). Obsolete.
2. Report on Nomenclature Dealing with Steric Regularity in High Polymers. *J. Polym. Sci.* **56**, 153–161 (1962). Superseded by Ref. 3.
3. Report on Nomenclature Dealing with Steric Regularity in High Polymers. *Pure Appl. Chem.* **12**, 643–656 (1966). Superseded by Ref. 10.
4. Report of the Committee on Nomenclature of the International Commission on Macromolecules. *J. Polym. Sci. Part B* **6**, 257–260 (1968). Obsolete.
5. Basic Definitions of Terms Relating to Polymers 1974. *Pure Appl. Chem.* **40**, 477–491 (1974). Reprinted as Chapter 1 of Ref. 30. Superseded by Ref. 22.
6. List of Standard Abbreviations (Symbols) for Synthetic Polymers and Polymer Materials 1974. *Pure Appl. Chem.* **40**, 473–476 (1974). Superseded by Ref. 7.
7. Use of Abbreviations for Names of Polymeric Substances (Recommendations 1986). *Pure Appl. Chem.* **59**, 691–693 (1987). Reprinted as Chapter 9 of Ref. 30.
8. Nomenclature of Regular Single-Strand Organic Polymers (Rules Approved 1975). *Pure Appl. Chem.* **48**, 373–385 (1976). Reprinted as Chapter 5 of Ref. 30.
9. Stereochemical Definitions and Notations Relating to Polymers (Provisional). *Pure Appl. Chem.* **51**, 1101–1121 (1979). Superseded by Ref. 10.
10. Stereochemical Definitions and Notations Relating to Polymers (Recommendations 1980). *Pure Appl. Chem.* **53**, 733–752 (1981). Reprinted as Chapter 2 of Ref. 30.
11. Nomenclature for Regular Single-Strand and Quasi-Single-Strand Inorganic and Coordination Polymers (Provisional). *Pure Appl. Chem.* **53**, 2283–2302 (1981). Superseded by Ref. 12.
12. Nomenclature for Regular Single-Strand and Quasi-Single-Strand Inorganic and Coordination Polymers (Recommendations 1984). *Pure Appl. Chem.* **57**, 149–168 (1985). Reprinted as Chapter 6 of Ref. 30 and as Chapter II-7 of Ref. 32.
13. Note on the Terminology for Molar Masses in Polymer Science. *Makromol. Chem.* 185 (Appendix to No. 1) (1984); *J. Polym. Sci., Polym. Lett. Ed.* **22**, 57 (1984); *J. Colloid Interface Sci.* **101**, 277 (1984); *J. Macromol. Sci., Chem. A* **21**, 903–904 (1984); *Br. Polym. J.* **17**, 92 (1985).
14. Source-Based Nomenclature for Copolymers (Recommendations 1985). *Pure Appl. Chem.* **57**, 1427–1440 (1985). Reprinted as Chapter 7 of Ref. 30.

15. Definitions of Terms Relating to Individual Macromolecules, Their Assemblies, and Dilute Polymer Solutions (Recommendations 1988). *Pure Appl. Chem.* **61**, 211–241 (1989). Reprinted as Chapter 3 of Ref. 30.
16. Definitions of Terms Relating to Crystalline Polymers (Recommendations 1988). *Pure Appl. Chem.* **61**, 769–785 (1989). Reprinted as Chapter 4 of Ref. 30.
17. A Classification of Linear Single-Strand Polymers (Recommendations 1988). *Pure Appl. Chem.* **61**, 243–254 (1989). Reprinted as Chapter 8 of Ref. 30.
18. Nomenclature of Regular Double-Strand (Ladder and Spiro) Organic Polymers (IUPAC Recommendations 1993). *Pure Appl. Chem.* **65**, 1561–1580 (1993).
19. Structure-Based Nomenclature for Irregular Single-Strand Organic Polymers (IUPAC Recommendations 1994). *Pure Appl. Chem.* **66**, 873–889 (1994).
20. Graphic Representations (Chemical Formulae) of Macromolecules (IUPAC Recommendations 1994). *Pure Appl. Chem.* **66**, 2469–2482 (1994).
21. Basic Classification and Definitions of Polymerization Reactions (IUPAC Recommendations 1994). *Pure Appl. Chem.* **66**, 2483–2486 (1994).
22. Glossary of Basic Terms in Polymer Science (IUPAC Recommendations 1996). *Pure Appl. Chem.* **68**, 2287–2311 (1996). Available on the world wide web at: [http://www.iupac.org/reports/1996/6812jenkins/index.html].
23. Definitions of Terms Relating to Degradation, Aging, and Related Chemical Transformations of Polymers (IUPAC Recommendations 1996). *Pure Appl. Chem.* **68**, 2313–2323 (1996).
24. Source-Based Nomenclature for Non-Linear Macromolecules and Macromolecular Assemblies (IUPAC Recommendations 1997). *Pure Appl. Chem.* **69**, 2511–2521 (1997).
25. Definitions of Terms Relating to the Non-Ultimate Mechanical Properties of Polymers (IUPAC Recommendations 1998). *Pure Appl. Chem.* **70**, 701–754 (1998). Available on the world wide web at: [http://www.iupac.org/reports/1998/7003kaye/index.html].
26. Definitions of Basic Terms Relating to Low-Molar-Mass and Polymer Liquid Crystals (IUPAC Recommendations 2001). *Pure Appl. Chem.* **73**, 845–895 (2001).
27. Generic Source-Based Nomenclature for Polymers (IUPAC Recommendations 2001). *Pure Appl. Chem.* **73**, 1511–1519 (2001). Errata. *Pure Appl. Chem.* **74**, 2019 (2002).
28. Definitions Relating to Stereochemically Asymmetric Polymerizations (IUPAC Recommendations 2002). *Pure Appl. Chem.* **74**, 915–922 (2002).
29. Nomenclature of Regular Single-Strand Organic Polymers (IUPAC Recommendations 2002). *Pure Appl. Chem.* **74**, 1921–1956 (2002).
30. W. V. Metanomski, ed., *Compendium of Macromolecular Nomenclature* (The Purple Book), Blackwell Scientific Publications, Oxford, 1991.
31. R. Panico, W. H. Powell, and J.-C. Richer, eds., *A Guide to IUPAC Nomenclature of Organic Compounds (Recommendations 1993)* (The Blue Book), Blackwell Scientific Publications, Oxford, 1993. Errata: *Pure Appl. Chem.* **71**, 1327–1330 (1999).
32. J. A. McCleverty and N. G. Connelly, eds., *Nomenclature of Inorganic Chemistry II. Recommendations 2000* (The Red Book II), Royal Society of Chemistry, Cambridge, 2001.
33. Chemical Abstracts *CA Index Guide*, Appendix IV. Chemical Abstracts Service, Columbus, Ohio, 2002. See especially Section 222 for polymer indexing principles. Reprints of Appendix IV are available gratis under the title "*Naming and Indexing of Chemical Substances for Chemical Abstracts*." Inquiries should be addressed to: Marketing Communications, Chemical Abstracts Service, P.O. Box 3012, Columbus, Ohio 43210-0012.
34. Nomenclature Committee, Division of Polymer Chemistry, American Chemical Society. *Macromolecules* **1**, 193–198 (1968).
35. M. Johnson and E. A. Grulke, in J. Brandrup, E. H. Immergut, and E. A. Grulke, eds., *Polymer Handbook*, 4th edition John Wiley & Sons, Inc., New York, 1999, Vol. **VIII**, pp. 25–52.

36. M. Ash and I. Ash, *Encyclopedia of Plastics, Polymers, and Resins*, Chemical Publishing, New York, 1982.
37. H.-G. Elias and R. A. Pethrick, eds., *Polymer Yearbook*, Harwood Academic Publishers, New York, 1984, p. 113.
38. L. A. Utracki, *Polymer Alloys and Blends: Thermodynamics and Rheology*, Carl Hanser Verlag, Munich, 1989 (distributed in USA by Oxford University Press, New York).
39. M. Hough, ed., *The Plastics Compendium: Volume 1—Key Properties and Sources*, RAPRA Technology Ltd., Shawbury, Shrewsbury, Shropshire, UK, 1995.
40. S. Allen, ed., *New Trade Names in the Rubber and Plastics Industries*, RAPRA Technology Ltd., Shawbury, Shrewsbury, Shropshire, UK, 1996.
41. F. W. Billmeyer, *Textbook of Polymer Science*, 3rd ed. John Wiley and Sons, Inc., New York, 1984
42. M. Ash and I. Ash, *Chemical Tradename Dictionary*, VCH Publishers, New York, 1993.
43. A. Masterson and M. Miller, eds., *Rubber Directory and Buyer's Guide*, 23rd ed. Rubber and Plastics News, Akron, Ohio, 1999.
44. Plastics—Symbols and Abbreviated Terms—Part 1: Basic Polymers and Their Special Characteristics, International Standard ISO 1043-2001, The International Standardization Organization, Geneva, Switzerland, 2001.
45. Nomenclature Committee, Division of Polymer Chemistry, American Chemical Society. *Polym. News* **9**, 101–110 (1983); **10**, 169–172 (1985).
46. H.-G. Elias, J. Brandrup, E. H. Immergut, and E. A. Grulke, eds., in *Polymer Handbook*, 4th ed. John Wiley & Sons, Inc., New York, 1999, Vol **VIII**, 1–24.
47. Polymer Trade Names http://www.123plastics.com/polytradename.asp http://www.polymerweb.com/_misc/tradenam.html http://www.plasticsusa.com/tradenam.html
48. Index of Polymer Trade Names (2nd ed.) (A listing of 35,000 trade names, available as printed handbook or CD-ROM). WILEY-VCH, Weinheim, or WILEY-VCH, New York: http://www.fiz-chemie.de/katalog/polymers/polym_polymer_index.html
49. Matweb Material Property Data (American Precision Products); data on 29,500 substances, including polymers: www.matweb.com or http://www.matweb.com/index.asp?ckck=1 http://www.matweb.com/search/SearchTradeName.asp http://www.matweb.com/polymertradename.htm
50. Polymer Doctor Trade Name Directory: http://www.polymerdoctor.com/fine/plsql/tradename_link_new
51. Guide to Polymer Trade Names: http://www.geocities.com/~spanoudi/tradname.htmb.
52. Plastics, Polymer Tradenames and Suppliers: http://www.plastics-market.net/information.htm
53. Plastics Technology Online: http://www.plasticstechnology.com/ To access the Materials Database, see http://66.192.79.234/.

J. L. SCHULTZ
E. S. WILKS
E. I. Du Pont de Nemours

NOVOLAKS. See PHENOLIC RESINS.

NUCLEIC ACIDS. See POLYNUCLEOTIDES.

NYLON. See POLYAMIDES.

OPTICAL PROPERTIES

Introduction

Three phenomena take place when light interacts with polymeric materials: absorption, scattering, and transmission through the bulk of the material. In the case of absorption it is possible that emission may take place of some or all of the absorbed energy. In the case of scattering, the light vector changes direction. This change may happen either with a change in energy (inelastic scattering) or without (elastic scattering). The scattered intensity depends on the refractive index variation. In the case of transmission the light propagates through the material and its state of polarization may change.

Polymers have many important optical properties, such as refractivity, reflection, scattering, absorption, clarity, haze, birefringence, stress–optical coefficient, optical configuration parameter, yellowness index, light transmission, gloss, color, and surface texture among others (1).

One application related to polymer rheology is stress field visualization. It relies on birefringence techniques to examine the spatial and temporal evolutions of stress in a polymer melt (see Fig. 1) (2). In this particular example the picture shows the isochromatic fringe patterns of a high density polyethylene melt in the entrance region in capillary flow experiment at 200°C. Techniques such as the application of birefringence to polymer flow problems are very useful in understanding polymer processing.

Extensional flow and structure–property relationships may also be studied by birefringence. A particularly interesting application from transient flow is presented in Figure 2, where phenomena such as overshoot and ringing are observed (3). In this example we see results for 1.5% polyethylene oxide solution for three different velocity gradients. Birefringence detects the presence of an overshoot,

Encyclopedia of Polymer Science and Technology. Copyright John Wiley & Sons, Inc. All rights reserved.

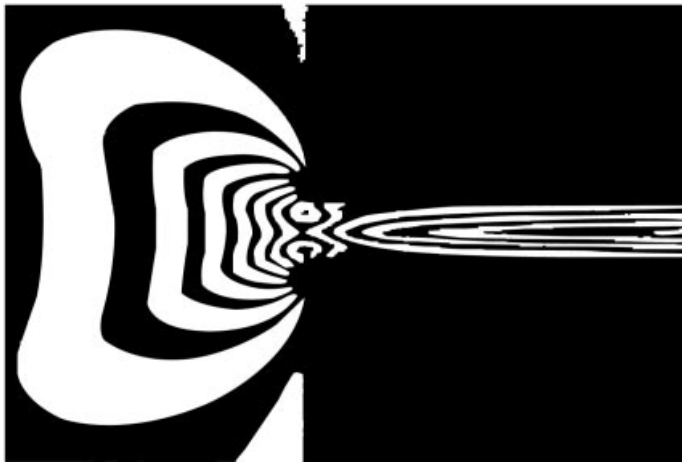

Fig. 1. Stress field visualization through birefringence (From Ref. 2).

whose magnitude increases with the velocity gradient while the time needed to attain the maximum has decreased. Phenomena such as those are observed after start-up of an extensional flow in a four-roll mill at various strain rates. Theories of polymer rheology can be improved with the insight provided by such experiments.

Market applications based on optical properties of polymers are countless. Polymer optical lenses, CDs, DVDs, and packaging applications for the medical, electronic, food, and cosmetic markets are just a small sampling where optical properties of polymers play a dominant role.

Emerging high technology areas such as optical computing, optoelectronics, and fiber optics are some others. Transitioning from traditional copper wire to fiber-optic cables for faster information transfer, light switches of very high speed, or intensity modulators up to 40 GHz are areas of immense interest in today's market. Altering the frequency of light from red to blue for laser applications and the associated increase of the density of data stored on an optical disk because of the shorter wavelength of blue light has recently been accomplished. Polymers can play a vital role in developing new electrooptical devices, optical waveguides, display screens, optical integrated circuits, amplifiers, attenuators, and photonic switching systems.

Applications in the biomedical area are also very important. Contact lenses, transparent medical tubing, and films for packaging are just few examples. There is literally no area of our life that has not been positively affected by the usefulness of the optical properties of polymers.

Basic Definitions and Computational Prediction of Fundamental Optical Properties of Polymers

Reliable prediction of optical properties allows a better, clearer understanding of the underlying structure–property relationships. This in turn opens new avenues for designing new polymers with desired optical properties. One may rely on

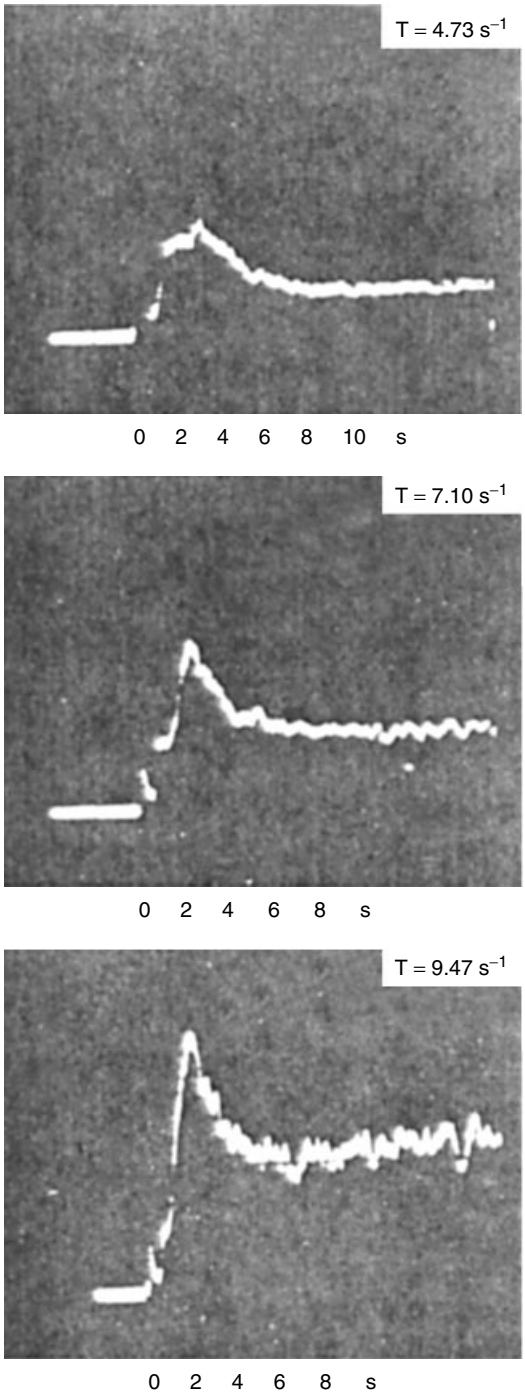

Fig. 2. Overshoot and ringing as observed through flow–birefringence experiments. In this example we see results for 1.5% polyethylene oxide solution for three different velocity gradients. (From Ref. 3).

ab initio (from first principles) and semiempirical models to study polymer fragments and monomers (4). Monte Carlo, molecular dynamics, and QSPR (quantitative structure–property relationships) are also being extensively used to study single chains and multichain polymer systems in bulk and in solution (5). Here we very briefly review the theory and qualitatively look at some of the available methods for predicting optical properties.

Optical Polarizability and Its Anisotropy. The polarizability, α, the constant of proportionality between the induced dipole moment, μ', and the intensity of the applied electric field, E, is of primary importance and is given by (6)

$$\mu' = \mu + \alpha E + \frac{1}{2}\beta E^2 + \frac{1}{6}\gamma E^3 + \cdots \tag{1}$$

where μ is the permanent dipole moment and the parameters β and γ in the nonlinear terms are the hyperpolarizabilities (see also under Nonlinear Optical Properties). Qualitatively, polarizability is the "ease" of the displacement of the electrons around the nuclei because of the presence of the field.

Application of perturbation theory allows the calculation of the electronic polarizability according to

$$\alpha = \frac{2}{3}\sum_n \frac{|\langle 0|\mu|n\rangle|^2}{E_n - E_0} \tag{2}$$

where the numerator is proportional to the square of the electric transition dipole moment μ from the ground (eg 0) to the excited (eg n) states. Dynamic polarizabilities far from an absorption band may be calculated from

$$\alpha(\omega) = \frac{2}{3\hbar}\sum_n \frac{\omega_{n0}|\langle 0|\mu|n\rangle|^2}{\omega_{n0}^2 - \omega^2} \tag{3}$$

where $\hbar = h/2\pi h$ being the Planck's constant and ω the frequency.

It is common to divide the polarizability by $4\pi\varepsilon_0$ to obtain what is called the polarizability volume, which typically has units of $\mathring{A}^3$. According to equation 1, if the two vector quantities μ and E are not of the same direction, then α must be a tensor. Generally for a molecule one may write the polarizability tensor as (7)

$$\alpha = \begin{bmatrix} \alpha_{xx} & \alpha_{xy} & \alpha_{xz} \\ \alpha_{yx} & \alpha_{yy} & \alpha_{yz} \\ \alpha_{zx} & \alpha_{zx} & \alpha_{zz} \end{bmatrix} \tag{4}$$

from which through diagonalization one obtains

$$\alpha = \begin{bmatrix} \alpha_X & 0 & 0 \\ 0 & \alpha_Y & 0 \\ 0 & 0 & \alpha_Z \end{bmatrix} \tag{5}$$

where X, Y, and Z are now the principal axes of the molecule. In the case of spherical symmetry, $\alpha_X = \alpha_Y = \alpha_Z$. Carbon tetrachloride, an optically isotropic

solvent used routinely in depolarized Rayleigh scattering experiments, is a typical molecule with spherical symmetry. For cylindrical symmetry, it holds that $\alpha_Y = \alpha_Z$. This will be true, for example, for the bonds of a polymer chain that is being treated in the freely jointed chain limit.

The anisotropic part of the polarizability tensor is defined as

$$\hat{\alpha} = \alpha - \frac{1}{3}\,\mathrm{Tr}(\hat{\alpha}\hat{\alpha})E_3 \tag{6}$$

where E_3 is the identity matrix of order 3. The quantity $\frac{1}{3}\,\mathrm{Tr}(\hat{\alpha}\hat{\alpha})$ is equal to the mean polarizability.

In some cases it is convenient to employ the following two relationships:

$$\alpha_{||} = \alpha_X - \frac{\alpha_Y + \alpha_Z}{2} \tag{7}$$

and

$$\alpha_{\perp} = \alpha_Y - \alpha_Z \tag{8}$$

where the symbols $\alpha_{||}$ and $\alpha_{\perp}$ denote the longitudinal and transverse anisotropies of the polarizability, respectively.

***Ab Initio* and Semiempirical Approximations and Models.** The general formulas of *ab initio* methods can be used for calculations directly and without approximation, only if the set of wave functions and eigenenergies is known with sufficient accuracy. This is true only in the case of the very simplest atoms and molecules. The "from first principles" approach is to calculate the wave functions by solving the Schrödinger equation exactly. For large molecules, such as polymer fragments and chains, it is currently impossible to produce a set of exact wave functions or to obtain sufficient spectroscopic data. Therefore various assumptions are introduced to alleviate the complexity of the calculations; semiempirical models contain such assumptions—which are beyond the scope of this chapter. However one may rely on semiempirical quantum-mechanical methods to predict (at least qualitatively) properties of polymer chain fragments.

Linear optical properties such as linear polarizabilities can be calculated relying on the theory mentioned above. For nonlinear optical properties there are several approximate methods available too. Some of the most basic ones are given below in a qualitative manner. For further reading a number of excellent books on the subject is suggested (8–10).

Resonant Case. The greatest simplification of the general formulas for the susceptibilities (see under Nonlinear Properties) can be made in the case when the nonlinear process under study is resonantly enhanced. In this case one aims to extract the significant resonant terms from the full expression for susceptibility, $\chi^{(n)}$, and then piece together the contributions from all the other levels into a negligible term. The resonant contribution may then be calculated using the best available wave functions for the resonant levels. One could also choose to use experimental data for the selected transition frequencies and oscillator strengths. In the case when one pair of levels provides the dominant resonant contribution, a two-level model is appropriate.

Resonant Two-Level Atom Systems. The description of resonant optical processes is greatly simplified by focusing on the dominant resonant transition. The model is based on a concept of an ensemble consisting of many two-level atoms that are identical and noninteracting. By "two-level," one refers to two energy eigenstates that are used to describe the atom. An alternative approach is to consider the eigenstates of the system and the optical field taken together (often called "dressed" atoms approach).

Unsoeld Approximation and Charge Models. In the case when all the combinations of optical frequencies involved are far removed from molecular resonances the hyperpolarizabilities do not depend on the details of the energy structure but only on the chemical bonding. The hyperpolarizabilities depend on the detailed distribution of charges in the ground state *only*, together with statistical averages of the frequencies and oscillator strengths of transitions to the excited states.

For saturated molecules in which the electrons are localized in bonds, the moments can be estimated using the vector sum of the polarizabilities of the individual bonds, and the interaction between bonds is neglected (bond additivity scheme).

Sum Over States (SOS). This method computes molecular orbitals, from which values for transition frequencies may be calculated. First the electronic ground state of the molecular system is determined, after which one may apply either the Hartree–Fock–Roothan method or the LCAO (linear combination of atomic orbitals) approximation. Then one accounts for correlations by configuration interaction calculations to form the lowest-energy excited states and transition dipole moments of the molecule. Finally transition frequencies and dipole moments are employed along with the formulas for the hyperpolarizabilities. The SOS method needs as input, energies and transition moments for excited states. It yields $\beta(\omega)$ directly (eq. 1); identification of contributing excited states is important.

Finite-Field Method. This method relies on deriving the various terms in the power series for the static-induced molecular dipole moment in terms of derivatives with respect to the local field. Therefore, if the molecular dipole moment can be calculated as a function of local electric field E then β_{ijk} is obtained from the second derivative of this function at $E = 0$.

The Local Field

The role of local field is very important in determining optical properties of polymers, both in solution and in the bulk (11). It becomes particularly critical in measurements where polarized light is involved. It is therefore reasonable to include a short description in this chapter.

In a vacuum the electric field E is defined in terms of the force experienced by an infinitesimal test charge that can be placed at any point in space. However this cannot be done within systems like a polymer melt or a polymer solution, since, by definition, the space where we would like to measure the field is already occupied by either a polymer fragment or a solvent molecule.

Typically, the standard definition of E at a point in a polymer system proceeds analogously to the procedure in vacuum except that one first creates a needle-shaped cavity oriented along the field direction. This definition has its own limitations: the shape of the cavity in which E is defined will probably be different from that of the definition; real charges will probably not have an appropriately shaped cavity around them. The actual field must be modified by allowance of the real shape of the molecule to which the charge belongs. The definition neglects the fields due to the other charges that belong to the molecule under consideration. E is defined in the absence of the other charges that belong to the molecule. Even if the interaction of these charges is already taken into account in the quantum-mechanical calculation of the molecular states in vacuum, there are contributions mediated through material outside the cavity that must be included.

Lorenz–Lorentz theory addressed the issue by extending the approach of Clausius–Mossotti to optical frequency fields (12,13). This extension relies on a spherical cavity (compare with the need for a needle-shaped cavity) and takes into account the effect of other charges. The only thorny issue is that a spherical cavity is not the best choice for anisotropic molecules. Nevertheless, the Lorenz–Lorentz approach has been widely used in studying optical properties of polymers (14). The expression of the local field is given by

$$L = \frac{n^2 + 2}{3} E \tag{9}$$

Using the molecular shape as a guide to develop the anisotropic cavity field may be a more realistic way of dealing with the issue. Boundary conditions could be a needle-shaped cavity and a disk-shaped one.

For polarized measurements the relationship between refractive index and absorbance is critical. Directional absorbance changes lead to birefringence, which in turn will affect strongly the nature of polarized light. The Kramers–Kronig relations come into play for cases like this one (15). They relate the complete electromagnetic absorption spectrum of a material to its refractive index at all frequencies and vice versa. A form of the relation is

$$\Delta n = \frac{2.303Cc}{2\pi^2} P \int_0^\infty \frac{\varepsilon(\nu')d\nu}{\nu'^2 - \nu^2} \tag{10}$$

Δn is the contribution to the refractive index due to the solute whose concentration is C (mol/L), c is the speed of light, and $\varepsilon(\nu')$ is the molar extinction coefficient. Δn is the difference between the refractive indexes of the solution and the solvent. Δn is essentially the isotropic contribution to the refractive index by the solute whose absorption spectrum determines $\varepsilon(\nu')$. It should not be confused with birefringence, which uses the same symbol (see under Birefringence). A common application of the Kramers–Kronig relation appears in light scattering, especially when one is interested in the effects of scattering on absorbance measurements.

Refractive Index

According to the ISO definition (16), refractive index is the ratio of electromagnetic radiation *in vacuo* to the phase velocity of electromagnetic radiation of a specified frequency in the medium. The refractive index is always greater than unity and it is dimensionless. For anisotropic materials the state of polarization of the light and its direction must be defined relative to a reference axis in the sample.

The two experimental methods recommended by ISO-489 are the Abbe refractometer technique and the Becke line technique. The latter is more useful with powdered or granulated transparent material or even with small flakes of material taken from a larger sample. ASTM D542 method includes only the Abbe method and it is widely used for the characterization of refractive index of polymers.

The refractive index decreases with increasing wavelength. The term *dispersion curve* refers to the graphical representation of that dependence (Fig. 3) (17).

One may estimate the refractive index in terms of the molar refraction R, which quantifies the intrinsic refractive power of the structural units constituting the polymer. According to Refs. 18 and 19 the molar refraction R_{LL} is given as

$$n = \sqrt{\frac{(V + 2R_{LL})}{(V - R_{LL})}} \tag{11}$$

According to another definition, by Gladstone, molar refraction R_{GD} is given by

$$n = 1 + \frac{R_{GD}}{V} \tag{12}$$

The value of n increases with the refractive power of the polymer. There is no simple correlation between high mass density and high refractive index for all polymers. For example, the densities of many polymers containing aromatic rings are not especially high, but these polymers usually have high refractive indexes.

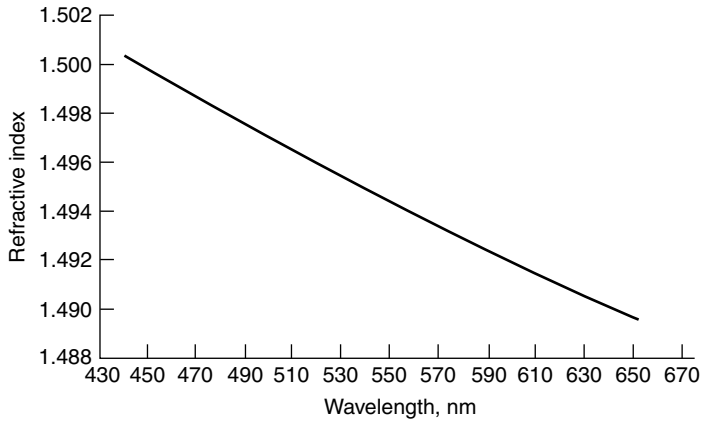

Fig. 3. Dispersion curve for an acrylic cast sheet (From Ref. 17).

Both the intrinsic refractivity and the density are key physical factors determining the refractive index.

Both R_{LL} and R_{GD} have relatively little dependence on temperature and crystallinity. On the other hand the molar volume V changes drastically with both of those properties. In particular, volume increases with temperature while it decreases with increasing crystallinity. As a result the refractive index decreases with increasing temperature and increases with crystallinity. The refractive index undergoes a change at the glass-transition temperature.

The temperature dependence of n is quite similar for all polymers. An empirical rule for glassy polymers (21) is that n decreases by about 1×10^{-4} to 2×10^{-4} per degree Kelvin increase of temperature. For isotropic amorphous polymers above T_g that value changes to about 3×10^{-4} to 5×10^{-4} per degree Kelvin, at typical temperatures. Since n can never be less than unity the rate of decrease with increasing temperature above T_g eventually levels off and asymptotically approaches zero. However, most polymers will degrade long before reaching temperatures high enough to for such a phenomenon be observed. Therefore the empirical rule mentioned above is valid for (moderate) temperatures of practical interest.

Typically one aims to predict the refractive index of the amorphous limit for a semicrystalline polymer. After that the effect of crystallinity may be calculated by using either R_{LL} or R_{GD} combined with an estimate of the change in volume due to crystallization. A large collection of refractive index data on polymers may be found in *Physical Properties of Polymers Handbook* by the American Institute of Physics (22). A representative albeit necessarily short list is given below in Table 1.

Bicerano, in his book *Prediction of Polymer Properties*, proposes the following predictive equation for the refractive index at room temperature (23):

$$n = 1.885312 + 0.024558(17^0\chi^v - 20^0\chi - 12^1\chi^v - 9N_{rot} + N_{ref})/N \qquad (13)$$

χ^0, $^0\chi^v$, and $^1\chi^v$ are the connectivity indexes; N_{rot} and N_{ref} are correction factors that account for crystallinity and for contributions of certain atoms such as F, Si, and ring structures.

The graphical representation of the correlation is given in Figure 4.

Specific Refractive Index Increments. The rate of change of refractive index n of a dilute solution with changing polymer concentration C plays an

Table 1. Refractive Indexes for Some Polymers

Polymer	Refractive index	Temperature, °C
Nylon 6,6	1.566	See Ref. 22
Poly(butyl acrylate)	1.3900	25
Poly(methyl acrylate)	1.5750	25
PMMA	1.49	See Ref. 22
Poly(carbonate)	1.5570	25
Polyethylene (0.914 g/cc)	1.5050	25
Poly(tetrafluoroethylene)	1.555	20

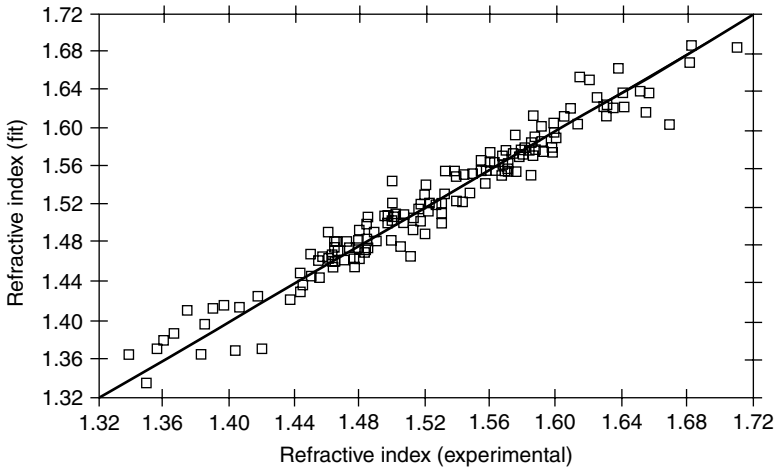

Fig. 4. Refractive index correlation for a series of polymers. Standard deviation: 0.0157; correlation Coefficient: 0.9770. The line denotes $y = x$. (From Ref. 23). □, $n(298\ \mathrm{K}) \approx 1.885312 + 0.024558(17.0\chi \mathrm{v} - 20.0\chi - 12.1\chi \mathrm{v} - 9N_{\mathrm{rot}} + N_{\mathrm{ref}})/N$.

important role in the extraction of information from light-scattering experiments, in particular for the determination of weight-average molecular weights (see Fig. 5). That change depends on the polymer, solvent, and temperature (20).

$$\frac{dn}{dC} \approx \frac{(n_{\mathrm{polymer}} - n_{\mathrm{solvent}})}{\rho_{\mathrm{polymer}}} \tag{14}$$

The correlation outlined above relies on values of refractive index and of density for the amorphous phase. All results are for room temperature.

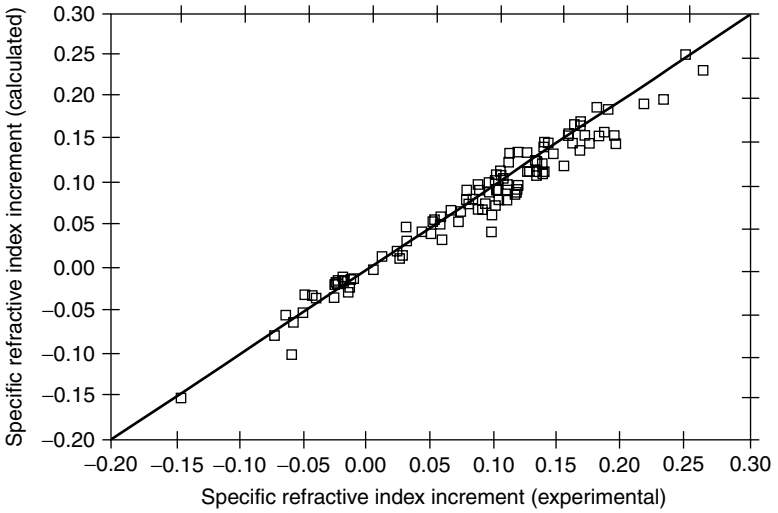

Fig. 5. Correlation for specific refractive index increments for a series of polymers. Standard deviation: 0.0158; Correlation coefficient: 0.9796. The line denotes $y = x$. (From Ref. 23).

Refractive Index Fluctuations in Glassy Polymers. Fluctuations in the refractive index within the bulk of a polymer can arise because of various optical inhomogeneities. Those fluctuations may be described by a radial correlation function, defined as

$$\gamma(r) = \frac{\langle \eta_i \eta_j \rangle_r}{\langle \eta^2 \rangle_{\text{av}}} \tag{15}$$

where η_j and η_i are the refractive indexes at positions i and j respectively, being at a distance r from each other. The brackets denote averages at all pairs of points at distance r apart.

At $r = 0$ the correlation function approaches unity. A common expression is

$$\gamma(r) = \exp(-r/a) \tag{16}$$

constant α being the correlation length. For PMMA, for example, α is at 100–200 nm.

Fluctuation in the refractive index will affect the intensity of the scattered light. According to Debye–Bueche (24) the scattered intensity at an angle θ to the incident beam has intensity I, given by

$$I \sim \langle \eta^2 \rangle_{\text{av}} \int_0^\infty \gamma(r) r^2 \frac{\sin Sr}{Sr} dr \tag{17}$$

with

$$S = 4\pi/\lambda \sin(\theta/2) \tag{18}$$

For PMMA the root mean square refractive index fluctuation is around 2×10^{-4}. The larger the fluctuations, the larger is the scattering intensity. This is critical for applications such as fiber optics, where transmission distances are critical.

Refractive Index and Orientation Fluctuations in Semicrystalline Polymers. The crystals of semicrystalline polymers are optically anisotropic. The simplest spherulite-based model for predicting light scattering is a sphere of radius r with a different polarizability in the radial direction α_r than in the tangential direction α_t (25). Assuming vertically polarized incident light, the intensities of the two scattered components (vertical and horizontal) are

$$I_{\text{VV}} \sim \cos^4 \mu_A (\alpha_t - \alpha_r)^2 + \cdots \tag{19}$$

$$I_{\text{HV}} \sim \sin^2 \mu_A \cos^2 \mu_A (\alpha_t - \alpha_r)^2 \tag{20}$$

where μ_A is the azimuthal angle in the scattering pattern. The HV component will have a maximum intensity in the θ direction at

$$\sin\left(\frac{\theta_m}{2}\right) = \frac{1.025}{\pi}\left(\frac{\lambda}{r}\right) \tag{21}$$

Therefore the scattering maximum moves to larger θ values as the mean spherulite radius decreases. For unpolarized incident light the scattering pattern becomes axially symmetric, with intensity independent of the angle μ_A.

There is always a concern when one tries to optimize properties such as transparency and toughness, because the requirements for those two in terms of particle size conflict with each other. For example, rubber-toughened ABS is opaque because the particle size of the rubber particles is kept at 1 μm in order to optimize toughness.

Another example is that of isotactic PP film produced on a cast film line. Its optical properties can change considerably by changing line conditions such as die temperature and chill roll temperature. Line speed affects cooling time and is therefore important too in affecting optical properties. All those conditions affect the development of the crystalline structure of the film, which in turn is related to its optical properties. Random copolymers of PP will have better optical properties than homopolymers, because of their inherently lower crystallinity.

Particulate Scattering from Isolated Irregularities. A model that addresses the issue of particulate scattering on the surface is the following: if the scattering centers are sufficiently separated from each other, the total scattering is the sum of those calculated individually from each particle. Mie light-scattering theory (26,27) uses spherical particles of diameter d and relative refractive index n (which is the ratio of the refractive index of the sphere to that of the matrix) (28).

The scattering efficiency factor K is defined as the total scattered energy divided by the energy incident on the surface of the particle. The size of the sphere will affect the values of K (Fig. 6). In general there are three regions of interest:

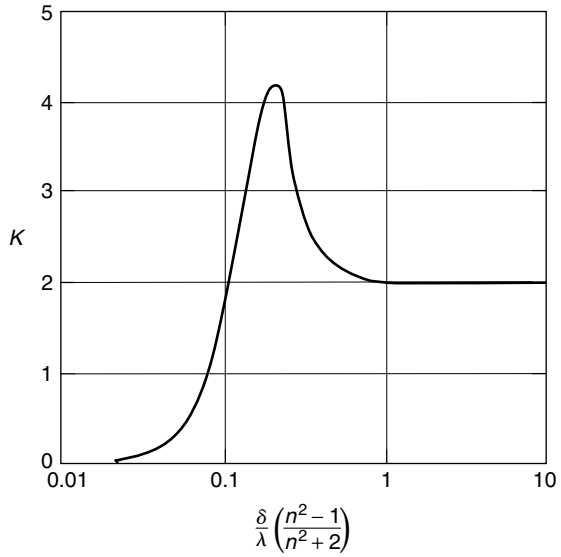

Fig. 6. Scattering coefficient K for a single sphere of relative refractive index n versus the ratio of the sphere diameter to the wavelength of the light (From Ref. 26).

When the particle diameter is less than 10% of the wavelength of light, Rayleigh scattering is observed, in which the efficiency factor is given by

$$K = \frac{8}{3}\pi^4 \left(\frac{d}{\lambda}\right)^4 \left(\frac{n^2-1}{n^2+2}\right)^2 \tag{22}$$

When the diameter is of the same order of magnitude as the wavelength of light, a peak in the value of K is observed. When the diameter is larger the scattering efficiency is around 2.

Internal Absorption. Internal absorption causes the transmitted intensity I to fall exponentially as the path length L increases through the polymer:

$$I = (1-R)^2 I_0 e^{-AL} \tag{23}$$

I_0 is the incident intensity and A is the attenuation coefficient. All polymers absorb strongly in the UV region.

Transmission and Haze

The degree of optical transparency of a polymeric material is determined by its luminous transmittance, haze, and clarity. Total luminous transmittance is the ratio of the transmitted luminous flux to the incident luminous flux. Regular transmittance is the ratio of undiffused transmitted flux to incident flux. Typically it encompasses the flux that deviates from the incident beam no more than 2.5°.

A breakdown of the factors affecting the appearance of a transparent polymer appears in the chart below:

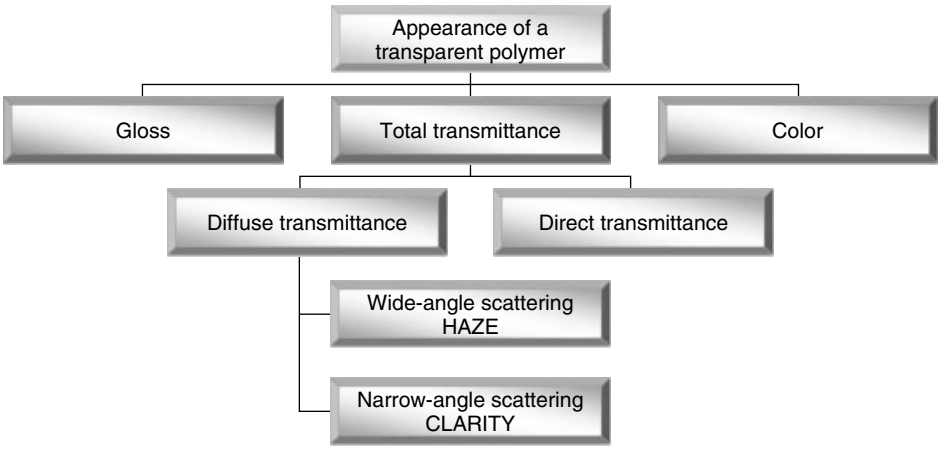

The term "haze" is used to describe the slightly cloudy appearance of film material resulting from the forward scattering of light. ASTM D1003 defines *haze* as the "percentage of transmitted light which in passing through the specimen deviates from the incident beam by forward scattering." For the purposes of this method only light flux deviating more than 2.5° on the average is considered to be haze.

Haze can be caused from a variety of sources found at the surface or in the bulk of the material. Some of them could be impurities, voids, bubbles, and filler particles. Regions of different refractive indexes brought about by crystallization can also be a cause of haze. Surface roughness could also be a reason for haze. For example, abrasion and/or weathering will affect haze by altering the surface of a polymer sample.

Haze characterizes the loss of contrast that results when objects are viewed through a scattering medium. The deterioration of contrast is due mainly to light scattered forward at large angles to the undeviated transmitted beam and is usually expressed through the forward-scattered fraction.

It is important to distinguish between surface and bulk scattering; for testing purposes the former is minimized by wetting the surface with a liquid of similar refractive index. That way the two effects (surface vs bulk) can be decoupled. The "milk-like" appearance of translucent polymer samples viewed from the side on which light is incident is due to back scattering.

It is customary to calculate the total luminous transmittance of the sample, T_t, as well as Haze, H. The ASTM method uses the following equations:

$$T_1 = 100\left(\frac{T_2}{T_1}\right) \tag{24}$$

and

$$H = 100\left[\left(\frac{T_4}{T_2}\right) - \left(\frac{T_3}{T_1}\right)\right] \tag{25}$$

The various transmittances are defined as follows (29):

Measurement	Position A	Position B
T1	No sample	White standard
T2	Sample	White standard
T3	No sample	Light trap
T4	Sample	Light trap

A simple hazemeter schematic is shown in Figure 7.

ISO CD14872, on the determination of haze of transparent material, specifies instrumentation similar but not identical to ASTM. While both methods require four measurements each, the sphere geometry employed is different.

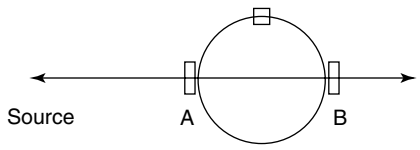

Fig. 7. Simple hazemeter (From Ref. 29).

Polymer morphology and its response to processing parameters will affect haze values. For example, polypropylene homopolymers have higher haze than random copolymers, with ethylene. The haze values of PP copolymers, in cast film operations, will be affected by such parameters as die temperature, chill roll temperature, line output, and sample thickness.

Transparency and Clarity

Transparency is a property that depends mainly upon the optical homogeneity of the polymer both in the bulk and at the surface. The variation of the refractive index in the material has the following effects:

(1) It produces changes in the phase and the amplitude of the light wave.
(2) It removes from the incident wave part of its energy through scatter within a certain solid angle.

The first effect is responsible for the aberration of the image formed by the optical system, for example, films, sheets, or optical lens. Typically, loss of clarity is associated with the confusion in the image plane of two distinct points in the object plane.

The second effect is responsible for the deterioration of contrast of the formed image. The two effects are closely interrelated and together constitute the two different aspects of what is typically termed as transparency.

Consider a monochromatic parallel beam of unpolarized flux ϕ incident perpendicularly on a polymer film immersed in a liquid of matching refractive index. A certain amount of the flux, ϕ_{sc}, will be scattered in all directions; another part, ϕ_{ab}, will be absorbed by the material. The remainder, ϕ_{under}, will be transmitted without any deviation (Fig. 8) (30):

$$\phi_{under} = \phi - \phi_{ab} - \phi_{sc} \tag{26}$$

The specular transmittance T is defined as

$$T = \phi_{under}/\phi \tag{27}$$

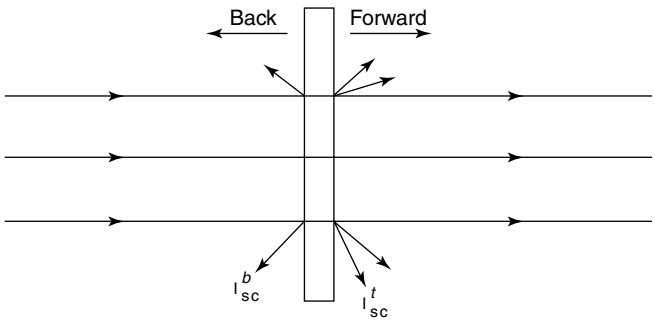

Fig. 8. Transmission of light through a sheet (From Ref. 30).

T is a function of the wavelength of the incident light and of the thickness of the sample. Immersion of the sample in a liquid of matching refractive index avoids having to take into account the reflective losses at the incident and emerging surfaces.

For materials of fairly high transparency, the relationship between specular transmittance and sample thickness Z is given by

$$T = \exp\{(-\sigma + \mathrm{K})Z\} \tag{28}$$

An expression based on the extinction index n'' is

$$(\sigma + \mathrm{K}) = (4\pi/\lambda)n'' \tag{29}$$

The sum $\sigma + K$ is equivalent to the attenuation factor α:

$$\alpha \simeq 54.6(n''/\lambda) \tag{30}$$

σ is known as the scattering coefficient and is a measure of the amount of scattered light. K is the absorption coefficient and represents the amount of light absorbed. Both quantities have units of m^{-1}. Typically, for polymers, K is fairly small when compared to σ. Therefore the attenuation coefficient may be taken to be equal to the scattering coefficient, which leads to the following expression for the total flux transmitted, ϕ_T:

$$\phi_\mathrm{T} = \phi_\mathrm{under} + \phi_\mathrm{sc} \tag{31}$$

Clarity is the ability of the sample to transmit the fine details of an object viewed through it. Maximum clarity is therefore achieved by minimizing the size of scattering centers as it is strongly related to the angular distribution of the scattering intensity. It is also affected by the distance between the object viewed and the sample (31).

Fresnel's law allows calculation of the maximum transparency τ_i of a plastic material.

$$\tau_i = 1 - R_0 \tag{32}$$

with

$$R_0 = \frac{(n-1)^2}{(n+1)^2} \tag{33}$$

Maximum transparency of a polymer can range between 98% (for a refractive index of 1.33) and 92.8% (for a refractive index of 1.73). However none of these values can be achieved in practice because there is always absorption and/or scattering of light by the sample.

For example, poly(methyl methacrylate) (PMMA), one of the most transparent plastics, never exceeds a transparency of around 93% for wavelengths between

430 and 1100 nm. In theory however PMMA could achieve a transparency of 96.1%. PMMA's transparency decreases above 1150 nm and below 380 nm.

Transparent polymers have values of τ_i higher than 90%. On the other hand polymers with τ_i less than 90% appear clear as only thin films. These are called translucent or contact-clear because films look clear when in contact with an object but hazy when viewed alone.

Clarity is negatively affected by light absorption and scattering. As we saw earlier, loss of contrast by forward scattering causes haze. The combined loss by scattering (both forward and backward) causes a "milk-like" appearance.

Local fluctuations of refractive index and/or orientation of anisotropic volume elements cause a polymer to be opaque. The various volume elements must be at least equal to the wavelength of the incident light. The clarity of the material can thus be increased considerably if elements such as microdomains are decreased. For example, spherulites are more homogeneous optically than lamellar structures of similar diameter.

Adjustment of refractive indexes of phases within a polymer blend can somewhat improve the clarity of the polymer. For example, ABS-modified PVC has a milky/yellowish appearance if the ABS is dispersed in PVC. The blend looks bluish milky if PVC is dispersed in ABS. If the dispersed materials have core-shell morphology then one can get transparent material if the mean refractive index of the core-shell particles matches that of the matrix.

Processing conditions strongly influence the morphology of polymers, thus affecting their transparency. For example, for injection/blow-molded PET, nonspherulitic structure and a limited range of crystal orientations can be achieved by (*1*) imparting crystallization at a low temperature upon heating from a glassy or partially disordered state, (*2*) cooling the preforms very rapidly so they are glassy, and (*3*) subsequent reheating to 100°C, so very small crystals form. Biaxial stretching before the occurrence of crystallization results in the desired microstructure.

Minimization of the refractive index difference between the crystalline and amorphous phases will also yield in higher transparency of articles. For example, poly(4-methyl-1-pentene) will yield transparent injection-molded products because of the small difference in refractive index for the two phases.

The hiding power of a polymer surface is related to inhomogeneities (such as fillers or more than one phase) that cause strong reflections.

$$R_{0,h} = \frac{(n_1 - n_2)^2}{(n_1 + n_2)^2} \tag{34}$$

The refractive index of the polymer is given by n_1 and that of the inhomogeneity (eg filler) by n_2.

The hiding power of a polymer is also affected by light scattering. High filler concentrations lead to multiple scattering, which reduces the hiding power through reduction of the relative scattering intensity. If one wishes to increase the hiding power one must look into increasing the backward scattering. Increasing the size of the filler particles would be one way to accomplish that. Typically though, one finds that the hiding power reaches a maximum at certain filler size and then it decreases.

ASTM D-1746 correlates see-through clarity with regular transmittance. However the correlation is not very strong for highly diffusing materials. There is no method widely accepted for this property. The work of Webber is often cited as a popular approach (32).

Reflection and Gloss

Reflectivity is defined as the ratio of the intensity of reflected to incident light. Both of those depend on the angles of incidence, alpha (α), and refraction, beta (β):

$$R = \frac{I_r}{I_0} = \frac{1}{2}\left[\frac{\sin^2(\alpha-\beta)}{\sin^2(\alpha+\beta)} + \frac{\tan^2(\alpha-\beta)}{\tan^2(\alpha+\beta)}\right] \tag{35}$$

Gloss is the ratio of the reflectivity of a sample to the reflectivity of a standard. The gloss increases with increasing refractive index and with sample of incidence. In the polymer film industry, three different angles are employed: 20°, 45°, and 60°. A test at an angle of 85° may also be performed in certain cases.

Gloss decreases when the sample has a rough surface because of the scattering. Optical inhomogeneities just below the surface also affect the values of gloss in a negative way.

Differences in local gloss on a surface cause "glitter" as a result of high directed light reflections. For example, polymer fibers show glitter if their cross sections are triangular or trilobal.

Gloss can also be defined as the degree to which a surface simulates a perfect reflecting material in its capacity to reflect light. Specular gloss is the term used for the proportion of light reflected in the mirror direction. The typical standard for gloss is optically flat, black glass. However, the assigned values of gloss depend on the refractive index of the glass employed, so comparisons between tests must take that into account.

According to ASTM D523 an angle of 60° is recommended for general use, 20° for high gloss materials, and 85° for low gloss materials. ASTM D2457 suggests measurements at 20°, 45°, and 60°.

Polymer surface morphology will affect the value of gloss. Processing parameters as well as mold finish (for various molding operations) or chill roll finish (in cast film operations) will also affect gloss values. Typically, rubber-modified polyolefins have a lower gloss than highly crystalline polyolefins.

Birefringence

Birefringence is the optical phenomenon in which a polymer sample exhibits different refractive indexes for light with plane polarization in two perpendicular directions. In other words an unequal retardation of orthogonal components is observed. Crystalline phases in a polymer are birefringent. Birefringence may also be induced in the unordered phase by applying an orientation field, be that mechanical or electromagnetic. Orientation birefringence is a result of physical

ordering of optically anisotropic elements along some preferential dimension. For uniaxially oriented samples there will be two refraction indexes $n_{\parallel}$ and $n_{\perp}$ corresponding to the polarization of light parallel and perpendicular to the sample symmetry axis. In a Cartesian coordinate system the birefringence for uniaxial symmetry will be given as

$$\Delta n = n_{\parallel} - n_{\perp} \tag{36}$$

Its individual components, along the axis, are given by

$$\Delta n_x = \Delta n_y \quad \text{and} \quad \Delta n_z = 0 \tag{37}$$

A macroscopic, quantitative way to analyze birefringence is through Jones (33–40) and Mueller (41) calculus and the Poincaré sphere (42). Those tools are widely used in the optical industry and references on them abound. Another active field of birefringence applications is the combination of the technique with polymer rheology, called flow–birefringence (43,44).

Birefringence of the Single-Chain and the Rotational Isomeric State (RIS) Model

The optical behavior of a single isolated chain is central in building optical molecular theories for polymers. Application of the RIS model to strain-birefringence is a well-known technique that has been around for the last 30 years. We focus on the mechanics of calculating the optical configuration parameter of a chain. The optical-configuration parameter is central to the structure–property optical relationships in polymers. This will help us to better understand the behavior of polymer networks later on. Flory and Nagai have shown how to evaluate the optical-configuration parameter in terms of the RIS model, thereby obtaining the following equation (7,45,46):

$$\Delta\alpha_s = \frac{3}{2}\sum \frac{\langle r^T \hat{a}_i r\rangle_0}{\langle r^2\rangle_0} \tag{38}$$

where $\boldsymbol{r}^{\mathrm{T}}$ is the transpose (ie, the row form) of the end-to-end vector $\boldsymbol{r}$ and $\hat{\boldsymbol{a}}_{\mathrm{i}}$ is the traceless tensor representing the anisotropy of the polarizability of bond i defined by

$$\hat{a}_i = a_i - \bar{a}_i \mathrm{E}_3 \tag{39}$$

where $\boldsymbol{a}_i$ is the polarizability tensor, $\bar{\boldsymbol{a}}_i$ is the mean polarizability, and $\boldsymbol{E}_3$ is the identity matrix of order 3. The angle brackets denote averages over the free unperturbed chain.

Application of the RIS model transforms the sum to a serial matrix multiplication scheme as follows:

$$\sum_{i=1}^{n} \langle r^{\mathrm{T}} \alpha_i r \rangle_0 = 2Z^{-1} J^* \left(\prod_{i=1}^{n} \mathrm{Q}_i \right) J \tag{40}$$

The configuration partition function is denoted by Z. The matrix $\boldsymbol{Q}_i$ is the generator matrix, for the quantity $\langle \boldsymbol{r}^{\mathrm{T}} \alpha_i \boldsymbol{r} \rangle_0$ is a rather large expression. The interested reader is encouraged to consult Flory's work on the subject (7).

Matrix $\boldsymbol{T}_i$ transforms a vector from its representation in local coordinate system $i + 1$ into its representation in local coordinate system i. The row and column operators $\boldsymbol{J}$ and $\boldsymbol{J}*$ in equation 40 are given by the first and last columns, respectively, of the matrix $\boldsymbol{Q}_i$.

Birefringence of Semicrystalline Polymers. For semicrystalline polymers the birefringence is the sum of the following terms:

$$\Delta n = v_{\mathrm{c}} \Delta n_{\mathrm{c}} + (1 - v_{\mathrm{c}}) \Delta n_{\mathrm{a}} + \Delta n_{\mathrm{f}} \tag{41}$$

v_{c} is the volume-fraction crystallinity determined from density measurements, Δn_{c} is the contribution to birefringence from the crystalline phase, Δn_{a} the contribution of the amorphous phase, and Δn_{f} the contribution from the boundaries between the two phases. An alternative expression, using the degree of crystallinity χ_{c}, as it is determined from X-ray diffraction, is

$$\Delta n = \chi_{\mathrm{c}} \Delta n_{\mathrm{c}} + (1 - \chi_{\mathrm{c}}) \Delta n_{\mathrm{a}} + \Delta n_{\mathrm{f}} \tag{42}$$

The value of Δn_{f} depends on the shape of the boundary between the phases as well as the difference in the average refractive indexes of the two phases. If that difference is small enough one could neglect its contribution. One way to determine its value is to swell the oriented polymer in solvents of varying refractive index. The solvent should swell the amorphous phase only and alter its refractive index. Thus the refractive index difference between the crystalline and the swollen amorphous phase may be altered (47).

Deformation birefringence arises as a result of an external deformation applied to the polymer sample. It could result from chain-packing changes or even bond-angle or bond-length deformations. Applying an external deformation is one way to make a normally optically isotropic sample optically anisotropic.

Deformation birefringence of a semicrystalline polymer is given by

$$\Delta n = v_{\mathrm{c}} \Delta n_{\mathrm{c}}^0 f_{\mathrm{c}} + (1 - v_{\mathrm{c}}) \Delta n_{\mathrm{a}}^0 f_{\mathrm{a}} + \Delta n_{\mathrm{f}} \tag{43}$$

$\Delta n_{\mathrm{c}}{}^0$ is the intrinsic birefringence of a crystalline phase, where the axis of the crystal is most nearly parallel to the chain axis.

The strain-induced birefringence in the amorphous region of a semicrystalline polymer disappears at the glass-transition temperature, as the chains assume isotropic configurations.

The deformation birefringence for graft or block copolymers is

$$\Delta n = v_{\mathrm{A}} \Delta n_{\mathrm{A}}^0 f_{\mathrm{A}} + v_{\mathrm{B}} \Delta n_{\mathrm{B}}^0 f_{\mathrm{B}} + \Delta n_{\mathrm{f}} \tag{44}$$

The volume fractions of the individual components A and B are denoted by ν_A and ν_B. Their respective orientation functions are denoted by f_A and f_B.

Birefringence of Polymer Networks. Elastomeric polymer networks deserve special mention because their cross-linked structure gives them unique physical properties, unlike those of other polymers. Covalently bonded networks are insoluble in any solvent, even in those that dissolve their precursor polymers. Optical techniques such as strain-induced birefringence allow the development of structure–property relationships as well as the study of their optical properties. Here we review some of the classical theories as well as some of the latest developments in the field.

The Theory of Kuhn and Grün. The theory of birefringence of deformed elastomeric networks was developed by Kuhn and Grün and by Treloar on the basis of the same procedure as that used for the development of the classical theories of rubber-like elasticity (48,49). The pioneering theory of Kuhn and Grün is based on the affine network model: that is, upon the application of a macroscopic deformation the components of the end-to-end vector for each network chain are assumed to change in the same ratio as that of the corresponding dimensions of the macroscopic sample.

Kuhn and Grün proceeded to calculate the length of the deformed chain vector and its angular coordinates in terms of the original length and orientation and the macroscopic elongation of the sample. Their assumptions allow the calculation of the contribution of a given chain to the total polarizability referred parallel to the principal axes of strain. Integration over all network chains allows the determination of the total polarizability for the network.

The chain model adopted by Kuhn and Grün is not based on the detailed chemical structure of the chain repeat units. Instead, the chain is composed of anisotropic statistical segments that become oriented as the network is deformed. Each segment is free to assume any orientation without any correlation to the orientation of the neighboring segments. The chain is considered to follow Gaussian statistics. Each link is assigned two polarizability components for light polarized parallel (symbol: $\alpha_\parallel$) and perpendicular (symbol: $\alpha_\perp$) to the segment axis. The difference in the refractive indexes is in general given by

$$n_i - n_j = \Delta n_0 \Psi_{i\,j} \quad \text{i, j} = 1, 2, \text{ or } 3 \tag{45}$$

where Ψ_{ij} is an orientation function depending on the angles θ and ϕ. The angle between the axis of the segment and the 3-direction is denoted by θ. The angle between the projection of the segment on the 1,2-plane and the 3-axis is denoted by ϕ. The Hermans orientation function is then given by

$$f = \frac{3\langle \cos^2\theta \rangle - 1}{2} \tag{46}$$

where $\langle \cos^2\theta \rangle$ is over the orientation of all segments.

On the basis of this model Kuhn and Grün develop the following expression for the stress–optical coefficient C for the case of uniaxial elongation:

$$C = \frac{\Delta n}{\tau}\frac{2\pi}{45kT}\frac{(\bar{n}^2+2)}{\bar{n}}\Delta\alpha_s \tag{47}$$

where Δn is the birefringence of the uniaxially stretched sample subjected to a stress τ (per unit area in the stretched state), k is Boltzmann constant, T is the absolute temperature, and $\bar{n}$ is the average refractive index of the network. The stress–optical coefficient is essentially the proportionality constant between the birefringence and the difference between the true stresses along the same axes. It is predicted to be independent of the degree of cross-linking and proportional to the anisotropy of the statistical segment. Experimentally it is found that this conclusion captures only part of the actual physics of the network. The anisotropy of the statistical segment $\Delta\alpha_s$ is given by

$$\Delta\alpha_s = (\beta_1 - \beta_2)_s \tag{48}$$

where β_1 and β_2 are the polarizabilities parallel and perpendicular, respectively, to the axis of the segment.

One crucial assumption here is that the local field on a segment is given by the Lorentz–Lorenz equation, which implies that the environment of a segment is optically isotropic (see also under Local Field). The treatment also involves the assumption of tensor additivity of polarizabilities of noninteracting segments (Valence Optical Scheme).

The anisotropy of a segment may be related to the anisotropy of the constituent bonds, again assuming polarizability additivity, by using

$$\Delta\alpha_s = \sum\left\{(\beta_1 - \beta_2)_i\left[3\cos^2\theta_i - 1\right]/2\right\} \tag{49}$$

where β_{1i} and β_{2i} are the polarizabilities of the ith bond along and perpendicular to the bond axis respectively, and θ_i is the angle between the bond axis and the segment axis.

According to the theory the orientation of the statistical links is predicted to be proportional to the stress difference, $\tau_i - \tau_j$

$$\Psi_{ij} = \frac{1}{5}\frac{\nu_c}{\nu_L}\left(\alpha_i^2 - \alpha_j^2\right) = \frac{\tau_i - \tau_j}{5\nu_L kT} \tag{50}$$

where ν_c is the number of network chains per unit volume and ν_L is the number of statistical segments per unit volume.

Birefringence of Phantom Networks. This theory is the basis for all theories that deal with birefringence of elastomeric polymer networks. It is based on the phantom network model of rubber-like elasticity. This model considers the network to consist of "phantom" (ie, non-interacting) chains. Consider the instantaneous end-to-end distance r for the ith network chain at equilibrium and at fixed strain. For a perfect (ie, no-defects) phantom network the birefringence induced

because of a deformation is defined as (50)

$$\Delta n = \left(\frac{2\pi}{27}\right)\left(\frac{\nu}{V}\right)\left[\frac{(n^2+2)^2}{n}\Gamma_2\right]\left[\Lambda_x^2 - \frac{\left(\Lambda_y^2+\Lambda_y^2\right)}{2}\right] \tag{51}$$

$\Lambda_t{}^2$s are the components of the molecular deformation tensor, which is given by

$$\Lambda_t^2 = \left[1-\frac{2}{\varphi}\right]\lambda_t^2 + \frac{2}{\varphi} \quad t = x, y, z \tag{52}$$

where $\lambda_t{}^2$ are the components of the macroscopic deformation tensor.

As we saw previously the quantity Γ_2 is defined as

$$\Gamma_2 = \frac{9}{10}\sum_i \frac{\langle r^{\mathrm{T}}\hat{a}_i r\rangle_0}{\langle r^2\rangle_0} \tag{53}$$

The summation is over all the units forming the chain. $\hat{\boldsymbol{a}}_i$ is the anisotropic part of the polarizability tensor for the unit with index i. $\boldsymbol{r}^{\mathrm{T}}$ is the transpose vector of the end-to-end vector $\boldsymbol{r}$, and the subscript 0 signifies that the average is over all configurations of the free chain. It is assumed that the polarizability tensor for the chain with a given configuration is obtained as the sum of the polarizability tensors of the groups forming the chain.

The connection between the polarizability tensor and the parameter Γ_2 given by

$$\left[\alpha_{xx} - \frac{(a_{yy}+a_{zz})}{2}\right]_r = \Gamma_2\frac{x^2 - [(y^2+z^2)/2]}{\langle r^2\rangle_0} \tag{54}$$

and $\langle r^2\rangle_0$ is the mean square end-to-end distance of a free chain. a_{xx}, a_{yy}, and a_{zz} are the x, y, and z components of the tensor $\hat{a}_{\mathrm{i}}$ for the chain averaged over all configurations. The subscript r on the left side of equation 54 signifies that the averaging is for the chain with fixed ends.

Combining equations 51 and 52, we obtain for the birefringence of a phantom network,

$$\Delta n_{\mathrm{ph}} = \left(\frac{\xi}{V}\right)kTC\left[\lambda_x^2 - \frac{\left(\lambda_y^2+\lambda_z^2\right)}{2}\right] \tag{55}$$

Focusing on the birefringence along the two principal axes x and y (typical for uniaxial deformation experiments), we obtain

$$\Delta n_{xy} = \left(\frac{2\pi\nu}{27V}\right)\left(1-\frac{2}{\varphi}\right)\left[\frac{(n^2+2)^2\Gamma_2}{n}\right]\left(\lambda_x^2 - \lambda_y^2\right) \tag{56}$$

For the development of equation 56 we have used the expression for the quantity C, the stress–optical coefficient, which is given by (compare to eq. 47)

$$C = \frac{2\pi}{27kT}\frac{(n^2+2)^2}{n}\Gamma_2 \tag{57}$$

and n is the mean refractive index of the network.

The Real Network. The total birefringence for a real network is the linear combination of the contributions resulting from the phantom network and the contributions arising from the constraints (51).

$$\Delta n_{xy} = \Delta n_{xy,\mathrm{ph}} + \Delta n_{xy,\mathrm{c}} \tag{58}$$

Flory has defined a reduced birefringence in a way similar to the reduced stress:

$$[\Delta n_{xy}] = [\Delta n_{xy,\mathrm{ph}}]\left[1 + \frac{\Delta n_{xy,\mathrm{c}}}{\Delta n_{xy,\mathrm{ph}}}\right] \tag{59}$$

where

$$[\Delta n] = \Delta n\left(\frac{V}{V_0}\right)^{1/3}(\alpha^2 - \alpha^{-1})^{-1} \tag{60}$$

The contribution from topological constraints is based on the various theories of rubberlike elasticity (52).

Birefringence Measurements. Birefringence measurements rely on placing a birefringent object between crossed polarizers (53,54). The basic concept is depicted in Figure 9.

Placing the sample at 45° to the plane of light polarization causes the object to stand out on a dark background. The two components of the polarized light A and B correspond to the principal planes of the sample. These two components travel the sample at different speeds, thus causing the emerging beams A1 and B1 to be out of phase. Each of those components reaches the analyzer, where they may be resolved into components parallel and perpendicular to the analyzer direction. One can see the interference results since they cause bright colors (typically called interference patterns). A photosensor may also be used to help quantify the results. Advances in technology of photoelastic modulators (PEM) and digitizing image software are helping in the design of new instruments that measure birefringence.

Nonlinear Optical Properties of Polymers

All the properties dealt with up until now involve linear interactions between light and polymer. Interaction of light with polymers in the nonlinear region involves second- and third-order effects as well as the phenomenon of photorefractivity (55,56). An optical nonlinear optical (NLO) polymer is one that, in response to an externally applied electric field, can either vary the speed of incoming light or alter its frequency. Varying the speed of light involves a change in the refractive

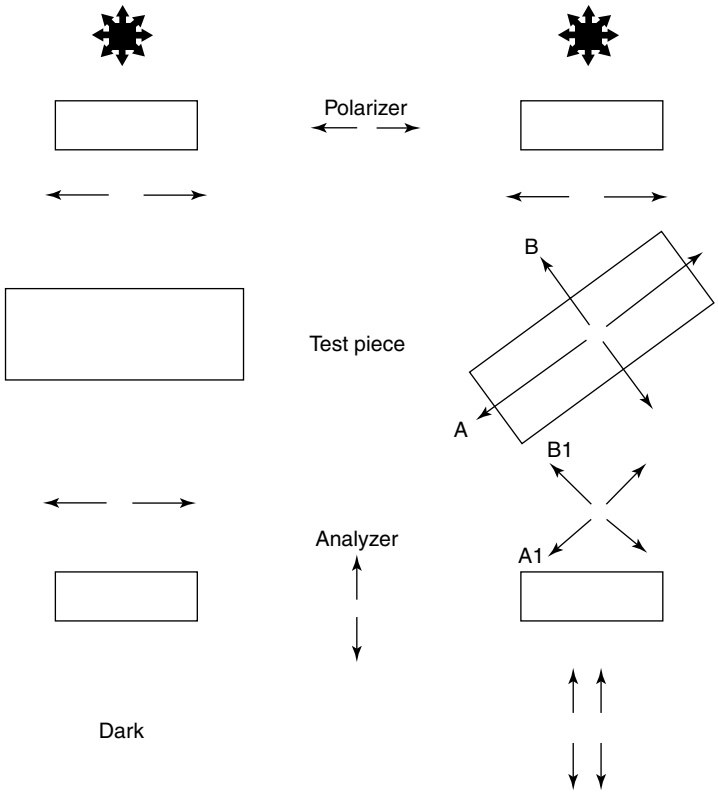

Fig. 9. Basis for birefringence setup (From Ref. 54).

index of the material. An optically nonlinear polymer has two components: the polymer itself and an optically nonlinear molecule (chromophore), which is either chemically attached to the polymer or dissolved in it.

The induced polarization P of a polymer is given by

$$P = \chi^{(1)}E + \chi^{(2)}EE + \chi^{(3)}EEE + \cdots \tag{61}$$

Linear optical phenomena involve the first-order susceptibility $\chi^{(1)}$, and in that case only the first term in the equation above is important. Higher order susceptibilitites are involved in nonlinear optical phenomena. Susceptibilities are a function of wavelength.

An equivalent equation but at the molecular level is the following:

$$\Delta\mu = \alpha E + \beta EE + \gamma EEE + \cdots \tag{62}$$

which gives the change in dipole moment μ when the field E is applied. Molecular polarizability is given by the term α. We saw equation 62 in a similar form earlier as equation 1. Higher order polarizabilities (hyperpolarizabilitites) are given by β (second-order), γ (third-order), etc.

In order for the polymer–chromophore system to be optically nonlinear the chromophores must be aligned so that on average they are all pointing in the same direction within the polymer. This alignment is achieved through a process called poling. The polymer is placed in a strong electric field and its temperature is raised above its T_g. Above this temperature the chromophores become mobile and can orient themselves in the external field. After orientation the polymer is cooled back down to room temperature and the orientational ordering is "frozen in."

Polymer NLOs are easily formed into thin films for guiding light in the optical equivalent of integrated circuits. These can potentially be operated at very high data rates, much higher than those possible for inorganic systems. However, inorganic systems don't need poling to achieve non-linearity. In polymer systems orientation degradation occurs as a result of thermal noise. Cross-linking has been considered as one method to stabilize the orientation of the chromophores. Another method is the use of high T_g polymer matrices.

The area of applications of nonlinear optics has not matured yet and the opportunities for creative work, both theoretical and experimental, abound. Here we have only covered some very introductory concepts.

BIBLIOGRAPHY

"Optical Properties" in *EPST* 1st ed., Vol. 9, pp. 525–623, by Robert Zand, University of Michigan; "Optical Properties" in *EPSE* 2nd ed., Vol. 10, pp. 493–540, by N. J. Mills, University of Birmingham, U.K.

1. G. H. Meeten, ed., *Optical Properties of Polymers*, Elsevier, London, 1986.
2. C. D. Han, *J. Rheol.* **25**, 139 (1981).
3. G. G. Fuller and L. G. Leal, *J. Polym. Sci., Polym. Phys. Ed.* **19**, 557 (1981).
4. V. Galiatsatos, K. B. Lipkowitz, and D. B. Boyd, eds., *Reviews in Computational Chemistry*, VCH Publishers, Inc., New York, N.Y., 1995, pp. 6, 149.
5. V. Galiatsatos, *Polym. Eng. Sci.* **33**, 285 (1993).
6. P. W. Atkins, *Quanta*, 2nd ed., Oxford University Press, New York, 1991.
7. P. J. Flory, *Statistical Mechanics of Chain Molecules*, Interscience Publishers, New York, N.Y., 1969.
8. C. P. Wong, ed., *Polymers for Electronic and Photonic Applications*, Academic Press, Inc., San Diego, Calif., 1993.
9. P. N. Butcher and D. Cotter, *The Elements of Nonlinear Optics*, Cambridge University Press, New York, N.Y., 1990.
10. A. C. Newell and J. V. Moloney, *Nonlinear Optics*, Addison-Wesley Publishing Co., Redwood City, Calif., 1992.
11. S. Sen, V. Galiatsatos, and G. D. Patterson, *J. Chem. Phys.* **103**, 892 (1995).
12. P. Lorrain and D. R. Corson, *Electromagnetic Fields and Waves*, W. H. Freeman, New York, N.Y., 1970.
13. W. Kauzmann, *Quantum Chemistry*, Academic Press, New York, N.Y., 1957.
14. L. Onsager, *J. Am. Chem. Soc.* **58**, 1486 (1936).
15. R. W. Christy, *Am. J. Phys.* **40**, 1403 (1972).
16. ISO 31/6 (1980), Quantities and units of light and electromagnetic radiations.
17. G. Ross and A. W. Birley, *Thermoplastics: Properties and Design*, John Wiley & Sons, Inc., London, 1974.

18. H. A. Lorentz, *Wied. Ann. Phys.* **9**, 641 (1880).
19. L. V. Lorenz, *Wied. Ann. Phys.* **11**, 70 (1880).
20. J. H. Gladstone, T. P. Dale, *Trans. R. Soc. (London) A* **418**, 887 (1858).
21. J. C. Seferis, in J. Brandrup and E. H. Immergut, eds., *Polymer Handbook*, 3rd ed., John Wiley & Sons, Inc., New York, 1989.
22. V. Galiatsatos, B. J. Sherman, S. Sen, and R. O. Neaffer, in J. E. Mark, ed., *Physical Properties of Polymers Handbook*, AIP Press, New York, N.Y., 1996.
23. J. Bicerano, *Prediction of Polymer Properties*, Marcel Dekker, Inc., New York, 1993.
24. P. Debye and A. M. Bueche, *J. Appl. Phys.* **20**, 518 (1949).
25. R. S. Stein, in R. W. Lenz and R. S. Stein, eds., *Structures and Properties of Polymeric Films*, Plenum Publishing Corp., New York, 1973.
26. H. E. Bennet, *Opt. Eng.* **17**, 480 (1978).
27. M. Kerker, *The Scattering of Light*, Academic Press, Inc., Orlando, Fla., 1969.
28. J. M. Elson, H. E. Bennett, and J. M. Bennett, *Applied Optics and Optical Engineering*, Academic Press, Inc., Orlando, Fla., 1979.
29. F. W. Billmeyer Jr. and Y. Chen, *Color Res Appl.* **10**, 219 (1985).
30. L. Mascia, *Thermoplastics: Materials Engineering*, 2nd ed., Elsevier Applied Science, New York, 1989.
31. H. Bender, *Kunststoffe* **59**, 501 (1969).
32. A. C. Webber, *J. Opt. Soc. Am.* **47**, 785 (1957).
33. R. Clark *Jones, J. Opt. Soc. Am.* **31**, 488 (1941).
34. Ref. 33, p. 493.
35. Ref. 33, p. 500.
36. R. Clark Jones, *J. Opt. Soc. Am.* **32**, 486 (1942).
37. R. Clark Jones, *J. Opt. Soc. Am.* **37**, 107 (1947).
38. R. Clark Jones, *J. Opt. Soc. Am.* **37**, 110 (1947).
39. R. Clark Jones, *J. Opt. Soc. Am.* **38**, 671 (1948).
40. R. Clark Jones, *J. Opt. Soc. Am.* **46**, 126 (1956).
41. H. Mueller, *J. Opt. Soc. Am.* **38**, 661 (1948).
42. H. Poincaré, in Georges Carré, ed., *Théorie Mathématique de la Lumière II*, Paris, 1892.
43. H. Janeschitz-Kriegl, *Polymer Melt Rheology and Flow Birefringence*, Springer Verlag, Berlin, 1983.
44. V. N. Tsvetkov, *Rigid-Chain Polymers; Hydrodynamic and Optical Properties in Solution* Consultants Bureau, New York, 1989.
45. K. Nagai, *J. Chem. Phys.* **40**, 2818 (1964).
46. K. Nagai, *J. Chem. Phys.* **47**, 2052 (1967).
47. A. N. Gent, *Macromolecules* **2**, 262 (1969).
48. W. Kuhn, *F. Grun Kolloid Z.* **101**, 248 (1942).
49. L. R. G. Treloar, *The Physics of Rubber Elasticity*, 3rd. ed., Clarendon Press, Oxford, 1975.
50. R. O. Neaffer, V. Galiatsatos, *Macromolecules* **26**, 4013 (1993).
51. J. E. Mark and B. Erman, *Rubberlike Elasticity, A Molecular Primer*, John Wiley & Sons, Inc., New York, 1989.
52. B. Erman and J. E. Mark, *Structures and Properties of Rubberlike Networks*, Oxford University Press, New York, N.Y., 1997.
53. E. Riande and E. Saiz, *Dipole Moments and Birefringence of Polymers*, Prentice Hall, Englewood Cliffs, N. J., 1992.
54. R. Brown, ed., *Handbook of Polymer Testing—Physical Methods*, Marcel Dekker, Inc., New York, 1999.

55. P. N. Prasad and D. J. Williams, *Introduction to Nonlinear Optical Effects in Molecules and Polymers*, John Wiley & Sons, Inc., New York, 1990.
56. S. R. Marder, J. E. Sohn, and G. D. Stucky, eds., *Materials for Nonlinear Optics* (ACS Symposium Series No. 455), American Chemical Society, Washington, D.C., 1991.

VASSILIOS GALIATSATOS
Equistar Chemicals, L.P.

ORGANOMETALLIC POLYMERS. See METAL CONTAINING POLYMERS.

ORIENTED FILMS. See FILMS, ORIENTATION.

PHENOLIC RESINS

Introduction

Phenolic resins are a large family of polymers and oligomers, composed of a wide variety of structures based on the reaction products of phenols with formaldehyde. Phenolic resins are employed in a wide range of applications, from commodity construction materials to high technology applications in electronics and aerospace. Generally, but not exclusively, thermosetting in nature, phenolic resins provide numerous challenges in the areas of synthesis, characterization, production, product development, and quality control.

As a family of resins originally developed in the early twentieth century, the nature and potential of phenolic resins have been explored thoroughly to produce an extensive body of technical literature (1–9). A symposium sponsored by the American Chemical Society commemorated 75 years of phenolic resin chemistry in 1983 (10), and in 1987 the Phenolic Molding Division of the Society of the Plastics Industry (SPI) sponsored a conference on phenolics in the twenty-first century (1). Exciting new developments continue as new systems are developed for carbon–carbon composites, aramid honeycombs, and new derivative chemistries such as cyanate esters and benzoxazines. New U.S. patents with phenolic resins in the claims are growing at about 150 patents per year.

Phenolic resins are prepared by the reaction of phenol or substituted phenol with an aldehyde, especially formaldehyde, in the presence of an acidic or basic catalyst. Their thermosetting character and the exotherm associated with the reaction presented technical barriers to commercialization. In 1900, the first U.S. patent was granted for a phenolic resin, using the resin in cast form as a substitute for hard rubber (11).

Work on the first commercially viable product was initiated by Baekeland in 1905. Using phenol and formaldehyde as starting materials, he established not only the differences between acid- and alkali-catalyzed products, but also the importance of excess phenol or formaldehyde made in producing intermediates.

Encyclopedia of Polymer Science and Technology. Copyright John Wiley & Sons, Inc. All rights reserved.

However, producing the resin was only part of the challenge. Baekeland also developed the technology to convert the reactive resins, which had a severe tendency to foam and cure to a brittle product, into useful molded articles by adding wood or mineral fibers and molding under heat and pressure. The final molded parts were tough, temperature resistant, and had a low void content (12). The first commercial phenolic resin plant was Bakelite GmbH, started in Germany in 1910; in the same year, the General Bakelite Co. was founded in the United States.

Early phenolic resins consisted of self-curing, resole-type products made with excess formaldehyde, and novolaks, which are thermoplastic in nature and require a hardener. The early products produced by General Bakelite were used in molded parts, insulating varnishes, laminated sheets, and industrial coatings. These areas still remain important applications, but have been joined by numerous others such as wood bonding, fiber bonding, and plywood adhesives. The number of producers in 2001 is approximately 15 in the United States and over 50 worldwide. Overall the number of producers is declining as the industry continues to undergo consolidation.

Monomers

Phenol. This is the monomer or raw material used in the largest quantity to make phenolic resins (Table 1). As a solid having a low melting point, phenol, C_6H_5OH, is usually stored, handled in liquid form at 50–60°C, and stored under nitrogen blanket to prevent the formation of pink quinones. Iron contamination results in a black color.

The most widely used process for the production of phenol is the cumene process developed and licensed in the United States by Honeywell (formerly AlliedSignal). Benzene is alkylated with propylene to produce cumene (isopropylbenzene), which is oxidized by air over a catalyst to produce cumene hydroperoxide (CHP). With acid catalysis, CHP undergoes controlled decomposition to produce phenol and acetone; α-methylstyrene and acetophenone are the by-products (13). Other commercial processes for making phenol include the Raschig process, using chlorobenzene as the starting material, and the toluene process, via a benzoic acid intermediate. In the United States, ~35–40% of the phenol produced is used for phenolic resins.

Table 1. Properties of Phenol

Property	Value
mol wt	94.1
mp, °C	40.9
bp, °C	181.8
Flash point, °C	79.0
Autoignition temperature, °C	605.0
Explosive limits, vol%	2–10
Vapor pressure at 20°C, Pa[a]	20

[a] To convert Pa to mm Hg, multiply by 7.5×10^{-3}.

Table 2. Substituted Phenols Used for Phenolic Resins

Substituted phenol	Resin application
Cresol (*o*-, *m*-, *p*-)	Coatings, epoxy hardeners
p-*t*-Butylphenol	Coatings, adhesives
p-Octylphenol	Carbonless paper, coatings
p-Nonylphenol	Carbonless paper, coatings
p-Phenylphenol	Carbonless paper
Bisphenol A	Low color molding compounds, coatings
Resorcinol	Adhesives
Cashew nutshell liquid	Friction particles

Substituted Phenols. Phenol itself is used in the largest volume, but substituted phenols are used for specialty resins (Table 2). Substituted phenols are typically alkylated phenols made from phenol and a corresponding α-olefin with acid catalysts (14). Acidic catalysis is frequently in the form of an ion-exchange resin (IER) and the reaction proceeds preferentially in the para position. For example, in the production of *t*-butylphenol using isobutylene, the product is >95% para-substituted. The incorporation of alkyl phenols such as cresol into the resin reduces reactivity, hardness, cross-link density, and color formation, but increases solubility in nonpolar solvents, flexibility, and compatibility with natural oils.

Formaldehyde. In one form or another, formaldehyde is used almost exclusively in the production of phenolic resins, regardless of the type of phenol (Table 3). It is frequently produced near the site of the resin plant by either of two common processes using methanol (qv) as the raw material. In the silver catalyst process, the reaction takes place at 600–650°C and produces water and hydrogen as by-products. The more common metal oxide process operates at 300–400°C. The gaseous formaldehyde is absorbed in water, and the final product is a formalin solution containing 36–50% formaldehyde. Of the various chemical forms of formaldehyde, the aqueous form is preferred for making phenolic resins, even though at least half of this form is water. The water serves to moderate the reaction and is readily removed in processing equipment (15).

Aqueous Formaldehyde. Water solutions of formaldehyde consist mainly of telomers of methylene glycol having <100 ppm of the formaldehyde as CH_2O (5). Alcohols form hemiformals with aqueous formaldehyde according to the following, where $n = 1, 2, 3$, etc.

$$ROH + HOCH_2OH \rightleftharpoons ROCH_2OH + H_2O$$

$$RO(CH_2O)_nH + HOCH_2OH \rightleftharpoons RO(CH_2O)_{n+1}H + H_2O$$

However, a second mole of alcohol or hemiformal does not add at the ordinary pH of such solutions. The equilibrium constant for hemiformal formation depends on the nature of the R group of the alcohol. Using NMR spectroscopy, a group of alcohols including phenol has been examined in solution with formaldehyde (16,17). The spectra indicated the degree of hemiformal formation in the

Table 3. Forms of Formaldehyde

		Resin preparation	
Type	Chemical formula	Advantages	Disadvantages
Gaseous	CH_2O		Unstable
Formalin			
36%	$HO(CH_2O)_nH$[a]	Easy handling, moderate, reactivity, stable at RT	High water content
50%	$HO(CH_2O)_nH$[b]	Increased capacity	Elevated temperature storage, formic acid formation
Paraformaldehyde	$HO(CH_2O)_nH$[c]	Increased capacity, water-free	Dangerously high reactivity, solids handling
Trioxane	$(CH_2O)_3$	Water-free	Catalyst requirements, high cost
Hexamethylenetetramine	$(CH_2)_6N_4$	Autocatalytic	Amine incorporation

[a] $n \approx 2$.
[b] $n \approx 3$.
[c] $n = 20$–100.

order of methanol > benzyl alcohol > phenol. Hemiformal formation provides the mechanism of stabilization; methanol is much more effective than phenol in this regard.

The large value for the hemiformal formation constant of methanol and its low molecular weight explains the high efficiency of methanol in stabilizing formalin solutions. Phenol, on the other hand, is inefficient, and phenol hemiformals are only formed by careful removal of water (18).

Other Aldehydes. The higher aldehydes react with phenol in much the same manner as formaldehyde, although at much lower rates. Examples include acetaldehyde, CH_3CHO; paraldehyde, $(CH_3CHO)_3$; glyoxal, OCH—CHO; and furfural. The reaction is usually kept on the acid side to minimize aldol formation. Furfural resins, however, are prepared with alkaline catalysts because furfural self-condenses under acid conditions to form a gel.

Hexamethylenetetramine. Hexa, a complex molecule with an adamantane-type structure, is prepared from formaldehyde and ammonia, and can be considered a latent source of formaldehyde. When used either as a catalyst or as a curative, hexa contributes formaldehyde-residue-type units as well as benzylamines. Hexa [100-97-0] is an infusible powder that decomposes and sublimes above 275°C. It is highly soluble in water, up to ca 45 wt% with a small negative temperature solubility coefficient. The aqueous solutions are mildly alkaline at pH 8–8.5 and reasonably stable to reverse hydrolysis.

Other Reactants. Other reactants are used in smaller amounts to provide phenolic resins that have specific properties, especially coatings applications. Aniline had been incorporated into both resoles and novolaks but this practice has been generally discontinued because of the toxicity of aromatic amines. Other materials include rosin (abietic acid), dicyclopentadiene, unsaturated oils such as tung oil and linseed oil, and polyvalent cations for cross-linking.

Polymerization

Phenolic resins are prepared with strong acid or alkaline catalysts. Occasionally, weak or Lewis acids, such as zinc acetate, are used for specialty resins.

Strong-Acid Catalysts, Novolak Resins. Phenolic novolaks are thermoplastic resins having a molecular weight of 500–5000 and a glass-transition temperature T_g of 45–70°C. The phenol–formaldehyde reactions are carried to their energetic completion, allowing isolation of the resin; formaldehyde–phenol molar ratios are between 0.5:1 and 0.8:1. Methylene glycol [463-57-0] (**1**) is converted to the corresponding hydrated carbonium ion **2**, which adds to the ortho and para positions of phenol with the elimination of water to form the corresponding ortho (**3**) and para (**4**) benzylic ions. The benzylic carbonium ions are in equilibrium with the corresponding benzylic alcohols, observed by NMR as transient species in the formation of novolak resins (16).

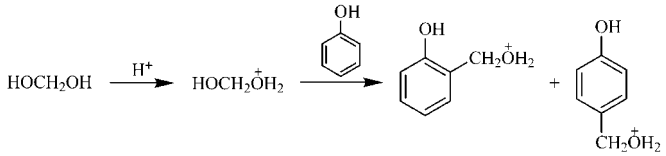

1 **2** **3** **4**

In the next step the hydrated benzylic carbonium ions **3** and **4** react with free ortho and para positions on phenols to form methylene-linked bisphenols, 2,2′(**5**), 2,4′(**6**), and 4,4′(**7**).

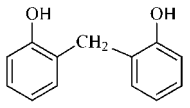

5

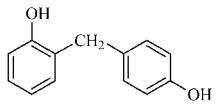

6

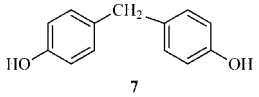

7

Table 4. Novolak Resin Properties

Property	Catalyst	
	Acid	Zn acetate[a]
Formaldehyde/phenol molar ratio	0.75	0.60
NMR analysis, %		
2,2′	6	45
2,4′	73	45
4,4′	21	10
GPC analysis		
Phenol, %	4	7
M_n	900	550
M_w	7300	1800
Water, %	1.1	1.9
T_g, °C	65	48
Gel time, s	75	25

[a]High ortho.

Continued reaction leads to the formation of novolak polymers having a molecular weight of up to 5000. Acid-catalyzed resins contain 50–75% 2,4′ linkages (**6**). The reaction rate is proportional to catalyst, formaldehyde, and phenol concentrations, and inversely proportional to the concentration of water. The rate of formation of the benzyl alcohol intermediate is 5–10 times lower than the rate to form the methylene-linked bisphenol (**3**). At typical molecular weights of 500–1000, novolak molecules are essentially linear because of the much lower reactivity of doubly-reacted phenolic units. In higher molecular weight polymers, the low concentration of end groups and unreacted phenol causes branching. Above 1000 molecular weight, branching has been observed by ^{13}C NMR; about 20% branching has been predicted in computer simulations (14,19,20). In the curing process, end groups are more reactive than the backbone groups. Thus a branched resin having a higher content of end groups than a corresponding linear equivalent may gel sooner and cure faster because of the higher resin functionality. The properties of an acid-catalyzed phenolic resin are shown in Table 4.

The typical acid catalysts used for novolak resins are sulfuric acid, sulfonic acid, oxalic acid, or occasionally phosphoric acid. Hydrochloric acid, although once widely used, has been abandoned because of the possible formation of toxic chloromethyl ether by-products. The type of acid catalyst used and reaction conditions affect resin structure and properties. For example, oxalic acid, used for resins chosen for electrical applications, decomposes into volatile by-products at elevated processing temperatures. Oxalic acid catalyzed novolaks contain small amounts (1–2% of the original formaldehyde) of benzodioxanes formed by the cyclization and dehydration of the benzyl alcohol hemiformal intermediates.

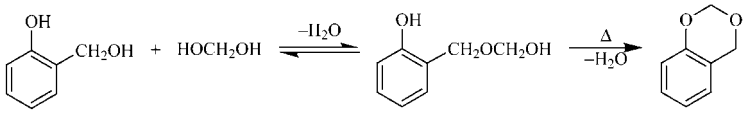

Benzodioxane is reasonably stable at neutral pH, but may decompose when the resin is cured, serving as a source of labile formaldehyde. Benzodioxanes are not found in sulfuric or sulfonic acid catalyzed resins, since the stronger acid readily catalyzes the second step in the reaction sequence.

Neutral Catalysts, High Ortho Novolaks. In the range of pH 4–7, formaldehyde substitution of the phenolic ring is possible, using divalent metal catalysts containing Zn, Mg, Mn, Cd, Co, Pb, Cu, and Ni; certain aluminum salts are also effective. Organic carboxylates are required as anions in order to obtain sufficient solubility of the catalyst in the reaction medium, as well as to provide a weak base. Acetates are most convenient and economical. Although lead acetate is highly effective because of its excellent solubility properties, it has been largely eliminated because of lead toxicity. Zinc and calcium salts are probably the most widely used catalysts (21).

Novolaks produced from these catalysts exhibit a high content of 2,2′-methylene units. The mechanism proposed for the ortho-directing effect involves chelation of the phenolic unit with the metal ion.

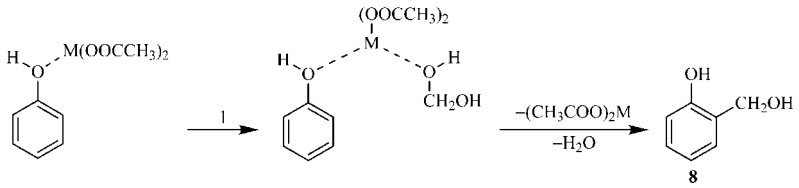

8

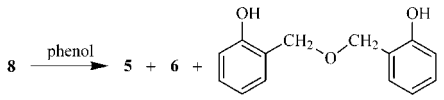

9

Zinc acetate catalyst produces essentially 100% *o*-methylol phenol (**8**) in the first step. The second step gives an approximately equal quantity of 2,2′- (5, 45%) and 2,4%-diphenylmethylene (6, 45%) bridges, indicating little chelate-directing influence. In addition, a small quantity (10%) of methylene ether units (**9**) (dibenzyl ether) is observed at moderate reaction temperature.

High ortho novolaks have faster cure rates with hexa. Typical properties of a zinc acetate catalyzed high ortho novolak are also shown in Table 4. The gel time with hexa is one-third of that with a strong acid catalyzed novolak.

Alkaline Catalysts, Resoles. Resole-type phenolic resins are produced with a molar ratio of formaldehyde to phenol of 1.2:1 to 3.0:1. For substituted phenols, the ratio is usually 1.2:1 to 1.8:1. Common alkaline catalysts are NaOH, $Ca(OH)_2$, and $Ba(OH)_2$. While novolak resins and strong acid catalysis result in a limited number of structures and properties, resoles cover a much wider spectrum. Resoles may be solids or liquids, water-soluble or -insoluble, alkaline or neutral, slowly curing or highly reactive. In the first step, the phenolate anion is formed by delocalization of the negative charge to the ortho and para positions. Alkaline catalysts are also effective in the polymerization–depolymerization of methylene

glycol. The mechanism of the formaldehyde addition to the phenolate is still not completely understood. The most likely mechanism involves the contribution of phenol hemiformals (**10**) (5).

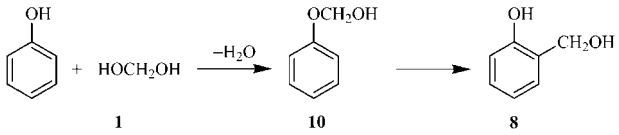

Rate studies show that base-catalyzed reactions are second order and depend on the phenolate and methylene glycol concentrations. The most likely path involves a nucleophilic displacement by the phenoxide on **1**, with the hydroxyl as the leaving group. In alkaline media, the methylolated quinone intermediate is readily converted to the phenoxide by hydrogen-ion abstraction (22).

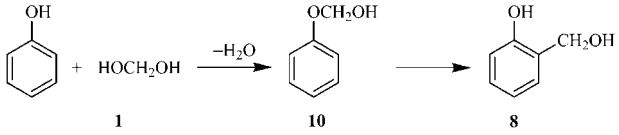

The ratio of ortho-to-para substitution depends on the nature of the cation and the pH. Para substitution is favored by K^+ and Na^+ ions and higher pH, whereas ortho substitution is favored at lower pH and by divalent cations, such as Ba^{2+}, Ca^{2+}, and Mg^{2+} (23).

Several extensive kinetic studies on the polymethylolation of phenol have been reported (22,24,25). For the reaction scheme shown in Fig. 1, seven different rate constants must be determined. Despite different solution concentration, temperatures, and methods of analysis, comparing reaction rates (26–28) from each study using an NaOH catalyst gave fairly close agreement that rate constants increase with methylol substitution. In fact, dimethylol-substituted phenols react with formaldehyde two to four times faster than phenol. As a result, unreacted phenol remains high in resole resins (5–15%) even though the formaldehyde/phenol ratio is as high as 3:1.

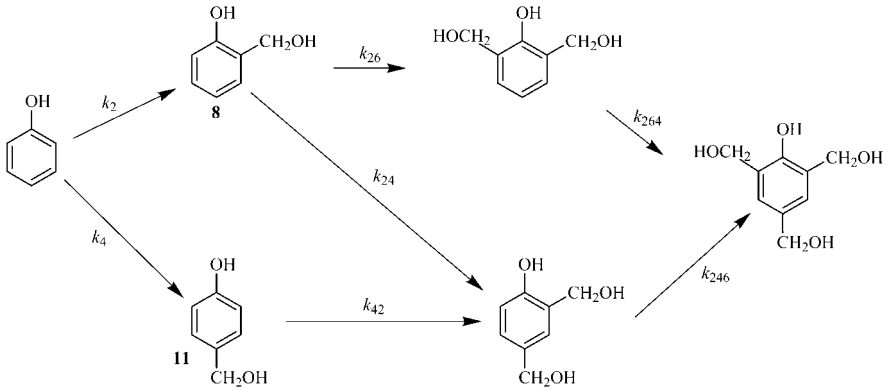

Fig. 1. Possible pathways and rate constants for the methylolation of phenol.

The rate studies show that k_{264} is by far the fastest reaction (by a factor of 4–6) than k_2 or k_4, with k_{24} the second fastest (by a factor of 2–4) (22,25).

Although monomeric methylolated phenols are used in certain applications, such as in fiber bonding, higher molecular weight resins are usually desirable. Molecular weight is increased by further condensation of the methylol groups, sometimes after the initial pH has been reduced. Dibenzyl ether (**9**) and diphenylmethylene formation are shown in the following. The formation of diphenylmethylene bridges is favored above 150°C and under strongly alkaline conditions; dibenzyl ether formation is favored at lower temperatures and near neutral pH.

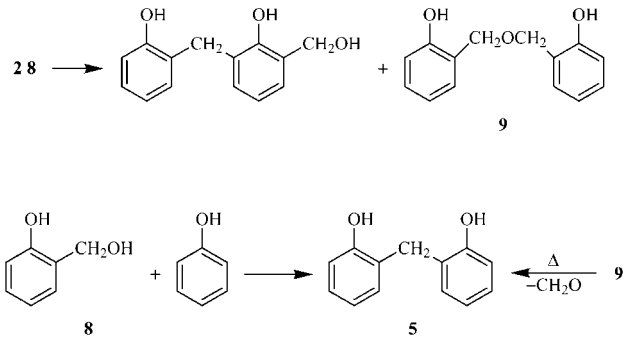

Special resoles are obtained with amine catalysts, which affect chemical and physical properties because amine is incorporated into the resin. For example, the reaction of phenol, formaldehyde, and dimethylamine is essentially quantitative (29).

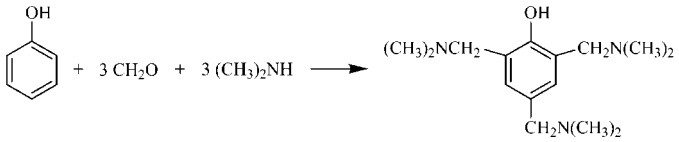

In practice, ammonia is most frequently used. With hexa, the initial reaction steps differ, but the final resole resins are identical, provided they contain the same number of nitrogen and CH_2 groups. Most nitrogen from ammonia or hexa is incorporated as dibenzylamine with primary, tertiary, and cyclic amine structures as minor products.

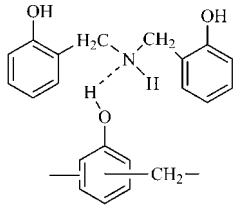

The physical properties of a resole resin prepared with hexa catalyst are shown in Table 5. Compared to the resin catalyzed with NaOH, this resin has higher molecular weight, less free phenol, lower water solubility, and a higher T_g.

Table 5. Properties of Resole Resins

	Catalyst	
Property	NaOH	Hexa
Concentration, pph	3	10
Formaldehyde/phenol ratio	2.0	1.5
Water solubility, %	100	Swells
GPC analysis		
Phenol, %	6	8
M_n	280	900
M_w	500	3000
T_g, °C	35	47
Gel time, s	65	110

Table 6. Methylene Group Distribution, % in Resoles

	Catalyst	
Methylene group	NaOH	Hexa[a]
2-CH_2OH	30	24
2-CH_2OCH_2OH	24	1
2-CH_2OR	2	4
4-CH_2OH	12	9
4-CH_2OCH_2OH	16	0
4-CH_2OR	2	4
2,2′-CH_2	0	0
2,4′-CH_2	7	12
4,4′-CH_2	7	10
2-CH_2N	0	27
4-CH_2N	0	7
Benzoxazine	0	2

[a] 6 pph.

This increase in T_g is higher than that expected if only phenol and formaldehyde were used, and is a result of the hydrogen-bonding interaction between the backbone amine units and the phenolic hydroxyls. Taking advantage of this effect, hexa and ammonia have been frequently used to produce solid, grindable, and water-insoluble resoles for molding compounds.

The methylene-isomer distributions of NaOH and hexa-catalyzed resoles are shown in Table 6. The distribution of amine structures is

$$\text{secondary} > \text{primary} \approx \text{tertiary}$$

and most benzylamines are ortho in the phenol ring from early steps in the reaction sequence.

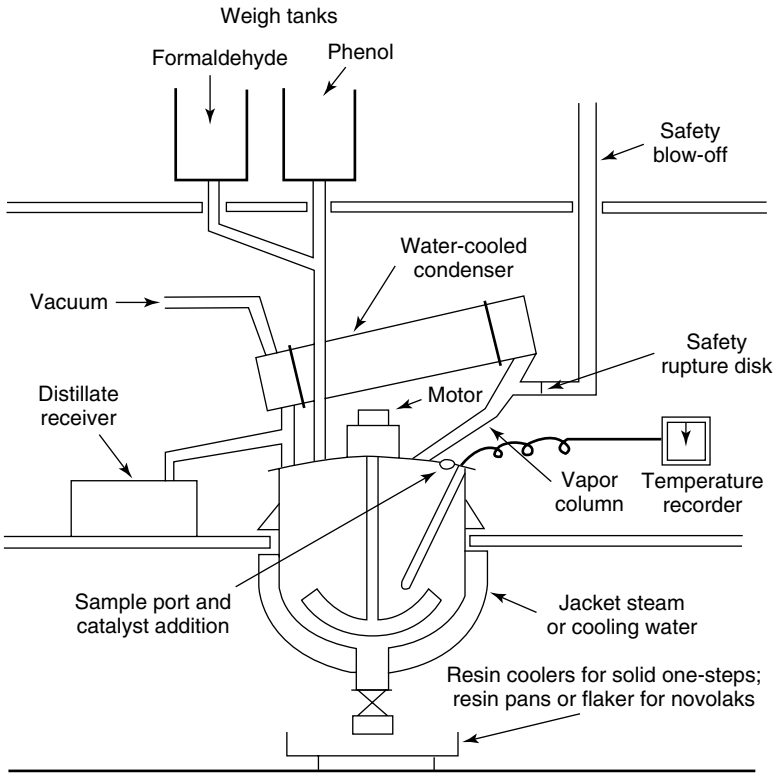

Fig. 2. Typical phenolic resin production unit.

Manufacture

The final state of a phenolic resin varies dramatically from thermoplastic to thermoset and from solid to liquid, and includes solutions and dispersions. With a bulk process, resole resins, in neat or concentrated form, must be produced in small batches ($\approx$ 2–10 m^3) in order to maintain control of the reaction and obtain a uniform product. On the other hand, if the product contains a large amount of water, such as liquid plywood adhesives, large reactors (20 m^3) can be used. Melt-stable products such as novolaks can be prepared in large batches (20–40 m^3) if the exotherms can be controlled. Some reactors are reportedly as large as 60 m^3 (Ref. 9, p. 83).

Batch processes for most phenolic resins employ the equipment shown in Fig. 2. Liquid reactants are metered into the stirred reaction vessel through weigh tanks, whereas solid reactants such as bisphenol A and $Ba(OH)_2$ present handling problems. Facilities are provided to carry out the reaction under vacuum or an inert gas.

Materials of Construction. Compatibility of the materials of construction and the process chemicals is extremely important. The reactors are usually made of stainless steel alloys. Copper is avoided because of the possible presence

of amines. Glass-lined reactors are occasionally used for nonalkaline resins. Because the use of HCl has been largely discontinued, material requirements are less stringent. The reactor contains a bottom discharge, which for solid heat-reactive resins must be large. Solid resole resins are discharged for rapid cooling in order to quench the thermosetting reactions. Resin coolers are made up of vertical plates with internally circulating water. The product can also be discharged to a large cooled surface. Discharges to belt and drum flakers are highly automated; however they can only be used for less-reactive resins.

Novolak resins can be stored molten in heated holding tanks under nitrogen. Because novolaks are used mainly in pulverized form with hexa and additives, a process that includes belt flaking and feeding directly into the blending and pulverizing system is preferred. Liquid and solution resole resins are cooled in the reactor by using jacket cooling and vacuum refluxing. Discharged products are filtered and pumped to refrigerated intermediate holding areas or packaged for shipping. The stability of liquid resole products varies greatly from product to product and depends on the storage temperature. The viscosity of a liquid resole resin increases but the water miscibility decreases as time and temperature increase. Generally, resoles, both liquids and solids, must be refrigerated.

Novolak Resins. In a conventional novolak process, molten phenol is placed into the reactor, followed by a precise amount of acid catalyst. The formaldehyde solution is added at a temperature near 90°C and a formaldehyde-to-phenol molar ratio of 0.75:1 to 0.85:1. For safety reasons, slow continuous or stepwise addition of formaldehyde is preferred over adding the entire charge at once. Reaction enthalpy has been reported to be above 80 kJ/mol (19 kcal/mol) (30,31). The heat of reaction is removed by refluxing the water combined with the formaldehyde or by using a small amount of a volatile solvent such as toluene. Toluene and xylene are used for azeotropic distillation. Following decantation, the toluene or xylene is returned to the reactor.

The reaction is completed after 6–8 h at 95°C; volatiles, water, and some free phenol are removed by vacuum stripping up to 140–170°C. For resins requiring phenol in only trace amounts, such as epoxy hardeners, steam distillation or steam stripping may be used. Both water and free phenol affect the cure and final resin properties, which are monitored in routine quality control testing by gas chromatography (GC). Oxalic acid (1–2 parts per 100 parts phenol) does not require neutralization because it decomposes to CO, CO_2, and water; furthermore, it produces milder reactions and low color. Sulfuric and sulfonic acids are strong catalysts and require neutralization with lime; 0.1 parts of sulfuric acid per 100 parts of phenol are used. A continuous process for novolak resin production has been described (32,33). An alternative process for making novolaks without acid catalysis has also been reported (34,35), which uses a peroxidase enzyme to polymerize phenols in an aqueous solution. The enzyme can be derived from soybeans or horseradish.

High Ortho Novolaks. The process for high ortho novolaks is similar to the one used for those catalyzed by strong acid. Zinc acetate is used at concentrations higher than the acids, typically 2% or more. The formaldehyde/phenol ratio is similar (0.75–0.85) but yields are 5–10% lower than those produced with strong acids, and reaction times are longer. Problems with gel particles and bulk gelation occur more frequently because small amounts of reactive dibenzyl ether

groups are present. Overall, the process is more expensive because of higher raw material costs, lower yields, and longer cycle times.

Another process employs a pH maintained at 4–7 and a catalyst that combines a divalent metal cation and an acid. Water is removed continuously by azeotropic distillation and xylene is recycled. The low water content increases the reaction rate. The dibenzyl ether groups are decomposed by the acid; the yield of 2,2′-methylene can be as high as 97% (36).

Resoles. Like the novolak processes, a typical resole process consists of reaction, dehydration, and finishing. Phenol and formaldehyde solution are added all at once to the reactor at a molar ratio of formaldehyde to phenol of 1.2–3.0:1. Catalyst is added and the pH is checked and adjusted if necessary. The catalyst concentration can range from 1 to 5% for NaOH, 3 to 6% for $Ba(OH)_2$, and 6 to 12% for hexa. A reaction temperature of 80–95°C is used with vacuum-reflux control. The high concentration of water and lower enthalpy compared to novolaks allows better exotherm control. In the reaction phase, the temperature is held at 80–90°C and vacuum-refluxing lasts from 1 to 3 h as determined in the development phase. Solid resins and certain liquid resins are dehydrated as quickly as possible to prevent overreacting or gelation. The endpoint is found by monitoring the gel time, which decreases as the reaction progresses. Automation includes on-line viscosity measurement, GC, and gel-permeation chromatography (GPC).

Phenolic Dispersions. These systems are predominantly resin-in-water systems in which the resin exists as discrete particles. Particle size ranges from 0.1 to 2 μm for stable dispersions and up to 100 μm for dispersions requiring constant agitation. Some of the earliest nonaqueous dispersions were developed for coatings applications. These systems consist of an oil-modified phenolic resin complexed with a metal oxide and a weak solvent.

In the postdispersion process, the solid phenolic resin is added to a mixture of water, cosolvent, and dispersant at high shear mixing, possibly with heating. The cosolvent, frequently an alcohol or glycol ether, and heat soften the resin and permit small particles to form. On cooling, the resin particles, stabilized by dispersant and perhaps thickener, harden and resist settling and agglomeration. Both resole and novolak resins have been made by this process (26).

The *in situ* process is simpler because it requires less material handling (37); however, this process has been used only for resole resins. When phenol is used, the reaction system is initially one-phase; alkylated phenols and bisphenol A present special problems. As the reaction with formaldehyde progresses at 80–100°C, the resin becomes water-insoluble and phase separation takes place. Catalysts such as hexa produce an early phase separation, whereas NaOH-based resins retain water solubility to a higher molecular weight. If the reaction medium contains a protective colloid at phase separation, a resin-in-water dispersion forms. Alternatively, the protective colloid can be added later in the reaction sequence, in which case the reaction mass may temporarily be a water-in-resin dispersion. The protective colloid serves to assist particle formation and stabilizes the final particles against coalescence. Some examples of protective colloids are poly(vinyl alcohol), gum arabic, and hydroxyethylcellulose.

For products intended to remain stable dispersions for an extended period, a particle size of 2 μm or less is desirable. A thickening agent is usually added after the reaction has been completed and the mixture is cooled in order to prevent

settling and agglomeration. Examples of thickeners are guar gum, xanthan gum, and hydroxyethylcellulose. The final products are generally between 40 and 50% solids, with a viscosity of 1500–5000 mPa·s (=cP).

Resole dispersions intended for isolation as discrete particles (27) can be used as flatting agents in coatings (28). Particles larger than 1000 μm are used in friction-element compositions. A-stage, thermosetting phenolic particles have been isolated from dispersion (27,38). With a hexa catalyst (6–12 parts) and a formaldehyde/phenol ratio of 1.5:1, the reaction is carried out at 50% solids for $\approx$90 min at 85°C. Poly(vinyl alcohol) and gum arabic are the preferred protective colloids. The particles (20–80 μm) are isolated from the mixture by filtration and, in the patent examples, by fluid-bed drying. These A-stage products (gel time at 150°C, 50–100 s) are suitable in applications where pulverized phenolic resins are being used, as well as in applications that take advantage of their spherical nature. One patent describes a sinter-resistant product for wood-bonding applications (39). In another patented process, both the production of particulate novolak resins and the aqueous dispersions of these resins are described (40).

Spray-Dried Resins. Spray drying produces resins in particulate form. Spray-drying a resole solution containing a blowing agent (41) produces phenolic microballoons. Spray drying also produces A-stage resins (42). The resins, prepared with a high NaOH content, are spray dried to give a final particle size of 40–60 μm. The particles are hygroscopic because of the high caustic content, but are sinter-resistant when kept dry. The principal application for this type of product is believed to be wood binding, especially for waferboard applications.

Cyanate Ester Resins. Cyanate ester resins, sometimes called triazines or cyanurates after the cured structure that they produce, are derived from phenols and phenolic resins. Specifically the starting phenols are reacted with cyanogen chloride, ClCN, and base to give the resins. In the cure step the cyanate groups trimerize to form triazine rings when heated in the range 180–250°C. Performance is generally intermediate between aromatic amine cured epoxides and toughened bismaleimides. Glass transition temperature T_g is about 250°C and the heat distortion temperature is about 250°C dry and 175°C wet. Electrical properties are excellent due to very low residual chlorine content. Principal applications are printed wiring boards and structural composites (Fig. 3) (43).

Benzoxazine Resins. Benzoxazine resins are prepared by the reaction of phenol, formaldehyde, and an amine. In one particular example a benzoxazine is prepared from bisphenol A, formaldehyde, and aniline to give 2,2′-bis(3-phenyl-4-dihydro-1,3,2-benzoxazine) propane. When heated to about 200°C the methylene bond to oxygen breaks and reforms onto the available ortho positions of adjacent moieties to give dibenzylamine structures. Resin formulations have been developed and formulated, in some cases with epoxy and phenolic resins to give ternary systems with T_g as high as 170°C (Fig. 4) (43–46).

Cure

A typical resin has an initial molecular weight of 150 to perhaps 1500. For systems of unsubstituted phenols, the final cross-link density is 150–300 amu

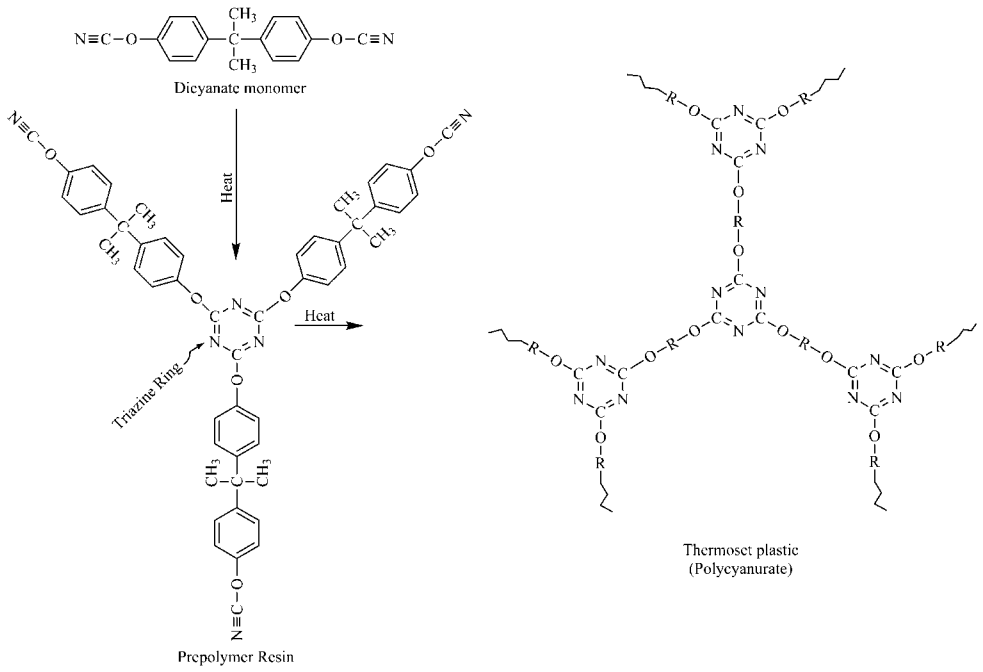

Fig. 3. Curing via cyclotrimerization; R = bisphenol unit. From Ref. 43.

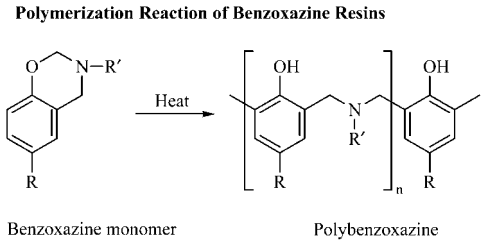

Fig. 4. Polymerization reaction of benzoxazine resins.

per cross-link. In other words, 25–75% of the ring-joining reactions occur during the cure phase.

Resoles. The advancement and cure of resole resins follow reaction steps similar to those used for resin preparation; the pH is 9 or higher and reaction temperature should not exceed 180°C. Methylol groups condense with other methylols to give dibenzyl ethers and react at the ortho and para positions on the phenol to give diphenylmethylenes. In addition, dibenzyl ethers eliminate formaldehyde to give diphenylmethanes.

In some resole applications, such as foam and foundry binders, a rapid cure of a liquid resin is obtained at room temperature (RT) with strong acid. The reactions proceed in the same manner as those of novolak resin formation. Methylol groups react at ortho and para phenolic hydrogen to give diphenylmethane units (47).

At pH 4–6, the cure is slower than it is at pH 8 and higher, and much slower than at pH 1–3. Reactions at pH 4–6 resemble those on the more alkaline side,

but with a substantial increase in side products. This is partly the result of the low rates of the main reactions and partly the result of stable intermediates at this pH range.

Some resoles contain latent acid catalysts, which on heating generate moderately strong acids. Examples include aryl phosphites such as diphenyl hydrogen phosphite and ammonium sulfate (48,49). The use of latent acid catalysis broadens the range of applications of phenolic resins to include areas such as liquid composite molding and pultrusion. Also resoles, which can contain so-called free formaldehyde, can be formulated with formaldehyde scavengers in form of amines such as melamine.

Novolaks. Novolak resins are typically cured with 5–15% hexa as the cross-linking agent. The reaction mechanism and reactive intermediates have been studied by classical chemical techniques (3,4) and the results showed that as much as 75% of nitrogen is chemically bound. More recent studies of resin cure (50–53) have made use of TGA, DTA, GC, IR, and NMR (16). They confirm that the cure begins with the formation of benzoxazine (**12**), progresses through a benzyl amine intermediate, and finally forms (hydroxy)diphenylmethanes (DPM).

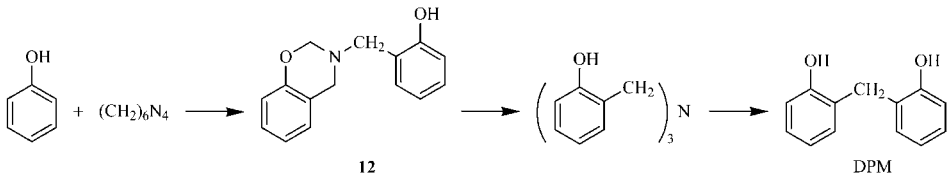

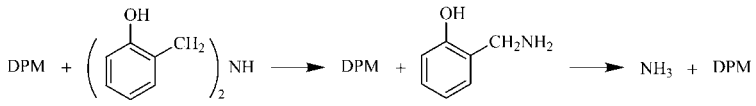

In the reaction of phenol and bisphenol F with hexa, NMR spectra show the transient appearance of benzoxazine intermediates; after 2 h at 103°C, all the benzoxazine decomposed to the diphenylmethylene and benzylamine intermediates (16).

The cure of novolaks with hexa has been studied with differential scanning calorimetry (DSC) and torsional braid analysis (TBA) (54); both a high ortho novolak and a conventional acid catalyzed system were included. The DSC showed an exothermic peak indicating a novolak–hexa reaction ≈20°C higher than the gelation peak observed in TBA. Activation energies were also calculated.

The resin rich in 2,2′-methylene exhibited the lowest activation energy, gel temperature, and DSC exotherm. The high concentration of the slightly acidic 2,2′-diphenylmethane end groups may account for the higher reactivity. These end groups should react with hexa to form benzoxazine intermediates first, which then decompose to react with vacant positions throughout the novolak molecule.

An isothermal method for studying the cure of phenolics employs dynamic mechanical analysis (DMA) (Table 7). The problems associated with programmed

Table 7. Isothermal DMA Results

Sample	Rate, min^{-1}		Activation energy, kJ/mol[a]
	At 150°C	At 185°C	
Hexa-catalyzed resole	0.22	1.00	71.1
Novolak			
6% hexa	0.07	0.09	8.8
12% hexa	0.12	0.19	18.8

[a]To convert kJ to kcal, divide by 4.184.

heating rates are avoided and mathematical treatment of the results is simplified. Although a more complex treatment is possible, a simple first-order dependence of modulus with time and an Arrhenius-type temperature dependence are sufficient. The rate studies of Table 7 indicate that doubling the amount of hexa doubles the rate at which the modulus approaches its long-term value. The novolak – 12% hexa cures substantially slower than the resole. In addition, they differ in temperature dependence of cure rates; the resole has an activation energy approximately four times greater than that of the novolak – 12% hexa (55).

Decomposition of Cured Resoles and Novolaks. Above 250°C, cured phenolic resins begin to decompose. For example, dibenzyl ethers such as **9** disproportionate to aldehydes (salicylaldehyde) and cresols (*o*-cresol). The aldehyde group is rapidly oxidized to the corresponding carboxylic acid. In an analogous reaction in hexa-cured novolaks, tribenzylamines decompose into cresols and azomethines, which cause yellowing.

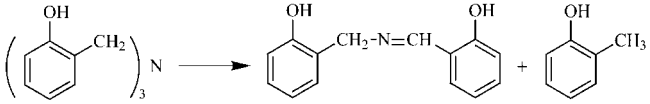

Substantial decomposition of phenolic resins begins above 300°C. In the presence of oxygen, the methylene bridging group is converted to a hydroperoxide, which, in turn, yields alcohols and ketones on decomposition.

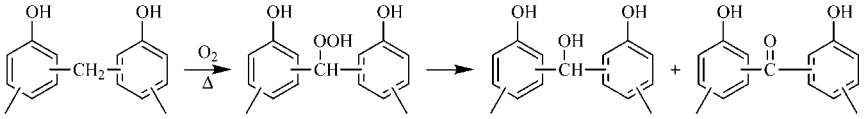

The ketone is especially susceptible to random chain scission. Decomposition continues up to ≈600°C; the by-products are mostly water, CO, CO_2, and phenols. The first stage of decomposition produces a porous structure having minimal shrinkage. The second stage begins near 600°C and is accompanied by shrinkage and substantial evolution of CO_2, H_2O, methane, and aromatics. The resulting polyaromatic chars represent ≈60% of the original resin when the atmosphere is inert, but this may be substantially less in the presence of air. The char ignites in air above 900°C.

The controlled decomposition of phenolic resins, in an inert atmosphere, is a method used to make carbon–carbon composites. In this case the resin is combined with other forms of carbon, such as carbon fibers, coke, and synthetic graphite, and cured under heat and pressure. Further heating to about 900°C converts the resin to a glassy form of carbon that can serve as a binder for the other carbon forms. The carbon yield from the phenolic resins can be in the range of 60–70% of the initial weight (see under CARBON–CARBON COMPOSITES).

Analysis and Characterization

The principal techniques for determining the microstructure of phenolic resins include mass spectroscopy (MS), proton and ^{13}C NMR spectroscopy, as well as GC, LC, and GPC. The softening and curing processes of phenolic resins are effectively studied by using thermal and mechanical techniques, such as TGA, DSC, and DMA. Infrared (IR) and electron spectroscopy are also employed. Recently matrix-assisted laser desorption-ionization mass spectrometry (MALDI-MS) has been used for the determination of molecular weight and end-group analysis (see MASS SPECTROMETRY). MALDI-MS is a soft ionization technique that has been applied to the determination of mass of large biomolecules and synthetics resins. The approach is useful for molecular weight determination and end-group analysis. Both novolaks and resoles have been studied and individual fragments with *m/z* up to about 2000 specifically identified. For resoles the technique is even able to resolve the various hemiformal structures that can occur. (Ref. 9, p. 92; 56–58).

Spectroscopy. Infrared spectroscopy (59) permits structural definition, eg, it resolves the 2,2′- from the 2,4′-methylene units in novolak resins. However, the broad bands and severely overlapping peaks present problems. For uncured resins, NMR rather than IR spectroscopy has become the technique of choice for microstructural information. However, Fourier transform infrared (FTIR) gives useful information on curing phenolics (60). Nevertheless, IR spectroscopy continues to be used as one of the detectors in the analysis of phenolics by GPC. (see VIBRATIONAL SPECTROSCOPY)

A great wealth of microstructural information is provided by Fourier transform ^{13}C NMR. Using the much greater chemical-shift range of this technique, detailed structural information is provided for both the aliphatic and the aromatic carbons (Table 8). Current techniques provide highly reliable quantitative data and relative peak areas (19,61–65) and make possible a quantitative measure of the numbers of branch points and end groups. Branching can cause early gelation in a novolak resin, and end groups usually have greater reactivity in the thermosetting reaction than do the backbone units. Another important advantage of ^{13}C NMR is the parametric predictability of the chemical-shift values. As a result, unknown peaks can be assigned to a hypothetical structure with reasonable certainty. At the same time, the process can be reversed and a computer can provide detailed structural analysis. ^{13}C NMR has been applied to cured phenolic resins (63). (see NUCLEAR MAGNETIC RESONANCE).

Chromatography. Gel-permeation chromatography (GPC) is an invaluable technique for determining the molecular size distribution of polymers. Phenolic resins, which have molecular weight components ranging from 100 to rarely

Table 8. Chemical Shifts of Methylene Carbons in Liquid Resoles

Structure[a]	Chemical shift,[b] ppm
Methylol C in **8**	61.3
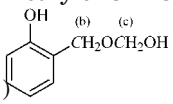	65.4 (b)
	88.0 (c)
Benzyl C in **9**	68.9
Methylol C in **11**	63.8
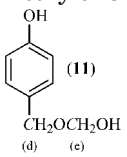 (**11**)	68.5 (d)
	88.0 (e)
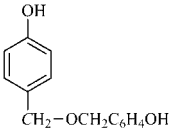	71.5
Methylene C in **5**	31.5
Methylene C in **6**	35.0
Methylene C in **7**	40.4

[a] Designated carbon is shown in italic or described.
[b] From tetramethylsilane in d_6-acetone solution.

more than 5000, require special column arrangements to optimize resolution. By using proper instrument calibration, it is possible to obtain number-average (M_n) and weight-average (M_w) molecular weight as well as quantitative information on free monomer and certain other low molecular weight species (66–68) (see CHROMATOGRAPHY, SEC).

Many resole resins exist as phenolate salts in solution. Because these ionic species are sparingly soluble in carrier solvents such as tetrahydrofuran, careful neutralization and filtration are required. Although GPC is an excellent technique for examining medium and high molecular weight fractions, GC and high performance LC are more effective for analyzing low molecular weight species.

Gas chromatography (GC) has been used extensively to analyze phenolic resins for unreacted phenol monomer as well as certain two- and three-ring constituents in both novolak and resole resins (69). It is also used in monitoring the production processes of the monomers, eg, when phenol is alkylated with isobutylene to produce butylphenol. Usually, the phenolic hydroxyl must be derivatized before analysis to provide a more volatile compound. The GC analysis of complex systems, such as resoles, provides distinct resolution of over 20 one- and two-ring compounds having various degrees of methylolation. In some cases, hemiformals may be detected if they have been properly capped (61).

The combined techniques of GC/MS are highly effective in identifying the composition of various GC peaks. The individual peaks enter a mass spectrometer

Table 9. Resole Components by HPLC and GC

Resin[a]	Components
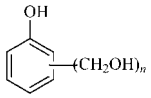	2; 4; 2,4; 2,6; 2,4,6
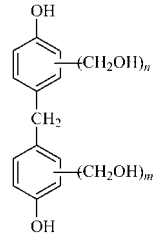	2; 2,6; 2,2′; 2,6,2′; 2,6,2′, 6′
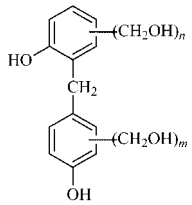	2′; 6; 4; 2′, 6′; 6,2′; 4,2′; 4,6; 4,2′, 6′; 4,6,2′; 4,6,2′,6′

[a]Also, **5**, **6**, and **7**, ie. 2,2′-, 2,4′-, and 4,4′-DPM.

in which they are analyzed for parent ion and fragmentation patterns, and the individual components of certain resoles are completely resolved.

High performance liquid chromatography (HPLC) is extremely effective in separating individual resin components up to a molecular weight of 1000 according to size and polarity. Dilute-solution conditions and low temperatures preserve the structure of unstable components. The resins are usually not derivatized. Gradient solvent elution gives excellent peak separation (69,70). In one study, resoles catalyzed by sodium and barium hydroxide were compared, and the components were separated up to and including methylolated four-ring compounds (61). Resole components resolved by GC and HPLC techniques are shown in Table 9. Like GC, HPLC is most effective when combined with other analytical tools, such as mass and UV spectroscopy. By using preparative-scale HPLC, individual peaks can be analyzed by proton and ^{13}C NMR spectroscopy.

Thermal Analysis. The main thermal analysis techniques applied to phenolic resins are TGA and DSC. In TGA, the sample weight is monitored microanalytically with time and temperature in air or nitrogen. When applied to resins and molding compounds, the scans indicate cure and decomposition temperatures accompanied by a measurable loss in weight. Resoles and novolaks lose from 5 to 20% of their weight on curing at 100–200°C. Weight loss provides information on shrinkage, void formation, and density change of composites.

Phenolic resins give a high char yield on combustion and TGA provides a measure of the expected yield. Typical values are between 40 and 65% in nitrogen. Decomposition begins at 350°C and continues up to 600°C. Autoignition temperature in air is above 900°C. Thermogravimetric analyses have played an important part in the development of carbon–carbon and carbon–graphite-fiber composites

containing phenolic resins. These composites are used in aircraft brake linings and carbon-pipe applications. In DSC and DTA, heat flow and sample temperature are compared to a reference material. Glass-transition temperature T_g is determined by DSC. The T_g of liquid resoles is below RT, that of friable novolaks is in the range of 50–75°C, and that of lightly cross-linked phenolics is between 150 and 225°C.

Cure kinetics of thermosets are usually determined by DSC (71,72). However, for phenolic resins, the information is limited to the early stages of the cure because of the volatiles associated with the process. For pressurized DSC cells, the upper limit on temperature is ≈170°C. Differential scanning calorimetry is also used to measure the kinetics and reaction enthalpies of liquid resins in coatings, adhesives, laminations, and foam. Software packages that interpret DSC scans in terms of the cure kinetics are supplied by instrument manufacturers.

Dynamic Mechanical Analysis. In DMA, a vibrating or oscillating sample is heated at a programmed rate or held isothermally at elevated temperature. The frequency and damping characteristics of the sample are monitored with time. A change such as gelation or passage through the T_g causes abrupt changes in the fundamental oscillation frequency of the sample and the damping ability of the specimen. The oscillation frequency can be related to the storage modulus of the sample, whereas the damping contains information related to the loss modulus.

Softening and cure are examined with the help of a torsional pendulum modified with a braid (73), which supports thermosets such as phenolics and epoxies that change from a liquid to a solid on curing. Another method uses vibrating arms coupled to a scrim-supported sample to measure storage and loss moduli as a function of time and temperature. An isothermal analytical method for phenolic resins provides data regarding rate constants and activation energies and allows prediction of cure characteristics under conditions of commercial use (55).

DSC and DMA scans of a novolac cure are shown in Figures 5a and 5b (74). The sample is a glassy solid initially and the DMA shows the distinctive T_g at 65°C followed by the appearance of a liquid state. From 110 to 125°C, the resin is a liquid and the chemical curing reactions begin, and it is followed by gelation at 140°C. Further reaction continues until 200°C, when a highly cross-linked, infusible solid is obtained. As the sample is cooled to RT, a slight increase in storage modulus is observed. The peak in the damping curve indicates the T_g of the cross-linked system at about 185°C.

Dynamic mechanical analysis provides a useful technique to study the cure kinetics and high temperature mechanical properties of phenolic resins. The volatile components of the resin do not affect the scan or limit the temperature range of the experiment. However, uncured samples must be supported by a braid, a scrim, or paper. This does not influence the kinetic results and can be corrected in the calculations of dynamic mechanical properties (qv). Recent DMA work on phenolic resins has been used to optimize the performance of structural adhesives for engineered wood products and determine the effect of moisture in wood product on cure behavior and bond strength (75–77).

Control Tests. Numerous chemical and physical tests are used in the manufacture of phenolic resins to ensure correct properties of the finished resins,

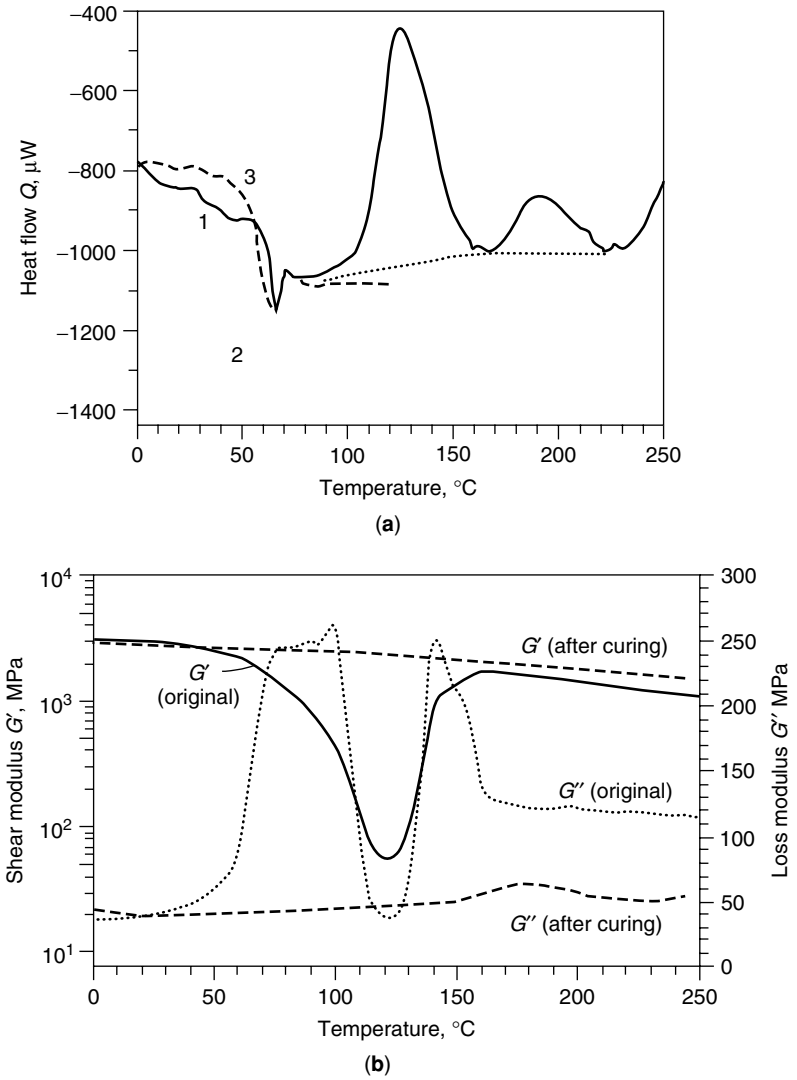

Fig. 5. DSC and DMA of novolac resin. (**a**) DSC Measurement of (1) original PF resin, (2) cured PF resin, and (3) novolac. (**b**) Torsion pendulum measurement of original and cured PF. To convert MPa to psi, multiply by 145. From Ref. 74.

including the following: refractive index is used to estimate the dehydration during manufacture and is proportional to the solids content; viscosity is used to determine molecular weight and solids content; nonvolatiles content is roughly proportional to polymer content; miscibility with water depends on the extent of reaction in resoles; specific gravity is measured for liquid resins and varnishes; melting point of novolaks and solid resoles affects application performance; gel times determine the reactivity of the resins; resin flow is a measure of melt viscosity and molecular weight; particle size affects performance and efficiency; and flash point and autoignition temperature provide flammability-characteristic measurements

required by government agencies regulating safety and shipping. ASTM D4706-93 (1998) describes the standard test method for qualitative determination of methylol group in phenolic resins.

Health, Safety, and Environmental Factors

The factors contributing to the health and safety of phenolic resin manufacturing and use are those primarily related to phenol (qv) and formaldehyde (qv). Unreacted phenol in a resin can range from ~5% for liquid resoles used in impregnation processes to well below 1% for novolaks intended for use as epoxy hardeners. Free formaldehyde can be <1% in liquid adhesives. Novolaks are usually free of formaldehyde. The toxicity of the resins is significantly lower than that of the phenol and formaldehyde starting materials. No detrimental toxicological effects have been reported for cured phenolic resins, which can be used in direct contact with food as in can coatings.

Uncured resins are skin sensitizers and contact should be avoided, as well as breathing the vapor, mist, or dust. Novolak-based pulverized products generally contain hexamethylenetetramine, which may cause rashes and dermatitis. Phenolic molding compounds and pulverized phenolic adhesives must be controlled as potentially explosive dusts. In addition, they contain irritating or toxic additives. ASTM test method D4639-86 (1996) describes the method for volative content in phenolic resins.

Phenol. Phenol is highly irritating to the skin, eyes, and mucous membranes in humans after acute inhalation or dermal exposures. Phenol is considered to be quite toxic to humans via oral exposure, with blood changes, liver and kidney damage, and cardiac toxicity reported. Chronic inhalation exposure to phenol in humans has been associated with gastrointestinal irritation, liver injury, and muscular effects. No data are available on the developmental or reproductive effects of phenol on humans. EPA has classified phenol as a Group D, not classifiable as to human carcinogenicity. The NIOSH threshold limit value (TLV) and Occupational Safety and Health Administration (OSHA) permissible exposure limit for phenol is 19 mg/m^3 (78). The health and environmental risks of phenol and alkylated phenols, such as cresols and butylphenols, have been reviewed (79).

Formaldehyde. Acute and chronic inhalation exposure to formaldehyde in humans can result in eye, nose, and throat irritation and respiratory symptoms. Reproductive effects have been reported in women workers exposed to formaldehyde. Limited human studies have reported an association between formaldehyde exposure and lung and nasopharyngeal cancer. The EPA has classified formaldehyde as a Group B1, probable human carcinogen of medium carcinogenic hazard. The OSHA has set its permissible exposure limit (PEL) at 4.5 mg/m^3 and the American Conference of Governmental and Industrial Hygienists have set the TLV at 1.5 mg/m^3 (80).

Wastewater. Phenol is a toxic pollutant to the waterways and has an acute toxicity (~5 mg/L) to fish. Chlorination of water gives chlorophenols, which impart objectionable odor and taste at 0.01 mg/L. Biochemical degradation is most frequently used to treat wastewater containing phenol. Primary activated sludge, along with secondary biological treatment, reduces phenol content to below

0.1 mg/L (81). ASTM D1783-01 describes the standard test methods for phenolic compounds in water.

Flammability. Phenolics have inherently low flammability and relatively low smoke generation. For this reason they are widely used in mass transit, tunnel building, and mining. Fiber-glass reinforced phenolic composites are capable of attaining the 1990 U.S. Federal Aviation Administration (FAA) regulations for total heat release and peak heat release for aircraft interior facings (1,82). They are also used as "fire restricting material" on cruise ships, high speed ferries, and commercial submarines. The self-ignition temperature is about 600°C and limiting oxygen index (LOI) is in the range 40–49%. (83).

Recycling. Thermosets are inherently more difficult to recycle than thermoplastics, and thermosetting phenolics are no exception. However, research in this area has been reported, and molded parts have been pulverized and incorporated at 10–15% in new molding powders. Both German and Japanese groups had instituted this type of practice in 1992 (84,85) (see RECYCLING).

A number of alternatives will have to be developed in order to effectively utilize cured phenolic material (86). One approach is the "thermoset recycling pyramid," a preferred order of execution that includes

(1) Tier 1: Reintroduction of the used material into the original material at relatively low levels (∼10%) in the raw material mix (this approach is used widely to recycle SMC and BMC thermoset polyesters)
(2) Tier 2: Reuse of the material in a lower performance thermoset product at relatively high levels (40–50%)
(3) Tier 3: Reuse of the product in alternative materials such as asphalt, roofing materials, concrete, and other construction products
(4) Tier 4: Pyrolysis of the material to generate raw material feed stocks and incineration for energy recovery. Phenolic molding compounds can yield a caloric value of 14,000–23,000 kJ/kg, depending on the type of filler.

Plenco and other companies have been working with the SPI's Phenolic Division to produce a "Recycling Blueprint" shown in Figure 6 below (87).

Biomass and Biochemical Processes. Phenolic resins have been produced from biomass and using biochemical processes in various ways. In Japan biomass from wood waste or waste from the food industry is treated with phenols and strong acid catalysis and heat to produce phenolic resins (88). Research at the National Renewable Energy Laboratory has shown that ablative fast pyrolysis can be used to convert a wide variety of biomass feedstocks into a liquid oil. The phenolic rich component can be extracted from this oil and used as a low cost replacement for synthetic phenol in phenolic resins (89). In another approach, soybean peroxidase enzymes have been used to prepare resins from phenolic moieties without the use of formaldehyde (90).

Economic Aspects. In 2000, worldwide consumption of phenolic resins exceeded 4×10^6 t; slightly less than half of the total volume was produced in the United States (91). The largest-volume application is in plywood adhesives, an area that accounts for ≈49% of U.S. consumption (Table 10). All wood bonding applications account for about two-third of phenolic resin use. During the early

Table 10. Long-Term Use of Phenolic Resins,[a] 10^3 t

End use market	1983	1993	2001
Bonding	295	454	645
Laminating	67	78	111
Plywood	580	687	976
Other	173	173	248
Total	*1115*	*1392*	*1980*

[a] Ref. 91.

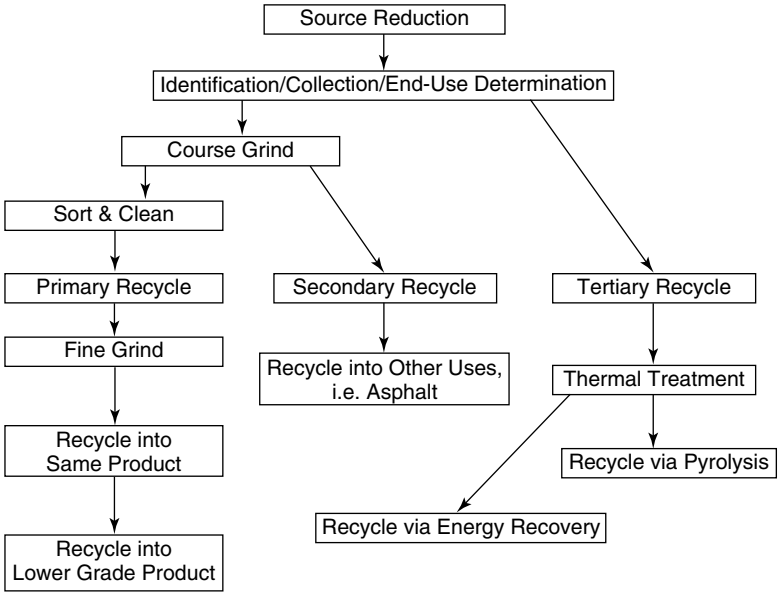

Fig. 6. SPI Blueprint for the reclamation of molded phenolics.

1980s, the volume of this application more than doubled as mills converted from urea–formaldehyde (UF) to phenol–formaldehyde adhesives because of the release of formaldehyde from UF products.

As a mature industry, U.S. production and application of phenolic resins have paralleled the growth in the GNP and the housing industry. The consumption of phenolic resins for coatings and molding powders has continued its decrease. The driving force behind coatings has been the need to reduce the volatile organics content (VOC) and the growth in alternative coatings such as waterborne, powder, and radiation-cured coatings. In the area of molding powders, numerous new engineering thermoplastics and alloys having superior properties have been introduced since the 1970s; however, phenolic molding powders continue to be used extensively in electrical, electronic, and machinery and underhood parts applications.

U.S. phenolic resin manufacturers include Ashland, Borden Chemical, Cytec Fiberite, Durez, FiberCote Industries, H.B. Fuller, P.D. George, Georgia-Pacific,

International Paper, Lockport Thermosets, Maruzen America, Plastics Engineering, Resinoid, Sumitomo America, TriQuest, and Vantico (92).

Prices of phenolic resins vary substantially depending on the application. In 2001, the price of general-purpose and semisolids was $1.50–1.80/kg, whereas epoxy-hardener grades can exceed $2.20/kg. Because raw materials of phenolic resins are derived from crude oil and natural gas, the prices of phenolic resins depend on the prices of these resources.

Applications

Coatings. For coatings applications, phenolic resins are grouped into four classes, depending on heat reactivity and the type of phenol. Substituted phenols are more compatible with oil and hydrocarbons, whereas heat-reactive resins require polar solvents. Depending on its nature, the resin can be used alone or as a modifying resin that acts as an adhesion promoter, a chemical cross-linker, or a hardening agent. In these cases the primary resin may be an alkyd, polyester, or epoxy (93).

Unsubstituted heat-reactive resins are designed for baked-on coatings and are usually not oil-soluble. They require strong solvents and although most are not water-miscible, their low molecular weight, high formaldehyde content promotes water miscibility. These resins are available as solids, viscous liquids, and solutions. Resins prepared with an alkaline catalyst and a slight excess of formaldehyde over phenol are heat-reactive, but not as much as resole resins designed for fiber bonding and paper impregnation. Recommended cure conditions are 30 min and 150°C.

Heat-reactive resins are more compatible than oil-soluble resins with other polar-coating resins, such as amino, epoxy, and poly(vinyl butyral). They are used in interior-can and drum linings, metal primers, and pipe coatings. The coatings have excellent resistance to solvents, acids, and salts. They can be used over a wide range of temperatures, up to 370°C for short periods of dry heat, and continuously at 150°C. Strong alkalies should be avoided.

The maximum recommended film thickness is 25 μm. At greater thicknesses, volatiles from the curing reaction, mainly water and some formaldehyde and phenol, can cause defects. These coatings have excellent electrical insulation properties, ie, up to 20 V/μm, because of low moisture absorption and low conductance. The coatings are hard with low flexibility, depending on curing conditions and film thickness.

Phenolic baking coatings can be used for metal, ceramic, and plastic surfaces. Applications include equipment for heating and air conditioning, chemical processing, petroleum refining, and water treatment. Some types are used in oil-well pipes and marine environments (94). Certain coatings can be used in food and beverage processing, subject to regulations.

The largest use of novolak resins in coatings is as a hardener for epoxy resins. The epoxy is frequently based on bisphenol A or epoxidized novolaks. Basic catalysts such as benzyldimethylamine are required for moderate baking conditions, such as 2 h at 180°C. The phenolic/epoxy ratio is adjusted to be stoichiometrically equivalent in order to give a highly cross-linked coating that has moderate

flexibility and excellent resistance to chemicals, heat, and moisture. Powder coating of pipes continues to be a growing application, especially when corrosion resistance is required. In solution form, the epoxy–phenolic systems are used as metal primers and in pipe coating.

Substituted heat-reactive resins are most widely used in contact-adhesive applications and, to a lesser extent, in coatings (95,96); *p*-butylphenol, cresol, and nonylphenol are most frequently used. The alkyl group increases compatibility with oleoresinous varnishes and alkyds. In combination with these resins, phenolics reduce water sensitivity. Common applications include baked-on and electrical insulation varnishes, and as modifiers for baking alkyds, rosin, and ester gum systems. Substituted heat-reactive resins are not used for air-dry coatings because of their soft, tacky nature in the uncured state; substituted nonheat-reactive phenolics are the modifying resin of choice in this case.

Substituted nonheat-reactive resins do not form a film and are not reactive by themselves, but are excellent modifier resins for oleoresinous varnishes and alkyds. Their high T_g and molecular weight provide initial hardness and reduce tack; oxygen-initiated cross-linking reactions take place with the unsaturated oils.

Early phenolic resin drying-oil varnishes were cooked in order to incorporate the phenolic resin into the formula. These resins have been replaced by cold-cut resins that reduce atmospheric emission by permitting direct incorporation of the phenolic after the oleoresinous varnish has been prepared. High solids systems enable coatings to meet the VOC standards required by regulatory agencies. Newer phenolic varnishes, developed in the 1980s, may contain as high as 80% nonvolatile solids (97).

Oleoresinous phenolic varnishes are excellent coatings that dry in 2–4 h and show exterior durability, corrosion resistance (especially when aluminum-modified), compatibility, solubility, and good package stability. Recoatability and intercoat adhesion are also excellent. The films are sensitive, however, to strong solvents and concentrated acids and alkalies. Unlike systems containing cross-linking phenolics, films containing these resins remain flexible.

Phenolics that are not heat-reactive may be incorporated into both air-dried and baked oleoresinous coatings. Applications vary widely and include clear and pigmented exterior varnishes, aluminum-maintenance paints, zinc-rich primers, can coatings, insulation varnishes, and concrete paints. As modifiers in a great variety of applications, they enhance the performance of oleoresinous and alkyd coatings.

Dispersions. In phenolic resin dispersions, the continuous phase is water or a nonpolar hydrocarbon solvent. The resin exists as droplets that have particle sizes of 1–20 μm and are dispersed in the continuous phase. Aqueous dispersions are prepared either *in situ* during the preparation of the resin itself or by high shear mixing (26,37).

Aqueous dispersions are alternatives to solutions of liquid and solid resins. They are usually offered in 50% solids and may contain thickeners and cosolvents as stabilizers and to promote coalescence. Both heat-reactive (resole) and nonheat-reactive (novolak) systems exist that contain unsubstituted or substituted phenols or mixtures. A related technology produces large, stable particles that can be isolated as discrete particles (52). In aqueous dispersion, the resin structure is

designed to produce a hydrophobic polymer, which is stabilized in water by an interfacial agent.

Aqueous dispersions are used in fiber bonding, paper coating, friction and abrasive applications, and laminates and wood bonding. Phenolic dispersions improve the strength of latex-contact adhesive applications. Epoxy-modified phenolic dispersions are prepared by dispersion of the phenolic epoxy resin. The systems are used for baked primer applications and bonding requirements. Minimum baking conditions are 20 min at 150°C (26).

Adhesives. Contact adhesives are blends of rubber, phenolic resin, and additives supplied in solvent or aqueous dispersion form; they are typically applied to both surfaces to be joined (98). Evaporation of the solvent leaves an adhesive film that forms a strong, peel-resistant bond. Contact adhesives are used widely in the furniture and construction industries and also in the automotive and footwear industries. The phenolic resins promote adhesion and act as tackifiers, usually at a concentration of 20–40%. In solvent-based contact adhesives, neoprene is preferred, whereas nitrile is used in specialty applications. The type and grade of phenolic resin selected control tack time, bond strength, and durability.

Neoprene–phenolic contact adhesives, known for their high green strength and peel values, contain a resole-type resin prepared from 4-*t*-butylphenol. The alkyl group increases compatibility and reduces cross-linking. This resin reacts or complexes with the metal oxide, eg, MgO, contained in the formulation, and increases the cohesive strength of the adhesive. In fact, the reactivity with MgO is frequently measured to determine the effectiveness of heat-reactive phenolics in the formulation.

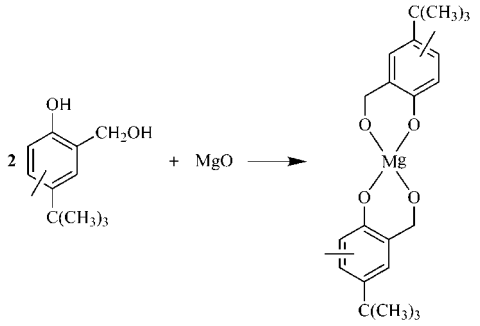

Phenolic resins substantially increase open time and peel strength of the formulation (98). For example, higher methylol and methylene ether contents of the resin improves peel strength and elevated temperature resistance. Adhesive properties are also influenced by the molecular weight distribution of the phenolic; low molecular weight reduces adhesion (99).

Waterborne contact adhesives contain an elastomer in latex form, usually an acrylic or neoprene-based latex, and a heat-reactive, cross-linkable phenolic resin in the form of an aqueous dispersion. The phenolic resin improves metal adhesion, green strength, and peel strength at elevated temperature. A typical formulation contains three parts latex and one part phenolic dispersion (dry weight bases). Although metal oxides may be added, reaction of the oxide with the phenolic resin does not occur readily.

Bonding properties of water-based contact adhesives are similar to those of solvent-based systems, but are free of flammability hazards. However, drying times are longer and the bond is sensitive to moisture.

Carbonless Copy Paper. In carbonless copy paper, also referred to as pressure-sensitive record sheet, an acid-sensitive dye precursor, such as crystal violet lactone or *N*-benzoylleucomethylene blue, is microencapsulated with a high boiling solvent or oil within a cross-linked gelatin (94,100,101) or in synthetic mononuclear microcapsules. Microcapsules that have a starch binder are coated onto the back of the top sheet. This is referred to as a coated-back (CB) sheet. The sheet intended to receive the image is treated on the front (coated-front (CF)) with an acid. When the top sheet is mechanically impacted, the dye capsules rupture and the dye solution is transferred to the receiving sheet where the acid developer activates the dye.

The original acid–clay developers have been largely replaced by phenolic compounds, such as para-substituted phenolic novolaks. The alkyl group on the phenolic ring is typically butyl, octyl, nonyl, or phenyl. The acidity is higher than that of a typical unsubstituted novolak because of the high concentration of 2,2′-methylene bridges.

Color intensity and permanence are improved by metal carboxylate salts, especially zinc salts (100), which catalyze the dye development and stabilize the dye in its colored form. The substituted novolak resin, along with extender and binder, can be applied to the receiving sheet as a solution or aqueous dispersion. Aqueous dispersions are probably the most widely used; they are manufactured by the resin supplier or the user from the base resin.

A typical coating composition for the CF component is shown in Table 11. It is dried in a high velocity air oven at 93°C.

Molding Compounds. Molding compounds were among the earliest applications for solid phenolic resins. Molding neat phenolic resin was almost impossible and the strength, especially on impact, was poor without reinforcement. Combining the resin, usually a novolak, with hexa, wood-flour, or asbestos reinforcement, as well as pigments and additives, gave a moldable thermoset. The molded articles exhibit high temperature, flame, and chemical resistance, retention of modulus at elevated temperature, and hardness. Systems that have good electrical properties can be formulated at low cost. Resins can be compounded with a choice of fillers for a variety of applications.

ASTM D4617-96 is the specification that covers phenolic molding compounds. The general-purpose compounds, having good strength and electrical properties,

Table 11. CF Coating Slurry Formulation

Constituent	Parts
Kaolin clay	64
$CaCO_3$	3
Colloidal silica	5.4
Hydroxyethyl starch	3
Styrene–butadiene latex	12
Novolak resin dispersion	12

Table 12. Applications for Molded Phenolic Parts[a]

Market	Key features	Examples
Appliances	Heat, moisture and chemical resistance; thermal and electrical insulation	Coffee pot handle and base; steam iron parts
Automotive and transportation	Heat, moisture, and hydrocarbon resistance; dimensional stability	Disc brake caliper pistons, transmission parts; water pump parts, torque converters; oil pump covers
Electrical	Heat and wear resistance; thermal and electrical insulation	Circuit breakers; motor control parts; commutators and alternators
Aerospace	Heat and chemical resistance; rigidity	Interior partitions; ablative surfaces
Packaging	Dimensional stability; chemical resistance	Closures

[a]Ref. 102.

are used in electrical appliances, automotive ignitions, and handles. Impact-resistant grades contain longer glass and textile fibers and rubber modifiers. Applications include pump housing and switches. Heat resistance is improved by incorporating mineral and glass fillers. Electrical-grade compounds contain mica and fiber glass fillers, and are used in specialty switches and cases. Graphite filler reduces the coefficient of thermal expansion. Although phenolic molding compounds compete with a wide variety of thermoset and thermoplastic compounds, they continue to be the preferred material in numerous applications, such as reinforced phenolic pistons in automotive disk brakes and transmission torque converters. Table 12 lists several applications for molded phenolic parts.

Phenolic molding materials are prepared by first blending the pulverized raw materials. In a compounding operation, the blend is passed through heated rolls to form a sheet as the resin melts. The compounded mixture remains on heated rolls until the desired flow and viscosity are reached. At this point, it is discharged as a thin sheet and allowed to cool. The product is then granulated and packaged. Alternatively, a Banbury-type mixer can be used for the initial mixing; the mix is then fed to a roll mill for finishing and sheeting. Compounding extruders are also used and through a continuous process provide a pelletized product.

Phenolic resins used in molding materials are predominantly novolaks with hexa as the curing agent. Oxalic acid catalyzed novolaks and high ortho resins are used. Resole resins may be used in place of hexa as the curing agent in certain electrical applications in which the NH_3 generated from the hexa can adversely affect metals such as copper and silver. Typically, the compound contains 40–50 wt% resin binder, 40–45% filler, and 5–10% pigment and additive. Fillers and reinforcements include wood flour, nutshell flour, cellulose fiber, mica (qv), wollastonite, mineral wool, mineral flour, glass fiber, organic fiber, carbon fiber, clay, and talc. Additives and pigments are magnesium oxide, graphite, molybdenum

sulfide, stearates, calcium carbonate, carbon black, nigrosine, lime, fluoropolymers, and salicylic acid.

Molding materials are fabricated into articles by compression, transfer, and injection molding processes. For compression molding, the powder is poured into the mold cavity or a preform heated prior to molding. Temperature ranges from 140 to 190°C and pressures from 13.8 to 55.5 MPa (2000–8000 psi). Because the material is more fluid in the mold, transfer molding is suitable for molding around inserts or for intricate shapes. In injection molding, cross-linking in the barrel and sprues must be avoided.

Abrasives. Abrasive materials are either bonded or coated. Bonded phenolic abrasives have superior strength and shock resistance compared to sintered ceramic compositions. The higher stability permits higher rotational speeds for resin-binder wheels; however, temperatures are lower than with ceramic wheels.

Synthetic aluminum oxide and silicon carbide are the principal inorganic abrasive materials. They are used in grit sizes from 44 or finer to 1680 μm (12–325 mesh). The coarser grit sizes are used for rough work when wheels are as large as 60 cm in diameter and 7.5-cm thick. These wheels are mounted in swinging-frame grinders and used to remove surface imperfections from stainless steel billets. Finer grit (250 μm (60 mesh)) may be used in 45-cm-dia cutoff wheels mounted in automatic grinders. These wheels can slice through a solid 2.5-cm steel bar in 4 s, leaving a clean, shiny cut surface.

In the usual method of manufacture, the grit is first wetted with a low viscosity liquid resole phenolic resin or furfural, using 1–3 wt% of the grit. A dry mixture of phenolic resin and fillers is added and the combination of wet grit and powder is tumbled until each grit particle is coated. The mix is temporarily dry and free-flowing. The powdered phenolic resin varies from 6 to 10% of the weight of the grit. The quantity and type of filler (alumina, cryolite, iron oxide, silicate) depend on the intended use of the wheel, whose grinding characteristics are affected by the filler. The free-flowing grit resin mix is placed into the mold and pressed at RT for 1–2 min at 13.8–34.5 MPa (2000–5000 psi). The dense form is removed and cured for 12–24 h; temperatures are increased gradually to 185°C for 8–12 h. Pressing temperatures may be increased for high density structures.

Heat resistance is an important characteristic of the bond. The strength of typical abrasive structures is tested at RT and at 300°C. Flexural strengths are between 24.1 and 34.4 MPa (3500–5000 psi). An unmodified phenolic resin bond loses about one-third of its RT strength at 298°C. Novolak phenolic resins are used almost exclusively because these offer heat resistance and because the moisture given off during the cure of resole resins results in undesirable porosity. Some novolaks modified with epoxy or poly(vinyl butyral) resin are used for softer grinding action.

Coated abrasives, such as sheets, disks, and drums, are used for polishing and finishing. Here, too, the abrasives, such as aluminum oxide and silicon carbide, have replaced the flint and garnet of common sandpaper. These industrial coated abrasives are manufactured from cloth or tough paper base. First, a coat of medium viscosity liquid resole resin is laid down on a continuous web of the backing. The web passes wet-side-down over a pan of grit, which adheres to it electrostatically and remains embedded in the resin layer. Altering the strength of the applied electrostatic field and the speed of the web can control the amount of grit deposited,

which varies from an open to a closed dense mass of abrasive. The uncured coated sheet is partially dried in a low temperature oven at 60°C, and a second, thinner coating of lower viscosity liquid resole resin is applied as a top to anchor the grit thoroughly. The coated web is taken off in rolls to be cured at 107–120°C for 3–4 h.

The resins should dry quickly and cure well at low temperatures. They usually are made at a high pH with high ratios of formaldehyde to phenol and held to fairly low molecular weight. Typical viscosities are 15,000 mPa·s (=cP) at 75% solids content for a first coat and 1000 mPa·s (=cP) at 50% solids for the top resin. For dense backing materials, such as fiber disks, a typical resin has a viscosity of 50,000 mPa·s (=cP) at 80% solids and is cured at 148°C. New opportunities are arising for coated abrasive belts in high pressure grinding. High strength backing has been developed and zirconia media are available for grinding.

Friction Materials. Phenolic friction materials are made from molding compounds developed to meet the extraordinary demands required by friction elements in the transportation industries. Friction materials are used for brake linings, clutch facings, and transmission bands. A moderately high coefficient of friction, which is temperature-independent, is needed. In addition, the material must be high in strength, low in wear and abrasion, and resistant to moisture and hydraulic fluids.

In the 1980s, significant changes occurred in automotive brake elements. Reformation of friction elements eliminated asbestos and increased employment of disk brakes. These developments required binder resins that have higher temperature performance without affecting the coefficient of friction and wear. Alternatives to asbestos include mineral, carbon, aramid, and metal fibers, especially iron. Semimetallic linings contain as much as 70% iron fibers. Other inorganic fillers include barites, alumina, lime, magnesia, and clay. Graphite and molybdenum disulfide are used to reduce scoring.

The resins can be a novolak–hexa or a resole–novolak blend. In some applications liquid resoles are used. Addition of alkylated phenol, oil, or cashew nutshell liquid (CNSL) reduces hardness and increases abrasion resistance. Modification by rubber improves the coefficient of friction and reduces brake fading.

Many friction material formulations contain 5–15 wt% of friction particles, the granulated cross-linked products of the reaction of CNSL, a phenol substituted at the meta position with a C_{15}, unsaturated side chain, and formaldehyde. Friction particles range in size from 50 to 500 μm. They reduce frictional wear and increase pedal softness (103).

Manufacture of friction elements includes the impregnation of fabrics and subsequent lamination, the wet-dough process, and the dry-mix process. Elements from the last two are prepared by compression-molding the formulation for up to an hour at 150–175°C. Thick brake elements require a carefully controlled heating-and-cooling cycle to minimize stresses created by expansion and contraction.

Foundry Resins. In the foundry industry, phenolic resins are used as the binder for sand in the manufacture of shell molds and cores. The two mating halves are joined by clamps or a bonding agent to form a shell mold into which the molten metal is poured for castings. The shell is formed by depositing a resin–sand mix on a hot metal pattern plate. After a certain period the pattern is inverted and

the excess resin–sand is removed. The sand particles are bonded by an oven cure, and the shell is ejected from the pattern plate.

Iron is the preferred metal for casting; steel and nonferrous metals are used in smaller amounts. Most castings are made in green sand molds, ie, uncured molds of sand, clay, and water. However, the use of shell moldings is growing, because such moldings permit reproducibility of castings with close dimensional accuracy. In addition, the simplicity of equipment procedures reduces costs.

The shell-molding process, introduced in the United States in 1948, is an important market for phenolic resins. In the original process, dry sand and powdered resin (6–8%) are blended. However, because of the high binder content and the difficulty in obtaining a uniform mix, precoating methods were developed.

Both cold- and warm-coating processes employ solutions of phenolic resins. The principal process used for foundry resins is the hot-coating process. It is the fastest, least expensive, and safest process, and it requires no volatile removal. The sand is heated to 135–170°C in a muller, and solid novolak resin in flake form is added, which melts quickly and coats the sand. A lubricant may be added at this point. After 1 min of mulling, the batch is cooled by adding water, which evaporates rapidly.

Hexa, which is not supplied with the resin, is usually added either with the water as a solution or just before or immediately after the water addition. By quenching the mix with water, the resin-coated sand is cooled to a point where there is no significant reaction with the curing agent. Any reaction between the resin and the hexa in the muller affects the bonding properties of the coated sand. As the batch cools and begins to break up, more lubricant may be added, which remains on the outside of the coated grains where it is most effective.

The total cycle time for most production batches is 2.5–3.5 min, considerably shorter than the cold- or warm-coating processes. Although a few available units have large capacity per batch, high production rates are possible because of the short cycle. While one batch is being mulled, sand for the next batch can be heated. The typical flake phenolic is an intermediate melting-point novolak containing 4% lubricant.

Laminates. Laminate manufacture involves the impregnation of a web with a liquid phenolic resin in a dip-coating operation. Solvent type, resin concentration, and viscosity determine the degree of fiber penetration. The treated web is dried in an oven and the resin cures, sometimes to the B-stage (semicured). Final resin content is between 30 and 70%. The dry sheet is cut and stacked, ready for lamination. In the curing step, multilayers of laminate are stacked or laid up in a press and cured at 150–175°C for several hours. The resins are generally low molecular weight resoles, which have been neutralized with the salt removed. Common carrier solvents for the varnish include acetone, alcohol, and toluene. Alkylated phenols such as cresols improve flexibility and moisture resistance in the fused products.

Industrial laminates are composed of two or more webs in sheet form that have been impregnated with a thermosetting resin and molded under heat and pressure. The web is usually made of cellulose paper, cotton fabric, glass cloth, glass mat, asbestos paper, wood veneer, and similar materials. Laminates are manufactured in sheets, rods, tubes, and special shapes, which can be machined by

common methods to produce parts for a wide range of uses. An important example is in printed-circuit applications, which require varnishes that impart electrical properties, punchability, machinability, and hot-solder and solvent resistance to the laminate. General-purpose laminates are used in gears, spacers, cams, ball-bearing retainer rings, and other structural parts requiring machinability as well as moisture, oil, and impact resistance.

A decorative laminate is composed of layers of resin-impregnated paper, which have been molded together under heat and pressure to form a solid homogeneous sheet. The component parts are composed of corestock impregnated with phenolic, print, and overlay. The corestock confers body and strength. The print sheet provides the design characteristic; it is impregnated with melamine resin, as is the overlay sheet that imparts abrasion protection to the print sheet. Approximately seven sheets of phenolic-impregnated corestock are covered with one print sheet, which, in turn, is covered with one overlay sheet. This combination is molded against polished steel plates to obtain the desired finish, usually satin or gloss.

The type of varnish used in the process depends on the kraft paper manufacturer and basis weight of the papers; the machine, temperature, and control (scraper bars, squeeze rolls) used; the method of cutting the paper to size; the laminate being produced (post-forming or regular); and the press-cure cycle.

Air and Oil Filters. Liquid resole resins are used to coat and penetrate the cellulose fibers of filters and separators in order to increase strength and stiffness and protect against attack by the environment. The type of phenolic to be used depends on both the final property requirements and the papermaking process.

Air and oil filters are made by a dry-web process in which the filter paper is dried over heated metal drums. The paper is saturated with the phenolic resin solution, either off- or on-line, and dried in an oven advancing the resin to the B-stage (semicured). The sheet, containing 20–30% resin, is rolled and shipped to the filter-unit manufacturer, where the sheet is convoluted and the filter assembled and cured to the C-stage (fully cured).

The resins used in air and oil filters are moderate-to-low molecular weight, catalyzed by caustic in one step; 10–20% alcohol is added; solids content is in the range of 50–60%. These resins are designed to penetrate the sheet thoroughly, yet not to affect the porosity of the paper. In the B-stage, the resin must have sufficient flexibility to permit pleating; the C-stage should have stiffness and resistance to hot oil.

Wood Bonding. This application requires large volumes of phenolic resins (5–25% by weight) for plywood, particle board, waferboard, and fiberboard. Initially, phenolic resins were used mainly for exterior applications, whereas UF was used for interiors. However, the concern over formaldehyde emission has caused the replacement of UF by phenol–formaldehyde adhesives.

Different phenolic resins are used for different types of wood; for example, plywood adhesives contain alkaline-catalyzed liquid resole resins. Extension with a filler reduces cost, minimizes absorption, and increases bond strength. These resins have an alkaline content of 5–7% and are low in free phenol and formaldehyde. Because many resins have a high water content and limited storage stability, they are frequently made at or near the mill producing the plywood product. The

plywood veneers are dried, coated with resin, stacked for pressing, and cured at 140–150°C.

Particle board and wood chip products have evolved from efforts to make profitable use of the large volumes of sawdust generated annually. These products are used for floor underlayment and decorative laminates. Most particle board had been produced with UF adhesive for interior use; resin demand per board is high due to the high surface area requiring bonding. Nevertheless, substantial quantities of phenol–formaldehyde-bonded particle board are produced for water-resistant and low formaldehyde applications.

The phenolic resins used for particle board are NaOH-catalyzed resoles of low viscosity and high water miscibility, similar to the liquid resole adhesives used in plywood manufacture. The higher resin and caustic content of the board frequently necessitates the addition of hydrophobic agents such as wax emulsions to increase the barrier properties of the board. The adhesive is applied to the particles in thin streams using high agitation to maximize material usage. Boards are cured in presses for 5–10 min at 150–185°C.

Waferboard, a more recent wood construction product, competes more with plywood than with particle board. Waferboard and strand board are bonded with solid, rather than liquid, phenolic resins. Both pulverized and spray-dried, rapid-curing resins have been successfully applied. Wafers are dried, dusted with powdered resin and wax, and formed on a caul plate. A top caul plate is added and the wafers are bonded in a press at ≈180°C for 5–10 min. Physical properties such as flexural strength, modulus, and internal bond are similar to those of a plywood of equivalent thickness.

Fiberboard or hardboard is made of low grade wood and wood waste. In the wet production process, a sheet is produced on a papermaking machine, such as a fourdrinier. A liquid resole is usually added to the beater section and precipitated onto the wood fibers by adjusting the pH. The moderately dry felt is further dried and cured in an off-line press.

Fiber Bonding. In fiber bonding, the resin is used as a binder in such products as thermal insulation batting, acoustic padding, and cushioning materials. All these materials consist of long fibers (glass or mineral fiber, cotton, polyester) laid down in a randomly oriented, loosely packed array to form a mat. They are bonded with resin to preserve the special insulating or cushioning quality of the mat.

In the dry-bonded process, fibers are reclaimed from woven textile scraps and powdered resin. Automotive acoustical padding (cotton and synthetic organic fiber) and thermal insulation batting (glass fiber) are made by this process. Inorganic and/or organic fibers are picked open to allow distribution of the phenolic resin among individual fibers. The fiber–resin mixture is formed into a blanket by cross-lapping a series of webs or by being blown into a chamber for deposition. The blanket is oven-cured to fuse the resin. Oven temperatures, dwell times, molding temperatures, and cycle times vary, depending on the type of fiber and curing characteristics of the resin.

The wet-bonded process uses virgin fiber spun from molten glass and liquid water miscible resin. High grade, thermal insulation batting is made by this process. The most common wet-bonded process for manufacturing glass or rock-wool, thermal insulation batting employs steam- or air-blowing. A stream of molten glass falls from the melting furnace into a rapidly spinning platinum

cylinder. Centrifugal force causes the glass to be extruded through many small holes in the cylinder wall. At the outside, the fibers are attenuated (drawn) by the action of a jet flame from burners located around the spinning cylinder. Spray nozzles located just below this unit apply liquid binder resin to the fibers, which are sucked onto a moving screen to form a continuous mat. The mat is conveyed through a forced hot-air curing oven similar to that used in the dry-bonded process. Curing is followed by cool-down, trimming, slitting, and roll-up.

Fiber bonding resins are marketed in the form of finely pulverized powders of novolak/hexa mixtures or resoles and water-miscible liquids. Resole resins are the standard for the fiber bonding industry. They have excellent curing properties and low content of solvent extractables after curing. Bond strength to the fiber is high and resin usage is low. Solid resole resins must be stored cool to reduce sintering and aging.

Novolak-based resins are primarily used for organic fibers. They require a cross-linking reagent, usually hexa, for cure. Bond strength is good, producing bonded mats that have high tensile strengths. The storage stability is also good, so that refrigeration is rarely required. A typical binder mix produced by the customer consists of phenolic resin, urea, hydrocarbon oil or wax emulsion, ammonium sulfate, and occasionally a silane adhesion promoter; it is diluted with water to 5–10% solids content. The urea acts as a scavenger for the free formaldehyde (5–8%) invariably present, both as an inexpensive extender and, owing to its high nitrogen content, as an antismoldering agent. The oil or wax emulsion acts as a fiber lubricant and dust suppressant, the ammonium sulfate as a cure accelerator, and the silane as an adhesion promoter. The large volume of water in the binder mix cools the newly spun fibers, thus preventing premature resin cure, ie, before the mat has been formed and compressed to the proper thickness. All water-miscible resins must be stored under refrigeration.

Composites. There has been substantial progress in improving the processability of phenolics in composite materials (104–106) to the point where a variety of materials are available for pultrusion, filament winding, and resin-transfer molding (see COMPOSITES, FABRICATION). More complicated composite systems are based on aramid and graphite fibers.

Epoxy resins are usually superior to phenolics because of better adhesion, lower shrinkage on curing, and a much lower volatile content. Nevertheless, there are many specific applications for phenolic resins, including formable laminates and sheet-molding compounds having low flammability and smoke generation. These systems are suitable for aircraft interiors. Another area is in binders for carbon–carbon composites for applications such as in ablative coatings of reentry vehicle and aircraft brakes. The high char yield and the strength and porosity of the char are important in these applications. Finally, phenolic novolaks are effective curing agents for epoxies, and epoxidized novolaks are being used in applications requiring high functionality and high cross-link density.

Glass-Reinforced Composites. These composites are prepared from SMC and by liquid injection molding, (LIM). Phenolic resins are usually not amenable to LIM because of the volatiles generated. However, a resin suitable to LIM has been prepared (107). The properties of the 60% glass-mat-reinforced product obtained from this resin were compared to conventional isophthalic polyester and vinyl ester sheet-molding compounds at equivalent glass loading; the mechanical

Table 13. Mechanical Properties of Composites[a]

Matrix resin	Flexural strength,[b] MPa[c]	Elongation, %	Notched Izod, J/m[d]	UL-94
Phenolic	228	2	1868	V0
Polyester	276	1.75	960	Burns
Vinyl ester	310	2	1227	Burns

[a]Glass content, 60%.
[b]For all three matrix resins, the flexural modulus is 12 GPa (1.7×10^6 psi).
[c]To convert MPa to psi, multiply by 145.
[d]To convert J/m to ft·lbf/in., divide by 53.38.

properties are shown in Table 13 (108,109). The phenolic resin systems have slightly lower strength values but measurably higher impact resistance. In addition, the phenolic glass composite has a UL-94 V0 rating, whereas the polyester SMC burns.

A patent describes the glass-reinforced pultrusion of phenolic resin composites (110). In pultrusion, bundles of continuous fiber are wetted with resin and shaped and cured through a series of heated dies. A sulfonic acid accelerates the cure rate, which must be high. The mechanical properties are reported to be equivalent to those obtained from conventional unsaturated polyesters, but the heat-distortion temperature and flammability resistance are superior. An acid-free phenolic pultrusion system has been announced that can produce large panels for buildings, ships, aircraft, and mine ducts. The system involves an injection-type die rather than conventional dip tanks, and up to 70% glass loadings can be attained (111).

Phenolic sheet-molding compound is seeing increased use in interior and exterior applications in mass transit. The trains in service on the English Channel tunnel have several panels made from phenolic SMC, which had to meet the strict European safety standards for fire and smoke generation.

Phenolic resin prepregs on glass fibers are prepared from alcohol solution and occasionally from aqueous solutions. The glass web is dipped in a tank containing resin solution; the resin content in the web is controlled by metering rolls. The wet web is dried in a horizontal or vertical oven arrangement and cured to B-stage of the resin. The dry web is cut, stacked, and stored under refrigeration until used in a laminate. Depending on the application, the prepreg can be rigid, similar to the epoxy-type prepregs used in laminated circuit boards, or soft and flexible, which provides the tack and drape required to conform to a shaped article. Autoclave molding is essential for shaped articles to reduce void formation by trapped air and volatiles. Examples of shaped articles include interior parts of commercial airplanes such as the composite duct assembly, based on wrapped phenolic – fiber glass, being used on the Boeing 737. Although not equal to epoxy-prepreg systems in strength, phenolic resins provide superior flammability resistance and lower smoke toxicity, because antimony and halogens are absent.

Carbon-Fiber Composites. Cured laminates of phenolic resins and carbon-fiber reinforcement provide superior flammability resistance and thermal resistance compared to unsaturated polyester and epoxy. Table 14 shows the dependence of flexural strength and modulus on phenolic–carbon-fiber composites at 30–40% phenolic resin (112). These composites also exhibit long-term elevated temperature stability up to 230°C.

Table 14. Strength Properties of Phenolic–Carbon-Fiber Composites

	Resin, %		
	Phenolic		
Property	40	35	Epoxy novolak, 27
Tensile strength, MPa[a]	115	63	64
Flexural strength, MPa[a]	183	126	110
Flexural modulus, GPa[b]	15.8	6.3	6.4

[a] To convert MPa to psi, multiply by 145.
[b] To convert GPa to psi, multiply by 145,000.

Carbon–Carbon Composites. Above 300°C, even such polymers as phenolics and polyimides are not stable as binders for carbon-fiber composites. Carbon–carbon composites are used at elevated temperatures and are prepared by impregnating the fibers with pitch or synthetic resin, followed by carbonization, further impregnation, and pyrolysis (112).

Carbon–carbon composites are used in high temperature service for aerospace and aircraft applications as well as for corrosion-resistant industrial pipes and housings. Applications include rocket nozzles and cases, aircraft brakes, and satellite structures. Carbonized phenolic resin with graphite fiber functioned effectively as the ablative shield in orbital reentry vehicles for many years (113).

Phenolic and furfuryl alcohol resins have a high char strength and penetrate into the fibrous core of the fiber structure. The phenolic resins are low viscosity resoles; some have been neutralized and have the salt removed. An autoclave is used to apply the vacuum and pressure required for good impregnation and sufficient heat for a resin cure, eg, at 180°C. The slow pyrolysis of the part follows; temperatures of 1000–1800°C are recommended for the best properties. On occasion, temperatures above 1800°C are used and constant weight is possible even up to 2760°C (114). A new process for carbon–carbon composite has been developed for engine components using phenolic resin and PAN fiber to produce near netshape parts (115,116).

Nanocomposites. Work conducted at Toyota in nylon-6 nanocomposites has generated several commercial products and stimulated substantial interest in a variety of polymer/nanoclay systems (see NANOCOMPOSITES, POLYMER-CLAY). The melt intercalation and curing behavior of phenolic resin were investigated using layered silicates such as montmorillonite and alkyl ammonium modified layered silicates. It was found by X-ray diffraction that the uncured phenolic was effectively intercalated. Depending on the surface treatment, the resulting interaction between organic modifier and phenolic resin played an important role in determining the stable nauostructure and the final morphology of the layered silicate composite (117,118).

The diagram below shows a representation of a polymer–clay, nanocomposite (qv).

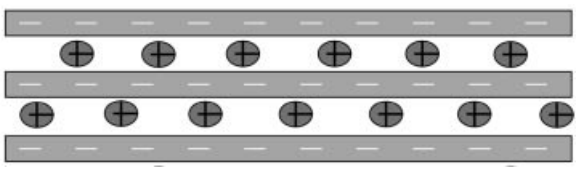

Liquid-Injection Molding. In LIM, monomers and oligomers are injected into a mold cavity where a rapid polymerization takes place to produce a thermoset article. Advantages of these processes are low cost, low pressure requirement, and flexibility in mold configuration. Conventional systems, such as isocyanate with polyol, release little or no volatiles. The generation of substantial volatiles in the mold is obviously undesirable and has represented a significant obstacle to the development of a phenolic-based LIM system. A phenolic LIM system based on an anhydrous high ortho liquid resole has been reported (119,120). Formaldehyde is present in the form of both methylol and phenolic hemiformals. A formaldehyde/phenol ratio of ≈1.5–1.0 is used at a pH of 4–7. Divalent salts catalyze the reaction at 80–90°C for 5–8 h and the water is removed by an azeotropic solvent. Uncatalyzed resoles have excellent storage stability.

An important aspect of this procedure is the use of latent acid catalysts, such as phenyl hydrogen maleate, phenyl trifluoracetate, and butadiene sulfone. These catalysts reduce the peak exotherm from over 200°C to 130–160°C. The resin catalyst mixture has a working life of up to several days at RT. The elevated temperature of molding these latent catalysts generates the corresponding acids, namely, maleic, trifluoracetic, and phenolsulfonic, which catalyze the resole reaction. Typically, a cycle time of 1–2 min is required for a mold temperature of ∼150°C.

The water liberated during the cure has no apparent effect on the composite properties. Glass-filled composites prepared in this manner retain mechanical properties at elevated temperatures as well as solvent and flammability resistance (108,109). Phenolic–graphite-fiber composites that exhibit superior mechanical properties have also been prepared by this process.

Foam. Phenolic resin foam is a cured system composed of open and closed cells with an overall density of 0.16–0.80 g/cm^3. Principal applications are in the areas of insulation and sponge-like floral foam. The resins are aqueous resoles catalyzed by NaOH at a formaldehyde/phenol ratio of ≈2:1. Free phenol and formaldehyde content should be low, although urea may be used as a formaldehyde scavenger.

The foam is prepared by adjusting the water content of the resin and adding a surfactant (eg, an ethoxylated nonionic), a blowing agent (eg, pentane, methylene chloride, or chlorofluorocarbon), and a catalyst (eg, toluenesulfonic acid or phenolsulfonic acid). The sulfonic acid catalyzes the reaction, while the exotherm causes the blowing agent, emulsified in the resin, to evaporate and expand the foam (121). The surfactant controls the cell size as well as the ratio of open-to-closed cell units. Both batch and continuous processes are employed. In the continuous process, the machinery is similar to that used for continuous polyurethane foam.

The properties of the foam depend mainly on density and the cell character. For insulation, a high content of closed cells, along with an encapsulated fluorocarbon blowing agent, is desired. The foam must have sufficient strength and be able to resist smoldering, ie, a glowing combustion characteristic of early foams. Smoldering is controlled by additives and foam structure. For floral foam, lower density and an open-cell structure having low toughness are desirable. Floral foam usually contains a wetting agent in the formulation to ensure the rapid uptake of water.

An all-phenolic sandwich structure for aircraft interior applications has been developed using syntactic and expandable semisyntactic phenolic foam. The

parts have outstanding fire behavior and are moldable to complex sandwich cores (117,118).

When smoldering is eliminated, phenolic foams exhibit excellent flammability resistance. Their LOI is 32–36%, and their smoke density is lower than that of polyisocyanurate foam of similar density. High thermal insulation K values have been obtained on foams of small cell size containing fluorocarbon blowing agents. Phenolic foams are used for building products and warehouse insulation and ASTM C1126-00 is the standard for faced or unfaced rigid cellular phenolic thermal insulation.

Honeycombs. Honeycomb structures usually involve resin-treated papers and fiberglass, sometimes with a core filler and surface skins bonded to the honeycomb. Uses can be in aircraft interior panels as well as more demanding parts. Phenolic resin-impregnated aramid paper honeycomb cores have been developed for fighter aircraft applications. These new honeycomb structures provide greater structural strength than other honecomb products currently available. One particular part application is the inlet cowl, which incorporates a complex structure, core machining, and core forming (122).

Spheres. Hollow spherical fillers have become extremely useful for the plastics industry and others. A wide range of hollow spherical fillers are currently available, including inorganic hollow spheres made from glass, carbon, fly ash, alumina, and zirconia; and organic hollow spheres made from epoxy, polystyrene, UF, and phenol–formaldehyde. Although phenol–formaldehyde hollow spheres are not the largest volume product, they serve in some important applications and show potential for future use.

In an early process by Sohio, a variety of compositions were produced by dissolving a film-forming polymer in a solvent (or water), adding a blowing agent, and spray drying the resulting solution under carefully controlled conditions. The use of spray drying to produce discrete, uniform hollow spheres, organic or inorganic, requires high skills in formulation, process control, and engineering. Some of the organic materials described include phenolic resins, poly(vinyl alcohol), polystyrene, methylcellulose, and protein. In the case of the phenolic resins, water-miscible resoles were used; water was the solvent and ammonium carbonate – ammonium nitrate or dinitrosopentamethylenetetramine was the blowing agent. Hollow phenolic spheres in sizes of 5–50-μm dia were obtained. The principal intended use was as a floating cap on petroleum naphtha and crude oil to retard evaporation.

Emerson & Cumming, Inc., eventually bought the rights to the Sohio process and produced a variety of microspheres. Union Carbide was licensed to produce the phenolic microspheres offered under the name Phenolic Microballoons (Table 15). When Phenolic Microballoons are introduced into a crude-oil storage tank, they form a fluid seal that rises and falls with the level of the oil. A continuous vapor-barrier seal is formed, which reduces evaporational losses up to 90%. Tests have been conducted under various mechanical and weather conditions and with crude oils of varying vapor pressure.

Phenolic Microballoons applications in plastics take advantage of low density, porosity, and surface-to-volume ratio to produce lightweight parts. Probably the most notable example is the syntactic foam.

Table 15. Physical Properties of Phenolic Microballoons

Property	Value
Average particle size, μm	43
Typical particle range, μm	20–120
Liquid displacement density, g/cm^3	0.15–0.35
Bulk density, g/cm^3	0.07–0.15
Toluene flotation, %	~90

While a conventional foam uses a blowing agent to form a cellular structure as the resin sets, syntactic foams are made by incorporating hollow spheres into liquid resins, especially epoxy resins in the case of Phenolic Microballoons, although urethanes and polyesters are also used. Having a continuous polymer phase and taking advantage of the high compressive strength of the spheres, syntactic foams can be made much stronger than conventional foams. In addition, they are being formed in place. As a result, syntactic foams have become widely used as a modeling, styling, and structural core material in automotive, marine, and aerospace applications.

A mixture of Phenolic Microballoons and resin binder has a putty-like consistency. It can be molded to shape, trowelled onto surfaces, or pressed into a core. Curing gives a high strength, low density (0.144 g/cm^3) foam free of voids and dense areas, and without a brittle skin. Syntactic foams are used in widely diverse applications, including boat flotation aids; structural parts in aircraft, submarines, and missiles; structural cores for wall panels; and ablative heat shields for reentry vehicles and rocket test engines.

Microballoons have been used for gap filling, where the spheres dampen sound or vibration in the structure. In the medical area, microballoons have been evaluated as a skin replacement for burn victims and phantom tissue for radiation studies. An important application is in nitroglycerin-based explosives, in which microballoons permit a controlled sequential detonation not possible with glass spheres.

In the 1990s, carbon microbeads have been produced by a proprietary process using phenolic resin. Potential applications are lubricants, adhesives, and conductive fillers for plastics, rubbers, and coatings (123).

Fibers. The principal type of phenolic fiber is the novoloid fiber (124). The term novoloid designates a content of at least 85 wt% of a cross-linked novolak. Novoloid fibers are sold under the trademark Kynol, and Nippon Kynol and American Kynol are exclusive licensees. Novoloid fibers are made by acid-catalyzed cross-linking of melt-spun novolak resin to form a fully cross-linked amorphous network. The fibers are infusible and insoluble, and possess physical and chemical properties that distinguish them from other fibers. Applications include a variety of flame- and chemical-resistant textiles and papers as well as composites, gaskets, and friction materials. In addition, they are precursors for carbon fibers.

The fibers are prepared from a high molecular weight novolak resin. Uncured fibers are prepared by melt-spinning the novolak. These fibers are then immersed in aqueous formaldehyde solution containing an acidic catalyst. As heat is applied, curing commences and the novolak resin is transformed into a cross-linked

network through the formation of methylene and dibenzyl ether linkages. The final cross-linked structure is free of molecular orientation, and the density of cross-linking is low. The fiber contains ≈5 wt% unreacted methylol groups, which can be utilized in the formation of novoloid-fiber composites, or be reduced by heating the cured fiber to 180°C.

Optimum mechanical properties of the fibers are developed provided the precursor novolak filaments are less than 25 μm in diameter to ensure sufficient diffusion of the formaldehyde and catalyst into the fiber. The individual fibers are generally elliptical in cross section. Diameters range from 14 to 33 μm (0.2–1.0 tex or 2–10 den) and fiber lengths are 1–100 mm. Tensile strength is 0.11–0.15 N/tex (1.3–1.8 g/den) and elongation is in the 30–60% range. Elastic recovery is as high as 96%.

The LOI of novoloid materials varies with the particular structure (fiber, felt, fabric) being evaluated; it is generally in the 30–34% range. By comparison, aramid fiber has a LOI of 28–31 and wool of 24. When exposed to flame, novoloid materials do not melt but gradually char until completely carbonized. The high strength of the phenolic char results in the fiber retaining its original fiber structure, and the char effectively absorbs heat from the materials. When novoloid products are exposed to flame, the products of combustion are principally H_2O, CO_2, and carbon char. Smoke emission is minimal, less than that of any other organic fiber.

Applications for novoloid fibers include a variety of flame-resistant protective clothing, safety accessories, and flame barriers for upholstered furniture. As an asbestos replacement, novoloid fibers have been used in gasketing, packings, brake linings, and clutch facings. In electrical applications, novoloid fibers and papers can be used as flameproof coatings and as wrapping tapes in wire and cable applications.

The novoloid molecular structure includes methylol groups, which are available for cross-linking with reactive sites in the matrix material. The ability of the fibers to react with matrix resins yields synergistic improvements in the properties of the composite. Novoloid fibers have been incorporated into composites with thermoplastic resins such as polypropylene, PVC, and polyamide polyesters. Thermosetting resins include phenolics, epoxies, and melamines. In certain elastomers, the methylol reactivity can be used to upgrade the high temperature performance, for example, in chlorinated polyethylene. A process has been announced that produces carbonized Kynol fiber having extremely high surface area (125).

BIBLIOGRAPHY

"Phenolic Resins" in *EPST* 1st ed., Vol. 10, pp. 1–73, by W.A. Keutgen, Union Carbide Corp.; "Phenolic Resins" in *EPSE* 2nd ed., Vol. 11, pp. 45–95, by Peter W. Kopf, Arthur D. Little, Inc.

1. *SPI Phenolic Molding Division Technical Conference*, Cincinnati, Ohio, June 1987.
2. S. R. Sandler and W. Caro, *Phenol Aldehyde Condensation*, Vol. **1**, Academic Press, Inc., New York, 1977, Chapt. "2".
3. R. W. Martin, *The Chemistry of Phenolic Resins*, John Wiley & Sons, Inc., New York, 1956.

4. N. J. L. Megson, *Phenolic Resin Chemistry*, Butterworth & Co. Ltd., Kent, U.K., 1958.
5. J. F. Walker, *Formaldehyde*, Van Nostrand Reinhold Co., Inc., New York, 1974.
6. T. S. Carswell, *Phenoplasts*, Interscience Publishers, New York, 1947.
7. A. Knop and W. Scheilb, *Chemistry and Applications of Phenolic Resins*, Springer, Berlin, 1979.
8. A. Knop and L. Pilato, *Phenolic Resins*, Springer, Berlin, 1985.
9. A. Gardziella, L. A. Pilato, and A. Knop, *Phenolic Resins*, Springer, Berlin, 1999.
10. *ACS Symposium on Phenolic Resins*, Washington, D.C., Aug. 1983.
11. U.S. Pat. 643,012 (Feb. 6, 1900), A. Smith.
12. U.S. Pats. 939,966 (Nov. 15, 1909) and 942,852 (Dec. 12, 1909), L. H. Baekeland.
13. J. B. Flemming, *Hydrocarbon Process.* **55**(1), 185 (Jan. 1976).
14. K. Kamide and Y. Miyakawa, *Makromol. Chem.* **179**, 359 (1978).
15. *Hydrocarbon Process.* 90 (Mar. 1976); 216 (Nov. 1965); 183 (Nov. 1969); 150 (Nov. 1975); 135 (Nov. 1973).
16. P. Kopf and E. Wagner, *J. Polym. Sci., Polym. Chem. Ed.* **11**, 939 (1973).
17. Y. Ihashi, K. Sawa, and S. Morita, *Kogyo Kagaku Zasshi* **68**, 1427 (1965).
18. U.S. Pats. 4,433,119 and 4,433,129 (Feb. 21, 1984), S. W. Chow and G. L. Brode (to Union Carbide Corp.).
19. S. Sojka, *Macromolecules* **12**, 767 (1979).
20. S. Ishida, Y. Tsutsumi, and K. Katsumasa, *J. Polym. Sci., Polym. Chem. Ed.* **19**, 1609 (1981).
21. H. Bender, *Ind. Eng. Chem.* **44**, 1619 (1952).
22. A. Zsavitsas and A. Beaulieu, *Am. Chem. Soc., Div. Org. Coat. Plast. Chem.* **27**, 100 (1967).
23. H. Peer, *Rec. Trat. Chim.* **78**, 851 (1959). *Rec. Trat. Chim.* **79**, 825 (1960).
24. J. H. Freemann and C. Lewis, *J. Am. Chem. Soc.* **76**, 2080 (1954).
25. K. Eapen and L. Yeddanapalli, *Makromol. Chem.* **4**, 119 (1968).
26. U.S. Pat. 4,124,554 (Nov. 7, 1978), J. Fry (to Union Carbide Corp.).
27. U.S. Pat. 4,206,095 (June 3, 1980), J. Wynsta and S. Schultz (to Union Carbide Corp.).
28. U.S. Pat. 3,943,080 (Mar. 9, 1976), M. Wismer (to PPG Industries).
29. H. A. Bruson and C. W. MacMullen, *J. Am. Chem. Soc.* **63**, 270 (1941).
30. T. T. Jones, *J. Soc. Chem. Ind. London* **65**, 264 (1946).
31. O. Vlk, *Plaste Kautsch.* **4**, 127 (1957).
32. U.S. Pat. 3,687,896 (Aug. 29, 1972), S. Vargia and U. Nistri (to Societa Italiana Resine SpA).
33. *Mod. Plast. Int. Ed.* **58**(4), 45 (Apr. 1981).
34. *Chem. Eng.* **99**(6), 19 (June 1992).
35. U.S. Pat. 4,900,671 (1990), A. Pokora (to Mead Corp.); U.S. Pat. 5,153,298 (1992), A. Pokora (to Mead Corp.).
36. U.S. Pat. 4,113,700 (1978), W. Aubertson (to Monsanto Co.).
37. U.S. Pat. 3,823,103 (July 9, 1979), J. Harding (to Union Carbide Corp.).
38. G. Brode, T. Jones, and S. Chow, *Chem. Technol.* **13**, 676 (1983).
39. U.S. Pat. 4,366,303 (Dec. 28, 1982), P. W. Kopf (to Union Carbide Corp.).
40. U.S. Pat. 4,788,236 (Nov. 29, 1988), P. W. Kopf (to Union Carbide Corp.).
41. U.S. Pat. 2,797,201 (July 11, 1957), F. Veatch (to Sohio).
42. U.S. Pat. 4,098,770 (July 4, 1978), A. Berchem, K. Sudan, and E. Gres (to Reichhold Chemicals, Ltd.).
43. R. B. Graver, in S. Lee, ed., *International Encyclopedia of Composites*, 2nd ed., SAMPE Publisher 2000, p. 176.
44. H. Ishida and Y. Rodriquez, *Polymer* **36**, 3151 (1995).
45. H. Ishida and Y. Rodriquez, *J. Appl. Polym. Sci.* **58**, 1751 (1995).

46. U.S. Pat. 6,207,786 (Mar. 27, 2001), H. Ishida and S. Rimdusit (to Edison Polymer Innovation Corp.).
47. K. Hultzsch, *Kunstostoffe* **37**, 205 (1947).
48. U.S. Pat. 5,334,675 (Aug. 2, 1994), A. Gerber (to Borden, Inc.).
49. U.S. Pat. 5,952,440 (Sept. 14, 1999), W. Walisser and C. Johnson (to Borden, Chemical).
50. E. Orrell and R. Burns, *Plast. Polym.* **68**, 469 (Oct. 1968).
51. V. Pshenitsyna and M. Kotrelev, *Polym. Sci. U.S.S.R.* **11**, 829 (1969).
52. V. Kurachenkov and L. Igonin, *J. Polym. Sci., Part A: Polym. Chem.* **1**, 2283 (1971).
53. M. Yamao, N. Yoshimi, and S. Tanaka, *Kogyo Kagaku Zasshi* **74**, 1938 (1971).
54. J. Gillham, *Polym. Prepr. (Am. Chem. Soc., Div. Polym. Chem.)* **22**(2), 131 (1981).
55. R. Young, P. Kopf, and O. Salgado, *Tappi* **64**(4), 127 (1981).
56. M. Karas and F. Hillenkamp, *Anal. Chem.* **60**, 2299 (1988).
57. H. Paschy, K. Rode, R. Ghahary, and D. Braun, *Die Angew. Makromol. Chemie* **241**, 95 (1996).
58. H. Mandal and A. Hay, *Polymer* **38**, 6267 (1997).
59. H. L. Bender, *Mod. Plast.* **30**, 136 (1953).
60. D. Boeschel, M. Fedtke , and W. Geyet, *Polymer* **38**, 1291 (1997).
61. B. Mechin, D. Hanton, V. Le Geoff, and J. Tanneur, *Eur. Polym. J.* **20**, 333 (1984).
62. J. Shaefer, *J. Am. Chem. Soc.* **98**, 1031 (1976).
63. R. Bryson, G. Hatfield, T. Early, A. Palmer, and G. Maciel, *Macromolecules* **16**, 1669 (1983).
64. C. Fyfe, *Macromolecules* **16**, 1216 (1983).
65. G. Maciel, I. Chuang, and L. Gollob, *Macromolecules* **17**, 1081 (1984).
66. E. Wagner and R. Greff, *J. Polym. Sci., Part A: Polym. Chem.* **1**, 2193 (1971).
67. D. Braun and J. Arnelt, *Angew. Makromol. Chem.* **73**, 133 (1978).
68. A. Rudin, C. Fyfe, and S. Vines, *J. Appl. Polym. Sci.* **28**, 2611 (1983).
69. E. Tesarova and V. Pacakova, *Chromatographia* **17**, 269 (1983).
70. W. Werner and O. Barber, *Chromatographia* **15**, 101 (1982).
71. L. Taylor, *Anal. Chem.* **42**, 297 (1970).
72. M. Kamal and S. Sourour, *Polym. Eng.* **13**, 59 (1973).
73. J. Enns and J. Gillham, *J. Appl. Polym. Sci.* **28**, 2567 (1983).
74. W. Stark, J. Döring, V. Bovtun, and C. Kürten, *NDT. net* **3**(11), 141 (Nov. 1998).
75. L. Lorenz, and A. Christiansen, *Ind. Eng. Chem. Res.* **34**, 4520 (1995).
76. X.-M. Wan, B. Riedl, R. Geimer, and A. Christiansen, *Wood Sci. Technol.* **30**, 423 (1996).
77. R. Geimer and A. Christiansen, *For. Prod. J.* **46**, 67 (1996).
78. U.S. Environmental Protection Agency, Technology Transfer Network, www.epa.gov, see phenol (108-95-2), May 17, 2001.
79. H. Babich and D. Davies, *Reg. Tox. Pharm.* **1**(1), 90 (1981).
80. U.S. Environmental Protection Agency, Technology Transfer Network, www.epa.gov, see formaldehyde (50-00-0), May 17, 2001.
81. A. Housden, *Water Pollut. Control* **80**, 490 (1981).
82. *Reinforced Plast.* **35**(7/8), 17 (1992).
83. *Rogers Corp., Molding Material Division, Manchester, Conn. Product Literature*, 2001.
84. *Plast. Week* 2 (Mar. 23, 1992).
85. *Plast. Environ.* 5 (July 10, 1992).
86. B. Olson and H. De Keyser, *Recycling Cured Phenolic Material*, Rogers Corp. Molding Materials Division, Manchester, Conn. Copyright 2001 and SAE International Congress and Exposition, 1992.
87. *Recycling Special Report, Phenolic Division of The Society of the Plastics Industry*, Copyright 2001.
88. *Chem. Eng. News* 21 (Jan. 22, 2001).

89. S. Kelley, M. Myers, D. Johnson, X.-M. Wang, and M. Davis, *Production of Chemicals and Materials from Renewable Resources*, (ACS Symposium Series), American Chemical Society, Washington D.C., 2001, p. 784,
90. U.S. Pat. 5,367,043 , J. Butter and R. Brandon (to Enzymol, Inc.).
91. mican Plastics Councilcos, 2000 Sales and Production Data, Arlington, Va.
92. *Plastics Technology Online Supplier Directory for Phenolic Resins*, Oct. 2001.
93. G. Bosshard, *Prog. Org. Coat.* **10**, 205 (1982).
94. U.S. Pats. 3,723,156 (Mar. 27, 1973) and 3,732,120 (May 8, 1973), B. Brockett; 3,737,410 (June 5, 1973), H. Mueller; 3,936,573 (Feb. 3, 1976), B. Brockett; and 4,165,102 (Aug. 21, 1979), J. Bodmer (to National Cash Register).
95. W. A. Boyd, C. Merriam, and J. Fry, in R. Tess and G. Behlein, eds., *Applied Polymer Science*, (ACS Symposium Series), 2nd ed., American Chemical Society, Washington, D.C., 1985, pp. 1141–1158.
96. D. M. Berger, *Met. Finish.* **74**(9), 52 (1976).
97. J. Fry, C. Merriam, and G. Misko, *Am. Chem. Soc., Div. Org. Coat. Plast. Chem.* **47**, 540 (1982).
98. B. Barth, in E. Skeist, ed., *Handbook of Adhesive*, Van Nostrand Reinhold Co., Inc., New York, 1977, Chapt. "23", p. 382.
99. H. Kollek, H. Brockmann, and H. Mueller, *Int. J. Adhesion Adhes.* **6**(1), 37 (1986).
100. U.S. Pat. 4,025,490 (May 24, 1977), F. Weaver (to Mead Corp.).
101. J. Perry, *Pulp Pap.* **46**, 93 (Aug. 1973); *Pulp Pap.* **46**, 116 (Oct. 1973).
102. G. Elbe, *Plastics Design Forum*, 66 (Nov./Dec. 1993).
103. U.S. Pats. 4,316,827 (Feb. 23, 1982) and 4,420,571 (Dec. 13, 1983), L. Pacala and J. Blickensderfer (both to Union Carbide Corp.).
104. J. Taylor, *44th International SAMPE Symposium*, Long Beach, Clif., 1999, p. 1123.
105. S. Qureshi, 51st Annual Conference, Composites Institute, SPI, 1996.
106. K. Yoshioka and J. Seferis, 46th International SAMPE Symposium, Long Beach, Clif. 2001.
107. U.S. Pat. 4,403,066 (Sept. 6, 1983), G. L. Brode, S. Chow, and W. Hale (to Union Carbide Corp.).
108. *ACS National Meeting*, Washington, D.C., Aug. 1983.
109. G. L. Brode, *Polym. Prepr.* **24**(2), 194 (1983).
110. U.S. Pat. 4,419,400 (Dec. 6, 1983), R. Hindersinn (to Occidental Petroleum).
111. *Plast. World* **47**(6), 42 (1989).
112. J. Delmonte, *Technology of Carbon and Graphite Fiber Composites*, Van Nostrand Reinhold Co., Inc., New York, 1981.
113. E. F'itzer and W. Schafer, *Carbon* **8**, 353 (1970).
114. S. Siebold, *SAMPE Symp.* **20**, 327 (Apr. 1975).
115. W. Kowbel, J. Webb and J. Withers, 44th International SAMPE Symposium, Long Beach, Clif., 1999, p. 1878.
116. U.S. Pat. 6,051,167 (Apr. 18, 2000), J. Withers, R. Loutfy, W. Kowbel, C. Bruce, and R. Vaidyanathan.
117. M. Chio, I. Chung, and J. Lee, *Chem. Mater.* **12**, 2977 (2000).
118. I. Kleba and E. Haberstroh, 46th International SAMPE Symposium, Long Beach, Clif., 2001.
119. U.S. Pat. 4,395,521 (July 26, 1983), S. W. Chow (to Union Carbide Corp.).
120. G. L. Brode, S. W. Chow, and M. Michno, *Polym. Prepr. (Am. Chem. Soc., Div. Polym. Chem.)* **24**(2), 192 (Aug. 1983).
121. U.S. Pats. 4,423,163 (Dec. 27, 1983), H. Doerge; 4,165,413 (Aug. 21, 1979), R. Sefton; and 444,912 (Apr. 24, 1984), J. Carlson (to Koppers Co., Inc.).
122. S. Linder and B. Brailsford, Phenolic Resin-Impregnated Aramid Paper Honeycomb Core Program, Navy Mantech Program, Office of Naval Research, FY96-98, 1998.

123. K. Esumi, S. Eshima, Y. Murakami, H. Honda, K. Esumi, and H. Oda, *Colloids Surf.* **108** 113 (1996).
124. U.S. Pats. 3,650,102 (Mar. 21, 1972) and 3,723,588 (Mar. 27, 1973), J. Economy and R. Clark (to Carborundum Co.).
125. *J. Chem. Week*, 5 (Aug. 10, 1989).
126. J. Woodbrey, H. Higginbottom, and H. Culbertson, *J. Polym. Sci., Part A: Polym. Chem.* **3** 1079 (1965).
127. R. Hirst and co-workers, *J. Polym. Sci., Part A: Polym. Chem.* **3**, 2091 (1965).
128. T. Yoshikawa and J. Kumanotani, *Makromol. Chem.* **131**, 273 (1970).
129. T. Sterling and J. Weinkam, *J. Occup. Med.* **30**, 895–901 (Nov. 1988).
130. U.S. Pat. 3,595,821 (July 27, 1971), S. Spector (to PPG Industries).

GENERAL REFERENCES

E. Dradi and G. Casiraghi, *Macromolecules* **11**, 1295 (1978).
T. Liu and S. Rhee, *Wear* **76**, 213 (1978).

PETER W. KOPF
TIAX, LLC

PHOSGENE. See Volume 3.

PHOSPHORUS–CONTAINING POLYMERS AND OLIGOMERS. See Volume 3.

PHOTORESISTS. See LITHOGRAPHIC RESISTS.

PIEZOELECTRIC POLYMERS. See Volume 3.

PLASTICIZERS. See Volume 3.

PMMA. See METHACRYLIC ESTER POLYMERS.

POLYACETAL. See ACETAL RESINS.

POLYACRYLAMIDE. See ACRYLAMIDE POLYMERS.

POLYACRYLATES. See ACRYLIC ESTER POLYMERS.

POLY(ACRYLIC ACID). See ACRYLIC (AND METHACRYLIC) ACID POLYME.

POLYACRYLONITRILE. See ACRYLONITRILE POLYMERS.

POLYAMIDES, AROMATIC. See Volume 3.

POLYAMIDES, FIBERS. See Volume 3.

POLYAMIDES, PLASTICS. See Volume 3.

POLY(*p*-PHENYLENEVINYLENE)

Introduction

Poly(*p*-phenylenevinylene) (PPV) and its derivatives are polymers that have been widely studied because of their potential applications in optoelectronic devices. PPV is a conjugated polymer, with a backbone consisting of alternating single and double bonds. Many conjugated polymers are known and exhibit remarkably high electrical conductivities when oxidatively or reductively doped (1) (see ELECTRICALLY ACTIVE POLYMERS). Much of the early research on PPV focused on the relatively disappointing properties of the doped material; however, interest in this material was reawakened in 1990 when Friend and co-workers in Cambridge discovered that films of undoped PPV could be used as the emitting layer in organic electroluminescent (EL) devices (2). This discovery stimulated intense research in the area, including many fundamental studies into the properties of PPV and its derivatives, as well as extensive academic and industrial interest on the applications of the materials (see LIGHT-EMITTING DIODES).

This article seeks to provide an overview of the methods by which PPV and some of its derivatives may be prepared, the physical and electronic properties of these materials, and the applications that are being explored. The reader who seeks a deeper and more detailed understanding of this fascinating material is referred to several excellent and comprehensive reviews that have been published on the synthesis, properties, and applications of PPV (3–7).

Methods of Preparation

Unsubstituted PPV. Many methods have been devised to prepare PPV for fundamental and applied studies. Because of its rigid conjugated backbone,

Encyclopedia of Polymer Science and Technology. Copyright John Wiley & Sons, Inc. All rights reserved.

unsubstituted PPV and even short oligomers are insoluble and intractable materials. An important consideration in all preparative routes that seek to prepare high molecular weight material, therefore, is the solubility of the growing polymer chain. One of the most successful approaches to high molecular weight (10,000–100,000) PPV is the Wessling or sulfonium precursor route, which proceeds via a soluble precursor polymer that is subsequently thermally converted to fully conjugated PPV. Other methods are available but generally produce low molecular weight material.

Sulfonium Precursor Route. In this route, polymerization of the bis sulfonium salt **1** with base yields a soluble polyelectrolyte **2** (8,9). This intermediate may then be purified, processed, and finally thermally converted to PPV. Both the nature of the sulfide used in the sulfonium salt and the counterion affect the conditions required in the preparation, as well as the molecular weight and structure of the resulting polymer (9,10). When dodecylbenzenesulfonate is used as a counterion, conversion to PPV is achieved in 3 min at only 115°C (11). A modified sulfonium precursor route has also been developed, in which the soluble methoxy-substituted polymer **3** is converted to PPV in the presence of HCl gas (12).

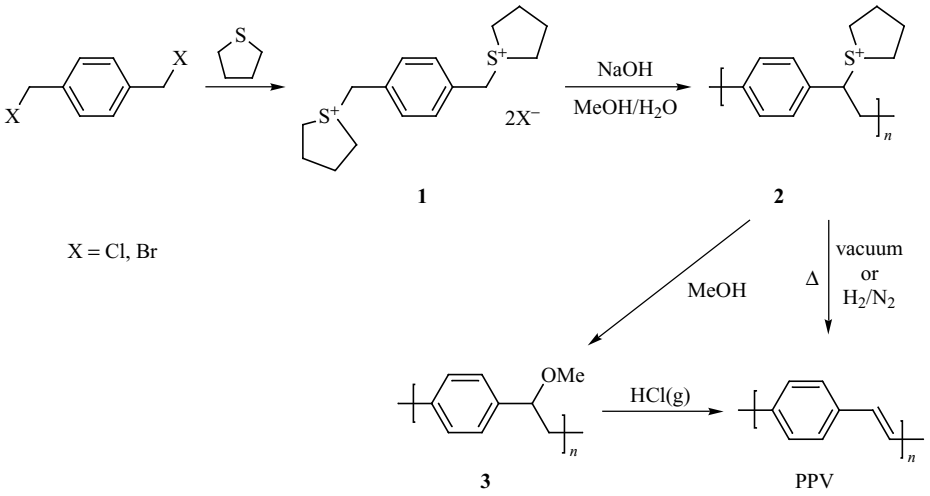

The mechanism of the polymerization has been the subject of some debate in the literature, with both radical and anionic mechanisms proposed. The presence of oxygen during the polymerization results in lower molecular weight polymer consistent with a radical mechanism (8). A *p*-xylylene or *p*-benzoquinodimethane intermediate is postulated and has been observed spectroscopically. Other studies have suggested that this intermediate polymerizes via an anionic mechanism (13, 14). Despite these conflicting results, the polymerization is typically carried out in the absence of oxygen, and the thermal conversion step done either in vacuum or under an inert or forming gas atmosphere.

Other Routes. Other synthetic routes to PPV include the Wittig reaction (eq. 1) (15), Pd-catalyzed Heck reaction (eq. 2) (16), and McMurry coupling (eq. 3) (17). Reaction of α,α'-dichloro-*p*-xylene with potassium *tert*-butoxide yields PPV

(eq. 4); this procedure was discovered by Gilch and Wheelwright and is referred to as the Gilch route (18). All of these methods yield PPV directly from soluble monomers, and thus produce primarily low molecular weight oligomers.

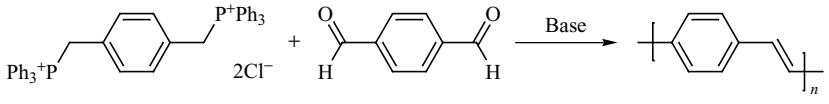

(1)

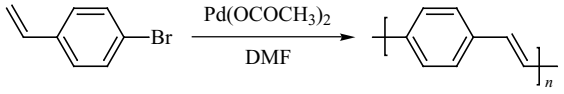

(2)

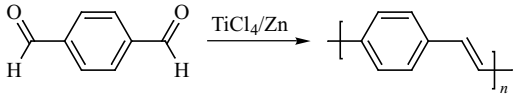

(3)

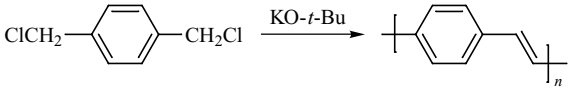

(4)

Electropolymerization is a convenient method for the preparation of insoluble conjugated polymers such as PPV because it yields thin films directly on an electrode surface. Such a film may then be directly utilized in an application requiring a conducting contact, such as electroluminescence. Several methods have been reported for the electrochemical preparation of PPV films. Electrochemical reduction of **4**,**5**,**6** has been shown to yield PPV films on metal and indium tin oxide (ITO) electrodes (19–21). Another direct route to thin-films is chemical vapor deposition (CVD) from precursors such as **7** or **8** (22,23).

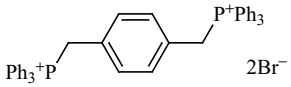

4

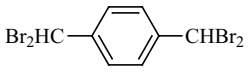

5

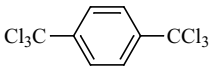

6

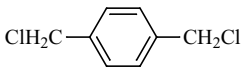

7

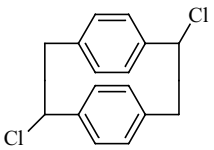

8

Ring-opening metathesis polymerization (ROMP) has been used to prepare unsubstituted PPV via a soluble precursor. Substituted paracyclophan-1-ene (**9**) (24) and norbornadiene derivatives (**10**) (25) have been used as monomers, with

$Mo(NAr)(CHC(CH_3)_2C_6H_5)[OCCH_3(CF_3)_2]_2$ (Ar = 2,6-diisopropylphenyl) used as the catalyst in the polymerization. This route proceeds via a living polymerization and consequently yields a relatively narrow molecular weight distribution.

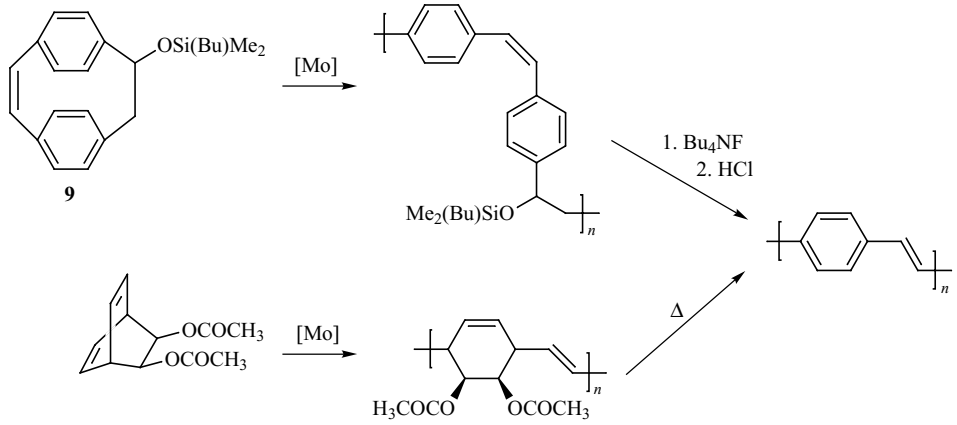

9 **10**

Substituted PPV. In order to increase the solubility and processibility of PPV in the conjugated form, substituents such as alkoxy or phenyl groups have been added to the backbone structure. In addition to enhancing the solubility, these substituents also change the electronic properties of the polymer via both inductive and conjugative effects. An additional benefit of soluble derivatives of PPV is that techniques for polymer characterization that require soluble material may be brought to bear on, and provide direct information about, molecular weights and higher-order structure.

Sulfonium Precursor Route. The Wessling route has also been used to produce soluble derivatives from monomers containing solubilizing substituents on the phenyl ring. For example, dialkoxy-substituted monomers yield **11**, which is soluble in organic solvents such as chloroform and chlorobenzene (26), as well as poly[2-(2-ethylhexyl)oxy-5-methoxy-*p*-phenylene)vinylene], or MEH–PPV (**12**) (eq. 5) (27). The branched side chains in MEH–PPV improve the solubility of this derivative over unbranched analogs, and this polymer is one of the most popular for use in electroluminescence applications.

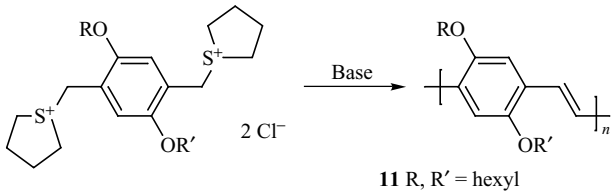

11 R, R′ = hexyl
12 R = methyl, R′ = 2-ethylhexyl (MEH-PPV) (5)

Other Routes. Substituted PPV derivatives have also been prepared by several other routes. In cases where the resulting polymers are soluble, these methods are often successful in preparing high molecular weight material. The Gilch route has been used to prepare phenyl and crown ether substituted polymers

(**13** and **14**) (eqs. 5 and 6) (28,29), and McMurry coupling has been used to yield a dihexyl-substituted polymer (**15**) that is soluble in a range of organic solvents (eq. 7) (30).

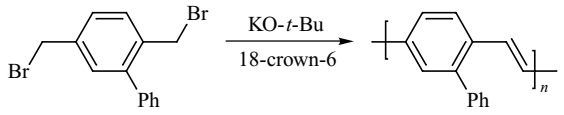

13 (6)

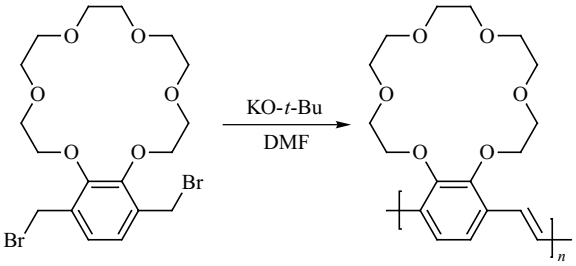

14 (7)

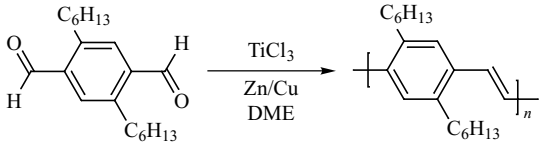

15 (8)

Copolymers. A number of studies have focused on the preparation of copolymers containing fully conjugated backbones, as well as those containing both conjugated and nonconjugated blocks. This work has been motivated by the desire to prepare materials having a range of electronic properties that can easily be tuned by variations in the proportion and nature of the monomers used in the copolymer synthesis. In addition, local variations in the π–π^* energy gap can be introduced in this way, which has been shown to result in dramatic improvements in the performance of these copolymers in electroluminescent devices.

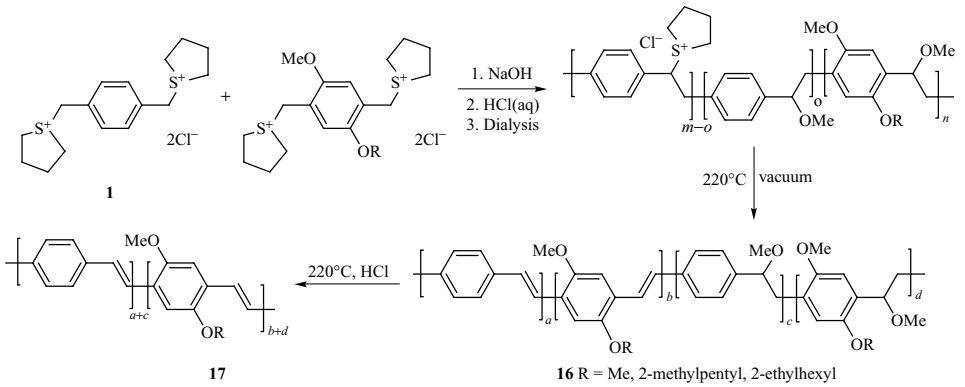

1

16 R = Me, 2-methylpentyl, 2-ethylhexyl

17

The sulfonium precursor route has been used to prepare copolymers by using various proportions of different monomers in the synthesis. This method has yielded both partially conjugated (**16**) and fully conjugated polymers (**17**) (31,32), as well as copolymers containing other aromatic groups in the backbone in addition to phenylenevinylene moieties such as in copolymer **18** (33).

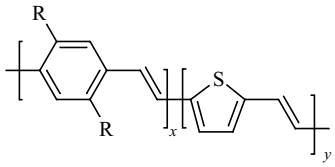

18 R = H, OMe Cl

The Wittig reaction has also been successfully used to prepare soluble copolymers with substituents such as alkoxy groups on the backbone (**19**) (34), as well as copolymers containing flexible, nonconjugated spacers (**20** and **21**) (35,36). Heck chemistry has been applied to prepare copolymers such as **22** (37).

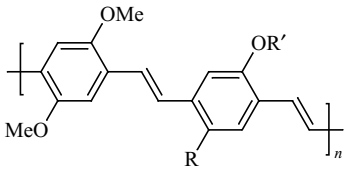

19 R = H, OR′; R′ = $(CH_2)_{15}CH_3$, $(CH_2)_{11}CH_3$, $(CH_2)_7CH_3$

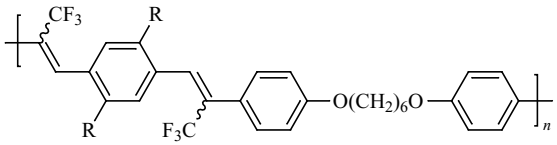

20 R = OC_8H_{17}

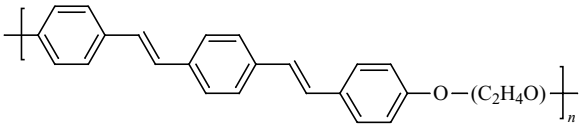

21

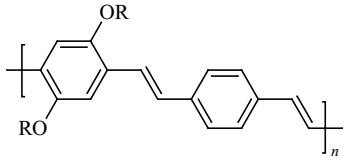

22 R = C_nH_{2n+1} (n = 4–16)

Composites and Blends. The mechanical and optoelectronic properties of PPV and its derivatives may be optimized for specific applications through the use of polymer blends (qv) and Composite materials (qv). Blends of MEH–PPV and polyethylene have been used to significantly enhance the degree to which the conjugated polymer chains are aligned upon stretching (38). The density of entanglements in gels of polyethylene is much lower than in spin-cast polymer solutions, and this effect remains after removal of the solvent. This allows tensile drawing of such blends to large draw ratios (>200), which causes the conjugated polymers to align to a degree normally expected in single crystals. Charge transport through blends can also be controlled by using a host polymer with specific properties. Blue emitters have been prepared from blends of poly(*p*-phenylphenylenevinylene) (PPPV) in poly(9-vinylcarbazole) (PVK), a hole-transporting polymer (28). In addition to enhancing the processibility of the PPPV, the PVK blue-shifts the electroluminescence, enhances hole-transport, and increases the probability of radiative recombination because of the dilution effect.

Composites of PPV with silica (SiO_2) and vanadium oxide (V_2O_5) have been prepared for use in nonlinear optical applications (39–41). These composites are prepared via sol–gel processing methods, and allow the superior nonlinear optical properties of the conjugated polymers to be combined with the very low optical losses found in inorganic glasses. In homogeneous nanocomposites of PPV with SiO_2, inter- and intrachain disorder in the polymer chains is disrupted when the silica interparticle separation is comparable to the coherence distance in the polymer. This influences the absorption and emission spectra, and results in reduced electronic conductivity (42). Composites of PPV with gold-coated silica nanoparticles showed enhanced stability to photo-oxidation, an effect attributed to an electronic interaction of the metal particles with the triplet excitons in PPV (43). Composite films of insulating SiO_2, TiO_2, and Al_2O_3 nanoparticles with MEH–PPV were prepared and result in more efficient charge injection and transport in electroluminescent devices formed from them, as well as enhanced emission intensities (44,45). Photovoltaic and time-resolved microwave conductivity measurements were also used to study nanocrystalline TiO_2/PPV composites, showing that excitons generated in the polymer are dissociated at the polymer/TiO_2 interface, with the electrons transferred to the nanocrystals (46). Indium arsenide-zinc selenide nanocrystals have been blended with MEH–PPV, giving materials emitting in the near-IR region (1–1.3 μm). External efficiencies of devices made from these composites were ∼0.5% (47).

Composites of PPV in films of the polyelectrolyte Nafion have been synthesized by electrostatically binding the dicationic monomer to the film, followed by treatment with base and thermal conversion (48). Ordered nanocomposites of PPV have been synthesized from mixtures of polymerizable lyotropic liquid crystals with PPV precursors (49). Photopolymerization of the host results in a hexagonal architecture, which can be fabricated into fibers and thin-films. A significant enhancement in photoluminescence of the composite relative to PPV was found.

Properties

Absorption and Emission. Films of PPV show three absorption bands, with maxima at 6.12, 5.06, and 3.09 eV respectively (50). The two higher-energy bands are attributed to localized molecular states, while the lower-energy band is due to a delocalized electronic excitation. The emission spectrum of PPV upon excitation at 355 nm is resolved into three lines with a spacing of 0.16 eV because of vibronic coupling (51). Migration of the excited state to the longest conjugation length segments in the polymer appears to occur prior to radiative decay, since smearing out of the vibrational fine structure is expected if emission from a distribution of sites within the polymer occurs. The photoluminescence efficiency varies between 5 and 25%, depending on the synthetic route used and the conversion conditions (52).

Two descriptions of the excited state have been applied to organic semiconductors, the exciton and the band model. The appropriate model depends on the extent of coupling between sites, with strong coupling yielding uncorrelated electrons and holes, while weak coupling favors correlated electron–hole

pairs (excitons). Time-resolved fluorescence and polarized fluorescence experiments suggest that the exciton model is appropriate in PPV (53). Rothberg and co-workers have examined the relative effects of interchain vs. intrachain excitations in MEH–PPV by comparing excited-state lifetimes and quantum yields in films to dilute solutions (54). They observed significantly lower quantum yields for emission in the films, and attributed this to the formation of nonemissive interchain excitons, which are not formed in dilute solution. They have also concluded that film morphology can play a significant role in the photophysical behavior of PPV (55). The presence of trace oxygen in the conversion of precursor polymer to PPV reduces the photoluminescence of the resulting material (56). This was shown to be correlated to the formation of carbonyl groups in the polymer backbone, and can be prevented by carrying out the conversion in a reducing atmosphere.

Photoconductivity. The first measurements of photoconductivity in PPV were carried out in the early (57). A later study revealed low dark conductivities for PPV films ($<10^{-15}$ S/cm), but significant photoconductivity upon irradiation at 440 nm. Significant conductivity was also found upon irradiation of the film in the near-IR region, despite insignificant optical absorption in this region. This was attributed to a charge-transfer mechanism involving trace oxygen (58). Oriented films of PPV showed enhancements in the photoconductivity with light polarized parallel to the direction in which the films were stretched (59). Transient photoconductivity measurements have also been used to address the question of the nature of the charge carriers in MEH–PPV films. The exciton model predicts a strong dependence of photoconductivity on temperature, and this is indeed observed for films greater than 120 nm in thickness. For thinner samples, both steady-state and fast time-resolved photoconductivity measurements demonstrate that photoconductivity is independent of temperature. These results are inconsistent with the exciton model (60).

Doping and Electrical Conductivity. Pristine PPV films are insulators at room temperature; however, exposure to oxygen causes an increase in conductivity to 10^{-11} S/cm—an effect attributed to reversible doping, with the oxygen acting as an electron acceptor (61). Irreversible doping of PPV films with strong oxidants such as $FeCl_3$ or H_2SO_4 produces black films with very high conductivities relative to the pristine material (62). Films doped with sulfuric acid showed conductivities of $\sim 10^4$ S/cm that were only weakly temperature-dependent, indicative of metallic behavior. The conductivity of films doped with $FeCl_3$ was slightly lower (10^3 S/cm) and decreased with temperature. The doped films are stable in oxygen, but are moisture-sensitive. Copolymers of PPV derivatives containing electron-donating groups, such as poly(1,4-phenylenevinylene-*co*-2,3,5,6-tetramethoxy-1,4-phenylenevinylene) (**23**), can also be doped with weaker oxidants such as I_2 to give materials with conductivities as high as 7×10^{-2} S/cm (63).

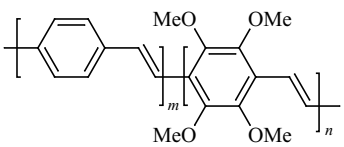

23

Microstructure and Liquid Crystallinity. The degree of structural order in PPV films depends greatly on the method of preparation. The degree of broadening in electron diffraction patterns has been used to assess the extent of ordering in different PPV samples (64). High resolution transmission electron microscopy revealed crystalline regions approximately 7 nm in size in oriented PPV films, and these crystallites are retained upon doping the films with H_2SO_4 (65). Substituents also have an effect on the structural order of PPV derivatives. Methoxy substituents allow chains to interlock and form a more ordered three-dimensional structure, while methyl groups cause the backbone to distort because of repulsive interactions between the backbone and side groups, resulting in a more disordered material (66). X-ray diffraction studies on MEH–PPV films cast from different solvents have shown that the chain orientation is anisotropic, and the aromatic rings are oriented predominantly parallel to the film plane (67). The crystallinity of films cast from THF is highest, and the crystalline domains largest, compared with films prepared from other solvents.

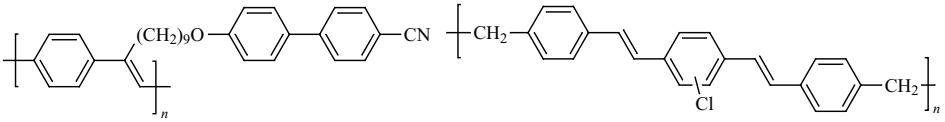

24

25

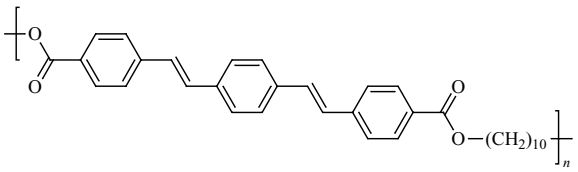

26

Liquid crystallinity has been observed in derivatives of PPV bearing mesogenic substituents, as well as in copolymers containing phenylenevinylene segments in the main chain. Copolymers in which some of the phenyl rings have alkoxy side chains (**22**) exhibit a nematic liquid crystalline phase, which has been characterized by polarized microscopy and differential scanning calorimetry (36). The temperature range between the melting point and the nematic–isotropic phase transition was found to depend on the length of the alkoxy group. A PPV derivative (**24**) bearing the well-known cyanobiphenyl mesogen as a side chain has both nematic and smectic mesophases (68). This polymer was oriented by rubbing a film with a Teflon stick, and a significant degree of orientation observed by polarized UV/vis and IR spectroscopies. Several examples of main-chain liquid crystalline polymers containing phenylenevinylene moieties bridged by saturated linkers are known. The thermotropic polymer **25** was prepared using a Wittig procedure, and was found to melt anisotropically (69). A related main-chain polymer (**26**) has a mesophase that exists between 218 and 275°C (70).

Nonlinear Optical Properties. For many optical signal processing applications, it is desirable for materials to have large optical nonlinearities and fast response times. For example, third-order nonlinear optical properties (qv) result in laser-pulse–induced refractive index changes that occur on the femtosecond

timescale. These changes could potentially be exploited in fast optical switches. Conjugated polymers are expected to be good candidates for such applications because of the delocalization of charge in the polymer backbone (71).

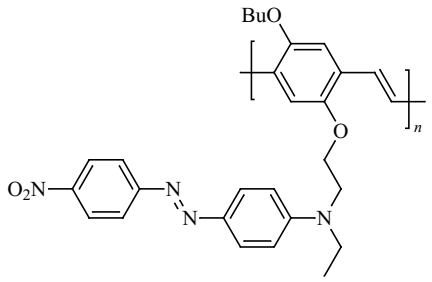

27

PPV has many of the characteristics desired in an NLO material, including good transparency, high π-electron density, and optical quality films that may be oriented and ordered. PPV has a third-order nonlinear optical susceptibility ($\chi^{(3)}$) of 7.8×10^{-12} esu (72), while $\chi^{(3)}$ for a substituted derivative, poly(2,5-dimethoxy-*p*-phenylenevinylene), is 5.4×10^{-11} esu at 1.85 μm (73). The higher value for the dimethoxy-substituted derivative may be due to more extended conjugation in this material. An alternative strategy that has been investigated is to introduce an NLO-active moiety pendent to a PPV backbone. For example, Disperse Red 1 has been tethered in this way (**27**), and the resulting polymer has a $\chi^{(3)}$ value of 2.5×10^{-12} esu (74).

Applications

Photovoltaics. Heterojunctions between conjugated polymers and films of electron acceptors behave as rectifying *p*–*n* junctions and may be used in photovoltaic devices. Such junctions have been prepared by vacuum evaporation of *n*-type buckminsterfullerene (C_{60}) onto spin-cast films of *p*-type MEH–PPV on ITO/glass substrates (Fig. 1) (75). These devices behave as rectifiers in the dark, and pass a photocurrent upon illumination with visible light. The open circuit voltage (V_{oc}) saturates at 0.53 V, with a fill factor of 0.48 and a power conversion efficiency of 0.04%. Photovoltaic devices made from blends of PPV with a processible methanofullerene showed power efficiencies of 0.25% under white light (76). The Cambridge group has also reported photovoltaic devices in which a heterojunction between bis(phenethylimido)perylene and PPV is sandwiched between ITO and Al. These devices had a somewhat greater fill factor (0.6) and V_{oc} approaching 1 V, with a quantum yield of 6% (electrons per incident photon) (77). A related approach involves using a blend of MEH–PPV and bis(phenethylimido)perylene, giving a fill factor of 0.27 at an open circuit voltage of 0.58 V; however improvements to these devices are limited by the poor solubility of the bis(phenethylimido)perylene (78).

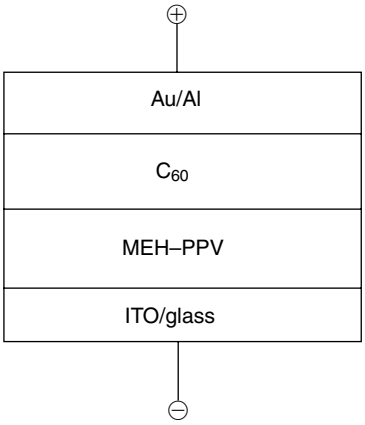

Fig. 1. Schematic of a MEH–PPV-based photovoltaic cell.

Photovoltaic cells have also been constructed from light-emitting electrochemical cells (LECs, see below) (79). In these devices, a phase-separated blend of MEH–PPV and cyano-PPV is used along with a solid electrolyte consisting of a mixture of polyethylene oxide (PEO) and $LiCF_3SO_3$. Sandwich photovoltaic cells using Al and ITO as the electrode contacts were doped using a prebias of 3 V, resulting in a V_{oc} of 1.0 V and a power conversion efficiency of 0.1%, assuming a fill factor of 0.25. The built-in potential is determined by the chemical potential difference between the *p*-doped and *n*-doped layers, rather than the work function of the electrodes, thus air-stable electrodes can be used in these cells.

Optical Memory. The permanent storage of data in films of PPV derivatives has been accomplished by irradiating films of the sulfonium precursor polymers with either a Xe arc lamp or Ar ion laser (488 nm) (80). Subsequent heating of the films resulted in the formation of colored, conjugated films only in regions that were not irradiated. Photochemical scission of the polymer chains leaves a water-soluble residue, which is readily removed by rinsing the heat-treated films with water. This process may also be used for the lithographic patterning of PPV films onto substrates.

Light-Emitting Devices. In the late 1980s Tang and VanSlyke reported electroluminescent devices that utilized thin films of 8-hydroxyquinoline aluminum (Alq_3) as the emitting material (81). They distinguished these devices from those based on conventional inorganic semiconductors by calling them "organic," despite the fact that the emissive compound is actually an inorganic coordination complex. The devices consisted of a layer of a hole-transporting aromatic amine on an ITO electrode, 60 nm of the luminescent Alq_3 and a Mg/Ag electrode. The devices behaved like rectifiers, and emitted light with a peak intensity at 550 nm, with a forward bias of as little as 2.5 V. In a subsequent publication, Tang and VanSlyke showed that doping of the Alq_3 layer with other highly fluorescent molecules, such as coumarin 540, increases the electroluminescence efficiency and allows tuning of the color from blue-green to orange-red (82).

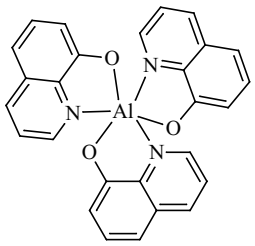

Alq_3

In 1990, the discovery that PPV could be utilized as the emitter in an electroluminescent device was reported by Friend and co-workers at the Cavendish Laboratory in Cambridge (2). The devices consisted of a PPV film, prepared using the sulfonium precursor route, sandwiched between an ITO and an Al electrode, and emitted green-yellow light under forward bias of 14 V, with a quantum efficiency of up to 0.05%. Shortly after this initial publication, Braun and Heeger demonstrated that MEH–PPV could also be used to fabricate EL devices in which the polymer was directly cast in the conjugated form from solution. They used both indium and calcium cathodes, and observed visible light at 4-V forward bias with the calcium cathode, with an efficiency of 1%.

Device Operation. Single-layer devices consist of an electroluminescent layer sandwiched between an electron-injecting cathode (usually a low work function material such as Ca or Al) and a hole-injecting anode (most commonly the transparent conductor ITO on glass).

The operation of the device under forward bias may be understood using a simple band diagram (Fig. 2**a**). The anode and cathode materials are chosen to provide low barriers to electron and hole injection by matching the valence and

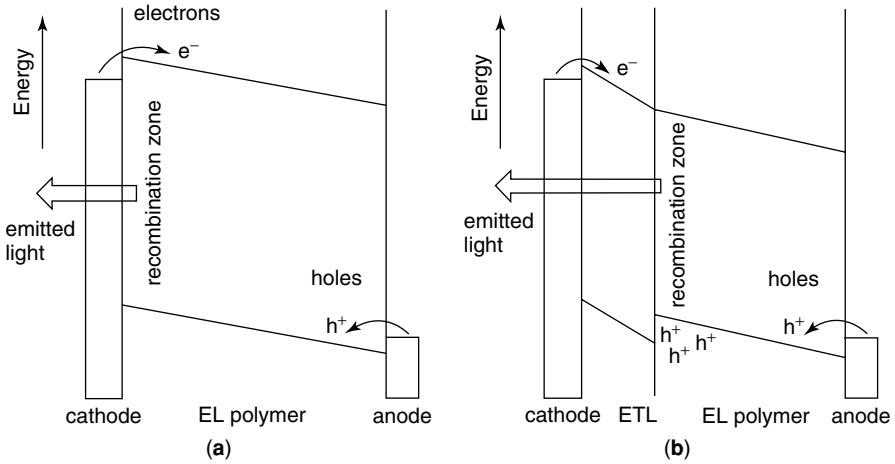

Fig. 2. Band diagram for (**a**) single-layer and (**b**) two-layer polymer EL devices (ETL = electron transporting layer).

conduction band energies of the polymer to the electrode work functions. A disadvantage of the single-layer device configuration is that charge recombination often occurs close to the cathode, since most EL polymers are better hole conductors than they are electron conductors. The metal electrodes are able to quench excitons in close proximity, thus reducing the EL efficiency.

An approach that has been used successfully to move the emitting zone away from the electrodes is the construction of two-layer cells in which recombination occurs at the interface between the two organic layers (Fig. 2**b**). Here, the material in the layer adjacent to the cathode is selected to have a high electron mobility but a lower hole mobility than the EL polymer that is located adjacent to the anode. Thus, electrons and holes are readily injected into the adjacent layers contacting the respective electrodes and accumulate at the interface between the two layers. A number of materials have been exploited for use as the electron-transporting layer (ETL), including 2-(4-biphenylyl)-5-(4-*tert*-butylphenyl)-1,3,4-oxadiazole (butyl PBD) **28** (83). Two-layer devices constructed with PPV as the emitting layer and butyl PBD dispersed in poly(methylmethacrylate) (PMMA) as the ETL showed a tenfold improvement in efficiency relative to analogous single-layer devices constructed using only PPV. Polymers containing oxadiazole moieties pendent to the backbone, as well as in the main chain, have been synthesized and tested as ETLs, and also act to improve external quantum efficiencies in two-layer devices (84). The EL efficiency was found to be temperature-independent in these devices, suggesting that charge injection from both electrodes is well-balanced. Multiwalled carbon nanotubes have been used as the ETL in devices, leading to an increase in brightness (85).

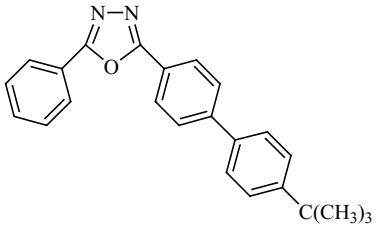

28

Hole injection from the anode can be improved via the use of a hole-transporting layer, which functions by improving hole injection into the electroluminescent layer and maximizing recombination of injected charges. Optimally, these materials should possess high glass-transition temperatures (T_g) and low ionization potentials. A large variety of triaryl amines have been investigated for use as hole-transport materials, including *N,N′*-diphenyl-*N,N′*-di-*m*-tolyl-1,1′-biphenyl-4,4′-diamine (TPD) (**29**) (86), *N,N′*-1-naphthyl-*N,N′*-diphenyl-1,1′-biphenyl-4,4′-diamine (NPD) **30** (87), 1,3,5-tris(2′-anthracyl-4″-methoxyphenylamino)benzene (**31**) (88), and the atropisomeric *cis*- and *trans*-5,11-dihydro-5,11-di-1-napthylindolo[3,2-*b*]carbazole (**32**) (89).

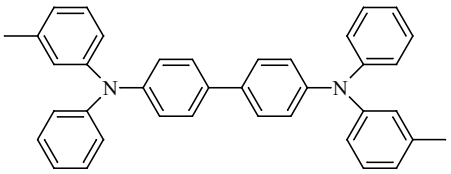

29

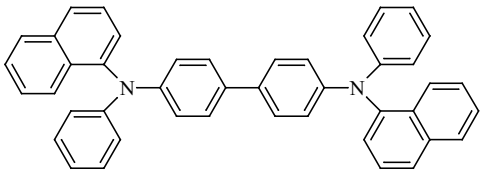

30

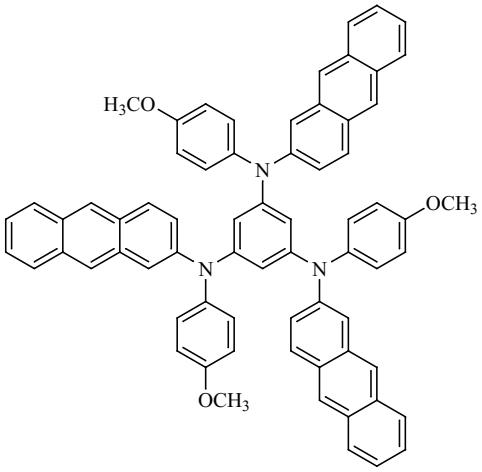

31

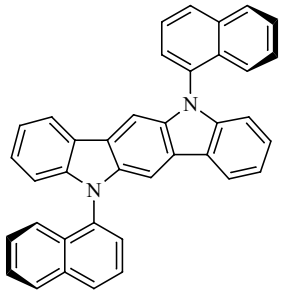

trans-**32**

The brightness of EL polymer based devices varies depending on the device configuration and polymer used. Uniax Corporation has reported ITO/PANI–CSA/MEH–PPV/Ca (PANI–CSA = polyaniline–camphor sulfonic acid) devices with a brightness as high as 10,000 cd/m^2 for bias voltages >5 V, over twice the brightness of a fluorescent lamp (90). Device brightness can be increased by using short drive pulses, which permit high current operation (91). Luminous efficiencies as high as 0.8 cd/A could be achieved in this way using current densities of 1 kA/cm^2 in single-layer PPV-based devices. Poly(3,4-ethylenedioxythiophene) (PEDOT) doped with polystyrene sulfonic acid (PSS) has also been investigated as a polymeric anode, and has been shown to result in increases in efficiency, brightness, and lifetime for devices based on MEH–PPV (92). When PPV is thermally converted with a PEDOT/PSS overlayer a large surface area interface results because of interpenetration of the two layers, possibly contributing to the improvement in quantum efficiency measured for these devices (93).

An application for which polymer-based EL devices may be uniquely suited is as flexible emitting materials. Such devices were first reported in 1992 by workers at Uniax, using a thin layer of PANI–CSA on flexible poly(ethylene terephthalate) (PET) as the anode, an MEH–PPV film as the emitter and vacuum-deposited Ca as the cathode (94). The PANI–CSA film is light green in color; however the absorption is low in the region of the spectrum where MEH–PPV emits (500–700 nm), so emission is readily observed through the anode.

Doped silicon has also been used as a hole-injecting electrode material (95). Devices consisted of an MEH–PPV film on a thin SiO_2 layer atop a heavily *p*- or

n-doped Si substrate. The top contact was a semitransparent Ca or Au electrode, and light emission was observed through this layer. The insulating SiO_2 layer allows the electrode Fermi level to be matched to the conduction band of the polymer, thus permitting the devices to operate in reverse bias with a high work function cathode material such as Au. The Cambridge group has also investigated the effect of separating the polymer layer from the Al cathode with a thin SiO_2 layer. This results in an increase in PL quantum efficiency since the emission zone is brought away from the metal interface (96).

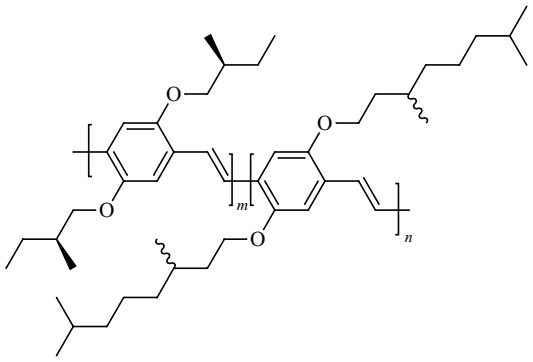

33

Circularly polarized electroluminescence (CPEL) has been obtained from a single-layer device in which the emitter is a PPV derivative with chiral pendent groups (**33**) (97). The CPEL is due to the inherent chirality of the polymer, since polymers containing racemic side groups did not show any effect; however aggregation of the polymer chains in the solid state is believed to enhance the magnitude of the effect.

The external efficiencies of electroluminescent devices based on PPV derivatives are typically between 0.2 and 4% (4), comparable to the efficiencies of inorganic EL devices. In addition to the use of electron- and hole-transporting layers to enhance efficiencies, other strategies have also been used. Son and co-workers reported polymers in which cis linkages were intentionally introduced into the PPV backbone (98). These defects prevent the polymer chains from packing efficiently in the solid state, thus producing amorphous PPV films. Both single- and two-layer devices prepared from this material had significantly higher efficiencies than comparable devices fabricated using PPV synthesized in the conventional fashion (high trans content). This improvement in efficiency may result from better chain separation in the amorphous material.

Degradation of polymer EL devices leading to limited lifetimes is a serious problem, particularly for commercial applications that typically demand lifetimes of $>10{,}000$ h. The low work function metals used as cathode materials (Al, Ca, In) are all air- and moisture-sensitive to varying degrees. Encapsulation to prevent intrusion of air and water is necessary for practical devices. The polymer layer has also been shown to be susceptible to degradation by singlet oxygen, which can form from oxygen impurities in the film by energy transfer from a nonradiative exciton in the polymer (99). Strict removal of oxygen in the film preparation process thus

results in longer device lifetimes. Oxidation of MEH–PPV has been shown to result in reduced fluorescence because of the formation of carbonyl groups, along with reduced carrier mobility as a consequence of chain scission. Localized shorts also form in these devices, which are initially isolated by melting of the cathode; however these eventually coalesce, causing device failure (100).

Although most studies have been carried out on PPV prepared using solution processing, EL devices have also been prepared from PPV prepared by chemical vapor deposition (101). The advantage of this approach is that many of the side reactions that typically occur during solution processing are eliminated, and this method is also compatible with existing methods for processing of inorganic LEDs. Single-layer devices prepared in this way had turn-on voltages as low as 4.5 V, with a brightness of 20 cd/m^3.

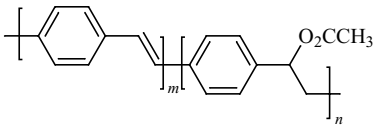

34

Modifications of the PPV structure have also been demonstrated to have an effect on the performance of EL devices (102). A PPV copolymer bearing acetate side groups (**34**), which disrupt the conjugation in the backbone, has been used to fabricate encapsulated single-layer devices with Al cathodes and ITO anodes, which operated continuously in air without degradation for 12,000 h. The devices were encapsulated by gluing a glass slide over the top of the device with epoxy resin.

For many display applications it is useful to pattern the emitting area of a device. Several successful approaches have been developed in this vein, including inkjet printing and solvent-assisted micromolding. In the inkjet approach, a conventional printer was modified to spray a solution of PEDOT onto defined areas of an ITO electrode (103). The whole area was then coated with an MEH–PPV film and a Ca cathode deposited to complete the device. Emission occurs only in the areas defined by the PEDOT layer because of the enhanced charge injection from this polymer relative to the ITO layer. Typical pixel sizes ranged from 180 to 400 μm, and the density of the dots could be used to control the brightness of emission from a given area. Solvent-assisted micromolding involves wetting a polydimethylsiloxane mold with methanol and allowing a solution of PPV precursor polymer to wick into the recessed regions of the mold (104). The mold is initially prepared by casting and curing a prepolymer against a lithographically prepared relief structure. When the methanol evaporates, the mold is removed, leaving the PPV precursor polymer patterned on the surface. Curing yields PPV, and devices are completed by deposition of Ca or Al. Emitting features as small as 800 nm can be prepared using this method. Inkjet patterning has also been used to produce a three-color (red–green–blue) display, using PPV derivatives and molecular dopants to achieve the various colors (105).

Color Range and Tuning. Variations in polymer structure allow tuning of the emission color over the entire visible spectrum. Polymers in which the

conjugation is broken because of the presence of the methoxy groups (as in **16**) show blue-shifted electroluminescence relative to unsubstituted PPV, with an emission maximum at 508 nm (106). Blue emission was also obtained from a copolymer containing short methoxy-substituted phenylenevinylene segments (**35**) (107). Single-layer devices containing this polymer sandwiched between Al and ITO have a maximum in the EL spectrum at 465 nm. A PPV derivative with Si groups in the backbone (**36**) emits blue light in both single- and two-layer device configurations (108). Green light was obtained from multilayer devices with poly(2-methyloctylsilyl-1,4-phenylenevinylene) (DMOS-PPV) (**37**) as the emitter combined with an electron-conducting and hole-blocking layer of either butyl PBD or a polymeric oxadiazole derivative (109). A low bandgap, cyano-substituted thienylene phenylenevinylene copolymer **38** was shown to emit in the near-IR region. The maximum in the EL spectrum is at 740 nm, and emission tails down to 1000 nm (110).

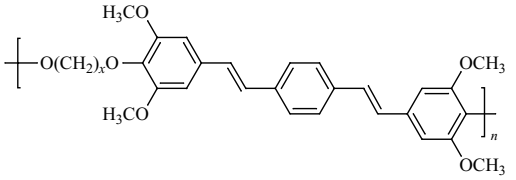

35

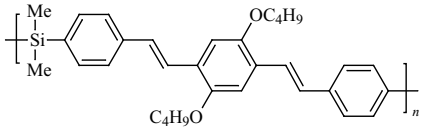

36

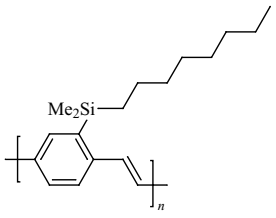

37

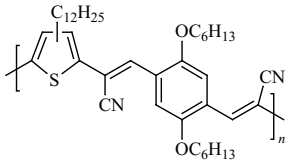

38

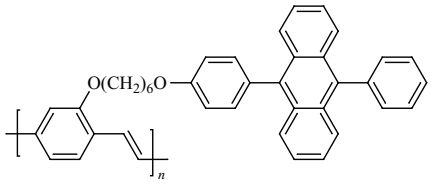

39

Several groups have developed polymer LEDs that emit light over a broad wavelength range, resulting in white light. Photoluminescence from polymer **39** arises from both the pendent diphenylanthracene units and the polymer backbone, thus covering much of the visible spectrum (111). However, electroluminescence from single-layer devices containing this polymer is significantly red-shifted relative to the photoluminescence, emitting green–red light apparently only from the main chain. Another approach that has produced white electroluminescence involves CdSe/PPV multilayer structures (112). These structures were prepared by alternate absorption of PPV precursor polymer and negatively charged CdSe

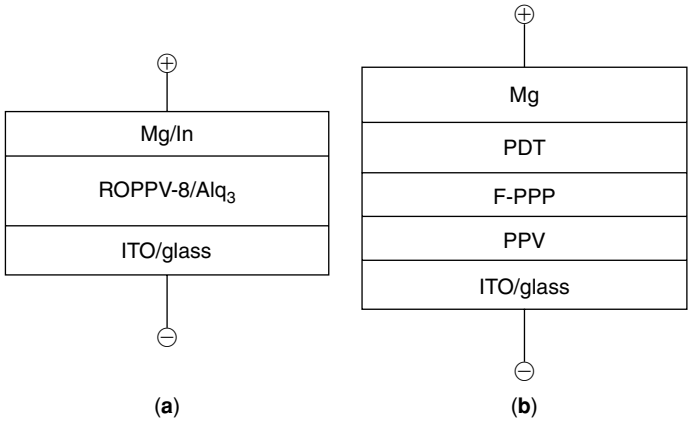

Fig. 3. Schematics of tunable color light-emitting devices.

particles onto an ITO substrate. In these devices, electroluminescence arises exclusively through charge recombination on the CdSe particles, and has a maximum intensity at 650 nm. The PPV is believed to act only to transport charge, thus significantly reducing the turn-on voltage in these devices compared with those using insulating poly(allylaminehydrochloride) as the host.

Polymer-based light-emitting devices in which the emission color may be tuned by varying the bias voltage have been fabricated. In one approach, the emitting layer consists of a mixture of poly(2,5-dioctyl-*p*-phenylenevinylene) (ROPPV-8) and Alq_3 sandwiched between a Mg/In cathode and an ITO anode (Fig. 3**a**) (113). The electroluminescence from this device varies from orange to greenish yellow as the bias voltage is increased from 15 to 22 V. Increasing the voltage increases the proportion of the emitted light arising from the Alq_3. Devices in which ROPPV-8 and Alq_3 are in separate layers emit only from the polymer layer regardless of applied voltage. Another approach uses a three-layer device, consisting of PPV, perfluoropropylated poly(*p*-phenylene) (F-PPP), and poly(3-dodecylthiophene) (PDT) (Fig. 3**b**) (114). The F-PPP acts as an electron-blocking layer, confining emission only to the side of the device to which a negative bias is applied. Thus, green light is emitted when the negative bias is on the PPV side, and red light is emitted when it is applied to the PDT side. Doping a PPV derivative with a dinuclear ruthenium complex, that acts both as electron-transfer mediator and triplet emitter, gives a material that exhibits reversible, voltage-dependent switching from red to green emission. Under forward bias, the excited state of the ruthenium complex is populated, giving red light, while under reverse bias, the lowest singlet state of the polymer is generated, giving green emission (115).

Self-Assembled Devices. Rubner and co-workers at MIT have developed a self-assembly approach to constructing PPV-containing heterostructures for use in EL devices (116). The heterostructures are built up by alternately dipping a substrate in solutions of the sulfonium PPV precursor polymer and anionic polyelectrolytes such as the sodium salts of poly(styrenesulfonate) (PSS) or poly(methacrylic acid) (PMA). The layers are then heated to convert the PPV to the fully conjugated form. This method allows for very precise control of thickness,

as well as manipulation of the nature of the surface (cationic or anionic) in contact with the anode and cathode. Device efficiency is very sensitive to the chemical nature of the interface, and the PMA/Al interface consistently yielded efficiencies greater by a factor of 2 relative to devices with a PPV/Al interface.

Light-Emitting Electrochemical Cells. Recently, Heeger and co-workers have developed light-emitting devices in which a blend of a semiconducting, luminescent polymer with a solid-state electrolyte is used in the emitting layer (117). These devices function as solid-state electrochemical cells, and charge injection results in the formation of a *p–i–n* junction through electrochemical doping. Many of the requirements in conventional polymer LEDs, such as a match between the electrode work function and the polymer valence and conduction bands, are circumvented in such light-emitting electrochemical cells (LECs).

Polymer LECs have been demonstrated to function in a dynamic-junction mode, in which ions move under the external bias to create the junction. These devices degrade when the drive voltage is beyond the window of electrochemical stability. When polyethylene oxide (PEO) is used as the ion-transport medium, the devices can operate in a frozen-junction mode at 100 K. In this mode, response times are comparable to those of polymer LEDs. An improvement on this approach allows the frozen junction to function at room temperature (118). In these single-layer devices a PPV derivative such as poly(2-butyl-5-{2-ethyl(hexyl)}-1,2-phenylenevinylene) was blended with an electrolyte containing a crown ether and lithium triflate. The devices were activated by applying a small voltage while heating to 60–80°C, creating the *p–i–n* junction, and functioned at room temperature with a turn-on voltage of 2.1 V and an external EL efficiency of 2–3%.

Stimulated Emission and Lasers. In 1996, Friend and co-workers demonstrated optically driven lasing from thin films of PPV sandwiched between a distributed Bragg reflector and an Ag mirror (119). Excitation was with a Nd:YAG laser, frequency-tripled to 355 nm. Emission occurs in three cavity modes, equally distributed at low excitation energy; but the 545-nm emission dominates at higher excitation energy, indicating that the device is lasing. The same year the Santa Barbara group reported laser emission from solutions and films of MEH–PPV and TiO_2 nanocrystals. The nanoparticles multiply scatter photons in the composite material, resulting in the scattering length exceeding the gain length (120). Stimulated emission has also been observed from crystalline films of an oligomer of phenylene vinylene substituted with octyloxy groups (**40**) (121).

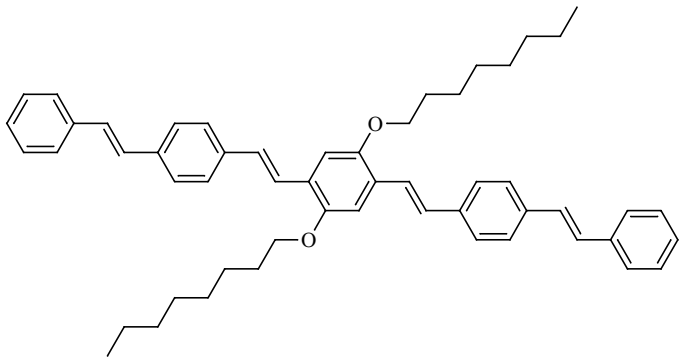

40

Future Considerations

The last 10 years have seen an explosion of research interest in PPV and its derivatives, driven by the potential of these materials as emitters in EL devices. Companies such as Philips, Uniax (DuPont Displays), Cambridge Display Technology, and Covion are engaged in bringing low information content display applications (cell phone and alphanumeric displays) based on organic emitters to market, and in late 1999 Pioneer Electronics had already begun selling a monochrome display for use in vehicles. Higher-information content applications, such as computer and television displays may be developed in the near future.

Although many of the problems that are of concern for optoelectronic applications of organic materials have been overcome, there are still many challenges ahead in the field. Many of the polymers that have been made recently have not yet been investigated in detail, and more work is needed to optimize these materials for specific applications. Fundamental questions also remain, such as the exact nature of the charge carriers in PPV films, and further studies on the photophysical behavior of these polymers are required.

Perhaps the most exciting prospect that has arisen from the intense research activity on PPV is the realization that organic materials and polymers can be used in real world optoelectronic applications. This will hopefully stimulate efforts to make and study more novel materials and to find new applications for them. In particular, any integration of conventional and molecular electronics will require many advances. The success of PPV and other organic EL materials has demonstrated that research in this field is a worthwhile enterprise, and the development of entirely new classes of materials with as yet unknown properties may be on the horizon.

BIBLIOGRAPHY

1. T. Skotheim, R. L. Elsenbaumer, and J. R. Reynolds, *Handbook of Conducting Polymers*, Marcel Dekker, Inc., New York, 1988.
2. J. H. Burroughes, D. D. C. Bradley, A. R. Brown, R. N. Marks, K. Mackay, R. H. Friend, P. L. Burns, and A. B. Holmes, *Nature* **347**, 539 (1990).
3. F. R. Denton III and P. M. Lahti, *Plast. Eng.* **49**, 61 (1998).
4. A. Kraft, A. C. Grimsdale, and A. B. Holmes, *Angew. Chem. Int. Ed.* **37**, 403 (1998).
5. J. Salbeck, *Ber. Bunsen-ges. Phys. Chem.* **100**, 1667 (1996).
6. J. R. Sheats, H. Antoniadis, M. Hueschen, W. Leonard, J. Miller, R. Moon, D. Roitman, and A. Stocking, *Science* **273**, 884 (1996).
7. J. R. Sheats, Y.-L. Chang, D. B. Roitman, and A. Stocking, *Acc. Chem. Res.* **32**, 193 (1999).
8. R. A. Wessling, *J. Polym. Sci., Polym. Symp.* **72**, 55 (1985).
9. R. W. Lenz, C. C. Han, J. Stenger-Smith, and F. E. Karasz, *J. Polym. Sci., Part A: Polym. Chem.* **26**, 3241 (1988).
10. R. O. Garay, U. Baier, C. Bubeck, and K. Muellen, *Adv. Mater.* **5**, 561 (1993).
11. A. Marletta, D. Goncalves, O. N. Oliveira, R. M. Faria, and F. E. Guimaraes, *Adv. Mater.* **12**, 69 (2000).
12. P. L. Burn, D. D. C. Bradley, R. H. Friend, D. A. Halliday, A. B. Holmes, R. W. Jackson, and A. Kraft, *J. Chem. Soc., Perkin Trans. 1* 3225 (1992).

13. P. M. Lahti, D. A. Modarelli, F. R. Denton III, R. W. Lenz, and F. E. Karasz, *J. Am. Chem. Soc.* **110**, 7258 (1988).
14. B. R. Cho, M. S. Han, Y. S. Suh, K. J. Oh, and S. J. Jeon, *J. Chem. Soc., Chem. Commun.* 564 (1993).
15. R. N. McDonald and T. W. Campbell, *J. Am. Chem. Soc.* **82**, 4669 (1969).
16. W. Heitz, W. Bruegging, L. Freund, M. Gailberger, A. Greiner, H. Jung, U. Kampschulte, N. Niessner, and F. Osan, *Makromol. Chem.* **189**, 119 (1988).
17. A. W. Cooke and K. B. Wagener, *Macromolecules* **24**, 1404 (1991).
18. H. G. Gilch and W. L. Wheelwright, *J. Polym. Sci., Part A-1* **4**, 1337 (1966).
19. H. Nishihara, M. Tateishi, K. Aramaki, T. Ohsawa, and O. Kimura, *Chem. Lett.* 539 (1987).
20. W.-P. Chang, W.-T. Whang, and P.-W. Lin, *Polymer* **37**, 1513 (1996).
21. M. Tateishi, H. Nishihara, and K. Aramaki, *Chem. Lett.* 1727 (1987).
22. E. G. J. Staring, D. Braun, G. L. J. A. Rikken, R. J. C. E. Demandt, Y. A. R. R. Kessener, M. Bouwmans, and D. Broer, *Synth. Met.* **67**, 71 (1994).
23. S. Iwatsuki, M. Kubo, and T. Kumeuchi, *Chem. Lett.* 1071 (1991).
24. Y.-J. Miao and G. C. Bazan, *J. Am. Chem. Soc.* **116**, 9379 (1994).
25. V. P. Conticello, D. L. Gin, and R. H. Grubbs, *J. Am. Chem. Soc.* **114**, 9708 (1992).
26. S. H. Askari, S. D. Rughooputh, and F. Wudl, *Synth. Met.* **29**, E129 (1989).
27. F. Wudl, P. M. Allemand, G. Srdanov, Z. Ni, and D. McBranch, *Polymers and an Unusual Molecular Crystal with Nonlinear Optical Properties* (ACS Symposium Series, 455), American Chemical Society, Washington, D. C., 1991, p. 683.
28. C. Zhang, H. von Seggern, K. Pakbaz, B. Kraabel, H. W. Schmidt, and A. J. Heeger, *Synth. Met.* **62**, 35 (1994).
29. H. Liu, S. Want, Y. Luo, W. Tang, G. Yu, L. Li, C. Chen, Y. Liu, and F. Xi, *J. Mater. Chem.* **11**, 3063 (2001).
30. M. Rehahn and A.-D. Schlüter, *Makromol. Chem., Rapid Commun.* **11**, 375 (1990).
31. P. L. Burn, A. Kraft, D. R. Baigent, D. D. C. Bradley, A. R. Brown, R. H. Friend, R. W. Gymer, A. B. Holmes, and R. W. Jackson, *J. Am. Chem. Soc.* **115**, 10117 (1993).
32. P. L. Burn, A. B. Holmes, A. Kraft, D. D. C. Bradley, A. R. Brown, R. H. Friend, and R. W. Gymer, *Nature* **356**, 47 (1992).
33. R. M. Gregorius, P. M. Lahti, and F. E. Karasz, *Macromolecules* **25**, 6664 (1992).
34. G. Kossmehl and M. Samandari, *Makromol. Chem.* **186**, 1565 (1985).
35. A. Lux, A. B. Holmes, R. Cervini, J. E. Davies, S. C. Moratti, J. Gruener, F. Cacialli, and R. H. Friend, *Synth. Met.* **84**, 293 (1997).
36. F. Cacialli, R. H. Friend, W. J. Feast, and P. W. Lovenich, *Chem. Commun.* 1778 (2001).
37. Z. Bao, Y. Chen, R. Cai, and L. Yu, *Macromolecules* **26**, 5281 (1993).
38. T. W. Hagler, K. Pakbaz, K. F. Voss, and A. J. Heeger, *Phys. Rev. B: Condens. Matter* **44**, 8652 (1991).
39. Y. Pang, M. Samoc, and P. N. Prasad, *J. Chem. Phys.* **94**, 5282 (1991).
40. C. J. Wung, Y. Pang, P. N. Prasad, and F. E. Karasz, *Polymer* **32**, 605 (1991).
41. C. J. Wung, W. M. Wijekoon, and P. N. Prasad, *Polymer* **34**, 11174 (1993).
42. P. K. H. Ho and R. H. Friend, *J. Chem. Phys.* **116**, 6782 (2002).
43. Y. T. Lim, T.-W. Lee, H.-C. Lee, and O. O. Park, *Opt. Mater.* **21**, 585 (2003).
44. L. Bozano, S. E. Tuttle, S. A. Carter, and P. J. Brock, *Appl. Phys. Lett.* **73**, 3911 (1998).
45. S. A. Carter, J. C. Scott, and P. J. Brock, *Appl. Phys. Lett.* **71**, 1145 (1997).
46. J. S. Salafsky, W. H. Lubberhuizen, and R. E. I. Schropp, *Chem. Phys. Lett.* **290**, 297 (1998).

47. N. Tesster, V. Medvedev, M. Kazes, S. Kan, and U. Banin, *Science* **295**, 1506 (2002).
48. T. A. E. Loss, C. W. Rogers, and M. O. Wolf, *Can. J. Chem.* **76**, 1554 (1998).
49. R. C. Smith, W. M. Fischer, and D. L. Gin, *J. Am. Chem. Soc.* **119**, 4092 (1997).
50. J. Obrzut and F. E. Karasz, *J. Chem. Phys.* **87**, 2349 (1987).
51. R. H. Friend, D. D. C. Bradley, and P. D. Townsend, *J. Phys. D: Appl. Phys.* 1367 (1987).
52. M. Meier, E. Buchwald, S. Karg, P. Posch, M. Greczmiel, P. Strohriegl, and W. Riess, *Synth. Met.* **76**, 95 (1996).
53. U. Rauscher, H. Bässler, D. D. C. Bradley, and M. Hennecke, *Phys. Rev. B: Condens. Matter* **42**, 9830 (1990).
54. M. Yan, L. J. Rothberg, E. W. Kwock, and T. M. Miller, *Phys. Rev. Lett.* **75**, 1992 (1995).
55. L. J. Rothberg, M. Yan, E. W. Kwock, T. M. Miller, M. E. Galvin, S. Son, and F. Papadimitrakopoulos, *IEEE Trans. Electron Devices* **44**, 1258 (1997).
56. F. Papadimitrakopoulos, K. Konstadinidis, T. M. Miller, R. Opila, E. A. Chandross, and M. E. Galvin, *Chem. Mater.* **6**, 1563 (1994).
57. H.-H. Horhold and J. Opfermann, *Makromol. Chem.* **131**, 105 (1970).
58. S. Tokito, T. Tsutsui, R. Tanaka, and S. Saito, *Jpn. J. Appl. Phys.* **25**, L680 (1986).
59. T. Takiguchi, D. H. Park, H. Ueno, K. Yoshino, and R. Sugimoto, *Synth. Met.* **17**, 657 (1987).
60. D. Moses, J. Wang, G. Yu, and A. J. Heeger, *Phys. Rev. Lett.* **80**, 2685 (1998).
61. S. Tokito, T. Tsutsui, S. Saito, and R. Tanaka, *Polym. Commun.* **27**, 333 (1986).
62. M. Ahlskog, M. Reghu, T. Noguchi, and T. Ohnishi, *Synth. Met.* **89**, 11 (1997).
63. J.-I. Jin, C.-K. Park, and H. K. Shim, *Macromolecules* **26**, 1799 (1993).
64. J. H. F. Martens, D. A. Halliday, E. A. Marseglia, D. D. C. Bradley, R. H. Friend, P. L. Burn, and A. B. Holmes, *Synth. Met.* **55**, 434 (1993).
65. M. A. Masse, D. C. Martin, E. L. Thomas, F. E. Karasz, and J. H. Petermann, *J. Mater. Sci.* **25**, 311 (1990).
66. J. H. F. Martens, E. A. Marseglia, D. D. C. Bradley, R. H. Friend, P. L. Burn, and A. B. Holmes, *Synth. Met.* **55**, 449 (1993).
67. C. Y. Yang, F. Hide, M. A. Diaz-Garcia, A. J. Heeger, and Y. Cao, *Polymer* **39**, 2299 (1998).
68. B. Winkler, S. Tasch, E. Zojer, M. Ungerank, G. Leising, and F. Stelzer, *Synth. Met.* **83**, 177 (1996).
69. W. Memeger, *Macromolecules* **22**, 1577 (1989).
70. M. Suzuki, J.-C. Lim, and T. Segusa, *Macromolecules* **23**, 1574 (1990).
71. A. Samoc, M. Samoc, M. Woodruff, and B. Luther-Davies, *Plast. Eng.* **49**, 373 (1998).
72. T. Kaino, K. Kubodera, S. Tomaru, T. Kurihara, S. Saito, T. Tsutsui, and S. Tokito, *Electron. Lett.* **23**, 1095 (1987).
73. T. Kaino, H. Kobayashi, K. Kubodera, T. Kurihara, S. Saito, T. Tsutsui, and S. Tokito, *Appl. Phys. Lett.* **54**, 1619 (1989).
74. C.-B. Yoon and H.-K. Shim, *J. Mater. Chem.* **8**, 913 (1998).
75. N. S. Sacriciftci, D. Braun, C. Zhang, V. I. Srdanov, A. J. Heeger, G. Stucky, and F. Wudl, *Appl. Phys. Lett.* **62**, 585 (1993).
76. C. J. Brabec, A. Cravino, G. Zerza, N. S. Sariciftci, R. Kiebooms, D. Vanderzande, and J. C. Hummelen, *J. Phys. Chem. B* **105**, 1528 (2001).
77. J. J. M. Halls and R. H. Friend, *Synth. Met.* **85**, 1307 (1997).
78. J. J. Dittmer, K. Petritsch, E. A. Marseglia, R. H. Friend, H. Rost, and A. B. Holmes, *Synth. Met.* **102**, 879 (1999).
79. J. Gao, G. Yu, and A. J. Heeger, *Adv. Mater.* **10**, 692 (1998).
80. K. Yoshino, T. Kuwabara, T. Iwasa, T. Kawai, and M. Onoda, *Jpn. J. Appl. Phys.* **29**, L1514 (1990).
81. C. W. Tang and S. A. VanSlyke, *Appl. Phys. Lett.* **51**, 913 (1987).

82. C. W. Tang, S. A. VanSlyke, and C. H. Chen, *J. Appl. Phys.* **65**, 3610 (1989).
83. A. R. Brown, D. D. C. Bradley, J. H. Burroughes, R. H. Friend, N. C. Greenham, P. L. Burn, A. B. Holmes, and A. Kraft, *Appl. Phys. Lett.* **61**, 2793 (1992).
84. M. Meier, E. Buchwald, S. Karg, P. Posch, M. Greczmiel, P. Strohriegl, and W. Riess, *Synth. Met.* **76**, 95 (1996).
85. P. Fournet, D. F. C. O'Brien, J. N. Horhold, H.-H., and W. J. Blau, *Synth. Met.* **121**, 1683 (2001).
86. K. Naito and A. Miura, *J. Phys. Chem.* **97**, 6240 (1993).
87. D. R. O'Brien, P. E. Burrows, S. R. Forrest, B. E. Koene, D. E. Loy, and M. E. Thompson, *Adv. Mater.* **10**, 1108 (1998).
88. M. Thelakkat and H.-W. Schmidt, *Adv. Mater.* **10**, 219 (1998).
89. N.-X. Hu, S. Xie, Z. Popavic, B. Ong, A.-M. Hor, and S. Wang, *J. Am. Chem. Soc.* **121**, 5097 (1999).
90. G. Yu, *Synth. Met.* **80**, 143 (1996).
91. N. Tessler, N. T. Harrison, and R. H. Friend, *Adv. Mater.* **10**, 64 (1998).
92. S. A. Carter, M. Angelopoulos, S. Karg, P. J. Brock, and J. C. Scott, *Appl. Phys. Lett.* **70**, 2067 (1997).
93. A. C. Arias, M. Granström, D. S. Thomas, K. Petritsch, and R. H. Friend, *Phys. Rev. B* **60**, 1854 (1999).
94. G. Gustafsson, Y. Cao, G. M. Treacy, F. Klavetter, N. Colaneri, and A. J. Heeger, *Nature (London)* **357**, 477 (1992).
95. I. D. Parker, and H. H. Kim, *Appl. Phys. Lett.* **64**, 1774 (1994).
96. H. Becker, S. E. Burns, and R. H. Friend, *Phys. Rev. B: Condens. Matter* **56**, 1893 (1997).
97. E. Peeters, M. P. T. Christiaans, R. A. J. Janssen, H. F. M. Schoo, H. P. J. M. Dekkers, and E. W. Meijer, *J. Am. Chem. Soc.* **119**, 9909 (1997).
98. S. Son, A. Dodabalapur, A. J. Lovinger, and M. E. Galvin, *Science* **269**, 376 (1995).
99. B. H. Cumpston, I. D. Parker, and K. F. Jensen, *J. Appl. Phys.* **81**, 3716 (1997).
100. J. C. Scott, J. H. Kaufman, P. J. Brock, R. DiPietro, J. Salem, and J. A. Goitia, *J. Appl. Phys.* **79**, 2745 (1996).
101. K. M. Vaeth and K. F. Jensen, *Appl. Phys. Lett.* **71**, 2091 (1997).
102. J. C. Carter, I. Grizzi, S. K. Heeks, D. J. Lacey, S. G. Latham, P. G. May, O. Ruiz de los Panos, K. Pichler, C. R. Towns, and H. F. Wittmann, *Appl. Phys. Lett.* **71**, 34 (1997).
103. J. M. Bharathan and Y. Yang, *Appl. Phys. Lett.* **72**, 2660 (1998).
104. J. A. Rogers, Z. Bao, and L. Dhar, *Appl. Phys. Lett.* **73**, 294 (1998).
105. H. Kobayashi, S. Kanbe, S. Seki, H. Kigchi, M. Kimura, I. Yudasaka, S. Miyashita, T. Shimoda, C. R. Towns, J. H. Burroughes, and R. H. Friend, *Synth. Met.* **111/112**, 125 (2000).
106. P. L. Burn, A. B. Holmes, A. Kraft, D. D. C. Bradley, A. R. Brown, and R. H. Friend, *J. Chem. Soc., Chem. Commun.* 32 (1992).
107. I. Sokolik, Z. Yang, F. E. Karasz, and D. C. Morton, *J. Appl. Phys.* **74**, 3584 (1993).
108. F. Garten, A. Hilberer, F. Cacialli, E. Esselink, Y. Van Dam, B. Schlatmann, R. H. Friend, T. M. Klapwijk, and G. Hadziioannou, *Adv. Mater.* **9**, 127 (1997).
109. S. T. Kim, D. H. Hwang, X. C. Li, J. Gruener, R. H. Friend, A. B. Holmes, and H. K. Shim, *Adv. Mater.* **8**, 979 (1996).
110. D. R. Baigent, P. J. Hamer, R. H. Friend, S. C. Moratti, and A. B. Holmes, *Synth. Met.* **71**, 2175 (1995).
111. S. J. Chung, J. I. Jin, and K. K. Kim, *Adv. Mater.* **9**, 551 (1997).
112. M. Gao, B. Richter, and S. Kirstein, *Adv. Mater.* **9**, 802 (1997).
113. M. Uchida, Y. Ohmori, T. Noguchi, T. Ohnishi, and K. Yoshino, *Jpn. J. Appl. Phys.* **32**, L921 (1993).
114. M. Hamaguchi and K. Yoshino, *Appl. Phys. Lett.* **69**, 143 (1996).

115. S. Welter, K. Brunner, J. W. Hofstraat, and L. De Cola, *Nature* **421**, 54 (2003).
116. O. Onitsuka, A. C. Fou, M. Ferreira, B. R. Hsieh, and M. F. Rubner, *J. Appl. Phys.* **80**, 4067 (1996).
117. Q. Pei, G. Yu, C. Zhang, Y. Yang, and A. J. Heeger, *Science* 1086 (1995).
118. G. Yu, Y. Cao, M. Andersson, J. Gao, and A. J. Heeger, *Adv. Mater.* **10**, 385 (1998).
119. N. Tessler, G. J. Denton, and R. H. Friend, *Nature* **382**, 695 (1996).
120. F. Hide, B. J. Schwatz, M. A. Diaz-Garcia, and A. J. Heeger, *Chem. Phys. Lett.* **256**, 424 (1996).
121. H.-J. Brouwer, V. V. Krasnikov, T.-A. Pham, R. E. Gill, and G. Hadziioannou, *Appl. Phys. Lett.* **73**, 708 (1998).

MICHAEL O. WOLF
The University of British Columbia

POLYANHYDRIDES

Introduction

The first report on the formation of polyanhydrides appeared in 1909 (1) and the detailed synthesis of a range of polyanhydrides was reported in 1930s (2,3). Polyanhydrides derived from aromatic diacids were hydrolytically stable and had excellent film- and fiber-forming properties (4). A large number of aromatic polyanhydrides were studied and characterized. They had glass-transition temperatures in the range of 50–100°C, appeared as opaque porcelain-like solids, and were resistant to hydrolysis even upon exposure to an alkaline solution (4). The mechanical properties of aromatic polyanhydrides were exemplified by the measurements carried out on stretched fibres of poly(di-(*p*-carboxyphenoxy)-1,3-propane) annealed at 110°C under constant load. The fibres showed a tensile strength of 40 kg/mm^2 with an elongation of 17.2% and a Young's modulus of 505 kg/m^2 (4). Concurrently, various types of heterocyclic polyanhydrides were synthesized from five-member ring heterocyclic diacids with acetic anhydride at 200–300°C under vacuum and nitrogen atmosphere, which had melting points in the range 70–190°C (5,6). It is thus clear that all the early research efforts were devoted to enhancing the stability of polyanhydrides against hydrolysis to get a good fiber- and film-forming polymer. Unfortunately, polyanhydrides were not commercially successful textile materials due to their unstable nature against hydrolysis, especially for aliphatic polyanhydrides. In contrast, their hydrolytic instability make them potentially useful for biomedical and pharmaceutical applications, where the hydrolytic instability of a polymer is a desired feature rather than a weakness. Langer and co-workers (7) were the first researchers to exploit the hydrolytically labile nature of polyanhydrides for controlled drug delivery through a medical device. This article will mainly focus on summarizing the synthesis and characterization of polyanhydrides used for pharmaceutical and medical device applications.

Encyclopedia of Polymer Science and Technology. Copyright John Wiley & Sons, Inc. All rights reserved.

The main advantage of using polyanhydrides for medical applications is that they gradually degrade into nontoxic, small molecular weight products after their intended use in drug delivery, obviating the need for retrieval (see BIODEGRADABLE POLYMERS, MEDICAL APPLICATIONS). A large number of polyanhydrides synthesized to date have been found biocompatible (8) and have excellent controlled release characteristics (9,10). The control over drug release kinetics and matrix degradation rate can be achieved through manipulation of the polymer compositions (11). Among the most useful diacid monomers for making polyanhydrides used in pharmaceutical applications are sebacic acid (SA), 1,3-bis(*p*-carboxyphenoxy)propane (CPP), and erucic acid dimmer (EAD). The copolymers poly(CPP-SA) and poly(EAD-SA) have been used in the clinic for the delivery of the anticancer agent *N*,*N*-bis(2-chloroethyl)-*N*-nitrosourea (BCNU) and the antibiotic gentamicin sulfate and in the United States, Food and Drug Administration (FDA) approved BCNU-poly(CPP-SA) as treatment for brain tumors (12).

Synthesis

Polyanhydrides have been synthesized by various techniques such as melt polycondensation, ring-opening polymerization, interfacial polycondensation, dehydrochlorination, and dehydrative coupling (13,14). The most widely used technique for polyanhydride synthesis is melt polycondensation, which occurs in two steps. In the first step, dicarboxylic acid monomers react with excess acetic anhydride to form acetyl-terminated anhydride prepolymers (**1**) with a degree of polymerization (DP) ranging from 1 to 20 (eq. 1).

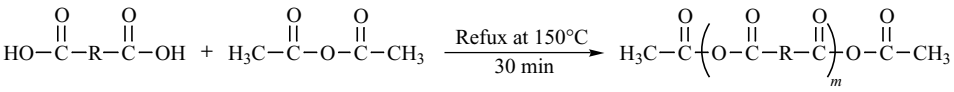

(1)

The activated monomers are then polymerized at an elevated temperature (if necessary) under vacuum to yield polyanhydrides with DP ranging from 100 to over 1000 (eq. 2).

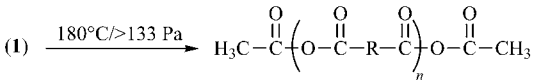

(2)

Purification of the prepolymers, using methods such as recrystallization, is a crucial step to increase the molecular weight (M_w) of polymers (15). It is important to carefully monitor the kinetics of the prepolymer reaction to prevent the formation of high molecular weight oligomers, which may have high T_m and are difficult to purify. In general, the melt polycondensation commences readily under low pressure and is completed in several hours at grams to kilograms scale. In comparison to the preparation of polyesters, in general, polycondensation of polyanhydrides proceeds more rapidly (11,16), for example, ester polycondensation completes in 12–24 h while polyanhydride takes less than 2 h to complete the reaction, depending on the molecular weight required. This reaction to form anhydrides is weakly

Table 1. Melt Polymerization of Poly(CPP-SA) (20:80) Using Coordination Catalysts[a]

Catalyst	Polymerization time, min	Viscosity[b] $[\eta]$, dL/g	Molecular weight[c] M_w	Molecular weight[c] M_n	Reaction[d] type
No catalyst	90	0.92	116,800	18,200	
Metal salts					
Cadmium acetate	31	1.25	245,010	29,420	A
Zinc acetate	50	0.31	33,440	8,020	A
Earth metal oxides					
Calcium oxides	20	0.88	140,935	14,877	A
Barium oxides	30	0.96	185,226	22,500	A
Calcium carbonate	28	0.90	141,600	15,500	A
Alkoxy metals					
Titanium isopropoxide	30	0.26	23,678	6,749	B
Titanium *n*-butoxide	30	0.20	21,785	7,211	B
Aluminium isopropoxide	32	0.64	63,247	17,081	A
Aluminium *t*-butoxide	32	0.68	75,387	18,509	A
Organometals					
$Zn(C_2H_5)_2$	60	0.62	85,060	15,287	B
$Zn(C_2H_5)_2$–H_2O (1:1)	60	1.18	199,060	25,312	A
Iron compounds					
Ferric acetylacetonate	30	0.36	26,850	8,910	B
Ferric chloride	30	0.41	29,340	9,100	B
Ferric hydroxide	30	0.30	27,500	6,920	A

[a]Polymerization was done at 180°C using 2 mol% catalyst. Ref. 13.
[b]Chloroform, 23°C.
[c]GPC; calibrated with polystyrene standards.
[d]A, heterogeneous catalysis; B, homogeneous catalysis.

exothermic (17), and hence, the equilibrium constant decreases with an increase in temperature. All the things being equal, a low polymerization temperature should afford a higher molecular weight. Excessive heating at 180°C appears to cause decarboxylation or decarbonylation (18). However, prolonged distillation of the initial reaction mixture, up to 72 h, improves the molecular weight. The condensation reaction of diacetyl mixed anhydrides of aromatic and aliphatic diacids is carried out in the temperature range of 150–200°C (19). In addition to acetic anhydride, a variety of catalysts have been included in the synthesis of polyanhydrides. Particularly, coordination catalysts facilitate the anhydride interchange in the polymerization and enhance the nucleophilicity of the carbonyl carbon (20). Table 1 shows the highest molecular weight obtained by using coordination catalysts in the synthesis of polyanhydride copolymer of bis(carboxyphenoxy)propane and sebacic acid (CPP-SA) (13). Except calcium carbonate, which is a naturally occurring material, the use of most catalysts for the production of medical grade polymers is undesirable because of their potential toxicity (15). Ring-opening polymerization (ROP) can also be used for the synthesis of polyanhydrides used for medical applications. For example, adipic acid polyanhydrides were prepared from cyclic adipic anhydride (oxepane-2,7-dione) by using cationic (e.g., $AlCl_3$ and $BF_3{\cdot}(C_2H_5)_2O$), anionic (e.g., $CH_3COO^-K^+$ and NaH), and coordination-type (e.g., stannous-2-ethylhexanoate and dibutyltinoxide) catalysts (21).

Because melt polycondensation often requires a high temperature, it is not suitable for making heat sensitive polymers. A variety of solution polymerizations at ambient temperature have been reported (18,22). Polyanhydride formation can be effected at room temperature by a dehydrochlorination between a diacid chloride and a dicarboxylic acid (eq. 3).

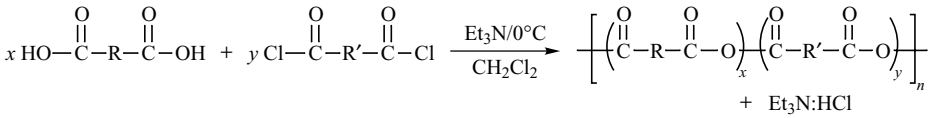

(3)

In an attempt to prepare copolyanhydrides of regular structures, polycondensation was conducted in organic solvent pairs such as pyridine–benzene and pyridine–ether. A polycondensation was reported between an acylchloride and a carboxylic acid in a single solvent system in the presence of an acid acceptor such as triethylamine (18). The polymerization took place on contact of the two monomers and was essentially complete within an hour as monitored by gel permeation chromatography (GPC). The DP was in the range of 20–30 as determined by vapor pressure osmometry. Comparable M_w and yields were obtained for polymerization conducted in solvents such as dichloromethane, chloroform, benzene, and diethyl ether (18). The DP was influenced by the order of addition. Adding the diacid solution dropwise to the diacid chloride solution consistently produced higher M_w polymers and yields as compared to the reverse order of addition (22). Adding the acyl chloride in a single portion, however, yields satisfactory results, suggesting that the rate of dehydrochlorination is comparable to the rate of acid chloride–amine complexation. The inconvenience of this homogeneous Schotten–Baumann condensation in solution is outweighed by the need to obtain the highly purified diacid chloride monomer. The formation of polyanhydrides by this method can be effected by using diacid chlorides, which upon controlled hydrolysis with a half equivalent of water form the acid that condense to anhydride bonds (eq. 4).

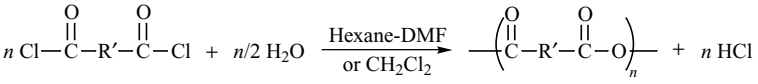

(4)

Low molecular weight polyanhydrides were prepared from the reaction of diacid with dehydrating agents such as *N*,*N*-bis[2-oxo-3-oxazolidinyl]phosphoramidoyl chloride and phenyl-*N*-phenylphosphonamidoyl chloride (18) or by direct condensation at elevated temperature under vacuum and acid catalysis (eq. 5).

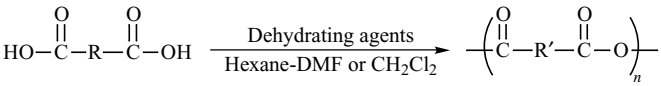

(5)

A one-step polymerization using diacyl chloride, phosgene, or diphosgene as coupling agents was also developed (eq. 6).

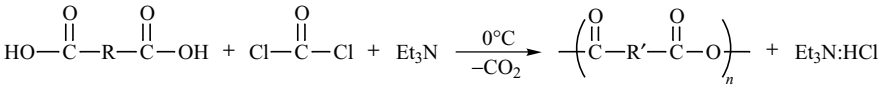

(6)

The results of polymerization between sebacic acid and fumaric acid, using either phosgene or diphosgene as coupling agents with various acid acceptors, were reported (22). Although phosgene and diphosgene are equally efficient, diphosgene as a liquid is preferred because of its ease of handling and lower vapor toxicity. The polymers have similar M_w when the same type of amine base was used. For example, the heterogeneous acid acceptor poly(4-vinylpyridine)(PVP) produced satisfactory results, whereas a nonamine heterogeneous base (e.g., K_2CO_3) yielded a lower M_w. This effect may be explained by the observation that pyridine forms a 1:1 complex with acid chlorides prior to their reaction with hydroxyl-bearing molecules. In the same way, the amines formed a soluble intermediate complex of acid–amine that improved the interaction with the coupling agent under homogeneous conditions. Although PVP is insoluble in the reaction medium, it swells and forms a similar acid-PVP complex. Carbonates, however, form a heterogeneous mixture with the acid and presumably react more slowly with the coupling agents to form the polymer (22).

Polyanhydride Structure

Since the introduction of polyanhydrides in the regime of polymers, hundreds of polyanhydride structures have been reported for the past century (23). A representative list of polyanhydrides is shown in Table 2. On the basis of their monomers, polyanhydrides can be categorized as the following types:

Aliphatic Polyanhydrides. Aliphatic polyanhydrides of saturated diacid monomers are crystalline, melt at temperatures below 100°C, and are soluble in chlorinated hydrocarbons. They degrade and are eliminated from the body within weeks (11).

Unsaturated Polyanhydrides. A series of unsaturated polyanhydrides were prepared by melt or solution polymerization of fumaric acid (FA), acetylenedicarboxylic acid (ACDA), and 4,4′-stilbenedicarboxylic acid (STDA). The double bonds remain intact throughout the polymerization process as noted by IR spectroscopy and were available for a secondary reaction to form a cross-linked matrix (27). The unsaturated homopolymers were crystalline and insoluble in common organic solvents, whereas copolymers with aliphatic diacids were less crystalline and soluble in chlorinated hydrocarbon solvents (27). Branched and crosslinked polyanhydrides were synthesized in the polymerization reaction of diacid monomers with tri- or polycarboxylic acid branching monomers (48). The molecular weights of the branched polymers were significantly higher (250,000 Da) than those of the respective linear polymers (80,000 Da). The specific viscosities of the branched polymers were lower than those of linear polyanhydrides with similar molecular weights. Except for the difference in molecular weights, there were no noticeable changes in the physicochemical or thermal properties of the branched polymers as compared to the linear polymers.

Table 2. Representative Polyanhydride Structures

Polymer type	General structure	Examples	Melting point, °C	Ref.
Aliphatic polyanhydrides	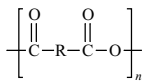 R = Aliphatic chain and X and n are the number of its unit	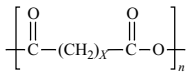 $x = 8$, PSA; 4, PAA	50–90	(24–26)
Unsaturated polyanhydrides	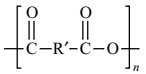 R' is unsaturated and remain intact during polymerization	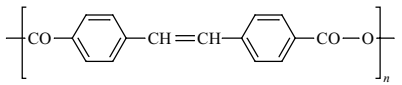 Poly(STDA) 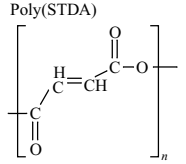 Poly(FA) 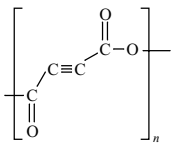 Poly(ACDA)	>200	(27,28)

Table 2. (Continued)

Polymer type	General structure	Examples	Melting point, °C	Ref.
Aromatic polyanhydrides	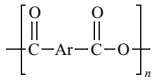 Homopolymers	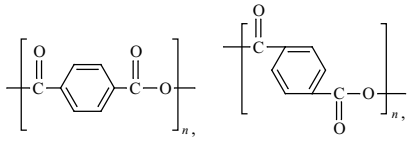 Poly(TA) Poly(ITA) 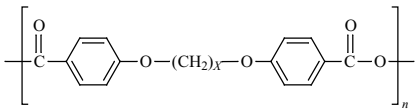 $X = 3$, poly(CPP); 6, poly(CPH)	>200	(4,29,30)
	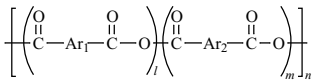 Copolymers	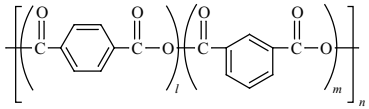 Poly(TA-ITA)	<100	
Aliphatic–aromatic polyanhydrides	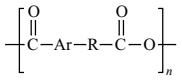 R and Ar are aliphatic and aromatic moieties respectively	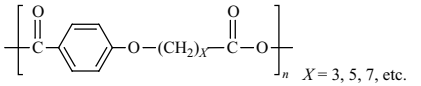 poly((*p*-carboxyphenoxy)alkanoic anhydride)	50–120	(19,31, 32)
	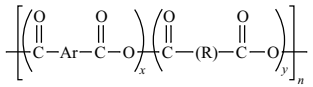 R and Ar are aliphatic and aromatic moieties respectively	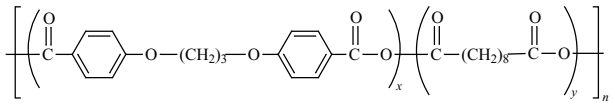 poly(CPP-SA)	50–240	(29)

Poly(ester anhydride) and poly(ether anhydride)	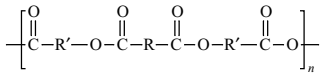 R' and R are aliphatic or aromatic moiety	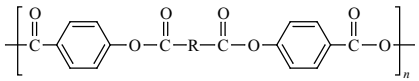 R = $(CH_2)_{2-8}$; {$(CH_2)_2$—O—(CH_2—CH_2—O)$_2$—$(CH_2)_2$}	98–176	(16,33–35)
Fatty acid based polyanhydrides	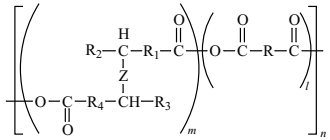 Z = —COO, —NH, CH_2, —$CONH_2$ R, R_1, R_2, R_3, R_4 are saturated or unsaturated alkyl groups. *l*, *m*, and *n* are the number, may be same or different	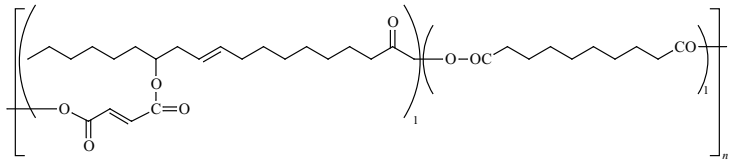 Copolymer of recinoleic acid and sebacic acid anhydride	20–90	(36–39)
Amino acid based polyanhydrides	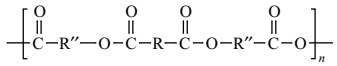 R" is amino acid moiety	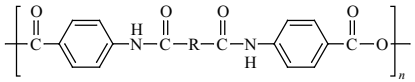 R = $(CH_2)_3$; {$(CH_2)_2$—O—$(CH_2)_2$}	58–170	(40–43)
Blends	Blends of two or more polyanhydrides or one polyanhydride with other like polyesters, polycarbonates, etc.	PSA-blend-PLA, poly[bis(glycine ethyl ester) phosphazene]-blend-(PSA or PSTP)		(44–47)

Aromatic Polyanhydrides. Aromatic homopolyanhydrides are insoluble in common organic solvents and melt at temperatures above 200°C (29). These properties limit the use of purely aromatic polyanhydrides, since they cannot be fabricated into films or microspheres using solvent or melt techniques. Fully aromatic polymers that are soluble in chlorinated hydrocarbons and melted at temperatures below 100°C were obtained by copolymerization of aromatic diacids such as isophthalic acid (IPA), terephthalic acid (TA), 1,3-bis(carboxyphenoxy)propane (CPP), or 1,3-bis(carboxyphenoxy)hexane (CPH).

Aliphatic-Aromatic Polyanhydrides. Polyanhydrides of diacid monomers containing aliphatic and aromatic moieties, such as poly-((*p*-carboxyphenoxy)alkanoic anhydride), were synthesized by either melt or solution polymerization, with molecular weights reaching up to 44,600 Da (19). The polymers of carboxyphenoxy alkanoic acid having methylene groups ($n = 3$, 5, and 7) were soluble in chlorinated hydrocarbon solvents and melted at temperatures below 100°C. These polymers displayed a zero-order hydrolytic degradation profile for 2–10 weeks. The length of the alkanoic chain positively correlates to the degradation time (19).

Poly(ester-Anhydrides) and Poly(ether-anhydrides). 4,4′-alkane- and oxa-alkanedioxydibenzoic acids were used for the synthesis of polyanhydrides. These polyanhydrides melted at a temperature range of 98–176°C and had M_w up to 12,900. Di- and triblock copolymers of poly(caprolactone) (PCL), poly(lactic acid) (PLA), and poly(hydroxybutyrate) (PHB) have been prepared from carboxylic acid terminated low M_w prepolymers copolymerized with SA prepolymers by melt condensation (49). Similarly, di-, tri-, and brush copolymers of poly(ethylene glycol) (PEG) with poly(sebacic anhydride) (PSA) have been prepared by melt copolymerization of carboxylic acid terminated PEG (50).

Fatty Acid Based Polyanhydrides. These polyanhydrides were synthesized from dimer and trimer unsaturated fatty acids (36,37,51). The dimers of oleic acid and eurecic acid are liquid oils containing two carboxylic acids, which are available for polymerization; correspondingly, the homopolymers are viscous liquids. Copolymerization with increasing amounts of SA forms solid polymers with increased melting points. The polymers are soluble in tetrahydrofuran, 2-butanone, and acetone. Polyanhydrides synthesized from nonlinear hydrophobic fatty acid esters based on ricinoleic acid, maleic acid, and SA, possessed desired physicochemical properties such as low melting point and hydrophobicity, and good flexibility (52) in addition to biocompatibility (53) and biodegradability (54).

Amino Acid Based Polyanhydrides. Amino acid based polymers were synthesized from dicarboxylic acids prepared by amidation of the amino group of an amino acid with a cyclic anhydride, or by the amide coupling of two amino acids with a diacid chloride (55). Low molecular weight polymers from methylene bis(*p*-carboxybenzamide) were synthesized by melt condensation (56). A series of amido-containing polyanhydrides based on *p*-aminobenzoic acid were synthesized by melt condensation (56). These polymers melted from 58 to 177°C and had molecular weights from 2500 to 12,400 Da. The homopolymers of all *N*-trimellitylimido acids containing amino acids were rigid and brittle with M_w below 10,000 Da (57). Higher molecular weight polymers were obtained by incorporation of flexible segments, ie, copolymers with aliphatic diacids, in the polymer backbone. Copolymers of *N*-trimellitylimido-glycine or aminodecanoic acid with either sebacic acid

(SA) or 1,6-bis(*p*-carboxyphenoxy)hexane (CPH) were prepared in defined ratios. High molecular weight copolymers (>100,000 Da.) were generally obtained with an increasing content of the SA or CPH comonomer relative to the trimellitylimidoglycine.

Blends. Blending, or mixing, appropriate polymers can alter the physical and mechanical properties of polyanhydrides. Blends of poly(trimethylene carbonate) (PTMC) with poly(adipic anhydride) (PAA) were found biocompatible in both *in vitro* and *in vivo* experiments (44). Blends were prepared by dissolving each polymer in methylene chloride followed by separately mixing in varying proportions using solvent-mixing technique (45). The results indicate that the blend may be a promising candidate for controlled drug delivery (44,46) and varying the proportion of PTMC and PAA can control the erosion rate of the polymer blend. Low molecular weight polyesters such as PLA, PHB, and PCL are miscible with polyanhydrides, whereas high molecular weight polyesters (M_w > 10,000 Da) are not compatible with polyanhydrides. Uniform blends of PCL with 10–90% by weight of poly(dodecanedioic anhydride) (PDD) were prepared by melt mixing at 120°C and exhibited good mechanical strength. Hydrolysis studies indicated that the anhydride component degraded and was released from the blend composition without affecting the PCL degradation (45).

Properties

Thermal. Because crystallinity is an important factor in controlling polymer erosion, the effect of polymer composition on crystallinity was studied (40,41). Almost all polyanhydrides show some degree of crystallinity as manifested by their crystalline melting points. Polymers based on SA, CPP, CPH, and FA were particularly investigated. Homopolyanhydrides of aromatic and aliphatic diacids, for example, poly(CPP) and poly(FA), were crystalline (>50% crystallinity) (29), whereas the copolymers possess a less degree of crystallinity, which increases by enhancing the mole ratio of either aliphatic or aromatic diacid monomers (29). The heat of fusion (H_f) values for poly(CPP-SA) demonstrated a sharp decrease from 36.6 to 2.0 cal/g as CPP is gradually added upto 40%, while an increase in H_f value was observed upto 26.5 cal/g on further addition of CPP (58). The trend of decreasing crystallinity, as one monomer is added, was noted using X-ray diffraction or differential scanning colorimeter (DSC) methods. The decrease in crystallinity is a direct result of the random presence of other units in the polymer chain. A detailed analysis of the copolymers of SA with the aromatic and unsaturated monomers, CPP, CPH, FA, and trimellitic-amino acid derivative, showed that copolymers with high ratios of SA and CPP, TMA-gly, or CPH were crystalline while copolymers with equal ratios of SA and CPP or CPH were amorphous (40). In contrasts, the poly(FA-SA) series displayed high crystallinity regardless of comonomer ratio (27).

The melting points of a large number of polymers have been determined and are shown in Table 2. Aliphatic polyanhydrides generally melt at lower temperatures than do aromatic polyanhydrides. The melting point of aromatic–aliphatic copolymers is proportional to the aromatic content in the copolymer. Introduction of fatty acids in copolymers also lowers the melting point of the bulk polymer.

Inclusion of an aromatic amide linkage in the backbone is found to increase the transition temperatures (55). The formation of intermolecular hydrogen bonds is believed to cause this high crystallinity. Poly(anhydrides-*co*-amide) also have high thermal stability (55).

Mechanical. Polyanhydrides show poor mechanical properties in comparison with other polymers such as polyesters. Mechanical properties of various polyanhydrides and their copolyanhydrides were tested as transparent and flexible films made by melt compression and solvent casting. It was observed that increasing the CPP content in copolymer composition increases the tensile strength as well as elongation of various polyanhydrides tested (13). Despite the low molecular weight ($M_n = 6400$) of poly(CPP-SA) (60:40), it has a higher tensile strength of 981 MPa (100 kgf/cm^2) than it has in the 20:80 composition ($M_n = 18{,}900$), 441 MPa (45 kgf/cm^2). Decreasing the M_n of films of the same CPP content (60%) from 12,100 to 6,400 results in lower tensile strength. The elongation at break of these films ranges from 17 to 23%.

Table 3 shows the mechanical properties of fatty acid based polyanhydrides. Films of fatty acid polyanhydrides were transparent and flexible with a tensile strength of 4–19 MPa and elongation at break in the range of 77–115%. The terpolymer of (fatty acid trimer (FAT)-CPP-SA) in a 1:1:1 weight ratio formed the strongest film. Figure 1 shows the stress–strain curve for polyanhydrides derived from natural fatty acids (54). The polymer had a tensile strength of 2.5–3.2 MPa and yield stress at break around 20% in comparison to poly(EAD-SA) (1:1) and PSA, which had tensile strengths of 5.7 and 7.2 MPa and yield stress at break of 10 and 1.5%, respectively. Thus, introduction of nonlinear fatty acid structures in polyanhydrides provides hydrophobicity and flexibility to the polymers.

Stability. The stability of polyanhydrides in solid state and dry chloroform solution was studied (20). Aromatic polymers such as poly(CPP) and

Table 3. Physical Properties of Fatty Acid Polyanhydrides[a]

Polymer[b,c]	Molecular weight		T_m[d], °C	ΔH, J/g	Crystallinity[e], %
	M_w	M_n			
Poly (SA)	465,800	23,400	89	132	50
Poly(RAM)	27,800	11,400	Viscous oil	—	—
Poly(RAM-SA) (50:50)	135,200	12,900	66	65	16
Poly(RAM-SA) (40:60)	6,200	5,000	77	66	∼20
Poly(RAM-SA) (30:70)	14,000	10,800	79	103	
Poly(RAM-SA) (20:80)	8,500	6,200	81	109	
Poly(RAM-SA) (10:90)	10,500	7,200	86	119	
Poly(HSAM)	29,500	9,400	Semisolid	—	—
Poly(HSAM-SA) (50:50)	32,000	11,600	67	51	18
Poly(HSAS)	15,200	8,700	Semisolid	—	—
Poly(HSAS-SA) (50:50)	28,700	13,000	70	79	20

[a] Ref. 54.
[b] Polymers were synthesized by melt condensation. RAM: ricinoleic acid maleate; SA: sebacic acid; HSAM: hydroxy stearic acid maleate; HSAS: hydroxy stearic acid succinate.
[c] Values in parentheses denote mole ratio.
[d] Melting transition temperature (T_{max}) was determined by DSC.
[e] Degree of crystallinity was obtained from X-ray analysis.

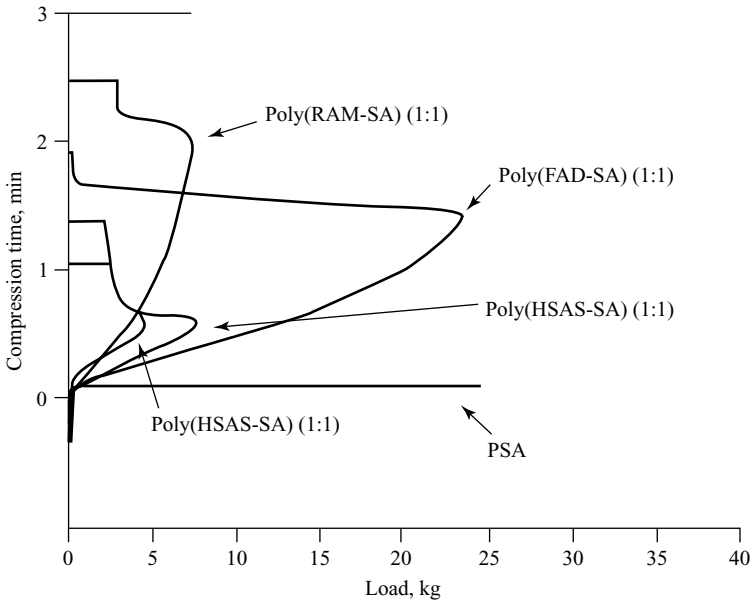

Fig. 1. Stress–strain curves for ricinoleic acid derived polymers (38).

poly(1,1-bis(*p*-carboxyphenoxy) methane) maintained their original molecular weight for at least 1 year in the solid state. In contrast, aliphatic polyanhydrides, such as PSA, showed decreased molecular weight over time. The decrease in molecular weight shows a first-order kinetics, with activation energies of 7.5 Kcal/(mol·K). The decrease in molecular weight was explained by an internal anhydride interchange mechanism, as revealed from elemental and spectral analyses. This mechanism was supported by the fact that the decrease in molecular weight was reversible and heating the depolymerized polymer at 180°C for 20 min yielded the original high molecular weight polymers. However, under similar conditions the hydrolyzed polymer did not increase in molecular weight (20). In many cases, it was observed that the stability of polymers in the solid state or in organic solution did not correlate with its hydrolytic stability (20). A similar decrease in molecular weight as function of time was also observed among the aliphatic–aromatic copolyanhydrides and imide-containing polyanhydrides (19,57).

Gamma-irradiation technique is typically used to sterilize polyanhydrides (59). Aliphatic and aromatic homo- and copolymers were irradiated at 2.5 Mrad dose and the change in properties was monitored before and after irradiation. Properties such as molecular weight, melting temperature, and heat of fusion remained the same, and ^{1}H NMR and FT-IR spectra of the polymer were also similar before and after irradiation (60,61). Using the same concept, these studies were extended for saturated and unsaturated polyanhydrides (28). Ricinoleic acid based copolymers with SA and poly(CPP:SA) were irradiated under dry ice and at room temperature while poly(FA:SA) was irradiated only at room temperature. Saturated polyanhydrides are stable enough during irradiation; however, the presence of double bonds conjugated to an anhydride bond creates an unstable structure

and leads to the formation of free radicals (28). These free radical polyanhydrides degrade into less conjugated polyanhydrides. The outcome of this process is self-depolymerization via inter- and/or intramolecular anhydride interchange to form polymers with lowered molecular weight. In general, polymers with high melting points and crystallinity give the highest yield of room temperature observable radicals. These endogenous free radicals were used to study processes of water penetration and polymer degradation *in vivo* (59). The detection of gamma sterilization induced free radicals *in vivo* using EPR could be of significance because changes in the mobility of the radicals can be used to study drug release kinetics in a non-invasive and continuous fashion, without introducing paramagnetic species (61).

***In Vitro* Degradation and Drug Release.** Degradation of polyanhydride matrices depends on many factors including the (*1*) chemical nature and hydrophobicity of the monomers; (*2*) shape, geometry, and surface area of the implants; (*3*) porosity; (*4*) level of drug loading in the polymer matrix; and the (*5*) pH of the media (polymers degrade faster in alkaline media (Fig. 2)) and drug solubility. As the degradation of polyanhydrides follows erosion and pH plays an important role in the solubility of its monomers in the medium (63), degradation of the polymer becomes faster on increasing the pH of the medium (Fig. 2) and porosity increases gradually on its surface as well as in bulk (63). Notably, the porosity of the implant can be changed by change in method of fabrication. For example, a compression-molded device will degrade faster than an injection-molded device (64,65) due to a higher porosity in the polymer mass. A large number of examples on the degradation behavior of various types of polyanhydrides exists, but the clinically tested polyanhydrides such as poly(CPP-SA), poly(FA-SA), and poly(EAD-SA) have been most scrutinized. In general, during the initial 10–24 h of incubation in aqueous medium, the molecular weight dropped rapidly with no loss in wafer mass (66). This incubation period was followed by a fast decrease in wafer mass, accompanied with a small decrease in polymer molecular weight. The period of extensive mass loss starts when the number-average molecular weight (M_n) of polymer approaches 2000 (DP $\sim$ 10 units) regardless of the initial molecular weight of the polymer. For example, SA, a slightly water-soluble comonomer, is released from the wafer over a 1-week time frame, leaving the less soluble comonomer, CPP

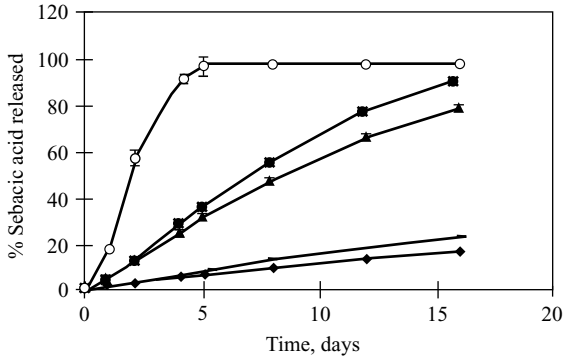

Fig. 2. Polymer degradation as a function of pH performed on the EAD:SA copolymer placebo (62). —♦—, pH 3; —, pH 5; —▲—, pH 7; —■—, pH 9; —○—, pH 11.

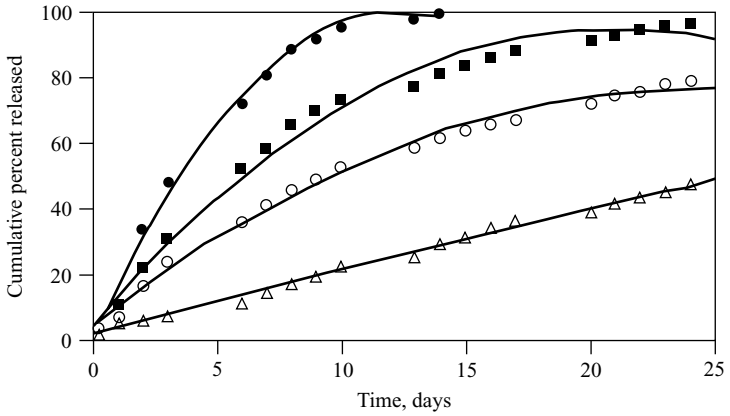

Fig. 3. Bupivacaine release from various poly(EAD-SA) compositions. Bupivacaine was released from polymer slabs in phosphate buffer (pH 7.4) at 37°C and determined by HPLC (36). ●, 10% FAD; ■, 20% FAD; ○, 30% FAD; △, 80% FAD.

or EAD, which is slower to solublize (66). Increasing the content of SA in the copolymer increases the hydrophilicity of the copolymer, which results in a higher erosion rate and hence higher drug release rate. The water uptake depends on the hydrophobicity of the polymer and therefore, the hydrophobic polymers that prevent water uptake have slower erosion rates and lower drug release rates. Because of this property, one can alter the hydrophobicity of the polymer by altering the structure and/or the content of the copolymer, and consequently alter the drug release rate. Increase of methotrexate (MTX) release upon increasing SA content in the fatty acid terminated polyanhydrides was reported recently (67). In the poly(CPP-SA) and poly(EAD-SA) series of copolymers, a 10-fold increase in bupivacaine release rate was achieved by alteration of the ratio of the monomers, and thus, both polymers can be used to deliver drugs over a wide range of release rates (Fig. 3).

Thus, there is no correlation between the drug release rate and polymer degradation expressed as percent decrease in the molecular weight, which might appear to be contradictory (68). On closer examination, it appears that drug dispersed in the polymer matrix is released when the eroding polymer brings the drug into contact with the solution. Drug release depends on the rate of erosion expressed as volume of the matrix dissolved per unit time, times the drug load rather than the rate of polymer degradation. The implication is that drug release should correlate with mass loss, which is a more appropriate indicator of the erosion rate than the decrease in molecular weight. Another feature of surface erosion is that the molecular weight of the polymer may decrease at the surface while the interior of the device still retains its initial molecular weight. Furthermore, lower molecular weight fragments so formed may not diffuse out or dissolve into the release medium. Therefore, it is not the decrease in molecular weight but the subsequent mass loss to the diffusion and erosion of molecular weight fragments which should correlate with drug release. This phenomenon also explains why drug release from these polymer devices was independent of the initial molecular weight of the copolymer (68).

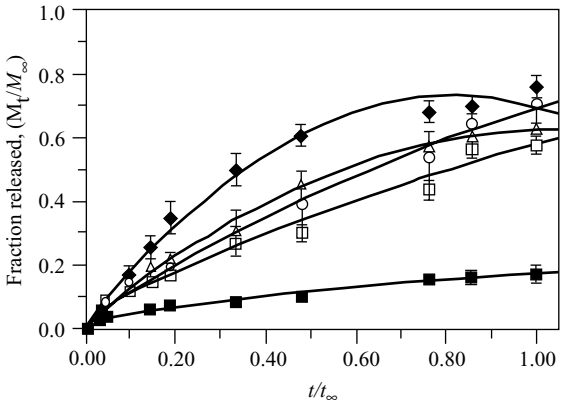

Fig. 4. *In vitro* release of ciprofloxacin from ricinoleic acid derived polymers. Release time (t_∞) was 460 h and the total drug load (M_∞) was 10 mg (38). □, SA; ●, RAM; ○, HSAM; (▲), HSAS; ■, FAD.

Recently, Stephans and co-workers (62) investigated the *in vitro* release behavior of gentamicin sulfate from a poly(EAD-SA) matrix and found that drug release rate was faster in a water than in a phosphate buffer of pH 7.4. Sulfate release was monitored along with drug release and the results indicated that an exchange of ions occurred during the *in vitro* drug release at pH 7.4. It was subsequently demonstrated that gentamicin could form an insoluble salt with EAD. This salt formation explains the slower drug release in pH 7.4 phosphate buffer. The release of indomethacin from poly(CPP-SA) and poly(EAD-SA) was studied and was found to be independent of drug loading (69). Moreover, more hydrophobic components reduce the water penetration into the polymers and this reduces the drug release rate. Figure 4 is one example of *in vitro* ciprofloxacin release with copolymers of various fatty acids components. A simple model that takes into account the following kinetic steps, namely, the spontaneous degradation of polymer to crystallized monomer, the creation of pores, the dissolution of monomers inside the pores, and the final release of monomer via diffusion through the pore network, was put forth by Gopferich and Langer to explain this unusual release behavior (69,70). Erosion was then simulated using a Monte-Carlo method that describes these morphological changes during erosion.

Characterization

Polyanhydrides have been characterized with regard to their chemical composition, structure, crystallinity and thermal properties, mechanical properties, thermodynamic properties, and hydrolytic stability. A representative set of analysis data has been summarized for the polyanhydrides poly(EAD-SA) and poly(CPP-SA) (Table 4). ^{1}H NMR spectroscopy indicates the degree of randomness that suggests whether the polyanhydrides is either a random or a block copolymer; the average length of sequence (L_n); and the frequency of occurrence of specific comonomers sequences (58). The anhydride bond presents characteristic peaks in

Table 4. A Representative Data Analysis for Polyanhydrides

Analysis	Instruments	Units	Conditions	Typical data/information								Ref.
				Poly(EAD-SA)[a]				Poly(CPP-SA)[b]				
Thermal properties	Perkin-Elmer DSC 7	Mol %	DSC – 10°C min	0:100	8:92	22:78	100:0	0:100	22:78	46:54	100:0	(29,68)
	Differential scanning	K	T_m	358.0	348.0	337.0	293.0	359.0	339.0	458.0	513.0	
	calorimeter (DSC)	K	T_g	333.1	283.0	283.0	273.0	333.1	320.0	274.8	369.0	
		kJ/kg	ΔH	150.7	250.2	13.0	4.0	150.7	64.0	13.0	110.9	
Crystallinity	X-ray diffraction	%	W_c	0:100	8:92	22:78	100:0	0:100	22:78	46:54	100:0	
	(XRD)			66	54	35	<5	66.0	35.0	14.2	61.4	
Mechanical				Poly(EAD-SA) (22:78)				Poly(CPP-SA) (40:60)				(24,36)
Tensile strength	Instron Tensile Tester	MPa	Film by melt	42				14.9				
Tensile modulus	Model 1122	MPa	22:78, M_w = 155 kDa	4.5								
Elongation yield		%		14								
Elongation at break		%		85								
Spectral												(36,71,72)
^{1}H NMR	GE Omega-PSG 600 Perkin–Elmer 1310	ppm	1% w/v in $CDCl_3$, 22°C	2.33 (t,4H), 1.32 (m, 8H), 1.23 (s, 60H), 0.8-0.9 (T, 8H)								
FT-IR	spectrophotometer	cm^{-1}	Film on NaCl plate	1,740; 1810				1,740; 1,770; 1,810				
Raman		cm^{-1}						1,723; 1,765; 1,804				
UV-wavelength		nm		253				265				
Molecular weight	Waters GPC system	10^4g/mol	GPC- polystyrene	M_w = 3–30; M_n = 1–3				M_w = 3–20, M_n = 0.5–3				(68,73)
Viscosity	Ubbelohde viscometer	dl/g	25°C, in CH_2Cl_2	η_{sp} = 0.2–1.4				ηsp = 0.2–0.9				
Mark–Houwink constants	Ubbelohde viscometer	ml/g	23°C, in CH_2Cl_2	k = 3.46; a = 0.634				k = 3.88; a = 0.658				
Surface and bulk			Film by spin casting	Quantitative elemental and				Quantitative elemental and				(74,75)
XPS			on aluminium sheet,	functional group information,				functional group				
TOF-SIMS			0.1% w/v in $CHCl_3$	molecular specificity, surface				information, molecular				
AFM	DI - instrument			morphology of polymer.				specificity, surface morphology of polymer				

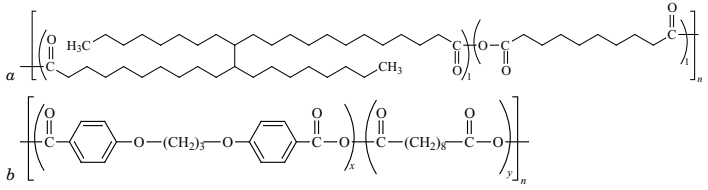

the IR and Raman spectra. In general, the carbonyl of aliphatic polymers absorbs at 1740 and 1810 cm^{-1}, and aromatic polymers at 1720 and 1810 cm^{-1} (72). The presence of carboxylic groups in the polymers can be determined from the presence of a peak at 1700 cm^{-1}. Thus, the degradation of polyanhydrides is determined from the ratio of the subsequent peaks at 1810 and 1700 cm^{-1}.

Fourier-Transform Raman Spectroscopy (FTRS) was used to characterize an homologous series of aliphatic poly(anhydrides), poly(carboxyphenoxy)alkanes, and copolymers of CPP and SA (72). All anhydrides show two diagnostic carbonyl bands, the aliphatic polymers have the carbonyl pairing at 1803/1739 cm^{-1}, and the aromatic polymers have the band pair at 1764 and 1712 cm^{-1} (72). FTRS was used to study the hydrolytic degradation of PSA rods exposed to water for 15 days. The carbonyl anhydride band pair (1803/1739 cm^{-1}) diminished in intensity from Day 0 to 15, with the emergence of the complimentary acid carbonyl band (1640 cm^{-1}) which increased in intensity over the same period. Similarly, the increase in the intensity of the C—C deformation at 907 cm^{-1} with hydrolysis reflects the increased freedom of the methylene chain in the low molecular weight oligomers.

The molecular weights of polyanhydrides were determined by viscosity measurements and GPC (58). The weight-average molecular weight (M_w) of polyanhydrides ranges from 5,000 to 300,000 with a polydispersity of 2–15 that increases with increased M_w. The intrinsic viscosity [η] increases with the increase in M_w. The Mark–Houwink relationship for poly(CPP-SA) was calculated from the viscosity data and the M_w values as determined by universal calibration of the GPC data using polystyrene standards.

$$[\eta]^{23^\circ C}_{CH_3Cl} = 3.88 \times 10^{-7} M_w^{0.658}$$

Crystallinity was determined by X-ray diffraction, a combination of X-ray and DSC, and data generated from ^1H NMR spectroscopy and Flory's equilibrium theory (40).

The morphology of polyanhydrides was studied by scanning electron microscope (SEM) to elucidate the mechanism of polymer degradation and drug release from polyanhydrides. The surface chemical structure of aliphatic polyanhydride films was examined using time-of-flight secondary ion mass spectroscopy (ToF-SIMS) and X-ray photoelectron spectroscopy (XPS) (24,76). The main peak at 285 eV corresponds to C—H. The peak at 289.5 eV arises from O—C=O. The XPS data confirmed the purity of the surface, and the experimental surface elemental ratios were in good agreement with the known stoichiometry of the examined polyanhydrides. The ToF-SIMS spectra of the polyanhydrides reflected the polymer structure. The SIMS data confirms a systematic fragmentation, in both negative- and positive-ion SIMS spectra, occurring throughout the entire series of the polyanhydrides examined. Radical cations were observed in the positive-ion spectra. The ion at *m/z* 71, which may arise from the fragmentation of the anhydride unit, CH_2=CHCOO—, was seen for all polyanhydrides. The combined use of ToF-SIMS and XPS provides a detailed insight into the interfacial chemical structure of polyanhydrides. Atomic force microscopy (AFM) was used to follow the degradation of poly(SA) and its blends with poly(lactide) (73,77). AFM was suitable to visualize polymer degradation without the need to dry the samples.

Biocompatibility and Elimination

Several tests to evaluate new biomedical materials were used to assess the safety of polyanhydrides (53,78). In these studies, poly(bis(*p*-carboxy-phenoxy)propane anhydride) poly(CPP) and its copolymers with SA were tested. Neither mutagenicity and cytotoxicity nor teratogenicity was associated with the polymers or their degradation products, as evaluated by mutation assays. The tissue response of these polyanhydrides was studied by subcutaneous implantation in rats and in the cornea of rabbits. The polymers did not provoke inflammatory responses in the tissues over a 6- week implantation period. Histological evaluation indicated relatively minimal tissue irritation with no evidence of local or systemic toxicity (53). Systemic response to the polymer was evaluated by monitoring of blood chemistry and hematological values, and by comprehensive examination of organ tissues. Both methods revealed no significant response to the polymer. Recently, biocompatibility of ricinoleic acid based polymer was tested in rats and compared to Vicryl (Ethicon) surgical suture and sham surgery (37). No abnormal gross pathological finding was observed at the implantation site after 3, 7, and 21 days of implantation. Blood chemistry and blood counting levels were similar for treated and untreated rats. The polymer was degraded into ricinoleic acid with constant release of incorporated drug while the inflammatory response after subcutaneous implantation was minimal to mild and comparable with clinically used Vicryl absorbable sutures.

CPP-SA copolymer was designed to deliver an anticancer agent directly into the brain for the treatment of brain neoplasm and *in vivo* safety evaluations and brain biocompatibility were assessed in rats (79), rabbits (8), and monkeys (80). In the rat brain study, the tissue reaction of the polymer (P(CPP-SA) (20:80)) was compared to the reaction observed with two standard materials used in surgery, which have been extensively studied, Gelfoam (absorbable gelatin sponge; Becton Dickenson) and Surgicel (oxidized cellulose absorbable hemostat; Ethicon). Histological evaluation of the tissue demonstrated a small rim of necrosis around the implant, and a mild to marked cellular inflammatory reaction limited to the area immediately adjacent to the implantation site. The pathological response associated with poly(CPP-SA) copolymer was slightly more pronounced than with Surgicel at the earlier time points, but noticeably less marked than with Surgicel at the later times. The reaction to Gelfoam was essentially equivalent to that observed in control rats. In a similar brain biocompatibility study carried out in monkeys, no tissue abnormalities were noted either in computerized tomography and magnetic resonance imaging. Furthermore, no abnormalities were observed either in the blood chemistry or hematology evaluations (81). There appeared to be no adverse systemic effects caused by the implants as determined by histological evaluation of tissues. Overall, no unexpected or untoward reaction to the treatment was observed. Copolymers of SA with several aliphatic comonomers such as EAD, FA, and IPA were also tested subcutaneously and in the rat brain and were found to be biocompatible as well (82). The hydrolysis and elimination processes of polyanhydrides have been studied using a series of polyanhydrides derived from different linear aliphatic diacids (83). These polymers degrade into their monomer or oligomers units at about the same rate but differ in the water solubility of their degradation products. Polymers based on natural diacids of

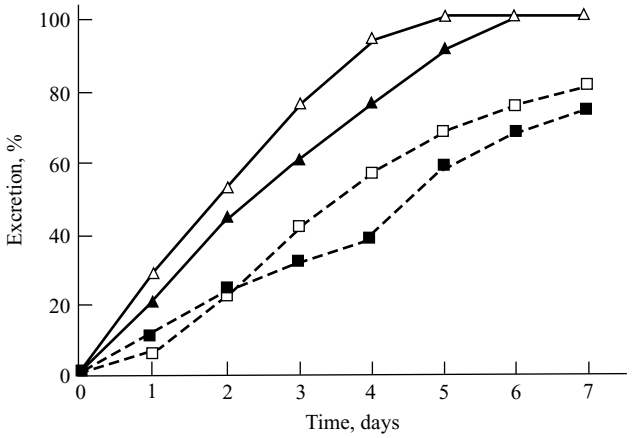

Fig. 5. *In vivo* and *In vitro* degradation of poly(CPP-SA) (20:80). The radioactive excretion data were used to determine the *in vivo* of SA and BCNU. *In vitro* hydrolysis was evaluated on compression-molded wafer in 0.1 *M* phosphate buffer, pH 7.4, at 37°C. SA and BCNU concentrations were determined by HPLC. △, BCNU, *in vitro*; ▲, SA, *in vitro*; □, SA, *in vivo*; ■, BCNU, *in vivo* (84).

the general structure —(OOC—$(CH_2)_x$—CO)— (where x is between 4 and 12) were implanted subcutaneously in rats and the elimination of the polymers from the implantation site was studied (83). The *in vitro* hydrolysis of this polymer series was studied by monitoring the mass loss, release of monomer degradation products, and the changes in content of anhydride bonds as a function of time. Both *in vitro* and *in vivo*, the rate of polymer elimination was a function of monomer solubility. The elimination time for polymers based on soluble monomers ($x = 4$–8) was 7–14 days, while the polymers based on monomers with lower solubility ($x = 10$–12) were eliminated only after 8 weeks. All polymers were found to be biocompatible and useful as carriers of drugs.

The elimination of poly(CPP-SA)-based implant (Gliadel (Guilford Pharmaceuticals)), which has been approved for the treatment of brain cancer, was studied in rabbit and rat brains using radioactive polymer and drug (Fig. 5) (84,85). The implant is composed of BCNU dispersed in a copolyanhydride matrix of 1,3-(*p*-carboxy)phenoxypropane (CPP) and sebacic acid (SA). Four groups of rabbits were implanted with wafers loaded with BCNU, one in a ^{14}C-SA-labeled polymer, another in a ^{14}C-CPP-labeled polymer, and two groups with ^{14}C-BCNU in a nonlabeled polymer, in which one group was for BCNU disposition study and the other was for residual drug study. In the rabbits implanted with the 14C-SA-labeled polymer, approximately 10% of the radioactivity was found in the urine and 2% in the feces, and about 10% remained in the device after 7 days of implantation. In contrast, only 4% of the radioactivity associated with the ^{14}C-CPP-labeled polymer was found in urine and feces during this period. However, a drastic increase in the CPP excretion was found after 9 days, and at 21 days, during this period, 64% of the implanted ^{14}C-CPP was recovered in the urine and feces, and 29% was still in the recovered wafers. Studies with radiolabeled BCNU in rabbit brain revealed that approximately 50% of the BCNU in the wafers was released in

3 days, and over 95% was released after 6 days in the rabbit brain. Excretion of this polymer after implantation in the rat brain using radiolabeled polymers showed that over 70% of the SA comonomer was excreted in 7 days, with about 40% of the SA metabolized to CO_2 (85). The elimination of poly(EAD-SA) rods loaded with 0, 10, and 20 wt% of gentamicin sulfate after implantation in the femoral muscle and bone of dogs was studied as part of the preclinical studies for Septacin-bone implant (86). Most of the polymer implant was gradually eliminated from bone and muscle within 4–8 weeks post implantation, with elimination from bone being faster leading to new bone formation in the implant site without any polymer entrapment. The elimination rate was dependent mainly on the amount of polymer implanted. Gentamicin was released for a period of about 3 weeks, with no residual drug detected in the polymer remnants 8 weeks postimplantation. In all experiments, no local or systemic toxicity was observed.

Fabrication of Delivery Systems

Polymers having low melting point and good solubility in common organic solvents such as methylene chloride, allow for the easy dispersion of a drug into their matrix. For example, drugs can be incorporated into a slab either by melt mixing the drug into the melted polymer, or by solvent casting (87). Polymer slabs loaded with drug can also be prepared by compression molding a powder containing the drug (88). Similarly, one can injection mold the drug-polymer formulation into beads or rods (89). Polymer films can be prepared by solvent casting the polymer solution containing the drug onto Teflon-coated dish (67). Microsphere-based delivery systems can be formulated by the common techniques including solvent removal, hot-melt encapsulation, and spray drying (90–92). However, it is essential that all processes be performed under anhydrous conditions to minimize hydrolysis of the polymer (see CONTROLLED RELEASE TECHNOLOGY).

Production and World Market

Polyanhydrides are not commercially available. One polyanhydride composition, poly(CPP-SA) (20:80), is manufactured at Guilford Pharmaceuticals in Baltimore on a kilogram scale, as part of the Gliadel implant for the treatment of brain tumors. Poly(dimer eurecic acid-co-sebacic acid) was developed for large scale production by Abbott Lab (Chicago) for the fabrication of the Septacin implant for prevention of bone infections. The Septacin product was manufactured by injection molding of the polymer–drug composition. The development of this product was stopped for marketing reasons. Samples of polyanhydrides may be obtained by a request from the corresponding author.

Pharmaceutical Applications

Polyanhydrides have been investigated as a candidate for controlled release devices of drugs for treating eye disorders (93), chemotherapeutic agents (94,95),

local anesthetics (88,96), anticoagulants (97), neuroactive drugs (98), and anticancer agents (99). Polyanhydrides were loaded with carmustine and implanted in the brains of rats, rabbits, and monkeys and studied. These were found to be biocompatible and efficacious against brain tumors (100,101). Based on the foundation of these laboratory studies, phases I and II were completed, which showed that treatment was well tolerated in all patients and did not appear to produce systematic side effects (81). Phase III human clinical trails demonstrated that the site-specific delivery of BCNU (carmustine) from a poly(CPP-SA) (20:80) wafer (Gliadel) in patients with recurring brain cancer (glioblastoma multiforme) significantly prolongs patients' survival (100). On the basis of result of a 4–5-years-long clinical trial, FDA has given the approval for a new treatment of brain tumors (94). Gliadel subsequently has been approved in Canada, South America, Israel, South Korea, and Europe for brain tumor treatment. Masters and co-workers (102,103) have used a polyanhydride cylinder for the delivery of local anesthetics in close proximity to the sciatic nerve to produce a neuronal block for several days. The use of polyanhydrides in oral delivery of insulin and plasmid DNA has been investigated (104). In the past 5 years, investigations have expanded to newer polymers and other drugs such as 4-hydroperoxy cyclophosphamide, cisplatin, carboplatin, and paclitaxel, and several alkaloid drugs in an effort to develop a better system for treating brain tumors (80,105–107). Carboplatin incorporated in poly(EAD-SA), prepared by mixing the drug in the melted polymer, has been evaluated for the treatment of brain tumors in laboratory animals, and has shown promising results (107). Poly(CPP-SA) has also been used to develop a delivery system for gentamicin sulfate for the treatment of osteomyelitis (105,108). A sustained release of gentamicin sulfate over a period of few weeks was obtained both *in vivo* and *in vitro* using this system. This delivery device was used in human clinical trials in the United States. The effect of long-term glutamic acid stimulation of trigeminals motoneurons, using poly(EAD-SA) microspheres, has also been explored. This study was undertaken to determine the role of glutamate in possible growth disorders of the craniofacial skeleton. Pronounced skeletal changes in the snout region were observed in rats that received glutamate, indicating a sustained release of glutamic acid *in vivo* can affect the development of skeletal tissue in growing rats (109). Recently, the use of polyanhydrides for the delivery of heparin and treatment of osteomyelitis has been reported (62,67).

Outlook

Polyanhydrides, especially the copolymers of aliphatic and aromatic anhydrides, are a versatile class of biodegradable polymers. The desired physicochemical properties of these polymers can be obtained by carefully adjusting the composition of the monomers and molecular weight of the final polymer. Polyanhydrides degrade gradually into nontoxic monomers after their intended uses. Another attractive feature of polyanhydrides is the erosion-dominated degradation mechanism, and accompanied controlled release of drugs from the matrices. Gliadel is the only regional drug therapy approved by FDA for treating brain cancer in the past 20 years. Given their structural and physicochemical versatility, polyanhydrides are

likely finding more applications in other novel drug delivery systems, medical devices, and tissue engineering products.

The advantages and disadvantages of these polymers are the hydrolytic instability of the anhydride bond. The main advantages of this class of polymers are as follows:

(1) prepared from easily available, low cost resources and generally regarded as safe dicarboxylic acid building blocks, many of them are body constituents or metabolites
(2) prepared in a one-step synthesis with no need for purification steps to yield, well-defined polymer structure with controlled molecular weight
(3) can be manipulated to release bioactive agents at a predictable rate for periods of weeks, as a function of polymer composition
(4) processable by low temperature injection-molding or extrusion for mass production, versatile properties, obtained by appropriate monomer selection, composition, surface area, and additives
(5) degrade to their respective diacids and completely eliminate from the body within a period of weeks to months
(6) sterilized by gamma-irradiation without any effect on polymer properties

Apart from these advantages, the main disadvantages of these polymers are their short-term degradation and release period, and the need for special storage conditions (refrigeration, dry conditions). Thus, these polymers are most suitable for short-term (days to weeks) controlled delivery of bioactive agents in the form of solid implants or injectable microspheres.

BIBLIOGRAPHY

"Polyanhydrides" in *EPST* 1st ed., Vol. 10, pp. 630–653, by Naoda Yoda, Toyo Rayon Company, Ltd.; "Polyanhydrides" in *EPSE* 2nd ed., suppl. Vol., pp. 648–665, by Kam Leong, Johns Hopkins University, and A. Domb, E. Ron, and R. Langer, Massachusetts Institute of Technology.

1. J. E. Bucher and W. C. Slade, *J. Am. Chem. Soc.* **31**, 1319 (1909).
2. J. W. Hill, *J. Am. Chem. Soc.* **52**, 4110 (1930).
3. J. W. Hill and H. W. Carothers, *J. Am. Chem. Soc.* **54**, 5169 (1932).
4. A. Conix, *J. Polym. Sci., Part A* **29**, 343 (1958).
5. N. Yoda, *J. Polym. Sci., Part A* **1**, 1323 (1963).
6. N. Yoda, *Makromol. Chem.* **55**, 174 (1962).
7. H. B. Rosen, J. Chang, G. E. Wnek, R. J. Linhardt, and R. Langer, *Biomaterials* **4**, 131 (1983).
8. H. Brem, A. Kader, J. I. Epstein, R. J. Tamargo, A. Domb, R. Langer, and K. W. Leong, *Sel. Cancer Ther.* **5**, 55 (1989).
9. M. Chasin, D. Lewis, and R. Langer, *BioPharm. Manuf.* **1**, 33 (1988).
10. E. Vasheghani-Farahani and M. Khorram, *J. Appl. Polym. Sci.* **83**, 1457 (2002).
11. N. Kumar, A.-C. Albertsson, U. Edlund, D. Teomim, A. Rasiel, and A. J. Domb, in A. Steinbuchel and Y. Doi, eds., *Polyesters-II*, Vol. **4**, Wiley-VCH, New York, 2002, p. 203.
12. W. B. Dang, T. Daviau, and H. Brem, *Pharm. Res.* **13**, 683 (1996).

13. A. J. Domb and R. Langer, *J. Polym. Sci., Part A: Polym. Chem.* **25**, 3373 (1987).
14. K. W. Leong, A. Domb, and R. Langer, in H. F. Mark and J. I. Kroschwitz, eds., *Encyclopedia of Polymer Science and Technology*, John Wiley & Sons, Inc., New York, 1989, p. 648.
15. A. J. Domb and R. Langer, *Polym. Mater. Sci. Eng.* **55**, 746 (1986).
16. V. R. Shastri, P. P. Hildgen, R. Langer, Y. Najajrah, I. Ringel, and A. J. Domb, in A. J. Domb, J. Kost, and D. M. Wiseman, eds., *Handbook of Biodegradable Polymers* Vol. **7**, Harwood Academic Publishers, Amsterdam, 1997, p. 119.
17. O. Hinterhofer, *Makromol. Chem.* **181**, 83 (1980).
18. K. W. Leong, V. Simonte, and R. Langer, *Macromolecules* **20**, 705 (1987).
19. A. J. Domb, C. F. Gallardo, and R. Langer, *Macromolecules* **22**, 3200 (1989).
20. A. J. Domb and R. Langer, *Macromolecules* **22**, 2117 (1989).
21. A.-C. Albertsson and S. Lundmark, *J. Macromol. Sci., A: Chem.* **25**, 247 (1988).
22. A. J. Domb, E. Ron, and R. Langer, *Macromolecules* **21**, 1925 (1988).
23. R. Subramanyam and A. G. Pinkus, *J. Macromol. Sci., A: Chem.* **22**, 23 (1985).
24. M. C. Davies, M. A. Khan, A. Domb, R. Langer, J. F. Watts, and A. J. Paul, *J. Appl. Polym. Sci.* **42**, 1597 (1991).
25. A. C. Albertsson and M. Eklund, *J. Polym. Sci., Part A: Polym. Chem.* **34**, 1395 (1996).
26. C. E. Carraher Jr. and R. J. Linville, *Polym. Prepr. (ACS)* **25**, 31 (1984).
27. A. J. Domb, E. Mathiowitz, E. Ron, S. Giannos, and R. Langer, *J. Polym. Sci., Part A: Polym. Chem.* **29**, 571 (1991).
28. D. Teomim, K. Maeder, A. Bentolila, A. Magora, and A. J. Domb, *Biomacromolecules* **2**, 1015 (2001).
29. A. J. Domb, *Macromolecules* **25**, 12 (1992).
30. M. Krishnan and D. R. Flanagan, *J. Controlled Release* **69**, 273 (2000).
31. C. E. Carraher Jr. and R. J. Linville, *Polym. Sci. Technol.* **31**, 187 (1985).
32. H. L. Jiang, K. J. Zhu, and L. J. Dai, *Macromol. Rapid Commun.* **22**, 414 (2001).
33. A. Merkli, C. Tabatabay, and R. Gurny, *Eur. J. Pharm. Biopharm.* **41**, 271 (1995).
34. H. R. Kricheldorf, *Makromol. Chem., Macromol. Symp.* **54**, 365 (1992).
35. L. Erdmann, B. Macedo, and K. E. Uhrich, *Biomaterials* **21**, 2507 (2000).
36. A. J. Domb and M. Maniar, *J. Polym. Sci., Part A: Polym. Chem.* **31**, 1275 (1993).
37. D. Teomim, A. Nyska, and A. J. Domb, *J. Biomed. Mater. Res.* **45**, 258 (1999).
38. A. J. Domb and R. Nudelman, *J. Polym. Sci., Part A: Polym. Chem.* **33**, 717 (1995).
39. H. Brem, A. Domb, D. Lenartz, C. Dureza, A. Olivi, and J. I. Epstein, *J. Controlled Release* **19**, 325 (1992).
40. A. Staubli, E. Mathiowitz, M. Lucarelli, and R. Langer, *Macromolecules* **24**, 2283 (1991).
41. K. E. Uhrich, A. Gupta, T. T. Thomas, C. T. Laurencin, and R. Langer, *Macromolecules* **28**, 2184 (1995).
42. J. Hanes, M. Chiba, and R. Langer, *Biomaterials* **19**, 163 (1998).
43. K. E. Uhrich, T. T. Thomas, C. T. Laurencin, and R. Langer, *J. Appl. Polym. Sci.* **63**, 1401 (1997).
44. U. Edlund and A.-C. Albertsson, *J. Appl. Polym. Sci.* **72**, 227 (1999).
45. A. J. Domb, *J. Polym. Sci., Part A: Polym. Chem.* **31**, 1973 (1993).
46. U. Edlund, A.-C. Albertsson, S. K. Singh, and I. Fogelberg, *Biomaterials* **21**, 945 (2000).
47. L. Y. Qiu and K. J. Zhu, *Polym. Int.* **49**, 1283 (2000).
48. M. Maniar, X. Xie, and A. J. Domb, *Biomaterials* **11**, 690 (1990).
49. E. Abuganima, Ph.D. dissertation, The Hebrew University of Jerusalem, 1996.

50. R. Gref, A. Domb, P. Quellec, T. Blunk, R. H. Mueller, J. M. Verbavatz, and R. Langer, *Adv. Drug Delivery Rev.* **16**, 215 (1995).
51. D. Teomim and A. J. Domb, *J. Polym. Sci., Part A: Polym. Chem.* **37**, 3337 (1999).
52. T. Zhang, M. Gu, and X. H. Yu, *J. Biomat. Sci., Polym. Ed.* **12**, 491 (2001).
53. C. Laurencin, A. Domb, C. Morris, V. Brown, M. Chasin, R. McConnell, N. Lange, and R. Langer, *J. Biomed. Mater. Res.* **24**, 1463 (1990).
54. A. J. Domb and R. Nudelman, *J. Polym. Sci., Part A: Polym. Chem.* **33**, 717 (1995).
55. A. J. Domb, *Biomaterials* **11**, 686 (1990).
56. M. Hartmann, A. Geyer, K. Wermann, V. Schulz, C. Knips, and P. Pinther, *J. Macromol. Sci., Pure Appl. Chem.* **A30**, 91 (1993).
57. A. Staubli, E. Ron, and R. Langer, *J. Am. Chem. Soc.* **112**, 4419 (1990).
58. E. Ron, E. Mathiowitz, G. Mathiowitz, A. Domb, and R. Langer, *Macromolecules* **24**, 2278 (1991).
59. K. Mader, A. Domb, and H. M. Swartz, *Appl. Radiat. Isot.* **47**, 1669 (1996).
60. K. Maeder, G. Bacic, A. Domb, O. Elmalak, R. Langer, and H. M. Swartz, *J. Pharm. Sci.* **86**, 126 (1997).
61. K. Maeder, Y. Cremmilleux, A. J. Domb, J. F. Dunn, and H. M. Swartz, *Pharm. Res.* **14**, 820 (1997).
62. D. Stephens, L. Li, D. Robinson, S. Chen, H. C. Chang, R. M. Liu, Y. Q. Tian, E. J. Ginsburg, X. Y. Gao, and T. Stultz, *J. Controlled Release* **63**, 305 (2000).
63. A. Gopferich, L. Schedl, and R. Langer, *Polymer* **37**, 3861 (1996).
64. K. W. Leong, B. C. Brott, and R. Langer, *Polym. Prepr. (ACS)* **25**, 201 (1984).
65. K. W. Leong, B. C. Brott, and R. Langer, *J. Biomed. Mater. Res.* **19**, 941 (1985).
66. W. B. Dang, T. Daviau, P. Ying, Y. Zhao, D. Nowotnik, C. S. Clow, B. Tyler, and H. Brem, *J. Controlled Release* **42**, 83 (1996).
67. D. Teomim, I. Fishbien, G. Golomb, L. Orloff, M. Mayberg, and A. J. Domb, *J. Controlled Release* **60**, 129 (1999).
68. A. D'Emanuele, J. Hill, J. A. Tamada, A. J. Domb, and R. Langer, *Pharm. Res.* **9**, 1279 (1992).
69. A. Gopferich and R. Langer, *J. Polym. Sci., Part A: Polym. Chem.* **31**, 2445 (1993).
70. A. Gopferich, D. Karydas, and R. Langer, *Eur. J. Pharma. and Biopharm.* **41**, 81 (1995).
71. D. L. McCann, F. Heatley, and A. D'Emanuele, *Polymer* **40**, 2151 (1999).
72. A. M. Tudor, C. D. Melia, M. C. Davies, P. J. Hendra, S. Church, A. J. Domb, and R. Langer, *Spectrochim. Acta, Part A* **47A**, 1335 (1991).
73. K. M. Shakesheff, M. C. Davies, A. Domb, D. E. Jackson, C. J. Roberts, S. J. B. Tendler, and P. M. Williams, *Macromolecules* **28**, 1108 (1995).
74. K. M. Shakesheff, X. Chen, M. C. Davies, A. Domb, J. Heller, C. J. Roberts, S. J. B. Tendler, and P. M. Williams, in Proc. 22nd Int. Symp. Controlled Release Bioact. Mater., 384 (1995).
75. A. G. Shard, K. M. Shakesheff, C. J. Roberts, S. J. B. Tendler, and M. C. Davies, in A. J. Domb, J. Kost, and D. M. Wiseman, eds., *Handbook of Biodegradable Polymers*, Vol. **7**, Harwood Academic Publishers, Amsterdam, 1997, p. 417.
76. M. C. Davies, K. M. Shakesheff, A. G. Shard, A. Domb, C. J. Roberts, S. J. B. Tendler, and P. M. Williams, *Macromolecules* **29**, 2205 (1996).
77. K. M. Shakesheff, M. C. Davies, C. J. Roberts, S. J. B. Tendler, A. G. Shard, and A. Domb, *Langmuir* **10**, 4417 (1994).
78. K. W. Leong, P. D'Amore, M. Marletta, and R. Langer, *J. Biomed. Mater. Res.* **20**, 51 (1986).

79. R. J. Tamargo, J. I. Epstein, C. S. Reinhard, M. Chasin, and H. Brem, *J. Biomed. Mater. Res.* **23**, 253 (1989).
80. H. Brem, R. J. Tamargo, A. Olivi, M. Pinn, J. D. Weingart, M. Wharam, and J. I. Epstein, *J. Neurosurg.* **80**, 283 (1994).
81. H. Brem, S. Mahaley, N. A. Vick, K. L. Black, S. C. Schold, P. C. Burger, A. H. Friedman, I. S. Ciric, T. W. Eller, J. W. Cozzens, and J. N. Kenealy, *J. Neurosurg.* **74**, 441 (1991).
82. M. Rock, M. Green, C. Fait, R. Geil, J. Myer, M. Maniar, and A. Domb, *Polym. Prepr. (ACS)* **32**, 221 (1991).
83. A. J. Domb and R. Nudelman, *Biomaterials* **16**, 319 (1995).
84. A. J. Domb, M. Rock, J. Schwartz, C. Perkin, G. Yipchuk, B. Broxup, and J. G. Villemure, *Biomaterials* **15**, 681 (1994).
85. A. J. Domb, M. Rock, C. Perkin, G. Yipchuck, B. Broxup, and J. G. Villemure, *Biomaterials* **16**, 1069 (1995).
86. A. J. Domb and S. Amselem, in A. J. Domb, ed., *Polymeric Site-Specific Pharmacotherapy*, John Wiley & Sons, Inc., Chichester, New York, 1994, p. 242.
87. A. J. Domb, in *Polymeric Site-Specific Pharmacotherapy*, John Wiley & Sons, Inc., Chichester, New York, 1994, p. 1.
88. D. B. Masters, C. B. Berde, S. Dutta, T. Turek, and R. Langer, *Pharm. Res.* **10**, 1527 (1993).
89. J. S. Deng, L. Li, Y. Q. Tian, M. Meisters, H. C. Chang, D. Stephens, S. Chen, and D. Robinson, *Pharm. Dev. Tech.* **6**, 541 (2001).
90. K. J. Pekarek, J. S. Jacob, and E. Mathiowitz, *Adv. Mater.* **6**, 684 (1994).
91. C. Bindschaedler, K. Leong, E. Mathiowitz, and R. Langer, *J. Pharm. Sci.* **77**, 696 (1988).
92. E. Mathiowitz and R. Langer, *J. Controlled Release* **5**, 13 (1987).
93. A.-C. Albertsson, J. Carlfors, and C. Sturesson, *J. Appl. Polym. Sci.* **62**, 695 (1996).
94. H. Brem and H. C. Lawson, *Cancer* **86**, 197 (1999).
95. A. H. Shikani and A. J. Domb, *Laryngoscope* **110**, 907 (2000).
96. M. Maniar, A. Domb, A. Haffer, and J. Shah, *J. Controlled Release* **30**, 233 (1994).
97. D. Chickering, J. Jacob, and E. Mathiowitz, *Biotechmol Bioeneg.* **52**, 96 (1996).
98. M. J. Kubek, D. Liang, K. E. Byrd, and A. J. Domb, *Brain Res.* **809**, 189 (1998).
99. A. Domb, S. Bogdansky, A. Olivi, K. Judy, C. Dureza, D. Lenartz, M. L. Pinn, M. Colvin, and H. Brem, *Polym. Prepr. (ACS)* **32**, 219 (1991).
100. H. Brem, M. G. Ewend, S. Piantadosi, J. Greenhoot, P. C. Burger, and M. Sisti, *J. Neurooncol.* **26**, 111 (1995).
101. A. J. Domb, Z. H. Israel, O. Elmalak, D. Teomim, and A. Bentolila, *Pharm. Res.* **16**, 762 (1999).
102. D. B. Masters, C. B. Berde, S. K. Dutta, C. T. Griggs, D. Hu, W. Kupsky, and R. Langer, *Anesthesiology* **79**, 340 (1993).
103. D. B. Masters and A. J. Domb, *Pharm. Res.* **15**, 1038 (1998).
104. G. P. Carino, J. S. Jacob, and E. Mathiowitz, *J. Controlled Release* **65**, 261 (2000).
105. C. T. Laurencin, T. Gerhart, P. Witschger, R. Satcher, A. Domb, A. E. Rosenberg, P. Hanff, L. Edsberg, W. Hayes, and R. Langer, *J. Orthop. Res.* **11**, 256 (1993).
106. K. D. Judy, A. Olivi, K. G. Buahin, A. Domb, J. I. Epstein, O. M. Colvin, and H. Brem, *J. Neurosurg.* **82**, 481 (1995).
107. A. Olivi, M. G. Ewend, T. Utsuki, B. Tyler, A. J. Domb, D. J. Brat, and H. Brem, *Cancer Chemother. Pharmacol.* **39**, 90 (1996).

108. A. J. Domb and S. Amselem, in *Polymer Site-Specific Pharmacotherapy*, John Wiley & Sons, Inc., Chichester, New York, 1994, p. 243.
109. E. L. Hamilton-Byrd, A. J. Sokoloff, A. J. Domb, L. Terr, and K. E. Byrd, *Polym. Adv. Technol.* **3**, 337 (1992).

NEERAJ KUMAR
The Hebrew University of Jerusalem
ZHONG ZHAO
Guilford Pharmaceuticals, Inc.
ABRAHAM J. DOMB
The Hebrew University of Jerusalem

POLYARYLATES

Introduction

Polyarylate resins are heat-resistant thermoplastics with excellent toughness, uv stability, flexural recovery, dimensional stability, and electrical properties.

Polyarylate polymer properties can be tailored by compositional variation, alloying with other high performance thermoplastics, and reinforcement. This flexibility renders polyarylate one of the more versatile high temperature polymers for current and emerging markets served by engineering thermoplastics.

Chemistry

Polyarylate polymers are aromatic polyesters derived from aromatic dicarboxylic acids and diphenols. In contrast to liquid crystalline aromatic polyester (derived from dicarboxylic hydroxy acids), polyarylates exhibit amorphous character on molding; T_g is ca 198°C. Polyarylates present a competitive cost/performance profile in the context of amorphous engineering thermoplastics, delivering an excellent balance of mechanical properties, particularly practical heat resistance which substantially exceeds that of polycarbonates (qv).

The preferred aromatic diphenol based on current commercial offerings is bisphenol A; the aromatic dicarboxylic acid is proportioned between isophthalic acid and terephthalic acid (eq. (1)). The election of a particular isophthalic acid/terephthalic acid ratio is influenced by both the commercial manufacturing process and market orientation (1). The ratio of x, y in the product of equation (1) is close to one for U-Polymer, produced by Unitika, the only current commercial polyarylate.

Encyclopedia of Polymer Science and Technology. Copyright John Wiley & Sons, Inc. All rights reserved.

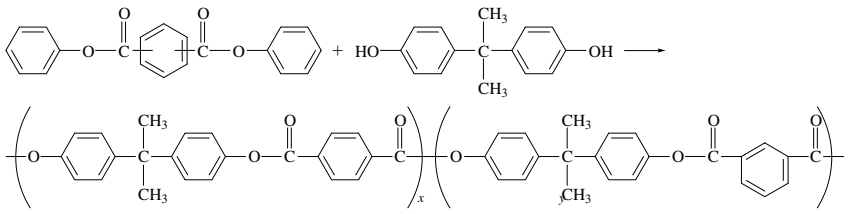

(1)

Diphenols are scarcely reactive towards aromatic diacids (2) and only low molecular weight polymers can be achieved through their direct reaction. To increase the reactivity and promote the polycondensation, at least one of the monomers has to be properly activated. Thus, two processes have been conceived for polyarylate synthesis: interfacial polycondensation (preferred over the solution process) between diacyl chlorides and alkali metal diphenate, and the high temperature metal-catalyzed melt polycondensation between either diphenol acetates and aromatic diacids, or diphenols and diacid diphenyl esters.

Properties

Polyarylates deliver excellent thermal performance with heat-deflection temperatures ranging from 154 to 174°C at 1.82 MPa (264 psi) and a UL thermal index of 130°C. In addition, a very low coefficient of thermal expansion [5.0–6.2 $\times$ 10^{-6} mm/(mm·°C) (60–130°C)] allows for superior performance in polyarylate/metal assemblies. The inherent uv resistance of polyarylate polymers results in excellent retention of mechanical properties under prolonged weathering conditions. As a coating or laminate, polyarylate provides a uv barrier for other performance plastics.

Mechanical properties compare favorably with other high performance amorphous and semicrystalline thermoplastics, where strength and toughness requirements are rigorous (Table 1). The flexural recovery (resilience) of polyarylate is excellent over a wide temperature range, which suggests applications where snap-fit action is required.

Polyarylate resins exhibit good combustion resistance in terms of low flame spread, a high oxygen index, and low smoke generation.

Unmodified polyarylates exhibit sufficient fire-retardant characteristics for many applications, whereas more stringent combustion requirements can be achieved with the proper selection of additives. The electrical properties of polyarylate polymers are reasonably constant over a broad temperature range and present a competitive profile for high performance electrical applications.

The amorphous character of polyarylates renders this class of polymer susceptible to stress-cracking tendencies in solvents such as ketones, aromatic hydrocarbons, esters, and chlorinated hydrocarbons. In applications where chemical resistance is critical, alloying polyarylate with other high performance materials can often meet the requirement.

Polyarylates are transparent and range in color from light yellow to amber. The transparent character can be maintained in alloying with other reactive

Table 1. Properties of Polyarylates

Property	Value
Density, g/mL	1.21
Flammability	V0
Oxygen index (LOI), %	36
Refractive index	1.64
Water absorption (24 h, 23°C)	0.26
Dielectric constant (1 MHz)	1.64
Dielectric strength, kV/mm	0.4
Dissipation factor (1 kHz)	0.004
Volume resistivity (23°C, dry), Ω·cm	2×10^{14}
Heat-deflection temperature at 1.8 MPa, °C	174
Thermal conductivity (23°C), W/(m·K)	0.21
Elastic modulus, GPa[a]	2.1
Tensile strength, MPa[b]	70
Flexural modulus, GPa[a]	2.1
Flexural strength, MPa[b]	75
Compressive strength, MPa[b]	84
Elongation at break, %	60
Notched Izod (3.2 mm), J/m[c]	205
Hardness (Rockwell)	R125

[a]To convert GPa to psi, multiply by 145,000.
[b]To convert MPa to psi, multiply by 145.
[c]To convert J/m to lbf·ft/in, divide by 53.38.

polyesters while mechanical properties can be tailored to end-use applications. Additional property modification is achieved by targeting mechanically compatible blends.

Processing

Polyarylates can be processed by most conventional melt processes, including injection molding, extrusion, blow molding, and thermoforming. Processing characteristics are similar to that of polycarbonate with the exception that higher melt temperatures are required.

Injection molding is the processing technique that is most widely employed, and resins are available that fill complex mold designs. Recommended melt temperatures range from 260 to 382°C depending on the composition, and mold temperatures can range from 65 to 149°C. Additionally, extrusion and blow-molding grades offer good melt strength combined with high throughput rates that are essential for blow molding, profile extrusions, and thermoforming operations.

Successful processing of polyarylates requires moisture levels below 0.02%, which is similar to requirements for other polyesters (ie, PET). All polyarylates are unstable in the presence of moisture at the processing temperatures described earlier; unsatisfactory part properties result from processing poorly dried resin.

Applications

Polyarylates are presently used in a wide variety of end-use applications and also show potential for future applications. Presently, polyarylates find use in the automotive, safety, electrical and electronics, and exterior construction and lighting areas.

Automotive. Properties of polyarylates, such as high heat resistance, dimensional stability, and capability for high gloss surface metallization of parts, allow these resins to be used in headlight housings and brake light reflectors. For exterior trim parts such as mirror housings, window trim, and door handles, the good uv resistance and weatherability of polyarylate eliminate the need for painting. In brackets and fasteners, the resin's creep resistance and dimensional stability are advantageous. Polyarylate alloys are being evaluated for use in body panel applications.

Safety Equipment. Polyarylates are used in fire helmets and fire shields because of their inherent resistance to hot and cold temperatures, impact and flammability resistance, colorability, and transparency. Polyarylates can also be used in other safety-related applications such as mining light covers and lenses for traffic signals.

Electrical and Electronic. Polyarylates provide the excellent temperature resistance and flame retardancy needed for electrical connectors, relay housings, coil bobbins, and switch and fuse covers.

Exterior Applications. Because of the excellent uv resistance of polyarylates, end use is found in such outdoor applications as glazing, skylights, and transparent panels. Polyarylates can be used alone or in multilayer constructions with other polymers. Properties such as transparency, impact and heat resistance, and low haze levels after long-term exposure have suited this resin for use in globes and other lighting components.

Producers

Currently, Unitika Corp. Ltd. is the only producer of this material in the world. The trade name of Unitika's polyarylate is U-Polymer. Polyarylate is marketed in North America by Toyota Tsusho America, Inc. World production is about 1000 t/year.

BIBLIOGRAPHY

1. A. Bettelheim, *Plast. Technol.* **31**, 20, 22 (1985).
2. B. D. Dean, M. Matzner, and J. M. Tibbitt, in G. Allen, C. Bevington, G. C. Eastmond, A. Ledwith, S. Russo, and P. Sigwalt, eds., *Comprehensive Polymer Science*, Vol. **5**, Pergamon Press, Oxford, 1989, Chapt. "18".

YUTAKA SHIRAHAMA
Unitika America Corporation
FUMIO OHAMA
Unitika Corporation Ltd.

POLYBENZIMIDAZOLE POLYMERS (PBI). See RIGID ROD POLYMERS.

POLYBENZOTHIAZOLES (PBT). See RIGID ROD POLYMERS.

POLYBENZOXAZOLES (PBO). See RIGID ROD POLYMERS.

POLYBUTADIENE. See BUTADIENE POLYMERS.

POLYBUTENES. See BUTENE POLYMERS.

POLYCARBONATES

Introduction

Polycarbonates are an unusual and extremely useful class of high heat polymers known for their toughness and clarity. The vast majority of polycarbonates are based on bisphenol A (BPA), and sold under the trade names Lexan (GE), Makrolon (Bayer), Caliber (Dow), Panlite (Teijin), and Iupilon (Mitsubishi). Many other producers and suppliers are available. BPA polycarbonates have glass-transition temperatures (T_g) in the range of 140–155°C and are widely regarded for their optical clarity and exceptional impact resistance and ductility at or below room temperature. Other properties such as modulus, dielectric strength, and tensile strength are comparable to other amorphous thermoplastics at similar temperatures below their respective T_gs. However, while most amorphous polymers are stiff and brittle below their T_gs, polycarbonates retain their ductility. Polycarbonates are prepared commercially by two completely different processes: Schotten–Baumann reaction of phosgene (qv) and an aromatic diol in an amine-catalyzed interfacial condensation reaction, or via base-catalyzed transesterification of a bisphenol with a monomeric carbonate such as diphenyl carbonate. Each process has its own inherent advantages and disadvantages. Many important products are also based on polycarbonate in blends with other materials, copolymers, branched resins, flame-retardant compositions, foams, and other materials. Polycarbonates are produced by more than a dozen companies, with global manufacture currently just over 2 million tons annually. Polycarbonate is also the object of both industrial and academic research because of its widespread utility and unusual properties. Research on polycarbonates has steadily increased over the past two decades, with over 5000 publications on the topic since 1995 and nearly 20,000 patents having appeared globally (more than 8000 since 1995). Japanese companies lead

Encyclopedia of Polymer Science and Technology. Copyright John Wiley & Sons, Inc. All rights reserved.

the number of patent holders, including Teijin Chemicals, Teijin Limited, Sekisui Chemical, Asahi Chemical, Idemitsu Petrochemical, Toray Ind., and Mitsubishi Gas Chemical Co. Other companies with significant patent portfolios include General Electric, Bayer AG, and Dow Chemical. Polycarbonate has been the subject of three monographs, one of them published in 2000 (1,2).

Historical Development

The first polycarbonates were prepared by Einhorn in the late 1890s via reaction of hydroquinone or resorcinol with phosgene, using pyridine as solvent (3). Attempts to prepare the polycarbonate of catechol led only to the cyclic five-membered carbonate. A few years later, the same materials were prepared by Bischoff via solventless transesterification using diphenyl carbonate (4). The hydroquinone polymer is brittle, crystalline, insoluble in most solvents, and melted at >280°C. The polymer from resorcinol is glassy and brittle, although it crystallizes from solution and melts at about 190–200°C. Both of these polymers were apparently of low molecular weight and owing to difficulties of processing and characterization, were not developed further. In fact, no research on polycarbonates appeared in the literature for about 30 years after their initial discovery. In the early 1930s, the preparation of *aliphatic* carbonates was studied during the investigation of the preparation and properties of polyesters (5). Because the reactions of aliphatic alcohols and phosgene proceed more slowly than those of phenols, two other methods were used to prepare the aliphatic polycarbonates: direct transesterification reactions and ring-opening polymerization of low molecular weight cyclic polycarbonates prepared by a distillative transesterification–depolymerization. Further work was carried out in the 1940s. 1,6-Hexanediol polycarbonates were prepared via transesterification using dibutyl carbonate (6). The aliphatic polycarbonates had low melting points and did not prove interesting commercially. In 1941, the Pittsburgh Plate Glass Co. (PPG) introduced a liquid casting resin designated as CR-39 (7). This material, formally a polycarbonate, was a cross-linked thermoset resin prepared by a peroxide-initiated radical polymerization of the bisallyl carbonate of diethylene glycol. The starting material was prepared from allyl alcohol and diethylene glycol bischloroformate (eq. (1)). Once polymerized, CR-39 was a colorless, transparent, scratch-resistant plastic which was used in optical applications. These materials differ markedly from the current thermoplastic polycarbonates. Although its nature and chemical makeup are completely different from modern polycarbonates, CR-39 was the first commercially available polycarbonate.

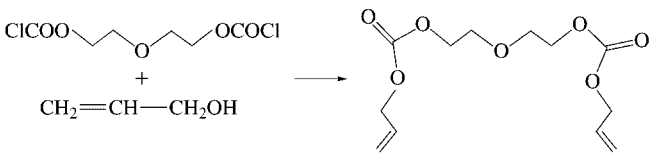

(1)

A reexamination of aromatic polycarbonate chemistry was carried out about 50 years after the first polycarbonates of resorcinol and hydroquinone were

discovered. In independent investigations by Schnell at Bayer AG and by Fox at General Electric, it was discovered that the polycarbonates of BPA could be prepared (eq. (2)). Unlike the aliphatic polycarbonates prepared earlier, which were either liquids or low melting solids, the aromatic polycarbonates were tough, amorphous solids having elevated T_gs. Owing to the unusual properties of the BPA polycarbonate, ie, toughness, transparency, and thermal stability, each company began development programs. Bayer AG, the first to report the properties of a series of polycarbonates (8), had patents issuing as early as 1954 (9). Commercial production of polycarbonate by Bayer AG began in Germany in 1958 and in the United States in 1960. General Electric (GE) started U.S. commercial production in 1960. After a period of litigation, U.S. patents were issued to Bayer AG, which claimed an interfacial process for preparation of polycarbonates, and had multiple claims to various polycarbonates (10). The basic GE patent claimed the transesterification process and the polycarbonate product so formed (11). Since that time extensive research has been carried out on polycarbonates. Several manufacturers have developed many niches of new products, blends, or processes for the production of these materials. Although GE and Bayer AG remain the principal producers, at least 50 companies have patented some aspect of polycarbonate chemistry. Over a dozen producers exist worldwide.

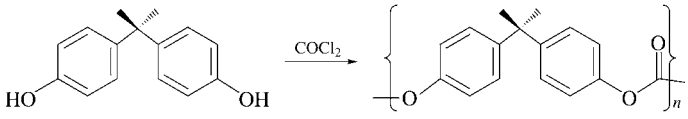

(2)

Solubility and Solvent Resistance. The majority of polycarbonates are prepared in methylene chloride solution. Other chlorinated solvents such as chloroform, *cis*-1,2-dichloroethylene, *sym*-tetrachloroethane, and methylene chloride are also good solvents for polycarbonates. The polymer is soluble in chlorobenzene or *o*-dichlorobenzene when warm, but crystallization may occur at lower temperatures. Methylene chloride is most commonly used because of the high solubility of the polymer (350 g/L at 25°C) and also because this solvent has low flammability and toxicity. Nonhalogenated solvents include tetrahydrofuran, dioxane, pyridine, and cresols. Hydrocarbons and aliphatic alcohols, esters, or ketones do not dissolve polycarbonates. Acetone promotes rapid crystallization of the normally amorphous polymer and causes catastrophic failure of stressed polycarbonate parts. In general, polycarbonate resins have fair chemical resistance to aqueous solutions of acids or bases, as well as to fats and oils, although prolonged exposure to high or low pH conditions can lead to loss of molecular weight. Chemical attack by amines or ammonium hydroxide occurs readily, and aliphatic and aromatic hydrocarbons promote crazing of stressed molded samples. For these reasons, care must be exercised in the choice of solvents for painting and coating operations. For sheet applications, polycarbonate is commonly coated with a silicone-silicate or acrylate hardcoat, which provides abrasion resistance as well as increased solvent resistance. Coated films are also available. Certain blends and copolymers of polycarbonate demonstrate dramatically improved solvent resistance. The blend of polycarbonate and poly(butylene terephthalate), eg, Xenoy

(GE) or Makroblend (Bayer), combines the toughness of polycarbonate with the solvent resistance of the semicrystalline polyester and is used in automotive applications. Hydroquinone polycarbonates were reinvestigated in the late 1980s (12). Several binary and ternary copolycarbonates were prepared using monomers such as hydroquinone, biphenol, and substituted hydroquinones. However, no thermal transitions other than the T_g were noted, and the copolymer with hydroquinone had a very low molecular weight ($\eta_{inh} = 0.09–0.10$). Difficulty in preparation of hydroquinone polycarbonates, owing to the insolubility of the oligomers, had been noted in the 1950s (13). Copolycarbonates of BPA and hydroquinone can be prepared via the intermediacy of oligomeric cocyclics (eq. (3)) (14). Although hydroquinone linear oligomers having degrees of polymerization greater than 2 are insoluble in CH_2Cl_2, the cyclic analogues remain soluble when randomly cyclized with BPA. Polymerization of the hydroquinone–BPA cocyclics via anionically initiated, ring-opening polymerization leads to high molecular weight semicrystalline polymers. Using this methodology, hydroquinone can be incorporated into the polycarbonate in levels up to 60%. The copolycarbonates show dramatically increased solvent resistance and are insoluble in all common polycarbonate solvents such as methylene chloride or tetrahydrofuran. Furthermore, when molded bars of the polycarbonate are exposed to gasoline while under stress, impact properties are retained, whereas standard polycarbonate grades fail.

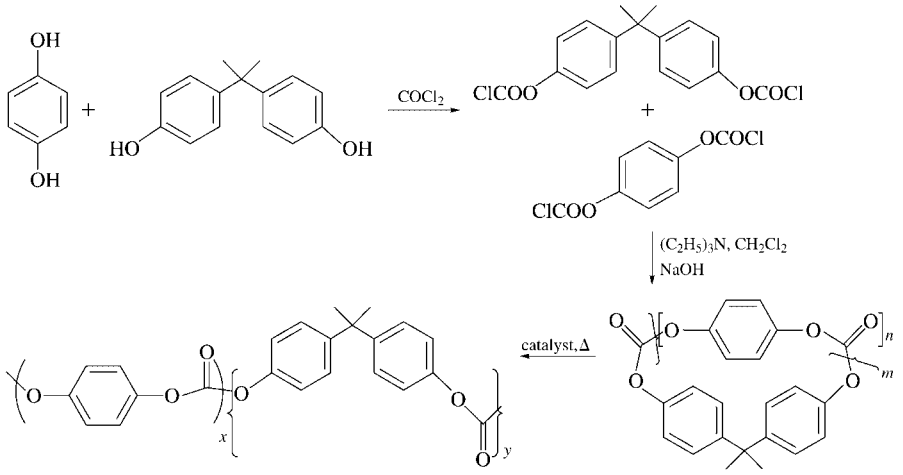

Hydroguinone HQ – BPA copolycarbonate (3)

BPA polycarbonate has excellent resistance to hydrolysis. Prolonged contact with water at 60°C or moderate-term (months) contact at 100°C has little effect on polycarbonate, but extended contact can eventually lead to embrittlement. For example, exposure of polycarbonate film to steam at 101 kPa (1 atm) at 100 and 150°C showed failure of the film after 700 and 200 h, respectively (15). Additives can accelerate the degradation by catalyzing hydrolysis. Although acids have little effect, aqueous base can lead to etching. Hydrolysis occurs at the surface. The hydrolytic stability can be attributed to the low water solubility in the resin (~0.3%), which leads to essentially no swelling, and to the high glass-transition temperature of

the resin. Heating at elevated temperatures (eg, during molding), however, can lead to degradation owing to hydrolysis. Drying of all grades of polycarbonate is recommended prior to molding so as to avoid hydrolysis to lower molecular weight materials. Hydrolysis of polycarbonate has been extensively studied (16).

Molecular Weight and Viscosity. BPA polycarbonates are commercially available in a wide range of molecular weights. As the molecular weight increases, melt and solution viscosities increase proportionally. Molecular weights may be determined or inferred by several means, including gel-permeation chromatography (gpc), light-scattering size-exclusion chromatography, measurement of intrinsic or inherent viscosity, and measurements of melt viscosity and flow. Correlation of intrinsic viscosity (IV), or inherent viscosity [η_{inh}], with weight-average molecular weight (M_w) has been carried out on carefully characterized polycarbonate samples (17). The following relationship exists when [η_{inh}] is in mL/g.

$$[\eta] = (41.2 \times 10^{-3})\left(M_w^{0.69}\right)$$

For chemical studies, the chromatographic methods or solution viscosities are methods of preference, but for practical applications, melt flow is most important. Standard injection-molding grades of polycarbonate have intrinsic viscosities in the range of 0.50–0.55 dL/g in chloroform at 30°C, with M_w of 35,000–70,000 and number-average molecular weight (M_n) of 15,000–24,000, as determined by gpc using polystyrene standards, or M_w of 18,000–30,000 as determined by light scattering. The polydispersity ratio (M_w/M_n) of polycarbonate is about 2.3–2.7. The range of molecular weights and viscosities available is shown in Table 1.

The mechanical properties of polycarbonate, eg, tensile strength, impact resistance, flexural strength, elongation, etc, improve dramatically with increasing polymer intrinsic viscosity up to a value of about 0.45 dL/g (Table 2). After that point, only slight increases in mechanical properties are seen with increasing molecular weight, but melt viscosity continues to climb. At IV values greater than

Table 1. Molecular Weight and Viscosity of Lexan Resins

Grade	Description	MFI[a]	IV[b]	M_w[c]	M_n[c]	PDI[d]	M_w[e]
131	Ultrahigh viscosity	3.1	0.629	72,600	28,100	2.58	35,500
1881	Very high viscosity	4.9	0.581	66,100	25,400	2.6	32,000
101	High viscosity	6.5	0.551	62,000	25,400	2.44	29,000
161	Medium high viscosity	7.4	0.538	60,600	24,400	2.48	27,900
141	Medium viscosity	9.2	0.510	57,000	23,900	2.38	26,300
141L	Medium low viscosity	11.2	0.493	54,500	22,700	2.40	27,400
121	Low viscosity	16.2	0.454	49,800	20,400	2.44	21,200
HF1110	High flow	20.9	0.434	46,900	18,400	2.55	22,700
SP1110	Superior flow	22	0.53	60,000	24,000	2.50	27,500
OQ1020	Optical quality	78	0.35	35,800	13,900	2.57	16,600

[a]MFI = melt-flow index.
[b]IV = intrinsic viscosity in CH_2Cl_2 at 25°C.
[c]From gel-permeation chromatography using polystyrene standards.
[d]PDI = polydispersivity ratio, M_w/M_n.
[e]Molecular weight from light scattering.

Table 2. Bisphenol A Polycarbonate Properties

Property	Lexan 141	Lexan 3414[a]	ASTM method
Physical properties			
Specific gravity	1.52	1.20	D792
Water absorption (23°C), %			
24 h	0.15	0.12	D570
Equil	0.35	0.23	D570
Melt-flow rate (300°C, 1.2 kgf), g/10 min	10.5		D1238
Mold shrinkage (3.2-mm part), %	0.1–0.2	0.5–0.7	D955
Light transmittance (550 nm), %	86–89		D1003
Haze, %	1–1.5		D1003
Refractive index	1.586		
Mechanical properties			
Tensile strength (Type I), MPa[b]			
Yield	60		D638
Break	70	160	D638
Tensile elongation at break (Type I), %	130	3.0	D638
Flexural strength, MPa[b]	97	190	D790
Flexural modulus, MPa[b]	2,300	9,600	D790
Compressive strength, MPa[b]	86	140	D695
Compressive modulus, MPa[b]	2,400	10,300	D695
Shear strength, MPa[b]			
Yield	41	75	D732
Break	695		D732
Shear modulus, MPa[b]	785	2,200	D732
Hardness (Rockwell R)	118	119	D785
Fatigue limit (2.5×10^6 cycles), MPa[b]	6.9	50	D671
Deformation under load (27 MPa[b]), %			
at 23°C	0.2	0.1	D621
at 70°C	0.5	0.2	D621
Impact properties			
Izod impact, J/m[c]			
Notched	801	133	D256
Unnotched	No break	1300	D256
Tensile impact (Type S), kJ/m^2[d]	578	67	D1822
Thermal properties			
Softening temperature (Vicat), °C	154	166	D1525
Heat deflection, °C			
at 0.45 MPa[b]	138	154	D648
at 1.8 MPa[b]	134	146	D648
Specific heat, J/(g·°C)[e]	1.25	1.0	C351
Coefficient of thermal expansion (−40 to 95°C), %	6.75×10^{-3}	1.67×10^{-3}	E831
Thermal conductivity, W/(m·K)	0.19	0.22	C177
Brittle temperature, °C	−129		D746
Continuous use temperature, °C	121		
Electrical properties			
Dielectrical strength, mV/m	15	17.7	D149
Dielectric constant			
60 Hz	3.17	3.53	D150
1 MHz	2.96	3.48	D150

Table 2. (Continued)

Property	Lexan 141	Lexan 3414[a]	ASTM method
Dissipation factor			
60 Hz	0.0009	0.0013	D150
1 MHz	0.010	0.0067	D150
Flame classifications			
100 Series 94, mm			
V-0 rating	6.10	3.05	UL 94
V-2 rating	1.14		UL 94
Oxygen index, %	26	30	D2863

[a] This polycarbonate is 40% glass reinforced.
[b] To convert MPa to psi, multiply by 145.
[c] To convert J/m to ft·lbf/in., divide by 53.38.
[d] To convert kJ/m^2 to ft·lbf/in.^{2}, divide by 2.10.
[e] To convert J to cal, divide by 4.184.

0.6 dL/g, the melt viscosity becomes so high that processing is very difficult. Because some compromise between polymers having high molecular weight and good mechanical properties must balance the processibility of the resin, newer formulations having increased melt flow are being marketed. Lexan SP copolyestercarbonates (GE), for example, demonstrate enhanced flow rates as measured by melt-flow index (10–22 g/min) compared to standard grades of resin (6–16 g/min), yet retain excellent impact resistance, eg, notched Izod of 642–910 J/m (12–17 ft·lb/in.). A variety of strategies have been used for improvement in the melt flow of polycarbonate, usually sacrificing thermal resistance (ie, lower T_g), while maintaining good impact strength. Ultrahigh molecular weight polycarbonates can be prepared via ring-opening polymerization of cyclic aromatic oligomeric carbonates. These materials, which are not commercially available, can lead to polycarbonates having IV > 1.0 dL/g and molecular weights of 300,000–500,000 (18).

Spectroscopy and Analysis. Polycarbonates have a strong C=O stretching band at 1770 cm^{-1}, and strong C—O stretching bands at 1220 and 1235 cm^{-1}, distinguishing them from polyesters. The amount of phenol end groups can be determined from the O—H absorption at 3595 cm^{-1}. Proton nmr spectroscopy shows a symmetrical A_2B_2 aromatic pattern at 7.16 and 7.24 ppm, and absorption for the *gem*-dimethyl at 1.68 ppm, relative to $(CH_3)_4Si$. The ^{13}C nmr shows seven distinct absorptions: 152.1, attributable to C=O; 148.9; 148.2; 127.9; 120.3; 42.5; and 30.9. X-ray spectroscopy shows a weak absorption at 725 cm^{-1}, related to crystallinity, and a band at 917 cm^{-1}, independent of crystallinity. Differential scanning calorimetry reveals a T_g at around 154°C, shifting somewhat with molecular weight or level of branching. End group and impurity analysis is best revealed by hydrolysis of the polycarbonate using KOH-methanol in tetrahydrofuran under nitrogen, followed by reversed-phase hplc analysis or by spectroscopic techniques. Trace levels of impurities, such as methylene chloride, amine, chloride, and sodium, are determined by standard analytical techniques, eg, atomic absorption or titration.

Structure and Crystallinity. The mechanical–optical properties of polycarbonates are those common to amorphous polymers. The polymer may be

crystallized to some degree by prolonged heating at elevated temperature (8 days at 180°C) (19) or by immersion in acetone. Recently, an extensive amount of work has appeared on solid-state polymerization of polycarbonate oligomers. The oligomers or low molecular weight polycarbonate can be crystallized by a variety of methods, typically treatment with an antisolvent vapor. Amorphous powder appears to dissolve partially in acetone, initially becoming sticky, then hardening and becoming much less soluble as it crystallizes. Enhanced crystallization of polycarbonate can also be caused by the presence of sodium phenoxide end groups (20). Film or fibers derived from low molecular weight polymer tend to embrittle on immersion in acetone; those based on higher molecular weight polymer (>0.60 dL/g) become opaque, dilated, and elastomeric. When a dilated sample is stretched and dried, it retains orientation and is crystalline, exhibiting enhanced tensile strength. The tensile heat-distortion temperature of the crystalline file is increased by about 20°C, and the gas permeability and resistance to solvent attack is increased.

Thermotropic polycarbonates have been prepared from mixtures of 4,4-dihydroxybiphenyl and various diphenols (12). Nematic melts were found for copolycarbonates prepared from methylhydroquinone, chlorohydroquinone, 4,4-dihydroxydiphenyl ether, and 4,4-dihydroxybenzophenone. Slightly crystalline polycarbonates have been prepared from mixtures of hydroquinone and BPA (14) [$T_g = 154°C$, $T_m = 313°C$, $\Delta H = 11.0$ J/g (2.63 cal/g)], and a highly crystalline, high heat polycarbonate has been prepared from methylhydroquinone (21) [$T_g = 155°C$, $T_m = 289°C$, $\Delta H = 31.0$ J/g (7.41 cal/g)]. While the former (hydroquinone–BPA) copolymer has only been prepared via cyclic oligomers, the methylhydroquinone polycarbonate can be prepared via a melt process.

Experimental and theoretical studies on the structure of BPA polycarbonates have been the object of considerable interest since the work of Williams and Flory in the late 1960s (22). Because of the low conformational barriers to rotation, phenyl ring-flipping and cis–trans isomerization about the carbonate group have been invoked as mechanisms for energy absorption, providing polycarbonates with low temperature impact strength. Crystal structures of diphenyl carbonate, described in detail, have been published (23,24). The crystal structures of a model carbonate (the bisphenyl carbonate of BPA) has also appeared (25). All of the published structures indicate that the thermodynamically preferred backbone conformation about the carbonate functionality is a trans–trans conformation. In this form, the dihedral angles of the aromatic rings with the carbonyl oxygen, C—O—C(=O)—O (174.8° and 176.5°), are nearly eclipsed, and as a consequence, the planes of the carbonyl groups are skewed from the planes of the aromatic rings by 59.1° and 53.2°. A cis–trans relationship about the carbonyl group was first seen in a complex of the bisphenyl carbonate of BPA with two molecules of a thiopyrilium salt (26). The cyclic dimer carbonate of BPA also shows only a cis–trans relationship of aromatic rings about the carbonyl (24). The crystal structure of the cyclic tetramer has also been described (24), showing two distinct types of aromatic conformations about the carbonyl. Several mathematical (27) and physical (28) methods have been used to analyze the conformational features of BPA polycarbonate. Estimations of the energy differences between conformations have been investigated by a variety of techniques, including ab initio calculations, (29) nmr spectroscopy, (30) and infrared spectroscopy (31). Molecular

simulation studies on the conformation of cyclic oligomers have also appeared (32).

Glass-Transition Temperature and Melt Behavior. The T_g of BPA polycarbonate is around 150°C, which is unusually high compared to other thermoplastics such as polystyrene (100°C), poly(ethylene terephthalate) (69°C), nylon-6,6 (45°C), or polyethylene (−45°C). The high T_g can be attributed to the bulky structure of the polymer, which restricts conformational changes, and to the fact that the monomer has a higher molecular weight than the monomer of most polymers. The high T_g is important for the utility of polycarbonate in many applications because, as the point which marks the onset of molecular mobility, it determines many of the polymer's properties such as dimensional stability, resistance to creep, modulus, and ultimate use temperature. Polycarbonates of different structures may have significantly higher or lower T_gs (see Table 3).

BPA polycarbonate becomes plastic at temperatures of around 220°C. The viscosity decreases as the temperature increases, exhibiting Newtonian behavior, with the melt viscosity essentially independent of the shear rate. At the normal injection-molding temperature of 270–315°C, the melt viscosity drops from 1100 to 360 Pa·s (11,000–3600 poise), which is about five times the viscosity of poly(ethylene terephthalate) of similar molecular weight over the same temperature range. Because the viscosity of polycarbonate can only be reduced by increasing the temperature, the ultimate limit on molecular weight is controlled by the processing conditions and the thermal stability of the polymer. Branched polycarbonates can be prepared by incorporation of small amounts of tri- or tetrafunctional phenols or carboxylic acids. The rheological properties of the branched resin are different from those of the linear resins. The branched resins demonstrate non-Newtonian behavior, and viscosity depends on shear rate. The melt viscosity of branched resins decreases with increasing shear, allowing extrusion at lower temperatures of materials with exceptional melt strength for blow-molding applications (Fig. 1). Polycarbonate melt rheology has recently been summarized in a review (55).

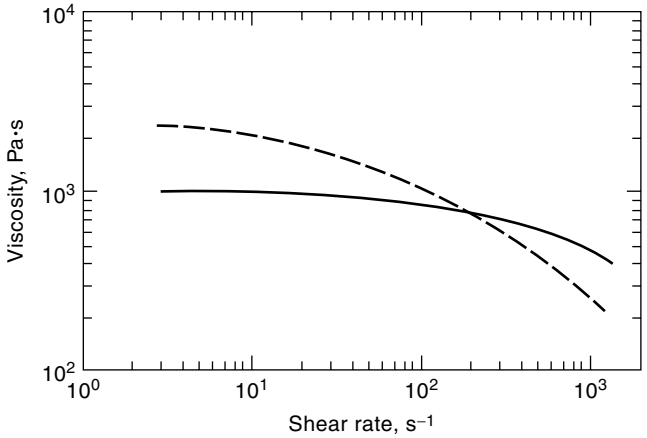

Fig. 1. Melt viscosity as a function of shear rate for (—) linear BPA polycarbonate and (- - -) branched polycarbonate. To convert Pa·s to Poise, multiply by 10.

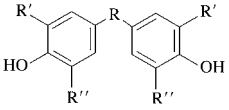

Table 3. Aromatic Polycarbonates Derived from Bisphenols

Monomer	Monomer mp, °C	T_g, °C	Melt range	References
When R′ = R″ = H; R =				
	163[a]	147	>300	7, 33,34
	161	145	230–235	7, 33,34
	152	113	220–240	7, 33,34
	249		200–210	7, 35
	213–215			36
	214–215[b]	168	230–260	37, 38
	122	130	185–195	7, 33,34
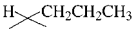	129	123	150–170	7, 33,34
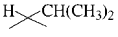	155	149	170–180	7, 33,34
	224	190		39
	161	121	200–215	39
	157[c]	149	215–230	7, 33,34
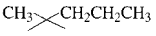	149	137	200–220	7, 33,34
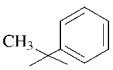	188	176	210–230	7, 33,34
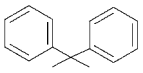	295	220	240	7, 33,34
	161[d]	149		40
	170	200		41
	147	186		41
	190[e]	179	250–260	7, 33,34
	157	167	240–250	7, 33,34
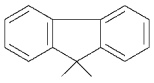	224	275	390	42,43
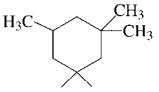	239	239		44

Table 3. (Continued)

Monomer	Monomer mp, °C	T_g, °C	Melt range	References
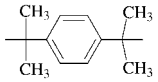	304	228		45
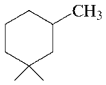	207			46
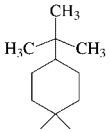	221			47
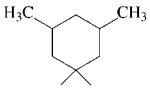	229			48
$R = C(CH_3)_2$; $R' = R'' = CH_3$	165[f]	207		49
$R = C(CH_3)_2$; $R' = R'' = Br$	178–80[g]	265		7, 33,34
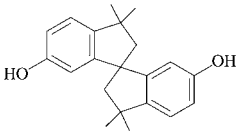	[h]	230		50,51
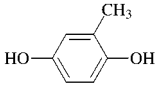	128–130[i]	155		13
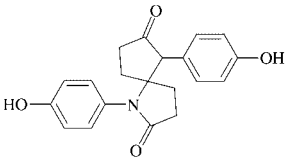		223		52
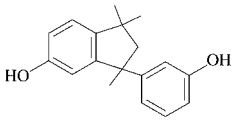				53
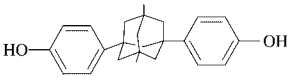		243		54

[a] Crystalline and insoluble.
[b] Bisphenol C; flame retardant.
[c] Bisphenol A.
[d] Flame retardant.
[e] Bisphenol Z.
[f] TMBPA; hydrolytically stable.
[g] TBBPA; flame retardant.
[h] SBI; low birefringence.
[i] $T_m = 289°C$; crystalline.

Thermal, Flame-Retardant, and Hydrolytic Behavior. BPA polycarbonate exhibits excellent thermal stability, especially in the absence of oxygen and water. The dry polymer may be heated to 320°C for several hours, or for short times to as high as 330–350°C with only minimal degradation. At these high temperatures, thermal-oxidative degradation leads to slight yellowing, requiring color stabilization. Low levels (usually <5000 ppm) of stabilizers (phosphites, phosphonites, phosphines, epoxide compounds, and organosilicon compounds) are usually added during processing. At temperatures above 400°C, rapid decomposition and cracking occur. BPA polycarbonate has an oxygen index of 26 according to ASTM D2863-70, indicating that under test conditions, an atmosphere of 26% oxygen is required to sustain combustion. Owing to thermal-oxidative stability, polycarbonate has some inherent flame-resistant properties and can be classified as V-2 according to UL94 of the Underwriters Laboratory. Several polycarbonate grades include additives to increase the flame-retardant properties, and to decrease smoke. Flame-retardant agents include brominated oligomers or polymer from tetrabromo-BPA, alkali metal salts, usually alkali sulfonates, and polytetrafluoroethylene (PTFE). The flame-retardant grades are classed as V-0 according to UL94 testing procedures, using a wall thickness of 3.2 mm. Recently, several so-called Eco-FR grades have appeared, which contain no halogenated or phosphorus additives, yet which still retain the V-0 rating.

Because of the low solubility of water in the resin, BPA polycarbonates are inherently resistant to aqueous acid and base, although strong nucleophilic bases can catalyze hydrolysis. Prolonged contact with water at 100°C can lead to reduced impact strength as a result of microcrack formation. In autoclave testing under steam pressure, water can be forced into the resin, forming pockets that eventually lead to haze, microcracks, and loss of properties. The formation of water-filled pockets has been confirmed experimentally (56). Although many additives have a deleterious effect on hydrolytic stability by acting as hydrolysis catalysts, some stabilizers, especially epoxides, can increase the hydrolytic stability. Polycarbonates should always be dried prior to melt processing because even the low levels of water present in the resin at equilibrium can lead to partial hydrolysis and lowering of the molecular weight of the molded parts. The equilibrium water content at 60% relative humidity is 0.26 wt% at ambient temperature, and 0.9 wt% at 100°C in water.

Optical Properties. Polycarbonate is a transparent, nearly colorless polymer, making it attractive as a glass replacement. Visible light transmission is about 90%, and haze is only 1–2% in typical commercial products. Absorption in the uv regions accounted for by the aromatic structure reaches a maximum at around 255 nm. Polycarbonate has a high refractive index (1.588) and a lower density than glass (1.52 g/mL), making it an attractive material for eyewear. Exposure of non-uv stabilized polycarbonate to strong uv or outdoor sunlight conditions can lead to photoyellowing of the survace. uv screens can be combined with hard coats to protect the surface of polycarbonate and also to provide resistance to chemical attack in sheet products used for glazing applications. Polycarbonate eyewear is usually available with a scratch-resistant coating.

Special polycarbonate grades have been developed for the rapidly growing optical information storage markets. Compact discs (CDs) utilize the transparency, low birefringence, mechanical and dynamic stability, and good heat-distortion

properties of polycarbonate. Polycarbonate prepared by the melt technique can be made especially free of contamination and with a controlled low molecular weight, and is the preferred substrate. The use of *p*-alkyl phenols with branched alkyl groups containing eight or nine carbon atoms result in extremely high melt flow polycarbonates having sustained impact strength. A number of other agents for increasing melt flow have also been patented. Typically, polycarbonate as molded is highly anisotropic and exhibits birefringence. Although the birefringence can be minimized using the appropriate processing conditions, only modification of the backbone can be used to reduce birefringence to zero. Use of the high flow resins leads to lower birefringence in the molded parts and also decreases the molding cycle times to only a few seconds. New polycarbonates with inherently lower birefringence have also been studied recently. A number of polymers with the phenyl rings out of the plane of the polycarbonate backbone are effective at reducing birefringence; the spirobiindane bisphenol (SBI) is a notable example. A copolymer of BPA with SBI can lead to zero orientational birefringence. This work has been reviewed (57,58).

Mechanical Properties. Mechanical and other properties of BPA polycarbonate are listed in Table 2. The room temperature modulus and tensile strength are similar to those of other amorphous thermoplastics, but the impact strength and ductility are unusually high. While most amorphous polymers are glass-like and brittle below their T_gs, polycarbonate remains ductile to about -10°C. The stress–strain curve in uniaxial tension (Fig. 2) is typical of ductile materials, having an initial Hookean region, followed by shear-induced yielding and plastic deformation. Breakage occurs at about 120% elongation. The area under the stress-strain curve is a measure of energy absorption per unit volume, and is about 65 J/m^3 (15.5 cal/m^3). That value is about 8.5 times higher than the energy

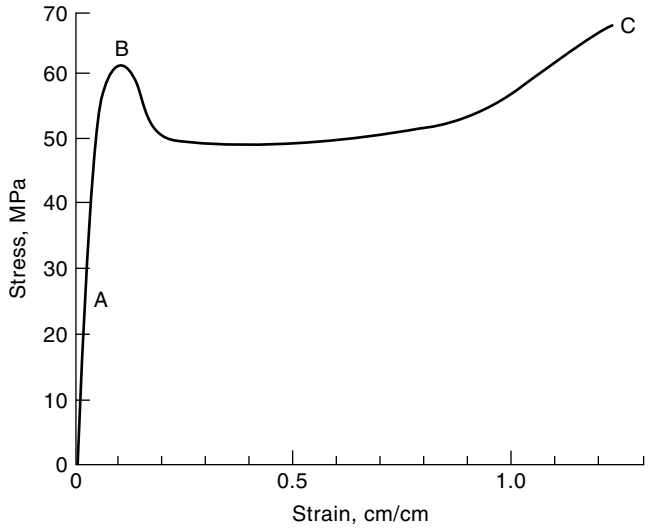

Fig. 2. Stress–strain curve for standard polycarbonate resin at 23°C where the points A, B, and C correspond to the proportional limit (27.6 MPa), the yield point (62 MPa), and the ultimate strength (65.5 MPa), respectively. To convert MPa to psi, multiply by 145.

absorption of cast aluminum, and 60% that of carbon steel, placing polycarbonate in an ideal position for use as a metal replacement. Weight savings as a metal replacement are substantial because polycarbonate is only 44% as dense as aluminum and one-sixth as dense as steel.

Impact strength can be measured by a variety of methods including notched Izod, tensile impact, and falling dart impact. The notched Izod test is most widely used to measure the toughness of a resin. This test involves measuring the energy absorption under impact conditions on a sample in which a notch has been cut to serve as a stress concentrator. Polycarbonates are among the highest rated engineering polymers for impact resistance and are the toughest transparent materials known. Under high strain rate conditions (impact), polycarbonates are sensitive to the nature of the stress concentrator, and different results can be obtained depending on how the notch is cut and on the thickness of the sample. At room temperature, decreasing the radius of the notch tip from 0.038 to 0.020 mm reduces the notched impact strength from 960 to 130 J/m (230–31 cal/m). A similar transition is noted when samples are tested over a range of temperatures, showing a transition from ductile to brittle behavior at temperatures around -20°C. As the thickness of the specimen is increased from 3.18 to 6.35 mm, a similar transition occurs, with brittle failure of thicker samples. The critical thickness phenomenon as well as the low temperature embrittlement can be alleviated by use of copolymers or blends.

Glass-reinforced polycarbonates are sold as high modulus materials having properties approaching those of metals while retaining the basic plastic attributes of low cost processing, dielectric character, resistance to corrosion, light weight, and inherent color. As the level of glass is increased, tensile and flexural strength and modulus increase to almost double their original values. Compressive strength increases by about 65%. Fatigue endurance increases dramatically to 7 times the value of the neat resin; deformation under load drops to 0.1% under 27 MPa (6800 psi) at 23°C. Both the coefficient of thermal expansion and mold shrinkage drop in glass-reinforced resins. As expected for a stiffer resin, the impact properties drop as well, to a notched Izod impact value of 133 J/m (32 cal/m). Properties of a 40% glass-reinforced resin are compared to a standard injection-molding resin in Table 2.

Preparation

The historical direct reaction route, which utilized phosgenation of a solution of BPA in pyridine proved inefficient commercially because of the need for massive pyridine recycle. Calcium hydroxide was used as an HCl scavenger for a brief period of time, but again, recycle was an issue. Although both solution and melt processes were piloted through the early and mid 1960s, the industry settled on an amine-catalyzed interfacial phosgenation process. In this process, the BPA is phosgenated in a solvent such as CH_2Cl_2 using a tertiary amine catalyst, while maintaining pH via the addition of NaOH. The by-product NaCl is then recycled back to chlorine (used to make phosgene in combination with carbon monoxide) and NaOH. The melt transesterification process simply involves base-catalyzed reaction of BPA with diphenyl carbonate. After sporadic work on the melt process

over many years, GE Plastics first commercialized this technology in a joint venture with Mitsui Petrochemical Industries, now called GE Plastics Japan. The small plant (35,000 ton/year) validated the technology and led to large-scale commercialization of the melt process in a full-scale plant (150,000 ton/year) in Cartagena, Spain.

Interfacial Polymerization. Most BPA polycarbonates are produced by an interfacial polymerization process utilizing phosgene. The interfacial process for polycarbonate preparation involves stirring a slurry or solution of BPA and 1–5% of a chain stopper such as phenol, *p*-*t*-butylphenol, or *p*-cumylphenol in a mixture of methylene chloride and water, while adding phosgene in the presence of a small amount (0.1–3%) of a tertiary amine catalyst (eq. (4)). Sodium hydroxide solution is added concurrently to maintain the appropriate reaction pH (typically 10–12). Efficient mixing is important to ensure contact between the four phases present [solid BPA, gaseous phosgene, methylene chloride (into which the polymer dissolves), and the aqueous phase (in which the by-product sodium chloride becomes concentrated)]. Phosgene addition is continued until the presence of free phenolic groups can no longer be detected. Interfacial reactions are often overphosgenated to ensure complete reaction, and the excess phosgene becomes hydrolyzed, forming sometimes significant amounts of sodium carbonate. When the reaction is complete, and after the brine phase has been separated, the methylene chloride solution of polymer is washed first with acid to remove residual base and amine and then with water. Many variations of this basic interfacial process have been patented including continuous or semicontinuous processes, various workup procedures, many types of catalysts (including phase transfer catalysts and bifunctional catalysts), methods which rely on the intermediacy of bischloroformate oligomers, and various schemes to control the formation of low molecular weight oligomeric species or cyclics.

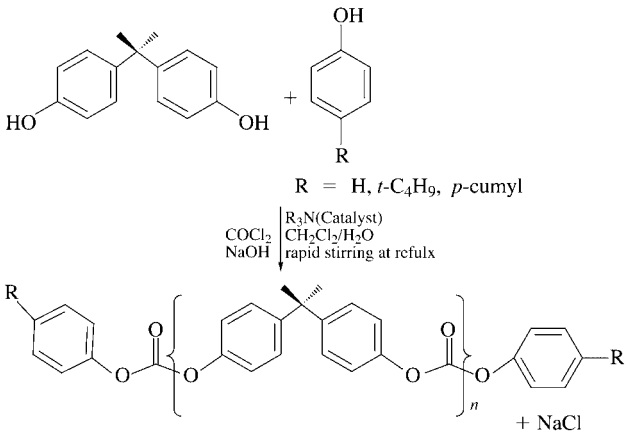

(4)

Studies on the mechanism of interfacial polycarbonate formation are complicated by its interfacial nature, involving four phases. In addition, effects such

as stirring rate, interfacial volume, and acid–base equilibria of BPA with NaOH are involved. Although some authors still believe that the tertiary amine acts solely as a base (59) (and hence as a phase-transfer agent, with $R_3N\text{-}H^+$ as the cationic species), other experimental kinetic evidence supports the importance of formation and reaction of acyl ammonium salts as intermediates (60). Assuming that acyl ammonium salts are formed, the sequence of reactions shown in equations 567 would occur. In the first step, the bisphenol reacts with phosgene to form a chloroformate (eq. (5), Ar = aryl group). Although this reaction can proceed in the absence of a catalyst, it is accelerated both by phase transfer and by nucleophilic catalysts. The reaction occurs quickly enough to compete effectively with phosgene hydrolysis, even at the reaction pH of 10–12. Reaction of a chloroformate functionality with a phenol to form a carbonate functionality requires a catalyst to proceed effectively (eq. (6)). In the absence of a catalyst, the reaction takes several hours, even at high pH (60). Tertiary amines provide a substantial rate acceleration, but phase-transfer catalysts [such as $(C_4H_9)_4NOH$ or $(C_4H_9)_3NCH_3OH$] are also very effective (61). The amines function by nucleophilic catalysis, forming an acyl ammonium salt in an equilibrium reaction with chloroformate, which is more susceptible toward attack by a phenol. The effects of tertiary amines on the formation and reactions of aryl chloroformates using model compounds have been studied (60). These studies, which used stop flow ftir techniques to measure kinetics, clearly showed that very slight changes in the nature of the tertiary amine structure can lead to dramatic changes in both the rate at which equilibrium is achieved and the position of equilibrium; both the rate and position of equilibrium can be affected by a factor of 4000–5000, simply by changing the amine from triethylamine to diethylmethylamine. Other investigators have shown that those changes effectively account for dramatic changes in product formation (62). Less hindered amines such as methyldiethylamine afford very fast reactions but significant hydrolysis of chloroformate, while more hindered amines, such as tributyl amine afford less hydrolysis, but also slower rates. Phase-transfer catalysts cannot involve intermediacy of an acyl ammonium salt, yet also provide fast rates. These catalysts function by solubilizing the phenoxide anion, making reaction in the organic phase more facile. Phase-transfer catalysts also provide the advantage that hydrolysis of both phosgene and chloroformates is greatly reduced. In highly phosgene-efficient cases, however, a small amount of tertiary amine is required to catalyze chloroformate hydrolysis (63). It is believed that the main route to hydrolysis, a largely undesired reaction, is via the acyl ammonium salt which, as it becomes less lipophilic, enters the water-rich interfacial region. Normally, polycarbonate reactions are overphosgenated to ensure complete conversion of bisphenol to product, forming slight stoichiometric excesses of chloroformate. Some hydrolysis of the chloroformate so formed is then necessary to complete the reaction, by converting the chloroformate to a phenoxide so that condensation to a carbonate can occur (eq. (7)). The use of bifunctional catalysts containing both a tertiary amine and a quaternary ammonium salt on the same molecule for polycarbonate synthesis has recently been patented (64). A side reaction that can also occur during interfacial phosgenation is the formation of urethanes. Under conditions of long reaction time or high amine level, acyl ammonium salts undergo a first-order reaction to form dialkyl urethanes (eq. (8)) (65).

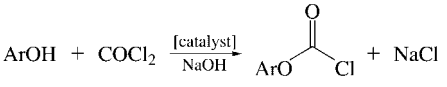

(5)

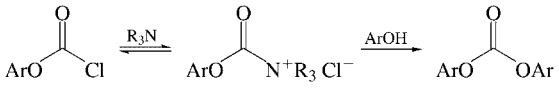

(6)

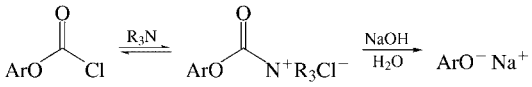

(7)

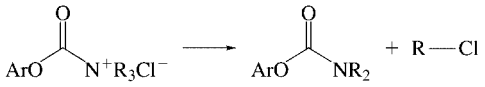

(8)

Methods for isolation of the product polycarbonate remain trade secrets. Feasible methods for polymer isolation include antisolvent precipitation, removal of solvent in boiling water, spray drying, and melt devolatilization using a wiped film evaporator or similar equipment. Regardless of the technique, the polymer must be dried, to avoid hydrolysis, and essentially be devoid of methylene chloride. Most polycarbonate, whether isolated as pellets or powder, is extruded at which point stabilizers, additives, and colors may be formulated.

Transesterification or Melt Process. There has recently been much renewed interest in the transesterification process for the preparation of polycarbonate because of the desire to transition technology to environmentally friendly processes. Three hundred and fifty patents on the melt process have appeared since 1995. The transesterification or melt process utilizes no solvent during polymerization, producing neat polymer directly, and so chlorinated solvents may be entirely eliminated. GE Plastics operates two melt polycarbonate plants, one in Chiba, Japan, and the other in Cartagena, Spain. The melt polymerization process involves the base-catalyzed transesterification reaction of a bisphenol with a source of carbonate functionality, such as diphenyl carbonate. During the reaction, the by-product phenol is removed, and polycarbonate forms directly. In the first stage of the reaction, diphenyl carbonate and BPA are combined with small amounts (usually <0.01 mol%) of basic catalysts (Na, Li, K, tetraalkylammonium, or tatraalkylphosphonium hydroxides or carbonates) in a melt reactor. Phenol is liberated in an equilibrium reaction, as shown in equation (9). As the raw materials pass through the stages of reaction, the reaction temperature is increased and higher vacuum is provided to facilitate removal of the phenol, driving the equilibrium toward polycarbonate. In the later stages of reaction, the polymer melt becomes very viscous and specialized equipment such as wiped film evaporators, helicone reactors, or multiple vacuum-vented extruders are necessary to expedite mass transfer of by-product phenol via good surface renewal of the melt.

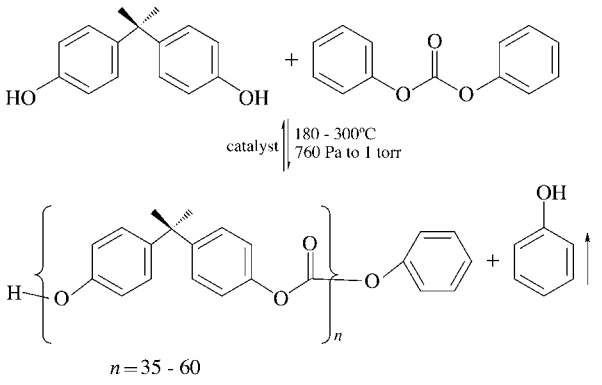

(9)

The polymer is exposed to an extensive heat history in the melt process. Early work on transesterification technology was troubled by thermal-oxidative reactions of the polymer, especially in the presence of basic catalysts (8–11). Early polycarbonates prepared by Fox and others via the melt process had noticeable brown colors. More recent work on catalyst systems, more reactive carbonates, and modified processes have improved the process to the point where formation of color and product decomposition can be effectively suppressed. Polymers with color at least as good as interfacially prepared materials can now be prepared commercially. One of the key requirements for the transesterification process is the use of clean starting materials. Methods for the purification of both BPA and diphenyl carbonate have been developed and patented. Activated carbonates that form high molecular weight polycarbonate at equilibrium in solution at or below room temperature have also been reported, although they are chiefly only of academic interest (66,67).

Initially, diphenyl carbonate to be used for the transesterification process was prepared by reaction with phosgene. The phosgenation can be carried out in CH_2Cl_2, or in water, which avoids the use of organic solvents in the polycarbonate process altogether (68). More recently, other methods for the preparation of diphenyl carbonate have been developed, which avoid the use of phosgene. GE Plastics uses a process commercialized by Enichem for the preparation of diphenyl carbonate, utilizing a two-step process. In the first step (eq. (10)), methanol is carbonylated using carbon monoxide in the presence of a catalyst to produce dimethyl carbonate. Reaction of dimethyl carbonate and phenol under specific transesterification conditions produces diphenyl carbonate. The by-product is methanol, which can be recycled. Because the transesterification reaction from dimethyl to diphenyl carbonate is a thermodynamically unfavorable equilibrium process, the reaction is normally carried out in two stages: first, formation of a mixed carbonate (eq. (11)), then disproportionation to dimethyl carbonate and diphenyl carbonate (eq. (12)). An alternative method for formation of diphenyl carbonate is the direct carbonylation of phenol, using palladium catalysts (69). Although this latter chemistry works well for formation of diphenyl carbonate, it has not proved efficient enough for the formation of high molecular weight polycarbonate directly from BPA.

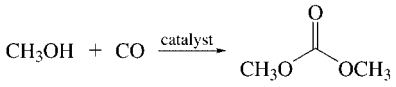

(10)

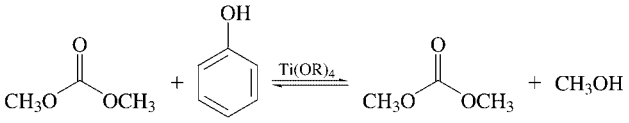

(11)

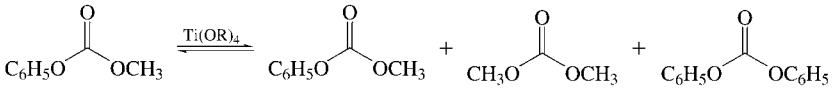

(12)

Preparation of polycarbonate via the melt process offers several processing advantages, including elimination of solvents and phosgene. The principal *product* advantage of melt-prepared polycarbonate is the fact that as an equilibrium product, the resin is stable. No changes in polydispersivity, oligomers, etc will be seen upon further processing (unless monomers are introduced). Additionally, the equilibrium levels of low molecular weight species (cyclic and linear oligomers, diaryl carbonates formed from chain stopper) are much lower than typically found in interfacially prepared polymer, and hence the polydispersivity (M_w/M_n) is narrower. Other impurities are also minimized, since there are no sources for contaminants such as solvent, amine, or NaCl to enter the process. One other major difference from interfacially prepared polycarbonate is the fact that the polymer is typically *not* completely end-capped; some level of phenol-terminated polymer will usually be present, which should be recognized in subsequent formulations.

Recent patent literature from Asahi describes novel polymerization processes that involve equipment with no moving parts, where the molten prepolymer is allowed to fall through holes and descend either freely or along a wire as a molten strand (70). The molten polymer from the bottom of the reactor is recycled to the top to reach the desired molecular weights. The setup provides a method to overcome mass transfer resistances and allows for removal of phenol from the system. Another process which has been an area of patent activity from GE and Asahi is in the area of solid-state polymerization of polycarbonate, wherein the prepolymer is converted to flakes/powder/particles and crystallized. The solids are then polymerized at a lower temperature than in conventional melt polymerization. Both methods seem to be in the development stage.

A spinoff of the melt process is "redistribution" technology, patented by GE (71). In the redistribution process, high molecular weight polycarbonate is extruded in the presence of a transesterification catalyst and, optionally, other monomeric or oligomeric materials. At the extrusion temperature, equilibrium transesterification occurs, leading to products similar to melt-prepared polycarbonate, even though the polymer may have originally been prepared by interfacial phosgenation. This technique is very useful for lowering the amounts of oligomers

in interfacial resin, and for forming very low M_w polycarbonate or branched polycarbonates.

Other polymerization techniques. An analogue of the transesterification process has also been demonstrated, using the diacetate of BPA (72). Transesterification of the diacetate with dimethyl carbonate using a titanate catalyst produces polycarbonate with methyl acetate as the by-product. Removal of the methyl acetate from the equilibrium drives the reaction to completion. Because of the problem of recycling methyl acetate back to BPA-diacetate, the process has not been commercialized.

Another technique for the preparation of polycarbonates which can lead to many novel applications is the ring-opening polymerization of cyclic oligomers. Although discrete cyclic oligomers of BPA and other bisphenols were isolated in the early 1960s, exploitation of this chemistry was not possible, owing to the difficulty of their preparation and purification (73). Furthermore, the cyclic tetramer of BPA, the most easily isolated, in about 25% yield, was a high melting, crystalline solid with a melting point of about 375°C, making melt polymerization difficult.

A newer process for the preparation of mixtures of cyclic oligomers has recently been discovered (18,62). This process utilizes a triethylamine-catalyzed hydrolysis and condensation of BPA bischloroformate in a pseudo-dilution reaction. This reaction efficiently provides 85–95% of a mixture of cyclic oligomers having a degree of polymerization of 2 to about 12, with good productivity [10–20% solids reactions (eq. (13))]. Three important features distinguish this work from the previous preparation of cyclic tetramer. First, the reaction is extremely selective toward formation of cyclic oligomers: less than 0.01% linear oligomers are formed. Because any linear oligomers which might be present would reincorporate into the polymer via chain-transfer reactions during ring-opening polymerization, their presence would limit ultimate molecular weight and so it is important to limit their level. Second, a *mixture* of cyclics is formed. The fact that a broad mixture of cyclics is formed results in depression of the melting point of the cyclics, allowing a clear melt to form at 200–210°C from BPA carbonate cyclic oligomers. The melting point can be depressed further by the incorporation of long-chain bisphenols (74). Lastly, the reaction can be carried out at concentrations similar to conventional polycarbonate processes, rather than under very high dilution (eg, $<0.01\,M$) conditions, allowing good productivity in large-scale equipment.

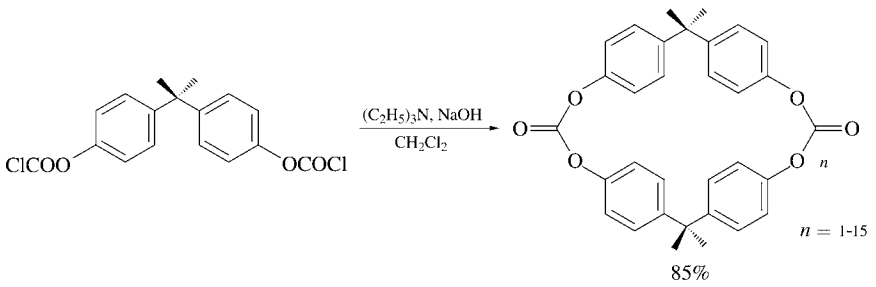

(13)

Melt polymerization of the cyclic oligomers can be achieved at 200–300°C, and solution polymerization is possible at ambient temperature (75). The ring-opening polymerization is driven almost entirely by entropy, in a reaction with

almost no exotherm, leading to the highest molecuar weight polycarbonates achievable by any process. Because the viscosity of the cyclic oligomers is about 10^5 times lower than the ultimate polymer, a variety of processing techniques become possible, including pultrusion, resin-transfer molding, and other techniques for the fabrication of fiber-reinforced composites. The use of cyclic oligomer technology also makes it possible to prepare polycarbonates that had been unattainable by other means, eg, hydroquinone–BPA copolymers. Although scaling to hundreds of kilograms has been carried out, this technology has not yet been commercialized.

Solid-state polymerization of BPA-polycarbonate oligomers has received much recent attention, with over 160 patents since 1995 (76,77). Typically, one prepares oligomeric or low molecuar weight polycarbonate (η_{inh} = 0.2–0.3 dL/g, $T_g \sim$ 120–135°C) via a melt process. After isolation of the oligomer, and enhancing crystallization by various techniques, additional basic catalyst is blended. Using solid-state polymerization techniques, the solid is then heated above its T_g, but below the melting point of crystalline polycarbonate, using a variety of techniques to remove by-product phenol. Vacuum and nitrogen purge conditions have been demonstrated, as well as methods involving supercritical or liquid carbon dioxide (78). After prolonged heating, the molecular weight increases to a useful range (η_{inh} = 0.44–0.8 dL/g). The polycarbonate is then processed as usual, losing the crystallinity and leading to an amorphous product, as in conventional melt processes. Despite many patents, the process has not yet been commercialized.

Processing. Polycarbonates may be fabricated by all conventional thermoplastic processing operations, of which injection molding is the most common. Recommended operating conditions are stock temperatures of 275–325°C and molding pressures of 69–138 MPa (10,000–20,000 psi). Thorough predrying is necessary to prevent hydrolysis of the polymer by dissolved water at the high processing temperatures. Inadequate drying may lead to surface-streaked parts and loss of molecular weight. Extrusion produced film, sheet and stock shapes, and higher molecular weights than those used for injection molding are preferred. Temperatures for extrusion vary between 285 and 315°C.

Structural foam molding is also a valuable commercial technique. The molding compound is charged with an inert gas under pressure and at the same time thermally plasticized in an extruder. Nitrogen gas may be pumped into the melt, or the molding compound may contain a chemical blowing agent that decomposes with gas generation at the plasticizing temperature. The pressurized plasticized melt is injected into a low pressure mold with a volume change taking place, causing the polymer to expand and fill the mold cavity. Very large parts having relatively low clamping pressures can be produced with this process.

Injection blow molding of polycarbonates produces an assortment of containers, from 20-L water bottles and 0.25-L milk bottles to outdoor lighting protective globes. The polymer normally contains a small amount of polyfunctional monomer that serves as a branching agent. Low level branching enhances the melt strength, as well as inducing non-Newtonian flow behavior (sensitivity of melt viscosity to shear).

Conventional thermoforming of sheet and film is applicable to the production of skylights, radomes, signs, curved windshields, body parts for automobiles,

skimobiles, boats, etc. Because BPA-polycarbonate is malleable, it can be cold-formed like metal, and may be cold-rolled, stamped, or forged.

Production. Production of polycarbonate has steadily increased since the first commercial scale plants were built in the early 1960s. Current annual capacities are edging close to the 4.5 billion pound mark. Demand forecasts continue to be in the 8–12% range, with the Far East showing the greatest growth potential. A number of joint ventures have been announced over the last few years, namely Dow/Sumitomo, Asahi/Chi Mei, Idemitsu/Formosa, to name a few. Plants have also opened in several countries and several more have been announced. Production of polycarbonate is approaching a fairly even split between the Americas, Europe, and Asia. Polycarbonate enjoys a comfortable niche between high priced specialty polymers and lower priced commodity resins.

GE Plastics is the largest polycarbonate producer, accounting for approximately 44% of the worldwide capacity (2 billion pounds). Bayer AG has a worldwide capacity of about 900 million pounds. Dow and the Dow/Sumitomo joint venture account for about 500 million pounds of annual capacity. Other producers include Mitsubishi and associated joint ventures (475 million pounds), Teijin (200 million pounds), and Idemitsu (100 million pounds). Capacity announcements have been made for the near future by Teijin (in Singapore; about 150 million pounds), Asahi/Chi Mei (in Taiwan; about 100 million pounds), Idemitsu/Formosa (100 million pounds), and General Electric (in Spain and in the United States). Normal grades of polycarbonate sold in 2000 for $1.40–$1.50/lb ($3–$3.30/kg). Many specialty grades demanded significantly higher prices. Over the last few years, growth of optical quality polycarbonate has been extremely strong.

Health and Safety Factors

BPA polycarbonate is an amorphous solid, supplied as extruded pellets averaging 2.5 mm in diameter and 3.2 mm long, or as a powder. Polycarbonate is considered a slight or nonexistent fire hazard. The ignition temperatures are quite high; flash ignition is at 449°C and autoignition is at 632°C, according to ASTM D1929. Odor and volatiles are negligible. Processing fumes, which include water, carbon dioxide, diphenyl carbonate, methylene chloride, and phenol are not formed in levels considered to be hazardous. Nonetheless, good housekeeping and industrial hygiene techniques should be followed. Polycarbonate has very low acute oral and dermal toxicity, is not a primary skin irritant, and does not cause systemic or local sensitization. In a finely divided form, polycarbonate is a mile eye irritant, consistent with the abrasive nature of the ground resin particle. Polycarbonate does not degrade during storage, and no heating or cooling requirements are necessary. For transportation purposes, polycarbonate is not classified as a hazardous material by U.S. Department of Transportation code, Title 49.

Uses

Extreme toughness, transparency, low color, resistance to burning, and maintenance of engineering properties over a wide thermal range are the outstanding properties of polycarbonate that make it useful for a variety of aplications. Glazing

and sheet are the largest markets for polycarbonate resins. About 80,000 t are used in these markets annually in the United States, nd 150,000 t worldwide. Clarity and an impact resistance 250 times greater than glass and 30 times greater than acrylic sheet makes polycarbonate the natural choice for window replacement in areas where breakage is common. Windows in airplanes, trains, and schools commonly use polycarbonate. Exotic applications include military use, for example in high speed aircraft canopies, where tests have shown polycarbonate to withstand impact with fowl at Mach 2. Polycarbonate is also used for security applications as laminates with glass or other materials. Polycarbonate offers unsurpassed projectile-stopping capability, as the material softens upon impact with a bullet, absorbing the projectile's energy. A large volume in laminated products also exists. The soft inner layer may be a urethane, acrylic, or siloxane–polycarbonate copolymer.

Automotive applications account for about 150,000 t of worldwide consumption annually, with applications for various components including headlamp assemblies, interior instrument panels, bumpers, etc. Many automotive applications use blends of polycarbonate with acrylonitrile–butadiene–styrene (ABS) or with poly(butylene terephthalate) (PBT). A large effort is currently under way to commercialize automotive window glazing from coated polycarbonate. Both large and small appliances also account for large markets for polycarbonate. Consumption is about 75,000 t annually. Polycarbonate is attractive to use in light appliances, including houseware items and power tools, because of its heat resistance and good electrical properties, combined with superior impact resistance and the ability to produce a wide variety of colors.

Packaging is a growing segment of the polycarbonate market, accounting for about 30,000 t of consumption annually. Polycarbonate has been the preferred choice for large returnable, refillable 20-L water bottles because of its light weight and impact resistance. GE Plastics has also introduced returnable, refillable 0.25-L milk bottles for use in schools. These bottles, which can be refilled 50–100 times, are attractive alternatives to nonreusable paper milk cartons in communities that are concerned about waste.

Electrical, electronic, and technical applications use polycarbonates for a variety of purposes. The worldwide market is about 160,000 t annually. Because of excellent electrical properties (dielectric strength, volume resistivity) and resistance to heat and humidity, polycarbonate is used for electrical connectors, telephone network devices, outlet boxes, etc. Polycarbonate had been popular for use in computer and business machine housings, but the use of neat resin was largely supplanted by blends of polycarbonate with ABS. However, new, highly colored and special effect resins (translucents, flip-flop colors, speckles, etc) have recaptured a significant portion of that market. A total of 25,000–30,000 t of resin is used annually. Polycarbonate also has many technical uses in instrument panels and devices, especially for membrane switches and insulators. Optical quality polycarbonate is the only suitable material for the compact disc market. Since their introduction in 1983, compact discs have shown explosive growth in the consumption of polycarbonate, with utility for audio, video, and computer applications, reaching about 25,000 t of annual production.

Medical and health-care related applications consume about 30,000 t of polycarbonate annually. Polycarbonate is popular because of its clarity, impact

strength, and low level of extractable impurities. Special grades have been developed to maintain clarity and resistance to yellowing upon gamma radiation sterilization processes. Leisure and safety applications are many and varied, accounting for about 30,000 t of consumption annually. The largest markets are for protective headgear such as football and motorcycle helmets, and safety helmets for firefighters and construction workers. Protective eyewear also uses polycarbonate because of its clarity and impact resistance.

Other Polycarbonates, Blends, and Copolymers

During the early development of polycarbonates, many bisphenols were investigated for potentially useful products. Some of these monomers and polymers are listed in Table 3. Despite this intensive research, however, no homopolycarbonates other than that of BPA have been produced commercially in any significant volume. Copolymers and blends, on the other hand, have been quite successful. Copolymer research constitutes a large portion of polycarbonate patents, with nearly 6000 patents since 1995. An excellent review of many types of polycarbonate homo- and copolymers arranged according to utility has recently appeared (79). Blends of polycarbonate with ABS and with PBT, in particular, have shown significant growth since the mid-1980s.

Copolymers. The copolymer of tetrabromo-BPA and BPA was one of the first commercially successful copolymers (80). Low levels of the brominated comonomer lead to increased flame resistance (V-0 rating by UL-94), while having little effect on other properties. The homopolymer of tetrabromo-BPA can also be prepared (81,82), but only the oligomeric version has been commercialized. The polycarbonate of bis-4-hydroxyphenyl-1,1-dichloroethylene, prepared from chloral and phenol, followed by dehydrohalogenation, was investigated as another inherently flame-resistant polymer that retained good impact properties (83).

For utility in compact discs and other laser-readable and especially in read–write data storage systems, polycarbonates of low birefringence are advantageous. Birefringence can be reduced by using bulky polarizable side groups, or eliminated entirely in structures such as the spirobiindane bisphenol (84) (SBI) shown in Table 3. Efforts to reduce the birefringence of polycarbonate by modifying the bisphenol have been reviewed (57,58). Numerous alkyl-substituted bisphenols have also been used (85). Aliphatic groups do not contribute to birefringence, and also lead to less water absorption in the polymer. Birefringence can also be reduced by eliminated molded-in stresses via the use of high flow resins. Many techniques for achieving high flow polycarbonates have been reported, including incorporation of aliphatic diesters into the backbone, modification of the bisphenol with aliphatic groups, and changing the polymer end groups. Incorporation of aliphatic diacids to form aliphatic ester carbonates can provide nearly twice the melt flow with little sacrifice in ductility.

Polyester carbonates can be prepared by the copolymerization of BPA with diacyl chlorides such as iso- or terephthaloyl chloride (eq. (14)) (86). These polymers have been commercialized by Bayer AG, GE, Dow Chemical, and Mitsubishi Chemical, Ltd. Melt processes to prepare these materials have also been demonstrated. In some cases, a diacid can be used directly because reaction with phosgene

converts it into an acid chloride prior to reaction with the bisphenol. The polyester carbonates prepared using aromatic diacids are useful as high heat materials. Although the polyarylate esters are crystalline as homopolymers, copolymerization as copolyestercarbonates allows formation of amorphous resins, which have impact strength similar to BPA polycarbonate, with the glass-transition temperature elevated to about 190°C. Incorporation of aliphatic esters into polycarbonate leads to elastomeric materials or copolymers with depressed T_g, but with dramatically increased melt flow (eq. (15)) (35). Some of these block copolymers also have improved low temperature impact strength and higher stress-crack resistance than neat BPA polycarbonate.

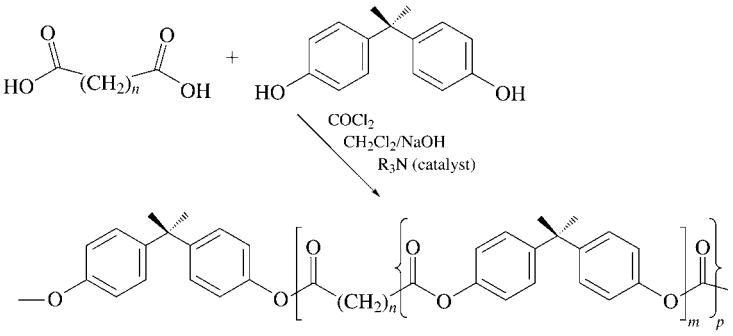

(14)

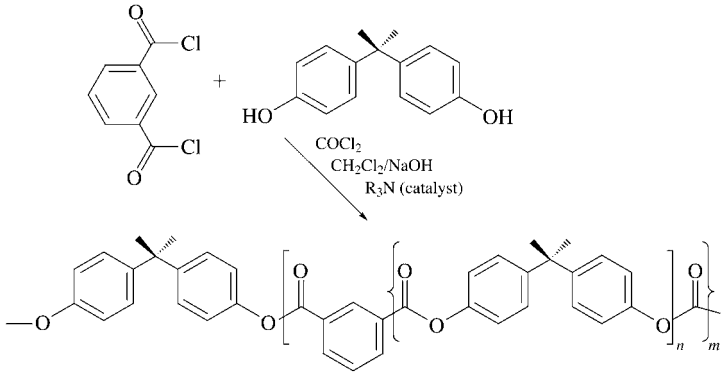

(15)

A variety of methods have been developed for the preparation of polydimethylsiloxane-*co*-BPA polycarbonates (87). These polymers differ greatly from conventional polycarbonate in that they have very low glass-transition temperatures ($T_g = -123$°C), and yet have excellent thermal stability and good weathering properties. Phosgenation of silanol-terminated siloxane oligomers in the presence of BPA, or reaction of BPA sodium salt with chlorosilane-stopped siloxane oligomers, followed by phosgenation with BPA are two of the described procedures (eqs. (16) and (17)) (88). Hydrosilation methods are also used (89). Use of cyclic oligomers for the preparation of these copolymers has also been described

(90). These materials display a wide range of properties, depending on the block length of the individual polymers and on the weight level of silicone present. Some of the block copolymers having low levels of silicone have outstanding low temperature impact strength; those having higher levels of silicone are thermoplastic elastomers. The enhanced ductility at low temperature was reported in the 1970s; incorporating 25% silicone into BPA polycarbonate lowers the ductile-brittle transition temperature from $\sim -15^{\circ}$C to -110°C (91).

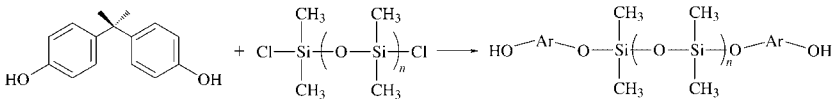

(16)

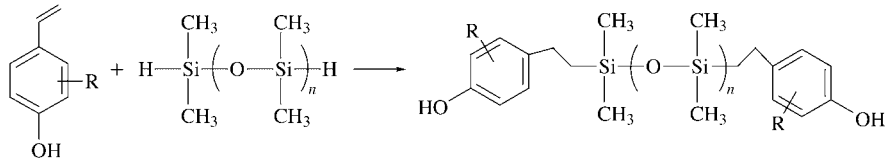

(17)

In 1991, Bayer reported the preparation of a family of polycarbonates (Apec) using a monomer based on the condensation of a hydrogenated isophorone with phenol (74,92). Because the bulky structure leads to rigidity derived from hindered rotational freedom, the polycarbonate retains the low temperature loss modulus of BPA polycarbonate, which affords low temperature impact strength, yet has a high glass-transition temperature. The homopolymer has a T_g of 239°C, and copolymers with BPA provide intermediate glass-transition temperatures. A variety of other monomers also provide high heat polycarbonates, but often at the expense of limited ductility (78).

Blends. The concept of blending two or more commercially available materials to create a new material having properties different from either starting material has generated a great deal of interest over the past few decades. One of the fastest growing market segments within the polycarbonate industry is this arena of blends. Polycarbonate blends are used to tailor performance and price to specific markets. Despite its strengths, polycarbonate suffers from shortcomings with regard to flow characteristics and solvent resistance. The two principal blends are produced to improve those characteristics. Polycarbonate–ABS blends (GE, Cycoloy; Bayer, Bayblend; Dow, Pulse; and Monsanto, Triax 2000) have improved flow and lower cost, and polycarbonate-polyesters which use either PBT or PET (GE, Xenoy, Bayer, Makroblend; Dow, Śabre, and Hoechst Celanese, Vandar) utilize semicrystalline polymers to improve chemical resistance, especially for automotive applications.

Fundamental studies of blends of polycarbonate with ABS indicate that the presence of ABS greatly decreases the melt viscosity in the blend, enhancing processibility. Even as little as 20% ABS provides a decrease in melt viscosity by a factor of 4–5 (93). A synergistic improvement of the notched impact strength at low temperature is also seen for polycarbonate–ABS blends (Fig. 3). About

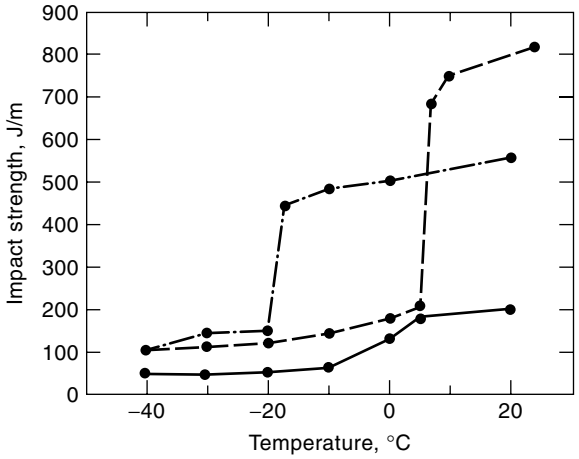

Fig. 3. Dependence of Izod impact strength on temperature for (- - -) polycarbonate, (—) ABS, and (-·-) polycarbonate–ABS blends. To convert J/m to ft·lbf/in., divide by 53.38.

35,000 t of these blends are produced annually, and significant growth in the market has been seen, with a yearly growth rate of 12–13%. More than half of the blends produced are used in the automotive market, mostly on instrument panels. The other large use for polycarbonate blends is in office and business machines, such as computer and printer housings.

Polycarbonate–polyester blends were introduced in 1980 and have steadily increased sales to a volume of about 70,000 t. This blend, which is used on exterior parts for the automotive industry, accounting for 85% of the volume, combines the toughness and impact strength of the polycarbonate with the crystallinity and inherent solvent resistance of PBT, PET, and other polyesters. Although not quite miscible, polycarbonate and PBT form a fine-grained blend, which upon analysis shows the T_g of the polycarbonate and the T_m of the polyester.

Other blends of polycarbonate have limited markets so far. The most significant blends are with polyurethane, polyetherimides, acrylate–styrene–acrylonitrile (ASA), acrylonitrile–ethylene–styrene (AES), and styrene–maleic anhydride (SMA).

BIBLIOGRAPHY

"Polycarbonates" in *EPST* 1st ed., Vol. 10, pp. 710–764, by L. Bottenbruch, Farbenfabriken Bayer AG; "Polycarbonates" in *EPSE* 2nd ed., Vol. 11, pp. 648–718, by D. Freitag, U. Grigo, P. R. Müller, and W. Nouvertné, Farbenfabriken Bayer AG.

1. W. F. Christopher and D. W. Fox, *Polycarbonates*, Reinhold Publishing Corp., New York, 1962; H. Schnell, *Chemistry and Physics of Polycarbonates*, Wiley-Interscience, New York, 1964.
2. D. G. LeGrand and J. T. Bendler, eds., *Handbook of Polycarbonate Science and Technology*, Marcel Dekker, Inc., New York, 2000.
3. A. Einhorn, *Liebigs Ann. Chem.* **300**, 135 (1898).

4. C. A. Bischoff and A. von Hedenstroem, *Chem. Ber.* **35**, 3431 (1902).
5. W. H. Carothers and F. J. Van Natta, *J. Am. Chem. Soc.* **52**, 314 (1930); J. W. Hill and W. H. Carothers, *J. Am. Chem. Soc.* **55**, 5031 (1933); E. W. Spanagel and W. H. Carothers, *J. Am. Chem. Soc.* **57**, 929 (1935).
6. U.S. Pat. 2210817 (1940), W. R. Peterson (to E. I. du Pont de Nemours & Co., Inc.).
7. R. L. Wakeman, *The Chemistry of Commercial Plastics*, Reinhold Publishing Corp., New York, 1947, p. 518.
8. H. Schnell, *Ang. Chem.* **68**, 633 (1956).
9. Belg. Pat. 532543 (1954), H. Schnell, L. Bottenbruch, and H. Krimm (to Bayer AG).
10. U.S. Pat. 3028365 (1962), H. Schnell, L. Bottenbruch, and G. Grimm (to Bayer AG).
11. U.S. Pat. 3153008 (1964), D. W. Fox (to GE).
12. H. R. Kricheldorf and D. Lübbers, *Makromol. Chem., Rapid Commun.* **10**, 383 (1989).
13. H. Schnell, *Angew. Chem.* **68**, 633 (1956).
14. D. J. Brunelle, H. O. Krabbenhoft, and D. K. Bonauto, *Polym. Prepr.* **34**(1), 73 (1993); D. J. Brunelle, H. O. Krabbenhoft, and D. K. Bonauto, *Makromol. Chemie* **194**, 1249 (1993).
15. R. Myers and J. Longs, eds., *Treatise on Coatings*, Marcel Dekker, Inc., New York, 1972, p. 283.
16. R. J. Gardner and J. R. Martin, *J. Appl. Poly. Sci.* **24**, 1269 (1979); C. A. Pryde and co-workers, *Poly. Eng. Sci.* **22**, 370 (1982).
17. C. Bailly and co-workers, *Polymer* **27**(9) 1410 (1986).
18. D. J. Brunelle and T. G. Shannon, *Macromolecules* **24**, 3035 (1991).
19. G. Kampf, *Kolloid Z.* **172**, 50 (1960).
20. Ch. Bailly, R. Legras, and J. P. Mercier, *Polym. Prepr.* **26**(2), 170 (1985).
21. U.S. Pat. 5767225 (1998), D. J. Brunelle and S. A. Serth-Guzzo (to GE).
22. A. D. Williams and P. J. Flory, *J. Polym. Sci., Polym. Phys. Ed.* **6**, 1945 (1968).
23. B. Erman and co-workers, *Macromolecules* **15**, 664 (1982).
24. D. J. Brunelle and M. A. Garbauskas, *Macromolecules* **26**, 2724 (1993); J. A. King and G. L. Bryant Jr., *Acta Cryst Allogr. C*, **49**, 550 (1993).
25. S. Perez and R. P. Scaringe, *Macromolecules* **20**, 68 (1987); P. M. Henricks, H. R. Luss, and R. P. Scaringe, *Macromolecules* **22**, 2731 (1989).
26. W. J. Dulmage and co-workers, *J. Appl. Phys.* **49**, 5543 (1978).
27. M. Hutnik, A. S. Argon, and U. Suter, *Macromolecules* **24**, 5870 (1991); M. Hutnik and co-workers, *Macromolecules* **24**, 5962 (1991); M. Hutnik, A. S. Argon, and U. W. Suter, *Macromolecules* **24**, 5956 (1991); M. A. Mora, M. Rubio, and C. A. Cruz-Ramos, *J. Polym. Sci., B: Polym. Phys.* **24**, 239 (1986).
28. F. J. Hoerth and co-workers, *Polymer* **33**, 1223 (1992); L. B. Liu, A. F. Yee, and, D. W. Gidley, *J. Polym. Sci., B: Polym. Phys.* **30**, 221 (1992); L. B. Liu and co-workers, *Mater. Res. Soc. Symp. Proc.* **61**, 61–70 (1991).
29. B. C. Laskowski and co-workers, *Macromolecules* **21**, 1629 (1988).
30. P. M. Henrichs and H. R. Luss, *Macromolecules* **21**, 860 (1988); P. M. Henrichs and V. A. Nicely, *Macromolecules* **23**, 3193 (1990).
31. P. Schmidt and co-workers, *Polymer* **32**, 1862 (1991).
32. K. R. Stewart, *Polym. Prepr.* **30**(2), 140 (1989).
33. H. Schnell, *Polym. Rev.*, Vol. **9**, Wiley-Interscience, New York, 1964.
34. H. Schnell, *Ind. Eng. Chem.* **51**, 157 (1959).
35. U.S. Pat. 5494997 (1996), L. P. Fontana, P. W. Buckley, and E. P. Boden (to General Electric).
36. Ger. Pat. 2746141 (1979), S. Aldelmann, D. Margotte, and H. J. Rosenkranz (to Bayer AG).
37. Z. Sobiczewski and Z. Wielgosz, *Plaste. Kautsch* **15**, 176 (1968).
38. M. R. MacLaury and co-workers, *J. Polym. Sci., Polym. Chem. Ed.* **18**, 2501 (1980).

39. W. J. Jackson Jr. and J. R. Caldwell, *Ind. Eng. Chem. Prod. Res. Dev.* **2**, 246 (1963).
40. WO Pat. 82/02402 (1982), V. Mark and C. V. Hedges (to GE).
41. E. G. Banucci, *J. Polym. Sci., Polym. Chem. Ed.* **11**, 2947 (1973).
42. P. W. Morgan, *Macromolecules* **3**, 536 (1970).
43. R. P. Kambour and co-workers, *J. Appl. Polym. Sci.* **20**, 3275 (1976); R. P. Kambour, W. V. Ligon, and R. R. Russell, *J. Polym. Sci., Polym. Lett. Ed.* **16**, 327 (1978).
44. D. Freitag, G. Fengler, and L. Morbitzer, *Angew Chem. Int. Ed. Engl.* **30**, 1598 (1991).
45. Ger. Pat. 2746141 (1975), D. Neuray, E. Tresper, and D. Freitag (to Bayer AG).
46. Ger. Offen. DE 3926768 (1991), V. Serini and co-workers (to Bayer AG).
47. Eur. Pat. Appl. EP 374656 (1991), V. Serini and co-workers (to Bayer AG).
48. Eur. Pat. Appl. EP 374623 (1990), V. Serini and co-workers (to Bayer AG).
49. V. Serini, D. Freitag, and H. Vernaleken, *Angew. Makromol. Chem.* **55**, 175 (1976).
50. K. C. Stueben, *J. Polym. Sci., A: Gen. Pap.* **3**, 3209 (1965).
51. Eur. Pat. Appl. 287887 (1988), G. R. Faler and J. C. Lynch (to GE).
52. U.S. Pat. 4906725 (1990), P. C. Wang (to Shell Oil Co.).
53. L. H. Tagle and F. R. Diaz, *J. Thermal Anal.* **38**, 2385 (1992).
54. G. Sh. Papava and co-workers, *Svobsch. Akad. Navk Grut. SSR*, **88**, 597 (1977).
55. T. C. Jordan and W. D. Richards, in Ref. 2, Chapt. "9".
56. M. Narkis and co-workers, *Poly. Eng. Sci.* **24**, 211 (1984).
57. G. Koempf, D. Freitag, and A. Witt, *Angew. Makromol. Chem.* **183**, 243 (1990).
58. G. Koempf and co-workers, *Polym. Adv. Technol.* **3**, 169 (1992).
59. J. A. King Jr., in Ref. 2, Chapt. "2".
60. E. Aquino, W. J. Brittain, and D. J. Brunelle, *Polym. Int.* **33**, 161 (1994); E. Aquino, W. J. Brittain, and D. J. Brunelle, *J. Polym. Sci., A: Polym. Chem.* **32**, 741 (1994).
61. U.S. Pats. 5300623 (1994) and 5391692 (1995), E. P. Boden and co-workers (to GE).
62. D. J. Brunelle, E. P. Boden, and T. G. Shannon, *J. Am. Chem. Soc.* **112**, 2399 (1990).
63. U.S. Pats. 5519105 (1996), 5804525 (1998), and 5739257 (1998), E. P. Boden and co-workers (to GE).
64. U.S. Pat. 5821322 (1999), D. J. Brunelle and co-workers (to GE).
65. P. G. Kosky and E. P. Boden, *J. Polym. Sci., Polym. Chem. Ed.* **28**, 1507 (1990).
66. U.S. Pats. 4321356 (1982) and 4363905 (1982), D. J. Brunelle and co-workers (to GE).
67. D. J. Brunelle, *Macromol. Rep., A* **28**, 95 (1991).
68. Eur. Pat. Appl. 228672 (1986), M. Janatpour and S. J. Shafer (to GE).
69. J. E. Hallgren and R. O. Matthews, *J. Organomet. Chem.* **175**, 135 (1979); J. E. Hallgren, G. M. Lucas, and R. O. Matthews, *J. Organomet. Chem.* **204**, 135 (1981).
70. U.S. Pat. 5589564 (1996), K. Komiya, Y. Kawakami, and H. Okamoto (to Asahi).
71. U.S. Pat. 5414057 (1995), A. J. Campbell and co-workers (to GE).
72. J. E. Hallgren and R. O. Matthews, *J. Organomet. Chem.* **175**, 135 (1979); J. E. Hallgren, G. M. Lucas, and R. O. Matthews, *J. Organomet. Chem.* **204**, 135 (1981).
73. H. Schnell and L. Bottenbruch, *Makromol. Chem.* **57**, 1 (1962).
74. D. J. Brunelle, *Makromol. Chem., Macromol. Symp.* **64**, 65–74 (1992).
75. T. L. Evans and co-workers, *Polym. Prepr.* **30**, 573 (1989).
76. V. S. Iyer and co-workers, *Macromolecules* **26**, 1186 (1993).
77. U.S. Pat. 5266659 (1993), S. Sivaram and co-workers (to Council of Sci. and Ind. Res.) DE Pat. 3941014 A1 (1991), U. Westeppe and co-workers (to Bayer AG).
78. M. D. Goodner and co-workers, *Polym. Prepr.* **40**(1), 97 (1999).
79. J. Schmidhauser and P. D. Sybert, in Ref. 2, Chapt. "5".
80. M. J. Marks and J. K. Sekinger, *J. Polym. Sci., A: Polym. Chem.* **32**, 1885 (1994).
81. U.S. Pat. 4794156 (1988), T. H. Ho and co-workers (to The Dow Chemical Company).
82. J. T. Gu, W. C. Luo, and C. S. Wang, *Angew. Makromol. Chem.* **208**, 65 (1993).
83. A. Factor and C. M. Orlando, *J. Polym. Sci., Polym. Chem. Ed.* **18**, 579 (1980).
84. U.S. Pat. 4950731 (1990), G. R. Faler and J. C. Lynch (to GE).

85. Jpn. Kokai Tokkyo Koho JP 63199729-34 (1988), K. Sasaki, I. Takahashi, and T. Sugano (to Daicel Chemical Co.).
86. D. C. Prevorsek, B. T. Debonna, Y. Kesten, *J. Polym. Sci., Polym. Chem. Ed.* **18**, 75 (1980).
87. U.S. Pats. 3189662 and 3419634 (1961), H. A. Vaughn Jr. (to General Electric).
88. D. W. Dwight and co-workers, *Polym. Prepr.* **29**, 702 (1979).
89. U.S. Pat. 5025074 (1991), G. C. Davis, B. E. McGrath, and K. M. Snow (to General Electric).
90. T. L. Evans and J. C. Carpenter, *Makromol. Chem., Macromol. Symp.* **42/43**, 177 (1991).
91. R. P. Kambour and co-workers, in R. D. Deanin and A. M. Crugnola, eds., *Toughness and Brittleness of Plastics*, American Chemical Society, Washington D.C., 1976.
92. D. Freitag, G. Fengler, and L. Morbitzer, *Angew Chem. Int. Ed. Engl.* **30**, 1598 (1991).
93. J.-S. Wu, S.-C. Shen, and F.-C. Chang, *J. Appl. Polym. Sci.* **50**, 1379 (1993).

DANIEL J. BRUNELLE
GE Corporate R&D

POLYCARBOSILANES

Introduction

Polycarbosilanes (**1**) have a polymeric backbone composed of silicon atoms and difunctional organic groups that connect the silicon atoms (1–4).

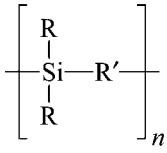

1

The side groups R can be alkyl, aryl, or alkoxy groups, and hydrogen or halogen atoms. The bridging group R′ can vary widely from methylene to alkenylene, alkynylene, arylene, and a combination of these groups. Because of this structural variation, polycarbosilanes can exhibit various interesting properties that neither polysiloxanes nor the usual hydrocarbon polymers can achieve. Polycarbosilanes generally have a very flexible and chemically stable backbone derived from Si—C bonds. Applications to ceramic precursors, conductive polymers, heat-resistant materials, and side-chain liquid crystalline polymers have been widely investigated. Methods commonly applied to prepare polycarbosilanes are ring-opening polymerization (ROP) of silacarbocycles, cross-condensation of dihalosilanes with difunctional organometallic compounds, and self-condensation of difunctional silicon compounds.

Encyclopedia of Polymer Science and Technology. Copyright John Wiley & Sons, Inc. All rights reserved.

Table 1. T_g's of Poly(silylenemethylene)s and Related Hydrocarbon Polymers

Polymers	T_g, °C
$[Si(CH_3)_2CH_2]_n$	−87
$[Si(CH_3)(CH_2CH_3)CH_2]_n$	−78
$[Si(CH_3)(n\text{-}C_4H_9)CH_2]_n$	−63
$[Si(CH_3)(n\text{-}C_6H_{13})CH_2]_n$	−71
$[SiH(CH_3)CH_2]_n$	−112
$[SiH(n\text{-}C_6H_{13})CH_2]_n$	−91
$[SiH(C_6H_5)CH_2]_n$	−37
$[CH(CH_3)CH_2]_n$	−10 to −20
$[CH(n\text{-}C_6H_{13})CH_2]_n$	−65
$[CH(C_6H_5)CH_2]_n$	100

Poly(silylenemethylene)s

Poly(silylenemethylene)s, $(SiR_2(CH_2))_n$, polymers composed of alternating SiR_2 and CH_2, are the simplest and the most extensively investigated polycarbosilanes. They can be regarded as the carbon analogues of polysiloxanes. They have been known for almost half a century, but keen interest has been paid since Yajima discovered that poly(silylenemethylene)s can be SiC ceramic precursors in 1975 (5–7). Poly(silylenemethylene)s have quite low glass-transition temperatures (T_g) owing to the relatively long Si—C backbone bonds, as shown in Table 1. A direct comparison of T_g's between asymmetrically substituted poly(silylenemethylene)s and the corresponding carbon analogues revealed the high flexibility of the poly(silylenemethylene)s (8,9). Poly(1,1-dimethylsilylenemethylene) (**2**) was first synthesized by reaction of $ClCH_2Si(CH_3)_2Cl$ with sodium metal (eq. 1) (10), but the molecular weight of the polymer was relatively low ($M_w = 850$).

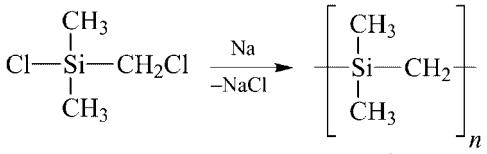

2 (1)

Higher molecular weight poly(silylenemethylene)s (**3**) can be prepared by ROP of 1,3-disilacyclobutanes (eq. 2).

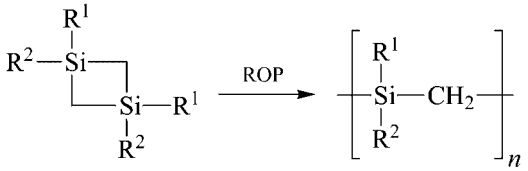

$R^1, R^2 = H, CH_3, (CH_2)_nCH_3, C_6H_5, Cl, OCH_2CH_3$ **3** (2)

Heating of 1,1,3,3-tetramethyl-1,3-disilacyclobutane to 300°C gave poly(dimethylsilylenemethylene) (M_w = 15,000) (11). On the other hand, platinum-catalyzed ROP of 1,1,3,3-tetramethyl-1,3-disilacyclobutane was reported in 1965 (12). Later, several researchers investigated other transition-metal-catalyzed ROP of 1,3-disilacyclobutane derivatives (13–19). Platinum-catalyzed ROP of 1,1,3,3-tetrachloro-1,3-disilacyclobutane (20,21) and 1,1,3,3-tetraalkoxy-1,3-disilacyclobutane has been reported (22). The platinum-catalyzed ROP is thought to be the most efficient and convenient way so far to obtain high molecular weight poly(silylenemethylene)s. Successive transformations of preformed polymers containing Si–X (X = H, Cl, OR) groups have been used to prepare a wide range of functionalized poly(silylenemethylene)s (eq. 3) (23–25).

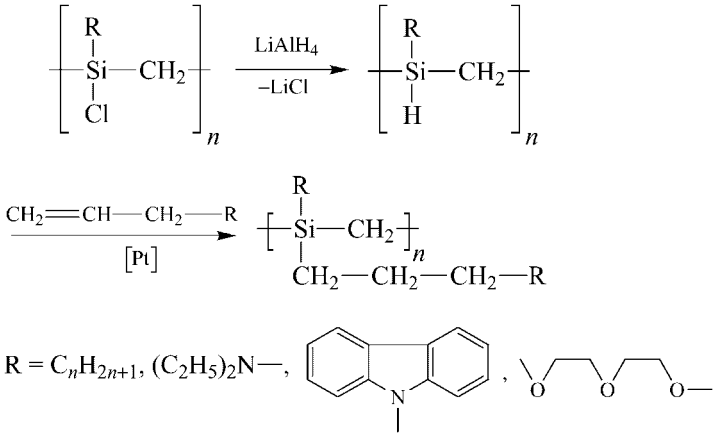

(3)

Polymers with mesogenic groups on silicon atoms have also been synthesized (26).

Poly(silyleneethylene)s

Poly(silyleneethylene)s, composed of alternating SiR_2 and $(CH_2)_2$, are synthesized by a catalytic hydrosilation of $HSi(CH_3)_2CH{=}CH_2$ (27,28). There are naturally copolymers of $-(Si(CH_3)_2{-}CH_2CH_2)-$ and $-(Si(CH_3)_2{-}CH(CH_3))-$, owing to α- and β-addition. More efficient synthesis of this series of polymers is attained by hydrosilation of $HSiCl_2CH{=}CH_2$ (29–31). In this case, the obtained poly(dichlorosilyleneethylene) (**4**) can be transformed into poly(dihydrosilyleneethylene) (**5**) by treatment with $LiAlH_4$ (eq. 4), which can be converted to SiC ceramics in high yield.

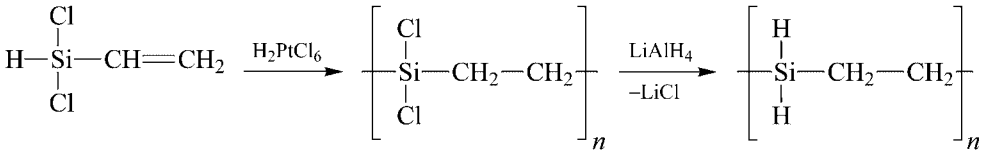

4 **5**

(4)

Poly(silylenetrimethylene)s

Poly(silylenetrimethylene)s (**6**), consisting of a —Si—$(CH_2)_3$— backbone, are most easily synthesized by the ROP of silacyclobutanes (eq. 5).

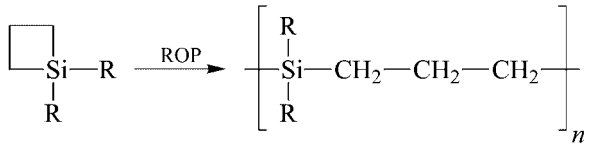

R = H, CH_3, CH_2CH_3, —*n*-C_3H_7, —CH═CH_2, C_6H_5, OCH_3, Cl **6**

(5)

Thermal ROP of 1-methylsilacyclobutane proceeds at 50°C (32), but those of 1,1-dimethylsilacyclobutane and 1-chloro-1-methylsilacyclobutane need high temperatures like 150–200°C (33) and 230°C (34), respectively. Platinum-catalyzed ROP of silacyclobutanes has also been reported (12,35). Other transition-metal-catalyzed ROPs have also been investigated (36). Very efficient Pt catalysts for the ROP of 1,1-dimethylsilacyclobutane has been recently reported (37). Polymers with oligooxyethylene pendant groups (38) or liquid crystalline mesogenic groups (26,39) are synthesized by utilizing the Pt-catalyzed polymerization. Anionic ROP of silacyclobutanes, which was first reported (40,41) in 1964, is also a powerful method for the preparation of poly(silylenetrimethylene)s (42,43). Recently, butyllithium-induced anionic polymerization of vinyl- (44) or hydride-substituted (45) silacyclobutanes was accomplished in THF at −78°C in the presence of hexamethylphosphoramide (HMPA). The produced poly(hydrosilylenetrimethylene) can be transformed to other poly(silylenetrimethylene)s having various pendant groups by hydrosilation with olefinic compounds such as allyl cyanide and allyl pentafluorobenzene (46). Organolithium-induced living anionic polymerization of 1,1-dialkylsilacyclobutanes was reported (47–51). This method is very attractive because it is applicable for synthesis of various block copolymers (eq. 6) (52,53).

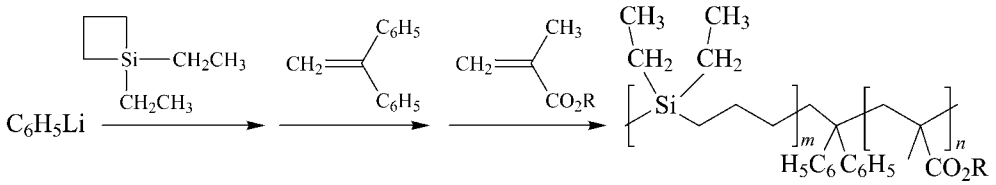

R = CH_3, *t*-C_4H_9, $CH_2CH_2OSi(CH_3)_2$*t*-C_4H_9

(6)

Self-assembly of amphiphilic block copolymers can be a new research area for applications of polycarbosilanes (54–56). An alternative route to prepare poly(silylenetrimethylene)s is hydrosilation of allylsilane derivatives bearing a Si—H group. $[C_6H_5SiCl(CH_2)_3]_n$ was synthesized by self-hydrosilation of allylchlorophenylsilane with Karstedt's catalyst (57). The synthesis of

poly(silylenetrimethylene) was reported, with a high degree of stereoregularity. Poly(methylphenylsilylenetrimethylene) rich in isotacticity was obtained by polyaddition of optically active allylmethylphenylsilane using platinum catalyst (58).

Other Polycarbosilanes with One Silicon and Three Carbons in the Repeating Unit. Various polymers consisting of one silicon and three carbons in the repeating backbone unit can be prepared by ROP of silacyclobutane derivatives. For instance, poly(silylenemethylene-1,2-phenylene), $(Si(CH_3)_2CH_2\text{-}o\text{-}C_6H_4)_n$, can be synthesized from 1,1-dimethyl-2,3-benzosilacyclobutene (59,60). Poly(silylene-2-propenylene), $(Si(CH_3)_2CH_2CH{=}CH)_n$ was synthesized from 1,1-dimethylsilacyclobutene (61). Poly(silylene-2-methylenetrimethylene), $(Si(CH_3)_2CH_2(C{=}CH_2)CH_2)_n$, was obtained from 1,1-dimethyl-3-methylenesilacyclobutane (62). Self-hydrosilation of propargylsilane also provides poly(silylene-2-propenylene). Optically active poly(methylphenylsilylene-2-propenylene) was synthesized by stereoselective polyaddition of (*R*)-methylphenylpropargylsilane using platinum catalyst (63).

Poly(silylene-2-butenylene)s

Poly(silylene-2-butenylene)s, $(SiR_2CH_2CH{=}CHCH_2)_n$ (**7**), can be readily prepared by butyllithium-induced anionic ROP of silacyclopent-3-ene derivatives in THF at −78°C in the presence of HMPA (eq. 7) (64).

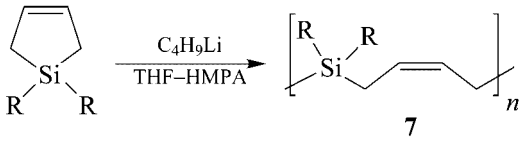

7

$R = CH_3, C_6H_5, H, —CH{=}CH_2$ (7)

The polymerization proceeds with high stereoselectivity to provide polymers having Z geometry around C=C double bonds with relatively narrow molecular weight distributions. Vinyl (65) groups and hydride (66) on the silicon atom are tolerant to the polymerization conditions and functional polymers bearing various pendant groups such as oligooxyethylene (67) or liquid crystalline mesogenic group (68) can be prepared. Another method to prepare poly(silylene-2-butenylene)s is acyclic diene metathesis (ADMET) polymerization of diallylsilanes, $(CH_2{=}CHCH_2)_2SiRR'$ (where R, R′ = CH_3 or Cl) catalyzed by tungsten carbene complex, $[\{(CF_3)_2CH_3CO\}_2(N\text{-}2,6\text{-}C_6H_3\text{-}(i\text{-}(C_3H_7)_2)Pr_2)W{=}CHC(CH_3)_2R]$ (where R = CH_3 or C_6H_5) (69,70).

Poly(silylenevinylene)s

In 1962, it was reported that platinum-catalyzed condensation of methylphenylsilane and diethynylmethylphenylsilane gave low molecular weight

poly(methylphenylsilylenevinylene) $(SiCH_3C_6H_5CH{=}CH_2)_n$ (71). High molecular weight poly(silylenevinylene)s, $(SiR^2CH{=}CH_2)_n$ (**8**), can be prepared by platinum-catalyzed hydrosilation of dialkyl-substituted ethynylsilane. For instance, poly(dimethylsilylenevinylene) (M_w = 30,380), poly(diethylsilylenevinylene) (M_w = 110,700), and poly(methylphenylsilylenevinylene) (M_w = 11,400) can be synthesized by hydrosilation of the corresponding dialkylethynylsilane, $HSiR^1R^2C{\equiv}CH$ (eq. 8) (72).

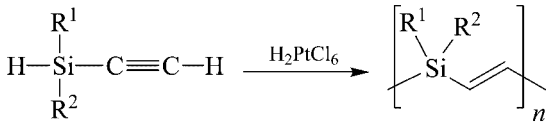

8

$R^1, R^2 = CH_3, CH_2CH_3, C_6H_5$ (8)

Melt-spun fibers from these polymers are thermally converted to SiC fibers in good ceramic yield. Another way to synthesize poly(silylenevinylene) is ruthenium- or rhodium-catalyzed polycondensation of dimethyldivinylsilane (73).

Poly(silylenealkynylene)s

Because silicon is able to conjugate electronically with adjacent alkyne π bonds, poly(silylenealkynylene)s, $(SiR_2C{\equiv}C)_n$ (**9**), can be expected to exhibit conducting or nonlinear optical properties. A very efficient method to synthesize poly(silyleneethynylene) has been reported. Dilithium acetylide prepared from trichloroethylene and butyllithium was treated with Cl_2SiR_2 to give high molecular weight polymers (M_w = 30,000, when R = C_6H_5; M_w = 20,000, when R = C_6H_5, CH_3) (eq. 9) (74).

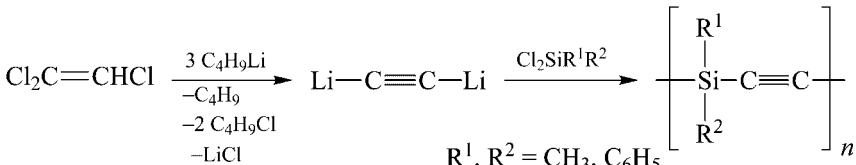

$R^1, R^2 = CH_3, C_6H_5$

9 (9)

However, these polymers were found to be very poor conductors, even after doping with iodine. Another type of acetylenic polymer, poly(silylenediethynylene), $(SiR_2C{\equiv}C{-}C{\equiv}C)_n$ (**10**), can be synthesized by condensation of $Cl_2SiR^1R^2$ (R^1, R^2 = CH_3, C_2H_5, or C_6H_5) and 1,4-dilithio-1,3-butadiyne prepared from 1,4-bistrimethylsilylbut-1,3-diyne and methyllithium (eq. 10) (75).

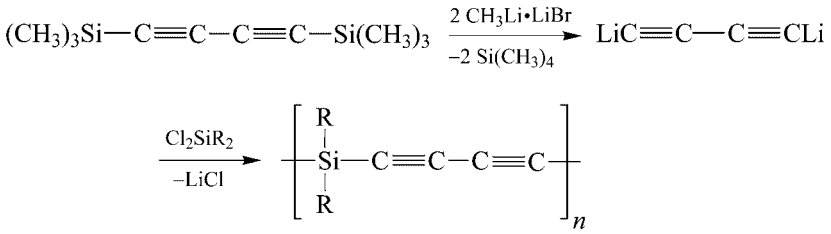

R = CH_3, CH_2CH_3, C_6H_5 **10** (10)

These polymers exhibit conductivity (10^{-5} – 10^{-3} S·cm^{-1}) after oxidation with $FeCl_3$, which is in the range of semiconductors. Application of polymer **10** as SiC ceramic precursors has also been investigated (76).

Poly(silylenearylene)s

Poly(dimethylsilylene-*p*-phenylene), $(Si(CH_3)_2\text{-}p\text{-}C_6H_4)_n$ (**11**), is successfully synthesized via condensation of *p*-chlorophenyldimethylchlorosilane and sodium (eq. 11).

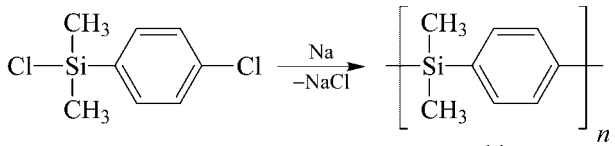

11 (11)

The polymer showed significantly high thermal stability and was not decomposed even at 400°C (77). It was reported that poly(silylenephenylene)s can be synthesized from the reaction of dichloromethylsilane or dichlorophenylsilane with *p*- and *m*-dilithiobenzene (78). An efficient method to prepare poly(silylene-*m*-phenylene) (**12**)(M_w = 4000–20,000), that is, a ruthenium-catalyzed desilylative condensation of *m*-bis(trihydrosilyl)benzene (eq. 12), was reported (79).

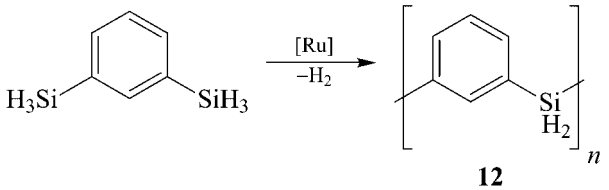

12 (12)

The synthesis and the high heat-resistant property of poly{[bis (ethynylphenyl)silylene]phenylene} have also been reported (80). Poly [(diethoxysilylene)phenylene] was first synthesized by a reaction of (3-bromophenyl)triethoxysilane with magnesium. Then the polymer was treated with (trimethylsilylethynyl)phenyllithium, followed by deprotection of the trimethylsilyl groups.

Poly(silylenealkenylenearylene)s. Poly(dimethylsilyenephenyleneviny lene)s were synthesized by chloroplatinic acid catalyzed self-hydrosilation of *o*-, *m*-, and *p*-(dimethylsilyl)phenylacetylene (81). These polymers are interesting as not only ceramic precursors but also blue-light-emitting materials. Poly(methylphenylsilyelenephenylenevinylene) and poly (diphenylsilyelenephenylenevinylene) were also prepared by chloroplatinic acid-catalyzed hydrosilation of methylphenylsilane or diphenylsilane with 1,4-diethynylbenzene (82). These polymers had both β- and α-hydrosilation addition structures in the vinylene moieties.

Poly(silylenealkynylenearylene)s. The first poly(silylenealkynylene arylene) to be reported was poly(dimethylsilyleneethynylene-*p*-phenyleneethynylene), $(Si(CH_3)_2C{\equiv}CC_6H_4C{\equiv}C)_n$, which was prepared by polycondensation of the disodium salts of *p*-diethynylbenzene with dimethyldichlorosilane (83). A more efficient method was reported, which is a palladium-catalyzed polycondensation of dihaloaromatics and diethynyldiphenylsilanes (eq. 13).

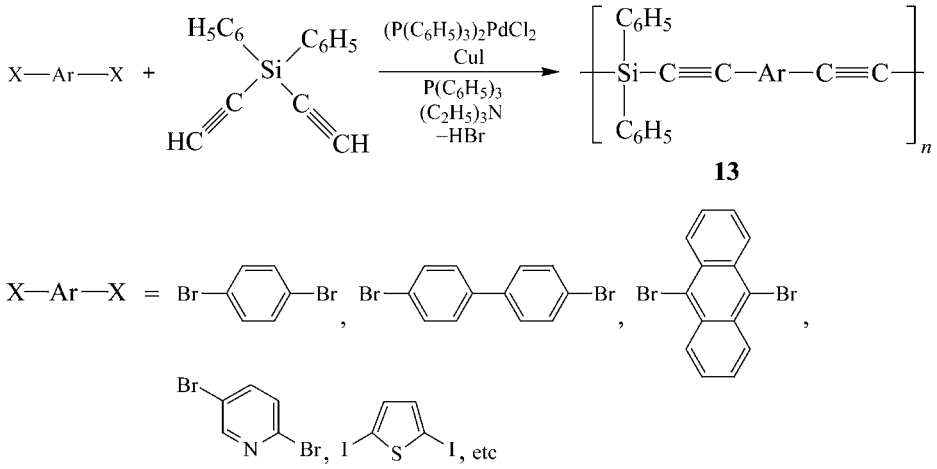

(13)

This polymerization can be applied to a wide range of condensations between diethynyldiphenylsilane and aromatic halides including pyridine and thiophene derivatives (**13**) (84). It was reported that dehydrogenative coupling of phenylsilane with *m*-diethynylbenzene in the presence of MgO to provide poly(silylene-*m*-diethynylenephenylene) (**14**) (eq. 14) (85,86).

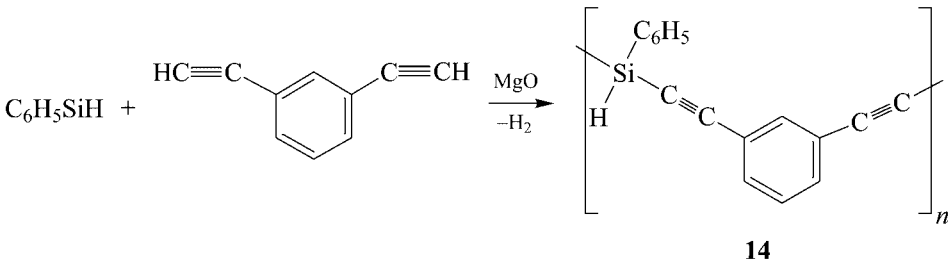

(14)

This polymer exhibited significantly high heat-resistant and burn-resistant properties, which is due to cross-linking of the polymer backbone through Si—H and C≡C bonds (85,86).

Poly(methylene(silacylohexanylene))s

Polycarbosilanes with silicon-containing six-membered rings in the backbone can be synthesized by cyclopolymerization of organosilicon monomers bearing two olefinic substituents. Poly(methylene-(1-sila-3,5-cyclohexanylene))s (**15**) are obtained by cyclopolymerization of dialkyldiallylsilanes. Coordination polymerization by Ziegler-type catalysts (87–89), cationic polymerization by $AlBr_3$ (90–92), and radical polymerization induced by AIBN (93) have been reported (eq. 15).

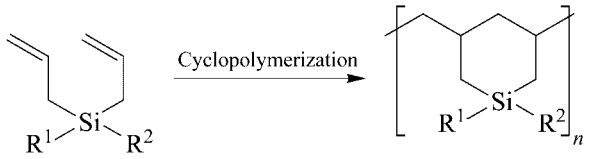

R^1, R^2 = CH_3, C_6H_5

15 (15)

Cyclopolymerization of another type of organosilicon monomer has been reported. Poly(methylene-4,6-disila-1,3-cyclohexanylene) (**16**) was prepared by an anionic polymerization of bis(dimethylvinylsilyl)methane in the presence of tetramethylethylenediamine (TMEDA) (eq. 16).

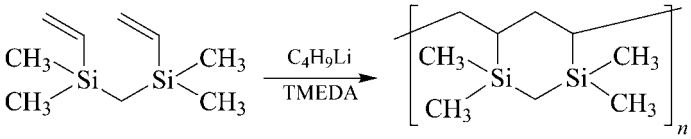

16 (16)

The polymerization can be controlled well to provide a sufficiently high molecular weight polymer (M_w = 12,400) having a six-membered ring structure in a very high yield (94,95).

Carbosilane Dendrimers

In 1992, the synthesis of a carbosilane dendrimer was reported (96). Starting from tetrachlorosilane, allylations of Si—Cl groups by allyl Grignard reagents and hydrosilations of the allyl groups with trichlorosilane were alternately repeated to give a dendrimer composed of silylenetrimethylene units up to the fifth generation (**G5**) (eq. 17) (96).

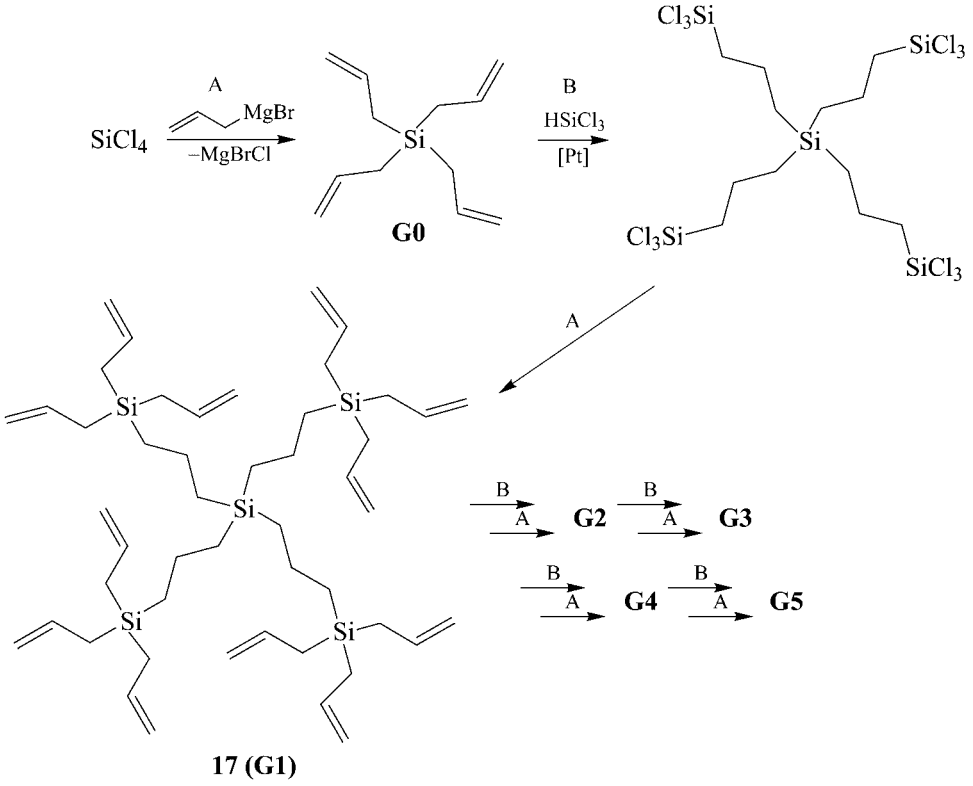

(17)

Other carbosilane dendrimers composed of silyleneethylene units, such as **18** and **19**, can be synthesized analogously by applying vinylations of Si—Cl groups instead of the allylations (97,98).

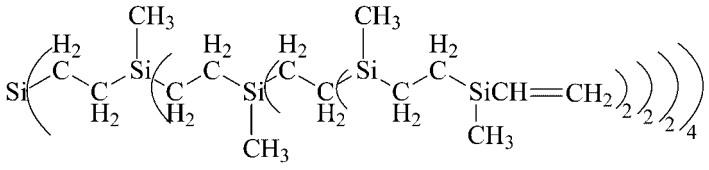

18

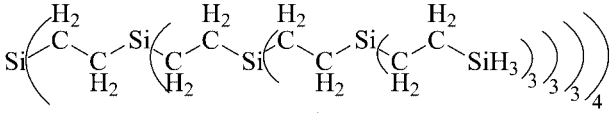

19

Many researchers employed these dendrimers as frameworks to attach other functional groups. For instance, dendrimers with mesogenic cholesteryl (99), perfluoroalkyl (100,101), hydroxyl, dimethylamino, sodium sulfonate,

trimethylammonium groups (102), palladium complexes (103–105), iron/gold clusters (106), and cyclopentadienyltitanium complexes (107) were synthesized.

BIBLIOGRAPHY

"Polysilanes and Polycarbosilanes" in *EPSE* 2nd ed., Vol. 13, pp. 162–186, by P. Trefonas, Monsanto Electronic Materials Co.

1. D. Seyferth, in M. Zeldin, K. J. Wynne, and H. R. Allcock, eds., *Inorganic and Organometallic Polymers*, (ACS Symposium Series No. 360), Washington, D.C., p. 21, 1988.
2. P. Kochs, in H. R. Kricheldorf, ed., *Silicon in Polymer Synthesis*, Springer, Berlin, 1996, Chapt. "4", p. 223.
3. M. A. Brook, *Silicon in Organic, Organometallics, and Polymer Chemistry*, John Wiley & Sons, Inc., New York, 2000, Chapt. "11", p. 340,
4. L. V. Interrante and Q. Shen, in R. G. Jones, W. Ando, and J. Chojnowski, eds., *Silicon-Containing Polymers: The Science and Technology of Their Synthesis and Applications*, Kluwer, Dordrecht, 2000, Chapt. "10", p. 247.
5. S. Yajima, J. Hayashi, and M. Omori, *Chem. Lett.* 931 (1975).
6. S. Yajima, K. Okamura, and J. Hayashi, *Chem. Lett.* 1209 (1975).
7. S. Yajima, *Ceram. Bull.* **62**, 893 (1983).
8. F. Koopmann and H. Frey, *Macromolecules* **29**, 3701 (1996).
9. Q. H. Shen and L. V. Interrante, *J. Polym. Sci., Part A: Polym. Chem.* **35**, 3193 (1997).
10. U.S. Pat. 2,483,972 (1948), J. T. Goodwin (to Dow Corning Corp.).
11. U.S. Pat. 2,850,514 (1958), W. H. Knoth (to E. I. Du Pont de Nemours Co., Inc.),
12. D. R. Weyenberg and L. E. Nelson, *J. Org. Chem.* **30**, 2618 (1965).
13. W. A. Kriner, *J. Polym. Sci., Part A-1* **4**, 444 (1966).
14. G. Levin and J. B. Carmichael, *J. Polym. Sci., Part A-1* **6**, 1 (1968).
15. V. A. Poletaev, V. M. Vdovin, and N. S. Nametkin, *Dokl. Akad. Nauk SSSR* **203**, 1324 (1972).
16. V. A. Poletaev, V. M. Vdovin, and N. S. Nametkin, *Dokl. Akad. Nauk SSSR* **208**, 1112 (1973).
17. T. Ogawa and co-workers, *J. Polym. Sci., Part A: Polym. Chem.* **33**, 2821 (1995).
18. T. Ogawa and M. Murakami, *Chem. Mater.* **8**, 1260 (1996).
19. F. Koopmann and H. Frey, *Macromol. Chem. Phys.* **199**, 2119 (1998).
20. H.-J. Wu and L. V. Interrante, *Macromolecules* **25**, 1840 (1992).
21. L. V. Interrante and co-workers, *J. Am. Chem. Soc.* **116**, 12085 (1994).
22. I. L. Rushkin and L. V. Interrante, *Macromolecules* **28**, 5160 (1995).
23. L. V. Interrante, Q. L. I. Rushkin, and Q. Shen, *J. Organomet. Chem.* **521**, 1 (1996).
24. W. Uhlig, *J. Polym. Sci., Part A: Polym. Chem.* **36**, 725 (1998).
25. M. Lienhard and co-workers, *J. Am. Chem. Soc.* **119**, 12020 (1997).
26. T. Ganicz and co-workers, *Polymer* **37**, 4167 (1996).
27. J. W. Curry, *J. Am. Chem. Soc.* **78**, 1687 (1956).
28. J. W. Curry, *J. Org. Chem.* **26**, 1308 (1961).
29. K. I. Kobrakov and co-workers, *Dokl. Akad. Nauk SSSR* **191**, 607 (1970).
30. B. Boury and co-workers, *Organometallics* **10**, 1457 (1991).
31. R. J. P. Corriu and co-workers, *Orgaonmetallics* **12**, 454 (1993).

32. U.S. Pat. 3,046,291 (1962), L. H. Sommer, (to Dow Corning Corp.).
33. N. S. Nametkin, V. M. Vdovin, and V. I. Zav'yalov, *Izv. Akad. Nauk SSSR, Ser. Khim.* 1448 (1965).
34. V. M. Vdovin, K. S. Pushchevaya, and A. D. Petrov, *Dokl. Akad. Nauk SSSR* **141**, 843 (1961).
35. N. S. Nametkin, V. M. Vdovin, and P. L. Grinberg, *Izv. Akad. Nauk SSSR, Ser Khim.* 1133 (1964).
36. C. S. Cundy, C. Eaborn, and M. F. Lappert, *J. Organomet. Chem.* **44**, 291 (1972).
37. H. Yamashita, M. Tanaka, and K. Honda, *J. Am. Chem. Soc.* **117**, 8873 (1995).
38. C. X. Liao and W. P. Weber, *Macromolecules* **26**, 563 (1993).
39. K. Komuro and Y. Kawakami, *Polym. Bull.* **42**, 669 (1999).
40. N. S. Nametkin, V. M. Vdovin, and V. I. Zav'yalov, *Izv. Akad. Nauk SSSR, Ser. Khim.* 203 (1964).
41. N. S. Nametkin and co-workers, *Dokl. Akad. Nauk SSSR* **209**, 621 (1973).
42. K. Komuro, S. Toyokawa, and Y. Kawakami, *Polym. Bull.* **40**, 715 (1998).
43. K. Komuro and Y. Kawakami, *Polym. J.* **31**, 138 (1999).
44. C. X. Liao and W. P. Weber, *Macromolecules* **25**, 1639 (1992).
45. C. X. Liao and W. P. Weber, *Polym. Bull.* **28**, 281 (1992).
46. C. X. Liao and W. P. Weber, *Macromolecules* **26**, 563 (1993).
47. K. Matsumoto and H. Yamaoka, *Macromolecules* **28**, 7029 (1995).
48. K. Matsumoto and co-workers, *J. Polym. Sci., Part A: Polym. Chem.* **35**, 3207 (1997).
49. R. Knischka and co-workers, *Macromol. Rapid Commun.* **19**, 455 (1998).
50. K. Matsumoto, M. Shinohata, and H. Yamaoka, *Polym. J.* **32**, 354 (2000).
51. K. Matsumoto, M. Shinohata, and H. Yamaoka, *Polym. J.* **32**, 1022 (2000).
52. K. Matsumoto and co-workers, *J. Polym. Sci., Part A: Polym. Chem.* **36**, 2699 (1998).
53. K. Matsumoto and co-workers, *J. Polym. Sci., Part A: Polym. Chem.* **39**, 86 (2001).
54. M. Nakano and co-workers, *Macromolecules* **32**, 6088 (1999).
55. M. Nakano and co-workers, *Macromolecules* **32**, 7437 (1999).
56. K. Matsumoto and co-workers, *Macromolecules* **35**, 555 (2002).
57. M. Chai and co-workers, *Macromolecules* **30**, 1240 (1997).
58. Y. Kawakami and co-workers, *Macromolecules* **31**, 551 (1998).
59. N. S. Nametkin and co-workers, *Vysokomol. Soedin, Ser. B* **11**, 207 (1969).
60. M. Theuring and co-workers, *Macromolecules* **25**, 3834 (1992).
61. M. Theuring and W. P. Weber, *Polym. Bull.* **28**, 17 (1992).
62. K. Matsumoto, K. Miyagawa, and H. Yamaoka, *Macromolecules* **30**, 2524 (1997).
63. Y. Kawakami and co-workers, *Macromolecules* **32**, 6874 (1999).
64. X. Zhang and co-workers, *Macromolecules* **21**, 1563 (1988).
65. S. J. Sargeant and co-workers, *Macromolecules* **25**, 2832 (1992).
66. S. Q. Zhou and co-workers, *Polym. Bull.* **23**, 491 (1990).
67. L. Wang and W. P. Weber, *Macromolecules* **26**, 969 (1993).
68. S. J. Sargeant and W. P. Weber, *Macromolecules* **26**, 2400 (1993).
69. K. B. Wagner and D. W. Smith Jr., *Macromolecules* **24**, 6073 (1991).
70. S. Cummings, J. Anderson, and K. Wagner, *Macromol. Rapid Commun.* **16**, 347 (1995).
71. V. V. Korshak, A. M. Sladkov, and L. K. Luneva, *Izv. Akad. Nauk SSSR, Otd. Khim. Nauk* 2251 (1962).
72. Y. Pang, S. Ijadi-Maghsoodi, and T. J. Barton, *Macromolecules* **26**, 5671 (1993).

73. B. Marciniec and M. Lewandowski, *J. Polym. Sci., Part A: Polym. Chem.* **34**, 1443 (1996).
74. S. Ijadi-Maghsoodi, Y. Pang, and T. J. Barton, *J. Polym. Sci., Part A: Polym. Chem.* **28**, 955 (1990).
75. J. L. Bréfort and co-workers, *Macromolecules* **11**, 2500 (1992).
76. R. J. P. Corriu and co-workers, *Macromolecules* **11**, 2507 (1992).
77. J. G. Noltes and G. J. M. van der Kerk, *Recl. Trav. Chem.* **81**, 565 (1962).
78. J. Ohshita and co-workers, *Macromolecules* **27**, 5583 (1994).
79. T. Sakakura and co-workers, *J. Chem. Soc., Chem. Commun.* 193 (1995).
80. J. Ohshita, A. Shinpo, and A. Kunai, *Macromolecules*, 32 (1999).
81. D. S. Kim and S. C. Shim, *J. Polym. Sci., Part A: Polym. Chem.* **37**, 2263 (1999).
82. D. S. Kim and S. C. Shim, *J. Polym. Sci., Part A: Polym. Chem.* **37**, 2933 (1999).
83. V. V. Korshak, A. M. Sladkov, and L. K. Luneva, *Izv. Akad. Nauk SSSR, Otd. Khim. Nauk* 728 (1962).
84. R. J. P. Corriu, W. E. Douglas, and Z.-X. Yang, *J. Polym. Sci., Part C: Polym. Lett.* **28**, 431 (1990).
85. M. Itoh and co-workers, *Macromolecules* **27**, 7917 (1994)
86. M. Itoh and co-workers, *Macromolecules* **30**, 694 (1997).
87. G. S. Kolesnikov, S. L. Davydova, and T. I. Ermolaeva, *Vysokomol. Soedin.* **1**, 1493 (1959).
88. C. S. Marvel and R. G. Woolford, *J. Am. Chem. Soc.* **82**, 1641 (1960).
89. G. B. Butler and R. W. Stackman, *J. Am. Chem. Soc.* **82**, 1643 (1960).
90. N. C. Billingham and co-workers, *J. Polym. Sci., Polym. Chem. Ed.* **15**, 675 (1977).
91. R. H. Cragg, R. G. Jones, and A. C. Swain, *Eur. Polym. J.* **27**, 785 (1991).
92. R. G. Jones, R. H. Cragg, and A. C. Swain, *Eur. Polym. J.* **28**, 651 (1992).
93. K. Saigo, K. Takeishi, and H. Adachi, *J. Polym. Sci., Part A: Polym. Chem.* **26**, 2085 (1988).
94. Y. Suga, J. Oku, and M. Takai, *Macromolecules* **27**, 7930 (1994).
95. Y. Suga and co-workers, *Macromolecules* **32**, 1362 (1999).
96. A. W. van der Made and P. W. N. M. van Leeuwen, *J. Chem. Soc., Chem. Commun.* 1400 (1992).
97. L.-L. Zhou and J. Roovers, *Macromolecules* **26**, 963 (1993).
98. D. Seyferth and D. Y. Son, *Organometallics* **13**, 2682 (1994).
99. M. C. Coen and co-workers, *Macromolecules* **29**, 8069 (1996).
100. K. Lorenz and co-workers, *Macromolecules* **30**, 6860 (1997).
101. B. A. Omotowa and co-workers, *J. Am. Chem. Soc.* **121**, 11130 (1999).
102. W. Shane and D. Seyferth, *J. Am. Chem. Soc.* **120**, 3604 (1998).
103. J. L. Hoare and co-workers, *Organometallics* **16**, 4167 (1997).
104. N. J. Hovestad and co-workers, *Organometallics* **18**, 2970 (1999).
105. E. B. Eggeling and co-workers, *J. Org. Chem.* **65**, 8857 (2000).
106. M. Benito and co-workers, *Organometallics* **18**, 5191 (1999).
107. S. Arévalo and co-workers, *Organometallics* **20**, 2583 (2001).

KOZO MATSUMOTO
Kyoto University

POLYCHLOROPRENE. See CHLOROPRENE POLYMERS.

POLYCYANOACRYLATES. See Volume 3.

POLY(CYCLOHEXYLENE TEREPHTHALATE).
See CYCLOHEXANEDIMETHANOL POLYESTERS.

POLYDIACETYLENE. See DIACETYLENE AND TRIACETYLENE POLYMERS.

POLYELECTROLYTES

Introduction

Polyelectrolytes are polymers that develop substantial charge when dissolved or swollen in a highly polar solvent such as water. These polymers are also commonly termed *polyions* because their charge arises from many ionized functional groups positioned along the chain contour. Electrostatic interactions between the ionized groups, as well as the presence of small electrolyte ions in the nearby solution, convey to polyelectrolyte systems a host of properties distinct from those displayed by neutral polymer systems. Unfortunately, describing and modeling these properties has proven difficult, and many key properties remain poorly understood. Industrial applications and academic interests focus on polyelectrolyte behavior in solutions, gels, adsorbed layers, and grafted brushes. Polyelectrolytes frequently form complexes with cosolutes such as multivalent ions, surfactants, other polymers, or small colloidal particles.

Even in water, which possesses a high dielectric constant, electrostatic forces strongly oppose the dissociation and physical separation of unlike charges. Thus, a diffuse cloud of small counterions closely surrounds a dissolved polyelectrolyte chain, and this cloud accumulates sufficient charge to compensate for the polyelectrolyte's fixed charge. Ions within the diffuse cloud dynamically exchange with small ions present as added or ambient low molecular weight electrolyte in the surrounding solution, but this exchange does not affect the net excess of countercharge the cloud accumulates. The size of the diffuse cloud reflects a balance between electrostatic energy, favoring the cloud's collapse onto the oppositely charged chain, and entropy, favoring the cloud's unbounded expansion. Counterions in the diffuse cloud, as well as other small ions of an added electrolyte, screen electrostatic interactions, a phenomenon reducing the length scales over which

Encyclopedia of Polymer Science and Technology. Copyright John Wiley & Sons, Inc. All rights reserved.

electrostatic interactions remain important. Adding electrolyte to a polyelectrolyte solution contracts the counterion cloud, and at sufficiently high electrolyte concentrations, the cloud's shrinkage onto the chain transforms many polyelectrolyte properties to those of a neutral polymer. Conversely, with no added electrolyte and thus only liberated counterions present, a special condition termed *salt free*, distinctive polyelectrolyte behaviors are strongly magnified.

Borrowing from the terminology of simple electrolytes, if the extent of dissociation of a polyelectrolyte's ionic groups depends on solution conditions, particularly pH or concentration, the polyelectrolyte is labeled "weak." On the other hand, if a polyelectrolyte's charge is relatively insensitive to solution conditions, the polyelectrolyte is labeled "strong." Weak and strong classifications can be ambiguous. Polyampholytes simultaneously contain both positive and negative charge units. These molecules may display an *isoelectric point*, a pH or solution condition at which the magnitudes of positive and negative charge are equal. Many proteins, for example, behave as weak polyanions at high pH, weak polycations at low pH, and neutral at some well-defined intermediate pH.

The electrostatic interactions of polyelectrolytes with nearby small ions have frequently been addressed using theoretical methods and approximations adapted from studies of colloids or simple electrolytes. However, polyelectrolytes introduce new and complicating features, most notably, molecular flexibility/orientation, chain entanglement, and a necessity for modeling electrostatic interactions consistently over a large range of length scales. Additional theoretical difficulties may include specific ion interactions, hydrogen bonding of water, unknown values of the local dielectric constant, and ordered placement of charges along the backbone.

Polyelectrolytes sometimes are categorized according to the solubility of their uncharged backbone. Polyelectrolyte species that would not dissolve in the absence of charge are termed *hydrophobic*, while those that would are termed *hydrophilic*. The distinction is only conceptual, as even if possible, removal of charge will normally modify nonelectrostatic interactions that affect polyelectrolyte solubility. Amphiphilic polyelectrolytes or "polysoaps" contain, in addition to charged chain sequences, well-defined hydrophobic units either in the backbone or attached as branches. *Ionomers* are charged polymers possessing along their backbones only a low density of charged units, with the fraction of these units typically less than about 15% on a mole basis. The remaining units are nonpolar and water-insoluble, and so ionomers do not dissolve readily in high dielectric constant solvents, and in more suitable lower dielectric constant solvents, the ionizable units interact mainly through dipole–dipole rather than direct electrostatic forces. Ionomers as a class are therefore distinct from polyelectrolytes.

Although DNA is perhaps the best-known biological polyelectrolyte, many additional examples are found among common proteins and polysaccharides. Polyelectrolytes are produced synthetically by polymerization of charged monomers or by chemical functionalization of both natural and synthetic neutral polymers. An increasing number of neutral polymers have been observed to behave much as polyelectrolytes as a result of association in solution with charged cosolutes such as surfactants and small ions. Such materials may be termed *pseudopolyelectrolytes*.

Outside of natural systems, where polyelectrolytes perform an enormous number of biological functions, polyelectrolytes are mostly employed to modify

solution rheology, control the aggregation of colloidal particles, or alter the nature of surfaces by adsorption. However, the number of applications for synthetic polyelectrolytes is large and growing, and no single use or class of uses dominates.

Examples of Polyelectrolyte

A vast number of chemical structures have been reported for polyelectrolytes. Table 1 illustrates a few of the more important and commonly encountered polyelectrolyte chemical structures. Although the table divides polyelectrolytes according to chemical origin, the division can be arbitrary. For example, poly(glutamic acid) can be prepared by either traditional organic synthesis or biosynthesis in genetically modified bacteria. Poly(styrene sulfonate) is an example of a synthetic polymer made equally by polymerization of charged monomer, styrene sulfonate, or by modification of neutral polymer, sulfonation of polystyrene. The ionic groups that endow polyelectrolytes with charge are no different than those found in small organic molecules bearing charge. The list of anionic groups includes sulfate, phosphate, sulfonate, and carboxyl, while that of cationic groups includes protonated ammonium, quaternized ammonium, sulfonium, and phosphonium. Polyelectrolytes in solid form are frequently available as either the salt or the acid/base, and the two forms can usually be interchanged after dissolution in solution by appropriate methods of ion exchange or dialysis. When dissolved in an aqueous environment containing small ions, the form of the starting material is irrelevant, as the system properties depend only upon the mixture of small ions present and not their source. The multivalent salts of a polyelectrolyte are often sparingly soluble or insoluble.

Basic Description of a Polyelectrolyte System

The Polyelectrolyte Chain. The presence of covalently attached ionic groups fundamentally distinguishes polyelectrolytes from neutral polymers, and so a description of polyelectrolyte properties begins with parameterization of polyelectrolyte charge. The projected number of elementary charges of magnitude e (1.602×10^{-19} C) per unit backbone length defines a polyelectrolyte's linear charge density. The inverse of this quantity, given the symbol b, represents the average axial spacing between charges. Important assumptions are implicit in the capturing of polyelectrolyte charge in b. First, charge units that are physically positioned at some radial distance from the backbone on side groups or ordered about the backbone as a helix are treated as equivalent to hypothetical charge units positioned along the chain axis. Second, the discrete axial spacing of charges present in the real chemical structure is smeared along the chain contour, eliminating local charge correlations. Finally, the radial mispositioning of charge implicit in specification of b supposes that the dielectric properties of the backbone are irrelevant to the polymer's electrostatic properties. The combined impact of all of these assumptions is unclear; at best, b should be understood to describe polyelectrolyte charge and its effects at large enough length scales so that local structural detail is unimportant. When local detail cannot be ignored, other measures of charge

Table 1. Typical Polyelectrolytes

Name	Repeat Unit
Synthetic polyelectrolytes	
Poly(acrylic acid)	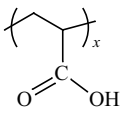
(6,6-ionene)	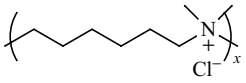
Poly(2-vinyl-pyridine)	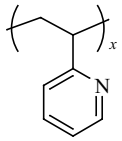
Poly(lysine)	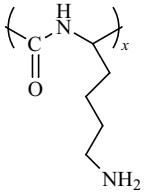
Poly(diallyldimethylammonium chloride)	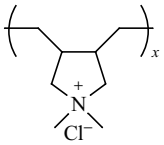
Poly(dimethylaminoethyl acrylate)	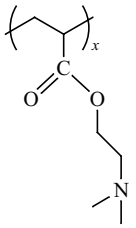
Poly(methacrylic acid)	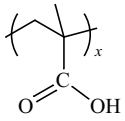
Poly(ethyleneimine)	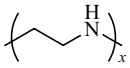
Poly(styrene sulfonic acid)	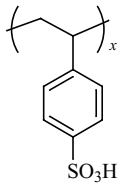

Table 1. (Continued)

Name	Repeat Unit
Poly(glutamic acid)	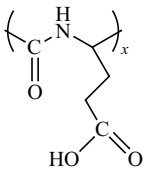
Poly(vinyl sulfate)	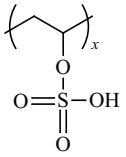
Poly(acrylamide-*co*-acrylic acid)	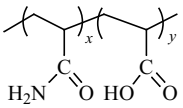
Natural polyelectrolytes	
Hyaluronic acid	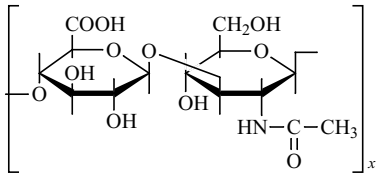
Chitosan	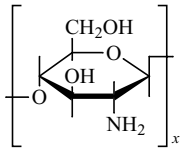
Carboxymethyl cellulose	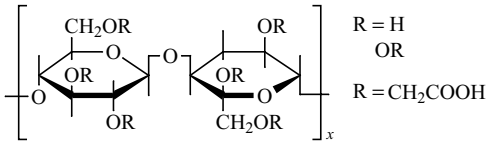
DNA (single stranded)	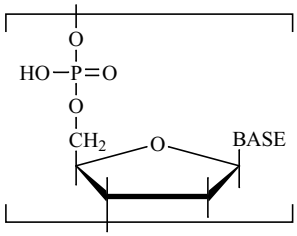

are needed. For example, to understand some behaviors of DNA, one might characterize the polymer's charge via a surface charge density rather than a linear charge density, or even further, via the helical placement of phosphate groups relative to a finite dielectric constant backbone. More complex polyelectrolyte charge descriptions require additional and often unavailable molecular details.

Even in the absence of charge, the characterization of an ordinary flexible polymer chain requires at least three physical parameters, chosen as the persistence length l_p (measuring chain stiffness), contour length L (measuring chain length), and excluded volume strength ν (measuring segmental interactions or solvent quality). The same quantities or their equivalents are also necessary to characterize a linear, flexible polyelectrolyte chain. Thus, the most basic polyelectrolyte chain description incorporates four parameters: b, L, l_p, and ν. Different and/or additional parameters will appear in the description of structurally complex polyelectrolytes such as globular proteins and dendrimers.

The Electrolyte Environment. The electrolyte environment also needs to be described to characterize a polyelectrolyte system. Polyelectrolytes dissolved or swollen in a solvent are bathed in a dielectric medium that typically includes, in addition to other polymer chains and liberated counterions, some level of added or ambient low molar mass electrolyte. A full system description therefore includes information about the solvent medium and any added electrolyte.

The interaction of thermally equilibrated charges across a medium of dielectric constant ε introduces to electrolyte solutions a fundamental length scale l_b, the Bjerrum length. This length characterizes the distance over which two bare charges of magnitude e experience an electrostatic interaction energy equal to the medium's thermal energy kT, ie,

$$l_b = \frac{e^2}{4\pi\varepsilon\varepsilon_0 kT} \tag{1}$$

where ε_0 is the permittivity of vacuum (8.854×10^{-12} $(A^2 \cdot S^4)/(kg \cdot m^3)$). (SI units will be employed here, although most of the polyelectrolyte literature uses CGS units.) At 25°C, l_b in water ($\varepsilon = 78$) is about 0.71 nm.

The introduction of counterions and added electrolyte introduces yet another length scale to electrolyte solutions, one that manifests the enhanced decay of electrostatic interactions in the presence of screening charges. When electrostatic effects are treated within the standard Poisson–Boltzmann approximation, the Debye length κ^{-1} governs the screening length of electrostatic interactions by these ions:

$$\kappa^{-1} = \left(\frac{\varepsilon\varepsilon_0 kT}{\sum_i c_{0,i} (ez_i)^2} \right)^{1/2} \tag{2}$$

where $c_{0,i}$ is the bulk concentration (number per volume) of the ith ion species of valence z_i. Relating the denominator of the term in parentheses to the ionic strength I (expressed in moles per volume) through

$$I = \frac{1}{2N_a} \sum_i c_{0,i} (z_i)^2 \tag{3}$$

where N_a is Avogadro's number, the expression for κ^{-1} can be rewritten as

$$\kappa^{-1} = \left(\frac{\varepsilon\varepsilon_0 kT}{2N_a e^2 I}\right)^{1/2} = \left(8\pi N_a I l_b\right)^{-1/2} \tag{4}$$

In water at 25°C, the last formula simplifies to $\kappa^{-1} = 0.304 I^{-1/2}$ nm when I is expressed in mole per liter (M). When $I = 1.0\,M$, for example, κ^{-1} is about 0.3 nm, and when $I = 0.001\,M$, κ^{-1} is about 10 nm. The largest experimentally obtainable values of κ^{-1} are in the range of tens to hundreds of nanometers, values characteristic of dilute, essentially salt-free polyelectrolyte solutions. For these extreme cases, I is dominated by the bulk concentration of counterions dissociated as the polymer dissolves. How this concentration can be estimated is discussed later; for highly charged polyelectrolytes, not all dissociated counterions contribute to I.

The basic description of the solvent medium thus provides two additional length scales, l_b and κ^{-1}, the former characterizing the spatial attenuation of electrostatic interactions according to the medium's dielectric constant and the latter characterizing the spatial attenuation of electrostatic interactions according to the medium's concentration of thermally equilibrated small ions. The Poisson–Boltzmann equation provides a consistent, albeit approximate, framework for describing the role of electrostatic interactions within a polyelectrolyte–solvent system, incorporating effects associated with both l_b and κ^{-1}. The diffuse counterion cloud described by the Poisson–Boltzmann equation is often termed the *Gouy–Chapman layer*. Some models for charged surfaces and polymers suppose that beneath the Gouy–Chapman layer lies an immobilized layer of adsorbed ions termed the *Stern layer*. Electrostatic models that address the electrolyte solution but ignore the nature of the charged substrate cannot predict the presence or properties of a Stern layer. The Poisson–Boltzmann equation suffers from numerous well-known deficiencies, and the full nonlinear equation can be difficult to solve analytically. The linearized version of the Poisson–Boltzmann equation, obtained via the Debye–Hückel approximation, is much easier to analyze and offers much qualitative, if not quantitative, insight into polyelectrolyte phenomena. Nevertheless, the Debye–Hückel approximation imposes a severe constraint, requiring that the electrostatic potential ψ be everywhere small compared to kT/e, a questionable condition for most polyelectrolyte systems. At typical polyelectrolyte charge densities, ψ is much in excess of kT/e near the chain backbone.

In the Debye–Hückel approximation, the electrostatic interaction energy of two point charges of magnitude e separated by distance r across a dielectric medium containing equilibrated small ions is expressed as

$$U(r) = kT\,\frac{l_b}{r}\,\exp(-\kappa r) \tag{5}$$

This simple Debye–Hückel or Yukawa potential captures the essence of electrostatic interactions in many polyelectrolyte systems, and as the outcome of a linear analysis, provides discrete interaction terms that can be directly summed to obtain the net electrostatic energy associated with the multiple charges of a polyelectrolyte system. When rigor beyond the Debye–Hückel approximation is mandatory, electrostatic energies must be evaluated through the full

Poisson–Boltzmann equation, more sophisticated analytical alternatives, or computer simulation. Both Debye–Hückel and Poisson–Boltzmann approaches offer a mean-field description of electrostatic screening by small (point-like), thermally equilibrated ions; such descriptions fail to address the spatial correlations in placement of these ions that may be important in real polyelectrolyte systems.

The various properties characterizing a polyelectrolyte chain and its surrounding solution combine to form a set of dimensionless parameters. Most importantly, the combination of b and l_b leads to the dimensionless charge density parameter ξ:

$$\xi = \frac{l_b}{b} = \frac{e^2}{4\pi\varepsilon\varepsilon_0 kTb} \tag{6}$$

In the study of polyelectrolytes, ξ plays a crucial role, as it provides the simplest well-defined physical property that can distinguish one polyelectrolyte from another or from a neutral polymer. Most polyelectrolytes possess a substantial charge density, a condition associated with ξ of order unity or greater. For a polyelectrolyte with a vinyl backbone and one charge per monomer unit, b is about 0.25 nm, and the value of ξ in water at room temperature is about 2.84; for DNA at the same solution conditions, b is about 0.17 nm (two phosphate charges per base pair step of 0.34 nm), and the value of ξ is about 4.2.

Counterion Condensation

In a variety of contexts, highly charged polyelectrolytes behave as if their net charge, or equivalently their average effective charge density, is less than the value determined by the number of ionizable units in the chain's chemical structure. Such behaviors imply that for energetic reasons some fraction of the counterions resides near or at the polyelectrolyte's "surface" where this opposite charge compensates for some of the charge associated with the chain's covalently attached ionic units. The hypothesized "condensation" of oppositely charged small ions reduces the polyelectrolyte's "apparent" or "effective" charge even when the polyelectrolyte's charge moieties are known to dissociate at the specified bulk solution conditions. Because the binding of condensed counterions arises from electrostatic forces in the solution phase, the condensed counterions do not form a classical Stern layer.

Although similar ideas were presented earlier and less rigorously (1–10), Oosawa (11,12) and Manning (13–16) independently formalized counterion condensation in the 1960s. Manning subsequently clarified and extended the original proposition to such a degree that the phenomenon is now frequently referenced as *Manning condensation* (17–24). Counterion condensation in its simplest form balances the entropy and electrostatic energy of small counterions located near a line or thin cylinder representation for a polyelectrolyte chain. Such descriptions for the local conformation of a polyelectrolyte chain have a long history (2,25); unfortunately, these geometric representations often muddy the extrapolation of theoretical predictions to flexible polyelectrolytes (26). Manning's first theoretical treatment of counterion condensation assumed that the polyelectrolyte's fixed

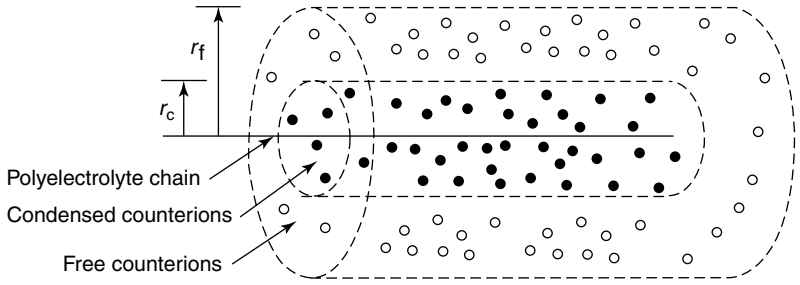

Fig. 1. Sketch of the two-phase model for counterion distributions near a line charge representation of a polyelectrolyte chain. Condensed (darkened circles) and free (open circles) ions occupy distinct regions bounded by r_c and r_f, respectively.

charge was smeared along the backbone (13–15), while later he developed an analogous treatment that assumed the charge was present as discrete point charges (19); the two treatments, both treating the chain as a line charge, produce nearly the same results.

Counterions released into solvent from a line charge sample a larger volume than before release, and therefore their entropy rises. However, entropy enhancement comes at a cost, as the further in outlying space the counterions explore the greater is their electrostatic energy. The condensation model splits counterions into two populations or states, those that are *condensed* and those that are *uncondensed* or *free*. The condensed ions possess only the freedom to move along and near the chain backbone while the free ions can move in a more or less unconstrained fashion within the solvent domain away from the backbone. Figure 1 provides a schematic of the postulated counterion populations near a line charge. The key issues for counterion condensation theories are the fraction of free ions and the extent to which condensed ions are localized. Some authors have found it useful to define two subpopulations of condensed ions (27): *site-bound condensed ions* are those in direct contact with a fixed charged group of the polyelectrolyte (no intervening water molecules) and *territorially-bound* condensed ions are those nonspecifically attached to the polyelectrolyte backbone, perhaps with their hydration layers intact. Only territorially bound condensed ions are able to wander readily along the chain's contour. Univalent condensed counterions are nearly always envisaged as territorially bound.

For univalent polyelectrolyte charge units and univalent counterions, Oosawa (12) argued that the concentrations of condensed and free counterions are related by an appropriate Boltzmann factor:

$$n_c = n_f \exp\left[\frac{-e\Delta\psi}{kT}\right] \tag{7}$$

where $\Delta\psi$ is the electrostatic potential difference between the regions containing the condensed and free ions (the potentials in both regions are assumed constant), and n_c and n_f are the respective (uniform) counterion concentrations (number per volume) in these regions. The bare charge density of the line charge is given

by e/b, but with condensation, the effective linear charge density is reduced to $\beta e/b$, where β is the fraction of free counterions. The electrostatic potential field near an infinitely long line charge in a dielectric (unscreened) medium decays logarithmically with radial distance from the line. Letting the outer radius of the region containing condensed ions be denoted r_c and the outer radius of the region containing free ions be denoted r_f, $\Delta\psi$ is estimated to be

$$\Delta\psi = -\frac{\beta e}{2\pi\varepsilon\varepsilon_0 b}\ln\left(\frac{r_f}{r_c}\right) = -\frac{\beta e}{4\pi\varepsilon\varepsilon_0 b}\ln\left(\frac{V_f+V_c}{V_c}\right) \tag{8}$$

where V_c and V_f are the volumes of the regions containing condensed and free counterions, respectively. Equations 7 and 8 can be combined to eliminate $\Delta\psi$:

$$\ln\frac{n_c}{n_f} = -\frac{e\Delta\psi}{kT} = \frac{\beta e^2}{4\pi\varepsilon\varepsilon_0 kTb}\ln\left(\frac{V_f+V_c}{V_c}\right) = \beta\xi\ln\left(\frac{V_f+V_c}{V_c}\right) \tag{9}$$

Counting the condensed and free ions located in volumes V_c and V_f,

$$\ln\left(\frac{1-\beta}{\beta}\right) = \ln\left(\frac{n_c V_c}{n_f V_c}\right) = \ln\frac{n_c}{n_f} + \ln\frac{V_c}{V_f} \tag{10}$$

Designating ϕ as the volume fraction of space containing only condensed ions, the two previous equations can be combined into an expression relating φ and β:

$$\ln\frac{1-\beta}{\beta} = \ln\frac{\varphi}{1-\varphi} - \beta\xi\ln\varphi \tag{11}$$

In the limit $\varphi \to 0$, the space occupied by condensed ions is small, and Oosawa demonstrated the existence of two types of solutions for this expression. When $\xi \leq 1$, a solution exists for $\beta \to 1$, and when $\xi > 1$, a solution exists for $\beta = 1/\xi$. The second statement establishes the presence of condensed counterions on a highly charged polyelectrolyte modeled in this fashion.

Counterion condensation offers the following quantitative predictions for effective polyelectrolyte charge: when $\xi < 1$, no ions condense and the effective charge density parameter ξ_{eff}, defined as the product $\beta\xi$, and the bare charge density parameter ξ are equal; when $\xi > 1$, sufficient counterions will condense onto the polyelectrolyte to lower its effective charge density parameter ξ_{eff} to unity. The condition $\xi_c = 1$ is viewed as the critical condition for the onset of counterion condensation for a polyelectrolyte in the presence of univalent counterions. The same trends apply to higher valence counterions except that the onset of counterion condensation is lowered to $\xi_c = |z_i|^{-1}$, and for $\xi > \xi_c$, $\beta = 1/|z_i|\xi$. Figure 2 sketches these predictions.

Although reaching the same predictions for the fraction of condensed counterions, Manning's derivations of counterion condensation are superior to the one just given (Oosawa's) in the sense that Manning's derivations allow ψ in the region of free ions to be screened in the Debye–Hückel approximation according to

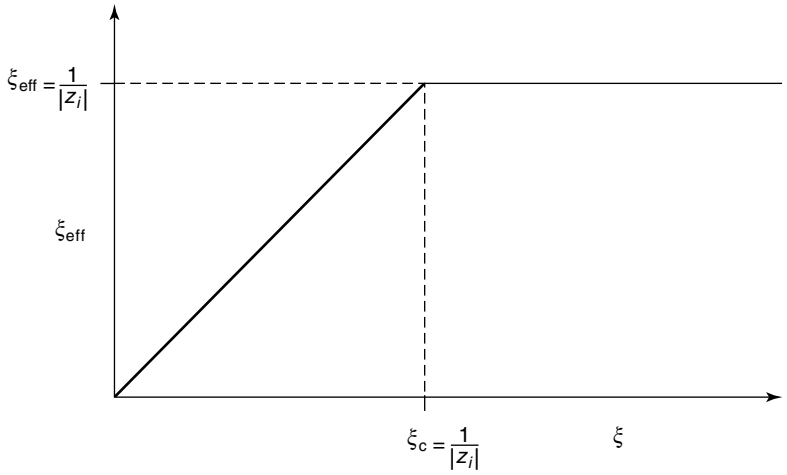

Fig. 2. Relationship of the effective linear charge density ξ_{eff} to the fixed linear charge density ξ as predicted by counterion condensation. The onset point of condensation ξ_c and the value of ξ_{eff} for $\xi > \xi_c$ both depend on the counterion valence z_i.

the value of κ^{-1}. Uncondensed ions accordingly contribute to screening, being included in the calculation of κ^{-1}, while condensed ions do not. Indeed, in a salt-free solution, only uncondensed ions create electrostatic screening, and accounting for counterion condensation, κ^{-1} is given as

$$\kappa^{-1} = \begin{cases} \left(4\pi N_a l_b f c_p\right)^{-1/2}, & \xi < 1 \\ \left(4\pi N_a b f c_p\right)^{-1/2}, & \xi > 1 \end{cases} \tag{12}$$

where c_p is the concentration (mole/volume) of polymer repeat units, and f is the fraction of these repeat units that bear charge; f equals unity for a polyelectrolyte homopolymer and less than unity for a copolymer possessing both charged and neutral repeat units. When I is small but nonzero and fc_p is large, κ^{-1} manifests contributions from both added electrolyte and dissociated counterions. Manning argued that the phenomenon of counterion condensation, although rigorously derived as a limiting law (all components infinitely dilute), satisfactorily describes polyelectrolyte solutions up to ordinary electrolyte concentrations.

Counterion condensation has detractors (28–34), who point to flaws in the concept's derivation, such as artificial subdivision of the counterions into two populations, inappropriate extrapolation of the Debye–Hückel approximation to regions of high electrostatic potential, and inconsistent treatment of counterions. The full nonlinear Poisson–Boltzmann equation offers a more rigorous way to interpret electrostatic phenomena in electrolyte solutions, but the physical picture obtained through this equation is different in some ways from the one suggested by condensation (21,34,35). In particular, a Poisson–Boltzmann analysis does not readily identify distinct populations of condensed and free counterions but rather a smoothly varying Gouy–Chapman layer. Nevertheless, Poisson–Boltzmann-based

analyses do find that in salt-free solutions there is a fraction of counterions equal to $1-\beta$ that cannot be fully diluted away from the chain at infinite chain dilution; the volume occupied by this trapped fraction is predicted by the Poisson–Boltzmann equation to be rather large, a feature inconsistent with the physical picture on which condensation is based (32). Zimm has pointed out that by applying this dilution criterion to identify condensed ions in salt-free solutions, all counterions are condensed on plane, none on a sphere, and some on a cylinder (36). Many experimental and theoretical studies support the general picture, if not the details, of the original counterion condensation concept (26,37–50).

Subdivision of counterions into condensed and uncondensed populations according to the Manning/Oosawa depiction is not unique. For example, a hypothetical "thermodynamically bound" counterion population can be defined to account for the deviations of polyelectrolyte solutions from thermodynamic ideality (35); this population is not equal to the condensed population. One can also use different definitions of *condensed*. The inflection point in the radial ion distribution, the Bjerrum length, and the radial distance over which the electrostatic interaction energy decays to kT have all been employed as alternative criteria for defining a condensed fraction (50).

According to a nonlinear Poisson–Boltzmann analysis, the initial radial decay of ψ from a cylindrical chain segment is much steeper than predicted by a Debye–Hückel analysis; see Figure 3 (28). The steep decay lessens at large distance, and ψ eventually adopts an asymptotic functional form compatible with a Debye–Hückel approximation. However, to superimpose across this distant region the predictions of the Poisson–Boltzmann analysis onto those formulated

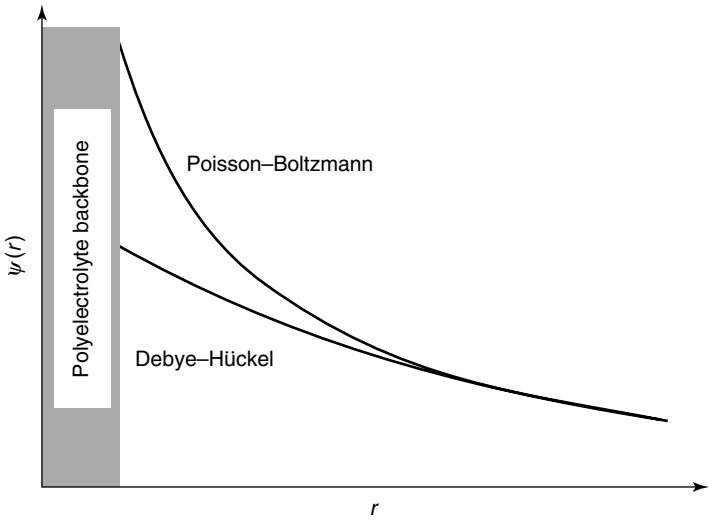

Fig. 3. Schematic plots of the decay of the electrostatic potential $\psi(r)$ near a polyelectrolyte chain of unspecified chain radius. The potential decay predicted by a nonlinear Poisson–Boltzmann analysis can be superimposed onto one predicted by a linearized Debye–Hückel approximation in the far field region if the surface potential of the Debye–Hückel is appropriately adjusted. However, in this case there remains strong deviation between the two approaches in the region nearer the chain.

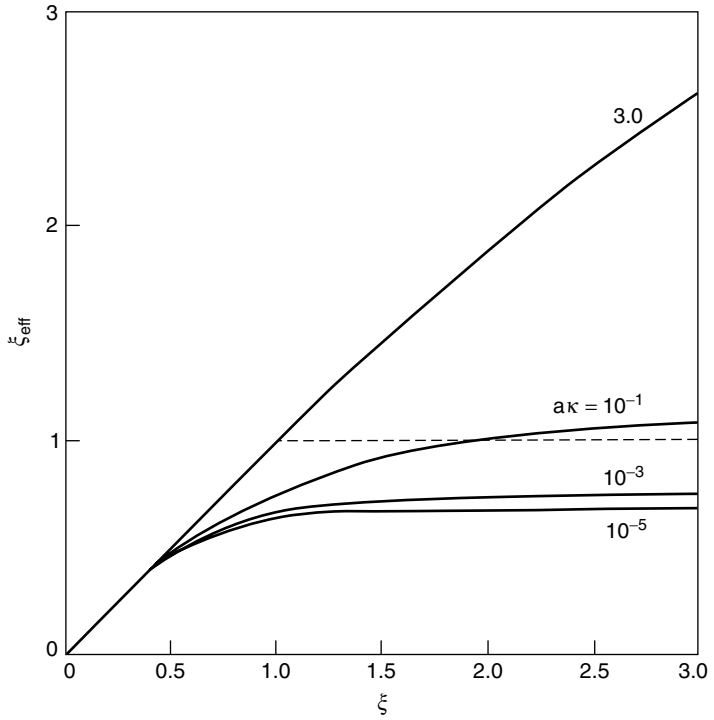

Fig. 4. Effective linear charge density ξ_{eff} of a charged cylinder derived by superimposing the far field (large r) Poisson–Boltzmann potential field onto the potential field predicted by use of the Debye–Hückel approximation. The solid lines correspond to different values of $a\kappa$, where a is the cylinder radius and κ^{-1} is the Debye length; the electrolyte is monovalent. For comparison, the counterion condensation prediction for ξ_{eff} is shown as a dotted line. Adapted from Ref. 51.

within the Debye–Hückel approximation, the linear charge density in the Debye–Hückel calculated must be reduced from the linear charge density in the Poisson–Boltzmann analysis. This reduced Debye–Hückel linear charge density can be interpreted, from the perspective of a distant observer, as defining the polyelectrolyte's "effective" or renormalized linear charge density (29,51); the same renormalization approach can be extended to other highly charged solutes (52). Figure 4 compares the effective linear charge density, as determined for a charged cylinder of radius a, to the effective linear charge density predicted by the Manning line charge model with counterion condensation. The two approaches agree in only the most qualitative manner, notably for $\xi \ll 1$. In this limit, where $\xi_{\text{eff}} = \xi$ according to both approaches, the Debye–Hückel approximation is valid throughout the entire solvent domain surrounding the polyelectrolyte. For $\xi \geq 1$, the effective linear charge and associated Debye–Hückel predictions apply only to phenomena associated with distant portions of the potential field.

Despite the nonrigorous theoretical status of counterion condensation, many of its predictions find direct support in experiment. As will be seen, properties such as osmotic pressure, ion activity coefficients, and counterion diffusion coefficient

can readily be understood if condensation is assumed. However, the same properties can almost always be successfully interpreted without the assumption of counterion condensation, perhaps after the greater analytical difficulty of a Poisson–Boltzmann analysis. Unfortunately, experiments designed to detect condensed counterions or to measure ξ_{eff} have led to ambiguous results. The status of counterion condensation in nondilute solutions remains an active area of research (48).

Single Chain Conformation in Dilute Solution

As reflected in size measures such as the mean radius of gyration R_g or mean-square end-to-end distance $\langle R^2 \rangle^{1/2}$, an isolated polyelectrolyte chain in dilute solution expands relative to an analogous neutral chain because of electrostatic repulsions between its similarly charged chain segments. Low molar mass electrolyte and counterions screen these repulsions, and in consequence, a flexible polyelectrolyte chain contracts as electrolyte is added (assuming the electrolyte does not contain ions that specifically bind to the chain, affecting the chain's charge in an unexpected way). At high enough electrolyte concentrations, the suppression of segment–segment repulsions suffices, at least for some polyelectrolytes, to transform a good solvent into one of marginal or poor quality. In the latter instance, precipitation or coacervation of the polymer may ensue, a process referred to as "salting out." Higher valence ions more effectively screen electrostatic repulsions and induce this phase separation at lower salt concentrations. Across the I range where flexible polyelectrolytes are normally used, 0.001–1.0 M, changes in chain conformation are significant, leading to variations of R_g of up to an order of magnitude. Polyelectrolyte expansion has immediate significance to numerous solution properties such as viscosity and diffusion coefficient.

Even the earliest discussions of polyelectrolyte conformation recognized that long-range electrostatic repulsions could induce chain stiffening and coil swelling (see CONFORMATIONS AND CONFIGURATION). In 1951, for example, Katchalsky wrote "...at low degrees of ionization the molecules are more or less hypercoiled rigid spheres ...they open up with increasing ionization and assume the form of kinked threads at about 10% ionization and, finally, at high degrees of ionization, stretch to rodlike filaments" (53). In a solution containing little added electrolyte, many investigators initially expected a conformational crossover, from electrostatically stiffened rod to electrostatically swollen Flory-like coil, when chain length exceeds κ^{-1} (2,54–57). Later investigations showed that polyelectrolyte size and conformation in solution present subtle complexities. Although there have been important recent theoretical contributions by Odijk, Skolnick, and Fixman (OSF) (58–63), Joanny and Barrat (64,65) and Muthukumar and co-workers (66–68), the quantitative matching of experimental data to theoretical predictions remains inconclusive except in a few limiting cases.

OSF Model. Extending two-parameter theories for neutral polymers to polyelectrolytes, the OSF approach envisages that electrostatic forces within a polyelectrolyte chain operate at two well separated length scales (51,58–63). At the short or segmental level, as sketched in Figure 5a, electrostatic repulsions between neighboring backbone charges increase l_p, stiffening the chain locally, while at the large or coil size level, as sketched in Figure 5b, electrostatic repulsions between

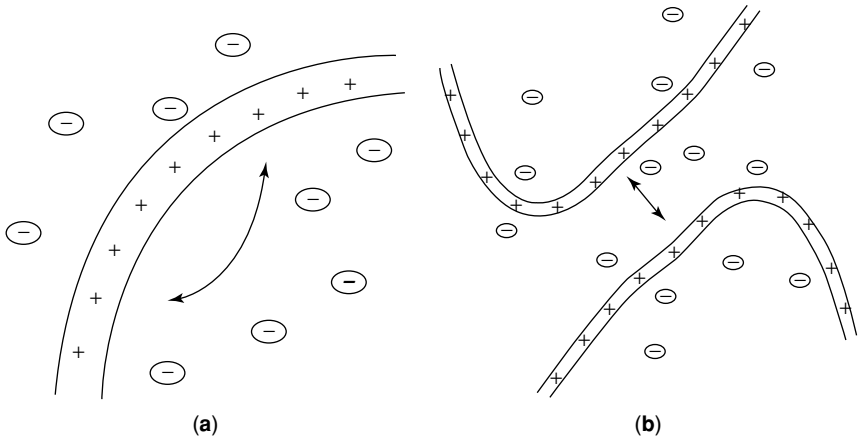

Fig. 5. Sketches illustrating the decomposition of electrostatic interactions into local and global impacts. In part **a**, repulsive forces between neighboring fixed charges on the chain cause backbone stiffening. In part **b**, repulsive forces between distant fixed charges on the chain backbone cause coil swelling. The presence of screening electrolyte ions reduces the magnitude of the repulsive forces.

segments widely separated along the backbone increase excluded volume, swelling the chain globally.

To model the first of these effects the OSF approach splits l_p into two contributions, one assigned from the equivalent neutral chain, defining the bare or intrinsic persistence length l_0, and one defined by electrostatic interactions, defining the electrostatic persistence length l_e,

$$l_p = l_0 + l_e \tag{13}$$

The value of l_0 is external to the OSF model while the value of l_e is determined by evaluating how local electrostatic interactions raise the bending energy of an extended chain segment of length L_s. The model defines the curvature of this segment through a function $\theta(s)$, where s is contour coordinate spanning $-L_s/2 < s < L_s/2$, and $\cos\,\theta(s)$ is given by the product $\boldsymbol{t}(s)\cdot\boldsymbol{t}(0)$, where $\boldsymbol{t}(s)$ is a unit vector tangent to the segment at position s. Allowing only small departures of the chain configuration from rod-like and imposing the Debye–Hückel approximation, the OSF treatment balances thermal fluctuations, intrinsic bending rigidity, and screened electrostatic interactions. At large s, the flexibility of the curve is captured in the mean-squared angle $\langle\theta(s)^2\rangle$:

$$\langle\theta(s)^2\rangle = \frac{s}{l_0 + l_e} \tag{14}$$

where

$$l_e = \frac{l_b}{4b^2\kappa^2} \tag{15}$$

The Debye–Hückel approximation strictly limits the OSF analysis to $\xi \ll 1$, but the analysis can reasonably be extended to more highly charged polyelectrolytes by invoking counterion condensation and substituting l_b for b. Then, for $\xi > 1$,

$$l_e = \frac{1}{4 l_b \kappa^2} \tag{16}$$

If the fluctuations in $\theta(s)$ are too great, ie, if the chain is too flexible, the perturbation approach of OSF fails. This breakdown occurs when $l_0 < b^2/l_b$. Consequently, the OSF model rigorously applies only to intrinsically stiff and highly charged polyelectrolytes such as DNA ($l_0 \approx 50$ nm). The original OSF calculation predicts l_e decays in inverse proportion to κ^2. Le Bret (69) and Fixman (70) improved the OSF model by evaluating electrostatics of a bendable chain segment within the broader framework of the Poisson–Boltzmann equation, finding that the decay of l_e at large I follows roughly κ^{-1} rather than κ^{-2}.

In addition to the local electrostatic stiffening manifested in l_e, the OSF approach considers how long range electrostatic repulsions impact excluded volume. Fixman and Skolnick (63) and Odijk and Houwaart (60) independently calculated an electrostatic contribution to excluded volume by adding a term to the binary cluster integral β_c associated with screened interaction between two charged, cylindrical chain segments. They both found that the electrostatic contribution to β_c is proportional to l_e^2/κ. From β_c, the expansion coefficient α, expressing the ratio of swollen chain size to unswollen chain size in the theta state, can be evaluated via the same expressions applied for neutral polymers.

Variational Models. Variational models address the conformations of inherently flexible polymers better than the OSF model. In the variational approach, a polyelectrolyte chain is postulated to conform to a simple flexible chain model that constrains how the conformation can rearrange; the overall free energy of the model is then minimized with respect to model parameters such as persistence length and chain size to obtain a mean-field chain description (71). The final result hinges on the choice of an appropriate chain model. Early studies assumed that a polyelectrolyte's segment distribution remains Gaussian or spherical as the molecule expands or contracts from a hypothetical uncharged theta state. Using these depictions, the free energy was expressed as a sum of terms arising from entropic elasticity and electrostatic segment–segment repulsions, the latter most often modeled using the Debye–Hückel potential.

More recently, Barrat and Joanny depicted a weakly charged, flexible polyelectrolyte as a semiflexible string of electrostatic subunits or "blobs" (64,65). Each blob is associated with a chain segment of sufficient length to balance electrostatic and elastic energies. Within a blob, the local chain statistics are unperturbed by electrostatic repulsions, but over larger length scales, blobs interact electrostatically, and the chain becomes extended if these interactions are strong. At values of κ^{-1} appropriate to salt-free solutions, the blobs arrange linearly in space to reduce electrostatic energy, and Barrat and Joanny argued that the chain radius R obeys the scaling relationship

$$R \sim l_b^{1/3} N \tag{17}$$

where the symbol $\sim$ implies proportionality. At small κ^{-1}, which imposes electrostatic screening between blobs, their variational calculation leads to the following relationships for l_p and R:

$$l_p \approx \kappa^{-1} \tag{18}$$

and

$$R \sim N^{3/5} \kappa^{-2/5} \tag{19}$$

In this instance, l_p can be termed only an "apparent" electrostatic persistence length since the variational procedure self-consistently calculates l_p and R. Muthukumar and co-workers approached the conformation of a flexible polyelectrolyte slightly differently, employing a variational procedure that combines the Debye–Hückel approximation with the Edward's path integral formalism (66–68). A similar formula was found for R in the limits of large and small κ^{-1} along with a crossover formula appropriate for intermediate κ^{-1}. At small values of κ^{-1}, the approach of Muthukumar and co-workers (66–68) can be rearranged to show an apparent persistence length

$$l_p \sim \kappa^{-4/5} \tag{20}$$

with a different dependence on κ^{-1} than predicted by Barrat and Joanny (64,65).

The large κ^{-1} result of both groups corresponds to an intuitive picture that a polyelectrolyte chain unravels into an extended linear conformation when electrostatic repulsions between segments are strong enough. Although unraveled, the chain retains local conformational freedom and remains less than fully stretched ($R \ll L$). The large κ^{-1} formula given above was first suggested in 1948 by Katchalsky and co-workers (54,72) and Hermans and Overbeek (56) and later clarified by de Gennes and co-workers (73) and Pfeuty (57). Similarly, the low κ^{-1} formula result shows that strongly screened electrostatic repulsions between segments can be interpreted as an increase in the chain's excluded volume (67,74). Indeed, using variational procedures, Hermans and Overbeek (56) and Flory (55) half a century ago derived the same small κ^{-1} formula for R; Richmond (74) and Pfeuty (57) more recently reported derivations.

Electrostatic stiffening dictates the persistence length of an inherently flexible polyelectrolyte, and so both the Joanny and Barrat as well as the Muthukumar values of l_p can legitimately be compared to the OSF value of l_e. Note the different dependences of the quantities on κ. Li and Witten criticized variational approaches (75), arguing that short wavelength bending modes should not alter the OSF formula for l_p except to the extent there may be weak logarithmic corrections. Other variational approaches have been described, leading to somewhat different formulas for l_p and R (76–81). Dobrynin and co-workers recently developed a scaling theory for the dilute and semidilute solution conformations of hydrophobic polyelectrolytes, those that dissolve solely because of their charges; these polyelectrolytes were predicted to decompose into a necklace-like shape of compact beads separated by narrow strings (82–84). Simulation results relevant to polyelectrolyte conformation are discussed in a later section.

The same electrostatic forces that influence chain conformation in dilute solution affect the thermodynamic interactions between chains, and these alterations are most directly reflected in the magnitude of the second virial coefficient A_2. As expected, when repulsive interactions are heightened, A_2 in polyelectrolyte solutions is large and positive. The magnitude of A_2 falls sharply upon increasing addition of electrolyte. Values of A_2 derived via an OSF-type model for polyelectrolyte conformation compare well to experimental data for both stiff and flexible polyelectrolytes when two closely approaching polyelectrolyte chains are allowed to reduce their mutual overlap by flattening (85,86).

Numerous scattering methods, along with diffusion, viscosity, birefringence, spectroscopy, and microscopy methods, have been employed to measure the structure of polyelectrolyte chains in dilute solution. A discussion of these methods is not attempted here. Most methods are employed in the same way as for neutral polymers. Neutron scattering makes accessible measurements of polyelectrolyte chain structure in nondilute solutions (87).

Figure 6 displays experimental measurements of l_e for two well-characterized samples of the inherently flexible cationic polyelectrolyte poly(2-vinyl-pyridiniumbenzyl bromide) (80). Data for l_e vs concentration c_s of an added 1:1 electrolyte are compared to predictions of the OSF model and a numerically evaluated variational model that yields l_p slightly dependent on chain length. Clearly, none of the proffered models offer quantitative agreement with experimental data. As noted by several investigators (88–90), the OSF model overpredicts the drop of l_p as electrolyte is added to a flexible polyelectrolyte solution. For

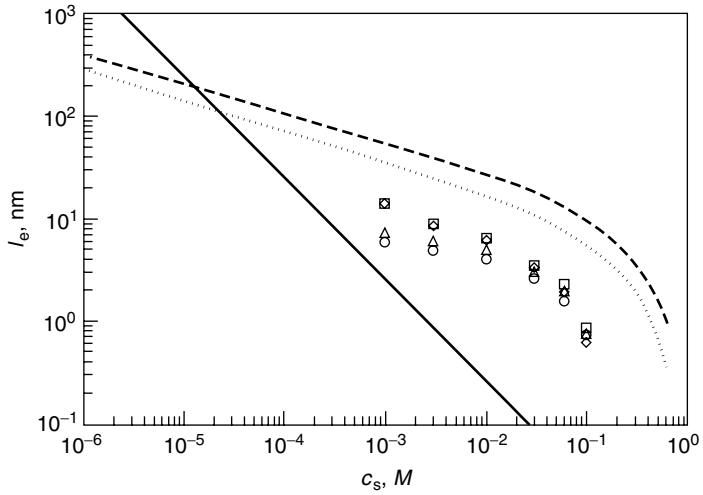

Fig. 6. Experimental data and theoretical predictions of the influence of added monovalent electrolyte at concentration c_s on the electrostatic persistence length l_e of poly(2-vinyl-pyridiniumbenzyl bromide). The data were obtained for chains of length L equal to 885 nm (circles from dynamic light scattering and diamonds from static light scattering) and 2240 nm (triangles from dynamic light scattering and squares from static light scattering), although no systematic influence on L is noted. The solid line represents the OSF theory for both chain lengths, and the dotted ($L = 885$ nm) and dashed ($L = 2240$ nm) curves provide l_e predictions from a variational calculation. Adapted from Ref. 80.

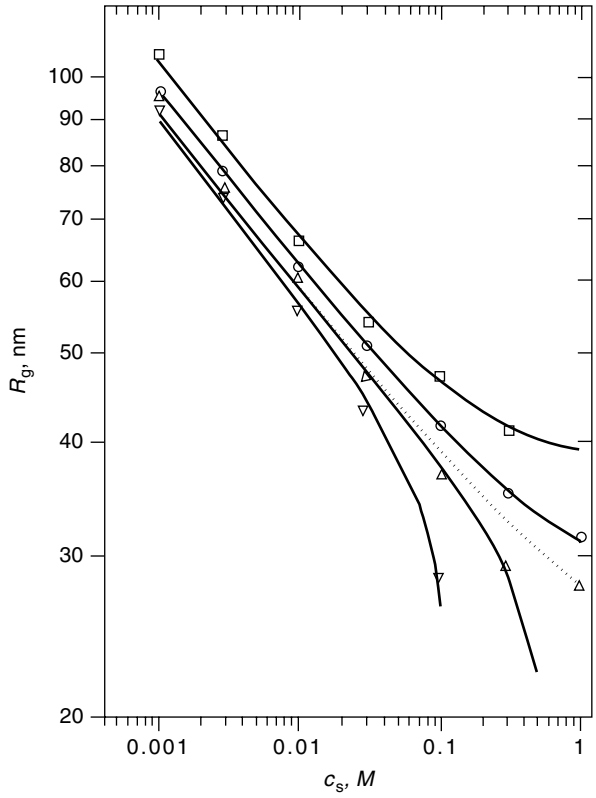

Fig. 7. Dependence of radius of gyration R_g on added electrolyte concentration c_s for 55–58% ethyl quaternized poly(2-vinyl pyridine) of chain length $L = 1000$ nm. Different symbols correspond to different counterions: F^- (squares), Cl^- (circles), Br^- (upward triangles), and I^- (downward triangles); the co-ion in each case is Na^+. The curves are fits to a theory described in the original reference. Adapted from Ref. 67.

low values of I, data for flexible polyelectrolytes approximately follow $l_p \sim \kappa^{-1}$ rather than $l_p \sim \kappa^{-2}$, a feature successfully captured in many variational calculations. Comparison of theoretical and experimental values of l_p for an inherently stiff polyelectrolyte is presented later; in this instance, the OSF model provides an excellent theoretical description.

The dependence of R_g on c_s is shown in Figure 7 for a high M sample of poly(2-vinyl-pyridiniumethyl bromide) (67). During a 3-orders-of-magnitude increase of c_s, R_g drops by approximately a factor of 4. The drop is sensitive to counterion identity, especially when c_s exceeds 0.1 M. The same investigation found that co-ion identity was unimportant to R_g over the same c_s range. Variational models that allow for hydrophobicity of segments and variable fractions of condensed counterions were reported to capture these trends well (67). Other investigators (89,91,92), however, were able to explain similar trends successfully through the OSF model, and still others reported trends inexplicable through any of the existing models (93); so the correct approach for flexible polymers remains uncertain.

Structure of Semidilute and Concentrated Polyelectrolyte Solutions

The properties of a single polyelectrolyte chain can be readily examined only in dilute solution, where on average, individual polymer molecules are widely separated. Most technological applications employ polyelectrolytes in semidilute or concentrated solutions, environments in which the polyelectrolyte coils overlap and perhaps entangle with one another. Unfortunately, many of the properties of semidilute and concentrated polyelectrolyte solutions are not well understood. The crossover from dilute to semidilute occurs at a value of c termed the critical overlap concentration c^*. As with neutral polymer solutions, the crossover is not abrupt, and so c^* is properly interpreted as a mean value characterizing a broad c range. The overlapping of polyelectrolyte chains at c larger than c^* causes solution thermodynamic properties to lose their dependence on polyelectrolyte molecular weight M, and instead, these properties depend on the solution's correlation length ξ_s, effectively the average mesh size of the fluctuating network formed by overlapping chains (94). At c^*, $\xi_s \approx R$, and above c^*, $\xi_s < R$. In semidilute or concentrated polyelectrolyte solutions, interactions between segments along the chain backbone separated by distances greater than ξ_s are screened by the presence of interposing segments attached to other chains.

Closely packed but nonoverlapped chains fully occupy a polymer solution at c^*, and so the concentration of segments inside any one chain domain approximately matches the solution's bulk segment concentration. The value of c^* thus can be estimated as the ratio of M to the average volume pervaded by a chain in dilute solution. Ignoring unimportant order unity geometric prefactors,

$$c^* \approx \frac{M}{N_a R^3} \tag{21}$$

The strong dependence of R on added electrolyte concentration implies that c^* for polyelectrolytes can vary greatly with solution conditions. Especially for salt-free polyelectrolyte systems, electrostatically driven chain swelling can strongly lower c^* from values expected for a neutral polymer. Dilute, salt-free polyelectrolyte systems are for this reason rarely examined. Dautzenberg (95) provided a model calculation of c^* for sodium poly(styrene sulfonate) of degree polymerization 10^4 dissolved in water without any added low molar mass electrolyte; using versions of equations 17 and 21 with added prefactors (73), he found $c^* \approx 6 \times 10^{-7}$ g/cm^3. However, applying the OSF model (58) in a similar calculation for a solution containing a relatively modest level of added monovalent electrolyte, $I = 0.01\ M$, he obtained $c^* \approx 6 \times 10^{--4}$ g/cm^3, an enhancement of c^* by 3 orders of magnitude.

As the previous section illustrated, different theories provide different values of R, making a theoretical assessment of c^* problematic. Substituting measured value of M and R into equation 21 offers the best way to determine c^*. Although flexible polyelectrolyte coils overlap above c^*, these coils are not necessarily entangled. As demonstrated by Boris and Colby (96) through measurements of the c dependence of viscosity, the polyelectrolyte concentration c_e required for onset of entanglement may be substantially higher than c^*.

To understand how chain–chain interactions affect polyelectrolyte solution properties at concentrations above c^*, many investigators have developed "cell" models that assign to each polyelectrolyte chain a nonoverlapping, concentration-dependent volume (7,25,41,97). Most often, the chains are regarded as infinitely long thin cylinders or lines spread uniformly in space but mutually aligned. Each chain then lies on the centerline of a cylindrical volume that possesses an outer radius inversely proportional to $c^{-1/2}$. For one common model, the Poisson–Boltzmann cell model, the potential field and ion distributions are solved within a single cell by assuming that radial gradients vanish at the volume's outer radial surface. From these distributions, both thermodynamic and dynamic properties of the polyelectrolyte and its surrounding electrolyte ions can be solved without further consideration of neighboring chains. Although providing insights and qualitative trends, cell models have a major drawback in their assumption that polyelectrolytes assemble into identical, space-filling cells. Such ordered structures are rarely, if ever, found in real polyelectrolyte solutions.

The understanding of structure in dilute, semidilute, and concentrated polyelectrolyte solutions remains incomplete. For polyelectrolyte systems that do not develop long-range order (ie, form mesophases) Odijk (98), Pfeuty (57), and de Gennes and co-workers (73,99) first proposed theoretical models for electrostatically induced solution structure, and others subsequently built upon their works (77,83,100–106). Dobrynin and co-workers developed a generalized scaling formalism for predicting thermodynamic and transport properties of both dilute and semidilute solutions of flexible polyelectrolytes (83). Rather complicated state diagrams distinguishing a variety of solution regimes (up to 10) were proposed by these investigators and others (49,65,77,84,107,108). The complexity of such diagrams arises from the interplay of intrinsic chain stiffness, electrostatic chain stiffness, chain entanglement, screening by electrolyte, intrinsic backbone hydophobicity, concentration of dissociated counterions, etc, as temperature, polymer concentration, and electrolyte concentration vary. At the current time, experimental methods have not caught up with theory, and the proposed state diagrams have not been confirmed.

Electrostatic repulsions in nearly salt-free solutions create sufficient order for the appearance of a well-defined peak in the low angle scattered intensity (107–114). In a plot of scattered intensity versus scattering vector q, Figure 8 displays how these peaks vary with c (114). Analogous peaks do not occur for flexible neutral polymers. When polyelectrolyte chains are dilute (but for c not too far below c^*), the angular position of the peaks is associated with the average distance d between physically separated chains; d is measured and predicted to be proportional to $c^{-1/3}$ (73,107,115). The spacing arises from the electrostatically induced liquid-like order in chain locations created when the electrostatic energy imposed through neighboring chains exceeds any given chain's thermal energy. When the polyelectrolyte chains are semidilute, the scattering peak's angular position reflects the value of ξ_s; ξ_s is measured and predicted to be proportional to $c^{-1/2}$ (57,73,99,101,107,110,111,113,115,116). In the so-called isotropic model, the scattering peak for a semidilute polyelectrolyte solution is attributed to the presence of a correlation hole of size κ^{-1} about each chain segment.

Considerable experimental evidence points to the presence of attractive electrostatic interactions between like-charged polyelectrolytes in simple electrolyte

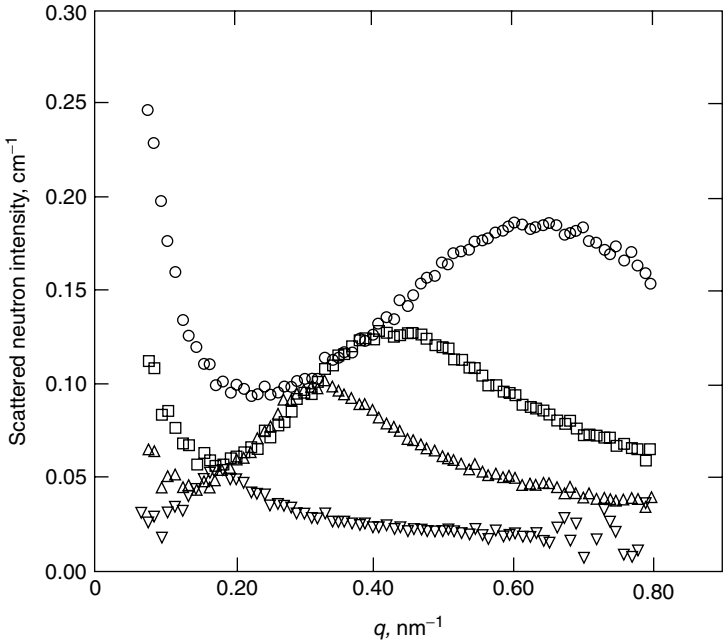

Fig. 8. Small-angle neutron scattered intensity plotted versus scattering vector q for salt-free deuterium oxide solutions of poly(2-vinyl pyridine), which possessed a molecular weight $M = 281{,}000$ g/mol prior to 45% methyl quaternization. Four different polymer concentrations were examined: 22 g/L (circles), 8.8 g/L (squares), 4.5 g/L (upward triangles), and 2.2 g/L (downward triangles). Adapted from Ref. 114.

solutions (114,117,123). One type of evidence is an upturn in scattered intensity in the low q range, as demonstrated in Figure 8. Attractive interactions would explain the aggregates or ordered domains that are often reported in semidilute and concentrated polyelectrolyte solutions. Because attractive interactions are not consistent with standard mean-field formalisms (Poisson–Boltzmann, Debye–Hückel) for electrostatic interactions, numerous efforts have been undertaken to augment these formalisms so as to admit such interactions (11,33,104,124–134). No consensus has yet been reached about the validity of extended formalisms. Indeed, the existence of attractive interactions between polyelectrolytes in a solvent containing only monovalent electrolyte ions remains a subject of debate. Experimental evidence for attractive electrostatic interactions in a solvent containing multivalent electrolyte ions, however, is overwhelming. For the multivalent case, attractions have been explained through coupled fluctuations in ion density (11,12,124) or short-range correlated order in condensed ions (132). Several theories predict that in more concentrated polyelectrolyte systems attractive electrostatic interactions might derive from potentials of mean force even when the pairwise interaction potentials are purely repulsive (104,133).

Understanding of structure in polyelectrolyte solutions at c well above c^* is poor, with many predictions but little experimental support for additional transitions as c increases (65,108). Characteristic features in rheology and scattering

data reveal transitions associated with the onset of chain entanglement and the crossover from semidilute to concentrated (96,108). Even under salt-free conditions, electrostatic interactions in concentrated solutions will be screened heavily by liberated counterions, leading to structure and properties comparable to a swollen neutral polymer solution. Experimentally, preparing concentrated, homogeneous polyelectrolyte solutions is usually difficult.

Solubility and Phase Behavior of Polyelectrolyte Solutions

Polyelectrolyte solutions can display a complex phase diagram strongly affected by the type and concentration of any added electrolyte (135–141). Figure 9 plots the phase behavior of sodium poly(vinyl sulfonate) in aqueous solutions varying in the concentration of added sodium chloride (135); the ordinate of the plot is the cloud point temperature T_p, indicating the first appearance of cloudiness as the solution is cooled. In this monovalent electrolyte, the polymer roughly obeys a standard, Flory–Huggins-type phase behavior, as indicated by the presence of

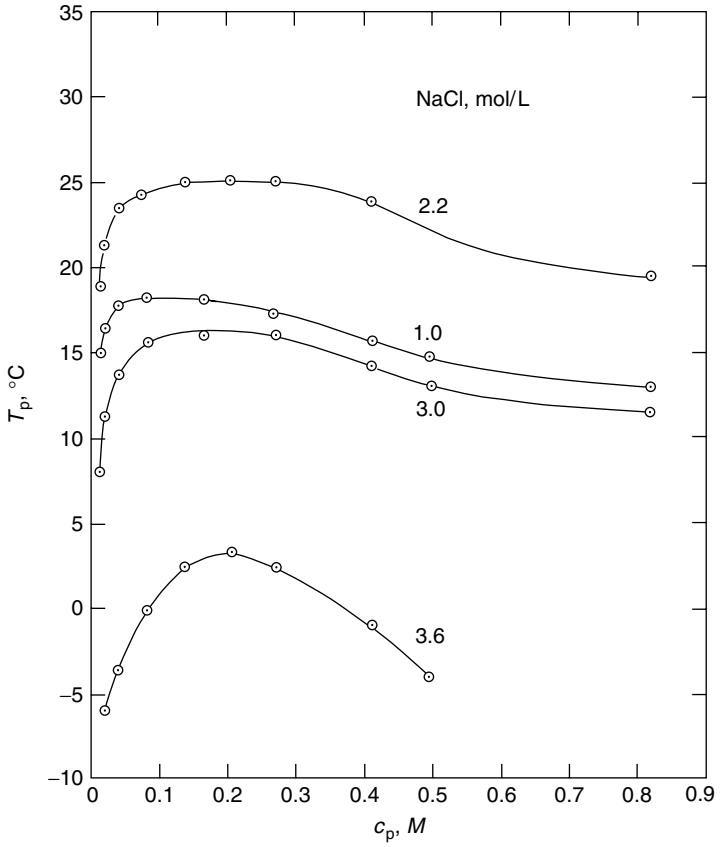

Fig. 9. Phase separation temperatures T_p plotted versus the concentration c_p of sodium poly(vinyl sulfate) at constant concentrations of NaCl. Adapted from Ref. 135.

an upper critical solution temperature at all electrolyte concentrations. A closer examination reveals less expected trends, such as an increase and subsequent decrease of the critical temperature with increasing electrolyte concentration. The rise of the critical temperature with increasing electrolyte concentration can be rationalized in terms of weakened electrostatic repulsions between polyelectrolyte chains when the electrolyte concentration is high. As electrostatic repulsions weaken, the core attractive segment–segment interactions of the uncharged polymer begin to dominate and polyelectrolyte insolubility eventually ensues (ie, salting out). In the absence of charge, most polyelectrolytes are hydrophobic, and so this sort of insolubility is expected but not always observed. The resolubilization or "salting in" of this polymer at higher sodium chloride concentration is more difficult to explain, although such resolubilization is not rare. Resolubilization may reflect specific chemical interactions of electrolyte ions with polyelectrolyte or development of a dense counterion layer near the backbone that overcompensates the polyelectrolyte's fixed charge. Computer simulations of ion distributions near polyelectrolytes often observe spontaneous overcharging at high electrolyte concentrations due to short-range correlations in ion placement.

Reliable theories that accurately correlate or predict polyelectrolyte phase diagrams are lacking. Letting electrostatic excluded volume between chain segments be modeled at the level of the Debye–Hückel approximation, a modified or effective Flory–Huggins parameter χ_{eff} can be determined via the random phase approximation (141):

$$\chi_{\text{eff}} = \chi_0 - \frac{\pi l_b f^2}{2\kappa^2 l_0^3} \tag{22}$$

where χ_0 is the interaction parameter in the absence of electrostatic interactions, a large and positive quantity for a polyelectrolyte with a hydrophobic backbone. The negative sign of the second term, which accounts for the added excluded volume derived from electrostatic interactions, confirms the tendency of repulsive forces among chain segments to heighten solubility. Substituting χ_{eff} into the standard Flory–Huggins model, shifts in the phase envelope of the type noted in Figure 9 at low electrolyte concentration can be qualitatively predicted. However, the same approach does not predict the observed change of phase envelope shape or the salting-in effect found at higher electrolyte concentrations. The Flory–Huggins model tacitly assumes the presence of only short-range forces, and so discrepancies arising from use of the model in the presence of long-range forces are not surprising.

Relatively few complete polyelectrolyte phase diagrams have been determined, and thus the universality of experimental trends remains uncertain. Even neutral water-soluble polymers display diverse phase diagrams, exhibiting in many instances a lower critical solution temperature due to entropy changes of solvent associated with hydrogen bonding; similar phenomena might be expected of polyelectrolytes. By plotting c_s vs c_p at fixed temperature, Ikegami and Imai identified two types of solubility behavior in polyelectrolyte solutions containing added electrolyte (137). In the first type, values of c_s required for phase separation are nearly independent of c_p (H-type). In the second, values of c_s at the onset of phase separation increase linearly with c_p (L-type). Subsequently, Axelos and

co-workers found that some systems exhibit intermediate behavior, the phase separation onset displaying a minimum on a c_s vs c_p plot (I-type) (138). More vexing, Prabhu and co-workers observed H-type behavior at low c_p and L-type behavior at high c_p (141), while Eisenberg and Ram Mohan reported still more complex trends (135). The phase-separated region can be characterized by the appearance of a transparent, polymer-poor liquid phase in equilibrium with a polymer-rich phase variously possessing the character of a solid precipitate, liquid, dispersion of microgel aggregates, or uniformly dense gel.

Trends in polyelectrolyte phase behavior and solubility are more complicated when solutions contain multivalent counterions. For poly(styrene sulfonate), Delsanti and co-workers demonstrated that both salting out and salting in occur for a wide range of added multivalent electrolyte types (139). The two-phase region they observed at intermediate concentrations of multivalent ion widened as valence increased and narrowed (and even vanished) as the concentration of a second, added monovalent electrolyte increased. Many investigators have discussed the possibility that multivalent counterions have an ability to form inter- and/or intramolecular ionic bridges or cross-links between polymer segments (95,136,142–144). However, phase separation requires an attractive force between chains, and the origin of this attraction remains mysterious. In addition, factors such as the intrinsic solubility of the analogous small electrolyte species, as defined by the chemical identity of the fixed charged unit and the multivalent counterion, are obviously also relevant (142). The solubility of polyelectrolytes, regarded as the maximum polyelectrolyte concentration before a gel or precipitate first forms, is nearly always lowered substantially in the presence of a substantial concentration of multivalent counterion.

Certain polyelectrolyte interactions induced by multivalent ions appear special. An important example is the condensation of dilute DNA chains by multivalent ions such as manganese, cobalt hexamine, and oligomeric polyamines (spermidine, spermine) (144–148). In this context, *condensation* refers to the compaction of a swollen DNA coil into a dense globule or toroid. The same multivalent ions cause DNA solutions to gel when DNA concentrations are high. Although some argue that periodic ordering of multivalent counterions in the space between aligned chains drives DNA to condense, others maintain that correlated ion fluctuations in this region cause condensation (11,128,130,149). A second special polyelectrolyte interaction is that between polyelectrolytes and oppositely charged organic dyes, which can either stack along the backbone or occupy preferred chain binding sites (150). A large photochromic shift in the dye's adsorption spectra often arises from stacking. Lastly, oppositely charged surfactants induce polyelectrolyte precipitation when the net surfactant charge approximately matches the net polyelectrolyte charge. Polyelectrolyte complexations resulting from these special interactions appear fundamentally different than the more universal electrolyte effects discussed here.

Thermodynamic and Transport Properties of Polyelectrolyte Solutions

Viscosity. At low c, the solution viscosity η can follow remarkably different trends for a polyelectrolyte than for a neutral polymer. With a neutral polymer,

the c dependence of specific viscosity η_s, defined as

$$\eta_s = \frac{\eta - \eta_0}{\eta_0} \tag{23}$$

where η_0 is the solvent viscosity, obeys the standard Huggins formula

$$\frac{\eta_s}{c} = [\eta] + k_H[\eta]^2 c \tag{24}$$

where $[\eta]$ is the intrinsic viscosity and k_H is the Huggins coefficient. The contribution to η_s/c due to isolated polymer chains is captured in $[\eta]$, while the contribution due to binary chain–chain interactions is captured in k_H. Contributions from higher order chain–chain interactions are neglected in the Huggins formula but can safely be ignored when c is below c^*. Molecular theories show that for neutral chains $[\eta]$ is proportional to the average hydrodynamic volume V_h pervaded by a single chain divided by the chain's molecular weight M, ie, $[\eta] \sim V_h/M$ (151). Further, V_h is proportional to the cube of the chain's hydrodynamic radius: $V_h \sim {R_h}^3$. Finally, R_h can often be expressed as a power law in M, ie, $R_h \sim M^\nu$, when M is sufficiently large. Putting these statements together, $[\eta]$ can generally be connected to M as $[\eta] \sim M^{3\nu-1}$. At large M, the excluded volume parameter ν provides an indication of chain conformation: for a dense spherical globule, $\nu = 1/3$; for a flexible chain in a theta solvent, $\nu = 1/2$; for a flexible chain in a good solvent, $\nu \approx 3/5$; and for a rod-like chain, $\nu = 1$.

At high concentrations c_s of added electrolyte, electrostatic interactions between polyelectrolyte chain segments are heavily screened, and polyelectrolyte solutions behave similarly to neutral polymer solutions, with the c dependence of η_s/c in accord with the Huggins formula. At somewhat smaller values of c_s, the expansion of polyelectrolyte chains by intramolecular electrostatic repulsions is reflected in elevated values of $[\eta]$, but again, η_s/c follows the Huggins formula. When there is little or no added electrolyte, the situation becomes more complex. As shown in Figure 10, plots of η_s/c vs c for solutions of poly(styrene sulfonate) containing low concentrations of sodium chloride display a pronounced maximum. The presence of the maximum is inconsistent with the Huggins formula. As shown in the same figure, varying c_s causes the position of the maximum to move in a way that maintains rough equality between the concentrations of liberated counterions and added electrolyte.

To model the anomalous behavior of η_s/c at low c_s, Fuoss and Strauss (154–157) long ago proposed an empirical relationship to replace the Huggins formula:

$$\frac{\eta_s}{c} = \frac{A}{1 + Bc^{1/2}} \tag{25}$$

where A and B are constants. Diluting a polyelectrolyte solution with solvent aliquots containing a low but constant value of c_s reduces I because polyelectrolyte solutions at lower c contain correspondingly fewer counterions. Configuration-based models for trends in η_s/c attribute the anomalous polyelectrolyte viscosity behavior to electrostatically driven chain expansion as I changes (157–162). In

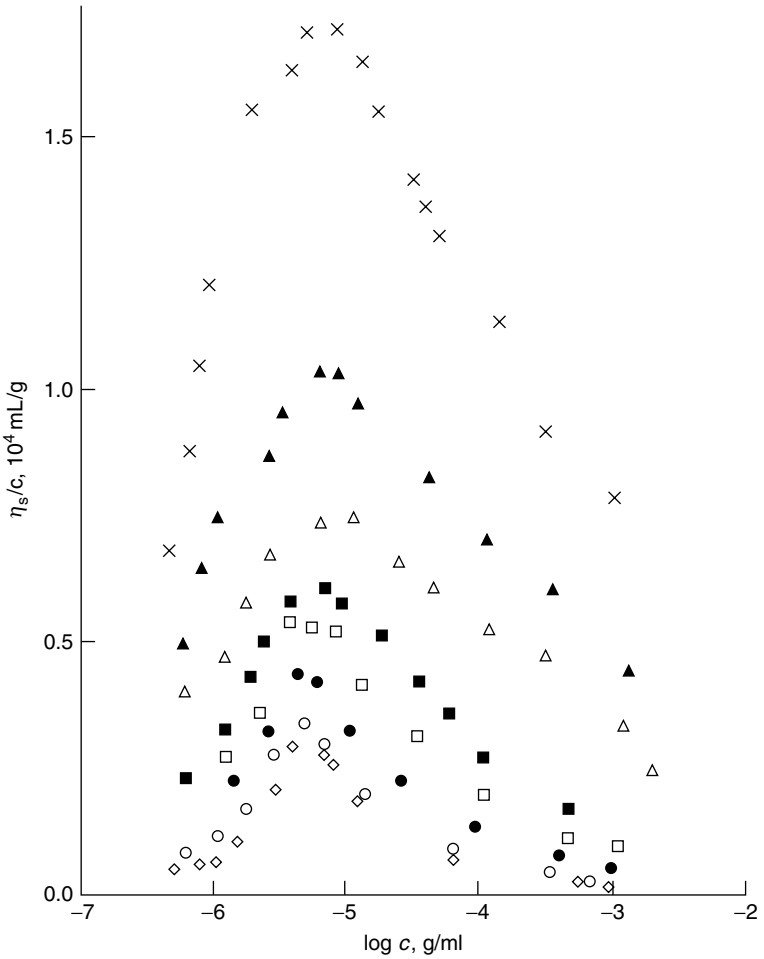

Fig. 10. Molecular weight M dependence of reduced viscosity η_s/c plotted against polymer concentration c_p for sodium poly(styrene sulfonate) in nearly salt-free solution. M, g/mol: × 690,000; ▲ 345,000; △ 212,000; ■ 177,000; □ 138,000; ● 88,000; ○ 31,000; ◇ 16,000. Adapted from Ref. 152, which uses data from Ref. 153.

the limit of infinitely small c, some have suggested that chains in salt-free solution become rod-like (157–159). This expectation is supported by the observed proportionality of A with the second power of M (163), a feature consistent with a solution containing rods. Also, the configuration-based models suggest that the maximum in η_s/c can be eliminated by adding sufficient electrolyte ions during dilution to compensate for the loss of liberated counterions, a procedure termed *isoionic dilution*. Indeed, the maximum disappears when isoionic dilution is followed (164,165). This last observation is important, as measurements of $[\eta]$ are important for polyelectrolyte characterization, and isoionic dilution appears the only method that can provide reliable values of $[\eta]$ at low c_s.

The Fuoss–Strauss formula has obvious flaws, perhaps most significantly, it does not predict the observed maximum in plots of η_s/c vs c. Strong evidence also

suggests that polyelectrolytes in salt-free solution do not fully extend at low c and that electrostatic interactions between chains influence η significantly (166–168). Other configuration-based models have subsequently appeared, incorporating increasingly sophisticated molecular dynamics to explain the drop of η_s/c at finite c (73,83,100,103,162). Many of these models recognize that in the region where η_s/c drops, c lies near or above c^*, and so an accounting of configurational constraints associated with chain–chain interactions may be needed.

Competing, nonconfiguration-based models for polyelectrolyte viscosity also have appeared, motivated largely, but not entirely, by observations that rigid, charged colloids also display a maximum in plots of η_s/c vs c (169–176). In the colloidal systems, the maximum is attributed to the impact on viscosity of long-ranged interparticle electrostatic interactions, a phenomenon sometimes termed the *secondary electroviscous effect*, which can be assessed at various levels of approximation by mode-coupling theories (177). From this perspective, the linear Huggins equation fails at low c_s because the primary interactions between chains are electrostatic, not hydrodynamic as this equation assumes; the interpretation is also consistent with the appearance and c dependence of the small-angle scattering peak observed for dilute polyelectrolytes under the same solution conditions. Transforming the mode-coupling principles to polyelectrolytes, Rabin and co-workers (153,170–172) proposed a phenomenological equation:

$$\frac{\eta_s}{c} = \frac{Ac}{\kappa^3} \tag{26}$$

where A is a constant proportional to the product $R_h l_b^2$. In this equation, a maximum in η_s/c derives from the c dependence of κ^{-1}. At low c, most electrostatic screening is by added or ambient electrolyte, but at high c, most electrostatic screening is by liberated counterions; the maximum in η_s/c occurs in the crossover region where both contributions are almost equal. For c below the maximum, the invariance of κ^{-1} implies that meaningful extrapolations to obtain $[\eta]$ are possible although perhaps difficult. For c above the maximum, a decay of η_s/c proportional to $c^{-1/2}$ is found, consistent with the Fuoss–Strauss formula. The location of the maximum itself is independent of M, consistent with experiment. Although lacking in rigor, the preceding formula accounts for most observed trends. The formula may fail to predict the impact of chain topology on η_s/c in the low c regime (161,178). Newer conformational models that do not rely on the secondary electroviscous effect can also rationalize a peak in η_s/c under certain conditions (160,162).

The dependence of $[\eta]$ on c_s has been correlated with various theoretical and phenomenological expressions, of which two are shown below (76,164,179,180):

$$[\eta] = [\eta]_\infty + Bc_s^{-1/2} \tag{27}$$

$$[\eta] = [\eta]^0 \left(\frac{c_s}{c_s^0}\right)^{-m} \tag{28}$$

where $[\eta]_\infty$ is the asymptotic value of $[\eta]$ at high c_s, and $[\eta]^0$ is the value of $[\eta]$ at an arbitrary reference value of c_s designated $c_s{}^0$. The constant B incorporates

nonelectrostatic contributions to excluded volume and chain stiffness. Values of the parameter m measured by experiment vary between 0.06 and 0.6, with higher values associated with more flexible polyelectrolytes (152). The two expressions obviously can lead to significantly different dependences of $[\eta]$ on c_s. At large enough M, relationships between $[\eta]$ and M for polyelectrolytes follow the standard Mark–Houwink formula

$$[\eta] = kM^a \tag{29}$$

which introduces the semiempirical Mark–Houwink coefficients k and a ($=3\nu-1$). At lower values of M, the complex conformational trends of polyelectrolytes make a simple scaling formula of this type less useful. As per the previous discussion, for characterization purposes, $[\eta]$ should be measured at high c_s, if possible, or alternatively by isoionic dilution at low c_s. Many values of k and a have been tabulated for polyelectrolytes (181), facilitating the determination of M by measurements of $[\eta]$; experimental methods and analysis are exactly as for neutral polymers. At large M, extreme care in the experiment may be needed to avoid artifacts due to shear-thinning of η; such shear-thinning is a larger problem for polyelectrolytes than neutral polymers, especially when c_s is small (165,168).

Little effort has been expended for polyelectrolytes to measure rheological properties other than η at values of c near and below c^*. Several measurements of the storage and loss modulus for dilute flexible polyelectrolyte solutions have been interpreted in terms of shifts in the longest chain relaxation time as the polyelectrolyte expands and contracts (182,183). The c dependence of η reflects the onset of chain entanglement well above c^* through a sharp upward transition in slope (96,184). In the semidilute but unentangled region, measured linear viscoelastic properties can be interpreted via a modified Rouse theory, and at the higher concentrations associated with chain entanglement, these properties can be interpreted via a modified reptation theory (184). Conditions that govern polyelectrolyte entanglement, however, are not understood.

Titration. Polyelectrolytes that dissociate as polyvalent weak acids or bases in an aqueous medium can be titrated with strong acid or base for the purpose of characterizing or varying the charge density. For a low molecular weight monoprotic acid, the degree of dissociation α closely follows the classic Henderson–Hasselbalch equation

$$pK_a = pH + \log\frac{1-\alpha}{\alpha} \tag{30}$$

where pK_a is the negative logarithm of the acid equilibrium constant K_a. This equation predicts that α rises sharply from zero to unity over a narrow pH window straddling the value of the acid's pK_a. Titration curves for diprotic acid and triprotic acid are not so simple, and thus complex trends are not be unexpected for polyelectrolytes, which possess a much greater number of dissociating sites. Indeed, α for polyelectrolytes typically varies across a large range of pH, and unlike low molecular weight acids or bases, depends strongly on I. With such interfering features, assigning a unique pK_a to a polyelectrolyte becomes problematical, and the well-defined pK_a of the low molecular weight acid or base corresponding to the repeat unit has little direct relevance.

Complexities arise in polyelectrolyte titration for a simple reason: the charge density of the chain changes during titration, altering the attractive electrostatic interactions between charged chain and oppositely charged titrant ion (185). For instance, if the fully ionized form of a polyelectrolyte such as poly(acrylic acid) is titrated with H^+, the strong attraction of the negatively charged polymer for H^+ at high pH weakens as more H^+ ions associate with the chain. Indeed, because the fully ionized chain is so negatively charged, H^+ associates with the polymer at pH values much above those at which H^+ associates with a hypothetical, isolated repeat unit. Although the pK_a of acrylic acid is 4.25, poly(acrylic acid) at pH 6.0 is about 20% protonated; by comparison, at the same pH acrylic acid is essentially unprotonated.

Extending the Henderson–Hasselbalch equation for a polyelectrolyte containing weak acid units, the negative logarithm pK_{app} of an apparent polyelectrolyte dissociation constant K_{app} can be determined from titration measurements using the following definition (186):

$$pK_{app} = pH + \log\frac{1-\alpha}{\alpha} \tag{31}$$

The value of K_{app} lies below the intrinsic dissociation constant K_a of an isolated acidic repeat unit, and as described above, typically decreases with increasing α because of enhanced electrostatic attractions between H^+ and negatively charged polyelectrolyte. A relationship between pK_{app} and pK_a was derived by Overbeek and others (53,185,187,188) through introduction of $dG_{el}/d\alpha$, the electrostatic contribution to the free energy change associated with transfer of a proton from infinity to the charged chain backbone:

$$pK_{app} = pK_a + 0.4343\left(dG_{el}/d\alpha\right)/RT \tag{32}$$

If all ions dissociated independently, $dG_{el}/d\alpha$ would be zero, while in the Debye–Hückel approximation, $dG_{el}/d\alpha$ is linear in α. In the preponderance of cases, $dG_{el}/d\alpha$ increases with α, the rate of the rise lessened at larger I (189,190); the variation of $dG_{el}/d\alpha$ with I in these situations mainly reflects the screening of electrostatic interactions between protons and the chain. A few polyelectrolytes display different behavior, pK_{app} showing a maximum followed by a minimum as α increases (186). A sharp conformational change such as helix-to-coil transition typically underlies a nonmonotonic dependence of pK_{app} on α.

Deriving a theoretical expression for pK_{app} requires evaluation of an electrostatic model for the polyelectrolyte chain, a procedure with significant uncertainties and much analytical and/or computational difficulty. Consequently, two empirical approaches are often employed to treat experimental data. In the first, one considers a modified Henderson–Hasselbalch equation, as for example, the form shown below which includes a single empirical parameter n (187,191):

$$pK_{app} = pH + n\log\frac{1-\alpha}{\alpha} \tag{33}$$

Values of pK_{app} and n obtained by fitting experimental titration data can reasonably correlate such data accurately over a range of α near 0.5, but the

fitted values vary strongly with c_s. Other modifications that also introduce fitting parameters to the Henderson-Hasselbalch equation have been proposed (192). The second approach represents titration data as the difference

$$\Delta pK(\alpha) = pK_{app} - pK_a \tag{34}$$

with the constant pK_a determined by extrapolation to $\alpha = 0$ (189). The function $\Delta pK(\alpha)$ is sometime replaced by $\Delta G_{el}(\alpha)$, obtained by integrating equation 32 (186):

$$G_{el}(\alpha) = 2.303RT\int_0^\alpha \Delta pK(\alpha)\ d\alpha \tag{35}$$

The second approach represents titration data in the form of a constant (pK_a) and a function [either $\Delta pK(\alpha)$ or $G_{el}(\alpha)$] rather than by two or more constants, as done in the first approach. Multiplying $G_{el}(\alpha)$ by the number of charges on the chain provides the total electrostatic contribution to the chain's free energy.

Viewing titration as a chain-charging process, one can derive a formula relating $\Delta pK(\alpha)$ to the electrostatic potential $\psi_s(\alpha)$ at chain sites where protons are bound (38,186,190):

$$\Delta pK(\alpha) = 0.4343\frac{e\psi_s(\alpha)}{kT} \tag{36}$$

Under the assumption that free energy changes during titration are purely electrostatic, this formula allows titration data to be assessed against electrostatic chain models that predict $\psi_s(\alpha)$. However, to interpret a polyelectrolyte's titration curve quantitatively requires a full understanding of how the chain's overall free energy varies upon association with protons, and this understanding may incorporate nonelectrostatic factors such as the local spacing of charge groups, chain flexibility and local conformation, and counterion hydrophobicity and size. A counterion condensation model incorporating some of these effects has been proposed by Manning (38,193).

Nonelectrostatic factors do not affect the end points of a titration, and thus when performed properly, titrations provide unequivocal information concerning the number of fixed charges on a polyelectrolyte just as they do for low molecular weight compounds.

Osmotic Pressure. The osmotic pressure π is a fundamental thermodynamic property that measures the activity of solvent in solution after the solution is equilibrated across a solute-impermeable membrane against a reservoir of pure solvent. For a neutral polymer solution, π can be expanded in c according to the well-known formula

$$\frac{\pi}{c} = RT\left(\frac{1}{M_n} + A_2c + \cdots\right) \tag{37}$$

where M_n is the polymer's number-average molecular weight, and A_2 is the second virial coefficient, reflecting nonideal chain mixing when its value is nonzero. With

nonideal mixing, chain locations in solution are correlated by either attractive or repulsive chain–chain interactions. Extrapolated to $c = 0$ or evaluated at theta conditions where $A_2 = 0$, measurements of π frame an absolute method for determining an unknown polymer's average molecular weight. Equally important, these measurements provide a means to evaluate A_2, and thus solvent quality, if π is obtained as a function of c at constant M_n.

For a polyelectrolyte solution, the situation is entirely different, as each dissociated counterion can contribute nearly as much to π as the polymer itself. If each chain dissolved in a salt-free solution dissociates Z^* monovalent counterions, the value of π can be written as, in the limit of ideal mixing (an inappropriate approximation),

$$\frac{\pi}{c} = \frac{RT}{M_n}\left(1 + Z^*\right) \tag{38}$$

In the usual case, with $Z^* \gg 1$ and $Z^* \sim M_n$, measurements of π extrapolated to zero c do not offer a way to measure M_n, as even a small variation or uncertainty in Z^* will obscure the polyelectrolyte chains' contribution to π. In general, Z^* is less than Z, the total number of fixed charges on the chain, owing to effects such as counterion condensation that reduce counterion activity. The reduction of π as a consequence of reduced counterion activity defines the osmotic coefficient ϕ_o (95,194):

$$\frac{\pi}{c} = \frac{RT}{M_n}\phi_o\left(1 + Z\right) \tag{39}$$

The same concepts apply to a polyelectrolyte solution containing added electrolyte. In the presence of a monovalent electrolyte at concentration c_s,

$$\pi = \phi_o RT\left[\left(1 + Z\right)c_m + 2c_s\right] \tag{40}$$

where c and M_n from the previous expression have been replaced by c_m, the molar concentration of polymer molecules. When the first term exceeds the second for a highly charged polyelectrolyte, experimentally determined values of ϕ_o are much less than unity (as small as 0.1), indicating that solutions at low electrolyte levels or high polymer concentration are strongly nonideal.

Although their theories differ, Lifson and Katchalsky (97) and later Manning (13) presented identical predictions for ϕ_o in dilute, salt-free polyelectrolyte solutions. Extrapolating ϕ_o to its value at zero c_p, experimental values consistent with their limiting theoretical predictions were obtained for both univalent and divalent counterions, as shown in Figure 11 (195–198). Experimentally, when M is large, values of ϕ_o depend little, if at all, on M. Low values of ϕ_o demonstrate that highly charged polyelectrolytes strongly suppress the activity of counterions, a finding in accord with counterion condensation, or more generally, the strong electrostatic interaction of counterions with polyelectrolyte chains. Experimentally, values of ϕ_o in salt-free solution slightly increase with c_p (195–198), as qualitatively captured by the Poisson–Boltzmann cell model of Lifson and Katchalsky (97). However, this and other simple electrostatic models cannot predict observed

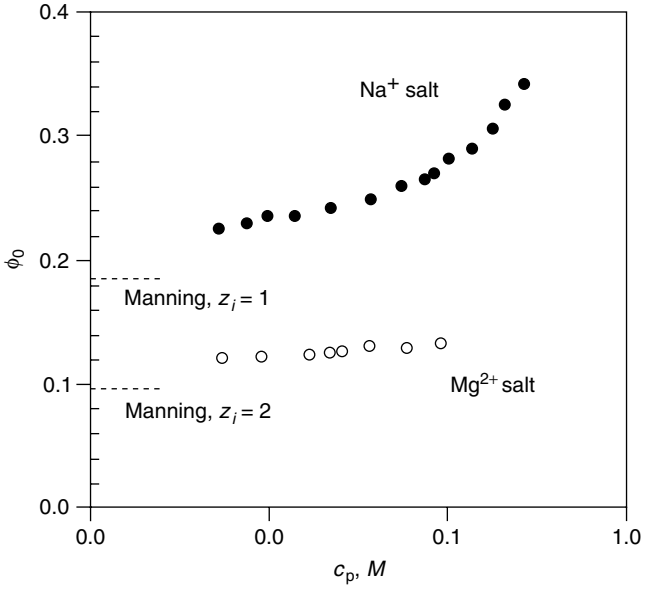

Fig. 11. Osmotic coefficients ϕ_o of poly(styrene sulfonate) with $M = 40{,}000$ g/mol plotted against polymer concentration c_p for salt-free solutions. Darkened and opened circles are for the Na^+ and Mg^{2+} salts of the polymer, respectively. The parameter z_i is the counterion valence. Data are from Refs. 195 and 196.

changes in ϕ_o when ε varies, a finding arguing for the presence of additional interactions between polyelectrolyte and counterion, such as ion pairing (199). Also, experimental data indicate that small counterions associate with polyelectrolytes to a greater extent than larger ones, a feature not explainable through a mean-field ion cloud description.

The osmotic pressures of polyelectrolyte solutions are most often measured in the presence of a membrane permeable to solvent and small ions but not to polyelectrolyte. The chemical potentials of the added electrolyte and solvent on each side of the membrane in this instance match, a condition defining Donnan equilibrium (200). Assuming ideal chain mixing, the quantity measured here is the Donnan osmotic pressure π_d, which can be equated to the difference of the osmotic pressures π and π', as defined above, between the inner (polymer-containing) and outer (polymer-free) compartments equilibrated in the presence of the electrolyte across the membrane:

$$\pi_d = RT\{\phi_o[(1+Z)c_m + 2c_s] - \phi_o' 2c_s'\} \tag{41}$$

where unprimed and primed quantities are evaluated at conditions of the inner and outer compartments, respectively. The need for electroneutrality establishes that $c'_s \neq c_s$, a feature referred to as the Donnan effect. Balancing the appropriate chemical potentials and imposing electroneutrality, the expression for π_d can be rearranged to a simpler form (95,200)

$$\frac{\pi_{\mathrm{d}}}{c} = RT\left(\frac{1}{M_{\mathrm{n}}} + \mathrm{A}_2^{\mathrm{d}}c + \cdots\right) \tag{42}$$

of similar appearance to the expression for the osmotic pressure π of a neutral polymer solution. The quantity $A^{\mathrm{d}}{}_2$ is the Donnan second virial coefficient (200):

$$A_2^{\mathrm{d}} = \frac{\phi_{\mathrm{o}}^2 Z^2}{4M_{\mathrm{n}}^2 c_{\mathrm{s}}} \tag{43}$$

The major contribution to $A_2{}^{\mathrm{d}}$ is the mismatch between c'_{s} and c_{s}, and as one consequence, $A_2{}^{\mathrm{d}}$ is independent of M_{n} (remembering that $\mathrm{Z} \sim M_{\mathrm{n}}$). The asymmetric distribution of small ions is such that the added electrolyte ion bearing the same charge as the polyelectrolyte is concentrated in the outer compartment while the converse is true for the added electrolyte ion of opposite charge.

The value of π for a polyelectrolyte solution will generally manifest nonideal chain mixing as well as the Donnan effect. Because of intermolecular electrostatic repulsions, A_2 is nearly always positive and large for polyelectrolytes. When $A_2 \neq 0$, an approximate expression corresponding to equation 37 for a polyelectrolyte solution in Donnan equilibrium can be written as (33,37)

$$\frac{\pi}{c} = RT\left(\frac{1}{M_{\mathrm{n}}} + A_2 c + A_2^{\mathrm{d}} c + \cdots\right) \tag{44}$$

Values of $A_2{}^{\mathrm{d}}$ are experimentally found to exceed substantially those of A_2 (95).

Equation 44 demonstrates that membrane osmometry can be employed to determine M_{n} for polyelectrolytes much as the method does for neutral polymers. The experiment works best when c_{s} is high and M_{n} is low, conditions that enhance the first term of equation 42. Although polyelectrolyte molecular weights of up to 10^5 g/mol have been successfully determined by membrane osmometry (95), the application of membrane osmometry for the measurement of polyelectrolyte molecular weight remains rare. More often, researchers exploit the technique to understand the interactions of electrolyte ions with polyelectrolyte chains. Recent attention has focused on measurements of π at values of c above c^*, and investigators have shown that polyelectrolytes in the presence of added salt behave similarly to neutral polymers at these concentrations (201). Without salt, experimental trends are more complex; however, when sufficiently concentrated in polyelectrolyte, solution behavior typical of neutral polymers is again observed (202).

Diffusion. The translational diffusion coefficient D is the most commonly measured transport property of polymer solutions, but as there are several distinct types of diffusion, care must be taken to interpret D properly. For $c \ll c^*$, Brownian motion of isolated chains in a homogeneous solvent defines the dilute solution diffusion coefficient D_0. As c increases toward c^* and above, chain–chain interactions modify the friction felt during chain motion. Under these conditions, the tracer- or self-diffusion coefficient D_{tr} is measured by tracking the path of a single chain in a macroscopically uniform mixture of chains and solvent. To distinguish the test chain from neighbors so that its path can be identified, the chain

must be labeled in a way that does not modify its motion. Chain–chain interactions typically increase friction and cause D_{tr} to fall with increasing c. The Brownian motion of highly diluted chains in a gel or similar medium defines a different type of tracer diffusion experiment, one in which labeling may not be necessary to follow chain motion. When diffusion is driven by a gradient of solute concentration (more properly, solute chemical potential), the situation envisaged by Fick's law of diffusion, a diffusion experiment yields the cooperative- or mutual-diffusion coefficient D_m. In a polyelectrolyte solution, D_m must be measured in the presence of a spatial gradient only in the polyelectrolyte component, holding the chemical potentials of other components everywhere uniform. Hypothetically, one might imagine the mutual diffusion of polyelectrolyte being measured by contacting two baths of different c that had previously been brought into Donnan equilibrium (8). As does D_{tr}, D_m in a sufficiently dilute solution superimposes on D_0, but unlike D_{tr}, D_m usually increases with c.

The value of D_{tr} can be obtained from the expression governing a solute's thermally driven root-mean-square displacement $\langle r^2 \rangle$ in time interval t. In three dimensions,

$$D_{tr} = \frac{\langle r^2 \rangle}{6t} = \frac{kT}{f_{tr}} \tag{45}$$

The second half of the equality defines f_{tr}, the tracer- or self-friction coefficient. Unlike D_{tr}, which reflects only solute friction, D_m manifests both solute friction and solute thermodynamics. For a binary system of neutral polymer and solvent, the following formulas apply:

$$D_m = \frac{c_m}{N_a f_m} \left(\frac{\partial \mu_p}{\partial c_m} \right)_{T,\mu_0} = \frac{1}{N_a f_m} \left(\frac{\partial \pi}{\partial c_m} \right)_{T,\mu_0} \tag{46}$$

where μ_p and μ_0 are the polymer and solvent chemical potentials, respectively, and f_m is the solute's mutual friction coefficient. For $c < c^*$, f_m and f_{tr} both vary nearly linearly with c, obeying expressions of the type

$$f_{m,}\, f_{tr} = f_0 \left(1 + k_p c\right) \tag{47}$$

where f_0 is the friction coefficient of an isolated chain with its ion cloud, and k_p is a positive coefficient.

Assuming sufficient added electrolyte in the asymptotic limit of small c, no distinction is made between D_0, D_{tr}, and D_m. In this limit, inserting f_0 for a sphere of radius R into the expression for D_0, the Stokes–Einstein formula is obtained:

$$D_0 = \frac{kT}{f_0} = \frac{kT}{6\pi \eta_0 R} \tag{48}$$

Often, the results of diffusion experiments in dilute solution are reported in terms of the hydrodynamic radius R_h, defined through the Stokes–Einstein expression by solving for R after D_0 is measured. The reporting of R_h is common even when solute shape is far from spherical.

At large values of I, D_m is found by experiment to obey

$$D_m = D_0\left(1 + k_D c\right) \tag{49}$$

where k_D is sometimes called the virial coefficient of diffusion. This form that can be theoretically rationalized by combining equations 43, 44, 46, and 47 and then expanding for small c (8,37,203),

$$D_m = D_0\left[1 + \left(2A_2M_n + \frac{\phi_0^2 Z^2}{2M_n c_s} - k_p\right)c + \cdots\right] \tag{50}$$

The first and third terms in parentheses are usually smaller than the second, and so k_D is expected to be approximately proportional to ${c_s}^{-1}$, as indeed is observed experimentally (37,92,203–206). The primary c_s influence on D_m at large I is through D_0; increasing c_s causes polyelectrolyte coils to contract, raising D_0 (91,92,206). The strong dependence of D_0 on c_s is shown for poly(styrene sulfonate) in Figure 12 (92). Equation 50 remains suspect, since polyelectrolyte solutions at large I contain at least two additional components, the counterions and the coions, not considered in equation 46, one of the relationships on which equation 50 is based. Polyelectrolyte motions are strongly influenced by nearby ions because the polyelectrolyte and the ions move within a common electrostatic field.

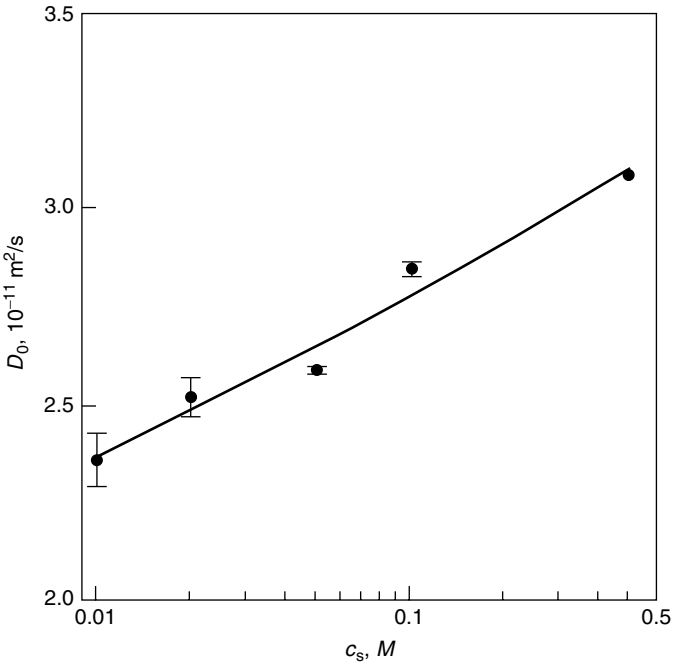

Fig. 12. Dilute solution diffusion coefficient D_0 of sodium poly(styrene sulfonate) as a function of added concentration c_s of NaCl. The polymer molecular weight M is 77,400 g/mol. Adapted from Ref. 92.

Fluctuations in ion density near a polyelectrolyte impose fluctuating electrostatic forces on the chain that can affect the chain's diffusion. As described by Sedlák (207), polyelectrolyte diffusion in dilute solution is "fast diffusion" because counterions cause more rapid motion in a polyelectrolyte than would be noted in an equivalent neutral chain. Several investigators have modified equation 50 to include this Nernst–Hartley-type diffusion in a consistent manner (203,206). Tivant and co-workers suggested that in a monovalent electrolyte solution at large I the enhancement of D_m by polyelectrolyte–electrolyte coupling should be expressed as (208)

$$D_m \cong D_0 \left[1 + \left(1 - \frac{2D_0}{D_1 + D_2} \right) \frac{\phi_0^2 Z^2}{2M_n c_s} c + \cdots \right] \tag{51}$$

where D_1 and D_2 are the diffusion coefficients of the counterion and co-ion, respectively. The factor in parentheses is typically close to unity at large I, allowing polyelectrolyte mutual diffusion to mimic roughly neutral polymer diffusion, albeit with the thermodynamic contribution to diffusion dominated by the Donnan effect. For small ion motions infinitely fast compared to polymer motions, equation 50 is recovered from equation 51.

At low I, the understanding of polyelectrolyte diffusion remains unsettled. Most diffusion experiments in polyelectrolyte solutions are conducted by dynamic light scattering, a method sensitive to the relaxation of the microscopic concentration fluctuations that spontaneously occur in a macroscopically homogeneous polyelectrolyte solution. The relaxation of these fluctuations is governed by mutual diffusion of polymer chains. The light scattering method can detect whether the relaxation is by a single diffusive process, and thereby monomodal, or by multiple diffusive process, and thereby multimodal. Schurr and co-workers (204) first discovered that when c is high and I is low, multimodal relaxation can occur over widely separated time scales. When two distinct diffusive modes are detected, the one that decays more rapidly is termed the *fast* mode and its effective diffusion coefficient designated D_f, while the second, less rapid mode is termed the *slow* mode and its effective diffusion coefficient designated D_s. Schurr referred to the region of solution conditions corresponding to monomodal behavior as the "ordinary phase" and that corresponding to multimodal behavior as the "extraordinary phase" (204). Equation 51 captures trends in diffusion for the ordinary phase when c is low. Figure 13 shows the emergence of two diffusive modes as a function of c.

By dynamic light scattering, a sharp shift in the intensity of scattered light and the appearance of two (or more) diffusive modes mark the onset of the extraordinary phase as c_p increases at constant c_s (118,120,204,209–215). Various empirical criteria for locating the boundary between ordinary and extraordinary phases have been proposed, the most successful establishing a threshold dependent on the ratio of c_p to c_s; the extraordinary phase normally appears when these two concentrations are roughly similar (112,118,210). However, the proposed criteria are not robust or universal (207,215,216). The fast mode originates in the electrostatic coupling of polyelectrolyte and counterions, as just described for the ordinary phase under conditions of low c and large c_s. The rapid diffusive motions of the small counterions are moderated by the slower polyelectrolyte, and

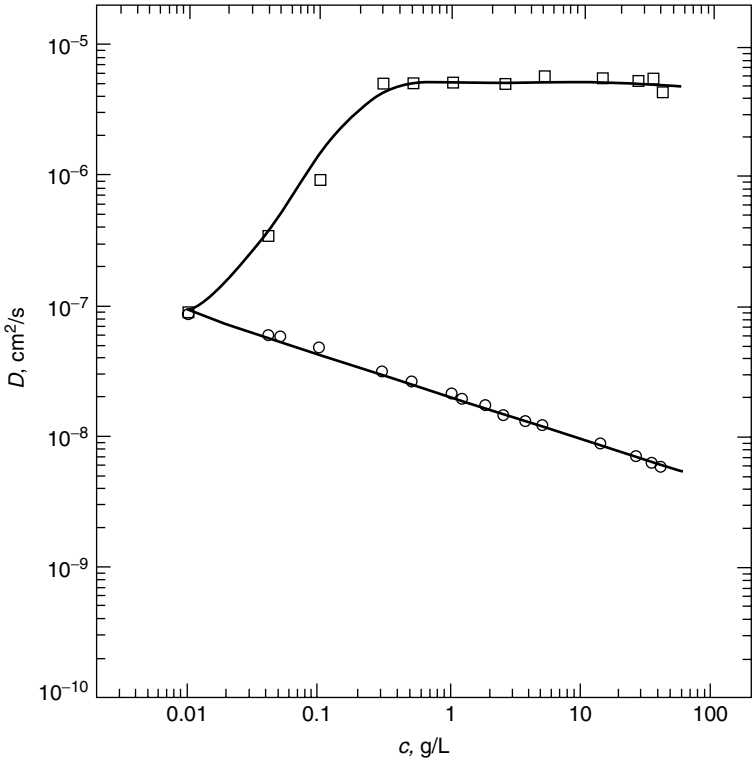

Fig. 13. Dependence of the fast (squares) and slow (circles) diffusion coefficients D of salt-free solutions of poly(styrene sulfonate) varying in polymer concentration c_p. The polymer molecular weight M is 100,000 g/mol. Adapted from Ref. 209.

simultaneously, the slow diffusive motions of the polyelectrolyte are enhanced by the faster counterions. A generalized version of equation 51 successfully explains the observed independence of D_f on M and c_p when M is large and $c_p/c_s \gg 1$. The same equation also successfully predicts values for D_f of the order 10^{-6} cm^2/s, a magnitude more typical for small molecule diffusion than for polymer diffusion. Values of Z needed to match experiment with theory, however, are often not much greater than unity, orders of magnitude smaller than the actual or effective (condensed) charge of the polyelectrolyte being studied (210,212,216,217).

The physics underlying the slow mode remain unclear, although many ideas have been suggested, such as the presence of an ordered phase, temporal aggregates, self-diffusion, or undissolved polymer (120,209,211–213,218). The structures responsible for D_s are larger than individual polymer chains, a feature taken by some to manifest the presence of attractive forces between chains. Others argue that filtration or long equilibration eliminates the slow mode, and thus its origins must be sought in kinetic rather than thermodynamic factors (207,219–221).

Techniques such as forced Rayleigh scattering, pulsed gradient NMR, and fluorescence recovery after photobleaching have recently made information concerning self-diffusion available for polyelectrolyte across the range of solution concentrations. The complex diffusion dynamics uncovered for D_m by dynamic

light scattering are not reflected in D_{tr}. As electrolyte levels rise from 0 to 1.0 M in a semidilute polyelectrolyte solution, D_{tr} usually increases by roughly a factor of about 2, reflecting alterations in coil size. Likewise, D_{tr} decreases with M and c across this range in a manner analogous to the trends expected of an unentangled polymer melt (180,212,222,223).

In polyelectrolyte systems, diffusion coefficients for species other than the polyelectrolyte may be important, especially those of counterions. In a salt-free solution, the counterion diffusion coefficient D_c at low c is depressed by the presence of polyelectrolytes, demonstrating that inherently faster counterion motions are attenuated by electrostatic interactions with slower moving polyelectrolyte. Manning developed a counterion condensation theory describing this attenuation for a salt-free solution in the limit of small c; he predicted that the ratio of D_c in the polyelectrolyte's presence to D_c in the polyelectrolyte's absence equals $0.866/|z_i|\xi$ (14). Experiments verify the predicted ξ dependence (42), but unexpectedly, the ratio also depends on c (224–226). The ratio falls rapidly from unity at low c to a broad minimum and then rises slightly to achieve a broad maximum. The maximum has been explained via a cylindrical cell model that shows increasing c electrostatically favors a shifting of the counterion distribution toward spaces between polyelectrolyte chains, a factor increasing D_c (226). However, beyond a c threshold, the density of chains become so great that counterion diffusion is physically obstructed, a factor then decreasing D_c. These shifts all occur at semidilute polymer concentrations. If the polyelectrolyte–electrolyte coupling ideas that explain D_f are correct, then D_c and D_f must be related, as recently theoretically demonstrated by Sasaki and Schipper (227).

Electrophoresis. As charged molecules, polyelectrolytes in solution migrate toward regions of lower electrostatic potential when an external electric field is applied. This electrophoretic migration can be monitored either in free solution (228) or in the presence of a separation medium imposing molecular-level geometric hindrances (229); the hindrances reduce the rate of migration compared to that in free solution. Gels, neutral polymer solutions, and other porous materials can act as effective separation media, with hindrances tailored to attenuate the migration of polyelectrolytes best according to chain size. A variety of experimental methods allow migration rates to be measured. Recently, the number of accessible medium types has expanded greatly owing to the development of capillary electrophoresis, a method allowing measurements of polyelectrolyte electrophoresis in a variety of both fluid-like and solid-like environments. The ratio of steady-state drift velocity v to the electric field strength E defines the electrophoretic mobility μ, the polyelectrolyte property measured by electrophoresis:

$$\mu = \frac{v}{E} \tag{52}$$

To distinguish results for a free solution experiment, one conducted without a separation medium, the mobility in free solution is usually written as μ_0. When the value of E is low enough to avoid field-induced distortion of the polyelectrolyte's configuration, μ is independent of E. Measurements of μ have long been a cornerstone of polyelectrolyte characterization, especially for polyelectrolytes of biological origin.

A uniform, externally applied electric field imposes four types of forces on a polyelectrolyte in free solution (228,230–232). First, the field acts directly on the fixed charge of the polyelectrolyte, producing on the chain a direct electric force F_e of magnitude EZe. Second, the field acts directly on the local excess of counterions, and since the charge of the counterion cloud is equal and opposite to that of the polyelectrolyte, produces on these ions an opposite, spatially distributed force of magnitude $-EZe$. However, because of the physical separation of counterions from polyelectrolyte, the force experienced by each ion is transmitted to the polyelectrolyte through intervening solvent only as a velocity disturbance. During the transmission, the disturbances are attenuated by viscous dissipation. Thus, the polyelectrolyte chain experiences the electric forces on counterions only vicariously, as dampened hydrodynamic forces distributed along the chain backbone. The magnitude of the overall transmitted force F_c, termed the retardation force, can be significantly less than $-EZe$. Indeed, F_c depends strongly on the spatial disposition of the counterions and thereby on κ^{-1}. When κ^{-1} is large, F_c is much reduced because the velocity disturbances propagate a long distance through solvent before impact on the chain. Third, the viscous character of the solvent resists chain translation, creating a drag force of magnitude F_d. This force is calculated as the product of v with the chain friction coefficient ζ: $F_d = -\zeta v$. Fourth, the field can distort and polarize the counterion cloud surrounding the polyelectrolyte, modifying two of the forces already described. With polarization, the force transmitted to the chain from counterions no longer can be calculated using the equilibrium structure of the counterion cloud, and the local dipole field associated with polarization reduces the electric force on the chain's fixed charges. Together, the two corrections comprise the relaxation force F_r. Summing forces on the chain at steady state (228),

$$F_e + F_c + F_d + F_r = 0 \tag{53}$$

While F_e is positive, F_c, F_d, and F_r are negative, ie, directed against the polyelectrolyte's migration. Interpreting μ_0 for a charged colloidal particle or a small electrolyte ion requires the same force balance (230).

Complications for polyelectrolytes arise from the complex architecture of the chain, poor understanding of the electrostatic interactions between counterions and polyelectrolyte, and chain flexibility. Notwithstanding complications, several observed trends in μ_0 for polyelectrolytes can readily be explained in terms of the force balance just described. For instance, irrespective of I, as seen in Figure 14, μ_0 is independent of M for high M polyelectrolytes (228,233). This trend has often been incorrectly rationalized by balancing F_e and F_d, assuming that both are proportional to M. Forcing the equality immediately leads to

$$\mu_0 = \frac{Ze}{f_0} \tag{54}$$

which is recognized as the standard Einstein formula for electrophoretic mobility of a small ion. With $Z \sim M$, constancy of μ_0 mandates that $f_0 \sim M$. However, f_0 is not proportional to M for polyelectrolytes of any conformation, as polyelectrolytes never behave as "free-draining" objects, an assumption of the Einstein formula.

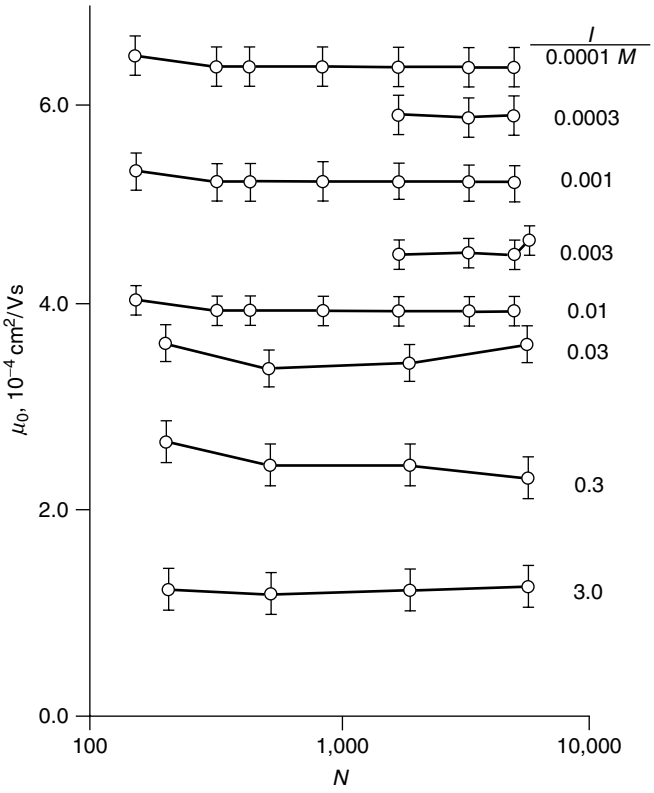

Fig. 14. Dependence of the free solution electrophoretic mobility μ_0 on degree of polymerization N for poly(styrene sulfonate) chains dissolved in NaCl solutions of varying ionic strength I. Adapted from Ref. 228.

The independence of μ on M more properly can be traced to the screening by counterions of long-ranged hydrodynamic interactions that ordinarily exist between distant chain segments. This screening has roots in F_c. The velocity disturbance propagated through solvent due to electric force acting on one chain segment is always accompanied by a comparable disturbance transmitted through solvent due to the force acting on a nearby counterion. At distances large compared to κ^{-1}, the two disturbances cancel, and for this reason, the polyelectrolyte gains apparent free-draining character. The same polyelectrolyte will not display free-draining character in a diffusion experiment (ie, D_0 will not be proportional to M^{-1}), and Z inferred by application of equation 54 to actual data is much too small (234).

A second important experimental trend interpretable through the force balance of equation 53 is the dependence of μ_0 on I at fixed M (228). As displayed in Figure 14, μ_0 drops significantly with increasing I. Again, the explanation lies in F_c. As I increases, κ^{-1} becomes smaller, and the hydrodynamic coupling of counterions to polyelectrolyte is enhanced, reducing μ_0 as F_c grows. Still another important trend, one not yet fully understood, is the dependence of μ_0 on ξ (43,46,235). Figure 15 shows that at low ξ, $\mu_0 \sim \xi$, but at high ξ, $\mu_0 \approx$ constant. One explanation for the loss of ξ dependence at high ξ is counterion condensation,

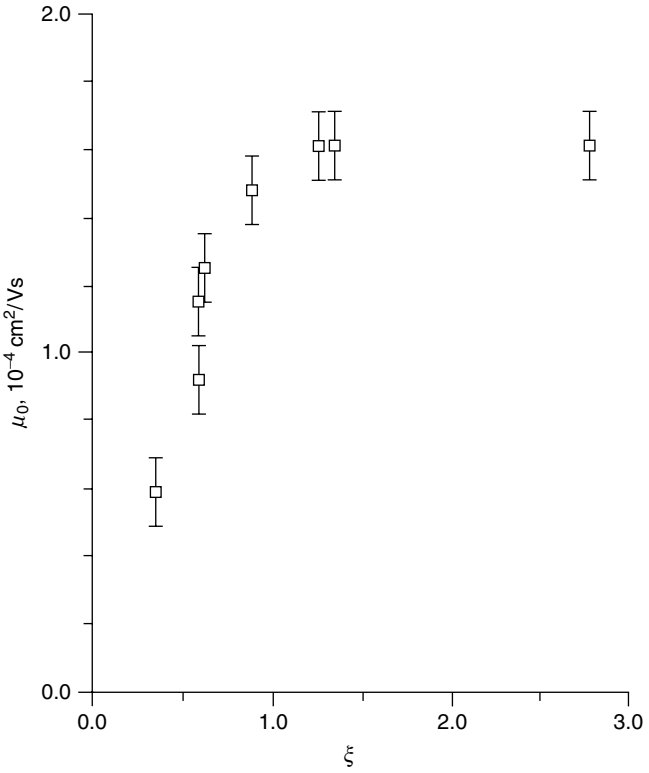

Fig. 15. Dependence of the free solution electrophoretic mobility μ_0 on dimensionless charge density ξ for equal M copolymers of acrylic acid and acrylamide. The charge density is controlled by varying copolymer composition while holding the pH high enough (pH 10.5 phosphate electrolyte) to ionize the acrylic acid units fully. From Ref. 46.

but nonlinear effects associated with F_r frame a plausible alternative explanation that remains to be explored fully.

In a separation medium such as a gel, the dependence of F_d on M is affected by the polyelectrolyte's configurational interactions with the medium, and consequently, μ becomes M dependent. Various sorts of interactions have been proposed, ranging from sieving to reptation to entropic barriers transport (229,236,237). Which type of interaction dominates depends on the heterogeneity and pore size of the medium, the size and flexibility of the polyelectrolyte, and the magnitude of the electric field. In recent years, characterization of polyelectrolytes by the traditional method of gel electrophoresis has slowly been supplanted by various capillary electrophoresis techniques, including many that exploit nongel separation media (229). In the future, characterizations may be performed in microfluidic, chip-based devices that allow precise tailoring of a patterned separation medium.

Electric and Magnetic Birefringences. In addition to causing polyelectrolyte migration, external fields can also make polyelectrolyte solutions become optically birefringent due to partial or even complete chain orientation (238,239). The birefringence Δn of a transparent medium measures how the refractive index n varies with respect to the polarization plane of propagated light. The difference

in n between light polarized parallel and perpendicular to an external alignment field defines Δn. If Δn is positive, n in the field direction is greater than n in the direction perpendicular to the field. For a polymer solution, finite values of Δn manifest preferential alignment of anisotropic chain segments. For many polyelectrolytes such as poly(styrene sulfonate), the optical polarizability of chain segments is larger perpendicular to the backbone than parallel to the backbone; in this case, the alignment of chains with respect to an electric field produces negative Δn.

Held for sufficient time in a steady field, polymer chains reach a saturating level of segmental orientation associated with their stationary birefringence Δn_s. For low magnitudes of E, Δn_s rises as the square of E, the ratio $\Delta n_s/E^2$ defining the Kerr constant K. At high enough E, Δn_s reaches an E-independent plateau corresponding to complete segment alignment. Achieving any level of segmental alignment implies the presence of permanent or induced dipoles that impose torque on the chain as the field is applied. For most polyelectrolytes, which possess no permanent dipole, the polarization of the counterion cloud by the electric field is responsible for providing the necessary induced dipole.

Several theories for the longitudinal polarizability of a counterion cloud surrounding a charged cylinder or rod have been developed, each employing a different treatment of the counterions (16,240,241). All results indicate that the polarizability of such a cylinder or rod increases approximately as the second or third power of length, a trend consistent with experiments performed on flexible polyelectrolytes under salt-free conditions (242). Worm-like chain theories, incorporating the average polarizability and optical anisotropy per segment as independent parameters, find that K/c_p in a sufficiently dilute solution has a significant dependence on l_p, and this fact allows l_p to be calculated from measurements of K/c_p (243–245). Analogously, l_p can be determined by a magnetic field alignment experiment using the measured value of CM, the Cotton–Mouton constant, which plays an analogous role to K (245–247). Figure 16 shows values of l_p as a function I for DNA examined by magnetic birefringence; data from other methods are plotted alongside, as are predictions made by the OSF model for various values of l_0. The agreement between theory and experiment and between data sets appears good.

Transient electric birefringence, the study of polyelectrolyte solutions by birefringence as a pulsed or oscillating electric field is applied, offers a powerful tool for examining both polyelectrolyte chain dynamics and structure (248–251). An external electric field can be manipulated and Δn measured over times scales short compared to those associated with chain reorientation and deformation. Thus, chain conformation can be inferred from the build up and decay of Δn as a time-dependent electric field of prescribed magnitude is abruptly applied and then removed. The field free Δn decay curves are typically fitted as a sum of exponentials, the largest of which is assigned to the longest conformational relaxation time τ_1 of the chains. According to the extended Zimm theory, the longest relaxation time of an isolated chain in a good solvent obeys

$$\tau_1 = \left(\frac{6^{3/2}}{2.38}\right)\frac{\Phi_0\eta_0}{N_a kT}R_g^3 \tag{55}$$

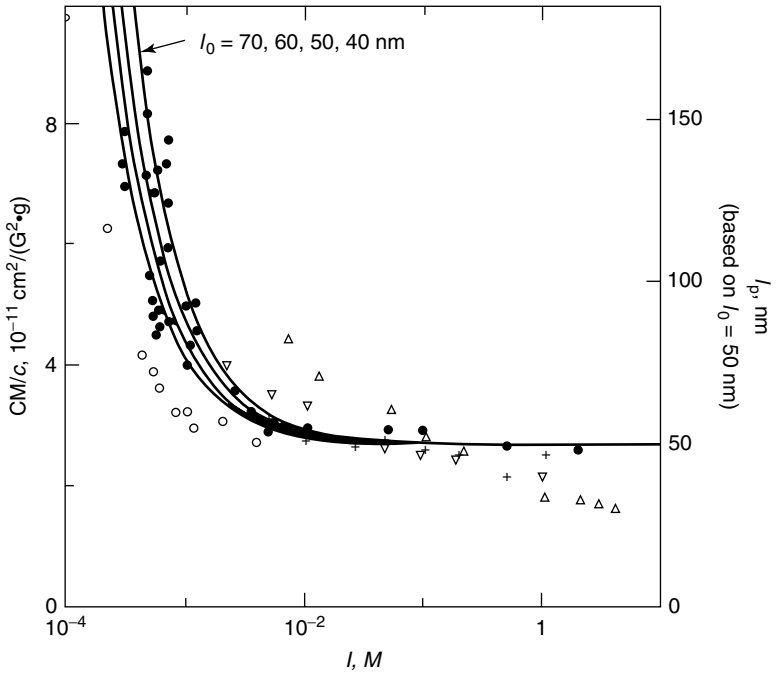

Fig. 16. Comparison of experimental values of the Cotton-Mouton constant CM (darkened circles) with theoretical (lines) and independently measured values (open symbols) of the persistence length l_p. The left and right axes have been shifted so that measured values of CM can be referenced against l_p. Theory curves are for the OSF model with l_0 between 50 and 70 nm, and l_e values from independent measurements were adjusted to the plotted l_p values by adding 50 nm. Adapted from Ref. 247.

where Φ_0 is a constant draining parameter of value 1.81×10^{23}. Values calculated by this formula agree with remarkable precision to those measured for flexible polyelectrolytes by transient electric birefringence (250). In addition, as c increases the observed values of τ_1 grow in predictable fashion (249). Figure 17 shows a sharp upward turn in τ_1 as c exceeds c^*. The presence of polydispersity, field-induced chain aggregation, or high levels of added electrolyte sometimes make electric birefringence measurements difficult.

Electric and magnetic birefringences are but two examples from a class of experimental methods that probe molecular structure and dynamics while external fields are applied to a homogeneous polyelectrolyte solution. Another important member of this class, one that remains poorly understood, is dielectric relaxation, which for a polyelectrolyte measures polarization of the counterion cloud as a function of frequency (45,252,253). Multiple relaxations are noted, including a low frequency mode associated with polarization of free ions over the whole length of the chain and a faster mode variously associated with polarization of condensed ions over a single segment, motion of counterions perpendicular to a segment, segmental reorientation, or motion of counterions over the screening length.

Conductivity. Polyelectrolyte solutions contain a variety of ionic species, including the polyelectrolyte itself, which move electrophoretically toward either

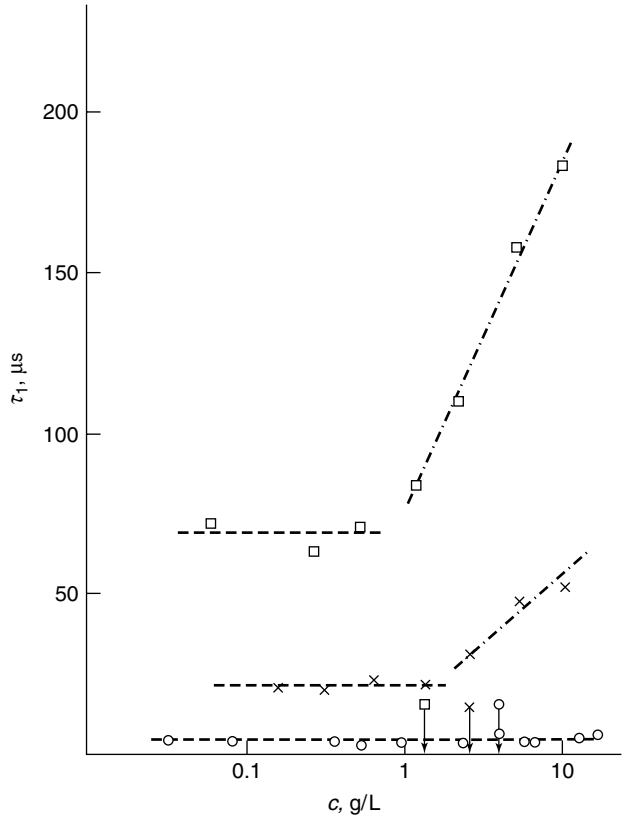

Fig. 17. Variation of the experimentally determined longest decay time τ_1 with polymer concentration c for three different molecular weight M poly(styrene sulfonate)s dissolved in 0.01 M NaCl [$\boldsymbol{M}$ (g/mol): ○ 177,000; × 400,000; □ 650,000]. Arrows directed toward the c axis indicate the theoretical value of c^* derived from the OSF chain model. Adapted from Ref. 249.

anode or cathode when an electric field is applied, and as a consequence of these motions, the solutions carry current. The specific conductance χ, characterizing the current-carrying ability of a solution, is defined as the reciprocal of the specific resistance; the specific resistance is the resistance in ohms across 1 cm of solution that has a cross section of 1 cm^2; the units of χ are $ohm^{-1} \cdot cm^{-1}$. In the discussion that follows, any contribution to χ from pure solvent is ignored; experimentally, any solvent contribution can simply be subtracted from the solution measurement. The equivalent conductance Λ for a polyelectrolyte solution is calculated from χ by multiplying by $1000/c_p$:

$$\Lambda = \frac{1000\chi}{c_p} \tag{56}$$

The factor 1000 allows c_p to be expressed in molar units so that Λ has the standard units of $cm^2/(\Omega \cdot mol)$.

The equivalent conductance of a polyelectrolyte solution is conventionally apportioned to the various ionic species present. If the solution is salt-free, the apportioning suggests the following empirical equation:

$$\Lambda = f_c \left(\bar{\Lambda}_p + \Lambda_c^0 \right) \tag{57}$$

where f_c is an interaction parameter dependent in part on the fraction of dissociated counterions, and $\bar{\Lambda}_p$ and $\Lambda_c{}^0$ are the equivalent conductances of polyelectrolyte and counterion, respectively (the latter defined at infinite dilution in absence of polyelectrolyte). The same type of apportioning can be more rigorously written as

$$\Lambda = F \frac{Z^*}{Z} (\mu_0 + \mu_c) \tag{58}$$

where F is the Faraday constant, representing a mole of elementary charges e, and μ_0 and μ_c are the mobilities of polymer and counterion, respectively, evaluated together in solution; the parameters Z^* and Z have the same meanings as before, representing the number of counterions released upon dissolution and the number of ionized sites on the chain, respectively. Relating f_c and Z^*/Z is not without ambiguity, clouding interpretations of the meaning of f_c and $\bar{\Lambda}_p$. The value of f_c relates to the fraction of uncondensed ions β within the counterion condensation model but also incorporates how these ions electrostatically interact with the chain.

Manning determined values of f_c and $\bar{\Lambda}_p$ for a line charge model with counterion condensation (18). Above ξ_c,

$$f_c = \frac{0.866}{|z_i|\xi} \tag{59}$$

The right-hand side is recognized as equivalent to the formula Manning presented for the attenuation of D_c in the presence of polyelectrolyte. The reduction of f_c below β demonstrates that polyelectrolytes suppress uncondensed counterion motions, but in this instance, in the context of counterion electrophoretic mobility and not counterion diffusion constant. Likewise, the value of $\bar{\Lambda}_p$ predicted by Manning reflects the influence of counterions on polyelectrolyte mobility. His model for Λ assumes that condensed counterions migrate rigidly with the polyelectrolyte line charge to which they have condensed.

Measurements of Λ in salt-free or nearly salt-free polyelectrolyte solutions reveal complex and seemingly nonuniversal trends (254–258). If Λ is measured as a function of c_p, a maximum is sometimes seen at very small values of c_p, and the maximum is usually followed at higher c_p by a broad minimum. For c_p below the minimum, M strongly affects Λ, but above the minimum, little impact of M on Λ is noted. At high M, the initial maximum may disappear. A schematic of typical behavior is presented in Figure 18. Wandrey correlated the position of the maximum with $c_p \sim c_s$ and the height of the maximum with $L \sim \kappa^{-1}$ but why these conditions lead to a maximum in Λ is unclear (257). The decrease of Λ after the

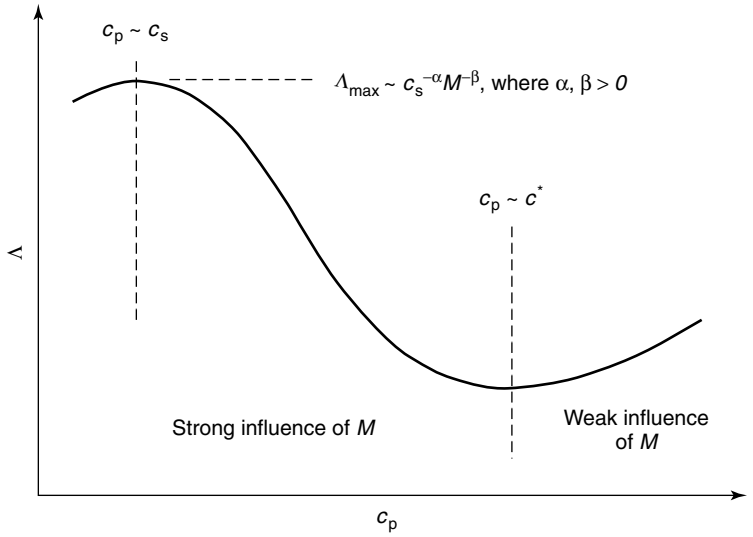

Fig. 18. Schematic depiction of the variation of polyelectrolyte equivalent conductance Λ with polyelectrolyte concentration c_p for salt-free solutions. Adapted in part from Ref. 257.

maximum can be explained through the continuous strengthening of electrostatic coupling between polyelectrolyte and counterions as κ^{-1} falls with increasing c_p; electrophoretic mobilities of both polyectrolyte and counterion decrease in consequence. To fit Λ data across the dilute polymer regime via the Manning model, Wandrey found it necessary to adjust f_c to smaller values at higher c_p. This trend can be rationalized as a shift toward more condensed counterions when κ^{-1} drops below the polyelectrolyte's molecular size. Shaaban and co-workers had earlier reached much the same rationalization (258). The need to vary f_c reflects that Λ falls too steeply with c_p for fitting to the unmodified (constant f_c) Manning model. Colby and co-workers considered the c range over which Λ decreases as semidilute in polyelectrolyte and thus developed a model for Λ based on a different description for the polyelectrolyte's mobility (259). The alternative model also does not capture well the steep drop of Λ with c. Interestingly, the growth of Λ above the broad minimum was explained by Colby and co-workers as possibly due to an increase in f_c with rising c_p, exactly opposite to the argument used by Wandrey to explain behavior at lower c_p. No rigorous theoretical model has yet predicted either the maximum or the minimum in Λ, but one might speculate that both trends in Λ for salt-free solutions might be connected to somewhat analogous anomalous trends in D_c or counterion activity (260).

With added electrolyte, the polyelectrolyte conductance can be derived from the measured solution conductance by subtracting the measured conductance of a polyelectrolyte-free solution containing the same level of added electrolyte. The polyelectrolyte equivalent conductance is then defined exactly as before, substituting the corrected polyelectrolyte conductance into equation 56. Trends in Λ vs c_p in this case do not match those of a salt-free solution, demonstrating that electrostatic interactions disallow additivity laws; in this case, additivity would suppose that the solution conductivity is simply the sum of independent conductances of

each component. Kowblansky and Ander proposed a modified additivity relationship, accounting for the impact of polyelectrolyte on electrolyte conductance, and this relationship correlates Λ reasonably well (261). At constant c_s, Λ usually grows or decreases more or less linearly with c_p in the dilute regime, allowing orderly extrapolation of Λ to Λ_0, the limiting equivalent conductance at zero c_p. Values of Λ_0 decrease with decreasing c_s, as might be expected in light of the previous discussion of how μ_0 varies with I.

Polyelectrolyte Gels

The placement of fixed charges in a swellable polymer network can endow the network with a variety of useful properties, perhaps the most important of which is a discontinuous swelling transition (262). For example, the volume of a polyelectrolyte gel may abruptly expand by several hundred times as the electrolyte concentration of a bathing solution decreases below a critical value (263). This property underlies the "superabsorbency" of many polyelectrolyte gels. A discontinuous swelling transition can be understood in terms of concepts already discussed, with attention focused on counterions and their impact on osmotic pressure.

The volume change of a polyelectrolyte gel is usually expressed in terms of the swelling ratio α, defined as the charged gel's volume V divided by the gel's volume V_0 when the constituent network strands adopt electrostatically unperturbed random walk configurations. At equilibrium, the charged gel adopts the value of α that minimizes the gel's total free energy $G(\alpha)$. Although slightly different forms have been proposed, expressions for $G(\alpha)$ generally assume separate additive contributions from network elasticity $G_{\text{elasticity}}$, which disfavors swelling, thermodynamics of polymer–solvent mixing G_{mixing}, which either favors or disfavors swelling depending on temperature, and counterion osmotic pressure G_{osmotic}, which favors swelling (263–266). Writing $G(\alpha)$ as a sum,

$$G(\alpha) = G_{\text{elasticity}} + G_{\text{mixing}} + G_{\text{osmotic}} \tag{60}$$

Sometimes included is another term accounting for electrostatic repulsions between the fixed charges of the network, but this term in most instances is small enough to be neglected. The first two terms explain the equilibrium swelling of neutral polymer networks. The elasticity term arises from the stretching of network strands as the gel expands. Such stretching can be analyzed by approximating network strands as Gaussian, or more accurately, via configurational models limiting strand extensibility. The mixing of solvent with network strands allows these strands to sample a larger range of conformations, which raises their entropy. The same mixing, however, increases solvent-segment contact, which nearly always raises enthalpy. The overall balance of entropy and enthalpy represented in the first two terms of equation 60 is captured in the standard Flory–Huggins theory for neutral polymer gels.

The most distinctive features of polyelectrolyte gels come from the third term, G_{osmotic}. Because the gel's fixed charges cannot escape the network, polyelectrolyte gels establish Donnan equilibrium with a bathing solution containing

only electrolyte and solvent. As noted earlier, the Donnan effect is a mismatch in c_s established across the boundary between two compartments held in Donnan equilibrium. The mismatch here can be traced to electroneutrality, which requires a sufficient number of counterions in the network to neutralize the fixed charges held there. The excess counterions inside the gel can be considered to apply a pressure at the gel–solution interface that causes the gel to swell. Ions in the external electrolyte solution apply an opposing pressure that causes the gel to shrink. The difference in the two pressures equals the Donnan osmotic pressure discussed earlier. Polyelectrolyte gels swell until their elastic modulus counters the Donnan osmotic pressure. The latter falls as the concentration of electrolyte ions in the external solution rises and at a critical concentration becomes too small to stabilize the swollen state of the gel against elastic contractile forces. For univalent fixed charges and monovalent electrolyte, the critical electrolyte concentration approximately matches the concentration of fixed charges in the swollen network (265). Above the critical electrolyte concentration, the gel shrinks, as only the first two terms of the expression for G remain important. The abrupt shrinkage with addition of electrolyte corresponds to a first-order phase transition if the reduced temperature is low enough.

Figure 19 displays the volume changes observed for *N*-isopropylacrylamide gels containing a small fraction of charged sodium acrylate units. Uncross-linked poly(*N*-isopropylacrylamide) solutions display a lower critical solution temperature slightly above room temperature. Upon heating, the cross-linked copolymer gel displays a discontinuous volume change as temperature is raised above 33°C, in some instances, with the gel shrinking by a factor of nearly 100. The presence of the charged units increases the transition temperature and expands the magnitude of the discontinuous volume change. Without the charged repeat units,

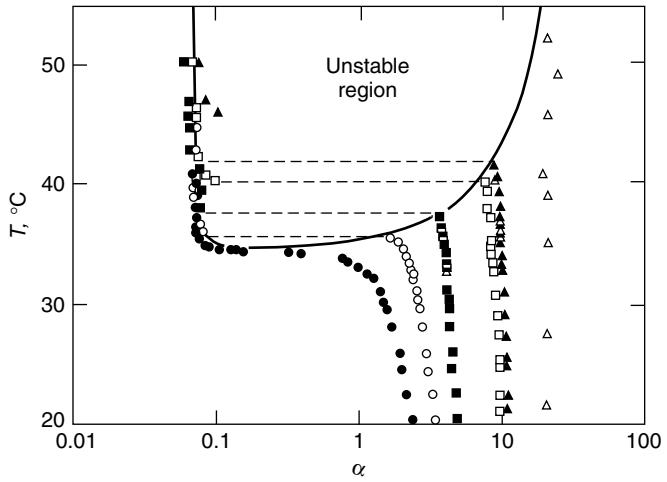

Fig. 19. Temperature T dependence of the degree of coil swelling α for copolymer gels of *N*-isopropylacrylamide and sodium acrylate in water. The total monomer concentration of gels at preparation was 700 mM, and the different plot symbols provide the concentration at preparation of sodium acrylate: ● 0 mM; ○ 8 mM; ■ 32 mM; □ 50 mM; ▲ 70 mM; △ 128 mM. Adapted from Ref. 263.

the volume change is continuous. Barrat and co-workers (266) and Rubinstein and co-workers (267) recently discussed many of the scattering, relaxation, and mechanical properties of swollen polyelectrolyte gels.

Polyelectrolyte Adsorption

The Adsorption (qv) of polyelectrolytes from solution onto solid, liquid, or gas interfaces defines a vast field, one that encompasses innumerable phenomena and many technologies. To simplify, only the grossest and most common issues are introduced here (268–270). Figure 20 displays pictorially how flexible polyelectrolyte homopolymers interact with a flat, charged surface (269). The left-hand side of this cartoon indicates behavior at low c_s, a condition typically dominated

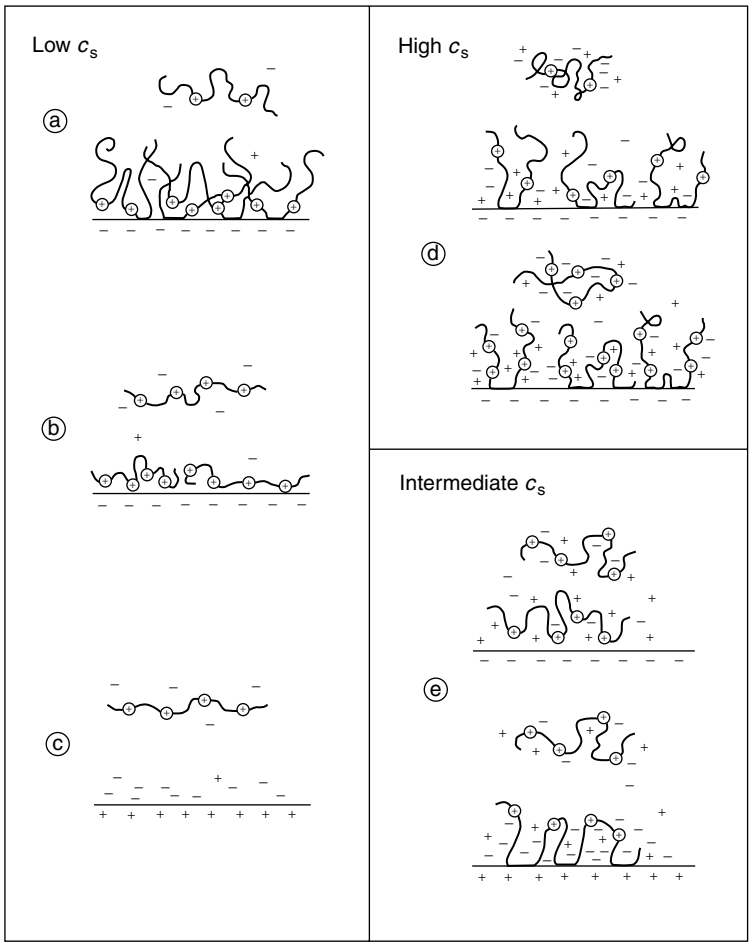

Fig. 20. Pictorial representations of polyelectrolyte adsorption under various conditions of surface charge density, polymer charge density, and ionic strength. The text discusses the specific conditions relevant to sketches **a-e**. Reprinted from Ref. 270.

by electrostatic interactions, while the right-hand side illustrates behavior at high c_s, a condition requiring additional consideration of the segment–surface interaction energy χ_s and possibly the segment–solvent interaction energy χ. Diagram **a** represents the adsorption of a lightly charged electrolyte from dilute solution onto an oppositely charged surface. In this instance, there is compensation by polyelectrolyte of surface charge, the adsorbed amount is high, and the adsorbed layer is thick (thickness $\sim R_g$). When the polyelectrolyte is more highly charged, as sketched in diagram **b**, there is again charge compensation, but the adsorbed amount is lower and the adsorbed layer is much thinner (thickness $\ll R_g$). The trend reflects the increased electrostatic attraction between polyelectrolyte and surface charges, resulting in a larger fraction of polyelectrolyte segments in contact with the surface. Diagram **c** shows that polyelectrolytes typically do not adsorb onto similarly charged surfaces when c_s is low; electrostatic repulsions cannot be overcome by even a large positive segment–surface contact energy.

Turning to the right-hand side of the figure, the top portion of diagram **d** shows adsorption at high c_s for a lightly charged polyelectrolyte attracted to an oppositely charged surface by a positive segment–surface interaction energy. The bottom portion of the same diagram shows the analogous situation for a more strongly charged polyelectrolyte. The strong screening of electrostatic interactions makes features in the two cases similar, including adsorbed amounts and layer thicknesses. Electrostatic interactions are essentially irrelevant. The bottom of the right-hand side, diagram **e**, describes behavior at intermediate c_s. Either electrostatics (top portion) or segment–surface interaction energy (bottom portion) can dominate. In the latter case, a polyelectrolyte adsorbs to a similarly charged surface with its fixed charges positioned as far away from the surface as is possible.

Sufficiently large χ_s can drive polyelectrolytes to adsorb on uncharged surfaces. Factors that enhance electrostatic repulsions within and between chains will oppose adsorption, as these interactions grow in step with the enhancement of segment concentration within an adsorbed layer. The adsorbed amount thus increases with c_s and decreases with ξ. Many studies show that polyelectrolyte adsorption is irreversible, just as with neutral polymers (*irreversible* implying undetectable desorption into polymer-free solvent) and that adsorbed layers equilibrate slowly, over time scales much longer than would be ordinary with neutral polymers (269,271). Because relaxation within layers is so slow, metastable states may persist over all practical time scales, with properties reflecting not just current conditions but the entire layer history.

To create polyelectrolyte brushes, which share many properties with adsorbed layers, chains are terminally attached to a surface through the hydrophobic association of a neutral end block or the covalent linkage of an end functionality (272–276). Many natural polymers are *polyampholytes*, polymers that can adsorb to a charged surface through segments of opposite charge even when the net charge interaction appears repulsive (277). Another adsorption phenomenon, of recent discovery and not yet fully understood, is *layer-by-layer* polyelectrolyte deposition (278–285). The *layer-by-layer* method capitalizes on the overcompensation of charge noted when polyelectrolytes are exposed to oppositely charged surfaces. Thus, a surface with inherently negative charge, such as a silicon oxide in contact with water, will adsorb sufficient cationic polyelectrolyte to become positively charged. This positive charge, in turn, can be overcompensated by adsorption of

an anionic polyelectrolyte. The process continues through alternating, sequential exposures of the surface to solutions of anionic and cationic polyelectrolyte. The final film may consist of hundreds of interpenetrated but identifiable polyelectrolyte layers; desirable properties included high uniformity, good stability in aqueous environments, and precise control of final layer thickness.

Adsorption or attachment of polyelectrolytes to dispersed colloidal particles underlies a number of technologies requiring particle stabilization or destabilization. Among these are paper manufacturing, paint formulation, mineral separation, water purification, and wastewater treatment. Stabilization prevents attractive interparticle forces, particularly short-range van der Waals forces, from causing particle aggregation, while destabilization, by exploiting new or enhanced attractive interparticle forces, accomplishes the opposite. Although terminologies and definitions vary, the aggregation of colloidal particles by added agents is usually termed *flocculation*. Permanent particle aggregates are called *flocs*, which typically possess a fractal structure that incorporates a considerable solvent fraction. By increasing effective particle size, flocculation plays an important role in solid–liquid separation processes such as filtration, flotation, and sedimentation.

Combining steric (ie configurational), osmotic, and electrostatic contributions, adsorbed/attached polyelectrolytes can modify interparticle forces in complex ways (286–291). Stabilization typically ensues when polyelectrolytes are irreversibly adsorbed/attached to particle surfaces at high density and in such a way that the chains extend significantly into the solution phase. High molecular weight polyelectrolyte brushes at large grafting density offer perhaps the most effective stabilization, but the same outcome often may be achieved more simply, for example, by the charge reversal created when polyelectrolytes adsorb to saturation on lightly charged particles. It is important for stabilization that the thickness of the adsorbed/attached polyelectrolyte layer exceeds the distance to the primary minimum of the van der Waals attraction. The irreversibility of polyelectrolyte stabilization contrasts with the reversibility of similar stabilization by surfactants.

Two distinct mechanisms have been identified for particle flocculation by added polyelectrolyte, *bridging* and *charge neutralization*. Bridging is effective when a high molecular weight, lightly charged polyelectrolyte is introduced to a dense dispersion of particles onto which the polymer adsorbs. The polyelectrolyte chains are long enough and the interparticle distances small enough for chains to link two or more particles. A loose polyelectrolyte layer structure favors bridging, as does a low adsorbed amount that leaves free a large fraction of the particle surface area. With a high adsorbed amount, the surface areas needed for bridging contacts become sparse, and stabilization arises rather than flocculation. Charge neutralization is effective when a polyelectrolyte of low molecular weight and high charge density is introduced to a dispersion of oppositely charged particles. The chains adsorb as a thin layer to an adsorbed amount that effectively compensates for the particle charge. The electrostatic stabilization of the bare particles is lost, causing flocculation. Since additional adsorption can recover electrostatic stabilization, charge neutralization is observed over a narrow window of polyelectrolyte concentration. In one variant of charge neutralization, termed the “electrostatic patch” mechanism, the point of charge compensation is achieved when the adsorbed polyelectrolyte has not yet fully covered the particle surface. The resulting

heterogeneity of surface charge induces attractive particle forces above those expected with uniform coverage. Bridging produces mechanically stronger flocs than charge neutralization.

Polyelectrolyte Complexes

Polyelectrolyte complexation forms a field as vast as polyelectrolyte adsorption, and so again, only the most salient features are mentioned. Complexes spontaneously form when polyelectrolytes are added to systems containing certain multivalent counterions (144,145,147), organic dyes with ionic groups (150), charged surfactants (292–295), oppositely charged polyelectrolytes (95,296–299), charged dendrimers (300,301), and charged colloids (95); the latter was discussed in the previous section. In addition to the systems listed, there are many examples of polyelectrolytes forming complexes with species such as neutral polymers, neutral surfactants, monovalent counterions, as well as proteins, viruses, and other biological structures.

Cooperative interactions among chain segments distinguish polyelectrolyte complexes from the complexes formed by low molecular weight compounds (302). As polyelectrolyte molecular weight decreases, the cooperativity is lost, and eventually complexation itself may disappear. Direct charge–charge interactions between polyelectrolyte "host" and oppositely charged "guest" drive polyelectrolyte complexations but so too does the entropy gain associated with the release of small counterions. Host–guest complexes characterized by 1:1 charge ratio are common. Most of these stoichiometric complexes are effectively insoluble, although at extremely low concentration solubility may be recovered. Nonstoichiometric complexes, on the other hand, are usually soluble or at least dispersible as charged aggregates or assemblies.

While polyelectrolyte charge density and solution ionic strength play a role in the final properties of soluble complexes, their greatest impacts are felt during complex formation and dissociation. Newly formed complexes are rarely ordered, and if mobilities of components are low, will remain disordered forever (302). There seems to be no universal approach for describing kinetic processes within a complex or predicting whether order will eventually appear. Complexes with smaller, less charged, and more mobile species, such as counterions, organic dyes, and surfactants, more often organize into well-defined structures, while polyelectrolyte–polyelectrolyte complexes usually possess a permanent "scrambled egg" morphology (95). Complexation at higher concentrations leads to structures reminiscent of thermoreversible gels. Such systems can frequently be disrupted or dissociated by altering parameters such as ionic strength so as to weaken electrostatic interactions.

Two complex types are given special attention. When charged surfactants are added to a solution of oppositely charged polyelectrolyte, the surfactant molecules begin to form micelles at a well-defined surfactant concentration that can be several orders of magnitude below the usual critical micelle concentration; this new concentration threshold is usually termed the *critical aggregation concentration*. The micelles formed under this condition may bind to the polyelectrolyte chains to form soluble complexes that have been described as possessing the "necklace

of beads" morphology (303–307); in other instances, spherical or cylindrical surfactant micelles apparently cluster into larger, dense aggregates surrounded or interpenetrated by polyelectrolyte (307). Bound micelles are smaller than free micelles formed above the critical micelle concentration in the absence of polyelectrolyte.

The thermodynamic factors governing the local organization of polyelectrolyte–surfactant complexes remain uncertain, but some have speculated that the polyelectrolyte chains stabilize smaller micelles by adsorbing to their surfaces. Stabilization clearly combines both electrostatic and hydrophobic interactions, making the outcome of complexation dependent on the chemistry of both polymer and surfactant. As the surfactant concentration increases, reaching a level at which enough micelles bind on the polyelectrolyte to raise the complex stoichiometry to approximately 1:1, solubility is lost and an ordered polymer–micelle precipitate appears (294); the unique solid-state structures so-formed are being intensely investigated for applications ranging from nonwetting coatings to drug delivery. Only as more surfactant is added to the phase-separated mixture do free surfactant micelles begin to appear. In some instances, even greater levels of added surfactant can resolubilize the precipitated complex. All of these behaviors depend strongly on ionic strength.

Polyelectrolytes form insoluble, stoichiometric (1:1 charge ratio) complexes when mixed with oppositely charged polyelectrolytes (95), especially if the mixing is performed under salt-free conditions at polymer concentrations that are neither extremely low nor high. The complex formation is fast and nearly molecular weight independent beyond the oligomer range. Soluble, nonstoichiometric complexes can be formed in two ways, by mixing oppositely charged polyelectrolytes of highly different molecular weights at nonstoichiometric mixing ratios (296) or by mixing oppositely charged polyelectrolytes at very low polymer concentrations (298). As opposed to polyelectrolyte–surfactant complexes, polyelectrolyte–polyelectrolyte complexes have little, if any, order, a feature probably reflecting the low mobility of their constituent chains. The driving forces for complexation is principally counterion release into a polyelectrolyte-depleted solution phase, a release that raises the entropy of the complexed system. Dependent on levels of added electrolyte, polyelectrolyte–polyelectrolyte complexes can undergo swelling, flocculation, and dissolution. When mixed at high polymer concentrations, oppositely charged polyelectrolytes may form an optically clear, one-phase system.

Polyelectrolyte Simulations

Serious difficulties abound in formulating analytical theories able to describe polyelelectrolyte phenomena, and so it is unsurprising that molecular simulation of these phenomena has seen much activity and development over the past decade. Unfortunately, few consensus judgments have as yet emerged about the relevance of simulation results to the properties of real polyelectrolytes. This situation will certainly change in the near future. A major issue in simulating polyelectrolytes is the long-range nature of electrostatic interactions. For a salt-free system containing a single flexible N-unit chain bearing a charge on each unit, the calculation of the electrostatic energy for each chain configuration requires

a computation time proportional to N^2. Thermally equilibrating this chain so as to explore configuration space fully requires the same step be repeated N^2 times. Thus, the total computation time for a simulation of equilibrium chain structure is proportional to N^4. A comparable calculation involving only short-range interactions, such as would be needed for the same chain without its charges, would entail a computation time proportional only to N^3. Various schemes have been devised to make polyelectrolyte simulations more computationally tractable, and each makes debatable physical approximations. Simulations attacking three general problems have been reported: the structure of the ion cloud near a polyelectrolyte segment (308–318), the overall configurational properties of a single flexible chain (311,312,317–331), and the structure of a system containing many polyelectrolyte chains (317,318,326,328,329,331).

Le Bret and Zimm (308), and later Vlachy and Haymet (309), Valleau (311), Christos and Carnie (312), and Stevens and Plimpton (317) examined ion distributions near polyelectrolyte segments by applying Monte Carlo or molecular dynamics methods that explicitly account for finite counterion size, treat electrostatic interactions at the level of full (not screened) Coulombic potentials, and represent water as a dielectric continuum. These constraints define the "primitive" model, which allows local correlations to develop in the placement of small ions. Two effects create such correlations, excluded volume (finite ion size) and electrostatics; mean field models (Poisson–Boltzmann, counterion condensation) incorporate neither of these effects. Within some simulations, limited structural or even molecular detail has been given the polyelectrolyte segment (332). In fewer cases, the standard primitive model was modified to account for the spatial variation of the dielectric constant near the chain backbone, recognizing that the high electric fields developed in this region can polarize the solvent (313,333). Adding even greater sophistication, Siebel and co-workers (334), Gordon and Goldman (335), Forester and McDonald (336), and Beveridge and Jayaram (337) performed simulations of ion distributions that replace the dielectric continuum of the primitive model with explicit solvent molecules. Many of these investigators specifically formulated simulation appropriate to DNA by assuming cylindrical or helical descriptions of the polyelectrolyte, while others formulated simulations appropriate to more flexible polyelectrolytes.

Le Bret and Zimm (308), modeling DNA as a dielectric cylinder within the primitive model, noted significant deviations from Poisson–Boltzmann predictions when either multivalent counterions or an large excess of positive and negative small ions are present. Also, they found strikingly large counterion concentrations, exceeding 1 M, at the model DNA surface, reminiscent of the oft-hypothesized condensed counterions. Others confirmed the findings (337), and in most instances, reported that the high counterion surface concentration persists as the bulk electrolyte concentration is varied, as predicted by counterion condensation but not Poisson–Boltzmann theory. Several investigations observed by simulation that screening of charges for flexible polyelectrolytes is much stronger than predicted by the Debye–Hückel approximation because counterions preferentially place themselves so as to heighten screening effects (311,312). Vlachy and Haymet deduced that the Poisson–Boltzmann equation retains semiquantitative utility for monovalent added electrolyte up to concentrations of $\sim$ 1 M. In the presence of divalent ions, the same investigators observed a cloud of counterions

clustered close to the chain of sufficient density to invert overall charge, another effect not predictable by Poisson–Boltzmann theory (309). More recently, the same overcompensation was reported for monovalent electrolyte at high concentration (316). Simulation studies have offered limited support for the classical counterion condensation depiction but interpretation of this concept within the context of simulation models is not unambiguous. Gonzales-Tovar and co-workers evaluated ion distributions through the hypernetted chain approximation, an analytical screening formalism of greater accuracy than the Poisson–Boltzmann equation, and identified several failings of counterion condensation (338) that others have identified through simulation.

Numerous simulations assessing the configurational properties of a single polyelectrolyte chain bathed in salt-free or electrolyte-containing solutions have been reported. Except for intrinsically stiff chains, nearly all studies have indicated that the OSF model overestimates the local stiffness of a highly charged, flexible polyelectrolyte as well as the dependence of this stiffness on electrolyte concentration. With intrinsically stiff chains, the OSF model appears to be quantitative. Molecular dynamics simulations by Stevens and Kremer suggested that the local structure of a flexible polyelectrolyte under salt-free conditions is not worm-like (326,327). Rather, these authors concluded that local counterions fluctuations cause the stiff (but not rod-like) chain segments to kink. Similarly, Micka and Kremer argued from simulation results that l_p is an inadequate measure by which to describe the conformation of a polyelectrolyte chain (330). Most simulations focused on polyelectrolyte coil size have assumed a priori a screening formula for electrostatic interactions between chain segments; commonly, screening has been applied using the form predicted by Debye–Hückel linearization. Irrespective of formalism, trends reported for the molecular weight dependence of coil size in the presence of electrolyte are reasonably consistent, although dispute persists about the precise dependence on c_s and whether simulated trends reflect asymptotic high M behavior (318,321,323,331,339). Under salt-free conditions, several simulations showed that polyelectrolyte chains are extended by repulsive segment–segment interactions such that $R \sim M$, but nonetheless, R_g remains less, by perhaps an order of magnitude, than it would be for a totally extended, rod-like configuration (311,326).

Simulation studies of polyelectrolyte–polyelectrolyte interactions appropriate to nondilute polyelectrolyte solutions are in their infancy. Stevens and coworkers performed a multiple chain, explicit counterion simulation demonstrating an extended-to-coiled conformational transition during passage from dilute to semidilute in a salt-free solution; this contraction unexpectedly began at c significantly below c^* (317,326). The same investigators found that simulated osmotic pressures during the c to c^* transition are reasonably consistent with experimental data but not with simulation results relying on Debye–Hückel linearization (328). For systems below coil overlap, Chu and Mak discovered by molecular dynamics simulation the presence of inter- and intrachain attractions that strengthen with increasing polymer concentration and Bjerrum length (318).

Many simulations of dynamic phenomena such as adsorption, electrophoretic motion, complexation, dilute solution viscosity, and electric birefringence have also been reported for polyelectrolytes, often for the purpose of gaining insight into experimental situations too complex for analytical theory. These

application-specific simulations usually apply polyelectrolyte models that ignore properties such as excluded volume, high charge density, or solvent viscosity. Such simulations guide physical understanding but normally do not offer any quantitative predictions other than scaling laws.

BIBLIOGRAPHY

"Polyelectrolytes" in *EPST* 1st ed., Vol. 10, pp. 781–861, by R. W. Armstrong and U. P. Strauss, Rutgers, The State University; "Polyelectrolytes" in *EPSE* 2nd ed., Vol. 11, pp. 739–829, by M. Mandel, University of Leiden.

1. J. R. Huizenga, P. F. Grieger, and F. T. Wall, *J. Am. Chem. Soc.* **72**, 2636–2642 (1950).
2. R. M. Fuoss, A. Katchalsky, and S. Lifson, *Proc. Natl. Acad. Sci., U.S.A.* **37**, 579–589 (1951).
3. F. Oosawa, N. Imai, and I. Kagawa, *J. Polym. Sci.* **13**, 93–111 (1954).
4. F. Oosawa, *J. Polym. Sci.* **23**, 421–430 (1957).
5. N. Imai and T. Onishi, *J. Chem. Phys.* **30**, 1115–1116 (1959).
6. T. Ohnishi, N. Imai, and F. Oosawa, *J. Phys. Soc. Jpn.* **15**, 896–905 (1960).
7. Z. Alexandrowicz, *J. Polym. Sci.* **56**, 97–114 (1962).
8. Z. Alexandrowicz and E. Daniel, *Biopolymers* **1**, 447–471 (1963).
9. A. Ikegami, *J. Polym. Sci., Part A* **2**, 907–921 (1964).
10. A. D. MacGillivray and J. J. Winkleman Jr., *J. Chem. Phys.* **45**, 2184–2188 (1966).
11. F. Oosawa, *Biopolymers* **6**, 1633–1647 (1968).
12. F. Oosawa, *Polyelectrolytes*, Marcel Dekker, New York, 1971, 160 pp.
13. G. S. Manning, *J. Chem. Phys.* **51**, 924–933 (1969).
14. G. S. Manning, *J. Chem. Phys.* **51**, 934–938 (1969).
15. G. S. Manning, *J. Chem. Phys.* **51**, 3249–3252 (1969).
16. G. S. Manning, *Q. Rev. Biophys.* **11**, 179–246 (1978).
17. G. S. Manning, *Annu. Rev. Phys. Chem.* **23**, 117–140 (1972).
18. G. S. Manning, *J. Phys. Chem.* **79**, 262–265 (1975).
19. G. S. Manning, *Biophys. Chem.* **7**, 95–102 (1977).
20. G. S. Manning, *Ber. Bunsen-Ges. Phys. Chem.* **100**, 909–922 (1996).
21. G. S. Manning, *Physica A* **231**, 236–253 (1996).
22. J. Ray and G. S. Manning, *Macromolecules* **32**, 4588–4595 (1999).
23. M. O. Fenley, W. K. Olson, and G. S. Manning, *Macromolecules* **33**, 1899–1903 (2000).
24. G. S. Manning, *Macromolecules* **34**, 4650–4655 (2001).
25. T. Alfrey Jr., P. W. Berg, and H. Morawetz, *J. Polym. Sci.* **7**, 543–547 (1951).
26. P. J. Heath and J. M. Schurr, *Macromolecules* **25**, 4149–4159 (1992).
27. G. S. Manning, *Acc. Chem. Res.* **12**, 443–449 (1979).
28. D. Stigter, *J. Phys. Chem.* **82**, 1603–1606 (1978).
29. M. Fixman, *J. Chem. Phys.* **70**, 4995–5005 (1979).
30. M. Guéron and G. Weisbuch, *Biopolymers* **19**, 353–382 (1980).
31. M. Mandel, *Eur. Polym. J.* **19**, 911–918 (1983).
32. M. Le Bret and B. H. Zimm, *Biopolymers* **23**, 287–312 (1984).
33. K. S. Schmitz, *Macroions in Solution and Colloidal Suspension*, VCH Publishers, New York 1993, 401 pp.
34. D. Stigter, *Biophys. J.* **69**, 380–388 (1995).
35. C. F. Anderson and M. T. Record Jr., *Ann. Rev. Phys. Chem.* **33**, 191–222 (1982).
36. B. H. Zimm, in A. Eisenberg and F. E. Bailey, eds., *Coulombic Interactions in Macromolecular Systems* (ACS Symposium Series 302), American Chemical Society, Washington, D.C., 1986, pp. 212–215.

37. E. Daniel and Z. Alexandrowicz, *Biopolymers* **1**, 473–495 (1963).
38. G. S. Manning and A. Holtzer, *J. Phys. Chem.* **77**, 2206–2212 (1973).
39. G. E. Boyd, D. P. Wilson, and G. S. Manning, *J. Phys. Chem.* **80**, 808–810 (1976).
40. K. Iwasa, *J. Phys. Chem.* **81**, 1829–1833 (1977).
41. B. K. Klein, C. F. Anderson, and M. T. Record Jr., *Biopolymers* **20**, 2263–2280 (1981).
42. P. Ander and M. Kardan, *Macromolecules* **17**, 2431–2436 (1984).
43. J. W. Klein and B. R. Ware, *J. Chem. Phys.* **80**, 1334–1338 (1984).
44. C. F. Wu, H. Chen, L. B. Shih, and J. S. Lin, *J. Appl. Crystallogr.* **21**, 853–857 (1988).
45. L. M. Penafiel and T. A. Litovitz, *J. Chem. Phys.* **97**, 559–567 (1992).
46. D. A. Hoagland, D. L. Smisek, and D. Y. Chen, *Electrophoresis* **17**, 1151–1160 (1996).
47. U. Mohanty, B. W. Ninham, and I. Oppenheim, *Proc. Natl. Acad. Sci. U.S.A.* **93**, 4342–4344 (1996).
48. R. M. Nyquist, B.-Y. Ha, and A. J. Liu, *Macromolecules* **32**, 3481–3487 (1999).
49. H. Schiessel, *Macromolecules* **32**, 5673–5680 (1999).
50. M. Deserno, C. Holm, and S. May, *Macromolecules* **33**, 199–206 (2000).
51. R. M. Davis and W. B. Russell, *J. Polym. Sci., Part B: Polym. Phys.* **24**, 511–533 (1986).
52. L. Belloni, *Colloids Surf.* **140**, 227–243 (1998).
53. A. Katchalsky, *J. Polym. Sci.* **7**, 393–412 (1951).
54. W. Kuhn, O. Künzle, and A. Katchalsky, *Helv. Chim. Acta* **31**, 1994–2037 (1948).
55. P. J. Flory, *J. Chem. Phys.* **21**, 162–163 (1953).
56. J. J. Hermans and T. T. G. Overbeek, *Recl. Trav. Chim. Pays-Bas* **67**, 761–776 (1948).
57. P. Pfeuty, *J. Phys. Colloq.* **39**, C2–C149 (1978).
58. T. Odijk, *J. Polym. Sci., Polym. Phys. Ed.* **15**, 477–483 (1977).
59. T. Odijk, *Polymer* **19**, 989–990 (1978).
60. T. Odijk and A. C. Houwaart, *J. Polym. Sci., Polym. Phys. Ed.* **16**, 627–639 (1978).
61. T. Odijk, in K.-H. Brennemann, F. Brouers, and D. Quitmann, eds., *Ionic Liquids, Molten Salts, and Polyelectrolytes* (Lecture Notes in Physics 172), Springer-Verlag, New York, 1982, pp. 184–198.
62. J. Skolnick and M. Fixman, *Macromolecules* **10**, 944–948 (1977).
63. M. Fixman and J. Skolnick, *Macromolecules* **11**, 863–867 (1978).
64. J.-L. Barrat and J.-F. Joanny, *Europhys. Lett.* **24**, 333–338 (1993).
65. J.-L. Barrat and J.-F. Joanny, in I. Prigogine and S. A. Rice, eds., *Advances in Chemical Physics*, Vol. **94**, John Wiley & Sons, Inc., New York, 1996, pp. 1–66.
66. M. Muthukumar, *J. Chem. Phys.* **86**, 7230–7235 (1987).
67. M. Beer, M. Schmidt, and M. Muthukumar, *Macromolecules* **30**, 8375–8385 (1997).
68. K. Ghosh, G. A. Carri, and M. Muthukumar, *J. Chem. Phys.* **115**, 4367–4375 (2001).
69. M. Fixman, *J. Chem. Phys.* **76**, 6346–6353 (1982).
70. M. Le Bret, *J. Chem. Phys.* **76**, 6243–6255 (1982).
71. S. Förster and M. Schmidt, *Adv. Polym. Sci.* **120**, 51–133 (1995).
72. A. Katchalsky, O. Künzle, and W. Kuhn, *J. Polym. Sci.* **5**, 283–300 (1950).
73. P. G. de Gennes, P. Pincus, R. M. Velasco, and F. Brochard, *J. Phys.* **37**, 1461–1473 (1976).
74. P. Richmond, *J. Phys. A: Math., Nucl., Gen.* **6**, L109–L111 (1973).
75. H. Li. and T. A. Witten, *Macromolecules* **28**, 5921–5927 (1995).
76. M. Fixman, *J. Chem. Phys.* **41**, 3772–3778 (1964).
77. A. R. Khokhlov and K. A. Khachaturian, *Polymer* **23**, 1742–1750 (1982).
78. C. Qian and A. L. Kholodenko, *J. Chem. Phys.* **89**, 2301–2311 (1988).
79. M. Schmidt, *Macromolecules* **24**, 5361–5364 (1991).
80. S. Förster, M. Schmidt, and M. Antonietti, *J. Phys. Chem.* **96**, 4008–4014 (1992).
81. B. Y. Ha and D. Thirumalai, *Macromolecules* **28**, 577–581 (1995).

82. A. V. Dobrynin, M. Rubinstein, and S. P. Obukhov, *Macromolecules* **29**, 2929–2974 (1996).
83. A. V. Dobrynin, R. H. Colby, and M. Rubinstein, *Macromolecules* **28**, 1859–1871 (1995).
84. A. V. Dobrynin and M. Rubinstein, *Macromolecules* **32**, 915–922 (1999).
85. D. Stigter and K. A. Dill, *Macromolecules* **28**, 5325–5337 (1995).
86. D. Stigter and K. A. Dill, *Macromolecules* **28**, 5338–5346 (1995).
87. E. Dubois and F. Boué, *Macromolecules* **34**, 3684–3697 (2001).
88. M. Tricot, *Macromolecules* **17**, 1698–1704 (1984).
89. W. F. Reed, S. Ghosh, G. Medjahdi, and J. François, *Macromolecules* **24**, 6189–6198 (1991).
90. K. Nishida, K. Kaji, T. Kanaya, and N. Fanjat, *Polymer* **43**, 1295–1300 (2002).
91. L. Wang and H. Yu, *Macromolecules* **21**, 3498–3501 (1988).
92. J. J. Tanahatoe and M. E. Kuil, *Macromolecules* **30**, 6102–6106 (1997).
93. K. Kassapidou, W. Jesse, M. E. Kuil, A. Lapp, S. Egelhaaf, and J. R. C. van der Maarel, *Macromolecules* **30**, 2671–2684 (1997).
94. P.-G. de Gennes, *Scaling Concepts in Polymer Physics*, Cornell University Press, Ithaca, N.Y., 1979, 324 pp.
95. H. Dautzenberg, W. Jaeger, J. Kötz, B. Philipp, C. Seidel, and D. Stscherbina, *Polyelectrolytes: Formation, Characterization, and Application*, Hanser Publishers, New York, 1994, 343 pp.
96. D. C. Boris and R. H. Colby, *Macromolecules* **31**, 5746–5755 (1998).
97. S. Lifson and A. Katchalsky, *J. Polym. Sci.* **13**, 43–55 (1954).
98. T. Odijk, *Macromolecules* **12**, 688–693 (1979).
99. J. Hayter, G. Janninck, F. Brochard-Wyart, and P. G. de Gennes, *J. Phys. Lett.* **41**, L451–L454 (1980).
100. T. A. Witten and P. Pincus, *Europhys. Lett.* **3**, 315–320 (1987).
101. G. Weill, *J. Phys.* **49**, 1049–1054 (1988).
102. M. Mandel, in M. Hara, ed., *Polyelectrolytes: Science and Technology*, Marcel Dekker, New York, 1993, pp. 1–75.
103. M. Rubinstein, R. H. Colby, and A. V. Dobrynin, *Phys. Rev. Lett.* **73**, 2776–2779 (1994).
104. M. Muthukumar, *J. Chem. Phys.* **105**, 5183–5199 (1996).
105. J. P. Donley, J. Rudnick, and A. J. Liu, *Macromolecules* **30**, 1188–1193 (1997).
106. A. V. Dobrynin and M. Rubinstein, *Macromolecules* **34**, 1964–1972 (2001).
107. K. Kaji, H. Urakawa, T. Kanaya, and R. Kitamaru, *J. Phys.* **49**, 993–1000 (1988).
108. K. Nishida, K. Kahi, and T. Kanaya, *J. Chem. Phys.* **114**, 8671–8677 (2001).
109. J.-P. Cotton and M. Moan, *J. Phys. Lett.* **37**, L75–L77 (1976).
110. M. Moan, C. Wolff, J.-P. Cotton, and R. Ober, *J. Polym. Sci., Polym. Symp.* **61**, 1–8 (1977).
111. M. Nierlich, C. E. Williams, F. Boué, J. P. Cotton, M. Daoud, B. Farnoux, G. Jannik, C. Picot, M. Moan, C. Wolff, M. Rinaudo, and P. G. de Gennes, *J. Phys.* **40**, 701–704 (1979).
112. M. Drifford and F. Dalbiez, *J. Phys. Chem.* **88**, 5368–5375 (1984).
113. M. Nierlich, F. Boué, A. Lapp, and R. Overthür, *Coll. Polym. Sci.* **263**, 955–964 (1985).
114. B. D. Ermi and E. J. Amis, *Macromolecules* **30**, 6937–6942 (1997).
115. R. Koyama, *Macromolecules* **19**, 178–182 (1986).
116. R. Koyama, *Macromolecules* **17**, 1594–1598 (1984).
117. N. Ise, T. Okubo, S. Kunugi, H. Matsuoka, K. Yamamoto, and Y. Ishii, *J. Chem. Phys.* **81**, 3294–3306 (1984).
118. S. Förster, M. Schmidt, and M. Antonietti, *Polymer* **31**, 781–792 (1990).

119. H. Matsuoka, D. Schwahn, and N. Ise, *Macromolecules* **24**, 4227–4228 (1991).
120. M. Sedlák and E. J. Amis, *J. Chem. Phys.* **96**, 817–825 (1992).
121. P. Wissenburg, T. Odijk, P. Cirkel, and M. Mandel, *Macromolecules* **27**, 306–308 (1994).
122. N. Ise, *Ber. Bunsen-Ges. Phys. Chem.* **100**, 841–848 (1996).
123. B. D. Ermi and E. J. Amis, *Macromolecules* **31**, 7378–7384 (1998).
124. T. L. Hill, *An Introduction to Statistical Thermodynamics*, Addison-Wesley, Reading, Mass., 1960, pp. 359–363.
125. I. Sagami and N. Ise, *J. Chem. Phys.* **81**, 6320–6332 (1984).
126. T. Odijk, *Macromolecules* **27**, 4998–5003 (1994).
127. J. Ray, *Langmuir* **10**, 2450–2461 (1994).
128. I. Rouzina and V. A. Bloomfield, *J. Phys. Chem.* **100**, 9977–9989 (1996).
129. R. Kjellander, *Ber. Bunsen-Ges. Phys. Chem.* **100**, 894–904 (1996).
130. B. J. Ha and A. J. Liu, *Phys. Rev. Lett.* **79**, 1289–1292 (1997).
131. J. Ray and G. S. Manning, *Macromolecules* **30**, 5739–5744 (1997).
132. N. Grønbech-Jensen, R. J. Mashl, R. F. Bruinsma, and W. M. Gelbart, *Phys. Rev. Lett.* **78**, 2477–2480 (1997).
133. K. S. Schmitz, *Langmuir* **13**, 5849–5863 (1997).
134. H. Greberg and R. Kjellander, *J. Chem. Phys.* **108**, 2940–2953 (1998).
135. H. Eisenberg and G. Ram Mohan, *J. Phys. Chem.* **63**, 671–680 (1959).
136. I. Michaeli, *J. Polym. Sci.* **48**, 291–299 (1960).
137. A. Ikegami and N. Imai, *J. Polym. Sci.* **56**, 133–152 (1962).
138. M. A. V. Axelos, M. M. Mestdagh, and J. Francois, *Macromolecules* **27**, 6594–6602 (1994).
139. M. Delsanti, J. P. Dalbiez, O. Spalla, L. Belloni, and M. Drifford, in K. S. Schmitz, ed., *Macro-ion Characterization: From Dilute Solutions to Complex Fluids* (ACS Symposium Series 548), American Chemical Society, Washington, D.C., 1994, pp. 381–392.
140. M. Olvera de la Cruz, L. Belloni, M. Delsanti, J. P. Dalbiez, O. Spalla, and M. Drifford, *J. Chem. Phys.* **103**, 5781–5791 (1995).
141. V. M. Prabhu, M. Muthukumar, G. D. Wignall, and Y. B. Melnichenko, *Polymer* **42**, 8935–8946 (2001).
142. K. A. Narh and A. Keller, *J. Polym. Sci., Part B: Polym. Phys.* **31**, 231–234 (1993).
143. J. Wittmer, A. Johner, and J. F. Joanny, *J. Phys. II* **5**, 635–654 (1995).
144. E. Raspaud, M. Olvera de la Cruz, J.-L. Sikorav, and F. Livolant, *Biophys. J.* **74**, 381–393 (1998).
145. V. A. Bloomfield, C. Ma, and P. G. Arscott, in K. S. Schmitz, ed., *Macro-ion Characterization: From Dilute Solutions to Complex Fluids* (ACS Symposium Series 548), American Chemical Society, Washington, D.C., 1994, pp. 195–209.
146. V. Bloomfield, *Curr. Opin. Struct. Biol.* **6**, 334–341 (1996).
147. E. Raspaud, I. Chaperon, A. Leforestier, and F. Livolant, *Biophys. J.* **77**, 1547–1555 (1999).
148. M. O. Khan, S. M. Mel'nikov, and B. Jönsson, *Macromolecules* **32**, 8836–8840 (1999).
149. W. M. Gelbart, R. F. Bruinsma, P. Pincus, and V. A. Parsegian, *Phys. Today*, 38–44 (2000).
150. V. Vitagliano, in E. Wyn-Jones and J. Gormally, eds., *Aggregation Processes in Solution*, Elsevier, New York, 1983, pp. 271–308.
151. P. J. Flory, *Principles of Polymer Chemistry*, Cornell University Press, Ithaca, N.Y., 1953, pp. 595–639.
152. D. F. Hodgson and E. J. Amis, in M. Hara, ed., *Polyelectrolytes: Science and Technology*, Marcel Dekker, New York, 1993, pp. 127–191.
153. J. Cohen, Z. Priel, and Y. Rabin, *J. Chem. Phys.* **88**, 7111–7116 (1988).

154. R. M. Fuoss and U. P. Strauss, *J. Polym. Sci.* **3**, 246–263 (1948).
155. R. M. Fuoss and U. P. Strauss, *J. Polym. Sci.* **3**, 602–603 (1948).
156. R. M. Fuoss, *J. Polym. Sci.* **3**, 603 (1948).
157. R. M. Fuoss, *Discuss. Faraday Soc.* **11**, 125–134 (1951).
158. A. Katchalsky and H. Eisenberg, *J. Polym. Sci.* **6**, 145–154 (1951).
159. A. Oth and P. Doty, *J. Phys. Chem.* **56**, 43–50 (1952).
160. D. F. Hodgson and E. J. Amis, *J. Chem. Phys.* **91**, 2635–2642 (1989).
161. D. F. Hodgson and E. J. Amis, *J. Chem. Phys.* **95**, 7653–7663 (1991).
162. W. Reed, *J. Chem. Phys.* **101**, 2515–2521 (1994).
163. U. P. Strauss and E. H. Smith, *J. Am. Chem. Soc.* **75**, 6186–6188 (1953).
164. D. T. F. Pals and J. J. Hermans, *Recl. Trav. Chim. Pays-Bas* **71**, 433–457 (1952).
165. R. M. Davis and W. B. Russell, *Macromolecules* **20**, 518–525 (1987).
166. H. Eisenberg and J. Pouyet, *J. Polym. Sci.* **13**, 85–91 (1954).
167. H. Fujita and T. Homma, *J. Colloid Interface Sci.* **9**, 591–601 (1954).
168. H. Vink, *Makromol. Chem.* **131**, 133–145 (1970).
169. T. Okubo, *J. Chem. Phys.* **87**, 6733–6739 (1987).
170. Y. Rabin, J. Cohen, and Z. Priel, *J. Polym. Sci., Part C: Polym. Lett.* **26**, 397–399 (1988).
171. J. Cohen, Z. Priel, and Y. Rabin, *Polym. Comm.* **29**, 235–236 (1988).
172. J. Cohen and Z. Priel, *Macromolecules* **22**, 2356–2358 (1989).
173. J. Yamanaka, H. Matsuoka, H. Kitano, and N. Ise, *J. Colloid Interface Sci.* **134**, 92–106 (1990).
174. J. Yamanaka, H. Matsuoka, H. Kitano, M. Hasegawa, and N. Ise, *J. Am. Chem. Soc.* **112**, 587–592 (1990).
175. J. Yamanaka, H. Araie, H. Matsuoka, H. Kitano, N. Ise, T. Yamaguchi, S. Saeki, and M. Tsubokawa, *Macromolecules* **24**, 3206–3208 (1991).
176. M. Antonietti, A. Briel, and S. Förster, *J. Chem. Phys.* **105**, 7795–7807 (1996).
177. B. Klein and W. Hess, in K.-H. Brennemann, F. Brouers, and D. Quitmann, eds., *Ionic Liquids, Molten Salts, and Polyelectrolytes* (Lecture Notes in Physics 172), Springer-Verleg, New York, 1982, pp. 199–211.
178. M. Antonietti, A. Briel, and S. Förster, *Macromolecules* **30**, 2700–2704 (1997).
179. R. A. Cox, *J. Polym. Sci.* **47**, 441–445 (1960).
180. I. Noda, T. Tsuge, and M. Nagasawa, *J. Phys. Chem.* **74**, 710–719 (1970).
181. J. Brandrup and E. H. Immergut, eds. *Polymer Handbook*, 3rd ed., John Wiley & Sons, Inc., New York, 1989.
182. R. W. Rosser, N. Nemoto, J. L. Schrag, and J. D. Ferry, *J. Polym. Sci., Polym. Phys. Ed.* **16**, 1031–1040 (1978).
183. D. F. Hodgson and E. J. Amis, *J. Chem. Phys.* **94**, 4581–4586 (1991).
184. I. Noda and Y. Takahashi, *Ber. Bunsen-Ges. Phys. Chem.* **6**, 696–702 (1996).
185. J. T. G. Overbeek, *Bull. Soc. Chim. Belg.* **57**, 252–261 (1948).
186. M. Nagasawa, *Pure Appl. Chem.* **26**, 519–536 (1971).
187. A. Katchalsky and J. Gillis, *Recl. Trav. Chim. Pays-Bas* **68**, 879–897 (1949).
188. R. Arnold and J. T. G. Overbeek, *Recl. Trav. Chim. Pays-Bas* **69**, 192–206 (1950).
189. T. Kitano, S. Kawaguchi, K. Ito, and A. Minakata, *Macromolecules* **20**, 1598–1606 (1987).
190. M. Ullner and B. Jönsson, *Macromolecules* **29**, 6645–6655 (1996).
191. A. Katchalsky and P. Spitnik, *J. Polym. Sci.* **2**, 432–446 (1947).
192. M. Mandel, *Eur. Polym. J.* **6**, 807–822 (1970).
193. G. S. Manning, *J. Phys. Chem.* **85**, 870–877 (1981).
194. M. Mandel, in J. I. Kroschwitz, ed., *Encyclopedia of Polymer Science and Engineering*, Vol. **11**, John Wiley & Sons, Inc., New York, 1988, pp. 739–829.
195. M. Reddy and J. A. Marinsky, *J. Phys. Chem.* **74**, 3884–3891 (1970).

196. M. Reddy, J. A. Marinsky, and A. Sarkar, *J. Phys. Chem.* **74**, 3891–3895 (1970).
197. D. Kozak and D. Dolar, *Z. Phys. Chem.* **76**, 85–92 (1971).
198. D. Kozak and D. Dolar, *Z. Phys. Chem.* **76**, 93–97 (1971).
199. N. T. M. Klooster, F. van der Touw, and M. Mandel, *Macromolecules* **17**, 2078–2086 (1984).
200. T. L. Hill, *Disc. Faraday Soc.* **21**, 31–45 (1956).
201. L. Wang and V. A. Bloomfield, *Macromolecules* **23**, 194–199 (1990).
202. L. Wang and V. A. Bloomfield, *Macromolecules* **23**, 804–809 (1990).
203. Y. Suzuki, I. Noda, and M. Nagasawa, *J. Phys. Chem.* **73**, 797–803 (1969).
204. S.-C. Lin, W. I. Lee, and J. M. Schurr, *Biopolymers* **17**, 1041–1064 (1978).
205. N. Nemoto, H. Matsuda, Y. Tsunashima, and M. Kurata, *Macromolecules* **17**, 1731–1735 (1984).
206. R. G. Smits, M. E. Kuil, and M. Mandel, *Macromolecules* **26**, 6808–6816 (1993).
207. M. Sedlák, *Langmuir* **15**, 4045–4051 (1999).
208. P. Tivant, P. Turq, H. Magdelenat, and R. Menez, *Biopolymers* **22**, 643–662 (1983).
209. M. Sedák and E. J. Amis, *J. Chem. Phys.* **96**, 826–834 (1992).
210. M. Drifford and J.-P. Dalbiez, *Biopolymers* **24**, 1501–1514 (1985).
211. J. M. Schurr and K. S. Schmitz, *Annu. Rev. Phys. Chem.* **37**, 271–305 (1986).
212. L. Wang, M. M. Garner, and H. Yu, *Macromolecules* **24**, 2368–2376 (1991).
213. M. Sedlák, *Macromolecules* **26**, 1158–1162 (1993).
214. E. J. Amis, D. E. Valachovic, and M. Sedlák, in K. S. Schmitz, ed., *Macro-ion Characterization: From Dilute Solutions to Complex Fluids* (ACS Symposium Series 548), American Chemical Society, Washington, D.C., 1994, pp. 322–336.
215. A. Sehgal and T. A. P. Seery, *Macromolecules* **31**, 7340–7346 (1998).
216. A. Topp, L. Belkoura, and D. Woermann, *Macromolecules* **29**, 5392–5397 (1996).
217. M. E. Ferrari and V. A. Bloomfield, *Macromolecules* **25**, 5266–5276 (1992).
218. R. G. Smits, M. E. Kuil, and M. Mandel, *Macromolecules* **27**, 5599–5608 (1994).
219. S. Ghosh, R. M. Peitzsch, and W. F. Reed, *Biopolymers* **32**, 1105–1122 (1992).
220. K. S. Schmitz, *Biopolymers* **33**, 953–959 (1993).
221. M. Sedlák, *Macromolecules* **28**, 793–794 (1995).
222. M. G. Oostwal, M. H. Blees, J. de Bleijser, and J. C. Leyte, *Ber. Bunsen-Ges Phys. Chem.* **94**, 379–381 (1990).
223. M. G. Oostwal, M. H. Blees, J. de Bleijser, and J. C. Leyte, *Macromolecules* **26**, 7300–7308 (1993).
224. P. Ander and W. Lubas, *Macromolecules* **14**, 1058–1061 (1981).
225. F. J. M. Schipper, K. Kassapidou, and J. C. Leyte, *J. Phys.: Condens. Matter* **8**, 9301–9308 (1996).
226. F. J. M. Schipper, J. G. Hollander, and J. C. Leyte, *J. Phys.: Condens. Matter* **9**, 11179–11193 (1997).
227. S. Sasaki and F. J. M. Schipper, *J. Chem. Phys.* **115**, 4349–4354 (2001).
228. D. A. Hoagland, E. Arvantidou, and C. Welch, *Macromolecules* **32**, 6180–6190 (1999).
229. G. W. Slater, T. B. L. Kist, H. Ren, and G. Drouin, *Electrophoresis* **19**, 1–17 (1998).
230. S. S. Dukhin and B. V. Derjaguin, *Electrokinetic Phenomena* (Surfaces and Colloid Science, Vol. 7), John Wiley & Sons, Inc., New York, 356 pp.
231. D. Stigter, *J. Phys. Chem.* **82**, 1424–1429 (1978).
232. G. S. Manning, *J. Phys. Chem.* **85**, 1506–1516 (1981).
233. B. M. Olivera, P. Baine, and N. Davidson, *Biopolymers* **2**, 245–257 (1964).
234. G. S. Manning, *J. Phys. Chem.* **84**, 1059–1060 (1980).
235. L. R. Whitlock, in J. W. Jorgenson and M. Phillips, eds., *New Directions in Electrophoretic Methods* (ACS Symposium Series 335), American Chemical Society, Washington, D.C., 1987, pp. 222–246.

236. E. Arvanitidou and D. A. Hoagland, *Phys. Rev. Lett.* **67**, 1464–1466 (1991).
237. G. W. Slater, P. Mayer, and G. Drouin, *Methods Enzymol.* **270**, 272–295 (1996).
238. E. Fredericq and C. Houssier, *Electric Dichroism and Electric Birefringence*, Clarendon Press, New York, 1973, 219 pp.
239. C. T. O'Konski, *Molecular Electro-Optics*, Parts 1 (Theory and Methods) and 2 (Applications to Biopolymers), Marcel Dekker, New York, 1976, 868 pp.
240. M. Mandel, *Mol. Phys.* **4**, 489–496 (1961).
241. M. Fixman, *Macromolecules* **13**, 711–716 (1980).
242. M. Tricot and C. Houssier, *Macromolecules* **15**, 854–865 (1982).
243. K. Nagai and T. Ishikawa, *J. Chem. Phys.* **43**, 4508–4515 (1965).
244. R. W. Wilson, *Biopolymers* **17**, 1811–1814 (1978).
245. C. Johner, H. Kramer, C. Martin, J. Biegel, R. Deike, and R. Weber, *J. Phys. II* **5**, 721–732 (1995).
246. G. Weill and G. Maret, *Polymer* **23**, 1990–1993 (1982).
247. G. Maret and G. Weill, *Biopolymers* **22**, 2727–2744 (1983).
248. P. J. Hagerman, *Biopolymers* **20**, 1503–1535 (1981).
249. S. Wijmenga, F. van der Touw, and M. Mandel, in B. Sedlacek, ed., *Physical Optics of Dynamic Phenomena and Processes in Macromolecular Systems*, Walter de Gruyter & Co., New York, 1985, pp. 87–105.
250. S. Wijmenga, F. van der Touw, and M. Mandel, *Macromolecules* **19**, 1760–1768 (1986).
251. Z. Wang, R. Xu, and B. Chu, *Macromolecules* **23**, 790–796 (1990).
252. M. Mandel and T. Odijk, *Annu. Rev. Phys. Chem.* **35**, 75–108 (1984).
253. B. Saif, R. K. Mohr, C. J. Montrose, and T. A. Litovitz, *Biopolymers* **31**, 1171–1180 (1991).
254. J. C. T. Kwak and R. C. Hayes, *J. Phys. Chem.* **79**, 265–269 (1975).
255. J. Szymczak, P. Holyk, and P. Ander, *J. Phys. Chem.* **79**, 269–272 (1975).
256. H. Vink, *Makromol. Chem.* **183**, 2273–2283 (1982).
257. C. Wandrey, *Langmuir* **15**, 4069–4075 (1999).
258. A. H. Shaaban, K. Behilo, and P. Ander, in K. S. Schmitz, ed., *Physical Optics of Dynamic Phenomena and Processes in Macromolecular Systems* (ACS Symposium Series 548), American Chemical Society, Washington, D.C., 1994, pp. 180–194.
259. R. H. Colby, D. C. Boris, W. E. Krause, and J. S. Tan, *J. Polym. Sci., Part B: Polym. Phys.* **35**, 2951–2960 (1997).
260. C. Wandrey, D. Hunkeler, U. Wendler, and W. Jaeger, *Macromolecules* **33**, 7136–7143 (2000).
261. M. Kowblansky and P. Ander, *J. Phys. Chem.* **81**, 2024–2032 (1977).
262. R. S. Harland and R. K. Prud'homme, eds., *Polyelectrolyte Gels: Properties, Preparation, and Applications* (ACS Symposium Series 480), American Chemical Society, Washington, D.C., 1992, 316 pp.
263. S. Hirotsu, Y. Hirokawa, and T. Tanaka, *J. Chem. Phys.* **87**, 1392–1395 (1987).
264. A. Katchalsky and I. Michaeli, *J. Polym. Sci.* **15**, 69–86 (1955).
265. I. Ohmine and T. Tanaka, *J. Chem. Phys.* **77**, 5725–5729 (1982).
266. J.-L. Barrat, J.-F. Joanny, and P. Pincus, *J. Phys. II* **2**, 1531–1544 (1992).
267. M. Rubinstein, R. H. Colby, A. V. Dobrynin, and J.-F. Joanny, *Macromolecules* **29**, 398–406 (1996).
268. M. A. Cohen Stuart, *J. Phys.* **49**, 1001–1008 (1988).
269. M. A. Cohen Stuart, G. J. Fleer, J. Lyklema, W. Norde, and J. M. H. M. *Scheutjens, Adv. Colloid Interface Sci.* **34**, 477–535 (1991).
270. G. J. Fleer, M. A. Cohen Stuart, J. M. H. M. Scheutjens, T. Cosgrove, and B. Vincent, *Polymers at Interfaces*, Chapman & Hall, London, 1993, pp. 343–373.
271. W. Barford, R. C. Ball, and C. M. M. Nex, *J. Chem. Soc., Faraday Trans.* **1**, 82, 3233–3244 (1986).

272. P. Pincus, *Macromolecules* **24**, 2912–2919 (1991).
273. O. V. Borisov, E. B. Zhulina, and T. M. Birshtein, *Macromolecules* **27**, 4795–4803 (1994).
274. C. Amiel, M. Sikka, J. W. Schneider Jr., Y.-H. Tsao, M. Tirrell, and J. W. Mays, *Macromolecules* **28**, 3125–3134 (1995).
275. E. B. Zhulina, T. M. Birshtein, and O. V. Borisov, *Macromolecules* **28**, 1491–1499 (1995).
276. Y. Tran, P. Auroy, and L.-T. Lee, *Macromolecules* **32**, 8952–8964 (1999).
277. T. J. Maternaghan and R. H. Ottewill, *J. Photo. Sci.* **22**, 279–285 (1974).
278. G. Decher, J. D. Hong, and J. Schmitt, *Thin Solid Films* **210/211**, 831–835 (1992).
279. Y. Lvov, G. Decher, and H. Möhwald, *Langmuir* **9**, 481–486 (1993).
280. G. Decher, *Science* **277**, 1232–1237 (1997).
281. G. B. Sukhorukov, E. Donath, H. Lichtenfeld, E. Knippel, M. Knippel, A. Budde, and H. Möhwald, *Colloids Surf., A: Physicochem. Eng. Aspects* **137**, 253–266 (1998).
282. S. S. Shiratori and M. F. Rubner, *Macromolecules* **33**, 4213–4219 (2000).
283. S. Y. Park, C. J. Barrett, M. F. Rubner, and A. M. Mayes, *Macromolecules* **34**, 3384–3388 (2001).
284. X. Arys, A. Laschewsky, and A. M. Jonas, *Macromolecules* **34**, 3318–3330 (2001).
285. S. T. Dubas and J. B. Schlenoff, *Macromolecules* **34**, 3736–3740 (2001).
286. J. Gregory, *Crit. Rev. Environ. Control* **19**, 185–230 (1989).
287. D. A. Mortimer, *Polym. Int.* **25**, 29–41 (1991).
288. H. W. Walker and S. B. Grant, *Colloids Surf., A: Physicochem. Eng. Aspects* **119**, 229–239 (1996).
289. H. W. Walker and S. B. Grant, *J. Colloid Interface Sci.* **179**, 552–560 (1996).
290. M. B. Hocking, K. A. Klimchuk, and S. Lowen, *J. Macromol. Sci., C: Rev. Macromol. Chem. Phys.* **39**, 177–203 (1999).
291. A. Fuchs and E. Killmann, *Colloid Polym. Sci.* **279**, 53–60 (2001).
292. P. Ilekti, L. Piculell, F. Tournilhac, and B. Cabane, *J. Phys. Chem. B* **102**, 344–351 (1998).
293. S. Zhou, C. Burger, F. Yeh, and B. Chu, *Macromolecules* **31**, 8157–8163 (1998).
294. C. K. Ober and G. Wegner, *Adv. Mater.* **9**, 17–31 (1997).
295. M. Antonietti, S. Förster, M. Zisenis, and J. Conrad, *Macromolecules* **28**, 2275–2279 (1995).
296. V. A. Kabanov and A. B. Zezin, *Pure Appl. Chem.* **56**, 343–354 (1984).
297. N. Karibyants, H. Dautzenberg, and H. Cölfen, *Macromolecules* **30**, 7803–7809 (1997).
298. H. Dautzenberg, J. Koetz, K.-J. Linow, B. Philipp, and G. Rother, in P. Dubin, J. Bock, R. Davis, D. N. Schulz, and C. Thies, eds., *Macromolecular Complexes in Chemistry and Biology*, Springer-Verlag, New York, 1994, pp. 119–134.
299. H. Dautzenberg, *Macromolecules* **30**, 7810–7815 (1997).
300. P. Welch and M. Muthukumar, *Macromolecules* **33**, 6159–6167 (2000).
301. Y. Li, P. L. Dubin, R. Spindler, and D. A. Tomalia, *Macromolecules* **28**, 8426–8428 (1995).
302. K. Petrak, in M. Hara, ed., *Polyelectrolytes: Science and Technology*, Marcel Dekker, New York, 1993, pp. 265–297.
303. M. Almgren, P. Hansson, E. Mukhtar, and J. van Stam, *Langmuir* **8**, 2405–2412 (1992).
304. J. Xia, H. Zhang, D. R. Rigsbee, P. L. Dubin, and T. Shaikh, *Macromolecules* **26**, 2759–2766 (1993).
305. B. Lindman and K. Thalberg, in E. D. Goddard and K. P. Ananthapadmanabhan, eds., *Interactions of Surfactants with Polymers and Proteins*, CRC Press, Boca Raton, Fla., 1993, pp. 205–271.

306. S. H. Chen and J. Teixeira, *Phys. Rev. Lett.* **57**, 2583–2586 (1986).
307. K. Kogej, G. Evmenenko, E. Theunissen, H. Berghmans, and H. Reynaers, *Langmuir* **17**, 3175–3184 (2001).
308. M. Le Bret and B. H. Zimm, *Biopolymers* **23**, 271–285 (1984).
309. V. Vlachy and A. D. J. Haymet, *J. Chem. Phys.* **84**, 5874–5880 (1986).
310. P. Mills, C. F. Anderson, and M. T. Record Jr., *J. Phys. Chem.* **90**, 6541–6548 (1986).
311. J. P. Valleau, *Chem. Phys.* **129**, 163–175 (1989).
312. G. A. Christos and S. L. Carnie, *J. Chem. Phys.* **92**, 7661–7677 (1990).
313. B. Jayaram, S. Swaminathan, D. L. Beveridge, K. Sharp, and B. Honig, *Macromolecules* **23**, 3156–3165 (1990).
314. P. A. Mills, A. Rashid, and T. L. James, *Biopolymers* **32**, 1491–1501 (1992).
315. T. Das, D. Bratko, L. B. Bhuiyan, and C. W. Outhwaite, *J. Phys. Chem.* **99**, 410–418 (1995).
316. J. C. G. Montoro and J. L. F. Abascal, *J. Chem. Phys.* **103**, 8273–8284 (1995).
317. M. J. Stevens and S. J. Plimpton, *Eur. Phys. J. B* **2**, 341–345 (1998).
318. J. C. Chu and C. H. Mak, *J. Chem. Phys.* **110**, 2669–2679 (1999).
319. S. L. Carnie, G. A. Christos, and T. P. Creamer, *J. Chem. Phys.* **89**, 6484–6496 (1988).
320. G. A. Christos and S. L. Carnie, *J. Chem. Phys.* **91**, 439–453 (1989).
321. G. A. Christos, S. L. Carnie, and T. P. Creamer, *Macromolecules* **25**, 1121–1124 (1992).
322. J.-L. Barrat and D. Boyer, *J. Phys. II* **3**, 343–356 (1993).
323. H. H. Hooper, H. W. Blanch, and J. M. Prausnitz, *Macromolecules* **23**, 4820–4829 (1990).
324. C. Reed and W. Reed, *J. Chem. Phys.* **92**, 6916–6926 (1990).
325. C. E. Reed and W. F. Reed, *J. Chem. Phys.* **94**, 8479–8496 (1991).
326. M. J. Stevens and K. Kremer, *Phys. Rev. Lett.* **71**, 2228–2231 (1993).
327. M. J. Stevens and K. Kremer, *Macromolecules* **26**, 4717–4719 (1993).
328. M. J. Stevens and K. Kremer, *J. Chem. Phys.* **103**, 1669–1690 (1995).
329. M. J. Stevens and K. Kremer, *J. Phys. II* **6**, 1607–1613 (1996).
330. U. Micka and K. Kremer, *J. Phys.: Condens. Matter* **8**, 9463–9470 (1996).
331. M. Ullner, G. Staikos, and D. N. Theodorou, *Macromolecules* **31**, 7921–7933 (1998).
332. B. J. Klein and G. R. Pack, *Biopolymers* **22**, 2331 (1983).
333. J. Mazur and R. L. Jernigan, *Biopolymers* **31**, 1615 (1991).
334. G. L. Siebel, U. C. Singh, and P. A. Kollman, *Proc. Natl. Acad. Sci. U.S.A.* **82**, 6537 (1985).
335. H. L. Gordon and S. Goldman, *J. Phys. Chem.* **96**, 1921–1932 (1992).
336. T. R. Forester and I. R. McDonald, *Mol. Phys.* **72**, 643 (1991).
337. B. Jayaram and D. L. Beveridge, *Annu. Rev. Biophys. Biomol. Struct.* **25**, 367–394 (1996).
338. E. Gonzales-Tovar, M. Lozada-Cassou, and D. Henderson, *J. Chem. Phys.* **83**, 361–372 (1985).
339. C. Y. Kong and M. Muthukumar, *J. Chem. Phys.* **109**, 1522–1527 (1998).

GENERAL REFERENCES

H. Dautzenberg, W. Jaeger, J. Kötz, B. Philipp, Ch. Seidel, and D. Stscherbina, *Polyelectrolytes: Formation, Characterization and Application*, Hanser Publishers, New York, 1994.

M. Mandel, *Physical Properties of Polyelectrolyte Solutions: An Introduction*, Pacini Editore, Pisa, Italy, 1999.
K. S. Schmitz, *Macroions in Solution and Colloidal Suspension*, VCH Publishers, New York, 1993.
M. Hara, ed., *Polyelectrolytes: Science and Technology*, Marcel Dekker, New York, 1993.
A. Rembaum and E. Sélegny, eds., *Polyelectrolytes and Their Applications*, D. Reidel Publishing, Boston, 1975.

DAVID HOAGLAND
University of Massachusetts

POLYESTERS, FIBERS. See Volume 3.

POLYESTERS, THERMOPLASTIC

Introduction

Polyesters enter our lives in a most ubiquitous manner as textiles, carpets, tire cords, medical accessories, seat belts, automotive and electronic items, photographic film, magnetic tape for audio and video recording, packaging materials, bottles, and so on. Their utility is illustrated by the vast range of their applications. This article describes the properties, synthesis, manufacture, and raw materials for the two most widely used thermoplastic polyesters: poly(ethylene terephthalate) (PET) [25038-59-9] and poly(butylene terephthalate) (PBT) [26062-94-2]. In order of volume, PET comes first by virtue of its enormous market tonnage in polyester fibers and films, as well as the resin for blow-molded bottles, containers, and food packaging.

Polyesters are linear polymeric molecules containing in-chain ester groups, formally derived by condensation of a diacid with a diol. The earliest commercial polyesters were the alkyd resins (qv), nonlinear polymers developed for surface coatings shortly after World War I. It was not until the 1930s that the classic studies of Carothers examined main-chain polyesters in a rigorous and systematic fashion (1). Although he studied a wide range of polyesters, made both from aliphatic diacids and diols (AA-BB) type and from ω-hydroxyacids (ABAB type), for various reasons, Carothers did *not* pursue polyesters derived from aromatic diacids and alkylene diols. All his aliphatic polymers were low melting ($<100^{\circ}$C) and were easily soluble in common organic (dry cleaning) solvents. They had little utility as textile fibers, which largely explains why Carothers turned his attention to polyamides. The first successful synthesis of satisfactory high molecular weight poly(ethylene terephthalate), 2GT, was made in England in 1942, during the early days of World War II. The inventors were J. Rex

Encyclopedia of Polymer Science and Technology. Copyright John Wiley & Sons, Inc. All rights reserved.

Whinfield and W. Dickson, working at the Calico Printers' Association (2,3). Other polymers pioneered by these workers included poly(1,3-propylene terephthalate), 3GT, poly(1,4-butylene terephthalate), 4GT, and the polyester from ethylene glycol and 1,2-*bis*(4-carboxyphenoxy)ethane, known as CPE-2G or "Fiber-O" (4). Of these materials, PET was selected for development as a melt-spinnable synthetic fiber, but commercialization was impossible until after the end of World War II. Eventually, when the various national economies were back on a peacetime footing, PET polymer and fibers derived from it were put into production. The whole market-driving force for polyester at this time was in the form of synthetic fibers. In the United Kingdom, the new material was manufactured by Imperial Chemical Industries Ltd. under the trade name Terylene, while DuPont introduced it to the United States in 1953 as Dacron (see POLYESTERS, FIBERS).

In the early 1950s, additional poly(alkylene terephthalate)s were examined in both United States and Europe for synthetic fiber applications. One of these, poly(1,4-butylene terephthalate), 4GT or PBT, had (and still has) some very attractive *fiber* properties. Notably, it was white and resisted photooxidative yellowing much better than nylon. It accepted disperse dyes much more readily than PET. It had excellent resilience and elastic recovery. All these features made it attractive for such fiber end uses as women's wear, hosiery, and carpet fiber. However, the twin criteria of pleat-retention and crease-resistance in apparel fabrics were commercially important at the time (it was an era when accordion pleats were highly fashionable in women's wear) and PET was superior on these counts. Only later was it realized that PBT polymer was highly suited to injection-molded applications. Not only was it highly crystalline, it had a *high rate of crystallization*, so that parts could be molded in a fully crystallized state and therefore free from distortion or warping. Unlike nylon, it had a low moisture uptake and was much more dimensionally stable to changes in atmospheric humidity. Molding-grade PBT resins were introduced in 1970 by Celanese Corp. as Celanex and others followed.

In contrast, PET was not successful as a molding resin because of its low rate of crystallization in a cold mold. The mold has to be heated to 130–140°C, well above the PET glass–rubber transition temperature (T_g) to obtain adequate crystallization rates. Satisfactory moldings were still not obtained because of uncontrollable crystal morphology. During the late 1960s, fast-crystallizing grades of PET were developed which had uniform morphology because of the presence of specific nucleating agents (5–7). Akzo and DuPont were early entrants in the field with their Arnite and Rynite range of PET resins; other manufacturers followed and PET molding resins are now widely used, particularly in the auto industry. However, the biggest single market for moldable PET today is in blow-molded bottles, which exceeds every other single end use for PET polymer except polyester fibers. In 1990, the annual world production of PET fibers (8) was about 9 million tons; according to Table 2 (see later) the annual production of PET bottle resin in 2000 was 1.4 million ton and growing rapidly. It is worth noting that poly(ethylene-2,6-naphthalenedicarboxylate) (PEN) was another important polyester also synthesized first by ICI workers in 1948 (9) (see POLY(ETHYLENE NAPHTHANOATE).

Manufacture of Raw Materials and Monomers

PET and PBT are both made from terephthalic acid and its dimethyl ester. Terephthalic acid (TA) is made by air-oxidation of *p*-xylene [106-42-3] in acetic acid under moderate pressure in the presence of catalysts such as divalent cobalt and manganese bromides (10). *p*-Xylene is the highest melting of three isomeric dimethylbenzenes and is separated by fractional crystallization from the C_8-aromatic fraction (including ethylbenzene) during petroleum refining (11). Alternatively it may be separated by selective adsorption on a zeolite bed combined with an isomerization process (12). For PET fiber production, very pure TA is required and in the early days, when the oxidation of *p*-xylene was achieved with 50% aqueous nitric acid under pressure, the process left some highly undesirable by-products such as nitroaromatics and carbazoles in the crude TA. Because of the great insolubility of TA, it was not easily purified by recrystallization and so it was converted to its dimethyl ester (dimethyl terephthalate, DMT), and the DMT in turn purified by redistillation under reduced pressure and a final recrystallization. PET was made by the reaction of DMT with excess ethylene glycol in the presence of catalysts to promote ester-interchange and polymerization. When the direct air-oxidation process of *p*-xylene became the process of choice, the DMT purification route was still used as an interim process, even though major undesirable impurities had been eliminated by the new oxidation route.

During the 1967–1972 period, pure TA became available in large quantities (13) because of the improvements in the process and purification of TA. Harmful incomplete oxidation products in crude TA such as *p*-toluic acid and 4-carboxybenzaldehyde (4-CBA) were eliminated by recrystallization from water under pressure with concomitant hydrogenation. Under these conditions, *p*-toluic acid is highly water-soluble and 4-CBA is hydrogenated to toluic acid (14). The availability of pure TA caused a major change in production methods for PET. Direct esterification (DE) processes using pure TA superseded the former ester-interchange (EI) process based on DMT. Interestingly, in recent years DMT has made something of a comeback, ostensibly because of the recycling of waste PET. Production of pure DMT derived from the methanolysis and glycolysis of PET waste is carried out on a significant scale (15,16). Manufacture of TA from *p*-xylene has undergone a constant process of improvement over the years and innumerable patents have been filed on small improvements, new oxidation catalysts, etc. A very recent article describes an experimental "Green Chemistry" *p*-xylene oxidation process using hydrogen peroxide and a manganese dibromide catalyst in supercritical water as a solvent. Under these conditions, the TA remains in solution (17).

Turning now to the diol components, ethylene glycol (ethane-1,2-diol) is made from ethylene in essence by direct air-oxidation to ethylene oxide and ring opening with water to give the 1,2-diol (18). Butane-1,4-diol is still made by the old Reppe process. Acetylene reacts with formaldehyde in the presence of a catalyst to give 2-butyne-1,4-diol, which is hydrogenated to butanediol. The ethynylation step depends on a special cuprous acetylide-bismuth salt catalyst, which minimizes side reactions (19). The hydrogenation step is best done in two stages over special catalysts (20). Another butanediol route starts from butadiene. In a process due to Mitsubishi Chemical Industries, butadiene reacts with acetic acid and

oxygen in the presence of a palladium catalyst to give 1,4-diacetoxy-2-butene (21), and the latter is hydrogenated over a special catalyst (22) and finally hydrolyzed to 1,4-butanediol. It is not known whether this process is in commercial use at the time of writing. Although Reppe plants still operate, the process has been replaced in newer plants by a route based on hydroformylation of allyl alcohol (from propylene oxide) over a rhodium catalyst (23) to give 4-hydroxybutyraldehyde. This is reduced to butanediol using a two-stage hydrogenation route (24) to minimize side reactions. The ethynylation route is still an important one but new plants use the Arco hydroformylation process, which was purchased by Lyondell.

Polymerization Processes

Thermoplastic polyesters are step-growth polymers which need to be made to high molecular weight (12,000–50,000) to be useful (25). The first stage is an esterification or ester-exchange stage where the diacid or its dimethyl ester reacts with the appropriate diol to give the bis(hydroxyalkyl)ester and some linear oligomers. Water or methanol is evolved at this stage and is removed by fractional distillation, often under reduced pressure at the conclusion of the cycle. For EI, weakly basic metallic salt catalysts are used: the list is extremely long, and many recipes are proprietary, but such salts as calcium, zinc and manganese acetates, tin compounds, and titanium alkoxides have been widely used (26–28). Certain EI-catalysts have the undesirable effect of promoting thermal degradation at high temperatures (29) encountered during the latter stages of high polymerization. A McClafferty rearrangement of the ester unit is often deemed responsible. To overcome this, EI-catalysts are sequestered at the end of ester-interchange by adding phosphorus compounds such as triphenyl phosphite, triphenyl phosphate, or polyphosphoric acid in stoichiometric amounts (30). Again, such recipes are often proprietary. Titanium and tin compounds [eg $Ti(OR)_4$ or R_2SnO] act as powerful universal catalysts for both EI and polymerization reactions and are left unchanged. They are not suitable for 2G-derived polyesters because of formation of a yellow color, although recipes are under development in Japan which claim to obviate this problem. For PBT, ester-exchange using DMT and a titanium alkoxide catalyst is the route of choice, since butanediol cyclizes to tetrahydrofuran (THF) in the presence of acids (31). Nevertheless, the direct polycondensation of butanediol with terephthalic acid using special reaction catalysts and conditions to minimize THF formation has been described (32–35).

Batch polymerization is usually done in an autoclave fitted with a powerful mechanical stirrer to handle the viscous melt, under high vacuum at a temperature above the melting point of the final polymer. During this critical stage, it is very important to eliminate oxygen and blanket the process with inert gas, nitrogen, or argon. During the polycondensation stage, the linear oligomers and the bis-hydroxyalkylterephthalate esters undergo a succession of ester-exchange reactions, eliminating the diol, which is removed under high vacuum, and thus increasing the molecular weight steadily. A polymerization catalyst is needed, whether the initial process is EI-based or DE-based. As already mentioned, tin

and titanium catalysts are suitable for both ester-interchange and polymerization, but for PET, antimony trioxide is the usual polymerization catalyst (36). It only becomes active at high temperatures and thus can be added at the start of the reaction along with the other catalysts. More recently, there has been a move away from heavy metals like antimony, particularly in Europe, where they are viewed with increasing disfavor on environmental grounds. Even in the United States, problems can arise with heavy metal contaminants (which include antimony) in waste glycolysis still-bottoms. These cannot be landfilled for environmental reasons and their safe disposal causes added expense. A less toxic metal would clearly be advantageous. However, alternatives are not universally satisfactory. Titanium alkoxides cause unacceptable yellowing of PET, apparently because of reaction with vinyl ester chain ends. This cannot occur with PBT. Germanium compounds, either as the dioxide, tetraalkoxide, or glycoloxide, are good catalysts, nontoxic, and give very white polymers. However, they are usually considered to be too expensive because of the relative scarcity of germanium. Another problem is loss of germanium by volatilization. The use of a germanium/titanium mixed catalyst is disclosed in a patent relating to PET bottles (37). Antimony trioxide is a robust polymerization catalyst, but in PET it is susceptible to reduction to antimony metal, which can cause an undesirable gray-blue color in the polymer.

As the polymer molecular weight increases, so does the melt viscosity, and the power input to the stirrer drive is monitored by a wattmeter so that an end point can be determined for each batch. When the desired melt viscosity is reached, the molten polymer is discharged through a bottom valve, often under positive pressure of the blanketing gas, and extruded as a ribbon or as strands, which are water-quenched and chopped continuously by a set of mechanical knives. Large amounts of PET are also made by continuous polymerization processes. PBT is made by both batch and continuous polymerization processes (38–40).

The polymer is then dried thoroughly and stored for subsequent processing. Whenever a polyester is made by melt polycondensation, a small amount of cyclic oligomer is formed which is in equilibrium with the polymer. This can be extracted with solvents from solid polymer but when the extracted polymer is remelted, more oligomer forms until the equilibrium is reestablished. The level of such oligomers is about 1.4–1.8% by weight for both PET and PBT. Thus it is impossible to completely remove cyclic oligomers from any melt-processed polyesters. In the case of PET, the main oligomer is a cyclic trimer (41,42) while in the case of PBT, the oligomers comprise roughly an equal mixture of cyclic dimer and trimer, together with much smaller amounts of higher oligomers (43). The presence of such oligomers usually does little harm, but under certain conditions they can exude to the surface. This is a problem with polyester *fibers* with their high surface/volume ratio. For example cyclic trimer can interfere with the fiber dyeing process. It is also a nuisance in bottle production as the trimer coats the preform injection molds.

It is often necessary to make polymer of much higher molecular weight than would be practicable in the melt, either by reason of excessively high melt viscosity or because degradation reactions would begin to overtake the rate of polymerization and limit molecular weight. For this reason, solid-state polymerization (SSP) is frequently used. Dried polymer chip of moderate molecular weight is heated at a temperature roughly 20°C below its softening point, either in a high vacuum or

in a stream of hot inert gas in a device which agitates the solid. Typical devices might be a twin-cone rotary vacuum drier or a fluidized-bed unit. There are many types of commercial SSP units available.

One very important practical consideration with PET is that the polymer chips must be fully crystallized by careful annealing before the solid-phase polymerization process begins. Usually the polymer has been water-quenched before cutting and will be largely amorphous. If not precrystallized, the chips may sinter together on attempted solid-phase polymerization. The difficulties caused by several tons of polymer setting to a solid mass can well be imagined! It is possible by careful annealing to raise the T_m of the PET considerably above the usual figure (44), thus allowing the solid-phase polymerization to take place at higher temperatures and shorter reaction times. Various agitation devices (45) and polymer chip treatments (46) have been described to prevent sticking. An integrated crystallizing and solid-state polymerization process has been described (47) in the patent literature.

In the solid-state process, the volatile by-products of the polycondensation reaction (traces of water, methanol, excess diol, etc) escape by vapor diffusion through the solid chip and are rapidly removed from the chip surface instead of being limited by viscous diffusion through a bulk melt. Esters of aliphatic diols and aromatic diacids begin to decompose thermally even in an inert atmosphere at around 250°C (48). In the polymer melt, local mechanical heating caused by viscous shear during agitation can cause thermal degradation. SSP eliminates this and the molecular weight rises within a few hours to the desired figure.

During the polymerization reaction, various by-products are formed. In the case of PBT, the major one is THF formed by dehydration of butanediol or by internal cyclization of the C_4-ester units. This is a harmless by-product, as far as the polymerization is concerned, since it is nonreactive under polymerization conditions and quickly volatilizes away. However, its formation is commercially undesirable because it constitutes an air pollution problem as a volatile organic emission, and represents the loss of valuable starting material (butanediol). PET, by contrast, has two major troublesome by-products. One is the generation of diethylene glycol (DEG) units in the chain by dehydration of 2-hydroxyethyl ester chain ends to form an ether link. This process cannot be entirely prevented, although addition of alkalis can reduce it, and it is further mitigated by restricting those time/temperature combinations that tend to favor DEG formation. DEG content is related to the change in softening point (ΔT_m) by the empirical relation (49)

$$\Delta T_m = (-2.2)m(^\circ C)$$

where m is the molar % concentration of DEG.

In addition to depressing melting point, DEG units adversely affect the crystallinity of the polymer, reduce the strength of both fibers and oriented films, and increase the susceptibility of the polymer to chemical attack and aqueous hydrolysis.

The other major by-product is acetaldehyde, which is produced by thermal degradation of the PET unit. Random oxygen–alkyl scission of ester units leaves a vinyl ester end and a carboxyl-ended chain. The vinyl ester reacts with a polymer

end-group to form a new polymer link and expels acetaldehyde, the tautomer of vinyl alcohol (50). The vinyl ester end can also thermally polymerize to give chain-branched and cross-linked products and gel-particles, and further thermal degradation of these polyvinyl units gives rise to colored polyenes (51,52). Although acetaldehyde is highly volatile, its presence is particularly objectionable in PET bottle resin used for soda bottles. Its presence may not exceed 3 ppm in the final container if used for potable substances, as it imparts an off-taste to popular cola drinks (53). Every time PET is melted during its processing, more acetaldehyde is generated. One reason for bottle resin undergoing a final solid-phase polymerization before stretch blow molding is to remove the last traces of acetaldehyde.

Physical Properties of PET

The full crystal structure of PET has been established by x-ray diffraction (54–57). It forms triclinic crystals with one polymer chain per unit cell. The original cell parameters were established in 1954 (54) and numerous groups have reexamined it over the years. One difficulty is determining when crystallinity is fully developed. One researcher (57) annealed PET at up to 290°C for 2 years.

Cell parameters are $a = 0.444$ nm; $b = 0.591$ nm; $c = 1.067$ nm; $\alpha = 100°$; $\beta = 117°$; $\gamma = 112°$; density = 1.52 g/cm^3

Thermochemical data depends on the degree of crystallinity in the polymer, and a very highly annealed polymer sample can have $T_m = 280°C$, much higher than the usual value of 260–265°C (58). The heat of fusion (59) is about 140 J/g, (33.5 cal/g). The glass–rubber transition temperature (T_g) depends on both the method of measurement and the state of the polymer. A solid chip sample as measured by differential scanning calorimetry (dsc) gives a value around 78°C (60) but a highly oriented and crystalline-drawn fiber measured by the dynamic loss method will give values as high as 120°C (61). The specific gravity of undrawn amorphous PET is 1.33, whereas crystalline-drawn fiber has a value of 1.39 (62).

As a step-growth polymer made under equilibration conditions, PET has a molecular weight distribution very close to the theoretical value of 2.0. The Mark–Houwink equation relates the intrinsic solution viscosity $[\eta]$ to the molecular weight as $[\eta] = KM_v^{\alpha}$, where M_v is the viscosity average molecular weight and K and α are the Mark–Houwink coefficients determined experimentally for individual solvents. The usual solvents historically used for PET are 60/40 w/w phenol/tetrachlorethane (P/TCE) and 2-chlorophenol (OCP). Neither solvent system is entirely satisfactory and better results have been obtained using either hexafluoroisopropyl alcohol (HFIP) or a 50/50 v/v mixture of HFIP and pentafluorophenol (PFP) at 25°C (63). Although expensive, these acidic fluorinated solvents readily dissolve even highly crystalline samples of PET at moderate temperatures, *thus avoiding the degradation problems commonly encountered with the older solvents at high temperatures*. Thus the results are more likely to be reliable, since degradation under normal conditions is minimal. The Mark–Houwink coefficients for PET for a range of solvent systems are shown in Table 1.

PET is a strong, stiff polymer. High tenacity tire-cord fibers with a tensile strength (tenacity) of up to 0.9 N/tex (10 g/den) and a tensile modulus of 11 N/tex

Table 1. Mark–Houwink Coefficients for PET in Various Solvents at 25°C

Solvent	K, 10^{-4} dL/g	α
OCP	6.31	0.658
P/TCE	7.44	0.648
HFIP	5.20	0.723
PFP/HFIP	4.50	0.705

(125 g/den) are readily obtained. Normal (ie apparel) textile fibers usually have tenacity around 0.5 N/tex (5.6 g/den) with a modulus of 7 N/tex (80 g/den). The tensile modulus of PET is significantly higher than that of either PBT (4GT) or PPT (3GT) polyester fibers.

Applications of PET

The applications of PET are almost too numerous to mention and new uses appear constantly. Historically, PET was first commercialized in the early 1950s as a *fiber-forming* polymer. Staple (noncontinuous) fiber for blending with wool (qv) and cotton (qv) for increased fabric performance was the first product and as such was highly successful. Later, continuous filament yarn, frequently bulked mechanically, for knitwear and especially for women's apparel was introduced. The high T_g and low moisture regain (0.4%) gave excellent wash-wear fabric properties with significantly reduced tendencies to wrinkle. Industrial high strength fibers were then developed, notably tire cords for automobile tires. These were usually made from high intrinsic viscosity (IV) polymer (ca 0.75) and spun as continuous filament yarn. When automobile seat belts became the norm, they were also made from polyester because, unlike nylon, it had a high modulus and low tendency to stretch. The whole topic of polyester fibers is a very large one and for a more comprehensive treatment, see Ref. 64 and Polyesters, Fibers.

Another market where PET proved of great value was in the form of *polyester films*, which were made by extrusion through a slit die, followed by a biaxial drawing process. They are used for photographic film backing and for magnetic audiotape and videotape substrates. Another market is drafting film. In all of these outlets the high strength and high modulus of PET, particularly for biaxially drawn films, give the desired dimensional stability and low stretch. For further details of film fabrication and processing, see Ref. 65 and films, manufacture; films, orientation.

One of the largest uses of PET resin and certainly the most dramatic in growth during the last 20 years is the stretch blow-molded *PET bottle*; annual consumption runs into billions of units in United States alone with corresponding rapid expansion on a worldwide scale. The advantages of a thermoplastic bottle are self-evident: it is light-weight, shatterproof, and recyclable. The early market driver was weight, which reduced transportation costs compared with glass during a severe energy shortage. Improved product safety associated with shatter-proof plastic bottles was another factor: recycling did not become a factor until later.

The major technical problem facing any thermoplastic bottle manufacturer is the permeability of the plastic bottle wall to oxygen and carbon dioxide, which affect the shelf-life of the contents. The average 2-L soda bottle maintains an internal pressure of CO_2 of ca 520 kPa (75 psi). To stop the product going "flat," carbon dioxide pressure must be retained during storage before unsealing for several weeks. Likewise, oxygen must not diffuse in through the bottle walls to oxidize the contents, spoiling the flavor of the product. PET is semipermeable to such gases. At one time, attempts were made to coat PET with impermeable layers but safety, cost, and recycling difficulties defeated them, although more recent processes appear promising.

The basic enabling invention in 1973 was the stretch blow-molded PET bottle process (66,67). In this process, the polymer bottle wall is subjected to a rapid biaxial drawing, which greatly increases the molecular orientation of the bottle wall. Not only does this increase the mechanical strength of the bottle but it also reduces the permeability of the walls (68). Blow-molding thermoplastic hollow articles is a highly specialized process and for more details the reader should consult a specialist publication (69). However, the process will be outlined so that the reasons for certain polymer properties will become apparent. A typical process is the two-stage blow-molding process. A bottle "preform" is molded by a conventional injection-molding process with thick walls and the neck with screw-cap threads in place. This preform is amorphous and clear. Multiple cavity dies are used to increase productivity. In the second stage, the preforms are heated in a mold to a carefully controlled temperature above the glass–rubber transition temperature, typically to 90–100°C. The inside of the mold cavity is the size and shape of the finished bottle. The preform is subjected to a combined axial and radial stretching process. A hollow metal mandrel passes into the preform and partially elongates it in the axial direction while dry air at about 345–690 kPa (50–100 psi) blows the walls of the softened preform outward to fill the mold, giving radial stretching. The mold opens to allow the bottle to cool. This combined process results in both radial and axial drawing of the bottle walls, which causes strain-induced crystallization and gives a container superior strength, clarity, and no environmental stress-cracking.

The usual 2-L bottle preforms weigh about 50 g and the final blown bottle has a wall thickness of about 0.38 mm (0.015) in. (70). In view of the enormous number of bottles produced annually, the processes are constantly being modified to raise throughput rates and are all highly automated. Several large machinery manufacturers (eg Cincinnati-Milacron, Sidel) specialize in building the complex blow-molding equipment. Typical cycle times for the actual blow molding are 3–6 s. This process had one serious drawback in the early days—it gave a bottle with a hemispherical base, which is clearly not capable of standing upright. A flat base could not be fully oriented, so gases would permeate out through it. For several years, PET soda-bottles were fitted with separate flat-bottomed basecaps, usually molded from high density polyethylene (HDPE) and secured with a hot-melt adhesive. This meant extra cost because of extra material and processing steps and interfered with recycling. The invention by the Continental Group of the so-called petaloid base bottles with a five- or six-lobed pattern base was a major advance: it made possible a one-piece, fully biaxially oriented bottle which could stand up by itself (71).

PET Bottle Resin. Stretch blow-molding is a mechanically severe operation with very high deformation rates. The consumer wants a glass-clear bottle: any opacity caused by strain-induced crystallization is highly undesirable. PET bottle resins are usually made to high molecular weight ($M_n = 22{,}000$–$40{,}000$; IV 0.75–0.90 dL/g) so as to withstand the severe blow-molding operation. Such an intrinsic viscosity is too high for melt-polymerization, and solid-stage polymerization is required. The process has been reviewed (72). PET bottle resin is made in a continuous melt-polymerization plant either by direct esterification using TA/glycol, or by EI using purified DMT, often recovered from recycled PET bottles. The process to be described is a direct esterification process. Firstly, the acid and glycol are thoroughly mixed to a paste and catalyst and stabilizers are added. The paste is pumped to the esterifiers where water is driven off. The molten mixture of low polymer and oligomers passes through various polymerization stages: a prepolymerizer, an intermediate polymerizer, and finally the melt arrives at the high polymerizer or finishing stage where the final IV is about 0.65 dL/g. During the various successive stages, the melt grows increasingly viscous and high vacuum is applied at the finisher to complete the reaction. The agitators used in the polymerizers are designed to disengage volatiles without high shear-rates and to obviate dead spots where polymer melt could stagnate and undergo degradation. A series of DuPont patents (73–75) describes a process whereby no vacuum is needed to build molecular weight to the desired level. By use of specially designed mechanical agitators and an ingenious reactor design, which continually generates thin films of polymer melt, a brisk stream of inert gas (nitrogen or CO_2) is sufficient to cause efficient disengagement of the excess glycol and thus drive the reaction to the desired IV. The entrained glycol can be recovered from the exit gas stream and the inert gas recycled. Clearly, the absence of vacuum equipment reduces capital costs and, it is claimed, the process can be operated both batchwise and continuously and is suitable for several commercial polyesters including PET, PEN, and PBT.

Returning to the original process description, at the exit from the high polymerizer, the molten polymer is extruded into a water-bath and continuously diced to small chips about 2.5–3.5 mm across. The chips are dried and passed to the crystallizers where they are annealed in the solid state above T_g, gradually rising to a temperature close to the point of maximum crystallization rate (approx. 40–160°C). They are slowly agitated to prevent them from sintering together as they move to the solid-state polymerizer. During the crystallization stage, the chip density increases from 1.33 to about 1.37 g/cm^3. Finally the chips pass into the solid-phasing towers. Here they descend slowly under gravity in a plug-flow mode through a long hot zone under a countercurrent flow of inert gas to sweep away the volatile by-products. The speed of descent is controlled so that an optimum time/temperature profile is maintained for the desired final IV. The scale of operation is impressive: typical melt-continuous polymerizers run at 10 tons/h, which implies a capacity of approximately 70 million kg/year; a large manufacturer may have several such units and each one provides enough polymer for well over one billion 2-L soda bottles. Newer plant capacities are even more remarkable: a new plant in South Carolina has a capacity of 182 million kg/year *in a single line*.

The number-average molecular weight for typical bottle resin is between 24,000 and 31,000 Da/molecule. One of the most objectionable by-products of

PET polymerization is acetaldehyde, which affects the taste of cola drinks at concentrations as low as 60 ppb. The specification for acetaldehyde in the final product must not exceed 3 μg of acetaldehyde per liter of headspace. The bulk of the acetaldehyde produced in the polymerization process is removed during the final solid-phase polymerization stage. Since blow molding is carried out well below 200°C, only minute amounts of fresh aldehyde are formed by thermal degradation at the last stage. Originally, bottle preforms weighed 60–70 g but this has now been reduced to about 50 g. The lighter weight bottles have thinner walls so that during biaxial drawing, excessive strain-crystallization (opacity) becomes a problem. Most manufacturers (76,77) have introduced copolymers of PET containing minor amounts (2–5 mol%) of such comonomers as isophthalic acid (PET-A) or cyclohexanedimethanol (PET-G) to reduce the polymer melting point by about 4–12°C with a lower tendency to crystallize. Polyesters hydrolyze very rapidly at 280°C in the melt. Rigorous polymer-drying to a chip moisture content below 50 ppm moisture is necessary before the injection molding of bottle preforms. (PET stored under ambient conditions can easily have a moisture content of 2000 ppm). Melt-dyed polymers using FDA-approved dyes are used to mold preforms for colored bottles where the customer requires them.

In recent years, more and more potables have been packed in PET bottles—one of the most rapidly growing areas, first in Europe but now in the United States as well, is bottled drinking water, both noncarbonated and name brand spa waters. Interestingly, for such potables, acetaldehyde must be even more stringently excluded than for cola drinks. A major market prize would be a bottle sufficiently impermeable to oxygen for packaging beer and wine without spoiling the flavor. This is a much more difficult task than packaging carbonated soft drinks. Numerous designs and bottle coatings have been explored but recycling must not be impaired. Plasma-coating of PET bottles with inorganic materials such as silica and glass to bring about a fivefold reduction in oxygen permeability has been disclosed (78,79). Sidel Corp. (80) has gained FDA approval for a process which plasma-coats amorphous carbon on the insides of 600-mL PET beer bottles at a rate of 10,000 bottles/h. The bottles, which are amber-colored, are said to be fully recyclable.

Other PET Packaging Products. In addition to blow-molded bottles, a packaging market has appeared in recent years for other types of PET polymer. One is amorphous PET (APET) which uses a comonomer (isophthalic acid is one) to minimize crystallinity. Such polymers are used in clear bubble and blister packs for a variety of pharmaceutical products and medical devices (81). Food packaging is also a rapidly growing market for APET and clear heat-sealable thermoformed packages are widely used. By use of blowing agents, foamed PET with a specific gravity of as little as 0.05 g/cm^3 can be made. Markets include baking trays and the very light foams can be used in food packaging. PET bottle resin is the feedstock and the foams can be recycled. One ingenious process uses the hydrocarbon heptane at 249°C as a PET blowing agent (82). These products are largely spin-offs from the vast and rapidly growing bottle resin process and provide new opportunities and markets for resin manufacturers. PET is regarded as a premium packaging material and its recyclability is both a market and an environmental advantage (83).

Table 2. World Nonfiber Polyester Resin Consumption Patterns 1999–2000, [a,b] 10^3 t

	PET				
Country or region	Bottles	Film and sheet	Molded	Total	PBT
USA and Canada	1299	136	423[c]	2132	67
	1389	**148**	**454**[c]	**2317**	**71**
Western Europe	1211	79[d]	NA	1520	116
	1352	**83**[d]	**NA**	**1703**	**129**
Japan	370	242	20	632	119
	380	**250**	**20**	**650**	**130**
China	NA	NA	NA	NA	36
	NA	**NA**	**NA**	**NA**	**37**

[a] Ref. 84.
[b] The values in bold are for the year 2000.
[c] Compounded resin.
[d] Does not include recording film.

PET Molding Resins. It is difficult to establish accurately the world market size for PET as a molding resin. The total tonnage is small compared with the vast amounts used for fibers and bottle resin. However Table 2 shows estimates for 1999–2000 consumption of nonfiber PET and PBT resin, broken down into end uses in several major world markets. The bulk of the U.S. market for PET molding resin is the auto industry. Its T_m and heat distortion temperature are higher than the corresponding values for PBT, and its low moisture uptake and dimensional stability with respect to changes in humidity make it superior to nylon. Both PET and PBT engineering resins have good resistance to chemicals and being crystalline, do not suffer from the solvent stress-cracking problems that plague amorphous materials such as polycarbonate. Polyesters are only attacked by powerful acidic or phenolic solvents, hot strong aqueous alkali, and certain bases such as hydrazine.

In the unfilled state, PET is not a good molding resin and all commercial grades are filled with either chopped glass strand (typically 3–4 mm long) or mineral fillers (usually mica) or a mixture of the two. Various proprietary nucleating agents added are often sodium salts of various organic carboxylic acids (see Ref. 5). Some manufacturers supply fire-retardant (FR) polymer grades as well. Such formulations often involve a synergistic mixture of an aryl halide with antimony oxide. One difficulty with flame-retardant PET polymer is that recipes which contain antimony trioxide can suffer severe polymer degradation at molding temperatures around 280–290°C. As has been discussed earlier, antimony trioxide is a polymerization catalyst and can also act as prodegradant at high temperatures. This is a less serious problem with FR grades of PBT because of lower processing temperatures (240–250°C). To mitigate the effect on PET, pentavalent antimony compounds such as sodium antimonate is used in some FR formulations. The halogenated species is often a ring-brominated polystyrene (85–90). These materials

are approved for Underwriters Laboratory V-0 classification and are nonfugitive and less likely to be environmentally harmful than are small molecule additives like decabromodiphenyl oxide. In Europe there has recently been a move to eliminate organohalogen compounds from FR formulations for environmental reasons. As a result, organophosphorus derivatives such as triarylphosphine oxides are being introduced (91).

Since the early 1990s in the United States, there has been pressure on manufacturers from the automotive industry, led notably by the Ford Motor Co., to use at least 25 wt% of post consumer recycled (PCR) material in their resins rather than 100% virgin polymer. In the case of PET, this is readily achievable, because of the large volume of recovered PET bottle polymer chip now available in the United States and in Europe. A recent article (82) states that during 1998–1999, 273,000 t of PET waste was recycled in the United States. Some suppliers use 100% recycled polymer in their compounded PET resins. The PCR recovery process and subsequent melt-compounding and reformulation reduce the initial IV of the original resin from around 0.75–0.85 dL/g to values around 0.62–0.65 dL/g, but this is still in the range of virgin melt-polymerized resin (as opposed to SSP resin). In the automobile industry, components are often pigmented black, so that differences in feedstock PCR chip color are minimized.

Initially, PET moldings were used in small components, typically electrical connectors and covers for fuses, etc (see Figs. 1 and 2). This is still the case, even

Fig. 1. Electrical automotive connectors molded from CelanexR PBT, Grote & Hartmann (Germany). Courtesy of Ticona, A business of Celanese AG.

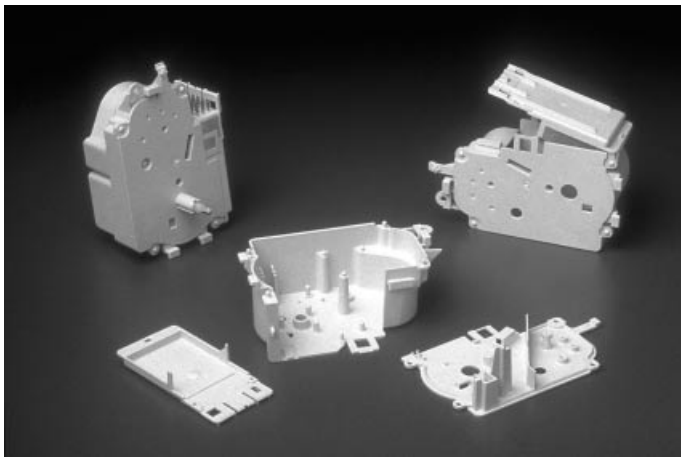

Fig. 2. Appliance timer housings molded from CelanexR PBT, Mallory (USA). Courtesy of Ticona, A business of Celanese AG.

Fig. 3. Healthcare inhaler for asthma patients molded from CelanexR PBT, Astra Turbohaler(tm). Courtesy of Ticona, A business of Celanese AG.

more so with the growing complexity of the modern automobile with its numerous on-board electronics, but recently the trend has been to use PET moldings more and more for non-load-bearing structural parts, such as radiator grille supports and headlamp mountings (Fig. 4). Glass/mineral filled PET moldings do not have

Fig. 4. Automotive, electroplatable grill-opening retainer molded from ImpetR PET, Mercury Sable. Courtesy of Ticona, A business of Celanese AG.

a smooth enough surface for exterior body-parts. However, they are very suitable for internal structural components. This trend is part of the drive to reduce automobile weight to improve gas-mileage or boost the range and performance of electric cars. Some moldings are dimensionally quite large, weighing well over 5 kg per shot. Improvements in mold design and better understanding of melt-flow behavior in molds, brought about by increasing use of computer-aided design and flow-simulation programs, have helped to make these large moldings possible on a routine production basis. Figures 5 and 6 show an experimental concept car where the bulk of the body/chassis pan is molded in a PET formulation. As stated, PET

Fig. 5. Chrysler composite concept vehicle (CCV) with large body parts molded from ImpetR PET, Daimler Chrysler. Courtesy of Ticona, A business of Celanese AG.

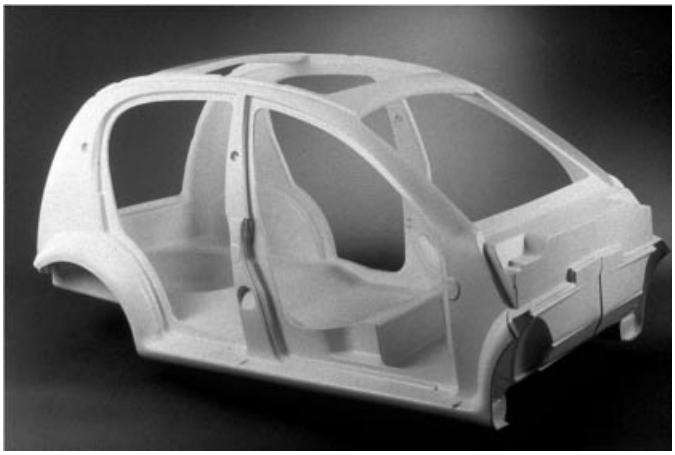

Fig. 6. Large body parts for Chrysler composite concept vehicle (CCV) molded from ImpetR PET, Daimler Chrysler. Courtesy of Ticona, A business of Celanese AG.

does not crystallize well in the unoriented state even in a hot mold unless nucleating agents and/or plasticizers (qv) are added. Commercial PET molding-grade polymers are nearly always filled. Typical compounded polymer properties are shown in Table 3.

Table 3. Typical Properties of PET Molding Resins[a]

Property	ASTM method	Glass 30%	Glass 45%	Glass 35%	(mineral filler)
Specific gravity	D792	1.58	1.70	1.60	1.60
Tensile strength, MPa[b]	D638	166	197	97	103
Elongation at break, %	D638	2.0	2.0	2.2	2.1
Flexural strength at 5%, MPa[b]	D790	245	310	148	152
Flexural modulus, GPa[c]	D790	9.66	14.5	9.66	9.66
Notched Izod, J/m[d]	D256	80.1	107	58.7	58.7
Heat deflection	D648	224	229	202	216
Temperature at 1.82 MPa[b], °C					
Flammability[e]	UL-94	HB	HB	HB	HB
Dielectric strength, V/25 μm	D149				
5.2 mm		565	540	500	450
1.6 mm		904	631	550	575
0.8 mm		975	951	810	860
Volume resistivity at 23°C, 50% rh, Ω·cm	D257	3.0×10^{15}		1.0	1.0
Dielectric constant ε, H_2	D150				
10^3		3.2	3.5	3.8	3.8
10^5		3.1	3.4	3.6	3.7

[a] Ref. 92.
[b] To convert MPa to psi, multiply by 145.
[c] To convert GPa to psi, multiply by 145,000.
[d] To convert J/m to ft·lbf/in., divide by 53.38.
[e] HB = Brinell hardness.

Economic Aspects of PET

The total world market for nonfiber PET polymer is still growing because of the demand for bottle resin. This grew worldwide from 1993 to 2000 at about 15%/year, although overproduction led to a falling-off recently. A published article (93) stated that the global consumption of PET grew at 19% during 1992 to a world total of 1,719,000 ton (3.79 billion lbs). Adding up the bottle resin figures from Table 1 given an estimated total of 3,121,000 ton, a 181% increase in 7 years. The world total devoted to beverage bottles is astonishing, but it is significant that Europe had by the year 2000 almost caught up with the United States in total bottle resin tonnage. There are interesting regional variations, notably the strong demand for packaging for mineral waters in Europe and the large hot-fill market in Japan. Looking ahead, the future growth of PET looks to be assured, its balance of properties and ability to be recycled being extremely favorable factors. New outlets for PET packaging are constantly appearing.

One significant trend in recent years has been the complete disappearance of some well-known major producers of PET polymer and the emergence of new ones. In the late 1990s, several major chemical companies sold off commodity chemical and polymer businesses to concentrate on other more profitable market areas such as pharmaceuticals and life-sciences. In 1998–1999, Hoechst Celanese split into Celanese AG and Aventis, a pharmaceutical company. It sold its large PET interests to the Koch-Saba group, now called Kosa, and headquartered in Houston, Tex. Celanese's remaining engineering polymer interests were taken over by its subsidiary Ticona. During 1998–2000, Shell gave up its polymer business and sold some 300,000 ton of PET capacity to the Mossi & Ghisolfi Group of Milan, Italy (94). ICI sold its PET plants in Europe to DuPont, and Dow in 1996 became a major PET manufacturer by acquiring 270,000 ton of plant capacity. Dow is also in the process of buying Union Carbide. Allied-Signal became Honeywell and were then almost acquired by GE until (2001) the European Union prevented the sale on antitrust grounds. Table 4 shows major world manufacturers of PET resin in late 1998, a situation that has now changed again with the removal of Shell and Hoechst Celanese as PET producers.

Table 4. Major World PET Producers[a]

Manufacturer	Nameplate capacity, 10^3 t
Eastman	1556
Kosa	840
DuPont	758
Shell	750
Nan Ya	540
Wellman	490
Rhodia-Ster	280
Hoechst-Celanese	250
Sunkyong	240
Far Eastern	200
Total	*5904*

[a] Ref. 83.

Commercial PET Engineering Resins. The first company to introduce nucleated PET molding resins was Akzo Plastics BV with their Arnite® range, later acquired by DSM NV. DuPont introduced their Rynite® fast-crystallizing materials in 1978, followed by other manufacturers. The present North American market is still dominated by DuPont, but there are other notable suppliers like Honeywell (Allied-Signal) with Petra® and Ticona with Impet®. Eastman also markets PET injection-molding grades under the tradename Thermx. In Europe the situation with PET is confined primarily to two suppliers, DSM NV and DuPont, while in Japan the main suppliers are Teijin, Toray, and Toyobo. The market prices for PET molding resins at the time of writing in the United States are \$2.90–3.15/kg for 30% glass-filled PET, \$3.26–3.41/kg for 55% glass-filled PET, and \$3.23–3.45/kg for 30% glass-filled FR grade PET (95). These compare with a current commodity price for PET bottle resin of \$1.36–1.50/kg (see ENGINEERING THERMOPLASTICS).

Safety and Environmental Factors

PET. PET polymer is safe and poses no threat to animals or humans. PET fibers have been in use for nearly 50 years and PET has U.S. Food and Drug Administration (FDA) approval for use as a food-packaging material. PET fibers have been used in internal arterial prostheses. The only significant hazard in handling PET resins is the dust hazard associated with mineral or glass fillers during chip grinding or compounding operations. Appropriate protective equipment must be worn. All extruders or machinery handling molten polymer should be properly ventilated to remove harmful fumes from the decomposition of molten polymer. Molten PET can cause serious contact thermal burns: it has a high heat capacity and sticks to the flesh. Adequate protection must always be worn when handling hot polymer.

PBT. PBT resins are not harmful or hazardous when handled at room temperature under normal conditions according to their Materials Safety Data Sheets. No problem with contact with the pellets has been encountered under normal conditions. Glass fines can however cause skin irritation, and if glass-filled resins are being ground or reground, due precautions must be taken. Inhalation of dust must be guarded against, as is true for grinding any glass-filled resin. During the molding, the temperature must not exceed 520°F and never over 550°F as decomposition with the evolution of harmful vapors can occur. As with all thermoplastics, adequate ventilation must be provided around injection-molding machines.

PBT Molding Resins

Poly(butylene terephthalate) is historically the oldest of the crystalline thermoplastic polyester molding resins, having been introduced by Celanese Corp. in 1970 under the trade name Celanex. General Electric Co. then brought out their own version Valox®, and today there are numerous suppliers including BASF, Bayer AG, and DSM. Celanese have recently become Ticona. In Japan,

the major manufacturers are Polyplastics, Toray, Teijin, and Mitsubishi (see ENGINEERING THERMOPLASTICS). As already explained, unlike PET, PBT has the ability to crystallize very rapidly (like nylon-6,6) even in a cold mold. It gives tough, distortion-free moldings without special additives or nucleants. Although the unmodified polymer has very good flow properties, and is used in electrical connectors and fiber-optical cable buffer tubes, it performs even better if reinforced with inorganic fillers, notably ∼3 mm (1/8 in) chopped glass fiber. Additional mineral fillers are incorporated for special applications where high heat-deflection temperature and stiffness are important. These mineral fillers include mica, talc, wollastonite, and even barium sulfate, the latter for special applications such as countertops.

The filled grades of PBT are tougher, stiffer, and stronger materials and they have improved notched Izod impact strength, since unfilled PBT is notch-sensitive (96,97). Even when unfilled, the plastic has good strength, rigidity and toughness, low creep, minimal moisture absorbance, and does not undergo dimensional changes with changes in humidity. It is characterized by excellent electrical and dielectric properties and a high surface finish. It has found wide acceptance in a variety of end uses where precision molding and a high quality finish are required. Typical are the electrical and electronic markets where it is widely used in such parts as connectors, plugs, switches, typewriter and computer keyboard components, printed circuit boards, and small electric motor components. PBT is widely used in the automotive industry for electrical components such as distributor caps, coil-formers, rotors, windshield wiper arms, headlight mountings, and other fittings. In the auto market, "under the hood" components have to maintain their dimensional stability at elevated temperatures as well as resist various automotive fluids. Other uses for PBT are home appliances, such as food mixers, hair dryers, coffee makers, toasters, and camera parts. PBT is used in industrial machinery, for example in molded conveyor-belt links and in medical devices such as nasal sprays and nebulizers. An appreciable quantity is used in polymer alloys and blends with other polymers. PBT is marketed in both standard and flame-retardant grades, the latter being essential in the United States to meet Underwriters' Laboratory 94V-0 standards in thin-walled sections.

Properties of PBT

Physical Properties. Unlike PET, the polymer PBT exists in two polymorphs, the α and β forms, which have distinctly different crystal structures. The two forms are interconvertible under mechanical stress (98–100). Both crystal forms are triclinic and the crystal parameters are shown in Table 5.

The change in the two forms mainly involves the c lattice dimension, which lengthens from 1.174 to 1.300 nm. It is believed that the relaxed α-form has a gauche–trans-gauche conformation of the three C—C bonds in the C_4-glycol unit, and the extended β-form exists in an all-trans form (62). The melting point of PBT is 222–224°C, depending on the degree of crystallization and annealing conditions. The heat of fusion is about 140 J/g (101) and the T_g is usually quoted at about 45°C, although this depends on the physical nature of the sample (102). PBT crystallizes

Table 5. Crystal Parameters for the Two Forms of PBT

Cell parameter	α form (unstretched)	β form (stretched)
a, nm	0.482	0.469
b, nm	0.593	0.580
c, nm	1.174 (1.165)[a]	1.300
α, degrees	100 (98.9)[a]	102
β, degrees	115.5 (116.6)[a]	120.5
γ, degrees	111	105
Volume, nm^3	0.260	0.267
density, g/cc	1.41	1.37

[a]Results given in Ref. 100.

Table 6. Mark–Houwink Parameters for PBT

Solvent	K, dL/g	α
P/TCE (at 30°C)	1.17×10^{-4}	0.87
OCP (at 25°C)	6.62×10^{-5}	0.915

very readily from the melt and it is difficult to obtain a truly amorphous sample. Its crystallization kinetics are thus not easy to determine (103). The density of the annealed crystalline unfilled polymer is 1.33 g/cm^3 whereas the amorphous material has a value of 1.26 g/cm^3 (104). Like PET, PBT is made to various molecular weights, the M_n values being in the 20,000–50,000 range. Intrinsic viscosities are usually measured in *o*-chlorophenol (OCP) or a phenol/tetrachlorethane mixture. The Mark–Houwink parameters are shown in Table 6 (105,106).

Flame-retardant grades of PBT usually consist of synergistic mixtures of antimony trioxide with various halogenated (brominated) aromatic compounds. A typical recipe for PBT might be 10 wt% decabromodiphenyl oxide and 5 wt% antimony oxide. Recently the trend has been to use polymeric or oligomeric brominated additives. A typical additive is an end-capped polycarbonate derived from tetrabromobisphenol-A [94334-64-2]; another is a mixture of epoxy oligomers derived from the diglycidyl ether of tetrabromobisphenol-A [68928-70-1]. The brominated polystyrenes (*loc. cit.*) have only limited usefulness in PBT as they have a low melt compatibility (107).

Chemical Properties. PBT is highly crystalline and does not suffer from solvent stress corrosion cracking as do amorphous materials. It is resistant at room temperature to most common chemicals and solvents, lubricants, greases, and automotive fluids. Ketones will attack it at elevated temperatures. Parts made from PBT are dishwasher-safe, but will not withstand repeated steam autoclaving. PBT is attacked by aqueous alkali and other strong bases and by dilute acids, particularly at elevated temperatures. PBT has very good resistance to weathering, and black pigmented grades with uv-stabilizers have excellent outdoor stability. Like all polyesters, PBT is susceptible to hydrolytic attack by moisture in the melt. Injection-molding screw temperatures are usually about 250°C and IV drop is rapid unless the polymer chip is dried to below 50 ppm moisture content and kept dry. Inadequate drying is the cause of most molding

Table 7. Mechanical Properties of PBT[a]

Property	Unfilled, grade, low mol. wt.	30% glass		
		General purpose	Flame retardant	High impact
Specific gravity	1.31	1.54	1.66	1.53
Tensile strength, MPa[b]	57	135	135	97
Tensile modulus, GPa[c]	2.5	9.7	11.7	8.3
Elongation, %	5	2	1.5	3.1
Flexural strength, MPa[b]	85.5	193	193	152
Flexural modulus, GPa[c]	2.5	8.3	10.3	6.9
Notched Izod, J/m[d]	37.4	90.7	69.4	160
Unnotched Izod, J/m[d]	1228	240	214	641
HDT at 1.82 MPa[b], °C	51	206	208	191
Volume resistivity, Ω·cm	10^{15}	10^{16}	5×10^{15}	4×10^{14}
Dielectric strength, V/25 μm	420	560	490	500
Dielectric constant ε, 100 Hz	3.2	3.7	3.9	4.3
Flammability UL94, at 0.8 mm	HB	HB	V0	HB

[a]Ref. 108.
[b]To convert MPa to psi, multiply by 145.
[c]To convert GPa to psi, multiply by 145,000.
[d]To convert J/m to ft·lbf/in., divide by 53.38.

problems. As the PBT melt is quite fluid, drooling from nozzles is sometimes a problem.

Mechanical Properties. Properties of typical grades of PBT, either as unfilled neat resin or glass-fiber filled, and FR grades are set out in Table 7. This table also includes impact-modified grades which incorporate dispersions of elastomeric particles inside the semicrystalline polyester matrix. These dispersions act as effective toughening agents which greatly improve impact properties. The mechanisms are not fully understood in all cases. The subject has been discussed in detail (109), and the particular case of impact-modified polyesters such as PBT has also been discussed (110,111).

Economic Aspects of PBT

According to information published between 1999 and 2000 the market for PBT in the United States and Canada increased from 67,000 to 71,000 t (147.6–156.6 million lbs), as shown in Table 2. The European and Japanese markets also use large amounts of PBT. The main outlets are electrical, electronic, and automotive components. The major manufacturers of PBT in North America, Europe, and Japan are shown in Table 8.

A more detailed analysis of end uses for PBT in North America, Europe, and Japan are shown in Table 9.

The future prospects for economic growth for PBT look good. It is still displacing thermosets from some markets and its versatility, excellent flow properties, and ease of molding will assure it a prominent place in the world for years to

Table 8. Principal World Manufacturers of PBT According to Region

USA	Europe	Japan
BASF – ULTRADUR®	Bakelite AG	General Electric
DuPont – CRASTIN®	BASF	Mitsubishi Eng. Plastics
General Electric – VALOX®	Bayer AG	Polyplastics[a]
Ticona – CELANEX®	DSM NV	Teijin[a]
	DuPont	Toray
	General Electric	Toyobo

[a]These two companies merged in 2000 to form Wintech which will produce both PET and PBT molding resins.

Table 9. End Uses of PBT for 1999–2000, ton

Market	1999	2000
United States and Canada[a]		
Appliances	7,020	7,392
Consumer/recreation	2,267	2,267
Electrical/electronic	14,286	15,420
Industrial	7,165	7,392
Transportation	33,559	35,827
Others	2,494	2,721
TOTAL	*66,971*	*71,019*
Western Europe[b]		
Appliances	11,000	12,500
Consumer/recreation	9,000	9,900
Electrical/electronic	36,700	39,700
Industrial	8,700	9,800
Transportation	43,300	48,200
Other	7,300	8,900
TOTAL	*116,000*	*129,000*
Japan[c]		
Automotive and vehicle	30,000	33,000
Electrical/electronic	38,000	44,000
Other	19,000	19,000
Total domestic	*87,000*	*96,000*
Exports	32,000	34,000
TOTAL	*119,000*	*130,000*

[a]Ref. 112.
[b]Ref. 113.
[c]Ref. 114.

come. Quoted prices (Nov. 1995) for PBT resins were $3.61–3.85/kg for unfilled resin, $3.74–4.18/kg for 30% glass-filled FR grades, and $4.29–4.51/kg for high impact grades (115).

BIBLIOGRAPHY

"Polyesters, Thermoplastic" in *EPST* 1st ed., Suppl. Vol. 1, pp. 444–467, by J. R. Caldwell, W. J. Jackson Jr., and T. F. Gray Jr., Tennessee Eastman Co., Division of Eastman Kodak

Co.; "Polyesters, Thermoplastic" in *EPSE* 2nd ed., Vol. 12, pp. 217–256, by J. Y. Jadhav and S. W. Kantor, University of Massachusetts. "Polyesters" in *EPSE* 2nd ed., Vol. 12, pp. 1–75, by I. Goodman.

1. H. Mark and G. S. Whitby, eds., *The Collected Works of W H Carothers on High Polymeric Substances*, Interscience Publishers Inc., New York, 1940.
2. U.K. Pat. 578,079 (June 14, 1946), J. R. Whinfield and J. T. Dickson (to ICI Ltd.).
3. U.S. Pat. 2,465,319 (Mar. 22, 1949), J. R. Whinfield and J. T. Dickson (to E. I. du Pont de Nemours & Co., Inc.).
4. J. Shimizu and co-workers, *J. Polym. Sci., Polym. Phys. Ed.* **21**, 275–284 (1983).
5. U.K. Pat. 1,239,751 (July 21, 1971), A. J. Dijkstra, J. A. W. Reid, and I. Goodman (to ICI Ltd.).
6. U.S. Pat. 4,393,178 (July 12, 1983), R. M. H. Legras and co-workers, (to Imperial Chemical Industries plc).
7. U.S. Pat. 4,380,621 (Apr. 19, 1983), E. Nield, D. E. Higgins, and M. W. Young (to Imperial Chemical Industries plc).
8. S. M. Hansen and P. B. Sargeant, *Kirk-Othmer Encyclopedia of Chemical Technology*, 4th ed., Vol. **10**, John Wiley & Sons, Inc., New York, Figure 8, p. 679.
9. Br. Pat. 604,073 (1948), J. G. Cook, H. P. W. Hugill, and A. R. Low (to I.C.I. Ltd.).
10. W. S. Witts, *Chem. Process. Eng.* **51**, 55 (1970).
11. U.S. Pat. 3,467,724 (Sep. 16, 1969), S. A. Laurich (to Chevron Research Co.).
12. U.S. Pat. 3,636,180 (Jan. 18, 1972), D. B. Broughton (to Universal Oil Products Co.).
13. U.K. Pat. 994,769 (June 10, 1965) (to Standard Oil Co.).
14. U.S. Pat. 3,584,039 (June 8, 1971), D. H. Meyer (to Standard Oil Co.).
15. J. Milgrom, *Outlook for Plastics Recycling in the United States*, Decision Resources Inc., 1993, pp. 25–27.
16. K. A. Domeshek, in D. Brunnschweiler and J. Hearle, eds., *Tomorrow's Ideas and Profits: Polyester: Fifty Years of Achievement*, The Textile Institute, Manchester, England, 1993, pp. 288–290.
17. M. Poliakoff and co-workers, *Chem. Eng. News* 30, (July 16, 2001).
18. G. O. Curme and F. Johnston, *Glycols* (ACE Monograph No. 114), Reinhold Publishing Corp., New York, 1952, Chapt. "2".
19. U.S. Pat. 3,920,759 (Nov. 18, 1975), E. V. Hort (to GAF Corp.).
20. U.S. Pat. 3,950,441 (Apr. 13, 1976), S. Rudolf and W. DeThomas (to GAF Corp.).
21. U.S. Pat. 3,922,300 (Nov. 25, 1975), T. Onoda and co-workers, (to Mitsubishi Chemical Industries Ltd.).
22. U.S. Pat. 4,010,197 (Mar. 1, 1977), M. J. Toriya and K. Shiraga (to Mitsubishi Chemical Industries Ltd.).
23. U.S. Pat. 4,064,145 (Dec. 20, 1977), P. D. Taylor (to Celanese Corp.).
24. U.S. Pat. 4,356,125 (Oct. 26, 1982), N. A. de Munck and J. F. Scholten (to Stamicarbon BV).
25. W. L. Hergenrother and C. J. Nelson, *J. Polym. Sci., Polym. Chem. Ed.* **12**, 2905 (1974).
26. R. E. Wilfong, *J. Polym. Sci.* **54**, 388 (1961).
27. Fr. Pat. 1,169,659 (1959) (to ICI Ltd.).
28. Can. Pat. 573,301 (1959), W. K. Easley and co-workers, (to Chemstrand Corp.).
29. H. Zimmerman and N. T. Kim, *Polym. Sci. Eng.* **20**, 680–683 (1980).
30. U.S. Pat. 4,501,878 (Feb. 26, 1985), L. J. Adams (to Eastman Kodak Co.).
31. U.S. Pat. 2,822,348 (1958), J. H. Haslam (to E. I. du Pont de Nemours & Co., Inc.).
32. U.S. Pat. 4,439,597 (Mar. 27, 1984), H. K. Hall and A. B. Padias (to Celanese Corp.).

33. U.S. Pat. 4,824,930 (Apr. 25, 1989), M. L. Doerr (to Celanese Fibers Inc.).
34. U.S. Pat. 4,511,708 (Apr. 16, 1985), T. Kasuga and co-workers, (to Polyplastics Co. Ltd.).
35. U.S. Pat. 4,656,241 (Apr. 7, 1987), H. Iida, K. Azuma, and M. Hayashi (to Toray Industries Inc.).
36. C. M. Fontana, *J. Polym. Sci., Part A-1* **6**, 2343–2358 (1968); Ref. 10 in this paper lists numerous U.S. patents relating to antimony oxide as a polymerization catalyst.
37. U.S. Pat. 4,820,795 (Apr. 11, 1989), S. Hirata and Y. Watanabe (to Toyo Seikan Kaisha).
38. U.S. Pat. 4,499,261 (Feb. 12, 1985), H. Heinze and co-workers, (to Davy McKee AG).
39. U.S. Pat. 4.973,655 (Nov. 27, 1990), G. Pipper and co-workers, (to BASF AG).
40. U.S. Pat. 5,064,935 (Nov. 12, 1991), R. Jackson, D. J. Lowe, and C. A. Stewart (to E. I. du Pont de Nemours & Co., Inc.).
41. I. Goodman and B. F. Nesbitt, *J. Polym. Sci.* **48**, 423–433 (1960).
42. S. Shiono, *J. Polym. Sci., Polym. Chem. Ed.* **17**, 4123 (1979).
43. G. C. East and M. Girshab, *Polymer* **23**, 323–324 (1982).
44. U.S. Pat. 3,718,621 (Feb. 27, 1973), W. K. Wilson (to Goodyear Tire & Rubber Co.).
45. U.S. Pat. 3,816,377 (June 11, 1974), Y. Okuzumi (to Goodyear Tire & Rubber Co.).
46. U.S. Pat. 4,064,112 (Dec. 20, 1977), H. J. Rothe and co-workers, (to Zimmer AG).
47. U.S. Pat. 4,161,578 (July 17, 1979), D. J. Herron (to Bepex Corp.).
48. L. H. Buxbaum, *Angew. Chem., Int. Ed.* **7**, 182–190 (1968).
49. Ref. 1, p. 22.
50. H. Zimmerman and N. T. Kim, *Polym. Eng. Sci.* **20**, 680–683 (1980).
51. E. P. Goodings, *Soc. Chem. Ind. London., Chem. Eng. Group* (Monograph 13), Society of Chemical Industry, London, 1961, 2112.
52. K. Tomita, *Polymer* **18**, 295 (1977).
53. A. von Hassell, *Plast. Technol.* 70 (Jan. 1979).
54. R. de P. Daubeny and C. W. Bunn, *Proc. R. Soc. London, Ser. A* **226**, 531 (1954).
55. S. Fakirov, E. W. Fischer, and G. F. Schmidt, *Makromol. Chem.* **176**, 2459 (1975).
56. E. Bornschegl and R. Bonart, *Colloid Polym. Sci.* **258**, 319 (1980).
57. Y. Kitano, Y. Kinoshita, and T. Ashida, *Polymer* **36**, 10, (1995).
58. M. Droscher, *Makromol. Chem.* **181**, 789 (1980).
59. H. W. Starkweather, P. Zoller, and G. A. Jones, *J. Polym. Sci., Polym. Phys. Ed.* **21**, 295 (1983).
60. J. Menczel and B. Wunderlich, *J. Polym. Sci., Polym. Lett. Ed.* **19**, 261 (1981).
61. K. H. Illers and H. Breuer, *J. Colloid Sci.* **18**, 1–31 (1963); J. H. Dumbleton, T. Murayama, and J. P. Bell, *Kolloid Z. Z. Polym.* **228**, 54–58 (1968).
62. D. B. G. Jaquiss, W. F. H. Borman, and R. W. Campbell, Kirk-Othmer Encyclopedia of Chemical Technology, 3rd ed., Vol. **18**, p. 552.
63. S. Berkowitz, *J. Appl. Polym. Sci.* **29**, 4353–4361, (1984).
64. Ref. 8, pp. 662–685.
65. K. J. McKenzie, in Ref. 8, pp. 761–787.
66. U.S. Pat. 3,733,309 (May 15, 1973), N. C. Wyeth and R. N. Roseveare (to E. I. du Pont de Nemours & Co., Inc.).
67. U.S. Pat. 3,778,214 (Dec. 11, 1973), N. C. Wyeth and co-workers (to E. I. du Pont de Nemours & Co., Inc.).
68. R. W. Tock and co-workers, *Adv. Polym. Technol.* **4**, 307–315 (1984).
69. E. A. Muccio, *Plastics Processing Technology*, Materials Information Society, 1994, Chapt. "5".
70. A. von Hassell, *Plast. Technol.*, 74 (Jan. 1979).

71. A. von Hassell, *Plast. Technol.*, 76 (Jan. 1979).
72. D. G. Callander, *Polym. Eng. Sci.* **25**, 453–457 (1985).
73. U.S. Pat. 5,552,513 (Sept. 3, 1996), K. K. Bhatia (to E. I. du Pont de Nemours & Co., Inc.).
74. U.S. Pat. 5,677,415 (Oct. 14, 1997), K. K. Bhatia (to E. I. du Pont de Nemours & Co., Inc.).
75. U.S. Pat. 5,865,423 (Jan. 5, 1999), K. K. Bhatia (to E. I. du Pont de Nemours & Co., Inc.).
76. U.S. Pat. 4,578,437 (Mar. 25, 1986), R. R. Light (to Eastman Kodak Co.).
77. P. A. Aspy and E. E. Denison, *Mod. Plast.* 74–76 (Aug. 1983).
78. nant Surface Technology SAcos, *Mod. Plast.* 12 (June 2000).
79. res AGcos, *Mod. Plast.* 12 (Dec. 2000).
80. il Corpcos, *Mod. Plast.* 10 (Sept. 2000).
81. *Modern Plastics Encyclopedia*, 2000, p. A-196.
82. *Plast. Technol.* 100 (Sept. 2000).
83. *Mod. Plast.* 58 (Jan. 1999).
84. *Mod. Plast.* 42–49 (Feb. 2001).
85. U.S. Pat. 4,074,032 (Feb. 14, 1978), H. Naarman and co-workers, (to BASF AG).
86. U.S. Pat. 4,143,221 (Mar. 6, 1979), H. Naarman and co-workers, (to BASF AG).
87. U.S. Pat. 4,200,703 (Apr. 29, 1980), K. Diebel and co-workers, (to Chemische Werke Huls AG).
88. U.S. Pat. 4,360,455 (Nov. 23, 1982), G. Lindenschmidt and co-workers, (to BASF AG).
89. U.S. Pat. 4,352,909 (Oct. 5, 1982), H. J. Barda and S. L. Gray (to Ferro Corp.).
90. U.S. Pat. 4,879,353 (Nov. 7, 1989), D. C. Sanders and co-workers, (to Great Lakes Chemical Corp.).
91. Eur. Pat. 664296 (July 26, 1995), V. Carletti and co-workers (to Great Lakes Chemical Italia).
92. *Technical Data, IMPET Resins, Hoechst-Celanese Corp.*, Summit N.J., 1994.
93. A. K. Mitchell, *Mod. Plast.* **71**(12), B48–B50 (1994).
94. *Mod. Plast.* 14 (Mar. 2000).
95. L. M. Sherman, *Plast. Technol.* 77 (May 1995).
96. Ger. Offen. 2,042,447 (Apr. 15, 1971) and U.S. Appl. (Aug. 29, 1969), D. D. Zimmerman and R. B. Isaacson, (to Celanese Corp.).
97. Ger. Offen. 2,533,358 (Feb. 26, 1976) and U.S. Appl. 496,607 (Aug. 12, 1974), F. M. Berardinelli (to Celanese Corp.).
98. E. Bornschegl and R. Bonart, *Colloid Polym. Sci.* **258**, 319 (1980).
99. I. H. Hall and M. G. Pass, *Polymer* **17**, 807 (1976).
100. R. Jakeways, I. M. Ward, and M. A. Wilding, *J. Polym. Sci., Polym. Phys. Ed.* **13**, 807–809 (1973).
101. K. H. Illers, *Colloid Polym. Sci.* **258(2)**, 117 (1980).
102. S. Z. D. Cheng, R. Pan, and B. Wunderlich, *Makromol. Chem.* **189**, 2443 (1988).
103. C. F. Pratt and S. Y. Hobbs, *Polymer* **17**, 12 (1976).
104. K. Tashiro and co-workers, *Macromolecules* **13**, 137 (1980).
105. W. F. H. Borman, *J. Appl. Polym. Sci.* **22**, 2119 (1978).
106. Ho Nan Sung, *Hoechst Celanese Corp.*, Summit N.J., private communication, 1994.
107. J. C. Gill, *Plast. Compd.*, 77–81 (Sept.–Oct. 1989).
108. Ref. 92, Table 8.
109. C. B. Bucknall, *Toughened Plastics*, Applied Science, London, 1977.
110. C. B. Bucknall and C. J. Page, *J. Mater. Sci.* 808 (1982).
111. D. J. Hourston, S. Lane, and H. X. Zhang, *Polymer* **32**, 2215–2220 (1991).
112. *Mod. Plast.* 43 (Feb. 2001).
113. *Mod. Plast.* 46 (Feb. 2001).

114. *Mod. Plast.* 49 (Feb. 2001).
115. L. M. Sherman and J. DeGaspari, *Plast. Technol.*, 71 (Nov. 1995).

ANTHONY J. EAST
Consultant

POLYETHERETHERKETONES (PEEK). See ENGINEERING THERMOPLASTICS.

POLYETHYLENE. See ETHYLENE POLYMERS.

POLY(ETHYLENE-NORBORNENE). See ETHYLENE-NORBORNENE COPOLYMERS.

POLY(3-HYDROXYALKANOATES). See Volume 3.

POLYIMIDES

Introduction

Polyimides are a class of high performance, highly versatile resins that can be tailored for application through the use of chemistry, processing, molecular weight control, and reaction conditions. Polyimides display excellent thermal, mechanical, and physical properties that place them in a general use category as material systems that can compete with other structural materials, mechanical fasteners, higher voltage connectors, and chemically resistant parts. As the requirements for lighter weight, broader temperature performance, increased strength, durability, and inertness continue to drive technology, polyimides will play an increasing role in the innovations of the future.

The first reported synthesis of an aromatic polyimide was in 1908 (1). However, much of the credit for the development and commercialization of polyimide products goes to DuPont, who benchmarked this endeavor in the 1960s with the release of Kapton H film, Vespel molded parts, and Pyre-ML wire varnish (2). This effort inspired other researchers in academia, industry, and government laboratories to pursue the chemistry, fabrication, and applications of polyimides not envisioned several decades ago. There are several excellent books that address the extensive topic of polyimides (3–6). This article provides an overview of the field of polyimides from synthesis and basic kinetic behavior to fabrication and articles of manufacture.

Polyimide Synthesis

The synthetic approach to the formation of polyimides is divided into three groups. The first group involves the synthesis of the polyimide by increasing the molecular

Encyclopedia of Polymer Science and Technology. Copyright John Wiley & Sons, Inc. All rights reserved.

weight of the monomer(s) through the formation of the imide ring via the amic acid/ester route. The second approach involves increasing the molecular weight of a precursor already containing the imide ring. The last method involves the conversion of a polymer into a polyimide.

Polyimides via Imide Ring Formation. The two-step approach is the most general approach used in the synthesis of linear polyimides (7–9). The first step involves the treatment of a diamine with either a dianhydride (the most popular), a tetracarboxylic acid, a diester diacid, a diester diacid-chloride or a trimellitic anhydride chloride (TAC) as in the case of polyamide-imides (Amoco's Torlon) (10,11). These reaction schemes are generally carried out in a high boiling polar protic (phenolic) or aprotic (NMP, DMAc, DMF, etc) solvent at low to moderate temperatures, resulting in the formation of the polyamic acid (or polyamide acid), amic ester, amic acid ester, etc via nucleophilic attack by the amine on the carbonyl carbon (12). Next the formation of the imide ring is brought about through thermal treatment, chemical dehydration, or both by a second nucleophilic attack, occurring at the adjacent carbonyl carbon, by the amide nitrogen, followed by the elimination of a condensate (typically water or alcohol). Removal of this condensate forces the equilibrium toward the right, driving the polymerization to completion (Le Chatelier's principle), thus forming the imide ring (8,13). Alternatively, a "one-step" method or direct conversion is used where a diamine and a dianhydride are placed in a solvent and heated to a temperature where the amic acid moiety formed dehydrates rapidly to the resulting imide. Thus, the polyimide is formed in "one step" (14).

Polyamic Acid Formation. To successfully carry out this synthetic approach, the following requirements must be met: chemical purity; the proper type and percent solids of reaction medium (facilitating solubility of the resulting polyamic acid); reaction temperature; and a method allowing for the removal of any by-products of polymerization (heat, condensates, etc) (13,15). Most commonly, a bifunctional compound is treated with a diamine to afford the amic acid, followed by imide ring formation during the final polymerization step. The routes to achieving a high molecular weight polyimide starting from the monomers via the polyamic acid are shown in Figure 1 (16). When a diamine (**1**) is treated with either a dianhydride (**2**), or a tetraacid or diacid-ester (**3**), alternative routes may occur depending on the reaction kinetics, where k_1 and k_3 are desirable and k_2 and k_4 are not. Table 1 summarizes the approximate kinetic "k_x" values. The pathway to k_4 depends on the amount of water or alcohol in the reaction medium; the reactivity (electrophilicity) of the dianhydride or tetraacid/diacid-ester; and the

Table 1. Typical Rate Constants for Polyamic Acid Synthesis[a]

Reaction	Rate constants
Propagation (k_1)	0.5–6.01 $mol^{-1} \cdot s^{-1}$
Depolymerization (k_2)	10^{-5}–10^{-6} s^{-1}
Imidization (k_5)	10^{-8}–10^{-9} s^{-1}
Anhydride hydrolysis (k_4)	0.1–0.41 $mol^{-1} \cdot s^{-1}$
Amine hydrolysis ($-k_3$)	0–10^{-6} s^{-1}

[a]Refs. 5,17, and 18.

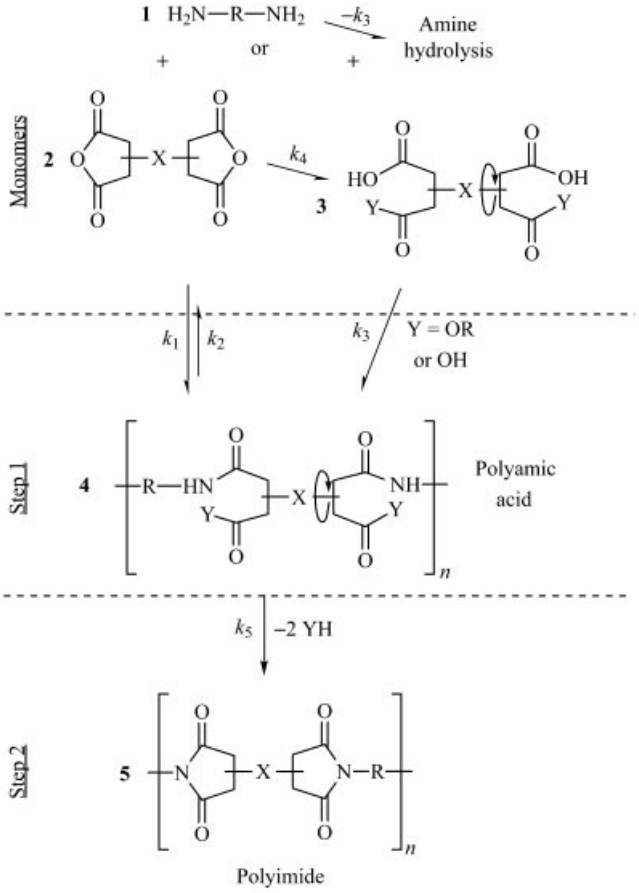

Fig. 1. Reaction Scheme for thermal imidization via polyamic acid/ester.

nucleophilicity of the diamine (Table 2). Steric hindrance and isomerization; polarity and autocatalytic effects of the solvent; and the time/temperature profile during the polyamic acid formation also affect the pathway to k_4 (17,18,20). Conversion of the anhydride moiety, k_4, has the effect of introducing another chemical functionality with a different reactivity that can affect both k_1 and k_3 via resonance. As shown on the reaction coordinate (Fig. 2), the effect of k_2 competes with k_1 and k_3 when the reaction temperature is raised and the thermal dehydration (k_5 conversion) to imide is occurring. Once the imide ring is formed, depolymerization is severely limited through removal of the condensate by-product. The choice of diamine and dianhydride affects the rate of polyamic acid formation both sterically, and through the electronic interactions of the monomers (affinity and basicity). PMDA is the dianhydride with the highest E_a value in Table 2. Any diamine that is treated with PMDA should polymerize faster than if it is treated with a dianhydride having a lower affinity. However, once one of the anhydride units of PMDA has reacted, the second anhydride moiety will display a lower reactivity because the former anhydride group has less electronic withdrawing ability since it ceases to exist with the progress of the reaction. This effect on other dianhydrides is less

Table 2. Electron Affinity and Basicity Values of Several Common Dianhydrides and Diamines Used in the Synthesis of Polyimides[a]

Dianhydride	Abbreviated name	E_a, eV	Diamine	Abbreviated name	pK_a (H_2O)
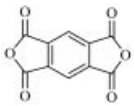	PMDA	1.9	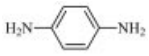	pDA	6.08
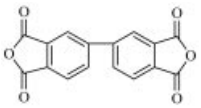	BPDA	1.38	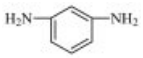	mDA	4.08
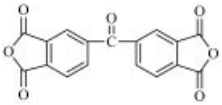	BTDA	1.55	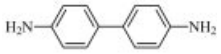	DAB	4.60
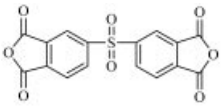	DSDA	1.57	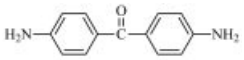	DABP	3.10
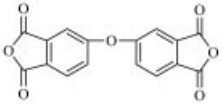	ODPA	1.30	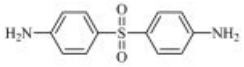	$DDSO_2$	2.15
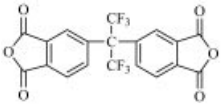	6FDA	ND[b]	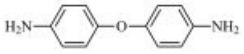	ODA or DAPE	5.20
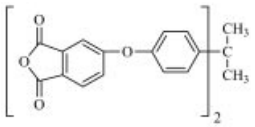	BPADA or ULDA	1.12	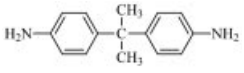	Bis-DA	ND[b]

[a]Ref. 19.
[b]ND = not determined.

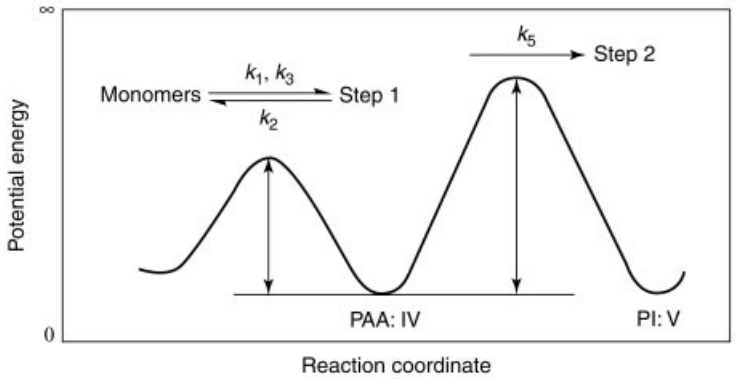

Fig. 2. Qualitative reaction coordinate diagram for polyimde synthesis via polyamic acid. From Ref. 21.

pronounced as the anhydride groups are separated by additional moieties that decrease the impact of the reacted anhydrides (20). A similar trend is seen with diamines. The more basic the amine, the faster it can react with a moiety that is susceptible to nucleophilic attack. Additionally, depending on type, the larger the number of chemical groups separating the amines, the less of an effect the conversion of one amine will have on the reactivity of the other (22).

Solvent effects depend on several factors, including the polarity of the medium, the percent solids, and the solubility of the reactants. As the polarity of the medium changes with conversion to polyamic acid, the viscosity and potential autocatalytic effects (kinetic conversion to polyamic acid) are observed (23). These effects are caused by the increasing molecular weight of the polyamic acid, which results in the buildup of carboxylic acid. The hydroxyl portion of the amic acid can form additional hydrogen bonds to adjacent polyamic acid groups, artificially increasing the observed viscosity (13). These additional carboxyl acid protons can assist nucleophilic attack (on the carbonyl carbon) via coordination with the anhydride carbonyl oxygen, increasing the step growth kinetics to polyamic acid formation. An accurate kinetic profile has been difficult to obtain as a result of the solvent effects and the changing reaction medium. Some investigators claim that irreversible second-order kinetics is followed, while others have observed reversible autocatalytic kinetics when THF is the solvent. Typically, polymerizations carried out in amide solvents (polar aprotic) do not display autocatalytic behavior (23,24). These solvent molecules closely associate with the hydroxyl protons, effectively isolating them from interacting with other anhydrides and amic acids. The reaction rate generally increases as the solvents become more polar and more basic (25,26). A model compound study showed that the acylation rate increased in the order THF < acetonitrile < DMAc < *m*-cresol. The polar protic solvent *m*-cresol was claimed to increase the rate because it functions as an acidic catalyst (23,24). Similar observations were noted when acids (benzoic acid) were introduced into a polyamic acid medium employing an amide solvent. THF, not being very basic, does not associate with the polyamic acid and some reversal occurs. This "retro" reaction (k_2) occurs when a proton is transferred from a carboxylic acid to an amide nitrogen (or any other basic species), followed by the subsequent attack of the carboxylate oxygen on the adjacent carbonyl carbon to re-form the anhydride or the rare isoimide (25,27). This reverse reaction can be prevented by replacing the hydroxyl proton of the polyamic acid with amine salts or esters, causing a marked decrease in conversion to monomeric species (28–30).

The effects of adventitious water on both the starting anhydride and polyamic acids have been shown to decrease their molecular weight over time via conversion to diacid and hydrolytic cleavage, respectively (16,31–33). This drop in molecular weight appears to be more dramatic the more dilute the solution, which is caused by the apparent increase in water content as the percent polyamic acid decreases. Additionally, the conversion from polyamic acid to monomer moieties is unimolecular, whereas the reverse reaction is bimolecular, shifting the equilibrium to the left toward the reactants (8). Evidence has indicated that further imidization of the polyamic acid occurs upon standing over time, having the effect of releasing water into the solution, resulting in further hydrolysis of the polyamic acid (16,34).

Lastly, monomer addition (sequence and rate) has been shown to affect both thermodynamic equilibrium, and the resulting molecular weight of the

polyamic acid. This condition is due to the difference in solubility of the monomers (dianhydride and diamine) in the polymerization solvent (8,16). As the dianhydride slowly dissolves in a medium containing the faster dissolving diamine, it maintains stoichiometric balance with the diamine, setting the condition for an infinite degree of polymerization. This "pseudo-interfacial" polymerization generates high molecular weight polyamic acid until one of the monomers is consumed. Thus, near the completion of the reaction, the medium contains a wide bimodal distribution. As the unreacted or excess monomer has time to come in contact with the high molecular weight polyamic acid, thermodynamic equilibrium (k_1/k_2) occurs and the molecular weights redistribute toward a unimodal distribution (35–37).

Polyimide Formation via the Polyamic Acid. The three methods to form the polyimide from the polyamic acid are thermal, chemical, and a combination of both. The thermal conversion of polyamic acid to polyimide requires the removal of the condensate produced during cyclodehydration (Fig. 1). This is achieved by elevated temperatures and, whenever possible, the addition of a solvent that facilitates azeotropic removal of the condensate. A typical solution for the thermal conversion reaction setup contains approximately 30% solids polyamic acid in NMP and 10% solids xylenes (azeotrope to remove water), and the reaction temperature is maintained at about 165°C for several hours, with water distilling out rapidly early in the reaction (8,38,39). Thermal conversion of polyamic acid in solution is fairly straightforward and becomes complex only when the resulting polyimide precipitates out of solution prior to complete imidization. The kinetics are more complex when the polyamic acid is isolated as a powder, spun as fiber, or cast as a film prior to imidization (40). Generally, the azeotropic cosolvent is not present in these "solid state" preforms, and the effects of the advancing T_g, solvent evaporation rate, percent solids, steric effects, side reactions, cure temperature, and surface-to-volume ratio of the polymeric preform affect the overall kinetics (9,41–43). Thus, attempts to follow the imidization rates using spectroscopy have been confusing as these factors are difficult to account for. One reaction that does not occur during thermal imidization is cross-linking between diamide groups (21,44,45). This is not surprising since there are soluble polyimides cited in the literature, and no spectral evidence exists that support this mechanism. However, thermal aging above 350°C for a period of time may result in cross-linking, but this is most likely due to a free-radical mechanism (thermal degradation) and is influenced by film thickness and the casting surface (46–48). Two pathways of thermally induced imidization are loss of proton on the carboxylic acid group after cyclization (the amide nitrogen initiates the attack on the adjacent carbonyl carbon) or removal of the proton on the carboxylic acid prior to or during ring closure. Since the conjugate base of the amide is more nucleophilic than the amide itself, ring closure should be faster in the latter case (9). When thermal imidization occurs in the presence of an amide solvent, the conversion to polyimide proceeds more readily because the loss of amic acid proton is facilitated through solvent hydrogen bonding. In some cases, the thermal imidization occurs in two steps (9,41). The first step is the rapid conversion to imide above 150°C, and the second step is a slower process during the latter stages of imidization. The following scenario can explain this. During the early stages of imidization, more solvent is present to assist ring closure and the T_g of the polymer is low (9). As the thermal conversion continues, the T_g is increased and the solvent content decreases (41). Chain mobility and

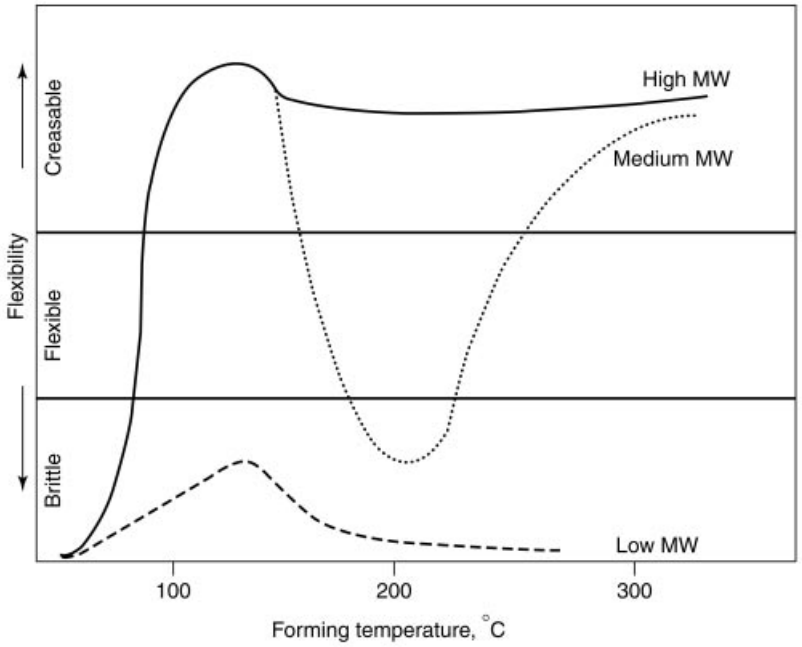

Fig. 3. Qualitative physical properties vs. molecular weight for thermally formed polyimide films (16).

solubility is decreased with increasing conversion, especially if the growing polyimide is semicrystalline. Additionally, as the amount of solvent decreases, the amount of solvent–polymer complexation, which normally facilitates the rate of ring closure, also decreases (9). This two-step rate effect is seen for fibers (high surface area) and cast films where solvent is lost during the processing. It has been shown that thicker films cure at faster initial rates as these films retain the solvent longer, due to extended migration/evaporation time, allowing the chains more mobility to undergo conversion (49). However, the effects of the surface imidizing faster (skinning) than the bulk must be taken into account for thermal convection curing (16). Dry polyamic acid powders with the highest surface-to-volume ratio imidize the slowest. The resulting molecular weight of the polyimide depends, in part, on the molecular weight of the polyamic acid (16). Although the kinetics follow Figure 2, the resulting physical properties of the polyimide films are displayed in Figure 3. Three molecular weight divisions are plotted as a function of temperature versus qualitative physical properties, demonstrating the effect of the polyamic acid molecular weight on the polyimide during conversion. This effect can be rationalized knowing that the amount of chain scission is independent of molecular weight, resulting in a more dramatic effect on lower molecular weight polyamic acids. The lower molecular weight polyamic acids can be reduced to monomers, where these units may be thermally unstable and susceptible to oxidation. When this occurs, the adulterated monomers upset the stoichiometric balance resulting in low molecular weight polyimide. Higher molecular weight polyamic acids are less likely to be converted down to monomeric levels, and the

oligomers will repolymerize to form medium or high molecular weight polyimide as stoichiometry is maintained.

Chemical imidization is not widely used because it employs additional reagents. However, it has the advantage of low temperature imidization and can be used to directly form fine polyimide molding powder (16,50). A typical chemical imidization reaction employs a 20–30% solids polyamic acid in an amide solvent with a slight molar excess of acetic anhydride and a molar equivalent of a triamine (triethyl amine, pyridine, or β-picoline) (51–54). The percent conversion for chemical imidization is a function of polyimide solubility. If the polymer crystallizes and/or precipitates from the reaction medium, imidization will be incomplete (16,50). Those systems that remain soluble must undergo thermal treatment to convert any isoimide, and remove residual solvent. The mechanistic routes of chemical imidization are shown in Figure 4, and involve the use of a triamine

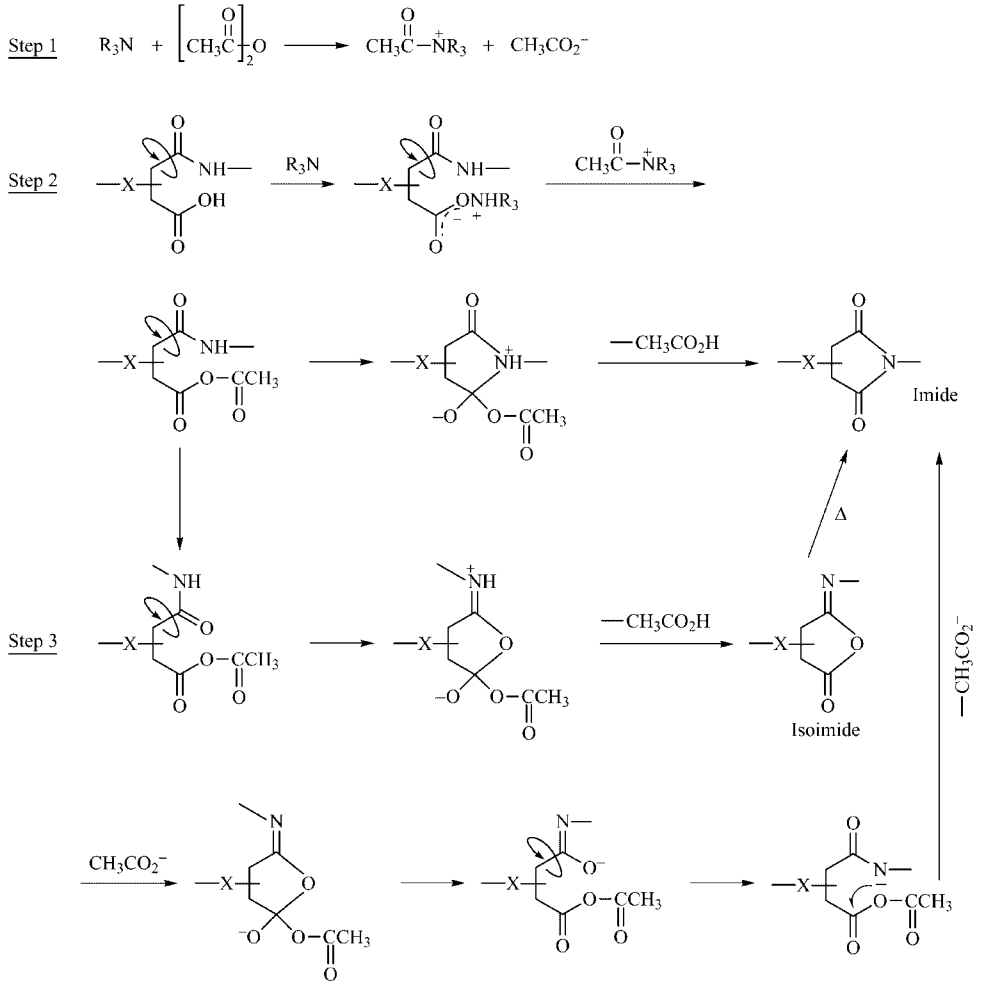

Fig. 4. Reaction Scheme for chemical imidization via polyamic acid.

to form the amine salt from acetic anhydride (step 1) and the amine salt of the polyamic acid (step 2). Next, the salt is replaced with the acetyl group (from the dianhydride salt) to form a mixed anhydride. The acetate group from the mixed anhydride group leaves as the amide nitrogen attacks the carboxylic acid carbonyl. The acetate group picks up the amide proton to form acetic acid resulting in the formation of the imide ring. If the polyamic acid is not in the proper conformation (ie the amide group may be rotated out of position) the carbonyl oxygen may attack the mixed anhydride to form the corresponding isoimide (step 3). The isoimide is readily converted to the imide thermally or by the presence of acetate ions that attack the ester carbonyl carbon, closely following the later stages of step 2. The important step is the conversion of the polyamic acid's hydroxyl group into a better leaving group, the acetate (55,56).

One system that takes advantage of both the chemical and thermal imidization is the gel casting of PMDA–ODA. This system starts as polyamic acid in NMP or DMAc to which is added β-picoline and acetic anhydride. This mixture starts to imidize and forms a gel as it is coated onto a rotating heated drum. The swollen gel film has mechanical integrity that allows it to be stripped off the drum and gripped by a tenter frame. Final conversion and solvent removal is achieved thermally (infrared and convection) while the film is undergoing mechanical orientation (57).

One-Step Formation of Polyimides. Polyimides that are soluble in high boiling organic solvents can be directly converted from their corresponding monomers. This is done by mixing a diamine and a dianhydride into a solvent above 180°C. Typically, solvents such as *m*-cresol with catalytic isoquinoline, nitrobenzene, or NMP are used depending on the polyimide formed (14,58,59). This system is useful for diamines and dianhydrides having low reactivity and those that are sterically hindered, such as perylenic dianhydrides (60,61). The conversion of monomer to polyimide proceeds rapidly with the intermediate polyamic acid being short-lived to the point that it is virtually undetectable. The degree of imidization is nearly 100% (62,63).

Synthesis of Polyimides Using Imide-Containing Monomers. Two methods may be employed to form a polyimide when the imide ring is intact. The first method uses a high yield organic reaction where imide-containing monomers polymerize via a different mechanism (aromatic nucleophilic displacement). The second approach involves thermosetting imide oligomers.

Polyimides via Aromatic Nucleophilic Displacement. Aromatic nucleophilic displacement is used in the synthesis of polyarylene ethers. Halogenated bisimides are polymerized with bisphenolates and activated A–B phthalimides to form polyetherimides (64–67). The reaction proceeds through the Meisenheimer-type transition lowering the activation energy of the displacement reaction. Table 3 shows the relative rates of displacement on substituted phthalimides with phenoxide (eq. 1), and it is worth noting that the displaced nitro group may affect the growing polyimide if not handled properly (66–68). A related synthetic method has been employed specifically for both bisphenols and halogenated diimides or the halogen containing A–B phenolated phthalimide monomers. Bisphenol or the *N*-phenol unit of the fluorinated phthalimide is converted to its corresponding trimethylsylated analogue. Polymerization of these sylated monomers

Table 3. Relative Reactivities of Substituted Phthalimides with Phenoxide[a] in DMSO at RT[b]

	Reactivities	
Position-X	R = Me	R = Ph
3-CI	1	—
3-F	4	20
3-NO_2	37	130
4-F	—	65
4-NO_2	170	520

[a]Equation 1.
[b]Ref. 68.

into polyimides is achieved in the melt at high temperature using cesium fluoride as a catalyst (69).

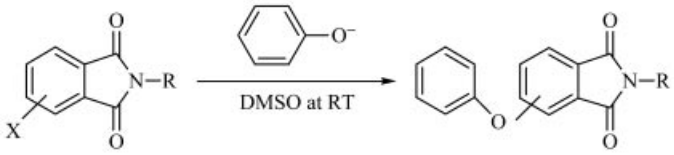

(1)

Polyimides via Addition Reactions. A second approach involves using maleimide-terminated monomers (bismaleimides or BMIs) in equal molar ratios with a dinucleophile, such as a diamine, or a diene like dibenzocyclobutane (BCB) and substituted dicyclopentadienes to form the corresponding linear polyaspartimides via Michael-type addition or the polyimides via a Diels–Alder [4 + 2] cycloaddition (Table 4) (104–115). Linear polyimides can be synthesized directly from the A–B maleimidobenzocyclobutane monomers (116). These reactions proceed without volatile evolution, but undergo thermally initiated retrograde reactions that lead to change in physical properties, chemical cross-linking, and aromatization of the cyclohexene ring (BCBs). Reactions involving BMIs with dicyclopentadieneones also proceed by a cycloaddition mechanism (114,115). This has the same advantage inherent to all Diels–Alder reactions in that no volatiles are generated. However, with these pentadieneone dieneophiles, CO is eliminated forming a cyclohexadiene moiety. The cyclohexadiene can undergo further addition reactions or aromatize with the abstraction of two hydrogen atoms, depending on the reaction conditions and the added stability of any pendent substituents (114,115). This type of chemistry can be used to create photosensitive polyimides for imaging. The last approach utilizes free-radical polymerization of substituted maleimides to afford ethylenic-type imide polymers (117,118). Maleimide groups are copolymerized with styrene and other maleimides to afford copolyimides. Polymerization of these systems is typically carried out with AIBN in polar solvents such as THF (119). These types of polyimides can be used for a variety of applications depending on the selection of the N-substituent.

Thermosetting systems involve the placement of reactive moieties on the imide containing molecule (1 part), and these oligomers can be blended with other reactive oligomers (2+ part) to provide additional benefits (Table 4). These

Table 4. Chemical Groups Used for Functionalizing or Reacting with Polyimides[a]

Reactive group	Onset cure temp., °C	Comments on long-term stability at 177°C
—O C≡N (Cyanate)	200–230	Poor thermal stability
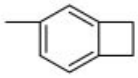 (Benzocyclobutene)	200–250	Coreacts with maleimide, poor long-term stability
—OCF═CF_2 (Trifluorovinylether)	250	Small processing window, unknown thermal stability
—C≡CH (Ethynyl)	200	Small processing window, unknown thermal stability
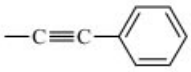 (Phenylethynyl)	320–370	Excellent thermal stability
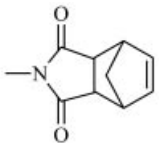 (Nadimide)	300–350	Cyclopentadiene evolution, low toughness
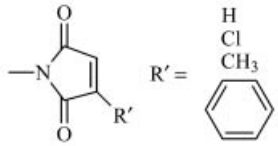 (Maleimide) (Chloromaleimide) (Methylmalimide)	200–230	Poor thermal stability
200–230	Poor thermal stability	
220–250	Poor thermal stability	
340–370	Unknown thermal stability	

[a]Refs. 70–103.

systems contain maleimide, norbornene (nadic), vinyl and allylic, acetylenic, phenylethynyl, or other types of unsaturated groups that react to cross-link the polyimide (70–99). When bismaleimides are used alone or in excess with a difunctional (at least) nucleophilic monomer, the resulting system is thermosetting, with chain extension (via Michael-type addition) occurring prior to the thermal

cross-linking of the maleimide functionality (via Michael addition) (120–124). Although the cross-linking of the maleimide group is thermally initiated, it is catalyzed with both free radicals and bases (72,73,118). Typical synthesis involves 30% (or more) total solids diamine and two equivalents of maleic anhydride in acetone at ambient temperature. After the bismaleamic acid precipitates (several hours), triethyl amine (approximately 0.5 equiv) is slowly added to the mixture until dissolution occurs. Acetic anhydride (slightly over 1 equiv) is added and the mixture is heated at reflux for several hours and the crude product is isolated by water precipitation. The intermediate maleamic acid is susceptible to isomerization during cyclodehydration, resulting in the production of the less desirable acetanilide (72,115). Metal acetate catalysts have been known to increase the yields of BMI (125). However, it has been the author's experience that these catalysts tend to be difficult to remove and provide marginal benefit. Blends of BMIs with aromatic allyls and phenylpropenyl oligomers, such as a bisallylphenol, have been used as thermosetting systems that undergo a complex reaction involving ene addition followed by Diels–Alder addition, respectively (90,91,93,95,98,99,126,127). The nadic group has been extensively explored for creating polyimide thermosetting resins including the "PMR" materials. These nadic-terminated oligomers are formed from nadic anhydride (NA), a diamine, and a dianhydride (87,88,128–133). These systems (like their aromatic counterparts) do not exhibit the same behavior as maleamic acid does during imidization as structural conformation remains in place. Unfortunately, the nadimides generate cyclopentadiene at the elevated temperatures required to cure them. Hence, these systems must be cured under pressure to avoid volatilization of the cyclopentadiene, which copolymerizes with itself, other nadic moieties, and the resulting maleimide (134–136). In an attempt to create a high temperature thermosetting imide system that can be handled as a room temperature liquid, the PMR approach was developed (polymerization of monomeric reactants). Here, the dianhydride and NA are treated with molar equivalents of an aliphatic alcohol and allowed to form the liquid diacid-ester isomers. The diamine and the diacid-esters are then dissolved in methanol, and the liquid system is solution cast or coated onto a preform to create a prepreg that is dried and cured under pressure to form a composite part. The advantage of this system is that the monomers remain intact at or below room temperature (89,137–139). The molar ratios of the diacid-methylester of BTDA, 4,4′-methylenedianiline (MDA), and the acid-methylester of NA of 2.087:3.087:2 are used to make a 1500 g/mol imidized reactive oligomer referred to as PMR-15. Acetylenic groups on polyimides are used to induce thermal cross-linking (76,140). The actual chemical structures developed during the acetylenic cross-linking can vary, as the reactivity of these groups is high enough to allow attack on chemical moieties other than acetylenic units (141). National Starch's Thermid IP-600 is an acetylene-terminated thermoset that has enhanced solubility, as it is an isoimide that thermally converts to imide when cured (142,143). The highest temperature matrix resin/structural adhesives were those based on phenylacetylene (phenylethynyl) (94,144,145). NASA's PETI (*p*henylethynyl-*t*erminated *i*mide) series consist of systems that cure at temperatures above 320°C (100–103,146–149).

Polyimides via Polymer Conversion. One method has already been introduced through the chemistry of isoimide synthesis and conversion. If the isoimide is desired directly, a polyamic acid is dissolved in a solvent system that

facilitates removal of the by-product and a molar equivalent of dicyclohexylcarbodiimide "DCC" or similar cyclodehydrating agent. These isoimides are then converted by thermal conversion to the corresponding imide (150). Other methods involve transimidation and treatment of dianhydrides with diisocynates. Transimidation involves the exchange of one imide nitrogen functionality (as the amine) for another. This type of reaction is favored when the attacking amine is more basic than the amine that comprises the imide ring. Because of the lower reactivity of aromatic amines, in comparison to aliphatic amines, this type of reaction offers certain advantages. When the less basic 2-aminopyridine terminates imide oligomers, this amine can be readily exchanged for other aromatic diamines to form a high molecular weight polyimide through proper stoichiometric control (151–154). This scenario allows for the formation of otherwise infusible polyimides, via melt processing techniques, and also permits the incorporation of chemical moieties that are susceptible to hydrolysis via the polyamic acid route. Another conversion route involves the reaction of diisocyanates with dianhydrides to form the polyimide followed by elimination of CO_2 (155–162). There is not a general consensus on the mechanism of this reaction. Some researchers contend that the isocyanate reacts with water to form the amine or alcohol to form the urethanes that react with the dianhydride to form the polyimide (157). Others favor a seven-membered ring formation that liberates CO_2 forming the imide ring (155). Metal salts have catalyzed these imide-forming reactions, and some have been polymerized in the melt (163,164).

Polyimide Structure–Property Relationships

One of the features of polyimides is that the polyimide macromolecules interact with themselves and with each other by either an electronic polarization or charge-transfer mechanisms (165,166). The degree to which these mechanisms play a role depends on the electron affinity of the imide ring (deficiency) and the electron donating ability of the N-substituent (ionization potential) (19). The extent to which these electronic interactions affect the neighboring polymer molecules influences the polyimide's color, glass-transition temperature, crystallinity, mechanical properties, and chemical resistance (167,168). It is apparent that the intrachain electronic polarization affords the yellow to dark orange color that arises in polyimides (167,168). The amount of chromophores present can be controlled to some extent by the selection of the cyclodehydration environment choice of monomers, polymerization conditions, and especially processing methods; and is not related to the presence of unconverted isoimide (167). Generally, the bulk structure–property relationships that apply to most polymers apply to polyimides. The thermal transitions are influenced by the selection of monomers and processing techniques (169–171). Monomers that have kinks, offsets, swivel units, pendent substituents, aliphatic moieties, and bulky units tend to lower the T_g, melt viscosity, and crystallinity and increase the solubility, as these units take up more free volume and introduce a more random structure than their symmetric counterparts (50,172–185). The proper selection of monomers has produced soluble nearly colorless polyimides by the introduction of fluorine-containing monomers (167,168). One interesting and unique polyimide developed by NASA, LaRC-SI,

does not use the standard approaches to develop solubility. This polyimide starts from a mixture of two dianhydrides BPDA and ODPA and a diamine 3,4′-ODA to afford an amorphous high molecular weight polyimide that is soluble in common high boiling amide solvents (38,182,186). What is intriguing is that the two homopolymers, ODPA/3,4′-ODA (LaRC-IA) and BPDA/3,4′-ODA, and the copolymer using ODPA/BPDA/4,4′-ODA are all insoluble and semicrystalline (182).

Aromatic polyimides are highly thermally stable because of their degree of aromaticity and ring structure. Typical decomposition points for polyimides, not subject to thermally initiated retro reactions, are above 450°C in air and above 500°C in nitrogen (187). Endcapping a polyimide with a stable monofunctional unit also enhances thermal stability by protecting chemically active chain ends that are subject to thermal and chemical instability (188,189). As a class, polyimides are resistant to chemical attack and moisture. An exception is the PMDA-containing polyimides that are hydrolyzed under basic conditions (190–192). The effect of degradation of one imide ring, in PMDA, changes the characteristics of the other ring via resonance through the common aromatic ring. This is also the case with monoaromatic diamines like pDA. However, most polyimides are highly resistant to caustics, acids, organic solvents, specialty fluids, and salts, even at elevated temperatures (38,100,103,175). The electrical properties of polyimides have led to their widespread use as dielectrics, flexible substrates, and wire insulation for the electronics industry (193–198). Although the imide ring is polar and electron deficient, the two dipoles of the carbonyl groups oppose each other and the imide rings along the polyimide backbone also directionally oppose each other. This simulates the bulk effect of a nonpolar polymer. Thus, polyimides make good dielectric materials when combining these properties with their high temperature and chemical stability (196,199–202). As expected, fluorinated polyimides display the best dielectric properties (low dielectric constant) as the fluorine atom imparts low polarizability, water uptake, and surface energy (200–202). Similar comparisons can be made from PTFE systems and their corresponding hydrocarbon analogues. The bulk mechanical properties of aromatic polyimides are among the best for commercial plastics (203). This is due to the interchain interactions of polyimides and their structural integrity imparted by their aromatic character (166,204). Additionally, those polyimides that can undergo melt processing tend to make excellent hot melt adhesives.

Photoimageable Polyimides

There are several ways (see Fig. 5) in which polyimides have been used in applications where "photoimaging" is required to produce a pattern on a substrate (typically silicon, or other materials including polyimide itself) (205). The first method is reactive ion etching (RIE) (includes plasma etching) or photoablation. This method does not require a photosensitive material, only a mask that can withstand the reactive ion gas or photons, and the material to be patterned, which is protected by the mask. In RIE, the reactive ions, generated by an RF field, attack the exposed polyimide to etch out the pattern of the mask. This process can be used with conventional polyimide film and requires few steps, but is not highly accurate and requires a hard (metal, silicon, etc) mask. The other methods

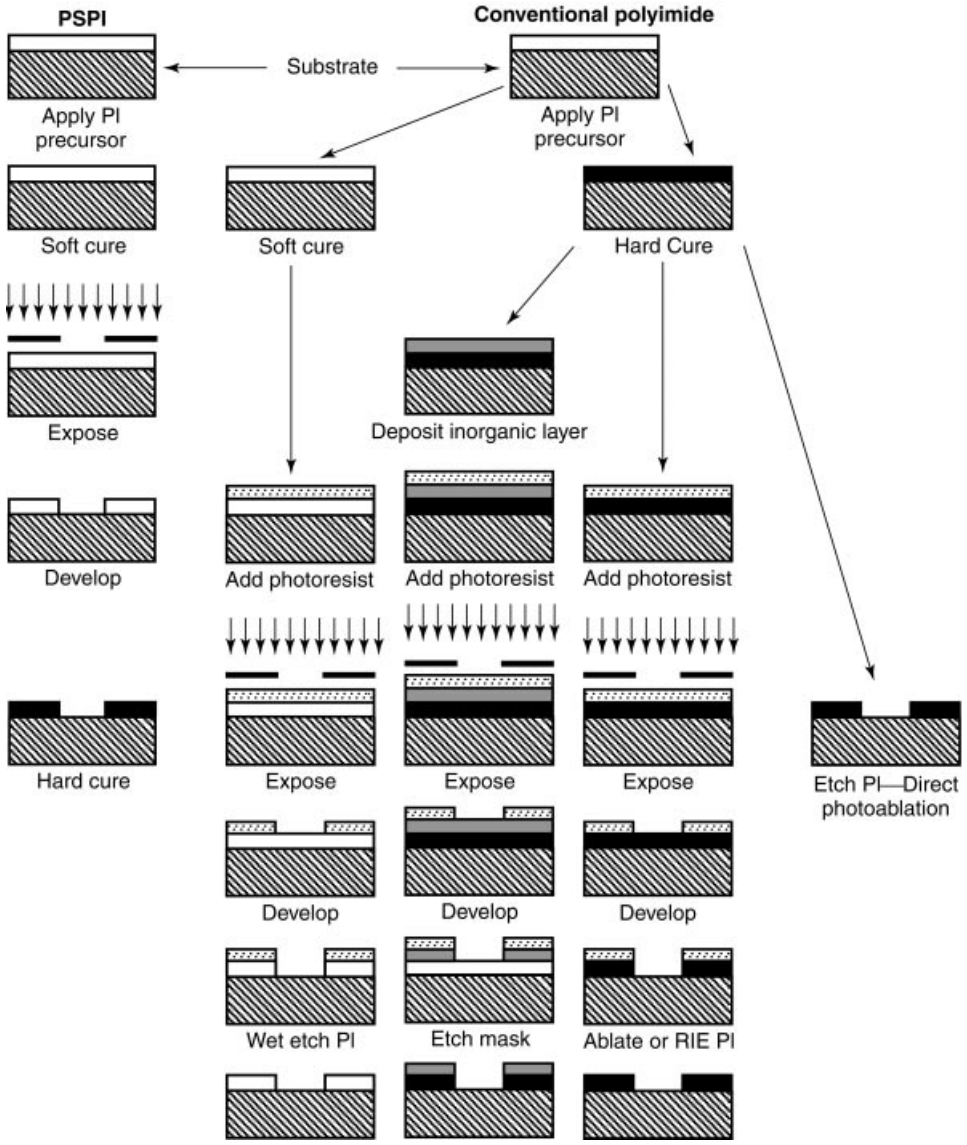

Fig. 5. Chart of various photoimaging processes. Reprinted from Ref. 205 p. 744, by courtesy of Marcel Dekker, Inc.

involving the conventional polyimide, as a dielectric, require an additional photosensitive material as the overcoat. The method is very much the same as using a mask, but higher degrees of accuracy are obtained as the photosensitive material's exposure and development are done with coherent short wavelength light. The combination of step reduction, increased accuracy, and less complexity while maintaining good dielectric, mechanical, and thermal properties have spurred the development of photosensitive polyimides (PSPIs) used with these photoimaging methods (206,207).

Photosensitive polyimides are often used in their soluble polyamic acid form and are of the negative resist type (forms a negative image on exposure). The polyamic acid has photosensitive units either attached to the polymer backbone, in conjugation with the carboxyl unit of the polyamic acid, or incorporated into the polyimide structure. Specific areas of the cast photosensitive film are exposed to light, thereby becoming insoluble, and the masked portions (unexposed areas) are washed away with solvent. The remaining cross-linked (exposed area) is then baked to thermally cure the polyamic acid and remove the photosensitized units. There are several approaches used to create PSPIs, with the more popular being those of the covalent, ionic, and intrinsic types (208). The covalent type was one of the first and still widely used commercial approaches. A photosensitive unit is attached to the carboxyl group of the starting dianhydride prior to polymerization with a diamine (Fig. 1, k_4 followed by k_3). The resulting sensitized polyamic acid is then exposed and the resulting sensitized ester unit photo-cross-links. The exposed film is then developed and baked (Fig. 1, k_5). Such photosensitive units are of the methacrylate or cinamyl variety. The ionic type is similar to the covalent type but instead the premade polyamic acid is sensitized using a tertiary amine having a photoreactive group and a photoinitiator. The interaction of the tertiary amine and the polyamic acid hydroxyls forms a photosensitized salt that is ionically bound to the polyamic acid (similar to Fig. 4, step 2). The ionic PSPI is then exposed, washed, and baked to develop the image. The last type is the intrinsic PSPIs, meaning that they are photosensitive as made. These PSPIs are generally based on BTDA and orthoalkylated diamines. When these intrinsic systems are exposed to a 365 nm wavelength, the hydrogen atoms of these pendent alkyls are abstracted through the excitation (C=O diradical formation) of the benzophenone radicals, inducing cross-linking of the pendent methylene radicals. Overall resolution of PSPIs is controlled by several factors including film thickness, exposure wavelength, and the selectivity of the developer. These drawbacks manifest themselves through pattern distortion, shrinkage, pinhole formation, and thermal stability effects during wafer processing. Most of these developed PSPIs have mechanical properties close to that of a standard polyimide film, demonstrating excellent planarity (surface flatness) and good breakdown voltage resistance.

Applications

Polyimides are manufactured in a variety of forms, finding utility ranging from electronics and medical to structural and adhesive applications. One of the more prevalent forms of polyimides is films. The most popular films are Dupont's Kapton, Ube Industries' Upilex, and GE's Ultem, and Kanekafuji's Apical, to name a few. In film form, some of these materials do not display a T_g, have good radiation resistance, and are used as bagging materials for composites, belts, and wire wrapping. Polyimide films have excellent mechanical properties with elongations from 30 to 120%, and tensile strengths and moduli 170–270 MPa and >3 GPa, respectively. They are coated with acrylics and silicones to make pressure-sensitive tape (209). They are also coated with an adhesive to bond metal foil (copper) on one or both sides, and sold to PCB manufactures for flexible cabling and circuits (examples include DuPont's Pyralux and clad derived from Kaneka's Apical series

of PI films). Metal is also vapor deposited onto polyimide films for applications requiring thin copper (less than 0.5 oz/12 μm) and where the additional adhesive is undesirable. Since these films and clads serve as dielectric materials, they are tested under IPC TM-650 tests and display breakdown voltages above 200 V/μm (5 kV/mil) and 1 MHz dissipation factors of 3.2 on average (198). Another method to create metallic coatings is an *in situ* method involving the introduction of silver organic salts [complexed silver(I) acetates] or other metallic complexes into the polyamic acid; through thermal imidization, the silver metal is reduced and migrates to the surface to form a reflective coating (9,210–213). For years, the electrical and aerospace industry has used polyimides as high performance wire insulation. These coatings are used in combination with other materials and may be either biaxially wrapped onto the wire, solution coated, and dried in multiple passes to form a varnish, or directly extruded over the wire. The polyimide insulation must survive tight radial bends, chaffing, and electrically induced oxidation and carbon tracking (193,214–216). A similar method to that of the wire varnish process is the fabrication of microporous membranes, thin walled tubes, and fibers. Flat or hollow fiber membranes are made by selective solution blending and thermal evaporation techniques and may also consist of rolled multiwalled structures (217–220). Similar methods are also used when creating open cell polyimide foams of varying density (221–225). Thin walled polyimide tubes created from PMDA and BPDA–ODA polyimides cannot be made via melt processing and are created by successive layering and drying to build up thickness and then removal of the internal wire or mandrel (via rapidly applied mechanical strain) that was used to provide the prerequisite form. These polyimide tubes find use as GC columns for chemical separation and as catheter medical tubing (226). The requirement of the preform selected is that it must release cleanly and uniformly from the cured polyimide. Continuous fibers, solution spun and dried from polyamic acid or as the polyimide, present a challenge as the solvent, cyclodehydration, and shrinkage problems associated with curing the fiber result in a technical challenge. Although the properties of these fibers are excellent when the proper draw ratio is used, they have not achieved a high performance niche market able to economically compete with polyesters or polyaramides (215,227,228).

Melt-Processable Polyimides. Polyimides that display a T_g and T_m well below their decomposition or thermosetting temperatures are candidates for melt-processing techniques that include extrusion, injection, and compression molding. Several other factors play into the selection of melt-processable polyimides and include melt viscosity, work time or pot life at temperature, and the ability to carry fillers or blends. Melt viscosity is crucial as it directly relates to molecular weight, affecting the processing temperature (189,229–231). The higher the molecular weight, the higher the temperature and pressure needed to create the part. As the polymer's molecular weight increases, the mechanical properties increase until a critical molecular weight is obtained, where the melt viscosity increases while the mechanical properties start to level out. This "knee" or bend in the mechanical and physical properties versus molecular weight curve is where any further increase in molecular weight increases the complexity of the melt forming without a significant improvement in the overall properties of the neat resin (229–231). The influence of molecular weight and its relationship to melt viscosity are affected by the structure of the polyimide in a fashion similar to the basic structure–property

relationships discussed earlier. Several resin systems developed by GE, NASA Langley, Furon, Mitsui, and others have found utility as thermoplastic molding resins. The T_g for these thermoplastic polyimides are in the range of 210–270°C and are processed 50–150°C above their glass transition temperature (229,230). The molecular weights of these resins range from several thousand to above 25,000 g/mol. These systems display excellent fracture toughness and high modulus and have been extruded, compression molded, machined and polished neat, or filled with graphite, PTFE, and metal and ceramic powders. These thermoplastic polyimides are sold as rod, sheet, and film stock or as final stock parts and composites (232–238).

Thermosetting polyimides solve the molecular weight effect on melt viscosity, but add the additional problems associated with curing exotherms and time/temperature limited processing windows. Thus, a wide processing window from the melt flow of the monomer(s) to the onset cure temperature should be selected. The melt-processable thermosetting systems are typically BMIs, PMRs, or BCB–maleimides, and these can blended with chopped fibers or other fillers, ground, or extruded and pelletized for moldings (239,240). These imide oligomers are then cured into high performance PCB substrates and composite forms. Recently, NASA Langley has developed several PETI-based low viscosity thermosetting resins that can be injection molded or resin infused into carbon fiber performs and then cross-linked at elevated temperatures (241).

Directly Formed Polyimides. There are several polyimides that do not undergo melt flow, but are directly formed into parts requiring performance under extremely harsh conditions (242,243). These direct formed polyimides include DuPont's Vespel (includes the SP product line), Ube's Upimol-S, and Imitec's I-903 and I-772. These polyimides undergo a forming process similar to that of ceramic sintering. The starting fine particle polyimide powder is either hot isostatically pressed (HIPed) or ram extruded and hot formed to generate a polyimide stock shape with a density in the range of 1.4–1.5 g/cm^3. These polyimide powders have also been blended with graphite, PTFE, and boron nitride for dry lubrication. These parts have very low CTE and do not smear under load at elevated temperatures, making them excellent choices for high temperature pressure–velocity requirements. These molded parts have found utility in rotating equipment, silicon wafer and chip processing, machine tooling, and chemical and material processing.

Polyimide Matrix Composites and Adhesives. Polyimides display properties that make the resulting advanced composites excellent choices as primary structural members for aerospace applications (244). The fibers in the composite are the load carrying members and the resin serves to transfer the load to the fibers and hold them in place. The composite is only as good as the resin. Thus, the selected matrix resin must have excellent thermal, chemical, and mechanical toughness, and high compressive strength and adhesive properties. One of the key elements in creating a strong composite is the wetting out of the fibers with the proper amount of resin. This is achieved by two methods, dry and wet (or solution) prepregging (245). The dry-coating method may consist of coating the fibers with fine polyimide powder and melt shearing the powder to form a film about the fibers (246). Another dry process involves melt-infusing a polyimide film into a fiber matrix affording prepreg tape. Solution prepregging involves the coating of the fibers with a solution containing the polymer or reactive monomers and

removing the solvent at a later stage to form the prepreg tape. The resulting prepreg should display tack and drape, ie, tack to allow it to remain in place prior to and during consolidation, and drape to allow it to contour to the tooling surface. These prepregs are then cut into the desired shapes, stacked, and laminated together on a tool in a hot press or autoclave to form the composite part. In order to achieve excellent consolidation, these polyimide laminates must undergo melt flow and adhere (240). Hence, the polyimides must display high adhesive strength under a variety of conditions. Initial Criteria for screening the hot melt aerospace polyimides is the titanium–titanium or aluminum–aluminum lap shear test (ASTM D1002); for the electronic industry, the T-peel and 180° peel tests are used (ASTM D1976 and D3330). Titanium lap shear strengths for polyimide adhesives range from 2000 psi to over 8000 psi under ambient conditions. It is worth noting that surface preparation plays a key role in determining the adhesive strength of the resin system. The polyimide resin systems that have been used for aerospace composite programs include BMIs, PMR-15, DuPont's Avimide series (based on the PMR approach), and NASA's PETI-5 (developed under the HSR program) that exceeds the performance criteria for the High Speed Civil Transport as a structural adhesive and matrix resin for this advanced composites program (240,247,248).

BIBLIOGRAPHY

"Polyimides" in *EPST* 1st ed., Vol. 11, pp. 247–272, by C. E. Sroog, E. I. du Pont de Nemours & Co., Inc.; "Polyimides" in *EPSE* 2nd ed., Vol. 12, pp. 364–383, by J. W. Verbicky Jr., General Electric Co.

1. T. M. Bogert and R. R. Renshaw, *J. Am. Chem. Soc.* **30**, 1140 (1908).
2. U.S. Pats. 3,179,614 and 3,179,634 (1965) and Br. Pat. 898,651 (1959), W. M. Edwards (all to E. I. Du Pont de Nemours & Co., Inc.).
3. M. W. Ranney, *Polyimide Manufacture*, Noyes Data Corp., Park Ridge N.J., 1971.
4. M. K. Ghosh and K. L. Mittal, eds., *Polyimides: Fundamentals and Applications*, Marcel Dekker, Inc., New York, 1996.
5. M. I. Bessonov, M. M. Koton, V. V. Kudryavtsev, and L. A. Laius, *Polyimides: Thermally Stable Polymers*, Plenum Publishing Corp., New York, 1987.
6. D. Wilson, H. D. Stenzenberger, and P. M. Hergenrother, eds., *Polyimides*, Blackie, London, 1990.
7. U.S. Pats. 2,710,853 (1955) and 2,867,609 (1959), W. M. Edwards and I. M. Robinson (both to E. I. du Pont de Nemours & Co., Inc.).
8. C. E. Sroog, A. L. Endrey, S. V. Abramo, C. E. Berr, W. M. Edwards, and K. L. Oliver, *J. Polym. Sci., Part A* **3**, 137 (1965).
9. J. A. Kreuz, A. L. Endrey, F. P. Gay, and C. E. Sroog, *J. Polym. Sci., Part A-1* **4**, 2607 (1966).
10. Y. Imai, in Ref. 4, Chapt. 3.
11. J. F. Dezern, *SAMPE J.* **24**(2), 27 (1988).
12. F. W. Harris, in Ref. 6, Chapt. 1.2.
13. G. M. Bower and W. L. Frost, *J. Polym Sci., Part A* **1**, 3135 (1963).
14. U.S. Pats. 4,324,884, 4,324,885, and 4,330,666 (1982), D. M. White (all to General Electric Co.).

15. M. L. Wallach, *Polym. Prepr.* **6**(1), 53 (1965).
16. R. A. Dine-Hart and W. W. Wright, *J. Appl. Polym. Sci.* **5**, 609 (1967).
17. V. I. Kolegov and S. Ya. Frenkel, *Polym. Sci. U.S.S.R., A* **18**, 1919 (1976).
18. V. I. Kolegov, *Polym. Sci. U.S.S.R., A* **18**, 1929 (1976).
19. Ref. 5, Chapt. 1, Tables 1.2 and 1.5.
20. V. W. Svetlichnyi, K. K. Kalnin'sh, V. V. Kudryavtsev, and M. M. Koton, *Dokl. Akad. Nauk SSSR (Engl. Trans.)* **237**, 693 (1977).
21. F. W. Harris and L. H. Lanier, in F. W. Harris and R. B. Seymour, eds., *Structure-Solubility Relationships in Polymers*, Academic Press, New York, 1977, pp. 183–198.
22. V. A. Zubkov, M. M. Koton, V. V. Kudryavtsev, and V. M. Svetlichnyi, *Zh. Org. Khim. (Engl. Trans.)* **17**, 1501 (1982).
23. V. A. Solomin, I. E. Kardish, Y. S. Snagovskii, P. E. Messerle, B. A. Zhubanov, and A. N. Pravendnikov, *Dokl. Akad. Nauk SSSR (Engl. Trans.)* **236**, 510 (1977).
24. R. L. Kaas, *J. Polym. Sci., Polym. Chem. Ed.* **19**, 2255 (1981).
25. A. Ya. Ardashnikov, I. Ye. Kardash, and A. N. Pravednikov, *Polym. Sci. U.S.S.R., A* **13**, 2092 (1971).
26. Ya. S. Vygodskii, T. N. Spirina, P. P. Nechayev, L. I. Chudina, G. Ye. Zaikov, V. V. Korshak, and S. V. Vinogradova, *Polym. Sci. U.S.S.R., A* **19**, 1738 (1977).
27. A. N. Pravednikov, I. Ye. Lordash, N. P. Glukhoyedov, and A. Ya. Ardashnikov, *Polym. Sci. U.S.S.R., A* **15**, 399 (1973).
28. P. P. Nechayev, Ya. S. Vygodskii, G. Ye. Zaikov, and S. V. Vinogradova, *Polym. Sci. U.S.S.R., A* **18**, 1903 (1976).
29. R. J. W. Renyolds and J. D. Sheldon, *J. Polym. Sci., Part C* **23**, 45 (1968).
30. J. B. Haung and B. M. Gong, *J. Vac. Sci. Technol., B* **3**, 253 (1985).
31. M. L. Bender, *J. Am Chem. Soc.* **79**, 1258 (1957); *J. Am Chem. Soc.* **80**, 5380 (1958).
32. E. J. Soichi, S. J. Havens, P. R. Young, and P. M. Hergenrother, *High Perform. Polym.* **7**, 55 (1995).
33. E. J. Soichi, NASA/CR-1998-207633, May 1998.
34. L. W. Frost and I. Kesse, *J. Appl. Polym. Sci.* **8**, 1039 (1964).
35. R. A. Orwoll, T. L. St. Clair, and K. D. Dobbs, *J. Polym. Sci., Polym. Phys. Ed.* **19**, 1385 (1981).
36. C. C. Walker, *J. Polym. Sci., Part A: Polym. Chem.* **26**, 1649 (1988).
37. W. Volksem and P. M. Cotts, in K. L. Mittal, ed., *Polyimides: Synthesis, Characterization and Properties*, Vol. **1**, Plenum Press, New York, 1984, pp. 163–179.
38. R. G. Bryant, *High Perform. Polym.* **8**, 607 (1996).
39. H. Furutani, J. Ida, K. Tanaka, and H. Nagano, *High Perform. Polym.* **12**, 461 (2000).
40. Ref. 5, p. 75, Table 1.20.
41. L. A. Laius, M. I. Bessonov, Ye. V. Kallistova, N. A. Adrova, and F. S. Florinskii, *Polym. Sci. U.S.S.R., A* **9**, 2470 (1967).
42. K.-M. Chen, T.-H. Wang, J.-S. King, and A. Hung, *J. Appl. Polym. Sci.* **48**, 291 (1993).
43. J. W. Verbicky Jr. and L. Williams, *J. Org. Chem.* **46**, 175 (1981).
44. S. V. Vinogradova, V. V. Korshak, and Ya. Vygodskii, *Polym. Sci. U.S.S.R., A* **8**, 888 (1966).
45. C. A. Pryde, *J. Polym. Sci., Part A* **27**, 711 (1989).
46. S. Kuroda, K. Terauchi, K. Nogami, and I. Mita, *Eur. Polym. J.* **25**, 1 (1989).
47. J. A. Cella, *Polym. Degrad. Stab.* **36**, 99 (1992).
48. M. I. Bessonov, in Y. Tabata, ed., Proc. Int. Symp. Polym. Microelectron., Kodansha, Tokyo, 1990, pp. 721–734.

49. R. Ginsburg and J. R. Susko, in K. L. Mittal, ed., *Polyimides: Synthesis, Characterization and properties*, Vol. **1**, Plenum Press, New York, 1984, pp. 237–247.
50. D. P. Heberer, S. Z. D. Cheng, J. S. Barley, S. H.-S. Lien, R. G. Bryant, and F. W. Harris, *Macromolecules* **24**, 1890 (1991).
51. U.S. Pats. 1,379,630, 1,379,631, and 1,379,633 (1965) and Can. Pat. 659,328 (1963), A. L. Endry (all to E. I. du Pont de Nemours & Co., Inc.).
52. U.S. Pat. 3,179,632 (1965), W. R. Hendrix (to E. I. du Pont de Nemours & Co., Inc.).
53. U.S. Pat. 3,282,898 (1966), R. J. Angelo (to E. I. du Pont de Nemours & Co., Inc.).
54. S. V. Vinogradova, Ya. S. Vygodskii, V. D. Vorob'ev, N. A. Churochkima, L. I. Cludina, T. N. Spirina, and V. V. Korshak, *Polym. Sci. U.S.S.R., A* **16**, 584 (1974).
55. M. M. Koton, T. K. Meleshko, V. V. Kudryavtsev, P. P. Nechayev, Ye. V. Kamzolkina, and N. N. Bogorad, *Polym. Sci. U.S.S.R., A* **24**, 791 (1982).
56. R. J. Cotter, C. K. Sauers, and J. M. Whelan, *J. Org. Chem.* **26**, 10 (1961).
57. J. G. Stephanie and P. G. Rickerl, in Ref. 4, Chapt. 9.
58. S. V. Vinogradova, G. L. Slonimskii, Ya. S. Vygodskii, A. A. Askadskii, A. I. Mzhef'skii, N. A. Churochkina, and V. V. Korshak, *Polym. Sci. U.S.S.R., A* **11**, 3098 (1969).
59. S. V. Vinogradova, Ya. S. Vygodskii, and V. V. Korshak, *Polym. Sci. U.S.S.R., A* **12**, 2254 (1970).
60. F. W. Harris and S. L.-C. Hsu, *High Perform. Polym.* **1**(1), 3 (1989).
61. D. Dotcheva, M. Klapper, and K. Muller, *Macromol. Chem. Phys.* **195**, 1905 (1994).
62. S. V. Vinogradova, Z. V. Gersashehenko, Ya. S. Vygodskii, F. B. Sherman, and V. V. Korshak, *Dokl. Akad. Nauk SSSR (Engl. Trans.)* **203**, 285 (1972).
63. Z. V. Gersashehenko, Ya. S. Vygodskii, G. L. Slonimskii, A. A. Askadskii, V. S. Papkov, S. V. Vinogradova, V. G. Dashevskii, V. A. Klimova, F. B. Sherman, and V. V. Korshak, *Polym. Sci. U.S.S.R., A* **15**, 1927 (1973).
64. U.S. Pats. 3,787,364 and 3,838,097 (1974), J. G. Wirth and D. R. Heath (both to General Electric Co.).
65. U.S. Pat. 3,847,869 (1974), F. J. Williams (to General Electric Co.).
66. T. Takekoshi, J. G. Wirth, D. R. Heath, J. E. Kochanowski, J. S. Manello, and M. J. Webber, *J. Polym. Sci., Polym. Chem. Ed.* **18**, 3069 (1980).
67. D. M. White, T. Takekoshi, F. J. Williams, H. M. Relles, P. E. Donahue, H. J. Klopher, G. R. Louks, J. S. Manello, R. O. Mathews, and R. W. Schluent, *J. Polym. Sci., Polym. Chem. Ed.* **19**, 1635 (1981).
68. F. J. Williams and P. E. Donahue, *J. Org. Chem.* **42**, 3414 (1977).
69. R. G. Bryant and T. L. St. Clair, in Abstracts of the 4th Int. Conf. on Polyimides, Ellenville, N.Y., Oct./Nov. 1991, p. II–69.
70. U.S. Pat. 2,444,536 (1948), N. E. Searle (to E. I. du Pont de Nemours & Co., Inc.).
71. U.S. Pat. 3,929,713 (1975), G. F. D. Alelio (to E. I. du Pont de Nemours & Co., Inc.).
72. C. E. Sauers, *J. Org. Chem.* **34**, 2275 (1969).
73. D. Kumar, *Chem. Ind.* **21**(2), 189 (1981).
74. C. P. Reghumadhan Nair, T. V. Sebastian, S. K. Nema, and K. V. C. Rao, *J. Polym. Sci., Polym. Chem. Ed.* **24**, 1109 (1986).
75. L. C. Cessna and H. H. Jablomer, in *31st SPE Techn. Conf.*, 1973, p. 57.
76. U.S. Pat. 3,845,018 (1974), N. Bilow, A. L. Landis, and L. J. Miller (to Hughes Aircraft Co.).
77. A. L. Landis, N. Bilow, R. H. Boschan, R. E. Lawrence, and T. J. Aponyl, *Polym. Prepr.* **15**, 533, 537 (1974).

78. N. Bilow and A. L. Landis, *Polym. Prepr.* **19**(2), 23 (1978).
79. N. Bilow, L. B. Keller, A. L. Landis, R. H. Boschen, and A. A. Castillo, *Sci. Adv. Mater. Proc. Eng. Ser.* **23**, 791 (1978).
80. A. O. Hardy and T. L. St. Clair, *Sci. Adv. Mater. Proc. Eng. Ser.* **28**, 711 (1983).
81. F. W. Harris, A. Pamidimukka, R. Gupta, S. Das, T. Wu, and G. Mock, *Polym. Prepr.* **24**, 324 (1983).
82. P. M. Hergenrother, *Polym. Prepr.* **21**(1), 81 (1980).
83. U.S. Pat. 4,220,750 (1980), F. E. Arnold and B. A. Reinhardt (to U.S. Air Force).
84. B. A. Reinhardt and F. E. Arnold, *J. Appl. Polym. Sci.* **26**, 2679 (1981).
85. L.-S. Tan and F. E. Arnold, *Polym. Prepr.* **26**(2), 176 (1985).
86. M. A. Chandhari, *32nd Int. SAMPE Symp.* **32**, 597 (1987).
87. E. A. Burns, H. R. Lubowitz, and J. F. Johns, NASA CR72460, 1968.
88. U.S. Pat. 3,528,950 (1970), H. R. Lubowitz (to TRW, Inc.).
89. T. T. Serafini, P. Delvigs, and G. R. Lightsey, *J. Appl. Polym. Sci.* **16**, 905 (1972).
90. J. King, M. Chaudhari, and S. Zahir, *29th Natl. SAMPE Symp.* **29**, 392 (1984).
91. H. D. Stenzenberger, M. Herzog, W. Römer, S. Pierce, and M. Camming, *29th Natl. SAMPE Symp.* **29**, 1043 (1984).
92. W. Vaucracynest and J. K. Stille, *Macromolecules* **13**, 1361 (1980).
93. H. D. Stenzenberger, P. Konig, M. Herzog, W. Römer, S. Pierce, and M. Camming, *18th Int. SAMPE Techn. Conf.* **18**, 500 (1986).
94. T. Takekoshi and J. M. Terry, *Polymer* **35**, 4875 (1994).
95. H. D. Stenzenberger, P. Konig, M. Herzog, W. Römer, S. Pierce, and M. Camming, *32th Int. SAMPE Symp.* **32**, 44 (1987).
96. U.S. Pats. 5,344,962 (1994) and 5,498,803 (1996), P. M. Hergenrother and B. J. Jensen (both to NASA).
97. R. Chandra and L. Rajabi, *J. Macromol. Sci., C: Rev. Macromol. Chem. Phys.* **37**(1), 61 (1997).
98. C. Gouri, C. P. Reghumadhan Nair, and R. Ramaswarmy, *High Perform. Polym.* **12**, 497 (2000).
99. H. Furutami, J. Ida, and H. Nagano, *High Perform. Polym.* **12**, 471 (2000).
100. P. M. Hergenrother, R. G. Bryant, B. J. Jensen, and S. J. Havens, *J. Polym. Sci., Part A* **32**, 3061 (1994).
101. P. M. Hergenrother and J. G. Smith Jr., *Polymer* **35**, 4857 (1994).
102. P. M. Hergenrother, R. G. Bryant, B. J. Jensen, J. G. Smith Jr., and S. P. Wilkinson, *39th Int. SAMPE Symp.* **39**, 961 (1994).
103. R. G. Bryant, B. J. Jensen, and P. M. Hergenrother, *J. Appl. Polym. Sci.* **59**, 1249 (1996).
104. B. C. Trivedi and B. M. Culbertson, *Maleic Anhydride*, Plenum Publishing Corp., New York, 1982, Chapt. "12".
105. V. L. Bell and P. R. Young, *J. Polym. Sci., Part A* **24**, 2647 (1986).
106. C. Digiulio, M. Gauther, and B. Jasse, *J. Appl. Polym. Sci.* **29**, 1771 (1984).
107. V. S. Volkov, S. A. Dolmatov, L. V. Yudina, V. S. Levshanov, L. I. Marinyuk, and L. A. Sholokhova, *Polym. Sci. U.S.S.R., A* **25**, 404 (1983).
108. J. V. Crivello, *J. Polym. Sci., Polym. Chem. Ed.* **11**, 1185 (1973).
109. J. E. White, M. D. Scala, and D. A. Snider, *J. Appl. Polym. Sci.* **29**, 891 (1984).
110. W. Oppolzer, *Synthesis* 793 (1978).
111. L.-S. Tan, E. J. Soloski, and F. E. Arnold, *Polym. Prepr.* **27**, 240, 453 (1986).
112. L.-S. Tan, F. E. Arnold, and E. J. Soloski, *J. Polym Sci., Polym. Chem. Ed.* **26**, 3103 (1988).
113. U.S. Pats. 2,890,206 and 2,890,207 (1959), E. A. Kraiman (both to Union Carbide Corp.).
114. F. W. Harris and S. O. Norris, *J. Polym. Sci., Polym. Chem. Ed.* **11**, 2143 (1973).

115. J. K. Stille, F. W. Harris, H. Mukamal, R. O. Rakutis, C. L. Schilling, G. K. Norem, and I. A. Reeds, *Am. Chem. Soc., Adv. Chem. Ser.* **91**, 628 (1969).
116. K. J. Bruza, K. A. Bell, M. T. Bishop, and E. P. Woo, *Polym. Prepr.* **35**, 373 (1994).
117. Ref. 104, pp. 265–267.
118. P. O. Towney, R. H. Snyder, R. P. Conger, K. A. Leibbrand, C. H. Stitteler, and A. B. Williams, *J. Org. Chem.* **26**, 15 (1961).
119. C. Hulubei and S. Morario, *High Perform. Polym.* **12**, 525 (2000).
120. U.S. Pat. 3,562,223 (1971), M. Bargain, A. Combet, and P. Grosjean (to Rhone-Poulenc).
121. C. M. Tung, C. L. Long, and T. T. Liar, *Polym. Mater. Sci. Eng.* **52**, 138 (1983).
122. U.S. Pat. 3,669,930 (1972), T. Asahara, N. Yoda, and N. Minami (to Toray Industries, Inc.).
123. T. M. Donnellan and D. Roylance, *Polym. Eng. Sci.* **32**, 409, 415 (1992).
124. A. V. Tungare and G. C. Martin, *Polym. Eng. Sci.* **33**, 614 (1993).
125. U.S. Pat. 4,154,737 (1979), G. G. Orphanides (to E. I. du Pont de Nemours & Co.).
126. H. D. Stenzenberger, K. U. Heinen, and D. O. Hummel, *J. Polym. Sci., Polym. Chem. Ed.* **14**, 2911 (1976).
127. K. A. Barrett, M. A. Chaudhari, and B. H. Lee, *SAMPE J.* **25**(2), 17 (1989).
128. H. R. Lubowitz, *Org. Coat. Plast. Chem.* **31**, 561 (1971).
129. R. W. Vaughan, J. F. Jones, and H. R. Lubowitz, *15th Natl. SAMPE Techn. Conf.* **15**, 59 (1969).
130. R. H. Pater, *SAMPE J.* **17**(6), 17 (1981).
131. R. H. Pater, *Polym. Eng. Sci.* **31**(1), 20, 28 (1991).
132. K. C. Chuang, J. E. Waters, and D. Hardy-Green, *42nd Int. SAMPE Symp. Expo.* **42**, 1283 (1997).
133. M. A. Meador, M. A. B. Meador, J. Petkovsek, T. Oliver, D. A. Scheiman, C. Gariepy, B. Nguyen, and R. K. Eby, *46nd Int. SAMPE Symp. Expo.* **46**, 497 (2001).
134. A. C. Wang and M. M. Ritchey, *Macromolecules* **14**, 825 (1981).
135. D. Wilson, *Brit. Polym. J.* **20**, 405 (1988).
136. P. R. Young, NASA TM-83192, 1981.
137. R. D. Vanucci and W. B. Alston, NASA TMX-71816, 1976.
138. T. L. St. Clair and R. A. Jewell, *23rd Natl. SAMPE Symp. Exhib.* **23**, 320 (1978).
139. R. H. Pater, in Proc. Conf. High Temp. Polym. Matrix Comp., NASA Lewis Research Center, Mar. 1983, p. 23.
140. S. Alan, L. D. Kandpul, and I. K. Varma, *J. Macromol. Sci., C: Rev. Macromol. Chem. Phys.* **33**, 291 (1993).
141. M. D. Sefcik, E. O. Stejskal, R. A. McKay, and J. Shaefer, *Macromolecules* **12**, 423 (1979).
142. N. Bilow, A. L. Landis, R. H. Boschan, and J. G. Fasold, *SAMPE J.* **18**(1), 8 (1982).
143. A. L. Landis and A. B. Naselow, *Nat. SAMPE Techn. Conf. Ser.* **14**, 236 (1982).
144. J. A. Johnston, F. M. Li, F. W. Harris, and T. Takekoshi, *Polymer* **35**, 4865 (1994).
145. R. G. Bryant and P. M. Hergenrother, *High Perform. Polym., Commun.* **7**, 121 (1995).
146. R. G. Bryant, B. J. Jensen, and P. M. Hergenrother, *Polym. Prepr.* **34**, 566 (1993).
147. S. J. Havens, R. G. Bryant, B. J. Jensen, and P. M. Hergenrother, *Polym. Prepr.* **35**, 553 (1994).
148. U.S. Pat. 5,412,066 (1995), P. M. Hergenrother, R. G. Bryant, B. J. Jensen, and S. J. Havens (to NASA).
149. U.S. Pat. 5,644,022 (1977), B. J. Jensen (to NASA).
150. A. Mochizuki, T. Tadashi, and M. Ueda, *Polymer* **35**, 4022 (1994).
151. Neth. Pat. Appl. 6,413,552 (1965) (to E. I. du Pont de Nemours & Co., Inc.).

152. Y. Imai, *J. Polym. Sci., Part B* **8**, 555 (1970).
153. M. E. Rogers, D. Rodrigues, G. L. Wilkes, and J. E. McGrath, *Polym. Prepr.* **32**, 176 (1991).
154. Z. Y. Wang, T. P. Bender, H. B. Zheng, and L. Z. Chen, *Polym. Adv. Technol.* **11**, 652 (2000).
155. W. J. Farrissey, J. S. Rose, and P. S. Carleton, *Polym. Prepr.* **9**, 1581 (1968).
156. R. A. Meyers, *J. Polym. Sci., Part A-1* **7**, 2757 (1969).
157. P. S. Carleton, W. J. Farrissey, and J. S. Rose, *J. Appl. Polym. Sci.* **16**, 2983 (1972).
158. N. D. Ghatge and U. P. Mulik, *J. Polym. Sci., Polym. Chem. Ed.* **18**, 1905 (1980).
159. G. D. Khune, *J. Macromol. Sci., Part A: Chem.* **14**, 687 (1980).
160. U.S. Pat. 3,708,458 (1973), L. M. Alberino, W. J. Farrissey, and J. S. Rose (to UpJohn Co.).
161. U.S. Pat. 3,562,189 (1971), W. J. Farrissey, A. McLaughlin, and J. S. Rose (both to UpJohn Co.).
162. U.S. Pats. 3,314,923 (1967) and 3,445,477 (1969), G. Mueller and R. Merten (both to Bayer Corp.).
163. U.S. Pat. 4,001,186 (1977), B. K. Onder (to UpJohn Co.).
164. U.S. Pat. 3,833,544 (1974), T. Takekoshi and J. S. Manello (to General Electric Co.).
165. T. L. St. Clair, in Ref. 6, Chapt. 3.
166. B. V. Kotov, T. A. Gordina, V. S. Voischev, O. V. Kolninov, and A. N. Pravednikov, *Vysokomol Soedin. A* **19**(3), 614 (1977).
167. A. K. St. Clair and W. S. Slemp, *SAMPE J.* **21**(4), 28 (1985).
168. U.S. Pats. 4,595,548 and 4,603,061 (1986), A. K. St. Clair and T. L. St. Clair (both to NASA).
169. T. Hou, N. T. Wakelyn, and T. L. St. Clair, *J. Appl. Polym. Sci.* **25**, 1731 (1988).
170. K.-M. Chen, T.-H. Wang, J.-S. King, and A. Hung, *J. Appl. Polym. Sci.* **48**, 291 (1993).
171. J. B. Friler and P. Cebe., *Polym. Eng. Sci.* **33**, 587 (1993).
172. V. L. Bell, B. L. Slump, and H. Gager, *J. Polym. Sci., Polym. Chem. Ed.* **14**, 2275 (1976).
173. H. H. Gibbs and C. V. Breder, *Polym. Prepr.* **15**, 775 (1974).
174. F. W. Harris, W. A. Feld, and L. H. Lanier, *Polym. Prepr.* **16**, 520 (1975).
175. T. L. St. Clair and D. J. Progar, *Polym. Prepr.* **16**, 538 (1975).
176. P. M. Hergenrother, T. Wakelyn, and S. J. Havens, *J. Polym. Sci.* **25**, 1093 (1987).
177. M. K. Gerber, J. R. Pratt, and T. L. St. Clair, in C. Feger, M. M. Khojasteh, and J. E. McGrath, eds., *Polyimides: Materials, Chemistry and Characterization*, Elsevier Science Publishing B.V., Amsterdam, the Netherlands, 1989, pp. 487–496.
178. J. R. Pratt, T. L. St. Clair, M. K. Gerber, and C. R. Gautreaux, in Proc. 3rd Int. Conf. on Polyimides, 1988, p. 223.
179. C. Koning, L. Teuwen, E. W. Meijer, and J. Moonen, *Polymer* **35**, 4889 (1994).
180. C. E. Lee, *J. Macromol. Sci., C: Rev. Macromol. Chem. Phys.* **29**, 431 (1989).
181. F. E. Arnold Jr., K. R. Bruno, D. Shen, M. Eashoo, C. Lee, F. W. Harris, and S. Z. D. Cheng, *Polym. Eng. Sci.* **33**, 1373 (1993).
182. R. G. Bryant, *Polym. Prepr.* **35**, 517 (1994).
183. A. Morikawa and T. Hatakeyama, *Polym. J.* **31**(1), 76 (1999).
184. M. Nishikawa, *Polym. Adv. Technol.* **11**, 404 (2000).
185. U.S. Pat. 6,166,174 (2000), B. J. Jensen (to NASA).
186. U.S. Pats. 5,639,850 (1997), 5,741,883 (1998), and 6,048,959 (2000), R. G. Bryant (all to NASA).
187. Ref. 5, Chapt. 2.

188. U.S. Pat. 3,234,181 (1966), K. L. Olivier (to E. I. du Pont de Nemours & Co., Inc.).
189. D. A. Scola, R. A. Pike, J. H. Vontell, J. P. Pinto, and C. M. Brunette, *High Perform. Polym.* **1**(1), 17 (1989).
190. R. Delasi, *J. Appl. Polym. Sci.* **16**, 2909 (1972).
191. J. Seo, A. Lee, J. Oh, and H. Han, *Polym. J.* **32**, 583 (2000).
192. C. I. Croall and T. L. St. Clair, *J. Plastic Film Sheeting* **8**, 172 (1992).
193. C. J. Wolf and R. S. Soloman, *SAMPE J.* **20**(1), 16 (1984).
194. J. Munson, in K. Gilleo, ed., *Handbook of Flexible Circuits*, Van Nostrand Reinhold Co., Inc., New York, 1992, Chapt. "2.2.1".
195. D. D. Denton, D. R. Day, D. F. Priore, S. D. Senturia, E. S. Anolick, and D. J. Scheider, *J. Electron. Mater.* **14**, 119 (1985).
196. M. C. Tucker, *Hybrid Circuit Technol.* **8**(10), 23 (1991).
197. J. Fjelstad, *An Engineer's Guide to Flexible Circuit Technology*, Electrochemical Publishing Ltd., Isle of Man, British Isles, 1993, p. 23.
198. Technical Literature: DuPont, http:/www.dupont.com/kapton/; Kaneka, http:/kanekahightech.com/apicalworld.html; Ube, http://www.orbital-e.co.jp/page-3.html; General Electric, http://www.geplastics.com.
199. L. V. Ng, H. J. Fick, and M. Bui, *Adv. Packaging* 29 (Nov./Dec. 2000).
200. A. K. St. Clair, T. L. St. Clair, and W. P. Winfree, *Polym. Mater. Sci. Eng.* **59**, 28 (1988).
201. T. Chino, S. Saski, T. Matsura, and S. Nishi, *J. Polym. Sci., Polym. Chem. Ed.* **28**, 323 (1990).
202. M. K. Gerber, J. R. Pratt, A. K. St. Clair, and T. L. St. Clair, *Polym. Prepr.* **31**, 340 (1990).
203. C. E. Sroog, in Ref. 6, Chapt. 9.
204. V. M. Svetlichnyi, K. K. Kalninish, V. V. Kudryavtsev, and M. M. Koton, *Dokl. Akad. Nauk* **237**, 612 (1977).
205. J.-M. Bureau and J.-P. Droguet, in Ref. 4, Chapt. 23.
206. T. O. Herndon, R. L. Burke, and J. A. Yasaitis, *Solid State Technol.* **27**(11), 179 (1984).
207. S. Fujimura, J. Komo, K. Hikazutani, and H. Yano, *Jpn. J. Appl. Phys.* **28**, 2310 (1989).
208. N. Yoda and H. Hiramoto, *J. Macromol. Sci., Part A: Chem.* **21**(13/14), 1641 (1984).
209. 3M Technical Data Sheets, 5413 (1994), 5419 (1995), and 5433 (1994), 3M Corp., St. Paul, Minn.
210. R. E. Sowthward, D. S. Thompson, D. W. Thompson, and A. K. St. Clair, *Chem. Mater.* **9**, 1691 (1997).
211. R. E. Sowthward, D. W. Thompson, and A. K. St. Clair, *Polym Prepr.* **39**, 423 (1998).
212. R. E. Southward and D. M. Stoakley, *Prog. Org. Coat.* **41**, 99 (2000).
213. R. E. Sowthward, J. Dean, J. L. Scott, S. T. Broadwater, and D. W. Thompson, *Polym. Mater. Sci. Eng.* **84**, 339 (2001).
214. F. Li, Z.-Q. Wu, E. P. Savitski, X. Jing, Q. Fu, F. W. Harris, S. Z. D. Cheng, and R. E. Lyon, *42nd Int. SAMPE Symp.* **42**, 1306 (1997).
215. T. J. Stueber and C. Mundson, *38th Int. SAMPE Symp.* **38**, 641 (1993).
216. P. R. Young, A. K. St. Clair, and W. Slemp, *38th Int. SAMPE Symp.* **38**, 664 (1993).
217. U.S. Pat. 4,512,893 (1985), H. Makino (to Ube Industries Ltd.).
218. W. J. Koros, G. K. Flemming, S. M. Jordon, T. H. Kim, and H. H. Hoehn, *Prog. Polym. Sci.* **13**, 339 (1988).
219. W. J. Koros and D. R. B. Walker, *Polym. J.* **23**, 481 (1991).

220. K. Matsumoto, K. Ishii, T. Kuroda, K. Inoue, and A. Iwama, *Polym. J.* **23**, 491 (1991).
221. U.S. Pat. 4,535,101 (1985), R. Lee, U. A. K. Sorathia, and D. A. Okey (to Imi-tech Corp.).
222. U.S. Pats. 4,539,342, 4,535,099, and 4,562,112 (1985), R. Lee, G. A. Ferro, and D. A. Okey (all to Imi-tech Corp.).
223. U.S. Pat. 4,980,102 (1990), F. U. Hill (to Sorrento Eng. Co.).
224. U.S. Pat. 4,900,761 (1990), R. Lee and M. D. O'Donnell (to Imi-tech Corp.).
225. E. W. Weiser, T. F. Johnson, T. L. St. Clair, Y. Echigo, H. Kaneshiro, and B. W. Grimsley, *High Perform. Polym.* **12**, 1 (2000).
226. R. Roth, *Med. Dev. Diag. Ind.* **23**(1), 102 (2001); see also, http://www.hvtechnologiesinc.com.
227. M. Eashoo, Z. Wu, A. Zhang, D. Shen, C. Tse, F. W. Harris, and S. Z. D. Cheng, *Macromol. Chem. Phys.* **199**, 2207 (1994).
228. S. K. Park and R. J. Farris, *Polymer* **42**, 10087 (2001).
229. L. M. Nicholson, K. S. Whitley, T. S. Gates, and J. A. Hinkley, *J. Mater. Sci.* **35**, 6111 (2000).
230. L. M. Nicholson, K. S. Whitley, and T. S. Gates, *Mech. Time-Depend. Mater.* **5**, 199 (2001).
231. E. J. Siochi, P. R. Young, and R. G. Bryant, *40th Int. SAMPE Symp.* **40**, 11 (1995).
232. T. H. Hou, E. J. Soichi, N. J. Johnston, and T. L. St. Clair, *Polymer* **35**, 4956 (1994).
233. T. H. Hou, N. J. Johnston, and T. L. St. Clair, *High Perform. Polym.* **7**, 104 (1995).
234. B. J. Jensen, T. H. Hou, and S. P. Wilkinson, *High Perform. Polym.* **7**, 11 (1995).
235. T. H. Hou and R. G. Bryant, *High Perform. Polym.* **8**, 169 (1996); *High Perform. Polym.* **9**, 437 (1997).
236. M. Namkung, R. G. Bryant, B. Wincheski, and A. Buchman, *J. Appl. Phys.* **81**, 4112 (1997); *J. Appl. Phys.* **83**, 6474 (1998).
237. M. Angelovici, R. Bryant, B. Northam, and S. Roberts, *Mater. Lett.* **36**, 254 (1998).
238. A. Buchman and R. G. Bryant, *Appl. Comp. Mater.* **6**, 309 (1999).
239. L. J. Laursen, M. T. Bishop, D. R. Calhoun, S. A. Laman, W. W. Lee, S. R. Wood, and P. C. Yang, *39th Int. SAMPE Symp.* **39**, 951 (1994).
240. D. Wilson, in Ref. 6, Chapt. 7.
241. B. J. Jensen, S. E. Lowther, and A. C. Chang, *Polym. Prepr.* **38**, 305 (1999).
242. U.S. Pat. 3,413,394 (1968), T. F. Jordan (to E. I. du Pont de Nemours & Co., Inc.).
243. Technical Literature: DuPont, http://www.dupont.com/vespel/; Ube, http://www.ube-ind.co.jp/english/hb/shohin/c_203/index_e.htm; Mitsui, http://mitsuichemicals.com/spep/aurum.
244. S. P. Wilkinson, J. M. Marchello, D. Dixon, and N. J. Johnston, *38th Int. SAMPE Symp.* **38**(1), 1 (1993).
245. A. Ramasamy, Y. Wang, and J. Muzzy, *38th Int. SAMPE Symp.* **38**(2), 1, (1993).
246. B. J. Jensen, R. G. Bryant, J. G. Smith Jr., and P. M. Herrgenrother, *J. Adhesn.* **54**, 57 (1995).
247. T. H. Hou, B. J. Jensen, and P. M. Hergenrother, *J. Comp. Mater.* **30**(1), 109 (1996).
248. T. H. Hou, S. P. Wilkinson, N. J. Johnston, R. H. Pater, and T. L. Schneider, *High Perform. Polym.* **8**, 491 (1996).

ROBERT G. BRYANT
NASA Langley Research Center

POLYISOBUTYLENE. See BUTYL RUBBER.

POLYISOPRENE. See ISOPRENE POLYMERS.

POLYKETONES. See Volume 3.

POLYMERIC DRUGS

Introduction

The use of functional polymers in medicine has seen considerable growth during the past two decades (1). Polymers as biomaterials have found applications in such areas as artificial organs, tissue engineering, components of medical devices, and dentistry. A growing aspect of the field is the recognition of polymers as useful therapeutic agents, ie, either polymers that exhibit pharmacological properties themselves, or that can be utilized as carriers for selective and sustained delivery vehicles for small molecule or macromolecular (eg proteins, genetic materials, etc) pharmaceutical agents.

There has been a growing literature pertaining to the use of functional polymers as delivery agents for therapeutics against a variety of disease states. They include delivery of drugs at a sustained rate, targeted delivery of drugs at specific sites (to minimize toxicity and enhance selectivity for certain antitumor agents), as well as macromolecular prodrugs with polymers acting as carrier molecules (2–4). More recently, polymers have been used as nonviral vectors for the delivery of genetic materials for gene therapy (5). There have been significant advancements in the area of polymeric drug delivery systems (including commercial products). Numerous research papers and excellent review articles dealing with this aspect of biomedical polymers have been published over the last two decades (6,7) (see CONTROLLED RELEASE TECHNOLOGY; GENE-DELIVERY POLYMERS).

Although polymers are used extensively as drug delivery agents, *intrinsically* bioactive polymers (polymers as active pharmaceutical ingredients) are a relatively recent development (8). Partly because of their high molecular weight, polymers would appear to offer several advantages over low molecular weight agents as potential therapeutic agents. These benefits may include lower toxicity, greater specificity of action, and enhanced activity due to multiple interactions (polyvalency). Nevertheless, the concept of polymeric drugs has been a subject of considerable skepticism, with medicinal chemists long considering synthetic

Encyclopedia of Polymer Science and Technology. Copyright John Wiley & Sons, Inc. All rights reserved.

polymers uninteresting as a class of potential pharmacophores. Some of the underlying concerns include the issue of polydispersity in molecular weight, and compositional heterogeneity (copolymers in particular) that could complicate process development. The high molecular weight characteristics of polymers make their systemic absorption through oral administration less likely. However, as we show below, these potentially limiting pharmacological characteristics of polymers can in fact be exploited to design and develop therapeutic agents for disease conditions where low molecular weight drugs have either failed or produced inadequate therapeutic profiles (9).

The fact that high molecular weight polymers are not (typically) absorbed from the gastrointestinal (GI) tract may be a decided advantage where it is desirable to deter a therapeutic from systemic exposure. For example, by combining this characteristic with the ability of polymers to selectively bind molecular and macromolecular components in intestinal fluids, it has become possible to develop a powerful new class of therapeutic agents that can selectively bind and remove detrimental species from the GI tract. As with any pharmaceutical, sequestration of each target molecule or pathogen requires a unique strategy and this strategy depends on not only the chemical nature of the target but also the location, concentration, and quantity of the target requiring removal.

Since several books and review articles have been published covering the area of polymeric drug *delivery* systems (2–7), this article has been limited to case studies where polymers act as active drugs. This article focuses on some of the most recent efforts in this regard and concentrates on the development of polymeric drugs for the sequestration of low molecular weight species such as bile acids, phosphate, and iron as well as polyvalent interactions to bind toxins, viruses, and bacteria. Of additional note is the use of polymers for the treatment of autoimmune diseases by inhibiting specific biological antigen binding events, and the use of conjugates of therapeutically active proteins with polymers as hybrid polymeric drugs. The latter approach to novel biopharmaceuticals overcomes possible antigenic properties of the therapeutic proteins in addition to protecting them from degradation by peptidases.

Polymeric Drugs as Specific Molecular Sequestrants

A number of potentially detrimental substances are present in the GI tract. These molecules and pathogens are implicated for various disease conditions. These species can be exogenic, that is, they enter the body with food, drinks, or from the environment or they may be produced endogenously as a result of metabolic processes. Effective removal of these species in a selective manner offers a promising prophylactic and therapeutic approach for the treatment of a number of disease states. Biocompatible polymeric sequestrants represent an ideal class of agents for this purpose. Their nonabsorption through the intestinal wall should offer minimal toxicity, while the incorporation of appropriate functional groups and manipulation of polymer physicochemical characteristics provides opportunities to tailor-make polymers with high selectivity and capacity.

Polymeric Sequestrants for Inorganic Ions. Electrolytes play a key role in regulating distribution of different inorganic anions and cations between

the intracellular and extracellular fluid compartments (homeostasis), and are vital in maintaining myocardial and neurological functions, fluid balance, oxygen delivery, and acid–base balance. Electrolyte imbalance, caused by either excessive ingestion or impaired elimination of an electrolyte from the body, has important physiological effects. Although certain nonrenal tissues (eg, muscle and liver) contribute to maintaining electrolyte balance, the kidney plays the predominant role in maintaining electrolyte balance (10). Therefore, renal impairment is the most common reason for electrolyte imbalance and can lead to critical health conditions. Conceptually, nonabsorbed polymeric sequestrants could be used to bind these excessive ions (implicated in various pathologic conditions) selectively in the GI tract.

Polymeric Potassium Sequestrants: Nonabsorbed Therapy for Hyperkalemia. Since the transmembrane potential is a major regulator of cell function, the ratio of potassium between intra- and extracellular fluids is critically important to all living cells (11). Hyperkalemia (elevated level of serum potassium, usually greater than 5.0 meq/L) can result from burn and crush muscle injuries, acidosis, or through the use of antihypertension drugs (angiotensin converting enzyme inhibitors). A rise in serum potassium can manifest moderate to serious health problems including paresthesias, areflexia, respiratory failure, and bradycardia (12). Since the kidney is responsible for elimination of most excess potassium, patients with impaired renal function are incapable of maintaining potassium homeostatis. Traditional approaches to treat hyperkalemia include use of insulin, glucose, sodium bicarbonate, and calcium chloride. However, these treatments have their own shortcoming. For example, excess calcium could lead to hypercalcemia, that in turn leads to myocardial infarction, kidney stones, and a variety of other conditions.

Use of an insoluble polyanionic resin to sequester excess potassium in the GI tract with elimination in the feces could enable patients to excrete potassium despite impaired kidneys. There are a number of low molecular weight ligands, which complex potassium ions (13). Utilizing this principle, a cation-exchange resin based on sodium polystyrene sulfonate (**1**) was developed to sequester potassium ion in the GI tract. This polymer, marketed under the brand name Kayexalate (Sanofi-Synthelabo) (14), was approved in the United States for the treatment of hyperkalemia in 1975, and is administered orally or rectally. A potential problem with its use is induction of hypernatremia (elevated serum sodium), since the material exchanges 1.0 equiv. of potassium for 1.5 equiv. of sodium. Furthermore, cases of intestinal necrosis have been attributed to Kayexalate (15). The adverse effects associated with Kayexalate may provide an opportunity for developing new generations of potassium sequestering polymers.

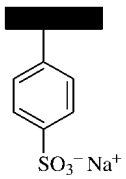

1

Polymeric Phosphate Sequestrants: Nonabsorbed Therapy for Chronic Renal Failure

Management of hyperphosphatemia (elevated serum phosphate) is a severe issue for patients suffering from chronic and end-stage renal failure (16,17). The major route for the excretion of phosphate in a healthy human is through the kidney, whereas patients with an impaired renal system accumulate phosphate ion through an imbalance in ingestion and excretion. This accumulation of phosphate leads to various pathologies of clinical importance including soft tissue calcification (leading to increased cardiovascular risk) and renal osteomalacia leading to bone pain, reduced bone density, and eventually fracture. The conventional treatment for hyperphosphatemia involves formation of insoluble calcium or aluminum phosphate in the GI tract by the administration of calcium and aluminum salts (18,19). However, since aluminum and calcium salts have the propensity to be absorbed through the GI wall, they can lead to undesirable toxic and metabolic side effects in patients with impaired renal function. Design and development of nonabsorbed cationic polymers as sequestrants for phosphate ions offer an ideal approach to treat hyperphosphatemia in renal failure patients.

The known binding of phosphate by polycationic species has long been a well-studied phenomenon. Polycationic compounds such as macrocyclic oligomeric amines and oligomeric guanidinium compounds (eg, **2** and **3**) have been used as receptors to study molecular recognition events involving phosphate and phosphonate anions as guests (20,21).

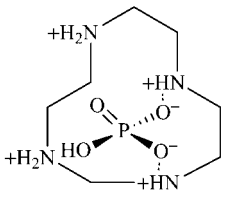

2

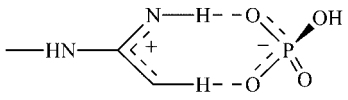

3

Electrostatic interaction is the primary governing force for this complexation and hydrogen bonding is considered to lend additional binding strength. Utilization of this principle of physical organic chemistry has led, in our hands, to the discovery of a series of nonabsorbed polymeric amine compounds that show affinity toward dietary phosphate (22) and to an effective therapeutic approach to hyperphosphatemia. Amine-functionalized polymer hydrogels (qv) were prepared either by the cross-linking of amine polymers or by the cross-linking polymerization of amine containing vinyl monomers (23–25) (see HYDROGELS). A variety of polymer gels were initially prepared, including materials bearing primary, secondary, and tertiary amine groups, in addition to polymers containing quaternary ammonium and guanidinium groups. Figure 1 illustrates the structural repeat units of a selection of these polymers; the phosphate binding capacities of the materials are summarized in Table 1. From several polymers investigated in detail, polyallylamine cross-linked with epichlorohydrin (**4**) was found to exhibit maximum phosphate

Table 1. Phosphate Binding Properties of Various Amine Functional Polymers at 5 m*M* Phosphate

Polymer type	Phosphate bound to polymer, meq/g
Polyallylamine/epichlorohydrin	3
Polyethyleneimine/acryloyl chloride	1.2
Diethylenetriamine/epichlorohydrin	1.5
Poly(dimethylaminoethylacrylamide)	0.8
Poly(4-trimethylammoniummethyl)styrene chloride	0.7

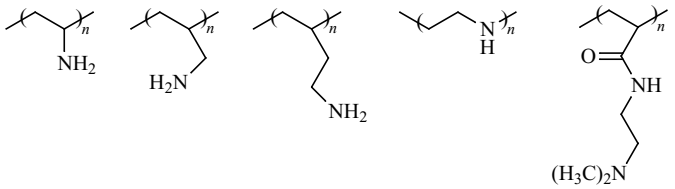

Fig. 1. Structural repeat units of some phosphate-binding polymers.

capacity, binding, it is believed, through electrostatic and possibly through hydrogen-bonding interactions.

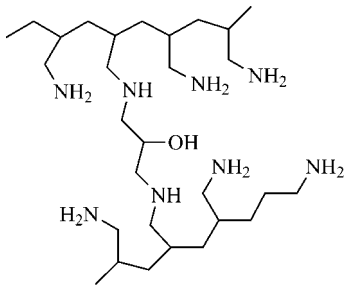

4

As with low molecular weight receptors for phosphate, the binding strengths and capacities of these polymers were found to depend on the pH of the medium. Since more ammonium groups are present at lower pH, the polymers exhibit higher binding capacity at lower pH. Because of higher concentration of amine groups in a polymer chain, and the divalent (and possibly trivalent) nature of phosphate anions, polymeric amines probably also exhibit stronger affinity over small molecule binders as a result of a chelating effect, although that phenomenon has not been examined in detail. Furthermore, assuring an appropriate spacing between the positive charges of the amine groups in the polymer chain and the backbone are key to the phosphate binding capacities of these polymers (26). Finally, polymers containing primary amines were found to be better phosphate sequestrants than polymers bearing secondary and tertiary amines, while polymers containing quaternary amines were found to be the poorest.

A systematic investigation taking these factors into account suggested that cross-linked polyallylamine gels are the most potent phosphate-binding polymers and possess properties suitable for pharmaceutical applications. This class of polymers exhibited maximum phosphate binding in the pH range encountered in the small intestine, while the polymer gel was found to be nontoxic and is essentially nonabsorbed. It was furthermore very well tolerated in end-stage renal failure patients undergoing hemodialysis (27).

A cross-linked polyallylamine has been developed commercially as a treatment for hyperphosphatemia under the generic name of sevelamer hydrochloride. Approved in the United States by the FDA in 1998, it has been marketed since under the brand name Renagel by Genzyme Corp. Renagel has been found to offer several advantages over and above traditional agents for the management of hyperphosphatemia in renal failure patients (28). It remves the need for exposure to toxic metal ions like aluminum and eliminates the intake of additional calcium, thereby alleviating the possibly serious issue of hypercalcemia. Furthermore, Renagel has been found to reduce serum parathyroid hormone and also reduce total and low density lipoprotein (LDL) cholesterol in hemodialysis patients. Since cardiovascular events are the most common causes of mortality of dialysis patients, Renagel offers a very promising treatment in the management of renal failure, and represents one of the first tailor-made, polymeric drug that exhibits its prophylactic and therapeutic properties through selective adsorption of unwanted dietary components in the GI tract.

Iron-Binding Polymers for the Treatment of Iron Overload Disorders

Although iron is essential for the proper functioning of all living cells, it is toxic if present in excess (29). In the presence of molecular oxygen, excess iron can produce oxygen-derived free radicals such as hydroxyl radical. These reactive free radicals interact with many biological molecules, resulting in peroxidative tissue or organ damage that forms the basis for several pathological conditions. Under normal conditions, iron metabolism is highly conserved, with the majority of the iron being recycled within the body. There is no normal iron loss mechanism; iron is not normally present in urine, feces, or bile. Its loss occurs only through bleeding or normal sloughing of epithelial cells. Certain genetic disorders can, however, lead to increased absorption of dietary iron (as in the case of hemochromatosis) or transfusion-induced iron overload (as in the case of β-thalassemia and sickle cell anemia) (30,31).

Although excess iron can be removed by venesection (especially in hemochromatosis patients), removal of iron using an iron chelator is the only effective way to relieve iron overload in patients with β-thalassemia or sickle cell anemia (32). The current standard of care is desferrioxamine (**5**), the only approved iron chelator for this condition in the United States. This drug has several drawbacks including a narrow therapeutic window and, being orally inactive, requiring administration by 8–12 h/day of parenteral infusions (33). Thus, there is a need for the discovery and development of orally active iron chelating agents for the treatment of iron overload.

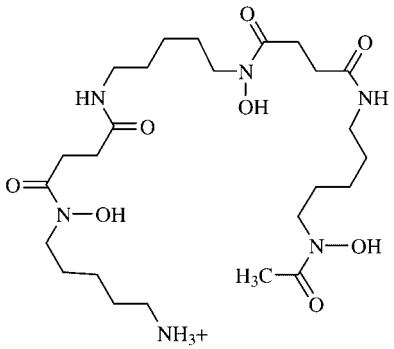

5

Development of nonabsorbed polymeric ligands to selectively sequester and remove dietary iron from the GI tract is an attractive method for the treatment of iron overload. Clinically useful polymeric iron chelators need to possess several features. The polymeric ligand must possess high affinity, capacity, and selectivity toward iron. Furthermore, the chelator should be biocompatible, and should not be absorbed from the GI tract. Design of polymeric chelators has been based on the knowledge of low molecular weight chelators. For clinical applications, the properties of chelators in terms of metal ion selectivity and ligand–metal complex stability is important. Since iron exists in two oxidation states (ferrous, +2, and ferric, +3), chelators can be designed for both the forms. For Fe(II), soft donor atoms [eg, nitrogen-containing ligands such as bipyridine (**6**) and phenanthroline (**7**) can be employed. Although these ligands are selective for Fe(II), they also possess affinity for other biologically important divalent metal ions such as Zn(II) and Cu(II). On the other hand, oxyanions like hydroxamates and catecholates are selective toward Fe(III), and these ligands in general show higher selectivity toward trivalent metal ions over divalent metal ions. Natural iron chelators like siderophores such as enterobactin (**8**) and desferrioxamine (**5**) contain catechol and hydroxamate groups respectively, and are selective for Fe(III) (34).

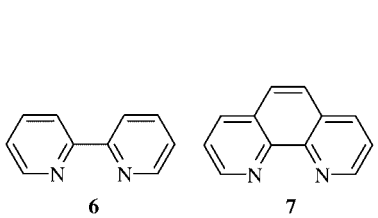

6

7

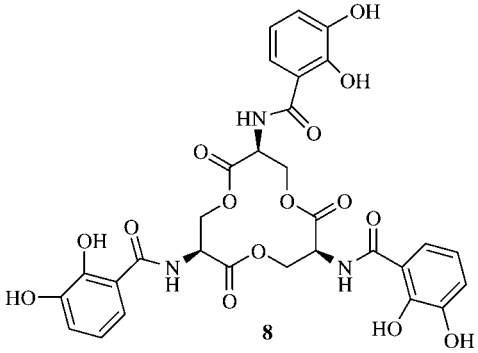

8

By considering these criteria, cross-linked polymeric hydrogels containing hydroxamic acid and catechol moieties (**9** and **10**) as well as cross-linked

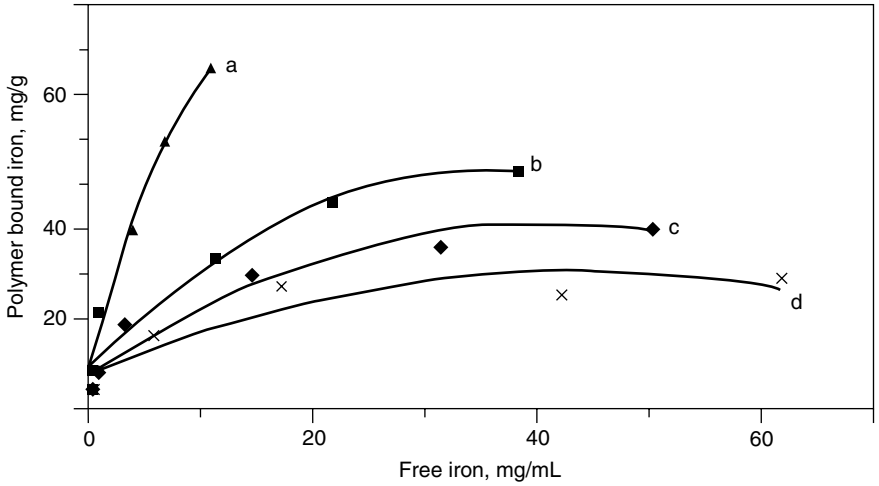

Fig. 2. Iron binding behavior of a poly(hydroxamic acid) hydrogel at different pH values: 8.0 (a), 7.0 (b), 5.7 (c), and 2.3 (d).

polyamines were prepared and were tested for their iron binding properties (35). Under *in vitro* conditions, all of these polymers sequester iron at high pH. At lower pH, the polymers containing hydroxamic acids maintained their iron binding properties, while other polymers showed reduced iron binding. Figure 2 shows the iron binding isotherms for a hydroxamic acid containing hydrogel at different pH values. *In vivo* studies using rodents have shown a decrease in absorption of dietary iron using this polymer (36). However, no human clinical data on the iron chelating polymers is available.

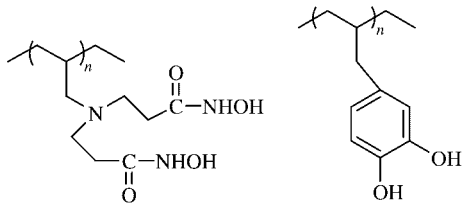

9 **10**

Bile Acid Sequestrants: Polymeric Drugs as Cholesterol-Lowering Agents

Increased plasma total cholesterol and low density lipoprotein cholesterol (LDLc) are established risk factors for antherosclerosis, which is the underlying cause of coronary heart disease and most strokes (37). The reduction of elevated LDLc is one of the most common therapeutic treatments for this disease, with the majority of the individuals at risk requiring only a modest (20–30%) reduction in LDLc level

to minimize this serious health risk (38). HMG-CoA reductase inhibitors (more commonly known as statins) are the most widely used drugs for reducing blood levels of LDLc and have been shown to significantly reduce the risk of coronary events and strokes. These findings have led to recent guidelines for expanding the use of cholesterol-lowering drug therapies to more patients (39), with an estimated 36 million people in the United States alone who are candidates for cholesterol-lowering drug therapy.

Despite the success with statins, there is still a need for new therapies to reduce blood LDLc. Statins are, for example, not indicated for pregnant women, for pedriatic use, or for patients with liver disease. Moreover, some patients do not achieve the LDLc goal with statin therapy alone. There are also long-term potential safety issues associated with statins such as liver dysfunction and musculoskeletal symptoms, illustrated by the recent withdrawal of a statin, cerevastatin (Baycol by Bayer), from the market as a result of several cases of rhabdomyolysis (40).

The molecular regulation of cellular cholesterol metabolism was elucidated by Brown and Goldstein (41). Cholesterol is synthesized in the liver by the enzyme HMG-CoA reductase. Subsequently, it is transformed into a bile acid in the liver and secreted to the gall bladder. The statins inhibit HMG-CoA reductase, which is the rate-limiting enzyme in cholesterol biosynthesis. The presence of bile acid in the cholesterol metabolism pathway suggests that another approach to reduce plasma LDLc is through effective removal of the bile acid from the bile pool, resulting in upregulation of bile acid biosynthesis and leading to a corresponding drop in plasma cholesterol levels (42).

Bile acid sequestrants (BAS) are cross-linked polymeric cationic gels that bind anionic bile acids in the GI tract and result in elimination of bile acid from the body (43). The use of these polymeric gels for sequestering bile acids is an established approach for treating elevated cholesterol (44). Being nonabsorbed, these polymeric drugs do not exhibit the systemic side effects that are associated with statins, and the BAS have over 30 years of clinical experience with a good safety record. Until recently, two cationic polymers, namely cholestyramine (**11**) and colestipol (**12**) have been the only approved BAS on the market. Despite the appeal of their safety profiles, these two first-generation BAS have, despite their high *in vitro* capacity, low clinical potency, which has led to reduced patient compliance and hence limited use. For example, the doses required for a 20% cholesterol reduction with cholestyramine and colestipol are typically 16–24 g/day (45). This low clinical efficacy of BAS has been ascribed to competition for bile acids with the active bile acid transporter system of the GI tract (46). It appears that, for a cationic polymer to be a potent BAS, it must have high binding capacity, strong binding strength, and selectivity toward bile acids in the presence of competing desorbing forces of the GI tract. Thus a potent BAS needs to exhibit slow off-rates of bound bile acids from the polymer resin to effectively overcome the active transport of bile acids from the GI tract. The design rules for making BAS of improved potency need to take into consideration the physicochemical features of bile acids (**13**). A typical bile acid possesses an anionic group and a hydrophobic core. Therefore, while electrostatic interaction is the primary force for bile acid binding by cationic polymers, a second attractive force that needs to be considered is the hydrophobic interaction between binder and bile acid. Furthermore,

favorable swelling characteristics of these cationic hydrogels in physiological environments are required for attaining high capacity. Thus, a balanced combination of hydrophilicity (high capacity) and hydrophobicity (to slow down the rate of desorption), along with optimum density of cationic groups, would constitute key features of the most potent BAS (47).

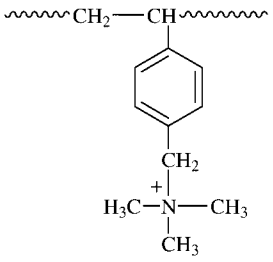

11

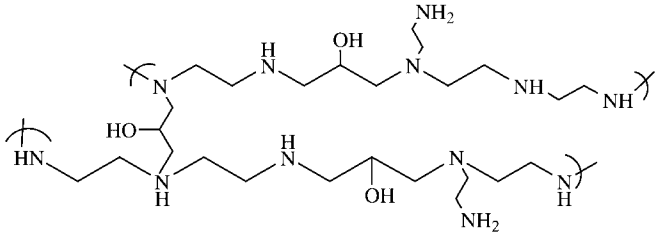

12

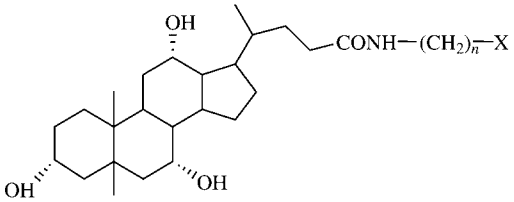

13

a: n = 1, X = COOH
b: n = 2, X = SO_3H

Consideration of these desired features has led to the discovery of a number of BAS over the last decade from our laboratories as well as from other groups (48–52). Figure 3 illustrates structures representative of these new BAS, with common features of these hydrogels being the presence of amine/ammonium groups. Additional structural features of these polymers include the presence of hydrophobic chains. A variety of polymer backbones including vinyl and allyl amine polymers, (meth)acrylates, (meth)acrylamide, styrene, carbohydrates, polyethers, and other condensation polymers have been considered (53,54). While a number of polymers have been synthesized and tested in preliminary *in vitro* and *in vivo* studies, very few have entered preclinical development and clinical trials. Some of these promising BAS include DMP-504 (**14**), colestimide (**15**), SK & F 97426-A (**16**), and colesevelam hydrochloride (**17**). Structural features of these polymers comprise

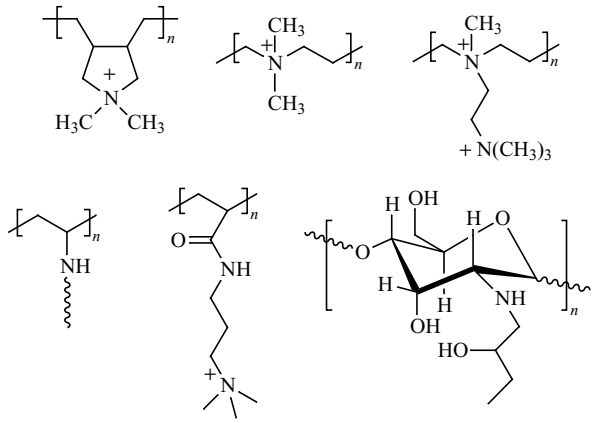

Fig. 3. Chemical structures of some representative bile acid sequestrants.

an optimum combination of charge density, hydrophobic tails, and water swelling properties. From this new generation of BAS that entered clinical trials, only two have been approved for marketing. Colestimide has been approved for marketing in Japan and is sold under the trade name Cholebine (Tokyo Tanabe) while colesevelam hydrochloride has been approved for marketing in the United States and is being sold under the trade name WelChol (Sankyo) (55,56). Both the polymers exhibit lower rates of side effects and better tolerated than previously marketed BAS. These BAS can be used as monotherapy or in combination therapy by coadministration with statins.

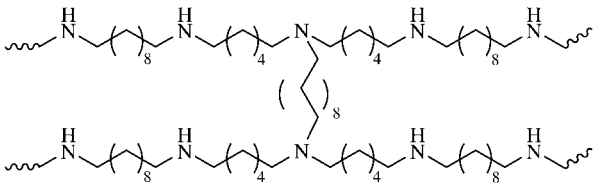

14

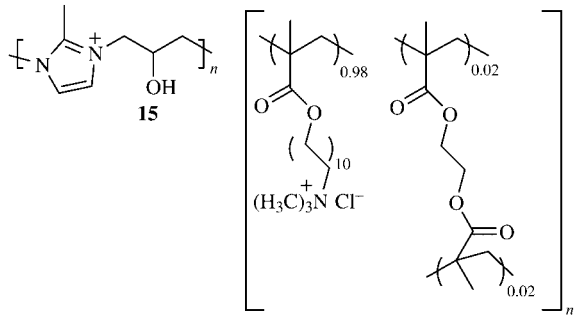

15

16

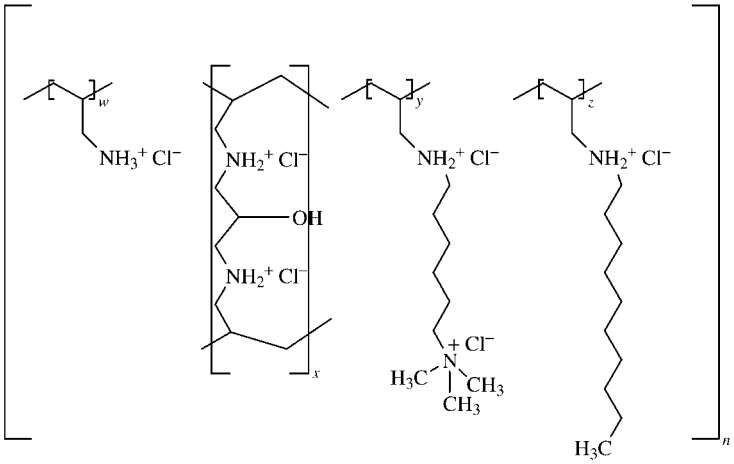

17

Polyvalent Ligands: Polymeric Drugs for the Sequestration of Macromolecular Pathogens

Polyvalent interactions are characterized by the simultaneous binding of multiple ligands on one molecular entity to multiple receptors on another (cells, viruses, proteins, etc). These interactions are widely prevalent in biological systems and they form the initiation steps for a great variety of cellular processes such as cell-surface or receptor-ligand recognition events. Polyvalent interactions can be collectively much stronger than corresponding monovalent interactions. They can provide the basis for mechanisms of both agonizing and antagonizing biological interactions that are fundamentally different from those available in monovalent systems. A schematic illustration of the principle of polyvalent interaction is shown in Figure 4. The theoretical framework of polyvalency and its role in biological processes have been reviewed by Whitesides and co-workers (57).

An appreciation of this important interaction in biological systems has been considered in the design and discovery of a new generation of novel therapeutic agents (58), and is particularly relevant when the interaction between a monovalent ligand and a polyvalent receptor is weak since polyvalency can significantly enhance the binding strength. Thus, a polyvalent inhibitor containing two or more linked ligands can bind at two more receptor sites on a target pathogen, leading to enhanced inhibition and/or sequestration of the target. This concept can obviously be extended further in polymeric systems wherein a collection of similar or different ligands can be covalently linked together to a single polymer chain. The flexibility to choose different polymer architectures (eg, random, alternate, block, graft, hyperbranched, etc), monomer types, and the ease of polymer synthesis and modification enables the synthesis of a wide variety of well-defined polyvalent species with desired features such as controlled ligand density, optimum binding strength/capacity, hydrophilicity/ hydrophobicity, and the incorporation of ancillary groups to enhance binding. Interplay of these features in polyvalent ligands

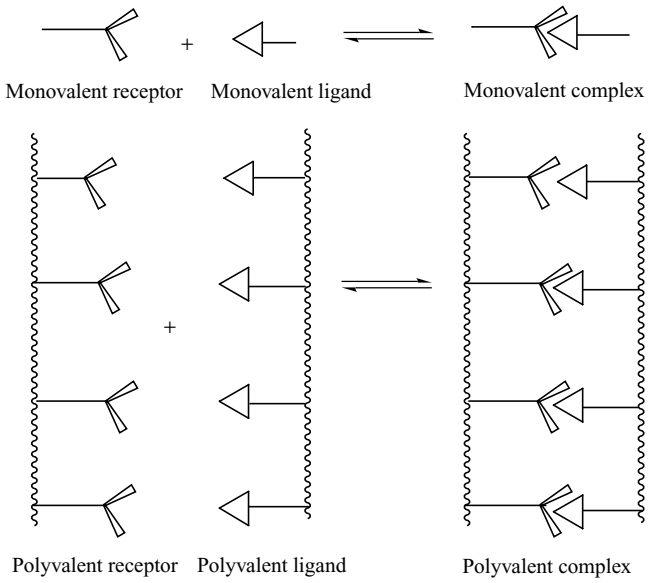

Fig. 4. Ligand–receptor interaction in monovalent (top) and polyvalent (bottom) systems.

can, in principle, lead to therapeutic agents with high potency as well as modulated biodegradability and bioavailability characteristics. This new concept of ligand–substrate interaction has led in recent years to the discovery of a variety of polymeric drugs that have been found to sequester/inhibit toxins, viruses, and bacteria.

Polyvalent Ligands as Sequestrants of Toxins. Toxins, produced by pathogenic microorganisms in the host body can generically be classified under two headings: exotoxins and endotoxins (59,60). *Exotoxins* are generally proteinous materials released by pathogenic species. *Endotoxins* are lipopolysaccharides and consist of polysaccharide segments and glycolipid segments that constitute the outer cell membranes of all Gram-negative bacteria.

After being secreted by microorganisms, these toxins can travel within the body of the host organism and can cause damage in regions of the body far removed from the infection site. The pathogenic effects of these toxins may include hemolysis, destruction of leucocytes, paralysis, diarrhea, and septic shock (61). Some of the pathogens that produce life-threatening toxins in the GI tract are the food-poisoning organisms *Staphylococcus aureus, Clostridium perfringens*, and *Bacillus cereus*, and the intestinal pathogens *Vibrio cholerae, Escherichia coli*, and *Salmonella enteritidis*. Furthermore, anthrax toxin is produced by *Bacillus anthracis*. In almost all cases, the causative agents responsible for major symptoms of diseases associated with these pathogens are the exotoxins produced by the organisms (62,63).

Clostridium difficile Toxin. Clostridium *difficile* (*C. difficile*) is responsible for large numbers of episodes of diarrhea that arise from antibacterial treatment in nosocomial settings (58). Since normal colonic flora inhibit the growth of *C. difficile*, the outbreak of this disease has been attributed to the disruption of normal

colonic flora by antibiotic treatment, allowing colonization of the gut by *C. difficile* that is ubiquitous in hospital settings. Two high molecular weight proteins (toxins A and B) released by *C. difficile* are primarily responsible for causing the diarrhea (64,65). The traditional approach to treat *C. difficile* associated diarrhea is the use of one of two antibiotics, metronidazole or vancomycin. The use of antibiotics, while effective in eliminating the initial *C. difficile* infection, can allow for repeat infection by *C. difficile* by sterilizing the gut. In many cases, repeated cycles of antibiotic treatment, followed by reinfection by *C. difficile*, leads to long hospital stays and debilitating effects on patients. There are also increasing reports of growing antibiotic resistance to *C. difficile* (66).

Since toxins are responsible for disease symptoms, and recolonization of *C. difficile* results from the inhibition of normal microbial flora growth by antibiotic treatment, selective sequestration and neutralization of these toxins by a polymeric sequestering agent would appear to offer an attractive nonantibiotic therapy for this disease. Being protein-based, *C. difficile* toxins possess multiple binding sites that can effectively interact with polymeric ligands bearing complementary binding sites through simultaneous polyvalent interactions. Anion exchange resins like cholestyramine and colestipol (the BAS described above) were the first group of polymeric ligands to be examined as sequestrants for *C. difficile* toxin. However, the effectiveness of these polymeric ion-exchangers to bind and remove *C. difficile* toxin was found to be modest (67).

Recent research has led to the discovery of some novel polymeric multivalent ligands as nonantimicrobial sequestrants for binding and neutralization of these toxins. One class of particularly effective materials has proven to be high molecular weight water-soluble anionic polymers (**18–20**) (68,69). In our hands, an anionic polymer, GT 160–246, was found to be very effective in treating this infection in hamsters (70). *In vitro* studies using pulsed ultrafiltration and fluorescence polarization spectroscopy revealed that the binding constants of complexes between this polymer and toxins A and B were 133 nM and 8.7 μM respectively (71). Furthermore, from fluorescence polarization data, it was estimated that one molecule of toxin A interacts with 600–1000 monomer units of GT 160–246, suggesting large polyvalent interactions between the polymer and protein surface. This polymer is currently in human clinical trials.

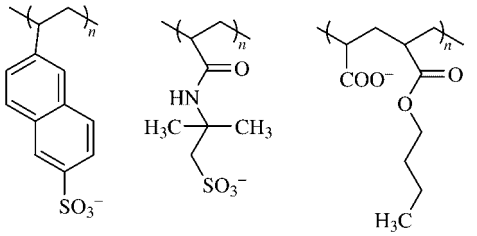

18 **19** **20**

Polymers bearing pendant oligosaccharide groups have also been investigated as possible sequestrants for *C. difficile* toxins (72,73). This approach is based on the principle that toxin A has shown a lectin-like activity, which allows it to bind to an oligosaccharide receptor on epithelial cells. Furthermore, toxin B has

been found to bind erythrocytes, implying that a carbohydrate receptor may be involved for its binding. After identifying appropriate oligosaccharide sequences, oligosccharide molecules (specific for toxins A and B) were covalently attached to polymer carriers. Compatible spacer arms of appropriate length between polymer backbones and oligosaccharide moieties were utilized to maximize the polymer–toxin interaction (**21**). Specific oligosaccharide sequences that are useful in this context are maltose, cellobiose, isomaltotriose, and chitobiose. Polymeric carriers examined include substituted polystyrene and other olefin backbones. Inorganic carriers such as biogenic silica and kaolinite were also used. These classes of sequestrants [under the trade name SYNSORB (Syn Sorb Biotech, Inc.)] were found to be effective in neutralizing toxins and in controlling diarrhea in animal models. One of these materials progressed to human trials, but was withdrawn after a phase II clinical trial.

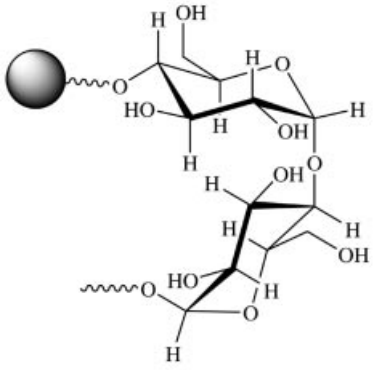

21

Anthrax Toxin. Anthrax toxin is produced by *Bacillus anthracis* and is the primary cause for the major symptoms of the disease (74). While the occurrence of anthrax in clinical settings is rare, growing concern over bioterrorism and biological warfare using *B. anthracis* has made development of agents active against anthrax a high priority. Although vaccines against anthrax exist, various factors make mass vaccination difficult. Furthermore, the course of the toxin-induced damage after symptoms are evident makes antibiotic treatment of limited utility. Therefore, development of agents that can sequester anthrax toxin (thereby inhibiting its action) might prove to be a valuable adjunct to antibiotic therapy.

Anthrax toxin consists of a single receptor-binding moiety, termed protective antigen (PA), and two enzymatic moieties, termed edema factor (EF) and lethal factor (LF). Upon release from bacteria as nontoxic monomers, these three proteins combine and undergo a cascade of processes through the formation of a cell-bound heptameric fragment called PA63, finally resulting in attack on macrophages (75). By utilizing phage-display library screening, a dodecameric peptide was identified that binds PA63 and inhibits its interaction with the protease enzyme. By attaching multiple copies of this dodecameric peptide sequence to a polyacrylamide-based polymer backbone, the corresponding polyvalent ligand was obtained. This polymer strongly inhibits ligand binding by PA63, toxin activity in cell culture, and toxicity in an animal intoxication model (76). The efficacy of this polyvalent

ligand in blocking the anthrax toxin *in vivo* suggests that this approach could be useful in developing therapeutically relevant agents for this life-threatening condition.

Polyvalent Ligands as Antiviral Agents. The use of polyvalent ligands to inhibit viral infection is the most extensively studied of all polyvalent interactions. This platform has in fact served as the prototypical system to validate the fundamental concept of polyvalent ligands as a new class of polymeric pharmaceutical agents.

Viral infection is initiated by the attachment of viruses to specific cellular receptors, which is mediated by viral attachment proteins (VAPs) (77). It has been postulated that by inhibiting the receptor-binding epitopes of VAPs with synthetic analogs of cellular receptors, novel antiviral agents can be designed. It has been calculated that many viruses, when binding to cell surfaces, interact with at least 10 (or more) monomeric cellular receptor units that are organized into polymeric cellular receptor units (78). The characteristic feature of such polyvalent cooperative binding is that high avidity of binding may be mediated by multiple low affinity individual contacts. Therefore, by presenting polymeric ligands containing multiple copies of the cellular receptor analogs, competitive inhibitors for viruses can be developed. This design principle has been utilized to develop prototype antiviral agents against viruses such as influenza and rotavirus.

Inhibition of Influenza Virus. Influenza virus A is the primary agent responsible for serious cases of human influenza. The infection of cells by this virus is initiated by attachment of the virus to the cell membrane. The attachment occurs through the interaction of hemagglutinin [a sialic acid (*N*-acetylneuraminic acid) receptor on the virus] with multiple sialic acid groups present on the surface of the mammalian epithelial cell (Fig. 5). This process is called hemagglutination (79). One of the strategies to treat such viral infection is to block the adhesion of the virus to cells by presenting sialic acid derivatives as competitors for cell-surface ligands (80). Although individual viral surface hemagglutinin (HA) binds individual cell-surface sialic acids (SA) weakly, the virus attaches to the cellular surface through multiple interactions between clusters of HA and SA residues. While an individual HA–SA interaction has a KdHA of $\sim 2.5 \times 10^{-3}\ M$, the interaction between the virus and an erythrocyte has a KdHA of $\sim 10^{-12}\ M$. Thus, the polyvalent interaction of the latter system is about a billionfold stronger than the

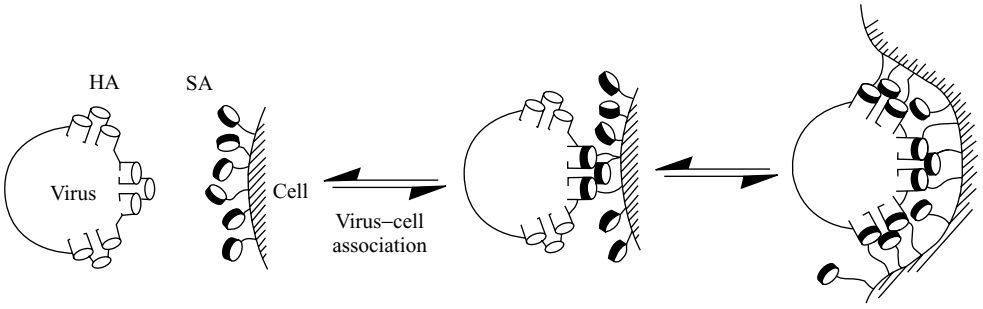

Fig. 5. Attachment of a virus to a host cell by interaction of viral hemagglutinin (HA) with cell-surface sialic acid (SA).

corresponding individual monovalent interaction. In theory, one approach to prevent viral infection may be to design polymeric SA derivatives containing multiple copies of SA. A number of groups have designed and synthesized such polyvalent inhibitors containing side-chain SA groups (81–84). Different kinds of polymer backbones were employed for this purpose (57). The most effective inhibitor among these polymers is a linear polyacrylamide derivative containing, on a side chain, the C-glycoside of SA (**22**). This polymeric ligand prevents hemagglutination at a concentration of 35 p*M*, while the corresponding monomeric α-methylsialoside inhibits hemagglutination at a concentration greater than 2 m*M* (85). A systematic investigation to elucidate the mechanism of this polyvalent interaction between influenza virus and polymeric ligands shows that a balanced combination of several factors including high affinity multiple ligand density, steric stabilization, and entropically driven enhanced binding is believed to contribute to the effectiveness of these polyvalent inhibitors in preventing viral attachment (86).

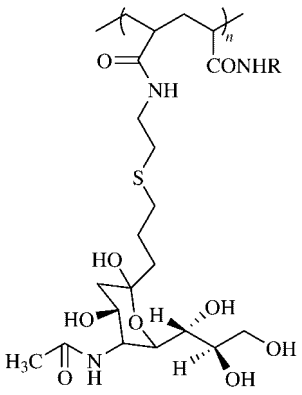

22

Although a wealth of information is available through *in vitro* studies, *in vivo* assays exhibiting the success of these polyvalent ligands in protecting animals against influenza infection has yet to be demonstrated. The success of this approach to develop antiviral agents for influenza would also depend on their favorable toxicity and activity profile *in vivo*.

Polyvalent Ligands as Antimicrobial Agents

Emergence of bacterial resistance to a number of antimicrobial agents is becoming a major worldwide health problem. The most significant problem in clinical practice is the increasing occurrence of methicillin-resistant *Staphylococcus aureus* (MRSA) strains (87). The majority of these strains have been found to carry multiple drug resistance factors. At present, the only effective treatment for multiply resistant MRSA infections is vancomycin. However, vancomycin resistance itself is a growing problem (88). This rapid emergence of multidrug-resistant bacterial strains and the potential threat they pose to human life means that development of novel antibacterial agents to overcome these shortcomings is critically important.

Use of polyvalent ligands as antibacterial agents have been considered to provide several advantages. Cluster effects from polyvalency would result in enhancement of weak nonbonding interaction between the bacterial surface receptors and the polymeric ligand. Furthermore, the use of polyvalent ligands could enhance lysis of the bacterial cell membrane/wall more rapidly.

As with viruses, most bacterial infections are also initiated by adhesion of microorganisms to the mucosal surfaces of host, mediated in part by bacterial protein adhesins (89). These adhesins interact with carbohydrate determinants of host cell glycolipids or glycoproteins. This fact suggests the use of specific polyvalent sugar constructs to competitively block the microbial adhesin and to protect against infection. This concept has been explored in our laboratories through the synthesis of a number of polymers bearing acid-functionalized glycoside moieties. Olefinic monomers containing glycoside moieties and acid functional groups such as *O*-sulfo and *O*-carboxymethyl groups were prepared and converted to various copolymers. These polymers were found to be effective *in vitro* against a number of bacterial targets (90).

A second approach to design polyvalent ligands as antimicrobial agents based on cationic polymers has also been developed in our laboratories. The mechanism of the antimicrobial action of these polymers is based on cell lysis. These polymers were designed as mimetics of certain cationic amphiphilic peptides containing multiple arginine and lysine residues. These cationic peptides, known as antimicrobial peptides, cause cell lysis through interaction of the positive charges of the peptides with negative phosphate head groups of cell membrane phospholipids (91). A series of amphiphilic cationic polymers were prepared bearing amine and ammonium groups as well as hydrophobic tails. These polymers were found to exhibit an inhibitory effect on a broad spectrum of microbes (92). In particular, some of these polymers (**23–25**) were found be very effective against *Cyptosporadium parvum*, which was, until the advent of protease inhibitors, a primary cause of GI tract infections in individuals with HIV infection (93). Some of these polymers were found to be superior to the commonly prescribed antibiotic, paromomycin.

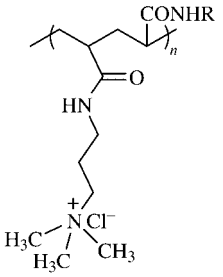

23

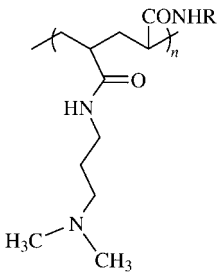

24

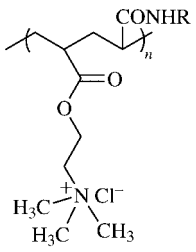

25

Synthesis of a multivalent vancomycin derivative exhibiting significantly enhanced antibacterial activity against vancomycin-resistant *enterococci* has been recently reported (94). This work was built upon the finding that dimeric vancomycin showed enhanced affinity toward the L-lysyl-D-alanyl-D-alanine peptidoglycan precursor that is responsible for the growth of the bacterial cell wall (95). A

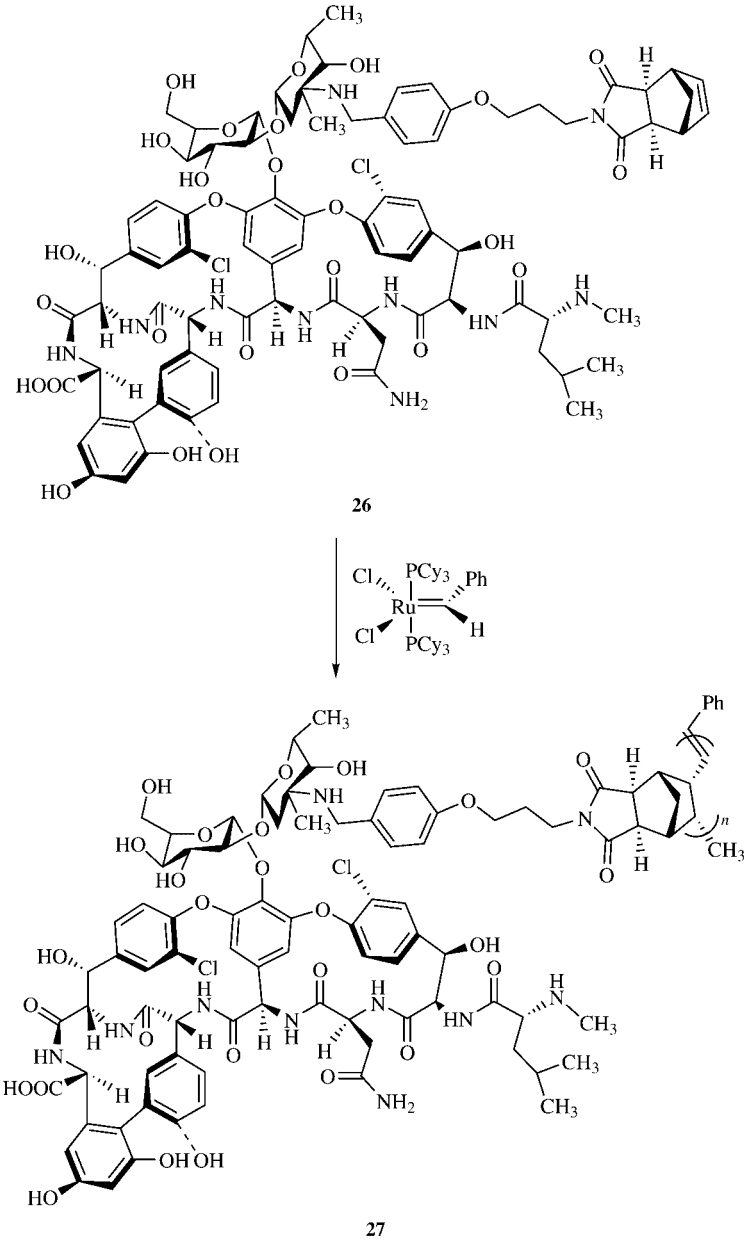

Fig. 6. Synthesis of polymeric vancomycin derivative.

polymeric vancomycin derivative was obtained by ring-opening metathesis polymerization of a functional cyclic olefin monomer containing the vancomycin moiety (Fig. 6). The antimicrobial property of the monomer (**26**) was similar to native vancomycin. Upon incorporation into the polymer backbone, the activity of the corresponding polymeric vancomycin derivative (**27**) was found to have increased

by nearly 60-fold, when tested against *S. aureus* and *S. enterococci*. This result further supports the importance of multivalency in the discovery of novel therapeutic agents.

Polymeric Drugs for the Treatment of Autoimmune Diseases

Simplistically, autoimmune diseases arise when the immune system mistakenly attacks itself. Ordinarily the immune system uses a number of defense mechanisms to prevent the development of autoimmune responses by directing T-cells (defense cells) to distinguish foreign invaders (96). Bypassing of the protection against autoimmunity leads to inflammation in various parts of the human body. Multiple sclerosis (MS) and rheumatoid arthritis (RA) are two of the most common autoimmune diseases.

MS is an autoimmune disease associated with immune activity directed against central nervous system antigens, thus affecting the brain and the spinal cord. Destruction of the regulatory mechanism that guards against autoimmunity leads to inflammation of the central nervous system. This disabling disease affects over 2.5 million people, particularly young adults (97). In general, immunosuppression and immunomodulation have been the mainstays of therapeutics strategies for the treatment of MS. One of the most popular treatments for relapsing–remitting MS is the use of recombinant beta interferon (eg Avonex) (98).

The development of a synthetic amino acid copolymer (glatiramer acetate) as an alternative to beta interferon for the treatment of relapsing-remitting form of MS represents a significant breakthrough in polymeric drug discovery (99). Glatiramer acetate is a random copolymer composed of four L-amino acids (alanine, lysine, glutamic acid, and tyrosine in a molar ratio of 4.2:3.4:1.4:1.0). This copolymer is prepared by the ring-opening random copolymerization of the corresponding *N*-carboxy-α-amino acid anhydrides (100). Systematic *in vitro* (using murine T-cell lines) and *in vivo* (using experimental allergic encephalomyelitis animal models) studies have established the possible mode of action of the polymer to its ability to mimic the myelin basic protein (MBP), one of the major autoantigens implicated in the pathogenesis of MS. MBP is known to sensitize autoreactive T-cells. The autoreactive cells migrate into the central nervous system and mediate the pathogenesis process of MS. The composition of glatiramer acetate is postulated to resemble a portion of MBP. The copolymer therefore competes with MBP for binding with T-cells (through cross-reaction) leading to antigen-specific intervention of the autoimmune process. In human clinical trials, glatiramer acetate demonstrated remarkable decrease in the number of relapses and rate of progression of the disease. Glatiramer acetate has been approved by FDA and European agencies for the treatment of relapsing-remitting form of MS in the United States and Europe, and is marketed under the brand name Copaxone by Teva Pharmaceutical Industries. Copaxone is the first synthetic polymeric drug approved for systemic treatment.

Since Copaxone works by antigen-specific intervention against MS, utility of this class of polymeric drugs can be expanded to treat other autoimmune diseases. Recently, Fridkis-Hareli and co-workers (101) have reported that glatiramer

acetate and other related copolymers (containing three amino acids) compete with type II collagen peptide 261-273, a candidate autoantigen in rheumatoid arthritis (RA) for binding to RA associated T-cells. This suggests the possible utility of these polymers in the treatment of RA and other autoimmune diseases (101).

Hybrid Polymeric Drugs Based on Polymer–Protein Conjugates

Biotechnology has offered the means to develop protein-based human therapeutics by recombinant DNA technology. However, the mode of delivery of these macromolecular drugs is not trivial. Furthermore, these proteins also have propensity to present toxic immunological responses. Design of polymer conjugates of proteins offers an opportunity to improve the therapeutic properties of the latter (102). The advantages of polymer–protein conjugates include reduction or nullification of the antigenicity of protein-based drugs, prolongation of their *in vivo* circulating half life, and enhancing delivery to the target site.

A variety of functional polymers have been used to conjugate therapeutic proteins, with the selection of polymers requiring stringent criteria. The polymers need to be nonantigenic, biocompatible, and intrinsically nondenaturing toward the therapeutic protein. A number of reactive polymers including copolymers of maleic anhydride with divinyl ether and styrene, poly(vinyl alcohol), poly(vinylpyrrolidinone), and poly(ethylene glycol) (PEG) have been utilized for this purpose (103). Amongst various polymers, PEG has been found to be most suitable for this purpose. Conjugation of enzymes using *multifunctional* polymers can lead to inter- and intramolecular cross-links leading to insoluble and/or complex aggregates of proteins. On the other hand, *monofunctional* PEG derivatives are nonantigenic and their conjugates with proteins produce more homogeneous products (104). This property is largely responsible for the success of PEG as the current polymer of choice for preparing polymer–protein hybrid biopharmaceuticals. With regard to architectures of PEG molecules, branched PEG derivatives are generally found to be superior to linear. Protein conjugates prepared using branched PEG were found to be less immunogenic and antigenic, more stable to proteolysis, and enzymatic activities tend to be better preserved. The superior properties of branched PEG are thought to be due to the "umbrella-like" spatial arrangement of polymer chains that protects the protein surfaces (105).

A number of therapeutic proteins such as agents for enzyme-replacement therapy, human growth hormones, and receptor binding proteins have been utilized for to prepare polymer–protein hybrid therapeutics. These polymeric conjugates have shown promising *in vitro* and *in vivo* properties. Most interestingly, some of these conjugates have entered human clinical trials or have already received regulatory approval. Some of these approved products are PEG-INTRON (Schering-Plough) (PEG–recombinant alpha interferon conjugate) for the treatment of hepatitis C, ONCASPAR (PEG–L-asparginase conjugate) for the treatment of acute lymphoblastic leukemia, and ADAGEN (PEG–adenosine deaminase conjugate) as an enzyme-replacement therapy for immune deficiency disease (106–108).

Conclusions and Future Prospects

Although polymeric materials have been developed to produce useful biomaterials and drug delivery systems, polymers acting as inherently therapeutic agents have largely remained unappreciated. In the present article we have attempted to illustrate that, through appropriate consideration of both disease targets and the unique properties of polymers, novel polymeric pharmaceutical products may be developed. These materials have, in many cases, therapeutic properties that cannot be achieved by traditional small molecules. Sequestrants that are confined to the GI tract are a case in point. An appreciation of the polyvalent interactions that drive the initial steps in many biological processes, both benign and pathogenic, also provides a rich source of potential therapeutic applications for polymeric materials. The case studies cited here illustrate that polymeric drugs are not solely an academic curiosity, but have produced novel and valuable therapeutic responses to important diseases.

BIBLIOGRAPHY

1. J. Jagur-Grodzinki, *React. Funct. Polym.* **39**, 99 (1999).
2. R. M. Ottenbrite, in R. L. Dunn and R. M. Ottenbrite, eds., *Polymeric Drugs and Drug Delivery Systems* (ACS Sympoisum Series 469), American Chemical Society, Washington, D.C., 1991, p. 3.
3. K. Ulbrich, M. Pechar, J. Strohalm, and V. Subr, *Macromol. Symp.* **118**, 577 (1997).
4. R. Duncan and J. Kopecek, *Adv. Polym. Sci.* **57**, 51 (1984).
5. S. C. DeSmedt, J. Demeester, and W. E. Hennink, *Pharm. Res.* **17**, 113 (2000).
6. R. Langer, *Nature* **392**, 5 (1998).
7. M. Ahlers, W. Muller, A. Reichert, H. Ringsdorf, and J. Venzmer, *Angew. Chem., Int. Ed. Eng.* **29**, 1269 (1990).
8. R. Duncan, in K. Park and R. J. Mrsny, eds., *Controlled Drug Delivery* (ACS Symposium Series 752), American Chemical Society, Washington, D.C., 2000, p. 350.
9. S. R. Holmes-Farley, *Polym. Mater. Sci. Eng.* **80**, 246 (1999).
10. M. Horne and P. Swearingen, *Pocket Guide to Fluids and Electrolytes*, The C. V. Mosby Co., St. Louis, Mo., 1989.
11. R. M. Rosa, M. E. Williams, and F. H. Epstein, in D. W. Seldin and G. Giebisch, eds., *The Kidney: Physiology and Pathophysiology*, Raven Press Ltd., New York, 1992, p. 2165.
12. G. O. Perez, J. R. Oster, R. Pelleya, P. V. Catalis, and D. C. Kem, *Nephron* **36**, 270 (1984).
13. T. J. Marrone and K. M. Terz, *J. Am. Chem. Soc.* **114**, 7542 (1992).
14. G. W. Gardiner, *Can. J. Gastroenterol.* **11**, 573 (1997).
15. B. B. Gerstman, R. Kirkman, and R. Platt, *Am. J. Kidney Dis.* **20**, 159 (1992).
16. J. Delmez and E. Slatopolsky, *Am. J. Kidney Dis.* **4**, 303 (1992).
17. J. W. Coburn and E. Slatopolsky, in B. M. Brenner and F. C. Rector Jr., eds., *The Kidney*, Saunders, Philadelphia, Pa., 1991, p. 2036.
18. S. M. Ott, N. A. Maloney, J. W. Coburn, C. Alfrey, and D. J. Sherrard, *N. Engl. J. Med.* **307**, 709 (1982).
19. F. Meric, P. Yap, and M. J. Bia, *Am. J. Kidney Dis.* **16**, 459 (1990).

20. F. P. Schmidtchen and M. Berger, *Chem. Rev.* **97**, 1609 (1997).
21. B. Dietrich, D. L. Fyles, T. M. Fyles, and J. M. Lehn, *Helv. Chim. Acta.* **62**, 2763 (1979).
22. G. M. Chertow, S. K. Burke, J. M. Lazarus, K. H. Stenzel, D. Wombolt, D. Goldberg, J. V. Bonverte, and E. Slatopolsky, *Am. J. Kidney Dis.* **29**, 66 (1997).
23. U.S. Pat. 5,496,545 (Jan. 1996), S. R. Holmes-Farley, W. H. Mandeville, and G. M. Whitesides (to GelTex Pharmaceuticals, Inc.).
24. U.S. Pat. 5,667,775 (Sept. 1997), S. R. Holmes-Farley, W. H. Mandeville, and G. M. Whitesides (to GelTex Pharmaceuticals, Inc.).
25. U.S. Pat. 5,698,190 (Dec. 1997), R. C. Hider and A. Canas-Rodriguez (to British Technology Group Ltd.).
26. S. R. Holmes-Farley, W. H. Mandeville, J. Ward, and K. L. Miller, *J. Macromol. Sci., Pure. Appl. Chem. A* **36**, 1085 (1999).
27. E. A. Slatopolosky, S. K. Burke, and M. A. Dillion, *Kidney Int.* **55**, 299 (1999).
28. A. J. Collins, W. L. St. Peter, F. W. Dalleska, J. P. Ebben, and J. Z. Ma, *Clin. Nephrol.* **54**, 334 (2000).
29. R. R. Crichton, *Inorganic Biochemistry of Iron Metabolism*, Ellis Harwood, New York, 1991.
30. G. M. Brittenham, in R. Hoffman, E. Benz, S. Shattil, B. Furie, and H. Cohen, eds., *Hematology: Basic Principles and Practice*, Churchill Livingstone, New York, 1991, p. 327.
31. D. J. Weatherall and J. B. Clegg, *The Thalassaemia Syndromes*, 3rd ed., Blackwell Scientific Press, Oxford, U.K., 1981.
32. Z. D. Liu and R. C. Hider, *Med. Res. Rev.* **22**, 26 (2002).
33. J. B. Porter, *Drug Safety* **17**, 407 (1997).
34. K. N. Raymond, G. Muller, and B. F. Matzanke, *Top. Curr. Chem.* **58**, 49 (1984).
35. U.S. Pat. 5,487,888 (Jan. 1996), W. H. Mandeville and S. R. Holmes-Farley (to GelTex Pharmaceuticals, Inc.).
36. P. K. Dhal, P. Cannon, S. R. Holmes-Farley, W. H. Mandeville, S. R. Polomoscanik, and T. X. Neenan, Conference Abstract, Gordon Research Conference on Reactive Polymers, Ion Exchangers and Sorbents, Henniker, N.H., Aug. 1999.
37. S. M. Grundy, *Circulation* **97**, 1436 (1998).
38. C. T. Sempos, J. I. Cleeman, M. D. Carroll, C. L. Johnson, P. S. Bachorik, D. J. Gordon, V. L. Burt, R. R. Briefel, C. D. Brown, and K. Lippel, *JAMA* **269**, 3009 (1993).
39. Executive summary of the third report of the "National Cholesterol Education (NCEP) Expert Panel on Detection, Evaluation, and Treatment of High Blood Cholesterol in Adults." *JAMA* **285**, 2486 (2001).
40. D. J. Rader, *Nat. Med.* **7**, 1282 (2001).
41. M. S. Brown and J. L. Goldstein, *Proc. Natl. Acad. Sci. U.S.A.* **96**, 11041 (1999).
42. S. M. Grundy, in R. Fears, ed., *Pharmacological Control of Hyperlipdaemia*, Prous Science Publishers, S.A., Barcelona, Spain, 1986, p. 3.
43. E. R. Stedronsky, *Biochim. Biophys. Acta* **1210**, 255 (1994).
44. W. H. Mandeville and C. Arbeeny, *IDrugs* **2**, 237 (1999).
45. G. M. Benson, C. Haynes, S. Blanchard, and D. Ellis, *J. Pharm. Sci.* **82**, 80 (1993).
46. M. Ast. and W. H. Frishman, *J. Clin. Pharmacol.* **30**, 99 (1990).
47. W. H. Mandeville, W. Braunlin, P. Dhal, A. Guo, C. Huval, K. Miller, J. Petersen, S. Polomoscanik, D. Rosenbaum, R. Sacchiero, J. Ward, and S. R. Holmes-Farley, *Mater. Res. Soc. Symp. Proc.* **550**, 3 (1999).
48. U.S. Pat. 5,607,669 (Mar. 1997), S. R. Holmes-Farley and W. H. Mandeville (to GelTex Pharmaceuticals, Inc.).
49. U.S. Pat. 5,919,832 (July 1999), S. R. Holmes-Farley and W. H. Mandeville (to GelTex Pharmaceuticals, Inc.).

50. U.S. Pat. 6,248,318 (1997), C. C. Huval, S. R. Holmes-Farley, J. S. Petersen, and P. K. Dhal (to GelTex Pharmaceuticals, Inc.).
51. G. M. Benson, D. R. Alston, D. M. B. Hickey, A. A. Jaxa-Chamiec, C. M. Whittaker, C. Haynes, A. Glen, S. Blanchard, S. R. Cresswell, and K. E. Suckling, *J. Pharm. Sci.* **86**, 76 (1997).
52. C. C. Huval, M. J. Bailey, S. R. Holmes-Farley, W. H. Mandeville, K. Miller-Gilmore, R. J. Sacchiero, and P. K. Dhal, *J. Macromol. Sci., Pure. Appl. Chem. A* **38**, 1559 (2001).
53. W. H. Mandeville and D. I. Goldberg, *Curr. Pharm. Des.* **3**, 15 (1997).
54. P. Zarras and O. Vogl, *Prog. Polym. Sci.* **24**, 485 (1999).
55. B. Gaudilliere and P. Berna, *Ann. Rep. Med. Chem.* **35**, 331 (2000).
56. B. Gaudilliere, P. Bernardellli, and P. Berna, *Ann. Rep. Med. Chem.* **36**, 293 (2001).
57. M. Mammen, S.-K. Choi, and G. M. Whitesides, *Angew. Chem., Int. Ed. Engl.* **37**, 2754 (1998).
58. L. L. Kiessling, L. E. Strong, and J. E. Gestwicki, *Ann. Rep. Med. Chem.* **35**, 321 (2000).
59. B. Henderson, M. Wilson, and B. Wren, *Trends Microbiol.* **5**, 454 (1997).
60. M. Rauchhaus, A. J. Coats, and S. D. Anker, *Lancet* **356**, 930 (2000).
61. B. Beutler and A. Poltorak, *Crit. Care Med.* **29**, 52 (2001).
62. Y. Gasche, D. Pittet, and P. Sutter, in W. J. Sibbald and J. L. Vincent, eds., *Clinical Trials for Treatment of Sepsis*, Springer, Berlin, Germany, 1995, p. 35.
63. T. C. Dixon, M. Meselson, J. Guillemin, and P. C. Hanna, *N. Engl. J. Med.* **341**, 815 (1999).
64. J. G. Bartlett, *Clin. Infect. Dis.* **18**(Suppl. 4), S265 (1994).
65. C. P. Kelly and T. LaMont, *Annu. Rev. Med.* **19**, 375 (1998).
66. D. Levy, *Clin. Ther.* **22**, 91 (2000).
67. N. S. Taylor and J. G. Bartlett, *J. Infect. Dis.* **141**, 92 (1980).
68. U.S. Pat. 6,290,946 (Sept. 2001), C. Bacon-Kurtz and R. Fitzpartick (to GelTex Pharmaceuticals, Inc.).
69. U.S. Pat. 6,270,755 (Aug. 2001), C. Bacon-Kurtz and R. Fitzpartick (to GelTex Pharmaceuticals, Inc.).
70. C. B. Kurtz, E. P. Cannon, A. Brezzani, M. Pitruzzelo, C. Dinardo, E. Rinard, D. W. K. Acheson, R. Fitzpatric, P. Kelly, K. Shacket, A. T. Papoulis, P. J. Goddard, R. H. Barker, G. P. Palace, and J. D. Klinger, *Antimicrob. Agents Chemother.* **45**, 2340 (2001).
71. W. Braunlin, Q. Xu, R. Fitzpatrick, C. B. Kurtz, R. Burrier, and J. D. Klinger, *Biophys. Soc. J.*, submitted.
72. U.S. Pat. 6,013,635 (Jan. 2000), L. D. Heerze and G. D. Armstrong (to Synsorb Biotech, Inc.).
73. L. D. Heerze, M. A. Kelm, J. A. Talbot, and G. D. Armstrong, *J. Infect. Dis.* **169**, 1291 (1994).
74. N. S. Duesbery and G. F. Vande-Woude, *Cell. and Mol. Life Sci.* **55**, 1599 (1999).
75. N. S. Duesbery, C. P. Webb, S. H. Leppla, V. M. Gordon, K. R. Klimpel, T. D. Copeland, N. G. Ahn, M. K. Oskarsson, K. Fukasawa, K. D. Paull, and G. F. Vande Woude, *Science* **280**, 734 (1998).
76. M. Mourez, R. S. Kane, J. Mogridge, S. Metallo, P. Deschatelets, B. R. Sellman, G. M. Whitesides, and R. J. Collier, *Nat. Biotechnol.* **19**, 958 (2001).
77. A. G. Bukrinskaya, *Adv. Vir. Res.* **27**, 141 (1982).
78. M. N. Matrosovich, *FEBS Lett.* **252**, 1 (1989).
79. D. C. Wiley and J. J. Skehel, *Annu. Rev. Biochem.* **56**, 356 (1987).
80. E. G. Weinhold and J. R. Knowles, *J. Am. Chem. Soc.* **114**, 9270 (1992).
81. S.-K. Choi, M. Mammen, and G. M. Whitesides, *J. Am. Chem. Soc.* **119**, 4103 (1997).

82. M. Mammen, G. Dahmann, and G. M. Whitesides, *J. Med. Chem.* **38**, 4179 (1995).
83. R. Roy, D. Zanini, S. J. Meunier, and A. Romanowska, *J. Chem. Soc., Chem. Commun.* 213 (1993).
84. M. N. Matrosovich, L. V. Mochalova, V. P. Marinina, N. E. Byramova, and N. V. Bovin, *FEBS Lett.* **272**, 209 (1990).
85. G. B. Sigal, M. Mammen, G. Dahmann, and G. M. Whitesides, *J. Am. Chem. Soc.* **118**, 3789 (1996).
86. S.-K. Choi, M. Mammen, and G. M. Whitesides, *Chem. Biol.* **3**, 97 (1996).
87. M. L. Cohen, *Trends Microbiol.* **2**, 422 (1994).
88. D. T. W. Chu, J. J. Plattner, and L. Katz, *J. Med. Chem.* **39**, 3853 (1996).
89. G. Reid and J. D. Sobel, *Rev. Infect. Dis.* **9**, 470 (1987).
90. U.S. Pat. 5,821,312 (Oct. 1998), W. H. Mandeville and V. R. Garigapati (to GelTex Pharmaceuticals, Inc.).
91. W. L. Maloy and U. P. Kari, *Biopolymers* **37**, 105 (1995).
92. U.S. Pat. 6,034,129 (Mar. 1998), W. H. Mandeville, T. X. Neenan, and S. R. Holmes-Farley (to GelTex Pharmaceuticals, Inc.).
93. J. M. Matukaitis, *J. Community Health Nurs.* **14**, 135 (1997).
94. H. Arimoto, K. Nishimura, T. Kinuki, I. Hayakawa, and D. Uemura, *J. Chem. Soc., Chem. Commun.* 1361 (1999).
95. U. N. Sundram, J. H. Griffin, and T. I. Nicas, *J. Am. Chem. Soc.* **118**, 13107 (1996).
96. L. Klein, M. Klugman, K. Nave, V. Tuohy, and B. Kyewski, *Nat. Med.* **6**, 56 (2000).
97. A. Compston and A. Coles, *Lancet* **359**, 1221 (2002).
98. G. L. Hall, A. Compston, and N. J. Scolding, *Trends Neurosci.* **20**, 63 (1997).
99. J. Fricker, *Lancet* **351**, 1792 (1998).
100. M. Sela, *Acta Polym.* **49**, 523 (1998).
101. M. Fridkis-Hareli, E. F. Rosloniec, L. Fugger, and J. L. Strominger, *Proc. Natl. Acad. Sci. U.S.A.* **95**, 12528 (1998).
102. C. Delgrado, G. E. Francis, and D. Fisher, *Crit. Rev. Ther. Drug Carrier Syst.* **9**, 249 (1992).
103. F. M. Veronese, P. Caliceti, and O. Schiavon, in J. M. Harris and S. Zalipsky, eds., *Poly(ethylene glycol) Chemistry and Biological Applications* (ACS Symposium Series 680), American Chemical Society, Washington, D.C., 1997, p. 182.
104. G. Fortier, *Biotechnol. Genet. Eng. Rev.* **12**, 329 (1994).
105. M. G. P. Saifer, R. Somack, and L. D. Williams, *Adv. Exp. Med. Biol.* **366**, 377 (1994).
106. K. Patel and J. McHutchison, *Expert Opin. Pharmacother.* **2**, 1307 (2001).
107. H. J. Muller, R. Beier, J. C. da Palma, C. Lanvers, E. V. Ahlke, V. Scutz, M. Gunkel, A. Horn, M. Schrappe, G. Henze, K. Kranz, and J. Boos, *Cancer Chemother. Pharmacol.* **49**, 149 (2002).
108. M. S. Hershfield, *Clin. Immunol Immunpathol* **76**, S228 (1995).

PRADEEP K. DHAL
S. RANDALL HOLMES-FARLEY
W. HARRY MANDEVILLE
THOMAS X. NEENAN
GelTex Pharmaceuticals, Inc., A Genzyme General Business

POLYMETHACRYLATES. See METHACRYLIC ESTER POLYMERS.

POLY(METHACRYLIC ACID). See ACRYLIC (AND METHACRYLIC) ACID POLYME.

POLYNUCLEOTIDES. See Volume 3.

POLYOXYMETHYLENE. See ACETAL RESINS.

POLYPHENYLENE ETHER. See POLYETHERS, AROMATIC.

POLYPHOSPHAZENES

Introduction

Polyphosphazenes (1–9) belong to the class of inorganic polymers (qv). They have a heteroatomic backbone consisting of alternating phosphorus and nitrogen atoms, with two side groups attached to each phosphorus atom (Fig. 1). The side groups can be organic, inorganic, or organometallic. Perhaps the most attractive feature of polyphosphazene chemistry is the very broad range of groups that can be easily incorporated into the macromolecular chain, which opens up unlimited possibilities for derivatization. The number of different polyphosphazenes that have been synthesized will soon approach 1000; no other polymer synthesis has been studied so extensively. The ability to control the macromolecular architecture and to fine-tune properties of the resultant polymer has attracted the attention of many research groups throughout the world. The initial application of polyphosphazenes as high performance elastomers has expanded into solid polymer electrolytes, membranes for gas and liquid separations, optically active polymers, biomaterials, and proton-exchange membranes for fuel cells. Polyphosphazenes are strong competitors for their isoelectronic analogues, polysiloxanes, which are considered the most important of all inorganic polymers with regard to commercial applications (see SILICONES).

History. The history of polyphosphazenes dates back to 1897, when Stokes (8) reported that phosphonitrilic chlorides could be converted by heating into "the rubber-like polyphosphonitrilic chloride." He described it as a "body, or a mixture of bodies, of very high molecular weight, that is highly elastic and insoluble in all neutral solvents, but which swells enormously in benzene". Since then there have been a number of studies devoted to polymerization of phosphonitrilic chlorides. Attempts to carry out the polymerization in organic solvents containing hydrogen

Encyclopedia of Polymer Science and Technology. Copyright John Wiley & Sons, Inc. All rights reserved.

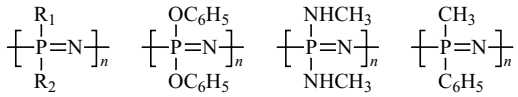

(**a**) (**b**) (**c**) (**d**)

Fig. 1. General formula (**a**) and three examples of polyorganophosphazenes with phenoxy (**b**), methylamino (**c**), and methyl/phenyl (**d**) substituents.

were unsuccessful. Later studies performed in halogenated solvents showed some moderate success: a soluble fraction of 18–50% with a polymerization degree of 300 was reported (11). Any effort to increase the molecular weight of the polymer resulted in formation of cross-linked, insoluble "inorganic rubber". To overcome the problem of cross-linking, Kauth (12) proposed a two-step synthesis. In the first step the monomer was heated for $\frac{1}{2}$ h at 150–200°C, which resulted in a partially polymerized oil that could be dissolved in a suitable solvent. This solution was used to "saturate some material," and the final polymerization was accomplished by an additional heating step. The struggle to obtain a soluble, long-chain polymer continued until the mid-1960s when Allcock and Kugel (13) reported that linear polydichlorophosphazene could be obtained. Optimization of the polymerization conditions and macromolecular substitution of chlorines with organic nucleophiles led to hydrolytically stable polyorganophosphazenes. Since then, interest by the military and polymer industries has led to an enormous growth in polyphosphazene science.

Nomenclature. Of the several naming systems related to phosphorus–nitrogen compounds: phosphonitrile (the oldest one), azaphosphorine, phosphorus-μ-nitrido, nitrilo-phosphoranylidyne, and phosphazene (14), only the last one has been generally accepted and adopted by the macromolecular research community. To comply with IUPAC nomenclature, a polyphosphazene with the common name poly(diphenoxyphosphazene) should be named catena-poly[(diphenoxyphosphorus)-μ-nitrido], if rules for "inorganic and coordination polymers" (15) were applied. If on the other hand, rules for "organic polymers" (16) were used, then the preferred constitutional repeating unit should be reoriented and the polymer should be named poly[nitrilo(diphenoxyphosphoranylidyne)].

Synthesis

There are three general methods to synthesize polyphosphazenes. One is the ring-opening polymerization of hexachlorocyclotriphosphazene, followed by a macromolecular substitution of chlorine atoms with a desired nucleophile or a combination of nucleophiles. As a result, the side groups are bonded to phosphorus through oxygen or nitrogen linkages. This is the primary method for polyphosphazene synthesis. The second method, called a "single-pot synthesis," is based on direct reaction of ammonium and phosphorus salts. The product, poly(dichlorophosphazene), then reacts with an appropriate nucleophile to give a poly(organophosphazene). It is claimed that production costs for this second method are low. The third method is condensation polymerization of phosphoranimines. Here the substituents are

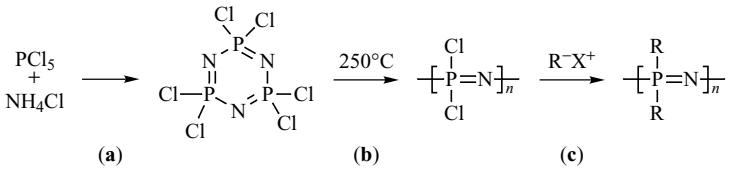

Fig. 2. (**a**) Trimer synthesis, (**b**) the ring-opening polymerization, and (**c**) the macromolecular substitution.

usually attached to phosphorus atoms prior to the polymerization. Very high molecular weights ($M_w = 10^6$) can be reached with ring-opening polymerization but the molecular weight distribution is very broad. Only moderate molecular weights ($M_w = 10^4$–10^5) are accessible via the condensation method; however, polydipersity in this case is usually <2.

Ring-Opening Polymerization. There are two variants of the method: melt polymerization and solution polymerization. The first method was developed by Allcock (13,17,18) and is shown schematically in Figure 2. It starts with the reaction of phosphorus pentachloride and ammonium chloride that leads to hexachlorocyclotriphosphazene. Following a multistep purification involving sublimation, this compound is polymerized by heating at 250°C in an evacuated and sealed glass tube for 24–48 h. After termination of the reaction, the linear poly(dichlorophosphazene) is isolated, by either sublimation or extraction of low molecular weight species, or by dissolution and precipitation. The molecular weight of the polymer is often very high, $M_w \sim 10^6$, but the molecular weight distribution is very broad. In the final step, the polydichlorophosphazene, dissolved in an inert solvent, is added to a suitable nucleophilic reagent. The product, usually polyorganophosphazene, is isolated by multiple precipitations. There are variants of the above method where partially substituted trimer is polymerized (Fig. 3) (19). Here a nucleophilic substitution is carried out on cyclochlorophosphazene and then the substituted trimer undergoes thermal ring-opening polymerization. This approach allows for the preparation of polyphosphazenes with substituents that cannot be incorporated through a classical macromolecular substitution route. There are, however, limitations imposed by both steric and mechanistic factors on the extent of substitution that makes the trimer polymerizable. Unless the substituted ring is highly strained as, for example, in the presence of transannular ferrocenyl (20), polymerization is generally feasible when no more than three nongeminal chlorines in hexachlorocyclophospazene are substituted. Fully methyl- or phenyl-substituted trimers undergo ring–ring equilibration but no polymers are formed (21,22). Ring-opening polymerization of some mixed ring

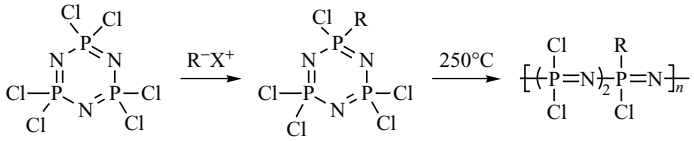

Fig. 3. Trimer substitution and the ring-opening polymerization of the substituted trimer.

systems, eg, $(NPCl_2)_2NSCl$, $(NPCl_2)_2NSOCl$, and $(NPCl_2)_2NSOF$, has been reported (23–25). These polymerizations were carried out at much lower temperatures 90–180°C) than that required for $(NPCl_2)_3$ alone.

The alternative method, solution ring-opening polymerization, was developed by several researchers (26–29), but most of the work is by Magill and co-workers (30). The polymerization of $(NPCl_2)_3$ is carried out in 1,2,4-trichlorobenzene using sulfamic or toluenesulfonic acid as a catalyst and $CaSO_4 \cdot 2H_2O$ as a promoter. The reaction is fast and yields poly(dichlorophosphazene) of high molecular weight with narrow and monomodal molecular weight distribution. From the poly(dichlorophosphazene) precursor, the desired poly(organophosphazene) is obtained by reaction with a suitable nucleophile. This last step is common to both the melt polymerization and the solution polymerization methods.

"Single-Pot" Synthesis. In order to simplify the synthesis of poly(dichlorophosphazene), Allen and co-workers (31,32) developed a method based on "two-step, single-pot" reaction of ammonium sulfate with phosphorus pentachloride (PCl_5). Both reactants are heated until a liquid monomer, *P*-trichloro-*N*-(dichlorophosphoryl)monophosphazene, is formed, which is then bulk-polymerized by further heating under inert atmosphere. After distilling off oxyphosphoryl chloride, the product, poly(dichlorophosphazene), is isolated. The authors claim that the method offers good yields, short reaction time, elimination of halogenated solvents, and leads to a polyphosphazene of high molecular weight and lower polydispersity.

Another method of direct synthesis of poly(dichlorophosphazene) developed by Carriedo and co-workers (33) has been disclosed. NH_4Cl and PCl_5 react in the presence of $CaSO_4 \cdot H_2O$ and NH_2HSO_3 as promoters, leading to polyphosphazenes of molecular weight on the order of 2×10^6. The yields are 30–40% on the basis of PCl_5.

Condensation Polymerization. Several procedures for the condensation polymerization of polyphosphazenes are known. In 1982, De Jaeger and coworkers (34) published an alternate synthetic route to poly(dichlorophosphazene) on the basis of thermal elimination of phosphoryl chloride from a P—N=P precursor. Important advantages of the reaction, as compared to the ring-opening polymerization, were the possibility to control the molecular weight of the polymer and to reduce the amount of cyclic oligomers in the product. The first successful condensation polymerization of substituted polyphosphazene was reported by Neilson and Wisian-Neilson (35–37). The reaction scheme is shown in Figure 4. The sequence begins with the synthesis of a *N*-silylphosphoranimine monomer containing the desired side groups and two leaving groups (trimethylsilyl and trifluoroethoxy). The product is isolated by a fractional distillation with an overall yield of ca 75%. The monomer is then polymerized by heating in a sealed glass

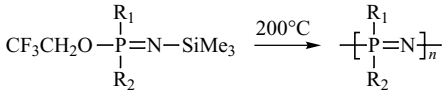

Fig. 4. The thermal condensation polymerization of phosphoranimine.

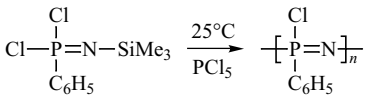

Fig. 5. The "living" cationic condensation polymerization of phosphoranimine.

ampule at 180–200°C for 7–12 days. This method allows for the synthesis of symmetrical and unsymmetrical homopolymers as well as random copolymers, but selection of the monomers is limited to either dialkyl- or alkyl–aryl-substituted. An improvement over the thermal process was proposed by Matyjaszewski's group (38,39). They prepared homo- and copolymers by tetrabutylammonium fluoride (TBAF) catalyzed anionic polymerization of phosphoranimines bearing trifluoroethoxy and alkoxyalkoxy substituents. The conditions of the reactions were relatively mild (100°C for 3–4 h) and it was possible to quantitatively produce linear polyphosphazenes with a narrow molecular weight distribution. The method, however, could be used in a very limited number of cases. The most promising condensation route was reported by Allcock and co-workers (40–43). It was based on PCl_5-induced, room temperature "living" cationic polymerization of *N*-(trimethylsilyl)-phosphoranimine. The reaction scheme is presented in Figure 5. For example, polymerization of *N*-(trimethylsilyl)-trichlorophosphoranimine leads to poly(dichlorophosphazene). Generally, if the monomer contained less then two organic substituents at the phosphorus, then an additional step, namely macromolecular nucleophilic substitution of the remaining chlorines, was necessary. The potential advantage of the method is that it allows for the synthesis of polyphosphazenes with controlled molecular weight and low polydispersity, with sophisticated architectures (eg block copolymers, hybrid organic/phosphazene copolymers, or star-branched polymers).

Polymeric Material Types

Phosphazene Homopolymers. Macromolecular substitution of poly(dichlorophosphazene) with use of a single kind of nucleophile leads to a symmetrical homopolymer. Symmetrical or unsymmetrical phosphazene homopolymers can also be obtained by condensation methods. If the bulkiness of the substituents do not impose any sterical constraints, then the resultant polyphosphazene is a crystalline material. Otherwise, glasses are obtained with a T_g of 150–250°C, as is the case for poly(spirophosphazenes) (44,45).

Copolymers. When two or more nucleophiles are used during the macromolecular substitution of poly(dichlorophosphazene), a mixed substituent system (46), ie a random copolymer, is obtained. There exists numerous data on the preparation and characterization of various random copolymers (47–53). To synthesize a block copolymer (or unsymmetrical homopolymer) condensation polymerization needs to be employed. Matyjaszewski and co-workers (54) synthesized block copolymers bearing various combinations of trifluoroethoxy and alkoxyalkoxy groups, by adding a second phosphoranimine after the first converted completely. Significant differences were found between random and block

copolymers with respect to their thermal properties and morphology. The T(1) transition of the random materials decreased dramatically when the fraction of units bearing alkoxyalkoxy groups increased, while the T(1) of the block copolymer was unaffected by the composition. Also, densities of the random copolymers decreased more rapidly than densities of the block materials when the fraction of the alkoxyalkoxy-bearing units was increased. Allcock and co-workers (55–57) synthesized copolymers with controlled molecular weights through a PCl_5-catalyzed cationic polymerization. First a *N*-(trimethylsilyl)-trichlorophosphoranimine was polymerized into a "living" poly(dichlorophosphazene). Next a second phosphoranimine, eg *N*-(trimethylsilyl)dichlorophenyl phosphoranimine was copolymerized using the "living" terminus. Subsequent replacement of the chlorine atoms with an appropriate side group resulted in a hydrolytically stable copolymer. A similar method was used to prepare a hybrid di- and triblock poly(phosphazene–ethylene oxide) and poly(phosphazene-siloxane) copolymers (58–61). Amphiphilic diblock copolyphosphazene with methoxyethoxyethoxy/methoxyethoxyethoxy and methoxyethoxyethoxy/phenyl units was synthesized by Chang and co-workers (62) and its micellar characterization was examined. The most voluminous literature on polyphosphazene copolymers relates to grafting. Wisian-Neilson and co-workers (63) prepared copolymers of poly(methylphenylphosphazene) with polystyrene, polymethylmethacrylate and with silicone grafts using anionic polymerizations. Chang and co-workers (64) grafted poly(2-methyl-2-oxazoline) onto partially brominated poly[bis(4-methylphenoxy)phosphazene] of low molecular weight ($M_w = 6200$) via cationic polymerization. When a high molecular weight polyphosphazene was used ($M_w > 10^5$), severe gelation resulted and the copolymer was insoluble in available solvents. Gleria and co-workers (65) synthesized several copolymers by thermal or photochemical grafting of various vinyl polymers onto polyphosphazene matrices. The free-radical process was initiated by hydrogen abstraction from a primary, secondary, or tertiary carbon of the alkylphenoxy substituent. Monomers such as maleic anhidride (66), methylmethacrylate (67), *N*,*N*′-dimethyl-acrylamide (68), meth(acrylic) acid (69), styrene (70), and vinyl acetate or alcohol (71,72) were used. Welker and co-workers (73,74) studied radiation-induced grafting onto allylamino-substituted polyphosphazenes and Prange and co-workers (75) prepared graft copolymers from polyphosphazene and polystyrene macromonomers.

An interesting example of a phosphazene random copolymer containing thiophenoxy groups was synthesized by Carriedo and co-workers (76). Although very long reaction times were required and low yields (ca 25%) were observed, it was the first time that a thiophenoxy-substituted poly(phosphazene) was obtained.

Polyphosphazene Blends. Polyphosphazene blends were investigated for thermal stabilization of organic polymers, biochemical applications, and membrane preparation. Poly[bis(carboxylatophenoxy)phosphazene]–polyurethane blends (77) were prepared through reactive mixing of the polyphosphazene with diisocyanate and diol prepolymers, and their flame-retarding potential was analyzed. Chen-Yang and co-workers (78) prepared blends of poly[bis(*p*-chlorophenoxy)phosphazene] and polystyrene, and studied their morphology, thermal properties, and flammability. Partial compatibility was observed when the polyphosphazene content was less than 50%. Ambrosio and co-workers (79) studied degradable polyphosphazene/polyester blends with self-neutralizing potential.

Herrero and Acosta (80) investigated the microstructure of poly(ethylene oxide)–poly[(octafluoropentoxy)(trifluoroethoxy)phosphazene] blends. Limited miscibility of both components was inferred, based on the observed shift of the components' glass-transition temperatures. Wycisk and co-workers (81) prepared membranes from blends of sulfonated poly[bis(3-methylphenoxy)phosphazene] with polyimides, polyacrylonitrile, and Kynar FLEX PVDF. Morphology, electrochemical performance, and methanol permeabilities of the membranes were then evaluated as part of a program to investigate such blends in direct methanol fuel cells. The polymers were immiscible and a domain-type structure was observed. The best compatibility resulted when the tetrabutylammonium or sodium salt of the polyphosphazene was used (82).

Cross-Linked Polyphosphazenes. Many applications require some level of cross-linking to be incorporated into the polymer to obtain an elastomer or to make it stronger, insoluble, or more thermally/chemically stable (83). Three kinds of cross-links are generally distinguished: physical (through crystallites or glassy microdomains), ionic complexes, and finally, covalent cross-links. The most stable are covalent bonds and these are of utmost importance. Two general methods, both of the radical nature, were generally used to induce covalent cross-linking in polyphosphazenes. One was based on incorporating some number of unsaturated functions like vinyl or allyl groups into the polyphosphazenes. This approach was generally adopted for vulcanization of polyphosphazene elastomers (84,85). The second method relied on labile hydrogen abstraction from secondary or tertiary carbons in the side groups (86–89). In Figure 6, an example is presented of photo-cross-linking of poly[(4-ethylphenoxy)(phenoxy)phosphazene] (90). Here, irradiation with UV light of wavelength 340 nm causes excitation of the benzophenone photoinitiator, which then abstracts hydrogen from a benzylic carbon of the polyphosphazene side groups. As a result, a macroradical is formed, where recombination of two macroradicals results in formation of a covalent cross-link. Electron beam irradiation or γ-ray exposure was also used to induce cross-linking of alkylaryloxy- or oligoethoxy-substituted polyphosphazenes (74,91–95). Interesting results were obtained with ionic cross-links. Allcock described the use of poly[bis(carboxylatophenoxy)phosphazene] for a microencapsulation of

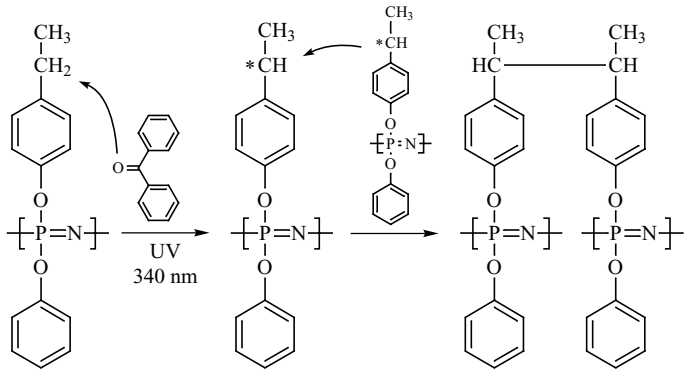

Fig. 6. The photo-cross-linking of poly[(4-ethylphenoxy)(phenoxy)phosphazene] with benzophenone photoinitiator.

mammalian cells (96). Acid–base complexation was also employed for cross-linking (97). In this way a poly[bis(3-methylphenoxy)phosphazene] sodium sulfonate was blended with polybenzimidazole into a membrane. Insoluble films were obtained after conversion of the sulfonate groups into sulfonic acid moieties and heat treatment of the polymer (98). The cross-linking degree and water swelling were controlled by adjusting the polybenzimidazole content.

Functional Polyphosphazenes. Functionalization can be defined as the introduction of chemical groups into the polymer chain that exert a specific function (eg chemical, physical, or biological) (99). Introduction of reactive groups into a polyphosphazene via the general macromolecular substitution route usually requires use of protected reagents, otherwise cross-linking and precipitation of the partially substituted polydichlorophosphazene may result (100,101). Derivatives containing hydroxylic (102–104), amine (105–108), and carboxylic (109) groups were prepared in this way.

Carriedo and co-workers (110,111) developed an interesting method of synthesizing various poly(aryloxyphosphazenes) using K_2CO_3 or Cs_2CO_3 as proton abstractors to substitute for chlorine atoms in poly(dichlorophosphazene). Even if bifunctional nucleophiles were used, no cross-linking was observed when the carbonates were present and the resultant polyphosphazene was soluble. Using this method, novel poly(spirophosphazenes) (112) and the chiral poly(dioxybinaphtylphosphazenes) (45) were synthesized.

A significant amount of research was devoted to post-functionalization of aryloxy- or methyl-substituted polyphosphazenes. In the first case, electrophilic aromatic substitution reactions were used to obtain sulfonated (113–116), carboxylated (117) nitrated (aminated) (118,119) and phosphonated (120,121) products (Fig. 7a). Alternatively, methyl substituents were deprotonated with *n*-BuLi and subsequently treated with a desired nucleophile (Fig. 7b). Using this method, polyphosphazenes bearing carboxylic (122), alcohol (123,124), ester (125), and other (63,126) groups became available. Numerous studies have been devoted

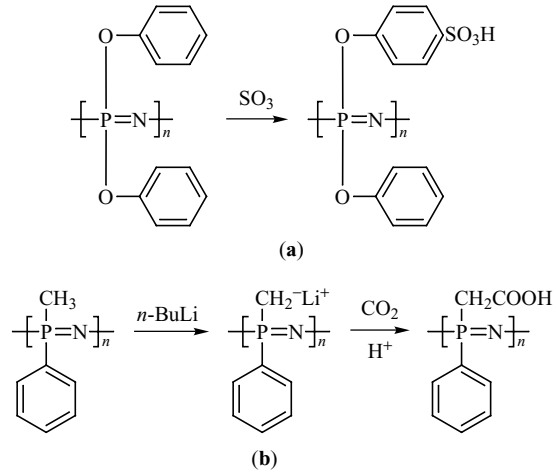

Fig. 7. (**a**) Sulfonation of the phenoxy substituents of the poly[bis(phenoxy)phosphazene] and (**b**) lithiation/carboxylation of the methyl group of poly[(methyl)(phenyl)phosphazene].

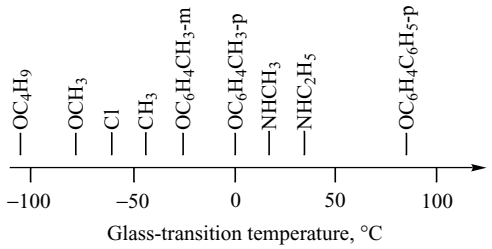

Fig. 8. The dependence of glass-transition temperature on the type of side group R in symmetrically substituted polyphosphazenes, $[R_2PN]_n$.

to a surface modification of polyphosphazenes (98,100). The most important objectives were balancing hydrophobicity or hydrophilicity, and immobilization of biologically active compounds (113,127–130).

Properties

Polyphosphazenes, owing to their inorganic backbone, are characterized by properties that are not common to organic polymers, namely low temperature flexibility, nonflammability, good thermal stability, and biocompatibility.

Backbone Flexibility. A characteristic feature of all the polyphosphazenes is their high skeletal flexibility, which is reflected in their very low glass-transition temperatures (Fig. 8). The high segmental mobility of the chain was explained by Allcock (4) as originating from cylindrical symmetry of the P—N bond because of broad overlapping of the nitrogen *p*-orbital with any of the five *d*-orbitals of the phosphorus (131). For example, the backbone torsional barrier in poly(difluorophosphazene) was found to be as low as 0.1 kcal per repeat unit (1). Although the formal structure of the polymers comprised a system of alternating single and double bonds, no electron delocalization was evidenced and an "island" pi-bond structure was postulated. Structural studies on poly(dichlorophosphazene) suggested a slight alternation in P—N bond lengths in the polymer backbone with values of 0.144 and 0.168 nm (132).

Crystallinity. Polyphosphazenes with a single substituent that is either small or rigid are semicrystalline. Their melting behavior consists of two first-order transitions, T(1) and T_m, separated by a 150–200°C gap. Optical microscopy showed that the crystalline structure was not lost at T(1), but rather existed as a mesophase until T_m was reached (2). Most fluoroalkoxy and aryloxy derivatives exhibited very high thermal stability with decomposition temperatures of 300–400°C.

Applications

Elastomers. An elastomer is a material that can be stretched repeatedly to a high extent (elongation greater than 200%) and always retracts to its original dimensions when the stress is released. Chain flexibility resulting from a freedom of

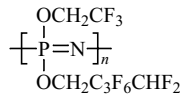

Fig. 9. An example of a typical polyphosphazene elastomer (EYPEL-F).

bond rotation within the polymer backbone is the main prerequisite for achieving elastomeric properties. Polyphosphazenes with low glass-transition temperatures proved to be best suited as high performance elastomers (61,133,134), especially for military applications. Substitution of two different types of fluoroalkoxy side groups on the same chain gave phosphazene polymers that were elastic at temperatures as low as −60°C, nonflammable, and resistant to hydrocarbon solvents, oils, and hydraulic fluids. A representative structure is shown in Figure 9 (135). Several polyphosphazene fluoroelastomers were commercialized under the trade name PNF or EYPEL-F. Polyphosphazenes were also used for toughening of thermosetting resins (136). Polydialkoxyphosphazenes were tested as low temperature greases and sealants (137). These materials proved to have high plasticity over a wide temperature range (−100°C to +100°C) with a decrease in the compressive/tensile modulus as the temperature was lowered.

Solid Polymer Electrolytes. Poly(ethylene oxide) (PEO) doped with a lithium salt has been used as the solid polymer electrolyte in rechargeable lithium batteries. The oxygen atoms in the PEO backbone coordinate metal cations, thus facilitating dissociation of the dissolved salts. However, because of its crystallinity, high conductivity could only be achieved when heated above 65°C. In 1984 Allcock and co-workers (138) found that poly[bis(methoxyethoxyethoxy)phosphazene] (MEEP, Fig. 10) doped with certain lithium and silver salts exhibited a room temperature ionic conductivity that was 2–3 orders higher than that of doped PEO. The repeat unit of MEEP has six oxygen atoms for cation coordination. The side groups are very flexible, which together with the inherent backbone flexibility, contributed to a glass-transition temperature being as low as −84°C. The polymer, however, was totally amorphous, which resulted in problems with its dimensional stability (139). A significant amount of research was directed to overcome this disadvantage. There were reports on cross-linking (140–142), blending with PEO (143,144), composites with silicates (145,146), and synthesis of poly(phosphazene-ethylene oxide) block copolymers (59). A new mechanical stabilization strategy, based on ceramic composites, was invented and developed at the Idaho National Engineering and Environmental Laboratory (147). Polyphosphazenes bearing crown ethers (148), sulfone or sulfoxide (149), or sulfonate (150) groups were also tested as potential Li^+ ion conducting solid polymer electrolytes.

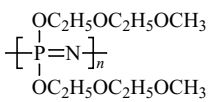

Fig. 10. Poly[bis(methoxyethoxyethoxy)phosphazene] (MEEP), a solid polymer electrolyte that was studied for use in lithium batteries.

Membranes for Gas Separation. Many linear polyphosphazenes have been tested as membranes for gas separation (151). Derivatives with phenoxy, trifluoroethoxy, or *n*-alkoxy were of most interest. Some of the work focused on O_2 and N_2 permeability (152–155) but other gases were also investigated (156–160). The literature data show a wide scatter of measured permeabilities for the same polymers. Most of the confusion can be attributed to the quality of the polymer samples, their thermal history, and experimental factors. Nevertheless, some trends are apparent. In general, low-T_g polyphosphazenes with alkoxy substituents have very high oxygen permeabilities, comparable to those of siloxane polymers, but with better selectivities (151). Also, polyphosphazenes showed a very high permeability for CO_2. Polyphosphazene membranes were applied to the recovery of helium from natural gas (158). Poly[bis(phenoxy)phosphazenes] have been tested in mixed gas separations where SO_2/N_2 separation factors as high as 17.2 were observed at 190°C (161). The effect of trimethylsilyl substituents on the gas transport properties of a series of polyphosphazenes has also been reported (162). When substituted at the para position of the phenoxy side groups, the polymers promoted an increase in selectivity accompanied by a decrease in gas permeability. Alternatively, incorporation of the trimethylsilyl group on the methyl group of poly[(methyl)(phenyl)phosphazene] resulted in an increase of both permeability and selectivity. While searching for chemoselective membranes, Orme and co-workers (163) incorporated three pendant groups into a polyphosphazene chain: 2-(2-methoxyethoxy)ethanol, 4-methoxyphenol, and 2-allylphenol. The first group gave the polymer proper hydrophilic character, the second group provided hydrophobic counterbalance and film-forming abilities, and finally, the third group enabled cross-linking (Fig. 11). The membranes showed some promise for CO_2 separation. The gas permeability of poly(organophosphazenes) was also the subject of theoretical studies and atomistic simulations (164).

Pervaporation. Separation of water–organic and organic–organic solutions by pervaporation is another area for potential applications of polyphosphazene membranes (151). Selectivities as high as 10^4 have been reported for the separation of dichloromethane from water by pervaporation, using a membrane prepared from poly[bis(trifluoroethoxy)phosphazene] (161,165). High selectivities for the separation of toluene and heptane were observed with a similar membrane (166). Pervaporation of water and alcohols was also investigated (167–169).

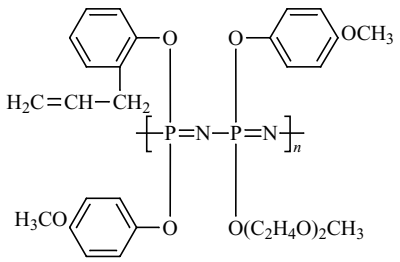

Fig. 11. Polyphosphazene with methoxyethoxyethoxy, 4-methoxyphenoxy and 2-allylphenoxy substituents used by Orme and co-workers (144) for gas separation studies.

Separation of Tritiated Water. Aromatic polyphosphazene membranes were investigated in the separation of tritiated water from normal water, because of their excellent radiological, thermal, and chemical stability (170,171). For these experiments carboxylated poly(diaryloxy)phospohazenes were used. A tritium depletion as high as 33% was reported.

Proton-Exchange Membranes for Fuel Cells. Fuel cells are a promising power source of the future. In current hydrogen/air PEM fuel cells, Nafion perfluorinated membranes are used as the proton-conducting separator of the anode and cathode half-cells. In addition to its high price, Nafion has two serious drawbacks that limit its use: high methanol crossover in direct methanol fuel cells (DMFC) and loss of conductivity (dehydration) at temperatures above 100°C in hydrogen/air fuel cells. Polyphosphazenes are a serious alternative to Nafion. Preliminary studies showed that films from sulfonated and UV-cross-linked poly[bis(3-methylphenoxy)phosphazene] possessed high proton conductivity, low methanol diffusivity, and good thermo-oxidative stability (172–174). Blends of sulfonated polyphosphazene and an inert organic polymer like a polyimide, poly(vinylidene fluoride), or polyacrylonitrile (PAN) were also investigated (175). The polyphosphazene component of the blend was stabilized by UV or e-beam cross-linking. The resultant membranes had conductivities from 0.01 to 0.06 S/cm (in water, 25°C) and an equilibrium water swelling from 20 to 60% (25°C). Direct methanol fuel cell (DMFC) tests were performed using membrane-electrode assemblies (MEA) prepared from SPOP/PAN and SPOP/Kynar FLEX (copolymer of vinylidene fluoride and hexafluoropropylene) blends. With a three-layer composite MEA (a methanol blocking film sandwiched between two high-conductivity membranes), a significant reduction in methanol crossover was observed with a modest decrease in current–voltage behavior, as compared to Nafion 117 (176). Phosphonated polyaryloxyphosphazenes were synthesized by Alcock and co-workers (120,121) and investigated as potential membrane materials for use in direct methanol fuel cells. The membranes cast from *N*,*N*-dimethylformamide were found to have conductivities between 0.01 and 0.1 S/cm and methanol diffusion coefficients (in 3 *M* MeOH) between 0.14×10^{-6} and 0.27×10^{-6} cm^2/s. Phenyl phosphonic acid functionalized poly[aryloxyphosphazenes] were prepared and evaluated as proton-conducting membranes in DMFC tests (177). Sulfonated derivatives of polyphosphazenes were also tested but their methanol barrier properties were found to be less attractive (178). Polyphosphazenes bearing sulfonimide groups were examined in a H_2/O_2 fuel cell at temperatures above 80°C. Less deactivation of the membrane due to dehydration (as compared to Nafion) was observed (179,180), which is a significant finding if these polymers are to be used in high temperature PEM fuel cells.

Biomedical Applications. Biomedical applications were investigated by a number of polyphosphazene research groups (181). The most important studies concerned biocompatibility, biodegradation, enzyme immobilization, and drug delivery (182,183). Polyphosphazene implants and prostheses were also examined. Biocompatibility through appropriate manipulation of surface or bulk chemistry was studied extensively (184). Works on the synthesis and cross-linking of amphiphilic polyphosphazenes (94), heparin immobilization (185–187), and other surface functionalizations (4,101) were reported.

Trypsin and glucose-6-phosphate dehydrogenase were immobilized on surface-aminated poly[bis(phenoxy)phosphazene] and successfully tested in continuous-flow reactors (130). Biodegradable polyphosphazene/poly(lactite-*co*-glycolide) blends were tested for controlled drug delivery using *p*-nitroaniline as a model release agent (188). Other polyphosphazenes that were susceptible to erosion under physiological conditions were also investigated; they contained amino acid ester (189–193), imidazolyl (194,195), glyceryl (104), or glucosyl (103) groups. *In vivo* performance under clinically relevant conditions were planned for poly[(*p*-methylphenoxy)-*co*-(ethylglicinato)phosphazene] matrices (196). Water-soluble methoxyethoxy–aminoaryloxy co-substituted polyphosphazenes were synthesized and tested as carriers for *N*-acetylglycine (106). Synthetic vectors for gene delivery based on polyphosphazenes were also reported (197). Song and co-workers (198,199) investigated the synthesis and antitumor activity of poly(organophosphazene)/diamineplatinum and poly(organophosphazene)/deoxorubicin conjugates. Only the first conjugate exhibited high antitumor activity due to controlled release of diamineplatinum(II). Polyphosphazene membranes and microspheres were investigated for the treatment of periodontal diseases (200). Antibacterial drugs, useful in periodontal tissue regeneration, could be entrapped in the membranes and released at appropriate rates to ensure therapeutic concentrations in the tissue. A hydroxyapatite–polyphosphazene composite was tested as a possible artificial bone-replacement material (201). Peripherial nerve regeneration with a poly[(organo)phosphazene] tubular prosthesis was presented as an alternative to silicone tubes usage (30). In other studies mammalian liver cells were encapsulated using calcium-cross-linked polyphosphazene (96), and polyphosphazene microspheres for insulin delivery were prepared (203) and their release behavior were evaluated. The use of polyphosphazenes as resilient denture liners and maxillofacial prostheses was also reported (204). Water-soluble phosphazene polymers were used to enhance the immunogenicity of HIV-1 secreted viral antigens (205). The system was found to have potential as a new HIV-1 vaccine candidate for human trials.

Flame Retardants. The high phosphorus and nitrogen content of polyphosphazenes make them nonflammable (206). Their properties are characterized by a high oxygen index (2), low smoke emission, noncorrosiveness, and low toxicity of combustion gases. Several polyphosphazenes were tested as coatings, foams, and coverings for electric cables. In flaming combustion, a commercially viable polyphosphazene exhibited a 75% reduction in heat release rate compared to the polyurethane rubber currently used in fire-blocked aircraft seat cushions (207). Cyclic, oligomeric, and polymeric phosphazenes have been investigated as flame-retarding additives and blends for several commodity polymers. For example, flame retardation improvement of polyurethane has been achieved by the use of aziridinyl substituted cyclotriphosphazene (208). The trimer served a dual function as cross-linker and as flame-retardant. Improvement of flame resistancy by incorporation of cyclic phosphazenes into organic polymers was the subject of many studies (209–213). Chen-Yang and co-workers (78) showed that blends of poly[bis(*p*-chlorophenoxy)phosphazene] and polystyrene had thermal stability and flame resistance significantly better than those of a pure polystyrene. Reed and co-workers (214) blended poly[bis(carboxylatophenoxy)-phosphazene] with structural polyurethane using reactive mixing and analyzed the thermal

stabilities of the resultant foams. An increase in flame resistance at loadings equal to or greater than 20 wt% was observed. Chen-Yang described the syntheses of an epoxy resin (215) and polyimides (216) containing flame-retarding cyclophosphazene.

Optical Devices. Of most interest in this application are those studies related to the nonlinear optical effects in polyphosphazene derivatives bearing aromatic azo units (217–219) and the photorefractive effect with polyphosphazenes bearing carbazolyl substituents (220). Possible applications include optical switches, frequency doublers for lasers, holographic data storage, and real-time image processing.

Hybrid Polyphosphazenes

In the last decade a number of hybrid polyphosphazenes containing backbone elements such as carbon, sulfur, or metal, in addition to phosphorus and nitrogen, have been synthesized and studied. Ring-opening polymerization of appropriate cyclic heterophosphazene has led to polymers like polycarbophosphazenes, polythiophosphazenes and polythionylphosphazenes (Fig. 12). Several polycarbophosphazenes have been synthesized (221,222). The general observation is that the polymers have a higher glass-transition temperature than the corresponding polyphosphazenes, which attributed to the lower rotational freedom of the C=N bond as compared to P=N. The first well-characterized examples of polythiophosphazenes, were reported by Dodge and co-workers (223). The polymers were moisture-sensitive and degradation was retarded only when bulky substituents such as o-phenylphenoxy were present. It was found that the S–Cl bond was more reactive than the P–Cl bond, which allowed for a regioselective substitution to yield polythiophosphazenes with different aryloxy substituents at the sulfur and phosphorus atoms. Synthesis of polythionylphosphazenes was reported by Liang and Manners (224). The perchlorinated polymers were moisture-sensitive, but reactions with aryloxy nucleophiles or primary amines converted them into stable poly(aryloxythionylphosphazenes) and poly(aminothionylphosphazenes), respectively (225,226). The substitution with aryloxides was regioselective but, contrary to the situation observed with polythiophosphazenes, only substitution of the P–Cl bonds was observed and the S–Cl bonds were intact. On the other hand, amines

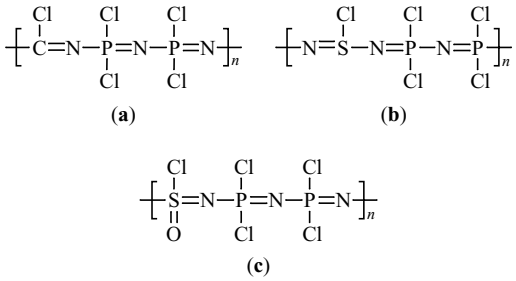

Fig. 12. (**a**) Polycarbophosphazene, (**b**) polythionylphosphazene, and (**c**) polythionylphosphazene, as examples of hybrid polyphosphazenes.

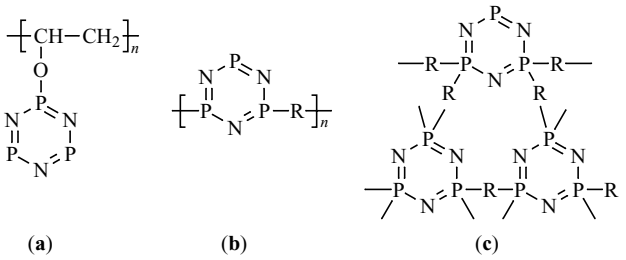

Fig. 13. Polymers containing cyclic phosphazene trimers: (**a**) poly(alkenylcyclophosphazene), (**b**) cyclolinear polyphosphazene, and (**c**) cyclomatrix material.

substituted easily at both phosphorus and sulfur atoms. Depending on the type of substituent, the polythionylphosphazenes showed properties typical of elastomers or glasses. Condensation routes to sulfur–nitrogen–phosphorus polymers were also reported (227,228).

Polymers Containing Cyclophosphazenes. Besides linear polyphosphazenes, three other macromolecular structures can be obtained based on the cyclic trimer: organic polymers with cyclophosphazene side groups, cyclolinear polymers, and cyclomatrix materials (Fig. 13). Poly(alkenylcyclophosphazenes) were studied in Allen's group (210). His approach involved the synthesis of cyclophosphazenes with an unsaturated group and subsequent radical copolymerization with various organic monomers, eg styrene or methyl methacrylate (229–232). The polymers consisted of an organic backbone, with the phosphazene rings as side groups. Other approaches involved either incorporation of phosphazene trimers into condensation polymers (233,234) or linkage to preformed organic polymers (213,235). Lately, Allcock presented the synthesis of cyclolinear-phosphazene-containing polymers via ADMET polymerization (236,237). Phosphazene–triazine cyclomatrix polymers were prepared by Mathew and co-workers (238). The group of Kumar and Gupta (239–241) developed several cyclolinear and cyclomatrix derivatives of polyimides. These materials showed good thermo-oxidative stability and a high char yield of 50–60% in air at 800°C.

BIBLIOGRAPHY

"Polyphosphonitrilic Polymers" under "Phosphorus-Containing Polymers" in *EPST* 1st ed., Vol. 10. pp. 139–144, by H. R. Allcock, The Pennsylvania State University; "Polyphosphazenes" in *EPSE* 2nd ed., Vol. pp. 31–41, by H. R. Allcock, Pennsylvania State University.

1. H. R. Allcock, *Phosphorus–Nitrogen Compounds*, Academic Press, Inc., New York, 1972, p. 337.
2. R. E. Singler, N. S. Schneider, and G. L. Hagnauer, *Polym. Eng. and Sci.* **15**, 321 (1975).
3. Ph. Potin and R. De, *Jaeger, Eur. Polym. J.* **27**, 341 (1991).
4. H. R. Allcock, in J. E. Mark, H. R. Allcock, and R. West, eds., *Inorganic Polymers*, Prentice Hall, Englewood Cliffs, 1992, p. 61.
5. H. R. Allcock, in P. Wisian-Neilson, H. R. Allcock and K. J. Wynne, eds., *Inorganic and Organometallic Polymers II* (ACS Symposium Series 572), American Chemical

Society, Washington, D.C., 1994, p. 208.
6. H. R. Allcock, in K. Hatada, T. Kitayama, and O. Vogl, eds., *Macromolecular Design of Polymeric Materials*, Marcel Dekker, Inc., New York, 1997, p. 475.
7. M. Gleria and R. De Jaeger, *J. Inorg. Organomet. Polym.* **11**, 1 (2001).
8. H. R. Allcock, *Chemistry and Applications of Polyphosphazenes*, John Willey & Sons, Inc., Hoboken, N. J., 2002.
9. R. De Jaeger and M. Gleria, eds., *Phosphazenes: A Worldwide Insight*, NOVA Science Publishers, Happauge, N. Y., 2002.
10. H. N. Stokes, *Am. Chem. J.* **19**, 782 (1897).
11. E. L. Gefter, *Organophosphorus Monomers and Polymers*, Associated Technical Services, Inc., Glen Ridge, 1962, p. 230.
12. U.S. Pat. 2,382,423 (Aug. 14, 1945), H. J. Kauth (to General Cable Corp.).
13. H. R. Allcock and R. L. Kugel, *J. Am. Chem. Soc.* **87**, 4216 (1965).
14. K. Matyjaszewski and W. V. Metanomski, *ACS Polym. Prepr.* **43**, 755 (2002).
15. *IUPAC, Pure Appl. Chem.* **57**, 149 (1985).
16. *IUPAC, Pure Appl. Chem.* **48**, 373 (1976).
17. H. R. Allcock, R. L. Kugel, and K. J. Valan, *J. Inorg. Chem.* **5**, 1709 (1966).
18. H. R. Allcock and R. L. Kugel, *Inorg. Chem.* **5**, 1716 (1966).
19. H. R. Allcock, *Polymer* **21**, 673 (1980).
20. I. Manners, G. H. Riding, J. A. Dodge, and H. R. Allcock, *J. Am. Chem. Soc.* **111**, 3067 (1989).
21. H. R. Allcock, G. H. Riding, I. Manners, J. A. Dodge, G. S. McDonnell, and J. L. Desorcie, *Polym. Prepr.* **31**, 48 (1990).
22. H. R. Allcock and D. B. Patterson, *Inorg. Chem.* **16**, 197 (1977).
23. J. A. Dodge, I. Manners, H. R. Allcock, G. Renner, and O. Nuyken, *J. Am. Chem. Soc.* **112**, 1268 (1990).
24. M. Liang and I. Manners, *J. Am. Chem. Soc.* **113**, 4044 (1991).
25. M. Liang and I. Manners, *Makromol. Chem., Rapid Commun.* **12**, 613 (1991).
26. U.S. Pat. 4,005,171 (Jan. 25, 1977), K. A. Reynard and A. H. Gerber (to Horizons Inc.).
27. U.S. Pat. 4,242,316 (Dec. 30, 1980), D. P. Sinclair (to Standard Oil Co.).
28. A. N. Mujumdar, S. G. Young, R. L. Merker, and J. H. Magill, *Makromol. Chem.* **190**, 2293 (1989).
29. U.S. Pat. 4,946,938 (Aug. 7, 1990), J. H. Magill and R. L. Merker (to University of Pittsburgh).
30. A. N. Mujumdar, S. G. Young, R. L. Merker and J. H. Magill, *Macromolecules* **23**, 14 (1990).
31. C. W. Allen and A. S. Hneihem, *Phosphorus, Sulfur and Silicon Relat. Elem.* **144**, 213 (1999).
32. U.S. Pat. 6,309,619 (Oct. 30, 2001), C. W. Allen, A. S. Hneihen, and E. S. Peterson (to Bechtel BWXT Idaho, LLC).
33. Span. Pat. ES 2,166,272 (2002), G. A. Carriedo, F. J. Garcia Alonso, and P. Gomez Elipe (to Universidad de Oviedo).
34. M. Helioui, R. De Jaeger, E. Puskaric, and J. Heubel, *Makromol. Chem.* **183**, 1137 (1982).
35. P. Wisian-Neilson and R. H. Neilson, *J. Am. Chem. Soc.* **102**, 2848 (1980).
36. R. H. Neilson and P. Wisian-Neilson, *Chem. Rev.* **88**, 541 (1988).
37. R. H. Neilson, P. Wisian-Neilson, J. J. Meister, A. K. Roy, and G. L. Hagnauer, *Macromolecules* **20**, 910 (1987).
38. K. Matyjaszewski, U. Franz, R. A. Montague, and M. L. White, *Polymer* **35**, 5005 (1994).
39. M. L. White and K. Matyjaszewski, *Macromol. Chem. Phys.* **198**, 665 (1997).
40. H. R. Allcock, C. A. Crane, C. T. Morrissey, J. M. Neilson, S. D. Reeves, C. H. Honeyman

and I. Manners, *Macromolecules* **29**, 7740 (1996).
41. J. M. Neilson and H. R. Allcock, *Macromolecules* **30**, 1854 (1997).
42. H. R. Allcock, C. A. Crane, C. T. Morrissey, and M. A. Olshavsky, *Inorg. Chem.* **38**, 280 (1999).
43. H. L. Allcock, S. D. Reeves, C. R. Denus, and C. A. Crane, *Macromolecules* **34**, 748 (2001).
44. G. A. Carriedo, F. J. Garcia Alonso, P. A. Gonzales, and J. L. Garcia Alvarez, *Macromolecules* **31**, 3189 (1998).
45. G. A. Carriedo, F. J. Garcia Alonso, P. Gomez Elipe, J. L. Garcia Alvarez, M. P. Tarazona, M. T. Rodriguez, E. Saiz, J. T. Vazquez, and J. I. Padron, *Macromolecules* **33**, 3671 (2000).
46. S. H. Rose, *J. Polym. Sci., Part B: Polym. Phys.* **6**, 837 (1968).
47. D. P. Tate, *J. Polym. Sci., Polym. Symp.* **48**, 33 (1974).
48. R. E. Singler, G. L. Hagnauer, and R. W. Sicka, *ACS Symp. Ser.* **260**, 143 (1984).
49. H. R. Penton, *Kautch. Gummi, Kunstat.* **39**, 301 (1986).
50. M. Gleria, F. Minto, L. Flamigni, and P. Bortolus, *J. Inorg. Organomet. Polym.* **2**, 329 (1992).
51. U.S. Pat. 5,260,103 (1993), M. Gleria, F. Minto, and L. Flamigni (to Consiglio Nazionale delle Ricerche).
52. H. R. Allcock and Y. B. Kim, *Macromolecules* **27**, 3933 (1994).
53. F. Minto, M. Gleria, A. Pegoretti, and L. Fambri, *Macromolecules* **33**, 1173 (2000).
54. M. L. White and K. Matyjaszewski, *Macromol. Chem. Phys.* **198**, 665 (1997).
55. H. R. Allcock, S. D. Reeves, J. M. Nelson, and C. A. Crane, *Macromolecules* **30**, 2213 (1997).
56. J. M. Nelson and H. R. Allcock, *Macromolecules* **30**, 1854 (1997).
57. H. R. Allcock, S. D. Reeves, J. M. Nelson, and I. Manners, *Macromolecules* **33**, 3999 (2000).
58. J. M. Nelson, A. P. Primrose, T. J. Hartle, and H. R. Allcock, *Macromolecules* **31**, 947 (1998).
59. H. R. Allcock, R. Prange, and T. J. Hartle, *Macromolecules* **34**, 5463 (2001).
60. R. Prange and H. R. Allcock, *Macromolecules* **32**, 6390 (1999).
61. H. R. Allcock and R. Prange, *Macromolecules* **34**, 6858 (2001).
62. Y. Chang, S. C. Lee, K. T. Kim, C. Kim, S. D. Reeves, and H. R. Allcock, *Macromolecules* **34**, 269 (2001).
63. P. Wisian-Neilson in P. Wisian-Neilson, H. R. Allcock, and K. J. Wynne, eds., *Inorganic and Organometallic Polymers II* (ACS Symposium Series 572), American Chemical Society, Washington, D.C., 1994 p. 246.
64. J. Y. Chang, P. J. Park, and M. J. Han, *Macromolecules* **33**, 321 (2000).
65. M. Gleria, F. Minto, P. Bortolus, G. Facchin, and R. Bertani, in P. Wisian-Neilson, H. R. Allcock and K. J. Wynne, eds., *Inorganic and Organometallic Polymers II* (ACS Symposium Series 572), American Chemical Society, Washington, D. C., 1994, p. 279.
66. M. Gleria, F. Minto, M. Scoponi, F. Pradella, and V. Carassiti, *Chem. Mater.* **4**, 1027 (1992).
67. F. Minto, M. Scoponi, L. Fambri, M. Gleria, P. Bortolus, and F. Pradella, *Eur. Polym. J.* **28**, 167 (1992).
68. F. Minto, M. Scoponi, M. Gleria, F. Pradella, and P. Bortolus, *Eur. Polym. J.* **30**, 375 (1994).
69. F. Minto, M. Gleria, P. Bortolus, L. Fambri, and A. Pegoretti, *J. Appl. Polym. Sci.* **56**, 747 (1995).
70. M. Gleria, A. Bolognesi, W. Porzio, M. Catellani, S. Destri, and G. Audisio, *Macromolecules* **29**, 469 (1987).
71. F. Minto, L. Fambri, and M. Gleria, *Macromol. Chem. Phys.* **197**, 3099 (1996).

72. L. Fambri, F. Minto, and M. Gleria, *J. Organomet. Polym.* **6**, 195 (1996).
73. M. F. Welker, H. R. Allcock, G. L. Grune, R. T. Chern, and V. T. Stannett, *Polym. Mater. Sci. Eng.* **66**, 259 (1992).
74. M. F. Welker, H. R. Allcock, G. L. Grune, R. T. Chern, and V. T. Stannett, in L. F. Thomson, C. G. Wilson, and S. Tagawa, eds., *Polymers for Microelectronics* (ACS Symposium Series 537), American Chemical Society, Washington, D. C., 1994, p. 293.
75. R. Prange, S. D. Reeves, and H. R. Allcock, *Macromolecules* **33**, 5763 (2000).
76. G. A. Carriedo, J. Jimenez, P. Gomez-Elipe, and F. J. Garcia Alonso, *Macromol. Rapid Commun.* **22**, 444 (2001).
77. C. S. Reed, J. P. Taylor, K. S. Guigley, M. M. Coleman, and H. R. Allcock, *Polym. Eng. Sci.* **40**, 465 (2000).
78. Y. W. Chen-Yang, H. F. Lee, and T. T. Wu, in P. Wisian-Neilson, H. R. Allcock and K. J. Wynne, eds., *Inorganic and Organometallic Polymers II* (ACS Symposium Series 572), American Chemical Society, Washington, D.C., 1994, p. 295.
79. A. M. A. Ambrosio, H. R. Allcock, and C. T. Laurencin, *Proc. Soc. Biomater.* **25**, 9 (1999).
80. C. R. Herrero and J. L. Acosta, *Polym. Int.* **32**, 349 (1993).
81. R. Wycisk, R. Carter, and P. Pintauro, in 12th Annual Meeting of the North American Membrane Society, Lexington, May 15–20, 2001.
82. R. Wycisk, R. Carter, P. N. Pintauro, and C. Byrne, in ACS 222nd National Meeting, Chicago, August 26–30, 2001.
83. R. A. Dickie, R. S. Bauer, and S. S. Labana, eds., *Cross Linked Polymers Chemistry, Properties, and Applications* (ACS Symposium Series 367), American Chemical Society, Washington, D. C., 1988.
84. U.S. Pat. 3,702,833 (1972), S. H. Rose and K. A. Reynard (to Horigons, Inc.).
85. H. R. Penton, *Kautsch. Gummi, Kunstst.* **39**, 301 (1986).
86. M. Gleria, F. Minto, L. Flamigni, and P. Bortolus, *J. Inorg. Organomet. Polym.* **2**, 329 (1992).
87. M. Gleria, F. Minto, L. Fambri, and A. Pegoretti, *Eur. Polym. J.* **31**, 791 (1995).
88. F. Minto, M. Gleria, A. Pegoretti, and L. Fambri, *Macromolecules* **33**, 1173 (2000).
89. R. Graves and P. N. Pintauro, *J. Appl. Polym. Sci.* **68**, 827 (1998).
90. R. Wycisk, P. N. Pintauro, W. Wang, and S. O'Connor, *J. Appl. Polym. Sci.* **59**, 1607 (1996).
91. D. Babic, D. M. Souverain, V. T. Stannett, D. R. Squire, G. L. Hagnauer, and R. E. Singler, *Radiat. Phys. Chem.* **28**, 169 (1986).
92. H. R. Allcock, S. Kwon, G. H. Riding, R. J. Fitzpatrick, and J. L. Bennett, *Biomaterials* **19**, 509 (1988).
93. V. T. Stannett, G. L. Grune, R. T. Chern, and H. R. Allcock, *Polym. Prepr. (Am. Chem. Soc., Div. Polym. Chem.)* **35**, 876 (1994).
94. H. R. Allcock, M. Gebura, S. Kwon, and T. X. Neenan, *Biomaterials* **9**, 500 (1988).
95. F. F. Steward, R. E. Singler, M. K. Harrup, E. S. Peterson, and R. P. Lash, *J. Appl. Polym. Sci.* **76**, 55 (2000).
96. S. Cohen, M. C. Bano, K. B. Visscher, M. Chow, H. R. Allcock, and R. Langer, *J. Am. Chem. Soc.* **112**, 7832 (1990).
97. J. Kerres, A. Ullrich, F. Meier, and T. Haring, *Solid State Ionics* **125**, 243 (1999).
98. R. Wycisk, R. Carter, and P. N. Pintauro, unpublished results (2001).
99. H. R. Allcock, in A. O. Patil, D. N. Schulz, and B. M. Novak, eds., *Functional Polymers* (ACS Symposium Series 704), American Chemical Society, Washington, D. C., 1998, p. 261.
100. H. R. Allcock, *Chem. Mater.* **6**, 1476 (1994).
101. H. R. Allcock, *Appl. Organomet. Chem.* **12**, 659 (1998).
102. M. A. Olshavsky and H. R. Allcock, *Chem. Mater.* **9**, 1367 (1997).
103. H. R. Allcock and A. G. Scopelianos, *Macromolecules* **16**, 715 (1983).

104. H. R. Allcock and S. Kwon, *Macromolecules* **21**, 1980 (1988).
105. H. R. Allcock, E. H. Klingenberg, and M. F. Welker, *Macromolecules* **26**, 5512 (1993).
106. S. K. Kwon, *Bull. Korean Chem. Soc.* **21**, 969 (2000).
107. S. K. Kwon, *Bull. Korean Chem. Soc.* **22**, 1243 (2001).
108. G. A. Carriedo, J. I. F. Martinez, F. J. G. Alonso, E. R. Gonzalez, and A. P. Soto, *Eur. J. Inorg. Chem.* 1502 (2002).
109. H. R. Allcock, S. Kwon, *Macromolecules* **22**, 75 (1989).
110. G. A. Carriedo, F. J. Garcia Alonso, and P. A. Gonzalez, *Macromol. Rapid. Commun.* **18**, 371 (1997).
111. G. A. Carriedo, F. J. Garcia Alonso, P. A. Gonzalez, J. L. Garcia, and P. Gomez-Elipe, *Phosphorus, Sulfur Silicon Relat. Elem.* **146**, 73 (1999).
112. G. A. Carriedo, L. Fernandez-Catuxo, F. J. Garcia Alonso, P. Gomez-Elipe, and P. A. Gonzalez, *Macromolecules* **29**, 5320 (1996).
113. H. R. Allcock and R. J. Fitzpatrick, *Chem. Mater.* **3**, 1120 (1991).
114. E. Montoneri, M. Gleria, G. Ricca, and G. C. Pappalardo, *Makromol. Chem.* **190**, 191 (1989).
115. E. Montoneri, M. Gleria, G. Ricca, and G. C. Pappalardo, *J. Macromol. Sci., Chem.* **A26**, 645 (1989).
116. R. Wycisk and P. N. Pintauro, *J. Membr. Sci.* **119**, 155 (1996).
117. H. R. Allcock, R. J. Fitzpatrick, and L. Salvati, *Chem. Mater.* **4**, 769 (1992).
118. H. R. Allcock, P. E. Austin, and T. F. Rakowsky, *Macromolecules* **14**, 1622 (1981).
119. H. R. Allcock and J. Y. Chang, *Macromolecules* **24**, 993 (1991).
120. H. R. Allcock, M. A. Hofmann, and R. M. Wood, *Macromolecules* **34**, 6915 (2001).
121. H. R. Allcock, M. A. Hofmann, C. M. Ambler, and R. V. Morford, *Macromolecules* **35**, 3484 (2002).
122. P. Wisian-Neilson, M. S. Islam, S. Ganapathiappan, D. L. Scott, K. S. Raghuveer, and R. R. Ford, *Macromolecules* **22**, 4382 (1989).
123. P. Wisian-Neilson and R. R. Ford, *Organometallics* **6**, 2258 (1987).
124. P. Wisian-Neilson and R. R. Ford, *Macromolecules* **22**, 72 (1989).
125. P. Wisian-Neilson, L. Huang, M. Q. Islam, and R. A. Crane, *Polymer* **35**, 4985 (1994).
126. P. Wisian-Neilson, C. Zhang, K. A. Koch, and J. Gruneich, *Phosphorus, Sulfur, Silicon* **69**, 144 (1999).
127. H. R. Allcock, J. S. Rutt, and R. J. Fitzpatrick, *Chem. Mater.* **3**, 442 (1991).
128. H. R. Allcock, R. J. Fitzpatrick, and K. B. Visscher, *Chem. Mater.* **4**, 775 (1992).
129. H. R. Allcock, C. T. Morrissey, W. K. Way, and N. Winograd, *Chem. Mater.* **8**, 2730 (1996).
130. H. R. Allcock and S. Kwon, *Macromolecules* **19**, 1502 (1986).
131. D. P. Craig and N. L. Paddock, *Nature* **181**, 1052 (1958).
132. Y. Chatani and K. Yatsuyanagi, *Macromolecules* **20**, 1042 (1987).
133. D. P. Tate, *J. Polym. Sci., Symp. Ser.* **48**, 33 (1974).
134. H. R. Penton, in M. Zeldin, K. J. Wynne, and H. R. Allcock, eds., *Inorganic and Organometallic Polymers* (ACS Symposium Series 360), American Chemical Society, Washington, D. C., 1988, p. 277.
135. J. H. Magill, *Polymer Data Handbook*, Oxford University Press, Oxford, 1999, p. 750.
136. O. L. Abu-Shanab, C. P. Chang, and M. D. Soucek, *High Perform. Polym.* **8**, 455 (1996).
137. V. S. Papkov, M. N. Ilina, V. P. Zhukov, D. J. Tsvankin, and D. R. Tur, *Macromolecules* **25**, 2033 (1992).
138. P. M. Blonsky, D. F. Shriver, P. E. Austin, and H. R. Allcock, *J. Am. Chem. Soc.* **106**, 6854 (1984).
139. H. R. Allcock, M. E. Napierala, D. L. Olmeijer, C. G. Cameron, S. E. Kuharcik, C. S. Reed, and S. J. M. O'Connor, *Electrochimica Acta* **43**, 1145 (1998).
140. J. S. Tonge and D. F. Shriver, *J. Electrochem. Soc.* **134**, 269 (1987).

141. J. L. Bennett, A. A. Dembek, H. R. Allcock, B. J. Heyen, and D. F. Shriver, *Chem. Mater.* **1**, 14 (1989).
142. G. A. Nazri and S. G. Meibuhr, *J. Electrochem. Soc.* **136**, 2450 (1989).
143. K. M. Abraham and M. Alamgir, *J. Power Source* **195**, 43 (1993).
144. K. M. Abraham, M. Alamgir, and R. K. Reynolds, *J. Electrochem. Soc.* **136**, 3576 (1989).
145. B. K. Coltrain, W. T. Ferrar, C. J. T. Landry, T. R. Molaire, and N. Zumbulayadis, *Chem. Mater.* **4**, 358 (1992).
146. C. Kim, J. S. Kim, and M. H. Lee, *Synth. Met.* **98**, 153 (1998).
147. J. DeGaspari, *Mech. Eng. Mag. Online* (Oct. 2002).
148. H. R. Allcock, D. L. Olmeijer, and S. J. M. O'Connor, *Macromolecules* **31**, 753 (1998).
149. H. R. Allcock and D. L. Olmeijer, *Macromolecules* **31**, 8036 (1998).
150. S. Ganapathiappan, H. C. Chen, and D. F. Shriver, *Macromolecules* **21**, 2299 (1988).
151. G. Golemme and E. Drioli, *J. Inorg. Organomet. Polym.* **6**, 341 (1996).
152. M. Kijiwara, in B. Sedlacek and J. Kahovec, eds., *Synthetic Polymer Membranes*, Walter de Gruyter, Berlin, 1987, p. 347.
153. M. Kijiwara, *J. Mater. Sci.* **23**, 1360 (1988).
154. F. A. Bittirova, V. V. Kireev, and A. K. Mikitaev, *Vysokomol. Seoedin. Ser. B* **23**, 30 (1981).
155. Jpn. Pat. 59154105 (1984), M. Yamabe, G. Kojima, and H. Wachi (to Asahi Glass Co.).
156. T. Hirose and K. Mizoguchi, *J. Appl. Polym. Sci.* **43**, 891 (1991).
157. E. Drioli, S. M. Zhang, A. Basile, G. Golemme, S. N. Gaeta, and H. C. Zhang, *Gas Sep. Purif.* **5**, 252 (1991).
158. E. S. Peterson and M. L. Stone, *J. Membr. Sci.* **86**, 57 (1994).
159. G. Golemme, E. Drioli, and F. Lufrano, *Polym. Sci.* **36**, 1647 (1994).
160. P. Wisian-Neilsen and G. F. Xu, *Macromolecules* **29**, 3457 (1996).
161. E. S. Peterson, M. L. Stone, R. R. McCaffrey, and D. G. Cummings, *Sep. Sci. Technol.* **28**, 423 (1993).
162. H. R. Allcock, C. J. Neilson, W. D. Coggio, I. Manners, W. J. Koros, D. R. B. Walker, and L. B. Pessan, *Macromolecules* **26**, 1493 (1993).
163. C. J. Orme, M. K. Harrup, T. A. Luther, R. P. Lash, K. S. Houston, D. H. Weinkauf, and F. F. Stewart, *J. Membr. Sci.* **186**, 249 (2001).
164. J. R. Fried and P. Ren, *Comput. Theor. Polym. Sci.* **10**, 447 (2000).
165. E. S. Peterson, M. L. Stone, W. F. Bowen, and A. K. Gianotto, *Recents Prog. Genie Proc.* **6**, 381 (1992).
166. D. Roizard, M. Pineau, A. Bac, J. J. Cuny, and P. Lochon, in W. R. Bowen, R. W. Field, and J. A. Howell, eds., Proceedings of the Euromembrane '95 Conference Bath, U. K., Sept. 18–20, 1995, p. II–239.
167. F. Suzuki, K. Onozato, H. Yaegashi, and T. Masuko, *J. Appl. Polym. Sci.* **34**, 2197 (1987).
168. Y. M. Sun, C. H. Wu, and C. L. Lin, *J. Polym. Res. (Taiwan)* **6**, 91 (1999).
169. C. J. Orme, M. K. Harrup, J. D. McCoy, D. H. Weinkauf, and F. F. Stewart, *J. Membr. Sci.* **197**, 89 (2002).
170. D. A. Nelson, J. B. Duncan, G. A. Jensen, and S. D. Burton, *Trans. Am. Nucl. Soc.* **71**, 82 (1994).
171. J. B. Duncan and D. A. Nelson, *J. Membr. Sci.* **157**, 211 (1999).
172. H. Tang and P. N. Pintauro, *J. Appl. Polym. Sci.* **79**, 49 (2000).
173. Q. H. Guo, P. N. Pintauro, H. Tang and S. O'Connor, *J. Membr. Sci.* **154**, 175 (1999).
174. R. Carter, R. Evilia, and P. N. Pintauro, *J. Phys. Chem. B* **105**, 2351 (2001).
175. R. Wycisk, R. Carter, H. Yoo, and P. N. Pintauro, NAMS 2002, 13th Annual Meeting, Long Beach, Calif., May 11–15, 2002.
176. R. Carter, R. Wycisk, H. Yoo, and P. N. Pintauro, *Electrochem. and Solid-State Lett.* **5**, A195 (2002).

177. H. R. Allcock, M. A. Hofmann, C. M. Ambler, S. N. Lvov, X. Y. Zhou, E. Chalkova, and J. Weston, *J. Membr. Sci.* **201**, 47 (2002).
178. M. F. Fedkin, X. Zhou, M. A. Hofmann, E. Chalkova, J. A. Weston, H. R. Allcock, and S. N. Lvov, *Mater. Lett.* **52**, 192 (2002).
179. M. A. Hofmann, C. M. Ambler, A. E. Maher, E. Chalkova, X. Y. Zhou, S. N. Lvov, and H. R. Allcock, *Macromolecules* **35**, 6490 (2002).
180. S. N. Lvov, NAMS 2002, 13th Annual Meeting, Long Beach, Calif., May 11–15, 2002.
181. A. G. Scopelianos, in W. S. W. Shalaby, ed., *Biomedical Polymers*, Hanser, New York, 1994, p. 153.
182. S. M. Ibim, A. A. Ambrosio, D. Larrier, H. R. Allcock, and C. T. Laurencin, *J. Controlled Release* **40**, 31 (1996).
183. A. K. Andrianov and L. G. Payne, *Adv. Drug Delivery Rev.* **31**, 185 (1998).
184. H. Kawakami, S. Kanezaki, M. Sudo, M. Kanno, S. Nagaoka, S. Kubota, *Artif. Organs* **26**, 883 (2002).
185. T. X. Neenan and H. R. Allcock, *Biomaterials* **3**, 78 (1982).
186. S. Lora, M. Carenza, G. Palma, G. Pezzin, P. Caliceti, P. Battaglia, and A. Lora, *Biomaterials* **12**, 275 (1991).
187. M. Carenza, S. Lora, G. Palma, G. Pezzin, and P. Caliceti, *Radiat. Phys. Chem.* **48**, 231 (1996).
188. C. T. Laurencin, S. E. Ibim, H. R. Allcock, A. M. Ambrosio, S. El-Amin, and M. S. Kwon, *Bioact. Mater.* **24**, 971 (1997).
189. H. R. Allcock, T. J. Fuller, D. P. Mack, K. Matsumura, and K. M. Smeltz, *Macromolecules* **10**, 824 (1977).
190. J. H. L. Crommen, E. H. Schacht, and E. H. G. Mense, *Biomaterials* **13**, 511 (1992).
191. P. Caliceti, S. Lora, F. Marsilio, A. Guiotto, F. M. Veronese, *Il Farmaco* **49**, 69 (1994).
192. H. R. Allcock, S. R. Pucher, and A. G. Scopelianos, *Biomaterials* **15**, 563 (1994).
193. L. Y. Qiu and K. J. Zhu, *J. Appl. Polym. Sci.* **77**, 2987 (2000).
194. H. R. Allcock, T. J. Fuller, and K. Matsumura, *Inorg. Chem.* **21**, 515 (1982).
195. H. R. Allcock and T. J. Fuller, *J. Am. Chem. Soc.* **103**, 2250 (1981).
196. J. H. Magill, *Polymer Data Handbook*, Oxford University Press, Oxford, 1999, p. 746.
197. J. Luten, J. H. van Steenis, N. M. E. Schuurmans-Nieuwenbroek, C. F. van Nostrumand, and W. E. Hennink, *Spring Meeting of the Belgian-Dutch Biopharmaceutical Society*, Gorleus Laboratoria, Leiden, the Netherlands, May 31, 2002.
198. S. C. Song, C. O. Lee, and Y. S. Sohn, *Bull. Korean Chem. Soc.* **20**, 250 (1999).
199. S. C. Song, C. O. Lee, and Y. S. Sohn, *Polym. Int.* **48**, 627 (1999).
200. F. M. Veronese, F. Marsilio, S. Lora, P. Caliceti, P. Passi, and P. Orsolini, *Biomaterials* **20**, 91 (1999).
201. K. A. Bernheim, C. S. Reed, and H. R. Allcock, *J. Invest. Med.* **47**, 42A (1999).
202. F. Langone, S. Lora, F. M. Veronese, P. Caliceti, P. P. Parnigotto, F. Valenti, and G. Palma, *Biomaterials* **16**, 347 (1995).
203. P. Caliceti, F. M. Veronese, and S. Lora, *Int. J. Pharm.* **211**, 57 (2000).
204. L. Gettleman, XIV International Conference on Phosphorus Chemistry, Cincinnati, Ohio, July 12–17, 1998.
205. L. Yichen, N. Touzjian, N. Kushner, C. Chutkowski, H. Qian, and S. Jenkins, XI International Conference on AIDS, Vancouver, Canada, July 7–12, 1996 (Abstract Mo. A.520).
206. W. C. Kuryla and A. J. Papa, ed., *Flame Retardancy of Polymeric Materials*, Vol. **I**, Marcel Dekker, Inc., New York, 1973.
207. R. E. Lyon, U. S. Department of Transportation, Federal Aviation Administration, Cabin and Fire Safety Reports, Fire-Resistant Elastomers, DOT/FAA/AR-TN01/104.

208. W. K. Huang, J. T. Yeh, K. J. Chen, and K. N. Chen, *J. Appl. Polym. Sci.* **79**, 662 (2001).
209. K. Inoue, S. Kaneyuki, and T. Tanigaki, *J. Polym. Sci., Part A: Polym. Chem.* **30**, 145 (1992).
210. C. W. Allen, *Trends Polym. Sci.* **2**, 342 (1994).
211. I. I. Selveraj and V. Chandrasekhar, *Polymer* **38**, 3617 (1997).
212. H. R. Allcock, W. R. Laredo, C. R. deDenus, and J. P. Taylor, *Macromolecules* **32**, 7719 (1999).
213. H. R. Allcock, T. J. Hartle, J. P. Taylor, and N. J. Sunderland, *Macromolecules* **34**, 3896 (2001).
214. C. S. Reed, J. P. Taylor, K. S. Guigley, M. M. Coleman, and H. R. Allcock, *Polym. Eng. Sci.* **40**, 465 (2000).
215. Y. W. Chen-Yang, H. F. Lee, and C. Y. Yuan, *J. Polym. Sci., Part A: Polym. Chem.* **38**, 972 (2000).
216. Y. W. Chen-Yang, H. F. Le, and S. F. Chen, *Phosphorus, Sulfur, Silicon Rel. Elem.* **75**, 109 (1996).
217. H. R. Allcock, C. G. Cameron, T. W. Skloss, S. Taylor-Meyers, and J. F. Haw, *Macromolecules* **29**, 233 (1996).
218. G. Rojo, F. Agullo-Lopez, G. A. Carriedo, F. J. Garcia Alonso, and J. I. Fidalgo, *Martinez, Synth. Met.* **115**, 241 (2000).
219. G. Rojo, F. Agullo-Lopez, G. A. Carriedo, F. J. Garcia Alonso and J. I. Fidalgo, *Martinez, Polym. Bull.* **45**, 145 (2000).
220. Z. Li, J. Li, and J. Qin, *React. Funct. Polym.* **48**, 113 (2001).
221. I. Manners, G. Renner, O. Nuyken, and H. R. Allcock, *J. Am. Chem. Soc.* **111**, 5478 (1989).
222. H. R. Allcock, S. M. Coley, and C. T. Morrissey, *Macromolecules* **27**, 2904 (1994).
223. J. A. Dodge, I. Manners, H. R. Allcock, G. Renner, and O. Nuyken, *J. Am. Chem. Soc.* **112**, 1268 (1990).
224. M. Liang and I. Manners, *J. Am. Chem. Soc.* **113**, 4044 (1991).
225. Y. Ni, A. J. Lough, A. L. Rheingold, and I. Manners, *Angew. Chem., Int. Ed.* **34**, 998 (1995).
226. Y. Ni, A. Stammer, M. Liang, J. Massey, G. J. Vancso, and I. Manners, *Macromolecules* **25**, 7119 (1992).
227. V. Chunechom, T. E. Vidal, and M. L. Turner, *Proc. Partner. Polym.* 50 (1996).
228. V. Chunechom, T. E. Vidal, H. Adams, and M. L. Turner, *Angew. Chem., Int. Ed.* **37**, 1928 (1998).
229. J. G. DuPont and C. W. Allen, *Macromolecules* **12**, 169 (1979).
230. C. W. Allen and R. P. Bright, *Macromolecules* **19**, 571 (1986).
231. J. C. Shaw and C. W. Allen, *Inorg. Chem.* **25**, 4632 (1986).
232. G. Bosscher and J. C. van de Grampel, *J. Inorg. Organomet. Polym.* **5**, 209 (1995).
233. U. Tunca and G. Hizal, *J. Polym. Sci., Part A: Polym. Chem.* **36**, 1227 (1998).
234. P. Radhakrishnan Nair, C. P. Reghunadhan Nair, and D. J. Francis, *Eur. Polym. J.* **32**, 1415 (1996).
235. T. J. Hurtle, N. J. Sunderland, M. B. McIntosh, and H. R. Allcock, *Macromolecules* **33**, 4307 (2000).
236. H. R. Allcock, E. C. Kellam III, and M. A. Hofmann, *Macromolecules* **34**, 5140 (2001).
237. H. R. Allcock and E. C. Kellam III, *Macromolecules* **35**, 40 (2002).
238. D. Mathew, C. P. R. Nair, and K. N. Ninan, *Polym. Int.* **49**, 48 (2000).
239. D. Kumar, A. D. Gupta, and M. Khullar, *J. Inorg. Organomet. Polym.* **3**, 259 (1993).

240. D. Kumar, A. D. Gupta, and M. Khullar, *J. Polym. Sci., Part A: Polym. Chem.* **31**, 2379 (1993).
241. D. Kumar and A. D. Gupta, *Macromolecules* **28**, 6323 (1995).

RYSZARD WYCISK
PETER P. PINTAURO
Case Western Reserve University

POLYPROPYLENE. See PROPYLENE POLYMERS.

POLYSACCHARIDES. See CARBOHYDRATE POLYMERS.

POLYSILANES

Introduction

Polysilanes or polysilylenes have catenated silicon backbone with two (organic) substituents on each silicon atom. Homopolymers (**1**) consist of single repeating silylene unit (R_2Si), and copolymers consist of two or more silylene units (**2**). Most are random block copolymers as in **2**, though several homopolymers with repeating disilylene ($R^1{}_2Si{-}SiR^2{}_2$) units have also been prepared. Materials prepared from trifunctional monomers are called "networked polysilanes (**3**)" or "ladder polysilanes (**4**)."

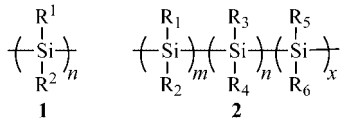

1 **2**

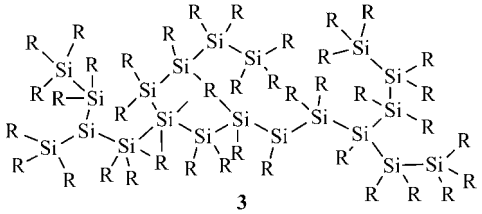

3

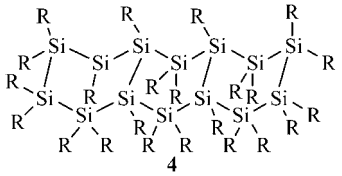

4

Encyclopedia of Polymer Science and Technology. Copyright John Wiley & Sons, Inc. All rights reserved.

Polysilanes bearing no specific chromophore in the side chain are colorless or white solids unless they contain substantial branching points. Most polysilanes are soluble in common organic solvents. But highly crystalline polymers $(CH_3)_2Si$, $(C_2H_5)_2Si$, $(C_6H_5)_2Si$) are insoluble. No specific toxicity has been reported. Polysilanes except those containing Si—H groups are air-stable below 300°C in the dark. Polymers involving halogen or triflate groups are moisture-sensitive and produce Si—O—H or siloxane bond on exposure to moisture. Weight loss begins around 350°C under vacuum or in inert gas. Black residue, mostly SiC, is observed after pyrolysis and this process is industrially used for SiC fiber production. Polysilanes are sensitive toward UV irradiation which induces polymer degradation mainly by Si—Si chain scission in vacuum or oxidation to siloxanes in air. A limited number of polysilanes [$(CH_3)_2Si)_n$, $(CH_3)_2Si)_m(CH_3—Si—C_6H_5)_n$, and $(CH_3—Si—C_6H_5)_n$] are commercially available in reagent quantity (Gelest, Inc., USA). The unique characteristics of polysilanes [strong absorption in UV region (300–400 nm), efficient fluorescence emission, high carrier mobility] originate from delocalized σ-electrons along their backbone, which yield similar physical properties to π-electrons in conjugated carbon polymers (1). The electronic state of polysilanes and ensuing physical characteristics are dependent on the following four factors: molecular weight (Si-catenation number), conformation (dihedral angle of the silicon backbone), substituents on silicon atom, and dimension of the backbone (branching points).

UV Absorption and Chromotropism

Strong absorption in the UV region is one of the most typical characteristics of σ-conjugated polysilanes. The λ_{max} and absorbance (ε) increases with increasing catenation number of silicon, which levels off around $n = 50$ (Fig. 1) (1). Poly(organosilanes) with $n > 50$ show λ_{max} at 300–400 nm (see Table 1). Polysilanes with aromatic substituents generally show longer λ_{max} than poly(alkylsilanes), which is attributed to σ–π conjugation (3). Poly{bis(butylphenyl)silane} shows λ_{max} at 400 nm, the longest absorption among linear polysilanes (1).

Because the silicon backbone is single bond in nature, the potential energy of polysilanes is dependent on the dihedral angle. The potential energy minima of polysilanes have been calculated to be $\omega = 180°$ (anti or trans) and ($\omega = \pm 60°$ (gauche). A more recent calculation (4), however, revealed that potential energy is dependent on the ratio of R^{vdxy}/R^{SiSi} where R^{vdxy} and R^{SiSi} are van der Waals radii of the substituents on silicon atom and $R^{SiSi} = \sim 2.36$ Å (0.236 nm), respectively. $\omega = 60°$ and 180° are the energy minima only for Si_nH_{2n+2}. Polysilanes with $R^{vdxy}/R^{SiSi} = 0.8$–1 have energy minima around $\omega = \pm 165°$ (transoid), $\pm 90°$ (ortho), $\pm 55°$ (gauche). These dihedral angles are found in permethylated oligosilanes in low temperature matrix (5) and Si_4Cl_{10} (11) in crystalline states. $Si_4(C_2H_5)_{10}$ has minima at $\omega = \pm 165°$ (T, transoid), $\pm 145°$, (D, deviant), $\pm 90°$ (O, ortho), $\pm 55°$ (G, gauche), and $\pm 45°$ (C, cisoid) (6).

Conformationally locked tetrasilanes and hexasilanes (7) confirmed that the all-anti conformer shows more intense absorption at the long wavelength than tetrasilanes containing other conformations. The combinations of the above possible dihedral angles make high molecular weight poly(organosilanes) complicated enantiomeric mixtures.

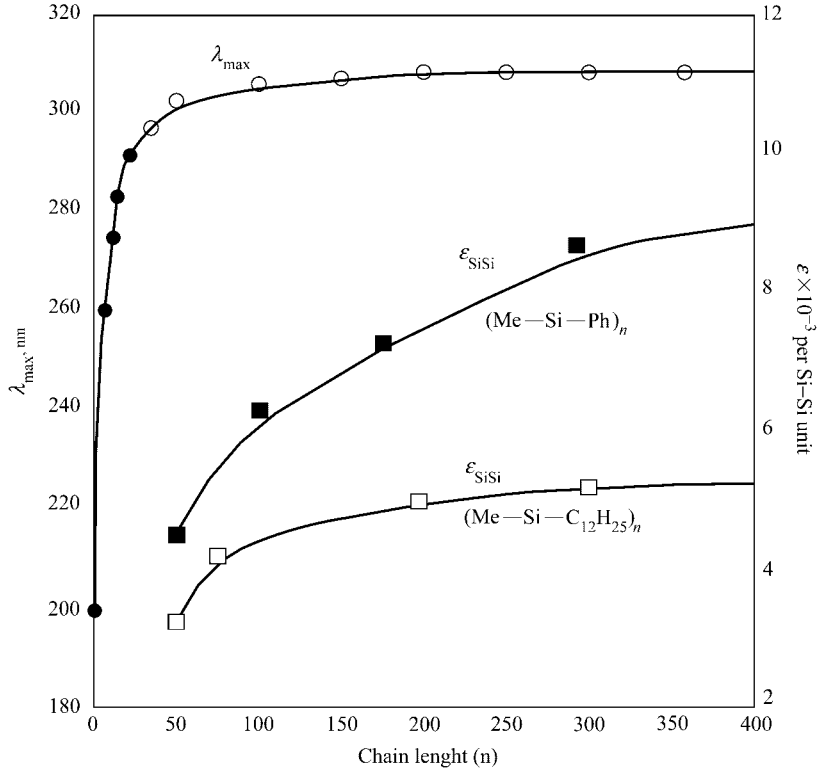

Fig. 1. Absorption wavelength maxima (λ_{max}) and extinction coefficients (ε_{SiSi}) as a function of oligomer chain length of n units $[SiR^1R^2]_n$. Reproduced with permission from Ref. 1, Copyright (1989), America Chemical Society.

UV spectroscopy is a convenient tool to examine the energy state of polysilanes. The silicon backbone of polysilanes is sensitive toward external stimuli and yields interesting chromotropic behavior both in solution and solid state (1,8). Thermochromism in dialkyl-substituted polysilanes has been studied intensively. Depending on the difference of the side-chain length, three types of spectral shift are induced on cooling in solution (Fig. 2) (9): (*1*) Continuous redshift to 320–330 nm is observed for polysilanes with very unbalanced side-chain length (Fig. 2a); (*2*) Continuous redshift to 350 nm with sharp intensification is observed for polysilanes with intermediately balanced side chains (Fig. 2b); (*3*) Discontinuous redshift to 355 nm for polysilanes with balanced long alkyl side chains (Fig. 2c). The absorption at 355 nm was once attributed to the most extended conformer (all-anti) but poly(didecylsilanes) and poly(didodecylsilanes) have recently been found to show absorption at 375 nm in solution (10). No spectral shift or a small hypsochromic shift is found for polysilanes bearing bulky substituents [$(C_6H_5{-}Si{-}CH_3)_n$, C_6H_5-Si-*c*-$C_6H_{11})_n$]. The molecular form of polysilanes in solution is conveniently estimated by the linear relationship $\varepsilon = 1130 \exp(-2.77\alpha)$ [α is the viscosity index in $[\eta] = kM^a$, and ε is the molar absorbance per Si unit] (11). Polysilanes with $\varepsilon = \sim 6000$ ($\alpha = 0.6$–0.7) are globular and those of $\varepsilon = \sim 10{,}000$

Table 1. UV–Vis Absorption Data for Typical Polysilanes[a,b]

R_1	R_2	λ_{max} (nm)	ε_{SiSi}
Me	*n*-Pr	306	5600
Me	*n*-Bu	304	
Me	*n*-Hex	306	5100
Me	*n*-$C_{12}H_{25}$	309	5000
Me	C_2H_4-Ph	303	9950
Me	*c*-Hex	326/320	7390
n-Pr	*n*-Pr	310	
n-Bu	*n*-Bu	314	8400
n-Hex	*n*-Hex	316/317	9700
n-$C_{14}H_{29}$	*n*-$C_{14}H_{29}$	318	8400
n-Pr	*n*-Hex	322	10600
n-Hex	*n*-Oct	318	8785
Me	Ph	341	9300
Me	*p*-C_6H_4Me	337/338	8600
Me	*p*-C_6H_4OMe	344	8180
Me	*p*-C_6H_4O*n*-Hex	354	5400
Me	*p*-C_6H_4Ph	352	4000
Me	β-naphthyl	350	2800
p-C_6H_4Et	*p*-C_6H_4Et	390	10200
p-C_6H_4*n*-Bu	*p*-C_6H_4*n*-Bu	395	26600
p-C_6H_4*s*-Pen	*p*-C_6H_4*s*-Pen	390	16200
p-C_6H_4*t*-Bu	*p*-C_6H_4*t*-Bu	376	3400
p-C_6H_4*n*-Hex	*p*-C_6H_4*n*-Hex	397	23300
m-C_6H_4*n*-Hex	*m*-C_6H_4*n*-Hex	400	21300
p-C_6H_4*n*-Hex	*p*-C_6H_4*n*-Hex	394	18600

[a] Refs. 1 and 2.
[b] All values were measure in THF.

($\alpha = 0.8$–1.0) are in an extended form. Rod-like polysilanes show $\varepsilon = 45{,}000$ ($\alpha = 1.6$ at -75°). The long persistence length of poly(bis(substituted-phenyl)silanes) determined by light scattering (>10 nm) is consistent with the strong absorbance ($\varepsilon > 2.5 \times 10^4$).

The thermochromic behavior of poly(dialkylsilanes) in the solid state is complicated by packing and mutual entanglement of the side groups. A discontinuous spectral shift of poly(dialkylsilanes) $[(R_2Si)_n]$ in the solid state occurs near the thermal phase transition temperature. Three conformations were determined by X-ray studies for uniaxially oriented poly(dialkylsilanes). Absorption maxima, thermochromic transition temperatures, and low temperature conformations of typical poly(dialkylsilanes) are listed in Table 2 (8). The absorptions at 375, 345, and 315 nm in Table 2 are related to all-trans (AT), TGTG′, and 7/3 helix conformations, respectively. Poly(dialkylsilanes) also show liquid crystalline behavior taking hexagonal columnar mesophase (*hcm*) (8,17). The thermochromic transition in the solid state is, however, independent of crystallization (18). Thermochromic behavior of poly(dialkylsilanes) is cooling rate dependent (19). Poly(dibutylsilane) and poly(dipentylsilane) show only a thermochromic blueshift in the solid state. However, they show a discontinuous type of shift either in solution or at high pressure (piezochromism) (20). Complexation with lithium ions

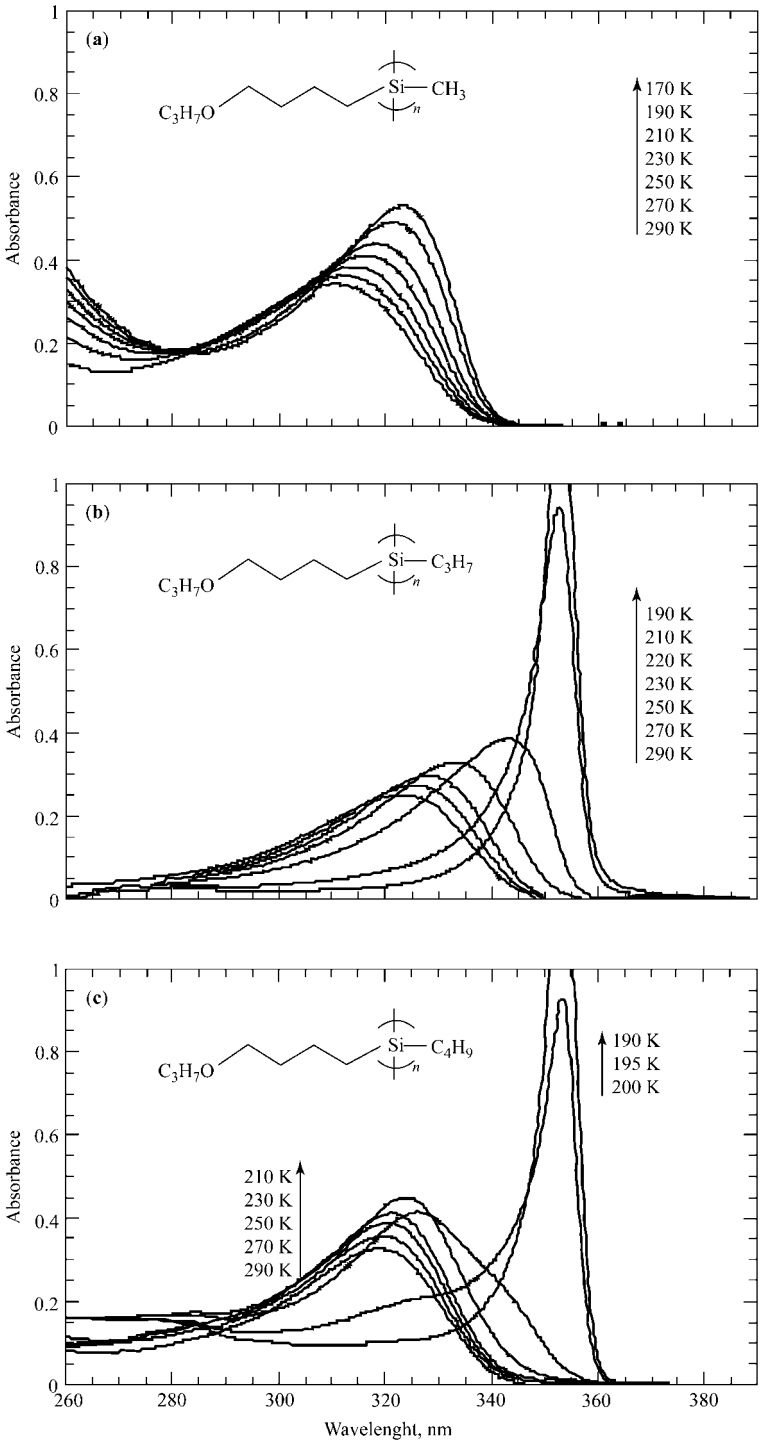

Fig. 2. Three types of temperature-dependent UV spectra of polysilanes in solution: (**a**) continuous, (**b**) intermediate, and (**c**) discontinuous shifts on cooling.

Table 2. Conformation, Thermochromic Transition Temperature, and Absorption Maxima of Polydialkylsilanes [(R—Si—R)$_n$] in Crystalline Phase

C-number in R	Low temperature conformation	T_d,[a] °C	λ_{max}(L),[b] nm	λ_{max}(H),[c] nm	Reference
C1	Trans		342	342	12
C2	Trans		316	316	13
C3	Trans		312	312	13
C4	7/3helix		313	320	14
C5	7/4helix		313	313	14
C6	Trans	42	374	317	14
C7	Trans	45	374	317	15
C8	Trans	43	374	317	15
C10	TGTG′	45	383	320	15
C14	TGTG′	54	347	322	16

[a] Transition temperature.
[b] λ_{max}(L) for low temperature form.
[c] λ_{max}(H) for high temperature form.

alters thermochromic behavior of [CH_3—Si—$(CH_2)_3$—$(OCH_2CH_2)_3$—OCH_3] (21) and [Oct—Si—$(CH_2)_4$—OCH_2CH_2—OC_2H_5] (ionochromism) (22). Electrochromism is reported only for poly{(3,3,3-trifluoropropyl)-methylsilane-*co*-methylpropylsilane}, which shows a blue shift when an electric field is applied (23).

Photoluminescence

A sharp fluorescence with small Stork shift is another characteristic of polysilanes. Fluorescence quantum yield (Φ) is generally high as summarized in Table 3 for typical polysilanes (1). Fluorescence lifetime is usually less than 1 ns. Temperature-dependent fluorescent spectra of poly(dialkylsilanes) correspond to thermochromic behavior. The fluorescence spectrum is also sensitive to structural defects; polysilanes having branching points (networked polysilanes **3** or ladder polysilanes **4**) show decreased fluorescence emission in the UV region but show an additional broad emission in the visible region (>430 nm) (24). The efficient emission makes polysilanes an emitting material of Light-Emitting Diodes (qv) (LEDs).

Ionization potential of polysilanes is in the range of 5–6 eV as determined by photoelectron spectroscopy (25,26), XPS (27) and xerographic surface analysis (28), which is due to a high HOMO level (29). Polysilanes behave as electron donors and form complexes with TCNE (30) and reduce metal ions (Au^{3+}, Ag^{+}, and Pd^{2+}) (31). The band gap of polysilanes is in the range of 3–4 eV as determined by the absorption edge.

Synthesis

Polysilanes are synthesized by following five methods: (*1*) reductive condensation of dichlorosilanes with alkali or alkali earth metals (Wurtz-type coupling), (*2*)

Table 3. Fluorescence of Polysilanes[a]

	Solution		Solid state	
Polysilane	λ_{max}, nm	Φ, %	λ_{max}, nm	Φ, %
$(CH_3—Si—C_6H_5)_n$	353	0.08–0.25	353	
$(CH_3—Si—C_6H_4OCH_3)_n$	362	0.2–0.5		
$\{CH_3—Si—Np(b)\}_n$	437			
$(CH_3—Si—C_3H_7)_n$	341	0.76	345	
$(CH_3—Si—C_6H_{13})_n$	337	0.61	343	
$(CH_3—Si—C_{12}H_{25})_n$	337	0.67	347	
$(C_6H_{13}—Si—C_6H_{13})_n$	342	0.42	371	
$(CH_3—Si—C_2H_4—C_6H_5)_n$			338	0.14
$(CH_3—Si—^iPr)_m(CH_3—Si—^nPr)_m$	340	0.69	342	
$(CH_3—Si—Si(CH_3)_3)_n$	335	0.026		
$(CH_3—Si—C_6H_4—Si(CH_3)_3)_n$	357	0.03		
$(CH_3—Si—C_6H_4CH_2Si(CH_3)_3)_n$	354	0.05		
$\{(p\text{-}BuC_6H_4)_2Si\}_n$	400	0.55		
$\{(p\text{-}BuOC_6H_4)_2Si\}_n$	412	0.6		

[a]From Ref. 1.

dehydrogenative coupling of hydrosilanes with transition-metal complexes (32), (*3*) anionic polymerization of masked disilenes (33–35), (*4*) ring-opening polymerization (ROP) of strained cyclic oligosilanes (36,37), and (*5*) redistribution polymerization of alkoxylated disilanes with base catalysts (38). Reductive condensation is a practical and general method to prepare a wide variety of polysilanes. The reaction is usually carried out in toluene with sodium. Yield and molecular weight are highly dependent on the dichlorosilane monomer and reaction condition. The reaction is believed to involve silyl anions and/or anion radials (eq. 1) (39). The reaction proceeds only on the surface of sodium (Fig. 3).

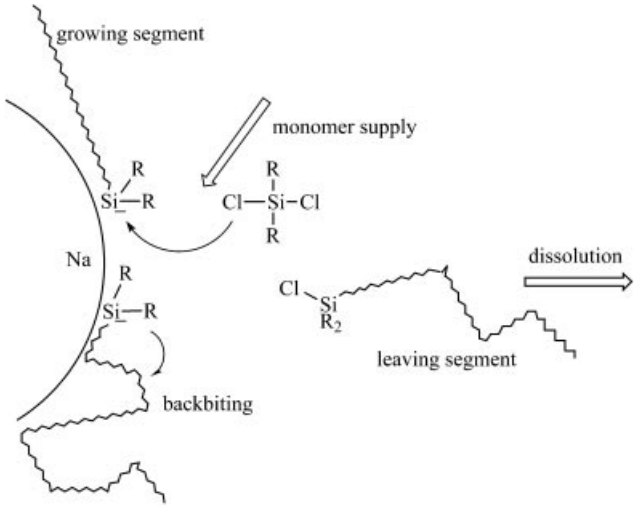

Fig. 3. Diffusion model of Wurtz coupling reaction.

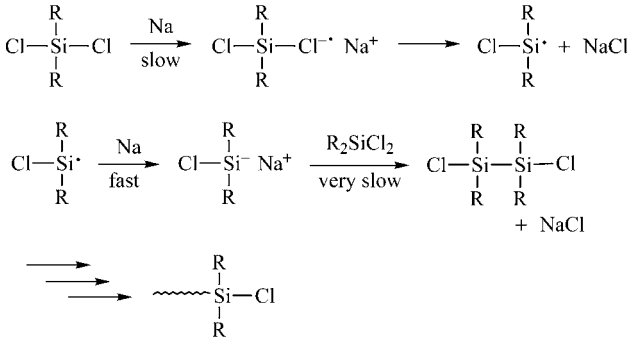

(1)

As a result of the severe reaction conditions (high temperature, alkali metals), the heterogeneous nature of the reaction, as well as a complicated reaction mechanism, polysilanes obtained by this method show polymodal molecular weight distribution. GPC peaks are found around $M_w > 10^6$, $\approx 10^5$, 10^4, and 10^3 and cyclic and linear oligomers ($M_w < 1000$). Reaction at relatively low temperature ($\approx 65^\circ$C) (40), reaction with sodium dispersion into monomer (41), reaction by rapidly adding monomers into sodium dispersion (42), reaction in the presence of sacrificing materials (43), reaction by using benzene as the solvent (44), and reaction under the presence of copper catalysts (42) are effective in obtaining polysilanes with high molecular weight ($M_w > 10^5$). High yield is achieved by the reactions of ultrasound agitation (45), using phase-transfer reagent (46), or using THF, diglyme, or HMPA as the solvent or additive (40). The obtained polysilanes in these high yield synthetic methods usually show monomodal molecular weight distribution. However, the molecular weight is not high ($< 1 \times 10^5$). Polymerization with potassium, Na/K alloy, and KC_8 are applied for less reactive monomers or low temperature polymerization but undesired cyclic and/or linear oligomers are also formed. Electrolysis with Mg electrodes under ultrasound irradiation affords a safe and controllable method but gives low molecular weight polymer ($M_n < 10^4$) (47).

Molecular weight of the product by dehydrogenative polymerization of hydrosilanes is low ($M_n < 10^4$) (48), but the reactive Si—H groups are further converted to diverse functional groups (Fig. 4) (49). Dehydrogenative polymerization

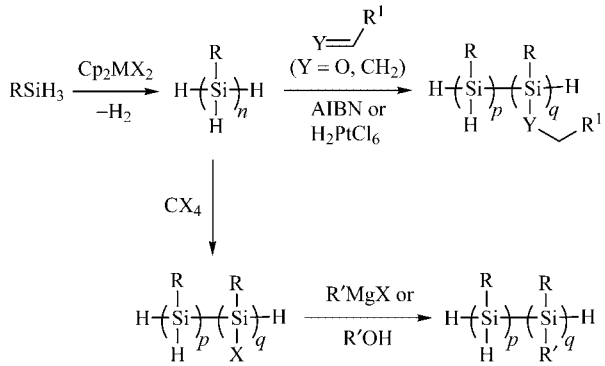

Fig. 4. Conversion of Si—H containing polysilanes.

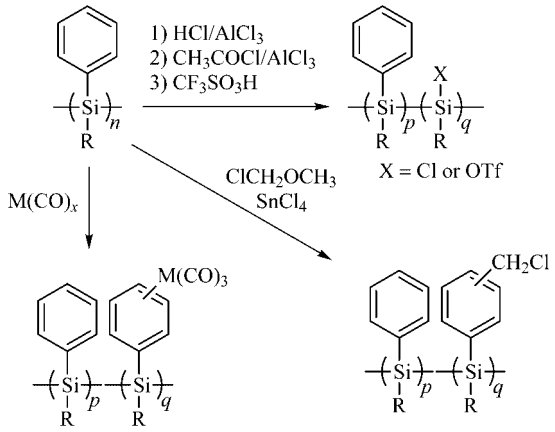

Fig. 5. Functional polysilanes derived from poly(alkylphenylsilane) by one step.

was also achieved under electrolytic conditions using Pt-electrodes (50) and this moderate reaction affords trifluoropropyl-substituted polysilanes (51).

Anionic polymerization of masked disilenes proceeds via a living condition to give polymers having controlled molecular weight (33). Head-to-tail polymers can selectively obtained and polysilanes with functional groups such as diethylamino groups are prepared. However, the masked disilene method is only applicable to the synthesis of non-aromatic-substituted polysilanes.

Ring-opening polymerization of cyclic monomers is initiated either thermally or anionically. Reactive monomers are obtained from $(C_6H_5)_8Si_4$ via dephenylation with HCl or TfOH (see Figs. 5 and 6) and subsequent substitution

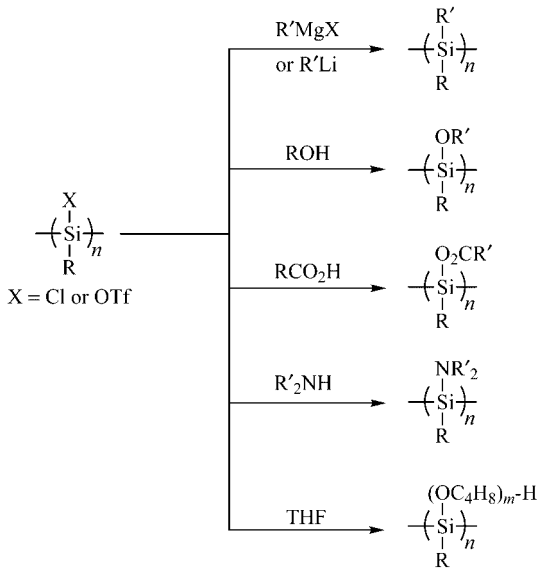

Fig. 6. Functional polysilanes from halogenated- or triflated-polysilanes.

reactions (37). Si_4Cl_8 prepared from $Si_4(C_6H_5)_8$ is found to afford crystalline polymer by thermal ROP (52). The starting monomer and final product can be used as the convenient starting material for polysilanes with functional side groups. ROP of silole-containing cycliopentasilane yields 1,1-silole-*co*-polysilane (53) and ROP of phenylnonomethylcyclopentasilane (54) gives a regular pentad polymer. Base-catalyzed redistribution polymerization of alkoxylated-disilanes is a simple method but offers only networked polymers (55).

Dendritic polysilanes have been prepared by stepwise reactions (56). Copolymerization of dichlorosilane and trichlorosilane yields ladder-type material (57).

Functional Polysilanes

Although severe Wurtz-type coupling reaction conditions destroy most functional groups, some functional polymers have been synthesized. The C=C bonds in the cyclohexenyl group react with HX to afford polysilanes possessing halogen groups (58). Several ethereal group substituted polysilanes (59) and 3,3,3-trifluoropropyl-substituted polysilanes have been prepared by Wurtz coupling at 150°C (60). *N*-carbazoyl-substituted polysilane (61), *p*-aminophenyl-substituted, and *N*-pyrolyl-substituted polysilanes are similarly prepared (62). Polysilanes bearing Si—H groups yield functional polysilanes via H_2PtCl_6-catalyzed hydrosilylation reaction (63) and free-radical reaction (64) or after conversion to Si—Cl groups by reaction with CCl_4, NCS, or $CuCl_2$ (65) (Fig. 4).

Phenyl-substituted polysilanes obtained in high yield are used as the staring material for functional polysilanes. Phenyl groups attached to silicon atoms are selectively replaced by halogen or triflate by $HCl/AlCl_3$ (66), $CH_3COCl/AlCl_3$ (67), or triflic acid (68) (Fig. 5). Functional polysilanes are obtained by the reaction of the halogen- or triflate-substituted polysilanes with nuclepophiles (Fig. 6). The poly(chloromethylphenylalkylsilanes) prepared by $SnCl_4$-catalyzed reaction (69) are useful substrates for diverse functional polysilanes (70) (Fig. 7). Reaction with amines gives polymers having ammonium substituents to prepare LB films (71) (see LANGMUIR–BLODGETT FILMS). Substantial decrease of molecular weight takes place during dephenylation and chloromethylation reactions. Aromatic groups in polysilanes have been studied to prepare arene-type complex with metal carbonyls (Cr, Mo, Mn) (72) but the products are unstable (Fig. 4).

Hybrid-Block Copolymer

Polysilanes are connected with carbon polymers to form A–B and A–B–A type block polymers. Reaction of Li-terminated polystyrene with cyclotetrasilanes (73) or halogen-terminated polysilanes (74), photolysis of polysilanes in carbon monomers (methacrylic monomers) (75), or reaction of halogen-ended polysilanes with poly(ethylene glycol) affords A–B and/or A–B–A type Block Copolymers (qv) (76) (Fig. 8). Comb-like Graft Copolymers (qv) have also been prepared by reaction of triflate-substituted poly(methylphenylsilane) with THF, 2-methyl-2-oxazoline, or isobutyl vinyl ether (77).

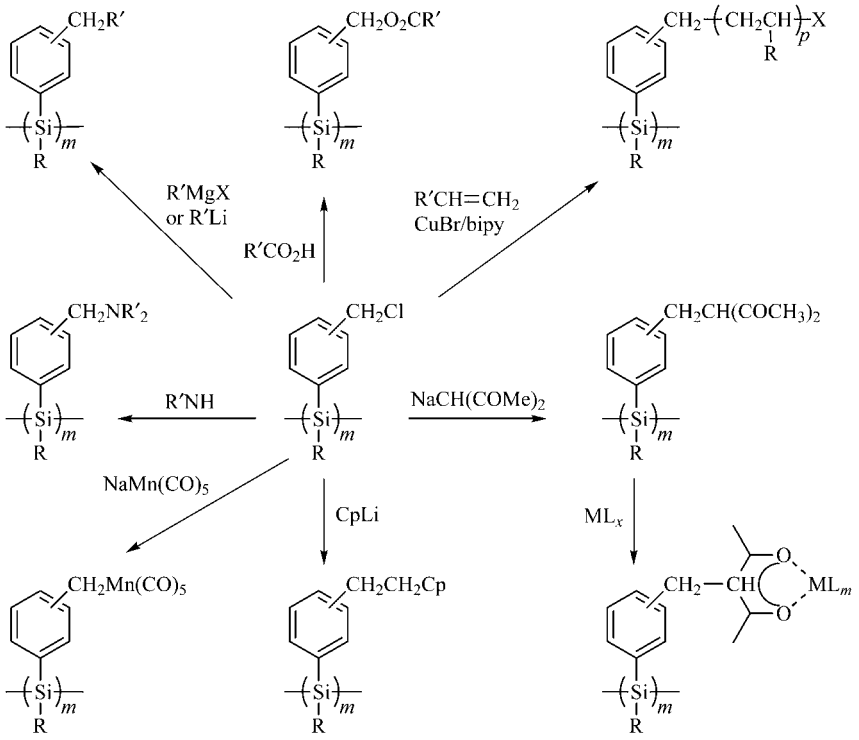

Fig. 7. Functional polysilanes from poly{(chloromethylphenyl)$_m$ethylsilanes}.

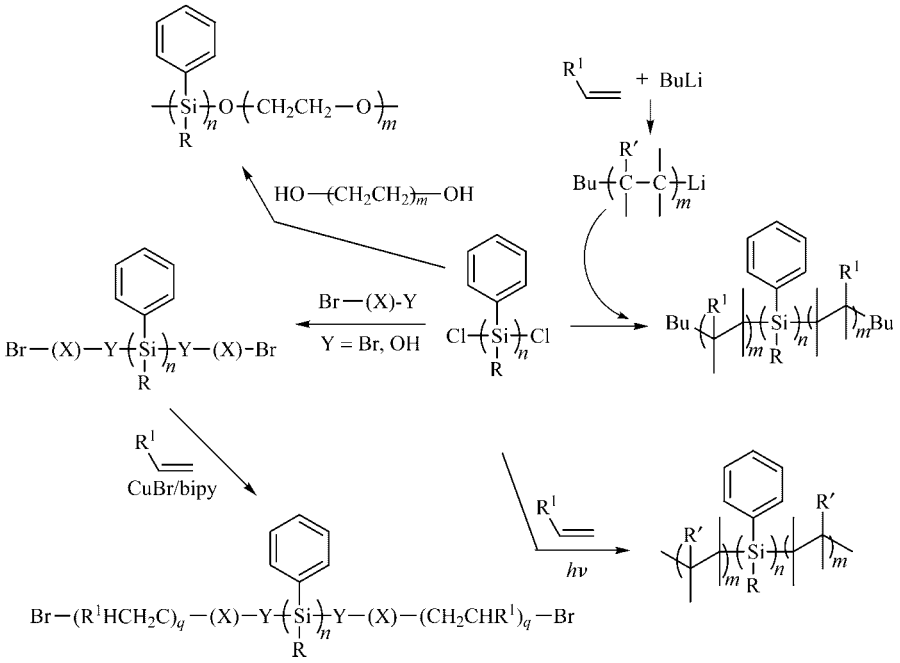

Fig. 8. Block copolymer from α,ω-dichloropoly(methylphenylsilane).

Unquenched product of masked disilene polymerization is used as the initiator of carbon monomers (78) (eq. 2).

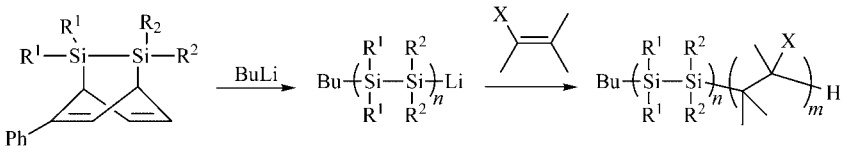

(2)

Atom transfer radical polymerization catalyzed by CuBr-bipyridyl is applied to polysilanes with chloromethylated-phenyl groups to prepare comb-like copolymer via the side groups (79) or 4-chloromethylphenylethyl-terminated polysilanes to give A–B–A type polymers (Fig. 8) (80).

Photoreactions

Strong absorption of polysilanes in the UV region makes these materials suitable for application to photo (81) and X-ray lithography (82). Photo-bleaching by UV irradiation indicates scission as the major process for most polysilanes; scission proceeds via silyl radical and/or silylene (R_2Si:) extrusion (Fig. 9) (83).

Dry process with oxygen plasma etching has been studied (84,85). UV-irradiation of polysilanes converts the Si—Si bonds to Si—O—Si bonds selective and efficiently. The resultant siloxane-bonded products are flexible and have different refractive indexes. They interact with polar materials and then are utilized for color filter and microlens production via a sol–gel process (86), depositing metals for electric circuits (87), wave guides, or optical recording (Fig. 10) (88).

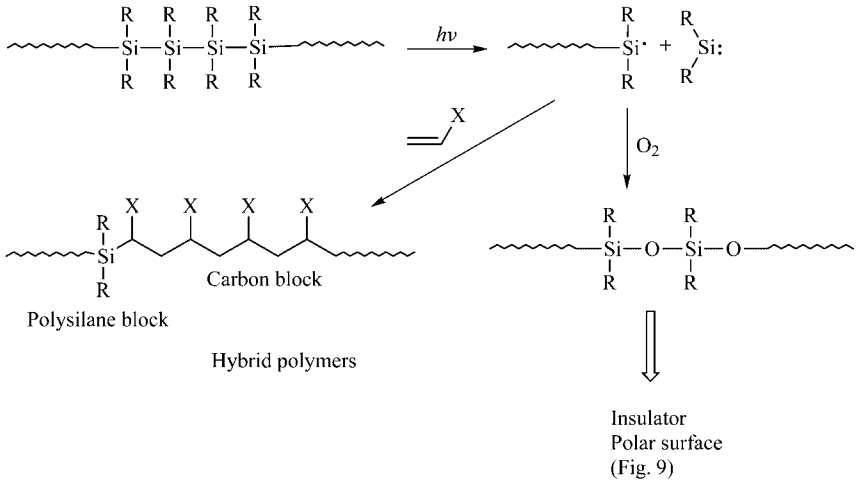

Fig. 9. Photochemical process of polysilanes.

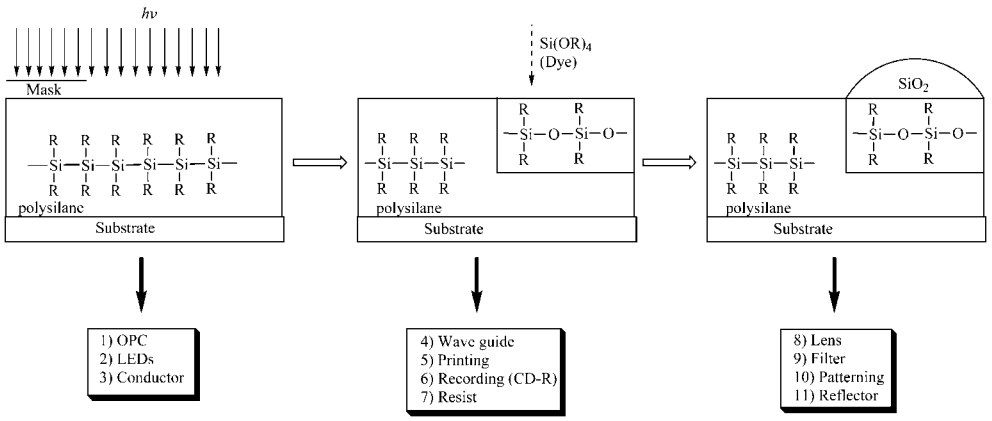

Fig. 10. Possible application of polysilanes.

Carrier Mobility and OPC

Most polysilanes show high photoconductivity, which has stimulated research of applications as organic photoconductors (OPC) in zerography. Carrier generation is, however, poor. Time-of-flight (TOF) studies revealed that holes are almost the sole carrier for most polysilanes (89) and the mobility ($\approx 10^{-4}$ cm^{-2}/V·s) is 2–3 order higher than most carbon polymers ($\approx 10^{-7}$cm^2/V·s) (Table 4).

Table 4. Ionization Potential and Hole Drift Mobility of Polysilanes

Polysilane	$10^{-3}\,M_w$	Ip,eV	μ, cm^2/V·s	Reference
$(CH_3—Si—CH_3)$		5.73		90
$(Bu)_2Si$		5.7	5.3	91
$(Pen)_2Si$		5.9		91
$(Hex)_2Si$		5.8	4.5	91
$(p\text{-}Bu—O—C_6H_5)_2Si$		5.5	4	91
$CH_3—Si—C_6H_5$	69	5.6	3.5×10^{-4}	92
$CH_3—Si—p\text{-}Tolyl$	9.5	5.45	32.3×10^{-5}	92
$CH_3—Si—C_6H_4—C_6H_5$	77	5.59	2.5×10^{-5}	92
$CH_3—Si—Pr$	71	5.66	1.4×10^{-4}	92
$CH_3—Si—CH_2CH_2C_6H_5$	210	5.64		92
$CH_3—Si\text{-}c\text{-}Hex$	120	5.59		92
$Pr—Si\text{-}Hex$	150	5.62		92
$CH_3—Si—Si(CH_3)_2C_6H_5$	180	5.85		92
$CH_3—Si—Si(CH_3)_2(p\text{-}Tolyl)$	19	5.52		92
$CH_3—Si—Si(CH_3)_2(o\text{-}Tolyl)$	8.4	5.57		92
$(CH_3—Si—CH_3)_n(CH_3—Si—C_6H_5)_m$	71	5.67	3.5×10^{-4}	92
$(CH_3—Si—CH_3)_n(CH_3—Si—CH_2CH_2C_6H_5)_m$	48	5.84	4.7×10^{-7}	92
$(CH_3—Si\text{-}c\text{-}Hex)_n(CH_3—Si—C_6H_5)_m$	3.7	5.79	1.3×10^{-5}	92
$CH_3—Si\text{-}c\text{-}Hex)_n(CH_3—Si\text{-}p\text{-}Tolyl)_m$	28	5.57		92
$CH_3—Si\text{-}Hex)_n(CH_3—Si—C_6H_5)_m$	2.9	5.77		92
$(CH_3—Si—C_6H_5)_n(CH_3—Si\text{-}p\text{-}Tolyl)_m$	2.9	5.79	4.5×10^{-5}	92
$((CH_3)_2Si—SiCH_3C_6H_5)_n$	900	5.64	$6.0 \times 10^{-}$	92

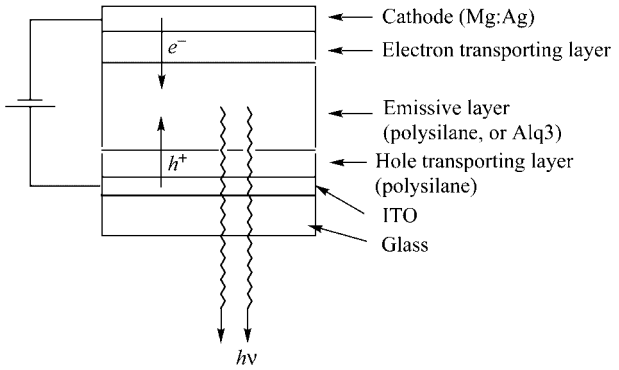

Fig. 11. Structure of LEDs. Polysilanes are used as hole transport layer or emissive layer.

Triarylamino-moieties as the side group or the additives enhance the mobility (93). However, electron mobility is observed only for poly{bis(butylphenyl)silane}, probably because of the localization of electrons along the main chain while holes are delocalized over side groups (94). Because carriers migrate by hopping among σ-conjugated domains (>10–15 Si units), the main-chain orientation (ordering) of the polysilane, in addition to maximizing σ-delocalization by controlling the conformation, is important for higher mobility (95). Ultra-drawing (96), mechanical deposition (97), the LB method (98), rubbing (99), dipping under constant air flow, vacuum deposition (100) as well as well as casting under strong electric field (101), weak electric field (102), or magnetic field (103) have been used to make oriented polysilane films (see FILMS, ORIENTATION).

Electroluminescence

High fluorescence quantum efficiency and high carrier mobility are advantages for the application of polysilanes as the emitting material of (LEDs). Single-layer LEDs by using poly(dimethylsilane) (104), poly(methylphenylsilane) (105), and poly(dialkylsilane) [$(C_4H_9)_2Si$, $(C_5H_{11})_2Si$, $(C_6H_{13})_2Si$] (106) have been reported. External quantum efficiency is, howevder, less than 10^{-4}%. Low efficiency is attributable to the poor efficiency of electron injection. Light is emitted from near polysilane–cathode interface because of low electron mobility. Most polysilane LEDs emit UV light only at low temperature (<200 K) and visible light is dominant in many cases (107). LEDs using carefully prepared poly(methylphenylsilane) (branching point-free) emit almost pure UV light similar to photoluminescence (108). Poly{bis(4-butylphenyl)silane-LEDs show high external quantum efficiency (0.1%) (109). Polysilanes are also used as the hole injection material for multilayer LEDs [anode: TPD:AlQ_3:polysilane:cathode] (110) or mixed with Eu^{3+} complex (111) or ALQ_3 (112) for full-color LEDs (Fig. 11).

Conductivity

Undoped polysilanes are insulating (113) [polysilastyrene ($<10^{-12}$S/cm), $(CH_3{-}Si{-}C_6H_5)_n$; 1×10^{-6} S/cm, $((CH_3)_2N{-}C_6H_4{-}Si{-}CH_3)$; 2×10^{-3} S/cm,

$\{(CH_3{-}Si{-}C_6H_4{-}N(CH_3)_2P)_m(CH_3{-}Si{-}CH_2CH_2{-}C_6H_4{-}NCH_3{}^P)_n\}$; 2×10^{-3} S/cm], ($C_6H_{13}{-}Si{-}C_6H_{13}$; 9×10^{-7} S/cm)]. Doping with a strong oxidant (AsF_5, SbF_5) increases conductivity up to 0.5 S/cm. Polysilanes with amino substituents (*p*-dimethylaminophenyl, pyrolylethyl, bis-pyrolylethyl) become conductive as high as 10^{-2} S/cm^2 on I_2-doping (114). Doped polysilanes are usually moisture- and air-sensitive and polymer degradation occurs.

BIBLIOGRAPHY

"Polysilanes and Polycarbosilanes" in *EPSE* 2nd ed., Vol. 13, pp. 162–186, by P. Trefonas, Monsanto Eletronic Materials Co.

1. R. D. Miller and J. Michl, *Chem. Rev.* **89**, 1359 (1989).
2. P. Trefonas, *Encycl. Polym. Sci. Eng.* **13**, 162 (1987).
3. C. G. Pitt, L. L. Jones, and B. G. Ramsey, *J. Am. Chem. Soc.* **94**, 3806 (1972).
4. F. Neuman, H. Teramae, J. W. Downing, and J. Michl, *J. Am. Chem. Soc.* **120**, 573 (1998).
5. S. Mazieres, M. K. Raymond, G. Raabe, A. Porodi, and J. Michl, *J. Am. Chem. Soc.* **119**, 6682 (1997); J. B. Lambert, J. L. Pflug, and J. M. Denari, *Organometallics* **15**, 615 (1996); A. Sekiguchi, M. Nanjo, C. Kabuto, and H. Sakurai, *J. Am. Chem. Soc.* **117**, 4196 (1995); H. Suzuki, Y. Kimata, S. Satoh, and A. Kuriyama, *Chem. Lett.* 293 (1995).
6. R. Zink, T. F. Magnera, and J. Michl, *J. Phys. Chem. A.* **104**, 3824 (2000).
7. K. Tamao, H. Tsuji, M. Terada, M. Asahara, S. Yamaguchi, and A. Toshimitsu, *Angew. Chem., Int. Ed. Engl.* **39**, 3287 (2000).
8. J. Michl and R. West, in R. G. Jones, W. Ando, and J. Chojnowski, eds., *Silicon Containing Polymers*, Kluwer Academic Publishers, Dordrecht, 2000, Chapt. "18".
9. F. H. Schilling, F. A. Bovey, A. J. Lovinger, and J. M. Zeigler, *Silicon-Based Polymer Science. A Comprehensive Resource* (Advances in Chemistry Series 224), American Chemical Society, Washington, D.C., 1990, Chapt. "21", p. 341.
10. K. Oka, T. Dohmaru, and R. West, 33rd Organosilicon Symposium, Saginaw, USA, 2000, Abstr. PA43.
11. M. Fujiki, *J. Am. Chem. Soc.* **118**, 7425 (1996).
12. A. J. Lovinger, D. D. Davis, F. C. Schilling, F. J. Padden Jr., and F. A. Bovey, *Polym. Prepr.* **31**, 263 (1990).
13. J. Lovinger, D. D. Davis, F. C. Schilling, and F. A. Bovey, and J. M. Zeigler, *Macromolecules* **22**, 356 (1989).
14. F. C. Schilling, J. Lovinger, J. M. Zeigler, D. D. Davis, and F. A. Bovey, *Macromolecules* **22**, 3055 (1989).
15. H. Kuzmany, J. F. Rabolt, B. L. Farmer, and R. D. Miller, *J. Chem. Phys.* **85**, 7417 (1986).
16. R. D. Miller, J. F. Rabolt, R. Sooriyakumaran, G. N. Ficks, B. L. Farmer, and H. Kuzmany, *Polym. Prepr.* **27**, 422 (1987).
17. T. Asuke and R. West, *J. Inorganic Organomet. Polym.* **4**, 45 (1994); S. S. Bukalov, L. A. Leites, R. West, and T. Asuke, *Macromolecules* **29**, 907 (1996).
18. C. H. Yuan and R. West, *Macromolecules* **27**, 629 (1994); C. H. Yuan and R. West, *Macromolecules* **26**, 2645 (1993).
19. S. S. Bukalov, L. A. Leites, R. West, and T. Asuke, *Macromolecules* **29**, 907 (1996); T. Kanai, H. Ishibashi, Y. Hayashi, T. Ogawa, S. Furukawa, R. West, T. Dohmaru, and K. Oka, *Chem. Lett.*, 650 (2000).

20. F. C. Schilling, F. A. Bovey, D. D. Davis, A. J. Lovinger, and R. B. Macgregor, *Macromolecules* **22**, 4645 (1989).
21. K. Oka, N. Fujiue, S. Nakanishi, T. Takata, T. Dohmaru, C. H. Yuan, and R. West, *Chem. Lett.* 253 (1997).
22. C. H. Yuan and R. West, *J. Chem. Soc., Chem. Commun.*, 2293 (1995).
23. M. Fujino, T. Hisaki, and N. Matsumoto, *Macromolecules* **28**, 5017 (1995).
24. M. Fujiki, *Chem. Phys. Lett.* **198**, 177 (1992); Y. Kanemitsu, K. Suzuki, S. Kyushin, and H. Matsumoto, *Synth. Met.* **69**, 585 (1995).
25. H. Ishii, A. Yuyama, S. Narioka, K. Seki, S. Hasegawa, M. Fujino, H. Isaka, M. Fujiki, and M. Matsumoto, *Synth. Met.* **69**, 595 (1995).
26. K. Seki, A. Yuyama, S. Narioka, H. Ishii, S. Hasegawa, H. Isaka, M. Fujino, M. Fujiki, and N. Matsumoto, *Polymeric Materials for Microelectronic Applications* (ACS Symposium Series 579), American Chemical Society, Washington, D.C., 1994, pp. 398–407, and references therein.
27. T. Kanai, S. Furukawa, Y. Maeda, Y. Hayashi, K. Oka, T. Dohmaru, and R. West, *J. Phys. Condens. Matter* **10**, 883 (1998).
28. T. Dohmaru, K. Oka, T. Yajima, M. Miyamoto, Y. Nakayama, and T. Kawamura, *Philos. Mag. B* **71**, 1069 (1995).
29. K. Takeda, N. Matsumoto, and M. Fukuchi, *Phys. Rev. B* **31**, 2114 (1984).
30. V. F. Trven and R. West, *J. Am. Chem. Soc.* **85**, 6824 (1973); H. Sakurai, M. Kira, and T. Uchida, *J. Am. Chem. Soc.* **95**, 6826 (1973).
31. M. Fukushima, Y. Hamada, E. Tabei, M. Aramata, S. Mori, and Y. Yamamoto, *Chem. Lett.* 347 (1998).
32. F. Gauvin, J. F. Harrod, and H. G. Woo, *Adv. Organomet. Chem.* **42**, 363 (1998); T. D. Tilley, *Acc. Chem. Res.* **26**, 22 (1993).
33. K. Sakamoto, K. Obata, H. Hirata, M. Nakajima, and H. Sakurai, *J. Am. Chem. Soc.* **111**, 7641 (1989).
34. H. Sakurai, and M. Yoshida, in R. G. Jones, W. Ando, and J. Chojnowski, eds., *Silicon Containing Polymers*, Kluwer Academic Publishers, Dordrecht, 2000, Chapt. "13", p. 375.
35. M. Went, H. Sakurai, and T. Sanji, in R. G. Jones, W. Ando, and J. Chojnowski eds., *Silicon Containing Polymers*, Kluwer Academic Publishers, Dordrecht, 2000, Chapt. "15", p. 415.
36. M. Cypryk, Y. Gupta, and K. Matyjaszewski, *J. Am. Chem. Soc.* **113**, 1046 (1991).
37. E. Fossum and K. Matyjaszewski, in R. G. Jones, ed., *Silicon-Containing Polymers*, The Royal Society of Chemistry, Cambridge, U.K., 1995, p. 115.
38. H. Watanabe, M. Abe, K. Sonoda, M. Uchida, Y. Ishikawa, and M. Inoyama, *J. Mater. Chem.* **1**, 483 (1991); K. Kabeta, S. Wakamatsu, and T. Imai, *Chem. Lett.* 835 (1994).
39. K. Matyjaszewski, *Polym. Prepr.* **28**, 224 (1987); S. Guthier and D. J. Worsfold, *Macromolecules* **22**, 2213 (1989).
40. R. D. Miller and P. K. Jenkner, *Macromolecules* **27**, 5921 (1994).
41. J. M. Zeigler, *Polym. Prepr.* **27**, 109 (1986).
42. K. Oka, M. Fukudome, T. Dohmaru, and R. West, *Electrophotography* **34**, 386 (1995).
43. P. K. Jenkner, H. Suzuki, and R. D. Miller, *Polym. Prepr.* **3**, 500 (1994).
44. J. M. Zeigler, L. I. McLaughlin, and R. J. J. Perry, *Inorg. Organomet. Polym.* **1**, 531 (1991).
45. G. J. Price, R. West, and J. Peter, *Polymer* **37**, 3975 (1996).
46. R. G. Jones, U. Budnik, S. Holder, W. K. Wong, and K. C. William, *Macromolecules* **29**, 8036 (1996).
47. S. Kashimura, M. Ishifune, N. Yamashita, H. B. Bu, M. Takebayashi, S. Kitajima, D. Yoshiwara, Y. Kataoka, R. Nishida, S. Kawasaki, H. Murase, and T. Shono, *J. Org. Chem.* **64**, 6615 (1999).

48. V. K. Dioumaev and J. F. Harrod, *J. Organomet. Chem.* **521**, 13 (1996).
49. H. Qui and Z. Du, *J. Polym. Sci., Part A: Polym. Chem. Ed.* **27**, 2861 (1989).
50. Y. Kimata, H. Suzuki, S. Satoh, and A. Kuriyama, *Chem. Lett.* **7**, 1163 (1994).
51. J. P. Banovetz, H. Suzuki, and R. M. Waymouth, *Organometallics* **12**, 4700 (1993).
52. J. R. Koe, D. R. Powell, J. J. Buffy, S. Hayase, and R. West, *Angew. Chem., Int. Ed. Engl.* **37**, 1441 (1998).
53. T. Sanji, T. Sakai, C. Kabuto, and H. Sakurai, *J. Am. Chem. Soc.* **120**, 4552 (1998).
54. M. Suzuki, J. Kotani, S. Gyobu, T. Kaneko, and T. Saegusa, *Macromolecules* **27**, 2360 (1994).
55. H. Watanabe, M. Abe, K. Sonoda, M. Uchida, Y. Ishikawa, and M. Inoyama, *J. Mater. Chem.* **1**, 483 (1991).
56. M. Nanjo, T. Sunaga, A. Sekiguchi, and E. Horn, *Inorg. Chem. Commun.* **2**, 203 (1999); J. B. Lambert, J. L. Pflug, and J. M. Denari, *Organometallics* **15**, 615 (1996).
57. S. Kyushin, H. Sakurai, H. Yamaguchi, and H. Matsumoto, *Chem. Lett.* 331 (1996).
58. H. Stuger and R. West, *Macromolecules* **18**, 2349 (1985).
59. J. S. Hrkach and K. Matyjaszewski, *J. Polym. Sci., Polym. Chem.* **32**, 1949 (1994); K. Oka, N. Fujiue, S. Nakanishi, T. Takata, T. Dohmaru, and R. West, *Chem. Lett.* 875 (1995); C. H. Yuan and R. West, *Macromolecules* **26**, 2645 (1993); L. A. MoSchwegler and M. Moller, *Acta Polym.* **48**, 319 (1997); T. J. Cleij, L. W. Jenneskens, and S. G. J. M. Kluijman, *Adv. Mater.* **9**, 961 (1997).
60. M. Fujino, T. Hisaki, M. Fujiki, and N. Matsumoto, *Macromolecules* **25**, 1079 (1992).
61. E. Tabei, M. Fukushima, and S. Mori, *Syntt. Met.* **73**, 113 (1995).
62. M. Fukushima, E. Tabei, M. Aramata, Y. Hamada, S. Mori, and Y. Yamamoto, *Synth. Met.* **96**, 239 (1998); M. Kakimoto, H. Ueno, H. Kojima, Y. Yamaguchi, and A. Nishiura, *J. Polym. Sci., Part A: Polym. Chem.* **34**, 2735 (1996).
63. H. Y. Qiu and Z. D. Du, *J. Polym. Sci., Part A: Polym. Chem.* **27**, 2849 (1989).
64. Y. Hsiao and R. M. Waymouth, *J. Am. Chem. Soc.* **116**, 9779 (1994).
65. J. P. Banovertz, Y. Hsiao, and R. M. Waymouth, *J. Am. Chem. Soc.* **115**, 2540 (1993).
66. R. West, *J. Organomet. Chem.* **300**, 327 (1986).
67. U. Herzog and R. West, *Macromolecules* **32**, 2210 (1999).
68. W. Uhlig, *J. Organomet. Chem.* **402**, C45 (1991); W. Uhlig, *J. Organomet. Chem.* **516**, 147 (1996); W. Uhlig, *Chem. Ber.* **129**, 733 (1996); K. Matyjaszewski, J. S. Hrkach, B. Marciniec, and M. Lewandowski, *J. Inorg. Organomet. Polym.* **5**, 183 (1995).
69. J. M. Zeigler, *Polym. Prepr.* **27**, 109 (1986).
70. R. G. Jones, R. E. Benfield, S. Holder, and A. C. Swain, in R. G. Jones, ed., *Silicon-Containing Polymers*, Royal Society of Chemistry, Cambridge, U.K., 1995, p. 132.
71. T. Seki, T. Tamaki, and K. Ueno, *Macromolecules* **21**, 3948 (1992); T. Seki, T. Tamaki, and K. Ueno, *J. Photopolym. Sci.* **6**, 113 (1993).
72. A. J. Wiseman, R. G. Jones, A. C. Swain, and M. J. Went, *Polymer* **37**, 5727 (1996).
73. E. Fossum, J. A. Love, and K. Matyjazeswki, *J. Organomet. Chem.* **499**, 253 (1995).
74. S. Demoustier-Champagne, A. F. de Mashiee, J. Devaux, and R. Fayt, *J. Polym. Chem.* **31**, 2009 (1993).
75. K. Matsukawa, S. Fukui, N. Higashi, M. Niwa, and M. Inoue, *Chem. Lett.* 1073 (1999); K. Matsukawa, M. Ishikawa, and H. Inoue, *Chem. Lett.* 332 (2000).
76. S. J. Holder, R. C. Hiorns, N. A. J. M. Sommerdijk, J. S. J. Williams, R. G. Jones, and R. J. M. Nolte, *J. Chem. Soc., Chem. Commun.* 1445 (1998).
77. K. Matyjaszewski, J. S. Hrkach, B. Marciniec, and M. J. Lewandowski, *J. Inorg. Organomet. Polym.* **5**, 183 (1995).
78. K. Sakamoto, Y. Fonada, M. Yoshida, and H. Sakurai, *J. Am. Chem. Soc.* **111**, 7641 (1989); T. Sanji, Y. Nakatsuka, F. Kitayama, and H. Sakurai, *Chem. Commun.* 2201 (1999); T. Sanji, Y. Nakatsuka, S. Ohnishi, and H. Sakurai, *Macromolecules* **33**, 1174 (2000).

79. R. G. Jones and S. J. Holder, *Macromol. Chem. Phys.* **198**, 3571 (1997).
80. L. Lutsen, G. P. G. Cordina, and R. G. Jones, *Eur. Polym. J.* **34**, 1829 (1998).
81. G. M. Wallraff, R. D. Miller, M. Baier, E. J. Ginsburg, and R. R. Kunz, *J. Photopolym. Sci. Technol.* **5**, 111 (1992).
82. A. Yamaguchi, T. Ogawa, H. Tachibana, H. Oizumi, T. Soga, M. Matsumoto, T. Matsuzaka, and E. Takeda, *J. Electrochem. Soc.* **143**, 657 (1996).
83. A. Wolf and R. West, *Appl. Organomet. Chem.* **1**, 7 (1987).
84. R. D. Miller, D. Hoofer, D. R. MaCKean, C. G. Willson, R. West, and P. Trefonas III, in L. Thompson, C. G. Willson, and J. M. Frechet, eds., *Materials for Microlithography* (ACS Symposium Series 266), American Chemical Society, Washington, D.C., 1984, p. 293.
85. J. M. Zeigler, L. A. Harrah, and A. W. Jonson, *SPIE* **539**, 166 (1985).
86. Y. Sakurai, Y. Tachibana, T. Koura, and M. Yokoyama, *Chem. Lett.* 167 (1996).
87. M. Fukushima, Y. Hamada, E. Tabei, M. Aramata, S. Mori, and Y. Yamamoto, *Chem. Lett.*, 347 (198).
88. N. Nagayama, Y. Tachibana, and M. Yokoyama, *Bull. Chem. Soc. Jpn.* **71**, 2205 (1998).
89. M. A. Abkowitz, M. Stolka, R. J. Weagley, K. M. McGrane, and F. E. Knier, *Silicon-Based Polymer Science* (Advances in Chemistry Series 224), American Chemical Society, Washington, D.C., 1990, p. 467.
90. K. Yokoyama and M. Yokoyama, *Solid State Commun.* **70**, 241 (1989).
91. N. Matsumoto, H. Suzuki, and H. Miyazaki, in B. R. G. Jones, W. Ando, and J. Chojnowski, eds., *Silicon-Containing Polymers*, Kluwer Academic Publishers, Dordrecht, 2000, pp. 531–552.
92. T. Dohmaru, K. Oka, T. Yajima, M. miyamoto, Y. Nakayama, T. Kawamura, and R. West, *Philos. Mag. B* **71**, 1069 (1995).
93. K. Yokoyama and M. Yokoyama, *Chem. Lett.* 1005 (1989).
94. J. Kumagai, H. Tachikawa, H. Yoshida, and T. Ichikawa, *J. Phys. Chem.* **100**, 16777 (1996).
95. H. Okumoto, T. Yatabe, M. Shimomura, A. Kaito, and N. Minami, *Synth. Met.* **121**, 1507 (2000).
96. G. P. van der Laan, M. P. de Haas, H. A. H. Frey, S. Sheiko, and M. Moeller, *Macromolecules* **27**, 1897 (1994).
97. N. Tanigaki, K. Yase, and K. Ueno, *Polymer* **36**, 2477 (1995).
98. F. W. Embs, G. Wagner, D. Neher, P. Albouy, and R. D. Miller, *Macromolecules* **24**, 5068 (1991); R. Kani, H. Yoshida, Y. Nakano, S. Murray, Y. Mori, Y. Kawaka, and S. Hayase, *Langmuir* **9**, 3045 (1993).
99. H. Tachibana, M. Matsumoto, and Y. Tokura, *Macromolecules* **26**, 2520 (1993).
100. S. Furukawa, M. Obata, M. Tamura, and H. Fujishiro, *Solid State Commun.* **84**, 475 (1992).
101. Y. Nakayama, K. Hirooka, and R. West, *Solid State Commun.* **100**, 759 (1996).
102. Y. Nakayama, K. Hirooka, and R. West, *Appl. Phys. Lett.* **67**, 638 (1995).
103. T. Nakamura, H. Nakagawa, K. Oka, H. Naito, I. Mogi, I. Watanabe, and T. Dohmaru, *Solid State Commun.* **106**, 447 (1998).
104. R. Hattori, T. Sugano, J. Shirafuji, and T. Fujiki, *Jpn, J. Appl. Phys.* **11B**, L1509 (1996).
105. H. Suzuki, *Adv. Mater.* **8**, 657 (1996).
106. N. Matsumoto, H. Suzuki, and H. Miyazaki, in R. G. Jones, ed., *Silicon-Containing Polymers*, Royal Society of Chemistry, Cambridge, U.K., 1995, Chapt. "19". p. 531.
107. Y. Kanemitsu, K. Suzuki, S. Kyushin, and H. Matsumoto, *Synth. Met.* **69**, 585–586 (1995); K. Suzuki, Y. Kanemitsu, S. Kyushin, and H. Matsumoto, *ACS Symp. Ser.* **579**, 425 (1994).
108. Y. Xu, T. Fujino, H. Naito, K. Oka, and T. Dohmaru, *Chem Lett.* 299 (1998).

109. C. H. Yuan, S. Hoshino, S. Toyoda, H. Suzuki, M. Fujiki, and N. Matsumoto, *Appl. Phys. Lett.* **71**, 326 (1997).
110. J. Kido, K. Nagai, Y. Okamoto, and T. Skotheim, *Appl. Phys. Lett.* **59**, 2760 (1991); H. Suzuki, H. Meyer, S. Hoshino, and D. Haarer, *J. Lumin.* **66/67**, 423 (1995).
111. J. Kido, *Chem. Lett.* 1267 (1991).
112. J. Kido, *Appl. Phys. Lett.* **59**, 2760 (1991).
113. R. West, *J. Organomet. Chem.* **300**, 327 (1986).
114. E. Tabei, M. Fukushima, and S. Mori, *Synth. Met.* **73**, 113 (1995); M. Fukushima, E. Tabei, M. Aramata, Y. Hamada, S. Mori, and Y. Yamamoto, *Synth. Met.* **96**, 239 (1998).

KUNIO OKA
Osaka Prefecture University

POLYSULFIDES. See Volume 3.

POLYSULFONES. See Volume 4.

POLYTETRAFLUORETHYLENE. See PERFLUORINATED POLYMERS.

POLYTRIACETYLENE. See DIACETYLENE AND TRIACETYLENE POLYME.

POLY(TRIMETHYLENE TEREPHTHALATE). See Volume 3.

POLYURETHANES. See Volume 4.

POLY(VINYL ACETATE). See VINYL ACETATE POLYMERS.

POLY(VINYL ALCOHOL). See VINYL ALCOHOL POLYMERS.

POLYVINYLCARBAZOLE. See VINYLCARBAZOLE POLYMERS.

POLY(VINYL CHLORIDE). See VINYL CHLORIDE POLYMERS.

POLY(VINYL ETHER). See VINYL ETHER POLYMERS.

POLY(VINYL FLUORIDE). See VINYL FLUORIDE POLYMERS.

POLY(VINYLIDENE CHLORIDE). See VINYLIDENE CHLORIDE POLYMERS.

POLY(VINYLIDENE FLUORIDE). See VINYLIDENE FLUORIDE POLYMERS.

POLYVINYLPYRROLIDINONE. See VINYL AMIDE POLYMERS.

POM. See ACETAL RESINS.

PRESSURE-SENSITIVE ADHESIVES. See Volume 4.

PROTEIN FOLDING

Introduction

Protein folding is one of the most important processes that are vital for the existence of every living system. The correctly folded state of proteins is essential for the tremendous array of protein functions at all levels of complexity, from the subcellular machinery to organs and macroscopic structural elements. A very incomplete list of protein functions includes their activity as enzymes (biocatalysts), sensors of chemical and physical signals, regulators of expression of the genetic information, structural building blocks (ranging from the microscopic cytoskeleton to the macroscopic fingernails and hair), and mediators of the immunological phenomenon (as antibodies, receptors, and antigen-presenting agents).

As correct protein folding is required for normal cell function, protein *mis*folding has grave consequences. An incorrect folded state of proteins is the hallmark of a large number of diseases of unrelated origin, some of which are the most common diseases in the western society. Such diseases include cystic fibrosis, the most common genetic disease in the Caucasian population, amyloid diseases, including Alzheimer's disease and Type II diabetes, and infectious prion diseases such as bovine spongiform encephalopathy—"the mad cow disease." Since amyloid diseases, are age-related, and the average age of the population will increase significantly in the next decades, the prevalence of such diseases is predicted to increase accordingly.

The "protein-folding problem" is related to the determination of how and why a protein of a given amino acid sequence adopts a certain three-dimensional structure. A recent extension to the problem includes the question of how and why a protein adopts the misfolded or unfolded conformations. This article describes the different hierarchies of protein folding, the classical models and current

Encyclopedia of Polymer Science and Technology. Copyright John Wiley & Sons, Inc. All rights reserved.

understanding of the folding process through defined pathways or funnels, the assistance of molecular chaperons in the folding process, the experimental methodologies that are being used for the study of protein folding, and the attempts and advances in the prediction of secondary and tertiary structures of proteins. Finally, the article will describe recent advancements in the understanding of protein unfolding and misfolding.

Proteins as Polymers

Proteins are generally composed of a linear combination of the 20 naturally occurring L-α-amino acids (see PROTEINS), and are thereby *polyamides*. The polymerization of the amino acids occurs through the formation of an amide linkage between the carboxyl group of given amino acid and the amino group of the next amino acid, with the resultant elimination of a molecule of water. This amide linkage is more commonly called a peptide bond and proteins are polypeptides. The molecular basis for the enormously diverse functions of the proteins is the significant diversity of their building blocks. The chemical nature of the 20 natural amino acids is extremely versatile. The side chain of the amino acids can be either negatively or positively charged, polar, aliphatic (branched or unbranched), or aromatic (substituted or nonsubstituted). It may include various functional groups such as thiol, amine, hydroxyl, carboxyl, phenyl, and amide groups. Furthermore, the properties of this biopolymer are a result of the amino acid sequence, that is, the linear arrangement of the building blocks, rather than the composition of the protein. Two proteins with the very same amino acid composition may be completely different in their folded-state and molecular properties.

Therefore, it is clear that the polymerization of a protein must be directed by a specific molecular plan, rather than a random polymerization process. The information for the polymerization of a linear sequence of a given protein is encoded in the DNA, which is transcribed to a messenger RNA, which is in turn translated into the protein polymer by cellular ribosomes (see POLYNUCLEOTIDES; GENETIC METHODS OF POLYMER SYNTHESIS). A typical length of a protein can range from tens to thousands of building blocks. Shorter polymers composed of amino acids (from 2 to around 40 amino acids long) are usually termed peptides. Some of the peptides are products of cleavage of longer ribosome-translated precursor. Other peptides (usually those shorter than 10 amino acids) may be synthesized by cellular enzymes, each devoted to the synthesis of one specific peptide. In many cases, those short peptides may be composed of amino acids that are different from the 20 naturally occurring amino acids. These peptides may be composed of nonnatural amino acids or D-α-amino acids. Moreover, ribosome-synthesized proteins may have building blocks that are different from the 20 natural amino acids. This is due to post-translational modifications (such as the enzymatic formation of hydroxyproline by the prolyl hydroxylase protein enzyme).

The incredible degree of diversity presented by proteins can be appreciated by the calculation of the number of linear combinations available even for very short proteins. For a very small protein of 50 amino acids, the number of linear combinations of the 20 natural amino acids is about 10^{65}. For a more typical-sized protein of 200 amino acids, the number of linear combinations is more than 10^{260}.

All these calculations are done without taking into account any post-translational modifications. This immense magnitude of structural diversity is the core of the central role of proteins in all living systems.

The Structures of Proteins

The structures of proteins are usually described in four levels of organization: primary, secondary, tertiary, and quaternary. In the context of the protein-folding question the secondary and tertiary structures are the most important.

Primary Structure. This is the linear amino acid sequence of the polypeptide chain as described above. Primary structure is usually denoted by either one- or three-letter conventional codes. Determination of the primary structure of proteins was performed for many years by the N-terminal sequencing that was developed by Frederick Sanger for which he received his first Nobel Prize in Chemistry in 1958. (His second Nobel Prize in 1980 was for the development of DNA-sequencing techniques.) This method is based on the Edman degradation reaction that removes the N-terminal amino acid of the protein chain, leaving a new N-terminus on the chain. The identity of the removed amino acid is then determined by HPLC analysis. In the last few years, there has been an increased tendency to use mass spectrometry techniques to determine the sequence of proteins. These sequencing procedures are based on tandem mass spectrometry (MS/MS) in which proteins, or more commonly protein fragments, are further fragmented in the mass spectrometer by collision with gas molecules. This results in an ensemble of many molecules with defined differences in mass. The high accuracy of the mass spectrometers and the ability to specifically select a precursor ion (through an ion trap or a quadrupole) allow the determination of the amino acid sequence of the chain. Only two amino acids could not be distinguished using conventional MS techniques. These are leucine and isoleucine, which have the same molecular mass. However, recent techniques such as TOF mass spectrometry identify side-chain fragmentations that allow the selective identification of leucine and isoleucine. Mass spectrometry (qv) is also a very powerful method for the determination of post-translational modifications.

The Secondary Structure. The arrangement of the amino acids in a protein into local structural elements is termed secondary structure. The two main structural elements that are seen in proteins are the α-helix and β-sheet structures. The α-helical structure, which was originally suggested by the Nobel Laureate Linus Pauling and Robert Corey (1), could be described as a spring coiled right-handed about an imaginary cylinder. The size of a helix can range from 5 to 50 amino acids. The helical structure has 3.6 residues per turn and the main forces that stabilize the structure are hydrogen bonds between amide hydrogens of peptide bonds and carboxyl oxygens of residues at the next turn of the helix. The β-sheet structure is formed by the stacking of individual β-strands. The β-strands are usually from 5 to 15 residues long and are in a fully extended conformation. This secondary structure is also stabilized by hydrogen-bonding amide hydrogens and carboxyl oxygens of stacked chains. The β-strands can be arranged either in a parallel manner (in each strand the amino acid sequence of the chain is arranged toward the same direction) or in an antiparallel manner, which is more stable

energetically. Other secondary structure elements are β-turns, short turns stabilized by a specific pattern of hydrogen bonds, and loops, which are flexible linkers that connect secondary structure elements.

Tertiary Structure. This is the three-dimensional structure of a protein. The tertiary structure is made up from the interaction of the secondary structure elements to form the overall folding pattern of the polypeptide chain. The tertiary structure of a protein is formally described by the coordinates in space of all (or most) atoms of the protein molecules [see description below of the protein databank (PDB)]. The tertiary structure is usually quite compact and after globular, but can also be elongated or possess other geometries. As with secondary structure elements, in spite of the fact that the number of possible folds (ie, the specific arrangement of secondary structure elements) is almost infinite, there is a basic set of a few thousand unique folds. This observation has a crucial role in our ability to predict the tertiary structure of proteins through fold-recognition methods as described below. The main driving force for formation of three-dimensional structures of proteins appears to be hydrophobic interactions (2–5). The arrangement of the protein in a way that minimizes the energetically unfavorable orientations (ie, hydrophobic moieties on the surface of the protein and hydrophilic moieties buried inside the core) appear to provide an overall structural pattern for the folded state. Interestingly, binary models of proteins, which present the protein as a linear arrangement of hydrophobic and hydrophilic elements, are quite successful in low resolution prediction of the three-dimensional structure of proteins and folding pathways (3–5). However, it is very clear that the fine structure of a protein is a result of much more complex interactions. Even the hydrophobic core could not be regarded purely as an unstructured entity, and there is certainly a core-packing process that may involve more specific interactions (eg, stacking of aromatic residues in a specific orientation within the hydrophobic core). Other elements like salt bridges, disulfide bonds, and hydrogen bonds are also very important in the stabilization of the folded proteins and fine-tuning of the folded state.

Figure 1 shows the primary, secondary, and tertiary structures of the bovine pancreatic trypsin inhibitor (BPTI). This small protein is being widely used as a model for folding studies, because of its small size (58 amino acids), the fact that it contains both α-helical and β-sheet structural elements, and its commercial availability.

Quaternary Structure. This is the spatial arrangement of non–covalently linked protein subunits to form a functional protein assembly. One of the best-known examples of a quaternary structure of protein is the assembly of functional hemoglobin that is made of four non–covalently linked subunits. Extensive discussion of the quaternary structure is beyond the scope of this article.

The Thermodynamic Hypothesis

A guiding principle in the study of protein folding is the "thermodynamic hypothesis" (6), established by Christian A. Anfinsen in the 1950s and early 1960s. The thermodynamic hypothesis suggests that a particular three-dimensional structure of a protein occurs because this molecular arrangement is the most stable

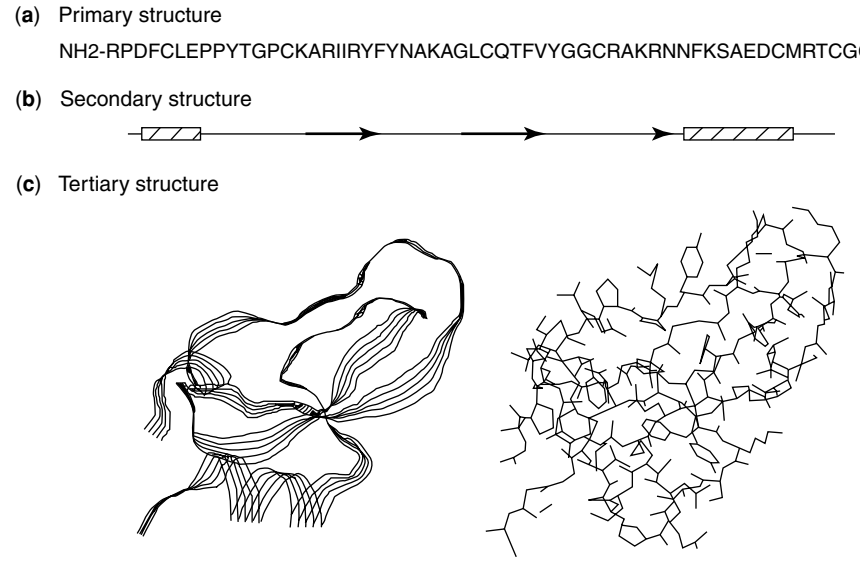

Fig. 1. Levels of structural organization of the BPTI protein. (**a**) Primary structure, the amino acid sequence of protein; (**b**) Secondary structure, α-helices are denoted by shaded boxes and β-strands are denoted by arrows. Secondary structure elements are presented according to their determination as they appear in the file containing the BPTI coordinates (1BPI) as deposited in the protein databank (PDB); (**c**). Tertiary structure, wireframe chemical structure (right), and schematic strand representation (left). The tertiary structures were prepared using rasmol software with BPTI coordinates.

thermodynamically. The development of the hypothesis was based on Anfinsen's experiments with the ribonuclease (Rnase) protein. The RNase is a relatively small protein of 124 amino acids that contains four disulfide bridges. Therefore, there are 105 ($7 \times 5 \times 3 \times 1$) possible combinations for the arrangement of the disulfide bond in the folded protein. However, only one orientation is enzymatically active. Anfinsen reduced the disulfide bridges of RNase and unfolded the protein under extreme chemical conditions using high concentrations of urea. Under these conditions the protein was completely unfolded and could be regarded as a random polymer. However, when the urea was removed, followed by oxidation of the disulfide bridges, the protein spontaneously refolded back into its original form. On the other hand, when the protein was oxidized in the presence of a high concentration of urea (that was only later removed), only about 1% activity was gained. This is consistent with a random formation of various 105 "scrambled" RNase structures, only one of which has enzymatic activity. The Anfinsen hypothesis could be best summarized in his own words from his 1972 Nobel Prize acceptance speech, "The native conformation is determined by the totality of interatomic interactions and hence by the amino acid sequence, in a given environment."

Chaperon-Assisted Protein Folding. The Anfinsen theory was a very clear turning point in our understanding of protein folding and it appears to be valid in the typical time frame of the folding process (milliseconds to seconds) for most studied proteins. However, more recent studies have clearly demonstrated

that in the cellular environment, the folding process may be assisted or may require the help of so-called molecular chaperons (7–9). The chaperons, which are large protein assemblies, are associated with the target protein during part of the folding process. However, once folding is complete (or even before), the correctly folded protein is released from the chaperon assembly into the cellular environment. The physiological role of the molecular chaperons is not fully understood. Chaperons are found in all living organisms including bacteria, but they are mainly expressed under conditions of stress (such as heat shock). It is widely speculated that the main role of these molecular assemblies is to avoid protein aggregation. They also seem to serve as "quality control" machinery under normal growth conditions. Nevertheless, for most cellular proteins the "thermodynamic hypothesis" seems to hold during their initial process of folding upon synthesis by the ribosome.

Levinthal's Paradox

The thermodynamic hypothesis describes the energetic end point of the folding process, but it does not deal with the pathway by which the molecule reaches its global energetic minimum. The rate of protein folding is usually in the order of milliseconds to seconds (10). However, the number of possible orientations of the dihedral angles of the various peptide bonds that compose the protein is astronomical. Assuming 10 possible conformations for each peptide bond in a very short 40 amino acid protein will result in 10^{40} possible conformations. The apparent contradiction between the number of possible configurations and the fast folding rate of proteins is known as "Levinthal's paradox" (11). Levinthal argued that if we consider an average rotation frequency around each bond, one could assume that a protein can sample about 10^{14} structures per second. Therefore, it would take 40 amino acids 10^{26} seconds or about 10^{18} years to examine all the possible conformations. This time scale is much larger than the present age of the universe. The clear conclusion from Levinthal's paradox is that folding cannot occur by sampling the entire conformational space and that there must be another way to reach the folded state of low energy. Indeed, Cyrus Levinthal suggested in the late 1960s, on the basis of his theoretical argument, that there are specific folding pathways.

Folding Pathways

It took several years after Levinthal's and others' theoretical arguments until folding pathways could actually be demonstrated. The very rapid folding reaction, that was proved to be highly instrumental in the conceptual realization of the folding pathways notion, made the observation of folding intermediates quite difficult. The first experimental proof for the existence of specific folding pathways came from experiments done by Thomas Creighton in the mid-1970s (12,13) on the folding of bovine pancreatic trypsin inhibitor (BPTI), the protein that is presented in Figure 1. BPTI has three disulfide bridges, and Creighton was able to trap folding intermediates of BPTI with one or two disulfide bridges formed, by irreversibly blocking all the free thiol groups at different folding stages.

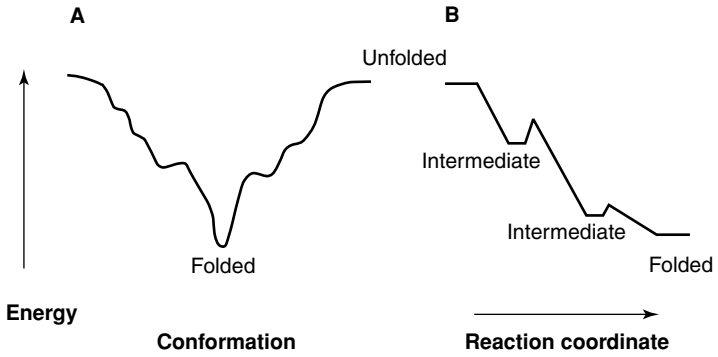

Fig. 2. Energy of folding reaction. **A**. Funnel view of the energetic landscape. The trajectory of the protein along the energy landscape is a probabilistic statistical mechanics function; **B**. A pathway view of the folding process. The folding process is represented as a chemical reaction. The reaction coordinate is deterministic and intermediates along the pathway are well-defined.

Analysis of the nature of the intermediates allowed the construction of a folding pathway of BPTI. Later experiments by Weissman and Kim (14)—using different methodologies—suggested that the nature of the folding intermediate might be different from that originally described. However, there was an agreement on the concept of intermediate species in the pathway from the unfolded to the folded state.

In more recent years, other groups have suggested that the pathway toward the minimum of free energy might be less deterministic than previously assumed (15–20). In this more modern point of view the folding process is seen as a multiplicity of routes down a folding funnel rather than a distinct pathway of discrete intermediates. This view is based on statistical mechanics rather than a chemical reaction view of the folding process (Fig. 2). This approach suggests that different partially folded species are distributed in the energetic landscape of the folding reaction according to the probability of occupation at a finite temperature in a way that is proportional to the Boltzmann factor. According to this view, the molecular dynamics within a folding funnel involves the progressive formation of an ensemble of partially ordered structures. The practical meaning of this approach is that there is no way to clearly know the folded state of a molecule during the folding process. Figure 2 presents a schematic view of the energetic landscape funnel and the folding pathway models.

The funnel approach does not contradict Levinthal's argument that a given protein does not sample the entire energy landscape of its various conformations. However, in spite of sampling only a small part of the energy landscape, the exact path is the result of a probability function rather than a deterministic function. Furthermore, since in a typical experiment of protein folding there is a very large number of molecules, there is no way to predict the exact conformation of each molecule, and they can only be represented as a probability function. Very recent studies that use single-molecule techniques should help further explore the energy landscape of protein folding (21).

Models for the Order of Events in the Folding Process

Regardless of the view of the folding process as discrete steps with defined intermediates or as an energetic funnel, one of the interesting questions that still remains open is the order of events during the folding pathways. The three major hypotheses for the order of events are (*1*) the framework model (22–24), (*2*) the nucleation-growth mechanism (25), and (*3*) the hydrophobic collapse model (3,4).

The framework model suggests that the first stage in the folding reaction involves the formation of elements of secondary structures without any significant compactization. These secondary structure elements are then assembled to form the compact and folded final structure of the protein. The nucleation-growth mechanism suggests that the first stage in the formation of the folded state involves the formation of a small nucleus that is well-folded and compact. This nucleus involves only a small fraction of the protein polypeptide chain. The formation of the nucleus is followed by hierarchical assembly of further structural elements to form the well-ordered three-dimensional structure. The hydrophobic collapse model suggests that the first stage of the folding process involves the rapid collapse of the protein chain into a compact conformation that does not have well-ordered secondary structures. The secondary structure elements then grow in the general framework of the collapsed structure. There is no clear indication which of the models correctly describes the folding mechanism. It may be that different protein molecules are being folded in different ways and/or that the actual sequence of events may be different from or a combination of the three models. The statistical mechanics model also may suggest that all three models are actually different discrete trajectories on the energy landscape and each one of them can occur even at the same folding reaction of an ensemble of protein molecules.

Experimental Methodologies

As described above, the folding reaction is a very rapid event (10). Therefore in order to be able to follow the kinetics of folding and sequence of events there is a need for rapid stopped-flow techniques. The properties that are usually monitored using these techniques are either aromatic residues fluorescence or circular dichroism spectra. The fluorescence of the aromatic residues (especially of tryptophan) is largely dependent on the dielectric constant of its environment. Furthermore, aromatic residues tend to be part of the hydrophobic core of the protein. Therefore, monitoring the change of fluorescence during folding and unfolding reactions allow insight into the reaction mechanism. Circular dichroism (CD) spectra of proteins provide direct information on the secondary structure of proteins. The CD spectrum of a protein in the far-UV region (180–250 nm) shows a clear indication of secondary structure (especially of α-helical structure). Thus it allows the direct observation of the formation of secondary structures. These two techniques can be used not only to study the kinetics of protein folding but also the thermodynamics. By steady-state determination of the fraction of folded protein upon titration with denaturating agent such as urea, the change in free energy (ΔG) of the folding reaction can be calculated.

Fourier-transformed infrared (FTIR) is another excellent method to study protein folding. Unlike the well-known use of FTIR as a method for the identification of functional groups, in terms of protein structure this method allows the determination of secondary structure. The frequency of vibration of the amide I band of the peptide chain (1500–1600 cm^{-1}) heavily depends on the structure of the protein. FTIR has the advantage of being more sensitive for the study of proteins that contain β-sheet elements as compared to CD. Furthermore, since FTIR spectroscopy can be applied to solids also, it allows the structural analysis of aggregated protein deposits. The availability of the rapid step-scan method for FTIR is also very useful for the study of rapid folding reactions (see VIBRATIONAL SPECTROSCOPY).

The Protein Databank (PDB). One of the most instructive tools available for researchers studying both basic and applied aspects of protein folding is the protein databank (PDB) (26,27). Databank data is freely available via the Internet (http://www.pdb.org) and it contains the coordinates of protein structures as determined by X-ray crystallography or nuclear magnetic resonance (NMR) spectroscopy. The rate of structure submission to the PDB has increased steadily over the years (Fig. 3). By the end of 2001 there were nearly 17,000 deposited structures in the PDB. The PDB was established at the Brookhaven National Laboratories (BNL) in the 1970s and maintained there for many years. Several years ago, the maintenance and development of the PDB was transferred to Rutgers, The State University of New Jersey; the San Diego Supercomputer Center at the University of California, San Diego; and the National Institute of Standards and Technology—three members of the Research Collaboratory for Structural Bioinformatics (RCSB).

Prediction of Protein Folding

The importance of the correct protein fold for the understanding of protein activity and design of novel proteins has led to much interest in the possibility of predicting correct protein folds. In spite of the great importance and interest in the prediction of the three-dimensional structure of proteins from the primary structure there are no such algorithms available to date. However, the attempts to predict secondary structures of proteins have been much more (although not fully) successful.

One of the earliest and most pivotal attempts to predict the secondary structure of proteins was made by Peter Chou and Gerald Fasman (28). The Chou–Fasman scale for secondary structure prediction is based on the statistical occurrences of amino acids in different secondary structure elements. Their classification was based on the structures of protein as deposited in the PDB, taking into account the relative occurrence of the different amino acids in various proteins (which can be quite diverse). The various amino acids were classified according to their ability to form or break the two major secondary structures. The categories were strong former (H), former (h), weak former (I), indifferent former (i), breaker (b), and strong breaker (B) of the specific secondary structure elements. Proteins are scanned through a fixed-size window and each area of the polymer is scaled for its tendency to form the various secondary structures. Further developments of the Chou–Fasman method, such as the GOR method (29), improved the prediction potential by taking into account not only the identity of the specific amino acid but

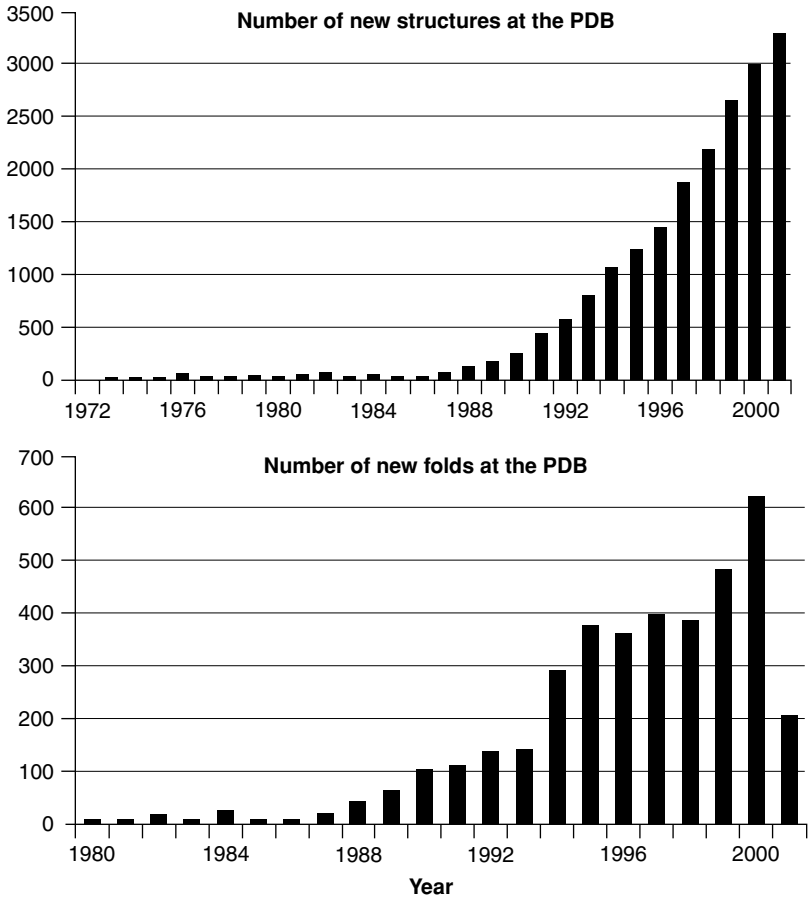

Fig. 3. New structures versus new folds in the PDB. There is a constant increase in the number of new structures submitted to the PDB. The number of new folds shows significantly different behavior, with a sharp decrease in 2001. The data was taken from the official PDB statistics.

also their context (ie, specific secondary structure patterns). Another approach for the prediction of secondary structures is based on neural networks analysis. According to this method, computational neural networks are trained by sequences of known secondary structures. One very successful example of the neural networks method is the development of the secondary structure prediction tool in a mail server called PHD (30).

Prediction of the three-dimensional structures of proteins is much more complex. The success rate of this process is formally determined by the a contest known as the Critical Assessment of Techniques for Protein Structure Prediction (CASP). The CASP contest showed a significant advance in the ability to predict three-dimensional structures of proteins over the years by homology modeling and fold recognition, as described below, but ab initio methods are still not very accurate. One of the major problems is finding a way to distinguish between the global minimum of free energy of a given protein molecule and local energetic minima. Most of the successful models of protein structures are based on homology modeling. Such

methods start by forcing the target sequence into the fold of its closest relative with a known folded state, followed by energy minimization of the structure using force fields. An Automated Comparative Protein Modeling Server, The Swiss Model, is available freely on-line (http://www.expasy.ch/swissmod/SWISS-MODEL.html). More advanced homology-modeling software is available commercially.

Another of the successful methods that is based on a reverse approach relies on protein fold recognition by "threading" (31). This method takes advantage of the fact that the number of folds is limited. Instead of trying to predict the fold of the protein on the basis of the amount of free energy, the method determines whether a given sequence can be fitted to a known fold. As the number of folds (Fig. 3) appears to be finite, it provides a way to look for the structure of new proteins using known folds. Another method for the prediction of three-dimensional structures of proteins is based on the *in silico* assembly of protein structure from shorter structural elements with more defined structures (32).

Protein Unfolding and Misfolding

There is an increased interest in recent years in protein unfolding and misfolding (33–37). For example, there is a clear realization that small but significant parts of protein molecules may be natively unfolded (38). Furthermore, the formation of misfolded protein aggregates is the hallmark of various unrelated diseases and therefore attracts much medical attention. Other research activities are directed toward the search for the physiological significance of the unfolding and misfolding phenomena. Indeed, recent studies have indicated that protein unfolding and misfolding might also have a physiological role. One instance is that of unstable and short-lived proteins, in which their instability is an integral part of a regulatory mechanism, as in the case of Toxin–Anitoxin systems (38). Another recent example is the formation of *curli* amyloid fibril in *Escherichia coli*, which is related to the formation of biofilms (39).

The formation of amyloid fibrils is probably one of the most important cases of protein misfolding. In this self-assembly process, soluble cellular proteins form large and ordered fibrillar structures. This process is also accompanied by a structural transition of the aggregated proteins from their native fold into a predominantly β-sheet secondary structure. The fibrillar structures are well ordered in the long axis direction, and X-ray fiber diffraction shows a clear 0.48-nm reflection on the meridian. Such reflection corresponds to the hydrogen bonding distance between β-strands. This is consistent with the secondary transition toward a β-sheet structure upon amyloid fibril formation as is observed using CD, and FTIR spectroscopy. There is also a correlation between the unfolded and misfolded states of proteins. Two amyloid-forming proteins, the diabetes-related islet amyloid polypeptide (IAPP) and the Parkinson's disease–related α-synuclein polypeptides, have clearly been shown to be natively unfolded.

The "Correctly Folded State" as a Metastable State

The folded state of protein, as determined by X-ray crystallography or NMR and deposited in the PDB, is considered the state of lowest free energy for a given

isolated protein molecule. However, recent studies have raised doubt about the validity of this assumption for concentrated ensembles of proteins in aqueous solution. Many (if not all) proteins may undergo a process of aggregation and misfolding at infinite time (35). For example, as described above, amyloid-related proteins tend to undergo spontaneous aggregation in solution. It is therefore assumed that the nonaggregated state of polypeptides such as IAPP is a kinetically trapped metastable state ["kinetic solubility," as coined by Jarrett and Lansbury (33)]. However, in recent years it has been realized that disease-related proteins are not the only ones to undergo an aggregation process in solution. It has been demonstrated that disease-unrelated proteins also, such as the SH3 domain, myoglobin, and a bacterial cold shock protein, form aggregated structures in solution. Aggregation is also noted in preparations of many protein solutions after long storage. This leads to the suggestion that the aggregated form, and most notably the amyloid form, of proteins may represent a generic form of proteins. Therefore if each protein molecule is not regarded as an independent thermodynamic system, but we consider the ensemble of proteins in aqueous solution as one large thermodynamic system, a solution of aggregation-prone but "correctly folded" proteins represent a system in a transient state that will eventually reach its global free-energy minimum of the aggregated state (35). It appears that many (or perhaps all) proteins will sooner or later undergo the aggregation process. For some proteins this may take minutes or hours and for others it can take months or years. For example, the fibrillation time of the aggregation-prone human calcitonin at physiological pH is 5 min at a concentration of 5 mg/mL, whereas the fibrillation time of non–aggregation-prone salmon calcitonin under the same condition is about 7 months (40), but after this long time it does form aggregated fibrillar structures.

BIBLIOGRAPHY

1. L. Pauling and R. B. Corey, *Proc. Natl. Acad. Sci. U.S.A.* **37**, 252 (1951).
2. G. D. Rose and R. Wolfenden, *Annu. Rev. Biophys. Biomol. Struct.* **22**, 381 (1993).
3. K. A. Dill, *Biochemistry* **24**, 1501 (1985).
4. K. A. Dill, *Biochemistry* **29**, 7133 (1990).
5. K. A. Dill, *Science* **250**, 297 (1990).
6. C. B. Anfinsen, *Science* **181**, 223 (1973).
7. F. U. Hartl and M. Hayer-Hartl, *Science* **295**, 1852 (2002).
8. R. J. Ellis, *Curr. Biol.* **11**, R1038 (2001).
9. T. K. Chaudhuri, G. W. Farr, F. A. Fenton, S. Rospert, and A. L. Horwich, *Cell* **107**, 235 (2001).
10. J. K. Myers and T. G. Oas, *Annu. Rev. Biochem.* **71**, 783 (2002).
11. C. Levinthal, *J. Chim. Phys.* **65**, 44 (1968).
12. T. E. Creighton, *J. Mol. Biol.* **87**, 563 (1974).
13. T. E. Creighton, *J. Mol. Biol.* **87**, 579 (1974).
14. J. S. Weissman and P. S. Kim, *Science* **256**, 112 (1992).
15. P. E. Leopold, M. Montal, and J. N. Onuchic, *Proc. Natl. Acad. Sci. U.S.A.* **89**, 8721 (1992).
16. P. G. Wolynes, J. N. Onuchic, and D. Thirumalai, *Science* **267**, 1619 (1995).
17. P. G. Wolynes, *Proc. Natl. Acad. Sci. U.S.A.* **93**, 14249 (1996).

18. K. A. Dill, K. M. Fiebig, and H. S. Chan, *Proc. Natl. Acad. Sci. U.S.A.* **90**, 1942 (1993).
19. E. M. Boczko and C. L. Brooks, *Science* **269**, 393 (1995).
20. J. N. Onuchic, P. G. Wolynes, Z. Luthey-Schulten, and N. D. Socci, *Proc. Natl. Acad. Sci. U.S.A.* **92**, 3626 (1995).
21. A. R. Fersht and V. Daggett, *Cell* **108**, 573 (2002).
22. O. B. Ptitsyn and A. A. Rashin, *Biophys. Chem.* **3**, 1 (1975).
23. P. S. Kim and R. L. Baldwin, *Annu. Rev. Biochem.* **51**, 459 (1982).
24. P. S. Kim and R. L. Baldwin, *Annu. Rev. Biochem.* **59**, 631 (1990).
25. A. R. Fersht, *Curr. Opin. Struct. Biol.* **7**, 3 (1997).
26. F. C. Bernstein, T. F. Koetzle, G. J. B. Williams, E. F. Meyer Jr., M. D. Brice, J. R. Rodgers, O. Kennard, T. Shimanouchi, and M. Tasumi, *J. Mol. Biol.* **112**, 535 (1977).
27. H. M. Berman, J. Westbrook, Z. Feng, G. Gilliland, T. N. Bhat, H. Weissig, I. N. Shindyalov, and P. E. Bourne, *Nucleic Acids Res.* **28**, 235 (2000).
28. P. Y. Chou and G. Fasman, *Biochemistry* **15**, 13222 (1974).
29. J. Garnier, D. J. Osguthorpe, and B. Robson, *J. Mol. Biol.* **120**, 97 (1978).
30. B. Rost and C. Sander, *Proc. Natl. Acad. Sci. U.S.A.* **90**, 7558 (1993).
31. D. Fischer, D. Rice, J. U. Bowie, and D. Eisenberg, *FASEB J.* **10**, 126 (1996).
32. C. D. Tsai, B. Ma, S. Kumar, H. Wolfson, and R. Nussinov, *Crit. Rev. Biochem. Mol. Biol.* **36**, 399 (2001).
33. J. T. Jarrett and P. T. Lansbury Jr., *Cell* **73**, 1055 (1993).
34. C. M. Dobson, *Trends Biochem. Sci.* **24**, 329 (1999).
35. E. Gazit, *Angew. Chem. Int. Ed.* **41**, 257 (2002).
36. E. Gazit, *FASEB J.* **16**, 77 (2002).
37. V. N. Uversky, *Protein Sci.* **11**, 739 (2002).
38. E. Gazit and R. T. Sauer, *J. Biol. Chem.* **274**, 2652 (1999).
39. M. R. Chapman, L. S. Robinson, J. S. Pinkner, R. Roth, J. Heuser, M. Hammar, S. Normark, and S. J. Hultgren, *Science* **295**, 851 (2002).
40. K. Kanaori and A. Y. Nosaka, *Biochemistry* **34**, 12138 (1995).

EHUD GAZIT
VERONICA GLATTAUER
JEROME A. WERKMEISTER
Tel Aviv University

PSA. See PRESSURE SENSITIVE ADHESIVES.

PULTRUSION. See COMPOSITES, FABRICATION.

PVC. See VINYL CHLORIDE POLYMERS.

PVDC. See VINYLIDENE CHLORIDE POLYMERS.

PVF. See VINYLCARBAZOLE POLYMERS.

PVK. See VINYLCARBAZOLE POLYMERS.

PVP. See VINYL AMIDE POLYMERS.

RECYCLING, PLASTICS

Introduction

The unabated growth in the use of plastics in recent years is of considerable concern because of the difficulties involved in waste disposal. Increasingly, plastics are replacing wood, glass, paper, and metal in numerous applications, especially in packaging. Items such as plastic cups, food utensils, and convenience containers such as "clam shells" (sandwich boxes) contribute substantially to the burgeoning municipal solid waste (MSW) stream. As a means of dealing with this waste, the recycling of plastics increased dramatically from about 1990, when the emphasis shifted from landfilling to recycling and energy recovery. To facilitate recycling, ever-revitalized infrastructures are needed for collecting, sorting, cleaning, reprocessing, and manufacturing new products to be marketed to end-users. This article focuses on recycling of thermoplastics in the MSW.

Plastics in MSW: The Americas. In the United States, plastic resin sales and captive use reached 46.2 million tons in 2001, a 4% decrease from 2000, according to the American Plastics Council (1). Resin production rose to 45.9 million tons in 2001, up 4.8% from the previous year. The U.S. plastics industry continues to expand into new markets as plastic products come to replace ones made of wood and metal (Fig. 1). In the United States, some 232 million tons of MSW were generated in 2000, an increase of 0.9 million tons over 1999 (Fig. 2). Of this stream, plastics constitute about 10.7 wt%. Plastic containers and packaging dominate, followed by materials in goods such as automobiles, appliances, electronics, furniture, and carpeting. Plastic resins used in containers and packaging include poly(ethylene terephthalate) (PET; in soft drink bottles with polypropylene [PP] caps), high density polyethylene (HDPE; in milk and water bottles), poly(vinyl

Encyclopedia of Polymer Science and Technology. Copyright John Wiley & Sons, Inc. All rights reserved.

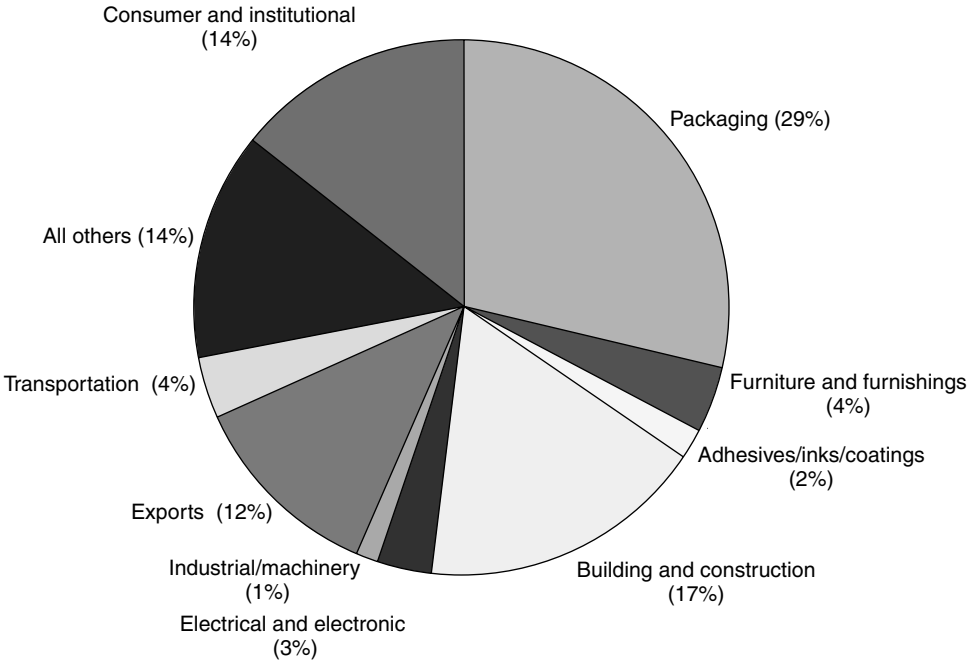

Fig. 1. Major market distribution for plastics (2001). From Ref. 2.

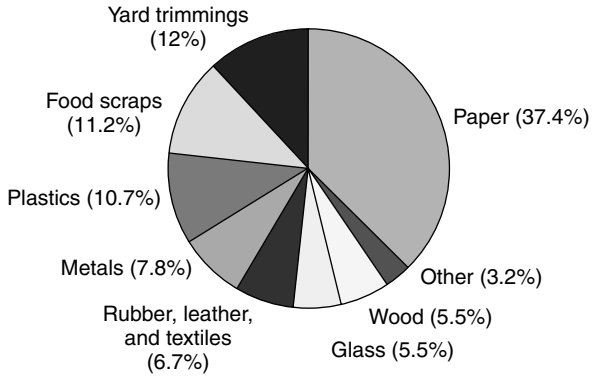

Fig. 2. Total waste generation in the United States (2000). From Ref. 2.

chloride) (PVC; in cooking-oil bottles), low density polyethylene (LDPE) and linear low density polyethylene (LLDPE; for bags, sacks, and wraps), and polystyrene (PS; in cups and containers). Table 1 shows the generation, recovery, and discard amounts for various resin types (see also POLYESTERS, THERMOPLASTIC; Ethylene Polymers; VINYL CHLORIDE POLYMERS; STYRENE POLYMERS).

Although the portion of plastics recovered by recycling in the United States is relatively small—1.34 million tons, or 5.4% of plastics generation in 2000—recovery of certain plastics has been increasing (2). Recently, 40% of discarded PET soft drink bottles and 31.9% of HDPE milk and water bottles were recovered (2). In

Table 1. Total Plastics in MSW (2000) by Resin Type[a]

Resin	Generation, 10^3 ton	Recovery, 10^3 ton	Generation, %	Discards, 10^3 ton
PET	2,490	430		2,060
HDPE	4,830	420		4,410
PVC	1,390			1,390
LDPE/LLDPE	5,740	150		5,590
PP	3,350	10		3,340
PS	2,280			2,280
Other resins	4,630	330		4,300
Total plastics in MSW	*24,710*	*1,340*	*5.4*	*23,370*

[a]Source: Ref. 2.

1960, an estimated 390,000 ton of plastics was discarded; by 1999, that figure had risen to 24.2 million tons. As a portion of MSW generation in the United States, plastics were less than 1% in 1960, increasing to 10.5% in 1999 (2). In Canada, the majority of collected plastic waste is represented by PET (54%) and HDPE (37%), followed by PP (6%) and PVC (3%). Post-consumer plastics recycling in Canada has focused on recycling of plastic packaging, employing manual sorting followed by reprocessing of resin-specific streams (eg, HDPE). In 1998, Canadians recycled almost all collected PET and HDPE waste (3,4). In Latin America, some countries have recently adopted regulations governing the MSW and have started to address recycling infrastructure issues. Brazil has adopted national take-back regulations on batteries and has passed laws regarding electronic scrap and end-of-life vehicles. In Mexico, legislation has been prepared regarding the recycling of lamps and batteries. In 2002, El Salvador, Jamaica, and Argentina considered regulations on batteries and printer cartridges.

Plastics in MSW: Europe, Asia, and the Pacific Rim. Consumption of plastics in Europe is predicted to grow about 4% annually from 24.9 million tons in 1995 to 36.9 million tons in 2006, with PP and PET showing the greatest increase (5). In the United Kingdom in 2000, only 8% of collected plastics was recycled instead of the targeted 15% (6). A related problem in the United Kingdom and elsewhere is the continued growth of the plastic portion in automotive shredded residue (ASR), which recently stood at about 40% of ASR. For Japan, plastics production and waste discharge data have been compiled by the Plastic Waste Management Institute, which reported that resin production in 1999 was 14,570,000 ton; total plastic waste discharge the same year was 9,760,000 ton (7). The breakdown of general waste and industrial waste in Japan in 1999 was 4,860,000 and 4,900,000 ton, respectively. In Australia, total plastic resin consumption in 2000 was 1,530,783 ton, of which 753,000 ton was landfilled and 167,673 ton was recovered (8). Between 1997 and 2000, plastics reprocessing increased by 80%, with packaging materials having the highest recovery (42.1%).

For many Asian countries as well as for Russia and other nations, data are either incomplete, of questionable reliability, or hard to come by. It has been reported that in India, the plastics share of the MSW is about 7% by weight (9). For 2000, the country's total production of plastics was estimated at 3 million tons. Although mechanical recycling (ie, grinding materials) is widely employed in India,

Fig. 3. SPI resin identification code. The seven symbols in the SPI Code can be found at the website http://grn.com/grn/library/symbols.htm (and elsewhere). However, the acronyms below the images are not part of the website images and have been added separately here.

feedstock recycling (ie, chemical depolymerization) is largely untried. In China, consumption of plastic products was estimated in 2000 to be growing about 20% annually (10). Around 50–60% of plastics waste in China is either uncollected or disposed of on land, in rivers, and in the sea. Although the remainder is available to recyclers, the actual rate of recycling has been declining steadily (from 20% to 5% in a recent period). This decrease in recycling of domestic materials is offset by the substantial business devoted to recycling waste imported from abroad, giving rise to allegations of "dumping" by foreigners.

Plastics Coding System and Terminology. In the United States, the Environmental Protection Agency (EPA) advocates Three R's: *Reduce* the amount of waste to be discarded, *Reuse* products or repair what is broken, and *Recycle* as much as possible, including buying products with recycled content. In the mid-1980s the Society of Plastics Industry (SPI) introduced a coding system using numbered triangles that are now found on containers around the world (Fig. 3). By accelerating the sorting of bottles and containers, the code greatly enhances recycling. This system also helps municipalities track plastics in their waste stream.

Terms related to the reprocessing of discarded materials include *recycling* (a process used to recover plastics waste); *recycled* (a reprocessed material containing some quantity of post-consumer plastic waste, usually more than 25 wt%); *reprocessing* (activity involving steps such as sorting, grinding, reextrusion, or remolding into a secondary material for remanufacturing of plastic goods); *recycled content* (the amount of plastics from the post-industrial and/or post-consumer waste stream that is added to a virgin resin); *post-industrial waste* (or preconsumer waste: off-spec parts, plant discards, and the like); and *post-consumer waste* (materials and products discarded after consumer use).

Challenges for Plastics Recycling

Plastics recycling presents numerous technical, economical, and marketing challenges. One such technical issue is the *variability of product composition and color*, because discarded products are made from a wide array of resins and additives. The *contamination* of the waste stream is aggravated by labels, glue, printing, product residue, and similar elements. Most waste streams include *immiscible polymers* (Table 2). Efforts to recover them via conventional melt processing without first sorting them will produce materials with uncontrolled coarse morphology, poor interfacial adhesion, and inferior physical properties (11–13). As is well known, the better the physical properties, the higher the quality of recycled

Table 2. Miscibility Chart for Commonly Used Thermoplastics[a,b]

Plastic type	PET	HDPE	PVC	LDPE	PP	PS	PA	PC
Poly(ethylene terephthalate)	M	IM	IM	IM	IM	IM	IM	IM
High density polyethylene		M	IM	IM	IM	IM	IM	IM
Poly(vinyl chloride)	IM	IM	M	IM	IM	IM	IM	IM
Low density polyethylene			IM	M	IM	IM	IM	IM
Polypropylene		IM	IM	IM	M	IM	IM	IM
Polystyrene		IM		IM	IM	M	IM	IM
Polyamide		IM	IM	IM	IM	IM	M	IM
Polycarbonate	M	IM		IM	IM	IM	IM	M

[a]Source: Polymer Technology Center—Northwestern University (Evanston, Ill.).
[b]Note: M = miscible; IM = immiscible.

products. Because all six major thermoplastics in the waste stream (PET, HDPE, PVC, LDPE, PP, and PS) are immiscible, they must be sorted before recovery for reuse can occur via melt processing. Also, reprocessing of mixed plastics with *different melting points* causes degradation, leading in turn to deteriorated physical properties. For example, PET and PVC cannot be melt processed together because PVC burns at the temperature where PET melts (270°C). If the same mixture is processed at 170°C—suitable for PVC—PET would remain unmelted, thus preventing the desired mixing.

The *difference in melt flow rates* of the various polymers originally selected for specific fabrication methods causes generation of heterogeneous mixtures (ie, low melt-flow rate plastics are used for blow molding, while high melt-flow rate plastics are needed for injection molding). Remelting mixed plastics usually lowers their properties, except for a few polymer blends such as HDPE/LLDPE or HDPE/PP (with 5–7% PP), which exhibit limited compatibility (14,15). To improve physical properties and processability of mixed plastic waste, an impact modifier and a compatibilizer are needed. Both of these can be added as premade ingredients, but only the compatibilizer can be generated *in situ* during reactive extrusion. The compatibilizer migrates to the interface, reducing the interfacial tension, improving adhesion, and stabilizing the blend morphology from coalescence and agglomeration of the dispersed particles. The most common compatibilizers are block or graft copolymers (ie, styrene–ethylene–butylene–styrene) and functionalized polymers (ie, maleated polyolefins). Although compatibilizers are used sparingly (1–5 wt%), they are expensive.

Although the additives (qv) *in the original product* can affect the physical properties and performance of recycled plastics, the extent of their cross-contamination remains unclear. Moreover, *multiple remelting cycles* cause thermal and oxidative degradation in thermoplastics, resulting in changes in molecular weight, discoloration, and sometimes cross-linking. Because of such adverse effects, 100% recycling cannot be achieved for plastic materials.

Successful recycling requires an *adequate supply* of a reasonably clean feedstock. Items such as PET soft drink bottles or natural HDPE milk bottles are abundant in the United States, where curbside collection and drop-off centers are common, and thus make ideal feedstocks. The collected plastics are sorted, ground, reclaimed as flakes or pellets, and sold to fabricators of new products. In Germany,

where the "Dual" system is operated by Duales System Deutschland GmbH, participants label their packaging with a green dot. Companies using this system are exempt from "take-back" programs. In 1994, the European Community published a directive that resembled the German Packaging Ordinance. Similar legislation known as Producer Responsibility Obligation was introduced in the United Kingdom in 1997. The primary obstacle to increased recycling in all venues, however, remains the imbalance between waste collection and potential end-use; far more plastic material is collected than can be recovered economically.

Economics

Plastics recycling is both an economic and an environmental activity. Possible outcomes of recycling include material recovery (via mechanical or chemical processes), energy recovery via incineration, or as a carbon source for blast furnaces (16). Of these, material recovery is the most ecologically beneficial. This nonpolluting method is applicable to both single and mixed polymeric waste that is generated either during product manufacture or from the MSW.

For plastics recyclers (reprocessors), the high costs of both transportation and processing are harsh economic realities. Because of the fuel and equipment expenses associated with transporting waste over long distances, most plastics recycling is best handled at the local level by municipalities. Sound management of processing costs suggests that energy recovery by incineration, landfilling, cracking plastics waste back into monomers, and use of biodegradable plastics are among the most feasible alternatives. The trend of virgin resin suppliers to become producers of recycled-content resins, which began in the United States and Europe, will continue in the new millennium. Some resin suppliers see this new market as an area for potential growth, especially with refined recycling technologies. For PET and HDPE bottles, for example, the cost of recycling (reprocessing) has been estimated at $100–150/ton, compared with incineration or energy recovery at $100/ton and landfilling at $30–50/ton (17). Waste-to-energy plants are more acceptable than incineration, which can produce undesirable toxic ash or fumes. The economics of post-consumer plastics recycling depends on the margin between product price and the cost of raw materials as well as the size of the recycling (reprocessing) facility. Crude oil prices also play a role in setting the cost of virgin resins.

Since the late 1980s, public awareness of the environmental benefits of recycling has increased, and governmental mandates for recycling have kept pace. Such legal requirements have kept the cost of materials from becoming the sole factor in determining the extent of recycling. These developments, however, do not ensure that recycling will be economically efficient. The cost of collection and separation of plastics remains high in contrast to that for aluminum and paper products. The task is further complicated for those plastics in the MSW that are pigmented in bright colors, contaminated, and/or multilayered. Although such products can be recycled using thermal processes such as pyrolysis, gasification, and hydrogenation (see below), mineral- or glass-filled materials and multilayered structures can be hard to recycle because of their complexity. The divergence among fabrication processes used to make plastic products also contributes to the

difficulty of sorting, cleaning, and reformulating materials cost-effectively. By the early 2000s in the United States and elsewhere, economical plastics recycling was limited to products made from HDPE and PET. Extending recycling to other plastics will require lowering recycling costs while improving physical properties and performance relative to those of virgin resins.

Technologies

Technologies for recycling post-consumer plastics were slow to develop until the 1990s (18). These technologies are usually divided into four categories: *primary* (regrind), *secondary* (mechanical), *tertiary* (feedstock), and *quaternary* (incineration). Each of these technologies has a viable role in recycling plastics while conserving natural resources and avoiding landfills.

In the most straightforward approach, *primary* recycling of regrind occurs in the manufacturing process, where regrind is simply added to virgin resin and the mixture is then reprocessed. *Secondary* recycling uses post-consumer sorted or unsorted plastics waste. When reprocessed, these materials are used in less demanding applications that do not require virgin resins. Manual sorting of plastics waste is still used to separate HDPE and PET. Figure 4 shows the layout of a manual sorting facility, with four people separating HDPE, PET, PP, and PVC. Automated sorting uses the differences in properties such as density, surface energy, low temperature behavior, and melting temperature (19). Frequently used

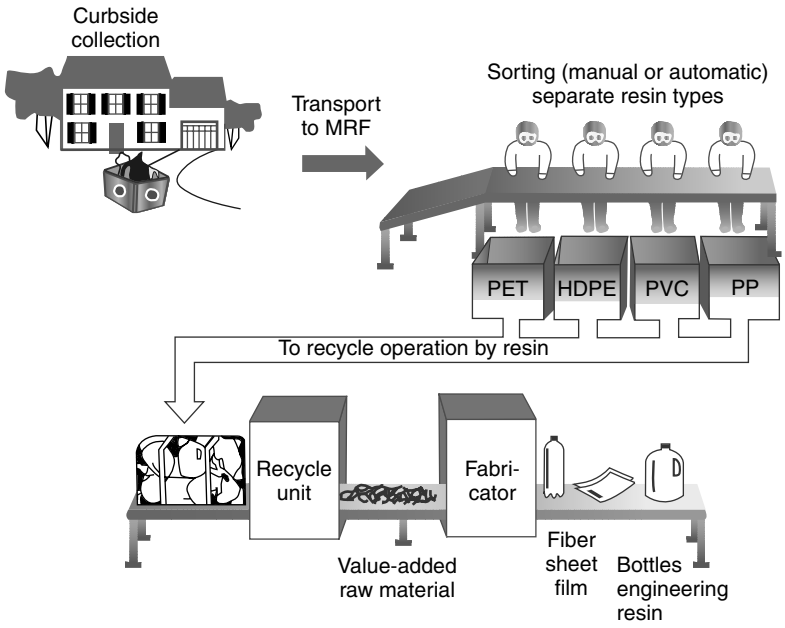

Fig. 4. Layout of a manual bottle-sorting line. Taken from http://www.plasticsrecycling.org/sort.htm.

Table 3. Density of Plastic Materials in the MSW[a]

Plastic material	Density, g/cm^3
PET	1.40
HDPE	0.95
PVC	1.40
LDPE	0.91
PP	0.90
PS	1.05

[a] Source: Polymer Technology Center—Northwestern University (Evanston, Ill.).

density separators divide materials into light and heavy fractions on the basis of plastic density (Table 3). Other methods include marking plastic products with one of the seven SPI codes, addition of unique organic markers to the polymer backbone, and solvent separation (selective dissolution) involving a solvent that dissolves one plastic followed by the use of another solvent at room temperature or higher in order to remove another plastic. Mixed plastics can be separated by froth flotation using surfactants.

As the plastics recycling industry matures, manual sorting will be replaced by automated techniques. One such approach has been developed by the Magnetic Separation System Co. (Nashville, Tenn.), which uses X ray, infrared (IR), and other sensors to separate PET and HDPE by type and by color (20). Their most recent automated sorting module, the Alladin, not only sorts plastic resins by type and color but can also create three outputs from one input (21). For example, clear PET, green PET, and blue PET (or PET, colored HDPE, and natural HDPE) could be sorted in one pass with the capacity of 4–6 ton/h. Other sorting methods include the use of solvents, X-ray fluorescence, near-IR, mid-IR, Fourier-transform Raman spectroscopy, and electrostatic sorting (22–25). The triboelectric pen (Tribopen), a compact device that senses the triboelectric charges of different plastics, can sort engineering resins such as polyamide and acrylonitrile–butadiene–styrene (ABS) from commodity plastics such as PP and PE (polyethylene) (26).

Another secondary recycling technology is the novel process called solid-state shear pulverization (S^3P), which does not require sorting of discarded plastics (27–29). The S^3P technology uses a pulverizer made by Berstorff GmbH (Hannover, Germany), that is based on a modified twin-screw extruder with intensive cooling. This mechanochemical process subjects plastics to simultaneous shear and compression, which results in unique changes in chemical structure because of *in situ* compatibilization and physical properties superior to those made by melt processing. Pulverization is accompanied by intimate mixing without melting, resulting in powder of unusual morphology, large surface area, and controlled particle size and distribution (Figs. 5–8).

Tertiary recycling involves thermal treatment of plastics waste resulting in chemical intermediates. Several technologies such as pyrolysis, gasification, and hydrogenation are being practiced (30–32). Pyrolysis converts polymers to a liquid in the absence of oxygen; gasification produces carbon monoxide and hydrogen in a limited-oxygen atmosphere, while during hydrogenation some hydrogen is added

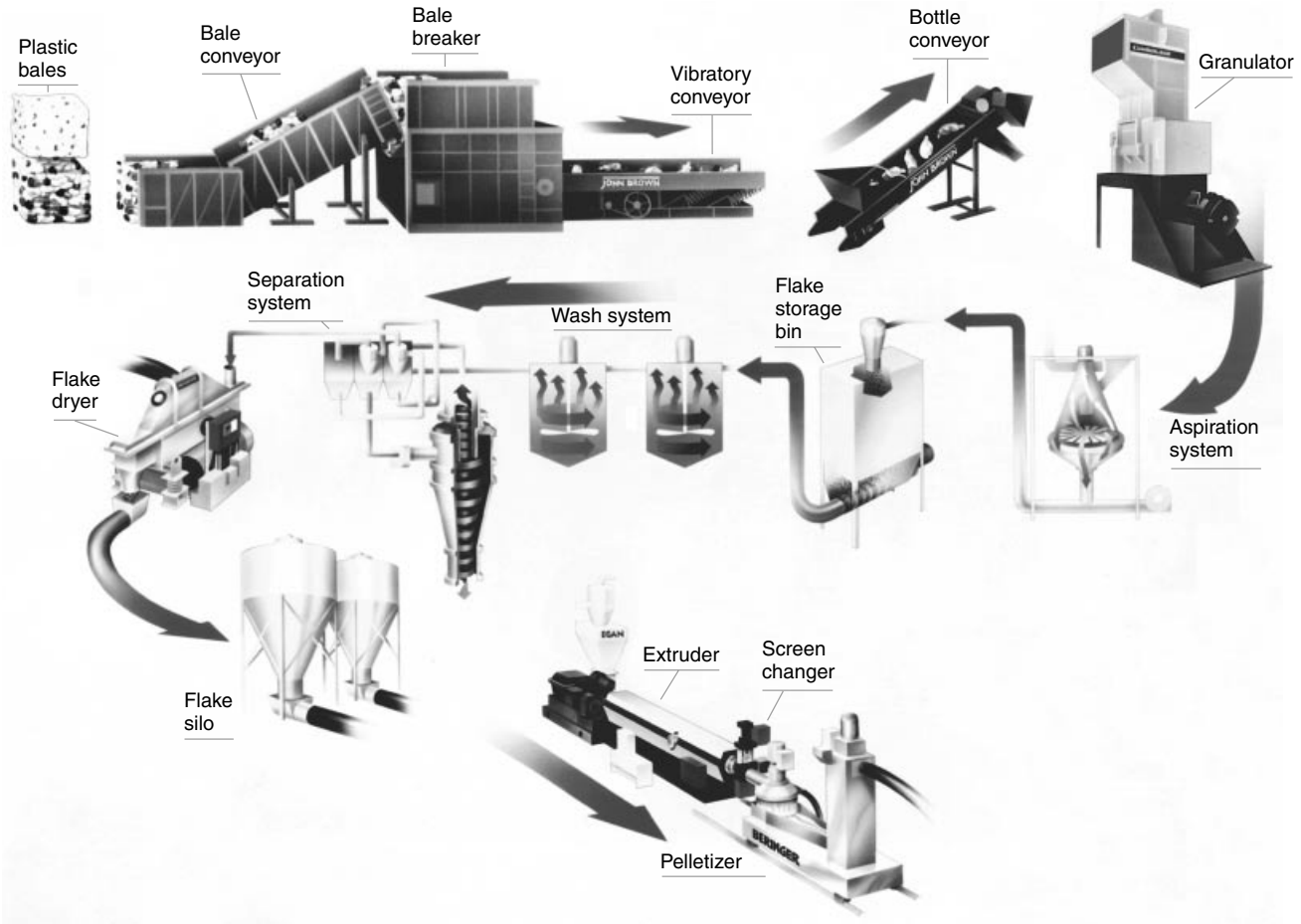

Fig. 5. Layout of a conventional plastics recycling line. Courtesy of Cumberland Engineering, South Attleboro, Mass.

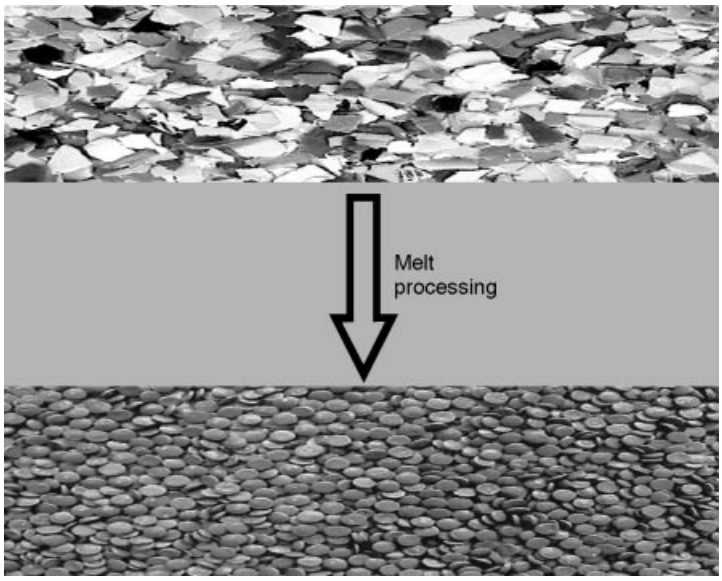

Fig. 6. Representative melt-processed pellets from corresponding post-consumer flakes.

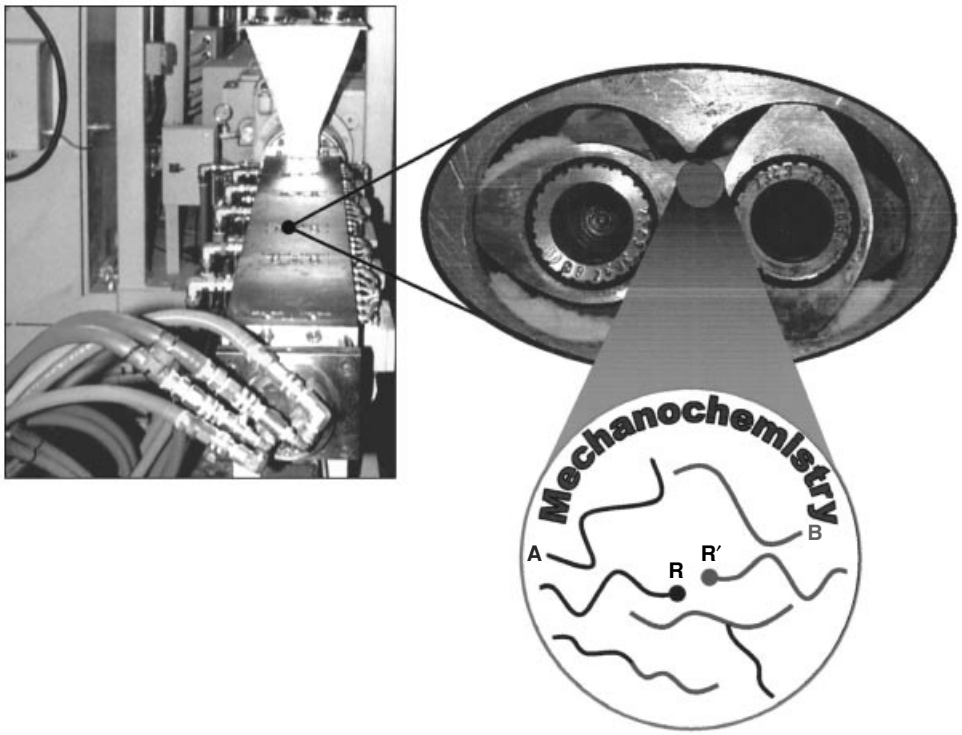

Fig. 7. Illustration of mechanochemsitry in a pulverizer during S^3P. Polymers A and B are compatibilized *in situ* to create AB block or graft copolymers.

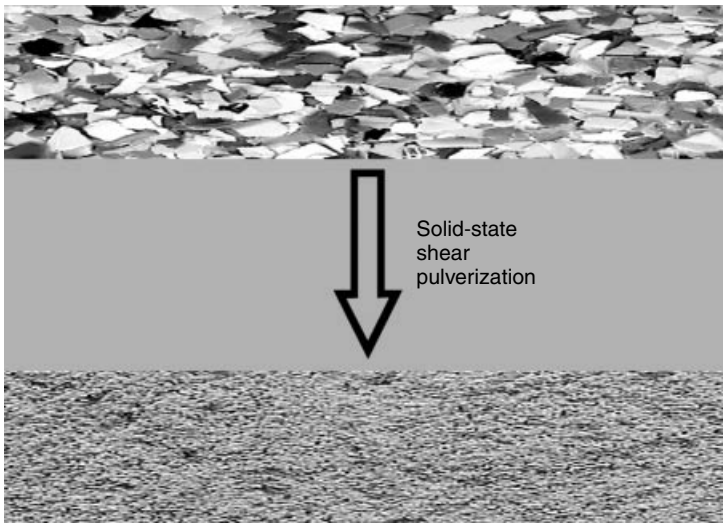

Fig. 8. Representative S^3P powder from corresponding post-consumer flakes.

in the cracking step. Heating plastics such as poly(methyl methacrylate) (PMMA), PS, and acetal homopolymers in the absence of oxygen produces monomers with very high yields (22). These monomers can be isolated, purified, and reused to make new polymers. Thermolysis, when carried out in the absence of air, produces synthetic crude oil. Gasification with controlled amounts of oxygen produces Syngas, which is used as a fuel. Hydrogenation by heat and pressure in an excess of hydrogen produces liquid fuel such as gasoline or diesel. Thermolysis is a versatile process that can handle contaminated medical waste, auto shredded residue, and other complex mixtures. Depolymerization of plastics by solvolysis produces monomers or oligomers (30).

Recycling approaches known as *advanced recycling technologies* (ART) reclaim feedstock value from discarded plastics through depolymerization. ART comprises two groups, depending on whether the depolymerization results in monomer or in hydrocarbon feedstock. The choice of recycling technique is influenced by factors such as the purity of the plastic stream, chemical makeup of the plastics, and the nature of additives. The type of plastic also helps to determine which depolymerization process is appropriate. Polyesters, polycarbonates (qv), polyamides, and polyurethanes (qv) undergo reverse polymerization and they can be converted to their respective monomers for use in making the same virgin resins (18,30). Plastics such as PE, PP, and PVC can be converted into petrochemicals and fuels through pyrolysis. ART processes do not require sorting and are integrated into existing refinery or petrochemical facilities (31).

Quaternary recycling involves waste-to-energy processes. Through combustion, plastics can generate energy amounts comparable to the range between Wyoming coal [22,080 kJ/kg (9600 Btu/lb)] and fuel oil [48,070 kJ/kg (20,900 Btu/lb)]. PE, PS, PET, and PVC yield 23,000, 39,000, 16,100, and 20,700 kJ/kg (10,000, 17,000, 7000, and 9000 Btu/lb) respectively (32). Post-consumer plastics (10–30%) mixed with paper (90–70%) are used as processed engineered fuel in

existing energy plants. Increasingly, automotive shredded residue is being co-combusted with the MSW in Europe and North America. Both environmentalists and citizens afflicted with the "not-in-my-back-yard" (NIMBY) syndrome are concerned about toxic fumes and ash by-products from incineration. Improvements in this process may render it more acceptable; a Japanese incinerator is already functioning alongside a public swimming pool in Tokyo.

Restabilization of Plastics for Recycling. To make recyclate suitable for reprocessing and reuse, it needs to be restabilized because of the partial consumption of the original stabilizers during the "first-life" application. During processing and end-use, plastics undergo an oxidative degradation that results in altered molecular weight by chain scission or by cross-linking, and in deterioration of properties and surface appearance (33). Once restabilized, recycled plastics can be used again despite many years of service. For example, 10- to 13-year-old pigmented HDPE crates that are restabilized with antioxidants (Irganox 1010, phosphite Irganox 168, and light stabilizers Tinuvin 327, including hindered amines Tinuvin 710) make them suitable for the manufacture of new crates (34). Recycled PBT/PC [PBT = poly(butyl terephthalate)] blends and talc-filled PP can be restabilized with Recyloblend 660 (35). Other restablized plastics that are successfully recycled include PP from battery cases, PS from yogurt cups, PVC from window frames, and EPDM/PP [EPDM = ethylene–propylene diene monomer] blends from car bumpers (34).

Single Waste Streams

Single streams consist of PET and HDPE bottles and are the most successfully recycled of all (36). Other types of plastics suffer from either insufficient quantities collected or lacking developed markets and favorable economics. In the United States in 2000, PET and HDPE represented about 50% of plastic bottle recovery, with bottles from PVC, LDPE/LLDPE, PP, and PS accounting for only about 5% (36). One advanced approach converts clear PET bottles into high quality regrind with low residual contamination (37). Labels and glue are removed in a mixture of hot water and steam that softens and separates them. After granulation, PET flakes are washed in a mixture of detergents and caustic soda at an elevated temperature for a few minutes. Possible heavy contaminants (glass, aluminum, sand, and product residue) are separated in a hydrocyclone. Lower density particles (ie, polyolefins) are separated by the sink/float method. Detergents are removed by washing followed by de-watering and drying to reach a moisture content ranging between 20% and 0.5%. The ability of PET to be converted to fiber has made the fiber market the largest U.S. outlet for recovered PET bottles. Other uses for recycled PET include strapping and film/sheet applications. PET can also be recycled by depolymerization to monomers that are used to make virgin PET (38).

HDPE recycling includes granulation, sorting from contaminants (labels, glue, and PP caps), washing, drying, and/or pelletizing. Because of odor retention, recycled HDPE is unsuitable for food packaging but can be used in motor oil bottles, pallets, crates, and plastic lumber (39). Unwashed HDPE can be compounded with fillers or glass fiber and pigments to be extruded only into low value products (14,15,40). LDPE/LLDPE used for packaging are recycled by blending with

Table 4. Physical Properties of 100% Post-Consumer PS[a]

Property	Value	Test method
Melt flow rate (g/10 min @ 200°C, 5-kg load)	5.0–8.0	ASTM D1238
Izod impact, J/m[b]	0.64–0.8	ASTM D256
Vicat softening point, °C	100	ASTM D638
Tensile strength at yield, MPa[c]	30.34	ASTM D638
Tensile elongation,%	25–45	ASTM D638

[a]Source: Ref. 41.
[b]To Convert J/m to ft · lb/in., multiply by 1.875.
[c]To Convert MPa to psi, multiply by 145.

virgin resins and reused mostly in films (2,3). PP from battery cases and caps, lids, and container packaging is reclaimed by blending with virgin PP. Recycled PP is used in auto parts, appliances, and consumer goods (15). Crystal PS from CD jewel cases and drinking cups is ground, washed, dried, and reprocessed by injection molding to be reused as hangers, trays, picture trays, and similar items (41). Physical properties of 100% post-consumer PS are shown in Table 4. Expanded PS (EPS) from discarded egg cartons, "clam shells" (sandwich boxes), and loose packaging is recycled by blending with virgin EPS at about a 25:75 ratio and reused in the same applications. PVC from wire and cable waste is recycled by a selective dissolution process called Vinyloop (42,43). Recovered pure PVC is used for garden hoses, vinyl wallpaper, and window frames.

Mixed Waste Streams

Polyolefins. One of the most common recycling activities involving mixed waste streams is the conversion of polyolefins to plastic lumber as a replacement for wood or concrete. Compositions of mixed plastics vary from 100% unwashed feedstock to refined, tailor-made mixtures containing mostly polyolefins, foaming and reinforcing agents, pigments, and other additives. The amount and type of polyolefins in these mixtures affect physical properties of the resultant plastic lumber. Higher LDPE content in mixed waste results in a product with low flexural modulus, while a higher PP content leads to a more brittle material, especially at subzero temperatures (44). Plastic lumber containing recycled HDPE, fiberglass, and wood flour exhibits increased stiffness without any significant reduction in tensile strength. The extrusion processes for making plastic lumber resemble those for fabricating thick-wall products such as park benches, railroad ties, and backyard decks. Mechanical recycling of mixed polyolefin waste is limited; products generally have a lower resale value than those from single plastics. Examples include pallets, containers, noise insulation walls, and landscape and garden items (13,45). Feedstock recycling for mixed plastics is gaining acceptance because they permit recovery of hydrocarbon components that are used in the manufacture of new chemicals and plastics.

Engineering Alloys and Blends. Many widely used thermoplastics are engineering alloys and blends created to meet an increasing demand for greater toughness, higher end-use temperature, and improved processability. This

combination of properties cannot be achieved by the use of single polymers but is made possible by alloying or blending of different polymers through the use of impact modifiers, compatibilizing agents, and other ingredients during blending. Modifiers and compatibilizing agents used in producing these blends, however, are sensitive to repetitive thermal history during melt reprocessing.

For example, impact-modified engineering alloys and blends with enhanced toughness are often susceptible to thermal and oxidative degradation because rubber degrades and cross-links, resulting in increased viscosity and processing difficulties. PC/ABS alloys where PC is the matrix require a higher processing temperature than ABS and are more vulnerable to thermal degradation (46). These alloys lose mechanical properties and exhibit increased melt viscosity after five injection molding rounds because of the cross-linking and oxidation of the rubber phase. Polyamide-6,6 (PA-66) and poly(2.6-dimethyl–1.4-phenylene oxide) (PPO) with a graft copolymer such as styrene–maleic anhydride as a compatibilizer and an elastomeric modifier such as styrene–butadiene–styrene block copolymer exhibit good stiffness at high temperature, and solvent resistance (47). Repetitive processing of these alloys at 280°C resulted in a significant loss of impact strength due to degradation. By contrast, reprocessing of a single polymer, PA-66 containing a thermally stable impact modifier, does not show a similar loss of impact strength. PC/PMMA alloy with an impact modifier used in auto lighting components shows a decrease in stiffness after repetitive reprocessing (46). PBT/PC [PBT = poly(butylene terephthalate)] blends exhibit a slight reduction in tensile properties after three reprocessing cycles attributed to a polybutadiene-based modifier. Engineering alloys and blends including PPO/PS, ABS/PC, and PC/PBT are blended with virgin materials and additives for reprocessing and reuse (with a minimum of 25 wt% of recycled material) (48). Thermoplastic polyurethanes (PUs) are recovered by mechanical recycling and are reprocessed by Injection Molding (qv) or Extrusion (qv).

Vehicle Recycling. Recycling of material from vehicles is limited to metals and plastics, with other nonmetallic materials going to landfills (49). After metals are separated, the remaining lighter fraction is called ASR. Of about 4 million tons of ASR produced annually in the United States, more than 1 million tons consist of PU foam and more than 750,000 ton consists of thermoplastics (50). Energy recovery from ASR via incineration is achieved by adding it to the MSW; stack emissions and ash composition show no measurable environmental impact (49). Argonne National Laboratory (Illinois) has developed a unique *froth flotation* process to separate high purity plastics such as ABS, HIPS (high impact polystyrene), and PP from the ASR. The process combines size reduction, two gravity-based separation steps, and a froth-flotation separation step. Froth-flotation recovers equal-density HIPS and ABS particles. When the particles are placed in a special aqueous mixture, HIPS particles float and ABS particles sink. Recovered plastics can be used again for computer parts, office equipment and accessories, and similar products. It has been estimated that this process could recover more than 136,000 ton of high purity plastics annually from scrapped autos and appliances, saving some 92 billion megajoules (87 trillion British thermal units) of energy and avoiding disposal costs of $10–40/ton (50). Another Argonne process separates flexible PU foam from ASR and cleans it to produce high quality foam for reuse.

Auto instrument panels that used to be made from 15 kinds of plastics are now 100% recyclable as a result of redesigning with mutually compatible plastics (51). Thermoplastic olefin elastomer (TOE), forms a skin, and PP foam and mineral-filled plasma-treated PP make up the core. Heat resistant and impact resistance are retained by increasing the amount of TOE and talc in the recyclate. New approaches to vehicle recycling include eco-design, employing design for disassembly (DFD), and design for recycling (DFR) (52). DFR involves designing for end-of-life, using both recycled and recyclable materials, reducing the number of materials, marking parts for material identification, and using compatible materials and DFD (53,54). In 1995, 24 different plastics were used in the average sedan made in the United States, for a total of 143 kg, or 9.3% of the vehicle. PU, PVC, and PP were the most common, followed by PA 66, ABS, and PE. Several of these plastics are recycled for various secondary applications, including reuse in new vehicles.

Electrical/Electronics Products Recycling. Electrical and electronics products such as computers, fans, stereos, TV housings, and vacuum cleaners make up about 1% of the MSW. End-of-life electronics are a fast-growing part of MSW. More than a dozen different resins are used in electrical/electronics products, including ABS, PMMA, polyamides, PC, PP, PS, flame-retardant (FR) HIPS, PU, PVC, blends of PC/ABS, and PET/PBT (55). The six most common resins are PS and HIPS (29%), ABS (14%), PP (12%), PU (9%), PC (8%), and phenol formaldehyde (5%). Several separation technologies are used to recover these polymers. MBA Polymers (Richmond, Calif.) has developed an automated process to recover PP, HIPS, ABS, PPO, FR HIPS, PC, and PVC (Fig. 9). The sorting of plastics from durable parts by plastic type is an important aspect of achieving high quality in recycled materials. Because the parts are made from engineering plastics (qv) with a wide variety of additives, fillers, and pigments, an identification by density is not reliable. Equipment for near-IR (NIR) and mid-IR (MIR) spectroscopy is sometimes used, although with limitations; NIR focuses on determining opacity, separating the mixed stream into clear (PET and PVC), translucent (HDPE and PP), and opaque (all colored materials)materials. Paints and coatings have to be removed for accurate identification; NIR systems cannot identify plastics filled with carbon black. Size reduction of parts involves high speed granulators and rotary grinders that produce particles of different sizes and liberate metal, labels, and other nonplastic materials. After metal and nonplastics removal and sorting, the engineering plastics are repelletized and formulated for manufacture of new parts and reuse in similar applications. About 7000 kJ/kg (3000 Btu/lb) are used to recover plastics with the MBA process, and no "raw material" energy is consumed. Using recovered plastic instead of additional virgin resin results in energy savings of 39,000 kJ/kg (17,000 Btu/lb) of raw material, or more than 85% of the energy needed to make virgin resin in the first place.

Carpet Recycling. By the beginning of the century, about 4.7 million tons of residential carpets were disposed of annually in the United States, with less than 5% being reused or recycled (56). Scrap carpet is bulky and difficult to collect. Efforts are underway in the United States to reduce landfilled carpets by 40% by 2012. Carpeting is a complex product consisting of 40–60 wt% of yarn from PA-6, PA-66, PET, and PP, 4–6% of primary backing made from woven PP, 38–52 wt% of adhesive made from styrene–butadiene latex with calcium carbonate as a filler,

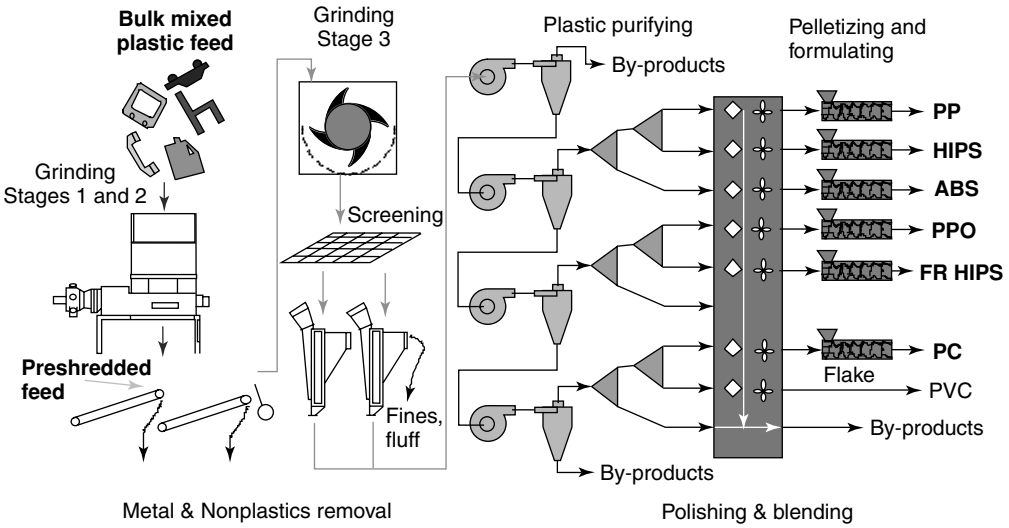

Fig. 9. Simple process flow diagram for recycling plastics from durable goods. Courtesy of MBA Polymers, Inc., Richmond, Calif.

and 3–5 wt% of secondary backing made from PP or jute (57). Carpets removed for disposal are often contaminated with dust and stains. In one method, carpets are chopped into small pieces that are fed into an extruder and then pelletized. The pellets are blended with virgin PP or LDPE for use in plastic lumber. Monsanto's patented process recycles PA-66 carpet without separation by using reactive extrusion and compatibilization (58). The resultant material is suitable for injection molding and extrusion. Yet another process produces interlocking floor tiles from vinyl-backed carpet with all the fibers of the carpet intact (59). The U.S. market for resilient flooring is about 1.5 billion square feet per year, representing a major outlet for recycled carpet.

Plastic Film Recycling

In contrast to the relative simplicity of recycling commodity resins, recycling plastic film has numerous facets, including the efficient consolidation of materials and the sorting and removal of contaminants. A significant aspect is the high volume-to-weight ratio of films, which translates into increased transportation cost. Films are more difficult to sort because most do not have identification codes. Some films like the pallet wrap contain plasticizers that make them tacky, and need to be handled separately from other films to prevent sticking. Different additives such as antislip agents and lubricants are used to manufacture films, and thus sorting is necessary. Agricultural film in the form of bags and shrink wrap can be hard to collect and to transport because of their bulk. A film used outdoors for a long time may be partially degraded, limiting its recyclability by melt extrusion. The S^3P technology discussed earlier allows recycling of densified agricultural film into

blown film without significant loss of physical properties. In Western Europe, the infrastructure for collecting and recycling PE film is more advanced than in the United States and Japan.

Biodegradable Plastics

Biodegradable plastics, designed to decompose through the action of living microorganisms, are an alternative to conventional plastics when recovery or recycling are impractical or not economically feasible. Biodegradable polymers, medical applications (qv) are of two types: naturally occurring and synthesized (64,65). The first group includes polysaccharides (qv) (starch, thermoplastic (qv); cellulose (qv)), protein (gelatin (qv); casein), and lignin (qv). Synthetic resins consists of polyalkylene esters, poly(lactic acid) and its copolymers, poly(vinyl alcohol), and others (see POLYLACTIDE; VINYL ALCOHOL POLYMERS). Some biodegradable polymers are commercial products: poly(lactic acid), starch-filled PE, poly(vinyl alcohol), plastics based on starch esters, and blends of starch esters with aliphatic polyesters, starch–poly(ε-caprolactone) blend, and others. Often, their cost prevents wide use of biodegradable plastics. Starch-based polymers are less expensive because starch is available from corn and other crops. Poly(vinyl alcohol) is widely used because of its solubility in water. Poly(lactic acid) is a low cost material used in medical implants and drug delivery. The mechanical properties of poly(lactic acid) are similar to those of PS, except for a lower glass-transition temperature and limited stability to hydrolysis. Like other plastics, biodegradable polymers can be processed by most conventional plastic processing methods such as injection molding and extrusion.

Biodegradable polymers offer unique advantages for the medical market (sutures, pins, implants) and for agriculture (mulch, seeding strips). In the United States, more than 125 million nontoxic biodegradable plastic sutures sutures (qv) are used each year in heart operations. Biodegradable polymers may also replace some hard-to-recycle contaminated products such as silage wrappings, plant pots, seed trays, and empty fertilizer bags containing chemical residue harmful to sewage treatment systems. Ongoing concern for a "green" environment has helped to increase production of biodegradable polymers from corn-derived sugar, beets, soybeans, rice bran, and potato peelings.

Life Cycle Assessment. The relatively new discipline called *life cycle assessment* (LCA) has considerable environmental implications with regard to plastic waste. LCA encompasses every phase from raw materials and resin manufacturers through transportation, processing, usage, recycling, and disposal (66). The life cycle of a plastic product embraces several steps (Fig. 10). Conversion of crude oil into petrochemicals is followed by a synthesis of virgin resins, which are then processed into products. When their useful life ends, products are either recycled or landfilled. By monitoring the qualities of a plastic throughout its life cycle, its performance value can be maintained at the highest possible level. Because only 5% of the consumed resources are transferred into useful products and 95% ends up as waste or by-products, most processes are resource-intensive (67). These may be modified in the future through LCA, which holds promise for emission studies and similar environmental aspects during the life cycle of a product.

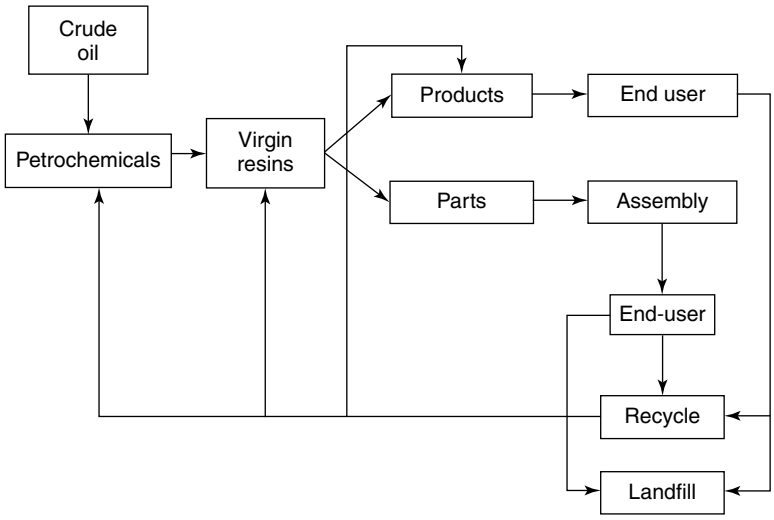

Fig. 10. Life cycle of plastics.

Overall, the reputation of plastics recycling has been a mixed one. On the one hand, many post-consumer products still cannot be recycled economically, and far too much plastic material is landfilled. On the other, emerging technologies and new attitudes are helping to brighten that picture. Increased commitments worldwide to a greener environment are reflected both in enhanced community participation and in stricter governmental regulations, raising expectations for improved plastics recycling in the future.

Other Economic Aspects

Extended Producer Responsibility. First introduced in Sweden in the early 1990s, the concept of Extended Producer Responsibility (EPR) has gained attention in Europe and elsewhere. EPR extends the manufacturer's responsibility regarding environmental impact of their products during the life cycle, recycling, and disposal. EPR was first mandated in Germany in 1991 as the "Green Dot" system. In the United States, EPR is defined more broadly as the shared responsibility of the government, consumers, and industry, rather than of the producer alone. Several American companies have voluntarily implemented EPR concepts: Xerox practices a maximum recovery of office equipment and takes back its products; Kodak takes back single-use cameras, and DuPont takes back and recycles PET film (60).

Eco-Design of Plastic Parts. Eco-design or "green design" of plastic parts involves minimizing the amount of material entering the MSW by reducing part weight and by extending the life of a part through improved performance. Reuse of a plastic for secondary applications is also practiced, along with *closed-loop recycling* (returning recycled plastic back into the same application) (61,62). Designers should choose compatible plastics to eliminate disassembly if possible,

because separation of materials is one of the critical elements in the economics of plastics recycling. Auto makers such as Peugeot (France) have adopted a "mono" material approach for large plastic parts such as bumpers in order to simplify recycling. Bumpers, fixtures, and fittings are made from one grade of PP, in contrast to the PP/EPDM blend usually used. Many manufacturers are still reluctant, however, to use recycled plastics or products with recycled content when designing their products because very little information about physical properties and long-term performance is available (63). Specifications such as size, weight, and wall thickness often constrain the use of recycled plastics. Certain products from recycled materials must be made thicker to compensate for the material's reduced properties.

BIBLIOGRAPHY

"Disposal and Reuse of Plastics" in *EPSE* 2nd ed., Vol. 5, pp. 103–128, by H. Alter, U.S. Chamber of Commerce.

1. The Resin Review: The Annual Report of the U.S. Plastics Industry, 2002 Edition, American Plastics Council (http://www.americanplasticscouncil.org/benefits/economic/economic.html).
2. Municipal Solid Waste in the United States—2002 Facts and Figures, U.S. EPA Report, EPA 530-R-02-001, Washington, D.C., June 2002.
3. *Directions for Recycling Plastics and Managing Plastics Residues*, Environment and Plastics Industry Council, Mississauga, Ont., 2002, pp. 1–18.
4. F. H. C. Edgecomb, in G. Akovali, C. A. Bernarbo, J. Leidner, L. A. Utracki, and M. Xanthos, eds., *Frontiers in the Science and Technology of Polymer Recycling*, Kluwer Academic Publishers, Dordrecht, the Netherlands, 1998, pp. 29–39.
5. Assessing the Potential for Post-Use Plastics Waste Recycling: Predicting Recovery in 2001 and 2006, Association of Plastics Manufacturers Europe Summary Report, Brussels, n.d.
6. R. Hooper, *Household Waste Plastics—A Future for Recovery*, Scientific and Technical Review, Institute of Waste Management, Brighton, England, Nov. 2000, p. 37.
7. Plastic Products, Plastic Waste, and Resource Recovery, Newsletter No. 22, Plastics Waste Management Institute, Tokyo, 1999.
8. Plastics Recycling Survey—2001, Plastics and Chemicals Industries Association, Melbourne, 2001.
9. Recycling of Plastics, Nilkamal Plastics, Ltd. (http://www.nilkamalplastics.com/news/newsdetail.asp?hlid=81&cat=Environment).
10. P. van Beukering, ed., Plastic Recycling in China—An International Life Cycle Approach, Report #W99/05, Institute for Environmental Studies, London, UK, May 1999, p. 147.
11. A. Utracki, in G. Akovali and co-workers, eds., *Frontiers in the Science and Technology of Polymer Recycling*, Kluwer Academic Publishers, Dordrecht, the Netherlands, 1998, pp. 123–152.
12. H.-F. Guo and co-workers, in Proceedings of SPE 3rd Annual Recycling Conference (ARC '96), Chicago, 1996, pp. 147–154.
13. T. Nosker and co-workers, in Proceedings of the SPE ANTEC '98, Atlanta, 1998, pp. 2912–2915.
14. J. F. Doyon and co-workers, in Proceedings of the SPE 52nd ANTEC '94, San Francisco, 1994, pp. 2876–2880.

15. M. Gibbs, in Proceedings of Polymeric Materials Science and Engineering, Vol. 63, Washington, D.C., 1990, pp. 1034–1042.
16. H.-J. Radusch and co-workers, in G. Akovali and co-workers, eds., *Frontiers in the Science and Technology of Polymer Recycling*, Kluwer Academic Publishers, Dordrecht, the Netherlands, 1998, pp. 153–189.
17. J. R. Ellis, in C. P. Rader and co-workers, eds., *Plastics, Rubber and Paper Recycling: A Pragmatic Approach* (American Chemical Society Symposium Series 609), American Chemical Society, Washington, D.C., 1995, pp. 62–69.
18. D. Mangaraj, *Comprehensive Polymer Science—Second Supplement*, Elsevier Science, Ltd., Oxford, 1996, pp. 605–667.
19. A. T. P. Zahavich and J. Vlachopoulos, in G. Akovali and co-workers, eds., *Frontiers in the Science and Technology of Polymer Recycling*, Kluwer Academic Publishers, Dordrecht, the Netherlands, 1998, pp. 271–295.
20. G. R. Kenny and D. Vaughan, in Proceedings of the SPE RETEC, Schaumburg, Ill., 1994, p. 59.
21. F. Hottenstein, private communication, Apr. 10, 2002.
22. R. J. Ehrig, ed., *Plastics Recycling, Products and Processes*, Hanser Publishing, Inc., New York, 1992, p. 29.
23. S. E. Selke, *Modern Plastics Handbook*, McGraw-Hill, New York, 1999, p. 124.
24. S. Smith, *Plast. News* 14 (Dec. 15, 1997).
25. I. Stambler, *R&D Mag.* **38**(11), 29–30 (Oct. 1996).
26. Br. Pat. PCT/GB94/00101 (n.d.), P. E. Mucci (to University of Southampton).
27. K. Khait, S. H. Carr, and M. Mack, *Solid-State Shear Pulverization: A New Polymer Processing and Powder Technology*, Technomic Publishing Co., Inc., Lancaster, Pa., 2001.
28. U.S. Pat. 5,814,623 (Sept. 29, 1998), K. Khait (to Northwestern University).
29. K. Khait and E. G. Riddick, in Proceedings of the SPE GPEC Detroit, 2002, pp. 293–299.
30. G. Mackey, in C. P. Rader and co-workers, eds., *Plastics, Rubber and Paper Recycling: A Pragmatic Approach* (American Chemical Society Symposium Series 609), American Chemical Society, Washington, D.C., 1995, pp. 161–169.
31. M. W. Meszaros, in C. P. Rader and co-workers, eds., *Plastics, Rubber and Paper Recycling: A Pragmatic Approach* (American Chemical Society Symposium Series 609), American Chemical Society, Washington, D.C., 1995, pp. 170–182.
32. American Plastics Council, http://www.plasticsresource.com/resource_conservation.
33. H. Herbst and co-workers, in G. Akovali and co-workers, eds., *Frontiers in the Science and Technology of Polymer Recycling*, Kluwer Academic Publishers, Dordrecht, the Netherlands, 1998, pp. 73–101.
34. F. A. Sitek, *Mod. Plast.* **70**(10), 64–88 (Oct. 1993).
35. J. Pospisil and co-workers, *Polym. Degrad. Stabil.* **48**, 357–358 (1995).
36. R. W. Beck, *2000 National Post-Consumer Plastics Recycling Report*, American Plastics Council, Arlington, V.I., Sept. 2001.
37. J. van den Brand, in Proceedings of the SPE 5th Annual Recycling Conference (ARC '98), Chicago, 1998, pp. 307–315.
38. "Breakthrough in PET Recycling Technology," PETCORE (PET Container Recycling—Europe), Vol. 3, no. 3, Haarlem, the Netherlands, 2001, p. 3.
39. S. D. George and S. H. Dillman, in Proceedings of the SPE 58th ANTEC, Orlando, 2000, pp. 2919–2921.
40. C. Tripodis and C. W. Brady, in Proceedings of the SPE 52nd ANTEC '94, San Francisco, 1994, pp. 2871–2873.
41. B. Kim and co-workers, in Proceedings of the SPE GPEC, Detroit, 2002, pp. 73–79.
42. J.-M. Yernaux and P. Crucifix, in Proceedings of the SPE GPEC, Detroit, 2002, pp. 193–199.

43. J. Milgrom, in Proceedings of the SPE 7th Annual Recycling Conference (ARC 2000), Detroit, 2000, pp. 93–99.
44. J. Scheirs, *Polymer Recycling: Science, Technology and Applications*, John Wiley & Sons, Inc., West Sussex, England, 1998, pp. 537–567.
45. V. E. Sperber, in Proceedings of the SPE 5th Annual Recycling Conference (ARC '98), Chicago, 1998, pp. 241–245.
46. T. S. Ellis, in D. R. Paul and C. B. Bucknall, eds., *Polymer Blends—Vol. 2: Performance*, John Wiley & Sons, Inc., New York, 2000.
47. J. T. Laverty and co-workers, *Polym. Eng. Sci.* **36**, 347–357 (Feb. 1996).
48. Ref. 44, pp. 304–334.
49. R. A. Pett and co-workers, in C. P. Rader and co-workers, eds., *Plastics, Rubber and Paper Recycling: A Pragmatic Approach* (American Chemical Society Symposium Series 609), American Chemical Society, Washington, D.C., 1995, pp. 47–59.
50. B. Jody, Recovering Usable Plastics from Automotive Scrap, http://www.transportation.anl.gov/ttrdc/recycling/plastics.html.
51. S. Itoh and K. Honjo, *Technical Notes, Japanese Society of Automotive Engineers Review 21*, Elsevier Science BV, Tokyo, 2000, pp. 385–415.
52. J. Staudinger and G. A. Keoleian, Management of End-of-Life Vehicles (ELVs) in the U.S., Report No. CSS01-01, Center for Sustainable Systems, University of Michigan, Ann Arbor, Mar. 2001.
53. Vehicle End-of-Life, Ford Motor Co. (http://www.ford.com).
54. K. Whitfield, Regulations/Economic and Plastics: The Uneasy Relationship, http://www.autofieldguide.com/colums/kermit/1101mat.html.
55. Plastics from Residential Electronics Recycling—Report 2000, American Plastics Council, Arlington, V.I. 2000.
56. A. Wilt and Garth Hickle, *Resour. Recycl.* Volume XXI, No. 2 pp. 9–12 (Feb. 2002).
57. J. Hagewood, "Carpet Recycling: An Overview," *Int. Fiber J.* http://www.hillsinc.net/carpet.htm, Apr. 1999.
58. C. G. Hagberg and J. L. Dickerson, *Plast. Eng.* **33**(4), 41–43 (Apr. 1997).
59. T. Ricciardelli and M. Lu, Development of a Class 1 Fire Rated Industrial Resilient Floor Tile Made from Post-Consumer Carpet Waste, Technical Report No. 24, Chelsea Center for Recycling and Economic Development, University of Massachusetts, Chelsea, Mar. 2000.
60. B. K. Fishbein, *Pollution Prevention Review*, Vol. **8**, John Wiley & Sons, Inc., New York, 1998, pp. 43–55.
61. D. T. Lintel and J. S. Smith, *Prog. Rubber Plast. Technol.* **12**, 221–235 (1996).
62. D. T. Lintel and J. S. Smith, *Prog. Rubber Plast. Technol.* **13**(2), 108–124 (1997).
63. D. T. Lintel and J. S. Smith, *Prog. Rubber Plast. Technol.* **13**(3), 189–202 (1997).
64. A.-M. M. Baker and J. Mead, in C. Harper, ed., *Modern Plastics Handbook*, McGraw-Hill, New York, 1999, p. 17.
65. R. Narayan, in Proceedings of the SPE GPEC 2002, Detroit, 2002, pp. 399–404.
66. M. Xanthos and A. L. Bisio, in G. Akovali and co-workers, eds., *Frontiers in the Science and Technology of Polymer Recycling*, Kluwer Academic Publishers, Dordrecht, the Netherlands, 1998, pp. 57–69.
67. L. Lundquist and co-workers, *Life Cycle Engineering of Plastics Technology, Economy and the Environment*, Elsevier Science, Ltd., Oxford, 2000, pp. 50–52.

GENERAL REFERENCES

J. Brandrup and co-workers, eds., *Recycling and Recovery of Plastics*, Hanser Publishers, Munich, 1995.

K. C. Frisch and co-workers, eds., *Recycling of Polyurethanes—Advances in Plastics Recycling*, Technomic Publishing Co., Inc., Lancaster, Pa., 1999.
V. Goodship, *Introduction to Plastic Recycling*, RAPRA Technology, Ltd., Shawburg, Shropshire, England, 2001.
C. D. Papaspyrides and J. G. Poulakis, in J. C. Salamone, ed., *Polymeric Materials Encyclopedia*, Vol. **10**, CRC Press, Boca Raton, Fl., 1996, pp. 7403–7419.

K. KHAIT
Northwestern University

REINFORCEMENT. See Volume 4.

RELEASE AGENTS. See Volume 4.

RHEOLOGICAL TESTING. See VISCOMETRY.

RIGID-ROD POLYMERS

Introduction

Scientists and technologists have aspired for a long time to produce high strength and high modulus synthetic polymeric fibers. The structural model for such fibers is made of densely packed and perfectly aligned straight polymers as shown in Figure 1. It was proposed many years ago by Staudinger (1) as the structure of polymer crystals. However, the actual development of such a fiber has been relatively slow. Figure 2 shows that the pace remained slow until DuPont revolutionized the field in the early 1970s with the commercial manufacture of an aromatic polyamide fiber under the trade name Kevlar (2–5) (see POLYAMIDES, AROMATIC).

The strongest motivation for exploring high performance fibers was provided by the aerospace industry. It generated needs for novel polymer fiber products with better properties and lower weight to be used in structural composites. Motivated by these needs, the field of high performance polymer fibers developed quickly in the 1970s and 1980s. For a long time, the U.S. Air Force worked to develop the so-called ordered polymers. Synthesis of high temperature resistant aromatic heterocyclic polymer systems began in the 1950s, and proceeded to the synthesis of ladder-like polymers, poly(6,9-dihydro-6,9-dioxobenzimidazo{2,1-*b*:1°,2′-*j*} benzo{1mn}{3,8} phenanthroline-3,12-diyl) (BBB) (**1**) and poly((7-0x0-7,1OH-bez{*de*} imidazo{4′5′:5,6} benzimidazo{2,1-*a*} isoquinoline-3,4:10,11-tetrayl)-10-carbonyl) (BBL) (**2**), in the early 1970s (6,7).

In pursuit of the general goal of producing polymers with better properties, but with easier processability than the ladder polymers, scientists in the Air Force Materials Laboratory successfully synthesized extended chain polymers, including poly((benzo{1,2-*d*:4,5′-d′} bisthiazole-2,6-diyl)-1,4-phenylene) (PBZT) (**3**), poly((benzo{1,2-*d*:4,5′-d′} bisoxazole-2,6-diyl)-1,4-phenylene) (PBZO) (**4**),

Encyclopedia of Polymer Science and Technology. Copyright John Wiley & Sons, Inc. All rights reserved.

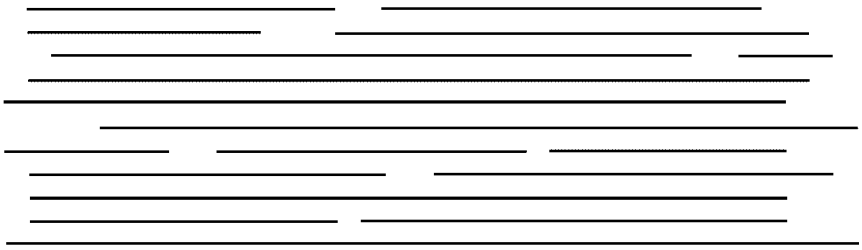

Fig. 1. The Staudinger model for crystals in polymers.

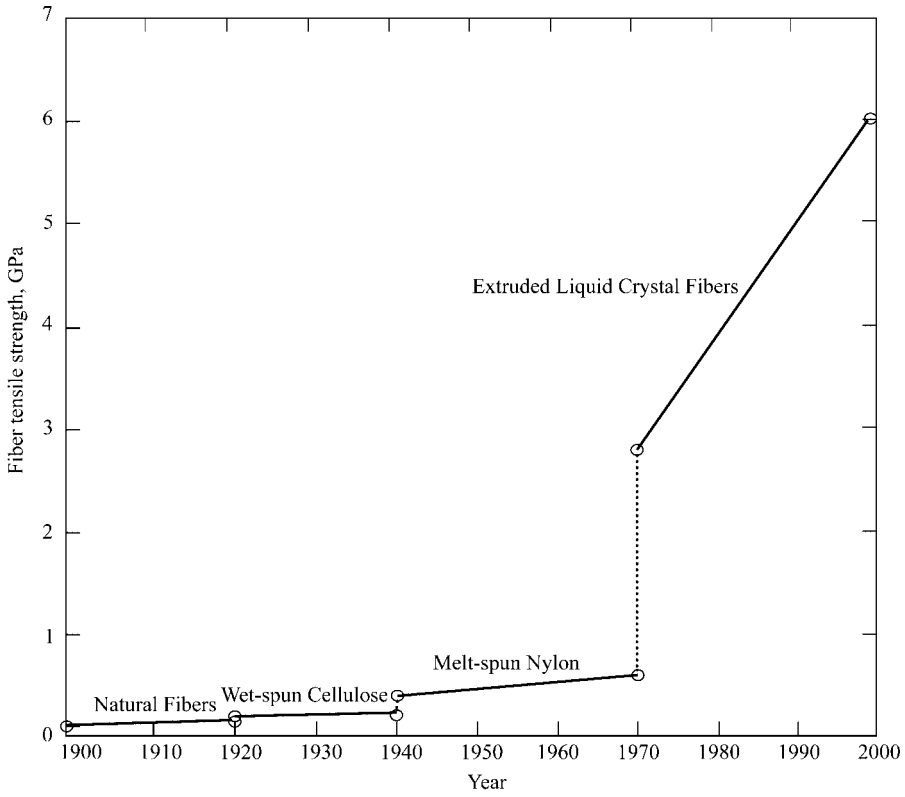

Fig. 2. History of the development of polymer fibers. To convert GPa to psi, multiply by 145,000.

poly(*p*-phenylene benzobismidazole) (PBZI or PBI) (**5**), poly(2,5 benzoxazole) (ABPBO) (**6**), poly(2,5 benzothiazole) (ABPBT) (**7**), and poly(2,5 benzimidazole) (ABPBI) (**8**) (shown in Fig. 3), commonly referred to as "rigid-rod polymers" (8,9). In this field, PBO is usually used to represent poly((benzo{1,2-*d*:4,5′-d′} bisoxazole-2,6-diyl)-1,4-phenylene). However, in the previous edition of the Encyclopedia, PBO was used for polybenzoxazole. Therefore, in order to avoid conflict with the current usage, PBZO is applied here as the acronym of poly((benzo{1,2-*d*:4,5′-d′} bisoxazole-2,6-diyl)-1,4-phenylene).

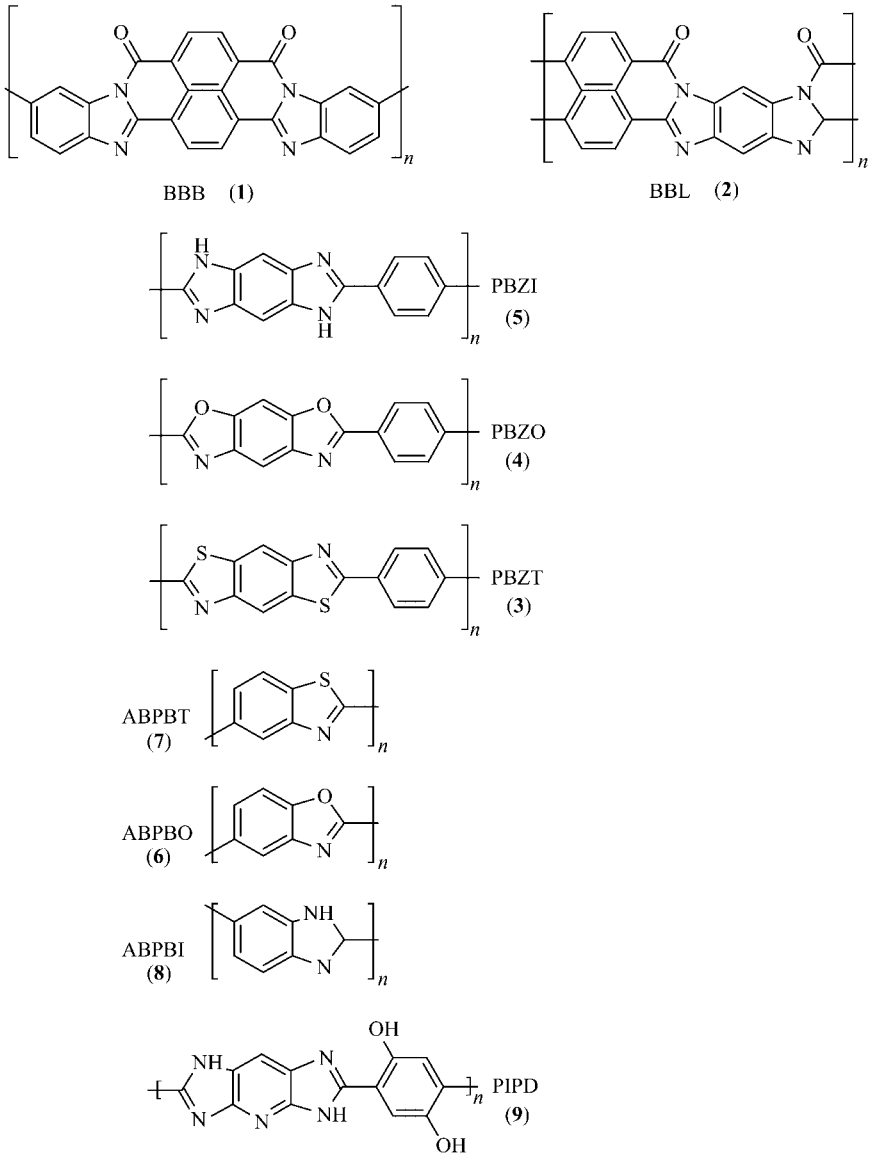

Fig. 3. Molecular structures of component members of PBZT, PBZO, PIPD, and other rigid-rod polymers.

In the 1970s and 1980s, an extensive Air Force-funded development program at SRI International, Celanese (now Hoechst Celanese Co.), DuPont, and several universities led to successful synthesis and fiber spinning from PBZT. In the mid-1980s, Dow Chemical Co. scaled up PBZO synthesis and pursued the commercialization of PBZO fibers and films (10), because they had shown excellent mechanical properties and could be synthesized more cheaply than PBZT (11,12). In 1991, the Toyobo Co. joined Dow in the Development of PBZO fibers. In 1994, Dow

decided to terminate its rigid-rod polymer program, and Toyobo was granted a license for production. In 1998, Toyobo announced success in the commercialization of PBZO fibers as the product Zylon. Recently, Akzo Co. claimed to have manufactured poly(2,6-diimidazo[4,5-b:4′5′-e] pyridinylene-1,4(2,5-dihydroxy)phenylene) (PIPD, also called M5) (**9**) fibers (13), another member of the PBX family, with improved compressive properties.

In addition to new derivatives from the PBZX family (14) and novel rigid-rod polymers such as rigid-rod polyimides (15,16) and aromatic poly(pyridinium salt)s (17), there are several special groups of rigid-rod polymers that have been studied and developed rapidly after the 1980s. Among them are polyphenylenes, poly(phenylene ethynylene), poly(*p*-phenylenevinylene) (qv), polythiophenes, polyanilines, polyquinolines, and some organometallic polymers (18–25) (see ELECTRICALLY CONDUCTIVE POLYMER; METAL–CONTAINING POLYMERS). All these are synthesized with conjugated structures and are primarily applied to optical and/or electrical usage. Recently, this field has become very active and many new rigid-rod polymers and their derivatives have emerged. It is very difficult to cover all the rigid-rod polymers, and in this article, we try to frame the research work and to construct a basic blueprint of these activities. The discussion begins with the properties, structures, syntheses, solution behavior, processing, and applications of the high performance fibers (and films) developed from the PBX family with PBZT and PBZO as the model compounds. Then other rigid-rod polymer systems are concisely reviewed.

Properties of PBZT and PBZO Fibers

The rigid-rod fibers, especially PBZO, display superior tensile properties (Table 1), thermal stability, flame resistance, barrier properties, and low smoke generation as well as low moisture sensitivity. Other good properties are cutting and abrasion resistance, chemical, oxidation, and radiation resistance, as well as a low dissipation factor (26,27). Furthermore, the rigid-rod fibers exhibit potentially useful electrical and nonlinear optical behavior. A shortcoming is the comparatively low axial compressive strength. For example, as shown in Table 1, PBZO (**4**) and PBZT (**3**) fibers exhibit tensile-to-compressive strength ratios around 15–20:1, tensile-to-shear strength ratios, 50:1, and tensile-to-shear modulus ratios, 200:1 (28). However, the newer PIPD fibers, commercialized by Akzo Nobel Co., exhibit improved compressive strength, closer to that of high performance carbon fibers (13).

Tensile Properties. Table 1 shows that the tensile properties of PBZT, PBZO, and PIPD fibers are about 55–60 times higher than that of high tenacity nylon, 25–30 times higher than polyester, 2 times higher than PPTA fibers (Kevlar 49), 4 times higher than glass fibers, and 1.5 times higher than steel. A plot of specific tensile strength and tensile modulus of fibers is given in Figure 4. It shows that PBZT, PBZO, and PIPD fibers are high due to their low density and superior tensile properties. Typical stress–strain curves of PBZT are shown in Figure 5. In general, for the rigid-rod polymer fibers, the tensile elongation at failure is about 1–2%, and heat-treated fibers are nearly linearly elastic.

Tensile properties of rigid-rod fibers, especially tensile strength, generally depend on molecular weight. With increasing molecular weight, tensile strength and

Table 1. Comparison of the Properties of Various Fibers

Materials (fibers)	Tensile modulus, GPa[a]	Tensile strength, GPa[a]	Compressive strength, GPa[a]	Density (kg/m^3) $\times 10^{-3}$
Steel	200	2.8	—	7.8
Al alloy	71	0.6	—	2.7
Ti Alloy	106	1.2	—	4.5
Alumina	350–380	1.7	6.9	3.7
Boron	415	3.5	5.9	2.5–2.6
SiC	200	2.8	3.1	2.8
S-glass	90	4.5	>1.1	2.46
E-glass	76	3.5	4.2	2.58
Pitch-based carbon				
P100	725	2.2	0.48	2.15
P120	827	2.2	0.45	2.18
PAN-based carbon				
M60J	585	3.8	3.8	1.94
T800	300	5.6	5.6	1.8
PPTA (Kevlar 49)	125	3.5	0.39–0.48	1.45
PPTA (Kevlar 149)	185	3.4	0.32–0.46	1.47
PPTA (Twaron)	115	3.2	0.58	1.45
Terlon A	135	3.8	0.4	1.45
PBZT	325	4.1	0.26–0.41	1.58
PBZO (Zylon)	360	6.0	0.2–0.4	1.56–1.58
PIPD	330	4	1.0–1.75	1.7
PE (Spectra 1000)	172	3	0.17	1.0
Vectran	65	2.9	—	1.4
Technora	70	3	—	1.39
Nylon	6	1.0	0.1	1.14
Textile PET	12	1.2	0.1	1.39

[a]To convert GPa to psi, multiply by 145,000.

elongation at break of PBZT and PBZO fibers increase (30,31). Of course, defects other than those associated with molecular ends also affect the strength of all polymer fibers. The defects include impurities, voids, surface damage, and misaligned crystals (32,33). When the intrinsic viscosity of PBZO/polyphosphoric acid (PPA) spinning solution reaches about 30 dL/g, the resulting fibers achieve the highest strength and modulus (31). After reaching a certain level, the fiber tensile modulus is independent of molecular weight (31). It is interesting that for different rigid-rod polymer fibers, the tensile molecular deformation process is similar even though these fibers have completely different chemical structures and processing. By monitoring the Raman band of the symmetrical vibrational mode of the *p*-phenylene ring, the tensile molecular deformation of different rigid-rod polymer fibers can be described with a modified series model. The Raman band shift is proportional to tensile stress (rather than tensile strain), and for all different rigid-rod polymer fibers, there is an identical slope of approximately $-4.0\ cm^{-1} \cdot GPa^{-1}$ (31). It was reported that PBZT fibers had two tensile failure modes. In Mode I, fibers with relatively higher average tensile strength exhibited little or no axial fibril splitting. In Mode II, significant splitting was observed with lower tensile strength. These two modes fit the Weibull statistical distribution (32,33).

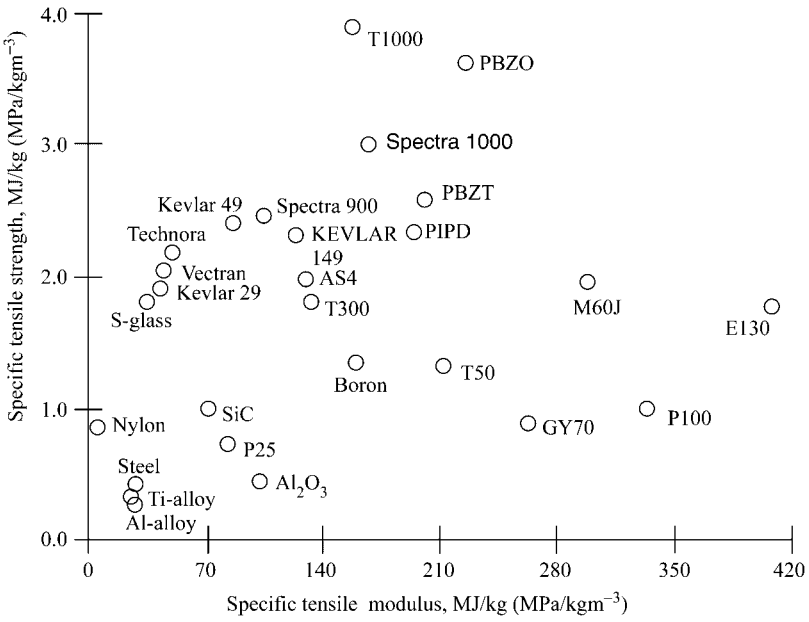

Fig. 4. The specific tensile strength and modulus of various fibers: The unit of specific strength or specific modulus (the fiber tensile strength or modulus divided by its density: Pa/(kg·m^{-3}) is equal to Nm/kg, namely J/kg).

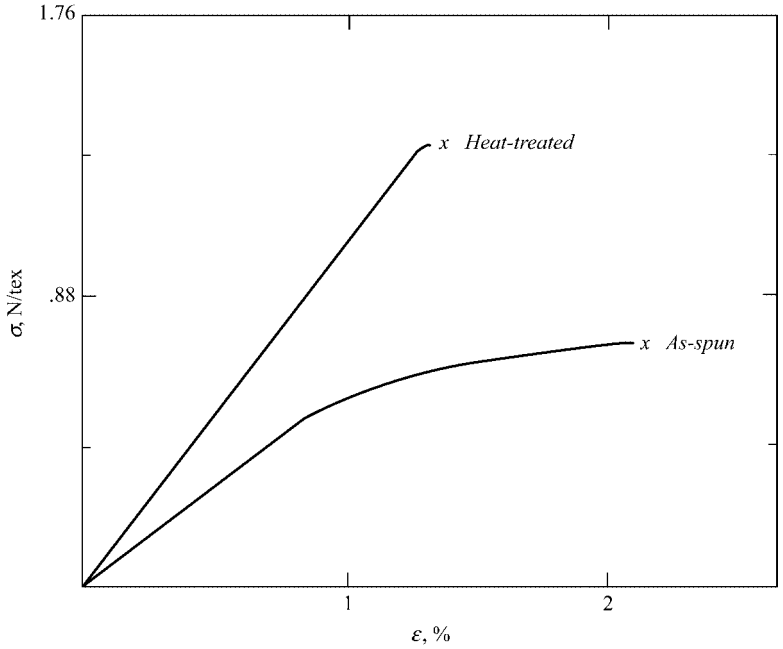

Fig. 5. Typical stress–strain curves of as-spun and heat-treated (HT) PBZT fibers. The unit conversion of fiber tenacity 1 N/tex = 0.102 kg/tex = 11.3 g/d, and the fiber tensile strength in pascal (SI unit) can be obtained as 1 N/tex = $\rho \times 10^9$ Pa = $\rho \times 1$ GPa, where ρ is the fiber density in g/cm^3. Reprinted from Ref. 29, by courtesy of Marcel Dekker, Inc.

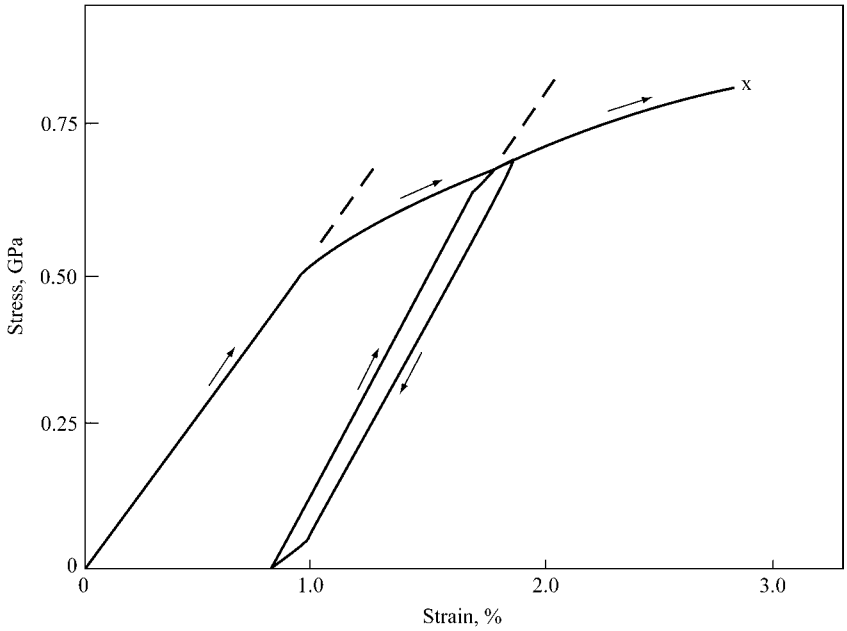

Fig. 6. Cyclic stress–strain behavior of as-spun PBZT fibers. Reprinted from Ref. 34, by courtesy of Marcel Dekker, Inc.

Cyclic stress–strain testing of as-spun (AS) PBZT fibers disclosed a nonlinear elastic–plastic behavior with strain hardening as shown in Figure 6. The tensile modulus of an AS fiber increases with repeated straining after an initial plastic deformation, which was estimated as about 2% (35,36), but the stress–strain curve of a heat-treated (HT) fiber exhibits almost no strain-rate dependence (35–38). The fatigue behavior of PBZT is similar to that of a completely elastic material. If it is perfectly elastic, the dissipation factor (tan δ) is zero. The fatigue lifetime of the HT fibers is about 13 times longer than that of the AS fibers, comparable to that of PPTA (Kevlar) fibers (39). The rigid-rod polymer fibers also have rather small creep and stress relaxation. Their creep and stress relaxation rates are extremely low compared with the conventional nylon and polyester fibers. Presumably this is caused by a combination of rigid chains and high order. Nevertheless, it was reported that the polymer fibers with rigid chains showed remarkable nonlinear dynamic viscoelasticity and poor fatigue behavior compared to those with flexible chains, especially under higher strain rate (40). The nonlinear elasticity of PBZT results from an inherent molecular nonlinear elasticity as well as crystal reorientation under an applied stress (41).

Temperature affects the nonlinear tensile elasticity. In general, the properties of the rigid-rod fibers are temperature-dependent. At 250°C, HT PBZT fiber retains approximately 80% of its room temperature tensile modulus and 70% of its room temperature tensile strength (28,37,42–46). However, fibers heated to 300°C for 65 h in air and then tested at room temperature did not show any loss of their tensile strength and modulus (47). Figure 7 shows both the strength and modulus retentions of PBZO fibers heated to 250°C under N_2 and in the

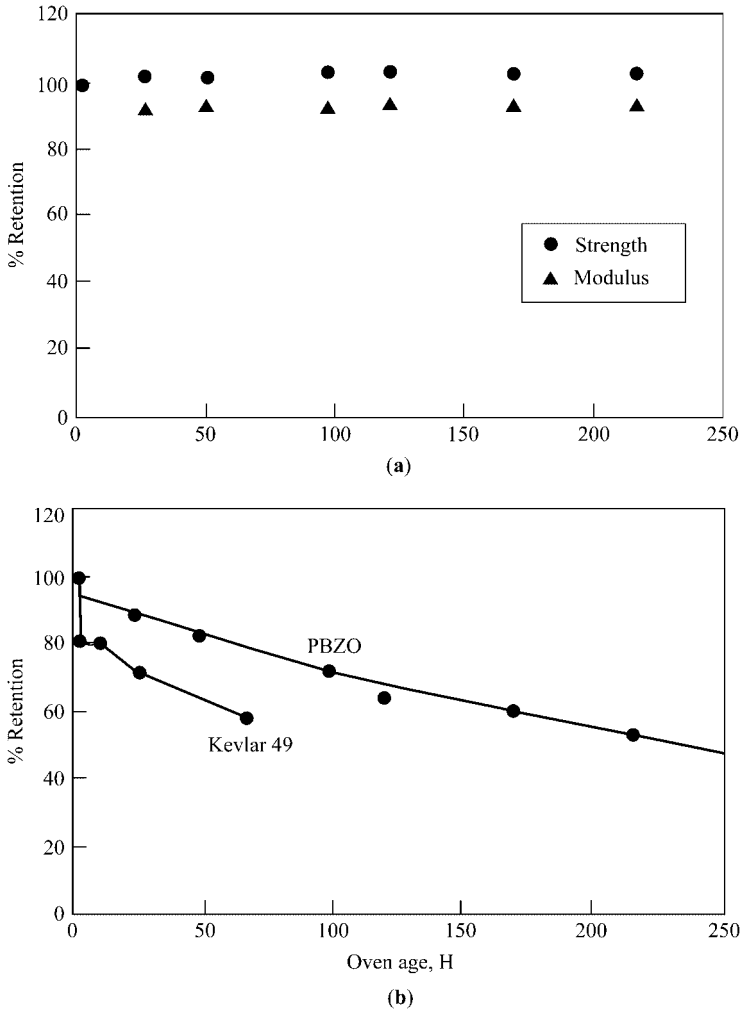

Fig. 7. (**a**) Tensile strength and modulus retention of PBZO fibers at 300°C in N_2. (**b**) Tensile strength retention of PBZO fibers with aging time at 300°C in the air, compared to that of PPTA (Kevlar 49) fibers. Reprinted from Ref. 34, by courtesy of Marcel Dekker, Inc.

air (27). Rigid-rod fibers clearly are more thermally stable than other synthetic polymer fibers (48). Jiang and co-workers reported a correlated relaxation around 300–400°C in both the laser-induced ultrasonic dynamic modulus (1 MHz) and the crystal *a*- and *b*-axis dimensions of PBZT fibers. This phenomenon is attributed to conformational oscillation around the single bond connecting the phenyl rings and bisthiazole moieties (37,49–52). A sharp increase was observed in the calculated X-ray diffraction intensity ratio of (200)/(010) around 300–400°C, which was also explained by the same oscillation using molecular dynamics simulations (50). The increase in the torsion angle was also considered to develop translational molecular motions in the direction parallel to chain axis, which brought about the decrease of the dynamic sonic modulus (53). Nakamae and co-workers recently reported that the static crystal modulus is constant in the range from

room temperature to 400°C (54). This indicates that the molecular motion suggested above is relaxed under a static force at room temperature and higher. Northolt proposed that the strong temperature dependence of the elastic tensile modulus of rigid-rod polymer fibers should be related to the rheological rotational displacement of the crystallites on account of strains in the intercrystallite interlayers (55,56). Based on the study of rigid-chain polymers (polyimides and Kevlar 49), Slutsker argued that the temperature dependence of elastic modulus should be associated with conformational defects in the crystallite lattices (54). The evolution of the conformational defects under load plays a key role in determining the static and dynamic elastic properties of the rigid chain polymer fibers. At low temperature, stretching a rigid chain polymer fiber causes an elastic extension of the covalent bonds and changes in the valence angles in the macromolecular skeleton, namely a true Hookean behavior. However, at high temperature, the fiber tensile elongation leads to a combination of the true elastic stretching and conformational transitions, an additional "non-Hookean" deformation, such as change from cis-conformation to trans-conformation. The conformational transitions are thermally activated and also reversible (57).

Compressive Properties. As listed in Table 1, the axial compressive strength of rigid-rod fibers is comparatively low, while isotropic boron, alumina, silicon carbide, E-glass, and some PAN-based carbon fibers are among the highest compressive strength fibers available. Figure 8 is a typical stress–strain curve of PBZO under tension and compression (47,58). The yield stress in compression is about one-tenth that in tension. However, the PIPD fiber shows improved compressive properties because of the intra- and intermolecular hydrogen bonds in its molecular structure (13). For PBZT fibers, no significant compressive strength dependence on either fiber tensile modulus or diameter was observed (32,33).

There is nonlinearity in compressive behavior for several rigid-rod polymer fibers (41,50,59–66). With increasing compressive stress the modulus decreases. This is the so-called modulus softening (or strain softening) phenomenon. The compressive modulus of PBZT fibers decreases up to 20% as determined with Raman spectroscopy (67), and up to 8% in a microtensile machine test (68–70). Under compression, the fiber birefringence decreases corresponding to crystal disorientation from the fiber axis (41,52,59,62–66). The crystal disorientation has also been observed by X-ray diffraction (65,66), which could contribute to the modulus decrease and even to the fiber compressive failure (52,62–66,71). It was reported that although under tension there was slight strain hardening at high strains, no strain softening behavior was observed during compression for PIPD fibers (72). However, under compression, a PIPD/epoxy composite still exhibits typical nonlinear behavior after yielding (73).

The compressive modulus (E_c) is suggested to be less than the tensile modulus (E_t). Some theoretical estimates predict it to be 70–90% of E_t (60). However, others reported that E_c appears approximately equal to E_t (41,59,62–64,70). The results of compression tests on unidirectional composites of rigid-rod fibers show that E_c is close to E_t (74,75). Improvement in the tensile modulus might not significantly change the compressive strength (76,77). By changing the spinning, coagulating, and drawing conditions, the tensile moduli of PBZO fibers varied from 130 to 210 GPa, but their compressive strengths were always in the range of 200–300 MPa. The small changes in compressive strength were considered within

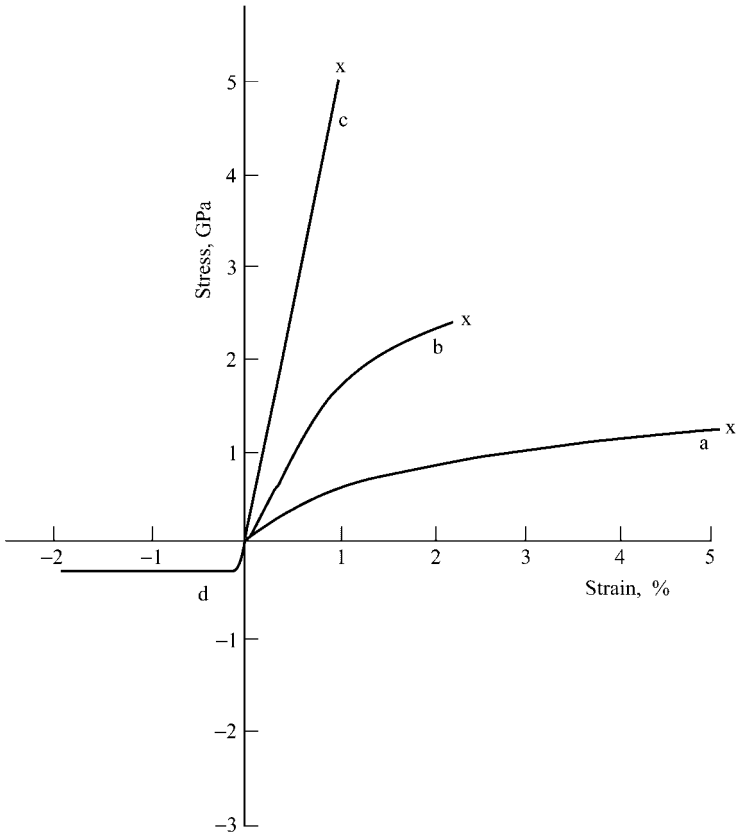

Fig. 8. Typical tensile (**a–c**) and compressive (**d**) stress–strain curves of PBZO fibers. (**a**) as-coagulated (wet), (**b**) as-spun (dried), (**c** and **d**) heat-treated. Reprinted from Ref. 34, by courtesy of Marcel Dekker, Inc.

the experimental error (78). Also, the compressive strengths of fibers made from PBZT and PBZO hardly change with variations in their tensile strengths (from 1.5 to 3.5 GPa). Conversely, the formation of compressive kink bands leads to only a small decrease in tensile strength (76,77,79–82). These results imply that no simple correlation exists between the tensile and compressive properties. For rigid-rod fibers, compressive failure may depend upon different structural factors from those controlling tensile strength. For example, in compression measurements based on bending, the fibrils/nanofibrils can play a role (83).

Based on shear mode buckling instability, a linear relation between compressive strength and torsional modulus of PBZT and ABPBO fibers was suggested, namely $\sigma_c = 0.3G$, where σ_c is the compressive strength and G the torsion modulus (84,85). However, results for a larger set of samples show departures from this relationship (85). For most rigid-rod fibers, the compressive strength is around one third to one fourth of the shear modulus (86). For example, the compressive strength value of PBZT fibers is approximately one fourth of the shear modulus (86). It was also reported that fiber axial compressive strength could be related to transverse tensile strength (87).

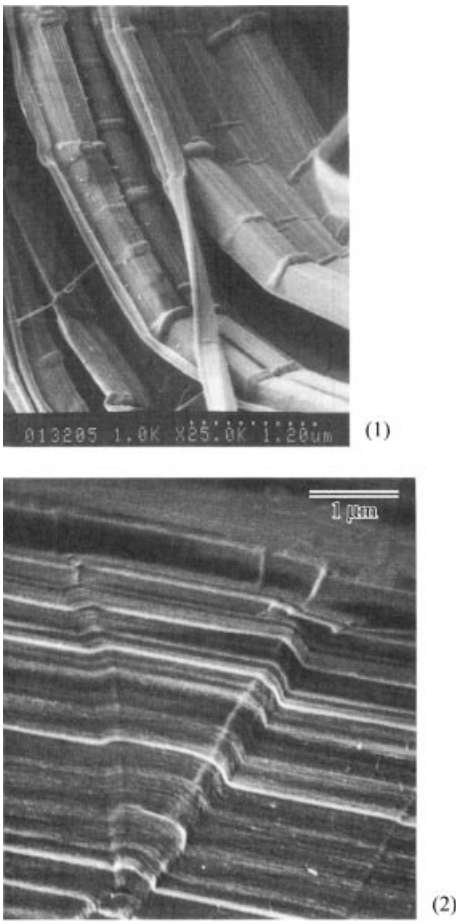

Fig. 9. Kink bands in PBZO fibers. Courtesy of D. Vezie.

For rigid-rod fibers, compressive failure is always associated with kink band formation (seen in Fig. 9) (85). Kinking is considered to be a localized axial deformation (88,89). Kink bands are nucleated locally, probably near the fiber surface. With the increase of compressive stress to a critical point, kink bands propagate and grow in toward the center and/or the other side of the fiber. Different fibers would have different critical strains for the formation of the first kink band (76,77) because of variations in structural order and defects. For PBZT fibers, no kinks are observed by optical microscopy up to 0.1% compressive strain. As the strain increases above 0.1%, kink bands suddenly appear and the number increases rapidly. Most of the new bands occur near the initial band and show some periodicity in kink concentration (90). In a limited range of strain, kink density is proportional to the compressive strain, but over the range (namely at larger strains), the density saturates (90,91). Upon the application of tensile strain after compressive kinking, many kink bands disappear, as observed by optical microscopy (65,66,90). This "reversibility" has also been confirmed by SEM examination (65,66,92). The kink band angle depends upon the fiber structure

and properties (58,93–97). For PBZO fibers, observed by TEM, kink bands are oriented at about $69 \pm 3^\circ$ to the fiber axis, with thickness from 45 nm to 1.8 μm. The thicker bands (1.2–1.8 μm) extend across the fiber with a comparatively uniform thickness. The thinner bands (0.1–0.3 μm) are usually wavy and nonuniform. Cracks and voids can develop in the bands, especially the thicker ones (>0.1 μm). When two bands intersect, a mutual shearing effect occurs, which can lead to the formation of voids. Also, the sheared region can be sheared with another intersection. The shear strain along kink bands is about 0.7%. Buckling may occur in regions of dense kink bands and intersections (98). In the crystals of PBZO fiber, a typical dimension of kinks in the fiber direction is 30–50 nm, shorter than an average PBZO molecule ($\approx$100 nm). The flux of chains through the kink boundary is apparently constant. This indicates that in a kink there is a cooperative local bending/reorientation of the covalently bonded molecules, rather than chain breakage (58,94,95). Computational modeling techniques have been used to study the possible mechanism for the reorientation, wherein compressive buckling might occur using a flipped state requiring a change of a single amide carbon–phenyl torsion angle (93,99).

There are various models for the mechanisms of kinking and compressive failure. Argon pointed out that for composite materials, kink bands form when the compressive stress along the orientation direction makes locally misaligned elements experience a relative shear stress that depends on the misorientation angle ϕ_o (100,101). DeTeresa suggested that for high performance polymer fibers, the kink formation should be determined by an elastic buckling instability in the fibers and that there is a correlation between compressive strength and the longitudinal shear modulus (79–81,83,85,86,102). Huh considered that the compressive strength is not limited by *fiber buckling*, but rather by Euler *fibril buckling* (90). Van der Zwaag argued that kink bands should form before elastic instability occurs, and may, therefore, be attributed to plastic deformation (76,77). Robinson and co-workers thought that compressive failure is related to crystallographic twinning (103), but there are counter-arguments that kinking is caused by slip (104,105). It was noted that for PBZT fibers, kink formation is associated with the $(010)\langle 001\rangle$ crystalline slip systems (91,106–110). Attenburrow and Basset thought that the extended chain deformation facilitates "fine" shear (111). Shigematsu proposed that both uniform *c*-axis shear and intercrystalline slip mechanisms should be involved in forming kink bands (112). However, many unanswered questions still remain. For example, different deformation processes, such as microbuckling, shearing, and bending, can produce kinking. It may be that kink band formation is a posteffect phenomenon and is not directly related to the material compressive strength. Many fibers kink in the mid-section of the compressive stress–strain curve.

Significant research activities have focused on enhancing the compressive properties of rigid-rod fibers (34,113). Most of these efforts have been related to increasing intermolecular interactions to improve the compressive strength (114–120). These efforts can be summarized as follows:

(1) Cross-linking PBZT fiber through post-heat-treatment in order to enhance lateral connectivity and improve the compressive strength (32,121,122);

(2) Cross-linking PBZT through creating free radicals
   a. by thermal elimination and/or irradiative degradation of activated aryl halogen followed by the combination of the aryl/benzyl free radicals (117);
   b. by incorporating a thermally reactive crosslinking fluorine moiety into PBZT (123,124);
(3) Cross-linking benzobisthiazole rigid-rod copolymers via labile methyl or dimethylephenoxy pendent groups (118,125–131);
(4) Cross-linking PBZO fibers with polyphenylene sulfide pendent groups (132);
(5) Making rigid-rod random copolymers of phenyl benzobisthiazole with phenyl benzobisthiazole pendent-*p*-terphenyl to change the packing order (115);
(6) Introducing benzocyclobutene (BCB) cross-linking moieties into PBZT (120, 126,133–136);
(7) Using Lewis acid complexation to change intermolecular interactions and influence compressive properties (137);
(8) Forming two-dimensional PBZT and PBZO films to increase compressive strength (121,138);
(9) Syntheses of tetramethylbiphenyl PBZT-*co*-PBZT systems (139), dihydroxy PBZT and dihydroxy PBZT/PBZT copolymers (140), and monomethyl-pendant-poly (*p*-phenylene benzobisimidazole) (141) to form intermolecular hydrogen bonding.

Unfortunately, so far, all these attempts at introducing stronger intermolecular or interfibrillar interactions in rigid-rod polymer fibers have not been very successful and no significant progress in enhancing compressive behavior has yet been achieved. In a few cases, compressive strengths of over 500 MPa were reported (123,127,141), but many were in the range of 25–400 MPa (78,116,141).

Recently, Sikkema reported a new rigid-rod polymer fiber, PIPD, which exhibits rather high compressive strength (13). Because of the presence of intermolecular hydrogen bonding (N—H···O) and intramolecular hydrogen bonding (O—H···N), PIPD forms either hydrogen-bonded sheets or a bidirectional hydrogen-bonding network. The hydrogen bonding produces a strong interaction between macromolecular chains and results in high shear modulus and compressive properties (13). With the Carr–Parrinello technique based on density functional theory, computer simulation shows that there exist hydrogen-bonding networks in PIPD fibers and the networks lead to an approximately three times stronger interchain interaction, which significantly improves the compressive strength of PIPD compared to PBZO and PBZT (142). For PIPD, a compressive modulus of over 300 GPa and a compressive strength of 1 GPa have been reached. Both of them are considerably higher than the corresponding values of all other rigid-rod polymer fibers and are the best compressive properties that have ever been reported for high performance polymer fibers (13,72,143,144).

There are several other approaches for improving the compressive strength:

(1) Coating a suitable ceramic, metal, or metal compound on the surface of rigid-rod fibers (2,61,67,113), such as immersion of PBZT fibers in molten

aluminum–silicon alloy or vapor-deposition of aluminum on the surface of the fibers (145). After forming a metal or ceramic layer, fiber tensile strength was decreased somewhat. Tensile fracture changed from fibrillar (for failure above 1.9 GPa) to planar (for failure below 1.9 GPa). An oxidized layer formed at the fiber surface, protecting PBZT from degradation. It is possible, therefore, to improve compressive strength of composites by the infiltration of liquid aluminum alloy into the reinforced rigid-rod fibers (143,144). On the basis of the theory of compressive failure caused by microbuckling of fibrils in shear, the critical buckling stress of rigid-rod fibers with stiff external coatings could be modeled (66). Recently it has been reported that coating Kevlar fibers with titanium nitride to a thickness of less than one-half micron by plasma-enhanced chemical vapor deposition technique suppressed the compressing buckling (146,147).

(2) Processing of PBZT/sol–gel and PBZO/sol–gel microcomposite fibers could improve the compressive properties (47,114,148).

(3) Imbedding thermoset polymers into PBZO fiber can enhance the resistance to compressive failure (149–151).

(4) By adding inorganic crystal whiskers (such as SiC and carbon nanotubes) into the spinning dopes to form composite fibers, the compressive properties of rigid-rod fibers could be improved (from 0.22–0.28 GPa for the original fibers to 0.31–0.6 GPa for the SiC-reinforced fibers). The volume percentage of the whiskers is controlled in the range of 1–20%, with sizes being $L =$ 2–20 μm, and $d = 0.1$–1.5 μm (152).

Thermal Properties. Rigid-rod fibers have good thermal stability because of the aromatic or aromatic heterocyclic (delocalized) backbones. PBZT, PBZO, and PIPD fibers in particular have good thermal behavior. Figure 10 shows the

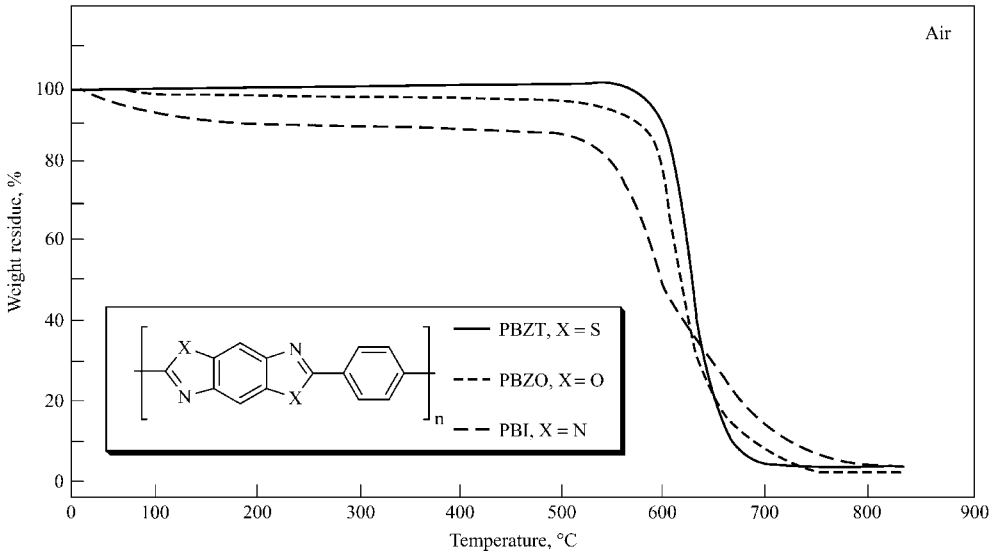

Fig. 10. Thermogravimetric analysis (TGA) diagram of PBX polymers in air. Reprinted from Ref. 34, by courtesy of Marcel Dekker, Inc.

thermogravimetric analysis (TGA) of PBX polymers (153). The thermal degradation of PBZT and PBZO occurs in air at about 600°C, and for PIPD, at around 530°C (13). At 371°C in air for 200 h, the weight retention for PBZO is reported to be 78%, and for PBZT, 70%. These fibers do not melt before decomposition occurs. They do not support combustion, but char at elevated temperature and generate small amounts of smoke while burning (154). The result of a fire fighter coat test (ASTM D4108-87, 2 cal/cm^2, 18-s exposure) demonstrated that the cloth made of aramid fibers formed brittle char while cloth made of the PBZO retained the texture integrity (27). The thermal weight-loss analysis of PBZO in air and helium shows hardly any weight loss up to 700°C in helium, and even at 850°C, 60% weight still remains (155,156). For PBZT, the main gases evolved are H_2S, HCN, and CS_2, which comprise 95% of the total ionization flow (155). The total loss of 28% at 1000°C is consistent with the loss of 1 mol of H_2S, 1 mol of HCN, and 0.25 mol of CS_2 per mole of PBZT repeat (157). For PBZO, oxygen-containing gases are the major released materials. These include CO, CO_2, and H_2O. Huang and So also discussed the mechanism of thermal decomposition for PBZT under elevated temperature (158,159).

The PBX polymer class has small negative axial coefficients of thermal expansion (CTE). For PBZT, the coefficient is approximately -1 to -2.5×10^{-6}/°C (43,160) and extrapolates to -7×10^{-6} at perfect orientation (156), or -2.9×10^{-6}/°C from 20 to 445°C (54). The negative values result from transverse vibration of the molecules as has been shown by molecular dynamics and molecular orbital calculations (52,53,71,161,162). Therefore, the fibers have good thermal dimensional stability. It was observed that under a given tension, the CTEs of PBZO fibers remain nearly the same for all heat cycles (10.8×10^{-6}/K with applied load of 1.2 MPa). The results from wet PBZO at low tension were also similar to those for their dry counterpart (43). Measured by adiabatic calorimetry, the specific heat capacities of PBZO and poly(*p*-phenylene) (PPP) at room temperature are 0.964 and 1.2 J/K·g, respectively, and above 50 K, the heat capacity shows a linear temperature dependence. Although there exists a significant difference between values of the heat capacity of PBZO and PPP, their heat capacity densities (heat capacity per unit volume) are approximately the same (1.5–1.6 J/K·cm^3) (163). Jenkins and co-workers reported a pronounced increase in thermal contraction for monomethyl pendent PBZT, which was observed at the temperatures (at about 350–450°C, varying with different fibers) where the pendent group cleaved, which was accompanied with a decrease in lattice parameters. Thermally induced chemical changes and crosslinking were considered the reasons for the accelerated shrinkage (141).

Optical and Electrical Properties. Nonlinear optics (NLO) is of interest because of its significance in providing novel optical processing approaches and applications in the area of photonics. The PBX polymer class has been recognized as candidates for NLO materials for photonic device applications (140,164–171). Owing to their orientability together with extensive conjugation given by the aromatic heterocyclic moieties, PBX polymers exhibit large third-order NLO response characterized by third-order susceptibility ($\chi^{(3)}$) derived dominantly from the delocalized π electrons (164,172). Table 2 lists the optical properties for PBZO and PBZT (173), and Table 3 exhibits the nonlinear optical third-order susceptibility of PBZT and thiophene-containing PBZT (MPBT) films (138,175,177–179). For

Table 2. Linear and Nonlinear Optical Properties of PBZO, PBZT, and Their Model Compounds[a]

Material	λmax,[b] nm	E_g,[b] eV	γ,[b] esu	$\chi^{(3)}$ (esu), resonance-enhanced (at 3 λ_{max})	$\chi^{(3)}$ (esu), off-resonance (at 2.4 μm)
PBZO	427	2.76		7.0×10^{-11}	8.1×10^{-12}
	401				
PBZT	468	2.48		8.3×10^{-11}	6.0×10^{-12}
	438				
	256				
cis-PBZO[c]	347.6		7.1×10^{-35}		7.3×10^{-13}
	331.8				
t-PBZT[c]	364.6		21×10^{-35}		20×10^{-13}
	347.2				
	332.6				

[a] Reprinted with permission from Ref. 173, copyright (1992) American Chemical Society.
[b] λ_{max} is the wavelength of the maximum absorption band, E_g, the optical band gap, and γ, the second hyperpolarizability.
[c] Data measured by degenerate four-wave mixing at 602 nm (174).

Table 3. Nonlinear Optical Third-Order Susceptibility ($\chi^{(3)}$) of PBZT and Thiophene-Containing PBZT (MPBT) Films[a]

Polymer	Processing solvent	$\chi^{(3)}$, esu	Reference
PBZT[b]	Polyphosphoric acid	3×10^{-11}	175
PBZT[c]	Methanesulfonic acid	$3.3–4.5 \times 10^{-10}$	176
MPBT[d]	Methanesulfonic acid	4.6×10^{-10}	177–179
MPBT[e]	Methanesulfonic acid	4.3×10^{-10}	177–179

[a] Copyright granted by Kluwer Academic/Plenum Publishers.
[b] Biaxial oriented film.
[c] Isotropic film.
[d] Value measured in the parallel orientation.
[e] Value measured in the perpendicular orientation.

PBZO, the nonresonant $\chi^{(3)}$ value at 2.4 μm was reported as 8.1×10^{-12} esu and for PBZT, 6.0×10^{-12} esu (measured with third-harmonic generation (THG) spectroscopy) (173). By improving the optical quality of PBZT, a $\chi^{(3)}$ of around $3.3–4.5 \times 10^{-10}$ esu was obtained (measured in a free standing film by degenerate four-wave mixing, as given in Table 3), nearly two orders larger than the former value (154,174,175,180). It has been observed that the magnitude of $\chi^{(3)}$ is essentially the same order for PBZO and PBZT, implying that there is no effect from the heteroatom on the NLO response of the heterocyclic rigid-rod polymers (173). It has also been reported that the NLO coefficient of the *trans*-PBZT monomer is larger (1.5-fold) than that of *cis*-PBZO monomer (174,181). The theoretical calculation disclosed that the geometrical isomerism (*cis vs. trans*) is a dominant factor affecting the NLO properties of the PBX family, compared to the nature of the heteroatom (O vs. S). The fully conjugated trans-isomers provide a better medium for NLO polarization than the partially conjugated cis-isomers (181). Heldmann suggested preparing electrooptical materials of rigid-rod polymers

with rigidly attached chromophores (22). Furthermore, PBZT molecular composites [with nylon-6,6 or poly(trimethyl hexamethyl eneterephthalamide) (PTMHT)] have nearly the same nonresonant third-order NLO coefficient as that of the pure PBZT (182), and molecular composites containing PBZT exhibited an enhanced NLO property (183,184). For PBZT/nylon (Zytel 330) molecular composite, $\chi^{(3)}$ is about 1.2–2.0 $\times$ 10^{-10} esu with an optical loss α of 1.2 $\times$ 10^3 cm^{-1}, compared to the α of 4.7 $\times$ 10^3 cm^{-1} for PBZT (154,175). Martin measured the linear and electroabsorption spectra of the PBZT films spin-coated from a Lewis acid complex, indicating that at least a three-level model must be used to describe their electrooptical behavior (185). The PBZT films showed an optical anisotropy with birefringence as large as 0.5 (186,187). The anisotropy of $\chi^{(3)}$ was also observed in biaxially oriented PBZT films, yielding values from 5.4 to 7.2 $\times$ 10^{-12} esu depending on the orientation degree (172).

Optical waveguide modes at wavelengths of 633 and 1300 nm have been induced in PBZT and PBZT/Mylar films. An in-plane optical loss ($\alpha_{\parallel}$) of 6.3 dB/cm and an out-of-plane optical loss ($\alpha_{\perp}$) of 300 dB/cm (at 700 nm) were determined, which also indicated strong optical anisotropy for PBZT (188). The PBZT thin films exhibit an out-of-plane optical attenuation coefficient (α_0) of 1300 dB/cm at 600-nm wavelength, and the optical loss is mainly due to intrinsic optical absorption of the polymer (169). Optical strength tests show that PBZT has a damage threshold higher than 10 GW/cm^2 with picosecond (ps) and shorter laser pulses (154,164,172,175,189). The threshold of PBZT films reaches 50 GW/cm^2 for ps laser pulses at 1.9 μm (183,184). The bilayer assemblies, consisting of a π-conjugated rigid-rod polymer layer (polybenzobisazoles) and a triarylamine-doped polycarbonate layer, were observed to be good photoconductors (190). Because of the photoinduced electron transfer and exiplex formation occurring at the bilayer interface, the intermolecular exciplexes work as the geminate ion-pairs, resulting in the enhancement of charge photogeneration and photoconductivity (190).

Today, many new conjugated rigid-rod polymers derived from the original rigid-rod molecules also have been synthesized in order to obtain special electrooptical and NLO properties (15,191,192). By way of example, a series of poly(benzobis(imidazole))s have been prepared to investigate the effect of molecular structure on the electrooptical properties (193). By replacing the *p*-phenylene ring in PBZT with a *trans*-divinylene moiety in the polymer backbone repeat unit (PBTDV), there is a 0.4-eV decrease in optical band gap. The longer the *trans*-polyacetylene segment introduced into the PBX mainframe, the lower the optical band gap (174,194).

It is well known that the rigid-rod polymer materials have good dielectric properties. However, it is interesting that because the extended π-conjugated structure provides extensive electron delocalization, the band gap calculated for PBZT in a coplanar conformation is 1.73 eV, which is close to that of polyacetylene (195,196). Therefore, although PBZT has low conductivity (about 10^{-12} S/cm) (197), because of the increase of nonplanarity that results in a significant increase in band gap, the conductivity of electrochemically doped PBZT can reach 20 S/cm (198). Substantial efforts have been made to produce electrical conducting conjugated rigid-rod polymers, including PBZT, PBZO, and their derivatives. PBZT fibers spun from nickel phthalocyanine solutions and followed by chemical

or electrochemical doping exhibited good electrical conductivity. In this fiber, PBZT was used as a component in alloys incorporating the molecular metal nickel phthalocyanine iodide (199). Electrically conducting PBZT fibers were also made by dispersing oxidized phthalocyanines (as synthetic metal phase) into the fibers (200). The experimental results of protonation of *cis*-PBZO in methanesulfonic acid solutions showed a dependence of electrical conductivity upon the *cis*-PBZO concentration (201). Rigid-rod benzobisthiazole, benzobisoxazole, and benzobisimidazole polymers containing 2,2′-bipyridine-5,5′ diyl moieties were synthesized, and displayed thin-film electrical conductivity of around 10^{-8} – 10^{-10} S/cm in the pristine state, and 10^{-4} – 10^{-5} S/cm upon filtration with $AgNO_3$ after $Ag^+ \rightarrow Ag^0$ reduction by $NaBH_4$ (170). By incorporating electroactive triarylamino moieties with insulating rigid-rod PBZT and following with iodine activation, the conductivity of the polymer reached 4.1×10^{-4} S/cm, about 5 orders of magnitude higher than previous reports. However, the activated conductivity did not have good stability (202,203). The longitudinal dc conductivity of lithium-doped sulfonated poly((1,7-dihydrobenzo {1,2-d:4,5-d′}dimidazole-2,6-diyl)-2-(2-sulfo)-*p*-phenylene) (PBI) was measured as high as 8.3×10^{-3} S/cm, but the transverse ac conductivity was lower. The observed conductivity was mainly ionic and no electronic component was detected (202,203).

Electrically conductive PBZT–Ag nanocomposite fibers were spun by two-step methods. First, PBZT fibers were spun with conventional dry-jet wet-spinning technology. Then the wet as-spun fibers were immediately immersed into a silver nitrate aqueous solution (30–70 wt%) at room temperature to allow silver ions to diffuse into the fibers. By means of chemical, thermal, or photo reduction methods, the silver salts in the fiber could be readily reduced to silver metal. The final products (silver-infiltrated fibers) have an optimal DC conductivity of 2.5×10^4 S/cm, about 16 orders greater than that of the pristine fibers (204). Tan synthesized polymers of benzobisthiazole (Bipy-PBZT), benzobisoxazle (Bipy-PBZO), and benzobisimidazole (Bipy-PyBI) containing 2,2′-bipyridine-5,5′diyl moieties. The thin films made out of these polymers displayed an electrical conductivity of 10^{-10} – 10^{-8} in the pristine state, 10^{-5} – 10^{-4} upon infiltration with $AgNO_3$, and 25–42 S/cm after $Ag^+ \rightarrow Ag^0$ reduction by $NaBH_4$ (205). In addition, Bipy-PyBI is the first conjugated rigid-rod polymer reported of this type that exhibits lyotropic behavior without any solubilizing pendents (170).

Du reported that thin films of PBZT, PBZO, and benzimidazobenzophenanthroline (BBL) polymers in the pristine state have an electrical conductivity of about 10^{-12} S/cm at room temperature (205). After high dosage ion implantation with Kr^+ (190 keV energy and 0.12 μA/cm^2 ion flux) on the surface of these polymer films, the conductivity increased by 6–9 orders of magnitude, reaching 10^2 S/cm. Table 4 is a comparison of the electrical conductivities of the pristine films and implanted layers of rigid-rod polymers (206). The ion implantation forms a sp^2-rich and three-dimensional interconnected carbon network on the surface of the polymer films, which exhibits semimetallic behavior (205,207). Wang reported that the conductivity of N^+-implanted poly(benzazole)s is about 0.1–10 S/cm at room temperature, which is significantly higher than that of corresponding pristine polymers. Based on the studies of electron paramagnetic resonance and Raman

Table 4. Electrical conductivities of the Krypton-Implanted Aggregated Films of Rigid-Rod Polymers[a]

	Thickness, μm		Conductivity, S/cm	
Polymer	Pristine film	Implanted layer	Pristine film	Ion-implanted layer
BBL[b]	13	0.38	1.1×10^{-9}	1.6×10^{-3}
DiOH-PBZT[c]	13	0.35	1.8×10^{-12}	2.4×10^{-3}
DiOH-PBZO[d]	13	0.38	2.5×10^{-12}	3.7×10^{-3}
DiOH-PBI[e]	15	0.32	2.2×10^{-9}	1.2×10^{-3}

[a]Reprinted with permission from Ref. 206, Copyright (1994), Plenum Press.
[b]BBL: poly[(7-oxo-7,10-*H*-benz[de]imidazo{4′,5′:5,6]-benzimidazo[2,1-a]isoquinoline-3,4:10,11-tetrayl)-10-carbonyl].
[c]DiOH–PBZT: poly{(benzo[1,2-d;4,5-d′]bisthiazole 2,6-diyl)-(2,5-dihydroxy 1,4-phenylene)}.
[d]DiOH–PBZO: poly{(benzo[1,2-d;4,5-d′]bisoxazole 2,6-diyl)-(2,5-dihydroxy 1,4-phenylene)}.
[e]DiOH–PBI: poly{(benzo[1,2-d;4,5-d′]bisimidazole 2,6-diyl)-(2,5-dihydroxy 1,4-phenylene)}.

vibrational spectroscopy, Wang suggested that the increase in conductivity should be attributed partially to the formation of a graphite laminar structure on the surface by the ion-implantation. This mechanism is significantly different from that of the doping-induced conductivity of polymer materials (208).

Other Properties. Rigid-rod fibers are hydrolytically stable and water has no significant effects on them. In addition, they have rather low moisture retention. The retention of PBZO fibers, after boiling in water, is only 0.5%, which is less than that of PPTA (Kevlar 49) fibers even at shorter desiccation times (43). After being dried at 250–300°C in vacuum, the moisture regain of PBZT fibers is less than 1 wt%, for PBZO fibers, 0.6%, and for PIPD fibers, 2% (13). Furthermore, most solvents have no effect on rigid-rod polymers. Only a few strong protic acids, such as PPA, methanesulfonic acid (MSA), chlorosulfonic acid (CSA), trifluoroacetic acid, and 100% sulfuric acid, can dissolve PBZT and PBZO.

Studies of radiation stability show that rigid-rod fibers are ranked as one of the best to resist electron radiation (46,49). For PBZT fibers, the critical dose (Q) of 100 keV damage is 1.6 C/cm^2, which is 1000 times that for PE (0.002 C/cm^2) (209). Under UV exposure, PBZT fiber can retain its tensile strength. As demonstrated by the GM's tests, for both as-spun and HT fibers there was little or no loss in tensile strength under UV exposure. It seems that the radiation would only disorder the macromolecule packing of PBZO, PBZT, and other rigid-rod fibers, rather than bring about bond scission or reorientation, because of the weak secondary intermolecular forces and the strong highly delocalized covalent bonding along the fiber axis (45).

Morphological Structure

PBZT, PBZO, and PIPD fibers are all spun by air-gap dry-jet wet spinning technology and have a round cross section. Their typical diameter ranges from 10 to 20 μm. A significant skin–core difference has been found for PBZT and PBZO (210,211). For PBZO, the skin thickness is on a scale of 10–100 nm (210). The skin has a relatively ordered structure and high orientation compared to the core

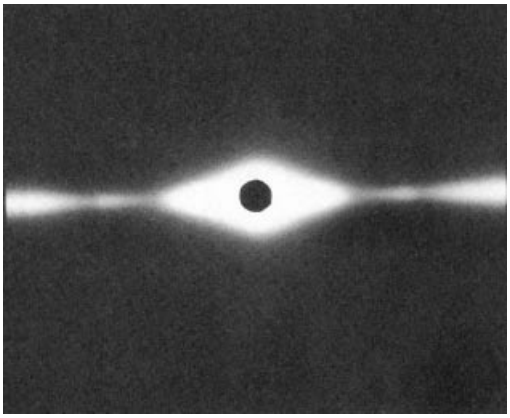

Fig. 11. SAXS photographs of PBZT fibers, showing strong equator scattering and no meridian layers. Reprinted from Ref. 34, by courtesy of Marcel Dekker, Inc.

(212,213). Heat treatment increases the crystallinity of the core (211,213). The magnitude of the skin–core differences is believed to result from the dry-jet wet spinning process involving diffusion of the solvent and fiber coagulation.

PBZT and PBZO fibers, especially the AS fibers, contain voids (44). For PBZT, the fibers spun from MSA have more pronounced voids (5–20% by volume) than fibers spun from PPA. Rates and conditions of coagulation are major factors affecting the porosity (29,44,214). After heat treatment, the SAXS of PBZT (Fig. 11) shows strong equatorial scattering, attributed either to voids elongated along the fiber or to nanofibrils. For PBZO fibers, the average diameter of the capillary-like microvoids is 2–3 nm, elongated in the fiber direction with a length of about 30 nm. Although inside the skin layer, the shape, size and frequency of microvoids are similar to those in the core of PBZO fibers, there is a void-free layer with thickness of approximately 0.2 μm in the surface region (215). Figure 12 presents the PBZO fiber structural models suggested by Martin (58) and Kitagawa (215).

A prominent structural feature found in PBZT and PBZO fibers is the oriented fibrils/nanofibrils. The Hermans–Stein orientation parameters are greater than 0.999. The axial disorder parameters are 0.53% for PBZT and 1.07% for PBZO, lower than that of Kevlar 49 fibers (1.7%) (210). However, local misorientation has been observed. Figure 13 is an image showing 3–4° misorientations between crystallites in PBZO fibers by high resolution electron microscopy (HREM) (94). The fibrils/nanofibrils are predominantly lath-shaped or ribbon-like (44,210). They are entwined and connected via Y-shaped junctions (216). It has also been reported that PBZT exhibits a lamellar appearance morphology (107). Figure 14 shows the fibril/nanofibril structure of PBZO fibers (203). For PBZT the diameter of nanofibrils is about 7–10 nm (216). The fibril dimension of PBZO is about 0.2 μm (210), and nanofibrils are of approximately 10–50 nm (210). Also, there are fibril bundles with diameters of about 5 μm. Some fibrils connect between larger fibril bundles (210). The fibrils/nanofibrils comprise discrete uniaxially oriented crystallites. It should be noted that the observed hierarchical fibril/nanofibril structures could be affected or even induced by the sample preparation techniques.

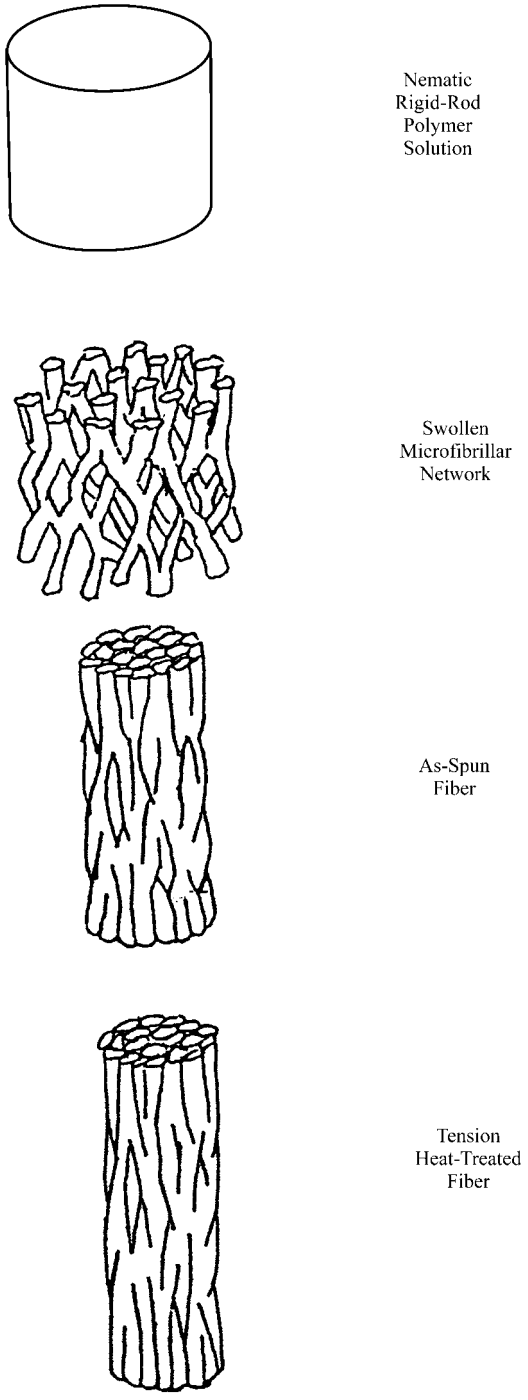

Fig. 12. Schematic diagrams of PBZO fiber structural model. (**a**) Evolution of fiber morphology suggested by Martin (58); (Reprinted from Ref. 28, by courtesy of Materials Research Society); (**b**) As-spun fiber structure suggested by Kitagawa (215) (Reprinted from Ref. 215, Copyright (1998), by permission of John Wiley & Sons, Inc.).

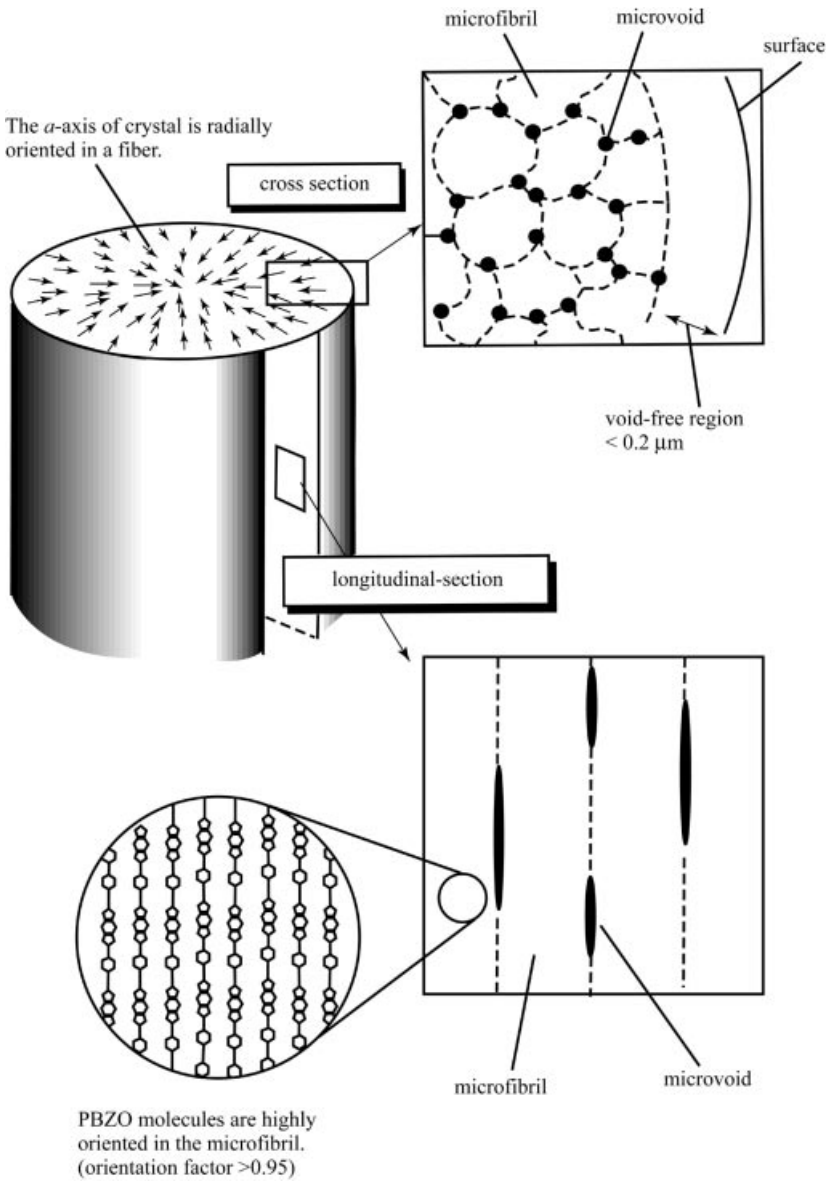

Fig. 12. (Continued).

Another unique characteristic of the rigid-rod fibers is that they are single-phase paracrystalline fibers, which is significantly different from many polymer fibers with a two-phase semicrystalline structure. Table 5 lists refined PBZT, PBZO, and PIPD crystal parameters. All of them have monoclinic crystal unit cells. For PBZT, two molecular chains pass through an oblique unit cell. Figure 15 shows the crystal structural models of PBZT suggested by Takahashi (218) and Fratini (217). In the Takahashi crystal model of PBZT, there is disorder

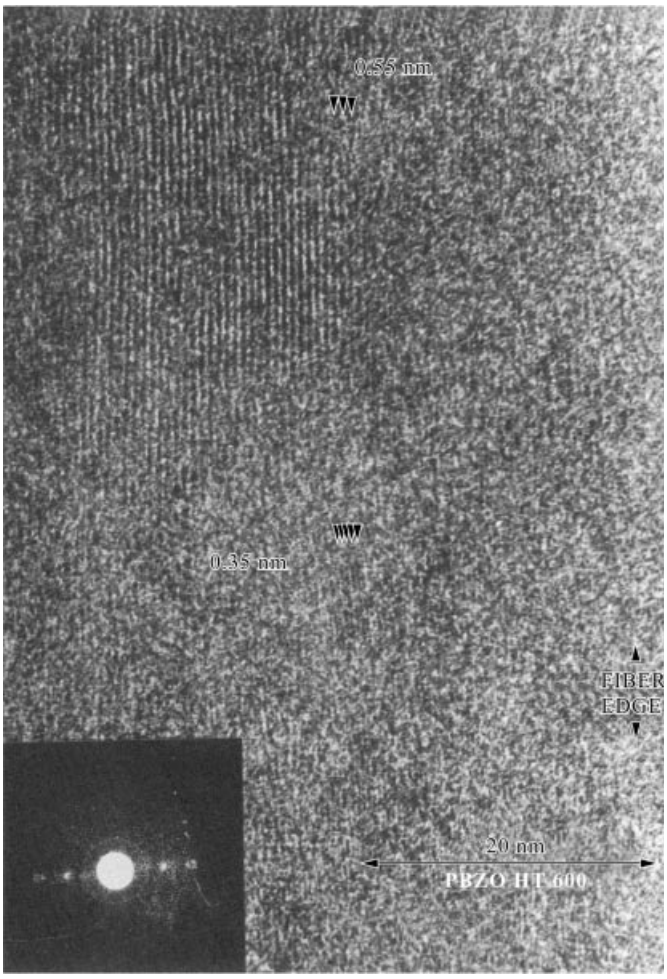

Fig. 13. HREM image of HT 600 PBZO fibers. Reprinted from Ref. 34, by permission of Marcel Dekker, Inc.

with respect to the molecular height. On the *ac* plane the molecular heights are disordered 1/2 and on the *bc* plane are disordered 1/5. Figure 16a is a PBZO crystal structure model suggested by Takahashi (225). For PBZO, two chains are packed in the unit cell and the height of PBZO molecules is disordered by a half of the fiber period, 1.205 nm. The neighboring chains are shifted by $c/4$ along the chain axis and an axial shift of chains is made by $+c/4$ or $-c/4$ randomly along the a-axis (94). Figure 16b gives the PBZO crystal structure proposed by Fratini and by Martin (96,217). In the recent report of the computer simulated modeling of the X-ray data, Tashiro and co-workers suggested that the chains form the layers extending along the (110) planes with the relative heights of neighboring chains in the sheets almost confined to either $+c/4$ or $-c/4$. These sheets are stacked together in b-axis direction with random heights along the chain axis (224).

Table 5. Comparison of Crystal Model Parameters of PBZT, PBZO, and PIPD

Authors	Material	Crystal density, g/cm^3	a-axis length, nm	b-axis length, nm	c-axis length, nm	γ angle, deg	Torsion angle between benzobisthiazole (or benzobisoxazole or pyridinylene) and phenyl rings, deg
Fratini (217)	PBZT	1.66 [85, 178]	1.179	0.354	1.251	94.0	46
Takahashi (218)			1.16	0.3588	1.251	92.0	20.5[a]
Fratini (217)		1.66 [85, 178]	1.12	0.354	1.205	101.3	13
Tashiro (224)	PBZO		1.115	0.360	1.213	100.0	—
Takahashi (225)			0.5651	0.357	0.603	101.4	25.7
Klop (144)	PIPD	1.77	1.26	0.348	1.201	$\alpha = 90$ $\beta = 108$ $\gamma = 90$	8.1

[a]This torsion angle is close to the calculated values of 27° (219,220), 20° (217), 21° (221), 29° (222), except for 55° (223).

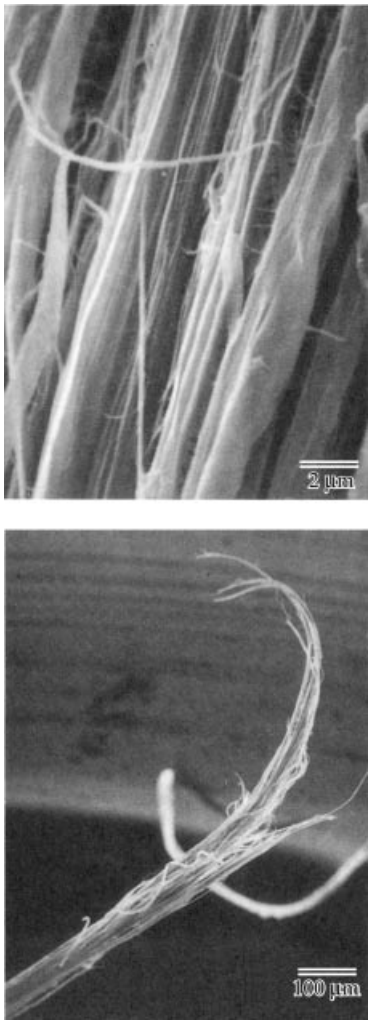

Fig. 14. Fibril/microfibril structure of PBZO fibers Reprinted from Ref. 34, by permission of Marcel Dekker, Inc.

For PIPD, two crystal unit cell models have been suggested, as shown in Figure 17 (142,144). In the monoclinic unit cell structure, the crystal lateral packing is rectangular and the cell contains two polymer chains located at its center and corners (Fig. 17a). As the *a*-axis is not perpendicular to the *c*-axis (chain direction), neighboring chains packed along the diagonals of the projection cell are shifted relative to each other in the *c*-axis direction by 0.2 nm. A distinguishing feature of the PIPD structure is that there are intramolecular (N—H···O) and intermolecular (O—H···N) hydrogen bonds. The intramolecular hydrogen bonds are located between the rigid moieties, contributing to the rigidity of the chains. The intermolecular N-H···O bonds form a bidirectional hydrogen-bonding network in which each polymer chain is linked to its four axially shifted neighbors.

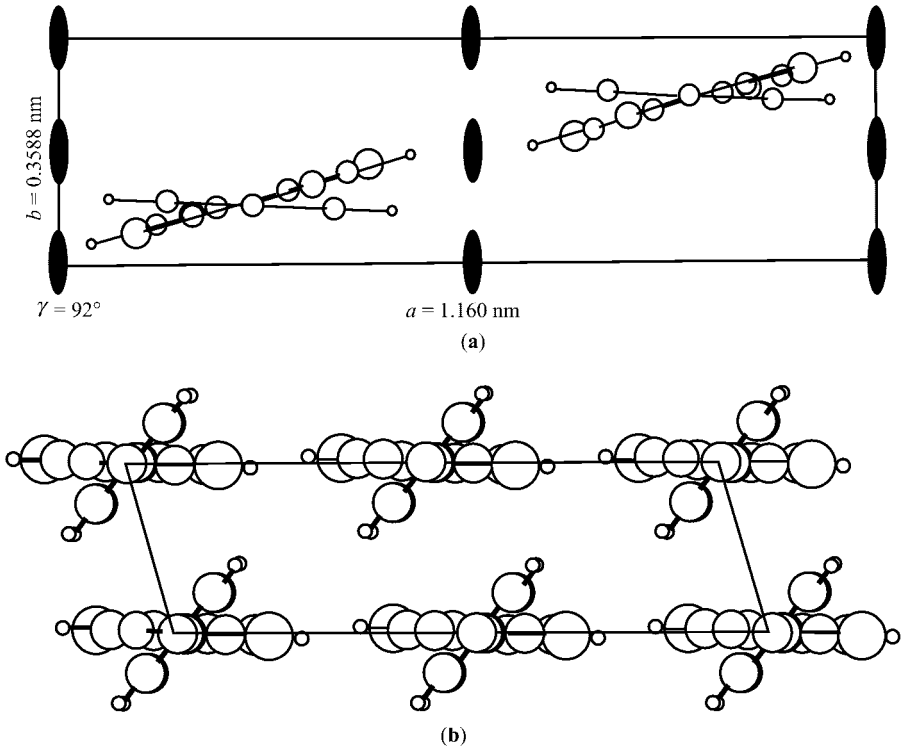

Fig. 15. Two crystal cell unit models of PBZT suggested by (**a**) Takahashi and Sul (218) (Reprinted from Ref. 218, Copyright (2000), by permission of John Wiley & Sons, Inc.); and (b) Fratini, the c-axis view of the molecular packing. The a-axis is horizontal (217). (Reprinted from Ref. 34, by permission of Marcel Dekker, Inc.).

Sheet structure may be present in a disorder model (namely a monoclinic model with sheet-like distortions), including sheets running parallel to the $(1\bar{1}0)$ but also sheets running parallel to the (110) planes (144). Computer simulation shows that for PIPD fibers, two possible crystal structures with hydrogen bonding networks may coexist: a sheet-like network for the triclinic structure and a two-dimensional network for the monoclinic structure, and there are negligible energy differences between them (142).

Benzimidazole polymers, such as PBDI, also can form a hydrogen-bonded network since they have two types of nitrogen atoms, one that is protonated as proton donors and the other that possesses the lone electron pair as proton acceptors. The variation in the strength of the hydrogen bonds in PBIs probably results in reversibility of water uptake, since some of the bonds can be more easily broken than others (226). However, PBZT and PBZO are not water-sensitive because they only have lone pair electron nitrogen atoms. In addition, the increased delocalization present in the heterocyclic rings may contribute to the lack of hydrogen bonding to water (226).

Heat-treated PBZO fibers have a three-dimensionally ordered crystal structure with limited long-range order (94,210). The structure exhibits a relatively

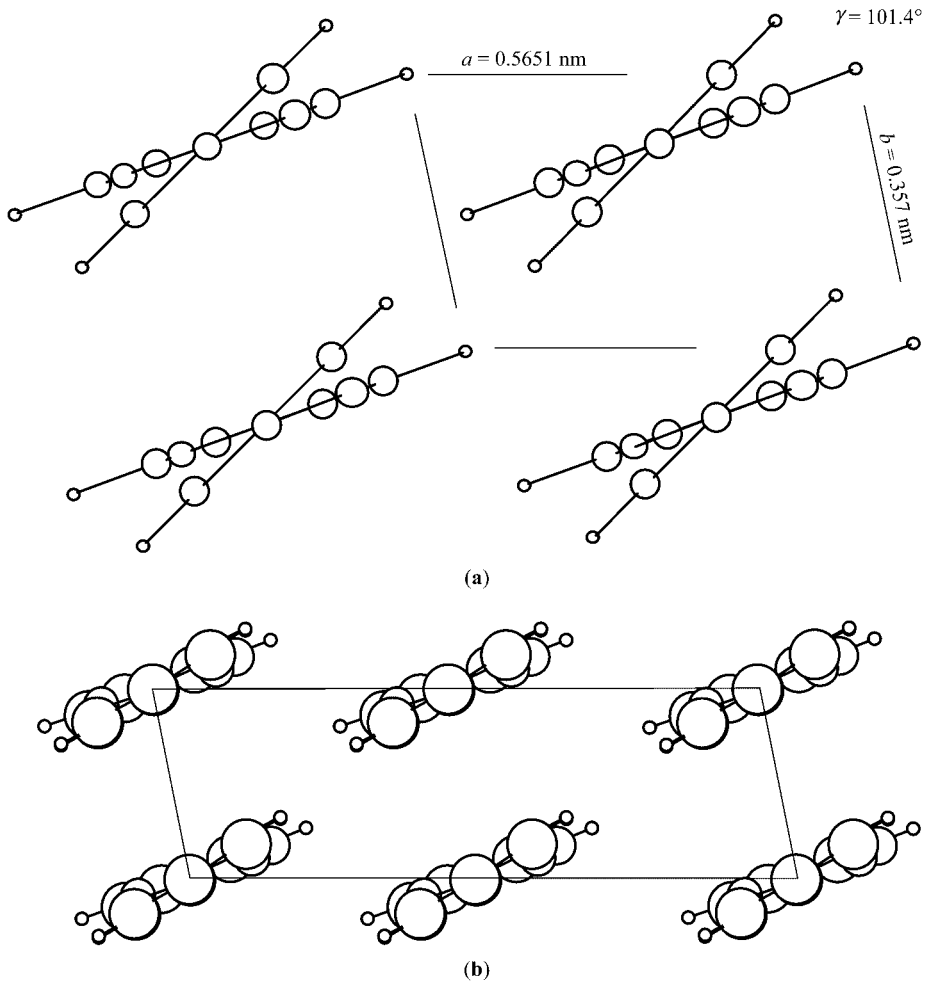

Fig. 16. Two crystal cell unit models of PBZO proposed by (**a**) Takahashi (Reprinted with permission from Ref. 225, Copyright (1999), American Chemical Society); and (**b**) Fratini (217) and Martin (96) (Reprinted from Ref. 34, by permission of Marcel Dekker, Inc.).

small crystal size of 16 nm in the longitudinal and 11 nm in the transverse directions, respectively (215). The average crystallite dimension of 15 nm (axial) $\times$ 50 nm^2 (transverse) for as-spun fibers grows to 20 nm (axial) $\times$ 150 nm^2 (transverse) for HT fibers. The planar molecules have improved registry, thus promoting three-dimensional crystallinity (210). In PBZT, the nonplanar molecules form only two-dimensional crystallites with less long-range periodicity (227) and with rather small crystal lateral size (L_a = 8.6 nm and L_b = 6 nm for HT fibers) (39). The crystallites of the as-spun fibers with a size of 3 nm^3 grow to 20 nm (axial) $\times$ 50 nm^2 (transverse) (39,210). With the synchrotron X-ray source, SAXS of as-spun PBZO fibers shows only an equatorial streak, which is generally attributed to elongated voids or fibrils. Heat-treated PBZO fibers exhibit a four-point pattern (Fig. 18) (228), which is indicative

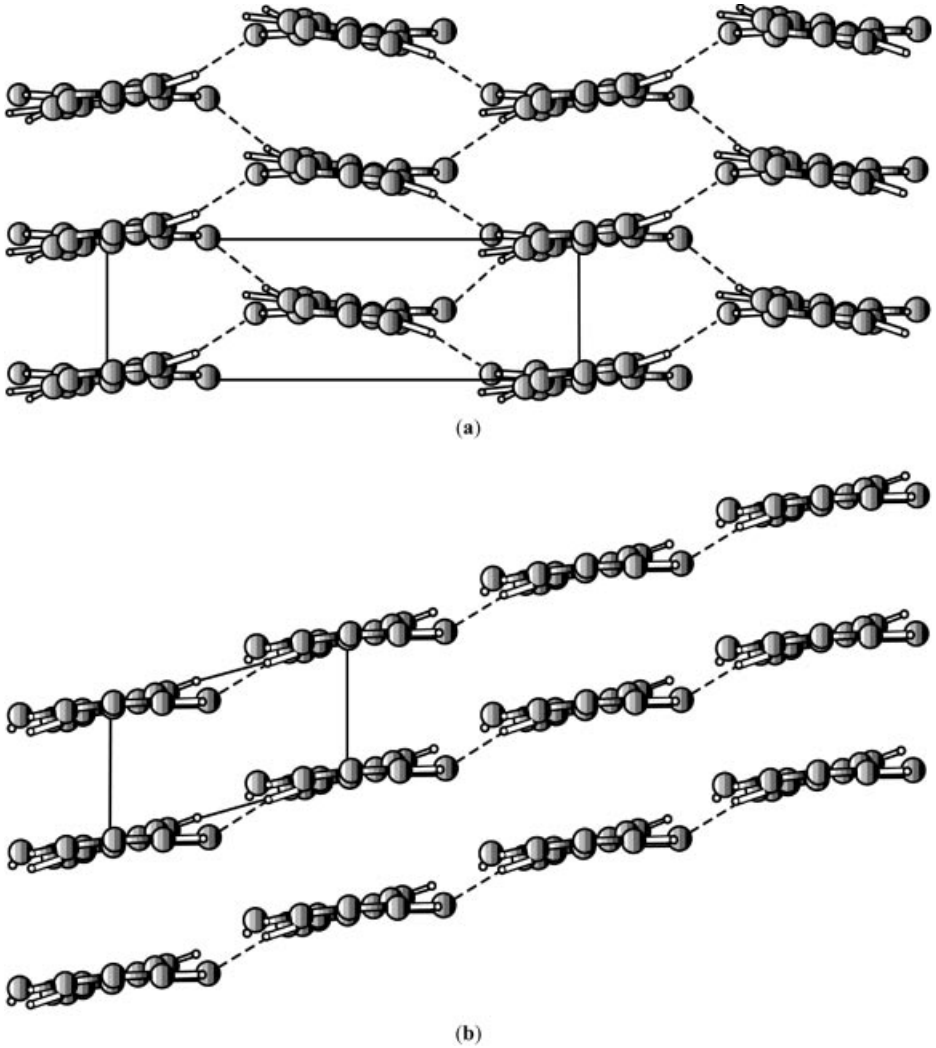

Fig. 17. Two crystal cell unit models of PIPD suggested by Klop and co-workers: (**a**) monoclinic unit cell and (**b**) triclinic unit cell. Both show the hydrogen-bonding network. Reprinted from Refs. 142 and 144, Copyright (1998, 1999 resp.), with permission from Elsevier Science.

of significant periodic density fluctuations along the fiber axis and is not seen in PBZT (Fig. 11) (94,188,210,228,229). It has been suggested that this SAXS pattern results from plate-like ordered regions with a tilt-angle from the fiber axis. For PBZT, because of the noncolinear and noncoplanar backbone, no radial 4-point pattern of SAXS has been observed (188,229). For PBZO, the long period and the radial spacing of the SAXS four-point pattern are 28 and 15 nm respectively (Fig. 18). The spacing keeps constant with varying the temperature of heat treatment. It is interesting that when the incident angle (with regard to the fiber sample) of the X-rays increases from normal (at 0°) to 30°, and then to 60° (by tilting the sample toward the beam), the four-point pattern

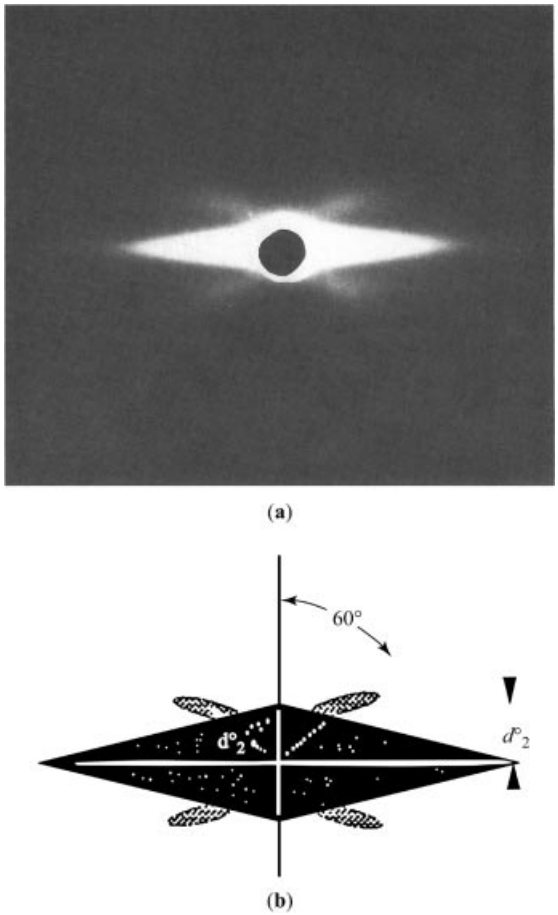

Fig. 18. SAXS pattern of PBZO (**a**) as-spun fibers, (**b**) schematic of HT fibers, exhibiting four-point scattering. Reprinted from Ref. 34, by courtesy of Marcel Dekker, Inc.

gradually changes to a two-point one (228). Figure 19 is a proposed structural model for PBZO to explain this result. In the model, crystal interfaces are at an angle to the fiber axis, giving a rhombohedral shape to the crystals (228). Also, this four-point pattern may result from arrangements of crystals that have a preferential shape. The axial grain boundaries of the crystals may have a tendency to orient at specific angles in regard to the axis. One could consider that the (302) crystal planes, working as axial grain boundaries, might serve an important function in the four-point pattern (94,96). HREM shows that PBZO fiber has large content of grain boundaries. Between adjacent crystal domains there may exist four different types of boundaries. In order of increasing energy, the four are lateral chain invariant, lateral chain rotation, axial chain invariant, and axial chain rotation (96). In addition, for PBZT and PBZO fibers containing small crystallites, there exist many structural defects such as grain boundaries between and dislocations within crystallites (94,95). Table 5 is a comparison of published crystal structural parameters of PBZT and PBZO fibers.

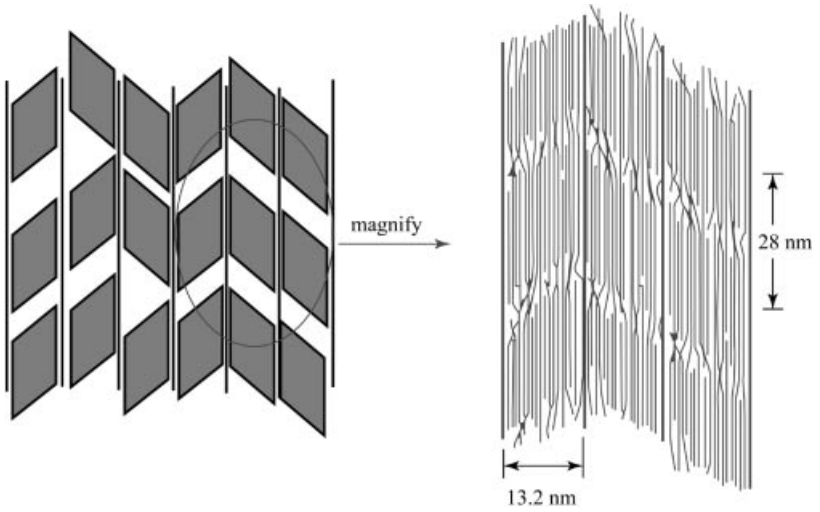

Fig. 19. Suggested structure model for PBZO Reprinted from Ref. 34, by permission of Marcel Dekker, Inc.

Lenhert first measured x-ray axial tensile modulas for PBZT and PBZO fibers with the results of 348, 395 GPa for BPZT as-spun and heat-treated fibers, and 387, 433 GPa for PBZO as-spun and heat-treated fiber, respectively (230). Recently.

Kitagawa also investigated the relation between applied stress and crystal structure of the as-spun (As-) and heat-treated (HM and HM+) PBZO (Zylon) fibers (231–234). The As-fibers have a slightly low tensile crystal modulus (430 GPa) compared to those of the HM and the HM+ (both are 460 GPa) (measured from the meridional X-ray diffraction peak of the PBZO fibers) (231–235). This difference is attributed to structure incompletion. In the rigid-rod polymer fibers, molecular ends, local molecular misorientation, and any inhomogeneities (density fluctuations) can cause the structure incompletion and the internal crystal disorder comes from the existence of density fluctuation along the fiber axis. Under extensional stress, the distribution of meridional diffraction spots becomes wider in the meridian, while the peak profile along the azimuthal direction becomes narrower. Kitagawa suggested that under the stress, the molecular orientation improvement alone should not affect interaction forces between molecules. Since the crystal size does not change but the ordering of periodicity in the crystal lattice decreases, it seems that the extensional stress affects only some local micro-region in the single-phase paracrystalline structure and crystalline disorder is increased (231–235). Davies reported that under axis extension stress, the peak of 1618 cm^{-1} Raman band broadened, which indicated that the stress and strain were distributed over the molecules (235,236).

The single crystalline structure in thin PBZT films has also been investigated (237–239). The PBZT thin films with single crystalline texture were processed from PBZT–MSA solution. In the three-dimensional oriented structure, the crystallographic c-axis is parallel to the shearing direction. The alignment of the a- and b-axes is driven by the self-assembling nature of the PBZT macromolecules

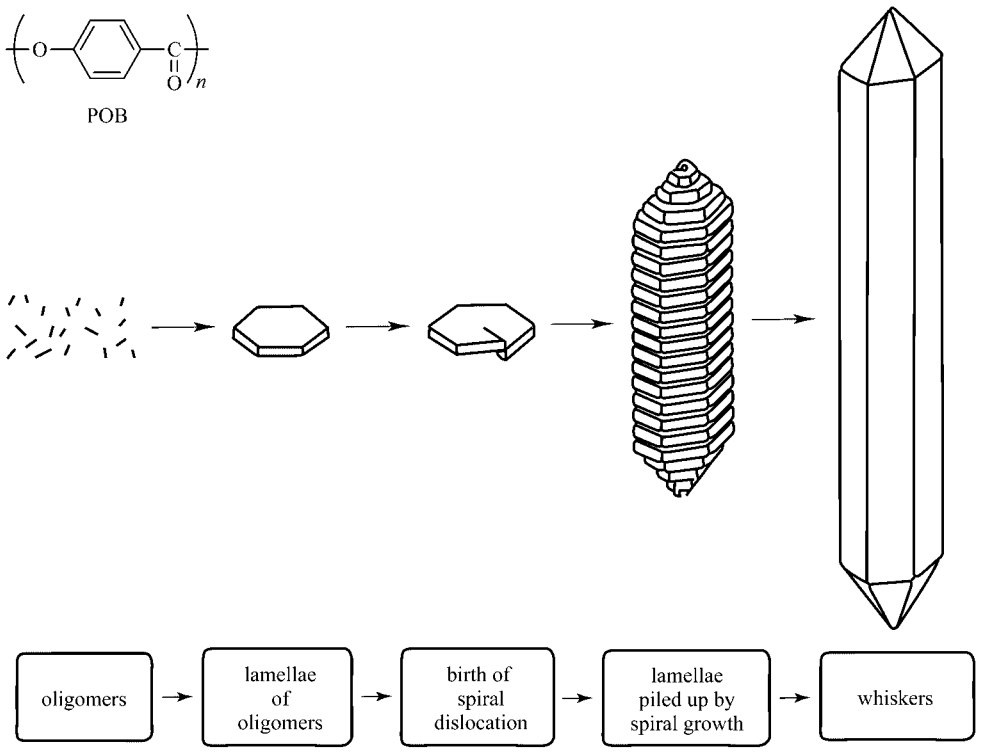

Fig. 20. A schematic diagram of the suggested POB whisker formation procedure. Reprinted from Ref. 247, Copyright (1993), with permission from Elsevier Science.

during the coagulation of the cast films, ie, the b-axis parallel to the transverse direction, and the a-axis perpendicular to the film surface (239,240).

The crystalline perfection of PIPD is similar to that of PBZO. The regular (ie nonrandom) c-axis shift of polymer chains in HT PIPD contrasts with the random $\pm c/4$ shift of polymer chains in PBZO fibers. Hence, the PIPD has a higher three-dimensional order than PBZO. This is a result of the presence of the hydrogen-bonding network, which also leads to good compressive performance (144). The crystal structure of as-spun PIPD fiber is characterized as a two-dimensionally ordered hydrate, which has a rectangular unit cell with $a = 1.685$ nm and $b = 0.338$ nm, containing planar macromolecules at its corners and center. Layers of polymer chains packed face to face are separated by layers of hydrogen-bonded water molecules. Upon heat treatment, the hydrate decomposes and the three-dimensional crystal structure develops. It is noteworthy that there exists some molecular flexibility in PIPD molecules, which is shown by the limited rotation that can exist between dihydroxyphenyl and heterocyclic moieties. The torsion angle between these two moieties may not be zero, but there is apparently some conjugation along the molecules with a closely planar conformation, because of the exhibition of metallic blue color of HT PIPD fibers (144).

There is another way of preparing extended chain crystals from rigid-rod chain polymers by means of crystallization during polymerization. The products

of this technique are called polymer whiskers. Many aromatic polyesters, such as poly(2-oxy-6-naphthoyl), poly(4′-oxy-biphenylcarbonyl), and poly(4-mercaptobenzoyl), can be used to make whiskers by means of the solid-state polymerization of the monomers and polymerization in solution to grow the crystal whiskers (241–249). Here, poly(oxy-1,4-benzenediylcarbonyl) (POB) is used as a model compound to concisely describe the typical procedure for preparing crystalline whiskers of the infusible rigid-rod polymers (188,238). The chemical structure of POB and the growth of whiskers are shown in Figure 20 (243–249). The process of POB whisker formation can be simply divided into three steps: (*1*) oligomers with low degree of polymerization are formed in a homogeneous polymerization. As soon as the degree of polymerization reaches a critical value, oligomers will crystallize from the solution (such as paraffin) to form lamellae; (*2*) if spiral dislocations can be created in the lamellae, then (*3*) needle-like crystals would be formed with the spiral growth, because of the progress of polymerization by transesterification in the interlamellar regions (as illustrated in Fig. 20). It is interesting that the final products do not have any lamellar structure but exhibit a smooth surface.

The POB whiskers can grow to 30–70 μm in length and 1–2 μm in diameter. The crystal whiskers have an identity period of 1.254 nm, corresponding to two structural residues. The observed density is about 1.50–1.51 g/cm^3, close to the theoretical density of 1.52 g/cm^3. The whiskers show high thermal stability. At about 350°C, the POB whiskers show a reversible first-order solid–solid transition caused by the rotation of 1,4-phenylene ring (250). At about 450°C, there is another phase transition associated with the nematic mesophase (251). The 5% weight loss temperature is at around 524°C (measured by TGA at a heating rate of 10°C per minute, in air). It seems that the whiskers display higher thermal stability than other POB crystals and the transition temperature is roughly correlated with the density of the crystals (243–251). In other words, the more densely the macromolecular chains pack in the whiskers, the higher the thermal stability they have. Since these whiskers have lower density than conventional ceramic whiskers, and excellent thermal and mechanical properties, they can be used as reinforcement materials for sports goods and dental materials, as well as replacement of asbestos (243–249).

Polymerization Reactions

The morphology and properties of the rigid-rod fibers are closely related to their molecular structure and processing. It is a difficult task to produce a stiff chain polymer by connecting rigid monomer units in a linear style because of the lack of solubility in many conventional solvents and a very high melting point. The synthesis of such a polymer might appear to be a simple condensation polymerization. However, it is difficult, as the long time from scientific discovery to commercialization shows. PBZT and PBZO are prepared by the reaction of terephthalic acid (TA) (**10**) or TA derivatives in PPA with aromatic tetra-amines (252–254). Equations 1 and 2 show the simplified synthetic routes to PBZT and PBZO. The detailed polymerization mechanism has been described elsewhere (254).

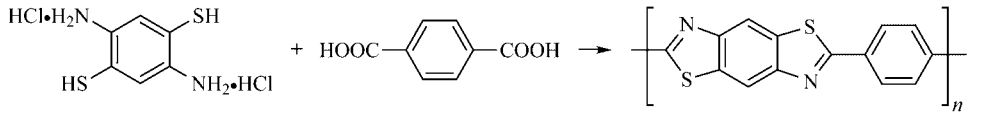

11 **10** **3**

(1)

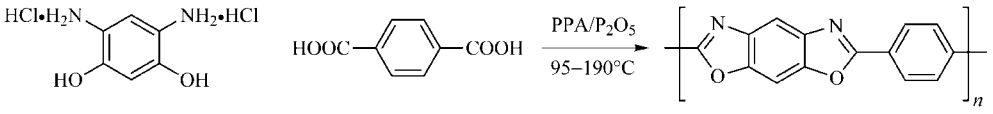

12 **10** **4**

(2)

The synthesis of *trans*-PBZT involves several steps (157,255): (*1*) first, *p*-phenylene diamine (PPD) is converted into bisthiourea with ammonium thiocyanate; (*2*) this compound is cyclized with bromine and then hydrolyzed to the oxidation-susceptible monomeric potassium salt; (*3*) the salt is isolated with HCl under reducing conditions. The bis-HCl salt is easily oxidized so that it should be handled with care. (*4*) The last step is a condensation reaction of 2,5-diamino-1,4-benzenedithiol dihydrochloride (DABDT) (**11**) with TA (**10**) in PPA (eq. 1). To completely remove hydrogen chloride before adding TA, the dehydrochlorination of amino monomers is performed under reduced nitrogen pressure, at 60–80°C (6). The particle sizes of the ultrahigh purity TA should be under 10 μm in order to assure dissolution. In the reaction, PPA has several functions, working as monomer solvent, dehydrating agent, and reaction catalyst. It is favorable to dehydration of PPA and drives polycondensation to completion (256). In order to obtain high molecular weight products, P_2O_5 is added. During the reaction, the phosphorus concentration is monitored and the P_2O_5 concentration is adjusted to about 82–84% (27). In adding the solid P_2O_5, the reaction is carried out with stirring, at 90°C, to completely dissolve the solids to form the mixture of monomers, PPA, and P_2O_5. Then, the mixture is slowly heated above 150°C (generally to 190–200°C) and the reaction kept at that temperature for 8–10 h (6). For *cis*-PBZO, polymerization in PPA is in the same manner as described above, except for using 4,6-diamino-1,3-benzenediol dihydrochloride (DABDO) (**12**) instead of DABDT (257,258). The monomer (4,6-diaminoresorcinol) can be prepared by first nitrating 1,2,3-trichlorobenzene. The second step is to prepare chlorodinitroresorcinol (**13**) through a displacement reaction using sodium hydroxide, followed by reduction to cause hydrogenolysis of the 2-chlorine atom and reduction of the nitro groups from this product (31) (eq. 3). Oxygen and moisture cause a rapid monomer decomposition. Therefore, the purity of the monomers has to be greater than 98.5% to obtain high molecular weight polymers. The procedure of monomer purification has been described (27). To keep the air-sensitive amino monomers away from side reactions, the polymerization is carried out under anhydrous conditions with inert gas protection. In addition, hydrochloride salts or other protective agents are added (6). At conversions of the reaction (eq. 2) in excess of 95%, there is a distinct decrease in the apparent polymerization rate, and the molecular weight distribution tends to broaden with increasing degree of

polymerization but the ratio of M_w/M_n never exceeds 1.8 (259,260). Furthermore, in order to control the molecular weight to the desired range, a monofunctional carboxylic acid (or its equivalent) is added to the polymerization reaction (256). During the reaction, the phosphorus concentration is adjusted so that the final P_2O_5 concentration is around 83% (25).

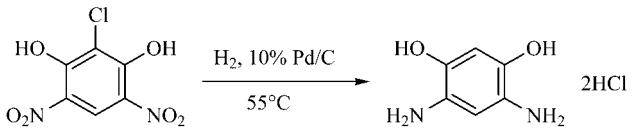

13 **12** (3)

Wolfe suggested that formation of the nematic liquid crystalline phase would increase the rate of polymerization as well as the molar mass of the final products (261). The reason is that ordering the molecules in the nematic domains increases the probability of making the reactive ends of oligomers align together thereby facilitating the reactivity. Ledbetter suggested that increasing shear on the system would also enhance the reactivity (31). The detailed polymerization mechanisms of PBZT and PBZO have been published elsewhere (113).

It has been reported that an alternate way to make the "PBX family" is by polymerizing dinitro difunctional nucleophilic monomers with terephthaloyl chloride, then reducing the nitro groups and cyclizing (262). The benefit of this is the improved oxidative stability of the dinitro monomers, but the disadvantage is the low conversion rate in reduction and cyclization. Recently, Likhatchev suggested a low temperature synthetic route for preparation of ladder poly(aroylenebenzimidazole)s (263). Hattori also reported a new two-step reaction to produce PBZT (264,265).

For PIPD, the synthetic route is different. The first step is to synthesize 2,6-diamino-3,5-dinitropyridine (DADNP) from the nitration of 2,6-diaminopyridine (DAP). With modification of the nitration medium (changing from concentrated sulfuric acid to oleum), degradation during the nitration reaction is stopped (13). Then, through the reduction of DADNP in phosphoric acid under the nitrogen and hydrogen atmosphere, more than 80% of polymer-grade crystals of 2,3,5,6-tetraaminopyridine·3HCl·1H_2O (TAP·3HCl·1H_2O) are prepared. Secondly, more than 90% polymer-grade 2,5-dihydroxyterephthalic acid (DHTA) can be produced by acid-mediated aromatization (in acetic acid refluxing with 30% aqueous H_2O_2 with a sodium iodide catalyst) of diethyl succinoylsuccinate followed by hydrolysis (13,266). Equation 4 is a simple schematic diagram of the synthesis of PIPD monomer and polymerization. Polymerization of the TAP (**14**) and DHTA (**15**) (1:1) complex or TD salt (2,3,5,6-tetraaminopyridinium 2,5-dihydroxyterephthalate) yields high quality PIPD polymers. The important improvement here is to use TAP phosphate (instead of its HCl salt), resulting in a much faster polymerization and eliminating corrosion during processing (13). Compared with PIPD, benzimidazole polymers, especially poly(*p*-phenylene benzobismidazole) (PBDI), are very hard to synthesize to high molecular weight (MW), because their low MW oligomers tend to crystallize out of PPA solution before the condensation polymerization is far advanced. This is due to preferential formation

of a stable hydrogen-bonded network in the presence of the excess water of condensation and this hydrogen network is more energetically favorable than the fully protonated molecular species dissolved in the solvent (226). Contrarily, PIPD can attain high MW via the formation of the TAP·DHTA (1:1) complex, the TD salt, which affords a fast polymerization cycle and eliminates low MW polymer that results when amine is polymerized with acid in PPA medium (13,226). By this route, high molecular weight PIPD polymers can be prepared in a routine of 4–5 h polymerization, with the relative viscosities of the products (0.25g/dL in MSA) greater than 20, even reaching as high as 300 (13).

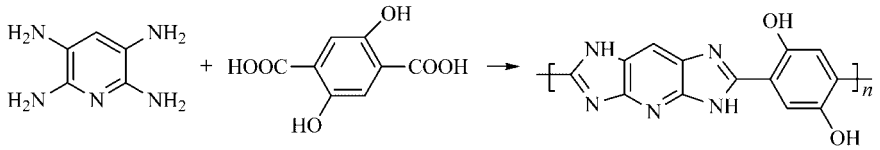

14 15 (4)

Lyotropic Liquid Crystal Polymer Solutions

It is well known that fibers spun from a lyotropic liquid crystal polymer solution can have good mechanical properties. In 1956, Flory predicted that liquid crystals would be readily formed from a rigid polymer solution at a critical concentration (267). The formation of the liquid crystal solution is dependent upon the solvent, temperature, molar mass, molecular length-to-diameter ratio, and especially, the macromolecular structure, which must be sufficiently rigid. For rigid-rod polymers, by using a suitable solvent, liquid crystals can be obtained, whereas their stiffness does not allow thermally induced liquid crystallinity (thermotropism) below their degradation temperature. However, because of their poor solubility in common solvents compared with flexible polymers, dissolution often requires using aggressive, strong protonating acids, which provide specific interactions (enthalpy), since the entropy change is small (268). Owing to the aromatic and heterocyclic molecular structure, for PBZT and PBZO, the rotation of bonds between the alternating phenylene and heterocyclic groups offers conformational flexibility to some extent. The nearly 180° catenation angle (between the two exocyclic bonds) in the repeat units leads to the overall conformation, which is nearly unaffected by the rotational conformation of the monomeric units. Also, the rotation can be confined by the interaction between the macromolecules. Therefore, they are highly rigid and, as described above, are able to form nematic liquid crystalline solution only in strong protonating acids, such as PPA, MSA, CSA, TFA, and 100% sulfuric acid (259,269,270).

The persistence length of molecules in solution is commonly defined as the average projection of the end-to-end distance of an infinite chain in the direction of the first link. It can be taken as a useful measure of their straightness and rigidity. Generally, the longer the persistence length, the lower the concentration needed for a polymer to form a liquid crystal (271,272). Table 6 lists the persistence lengths of PBZT, PBZO, and a few other polymers. Measured data for PBZT and PBZO agree qualitatively with calculations from molecular dynamics

Table 6. Measured Persistence Length for Various Polymers

Polymer	Experimental persistence length, nm
trans-PBZT	>50 (273)
cis-PBZO	>64 (224,274)
	10–117.5 (224)
PPTA	43.5 (275)
PBA	20–40 (276,277)
	41 (275)
X-500 (poly(amide hydrazide))	20–40 (276,277)
	7.5 (225)
Cellulose	4.2 (278)
PE	0.575 (275)

simulations (161,279). Such results can be subject to uncertainties arising from questions concerning the force fields and sampling all of phase space. Also, there is significant uncertainty in the persistence length measurement for rigid-rod polymers because of difficulty in finding suitable solvents. Another problem is that solvents and salts may change the conformation of the molecules, and thus the molecular rigidity (271,272,280,281). Furthermore, the salts may also change the phase diagram of the rigid-rod polymers. Therefore, the data in Table 6 should be used for relative comparison only.

In recent decades, the properties and structure of rigid-rod polymer concentrated solutions and their liquid-crystal phase formation have been extensively studied (157,259,282–284). To form a liquid crystal phase in MSA for ABPBT, ABPBO, PBZT, and PBZO, the solution concentration should be in the ranges of 13–21%, 15–18%, 5–18%, and 5–14%, respectively. Compared to PBZT and PBZO, the concentration ranges of ABPBT and ABPBO are narrower and higher (261,285). As shown in the phase diagram of the PBZO–H_2SO_4 system (Fig. 21) (286), upon adding the rigid-rod polymer, the viscosity increases but the solution remains isotropic and visually clear. With increasing polymer concentration, the rod-like molecules tend to cluster in bundles of quasi-parallel rods to form "domains." These domains are anisotropic and within them the rods form nematic order. However, there is little, if any, directional correlation among these domains. At this stage, the viscosity keeps increasing with concentration although the solution gradually changes from a single phase to biphasic. At the critical concentration, the solution becomes anisotropic and visually opaque. With further increase in polymer concentration, the viscosity drops sharply. This decrease is the result of the formation of monophase-oriented liquid crystal domains in which the chains align parallel to the flow direction, thus reducing the friction between the neighboring molecules. Temperature and solvent selection have significant effect on the critical concentration. Also it is a function of molar mass and the length-to-diameter ratio. With increasing molar mass and the length-to-diameter ratio of the polymer, the critical concentration tends to decrease. The solution viscosity also depends upon the alignment of the polymer molecules. Thus, external force fields, such as flow, electric, and magnetic fields, which affect the orientation, will influence the viscosity (5,271,272,282,287–290).

For rigid-rod polymers, the relation between intrinsic viscosity and molecular weight is (291):

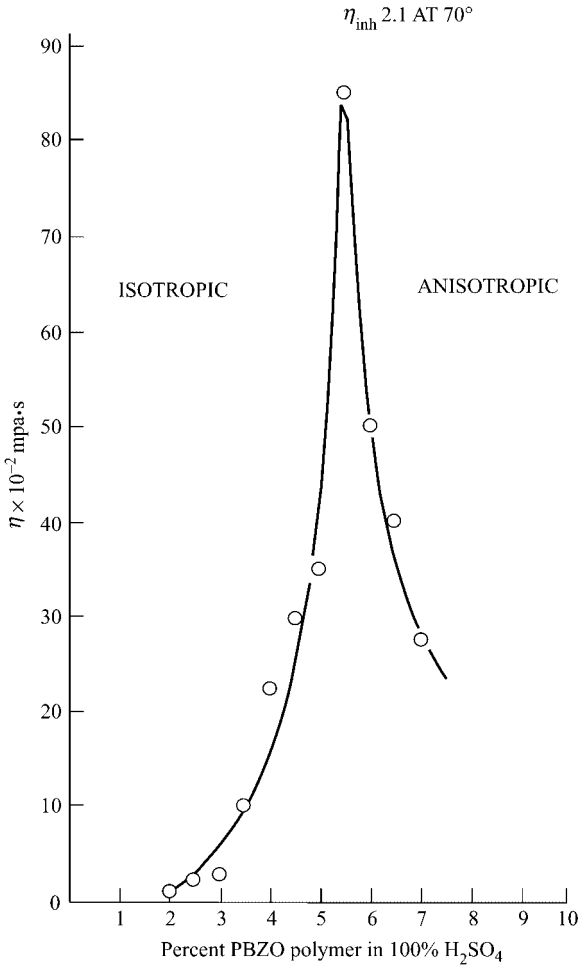

Fig. 21. A typical critical concentration curve for the rigid-rod polymers (PBZO) ($[\eta_{inh}]$: 2.1 dL/g) in 100% H_2SO_4 at 70°C (mPa·s = cP).

$$[\eta] = 5.81 \times 10^{20} \times (d_H)^{0.2} \times (M_n)^{1.8} / (M_1)^2 \quad (5)$$

where $[\eta]$ is intrinsic viscosity, d_H is hydrodynamic diameter of chain element, M_n is molecular weight, and M_1 is the mass per unit length (for PBZT, 2.15×10^9 Da/cm, and for PBZO, 1.83×10^9 Da/cm). A value of 4.86 instead of 5.81 also has been reported (259,261). If d_H is 10^{-7} cm (1 nm), the Mark–Houwink equations in MSA are

$$\text{for } \textit{trans}\text{-PBZT}, [\eta] = 1.65 \times 10^{-7} \times (M_w)^{1.8} \quad (6)$$

$$\text{for } \textit{cis}\text{-PBZO}, [\eta] = 2.77 \times 10^{-7} \times (M_w)^{1.8} \quad (7)$$

Figure 22 is the bilogarithmic plot of $[\eta]$ vs. M_w for PBZT–MSA solution (292). The slope, 1.8, agrees with equation 6. Viscosity measurements of low molecular

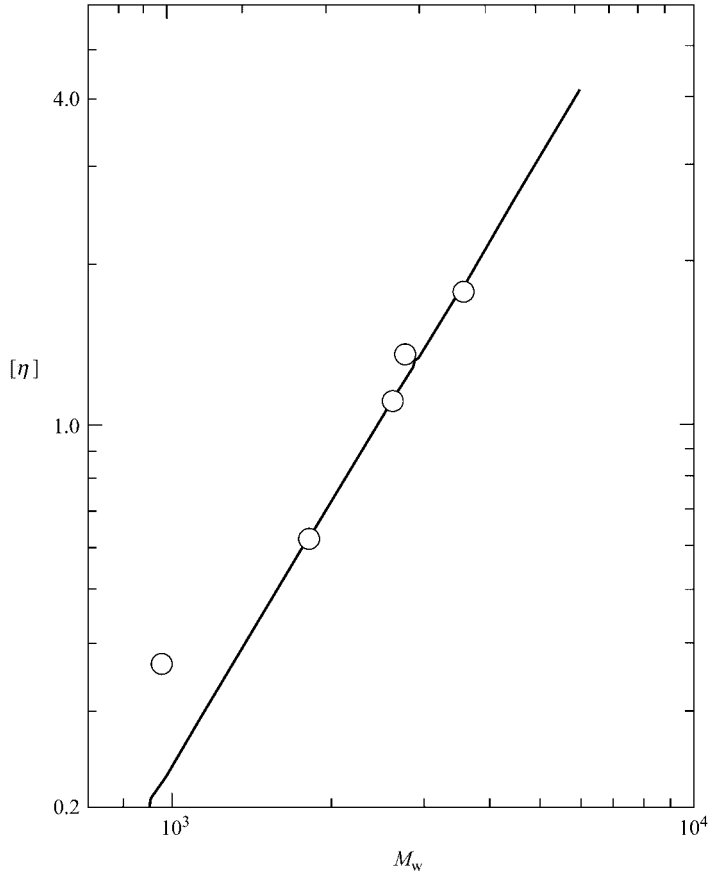

Fig. 22. Bilogarithmic plot of $[\eta]$ vs. M_w for PBZT–MSA solution. Reprinted from Ref. 34, by permission of Marcel Dekker, Inc.

weight PBZO solution in chlorosulfonic acid yield a Mark–Houwink exponent of 1.85 (292). The high Mark–Houwink exponents and persistence lengths both indicate high rigidity. Kwei (293) recently reported that for rigid-rod polymer solutions, in the general expression of the relation between specific viscosity η_{sp}, concentration C, and intrinsic viscosity $[\eta]$

$$\eta_{sp} = C[\eta]\left(1 + k_1 C[\eta] + k_2 (C[\eta])^2 + k_3 (C[\eta])^3 + \cdots\right) \tag{8}$$

the experimental k_1 value is approximately 0.5, which is lower than the theoretical estimation, 0.73–0.77 (294,295). It is possible that the long-range hydrodynamic interaction leads to a higher theoretical value (293).

The rigid-rod model based on the Smoluchowski equation has been proven successful in predicting the rheological behavior of rigid-rod polymers in the nematic phase (259,273,281,293,296–301). The flow birefringence technique has been used to characterize molecular weight, intrinsic viscosity, and optical anisotropy of different rigid-rod polymer solutions (274–276). Based on the rheo-optical flow birefringence data, the Doi–Edwards scaling law, $D_r \propto c^{-2}$ (where

D_r is a concentration-dependent rotational diffusion coefficient and c, the number concentration), holds only at very high concentrations (when $cL^3 > 150$, where L is the length of the rigid rod) for rigid-rod polymer solution. In semidilute solutions (when $cL^2d > 1$, where d is the diameter of the rigid rod), a modified Fixman model can be used to explain the temperature and concentration dependence of the rotational diffusivity (277). For PBZT and PBO, effects resulting from electrostatic interactions and molecular rheology have been studied actively (278,292,302–305). A dilute solution of these rigid-rod polymers in a low ionic strength acid shows high viscosity and small transitional diffusion. These behaviors could be attributed to a pseudo ordering of the solvent introduced by electrostatic repulsion between the protonated macromolecules. For PBZT–MSA, upon flow reversal, at low concentration and shear rate, the shear stress vs. strain shows no overshoot and a positive first normal stress transient. At high concentration and shear rate, damped oscillation in the shear stress (and a negative transient) is followed by oscillations in the first normal stress coefficient. The threshold shear rate dividing response to the flow corresponds to the onset of shear-induced variation in the polydomain texture (258). For PBZT–PPA, the oscillation in shear stress upon flow reversal and step shear persists for long times with very little damping (258). It appears that for PBZT liquid crystalline systems, anisotropic phase transient flow response is closely related to the selected solvent, rod concentration, flow-induced texture, and shear rates (258). With increasing temperature, in the concentrated PBZO– and PBZT–PPA solutions, the viscosity shows an asymmetric "V-shape" change. At high temperature, the viscosity increases markedly and the rigid-rod polymer crystallizes out of solution. This phase separation occurs near or above 230°C. It is argued that this effect is reversible, due to phase separation, not to an anisotropic-to-isotropic transition (306). In multielement systems (such as PBZT/nylon/MSA) the interaction between the rigid rod and coil molecules has a great influence on phase behavior of the systems (307–309). In addition, Fischer observed the belt-structure of PBZT liquid crystals with atomic force microscopy (310). Ding and Wu also studied the formation, transition, and texture of the liquid crystal phase of PBZT (311–313).

WAXD has been used to study the crystal solvate phase in PBZT–PPA and PBZO–PPA solutions (314–317). Upon exposure to moisture, several phases emerge in the liquid crystalline solutions, delineated as crystal solvate phases form I and form II, and the polymer crystalline phase. Form I is observed at low moisture level and ambient temperature. It may be a complex formed by the protonated macromolecules and solvent anions. This form has a three-dimensional structure and melts at around 70°C, a reversible transition. Form II is a crystalline phase observed at higher moisture content. Its behavior is different from that of form I. With increasing temperature, a gradual transition from form II to the crystalline polymer occurs in the temperature range of 250–300°C. This change is irreversible. At about 250°C, a new recrystallization occurs and the crystal spacing is close to that found in the crystalline polymer. In addition, for PBZO–PPA, form II still is a three-dimensional structure, but for PBZT–PPA, it lacks a distinct crystalline order (315–317). It was suggested that the form II of PBZT–PPA is composed of PBZT, PPA, and H_2O molecules with a range of compositions (316,318). During the transformation from form I to form II, thin nanofibrils with width less than 10 nm were formed. The results also indicated that no solvate

structures were formed during spinning and thermally induced crystal solvates which form in PBZO–PPA were not induced by extrusion. On the basis of study of the spinning extrudate and of the crystal solvates, it may be concluded that for rigid-rod fibers, the nanofibrillar/fibrillar morphology is probably determined by structures existing in the liquid crystalline spinning solution (extrudate) before fiber coagulation (316,319–322).

As to rigid-rod polymers, the properties of their dilute solutions have also been extensively studied (259,323,324). For the isotropic PBZT–MSA solution (2.5–8 wt% of PBZT, temperature from 0 to 100°C), the transient behavior from anisotropic to isotropic is qualitatively similar to that of flexible polymers (325). From the PBZT–MSA solution (3%), spherulites and co-crystals could be formed (326). Further, for PBZT–H_2SO_4 dilute solution (0.02–0.1 wt% of PBZT in 86.5–97.0 wt% H_2SO_4), quenching forms fibrillar crystals with the polymer chains parallel to the fibril direction. In addition, heat treatment of the solution can change the fibrils to shish-kebab structure. However, isothermal crystallization forms rod-like crystals (at 85–110°C). Usually the crystals are the same length and from 5 to 20 rod-like crystals align parallel to each other to form groups. Here, the polymer molecules are perpendicular to the rod-like crystals and the width of the crystals is related to the average molecular length, especially for the low molecular weight polymers (327). Shimamura reported that lath-shaped lamella crystals can form in dilute PBZO-concentrated H_2SO_4 solution. Decreasing the crystallization temperature or increasing the chain length changes the crystallites to flat fibrils (328,329).

Rigid-rod polymer–Lewis acid complexes, made by dissolving the polymer in an aprotic polar solvent such as nitromethane containing $AlCl_3$, BCl_3, or $GaCl_3$, have been studied to find new solvents and to improve processability of the rigid-rod polymers. PBZT was taken as a model compound to study this method (128,330–336). The Lewis acid, such as $AlCl_3$ or $GaCl_3$, must be in high molar ratio to obtain a relatively stable complex solution. Such a solution is suitable for film casting, and possibly fiber spinning. However, instability of the PBZT–Lewis acid complex in air is a problem for large-scale processing (335). In addition, Lewis acid coordination complexes of rigid-rod polymers have been used for a variety of applications including nonlinear optical materials (337). In order to increase the thermal plasticity of PBZX compounds in ordinary organic solvents, Reinhardt and others added fluoro-containing groups into the main chains (338–342). It has also been reported that the synthesis of PBZT with sulfur-groups leads to a new group of polyelectrolytes and an improvement of rigid-rod polymer film flexibility (343,344).

Fiber Spinning Process

By using high molecular weight polymers to form liquid crystal spinning solutions, combined with an optimal dry-jet wet spinning process and tension-heat-treatment, high quality rigid-rod polymer fibers can be produced. It has been observed that commonly, the higher the molecular weight of PBZO (with higher intrinsic viscosity (IV) of the spinning dope), the better the fiber mechanical properties, especially tensile strength. As shown in Figure 23, the fiber

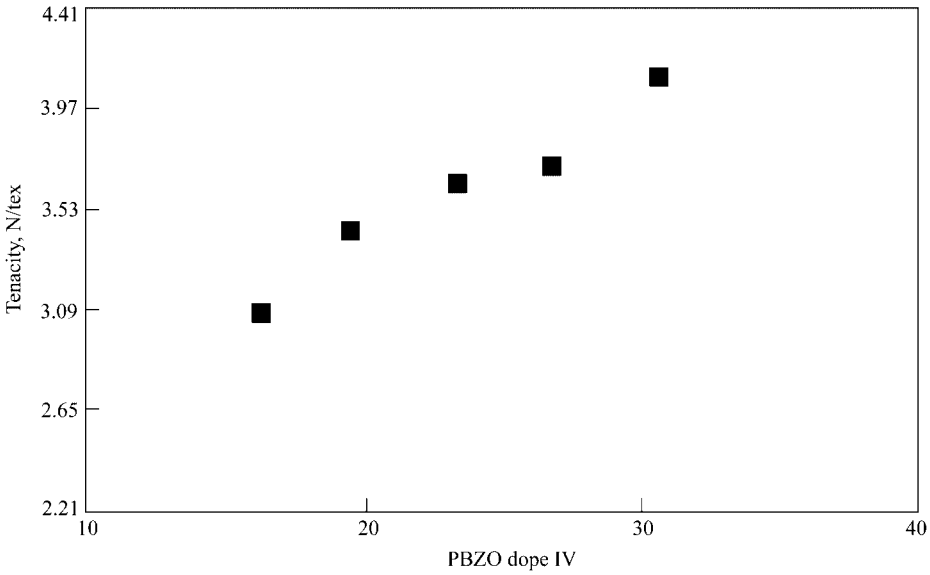

Fig. 23. Effect of dope IV (dL/g) on fiber tenacity (N/tex) of PBZO fibers. The unit conversion of fiber tenacity 1 N/tex = 0.102 kg/tex = 11.3 g/d, and the fiber tensile strength in pascal (SI unit) can be obtained as 1 N/tex = $\rho \times 10^9$ Pa = $\rho \times 1$ GPa, where ρ is the fiber density in g/cm^3. Reprinted from Ref. 34, by courtesy of Marcel Dekker, Inc.

tenacity is improved with the increase of IV (27). However, it is worth noticing that for rigid-rod fiber spinning, a single viscosity coefficient is not sufficient to completely describe the rheology of the dope solution. Because of the complicated rheological behavior of the liquid crystal solutions, there still exist some questions that haven't been answered well (272).

As mentioned above, PBZT and PBZO can be dissolved in only a few solvents. In general, PPA is chosen as the solvent for polymerization and to prepare the liquid-crystal spinning dope. There are several other solvents, such as MSA, 97.5% MSA/2.5% CSA, and 100% H_2SO_4, which can also be used (259,278). The polymer–PPA solutions offer several significant advantages over the solutions from other solvents (35,36): (*1*) Great improvement in process simplicity. After polymerization in PPA, PBZT–PPA or PBZO–PPA solution can be directly used as spinning solution. Therefore, the processes of separating the polymer from its polymerization solvent and then redissolving it into its spinning solvent were eliminated (345). (*2*) With PPA, the spinning dope can have higher viscosity, better spinnability, and higher draw-ratios. Therefore the fibers can have superior properties (35,36,286). In addition, compared to the fibers produced with PBZT–MSA spinning-solution, the fibers made from PBZT–PPA dope have fewer large voids (346).

The polymer concentration in a spinning dope is normally maintained within a factor of 2–3 of the concentration corresponding to the isotropic–anisotropic transition (347). For example, the transition from isotropic to anisotropic solution polymerization of PBZT occurs at 5 wt% (348) so that the polymer concentration in the spinning dope is about 10–15% (29,31). Generally, for both PBZT and PBZO

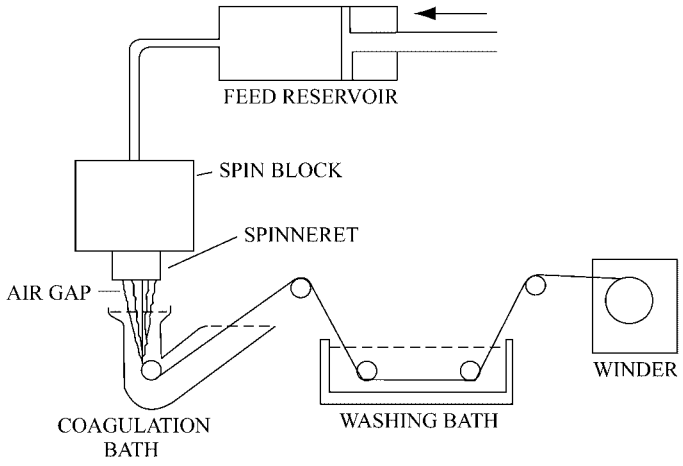

Fig. 24. A schematic chart of dry-jet wet spinning.

in PPA or MSA, 13–15% concentration polymer solutions with M_w over 10,000 are selected to prepare the spinning dopes (258,349).

It has been amply demonstrated that for lyotropic rigid-rod polymer solutions, the dry-jet wet spinning process can produce excellent fibers (29,35,36,44, 286,350). As schematically shown in Figure 24, this technique involves several steps: (*1*) the extrusion of a liquid crystal spinning solution under heat and pressure; (*2*) after passing the spinneret, the stream of the spinning solution goes through an air (or inert gases) gap into a coagulation bath; (*3*) this is followed by the processes of washing, drying, and tensioned heat treatment. The dry-jet wet spinning technique shows several advantages over a conventional wet spinning process: (*1*) owing to the use of a gap, a dope with a considerably higher temperature can be used to extrude the solution into a cold coagulation bath. Normally, the more concentrated the dope, and the higher the molecular weight of the polymer, the higher the achievable spinning rate, which leads to improved fiber mechanical properties and productivity. (*2*) The gap provides a region for extensional flow of the liquid crystalline solution, which allows a higher spin draw ratio (SDR, defined as the ratio of the take-up speed of the fiber to the extrusion speed of the spinning solution), which promotes higher molecular orientation. (*3*) Because of the travel in the air gap, a very thin sheath can be formed on the surface of the spinning solution (and newly formed fiber). Then in the coagulation bath, this sheath has the function of affecting (decelerating) the precipitant diffusion into the fiber, which results in good fiber quality. (*4*) This technique can facilitate a higher output per spinneret (in other words, more spinning dope can be extruded through a spinneret in a given period).

For these fiber-spinning systems, increasing the extrusion rate has only a limited effect upon the molecular orientation. Under constant draw ratio, the orientation parameter has little to do with the capillary die shear rate over the range of 25–5000 s^{-1} (119,319–321). However, the SDR has a significant effect on crystal size and molecular orientation. For PBZO, increasing the SDR increases the axial coherence length and decreases the lateral coherence length. The Hermans–Stein

orientation parameter of the as-spun fibers in the drawing zone increases from 0.9 at an SDR of 3 to 0.95 at an SDR of 20, and then levels off with further increase in SDR (321,349). It has been suggested, after SDR above 10, to adopt an affine deformation model to describe the spin-draw behavior for the PBZO–PPA system (319–321,351). Generally, for PBZT fiber spinning, an SDR greater than 3 is chosen. The commonly used spinning speed ranges from hundreds to thousands of meters per minute.

Several different coagulants, such as cool water, dilute PPA, methanol, and NH_4OH, have been studied for PBX fibers (352). During coagulation, the acid solvent diffuses out of the fiber such that initially about 90% of the solvent is removed (353). At the same time, the highly oriented crystallites in the as-spun fibers are fixed into the fibril/nanofibril network. This network constitutes the basic structure of the final products (47,354). The composition, pH, and temperature are three important parameters of the coagulation bath, which can influence the final structure and properties of the fibers. Generally, slower coagulation rates result in higher tensile strength and modulus, because the slow coagulation assists the formation of co-crystals of the polymer and solvent (216). A low nucleation density of crystal solvates leads to a lamellar structure but a high nucleation density tends to form nanofibrillar structure (47). It has been observed that by changing the composition of the coagulation bath, for example by using iodine/ethanol solution, a measurable variation in PBZT fiber structure and properties results (216,355).

For rigid-rod polymer fibers, the formation process is rather complicated because of the mixing of chemical reactions and physical variations by altering the processing parameters, such as forced external fields (stress and temperature). For example, both chemical quench and thermal quench during the process can change the material concentration and orientation. Owing to the complexity of the process, there exist different arguments about the fiber formation mechanisms. For instance, by means of a TEM study on PBZT fibers, it was proposed that one-dimensional nucleation and growth via axial diffusion during the process should be the mechanism for microstructure formation (356). However, it was argued that this hypothesis could not explain the formation of axial periodicity (10–35 nm). A spinodal decomposition-based clustering model of concentration and orientation rearrangement of macromolecular rods within a transient network has been proposed as the mechanism responsible for the formation of fibrils/nanofibrils, microvoids, and the periodicity (347). In the near future, with the progress in science and technology, as real time *in situ* experimental data become available, new mechanism models and/or modified existing concepts will gradually merge. For example, ribbons recently have been spun through a slit die and coagulated by drastically different conditions in an attempt to elucidate the mechanism by which the nanofibrils are formed (357).

Because of their excellent thermal stability, the subsequent heat treatment of rigid-rod fibers can be run in a wide temperature range. The HT temperature is chosen around 500–700°C and the HT residence time is from a few seconds to several minutes. It has been found that the HT time is closely associated with the HT temperature, and the optimum HT time should be inversly related to the employed temperature (31,358). Tension is necessary for the heat treatment to improve the fiber properties. With tension, during heat treatment chain orientation can be greatly improved, resulting in an increase in tensile properties, especially

Table 7. Changes in Structural and Property Prameters of PBZO Fibers through Heat Treatment at 600°C[a]

Structural or Property Parameters	As-spun PBZO	Heat-treated PBZO
Average lateral crystallite size, nm	7.5	12.6
Average axial crystallite size, nm	16	22
Misorientational angle, deg	6	4
Tensile modulus, GPa[b]	165	317
Tensile strength, GPa[b]	4.3	4.9
Breaking elongation, %	2.8–3.5	1.5–1.7
Density, g/cm^3	1.56	1.56–1.58
Equilibrium moisture, % (at 22°C, 65% RH)	2	<0.5

[a]From Refs. 94 and 210.
[b]To convert GPa to psi, multiply by 145,000.

for modulus (329). For PBZT, the fibers pass through an oven at a temperature of 550–650°C with resident time of 10–30 s, and tension of 140–410 MPa (44) in nitrogen (or air) atmosphere, and for PBZO fibers, 580°C, 10 s, and 480 MPa (69,600 psi) tension in nitrogen (27).

After the tensioned heat-treatment, the fibers have a significant improvement in overall axial orientation, crystal perfection, lateral order, as well as a decreased void content (359). Therefore, fiber tensile modulus has greatly increased, and fiber tensile strength, moderately increased. Taking PBZO as an example, Table 7 lists all these improvements through the tensioned fiber heat treatment: orientation (determined by X-ray azimuthal scans of the equatorial reflections), axial and lateral crystallite sizes (calculated from the equatorial diffraction peaks), tensile strength and modulus (94,210,229). Alternatively it was reported that the heat-treatment temperature has a great influence on the tensile strength but limited effect on the tensile modulus (28). As shown in Figure 25, with the increase in the temperature up to 700°C, the tensile strength is improved, but the modulus remains nearly constant. This could be due to the substantial enhancement of molecular lateral order. However, the applied stress during heat treatment affects both fiber tensile strength and modulus. Figure 26 shows that with the increase of applied stress, tensile strength and modulus both increase (28). Based on these facts, it was suggested that during heat treatment, the development of fiber tensile strength and modulus seems not directly dependent upon the processing parameters, but rather indirectly through the improvement of overall molecular orientation and chain lateral order (28,44).

PIPD and many other lyotropic polymers have also been spun by the dry-jet wet spinning technique (13,46,143,229). The spinning process is similar to that for PBZT and PBZO. The as-polymerized PIPD solution can be directly used to spin the fibers. The molecular weight of PIPD polymers is controlled in the range of 60–150 K. The spinning dope is maintained above 160°C (at 180°C, normally) with a concentration of 18 wt%. The spin-draw ratio can be adjusted from 5 to 15 in accordance with the selection of the spinning orifice diameter in order to manufacture fibers with a diameter in the range of 8–14 μm. Water or dilute phosphoric acid at room temperature is selected as the coagulation bath. After coagulation, the as-spun fibers are fully washed to remove the residual PPA, and

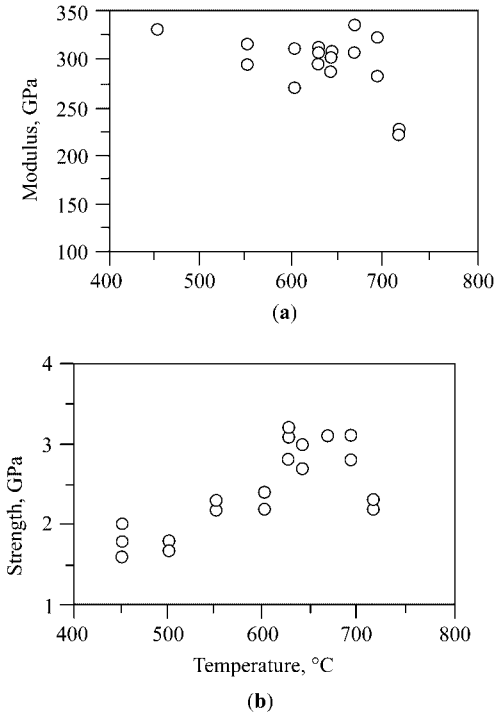

Fig. 25. Effect of heat-treatment temperature on tensile properties of PBZT fibers: (**a**) tensile modulus, (**b**) tensile strength. To convert GPa to psi, multiply by 145,000. Reprinted from Ref. 34, by courtesy of Marcel Dekker, Inc.

dried at a mild temperature. Subsequently the tension-heat treatment is carried out at a temperature over 400°C for about 20 s in nitrogen atmosphere to produce the final PIPD fiber (13,143,144).

Rigid-rod polymer films, including PBZT and PBZO, have also been produced from their solutions for various applications (114,156,345). Furthermore, scientists have been working to lower the melting points of rigid-rod polymers to enable new melt-spinning processes. Generally, the following approaches exist to lower the melting points: (*1*) appending flexible side-chain groups to the stiff main chains; (*2*) inserting flexible comonomer units into the stiff backbones; (*3*) inclusion of bent units of different sizes. Recently the preparation of new thermotropic liquid crystalline polymer fibers from rigid-rod polymers has been reported (248,360). A transition from solid phase to anisotropic melt phase in the temperature range of 280–450°C has been reported for the thermotropic PBZT with long alkyloxy side chains (C_n-PBZT). Longer side chains give lower transition temperatures. However, these polymers are not stable at high temperatures so that melt processing could not be investigated (248,360). A solid-state coagulation process was suggested to make high quality rigid-rod optical films (361). In this process, the rigid-rod polymer solution is rapidly frozen into a solid mixture and then is coagulated at a cryogenic temperature with a proper coagulate to extract the frozen solvent. PBZT thin films made by this technique had an optical attenuation coefficient (over 250–2500 nm range) of about 1300 dB/cm, significantly lower than

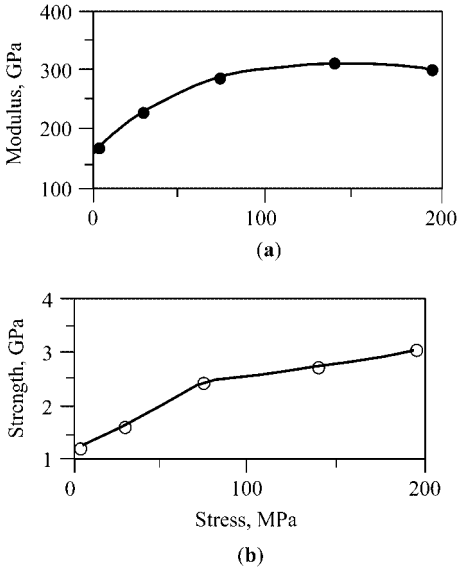

Fig. 26. Effect of applied stress during heat treatment on tensile properties of PBZT fibers: (**a**) tensile modulus, (**b**) tensile strength. To convert GPa to psi, multiply by 145,000. Reprinted from Ref. 34, by permission of Marcel Dekker, Inc.

that (4300 dB/cm) of the thin films prepared by conventional solution coagulation process. The reason for this improvement is that optically isotropic PBZT solution is first frozen into a transparent solid mixture to preserve the molecular dispersion of the polymer in the solvent. Then the solvent is extracted from the frozen mixture without disrupting the molecular distribution of the polymer, and phase aggregation in the final films is minimized (361).

Computer Simulation

Whether from either a practical purpose or from a theoretical viewpoint, it is useful to understand the molecular structure, its geometry, and the properties of a material. In the recent two decades, with the rapid progress in computer techniques, computer modeling has been systematically applied to test theories and to estimate the optimal properties for rigid-rod polymers (362,363). For estimation of the elastic properties of solid materials, computer modeling began by using empirical values for the forces between atoms, not values derived from quantum mechanics. One of the most common methods for calculating material elastic constants is molecular dynamics with the empirical valence field method, which is based on experimental data. Today, advances in computational materials science allow us to choose more accurate calculations to replace the empirical methods (364), but there are still serious limitations in computer techniques (see MOLECULAR MODELLING). The most accurate method, the quantum mechanical, is restricted to a single polymer chain, and nonbonded intermolecular interactions still cannot be explicitly calculated quantum-mechanically because most of

the methods derived from quantum mechanics are still beyond the capability of modern computers. Because of the limitations of computing power and calculation methods, the so-called semiempirical quantum approach has been chosen, which is a compromise, namely, using semiempirical procedures to approximate or simplify the quantum mechanical calculations (362,363).

For rigid-rod polymers, semiempirical quantum mechanical calculations have been applied to estimate the intrinsic axial tensile modulus of molecular chains (99,365–367), as well as strain and temperature dependence (52,71). Comparing PPTA (Kevlar) with typical rigid-rod polymer fibers, such as PBZT and PBZO, it is clear that the rigid rings in PBZT and PBZO are connected essentially coaxially by para-bonds along the chain axis. During axial tensile deformation, the deformation energy is consumed not by rotations, but by deformations of the stiff para-bonds and aromatic rings. Therefore, PBZT and PBZO have very high values of the theoretical chain modulus (368). Comparatively, the experimental tensile moduli of both PBZT and PBZO fibers approach the theoretical values. However, for tensile strength, few fibers exceed 50% of the theoretical values. PBZT and PBZO theoretical fiber tensile strengths are more than 20 GPa (369) and the theoretical strength of a single PBZO molecule is about 60 GPa (367). If the polymer chains in the tested fiber were actually as long as the gauge length, and perfectly oriented parallel to the fiber axis with no flaws, the measured fiber stress at break would equal the theoretical chain estimate. The value of the tensile strength determined primarily by covalent bonds and lateral chain packing density is estimated to be 10–15% of that of the theoretical chain modulus (370,371). Ab initio molecular dynamics has been used to simulate the PIPD crystal structure. The force necessary for the dynamics was calculated from the electronic structure using the Hellmann–Feynman theorem. The calculated chain modulus is in the range of 550–580 GPa, close to the experimental value (510 GPa) (142,143). Note that the current computer simulations of the tensile properties of rigid-rod polymer fibers serve only to establish an achievable upper limit for tensile modulus and show the prospect of future development possible by perfecting the fiber spinning and treatment processes. Liu and Yang did molecular simulation for PBZT molecular arrangements in the crystal structure with quantum mechanics and molecular mechanics, and found that PBZT can hardly form three-dimensionally ordered crystal structure with high regularity (372–374).

Computer simulation has also been used to study the solution properties of rigid-rod polymers (161,279,362). It has been found that the local structure and dynamics of different rigid-rod polymers may be quite different but global motions in dilute and semidilute solutions are expected to be very similar (375). Based on the Broersma and Tirado-de la Torre relations, the translational and rotational coefficients, D_t and D_r, of rigid-rod polymers in dilute (or semidilute) solutions can be written in the forms

$$D_t = (\kappa_B T/3\pi\eta_0 L)(\ln p + \nu) \tag{9}$$

and

$$D_r = \left(3\kappa_B T/\pi\eta_0 L^3\right)(\ln p + \delta) \tag{10}$$

where κ_B is Boltzmann constant, T, the absolute temperature, η_0, the pure solvent viscosity, ν and δ are "end effect" corrections, respectively, L, the length of the rigid-rod (polymer), and $p = L/d$, the length to cross-sectional diameter (d) ratio (376–378). The dimensions of the rigid-rod molecules in dilute solution may be obtained from the measurements of D_r and D_t (375). Teraoka and Hayakawa used a mean-field Green function theory to investigate the dynamics of entangled rigid-rod polymers in solutions, and the translational diffusion coefficient D_t was obtained:

$$D_t/D_{t0} = \left[1 + \gamma^{-\frac{1}{2}}(cL^3)\right]^{-2} \tag{11}$$

and the rotational diffusion coefficient D_r was

$$D_r/D_{r0} = \left[1 + \beta^{-\frac{1}{2}}(cL^3)\right]^{-2} \tag{12}$$

where γ and β are numerical constants, respectively, c, the number concentration of the polymer, L, the length of the rigid-rod (polymer), and D_{t0} or D_{r0}, the translational or rotational diffusion constant in a sufficiently dilute solution, respectively (379,380). Many new models and theories of simulating studies for rigid-rod polymers have been emerging. For example, Mondescu and Muthukumar investigated the steady-state transport properties of a heterogeneous suspension of rigid-rod polymers and spheres without excluded volume interaction, by applying the multiple scattering formalism and the effective medium theory (381). Yu used the Galerkin method to solve the diffusion equation of the distribution function for rigid-rod polymers, in order to simulate the interactions between the rigid-rod polymers and the coherent structure in a mixing layer (382). La Penna used a mode-coupling expansion of the Smoluchowski generalized diffusion equation with hydrodynamic interactions to calculate the time correlation functions of molecular configurational variables and found the results to be in good agreement with those obtained by an analytical solution of the rotational diffusion equation of rigid-rod polymers (383). For a linear rigid-rod, the second-order mode-coupling diffusion theory gave good hydrodynamic results for the bond time correlation function of the rigid-rod polymer solutions (384).

Farmer computed the effect of protonation on the behavior of PBZT and PBZO rigid-rod polymers. A significant portion of the charge deposited on the molecules was delocalized into the phenyl ring when it was coplanar with the heterocycle. The delocalization resulted in a higher torsional energy barrier for the protonated molecules and a lower barrier for out-of-plane bending. Thus the flexibility observed in previous molecular dynamic simulations of the neutral molecules in vacuo appears to be reasonable depiction of the stiffness of the rigid-rod polymers, even in strong acid solution (385).

Computer simulation has become a strong tool to understand the molecular structure and predict the properties of rigid-rod polymers. Furthermore, the understanding of the dynamics of rigid-rod polymers also helps give insight and aids investigation of structure–function relationships of DNA and many other biomaterials (375). However, the computer simulation of real polymers and their solutions (especially for the concentrated solutions) is rather complicated. Many

structural factors, such as chain length distribution, orientation of the chains, various bonding between atoms (such as covalent bonds in the chain and secondary forces between the chains), the nonuniformity and anisotropy of the structure, the interaction of macromolecules and solvents, as well as the presence of impurities, will affect the results. In different situations, various factors or combinations of them may be important. With further progress in computer techniques and calculation methods, more accurate simulation results will emerge in the future.

Molecular Composites

An interesting developing direction for rigid-rod polymers is to prepare "molecular composites." A molecular composite is a molecular-level (or nano-level) analogue of a chopped fiber-reinforced composite. The aim is to form a homogeneous mixture of a rigid-rod polymer, as the reinforcement, and a flexible chain polymer, as the matrix, with improved stiffness. The concept of molecular composites first appeared in the 1970s–1980s (386–389). Today, molecular composites have been developed as a new generation of high performance materials (390). Two key factors, the aspect ratio of the reinforcing rigid-rod polymer and its miscibility with the flexible polymer, control the mechanical and physical properties of the molecular composites. Owing to reinforcing at the molecular level, a molecular composite exhibits a single uniform thermal expansion coefficient and isotropic characteristics, which are greatly different from the conventional unidirectional fiber-reinforced composite materials (391).

There are several approaches to making molecular composites: (*1*) Takayanagi finely pulverized and then mixed rigid crystalline polymer microdomains (such as PPTA) with different flexible polymer matrices (including nitrile–butadiene rubber, nylon-6, and nylon-6,6) (386,392); (*2*) using guidance from solution thermodynamics (theoretical (393) and experimental (387,388), Hwang and co-workers codissolved the rigid-rod polymers (such as PBZT) with various semiflexible polymers [such as aromatic heterocyclic semiflexible polymers, ABPBI (poly(2,5(6′)-benzimidazole)) or ABPBT (oly(2,5(6′)-benzothiazole)), with coil-like polymers, nylon or poly(*p*-phenylene quinoxaline)] as matrix, in strong acids (such as methanesulfonic), and then rapidly coagulated the isotropic solution to "quench" the dispersed state (387,388,394–396); (*3*) Lenke and co-workers polymerized rigid-rod molecules (such as polyazomethine, polyimides, and polycarbodiimides) in thermoplastic precursors (such as nylon-6), or thermoset precursors (such as epoxies), and then polymerized the precursors (as the matrix) to form an *in situ* molecular composite (397–399); (*4*) using poly(amideimide) or other rigid polymers that can form melts, instead of the rigid-rod polymers which cannot be melted, molecular composites were prepared with a melt process (53).

Fibers and films made by molecular composite processing display good mechanical and thermal properties, chemical and environmental resistance, as well as interesting optical and electrical behaviors. The molecular composite made from articulated rigid-rod PBZT with a thermoplastic pendant, poly(etherketone) (PEK), has significantly higher T_g and tensile properties than the neat PEK homopolymer (400). A PBZT/BBB (poly(benzimidazobenzophenanthroline))

molecular composite demonstrates good thermal stability (401). The ABA copolymers of carboxy-terminated PBZT and 3,4-diaminobenzoic acids show much better tensile strength (up to 33% increase) than simple blends (402,403). Graft copolymers of PEK and PBZT also improved the composite processability (404) and prevented the segregation of PBZT molecules (405). Therefore, the toughness of the molecular composites increases with the increase of rigid-rod polymer content (406). It has also reported that fibers spun from molecular composites with PBZT/PBZO were strong and stiff (252,407,408). In addition, molecular composites can eliminate the detrimental interface issues with conventional fiber-reinforced composites, such as CTE mismatch between fibers and matrix (409,410).

It should be noted that unless care is taken, the rigid-rod molecules would not completely disperse in the molecular composites, but form small coacervated domains (410). There remain several problems. Among them, the most critical one is the inability to consolidate without phase separation (6). Several new molecular composite systems are suggested and activity has been concentrated on the improvement of processability (2,114,151,337,409,411–415). Recently, Wiff has proposed making recyclable "nano" thermoplastic/liquid crystal composites (416). By a special processing technology, the thermotropic liquid-crystalline (rigid-rod) polymers (TLCP) were blended with thermoplastic resins to keep the liquid crystalline domains small enough that their size approached that of microvoids in the thermoplastic polymer systems. The uniform dispersion and small size were achieved through use of static mixers at temperatures where the TLCP is in the nematic state and the thermoplastic is a melt. Therefore the mechanical properties, including flexural and tensile strengths and moduli, as well as low temperature impact strength, of the nano composites were greatly improved. In particular, the fracture toughness is doubled. The possible explanation is that the reinforcements are not needle- or fiber-shaped but rather form an interconnecting network of nanoscale platelets (416).

End Uses of Rigid-Rod Polymers and Fibers

With the rapid technological progress in many engineering fields, the use of high performance polymer fibers is required. Because of their superior properties, various rigid-rod polymers have been developed and their applications have been explored. Taking advantage of their low density, excellent tensile properties, hydrolytic and chemical resistance, thermooxidative stability, and dielectric behavior, rigid-rod polymer fibers have great potential to be widely applied for composite materials. The fields include anti-ballistics, fire protection, athletic equipment, strings, cables, ropes, cordage, sails, multilayer circuits, safety gloves and pulps, especially for many in space and marine environments.

Generally rigid-rod fiber composites can provide potential significant advantages: (*1*) retention of a large fraction of tensile properties under static and cyclic conditions; (*2*) low density; (*3*) a good balance between lamination properties and impact damage tolerance; (*4*) high working temperature. PBZT and PBZO composites compare favorably in tension to other composites reinforced with Kevlar 49 or S-glass. They also show better behavior than the conventional aluminum matrix

composites. The environmental stability of rigid-rod fiber composites is generally excellent (369–371,417,418). The thermal behavior of rigid-rod fibers result in composite materials with good thermal insulating properties, such as thermal insulating support straps for cryogenic applications in space (73). The rigid-rod fibers are one of the best precursor materials for manufacturing ballistic products. Ballistic products made with rigid-rod fibers have the special features of low density, high strength, and high energy-absorption capability. Recently, ballistic products based on Zylon (PBZO) fibers have been introduced (419).

Although normally many of the rigid-rod fibers have relatively low compressive strength, their composites do not catastrophically fail at high bending as do those made with graphite or glass-fiber composites. It has been reported that the interfacial shear strength was 75% increased by the addition of a functionalized additive into PBZO fibers (420). Also, through synthesizing new PBZO copolymers to add new functional groups on the fibers, the interfacial adhesion between fiber and resin matrices has been enhanced (150,420–422). In addition, plasma treatments have also been applied to improve the surface adhesion of PBZT fibers in composites (423). The recently reported PIPD fibers have shown very good compressive properties. This opens a new way for rigid-rod polymer fibers to compete with carbon fibers for high performance applications economically and efficiently, especially in fields requiring high electrical resistance, such as electrical insulating ladders and satellite solar panels (73). In addition, the polarity of PIPD fibers results in good adhesion with many polymer matrix materials, including epoxy, unsaturated polyester and vinyl ester resins. It has been reported that PIPD fibers have better adhesion than that of adhesion-activated Twaron 1001 (PPTA) fibers and much better than regular Twaron 1000 (nonactivated) (13).

Their thermal stability leads to the use of rigid-rod polymers as catalyst supports. Polybenzimidazole (PBI), another member of PBX rigid-rod polymer family, has been chosen as a catalyst support for both reduction and oxidation, such as supporting palladium catalysts for Wacker-type oxidation and hydrogenation and Mo(VI) catalysts for epoxidation of propene (424). PBI-supported palladium dichoride exhibited a thermooxidative stability up to 400°C. N-cyanomethylated PBI/$PdCl_2$ is the most active catalyst for ketonization of terminal alkenes using air as oxidant and will not form Pb(O) up to 120°C (425). PBI–molybdenum(VI) oxide diacetate is a highly active, stable, recyclable, and long-life catalyst for the Halcon process (426). PBI–Pd^0 is an effective catalyst for the reduction of nitro-compounds or alkenes, and PBI–Cr(VI) is an active oxidizing agent for alcohols (427–431). Sulfonated PBI can also be applied to making high temperature-resistant synthetic papers (432). It was marketed under the trade name of Celazole by Hoechst Celanese Co. and used as a nonflammable and nonsmoking high performance material (433).

Rigid-rod polymers have demonstrated their potential for space materials. The rigid-rod polymer films are applied as advanced space durable materials for inflatable structures and thermal control applications (433,434). Woven fabrics comprising PBZO fibers blended with other selected fibers have shown combinations of their properties and in some space applications (such as light-weight parts and structures for protecting spacecraft against micrometeoroids), could be superior to those made by the component materials alone. By blending PBZO yarns with other high performance materials, enhanced performance was observed (434). In

addition, polyarylene ether benzimidazoles (PAEBI), first synthesized by NASA scientists and now produced by Triton Systems, Inc. under trade names TOR and TOR-LM, show significant resistance to erosion caused by atomic oxygen (15 times higher) compared to other thermal control polymer materials such as Kapton (polyimides (qv)) and FEP Teflon. This is due to the incorporation of a phosphorus–oxygen linkage in the polymer backbone to form an *in situ* protective layer on the surface. These materials still keep many advantages of the rigid-rod polymers, such as high T_g and good mechanical properties, coupled with high optical transmission (435).

Rigid-rod polymer material is one of the best candidates for membrane technology (qv), such as gas separation and fuel cells (436). The high chemical and environmental resistance and mechanical properties lead to the choice of the rigid-rod polymers (such as PBI) as reverse-osmosis membranes, which show high efficiency and long work-life (437). Many rigid-rod polymers can form films with extremely high permeability and selectivity for water vapor, making them potentially useful as pervaporation and dehydration membranes (438). When PBI was used as a pervaporation membrane a higher selectivity of aromatic compounds, such as toluene and chlorobenzene, was achieved (437). Because of the high affinity for acidic compounds, PBI was used for separation of acidic compounds from mixtures, and microporous PBI was used for sorption of aqueous sulfur dioxide or separation of carbon dioxide (439–441). Chemically modified PBI with chelating ligands has also been used as metal-selective sorbents for hydrometallurgical applications (442–447). PBI resin modified with mercaptoacetic acid has resulted in high metal sorption capacity (440,441).

The high dielectric strength of rigid-rod polymers coupled with good heat and moisture resistance provides high insulation efficiency, preventing electrical current leakage. The excellent dielectric behavior accompanied with low thermal expansion and high dimensional stability make the rigid-rod polymers applicable in specialized electronic applications. For example, most transmissivity problems in composite radomes are due to the reflection of the electromagnetic waves at the interface between the two components with different dielectric constants. The less the difference in dielectric constant, the smaller the reflection of the electromagnetic radiation. Rigid-rod fibers have lower dielectric constant and lower loss tangent than carbon fibers; hence they have lower radar observability (34).

Rigid-rod polymers have potential to work as conductive materials. Conducting materials have been prepared from the conjugated rigid-rod polymers with techniques of chemical/electrochemical doping as well as ion implantation (448–450). After implanting with $^{84}Kr^{+}$, PBZT and PBZO are changed significantly in molecular and morphological structures, which strongly affect their electric behavior. However, they still retain their excellent thermal and mechanical properties. A major change in molecular composition is the reduction or elimination of heteroatoms, resulting in a substantial carbonization. Morphological change is the formation of brush-heaps, mainly determined by the processing conditions. Implanted polymers exhibit metallic absorption with absorption coefficients less than those of the original materials in the UV–visible range. The conductivity of implanted PBZT and PBZO reaches 80–200 S/cm, being stable with time and temperature (207). PBZT conductive fibers have also been produced by doping with phthalocyanine (Pc) compounds, such as NiPc and $(SiPcO)_n$ (199,451,452).

Unfortunately, conventional doping techniques did not result in high conductivity (207). However, recently it has been reported that PBZT/silver conductive fibers, made by infiltration during processing, have electric conductivity over 10^4 S/cm and at the same time have maintained good mechanical properties, with a tensile modulus of 52 GPa and a tensile strength of 1 GPa (204).

In addition to the applications as molecular composites mentioned in the earlier section, rigid-rod polymers have also been used to synthesize nanoporous polymer hosts. Dhal reported template polymerization using bis(imidazole)–Cu^{II} complexes as templates (453). These templated copper-complexing rigid-rod polymers have the properties of selective binding and substrate recognition (453). It is obvious that by adding some other abilities, such as orientation of anchoring sites and shape selectivity, the nanoporous rigid-rod polymer hosts could become a promising technology for nanophase materials (454). Furthermore, as described in the next section, rigid-rod polymers have great potential for organic opto-electronic devices.

Other Rigid-Rod Polymer Systems

Rigid-rod polymers have attracted much interest for photonic and electronic applications as a result of their unique conjugated structure and superior properties (22,167,455–457). Recently, these conjugated rigid-rod polymers, because of their conducting behavior, are called the fourth generation of polymeric materials (171,458–460).

As described above, rigid-rod polymers offer excellent optical, electrical, and mechanical properties, chemical resistance, as well as high temperature, environmental, and dimensional stabilities. In addition, many rigid-rod polymers have the ability to form lyotropic (in their concentrated solutions) or thermotropic (in bulk state at elevated temperature) liquid crystals (461). In the liquid-crystalline state, high order can be introduced by the interactions between external electric or magnetic field and molecular dipole moments, diamagnetic anisotropy, interactions with a planar surface or inhomogeneous flow pattern. Many new rigid-rod polymers have been synthesized and studied for the potential applications in electronic/optical devices, such as field effect transistors, Schottky diodes, light-emitting diodes, electrochromic devices, photoactive films, high efficiency solar cells, push–pull amplifiers, batteries, optical data storage, and second- or third-order NLO materials (462–470). Unfortunately, little real usage has been reported because most rigid-rod conjugated polymers are insoluble, nonfusible, and have poor processability. However, research activities have continued, and in recent decades, so many new rigid-rod polymers have been synthesized and studied, such as PPP, Poly(*p*-phenylene ethynylene) (PPE), poly(*p*-phenylenevinylene) (PPV) (qv), polythiophene (PTh), polypyrrole (PPy), polyaniline (PA), and polyacetylene (PAc), that it is beyond the scope of this article to cover all of them. Here several model rigid-rod polymers are listed for reference. (see ELECTRICALLY CONDUCTIVE POLYMERS)

PPP, PPE, PPV, and Their Derivatives. PPP, PPE, PPV, and their derivatives are potential candidate rigid-rod polymer materials for advanced optical/electrical applications (18,22,24,471,472). The molecular structure of PPP is represented as **16**. Electronic conduction needs an electron delocalization

associated with high electron mobility between molecules, while nonlinear optical properties need a large electron delocalization and optical transparency. The polarizable π-electrons of PPP (PPE or PPV) conjugated structures can meet these requirements. In order to increase electronic/nonlinear-optical response, the rigid-rod polymers should have strong intermolecular electronic interactions so that the macromolecular backbones have to possess extended conjugation lengths and be well oriented (473). However, this kind of structure results in the polymers being insoluble and infusible, and prevents the formation of well-defined, high molecular weight rigid-rod polymers. These seriously limit their applications. In order to synthesize rigid-rod polymers with good processability, two major synthetic strategies have been taken: (*1*) the desired functional groups are part of the monomers, and the functional polymers are obtained directly from polymerization process (468,474,475); (*2*) PPP, PPE, or PPV is synthesized and then the functional groups are added or changed to make the functional polymers (21,169,468,476,477). For example, some organometallic pendants are attached to their conjugated frames not only for increasing solubility but also for enhancing the optical/electrical properties (478). Different synthetic methods, such as the conventional wet-chemical methods (479–482), and the Langmuir–Blodgett (LB) molecular process (483) are used to execute these strategies.

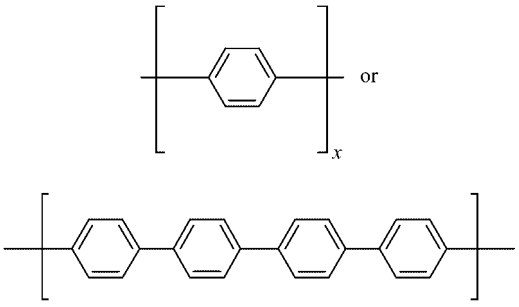

(**16**)

PPP, PPE, PPV, and their derivatives show high third-order susceptibility and electronic conductivity (474,484). The $\chi^{(3)}$ values of their oligomers and derivatives were measured in the range of 10^{-10} esu by Yamamoto and Moroni (485,486). As a result of triple bonds in the main chain, PPE and its derivatives (Fig. 27) have attracted special attention. The $\chi^{(3)}$ values of some PPE derivatives can reach the range of 10^{-10} esu (485), and even to 1.8×10^{-9} esu (487). In addition, rigid-rod PPP and its derivatives have also been studied as polyelectrolytes (19,488). One approach involves using PPP, as "hairy" rigid-rod reinforcing elements, with ethyleneoxide side chains (the "hairs"), as the separating liquid-like matrix, in which lithium salts are dissolved. This kind of material can offer the needed combination of ion conductivity and mechanical strength (471).

Polythiophene and Its Derivatives. Among many conductive rigid-rod polymers, such as PAc, PPP, PPE, PA, and PPy, PTh has rapidly become an intensively studied material for optical/electronic applications (20). The molecular structures of PTh and its derivatives are represented as **17** and **18**. Just like other conductive polymers, PTh has a π-conjugated electronic structure. Because of the

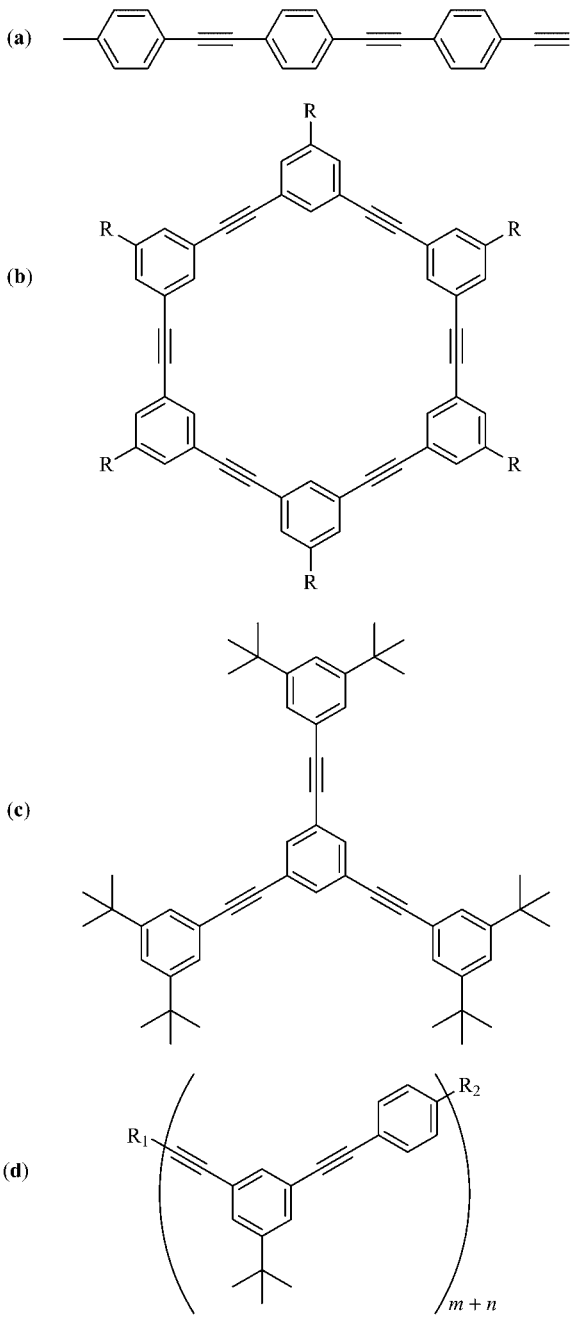

Fig. 27. Chemical structures of PPE and its derivatives: (**a**) molecular unit structure of PPE, (**b**) macrocycles, (**c**) dendrimers, and (**d**) nanoarchitecture.

high stability of both doped and undoped PTh and its derivatives, many electronic and optical applications can be developed (147,489,490). Because of the insoluble and infusible nature of PTh and some of its derivatives, chemical modification of their structures is necessary. This can be done by methods such as attaching

flexible side chains (or groups) to the rigid polymer backbone by synthesizing alkylated PThs or polyalkylthiophenes (PATs) (491), and introducing flexible or kinked spacer units into the main chain or preparing random copolymers (492). Furthermore, different synthetic methods, such as electrochemical synthesis (493–496) and plasma-enhanced chemical vapor deposition (PECVD) (497–500), have been studied for making rigid-rod polymer films. For example, poly(3-alkylthiophene)s changed from the original board-like structure of PTh to a sheet-like geometry, because the polymer adopts a configuration with the side chains extending preferentially within a plane (501,502). In this case, the planarity depends strongly on the nature of the substituent, temperature, or the solvent (468). Based on the study of a series of phenylene-based conjugated polymers, Dufresne suggested that thermochromic and solvatochromic phenomena in the conjugated rigid-rod polymers can be driven by a delicate balance between steric intramolecular interaction and attractive interchain interactions. For these polymers, no planar conformation is accessible if the steric interactions are too strong. In the absence of significant steric interactions, nearly planar conformation can be maintained, even at high temperatures. In addition, small changes in the repeat unit of these conjugated polymers can result in great differences in their chromic behavior (470). Therefore, the conformational analyses on model compounds can be a highly valuable tool to understand structure–property relation and design new functional rigid-rod polymers (470).

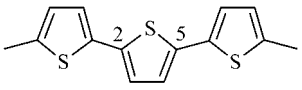

(**17**)

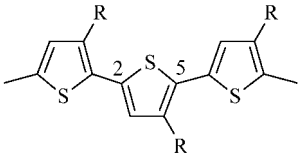

(**18**)

PThs are very poor electrical conductors unless they are partially oxidized (p-doped) or reduced (n-doped). The p-doped PTh materials are stable in the absence of atmospheric moisture whereas the n-doped are very air-sensitive. The conductivity of p-doped PTh is about 10–100 S/cm (503). The conductivity of soluble poly(3-alkylthiophenes) is about 10^{-2} S/cm and that of I_2- doped HT-coupled PATs can reach 5×10^3 S/cm (504). Jin and Xue reported that the electrochemically synthesized PTh films from the thiophene/BF_3-ethyl ether solution have shown excellent two-dimensional electric conductivity, 100 S/cm. The free-standing films are flexible and have good mechanical properties. Their tensile strength of 140 MPa is greater than that of aluminum sheets (100–110 MPa). These properties are due to their highly anisotropic and conjugated structure, high degree of polymerization, and compact morphology. The thiophene rings in the macromolecular chains are nearly parallel to the electrode plate, with high coplanarity (496). The template-mediated polymerization of thiophene and pyrrole monomers down a nucleopore channel can make nanofibers with enhanced electronic conductivity

(505,506). The conductivity increases with the decrease of fiber size. The reasons for the enhancement of the optical and electronic properties have yet to be established. They may be due to the preferential orientation of the polymer chains along the fiber axis or the surface layers of the polymer chains (505,506). The solutions and films of PTh and its derivatives can exhibit interesting thermochromic and solvatochromic behavior (507). Existence of the electrochemical reversibility of the transition between the doped and undoped states and the resulting color change can lead to many sensor applications in electronic, chemical, and biotech fields (508–510). PTh and its derivatives have been studied for use in rechargeable batteries. They have shown high voltage, high energy and power densities, although self-discharge exists (511).

Organometallic Polymers. In order to enhance the ion conductivity, electroluminescence, and/or nonlinear optical properties, many new organometallic polymers have been synthesized and studied (19,23,25,512–515) (see METAL–CONTAINING POLYMERS). As a result of the delocalization of electron density along the backbone of the organometallic polymers (qv) causing a strong intramolecular interaction, most of them belong to the rigid-rod polymer families. There are mainly two kinds of organometallic polymers: (*1*) pendant organometallic fragments attached to the functionalized side chains or moieties with the polymer backbone containing a delocalized π system (516); and (*2*) the metal center is an integral part of the polymer backbone (517).

Unfortunately only limited work relating to this topic has been reported. However, more and more research is associated with these polymers. It has been observed that metals embedded in the polymer backbone do not block the delocalization of the electrons, but greatly improve the processability, such as decreasing melting point or increasing solubility (518,519). One good example is the transition-metal-containing polymers (520–522). Organonickel polymers have a rigid-rod structure with trans-geometry around the metal centers. These polymers have remarkable environmental and thermal stability. All of the lower molecular weight nickel oligomers are soluble in common organic solvents. The solubility of nickel-containing polymers decreases as solvent polarity decreases. At the same time, these polymers showed interesting optical nonlinearity and/or electron conductivity (505). The organometallic polymers have potential to be used in electronic and NLO devices, as well as in reactive materials and polymer catalysts (523–525).

Summary. Rigid-rod polymers and their derivatives show great potential for electronic and optical applications and many new rigid-rod polymer systems have been emerging. However, there are still significant gaps in the understanding of the structure–property relationships. More profound research is needed to create the capability of predicting and controlling the molecular architecture and optical/electronic behavior of various rigid-rod polymer systems. In addition, more processing methods should be developed to prepare rigid-rod polymer films and other products. The techniques should be able to accurately control the processing parameters and easily manipulate the morphology. However, the popularly used spin-coating technique for the preparation of organic films is quite inadequate for rigid-rod polymer systems, since manipulation to a specific film morphology is almost impossible. Although Langmuir–Blodgett (LB) (526) self-assembly, electrochemical, PECVD, and other techniques have been studied to fabricate rigid-rod

polymer films, all these methods still have serious limitations. In addition, to make excellent optical devices, the light scattering caused by rigid-rod polymer systems should be addressed. The anisotropy in the microscopic polarizability of the rigid-rod polymers can cause considerable light scattering, which can seriously affect the efficiency of many linear and nonlinear optical devices. However, building on the many merits exhibited by the rigid-rod polymer materials, it is probable that in the near future, these problems will be gradually solved and the rigid-rod polymers will play an even more important role in optical/electronic applications.

The Future

This brief review of the field of rigid-rod polymers does not exhaustively cover the whole area, since many new rigid-rod polymers have been synthesized and studied recently. We have tried to use several typical rigid-rod polymers, such as PBZT, PBZO, and PPP, as model compounds to describe the history, polymerization, structure, properties, applications, and the developing directions of the rigid-rod polymers. A few areas of present or potential novel levels of performance have been described to interest the readers in the great scope of the polymers.

Apparently, the aerospace industry has traditionally driven research and development of new, lighter, stronger, stiffer, tough, durable, and processable polymer fibers for use in structural composites for airplanes and spacecraft. The growing percentage of composites in flying aircraft are a glowing testament to their continuing progress. In addition to the aerospace industry, other fields, such as automobiles, ships, machinery, sporting equipment, and construction materials, are also increasing the use of high performance polymer composites. Conservative predictions of the demand for advanced composites in the world project that in the twenty-first century, other industrial applications will expand their share to 55% while the occupation of aerospace applications will be decreased to 45% (2). A 10-fold increase in consumption of high performance fibers was predicted in the late 1990s and projections of worldwide requirements for advanced composites could reach 500 million tons per year in the first decade of the 21st century. It is likely that the markets for replacement of high density structural materials have not yet been fully identified (2). When polymer performance meets the application requirements, then reducing processing and manufacturing costs, and sometimes, even making new low cost (rigid-rod) polymers becomes critical. If the cost of high performance rigid-rod polymers can be reduced, the demand will be much higher. If the cost of rigid-rod fibers can be decreased to less than $10/kg, demand can increase by a factor of 10 (2). With continual rapid progress in the science, engineering, and technology of materials and their processing, new rigid-rod polymers and novel processing methods should emerge to advance the existing technology. Clearly, rigid-rod polymers have excellent potential as novel structural materials.

Furthermore, because of the extensive π-electron delocalization in the conjugated structure of rigid-rod polymers, many novel applications in the rapidly growing computer information industry, as well as many other physical and chemical industries have also been stimulated. Today many new patents apply rigid-rod polymers in sensors, conductors for electrons and/or ions, special membranes, polyelectrolytes, catalysis, electrochromic devices, holography, optical switching,

image techniques, and data storage. The high second-order and/or third-order optical nonlinearities, excellent insulating behavior or conducting properties (after doping), and many other unique electric/optical properties, combined with their excellent mechanical and chemical properties, make the rigid-rod polymers potential candidates for electrooptical and multifunctional applications.

However, there still remain fundamental scientific and technical problems to be solved in understanding and applying rigid-rod polymers. For example, we need to understand the mechanisms of strength, stiffness, and compressive failure so that we can design new rigid-rod molecules and/or new processes to overcome the current limitations. Rewards for overcoming technical limitations will be considerable for both scientific knowledge and technological achievement. The tailorability of rigid-rod polymers, with the resultant enormous variations in properties makes them quite attractive for research addressing specific property goals. Furthermore, with the rapid growth of the computer and information industry, rigid-rod polymers for conductivity and nonlinear optical applications have serious and exciting challenges and opportunities for next generation optical/electronic materials. The relatively new class of rigid-rod polymers will continue to offer exciting opportunities for scientists and engineers for many decades to come.

BIBLIOGRAPHY

"Polybenzothiazoles" in *EPST* 1st ed., Vol. 10, pp. 675–681, by Harold H. Levine, Whittaker Corporation; "Polybenzothiazoles and Polybenzoxazoles" in *EPSE* 2nd ed., Vol. 11, pp. 601–186, by James F. Wolfe, SRI International; "Polybenzimadazoles" in *EPSE* 2nd ed., Vol. 11, pp. 572–601, by Alan Buckley; and D. E. Stuetz, Celanese Research Center, and G. A. Serad, Celanese Specialty Operations.

1. H. Staudinger, in *Die Hochmolekularen Organischen Verbindungen*, Springer-Verlag, Berlin, 1932, p. 111.
2. Committee on High-Performance Synthetic Fibers for Composites, National Materials Advisory Board, National Research Council, High-Performance Synthetic Fibers for Composites, 1992.
3. E. E. Magat and R. E. Morrison, *CHEMTECH* 702 (1976).
4. W. B. Black, in W. B. Black and J. Preston, eds., *High-Modulus Wholly Aromatic Fibers*, Marcel Dekker, New York, 1973, p. 3.
5. Committee on Liquid Crystalline Polymers, National Materials Advisory Board, National Research Council, *Liquid Crystalline Polymers* (NMAB-453), 1990.
6. F. E. Arnold Jr. and F. E. Arnold, *Adv. Polym. Sci.* **117**, 257 (1994).
7. C. S. Marvel, *An Introduction to the Organic Chemistry of High Polymers*, John Wiley & Sons, Inc., New York, 1959.
8. W. W. Adams and T. E. Helminiak, in L. L. Hench and D. R. Ulrich, eds., *Science of Ceramic Chemical Processing*, John Wiley & Sons, Inc., New York, 1986.
9. H. Vogel and C. S. Marvel, in D. A. Tirrell, M. Sawamoto, and E. M. Pearce, eds., *A Half-century of Journal of Polymer Science*, John Wiley & Sons, Inc., New York, 1997, p. 117.
10. F. Flam, *Science* **251**, 874 (1991).
11. F. E. Arnold, in W. W. Adams, R. K. Eby, and D. E. McLemore, eds., *The Materials Science and Engineering of Rigid-Rod Polymers*, Vol. **134**, MRS (Materials Research Society), Boston, 1989, p. 75.
12. M. S. Reisch, *C&E News* **65**, 9 (1987).
13. D. J. Sikkema, *Polymer* **39**, 5981 (1998).

14. M. L. Keshtov, A. L. Rusanov, V. V. Kireev, A. A. Kirillov, S. V. Keshtova, and F. W. Harris, *Polym. Sci., Ser. B* **43**, 98 (2001).
15. M. Tomikawa, F. W. Harris, S. Z. D. Cheng, and E. Galentier, *Reactive Functional Polym.* **30**, 101–107 (1996).
16. F. W. Harris and S. L.-C. Hsu, *High Performance Polym.* **1**, 3 (1989).
17. S. A. X. Huang, K. C. Chuang, S. Z. D. Cheng, and F. W. Harris, *Polymer* **41**, 5001 (2000).
18. F. Wudl, in J. L. Bredas and R. R. Chance, eds., *NATO Advanced Research Workshop on Conjugated Polymeric Materials: Opportunities in Electronics, Optoelectronics and Molecular Electronics* (NATO ASI Series, Applied Science, No. 182), Kluwer Publishers, Mons, Belgium, 1989.
19. F. M. Gray, *Solid polymer Electrolytes: Fundamentals and Technological Applications*, VCH, New York, 1991.
20. J. Roncali, *Chem. Rev.* **92**, 711 (1992).
21. E. Harlev and F. Wudl, in W. R. Salaneck, I. Lundstrom, and B. Randy, eds., *81st Nobel Symposium*, Lulea, Sweden, 1993, p. 139.
22. C. Heldmann, D. Neher, H. J. Winkelhahn, and G. Wegner, *Macromolecules* **29**, 4686–4697 (1996).
23. M. Irwin, G. Jia, N. C. Payne, and R. J. Puddephatt, *Organometallics* **15**, 51 (1996).
24. P. Wautelet, M. Moroni, L. Oswald, J. Le Moigne, A. Pham, J.-Y. Bigot, and S. Luzzati, *Macromolecules* **29**, 446 (1996).
25. S. Kelch and M. Rehahn, *Chem. Commun.* 1123 (1999).
26. H. Jiang, W. W. Adams, and R. K. Eby, in E. L. Thomas, ed., *Materials Science and Technology, Vol. 12: Structure and Properties of Polymers*, VCH Publishers Inc., Weinheim, Germany, 1993, p. 597.
27. J. Im, Z. Lysenko, S. Martin, M. Mills, J. Jakubowski, and D. E. McLemore, in ESF'94, Yokohama, Japan, 1994.
28. S. R. Allen and R. J. Farris, in W. W. Adams, R. K. Eby, and D. E. McLemore, eds., *The Materials Science and Engineering of Rigid-Rod Polymers*, Vol. **134**, MRS, Boston, 1989, p. 297.
29. S. R. Allen, A. G. Filippov, R. J. Farris, and E. L. Thomas, in A. E. Zachariadas and R. S. Porter, eds., *The Strength and Stiffness of Polymers*, Marcel Dekker, New York, 1983, p. 357.
30. W. C. Uy and J. F. Mammone, *Can. Textile J.* (4), 54 (1988).
31. H. D. Ledbetter, S. Rosenberg, and C. W. Hurtig, in W. W. Adams, R. K. Eby, and D. E. McLemore, eds., *The Materials Science and Engineering of Rigid-Rod Polymers*, Vol. **134**, MRS, Boston, 1989, p. 253.
32. M. Sahafeyan and S. J. Kumar, *J. Appl. Polym. Sci.* **56**, 517 (1995).
33. R. Moreton, in W. Watt and B. V. Perov, eds., *Strong Fibers*, North Holland, Amsterdam, 1985, p. 452.
34. H. Jiang, W. W. Adams, and R. K. Eby, in M. Lewin and J. Preston, eds., *High Technology Fibers*, Marcel Dekker, New York, 1996, Chapt. "2", p. 171.
35. S. R. Allen, A. G. Filippov, R. J. Farris, E. L. Thomas, and E. C. Chenevey, *J. Appl. Polym. Sci.* **26**, 291 (1981).
36. S. R. Allen, A. G. Filippov, R. J. Farris, and E. L. Thomas, *Macromolecules* **14**, 1138 (1981).
37. H. Jiang, R. K. Eby, W. W. Adams, and G. Lenhert, in W. W. Adams, R. K. Eby, and D. E. McLemore, eds., *The Materials Science and Engineering of Rigid-Rod Polymers*, Vol. **134**, MRS, Boston, 1989, p. 341.
38. W.-Y. Yeh and R. J. Young, *Polymer* **40**, 857 (1999).
39. A. R. Bunsell, *J. Mater. Sci.* **10**, 1300 (1975).

40. T. Liang, A. Takahara, K. Saito, and T. Kajiyama, *Polymer* **39**, 5387 (1998).
41. P. E. Klunzinger, R. G. Ramirez, D. A. Thomas, and R. K. Eby, *Bull. Am. Phys. Soc.* **37**, p. 508 (1992).
42. H. Jiang, P. Arsenovic, R. K. Eby, J. M. Liu, and W. W. Adams, *Polym. Prepr. (Japan)* **36**, 5 (1987).
43. J. Im, P. A. Percha, and D. S. Yeakle, in W. W. Adams, R. K. Eby, and D. E. McLemore, eds., *The Materials Science and Engineering of Rigid-Rod Polymers*, Vol. **134**, MRS, Boston, 1989, p. 307.
44. S. R. Allen, R. J. Farris, and E. L. Thomas, *J. Mater. Sci.* **20**, 2727 (1985).
45. S. Kumar and W. W. Adams, *Polymer* **31**, 15 (1990).
46. S. Kumar, *Indian J. Fiber Test Res.* **16**, 52 (1991).
47. S. Kumar, in *International Encyclopedia of Composites*, Vol. **4**, VCH Publishers Inc., Weinheim, Germany, 1990, p. 51.
48. D. Rein and Y. Cohen, *J. Mater. Sci.* **30**, 3587–3590 (1995).
49. H. Jiang, R. K. Eby, and W. W. Adams, *Polym. News* **15**, 77 (1990).
50. K. S. Macturk, R. K. Eby, and W. W. Adams, *Polymer* **32**, 1782 (1991).
51. L. Feldman, A. Zihlif, R. J. Farris, and E. L. Thomas, *J. Mater. Sci.* **22**, 1199 (1987).
52. P. E. Klunzinger, R. K. Eby, and W. W. Adams, in I. Aksay, E. Bear, M. Sarikaya, and D. Tirrell, eds., *MRS Proceedings*, Vol. **255**, 1992, p. 119.
53. K. S. Macturk, R. K. Eby, and B. L. Farmer, *Polymer* **35**, 53 (1994).
54. K. Nakamae, T. Nishiro, Y. Gotoh, R. Matsui, and M. Nagura, *Polymer* **40**, 4629 (1999).
55. M. G. Northolt and J. J. Van Aarsten, *Polym. Symp.* **58**, 283 (1977).
56. M. G. Northolt and D. J. Sikkema, in A. A. Collier, ed., *Liquid Crystal Polymers: From Structures to Applications*, Elsevier, Oxford, U.K., 1992, p. 273.
57. A. I. Slutsker and O. Mirzoev, *Phys. Solid State* **38**, 851 (1996).
58. D. C. Martin and E. L. Thomas, in W. W. Adams, R. K. Eby, and D. E. McLemore, eds., *The Materials Science and Engineering of Rigid-Rod Polymers*, Vol. **134**, MRS, Boston, 1989, p. 415.
59. P. E. Klunzinger, K. S. Macturk, R. K. Eby, and W. W. Adams, *Polym. Prepr.* **32**, 187 (1991).
60. F. J. McGarry and J. E. Moalli, *Polymer* **32**, 1811 (1991).
61. F. J. McGarry and J. E. Moalli, *Polymer* **32**, 1816 (1991).
62. D. V. Mahony, *PhD Dissertation*, The University of Akron, Akron, Ohio, 1994.
63. R. G. Ramirez, *PhD Dissertation*, The University of Akron, Akron, Ohio, 1994.
64. M. G. Dobb, in W. Watt and B. V. Perov, eds., *Strong Fibers*, North Holland, Amsterdam, 1985, p. 684.
65. E. P. Socci, D. A. Thomas, D. T. Grubb, W. W. Adams, and R. K. Eby, *Bull. Am. Phys. Soc.* **40**, p. 351 (1995).
66. E. P. Socci, D. A. Thomas, R. K. Eby, D. T. Grubb, and W. W. Adams, *Polymer* **37**, 5005 (1996).
67. U. Santhosh, K. E. Newman, and C. Y.-C. Lee, *J. Mater. Sci.* **30**, 1894 (1995).
68. T. A. Doyne, A. N. Palazotto, T. Schuppe, Y.-C. Lee, and C. S. Wang, *Proceedings of ACS Polymer Material Science and Engineering*, Vol. **63**, 1990, p. 982.
69. S. A. Fawaz, A. N. Palazotto, and C. S. Wang, in W. W. Adams, R. K. Eby, and D. E. McLemore, eds., *The Materials Science and Engineering of Rigid-Rod Polymers*, Vol. **134**, MRS, Boston, 1989, p. 381.
70. S. A. Fawaz, A. N. Palazotto, and C. S. Wang, *Polymer* **33**, 100 (1992).
71. P. E. Klunzinger, K. A. Green, R. K. Eby, B. L. Farmer, W. W. Adams, and G. Czornyj, Technical Paper, XXXVII, Society of Plastics Engineering, 1991, p. 1532.
72. J. Sirichaisit and R. J. Young, *Polymer* **40**, 3421 (1999).
73. O. C. van der Jagt and A. Beukers, *Polymer* **40**, 1035 (1999).

74. S. L. Bazhenov, V. V. Kozey, and A. A. Berlin, *J. Mater. Sci.* **24**, 4509 (1989).
75. R. E. Wilfong and J. J. Zimmerman, *J. Appl. Polym. Sci. Polym. Symp.* **31**, 1 (1977).
76. S. Van der Zwagg and G. Kampschoer, in *Integration of Fundamental Polymer Science & Technology*, Vol. **2**, Elsevier Applied Sciences, London, 1988, p. 545.
77. S. Van der Zwagg, S. J. Picken, and C. P. Van Sluijs, in *Integration of Fundamental Polymer Science & Technology*, Vol. **3**, Elsevier Applied Sciences, London, 1989, p. 199.
78. S. Kumar and T. E. Helminiak, in W. W. Adams, R. K. Eby, and D. E. McLemore, eds., *The Materials Science and Engineering of Rigid-Rod Polymers*, Vol. **134**, MRS, Boston, 1989, p. 363.
79. S. J. DeTeresa, S. R. Allen, R. J. Farris, and R. S. Porter, *J. Mater. Sci.* **19**, 57 (1984).
80. S. J. DeTeresa, R. S. Porter, and R. J. Farris, *J. Mater. Sci.* **20**, 1645 (1985).
81. S. J. DeTeresa, AFWAL-TR-85-4013, 1985.
82. S. J. DeTeresa, R. S. Porter, and R. J. Farris, *J. Mater. Sci.* **23**, 1886 (1988).
83. S. Putthanarat, N. Stribeck, S. A. Fossey, R. K. Eby, and W. W. Adams, *Polymer* **41**, 7735 (2000).
84. S. R. Allen, *Polymer* **29**, 1091 (1988).
85. V. R. Mehta and S. Kumar, *J. Mater. Sci.* **29**, 3658 (1994).
86. S. J. DeTeresa and R. J. Farris, in W. W. Adams, R. K. Eby, and D. E. McLemore, eds., *The Materials Science and Engineering of Rigid-Rod Polymers*, Vol. **134**, MRS, Boston, 1989, p. 375.
87. V. V. Kozey and A. A. Berlin, *Japan-USSR Joint Symposium on Advanced Composites Materials*, Moscow, 1991, Paper N-22-p.
88. N. Melanitis and C. Galiotis, *J. Mater. Sci.* **25**, 5081 (1990).
89. C. Vlattas and C. Galiotis, *Polymer* **32**, 1788 (1991).
90. W. Huh, S. Kumar, T. E. Helminiak, and W. W. Adams, *SPE Annual Technical Conference Proceedings*, 1990, p. 1245.
91. T. Takahashi, M. Miwa, and S. Sukurai, *J. Appl. Polym. Sci.* **28**, 580 (1983).
92. D. A. Thomas, *PhD Dissertation*, The University of Akron, Akron, Ohio, 1994.
93. P. E. Klunzinger and R. K. Eby, *Polymer* **34**, 2431 (1993).
94. D. C. Martin and E. L. Thomas, *Macromolecules* **24**, 2224 (1991).
95. D. C. Martin and E. L. Thomas, *J. Mater. Sci.* **26**, 5171 (1991).
96. D. C. Martin and E. L. Thomas, *Phil. Mag.* **64**, 903 (1991).
97. D. Vezie, J. S. Speck, and E. L. Thomas, *APS Symposium Bulletin*, Vol. **37**, 1992, p. 516.
98. C. C. Chau, J. Blackson, and J. Im, *Polymer* **36**, 2511 (1995).
99. S. G. Wierschke, in W. W. Adams, R. K. Eby, and D. E. McLemore, eds., *The Materials Science and Engineering of Rigid-Rod Polymers*, Vol. **134**, MRS, Boston, 1989, p. 313.
100. A. S. Argon, *Glass Science & Technology*, 1980, Chapt. 3, p. 5.
101. A. S. Argon, *Proceedings of International Conference*, Gainesville, Fla., 1981, p. 393.
102. S. J. DeTeresa, R. J. Farris, and R. S. Porter, *Polym. Composites* **3**, 57 (1982).
103. I. M. Robinson, P. H. I. Yeung, C. Galiotis, R. J. Young, and D. J. Batchelder, *J. Mater. Sci.* **21**, 3440 (1986).
104. T. B. Hess and C. S. Barrett, *Trans. AIME J. Metals* **185**, 599 (1949).
105. J. J. Gilman, *J. Metals* **192**, 621 (1954).
106. T. Takahashi, C. F. Xiao, and K. Sakurai, *Sen-i Gakkaishi (Japanese)* **47**, 397 (1991).
107. T. Takahashi, K. Suzuki, T. Aoki, and K. Sakurai, *J. Macromol. Sci.-Phys., B* **30**, 101 (1991).
108. E. J. Roche, T. Takahashi, and E. L. Thomas, *ACS Symposium Series* **141**, p. 303. (1980).

109. M. Miwa, E. Tsushima, and J. Takayasu, *J. Appl. Polym. Sci., Polym. Symp.* **43**, 1467 (1991).
110. M. Miwa, E. Tsushima, and J. Takayasu, *Sen-i Gakkaishi (Japanese)* **47**, 171 (1991).
111. G. E. Attenburrow and D. C. Bassett, *J. Mater. Sci.* **14**, 2679 (1979).
112. K. Shigematsu, K. Imada, and M. Takayanagi, *J. Polym. Sci. Polym. Phys.* **13**, 73 (1985).
113. Y.-H. So, *Prog. Polym. Sci.* **25**, 137 (2000).
114. R. F. Kovar, R. R. Haghighat, and R. W. Lusignea, in W. W. Adams, R. K. Eby, and D. E. McLemore, eds., *The Materials Science and Engineering of Rigid-Rod Polymers*, Vol. **134**, MRS, Boston, 1989, p. 389.
115. C. S. Wang, J. Barkett, S. B. Bhattacharya, H. H. Chuah, and F. E. Arnold, *Proceedings of ACS Polymer Material Science and Engineering*, Vol. **60**, 1989, p. 767.
116. T. D. Dang, L. S. Tan, K. H. Wei, H. H. Chuah, and F. E. Arnold, *Proceedings of ACS Polymer Materials Science and Engineering*, Vol. **60**, 1989, p. 424.
117. W. Sweeny, *J. Polym. Sci. Part A: Polym. Chem.* **30**, 1111 (1992).
118. U. Santhosh, M. H. Dotrong, H. H. Song, and C. Y.-C. Lee, *Proceedings of ACS Polymer Material Science and Engineering*, Vol. **64**, 1991, p. 40.
119. I. K. Gillie, M. Newsham, S. J. Nolan, V. S. Jear, and R. A. Bubeck, *Bull. Am. Phys. Soc.* **38**, p. 292 (1993).
120. M.-C. G. Jones, T. Jiang, and D. C. Martin, *Bull. Am. Phys. Soc.* **39**, p. 697. (1994).
121. P. Bonk, S. J. Harris, J. H. Im, N. L. Madison, and S. Rosenberg, AFWAL-TR-88-4131, 1988.
122. J. F. Mammone and W. C. Uy, AFWAL-TR-82-4154, 1984.
123. S. Bhattacharya, H. H. Chuah, M. Dotrong, K. H. Wei, C. S. Wang, D. Vezie, A. Day, and W. W. Adams, *Proceedings of ACS Polymer Materials Science and Engineering*, Vol. **60**, 1989, p. 512.
124. M. Dotrong and R. Evers, *Proceedings of ACS Polymer Materials Science and Engineering*, Vol. **60**, 1989, p. 507.
125. M. Dotrong, M. H. Dotrong, and R. C. Evers, Proceedings of ACS Polymer Material Science and Engineering, Vol. **65**, 1991, p. 38.
126. T. T. Tsai and F. E. Arnold, *Polym. Prepr. (ACS)* **29**, 324 (1988).
127. H. H. Chuah, T. T. Tsai, K. H. Wei, C. S. Wang, and F. E. Arnold, *Proceedings of ACS Polymer Material Science and Engineering*, Vol. **60**, 1989, p. 517.
128. X. Hu, S. Kumar, M. B. Polk, and D. L. Vanderhart, *J. Polym. Sci., Part A: Polym. Chem.* **36**, 1407 (1998).
129. S. Jenkins, K. I. Jacob, and S. Kumar, *J. Polym. Sci., Part B: Polym. Phys.* **36**, 3087 (1998).
130. V. R. Mehta, S. Kumar, M. B. Polk, D. L. Vanderhart, and F. Arnold, *J. Polym. Sci., Part B: Polym. Phys.* **34**, 1881 (1996).
131. V. R. Mehta and S. Kumar, *J. Appl. Polym. Sci.* **73**, 305 (1999).
132. Y.-H. So, B. Bell, J. P. Heeschen, R. A. Nyquist, and C. L. Murlick, *J. Polym. Sci., Part A: Polym Chem.* **33**, 159 (1995).
133. L. J. Markoski, K. A. Walker, G. A. Deeter, G. E. Spilman, D. C. Martin, and J. S. Moore, *Chem. Mater.* **5**, 248 (1993).
134. T. D. Dang, C. S. Wang, W. E. Click, D. C. Martin, G. A. Deeter, J. S. Moore, D. M. Husband, and F. E. Arnold, *Polym. Prepr. (ACS)* **36**, 455 (1995).
135. T. D. Dang, C. S. Wang, W. E. Click, H. H. Chuah, T. T. Tsai, D. M. Husband, and F. E. Arnold, *Polymer* **38**, 621 (1997).
136. M. F. Farona, *Prog. Polym. Sci.* **21**, 505 (1996).
137. N. Venkatasubramanian and S. Kumar, *Proceedings of ACS Polymer Materials Science and Engineering*, Vol. **67**, 1992, p. 453.

138. M. Dotrong, M. H. Dotrong, and R. C. Evers, *Polym. Prepr. (ACS)* **34**, 408 (1993).
139. X. Hu, M. B. Polk, and S. Kumar, *Macromolecules* **33**, 3342 (2000).
140. L.-S. Tan, F. E. Arnold, T. D. Dang, H. H. Chuah, and K. H. Wei, *Polymer* **35**, 3091 (1994).
141. S. Jenkins, K. I. Jacob, and S. Kumar, *J. Polym. Sci., Part B: Polym. Phys.* **38**, 3053 (2000).
142. J. C. L. Hageman, J. W. van der Horst, and R. A. de Groot, *Polymer* **40**, 1313 (1999).
143. M. Lammers, E. A. Klop, M. G. Northolt, and D. J. Sikkema, *Polymer* **39**, 5999 (1998).
144. E. A. Klop and M. Lammers, *Polymer* **39**, 5987 (1998).
145. K. E. Newman, P. Zhang, L. J. Cuddy, and D. L. Allara, *J. Mater. Res.* **6**, 1580 (1991).
146. *MRS, Mater. Res. Soc. Bull.* 7 (1995).
147. N. Arsalani and K. E. Geckeler, *J. Prakt. Chem.* **337**, 1 (1995).
148. C. C. Chau, W. J. Harris, J. H. Im, N. L. Madison, S. Rosenberg, and Y.-H. So, WRDC-TR-90-4005, 1990.
149. H. H. Chauh, L. S. Tan, and F. E. Arnold, *Polym. Eng. Sci.* **29**, 107 (1989).
150. Y.-H. So, A. Sen, P. Kim, and V. St. Jeor, *J. Polym. Sci., Part A: Polym. Chem.* **33**, 2893 (1995).
151. R. L. McGee, Y.-H. So, S. J. Martin, C. F. Broomall, V. St. Jeor, J. J. Curphy, E. J. Swedberg, and D. G. Wetters, *J. Polym. Sci., Part A: Polym. Chem.* **35**, 2157 (1997).
152. U.S. Pat. 5,512,368 (1996), M. A. Harmer and B. R. Phillips (to E. I. du Pont de Nemours & Co., Inc.).
153. L. R. Denny, I. J. Goldfarb, and E. J. Soloski, in W. W. Adams, R. K. Eby, and D. E. McLemore, eds., *The Materials Science and Engineering of Rigid-Rod Polymers*, Vol. **134**, MRS, Boston, 1989, p. 345.
154. I. J. Goldfarb, H. Reale, S. Wierschke, and J. Medrano, in W. W. Adams, R. K. Eby, and D. E. McLemore, eds., *The Materials Science and Engineering of Rigid-Rod Polymers*, Vol. **134**, MRS, Boston, 1989, p. 609.
155. E. G. Jones and D. L. Pedrick, in W. W. Adams, R. K. Eby, and D. E. McLemore, eds., *The Materials Science and Engineering of Rigid-Rod Polymers*, Vol. **134**, MRS, Boston, 1989, p. 407.
156. R. W. Lusignea, in W. W. Adams, R. K. Eby, and D. E. McLemore, eds., *The Materials Science and Engineering of Rigid-Rod Polymers*, Vol. **134**, MRS, Boston, 1989, p. 265.
157. J. F. Wolfe, B. K. Loo, and F. E. Arnold, *Macromolecules* **14**, 915 (1981).
158. L. Huang, B. Shi, and X. Jin, *Gao-fen-zi Xue-bao (Chinese)* **3**, 338 (1999).
159. Y. H. So, S. W. Froelicher, B. Kaliszewski, and R. DeCaire, *Macromolecules* **32**, 6565 (1999).
160. L. A. Pottick, *Ph.D. dissertation*, University of Massachusetts, 1986.
161. B. L. Farmer, B. R. Chapman, D. S. Dudis, and W. W. Adams, *Polymer* **34**, 1588 (1993).
162. P. E. Klunzinger and R. K. Eby, *Polym. Prepr. (ACS)* **36**, 631 (1995).
163. K. Saito, Y. Takahashi, and M. Sorai, *J. Polym. Sci., Part B: Polym. Phys.* **38**, 1584 (2000).
164. P. N. Prasad, in W. W. Adams, R. K. Eby, and D. E. McLemore, eds., *The Materials Science and Engineering of Rigid-Rod Polymers*, Vol. **134**, MRS, Boston, 1989, p. 635.
165. B. A. Reinhardt, *Trends Polym. Sci.* **1**, 4 (1993).
166. M. A. Druy and L. H. Domash, in W. W. Adams, R. K. Eby, and D. E. McLemore, eds., *The Materials Science and Engineering of Rigid-Rod Polymers*, Vol. **134**, MRS, Boston, 1989, p. 653.
167. A. J. Heeger, in W. R. Salaneck, I. Lundstrom, and B. Randy, Lulea, eds., *81st Nobel Symposium*, Sweden, 1993, p. 27.
168. J. W. Lee and C. S. Wang, *Polymer* **35**, 3673 (1994).

169. J. W. Lee, C. S. Wang, S. Caracci, and D. M. Husband, *Polymer* **39**, 2765 (1998).
170. L.-S. Tan, J. L. Burkett, S. R. Simko, and J. Alexander M. D., *Macromol. Rapid Commun.* **20**, 16 (1999).
171. A. J. Heeger, *J. Phys. Chem. B* **105**, 8475 (2001).
172. D. N. Rao, J. Swiatkiewicz, P. Chopra, S. K. Ghoshal, and P. N. Prasad, *Appl. Phys. Lett.* **48**, 1187 (1986).
173. S. A. Jenekhe, J. A. Osaheni, J. S. Meth, and H. Vanherzeele, *Chem. Mater.* **4**, 683 (1992).
174. B. A. Reinhardt, M. R. Unroe, R. C. Evers, M. Zhao, M. Samoe, P. N. Prasad, and M. Sinsky, *Chem. Mater.* **3**, 864 (1991).
175. C. Y.-C. Lee, J. Swiatkiewicz, P. N. Prasad, R. Mehta, and S. J. Bai, *Polymer* **32**, 1195 (1991).
176. M. Dotrong, R. Mehta, G. A. Balchin, R. C. Tomlinson, M. Sinsky, C. Y.-C. Lee, and R. C. Evers, *J. Polym. Sci., Part A: Polym. Chem.* **31**, 723 (1993).
177. W. J. Bailey, in H. F. Mark and N. G. Gaylord, eds., *Encyclopedia of Polymer Science and Technology*, Vol. **8**, John Wiley & Sons, Inc., New York, 1968, p. 97.
178. P. E. Cassidy, *Thermally Stable Polymers: Synthesis and Properties*, Marcel Dekker, New York, 1980, Chapt. "9".
179. W. J. Bailey, in H. F. Mark, N. M. Bikales, C. G. Overberger, and G. Menges, eds., *Encyclopedia of Polymer Science and Engineering*, 2nd ed., Index volume, John Wiley & Sons, Inc., New York, 1990, p. 158.
180. J. W. Lee, C. S. Wang, H. H. Song, and G. E. Price, *Polymer* **36**, 955 (1995).
181. S. P. Karna, V. Keshari, and P. N. Prasad, *Chem. Phys. Lett.* **234**, 390 (1995).
182. M. F. Roberts and S. A. Jenekhe, *Chem. Mater.* **2**, 629 (1990).
183. S. A. Jenekhe, M. F. Roberts, H. Vanherzeele, and J. S. Meth, *Polym. Prepr. (ACS)* **32**, 140 (1991).
184. H. Vanherzeele, J. S. Meth, S. A. Jenekhe, and M. F. Roberts, *Appl. Phys. Lett.* **58**, 663 (1991).
185. S. J. Martin, D. C. Bradley, J. A. Osaheni, and S. A. Jenekhe, *Mol. Cryst. Liq. Cryst.* **256**, 583 (1994).
186. J. Swiatkiewicz, P. N. Prasad, F. E. Karasz, M. Druy, and P. Glatoski, *Appl. Phys. Lett.* **56**, 892 (1990).
187. S. J. Bai, R. J. Spry, D. E. Zelmon, U. Ramabadran, and J. Jackson, *J. Polym. Sci., Part B: Polym. Phys.* **30**, 1507 (1992).
188. S. J. Bai and G. E. Price, *Polymer* **33**, 2136 (1992).
189. I. J. Goldfarb and J. Medrano, in *Nonlinear Optical Effects in Organic Polymers*, Kluwer Academic Publishers, London, 1989, p. 93.
190. J. A. Osaheni, S. A. Jenekhe, and J. Perlstein, *J. Phys. Chem.* **98**, 12727 (1994).
191. D. W. Polis, L. R. Dalton, and D. J. Vachon, in W. W. Adams, R. K. Eby, and D. E. McLemore, eds., *The Materials Science and Engineering of Rigid-Rod Polymers*, Vol. **134**, MRS, Boston, 1989, p. 679.
192. J. K. Politis, M. D. Curtis, L. González-Ronda, and D. C. Martin, *Chem. Mater.* **12**, 2798 (2000).
193. J. A. Osaheni and S. A. Jenekhe, *Macromolecules* **28**, 1172 (1995).
194. J. A. Osaheni and S. A. Jenekhe, *Chem. Mater.* **4**, 1282 (1992).
195. D. Bhaumik and J. E. Mark, *Polym. Prepr. (ACS)* **23**, 23 (1982).
196. D. Bhaumik and J. E. Mark, *J. Polym. Sci., Part B: Polym. Phys.* **21**, 1111–2543 (1983).
197. R. E. Baker and D. Y. Chen, *Annu. Rep. Conf. Electr. Insul. Dielectr. Phenom.*, 1981, p. 35.
198. J. M. C. Redman, J. M. Giesler, W. R. Romanko, S. H. Carr, P. A. Cepra, T. J. Marks, H. O. Marcy, and C. R. Kannewurf, *Synth. Met.* **29**, F25 (1989).
199. A. DePra, J. G. Gaudiello, and T. J. Marks, *Macromolecules* **21**, 2295 (1988).

200. W. R. Romanko, P. A. McHatton, H. C. Marcy, C. R. Kannewurf, T. J. Marks, and S. H. Carr, *Synth. Met.* **41/43**, 947 (1991).
201. D. B. Roitman, J. Mcalister, M. Mcadon, and R. A. Wessling, *J. Polym. Sci., Part B: Polym. Phys.* **32**, 1157 (1994).
202. R. J. Spry, M. D. Alexander Jr., S. J. Bai, T. D. Dang, G. E. Price, D. R. Dean, B. Kumar, J. S. Solomon, and F. E. Arnold, *J. Polym. Sci., Part B: Polym. Phys.* **35**, 2925 (1997).
203. S. J. Bai, K. R. Srinivasan, L.-S. Tan, R. J. Spry, and G. E. Price, *J. Appl. Phys.* **85**, 280 (1999).
204. R. A. Vaia, J. W. Lee, C. S. Wang, B. Click, and G. Price, *Chem. Mater.* **10**, 2030 (1998).
205. G. Du, V. N. Prigodin, A. Burns, J. Joo, C. S. Wang, and A. J. Epstein, *Phys. Rev. B.* **58**, 4485 (1998).
206. L.-S. Tan, in P. N. Prasad, ed., *Frontiers of Polymers and Advanced Materials*, Plenum Press, New York, 1994, p. 493.
207. J. A. Osaheni, S. A. Jenekhe, A. Burns, G. Du, J. Joo, Z. Wang, A. J. Epstein, and C. S. Wang, *Macromolecules* **25**, 5828 (1992).
208. S. Wang, P. Wu, and Z. Han, *Polymer* **42**, 217 (2001).
209. W. W. Adams and R. K. Eby, *Bull. Mater. Res. Soc.* 22 (Nov./Dec. 1987).
210. S. J. Krause, T. B. Haddock, D. L. Vezie, P. G. Lenhert, W.-F. Hwang, G. E. Price, T. E. Helminiak, J. F. O'Brien, and W. W. Adams, *Polymer* **29**, 1354 (1988).
211. R. J. Young, D. Lu, R. J. Day, F. Knoff, and H. A. Davis, *J. Mater. Sci.* 27 (1992).
212. R. J. Young, R. J. Day, and M. Zakikhani, in W. W. Adams, R. K. Eby, and D. E. McLemore, eds., *The Materials Science and Engineering of Rigid-Rod Polymers*, Vol. **134**, MRS, Boston, 1989, p. 351.
213. R. J. Young, R. J. Day, and M. Zakikhani, *J. Mater. Sci.* **25**, 127 (1990).
214. T. A. Hancock, J. L. White, and J. E. Spruill, *Polym. Eng. Sci.* **20**, 1126 (1980).
215. T. Kitagawa, H. Murase, and K. Yabuki, *J. Polym. Sci., Part B: Polym. Phys.* **36**, 39 (1998).
216. M. A. Rakas and R. J. Farris, *J. Appl. Polym. Sci.* **40**, 823 (1990).
217. A. V. Fratini, P. G. Lenhert, T. J. Resch, and W. W. Adams, in W. W. Adams, R. K. Eby, and D. E. McLemore, eds., *The Materials Science and Engineering of Rigid-Rod Polymers*, Vol. **134**, MRS, Boston, 1989, p. 431.
218. Y. Takahashi and H. Sul, *J. Polym. Sci. Part B: Polym. Phys.* **38**, 376 (2000).
219. Y. Yang and W. J. Welsh, *Macromolecules* **23**, 2410 (1990).
220. W. J. Welsh, J. E. Mark, Y. Yang, and G. P. Das, in W. W. Adams, R. K. Eby, and D. E. McLemore, eds., *The Materials Science and Engineering of Rigid-Rod Polymers*, Vol. **134**, MRS, Boston, 1989, p. 621.
221. W. J. Welsh and Y. Yang, *Comp. Polym. Sci.* **1**, 139 (1991).
222. B. L. Farmer, S. G. Wierschke, and W. W. Adams, *Polymer* **31**, 1631 (1990).
223. W. J. Welsh, D. Bhaumik, and J. E. Mark, *J. Macromol. Sci. Phys. B* **20**, 59 (1981).
224. K. Tashiro, J. Yoshino, T. Kitagawa, H. Murase, and K. Yabuki, *Macromolecules* **31**, 5430–5440 (1998).
225. Y. Takahashi, *Macromolecules* **32**, 4010 (1999).
226. D. Tomlin, A. V. Fratini, M. Hunsaker, and W. W. Adams, *Polymer* **41**, 9003 (2000).
227. J. A. Odell, A. Keller, E. D. T. Atkins, and M. J. Miles, *J. Mater. Sci.* **16**, 3309 (1981).
228. S. Kumar, S. Warner, D. T. Grubb, and W. W. Adams, *Polymer* **35**, 5408 (1994).
229. M. E. Hunsaker, G. E. Price, and S. J. Bai, *Polymer* **33**, 2128 (1992).
230. P. G. Lenhert and W. W. Adams, in W. W. Adams, R. K. Eby, and D. E. McLemore, eds., *The Materials Science and Engineering of Rigid-Rod Polymers*, Vol. **134**, MRS, Boston, 1989, p. 329.

231. T. Kitagawa and K. Yabuki, *J. Polym. Sci.: Part B: Polym. Phys.* **38**, 2901 (2000).
232. T. Kitagawa and K. Yabuki, *J. Polym. Sci., Part B: Polym. Phys.* **38**, 2937 (2000).
233. T. Kitagawa, M. Ishitobi, and K. Yabuki, *J. Polym. Sci., Part B: Polym. Phys.* **38**, 1605 (2000).
234. T. Kitagawa and K. Yabuki, *Polymer Fibers 2000 Symposium*, Manchester, U.K., July 5–7, 2000.
235. T. Kitagawa, K. Yabuki, and R. J. Young, *Polymer* **42**, 2101–2112 (2001).
236. R. J. Davis, R. J. Young, and C. Riekel, *Polymer Fibers 2000 Symposium*, Manchester, U.K., July 5–7, 2000.
237. Y. Yamashita, Y. Kato, S. Endo, and K. Kimura, *Makromol. Chem., Rapid Commun.* **9**, 687 (1988).
238. K. Kimura, S. Endo, Y. Kato, and Y. Yamashita, *Polymer* **35**, 123 (1994).
239. H. H. Song and S.-K. Hong, *Polymer* **38**, 4241 (1997).
240. H. H. Song and C. S. Wang, *Polymer* **34**, 4793 (1993).
241. H. R. Kricheldorf and G. Schwarz, *Makromol. Chem.* **184**, 475 (1983).
242. Y. Yamashita, K. Akagi, K. Monobe, and K. Shimamura, *1983 Korea–Japan Joint Meeting on Textile Science and Technology*, 1983, p. 130.
243. Y. Yamashita, Y. Kato, S. Endo, and K. Kimura, *Koubunshi Ronbunshu (Japanese)* **44**, 41 (1987).
244. Y. Kato, Y. Yamashita, K. Kimura, and S. Endo, *Koubunshi Ronbunshu (Japanese)* **44**, 35 (1987).
245. Y. Kato, Y. Yamashita, K. Kimura, and S. Endo, *Koubunshi Ronbunshu (Japanese)* **45**, 973 (1988).
246. Y. Kato, Y. Yamashita, K. Kimura, and S. Endo, *Koubunshi Ronbunshu (Japanese)* **47**, 583 (1990).
247. K. Kiruma, S. Endo, Y. Kato, and Y. Yamashita, *Polymer* **34**, 1054 (1993).
248. K. Kiruma, S. Endo, Y. Kato, and Y. Yamashita, *Polymer* **35**, 123–3311 (1994).
249. K. Kiruma, S. Endo, Y. Kato, and Y. Yamashita, *Macromolecules* **28**, 255 (1995).
250. H. R. Kricheldorf and A. Conradi, *Macromolecules* **22**, 14 (1989).
251. J. Economy, W. Vollsen, C. Viney, R. Geiss, R. Siemens, and T. Karis, *Macromolecules* **21**, 2777 (1989).
252. Y.-H. So, J. P. Heeschen, and C. L. Murlick, *Macromolecules* **28**, 7289 (1995).
253. Y.-H. So and J. P. Heeschen, *J. Org. Chem.* **62**, 3552 (1997).
254. Y.-H. So, J. P. Heeschen, B. Bell, P. Bonk, M. Briggs, and R. DeCaire, *Macromolecules* **31**, 5229 (1998).
255. J. F. Wolfe, in W. W. Adams, R. K. Eby, and D. E. McLemore, eds., *The Materials Science and Engineering of Rigid-Rod Polymers*, Vol. **134**, MRS, Boston, 1989, p. 83.
256. U.S. Pat. 4,533,692 (1985), J. R. Sybert, P. D. Sybert, B. Wilson, and J. F. Wolfe (to SRI International).
257. R. J. Schmitt, D. S. Ross, J. R. Hardee, and J. F. Wolfe, *J. Org. Chem.* **53**, 5568 (1988).
258. A. W. Chow, J. F. Sandell, and J. F. Wolfe, *Polymer* **29**, 1307 (1988).
259. G. C. Berry, P. C. Metzger, S. Venkatramm, and D. B. Cotts, *Polym Prepr. (ACS)* **20**, 42 (1979).
260. D. B. Cotts and G. C. Berry, *Polym. Prepr. (ACS)* **20**, 571 (1979).
261. J. Wolfe, in H. F. Mark, ed., *Encyclopedia of Polymer Science and Engineering*, Vol. **11**, John Wiley & Sons, Inc., New York, 1988, p. 601.
262. A. L. Rusanov, *Polym. Sci. U.S.S.R.* **28**, 1745 (1986).
263. D. Likhatchev, S. Granados-Focil, R. Gavineo, M. Canseco, and L. Alexandrova, *High Perform. Polym.* **11**, 405 (1999).
264. T. Hattori, K. Kagawa, and M. Kakimoto, *Macromolecules* **26**, 4089 (1993).
265. T. Hattori, K. Kagawa, and M. Kakimoto, *Polym. J.* **26**, 930 (1994).

266. U.S. Pat. 5041522 (1991), T. D. Dang, H. H. Chuah, L.-S. Tan, and F. E. Arnold (to U.S. Airforce).
267. P. J. Flory, *Proc. Roy. Soc. A* **234**, 60–73 (1956).
268. A. N. Semenov and A. V. Subbotin, *Polym. Sci. U.S.S.R.* **31**, 2266–2273 (1989).
269. G. C. Berry, in W. W. Adams, R. K. Eby, and D. E. McLemore, eds., *Materials Science and Engineering of Rigid-Rod Polymers*, Vol. **134**, MRS, Boston, 1989, p. 181.
270. J. A. Odell, A. Keller, E. D. T. Atkins, M. J. Nagy, J. L. Feijoo, and G. Ungar, in W. W. Adams, R. K. Eby, and D. E. McLemore, eds., *Materials Science and Engineering of Rigid-Rod Polymers*, Vol. **134**, MRS, Boston, 1989, p. 223.
271. V. G. Kulichikhin, A. Y. Malkin, S. P. Papov, O. N. Korol'kova, V. D. Kalmykova, A. V. Volokina, and O. B. Semenov, *Polym. Sci., Ser. A* **41**, 1337 (1999); [*translated from Vysokomol. Soedin., Ser. A* **16**, 169 (1974) (in Russian)].
272. A. M. Donald and A. H. Windle, *Liquid Crystalline Polymers*, Cambridge University Press, Cambridge, U.K., 1992.
273. V. Faraoni, M. Grosso, and S. Crescitelli, *J. Rheol.* **43**, 829 (1999).
274. T. I. Garmonova, V. N. Artem'eva, and Y. M. Nekrasova, *Polym. Sci. U.S.S.R.* **32**, 1972 (1990).
275. T. I. Garmonova, *Polym. Sci. U.S.S.R.* **32**, 2315 (1990).
276. Y. R. Oh, Y. S. Lee, M. H. Kwon, and O. O. Park, *J. Polym. Sci., Part B: Polym. Phys.* **38**, 509 (2000).
277. A. Immaneni and A. J. Mchugh, *J. Polym. Sci., Part B: Polym. Phys.* **36**, 181 (1998).
278. G. C. Berry, M. Cotts, and S. Chu, *J. Brit. Polym.* **13**, 47 (1981).
279. R. Zhang and W. L. Mattice, *Macromolecules* **25**, 4937 (1992).
280. W. G. Miller, *Liquid Crystals Ordered Fluids*, Vol. **11**, Plenum Press, New York, 1974, p. 243.
281. A. Ciferri, *Polym. Eng. Sci.* **15**, 191 (1975).
282. A. Ciferri, *Int. J. Polym. Mater.* **6**, 137 (1978).
283. G. Petekidis, D. Vlassopoulos, G. Fytas, R. Rulkens, and G. Wegner, *Macromolecules* **31**, 6129 (1998).
284. G. Petekidis, D. Vlassopoulos, G. Fytas, R. Rulkens, G. Wegner, and G. Fleischer, *Macromolecules* **31**, 6139 (1998).
285. S.-F. Wang, P.-P. Wu, and Z.-W. Han, *Gao-feng-zi Tong-bao (Chinese)* (3), 16 (2001).
286. E. W. Won Choe and S. N. Kim, *Macromolecules* **14**, 920 (1981).
287. S. Y. Frenkel, *Theory of Man-Made Fibre Spinning (in Russian)*, Vol. **91**, Mytishchi, 1975, p. 111.
288. A. I. Kol'tsov, N. G. Bel'nikevich, A. V. Gribenov, S. P. Papkov, and S. Y. Frenkel', *Polym. Sci., Ser. A* **41**, 1334 (1999); [*translated from Vysokomol. Soedin., Ser. B* **15**, 645 (1973) (in Russian)].
289. G. Marrucci, *Polym. Eng. Sci.* **15**, 191 (1975).
290. P. J. Collings, *Liquid Crystals*, Princeton University Press, Princeton, N.J., 1990.
291. D. B. Cotts and G. C. Berry, *Macromolecules* **14**, 930 (1981).
292. C. P. Wong, H. Ohnuma, and G. C. Berry, *J. Polym. Sci.* **65**, 173 (1978).
293. T. K. Kwei, M. Nakazawa, S. Matsuoka, M. K. Cowman, and Y. Okamoto, *Macromolecules* **33**, 235 (2000).
294. J. Riseman and R. Ullman, *J. Chem. Phys.* **19**, 578 (1951).
295. R. Sima, *J. Colloid Sci.* **5**, 386 (1950).
296. G. Marrucci and P. L. Maffettone, *Macromolecules* **34**, 1217–1231 (1990).
297. S. Z. Hess, *Z. Naturforsch.* **31A**, 1034 (1976).
298. M. Doi, *J. Polym. Sci., Polym. Phys. Ed.* **19**, 229 (1981).
299. R. G. Larson, *Macromolecules* **23**, 3983 (1990).

300. J. J. Magda, S. G. Baek, L. de Vries, and R. G. Larson, *Macromolecules* **24**, 4460 (1991).
301. P. L. Maffettone and S. Crescitelli, *J. Rheol.* **38**, 1559 (1994).
302. U.S. Pat. 3,767,756 (1973), H. Blades.
303. G. C. Berry, *Polym. Prepr. (ACS)* **23**, 27 (1982).
304. Y. Cohen, Y. Saruyama, and E. L. Thomas, *Macromolecules* **24**, 1161–1167 (1991).
305. E. O. Shaffer II, C. J. Carriere, and R. A. Bubeck, *J. Polym. Sci., Part B: Polym. Phys.* **30**, 259 (1992).
306. K. H. Wei and W. W. Adams, personal communication, 1996.
307. W. Huh, C. Y.-C. Lee, and S. J. Bai, *Polymer* **33**, 789 (1992).
308. H. Fischer, J. A. Odell, and A. Keller, *J. Mater. Sci.* **29**, 1025 (1994).
309. S. Wang, G. Bao, P. Wu, and Z. Hen, *Eur. Polym. J.* **36**, 1843 (2000).
310. H. Fischer, M. J. Miles, and J. A. Odell, *Macromol. Rapid Commun.* **15**, 815 (1994).
311. J.-D. Ding, Y.-H. Hu, and Y.-L. Yang, *Gao-deng Xue-xiao Hua-xue Xue-bao (Chinese)* **17**, 996 (1996).
312. P. Wu, F. Sun, and B. Liao, *Gao-fen-zi Xue-bao (Chinese)* (2), 136 (1992).
313. P. Wu, Z. Hen, and M. Yan, *Gong-neng Gao-fen-zi Xue-bao (Chinese)* **1**, 61 (1988).
314. Y. Cohen and E. L. Thomas, *J. Polym. Sci., Part B: Polym. Phys.* **25**, 1607–1614 (1987).
315. Y. Cohen and E. L. Thomas, *Macromolecules* **21**, 433–436 and 437–441 (1988).
316. Y. Cohen, in W. W. Adams, R. K. Eby, and D. E. McLemore, eds., *The Materials Science and Engineering of Rigid-Rod Polymers*, Vol. **134**, MRS, Boston, 1989, p. 195.
317. Y. Cohen, S. Buchner, H. G. Zachman, and D. Davidov, *Polymer* **33**, 3811 (1992).
318. Y. Cohen and E. Cohen, *Macromolecules* **28**, 3631–3636 (1995).
319. S. J. Nolan, C. F. Broomall, R. A. Bubeck, B. G. Landes, P. R. Rudolf, M. J. Mills, and M. J. Radler, in R. K. Eby, R. C. Evers, M. A. Meador, and D. Wilson, eds., *High Performance Polymers and Polymer Matrix Composites*, Vol. **305**, 1993, p. 111.
320. C. F. Broomall, R. A. Bubeck, B. G. Landes, M. J. Mills, S. J. Nolan, M. J. Radler, and P. R. Rudolf, *Bull. Am. Phys. Soc.* **39**, 565 (1994).
321. M. J. Radler, B. G. Landes, S. J. Nolan, C. F. Broomall, T. C. Chritz, P. R. Rudolf, M. E. Mills, and R. A. Bubeck, *J. Polym. Sci., Part B: Polym. Phys.* **32**, 2567 (1994).
322. Y. Cohen and W. W. Adams, *Polymer* **37**, 2767–2774 (1996).
323. Y. Einaga and G. C. Berry, *Polym. Prepr. (ACS)* **23**, 27 (1982).
324. G. C. Berry, C. C. Wei, and R. Furukawa, *Polym. Prepr. (ACS)* **27**, 228 (1986).
325. C. C. Lee, S. C. Chu, and G. C. Berry, *J. Polym. Sci., Polym. Phys.* **21**, 1573 (1983).
326. E. L. Thomas, Y. Cohen, and H. H. Frost, *Polym. Prepr. (ACS)* **27**, 231 (1986).
327. K. Shimamura, H. Kobayashi, and T. Ikawa, *Sen-i Gakkaishi (Japanese)* **49**, 26 (1993).
328. K. Shimamura, T. Uchida, M. Suzuki, and C.-X. Zhang, *Sen-i Gakkaishi (Japanese)* **54**, 374 (1998).
329. K. Shimamura and T. Uchida, *Polymer Fibers 2000 Symposium*, Manchester, U.K., July 5–7, 2000.
330. U.S. Pat. 4,963,616 (1990), S. A. Jenekhe (to Honywell Inc.).
331. S. A. Jenekhe, P. O. Johnson and A. K. Agrawal, *Macromolecules* **22**, 3216 (1989).
332. S. A. Jenekhe and P. O. Johnson, *Macromolecules* **23**, 4419 (1990).
333. M. F. Roberts and S. A. Jenekhe, *Chem. Mater.* **5**, 1744 (1993).
334. M. F. Roberts, S. A. Jenekhe, and A. Cameron, *Chem. Mater.* **6**, 658 (1994).
335. N. Venkatasubramanian, M. B. Polk, S. Kumar, and T. Gelbaum, *J. Polym. Sci., Part B: Polym. Phys.* **31**, 1965 (1993).
336. J. W. Connolly, D. S. Dudis, S. Kumar, L. T. Gelbaum, and N. Venkatasubranmanian, *Chem. Mater.* **8**, 54 (1886).

337. M. F. Roberts and S. A. Jenekhe, *Chem. Mater.* **6**, 135 (1994).
338. B. A. Reinhardt, *Polym. Commun.* **31**, 453 (1990).
339. J. G. Hilborn, J. W. Labadie, and J. L. Hedrick, *Macromolecules* **23**, 2854 (1990).
340. W. D. Joseph, R. Mercier, and R. Prasad, *Polymer* **34**, 866 (1993).
341. W. D. Joseph, J. C. Abed, and R. Mercier, *Polymer* **35**, 3046 (1994).
342. W. D. Joseph, J. C. Abed, and T. H. Yoon, *Polym. Prepr. (ACS)* **35**, 551 (1994).
343. S. Kim, D. A. Cameron, and Y. Lee, *J. Polym. Sci., Part A: Polym. Chem.* **34**, 481 (1996).
344. R. A. Johnson and L. J. Mathias, *J. Polym. Sci., Part A: Polym. Chem.* **33**, 1901 (1995).
345. E. C. Chenevey and W. D. Timmons, in W. W. Adams, R. K. Eby, and D. E. McLemore, eds., *The Materials Science and Engineering of Rigid-Rod Polymers*, Vol. **134**, MRS, Boston, 1989, p. 245.
346. E. L. Thomas, R. J. Farris, and S. L. Hsu, AFWAL-TR-80-4045, 1980.
347. K. G. Beltsios and S. H. Carr, *J. Macromol. Sci. Phys. B* **29**, 71 (1990).
348. A. W. Chow, H. R. D., J. F. Sandell, and J. F. Wolfe, in W. W. Adams, R. K. Eby, and D. E. McLemore, eds., *The Materials Science and Engineering of Rigid-Rod Polymers*, Vol. **134**, MRS, Boston, 1989, p. 95.
349. S. J. Nolan, C. F. Broomall, R. A. Bubeck, M. J. Radler, and B. G. Landes, *Rev. Sci. Instrum.* **66**, 2652 (1995).
350. H. H. Yang, *Aromatic High-Strength Fibers*, John Wiley & Sons, Inc., New York, 1989.
351. S. J. Picken, S. Van der Zwaag, and M. G. Northolt, *Polymer* **33**, 2999 (1992).
352. M. A. Rakas and R. J. Farris, *Polym. Mater. Sci. Eng.* **58**, 1024 (1988).
353. K. Shimamura and A. Hashimoto, *Sen-i Gakkaishi (Japanese)* **47**, 325 (1991).
354. Y. Cohen and E. L. Thomas, *Mol. Cryst. Liq. Cryst.* **153**, 375–384 (1987).
355. M. A. Rakas and R. J. Farris, in W. W. Adams, R. K. Eby, and D. E. McLemore, eds., *The Materials Science and Engineering of Rigid-Rod Polymers*, Vol. **134**, MRS, Boston, 1989, p. 95.
356. Y. Cohen and E. L. Thomas, *Polym. Eng. Sci.* **25**, 1093 (1985).
357. Y. Tsabba, D. M. Rein, and Y. Cohen, *J. Polym. Sci., Part B: Polym. Phys.*, **40**, 1087 2002.
358. L. A. Pottick, R. J. Farris, and E. L. Thomas, *Polym. Eng. Sci.* **25**, 284 (1985).
359. Y. Cohen and E. Gartstein, *Polym. Eng. Sci.* **36**, 1355–1359 (1995).
360. M. G. Forest, H. Zhou, and Q. Wang, *SIAM J. Appl. Math.* **60**, 1177 (2000).
361. J. W. Lee, C. S. Wang, G. E. Price, and D. M. Husband, *Polymer* **38**, 1403 (1997).
362. K. Krember and F. Muller-Plathe, in M. Borowko, ed., *Computational Methods in Surface and Colloid Science*, Marcel Dekker, New York, 2000, p. 481.
363. D. T. Grubb, in E. L. Thomas, ed., *Materials Science and Technology, Vol. 12: Structure and Properties of Polymers*, VCH Publishers Inc., Weiheim, Germany, 1993, p. 301.
364. V. N. Shogenov, G. V. Kozlov, and A. K. Mikitayev, *Polym. Sci. U.S.S.R.* **31**, 1945–1950 (1989).
365. J. R. Shoemaker, T. Horn, P. Haaland, R. Pachter, and W. W. Adams, *Polymer* **33**, 3351 (1992).
366. W. J. Welsh, D. Bhaumik, H. H. Jaffe, and J. E. Mark, *Polym. Eng. Sci.* **24**, 218 (1984).
367. S. Wierschke, J. R. Shoemaker, P. Haaland, R. Pachter, and W. W. Adams, *Polymer* **33**, 3357 (1992).
368. K. Tashiro and M. Kobayashi, *Polymer* **32**, 454 (1991).
369. T. Ohta, T. Kunugi and K. Yabuki, *High Tenacity and High Modulus Fibers*, Kyo Pitsu Publisher Co. Ltd., Tokyo, 1988.
370. A. Kelly, *Strong Solids*, Clarendon Press, Oxford, 1973.
371. A. Kelly and N. H. MacMillan, in *Strong Solids*, Oxford Science Publications, Oxford, 1986, p. 21.

372. Y. Liu and X. Yang, *Chin. Chem. Lett.* **4**, 779 (1993).
373. Y. Liu and X. Yang, *Hua-xue Tong-bao (Chinese)* **4**, 32 (1996).
374. X. Yang, Y. Liu, and S. L. Hsu, *Chin. J. Polym. Sci.* **15**, 295 (1997).
375. M. A. Tracy and R. Pecora, *Annu. Rev. Phys. Chem.* **43**, 525 (1992).
376. M. M. Tirado and G. de la Torre, *J. Chem. Phys.* **71**, 2581 (1979).
377. M. M. Tirado and G. de la Torre, *J. Chem. Phys.* **73**, 1986 (1980).
378. S. Broersma, *J. Chem. Phys.* **74**, 6989 (1981).
379. I. Teraoko and R. Hayakawa, *J. Chem. Phys.* **89**, 6989 (1989).
380. I. Teraoko and R. Hayakawa, *J. Chem. Phys.* **91**, 2643 (1991).
381. R. P. Mondescu and M. Muthukumar, *J. Chem. Phys.* **105**, 4847 (1996).
382. Z. Yu, J. Lin and X. Fan, *J. Non-Newtonian Fluid Mech.* **83**, 1 (1999).
383. G. La Penna, R. Pratolongo, and A. Perico, *Macromolecules* **32**, 506 (1999).
384. A. Perico and R. Pratolongo, *Macromolecules* **30**, 5958 (1997).
385. B. L. Farmer, D. S. Dudis, and W. W. Adams, *Polymer* **35**, 3745 (1994).
386. M. Takayanagi, T. Ogato, T. Morikawa, and T. Kai, *J. Macromol. Sci-Phys., B* **17**, 591 (1980).
387. W.-F. Hwang, D. R. Wiff, T. E. Helminiak, and W. W. Adams, *Org. Coating Appl. Polym. Sci. (ACS)* **48**, 919 (1983).
388. W.-F. Hwang, D. R. Wiff, C. Verschoore, G. Price, T. E. Helminiak, and W. W. Adams, *Polym. Eng. Sci.* **23**, 784 (1983).
389. T. E. Helminiak, F. E. Arnold, and C. L. Benner, *Polym. Prepr. (ACS)* **16**, 659 (1975).
390. S. Palsule, *ESA J.* **17**, 133 (1993).
391. G. W. Adams and J. M. G. Cowie, *Polymer* **40**, 1993 (1999).
392. M. Takayanagi, in J. C. Seferis and P. S. Theocavis, eds., *Interrelations between Processing Structures and Properties of Polymeric Materials*, Elsevier Science Publishers, Amsterdam, 1984.
393. P. J. Flory, *Macromolecules* **11**, 1138 (1978).
394. U.S. Pat. 4, 207, 407 (1980), T. D. Helminiak (to U.S. Airforce).
395. U.S. Pat. 4,614,784 (1986), J. J. Kozakiewicz (to American Cyanamid Co.).
396. S. Kumar and C. S. Wang, *Polym. Commun.* **29**, 355 (1988).
397. U.S. Pat. 5, 068, 291 (1991), G. L. Gallaway and P. B. Foreman (to National Starch and Chemical Investment Holding Corp.).
398. L.-S. Tan and F. E. Arnold, *Polym. Prep. (ACS)* **32**, 51 and 636 (1991).
399. D. R. Wiff and G. M. Lenke, *37th International SAMPE Symposium*, 1992, p. 991.
400. S. J. Bai, M. Dotrong, and R. C. Evers, *J. Polym. Sci., Part B: Polym. Phys.* **30**, 1515 (1992).
401. M. F. Roberts and S. A. Jenekhe, *J. Polym. Sci., Part A: Polym. Chem.* **33**, 577 (1995).
402. T. T. Tsai, W.-F. Hwang, and F. E. Arnold, *J. Polym. Sci., Polym. Chem.* **27**, 2839 (1989).
403. K. L. Cooper, *Polym. Prepr. (ACS)* **33**, 1006 (1992).
404. U. M. Vakil, C. S. Wang, C. Y.-C. Lee, M. H. Dotrong, M. Dotrong, and R. C. Evers, *Polym. Prepr. (ACS)* **33**, 479 (1992).
405. M. Dotrong, M. H. Dotrong, and R. C. Evers, *Polym. Prepr. (ACS)* **33**, 477 (1992).
406. D. R. Wiff, T. E. Helminiak, and W.-F. Hwang, in A. E. Zachariadas and R. S. Porter, eds., *High Modulus Polymers*, Marcel Dekker, New York, 1988, Chapt. "8", p. 228.
407. D. R. Wiff, G. M. Lenke, and P. D. Fleming III, *J. Polym. Sci., Part B: Polym Phys.* **32**, 2555 (1994).
408. C. A. Gabriel, R. J. Farris, and M. F. Malone, *1986 Nonwovens Conference*, 1986, p. 255.
409. W. W. Adams and S. Kumar, in D. R. Uhlmann and D. R. Ulrish, eds., *Ultrastructure Processing of Advanced Materials*, John Wiley & Sons, Inc., New York, 1992, p. 343.

410. J. Maclachlan, M. Madey, R. K. Eby, and W. W. Adams, *Polym. Commun.* **28**, 326 (1987).
411. H. Akita, H. Kobayashi, T. Hatori, and K. Kagawa, *J. Polym. Sci., Part B: Polym. Phys.* **37**, 199 (1999).
412. H. Akita and H. Kobayashi, *J. Polym. Sci., Part B: Polym. Phys.* **37**, 189–209 (1999).
413. E. Ruckenstein and Y. Yuan, *Polymer* **38**, 3855 (1997).
414. D. F. Stamatialis, M. Sanopoulou, and J. H. Petropoulos, *J. Appl. Polym. Sci.* **65**, 317 (1997).
415. N. Venkatasubramanian, D. R. Dean, T. D. Dang, G. E. Price, and F. E. Arnold, *Polymer* **41**, 3213 (2000).
416. D. R. Wiff and R. J. Weinert, *Polymer* **39**, 5069 (1998).
417. N. H. Ladizesky and I. M. Ward, *Compos. Sci. Technol.* **26**, 129 (1986).
418. J. Scherf, Y. Cohen and H. D. Wagner, *Int. J. Adhesion and Adhesives* **12**, 251–256 (1992).
419. M. J. N. Jacobs and L. J. van Dingenen, *Polymer Fibers 2000 Symposium*, Manchester, U.K., July 5–7, 2000.
420. S. Yalvac, J. J. Jakubowski, and A. Sen, *Polymer* **37**, 4657 (1996).
421. Y. Qiu, S. Deflon, and P. Schwartz, *J. Adhes. Sci. Technol.* **7**, 1041 (1993).
422. R. F. Kovar, *J. Plast. Film Sheeting* **11**, 290 (1995).
423. Y. Qiu, S. Deflon and P. Schwartz, in M. Strobel, C. Lyons, and K. L. Mittal, eds., *Plasma Surface Modification of Polymers*, VSP, Utrecht, the Netherlands, 1994, p. 209.
424. M. A. Andrews and K. P. Kelly, *J. Am. Chem. Soc.* **103**, 2894 (1981).
425. H.-G. Tang and D. C. Sherrington, *J. Catal.* **142**, 540 (1993).
426. M. M. Miller and D. C. Sherrington, *Chem. Commun.* **1**, 55 (1994).
427. Y. P. Wang and D. C. Neckers, *React. Polym.* **3**, 191 (1985).
428. N. H. Li and J. M. J. Frechet, *Chem. Commun.* **16**, 1100 (1985).
429. N. H. Li and J. M. J. Frechet, *React. Polym.* **6**, 311 (1987).
430. J. M. J. Frechet and N. H. Li, *Polym. Prepr. (ACS)* **26**, 251 (1985).
431. J. M. J. Frechet, A. Deratani, and G. Darling, *Macromol. Chem., Macromol. Symp.* **1**, 96 (1986).
432. J. E. Ramirez and C. F. Dwigging, *Converting and Packaging* **1**, 12 (1985).
433. O. R. Hughes, P. N. Chen, W. M. Cooper, L. P. DiSano, E. Alvarez, and T. E. Andres, *J. Appl. Polym. Sci.* **53**, 485 (1994).
434. E. Orndoff, S. Clarke, and R. Dasgupta, NASA Tech Briefs, Nov. 2000, p. 54.
435. P. Schuler and R. Haghighat, *SAMPE J.* **35**, 37 (1999).
436. B. Sillion, *High Perform. Polym.* **11**, 417 (1999).
437. R. A. Sferrazza and C. H. Goodings, in R. A. Bakish, ed., *3rd Int. Conf. Pervaporation Processes Chem. Ind.*, Englewood, N.J., 1988, p. 97.
438. N. Sarkar and L. D. Kershner, *J. Appl. Polym. Sci.* **62**, 393 (1996).
439. R. D. Noble, J. J. Pellegrino, E. Grosgogeat, D. Sperry, and J. D. Way, *Sep. Sci. Technol.* **23**, 1595 (1988).
440. M. Chandra, K. F. O'Driscoll, and G. L. Pempel, *React. Polym. Ion Exch. Sorbents* **5**, 157 (1987).
441. M. Chandra, K. F. O'Driscoll, and G. L. Pempel, *React. Polym. Ion Exch. Sorbents* **7**, 25 (1987).
442. M. Chandra and G. L. Pempel, *J. Polym. Sci., Part A: Polym. Chem.* **27**, 3237 (1989).
443. M. Chandra and G. L. Pempel, *React. Polym.* **11**, 165 (1989).
444. M. Chandra and G. L. Pempel, *React. Polym.* **12**, 83 (1990).
445. M. Chandra and G. L. Pempel, *React. Polym.* **13**, 103 (1990).
446. M. Chandra and G. L. Pempel, *React. Polym.* **16**, 29 (1991).

447. M. Chandra and G. L. Pempel, *React. Polym.* **17**, 159 (1992).
448. S. A. Jenekhe, in *Encyclopedia of Polymer Science and Engineering, Suppl.*, John Wiley & Sons, Inc., New York, 1989, p. 352.
449. I. Belaish, C. Rettori, D. Davidov, M. R. McLean, L. Dalton, and H. Nalwa, in W. W. Adams, R. K. Eby, and D. E. McLemore, eds., *The Materials Science and Engineering of Rigid-Rod Polymers*, Vol. **134**, MRS, Boston, 1989, p. 689.
450. A. G. MacDiarmid and A. J. Epstein, *J. Chem. Soc., Faraday Discus.* **88**, 317 (1989).
451. S. H. Carr, *Polym. Prepr. (ACS)* **33**, 374 (1992).
452. K. G. Beltsios and S. H. Carr, *Polym. Prepr. (ACS)* **30**, 163 (1989).
453. P. K. Dhal and F. E. Arnold, *J. Am. Chem. Soc.* **113**, 7417 (1991).
454. G. Wulff, in C. G. Gebelein, ed., *Biomimetic Polymers*, Plenum Press, New York, 1990, p. 1.
455. L. Yu and L. R. Dalton, *J. Am. Chem. Soc.* **111**, 7417 (1989).
456. D. S. Chemla and J. Zyss, *Nonlinear Optical Properties of Organic Molecules and Crystals*, Academic Press, New York, 1987.
457. U. Lauter, W. H. Meyer, and G. Wegner, *Macromolecules* **30**, 2092 (1997).
458. C. K. Chiang, C. R. J. Fincher, Y. W. Park, A. J. Heeger, H. Shirakawa, and E. J. Louis, *Phys. Rev. Lett.* **39**, 1098 (1977).
459. H. Shirakawa, E. J. Louis, A. G. MacDiarmid, C. K. Chiang, and A. J. Heeger, *Chem. Commun.* 578 (1977).
460. A. G. MacDiarmid and A. J. Epstein, in P. N. Prasad, ed., *Frontiers of Polymers and Advanced Materials*, Plenum Press, New York, 1994, p. 251.
461. G. T. Pickett and K. S. Schweizer, *J. Chem. Phys.* **112**, 4881 (2000).
462. S. Lutun, B. Hasiak and D. Couturier, *Synth. Commun.* **29**, 111 (1999).
463. J. C. Gustafsson, O. Inganas, and A. M. Andersson, *Synth. Met.* **62**, 17 (1994).
464. F. Garnier, R. Hajlaoui, A. Yassar, and P. Srivastova, *Science* **265**, 1684 (1994).
465. W. R. Salaneck, D. T. Clark, and E. J. Samuelsen, *Science and Applications of Conducting Polymers*, Bristol, U.K. 1990.
466. T. Matsunaga, in P. N. Prasad and J. K. Nigam, eds., *Frontiers of Polymer Research*, Plenum Press, New York, 1991, p. 245.
467. C. H. McCoy and M. S. Wrighton, *Chem. Mater.* **5**, 914 (1993).
468. D. Neher, *Adv. Mater.* **7**, 691 (1995).
469. A. P. Davey, S. Elliott, O. O'Connor, and W. Blau, *J. Chem. Soc., Chem. Commun.*, 1433 (1995).
470. G. Dufresne, J. Bouchard, and M. Leclerc, *Macromolecules* **33**, 8252 (2000).
471. U. Lauter, W. H. Meyer, V. Enkelmann, and G. Wegner, *Macromol. Chem. Phys.* **199**, 2129–2140 (1998).
472. P. Baum, W. H. Meyer, and G. Wegner, *Polymer* **41**, 965–973 (2000).
473. C. Weder, M. S. Wrighton, R. Spreiter, C. Bosshard, and P. Gunter, *J. Phys. Chem.* **100**, 18931 (1996).
474. D. A. Halliday, P. L. Burn, D. C. Bradley, R. H. Friend, O. M. Gelsen, A. B. Holmes, A. Kraft, J. H. F. Martens, and K. Pichler, *Adv. Mater.* **5**, 40 (1993).
475. M. Moroni, J. Le Moigne, T. A. Pham, and J.-Y. Bigot, *Macromolecules* **30**, 1964 (1997).
476. R. Freudenberger, W. Claussen, A.-D. Schulter, and H. Wallmeier, *Polymer* **21**, 4496 (1994).
477. A. D. Child and J. R. Reynolds, *Macromolecules* **27**, 1975 (1994).
478. M. Wright, *Polym. Prepr. (ACS)* **29**, 294 (1988).
479. C. Weder and M. S. Wrighton, *Macromolecules* **29**, 5157 (1996).
480. G. Shi, S. Jin, G. Xue, and C. Li, *Science* **267**, 994 (1995).
481. V. Percec, M. Zhao, J.-Y. Bae, and D. H. Hill, *Macromolecules* **29**, 5157 (1996).
482. S. Jin, X. Liu, W. Zhang, Y. Lu, and G. Xue, *Macromolecules* **33**, 4805 (2000).
483. J. Kim, S. K. McHugh, and T. M. Swager, *Macromolecules* **32**, 1500 (1999).

484. L. Yu and L. Dalton, *Macromolecules* **23**, 3439 (1990).
485. T. Yamamoto, M. Tagaki, K. Kizu, K. Kubota, H. Kabara, T. Kirihara, and T. Kaino, *J. Chem. Soc., Chem. Commun.* 797 (1993).
486. M. Moroni, J. Le Moigne, and J. Luzzati, *Macromolecules* **27**, 562 (1994).
487. K. Kondo, M. Okuda, and T. Fujitani, *Macromolecules* **26**, 7382 (1993).
488. J. M. Tour, *Adv. Mater.* **6**, 190 (1994).
489. S.-C. Ng, T.-T. Ong, and H. S. O. Chan, *J. Mater. Chem.* **8**, 2663 (1998).
490. N. C. Billingham and P. D. Calvert, *Adv. Polym. Sci.* **90**, 1 (1989).
491. A. A. Berlin, G. A. Pagani, and F. Sannicolo, *J. Chem. Soc., Chem. Commun.* 1663 (1986).
492. H. Neugebauer, G. Nauer, A. Neckel, G. Tourillon, F. Garnier, and P. Lang, *J. Phys. Chem.* **88**, 652 (1984).
493. G. Tourillon and F. Garnier, *J. Electroanal. Chem.* **135**, 173 (1982).
494. A. R. Sorensen, L. Overgaard, and I. Johannsen, *Synth. Met.* **55/57**, 1626 (1993).
495. M. Onoda, T. TIwasa, T. Kawai, and K. Yoshino, *Synth. Met.* **55/57**, 1614 (1993).
496. S. Jin and G. Xue, *Macromolecules* **30**, 5753 (1997).
497. P. Haaland and H. Jiang, *MRS Symposium Proceedings*, Vol. **374**, 1995, p. 123.
498. N. V. Bhat and D. S. Wavhal, *J. Appl. Polym. Sci.* **70**, 203 (1998).
499. R. K. Sadhir and J. Schoch, K. F., *Thin Solid Films* **223**, 154 (1993).
500. K. Tanaka, K. Yoshizawa, T. Takeuchi, T. Yamabe, and J. Yamauchi, *Synth. Met.* **38**, 107 (1990).
501. M. Sato, S. Tanaka, and K. Kaeriyama, *J. Chem. Soc., Chem. Commun.* 873 (1986).
502. K. Y. Jen, G. G. Miller and R. L. Elsenbaumer, *J. Chem. Soc., Chem. Commun.* 1346 (1986).
503. J. L. Bredas and G. B. Street, *Acc. Chem. Res.* **18**, 305 (1985).
504. R. D. McCullough and S. P. Williams, *J. Am. Chem. Soc.* **11**, 11608 (1993).
505. C. R. Martin, L. S. Van Dyke, Z. Cai, and W. Liang, *J. Am. Chem. Soc.* **112**, 8976 (1990).
506. Z. Cai, J. Lei, W. Liang, V. Menon, and C. R. Martin, *Chem. Mater.* **3**, 960 (1991).
507. G. Gustafsson, O. Inganas, W. R. Salaneck, J. Laakso, M. Loponen, T. Taka, J.-E. Osterholm, H. Stubb, and T. Hjertberg, in J. L. Bredas and R. Silbey, eds., *Conjugated Polymers*, Kluwer Academic, the Netherland, 1991, p. 315.
508. E. M. Genies and M. Marchesiello, *Synth. Met.* **55/57**, 3677 (1993).
509. J. Roncali, R. Garreau, D. Delabouglise, F. Garnier, and M. Lemaire, *J. Chem. Soc., Chem. Commun.* 679 (1989).
510. M. Uchida, Y. Ohmori, C. Moroishima, and K. Yoshino, *Synth. Met.* **55/57**, 4180 (1993).
511. F. Li and W. J. Albery, *J. Electroanal. Chem. Interfacial Electrochem.* **302**, 279 (1991).
512. M. Irwin, G. Jia, J. Vittal, and R. J. Puddephatt, *Organometallics* **15**, 5321 (1996).
513. D. Fontin, M. Drouin, and P. D. Harvey, *J. Am. Chem. Soc.* **120**, 5351 (1998).
514. D. A. Mbi Egbe and E. Klemm, *Macromol. Chem. Phys.* **199**, 2683 (1998).
515. X. Wei and D. F. Shriver, *Chem. Mater.* **10**, 2307 (1998).
516. A. Sahver, I. S. Butler, and J. P. Gao, *Organometallics* **15**, 5321 (1989).
517. M. M. Zulu and A. J. Lees, *Organometallics* **8**, 955 (1989).
518. C. A. Tolman, *Chem. Rev.* **77**, 313 (1977).
519. M. C. Bohm, *One-Dimensional Organometallic Materials*, Springer-Verlag, New York, 1987.
520. W. Bruns and W. Kaim, *J, Organomet. Chem.* **390**, C45 (1990).
521. R. Gross and W. Kaim, *Inorg. Chem.* **25**, 498 (1986).
522. E. Keaton, *Organic Semiconducting Polymers*, Marcel Dekker, New York, 1968.
523. J. E. Sheats and C. U. Carraher Jr., *Metal-Containing Polymeric Systems*, Plenum Press, New York, 1985.
524. B. Cotts and Z. Reyes, *Electrically Conductive Organic Polymers for Advanced Applications*, Noyes Data, Park Ridge, N.J., 1986.

525. F. L. Carter, *Molecular Electronic Devices*, Marcel Dekker, New York, 1987.
526. H. Menzel and B. Rambke, *Macromol. Chem. Phys.* **198**, 2073 (1997).

HAO JIANG
Anteon Company
RONALD K. EBY
University of Akron
W. WADE ADAMS
Air Force Research Laboratory, Materials Research Society

RNA. See POLYNUCLEOTIDES

SEMICRYSTALLINE POLYMERS

Introduction

Although scientific explanation of crystals can be traced back to the fifteenth century, it is not until the beginning of the twentieth century that the determinations of the arrangements of the fundamental units and their detailed shapes were possible, after the discovery of x-ray diffraction on crystals. Motifs and repetition schemes have been utilized to describe the detailed arrangements of crystals. For a crystal formed by polymers, a motif only includes part of a molecule. The difference between polymer crystals and small-molecular crystals is twofold. First, crystals formed by small molecules commonly possess more or less identical chemical and physical bonds constructed in a three-dimensional unit cell, while in polymer crystals they are usually anisotropic because of different chemical and physical bonds involved in different directions of a unit cell. Second, polymer crystals are not in a single phase having 100% crystallinity, but are only partially crystallized; therefore, they are called semicrystalline polymers. In a bulk semicrystalline polymer sample, one can find both crystalline and amorphous regions, and the crystalline region may form different aggregates in shapes in different length scales. As a result, many macroscopic properties are critically associated with different structural and morphological levels to complicate structure-property relationships. If one considers these different length scales in semicrystalline polymers, there are at least four levels that can be identified: crystal unit cells in a length scale of a few tenth to one nanometer; single lamellar crystals having at least one dimension size less than a few tens of nanometers; lamellar aggregates in a length scale of a few hundreds of nanometers; and crystallinity is a concept in the macroscopic

Encyclopedia of Polymer Science and Technology. Copyright John Wiley & Sons, Inc. All rights reserved.

scale. This article focuses the discussion on these length scales in semicrystalline polymers; however, only some important concepts and experimental observations could be included here. Many detailed descriptions and discussions must be found in the references cited and other comprehensive books and reviews.

Crystal Unit Cells in Semicrystalline Polymers

Disregarding any detailed morphological models proposed for the lamellar crystals in semicrystalline polymers in the past half century, crystal unit cells in semicrystalline polymers exactly obey the rules of classical crystallography, which consist of 7 crystal systems and 14 Bravais lattices (more precisely, there are only 6 crystal systems in polymer crystals, and the cubic system does not exist). Most of the unit cell determinations of the semicrystalline polymers rely on the wide-angle x-ray diffraction (waxd) experiments on oriented polymer fibers and films. This is because of small crystal sizes in polymers, which lead to a difficult experimental task to obtain single-crystal waxd results on semicrystalline polymers. It is also possible to use electron diffraction (ed) method in transmission electron microscopy (tem) to determine polymer lamellar crystal unit cell structures, dimensions, and symmetries.

Chain Molecular Conformations. One of the most important exercises in studying polymer crystals is to determine what are the atomic positions in the crystal lattice. Since polymer chains are at least connected in one dimension via covalent bonds, polymer crystal unit cells are thus usually anisotropic and critically associated with chain conformations in the crystal lattices. It is believed that the chain conformations in a lattice must possess the lowest free energy after considering both intra and interchain interactions. The intrachain interactions of each chain conformation can be calculated using the rotational isomeric model of a single chain in vacuum (1), while interchain interactions require force fields of the chain molecules in crystal lattices (see CONFORMATIONS AND CONFIGURATION). All the chain conformations can be viewed to be helical conformations. In the case of polyethylene (PE), its zigzag conformation can be described as a 2_1 helical structure (2). The lowest free energy of the PE conformation is thus all trans conformation, although three possible conformations, trans, gauche+, and gauche−, can be identified in PE. Figure 1 shows the projected structures of the trans and gauche conformations and potential energy diagram for internal rotation around the C—C bond of *n*-butane. When PE crystallizes, its chain conformation adopts all trans conformation. This is also true in poly(vinyl alcohol) (PVA), where the replacing group of hydrogen (H) is hydroxy group (OH) that forms hydrogen bonding and is small enough not to disturb the trans conformation of the carbon backbones.

However, when all the H atoms in PE are replaced by fluorine (F) atoms, polytetrafluoroethylene (PTFE), the van der Waal's radius of the F is larger than that of the H and introduces steric hindrance. Therefore, a slight rotation of the C—C backbone has to take place (around 14° away from the trans conformation), which leads to a helical chain conformation (3,4). Usually, for a series of isotactic vinyl polymers having substituent groups, the lowest free energy conformations of individual chains are helical forms. One of their simplified forms, 3_1, is shown in Figure 2a. Figure 2b includes a series of 3_1 helical conformations in isotactic polypropylene (iPP), which possess an equal free energy (5). A general scheme

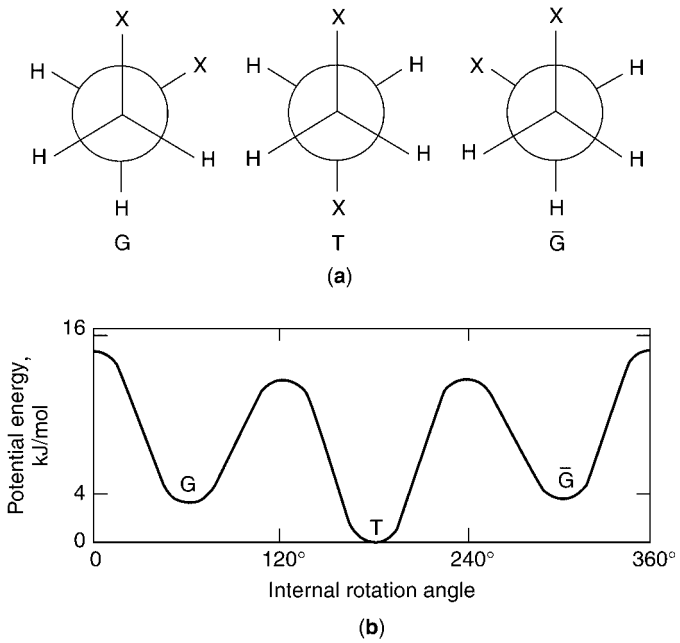

Fig. 1. (**a**). Projected conformations of the trans and gauche forms. (**b**). Potential energy of butane as a function of the rotation angle of the center bond C_2H_5—C_2H_5.

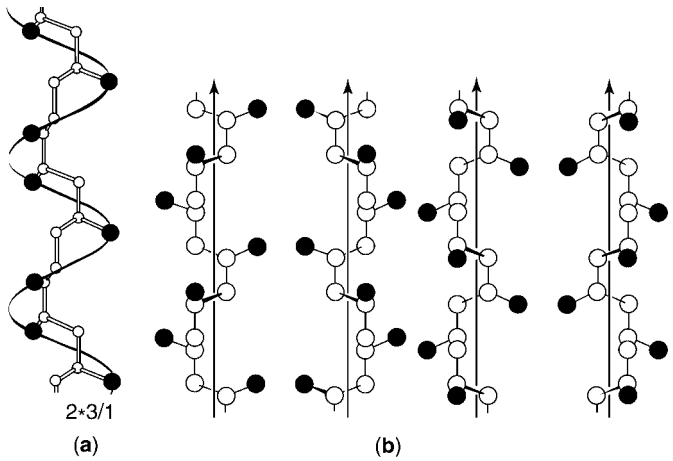

Fig. 2. (**a**). A 3_1 helical structure simplified using mathematical expression. (**b**). Projection of 3_1 helical at right angle to the helical axis for iPP. The filled circle represents CH_3. Therefore, four possible conformations exist with identical free energy: A. Right-handed *d* helix; B. Left-handed helical *l* helix; C. Left-handed *d* helix; and D. Right-handed *l* helix (6).

for discussing different helical conformations has been developed. Figure 3 shows examples of the point net projections of helical conformations (5).

Detailed atomic positions in polymer helical conformations can be determined using the rotational isomeric model developed (1). It helps to obtain a

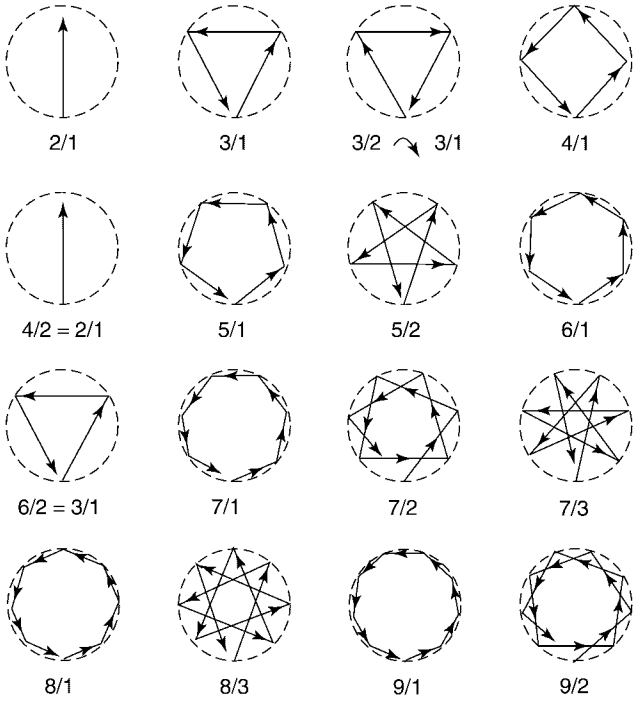

Fig. 3. Point net projections of different helical conformations (5).

free-energy minimum conformation for a specific macromolecule in vacuum. When one describes the lowest free-energy conformation of macromolecules, it is relatively easy to start with point group operations that originally represent the symmetry of low molecular weight (LMW) compounds. There are two different operations in point groups: rotation and inversion. However, it is also necessary to introduce space group operations such as screw axes and glide planes to illustrate chain conformations. Since macromolecular conformations are all considered as helical forms, the helical conformations can be distinguished as right- and left-handed helices. If there are distinct substituent groups on the backbones like in the cases of isotactic vinyl polymers, one may also have two different pointing directions of these groups if one artificially keeps all the C—C bonds in the trans conformation by looking along the long-chain direction (d and l). The total number of conformations is thus 4, which possess identical potential energies. A typical example is iPP, and its calculated potential energy is shown in Figure 4. It is evident that both angles of Φ_1 (rotation around CH_2—$CHCH_3$) and Φ_2 (rotation around $CHCH_3$—CH_2) possess two minima at $\Phi_1 = 120^\circ$ and $\Phi_2 = 0^\circ$ (right-handed helix) and $\Phi_1 = 0^\circ$ and $\Phi_2 = 240^\circ$ (left-handed helix) (6,7).

A nomenclature, which allows geometrically equivalent motifs of the four types of helices to be distinguished, has been proposed in a cylindrical coordinate (8). For each atom i of the repeating units, it can be described relative to its helical lattice point using three parameters: R_i (distance from the helix axis), $\Delta\Phi_i$ (rotation along the helical axis from the lattice point, which is defined as

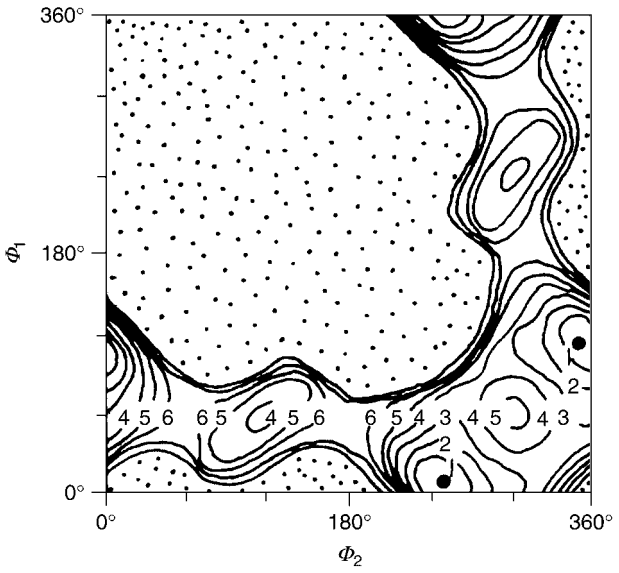

Fig. 4. Potential energy (kcal/mol) calculation of iPP as a function of rotation angles Φ_1 and Φ_2 (5).

$2\pi t/u$, where t is the number of turns of the helix and u is the periodicity about the helical rotational axis), and Δz_i (motion parallel to the helical axis from the lattice point, which is defined as c/u, where c is the crystallographic identity period along the z axis). Equivalent repeat units must have identical R_i for all atoms and can only differ in signs of $\Delta\Phi_i$ and Δz_i. When $\Delta\Phi_i$ and Δz_i are both same or both are of opposite sign for all atoms in two repeating units considered, they are isomorphous since they can be brought into coincidence with each other by simple translation and rotation. When they differ in sign in one coordinate only (either $\Delta\Phi_i$ or Δz_i), they are enantiomorphous since they can be brought into coincidence with each other only by reflection. All the atoms in two repeating units in which all Δz_i are of equal signs are called *isoclined*, while if they are of opposite signs, they are *anticlined*. Using this rule, one can identify clearly in Figure 2b that using the right-handed iPP *d* helix as a reference, helix A in Figure 2b, which is the right-handed isotactic *d* helix, is isomorphous isoclined; helix B is enantiomorphous isoclined; helix C, enantiomorphous anticlined, and helix D, isomorphous anticlined.

In general, as long as both directions of the macromolecule are identical, the repeat units of a single chain may be isoclined or anticlined to each other. In isotactic vinyl polymers, neighboring repeat units may be isomorphous isoclined or enantiomorphous anticlined without breaking the all-*d* or all-*l* sequence. In the latter case, however, the conformation must have planes of symmetry perpendicular to the chain axis, a condition only possible for the 2_1-planar zigzag conformation. For the same reason, successive repeat units in syndiotactic vinyl polymers may also be isomorphous anticlined or enantiomorphous isoclined. Macromolecules that are not identical in both directions of the chain can only consist of isoclined repeat units.

In summary, conformations of a regular sequence of equivalent motifs can only be generated in the following four specific ways:

(1) Isoclined isomorphous sequence can be generated only by the translation of c/u with simultaneous rotation by an angle of $2\pi t/u$ about an axis parallel to the direction of translation.
(2) Isomorphous pairwise anticlined sequence can be generated by helices that possess twofold axes of symmetry at right angles to the helical axis between adjacent motifs. By rotation with respect to the twofold axis of symmetry, the adjacent isomorphous anticlined motifs are generated.
(3) Enantiomorphous pairwise isoclined sequence can be generated only by repetition through a glide plane that contains the molecular chain axis. No helical repetition is possible in this case.
(4) Enantiomorphous pairwise anticlined sequence can be generated by successive centers of symmetry along the chain axis or by planes of symmetry at right angles to the chain axis. Both modes are incompatible with helical repetition.

Crystal Unit Cells. The crystal lattice is a purely imaginary construction that functions as a coordinate system and to which the actual structure is referred. There are six parameters used to construct the lattice: the three grid line directions a, b, and c to form a right-handed system and three angles α, β, and γ, each of which is between two axes (such as α is between the b and c axes). In forming a crystal unit cell, one has to deal with packing of macromolecules. In crystals, within a macromolecule, it must possess a regular, unique extended helical chain conformation of the lowest or near the lowest free energy (intrachain interaction). This structure is generally described by a single-chain conformation in the vacuum after certain modifications. Putting several helical chain conformations into a three-dimensional lattice to generate a crystal unit cell requires to consider interchain interaction among the chains, ie, the close packing energy. Generally speaking, intrachain interaction deals with rotational isomerism, and it possesses a higher energy compared with the packing energy. Specific cases may exist such as in the case of poly(ethylene oxide) (PEO) in which the interchain interaction is strong enough to distort the 7_2 helical PEO chain conformation (9).

A cylinder is the most symmetric body that approximates to some degree a macromolecule in its helical chain conformation. Close packing of cylinders leads to an array identical to a layer of spheres in cross section. The symmetry of this hexagonal packing with six coordination numbers is $6/mmm$, having a packing density of 90.7% (see Fig. 5a). Conversely, if more appropriately, one may consider the helical-shaped macromolecule that is similar to a solid screw. Now the handedness of the screws needs to be taken into account when they are closely packed together, as shown in Figure 5b. The close packing can be achieved between two screws only in the opposite handedness with almost rectangular threads. The coordination numbers for such close packing reduces to 4 and the maximum packing density that can be reached is 92%. However, these models cannot be precisely used to determine the macromolecular close packing in crystals. Detailed atomic positions in chain conformations and their interaction energies must be known before one can construct a crystal unit cell.

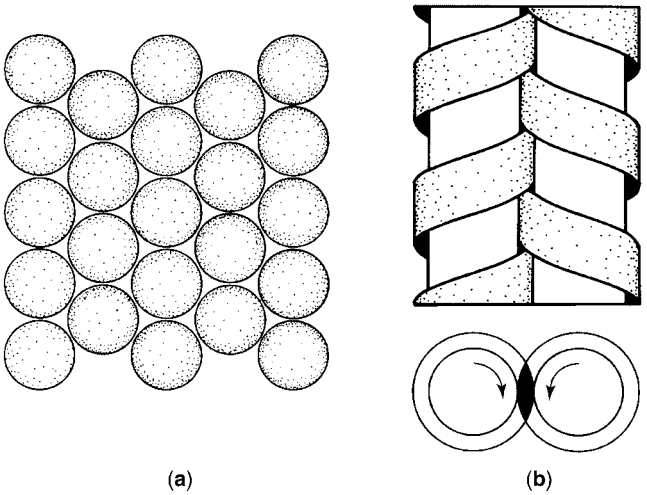

Fig. 5. (**a**). A hexagonal two-dimensional packing projected along both perpendicular and parallel to the cylindrical axis, and (**b**) a projection of a pair of close-packed screws having opposite handedness along both perpendicular and parallel to the long axis of the screws (5).

Three examples provided here are molecular packing, symmetry, and unit cells of orthorhombic form of PE (Fig. 6) (2,10), monoclinic α form of iPP (Fig. 7), (11), and orthorhombic form of syndiotactic polypropylene (sPP) crystals having antichiral packing in handedness (Fig. 8) (12).

Determination of Crystal Unit Cells. The most important technique to determine crystal unit cells is waxd. In these experimental procedures, a concept of reciprocal lattice has to be introduced. The relationships between the real and reciprocal lattices in three dimensions depend on the angles between the axes in the real lattice. Consider the cases of an orthorhombic cell, where the three real axes are mutually perpendicular to each other but the axial lengths are not the same. The planes (100), (010), and (001) are perpendicular to a, b, and c axes, respectively; their normals are thus along these axes. Hence, the reciprocal lattice point 100 can be considered to be on the a axis at a distance $1/a$ from the origin. The line connecting this point to the origin is one edge of the unit cell in reciprocal space and is thus a^*. In the same way the reciprocal axes b^* and c^* coincide with the corresponding real axes b and c, and all three reciprocal axes are also mutually perpendicular to each other. The result is a reciprocal unit cell with the relationships summarized in Table 1. (See further references for the relationship between real and reciprocal lattice.)

It should cause no surprise that for polymer crystals with very small sizes, a definitive structural analysis is difficult using only unoriented diffraction patterns. This is not only due to the small number of observable diffractions and their general broadening, but also to the fact that high angle diffraction rings often consist of the superimposition of several reflections of different indices. In certain special cases, eg, when a structural similarity to a known substance is suspected on the basis of chemical composition, it may be possible to make identification by comparison, but even this procedure contains possible errors.

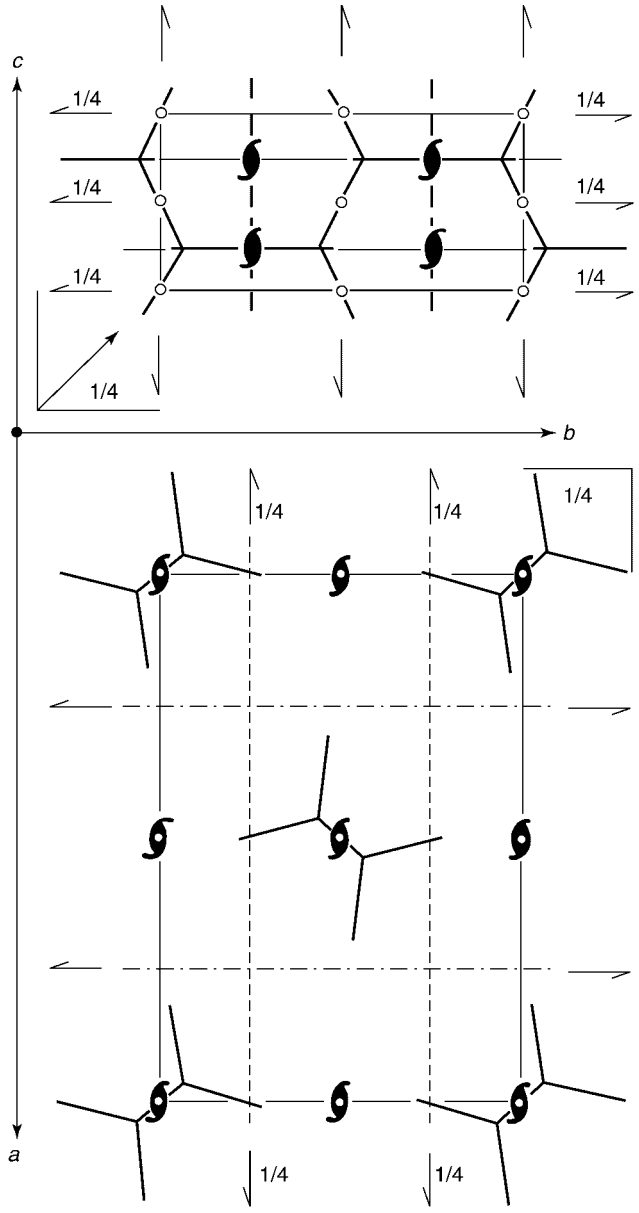

Fig. 6. Crystal unit cell of orthorhombic form of PE in three-dimensional real space (5).

In most cases, structural analysis of polymer crystals is carried out using uniaxially oriented samples (fibers or films). The basic procedures include (*1*) determination of the fiber period; (*2*) indexing (*hkl*) diffractions and determining the unit cell parameters; (*3*) determination of the space group symmetry; (*4*) structural analysis; and (*5*) Fourier transforms and syntheses and Patterson functions. The first three aspects of the procedure are discussed here, and the last two aspects are left for further references.

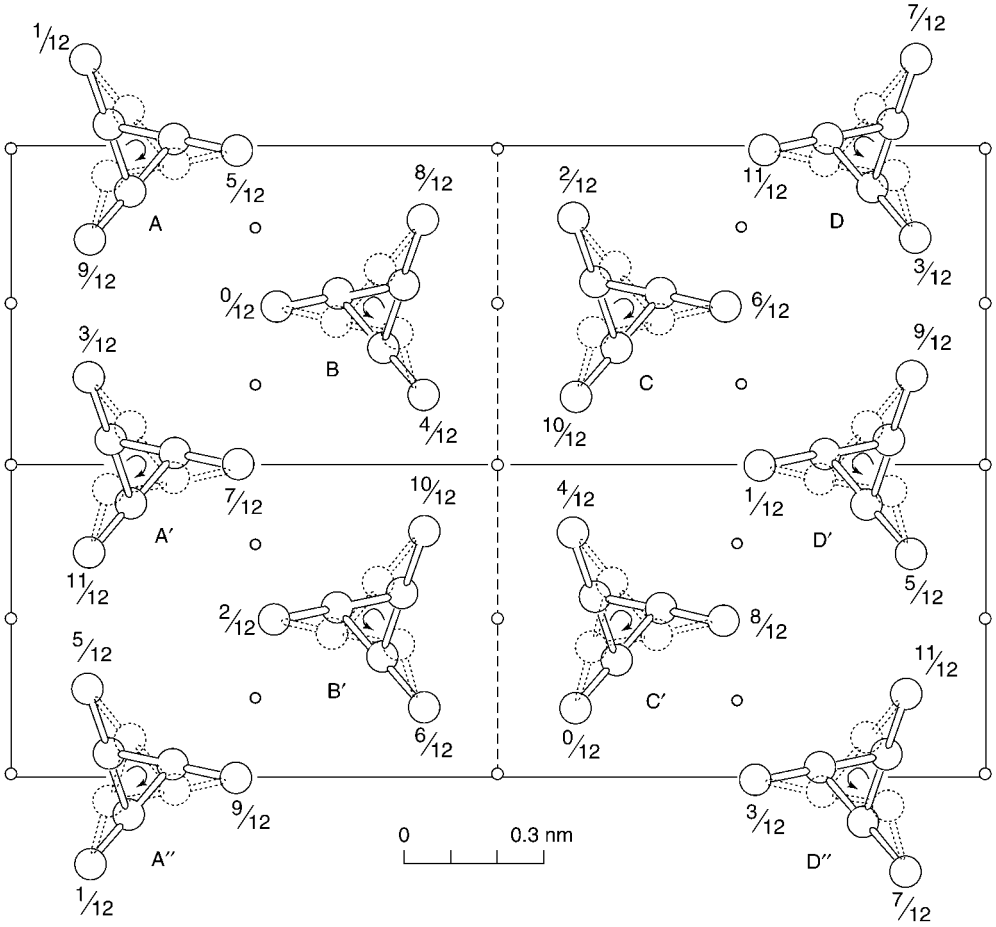

Fig. 7. Crystal unit cell of monoclinic α form of iPP in three-dimensional real space (11).

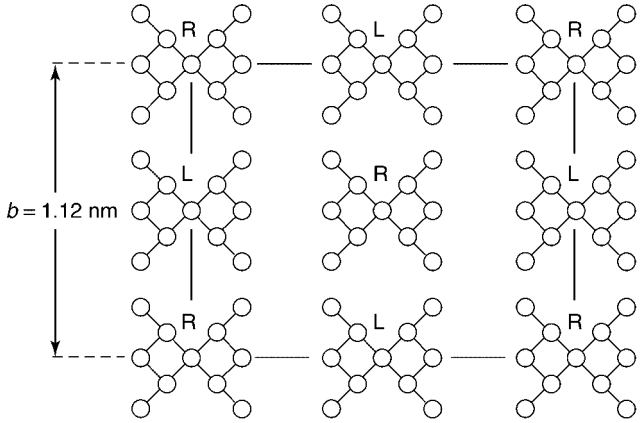

Fig. 8. Crystal unit cell of orthorhombic form of sPP having antichiral handedness packing projected along the chain direction (12).

Table 1. Real and Reciprocal Space Relationship in an Orthorhombic Unit Cell

$a^* = 1/a$	$a = 1/a^*$	$\alpha = \beta = \gamma = \alpha^* = \beta^* = \gamma^* = 90^\circ$
$b^* = 1/b$	$b = 1/b^*$	$V^* = 1/V = a^*b^*c^*$
$c^* = 1/c$	$c = 1/c^*$	$V = 1/V^* = abc$

Polymer chains usually align along the fiber axis during drawing and deformation, and the chain direction is commonly defined as the c axis [there are several exceptions due to hydrogen bonding, smectic domains in liquid crystals, and biopolymers (13–15)]. The fiber period for the fully extended conformation of the polymer by chain is calculated from the chemical structure of the repeat unit of the polymer by using standard bond angle and bond length data. The measured value of the fiber period can be compared with the calculated value. If the value agrees within the limit of experimental error, the chain is considered to be fully extended in the fiber. When the calculated period is slightly greater than the experimental value, this often indicates a twisted or loosely folded conformation of the molecular chains, and the degree of twisting or fold can be estimated from the discrepancy between the two values. Another possibility is that the chains are slightly inclined with respect to the principal axis of the unit cell. A large discrepancy often points to a helical conformation of the chains. Computer calculation of the chain conformation with the lowest free energy is a powerful tool to examine these discrepancies. However, in some cases, interchain interactions must also be taken into consideration. This may lead to complication in the crystal structure determination.

With perfect orientation, chain axis (usually, c axis) is aligned along the fiber direction, and a^* and b^* axes in the reciprocal space are perpendicular to the fiber axis. Therefore, diffraction spots on the equator come from $(hk0)$ planes. The first step to determine unit cell parameters is to index the diffraction peaks on the equator. Because in small-molecular single crystal rotating experiments several reflections close to the center are chosen, their distances to the center are measured to be ξ_1, ξ_2, ..., the smallest ξ, ie, ξ_1 is assumed to be on the a^* axis and is plotted on this axis to the right of the origin as the 100 reciprocal lattice point, at the appropriate distance on the chosen scale. An attempt is also made to find the b^* axis based on the second closest ξ_2, which is assumed to be the 010 reciprocal lattice point, and the third closest ξ_3, which is assumed to be representative of 110 reciprocal lattice point. A suitable combination of low index triangle reciprocal lattices may thus be constructed. Two sides of the triangle lattice are a^* and b^* axes, respectively. A complete two-dimensional lattice can thus be established by translating the triangle into the two-dimensional space. The crossover points in the reciprocal lattice, which represent 110, 210, 120, ..., reciprocal lattice points, must correspond to the diffractions observed along the equator direction (ξ_4, ξ_5, ...). It should be mentioned that reflection does not necessarily occur from all sets of planes associated with reciprocal lattice points, although they fulfill the conditions considered so far. There are other conditions, connected with the symmetry properties of the crystal, which may induce the systematic absence of certain reflections [extinction rule (16)].

The next step is to index the general reflections of the type hkl, which involves the c^* axis (the fiber period). The first layer reflections above and below the equator are the $hk1$ and $hk\bar{1}$ reflections, respectively. The indices to be determined in this case are h and k: if the third axis, ie, the c axis in this case, is normal to the ab plane, the c^* axis will coincide with the c axis, also being perpendicular to both a^* and b^* axes. In this case, the ξ values of all the reciprocal lattice points $hk1$ and $hk\bar{1}$ will be equal to the ξ values of the reciprocal lattice points having the same values of h and k in the equator plane. To index the points, therefore, a point whose ξ value is the same as that of an $hk0$ point is given the same indices h and k, and so becomes $hk1$ or $hk\bar{1}$. The indices h and k can be simply determined using the values of corresponding spots on the equator. If the third axis is not normal to the a^* and b^* axes, as in a triclinic unit cell, the procedure is more tedious. In this case the ξ values of the points on the layer lines are no longer the same as those of the $hk0$ points having the same values of h and k; namely, the projections of the lattice points on the equatorial plane do not coincide with the equatorial lattice points. However, since all the lattice layers are identical, provisional use of this equatorial plane can still be made. The origin (the point with both h and k zero) of the first layer of the reciprocal lattice is projected on the equatorial plane, and a new lattice is drawn about the projected point as lattice origin. It will therefore be slightly offset from the previous lattice. The original origin of the equatorial plane is taken as the center of the diffraction sphere, which is then rotated. The same result is obtained if the center of rotation of the diffraction sphere is moved from the origin by exactly the same amount as the offset of the points in the first layer, the diffraction sphere then being rotated in the usual manner. By repetition of this procedure for the first layer below the equator, and for the second, third, and other higher order layers, all the reflections hkl on the film can be indexed. Several examples of detailed determination in uniaxially oriented polymer unit cell parameters can be found in Reference 17.

X-ray diffractions from a crystal can only occur in directions defined by the reciprocal lattice points and with intensities that are governed by a structure factor of the form

$$F(hkl) = \sum_{j}^{N} f_j \exp[2\pi i(hx_j + ky_j + lz_j)] \tag{1}$$

where f_j is the atomic scattering factor of the jth atom in the unit cell, and x_j, y_j, and z_j are the coordinates of this atom in the unit cell. The summation is carried out over all the atoms in the unit cell. The atoms in the unit cell are not independent, but generally fall into groups within which the atoms are related by the symmetry of the crystal. Since comparatively simple relationships hold between the coordinates of the atoms in these groups, insertion of these relationships into equation simplifies the equation and reduces the number of terms in the summation. Certain symmetry operation will result in zero intensity for certain (hkl) planes, which is called extinction. Since it arises from the crystal symmetry, the space group of the crystal may be identifiable from the characteristic systematic absences. In an actual analysis, the indices of all the diffraction spots for the crystal are first tabulated. Regularities are then sought in the indices of observed

reflections. This is because sometimes a very weak reflection may not be observed owing to experimental limitations, obscuring the regularity of the indices of the completely missing reflections. The symmetry is determined by both the point and space groups, which include rotations, inversions, screw axes, and glide planes. They govern the extinction rules. Finally, the space group can be found by consulting International tables for x-ray crystallography.

It is difficult to determine the space group of polymer crystals, since the diffraction diagrams can often be obtained only for uniaxially oriented specimens. Quite often, it is impossible to verify the extinction rules because of difficulty of indexing due to overlapping of reciprocal lattice points, inability to observe the high order diffractions, etc. In such cases, one solution is to select a possible space group and carry out the analysis, assuming initially that the symmetry is high. If this fails, lower symmetries or other space groups are considered in an attempt to find the correct one. However, this is a trial and error method, and it is better to obtain as many independent $|F(hkl)|^2$ as possible, eg, by preparing biaxially drawn specimens, making inclined uniaxially oriented fiber photographs or Weissenberg photographs, or using x-rays of shorter wavelength, such as Mo radiation, to obtain data for higher order diffractions. Structural analysis and Fourier transform and Patterson functions are relatively complicated, and they are not discussed here.

In the modern waxd crystallographic analysis, waxd experimental results are always combined with conformational and packing energy calculations to obtain more precise crystal unit cell dimensions and atomic positions in a crystal lattice. Under constrained conditions, the least-square calculation reduces the error to a degree that the diffraction positions and intensities can be semiquantitatively fitted to the experimental observations. However, force fields between chain molecules in crystals are difficult to establishe and defects existing in real crystals limit the accuracy of the calculations.

Other experimental methods are also useful in determining crystal structures. Infrared–Raman vibration spectroscopy can, for example, be used in identifying atomic and molecular interactions. This method can detect local structural changes via force field changes. In a complete vibration spectrum of a semicrystalline polymer, there are two regions of vibration frequencies: the acoustic and optical regions. In general, the vibration bands in the acoustic region possess low frequencies, and therefore correspond to vibrations linked with molecular packing. The vibrations in this region are specifically characteristic of packing schemes and orders. For example, in PE, up to approximately 2×10^{13} Hz, the vibration motion can be visualized as a torsional and an accordion-like motion of the CH_2 backbones. These two vibration motions are generally associated with the skeletal vibrations. When the PE chain molecules are in crystals, crystal lattice vibration modes can also be determined, which are not seen in a vibration spectrum of an isolated chain. Both infrared and Raman-active lattice modes can be observed in the low frequency region. For example, in PE crystals, the infrared-active lattice mode is at 72 cm^{-1} with a perpendicular polarization at room temperature (18–20). The Raman-active vibration lattice mode at 137 and 108 cm^{-1} are also observed at very low temperatures (eg, at $-196^{\circ}C$) (21,22).

The vibration bands in the optical region are at higher frequencies, and they reflect specific modes of group vibrations. These vibration motions generally involve oscillations of relatively isolated groups of atoms along the polymer backbone

chains, such as stretching, bending rocking, wagging, and twisting between atoms and groups. In PE, between 2×10^{13} and 5×10^{13} Hz in the vibration frequency range, they are mainly associated with bending of the C—H bond and C—C stretching vibration. When the frequencies are above 8×10^{13} Hz, they correspond to the C—H stretching vibrations. Among these vibration frequencies in the optical region, one can find some vibrations that are observed only for crystals, ie, crystal-sensitive bands. For example, after annealing an amorphous PVA sample close to its melting temperature for a long period of time, the intensity of the stretching of PVA at 1141 cm^{-1} found in both infrared and Raman spectroscopic measurements increases with increasing crystal density as a result of annealing (23,24). This indicates that the crystal-sensitive band appears only when the PVA units along the chains are aggregated together to form regular conformational segments and/or when oscillators are arranged together in a regular way. The length of regular structural units necessary to detect the crystal-sensitive band can be determined by the relationship between the band intensity and the segmental length in copolymer samples (25).

In some cases, vibration bands are also conformation-sensitive. In particular, when a polymer exists in several crystal forms, different chain conformations may exist in these crystal modifications; one example is poly(vinylidene fluoride) (PVDF). At least four types of crystal modifications are known: forms I, II, II_{polar}, and III (26). Form I has nearly a zig-zag chain conformation. Forms II and II_{polar} exhibit the glide-type TGTG conformation, while form III has a $TTTGTTTG^-$ conformation. The ir spectra of these crystal modifications are shown in Fig. 9 (27). For example, the intensive bands observed in the spectra of form I are 1275, 840, and 510 cm^{-1}, and others correspond to the vibration modes intrinsic to long trans sequences of ...TTTT.... The bands at 800, 766, 610, and 530 cm^{-1} and others in the spectra of form II are attributed to the conformation sequence of TG. On the other hand, in form III, the TG and TT bands coexist in addition to the bands characteristic of the TTTG sequence (27).

In oriented polymer samples, polarized Infrared and Raman spectroscopy are also very useful in determining bond orientations in the crystals and oriented amorphous regions (28–34). Furthermore, surface enhanced Raman scattering techniques can also be used to obtain information regarding the molecular orientation at surfaces and interfaces.

Crystal Morphology: Polymer Single Crystals and Polycrystalline Aggregates

Although polymer crystals have been explained using the so-called "fringed micellar" model in the infant stage of polymer crystal physics, understanding of dendrites formed in solution and spherulites grown from the polymer melt, in close analogy with those in simple organic and inorganic substances, leads to a basic underlying building block—polymer single crystals. By using dilute polymer solutions, single crystals with regular shapes were observed first by optical microscopy and then by tem (35–37). The most well-known example is that of PE grown in dilute solutions, in which perfectly regular-facetted, lozenge-shaped single crystals with a thickness of about 10 nm are formed (38–41). Later, it was

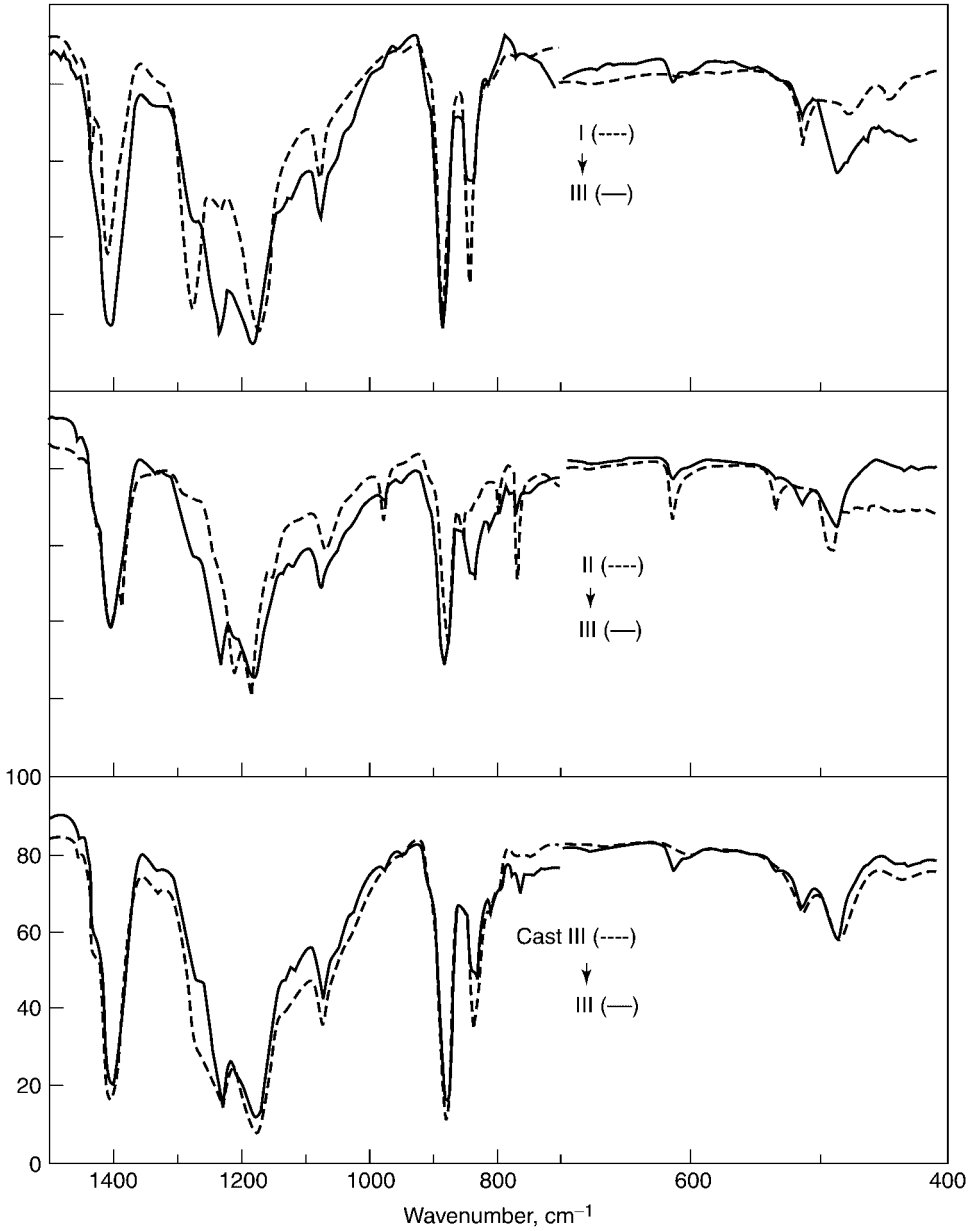

Fig. 9. Comparison of the ir spectra of PVDF forms I, II, and as-cast III (dashed lines) with that of form III (solid line) (27).

also observed that PE lamellar crystals are also the building blocks of melt-grown spherulites and other aggregates (41,42). The analysis of lamellar single crystals leads to the birth of the chain folding concept, which has been one of the most important advances in polymer crystal physics, and has been widely accepted in spite of some controversy. In the past half century, increasing numbers of

crystalline polymers were shown to form lamellar single crystals in dilute solution, blends, and the melt (see MORPHOLOGY).

The importance of observing polymer single crystals stems from their usefulness in analyzing crystal growth mechanisms. Crystallization of small molecules and polymers from solution or the melt on an existing crystal surface can be described using one of two mechanisms: lateral (layer) and normal growths (43,44). The former is nucleation-controlled, having an exponential dependence of growth rates with respect to undercooling (ΔT, having a nucleation barrier) and well-defined crystal habits. The latter implies a continuous growth with a rough surface (without an enthalpy barrier) having a linear relationship between growth rates and ΔT near the melting temperature. The crystal habit in this case is usually determined by temperature or concentration gradient, and thus the boundaries are curved. Therefore, the growth-rate dependence with ΔT and crystal growth habit become two important characteristics in distinguishing between these growth mechanisms. Furthermore, polymer single crystals are true crystals following any existing definition since they possess all the crystalline characteristics; yet, they are always chain folded and in a metastable state (45,46). This leads to a great interest in crystal metastability and its role in determining structure and properties of polymeric materials. It should be pointed out that polymer single crystals are important structural and morphological probes, which encompass broader length scales as compared with small molecular species. These probes include atomic positions and helical conformations (in most cases) in a close-packing scheme, lamellae, and aggregates. Lamellar single crystals in polymers are precursors in developing crystal aggregates such as dendrites and spherulites.

Observations of Single Lamellar Crystals. Polymer lamellar single crystals were first observed in PE crystals grown from dilute solution in the 1950s (35–41). Figure 10 shows a PE lamellar single crystal grown from a dilute solution and observed in tem. The crystal exhibits two large lateral dimensions and has a small thickness around 10 nm. The lozenge-shaped crystal reflects well-defined crystal growth fronts, and a so-called *sectorization*, which is associated with crystal planes. The four growth faces are the (110) planes. Besides PE, a number of crystalline polymers have since been reported to produce lamellar single crystals from dilute solutions. Some of them are highly facetted or nearly facetted, but others possess irregular shapes. Figures 11 and 12 represent two typical examples

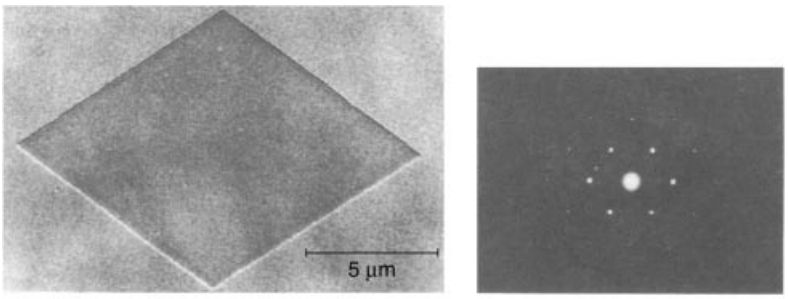

Fig. 10. Transmission electron micrograph of a PE single lamellar crystal grown from dilute solution. A [00*l*] zone electron diffraction of this single crystal is also included (47).

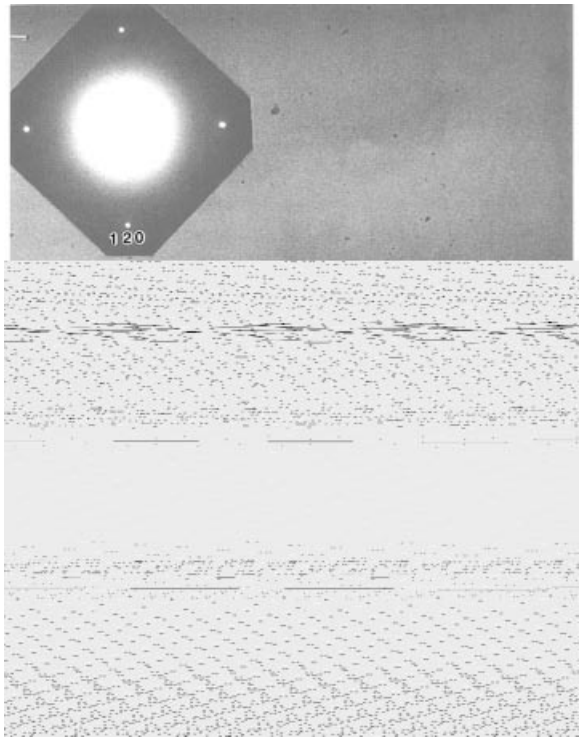

Fig. 11. Transmission electron micrograph of PEO single lamellar crystal grown from dilute solution. Note that this lamellar crystal exhibits a regular facetted square shape with four (120) growth faces. A [00*l*] zone electron diffraction of this single crystal is also included (48).

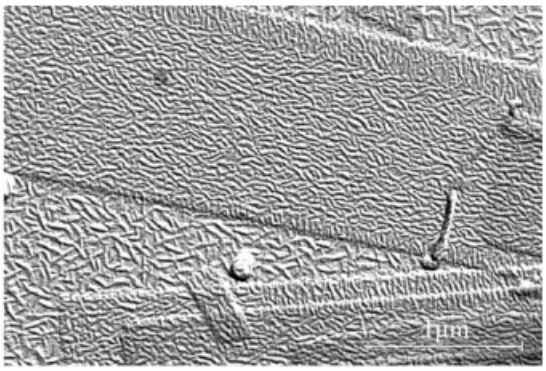

Fig. 12. Transmission electron micrograph of iPP single lamellar crystals grown from dilute solution (49). Note that this lamellar crystal exhibits an anisotropic elongated shape. PE decorations can be seen on the tops of these single crystals.

for PEO (48,50) and iPP (51,52). Note that these two examples possess very different single crystal shapes (isotropic vs anisotropic), which are discussed in the following section. Many crystalline vinyl and diene polymers, polyoxides, polyesters, and polyamides (5,47,53) form single crystals in dilute solutions.

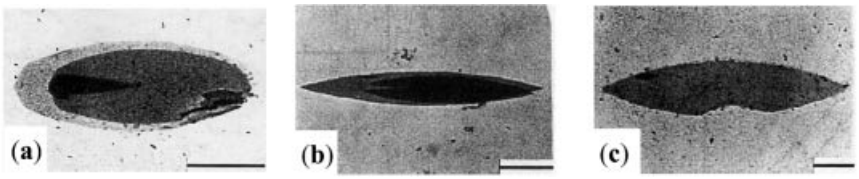

Fig. 13. PE single lamellar crystals grown from the bulk melt at different crystallization temperatures: (**a**) 123°C for 8 s; (**b**) 125°C for 30 s; (**c**) 128°C for 20 min (60,61). These single crystals were solvent extracted from the bulk sample.

Soon after the observation of solution-grown lamellar single crystals, it was found that lamellar crystals are also the basic building blocks of more complex crystal morphologies formed in melt-crystallized polymers. However, it was found that lamellar single crystals in polymers can also grow from the melt. One of the first examples in the 1970s is LMW PEO (54–58). For entangled polymers (ie, with reasonably high molecular weights), lamellar single crystals of PE were reported at the end of 1980s from both bulk samples and thin films (59–61). In bulk samples, PE was crystallized at low ΔT's and then quickly quenched to a low temperature cooling bath. Solvent extraction was used to dissolve the small and less stable PE crystals that were formed during the quenching process, the more stable lamellar single crystals with facetted shapes remain and can be observed under tem (Fig. 13). Lamellar single crystals of sPP were grown from the melt in thin-film samples, and the crystals showed an elongated rectangular shape (Fig. 14) (62–67). Other reports on lamellar single crystals include PVDF grown from blends (68–70), isotactic polystyrene (i-PS) grown from the melt on thin films (71,72), the poly(ethyl ketone) family grown from blends and the melt (73,74), and other polymers. It should be noticed that melt crystallization in the bulk and in thin films sometimes results in differences in single crystal morphologies. In fact, thin-film growth is one type of crystallization in confined geometrical space.

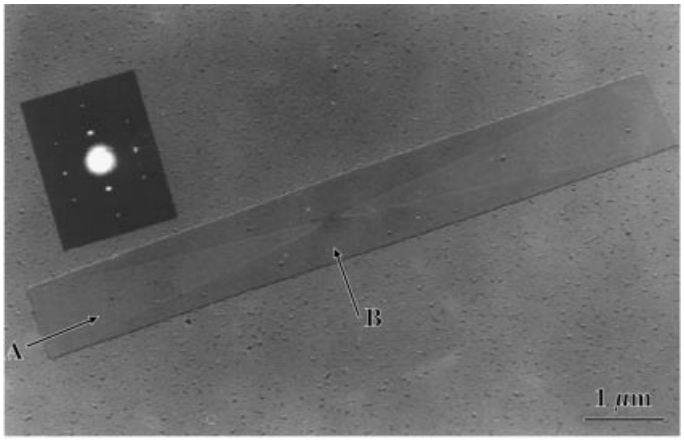

Fig. 14. Transmission electron micrograph of a sPP single lamellar crystal grown from the melt of thin film. Note that this lamellar crystal exhibits an anisotropic elongated shape with clear four sectors visible by the thickness difference in these sectors (63).

In general, a low symmetry unit cell generates a more anisotropic single crystal habit in the melt or in blends, as in the case for PE in the orthorhombic form (59–61,75), iPP in the monoclinic α-form (51,52), sPP in the high temperature orthorhombic form (62–67), PVDF in the orthorhombic α-form (68–70), and others, all of which show anisotropic single lamellae. This implies that the growth rate along one unique axis is much faster than along the other. On the other hand, polymers such as PE in the high pressure hexagonal form (76), polyoxymethylene (77,78), iPS in the hexagonal form (71,72), poly-4-methyl-1-pentene in the tetragonal form (79), and others possess higher rotational symmetry in their crystal unit cells, and thus exhibit more symmetric polygonal lamellar habits (80). These two types of lamellar single crystal precursors may follow different pathways to form transient aggregates that evolve into the ubiquitous spherulites (81).

In case of chain-folded lamellar crystals, it should not be forgotten that polymer single crystals can also be obtained in the form of extended chains. Ideally grown extended chain single crystals were first proposed by Sauter (82). Now it is known that under certain conditions, polymer chains can be extended to form extended chain single crystals. For example, PE at elevated pressures forms crystals having the hexagonal lattice as shown in Figure 15 (83). The chain molecules possess a large mobility along the chain direction in the crystals, and therefore the lamellar crystals thicken continuously to form extended chain single crystals (84,85). Extended chain single crystals can also be found for PTFE after annealing at elevated temperatures (86). Another type of extended chain single crystals is the so-called *whisker crystals*, which must not be confused with fibrous crystals. Note that the fibrous crystal may not be necessarily single crystalline. Examples of this class are *"shish" crystals* and whisker crystals obtained during polymerization from monomer vapors.

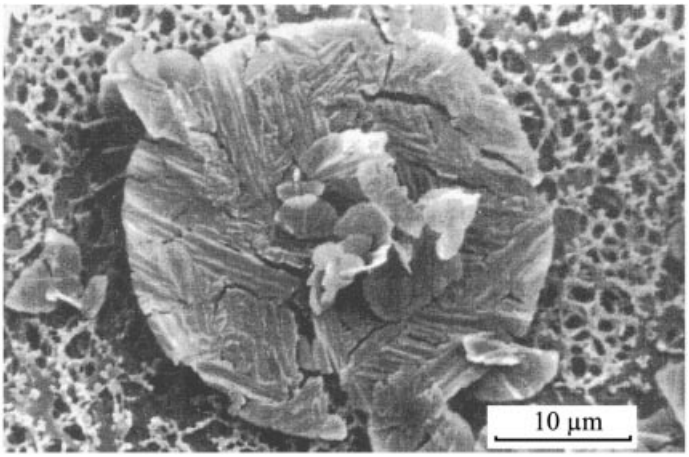

Fig. 15. Circular crystal of PE grown under an elevated pressure in the hexagonal structure, which has undergone a transition to the orthorhombic structure by reducing the pressure. The crystal was extracted from the bulk by a solvent extraction. The transformed crystal displays three sets of ridges, 60° apart, which indicate that three orientations of the *b* axis are generated by the hexagonal to orthorhombic transition (83).

Chain Folding Principle and Single Crystal Sectorization. How can a long-chain molecule be accommodated in this lamellar-shaped single crystals with a thickness of only 10–50 nm? Earlier, in an almost unnoticed paper by Storks (87), who is virtually unknown in the polymer field, noted that in gutta-percha thin films (of a 27-nm thickness) he could not directly see the crystals because an interferometer was used to measure the overall film thickness. However, he observed $hk0$ diffraction and stated that

> films of guttapercha are found to be composed of relatively large crystallites which are precisely oriented with their fiber axis direction normal to the film surface. It is presumed that the macromolecules are folded back and forth upon themselves in such a way that adjacent sectors remain parallel (87).

Since the late 1950s, ed experimental results on single crystals have clearly shown that the long chain direction is normal or close to normal direction since the chain direction is parallel to the electron beam (see the [00l] zone ed pattern of PE single crystals in Fig. 10). In agreement with Storks' conclusion, the only way to explain this experimental observation is that the chains are folded in the lamellar single crystals. This would also mean that what appears to be a single crystal should be composed of as many sectors as there are prism faces distinguished by the fold plane direction in each sector.

Following these early experimental observations and explanations of chain folding in solution-grown lamellar single crystals, several methodologies have been developed, which are specifically important in determining the chain folding. These include LMW PE decoration method (49,88), the breakage of single crystals under elongation (53,89), and lateral force mode in atomic force microscopy (afm) (90). For the LMW PE surface decoration, the basic principle is to use orientational ("soft") epitaxy of LMW species on a microscopically oriented surface. If chain folding possesses a uniform orientational direction, for example, in one growth sector, the chain direction of the LMW PE aligns parallel to the folding direction. PE molecules then crystallize into a needle-like shape with its long axis perpendicular to the folding direction of the lamellar single crystal. It was also shown that without folded chains such as in short n-alkanes, such orientational growth of the LMW PE crystals on the end surface of n-alkane single crystals is lost (49). This decoration experiments have been performed not only in PE, iPP (49), PEO (91), and other lamellar single crystals of polymers grown in solutions, but also in the lamellar crystals formed in the melt. After significant efforts of the past half century, now it is known that polymer crystallization from both solution and the melt can form sectors. Sectorization is a consequence of different crystal growth planes with individual chain-folding directions, as evidenced by the PE decoration experiments. Sectorization is also an indication of normal (nucleation) growth mechanism of polymer crystallization.

Later investigations showed a facetted crystal-habit dependence of the PE lamellar single crystals on different temperatures and solvents used. By changing from good solvents to poor ones, the single crystals with four (110) growth faces gradually changed to six planes having two extra (200) growth faces. The habit change continues and the four (110) growth faces gradually decrease in size

because of a faster growth rate along the [110] direction. This leads to a continuous change of the crystal's aspect ratio and curvature of the (200) planes with increasing crystallization temperature (92,93). A similar study for the melt growth of PE single lamellar crystals indicates an aspect ratio change with ΔT (see Fig. 12) (60,61,94). Some intriguing experimental observations related to sectorization involve lamellar single crystals of sPP. The sectorization takes place along diagonal directions in a lamellar crystal that possesses an anisotropic elongated shape. Four sectors are formed: the (010) [with the (010) free edge] and the (100) [with the (100) free edge] sectors, as observed by tem (see Fig. 14) and AFM. Although the crystals in both sectors are in the high temperature orthorhombic structure (62–65), direct observation of this sectorization is possible owing to a thickness difference of the sectors with different fold planes. AFM results show that the thickness difference depends on crystallization time. Similar but much smaller difference had been reported in PE solution-grown lamellar single crystals (95).

Epitaxy and Twinning in Polymer Single Crystals. *Epitaxy* and *twinning* are frequently observed in polymer single crystals. In most cases, they are always associated with traditional crystal defects. Epitaxy is generally applied to oriented growth of one crystalline substance on a substrate of a different substance. However, it is also common that epitaxy may occur within one crystalline substance at different (*hkl*) crystalline planes. By contrast, the twin contains an added element of symmetry over and above that which either component possesses. In other words, epitaxy only needs lattice match whereas twinning introduces an additional symmetry axis.

Extensive studies have been carried out regarding polymer crystallization on inorganic or organic (nonpolymeric) small-molecular crystal surfaces. The general rule is that at least one of the (*hkl*)—or more frequently the (*hk*0)—planes of the polymer crystal lattice must match with one of the crystallographic planes in the small-molecular crystals. Although most of the works do not provide polymer single crystals when they are epitaxially grown on the nonpolymeric crystals, they contribute to the development of nucleation agents, as in the case of the α-form of iPP (96). Using the epitaxy method to grow polymer single crystals with specific forms and orientations is, however, a powerful tool in understanding polymer crystallographic structures and its relationships with the nonpolymeric materials. One example is the β-form single crystal of iPP grown on substrates of γ-quinacridone and dicyclohexylterephthalamide that helps in analyzing the details of the β-form crystal structure (97).

For the polymers epitaxially grown on their own crystallographic planes, one example is the so-called *cross-hatching phenomenon*. The *daughter lamellae* (tangential lamellae in spherulites) are at about 80° or 100° with respect to the *parent lamellae* (radial lamellae along the radial direction in spherulites) observed in the α-form of iPP crystals. It is known that tangential lamellae grow epitaxially on the lateral (010) crystallographic plane of the radial lamellae by a satisfactory interdigitation of the methyl groups (the contact planes). This matching stems from the near identitical dimensions of the a and c axes in the α-form unit cell (98). A very special case, which reflects perfectly molecular epitaxy, is the γ-form of iPP. The real breakthrough in understanding the γ-form came (98) when it was realized that the chain axes in the unit cell are not parallel. Instead, the structure is made up of a succession of bilayers tilted 80° or 100° to each other, which is

similar to the cross-hatching crystals in the α-form but this time at the molecular chain-packing scale (99). This special relationship allows an epitaxial growth of the tilted γ-form on the α-form in iPP (100).

Lamellar single crystals can in some cases form epitaxially when two different ($hk0$) planes can be matched. This leads to a common chain direction (the c axis). An example is sPP lamellar single crystals grown from the melt in the thin-film form (101). This can also be found in the case of oligomer single lamellar crystals (102). Another example is shish–kebab structures. The kebab structure is generally made of lamellar crystals that grow along the orientation of the chain direction of the shish single crystals, and therefore, it is an epitaxy of a chain-folded polymer on its own extended chain crystals. Polymer crystals can also be epitaxially grown on other ordered polymer surfaces. A recent example is α-form of iPP epitaxially grown on PTFE and organic substrates (103), which may be recognized as some kind of morphological epitaxy. Detailed description can be found in a review article (104).

Twins in polymer single crystals have been observed as early as in the 1950s. In particular, when the self-seeding experiments were introduced, twinned lamellar single crystals were widely reported first in solution-grown PE and PEO single crystals (5). Melt-crystallized twin crystals were also found. An example is the PE crystallized at elevated pressure to form single crystals having the hexagonal structure, and thus its morphology possesses a rounded shape. With the release of pressure, the crystal structure undergoes a transition to orthorhombic structure; however, this rounded shape of the crystals cannot be changed. It thus forms an orthorhombic single crystal with three equivalent b axis orientations of the orthorhombic cell, 60° apart (see Fig. 15) (76), which is a very special case for generating twin crystals via a crystal–crystal transition. Twin crystals can also be found in oligomers crystallized from the melt (102). Molecular packing disturbances in the formation of the twin are usually invoked to explain these crystal defects (5).

Curved Crystals, Frustrated Crystals, and Helical Crystals in Polymers. Lamellar crystals are not always flat. Curved crystals have been observed and reported to form sometimes in dilute polymer solutions. The observations can be traced back to the early 1970s in poly-4-methyl-pentene-1 (P4MP) (105), polychlorotrifluoroethylene (PCTFE) (106), and polyoxymethylene (POM) (107). In particular, the crystals are more pronouncedly curved (they have a smaller radius of curvature), when the crystallization temperature decreases. It is believed that individual fold domains are nonplanar. A simple four or six sectored crystal is actually slightly conical in overall shape. Therefore, a hypothetical model pertaining to the origin of curved crystals in polymers has been proposed. In addition, scroll-like as opposed to curved- or band-like crystals were also observed, such as in nylon-6,6 (108), isotactic polybutene-1 (109), and recently, in chiral nonracemic (R)- and (S)-poly(epichlorohydrin) solution-grown single crystals (110). An interesting observation relates to PVDF lamellar crystals grown in the melt, although they are not strictly single crystals. The lamellar structures within PVDF spherulites in the γ-form have a curious architecture in which the lamellae adopt a highly curved "scroll-like" morphology, with the axis of the scroll parallel to the spherulite radius (111). It has been suggested that this scroll-like morphology results from an imbalance of the fold composition on opposite fold

surfaces. The imbalance reflects the polarity of the γ-phase crystal structure and the steric constraints on the fold conformation (112).

The concept of frustrated crystals was introduced in materials science to describe the mutual orientation of magnetic spins in antiferromagnetic systems (113). Frustration exists wherever vicinal requirements are incompatible with packing requirements (eg, antiparallelism of spins in a triangluar or close-packed hexagonal lattice) (114). This concept was introduced in polymer crystallographic systems in the middle of 1990s (115). These frustrated structures are based on trigonal unit cells that contain three threefolded isochiral helices and in which the (nearly) similar azimuthal setting of two helices differs significantly from that of the third helix. In most cases, triangular single crystal morphology can be observed. Some of the morphologies also possess a hexagonal shape. This is a local consequence of the different azimuthal settings, which create different nucleation sites on opposite sides of any given growth plane (116). Examples include the β-form of iPP (117), isotactic poly(2-vinylpyridine) (118), poly(*tert*-butylethylene sulfide) (119), poly(L-hydroxyproline) (120), and α''-superstructure of syndiotactic PS (121). Figure 16 shows triangular single crystals of poly(L-hydroxyproline) and poly(*tert*-butylethylene sulfide) (120).

Because of the introduction of biomacromolecules and the development of asymmetric synthesis, chiral nonracemic polymer aggregates and single crystals become a new research topic. In biomacromolecules, double-twisted packing is similar to a stack of twisted β-sheets as is the case in several biopolymers (122–125). These twisted sheets pack closely with a twist that is perpendicular to the helical axis of the sheets themselves. Many examples possessing the double-twisted helical packing are in liquid crystalline states. Examples include dinoflaggellate chromosomes (in *Prorocentrum micans*) in an *in vivo* arrangement (122), DNAs (126), and poly-γ-benzyl-L-glutamate (127,128). Helical single crystals of the β-modification grown from *Bombyx mori* silk fibroin solution have been reported (129). Many chiral nonracemic polymers have been synthesized by an asymmetric synthetic method. The most recent example is that of chiral main-chain liquid crystalline polyesters that can form helical single crystals as shown in Figure 17 (130–134). It has also been found that the chain orientation in this helical single crystal is double-twisted. Furthermore, PE decoration indicates that there is no sectorization and that the chain-folding direction is along the long helical axis. These crystals can thus only be true crystals in Riemannian space (130).

Polycrystalline Aggregates: Dendrites and Spherulites. When the building blocks of single lamellar crystals aggregate together, different polycrystalline morphologies are generated. This introduces another length scale, usually in a range of a fractional micrometers up to, in some cases, fractions of centimeters. Two major factors determine the final morphology. The first is the polymer characteristics such as chain flexibility, molecular weight, and molecular architecture. The other is the outside environment such as crystallization from solution or melt, undercooling and pressure of crystallization, and external field applied. The most common polycrystalline morphologies are dendrites and spherulites. Fibrous crystals may be polycrystalline or single crystals.

Dendrites are branched crystals which in some cases take on a tree-like shape. Typically, polymer dedritic crystals form in solution, as shown in Figure 18 (135): either in dilute solution at relatively high undercooling or in polymer

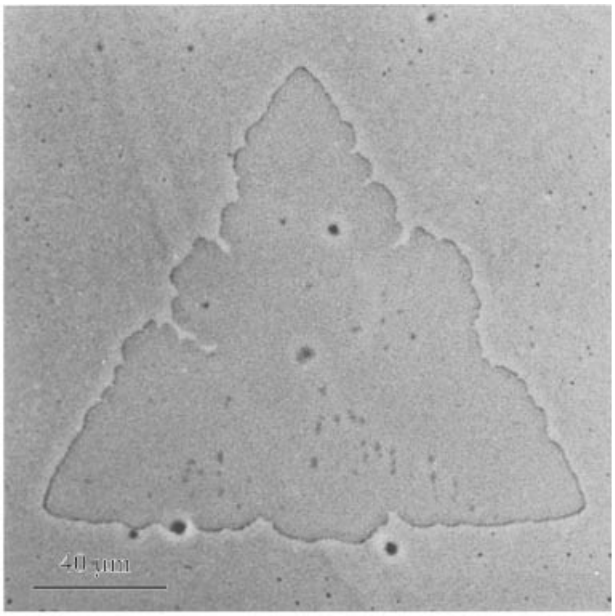

(a)

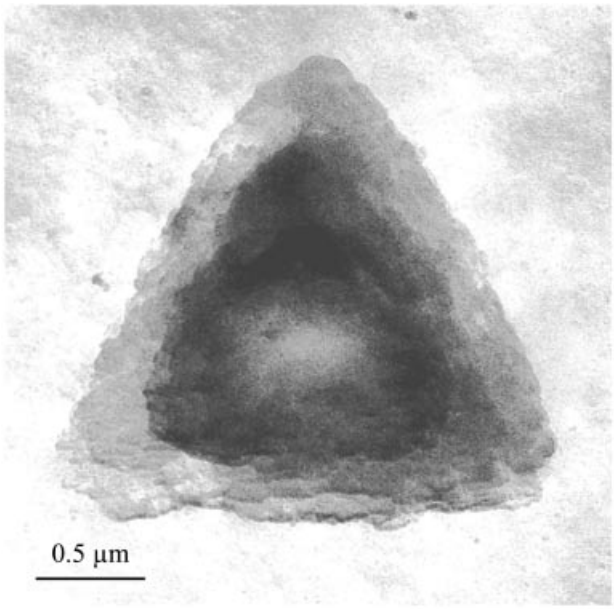

(b)

Fig. 16. (**a**). Phase contrast optical micrograph of a single crystal of iPKBES formed in thin film at 130°C (**b**). Transmission electron micrograph of poly(L-hydroxyproline) grown from a 0.1% solution in a 1/9 (v/v) mixture of formic acid and ethanol at room temperature (120).

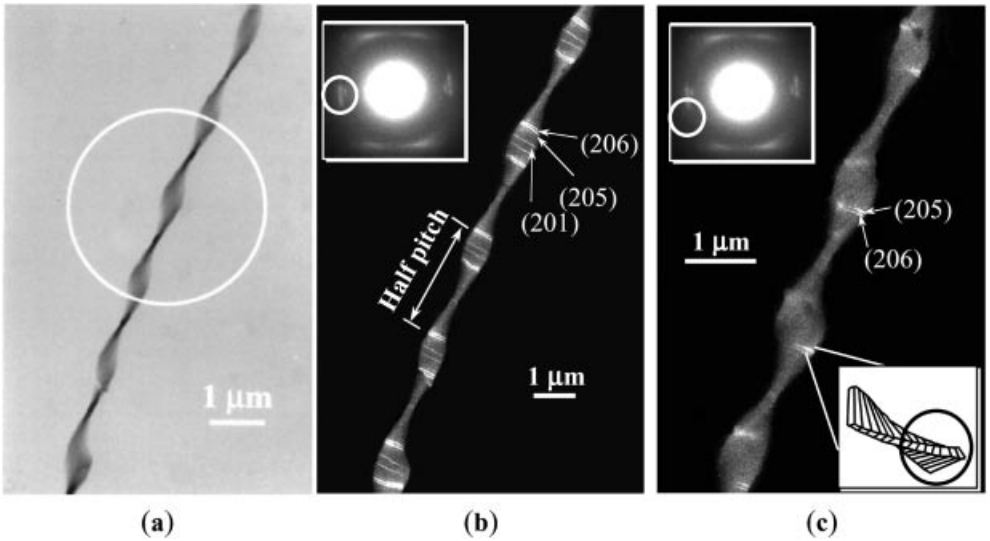

Fig. 17. Single helical lamellar crystal morphology of the nonracemic chiral main-chain polyester synthesized from (*R*)-(−)-4′-{omega-[2-(*p*-hydroxy-*o*-nitrophenyloxy)-1-propyloxy]-1-nonyloxy}-4-biphenyl carboxylic acid in the tem (**a**). The two dark field inserts are obtained from the full (**b**) and partial ed arcs (**c**) to illustrate that the chain orientation in this helical lamellar crystal is double-twisted (130,131).

solutions at slightly higher concentration. Although the branches in dendrites may sometimes show regular symmetry (see Fig. 18) or in most cases irregular growth, all of them possess crystallographic relationships. The formation of dendrites is linked with a local change in crystallization conditions. In principle, crystal growth can be influenced by concentration gradients caused by rejection of noncrystallizing species and temperature gradients generated by directional dissipation of the heat of crystallization. It is believed that the concentration effect is dominant (136,137). Using Fick's second law of diffusion, the concentration gradient at the crystal growth front can be represented quantitatively, which corresponds roughly to the ratio between crystal growth rate and diffusion coefficient. Only in the specific case of monoclinic α-form in iPP, the dendrites are due to a cross-hatching of the lamellae (138).

Spherulites, as first found to form in both organic and inorganic materials, are rounded crystalline bodies (5). They are circular in cross section and are composed of thin divergent crystal fibers that under polarized light microscopy (PLM) give rise to a Maltese cross pattern, with the arms parallel to the polarizer and analyzer. Spherulites in polymer crystals were first observed during the second world war. Figure 19 shows typical banded sperulites with Maltese cross of poly(trimethylene terephthalate) under PLM (139). The banded texture is due to lamellar crystals cooperatively twisting along the growth direction of spherulites, although the detailed mechanisms of twisting are still debated. Whatever the chain chemical structure and flexibility, almost all of the semicrystalline polymers form spherulites when they crystallize from the melt. Two general types of spherulites can be identified. Spherulitic radiation of the substructures can

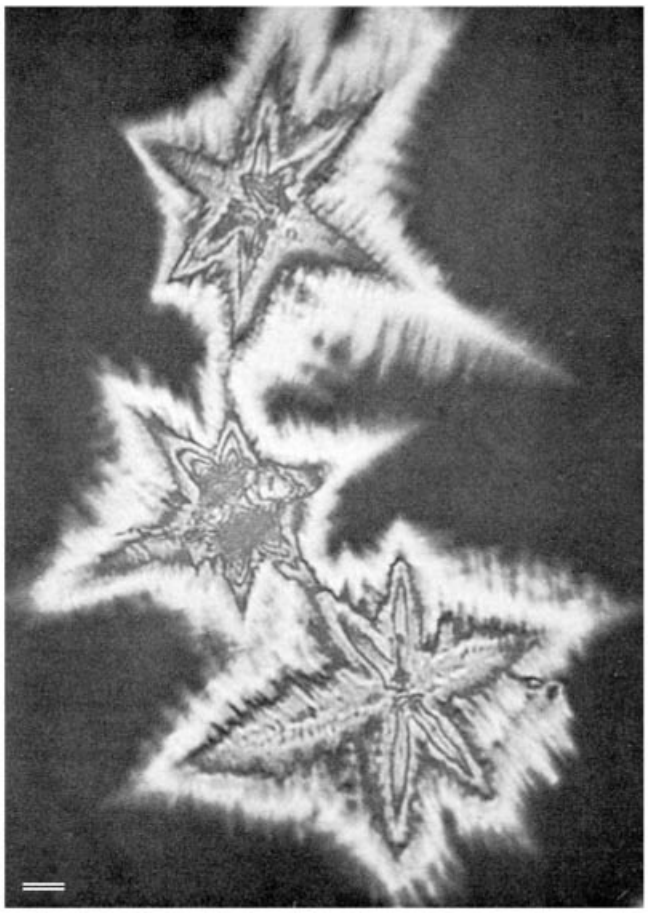

Fig. 18. Polyethylene dendrites grown from 0.05% solution in toluene at 70°C. They were observed under interference microscopy (135).

be achieved initially by a heterogeneous nucleus. The substructures then branch out in order to fill in space. However, the initial nucleus can be a simple one. In this case, lamellae initially start in two directions and then splay and diverge. The central portion has an inhomogeneous structure, commonly called the "eye" structure. It is readily apparent that the substructure in polymer spherulites is lamellar crystal. In fact, spherulites are aggregates of lamellar crystals cooperatively packed together. However, the mechanism of formation of polymer spherulites is complicated and actively discussed in the past several decades. In general, development of a spherulite from a single lamellar crystal must involve some sort of morphological instability.

It should be noted that dendrites and spherulitic aggregates are not completely crystalline. Certain amorphous regions remain even if macroscopically crystalline aggregates appear to have impinged. In some extreme cases of branched PE, the amorphous portions in spherulites can be as high as 90%. Two different types of amorphous regions can exist in these semicrystalline polymers,

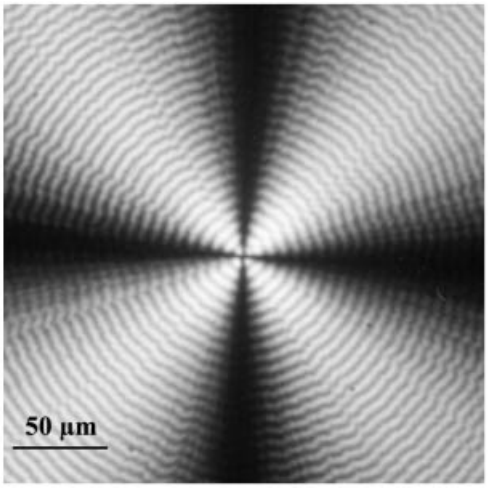

Fig. 19. Banded spherulite of poly(trimethylene terephthalate) crystallized from the melt at 150°C (139).

which are either located between neighboring lamellar crystals or segregated in separate pockets. These two types of regions are usually called microscopic and macroscopic amorphous regions. When linking these morphological observations with crystallinity concept, the usefulness and disadvantages of the two-phase model will be apparent.

Crystallinity Concept

The concept of the crystallinity of a semicrystalline polymer is based on the two-phase approximation of the polymer structure, which assumes that uniform crystalline and amorphous regions can be distinguished. It was adopted in the early years of polymer science with the first serious attempts to determine the ratio of the two phases in a polymer. The two-phase model successfully explained mechanical properties of semicrystalline polymers using continuous mechanics. Following the discovery of the chain folding, the two-phase concept was questioned. It seemed difficult to reconcile with the existence of layers with sharp folds at the interface between adjoining crystalline lamellae. Instead, the crystal defect model was proposed, according to which the amorphous phase is dispersed in the crystalline phase in the form of defects within the crystalline structure. As a result, the degree of crystallinity no longer had a direct obvious meaning, and other concepts such as "crystallinity index" or "degree of order" were proposed to quantify the phenomena associated with the presence of defects. However, as a result of increasing experimental evidence, the two-phase model was later restored, and was generally used to describe polymer morphology.

Crystallinity can vary widely in semicrystalline polymers. Three rough classes of polymers can be identified, which have high crystallinity (over 50%), medium crystallinity (between 20 and 50%), and low crystallinity (below 20%). High crystallinity polymers are seen in linear PE, iPP, PEO, etc; medium

crystallinity polymers are poly(ethylene terephthalate), poly(aryl ether ether ketone)s, poly(phenylene sulfide), and others; low crystallinity polymers are poly(vinyl chloride), some high temperature aromatic polyimides [poly(4,4′-oxydiphenylene pyromellitimide), etc] and ultralow density short-chain branched PEs, etc. Deviations from the two-phase model seem to occur in the sense that the phase boundary may occupy nonnegligible weight and volume in the materials, in which the structural order gradually changes between those of the crystalline and of the amorphous phase.

The crystallinity is thus apparently a meaningful quantity, and its determination is a matter of paramount importance in the investigation of semicrystalline polymer morphology. Either the weight w^c or the volume v^c fractions can be determined using the densities of the whole polymer, the crystalline phase, and the amorphous phase, given by ρ, ρ_c, and ρ_a, respectively. The following relations hold:

$$v^c = V_c/V \tag{2}$$

$$w^c = W_c/W \tag{3}$$

$$v^c = (\rho - \rho_a)/(\rho_c - \rho_a) \tag{4}$$

$$w^c = (\rho_c/\rho)v^c \tag{5}$$

To determine crystallinity in a semicrystalline polymer, diffraction, thermodynamic, and spectroscopic methods can be used. Diffraction method is mainly used with waxd methods. Thermodynamic methods include dilatometry, differential scanning calorimetry (dsc), etc, while ir and nuclear magnetic resonance (nmr), and other spectroscopic methods can also be used.

The most universal waxd method to determine crystallinity was developed by the introduction of a disorder function D (140).

$$4\pi \int_0^\infty s^2 I_c(s)\mathrm{d}s = w^c 4\pi \int_0^\infty s^2 \bar{f}^2 D\mathrm{d}s \tag{6}$$

In this equation, w^c represents the true weight fraction of crystals in the sample. The quantity $\bar{f}^2$ represents the mean square atomic scattering factor of the polymer summed over all atoms i (N_i is the number of atoms of type i)

$$\bar{f}^2 = \sum N_i f_i^2 / \sum N_i \tag{7}$$

The total scattering can be expressed as

$$4\pi \int_0^\infty s^2 I(s)\mathrm{d}s = 4\pi \int_0^\infty s^2 \bar{f}^2 \mathrm{d}s \tag{8}$$

and the weight fraction crystallinity that can be used to evaluate the experimentally obtained data is

$$w^c = \frac{\int_0^\infty s^2 I_c(s)\mathrm{d}s \int_0^\infty s^2 \bar{f}^2 \mathrm{d}s}{\int_0^\infty s^2 I \mathrm{d}s \int_0^\infty s^2 \bar{f}^2 D\mathrm{d}s} \tag{9}$$

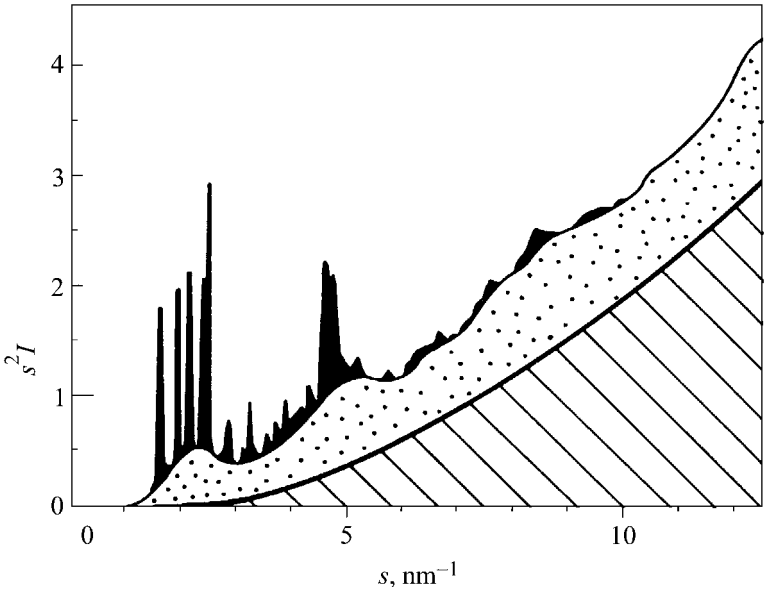

Fig. 20. Wide-angle x-ray diffraction crystallinity determination of iPP (5,140).

Application of the above equation requires either a sample with completely random orientation of crystals or a proper averaging of oriented samples. Averaging techniques have been described more than 30 years ago (141,142). Also, three-dimensional order is assumed to exist in the crystalline regions, so that the disorder is not strongly anisotropic. For the treatment of the anisotropic case, additional structural detail is needed to evaluate the amount of material which shows one- or two-dimensional order (143). An example of a $s^2I(s)$ curve computed directly from the experimental data of an iPP sample is shown in Figure 20 (5,144). Before using equation 9, the incoherent Compton scattering (shadowed area) must be subtracted. The crystalline portion $s^2I_c(s)$ can be delineated by subtraction of the undulating diffuse scattering area (drawn dotted). The separation line can be found by drawing a smooth curve through the minimum between the crystalline peaks along the general slope of the continuous scattering. According to Ruland, the procedure restricts the region counted as "crystalline" to sizes bigger that 2–3 nm.

A number of more approximate methods that avoid much of the complex computation described above have been used to estimate the crystallinity from x-ray diffraction data (145). A diffraction curve of an unoriented sample over a limited range of angle that contains most of the crystalline diffraction peaks and the major portion of the amorphous halo can typically be separated as indicated, for instance, in the case of iPP in Figure 21. A straight background line is drawn between the limits of the chosen interval of angles which should separate the incoherent scattering and others, largely not crystallinity-dependent, coherent scattering contributions. A line separating the sharp diffraction peaks is then drawn by connecting the minimum between well-separated crystalline reflections to a shape similar to that found (or expected) for a totally amorphous sample. The proportionality of the separated areas or amplitudes at suitably chosen angles to the crystalline or amorphous fraction is then determined by calibration. Much of the error introduced by integrating the diffraction intensity with respect to

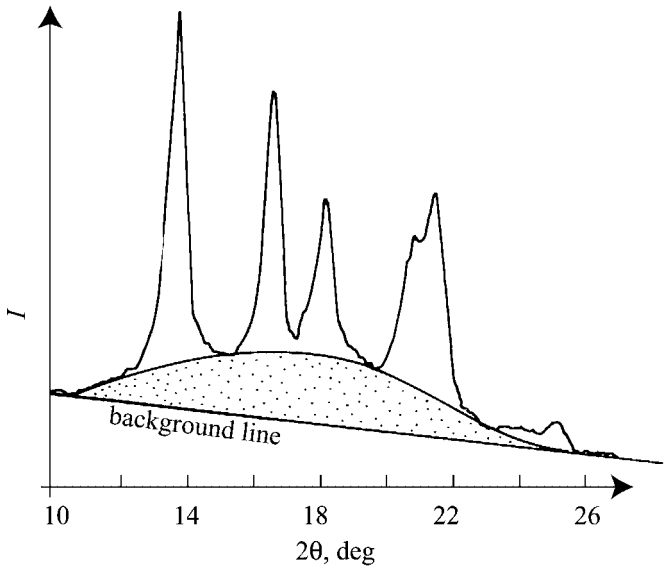

Fig. 21. Crystallinity of iPP determined using waxd method (144).

θ or using amplitudes at one angle rather than evaluating the integral over all reciprocal space is minimized by the calibration.

Thermodynamic approaches provide powerful tools to characterize the properties in identifying these metastable states to understand the effects of phase size, dimensionality, and composition on the materials properties. One well-known example is the density gradient column method to determine densities of semicrystalline polymers. Based on known equilibrium crystalline and amorphous densities, the crystallinity of a semicrystalline sample can be calculated by using equations 4 and 5. However, it should be noted that the determination of these equilibrium density data is not trivial. Proper extrapolations are necessary to ensure the equilibrium nature of the results. Detailed issues discussed can be found in Reference 146. Another commonly used method is to measure the heat of crystallization or fusion by using dsc. By knowing the equilibrium heat of fusion, the crystallinity of a sample can be easily calculated.

$$w^{c} = 1 - \frac{\Delta h_f(m)}{\Delta H_f} \tag{10}$$

where $\Delta\ h_f(m)$ is the measured heat of fusion and ΔH_f is the equilibrium heat of fusion of a specific polymer crystal. Again, this equilibrium heat of fusion can only be obtained using proper extrapolation methods, and corrected procedures and data treatments are necessary. Over 100 equilibrium heat of fusion data have been listed in Reference 147, which have been critically reviewed.

Spectroscopic methods like such as ir require finger printing vibration frequencies, which are specifically crystal- or amorphous-sensitive. The nmr method basically measures mobility of nuclei. Above the glass transition temperature of a semicrystalline sample, the amorphous part becomes mobile and the crystalline part is still rigid: the nuclei in these two parts possess different mobilities and thus can be detected by nmr (for detailed information, see Ref. 5).

However, if the two-phase model were strictly a precise description of a semicrystalline polymer, in which the crystalline and amorphous parts have sharp boundaries and do not have connections, its macroscopic mechanical response toward outside environments would be very weak. There must be some materials between these two parts, and therefore create interfaces. The characterization of the interfacial structures in semicrystalline polymers—identifying so-called *rigid amorphous fractions*—requires precise determination of crystallinity and the mobile amorphous portion of a semicrystalline sample. This concept can be traced back as far as 30 years ago. However, extensive studies have been carried out in the past 10–15 years only (148–155). On the other hand, researches on interface between crystalline and amorphous regions in bulk polymers have also been carried out using different experimental methods of small angle x-ray scattering, ^{13}C solid-state NMR, Raman spectroscopy, and tem (156–162). It is known that the crystallinity concept invokes the two-phase model, which simply divides the system into a perfectly ordered crystalline region and an amorphous region with sharp boundaries. In order to examine the validity of this two-phase (crystallinity) model, using for example, the dsc method, one needs first to establish the heat capacity data in solid and liquid states of the polymers. With these data, one could therefore predict that for a semicrystalline polymer

$$w^{c} = 1 - \frac{\Delta c_p(m)}{\Delta c_p(a)} \tag{11}$$

where w^c is the weight-fraction crystallinity and is usually obtained by dsc measurements, density determination, and/or waxd experiments. The terms $\Delta c_p(m)$ and $\Delta c_p(a)$ are the heat capacity increases at glass-transition temperature (T_g) for the semicrystalline sample and the amorphous sample, respectively. Surprisingly, a wide variety of behaviors that deviates from the ideal two-phase model exist. A positive heat capacity deviation is observed for practically all polymers long before the clearly recognized fusion endotherm begins. This has been linked to premelting and/or defect formation. For PE and PTFE, these positive deviations close to the melting temperatures are well-analyzed (147,163). The heat capacities of POM show, on the other hand, a negative deviation at somewhat lower temperatures relative to the melting temperature (T_m) (148,149). This reveals an extra fraction in the polymer that contributes neither to the glass transition at T_g nor to the heat of fusion at T_m. This fraction has been called the *rigid amorphous fraction*. In POM, this rigid amorphous fraction does not show any sign of softening up to the polymer melting. Similar measurements in iPP exhibit a rigid amorphous fraction that is gradually unfreezing, which in turn leads to the occasionally observed *double glass transition* (164). As a result, if a rigid amorphous fraction exists in a semicrystalline polymer, the two-phase model cannot be used to describe that system, and

$$w^{c} < 1 - \frac{\Delta c_p(m)}{\Delta c_p(a)} = f_r \tag{12}$$

The resulting difference between equations 10 and 11 is the rigid amorphous fraction in a polymer, $f_r - w^c$. Most of the thermoplastic engineering polymers such

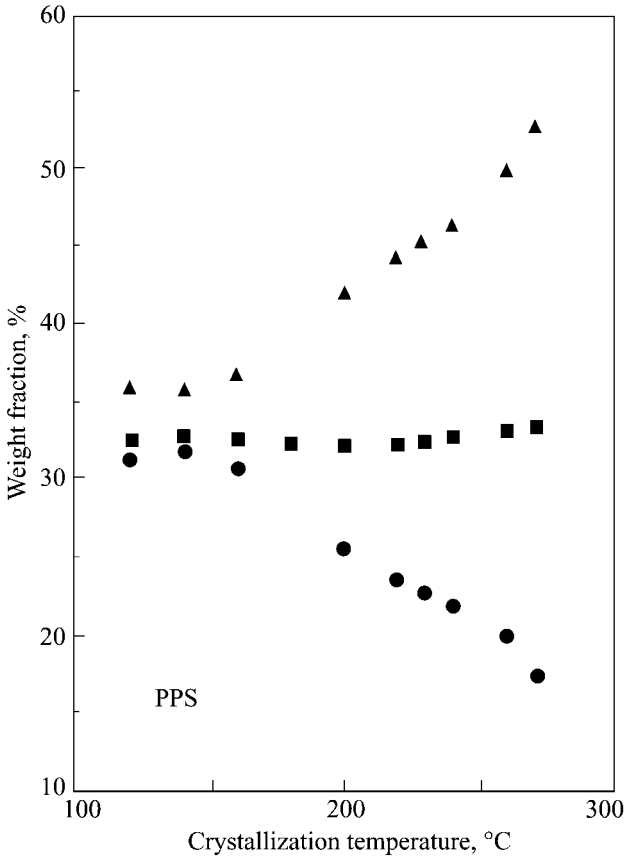

Fig. 22. Rigid amorphous, mobile amorphous, and crystallinity changes in PPS with crystallization temperatures (166). Mobile amorphous fraction;■ rigid amorphous fraction;● and weight fraction crystallinity ▲.

as PEEK (150), PPS (151), PPO (152), PET (165), PBT (154), PEN (153), and polyimides (155) show this kind of behavior that is critically dependent upon the thermal history of the samples. Figure 22 shows three fractions in a high molecular weight linear PPS sample, in which the nonmobile amorphous fraction above T_g represents the rigid amorphous fraction (166). More complicated situations may also be observed by combining both positive and negative deviations of heat capacities in a semicrystalline polymer. Other structural characterization methods are necessary to distinguish these deviations and to separate both effects.

Physical Properties Affected by Crystal Structures and Morphologies

Polymer crystals are always semicrystalline, and thus, they are far from perfect. Limited crystal sizes and complicated aggregates make the basic understanding of the structure-property relationships very difficult. To simplify, two types of properties in general exist for crystals of small molecules: structure-insensitive and structure-sensitive properties. The structure-insensitive properties include

density, heat of fusion, modulus, and refractive index whereas the structure-sensitive properties are deformation, chemical reactivity, electrolytic conductivity, etc. However, in polymer crystals, one needs to introduce morphology-insensitive and morphology-sensitive properties because of the existence of structures in different length scale. Although most of the properties in these two catalogs that were identified in small-molecular crystals are also more or less applicable in polymer crystals as recognized on the basis of morphological levels, the relationships obtained are certainly by far scattered.

The modulus of isotropic semicrystalline polymers is associated with crystallinity. Since the modulus is relatively morphology-insensitive, one can plot a relationship between modulus and crystallinity or density. Extensive studies have been carried out in linear PE and PE copolymers to establish structure-property relationships (167–175). Figure 23 shows such a relationship for a whole spectrum of PE over 9000 data points, including very low density branched PE and copolymers to high density PE (176). Interestingly, the data follow a consistent trend: lower density (crystallinity) samples have lower modulus and higher density (crystallinity) samples have high modulus. The deviation of the data is about ±50%. As the mechanical measurements are from very different sources, the correlation between density (crystllinity) and modulus can be viewed as excellent. The deviation may come from morphological dependence of the modulus with a constant density in addition to experimental errors in these measurements. However, this morphological dependence is weak, and therefore, this example provides a clear indication that the modulus is basically a morphology-less-sensitive, but crystallinity-more-sensitive property. However, no clear-cut correlation between the structure-sensitive property and crystallinity can be established. For example, these kinds of observations can be found in the measurements of heat of fusion. Although the melting temperature is crystal-size-dependent, which is closely

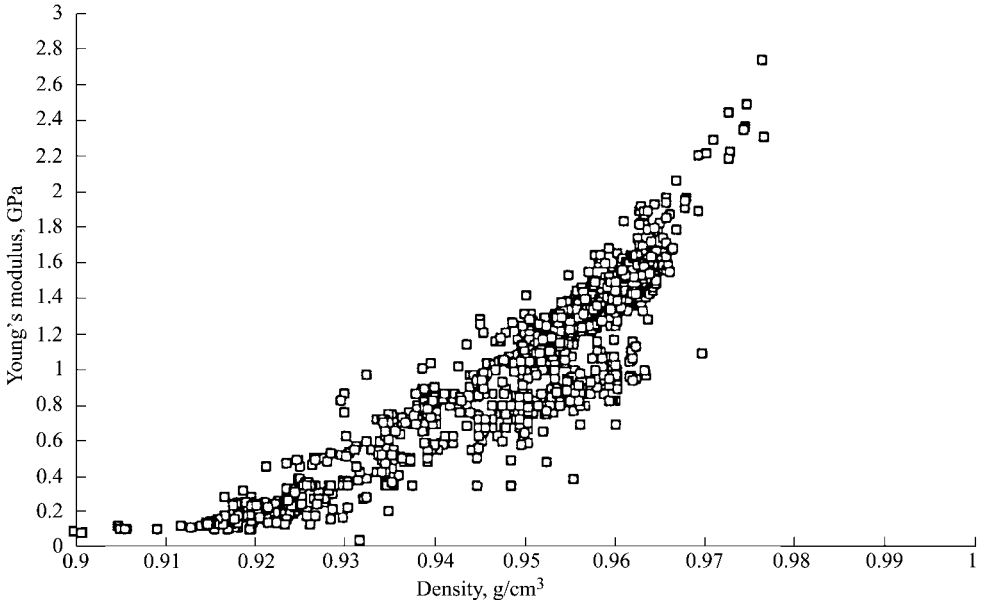

Fig. 23. Modulus versus density in various PE (176).

associated with crystal morphology, the amount of heat required to isotropize the crystal is a morphology-insensitive property.

Crystal modulus can also be associated with the molecular conformation in the polymer crystal. In order to determine the crystal modulus of polymers, oriented polymer samples are usually used. The basic assumption is that the stress applied on polymer samples is evenly transmitted through the sample. Various structural characterization methods are then applied to measure the lattice strain under stress, including waxd and Raman experiments. In waxd experiments, the d-spacing shift along the chain molecular direction can be observed at different tensile stress level. In Raman spectroscopic method, the vibration bands shift to lower frequencies with increasing tensile stress. Note that these types of measurements use macroscopic stress and microscopic strain to obtain Young's modulus. Other methods may also be applied, such as the velocity of acoustic phonon propagating within the polymer crystals from the frequency–dispersion curve measured by coherent inelastic neutron scattering. Table 2 shows crystalline modulus along the chain molecular direction for different semicrystalline polymers. The calculated modulus data in most cases are carried out using lattice dynamic treatment and deformation mechanism of the chain subjected to tensile stress (177–185).

Table 2. Crystallite Modulus (GPa[a]) along the Chain Axis

Form	Polymer[b]	Observed	Calculated
Planar-zigzag	PE	240 (290, 329)	316
	PVA	250	287
	Nylon-6 (α)	165 (20°C)	170
		270 (−150°C)	312
	PVDF (I)	177	237
	PDA (PDCHD)	45	40
Helix, glide	iPP	40	40
	POM	53 (75)	109
	PVDF (II)	59	77
	Nylon-6 (γ)	27	54
Aromatic polyester	PET	108	95
	PTMT (α)	13	10
	PTMT (β)	20	27
	PEOB (α)	6	2
	PEOB (β)		57
Rigid rod polymer	Kevlar	153, 200	182
	PBA	188	163 (GTGT)
			238 (TTTT)
	Nomex	88	117
	PBT	395	371
	P-p-P		275
	PBB		588
	PPPI		505
	Cellulose (I)	127	168
	Cellulose (II)	90 (109)	162

[a]To convert GPa to kbar, multiply by 10^5.

[b]PDA = polydiacetylene; PET = poly(ethylene terephthalate); PBA = poly(p-benzamide); P-p-P = poly(p-phenylene); PBB = polybenzobisthiazole; PPPI = poly(p-phenylenepyromellitimide).

In the past 50 years, substantial progresses in understanding of almost every aspect of semicrystalline polymers have been made. However, it is not a simple task, based on the knowledge of polymer crystal structures, to predict their macroscopic properties. This is because compared with crystals of small molecules, polymer crystals in bulk are generally in the form of polycrystalline aggregates. Their semicrystalline nature leads to broad structural length scales which in turn affect the final performances of the materials. Polymer single crystals are not only an essential step in understanding how long-chain molecules can be closely packed in three-dimensional space, but also are the most important step as a building block in the development and formation of the polymer aggregates in bulk materials.

BIBLIOGRAPHY

"Crystallinity" in *EPSE* 1st ed., Vol. 4, pp. 449–528, by R. L. Miller, Chemstrand Research Center, Inc.; "Crytalline Polymers" in *EPSE* 2nd ed., Suppl. Vol., pp. 187–231, by K. Tashiro and H. Tadokoro, Osaka University.

1. P. J. Flory, *Statistical Mechanics of Chain Molecules*, Wiley-Interscience, New York, 1969.
2. C. W. Bunn, *Trans. Faraday Soc.* **35**, 483 (1939).
3. T. Shimanouchi and S. Mizushima, *J. Chem. Phys.* **23**, 707 (1955); R. E. Hughes and J. L. Lauer, *J. Chem. Phys.* **30**, 1165 (1959).
4. E. S. Clark and L. T. Muus, *Z. Krist.* **117**, 119 (1962).
5. B. Wunderlich, *Macromolecular Physics, Crystal Structure, Morphology, Defects*, Vol. **1**, Academic Press, Inc., New York, 1973.
6. G. Natta, P. Corradini, and P. Ganis, *Makromol. Chem.* **39**, 238 (1960).
7. G. Natta, P. Corradini, and P. Ganis, *J. Polym. Sci.* **58**, 1191 (1962).
8. G. Nata and P. Corradini, *J. Polym. Sci.* **39**, 29 (1959); see also, *Nuovo Cimento Suppl.* **15**, 9 (1960).
9. Y. Takahashi and H. Tadokoro, *Macromolecules* **6**, 672 (1973).
10. P. Zugenmaier and H. J. Cantow, *Kolloid Z. Z. Polym.* **230**, 229 (1969).
11. G. Nata and P. Corradini, *Nuovo Cimento Suppl.* **15**, 40 (1960).
12. A. J. Lovinger, D. D. Davis, and B. Lotz, *Macromolecules* **24**, 552 (1991).
13. Y. Kinoshita, *Makromol. Chem.* **33**, 21 (1959).
14. M. E. Leland and co-workers, *Macromolecules* **30**, 5249 (1997).
15. R. D. B. Fraser and T. P. MacRae, *Conformation in Fibrous Proteins*, Academic Press, Inc., New York, 1973.
16. G. H. Stout and L. H. Jensen, *X-ray Structure Determination, A Practical Guide*, 2nd ed., Wiley-Interscience, New York, 1989.
17. P. Corradini and I. W. Bassi, *J. Polym. Sci., Part C* **16**, 3233 (1968); see also, M. Eashoo and co-workers, *Macromol. Chem. Phys.* **195**, 2207, (1994); J. J. Ge and co-workers, *Macromolecules* **30**, 6498 (1997).
18. A. O. Frenzel and J. P. Butler, *J. Opt. Soc. Am.* **54**, 1059 (1964).
19. S. Krimm and M. I. Bank, *J. Chem. Phys.* **42**, 4059 (1965).
20. J. E. Bertie and E. Whalley, *J. Chem. Phys.* **46**, 1271 (1967).
21. R. T. Harley, W. Hayes, and J. F. Twisleton, *J. Phys. C* **6**, L167 (1973).
22. M. Kobayashi, T. Uesaka, and H. Tadokoro, *Chem. Phys. Lett.* **37**, 577 (1976).
23. H. Tadokoro, S. Seki, and I. Nitta, *Bull. Chem. Soc. Jpn.* **28**, 559 (1955).
24. H. Tadokoro, *Bull. Chem. Soc. Jpn.* **32**, 775 (1959).
25. R. Iwamoto, M. Miya, and S. Mima, *J. Polym. Sci., Polym. Phys. Ed.* **17**, 1507 (1979).
26. K. Tashiro, M. Kobayashi, and H. Tadokoro, *Ferroelectrics* **32**, 167 (1981).
27. K. Tashiro, M. Kobayashi, and H. Tadokoro, *Macromolecules* **14**, 1757 (1981).

28. A. Elliott, E. J. Ambroso, and R. B. Temple, *Nature (London)* **163**, 567 (1949).
29. H. Tadokoro and co-workers, *J. Polym. Sci.* **28**, 244 (1958).
30. H. Tadokoro, K. Tatsuka, and S. Murahashi, *J. Polym. Sci.* **59**, 413 (1962).
31. H. Arimoto, *J. Polym. Sci., Part A-2* **1**, 2283 (1964).
32. K. Imada and co-workers, *Makromol. Chem.* **83**, 113 (1965).
33. T. C. Damen, S. P. S. Porto, and B. Tell, *Phys. Rev.* **142**, 570 (1966).
34. K. Tashiro, M. Kobayoshi, and H. Tadokoro, *Polym. Bull.* **1**, 61 (1978).
35. A. P. Yundt, *Tappi J.* **34**, 89 (1951).
36. W. Schlesinger and H. M. Leeper, *J. Polym. Sci.* **11**, 203 (1953).
37. A. Keller and J. R. S. Waring, *J. Polym. Sci.* **17**, 447 (1955).
38. R. Jaccodine, *Nature* **176**, 305 (1955).
39. A. Keller, *Philos. Mag.* **2**, 1171 (1957).
40. P. H. Till Jr., *J. Polym. Sci.* **24**, 301 (1957).
41. E. W. Fischer, *Z. Naturforsch., A: phys. Sci.* **12**, 753 (1957).
42. K. Kobayashi, *Kagaku (Chem.)* **8**(special issue), 203 (1962).
43. B. Mutaftschiev, ed., in Interfacial Aspects of Phase transformations, Proceeding of the NATO Advanced Study Institute, D. Reidel Publishing Company, Dordrecht, the Netherlands, 1982.
44. K. Armitstead and G. Goldbeck-Wood, *Adv. Polym. Sci.* **100**, 221 (1992).
45. A. Keller and S. Z. D. Cheng, *Polymer* **39**, 4461 (1998).
46. S. Z. D. Cheng and A. Keller, *Annu. Rev. Mater. Sci.* **28**, 533 (1998).
47. A. Keller, *Polym. Cryst., Rep. Prog. Phys.* **31**, 623 (1968).
48. J. Chen and co-workers, *J. Polym. Sci., Polym. Phys. Ed.* **33**, 1851 (1995).
49. J.-C. Wittmann and B. Lotz, *J. Polym. Sci., Polym. Phys. Ed.* **23**, 205 (1985).
50. B. Lotz and co-workers, *Kolloid Z. Z. Polym.* **209**, 115 (1966).
51. J. A. Sauer, D. R. Morrow, and G. C. Richardson, *J. Appl. Phys.* **36**, 3017 (1965).
52. B. Lotz and co-workers, *Polymer* **32**, 2902 (1991).
53. P. H. Geil, *Polymer Single Crystals*, Wiley-Interscience, New York, 1963.
54. A. J. Kovacs and A. Gonthier, *Colloid Polym. Sci.* **250**, 530 (1972).
55. A. J. Kovacs, A. Gonthier, and C. Straupe, *J. Polym. Sci., Polym. Symp.* **50**, 283 (1975).
56. A. J. Kovacs and C. Straupe, *Faraday Discuss. Chem. Soc.* **68**, 225 (1979).
57. S. Z. D. Cheng and co-workers, *J. Polym. Sci., Polym. Phys. Ed.* **29**, 287 (1991).
58. S. Z. D. Cheng and co-workers, *J. Polym. Sci., Polym. Phys. Ed.* **29**, 299 (1991).
59. H. D. Keith and co-workers, *Macromolecules* **22**, 2230 (1989).
60. A. Toda, *Colloid. Polym. Sci.* **270**, 667 (1992).
61. A. Toda and A. Keller, *Colloid. Polym. Sci.* **271**, 328 (1993).
62. B. Lotz, A. J. Lovinger, and R. E. Cais, *Macromolecules* **21**, 2375 (1988).
63. A. J. Lovinger and co-workers, *Macromolecules* **26**, 3494 (1993).
64. A. J. Lovinger, B. Lotz, and D. D. Davis, *Polymer* **31**, 2253 (1990).
65. A. J. Lovinger, D. D. Davis, and B. Lotz, *Macromolecules* **24**, 552 (1991).
66. Z. Bu and co-workers, *Macromolecules* **29**, 6575 (1996).
67. W. Zhou and co-workers, *Macromolecules* **33**, 6861 (2000).
68. R. M. Briber and F. A. Khoury, *J. Polym. Sci., Polym. Phys. Ed.* **31**, 1253 (1993).
69. A. Toda, T. Arita, and M. Hikosaka, *Polymer* **42**, 2223 (2001).
70. A. Toda, *Single Crystal Growth of PVDF*, Private communication.
71. H. D. Keith, *J. Polym. Sci., Part A* **2**, 4339 (1964).
72. H. D. Keith and F. J. Padden Jr., *J. Polym. Sci., Polym. Phys. Ed.* **25**, 2371 (1987).
73. A. J. Lovinger, S. D. Hudson, and D. D. Davis, *Macromolecules* **25**, 1752 (1992).
74. R. M. Ho and co-workers, *Macromolecules* **27**, 2136 (1994).
75. I. A. M. al Raheil, R. H. Olley, and D. C. Bassett, *Polymer* **29**, 1539 (1988).
76. J. A. Di Corleto and D. C. Bassett, *Polymer* **31**, 1971 (1990).
77. D. Patel and D. C. Bassett, *Proc. R. Soc. London, Ser. A.* **445**, 577 (1994).

78. P. H. Geil, N. K. J. Symons, and R. G. Scott, *J. Appl. Phys.* **30**, 1516 (1959).
79. D. C. Bassett, F. R. Dammont, and R. Salovey, *Polymer* **5**, 579 (1964).
80. H. D. Keith and F. J. Padden Jr., *Polymer* **27**, 1463 (1986).
81. F. Khoury, *Mechanisms of Polymer Spherulite Formation*, Private communication.
82. E. Sauter, *Z. Phys. Chem. B* **18**, 417 (1932).
83. D. C. Bassett and B. Turner, *Philos. Mag.* **29**, 925 (1974).
84. B. Wunderlich and L. Melillo, *Makromol. Chem.* **118**, 250 (1968).
85. M. Hikosaka and co-workers, *J. Macromol. Sci., B: Phys.* **31**, 87 (1992).
86. L. Melillo and B. Wunderlich, *Kolloid Z. Z. Polym.* **250**, 417 (1972).
87. K. H. Storks, *J. Am. Chem. Soc.* **60**, 1753 (1938).
88. J.-C. Wittmann and B. Lotz, *Makromol. Rapid Commun.* **3**, 733 (1982).
89. D. H. Reneker, *J. Polym. Sci., Part A* **3**, 1069 (1965).
90. T. Kajiyama, I. Ohki, and A. Takahara, *Macromolecules* **28**, 4768 (1995).
91. J. Chen and co-workers, *J. Polym. Sci., Polym. Phys. Ed.* **33**, 1851 (1995).
92. F. Khoury, *Aspect Ratio Changes in Solution Grown PE Single Crystal with Respect to Crystallization Temperatures and Different Solvents*, Private communication.
93. S. J. Organ and A. Keller, *J. Mater. Sci.* **20**, 1571 (1985); *J. Mater. Sci.* **20**, 1586 (1985); *J. Mater. Sci.* **20**, 1602 (1985).
94. A. Toda, *Faraday Discuss.* **95**, 129 (1993).
95. Y. Nakagawa and co-workers, *Jpn. J. Appl. Phys.* **33**, 3771 (1994).
96. C. Mathieu and co-workers, *Polymer* **41**, 7241 (2000).
97. B. Lotz and J.-C. Wittmann, *J. Polym. Sci., Polym. Phys. Ed.* **24**, 1541 (1986).
98. S. Bruckner and S. V. Meille, *Nature* **340**, 455 (1989).
99. B. Lotz, J.-C. Wittmann, and A. J. Lovinger, *Polymer* **37**, 4979 (1996).
100. B. Lotz and co-workers, *Polymer* **32**, 2902 (1991).
101. W. Zhou and S. Z. D. Cheng, unpublished results.
102. J. Liu and co-workers, *Macromolecules* **27**, 989 (1994).
103. S. Yan and co-workers, *Polymer* **41**, 2613 (2000).
104. J.-C. Wittmann and B. Lotz, *Prog. Polym. Sci.* **15**, 909 (1990).
105. F. Khoury and J. D. Barnes, *J. Res. Natl. Bur. Stand., A: Phys. Chem.* **76A**, 225 (1972).
106. F. Khoury and J. D. Barnes, *J. Res. Natl. Bur. Stand., A: Phys. Chem.* **78A**, 363 (1974).
107. F. Khoury and J. D. Barnes, *J. Res. Natl. Bur. Stand., A: Phys. Chem.* **78A**, 95 (1974).
108. P. H. Geil, *J. Polym. Sci.* **44**, 449 (1960).
109. V. F. Holland and R. L. Miller, *J. Appl. Phys.* **35**, 3241 (1964).
110. I. Saracovan and co-workers, *Macromolecules* **32**, 717 (1999).
111. A. S. Vaughan, *J. Mater. Sci.* **28**, 1805 (1993).
112. B. Lotz and co-workers, *C. R. Acad. Sci. IIC* **1**, 609 (1998).
113. G. Toulouse, *Commun. Phys.* **2**, 115 (1977).
114. I. Syozi, C. Domb, and M. S. Green, eds., *Phase Transitions and Critical Phenomena*, Academic Press, Inc., London, 1972, p. 269.
115. B. Lotz, S. Kopp, and D. L. Dorset, *C. R. Acad. Sci. (Paris)* **319**, 187 (1994).
116. L. Cartier, T. Okihara, and B. Lotz, *Macromolecules* **30**, 6313 (1997).
117. D. L. Dorset and co-workers, *Polymer* **39**, 6331 (1998).
118. T. Okihara and co-workers, *Polymer* **40**, 1 (1998).
119. L. Cartier, N. Spassky, and B. Lotz, *Macromolecules* **31**, 3040 (1998).
120. L. Cartier and B. Lotz, *Macromolecules* **31**, 3049 (1998).
121. L. Cartier, T. Okihara, and B. Lotz, *Macromolecules* **31**, 3303 (1998).
122. F. Livolant and Y. Bouligand, *Chromosoma* **80**, 97 (1980).
123. C. Chothia, *J. Mol. Biol.* **75**, 295 (1973).
124. M. Kleman, *Rep. Prog. Phys.* **52**, 555 (1989).
125. M. Kleman, *Adv. Phys.* **38**, 605 (1989).
126. F. Livolant and Y. Bouligand, *J. Phys.* **47**, 1813 (1986).
127. F. Rybnikar and P. H. Geil, *Biopolymers* **11**, 271 (1972).

128. E. T. Samulski and A. V. Tobolsky, *Liq. Cryst. Plast. Cryst.* **1**, 175 (1975).
129. B. Lotz and co-workers, *J. Mol. Biol.* **156**, 345 (1982).
130. C. Y. Li and co-workers, *Phys. Rev. Lett.* **83**, 4558 (1999).
131. C. Y. Li and co-workers, *J. Am. Chem. Soc.* **122**, 72 (2000).
132. C. Y. Li and co-workers, *Phys. Rev. B* **60**, 12675 (1999).
133. C. Y. Li and co-workers, *Macromolecules* **32**, 524 (1999).
134. C. Y. Li and co-workers, *Polymer* **41**, 8953 (2000).
135. B. Wunderlich, *Ind. Eng. Chem.* **56**, 18 (1964).
136. H. D. Keith and F. J. Padden Jr., *J. Appl. Phys.* **34**, 2409 (1963).
137. H. D. Keith and F. J. Padden Jr., *J. Appl. Phys.* **35**, 1270 (1964).
138. F. Khoury, *J. Res. Natl. Bur. Stand.* **70A**, 29 (1966).
139. B. Wang and co-workers, *Polymer* **42**, 7171 (2001).
140. W. Ruland, *Acta Cryst.* **14**, 1180 (1961).
141. C. R. Desper and R. S. Stein, *J. Polym. Sci., Part B* **5**, 893 (1967).
142. W. Ruland and A. Dewaelheyns, *J. Sci. Instrum.* **44**, 236 (1967)
143. W. Ruland, *Textiltechnik* **18**(2), 59 (1966).
144. J. W. Turley, *X-ray Diffraction Patterns of Polymers*, The Dow Chemical Company, Midland, Mich.
145. L. E. Alexander, *X-ray Diffraction Methods in Polymer Science*, Wiley-Interscience, New York, 1969.
146. B. Wunderlich, *Macromolecular Physics, Crystal Melting*, Vol. **3**, Academic Press Inc., New York, 1980.
147. B. Wunderlich, *Thermal Analysis*, Academic Press, New York, 1991.
148. H. Suzuki, J. Grebowicz, and B. Wunderlich, *Makromol. Chem.* **189**, 1109 (1985).
149. H. Suzuki, J. Grebowicz, and B. Wunderlich, *Br. Polym. J.* **17**, 1 (1985).
150. S. Z. D. Cheng, M.-Y. Cao, and B. Wunderlich, *Macromolecules* **19**, 1868 (1986).
151. S. Z. D. Cheng and B. Wunderlich, *Macromolecules* **20**, 1630 (1987).
152. S. Z. D. Cheng, Z. Wu, and B. Wunderlich, *Macromolecules* **20**, 2802 (1987).
153. S. Z. D. Cheng and B. Wunderlich, *Macromolecules* **21**, 789 (1988).
154. S. Z. D. Cheng, R. Pan, and B. Wunderlich, *Makromol. Chem.* **189**, 2243 (1988).
155. S. Z. D. Cheng and co-workers, *J. Polym. Sci., Polym. Phys. Ed.* **28**, 655 (1990).
156. G. R. Strobl and W. J. K. Hagedorn, *J. Polym. Sci., Polym. Phys. Ed.* **16**, 1181 (1978).
157. I. G. Voigt-Martin and co-workers, *J. Polym. Sci., Polym. Phys. Ed.* **27**, 957 (1989).
158. I. G. Voigt-Martin and L. Mandelkern, *J. Polym. Sci., Polym. Phys. Ed.* **27**, 987 (1989).
159. L. Mandelkern, R. G. Alamo, and M. A. Kennedy, *Macromolecules* **23**, 4721 (1990).
160. R. G. Alamo, B. D. Viers, and L. Mandelkern, *Macromolecules* **26**, 5740 (1993).
161. N. Striberk and co-workers, *Macromolecules* **28** 5029 (1995).
162. R. Kitamaru and co-workers, *Macromolecules* **29**, 6847 (1996).
163. S.-F. Lau, H. Suzuki, and B. Wunderlich, *J. Polym. Sci., Polym. Phys. Ed.* **22**, 379 (1984).
164. J. Grebowicz, S.-F. Lau, and B. Wunderlich, *J. Polym. Sci., Polym. Symp.* **71**, 19 (1984).
165. J. Menzel and B. Wunderlich, *J. Polym. Sci., Polym. Lett. Ed.* **19**, 261 (1981).
166. S. Z. D. Cheng, unpublished data.
167. B. Crist, C. J. Fisher, and P. R. Howard, *Macromolecules* **22**, 1709 (1989).
168. H. Swei, B. Crist, and S. H. Carr, *Polymer* **32** 1440 (1991).
169. M. D. Failla and L. Mandelkern, *Macromolecules* **26**, 7167 (1993).
170. J. Rhee and B. Crist, *J. Polym. Sci., Polym. Phys. Ed.* **32**, 159 (1994).
171. M. A. Kennedy, A. J. Peacock, and L. Mandelkern, *Macromolecules* **27**, 5297 (1994).
172. Z. Zhou, N. Brown, and B. Crist, *J. Polym. Sci., Polym. Phys. Ed.* **33**, 1047 (1995).
173. M. A. Kennedy and co-workers, *Macromolecules* **28**, 1407 (1995).
174. J. T. Graham, R. G. Alamo, and L. Mandelkern, *J. Polym. Sci., Polym. Phys. Ed.* **35**, 213 (1997).
175. A. J. Peacock and co-workers, *J. Mater. Sci.* **33**, 2255 (1998).

176. J. Janzen, *Polym. Eng. Sci.* **17**, 1242 (1992).
177. I. Sakurada and K. Kaji, *J. Polym. Sci., Part C* **31**, 57 (1970).
178. J. Clements, R. Jajeways, and I. M. Ward, *Polymer* **19**, 639 (1978).
179. B. Brew and co-workers, *J. Polym. Sci., Polym. Phys. Ed.* **17**, 351 (1979).
180. G. Wu, K. Tashiro, and M. Kobayashi, *Macromolecules* **22**, 758 (1989).
181. S. Jungnitz, R. Jakeways, and I. M. Ward, *Polymer* **27**, 1651 (1988).
182. K. Tashiro, G. Wu, and M. Kobayashi, *Polymer* **29**, 1768 (1988).
183. K. Tashiro, M. Kobayashi, and H. Tadokoro, *Macromolecules* **10**, 412 (1977).
184. K. Tashiro, M. Kobayashi, and H. Tadokoro, *Macromolecules* **11**, 908 (1978).
185. Z. Wu and co-workers, *J. Polym. Sci., Polym. Phys. Ed.* **28**, 2565 (1990).

CHRISTOPHER Y. LI
Drexel University
STEPHEN Z. D. CHENG
The University of Akron

SHAPE-MEMORY POLYMERS.

See Volume 4.

SILANE COUPLING AGENTS

Introduction

The term *silane coupling agent* generally applies to silicon-containing species capable of forming chemical linkages between dissimilar materials, especially in reinforced polymer composites. The materials to be linked are often organic polymers and inorganic fillers, though silane coupling agents can also be useful with other kinds of fillers and polymers. Small amounts of silane coupling agents, used at an interface, can greatly improve the mechanical properties of composite materials. They may also be used on formed parts as coatings to alter the surface properties of materials, or copolymerized into organic polymers. Silane coupling agents are found in a broad range of applications as varied as metal coatings, dental materials, and contact lenses. The present article is focused primarily on their use in polymer composites, where they are used as interfacial modifiers.

In their most common form, polymer-reinforced composite materials consist of an organic matrix and inorganic filler (here the term filler will be used in a general sense, and can include reinforcing fibers). The polymer typically forms the continuous phase that protects the filler from environmental damage and holds the composite together. The filler reinforces (improves the strength and modulus) or simply takes up space without degrading the properties of the polymer. The transfer of stresses between the fiber and filler is critical in achieving reinforcement. Binary mixtures of polymer and filler can have poor mechanical properties because of poor interactions between them, which result in weak interfaces. These interfaces are often the source of failure in composites through delamination. Failure at interfaces is especially acute in the presence of small-molecule chemical species, such as water.

Encyclopedia of Polymer Science and Technology. Copyright John Wiley & Sons, Inc. All rights reserved.

Given the widespread use of silane coupling agents, there have been a number of papers and reviews that have focussed on their chemistry, application, and effects. The cornerstone of these is the book by Plueddemann (1), which discusses most of the aspects of coupling agent application. A few symposium-based books have also been produced (2), as well as a few reviews (3,4). As Plueddemann points out, in many cases, with the use of the proper coupling agent under the proper conditions, the failure in composite materials no longer takes place at the interfaces between the dissimilar materials.

Chemical Composition and Reactions

Silane coupling agents generally have hydrolyzable and organofunctional ends. The general structure of the coupling agents can be represented as

$$X_3SiR$$

where the X represents the hydrolyzable groups that are typically chloro, ethoxy, or methoxy groups. The organo, R, group can have a variety of functionalities chosen to meet the requirements of the polymer. Chlorosilanes are very reactive; the liquids and vapors are extremely irritating to the body. There can be 1–3 X groups and the number of these can alter the way the silane bonds to an oxide surface or to other coupling agents. When the number of X groups are less than three, the remaining groups are replaced by additional (usually nonfunctional) alkyl groups such as methyl. Generally, coupling agents with three X groups are used in composite materials because of their greater stability on surfaces, but there are clearly other applications where it may be desirable to use one or two hydrolyzable X groups. In this report, we will focus on materials with three X groups. This trifunctionality is common for most coupling agents used in composites.

It should be noted that there are several generally accepted methods of naming silane coupling agents. No attempt will be made here to apply a systematic approach to the nomenclature (see SILICONES). A few common coupling agents are listed in Table 1 along with their Chemical Abstracts Registry Numbers and chemical formulas. For the species shown, the main differences in the coupling agents are the organo-functional groups. A variety of coupling agent species with different organo groups is available from commercial sources.

The choice of the coupling agent is typically based on the surface and the polymer used. It is of utmost importance that the organofunctional group is typically matched to the polymer. Tables of suggested coupling agents proposed for different resins are found in the literature from manufacturers (5) and will not be reproduced here.

The first step in the application of a silane coupling agent is the hydrolysis of the X groups. Generally water is required and the by-products are HCl or alcohol. The water for hydrolysis, which may be added intentionally, can be found as trace amounts in organic solvents, or can be located on the surface of the fillers. The hydrolysis of the alkyl groups may be acid- or base-catalyzed. In pH-neutral solutions, the reactions of alkoxysilanes can be quite slow. For many of the coupling agents, hydrolysis proceeds with the addition of the coupling agent

Table 1. Representative Silane Coupling Agents

Common name	CAS Registry Number	Formula
3-Aminopropyltriethoxysilane (APS)	919-30-2	$(CH_3CH_2O)_3Si(CH_2)_3NH_2$
4-Aminobutyltriethoxysilane (ABS)	3069-30-5	$(CH_3CH_2O)_3Si(CH_2)_4NH_2$
N-2-Aminoethyl-3-aminopropyltrimethoxysilane (AEAPS)	1760-24-3	$(CH_3O)_3Si(CH_2)_3NHCH_2CH_2NH_2$
Vinyltrimethoxysilane (VS)	2768-02-7	$(CH_3O)_3SiCH{=}CH_2$
3-Methacryloxypropyltrimethoxysilane (MPMS)	4369-14-6	$(CH_3O)_3SiCH_2CH_2CH_2OC(=O)CH{=}CH_2$
3-Acryloxypropyltrimethoxysilane (APMS)	160716-45-0	$(CH_3O)_3SiCH_2CH_2CH_2OC(=O)CH{=}CH_2$
3-Glycidoxypropyltrimethoxysilane (GPS)	2530-83-8	$(CH_3O)_3SiCH_2CH_2CH_2OCH_2CH(O)CH_2$

to a solvent (such as acetone) with water and acid (or base). In principle, there are three separate rate constants, one for each of the three X groups. The rates of hydrolysis can be followed by spectroscopic techniques such as NMR or FTIR. Many of the hydrolysis experiments have been reviewed with a special emphasis on how experimental conditions affect the rates of hydrolysis (6,7). Some coupling agents have functional groups that self-catalyze the hydrolysis, such as the amine group in 3-aminopropyltriethoxysilane (APS). Amine-functional coupling agents hydrolyze relatively quickly in the presence of water without the addition of acid or base.

Following hydrolysis, and in some cases competing with it, is the condensation of the silanols with other silanols or surface species. This typically occurs with the loss of water. Subsequent drying of the material may drive the reaction to completion. The ultimate condensed product of the coupling agents would have a formula $RSiO_{3/2}$. These compounds are called silsesquioxanes (8) and are highly cross-linked amorphous polymers. An idealized schematic representation of the resulting structures is shown in Figure 1 for the coupling agent 3-aminopropyltriethoxysilane. There are at least three separate hydrolysis reactions (one for each X group) and the condensation of the hydroxyl groups can occur before all three of the X groups are hydrolyzed. Thus, the kinetic scheme for hydrolysis and condensation is very complicated and is often described, not in terms of the individual species, but in terms of the total number of hydrolyzed or condensed groups.

Surface Reactions/Interactions

An additional level of complexity is encountered when silanes are added in the presence of solid surfaces. Hydrolyzed or unhydrolyzed coupling agents will interact with a variety of oxide surfaces. Even in the case of metal fillers, an oxide layer is often found at the surface. The presence of water at these interfaces may

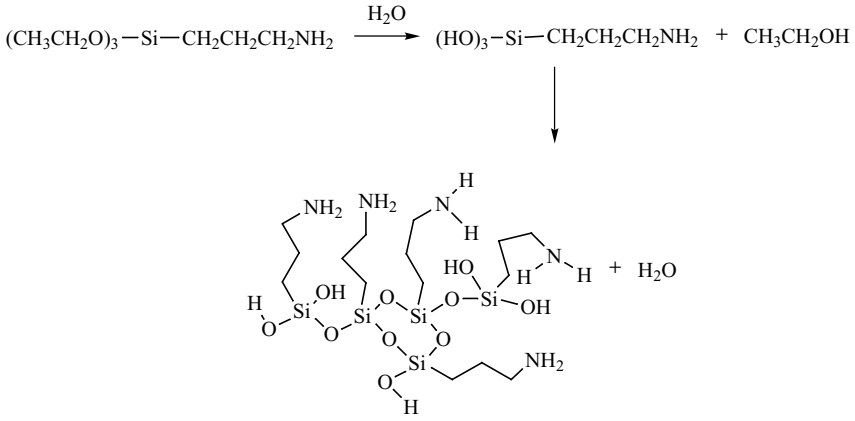

Fig. 1. Idealized representation of the hydrolysis and condensation of 3-aminopropyltriethoxysilane.

be sufficient to hydrolyze the coupling agents. Thus, the addition of "extra" water may not be necessary. Unless the concentration of the coupling agent in solution is very low, the adsorbed species will likely be small oligomers rather than monomers. There will be an attraction due to hydrogen bonding of oxide surfaces and the coupling agent's silanol groups. The organo group may also be attracted to the oxide surfaces. For example, APS appears to attach itself to oxide surfaces (alumina and silica), first via the amine group, then the molecule flips, allowing the silanols of the coupling agent to react (9). Presumably, this is why on iron, fresh films of APS can be rinsed off unless they are aged in some way (10). Generally, some kind of aging or heat treatment is required to fix the coupling agent to the surface. An idealized example of the ultimate surface structures formed is shown in Figure 2. It should be noted that the geometry of the surface is such that it is virtually impossible for all three of the SiO— bonds on the coupling agent to be attached directly to the silica. Bonding to other coupling agents or dangling hydroxyls is likely. There may be a mixture of physisorbed and chemisorbed species in thicker coupling agent layers.

The amount of coupling agent adsorbed on surfaces depends on the conditions present. Under highly controlled conditions and limited hydrolysis from very dilute solutions, "monolayers" may be produced (11). For 3-methacryloxypropyltrimethoxysilane (MPMS), it has been estimated that the surface area for the adsorbed molecule, lying flat on the surface and end adsorbed (functional group extending away from the surface), amounted to 55 and 24 Å^2,

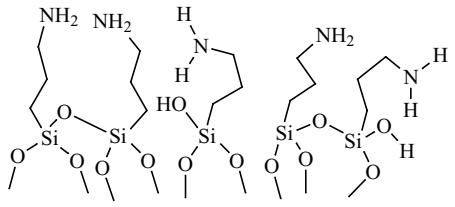

Fig. 2. Idealized structures of 3-aminopropyltriethoxysilane (APS) on a silica surface.

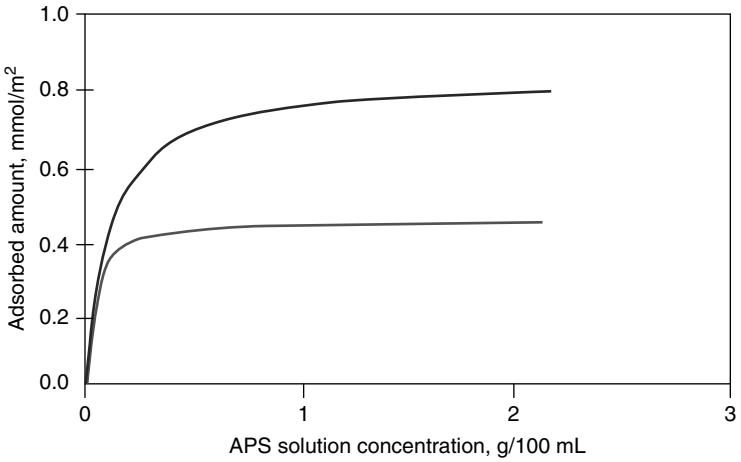

Fig. 3. Adsorption isotherms for 3-aminopropyltriethoxysilane in acetone/water mixtures. The two isotherms shown are indicative of the extremes in the measurements made at two different times on the same system.

respectively (12). Occupied areas for other coupling agents with similar structures are similar. For typical treatment conditions, the amount of coupling agent adsorbed depends on the state of the coupling agent in solution. Because of the complexity of the reactions and reaction conditions, this state is often difficult to control with great precision.

An example of an adsorption isotherm for solutions with oligomers present is shown in Figure 3 for APS adsorbed onto silica from acetone/water mixtures after washing. The two isotherms shown represent the extremes from a large number of replicate runs on the same system (see ADSORPTION) (7). Interestingly, the amount adsorbed does flatten out and has the shape of a typical polymer adsorption isotherm. The adsorption isotherm measurements had good precision within a single experiment, but maximum adsorbed amounts varied from run to run, possibly because of different levels of hydrolysis and condensation within the coupling agent solution. It was estimated that on average, about 0.65 mmol/100 m^2 of APS was adsorbed. The individual experimental results ranged between 0.4 and 0.8 mmol/100 m^2. The average amount corresponds to an area of about 25 $Å^2$ per coupling agent molecule, which is consistent with the coupling agent molecule standing on end. It is also roughly what one expects for one coupling agent molecule per surface silanol.

Silane coupling agents may also be directly used as coatings for a variety of applications (10,13,14). Coupling agents in coatings formulations can be used in either solvent- or water-borne systems, such as clear coats for automotive applications (13,15). Formulations can also be used to impart scratch and abrasion resistance to softer materials such as polycarbonate and poly(methyl methacrylate) (PMMA) (14). Applications of this type allow the use of materials whose bulk properties are desirable because the surface properties can be fine-tuned.

Often glass fiber or fabric can be treated in a continuous process by passing the glass through a solution (usually less than a few percent) of the coupling agent in a suitable solvent. The coated substrate is then heated and the coating dried and

reacted on the surface. This process normally puts much more coupling agent (an order of magnitude or more) on the surface than the "oligomeric monolayers" mentioned above. The equivalent of several monolayers may be required for optimal mechanical behavior of the resulting composites (see Mechanisms of Reinforcement). The multilayers (interphase) are likely to be fairly disorganized—more like highly cross-linked polymers than separate highly organized layers, though organized layers can be built with sequential deposition.

Analysis of Coupling Agents

The condensation of silanes on oxide surfaces occurs with the loss of water. The reactions, in principle, may be monitored by thermal gravimetric analysis (TGA) or spectroscopic means. The same technique can also assess the thermal stability of the resulting interphase. A TGA trace for 3-acryloxypropyltrimethoxysilane (APMS) condensed onto silica is shown in Figure 4. This analysis was done following an initial heat treatment to remove water and more fully condense the silanols. With a heating rate of 10°C/min, the organic portion of the coupling agent volatilizes off the surface between 300 and 600°C. At moderate temperatures, such as 100°C, the coupling agents are relatively stable. The SiO portions of the coupling agent molecule, along with the rest of the silica, remain intact on the surface (16). Knowledge of the beginning and ending weights provides a reasonable measurement of the amount of coupling agent bound to the surface. In the example below, the mass of coupling agent adsorbed is about 17% of the mass of the treated silica. With the knowledge of the specific surface area of the silica, the amount of coupling agent adsorbed corresponds to the equivalent of 4.5 monolayers in this case.

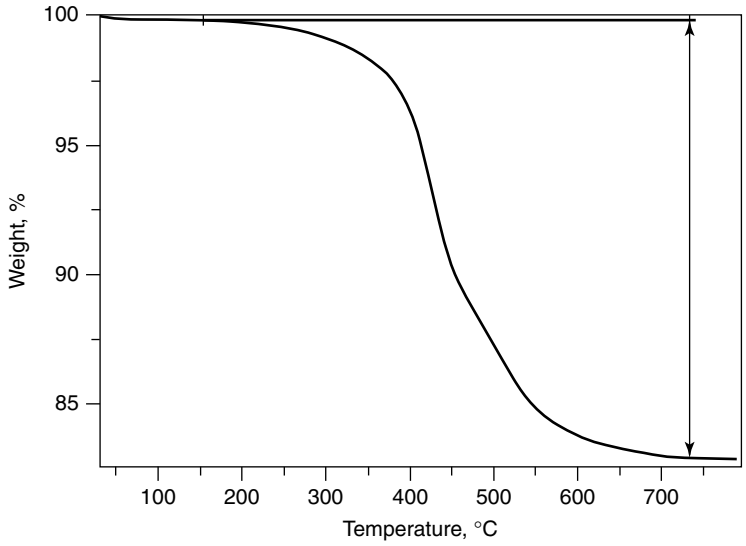

Fig. 4. Thermogravimetric analysis of surface-adsorbed 3-acryloxypropyltriethoxysilane on silica.

Although many forms of surface spectroscopy may be used for the characterization of the reactions of silanols, IR and NMR are perhaps the most informative, but are not reviewed here (3,4,17). Analyses of IR spectra provide a sensitive way of probing the state of the coupling agents from solution to on the surface. FTIR provides several advantages, including speed of measurement and high throughput. It also provides several different ways of probing the interfaces, such as transmission, diffuse reflectance, or internal reflectance. Some of the details that these studies have uncovered can be illustrated for APS. As early as the 1980s (18), FTIR was shown to identify the presence of internal hydrogen bonding, ring structures, and oligomers of this coupling agent in solution. On the surface, this material may also form ring structures, bicarbonate salts, and other species (11,19). These studies have been used to guide researchers in determining appropriate processing conditions.

NMR can be very informative relative to the details of the chemical species produced in solution and on the surfaces. Proton NMR has been used to follow hydrolysis reactions. It is especially easy to follow the alcohol produced. Proton NMR is not as useful in determining the exact nature of the species present during condensation, but silicon-29 NMR is, and it can provide information on the number of different groups attached to the silicon atom. The disadvantage is that the silicon-29 nucleus is not very abundant (4.7%), and so most of the silicon atoms are not NMR-active. For a model compound such as methyltrimethoxysilane, it is possible to identify all the different substituents on the silicon atoms at the early stages of hydrolysis and condensation. The relative amounts of the different components were shown to fit to a statistical model for hydrolysis (20).

Solid-state silicon NMR has also been a significant aid in the understanding of the reactions of the coupling agent with the surface of the filler. These investigations have been aided by detailed studies of the fillers alone (21). A number of studies have focused on the reactions with surface species and yield a detailed view of the species present, similar to that done for solutions, though with less resolution (22,23). More specifically, coupling agents with a single R group and three oxygen groups would be given the symbol T^i, with the superscript i denoting the number of O—Si species attached to the silicon in question. Thus, a T^3 species would represent a fully condensed silane. Under conditions of full hydrolysis, the other substituents would be expected to be hydroxyls. A silicon species with four oxygen atoms attached would be considered a Q^i species. Thus, a Q^4 would be a fully condensed silicon with no organic substituent.

The silicon-29 NMR spectra is shown in Figure 5 for adsorbed and heat-treated APMS on a silica surface (16). The spectra were taken with magic angle spinning and cross-polarization (CP-MAS). The clear separation of the T (-50 to -75 ppm) and Q (-90 to -115 ppm) groups is obvious in the spectra. For the 100°C heat-treated material, the coupling agent spectrum is dominated by the T^3 and T^2 species, showing a high degree of condensation. The Q region of the spectrum consists primarily of Q^3 and Q^4 species. It should be noted that the cross-polarization from protons increases the intensity of the Q^3 (surface hydroxyl containing) silicon atoms more than the Q^4 species. Upon heat treatment to 600°C, the Si-29 NMR spectrum shows the disappearance of the T resonances, and all of the silicon has been converted to Q species. The agreement between silicon NMR and gravimetric analysis is very good.

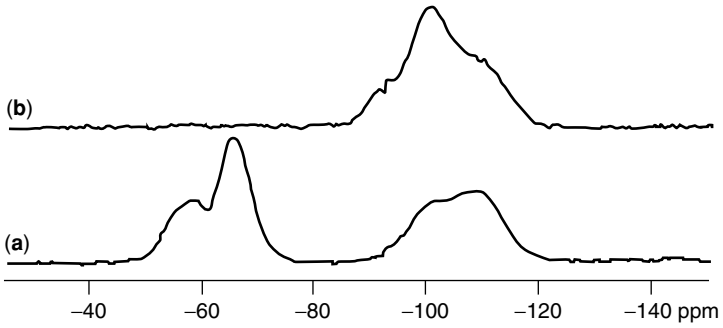

Fig. 5. Silicon-29 NMR spectra of 3-acryloxypropyltrimethoxysilane on silica (**a**) adsorbed and heated to 100°C and (**b**) after heating the sample in (**a**) to 600°C.

Mechanisms of Reinforcement

In principle, silane coupling agents can influence the mechanical properties of composites in several ways (see REINFORCEMENT). Without question, the adsorption and reaction of a silane with the surface changes the properties of the interface (see SURFACE PROPERTIES). The surface energies of inorganic fillers and polymers are likely to be rather different. A comparison of critical surface tensions for some polymers and coupling agent films (1,24) shows that the functional groups can vary the surface tension from very low (similar to polytetrafluoroethylene) to rather high (close to glass)(24). Indeed, the variation of surface energies and zeta potential with different treatments of the same coupling agent can even be large(25). The use of an appropriate coupling agent should allow the modification of a surface so that an organic polymer will wet it. In principle, this should ensure good contact between the polymer and filler at the interface (at least as far as the preparation of the composite is concerned). In addition, the choice of coupling agents with low surface tensions may help exclude high surface tension species (eg water from the interface). In spite of the matching of the surface tension between the polymer and the silane film, Plueddemann (26) has shown that when the composites were exposed to water, only reactive silanes gave high strengths in polyester–glass laminates. It seems reasonable to conclude that the presence of chemical bonds is very important for enhanced wet strengths in composites. The binding energy associated with chemical bonds, much greater than other interactions (eg van der Waals forces), is undoubtedly responsible for this effect.

It should be noted that surface energy and interactions can still play crucial roles in the production of composites. Many manufactures sell fibers and fillers with a variety of "sizings" deposited on the surfaces for compatibilization with resins and the protection of the fibers during production and handling. These sizings often contain silane coupling agents, and may also contain other chemical species. Discussion with the manufacturers or careful reading of their literature is important for selecting the proper filler with the proper surface treatment for a given application and polymer. Good dispersion of fibers is critical for effective reinforcement and this can be aided by the appropriate surface treatment.

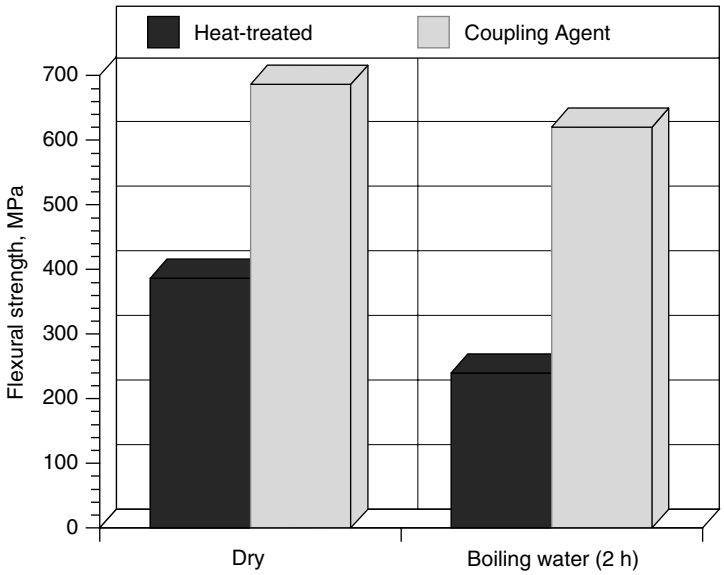

Fig. 6. Flexural strength of heat-treated and methacrylate coupling agent treated glass-fiber/polyester composites. The 2-h boiling-water test approximates longer-term water exposure (1).

In many cases, the mechanical properties of composites are compared for treated and untreated fibers. Generally, the preparation of an "untreated" fiber requires the removal of the sizing. Heat treatment is the most practical method of obtaining a bare fiber, especially with glass. Heat treatment can be followed with thermogravimetric analysis, which is also a convenient way of estimating how much coupling agent was adsorbed onto the surface, as mentioned previously.

An example of the effect of coupling agents in a polymer composite is illustrated in Figure 6, where the strength of a glass-fiber-reinforced polyester composite, with and without a coupling agent, is compared (1). Similar results can be found for other mechanical properties and other composite systems as well. It needs to be noted that the actual values of the strength are dependent on a number of parameters such as the amount of coupling agent and fiber geometry/content. The changes in mechanical properties are also especially dependent on the nature of the coupling agent. In fact, reductions in strength can be found with certain coupling agents (1). In any case, with the appropriate selection of a coupling agent, the main points are clear. Significant improvements can be found in dry strengths, with even more dramatic improvements found under conditions of water ingress. Clearly, the coupling-agent is able to withstand the effects of water.

Coupling agents are clearly effective at modifying the interface between the polymer and fillers. As noted by Plueddemann (1), with silane coupling agents, the failure mode of some composites can be altered so that failure no longer occurs at the interface. An example of the reinforcement of the interfaces is shown in Figure 7 for the fracture surfaces of a composite made of 3-AFMS-treated fibers with PMMA (27). The use of the coupling-agent increases the strength of the

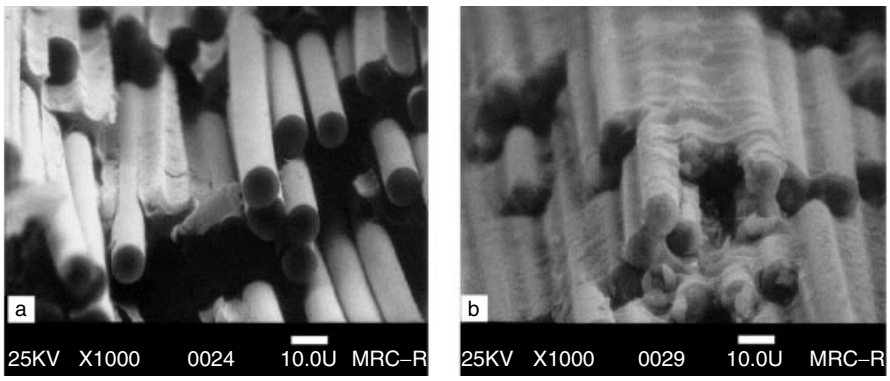

Fig. 7. Fracture surface for glass-fiber-reinforced PMMA for (**A**) untreated fibers and (**B**) 3-acryloxypropyltrimethoxysilane treated fibers.

composite. The fracture surface for the heat-treated fiber shows that the resin and fiber separated at the interface between them, resulting in the exposure of bare fiber. The fiber was pulled out of the resin. In contrast, the coupling agent-treated fiber shows a rough interface, with resin attached to the fiber, and the implication is that fracture occurred within the resin phase.

As previously noted in this section, the presence of a chemical bond is virtually required for improvements in mechanical properties. It is perhaps the most important requirement for enhancement of properties. One factor, not always recognized as important, is the mechanical properties of the adsorbed coupling agent layer. In most fiber and filler treatments, the coupling agent layers are the equivalent of many monolayers thick. They can be considered as an interphase. The mechanical properties of the interphase need to be considered in the optimization of the final properties.

The role of the physical nature of the interphase has been probed by comparing the properties of composites made with two coupling agents, APS and ABS. These two coupling agents have the same functional groups and are similar enough to have the same chemistry. NMR studies have shown that multilayers of each coupling agent on silica form an interphase that is graded in terms of mobility (28). The coupling agents bonded to or very near to the surface of the silica are more rigid than the coupling agents further away from the surface. Lower mobility correlates with a higher modulus and vice versa. Near the silica interface, both adsorbed APS and ABS behave similarly, but away from the surface, the outer layers of ABS are more mobile (lower modulus) than APS. The role that the different dynamics plays is apparent from mechanical property tests. In Figure 8, the critical energy release rate (fracture toughness) of the interphase for epoxy composites is compared. Both ABS and APS improve the properties of the composites over bare glass, but more improvement is found for APS (29). Qualitatively similar results are found for other mechanical property tests. It is believed that the APS interphase provides the best transition from the properties of the glass on one side of the interphase to that of the epoxy on the other. The ABS interphase was believed to be too flexible at the epoxy–ABS interface for optimum properties.

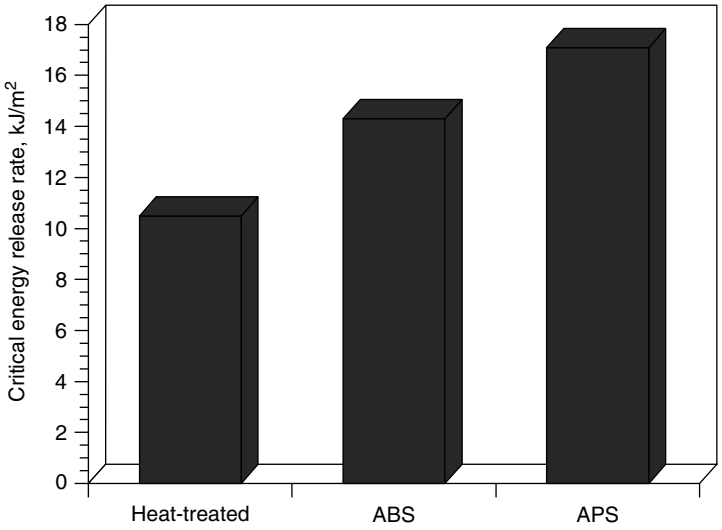

Fig. 8. Critical energy release rate (fracture toughness) of glass-fiber/epoxy composites, with the fibers being heat-treated (bare), and ABS- and APS-treated glass (29).

Application of Silanes in Advanced Materials

The silanes need not necessarily be linked to macroscopic fillers to be useful as coupling agents. For example, the fillers used do not necessarily need to be of large size. The use of hybrid materials goes back to the 1950s (15). Silane coupling agents are also useful in the production of organic/inorganic hybrid materials and some nanomaterials. In some cases, silane coupling agents can be used to functionalize nanomaterials made from different core structures.

There are a number of ways in which the coupling agent functionality can be incorporated into hybrid materials (8,14). Organic materials can be "embedded" in an inorganic matrix without chemical bonding. Interpenetrating networks may allow continuity of both species simultaneously. Covalent bonding between the two different materials on a nanometer scale can be achieved via coupling agents, which can be copolymerized or grafted with an organic polymer. Depending on the technique of integrating the dissimilar materials, property differences can be obtained in the final products.

Bridged polysilsesquioxanes are materials that have an organic moiety sandwiched between two silane functional species that can form the silsesquioxane linkages (30,31). These materials are effectively cross-linked by the inorganic moieties. The organo part can be changed readily, but is kept relatively short so that phase separation does not occur. Drying conditions and solvents can have a major effect on the porosity of the products formed, ranging from nonporous to microporous. These materials can have application in sensors, catalysts, optics, and coatings.

One final class of materials that is being increasingly considered for use in composites is that based on polyhedral oligomeric silsesquioxanes (POSS) (see HYBRID PLASTICS) (8,14,32–34). A variety of different cage structures have been discovered, but more recently the cubic structure is receiving increased attention

as its production costs are decreased. POSS molecules can be used to reinforce organic polymers with either functional or nonfunctional groups at any or all of the vertices of the cages. With the proper functionality, the POSS molecules can be incorporated into the backbone of organic polymers. With multifunctional reactive POSS species, the POSS material can also be effective as a cross-linking agent. The presence of the POSS in the polymer changes the glass-transition temperature, mechanical properties, and heat resistance. The small size of POSS means that it can be effectively dispersed in the polymer matrix.

Clearly, silicon-based building blocks are the foundation of a variety of materials. With other transition-metal species, these building blocks form a basic set of nanomaterials whose applications are still emerging (35,36).

BIBLIOGRAPHY

"Coupling Agents" in *EPSE* 2nd ed., Vol. 4, pp. 284–298, by E. P. Plueddemann, Dow Corning Corporation.

1. E. P. Plueddemann, *Silane Coupling Agents*, 2nd ed., Plenum Press, New York, 1991.
2. K. L. Mittal, ed., *Silanes and Other Coupling Agents*, VSP, Utrecht, 1992.
3. N. Suzuki and H. Ishida, *Macromol. Symp.* **108**, 19–53 (1996).
4. H. Ishida, *Polym. Compos.* **5**, 101–123 (1984).
5. B. Arkles, ed., *Silicon, Germanium, Tin and Lead Compounds, Metal Alkoxides, Diketonates and Carboxylates*, 2nd ed., Gelest, Inc., Tullytown, Pa., 1998.
6. F. D. Osterholtz and E. R. Pohl, *J. Adhes. Sci. Technol.* **6**, 127–149 (1992).
7. F. D. Blum, W. Meesiri, H. J. Kang, and J. E. Gambogi, *J. Adhes. Sci. Technol.* **5**, 479–496 (1991).
8. R. H. Baney, M. Itoh, A. Sakakibara, and T. Suzuki, *Chem. Rev.* **95**, 1409–1430 (1995).
9. C. W. Chu, D. P. Kirby, and P. D. Murphy, *J. Adhes. Sci. Technol.* **7**, 417–433 (1993).
10. W. J. van Ooij and T. Child, *CHEMTECH* **28**, 26–35 1998.
11. H. Ishida, S. Naviroj, S. K. Tripathy, J. F. Fitzgerald, and J. L. Koenig, *J. Polym. Sci., Polym. Phys. Ed.* **20**, 701–718 (1982).
12. J. D. Miller, K. P. Hoh, and H. Ishida, *Polym. Compos.* **5**, 18–28 (1984).
13. M. J. Chen, F. D. Osterholtz, E. R. Pohl, P. E. Ramdatt, A. Chaves, and V. Bennett, *J. Coat. Technol.* **69**(870), 43–51 (1997).
14. G. Schottner, *Chem. Mater.* **13**, 3422–3435 (2001).
15. B. Arkles, *Chemtech* **29**, 7–14 1999.
16. H. Jo and F. D. Blum, *Langmuir* **15**, 2444–2449 1999.
17. L. Britcher, S. Kempson, and J. Matisons, in K. L. Mittal and A. Pizzi, eds., *Adhesion Promotion Techniques*, Marcel Dekker, Inc., New York, 1999, pp. 347–385.
18. C.-H. Chiang, H. Ishida, and J. L. Koenig, *J. Colloid Interface Sci.* **74**, 396–404 (1980).
19. S. R. Culler, H. Ishida, and J. L. Koenig, *Polym. Compos.* **7**, 231–238 (1986).
20. T. M. Alam, R. A. Assink, and D. A. Loy, *Chem. Mater.* **8**, 2366–2374 (1996).
21. C. H. C. Liu and G. E. Maciel, *J. Am. Chem. Soc.* **118**, 5103–5119 (1996).
22. G. E. Maciel, and D. W. Sindorf, *J. Am. Chem. Soc.* **102**, 7606–7607 (1980).
23. K. P. Hoh, H. Ishida, and J. L. Koenig, *Polym. Compos.* **11**, 121–125 (1990).
24. B. Arkles, *CHEMTECH* **7**, 766–778 1977.
25. H. Watson, A. Norstrom, A. Torrkulla, and J. Rosenholm, *J. Colloid Interface Sci.* **238**, 136–146 (2001).
26. E. P. Plueddemann, *J. Paint Technol.* **40**(516), 1–9 (1968).
27. H. Jo and F. D. Blum, *Chem. Mater.* **11**, 2548–2553 (1999).
28. H. J. Kang and F. D. Blum, *J. Phys. Chem.* **95**, 9391–9396 (1991).
29. T. W. H. Wang, F. D. Blum, and L. R. Dharani, *J. Mater. Sci.* **34**, 4873–4882 (1999).

30. D. A. Loy, and K. Shea, *J. Chem. Rev.* **95**, 1431–1442 (1995).
31. K. J. Shea and D. A. Loy, *Chem. Mater.* **13**, 3306–3319 (2001).
32. G. Z. Li, L. C. Wang, H. L. Ni, and C. U. Pittman, *J. Inorg. Organomet. Polym.* **11**, 123–154 (2001).
33. J. D. Lichtenhan and J. Schwab, *J. Int. SAMPE Tech. Conf.* **32**, 185–191 (2000).
34. P. T. Mather, H. G. Jeon, A. Romo-Uribe, T. S. Haddad, and J. D. Lichtenhan, *Macromolecules* **32**, 1194–1203 1999.
35. C. Sanchez, G. Soler-Illia, F. Ribot, T. Lalot, C. R. Mayer, and V. Cabuil, *Chem. Mater.* **13**, 3061–3083 (2001).
36. U. Schubert, *Chem. Mater.* **13**, 3487–3494 (2001).

FRANK D. BLUM
University of Missouri-Rolla

SINGLE-SITE CATALYSTS.

See Volume 4.

SMART MATERIALS, MICROGELS

Introduction

The use of smart materials in the development of many technologically important devices and formulations is becoming increasingly widespread. However, as a result of their increased proliferation and relative novelty it is appropriate to ask: what are smart materials, how do they work, and what are their applications?

Smart materials may be broadly defined as any material that can respond to subtle changes in environmental conditions, eg, a change in temperature, pH, ionic strength, solvency, light intensity, or the influence of an applied electric field (1). One class of cross-linked polymers, often given the prefix of a "smart" or "intelligent" material, is colloidal microgel particles. These particles have been described as "smart" because of their ability to undergo, often quite dramatic, conformational changes in response to a change in their environmental conditions. Microgel particles have a high degree of sensitivity and they are capable of undergoing rapid changes in their physical properties, including changes in particle size and surface charge density. The rapidity of change comes about as a result of microgel particles having very high surface area-to-volume ratios, which allows rapid diffusion of a given stimulus, eg, a reduction in environmental pH, to facilitate a response throughout the matrix of a microgel over very short-time scales, typically of the order of a few seconds. This property has enabled particles of this type to find utility in many biomedical and industrial applications. This article aims to give the reader an understanding of how microgels may be prepared by outlining some of the synthetic strategies employed for microgel synthesis. Some of the techniques used in the characterization of these smart materials, such as calorimetry, light scattering, rheology, and neutron scattering, are also examined. Further, this article provides an overview of the diverse number of applications

Encyclopedia of Polymer Science and Technology. Copyright John Wiley & Sons, Inc. All rights reserved.

for which smart polymeric microgels are currently finding utility. These range from enhanced oil recovery to drug delivery through sophisticated additives in the paint and coating industries.

Colloidal microgels may be defined as a disperse phase of discrete polymeric gel particles, which are typically in the size range of 1 nm to 1 μm, uniformly dispersed in a continuous solvent medium (2). Microgels are dispersions of particles—in contrast to true single-phase solutions—and as such they often display typical colloidal characteristics, eg, turbidity. They are of considerable academic and commercial interest because of their "sponge-like" properties and their ability to change molecular conformation, ie, shrink and swell in response to a number of different external stimuli. Microgels have similar properties to polymers and water-swollen gels (usually termed hydrogels or macrogels) but are discrete particles with characteristics that are dependent on the method of synthesis, cross-link density, monomer concentration, monomer composition, and solvency conditions (3,4) (see HYDROGELS).

Microgel Preparation

Several methods have been reported in the scientific literature for the synthesis of microgel particles. These include emulsion polymerization (5), inverse microemulsion polymerization (6,7), and anionic copolymerization (8) (see HETEROPHASE POLYMERIZATION).

Emulsion Polymerization. The most widely used method for the preparation of microgel particles is emulsion polymerization (1,9,10). The major limitation of this technique is that only low particle concentrations (hence dilute dispersions) can be prepared; however, a high product yield (typically around 95%) can be achieved. A surfactant may be added to the reaction to increase the concentration of particles that may be synthesized. The disadvantage of adding a surfactant to the reaction mixture is that smaller particles having typical diameters of the order of 150 nm are commonly produced (5). This occurs as small particles, formed as intermediaries in the reaction process, become stabilized by electrostatic forces originating from the added surfactant molecules. The surfactant molecules stabilize the small particles, thus preventing them from growing into larger microgels. The removal of any residual surfactant at the termination of the polymerization process can also be problematic. Remaining surfactant can affect the physicochemical properties of the microgel and can also lead to a contamination of the surface, making it irregular in composition. This in turn can affect the microgel behavior, eg, irregular deposition because of the blocking of certain surface sites.

Surfactant-free emulsion polymerization is often used deliberately to produce larger particles. This method has been reported extensively for the preparation of poly(*N*-isopropylacrylamide), ie, [poly(NIPAM)] microgel particles (10). In this procedure the microgel particles are prepared in a one-pot reaction involving the free-radical polymerization of the monomer NIPAM. The reaction is carried out in an aqueous solution in the presence of a cross-linking agent (usually *N*′,*N*′-methylenebis acrylamide) and an initiator (such as potassium persulfate), which undergoes thermal decomposition on heating to yield an anion radical. The reaction is carried out under an inert atmosphere of nitrogen and at a temperature of $\sim$70°C (or higher) to ensure the decomposition of the initiator and maintain

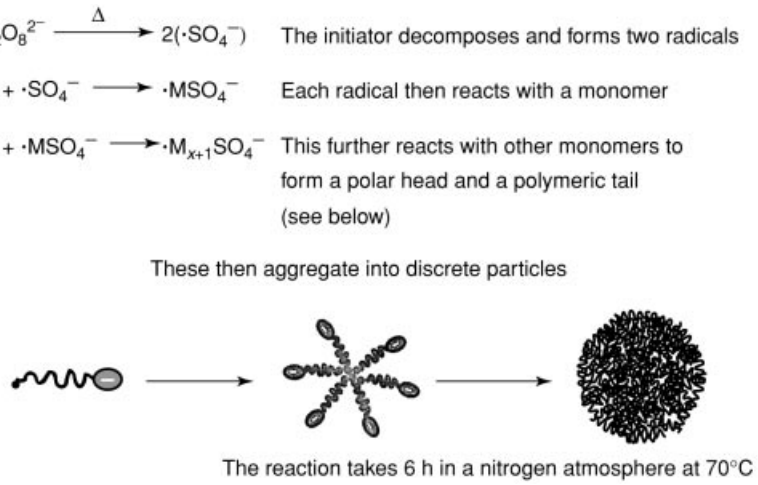

Fig. 1. Microgel preparation.

suitable reaction kinetics. The reaction is similar to that used in the preparation of a latex particle, such as polystyrene latex (11), but with the addition of a cross-linker.

The mechanism involved in the synthesis of microgel particles is shown in Figure 1 and starts with the thermal decomposition of the initiator to form free radicals. The free radicals are water-soluble and react with the monomer (across the double bond) to form monomeric radicals. These radicals participate in further reactions with other monomer units to form oligomeric radicals. The oligomeric radicals have polar end groups (originating from the initiator) and are solubilized in water until a critical chain length is reached. The oligomers aggregate and begin to mix with other oligomeric chains at which point small particles start to form. The particles grow in size until they are stabilized by electrostatic repulsion forces between charged groups on the surface of the particles. These charge repulsion forces originate from the ionic initiator. The particles continue to grow by the adsorption of further monomer units or other oligomers either until all of the monomer is used up or until another radical species enters the growing particle and terminates the reaction (10). This method yields microgels that are regular in both size and composition. Such particles are described as being monodisperse.

By the same mechanism reported for polystyrene latexes (11,12) anionic microgel particles can be prepared, with negative charges originating from a persulfate initiator, such as potassium persulfate or ammonium persulfate (1,9–13). The dominant surface charge group arising from the persulfate initiator is $-SO_3^-$, a strong acid group with $pK_a \sim 1.5$. Because of the low pK_a value the surface sulfate charges will remain ionized and hence the microgel will retain its negative charge over a wide pH range. Microgels having weaker acid surface groups, eg, $-COO^-$, may be prepared using, eg, 2,2′-azobiscyanovaleric acid as the initiator (11). The carboxyl groups have a $pK_a \sim 5$ as a result, at low dispersion pH, the microgel will have a lower charge density than at higher pH because of the lower dissociation of the carboxyl protons. This can have implications for microgel

interactions, both with themselves and with other surfaces, eg, during deposition where pH conceivably could be used to either enhance or diminish the extent of deposition which may occur through an increase or decrease in the charge density at the microgel surface. Cationic microgels can also be prepared by using a positively charged free-radical initiator [such as 2,2′-azobis-(2-amidio propane) dihydrochloride] (13–16), which gives the particles a positive charge in the form of amidine groups [ie, protonated amines (NR_3^+)].

Much of the work reported in the academic literature is based upon microgels prepared from poly(NIPAM), but there are, however, a number of microgels that have been prepared from other monomers. These include methyl methacrylate with other copolymers such as ethylene glycol dimethacrylate (17,18), methyl methacrylate with *p*-divinylbenzene (19), and methyl methacrylate with methacrylic acid (20). Other microgel particles have been prepared from poly(allylamine hydrochloride) (21), vinylpyrrolidinone and acrylic acid (22), acrylamide and acrylamide with methacrylamidopropyltrimethylammonium chloride (23), and acrylamide copolymerized with 2-acrylamido-2-methylpropanesulfonic acid (24).

Preparation of Microgel Particles Having Novel Morphologies. Some of the more recent research into novel microgels involves the synthesis of microgels having a structure resembling a flower (25). The preparation of one of these types of structures is shown in Figure 2. The flower microgels are prepared by using a suitable polymer having two distinctly different monomers. One

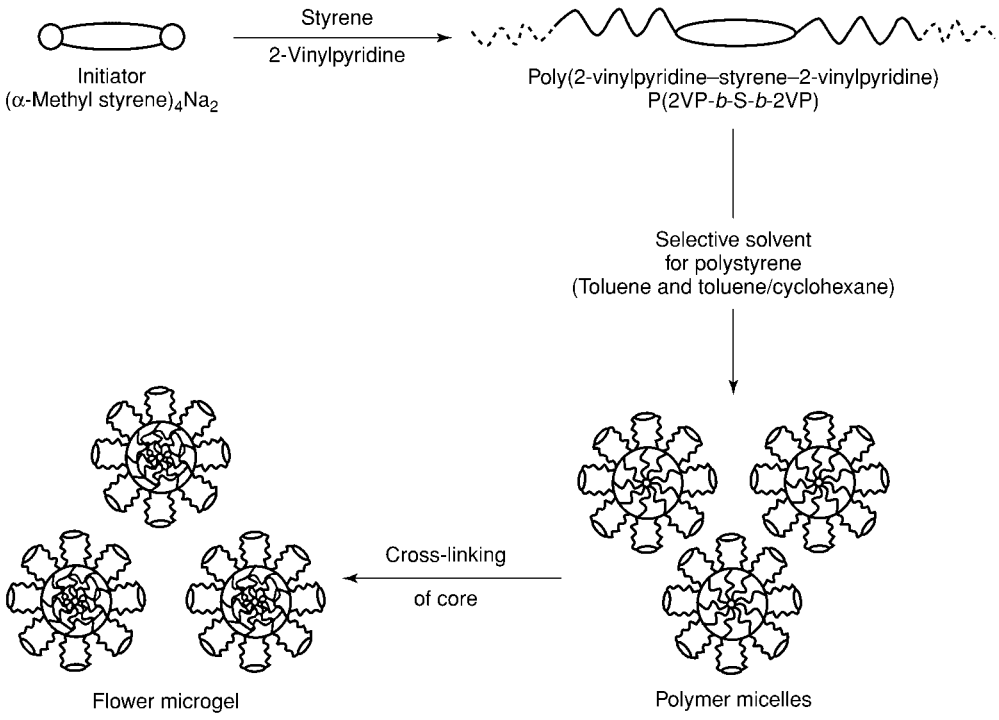

Fig. 2. Preparation of flower microgels. Redrawn from Ref. 26.

of the monomers is hydrophobic (A, which in this example is styrene) and the other is hydrophilic (B, vinylpyridine), which are copolymerized to form a triblock BAB copolymer. The resultant polymer chains are then exposed to a selective solvent, toluene and toluene/cyclohexane. In this particular case toluene is a good solvent for the A block and is a nonsolvent for the B block, which results in the formation of a polymer micellar structure. The central part of the flower micelle structure is then "fixed" by subsequent crosslinking with 1,4-diiodobutane, again using toluene as the solvent for the reaction.

The novel morphology and micellar structure of flower microgels allows them to be utilized as absorption centers for both hydrophilic and hydrophobic solutes. These structures permit the absorption of hydrophobic solutes into the hydrophobic domains within the microgel structure. It could be envisaged that a poorly water-soluble drug may be solubilized within the hydrophobic domains of the flower microgel structure. One advantage that flower microgels may offer over surfactant micelles is that their molecular structure is not concentration-dependent. Therefore, these materials may find application at concentrations lower than the critical micelle concentrations of many surfactants.

Poly(NIPAM) microgel particles have been used as a micromatrix for the polymerization of a second hydrophobic monomer, *N*-methylpyrrole (Mpy) (27). The microgel particles are synthesized first, and are then reacted with Mpy in the presence of an initiator (ammonium persulfate). The resultant poly(NIPAM)-*co*-poly(MPy) particles have a "raspberry" morphology, with poly(Mpy) particles located within the poly(NIPAM) structure. Small poly(Mpy) particles (15 nm) are found centrally, while larger 60-nm poly(Mpy) particles are located close to the poly(NIPAM) periphery. This is the first example of poly(NIPAM) microgel particles being used as a host for the preparation of particles from a second monomer. The poly(NIPAM)-*co*-poly(MPy) microgel particles are colloidally stable and exhibit a conformational phase transition at 32°C upon heating. Similarly to the poly(NIPAM) microgel particles described above, they also aggregate upon heating in an electrolyte solution (0.1 *M* NaCl).

Larger poly(NIPAM) microgels or "minigels" have been prepared by inverse suspension polymerization (28). These particles are much bigger than conventional microgel particles and are in the order of 2.5-μm diameter at 25°C and so have been given the name minigels. Minigels show physicochemical properties similar to those of microgels and have a reversible conformational phase transition as a function of temperature. Interestingly the reswelling of the minigels, on cooling, may take up to 15 min to reach a fully swollen state, showing the benefit of the rapid swelling/deswelling phase transition of microgel particles.

Preparation of Core–Shell Microgels. The preparation and electrokinetic and colloid stability behavior of styrene–*N*-isopropylacrylamide and styrene–*N*-isopropylacrylamide-*co*-aminoethyl methacrylate (AEM) core–shell latexes have been reported in Reference 29, where the particles having a core of polystyrene surrounded by layers of (*1*) poly(NIPAM) and (*2*) poly(NIPAM-*co*-AEM) were prepared. The particles were produced by first synthesizing the polystyrene core via a surfactant-free polymerization reaction and then, when the formation of the core was ~90% complete, the shell was generated by the addition of the NIPAM monomer and crosslinker N′,N′-methylenebisacrylamide (*1*). In the case of core–shell particles, NIPAM, aminoethyl methacrylate, and the

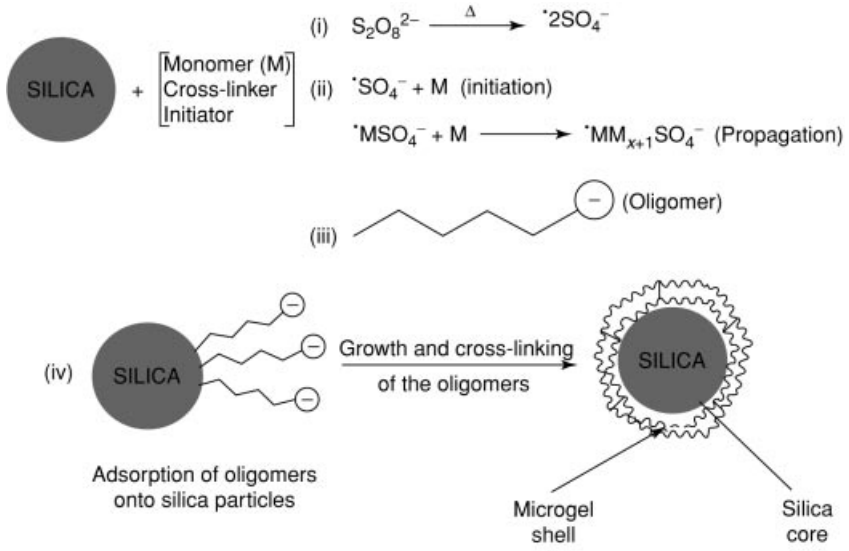

Fig. 3. Proposed mechanism for the preparation of core–shell microgels.

crosslinker were added (*2*) The thickness of the shell surrounding the core can be controlled by increasing or decreasing the environmental temperature of the dispersion, with the shell collapsing at a temperature above the critical solution temperature for poly(NIPAM). Under these conditions the particles could be made to destabilize and undergo an aggregation. A similar approach was adopted in Reference 30, where core–shell microgels were synthesized by polymerizing NIPAM and N′, N′-methylenebisacrylamide in the presence of potassium persulfate around a mondisperse silica core. The mechanism outlining the formation of core–shell particles is illustrated in Figure 3. The resultant particles formed via this process were found to be monodisperse. The thickness of the core was examined by a combination of neutron scattering and dynamic light scattering techniques, as a function of temperature. The distance over which the shell extended was also found to decrease with increasing temperature.

Characterization of Microgels

A number of techniques are commonly employed for the study of microgel dispersions. These include dynamic light scattering, differential scanning calorimetry, electron microscopy, nuclear magnetic resonance spectroscopy, and neutron scattering. These techniques provide information on particle size, shape and size changes, the thermodynamic processes which take place as the microgels undergo their conformational transitions, and fine detail regarding the polymer microstructure within the particles in addition to the relative hydrophobicity and hydrophilicity of the particles.

Dynamic Light Scattering. Dynamic light scattering is a particularly useful technique for monitoring the conformational behavior of microgels in different solvent environments. It allows the measurement of the hydrodynamic

diameter of the microgels by monitoring the diffusion coefficient (D) of the particles in dispersion:

$$D = \frac{kT}{6\pi\eta a}$$

where k is Boltzmann's constant, T is the temperature, η is the viscosity of the dispersion medium, and a is the hydrodynamic diameter.

There are numerous reports in the literature where dynamic light scattering has been used to follow microgel behavior (16,20,31,32). By comparing the hydrodynamic size before and after a transition it is possible to determine the swelling ratio of the microgel, which is useful in terms of potential applications including drug delivery and rheology modification.

Differential Scanning Calorimetry. The use of differential scanning calorimetry (dsc) to study microgel dispersions was pioneered at the University of Greenwich, London (33). The technique can be applied to microgel systems that undergo a thermally induced conformational transition. Poly(NIPAM) microgels, for example, undergo a thermal conformational transition at 34°C in water. A typical dsc output for the transition is shown in Figure 4. The instrumental output is an endotherm for the heating cycle and a mirror image exotherm for the cooling cycle. As the microgel is heated, a series of processes begin to take place. The major contribution to the calorimetric output is the expulsion of water from the

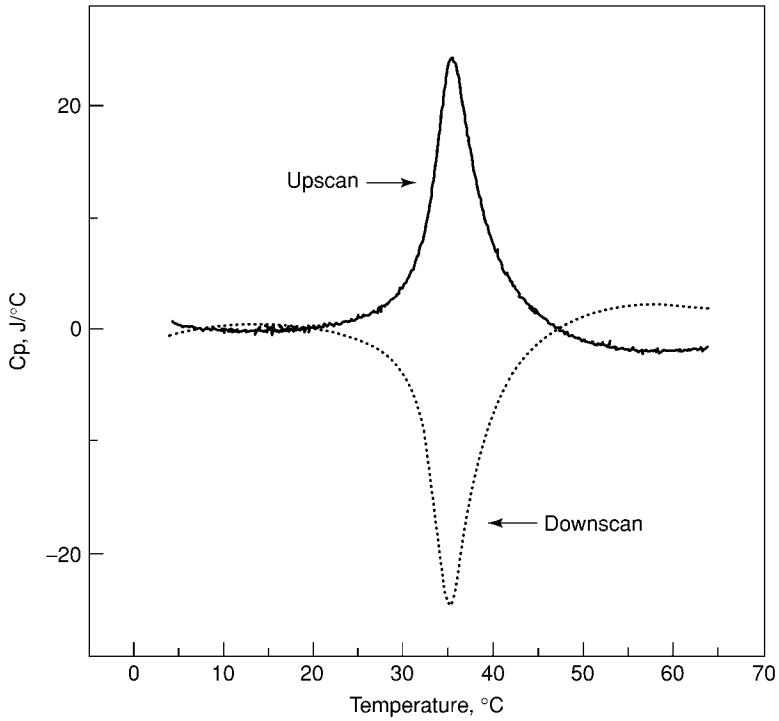

Fig. 4. A typical dsc output for a poly(NIPAM) microgel dispersion.

regions surrounding the polymer chains. This breaking of the polymer–solvent interaction is an endothermic process. In addition to the expulsion of water from the microgel structure some aggregation of the polymer chains will inevitably take place as the microgel structure collapses. From the calorimetric output information regarding the enthalpy change associated with the conformational transition, the precise temperature of the transition and some detail regarding the extent of chain aggregation within the microgel may be obtained.

Other Techniques. Small-angle neutron scattering has been used to study microgel behavior by a number of research groups (34,35). Fine details regarding the uniformity of the structure and the change in the dynamics of polymer–solvent interactions as a function of temperature may be determined using this technique. Further details regarding the nonuniform nature of microgel surfaces may also be obtained from neutron scattering measurements.

The diffusion and relaxation behavior of solvent both within and external to a microgel may be measured using nmr. The technique provides information regarding the internal environment of a microgel. For example, it has been reported that the internal environment of a microgel is considerably more hydrophobic than the exterior (36), a finding which may have application in the use of microgels as hosts for poorly water-soluble materials.

Transmission electron spectroscopy has been widely used to study microgel dispersions (37–39). The technique offers the advantage of being able to study a real image that illustrates both the size and the shape of the particles. One cautionary note, however, regarding the use of electron microscopy in studying microgels has been reported (40). In the electron microscopy chamber the microgels are exposed to high vacuum conditions and as a result the microgel particles, which are readily deformed, form pancake-like structures, thus misrepresenting their hydrodynamic shape which is much more spherical.

Properties of Microgels

Microgels differ from bulk gels in a number of fundamental ways. Some of these are illustrated in Figure 5, and include significant differences in bulk viscosity characteristics, rapidity of solution response, and surface area-to-volume ratios. Although bulk gels and microgels have very similar polymer chemistry, their physical molecular arrangement can give rise to the differences stated. This review focuses primarily on microgels; however, it is worth noting that some of the polymer chemistry behavior described may equally be as applicable to bulk gels as it is to microgels.

Microgels that are sensitive to pH, electrolyte concentration, light intensity, or the introduction of a cosolvent (nonsolvent) to their environment can be prepared. Table 1 shows a selection of different microgels reported in the scientific literature, which have been prepared to respond to specific external stimuli. The properties of some of these microgels are discussed below.

Effect of Temperature. Poly(NIPAM) microgels are by far the most widely investigated and reported systems (1,9,10). The first reported preparation of microgel particles of this type was by Pelton and Chibante in 1986 (13), where they used a surfactant-free emulsion polymerization process to produce a dispersion

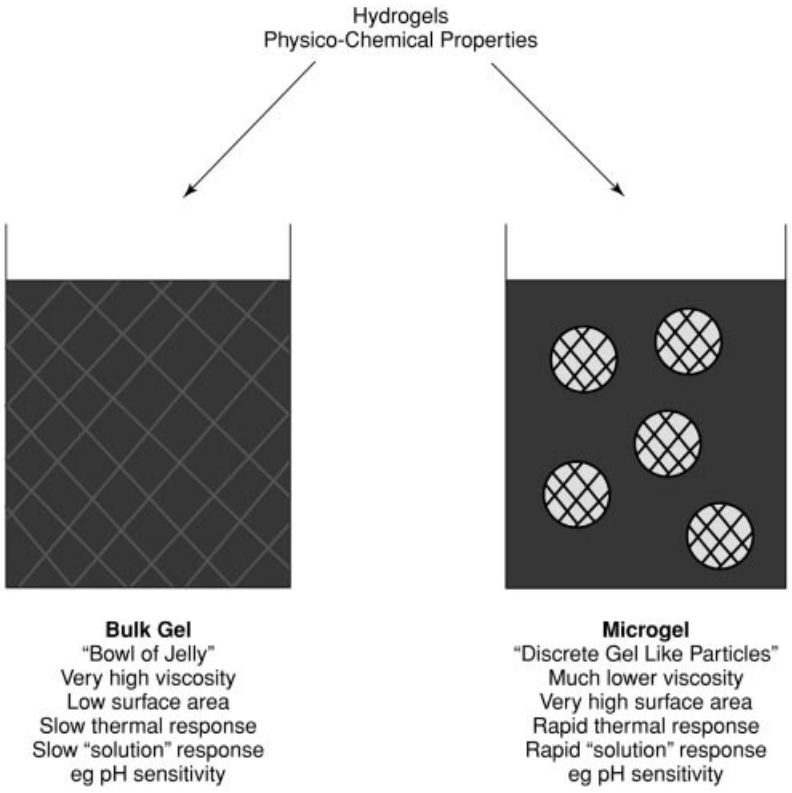

Fig. 5. A comparision of the physicochemical properties of bulk gels and microgels.

of monodisperse microgel particles. The particles formed were of interest because they showed a thermoreversible "conformational transition" in water at around 34°C. Below this temperature the microgels have a swollen conformation as a result of low van der Waals attractive forces and hydrogen bonding, with the interstitial spaces of the microgel being filled with water molecules. When the environmental temperature of the dispersion approaches the transition temperature of 34°C, the polymer–solvent interactions decrease dramatically and the particles begin to contract. The polymer chains collapse as polymer-polymer interactions dominate over polymer–solvent interactions. The polymer molecules now prefer to interact with themselves rather than with water molecules, and the hydrogen bonds that conferred stability are now disrupted. As the microgel shrinks, a high proportion of the entrapped water is excluded from the regions within the polymer matrix and the particle begins to form a hard sphere-like structure. When the microgel particles are in their collapsed state, they remain dispersed as a result of electrostatic repulsion between charged groups (originating from the initiator) on the microgel surface. The shrinking of microgel particles is a reversible process and so on cooling back to below 34°C, the polymer–solvent interactions ameliorate and the microgel returns to its original swollen conformation. Figure 6 shows the shrinking and swelling of poly(NIPAM) microgel particles.

Table 1. The Structure and Properties of Some Common Colloidal Microgels

Type	Structure	Specific environmental stimuli	References
Homopolymers	Poly(NIPAM), $[H_2C{=}CHCONHCH(CH_3)_2]_n$	Temperature (~34°C)	1,9,10
	Poly(*N*-ethylacrylamide), $[H_2C{=}CHCONHCH_2CH_3]_n$	Temperature (~78°C)	31
Copolymer microgels	Poly(NIPAM)–acrylic acid, $[H_2C{=}CHCO_2H]$	pH (swells between pH 4–6)	41
	Poly(NIPAM)–crown ether $[H_2C{=}CHCONHC_6H_3(O_6C_{10}H_{20})]$	Chemically responsive microgel (specifically K^+ and Na^+ ions)	42
	Poly(NIPAM)–vinyl imidazole $[H_2C{=}CH(NCH_2NCH_2)]$	Microgel behaves as a reaction centre	43
Flower microgel	Poly(2-vinylpyridine–styrene-2-vinylpyridine) 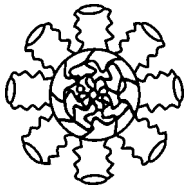	Solvent hydrophobicity	25
Ampholytic microgel	Poly(vinylbenzyl chloride–*tert*-methacrylate–trimethylamine)	Specifically designed to be used as a catalytic medium	44,45

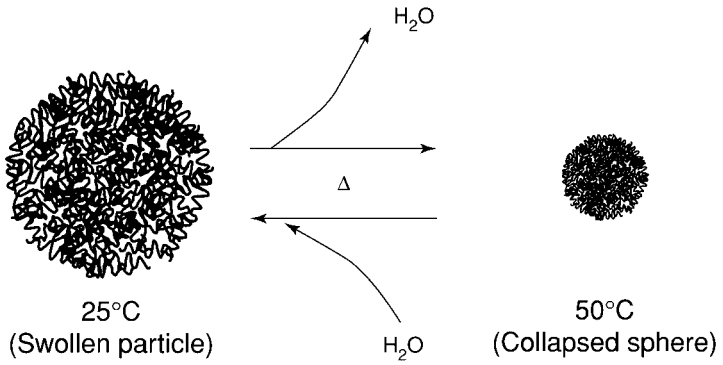

Fig. 6. Thermosensitive properties of a poly(NIPAM) microgel.

Microgel particles have also been prepared using poly(*N*-ethylacrylamide) [poly(NEAM)] (31), a monomer structurally similar to poly(NIPAM). Poly(NEAM) is less hydrophobic than poly(NIPAM), and the resulting microgel particles prepared from poly(NEAM) have a much higher transition temperature of 78.2°C. Therefore, the temperature at which the conformational transition occurs can be manipulated to suit a number of applications by simply changing the monomer used in the preparation. The more hydrophobic the monomer, the lower the temperature at which any conformational transitions will take place in water.

The advantage of using microgels over linear polymers and macrogels is the speed at which the conformational change occurs. It has been reported that the equilibration time for microgels is ∼1 s (26,46). This is much faster than the equilibration time needed for the typical swelling of polymers and macrogels in solution, which is in the order of hours or days. The cross-linking of the polymer chains in a microgel means that the distance between polymer chains in a microgel is a great deal shorter when compared with the distance between linear chains in solution, and this gives rise to the speed at which the polymer chains collapse. The large surface to volume ratio of microgels also aids rapid chain collapse, giving microgels an advantage over their macrogel and linear polymer counterparts. The phase transition of high concentrations of the linear polymer chains of poly(NIPAM) in solution have been shown to resemble the shrinking behavior of a microgel (47). At dilute polymer concentrations, the linear poly(NIPAM) has a phase transition resembling a random coil-to-globule collapse with a transition temperature of 34.1°C. However, at higher polymer concentrations linear poly(NIPAM) has a phase transition similar to that of a poly(NIPAM) microgel, where a transition resembling the diffusion of water from within the gel structure is observed.

Swelling Behavior. The extent of swelling (or deswelling) is the most useful property of microgel particles. The swellability of microgel particles is dependent on the cross-linker concentration (48) used in the preparation. High levels of cross-linker will result in a large microgel particle having a tight compact structure, with its center being difficult to penetrate. Higher concentrations of cross-linker will also give rise to a faster conformational transition as the polymer chains are closer together, thereby enabling a quicker collapse. However, at low cross-linker densities the microgel particles have properties resembling high

molecular weight polymers. Generally, microgels are prepared with an average cross-linker density somewhere between these two extremes, although the cross-linker density is usually uneven between each individual microgel particle and is given as an average cross-linker density per dispersion.

Colloid Stability. The stability of microgel particles in water at 25°C is a result of low van der Waals attractive forces coupled with some steric contributions from the polymeric chains at the periphery of the particles. The low van der Waals forces are a consequence of the particles being fully swollen with solvent molecules, and the microgel Hamaker constant resembles that of the solvent, thereby resulting in low van der Waals attractive forces. The Hamaker constant is the basis of the van der Waals attractive force. Its origins lie in the temporary and permanent dipoles, which exist within a macroscopic material. For a microgel-type particle, the macroscopic material consists of a combination of a polymer matrix and the water contained within its structure. In a swollen state, the fraction of water in the total structure is large and hence the Hamaker constant is much closer to that of bulk water, resulting in a negligibly small attractive force existing between the microgels. When the particle collapses, as a result, eg, of heating the dispersion, the fraction of water within the structure decreases and the Hamaker constant increases as it now reflects a larger percentage of polymer contributing to the overall structure. The van der Waals forces increase but the particles remain dispersed because stabilization is brought about by electrostatic repulsion between charged groups on the surface of the microgels. These originate from the initiator used during the preparation of the microgel particles.

The stability of microgel particles in electrolyte is somewhat different to that of other model colloids. Colloidal particles such as silica or polystyrene latex flocculate in electrolyte at room temperature when the concentration of electrolyte exceeds their critical flocculation concentration (49,50). Poly(NIPAM) microgels, however, are stable in electrolyte at room temperature but will reversibly flocculate when heated above their lower critical solution temperature (LCST) in an electrolyte solution. It has been shown that poly(NIPAM) microgel particles at 40°C flocculate at an NaCl concentration above 0.06 M (51). These particles were also found to redisperse on cooling back to 25°C. The stability of the microgel particles at 25°C in an electrolyte solution is, as a result of the low van der Waals forces, from the particles being swollen in solution. Therefore, the particles remain dispersed even though electrostatic repulsion has been reduced by the presence of electrolyte ions. At 40°C the solvent molecules are forced out of the microgel and van der Waals attractive forces subsequently increase. Since the ionic groups on the microgel are screened by electrolyte ions, the particles aggregate when heated, as van der Waals forces now dominate. This process is reversible and so on cooling, the particles reswell and the van der Waals attractive forces decrease, resulting in a stable dispersion.

Rheological Properties. The rheological behavior of microgel particles as a function of temperature has been investigated (52,53). Not surprisingly, the viscoelastic properties of poly(NIPAM) microgels change quite dramatically with temperature. At low temperatures poly(NIPAM) dispersions display a very elastic-type behavior. This, perhaps, is not surprising, as the particles are readily deformable below their critical phase-transition temperatures. A microgel can be envisaged as a sponge-like material having elastic properties when swollen.

Upon heating a dispersion above the critical phase-transition temperature, the dispersion becomes less elastic and displays the rheological characteristics typical of any particulate dispersion. The rheology of the dispersions as a function of the volume fraction of particles has also been examined (54), and the viscosity and shear thinning behavior increases as the volume fraction increases. This may be attributed to the microgel at elevated volume fractions effectively absorbing the dispersion solvent to within the polymer matrix, thus forming a putty-type material. The application of shear to this material results in a "squeezing" coupled with a deformation of the microgel, resulting in a reduction in volume and simultaneous solvent expulsion. This in turn causes the viscosity of the dispersion to decrease. Poly(NIPAM) microgels were shown to exhibit unusual behavior (55) when compared to the linear polymer poly(NIPAM). This difference comes about when the two systems are heated to their critical phase-transition temperature. The linear poly(NIPAM) is believed to undergo intermolecular aggregation, resulting in an effective increase in the molecular mass of the polymer, hence increasing its viscosity. Additional chain entanglement, around the LCST, will also contribute to an increase in viscosity. As the temperature rises further the linear polymer chains collapse; a sudden and dramatic reduction in viscosity is observed. In a microgel such behavior cannot readily take place as intramolecular aggregation is inhibited by the presence of the cross-links within the structure. Further, intermolecular aggregation is inhibited by increases in surface charge density above the critical phase-transition temperature, resulting in enhanced particle separation.

Osmotic Deswelling. Poly(NIPAM) particles have been reported to undergo osmotic deswelling in a good solvent by the addition of a nonadsorbing polymer to the microgel dispersion (56). The deswelling of the microgel particles in various polyethylene glycol–water solutions was found to be due to the loss of water from inside the microgel network so as to minimize the osmotic pressure of the solution outside the gel.

Addition of methanol to a poly(NIPAM) microgel dispersion has been shown to have a significant effect on microgel particle size (57,58). At 25°C, both pure water and pure methanol are good solvents for the microgel and the particles have a swollen conformation. The particles collapse in a volume fraction between 0.2 and 0.4 methanol, and then reswell at high volume fractions of alcohol. The decrease in particle size has been attributed to the removal of water molecules from within the microgel structure, to form distorted tetrahedral structures around the alcohol molecules. The hydrogen bonding and hydrophobic interactions within the microgel are disrupted and the microgel collapses. This is termed *co-non-solvency*. As the methanol volume fraction is further increased the microgel particles reswell. The alcohol molecules interact through hydrogen bonding and hydrophobic interactions, resulting in an increase in particle size.

Influence of Comonomers on Microgel Properties. The overall physicochemical properties of a microgel depend not only on the cross-linker concentration, but also on the concentration of monomer/comonomers used in the synthesis. The addition of a small amount of comonomer (typically 1–5 wt% monomer) can have a dramatic effect on the overall properties of the resultant microgel particles. For example, a pH- and temperature-sensitive microgel can be prepared by copolymerizing poly(NIPAM) with acrylic acid. These spherical particles undergo

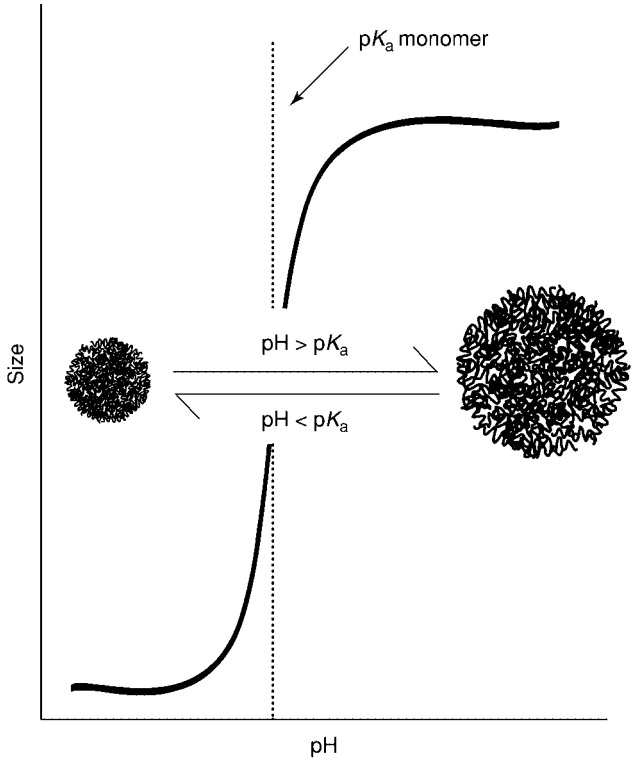

Fig. 7. Shrinking and swelling of a poly(NIPAM)-*co*-acrylic acid microgel.

a conformational transition in response to an environmental pH change (41). By selecting monomers that have pK_a values corresponding to the transition pH of interest, microgels having tailored pH-dependent transitions can be prepared. In the case of an acidic monomer (eg, acrylic acid), the microgels typically adopt a compact structure at a pH below the pK_a of the monomer. At a pH value above that of the pK_a, the polymer chains of the microgel become ionized, forcing the microgel to adopt a more extended conformation as a result of intramolecular charge repulsion. Under these conditions the microgel swells (Fig. 7).

When (NIPAM) is copolymerized with a vinyl crown ether monomer, the resultant microgel particles show a phase-transition dependency based upon the addition of certain metal ions (42). Addition of K^+ ions results in a notable increase in the phase-transition temperature, while the addition of Na^+ results only in a small increase (up to 7.5°C was observed for K^+ ions as compared to 1.5°C for Na^+ ions). This anomaly is attributed to the binding affinity and size of the metal ion used. Potassium ions have a higher affinity for the crown ether groups than the sodium ions, and can fit more easily into the cavity of the crown ether. Binding of the K^+ ions makes the microgel more hydrophilic, which increases the phase-transition temperature. Interestingly, Li^+ ions are not captured by the crown ether microgel and the phase-transition temperature in dispersions containing these ions remains unchanged.

Applications

Currently, microgels are being investigated for their potential use as drug delivery vehicles, binding/adsorption agents, catalytic media, and their ability to improve existing industrial formulations, eg, specialist paints. The next sections describe how microgels are utilized in these applications and also describe some of the newly investigated uses of these polymeric smart materials.

Drug Delivery Vehicles. The shrinking and swelling of microgel particles makes them particularly suited to applications such as drug delivery, where it can be envisaged that as a result of their porous matrix-like structure microgel particles can readily accommodate drug molecules. Drugs are known to partition into the interstitial regions of a microgel, especially if the drug has limited water solubility (59). It has been reported that ∼94% of the water inside a microgel is driven out during a phase transition (9) so that drug displacement, by solvent molecules, could occur following a triggered microgel conformational change. The period over which the drug is released will be dependent upon the size of microgel particles used and the level of crosslinker, which in turn affects the interstitial volume.

Copolymer microgels of poly(NIPAM)-*co*-acrylic acid-*co*-butyl methacrylate have been investigated with respect to their application for modulated insulin release (60). The butyl methacrylate within the microgel structure fulfills two roles. Firstly, butyl methacrylate confers improved mechanical properties onto the microgel. Secondly, the butyl methacrylate moiety gives rise to a high uptake efficiency of insulin as a consequence of the presence of specific insulin-binding regions on the butyl side chains of the butyl methacrylate. At low pH (pH 2), the rate of insulin release was found to be limited to ∼10 wt% of the loaded capacity of the microgel. However, upon raising the pH to 7.4 the majority of the remaining insulin was released. The acrylic acid component of the microgel facilitates an expansion of the microgel structure at higher pH, thereby enhancing the intramolecular pore dimensions and allowing a diffusion-mediated release of the insulin to take place. It is proposed that "polymeric beads" such as these may prove to be very useful vehicles for the delivery of peptides and proteins to the gastrointestinal tract. As the microgel will have a "closed" structure at the pH of the stomach (approximately pH 2), little or no diffusion of the encapsulated material will take place. On moving out of the stomach into the gastrointestinal tract, the pH will increase. This allows the pores of the microgel to open and the active material to be released into a much less acidic and aggressive environment, so that the higher order structure of the peptides/proteins may be maintained longer.

Microgel particles consisting of vinylpyrrolidinone copolymerized with acrylic acid have been prepared (61). These particles were designed to be used as an oral drug delivery vehicle. The microgel particles were loaded with a marker compound fluorescein isothiocyonate (FITC)-dextran and the release of this compound was monitored as a function of pH and temperature. The release of this compound was found to be slow in an acid solution but increased rapidly as the pH was increased. There was also a subsequent increase in FITC-dextran release when the particles were heated. At 4°C ∼18% of the FITC-dextrans were released while ∼50% was released at 37°C. The increase in the amount of FITC-dextran released is due to the microgel shrinking when heated.

Poly(methacrylic acid-*co*-acrylic acid) microgels (62) are also being investigated for their use as drug delivery vehicles. A study has been carried out on the influence of cross-linker density on the uptake and release of a drug/protein from these materials, for investigating the induced swelling of the microgels following changes in pH and NaCl concentration. This study concluded that the swelling ratio of the microgel increased as the mole fraction of the cross-linker decreased (ie, the microgel polymer chains become more restricted as the number of cross-links increases). The microgel therefore has less capacity to shrink and swell as the amount of cross-linker increases. The results also suggested that binding affinity, microgel dehydration upon loading, and drug packing were also important features in determining the uptake of the drugs/proteins. These microgels potentially show promise as uptake and release vehicles, but further experiments are needed to fully optimize and identify the types of substrates that will enable these materials to be fully utilized as controlled-release devices.

A review on the applications of thermally reversible polymers and hydrogels in therapeutics and diagnostics has been written (43). In this review, the author highlights a number of uses of poly(NIPAM) polymer and poly(NIPAM) gels. These include their use in the delivery or removal of drugs, toxins, pollutants, and dyes. They can also be used in combination with immobilized ligands for use in separations and diagnostics (see CHROMATOGRAPHY, AFFINITY). Finally, enzymes and other catalysts may be incorporated into the gels for use in therapeutics, diagnostics, bioreactors, chemical processes, and bioseparations.

Binding/Adsorption Agents. A new development of novel microgel structures involves the incorporation of low levels of a particular chemical entity within the polymer matrix at the preparation stage. By incorporating vinyl imidazole (63) as a comonomer with NIPAM during the synthetic reaction, it is possible to produce microgel particles that will specifically bind certain other molecules, eg, haems, at the derivative sites within their structure (Fig. 8). Under controlled environmental conditions, the microgel–haem complex may be investigated with respect to chemical reactions taking place at the immobilized haem groups. Such application has considerable potential with the highly specific functionalities within the structures, providing opportunity for chemistry to take place on a functional group immobilized within the microgel matrix. While this type of application remains in its infancy, it may find utility in sensor technology and/or as a model system, eg, for the study of drug-receptor binding.

Although not a microgel, poly(NIPAM) hydrogels have been prepared as a temperature-sensitive gel for use as a size-selective absorbant (44). Hydrogels are simply cross-linked polymer gels in aqueous solution. The poly(NIPAM) hydrogel swells by adsorbing water but does not adsorb large molecules such as proteins or other high molecular weight polymers/solutes (polyethylene oxide and gelatin). The dry gel is placed into a sample solution where it begins to swell, with water entering the microgel. Small solutes such as urea were found to be adsorbed; therefore, the separation efficiency in this solute is poor. However, high separation efficiency was observed for large solutes of polyethylene oxide, gelatin, and polyethylene glycol, showing that poly(NIPAM) hydrogels can be used as a size, selective separation process. Hydrogels (qv) offer an advantage over other separation techniques (such as silica gels) as they can be used in dilute solutions and can easily be reused. The swollen gel is removed by filtration and is warmed or dried

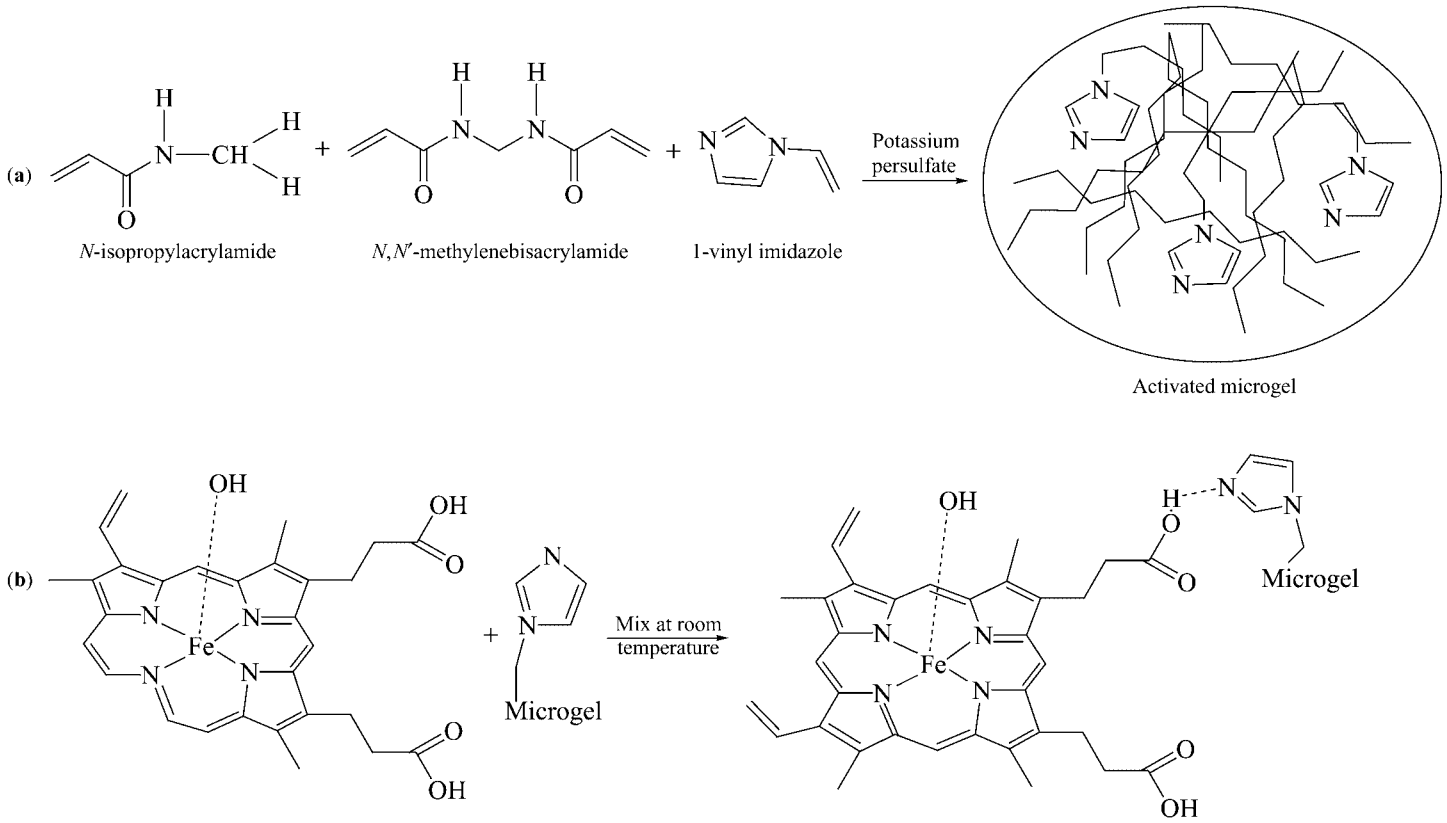

Fig. 8. Preparation and hydrogen bond formation of poly(NIPAM)-*co*-imidazole microgel particles. (**a**) Preparation of the microgel particles; (**b**) hydrogen formation: the modified microgel interacts with an aqueous solution of hematin to form a hydrogen bonded species.

to remove the water from within the hydrogel. The hydrogels behave like microgel particles, so that when heated, a hydrogel shrinks as a result of a decrease in solvent quality. The hydrogel is then ready for reuse.

Catalytic Media. Another class of microgel is a polyampholyte microgel, which has been studied with respect to its application as a colloidal catalytic media (45). For example, less than 1 mg/mL of a polyampholyte microgel based upon vinylbeznyl chloride–*tert*-butyl methacrylate–trimethylamine accelerates the rate of decarboxylation of 6-nitrobenzisooxazole-1-carboxylate ion 60–115 times faster than when carried out in water alone. The effect was reported to be similar to the catalytic activity of the more widely used hexadecyltrimethylammonium chloride micelles. These microgel particles were also found to be stable in a salt concentration of 4 *M* NaCl.

Microgel-bound oxzaborolidines have been prepared and used as catalysts in the enantioselective reduction of prochiral ketones (64). The selectivities of these microgel-supported catalysts are reported in most cases to be comparable to those achieved with low molecular weight polymers. The advantage of the application of microgel-bound catalysts is their good solubility, together with low viscosity characteristics. Microgels of this type can be easily removed by ultrafiltration because of their large size in comparison to linear polymers, making them particularly suitable for use in an on-line process system.

A further report concerning the use of microgels as catalytic centres involves microgel-stabilized palladium colloids (65). Microgels of this type can be conveniently loaded with Pd^{2+} ions, which become subsequently reduced. The resulting metal colloid can be readily precipitated out of solution and redispersed in suitable solvents for subsequent use. Preliminary experiments with these systems show them to be active catalysts for the vinyliation of aryl iodides and bromides.

Improving Existing Formations. Current industrial applications of microgels involve their use in the printing, pharmaceuticals, oil recovery, and coating technologies. Recent advances include the use of microgels in improving the coating properties of pigment particles (66). Negatively charged microgel particles have been shown to adsorb onto the surface of positively charged pigment particles, where they essentially have the role of stabilizers or dispersants. The use of microgels particles in this case promotes stability and also increases the shelf-life of these pigments. Microgels have also been added as a component in waterborne paints where they improve the film properties by increasing the tensile strength of the paint (67). Microgel dispersions are shear thinning and can be used to alter the rheological properties of a given formulation. The addition of microgels therefore fulfills a dual role within the paint, ie, acting as a strengthening agent and viscosity modifier.

New Applications. A new smart material that expands and contracts in response to certain proteins is being developed in Japan for use either as a drug delivery vehicle or as an artificial muscle (68). The material is a hydrogel prepared from two different types of polyacrylamide. At one end an immunoglobulin (IgG) protein, derived from rabbit, is attached and to the other end another antibody, derived from goat, is bound with a specific site for the rabbit IgG. In water, the two sets of molecules cross-link to each other via the IgG and antibody sites to form a tightly bound gel. The resultant gel swells in a solution of IgG because the free protein binds to the antibodies on the second type of polymer, thereby breaking the

cross-links and causing the structure to open. The gel has been designed for use in the treatment of cancer. Here, the gel could be forced to swell (release a cancer-treating drug) in the presence of cancer-specific proteins. But in the absence of the cancer protein, the gel stays in its contracted state, keeping the drug inside the gel. Therefore, these gels can be used to target and treat specific parts of the body that have been affected by cancer.

Researchers claim that they have "engineered a new class of gel with two levels of hierarchy." In fact, they have used microgels as building blocks to form macrogels with "new and unique" properties (69). They further suggest that such macrogels may lead to new technological applications, eg, in drug delivery, sensors, bioadhesives, and displays. A further novel development is the use of monodisperse hydrogel particles consisting of poly(NIPAM) chemically cross-linked with *N′*,*N′*-methylenebisacrylamide to form colloidal crystals and glasses in concentrated solution. This development is explored in an experimentally rigorous article (70).

A new possible application of colloidal microgels is as a support matrix for the immobilization of chemical entities. Solute molecules can freely enter the microgel structure, undergo a chemical reaction, and then the product can exit the polymer matrix. This offers a unique potential application for microgels as catalytic centers. Additionally, as the microgel can be used as an immobilized support and as a result of their characteristic high surface area-to-volume ratio (typically 10 m^2/g), they may find application for new approaches, eg, to peptide synthesis or combinatorial chemistry.

Conclusions

Microgels have become of enormous academic and commercial interest in recent years, with an exponential increase taking place in the number of published works on the subject. As the understanding of microgel structures and their physicochemical properties increases, their commercial utility expands simultaneously. Initial interest in these materials was suppressed because of their high manufacturing cost and limited availability. The development of high value products, such as cosmetics and specialist paints, incorporating microgels, allowed an expansion of their use. As the potential range of applications of these materials increases, the future utility of smart polymer matrixes seems unlimited, with innovation and invention being the controlling factor for their future utilization.

BIBLIOGRAPHY

1. M. Murray and M. J. Snowden, *Adv. Colloid Interface Sci.* **54**, 73 (1995); Y. Osada and S. B. Ross-Murphy, *Sci. Am.* **268**, 82 (1993).
2. M. J. Snowden and B. Z. Chowdhry, *Chem. Br.* **12**, 943 (1995).
3. M. Antonietti, *Angew. Chem. Int., Ed. Engl.* **27**, 1743 (1988).
4. W. Funke, *Br. Polym. J.* **21**, 107 (1989).
5. X. Wu and co-workers, *Colloid Polym. Sci.* **272**, 467 (1994).
6. Y. Hirose and co-workers, *Macromolecules* **20**, 1342 (1987).
7. S. Neyret and B. Vincent, *Polymer*, **38**, 6129 (1997).

8. M. Antonietti, T. Pakula, and W. Bremser, *Macromolecules* **28**, 4227 (1995).
9. R. Pelton, *Adv. Colloid Interface Sci.* **85**, 1 (2000).
10. B. R. Saunders and B. Vincent, *Adv. Colloid Interface Sci.* **80**, 1 (1999).
11. J. W. Goodwin and co-workers, *Br. Polym. J.* **5**, 347 (1973).
12. J. W. Goodwin, R. H. Ottewill, and R. Pelton, *Colloid Polym. Sci.* **257**, 61 (1979).
13. R. Pelton and P. Chibante, *Colloids Surf.* **20**, 247 (1986).
14. K. Tam, S. Ragaram, and R. Pelton, *Langmuir* **10**, 418 (1994).
15. A. Islam, B. Chowdhry, and M. Snowden, *J. Phys. Chem.* **99**, 14205 (1995).
16. A. Loxley and B. Vincent, *Colloid Polym. Sci.* **275**, 1108 (1997).
17. H. Tobita and Y. Uemura, *J. Polym. Sci.*, Part B: Polym. phys. **34**, 1403 (1996).
18. S. Zhu and A. Hamielec, *Makromol. Chem., Macromol. Symp.* **63**, 135 (1992).
19. K. Ishizu, M. Nunomura, and T. Fukutomi, *J. Polym. Sci.*, Part A: Polym. Chem. **25**, 1163 (1987).
20. B. Saunders, H. Crowther, and B. Vincent, *Macromolecules* **30**, 482 (1997).
21. M. Frank and W. Burchard, *Makromol. Chem., Rapid Commun.* **12**, 645 (1991).
22. S. Sahoo and co-workers, *J. Colloid Interface Sci.* **206**, 361 (1998).
23. H. Hooper and co-workers, *Macromolecules* **23**, 1096 (1990).
24. O. Okay, S. Sariisik, and S. Zor, *J. Appl. Polym. Sci.* **70**, 567 (1998).
25. R. Saito and K. Ishizu, *Polymer* **38**, 225 (1997).
26. C. Wu, *Polymer* **39**, 4609 (1998).
27. J. Mrkic and B. Saunders, *J. Colloid Interface Sci.* **222**, 75 (2000).
28. P. Dowding, B. Vincent, and E. Williams, *J. Colloid Interface Sci.* **221**, 268 (2000).
29. L. Nabzar and co-workers, *Langmuir* **14**, 5062 (1998).
30. N. Hatto, T. Cosgrove, and M. J. Snowden, *Polymer* **41**, 7133 (2000).
31. J. Lowe and co-workers, *Polymer* **39**, 1207 (1998).
32. K. Kratz, T. Hellweg, and W. Eimer, *Polymer* **42**, 6631 (2001).
33. M. Murray and co-workers, *J. Chem. Soc. Chem. Commun.* **15**, 1803 (1994).
34. K. Kratz, T. Hellweg, and W. Eimer, *Ber. Bunsen-Ges. Phys. Chem.* **102**, 1603 (1998).
35. H. M. Crowther and co-workers, *Colloids Surf., A* **152**, 327 (1999).
36. P. C. Griffiths and co-workers, *Colloid Polym. Sci.* **273**, 405 (1995).
37. R. Greenwood and co-workers, *J. Eur. Ceram. Soc.* **20**, 1707 (2000).
38. D. Kunz and W. Burchard, *Colloid Polym. Sci.* **264**, 498 (1986).
39. G. Morris, B. Vincent, and M. J. Snowden, *Prog. Colloid Polym. Sci.* **105**, 16 (1997).
40. B. R. Saunders and B. Vincent, *J. Chem. Soc., Faraday Trans.* **92**, 3385 (1996).
41. G. E. Morris, B. Vincent, and M. J. Snowden, *J. Colloid Interface Sci.* **190**, 198 (1997).
42. M. Irie, Y. Misumi, and T. Tanaka, *Polymer* **34**, 4531 (1993).
43. A. Hoffman, *J. Controlled Release* **6**, 297 (1987).
44. R. Freitus and E. Cussler, *Sep. Sci. Technol.* **22**, 911 (1987).
45. K. Hampton and W. Ford, *Abstract Papers of the American Chemical Society* **218**, 32 (COLL) (1999).
46. C. Wu and S. Zhou, *Macromolecules* **30**, 574 (1997).
47. I. Yamaoto, K. Iwasaki, and S. Hirotsu, *J. Phys. Soc. Jpn.* **58**, 210 (1989).
48. C. Wu and S. Zhou, *J. Macromol. Sci., B: Phys.* **36**, 345 (1997).
49. W. McPhee, K. Tam, and R. Pelton, *J. Colloid Interface Sci.* **156**, 24 (1993).
50. R. Iler, *The Chemistry of Silica: Solubility, polymerization, colloid and surface properties, and biochemistry*, Wiley-Interscience, New York, 1979.
51. D. Bastos and F. de las Nieves, *J. Colloid Polym. Sci.* **272**, 592 (1994).
52. M. Snowden and B. Vincent, *J. Chem. Soc., Chem. Commun.* **16**, 1103 (1992).
53. M. Wolfe, *Prog. Org. Coat.* **20**, 487 (1992).

54. D. Ole Kiminta, P. Luckham, and S. Lenon, *Polymer* **36**, 4827 (1995).
55. K. Tam, X. Wu, and R. Pelton, *Polymer* **33**, 436 (1992).
56. T. Ishidao and co-workers, *Macromolecules* **26**, 7361 (1993).
57. M. Mielke and R. Zimehl, *Prog. Colloid Polym. Sci.* **111**, 74 (1998).
58. H. Crowther and B. Vincent, *Colloid Polym. Sci.* **276**, 46 (1998).
59. P. F. Kiser, G. Wilson, and D. Needham, *Nature* 394, 459 (1998).
60. C. Ramkisson-Ganorkar and co-workers, *J. Controlled Release* **59**, 287 (1999).
61. S. Sahoo and co-workers, *J. Colloid Interface Sci.* **206**, 361 (1998).
62. G. Eichenbaum and co-workers, *Macromolecules* **32**, 4867 (1999).
63. G. Fern, J. Silver, M. J. Snowden, and R. Withnall, unpublished data, patent pending, (2002).
64. K. Hampton and W. Ford, *Abstract Papers of the American Chemical Society* **218**, 18 (POLY) (1999).
65. A. Biffis, *J. Mol. Catal. A* **165**, 303 (2001).
66. K. Ishii, *Colloids Surf., A* **153**, 591 (1999).
67. Y. Nakayama, *Prog. Org. Coat.* **33**, 108 (1998).
68. *Chem. Ind.* 494 (July 5, 1999).
69. Z. Hu and co-workers, *Adv. Mater.* **12**, 1173 (2000).
70. H. Senff and W. Richtering, *J. Chem Phys.* **111**, 1705 (1999).

L. S. BENEE
Pfizer Ltd
M. J. SNOWDEN
B. Z. CHOWDHRY
University of Greenwich

SOLUTION POLYMERIZATION. See BULK AND SOLUTION POLYMERIZATION.

S-POLYSTYRENE. See SYNDIOTACTIC POLYSTYRENE.

STABILIZATION. See Volume 4.

STATISTICAL THERMODYNAMICS

Introduction

The objective and mode of thinking of statistical thermodynamics, its elementary tools, and model building are directly relevant to polymer physics. This article introduces the subject and relevant key references from a modern point of view. Perhaps the best introductory material is the problem source book (1,2), while Reference 3 is a standard reference. Minimum prerequisites are the rudiments of thermodynamics (4,5), and mechanics (6,7). Understanding of probability is very helpful (8).

Encyclopedia of Polymer Science and Technology. Copyright John Wiley & Sons, Inc. All rights reserved.

Objective and Mode of Thinking

Macroscopic objects contain many atoms and molecules. Although these elements may obey the laws of (quantum) mechanics, it is extremely costly, and often meaningless, to know the mechanical motion of each element. Fortunately, these objects obey their own macroscopic laws, as demonstrated empirically. Typical examples of these laws are thermodynamics and hydrodynamics. These laws describe relations among macroscopic observables. They are usually called phenomenological laws and are often regarded as less fundamental than, eg, the laws of mechanics. However, the laws of, eg, thermodynamics are asymptotically exact, and should not be regarded as an inaccurate approximation of something more fundamental. It should not be forgotten that the laws of mechanics are also empirical laws. The founding fathers of statistical mechanics, including Gibbs and Einstein, tried to justify thermodynamics with mechanics, but the subsequent history tells us that the mechanics they relied on was less reliable than thermodynamics.

To understand systems consisting of many elements with the aid of thermodynamics and mechanics is the objective of statistical thermodynamics. The advent of single macromolecule experimental methods emphasizes the importance of the study of mesoscopic systems and fluctuations. Macroscopic and mesoscopic observables (henceforth simply called macro-observables) are interpreted as sums of many microscopic quantities or coarse-grained stochastic quantities. Thus, elucidating macroscopic or mesoscopic behavior in terms of the properties of elements inevitably becomes statistical. The laws of large numbers and the large deviation principle (8) become the key mathematical tools.

The problems in statistical thermodynamics fall into two categories. The first category involves the study of the structure of phenomenological framework and the interrelations among macro-observables without calculating their actual values. The second category involves the calculation of the actual values of parameters appearing in the phenomenology from more microscopic parameters. The first category concerns finding and explaining the relationships among macro-observables appearing in the description of a class of states of materials. The two main problems are to recognize well-defined classes of phenomena, called universality classes, and to construct suitable models (the so-called minimal models) for these classes. These models are statistical but their elements need not be molecules or atoms. There is a wide range of choice of elementary objects; truly atomistic pictures can even be counterproductive. A typical problem in the second category is to compute phenomenological parameters, eg, viscosities or phase-transition temperatures, which, by definition, reflect the specificity of the individual systems. For the second-category problems, the source of the microscopic parameters is delicate; they are often obtainable only through macroscopic comparisons. Thus, it is difficult to obtain model-free conclusions, although practically useful results may be obtained.

Equilibrium Problems

The main theoretical framework of the static aspect of statistical thermodynamics is Gibbs statistical mechanics. The universal behavior of macroscopic objects

can be described phenomenologically with the aid of equilibrium thermodynamics with five major laws [(4,5); those who are serious about thermodynamics must read Ref. 9]: the existence of thermal equilibrium and temperature (the zeroth law); the conservation of energy (the first law); the variational principle for entropy (the second law); the inaccessibility of the absolute zero temperature (the third law); and the clear distinction between extensive and intensive quantities (sometimes called the fourth law). The equilibrium states of macroscopic objects comprise a universality class characterized by equilibrium thermodynamics, and statistical ensembles should be understood as minimal models for this class.

All macroscopic observables are obtainable from the distribution of microscopic states (henceforth, microstates) of elements that obey mechanics. Strictly speaking, this is the most basic assumption of statistical thermodynamics. However, to elucidate macroscopic phenomena, it is not necessary to know the true distribution of microstates of the system. Boltzmann introduced the concept of orthodic ensembles that are compatible with thermodynamics. In practice, an orthodic ensemble is established by demonstrating that it is compatible with the laws of mechanics and with the laws of thermodynamics. Gibbs demonstrated that the canonical distribution function

$$P(\{q\}) = \frac{1}{Z}\, \mathrm{e}^{-H(\{q\})/k_{\mathrm{B}}T} \tag{1}$$

with the micro–macro relation dictated by the expression for the Helmholtz free energy A:

$$A = -k_{\mathrm{B}}T \log Z \tag{2}$$

satisfies the above compatibility requirement. Here, $\{q\}$ collectively denotes the microscopic coordinates, $H(\{q\})$ is the Hamiltonian of the system, k_{B} is the Boltzmann constant, and T is the absolute temperature. Z is the normalization constant of the distribution called the canonical partition function:

$$Z = \sum \mathrm{e}^{-H/k_{\mathrm{B}}T} \tag{3}$$

where the summation is the sum (integral) over all the microscopic states. A physical derivation of the canonical ensemble was given by Einstein, whose starting point was the principle of equal probability: the probability of finding a microstate on a constant-energy surface is independent of the microstate (the microcanonical ensemble). Einstein introduced the canonical ensemble as a subensemble of a microcanonical ensemble. Then, he identified heat as the energy imported to the microscopic degrees of freedom, and derived equation 2 (for a historical account see Ref. 10). There are many arguments demonstrating the naturalness of the canonical distribution. Lenard (11) demonstrated, crudely put, that the distribution of microstates as given by the canonical distribution is equivalent to

the second law in the form of "passivity", $\Delta A \leq W$, where W is the work done to the system to change it from an initial to a final equilibrium state at the same temperature, with ΔA being the free-energy change between these two states. A stronger statement is possible [Jarzynski's equality (12)]

$$\left\langle \mathrm{e}^{-W/k_B T} \right\rangle = \mathrm{e}^{-\Delta A/k_B T} \tag{4}$$

Here, $\Delta A = A_b - A_a$, where A_s is the Helmholtz free energy of the equilibrium state with the Hamiltonian H_s ($s = a$ or b) with the temperature T, and $\langle\ \rangle$ implies the average over many experiments, where W is the work in each run of the experiment changing the Hamiltonian from H_a to H_b according to a fixed protocol with the initial ensemble given by the canonical distribution $\propto \mathrm{e}^{-H_a/k_B T}$. Although it is not easy to use this equality for a macroscopic system, it is practically useful for single-molecule experiments (cf. 13).

Mathematically speaking, statistical mechanics must study a system in the thermodynamic (large system) limit. In this limit, the system Hamiltonian does not exist. Thus, we need an indirect way to introduce the distribution (measure) in the thermodynamic limit. This is the theory of the Gibbs measure (14,15). If we wish to understand phase transitions as mathematical singularities of thermodynamic potentials, we must take the thermodynamic limit. When the Gibbs measure for a system is not unique the system exhibits a phase transition.

If we look at a small portion of a macroscopic system or study a mesoscopic system, we must study fluctuations. The probability of fluctuations is phenomenologically described by the thermodynamic theory of fluctuations (5). From the ensemble theory point of view, the fluctuation theory is the study of large deviations from the expectation value. This is the reason why large deviation theory is becoming increasingly important in statistical thermodynamics. Standard works on large deviation theory are References 16 and 17; perhaps as accessible introduction to the topic may be found in Reference 18.

Nonequilibrium Problems

Even more challenging problems than those discussed above arise from the consideration of time-dependent and nonequilibrium properties of macroscopic systems. Unfortunately, there is no general theoretical framework tantamount to the Gibbs statistical mechanics. Most likely, there is no universality class that can be called the macroscopic nonequilibrium class. There is, however, a class that may be called the linear nonequilibrium class. Its phenomenological framework is the linear nonequilibrium thermodynamics, which contains several fundamental laws: the second law as the positivity of entropy produced inside the system as a result of dissipation; phenomenological linear force–flux relations; and the Onsager reciprocity stating the symmetry relations among kinetic coefficients (19,20). We also assume that thermodynamic relations hold locally in space (this is called the local equilibrium assumption).

The fundamental statistical thermodynamic idea for the linear nonequilibrium class is that fluctuations can spontaneously realize nonequilibrium states in

a (small) part of a large equilibrium system. A precise formulation was given as Onsager's regression hypothesis: the decay dynamics of fluctuations is on the average the macroscopic laws governing the time evolution of macro-observables. At least formally, for example, the Navier–Stokes equation (and the associated heat equation) may be derived as the equation governing the fluctuation of the velocity field (21). The statistical principle is given as Onsager's principle [so christened by Hashitsume (22)] that can be summarized, in modern terms, roughly as follows: the Lagrangian of the Onsager–Machlup path integral is given by the large deviation function for the microscopic fluctuations. This framework tells us that the response of an observable of a system to a small external disturbance is controlled by the fluctuation dynamics of the observable [fluctuation–dissipation relations (FDR) (23,24)]. The FDR of the first kind relates the flux–flux correlation function to the corresponding transport coefficient (the Green–Kubo relations), and the FDR of the second kind gives the relation between the autocorrelation of the noise and the mobility (25). The formula for the intrinsic viscosity in terms of polymer force flux may be a familiar example for polymer scientists (26). The FDR of the second kind is of supreme importance in the construction of minimal models to elucidate time-dependent properties of systems (27) close to equilibrium. Although FDR is often called the fluctuation–dissipation theorem, its derivation is always a combination of microscopic argument and phenomenological requirements, as clearly stressed by Nakano (24).

Needless to say, most interesting phenomena in nonequilibrium are not linear. These phenomena cannot be in the class considered above, but usually they are modeled in terms of nonlinear Langevin equations of the following form (Zwanzig's nonlinear Langevin equation):

$$\frac{\mathrm{d}A}{\mathrm{d}t} = v(A) - L\frac{\delta \mathcal{F}}{\delta A} + f \tag{5}$$

or the corresponding Fokker-Planck equation describing the time evolution of the distribution function (28–30). Here, $\boldsymbol{v}(\boldsymbol{A})$ is called the streaming term, L is the (bare Onsager) kinetic coefficient (matrix), $\mathcal{F}$ is the free-energy functional, and $\boldsymbol{f}$ is the noise satisfying the FDR of the second kind: $\langle \boldsymbol{f}\, \boldsymbol{f}(t)\rangle = 2k_{\mathrm{B}}TL\delta(t)$. It is assumed that the equilibrium distribution of $\boldsymbol{A}$ is described by the distribution function proportional to $\exp(-\mathcal{F}/k_{\mathrm{B}}T)$. The streaming term $\boldsymbol{v}$ in equation 5 is often expanded in terms of the polynomials of $\boldsymbol{A}$. When this expansion is truncated at the second order, equation 5 becomes the starting point of the mode-coupling theory and dynamical renormalization group theory, with a remarkable success in critical dynamics (31). The use of the mode-coupling theory for supercooled liquids and glasses seems to be an increasingly important topic with highly interesting results (32), but its microscopic foundation is still a difficult question.

It seems that all the successfully elucidated dynamical universality classes adopt as their minimal models the ones described in terms of nonlinear Langevin equations (33). This indicates the general correctness of Onsager's principle as a fundamental principle (beyond the linear regime). Just as equilibrium statistical mechanics is a statistical framework based on the principle (of equal

probability) compatible with the phenomenological laws (equilibrium thermodynamics), nonequilibrium statistical mechanics exhibits the same structure. Thus, to deepen our understanding of nonequilibrium phenomena and to go beyond the linear regime, we need clear phenomenological understanding of a wider class of phenomena. There are some attempts (34,35), but there is no consensus.

Synopsis and Examples

Statistical thermodynamics is a discipline that elucidates phenomenological laws of a class of phenomena (a universality class) from analyses of statistical models that capture the salient features of the class (minimal models). The principal objective of statistical thermodynamics is to recognize universality classes and to find corresponding minimal models. Examples follows from polymer solution theory.

Dilute Solution. If the interchain interactions can be ignored, the polymer solution is in the dilute regime. If we are interested in the global features of a polymer, we need not respect the discreteness of each bond; we may use the Wiener process to describe the chain [thanks to Donsker's invariance principle (36)]. The interaction among nonbonded monomer units gives the well-known excluded-volume interaction and is usually mimicked by a delta-function pseudopotential. Thus, a chain described by the Wiener process interacting with itself through a delta-function pseudopotential (with an interaction contour-range cutoff) is conceived as a minimal model for static properties of dilute solutions [the Edwards model (37)]. The partition function of a chain can be conveniently described in terms of the path integral (the Feynman–Kac formula) (38,39). RG theory (for general introduction, see Refs. 40–43) has given various quantitative results for universal properties; agreement with experiment looks satisfactory (44–46). That is, we can clearly recognize a universality class of dilute-solution statics with a good minimal model.

To understand dynamics and transport properties, a set of (nonlinear) Langevin equations describing the Edwards model and the solvent velocity field is proposed as a minimal model. Comparison of the outcome of the model with experimental results has revealed that this minimal model is reasonable (47); but closely studied, less than minimal. The importance of the direct chain–chain friction must not be underestimated (48). With this additional effect, the model seems minimal, but a more careful study may be needed.

Semidilute Systems. In more concentrated solutions, the interchain interactions (overlap) cannot be ignored. Even if the monomer number density of the solution is infinitesimal, long chains can overlap extensively. This regime is the semidilute solution recognized by des Cloizeaux. In this regime the interchain interactions may still be described by the delta-function pseudopotential. For equilibrium properties the many-chain version of Edward's minimal model seems appropriate (49,50). Thus, we have the universality class of semidilute solution statics with a reliable minimal model. For dynamics, since there is extensive chain overlap, the chain entanglement cannot be ignored. The straightforward

many-body version of the dilute-solution minimal Langevin model is intractable and it is fair to say that our understanding of semidilute-solution dynamics is incomplete (51). As a minimal model, a model of fluids with the strain field effect by Doi and Onuki should be studied seriously (33). To understand dynamics in polymer solutions in general, careful simulations would become increasingly important (52).

Beyond Semidilute Solutions. Further increase of concentration gives the concentrated regime and the melt regime. Beyond the semidilute regime, the minimal model mentioned above is not adequate, because the volume fraction is now finite and it really exerts entropic forces (53). If the static model is not in a good shape, it should be clear that we do not have a reliable minimal model for dynamics of nondilute solutions. We must take into account entanglement and direct friction as well as the hydrodynamic interactions. Thus, from the statistical thermodynamic point of view, real understanding of many polymer chain systems is still beyond our reach.

BIBLIOGRAPHY

"Statistical Thermodynamics" in *EPSE* 2nd ed., Vol. 15, pp. 614–625, by Y. Oono, University of Illinois.

1. M. Toda, R. Kubo, and N. Saito, *Statistical Physics I Equilibrium Statistical Mechanics*, Springer-Verlag, New York, 1983.
2. R. Kubo, H. Ichimaru, T. Usui, and N. Hashitsume, *Statistical Mechanics*, North Holland, Amsterdam, 1965.
3. L. D. Landau and E. M. Lifshitz, *Statistical Mechanics*, Pergamon Press, London, 1980.
4. R. Kubo, H. Ichimaru, T. Usui, and N. Hashitsume, *Thermodynamics*, North Holland, Amsterdam, 1968.
5. H. B. Callen, *Thermodynamics*, Interscience Publishers, New York, 1960.
6. L. D. Landau and E. M. Lifshitz, *Mechanics*, Pergamon Press, London, 1976.
7. G. A. Baym, *Lectures on Quantum Mechanics*, Benjamin/Cummings Publishing Co., Reading, Mass., 1973.
8. R. Durrett, *Probability: Theory and Examples*, Wadsworth & Brooks Cole, Pacific Grove, Calif., 1991.
9. E. H. Lieb and J. Yngvason, *Phys. Rep.* **310**, 1 (1999).
10. L. Navarro, *Arch. Hist. Exact Sci.* **53**, 147 (1998).
11. A. Lenard, *J. Stat. Phys.* **19**, 575 (1978).
12. C. Jarzynski, *Phys. Rev. Lett.* **78**, 2690 (1997).
13. J. Liphardt, S. Dumont, S. B. Smith, I. Tinoco Jr., and C. Bustamante, *Science* **296**, 1832 (2002).
14. D. Ruelle, *Statistical Mechanics, Rigorous Results*, Benjamin, New York, 1969.
15. R. B. Israel, *Convexity in the Theory of Lattice Gases*, Princeton University Press, Princeton, 1979.
16. J.-D. Deuschel and D. W. Strook, *Large Deviation*, Academic Press, New York, 1989.
17. R. S. Ellis, *Entropy, Large Deviations, and Statistical Mechanics*, Springer-Verlag, New York, 1985.
18. Y. Oono, *Prog. Theor. Phys. Suppl.* **99**, 165 (1989).

19. I. Prigogine, *Introduction to Thermodynamics of Irreversible Processes*, 2nd ed., Wiley-Interscience, New York, 1961.
20. S. R. de Groot and P. Mazur, *Nonequilibrium Thermodynamics*, North Holland, Amsterdam, 1969 [A Dover edition is also available].
21. K. Miyazaki, K. Kitahara, and D. Bedeaux, *Physica A* **230**, 600 (1996).
22. N. Hashitsume, *Prog. Theor. Phys.* **8**, 461 (1952).
23. R. Kubo, *Rep. Prog. Phys.* **29**, 255 (1966).
24. H. Nakano, *Int. J. Mod. Phys. B* **7**, 2397 (1993).
25. H. Mori, *Prog. Theor. Phys.* **33**, 424 (1965).
26. M. Bixon, *Annu. Rev. Phys. Chem.* **27**, 65 (1976).
27. B. J. Berne, ed., *Statistical Mechanics, Part B: Time-Dependent Processes*, Plenum Press, New York, 1977.
28. H. Risken, *The Fokker–Planck Equation*, 2nd ed., Springer-Verlag, Berlin, 1989.
29. C. W. Gardiner, *Handbook of Stochastic Methods for Physics, Chemistry and the Natural Sciences*, 2nd ed., Springer-Verlag, Berlin, 1985.
30. N. G. van Kampen, *Stochastic Processes in Physics and Chemistry*, North Holland, 1981.
31. K. Kawasaki, *Ann. Phys.* **61**, 1 (1970).
32. W. Götze and L. Sjögren, *Rep. Prog. Phys.* **55**, 241 (1992).
33. A. Onuki, *Phase Transition Dynamics*, Cambridge University Press, Cambridge, 2002.
34. D. Jou, J. Casas-Vásquez, and G. Lebon, *Extended Irreversible Thermodynamics*, Springer-Verlag, New York, 1993.
35. Y. Oono and M. Paniconi, *Prog. Theor. Phys. Suppl.* **130**, 27 (1998).
36. M. D. Donsker, *Mem. Am. Math. Soc.* **6** (1951).
37. S. F. Edwards, *Proc. Phys. Soc.* **85**, 613 (1965).
38. R. P. Feynman, *Statistical Mechanics*, Benjamin/Cummings Publishing, Co., Reading, Mass., 1972.
39. I. M. Gel'fand and A. M. Yaglom, *J. Math. Phys.* **1**, 48 (1960).
40. M. E. Fisher, in F. J. W. Hahne, ed., *Lecture Notes in Physics*, Vol. **186**, Springer-Verlag, New York, 1983.
41. M. Le Bellac, *Quantum and Statistical Field Theory*, Oxford University Press, Oxford, 1991.
42. N. D. Goldenfeld, *Lectures on Phase Transitions and the Renormalization Group*, Addison-Wesley Publishing Co., Inc., Reading, Mass., 1992.
43. Y. Oono, *Advances in Chemical Physics*, Vol. **61**, Wiley-Interscience, New York, 1985, Chapt. 5.
44. P. G. de Gennes, *Scaling Concepts in Polymer Physics*, Cornell University Press, Ithaca, N.Y., 1980.
45. M. Daoud, J. P. Cotton, B. Farnoux, G. Jannink, G. Sarma, H. Benoit, R. Duplessix, C. Picot, and P. G. de Gennes, *Macromolecules* **8**, 804 (1975).
46. J. des Cloizeaux and G. Jannink, *Polymers in Solution: Their Modelling and Structure*, Oxford University Press, Oxford, 1990.
47. W. Brown and T. Nicolai, in W. Brown, ed., *Dynamic Light Scattering*, Oxford University Press, Oxford, 1993, p. 272.
48. Y. Shiwa and Y. Tsunashima, *Physica A* **197**, 47 (1993).
49. T. Ohta and A. Nakanishi, *J. Phys. A* **16**, 4155 (1983); T. Ohta and Y. Oono, *Phys. Lett. A* **89**, 460 (1982).
50. L. Schäfer, *Excluded Volume Effects in Polymer Solutions, as Explained by the Renormalization Group*, Springer, Berlin, 1999.
51. G. C. Berry, *Adv. Polym. Sci.* **114**, 233 (1994).

52. B. Dünweg, D. Reith, M. Steinhauser, and K. Kremer, *J. Chem. Phys.* **117**, 914 (2002); P. Ahlrichs, R. Evraers, and B. Dünweg, *Phys. Rev. E* **64**, 040501(R) (2001).
53. Y. Shiwa, Y. Oono, and P. W. Baldwin, *Mod. Phys. Lett. B* **4**, 1421 (1990).

YOSHITSUGU OONO
University of Illinois

STRESS RELAXATION. See VISCOELASTICITY.

STRUCTURAL REPRESENTATION OF POLYMERS

Introduction

Since virtually the dawn of modern chemistry, scientists have found it desirable to represent chemical substances by name, and also, where possible, by a structure that shows how the atoms are connected. Storage of information about a substance, whether on paper or in a computer database, is of value only if a substance can be located, for example by use of its name, molecular formula, structure, or some combination of these; otherwise the substance record, together with any attached data, is essentially lost.

Knowledge of these three key properties of a substance affords versatility in its retrieval. This is relatively easy for substances that are nonpolymeric in nature; although the molecular formula of a substance is usually not unique, its molecular formula together with a unique systematic name, a unique structure, or both, are sufficient to distinguish a nonpolymeric substance from all other substances.

However, for polymers, these statements are not completely true. By its very nature, a polymer is usually not a single, discrete substance, but rather a mixture of somewhat different molecules. Although these have strong similarities to one another, at the molecular level probably no two individual molecules are identical in terms of such properties as chain length (molecular weight), linearity (degree of branching or cross-linking), arrangement of repeating units (alternating, block, random, statistical, etc), or conformation (spatial arrangement of atoms within a chain).

Thus, polymers are inherently different from nonpolymers, and many attempts have been made to define what constitutes a polymer. The International Union of Pure and Applied Chemistry (IUPAC), an international consortium

Encyclopedia of Polymer Science and Technology. Copyright John Wiley & Sons, Inc. All rights reserved.

composed of professional scientists who propose and recommend standards for chemical nomenclature and structure representation, defines a *polymer* as "a substance composed of molecules characterized by the multiple repetition of one or more species of atoms or groups of atoms (constitutional units) linked to each other in amounts sufficient to provide a set of properties that do not vary markedly with the addition or removal of one or a few constitutional units" (1).

A polymer may be assigned a unique name, eg, poly(oxy-1,2-ethanediyl) (structure-based) or poly(oxirane) (source-based), but since such nomenclature (see NOMENCLATURE) incorporates no properties such as molecular weight, these names per se are insufficient to distinguish one sample from another. Likewise, any single complete molecular formula that represents a discrete molecule within the polymer is inadequate to describe the whole polymeric mixture, and to write a molecular formula for every distinct molecule present in a polymer would be hopeless. Therefore, compromises must be made. This article describes the current situation with regard to structural representation of polymers.

General Discussion

Polymer structural representation has two purposes:

(1) identification—to distinguish a given polymer from all others
(2) description—to record structural details that will enable the polymer to be retrieved in all searches for appropriate classes of polymers.

The ideal representation of a polymer is perhaps one that includes all known structural information; that is, the structure of the polymer itself *and* the structures of the substance(s) from which it was formed. This is usually impracticable; most polymers are represented in just one of these two ways.

Structure-based polymer representation: the polymer is represented in terms of the structure of its constitutional or structural repeating unit. Two common expressions are in use: "constitutional repeating unit" (CRU)—preferred by IUPAC; and "structural repeating unit" (SRU)—preferred by Chemical Abstracts Service (CAS) (2) (see Chemical Abstracts Service Information System); the two are virtually synonymous, and SRU will be used in this article. For example, polyethylene can be represented by the SRU$-(-CH_2-)_n-$ (the largest fragment that can be written without repetition) or by the SRU$-(-CH_2-CH_2-)_n-$ (obtained by opening the double bond in ethylene). (IUPAC recommends that in printed communications the subscript "n" as well as any other letters denoting multiplicities of polymeric sequences be printed in italic type or, in the absence of italics, be underlined. This article, which addresses primarily database records and their retrieval, indicates subscripts in the upright style without underlining.)

Source-based polymer representation (also called product-by-process representation): the polymer is represented in terms of the names and structures (where known) of the substance(s) from which the polymer was formed. For example, polyethylene is represented by the expression $(CH_2{=}CH_2)_x$, because the structure of the monomer, ethylene, from which it is made is $CH_2{=}CH_2$.

Source-based polymer representation preceded structure-based representation because polymers were made before they were structurally characterized. The

introduction of structure-based representation, however, did not render source-based representation obsolete, and currently the two complementary systems coexist. Source-based representation continues to exist for several reasons:

(1) For some polymers the method is preferable to structure-based representation. For example, the source materials used to manufacture Bakelite™ or Melmac™ are, in practice, more important than their structures; even if all the SRUs present in these highly cross-linked polymers could be delineated, to represent them thus would serve little purpose.
(2) Many source-based names are sufficiently explicit for the structures to be instantly deducible by scientists; therefore it is unnecessary to state them.
(3) For condensation polymers prepared from three or more monomers, it is impossible to write a meaningful SRU unless special additional rules are formulated to create an artificial or stylized one.
(4) Source-based names often lend themselves more easily to verbal and written communications, eg, "polycaprolactone" versus "poly[oxy(1-oxo-6-hexanediyl)]".
(5) Some problems concerning structure-based representation remain unresolved in terms of their delineation in a computer database. For example, the structure representation of an SRU within a larger SRU still poses software problems for CAS. The CAS Registry System, designed over 30 years ago, cannot handle a structural representation like the one shown in Figure 1a (SRU within a larger SRU). It does provide a source-based representation, as shown in Figure 1b, with two monomers of the type $(A{\cdot}B)_x$, one of which is an SRU with two hydroxy end groups and the other a dicarboxylic acid (2).

Thus, CAS can register an SRU within a polymer, eg, $[U{-}(A)_n{-}V{\cdot}B]_x$, and a polymer within a polymer, eg, $[(A)_x{\cdot}B]_x$, but not an SRU within an SRU, eg, $[(A)_n{\cdot}B]_n$.

Such complex structure-based representations pose no problems for more recent systems such as MDL's ISIS™ program with features designed expressly for polymer structure storage and retrieval.

In contrast, for many polymer classes, especially those that result from considerable chemical transformation of starting materials, it is more useful to represent them by structure than in terms of the source materials used to prepare them.

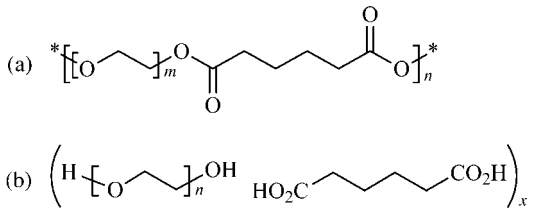

Fig. 1. Representations of polyester from hexanedioic (adipic) acid and poly(oxy-1,2-ethanediyl) [poly(oxyethylene)]; asterisks at ends of SRU denote unspecified end groups.

The structure of a polymer is generally displayed by representing it as a parenthesized expression with a subscript letter outside the closing parenthesis. Two such expressions are commonly used:

(1) For structure-based polymer representation, the expression used is $-(-A-)_n-$, where A represents the SRU of the polymer and the subscript n indicates that A is repeated an indefinite number of times. An SRU is an atom-by-atom or group-by-group representation of the smallest unit that, when repeated, in theory—and sometimes in reality—represents the polymer. Thus, poly(oxymethylene) can be expressed as $-(-O-CH_2-)_n-$.

(2) For source-based polymer representation, the expression used is $(A{\cdot}B{\cdot}\ldots)_x$, where A, B, etc, represent the atom-by-atom or group-by-group representation(s) of polymerizable substance(s) used to prepare the polymer and the subscript x indicates that A, B, etc, are repeated an indefinite number of times. Thus, nylon-6,6 can be expressed as $(H_2N-(CH_2)_6-NH_2{\cdot}HO_2C-(CH_2)_4-CO_2H)_x$.

Expressions such as $-(-O-CH_2-)_n-$ and $(H_2N-(CH_2)_6-NH_2{\cdot}HO_2C-(CH_2)_4-CO_2H)_x$ depict actual structures, not molecular formulae. Although expressions such as $(CH_2O)_n$ and $(C_6H_{16}N_2{\cdot}C_6H_{10}O_4)_x$ are used by CAS to represent the molecular formulae of poly(oxymethylene) and nylon-6,6 respectively, these expressions are, per se, neither structure-based nor source-based representations of these two polymers. There is a link, however, between the full structural representation and its molecular formula. The subscript n is used consistently for both an SRU and its molecular formula; similarly, the subscript x is used consistently for both a homopolymer (copolymer) structure expressed in terms of monomer(s) and its corresponding molecular formula.

These two types of representation, both of which are more theoretical than actual (although they can be actual), have advantages and disadvantages.

For structure-based polymer representation the advantages and disadvantages are as follows.

(1) **Advantages:**

a. The theoretical (which is sometimes the actual) repeating unit of the polymer is depicted precisely and unambiguously.

b. If structural irregularities in the polymer are ignored, there is presumably no doubt about the exact structure.

c. End groups may be indicated by modification of the expression $-(-A-)_n-$ to a format such as $U-(-A-)_n-V$, where U and V are structures of end groups; thus, α-methacryloyl-ω-methoxypoly(oxyethylene) is represented by the expression $CH_2{=}C(CH_3)-CO-(-O-CH_2-CH_2-)_n-OCH_3$. The corresponding molecular formula is written in the format $(A)_nW$, where A is the molecular formula of the SRU (exclusive of end groups) and W is the summation of molecular formulae of end groups U and V; thus, W (atom count) = U (atom count) + V (atom count). In the

latter case, however, without a name or structure, it is sometimes impossible to determine which atoms belong to U and which to V. Thus, the two SRUs α-methacryloyl-ω-methoxypoly(oxyethylene) and α-acryloyl-ω-ethoxypoly(oxyethylene) are represented by the same molecular formula expression $(C_2H_4O)_n\ C_5H_8O_2$.

(2) **Disadvantages:**

a. The method fails to indicate the monomers from which the polymer was prepared; for a polymer chemist this is frequently an important consideration.
b. For polymers prepared from asymmetrical monomers that give rise to a product containing several SRUs, the pedantry involved in naming every possibility can become tedious.

(3) For source-based polymer representation the advantage and disadvantages are as follows.

(4) **Advantage:**

a. A polymer can always be represented in terms of the monomers used to synthesize it, even if the structures of some of them are imprecisely defined (eg, castor oil). It must be pointed out, however, that monomers can never, per se, show the structure of a polymer containing them; the reader must use other knowledge to deduce it.

(5) **Disadvantages:**

a. The atom-by-atom structure of the polymer is not depicted, even when it can be deduced with some degree of certainty.
b. Scattering of information may occur from either or both of the following sources: (a) the same polymer may be synthesized from different monomers; (b) under different reaction conditions the same monomer(s) may give rise to more than one polymer structure.

Some polymers are traditionally represented by the structure-based method, some by the source-based method, and others by both methods, but always as separate expressions, rather than one all-encompassing expression.

Provided (*1*) both structure-based and source-based types of representation are stored, (*2*) all practical representational possibilities for both types are stored, and (*3*) the storage/retrieval system is capable of retrieving all stored representations when only one is specified, a key advantage of using separate expressions for representations of a polymer is that searchers can find a polymer by searching any possible representation. Currently, condition (*1*) is sometimes met, whereas conditions (*2*) and (*3*) are frequently not, which results in scattered data and frequent failure to retrieve critical information.

Seemingly random use of structure-based and source-based representations with no cross-referencing between them has resulted in decades of confusion.

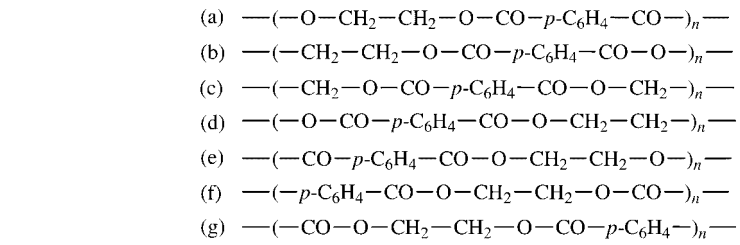

Fig. 2. "Phase-shift" versions of PET represented as an SRU. While it is possible to write seven structures, as far as CAS searching is concerned, both the human searcher and the CAS Messenger computer program recognize that (**a**) = (**e**), (**b**) = (**d**), and (**f**) = (**g**).

For even the simplest of polymers, a searcher is faced with three fundamental questions: (*1*) is the desired polymer represented as structure-based or source-based; (*2*) if it is structure-based, how is the structure drawn; (*3*) if it is source-based, what monomers were used? To take a polyester example, a question such as whether parent acids or simple derivatives (eg, methyl esters or phenyl esters or acid chlorides) were used is often far more important to a polymer scientist than the structure of the final polymer.

Any polymer representation used for identification must be predictable, ie, easily arrived at by a searcher applying a set of rational and invariable rules. Without knowledge of rules for determining the order of an atom-by-atom representation of an SRU, a searcher seeking information on poly(ethylene terephthalate) (PET), for example, would theoretically have to search for all seven structures shown in Figure 2.

Each of these would have a unique name, and so a search by name, vice one by structure, would not narrow the number of possibilities.

CAS (2) and IUPAC (3) have devised rules for the orientation of SRUs that, when followed, reduce a searcher's choices to one of the above seven; the preferred structure for PET is shown as Figure 2a.

Until September 2002, searchers faced an essentially insolvable problem in a search for source-based representations for PET. A searcher might think of searching only for the two representations shown as Figures 3a and 3b; the representation shown as Figure 3c, which represents PET synthesized by a modern, industrially significant route, would thus not be retrieved.

A search for source-based representations for a polymer therefore depended upon a searcher's ability to surmise how it might be represented; in other words, it was a guessing game.

The three above-listed questions arise for searches involving only simple polymers; for more complex polymers, further questions arise such as how many

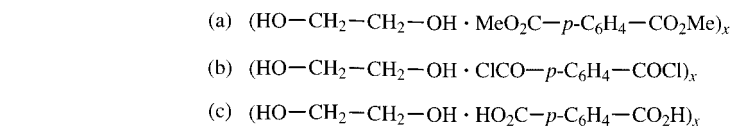

Fig. 3. Different expressions for source-based representations of PET.

comonomers were used to prepare them, whether end groups need to be considered, and whether the polymers are aftertreated (post-treated), block, branched, comb, cross-linked, dendritic, graft, star, etc.

To say that one polymer is or is not different from another will always require some arbitrary judgment of what is or is not significant in polymer identification. For example, are the two polymers represented by the source-based expressions shown as Figures 3a and 3c sufficiently "different" to be worthy of two separate representations? In terms of source-based polymer registration, CAS regards them as two separate polymers. Some industrial consumers of PET may find that the presence of carboxy end groups rather than methoxycarbonyl ones makes no difference for their particular application, while others may find that end group composition makes an appreciable difference to product properties; thus, the answer may depend upon many factors.

It must also be pointed out that neither structure-based nor source-based representation currently takes into account any structural irregularities. Real polymers, as synthesized, are seldom structurally perfect. Depending on the type of polymer, various kinds of structural irregularities may arise during a polymerization process.

Some examples are given below:

(1) PET may contain irregularities known as "ether defect," a colloquial name indicating the presence of some —O—CH_2—CH_2—O—CH_2—CH_2—O— moieties.

(2) Depending upon polymerization concentration, difunctional acrylic compounds (eg, ethylene diacrylate) may give polymers that are hyperbranched, hyper-cross-linked, or both.

(3) Low density polyethylene is irregularly branched.

(4) Polymers formed between simple diamines (eg, 1,5-pentanediamine) and simple dihalo compounds (eg, 1,5-dichloropentane) are frequently branched, cross-linked, or both.

Such irregularities, which may vary from batch to batch, can affect polymer properties appreciably.

Thus polymer structures represented on paper or stored in a database as ideal or theoretical representations are frequently not true representations of actual polymer structures. Before September 2002 all these problems and questions posed significant difficulties for the average polymer searcher. The following sections discuss what has been achieved to date in terms of organizing polymer structures and nomenclature, and of facilitating polymer searching.

In September 2002, CAS introduced a new on-line search-tool called POLYLINK, which is designed to solve the above problems regarding "phase-shift" and retrieval of structure-based representations and their source-based counterparts (4).

Organizations and Databases

Over the last 50 years, two major organizations, CAS and IUPAC, have tackled the daunting task of how best to represent polymer structures. Their achievements

are impressive, and the two organizations are in virtually complete agreement on structure-based and source-based representations of polymers, both on paper and in searchable on-line databases such as the CAS Registry File. However, much still remains to be done; some aspects of copolymer representation need enhancement, and such newer areas as aftertreated (post-treated), comb, dendritic, and star polymers are handled inadequately.

In addition to these organizations, computer software companies such as Daylight and MDL Information Systems, Inc. (MDL) offer for sale computer programs that are suitable for either mainframe or personal computers, and many companies use them to create their own proprietary databases containing agricultural chemicals, pharmaceuticals, polymers, etc. Some computer programs accommodate chemical structures only, while others accommodate textual data only. MDL's ISIS™/Host is a computer program that enables users to combine chemical structures from one file with textual data from another to produce an integrated product. MDL's ISIS program enables users to register a wide variety of polymer structures.

Storage and Retrieval of Polymer Structures

Storage of Polymer Structures. CAS has developed comprehensive sets of nomenclature rules and structure conventions that have become standards in the world of chemical literature (see Chemical Abstracts Service Information System). CAS selects polymers for indexing according to a set of rules (5). The Registry File records are created from chemical information published in books, patents, dissertations, scientific journal articles, etc.

MDL's ISIS program permits registration of polymer structure representations as source-based, structure-based, or both. Users who create their own databases with such a program are therefore free to store polymer representations in any way they wish within program limitations. The optionally available "duplicate detection" feature alerts a person registering a substance that the structure is already in the database. For example, the three possible representations of poly(oxy-1,2-ethanediyl) shown as Figures 4a–4c are "perceived" by MDL's ISIS program as being "phase-shift" versions of the same polymer; use of the duplicate detection feature during registration of any one of these three representations can alert a registrar that it is already registered as 4a, 4b, and 4c.

Retrieval of Polymer Structures. It is axiomatic that to conduct an efficient search, searchers need to know the rules of the database or file being searched. Although this article is not intended to be a teaching manual on how to search polymer files or databases, some basic differences between searching the CAS Registry File and searching an MDL database by means of the ISIS program merit discussion.

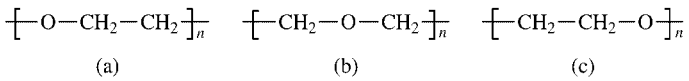

Fig. 4. "Phase-shift" versions of poly(oxy-1,2-ethanediyl).

Searchers who choose to search a publicly available file such as the CAS Registry File must learn the rules imposed on them by CAS (2). The CAS Registry File is remotely searchable via the Scientific and Technical Information Network (STN) in Columbus, Ohio. Anyone with an STN account and a computer equipped with the necessary hardware and software may access this file. As of September 2002, the Registry file contains names, structures, or both for over 42 million substances, of which nearly 934,000 are polymers.

Those who choose to search a private database such as one created with MDL's ISIS must learn a different set of search techniques. ISIS™/Draw, the ISIS chemical drawing package, is a presentation package for polymer structures. ISIS/Draw allows scientists to draw polymer structures with ease and speed, and then to search and share them. Researchers also have the enhanced capability of accessing 2D and 3D databases, with a wide range of search options and a link to global data. ISIS/Draw includes full annotation capabilities, which enable researchers to label collections of atoms or bonds with related function or process information (6).

To perform a polymer structure search using ISIS, the searcher uses ISIS/Draw to draw the desired structure, eg, a complete polymer or a fragment. Polymer structure queries may include any of the standard ISIS query properties, eg, atom lists, ring counts, substitution counts, or bond types. The searcher transfers the drawn structure to ISIS™/Base and initiates a search. Search modes are

(1) Current Mol (looks for the specific polymer only)
(2) Flexmatch (allows some flexibility in what is considered an "exact" match)
(3) SSS ("substructure search"; looks for all polymers that include the query structure)
(4) "Search by Form" (combines SSS with any other data provided in the query form, eg, physical properties).

MDL's ISIS program has an extremely valuable search feature: during a search for any given polymer, use of MDL's "flexmatch" program results in retrieval of all representations stored—both structure-based (regardless of "phase-shift") and source-based structures. Thus, for PET, assuming that the seven SRU structures shown as Figures 2a–2g and the three source-based structures shown as Figures 3a–3c were registered in a database, a search for any one of the 10 structures would retrieve all 10. The CAS Registry File added this feature in September, 2002 (4).

The rest of this article discusses structure representation for the types of polymers most commonly encountered. First, the principal CAS and IUPAC guidelines governing regular, single-strand, organic polymers are presented. This is followed by an overview of more complex substances–aftertreated (post-treated), alternating, block, comb, cross-linked, dendritic, graft, hyperbranched, hyper-cross-linked, star, and star-block polymers. There is also a section that summarizes stereochemistry in polymers, followed by another that reviews inorganic and quasi-inorganic polymers, double-strand (ladder) polymers, siloxanes and silicones, and oligomers and telomers.

Regular, Single-Strand, Organic Polymers

The word "regular" in the heading is used here to mean "ordinary", or, in the case of copolymers, random or statistical types with no special attributes such as "nonpolymeric spacer groups" (called junction units by IUPAC). As mentioned above, these are drawn usually as either structure-based, ie, —(—A—)$_n$—, or source-based, ie, —(A·B···)$_x$.

Structure-based versus Source-based Representation. There are no absolute rules that specify which types of polymers shall be represented as structure-based, which as source-based, and which by both methods. IUPAC makes no definitive statement about whether a polymer shall be represented as source-based or structure-based; thus, polymers may be represented both ways, and many examples of this can be found in both IUPAC's publications (1,6–13) and the CAS Registry File.

CAS states (2) that "specific polymers are named on the basis of the monomers from which they are formed and/or on the basis of their structure, as represented by an SRU." Since original documents do not always provide sufficient structural information to allow generation of the SRU name, the method most frequently used for describing polymeric substances is by citation of the component monomers. A few commercial polymers, each of which accounts for a large number of index entries, are indexed only at the SRU-based systematic polymer name. Systematic (SRU) nomenclature for polymers has been adopted from the system developed by the Committee on Nomenclature of the Division of Polymer Chemistry of the American Chemical Society (ACS) (14). Note: the IUPAC recommendations (*Pure Appl. Chem.* **48**, 373–385 (1976)) are in full agreement with CAS practice. Names derived by this system, in addition to monomer-based entries, are cited for polymers whose structural repeating units are well-documented or can confidently be assumed.

The "few commercial polymers" to which CAS refers (2,15) are the following:

(1) nylon-6
(2) nylon-6,6
(3) PET
(4) α-hydro-ω-hydroxypoly(oxy-1,2-ethanediyl) (polyethylene glycol)
(5) α-hydro-ω-hydroxypoly[oxy(methyl-1,2-ethanediyl)] (polypropylene glycol)

In accordance with CAS's policy (2,15), CAS assumes SRUs for such two-component condensation polymers as

(1) polyamides derived from a dibasic acid and a diamine
(2) polyesters derived from a dibasic acid and a dihydric alcohol
(3) polycarbonates from carbonic acid and a dihydric alcohol.

This is *not* limited to common polymers; as long as the criteria are met (15), uncommon polymers are also registered with both structure-based and source-based representations.

In contrast, CAS traditionally represents the following polymer types by only one method. These examples are illustrative only; the list is not meant to be exhaustive.

(1) **Source-based:**

a. Acetylenic
b. Acrylic and methacrylic
c. Alkyd
d. Ethylenic
e. Polyamic acids, polyamides, polyesters, polyimides, polyurethanes, and combinations of these types that are prepared from more than two monomers
f. Thermoset
g. Vinyl
h. Any other polymer for which the structure is unknown
Polymers in these eight groups are usually assigned source-based names, but these groups do not necessarily correspond to specific CAS polymer classes. A CAS publication (16) cites 42 specific polymer classes; an up-to-date list may be viewed by entering CAS Registry File online and executing the command: expand A/PCT.

(2) **Structure-based:**

a. Double-strand (ladder)

To take one example, the CAS principles—for both registration and searching—determine that a polymer such as poly(oxy-1,2-ethanediyl) is registered and named only as structure a in Figure 4; registration of structure 4b is forbidden by ordering rules. Structure 4c is the mirror image of structure 4a and is equated to structure 4a in the process of registration and naming.

It might therefore be assumed that retrieval of structures 4b and/or 4c during a search denotes incorrect indexing. However, owing to the way in which CAS's Messenger software operates, a search for structure 4c also retrieves the polymer with structure 4a. Some displayed images appear with the head atom on the left; others are mirror image when compared with the name. Regardless of which way round the on-screen image appears, retrieval of the desired polymer was historically likely to fail unless CAS's principles were followed. This search problem has been largely solved by the introduction in September 2002 of the POLYLINK search tool (4).

A comprehensive review of structure-based and source-based representations for regular, single-strand, organic polymers has been published (17).

Homopolymers.

Structure-based Method. The CAS principles (2,14) and IUPAC (3) recomendations for structure-based polymers are as follows. The descending order

of priority of citation (and of structuring the SRU) is (*1*) heterocyclic rings, (*2*) acyclic heteroatoms in the order O, S, Se, Te, N, P, As, Sb, Bi, Si, Ge, Sn, Pb, B, Hg, (*3*) carbocyclic rings, (*4*) acyclic carbon chains. If substituents are present, otherwise identical parent radicals in the SRU are chosen by the principles, in turn, of maximum number, lowest locants, and earliest alphabetic order of substituents. The shortest path (smallest number of atoms) is taken from the most preferred multivalent radical to another occurrence of the same radical (if present) within the SRU, then to the next most preferred radical, and so on. For SRUs containing more than one heterocyclic ring, there are further rules for determining heterocyclic ring seniority (18).

The complete registration process may be summarized as follows:

(1) *Step 1:* The atom sequence that defines the SRU is identified.
(2) *Step 2:* The "head" atom or senior bivalent radical of the sequence is defined.
(3) *Step 3:* The SRU is oriented, ie, a decision is made on which way to proceed along the atom sequence.
(4) *Step 4:* The SRU is named.

As an example, consider the 12-backbone-atom SRU sequence:

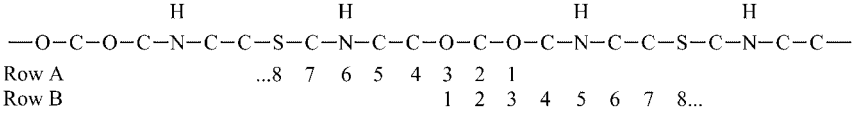

Determination of the head atom, and subunit citation order, is as follows: O is senior to S, and S is senior to N; therefore, one of the two oxygen atoms must be the head atom. The SRU must therefore be either row A, atoms 1 to 12, or row B, atoms 1 to 12. The row A sequence places the N atom in position 6, whereas the row B sequence places it in position 5; the latter is therefore correct, and the final SRU is $-(-O-C-O-C-NH-C-C-S-C-NH-C-C-)_n-$.

Essentially the same steps should be followed by searchers in order to conduct an effective search for structure-based polymers.

For polymers in SCION, a DuPont proprietary database, the same four basic steps are used for SRU identification and orientation. However, the rules that control these steps are different; this results in names and structures for SRUs that are sometimes different from SRUs as defined and oriented by CAS principles (19).

Source-based Method. For source-based representations, CAS structures homopolymers by an expression such as $(A)_x$, where A is a monomer. A typical CAS source-based homopolymer representation is shown as Figure 5.

IUPAC makes no recommendations for formal source-based, one-component homopolymer nomenclature or structural representation. However, IUPAC recognizes that for common idealized structural representations such as polyethylene, polypropylene, and polybutadiene, these semisystematic or trivial names are approved for use in scientific work. Where the semisystematic name is an obvious

REGISTRY COPYRIGHT 1995 ACS

RN 9003-01-4 REGISTRY
CN 2-Propenoic acid, homopolymer (9CI) (CA INDEX NAME)
OTHER CA INDEX NAMES:
CN Acrylic acid, polymers (8CI)
:
MF (C3 H4 O2)x[a]
CI PMS, COM
PCT Polyacrylic
:

CM 1

CRN 79-10-7
CMF C3 H4 O2

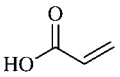

:

Fig. 5. Representation of acrylic acid homopolymer. [a]In on-line displays of CAS registry records, all subscripts–numerical (next to the atoms) and letter (outside parentheses)—appear on the same line.

source-based name, the polymer referred to is derived from the indicated source (see Appendix A in Ref. 3).

Copolymers.

Structure-based Method. CAS does not generally index *unterminated* copolymers of SRUs by the structure-based method. Formats such as poly(oxyethylene)/poly(oxytetramethylene) or poly[(oxyethylene)/(oxytetramethylene)] are not used. Instead, a source-based representation is used (see Fig. 9 below).

IUPAC states (7) that a comprehensive structure-based system of naming copolymers would be desirable, but that such a system presupposes a knowledge of the structural identity of all the SRUs as well as their sequential arrangements within the polymer. They suggest that when this information is available, the structure-based nomenclature used for single-strand polymers (3,13) can be extended to copolymers. A separate publication (8) depicts many structure-based copolymer representations.

Source-based Method. The source-based structural representation of a copolymer is in the format $(A{\cdot}B\cdots)_x$, where A, B, etc, are monomers. Figures 6–8 illustrate the method.

Although poly(oxyethylene) and poly(oxytetramethylene) are represented as structure-based homopolymers, the poly(oxyethylene/oxytetramethylene) copolymer is represented as a source-based polymer (see Fig. 9).

CAS does not use words such as “random” or “statistical” to describe random or statistical copolymers; copolymers without special attributes such as “block” are assumed to be random.

A comprehensive IUPAC publication (8) discusses nomenclature for source-based copolymers.

REGISTRY COPYRIGHT 1995 ACS
RN 27987-76-4 REGISTRY
CN Benzenamine, 4-ethenyl-, polymer with ethenylbenzene (9CI) (CA INDEX NAME)
OTHER CA INDEX NAMES:
CN Aniline, p-vinyl-, polymer with styrene (8CI)
:
MF (C8 H9 N . C8 H8)x
CI PMS, COM
PCT Polystyrene
:
CM 1

CRN 1520-21-4
CMF C8 H9 N

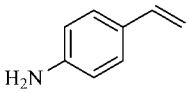

CM 2

CRN 100-42-5
CMF C8 H8

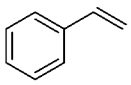

:

Fig. 6. Source-based representation of *p*-vinylaniline/styrene copolymer.

Complex Polymers

Space limitations preclude more than an overview of these types: aftertreated (post-treated), alternating, block, comb and graft, cross-linked, dendritic, hyperbranched, hyper-cross-linked, star, and star-block. Comprehensive reviews of structure-based and source-based representations for them have been published (20,21).

Aftertreated (Post-treated) Polymers. CAS describes *post-treated polymers* as those polymers that are modified, either partially or completely, after the basic polymer backbone or skeleton has been formed. These modifications may result from a reaction or series of reactions of the main chain, end groups, and/or pendent functional groups of the polymer. Post-treatment is indicated by modification terms after the polymer name that describe the nature of the post-treatment. CAS divides post-treated polymers into two types: structurable and registrable; and nonregistrable (15). A third category, registrable and referred to as "nameable but not structurable" (15), is now provided with structures, and the backfile is being updated on an ongoing basis with structure-based access. (A description of the indexing enhancements is also available from CAS Customer Service and is offered on the world wide web (WWW) at http://www.cas.org/EO/enhanc.html.)

IUPAC discusses post-treated polymers in a 1994 publication (12), and several examples of structure-based representations are given. As of September 2002, IUPAC has made no recommendations regarding nomenclature or structural representation for post-treated source-based polymers.

REGISTRY COPYRIGHT 1995 ACS
RN 24938-04-3 REGISTRY
CN 1,3-Benzenedicarboxylic acid, polymer with 1,4-benzenedicarboxylic acid and 1,2-ethanediol (9CI) (CA INDEX NAME)
:
MF (C8 H6 O4 . C8 H6 O4 . C2 H6 O2)x
CI PMS
PCT Polyester, Polyester formed
:

CM 1

CRN 121-91-5
CMF C8 H6 O4

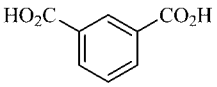

CM 2

CRN 107-21-1
CMF C2 H6 O2

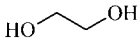

CM 3

CRN 100-21-0
CMF C8 H6 O4

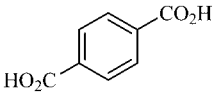

:

Fig. 7. Source-based representation of a three-component polyester.

Alternating (and Other Periodic) Polymers. Alternating and other periodic copolymers are viewed somewhat differently by CAS and IUPAC.

Neither "alternating" nor "periodic" is used as a modifier by CAS for alternating or periodic polymers named on the basis of their structure. The text descriptors "alternating" and "periodic" are not used with SRUs because any alternation or periodicity would be obvious in the structure and would not need to be differentiated from another similar structure by means of a text descriptor.

Registration by CAS of source-based representation of alternating copolymers with the term "alternating" as an integral part of the Registry record began with the 12CI (1987) (2). Alternating copolymers are distinguished in CA Registry File from random copolymers by including the term "alternating" in the Registry record of a given copolymer with its source-based name (see Fig. 10).

IUPAC recommends that an *alternating polymer* be named as a copolymer comprising two species of monomeric units (or monomers) distributed in alternating sequence (7). The arrangement ABABAB— or $(AB)_n$ thus represents an alternating copolymer. As far as possible, alternating and periodic polymers are treated as regular polymers (8). An alternating sequence arrangement of monomers is represented by (A-*alt*-B), and the corresponding polymer is named poly(A-*alt*-B).

For source-based representations, IUPAC recommends that alternating and periodic copolymer names contain the connectives -*alt*- and -*per*-, respectively.

REGISTRY COPYRIGHT 1995 ACS
RN 24937-74-4 REGISTRY
CN Formaldehyde, polymer with benzenamine and phenol (9CI) (CA INDEX NAME)
:
MF (C6 H7 N . C6 H6 O . C H2 O)x
CI PMS
PCT Amino resin, Phenolic resin
:

CM 1

CRN 108-95-2
CMF C6 H6 O

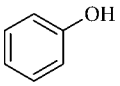

CM 2

CRN 62-53-3
CMF C6 H7 N

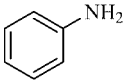

CM 3

CRN 50-00-0
CMF C H2 O

$H_2C{=}O$
:

Fig. 8. Source-based representation of aniline/formaldehyde/phenol terpolymer.

Table 1 lists the source-based connectives recommended by IUPAC for alternating, periodic, and several other polymer types. According to the above IUPAC recommendations, the source-based name for PET and the trivial name nylon-6,6 represent alternating copolymers.

Block Polymers. This section discusses structure-based and source-based nomenclature for ordered, segmented, and unordered block polymers, and polymers with "nonpolymeric spacer units" or "junction units." Star-block polymers are discussed under star polymers.

When CAS began to register polymers in 1967, no distinction was made between block and other copolymers. The information might have been part of the descriptive "index modification," but it was not part of the Registry record. Registration of block copolymers with the term "block" as an integral part of the Registry record began with the 12CI (1987).

CAS makes no distinction among ordered, segmented, and unordered block polymers. For source-based representation, block polymers are distinguished from random polymers by indexing as copolymers at the monomer names. The term "block" is cited in a special modification after all other structural information (2).

IUPAC has published recommendations for structure-based and source-based representations of block polymers (7,8,12).

REGISTRY COPYRIGHT 1995 ACS
RN 27637-03-2 REGISTRY
CN Furan, tetrahydro-, polymer with oxirane (9CI) (CA INDEX NAM
OTHER CA INDEX NAMES:
CN Ethylene oxide, polymer with tetrahydrofuran (8CI)
CN Furan, tetrahydro-, polymer with ethylene oxide (8CI)
CN Oxirane, polymer with tetrahydrofuran (9CI)
:
MF (C4 H8 O . C2 H4 O)x
CI PMS, COM
PCT Polyether, Polyether formed
:

CM 1

CRN 109-99-9
CMF C4 H8 O

CM 2

CRN 75-21-8
CMF C2 H4 O

:

Fig. 9. Source-based representation of poly(oxyethylene/oxytetramethylene) copolymer.

Comb and Graft Polymers. These two types of complex polymers are discussed together because there is overlapping technology, and it is not always possible to distinguish between them.

CAS does not recognize comb polymers as a type. Many (but not all) comb polymers are classified as graft polymers; for example, the comb polymer from

REGISTRY COPYRIGHT 1995 ACS
RN 108080-86-0 REGISTRY
CN Oxirane, (butoxymethyl)-, polymer with carbon dioxide, alternating (9CI) (CA INDEX NAME)
:
CM 1

CRN 2426-08-6
CMF C7 H14 O2

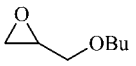

CM 2

CRN 124-38-9
CMF C O2

:

Fig. 10. Source-based representation of alternating (butoxymethyl)oxirane/carbon dioxide polymer.

Table 1. IUPAC Source-based Copolymer Classification

Type	Connective	Example
Unspecified	*-co-*	poly(A-*co*-B)
Statistical	*-stat-*	poly(A-*stat*-B)
Random	*-ran-*	poly(A-*ran*-B)
Alternating	*-alt-*	poly(A-*alt*-B)
Periodic	*-per-*	poly(A-*per*-B-*per*-C)
Block	*-block-*	polyA-*block*-polyB
Graft	*-graft-*	polyA-*graft*-polyB

acrylonitrile, polyethylene glycol monomethacrylate, and styrene is classified as a graft polymer, whereas comb polymers from homopolymers of macromonomers are not.

Registration of graft copolymers with the term "graft" as an integral part of the Registry record began with the 12CI (1987). When CAS began to register source-based representations of polymers in 1967, no distinction was made between graft and other copolymers. The information might have been part of the descriptive "index modification," ie, the word "graft" might appear somewhere in the text, but it was not part of the Registry record. Comb and graft polymers comprising an SRU backbone and an SRU side chain are represented as graft polymers with source-based names (see Fig. 11).

Differentiation between the polymeric substrate and the applied monomer is not made. For example, whether 1-hexene is grafted onto 1-heptene homopolymer or vice versa, the preferred name is "1-heptene, polymer with 1-hexene, graft" with an additional name "1-hexene, polymer with 1-heptene, graft" (2). Thus, CAS makes no distinction between poly(A-*graft*-B) and poly(B-*graft*-A).

Application of the text descriptor 8:PM, GRAFT to graft polymers began with the 12CI (1987); earlier records are not so designated, but this is of minor importance to searchers because this descriptor is currently displayable but not searchable. The term "graft", which *is* searchable, is also part of the name.

IUPAC has proposed that graft polymers be named in the same way as regular polymers (4) or irregular polymers (12) but with minor modifications. IUPAC also gives recommendations for irregular polymers in which polymer chains are attached to the main chain through a constitutional unit (linking unit) different from the constitutional unit of the side chain (8). Graphic representations of graft polymers have been published (8).

An IUPAC publication (11) discusses both structure-based and source-based representations of comb polymers; a *comb polymer* is described as a macromolecule comprising a main chain with trifunctional points from which linear side chains emanate. If the subchains between the branch points of the main chain and the terminal subchains of the main chain are identical with respect to constitution and degree of polymerization, and the side chains are identical with respect to constitution and degree of polymerization, the macromolecule is termed a regular comb macromolecule. If at least some of the branch points are of functionalities greater than three, the macromolecule may be termed a *brush macromolecule*.

Idealized representation:

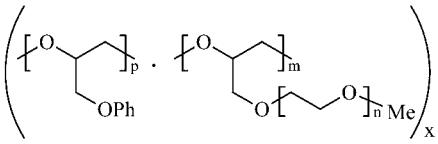

CAS Registry File record:
REGISTRY COPYRIGHT 1996 ACS
RN 154353-60-3 REGISTRY
CN Oxirane, (phenoxymethyl)-, polymer with α-methyl-ω-(oxiranylmethoxy)poly(oxy-1,2-ethanediyl), graft (9CI) (CA INDEX NAME)
:
DES 8:PM, GRAFT
CM 1

CRN 40349-67-5
CMF (C2 H4 O)n C4 H8 O2
CCI PMS

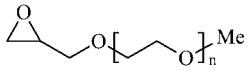

CM 2

CRN 122-60-1
CMF C9 H10 O2

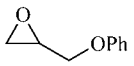

:

Fig. 11. CAS representation of an "all-SRU" comb (or graft) polymer.

Cross-linked Polymers. As the name indicates, these have two or more separate polymeric chains connected by a cross-link; it is *implied* that the cross-link is generally (*1*) relatively short (and not itself polymeric) and (*2*) at irregular intervals along the chains, but there seem to be no firm rules on these points. Ladder polymers comprising two linear strands cross-linked at regular intervals are discussed under Double-Strand (Ladder) Polymers.

The *Index Guide* (2) gives no information on how cross-linked polymers are indexed, because CAS treats them as copolymers.

IUPAC has published no specific recommendations on nomenclature or structural representations for cross-linked structure-based polymers. For source-based representations of polymers, IUPAC defines a cross-link as a small region in a macromolecule from which at least four chains emanate, which is formed by reactions involving sites or groups on existing macromolecules or by interactions between existing macromolecules (22). The small region may be an atom, a group of atoms, or a number of branch points connected by bonds, groups of atoms, or oligomeric chains. In the majority of cases a cross-link is a covalent structure but the term is also used to describe sites of weaker chemical interactions, portions of crystallites, and even physical interactions and entanglements.

Cross-links, the branch units of star macromolecules and other junction units, are optionally specified by their source-based names after the name of the

macromolecule, with the Greek connective ν separated by hyphens. When the content of the cross-linking monomer is high, the macromolecule is treated as a copolymer molecule (11).

Dendritic, Hyperbranched, Hyper-cross-linked, Star, and Star-Block Polymers. These groups of polymers are discussed together because there is overlapping technology that makes it difficult to discuss them separately. In the last decade there has been a sharp rise in interest of these types of polymers.

Tomalia and co-workers (23) describe a dendrimer as having three distinguishing architectural features: an initiator core, interior layers (generations) composed of repeating units radially attached to the initiator core, and an exterior or surface of terminal functionality attached to the outermost generation.

These dendrimers differ from classical monomers or oligomers by their extraordinary symmetry, high branching, and maximized (telechelic) terminal functionality. Dendrimer synthesis is accomplished by a variety of strategies involving time-sequenced propagation techniques. The resulting dendrimers grow in a geometrically progressive fashion. Chemical bridging of these dendrimers (24) leads to Starburst^{TM} [Dow Chemical Co. (25)] polymers. Tomalia and Durst have written a detailed account of Starburst/cascade dendrimers and hyperbranched structures (26).

Turner (27) considers hyperbranched polymers to be highly branched, noncross-linked polymers prepared by the step-growth polymerization of A_xB (or AB_x) polymers. Thus, A_2B means that for every two type A reactive groups there is one type B reactive group, while AB_2 means that for every one type A reactive group there are two type B reactive groups. AB_2 and AB_3 (or A_2B and A_3B) are the commonest; AB_x (or A_xB) types where $x > 3$ tend to be so sterically crowded that polymerization is difficult unless the reactive groups are well separated.

Voit (28) portrays the essential differences between dendrimers and hyperbranched polymers as follows:

(1) Dendrimers are prepared by a stepwise approach; they are structurally perfect or nearly perfect (ie, the branching ideality approaches 100%), their size is limited (ie, they cannot grow forever), and their molecular weight is dependent upon the number of generations.

(2) Hyperbranched polymers may be prepared by a one-step synthesis under conventional polycondensation conditions; their molecular weight is dependent upon the condensation reaction, not upon the number of generations, and the branching ideality is typically between 50 and 75%.

The terms "star polymer" and "star-shaped polymer" are used somewhat imprecisely. The same term is used to describe at least two physically different polymeric "clusters." A *star polymer* may be a polymer comprising a precise center of known structure from which radiate a known number of arms. The arms, which may contain one or more SRUs or polymerized monomers, may be random, statistical, or blocky; polymers containing the latter are usually called *star-block polymers*.

A star polymer may also comprise an unknown number of arms connected to the center of the cluster by addition to the reaction mass of a second, multifunctional monomer or SRU that ties all the linear growing polymer chains together

into a cross-linked (microgel) core. These are sometimes called *star-branch polymers* (29). Cloutet and co-workers (30) however, describe a star-branched polymer as a "dendritic block polymer." A third type of star polymer comprises a dendritic core from which emanate a known number of arms (31). In any of these types of star polymers, the arms may be all the same, or different arms may have different compositions; the latter known variously as heterostar (32), miktoarm star (33), or variegated star polymers (11).

CAS handles dendrimers as regular organic compounds or polymers, depending on the degree of polymerization. The number of nonhydrogen atoms is also a factor. Low generation dendrimers having 10 or fewer repeating units and a nonhydrogen atom count less than 253 are structured and named systematically as specific nonpolymeric compounds. Higher generation dendrimers having more than 10 repeating units or a nonhydrogen atom count greater than 253 (which thus forces a manual registration at a lower degree of polymerization) are structured and named as polymers.

Polymers having dendritic or starburst structure are indexed at the controlled term DENDRITIC POLYMERS, which was added as a new index heading starting with the CA 13th Collective Index Period in 1992. Additional index entries are made for specific dendrimers. The approach for preparing divergent or convergent dendrimers may be indicated in the text modification when so specified by the author of the source document. [Convergent and divergent refer to the two basic methods of forming dendrimers; as the names imply, convergent dendrimers (typified by the work of Fréchet and co-workers (34)) are built "inward," ie, from the periphery toward the core, whereas divergent dendrimers (typified by the work of Tomalia and co-workers (23,24)) are formed by building outward from the core.] Currently CAS has no specific nomenclature for polymeric dendrimers; they are named according to regular polymer nomenclature rules. The polyfunctional core used in either the divergent or convergent approach is not included in the polymer registration. CAS's policy on the indexing of dendrimers is described in more detail elsewhere (21).

IUPAC has addressed star and star-block polymer representations (8,11). As of September 2002, no specific recommendations on nomenclature or structure representation for dendrimers, hyperbranched, or hyper-cross-linked polymers have been published; an IUPAC document on this topic is close to completion. An IUPAC paper on source-based nomenclature (11) describes a star polymer as a macromolecule containing a single branch point from which linear chains (arms) emanate. In a regular star polymer all arms are identical with respect to constitution and degree of polymerization. A variegated star has different arms composed of different monomers.

Comprehensive reviews of nomenclature for structure-based and source-based representations for dendritic, hyperbranched, and hyper-cross-linked polymers (21,35–38), and for star and star-block polymers (21), have been published.

Stereochemistry in Polymers

CAS represents stereochemistry in polymers by text descriptor terms when the necessary information is reported; such terms include isotactic, syndiotactic,

threo-diisotactic, erythro-diisotactic, and disyndiotactic (2). The term "atactic" (for a random configuration) is not employed by CAS in indexing specific polymers. In addition to the special terms above, polymer stereochemistry is defined, when appropriate, by the stereo descriptors E, Z, R, S, R*, and S*.

The first extensive IUPAC publications on stereochemistry in high polymers were published in the early 1960s, and subsequently in 1966 as a single article (39). In addition to more conventional polymer names, eg, polyethylidene and polypropylene, the "-amer" nomenclature was introduced in 1952 (10). IUPAC basic definitions relating to stereochemistry, eg, tacticity and isotactic polymer, were published in 1974 (1).

A major 1981 IUPAC document (9) addresses polymer stereochemistry in depth. Key chapters of this document discuss basic definitions (configurational unit, configurational base and repeating units, stereorepeating unit, different types of tacticity, tactic block polymers, and stereoblock polymers); sequences; conformations; and supplementary definitions. Most of the illustrations use the rotated Fischer projections, but some three-dimensional representations are included.

Miscellaneous Polymer Types

These include inorganic and quasi-inorganic polymers, double-strand (ladder) polymers, siloxanes and silicones, and oligomers and telomers. A comprehensive review of structure-based and source-based representations for these types of polymers has been published (40).

Inorganic and Quasi-inorganic Polymers. A polymer need not be completely inorganic to be classified as an inorganic polymer; an inorganic backbone is sufficient, even if there are organic moieties attached to a backbone atom.

A regular linear polymer that can be described by a preferred SRU in which only one terminal constituent subunit is connected through a single atom to another identical SRU or to an end group is a *quasi-single-strand polymer*, ie, it does not fit the definition of a regular single-strand polymer, but it can be named in the same manner (13).

CAS represents single-strand inorganic polymers by both structure-based and source-based methods. Figure 12 shows a typical structure-based record;

REGISTRY COPYRIGHT 1995 ACS
RN 74418-71-6 REGISTRY
CN Poly[imino(aminophosphinylidene)] (9CI) (CA INDEX NAME)
:
MF (H3 N2 O P)n
CI PMS
PCT Polyother, Polyother only
:

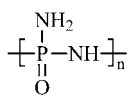

:

Fig. 12. Structure-based record; poly[imino(aminophosphinylidene)].

REGISTRY COPYRIGHT 1995 ACS
RN 56581-26-1 REGISTRY
CN 1,3,5,2,4,6-Triazatriphosphorine, 2,2,4,4,6,6-hexafluoro-2,2,4,4,6,6-hexahydro-, homopolymer (9CI) (CA INDEX NAME)
:
MF (F6 N3 P3)x
CI PMS
PCT Polyphosphazene, Polyphosphazene formed
:

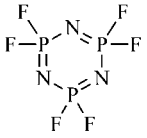

:

Fig. 13. Source-based record; homopolymer from hexafluorotriazatriphosphorine. Poly[nitrilo(difluorophosphoranylidyne)] [28655-96-1], the corresponding structure-based representation, is also registered in the CAS Registry file.

nitrogen is senior to phosphorus and might be expected to appear on the left but (as explained under Structure-based versus Source-based Representation) this may not always occur.

Source-based representations of polymers are typically recorded as shown in Figure 13.

Some references on phosphazenes (41) show the structures with nitrogen mostly on the left, although some are drawn with phosphorus on the left.

When SRUs are bridged only by metals, systematic polymer nomenclature is not used; instead, the substance is indexed either at the monomeric salt name or by coordination nomenclature, with a modification phrase, in either case, such as "homopolymer" or "polymer with. . ." (2).

IUPAC (13) presents a system of nomenclature for regular single-strand and quasi-single-strand inorganic and coordination polymers. The system is based on the selection and naming of an SRU defined (1) as the smallest structural unit the repetition of which describes the polymer structure. The name of the polymer is the name of this repeating unit prefixed by the terms "poly," "*catena*", or other structural indicator, and designations for end groups, if desired. IUPAC has created sets of rules for (*1*) determining an unambiguous, although not necessarily unique, name for each SRU; (*2*) a unique name; and (*3*) resolving situations when further choice is needed for selection of a senior subunit in an SRU.

Double-Strand (Ladder) Polymers. Double-strand ladder and spiro polymers contain no open-chain bonds in the backbone. Polymers containing some open-chain backbone bonds (called partial ladder, imperfect ladder, step-ladder, or block ladder polymers) are not considered to be true ladder or spiro polymers.

The CAS and IUPAC nomenclature and structure representation systems are very similar. CAS's rules for ladder polymers are published in the *Index Guide* (2). IUPAC defines a ladder or spiro polymer as a double-strand polymer, the molecules of which are formed by an uninterrupted sequence of rings with adjacent rings having one atom in common (spiro polymer) or two or more atoms in common (ladder polymer). A comprehensive system is presented for (*1*) identifying, (*2*) orienting, and (*3*) naming the preferred SRU, and subsequently (*4*) naming

the polymer (42). The nomenclature and structure representation system used in SCION, a DuPont proprietary database, is novel and radically different (43).

Other prominent articles on double-strand polymers include those by Overberger and Moore (44), DeWinter (45), and Bailey (46); the latter reference contains a short "proposed nomenclature" section that is essentially a reprint of part of an ACS publication (14).

Siloxanes and Silicones. Although IUPAC classifies polysiloxanes as inorganic polymers (13), there is sufficient interest and diversity in them as a group for them to warrant discussion separate from other inorganic polymers.

Polysiloxanes occupy a virtually unique position in the world of polymers. Many polysiloxanes comprise a partly or wholly inorganic backbone built from alternating silicon and oxygen atoms; in contrast, pendent groups or side chains attached to silicon atoms are usually organic. Types discussed in this section include regular single-strand, hyperbranched, ladder, and spiro polysiloxanes.

Prior to 1994, polysiloxanes prepared by hydrolytic polymerization of alkoxysilanes or halosilanes were indexed in CAS's CA File at the index heading "Siloxanes and Silicones" with no polymer registration. Polysiloxanes described by authors only in terms of SRUs were indexed at this heading with no polymer registration. [A description of the indexing enhancements is also available from CAS Customer Service and is offered on the world wide web (WWW) at http://www.cas.org/EO/silox.html.]

Beginning with volume 121 (1994) of CAS Chemical Abstracts, structural representation and machine registration was begun for polymers previously handled only as text terms in the CA File. Backfile conversion is not planned.

This policy change affects the following areas [CAS's exact phraseology (including use of parentheses, vice brackets, for SRUs) is used below; in most cases, when words such as siloxanes or silsesquioxanes are cited, what is meant is polysiloxanes or polysilsesquioxanes]:

(1) siloxanes or silsesquioxanes prepared by hydrolytic polymerization of alkoxysilanes or halosilanes
(2) siloxanes described only in terms of single-unit SRUs of the type $(—O—SiRR'—)_n$ (R, R′ = monovalent radical)
(3) siloxanes described only in terms of multiunit SRUs of the type $(—O—SiR_2—)_x$ $(—O—SiR'_2—)_y$ or $(—R_2SiO—)_x(—R'SiO_{1.5}—)_y$ (R, R′ = monovalent radical)
(4) ceramers (hybrid organic–inorganic networks) prepared by hydrolytic polymerization (sol–gel process) of tetraalkoxysilanes containing organic moieties, which may be trialkoxysilyl-terminated organic polymers
(5) end groups for siloxane SRUs
(6) copolymers containing siloxane components
(7) tradenames for siloxanes and silsesquioxanes
(8) silicone rubbers.

A more detailed discussion of siloxane nomenclature and structure representation (40) includes further information on the changes introduced by CAS (http://www.cas.org/EO/silox.html).

For linear polysiloxanes, an IUPAC document (13) states that if there is a choice for the central atom, the element occurring *later* in the general element

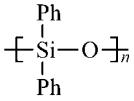

Fig. 14. Poly[(diphenylsilylene)oxy]. Polymer name: *catena*-poly[(diphenylsilicon)-μ-oxo]; Synonym: poly(diphenylsiloxane) (47).

sequence table (ie, the periodic table) is the central atom. Order of precedence begins in the top, right-hand corner of the periodic table and proceeds (in vertical columns) toward the bottom, left-hand corner; thus, atom seniority is F, Cl, Br, I, At, O, S, Se, Te, Po, N, P, As, Sb, Bi, C, Si, . . ., Li, Na, K, Rb, Cs, Fr, He, Ne, Ar, Kr, Xe, Rn.

The linear polysiloxane (diphenylsilylene)oxy is represented by the structure shown as Figure 14. The IUPAC name also differs appreciably from the CAS name. According to the rules for linear organic polymers, this polymer would be oriented and named poly[oxy(diphenylsilylene)] (13).

Lichtenwalner and Sprung (48) present some IUPAC nomenclature for polysiloxanes; most of their examples show silicon on the left. Other papers on polysiloxanes in a 1988 symposium publication (41) show the structures with silicon mostly on the left, although some are drawn with oxygen on the left.

Oligomers and Telomers. Qualitatively, *oligomers* are "short polymers", and *telomers* are "short polymers with specific end groups".

The terms "telogen" and "telomerization" were defined many years ago to describe an innovative method for the free-radical polymerization of ethylene (49,50). The essence of telomerization, described in a 1942 patent (50), involves reaction of a telogen XY (also called a chain-transfer agent) with an ethylenic molecule to give a telomer of structure X—$(A)_n$—Y. In the product telomer, fragments of the chain-transfer agent are attached to the termini of the molecule (49,50). Figure 15 illustrates the method.

CAS indexes oligomers of definite structures as specific compounds by the regular principles of organic nomenclature. When the precise structure is not known but the number of units is specific, "dimer", "trimer", etc, is expressed in the modification at the name of the monomer. The term "oligomeric" may be cited if this aspect is stressed in the original document (2). "Oligomeric," if applicable, is expressed in the text modification part of the index entry and is not part of the CAS Registry record, except for some records marked with an asterisk. [CAS Registry numbers appended with an asterisk (*) represent substances of unknown or variable composition, complex reaction products, or biological substances that do not meet the criteria for CA indexing. These substances generally have been registered for regulatory agencies and receive a CA Index Name. They have a special code of CTS or GRS in the Class Identifier (CI) field. The information in the Locator (LC) field and/or Source of Registration (SR) field provides an indication of the reason for registration.]

Telomers of unknown structure are indexed similarly to copolymers with the term "telomer with. . ." cited in the modification (see Fig. 15). Telomers with a definite structure are named systematically (2) rather than as telomers per se (see Fig. 16).

Chemical reaction:

$$CCl_4 + n\ H_2C{=}CH_2 \longrightarrow Cl_3C{-}\left[CH_2{-}CH_2\right]_n{-}Cl$$

Abbreviated CAS Registry record:
RN 25398-31-6
CN Ethene, telomer with tetrachloromethane
MF (C2H4)x.CCl4
Structure: (CH2=CH2)x.CCl4

Fig. 15. CCl_4 added as chain-transfer agent in ethylene polymerization.

Structure: Cl-[-CH_2-]$_6$-CCl_3
Name: heptane, 1,1,1,7-tetrachloro-

Fig. 16. Oligomeric poly(ethylene) telomer with CCl_4. The term "oligomeric" is part of the CAS Registry record name only in records marked with an asterisk (see text for details).

IUPAC defines an oligomer as "a substance composed of molecules containing a few of one or more species of atoms or groups of atoms (constitutional units) repetitively linked to each other for which the physical properties vary with the addition or removal of one or a few constitutional units from its molecules" (1). IUPAC defines "telomer" and "telomerization" essentially as follows (22):

(1) *telomer*: an oligomer obtained by a telomerization process
(2) *telomerization*: an oligomerization by chain reaction carried out in the presence of a large amount of chain-transfer agent, so that the end groups are essentially fragments of the chain-transfer agent.

No recommendations have been published on how oligomers and telomers are to be named and represented graphically by either structure-based or source-based methods.

IUPAC references to oligomers and telomers are rare, although examples of a telomer (51) and an oligomer have been published. (see Section 4.3, Example 4.3-E1, in Ref. 8). IUPAC uses subscript *a*, *vice* subscript *n*, to indicate oligomers.

Conclusions

Over a period of about 50 years, representation of polymer structures, both on paper and in databases, has developed from a virtually random system to a highly organized and sophisticated one. Polymers are represented sometimes by structure-based methods, sometimes by source-based methods, and sometimes by both. Both methods survive because each offers advantages and disadvantages. Both methods involve structural representation of polymers by a precisely defined set of rules developed over several decades by CAS, IUPAC, and the Committee on Nomenclature of the Division of Polymer Chemistry of the ACS. Areas still in need of improved representation are copolymers of unterminated SRU types: aftertreated (post-treated) polymers, and dendritic (52), hyperbranched, hyper-cross-linked, star, and star-block polymers. Also needed are hierarchical relationships between intellectually related polymers (53).

Abbreviations

ACS: American Chemical Society
CA: Chemical Abstracts
CRU: Constitutional repeating unit
IUPAC: International Union of Pure and Applied Chemistry
MDL: MDL Information Systems, Inc.
RN: Registry number
SRU: Structural repeating unit
SSS: Substructure search
STN: Scientific and Technical Information Network
8CI: CA Eighth Collective Index
9CI: CA Ninth Collective Index
12CI: CA Twelfth Collective Index

BIBLIOGRAPHY

1. IUPAC, *Pure Appl. Chem.* **40**, 477–491 (1974); reprinted as Chapt. 1 in Ref. 51. See also (a) V. Gold, K. L. Loening, A. D. McNaught, and P. Sehmi, *Compendium of Chemical Terminology/IUPAC Recommendations*, Blackwell, Oxford, 1987; (b) *Encyclopedia of Polymer Science and Engineering*, 2nd ed., Vol. **12**, John Wiley & Sons, Inc., New York, 1988, p. 398.
2. CAS 2002 *Index Guide*, ACS, Washington D.C., 2002; Appendix IV: Section 222.
3. IUPAC, *Pure Appl. Chem.* **48**, 373–385 (1976); reprinted as Chapt. 5 in Ref. 51.
4. CAS. "*Enhanced Polymer Searching in Registry.*", STNotes No. 30, July 2002. Available on the world wide web at http://www.cas.org/ONLINE/STN/STNOTES/stnotes30.pdf.
5. CAS 2002 *Index Guide*, ACS, Washington, D.C., 2002; Appendix II: Section 14A.
6. *MDL Information Systems*, Press release, San Leandro, Calif., Jan. 22, 1997.
7. IUPAC, *Pure Appl. Chem.* **57**, 1427–1440 (1985); reprinted as Chapt. 7 in Ref. 51.
8. IUPAC, *Pure Appl. Chem.* **66**, 2469–2482 (1994).
9. IUPAC, *Pure Appl. Chem.* **53**, 733–752 (1981); reprinted as Chapt. 2 in Ref. 51—see especially Refs. 1 and 4 cited therein.
10. IUPAC, *J. Polym. Sci.* **8**, 272–277 (1952).
11. IUPAC, *Pure Appl. Chem.* **69**, 2511–2521 (1997).
12. IUPAC, *Pure Appl. Chem.* **66**, 873–889 (1994).
13. IUPAC, *Pure Appl. Chem.* **57**, 149–168 (1985); reprinted as Chapt. 6 in Ref. 52.
14. ACS, *Macromolecules* **1**, 193–198 (1968).
15. CAS, Columbus, Ohio, *Searching for Polymer Information in CAS ONLINE*, Mar. 1990 (Publication C1EJ-0390).
16. STN International, *Registry File: Polymer Class Terms*, Chemical Abstracts Service, Jan. 1993 (Publication CAS6009-1192).
17. E. S. Wilks, *J. Chem. Inf. Comput. Sci.* **37**, 171–192 (1997).
18. CAS, Columbus, Ohio, *Chemical Substance Name Selection Manual (9CI)*, 1978 edition, Section A-130, A-187–A-192.
19. J. A. Patterson, J. L. Schultz, and E. S. Wilks, *J. Chem. Inf. Comput. Sci.* **35**, 8–20 (1995).
20. E. S. Wilks, *J. Chem. Inf. Comput. Sci.* **37**, 193–208 (1997).
21. E. S. Wilks, *J. Chem. Inf. Comput. Sci.* **37**, 209–223 (1997).
22. IUPAC, *Pure Appl. Chem.* **68**, 2287–2311 (1996).
23. D. A. Tomalia, H. Baker, J. Dewald, H. Hall, G. Kallos, S. Martin, J. Roeck, J. Ryder, and P. Smith, *Macromolecules* **19**, 2466–2468 (1986).

24. *Polym. J. (Tokyo)* **17**, 117–132 (1985).
25. L. R. Wilson and D. A. Tomalia, *Polym. Prepr.* **30**(1), 115–116 (1989).
26. D. A. Tomalia and H. D. Durst, in E. Weber, ed., *Topics in Current Chemistry, Vol. 165: Supramolecular Chemistry I—Directed Synthesis and Molecular Recognition*, Springer-Verlag, Heidelberg, 1993, pp. 197–307.
27. R. S. Turner, in 210th ACS National Meeting, Chicago, Ill., Aug. 20–24, 1995, (Paper PMSE-040).
28. B. I. Voit, *Acta Polym.* **46**, 87–99 (1995).
29. L. Wang, S. T. McKenna, and R. Faust, *Macromolecules* **28**, 4681–4685 (1995); D. Tian, Ph. Dubois, R. Jerome, and Ph. Teyssie, *Macromolecules* **27**, 4134–4144 (1994); J. A. Simms, *Prog. Org. Coat.* **22**, 367–377 (1993).
30. E. Cloutet, J.-L. Six, D. Taton, and Y. Gnanou, in 210th ACS National Meeting, Chicago, Ill. Aug. 20–24, 1995. (Paper PMSE-069).
31. H. A. M. van Aert, M. E. M. Burkard, J. F. G. A. Jansen, M. H. P. van Genderen, E. W. Meijer, H. Overing, and G. H. W. Bunig, *Macromolecules* **28**, 7967–7969 (1995).
32. D. Rein, P. Rempp, and P. J. Lutz, *Makromol. Chem., Macromol. Symp.* **67**, 237–249 (1993).
33. H. Iatrou and N. Hadjichristidis, *Macromolecules* **25**, 4649 (1992); H. Iatrou and N. Hadjichristidis, *Macromolecules* **26**, 2479–2484 (1993); H. Iatrou, E. Siakali Kioulafa, N. Hadjichristidis, J. Roovers, and J. Mays, *J. Polym. Sci., Part B: Polym. Phys.* **33**, 1925–1932 (1995).
34. J. M. J. Fréchet, C. J. Hawker, and K. L. Wooley, *J. Macromol. Sci., A: Pure Appl. Chem.* **31**, 1627–1645 (1994).
35. C. J. Hawker and J. M. J. Fréchet, in J. L. Hedrick and J. W. Labadie, eds., *Step-Growth Polymers for High-Performance Materials* (ACS Symposium Series 624), American Chemical Society, Washington, D.C., 1996, pp. 132–144.
36. A.-D. Schlüter, W. Claussen, B. Karakaya, and W. Lamer, in J. L. Hedrick and J. W. Labadie, eds., *Step-Growth Polymers for High-Performance Materials* (ACS Symposium Series 624), American Chemical Society, Washington, D.C., 1996, pp. 145–155.
37. H. R. Kricheldorf, O. Stöber, G. Löhden, T. Stuckenbrock, and D. Lübbers, in J. L. Hedrick and J. W. Labadie, eds., *Step-Growth Polymers for High-Performance Materials* (ACS Symposium Series 624), American Chemical Society, Washington, D.C., 1996, pp. 156–185.
38. C. J. Hawker and W. Devonport, in J. L. Hedrick and J. W. Labadie, eds., *Step-Growth Polymers for High-Performance Materials* (ACS Symposium Series 624), American Chemical Society, Washington, D.C., 1996, pp. 186–196.
39. IUPAC, *Pure Appl. Chem.* **12**, 643–656 (1966).
40. E. S. Wilks, *J. Chem. Inf. Comput. Sci.* **37**, 224–235 (1997).
41. M. Zeldin, K. J. Wynne, and H. R. Allcock, eds., *Inorganic and Organometallic Polymers* (ACS Symposium Series 360), American Chemical Society, Washington, D.C., 1988.
42. IUPAC, *Pure Appl. Chem.* **65**, 1561–1580 (1993).
43. J. L. Schultz and E. S. Wilks, *J. Chem. Inf. Comput. Sci.* **36**, 786–793 (1996).
44. C. G. Overberger and J. A. Moore, *Adv. Polym. Sci.* **7**, 113–150 (1970).
45. W. DeWinter, *Rev. Macromol. Chem.* **1**, 329–353 (1966).
46. W. J. Bailey, *Encyclopedia of Polymer Science and Engineering*, 2nd ed., Index Vol., John Wiley & Sons, Inc., New York, 1990, pp. 158–245.
47. IUPAC, *Pure Appl. Chem.* **61**, 243–254 (1989); reprinted as Chapt. 8 in Ref. 52.
48. H. K. Lichtenwalner and M. N. Sprung, *Encyclopedia of Polymer Science and Technology*, Vol. **12**, John Wiley & Sons, Inc., New York, 1970, pp. 467–468.
49. B. Gordon and J. E. Loftus, *Encyclopedia of Polymer Science and Engineering*, 2nd ed., Vol. **16**, John Wiley & Sons, Inc., New York, 1990, pp. 533–554.
50. U.S. Pat. 2,440,800 (Apr. 10, 1942), W. E. Hanford and R. M. Joyce (to E.I. du Pont de Nemours & Co., Inc.).

51. IUPAC, "Compendium of Macromolecular Nomenclature," in W. V. Metanomski, ed., *The Purple Book*, Blackwell, Oxford, 1991, Chapt. 5, p. 107.
52. J. L. Schultz and E. S. Wilks, *J. Chem. Inf. Comput. Sci.* **37**, 436–442 (1997).
53. J. L. Schultz and E. S. Wilks, *J. Chem. Inf. Comput. Sci.* **37**, 425–435 (1997).

JOHN L. SCHULTZ
EDWARD S. WILKS
E. I. Du Pont de Nemours

STYRENE–BUTADIENE COPOLYMERS.

See Volume 4.

STYRENE POLYMERS.

See Volume 4.

SULFUR–CONTAINING POLYMERS.

See Volume 4.

SUPERABSORBENT POLYMERS

Introduction

Superabsorbent polymers are very high molecular mass, cross-linked polyelectrolytes (qv) that can absorb or imbibe more than 10 times their mass of water or aqueous solutions. In order to absorb this large quantity of aqueous fluid, the polymers must be only slightly cross-linked so that the polymer chains can adopt widely spaced configurations. And in order to remain largely insoluble, while at the same time being highly expanded, the polymer chains must have very high molecular mass so that the small number of cross-links connect together all the chains. Cross-linked polyelectrolytes absorb more aqueous liquid than do neutral polymers as a result of the added osmotic, swelling pressure of the counterions that balance the high electric charge of the ionized functional groups spaced along the polymer chains (see POLYELECTROLYTES).

While any high molecular mass, cross-linked polyelectrolyte can function as a superabsorbent polymer, the commercially available superabsorbent polymers are alkali metal salts of poly(acrylic acid) cross-linked with multifunctional cross-linkers (see ACRYLIC (AND METHACRYLIC) ACID POLYMERS). Most often the cross-links are formed from comonomers that are incorporated into the polymer during the free-radical-initiated addition polymerization. Common cross-linkers are di- and triacrylates or methacrylates. The polymer chains can also be cross-linked after the main polymer chains have been formed. In this case, the cross-linker is multifunctional with groups that can react with the carboxylic acid or carboxylate groups present along the polymer chains. Examples of this type of cross-linker are polyols, polyepoxides, polyamines, and the like. Most commonly, the polymers are made by means of free-radical-initiated polymerization of an aqueous solution of the monomers, followed by drying the hydrogel that is formed and grinding the dry polymer to a granular powder.

Encyclopedia of Polymer Science and Technology. Copyright John Wiley & Sons, Inc. All rights reserved.

The principal use of superabsorbent polymers is as a liquid absorbent in disposable hygiene products, which include baby diapers, feminine hygiene products, and adult incontinence products. Smaller volume uses include liquid absorbent pads for packaged meats and water-blocking tapes and coatings for electrical and telecommunication cables.

Physical Properties of Monomers

The monomers useful for making superabsorbent polymers are water-soluble monomers such as those listed in Table 1. Acrylic acid, methacrylic acid, and 2-acrylamido-2-methylpropanesulfonic acid (1,2) are the principal ionizable monomers useful for making superabsorbent polymers. Other comonomers such as acrylamide and *N*-isopropylacrylamide can also be incorporated into the polymer chain. For example, *N*-isopropylacrylamide imparts temperature sensitivity into the superabsorbent polymer (3,4). The useful cross-linkers include a variety of multifunctional monomers, such as those shown in Table 2. They can

Table 1. Principal Monomers Used in the Preparation of Superabsorbent Polymers

Property	Acrylic acid	Methacrylic acid	Acrylamide	*N*-Isopropyl-acrylamide	2-Acrylamido-2-methylpropane-sulfonic acid
CAS registry number	79-10-7	79-41-4	79-06-1	2210-25-5	15214-89-8
Molecular formula	$C_3H_4O_2$	$C_4H_6O_2$	C_3H_5NO	$C_6H_{11}NO$	$C_7N_{13}NO_4S$
Molecular mass, g/mol	72.06	86.10	71.08	113.16	207.21
Melting point, °C	13.5	16	84.5	62	195
Boiling point, °C	139	163	136 (3330 Pa)	90 (267 Pa)	—
Flash point, °C	50	76	—	—	160
Density at 20°C, g/cm^3	1.040	1.015	1.122 (30°C)	—	—
ΔH_{polym}, kJ/mol	77.5	56.3	81.5	—	92.0

Table 2. Cross-linkers Used in Superabsorbent Polymers

Property	*N*,*N*′-Methylene bisacrylamide	Ethylene-diacrylate	1,1,1-Trimethylol-propanetriacrylate	Triallyl-amine	Tetra(allyloxy) ethane
CAS registry number	110-26-9	2274-11-5	15625-89-5	102-70-5	16646-44-9
Molecular formula	$C_7H_{10}N_2O_2$	$C_8H_{10}O_4$	$C_{15}H_{20}O_6$	$C_9H_{15}N$	$C_{14}H_{22}O_4$
Molecular mass, g/mol	154.17	170.16	296.32	137.23	254.33
Boiling point, °C	—	67 (267 Pa)	—	150	157 (3330 Pa)
Density at 20°C, g/cm^3	—	1.094	1.100	0.790	1.001
Flash point, °C	—	92	>110	30	>110

be di-, tri-, or tetrafunctional, and can have mixed types of polymerizable groups such as methacrylate and allyl, as in allylmethacrylate. Mixed types of functional groups provide olefins with varying reactivity toward the main monomer. The mixed-functional cross-linkers can be used to control the incorporation of the cross-links during the polymerization. For example, the gel point of the polymerization can be made at lower conversion of monomers by using a cross-linker that is more reactive than the main monomer. Conversely, the gel point can be delayed to higher conversion of monomers by using a less reactive monomer compared to the main monomer.

Manufacture of Monomer

The principal monomer used in the manufacture of superabsorbent polymers is acrylic acid. Acrylic acid is made by the oxidation of propene in two steps (5). First, propene is oxidized to acrolein, and then the acrolein is further oxidized to acrylic acid. Different mixed metal oxide catalysts are used for each step to optimize the yield and selectivity of the oxidation reactions. Technical-grade acrylic acid is isolated from the steam-quenched reaction gas by means of solvent extraction and distillation, and is used principally in the further preparation of acrylate esters. The technical-grade acrylic acid is further purified by distillation or by crystallization from the melt to afford the polymerization-grade monomer.

Properties of Polymers

The principal useful feature of superabsorbent polymers is their ability to absorb aqueous liquids and expand or swell in size. The swollen polymer—a cross-linked polymer solution—holds tightly to the liquid and prevents the liquid from being easily squeezed from the expanded structure. The two principal properties of the polymer that define their usefulness are the swelling ratio and the elastic modulus of the swollen polymer.

Swelling Ratio. The swelling characteristic of superabsorbent polymers has been described in several ways. A volumetric swelling ratio is equal to the volume of solvent absorbed per unit volume of the polymer. The gravimetric swelling ratio, or specific absorbency, is equal to the mass of solvent absorbed per unit mass of unswollen polymer. The gravimetric ratio is most commonly used in the measure of swelling in commercial practice. These volumetric and gravimetric ratios can be easily interconverted by multiplication with the ratio of densities of the solvent and polymer. The molecular theories of swelling and elasticity of cross-linked polymer networks use the volume fraction of polymer in the gel phase as a measure of swelling extent. The reciprocal of the volume fraction, equal to the ratio of gel volume to polymer volume, is an alternative volumetric swelling ratio. The theory (6) yields equation 1 for the swelling ratio q_{m} in terms of the essential structural and polymer synthesis parameters of the system.

$$q_m^{5/3} = \frac{\left(\frac{1}{2} - \chi\right) 2M_{\mathrm{c}}}{V_1 \rho_0 \upsilon_{2^0}^{2/3} (1 - 3M_c/M_n)} \tag{1}$$

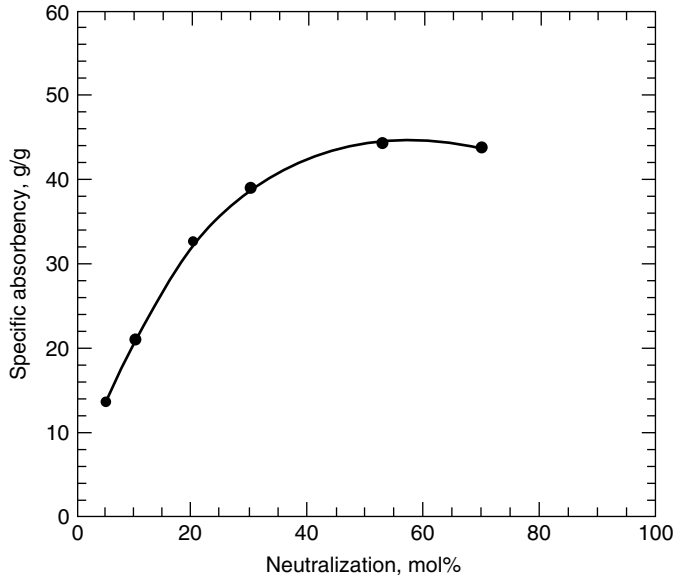

Fig. 1. Effect of neutralization on specific absorbency.

Assuming a randomly cross-linked, four-functional network, and including the ionic effects in an "apparent χ," the swelling ratio depends on the molecular mass of polymer chain between cross-links M_c, on the backbone molecular mass M_n, the molar volume V_1 of the solvent, and the density ρ_0 of the unswollen polymer. The volume fraction of monomer υ_{20} during polymerization influences the maximum swelling ratio through the term $\upsilon_{2^0}^{2/3}$.

Commercialized superabsorbent polymers are salts of weak polyacids; hence, their swelling varies with the pH of the swelling liquid or the ionization extent of the polymer, as shown in Figure 1. For superabsorbents made from strong acid monomer such as 2-acrylamido-2-methyl-1-propanesulfonic acid, the swelling extent does not depend on the pH of the swelling liquid (7).

The swelling ratio of any superabsorbent polymer depends directly on the cross-link density imposed during synthesis. The actual cross-link density often differs from the stoichiometry of reagents employed on account of inefficient incorporation of cross-linker, poor reactivity of cross-linker relative to acrylic acid, and the functionality (number of reactive olefinic groups) of the cross-linker molecule.

The swelling extent of all superabsorbent polymers is very sensitive to the salt concentration of the swelling liquid (8), as a direct result of their polyelectrolyte nature. The swelling extent decreases with increasing concentration of ions in solution. Divalent ions, such as calcium or magnesium, decrease the swelling of superabsorbent polymers much more than monovalent ions (per mole of ions) (9). The additional effect is so large that it has been erroneously believed that the divalent ions behave like cross-linkers. Measurements of both the swelling extent and elastic modulus of the swollen gels have disproved that notion (10). The gels, swollen in solutions of divalent ions, had equivalent modulus to the gels swollen

to the same volume fraction polymer in monovalent salt solution. However, many higher valence ions, such as ferric or chromic, add to the cross-link density of gels swollen in their solutions.

Modulus of Elasticity. When a swollen superabsorbent polymer particle is subjected to mechanical stress, it strains and changes shape. The elastic modulus of the material is the ratio of the applied stress to the resulting strain. For swollen superabsorbent polymers, the magnitude of the elastic shear modulus principally depends on the cross-link density established during synthesis of the polymer and on the extent of swelling during measurement of the modulus. Polymer swelling lowers the cross-link density by increasing the volume in which the cross-links reside.

The elastic modulus of the swollen superabsorbent polymer is important for several reasons. The powdered polymer is typically used in a physical blend with fibers such as cellulose and thermoplastic binder fibers. The resulting structure is called the absorbent core. The absorbent core relies on pore spaces between the fibers and polymer particles to provide liquid transport volume for the overall structure. When the swollen superabsorbent particles have low modulus, they are easily deformed by body pressures and can fill in the interfiber and interparticle pores. This prevents liquid flow and wicking of liquid into the drier portions of the core. Higher modulus limits the deformation of the particles and helps maintain the pore space.

The elastic modulus also influences the swelling kinetics of the superabsorbent polymer in the blend (11). For a cross-linked polymer, different shaped particles have different swelling kinetics. This results from the coupling between the diffusion of water into the polymer network through the surfaces of the particles, and the relaxation of the cross-linked polymer chains in the presence of the swelling agent. Of the simple shapes, spherical particles have the fastest kinetics whereas flat disks have the slowest kinetics. Spherical particles that are deformed into a disk-like shape swell more slowly, and therefore the more deformable swollen particles (lower elastic modulus) will be slower than similar sized particles with higher modulus that are less deformable.

The elastic modulus is controlled by the polymer network structure and synthesis conditions. The number of cross-links added per mole of main monomer helps define the molecular mass between cross-links. The molecular mass of the backbone polymer chain (obtained if no cross-linker was used) affects the effectiveness of the cross-links in forming a fully connected network with no soluble fraction and minimum content of dangling chains. The polymer volume fraction during cross-linking υ_{2^0} defines the extent of entanglement of the network chains, and therefore influences the elastic modulus.

From the molecular theory of networks, the shear modulus is given in terms of polymerization parameters according to equation (2)

$$G = \frac{\rho_0 RT}{2M_c}\left(1 - \frac{3M_c}{M_n}\right)\upsilon_{2^0}^{2/3}\upsilon_2^{1/3} \tag{2}$$

wherein the parameters have the same meanings as given above for the equation of the swelling ratio. The extent of swelling during measurement is expressed through the volume fraction of polymer in the gel υ_2. The gas constant R and the

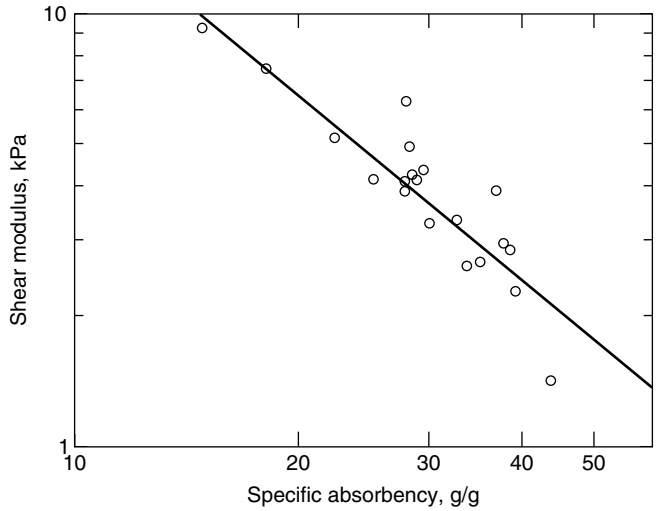

Fig. 2. Relationship of gel shear modulus to the specific absorbency. Polymers were swollen in 0.9% NaCl solution. To convert kPa to dyn/cm^2, multiply by 10^4.

temperature T also affect the magnitude of the modulus. By comparing equations 1 and 2, the swelling capacity and the elastic modulus are inversely related to the same structural parameters. This relationship is shown in Figure 2.

Swelling Kinetics. A first-order relaxation process in which the polymer chains relax and diffuse into the aqueous solution controls the swelling rate, which is given by equation 3:

$$\text{Rate of swelling} = \frac{dQ}{dt} = k(Q_{max} - Q(t)) \tag{3}$$

wherein Q_{max} and $Q(t)$ are the swelling ratios at equilibrium and at any time t, under the conditions of the experiment. The first-order rate (or relaxation) coefficient k depends on the diffusion coefficient of the polymer chains and on the particle radius. Integration over the total swelling time yields equation 4.

$$Q(t) = Q_{max}(1 - e^{-kt}) \tag{4}$$

The rate coefficient k depends on the elastic subchain length (between cross-links), decreasing with increasing chain length between cross-links (ie, lower cross-link density). The rate coefficient also decreases with increasing particle radius. Increasing the temperature hastens the thermal fluctuations of the chains, and hence increases the rate coefficient. The rate coefficients for the weak polyelectrolyte superabsorbent polymers vary with the pH (extent of neutralization) and the salt concentration as well. At higher pH, the chains adopt a stiffer conformation; hence, the rate coefficient increases with pH. Addition of monovalent salts has the reverse effect on conformation; hence, the rate coefficient decreases with increasing salt concentration.

Polymerization

Superabsorbent polyacrylates are prepared by means of free-radical-initiated copolymerization of acrylic acid and its salts with a cross-linker (12,13). Two principal processes are used: bulk, aqueous solution polymerization and suspension polymerization of aqueous monomer droplets in a hydrocarbon liquid continuous phase (14) (see BULK AND SOLUTION POLYMERIZATIONS REACTORS; HETEROPHASE POLYMERIZATION). In either process, the monomers are dissolved in water at concentrations of 20–40 wt% and the polymerization is initiated by free radicals in the aqueous phase (15). The initiators, freeradical (qv) used include thermally decomposable initiators, reduction–oxidation systems, and photochemical initiators and combinations. Redox systems include persulfate/bisulfite, persulfate/thiosulfate, persulfate/ascorbate, and hydrogen peroxide/ascorbate. Thermal initiators include persulfates, 2,2′-azobis(2-amidinopropane)-dihydrochloride, and 2,2′-azobis(4-cyanopentanoic acid). Combinations of initiators are useful for polymerizations taking place over a temperature range.

The copolymerization is conducted either at low pH with the acid-form monomers, which are neutralized after polymerization, or at roughly neutral pH with partially neutralized carboxylate salts. Sodium hydroxide and sodium carbonate typically are the neutralizing agents. The cross-linkers vary in functionality, from difunctional acrylate esters and methylenebisacrylamide, to trifunctional compounds, such as 1,1,1-trimethylol-propanetriacrylate and triallylamine, and to tetrafunctional compounds, such as tetra(allyloxy)ethane.

In the case of acrylic and methacrylic acids, the reactivity of the monomer toward polymerization is a complex function of the pH (extent of neutralization) and monomer concentration. The reactivity of ionized monomer being lower than the neutral carboxylic acid, polymerization proceeds more slowly as pH is increased (16–18). A minimum in the polymerization rate occurs at pH of 7 (19–21). Above pH of 7, the rate increases again because of electrostatic screening due to increased ionic strength.

Processing of Polymers

Gel Size Reduction. After polymerization, the gel intermediate must be dried. However, prior to drying, the size of the gel pieces must be reduced in order to increase surface area and speed drying. In some commercial processes, the gel size reduction is done in the polymerization vessel by means of high torque agitators or screws. In other processes, gel is sized in a separate unit operation of gel extrusion and cutting or mincing. Final gel particles are in the diameter range of 0.5–3 cm.

Drying. The water used as solvent in the polymerization is removed from the polymerized gel by evaporation in continuous-operation, hot-air convection dryers or in contact dryers such as steam-heated drum dryers. In hot-air convection dryers, the rate of moisture removal depends on the heating gas temperature, humidity and flow rate, and the diffusion characteristics of water from the gel. Drying occurs in three general stages. For high water content in the gel, the drying rate is constant, as the rate is limited by heat transfer into the gel. At low water

contents, the drying is limited by diffusion of water through the gel, and the drying rate falls as water is further depleted. In the intermediate or transition regime, some of the polymer is still in the constant-rate regime while other portions have entered the diffusion-controlled regime.

On rotating drum dryers, the drying energy is conductively transferred from the hot metal drum to the gel (22). The hydrogel must be applied to the drum in a sufficiently thin layer, accounting for the available heat transfer and drum size, so that it is thoroughly dry in about three quarters of a revolution of the drum roll, whereupon it is scraped from the drum with flaking knives. In order to spread the gel layer effectively onto the drum, the hydrogel must be soft enough to be deformable in the dryer nip.

Grinding and Sieving. Grinding or milling the very coarse dryer product, followed by sieving sets the particle size distribution of the dried superabsorbent polymer. The common polyacrylate superabsorbent polymers have a particle size distribution ranging from about 200 to 800 μm. Two-stage milling is frequently used in combination with sieving and recycle of the oversize particles in order to prepare a relatively narrow size distribution of the final granular powder. Knife mills, attrition mills, roll crushers, and the like are used in the first stage to provide a coarse but narrower particle size distribution feed for the second grinding stage. In the second stage, the final average particle size is attained. Sieving off both the coarse tail and the fine tail of the size distribution typically narrows the final size distribution further. The coarse tail is recycled to the grinder, and the fine tail may be used for other purposes or recycled back to the polymerization reactor.

Surface Cross-linking. Since small particles of hygroscopic polymer absorb water very fast, they can quickly form a thin, sticky layer of gel at the particle surface and then clump together or "gel block." The resulting interparticle adhesion causes the formation of large, sticky agglomerates with low interparticle porosity and drastically slower swelling rate. One remedy is to add a solution of multivalent cations to the surface of the dry particles, forming an ionically cross-linked surface layer (23). Alternatively, the particle surface can be coated with and reacted at elevated temperature with polyols, polyepoxides, linear or cyclic diesters or polyamines, as examples, forming a covalently cross-linked surface shell (24–26). This shell of higher cross-link density is less swellable, less sticky, more rigid than the untreated polymer surface, and prevents gel-blocking. This improves the permeability of the particle bed toward liquids.

A third method to produce these so-called structured particles is to first form a particle with higher cross-link density and then lower the cross-link density in the center of the particle. Cross-linked polymers made in the presence of oxidizing agents such as sodium or potassium chlorate have shown improvements in absorbency under load and swelling capacity after a high temperature heating step (27) wherein a portion of the polymer chains in the particle center are cleaved through the action of the oxidizers.

Economic Aspects

Cross-linked, partially neutralized poly(sodium acrylate) represents the overwhelming majority of the superabsorbents manufactured in the world today.

The global manufacturing capacity for these superabsorbent polymers in 2001 was estimated to be about 1.187 million metric tons per year. This quantity is split with 380 kt/year in Europe, 427 kt/year in the United States of America, and 380 kt/year in Asia. Total global usage of superabsorbent polymers in 2001 amounted to about 1093 kt, or just over 92% of the global manufacturing capability (28).

In 2001, there were six principal global manufacturers of superabsorbent polymers. BASF Aktiengesellschaft had about 305 kt/year of manufacturing capacity, followed by Degussa (Stockhausen division) with about 245 kt/year, Nippon Shokubai Kagaku Kogyo with about 230 kt/year, The Dow Chemical Co. with about 120 kt/year, SanDia (Sanyo and Mitsubishi joint venture) with about 95 kt/year, and Sumitomo Chemical with about 60 kt/year. Several more small manufacturers together made up another 132 kt/year of manufacturing capability. Included in this group of smaller companies are those who make slightly different superabsorbent polymers such as cross-linked, partially neutralized poly(potassium acrylate) and cross-linked, slightly ionized polyacrylamide, which are used mainly in the agricultural and horticultural industries.

Superabsorbent polymers are used mainly in disposable, personal care hygiene products. About 81% of total tonnage (885 kt/year) is used in infant diapers and child training pants. Another 14% of the total (157 kt/year) is used in adult incontinence products, and about 2% (22 kt/year) is used in feminine menstrual pads and napkins. The remaining 3% of total tonnage (32.8 kt/year) is used in other applications such as construction materials, cable wrapping tapes, agriculture, and horticulture.

Analytical and Test Methods

Swelling Capacity. Several methods have been used to measure the specific absorbency (mass of liquid absorbed per unit mass of superabsorbent polymer), swelling ratio, or swelling capacity (29). In the most common technique (30), a small quantity of superabsorbent polymer is placed in a porous, heat-sealable bag, which is then immersed in the desired aqueous liquid. The polymer is allowed to absorb liquid for a time long enough to reach maximum or equilibrium swelling, which is usually from 30 to 90 min. Then the porous bag and its contents are centrifuged under standard conditions to remove the unabsorbed liquid from the pore spaces between the swollen particles. The liquid absorbed is determined by gravimetry.

Elastic Modulus. The elastic shear modulus of swollen superabsorbent polymer is commonly measured by means of oscillatory rheometry, using any of a variety of commercially available instruments (31). The sample to be analyzed is screened to the desired particle size cut such that the swollen particle size is smaller than the gap between the measuring plates. The sample is swollen in the desired liquid, usually 0.9 wt% NaCl solution or synthetic urine. Excess liquid is removed from the swollen hydrogel by blotting to minimize interparticle slippage. The hydrogel typically is placed onto the lower circular plate. An upper conical plate is positioned at the proper sample gap, which is packed with the gel. An oscillating torque is applied at a known frequency to the upper plate and the

resulting angular displacement of the cone is determined. The shear modulus of the hydrogel is calculated from the ratio of the applied stress to the resulting strain (32).

Particle Size Distribution. The particle size distribution is determined by sieving. The Rotap sieving, similar to the ASTM method used for polymer powders (33) is typically used. The method consists of placing a known quantity of the powder in a stack of sieves that are shaken horizontally while being hit at the top with a hammer (34). Alternatively, vibrating sieve sets may be used. The mass of polymer on each sieve is measured gravimetrically. From this data, the size distribution may be plotted and the mass-median particle size calculated.

Bulk Density and Flowability. The polymer bulk density (35) and polymer flowability (36) affect conveying pipe and hopper design in the polymer manufacturing plants and dosing machine settings on diaper manufacturing lines. Flowability is typically evaluated by timing the flow of a 100-g granular sample from a funnel into a cylinder of known volume. The bulk density, taken from the same procedure, is the mass/volume ratio of polymer in the cylinder.

Swelling Kinetics Methods. Swelling kinetics for superabsorbent polymers may be measured by a viscometric method (37), based on the dependence of suspension viscosity on the volume fraction of the suspended particles. However, the swelling rate is most often measured by determining the specific absorbency as a function of time, for example, by means of the centrifuge capacity analysis. An absorption rate may also be obtained from data of swelling vs time using the demand absorbency method (38).

A simple, single-point measurement of kinetics has been used in the patent art (39–41) and its characteristics have been described (37). The method, referred to as the "vortex time" analysis, is based upon the earlier exponential kinetic equation, rearranged to obtain equation (5) for a characteristic swelling time in terms of the values of Q, Q_{max}, and the rate coefficient k.

$$t_v = -\frac{1}{k}\ln(1 - Q/Q_{max}) \tag{5}$$

When the relative swelling of the sample Q/Q_{max} is known or is held constant, then t_v is simply related to the rate coefficient.

In the original method (39), 2 g of polymer sample is mixed with 50 mL of the desired test fluid, which is stirred by means of a magnetic stirring bar in a small beaker. As the fluid absorption proceeds, the viscosity of the suspension increases until the stirring vortex disappears at time t_v. The volume fraction of swollen polymer in the suspension when the vortex disappears was estimated to be equal to 0.52 (42). For the most accurate and comparable results across samples with different swelling capacities, the mass of polymer added must be adjusted based on the value of the specific absorbency. As the specific absorbency increases, less polymer is used in the test so that each sample reaches the same relative swelling extent at time t_v (43).

Absorbency under Load. The absorbency under load is a commonly used measure of the performance of superabsorbent polymers in absorbent products

such as diapers. It is not so much a property of the superabsorbent polymer, but rather a swelling phenomenon of a compressed, packed bed of polymer particles. The test system consists of a short plastic cylinder with a fine mesh screen fixed over one end. A quantity of dry polymer particles is placed on the screen and covered with a loose-fitting plastic disk as a piston. A standard weight is placed on the plastic piston, and then the polymer is put into contact with a saline solution through the fine mesh screen. As the polymer absorbs liquid, the swelling particles fill the cylindrical cell and push up the piston. The gravimetric swelling ratio achieved in a standard time is determined. The test is thought to mimic the behavior of the polymer as it swells within the absorbent core, under compression applied by the baby's body. The test has been modeled in terms of the polymer properties and some characteristics of the particle bed (44).

Uses

The unique attributes of superabsorbent make them useful in many different applications. The liquid absorption and retention ability makes them useful in disposable hygienic products. These include infant diapers, feminine hygiene pads, and adult incontinence products. Other absorbent products suitable for superabsorbent polymers are paper towels, surgical sponges, meat trays, disposable mats for outside doorways, household pet litter, bandages, and wound dressings. Because the gels can slowly release water vapor to the atmosphere, they can be used in humidity controlling products or as soil conditioners. Superabsorbent polymers can also release water-soluble substances from within the network structure into surrounding solutions; hence, pharmaceuticals or fertilizers may be controllably released from within the gels. The rubbery nature of the swollen gels can control the consistency of cosmetics or concrete, and yield a soft and dry feel to hot or cold packs for sore muscles. The combination of swelling and soft rubber properties imparts sealing properties to products that may come into contact with water or aqueous solutions, such as, underground wires and cables. In the following paragraphs, additional details will be given of how the properties of superabsorbent polymers affect their utility in specific products.

Disposable Infant Diapers. A basic disposable diaper consists of an absorbent core sandwiched between a liquid permeable top-sheet and an impermeable back-sheet (45). The top-sheet, next to the baby's skin, allows urine to flow through it into the core. The back-sheet, made of impermeable plastic, helps keep the baby's clothing dry. The core takes in the liquid, distributes it within the core and holds the liquid under compression from the baby.

In a diaper, the polymer is mixed with 0.5–10 times its mass of cellulose pulp fluff (processed wood fiber) to make up the core (46–48). Cores containing superabsorbents are thinner because a smaller volume of dry superabsorbent polymer can absorb the same volume of aqueous liquid as a larger volume of fluff.

In addition to the specific absorbency of the superabsorbent polymer, the absorption rate of the diaper must be optimized to the urination rate of the baby. When the core absorbs too slowly relative to the urination rate, the liquid overflows

the core and leaks from the diaper. The absorption rate of the composite is influenced by the absorption rate of the superabsorbent polymer. Fast swelling of the polymer can contain the liquid quickly. However, in some diaper designs, fast swelling may cause the diaper to leak if the porosity and permeability of the composite is reduced too rapidly.

Adult Incontinence. Adult incontinence products include belted or fitted disposable garments and light incontinence pads, which are similar to feminine napkins. Similar design considerations are used as in baby diapers. In adults the liquid volume is larger and the urination rate is faster than in infants; therefore, polymers with larger specific absorbency and faster swelling rate are desired for this application (49). The market for these products is growing with the aging population.

Feminine Hygiene. The first personal-hygiene product commercialized with superabsorbent polymer was a feminine napkin in Japan. Perhaps the biggest challenge in using superabsorbent polymer in these products is the huge difference in properties between urine and menstrual fluid. Menstrual fluid is a complex, viscous mixture of water, salts, proteins, and cells. The cells are far too large to be absorbed into the superabsorbent polymer, and the proteins make the fluid very viscous and thereby slow the diffuse of liquid into the polymer. In other blood absorption applications, such as in surgery and surgical appliances, the polymers can be chemically modified to prevent undesired blood clotting (50). Incorporating similar additives into superabsorbent polymers may improve their performance in feminine hygiene products.

Agricultural and Horticultural Applications. Superabsorbents in agriculture and horticulture are used as a mulch, to help the soil retain moisture (51,52). To provide this function, the polymers optimally are mixed into soil at a concentration of about 0.1 wt%. The resulting mixture retains moisture longer than untreated soil and helps maintain optimum germination conditions. Superabsorbent polymer helps improve porosity in clay soils, as the polymer particles expand and contract during the moisture cycles. However, in wet and soggy soils with low oxygen content, superabsorbent polymers can prolong the unfavorable soil conditions. Salt-tolerant superabsorbent polymers may be more useful than the common polyacrylates for this application. An excellent review of superabsorbents in soil has been published (53).

Construction Materials. Superabsorbent polymers are used to control liquid water in a variety of construction-related products. Joint-sealing composites are made by blending superabsorbents into chloroprene rubber (54) or into poly(ethylene-*co*-vinyl acetate) (55). These composites are used like mortar in the concrete block walls of the structure. Gaps left during construction are subsequently filled as the superabsorbent swells in any water, and subsequent leaks are prevented. A water-blocking construction backfill has also been developed from cement, water absorbing polymer, and an asphalt emulsion (56).

The swelling property of superabsorbents also protects communication cables from water damage (57,58). Water-blocking tapes are wrapped around fiber-optic communication cables and power transmission cables to stop intrusion of water into the cables if the water-resistant coverings are cut or broken (59). The

swelling polymer seals the damaged area and slows water penetration further along the cable.

Food Packaging. Superabsorbent polymer can also absorb juice or water from raw chicken, shellfish and other meats, or from frozen foods as they thaw, reducing sogginess of the product (60). Chilled superabsorbent polymer gels can also be used as a dry-cooling medium to keep perishable foods cold (61). The humidity controlling property of superabsorbent polymer also can be used to maintain a constant humidity in vegetable and fruit storage and prevent water spotting on fruits (62).

Sensors. Superabsorbent polymers can be used in sensor systems by virtue of their swellability and rubbery nature, which are controllable by changes in water content, pH, and ionic strength. Because a small voltage may be induced in a soft hydrogel by applying mechanical stress to the gel, a pressure-sensitive switch is possible (63). The potential that develops between the stressed and unstressed parts of the gel generates a signal that can light a photo diode. The intensity of the light emitted by the diode depends on the magnitude of the applied stress. The application of a voltage across a polyelectrolyte gel conversely causes a volume change in the gel. This may be used to perform work in applications such as robotic fingers (64) or artificial muscle (65).

BIBLIOGRAPHY

1. O. Okay, S. B. Sariisik, and S. D. Zor, *J. Appl. Polym. Sci.* **70**, 567–575 (1998).
2. F. Rosa, J. Bordado, and M. Casquilho, *Polymer* **43**, 63–70 (2002).
3. H. Hirose and M. Shibayama, *Macromolecules* **31**, 5336–5342 (1998).
4. J. Zhang and N. A. Peppas, *Macromolecules* **33**, 102–107 (2000).
5. T. Ohara, T. Sato, N. Shimizu, G. Prescher, H. Schwind, O. Weiberg, and K. Marten, *Ullman's Encyclopedia of Industrial Chemistry*, 5th ed., Vol. A1, 1985. pp. 161–176
6. J. E. Mark and B. Erman, *Rubberlike Elasticity, A Molecular Primer*, John Wiley & Sons, Inc., New York, 1988.
7. O. Okay and S. Durmaz, *Polymer* **43**, 1215–1221 (2002).
8. E. Vasheghani-Farahani, J. H. Vera, D. G. Cooper, and M. E. Weber, *Ind. Eng. Chem. Res.* **29**, 554–560 (1990).
9. I. Ohmine and T. Tanaka, *J. Chem. Phys.* **77**, 5725–5729 (1982).
10. F. Horkay, P. J. Basser, A. Hecht, and E. Geissler, *Macromol. Symp.* **171**, 201–208 (2001).
11. C. Wang, Y. Li, and Z. Hu, *Macromolecules* **30**, 4727–4732 (1997).
12. F. Askari, S. Nafisi, H. Omidian, and S. A. Hashemi, *J. Appl. Polym. Sci.* **50**, 1851–1855 (1993).
13. F. L. Buchholz, *J. Chem. Educ.* **73**, 512–515 (1996).
14. U. Dayal, S. K. Mehta, M. S. Choudhary, and R. C. Jain, *J. Macromol. Sci., Rev. Macromol. Chem. Phys. C* **39**, 507–525 (1999).
15. H. Omidian, S. A. Hashemi, P. G. Sammes, and I. G. Meldrum, *Polymer* **39**, 3459–3466 (1998).
16. S. H. Pinner, *J. Polym Sci.* **9**, 282–285 (1952).
17. H. W. Melville, in Proceedings of the International Colloquium on Macromolecules, Amsterdam, 1949, Centen, Amsterdam, 1950, p. 376.
18. G. Blauer, *J. Polym. Sci.* **11**, 189–192 (1953).
19. H. Ito, S. Shoji, and S. Shigenari, *J. Chem. Soc. Jpn., Ind. Chem. Sect.* **58**, 194–196 (1955).

20. V. A. Kabanov, D. A. Topchiev, and T. M. Karaputadze, *J. Polym. Sci. Symp.* **42**, 173–183 (1973).
21. V. A. Kabanov, D. A. Topchiev, T. M. Karaputadze, and L. A. Mkrtchian, *Eur. Polym. J.* **11**, 153–159 (1975).
22. J. McKetta, *Encyclopedia of Chemical. Processing. and Design*, Vol. **17**, Marcel Dekker, Inc., New York, 1982, pp. 17–19.
23. U.S. Pat. 4,043,952 (1977), S. H. Ganslaw and H. G. Katz (to National Starch and Chemical Corp.).
24. Eur. Pat. Appl. 629,411 (1994), T. Sumiya, M. Date, and K. Tanaka (to Sanyo Chemical Industries, Ltd.).
25. Jpn. Kokai Tokkyo Koho 57-44,627 (1982), S. Oobayashi, M. Nakamura, T. Yamamoto, and M. Fujikake (to Seitetsu Kagaku Co., Ltd.).
26. Jpn. Kokai Tokkyo Koho. 58-42,602 (1983), T. Ito, F. Masuda, K. Tanaka, and K. Mita (to Sanyo Chemical Industries, Ltd.).
27. WIPO Int. Appl. 94-20,547 (1994), J. H. Burgert, F. L. Buchholz, S. B. Christensen, H. A. Gartner, A. T. Graham, and T. C. Johnson (to The Dow Chemical Company.).
28. R. May, unpublished data, The Dow Chemical Company, 2002.
29. S. Cutié, P. B. Smith, R. E. Reim, and A. T. Graham, in F. L. Buchholz and A. T. Graham, eds., *Modern Superabsorbent Polymer Technology*, Wiley-VCH, New York, 1998, p. 153.
30. U.S. Pat. 5,149,334 (1992), F. H. Lahrman, C. J. Berg, and D. C. Roe (to The Procter and Gamble Co.).
31. Eur. Pat. Appl. 530,438 (1993), D. R. Chambers, H. H. Fowler, Y. Fujiura, and F. Masuda (to Hoechst Celanese Corp.).
32. J. D. Ferry, *Viscoelastic Properties of Polymers*, 2nd ed., John Wiley & Sons, Inc., New York, 1970.
33. *Particle Size (Sieve Analysis) of Plastic Materials*, ASTM D1921 American Society of Testing and Materials, 1982.
34. B. H. Kaye, in P. J. Elving and J. D. Winefordner, eds., *Direct Characterization of Fine Particles*, John Wiley & Sons, Inc., New York, 1981, p. 69.
35. *Apparent Density of Free Flowing Metal Powders*, ASTM B212-82, American Society for Testing and Materials, 1982.
36. *Flow Rate of Metal Powders*, ASTM B213-77, American Society for Testing and Materials, 1977.
37. F. L. Buchholz, in L. Brannon-Peppas and R. Harland, eds., *Absorbent Polymer Technology*, Elsevier Science Publishers, New York, 1990, pp. 233–247.
38. E. Selic and W. Borchard, *Macromol. Chem. Phys.* **202**, 516–520 (2001).
39. U.S. Pat. 4,587,308 (1986), M. Makita and S. Tanioku (to Arakawa Kagaku Kogyo Kabushiki Kaisha).
40. U.S. Pat. 5,053,460 (1991), P. Mallo, M. Moreau, and J. Cabestany (to Societe Francaise Hoechst).
41. Eur. Pat. Appl. 615,736 (1994), M. K. Melius, S. M. Yarbrough, M. C. Putzer, S. R. Kellenberger, and S. K. Byerly (to Kimberly-Clark Corp.).
42. F. L. Buchholz, in L. Brannon-Peppas and R. Harland, eds., *Absorbent Polymer Technology*, Elsevier Science Publishers, New York, 1990, pp. 233–247.
43. S. Cutié, P. B. Smith, R. E. Reim, and A. T. Graham, in F. L. Buchholz and A. T. Graham, eds., *Modern Superabsorbent Polymer Technology*, Wiley-VCH, New York, 1998, p. 156.
44. F. L. Buchholz, in F. L. Buchholz and A. T. Graham, eds., *Modern Superabsorbent Polymer Technology*, Wiley-VCH, New York, 1998, p. 201ff.
45. U.S. Pat. 4,306,559 (1981), K. Nishizawa, T. Shirase, and H. Mizutani (to Kao Soap Co., Ltd.).

46. U.S. Pat. 5,147,343 (1992), S. R. Kellenberger (to Kimberly-Clark Corp.).
47. U.S. Pat. 5,149,335 (1992), S. R. Kellenberger, W.-H. Shih-Schroeder, and A. J. Wisneski (to Kimberly-Clark Corp.).
48. U.S. Pat. 5,021,050 (1991), M. J. Iskra (to Weyerhauser Co.).
49. U.S. Pat. 5,439,458 (1995), J. R. Noel and A. Ahr (to The Procter and Gamble Co.).
50. E. W. Merrill, R. W. Pekala, and N. A. Mahmud, in N. A. Peppas, ed., *Hydrogels in Medicine and Pharmacy, Vol. 3: Properties and Applications*, CRC Press, Boca Raton, Fla. 1987, pp. 1–16.
51. T. Yamaguchi and S. Tsukakoshi, *Chem. Express* **7**(2), 165–168 (1992).
52. M. Bakass, A. Mokhlisse, and M. Lallemant, *J. Appl. Polym. Sci.* **83**, 234–243 (2002).
53. K. S. Kazanskii and S. A. Dubrovskii, *Adv. Polym. Sci.* **104**, 97–133 (1992).
54. Jpn. Kokai Tokkyo Koho 62-149,335 (1987), T. Tsubakimoto, T. Shimomura, and H. Kobayashi (to Nippon Shokubai Kagaku Kogyo).
55. Jpn. Kokai Tokkyo Koho 06-157,839 (1994), S. Masakatsu, S. Eiji, N. Toshikazu, and I. Masatoshi (to Tonen Chemical Corp.).
56. A. Moriyoshi, I. Fukai, and M. Takeguchi, *Nature* **344**, 230–232 (1990).
57. Eur. Pat. Appl. 24,631 (1981), K. E. Bow (to The Dow Chemical Company).
58. K. Hogari and F. Ashiya, in F. L. Buchholz and N. A. Peppas, eds., *Superabsorbent Polymers: Science and Technology* (ACS Symposium Series 574), The American Chemical Society, Washington, D.C., 1994, pp. 128–140.
59. Eur. Pat. Appl. 375,685 (1990), H. Polle (to Siemens Aktiengesellschaft).
60. Eur. Pat. Appl. 68,530 (1983), A. M. DeGouw, J. Prins, and J. Dingermans (to Akzo N.V.).
61. Australian Pat. 8,777,327 (1988), P. Clerk.
62. T. Shimomura and T. Namba, in F. L. Buchholz and N. A. Peppas, eds., *Superabsorbent Polymers, Science and Technology* (ACS Symposium Series 573), American Chemical Society, Washington, D.C., 1994, pp. 112–115.
63. K. Sawahata, J. P. Gong, and Y. Osada, *Macromol. Rapid Commun.* **16**, 713–716 (1995).
64. K. Kurauchi, T. Shiga, Y. Hirose, and A. Okada, in D. DeRossi and co-workers, eds., *Polymer Gels*, Plenum Press, New York, 1991, pp. 237–246.
65. W. Kuhn, B. Hargitay, A. Katchalsky, and H. Eisenberg, *Nature* **165**, 514–516 (1950).

GENERAL REFERENCES

F. L. Buchholz and N. A. Peppas, eds., *Superabsorbent Polymers, Science and Technology* (ACS Symposium Series 574), American Chemical Society, Washington, D.C., 1994.

F. L. Buchholz and A. T. Graham, eds., *Modern Superabsorbent Polymer Technology*, Wiley-VCH, New York, 1998.

J. P. Cohen Addad, *Physical Properties of Polymeric Gels*, John Wiley & Sons, Inc., New York, 1996.

D. DeRossi, K. Kajiwara, Y. Osada, and A. Yamauchi, eds., *Polymer Gels, Fundamentals and Biomedical Applications*, Plenum Press, New York, 1991.

L. Brannon-Peppas and R. Harland, *Absorbent Polymer Technology*, Elsevier, New York, 1990.

P. K. Chatterjee, ed., *Absorbency*, Elsevier, New York, 1985.

K. Dusek, ed., *Responsive Gels: Volume Transitions 1* (Advances in Polymer Science 109), Springer-Verlag, Berlin, 1993.
K. Dusek, ed., *Responsive Gels: Volume Transitions 2* (Advances in Polymer Science 110), Springer-Verlag, Berlin, 1993.

FREDRIC L. BUCHHOLZ
The Dow Chemical Company

SURFACE PROPERTIES.

See Volume 4.

SUSPENSION (OR PRECIPITATION) POLYMERIZATION.

See HETEROPHASE POLYMERIZATION.

SYNCHROTRON RADIATION

Introduction

The application of x-ray scattering to elucidate the structure and phase behavior of biological and synthetic polymeric systems has been an established research field for a long time. Initially these experiments were performed with conventional x-ray sources such as sealed tube generators and later with rotating anode generators. Although polymers are in general weakly scattering, the pioneers of this field managed to resolve many problems by ingenious use of the existing equipment. However, when the higher intensity generated by synchrotron radiation (SR) sources became available, it did not take long for the huge potential of the highly collimated and intense x-ray beams generated by these machines to be recognized as extremely valuable. Not only can the morphology of polymers be elucidated to a higher degree of accuracy than with conventional x-ray sources, but also structural changes can be studied while varying parameters such as sample temperature, pressure, and shear field in a time-resolved way.

Fundamentally, there is no real difference between x-ray research performed with laboratory x-ray sources or with SR sources, apart from technical issues such as the higher x-ray flux, smaller x-ray beam divergence, or better collimation. The treatment and interpretation of data in both cases is consequently not fundamentally different. Therefore, this article focuses on issues that are related to those aspects in which the higher beam quality of SR beamlines is indispensable, although one should hasten to add that the use of SR should not be seen to be competitive with research performed with conventional x-ray generators, but a welcome complimentary extension of the experimental possibilities.

The higher flux, the wavelength tuneability, and the smaller beam sizes allow fast time-resolved experiments, the use of more complicated sample environments,

Encyclopedia of Polymer Science and Technology. Copyright John Wiley & Sons, Inc. All rights reserved.

the simultaneous combination of scattering experiments with other, non-x-ray-based techniques, and also a high throughput of samples.

At present, SR sources have become so powerful that it has become feasible not only to perform real-time experiments on conventional polymeric systems, but also to perform much more sophisticated experiments on extremely small samples. This includes experiments on a single silk fiber spun by a spider or the changes in the fiber diffraction pattern generated by the fibers in the muscles from a live drosophila fly, which was persuaded to flap its wings in an x-ray beam.

In this article some of the possibilities for conventional x-ray scattering experiments and the insight these experiments have shed on polymers with the use of SR are discussed. It is impossible to comprehensibly cover the whole field where SR and polymer research intermingle. At present there are approximately 20–30 SR beamlines that are being used for x-ray scattering experiments. Experience tells that a week of experiments on such a beamline provide on average ample data suitable for publishing. This means that around 20 publications appear per week in which synchrotron scattering experiments on polymers are being described.

Synchrotron Radiation

Synchrotron radiation is the name given to the electromagnetic radiation emitted when highly energetic charged particles are led through a magnetic field and are thus forced to change their direction. The existence of this radiation was first predicted by the theoretical work of Schwinger and others (1) and subsequently experimentally observed by researchers from General Electric in 1947. The production of SR is not limited to particle accelerators. Astrophysicists also have found that it is generated when charged particles are spiraling toward a celestial body is its magnetic field.

First treated as an unwanted side effect in high energy physics research, because of the electron energy loss involved in the emission that is detrimental to the efficiency of accelerators used for high energy physics research, it was soon recognized to be an extremely valuable tool for researchers wanting to use the broadband wavelength spectrum, which ranges from infrared to the hard x-ray domain (from a few electron volts to scores of kiloelectron volts). Consequentially, the first experiments using SR were performed in a parasitic mode on high energy physics machines. However, the requirements regarding the electron beam size between high energy physics and x-ray research are not completely compatible, which led to the construction of machines dedicated to the production of SR, the so-called storage rings, in which the electrons emitting the radiation were made to circulate while keeping their energy constant. This approach contrasts with high energy physics where the electrons are continuously accelerated and thus the SR spectrum is continuously changing.

In the history of SR research, one generally groups the laboratories which used the radiation of high energy physics machines in a parasitic mode in the category of the first generation machines (eg, Desy at Hamburg, the Cornell Synchrotron, Nina in Daresbury). The second generation machines are those that were dedicated to the production of SR and in which care was taken to optimize the electron beamsizes (NSLS at Brookhaven, Photon Factory in Tsukuba, SRS at

Daresbury). In these machines, most beamlines relied on the photons produced by bending magnets. In the third generation of machines, the electron beamsizes are even further reduced and a large number of beamlines are constructed, not only on bending magnets but also on undulators or multipole wigglers (ALS in Berkeley, APS in Argonne, ESRF in Grenoble, Spring8 in Harima). On most websites of SR laboratories, one can find pages listing other known laboratories (eg, www.esrf.fr, www.aps.anl.gov, or www.spring8.or.jp).

The x-ray wavelength spectrum and the number of photons that is generated is a function of the energy of the electrons in the storage ring and the magnetic fields that are used to keep the electrons in a closed orbit. A detailed treatment of these aspects is beyond the scope of this article. The interested reader can find a large amount of literature on these subjects (2,3).

A table with operational SR sources can be found in Reference 4 and a table with operational x-ray scattering beamlines can be found in Reference 5. Since SR-based research is still a rapidly expanding field, these tables might become outdated within several years.

The basic "workhorse" of the earlier generations of storage rings is the bending magnet in which electrons were forced to move in a circular path upon which they emitted radiation. This type of magnet generates a relatively broad cone of radiation with a relatively high divergence (see Fig. 1a). It should be remarked that even with these magnets the divergence and collimation is superior to that with conventional x-ray generators. A typical example of an intensity versus wavelength curve is given in Figure 1b, where the spectrum of a bending magnet of the European Synchrotron Radiation Facility (ESRF) is shown.

The more recent generation of SR sources still uses bending magnets since these are indispensable for the construction of a storage ring. However, modern accelerator technology allows for the insertion of devices in the straight sections between bending magnets. Of the different types of insertion devices, such as wigglers, wavelength shifters, and undulators, only the last ones are of interest for soft condensed matter research. These devices consist of arrays of permanent magnets which force the electrons (or positrons) in the storage ring over a sinusoidal path. By choosing the appropriate periodicity of the path, the x rays emitted by the electrons will be coherent from one position of the path with respect to the following equivalent position in the sinus. This causes interference effects between the succesive undulations. The result is that highly intense and extremely collimated x-ray beams are generated. See Figure 2a for a description of this process and Figure 2b for an example of the energy/intensity spectrum, which is generated by an ESRF undulator.

Beamlines. The greatest advantage of SR beamlines over conventional sources, when dealing with soft condensed matter research, is maybe not even the larger amount of photons which can be thrown onto the sample, but more so the fact that these photons are in less divergent beams. This means that optical elements can be used to condition the beam, which is not feasible with conventional sources. Obviously there are some drawbacks as well, but apart from the higher harmonic problem, which is discussed later, these mainly have consequences for the construction of the beamline and should not concern users of these beamlines. However, it is a fact of synchrotron life that most experimenters using these facilities will one day encounter some problems due to technical failures connected

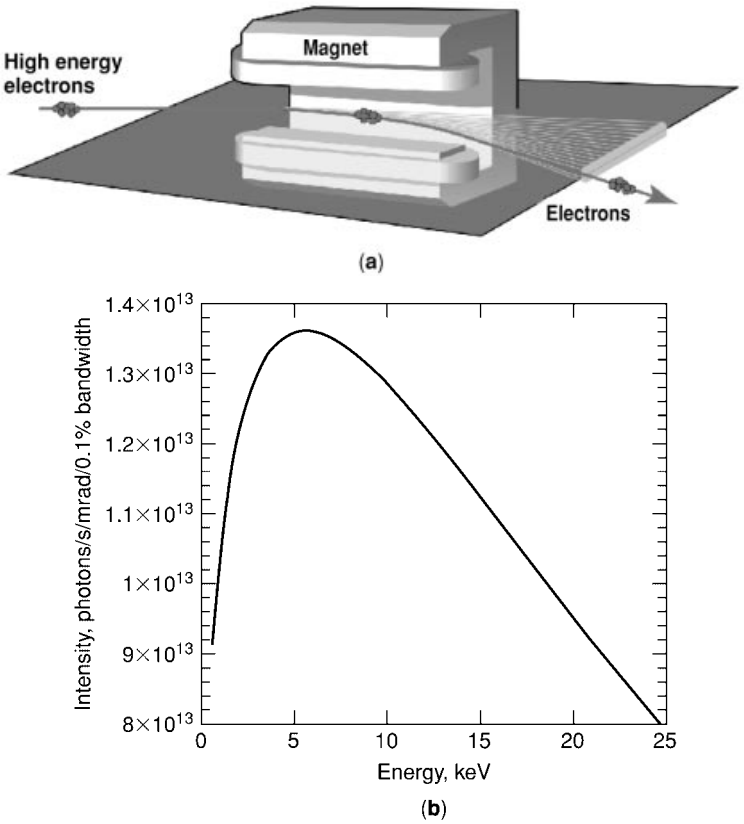

Fig. 1. (**a**) X rays are generated when charged particles with relativistic speeds are led through a homogeneous magnetic field. The Lorentz force forces the particles to follow a circular trajectory. In this process the particles emit radiation. (**b**) x-ray flux as function of energy generated by a bending magnet of the ESRF in Grenoble operating at 6 GeV and with a magnetic field of 0.8 T in the magnet. Similar curves of other third generation SR facilities can be shown. For second generation sources the flux is approximately a factor of 10 lower. However, even these second generation sources can generate a factor of 100–1000 more intensity when compared with conventional x-ray generators.

with the drawbacks. The mean time between failures of a beamline is shorter than that of a decent laboratory generator.

For conventional scattering beamlines there are three types of optical elements which are important. These are monochromators, mirrors, and slits. The functions of these are briefly discussed, since for an experimenter it is often detrimental if there is no basic understanding. Depending on the application, different types of elements can be used and they can be placed in different orders.

Monochromators. The x-ray spectrum emitted by a storage ring has been discussed in a previous section. For most scattering experiments the "white spectrum" emitted by the storage ring is not directly useful but one requires a monochromatic x-ray beam. Monochromators are available in several varieties with different properties. A conventional scheme uses a triangular monochromator which is circularly bent by clamping the base and pushing against the tip. This

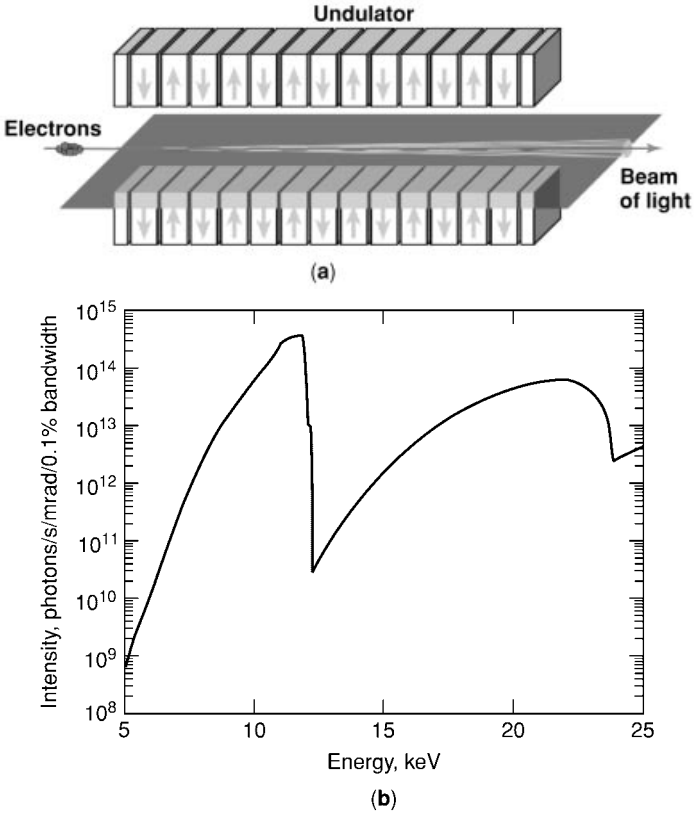

Fig. 2. (**a**) Undulators consist of a series of permanent magnets which are positioned to force the charged particles in the storage ring to follow an undulating path. With the appropriate period this radiation is coherent with respect to the radiation emitted by the next undulation. (**b**) Representative spectrum of an ESRF undulator. At the ESRF it is possible to place three of these undulators in series, thus enhancing the flux even further.

enables not only monochromatization but also focussing (6). Another commonly used design is the double crystal monochromator from which the second crystal is also sometimes bent for the same focussing purpose (*sagittal focussing*) (7). The monochromator material defines the bandwidth which is transmitted ($\Delta\lambda/\lambda$). One can use Si, with a narrow bandwidth, Ge, or alternatively monolayer systems. The last option allows a very high transmission at the expense of bandwidth. However, for x-ray scattering beamlines used for polymer research, the bandwidth is rarely an issue, not even with the monolayer systems in which the bandwidth is of the order of 0.01. In contrast with neutron scattering experiments, the raw data in general does not have to be treated for the bandwidth spread. The conventional energy range used in soft condensed matter research is 5–15 keV, which is equivalent to a wavelength range of 0.08–0.25 nm.

Mirrors. X rays can be focussed by letting the radiation impinge under grazing incidence upon a very smooth surface which is slightly bent. The material from which the mirror is made used to be special types of glass such as Zerodur or fused quartz but the tendency is to start using single crystal Si mirrors since these have

better mechanical and thermal properties. Other mirror substrates are in use as well. The angle of incidence lies somewhere between 1.0 and 10 mrad and, together with the substrate or coating material, determines the high energy cutoff. Over a certain energy, x rays are not reflected anymore. This property has become more important with the new generation of synchrotrons which operate at higher energies and therefore have a substantial amount of high energy radiation in the white spectrum. Monochromators transmit not only the primary energy but also the higher harmonics of these, and this has to be suppressed.

Average parameters for a mirror are a surface roughness of 0.15–0.4 nm and a slope error of 1–4 μrad. The dimensions can vary from several centimeters to 1.5 m. The surface quality is very important and therefore these mirrors are always mounted in a high vacuum vessel.

Slits. Slits are used to shape the beam and to reduce parasitic scatter around the primary beam. The latter is of overriding importance in small-angle scattering beamlines since it is the amount of parasitic scatter that is the most important factor in determining the possible low angle resolution and therefore the maximum size of the structures that can be observed (see Fig. 3).

Assembled Beamlines. The requirements for a beamline suitable for either wide-angle x-ray scattering (waxs) or small-angle x-ray scattering (saxs) do not differ much. One needs a beam size of around 0.5×0.5 mm^2 with a reasonable intensity ($>10^{10}$ photon/s). For saxs there is an extra requirement to reduce the parasitic scatter around the direct beam as much as possible. In time several design schemes, often dictated by the available x-ray source, have been used. These are based on a focussing element in the horizontal direction (often functionally combined with the monochromator) and a focussing element in the vertical direction (often a mirror). Examples of assembled beamlines can be found in References 8–12. This is a nonexhaustive list. A more extensive list can be found in Reference 5. A schematic description of a beamline can be seen in Figure 3. In this

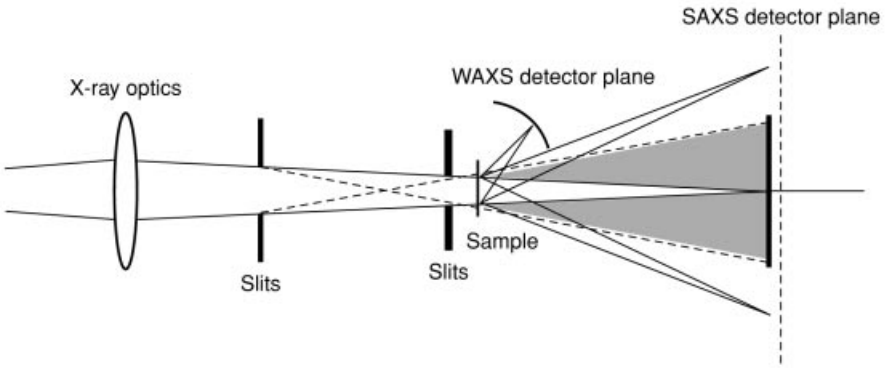

Fig. 3. Schematic description of an x-ray scattering beamline. The optical system is represented by a lens. The parasitic scatter cone is represented by the gray area. The scattering information which falls in this region is useless since the parasitic scatter is orders of magnitude more intense than the scattering pattern itself. The importance of the positioning of the slits in determining the extent of the parasitic scatter cone, which is the limiting factor in achieving low angle resolution, can be observed. Most beamlines are in fact equipped with three or more slit systems between the last optical element and the sample position.

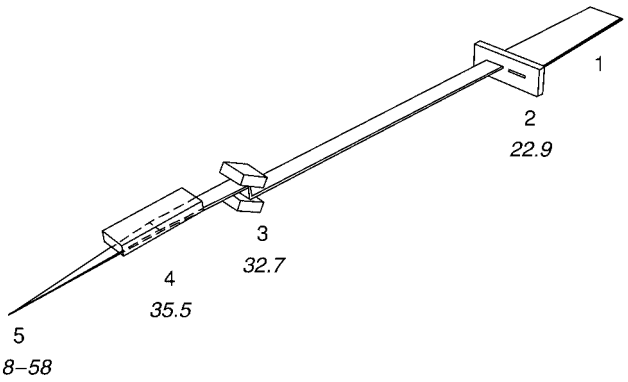

Fig. 4. Typical layout of the optical system of a scattering beamline constructed on a bending magnet source of the ESRF. The radiation fan (1) emitted by the bending magnet is used for two beamlines, each receiving 0.02 mGy of the total 0.09 mGy (2). A double crystal monochromator (3), from which the second crystal can be bent in order to allow horizontal focussing, is constructed in such a way that an energy range from 0.05 to 0.3 mGy can be covered. The long single crystal Si mirror (4) can also be bent in order to focus the beam in the vertical direction. Possibilities exist to insert an extra mirror in front of the monochromator which can be used to collimate the beam. This will enhance the energy resolution and will allow anomalous scattering experiments to be performed. The flux generated by this beamline is up to 10^{12} photons/s which can be focussed in a round 300-μm focal spot. Courtesy of I. Cerjah.

figure the optical system is represented as a lens ignoring the different schemes that exist. The most conventional systems at present are a combination of a vertically focussing mirror combined with an asymmetric-cut triangular monochromator that has the dual function of monochromatization and focussing in the horizontal plane (8,11) or, alternatively, a sagitally focussing double crystal monochromator combined with a vertical focussing mirror (12). A schematic example of one of the possible schemes to construct a saxs/waxs beamline is shown in Figure 4.

The use of optical elements that can focus the beam into a small spot is one of the main advantages of SR. This allows the user to generate a rather large x-ray flux on the sample in pseudo pinhole collimation. Until recently, the only other method to obtain sufficient flux was the use of a conventional generator equipped with a slit-collimated Kratky system (13). This unavoidably leads to the use of (mathematical) desmearing techniques. Nowadays, it has also become possible to utilize focussing elements such as Göbel mirrors on conventional generator equipment (14,15). In combination with efficient electronic detectors, one gains a lot in data quality, although the data quality obtained with SR is still unsurpassed.

A recent development is the use of helical undulators. These undulators can generate a very small beam size with a energy bandwidth of around 2%. For many scattering experiments this is still acceptable. This means that one can construct a beamline without further optics and thus without any flux losses. In this way it is possible to create a beamline that can generate 10^{17} photons/s on a sample (16).

However, in soft condensed matter such a beamline will only be useful in some special cases since technology to detect these enormous fluxes does not yet exist, and radiation damage on samples will be severe.

A rather special optical system, used when one wants to observe very small scattering angles, is the Bonse–Hart camera (17,18). This method is also sometimes called ultrasmall-angle x-ray scattering (usaxs) but this is rather arbitrary since in the literature one can find many examples where this term is used for data obtained with conventional beamlines. With the Bonse–Hart system one places the sample between two double crystal monochromators. The analyzing crystal behind the sample is (angular) step scanned over the transmitted beam. This technique requires a high photon flux and an x-ray beam with a very small divergence and is therefore most suitable to be used in third generation synchrotrons (19,20). Since the technique is step scanning, it is impractical to cover large angular ranges or time-resolved processes. Although the possibilities of Bonse–Hart cameras generate enthusiasm among users, the experience is that they do not reach a large audience. This is evidenced by the relatively small number of publications in this field. It is interesting to note that the number of neutron scattering experiments using the Bonse–Hart technique far outnumbers the x-ray scattering experiments.

X-ray Scattering

The most widely used x-ray techniques are saxs and waxs. The use of surface reflectivity is becoming more popular but will be treated in another article. There is a small niche for other techniques such as photon correlation spectroscopy in which one can study the dynamics of individual molecules. This technique is related to neutron spin echo experiments. However, the application is still fraught with difficulties and it is a very specialized subject.

The use of SR-based x-ray scattering on polymers was pioneered by H.G. Zachmann and co-workers in Hamburg around 1980 (21). This group was building upon the experience obtained with time-resolved experiments on biological materials such as contracting frog muscles and protein solution scattering (22). Initially the emphasis was on the static characterization of samples but soon time-resolved methods became more commonplace. When performing time-resolved experiments the role of the sample environment becomes more important. One needs to perturb the samples from the initial state in a controlled and homogeneously manner into another state. This is discussed in a later section.

Technology Detectors

One of the greatest problems that is encountered in SR-based experiments in soft condensed matter research is that the position-sensitive detector technology is lagging behind the development of beamlines by several generations. Different detectors can cope with different aspects but, at the time of writing, there is no detector that is capable of dealing with all the required aspects. For a better understanding of this problem it is convenient to first define the aspects that are important for performing experiments in soft condensed matter research: high count rate, time framing capacity, high dynamic range, large detection area, and spatial resolution.

At present the two main types of detectors that are used are based on either gas-filled wire chambers (23,24) or charge-coupled devices (CCDs) (25,26). In some cases, one uses photodiode arrays (27), and for static experiments the image plate detector can be utilized (28). However, only the two main types are discussed briefly.

Despite their obvious shortcomings, gas-filled wire chambers have been in use for a long time. This is because they have some very good properties. The most obvious shortcomings are that they have a limited count rate capacity and they require a good deal of maintenance. On the positive side they have a very large dynamic range, ie, the difference between the strongest and the weakest feature that can be detected, of more than six decades. The electronic time-frame rate can be as short as 10 μs/frame, and the dimensions of the active surface can be made large without incurring a penalty in the form of extreme costs. Also, they can be constructed in a variety of shapes—curved, quadrant—that can be suited to the experimental needs.

The CCD detectors have as main shortcomings the limited dynamic range, the slow time-frame rate, and the costs. The positive points of these detectors are that they can handle a large count rate, are relatively maintenance free, and the spatial resolution is superior to that of gas-based detectors.

To discuss these issues in detail is beyond the scope of this article. Practically, often one does not have the choice between different types of detectors since the cost of a detector system is so high that very rarely a beamline will be equipped with more than one system and so one has to accept what is offered. However, the experimental limitations imposed by the detector system can be assessed beforehand, as shown in the following section.

In Table 1 can be found a coarse summary of the properties of the two types of detectors.

An aspect that also requires some attention is the dimensionality of the detector. For a scattering pattern that is isotropic, ie, absence of orientational effects in the sample, in principle it is sufficient to utilize a linear, or one-dimensional, detector. Even in this case one often uses an area, or two-dimensional, detector since a polar integration over the diffraction pattern improves the statistics considerably. However, for fast time-resolved experiments, the larger data volume

Table 1. Properties of Two Types of Detectors

Property	Gas-filled wire chambers	Charge-coupled devices
	Counting	Integrating
Count rate	Relatively low	High
Spatial resolution	Low (200–300 μm)	High (25 μm)
Dynamic range	High (1:10^6 to 10^7)	Low (1:10^4 to 10^5)
Read-out noise	None	Weak signals will be influenced
Read-out speed detector	Fast (10 μs)	Slow (100 ms)
Maintenance	Not easy	Easy
Parallax problems	At wider angles	None
Efficiency	High (5–12 keV); low (>12 keV)	Low but much better than that of gas detector (>12 keV)

might be difficult to handle and unnecessarily complicate the experiment. In this case, one can revert to a so-called quadrant detector (24), which is essentially a linear detector but has an increasing, circular-shaped, active area as function of the radius. This provides the combined advantage of small data volumes while still retaining the benefits of the improved statistics at larger q-values. For (partially) oriented samples one requires a detector that can measure an anisotropic scattering pattern and one is obliged to use an area detector.

Time Resolution

When performing time-resolved experiments there are many experimental aspects that one has to consider. These range from the suitability of the x-ray equipment, such as detectors, to the sample environment that one is using. The latter especially deserves attention since in a time-resolved experiment one generally varies a physical or chemical parameter in order to study the response of the sample to this perturbation. The crucial aspect here is that this parameter should be varied in a controlled and uniform way. (See for this the section dealing with sample environments and technique combinations.)

Before starting to design a time-resolved experiment one has to check if it is possible to obtain the information that one needs with the available experimental equipment. Ultimately, this can only be determined empirically, but by carefully assessing the factors that influence the time resolution, it might be possible to see beforehand if there is not a parameter that inhibits the experimenter to perform the experiment at the time resolution needed in order to render relevant results, and thus avoid wasting the scarce time generally allocated to central SR facility users. The important parameters are

(1) **X-ray flux:**

With SR sources the flux is dependent on the photon energy. The higher the flux the faster an experiment can be performed.

(2) **Detector efficiency:**

Different types of detectors have different photon-energy-dependent efficiencies.

(3) **Maximum count rate a detector can handle:**

This is dependent on the physical process by which the photons are detected and on the detector electronics. If the value of this parameter is high, more photons can be detected in a single frame and will therefore have a positive effect on the time resolution.

(4) **Read-out time of the detector:**

This depends on the number of “pixels” to be read out and on the physical process by which the detector is read out.

(5) **Attenuation of x rays by windows around the sample and extra background scatter:**

In some cases, this factor can be eliminated by placing both sample and detector in a vacuum chamber. The smaller this number is the faster the experiment can be performed. However, even when x-ray flux is abundant, extra background scatter will have a negative impact on the quality of the data.

(6) **X-ray contrast:**

In an x-ray scattering experiment this is the electron density contrast giving rise to the scattering. If the contrast is high, one needs less time to obtain a statistically significant result.

(7) **Statistical accuracy:**

This parameter depends heavily on which parameters one wants to derive from the experiment, but in general this is also a human factor. Some people have "the eye of faith" and others do not. The higher this value, the better the data quality but the slower the time resolution.

(8) **Available memory to store the different time frames:**

This is a crucial consideration and might be a limiting factor in applications where it is crucial to use two-dimensional detectors. (Although computer memory is cheap nowadays it is still not trivial to store large data volumes rapidly.)

(9) **Dynamic range:**

The maximum intensity a detector can detect in comparison with the minimum is called the *dynamic range*. In scattering experiments, where the intensity generally falls as $1/q^4$, this is not a trivial issue. One should keep in mind that some types of detectors, such as CCDs, add dark current and read-out noise to the signal, which influences the dynamic range. A higher efficiency and low noise level will have a positive effect on the achievable time resolution.

(10) **Radiation damage:**

It is possible that the sample is destroyed by radiation damage before the statistical quality of the data is high enough.

All these parameters can be summarized in a symbolic formula as follows:

$$\text{Time resolution} = \frac{\text{readout} \times \text{statistics} \times \text{attenuation}}{\text{flux} \times \text{detector efficiency} \times \text{maximum count rate} \times \text{contrast} \times |\text{memory}| \times |\text{dynamic range}| \times |\text{radiation damage}|}$$

The higher the "value" of the time-resolution parameter, the longer the length of a time frame, and consequently the slower the experiment. In order to assess if an experiment is sensible, this "value" should, as mentioned in the previous section, be compared with the time scale on which it is possible to perturb the sample uniformly. The parameters "memory," "dynamic range," and "radiation damage" act as a type of delta functions. The fastest experiments, using conventional methods and noncyclic data collection, are at the moment limited to roughly 0.1 s/frame. When dealing with a process that can be accurately cycled, one can play different tricks and the time resolution can be pushed toward the millisecond/frame resolution at the expense of a very complicated experimental protocol (29).

Sample Environment

If one wants to measure samples at nonambient conditions, it is required to utilize a sample cell that can bring the sample in the required state. The most commonly and easily varied parameters are temperature and pressure. However, with the increasing degree of sophistication that SR users have brought to their experiments it is not uncommon to bring for instance reaction injection molding (RIM) or extrusion apparatus to the beamlines in order to mimic industrial processing conditions. Several examples of this are discussed in following sections. Also, the combination of time-resolved x-ray experiments with the other non-x-ray-based techniques, such as infrared spectroscopy or Raman scattering, has become more common. The often conflicting requirements of the different techniques increase the difficulties in constructing sample cells which are suitable for this type of experiment. A simple example of such conflicting requirements is the need for free x-ray access to a sample on which one wants to perform simultaneously differential scanning calorimetry (dsc). The latter technique requires the sample to be contained in an environment that inhibits uncontrolled heat flow toward or from the sample. This obviously is in conflict with the need for free x-ray access.

In the case of time-resolved experiments the sample has to be brought from an initial state to a final state. If this requires, for instance, a temperature change, it is crucial that during the experiment the temperature gradients over the sample are limited. This is illustrated in Figure 5. The problems that are depicted schematically in this figure can be of paramount importance in the interpretation of events occurring around a phase transition (30–32). It is obvious that an accurate knowledge of the actual temperature of the sample is of paramount importance. Often there is a difference between the set point of the temperature controller and that of the sample. Therefore, one often samples the read-out from a thermocouple attached to the sample at the same rate as the time frames of the scattering experiment. The same holds true for any other parameter that is used to initiate the sample condition.

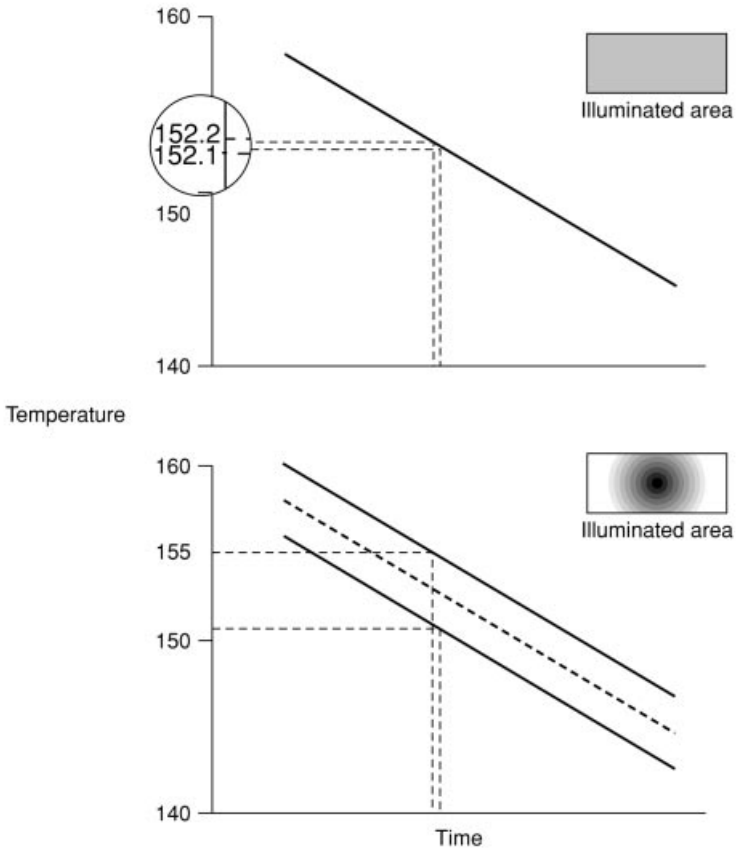

Fig. 5. The upper panel shows the ideal experiment in which the sample is cooled down and where the sample has an homogenoeus temperature. The inset, marked illuminated area, shows the temperature distribution over the sample in a gray scale. A small lapse in time corresponds to a minute change in the thermodynamic state of the sample, which therefore can be considered to be quasi-static. The accuracy is only limited by the length of the time frame. In the lower panel a situation is depicted where the sample does not have a homogeneous temperature over the x-ray region illuminated by the x-ray beam. It is now impossible to construct a temperature versus time diagram with the same accuracy as in the above panel. For every time frame, one will not observe the structure of a single thermodynamic state but a mixture of states. Obviously it will always remain of paramount importance to measure the exact temperature as well as being able to control the temperature gradients.

In the case where one wants to combine x-ray experiments with optical experiments, such as birefringence or light scattering, the problem of the quality of the sample windows is an important issue. This again is the case with high pressure experiments where the cell windows are made of diamond. Although this material contributes relatively small levels of parasitic scatter per unit window thickness, and is fairly transparent to x ray, the simple fact that one requires thick windows brings the parasitic scatter to a such level that the signal-to-noise ratio of the experiment becomes quite unfavorable. This is further discussed in the section on Pressure Cells.

The ideal window material for x-ray scattering experiments should have a high transparency for the x rays of the required wavelength, be an isotropic scatterer with no preferential orientation, be mechanically stable at the temperatures required, etc. This rules out many common materials. Al and Be windows, for instance, generate a large amount of parasitic scatter in the saxs region because of the presence of grain boundaries in the material. Ideal materials are composed of light elements either completely crystalline with a simple large unit cell, such as mica, or completely amorphous. However, this is only a rule of thumb since a material like amorphous (glassy) carbon has a very intense waxs pattern that can be order of magnitudes larger than that of the polymer under investigation. Unfortunately, no systematic study of this problem has been made so far.

Data Analysis

Data analysis for combined time-resolved experiments follows in principle the same path as that for non-time-resolved experiments. The difference is that there is often a nontrivial problem with respect to the amount of data that has to be analyzed. Careful data reduction (normalization, background subtraction, subtraction of the amorphous component from the crystalline peaks, etc) and analysis of a single scattering curve can take several hours. With time-resolved data it is nearly impossible to spend this much time on each individual frame. Although it is possible to develop software to automatically analyze time-resolved data, it is nontrivial and one cannot avoid many manual cross checks in order to obtain reliable results (33). An example of the problems that one can encounter is shown in Figure 6.

It is obvious that often the standards of analysis are lowered. This does not always have to be a problem. Much depends on what one wants to learn from the data. Static experiments for accurate determinations of the morphology is a minority class of experiments performed with SR beamlines. When kinetics are studied, it often suffices to concentrate on a small part of the data range and study the development of the scattered intensity in this region as a function of time and ignore, for instance, elaborate background subtraction routines that might be only second-order effects.

An aspect that is quite often overlooked in the analysis of data where a morphological change is taking place in the sample due, for instance, to crystallization or phase separation, is the fact that corrections that should be applied to the data often change in time. As an example, one can think of the situation in which a micellar system by a change in temperature converts to a cylindrical morphology. Then the so-called Lorentz correction for saxs data, required to calculate the real scattered intensity and compensate for the fact that calculations for the scattering profile are based upon one-dimensional projections in the direction of the periodicity, also changes. The terminology "Lorentz correction" is in principle not correct (34,35), but the use of it is so widespread that this article conforms to the standard practice. The correct Lorentz factors are for the different cases:

$I_c(q) = I(q)q^2$	for infinitely long and wide lamellae
$I_c(q) = I(q)q$	for long thin cylinders
$I_c(q) = I(q)$	for spherical particles

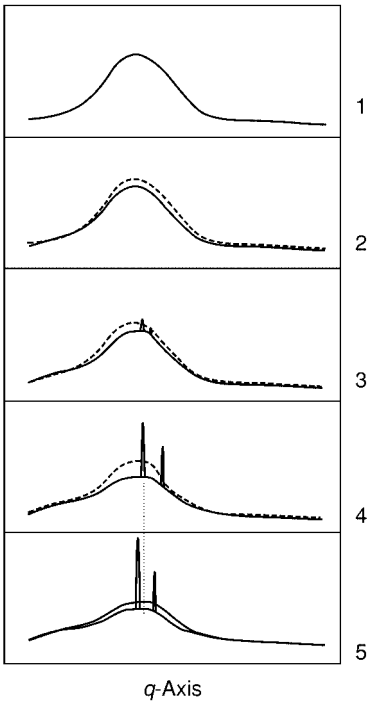

Fig. 6. This schematic diagram shows waxs patterns corresponding to the crystallization of a semicrystalline polymer. One can see the problems that one can encounter in the data analysis of time-resolved data. The first frame shows the amorphous ring characteristic of a molten polymer. In the second frame the previous frame is shown as a dotted line. The amorphous ring has slightly diminished in intensity and two small peaks have started to grow. In the following frames the diffraction peaks gain in intensity while the amorphous halo keeps diminishing. Between frames 4 and 5 the diffraction peaks move to lower q-values. If one now wants to follow the intensity of the diffraction peaks one has to subtract an ever changing background and also one has to take into account the peak movements. Mathematically this is a trivial problem but to do this in an automated way with software is nontrivial.

It is clear that to determine the point where one should cross over from the use of one correction to the other is a process which is not straightforward and is difficult to automatize.

Anomalous Scattering

In contrast to conventional x-ray generators, which only produce usable amounts of photons at discrete energies, SR beamlines can, when equipped with the appropriate monochromator, be tuned to any energy of the white spectrum generated by the storage ring. This has opened up the possibility to use the method of anomalous, or resonant, scattering. In this technique, one uses the property of x rays that the scattering cross section varies in the proximity of an elemental absorption

edge. This is not unlike the contrast variation in neutron scattering which is based on using different isotopes of the same element, notably hydrogen and deuterium in polymer research. Anomalous scattering is a technique that has become popular, for instance, protein in crystallography, where it is an important tool to solve the phase problem needed to solve the structure of a crystal unambiguously.

The x-ray scattering cross section is energy dependent and is given by

$$f(q,E) = f_0(q) + f_1(q,E) + if_2(q,E)$$

The first term is the Fourier transform of the electron density around the scattering atom, which is the only term to be considered in normal experiments. At small scattering angles this is equivalent to the number of electrons in the atom. The two other terms only have an appreciable magnitude at energies close to an absorption edge. The unfortunate fact is that the energy window practical for soft condensed matter experiments, 5–15 keV, does not contain absorption edges from the most common occurring elements in this type of research. This limits this type of research to polymers and colloids containing heavier elements, or, for instance, real-time experiments where catalysts are involved, or, for instance, liquid crystalline materials (36). In Figure 7 the variations in the scattering factors as function of the energy are shown. The elements with edges easily accessible are the elements with Z values between 20 and 36 for the K-edges and between 50 and 82 for the L-edges. It should be noted that the effects occurring in anomalous scattering are only small, unlike the large variations that are possible in neutron scattering when selective deuteration is applied.

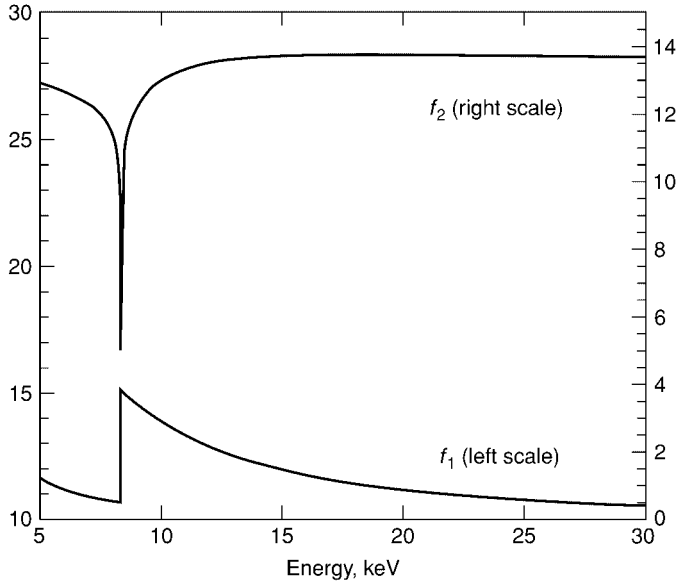

Fig. 7. Variations of the scattering factors f_1 and f_2 near the K-absorption edge of Ni (8.33 keV). The large variation in the parameter f_2 is responsible for the effects that can be used in anomalous scattering experiments.

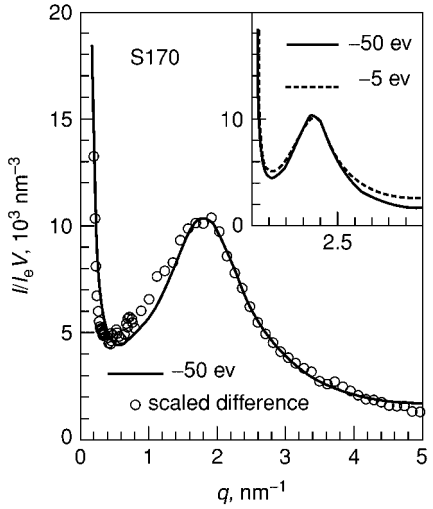

Fig. 8. Anomalous saxs data from a nickel-neutralized sulfonated polystyrene. The scattering curves were obtained at x-ray energies respectively 5 and 50 eV from the Ni K-edge (inset). The main figure shows the scattering curve obtained at 50 eV from the edge and the scaled difference pattern (open symbols). This illustrates the minute differences between the curves. This type of scattering data requires an energy tuneable x-ray source. Courtesy of R. Register.

An example of results of this technique is given in Figure 8 (37). This shows the minute differences between scattering curves taken at different energies close to the Ni K-edge from a nickel-neutralized sulfonated polystyrene. By using this technique, the authors could prove that the sample under investigation had an inhomogeneous distribution of ionic repeat units instead of explanations relying on artifacts due to precipitates or microvoids. Also, it was possible to determine the sign of the electron density difference between the crystalline and amorphous phases.

A more detailed treatment of contrast variation techniques, for both x ray and neutron scattering experiments, can be found in Reference 38 and in a book (39).

Another technique that makes use of the tuneability of SR sources is x-ray absorption spectroscopy (xas) (2). This is relatively rarely used in polymer research. One of the few examples found in the literature deals with *halato-telechelic ionomers* (40). These are short linear chains selectively terminated by a metal carboxylate or sulfonate ionic group. The local order of these groups could be determined by using extended x-ray absorption spectroscopy (exafs). More work using this technique applied to ionomer morphology is reported (41).

Radiation Damage

The damage to polymer samples by exposure to x rays is at present poorly documented. In biological research using SR, such as protein solution scattering and crystallography, this phenomenon is well known but unfortunately also rarely

quantitatively treated (42–46). With the advent of the third generation of SR sources that can generate very high fluxes of around $10^{12} - 10^{13}$ photons/s in a 0.1-mm^2 spot, this is not a problem that can be ignored by material scientists anymore. See for instance Reference 47, in which it is shown that starch samples are destroyed within 10 s of exposure to an x-ray beam of 10^{10} photons/s in a 2-μm spot, or the experiments in which it was shown that relaxation times in a coherent small-angle scattering experiment were influenced by the dose of x rays (48).

The exact mechanism that causes the radiation damage is not known. It is unlikely to be a local heating effect since a quick calculation shows that with the aforementioned fluxes a polyethylene sample can heat up by around 0.1°/s, assuming that no heat transfer takes place to the surrounding area. This might have implications for experiments in which one attempts to obtain isothermal conditions but in itself will not be the cause of the damage. More likely is that the ionizing radiation damages chemical bonds. This is supported by the observation that in carefully performed experiments on ionomers in solution it is possible to observe the effects due to the ionization of water (49).

Quite often the first sign of radiation damage is a discoloration of the sample surface. The occurrence of radiation damage in the bulk of the material can lead to loss of orientation in aligned samples and also diminishing intensity in diffraction (46). There are several methods to avoid radiation damage, but unfortunately all these require displacing the sample through the beam, which means that one is not continuously observing the same sample. For bulk polymers this is no problem, but when stretching or microfocus experiments are performed, one is well advised to use the most efficient detector available and reduce the intensity of the incoming beam. The interaction of x rays and radiation damage effects in the solid state are extensively treated in Reference 50.

A rather spectacular effect of radiation damage is shown in Figure 9. This example shows aligned rigid rod microtubule biopolymers in solution. Not only

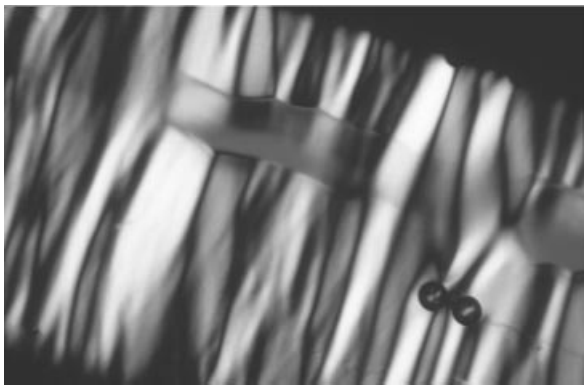

Fig. 9. An initially aligned sample of rigid rod microtubule biopolymers in solution after it has been hit by radiation. The sample is viewed between crossed polarizers. The burn mark is centrally placed. The alternating dark and light bands are domains that have a different orientation. The transition from uniform alignment to domains with different orientation takes place in seconds after the sample is irradiated. The burn mark has dimensions of roughly 0.5×3 mm^2. The shift of the domains with respect to each other is approximately 0.5 mm as witnessed by the distortions of the burn mark.

is the material at the spot where the beam hits the sample damaged, but also the previously homogeneously oriented region around it is broken up in several differently oriented domains many times larger than the actual burn mark itself. This is probably due to hydrodynamic instabilities (51).

The unfortunate fact is that serious studies of this problem would require large amounts of beam time and the subject itself is not very fashionable.

SAXS Experiments

SAXS experiments provide information on length scales from, arbitrarily, 1 nm and larger. This means that information regarding the long spacing in semicrystalline polymers, density fluctuations, interface shape, spherulite size, etc, can be accessed by this technique. On some conventional beamlines it is possible to observe dimensions comparable to small spherulites. However, in general one has to use a specialized Bonse–Hart usaxs camera to achieve this. The determination of the large-scale structure of a sample is a conventional way of using saxs. An example of this is the structure determination of a self-organized polyaniline sample that was doped with acid in order to create a conducting polymer. By attaching 4-hexylresorcinol via hydrogen bonding to the polyaniline salts, a supramolecular structure is formed. When the samples are heated above the crystallization temperature of 4-hexylresorcinol, the material self-organizes. On the basis of the saxs pattern it is possible to deduce that the organization is in the form of a hexagonal array of cylinders where the hexyl tails are microphase separated from the cylinders (52) (see Figs. 10a and 10b). The use of SR is crucial here since with conventional x-ray generators it would not be possible to obtain the required data quality in an acceptable time.

Solution Scattering. Solution scattering is a well-known saxs technique used to elucidate the shape and weight of molecules. It has been extensively used over the years (53).

The prerequisites for an accurate determination of the shape parameters are that the molecules in solution are monodisperse in size, identical in shape, and that the solution is sufficiently dilute so that no interparticle scattering is observed. In practice the first two conditions are rarely met, apart from the case where one deals with biological materials and more recently with some specially prepared colloids. The theoretical framework to deal with all the problems that one can encounter does not exist at the moment. The problem of interparticle scatter is especially hard to solve. Attempts to analyze the degree of polydispersity, assuming an identical shape function with a free parameter describing the size distribution of the particles, have been reported many times in the literature; see for instance References 54–57. The problem of interparticle scatter has attracted less attention probably because the problem is somewhat harder to solve; see for instance References 58 and 59.

The use of SR, with the higher intensity compared to that of conventional Kratky cameras, is indispensable in the accurate determination of saxs data at intermediate scattering angle (60). In the study of Kraton PS–PEP–PS (polystyrene–polyethylene–propylene) triblock copolymer in extender oil, although this complex is a gel, solution scattering methods can be applied to elucidate the structure. In

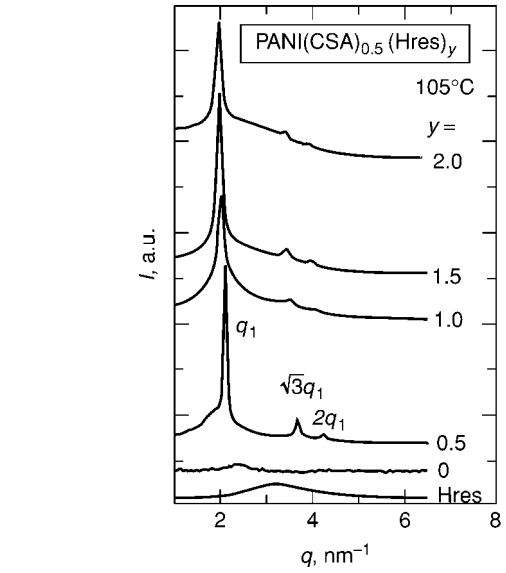

(a)

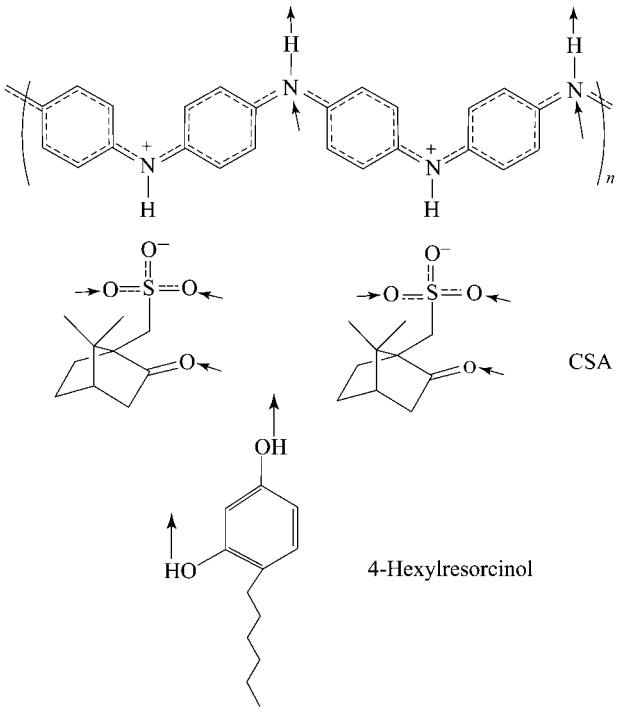

(b)

Fig. 10. Panel A shows saxs patterns obtained from a polyaniline salt–4-hexylresorcinol supramolecular arrangement in a hexagonal register, which is evident from the 1, $\sqrt{3}$, 2 q-spacing of the diffraction peaks. Panel B shows the structure that could be deduced from the diffraction patterns. The cylinders are formed of the polyaniline salt combined with the phenolic groups of the 4-hexylresorcinol. The hexyl tails microphase separate from the cylinders and act as spacers between them.

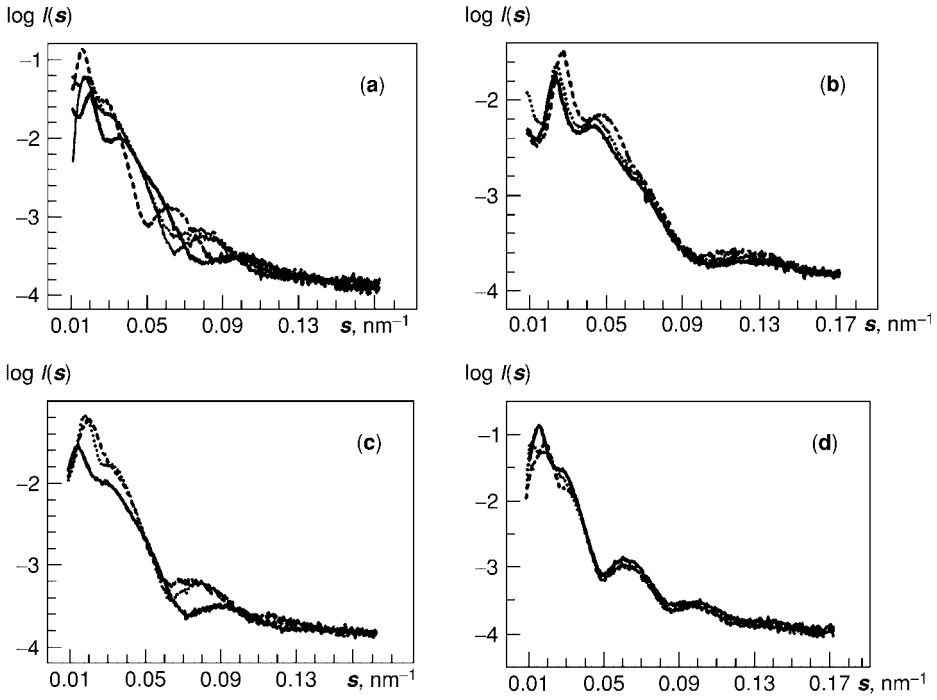

Fig. 11. SAXS curves for triblock copolymer gels with a PEP midblock and PS endblocks. The different tables represent curves obtained with molecular weights M_n = 100,000, 20,000, and 300,000 respectively. Clearly distinguishable are two scattering peaks at low angles due to interparticle scatter. The peak at wider angle is due to form factor scatter from the high electron density PS spheres which are insoluble in the extender oil. Only the use of SR allows one to obtain sufficiently accurate data in this scattering region to be able to perform a decent analysis. For further explanations one is referred to the text.

Figure 11 scattering patterns are shown from sample with a variable molecular weight and different PS contents. The scattering at low q is dominated by two peaks which are caused by interdomain scatter. The domains are being formed by the insoluble PS blocks. The distance between the domains is much larger than the domain size and so that the form factor intensity oscillations start at intermediate scattering vectors. The positive identification of the origin of these peaks was done by stretching the samples, which increased the interdomain spacing and thus moved the associated peaks to lower scattering angles, but left the form factor maxima at the same position. The analysis of this data was performed in two alternative ways. The first method starts from the assumption that there exists a short-range liquid-like order between the hard core domains with an equiprobable distribution around the central core. This is followed by the introduction of some nearest-neighbor coordination. The form factor of the domains is calculated according to classical methods (61). The equations to be fitted in this case are

$$I(s) = KN\langle P(s,r_0,\sigma)\rangle S(s,R,\eta)$$

$$\langle P(s,r_0,\sigma)\rangle = \int_0^\infty \frac{1}{\sigma\sqrt{2\pi}} \exp\left[-\frac{(r-r_0)^2}{2\sigma^2}\right] P(s,r)\,\mathrm{d}r$$

where $\boldsymbol{s} = 1/d$ is the scattering vector, $I(\boldsymbol{s})$ is the scattered intensity, K a constant, N the number of scattering particles, r_0 the mean domain radius, and σ the dispersion factor. $P(\boldsymbol{s}, r)$ is the averaged form factor and $S(\boldsymbol{s}, R, \eta)$ is the structure factor of a monodisperse system. The second method consisted of the modeling of the short-range order with the Debye formula:

$$I(s) = K\langle P(s,r_0,\sigma)\rangle\left[N + 2\sum_k Z_k \frac{\sin(2\pi s R_k)}{2\pi s R_k}\right]$$

In the above equation the sum in square brackets represents the interference function of a distribution of spheres. The distribution is characterized by a discrete set of distance, R_k, with a frequency Z_k. By now replacing the starting set Z_k with a new set defined by a Gaussian distribution around R_k, one can search the best fit to the data.

In this particular case both methods produced satisfactory agreement. It should be pointed out that both these methods rely to a great extent on a high data quality in the intermediate scattering angle range. To obtain sufficient intensity in this region one has to collect the data per sample for about 10 min, with an equal or longer time for the background scattering pattern, on an SR beamline which produces approximately 10^{11} photons/s. Assuming the use of a rotating anode generator and a detector with an equal sensitivity, this translates to an exposure of approximately 20 h to obtain the same data quality, with an additional 20 h for the background pattern.

An attempt to analyze data from a system in which several components with different shapes, each with different size distributions, is described in Reference 62. A microemulsion of oil-rich sodium bis(2-ethylhexyl) sulfosuccinate exhibits a continuous phase transition from the droplet to the cylinder state as a function of salt concentration and temperature. In this extensive work, dealing with more than 500 scattering curves from samples with different composition and/or temperature, the authors managed to obtain reasonable fits even after assuming some physically less attractive simplifications regarding the interparticle interactions.

It is probably still not an understatement to say that the in-depth analysis of solution scattering data on real, not idealized, samples is still a specialized field.

An experimental method, intermediate between solution scattering and fiber diffraction, is used to prepare well-oriented samples in a solvent. An example of this is the partial orientation of tobacco mosaic virus (TMV) by subjecting the sample to electric field pulses between 1.25 and 5.25 keV/cm (63). TMV is a model system for rigid rod-like molecules. The x-ray studies, combined with transient birefringence measurements, render valuable information on the orientational effect of electric fields on these macromolecules with a time resolution which can be as short as 2 ms/frame. A similar method is to self-assemble rigid rod molecules in a magnetic field. The interaction of the diamagnetic moment, present in nearly every molecule, with magnetic fields over 10 T induces orientation which is not lost upon removal from the magnetic field owing to steric hinderances inhibiting rotational diffusion. Thus one obtains a sample which, although still in solution, is nearly perfectly oriented. This allows the structural determination of these

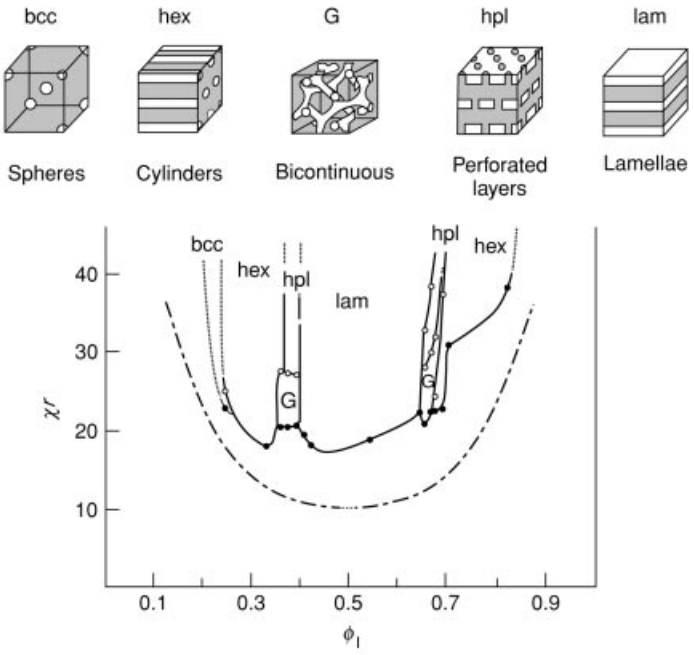

Fig. 12. Phase diagram of the PI–PS diblock copolymer system. The vertical axis is expressed in χN units (where χ the Flory–Huggins segment–segment interaction parameter and N the degree of polymerization). The determination of this phase diagram is based upon tem, saxs, and sans data. The α—. curve is the predicted order–disorder transition line. The open symbols are order-order transition points and the closed symbols order–disorder. The solid lines are drawn as guides for the eyes.

molecules in solution via fiber diffraction methods, which have an intrinsically higher information content than pure solution scattering (46).

Static Phase Diagrams. An example of the study of complicated phase diagrams in which synchrotron saxs experiments have been shown to be extremely useful is given in Reference 64. These authors have investigated the complex phase behavior of polyisoprene–polystyrene (PI–PS) diblock copolymers. In these experiments the compositional phase diagram was determined by heating samples with variable volume fractions of PI (Fig. 12). This type of experiment is also feasible with conventional x-ray sources. However, the data quality is much higher and the experiments can be performed in less than a day instead of many months required with conventional generators. It should be stressed that in principle it is possible to determine the phases unambiguously on the basis of saxs patterns alone in case the accessible q-range shows sufficient diffraction peaks. This is rarely the case because of the limited length of detectors, and therefore it is required to back up the conclusions by results from other techniques such as transmission electron microscopy (tem) and rheology. This underlines the complimentary nature of synchrotron experiments with other techniques which can be applied either independently or simultaneously.

Fiber Diffraction. Fiber diffraction is a well-known technique for the characterization of materials which possess fiber symmetry, ie, a one-dimensional

regular packing of subunits. In some cases this is a consequence of the production process but in other cases fiber diffraction can be used even if the sample under investigation is essentially not a fiber. This is the case when oriented objects are imbedded in a matrix and the interdistance between the objects is relatively large, such as in a composite material. The latter situation can be induced via several ways including shearing (65,66), electromagnetic fields (67,68), and centrifugation (69). The information content in such diffraction patterns is higher than in the case of randomly oriented objects. It should be noted that both saxs and waxs are being used for the study of fiber texture. In the 1950s and 1960s many polymer crystal structures and other crystallographic polymer problems were solved by using wide-angle fiber diffraction. However, this type of work, lacking the need for time resolution, is ideally suited to be carried out with conventional generators and therefore the research community occupying themselves with this type of work appears to have less demands for access to SR.

In the case where one performs time-resolved experiments on real fibers, be they natural or synthetic, the use of SR has some distinct advantages. Because of the nature of a fiber, the interaction section between the x-ray beam and the fiber, which determines to a great extent the quality of the diffraction pattern, is limited by the size of the fiber. It is clear that, for a fixed number of photons in the x-ray beam, the smaller the beam the better the experimental situation is.

The above is certainly the case in experiments where an extruder is placed on a beamline in order to survey the structural developments in the fiber as a function of the distance from the spinnerette. This specific subject is discussed in later sections. Complicated experiments on contracting muscles, gels containing viruses, oriented polymer nanocomposites, mechanically induced ordering in samples subjected to stress, etc, also fall under the remit of fiber diffraction.

A very elaborate theory exists for the analysis of fiber diffraction data, although no recent monographs on the subject exist; the book Diffraction of x-rays by Chain Molecules (70) contains still the most comprehensive treatment. A large part of the mathematical framework was developed for the famous studies that were done to unravel the structure of DNA (Fig. 13) (71). This subject has remained popular to this day (72). Unfortunately, although the theory exists, there are no standard data analysis packages. In the recent literature on SR-based synthetic polymer research, there are few examples to be found in which the authors extract more information than Hermans orientation functions or spacings of diffraction maxima from their data.

An example of analysis in which a more elaborate data analysis was performed is the analysis of stretched samples of poly(etherester) (PEE) (73,74). This material consists of hard and soft domains. By stretching this material the soft domains elongate and become needle shaped. The analysis performed here is in the form of projections which are, in this case, integral operators that map functions onto subspaces of the domain in which they are defined. The most well known of these projections is the one that maps the scattered intensity onto a zero-dimensional subspace, ie, a number or scalar. For instance,

$$\{I\}_0 = \int I(s) d^3 s$$

which is a mathematically correct way to define the well-known invariant.

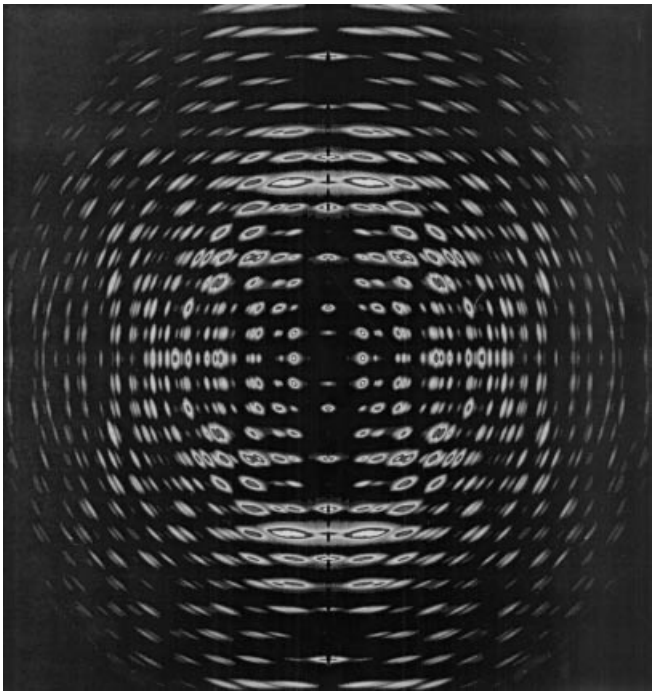

Fig. 13. X-ray fiber diffraction pattern recorded from polymeric DNA containing a well-defined alternating A-T repeat along each strand of the double helix. This conformation, known as the D conformation of DNA, has 8 bp per helix pitch. Diffraction pattern recorded on beamline 7.2 at the Daresbury SRS. At the center of the pattern one observes spacings up to about 3.5 nm while the edge of the pattern reveals structural details down to 0.22 nm. Pattern kindly provided by T. Forsyth.

In the case where one deals with fiber symmetry, one can express the three-dimensional fiber diffraction pattern in cylindrical coordinates with $I(\boldsymbol{s}) = I(\boldsymbol{s}_{12}, \boldsymbol{s}_3)$, where $\boldsymbol{s}_3$ is a vector parallel to the fiber axis and $\boldsymbol{s}_{12}$ the cylindrically symmetric direction at right angles to the fiber axis. The projection $\{I\}_1\,(\boldsymbol{s}_3) = 2\pi \int_0^\infty s_{12}\, I(\boldsymbol{s}_{12}, \boldsymbol{s}_3)\, \mathrm{d}_1$, which is a planar integration in the plane at right angles to the fiber axis, and therefore can be expressed as a function of $\boldsymbol{s}_3$, contains the information on the domain height and distribution of both the hard and soft blocks in the longitudinal direction. The projection $\{I\}_2\,(\boldsymbol{s}_{12}) = 2\int_0^\infty I(\boldsymbol{s}_{12}, \boldsymbol{s}_3)\, \mathrm{d}$ describes the fiber as a two-phase system in the direction at right angles (transverse) to the fiber axis. By using this methodology the author was able to comprehensively characterize the shape deformation of the soft domains as a function of the sample elongation. An illustration of this is given in Figure 14.

More examples of the use of fiber diffraction can be found in the following sections.

SAXS/WAXS Experiments

The combination of simultaneous saxs and waxs experiments has gained a widespread popularity in the last decade (11,21,75). As with many technique

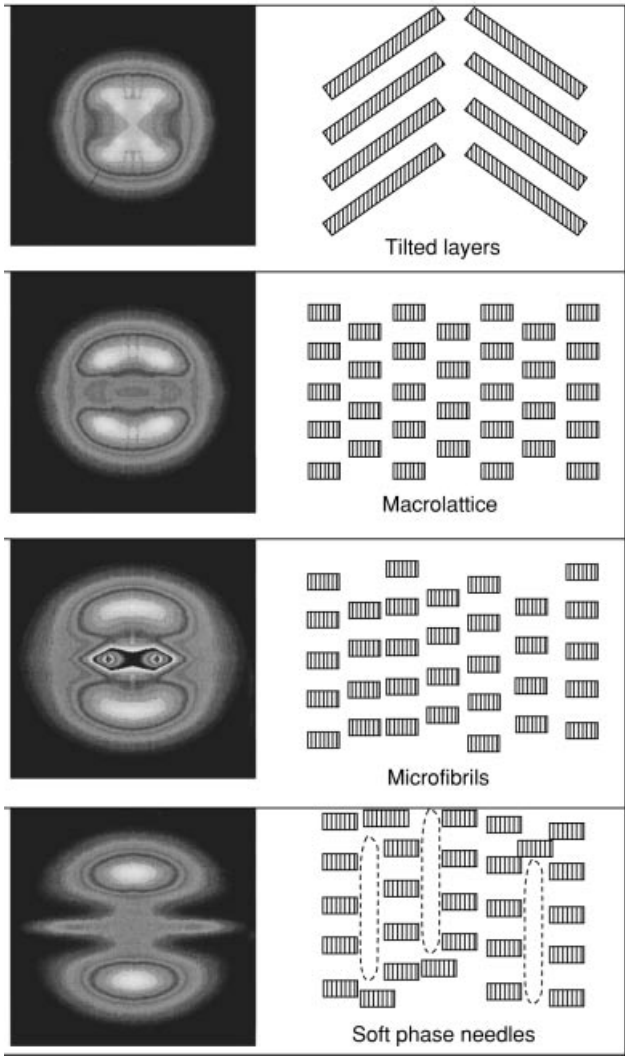

Fig. 14. Scattering patterns and derived structures from PEE under strain. The structures are derived using analyis methods given in Reference 73. Courtesy of N. Stribeck.

combinations it is unavoidable that the quality of the data obtained is not as good when compared with the quality that can be obtained when independent experiments are performed. In the case of combined saxs and waxs experiments, the main reason for this is that for optimized experiments one obtains the highest resolution when the x-ray beam is focussed on the detector. Apart from the special case when a microfocus beamline is used, one normally utilizes two detectors: one placed close to the sample, to collect the waxs, and the other one at several meters from the sample in order to collect the saxs. This means that one has to make a choice where to focus the beam. With modern beamlines the loss of data through over/under focus has become relatively unimportant. The intrinsically small beam

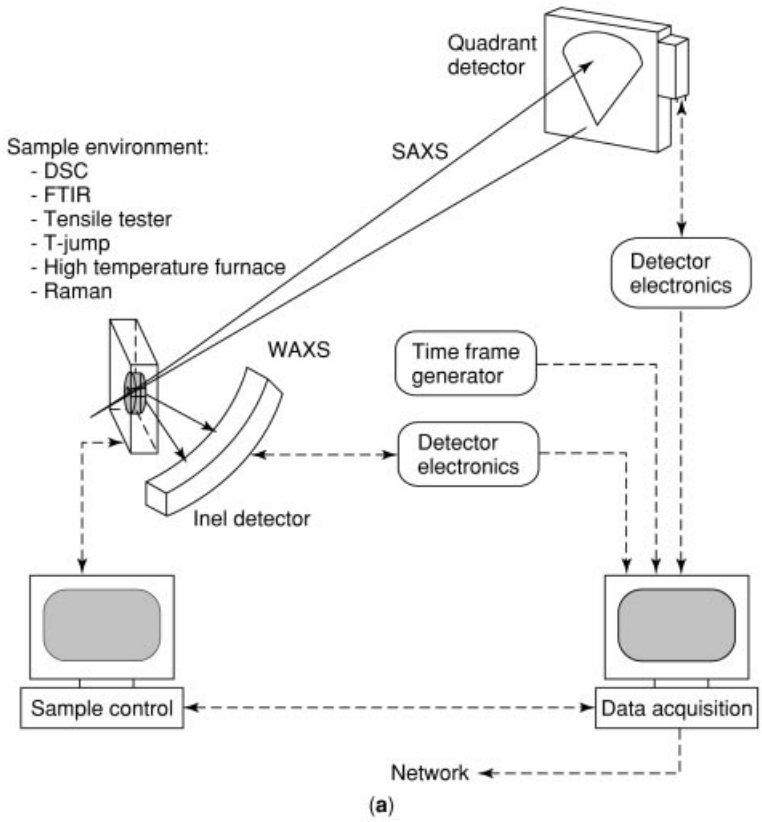

Fig. 15. Panel A shows a schematic diagram of a combined saxs/waxs experimental station suitable for time-resolved experiments. In this case the sample is placed at the center of a curved waxs detector which is placed such that the saxs scattering pattern is not obscured. The sample–saxs detector distance can be varied depending on the required q-range needed. The two independent detector systems are synchronized by the use of a single time frame generator. In panels B and C the simultaneously collected saxs and waxs curves, produced with the setup shown in panel A, from a heating/cooling experiment on HDPE are shown.

divergences allow the construction of scattering cameras with a very large depth of field.

An example of a saxs/waxs setup is given in Figure 15. In this example a curved detector is used to collect the waxs pattern. This has the advantage that no distortions in the scattering pattern can occur because of parallax problems. The distance between the sample and the saxs detector can be varied from 0.7 to 4 m, depending on the scattering vector range that one wants to study. The time resolution that can be practically achieved, without compromising with the data quality too much, is 0.1 s/frame, on a strongly scattering polymer sample. The q-range that can be observed depends on the particular beamline. A typical example is station 8.2 at the SRS in Daresbury, where it is possible to collect data in the range 0.06–30 nm^{-1}. This practically means that one covers the length scale of two hierarchical structural levels. The ordering of individual polymer

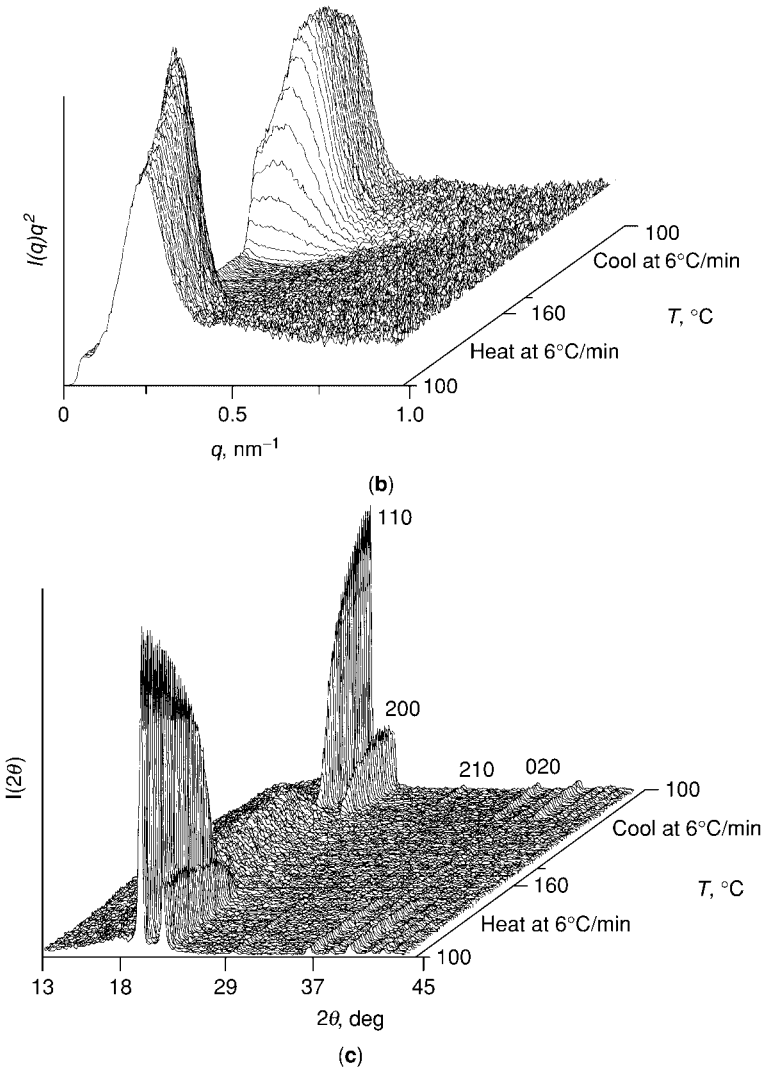

Fig. 15. (Continued).

chains with respect to each other and the level above where assemblies of ordered polymers, like lamellae, again exhibit ordering with respect to each other. The structural level above that, with length scales up to the micrometer range, such as spherulites, used to be the domain of light scattering (76,77) but on third generation SR sources it is sometimes possible to reach this level with x-ray scattering as well, although no systematic work in this field has been reported yet. The advantage of using x-ray scattering instead of small-angle light scattering (sals) in the study of spherulite formation is that the latter technique is limited to thin films while with the former bulk samples can be studied. However, this means that at present the data can only be obtained in two discrete q-ranges with a gap between them. There is no fundamental reason why this problem could not

be solved—only a financial one—since it requires the construction of a very large position-sensitive detector.

The simultaneous collection of waxs and saxs data has its obvious advantages. The most important is that one is able to correlate structural changes on different length scales with each other. In some cases there are extra advantages. In the case of a two-phase lamellar system, the invariant obeys the following relation:

$$Q = \int_0^\infty q^2 I(q) dq = \langle n_e^2 \rangle \phi(1-\phi)$$

with Q the invariant, n_e the electron density difference between the two phases, and ϕ the crystalline volume fraction. This clearly is an equation which is quadratic in ϕ and which has a maximum when the crystalline volume fraction reaches 50%. The crystalline volume fraction can be determined from the waxs data by conventional ways (55). In a recrystallization experiment one can, by coplotting the crystalline fraction together with the invariant, determine a linear scale based upon the 0 and 50% crystallinity points, which is internally completely consistent. [A minor correction might have to be applied for changes in n_e during crystallization (78)]. This procedure is illustrated in Figure 16.

In the case where one is not strictly dealing with a two-phase system because of, for instance, the polymer crystallizing in spherulites, a modification has to be made. The relative invariant is now given by

$$Q' = K X_s X_l (1 - X_l) \Delta\eta^2$$

where K is a constant, X_s is the volume fraction of spherulites, X_l the degree of crystallinity in the lamellar stacks, and $\Delta\eta$ the electron density difference between the crystalline and amorphous polymer. The relation $X_c = X_s X_l$ is valid in this case. In the molten state, $X_s = X_l = 0$. In isothermal primary crystallization it can be assumed that X_s varies approaching 1 while X_S is approximately constant. In the reverse situation, when heating the sample, it can be assumed that $X_s = 1$. This means that as limiting behaviors, upon crystallization X_l is a constant and Q' is a linear function of X_c while on melting X_S is a constant and Q' has a quadratic dependence on X_c. This method has been applied in crystallization studies of iPP (79). Referring back to the previous example on the melting of high density polypropylene (HDPE) it should be noted that at the point where $X_S = 1$, one has $X_c = 50\%$.

One of the topics that has generated heated debates (30–32,80–85) is the mechanism of primary crystallization in semicrystalline polymers which are, after a temperature quench, crystallized from the melt. According to the theories of Hoffmann and Lauritzen and Keller and co-workers (86,87), and references therein] the onset of crystallization is a nucleation and growth process. An alternative interpretation is that the process is more complicated than straightforward nucleation and growth and involves a mesophase characterized by behavior similar to spinodal decomposition. One of the implications of this latter scenario is that there should be long range order in the solidifying sample before one can observe crystalline structure. Combined saxs/waxs experiments can play a role here.

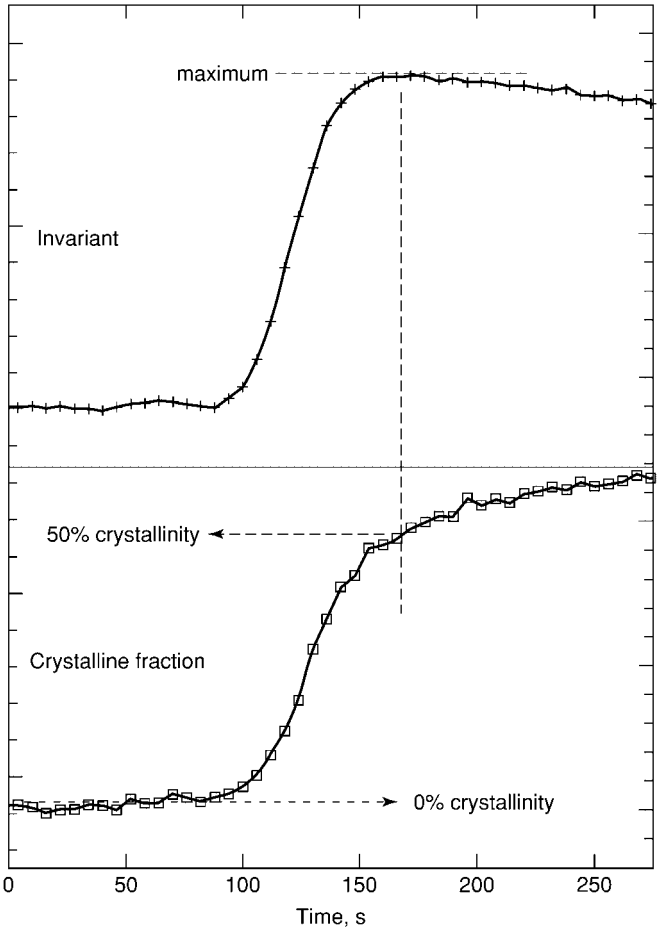

Fig. 16. Data obtained in a combined saxs/waxs experiment on the dynamic solidification of HDPE. The saxs invariant $Q = \int_0^\infty I(q)q^2 = \langle n_e \rangle^2 \phi(1-\phi)$ has a quadratic dependence on the crystalline volume fraction ϕ and reaches a maximum when the volume fraction reaches 50%. The integrated intensity of the waxs diffraction peaks has a linear relation with the degree of crystallinity. By taking the melt as the zero degree of crystallinity point and the maxium of the invariant as the 50% mark, it is possible to construct a degree of crystallinity scale which is internally consistent.

Small-angle scattering is an ideal tool to study the characteristic length scale of the long range density fluctuations occurring during phase-separation processes [eg, 88–91]. The crystalline structure can be observed with waxs.

That crystallization can occur via a spinodal mechanism in nonisotropic system, such as drawn poly(ethylene teraphtalate), is well known (92). The spinodal mechanism is characterized by the following development of the scattering intensity:

$$I(q,t) = I(q,0)\mathrm{e}^{2R(q)t}$$

in which $I(q, t)$ represents the time evolution of the scattered intensity and $I(q, 0)$ the scattered intensity at time $t = 0$. The factor $R(q)$ is the amplification factor (or growth rate constant) which is given by

$$R(q) = -Mq^2\left(\frac{\partial^2 G}{\partial \rho^2} + 2\kappa q^2\right)$$

with M the mobility term, G the Gibbs free energy, and κ a gradient free-energy term (31). However, this equation is not very useful in a scattering experiment. A more interesting derivable parameter is the effective diffusion coefficient D_{eff}, which can be derived from the growth constant as follows:

$$D_{\text{eff}} = \lim_{q \to 0} - \frac{2R(q)}{q^2}$$

Since $R(q)$ effectively has a q^4 dependence, one normally plots $R(q)/q^2$ vs q^2 to determine the effective diffusion coefficient (93).

The usefulness of SR becomes apparent when one realizes the important role that the amplification factors have in the spinodal formalism. To determine this factor properly one has to make a linear fit for every value of q to a $\log I(q, t)$ vs t plot. This requires many curves taken at different times with a reasonable fast framing rate matched to the transient nature of the phenomenon.

In Figures 17a and 17b, used to determine the D_{eff}, are shown data obtained from temperature quenches of quiescent iPP at different temperatures.

As mentioned earlier, one aspect of attempts to distinguish between a conventional nucleation and growth mechanism and a spinodal decomposition like mechanism in quiescent crystallising polymer is to investigate the absence or presence of a time lag between the onset of a rise in the invariant, which is dominated by data in the saxs regime, and the onset of the rise in crystallinity, which is evidenced by growing intensity of crystalline peaks in the waxs region. In Figure 18, in which one can see the results of a simultaneous saxs/waxs experiment on isothermal crystallization of iPP, one can clearly see that in this case the rise in the invariant precedes the rise in the crystalline peaks. This result highlights the question if the results of such an experiment are not influenced by the experimental method used. This influence can be twofold. In the first place one of the techniques can be intrinsically less sensitive than the other. In the second place the detector can introduce noise so that the real effects are hidden in the noise band. This is treated in somewhat more detail in a later section.

In crystallization experiments where one wants to study a short-lasting transient effect, with statistically relevant data, it is sometimes possible to translate the problem from the time domain to a spatial domain. In crystallization experiments this can be done very elegantly by using a scaled-down version of an industrial melt extruder. With appropriate extrusion rates one can obtain an unoriented melt just after the molten polymer has been extruded from the extrusion die. Further down the extruded film the polymer solidifies and crystallises. When mounted on an elevation platform it is now possible to choose the distance after the extrusion die where the x-ray beam intercepts the crystallising film. (Fig. 19). The distance from the die can be translated into a crystallization time. This method

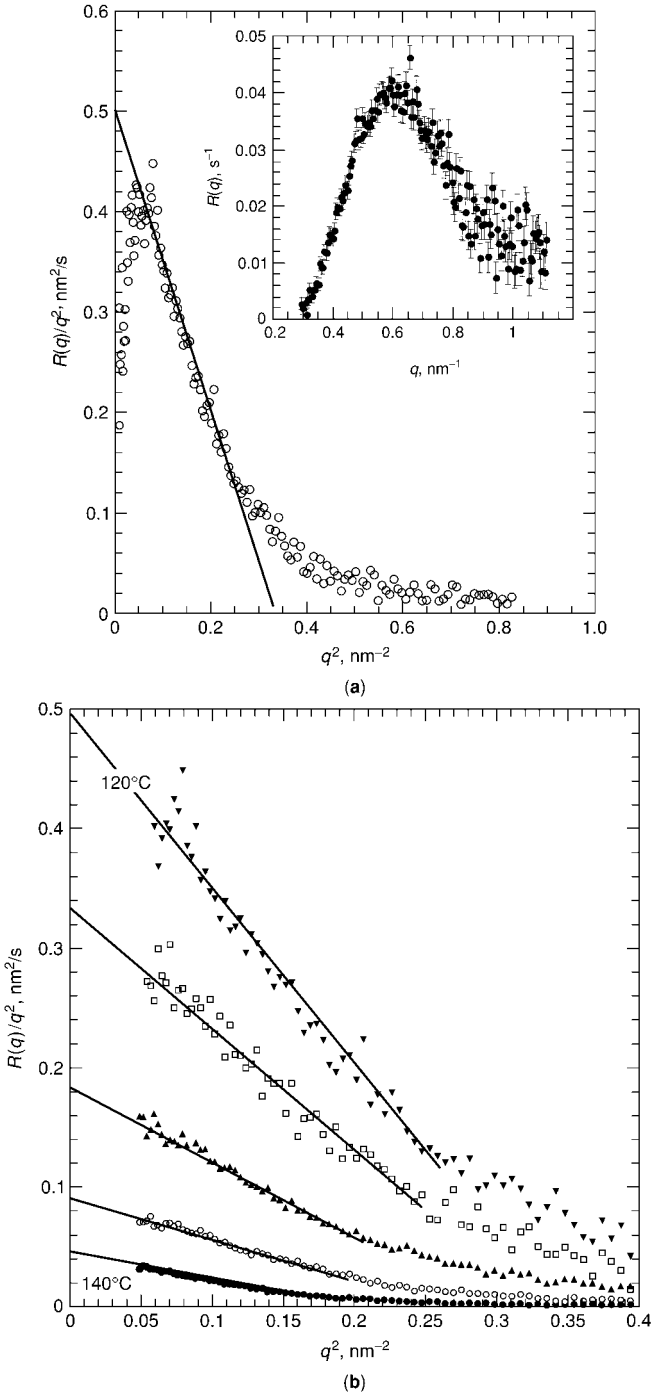

Fig. 17. Panel A shows a Cahn–Hilliard plot to estimate the effective diffusion constant D_{eff} from the intercept with the vertical axis for an isothermal crystallization experiment on iPP. The inset shows the $R(q)$ vs q. Panel B shows similar plots obtained at different crystallization temperatures from 120°C (top curve) to 140°C (bottom curve) in steps of 5°C (31).

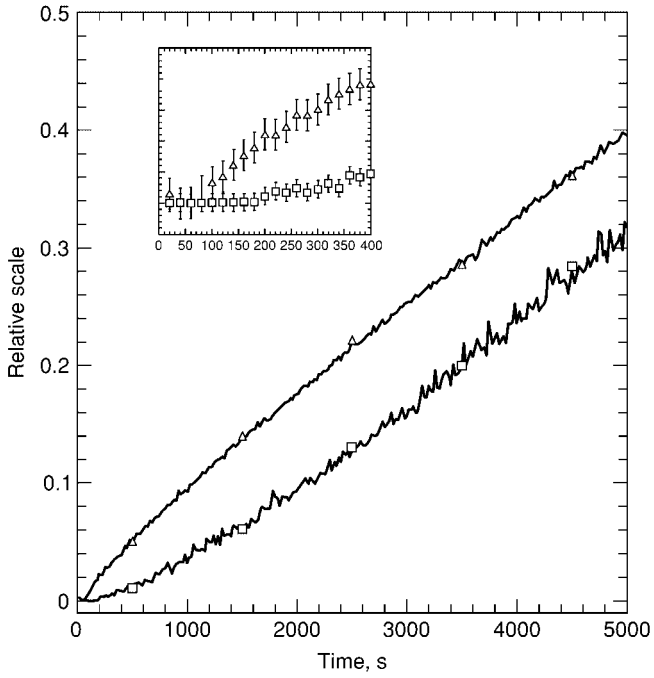

Fig. 18. SAXS/WAXS experiment on the isothermal crystallization of iPP. The saxs invariant and the crystallinity derived from the integrated intensity of the crystalline waxs peaks are coplotted with an arbitrary vertical axis. In this data set, the rise of the invariant precedes the rise of the crystallinity, which can indicate a spinodal-like crystallization mechanism. To base theories regarding crystallization solely on the outcome of such an experiment is dangerous since the results could be influenced by both instrumentation shortcomings and the physics behind the diffraction phenomena. —△— saxs invariant; —□— waxs crystallinity.

has been used (31,94) with the explicit goal of studying polymer crystallization. It is important to note here that in the latter case (31) one used similar detectors for the collection of the waxs and the saxs data. In principle it is not necessary to use two-dimensional detectors here, but in order to obtain the certainty that one is studying unoriented samples, area detectors are indispensable. For inappropriate flow rates one can obtain crystallization effects due to the sample deformation and shear.

The combination of saxs and waxs allows an experimenter to study hierarchical structural length scales from approximately 0.2 to 200 nm. The structural level above this is in some cases accessible with x-ray scattering by using the Bonse–Hart cameras, but this technique does neither provide time resolution nor a scattering vector range on an appreciable scale. Therefore equipment suitable for the combination of x-ray scattering experiments in combination with light scattering experiments has been developed (95,96). When using such a combination of techniques one encounters the situation where one has to make some concessions on the quality of the data for at least one of the techniques in order to be able to take any data at all. The optimum sample thickness for light scattering and for x ray scattering is considerably different. For polymers the optimum

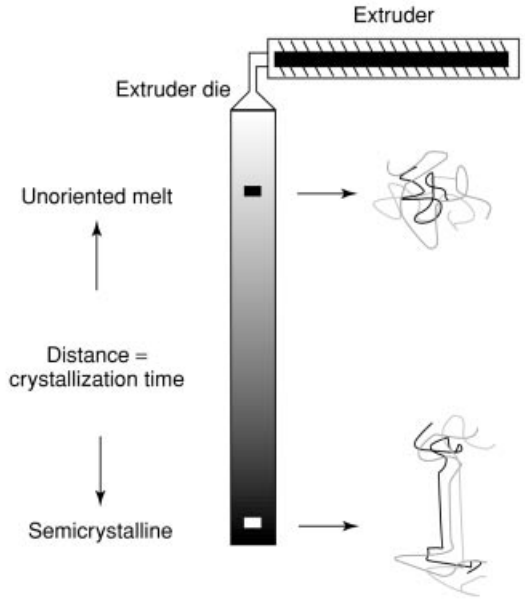

Fig. 19. Schematic description of experiments with an on-line extruder. The short transient phenomena are too short to be followed with a conventional scattering experiment. However, by prolonged measurements on different positions with respect to the extrusion die it is possible to obtain data with a good statistical significance in which the crystallization time is translated into the distance from the die.

thickness for x-ray scattering is around 1.5 mm (at $E = 8$ keV), and the optimum thickness for light scattering is around 10–100 μm. It is possible to obtain data from x-ray scattering with such thin samples but the signal-to-noise ratio from the data will not be very good. An alternative is to use a sample container that is tapered and in which one uses the thin end of the wedge for light scattering experiments and the thicker end for x-ray scattering. Care has to be taken that temperature gradients over the sample do not create essentially different thermodynamic states.

Microfocus

The third generation of SR sources allows the construction of beamlines with a very small beam size while still generating sufficient x-ray flux to be able to collect data on a reasonable time scale. Beam dimensions are still diminishing because of technological developments. At the time of writing it is possible to achieve a beam spot of 4 μm at the sample position for waxs experiments and down to 10 μm for saxs experiments. The reason for the larger beam size in the saxs experiments is that reduction in beam dimensions bears the penalty of a larger parasitic scatter cone which reduces achievable angular range at smaller scattering vector.

An interesting phenomenon in these experiments is that samples which appear to be completely homogeneous in experiments with a larger source size often

exhibit local orientational variations. This is most clearly seen in experiments on spherulite-forming polymers. By step scanning the sample through the beam it is possible to map the orientation of the lamellae inside the spherulite. This has been done on spherulites of poly(3-hydroxybutyrate) (97) (Figs. 20a and 20b). When viewed with a larger beam size one will only be able to probe the lamellar thickness averaged over all the orientations of the lamellar inside the spherulite.

Another advantage is that by using a detector with a high enough spatial resolution it is possible to observe on a single detector the long period as well as the region where the amorphous halo and crystalline peaks of a semicrystalline polymer are (Fig. 21). For time-resolved experiments this is not in all cases an option since the large number of photons hitting the sample in a small volume will unavoidably damage the sample. However, this method is useful when one wants to relate and calibrate the diffraction intensity of small-angle features with wide-angle features. A calibration sample measured both on a microfocus beamline and in a saxs/waxs setup with two independent detectors can be used for this. By using a combination of conventional saxs/waxs, microfocus saxs/waxs, and light microscopy, secondary crystallization during isothermal crystallization of iPP and PVF_2 has been studied (98). In the microfocus experiment a random point was chosen and this was illuminated till the growth front of a spherulite passed by. The increase in crystallinity during the following period was deemed to be due to secondary crystallization. These results were compared with the bulk measurements from the conventional experiments. The authors were able to show that the secondary crystallization was strongest directly behind the boundary between the virgin amorphous material and the spherulite.

Sample Environments and Technique Combinations

The early period of the application of SR in soft condensed matter research focussed mainly on structural determinations as function of easily varied parameters such as sample composition and temperature. Over the years the instrumentation has improved so much that one can state that this can now routinely be done. The challenge to extend the experimental possibilities by not only performing the scattering experiments, but also combining this simultaneously with techniques available in standard laboratories, was obviously felt by many experimenters. Doing these types of combined experiments has the advantage that for some samples the structural parameters can be correlated with thermodynamic or spectroscopic parameters obtained with the complimentary technique. These latter techniques can be repeated on a more extensive range of samples in the home laboratory. The combined experiments, obtained in the usually rather scarce experimental time allocated on the large-scale x-ray facilities, can then be used to extrapolate the structural information over the full sample range.

Combined experiments require a higher level of sophistication of the sample environment. Many examples can be found in the literature, for instance, fast stopflow cells (99), concentration gradient devices (100), and temperature jump cells (101). In the following sections some technique combinations and the implications for sample cell construction are discussed; see also Reference 5. Before treating

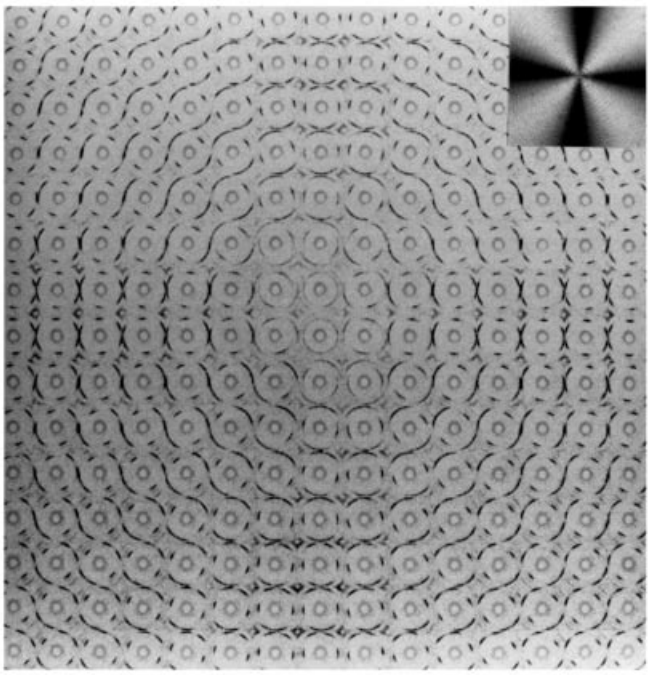

Fig. 20. In panel A diffraction patterns on different positions inside a spherulite of poly(3-hydroxybutyrate) are shown. The diffraction patterns are mapped onto the position inside the spherulite. The spherulite was mapped with a 10-μm beam on a microfocus beamline at the ESRF. The data presented here shows approximately 150 μm^2 of the spherulite. Panel B shows one of the diffraction patterns. It could be indexed to an orthorombic unit cell with dimensions $a = 0.576$, $b = 1.32$, and $c = 0.596$ nm. The degree of disorder increases toward the center of the spherulite. Courtesy of A. Mahendrasingam.

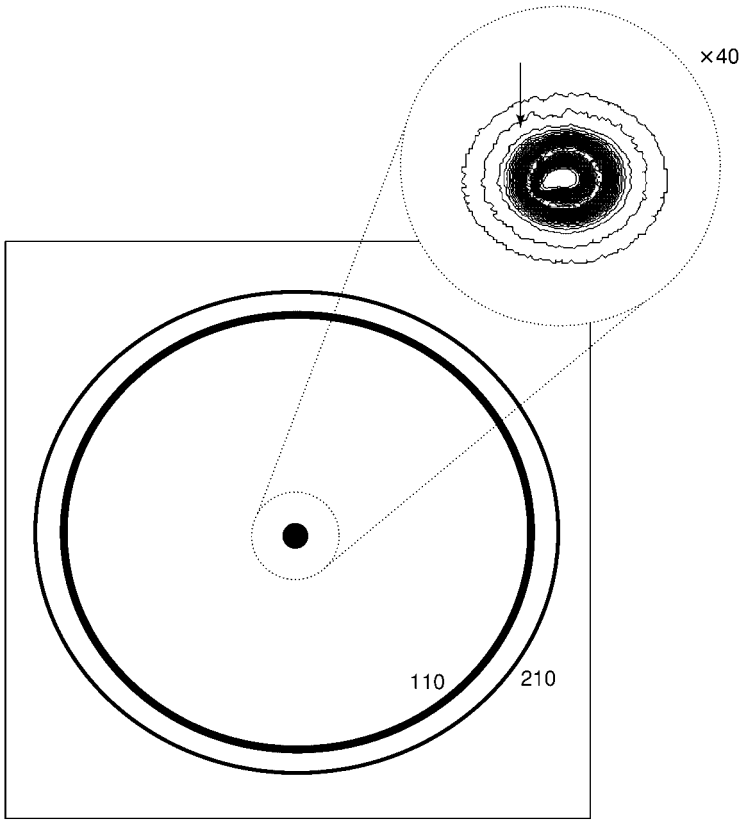

Fig. 21. Diffraction pattern and intensity trace of HDPE measured on a microfocus beamline. The diffraction intensity due to the lamellar thickness and the peaks due to the crystalline packing of the molecules can be obtained in a single diffraction pattern. The sample survives only a couple of minutes in the x-ray beam because of radiation damage. The photon flux can be as high as 1010 photons/s in a 10-μm diameter spot. Data taken in collaboration with M. Drakapopoulos/ESRF.

chosen subjects in more detail, some experiments that will highlight difficult experiments that require complicated sample environments and technique combinations are discussed. These examples include experiments performed either on second generation SR sources beamlines or on bending magnet beamlines of third generation sources, and therefore also serve to illustrate that by concentrating on sample environments it is not always required to have access to the superior quality of undulator beamlines at third generation SR sources.

The realignment process of liquid crystals in changing electric or magnetic fields has been studied in real time by techniques such as optical birefringence (102), nuclear magnetic resonance (nmr) (103), or x-ray diffraction (104). For samples requiring strong magnetic fields (>2 T) in combination with x-ray scattering, this is a nontrivial matter. In this case the field has to be generated by a superconducting magnet which, because of the cryogenic system required, has only limited possibilities for x-ray access. Split coil magnets with a large bore are expensive.

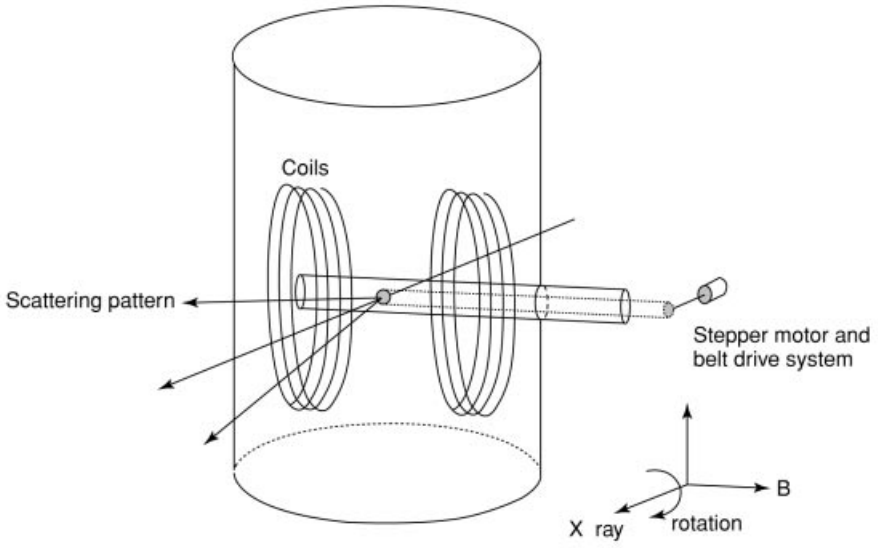

Fig. 22. Schematic representation of an experiment designed to study the reorienation mechanism of a smectic liquid crystal (8CB). The sample was placed in a magnetic field of 6 T at a temperature of 32°C. The magnetic field induces an alignment. By mechanically rotating the sample around the "x-ray axis" the reorientations due to the constant magnetic field can be studied.

The large bore is required since it allows thermal shielding between the cryogenic temperatures (≈4 K) required for cooling the coils and the sample temperature, which generally is >300 K. Moreover superconducting fields cannot be switched on time scales relevant for realignment studies (<100 ms). This implies that the sample has to be rotated in the field and so a rotation and temperature control mechanism has to be inserted in the coil (105). In Figure 22 the principle of this experiment is outlined. Experiments like this have been performed on a bending magnet beamline at the ESRF specifically designed to be able to accommodate large-scale sample environments for polymer processing experiments (12). In Figure 23 results of such experiments in a 5-T field on a smectic 8CB sample are shown. The sample temperature was set to 32°C. The sample was rotated in 70 ms and the realignment process was followed with a time resolution of 250 ms/frame. From these experiments it is clear that there is a transient phase occurring during the rotation in the magnetic field. The highest field that could be achieved in these experiments was 10 T. Such fields also allow the orientation of larger molecules with a small diamagnetic (46). In Figure 24 the fiber diffraction pattern of a biological microtubule polymer is shown. These polymers were self-assembled in the field by using a temperature jump from 4 to 37°C. The advantage of being able to perform such experiments is that one is able to obtain oriented diffraction patterns, which can be analyzed with fiber diffraction techniques, while the sample is contained in a buffer solution in which it retains its hydration and biological functionality.

The combination of saxs and waxs with light scattering has been discussed in the section on combined saxs and waxs experiments. However, light scattering

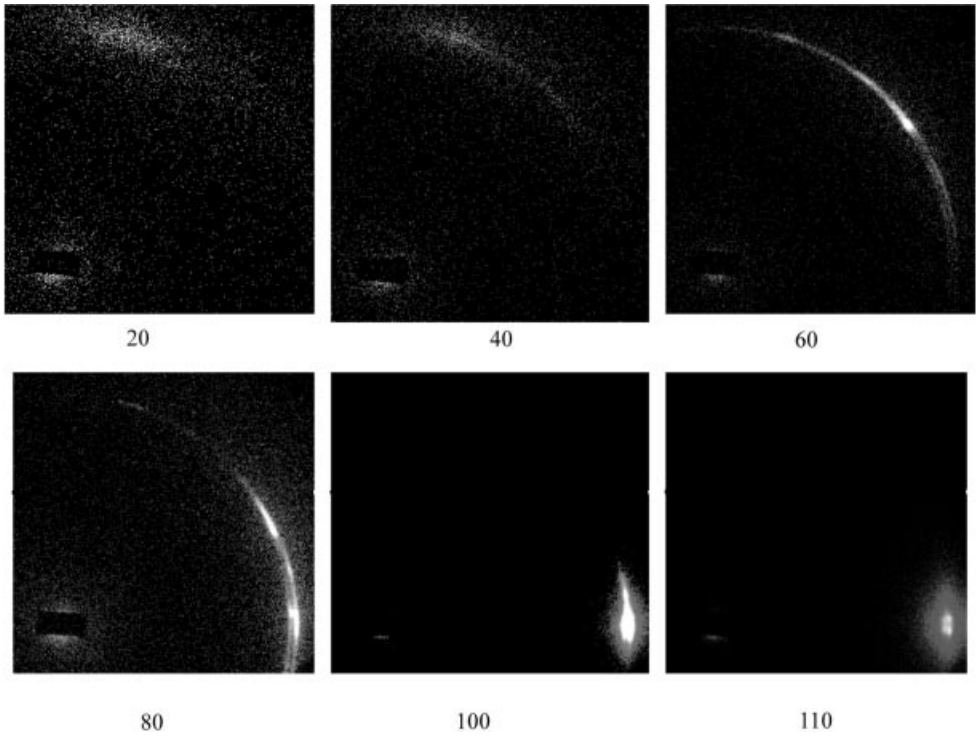

Fig. 23. Different stages of a realignment experiment on an 8CB liquid crystal oriented in a 6-T magnetic field. The unperturbed sample showed a diffraction peak in the lower right-hand corner. Once the sample is rotated inside the field the reflection moves to the top left-hand corner. The sample is forced to reorient to the original position by the magnetic field. The different time frames here show this reorientation effect. Interesting to notice is that when the sample is rotated back to about 50°, the x-ray reflection splits up in two discrete reflections. For this there is no explanation found yet. The time-frame rate was 0.25 s/frame. Unpublished data, courtesy of J. Seddon, B.A. Timimi, and W. Bras.

can be used for more complicated purposes or for obtaining a direct correlation between light transparency of a sample used in liquid crystal display units. In such a case one can correlate directly the transparency with the structural information contained in the x-ray scattering patterns. Strong electric fields are generated relatively easily. They are a common tool for the alignment of, for instance, liquid crystals. Modulated fields have found use both in the studies of liquid crystals and in solution scattering experiments (63). An example of a very complicated but elegant experiment can be found in Reference 106 which reports an experiment on a sample cell transparent to both optical and x-ray wavelengths used in the study of layer deformations in smectic liquid crystals during electric field induced switching. The electrooptic measurements provide information on the bulk motion of the liquid crystalline director while the saxs data is used to connect the liquid crystalline layer motion (Fig. 25). This experiment used bending magnet radiation from the SRS in Daresbury, which is a second generation SR source (107).

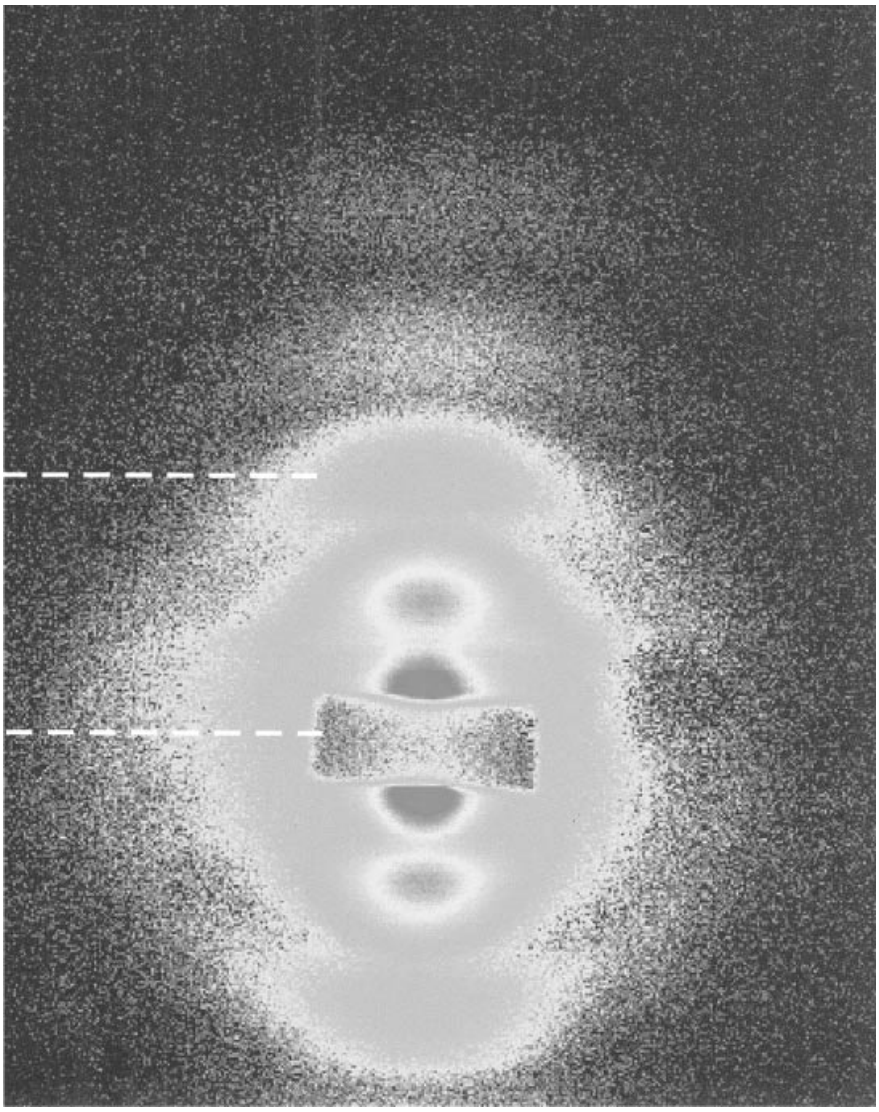

Fig. 24. Diffraction pattern of a magnetically aligned sample of microtubule biopolymers. The orientation was achieved by assembling the polymers, from the tubulin protein solution, in a 9 T on-line magnet. The diamagnetic moment of the tubulin protein is sufficiently high to induce orientation once several tubulin dimers have assembled. Unpublished data, courtesy of F. Díaz, G.R. Diakun, and W. Bras.

Temperature Control and Thermodynamic Experiments

Temperature control of the sample is one of the most basic requirements for an experiment. This is especially the case when one performs time-resolved experiments in which one wants to determine the structural phases in a temperature–composition diagram (64,108). The required accuracy is dependent

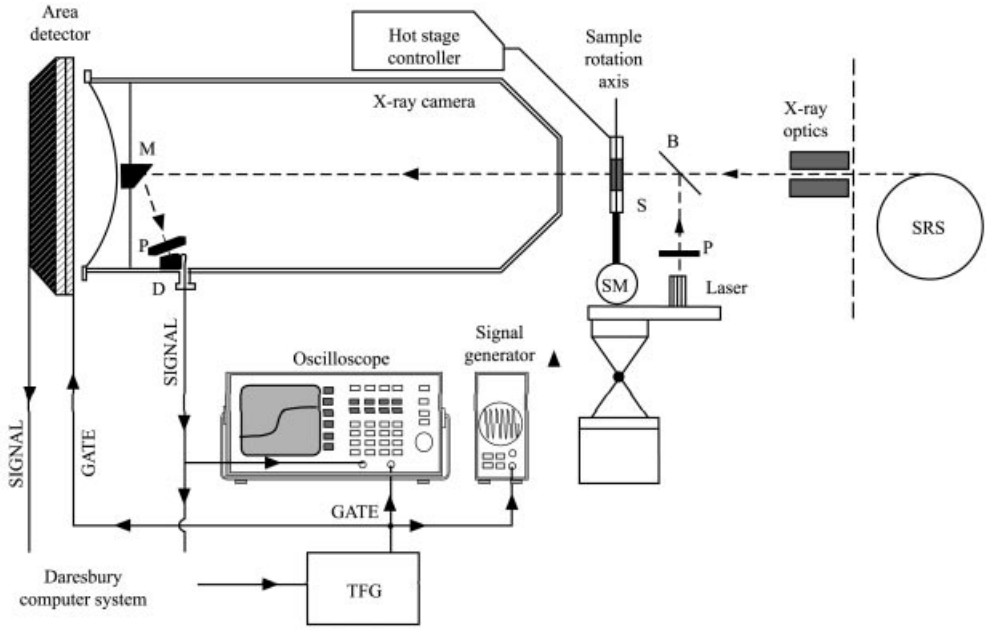

Fig. 25. Combined optical and x-ray experiment. By using a thin x-ray transparent mirror a polarized light beam is guided parallel to the x-ray beam through the sample. A second mirror mounted on the x-ray beam spot deflects the light onto a photodiode. The sample orientation can be influenced by using an electric field. Key: D = detector; P = polarizer; M = mirror; S = sample; B = beamsplitter; SM = stepper motor; TFG = time frame generator. Courtesy of N. Gleeson.

on the experiment but can be roughly 0.1°C in some cases. In principle this is no problem but one always has the complication that one requires access for the x-ray beam. This access often causes temperature gradients to develop. Also in processes where the temperature is changed as a function of time, not only spatial temperature gradients, but also temporal gradients exist, making an accurate control difficult.

A popular method for the investigations of crystallization kinetics is to rapidly quench the sample at a temperature below the melting point and then perform an isothermal crystallization experiment. Apart from the scientific merits, there is obviously an interest in such temperature quench techniques from an industrial point of view. The temperature control in a fast quench does not in general exist and only the start and final temperature can be controlled (109). An elegant way to perform a temperature quench experiment is to keep the sample above the beamline in a furnace at an elevated temperature and then, shoot, it into a second furnace which is mounted on the beamline (101). A time resolution of 0.1 s/frame is feasible at present (109). It should be stressed that the limitations here are more in the temperature control than in the SR beamlines.

Thermodynamic experiments on phase transitions by using differential scanning calorimetry (dsc) and differential thermal analysis (dta) are some of the most important tools of the polymer researcher which can be found in nearly every

laboratory. The accurate correlation of thermodynamic parameters with structural information increases the understanding of the basic phase transition under consideration. To be able to perform simultaneous experiments on a single sample for a set of reference samples, with, for instance, a variable content of copolymer, allows one to extrapolate these results to samples for which only dsc data is available. A data set obtained in the scarce time available on SR beamlines can thus be the basis for a full understanding in a systematic study in which the copolymer content can be varied more finely than in the time available on the SR beamline (110,111). Several manufacturers produce small thermal analysis instruments that have been designed to be used in combination with optical microscopy (5). With some slight modifications these instruments can be used in combination with x-ray scattering experiments.

However, it is a misunderstanding that one can obtain data from combined experiments that can compete with that obtained from independently performed and optimized experiments. Especially the thermodynamic results are often more qualitative than quantitative. The rationale behind combining experiments is that the thermodynamic data obtained with, for instance, an on-line dsc will still show the strong features. The correlation of specific thermodynamic features with time frames of the scattering data enables correlation with an independently obtained high quality dsc trace. In such a case the on-line dsc acts as an accurate thermometer.

A good example of the above statement are experiments with temperature-modulated dsc (TMDSC) on samples of linear PE (112). Here a programmable temperature controller is set up in such a way that the temperature/time profile follows exactly the profile that in an off-line modulated dsc instrument is applied to the sample. By carefully assessing the correlation between the temperature profile and the influence this exerts on the invariant Q, as well as on the crystallinity derived from the waxs, it is possible to show that reversible melting and crystallization take place at the lamellar fold surface and not on the lateral surfaces of the crystallites (see Figs. 26a and 26b).

Spectroscopy and Reactive Processing

In previous sections the combination of x-ray scattering with thermal analysis methods and light scattering was described. These techniques complement the structural information by adding either direct or indirect information regarding a higher hierarchical level of organization. Structural information on shorter length scales is not accessible by x-ray scattering experiments. For additional information regarding conformational changes in larger molecules and chemical bonds between molecules one has to utilize spectroscopic techniques such as infrared absorption or Raman scattering, depending on whether one wants to study bond orientations parallel or perpendicular to the polymer chain. Especially when one is dealing with reactive processing of polymers the approach to combine time-resolved synchrotron x-ray scattering experiments with spectroscopy can be fruitful.

The simultaneous combination of x-ray scattering with spectroscopic techniques is still in its infancy. As an example a combination of Fourier transform

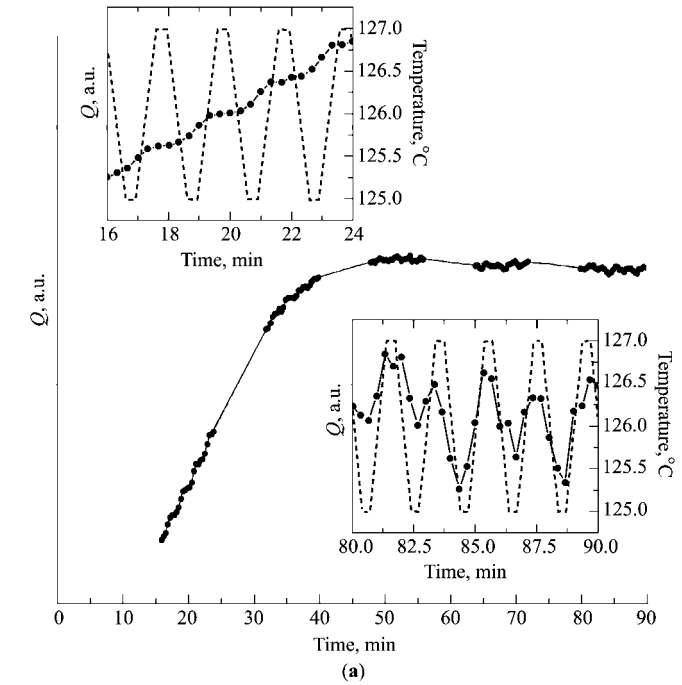

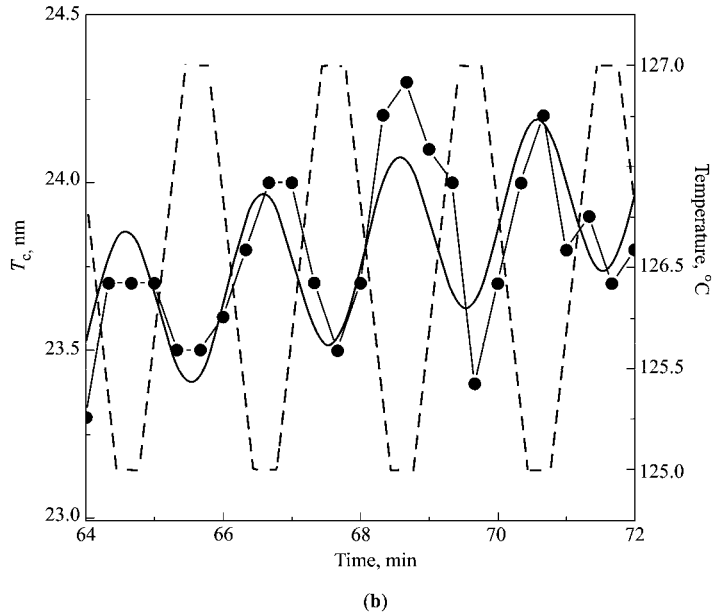

Fig. 26. Panel A shows the time development of the invariant Q in a temperature-modulated crystallization experiment on linear PE. The insets are magnified parts of the main figure at time 16–24 min (upper) and 80–90 min (lower). Panel B shows the thickness of the crystalline layer, T_c, as a function of temperature. The thick line represents a fit to the data points, and the dotted line is the applied temperature profile. The correlation between the two is obvious. Courtesy of B. Goderis

infrared spectroscopy (ftir) with saxs is discussed (113). In this example the information about vibration modes involving motions of chemical groups in molecules is used as a parameter directly linked to the chemical reaction during the formation of a polyurethane while the saxs pattern provides the information on the formation of structure in the sample.

One of the problems that one faces when combining ftir and x-ray scattering is that the optimum thickness for transmission experiments with both techniques differ by several orders of magnitude. For homogeneous samples the solution to this problem is to perform the x-ray scattering experiment in transmission and use of the method of attenuated total reflection (ATR) for the ftir experiment. With the ATR method the sample is mounted onto a zinc selenide or KRS5 crystal. This crystal acts as a prism and is illuminated with infrared radiation from the side. The infrared radiation is reflected several times in the crystal and upon each reflection penetrates superficially in the sample material. The multiple reentry enhances the absorption and increases the signal-to-noise ratio considerably. One can now choose to either provide x-ray access through the crystal or, the more elegant solution, extend the stainless steel support and temperature control. A small hole in this extension provides x-ray access (see Fig. 27).

An experiment describing the formation of polyurethane elastomers through the reaction of isocyanate with hydroxyl components is now discussed as a specific example. The experiment was set up to resolve the question whether hydrogen bonding between the carbonyl groups forced the structure formation or whether the hydrogen bonding was just a consequence of the formation of structure. The combined experiment showed unequivocally that the structure formation, as evidenced by the rise in the saxs invariant, preceded the hydrogen bonding, observed as a shift in the carbonyl absorbencies from 1720 cm^{-1} (free) to 1700 cm^{-1} (hydrogen bonded) (see Fig. 28). The importance of the simultaneous performance of the experiments on the same sample lies in the fact that with independently performed experiments the correlation between the time axis of the two experiments did not show this with sufficient degree of accuracy.

With the appropriate equipment the time resolution can be reduced to 1 s/frame. This improvement brings the time resolution inside the realm that is interesting for the combination with polymer processing techniques such as reaction injection molding (RIM). RIM processes have been studied independently by saxs and ftir (114,115). Here one faces the problem that the sample cell is rather large and has to be filled completely and homogeneously on a time scale which is short compared to that of the reaction that is taking place. Therefore time resolutions below 2–4 s/frame are not achievable. In Figures 29a–29c, the results from a similar reaction as described above, but now at industrially relevant temperatures and reaction rates, are shown. Having shown that these experiments are feasible from an experimental point of view, a remark can be made that every time that an experiment was done a new ATR crystal was required since they invariably break when one tries to free them from the formed polyurethane. This makes these experiments rather expensive.

Another spectroscopic technique which at times can be very useful to combine with x-ray scattering experiments is Raman scattering. This technique can

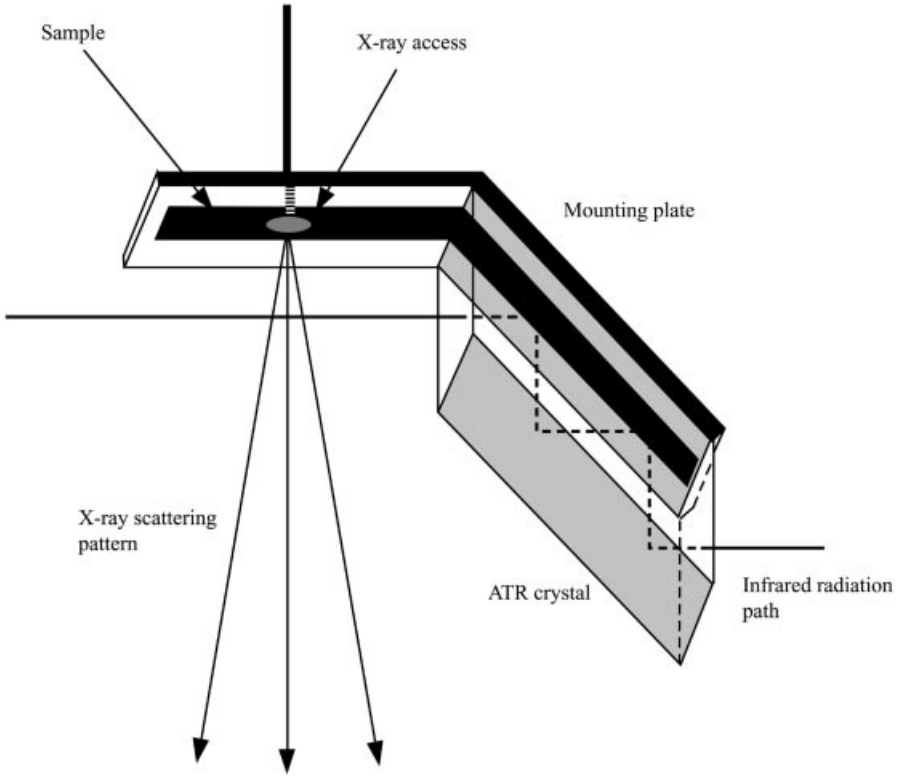

Fig. 27. Experimental layout for a combined ftir, saxs, and waxs experiment. By using the ATR method for the ftir it is possible to overcome the problem of incompatible optimum thicknesses for the different techniques. For slow reactions this method is suitable. For faster reactions, where it is more important that there is an exact coincidence of the positions on the sample where the data is obtained, one has to drill a hole in the ATR crystal in order to allow x-ray access.

be used in a similar fashion as ftir but is also usable with nontransparent samples and provides more information on the vibrations in the carbon chain of the polymer. This contrasts with ftir where the information content mainly relates to the substituents on the carbon chain.

In practice, the combination of Raman scattering with x-ray scattering is greatly facilitated by the possibilities of using fiber optics and microscopic techniques (116). One very elaborate study (117,118) used the combination of *in situ* saxs/waxs/Raman scattering to shed light on the very complex phase behavior of syndiotactic polystyrene (sPS) dissolved in reactive solvents. The verdict from this study was that it was crucial to combine these three techniques in a time-resolved way in order to obtain a clear picture of the complicated processes taking place in these systems. The changes in the crystalline conformation of sPS are monitored spectroscopically, the degree of crystallinity by the waxs experiments, and the phase separation process by saxs.

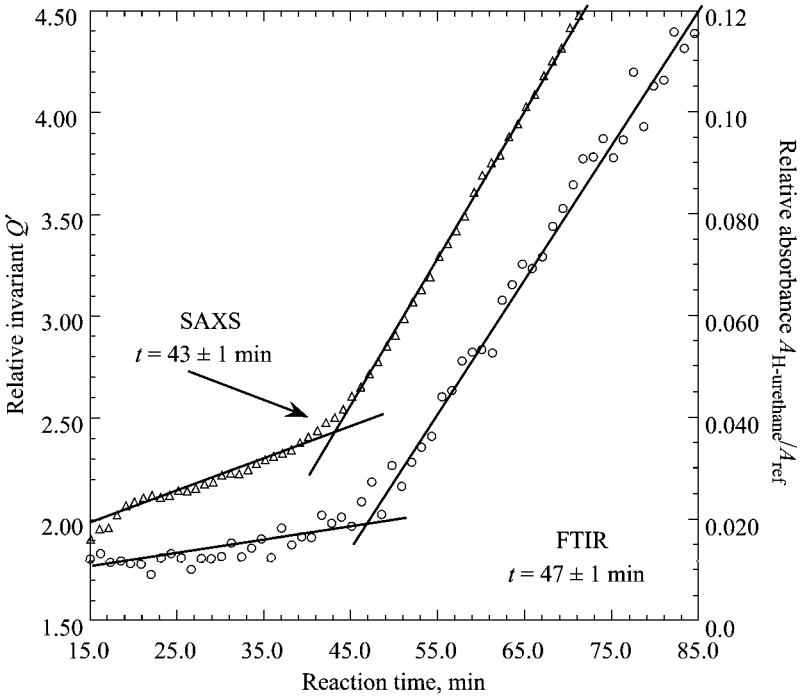

Fig. 28. Polyurethane elastomer formation studied by a combination of saxs and ftir. The chemical reaction forming the polyurethane can be monitored by following the changes in the infrared absorption bands. In this figure the intensity of the band associated with the hydrogen bonded urethane is coplotted with the saxs invariant. It is clear that the invariant increases before the ftir signal. By applying this method the possibility that structure formation is caused by hydrogen bonding could be excluded and it was shown that the hydrogen bonding is a consequence of the structure formation. △ Relative invariant Q'; ○ $A_{H-urethane}/A_{ref}$.

Deformation

In situ deformation of polymers via uniaxial drawing can be implemented on an SR beamline relatively easily (119,120). This was already mentioned in the section on Fiber Diffraction. In two-phase systems one can study the deformation of the constituent phases. Also of interest are damage effects due to cavitation and crazing (121,122). The main experimental problems with x-ray experiments on devices mounted in a tensile tester is to keep illuminating the same spot on the sample with the x rays and to properly normalize the scattering pattern since the transmission is continuously changing by the nature of the drawing process. Methods to keeping illuminating the same spot are in the first place by using devices which move both jaws with the same speed. Still the sample can slip in the jaws occasionally, causing a change in position of the material under investigation. This can be compensated by drawing small markers on the material and keeping a visual observation via a closed circuit television system.

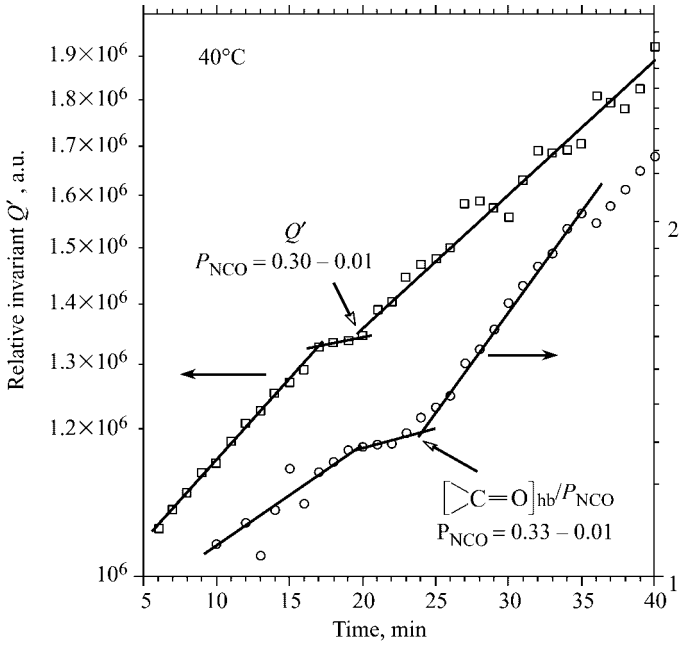

Fig. 29. Results from an on-line RIM/SAXS/FTIR experiment at different temperatures studying a similar reactive processing experiment on polyurethane formation. However, in this case the experiment was combined with an on-line RIM machine so that industrial processing conditions regarding temperature and reaction rate could be used. The ftir data was obtained via the ATR method. Shown are the isocyanate conversions (right-hand scales) and the invariants for different temperatures. From these experiments it can be concluded that at the microphase-separation point the chemical reaction kinetics change from second order to a diffusion control. Courtesy of M. Elwell.

The deformation of HDPE shows how a strain-induced phase transformation can be studied (122). In this experiment it is interesting to follow the large-scale changes induced by the strain and try to relate this to the changes in the crystalline unit cell of the material. In order to correlate these small- and large-scale events it is required to collect the saxs and the waxs data simultaneously. However, since we are dealing with a nonisotropic scatterer the use of area detectors over one-dimensional detectors is preferred. For simultaneous experiments this poses somewhat of a problem. In order not to intercept the saxs pattern the waxs detector has to be offset with respect to the direct beam which means that the complete scattering pattern can not be detected. Often the waxs detector will be tilted at an angle of 45° in order to intercept as large a q-range as possible. Such a mounting and the short sample–detector distance invariably creates a distorted pattern (see Fig. 30). As long as there are just geometrical distortions there is not a real problem, but in the case of gas-filled multiwire chambers one will encounter parallax effects as well. With CCD detectors one does not have this problem but, as mentioned in the section on Detectors, one has less dynamic range and might struggle to detect weak features (120). However, when one is interested in the order of events taking place, such a setup can be very useful. In Figure 30

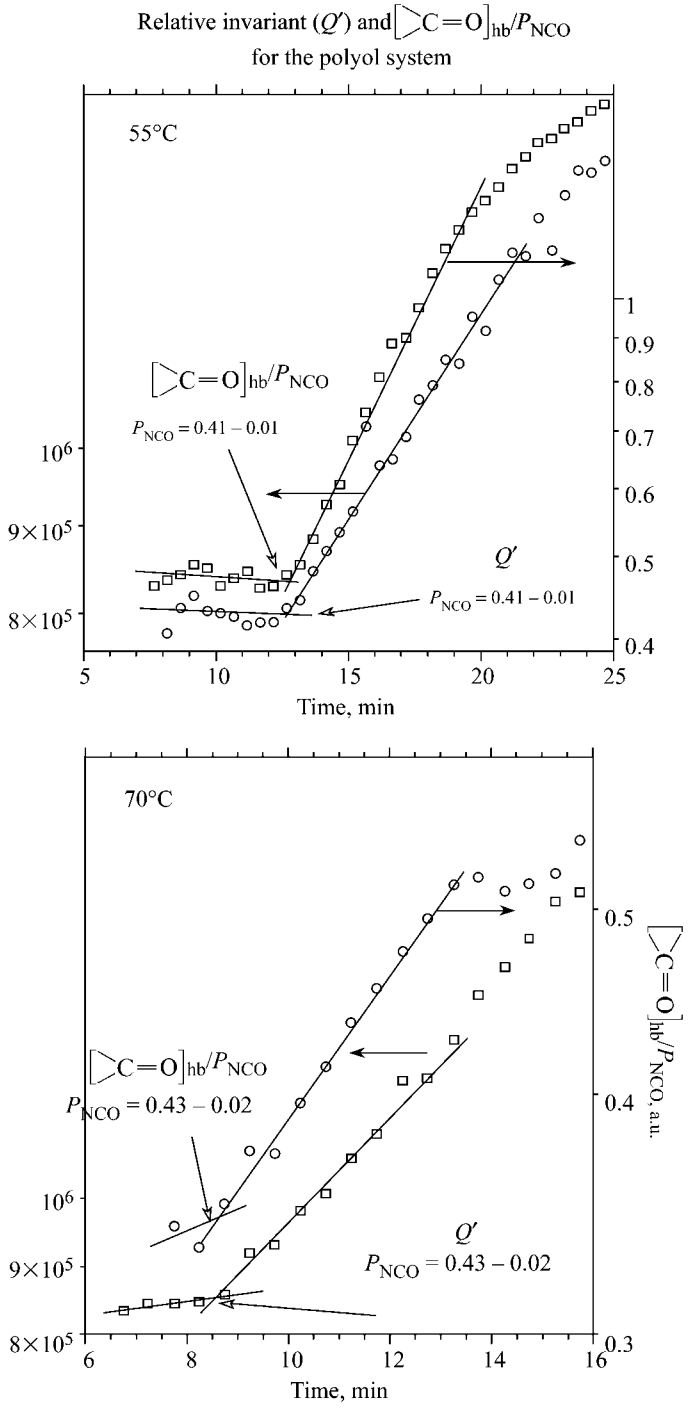

Fig. 29. (Continued).

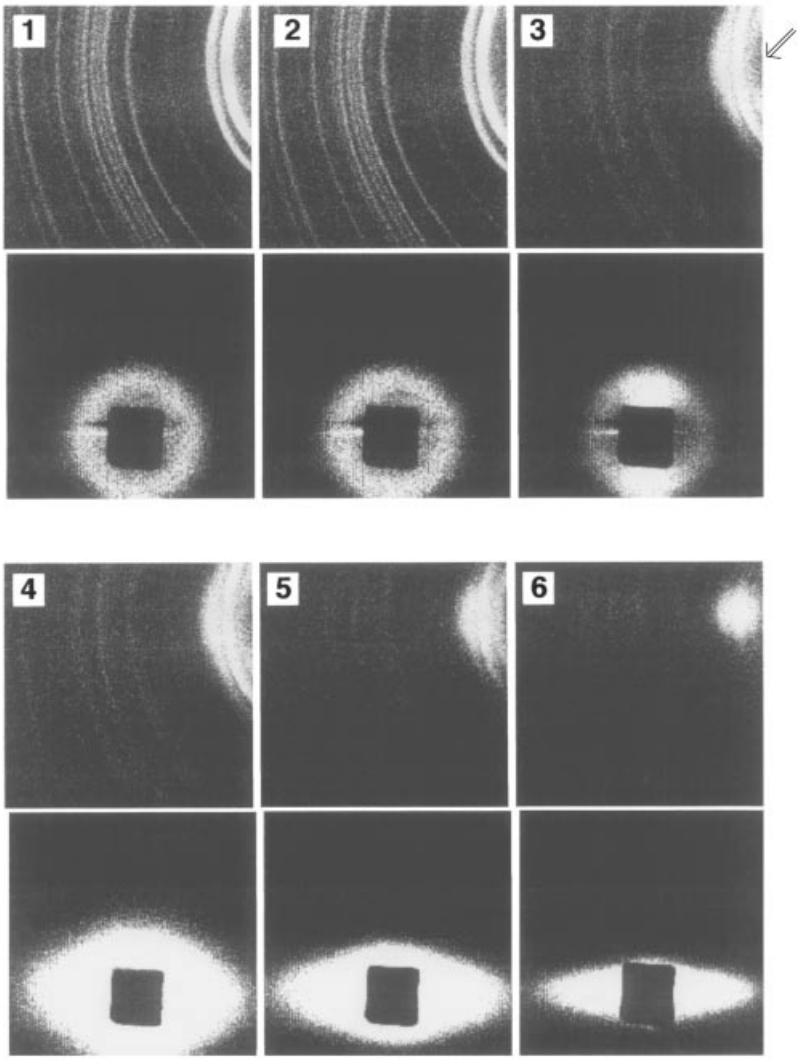

Fig. 30. A simultaneous saxs/waxs experiment on an oriented sample which requires both area detectors for the saxs and waxs region. An HDPE sample is stretched. The deformation induces a martensitic phase transformation as evidenced by the occurrence of extra reflections in the waxs region (top row of diagrams, see arrow). Void scattering is found in the saxs patterns (bottom row of diagrams). For a further explanation one is referred to the text and to References 122 and 123.

both saxs and waxs patterns are shown as a function of draw ratio (122). This data shows how the deformed HDPE first becomes oriented, as witnessed by the fact that the initially isotropic Debye Scherrer rings in the waxs pattern deform in noncontinuous arcs. At the same time the diffraction intensity in the saxs pattern, corresponding to the lamellar spacing, shows orientation. However, already at strains of 5% the intensity is dominated by very intense void scattering. Another interesting feature that can be observed is evidence of a martensitic phase

transition through the occurrence of extra reflections on either side of the 110 and 200 reflectons in the waxs pattern. This transition from a orthorhombic to monoclinic unit cell as already been discussed (124). With conventional x-ray sources it is very difficult to follow such transitions in real time. The high flux of an SR source and the associated instruments, such as high count rate detectors, are required here. An extensive study of deformation phenomena in polyethylene has been given (123). Crazing phenomena have been described quantitatively (121,125). The authors have made an attempt to elucidate the contributions that different effects might have on the anisotropically scattered intensity. Not all aspects of the interpretation of crazing data have been fully understood yet. A rigid mathematically acceptable framework is still lacking.

Biaxial drawing systems have been developed (126) but so far very few results can be found in the literature (127,128). The difficulties encountered in obtaining quantitative data have been described (126). However, most problems are not insurmountable and it can be expected that soon this technique will also be applied routinely. Complete uniform deformation, like in film blowing, is experimentally much more difficult to perform because of the fast changing thickness, and thus x-ray absorption of the sample, which makes normalization difficult. Also, one can expect the detector count rate to vary rapidly in unison with the sample thickness, thus requiring a detector with both a high count rate and a high dynamic range.

Pressure Cells

Pressure is undeniably one of the most interesting parameters that can be varied in real-time studies on polymeric samples. During processing polymers are often subjected to a combination of pressure and shear. Not only the industrial relevance makes structure/pressure studies interesting, but also the possibility to use pressure as a thermodynamic variable in time-resolved scattering experiments allows the structural determination of phases detected previously only by techniques with less direct information content, such as dsc. The application of pressure increases the melting temperature of the polymer, which facilitates a higher chain mobility. Thus a larger possibility exists, upon annealing at high P–T, for growing more perfect crystals or even forming new crystalline phases. In copolymers of polyethylene, side chains can crystallize in the more open hexagonal form, normally not stable at ambient pressure and temperature, instead of the normal orthorhombic form (129).

The problem with x-ray experiments at elevated pressures is the sample cell windows. These have to be able to withstand the high pressure and still be sufficiently transparent to x rays. In the general understanding there are some misgivings about the problems associated with these cell windows. The problem is not only a matter of absorption, as is often assumed, but also of signal-to-noise ratio and multiple scattering. In Figure 31 the transmission as function of energy of diamond and polypropylene is shown. There are two key issues:

(1) the sample plus windows still should show a decent x-ray transmission;
(2) the scattering signal of the sample should not be completely wiped out by the signal from the windows.

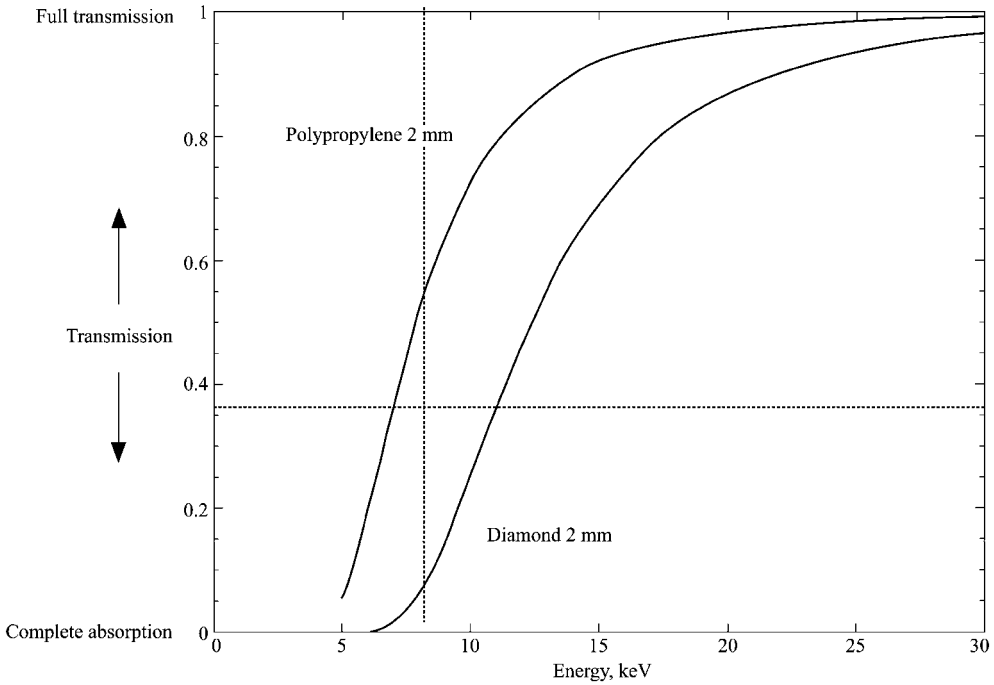

Fig. 31. Transmission of diamond, often used for x-ray windows in high pressure cells, compared with the transmission of PE as function of energy. Conventional x-ray generators most often use Cu Kα radiation (dotted vertical line). It is clear that the possibility to vary the x-ray energy is a most useful option when one needs to use less x-ray transparent windows. One is reminded that the optimum thickness for x-ray scattering is the one at which the ratio $I_t/I_0 = 1/e$.

From Figure 31 it can be seen that increasing the x-ray photon energy above the conventionally used 8 keV (ie, the Cu Kα line produced by most generators) allows a much higher transmission. The second point can be addressed by choosing a sample thickness that is matched to the thickness of the diamond windows in such a way that the sample signal is at least of the same order of magnitude as the signal from the windows. The reader is reminded that the optimum thickness for scattering is when the ratio of the transmitted beam, I_t, to the incoming beam, I_0, is

$$\frac{I_t}{I_0} = \frac{1}{e}$$

If the transmission is much lower than this value multiple scatter will occur and this gives rise to an uncorrelated background which can seriously affect the quality of the data. With too low a transmission, increasing the flux from the incoming beam is not going to be the solution since this will also increase the background proportionally. On most SR beamlines it is possible to vary the energy somewhat, and this explains why the field of high pressure diffraction has grown with the advent of SR and especially with the coming on line of the powerful third generation of SR sources.

An extensive study on the *P–T* phase diagram of polyethylene has been reported (130). This author has developed a cell which has been copied by several others (130). Pressures of up to 5 kbar can be reached with this *in situ* piston–cylinder sample cell, equipped with diamond windows. By using two cylinders it is possible to apply three-dimensional pressure which is regulated by pressurized nitrogen gas. One of the main conclusions of this work was that within the pressure and temperature range of this experiment the formation and growth of single crystals, in both the stable and metastable part of the phase diagram, took place in the mobile hexagonal phase. When allowed to transform from the metastable hexagonal to the orthorhombic phase all crystal growth stopped. Another very nice example of experiments using a similar type of pressure cell is given in Reference 131. These authors investigated the P–T phase diagrams of poly(4-methylpentene-1).

Rheology and X-ray Scattering

The response of a polymeric sample to an applied shear is obviously of interest since most industrial processing processes imply that the material is subjected to shear somewhere in the process before the final product is ready. Sometimes this induces crystallization (132), phase separation, or orientation in the final product. It is therefore not surprising that over the last decades extensive *in situ* studies of these induced structural changes whilst the shear is applied have been conducted, in preference over postmortem determinations of the structure. Independent of which type of shear geometry one uses, one encounters the problem that the sample has to be contained at a high temperature in a cell which is capable of withstanding the pressures intrinsic to the shear process (133). Optical microscopy has already been used for this type of work since the 1960s (134) but for length scales, only accessible via scattering, with wavelengths shorter than that of visible light, this type of studiys was till recently the domain of neutron scattering since the high penetration power of neutrons allowed the construction of sturdy cells whilst the high neutron scattering cross section for polymers enabled data collection with a reasonable signal-to-noise ratio (135,136). However, just as in the previous section in which pressure cells were discussed, nowadays it is possible to construct shear cells of many types which can be used in situ with x rays because of the availability of sufficient flux at shorter wavelengths (with sufficient penteration power) on the latest generation of SR sources. The intensity of the x-ray beam at these wavelenghts can be so high that it allows in some cases time-resolved experiments on time scales not accessible with neutron scattering experiments. This does not imply that x-ray scattering will replace neutron scattering experiments. They are essentailly complimentary tools in the toolbox available to soft condensed matter researchers.

A commercially available parallel plate shear device Linkam CSS (137) from which the windows were replaced with Kapton windows, in order to increase the x-ray transparency and reduce the parasitic scatter, was used in a study on the shear-induced crystallization behavior of iPP by saxs (138). By applying a short step shear it was found that the crystallization ratio could be increased by 2 orders of magnitude with respect to the quiescent mode. This increase can be attributed to orientation-induced primary nuclei. These are probably lamellae

(kebab) oriented parallel to the flow direction. After cessation of shear, strong x-ray scattering occurs indicative of the growth of crystals perpendicular to the flow direction (shish). This secondary crystallization growth is nucleated on the earlier formed shear-induced crystals. It is interesting to note that the final morphology, as observed by saxs and tem, does not show a full shish-kebab structure under most of the experimental conditions, ie, different shear step rates. The extended chain primary nuclei template the folded chain crystals but are apparently too tiny to be observed directly. This type of experiment can be performed with a time framing rate of approximately 10 s/frame using a CCD detector.

The parallel plate geometry is preferable from an x-ray scattering point of view (139). Only two x-ray windows are required to confine the sample. However, from a rheological point of view this is not the only required geometry. Couette cells have been used extensively in neutron scattering (140). With an appropriate material for the construction of the cylinders a similar approach can be used in saxs experiments (141). The absorption and scattering power of the cylinder material are of overriding importance since the x-ray beam has to traverse either four windows in the case where the incident x-ray wave vector is at right angles with the shear direction, or a considerable amount of material when the incident beam is parallel with the shear direction (Fig. 32). By using thin cylinders of polycarbonate this problem can be partially solved. However, that limits the usefulness of such a cell to a temperature range not exceeding the melting temperature of polycarbonate. An alternative can be to use very thin aluminum cylinders but this has as a consequence an increase in the background noise due to the crystalline grain boundaries in the aluminum which produce considerable small-angle scattering. The Couette geometry is not really useful for waxs experiments since the diffraction pattern is produced not by a single intersection of the beam with the sample but in two discrete spots separated by several centimeters. For saxs this is hardly a problem but in waxs, with the much smaller sample–detector distances, this difference is considerable.

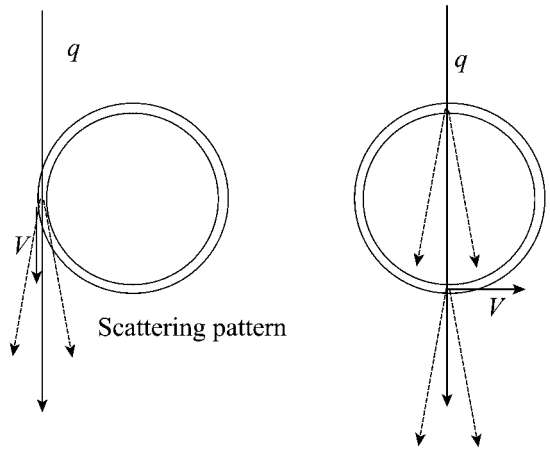

Fig. 32. Couette cell geometry used in on-line x-ray experiments. In the older generation SR sources, the use of a Couette cell is nearly impossible because of the lower x-ray flux which caused too much x-ray absorption. *V* indicates the flow direction.

The use of several other types of shear cells on x-ray beamlines has been reported in the literature. Recently the use of a 'cone and plate' type was reported (142). The other main type used in x-ray research is the reciprocating or oscillatory shear cell (143,144). This system can be mechanized in which the shear that can be applied is completely controlled. A charming example and result of improvisation, often required when using central facilities to which one has access for only a limited amount of time, can be seen in Figure 33. Only a small amount of shear and a slow cooling down was required to induce the hexagonal ordering in this diblock micellar system. This was achieved by drilling a hole in a stainless steel vacuum flange, gluing two pieces of mica as window material to the flange and a piece of brass, sandwiching the sample between the two windows, and reciprocally rubbing the sample for some seconds. The slow cooling was provided by heating the stainless steel flange with a hot air gun and letting the sample air cool so that the thermal mass of the flange allowed for a slow cool (145).

Industrial Polymer Processing Equipment

Real-time studies are, besides interesting for fundamental aspects of polymer behavior, obviously of interest for the polymer processing industries. How a material behaves and changes when subjected to flow, extension, pressure, temperature changes, etc, are all questions of great importance to processing. In these experiments the time resolution of the process is a parameter which can be influenced to a lesser extent than in more fundamental research. It is therefore not surprising that scaled down versions of processing equipment have been mounted on x-ray scattering beamlines where the higher flux enables a substantial part of these experiments to be performed.

In an earlier section the application of a scaled down version of an industrial-type extruder has already been mentioned in connection with crystallization experiments (30). This type of equipment can also be used for more applied experiments, where not the fundamental aspects of crystallization are studied, but more the influence of the spin rates, tension, and shape of the die heads on the final morphology that can be obtained (146,147). The importance of this is underlined by the fact that as early as 1964 researchers have attempted to do *in situ* experiments (148) using a rotating anode generator. Only in 1993 were these experiments taken to an SR source with consequently an increase in data quality (149). In this case the high photon flux is of crucial importance since what is required is that the cross section of the fiber with the x-ray beam remains unchanged over the complete time that one requires to obtain statistically significant data. With a higher photon flux this moment is reached much faster and thus the stability of the spin line does not have to be maintained over a period of days but rather over a period of up to 30 mins.

Experiments performed on poly(vinylidene fluoride) show a development of large-scale structure before a small-scale structure could be observed (149). The authors concluded that this was in agreement with earlier findings where in a nonquiescent sample, crystallization was initiated via spinodal decomposition. The final structure was reached via a two-step crystallization mechanism and resulted in a shish-kebab-like structure where it could be noted that there was

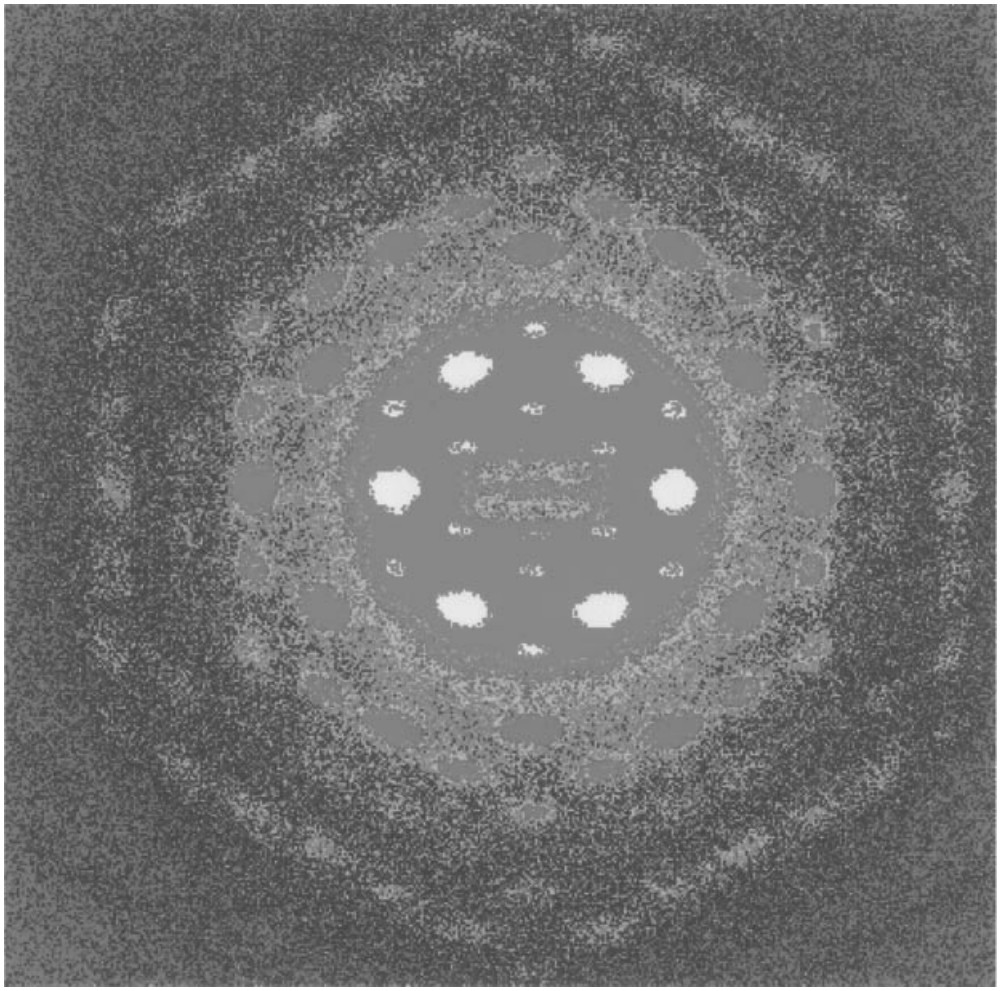

Fig. 33. Small-angle diffraction pattern of a sheared micellar-forming diblock copolymer. The sample was sheared and slowly cooled down on-line so that the formation of the hexagonal structure could be observed. The low angle resolution is about 120 nm. Unpublished results, courtesy of G.P.R Fairclough, R.N. Young, L.Messe, A.J. Ryan, W. Bras.

a noted increase in the *d*-spacing of the primary peaks in the saxs region with increased take-up speed from the fiber. However, this was not the case in the relaxed material from the final fiber.

Over the last decade the processing of polymers in supercritical CO_2 has gained some popularity (150). From a P–I phase diagram one learns that pressures in excess of 7 MPa (70 bar) are required to reach the supercritical state in CO_2. *In situ* experiments have therefore largely been restricted to neutron scattering experiments where the window thickness, when the appropriate materials are used, is not too large an issue. With x-ray scattering this is a problem, just as with the high pressure experiments discussed in an earlier section. However, again the

third generation of SR sources will allow the construction of cells suitable for fast time-resolved experiments. Shorter wavelengths will have to be used to maximize the penetration power and to minimize multiple scatter which will occur with the large sample path length in the windows and the sample (151–154).

RIM is a commonly used process in the production of polyurethane. Since the chemical process can be completed very rapidly it is necessary to use a scaled down RIM machine which can be mounted on a beamline in cases where one wants to follow the structure formation during the chemical reaction forming the polyurethane (Fig. 34). The design of such a setup requires some thought in order to have a bearing on the real industrial process (114). One of the experimental details to take care of is that in a real large-scale manufacturing plant the volume being formed is much larger with consequently different temperature distributions in the reaction chamber compared with a small-scale x-ray machine. This can be compensated by measuring the temperature development in a real plant and then mimicing this profile with programmable sample heaters in the x-ray equipment (155).

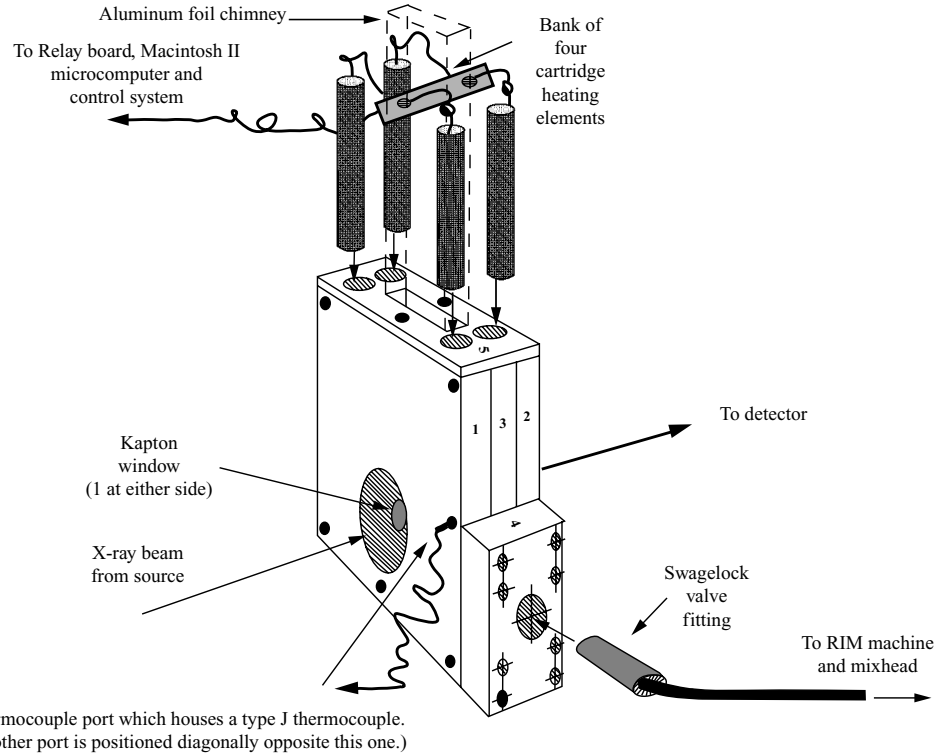

Fig. 34. Sample cell suitable for on-line experiments with a RIM machine. In a real RIM mold the temperature is determined by the thermal conduction in the reaction product and by the dimensions of the real mold. The temperature of this cell can be programmed to follow the temperature profile recorded in real RIM mold in order to obtain realistic results. Courtesy of M. Elwell.

The increasing quality of the x-ray beams that one can nowadays generate with SR beamlines and the increase in experimental infrastructure allows many experiments using processing equipment to be performed. Where some 15 years ago the insertion of a sample heater allowed time/temperature resolved experiments and was thus considered to be a novelty, one can now think of installing previously unthought of equipment, such as thin blown film lines, on SR beamlines.

Influence of Experimental Technique when Determining Simultaneity of Two Events

This section is inspired by the heated debate around the onset of primary crystallization in semicrystalline polymers (30–32,80–85) and the many discussions regarding experimental technique that have taken place because of this debate. Although this example will be used, the underlying idea is that many time-resolved experiments where technique combinations are used are performed to establish the relation between different parameters. This can be the order in which events happen but also differences in the time evolution of the values of parameters. The determination of the simultaneity of two events is typical of combined time-resolved techniques that are becoming more normal in SR experiments. Therefore some details in this specific experiment will be treated in a little more detail as an example of problems that can arise in time-resolved SR experiments. Another experiment where a similar question is addressed can be found in the section where spectroscopic techniques (ftir) in combination with saxs are discussed.

This primary stage of primary crystallization can be characterized either by the conventional nucleation and growth mechanism or by a spinodal decomposition like mechanism while the possibility cannot be excluded that yet another mechanism is involved. In this debate one of the distinguishing features between spinodal-like mechanisms and nucleation and growth is that the rise of the (saxs-dominated) invariant precedes the onset of the increase in the crystallinity as evidenced by the rise in the crystalline peaks in the waxs region.

There are two types of experimental problems that can influence the suitability of an experiment to determine if there is a time lag between the occurrence of two events. The first are the problems that are related to the experimental equipment used, and the second are the intrinsic problems related to the underlying physics of the problem. An example of each of these problems is described below.

An example of how the experimental equipment can influence the outcome of the experiment is in the choice of the appropriate detector system. More specific detector details have been discussed in the instrumentation section. When one is dealing with the onset of an effect one is generally dealing with a small effect on a large background. This means that one has to be very careful with the effects that a detector noise can have. In Figure 35 details of the isothermal crystallization experiment on iPP, described in an earlier section, are given. The two lower curves (open symbols) show the invariant and the degree of crystallinity obtained with low noise detectors. The time lag between the initial rise of the two curves is clear. The same data to which some background noise, not unlike the noise that will be introduced by an integrating detector or the statistical noise because of the

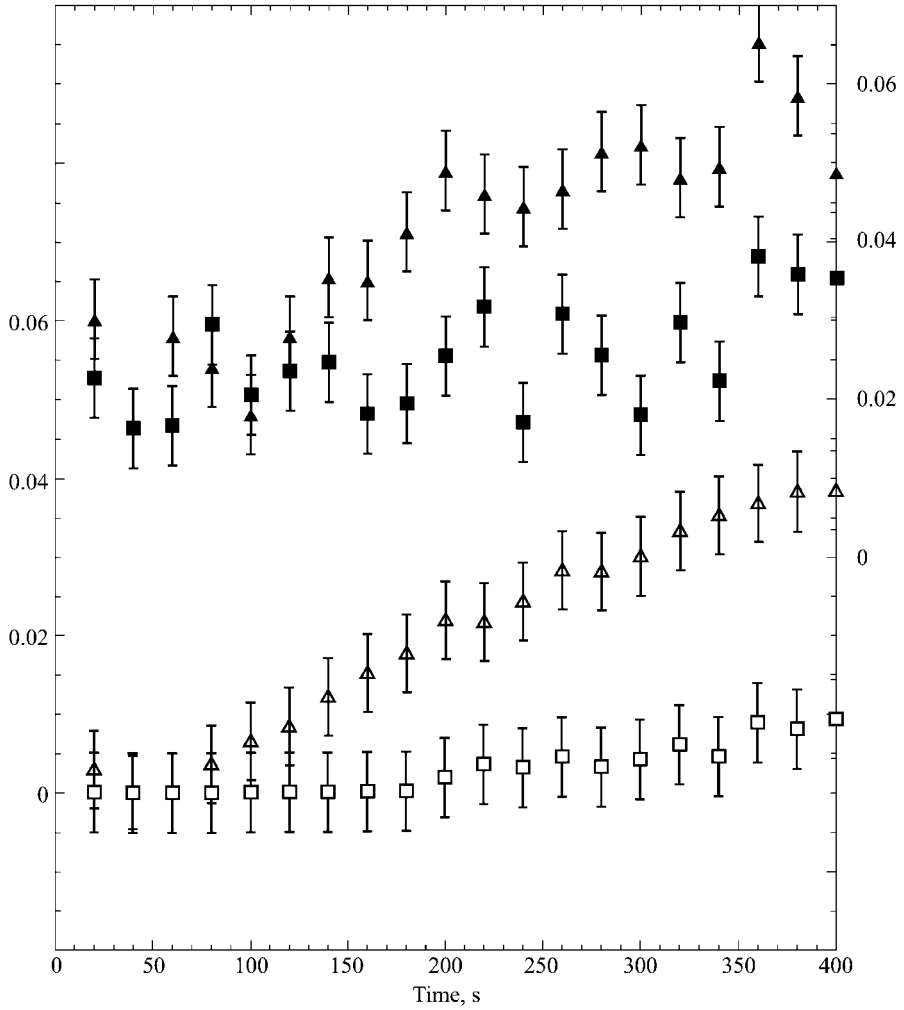

Fig. 35. Noise simulation on data intended to be used for the determination of which signal occurs first. This is a situation which is often encountered in time-resolved studies using technique combinations. The data represents the same event but with different levels of noise added. It is clear that the lower noise data is better suited fot this purpose. However, a higher noise level only invokes a larger experimental error in the determination of the point where the signals start to increase, but not a systematic tendency.

use of a low count rate detector, is added is shown by filled symbols. From these two curves it will be very difficult to assess if there indeed is a time lag.

A problem associated with the underlying physics is in the determination of the intensity of a crystalline peak in the waxs region. It is well known that below a certain threshold the size of a crystallite can influence the width of a diffraction peak (156). The broadening of a peak due to limited crystal size is given by

$$B = \frac{0.9\lambda}{t\cos\theta}$$

where B is the line broadening (in radians), λ the x-ray wavelength used, θ the scattering angle, and t the diameter of the crystalline particle. (t and λ should be in the same units.) In Figure 36, the relation of particle diameter with respect to line broadening at a fixed angle of $\theta = 20^\circ$ is given. For the type of experiments discussed here the use of a position-sensitive detector is indispensable. The best detectors of this type (157) have a spatial resolution that is roughly 0.1°. SR permits the elimination or reduction of most other causes of line broadening in diffraction so that the broadening due to the finite crystal size becomes the dominant factor. From Figure 36 it can now be deduced that for crystallites below a diameter of 80 nm the line broadening becomes measurable. Attempts to measure this effect can be found in the literature (112). The result of this is that the diffracted intensity, which is already small at the initial stages of crystallization, is smeared out over several detector channels at the onset of crystallization. The normal experimental background remains constant so that the signal-to-noise ratio becomes less favorable. Again it will be clear that any effect that the detector system might have on the signal-to-noise ratio should be eliminated as much as possible. It can be noted that crystallite size is not the only parameter affecting the width and

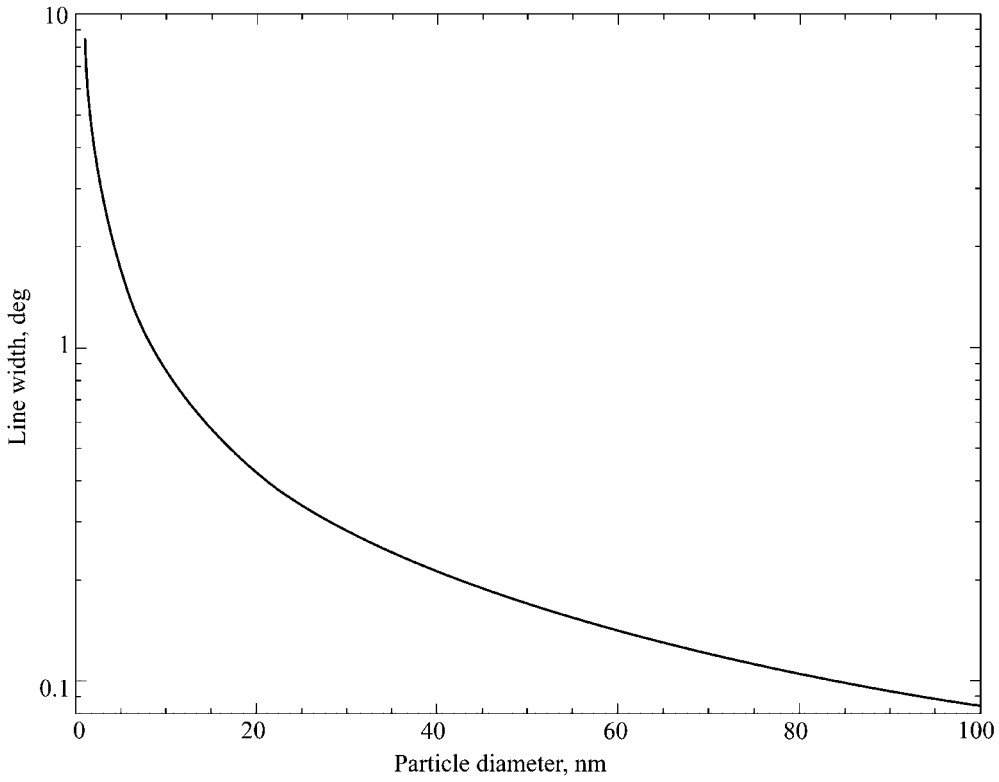

Fig. 36. The broadening of a diffraction line as a function of the particle size. This broadening is only relevant when one utilizes a detector and a sample–detector distance in which this is measurable. For most position-sensitive detectors this is not the case and the broadening is most of the times only measurable with a step-scanning diffractometer.

intensity of crystalline reflections. For a more detailed treatment one is referred to References 55,158, and 159.

The determination of the point where a curve changes slope is intrinsic to the problem sketched above. In the literature it is sometimes argued that a higher noise level could exert a systematic influence on the determination of such a point (32). Intuitively and visually one finds this correct. However, a closer inspection reveals some counterintuitive facts. Consider the case that a linear horizontal curve at a certain point in time starts to increase linearly with time. Now determine the exact moment in time where this occurs.

The horizontal part can be represented by

$$f(t) = c$$

and the other part by

$$g(t) = c + at$$

For the intercept

$$f(t) = g(t) \Rightarrow t = 0$$

If now a background or noise level Δc is added, it reads like

$$\begin{aligned} f(t) &= c \pm \Delta c_{\mathrm{f}}; \quad g(t) = c + at \pm \Delta c_{\mathrm{g}}; \\ f(t) &= g(t); \quad c \pm \Delta c_{\mathrm{f}} = c + at \pm \Delta c_{\mathrm{g}}; \\ \Rightarrow t &= \frac{\sqrt{2}}{a} \end{aligned}$$

Assuming the noise levels in both curves to be the same at the moment when the increase in intensity starts, apply conventional error analysis to this and estimate that the expected error margin is $\sqrt{2}$ times a single error margin. So variations in the position of the intercept are only due to the higher noise levels, which influence the accuracy of the linear fits and thus the position of the intercept. This ultimately leads to a larger error margin but not to a systematic tendency. This is easily verified by numerical simulations.

Summary

The advent of the third generation of SR sources has created many new options. To conclude this article two examples of highly sophisticated experiments, impossible to perform on earlier generations of SR sources, are discussed.

The first example refers back to the on-line melt-spinning experiments mentioned in an earlier section. These experiments are difficult to perform but the problems associated with this have been solved by different research groups. However, long before manufacturers were capable of spinning fibers, nature had developed several organisms which perform this feat. A spider is capable of routinely

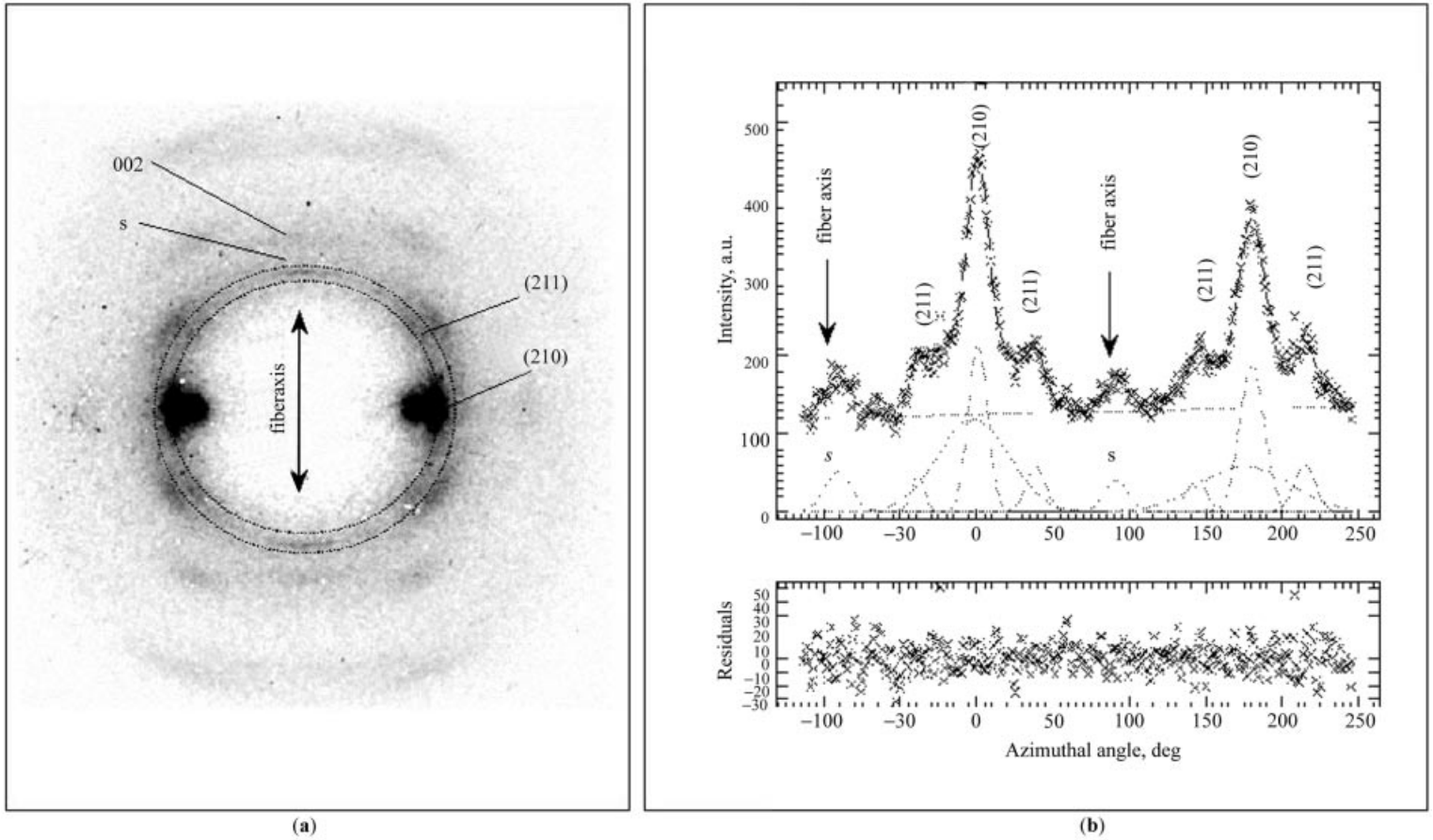

Fig. 37. Fiber diffraction pattern of spider silk obtained in real time by forced silking while the spider was placed close to the x-ray beam (panel A). The fiber is approximately 3.7 μm in diameter. The spot size of the x-ray beam is 7 μm. In panel B the diffraction intensity on the ring indicated in panel A is shown. The intensity can be fitted to Gaussian functions (160). Courtesy of C. Riekel.

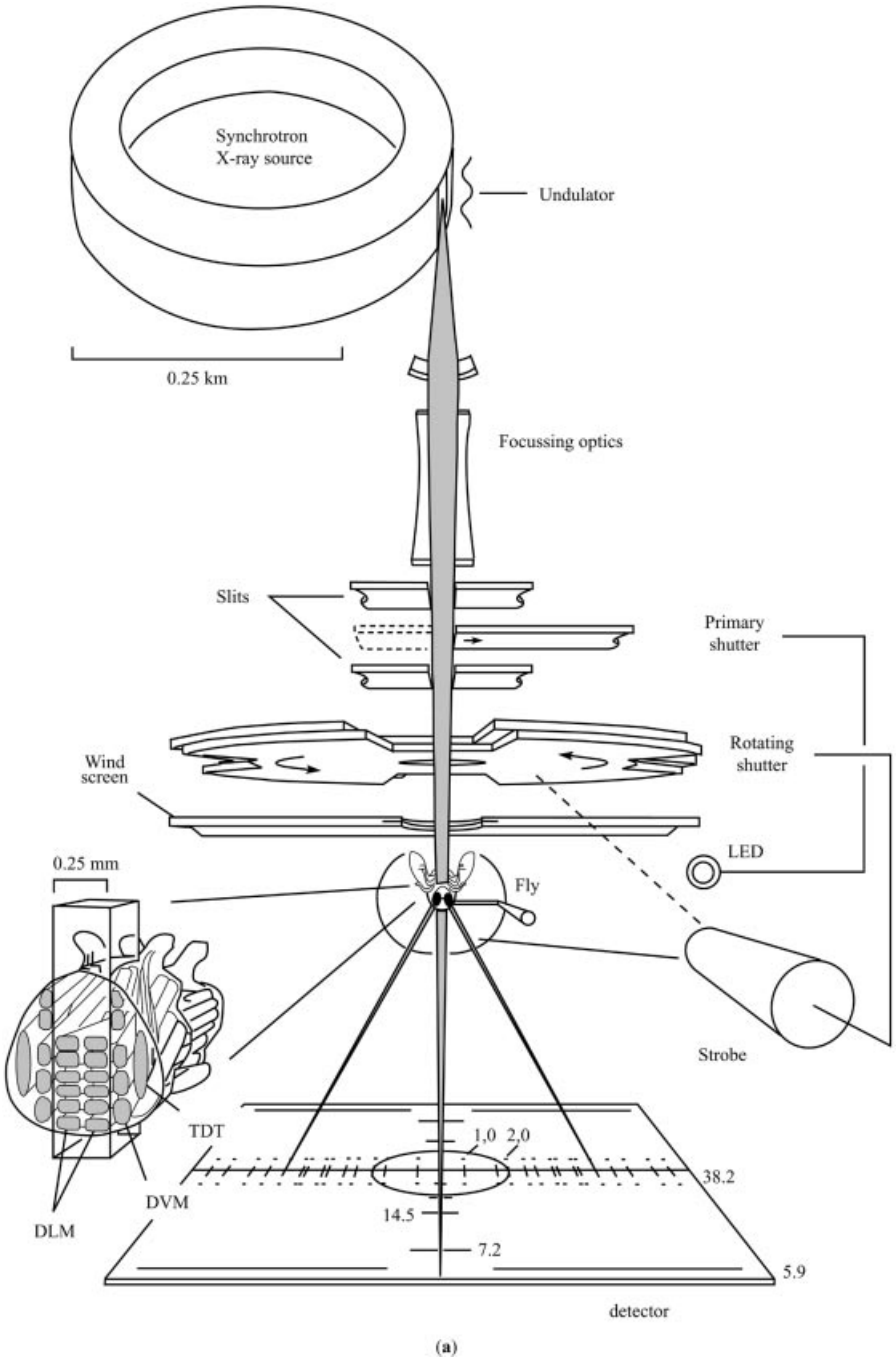

Fig. 38. Panel A shows the experimental layout for an experiment in which the changes in the diffraction pattern of the flight muscle of a fruitfly was studied in real time with a live fruitfly. The beat of the wings was synchronized with a fast shutter using a stroboscope. In panel B the difference pattern between the resting and active fruitfly muscle is shown (162). Courtesy of T. Irving.

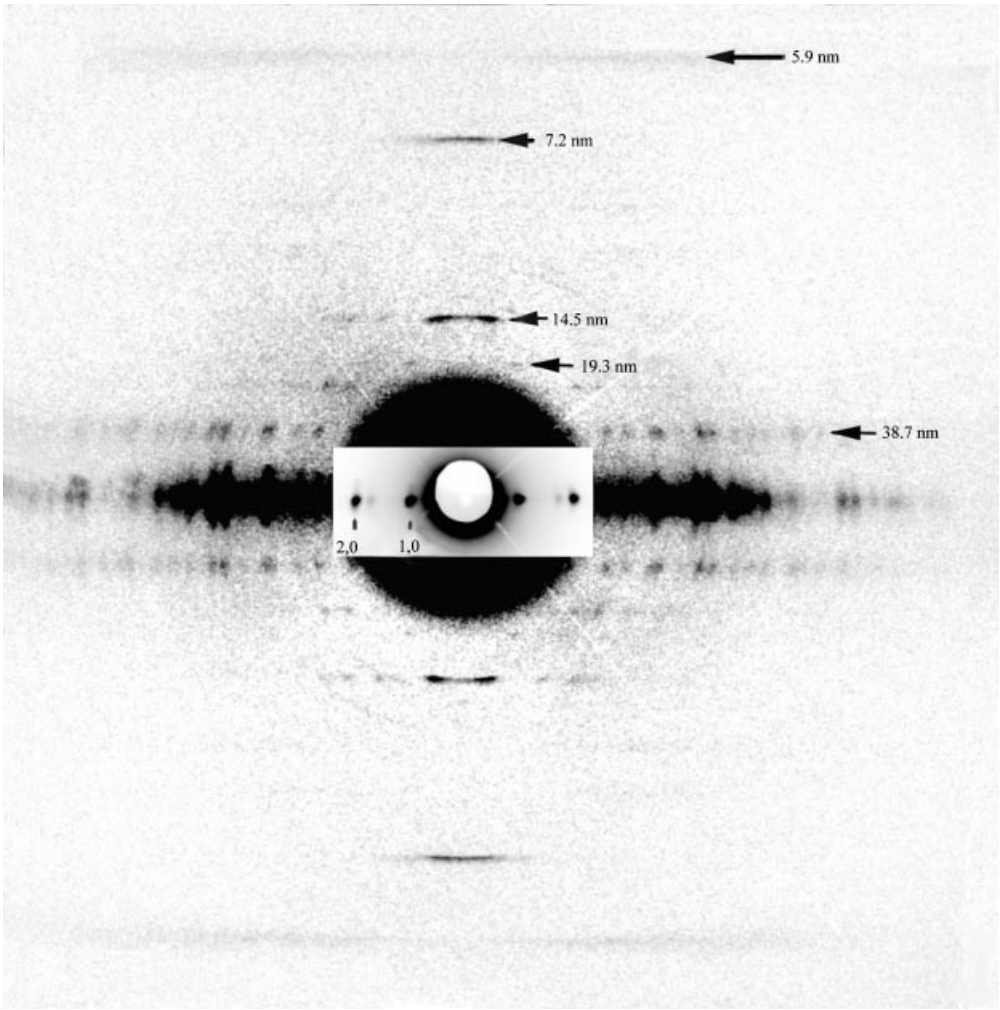

Fig. 38. (Continued).

spinning ultrastrong fibers with a diameter of around 10 μm. In a stunning experiment a spider was persuaded to play the role of extruder on a microfocus beamline (160). As such, it was possible to study the crystallization of natural silk (Fig. 37).

The second example is an echo of the earliest ground breaking time-resolved saxs experiments, performed in Hamburg, on muscles. The experience obtained with diffraction experiments on frog muscle fibers was gratefully absorbed by the polymer community. These experiments were later refined to the level that one could perform experiments on single frog muscle fibers (161). However, this is still a far cry from what has become feasible recently. In an experiment with a microfocus beamline it was possible to observe the changes in the diffraction pattern in the wing muscles of a live fruitfly. By carefully synchronizing the wing beat of the fly with the detector time frames one could observe the changes in the muscle diffraction pattern between the up and down stroke (162) (Fig. 38).

The ingenuity not only in the construction of the beamlines but also in the performing of these two experiments deserves to be applauded. The resilience of nature also can be applauded since both animals survived the experiment without apparent problems.

These two examples serve to remind the reader that it is possible to perform completely new experiments by using third generation SR sources and that one should see the beamlines there not only as a more powerful extension of the home laboratory but also as completely new tools suitable for experiments that so far were unthinkable.

BIBLIOGRAPHY

1. J. Schwinger, *Phys. Rev.* **70**, 798 (1946); D. Ivanenko and J. Pomeranchuk, *Phys. Rev.* **65**, 343 (1944).
2. G. Margaritondo, *Introduction to Synchrotron Radiation*, Springer-Verlag, New York.
3. P. J. Duke, *Synchrotron Radiation: Production and Properties*, Oxford Science Publications, Oxford, 2000.
4. S. S. Hasnain, J. R. Helliwell, and H. Kamitsubo, *J. Synchr. Radiat.* **1**(1), 1–106 (1994); S. S. Hasnain, H. Kamitsubo, and D. M. Mills, *J. Synchr. Radiat.* **8**, 1171 (2001).
5. W. Bras and A. J. Ryan, *Adv. Colloid Polym. Sci.* **75**, 1–43 (1998).
6. M. Lemonnier and co-workers, *Nucl. Instrum. Methods* **152**, 173–177 (1978).
7. A. Freund and co-workers, *SPIE* **3448**, 144–154 (1995).
8. M. H. J. Koch and J. Bordas, *Nucl. Instrum. Methods A* **208**, 461–469 (1983).
9. M. Capel, *Synchr. Radiat. News* **6**(2), 22–27 (1993).
10. Y. Amemiya and co-workers, *Rev. Sci. Instrum.* **60**(7), 1552–1556 (1989).
11. W. Bras and co-workers, *Nucl. Instrum. Methods A* **326**, 587–591 (1993).
12. W. Bras, *J. Macromol. Sci., B: Phys.* **37**(4), 557–565 (1998).
13. O. Kratky, in O. Glatter and O. Kratky, eds., *Small Angle X-ray Scattering*, Academic Press, Inc., New York, 1982.
14. A. Bergmann and co-workers, *J. Appl. Crystallogr.* **33**, 869–875 (2000).
15. A. Knoll and L. Brugemann, *J. Phys. IV* **6**, 385–391 (1996).
16. Spring8 Annual Report 1999. URL: www.spring8.or.jp.
17. U. Bonse and M. Hart in H. Brumberger, ed., *Small Angle x-ray Scattering*, Gordon and Breach, New York, 1967.
18. U. Bonse and M. Hart, *Z. Physik* **189**, 151 (1966).
19. O. Diat and co-workers, *Nucl. Instrum. Methods A* **356**, 566–572 (1995).
20. B. Chu and co-workers, *Rev. Sci. Instrum.* **65**, 3233–3237 (1994).
21. G. Elsner, C. Riekel, and G. Zachmann, *Adv. Polym. Sci.* **67**, 1–57 (1985).
22. G. Rosenbaum, K. C. Holmes, and J. Witz, *Nature* **230**, 434–437 (1971).
23. A. M. Petrascu, M. H. J. Koch, and A. Gabriel, *J. Macromol. Sci., B: Phys* **37**(4), 463–483 (1998).
24. R. A. Lewis and co-workers, *Rev. Sci. Instrum.* **63**, 642–647 (1991).
25. T. Fujisawa, Y. Inoko, and N. Yagi, *J. Synchr. Radiat.* **6**, 1106–1114 (1999).
26. A. Koch, *Nucl. Instrum. Methods A* **348**, 654–658 (1994).
27. G. B. Stephenson and co-workers, *Rev. Sci. Instrum.* **60**, 1537–1539 (1989).
28. Y. Amemiya and co-workers, *Rev. Sci. Instrum.* **60**, 1552–1556 (1989).
29. W. Bras, in W. Brown and K. Mortensen, eds., *Scattering in Polymeric and Colloidal Systems*, Gordon and Breach, New York, 2000, Chapt. “10”.

30. N. J. Terrill and co-workers, *Polymer* **39**, 2381–2385 (1998).
31. A. J. Ryan and co-workers, *Faraday Discuss.* **112**, 13–29 (1999).
32. Z. G. Wang and co-workers, *Polymer* **41**, 8825–8832 (2000).
33. B. S. Hsiao and R. K. Verma, *J. Synchr. Radiat.* **5**, 23–29 (1998).
34. P. Debye and P. Scherrer, *Phys. Z.* **19**, 481 (1918).
35. F. C. Blake, *Rev. Mod. Phys.* **5**, 169 (1933).
36. L. S. Matkin and co-workers, *Appl. Phys. Lett.* **76**, 1863–1865 (2000).
37. R. A. Register and S. L. Cooper, *Macromolecules* **23**, 310–317 1990; *Macromolecules* **23**, 318–323 (1990).
38. C. E. Williams, in P. Linder and Th. Zemb, eds., *Neutron, x-ray and Light Scattering*, North Holland, Amsterdam, 1991.
39. L. A. Feigin and D. I. Svergun, *Structure Analysis by Small Angle x-ray and Neutron Scattering*, Plenum, New York, 1987.
40. G. Vlaic and co-workers, *J. Phys. II (France)* **5**, 665–675 (1995).
41. R. A. Register and co-workers, *Macromolecules* **22**, 2224 (1984).
42. C. Nave, *Radiat. Phys. Chem.* **45**, 483–490 (1995).
43. A. Cheng and M. Caffrey, *Biophys. J.* **70**, 2212–2222 (1996).
44. A. Cheng, J. L. Hogan, and M. Caffery, *J. Mol. Biol.* **229**, 291–294 (1993).
45. R. B. G. Ravelli and S. McSweeney, *Struct. Fold. Des.* **8**, 315–328 (2000).
46. W. Bras and co-workers, *Biophys. J.* **74**, 1509–1521 (1998).
47. T. A. Waigh and co-workers, *Macromolecules* **30**, 3813–3820 (1997).
48. E. Geissler and co-workers, *Phys. Rev. E* **62**, 8308–8313 (2000).
49. C. E. Williams, Private communication, 2001.
50. P. Ehrhart, *J. Nucl. Mater.* **216**, 170–198 (1994).
51. W. Bras, F. Diaz, and G. R. Diakun, Unpublished results, 2001.
52. H. Kosonen and co-workers, *Macromolecules* **33**, 8671–8675 (2000).
53. I. W. Hamley, *The Physics of Block Copolymers*, Oxford Science Publications, Oxford, 1998, Chapt. "3".
54. A. Cumming and co-workers, *Phys. Rev. A* **45**, 885–897 (1992).
55. F. J. Balta-Calleja and C. G. Vonk, *X-ray Scattering of Synthetic Polymers*, Elsevier, Amsterdam, 1989, Chapt. "7.4".
56. D. I. Svergun, A. V. Semenyuk, and L. A. Feigin, *Acta Crystallogr. A* **44**, 244–250 (1988).
57. O. Glatter, *J. Appl. Crystallogr.* **13**, 7–11 (1980).
58. J. Brunner-Popela and O. Glatter *J. Appl. Crystallogr.* **30**, 431–442 (1997).
59. O. D. Velev, E. Kaler, and A. M. Lenhoff, *Biophys. J.* **75**, 2682–2697 (1998).
60. N. Mischenko and co-workers, *Macromolecules* **28**, 2054–2062 (1995).
61. O. Glatter, in Ref. 13.
62. D. I. Svergun and co-workers, *J. Chem. Phys.* **113**, 1651–1665 (2000).
63. M. H. J. Koch and co-workers, *Science* **240**, 194–196 (1988).
64. A. K. Khandpur and co-workers, *Macromolecules* **28**, 8796–8806 (1995).
65. V. R. Mhetas and L. A. Archer, *J. Polym. Sci., Part B: Polym. Phys.* **38**, 222–233 (2000).
66. D. K. Cinader and W. R. Burghardt, *Polymer* **40**, 4169–4180 (1999).
67. S. V. Lyukin, I. M. Neelov and Y. Y. Gotlieb, *Macromolecules* **33**, 9126–9135 (2000).
68. T. Kawai and T. Kimura, *Macromolecules* **33**, 8421–8425 (2000).
69. E. Mandelkow, J. Thomas, and C. Cohen, *Proc. Natl. Acad. Sci. U.S.A.* **74**, 3370–3374 (1977).
70. B. K. Vainshtein, *Diffraction of X-rays by Chain Molecules*, Elsevier, Amsterdam, 1966.
71. T. Forsyth, Private communication, 2001.

72. R. J. Greenall, C. Nave, and W. Fuller, *J. Mol. Biol.* **305**, 669–672 (2001).
73. N. Stribeck, in P. Cebe, B. S. Hsiao, and D. J. Lohse, eds., *Scattering from Polymers* (ACS Symposium Series, Vol. 739), ACS, New York, 1998.
74. N. Stribeck, S. Fakirov, and D. Sapoundjieva, *Macromolecules* **32**, 3368–3378 (1999).
75. Z. Wang and co-workers, *Macromolecules* **33**, 978–989 (2000).
76. R. S. Stein and J. Cronauer, *J. Mol. Struct.* **383**, 19–22 (1996).
77. C. Wutz and co-workers, *Rev. Sci. Instrum.* **66**, 1303–1307 (1995).
78. R. Gehrke, C. Riekel, and H. G. Zachmann, *Polymer* **30**, 1582 (1989).
79. A. J. Ryan and co-workers, *Polymer* **35**, 759–768 (1994).
80. B. Heck and co-workers, *Polymer* **41**, 8839–8848 (2000).
81. M. Muthukumar and P. Welch, *Polymer* **41**, 8833–8837 (2000).
82. P. D. Olmsted and co-workers, *Phys. Rev. Lett.* **81**, 373–376 (1998).
83. Y. A. Akpalu and E. J. Amis, *J. Chem. Phys.* **113**, 392–403 (2000); *J. Chem. Phys.* **111**, 8686–8695 (1999).
84. P. S. Dai and co-workers, *J. Appl. Crystallogr.* **33**, 714–717 (2000).
85. G. Hauser, J. Schmidtke, G. Strobl, and T. Thurn-Albrecht, in Ref. 73.
86. A. Keller, *Macromol. Symp.* **98**, 1–42 (1995).
87. J. D. Hoffman and R. L. Miller, *Polymer* **38**, 3151 (1997).
88. K. Binder, in R. W. Cahn, P. Haasen, and E. J. Kramer, eds., *Materials Science and Technology, Vol. 5: Phase Transformations in Materials*, VCH Publishers, New York.
89. J. S. Higgins, H. A. Fruitwala, and P. E. Tomlins, *Br. Polym. J.* **21**, 247–257 (1989).
90. T. Kyu and J. M. Saldanha, *Macromolecules* **21**, 10211–1026 (1988).
91. T. Hashimoto, M. Takenaka, and T. Izumitani, *J. Chem. Phys.* **97**, 679–689 (1992).
92. G. Strobl, *The Physics of Polymers*, Springer-Verlag, New York, 1996, Chapt. "4".
93. T. Hashimoto, M. Itakura, and N. Shimidzu, *J. Chem. Phys.* **85**, 6773–6786 (1986).
94. M. Cakmak and co-workers, *J. Polym. Sci., Part B* **31**, 371–381 (1993).
95. H. G. Zachmann and C. Wutz, in M. Dosière, ed., *Crystallization of Polymers*, Kluwer Academic Publishers, Boston, 1993, pp. 403–414.
96. C. Wutz and co-workers, *Rev. Sci. Instrum.* **66**, 1303–1307 (1995).
97. A. Mahendrasingam and co-workers, *J. Synchr. Radiat.* **2**, 308–311 (1995).
98. R. Kolb and co-workers, *Polymer* **42**, 5257–5266 (2001).
99. H. Tsuruta and co-workers, *Rev. Sci. Instrum.* **60**, 2356–2358 (1989).
100. M. Caffrey, *Biophys. J.* **55**, 47–52 (1989).
101. B. S. Hsiao and co-workers, *Polymer* **34**, 3986–3995 (1993).
102. Y. Takanishi and co-workers, *J. Mater. Chem.* **9**, 2771–2774 (1999).
103. G. R. Luckhurst, *Mol. Cryst. Liq. Cryst.* **347**, 121–135 (2000).
104. I. Dierking and co-workers, *Phys. Rev. E* **61**, 1593–1598 (2000).
105. C. J. Dunn and co-workers, *Mol. Cryst. Liq. Cryst.* **347**, 411–422 (2000).
106. H. F. Gleeson, C. Carboni, and A. S. Morse, *Rev. Sci. Instrum.* **66**, 3563–3568 (1995).
107. E. Towns-Andrews and co-workers, *Rev. Sci. Instrum.* **60**, 2346–2349 (1989).
108. S. Förster and co-workers, *Macromolecules* **27**, 6922–6935 (1994).
109. W. Bras and co-workers, *J. Phys. IV* **3**, 447–450 (1993).
110. T. P. Russell and J. T. Koberstein, *J. Polym. Sci., Polym. Phys. Ed.* **23**, 1109–1115 (1985).
111. W. Bras and co-workers, *J. Appl. Crystallogr.* **28**, 26–32 (1995).
112. B. Goderis and co-workers, *Macromolecules* **34**, 1779–1787 (2001).
113. W. Bras and co-workers, *Science* **267**, 996–999 (1995).

114. A. J. Ryan and co-workers, *Macromolecules* **24**, 2883 (1991).
115. M. Elwell, A. J. Ryan, and W. Bras, Unpublished results, 1998.
116. G. K. Bryant and co-workers, *Rev. Sci. Instrum.* **69**, 2114–2117 (1998).
117. S. Rastogi, J. G. P. Goossens, and P. J. Lemstra, *Macromolecules* **31**, 2983–2998 (1998).
118. J. G. P. Goossens, *Processing of Tractable Polymers using Reactive Solvents*, Ph. D. dissertation, Eindhoven University, 1998.
119. G. J. Salomons and co-workers, *Rev. Sci. Instrum.* **67**, 1748–1752 (1996).
120. D. J. Hughes and co-workers, *J. Synchr. Radiat.* **3**, 1196, 84–90
121. C. He and co-workers, *Polymer* **39**, 659–667 (1998).
122. W. Bras and co-workers, *J. Synchr. Radiat.* **2**, 87–92 (1995).
123. M. F. Butler and co-workers, *Macromolecules* **28**, 6383–6393 (1995).
124. I. L. Hay and A. Keller, *J. Polym. Sci. Part C* **30**, 289–293 (1970).
125. T. Pomper and co-workers, *J. Macromol. Sci., Part B: Phys.* **38**, 869–883 (1999).
126. C. Martin, Ph. D. dissertation, Keele University, 2001.
127. J. Sweeney and I. M. Ward, *Polymer* **36**, 299–308 (1995).
128. J. M. Matthews and co-workers, *Polymer* **38**, 4795–4802 (1997).
129. R. Androsch and co-workers, *Macromolecules* **32**, 3735 (1999).
130. M. Hikosaka and co-workers, *J. Macromol. Sci., B: Phys.* **31**(1), 87–131 (1992).
131. S. Rastogi, G. W. H. Hohne, and A. Keller, *Macromolecules* **32**, 8897 (1999).
132. C. Tribout, B. Monasse, and J. M. Haudin, *Colloid Polym. Sci.* **274**, 197 (1996).
133. K. Mortensen and co-workers, *Physica B* **213/214**, 682–684 (1995).
134. R. R. Lagasse and B. Maxwell, *Polym. Eng. Sci.* **16**, 189 (1976).
135. S. Fujii, T. Isojima, and K. Hamano, *Phys. Lett. A* **263**, 393–400 (1999).
136. Y. Y. Won and co-workers, *J. Phys. Chem. B* **104**, 7134–7143 (2000).
137. http://www/linkam.co.uk.
138. R. H. Somani and co-workers, *Macromolecules* **33**, 9385–9394 (2000).
139. P. Keates and co-workers, *J. Non-Newtonian Fluid Mech.* **52**, 197–215 (1994).
140. P. Lindner, in Ref. 38.
141. J. A. Pople, I. W. Hamley, and G. P. Diakun, *Rev. Sci. Instrum.* **69**, 3015–3021 (1998).
142. F. E. Caputo and W. R. Burghardt, *Macromolecules* **34**, 6684–6694 (2001).
143. J. A. Pople and co-workers, *Macromolecules* **30**, 5721–5728 (1997).
144. S. Okamoto, K. Saijo, and T. Hasimoto, *Macromolecules* **27**, 3753–3758 (1994).
145. G. P. R. Fairclough, A. J. Ryan, L. Messe, and W. Bras, Unpublished results.
146. S. J. Nolan and co-workers, *Rev. Sci. Instrum.* **66**, 2652–2657 (1995).
147. J. M. Samon and co-workers, *Polymer* **42**, 1547–1559 (2001).
148. F. P. Chappel and co-workers, *J. Appl. Chem.* **14**, 12–18 (1964).
149. M. Cakmak and co-workers, *J. Polym. Sci., Part B: Polym. Phys.* **31**, 371–381 (1993).
150. Y. B. Melnichenko and co-workers, *J. Appl. Crystallogr.* **33**, 682–685 (2000).
151. B. E. Warren, *X-ray Diffraction*, Dover Publications, New York, 1990, Chapts. "4.2" and "4.3".
152. M. Monkenbosch, *J. Appl. Crystallogr.* **29**, 591–592 (1996).
153. N. F. Berk and K. A. Hardman-Rye, *J. Appl. Crystallogr.* **21**, 645–651 (1988).
154. A. J. Allen and N. F. Berk, *J. Appl. Crystallogr.* **27**, 878–891 (1994).
155. A. N. Wilkinson and co-workers, *Polymer* **37**, 2021–2024 (1996).
156. B. D. Cullity, *Elements of X-ray Diffraction*, 2nd ed., Addison-Wesley Publishing Co., Inc., Reading, Mass., 1978.
157. V. Zhukov and co-workers, *Nucl. Instrum. Methods A* **392**, 83–88 (1997).
158. L. E. Alexander, *X-ray Diffraction Methods in Polymer Science*, Wiley-Interscience, New York, 1969.

159. R-J. Roe, *Methods of X-ray and Neutron Scattering in Polymer Science*, Oxford University Press, London, 2000.
160. C. Riekel, M. Muller, and F. Vollrath, *Macromolecules* **32**, 4464 (1999).
161. M. Linari and co-workers, *Proc. Natl. Acad. Sci. U.S.A.* **97**, 7226–7231 (2000).
162. T. C. Irving and D. W. Maughan, *Biophys. J.* **78**, 2511–2515 (2000).

WIM BRAS
Netherlands Organisation for Scientific Research (NWO)
Dubble & European Synchrotron Radiation Facility

SYNDIOTACTIC POLYSTYRENE.

See Volume 4.

TEST METHODS

Introduction

Plastics testing encompasses the entire range of polymeric material characterizations, from structure to material response to environmental effects. Whether the analysis or property testing is for quality control of an industrial plastic or for the determination of the relaxation response of a material to an imposed stress, a variety of test techniques is available for the researcher (see CHARACTERIZATION OF POLYMERS).

Polymer analysis continues to progress with improvements in instrumental techniques and computer-enhanced data analysis methods that allow detection of effects of side-chain rotations or localized variation in free volume of a polymer film. Combinations of instrumental analysis techniques such as pyrolysis–gas chromatography (pyrolysis–GC) or liquid chromatography–mass spectroscopy (LC–MS), used for separation and identification of polymer components and degradation products from complex systems have been further enhanced with the addition of thermal techniques that allow targeting narrow temperature ranges or microscopy techniques targeting localized areas of a sample for analysis. (See MASS SPECTROMETRY; CHROMATOGRAPHY, HPLC; CHROMATOGRAPHY, SIZE EXCLUSION.) Atomic Force Microscopy (AFM) allows determination of polymer morphology (qv) at the nano level (see ATOMIC FORCE MICROSCOPY). The use of microprocessors to capture transient signals from physical test methods, ie high speed impact, allows the observation of the complete impact event, while improvements in fracture mechanics techniques lead to increased understanding of material response to stress independent of geometry effects.

Encyclopedia of Polymer Science and Technology. Copyright John Wiley & Sons, Inc. All rights reserved.

Composition and Structure

Fourier transform infrared (FTIR) is one of the most commonly used analysis methods for determining the composition of polymers (see VIBRATIONAL SPECTROSCOPY). Other routine applications are in fingerprinting contaminants, characterizing chemical property gradients, or mapping physical property anisotropy (1). The FTIR technique, which corresponds to the vibrational energies of atoms or specific groups of atoms within a molecule as well as rotational energies, identifies components by comparing the spectrum of a sample to reference spectra. The infrared spectral region is commonly from 2 to 50 μm, and the region of 7–15 μm is capable of differentiating similar isomers (2). The 7–8.5-μm region has been used in model hydrocarbon studies to show that the absorption of methylene groups is dependent on the size of the methylene sequences in compounds (3). FTIR has been used to study structural modifications of polypropylene during aging (4), determine crystalline forms of syndiotatic polystyrene through spectral subtraction methods (5), simultaneously monitor polymerization and microphase separation in a polyurethane system through identification of reaction products formed (6), and to quantitate grafting levels of succinic anhydride onto polypropylene (7).

Some examples of composition determinations using IR analysis of polymers are as follows. The N stretching mode has been used for quantitative analysis of acrylonitrile in butadiene–acrylonitrile copolymers (8). [Residual catalyst support in commercial polyethylene can be detected at levels as low as 100 ppm (9).] The short-chain branching distribution of an ethylene 1-olefin copolymer across the molecular weight distribution was determined using a combination of size exclusion chromatography (SEC) with FTIR (10). There are several excellent sources of spectra both in print and on computer disk for comparing and matching the fingerprints obtained from a sample (11,12).

Tracking of trans conformers in sub-T_g annealed amorphous poly(ethylene terephthalate) (PET) films by FTIR indicated that closer interchain packing and formation of new cohesional entanglements along the chains occur that are not apparent in quenched or slowly cooled material (13). Step-scan FTIR photoacoustic analysis was used in determining surface stratification of components within a thermoplastic olefin. The IR bands were used as analytical depth-profiling probes to establish the orgin of photoacoustic (PA) signals (14). FTIR monitoring of the stress relaxation of polyurethanes led to the determination that differences in phase separation was related to the structure of the polymer (15). The combination of FTIR with *in situ* WAXS (wide-angle X-ray spectroscopy (qv)) measurements during the drawing and annealing of PET film allowed the study of the development of molecular orientation and crystallization (16). Specular reflectance FTIR–microscopy has been used in studies of several polymers: liquid crystalline polymers, sidechain (LCP) (17,18), polyurethanes (19), carbon-filled polymers (20,21), and poly(aryl ether ether ketone) (PEEK) (1). Progress has been made in the development of on-line IR equipment for monitoring the extrusion of polymers using the near-IR range rather than mid-IR with resultant lower sensitivity to molecular fragments (22). Some work has been done on calibration of these systems against dynamic rheological standards (23). Real-time quantitative

monitoring of the level of filler in extruded polymers has been reported using near-IR spectroscopy (24).

Combination techniques such as microscopy–FTIR and pyrolysis–IR have helped solve some particularly difficult separations and complex identifications. Microscopy–FTIR has been used to determine the composition of copolymer fibers (25); polyacrylonitrile, methyl acrylate, and a dye-receptive organic sulfonate trimer have been identified in acrylic fiber. Both normal and grazing angle modes can be used to identify components (2–7). Pyrolysis–IR has been used to study polymer decomposition (27).

Raman spectroscopy is an emission phenomenon as opposed to IR absorption, and results from vibrations caused by changes in polarizability (see VIBRATIONAL SPECTROSCOPY). Raman spectroscopy had limited use until the advent of lasers as the exciting source. It can be complementary to IR and may be more useful when the sample for analysis is a filled polymer or composite containing silica, clay, other similar inorganic filler, or a piece of polymer, but particularly thermosets or rubbery products requiring no further sample preparation. Additional advantages over IR are the intensity advantage for the C=C band and the determination of thiol groups in sulfur polymers (28). Fluorescence is a significant interference in Raman spectroscopy because it occurs simultaneously in several commercial plastic products. Fourier transform of Raman spectroscopy and other techniques for reducing fluoresence (29,30) have expanded its applicability. FT-Raman spectroscopy has been used as an alternative technique to thermal gravimetric analysis (TGA) of filler content up to 75 wt% of the polymer (1). It has also been used to determine the isotacticity of polypropylene giving good correlation to FTIR and ^{13}C NMR data (31).

Studies of blends using Raman imaging and Raman microscopy have been used to determine miscibility and phase behavior of blends (32) and morphology in blends of linear and branched polyethylene (33). On-line Raman was used to monitor copolymerization of styrene and *n*-butyl acrylate by monitoring monomer concentrations (34). Raman longitude acoustical mode (LAM) was used to study stress-induced states of a blend of polyethylenes in a microfilm. Structure appeared to be the formation of straight tie molecules localized in neighboring crystals with amorphous layers between the crystals. Presence of all-trans sequences with length exceeding the mean crystallite size appeared to be due to stress-induced gauche to trans formations in the amorphous phase (35).

Nuclear magnetic resonance (NMR) requires an atomic nucleus that can absorb a radio-frequency signal impinging it in a strong magnetic field to give a spectrum. The field strength at which the nucleus absorbs is a function of both the nucleus and its immediate electronic environment. The atoms normally used for NMR analysis are as follows (36): ^{1}H, ^{19}F, ^{31}P, ^{11}B, ^{14}N, ^{29}Si, ^{13}C, ^{2}H, ^{17}O, ^{33}S, and ^{15}N. Of these, the most commonly used in polymer analyses are ^{1}H and ^{13}C. Solid-state ^{13}C NMR utilizing proton spin-lattice relaxation time in the rotating frame has been used for determination of composition, phase, and compatibility (misciblity) of blends (37–40). In combination with SEC, ^{13}C NMR is capable of quantitating both long- and short-chain branching in polymers (41). The technique has also been used for characterizing molecular structure differences in reject ethylene vinyl alcohol polymer that correlated to changes in thermal and mechanical properties (42). A combination of ^{13}C NMR and deuterium NMR were

used to determine the effects of low molecular weight additives on secondary relaxation processes in PET. The additives were found to reduce the number of phenyl ring flips that were shown by the deuterium NMR to closely relate to the relaxation peak observed by dynamic mechanical thermal analysis (43). Fourier transform has also been applied to NMR, allowing increased sensitivity on microsamples. Spectra can be obtained on as little as 10 μg (44). NMR techniques were used to study the reactions and catalytic activity of different agents for transesterification reactions between polymers (45). Two-dimensional time-domain proton NMR identified and characterized relaxation components over a temperature range. Phase transitions and different phases were observed (46). Similar analysis of high density polyethylene (HDPE) showed three phases, which have been tentatively identified as a crystalline region, an area of chain loops on the surface of crystallites and entangled chain segments, and the third phase of chains in the amorphous phase (47). Molecular chain dynamics, chain orientation, and molecular packing differences were determined in HDPE and isotactic polypropylene (48). Microphase separation in polyureas that were prepared by RIM (reaction injection molding) techniques were determined with solid-state NMR (49).

An additional technique that has been found useful in analysis of the composition of polymers and blends is liquid chromatography. Pasch and Rode used the critical point of adsorption of the least polar component of a blend to determine the liquid chromatographic conditions for separating blends of polymethacrylates into components (50). High pressure liquid chromatography (HPLC) in combination with mass spectroscopy was used to analyze the components of an epoxy resin (51). HPLC has also been used with a precipitation–redissolution technique to separate polymer molecular weights for several polymers as a shorter technique compared to SEC (52). Reverse-phase liquid chromatography with UV detection was useful in qualitative determination of brominated flame retardants in polymeric waste materials (53).

Pyrolysis techniques for thermally degrading polymers have high sensitivity, allow trace analysis of all organics in liquid or solid state, require minimal sample preparation and small amounts of sample, and allow simultaneous identification and quantification in one run. However, they may have limited reproducibility and limited applicability where inorganic fillers are present (54). There have been various types of pre- and post-pyrolysis derivations done to simplify analysis by GC separation and reduce interferences from surrounding materials (55).

Many studies have been published on the use of pyrolysis–GC: Determination of the primary degradation products of polyacrylonitrile (56), number-average molecular mass using end-group analysis (57), kinetic measurements of the thermal degradation of polymers using sequential pyrolysis (58), determination of stereospecific sequencing in polypropylene (59), composition and microstructure of styrene maleic anhydride (SMA) copolymers (60) are examples in addition to frequent use in determination of additives. Combinations of pyrolysis–GC with FTIR techniques have been used in the characterization of branching in comb-like polymers (61) and analysis of butadiene–acrylonitrile copolymers (62). Additional examples of use of pyrolysis–GC for polymer systems can be found in Wampler's (63) and Bart's (54) reviews.

Additives to polymers are important components affecting the polymer's performance in processing, aging, and maintaining properties under adverse

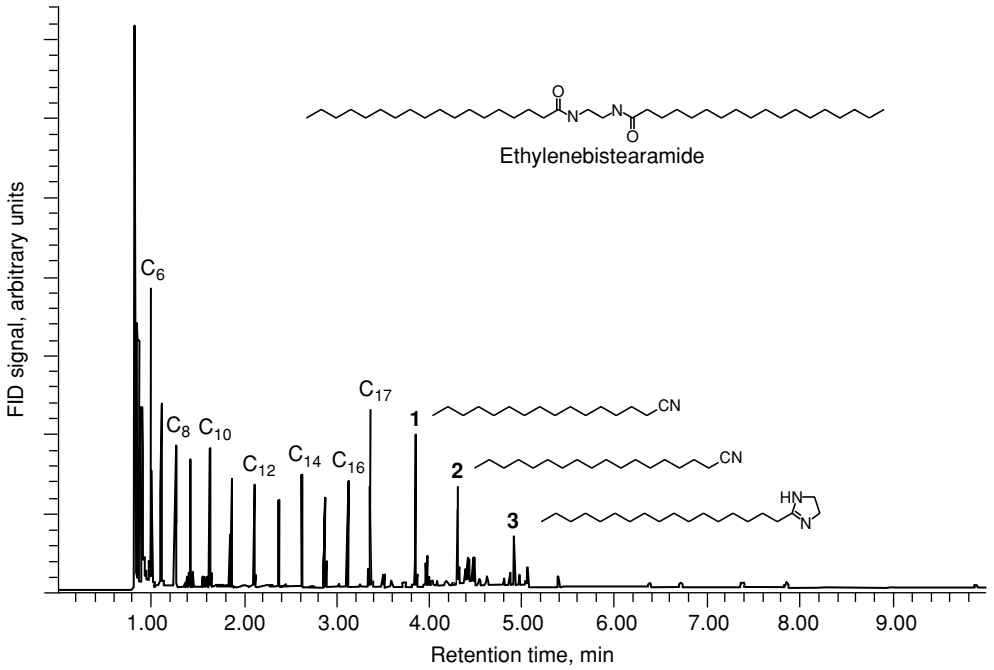

Fig. 1. The pyrogram of *N*,*N*′-ethylenebistearamide. The identification of peaks labeled in the pyrogram is 1 – hexadecanenitrile, 2 – octadecanenitrile, 3 – 1*H*-2-heptadecyl-4,5-dihydroimidazole. Reprinted from Ref. 67, Copyright (2000), with permission from Elsevier Science.

environmental conditions. In some cases it is possible to determine these in solid or molten polymer, but generally they must be separated from the polymer prior to analysis. Typical methods that have been used for obtaining a sample for additives analysis include solvent extracting, dissolving the polymer matrix, hydrolyzing the material, or thermally destroying the matrix. Samples are then analyzed using gas or liquid chromatography techniques alone or in combination with mass spectroscopy to identify specific components. pyrolysis–GC has been shown to be particularly useful for analysis of flame retardants (64,65), plasticizers (66), lubricants (67), antioxidants (68), and other stabilizers (69,70) in many polymer matrices. Figure 1 gives a pyrogram of a common lubricant, ethylenebistearamide.

Various techniques for extracting and analyzing low molecular weight components of polymers include static and dynamic heat extractions, headspace analysis, and thermochromatography (71). These are used primarily where solventless systems are required for analysis (72,73). Gas-phase mirage-effect spectroscopy has been used for measuring trace gases and organic volatiles up to parts per billion (ppb) levels during nondestructive characterization and photodecomposition studies (74). Packed column supercritical fluid chromatography (pSFC) with atmospheric pressure chemical ionization detection has been shown to detect and quantitate a variety of additives, including antioxidants, light stabilizers, and slip agents (75).

New technologies in the area of microscopy, such as atomic force microscopy (AFM) and electron spin resonance (ESR), have allowed the study of morphology of polymers and blends of polymers to extend to localized areas at interfaces of phases in semicrystalline polymers. Other techniques such as wide-angle and small-angle X-ray scattering (WAXS, SAXS), small-angle neutron scattering (SANS), small-angle light scattering (SALS), scanning and transmission electron microscopy (SEM, TEM) have been used for structure studies as well. WAXS has been used for examining the crystalline regions of semicrystalline polymers and composites (76–78). SAXS was used with linear correlation functions to determine the overall crystallinity and fraction of semicrystalline stacks during crystallization and melting of linear polyethylene (79) while crystallite size distributions were calculated from WAXS profiles in a similar polymer (80). By monitoring the surface structure of a PEEK composite, skin effects were observed using reflectance WAXS (81). SAXS allows the determination of morphology via domains and microstructure by varying electron density in different areas of a material or density differences between amorphous and crystalline phases (82,83). This has been shown to be useful in determining the phase behavior of blends of poly(vinyl methyl ether) with styrene–butadiene–styrene copolymers (84). Correlation of thermal and structural properties of a blend of polyamide with liquid crystal polymer over a range of compositions and thermal treatments (85) and determination of an ordered crystalline/amorphous lamellar structure in a blend of poly(ethylene oxide) and poly(vinyl acetate) (86) have used SAXS. This technique has also been used qualitatively in determining domains and component mixing with interpenetrating polymer networks (87). Other X-ray techniques were used to show the solid-state structures of aromatic copolyesters (88) and measure crystalline form transition under stress with poly(butylene terephthalate) (89).

Structure determinations in polymers have involved the use of SANS techniques to evaluate not only the radius of polymer molecule gyration where light or X-ray scattering is not usable, but also phase dimensions in multicomponent polymers and suggested mechanisms of phase separation (90). Applications in polymer melts as well as concentrated and dilute solutions of polymers and solid-state samples have investigated the nature of semicrystalline polymers, polymer blends, and the development of new theories of polymer solutions and networks (91). Another technique finding use in structure analysis is dielectric spectroscopy. A combination of X-ray scattering and dielectric spectroscopy has been used to study the noncrystalline regions of semicrystalline polymers; this technique uses semicrystalline and amorphous polymer blends in which the amorphous polymer, although miscible in amorphous regions, is excluded from the crystal–amorphous interphase region (92). SALS techniques have been able to distinguish between nucleation and growth and spinodal decomposition in phase separation mechanisms (93). SEM has been used to determine the location of compatibilizers at the interface of blends of thermoplastic urethanes and polypropylene (94).

AFM is used at the nanoscale to analyze structure of polymers. It has been used to determine spatial distribution of impact modifier in high impact polypropylene (95), follow pit growth in a film of a blend as a function of exposure time during degradation studies of coatings on metal (96), determine surface topography and molecular organization of liquid crystalline polymers (97), and observe

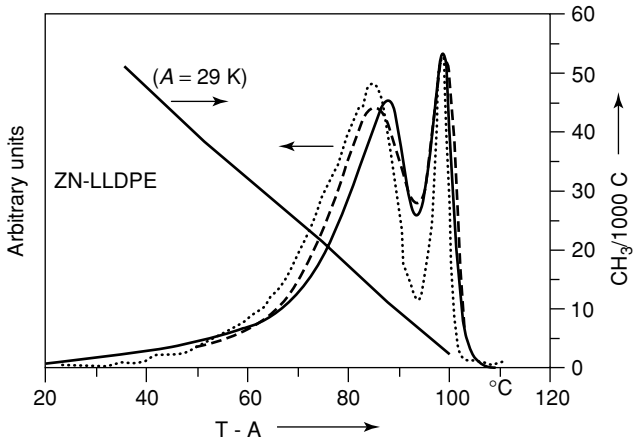

Fig. 2. Comparison of the short-chain branching distribution of ZN-LLDPE as obtained by TREE, CRYSTAF, and DSC. A calibration curve for the DSC data is plotted on the right axis. Reprinted from Ref. 101, Copyright (2000), with permission from Elsevier Science.

nanoparticles in polypropylene matrix (98). In combination with other techniques it allows the determination of composition versus depth of nano silica particles in a surface film, including the location of sub-surface nano silica particles (99). AFM in conjunction with SEM was used to study the influence of aging on morphology of polypyrrole films (100). The use of a vibrating, heating stage for mounting samples and observing the effects on the AFM cantilever allows the study of local elastic and viscoelastic properties (101). Figure 2 shows both topography and simultaneously acquired amplitude images with this technique. Scanning force microscopy of isotatic polypropylene under a moderate applied shear stress was used to study plasticity and damage mechanisms (102).

ESR techniques use nitroxyl radicals either dispersed in polymer matrix (spin probe) or covalently bonded to polymer chain (spin label) which are sensitive to the environment allowing molecular motion and microstructure of polymers to be identified from spectra (103). Quantitative methods of heterogeneous ESR spectra are divided into (*1*) outer hyperfine etrema, (*2*) signal intensities related to the relative concentration of the probe in different phases, and (*3*) simulation of the spectra. The presence of two well-separated outer maxima above the glass-transition temperature could be ascribed to two phases in natural rubber (104), miscible blends (105), immiscible blends (106), cross-linked polymers (107), and polyurethanes (108). ESR has used the measurement of the oxidation product to monitor the consumption of stabilizer in polypropylene (109).

Molecular Weight

The molecular weight and the distribution of multiple molecular weights normally found within a commercial polymer influence both the processibility of the material and its mechanical properties. For a few well-defined homopolymers,

an analysis of composition and molecular weight is sufficient to define the likely mechanical properties of the polymer.

Low-angle laser light scattering (turbidity) has been found to be the most accurate and reproducible technique for measuring polymer molecular weights (average molecular weight) as a primary method (110) (see MOLECULAR WEIGHT DETERMINATION). Most turbidimetric techniques use polymer solubility as a function of temperature for defining molecular weights (111). Dynamic light scattering has been used to obtain the distribution of hydrodynamic radius, which can be converted to molecular weight distribution with appropriate calibration. This technique can be performed in corrosive solvents or with polymers that dissolve only at high temperatures (112). Gel-permeation chromatography (GPC), although a secondary technique requiring careful calibration and interpretation of data, is the most frequently used commercial technique because of its ease of use, low cost, short time for analysis, and generation of excellent comparative data (113). Shifting of the polymer molecular weight peak or displacement in comparison to a standard or good material can indicate the presence of a higher molecular weight species by showing a shift to early elution, or a lower molecular weight species by showing a shift to later elution. These shifts can affect the processibility and physical performance of the material. Small sharp peaks that elute late from the GPC column may indicate the presence of low molecular weight oligomers, residual monomers, additives, or even residual moisture in the polymer.

A wide variety of polymers have been analyzed by gel-permeation or chromatography, size exclusion (SEC) to determine molecular weight distribution of the polymer and additives (114–117). Improvements in GPC include smaller crosslinked polystyrene beads having narrow particle size distributions, which allow higher column efficiency and new families of porous hydrophilic gels to be used for aqueous GPC (118). SEC in combination with FTIR has been used to monitor component content and compositional effects with changes in molar mass of HDPE and polypropylene (119). SEC fractionation followed by NMR and multiangle light scattering detector (MALDI) of random copolymers of acrylates with styrene maleic anhydride allowed determination of a model for composition and the ratio between number-average molecular weight (M_n) and weight-average molecular weight (M_w) of the SEC fraction (120). The combination of SEC with MALDI was also used to characterize branched polystyrene and poly(benzyl methacrylate) (121,122).

Temperature-rising elution fractionation (TREF) is a technique for obtaining fractions based on crystallizability independent of molecular weight effects (123,124) which allows qualitative analysis of short-chain branching in olefins. Determination of crystallizable lengths from TREF spectra led to the development of a quantitative method for short-chain branching (125). Single-step crystallization fractionation (CRYSTAF) has been developed for measuring composition or short-chain branching distribution by monitoring on-line polymer concentration in solution at decreasing temperatures (124). TREF, CRYSTAF, and differential scanning calorimetery (DSC) with specialized sample preparation were used to determine short-chain branching distribution and composition of blends of linear low density polyethylene (LLDPE). All three methods showed similar comonomer distribution (125) (see Fig. 3). Characterization of HDPE chain structure with SEC

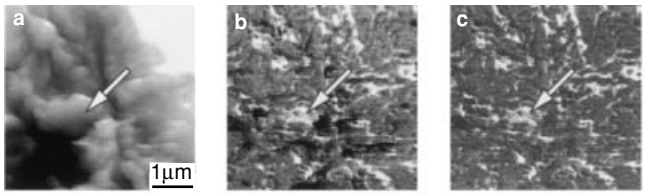

Fig. 3. (**a**) Topography, (**b**) amplitude (∼elasticity), and (**c**) phase (∼viscoelasticity) simultaneously acquired images of PES/SAN. The scale bar applies to all three images. Reprinted from Ref. 125, Copyright (2001), with permission from Elsevier Science.

and CRYSTAF methods was able to be correlated to environmental stress-crack resistance (126).

Thermal Properties

Thermal analysis involves techniques in which a physical property of a material is measured against temperature at the same time the material is exposed to a controlled temperature program. A wide range of thermal analysis techniques have been developed since the commercial development of automated thermal equipment as listed in Table 1. Of these the best known and most often used for polymers are thermogravimetry (TG), differential thermal analysis (DTA), differential scanning calorimetry (DSC), and dynamic mechanical analysis (DMA).

Thermogravimetric analysis (TGA), which monitors the change in the mass of a material during a controlled temperature ramp, is useful for both qualitative and quantitative analysis. It is used to help identify the types of polymers by comparison to degradation curves or when used with FTIR or pyrolysis–GC-MS (128–132), as well as identify and quantify additives such as carbon fillers, mineral fillers, plasticizers, antioxidants, stabilizers, UV absorbers, nucleating agents, and lubricants (133,134). Carbon black or graphite, which is commonly used as a colorant or filler in many plastics, may be analyzed using TGA by running the analysis in a nitrogen atmosphere to 600°C for measurement of the polymer component and then switching to an oxygen atmosphere and heating to 800 or 900°C to oxidize the carbon (133). The derivative curve of TGA can be used to improve the determinations of onset and end point of decomposition of low level components or in multipolymer systems (135). Refinements in computer control and instrument design have also led to commercial instruments having smooth changes in dynamic heating rate that varies as a function of weight loss, a low mass furnace for rapid response, and horizontal purge gas flow to better remove decomposition products, among other changes (136).

Differential thermal analysis (DTA) monitors the temperature difference between a specimen and a reference material, whereas differential scanning calorimetry (DSC) heats specimen and reference materials separately and measures the heat flow between the materials. DSC is the method of choice for determinations of melting point as well as the presence and level of crystalline phase

Table 1. A Survey of Common Thermal Analysis Techniques[a,b]

Technique	Abbreviation	Property measured (dependent variable)
Thermogravimety	TG	mass, m
Derivative thermogravimetry	DTG	dm/dt
Differential thermal analysis	DTA	dT/dt
Differential scanning calorimetry	DSC	dH/dt
Thermomechanometry		
Thermomechanical analysis	TMA	L, dL/dT
Thermal dilatometry	TDA	V, dV/dT
Dynamic mechanical analysis (including torsional braid analysis, TBA)	DMA	$G^*(\omega)$
Thermoelectrometry		
Thermally simulated conductivity	TSC	di/dt
Thermally stimulated polarization	TSP	
Thermally stimulated depolorization	TSD	
Dielectric thermal analysis	DETA	$Z^*(\omega)$
Thermophotometry		
Thermoluminescence (including oxyluminescence)	TL	dI/dt
Thermal microscopy	TM	
Emanation thermal analysis	ETA	Radioactive gas evolution
Thermosonimetry	TS	Acoustic emission
Evolved gas analysis	EGA	GC/MS/IR, etc
Thermomagnetometry	TM	Magnetic effect on TG

[a]From Ref. 127.

[b]Combined simultaneous techniques—many of these techniques can be combined to give simultaneous or sequential measurements on the same sample, eg, TG/MS, TG/IR, DSC/XDR, DSC/TG/MS, pyrolysis/GC, Differential photocalorimetry (DPC), etc.

in polymers. The effects of heating rate and oxygen flow rate on oxidative induction time of HDPE (137), applied strain during cooling (138), spherulitic crystal growth and crystalline structures (139,140), and curing of thermosets (141–143) have been studied using DSC techniques.

DSC has been found suitable for the determination of second-order transitions (T_g = glass transition) and, in some cases, β-transitions. Procedures for the determination of T_g are discussed in the literature (135,136), which includes data on the dependence of T_g on number-average molecular weight (M_n for polymers. This shows a significant effect until a critical M_n is reached with little or no effect beyond. A technique employing DSC to measure specific heat of rapidly quenched polyethylene samples, which are subsequently annealed at low temperatures, shows the formation of secondary crystals that melt near the annealing temperature with small endotherms. The endotherms increase and melting points rise as time increases, leading to the potential use of this technique for studying the thermal history of samples (144,145). Additional work on the correlation of enthalpy changes with the aging of samples has been completed on PBT (146). For amorphous polymers, changes in T_g can be used to determine aging that has

occurred below and near T_g. Accuracy is improved by matching the heating rates of DSC to cooling rates on specimen preparation (135,136). The T_g response to aging relates to the continued relaxation of frozen molecular structure that continues over time below T_g and results in changes in free volume (147). Reduction in free volume due to aging can be correlated to reduced impact strength and improved creep response at low strain rates for polymers.

The relative effectiveness of nucleating agents in a polymer can be determined by measuring recrystallization exotherms of samples molded at different temperatures (135). Effects of formulation change on the heat of rubber vulcanization can be determined by DSC; pressurized cells may be needed to reduce volatilization during the cure process (148).

Changes in heat capacity and measurement of T_g for blends have been used to determine components of copolymers and blends (149–152) although dynamic mechanical analysis has been found to give better resolution. Equations relating T_g of miscible blends and ratios of components have been developed from DSC techniques, eg, the Fox equation (eq. 1), where T_{g12} is the T_g of the blend, W_1 or W_2 is the weight fraction of component 1 or 2, and T_{g1} or T_{g2} is the T_g of the pure component 1 or 2 (153); the Gordon–Taylor–Wood (GTW) equation (eq. 2), where k is the best fit constant for empirical data (154); and the Couchman equation (eq. 3), where x_1 and x_2 are mass fractions and ΔC_p is heat capacity changes for neat polymers (155).

$$\frac{-1}{T_{g12}} = \frac{W_1}{T_{g1}} + \frac{W_2}{T_{g2}} \tag{1}$$

$$\mathrm{T_{g12}} = \frac{k(\mathrm{T_{g2}} - \mathrm{T_g})\mathrm{W_2}}{1 - \mathrm{W_2}} + \mathrm{T_{g1}} \tag{2}$$

$$\ln \mathrm{T_{g12}} = \frac{x_1 \Delta C_{p1} \ln \mathrm{T_{g1}} x_2 \Delta C_{p2} \ln \mathrm{T_{g2}}}{x_1 \Delta C_{p1} + x_2 \Delta \mathrm{C_{p2}}} \tag{3}$$

Modulated DSC has been used to evaluate correlations between polymer chain molecular characteristics and crystallization behavior in polyethylene (156). It has also been used in the study of thermal treatments of PET (157) and the kinetics of the T_g (158).

Thermomechanical analysis (TMA) measures the dimensional changes of a fabricated polymer part at a constant heating rate. First-order (T_m) and second-order (T_g) transitions may be measured from graphing length of specimen (L) versus temperature (T). This technique may also be used to determine the coefficient of linear thermal expansion (CLTE) for a material. TMA can be more sensitive to small changes in enthalpy typical of highly crystalline polymers than DSC (159). This technique has also been used for evaluating dimensional changes of polymers in fluid environments. Studies have been completed on water–nylon 6 at different temperatures (160), chlorobenzene–polyethylene (161), and elastomers in various fluid and oils.

DMA involves exciting a material with a periodic stress and monitoring the resultant strain for viscoelastic properties of the material with respect to temperature, humidity, vibration frequency, dynamic or static strain amplitude, or other parameter against time (162). The two primary uses are for determination of morphology including glass transitions and melts and checking polymer behavior at conditions simulating end use while maintaining temperature equilibrium. This method detects α- (first-order or glass) transitions, β- (side-chain motions) transitions, and γ- (crankshaft rotation of main-chain segments or single bond flips) transitions, and has about a 1000$\times$ greater sensitivity to DSC and about 100$\times$ greater sensitivity to modulated DSC for amorphous polymers. In this procedure, a specimen is placed under a fixed or free oscillatory stress and the strain with which the specimen responds is recorded. Polymers are typically viscoelastic in nature, and have a dynamic response to the oscillatory stress controlled by the viscous component, which results in a strain that continues to increase until the stress is removed, but is not recoverable. The other component is the elastic response, which reacts instantaneously to the applied stress and is completely recovered when the stress is removed. Polymers respond with elements of each, resulting in a strain with the same frequency as the applied stress, but out of phase by an amount, δ, dependent on the relative elastic and viscous nature of the material (see Fig. 4) (163). Samples can be tested under different stress configurations, ie, tensile, flexural, compressive, and shear, by using a varying resonance frequency under a constant temperature or constant rate of temperature change. The tangent of δ is known as the loss factor and is the ratio of E'', the loss modulus, over

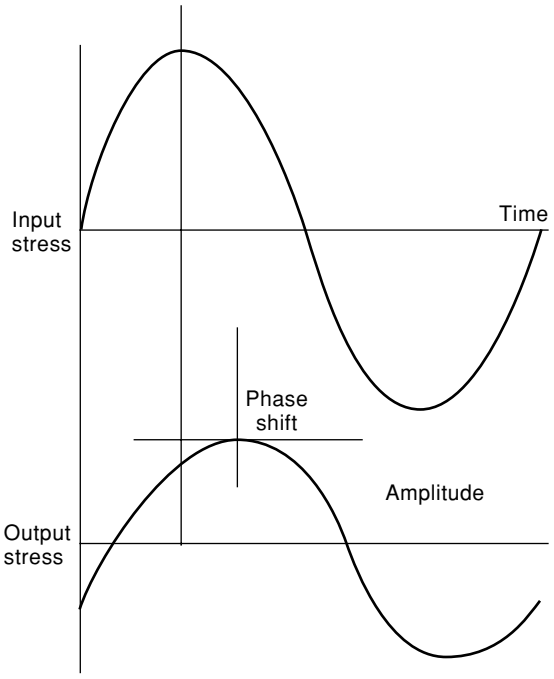

Fig. 4. Applied stress and resultant strain in DMA measurements.

E', the storage modulus; E is used for tensile (extensional deformation) whereas G is used for shear.

Stress levels are kept low within the elastic region of the material. Although solid-state testing is used most frequently, melt-state testing allows the examination of viscosity versus frequency at a set temperature and also shows the response of the shear storage and loss modulus (G' and G'') versus frequency. Solid-state testings of both amorphous and semicrystalline polymers by DMA have shown effects on tan δ values near the T_g for each type of material from differences in orientation by sample preparation method. For amorphous materials, the values of tan δ are higher in the temperature region slightly below the T_g as orientation increases in the sample; the same effect is seen for crystalline materials above the T_g (164). The interrelationship between temperature and frequency as well as time and frequency are well established (165). The equivalence of the effects of temperature and time in viscoelastic systems results in time–temperature superpositioning (166) and is related by the Williams–Landel–Ferry (WLF) equation (eq. 4) for amorphous polymers, where a_T is the shift factor, T is the measurement temperature, T_o is the reference temperature, and c_1 and c_2 are constants (167).

$$\log a_T = \frac{-c_1(T - T_0)}{c_2 + (T - T_0)} \tag{4}$$

This allows the production of master curves, which can be used to estimate changes in modulus or other properties over a long period of time by shorter tests over different temperatures. The Arrhenius relationship (eq. 5) for crystalline polymers or other transitions, where E_a is the activation energy and R the gas constant (8.3 J/mol), is as follows:

$$\text{Log } a_T = \frac{-E_a}{R(T - T_0)} \tag{5}$$

DMA of multiple frequency measurements over a range of temperatures allows the plotting of modulus versus time in similar master curves as generated by a series of short-term creep studies in a much shorter timeframe. There are potential problems with these predictions, such as internal stresses in amorphous polymers interfering in superpositioning loss modulus data near T_g (168), using data in temperature regions outside linear viscoelastic behavior (169), or strains outside the linear regions. Studies on blends have been documented on styrene block copolymers with poly(α-methylstyrene) (170), unsaturated polyesters with elastomers (171), polyethylene copolymers with low ethylene content (172), and polycarbonate–poly(butylene terephthalate) (173). Furthermore, DMA is used to study the curing of thermoset systems (174–176). DMA has also been used to study the effects of additives of filled polymers (177,178) and the relaxation mechanisms of polycarbonate, metallocene polyethylene, and polypropylene fibers (179–181). The nonlinear behavior and deformation mechanisms of closed cell olefin foams were determined with DMA techniques (182). There are series of established standards for a variety of DMA techniques available from both ISO and ASTM as shown in the table below.

Test area	Subject	ASTM	ISO
Physical properties	Specific gravity/density	D792, D1505	1183
	Water absorption	D570	62
Rheological properties	Melt flow rate	D1238	1133
	Capillary rheology	D3835	11443
	Capillary rheology-screw	D5422	
	Spiral flow-thermoset	D3132	
	Solution viscosity	D2857	1628 1-5
Mechanical properties	Tensile	D638	527 1-4
	Compressive	D695	604
	Flexural	D790	178
	Charpy impact	D6110	179
	Notched Izod impact	D256	180
	Instrumented dart impact	D3763	6603-2
	Gardner/dart drop	D5420	6603-1
	Tensile impact	D1822	8256
	Rockwell hardness	D785	2039-2
	Creep	D2990	899
	Fracture toughness	D5045, D5528, D6068	572
Thermal properties	Heat deflection temp.	D648	75 1-2
	Vicat softening temp.	D1525	306
	DSC	D5417	11357 1-3
	Dynamic mechanical analysis	D5279, D4065, D5023, D5418, D5024, D5026, D4440, D4092	6721 1-10
Optical properties	Haze	D1003	14782
	Transmittance	D1003	13648 1-2
	Color	D2244, D6290, D7729	
Electrical properties	Dielectric strength	D149	IEC 243-1
	Dielectric constant	D150	IEC 250
	Volume/surface resistivity	D257	IEC 93
Ignition properties	Flammability	D635, D560, D3801, D3814, D1929, E176 UL94	871, 1210
	Limited oxygen index	D2863	4589
	Avg. extent of burning	D635	2782, 1210
Environmental	Chemical resistance	D543	175, 4600, 6252, 4599
	Thermal aging	D5510	2578
	Weathering	D1435, D4364, G26, D5071, D4674, G152, G153, D6360	4607, 877, 4665, 4892, 11507, 4892
	Biodegradability	D5209, D5210, D5247, D5271, D5272, D5338, D5509, D5511, D5512, D5525, D5526, D5988, D6003	14851, 14852, 14853, 14855, 15985
	Fungi	G21	846
	Bacteria	G22	
	Radiation	E1027	

Recent developments have been in the area of microthermal analysis using thermal conductivity with thermal diffusivity signals or AFM to visualize specific areas or domains in the material and perform localized thermal analysis studies (183,184). Relaxational behavior over time and temperature is related to changes in free volume of the material. Positron annihilation lifetime spectroscopy (PALS) measurements of positron lifetimes and intensities are used to estimate both hole sizes and free volume within primarily amorphous phases of polymers. These data are used in measurement of thermal transitions (185,186) structural relaxation including molecular motions (187–189), and effects of additives (190), molecular weight variation (191), and degree of crystallinity (192). It has been used in combination with DSC to analyze the range of miscibility of polymethyl methacrylate poly(ethylene oxide) blends (193).

Another relatively recent development in thermal technique for polymers is equipment for reliable measurement of chemiluminescence. The luminescence is thought to be from the drop of an excited carbonyl group back to the neutral state after excitation from the termination of two peroxy radicals. Its use is primarily in determination of oxidation stability of polymers to determine an oxidative induction time (OIT) (194,195). It has also been used to monitor oxidation of polymers subjected to stress (196) and simulated weathering (197).

Another technique that is similar to DMA is dielectric thermal analysis which is covered under the Electrical Properties section.

Vicat softening temperature (ASTM D1525, ISO 306) uses a flat-ended needle penetration of 1 mm of the plastic specimen under controlled heating conditions to indicate short-term resistance to heat. For some plastics these curves can be extrapolated to zero force and zero rate of heat to give values in agreement with glass-transition data (198). Testing of deflection temperature under load (ASTM D648, ISO 75) determines bending resistance of plastic specimen under load and at a set rate of temperature increase. This test is highly influenced by the molded-in stresses and the thickness of the specimen tested. Annealing specimen to relieve stresses prior to testing improves reproducibility of the test but also results in higher values than unannealed specimen. Locati and co-workers have proposed monitoring of the complete deflection curve with both annealed and unannealed samples to obtain a $T_{0.25}$ that is a temperature characteristic of a material at zero stress (but dependent on deformation) and two stress sensitivity coefficients that are dependent on the thermomechanical history of the material to better indicate the material performance in applications (199).

Processing Properties

The flow properties of polymers, whether the viscosity of liquid thermosets prior to gelation or of molten thermoplastics, are important parameters for the proper processing of materials (see RHEOLOGY). Several test methods have been developed to predict or correlate to actual processing conditions or for quality control testing of polymers. For thermoplastics, the commonly used quality control method is melt flow rate (ASTM D1238 or ISO 1133). This technique can give values at melt index conditions that are inversely proportional to the molecular weight of homopolymers. However, the common addition of processing aids, lubricants, and

fillers makes this correlation highly unreliable. Procedures that determine melt flow under two loads have been used primarily with polyolefins as an indication of molecular weight distribution. Melt flow rate values, although useful for quality control, are not indicative of the actual response of the material during processing, primarily due to the viscoelastic nature of polymers. Because polymers are non-Newtonian in flow, large differences in shear rate of the melt flow rate test ($1–50\ s^{-1}$) versus that of processing equipment, eg, extrusion ($10^2–10^3\ s^{-1}$) and injection molding ($10^3–10^5\ s^{-1}$), can cause large changes in the viscosity of most polymers.

Because processing conditions cover a wide range of shear rates, tests that can simulate both temperature and shear rate conditions are more useful in predicting flow properties. Several studies have been conducted on correlating common processing techniques that use torque rheometers, capillary rheometers, high pressure capillary rheometers, and oscillating disk rheometers for both thermoplastics and thermosets (202–204). Capillary rheometers have been designed to reach shear rates of $10^7\ s^{-1}$ and are used to study flow behavior at high shear (202). A typical set of curves of viscosity versus shear rate is shown in Figure 5 (205). A study of flow testing of ABS resins showed similar flow ranking of different grades of resin by using capillary rheology (ASTM D3835, ISO 14133), spiral flow molding, and on-machine rheometry (206,207), the last technique using an injection-molding machine as a rheometer. Capillary rheology tests using a screw rheometer in place of a piston have been published as ASTM D5422. Work is in development at ISO for determining extensional viscosity data as well as drawing properties using a rheometer for improved understanding of extrusion processing (208). Some work has been completed on using capillary rheology

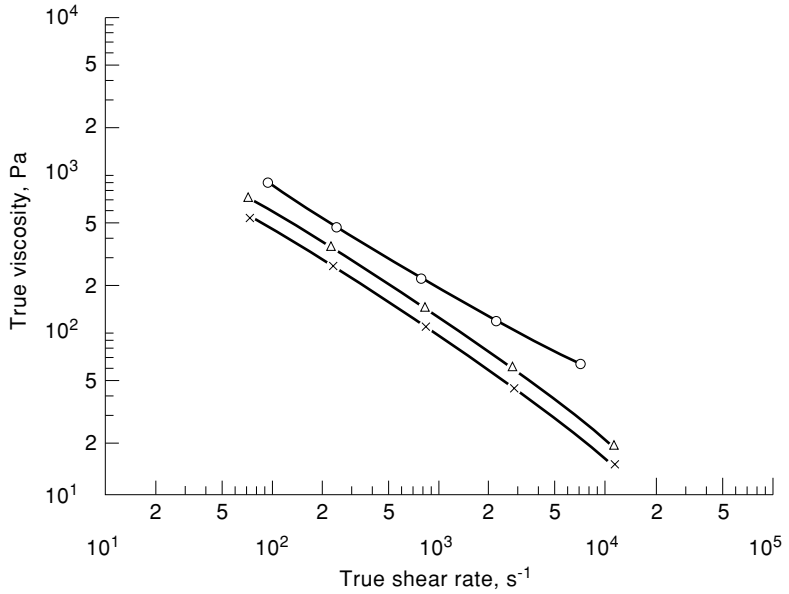

Fig. 5. Capillary melt viscosity; ○, = 300°C, △, = 320°C, and ×, = 340°C. Courtesy of The Dow Chemical Company.

measurments on-line to measure rheological properties during polymerization (209).

Flow tests designed for thermosetting resins include a cup flow mold for flash-molding of powdered phenolic and alkyd materials (ASTM D731), spiral flow for low pressure thermosets (ASTM D3123), and torque rheometer techniques (ASTM D3795). In addition to these, tests for measuring time to gelation (gel) are important for processors to understand usage time and pot life (210). Dilute solution viscosity testing of polymers requires complete dissolution in the solvent without degradation or interaction with the solvent within the chosen temperature range of the tests. Data from these tests have been used to determine relative molecular weight of polymers (211).

New standard tests for determining pressure–volume–temperature (PVT) properties of materials using rheometers and other techniques (212,213) are being established to discover the correlation for the fundamental properties of plastics. These in combination with no-flow temperature, ejection temperature, and capillary rheology data are useful in predicting the behavior of molten plastic as it enters and fills a mold. Several mold-filling prediction computer programs are commercially available (214,215) to assist mold designers and plastic processors in developing plastic parts that have reduced stresses from the molding process, and in improving productivity with easier start-up of new molds and fewer rejected parts.

Mechanical Properties

Mechanical properties of plastics can be determined by short, single-point quality control tests and longer, generally multipoint or multiple condition procedures that relate to fundamental polymer properties. Single-point tests include tensile, compressive, flexural, shear, and impact properties of plastics; creep, heat aging, creep rupture, and environmental stress-cracking tests usually result in multipoint curves or tables for comparison of the original response to postexposure response.

Tensile properties are those of a plastic being pulled in an uniaxial direction until sufficient stress is applied to yield or break the material. Standard tests are ASTM D638 and ISO 527 parts 1–4. For many materials, Hooke's law is valid for a portion of the stress–strain curve. If stress is relieved during this portion of the testing, any strain that has occurred is fully recovered. Elastomers generally do not show a linear response nor a true yield point. Tensile curves can be used as an indication of polymer strength and toughness. Figure 6 shows the relationship normally seen for the stress necessary for yield or break with strength, whereas elongation beyond yield shows ductility (toughness). Similar curves can be generated for tests in comparison, flex, shear, and some forms of impact.

Mechanical properties are determined on solid polymers in arbitrary forms defined precisely by standard test methods in ISO, ASTM, or other national standards organizations. Parts are formed by either injection molding, compression molding, or milling from extruded sheet or molded plaques. Viscoelasticity of polymers dictates that the technique used to make the part must have a significant effect on the mechanical behavior of the polymer. For valid comparison of materials, they should be prepared similarly and conditioned under the same

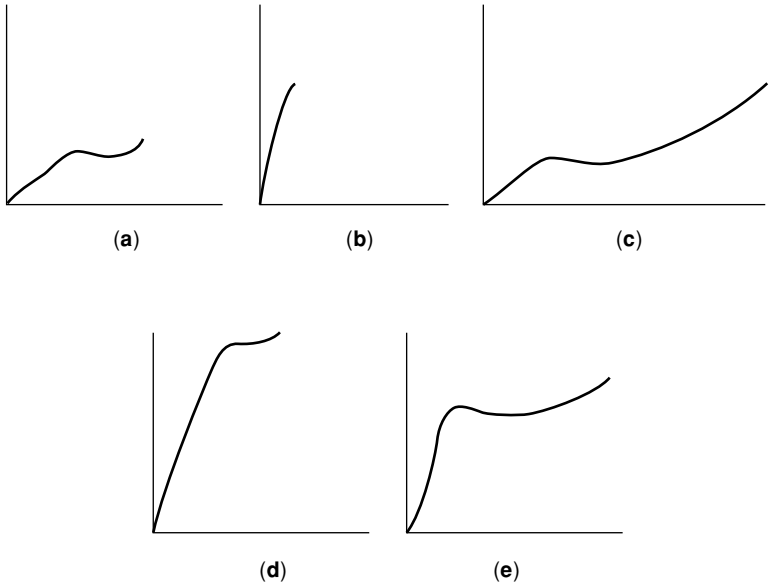

Fig. 6. Types of stress–strain curves: (**a**) soft and weak; (**b**) hard and brittle; (**c**) soft and tough; (**d**) hard and strong; and (**e**) hard and tough.

environment. Viscoelastic effects are also the reason for the rate of strain effects on the modulus values of materials under tensile, flexural, and compressive testing (216,217). The modulus of elasticity is also thickness-dependent, showing decreases as thickness increases in the plane-stress condition (0.1–2 mm) and the opposite effect at higher thicknesses where plane-strain conditions exist (218). Several types of impact testing have been developed to measure a plastic's response to a high rate of strain. Notched or Charpy Izod impact are pendulum impact tests essentially uniaxial in direction. Although both tests have been long established for quality control tests and material property data sheets, they are not useful in determining the impact response of a plastic in most applications. ASTM D256 lists multiple cautions on using data from these tests. Notched Izod's primary practical value in characterizing a plastic material is to establish notch-sensitivity of the material. Drop-weight impacts, either manual or instrumented, give more practical information because of the multiaxial stresses found in these test procedures which are closer to normal impact events. Instrumented impact allows the recording of the full impact event as a stress–strain curve, showing similar characteristics to tensile or other modes of stress–strain tests. Instrumented impact is preferred for monitoring ductile–brittle transitions and determining the effects of polymer composition on material toughness. Analysis of DMA analysis and impact properties of various compositions of impact-modified polypropylene showed a direct correlation between the loss tangent of DMA tests and impact properties (219).

Creep, creep rupture, and stress relaxation tests are multiple-point tests requiring long periods of time (1000 h minimum) to generate useful data; these are standard tests for determining more fundamental polymer properties. Data for

these tests are generated under several time–temperature–stress-level conditions in either tensile, flexural, compressive, or shear modes and combined into master curves using superpositioning theory (see AGING, PHYSICAL; VISCOELASTICITY). The low stress loads applied in creep tests, and thereby the low strain rates determined, require sensitive equipment for accurate measurements. Studies that normalize the stress required to produce a given strain in a given time to the stress producing that same strain after 24 h, have shown that plots of the normalized stress rates versus time over stress (24 h) give a single curve, which can be used with other short-term (days) creep tests at different stress levels to prepare master curves that can require up to 1 year for traditional data generation (220). Isometric curves can also be obtained similarly by using different temperatures for a given strain. Modulus values from these curves are used in plastic part design equations to predict part performance over the expected life of the part.

Fatigue testing of polymers may consist of static fatigue, ie creep rupture, or dynamic fatigue. Modes of cyclic fatigue include tension, compression, or shear, which use sinusoidal-, square-, and sawtooth-wave forms for applying stress, although varying strain can also be used in cyclic fatigue testing (see FATIGUE). Notching of specimen and high or low temperatures have been employed to accelerate the failure via embrittlement of the materials, but can lead to unwarranted extrapolation of the test data without additional tests (221).

Substantial work on the application of fracture mechanics techniques to plastics continues today (222–225) (see FRACTURE). The principle is based on failure stress proportionality to the square root of the energy required to create the new surfaces as a crack grows and inversely with the square root of the crack size originally determined with glasses. For the use of linear elastic fracture mechanics in plastics, certain assumptions must be met (226): (*1*) the material is linearly elastic; (*2*) the flaws within the material are sharp; and (*3*) plane strain conditions apply in the crack front region. The equation relating fracture toughness to modulus and energy release is given below for plane-stress and plane-strain conditions:

$$\text{Plane-stress} \qquad K_c = (E\ G_c)^{1/2} = Y\ \sigma_f a^{1/2}$$

where K_c = fracture toughness, E = Young's modulus, G_c = critical energy release rate per unit crack length, σ_f = nominal applied stress at fracture, a = crack length (or $\frac{1}{2}$ internal crack length), and Y = geometry factor.

$$\text{Plane-strain} \qquad K_c = \left(E/1 - \nu^2\ G_c\right)^{1/2}$$

where ν = Poisson's ratio.

ASTM D5045 has been accepted for the determination of the critical stress intensity factor, *KIC*. Although *KIC* is temperature- and rate-dependent and the dependence is specific for any material, it is relatively independent of specimen geometry. Single-edge-notched beams are typically used for the test, but other

geometries, eg, compact tension, short rod, and center-notched tension, have been used for the testing (227–231). Some plastics do not follow the mode outlined in D5045 at the thicknesses normally used in parts. These require the use of elastic plastic fracture mechanics using the *J*-integral parameter (232). More complex treatments of fracture incorporating nonlinear, viscoelastic effects have also been developed (233–235).

Hardness measurements such as Rockwell or Vicker's indentation properties are time-dependent as a result of the viscoelastic flow and relaxation processes (236) (see HARDNESS). Microhardness measurements have been used to correlate with other properties such as Young's modulus and compressive yield stress in polyethylenes (237) and glass-transition temperature of amorphous plastics (238). Scratch resistance in polyproplyene studies was found to have shear yielding as the main cause of plastic flow scratch pattern with tensile tear effects on the surface and shear-induced fracture on the subsurface (239).

Environmental Effects Tests

In practical applications of plastic materials, their mechanical properties can be significantly influenced by environmental factors of chemical exposure, temperature, radiation (photon and gamma ray), biological agents, and/or combinations of several of these factors at once. Few standard tests have been developed in these areas. Techniques and models used to extrapolate data from aging and environmental resistance tests on polymers have been proposed to predict service performance in various applications (240). This paper illustrates uses of Arrhenius, Avrami, WLF, and diffusion equations in evaluating exposure data and discusses their limitations. Mechanical properties can be determined by using ovens or cold-temperature chambers under the same procedures described in ASTM or ISO short-term tests to evaluate the effect of heat or cold. The length of exposure time, test conditions (at temperature or after being reconditioned to standard testing conditions after exposure), and reference material must all be stated to use these data. ISO 2578 addresses these variables, but allows the tester to choose the characteristic for testing and the threshold value (limit of decline in performance). It recommends testing for 20,000 h and performing the test under standard room temperature conditions after heat exposure. ASTM is developing a standard for comparative indexing of heat-aged materials to original properties, but does not indicate a minimum exposure time. Thermal expansion testing also addresses the physical dimensional changes in plastic parts exposed to temperature changes. The change must be measured in each orthogonal direction, because polymers are not generally isotropic or homogeneous. ASTM D696 has been used for coefficient of linear thermal expansion. Shrinkage measurements are not related to low temperature measurements, but refer to the dimensions of post-molded parts compared to the mold dimensions or to post-molding shrinkage that involves short-term, high heat exposure with post-exposure dimensional measurements. Melting points of crystalline materials may be determined by capillary tube or hot-plate techniques, whereas softening point (ISO 306, ASTM D1525) by penetration or deflection under load (ISO 75, ASTM D648) is generally used for amorphous and semicrystalline polymers.

Chemical exposure of plastics may exhibit a wide range of effects with one chemical and one type of polymer, depending on the concentration of chemical agent, temperature of exposure, molded-in stresses within the specimen, applied stress level to the part during exposure, and formulation of the specific polymer grade. Standardized tests have been developed to evaluate the effects of chemical agents on plastics with and without external stress. Tests such as ASTM D543 and ISO 175 propose procedures for evaluating the effects of suggested chemicals on dimensions, appearance, and mass of the polymer specimen after the specimen has been immersed for a set period of time. Mechanical properties may also be checked if the specimen has maintained sufficient integrity to test. Tests in which stress is externally applied include both stress and strain techniques. ASTM D1693 uses bent strips of polyethylene with a cut, exposed to an aggressive surfactant and exposed until failure or 48 h. Several improvements have been suggested, primarily in better defining specimen preparation (241) or control of the amount of strain used (242). For blow-molded polyethylene bottles, accelerated test conditions of higher temperature and pressure were found applicable (243). Amorphous poly(ethylene terephthalate) used aqueous sodium hydroxide and creep crack growth rates to determine environmental stress-crack performance (244).

The method of caustics has also been used to study the formation of cracks and crazes formed by exposure of PMMA to solvents (245). ISO 4599 has been developed to better control the application of stress using a jig having the curve of the arc of a circle for shaping the specimen and maintaining a set curvature during exposure to the agent. After a predetermined time the specimen is tested for tensile or flexural properties and compared to preexposure test values. ISO 4600 uses the technique of impressing an oversized ball or pin into a hole drilled in the specimen to apply a strain.

Tests using a constant stress (constant load) normally by direct tension have been described in ISO 6252. This test takes the specimen to failure, or a minimum time without failure, and frequently has a flaw (drilled hole or notch) to act as a stress concentrator to target the area of failure. This type of testing, as well as the constant strain techniques, requires careful control of specimen preparation and test conditions to achieve consistent results (246,247). Use of a slow strain rate with a four-point bend specimen configuration and constant load has been suggested as a method for ranking materials for environmental stress-crack resistance (248).

Weathering of plastic materials combines complex factors of temperature, radiation, oxidation, and moisture effects on a plastic part. Weathering effects vary with geography, time of year, and position of material being exposed. All of these effects make predicting the weatherability of a material extremely difficult. A recently completed study on the reproducibility of weathering data concluded that ranking of materials appears consistent although absolute data varies significantly from lab to lab (249). ISO 877 and ASTM G24 outline procedures for standardizing outdoor exposure of plastics under glass; ISO 4607 and ASTM D1435 are techniques for total exposure of plastic specimens to natural elements in racks and under specific climatic conditions. Frequently, only changes in physical appearance are measured after weathering; however, appropriate specimens can be exposed, mechanically tested, and compared to carefully stored control specimens

(250). The long time periods required for outdoor weathering studies have led to the development of several accelerated techniques. The use of extreme and consistent climates, eg, South Florida or Arizona, and intensifying techniques for natural sunlight have been suggested to accelerate tests. ASTM D4364 has established a method for the use of a follow-the-sun rack with flat mirrors to reflect sunlight uniformly onto the test specimen as an intensifying technique. Because these techniques still require long exposure times to obtain results, in-lab acceleration tests to weather materials artificially have been developed. Various lamp sources have been used, such as low and high pressure mercury, carbon arc, and xenon arc. Although carbon arc lamps are still used to weather materials, xenon arc lamps are the preferred lamp for plastics weathering. These lamps simulate sunlight closely when appropriate filters are used (Fig. 7). Various correlations have been reported between xenon testing and outdoor weathering. For several plastics, 500 h in xenon arc testing, provided high humidity and water spray are used, are equivalent to 1 year of outdoor exposure. Some equipment manufacturers indicate that the ratio is one hour of accelerated to 10 h of outdoor exposure, whereas experimenters have found that the ratio can range from 1 h accelerated/5 h outdoor to 1 h accelerated/9 h outdoor when evaluated by the change in plastic color. Accelerated tests should be used to compare the relative performance of materials and ranking resistance to exposure, rather than for any direct correlation to outdoor weathering. Both ISO and ASTM have established practices for the use of carbon arc and xenon arc accelerated equipment. Recently, suggestions have been made for use of higher temperatures and irradiance levels to further accelerate weathering (251).

Fluorescent UV lamps within an apparatus that allows condensation cycles rather than the water spray typical of xenon arc tests have been developed for

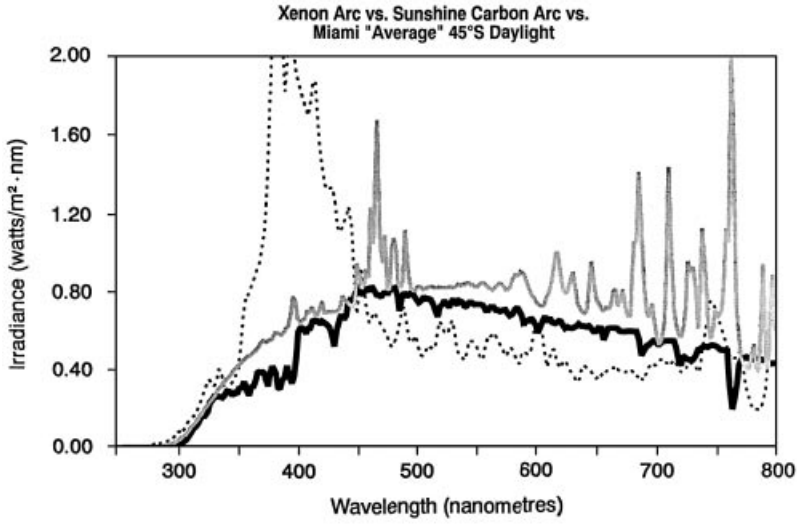

Fig. 7. Comparison of xenon arc, sunshine carbon arc, and Miami average 45°S daylight, where (▒) represents xenon with Type S high borate filters, 0.35 W/(m^2·nm) at 340 nm; (···) represents sunshine carbon arc with Corex; and (▬) represents daylight. Courtesy of Atlas Electric Devices Co.

plastics testing. The spectral cutoff wavelength of the lamps used in the apparatus determines the severity of the test. Ultraviolet B (UVB) 313 lamps allow a significant irradiance component below 290 nm, which is normally filtered out by the earth's atmosphere. Ultraviolet A (UVA) 340 lamps have shown better correlation to the spectral irradiance of natural sunlight, although the visible light range is missing.

Other environmental testing standards have been developed for evaluating the effects of biological agents, either strains of fungi (ISO 846 or ASTM G21) or bacteria (ASTM G22), on mold growth on the plastic material, or if the plastic material has a toxic effect on the fungi. Longer-term outdoor exposure tests for resistance to microbial attack require geographic locations favorable to microbial growth or burial of the material in soil. ASTM E1027 is used for exposure of polymers to ionizing radiation. This can be used for testing the resistance to gamma rays, electrons, neutrons, etc. These tests are important for plastics used in the medical area to determine the resistance to sterilization techniques. A set of standards have been introduced at ASTM and ISO for the evaluation of biodegradable plastic materials. These standards have recommended standard conditions for a variety of environments to substantiate environmental performance of this new type of plastic material.

Optical Properties

Transparency, gloss, color, refractive index, and reflectance are the properties normally associated with aesthetics of plastic materials. In some areas, changes in optical properties, increases in haze after abrasion testing, color differences after weathering, and birefringence analysis of residual stress within a transparent part (252) are all used to measure the effects of applied stresses. Measurements of color, gloss, refractive index, and haze apply to many products beyond plastics and use similar techniques. Reference should be made to this general topic for detailed information.

One of the most widely accepted measurements of color in plastics is based on standards developed by the Commission Internationale de l'Eclairage (CIE) for illuminants and observers to establish tristimulus values. A common color scale used to describe color in numeric terms of lightness and hue is the L-a-b tristimulus system, where L is scaled vertically from a perfect white with a value of 100 to a perfect black at 0; a is positive for red and negative for green; and b is positive for yellow and negative for blue. Spectrophotometers are used to measure the full reflectance of a colored material over the visible range and convert to the tristimulus values via microprocessors. Color as viewed under various CIE illuminants and/or observers can be determined by a single spectrophotometric analysis as the microprocessor computes the tristimulus values for each set of conditions. Color-matching of an object can be completed by comparing spectral curves generated through the use of the spectrophotometer. However, many factors, such as gloss, texture, opacity, and changes in illuminant and observer, complicate the visual appearance of a color with the spectral curve of a color. ASTM D1729 establishes procedures for visual evaluation of color and defines illuminant, viewing conditions,

and use of standards for comparison; ASTM D2244 describes instrumental color evaluation techniques. Specular gloss, the relative reflectance of a specimen in the specular direction, is usually measured at 60° angle of incidence for most plastics. High gloss materials may be measured at 20° incidence and low gloss specimens at 85° incidence using ASTM D523. For films, ASTM D2457 uses measurements at 20°, 60°, and 45° angles of incidence.

Electrical Properties

Dielectric analysis (DEA) or dielectric thermal analysis (DETA) is similar to DMA (see DIELECTRIC RELAXATION). In DEA, the movement of dipoles or other ionic species that can be electrically stimulated allows the monitoring of changes in ionic conductivity. Similar to DMA phase angle δ, in DEA this is related to the lag of the polarization induced in an insulator placed in an alternating electrical field. The energy dissipated as heat is proportional to the dielectric loss ε'', and the energy stored is the real part of the dielectric constant, ε'. The electrical technique is considered more sensitive to transitions below T_g than DMA (253). It is also more sensitive to β-transitions frequently linked to impact strength and long-term mechanical strength (254). Dielectric analysis has a broader and higher range of frequencies than DMA. Changes in permittivity with time in DEA measurements have been correlated with moisture content change in polymers (255) and have become an on-line technique for monitoring moisture in polymers. Thermally stimulated conductivity (TSC) uses the technique of polarizing a polymer at different temperatures, quenching the sample, and measuring the depolarizing current as the material is heated at a controlled rate (256). The rate of repolarization is related to the relaxation times of internal motions. When DEA was used to characterize the alpha relaxation process of an interphase formation in composite material, the process was found to be diffusional rather than a resin curing process (257). A combination of DMA and DEA in a study on the effects of low molecular weight additives in poly(ethylene terephthalate) was able to resolve that beta peak had two different relaxation processes correlating with different molecular motions in the polymer chain (258). DMA relaxation spectroscopy was also used to relate the structure of lateral groups of aromatic polyamides to molecular mobility (259). Inverse gas chromatography has been used to predict and measure diffusion coefficients using a method at finite concentration of solvent (260). It has also been used to examine surface properties of solid materials (261).

Excellent insulating properties, along with the ability to be structural components, make plastics the ideal candidate materials for electrical applications. Although generally used as insulators, carbon black or carbon fiber can be added to make plastic materials electrically conductive, thereby expanding their usefulness in the electronics area.

Standard testing of electrical properties of plastics includes dielectric strength, permittivity, dissipation factor, surface and volume resistivity, and arc resistance. Dielectric strength is the maximum voltage required for breakdown and is determined by one of three techniques: short-time, slow-rate or slow-rise, and step-by-step. The two last techniques use data from the short-time test to

determine a starting point. Dielectric strength is thickness-dependent with thin foils being used in specific space-saving devices.

Permittivity gives an indication of the electrical storage ability of a conductor (behaving as a capacitor). The thinner the material, the higher the permittivity or capacitance, allowing use of plastic foils in areas where high capacitance is required. However, when plastics are used as insulators, low permittivity is required. Resistivity testing can be either volume, relating to leakage of current through the body of the insulator, or surface, relating to a surface layer of moisture or contaminant leading to electrical loss.

Arc resistance or tracking resistance is the resistance of a material to a high voltage arc or discharge. ASTM has published three methods to test this phenomenon, depending on the conditions to be tested: D495 for high voltage, low current, dry arc resistance; D2132 for dust and fog tracking; and D2302 for liquid-contaminant inclined-plane tracking. A comparative tracking index (CTI) technique uses a low frequency, low level current applied between electrodes while allowing drops of aqueous solution to fall between electrodes at 30-s intervals. This technique is described in ASTM D3638. However, the results or values obtained from these tests cannot be used in design studies (262).

Electromagnetic interference (EMI) testing has become more prevalent for materials that either emit or are affected by EMI. Shielding efficiency (SE) of materials is determined by measuring electric field strength between a transmitter and receiver with or without the presence of the material under test.

Underwriters' Laboratories (UL) is an independent, nonprofit organization that develops standards for safety in electrical products. UL 746 A, B, and C describe tests and limits for materials used in electrical equipment; UL 746 D lists test requirements for the fabricated plastic parts (263).

Flammability Properties

Plastics have become an important material in the construction industry and are used in areas of insulation, wire coating, flooring materials, and piping; they are also considered for structural components as foam panels and plastic wood. As use in the industry has grown, so has concern about the fire properties of these materials. Tests to determine ignition resistance, flame spread, heat release, and smoke or toxic gas release have been developed. However, the results of these tests are not applicable to the performance of the materials under actual fire conditions. These small-scale tests are intended for quality control and potential hazard ranking. Several organizations that go beyond testing standard bodies such as ASTM or the International Electrotechnical Commission (IEC) have developed tests and/or regulations for the use of plastics in electrical appliances or buildings. A listing of some of these tests is given in ASTM D3814. General fire test terminology is given in ASTM E176. Ignition temperature tests ISO 871 and ASTM D1929 have procedures using small external pilot flames. The limiting oxygen index test has been used in quality control primarily for its good reproducibility, but cannot be used to predict fire performance. ISO 4589 and ASTM D2863 determine the minimum oxygen concentration required to support flaming combustion under set conditions.

UL 94 flame testing of plastics is similar to ASTM D635 for horizontal burn and ASTM D568 and D3801 for vertical burn. UL lists both materials and fabricated products meeting the various 94 requirements in a publication (264). Rate of heat release data are highly important in determining fire behavior, but few tests have been established. Equipment proposed by Factory Mutual has been used in fundamental fire modeling studies (265). The cone calorimeter as described by the National Institute of Standards Technology (NIST) utilizes both vertical and horizontal specimens (266). Refinements of this equipment have allowed testing in the reduced oxygen atmosphere typically found under fire conditions (267). Smoke generation tests have used changes in light absorption of a photoelectric cell within a confined chamber as the primary measurement. Results are reported as percent obscuration or smoke density. Flame or radiant panels can be used as the ignition source in these tests.

Nondestructive Testing

Nondestructive testing of materials is defined as any test that does not damage the plastic piece beyond its intended use. These can be visual and, in some cases, mechanical tests. However, the term is normally used to describe X-ray, nuclear source, ultrasonics, atomic emission, as well as some optical and IR techniques for polymers. Nondestructive testing is used to determine cracks, voids, inclusions, delamination, contamination, lack of cure, anisotropy, residual stresses, and defective bonds or welds in materials.

X-ray techniques can readily determine voids down to 1 mm in diameter and cracks (as long as the plane of the crack is close to the direction of the ray) (268). Nuclear sources and gamma and beta rays have been used to measure the thickness of extruded plastic sheet. For ultrasonics, the frequency used for plastics ranges between 0.5 and 5 MHz. However, isolated defects smaller than a wavelength are difficult to detect with this technique. Ultrasonics have also been used to determine elastic modulus, shear modulus, and Poisson's ratio via the relationship of sound wave velocities through a material (268,269). In studies with blends, the variation of the ultrasonic velocity with composition of a blend is nonlinear where the blend shows incompatibility and linear where it is compatible (270). Holographic interferometry uses an expanded beam of light from a laser source divided by a beam splitter, with one portion hitting the object and the other hitting a recording screen. When both beams are combined at the screen a unique interference pattern is formed. Comparison of this generated image with another of the object under stress produces a fringe pattern for analysis. The maximum depth/diameter ratio for a detectable defect is less than 0.2 (271).

Thermal imaging is sensitive to IR radiation that detects temperature changes over the surface of a part when heat has been applied. Thermal diffusion in a solid is affected by variation in composition or by the presence of cracks, voids, delaminations, etc; the effects are detected by surface temperature changes. Defects cannot be detected if their depth below the surface is more than two to three times their diameter. Nondestructive testing has been primarily used for composites and analysis of adhesive bonds or welds. Several studies are documented in the literature (272–274).

Other Tests

A variety of methods have been used to evaluate diffusion or permeability of gases and solvents with polymers: FTIR spectra of CO_2 allowed the determination of apparent diffusion coefficients of the gas in membranes of rubbery and glassy polymers from desorption kinetics (275); internal reflection FTIR was used to monitor water uptake by a polymer film (276); spin probe techniques have been used in the study of high permeability and high free volume glassy polymers (277); and an *in situ* gravimetric method using an electro-balance was used to determine solubility and diffusivity of gases in polymers over a range of temperatures and pressures (278).

There are other tests for polymers that are not included in this review including some density, filler analysis techniques and other physical tests. For convenience, a listing of ASTM and ISO standards for the major test in this work is provided in the references.

BIBLIOGRAPHY

"Test Methods" in *EPST*, 2nd ed., Vol. 16, pp. 570–576, by G. Neil Spokes, Consultant.

1. J. M. Chalmers and co-workers, *Analyst* **123**, 579–586 (1998).
2. P. C. Painter, M. M. Coleman, and J. L. Koenig, *Theory of Vibrational Spectroscopy with Application to Polymers*, John Wiley & Sons, Inc., New York, 1981.
3. G. Bucci and T. Simonazzi, *J. Polym. Sci. Part C-7* 203 (1964).
4. A. Rjeb and co-workers, *J. Appl. Polym. Sci.* **77**, 1742–1748 (2000).
5. P. Musto and co-workers, *J. Polym. Sci. Part B* **35**, 1055–1066 (1997).
6. M. J. Elwell and A. J. Ryan, *Polymer* **37**, 1353–1361 (1996).
7. J. M. Garcia-Martinez and co-workers, *J. Appl. Polym. Sci.* **73**, 2837–2847 (1999).
8. T. R. Crompton, *The Analysis of Plastics*, Elsevier Science, Inc., Elmsford, N.Y., 1986.
9. D. Battiste and co-workers, *Anal. Chem.* **53**, 2232 (1981).
10. P. J. DesLauriers and co-workers, *Polymer* **43**(1), 159–170 (2002).
11. D. O. Hummel and F. Scholl, *Atlas of Polymers and Plastics Analysis*, 2nd ed., Vol. **1**, Carl Hanover Verlag, Munich, 1978.
12. C. D. Craver, *Infra-Red Spectra of Plasticizers and Other Additives*, 2nd ed., The Coblentz Society, Kirkwood, Mo., 1980.
13. Y. Wang and co-workers, *J. Polym. Sci. Part B* **36**, 783–788 (1998).
14. B. R. Kiland and co-workers, *Polymer* **41**, 1597–1606 (2000).
15. E. E. C. Monteiro and J. Fonseca, *Polym. Test.* **18**, 281–286 (1999).
16. A. C. Middleton and co-workers, *J. Appl. Polym. Sci.* **79**, 1825–1837 (2001).
17. A. Kaito and K. Nakayama, *Macromolecules* **25**, 4882 (1992).
18. J. A. Jansen and co-workers, *Polymer* **35**, 2970 (1994).
19. M. Clayborn and co-workers, *J. Appl. Spectrosc.* **45**, 279 (1991).
20. J. M. Chalmers and co-workers, *Spectrosc. Int. J.* **8**, 13 (1990).
21. J. M. Chalmers and co-workers, *Micron* **27**, 315 (1996).
22. T. Rohe and co-workers, *Talanta* **50**, 283–290 (1999).
23. M. G. Hansen and S. Vedula, *J. Appl. Polym. Sci.* **68**, 859–872 (1998).
24. M. Shenton and co-workers, *Polym. Int.* **49**, 1007–1013 (2000).
25. M. G. Hansen, *SPE ANTEC* **37**, 840 (1991).
26. G. C. Pandey, *Analyst* **112**, 231–232 (1989).
27. F. Eng and C. Shebih, *SPE ANTEC* **35**, 1174 (1989).
28. D. Battiste and co-workers, *Anal. Chem.* **53**, 73 (1981).

29. D. Mathieu and A. Grand, *Polymer* **39**, 5011–5017 (1998).
30. J. P. Tomba and co-workers, *J. Polym. Sci. Part B* **38**, 1013–1023 (2000).
31. T. Sundell and H. Fagerholm, *Polymer* **37**, 3227–3231 (1996).
32. Y. Ward and Y. Mi, *Polymer* **40**, 2465–2468 (1999).
33. R. L. Morgan and co-workers, *Polymer* **42**, 2121–2135 (2001).
34. M. Van and co-workers, *J. Appl. Polym. Sci.* **79**, 426–436 (2001).
35. K. Kober and co-workers, *J. Polym. Sci. Part B* **36**, 2829–2833 (1998).
36. H. Buijs and co-workers, *Am. Lab.* **21**(2), 62–69 (1989).
37. E. Da Silva and M. Tavares, *J. Appl. Sci.* **67**, 449–453 (1999).
38. L. Mendes and co-workers, *Polym. Test.* **15**(1), 53–68 (1996).
39. M. Tavares and L. Mendes, *Polym. Test.* **19**, 399–404 (2000).
40. R. Wu and co-workers, *Polymer* **43**(1), 171–176 (2002).
41. A. Striegel and M. Krejsa, *J. Polym. Sci. Part B* **38**, 3120–3135 (2000).
42. M. Tavares and C. Mothe, *Polym. Test.* **17**, 289–295 (1998).
43. A. Maxwell and co-workers, *Polymer* **39**, 6835–6849 (1998).
44. K. Plochokca and H. Harwood, *ACS Div. Polym. Chem. Pap.* **19**, 240 (1978).
45. I. Pesneau and co-workers, *J. Appl. Sci.* **79**, 1556–1562 (2001).
46. W. Weglarz and co-workers, *J. Polym. Sci. Part B* **38**, 2487–2506 (2000).
47. C. Choi and co-workers, *J. Polym. Sci. Part B* **35**, 2551–2558 (1997).
48. M. Tavares, *Polym. Test.* **19**, 899–904 (2000).
49. S. Lehmann and co-workers, *J. Polym. Sci. Part B* **36**, 693–703 (1998).
50. H. Pasch and K. Rode, *Polymer* **39**, 6377–6383 (1998).
51. U. Fuchslueger and co-workers, *J. Appl. Polym. Sci.* **72**, 913–925 (1999).
52. M. Janco and co-workers, *J. Polym. Sci. Part A* **38**, 2767–2778 (2000).
53. M. Riess and R. van Eldik, *J. Chrom. A* **827**(1), 65–71 (1998).
54. J. C. J. Bart, *Polym. Test.* **20**, 729–740 (2001).
55. F. C.-Y. Wang, *J. Chrom. A* **843**, 413–423 (1999).
56. M. Minagawa and co-workers, *J. Appl. Polym. Sci.* **79**, 473–478 (2001).
57. F. C.-Y. Wang and D. Meunier, *J. Chrom. A.* **888**, 209–217 (2000).
58. R. Lehrle and co-workers, *Polym. Degrad. Stab.* **67**(1), 21–33 (2000).
59. H. Ohtani and co-workers, *Macromolecules* **17**, 465 (1984).
60. F. C. Wang and P. B. Smith, *Anal. Chem.* **68**, 3033 (1996).
61. R. Yang and co-workers, *J. Appl. Polym. Sci.* **81**, 359–363 (2001).
62. D. Weber, *Int. Lab.* **21**, 51 (1991).
63. T. Wampler, *J. Chrom. A* **842**, 207–220 (1999).
64. F. C. Wang, *Anal. Chem.* **71**, 2037 (1999).
65. F. C. Wang, *J. Chrom. A.* **886**, 225–235 (2000).
66. F. C. Wang, *J. Chrom. A.* **883**, 199–210 (2000).
67. F. C. Wang and W. Buzanowski, *J. Chrom. A.* **891**, 313–324 (2000).
68. F. C. Wang, *J. Chrom. A.* **891**, 325–336 (2000).
69. M. A. Robeson and co-workers, *J. Chromatogr.* **505**, 375 (1990).
70. T. Meyer-Dulheuer, Shimadzu Seminar, Duisburg, 1998.
71. J. C. J. Bart, *Polym. Test.* **20**, 729–740 (2001).
72. A. R. Berens and co-workers, *J. Appl. Polym. Sci.* **19**, 3169–3172 (1975).
73. S. W. Bigger and co-workers, Preprints 37th International Symposium on Macromolecules, Gold Coast, 1998, p. 377.
74. B. L. Zimmering and co-workers, *J. Appl. Polym. Sci.* **69**, 1875–1883 (1998).
75. M. J. Carrott and co-workers, *Analyst* **123**, 1827–1833 (1998).
76. J. Hay and co-workers, *Polym. Commun.* **26**(6), 175 (1984).
77. D. Rueda and co-workers, *Calliga. Polym. Lett.* **29**, 9, 258 (1983).
78. N. T. Wakelyn, *J. Polym. Sci., Polym. Lett.* **25**, 25 (1987).
79. B. Goderis and co-workers, *J. Polym. Sci. Part B* **37**, 1715–1738 (1999).

80. G. Bodor and co-workers, *J. Polym. Sci. Part B* **34**, 485–496 (1998).
81. P. Cebe, L. Lowry, and S. Chung, *SPE ANTEC* **35**, 1120 (1989).
82. O. Krathy, in O. Glatter and O. Krathy, eds., *Small-Angle X-Ray Scattering*, Academic Press, Inc., New York, 1982.
83. J. Barnes and F. Mopsik, *SPE ANTEC* **34**, 1178 (1988).
84. R. Xie, B. Yang, and B. Jiang, *J. Polym. Sci. Part B* **34**, 1489–1499 (1996).
85. I. Campoy, M. Gomez, and C. Marco, *Polymer* **41**, 2295–2299 (2000).
86. C.-I. Huang and J.-R. Chen, *J. Polym. Sci. Part B* **39**, 2705–2715 (2001).
87. M. Song and co-workers, *J. Appl. Polym. Sci.* **79**, 1958–1964 (2001).
88. M. Ishaq, J. Blackwell, and S. Chvalun, *Polymer* **37**, 477–483 (1996).
89. A. Kawaguchi and co-workers, *J. Polym. Sci. Part B* **38**, 838–845 (2000).
90. M. A. Jones, T. P. Russell, and D. Y. Yoon, Proceedings of Polymer Material Science & Engineering, San Diego, Calif., 1993, p. 394.
91. P. G. deGennes, *Scaling Concepts in Polymer Physics*, Cornell University Press, Ithaca, New York, 1979.
92. M. A. Jones, T. P. Russell, and D. Y. Yoon, Proceedings of Polymer Material Science & Engineering, San Diego, Calif., 1993, p. 396.
93. J. Maugey, T. Van Nuland, and P. Navard, *Polymer* **42**, 4353–4366 (2001).
94. K. Wallheinke and co-workers, *Polym. Test.* **17**, 247–255 (1998).
95. K. Swaminathan and D. Marr, *J. Appl. Polym. Sci.* **78**, 452–457 (2000).
96. D. Raghavan and co-workers, *J. Polym. Sci. Part B* **39**, 1460–1470 (2001).
97. S. Gould and co-workers, *J. Appl. Polym. Sci.* **74**, 2243–2254 (1999).
98. M. Zhang and co-workers, *J. Appl. Polym. Sci.* **80**, 2218–2227 (2001).
99. J. Feng and co-workers, *Polymer* **42**, 2259–2262 (2001).
100. G. Merle and co-workers, *Polym. Test.* **18**, 217–229 (1999).
101. F. Oulevey and co-workers, *Polymer* **41**, 3087–3092 (2000).
102. H. Oyama, T. Solberg, and J. Wightman, *Polymer* **40**, 3001–3011 (1999).
103. Z. Veksli, M. Andreis, and B. Rakvin, *Prog. Polym. Sci.* **25**, 949–986 (2000).
104. Z. Veksli, M. Andreis, and D. Campbell, *Polymer* **39**, 2083–2088 (1998).
105. G. Muller, R. Stadler, and S. Schlick, *Makromol. Chem. Rapid Commun.* **13**(2), 117–124 (1992).
106. G. G. Cameron and co-workers, *Eur. Polym J.* **27**, 1181–1186 (1991).
107. H. Tenhu and K. Voahtera, *Eur. Polym. J.* **27**, 717–722 (1991).
108. W. P. Chen and S. Schlick, *Polymer* **31**, 308–314 (1990).
109. S. Commereuc and co-workers, *J. Appl. Polym. Sci.* **69**, 1107–1114 (1998).
110. T. Dumelow, S. R. Holding, and L. J. Maisey, *Polymer* **24**, 307 (1983).
111. W. C. Taylor and L. H. Tung, Paper presented at 140th Meeting of the American Chemical Society, Chicago, Ill., 1961.
112. R. Russ, K. Guo, and L. Delong, *SPE ANTEC* **34**, 983 (1988).
113. V. Shah, *Handbook of Plastics Testing Technology*, John Wiley & Sons, Inc., New York, 1984, p. 179.
114. J. Choi, *SPE ANTEC* **34**, 1013 (1988).
115. J. M. Guenet and co-workers, *J. Appl. Polym. Sci.* **21**, 2181 (1977).
116. S. Mori, *Anal. Chem.* **61**, 1321–1325 (1989).
117. J. Sebastian and R. Register, *J. Appl. Polym. Sci.* **82**, 2056–2069 (2001).
118. J. L. Viony and J. Lesec, in A. Abe, ed., *Advances in Polymer Science*, Springer-Verlag, Berlin, 1994.
119. L. Verdurmen-Noel, L. Baldo, and S. Bremmers, *Polymer* **42**, 5523–5529 (2001).
120. M. Montaudo, *Polymer* **43**, 1587–1597 (2002).
121. S. Podzimek and T. Vlcek, *J. Appl. Polym. Sci.* **82**, 454–460 (2001).
122. S. Podzimek, T. Vlcek, and C. Johann, *J. Appl. Polym. Sci.* **81**, 1588–1594 (2001).
123. L. Wold and co-workers, *J. Polym. Sci., Polym. Phys.* **20**, 441 (1982).

124. L. Britto and co-workers, *J. Polym. Sci. Part B* **37**, 539–552 (1999).
125. B. Gabriel and D. Lilge, *Polymer* **42**, 297–303 (2001).
126. J. Soares, R. Abbott, and J. Kim, *J. Polym. Sci. Part B* **38**, 1267–1275 (2000).
127. A. R. McGhie, in R. G. Linford, ed., *Thermal Analysis Techniques in Electrochemical Science and Technology of Polymers-2*, Elsevier Publishing Co., Inc., New York, 1990, p. 202.
128. J. Chiu, *Appl. Polym. Symp.* **2**, 25 (1966).
129. L. H. Perng, *J. Polym. Sci. Part A* **38**, 583–593 (2000).
130. P. Moulinie and co-workers, *Polym. Test.* **15**(1), 75–89 (1996).
131. C. A. Wilkie, *Polym. Degrad. Stab.* **66**, 301–306 (1999).
132. L. H. Perng, *J. Appl. Polym. Sci.* **79**, 1151–1161 (2001).
133. J. J. Maurer, in E. Turi, ed., *Thermal Characterization of Polymeric Materials*, Academic Press, Inc., New York, 1981, p. 585.
134. H. E. Bair, in E. Turi, ed., *Thermal Characterization of Polymeric Materials*, Academic Press, Inc., New York, 1981, p. 845.
135. M. P. Sepe, in N. P. Cheremisinoff, ed., *Elastomer Technology Handbook*, CRC Press, Inc., Boca Raton, Fla., 1993, p. 139.
136. M. P. Sepe, in N. P. Cheremisinoff, ed., *Elastomer Technology Handbook*, CRC Press, Inc., Boca Raton, Fla., 1993, p. 148.
137. Rosa and co-workers, *Polym. Test.* **19**, 523–531 (2000).
138. J. Rodriguez-Cabello and co-workers, *J. Appl. Polym. Sci.* **60**, 1709–1717 (1996).
139. R. Phillips and J. A. Manson, *J. Polym. Sci. Part B* **35**, 875–888 (1997).
140. K. Jokela and co-workers, *J. Polym. Sci. Part B* **39**, 1860–1875 (2001).
141. J. L. Vilas and co-workers, *J. Appl. Polym. Sci.* **79**, 447–457 (2001).
142. S. Li, E. Vuorimaa and H. Lemmetyinen, *J. Appl. Polym. Sci.* **81**, 1474–1480 (2001).
143. K. de la Caba and co-workers, *Polym. Int.* **45**, 333–338 (1998).
144. J. H. Hou and J. M. Bai, *SPE ANTEC* **33**, 946 (1987).
145. B. Wunderlich, in E. Turi, ed., *Thermal Characterization of Polymeric Materials*, Academic Press, Inc., New York, 1981, Chapts. "2" and "3".
146. P. Soni, SPE Seminars, Chicago, Ill., June, 1991.
147. L. C. E. Struik, *Physical Aging in Amorphous Polymers and Other Materials*, Elsevier, Amsterdam, the Netherlands, 1978.
148. J. J. Maurer, in E. Turi, ed., *Thermal Characterization of Polymeric Materials*, Academic Press, Inc., New York, 1981, Chapt. "6".
149. S. W. Shalaby and H. E. Bair, in E. Turi, ed., *Thermal Characterization of Polymeric Materials*, Academic Press, Inc., New York, 1981, Chapt. "4".
150. H. E. Bair, *Polym. Eng. Sci.* **14**, 202 (1974).
151. M. Song, A. Hammiche, and H. Pollock, *Polymer* **37**, 5661–5665 (1996).
152. A. Vatalis and co-workers, *Thermochem. Acta* **372**(1/2), 33–38 (2001).
153. T. G. Fox, *Bull. Am. Phys. Soc.* **1**(2), 123 (1956).
154. M. Gordon and J. S. Taylor, *J. Appl. Chem.* **2**, 493 (1952).
155. P. R. Couchman, *Macromolecules* **11**, 1156 (1978).
156. J. Janimak and G. Stevens, *Thermochim. Acta* **332**(2), 125–142 (1999).
157. M. Song, *J. Appl. Polym. Sci.* **81**, 2779–2785 (2001).
158. I. Okazaki and B. Wunderlich, *J. Polym. Sci. Part B* **34**, 2941–2952 (1996).
159. M. P. Sepe, in N. P. Cheremisinoff, ed., *Elastomer Technology Handbook*, CRC Press, Inc., Boca Raton, Fla., 1993, p. 157.
160. M. P. Sepe, in N. P. Cheremisinoff, ed., *Elastomer Technology Handbook*, CRC Press, Inc., Boca Raton, Fla., 1993, p. 165.
161. R. W. Thomas and M. W. Cadwallader, Technical data, TA Instruments Hotline, Wilmington, Del., June, 1990.

162. J. Gearing, in R. Brown, ed, *Handbook of Polymer Testing*, Marcel Dekker, Inc., New York, 1999, p. 501.
163. A. R. McGhie, in R. Linford, ed., *Electrochemical Science and Technology of Polymers-2*, Elsevier Applied Science Publishers, Ltd., London, 1990, p. 218.
164. C. Rohm and P. Herh, *SPE ANTEC* **34**, 1135 (1988).
165. J. D. Ferry, *Viscoelastic Properties of Polymers*, 3rd ed., John Wiley & Sons, Inc., New York, 1980.
166. L. H. Sperling, *Introduction to Physical Polymer Science*, John Wiley & Sons, Inc., New York, 1986, p. 384.
167. A. R. McGhie, in R. Linford, ed., *Electrochemical Science and Technology of Polymers-2*, Elsevier Applied Science Publishers, Ltd., London, 1990, p. 266.
168. C. L. Rohn, *SPE ANTEC* **35**, 870 (1989).
169. A. R. McGhie, in R. Linford, ed., *Electrochemical Science and Technology of Polymers-2*, Elsevier Applied Science Publishers, Ltd., London, 1990, p. 204.
170. C. D. Han and co-workers, *Macromolecules* **22**, 3443–3451 (1989).
171. J. Sahai, K. Nakamura, and S. Inoue, *SPE ANTEC* **36**, 1912 (1990).
172. M. P. Sepe, in N. P. Cheremisinoff, ed., *Elastomer Technology Handbook*, CRC Press, Inc., Boca Raton, Fla., 1993, p. 220.
173. Y. Feng, X. Jin, and J. Hay, *J. Appl. Polym. Sci.* **68**, 395–401 (1998).
174. S. Simon, G. Mckenna, and O. Sindt, *J. Appl. Polym. Sci.* **76**, 495–508. (2000).
175. S. Markovic and co-workers, *J. Appl. Polym. Sci.* **81**, 1902–1913 (2001).
176. J. Hiltz, S. Kuzak, and P. Waitkus, *J. Appl. Polym. Sci.* **79**(3), 385–395 (2001).
177. K. Lozano and E. Barrera, *J. Appl. Polym. Sci.* **79**(1), 125–133 (2001).
178. S. Diez-Gutierrez and co-workers, *Polymer* **40**(19), 5345–5353 (1999).
179. M. D. Shelby and co-workers, *J. Polym. Sci. Part B* **39**(1), 32–46 (2001).
180. K.-H. Nitta and A. Tanaka, *Polymer* **43**, 1219–1226 (2001).
181. O. Fri cova and co-workers, *Acta Polym.* **49**, 495–501 (1998).
182. M. Rodriguez-Perez and J. de Saja, *Polym. Test.* **19**, 831–848 (2000).
183. W. Xie and co-workers, *Thermochem. Acta* **367–368**, 135/142 (2001).
184. M. Song and co-workers, *J. Appl. Polym. Sci.* **81**, 2136–2141 (2001).
185. A. Uedono and co-workers, *J. Polym. Sci. Part B* **36**, 1919–1925 (1998).
186. P. Ramachandra and co-workers, *Polymer* **37**, 3233–3239 (1996).
187. T.-T. Hsieh, C. Tiu, and G. Simon, *J. Appl. Polym. Sci.* **82**, 2252–2267 (2001).
188. W. J. Davis and R. A. Pethrick, *Polym. Int.* **45**, 395–402 (1998).
189. H. Higuchi, A. Jamieson, and R. Simha, *J. Polym. Sci. Part B* **34**, 1423–1426 (1996).
190. J. Borek and W. Osoba, *J. Polym. Sci. Part B* **34**, 1903–1906 (1996).
191. H. Mohamed and N. Abd El-Aziz, *Polymer* **42**, 8013–8017 (2001).
192. G. Dlubek and co-workers, *J. Polym. Sci. Part B* **40**(1), 65–81 (2002).
193. J. C. Machado and co-workers, *J. Polym. Sci. Part B* **38**, 1045–1052 (2000).
194. P. K. Fearon and co-workers, *J. Appl. Polym. Sci.* **79**, 1986–1993 (2001).
195. G. Ablblad and co-workers, *Polym. Test.* **16**(1), 59–73 (1997).
196. K. Jacobson and co-workers, *Polym. Test.* **18**, 523–531 (1999).
197. D. Kockott, *Polym. Test.* **20**, 725–727 (2001).
198. D. Crofts, RAPRA Research Report, No. 200, Rubber and Plastics Research Association, Shrewsburg, U.K., 1972.
199. G. Locati, S. Poggio, and J. Rathenow, *Polym. Test.* **16**, 363–377 (1997).
200. J. A. Brydson, *Flow Properties of Polymer Melts*, 2nd ed., Godwin/Plastics and Rubber Institute, 1981.
201. H. Takahashi, T. Matsuoka, and T. Kurauchi, *J. Appl. Polym. Sci.* **30**, 4669 (1985).
202. Dow Chemical Company, Technical data, Midland, Mich., 1993.
203. M. A. Couch and D. M. Binding, *Polymer* **41**, 6323–6334 (2000).

204. N. Sombatsompop and N.-T. Intawong, *Polym. Test.* **20**(1), 97–103 (2000).
205. J.-Z. Liang, *Polym. Test.* **20**(1), 29–31 (2000).
206. K. T. Paul, *RAPRA Bulletin*, Rubber and Plastics Research Association, Shrewsburg, U.K., Feb. 1972.
207. B. J. Furches and G. Kachin, *SPE ANTEC* **35**, 1663 (1989).
208. R. J. Groleau, *SPE ANTEC* **35**, 1183 (1989).
209. J. Covas, J. Nobrega, and J. Maia, *Polym. Test.* **19**(2), 165–176 (2000).
210. P. Starch and P. Kantla, *Kem-Kemi* **3**(2), 175–178 (1976).
211. Y. Mao and co-workers, *J. Appl. Polym. Sci.* **82**(1), 63–69 (2001).
212. R. Pantani and G. Titomanlio, *J. Appl. Polym. Sci.* **81**, 267–278 (2001).
213. J. Suhm and co-workers, *Acta Polym.* **49**(2/3), 80–87 (1998).
214. MOLDFLOW, Moldflow Australia, Victoria, Australia.
215. C-MOLD, AC Technology, Ithaca, N.Y., IDEAS, Structural Dynamics Research Corp., Cincinnati, Ohio.
216. F. Romani and co-workers, *Polymer* **43**, 1115–1131 (2002).
217. G. Dean and B. Read, *Polym. Test.* **20**, 677–683 (2001).
218. S. Bastida and co-workers, *Polym. Test.* **17**(2), 139–145 (1998).
219. S. Jafari and A. Gupta, *J. Appl. Polym Sci.* **78**, 962–971 (2000).
220. F. Ramsteiner, *Polym. Test.* **18**, 641–647 (1999).
221. A. V. Shenoy and D. R. Saini, *Polym. Test.* **6**(1), 37–45 (1986).
222. W. Grellmann and M. Che, *J. Appl. Polym. Sci.* **66**, 1237–1249 (1997).
223. W. Li, R. Li, and S. Tjong, *Polym. Test.* **16**, 563–574 (1998).
224. S. Seidler and W. Grellmann, *Polym. Test.* **14**, 453–469 (1995).
225. K. Kendall, W. J. Clegg, and R. D. Gregory, *J. Mater. Sci. Lett.* **10**, 671–682 (1991).
226. S. W. Hawley, *RAPRA Rev. Rep.* **5**(12), 14 (1992).
227. J. d'Almeida and S. Monteiro, *Polym. Test.* **18**, 407–414 (1999).
228. F. Ramsteiner and T. Armbrust, *Polym. Test.* **20**, 321–327 (2001).
229. A. Stearn, M. Novotny, and R. Lang, *Polym. Test.* **17**, 403–422 (1998).
230. A. Stearn, M. Novotny, and R. Lang, *Polym. Test.* **17**, 423–441 (1998).
231. F. Ramsteiner, *Polym. Test.* **15**, 573–584 (1996).
232. C. Bernal, P. Montemartini, and P. Frontini, *J. Polym. Sci. Part B* **34**, 1869–1880 (1996).
233. G. C. Adams and co-workers, *Polym. Eng. Sci.* **30**(4), 24–28 (1990).
234. D. B. Barry and O. Delatycki, *J. Appl. Polym. Sci.* **38**, 339–350 (1989).
235. Y.-W. Mai and P. Powell, *J. Polym. Sci., Polym. Phys.* **29**, 785–793 (1991).
236. I. Low, G. Paglia, and C. Shi, *J. Appl. Polym. Sci.* **70**, 2349–2352 (1998).
237. A. Flores and co-workers, *Polymer* **41**, 5431–5435 (2000).
238. S. Fakirov, F. Calleja, and M. Krumova, *J. Polym. Sci. Part B.* **37**, 1413–1419 (1999).
239. C. Xiang and co-workers, *J. Polym. Sci. Part B* **39**(1), 47–59 (2000).
240. R. Brown, *Polym. Test.* **14**, 403–414 (1995).
241. R. J. Roe and C. Gievewski, *Polym. Eng. Sci.* **15**(6), 197 (1975).
242. K. Takahashi, A. E. Abo-El-Ezz, and N. Takeda, Proceedings of the 7th International Conference, Cambridge, U.K., 1988, pp. 29/1–29/4.
243. J. Strebel, *Polym. Test.* **14**, 189–202 (1995).
244. E. Moskala, *Polymer* **39**, 675–680 (1998).
245. ISO 4599, Plastics: Determination of Resistance to Environmental Stress-Cracking, Bent Strip Method, ISO, Geneva, Switzerland, 1986.
246. R. P. Brown, ed., *Handbook of Plastics Test Methods*, 3rd ed., John Wiley & Sons, Inc., New York, 1988, p. 354.
247. D. Kiessling and W. Schaaf, *Plast. u. Kaut.* **33**, 310–313 (1986).

248. A. Turnbull, A. Maxwell, and S. Pillai, *Polym. Test.* **19**(2), 117–129 (2000).
249. I. Jakubowica and co-workers, *Polym. Test.* **19**, 729–753 (2000).
250. T. Kobayashi and co-workers, *Kobunshi Ronbun* **42**, 405–413 (1985).
251. J. Boxhammer, *Polym. Test.* **20**, 719–724 (2001).
252. Ref. 246, pp. 271–272.
253. J. M. Garcia and co-workers, *J. Polym. Sci. Part B* **35**, 457–468 (1997).
254. T. R. Manley, J. A. Stonebanks, and P. Laggon, *Polym. Commun.* **28**, 17 (1988).
255. R. Sharma and co-workers, *J. Appl. Polym. Sci.* **68**, 553–560 (1998).
256. A. Bernes and C. Locahanne, in S. E. Keithwath, ed., *Order in the Amorphous State of Polymers*, Plenum Publishing Corp., New York, 1987, p. 305.
257. P. Bartolomeo, J. Chailan and J. Vernet, *J. Polym. Sci. Part B* **38**, 2162–2169 (2000).
258. A. Maxwell, L. Monnerie, and I. Ward, *Polymer* **39**, 6851–6859 (1998).
259. R. Diaz-Calleja, J. De Abajo, and J. de la Campa, *J. Polym. Sci. Part B* **35**, 919–927 (1997).
260. F. Tihminlioglu and co-workers, *J. Polym. Sci. Part B* **35**, 1279–1290 (1997).
261. A. Voelkel and co-workers, *Polymer* **37**, 455–462 (1996).
262. Ref. 246, p. 258.
263. UL 746 A–D, Underwriters Laboratories, Chicago, Ill., 2000/2001.
264. UL 94, Underwriters Laboratories, Chicago, Ill., May 2001.
265. A. Tewarson and R. F. Pion, *Combust. Flame* **26**, 85 (1976).
266. V. Brabraushas, NBSIR 82-2611, U.S. Bureau of Commerce, National Bureau of Standards (now NIST), Washington, D.C., 1982.
267. N. Batho, personal communication, Dark Star Research, Penley, Clwyd, U.K., Mar. 1992.
268. W. N. Reynolds, *RAPRA Rev. Rep.* **3**(2), 30 (1990).
269. A. Sahnoune, F. Massines, and L. Piche, *J. Polym. Sci. Part B* **34**, 341–348 (1996).
270. G. V. Thomas and M. Nair, *J. Appl. Polym. Sci.* **69**, 785–790 (1998).
271. W. N. Reynolds, *RAPRA Rev. Rep.* **3**(2), 30/12 (1990).
272. Y. Bar-Cohen, C. C. Yin, and A. K. Mal, J. Adhesion, **29**, 257–274 (1989).
273. J. Summerscales, ed., *Nondestructive Testing of Fibre-Reinforced Plastic Composites*, Vol. **1**, Elsevier Applied Science Publishers, Ltd., Barking, U.K., 1987, pp. 278, 627–629.
274. W. N. Reynolds, *Mat. Des.* **5/6**, 256–270 (1985).
275. A. Higuchi and co-workers, *J. Polym. Sci. Part B* **34**, 2153–2160 (1996).
276. I. Linossier and co-workers, *J. Appl. Polym. Sci.* **66**, 2465–2473 (1997).
277. Y. P. Yampolskii and co-workers, *Polymer* **40**, 1745–1752 (1999).
278. B. Wong, Z. Zhang, and Y. Handa, *J. Polym. Sci. Part B* **36**, 2025–2032 (1998).

GENERAL REFERENCES

T. R. Crompton, *Analysis of Polymers, An Introduction*, Pergamon Press, Inc., Oxford, 1989.
D. O. Hummel and A. Solti, *Atlas of Polymer and Plastics Analysis*, Vol. **2**, VCH Publishers, New York, 1988.
M. P. Sepe, *Dynamic Mechanical Analysis for Plastics Engineering*, Plastics Design Library, Norwich, New York, 1998.
E. Turi, ed., *Thermal Characterization of Polymeric Materials*, Academic Press, Inc., New York, 1997.
R. P. Brown, ed., *Handbook of Polymer Testing*, Marcel Dekker, New York, 1998.

ASTM Volumes 8.01–8.03, Testing of Plastics, ASTM, Philadelphia, Pa. (published annually).
T. P. Wampler, ed., *Analytical Pyrolysis Handbook*, Marcel Dekker, New York, 1995.
F. A. Bovey and P. A. Miaree, *NMR of Polymers*, Academic Press, New York, 1996.
J. G. Williams, *Fracture Mechanics of Polymers*, John Wiley & Sons, Inc., New York, 1987.

BARBARA J. FURCHES
The Dow Chemical Company

TETRAFLUOROETHYLENE POLYMERS. See PERFLUORINATED POLYMERS.

THERMOFORMING

Introduction

Thermoforming is the art and science of forming commercial products by heating plastic sheet to a softened, pliable state, pressing the sheet against a cool mold, holding the formed sheet against the mold until rigid, and trimming the formed part from the web or skeleton surrounding it. Nearly all unfilled or unreinforced thermoplastics are formed in this manner on conventional equipment. Newer forming technologies are used to form filled and reinforced thermoplastics and certain thermosetting polymers. In general, thermoforming is used when large surface area-to-wall thickness parts are needed, when rapid evaluation of product designs are sought, when very high production rates of thin-walled parts are desired, and when a few to a few hundred thick-walled parts are needed.

Although commercial thermoforming, sometimes called *vacuum forming* or *swedging*, was not developed until the 1870s, when cellulose nitrate was first cut into thin sheets, Egyptians, Pacific natives, and American Inuits formed naturally occurring tortoise sheet and tree bark or natural cellulose into bowls and boats long before then (1).

In the 1870s, cellulose sheet was formed using metal molds and steam as the heating and forming medium (2,3). The earliest products were baby rattles, toys, mirror cases, and hairbrush backs. In the early 1900s, piano keys were drape-formed over captive wooden cores. In 1930, Fernplas Corp. patented a bottle fabricated from two thermoformed halves. Relief maps for the U.S. Coast and Geodetic Survey were thermoformed of cellulose acetate in the 1930s. The first automatic roll-fed thermoformer was sold by Clauss B. Strauch Co., in 1938, to manufacture cigarette tips and ice-cube trays. The heating, bending, and shaping of plastic sheet were taught in high school industrial art courses in the late 1930s (4).

Encyclopedia of Polymer Science and Technology. Copyright John Wiley & Sons, Inc. All rights reserved.

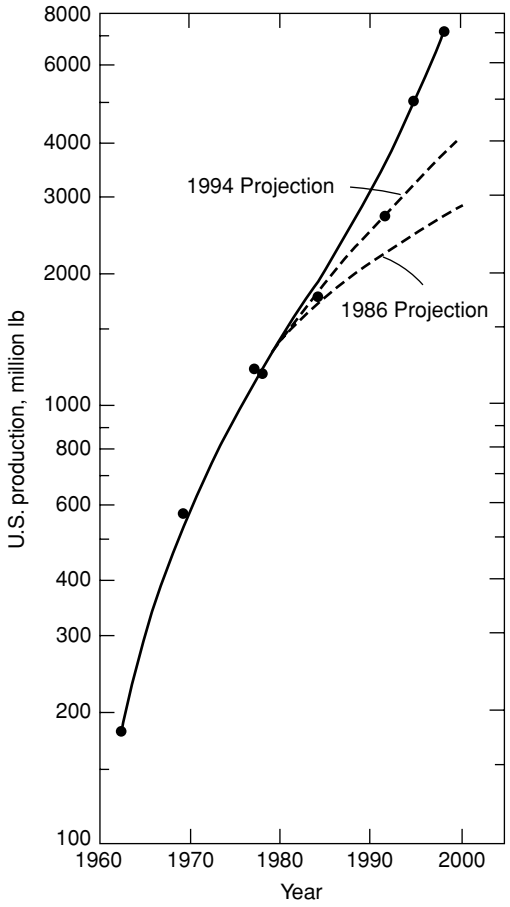

Fig. 1. Thermoforming production in the United States (7). 1 million lb = 455,000 t. Redrawn and used with permission of Hanser Publications.

The Second World War accelerated interest in thermoforming, with the demand for cast poly(methyl methacrylate) fighter/bomber windows, gun closure and windscreens (5).

By the mid-1950s, thermoformed blister packages and food containers of polystyrene were found in most grocery stores. In 1962, approximately 77,000 t of plastic was thermoformed in the United States. By 1998, approximately 2.9 million metric tons of plastic were thermoformed in North America (6) (Fig. 1). This is a sustained annual growth rate of about 10% over nearly four decades. An additional 4.55 million metric tons are thermoformed worldwide. The total world market is estimated to have a value of about US$ 35,000 million.

Thermoforming is typically bifurcated into thin-gauge thermoforming and heavy- or thick-gauge thermoforming. As seen in Table 1, thin-gauge thermoforming uses sheet 1.5 mm or less in thickness, with its primary products being packaging containers. Typical disposable products include blister packages, point-of-purchase containers, bubble packages, slip sleeve containers, auto/video

Table 1. Thermoforming Categorization[a]

Item	Thin-gauge	Heavy-gauge
Sheet thickness range	Less than 1.5 mm	Greater than 3.0 mm
Dominant products	Packaging, disposables	Cabinetry, industrial
Sheet handling	Rolls	Palletized cut sheet
Typical machine type	In-line former, trimmer	Shuttle or rotary press
Press size	To 0.8 × 2 m	To 4 × 6 m or more
Machine control aspects	Automated	Automated to manual
Controlling aspect, heating	Heater output	Conduction into sheet
Heater type	Electric, ceramic, quartz	Electric, catalytic gas, forced hot air
Pattern heating	Not usually done	Common
Part size tendency	Small	Medium to very large
Number of mold cavities	Many to a hundred	One or two, usually
Mechanical assist	Plug	Plug, billow, vacuum box
Mold type	Female, usually	Male, female, mixed
Mold materials	Aluminum, machined	Wood, plaster, syntactic foam, white metal, cast aluminum
Mold cooling	Active, controlled	Active to none for prototype
Free surface cooling	Ambient, usually	Forced air, fogging
Trimming aspects	Punch and die, rim roll	Multiaxis routing
Nonproduct trim level	About 50%	About 25–30%
Wall thickness tolerance, normal	20%	20%
Wall thickness tolerance, tight	10%	10%
Pressure forming application	Deep draw, formed rim	Textured surfaces, deep draw

[a]Ref. 8.

cassette cases, hand and power tool cases, cosmetic cases, meat and poultry containers, unit serving containers, convertible-oven food serving trays, wide-mouth jars, vending machine hot and cold drink cups, egg cartons, produce and wine bottle separators, medicinal unit dose portion containers, and form, fill, and seal (FFS) containers for foodstuffs, hardware supplies, medicine, and medicinal supplies.

Heavy-gauge thermoforming uses sheet 3 mm or more in thickness, with primary products being permanent or industrial products. Typical products include equipment cabinets for medical and electronic equipment, tote bins, single and double deck pallets, transport trays, automotive inner-liners, headliners, shelves, instrument panel skins, aircraft cabin wall panels, overhead compartment doors, snowmobile and motorcycle shrouds, fairings and windshields, marine seating, locaters and windshields, golf cart, tractor, and RV shrouds, skylights, shutters, bath and tub surrounds, lavys, single- and double-wall shipping containers and pallets, storage modules, exterior signs, swimming and wading pools, landscaping pond shells, luggage, gun and gulf club cases, boat hulls, animal carriers, and seating of all types.

There is a growing but very still limited market for products formed from sheet between about 1.5 mm (thin-gauge) and 3.0 mm (heavy-gauge) thickness. Usually, products of this thickness are either too expensive to be disposable or too thin to be industrial or permanent products. One major application is in the manufacturing of very large volume drink cups (1/2 L or more).

Currently thin-gauge thermoforming accounts for about three-quarters of all sheet formed, in both tonnage and dollar volume. Thin-gauge thermoforming companies tend to be very large with broad spectra of products. Furthermore, companies that manufacture products may also do in-house thin-gauge thermoforming for the packages for these products. Heavy-gauge thermoforming companies tend to be small with narrow product lines. As a result, there are many more heavy-gauge thermoforming companies than thin-gauge thermoforming companies. In 2001, it was estimated that there were about 500 heavy-gauge thermoforming companies and less than 200 thin-gauge thermoforming companies in North America (9).

As outlined in Table 1, there are substantial differences in the characteristics of these two thermoforming categories. In addition to the sheet thickness criterion, there is a difference in the way the sheet is presented to the thermoforming machine. Thin sheet is usually delivered in rolls of up to 3000 m in length, weighing up to 2300 kg and having diameters up to 1.5 m. The sheet is fed continuously into the thermoforming machines that are usually called roll-fed machines. Thick sheet is usually guillotine-cut to size and palletized. The individual sheets are then loaded manually or pneumatically into the thermoforming machines, known as cut-sheet machines.

Thermoforming is a competitive technology. In thin-gauge it competes with paper, paperboard, plastic-coated paper and paperboard, paper pulp, expanded polystyrene foam, aluminum foil, and roll-sheet steel. It also competes with plastics extrusion, compression molding, stretch-blow molding, injection molding, and injection-blow molding. In heavy-gauge, it competes with injection molding, rotational molding, blow molding, fiberglass-reinforced polyester resin spray-up molding and lay-up molding, compression molding, sheet compound molding, bulk compound molding, sheet metal forming, and metal die casting.

When compared to other technologies, thermoforming offers many advantages: there is a wide variety of polymers from which to choose; molds are single-sided and are thus less expensive than injection molds; the time from concept to final part acceptance is usually quite short; there are many available mold materials; aluminum—the mold material of choice—is lightweight, has a high thermal conductivity, is relatively inexpensive, and is easy to machine and cast; processing temperatures are low; processing pressures are very low; mold detail replication is good; part surface area-to-wall thickness is extremely high; and there are many excellent trimming techniques (10).

However, thermoforming has some serious limitations. Among others, the polymer of choice may not be extrudable or may sag too much during heating in the thermoforming machine; there is additional cost in producing sheet; the unused portion of the sheet—the trim, web, or skeleton—must be recycled to keep sheet costs reasonable; because of the end-use of the product (medical, pharmaceutical, foodstuffs), recycling of the trim may not be acceptable, it may not be possible to stretch the sheet sufficiently to achieve the desired part shape, part wall thickness is not well-controlled or predictable, and is not uniform across the part; wall thickness cannot be changed locally through design; surface texture may be required on both sides of the part; the part performance criteria may required reinforced or highly filled polymers; the part tolerance, edge radii, and draft angles may be unacceptably tight for the thermoforming process; and there

may be other processes that are more economically attractive. A general comparison of four thermoplastic processes is given in Table 2 (see INJECTION MOLDING; BLOW MOLDING).

Machinery

The specific details of thermoforming machinery depend on whether thin-gauge or heavy-gauge parts are fabricated. However, all machines include some form of sheet handling device, some way of moving the sheet from one station to another, a sheet heating oven, a vacuum system, a forming press containing the mold assembly, a formed part removal region, and a system for controlling the various elements of the machine that allow sheet transfer from one station to another. In addition, the machines may include some form of sheet prestretching, such as a preblowing step or mechanical pushers or plugs, a pressure system, a mold cooling system, a trimming press, and some form of trim removal.

Thin-Gauge Machines. The schematic in Figure 2 illustrates the most common thin-gauge thermoforming machine arrangement. The sheet, delivered as a roll, is indexed through the machine on pins that are arranged along parallel or near-parallel lengths of continuous link chains. The sheet is usually uniformly heated from both top and bottom with infrared heaters. Most commercial machines use ceramic bricks or tiles, metal plate heaters, metal rod heaters, quartz tubes, or quartz plate heaters as energy sources. Typically, the ovens accommodate two or more "shots" or forming stops. Once the sheet is at the forming temperature, it is indexed into the forming press. The forming press contains at least one platen with the desired mold assembly. If the parts being formed require matched forming, as is the case with low density foam sheet, a second platen contains the matching mold assembly. If not, the second platen may contain a pressure box, a

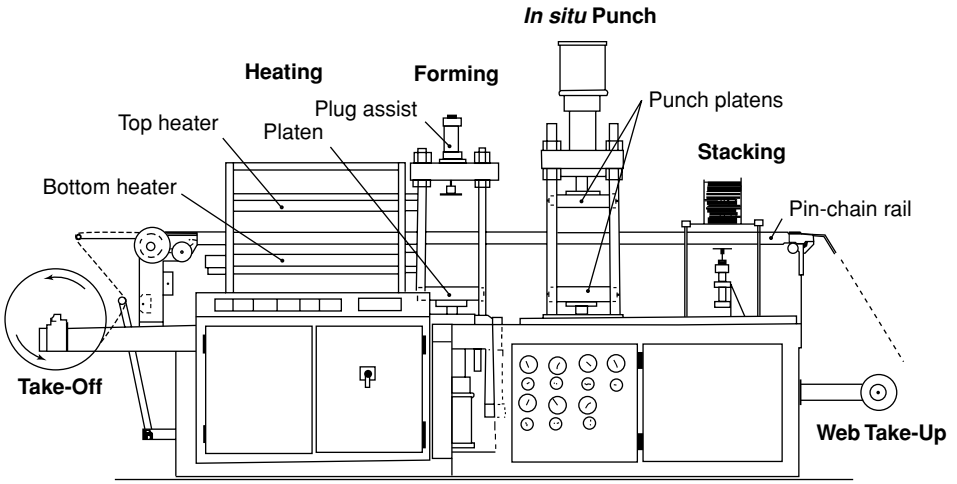

Fig. 2. Schematic of small thin-gauge thermoforming machine (Kiefel GmbH, Freilassing, Germany). Used with permission of Hanser Publications.

Table 2. Comparison of Four Thermoplastic Processes[a]

Characteristic	Thermoforming	Injection molding	Blow molding	Rotational molding
Polymer form	Sheet	Pellets	Pellets	Powder
Variety of polymer	Good to excellent	Excellent	Good	Fair to limited
Raw material cost	Polymer + sheet extrusion	Standard	Standard	Polymer + grinding
Variety of mold materials	Very many	Very limited	Limited	Many
Mold cost	Moderate to low	Highest	High	Moderate to low
Production mold material	Aluminum	Steel	Aluminum	Aluminum, steel
Thermal cycling of mold	Gentle	Moderate	Moderate	Severe
Process key	Rubbery solid sheet	Viscoelastic liquid	Elastic liquid	Melting Powder
Cycle time	Moderate to short	Very short	Moderate	Very long
Man/machine interaction	Normally high	Nil to low	Low	Very high
Part wall uniformity	Fair to poor	Excellent	Poor to fair	Good to excellent
Major design problems	3D corner, wall thickness uniformity	Gating, weld line	Pinch-off, wall uniformity	Porosity
Part failure mode	Thin corners, microcracks	Weld line	Thin side walls, poor pinch-off	Poor tensile strength
Operating pressure, MPa[b]	−0.1 to 0.5	10 to 100	0.5 to 2.5	0 to 0.1
Operating temperature, °C	50 to 250	150 to 300	100 to 250	200 to 350
Filling methods	Manual to automatic	Automatic	Automatic	Manual
Part removal methods	Manual to automatic	Automatic	Automatic	Manual
Flash, trim	Highest	Low to nil	Moderate to high	Moderate to low
Inserts	Possible	Feasible	Feasible	Usual
Orientation in part	Highest	Moderate to high	High to moderate	Unoriented
Stress retention	Highest	High	High to very high	None to little
Shrinkage, warpage	High to moderate	Controllable	Moderate to high	High
Part design advantage	Very thin walls	Wide variation in part wall thickness	Hollow parts	Very large hollow parts
Part characteristic	Single-sided	Both sides finished	Single-sided	Single-sided
Part surface finish	Good to very good	Excellent	Very good	Good
Surface texture	Good	Excellent	Very good	Good to fair

[a] Ref. 11.

[b] 1 MPa equals approximately 10 atm.

mechanical plug assist assembly, and/or a clamping grid assembly. There are several ways of opening and closing the forming press. Mechanical and pneumatic toggles have been used for decades. Electrically driven platens have become quite popular recently.

The majority of thin-gauge parts are formed into female or negative cavities. For deep cavities or multiple-compartmented cavities, mechanical assists, called plugs, are used to prestretch the sheet before vacuum and/or pressure is used to force the sheet against the mold surface. Air pressure to 5 bar is used, in conjunction with vacuum, for deeply drawn parts or for parts requiring high surface detail or sharp radii.

In thin-gauge forming, there are three common ways of removing the formed part from the web, skeleton, or unformed portion of the sheet. In-mold trimming employs steel rule dies that are a portion of the clamping assembly holding the sheet to the mold surface. Once the parts are formed, the steel rule die assembly is activated to cut the parts free of the web. In-machine trimming employs a separate trimming station that is situated downstream of the forming press, but still within the machine frame. The sheet containing the formed parts is indexed from the forming press directly into this trimming station, where steel rule dies separate the parts from the web. In-line trimming employs a separate trimming press that is downstream from the forming machine, as shown in Figure 3 (12). The sheet containing the formed parts is fed from the end of the forming machine pin-chain assembly into a separate indexer on the trimming press. The sheet containing the formed parts passes between a punch assembly and a die assembly. The punch pushes the formed parts against a trim die, cutting the parts away from the web and pushing them onto a collection table.

FFS machines are used in for packaging pharmaceuticals, foodstuffs, and medical supplies. As seen in Figure 4, thermoforming is a small portion of the process (13). In these machines, the sheet is usually pulled through the entire

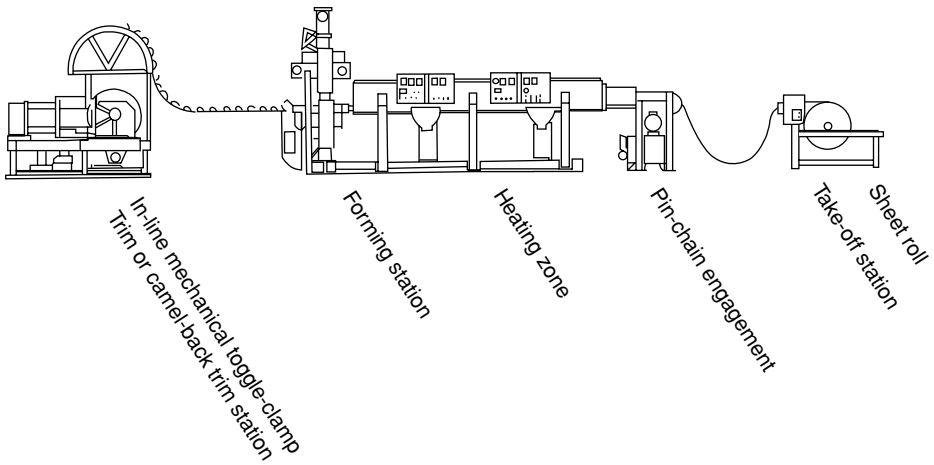

Fig. 3. Schematic of large thin-gauge thermoforming machine (Battenfeld—Glouster, Glouster, Mass.) (12). Used with permission of Hanser Publications.

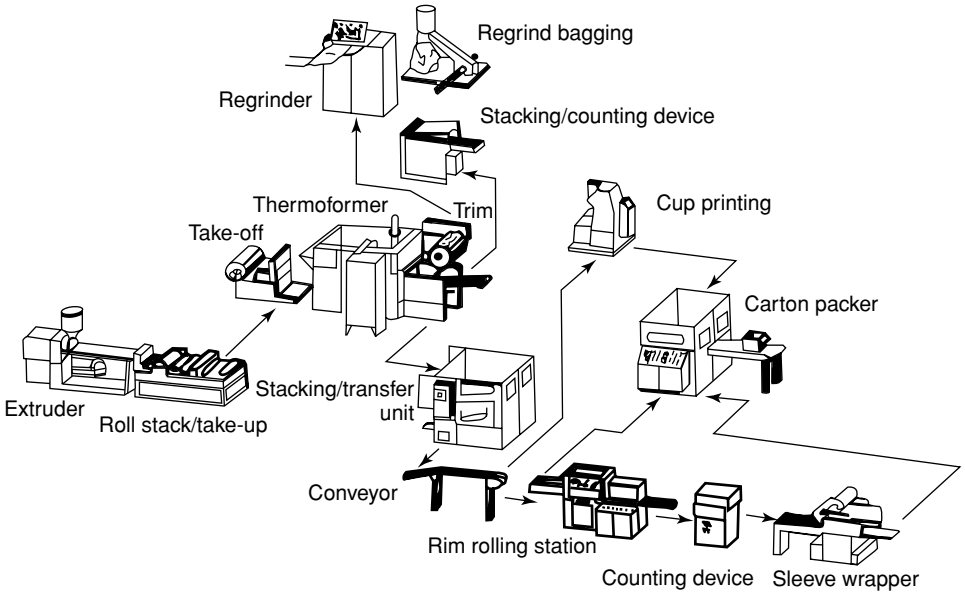

Fig. 4. Thermoforming as an integral part of thin-gauge container production line (13). Used with permission of Hanser Publications.

FFS sequence. The sheet is heated by contact with heated plates or rolls. FFS technology is most effective when the sheet is on the order of 250 μm or so.

For all roll-fed applications, it is economically necessary to collect the web for regrinding and reprocessing into sheet. For the in-line trimming press, the web is guillotined at the press and the chips are vacuum-collected for reprocessing.

Heavy-Gauge Machines. There are several common designs for heavy-gauge thermoforming machines. The simplest and most widely used is the shuttle machine (Fig. 5) (14), where the sheet, cut to size and palletized, is loaded, one

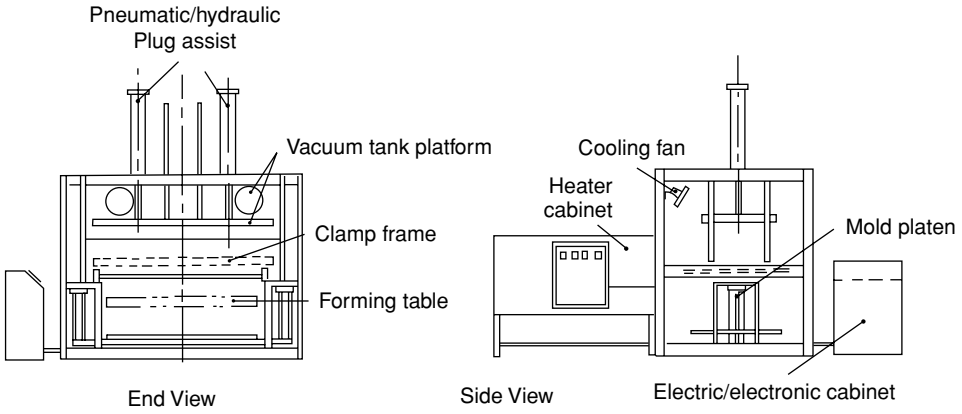

Fig. 5. Schematic of heavy-gauge shuttle thermoforming machine (Drypol/Zimco, no-longer in business) (14). Used with permission of Hanser Publications.

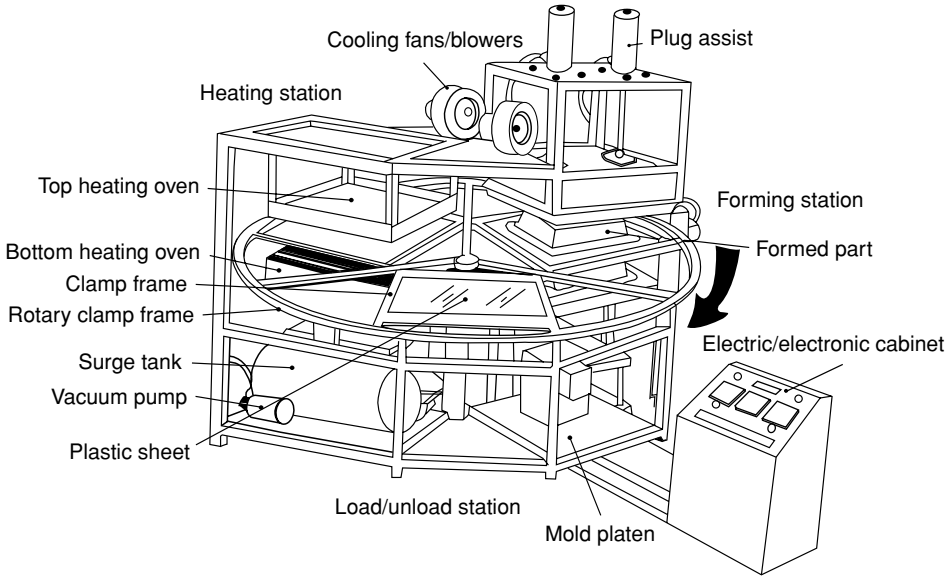

Fig. 6. Schematic of heavy-gauge rotary thermoforming machine (15). Used with permission of Hanser Publications.

sheet at a time, in a four-sided clamp frame and shuttled into the oven. When the sheet is at its forming temperature, it is shuttled to the forming press. When the sheet has been formed and cooled, it is removed from the clamp frame to a trimming fixture. Shuttle presses are very versatile and capable of forming parts of nearly unlimited dimensions. Shuttle presses with two forming stations and a central oven are used to overcome the economically inefficient operation of a single forming press machine. Rotary thermoforming machines, with either three or four stations, are quite energy efficient, but require more care in setting up. Figure 6 is a schematic of a three-station rotary machine (15). These machines are also limited in the size of the parts that can be formed.

A three-station machine has one heating station, in addition to the forming station and the load–unload station. The four-station machine has two heating stations. The sheet is usually uniformly heated from both top and bottom with infrared heaters. Most commercial machines use ceramic bricks or tiles, metal plate heaters, metal rod heaters, quartz plate heaters, or catalytic gas heaters as energy sources. As with thin-gauge thermoformers, once the sheet is at the forming temperature, it is indexed into the forming press. The forming press contains at least one platen with the desired mold assembly. The press may contain a second platen. For single-sheet forming, the second platen may contain a pressure box, a mechanical plug assist assembly, and/or a vacuum draw box to pneumatically prestretch the sheet. As with thin-gauge forming, the mold may be mounted on either the top or the bottom platen. The mold frame usually contains one to a few molds, which can be either male or female. Mechanical toggles or electrically driven chain with rack-and-pinion guides are used to raise and lower the platen. If a pressure box is used, the mold sections are mechanically locked and pressure bags are inflated to ensure an intimate seal against air pressures to 0.5 MPa.

Twin-sheet thermoforming is the method of forming hollow or semihollow parts such as pallets and door panels. Four-station machines are commonly used to form these parts. The first sheet is loaded in the clamp frame and rotated into the first oven. After a predetermined time, the second sheet is then loaded in the next clamp frame and rotated into the first oven. This action rotates the first sheet to the second oven. When the first sheet is at its forming temperature, it is rotated to the forming press and formed into the top mold cavity. When the part is sufficiently cooled, the clamp frames release the sheet. This allows the second sheet, in its clamp frame, to be rotated to the forming press, where it is formed into the top mold cavity. Then the platens close, are mechanically locked together, and air is forced under pressure between the two sheets. This forces the sheets against their respective molds and the clamping force provides for sealing of peripheral edges and any mating surfaces designed into the part. The welded-together sheets are then released from the clamp frame and removed to the trimming device (16).

There are many ways to trim the part from the surrounding plastic. Hand-held routers, band saws, and circular saws are commonly used. Hand-held drills are used for holes and slots. Computer numerical-controlled routers are used extensively for parts requiring dimensional accuracy along trim lines.

Process Characteristics

The Forming Process. Drape forming (*male* or *positive forming*; Fig. 7) and vacuum forming (*female* or *negative forming*; Fig. 8) are the earliest and simplest methods of thermoforming (17). Both methods yield parts with very nonuniform wall thicknesses. Free forming (*billow* or *free bubble forming*) uses no mold. The sheet is simply pneumatically stretched to the desired extent, and then allowed to cool in this shape.

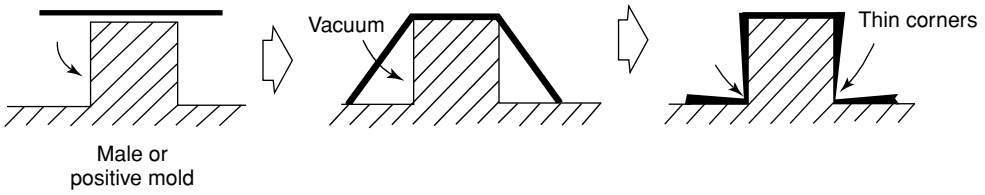

Fig. 7. Male or positive forming (17).

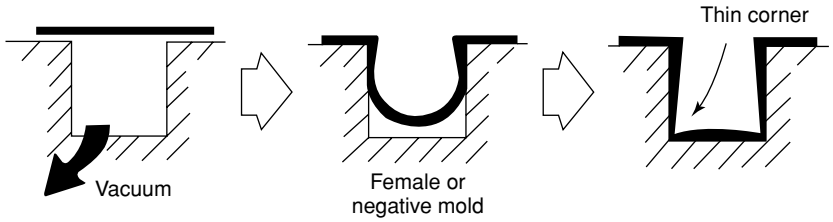

Fig. 8. Female or negative forming (17).

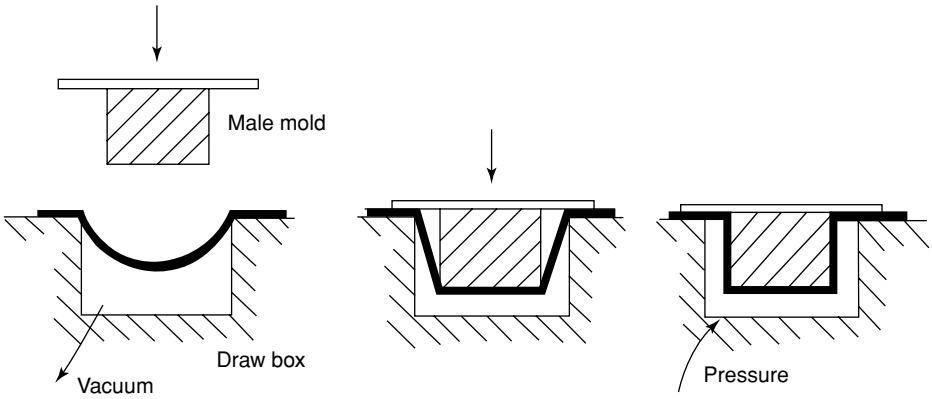

Fig. 9. Schematic of vacuum draw box prestretching, followed by male or positive mold insertion (18).

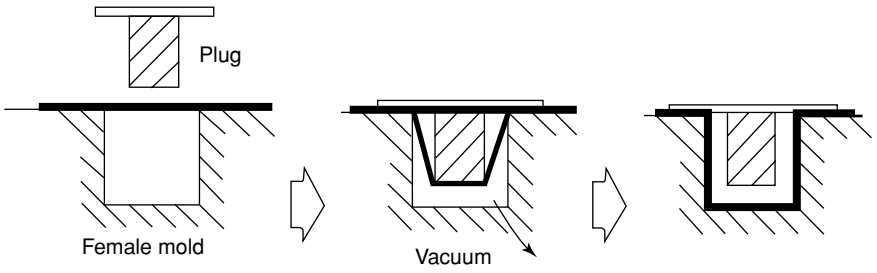

Fig. 10. Schematic of plug-assisted female or negative forming (18).

Prestretching is used to improve part wall thickness. Pneumatic stretching (*billow forming* or use of *vacuum draw box*; Fig. 9) is used with male molds. Mechanical stretching (*plug assist* or *push forming*) is frequently used with female molds (Fig. 10) (19). When the sheet has been stretched to near the bottom of the mold cavity, a combination of vacuum and compressed air is used to force the sheet off the plug and against the mold surface.

Pressure forming is used when the plastic is very stiff at the forming temperature, as with oriented polystyrene, when molded part requires surface detail and sharp radii or when the parts are deeply drawn. Thin-gauge pressure forming is commonly used for drink cups, deli containers, and pudding cups.

Matched mold forming is used when the plastic is very stiff at the forming temperature, as with highly filled or reinforced polymers or foamed polymers. Slip forming is used when the sheet cannot be easily stretched, as with continuous-glass reinforced polymers. During forming, the heated sheet is allowed to slide through the clamping frame. Diaphragm forming uses a heat-resistant neoprene or silicone membrane or bladder that carries the heated sheet into the mold cavity. The diaphragm is usually inflated with hot oil.

Twin-sheet forming produces hollow or semihollow parts. Both halves of a part are typically formed in female molds, and then pressed together to affect a

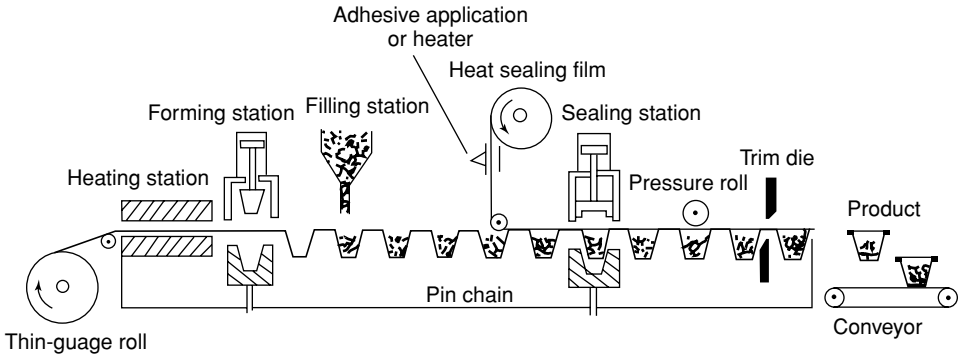

Fig. 11. FFS forming (19). Used with permission of Hanser Publications.

peripheral seal as well as internally welded regions. Both heavy-gauge and thin-gauge parts are twin-sheet formed.

Contact forming or trapped sheet forming is used primarily with thin-gauge FFS applications (Fig. 11) (19). The sheet is heated on one or both sides by direct contact with heated metal surface. The hot sheet is then drawn into the mold cavity. From that point, the sheet containing the formed parts is mechanically pulled through the filling, sealing, and trimming steps. Mechanical forming usually does not require a mold. The plastic sheet is machined to shape, and then locally heated and mechanically formed into the final part shape, where the open seams are glued. Cuspation also uses no mold. Instead the heated sheet is impaled at high speed with sharp projections (20). The product is a three-dimensional mat that competes with honeycomb and medium density foam.

In the 1970s, the Dow Chemical Co. developed a technique for forming shapes from sheet without the need to trim and regrind. In the scrapless thermoforming process (STP), the sheet is diced into squares (21). The squares are then coated with lubricant and heated in a conveyor oven. Each square is then placed in a forging press where it is formed into a disk. The disk is then pressure formed into an axisymmetric container. STP has merit when multilayer sheet trim cannot be successfully reprocessed. Billet forming also uses precut shapes, usually disks called billets. These are mechanically loaded into clamping fixtures that are then conveyed through an oven. Each tray containing the billets is then conveyed to a forming press where ring clamps secure the billets prior to plug-assist thermoforming into cavities. This technique is used to produce bottle liners, paint can liners, and condoms.

Heavy-gauge sheet stays at the forming temperature far longer than thin-gauge sheet or film. As a result, many more processing steps are possible with heavy-gauge sheet. The techniques are cataloged as to whether the mold is male or female, whether the sheet is prestretched with air or with a plug, and whether the stretching force is applied through pressure or vacuum (22).

Direct extrusion-to-forming is used in both thin- and heavy-gauge forming. Can lids and picnic plates are typical shallow-draw thin-gauge products produced by extruding sheet directly onto a wheel assembly that contains myriad molds. The key to quality wheel production is ensuring that the sheet is sufficiently cool

during stretching. In heavy-gauge forming, after exiting the extrusion die, the sheet is usually cooled until somewhat rigid, then reheated in the in-line thermoformer. Since the sheet is continuous, the thermoforming machine is similar to a traditional roll-fed thin-gauge thermoforming machine. This technology is employed when production runs are long, as with refrigerator door liners.

There are three essentially separate sequential phenomenological steps in thermoforming—heating, stretching, and trimming (technically mechanical breaking or fracture).

Heating. Three general methods of inputting energy to sheet are convection, conduction, and radiation.

Conduction is energy transfer by direct contact between the sheet and a heating source. Contact heating is used when the sheets are very thin. FFS machines frequently use contact heating with the forming station being integral to the heating plate. Polymer density, specific heat (enthalpy or heat capacity), thermal conductivity, and thermal diffusivity are important in conduction. Conduction is also the method by which energy moves through the plastic sheet. Polymers are thermal insulators when compared with metals. Conduction of heat from the sheet surface to its interior is a controlling factor for heavy-gauge plastic sheets.

Convection is energy transfer between moving air and the plastic sheet surface. Convective heat transfer is always present since the heating sheet is surrounded by ambient air, and the free surface of the formed part is in contact with ambient or fan-driven air. Typically, energy transfer is low when the air is quiescent and only slightly higher when air is positively moved across the sheet or formed part surface. Convective hot-air ovens are used to heat very thick sheet.

Radiation is electromagnetic energy interchange between hot and cold surfaces in view of each other. For most thermoforming processes, most of the radiant energy is in the far-infrared wavelength range, from about 2.5 μm to about 15 μm (Fig. 12) (23). Radiant heat transfer efficiency depends on the absorbing and emitting characteristics and the relative dimensions and spacing of the heating source and the polymer material. Radiation heat transfer provides the fastest and most versatile means for heating sheet in thermoforming. The energy output from

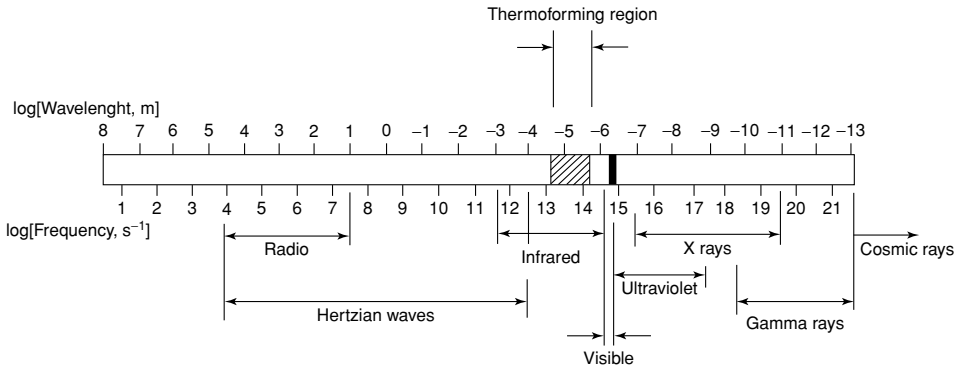

Fig. 12. Electromagnetic domain showing thermoforming region as portion of infrared band (23). Used with permission of Hanser Publications.

radiant heaters is typically in the range of 30–60 kW/m^2 with a temperature range of 150–900°C. The common thermoforming heating sources are as follows (24):

(1) Hot air (including convection toaster ovens)
(2) Hot water/steam
(3) Sun lamps (drugstore variety)
(4) Nichrome spiral wire (such as toaster wire)
(5) Steel rod heaters
(6) Steel or nichrome tape
(7) Quartz tube heaters (nichrome wire, tungsten wire or tape)
(8) Halogen heaters (halogen-gas filled quartz tubes with tungsten wire or tape)
(9) Steel plates with embedded resistance wire
(10) Ceramic plates with embedded resistance wire
(11) Ceramic bricks with embedded resistance wire
(12) Quartz cloth heaters backed with exposed nichrome wire
(13) Steel plates that reradiate combustion energy from gas flame
(14) Steel wire grids that reradiate combustion energy from gas flame
(15) Ceramic plates that reradiate combustion energy from gas flame
(16) Indirect gas combustion on catalytic beds
(17) Direct gas combustion

Only a portion of the energy emitted by the heater actually reaches the sheet, as seen in Figure 13 (25). The selection of an appropriate heater depends on several factors:

(1) *Day-to-day running costs*. Energy costs for gas combustion heaters are about one-fourth of those for electric heaters.
(2) *Maintenance costs*. Quartz tube heaters are fragile and must be carefully cleaned. Rod heaters are rugged but can rapidly lose efficiency.
(3) *Initial installation cost*. Plate and panel heaters require less electrical connections than ceramic brick heaters. Catalytic combustion heaters require both gas and electric connections.
(4) *Heater versatility*. Quartz and halogen heaters heat very rapidly, compared with panel and catalytic combustion heaters. Ceramic brick heaters allow ease of zoning or pattern heating.
(5) *Polymer characteristics*. The sheet thickness and the polymer infrared radiation absorption characteristics may influence the heating method. Polymers with high infrared radiant transmission levels heat slower than polymers with low levels. Thin polymer sheets heat slower than thicker sheets. Polymers with higher thermal diffusivity values heat more uniformly than those with lower values. Crystalline polymers such as polyethylene and polypropylene require more energy to reach forming temperature than amorphous polymers such as polystyrene and poly(vinyl chloride) (PVC). Crystalline polymers benefit by preheating, with the preheater being placed

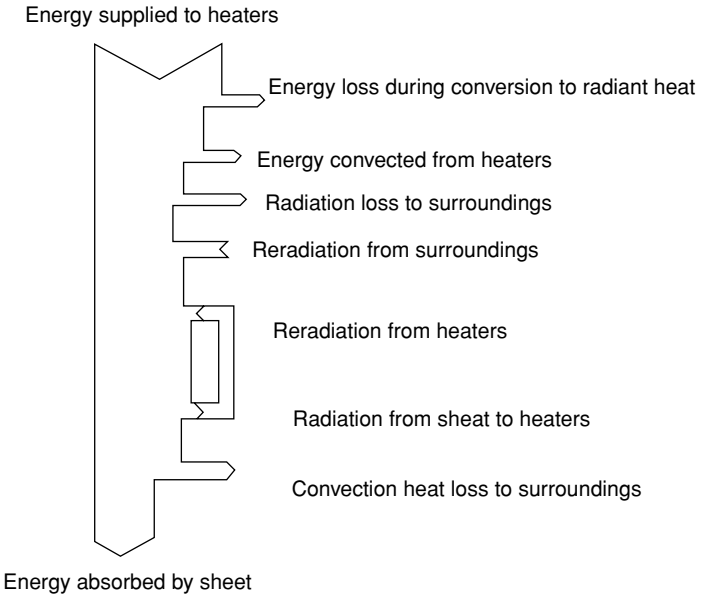

Fig. 13. Net energy transfer from heaters to sheet (25). Used with permission of Hanser Publications.

between the unroll stack and the pin-chain engagement on thin-gauge machines and as the first of two heaters on heavy-gauge four-station rotary thermoforming machines.

Most modern forming ovens heat sheet on both sides. Oven heater efficiency depends also on heater-to-sheet spacing, closed vs. open oven design, extent and reflective nature of nonheated surfaces, thermal protection of sheet clamping devices, heater-to-sheet area, and number of thin-gauge shots in the oven.

Sag bands or metal rods that run length of the thin-gauge oven have been used for polymers that sag excessively when heated. Some heavy-gauge shuttle thermoforming machines are equipped with ovens that completely seal the sheet between the heaters. These ovens are equipped with vacuum and compressed air, so that the sheet is lifted when it begins to sag.

Sheet Stretching. When the polymer sheet is at its forming temperature, it is transferred to the forming press where it is stretched against the mold surface. Technically, stretching is biaxial deformation of a nonisothermal rubbery elastic or viscoelastic membrane achieved through differential pressure across the sheet surface. Typical strain rates are up to 25 s^{-1}. The rubbery elastic characteristic of a polymer is described by its set of temperature-dependent stress–strain curves, as shown in schematic in Figure 14 (26).

The forming temperature region is the shaded portion. The polymer resistance to applied differential pressure and the polymer elongation at break determine the lower forming temperature. The level of sheet sag during heating determines the upper forming temperature. The maximum applied differential pressure is shown in Figure 14 as a horizontal line. The value represents the

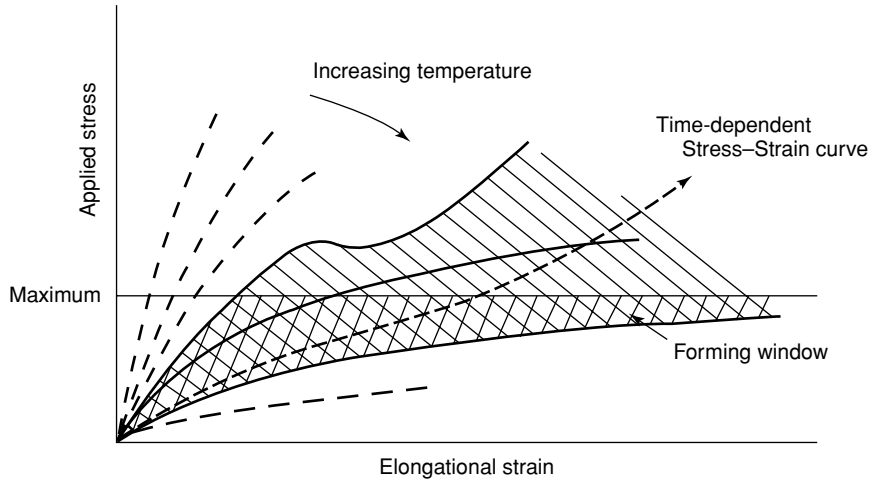

Fig. 14. Typical stress–strain schematic in thermoforming (26). Crosshatched region represents forming window. Used with permission of Hanser Publications.

applied vacuum in the case of vacuum forming or the extent of auxiliary air pressure used in pressure forming. The crosshatched area below this line represents the thermoforming window for a given polymer.

For most thermoforming operations using unfilled or unreinforced polymers, the differential pressure is less than 0.5–1.0 MPa (145 psi). Differential pressures of more than 3.0 MPa may be needed for high performance reinforced polymers.

Stretching against a mold surface is a differential process in that only that portion of sheet that is not in contact with the mold surface stretches. As a result, the part wall thickness varies substantially across the part surface, with the thinnest part being in the region where the sheet touches the mold last. There are two common ways of prestretching the sheet to improve wall thickness variation. In heavy-gauge thermoforming, the sheet may be prestretched using differential air pressure to inflate the sheet or draw it into a vacuum box. In both heavy-gauge and thin-gauge thermoforming, a solid shape or plug may be mechanically pressed into the sheet before differential pressure forces the sheet against the mold surface. The plug nearly uniformly draws the sheet between its bottom edge and the rim of the mold. As seen in Figure 15 (27), the effect is to pull material from the thicker regions of the part, thereby increasing the thickness of material in the region where the sheet touches the mold last.

Part wall thickness can now be predicted quite accurately with finite element analysis. The physical sheet is replaced with a two-dimensional mesh of triangular elements and nodes, which is then mathematically deformed under increasing load. When the nodes touch the electronic surface of the mold, they are affixed. Force continues to increase until all or most of the elements are rendered immobile. Currently the Ogden power-law model is used as the polymer elastic constitutive equation or response to applied load (28).

Although elastic stress–strain behavior describes sheet stretching for most thermoforming processes, sheet deformation during plug-assist prestretching is

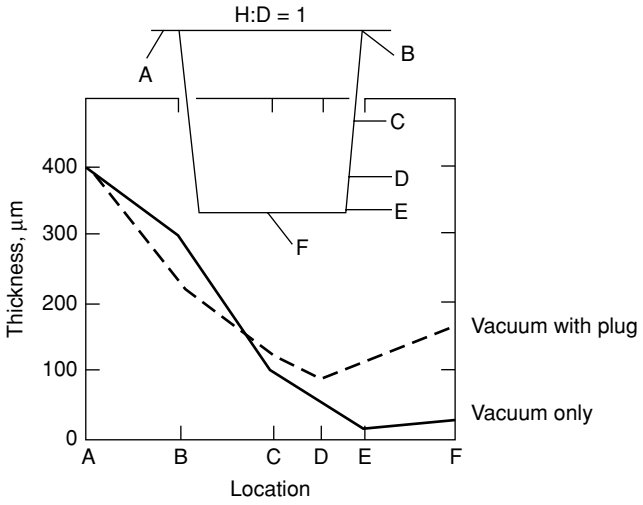

Fig. 15. Comparison of wall thickness variation with and without mechanical plug assist (27). Used with permission of Hanser Publications.

best described as viscoelastic. That is, the polymer responds as an elastic liquid with unrecoverable deformation occurring particularly in the contact region at the plug edge. Currently, the Kaye-Bernstein, Kearsley, Zapas model is used for the polymer viscoelastic response to applied load.

Rigidifying the Part. Commercial molds are temperature-controlled. In heavy-gauge thermoforming, cooling time on the mold surface may control the overall cycle time. Energy is removed from the polymer part by conduction through the single mold surface to recirculating coolant in the interior of the mold. Forced-air free-surface cooling helps reduce cooling time.

Trimming. *Trimming* is mechanical cutting or breaking of cooled plastic. Although there are many ways of cutting plastic, including laser and water jet cutting, most commercial thermoforming operations use either of two approaches (29). Compression cutting involves the mechanical pressing of a sharp metal edge against the plastic part. It is usually used to trim plastic less than 1.5 mm in thickness or low density foam plastic of any thickness. The sharp metal edge, usually a steel rule die, can either be pressed against an anvil or can squeeze the plastic between a forged die and a punch that has interference fit with the cutting edge (30).

Chip cutting involves mechanical breaking away of small pieces of plastic with a multitoothed blade or wheel, in a kerf between the desired part and the selvedge. It is generally used to trim plastic with thickness greater than 3 mm, and for filled and reinforced plastic. Bandsaws, hand-held drills and routers, and table-mounted circular saws are used for general cutting such as hogging the part from its trim. Computer-driven three-axis and five-axis routers are now used for more accurate trimming, especially where holes and slots must be cut into the part. The parts are usually tightly held with vacuum against a rigid fixture while being trimmed. The selection of the trim bits and the depth and speed of trimming depends strongly on the polymer being cut.

Process and Product Control. Machine control has steadily progressed from relay clock timers to programmable logic controllers controls to all-computer controls. On-board computers not only control the process variables but also are used extensively for inventory control. Even though infrared sensors have been used for years to measure single-point sheet temperatures during oven heating, exiting sheet on temperature alone is still novel. Recent line scanning of moving sheet has enabled operators to manually adjust heaters, but feedback heater temperature control has yet to find acceptance. Thermography or two-dimensional infrared imaging of hot surfaces is invaluable in determining heater performance, sheet temperature uniformity, effect of zone heating on sheet temperature, and mold temperature uniformity. The cost of these devices is a deterrent toward their wide acceptance as process monitors.

Thin-gauge all-electric machines were first developed for aseptic and clean-room medical packaging. In addition to minimizing lubricating and hydraulic oils, machine setup, including mold siting and in-press trim die adjustment, is far easier than with partially electric systems. Touch-screen setup programs and computer control have reduced setup time. For redoing previous jobs, these adjustments are automatic.

Incoming sheet quality control is of prime importance to the thermoformer. In addition to residual sheet orientation induced during extrusion, sheet quality monitoring must include gauge thickness, squareness for cut sheet, surface gloss or texture, color and color uniformity, identification and control of defects such as pits, gels, scratches, die lines, and optical distortion, melt flow characteristics of polyethylenes and polypropylenes, crystallinity level and intrinsic viscosity of poly(ethylene terephthalate), and mechanical properties such as impact strength, tensile strength and modulus, elongation at forming temperature, and tear resistance for thin-gauge sheet. In many cases, thermoformers may accept certification of many of these parameters from either the sheet extrusion house or the polymer supplier. In some cases, the thermoformer should run his/her own tests to ensure incoming product quality (31).

Mold design accuracy and part quality assurance have benefited from computerized coordinate measuring machines. Coordinate measuring machines provide valuable information on part reverse engineering and local part shrinkage value determination. Mold and plug design and fabrication now depend on computerized design and mold manufacture. And computer numerically controlled trimming devices in heavy-gauge forming have accelerated designer and user acceptance of thermoformed parts.

Material Characteristics

Usually if a polymer can be extruded or cast into sheet form, it can be thermoformed. Since the basic thermoforming processes use less than 1 MPa forming pressures, nearly all thermoformable polymers are unfilled or unreinforced. The thermoforming process relies on the “hot strength” of the polymer to minimize sagging during heating. As a result, most thermoformable polymers are amorphous (see AMORPHOUS POLYMERS). Styrenics,

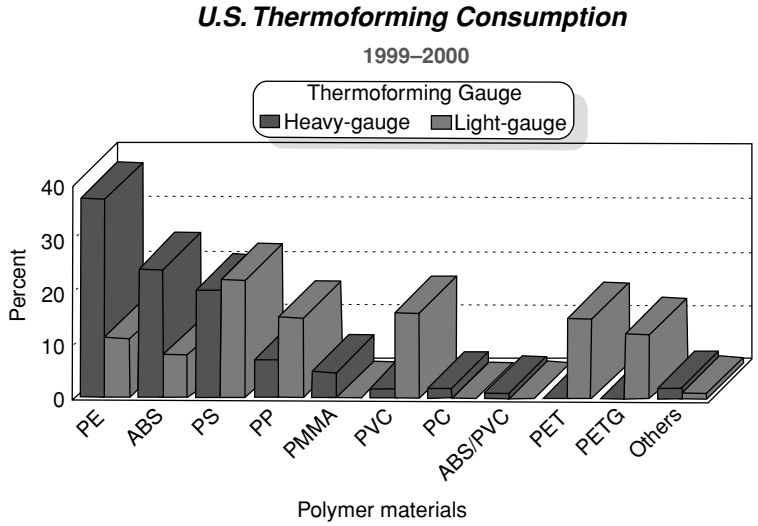

Fig. 16. U.S. plastic materials consumption for thin-gauge (2.1 million metric tons) and heavy-gauge (682,000 t) thermoforming (32). PE = Polyethylene; ABS = acrylonitrile–butadiene–styrene; PS = polystyrene; PP = polyproplyene; PMMA = poly(methyl methylacrylate); PVC = poly(vinyl Chloride); PET = poly(ethylene terephthalate). Redrawn and used with permission of SPE Thermoforming Division.

particularly polystyrene (see STYRENE POLYMERS) and ABS (see ACRYLONITRILE–BUTADIENE–STYRENE POLYMERS), amorphous poly(ethylene terephthalate) (see POLYESTERS, THERMOPLASTIC) [APET], PVC (see VINYL CHLORIDE POLYMERS), poly(methyl methacrylate) (see METHACRYLIC ESTER POLYMERS) [acrylic], and polycarbonates (qv) are commonly thermoformed. The only crystalline polymer in wide use is high density polyethylene, which has excellent elasticity in the melt state (see ETHYLENE POLYMERS, HDPE; SEMICRYSTALLINE POLYMERS). Newer grades of polypropylene are being designed specifically for thermoforming. Figure 16 shows current U.S. polymer usage in both thin-gauge and heavy-gauge thermoforming (32).

In addition to "hot strength" or elasticity at the forming temperature, other intrinsic polymer characteristics are important in thermoforming. The chemical makeup of the polymer dictates the extent of infrared energy absorption or its counterpart, infrared energy transmission. At the same thickness, polyethylene has a higher infrared transmission level and therefore lower radiant energy absorption than polystyrene. This is seen by comparing the infrared spectra of polyethylene (Fig. 17) and polystyrene (Fig. 18) (33). As expected, the fraction of energy transmitted through the polymer film decreases with increasing film thickness. Infrared energy transmission spectra are usually available from polymer material suppliers.

The forming window for a given polymer can be quantified by differential thermal mechanical analysis. Specifically, the temperature-dependent elastic modulus is key, as shown in Fig. 19, for typical thermoformable polymers (34). An adequate forming window is dictated if the modulus curve shows a flattening or

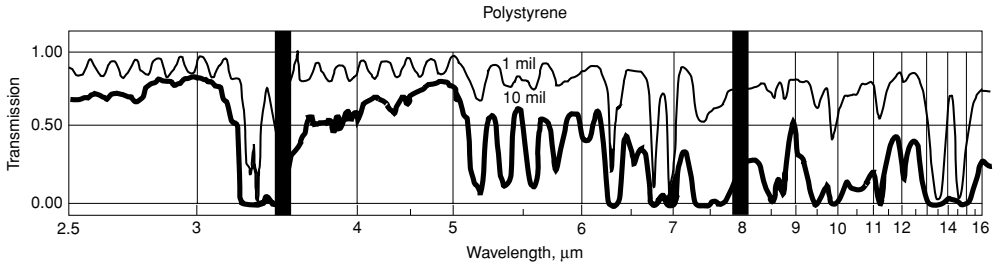

Fig. 17. Infrared transmission spectrum for two thicknesses of polystyrene (33). 1 mil = 25.4 μm. Used with permission of Hanser Publications.

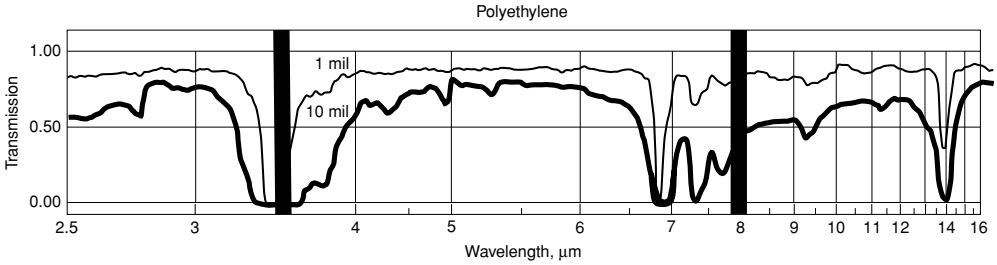

Fig. 18. Infrared transmission spectrum for two thicknesses of polyethylene (33). 1 mil = 25.4 μm. Used with permission of Hanser Publications.

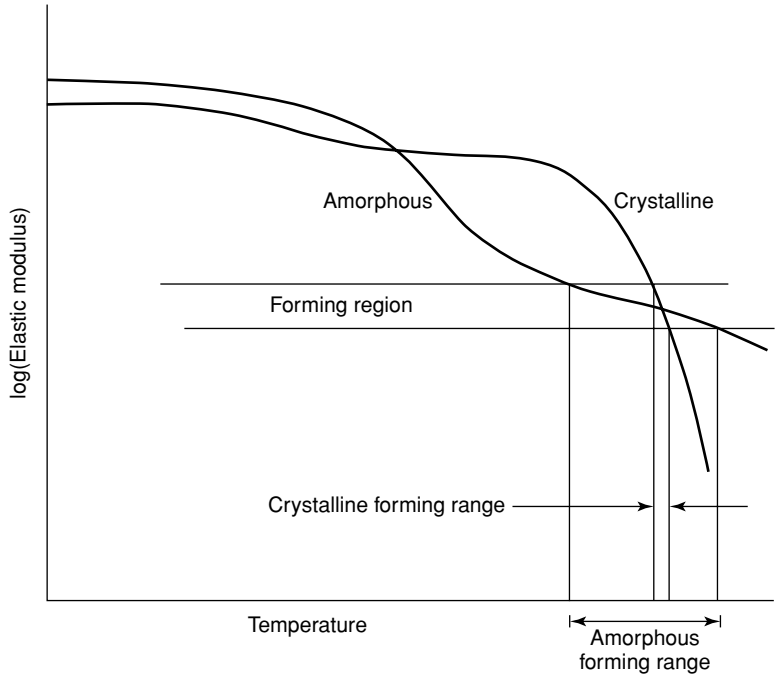

Fig. 19. Typical temperature-dependent elastic moduli of an amorphous and a crystalline polymer, showing forming regions for both (34).

plateauing at a value range consistent with normal thermoforming differential pressure. If the polymer modulus curve shows little flattening or if the flattening occurs at a very low value, the polymer may have a small forming window or none at all. If the flattening occurs at a very high value, normal forming pressures may be inadequate to stretch the polymer into detailed or complex molds.

Polymer thermal properties, such as temperature-dependent specific heat or enthalpy, thermal conductivity, and thermal diffusivity are also important. Although thermoforming is a thermally and mechanically gentle process insofar as the polymer is concerned, the general process of extrusion, thermoforming, regrinding, and potentially multiple reextrusions may lead to extensive molecular damage (35). This is particularly true with thermally sensitive polymers such as PVC and poly(ethylene terephthalate). Thus intrinsic polymer thermal stability and thermal and mechanical stability of the additives must be considered.

By far the majority of sheet formed does not contain fillers or reinforcing fibers. Fillers and fibers increase polymer stiffness but usually not polymer transition temperatures. Polymers containing up to 40 wt% talc, calcium carbonate, glass cullet, and diatomaceous earth are typically pressure formed at higher than usual temperatures. Polymers containing moderate levels of chopped glass and carbon fiber and certain types of nonwoven fibers are also pressure formed or matched mold formed. Fillers and fibers affect the radiative and thermal properties of the sheet. Organic dyes used to color transparent polymers usually do not affect the radiative characteristics of the polymers. Inorganic pigments have particle sizes that may interfere with volumetric radiant absorption.

And although thermoforming is basically a rubbery solid deformation process, the viscoelastic character of the polymer may need to be understood, particularly for the plug-assisted forming process. Computer-aided design programs also may need polymer viscoelastic properties. This may be particularly true for crystalline polymers such as polyethylene and polypropylene when formed above their melt temperatures. This is discussed below.

Excessive and/or inconsistent residual orientation in polymer sheet induced during the extrusion process can be a vexing problem in thermoforming. Thermoformers work with extruders to keep both machine-direction and cross-direction orientations to 5% or less. Table 3 gives advantages and disadvantages of several thermoformable polymers.

Mold Materials

Since thermoforming is a low pressure process, production molds are made of soft metals such as aluminum (36). Very large heavy-gauge molds and some thin-gauge molds are commonly sand-cast of A356 aluminum. Multicavity thin-gauge molds and some smaller heavy-gauge molds are machined from A6061 aluminum. For polymers requiring higher forming temperatures, such as polysulfones (qv) or polycarbonates (qv), machining grade A7075 aluminum is used. Machined 316 stainless steel is used on occasion for corrosive polymers such as rigid poly(vinyl chloride). Electroformed nickel molds are used when extreme mold detail is required. Regions far from cooling sources may be made of higher thermal conductivity metals such as copper–aluminum alloy or bronze. Pinch-off areas may be

Table 3. Advantages and Disadvantages of Thermoformable Polymers[a]

Polymer	Processing temperature range, °C	Advantage	Disadvantage
Polystyrene (TG)	150–190	Easily formed	Brittle
		Inexpensive	Tenacious trim dust
		Easily extruded	Plug mark-off
High-impact polystyrene (HG, TG)	160–205	Available	Limited elongation
		Good impact	Yellows at high temp
		Easily colored	May smoke
			Hazy, translucent
ABS HG)	150–205	Great toughness	Absorbs moisture
		Easily formed	Yellows at high temp
			Splitty at low temps
			FR grades stiff
Modified polyphenylene oxide (HG)	165–220	Forms like HIPS	Stiff at mod temps
		Fire-retardant	Odor at forming temp
		Great pressure-formed	Usually trim cold
			Tenacious trim dust
Oriented polystyrene (TG)	130–160	Superior surface gloss	Careful heating
		Great impact strength	Trimming difficult
		Great opticals	Expensive
			Direct contact heating
Poly(methyl methacrylate) (acrylic) (HG)	150–205	Great gloss	Somewhat moisture sensitive
		Readily formed	Easily scratched
		Excellent UV	Brittle in sharp corners
Poly(methyl methacrylate)/poly(vinyl chloride) (HG)	150–190	Great pressure-formed	Yellow at high temps
		Good fire retardancy	Brittle in trimming
			Good outdoor appl.
Extra tough polymer (hg, TG)	150–180	Good toughness	Expensive
		Good clarity	Not normally a stock item
		Good chem. resistance	
Flexible PVC (hg, TG)	105–150	Good drawability	Weak at high temps
		Fire retardant	Plasticizer odor
		Good automotive matl	Grain wash at high temps
Rigid PVC (HG)	120–180	Fire retardant	Yellows at high temps
		Easily colored	Low T_g
		Tough	Difficult prestretch
		Moderate transparency	Narrow processing window
		Outdoor appl.	Recycle times limited

Table 3. (Continued)

Polymer	Processing temperature range, °C	Advantage	Disadvantage
Low density polyethylene (TG)	125–175	Tough	Poor high temp char.
			Excessive sag
			Narrow forming window
			Haze at high temps
			Sticky on plugs
High density polyethylene (HG)	140–195	Tough	Excessive sag
		Good melt strength	Black heats fast
		Fractional melt index	
Polypropylene (hg, TG)	145–165	Tough	Narrow forming window
		High temp appl.	Excessive sag
		Can be transparent	Plug mark-off
		Best pressure-formed	Can be sticky
		Heavy-gauge matls now	Whiskers during trimming
EP copolymer (TG)	130–180	Forms like high denisty polyethylene	Sags at high temp
		Forms best cool	Clean trim difficult
Oriented polypropylene (TG)	145–160	Very low haze	Expensive
		High gloss	Must be heated very carefully
		Great impact strength	Sags, loses orientation
		Contact heat best	
Ethylene–vinyl acetate (TG)	135–150	Draws well	Easily torn
			Narrow forming window
Polypropylene – −20% talc (hg, TG)	150–205	Forms well	Stiff at forming temp
		Plug desired	Low elongation at high temp
		Best pressure-formed	Matte surface
Polypropylene – −40% glass-reinforced (HG, tg)	150–230	Best pressure-formed	Very stiff at forming temp
			Shallow draw best
			Plug assist questionable
Polycarbonate (HG)	180–230	Great UV resistance	Stiff at forming temp
		High temp appl.	Moisture sensitive
		Good forming window	Trim very difficult
		Good colors	

Table 3. (Continued)

Polymer	Processing temperature range, °C	Advantage	Disadvantage
Amorphous poly(ethylene terephthalate) (TG)	125–165	Tough thin-gauge	Sags, necks
		Orients, toughens	Crystallizes rapidly
		Transparent	Difficult cold trim
			Trim must be recrystallized
Crystallizable poly(ethylene terephthalate) (TG)	185–200	High temp appl.	Mold temp control
			Very stiff when hot
			Crystallinity control difficult
			Brittle when too crystalline
Glycol-modified poly(ethylene terephthalate) (HG, TG)	160–180	Good toughness	Somewhat costly
		Good colors	Limited sourcing
		Good forming window	Can yellow at high temp
			Not good outdoor matl
Cellulosics (TG)	140–165	Excellent clarity	Expensive
		Great toughness	Lost market to PVC, PET
		Good forming window	Somewhat moisture sensitive
			Limited availability
Thermoplastic elastomer (TG)	135–180	Draws well	Spring-back
		Many versions to choose	High rubber difficult
		Automotive darling	May tear at high temp
			Grain wash at high temp

[a]Key: HG = major heavy-gauge; TG = major thin-gauge; hg = minor heavy-gauge; tg = minor thin-gauge; no notation, not normally used.

made of carbon steel. Gaskets in pressure boxes are usually made of neoprene or silicone.

Thermoforming is one of the major processes used to produce prototype parts that may be made other ways, such as injection molding. Many materials are used to produce molds that are serviceable for a few to a few hundred parts. Traditional mold materials include wood, plywood, hard plaster such as Hydrocal (US Gypsum), and medium density fiberboard. Sprayed and cast white metal are used on occasion.

Recently, prototype molds are being fabricated from particle-filled polyurethane and epoxy syntactic foams using computer-aided multiaxis routers. Plugs, used to mechanically prestretch polymer sheet, are also usually machined from syntactic foams. For certain polymers, heated aluminum plugs or solid nylon plugs are desired.

Part Design

In general, thermoforming may be described as a differential stretching process. The sheet free of the surface continues to thin as it is drawn against the mold surface. As a result, the thickest portion of the part is where the sheet touches the mold first and the thinnest is where the sheet touches the mold last. Prestretching techniques move sheet from the thicker areas to the thinner ones, but in general, thermoformed parts have nonuniform wall thicknesses. Female parts tend to have thicker rims and thinner two- and three-dimensional corners. Male parts tend to have thicker two- and three-dimensional corners and bottoms and thinner rims. Multicompartment parts with both male and female sections, sometimes called androgynous parts, require careful mold design and proper sizing of plugs to minimize very thin sidewalls and internal webbing and to provide adequate internal draft angles.

Recently, computer-aided design programs have been devised that allow prediction of part wall thickness (37,39). These programs use finite element analysis, with the sheet being characterized as a two-dimensional mesh of nodes forming triangular elements. Although the earliest programs used Mooney-Rivlin constitutive equations of state to describe purely elastic polymer response to the applied differential load, current programs use the doubly infinite semiempirical Ogden model, with the series truncated at two or four elements. The K-BKZ constitutive model is used to describe viscoelastic behavior (39). An example of a computer-generated thickness profile is given as Figure 20.

Computer-aided wall thickness prediction is compromised by measured variation in actual part wall thickness due to the practical intrinsic variation in processing parameters, as seen in Figure 21 for thin gauge parts and Figure 22 for heavy-gauge parts (40).

Distortion-printed products have been used since World War II (41). Until recently, the standard technique involved thermoforming a polymer sheet to the desired shape, painting the desired design on the shape, and then reheating the shape to a flat sheet. This has been largely replaced with finite element computer programs that carry out the entire process electronically.

Most amorphous polymers linearly shrink about 0.4–0.6%. Crystalline polymers such as high density polyethylene and polypropylene linearly shrink about 2.0% (42). Thermoformed parts shrink away from female molds and onto male molds. Male molds must have typical draft angles of 2–5°, but sufficiently great enough to allow release of the formed parts. Female molds need minimal, if any, draft angles.

Many thermoformed parts contain undercuts. Detents and interlocking lugs are frequently used in thin-gauge packages with integral lids. Undercuts in

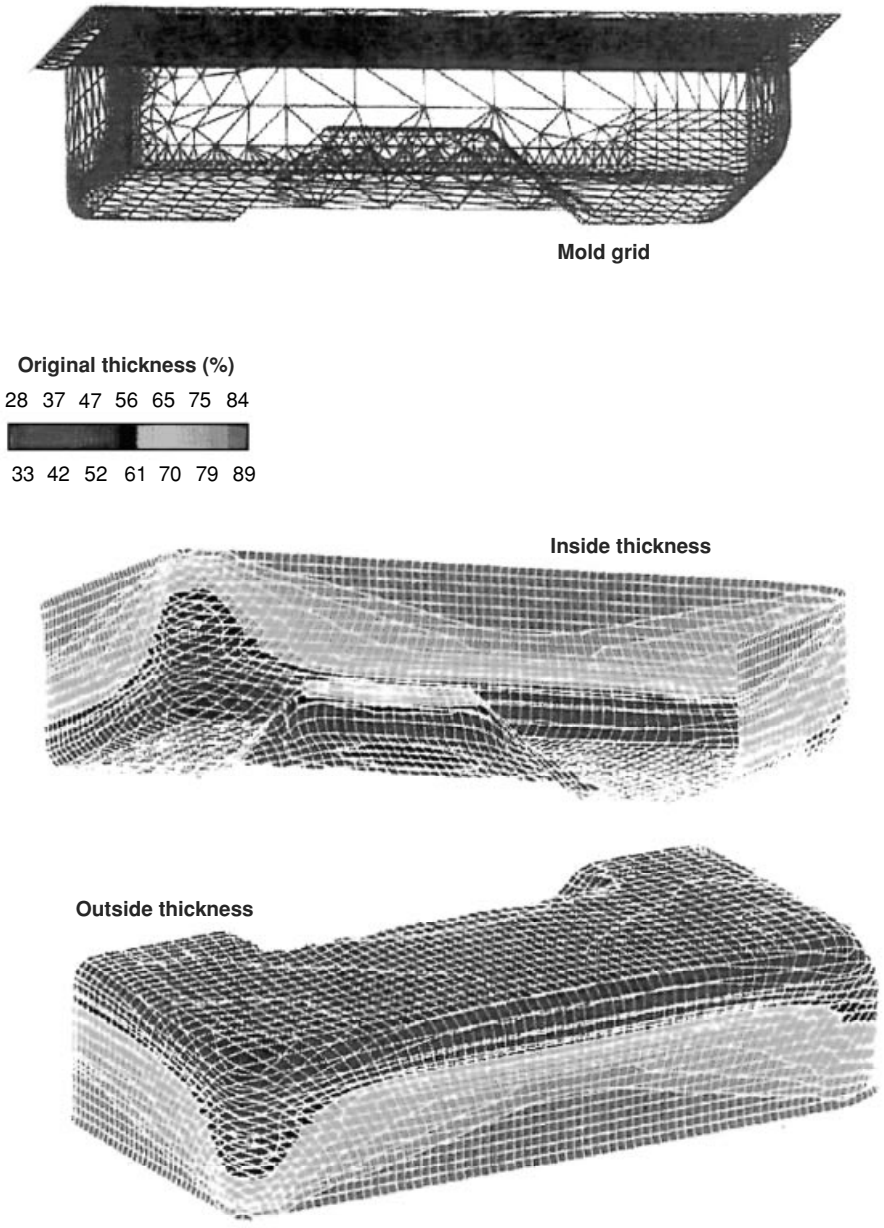

Fig. 20. Finite element analysis of local wall thickness for drawdown into negative mold (39). Used with permission of Institut für Kunststoffeverarbeitung, Aachen, Germany.

heavy-gauge parts are achieved with swing-away sections that are either manually or pneumatically activated (43).

Holes are machined into heavy-gauge parts in the post-forming, trimming operation. Holes are punched into thin-gauge parts just prior to cutting the parts from their web.

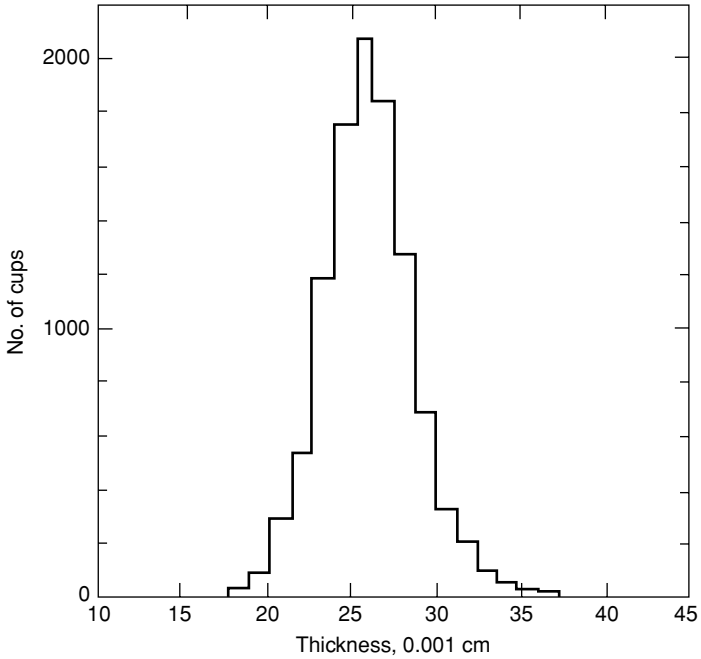

Fig. 21. Side wall thickness variation during normal production—thin-gauge thermoformed cup (40). Redrawn and used with permission of SPE Thermoforming Division.

Newer Technologies

Twin-sheet thermoforming is more than a century old. Recent interest in returnable shipping pallets has rekindled this heavy-gauge technology. The competition is rotational molding and blow molding, major technologies for producing hollow parts. Twin-sheet forming forte lies in manufacturing high aspect ratio parts with many welded areas, such as shipping pallets, backboards, tabletops, and door panels. The key to quality twin-sheet parts is the integrity of the seal area between the two formed plastic sheets. This is particularly important in sequential forming, where the first formed plastic sheet resides on its mold half while the second sheet is being formed. High density polyethylene is the preferred polymer, since it remains tacky throughout this interval. Rigid PVC and ABS have also been twin-sheet formed economically. Although the earliest twin-sheet parts were of thin gauge, interest is only recently been rekindled in this area, with commercial successes in medical devices and liquid containers.

Multilayer polymer film and sheet are thermoformed into packages when moisture, odor, and/or oxygen barriers are needed. A typical multilayer package consists of a rigid outer polymer such as polystyrene, followed by an adhesive layer, an oxygen barrier film such as ethylene vinyl alcohol, another adhesive layer, and a moisture barrier inner polymer such as polyethylene or polypropylene. Although multilayer films and sheets are relatively easy to thermoform, the growth in the market has been limited by the difficulty in reprocessing the trim.

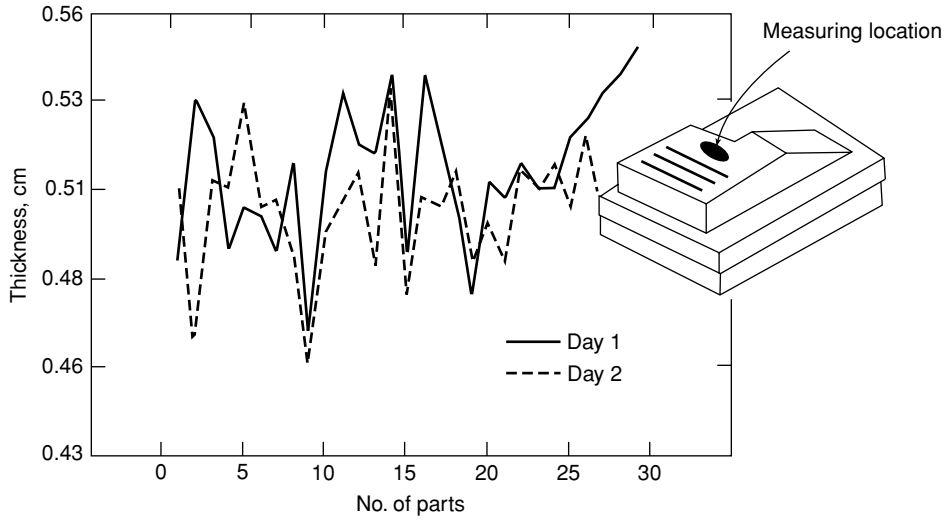

Fig. 22. Bottom wall thickness variation during normal production—heavy-gauge thermoformed part (41). Redrawn and used with permission of SPE Thermoforming Division.

Thermoplastic foam sheet of polystyrenics or polyolefins are thermoformed into impact resistant packages. Typically, care must be taken to avoid overheating low density foam sheet. Foams are usually quite stiff at forming temperatures and matched mold tooling is normally used to achieve reasonable draw ratios (44). For advanced applications where the packages must act as both rigid containers and moisture absorbers, mechanical, thermal, and phase separation means are used to open foam cells. These foams are usually formed at higher temperatures on single-surfaced molds. Even when foamed, polylactic acid and polystarch derivative polymers thermoform well into compostable or degradable containers.

Heavy-gauge thermoforming owes much of its continuing success against injection molding to the adaptation of computer numerically controlled routers from the woodworking industry (16). Computer-controlled routing has allowed accurate nonplanar trim lines, reproducible slotting, and accurate hole drilling.

Even though lightly filled polymers have been thermoformed for decades, the majority of the sheet formed contains no fillers or fibers. Recent developments in forming reinforced thermoplastic sheet include a thermoformed all-composite bumper assembly for BMW (Jacob Composite GmbH, Dresden, Germany, 2002) and composite bed leaf springs (45). Currently, glass-reinforced polypropylene and nylons are the preferred polymeric materials. This work is being spurred by newer technologies in heating and bending the less-extensible sheet.

BIBLIOGRAPHY

"Thermoforming" in *EPST* 1st ed., Vol. 13, pp. 832–843, by George P. Kovach, Koro Corporation; "Thermoforming" in *EPSE* 2nd ed., Vol. 16, pp. 807–432, by Joseph N. McDnald, Joseph McDonald Associates.

1. J. L. Throne, *Technology of Thermoforming*, Hanser Publishers, Munich, 1996, Table 1.1, p. 4.
2. J. H. DuBois, *Plastics History U.S.A.*, Cahners Books, Boston, 1972, Chapt. 2.
3. J. L. Throne, in Soc. Plast. Engrs. Annual Tech. Conf., Tech Papers, Vol. 60, No. 3, 2002, pp. 4089–4095.
4. D. E. Mansperger and C. W. Pepper, *Plastics: Problems and Processes*, International Textbook Co., Scranton, Pa., 1938, p. 116.
5. Anon., *Modern Plastics Catalog 1940*, Breskin Publishing Corp., New York, 1939, p. 52.
6. P. J. Mooney, *Understanding the Thermoforming Packaging Business*, Plastics Custom Research Services, Advance, N.C., 2002.
7. Ref. 1, Figure 1.1 (revised and redrawn), p. 6.
8. J. L. Throne, *Understanding Thermoforming*, Hanser Publishers, Munich, 1999, Table 1.2, p. 4.
9. P. J. Mooney, *Understanding the Industrial Thermoforming Business*, Plastics Custom Research Services, Advance, N.C., 2001, pp. 7–12.
10. Wm. K. McConnell Jr., *Ten Fundamentals of Thermoforming: Companion Volume*, Society of Plastic Engineers, Brookfield, Conn., 2001.
11. J. L. Throne, *Plastics Process Engineering*, Marcel Dekker, New York, 1979, pp. 850–859.
12. Ref. 8, Figure 4.2, p. 45.
13. K.-H. Hartmann, *Kunststoffe* **78**, 398–401 (1988), Bild 3.
14. Ref. 1, Figure 1.23, p. 33.
15. Ref. 1, Figure 1.25, p. 43.
16. K. J. Susnjara, *Three Dimensional Trimming & Machining: The Five Axis CNC Router*, Thermwood Corp., Dale, Ind., 1999.
17. Ref. 10, Figure 1-26, p. 1–15.
18. J. Florian, *Practical Thermoforming: Principles and Applications*, 2nd ed., Marcel Dekker, New York, 1996, pp. 140–146.
19. J. Frados, ed., *Plastics Engineering Handbook*, 4th ed., Van Nostrand Reinhold, New York, 1976, pp. 278–281.
20. D. G. Keith and A. E. Flecknoe-Brown, *Mod. Plast.* **56**(12), 62–64 (Dec. 1979).
21. Anon., *STP, Scrapless Forming Process*, Dow Chemical Co., Midland, Mich., 1976.
22. J. Penix, in M. L. Berins, ed., *SPI Plastics Engineering Handbook*, 5th ed., 1991, pp. 383–427.
23. F. Kreith, *Principles of Heat Transfer*, 2nd ed., International Textbook Co., Scranton, Pa., 1965, Figure 5-1, p. 199.
24. Ref. 8, Table 5.4, p. 62.
25. J. L. Throne and J. Beine, *Thermoformen: Werkstoffe-Verfahren-Anwendung*, Carl Hanser Verlag, Munich, 1999, Bild 5.22.
26. Ref. 8, Figure 6.5, p. 83.
27. A. Hoeger, *Warmformen von Kunststoffen*, Carl Hanser Verlag, Munich, 1971, Seite 98.
28. Ref. 1, pp. 226–242.
29. R. W. Ogden, *Non-Linear Elastic Deformations*, Dover, New York, 1997, Chapt. 7.
30. Ref. 18, pp. 237–247.
31. J. L. Throne, Advances in Thermoforming, Rapra Review Report, Vol. 8, No. 9, London, 1997, Table 4.
32. Anon., Thermoforming Quarterly, Society of Plastic Engineers, Thermoforming Division, Brookfield Center, Conn., Vol. 19, No. 3 (3rd Quarter 2000), cover.
33. G. Gruenwald, *Thermoforming: A Plastics Processing Guide*, 2nd ed., Technomic Publishing Co., Lancaster, Pa., 1998, Figure 2.2.

34. G. Kampf, *Characterization of Plastics by Physical Methods: Experimental Techniques and Practical Application*, Hanser Publishers, Munich, 1986, Section 6.2.
35. J. L. Throne, *Thermoforming*, Hanser Verlag, Munich, 1987, Appendix 2.I.
36. A. Buckel, *Thermoforming Tooling*, McConnell Co., Inc., Fort Worth, Tex., 2000, pp. 8–12.
37. K. Kouba, M. O. Ghafur, J. Vachopoulos, and W. P. Haessley, in Soc. Plast. Engrs. Annual Tech. Conf., Tech Papers, Vol. 40, 1994, pp. 850–853.
38. W. Michaeli and K. Hartwig, *Abschlussbericht zum DFG-Vorhaben, MI 192/30*, Inst. fur Kunststoffe Verarbeitung, RWTH Aachen, 1996.
39. J. F. Lappin, E. M. A. Harkin-Jones, and P. J. Martin, in Soc. Plast. Engrs. Annual Tech. Conf., Tech Papers, Vol. 45, 1999, pp. 826–830.
40. M. J. Stevenson, *Thermoforming Quarterly*, Society of Plastic Engineers, Thermoforming Division, Brookfield Center, Conn., Vol. 17, No. 4 (4th Quarter 1998), pp. 9–17.
41. J. N. McDonald, in J. I. Kroschwitz, ed., *Encyclopedia of Polymer Science and Engineering*, 2nd ed., Vol. **16**, John Wiley & Sons, Inc., New York, 1985, p. 809.
42. Ref. 27, Seite 163.
43. P. Schwarzmann (with A. Illig), *Thermoforming: A Practical Guide*, Hanser Publishers, Munich, 2001, pp. 162–165.
44. J. L. Throne, *Thermoplastic Foams*, Sherwood Publishers, Hinckley, Ohio, 1996, pp. 579–583.
45. Wm. Boerger, in *Thermoforming Conference Session*, National Plastics Exposition, Chicago, Ill., June 20, 2000.

JAMES L. THRONE
Sherwood Technologies, Inc.

TRANSITIONS AND RELAXATIONS.

See VISCOELASTICITY.

TRIBOLOGICAL PROPERTIES OF POLYMERS.

See ABRASION AND WEAR.

URETHANE COATINGS

Introduction

Polyurethanes (qv) are polymers containing urethane (—NH—COO—) linkages; carbamate is a synonym for urethane. Urethanes are usually formed by reaction of an alcohol with an isocyanate, but they can also be made by other methods. Commonly, urethanes made by a nonisocyanate route are called carbamates. To add to the confusing terminology, the terms *urethane* and *polyurethane* are applied to almost any binder derived from isocyanates even though only part, if any, of the reaction products are urethanes. The article on polyurethanes discusses synthesis and sources of various polyisocyanates.

An important advantage of most urethane coatings is the superior abrasion resistance of their films. The abrasion resistance results from the strong intermolecular hydrogen bonds between urethane groups. Under mechanical stresses, energy (about 20–25 kJ/mol of hydrogen bonds) may be absorbed by separation of hydrogen bonds, which re-form when the stress is removed (though probably in different positions). Energy absorption by this reversible process reduces the likelihood of irreversible breaking of covalent bonds, leading to degradation. This permits design of polyurethanes that are abrasion resistant while still resisting swelling with solvents. The isocyanate group is highly reactive, and so polyisocyanates can be used to make coatings that cure at ambient temperature or at moderately elevated temperatures. Coatings based on aliphatic diisocyanates exhibit exceptional exterior durability when stabilized with hindered amine light stabilizers (HALS). Resistance of urethane coatings to environmental etching is superior to that of many melamine–formaldehyde (MF) cross-linked coatings (1). The principal limitation of urethane coatings is cost relative to many other binders.

Encyclopedia of Polymer Science and Technology. Copyright John Wiley & Sons, Inc. All rights reserved.

Isocyanates react with alcohols and phenols to form urethanes. In general, rates of urethane formation decrease in the following order: primary alcohols > secondary alcohols > 2-alkoxyethanols > 1-alkoxy-2-propanols. Isocyanates can react with urethanes to form allophanates. This reaction is much slower than the reaction of isocyanate with alcohol. Isocyanates react rapidly with primary and secondary amines to form ureas. The reaction is much faster than the reaction of isocyanates with alcohols. Isocyanates can react with ureas to form biurets. Biuret formation is slower than urethane formation, but faster than allophanate formation. Isocyanates react with water to form unstable carbamic acids, which dissociate into carbon dioxide and an amine. The amine is so much more reactive that it reacts with another isocyanate (in preference to water) to form urea. The reactivity of water with isocyanates is somewhat slower than that of secondary alcohols, but much more rapid than that of uncatalyzed reaction with urethanes or ureas.

Imines act as blocked amines because they hydrolyze to yield free amines, which react with an isocyanate. Ketimines also react directly with isocyanates to yield a variety of products, depending on the particular reactants and conditions. Aldimines react analogously with isocyanates to yield unsaturated substituted ureas. Since aldimines are more stable to hydrolysis than ketimines, the fraction undergoing direct reaction with isocyanate in the presence of water is greater than that with ketimines. Carboxylic acids react relatively slowly to form amides and CO_2. Hindered carboxylic acid groups, such as in 2,2-dimethylolpropionic acid (3-hydroxy-2-(hydroxymethyl)-2-methylpropanoic acid) [4767-03-7], react very slowly.

Isocyanates also react with each other to form dimers (uretdiones) and trimers (isocyanurates). Formation of uretdiones is catalyzed by phosphines. Formation of isocyanurates is catalyzed by quaternary ammonium compounds; trimerization of aromatic isocyanates is catalyzed by tertiary amines. Uretdiones decompose thermally to regenerate isocyanates and are used as blocked isocyanates. Isocyanurates are stable and isocyanurates of diisocyanates are extensively used as multifunctional isocyanates.

Reactions of isocyanates with alcohols are catalyzed by a variety of compounds, including bases (tertiary amines, alkoxides, and carboxylates), metal salts and chelates, organometallic compounds, acids, and urethanes. The most widely used catalysts in coatings are organotin (IV) compounds, most commonly dibutyltin dilaurate (DBTDL) (dibutylbis[(1-oxododecyl)oxy]stannate) [77-58-7] and tertiary amines, commonly diazabicyclo[2.2.2]octane (DABCO). Combinations of DABCO and DBTDL often act synergistically.

DBTDL is soluble in a wide range of solvents, comparatively low in cost, colorless, and, in general, highly effective at levels of the order of 0.05 wt%. DBTDL promotes urethane formation without promoting allophanate formation (2) or trimerization (3). While aromatic isocyanates are more reactive than aliphatic isocyanates in uncatalyzed reactions with alcohols, the reactivity of aliphatics can be roughly equal with DBTDL. On the other hand, amine catalysts are more effective with aromatic than aliphatic isocyanates. Carboxylic acids inhibit catalysis by organotin compounds.

Isocyanates also react with water; if this happens in a solventborne coating during application, CO_2 is generated, which may reduce gloss or result in

bubbling. Catalyst selection affects the relative rate of reaction of isocyanates with hydroxyl groups and water. A zirconium acetoacetate complex [$Zr(AcAc)_4$] catalyst is reported to be more selective than DBTDL (4).

Isocyanates Used in Coatings

Both aromatic and aliphatic isocyanates are used in coatings; the former are less expensive and the latter provide films with better color retention and exterior durability. Diisocyanates are used in two broad types of ways: (*1*) as raw materials in the synthesis of resins and (*2*) as cross-linkers for resins with multiple substituent groups that are reactive with isocyanate groups. Isocyanates are toxic materials. When used as cross-linkers for coatings, they are reacted to form higher molecular weight isocyanate products with lower toxic hazards.

The aromatic isocyanates most widely used in coatings are bis(4-isocyanatophenyl)methane [101-68-8] (MDI) and 2,4-toluene diisocyanate (TDI) (2,4-diisocyanato-1-methylbenzene) [584-84-9]. MDI is available in several grades: a mixture of 90% of the 2,4′ isomer and 10% of the 4,4′ isomer; and several oligomeric (frequently called polymeric) MDI with longer chains of methylene phenyl groups. The cost is lower than TDI. When used as a cross-linker in coatings, the monomeric grade is converted to a low molecular weight prepolymer by reacting with a polyol such as trimethylolpropane. The polymeric grades have lower toxicity.

The most common grade of commercial TDI consists of a mixture of about 80% 2,4- and 20% 2,6-diisocyanato isomers. Nearly pure 2,4-TDI is also available at a premium price. Because of toxic hazards, TDI is not used as such in final coating formulations. For coatings in which unreacted isocyanate groups are needed, TDI is converted into derivatives of higher molecular weight and higher functionality. Higher molecular weight reduces the toxic hazard, and the higher functionality yields solvent-resistant films more rapidly. TDI has the advantage of a differential in reactivity between the ortho- and the para-isocyanate groups with alcohols, which makes possible synthesis of isocyanurates and prepolymers with narrower molecular weight distribution than with diisocyanates in which the isocyanate groups are equally reactive. A prepolymer prepared by the reaction of trimethylolpropane (TMP) (2-ethyl-2-(hydroxymethyl)-1,3-propanediol) [77-99-6] with a large excess of 2,4-TDI and then removal of excess TDI by using a vacuum wiped-film evaporator is widely used. The isocyanurate derived from TDI made by trimerizing TDI also has a lower toxic hazard than monomeric TDI; the reaction is almost exclusively at the 4-position.

The principal aliphatic isocyanates used are 1,6-hexamethylene diisocyanate (HDI) (1,6-isocyanatohexane) [822-06-0], bis(4-isocyanatocyclohexyl)methane (H_{12}MDI) [5124-30-1], and isophorone diisocyanate (IPDI) (3-isocyanato-1-isocyanatomethyl)-1,3,3-trimethylcyclohexane [4098-71-9]. Tetramethyl-*m*-xylidene diisocyanate (TMXDI) [2778-42-9] and *m*-isopropenyl-α,α-dimethylbenzyl-isocyanate (TMI) (1-(1-isocyanato-1-methylethyl)-3-(1-methylethenyl)benzene [2094-99-7] are specialty products used on a much smaller scale. Diisocyanates are only used as higher molecular weight derivatives in coatings to increase functionality and reduce toxic hazard.

HDI is especially hazardous and is handled on a large scale only in chemical plants. The first less hazardous derivative was a biuret, which can be made by reacting HDI with a small amount of water and then removing excess HDI. The presence of oligomeric biurets makes the average functionality higher than 3. These polyfunctional isocyanates give coatings with good color retention and weather resistance. The viscosity of an early commercial product was about 11.5 Pa·s (115 P) at 20°C. Grades with lower average molecular weights (and average functionalities nearer to 3) are available with viscosities as low as 1.4 Pa·s (14 P). HDI isocyanurates are used on a larger scale. The isocyanurate gives coatings with greater heat resistance and even better long-term exterior durability than HDI biuret. Commercial products contain oligomeric material, and average functionality is over 3. Grades with lower oligomer content with viscosities as low as 1 Pa·s (10 P) are available.

Allophanate derivatives of HDI and IPDI are another type of polyfunctional isocyanate. They are made by reacting an alcohol or diol with excess isocyanate, then removing unreacted diisocyanate with a wiped film evaporator giving an isocyanate-terminated allophanate (5). The properties can be varied by using different alcohols or diols to make the starting urethane. For example, the cetyl alcohol urethane from HDI yields an allophanate diisocyanate that is soluble in aliphatic hydrocarbons. Derivatives with higher functionality are made by reacting a glycol with excess diisocyanate.

The uretdione dimer of HDI also has lower volatility with low viscosity and can be used for cross-linking in ambient cure coatings. Very low viscosity grades, <100 mPa·s (=cP), are reported to permit formulation of very low VOC coatings (6).

H_{12}MDI is less volatile than HDI and is sometimes used as a free diisocyanate in coatings to be applied by roll coating, but not by spray coating. It is a mixture of stereoisomers; since both isocyanato groups are secondary, reactivity is lower than HDI or IPDI. Combined allophanate–isocyanurate derivatives are available with low free monomer content. Reference 7 covers the chemistry and uses of H_{12}MDI.

Commercial IPDI is a mixture of Z-(cis) and E-(trans) isomers in a 75:25 ratio. The isomers are difficult to separate. Isocyanurate derivatives of IPDI and prepolymers with TMP are widely used.

TMXDI and TMI have aromatic rings, but give color retention and exterior durability equivalent to aliphatic isocyanates. Since the isocyanato group is on a tertiary carbon, the reactivity is lower than that of less sterically hindered aliphatic isocyanates. This difference can be offset by using higher catalyst levels and sterically accessible tin catalysts such as dimethyltin diacetate (DMTDA) instead of DBTDL. TMXDI is offered as a low molecular weight, essentially diisocyanate-free, prepolymer with TMP. TMI is used as a comonomer with acrylic esters to make 2000–4000 molecular weight copolymers with 40–50 mol% TMI; thus each molecule has several isocyanate groups (8).

Two Package Urethane Coatings

The largest volume of urethane coatings is two package (2K) coatings that are mixed just before application. One package contains the polyol (or other

coreactant), pigments, solvents, catalyst(s), and additives; the other contains the polyisocyanate and moisture-free solvents. Sometimes, the catalyst is in a separate third package so that cure rate can be adjusted for variations in ambient conditions. While the major reaction is formation of urethane cross-links, some urea cross-links result from reaction of atmospheric water with the isocyanate.

Any hydroxy-functional coreactant can be used; hydroxy-terminated polyester and hydroxy-substituted acrylic resins are most common. In general terms, polyesters permit higher solids and give films with greater solvent resistance and better adhesion to metals. Acrylics provide faster dry, lower cost (since their equivalent weight is usually higher than that of polyesters, resulting in the need for less of the more expensive polyisocyanate), and better exterior durability, resulting from superior hydrolytic and photochemical stability. Since alkyd resins have unreacted hydroxyl groups, their rate of dry can be accelerated by adding a polyisocyanate such as the isocyanurate trimer of IPDI just before application. Nitrocellulose (shipped wet with plasticizer instead of ethyl or isopropyl alcohol) is used in formulating cross-linking furniture lacquers. Bisphenol A epoxy resins are also cross-linked with isocyanates through their hydroxyl groups. Hydroxy-terminated polyethers are used with aromatic polyisocyanates in flooring, roofing, and containment coatings.

Urethane coatings for maintenance paint applications are generally cured at ambient temperatures, while those for automobile refinishing and aircraft applications are cured at ambient or modestly elevated temperatures. If the T_g of the partially reacted system is near the temperature at which the cross-linking must occur, the rate of urethane formation becomes mobility controlled and cure rate is slow. If the T_g of the fully reacted system is significantly above the cure temperature, the reaction virtually stops before the cross-linking reaction has gone to completion (9). Water can continue to diffuse longer through such a matrix, and the last stages of reaction are predominately with water. Since in many ambient cure coatings, one wants a coating with a T_g somewhat above the curing temperature, selection of a combination of polyisocyanate and polyol that provides an appropriate final T_g is critical. A polyisocyanate with relatively flexible aliphatic chains (such as the isocyanurate of HDI) is used with a relatively high T_g acrylic or polyester. On the other hand, a polyisocyanate that yields relatively rigid cross-linked segments (such as the TMP/TMXDI prepolymer) requires a lower T_g acrylic or polyester.

An important variable in 2K polyisocyanate/polyol coatings is the ratio of available isocyanate groups to available hydroxyl groups (N=C=O/OH). In ambient cure systems, it is often found that a ratio of the order of 1.1:1 gives better film performance than a 1:1 ratio. A probable reason is that part of the N=C=O reacts with water from solvent, pigment, or air to give urea cross-links. The excess isocyanate assures that essentially all of the hydroxyl groups react, and subsequently all the remaining isocyanate groups react with water. Solvent resistance is improved. Some finishes, for example aircraft finishes, are formulated with N=C=O/OH ratios as high as 2:1. The resulting reduced hydroxyl concentration gives longer pot life. It is possible that the high mobility of water and the reactivity of amine groups resulting from the water/isocyanate reaction favor faster reaction rates at higher T_g values than possible with only the hydroxyl/isocyanate reaction.

There is always a compromise between pot life and curing time. Several formulating variables are available to increase pot life with little effect on cure time. Concentrations of reactive groups should be kept as low as possible; this becomes more difficult as one formulates to increasingly higher solids. As noted in the preceding paragraph, using mixed polyol/moisture curing systems helps. Since isocyanate/alcohol reactions proceed most slowly in media with high levels of hydrogen-bond accepting groups, solvents which are strong hydrogen-bond acceptors should be selected to the extent possible, and resins should be designed, if possible, with low levels of hydrogen-bond accepting groups. After application, as the solvent evaporates, the medium becomes less hydrogen-bond accepting and the reaction rate increases accordingly. This strategy serves the purpose of both extending pot life and promoting reactivity after application. However, it should be noted that solvents with greater hydrogen bond accepting strength tend to have higher viscosities, higher solids and longer pot lives are obtained with solvents having intermediate hydrogen-bond accepting strength (10).

Organotin catalysts are generally preferable to amine catalysts because reaction rates depend on alcohol concentration to the one-half power with organotin catalysts and to the first power with amine catalysts. Since the effectiveness of tin catalysts is reduced by carboxylic acids, one can add a volatile acid such as acetic or formic acid to the formulation. The acid inhibits reaction during the pot life stage, but evaporates during application so that the inhibiting effect disappears. 2,4-Pentadione increases pot life by chelating with organometallic catalyst compounds.

Availability of lower viscosity isocyanate cross-linkers makes possible formulation of higher solids 2K coatings. However, one must consider not just the viscosity of the cross-linker, but also that of the combination of polyol and cross-linker. In some cases, a lower viscosity cross-linker also has a lower equivalent weight; this means that the weight ratio of cross-linker to polyol must be reduced to maintain the same stoichiometric ratio of N═C═O/OH (11). Since the polyol often has a much higher viscosity, this reduced ratio can give a higher viscosity coating, in spite of the lower viscosity of the cross-linker. Higher solids can be obtained using a somewhat higher viscosity polyisocyanate with a higher equivalent weight.

If very fast cure at relatively low temperatures is needed, reactive coreactants and/or high catalyst levels are used, and the pot life is short. Such formulations can be applied using special spray equipment in which the two packages are fed to a spray gun by separate proportioning pumps and mixed inside the gun just before they are sprayed. Care is required to assure that the proper ratios are fed and thoroughly mixed; such spray equipment can be expensive and complex.

Most amines react too rapidly for use in 2K coatings; however, hindered amines have been developed that permit their use. Polyaspartic esters are hindered amines that are used in high solids coatings (12). The aminoesters are synthesized by the addition of a diamine such as 4,4′-(aminophenyl)methane to diethyl maleate. The pot life of these combinations is increased by addition of DBTDL. On the other hand carboxylic acids and water accelerate reaction rates. By proper selection of isocyanate and aspartate and adjustment of catalysts, it is possible to formulate very high solids 2K coatings with a reasonable pot life and fast curing.

Imines react directly with isocyanates or with water followed by the reaction of the free amine generated; the ratio of the two reactions depends on relative humidity, the time between application and cure, and the curing temperature (12). The reaction with water releases amine to react with isocyanate and carbonyl compound, which volatilizes. In the direct reaction, carbonyl compound from the imine is not released, and hence, VOC (volatile organic compound) emissions are lower. The ratio of the two reactions depends on the relative humidity and on the time between application and baking. The direct reaction is catalyzed more than the water reactions by carboxylic acids, and water and tertiary amines reduce the rate of reaction. The imines have very low viscosities; for example, the bis(methyl isobutyl ketone) ketimine of ethylene diamine has a viscosity of 5 mPa·s (=cP) and an equivalent weight of 112. Direct reaction is more favored with aldimines, especially above 60°C. Imines permit formulation of 2K coatings with very high solids, better pot life, and faster drying than with polyols (12). They can be used alone or in combination with a hydroxy-functional polyester or acrylic resin (13).

Blocked Isocyanates

In early work on isocyanates in coatings, it was recognized that there would be advantages to develop systems supplied in one package with minimal toxic hazard. One-package coatings do not require costly mixing equipment, and eliminate concerns over controlling the ratio of mixing of two components. These objectives led to work on *blocked isocyanates*, taking advantage of reversible reactions of isocyanates. A di- or polyisocyanate is reacted with a monofunctional active hydrogen compound, and the adduct (a blocked isocyanate) is formulated into a coating with a coreactant resin. The coating is stable at ambient temperature, but when baked, the monofunctional reactant is released (and usually volatilized), and the coreactant cross-links. Many blocked isocyanates are sufficiently stable in the presence of water at storage temperatures for use in waterborne systems. However, use of blocked isocyanates has two drawbacks: relatively high temperatures are required for cross-linking and, in some cases, release of the blocking agent can cause a pollution problem. An extensive review citing over 1700 references has been published covering the structure, reactions, catalysis, and applications of blocked isocyanates (14).

The blocking agents most widely used commercially are phenols, oximes, alcohols, ε-caprolactam (hexahydro-2*H*-azepin-2-one) [105-60-2], 3,5-dimethylpyrazole, 1,2,4-triazole, and diethyl malonate (propanedioic acid diethyl ester) [105-53-3]. It is common to see tables of "unblocking temperatures." The implication is that there is some "magic temperature" above which the various blocked isocyanates abruptly unblock; however, no such temperature exists. Published unblocking temperature data are based on some measurement of extent of reaction under a specific set of conditions. Examples of such criteria are the lowest temperature at which free isocyanate can be detected spectroscopically or the temperature required to achieve a specified degree of solvent

resistance in cross-linking a coreactant resin in a specified time. The values depend on rate of heating as well as the time at a temperature. A variety of catalysts is used: organotin compounds, DABCO, and zinc octanoate are among them.

Phenols were the first blocking agents used commercially, despite their environmental problems. Blocked isocyanates made with phenol or alkyl-substituted phenols are less thermally stable than those blocked with alcohols. Blocked aromatic isocyanates are more reactive than blocked aliphatic isocyanates. A typical curing schedule with a phenol blocked aromatic polyisocyanate and a hydroxy-functional resin is 30 min at 160°C. Phenol blocked isocyanates are used for wire coatings, applied by running the wire through a coating bath and then through an exit die appropriately larger than the diameter of the wire. This process requires a coating with one package stability. Since wire is small and can be heated to high temperatures without major energy cost, high cure temperature is not a major disadvantage. Phenols had been used for many years as solvents in wire coating, and ovens were already engineered to incinerate the phenol, eliminating the pollution problem and providing some fuel value. The excellent abrasion resistance of polyurethane wire coatings justifies the cost. Phenol blocked isocyanates react with amines at room temperature. They are used as flexibilizing reactive additives in amine cured epoxy coatings.

Oximes, such as methyl ethyl ketone oxime (MEKO) (2-butanone oxime) [96-29-7], form less thermally stable blocked isocyanates than phenols. Their reactivity is such that reasonably stable one package coatings can be formulated with hydroxy-functional resins that can be cured in 30 min at 130°C or somewhat lower. Oximes are used as blocking agents in magnetic metal oxide coatings for application to oriented polyester tape. Such coatings must be cured in a short time at temperatures no higher than 80°C to avoid distortion of the plastic tape and yet must have sufficient pot life (at least a few hours) to permit application with a roll coater. An oxime blocked diisocyanate with an amine-terminated polyamide coreactant gives sufficient pot life, but still cures rapidly at 80°C. The excellent abrasion resistance and flexibility of polyurethane coatings are major advantages in this application.

Steric crowding on either oxime or isocyanate enhances the dissociation rates. Isocyanates blocked with diisopropyl and diisobutyl ketoximes dissociate faster than the same isocyanates blocked with MEKO (15). Oxime blocked TMXDI dissociates faster than other less sterically crowded aliphatic isocyanates and with comparable rates to aromatic isocyanates. Blocked TMI cross-linkers can be synthesized by first copolymerizing the TMI with acrylate esters, and then reacting the polyfunctional acrylate with an oxime such as MEKO. Alternatively, one can react TMI with the oxime and then copolymerize the blocked monomer with acrylate esters (16).

Oximes oxidize at elevated temperatures to yield colored products. As a result, in some cases, films made with oxime blocked isocyanates yellow during baking. The yellowing can be minimized by including a reducing agent such as a hydrazide derivative, for example, an oligomeric hydrazine adipate, in the formulation (17). Isocyanates blocked with 3,5-dimethylpyrazole (DMP) yellow less than with MEKO and give somewhat faster curing (18). 1,2,4-Triazole and mixtures of

1,2,4-triazole and DMP are reported to give low curing temperatures and freedom from yellowing (19,20). Concerns about possible toxic hazards with MEKO are serving to increase emphasis on evaluating other blocking agents, such as DMP and triazole.

The largest volume coatings with blocked isocyanates are cationic electrodeposition primers. They must be stable in water indefinitely. Alcohols are the most widely used blocking agents. 2-Ethylhexyl alcohol (2-ethylhexanol) was the most widely used but is being replaced by half ethers of glycols to obtain lower curing temperatures. Amine groups on the coreactant resin are neutralized with weak acids, such as lactic or formic acid. During electrodeposition, the protonated amine groups are converted into free amines at the cathode, causing the polymer to form a uniform coating on the cathode. The coatings are subsequently cured at relatively high temperatures.

Tris(alkoxycarbonylamino)triazine (TACT), a mixed methyl and butyl carbamate derivative of melamine, acts as an alcohol blocked isocyanate (21). TACT is much more reactive than conventional alcohol blocked isocyanates, since it is activated by the triazine ring. It cross-links hydroxy-functional acrylics at 125°C in 30 min, comparable to (or lower than) oxime blocked isocyanates. The reaction is not catalyzed by tin compounds; it is catalyzed to a small extent by dodecylbenzene sulfonic acid.

Diethyl malonate blocked diisocyanates cross-link with polyols at low temperatures, a typical curing schedule of 120°C for 30 min. However, reaction of diethyl malonate blocked isocyanates with alcohols does not yield urethanes, but rather transesterification occurs (22). Correspondingly, reaction with amines yields amides, not ureas. The transesterification proceeds fairly rapidly at 120°C; storage stable coatings can be formulated by using monofunctional alcohol in the solvent mixture. The monofunctional alcohol extends the stability by competing with the polyols for reaction with the blocked isocyanate. After the coating is applied, the monofunctional alcohol evaporates, and reaction with polyol gives a cross-linked coating. The active hydrogen of malonic ester blocked isocyanates reacts with MF resins (23). Clear coats for automobiles have been formulated with a combination of a hydroxy-functional acrylic resin, malonic ester blocked HDI and IPDI trimers, and an MF resin (24). Cross-linking reactions result from reactions of isocyanates from the blocked isocyanate with hydroxyl groups, MF resin cross-linking of hydroxyl groups, and MF resin reaction with the malonic ester blocking groups.

A large scale use of blocked isocyanates is in powder coatings. The principal blocking agent is ε-caprolactam. The most widely used isocyanate has been IPDI isocyanurate. Use of caprolactam is decreasing because of the high temperatures required for curing and oven buildup that is difficult to clean. Oxime blocked isocyanates cure at lower temperature, but there is concern about possible toxic hazards. A blocked isocyanate derived from 1,2,4-triazole and a mixture of monomeric HDI and HDI isocyanurate permits relatively low temperature cure of acrylic powder coatings while giving good mechanical properties (25). Blocking with a mixture of 1,2,4-triazole and 3,5-dimethylpyrazole is reported to give non-yellowing and low temperature cure (19,20). Polyol derivatives of IPDI uretdiones are used as cross-linkers in powder coatings; some will permit curing at lower temperatures than does caprolactam. The uretdione groups disassociate

to isocyanates at curing temperatures, providing cross-linking with no volatile blocking agent (26).

Moisture Curing Urethane Coatings

Polyurethane moisture curing coatings cross-link under ambient conditions by reaction of isocyanates with atmospheric water. Most such coatings use isocyanate-terminated resins made from hydroxy-terminated polyesters by reacting the terminal hydroxyl groups with an excess of a diisocyanate such as oligomeric MDI or, if color retention is needed, IPDI. So the coating does not contain unreacted diisocyanate; the resin is prepared utilizing a ratio of N=C=O to OH that is significantly less than 2 to 1. The coatings are stable when stored in the absence of water, but cross-link after application by reaction of the isocyanates with water to form amines, which react with another isocyanate to form substituted urea cross-links. Cure rates depend on the water content of the air; at low temperatures, higher relative humidity is required than at higher temperatures, since the relative humidity decreases with increasing temperature. At high humidity and temperature, cure is rapid, but the carbon dioxide released by the reaction of isocyanate with water can be trapped as bubbles, especially in thick films. See Reference 27 for discussion of the effects of temperature and humidity and other application considerations. Moisture curing urethane coatings are used for applications such as floor coatings, for which abrasion resistance and hydrolytic stability are important. They are called urethane coatings even though these cross-links are urea groups rather than urethane groups. Since urea groups also form intermolecular hydrogen bonds, presumably, they can affect resistance to mechanical stress similarly to urethane groups. Hydrolytic resistance of coatings is affected by several variables, including cross-link density and free-volume availability, as well as the functional groups present. Ureas and urethanes from aliphatic isocyanates are somewhat more resistant to hydrolysis than those from aromatic isocyanates. Both urea and urethane groups are generally more stable to hydrolysis than unhindered ester groups.

Moisture curing coatings are less susceptible to error in application than 2K coatings, for which there is a chance of incorrect ratios of packages affecting the stoichiometric ratios. A disadvantage is that solvents, pigments, and other components must be essentially water free. Use of moisture cure coatings is primarily in clear, gloss coatings since it is expensive to remove adsorbed water from pigments. Molecular sieves can be used to adsorb water, but can reduce gloss. Pigmented moisture cure coatings can be made using a water scavenger such as an alkyl orthoformate or *p*-toluenesulfonylisocyanate. Such water scavengers, especially sulfonylisocyanates, must be handled with care because of toxicity. Oxazolidines are reported to be effective moisture scavengers for aliphatic isocyanate-based coatings, presumably with less toxic hazard and lower cost (28). 4-Ethyl-2-methyl-2-(3-methylbutyl)-1,3-oxazolidine provides rapid water removal, while not adversely affecting stability or performance of a coating. Monomeric diisocyanates such as IPDI can also be used to react with water in the pigment dispersion before mixing it with the rest of the formulation; excess diisocyanate can be scavenged with a polyol (29).

Waterborne Polyurethanes

VOC emission regulations have led to work on waterborne polyurethane systems; a variety of approaches have been investigated (30,31).

Thermoplastic Polyurethane Dispersions. Polyurethane dispersion resins are predominantly linear, relatively high molecular weight polyurethane polymers dispersed in water. Such materials are latexes, but they are generally called *polyurethane dispersions* (PUDs). One way to prepare such dispersions is by the *acetone process* (30). An isocyanate-terminated polymer is made in acetone solution from a diisocyanate and a diol (or mixture of diols). This resin is chain extended by reacting with a sulfonate-substituted diamine, $H_2NCH_2CH_2NHCH_2CH_2SO_3^- Na^+$. The acetone solution is diluted with water, and the acetone removed by distillation. The sulfonate salt substituent acts as a charge repulsion stabilizer for the aqueous dispersion. The average number of sulfonate groups per molecule can be adjusted by using mixtures of unsubstituted and sulfonate-substituted diamines. One can incorporate a small amount of trifunctional isocyanate in making the initial isocyanate-terminated polymer. The result is a dispersed polymer with a low degree of cross-linking—low enough that the particles can still coalesce to a continuous film, but high enough that film properties are superior to those obtained with linear polymers (32). Since urethanes hydrogen bond strongly with water, the particles are swollen with water, plasticizing the polymer and thereby permitting film formation with higher T_g polymers than is possible with acrylic latexes (33).

The acetone process has the disadvantage that the removal of acetone is a time-consuming and expensive step. PUDs can also be made using a low volatility solvent. *N*-methylpyrrolidinone (NMP) has been the most widely used solvent. The cost of manufacture is lower but the VOC is obviously higher and the low volatility of NMP requires baking to remove the solvent. There is also concern about the possible carcinogenicity of NMP.

Dispersions can also be made by solvent-free processes. For example, isophorone diisocyanate, polycaprolactone diol, polytetrahydrofurandiol, and dimethylolpropionic acid are reacted with an NCO:OH ratio of 1.6:1 to make an isocyanate-terminated prepolymer. The prepolymer is neutralized with triethylamine and dispersed in water. The prepolymer is then chain extended by reacting with hydrazine hydrate.

One can also make combined acrylic/urethane (hybrid) aqueous dispersions (33). Acrylic monomers are emulsion polymerized in the presence of an aqueous dispersion of a hydroxy-terminated polyurethane. The polyurethane stabilizes the aqueous dispersion, minimizing need for surfactant. Coalescence requires balance of the T_g of both the urethane and acrylic parts of the system. Compositions based on an IPDI/polypropylene glycol/DMPA urethane with styrene/methyl methacrylate/butyl acrylate are reported to form films at low temperatures.

Cross-Linkable PUDs. Cross-linkable PUDs are also made. For example, a hydroxy-functional polyurethane can be made using a diisocyanate, a diol, a triol, and 2,2-dimethylolpropionic acid (DMPA) in a *one-step process*. The sterically hindered carboxylic acid group on DMPA is so low in reactivity with isocyanate that few amide bonds are formed. After neutralization of carboxylic acid groups with an amine, the resin is diluted with water to yield a dispersion stabilized by

the salt groups on the surface of polymer aggregates. Commonly, NMP is used as a solvent to reduce the viscosity of the resin. Such resins do not have the hydrolytic stability problems of water-reducible polyesters; also, the probability of formation of low molecular weight, cyclic, nonfunctional molecules is low. Lower viscosity PUDs can be made by a *two-step process* (34). First, a linear isocyanate-terminated polyurethane is made using a diisocyanate, a diol, and DMPA; then, in a second step, the terminal isocyanate groups are reacted with aminoalcohols such as diethanolamine to yield a hydroxy-terminated polyurethane.

Polyurethane dispersions can also be prepared by a nonisocyanate process (35). An aliphatic polyester diol is reacted with a bis(2-hydroxypropyl carbamate), a triol, and a transesterification catalyst, such as dibutyltin oxide. Carboxy functionality is then introduced by reacting some of the remaining hydroxy groups with an anhydride.

The hydroxy-functional polyurethane dispersions can be cross-linked with MF resins or blocked isocyanates. Blocked isocyanates can also be used with water-reducible anionic acrylic or polyester resins instead of an MF resin; oxime blocked isocyanates are commonly used, owing to their high reactivity. Oxime blocked aliphatic isocyanates are more stable to hydrolysis than oxime blocked aromatic isocyanates (32). As mentioned earlier alcohol blocked isocyanates are used in cationic electrodeposition coatings.

2K Waterborne Coatings. Since isocyanates react relatively readily with water, it was assumed for many years that they could not be used directly in waterborne coatings; however, in the last few years, 2K waterborne coatings have been developed. The Bayer Corporation was awarded a Presidential Green Award in 2000 for its work in developing 2K waterborne urethane coatings. Reference 36 is a review of the work on 2K waterborne urethane systems.

It is relatively easy to make 2K coatings with good properties in the laboratory; however, production use is more difficult. There are several potential problems. In some systems, it is difficult to assure that uniform stoichiometric ratios are obtained throughout the film. As with solventborne 2K coatings, waterborne 2K coatings can be expected to have limited pot life. In solventborne coatings, pot life can be determined by monitoring viscosity increases. In many 2K waterborne coatings, viscosity does not increase as reactions between N=C=O and OH take place, since they change the viscosity inside the aggregate particles, but not the bulk viscosity. In fact, the generation of CO_2 by the reaction of isocyanate decreases the pH, leading to shrinking of the aggregate particles, which can result in viscosity reduction. If reaction occurs to a significant extent before application, coalescence will be inhibited, and therefore, film properties may be poor. If there is too much reaction before volatiles are evaporated, complete coalescence of the dispersion particles may not occur. Since isocyanates also react with water, full reaction of the polyols requires an excess of isocyanate. Furthermore, the reaction with water results in formation of CO_2, which can lead to *blistering*, especially as thicker films are applied.

One approach to solving these problems is to combine conventional polyisocyanates with conventional, amine neutralized, water-reducible resins in a water-miscible solvent and then add water. A similar process is used for water-reducible coatings cross-linked with MF resins. Conventional water-reducible acrylic resins in solvents such as 1-methoxy-2-propanol acetate have been used. Water-soluble

glycol ethers do not significantly interfere since they are primarily in the water phase, with little chance to interact with isocyanates. Tertiary amines such as triethylamine or *N*-alkylmorpholines are used to neutralize the resin rather than the dimethylethanolamine widely used in MF cross-linked coatings. 2-amino-2-methyl-1-propanol is a particularly poor choice, since the primary amines are very reactive with isocyanate. The amine is added to the resin solution before the polyisocyanate. Finally, the coating is reduced to application viscosity with water. Mixing the polyisocyanate into the acrylic solution requires good agitation, and with conventional polyisocyanates, erratic results are common. It is necessary to use a high NCO/OH ratio, often above 2, to compensate for nonproductive reactions of isocyanate with water; the high ratio increases cost. Since TMXDI reacts more slowly with water than other commercial isocyanates, successful use of this approach is reported with lower NCO/OH ratios (37).

Alternatively, a conventional polyisocyanate can be mixed in after reduction with water, just before spraying. Spray equipment designed to provide in-line intensive mixing of the two components has been used to apply polyisocyanate 2K water-reducible OEM automotive clear coats with properties comparable to those obtained with solventborne 2K coatings (38). A large fraction of the water evaporates during flash off and initial baking, reducing the extent of isocyanate reaction with water, minimizing CO_2 evolution, and permitting lower ratios of NCO/OH.

Mixing conventional polyisocyanates into the polyol after reduction with water can result in problems resulting from nonuniform stoichiometry. Hydrophilically modified polyisocyanates made by reacting a fraction of the —NCO groups on a polyisocyanate (such as HDI or IPDI isocyanurate) with a polyglycolmonoether are more easily mixed. The modified polyisocyanate is stirred into an aqueous dispersion of a coreactant to form a heterogeneous dispersion in which the polyisocyanate and coreactant are in separate dispersed particles (39–41).

Although alcohols react more rapidly with isocyanates than water, in a water system, there is a very large excess of water, and so a significant fraction of the isocyanate groups react with water; but these reactions also give cross-links. To assure reaction of most of the hydroxyl groups, NCO/OH ratios of 2 or greater are recommended. Some applications, such as wooden kitchen cabinets, do not require that cross-linking be complete; in such cases, lower NCO/OH ratios can be used, permitting lower cost and longer pot life (42). Results are dependent on the process used to mix the two packages together; high, but not excessive, shear is required to obtain relatively uniform particle size with an average diameter of about 150 nm. Two-component mixing spray guns are reported to give the most dependable results. Hydrophylically modifed polyisocyanate 2K coatings give films with adequate performance for many applications, but the reduction in functionality resulting from the reaction with the polyetherpolyol results in films with inadequate properties for such applications as automotive clear coats.

Carboxylic acid-functional PUDs can also be cross-linked with polyaziridines in 2K coatings. For example, a group of patents cover use of trifunctional aziridines, such as trimethylolpropane tris(2-aziridinylpropionate), in 2K coatings for plastics (43). Carboxylic acid-functional PUDs can also be cross-linked with polycarbodiimides (44).

Uralkyds

Uralkyds are also called *urethane alkyds* or *urethane oils*. They are alkyd resins (qv) in which a diisocyanate, usually 2,4(6)-toluene diisocyanate (TDI), has fully or partly replaced the phthalic anhydride (PA) usually used in the preparation of alkyds. One transesterifies a drying oil with a polyol such as glycerol or pentaerythritol to make a "monoglyceride" and reacts it with some PA (if desired) and then with somewhat less diisocyanate than the equivalent amount of N=C=O based on the free OH content. To assure that no N=C=O groups remain unreacted, methyl alcohol is added at the end of the process. Just like alkyds, uralkyds dry faster than the drying oil from which they were made, since they have a higher average functionality (more activated diallylic groups per average molecule). The rigidity of the TDI aromatic rings also speeds up the drying by increasing the T_g of the resin.

Two principal advantages of uralkyd over alkyd coatings are superior abrasion resistance and resistance to hydrolysis. Disadvantages are inferior color retention (when aromatic isocyanates used) of the films, higher viscosity of resin solutions at the same percent solids, and higher cost. Uralkyds made with aliphatic diisocyanates have better color retention, but are more expensive and have lower T_g. The largest use of uralkyds is in architectural coatings. Many so-called varnishes sold to the consumer today are based on uralkyds; they are not really varnishes in the original sense of the word. They are used as transparent coatings for furniture, woodwork, and floors; applications in which good abrasion resistance is important. Since they are generally made with aromatic isocyanates, they tend to turn yellow and then light brown with age; yellowing is acceptable in clear varnishes, but would be a substantial drawback in light colored pigmented paints.

Water-reducible polyunsaturated acid-substituted aqueous polyurethane dispersions are also being used (45). They can be made by reacting a diisocyanate with a polyol, monoglyceride of a drying oil, and dimethylolpropionic acid. The carboxylic acid groups are neutralized with a tertiary amine and dispersed in water. If aliphatic isocyanates are used, good color retention can be obtained. They are much more resistant to hydrolysis than conventional alkyd resins. Films also have excellent abrasion resistance. Cost can be reduced by blending in 10–20% of acrylic latex.

Hydroxy-Terminated Polyurethanes

Diisocyanates can react with diols and triols at an N=C=O/OH ratio of less than 1 to make hydroxy-terminated polyurethanes, which can be cross-linked with MF resins or with other cross-linkers that react with hydroxyl groups. Urethane groups also cross-link with MF resins. Compared to polyesters, hydrolytic stability is better and coatings provide the toughness and abrasion resistance associated with urethane coatings. However, the solids at equal molecular weight and viscosity are lower because of intermolecular hydrogen bonding, and the urethane groups increase moisture absorption. Compared to hydroxy-functional

acrylic resins, they offer the advantage of abrasion resistance and the possibility of using lower molecular weight resins.

Hydroxy-terminated polyurethanes with low molecular weight and viscosity have been synthesized by reaction of cyclic carbonates with diols (46). These *urethane diols*, as reactive diluents, permit formulation of higher solids acrylic/MF coatings with good properties. It was also suggested that they may be useful in water-reducible systems, reducing the organic solvent requirement.

Carbamate-Functional Reactants

MF resins react with carbamate groups under approximately the same conditions as when they react with hydroxyl groups. Carbamate-functional acrylics can be cross-linked with MF resins to give films with better environmental etch resistance than MF cross-linked hydroxy-functional acrylics while retaining the advantage of mar resistance as compared to conventional urethane coatings. Carbamate-functional acrylics can be prepared by reacting acrylic resins with urea (47). They can also be prepared by ester interchange between a hydroxyl group on a hydroxy-functional acrylic resin and the carbamate from propylene glycol monomethyl ether (48). Carbamate-functional polyester oligomers can be prepared by reacting glycidyl neodecanoate with dimethylolpropionic acid, followed by transesterification of the hydroxyl groups with methyl carbamate. Clear coats cross-linked with MF resins are reported to give films with excellent environmental etch resistance and mar resistance (49).

Another approach using carbamate-functional reactants is to react a polyisocyanate such as IPDI isocyanurate or HDI isocyanurate with hydroxypropyl carbamate (50). These carbamates are used in automotive clear coats with an MF resin that has been partially reacted with butyl carbamate to reduce its functionality. The remaining methoxymethyl groups of the melamine resin react with the carbamate groups of the isocyanurate-derived carbamate to give cross-linked films with outstanding environmental etch and mar resistance. The use of a combination of a carbamate-functional acrylic resin, a polycarbamate derived from a polyisocyanate, and an MF resin has also been patented (51).

Urethane Vehicles in UV Cure Coatings

Acrylated urethane oligomers are used with mono- and polyfunctional acrylic esters in uv cure coatings. Any polyol or hydroxy-terminated oligomer (HO-R-OH) can react with excess diisocyanate (OCN-R′-NCO) to yield an isocyanate-terminated oligomer. This oligomer then react with 2-hydroxyethyl acrylate (2-propenoic acid 2-hydroxyethyl ester) (HEA) at ambient or moderately elevated temperature to yield an acrylated urethane oligomer. Such urethane oligomers are particularly used in coatings that require excellent abrasion resistance such as clear topcoats for flooring. A coating for polycarbonate plastics is a recent example of such coatings. The coatings are based on HDI isocyanurate reacted with HEA dissolved in 1,6-hexanediol diacrylate (52).

Markets

The U.S. market for urethane coatings in 1997 was reported to be 270×10^6 L with a value of $1.6 billion (53). The same report forecast the market in 2002 to be 290×10^6 L with a value of almost $1.9 billion. These figures do not include $320 million of isocyanate activators and flex additives used with acrylic and alkyd enamels in automobile refinish coatings.

The largest market is reported to be architectural paints, consisting primarily of uralkyds used as varnishes for furniture and floors and in floor paints. The major advantage of these coatings over alkyd paints is their higher abrasion resistance. Acrylic/urethane aqueous dispersions are a growing part of this market.

The second largest market is reported to be OEM automotive coatings. The most important components of this market are cationic electrodeposition coatings, which are all formulated with blocked isocyanate cross-linkers. Blocked isocyanates are also used in chip-resistant primers. Waterborne urethane base coats are used in several assembly plants. Clear topcoat is a growing part of the market; 2K solventborne acrylic resins with a polyisocyanate have been used for many years as have blocked isocyanate cross-linked acrylic one component coatings. A small but rapidly growing class of coatings is 2K waterborne urethane coatings. Urethane coatings are extensively used on plastic components of automobiles.

Other important markets include automotive refinish coatings, maintenance coatings, aircraft finishes, camouflage coatings for military vehicles, wire enamels, magnetic tape, and coatings for plastics.

BIBLIOGRAPHY

1. J. D. Nordstrom and A. H. Dervan, in *Proc. Waterborne High-Solids Coat. Symp.*, New Orleans, 1993, p. 3.
2. I. Yilgor and J. E. McGrath, *J. Appl. Polym. Sci.* **30**, 1733 (1985).
3. S. W. Wong and K. C. Frisch, *J. Polym Sci., Part A: Polym. Chem.* **24**, 2867, 2877 (1986).
4. W. J. Blank, Z. A. He, and E. T. Hessell, *Prog. Org. Coat.* **35**, 19 (1999).
5. U.S. Pat. 5124427 (1992), T. A. Potter and W. E. Slack [to Miles, Inc. (now Bayer Corp.)].
6. R. T. Wojcik, *Polym. Mat. Sci. Eng.* **70**, 114 (1994).
7. R. S. Dearth, H. Mertes, and P. J. Jacobs, *Prog. Org. Coat.* **29**, 73 (1996).
8. U.S. Pat. 5254651 (1993), V. Alexanian, R. G. Lees, and D. E. Fiori [to American Cyanamid Co. (now Cytec Industries)].
9. D. E. Fiori and R. W. Dexter, in *Proc. Waterborne Higher-Solids Coat. Symp.*, New Orleans, 1986, p. 186.
10. N. Hazel, J. Biggin, J. Kersey, and C. Brooks, in *Proc. Waterborne High-Solids Powder Coat. Symp.*, New Orleans, 1997, p. 237.
11. S. A. Jorissen, R. W. Rumer, and D. A. Wicks, in *Proc. Waterborne Higher-Solids Powder Coat. Symp.*, New Orleans, 1992, p. 182.
12. D. A. Wicks and P. E. Yeske, *Prog. Org. Coat.* **30**, 265 (1997).
13. U.S. Pat. 5214086 (1993), P. J. Mormile and co-workers, (to BASF Corp.).

14. D. A. Wicks and Z. W. Wicks Jr., *Prog. Org. Coat.* **36**, 148–172 (1999); *Prog. Org. Coat.* **41**, 1–85 (2001).
15. J. S. Witzeman, *Prog. Org. Coat.* **27**, 269 (1996).
16. H. R. Lucas and K. J. Wu, *J. Coat. Technol.* **65**(820), 59 (1993).
17. U.S. Pat. 5504178 (1996), M. W. Shaffer and co-workers (to Bayer Corp.).
18. R. T. Wojcik and co-workers, in *Proc. Waterborne Higher-Solids Powder Coat. Symp.*, Part 2, New Orleans, 1994, p. 474.
19. Th. Engbert, E. Konig, and E. Jurgens, Farbe Lack, **102**, 51 (1996).
20. M. Sohoni and P. Figlioti, in *Proc. Waterborne High-Solids Powder Coat. Symp.*, New Orleans, 1998, p. 267.
21. A. Essenfeld and K.-J. Wu, in *Proc. Waterborne High-Solids Powder Coat. Symp.*, New Orleans, 1997, p. 246.
22. Z. W. Wicks Jr. and B. W. Kostyk, *J. Coat. Technol.* **49**(634), 77 (1977).
23. W. J. Blank and co-workers, *Polym. Mater. Sci. Eng.* **77**, 391 (1997).
24. U.S. Pat. 5516559 (1996), U. Rockrath, G. Wigger, and U. Poth (to BASF Lacke+Farben AG).
25. F. M. Witte, G. Kieft, W. H. A. van den Elshout, R. Baijards, and M. Houweling, in *Proc. Waterborne High-Solids Powder Coat. Symp.*, New Orleans, 1995, p. 32.
26. R. M. Guida, *Modern Paint Coat.* 34 (July 1996).
27. G. Gardner, *J. Protective Coat. Linings* 81 (Feb. 1996).
28. G. N. Robinson, J. F. Alderman, and T. L. Johnson, *J. Coat. Technol.* **65**(820), 51 (1993).
29. U.S. Pat. 4304706 (1981), B. R. Urs.
30. J. W. Rosthauser and K. Nachtkamp, in K. C. Frisch and D. Klempner, eds., *Advances Urethane Sci. Technol.*, Vol. **10**, Technomic Publishing Co., Westport, Conn., 1987, pp. 121–162.
31. J. C. Padget, *J. Coat. Technol.* **66**(839), 89 (1994).
32. P. L. Jansse, *J. Oil Colour Chem. Assoc.* **72**, 478 (1989).
33. R. Satguru and co-workers, *J. Coat. Technol.* **66**(830), 47 (1994).
34. C. R. Hegedus and K. A. Kloiber, *J. Coat. Technol.* **68**(860), 39 (1996).
35. W. J. Blank and V. J. Tramontano, *Prog. Org. Coat.* **27**, 1 (1996).
36. Z. W. Wicks Jr., D. A. Wicks, and J. Rosthauser, *Prog. Org. Coat., submitted for publication.*
37. D. E. Fiori, *Prog. Org. Coat.* **32**, 65 (1997).
38. M. Dvorchak and H. Bui, in *Proc. Waterborne High-Solids Powder Coat. Symp.*, New Orleans, 1998, p. 80.
39. P. B. Jacobs and P. C. Yu, *J. Coat Technol.* **65**(822), 45 (1993).
40. M. J. Dvorchak, *J. Coat. Technol.* **69**(866), 47 (1997).
41. C. R. Hegedus, A. G. Gilicinski, and R. J. Haney, *J. Coat. Technol.* **68**(852), 51 (1996).
42. H. Bui and co-workers, *Eur. Coat. J.* 476 (1997).
43. U.S. Pat. 4278578 (1981), D. Carpenter (to Hillyard Enterprises, Inc.); U.S. Pats. 4380596 (1983) and 4459329 (1984), G. R. Watchko (to General Electric Co.); U.S. Pat. 4493912 (1985), G. R. Watchko, C. D. Dudgeon, and M. R. Winstead (to General Electric Co.).
44. J. W. Taylor and D. R. Bassett, in J. E. Glass, ed., ACS Symposium Series, Vol. **663**: *Technology for Waterborne Coatings*, American Chemical Society, Washington, D.C., 1997, p. 137.
45. W. Liu, S. Wang, and T. Rende, *Western Coat. Symp.*, Reno, NV, 1999.
46. W. J. Blank, *Prog. Org. Coat.* **20**, 235 (1992).
47. U.S. Pat. 5605965 (1997), J. W. Rehfuss and D. L. St. Aubin (to BASF Corp.).
48. Int. Pat. Appl. WO 95/29947 (1995), S. V. Barancyk, C. A. Verardi, and W. A. Humphrey (to PPG Industries, Inc.).

49. M. L. Green, *J. Coat. Technol.* **73**(918), 55 (2001).
50. U.S. Pat. 5512639 (1996), J. W. Rehfuss and W. H. Ohrbohm (to BASF Corp.).
51. U.S. Pat. 6165618 (2000), W. H. Ohrbohm and co-workers, (to BASF Corp.).
52. U.S. Pat. 6232360 (2001), J. Meixner, W. Fischer, and J. Pedain (to Bayer Aktiengesellschaft).
53. *Coatings VI*, Skeist Inc., Whippany, N.J., 1998, pp. 874–897.

ZENO W. WICKS JR.
Consultant

URETHANE POLYMERS. See POLYURETHANES.

UV STABILIZERS

Introduction

Ultraviolet stabilizers extend the service life of plastics and coatings by the inhibition of degradative processes photoinitiated by UV light from the sun and other UV sources.

Of the various chemical classes of UV stabilizers that have been developed, the benzophenone and benzotriazole UV absorbers, the hindered amine light stabilizers (HALS), and their combinations continue to satisfy the UV stabilization requirements of most of the large-volume outdoor polymer applications. In addition, many new stabilizer chemistries, such as UV absorbers based on hydroxyphenyl triazines, have been developed for more demanding applications or to satisfy specific market needs. Light stabilizers together with other additives (qv), such as antioxidants (qv), impact modifiers, colorants (qv), fillers, heat stabilizers (qv) and plasticizers (qv), have enhanced the properties and extended the service life of polymeric materials, resulting in the replacement of traditional materials in a multitude of outdoor weatherable applications.

The effective use of light stabilizer products requires a basic understanding of polymer photodegradation processes, UV stabilization mechanisms, desired end-use properties, and weathering testing program design. This article will provide a brief review of these various elements, together with some current application examples (1–6).

Polymer Photodegradation Processes

In order for photodegradation to occur, absorption of UV light energy is required by UV-absorbing chemical groups in the polymer formulation. These light-absorbing

Encyclopedia of Polymer Science and Technology. Copyright John Wiley & Sons, Inc. All rights reserved.

groups are called *chromophores*. Excited states and radicals are generated from this photoinitiation process. In some polymers, such as polycarbonate, inter- or intramolecular reactions take place, resulting in appearance changes, such as the yellowing, and/or changes in physical properties, such as the loss in impact strength. In other polymers, such as polyolefins, the radicals react with oxygen, producing peroxy radicals which abstract hydrogens to generate hydroperoxides and new polymer radicals. Further photolysis of the hydroperoxides and carbonyl groups occurs, resulting in appearance changes, such as loss of surface gloss, and changes in physical properties, such as loss of elongation and tensile strength. This latter process is called photo-oxidation.

The sources of the UV-absorbing chromophores come from the chemical structure of the polymer, the thermal processing degradation products, colorants, fillers, other additives such as halogenated flame retardants, antioxidants and their transformation products, feedstock or process impurities, and residual catalyst.

The source of UV light energy is primarily from solar radiation. The UV light reaching the earth's surface ranges from 290 to 400 nm and consists of only 5% of the total solar radiation. However, the corresponding photon energy of 418–293 kJ/mol (100–70 kcal/mol) is sufficiently strong to break molecular bonds in most polymers and coatings. In Table 1, the relationship between the photon energy and the strength of many of the chemical bonds found in most plastics and coatings is given. Other environmental factors in polymer photodegradation are the surface temperature, moisture level, and atmospheric pollutants.

As shown in Table 2, the wavelength sensitivity of polymers has been measured using a series of UV light filters, confirming that each of the major polymers are sensitive to certain wavelengths within the 290–400-nm UV region (7,8). For example, the activation spectra maxima for polystyrene was found to be 310–325 nm, and for polypropylene there were three maxima at 290–300, 330, and 370 nm. Although a narrow wavelength maxima is reported for each polymer, the full polystyrene spectrum shown in Figure 1 illustrates that polymers are typically sensitive to a broader range of UV light energy.

As shown in Figure 2, the use of a UV filter to screen this harmful UV light energy can effectively prevent the photo-oxidation process and loss of breaking

Table 1. Relationship Between Photon Energy and Chemical Bond Strength

Wavelength, nm	Photon energy, kJ/mol[a]	Chemical bond	Bond strength, kJ/mol[a]
280	428	C═C	607
300	400	O—H	460
		C—H (primary)	444
		C—H (secondary)	398
		N—H	389
320	375	C—H (tertiary)	381
		C—O	364
340	353	C—C	347
360	333	C—Cl	326
380	316	C—N	285
400	300	O—O	268

[a]To convert kJ/mol to kcal/mol, divide by 4.184.

Table 2. UV Wavelength Sensitivity of Polymers[a]

Polymer	Activation spectra maxima, nm
Nylon	290–315
PMMA	290–315
SAN	290, 310–330
Polycarbonate	280–310
Polystyrene	310–325
Polyethylene	300–310–340
Polypropylene	290–300, 330, 370
ABS	300–310, 370–385
PVC homopolymer	320
PVC copolymer	330, 370
Polyarylate	350
PUR (aromatic)	350–415

[a]Samples exposed to Xenon Arc WOM or sunlight.

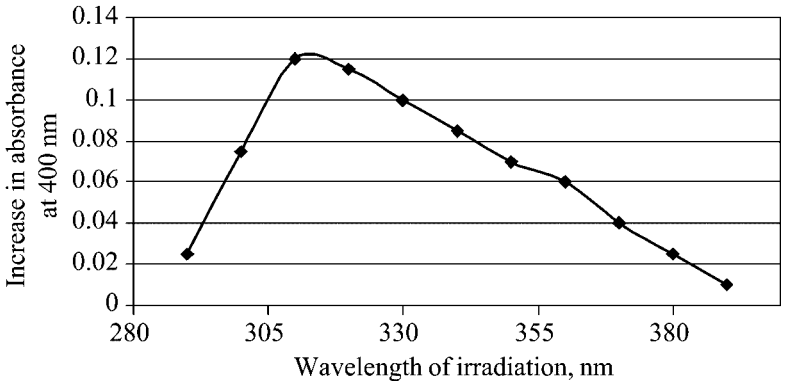

Fig. 1. Activation spectrum of polystyrene.

strength. Without the UV filter, the polypropylene monofilament degrades in only 600-h Xenon Arc Weather-O-Meter (WOM) exposure. This clearly shows the effect of UV light energy on the photo-oxidation process.

UV Stabilization Mechanisms and Strategies

The initial emphasis in light stabilizer development was the inhibition of the photoinitiation processes. This UV stabilization strategy consisted of the incorporation of additives into the polymer or coating formulation, which either absorbed UV light energy or acted as quenchers of the photoexcited states of the chromophores. In the former case the UV absorber competes with the chromophores for the harmful UV light energy, which is preferentially absorbed by the UV absorber and dissipated harmlessly as heat (9). In this competitive absorption mechanism, the UV absorber must have relatively high absorptivity at the wavelengths of UV light to which the polymer is photosensitive (activation spectra maxima). In the latter

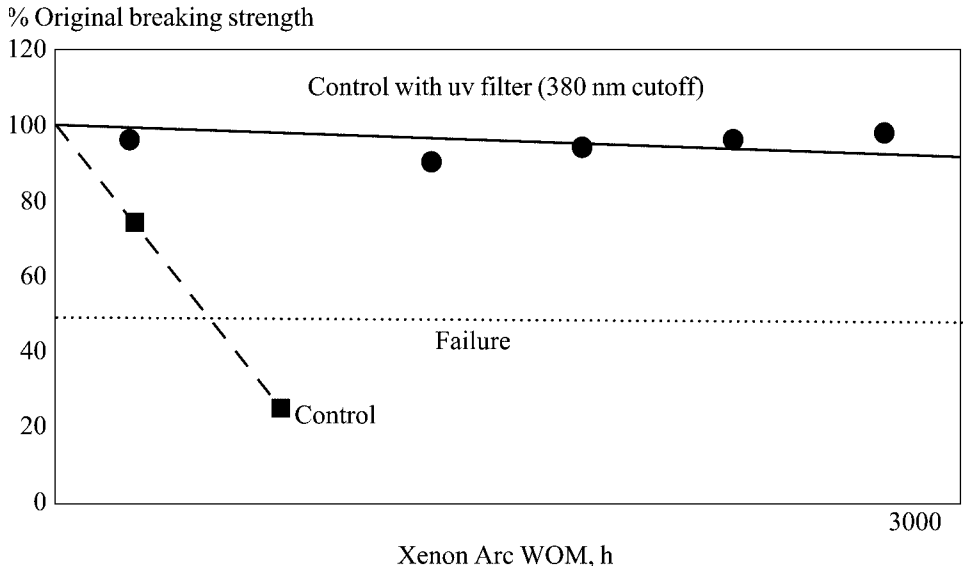

Fig. 2. Effect of a UV filter on the UV stability of polypropylene monofilament.

case, the quencher returns the excited states to ground states by energy transfer processes. In both cases, radical formation is inhibited and the outdoor service life of the polymer is extended, depending on the efficiency of these stabilization processes (see STABILIZATION).

Also, light stabilizers have been developed to inhibit the subsequent oxidative processes by radical scavenging and hydroperoxide decomposition mechanisms. In these processes, the light stabilizer molecules undergo chemical reactions with the propagating intermediates in the polymer photo-oxidation processes. In some cases the light stabilizer is gradually consumed and in others the stabilizing chemical groups are regenerated to some degree in the stabilization process. This latter process has been used to explain the effectiveness of HALS (10–12).

The third strategy is to combine a UV absorber with a radical scavenger or a hydroperoxide decomposer to provide more efficient and sometimes synergistic UV-stabilizing activity. Also, effective combinations of radical scavengers and hydroperoxide decomposers have been reported (13). And finally, as part of a total system strategy, melt-processing antioxidants can be added to the polymer formulation to minimize the formation of UV-absorbing chromophores from thermal oxidation during thermal processing.

An overview of stabilizer mechanisms and types of chemicals used for each mechanism is provided in Table 3. Further descriptions of these mechanisms follow. The three major classes of UV absorbers are 2-hydroxybenzophenones, 2-hydroxyphenylbenzotriazoles, and the newer 2-hydroxyphenyl-*s*-triazines. The nickel phenolates not only have excited state quenching capability, but also provide radical scavenging and hydroperoxide decomposing activity. The radical scavengers include hindered benzoates and hindered amines. The hindered amines have the added capability to decompose hydroperoxides. Another class of

Table 3. UV Stabilization Mechanisms and Chemical Stabilizers

Mechanism	Chemical agents
Competitive UV absorption	2-Hydroxy benzophenones
	2-Hydroxyphenyl benzotriazoles
	2-Hydroxyphenyl-*s*-triazines
	Other chemical classes
Excited state quenching	Nickel phenolates
Radical scavenging	Nickel phenolates
	Hindered amines
	Hindered benzoates
Hydroperoxide decomposition	Nickel phenolates
	Hindered amines
	Phosphites
Residual catalyst deactivation	Acid acceptors
	Metal deactivators

hydroperoxide decomposers are the phosphites. Residual catalyst deactivation has been reported (14,15) to be of some value in both thermal and light stabilization of polymers, and acid acceptors such as calcium stearate and metal chelators such as oxamides or hydrazides are the major chemical classes. Each of these mechanisms and stabilizer types can be applied depending on the photodegradation mechanism of the polymer and the performance requirements of the application.

Light stabilizers need to satisfy a number of technical, as well as commercial, requirements. Technical requirements include strong, broadband UV absorption (for UV absorbers), high inherent stability to UV light energy, good solubility–migration balance in the polymer substrate, low volatility and extractability, low color and odor, minimum adverse interactions with other system components, and good storage stability.

In addition to the primary light stabilization functional group, substituents are used to fine-tune performance as follows:

(1) To vary the molecular weight to change the volatility, solubility–migration balance, and extractability.
(2) To vary the chemical reactivity of the functional group.
(3) To enhance the UV absorption or the inherent light stability.
(4) To add a reactive group to achieve permanence.

Of course, commercial considerations, such as optimum cost–performance balance, food contact sanction, and technical support from suppliers are also important considerations in UV stabilizer selection.

There are numerous factors which will affect the performance of light stabilizers in each polymer and application. Therefore, although careful definition of specific application requirements can help to develop some initial stabilizer options, testing of these systems via accelerated weathering techniques is often required. Numerous useful references are available describing accelerated test

Table 4. UV Light Exposure Testing Methods

Accelerated weathering device
Xenon Arc WOM (ASTM D2656-92A, G26-92)
Carbon Arc WOM (ASTM D1499-92A)
Fluorescent Sunlamp (ASTM G53-93)
Accelerated outdoor weathering devices
EMMA Test Method (ASTM G90-91)
EMMAQUA Test Method (ASTM D4362-94, G90-91)
Natural outdoor exposure
Direct (ASTM D1435-85)
Under Glass (ASTM G24-87)

methods to predict weathering performance (16–21) (see WEATHERING). Table 4 lists some of the commonly used accelerated and natural outdoor UV exposure conditions and ASTM test methods. Generally, the Xenon Arc WOM provides the best correlation with outdoor data because of the spectral match with the UV portion of the sun's energy. The carbon arc and fluorescent sunlamp weathering units provide greater acceleration in testing but correlate to a lesser degree because of their spectral energy differences with sunlight. With regard to the fluorescent accelerated units, the newer 340A lamp provides a better spectral match with sunlight than the 313B lamp. Actual outdoor exposure should be performed to establish a correlation not only with regard to ranking the performance of the various light stabilizer systems but also to determine the number of months or years equivalent to a given number of hours (or dosage of incident light energy, expressed as kJ/m^2 or alternate units) of accelerated exposure. Arizona and Florida are the major outdoor weathering sites in North America. Accelerated outdoor weathering is also available whereby the sun's light energy is concentrated on the sample surface with mirrors and a mounting device which follows the sun across the horizon to maximize the light exposure. Again, correlation studies with actual outdoor exposure are recommended.

UV Light Absorbers

A UV light absorber is a type of light stabilizer which functions by competitive absorption of the UV light energy, causing the photodegradation of a polymer formulation. The UV absorber competes with all chromophores in the formulation and dissipates the absorbed energy as heat. The chromophores are UV light absorbing chemical groups in the polymer formulation. These may include the polymer itself and other additives, such as halogenated flame retardants, fillers, and pigments. In effect, the UV light absorber inhibits the first step in the polymer photodegradation process, which is photoinitiation. The UV light absorber can be used in combination with other types of light stabilizers which are designed to inhibit the other, subsequent steps in the photodegradation processes. Also, UV light absorbers may function as UV screeners in plastics, coatings, and cosmetic sunscreens to reduce or eliminate the transmission of UV light energy, protecting UV-sensitive substrates.

The factors involved in the effectiveness of the competitive UV light absorption stabilization mechanism are as follows:

(1) The UV wavelength region causing photodegradation of the polymer formulation.
(2) UV absorptivity of the polymer formulation in this region.
(3) UV absorptivity of the UV absorber in this region.
(4) Thickness of the polymer.
(5) Concentration and dispersion of the UV absorber.
(6) Inherent light stability of the UV absorber.
(7) Permanence of the UV absorber.
(8) Chemical reactivity of the UV absorber in the photodegradation process.
(9) The UV light and thermal exposure conditions of the polymer formulation.

Several chemical classes of UV light absorbers are currently available (see Table 5). The major chemical classes are the 2-hydroxybenzophenones (such as 2-hydroxy-4-*n*-octyloxybenzophenone; CYASORB® UV-531 light absorber) and the 2-hydroxyphenylbenzotriazoles (such as 2-(2-hydroxy-5-*tert*-octylphenyl)benzotriazole; CYASORB® UV-5411 light absorber). Other chemical classes consist of the 2-hydroxyphenyl-*s*-triazines (such as 2-[4,6-bis(2,4-dimethylphenyl)-1,3,5-triazin-2-yl]-5-(octyloxy) phenol; CYASORB® UV-1164 light absorber), the cyanoacrylates (such as ethyl 2-cyano-3,3-diphenylacrylate; UVINUL® 3035), the oxanilides (such as 2-ethyl,2′-ethoxy-oxanilide; SANDUVOR® VSU), the benzylidene malonates (such as 4-methoxybenzylidene-malonic acid, dimethyl ester; SANDUVOR® PR-25), and the benzoxazinones (such as 2,2′-(1,4-phenylene) bis[4*H*-3,1-benzoxazin-4-one]; CYASORB® UV-3638 light absorber).

The UV light absorber chemical structure consists of a functional group and substituents. The functional group gives the UV absorber its characteristic UV absorption properties. As noted previously, the substituents are added to the chemical structure to modify its UV absorption properties, and other properties such as compatibility with the polymer substrate, color contribution, thermal volatility, extractability, chemical reactivity, and permanence.

CYASORB® UV-531 light absorber is used primarily in polyolefin and flexible PVC outdoor applications. Figure 3 shows an application example for this product, namely the improvement in the color stability of a flexible PVC film during accelerated Xenon Arc WOM UV exposure. CYASORB® UV-1164, an example of the newer generation of triazine UV absorbers, has higher molecular weight and lower volatility for use at higher processing temperatures and for greater permanence in thin film applications. CYASORB® UV-5411 is used primarily in molding grade polycarbonate and other applications, such as styrenics and thermoset polyester. Figure 4 shows an application example for this product, namely the improvement in the color stability of a polycarbonate plaque during accelerated Xenon Arc WOM UV exposure. In all three UV light absorber examples, the octyl substituent is used to increase molecular weight, lower the volatility, and increase the compatibility with polymeric substrates.

Table 5. UV Absorbers

Chemical structure [CAS No.]	Chemical name	Trade name (producers)
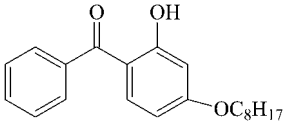 [1843-05-6]	2-Hydroxy-4-*n*-octyloxybenzophenone	CYASORB® UV-531 light absorber (Cytec Industries Inc.) Chimassorb 81 (Ciba Specialty Chemical) Hostavin ARO 8 (Clariant) Lowilite 22 (Great Lakes)
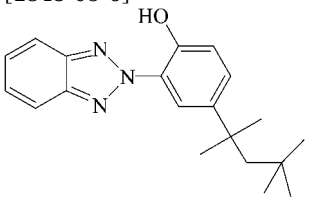 [3147-75-9]	2-(2′-Hydroxy-5′-*tert*-octylphenyl)benzotriazole	CYASORB® UV-5411 light absorber (Cytec Industries Inc.) Sumisorb 340 (Sumitomo) Tinuvin 329 (Ciba Specialty Chemical)
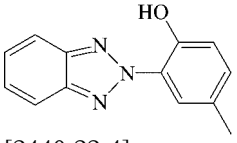 [2440-22-4]	2-(2′-Hydroxy-5′-methylphenyl)benzotriazole OR Phenol, 2-(2*H*-benzotriazole-2-yl)-4-methyl	CYASORB® UV-5365 light absorber (Cytec Industries Inc.) Tinuvin P (Ciba Specialty Chemical) Eversorb 71 (Everlight) Lowilite 55 (Great Lakes)
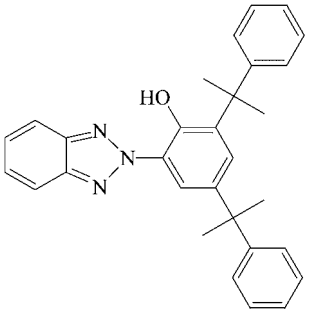 [70321-86-7]	2-(3′,5′-*bis*(1-methyl-1-phenylethyl)-2′-hydroxyphenyl)benzotriazole	Tinuvin 234, Tinuvin 900 (Ciba Specialty Chemical)

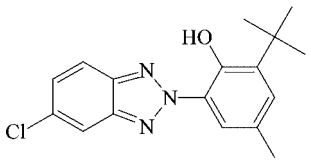

[3896-11-5]

Phenol, 2-(5-chloro-2*H*-benzotriazole-2-yl)-6-(1,1-dimethylethyl)-4-methyl

Tinuvin 326 (Ciba Specialty Chemical) Eversorb 73 (Everlight) Lowilite 26 (Great Lakes)

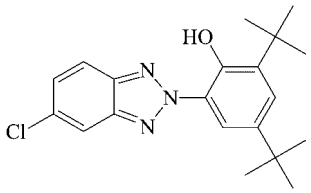

[3864-99-1]

Phenol, 2-(5-chloro-2*H*-benzotriazole-2-yl)-4,6-bis(1,1-dimethylethyl)-

Tinuvin 327 (Ciba Specialty Chemical) Lowilite 27 (Great Lakes)

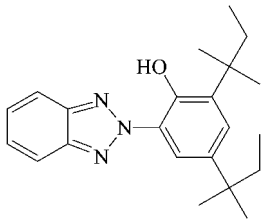

[25973-55-]

2-(2′-Hydroxy-3′,5′-di-*tert*-amylphenyl)benzotriazole OR Phenol, 2-(2*H*-benzotriazole-2-yl)-4,6-bis(1,1-dimethylpropyl)-

CYASORB® UV-2337 light absorber (Cytec Industries Inc.) Tinuvin 328 (Ciba Specialty Chemical) Lowilite 28 (Great Lakes)

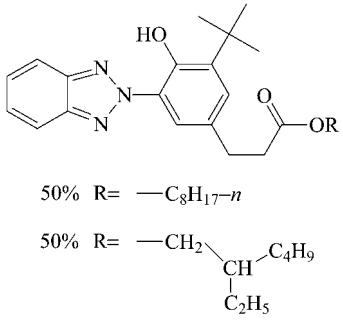

50% R= —C_8H_{17}–*n*

50% R= —CH_2—CH(C_2H_5)—C_4H_9

[127519-17-9]

Benzenepropanoic acid, 3-(2*H*-benzotriazol-2-yl)-5-(1,1-dimethylethyl)-4-hydroxy-, C7-9 branched alkyl esters

Tinuvin 384, Tinuvin 99 (Ciba Specialty Chemical)

Table 5. (Continued)

Chemical structure [CAS No.]	Chemical name	Trade name (producers)
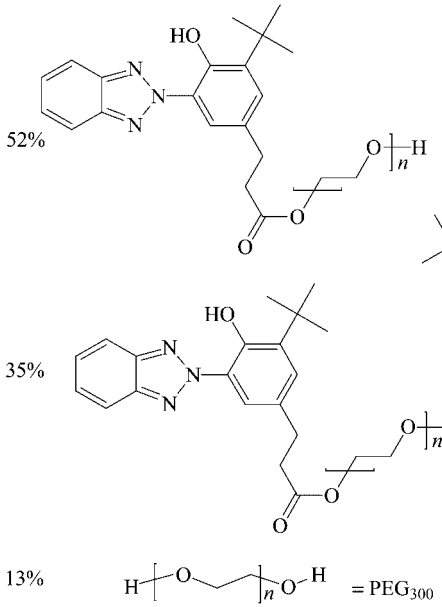 52% 35% 13% $= PEG_{300}$ [104810-48-2] + [104810–47–1]	Mixture of poly(oxy-1,2-ethanediyl)-α(3-(3-(2*H*-benzotriazol-2-yl)-5-(1,1-dimethylethyl)-4-hydroxyphenyl)-1-oxopropyl)-ω-hydroxy, poly(oxy-1,2-ethanediyl)-α-(3-(3-(2*H*-benzotriazol-2-yl)-5-(1,1-dimethylethyl)-4-hydroxyphenyl)-1-oxopropyl)-ω-(3-(3-(2*H*-benzotriazol-2-yl)-5-(1,1-dimethylethyl)-4-hydroxyphenyl)-1-oxopropoxy), and polyethylene glycol, MW = 300	Tinuvin 213, Tinuvin 1130 (Ciba Specialty Chemical)
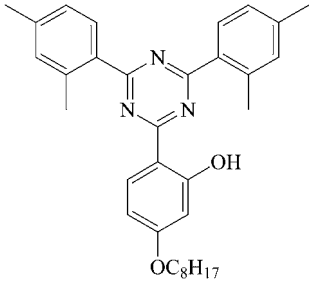 [2725-22-6]	2-[4,6-Bis(2,4-dimethylphenyl)-1,3,5-triazin-2-yl]-5-(octyloxy) phenol	CYASORB® UV-1164 light absorber (Cytec Industries Inc.)

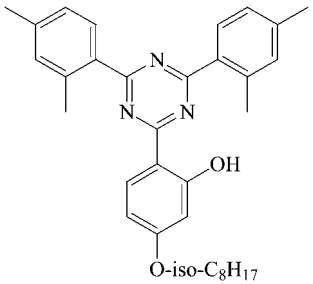

[137759-38-7]

1,3-Benzenediol, 4-[4,6-bis(2,4-dimethylphenylphenyl)-1,3,5-triazin-2-yl]-, C7-9 branched alkyl ethers, 65% in xylenes

CYASORB® UV-1164L light absorber (Cytec Industries Inc.)

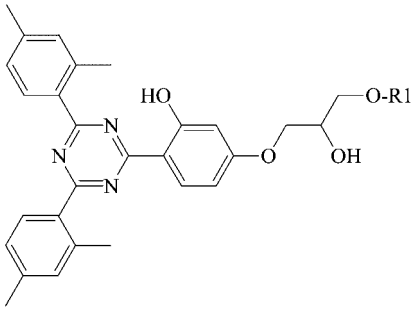

R1=$C_{10}H_{21}$-$C_{16}H_{33}$
Average $C_{12}H_{25}$-$C_{13}H_{27}$

[153519-44-9]

1,3-Benzenediol, 4-[4,6-bis(2,4-dimethylphenylphenyl)-1,3,5-triazin-2-yl]-, reaction products with [(dodecyloxy)methyl]oxirane and oxirane mono[(C10-16-alkyloxy) methyl] derivatives

Tinuvin 400 (Ciba Specialty Chemical)

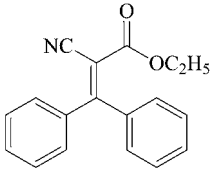

[5232-99-5]

Ethyl 2-cyano-3,3-diphenylacrylate

Uvinul 3035 (BASF)

Table 5. (Continued)

Chemical structure [CAS No.]	Chemical name	Trade name (producers)
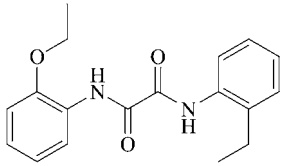 [23949-66-8] [23949-30-4]	2-Ethyl,2′-ethoxy-oxalanilide	Sanduvor VSU (Clariant) Tinuvin 312 (Ciba Specialty Chemical)
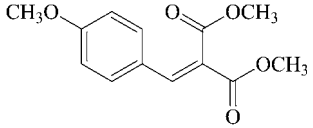 [7443-25-6]	Propanedioic acid, [(4-methoxyphenyl)-methylene]-, dimethylester	Hostavin PR-25 (Clariant)
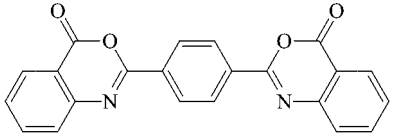 [18600-59-4]	2,2′-(1,4-Phenylene)bis[4*H*-3,1-benzoxazin-4-one]	CYASORB® UV-3638 light absorber (Cytec Industries Inc.)

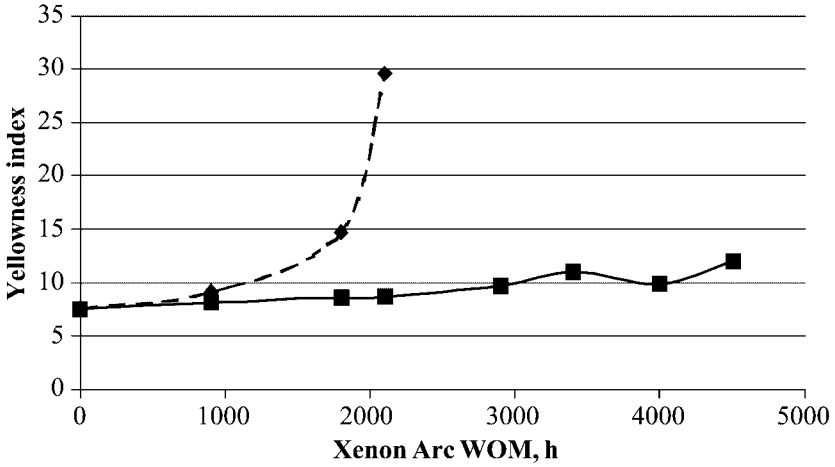

Fig. 3. UV stabilization of 250-μm flexible PVC films. —◆— Control, —■— UV-531 0.5 PHR.

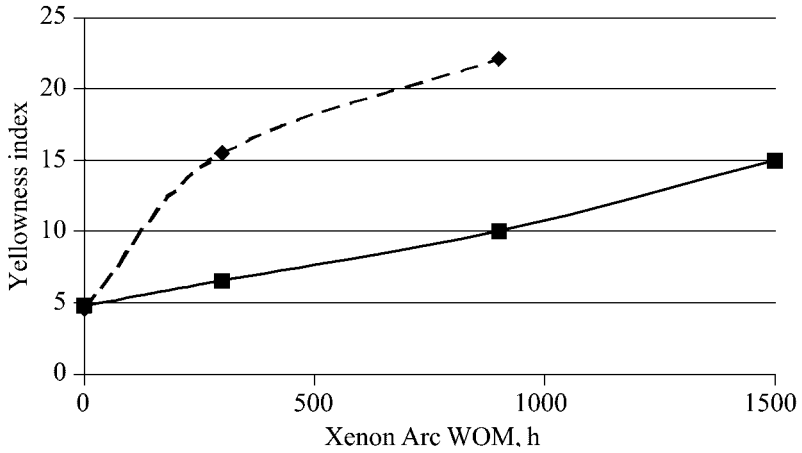

Fig. 4. UV stabilization of 1.5-mm injection-molded polycarbonate plaques. —◆— Control, —■— 0.35% CYASORB UV-5411.

The optimum amount of UV absorber varies with each chemical type and application, but in most cases is in the 0.25–1.0% concentration range. Other factors to consider while selecting the proper type and amount of UV absorber are color contribution, FDA sanction for food packaging applications, and, of course, add-on cost. The UV absorbers are incorporated into plastic substrates by dry blending, extrusion compounding, and then conversion into the final product by various processes such as injection molding, blown film extrusion, multifilament spinning, and sheet extrusion. Also, UV absorber dispersions can be prepared and dyed onto textile fabrics, which will not only UV-stabilize the polymer substrate but also improve the color stability of the dyes used to color the fabric.

The use of UV absorbers as UV screeners is practiced in a multitude of applications, such as sunglasses, interocular lenses, auto windshield films, solar control

glazing films, photographic products, greenhouse films, product packaging, and cosmetic sunscreens. In each application, the polymer type, the UV absorber type, the thickness of the plastic product, and the concentration of the UV absorber need to be considered to meet the reduced UV percentage transmission requirements of the application. The UV transmission properties of a plastic product are governed by the Beer–Lambert Law, which states that the absorbance (A) is proportional to the absorptivity (a) of the medium times the thickness (b) of the medium times the concentration (c) of the UV-absorbing compounds in the medium (eq. 1).

$$A = abc \tag{1}$$

Hindered Amine Light Stabilizers

Hindered amine light stabilizers (HALS) have been well recognized for more than 25 years to be the most proficient UV stabilizers for a large number of polymers. This is particularly true for the protection of polyolefins against the degradative effects of light energy. The protective effects of HALS has enabled the growing use of polypropylene (PP) in the automotive industry. The main protective effect is the strong improvement in light stability achieved with the use of HALS. These stabilizers also impart thermal stability to plastics at temperatures below 130°C. Although there are wide structural variations in commercial HALS products, all share the 2,2,6,6-tetramethylpiperidine ring structure (**1**).

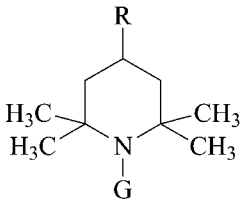

(1)

The nitroxide radical of this cyclic amine is the actual active light stabilizer. The nitroxide radical is generated *in situ* by photo-oxidation and photohydrolysis, depending on the substituent on the nitrogen atom. The mechanism of stabilization of hydrocarbons, eg PP, by HALS has been studied extensively (22–34). The kinetics of nitroxide generation and consumption in coating matrices has been studied by electron spin resonance (esr) (35–43). Nitroxide consumption in coatings has been used to measure photoinitiation rates for photo-oxidation. In a sequence of reactions known as the Denisov Cycle, the nitroxide radical combines with other radical species in the coating matrix to form amino ether intermediates, which further react with radical species to regenerate the nitroxyl radical and form nonradical chemical by-products. Thus the piperidinyl nitroxide radical may be thought of as a catalytic radical scavenger. An early representation of the Denisov Cycle is shown in Figure 5.

The knowledge of the degradation mechanisms of polyolefins has grown over the past few years owing to the scientific work of several industrial research groups

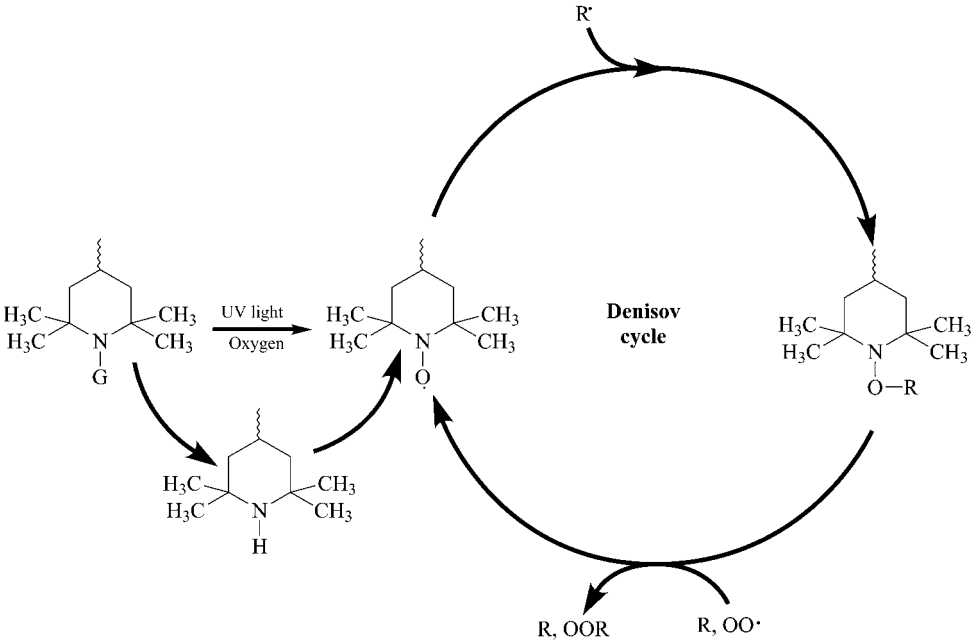

Fig. 5. Chemical mechanism of HALS activation and radical scavenging.

and universities. Concurrently, the influence of structural, chemical, and physicochemical characteristics of HALS has been understood and improvements in their performances made. These advancements have led to several generations of HALS intended to cover a wide variety of applications. With these improvements, the confidence in the correlation between accelerated and outdoor weathering has grown, thus reducing the time necessary for evaluation and approval of new stabilizing products and systems.

The consequence of this continuous growth in knowledge has been the appearance on the market of several generations of HALS, which can be historically summarized as follows: first generation – monomeric HALS; second generation – polymeric HALS; third generation – noninteractive HALS; and fourth generation – synergistic UV absorber – HALS combinations.

First Generation: Monomeric HALS. Several decades ago, physical organic chemists were entranced by the concept of stable free radicals and their potential as radical trapping agents. References on the use of nitroxyls as potential stabilizers for plastics had already been cited in the patent literature (44).

In pioneering work during the 1960s, 2,2,6,6-tetramethyl-4-oxy-piperidine *N*-oxyl (also known as *N*-OxylTAM) was synthesized (45), and found to be effective as a light stabilizer in plastics (46). See Table 6 for HALS structure. However, the molecule had a low melting point, had limited thermal stability, imparted color to substrates, and was highly migratory (47). Further improvements were needed. Subsequent studies by Sankyo Corp. led to the discovery that the amine analogs of the *N*-oxyl compounds were highly active as stabilizers, with fewer undesirable side reactions (48). Commercialization of the first HALS product, decanedioic acid

Table 6. Hindered Amine Light Stabilizers

Chemical structure [CAS No.]	Chemical name	Trade name (producers)
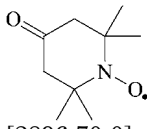 [2896-70-0]	2,2,6,6-Tetramethyl-4-oxy-piperidine *N*-oxyl	N-OxylTAM 4-Oxo-TEMPO (Nova Molecular Technologies)
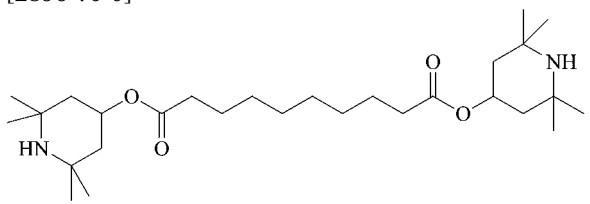 [52829-07-9]	Decanedioic acid, bis(2,2,6,6-tetramethyl-4-piperidinyl)ester	Tinuvin 770 (Ciba Specialty Chemicals) Sanol LK 77 (Sankyo) Sumisorb 577 (Sumitomo) Lowilite 77 (Great Lakes)
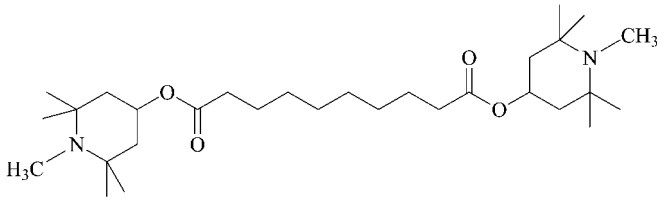 [41556-26-7]	Decanedioic acid, bis(1,2,2,6,6-pentamethyl-4-piperidinyl)ester	Tinuvin 765, Tinuvin 292 (Ciba Specialty Chemicals) Lowilite 76 (Great Lakes)
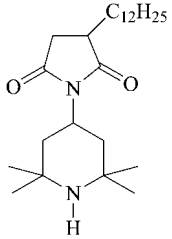 [79720-19-7]	3-Dodecyl-1-(2,2,6,6-tetramethyl-4-piperidinyl)-2,5-pyrrolidine-2,5-dione	CYASORB® UV-3581 Light Stabilizer (Cytec Industries Inc.) Sanduvor 3055 (Clariant)

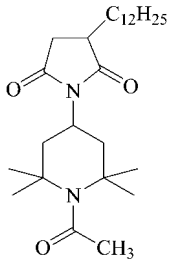

[106917-31-1]

3-Dodecyl-1-(1-acetyl-2,2,6,6-tetramethyl-4-piperidinyl)-2,5-pyrrolidinedione

Sanduvor 3058 (Clariant)

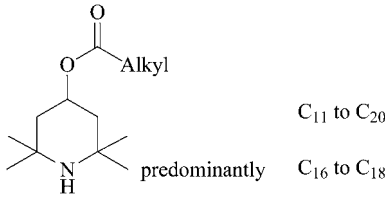

[167078-06-0]

Mixture of esters of 2,2,6,6-tetramethyl-piperidinol with higher fatty acids, mainly stearic and palmitic acids

CYASORB® UV-3853 Light Stabilizer (Cytec Industries Inc.) Hostavin 845 (Clariant)

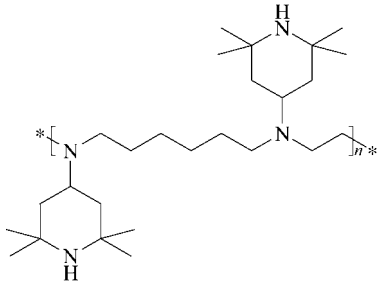

[61269-61-2]

N,*N*′Bis(2,2,6,6-tetramethyl-4-piperidyl)hexamethylendiamine polymer with ethane-1,2-dibromo

Spinuvex A-36 (Introduced by Montedison) - no longer commercially available

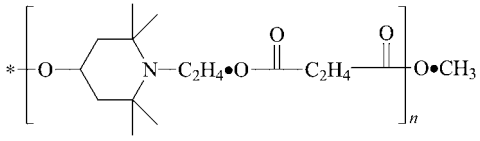

[65447-77-0]

Butanedioic acid, polymer with 4-hydroxy-2,2,6,6-tetramethyl-1-piperidine ethanol

Tinuvin 622 (Ciba Specialty Chemicals) Everlight (Eversorb 62) Lowilite 76 (Great Lakes)

Table 6. (Continued)

Chemical structure [CAS No.]	Chemical name	Trade name (producers)
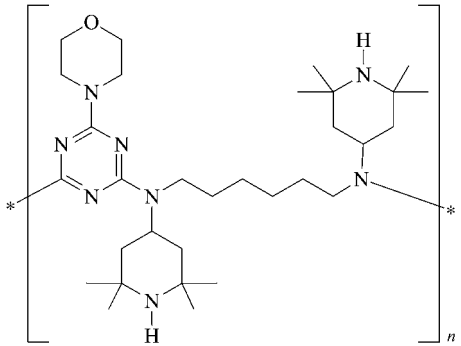 [82451-48-7]	1,6-Hexanediamine, *N*,*N*′-bis(2,2,6,6-tetramethyl)-4-(piperidinyl)-, polymers with 2,4-dichloro-6-(4-morpholinyl)-1,3,5-triazine	CYASORB® UV-3346 Light Stabilizer (Cytec Industries Inc.)
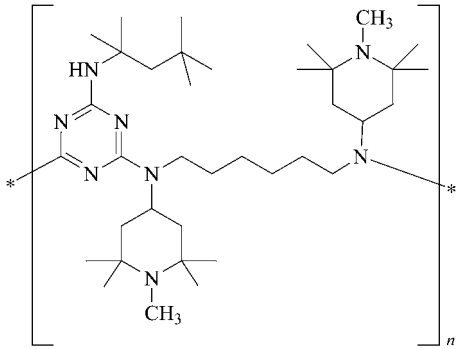 [71878-19-8] or [70624-18-9]	Poly-[[6-[(1,1,3,3-tetramethylbutyl)amino]-1,3,5-triazine-2,4-diyl][2-(2,2,6,6-tetramethyl-4-piperidinyl)imino]-1,6-hexanediyl [2,2,6,6-tetramethyl-4-(piperidinyl)-imino]]	Chimassorb 944 (Ciba Specialty Chemicals) Eversorb 91 (Everlight) Lowilite 94 (Great Lakes)

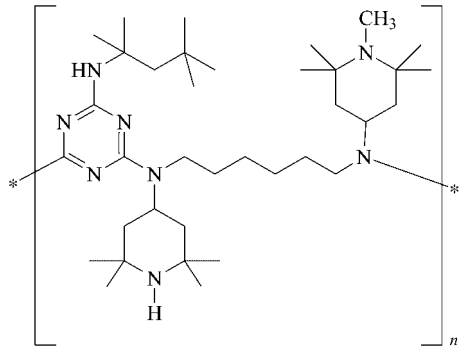

[193098-40-7]

1,6-Hexanediamine, *N*,*N*′-bis(1,2,2,6,6-pentamethyl-4-piperidinyl)-, polymers with 2,4-dichloro-6-(4-morpholinyl)-1,3,5-triazine

CYASORB® UV-3529 Light Stabilizer (Cytec Industries Inc.)

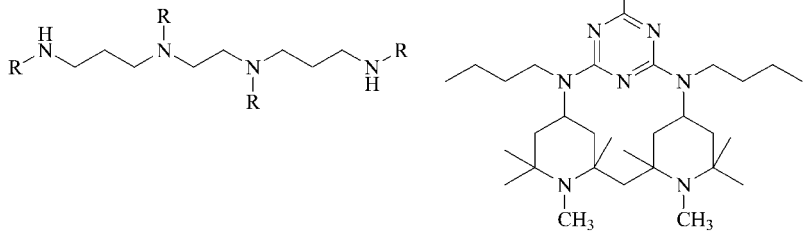

[106990-43-6]

1,3,5-Triazine-2,4,6-triamine,*N*,*N*″-[1,2-ethanediylbis[[[4,6-bis[butyl(1,2,2,6,6-pentamethyl-4-piperidinyl)amino]-1,3,5-triazine-2-yl]imino]-3,1-propanediyl]-bis[*N*,*N*″-dibutyl-*N*′,*N*″-bis(1,2,2,6,6-pentamethyl-4-piperidinyl]-

Chimassorb 119 (Ciba Specialty Chemicals)

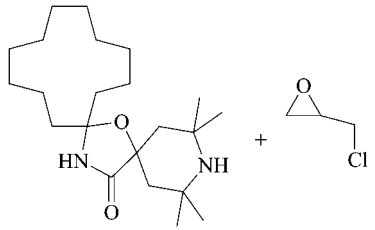

[64338-16-5] + [106-89-8]

Polymer of 2,2,4,4-tetramethyl-7-oxa-3,20-diaza-dispiro-[5.1.11.2]-heneicosan-21-on with epichlorohydrin

Hostavin N 30 (Clariant)

Table 6. (Continued)

Chemical structure [CAS No.]	Chemical name	Trade name (producers)
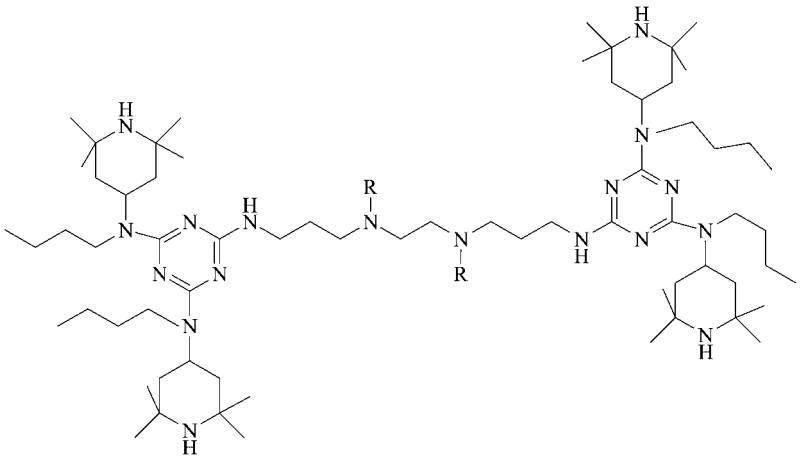 [154636-38-1]	1,3-propanediamine, *N*,*N*″-1,2-ethanediylbis-, polymer with *N*-butyl-2,2,6,6-tetramethyl-4-piperidinamine and 2,4,8-trichloro-1,4,5-triazine	Uvasorb HA88 (Sigma)
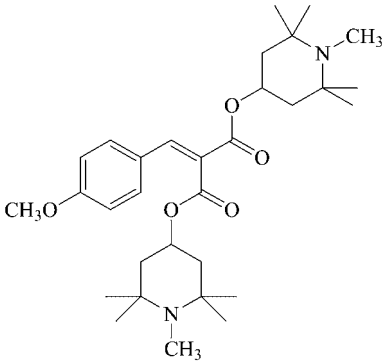 [147783-69-5]	Propanedioic acid, [(4-methoxyphenyl)methylene]-bis(1,2,2,6,6-pentamethyl-4-piperidinyl) ester	Hostavin PR-31 (Clariant)

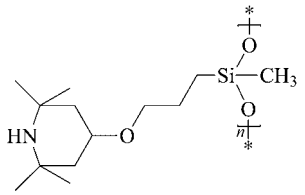

[164648-93-5] or [102089-33-8] or [137898-96-5]

Polymethyl[propyl-3-oxy(2′,2′,6′,6′-tetramethyl-44′-piperidinyl)]siloxane

Uvasil 299 (Great Lakes) Uvasil 299LM (1100-1300 MW) Uvasil 299HM (1800-2400 MW)

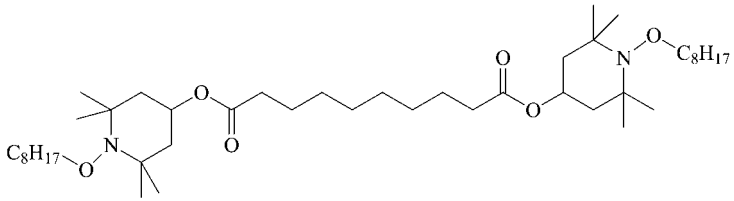

[122586-52-1] or [129757-67-1]

Decanedioic acid, bis(2,2,6,6-tetramethyl-4-piperidinyl)ester, reaction products with *tert*-butyl hydroperoxide and octane

Tinuvin 123 (Ciba Specialty Chemicals)

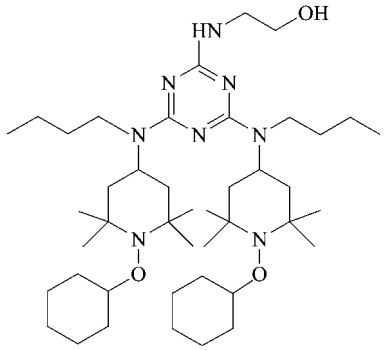

[150686-85-4]

2-[(2-Hydroxyethyl)amino]-4,6-bis[*N*-(1-cyclohexyloxy-2,2,6,6-tetramethylpiperidin-4-yl)]butylamino-1,3,5-triazine

Tinuvin 152 (Ciba Specialty Chemicals)

Table 6. (Continued)

Chemical structure [CAS No.]	Chemical name	Trade name (producers)
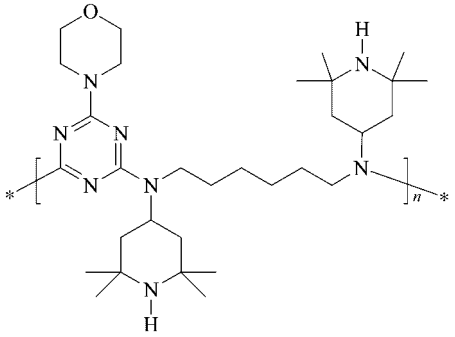 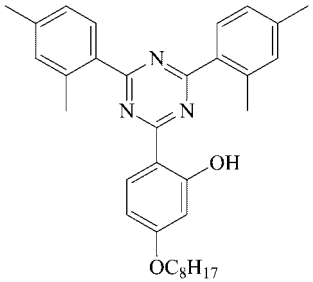 [82451-48-7] + [2725-22-6]	1,6-Hexanediamine, *N*,*N*′-bis(2,2,6,6-tetramethyl)-4-(piperidinyl)-, polymers with 2,4-dichloro-6-(4-morpholinyl)-1,3,5-triazine + 2-[4,6-Bis-(2,4-dimethylphenyl)-1,3,5-triazin-2-yl]-5-(octyloxy) phenol, proprietary mixture	CYASORB THT™ 4611 Light Stabilizer (Cytec Industries Inc.)

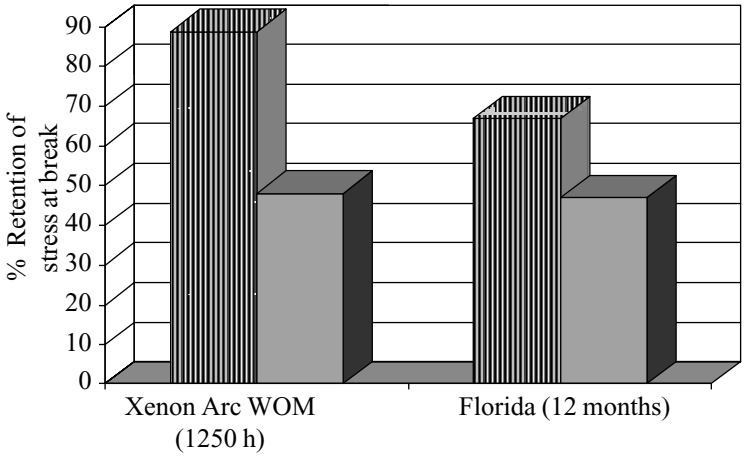

Fig. 6. UV stabilization of 1.5-mm injection-molded PP Homopolymer tensile bars. ▩ 0.15% CYASORB UV-3853, ▩ 0.15% Tinuvin 770. 0.1% CaSt, 0.075% Irganox 1010.

bis(1,2,2,6,6-pentamethyl-4-piperidinyl)ester (Tinuvin 770), occurred in 1974, and it has since become one of the most important monomeric HALS for the stabilization of plastics, especially PP. Its counterpart, Tinuvin 292 (same structure), is one of the most important HALS for coatings stabilization. This HALS is endowed with high mobility within polyolefins, owing to its small molecular size.

Another option, CYASORB® UV-3853 light stabilizer, is a mixture of three *n*-alkyl esters which affords enhanced polyolefin compatibility (reduced blooming) and solubility. These factors have been shown to have a dramatic effect on stabilization efficacy in some applications. For example, CYASORB® UV-3853 exhibits significantly better stabilization performance in PP despite only half the molar activity (piperidinyl groups per mole) as compared with Tinuvin 770 (Fig. 6). The comparable volatility of the products indicates that the difference in performance cannot be associated with that parameter. Also, in thick section parts, additive loss is generally controlled by diffusion and not by additive volatility. Since the products are similar in molecular weight (MW), one would expect their diffusion coefficients to be similar. If the solubility parameters of the products differed sufficiently, that could account for the performance differences; studies (49) have borne this out.

Second Generation: Polymeric HALS. One specific application that was of great interest in the development of higher MW HALS was PP fibers (50). PP fibers, by virtue of their high surface area-to-volume ratios and tendency to undergo postspinning treatments (tentering/backing) were often victims of stabilizer loss during processing. Economics and performance were compromised as a result of the fugitive nature of nonpolymeric, low molecular weight HALS. The necessity of a high molecular weight, low volatility HALS was, therefore, established.

In the early stages of commercialization of oligomeric HALS, the supporting structure for the piperidinyl functionality was clearly an area of focus. One product, Spinuvex A36 (no longer commercially available), had a polyamino backbone

with pendent piperidinyl groups. Another, butanedioic acid, a polymer with 4-hydroxy-2,2,6,6-tetramethyl-1-piperidine ethanol (Tinuvin 622), was a polyester, with the active sites incorporated into the backbone. With thermogravametric properties T-10% (defined as the temperature at which 10% of the molecule is lost gravimetrically) of 301 and 329°C for Spinuvex A36 and Tinuvin 622 respectively, versus 259°C for Tinuvin 770, both products satisfied the low volatility criterion (50). Still, further improvements were needed, as deficiencies in thermoxidative stability and UV performance after postspinning treatments were still evident in PP formulations containing these additives.

The introduction of triazine-type high performance HALS was the next leap in HALS technology. Triazine backbones made excellent carriers for piperidinyl groups, affording superior thermal and photochemical stability as well as low volatility. Two of the most commonly used HALS of this class are 1,6-hexanediamine, N,N'-bis(2,2,6,6-tetramethyl)-4-(piperidinyl)-, polymers with 2,4-dichloro-6-(4-morpholinyl)-1,3,5-triazine (CYASORB® UV-3346 light stabilizer) and poly-[[6-[(1,1,3,3-tetramethylbutyl)amino]-1,3,5-triazine-2,4-diyl][2-(2,6,6-tetramethyl-4-piperidinyl)imino]-1,6-hexane-diyl [2,2,6,6-tetramethyl-4-(piperidinyl)-imino]] (Chimassorb 944).

In the development of these high performance products, the optimal molecular weight for performance had to be defined. Significant effort was devoted to optimization. For example, in one study, oligomeric HALS with the empirical structure of CYASORB® UV-3346 were prepared, with different number- average MWs. The results indicated that oligomeric products with MWs in the 1600–1700 range afforded maximum performance under the test conditions (51). Molecular weight is a balance of acceptable volatility on the low end, and that of loss of translational mobility and matrix compatibility on the high end.

As an example, a Unipol (trademark of Union Carbide Corp.) LLDPE was compounded with a base stabilizer package, and 0.075% of CYASORB® UV-3346, Chimasorb 944, or Tinuvin 622. The resulting pellets were converted into tensile bars through injection molding. The tensile bars were exposed in a Xenon Arc WOM with water spray under ASTM G26 conditions, until failure. As expected, both high performance, triazine-class HALS outperformed the polyester HALS by a wide margin, as shown in Figure 7. The poor performance of the formulation containing Tinuvin 622 is thought to be directly related to its structure. In order to generate the active species for radical trapping, the backbone of the polyester HALS must first begin to cleave. Since the piperidinyl moieties are bonded to electron-withdrawing groups, the activation kinetics are not as favorable as they would be for a secondary or simply alkylated tertiary piperidinyl group (43,52,53). In addition, the polyester backbone is prone to photolytic and hydrolytic cleavage reactions, which can lead to additive loss. The latter reactions can be exacerbated in the presence of typical formulation components such as stearates.

A combination of monomeric and oligomeric products has shown improvement in UV performance as one might expect with a larger distribution of molecular weights. This distribution of molecular weights will give a better balance between mobility and efficiency in UV stabilization. Figure 8 demonstrates the improved performance that a 1:1 blend of a monomeric and a polymeric HALS can have compared with a single component system.

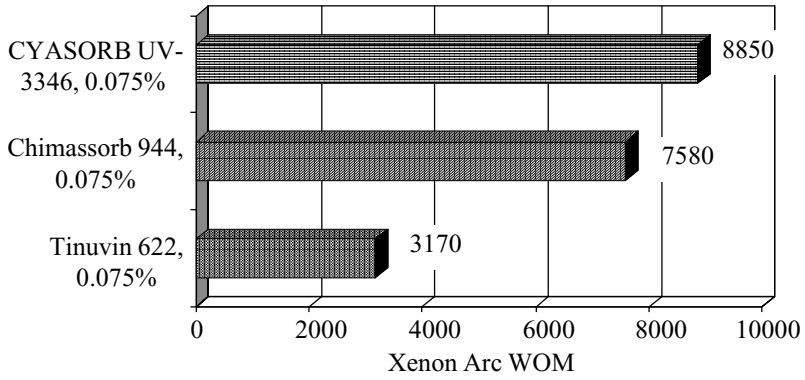

Fig. 7. UV stabilization of 1.5-mm injection-molded LLDPE tensile bars. X-axis in Hours to 50% retention of original elongation.

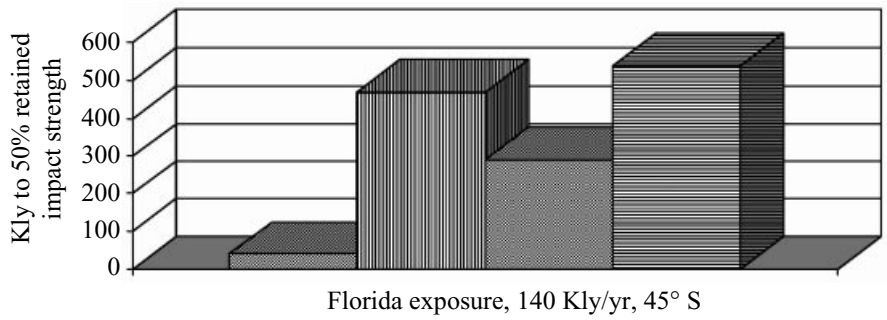

Fig. 8. UV stabilization of 2-mm injection-molded polypropylene plaques. ■ Control, ▩ 0.3% Tinuvin 770, ■ 0.3% Chimassorb 944, ▩ 0.15% Tinuvin 770 + 0.15% Chimassorb 944.

Third Generation: Noninteractive HALS. Although HALS have successfully displaced other types of UV stabilizers in many polyolefin applications, they are not without problems. In some applications, the basicity and nucleophilicity of secondary-amine HALS can sometimes contribute to undesirable side reactions. HALS can interact with other compounds in the stabilizer package and/or environmental agents to produce unanticipated and deleterious effects. Studies have shown that under certain conditions, HALS can be adsorbed to fillers in the polymer, resulting in a reduction in stabilization efficiency (54). A similar effect has been observed for some pigment classes. It has been proposed (55) that certain HALS can cause pigments to agglomerate, causing a reduction in color intensity. It was concluded (56) that in combination with certain antioxidants, some HALS will exacerbate the discoloration of polyolefins when exposed to oxides of nitrogen (gas fading). When used in agricultural films, HALS' effectiveness can be compromised by interactions with pesticides and fertilizers.

By alkylating the piperidinyl nitrogen, these interactions are minimized, and the basicity of the HALS is reduced. Tertiary HALS such as 1,6-hexanediamine, *N*,*N*′-bis(1,2,2,6,6-pentamethyl-4-piperidinyl)-, polymers with morpholine-2,4,

6-trichloro-1,3,5-triazine (CYASORB® UV-3529 Light Stabilizer) and 1,3,5-triazine-2,4,6-triamine,*N*,*N*″-[1,2-ethanediylbis[[[4,6-bis[butyl(1,2,2,6,6-pentamethyl-4-piperidinyl)amino]-1,3,5-triazine-2-yl]imino]-3,1 propanediyl]-bis[*N*′,*N*″-dibutyl-*N*′,*N*″-bis(1,2,2,6,6-pentamethyl-4-piperidinyl)] (Chimassorb 119) were developed to provide superior light stabilization performance while minimizing undesirable secondary interactions. Its lower basicity is also beneficial in controlling the discoloration rates of base-sensitive antioxidants like benzenepropanoic acid, 3,5-bis(1,1-dimethylethyl)-4-hydroxy-,2,2-bis[[3-[3,5-bis(1,1-dimethylethyl)-4-hydroxyphenyl]-1-oxopropoxy]methyl]-1,3-propanediyl ester (Irganox 1010), when the latter are exposed to exhaust gas fumes (NO_x).

It has been reported previously (57) that the light-stabilizing efficiency of CYASORB® UV-3529 is comparable to that of CYASORB® UV-3346 in most natural and pigmented PP fibers. The increased steric hindrance at the piperidinyl nitrogen in CYASORB® UV-3529 lowers the potential for interaction with pigments. With fewer tendencies for pigment agglomeration, color strength or yield is uncompromised when the HALS is added to the formulation.

Alkylating the piperidinyl nitrogen is also expected to reduce the HALS–pesticide interactions in greenhouse films. Figure 9 shows a comparison of the performance of CYASORB® UV-3346 and CYASORB® UV-3529 with Hostavin N-30, a reaction mixture of secondary and tertiary hindered amines, in acid-treated films. This test has been reported in the literature as a simulation for pesticide overspray. In this experiment, 50-μm LDPE greenhouse films were treated with 0.1 N sulfurous acid to simulate a sulfur-containing pesticide. The results show that substitution on the piperidinyl nitrogen alone is not sufficient to guarantee an elimination of undesirable secondary reactions. Differences in MW and MW distribution must also be considered.

Another class of low interactivity HALS is that based on NOR (alkoxyamine hindered amines) chemistry. These are also low basicity HALS which are claimed to provide stabilization efficiency and chemical resistance. Low MW products of this type, such as bis-(1-octyloxy-2,2,6,6,tetramethyl-4-piperidinyl) sebacate

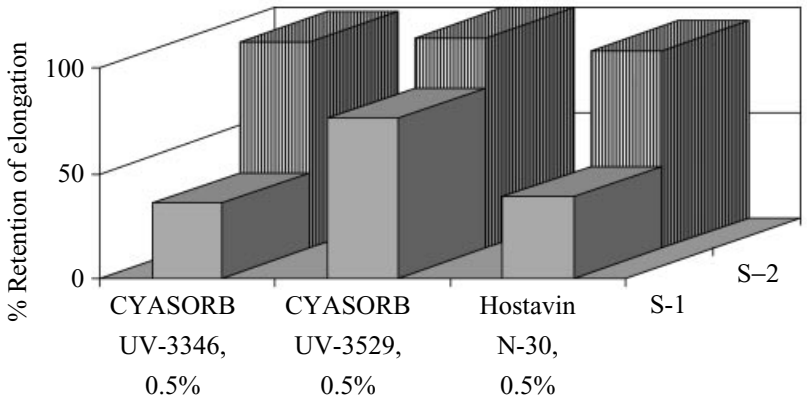

Fig. 9. UV stabilization of acid-treated 50-μm LDPE greenhouse films. S-1 (24-h dip-treated in 0.1 *N* H_2SO_3) vs S-2 (NON-TREATED). Xenon Arc WOM (1000 hours UV exposure).

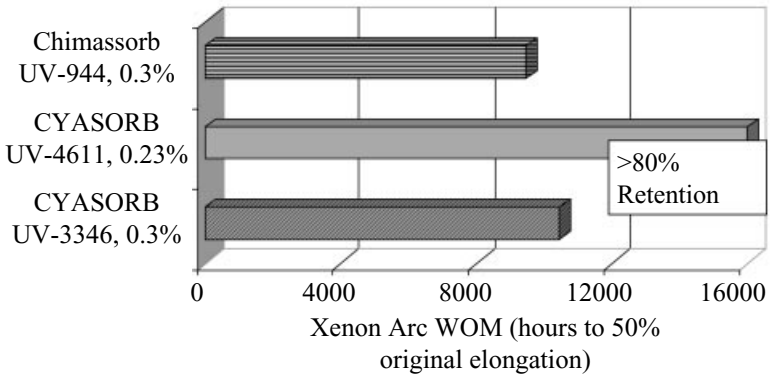

Fig. 10. UV stabilization of 1.5-mm injection-molded LLDPE tensile bars.

(Tinuvin 123), have been used extensively in automotive molding and coating applications. Higher MW versions have been developed and are targeted for greenhouse film applications (58), but commercial viability of these products is yet to be demonstrated.

Fourth Generation: Triazine–HALS Products. Combinations of triazine absorbers and HALS have recently been reported to show dramatic stabilization efficacy (59). Figure 10 shows a comparison of traditional oligomeric HALS with a Triazine–HALS blend (CYASORB THT^{TM}-4611 Light Stabilizer). These results demonstrate a significant performance advantage for the blend product. Investigations thus far have not discerned a mechanism consistent with the extent of synergism observed.

Other Light Stabilizer Types

In addition to UV absorbers and HALS, other types of UV stabilizers which inhibit degradation processes subsequent to photoinitiation are used. These include excited state quenchers, hydroperoxide decomposers, radical scavengers, and acid acceptors.

Excited State Quenchers. One of the first ideas beyond competitive UV absorption was to quench the excited states of the UV-absorbing chromophores, leading to radical formation. If the energy could be transferred to a molecule and dissipated harmlessly, radicals would not be formed. The nickel chelates have been reported to act primarily as excited state quenchers. However, most nickel UV stabilizers also have been found to provide hydroperoxide-decomposing or radical-scavenging activity. The nickel chelates usually add tan or green color to the polymer system. They perform better than UV absorbers in thin cross sections and in highly pigmented systems.

Nickel di-butyldithiocarbamate (Rylex NBC)(see Table 7) was introduced in the late 1950s. It had many drawbacks, such as high color contribution and volatility, but was a potent light stabilizer. It functioned mainly through hydroperoxide decomposition. It was used primarily in woven PP slit tape bags for the military. [2,2′-Thiobis(4-octylphenolato)]-*n*-butylamine nickel (CYASORB® UV-1084 Light

Table 7. Excited State Quenchers and Antioxidants

Chemical structure [CAS No.]	Chemical name	Trade name (producers)
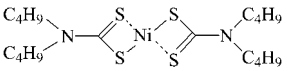 [13927-77-0]	Bis-*N*,*N*-di-*n*-butyldithiocarbamate, Nickel (II)	Rylex NBC (DuPont) UV-Chek AM 104 (Ferro) Vanox NBC (R. T. Vanderbilt) Antigene NBC (Sumitomo)
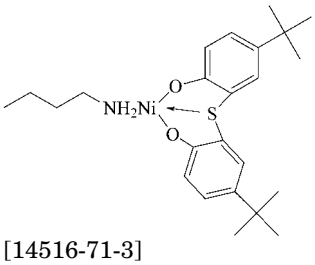 [14516-71-3]	[2,2-Thiobis(4-*tert*-octylphenolato)]-*n*-butylamine, Nickel (II)	CYASORB® UV-1084 Light Stabilizer (Cytec Industries Inc.) Chimassorb N 705 (Ciba Specialty Chemical)
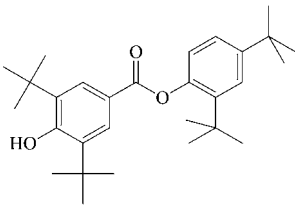 [4221-80-1]	3,5-Di-*tert*-butyl-4-hydroxybenzoic acid, 2,4-di-*tert*-butyl phenylester	Ionox 901 (Shell) UV-Chek AM 340 (Ferro) Tinuvin 120 (Ciba Specialty Chemical) Seesorb 712 (Shipro Kasei)
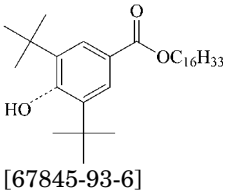 [67845-93-6]	3,5-Di-*tert*-butyl-4-hydroxybenzoic acid, hexadecyl ester	CYASORB® (UV-2908 Light Stabilizer (Cytec Industries Inc.)
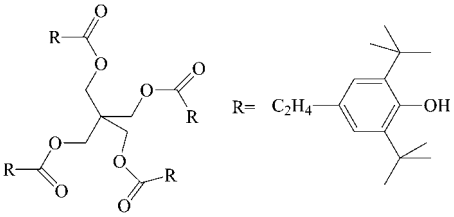 [6683-19-8]	3,5-Bis(1,1-dimethylethyl)-4-hydroxybenzene-propanoic acid, 2,2-bis[[3-[3,5-bis(1,1-dimethylethyl)-4-hydroxyphenyl]-1-oxopropoxy]methyl]-1,3-propanediyl ester	Irganox 1010 (Ciba Specialty Chemical)
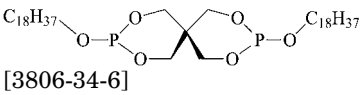 [3806-34-6]	Di-stearyl pentaerythritol diphosphite	Weston 618 (G. E. Specialty Chemical)
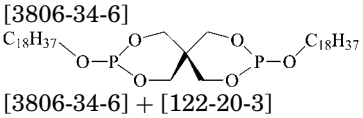 [3806-34-6] + [122-20-3]	Di-stearyl pentaerythritol diphosphite plus <1% triisopropanolamine	Weston 619 (G. E. Specialty Chemical)

Stabilizer) was introduced in the early 1960s. This product continues to be used extensively in agricultural film applications, where its main advantage is resistance to deactivation by pesticides and soil fumigants, while providing good light stability. It is used alone in white on black mulch film products. Also, it is used in combination with 2-(2-hydroxy-4-octyloxyphenyl)benzophenone (CYASORB® UV-531 light absorber) in greenhouse film products usually at a 2:1 ratio. In this latter case, a bright yellow-green color is formed partially from the formation of the nickel complex of CYASORB® UV-531, which was found to be a very effective light stabilizer by itself. CYASORB® UV-1084 is also used in the stabilization of PP slit tape artificial turf.

Hydroperoxide Decomposers. Hydroperoxides were found to be a key UV-absorbing chromophore and an intermediate in the thermal and photooxidative mechanisms of many polymers. Reducing the hydroperoxide to a stable alcohol before it was thermolized or photolized into radical fragments was recognized to be very beneficial to polymer stabilization. Phosphites, nickel dithiocarbamates, cobalt dithiophosphinates, amidothiophosphates, and nickel thiobisphenolates (eg, CYASORB® UV-1084 Light Stabilizer) all are capable of decomposing hydroperoxides, and provide a significant amount of light stabilizing activity.

Since hydroperoxides are decomposed by heat and light to generate radicals which feed the degradation processes, it is essential that they be decomposed into nonradical products. Phosphites, such as di-stearyl pentaerythritol diphosphite (Weston 618), and sulfur compounds, such as nickel dibutyl dithiocarbamate (Rylex NBC), provide this function and both provide UV-stabilizing activity in polyolefin formulations. Phosphites usually are used in combination with other UV stabilizer types.

Radical Scavengers. Reacting with the radicals generated from the excited states before they would react with oxygen or reacting with the peroxide radicals before they would abstract a hydrogen from the polymer would certainly be beneficial to the stabilization process. Hindered phenolic antioxidant radical scavengers developed for thermal stabilization of polymers were found to offer very little light-stabilizing activity. However, the unique hindered benzoate class of radical scavengers was soon discovered. First there was the photorearrangeable aromatic benzoate 3,5-di-*tert*-butyl-4-hydroxybenzoic acid, 2,4-di-*tert*-butyl phenylester (Ionox 901) developed by Shell (60) and later commercialized by Ferro as UV Check AM-340, by Ciba as Tinuvin 120, and by others such as Seesorb 712 from Shipro Kasei in Japan. The aliphatic benzoate *n*-hexadecyl 3,5-di-*tert*-butyl-4-hydroxybenzoate (CYASORB® UV-2908 Light Stabilizer) does not photorearrange (61) to a benzophenone UV absorber, but does offer superior light-stabilizing activity, alone or in combination with other classes of stabilizers (62,63).

For example, a high MW hindered amine (eg, CYASORB® UV-3346 Light Stabilizer) combined with CYASORB® UV-2908 provides synergistic performance in PP slit tape applications during Xenon ARC WOM exposure (Fig. 11) (64). The use of this combination also allows improved processability in production of the slit tapes because of reduction in water carryover compared with HALS alone. It has also been demonstrated that, in thick section PP, long-term stability can be dramatically improved with CYASORB® UV-3346 combined with CYASORB® UV-2908.

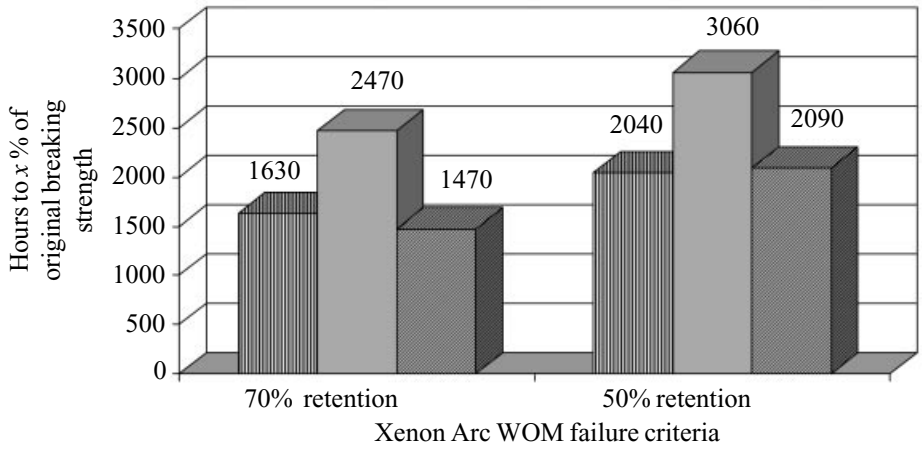

Fig. 11. UV stabilization of 65-μm PP slit tape. ▨ 0.3% CYASORB UV-3346; ▨ 0.2% CYASORB UV-3346, 0.1%. CYASORB UV-2908; ■ 0.3% Tinuvin 783.

Although HALS are recognized as one of the greatest advances in light stabilizer technology, their basicity and reactivity limits their use in many applications. Some examples are acid-catalyzed cross-linked automotive coatings, halogenated flame-retardant plastics, and interaction with pesticides in Ag films. Aliphatic benzoates can be substituted as radical scavengers in such applications where HALS cannot be used (65).

For example, the UV stabilization of blue, V-2 flame-retardant stadium seating was approached on the basis of the pigment and FR type. A benzophenone, 2-hydroxy-4-*n*-octyloxybenzophenone (CYASORB® UV-531 light absorber), was used at 0.5% to keep the blue pigment from fading and the aromatic bromine portions of the FR stable against UV radiation. CYASORB® UV-2908 was used at 0.5% in place of a HALS. An aliphatic phosphite (Weston 619) was incorporated at 0.5% to enhance the UV performance of UV-2 and to prevent degradation of the polypropylene during the extrusion and molding processes.

Pigments and Fillers. Other factors such as product cross-section and opacity affect UV stabilizer effectiveness, depending upon the chemical type and mechanism of action. In fact, carbon black and many white pigments, such as rutile titanium dioxide and zinc oxide, at sufficient concentration levels can limit the penetration of UV light energy, providing high levels of UV stabilization. In other situations, unfavorable interactions between pigments, fillers, and UV stabilizers result in reduced light stability.

Stabilization of Coatings

Coatings (qv) present a unique stabilization challenge because of their high surface-to-volume ratio. Coatings, like polymers, are classified as either thermoplastic or thermoset. Thermoplastic coatings are those that are composed mainly of individual polymer chains, sometimes partially branched. Examples of this type are acrylic latex paints, polyurethane dispersions, and nitrocellulose lacquers.

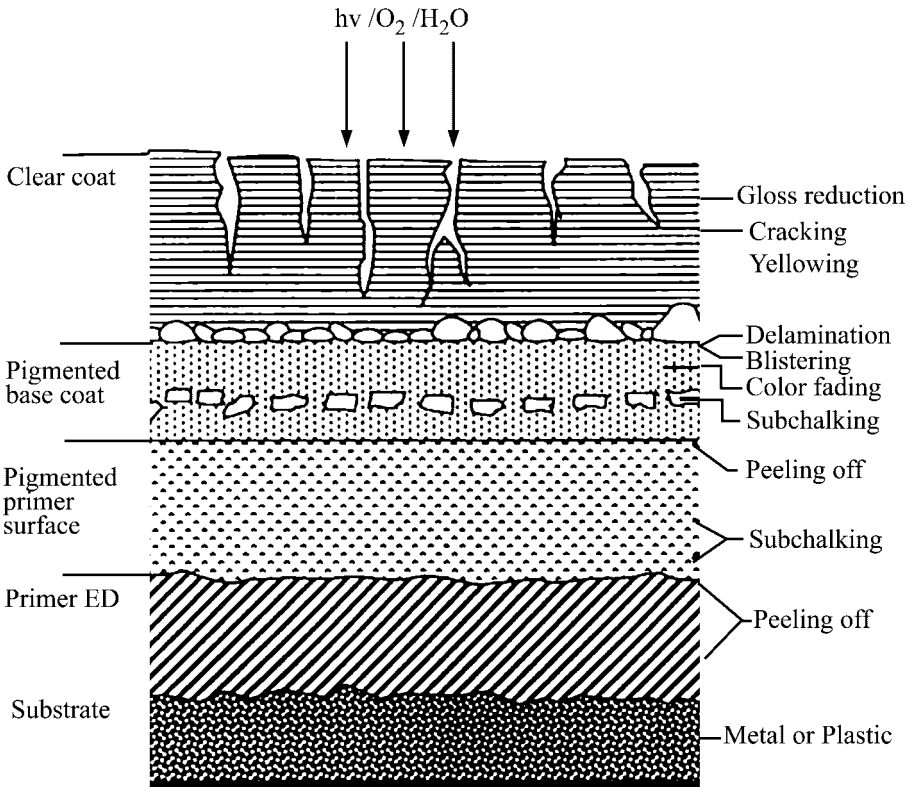

Fig. 12. Degradation phenomenon observed during weathering of a multilayer coating.

Thermoset coatings are those that are cross-linked to form an infinite polymer network. Examples of this type are acrylic melamines, two-component acrylic or polyester urethanes, alkyds, and epoxies. Coatings range in complexity from pigmented monocoats to multilayer coatings used on the exterior of automobiles. Any exterior coating is subject to degradation by the combined action of UV light, oxygen, and sometimes water, by the process of photo-oxidation. Modes of degradation of coatings are summarized in the idealized drawing of an automotive exterior coating of Figure 12. Before any organic coating film is applied, the steel is galvanized with a 0.2–0.6-μm layer of zinc, and then phosphated (0.3 μm). Then an E-coat (20 μm) is applied by electrodeposition (ED) and cured for corrosion resistance; a primer surfacer (25 μm) is applied for smoothing the surface and imparting adhesion; and a pigmented base coat (20 μm) is applied for the desired color. After a flash step (ambient or low temperature evaporation of solvent and/or water), a clear top coat (50 μm) is applied for an aesthetic high gloss appearance and the base coat/clear coat layers are simultaneously cured. UV radiation, oxygen, heat, and water have the following detrimental effects on the final coating film: reduction in gloss, yellowing, cracking, and blistering of the top coat; color fading of the base coat; and delamination at the base coat/top coat or other layer interfaces.

UV absorbers and HALS have found broad application in coatings for the slowing of these degradation processes, thereby extending the useful lifetime of

coatings. UV absorbers are most commonly used in clear coats, and also find use in pigmented coatings. UV absorbers can reduce pigment or dye fading, protect light-sensitive substrates from degradation, reduce blistering and delamination, and reduce yellowing. Benzotriazole is the most commonly used class of UV absorbers. 2-(2′-Hydroxy-3′,5′-di-*tert*-amylphenyl)benzotriazole (Tinuvin 328; CYASORB® UV-2337) is the largest volume UV absorber for coatings, followed by 2-(3′,5′-bis(1-methyl-1-phenylethyl)-2′-hydroxyphenyl)benzotriazole (Tinuvin 900) and benzenepropanoic acid, 3-(2*H*-benzotriazol-2-yl)-5-(1,1-dimethylethyl)-4-hydroxy-, C7-9 branched alkyl esters (Tinuvin 384). The use of benzophenones is restricted to some decorative and wood coatings. Recently, 2-hydroxy-phenyl-*s*-triazines have been introduced commercially. Examples are (i) 1,3-benzenediol, 4-[4,6-bis(2,4-dimethylphenylphenyl)-1,3,5-triazin-2-yl]-, C7-9 branched alkyl ethers (65% in xylenes) (CYASORB® UV-1164L light absorber) and (ii) 1,3-benzenediol, 4-[4,6-bis(2,4-dimethylphenylphenyl)-1,3,5-triazin-2-yl]-, reaction products with [(dodecyloxy)methyl]oxirane and oxirane mono[(C10-16-alkyloxy)methyl] derivatives (Tinuvin 400). This class of stabilizers exhibits strong UV-B (285–315 nm) absorptivity, low volatility, and synergy with HALS. In addition, it has the highest inherent light stability (66).

HALS play a major role in reducing the degradation that occurs on the coating surface, for example gloss reduction, cracking, and chalking (for pigmented coatings). They also help to reduce yellowing.

Monomeric HALS are almost exclusively used for coatings stabilization—polymeric HALS lack solubility in coatings and do not work as effectively as the monomeric type. Common HALS in commercial use for coatings stabilization include 3-dodecyl-1-(2,2,6,6-tetramethyl-4-piperidinyl)-2,5-pyrrolidine-2,5-dione (Sanduvor 3055; CYASORB® UV-3581 Light Stabilizer) and decanedioic acid, bis(1,2,2,6,6-pentamethyl-4-piperidinyl)ester (Tinuvin 292). These HALS are secondary (hydrogen-substituted) and tertiary (methyl-substituted) amines, respectively. Being basic in nature, these HALS interact with acid-curing catalysts commonly used in melamine-, benzoguanamine-, glycoluril-, and urea-formaldehyde resins, thereby interfering with curing. To overcome this limitation, nonbasic HALS were developed. Examples are 3-dodecyl-1-(1-acetyl-2,2,6,6-tetramethyl-4-piperidinyl)-2,5-pyrrolidinedione (Sanduvor 3058) and Tinuvin 123. Sanduvor 3058 has *N*-acetyl substitution (amide type HALS), and Tinuvin 123 has *N*-octyloxy substitution (amino ether type HALS). These HALS do not interfere with the curing of acid-catalyzed coatings.

Light stabilizers, including UV absorbers, HALS, and in some cases antioxidants, have been used to improve the weatherability of coatings and extend their useful lifetime. Unlike light stabilizers for plastics, light stabilizers for coatings must be soluble in common solvents used in solvent-borne paint, and compatible with the oligomeric and polymeric resins employed as paint binders. The ideal stabilizer is a liquid, for facile incorporation into the paint formulation. Example of liquid stabilizers are CYASORB UV-1164L (65% in xylenes) and Tinuvin 384. With the increased use of water-borne coatings, water-dispersible UV absorbers like a mixture of poly(oxy-1,2-ethanediyl)-α-(3-(3-(2*H*-benzotriazol-2-yl)-5-(1,1-dimethylethyl)-4-hydroxyphenyl)-1-oxopropyl)-ω-hydroxy, poly(oxy-1,2-ethanediyl)-α-(3-(3-(2*H*-benzotriazol-2-yl)-5-(1,1-dimethylethyl)-4-hydroxyphenyl)-1-oxopropyl-ω-(3-(3-(2*H*-benzotriazol-2-yl)-5-

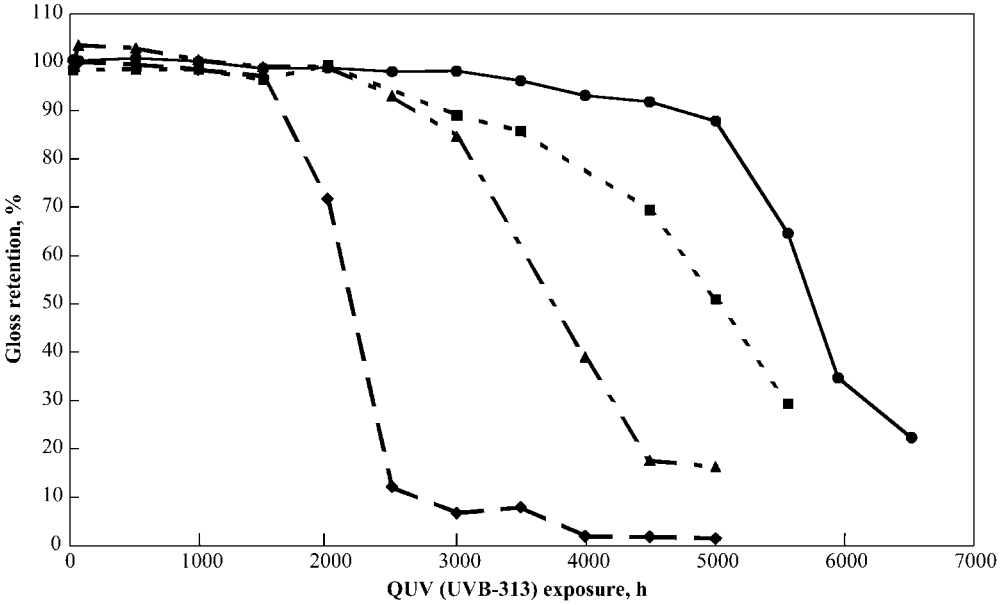

Fig. 13. Example of synergy between UV absorber and HALS. QUV weathering of Cymel® 303/Doresco® TA39-14 (styrene-free) acrylic clear coats. —◆ - Unstabilized; —▲ - 1% UV-1164; – ■- 1% UV-3581; —●— 0.5% UV-1164, 0.5% UV-3581.

(1,1-dimethylethyl)-4-hydroxyphenyl)-1-oxopropoxy, and polyethylene glycol, MW = 300 (Tinuvin 1130), are becoming increasingly important.

UV absorbers and HALS used in combination often exhibit a synergistic effect in coatings (67–70). 2-Hydroxyphenyl-*s*-triazines in particular also exhibit a synergistic effect (71,72). Thus they are typically used in combination. Figure 13 depicts an example of synergy between CYASORB UV-1164 and SANDUVOR 3055 under accelerated weathering conditions. In this case, the gloss retention of films containing 0.5% CYASORB UV-1164 and 0.5% SANDUVOR S-3055 is superior to films containing 1% of either stabilizer alone. The effectiveness of UV absorber/HALS combinations in Florida weathering has also been demonstrated. Florida weathering results for Joncryl® 510 (styrenated acrylic)/CYMEL® 303 acrylic melamine coatings containing 2% CYASORB UV-1164 in combination with SANDUVOR 3058 acetyl HALS over white base coats are given in Figures 14 and 15. The stabilized clear coats retain nearly 75% of their original gloss after 5 years of Florida weathering and exhibit a total color change (ΔE) of only 3 units after 6 years of Florida weathering.

Besides gloss and color changes, delamination is a major mode of failure, especially in multilayer coatings. For example, in an automotive original equipment manufacturer (OEM) multilayer coating as depicted in Figure 12, the ED primer coat is typically an aromatic epoxy resin. Aromatic epoxy resins are extremely light-sensitive, and decomposition of this layer can cause delamination at the ED primer/primer surfacer interface, or the ED primer/base coat interface. This was a major cause of automotive coating blistering and peeling in the 1980s. Although the real reasons will never be known, mechanisms of failure could have been any

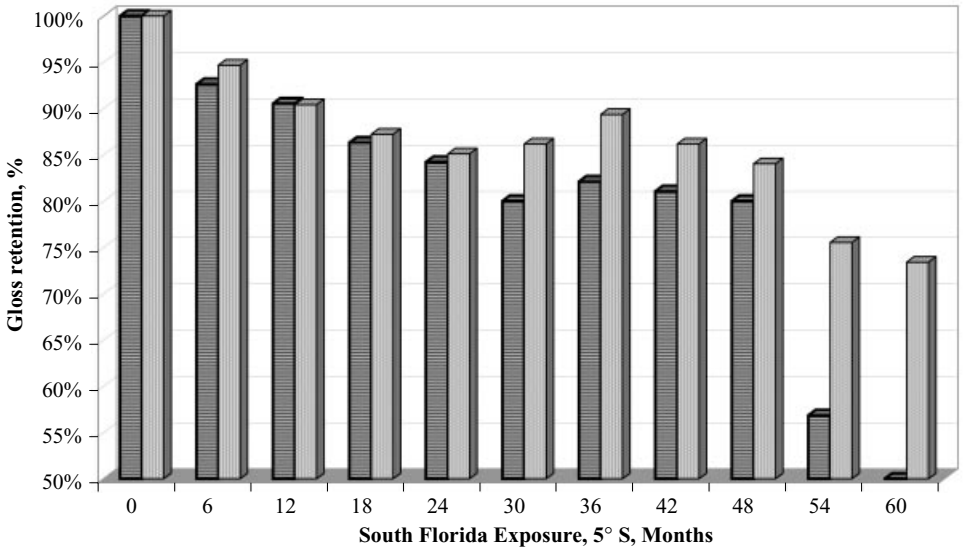

Fig. 14. % Gloss retention of 2% Cyasorb UV-1164L, 1% Sanduvor 3058, in Joncryl 510 (10% styrene acrylic)/Cymel 303 clear coat over white base coat. ■ Blank; ▨ 2% UV-1164L, 1% S-3058.

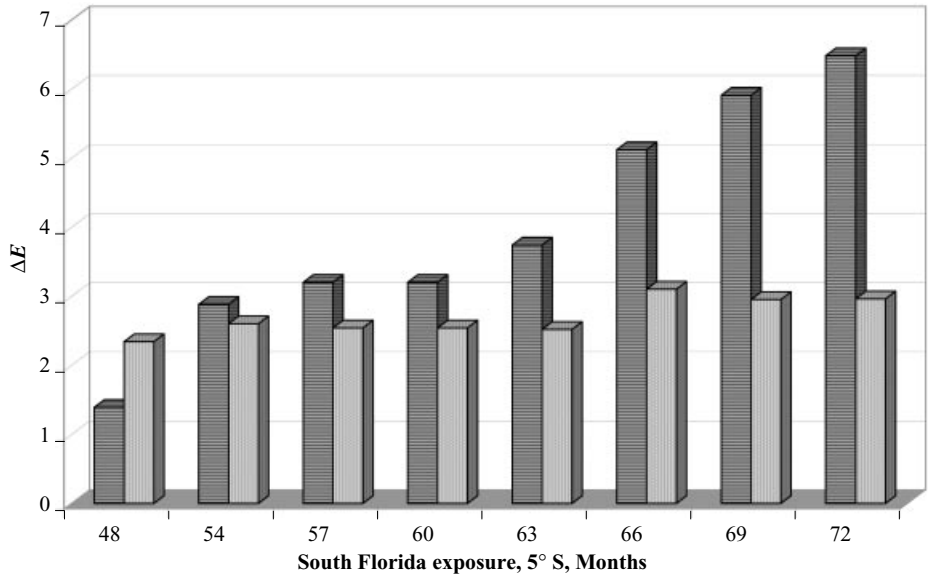

Fig. 15. ΔE with 2% Cyasorb UV-1164L, 1% Sanduvor 3058, in Joncryl 510 (10% styrene)/Cymel 303 clear coat over white base coat. ■ Blank; ▨ 2% UV-1164L, 1% S-3058.

one or a combination of (*1*) the absence of a heavily pigmented primer surfacer layer, (*2*) lower than normal film builds for the base coat and clear coat, affording less pigment screening of UV light (by the base coat) and less UV absorber screening of UV light (base coat and/or clear coat), (*3*) transmission of light in the

360-nm to visible regions due to UV absorbers with weak absorbance in this band, which also promotes degradation of epoxy resins, and (*4*) lower than normal UV absorber concentrations in the base coat and/or clear coat. Each of these conditions would lead to increased incidence of UV light onto the light-sensitive epoxy layer. Another mechanism of failure could have been over-bake conditions during curing, which would lead to thermal oxidation of the epoxy layer, the formation of radical species, and a "jump start" on photo-oxidation.

Since 1985 it has been recognized that light stabilizers can migrate in coatings, leading to concentration gradients as a function of depth. The concentration gradient can be across a single coating layer, between different layers of a multilayer coating, or between a coating and a permeable substrate such as plastic or wood. The microtome technique pioneered by Sandoz (now Clariant) chemists (73–77), and further utilized at Cytec Industries (78–83), involves the physical slicing of a coating film, parallel to its surface, in increments as small as 10 μm. The individual coating slices are then extracted with solvent or supercritical carbon dioxide and the extracts analyzed by glpc or hplc for stabilizer content. Alternatively, for clear films, UV absorber concentrations can be determined by UV spectroscopy. An example of migration of stabilizers between different coating layers is given in Figure 16 (80). The coating is an E-coat, base coat, and clear coat system. Only

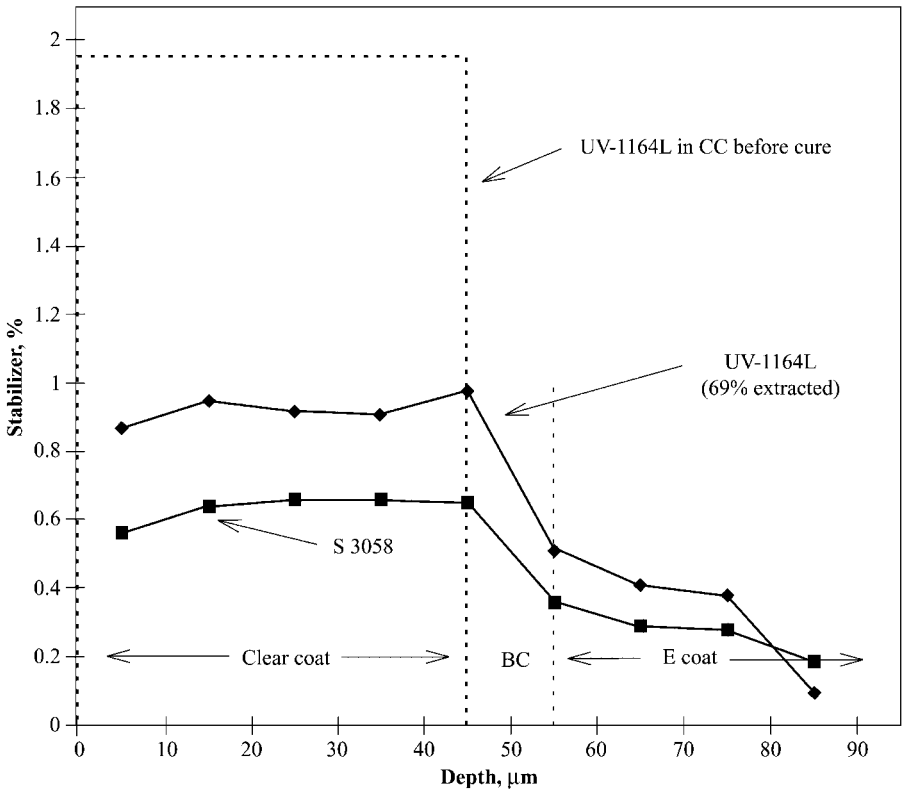

Fig. 16. Depth profile of stabilizer concentration in a clear coat/base coat/E coat system. Stabilizers were added to clear coat only prior to cure.

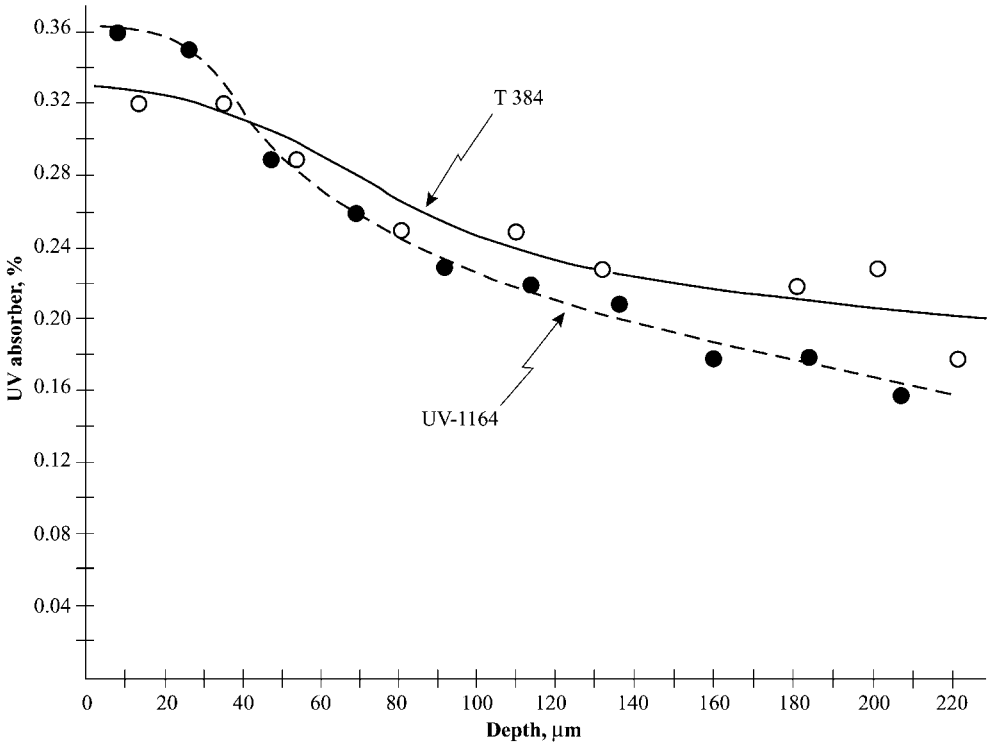

Fig. 17. Depth–concentration profile for Tinuvin® 384 and CYASORB® UV-1164L, showing migration into an RIM plastic substrate. A depth of 0 μm denotes the coating–RIM interface.

the clear coat was formulated with CYASORB UV-1164L and SANDUVOR 3058. But it can clearly be seen that during cure, both stabilizers have migrated not only into the base coat, but into the E-coat as well. Figure 17 depicts the results of two microtoming experiments of a RIM plastic, which had been painted with stabilized coatings (80). In one case, the RIM was coated with a film containing CYASORB UV-1164L, in the other, with a film containing Tinuvin 384. In each case, the coating–RIM interface is assigned a depth of 0 μm, and the stabilizers have migrated at least to a depth of 220 μm.

These data indicate that the amount of stabilizer actually present in any given coating film may be considerably less than originally formulated into the paint in multilayer coatings and coatings over plastics. This has led to a reevaluation of stabilization strategies for this application. One approach to minimize migration is to use a bondable light stabilizer. For example Tinuvin 400 has a secondary hydroxyl group, while 2-[(2-hydroxyethyl)amino]-4,6-bis[*N*-(1-cyclohexyloxy-2,2,6,6-tetramethylpiperidin-4-yl)butylamino-1,3,5-triazine (Tinuvin 152) has a primary hydroxyl group. With hydroxyl substituents, both stabilizers are capable of forming covalent bonds with typical coating cross-linkers, both melamine-formaldehyde resins and polyisocyanate resins, during cure. Thus they are locked into the coating matrix and prevented from migrating. Another novel

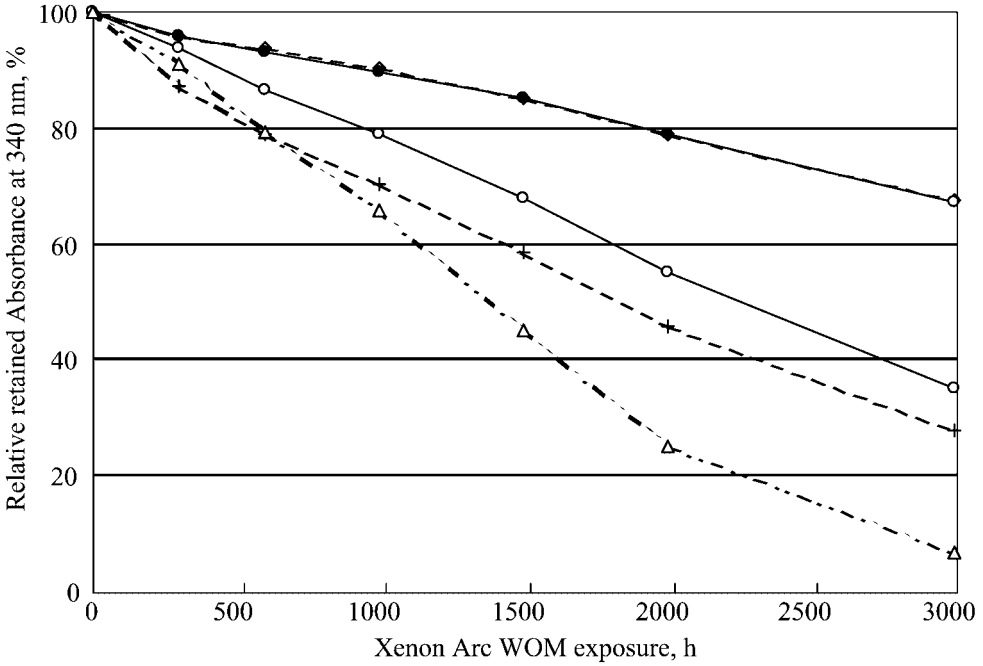

Fig. 18. Xenon weathering of UV absorbers in acrylic melamine clear coats (Copolymer N). – –◇– – CYASORB UV-1164, —●— CYASORB UV-1164L, —○— Tinuvin 1130, – –+– – Tinuvin 384, – -△– - Tinuvin 328.

approach is exemplified by propanedioic acid, [(4-methoxyphenyl)methylene]-bis(1,2,2,6,6-pentamethyl-4-piperidinyl) ester (SANDUVOR PR-31). This HALS forms a covalent bond with the coating matrix by a photochemical reaction upon exposure to light.

2-Hydroxyphenyl-*s*-triazines have excellent inherent light stability. This was demonstrated in an experiment in which acrylic melamine films containing various UV absorbers were drawn onto quartz slides and subjected to accelerated weathering (66). The loss of absorbance at the reference wavelength of 340 nm over time, an indication of UV degradation of the UV absorbers themselves, was measured. The stability of the UV absorbers in films containing a durable acrylic, Copolymer N, versus a less durable acrylic, Copolymer A, were compared. The results are given in Figures 18 and 19. In both cases, the 2-hydroxyphenyl-*s*-triazines CYASORB UV-1164 and CYASORB UV-1164L show the lowest rate of degradation compared with the other UV absorbers, all benzotriazoles. All of the UV absorbers had overall higher rates of degradation in the less durable acrylic, suggesting increased free-radical attack on the UV absorbers by the degrading coating matrix.

The ranking of stability of UV absorbers observed in the accelerated weathering studies was confirmed in Florida weathering of acrylic melamine automotive OEM coatings (84). The technique of microtoming was used to obtain 10-μm slices of the coating film (including both the top coat and base coat). Each slice was then analyzed by extraction and glpc for UV absorber content. UV absorber

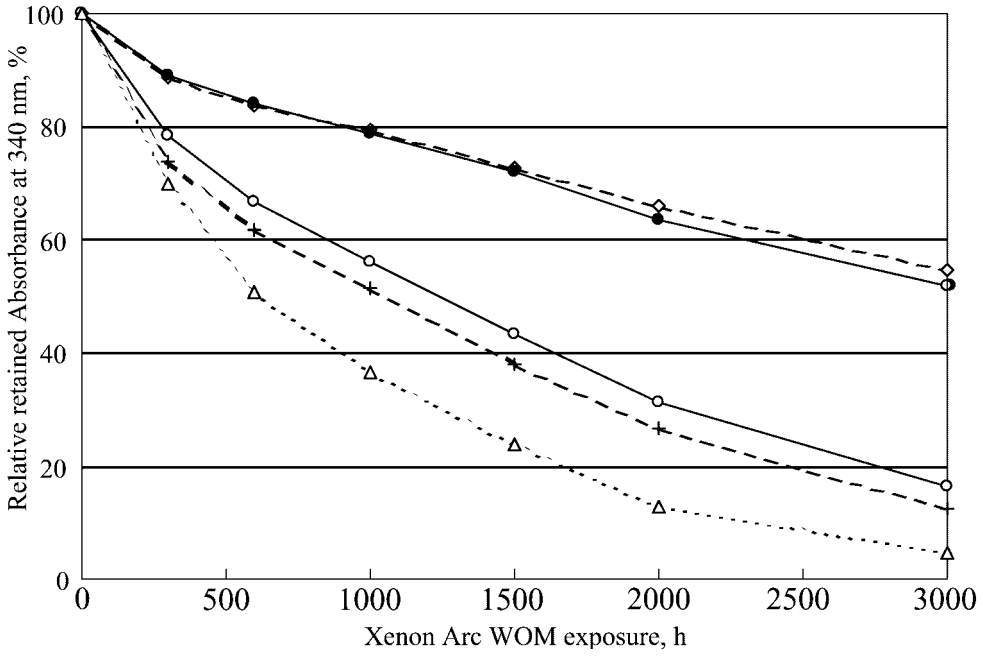

Fig. 19. Xenon weathering of UV absorbers in acrylic melamine clear coats (Copolymer A). – –◇– – CYASORB UV-1164, —●— CYASORB UV-1164L, —○— Tinuvin 1130, – –+– – Tinuvin 384, – -△– - Tinuvin 328.

concentration plotted as a function of depth for four coating films is shown in Figure 20. Two of the films contain CYASORB UV-1164L, microtomed after curing and after 3 years of Florida exposure, and two contain Tinuvin 900, likewise microtomed after curing and after 3 years of Florida exposure. It is evident from Figure 20 that additive concentration is not uniform throughout the coating film. The concentration of UV absorber tends to be less near the surface, because of volatilization during cure in the case of freshly cured films, and because of the combined effects of volatilization and degradation by UV light for the exposed coating films. Also, the loss of Tinuvin 900 is much greater than the loss of CYASORB UV-1164L after 3 years of Florida exposure, as predicted by the accelerated weathering experiment.

A series of papers published by the Research Staff at Ford Motor Co., Dearborn, Michigan, provides some insights into the photodegradation and stabilization of acrylic melamine and acrylic urethane coatings (35–43,85–97). These are the two most common thermoset (cross-linked) coating classes used for automotive OEM clear coats. These cross-linked materials derive their physical properties, eg hardness and chemical resistance, from chemical cross-links formed during the curing process between the backbone resin, usually a linear acrylic or polyester polyol, and a cross-linker (melamine-formaldehyde resin, or polyisocyanate), usually multifunctional. Conventional weathering of coatings to determine the durability of these coatings has its drawbacks. Outdoor weathering can take 5 years or more before physical failure. Accelerated weathering shortens the

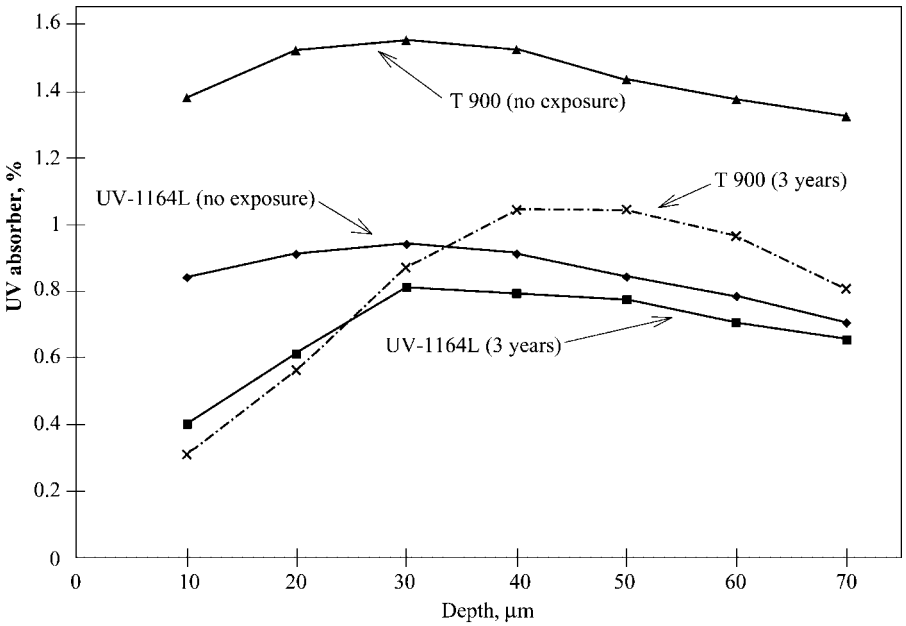

Fig. 20. Depth distribution of CYASORB® UV-1164L and Tinuvin® 900 in clear coat/base coat films after cure and after three years of florida exposure.

time to failure from years to several months, but the correlation of the results with outdoor weathering results depends upon the composition of the coating system. Since these cross-linked films can undergo a large amount of chemical changes (eg cross-link scission) before physical properties are affected, chemical tests have been used to rapidly track photodegradation without the use of artificially harsh accelerated exposure conditions. New chemical test protocols involving UV and ftir spectroscopy, iodometric titration, and esr have been used to assess coating weatherability.

BIBLIOGRAPHY

1. O. Cicchetti, *Adv. Polym. Sci.* **7**, 70 (1970).
2. D. J. Carlsson and D. M. Wiles, *J. Macromol. Sci., C: Rev. Macromol. Chem.* **14**(1), 65 (1976).
3. D. J. Carlsson and D. M. Wiles, *J. Macromol. Sci., C: Rev. Macromol. Chem.* **14**(2), 155 (1976).
4. N. S. Allen and J. F. McKellar, *Chem. Soc. Rev.* **4**, 533 (1975).
5. B. Ranby and J. F. Rabek, *Photodegradation, Photooxidation and Photostabilization of Polymers*, Wiley-Interscience, New York, 1975.
6. F. Gugumus, *Plastics Additives Handbook*, 5th ed., Carl Hanser, Munich, 2001, p. 141.
7. R. C. Hirt, N. A. Searle, and R. G. Schmitt, *SPE Trans. 1* (1) 21–25 (1961).
8. J. F. Rabek, *Polymer Photodegradation*, Chapman and Hall, New York, 1995.
9. D. M. Wiles, *Pure Appl. Chem.* **50**, 291 (1978).
10. P. P. Klemchuk, M. E. Gande, and E. Cordola, *Polym. Degrad. Stab.* **27**, 65 (1990).

11. G. Gueskens, M. N. Kanda, and G. Nedelkos, *Bull. Soc. Chim. Belg.* **99**, 1085 (1990).
12. E. N. Step and co-workers, *Macromolecules* **27**, 2529 (1994).
13. J. A. Stretanski, Polyolefins III SPE-RETEC, 1981.
14. S. P. Fairgrieve and J. R. MacCallum, *Polym. Commun.* **25**, 44 (1984).
15. J. Kresta, SPE-RETEC, Plastic Prog. Process, 1980, p. 470.
16. F. Gugumus, in G. Scott, ed., *Developments in Polymer Stabilization*, Vol. **8**, Elsevier, 1987, pp. 239–289.
17. R. M. Fischer, W. D. Ketola, and W. P. Murray, *Prog. Org. Coat.* **19** 151–163 (1991).
18. W. D. Ketola and D. Grossman, eds., *Accelerated and Outdoor Durability Testing of Organic Materials*, STP 1202, American Society for Testing and Materials, Philadelphia, Pa., 1995.
19. G. Wypych, *Handbook of Material Weathering*, 2nd ed., ChemTec Publishing, Toronto, 1995.
20. G. Wypych, ed., *Weathering of Plastics: Testing to Mirror Real Life Performance*, Plastics Design Library, Norwich, New York, 1999.
21. D. R. Bauer and J. W. Martin, eds., *Service Life Prediction of Organic Coatings* (ACS Symposium Series No. 722), Oxford University Press, Oxford, U.K., 1999.
22. T. Toda, E. Mori, and K. Murayama, *Bull. Chem. Soc. Jpn.* **45**, 1904 (1972).
23. T. A. B. M. Bolsman, A. P. Blok, and J. H. G. Frijns, *Recueil, J. Royal Netherlands Chem. Soc.* **97**, 313 (1978).
24. D. W. Grattan, D. J. Carlsson, and D. M. Wiles, *Polym. Degrad. Stab.* **1**, 69 (1979).
25. D. K. C. Hodgeman, *J. Polym. Sci., Polym. Chem. Ed.* **18**, 533 (1980).
26. J. Sedlar and co-workers, *Polymer* **21**, 5 (1980).
27. D. J. Carlsson and co-workers, *Pure Appl. Chem.* **52**, 389 (1980).
28. D. J. Carlsson, K. H. Chan, and D. M. Wiles, in S. R. Pappas and F. H. Winslow, eds., *Photodegradation and Photostabilization of Coatings*, (ACS Symposium Series No. 151), American Chemical Society, Washington, D.C., 1981, p. 51.
29. D. J. Carlsson and co-workers, *J. Polym. Sci., Polym. Chem. Ed.* **20**, 575 (1982).
30. T. Kurumada and co-workers, *J. Polym. Sci., Polym. Chem. Ed.* **22**, 277 (1984).
31. B. N. Felder, in P. P. Klemchuk, ed., *Polymer Stabilization and Degradation* (ACS Symposium Series No. 280), American Chemical Society, Washington, D.C., 1985, p. 69.
32. G. Geuskens and G. Nedelkos, *Polym. Degrad. Stab.* **19**, 365 (1987).
33. P. Gijsman, J. Hennekens, and D. Tummers, *Polym. Degrad. Stab.* **39**, 225 (1993).
34. F. Gugumus, *Polym. Degrad. Stab.* **40**, 167 (1993).
35. J. L. Gerlock, *Anal. Chem.* **54**, 1529 (1983).
36. J. L. Gerlock and D. R. Bauer, *J. Polym. Sci., Polym. Lett. Ed.* **22**, 477 (1984).
37. J. L. Gerlock and co-workers, *J. Coat. Technol.* **57** 37–46 (1985).
38. J. L. Gerlock, D. R. Bauer, and L. M. Briggs, in Ref. 31, p. 119.
39. D. R. Bauer, J. L. Gerlock, and L. M. Briggs, *Polym. Degrad. Stab.* **14**, 53 (1986).
40. J. L. Gerlock, D. F. Mielewski, and D. R. Bauer, *Polym. Degrad. Stab.* **20**, 123 (1988).
41. D. R. Bauer, M. J. Dean, and J. L. Gerlock, *Ind. Eng. Chem. Res.* **27**, 65 (1988).
42. D. R. Bauer and J. L. Gerlock, *Polym. Degrad. Stab.* **27**, 271 (1990).
43. D. R. Bauer, J. L. Gerlock, and D. F. Mielewski, *Polym. Degrad. Stab.* **28**, 115 (1990).
44. USSR Pat. 166,133.
45. M. B. Neiman, E. G. Rozantzev, and Yu. G. Mamedova, *Nature* **196**, 472 (1962).
46. Murayama, *Pharmacia* **10**, 573 (1974).
47. T. Toda and co-workers, in Ref. 31, p. 37.
48. Br. Pat. 1,196,224 (1967) (to Sankyo Co. Ltd.).

49. J. L. Malik, A. Hrivik, and E. Tomova *Polym. Degrad. Stab.* **35**, 61 (1992).
50. R. L. Tucker and P. Susi, *Stabilization of Polypropylene Filaments*, in *187th Meeting of the ACS*, St. Louis, 1984.
51. *Cytec Industries*, unpublished work, 1992.
52. F. Gugumus, *D. Angew. Makromol. Chem.* **190**, 111 (1991).
53. F. Gugumus, *Polym. Degrad. Stab.* **40**, 167 (1993).
54. Kikkawa, *Polym. Degrad. Stab.* **49**, 135 (1995).
55. J. Eng and K. Nolan, Polymer Stab. and Mod. '97 Conf., Hilton Head, S.C., 1997.
56. S. Samuels and co-workers, *SPE Polyolefins IX*, 1995.
57. K. Keck-Antoine, 53rd SPE-ANTEC **3**, 1995, p. 3615.
58. A. Thürmer, *Masterbatch 2000* (2000).
59. F. A. Cangelosi, L. H. Davis, and S. Samuels, *SPE Polyolefins XIII SPE-RETEC 2001* (2001).
60. U.S. Pat. 3,206,431 (1965), M. E. Doyle and co-workers (to Shell Oil Co.).
61. H. J. Hellar and H. R. Blattman, *Pure Appl. Chem.* **30**, 145 (1972).
62. U.S. Pat. 4,237,042 (1980), J. A. Stretanski (to American Cyanamid Co.).
63. U.S. Pat. 4,670,491 (1987), J. A. Stretanski and F. Loffelman (to American Cyanamid Co.).
64. J. A. Stretanski, *SPE-RETEC Polyolefins III*, 1981.
65. N. S. Allen and co-workers, *Polym. Degrad. Stab.* **7** (1984).
66. M. L. Cohen, Cytec Industries Inc., unpublished work, 1995.
67. U.S. Pat. 4,314,933 (1982), G. Berner, (to Ciba-Geigy Corp.).
68. U.S. Pat. 4,344,876 (1982), G. Berner (to Ciba-Geigy Corp.).
69. U.S. Pat. 4,426,471 (1984), G. Berner (to Ciba-Geigy Corp.).
70. U.S. Pat. 4,426,472 (1984), G. Berner, (to Ciba-Geigy Corp.).
71. U.S. Pat. 4,619,956 (1986), P. V. Susi, (to American Cyanamid Co.).
72. U.S. Pat. 4,740,542 (1988), P. V. Susi (to American Cyanamid Co.).
73. H. Böhnke, E. Hess, and L. Avar, *19th FATIPEC-Kongr.* **1**, 317 (1988).
74. K. Bechtold, E. Hess, and G. Ligner, *J. Coat. Technol.* **63**, 53 (1991).
75. G. Ligner and E. Hess, *Farbe Lack* **97**, 676 (1991).
76. H. Böhnke and E. Hess, *Adv. Org. Coat. Sci. Tech. Technol. Ser.* **13**, 49 (1991).
77. G. Ligner and E. Hess, *EuroCoat* **10**, 622 (1991).
78. G. Haacke and J. Brinen, *22nd FATIPEC-Kongr.* **3**, 182 (1994).
79. G. Haacke, J. S. Brinen, and P. J. Larkin, *J. Coat. Technol.* **67**, 29 (1995).
80. G. Haacke, F. F. Andrawes, and B. H. Campbell, *J. Coat. Technol.* **68**, 57 (1996).
81. G. Haacke and co-workers, *Prog. Org. Coat.* **34**, 75 (1998).
82. F. Andrawes and co-workers, *Anal. Chem.* **70**, 3762 (1998).
83. G. Haacke and co-workers, *J. Coat. Technol.* **71**, 87 (1999).
84. G. Haacke, Cytec Industries Inc., unpublished work, 1999.
85. D. R. Bauer, R. A. Dickie, and J. L. Koenig, *Ind. Eng. Chem. Prod. Res. Dev.* **25**, 289 (1986).
86. J. L. Gerlock, T. Riley, and D. R. Bauer, *Polym. Degrad. Stab.* **14**, 73 (1986).
87. D. R. Bauer and J. L. Gerlock, *Polym. Degrad. Stab.* **14**, 97 (1986).
88. J. L. Gerlock, D. R. Bauer, and L. M. Briggs, *Prog. Org. Coat.* **15**, 197 (1987).
89. K. R. Carduner and co-workers, *Macromolecules* **21**, 1598 (1988).
90. D. R. Bauer and co-workers, *Polym. Degrad. Stab.* **28**, 39 (1990).
91. D. F. Mielewski, D. R. Bauer, and J. L. Gerlock, *Polym. Degrad. Stab.* **33**, 93 (1991).
92. D. R. Bauer and co-workers, *Ind. Eng. Chem. Res.* **30**, 2482 (1991).
93. D. R. Bauer, J. L. Gerlock, and D. F. Mielewski, *Polym. Degrad. Stab.* **36**, 9 (1992).
94. D. R. Bauer, D. F. Mielewski, and J. L. Gerlock, *Polym. Degrad. Stab.* **38**, 57 (1992).
95. D. R. Bauer, *J. Coat. Technol.* **66**, 57 (1994).

96. J. L. Gerlock and co-workers, *Polym. Degrad. Stab.* **47**, 405 (1995).
97. J. L. Gerlock and co-workers, *Polymer Durability* (Advances in Chemistry Series 249), 1996, p. 335.

FRANK A. CANGELOSI
LEONARD H. DAVIS
ROBERT L. GRAY
JOSEPH A. STRETANSKI
DENNIS J. JAKIELA
Cytec Industries

VIBRATIONAL SPECTROSCOPY

Introduction

One of the most valuable realizations of a polymer scientist dealing with structural characterization is that use of many different techniques is required to fully understand polymer structures of different scales. Gel permeation chromatography, light scattering, and mass spectrometry (qv), particularly matrix assisted laser desorption mass spectrometry (MALDI), characterize overall molecular weight. Nuclear magnetic resonance can elucidate polymer chemical composition. Transmission electron microscopy is used to characterize density fluctuation within the sample to obtain detailed morphological features such as crystallite form and degree of phase separation in compatible systems. For information regarding atomic placement, X-ray and electron diffraction methods are generally utilized. Differential thermal calorimetric measurements provide insight regarding structural changes as functions of temperature and processing history. Vibrational spectroscopy is one of the oldest and most powerful technique for analyzing polymer composition and structure. In addition, the principal advantage for use of vibrational spectroscopy as a morphological tool is that it is extremely selective. Both crystalline and amorphous polymer structures can be characterized. Conformational order ranging from the shortest chemical repeat to several hundred angstroms can be measured. Unlike diffraction techniques which depend on long-range order or disorder, vibrational spectroscopy is characteristic of chain conformation at a more localized level. Although numerous techniques address polymer structure in the crystalline state, few provide information on the disordered state, a subject capable of being studied using vibrational spectroscopy. In fact, vibrational spectroscopy is routinely utilized to characterize polymer composition, segmental orientation, chain conformation, and intermolecular

Encyclopedia of Polymer Science and Technology. Copyright John Wiley & Sons, Inc. All rights reserved.

interactions. Because of significant advances in instrumentation and simulation software, most laboratories possesses instrumentation capable of producing excellent data. Fibers, films, solutions, and melts can be analyzed with great confidence. The sample under examination need not be static in nature. Time-dependent phenomenon can be measured with time resolution as short as microseconds. It is also possible to measure samples in the range of micrometers or smaller with dedicated accessories. Vibrational spectroscopy provides information complementary to other characterization techniques and has proven of enormous value to studies in polymer science and engineering.

Applications of vibrational spectroscopy of polymers are generally divided into two subsets: infrared absorption spectroscopy and Raman scattering. Each offers particular advantages. The physical origin of the infrared and Raman effects are quite different, however. One depends on the dipole change and the other on changes in polarizability tensor (1). Different vibrational modes are therefore active in Raman and infrared. The more symmetric the molecule, the greater the difference between Raman and infrared spectra (1). The two techniques are truly complementary, however. For both cases, although more so for infrared, substantial literature exists regarding their utility for polymer characterization (2–8). Infrared spectroscopy is more appropriate for studies of chemical composition and side groups. Raman scattering is more effective for structural characterization since intense Raman scattering is often associated with the significant polarizability changes of the all-carbon backbone of the polymer chain and can be used much more readily to analyze chain conformation. They can be implemented in a broad spectrum of configurations including remote sensing and for studying solids, liquids, and gases. Intractable samples can be studied without much preparation. The power of vibrational spectroscopy, ie its selectivity and sensitivity, cannot be overestimated. Most research laboratories possess an excellent Fourier transform infrared and/or Raman spectrometer. These instruments are accurate, sensitive, durable, versatile, easy to use, and inexpensive to purchase. Extensive software is available for instrument control and to correlate spectroscopic features to the possible molecular functional groups from which they originate.

Infrared, Raman, and Normal Mode

Molecular spectroscopy is now a mature field of study. It is, however, difficult to find references superior to the classic treatise written by Herzberg nearly 50 years ago (1). The origin of vibrational spectra is usually considered in terms of mechanical oscillations associated with mass of the nuclei and interconnecting "springs" (9). Vibrational spectroscopy considers the frequency, shape, and intensity of internuclear motions due to incident electromagnetic fields. In the harmonic approximation, the vibrational bands are associated with transitions between nearest vibrational states. When higher order transitions, resonance, and coupling between vibrational motions require analysis, quantum mechanical treatment is mandated (1). Improvements and advancements in polymer spectroscopy are driven by the many problems of interest in the polymer community.

Infrared Spectroscopy. Infrared absorption spectroscopy is among the oldest and most widely used characterization techniques available to polymer

scientists. Without exaggeration, nearly every laboratory has an excellent Fourier transform infrared spectrometer. Sample preparation does not require significant effort. Polymers mixed with potassium bromide and then pressed into pellets or films prepared from melt or cast from solution can be easily studied. For bulk samples or powders, or if a concentration profile is needed for a film, the reflectance technique is perhaps more suitable (10). With the recent improvements in instrumentation, quantitative spectroscopic analysis of polymer solutions is not difficult to achieve. The availability of small yet powerful computers attached to instruments has provided new and powerful analysis routines for structural characterization.

Normal vibrations related to a change in dipole moment are infrared active. Groups with large dipole moments, such as C=O and N—H, typically have strong infrared absorptions. The majority of reported spectroscopic studies by infrared spectroscopy focus on determination of polymer molecular composition by analysis of characteristic vibrations of functional groups. The power of vibrational spectroscopy, ie its selectivity and sensitivity, cannot be overestimated. With accurately defined band assignment, particularly if the transition dipoles are well established, quantitative analysis of sample anisotropy in terms of segmental orientation can be accurately established.

Virtually all instruments employ an interferometer for infrared spectroscopy (11,12). Extremely accurate positions, intensity, and shape can be obtained. An interferometer generates information from the entire range of a given spectrum during each scan. The instruments, which are routine and extremely reliable, collect large amounts of energy at high resolution. Data are obtained in a relatively short time scale. Time resolution of milliseconds can be carried out with ease. With additional modifications, high temporal resolution as short as microseconds can also be accomplished with commercial instrumentation. Instrument improvements make far- and near-infrared spectroscopy feasible for structural characterization.

Tremendous advancements in a number of applications have been made possible by infrared spectroscopy. Specialized accessories facilitate surface studies. Developments in imaging techniques make high spatial resolution spectroscopy possible (13). High temporal resolution to follow kinetic developments can be accomplished with great precision and signal-to-noise ratio. Specialized techniques such as time-resolved spectroscopy and two-dimensional spectroscopy have contributed significantly to the understanding of molecular dynamics (14–16). Structural variations such as degree of crystallinity, segmental orientation, and composition at surface or bulk, can all be analyzed with the use of different types of spectroscopies. The development of photoacoustic spectroscopy should also be noted (17). This technique has contributed significantly to analysis of polymer structure, both surface and bulk, with sensitivity and speed. These application-driven developments are discussed below in greater detail.

Raman Scattering. Although the Raman effect was first reported in 1928 (18,19), its utility as a characterization tool was not realized until the advent of lasers in the early 1960s (20). With the recent advances in lasers, detection systems, and spectrometer design, a tremendous potential exists for use of the Raman technique as a characterization technique. Since it is a scattering technique, samples such as powder, film, solid, filament, or solution can all be studied

with little sample preparation. Biological samples can also be characterized since scattering from water is extremely weak. As virtually all polymers used commercially are carbon based, the change in polarizability along the backbone is large. Raman scattering is therefore particularly suitable for characterization of polymer backbone conformation. Confocal Raman microscopes are available with spatial resolution approaching the diffraction limit of the focused laser beam. The lasers generally used for Raman scattering produce highly polarized excitation radiation. The polarized or depolarized scattered radiation collected are especially suitable for analysis of segmental orientation. In fact, various Raman techniques have been used on-line to elucidate effects of changing processing parameters on morphology development in uniaxial and biaxial polymers.

Despite its capability for delivering detailed structural information, Raman scattering has not yet achieved equal status with other characterization techniques. Its development has been slow because of the high initial investment and maintenance costs (high power lasers, sophisticated spectrometers, sensitive detectors, etc). The Raman effect is extremely weak, eg, only 1 in 10^4 or many fewer incident photons result in inelastic scattering (21). Intense excitation sources are needed which may also cause fluorescence that overwhelms the Raman signals. The earliest Raman studies on polystyrene and poly(methyl methacrylate) were possible only because the samples were totally clear and fluorescence free. Raman spectra can today be readily obtained from most polymers. Recrystallization or extraction has been effective in removing impurities that cause fluorescence. Another alternative is to use long wavelength excitation (1.06 μm) as in most Fourier transform instruments. Nevertheless, the Raman technique yields tremendous structural information and effectively complements other characterization techniques. Many Raman instruments are designed around a dispersive spectrometer. In comparison to infrared instruments, this type of spectroscopy is much slower. There are, however, distinct advantages. These are

(1) Since many excitation sources are in the visible range, the optical elements are generally much simpler to deal with in comparison to infrared.
(2) The photomultiplier exhibits much flatter quantum efficiency.
(3) Lower frequency vibrations can be studied with ease.
(4) Because of the shorter excitation wavelength, high spatial resolution can be achieved for imaging studies.

In addition, with the tremendous improvements in multichannel charge-coupled device (CCD) detectors, high quality Raman data can be obtained efficiently.

The Raman effect, an absorption and emission phenomenon, can be described in the following fashion. Imagine placing a molecule in an electric field. This molecule will be polarized by the electric field; in other words a dipole will be induced in the molecule such that the electrons are distorted away from the direction of the field. If the electric field is oscillating (with frequency ω_0), the induced dipole will oscillate with the same frequency, ω_0; this is typical Rayleigh scattering. Now imagine the case where the molecule is already vibrating with some other frequency ω_i (for example, bond stretching). The interaction between the oscillating

molecule and the incident radiation will result in both elastic (Rayleigh) and inelastic (Raman) scattering.

The polarizability of the oscillating molecule is described by

$$\alpha = \alpha_0 + \sum_{i=1}^{i=3N-6} \frac{\partial \alpha}{\partial Q_i} Q_i + \cdots = \alpha_0 + \sum_{i=1}^{i=3N-6} \alpha_i' Q_i + \cdots \tag{1}$$

where Q_i describes the vibration of the molecule. The interaction of the oscillating molecule with the incident radiation can be expressed as

$$I_{\text{scattered}} = \alpha E = \left(\alpha_0 + \sum_{i=1}^{i=3N-6} \frac{\partial \alpha}{\partial Q_i} Q_i + \cdots \right) E \tag{2}$$

The incident radiation is described by $E = E_0 \cos \omega_0 t$ and the vibrational mode is described by $Q_i = Q_i^0 \cos \omega_i t$. After substituting these two expressions into the above equation, we get a description for scattered light by an oscillating molecule.

$$\begin{aligned} I_{\text{scattered}} = \alpha E &= \left(\alpha_0 + \sum_{i=1}^{i=3N-6} \frac{\partial \alpha}{\partial Q_i} Q_i + \cdots \right) E \\ &= \alpha_0 E_0 \cos \omega_0 t + \sum_{i=1}^{i=3N-6} \frac{\partial \alpha}{\partial Q_i} Q_i^0 E_0 \cos \omega_i t \cos \omega_0 t \\ &= \alpha_0 E_0 \cos \omega_0 t + \sum_{i=1}^{i=3N-6} \frac{\partial \alpha}{\partial Q_i} Q_i^0 E_0 [\cos(\omega_0 + \omega_i)t + \cos(\omega_0 + \omega_i)t] \end{aligned} \tag{3}$$

The scattered light includes both elastically scattered radiation (ie Rayleigh scattering) and inelastic scattering (Stokes and anti-Stokes Raman scattering), is dependent on the change in polarizability and is described by a tensor. In general, the scattering tensor (real and symmetric) is defined as

$$\alpha_{\text{mol}} = \begin{pmatrix} \alpha_{11} & \alpha_{12} & \alpha_{13} \\ \alpha_{21} & \alpha_{22} & \alpha_{23} \\ \alpha_{31} & \alpha_{32} & \alpha_{31} \end{pmatrix} \tag{4}$$

Six independent elements need be determined. In this case, we designate α_{ij}'s to represent the change in polarizability elements in respect to the displacement relative to the equilibrium positions. The elements depend on the molecular symmetry, functional groups, and degree of orientational order in the sample. When the symmetry of the translational repeat of polymers is known, analysis of polarized Raman scattering yields significant structural information. The chain segment orientation distribution, the parameters needed to achieve the degree of anisotropy, and assignment of particular bands can all be obtained (22–27).

Unless the sample is an oriented macroscopic single crystal (almost never the case), some polarization information in the scattered light is lost. Partially

oriented systems can be either uniaxially oriented such as in fibers or planarly (biaxially) oriented films. Here the relationship between the molecular and laboratory frames is partially lost. Thus, specific information about each of the six elements is lost. Instead the tensor elements combine forming a new set of four elements, each being a linear combination of the previous six elements (24). These are useful for structural analysis and band assignment.

The molecular orientation with respect to the laboratory frame can be completely random as in liquids or melts. Each scattering center is randomly oriented relative to the laboratory frame such that the scattering tensor is reduced to the relationship between the isotropic and anisotropic portions. Even under these circumstances, information about the scattering tensor elements associated with various modes can be obtained through measurements of the *depolarization ratio* ρ, defined to be the ratio of the scattered light intensity obtained when the scattered and incident beams are linearly polarized perpendicular to each other to that obtained when they are polarized parallel to each other (20). Careful analysis of polarized Raman spectra can still yield information regarding the local chain conformation, interaction with solvents, degree of chain extension, or amorphous portions of semicrystalline polymers or glassy solids (28–34). Since most polymers of interest involve carbon backbones, the differential polarizability tensor elements have large isotropic elements. In many cases, only the isotropic spectrum is used for structural characterization, thus eliminating vibrations unrelated to conformational analysis (35–38).

Nature of Normal Vibrations. The vibrations observed using either infrared or Raman deal with oscillatory movements of nuclei vibrating about their equilibrium positions. This is based on the fact that in the presence of an exciting electromagnetic radiation, electronic and nuclei motions can be considered separately (1) and is generally referred as the Born Oppenheimer approximation (1). Quantum mechanics and associated wavefunctions need be considered in order to analyze the intensity of vibrational transitions. In addition, coupling of vibrations and other second-order effects can only be addressed using quantum mechanical formalisms. The classical picture involving masses and spring constants is the norm, however. In this case, the equilibrium geometry of molecules and polymers is the basis for studies on the optical activity of various infrared or Raman active modes (9,39). Both infrared and typical Raman spectra characterize the absorption of energy from the incident beam by the relative motions of nuclei associated with a polymer.

Vibrations are considered in terms of the classical expressions governing motion of nuclei vibrating about their equilibrium positions with a simple harmonic motion (40). The potential and kinetic potential energies of molecules are defined in terms of the coordinates most appropriate to the molecular structures. All relative motions of atoms about the center of mass (vibrations) are linear combinations of a set of coordinates, known as normal coordinates. For every normal mode of vibration, all coordinates vary periodically with the same frequency and pass through equilibrium simultaneously.

Application of vibrational spectroscopy depends extensively on characteristic vibrations associated with functional groups (5). For composition analysis, the software associated with various spectrometers is capable of searching the extensive reference library to yield the best match for the measured spectra. For more

quantitative analysis of sample composition, changes in chain conformation, or packing, it is often necessary to consider the relative band intensity or bandwidth. A normal coordinate analysis (described below) is helpful in band assignment and interpretation of observed features.

For a nonlinear small molecule of N nuclei, there are $3N$-6 vibrations. The 6 degrees of freedom associated with the overall molecular translations and rotations cannot be considered as vibrations. However, the spectra obtained for polymers are not as complicated as might be imagined considering the extremely high molecular weight of most polymers of interest. In fact, for infinite polymers of well-defined conformation, there are $3N$-4 optically active vibrations, where N now refers to the number of nuclei per translationally equivalent structural unit (8,39,41). In comparison to small molecules, 2 additional vibrational transitions exist because only the rotation about the chain axis can occur without being drawn back toward the equilibrium position. The optical activity of expected vibrations can be analyzed based on the helical chain structure (8,39,41). For polyethylene, the translational equivalent repeat is $-CH_2CH_2-$; N is 6. For polypropylene N is 27, since there are nine atoms per chemical repeat and three units form a translationally equivalent repeat unit. For highly ordered polymers or oligomers, symmetry analysis or group theory is a powerful tool for determining the number of expected vibrations and their optical activities (40). The infrared and Raman spectra obtained for a highly crystalline polyethylene film are shown in Figure 1. Numerous studies have been carried out to elucidate the vibrational features of polyethylene or n-alkanes (42–44). Note that in Figure 1, none of the bands present in the infrared are Raman active. This mutual exclusion reflects the fact that the polyethylene chain conformation has inversion symmetry (1,6,8,45–47).

Most polymer solids contain both crystalline and amorphous regions. The number of vibrations observed is generally higher than expected purely from symmetry considerations of well-defined chain conformation. In polyethylene, for example, by measuring a series of samples containing different degrees of crystallinity, vibrational transitions associated with irregular chain conformations, presumably in the amorphous regions, can be found in the 1300 cm^{-1} region (Fig. 2). Since the structures are irregular, transition assignments cannot be made from symmetry considerations and numerical analysis is required as demonstrated below.

Coupled Oscillator Model. The theory that vibrations couple (such as crystal field splitting in ordered polymers) is generally accepted. Individual chemical repeats may vibrate independent of each other. As polymer spectra do not significantly differ from the constituent monomers, this is the basis for analysis of composition analysis using "fingerprint" features. Information regarding chain conformation, configuration, or packing in the condensed state may reside in the band splitting, band shape or position of the observed vibrations. The degeneracy of the vibrations of functional groups in each chemical repeat may be lifted due to the covalent interconnecting bonds. This strong interaction may introduce additional features expected from consideration of a single monomer unit. The presence of secondary intermolecular interactions may introduce additional features (7). This can be demonstrated most clearly in spectra obtained for an oligomer with well-defined chain conformations arising from the connectivity of the chain of repeat units. These additional spectroscopic features, found in both infrared and

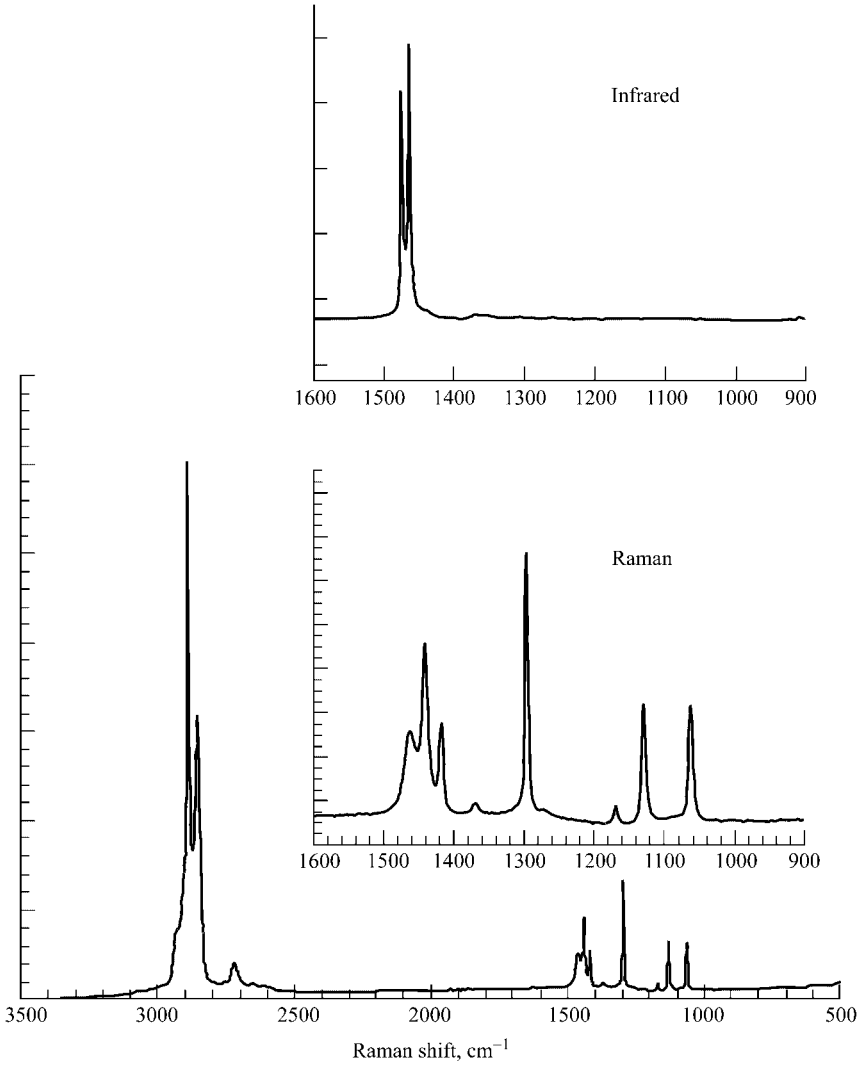

Fig. 1. Infrared and Raman spectra for polyethylene.

Raman spectra of oligomers, have been explained in terms of a coupled oscillator model (42,48). Detailed understanding of the vibrations found for oligomers yields considerable insight into vibrational spectra obtained for polymers.

The idea that vibrations can couple is quite general. For each vibration with frequency ω_0 found for the individual chemical repeat units, a series of vibrations arising from the backbone coupling may shift from the unperturbed value. For a chain with N chemical repeat units or N oscillators, instead of a set of N degenerate vibrations of frequency ω_0, a series or progression of vibrations may exist. Representative infrared and Raman spectra for $C_{20}H_{42}$ are shown in Figure 3. The frequency separation of the progression modes is inversely proportional to the unperturbed frequency ω_0. The localized vibration, such as the CH_2 stretching

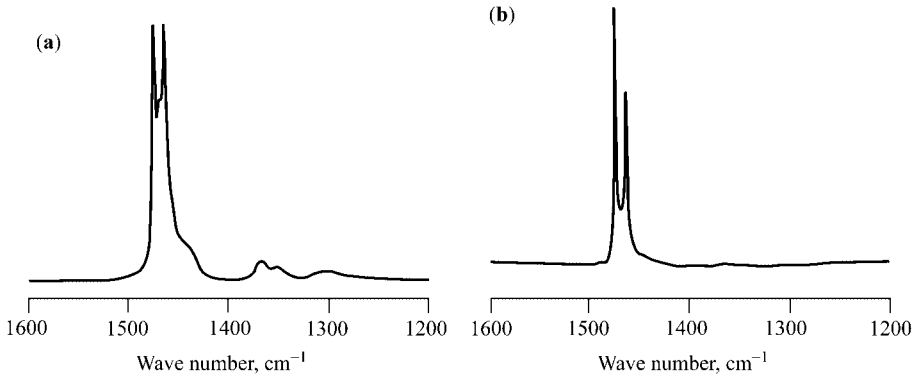

Fig. 2. Amorphous bands found for polyethylene: (**a**) polyethylene film quenched from melt; (**b**) same film after annealing.

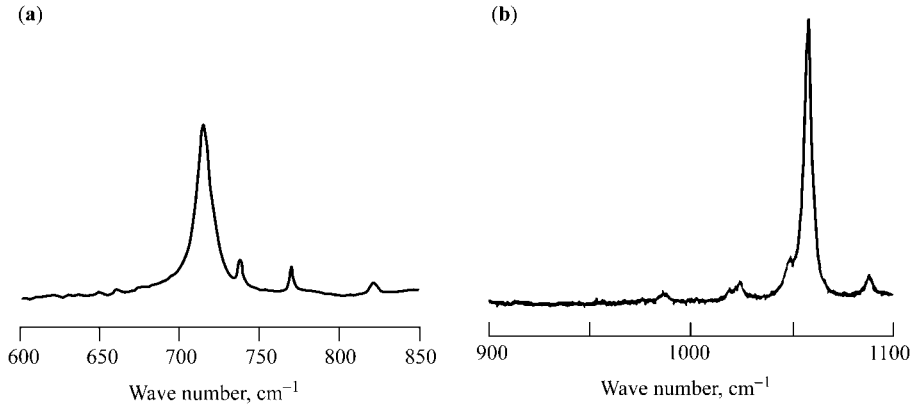

Fig. 3. Progression bands observed for $C_{20}H_{42}$: (**a**) infrared spectrum; (**b**) Raman spectrum.

vibration in the 3000 cm^{-1} region, is hardly perturbed by the interaction along the chain. In contrast, low frequency components such as the CH_2 rocking vibration at 700 cm^{-1}, can be perturbed significantly.

The frequency of individual vibrations can be expressed as

$$\omega_i^2 = \omega_0^2 + \Delta\omega_i^2 \tag{5}$$

where ω_0 is the unperturbed frequency of an oscillator in the chemical repeat. The ω_i is the frequency of the ith mode in the progression. $\Delta\omega_i^2$ is the perturbation dependent on geometric parameters (conformation) and interactions between adjacent units. Seldom is there a need to consider interactions beyond adjacent units. When molecular weight increases, the intensity is concentrated at the unperturbed position with an asymmetric band shape (7). For chains with well-defined conformation, the perturbing effects of coupling are clear and can be analyzed. Spectroscopic features can therefore be used to analyze chain conformation. For disordered structures, the vibrational spectra observed may be complex owing to

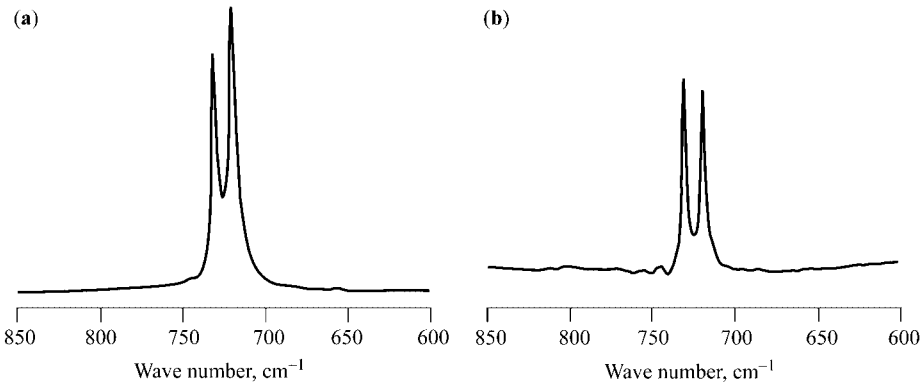

Fig. 4. Crystalline field splitting observed for polyethylene: (**a**) film quenched from melt; (**b**) film annealed at 80°C.

changes in both band frequency and shape. In this case, the vibrational mode can be quite complex because contributions of various internal coordinates to the vibration (character of the vibration) may change significantly as compared to an ordered structure. When understood, changing frequency and character of several vibrations provide tremendous insight into the structure of polymers in solution or melt.

Additional features are observed for highly crystalline polymers. The crystalline structure of polyethylene has been well characterized (45). There are two chains per crystalline unit cell. Just as strong coupling exists between vibrations along the polymer chain, coupling can also occur for equivalent vibrations in the crystalline unit cell. The nonbonded intermolecular coupling between the two chains effectively removes the degeneracy between the equivalent oscillators associated with the chemical units of the two individual chains. Instead of one component near 720 cm^{-1}, a doublet at 721 and 730 cm^{-1} is observed (Fig. 4). The magnitude of the splitting and the relative intensity of the two components depends on the specificity and magnitude of the nonbonded van der Waals interactions between the two chains in the unit cell. In *trans*-1,4-polybutadienes, the splitting, particularly at low temperatures, seen at 240 cm^{-1} is consistent with predictions from theoretical analysis (49). Similar observations have been found for crystalline structures of proteins and model polypeptides. There the hydrogen bonded amide units exhibit well-defined spectroscopic features due to transition dipole coupling (50,51). Similar effects in poly(lactic acid) have recently been observed (52,53). Even the isolated C=O stretching vibration is sufficiently perturbed to have at least three components. In this case, strong dipoles of the ester groups affect both chain conformation and chain packing.

The nature of intermolecular interactions can also be studied by analyzing the frequency and intensity of the external vibrations, or lattice modes, of the unit cell (49,54,55). The coupling of chains can be characterized by the whole chain segment movements which generally occur in the very low frequency region, ie, typically <100 cm^{-1}. These modes are in addition to the internal modes of each chain. The translatory modes can be seen in far-infrared absorption spectra. Fourier transform instruments have improved the signal-to-noise ratio, making

these measurements relatively painless. Since intermolecular interactions can be significantly increased by lowering the measurement temperature, the magnitude of crystal-field splittings may increase substantially and the shape of the lattice modes may narrow with an upward shift in frequency.

With a Raman instrument, measurement of these low lying bands is fairly straightforward. If the elastic Rayleigh scattering can be removed (for example the use of iodine gas filters (56) to selectively absorb the Rayleigh line), very low frequency vibrations in the range of a few cm^{-1} can be observed. Based on the unit cell parameters of polyethylene, a set of Raman active lattice vibrations has been observed for polyethylene and paraffins (57). Rotatory modes are seen in *trans*-1,4-polybutadiene (49). With analysis of these low lying vibrations in a quantitative fashion, a correlation between molecular and macroscopic properties such as heat capacity, thermal pressure, thermal expansion, P–V–T relations, and stress–strain behavior can all be established (58).

Normal Coordinate Analysis. Normal coordinate analysis provides information concerning the nature of vibrations. Accurate assignment is the basis for using characteristic frequencies of various functional groups. Detailed analysis of data obtained by normal coordinate analysis has traditionally been based on the symmetry of the equilibrium structure. The optical activity and characteristics of the normal vibration can be deduced from the constructed symmetry coordinates (9,40). Recent advances in computing have had a tremendous impact on analysis of vibrational spectroscopy. Vibrational modeling of polymers has traditionally involved use of a normal coordinate analysis (NCA) based on Wilson's GF matrices and force constants transferred from small molecules (42). Refinements in force field are often required to better fit the polymer system. Such analyses can only involve the specific chain conformation generated with well-established bond lengths and valence and torsional angles. The first computer programs, introduced in the 1960s, were followed by many variations (42,43,59,60). The generation of structures consistent with helical parameters obtained from diffraction data usually test the structural parameters. Only recently has calculation of vibrational spectra for all possible chain conformations sufficiently large to describe disordered chains become feasible.

A requisite for accurate NCA analyses is availability of a reliable force field. In general, only intramolecular potential energies are needed. The cartesian coordinate is most convenient to define all individual atoms in space. It is, however, most natural to consider the potential energy of the molecule in terms of bond, valence angles, and torsional angles, commonly referred to as internal coordinates. All force constants are defined in this coordinate system. The relationship between the two sets of coordinates is easily established (9). With few exceptions, such as polyethylene and *trans*-1,4-polybutadienes, explicit evidence of optically active intermolecular vibrations is unavailable (49). Therefore, interchain interactions are seldom considered, even though well-defined interatomic potentials can easily be incorporated (54,55). As the number of force constants (both diagonal and off-diagonal coupling) is much larger than the number of observations, few are determined with certainty. In both intra- and intermolecular interactions, the force fields are transferred from those established for small molecules. Among those refined for specific polymers, perhaps the most used are those for n-alkanes and polypeptides (42,43,59–61).

Analysis of disordered structures is of particular interest as these chains lack long-range order and may possess very specific chain conformational distribution depending on the environment. For example, changes in the solvent chain dimension can be monitored using the static light scattering technique. A detailed description of structural changes in this chain and specific interactions between chain and solvent can be accomplished only by use of vibrational spectroscopy.

Polymer conformation is often described using the concept of the rotational isomeric state (62). It is unrealistic to model polymers with randomly oriented bonds. Because of steric interaction of substituent atoms, some relative orientations of adjacent bonds are more favorable than others. The rotational isomeric model encompasses this idea and is generally used to describe polymer chain conformation. For example, the most favorable polyethylene chain conformation is the planar zigzag trans structure (rotational angle = 180°). Less favorable are the gauche and gauche′ states (60 and 240°). For polyethylene, the probability of obtaining the relative orientation of adjacent bonds in these states is much higher than others. An ensemble of chain conformation is most convenient to describe the amorphous structure. Vibrational spectroscopy is one of the few tools available for observation of both crystalline and amorphous structures. It should be noted that the marked increase in computing performance during the past few years has served, over the same time frame, as perhaps a prime impetus for progress of spectroscopy research. Experimental data are complemented by sophisticated calculations. In the past, large and challenging analyses of macromolecular systems were possible only on mainframe computers. The same calculations can be performed today and with greater speed on workstations or personal computers available in virtually every laboratory. With the support of simulation methods, spectroscopic analysis is again among the most useful characterization method of polymers.

Lack of a quantitative definition of disorder is a major obstacle in analysis of spectra from disordered polymeric chains. Rather than analyzing one specific chain conformation for an ordered chain, the analysis requires the vibrational spectrum of a conformational distribution. This problem is complex, even in relatively short-chain molecules. An extremely large number of possible conformers exist, each with a unique spectrum often only slightly different from another. The isotropic Raman spectrum for the disordered state was simulated as a composite of contributions from the ensemble of chains generated by a Monte Carlo procedure that assigned both a conformation and a total probability for each chain. The spectrum of each conformation is calculated from force constant and intensity data transferred from smaller molecules. These individual spectra are then weighted by their probabilities and combined into a composite spectrum. With a surprisingly small number of structural and intensity parameters (additivity in bond polarizability is always assumed), it is possible to accurately reproduce experimental infrared and Raman spectra of some *n*-alkanes (36). The same method has been applied to more complicated polymers lacking long-range order. The original code was designed for polymers with identical skeletal bonds. Subsequent program modifications were introduced to allow nonequivalent bonds along the chain (38,63). Disordered chains may include configurational defects. Generation of chains containing specific defect content is not as difficult as first envisioned. Flory developed methods for determining the probability of finding specific conformers along the

chain. These are incorporated into the programs. Polymeric chains containing both conformational and configurational defects can now be analyzed with confidence (64,65). In practice, rather large numbers (>2000) of finite chains are considered.

Structural Characterization

The use of vibrational spectroscopy to identify molecular functional groups of polymers has been historically successful. New types of problems and specific requirements demand that vibrational spectroscopy move beyond composition analysis to specific areas such as surface characterization, imaging at specific areas of interest, kinetics of phase transformation, and others. The examples presented below demonstrate the developments in the most basic structural characterization.

Chain Configuration. Infrared spectroscopy has many fingerprint bands characteristic of functional groups. Extensive collections of spectra have been published. In addition, libraries and efficient search routines can match experimental data to those in the collection and identify those present. Raman spectroscopy, unlike the infrared technique, has not been extensively utilized for composition analysis. For many functional groups, Raman scattering can, in fact, make composition analysis a relatively easy task. For example, cis–trans structures of polybutadienes, vinyl C=C stretching, compounds containing sulfurs, and perchlorates, all exhibit strong, easily identified Raman bands for analysis. Aromatic units typically exhibit strong Raman scattering.

Unique applications employ both types of spectroscopies for structural analysis. The complementary nature of infrared and Raman effects can be seen in the structure determination of 1:1 hexafluoroisobutylene and vinylidene fluoride copolymer. This problem is virtually impossible to solve with other techniques. The two monomers can be linked in two ways during polymerization, by formation of head-to-tail (normal linking) or head-to-head linkages. By comparing infrared and Raman spectroscopic data, it was concluded that the polymers formed are indeed alternating in nature (66). It was additionally concluded that only head-to-tail linkages were observed. The proposed chemical structure is shown below.

$$-(C(CF_3)_2CH_2CF_2CH_2)_n-$$

The CH_2 units are decoupled by the presence of a rather bulky CF_2 unit between them. If the copolymers were formed in a head-to-head linkage, considerable coupling of the stretching vibrations would be expected. In fact, in both infrared and Raman spectra, the CH_2 symmetric and antisymmetric vibrations were observed at 3040 and 2985 cm^{-1}. This coincidence provides proof that high frequency CH_2 vibrations are decoupled and thus degenerate. If the polymer were formed in a head-to-head linkage, mutual exclusion would be expected, contrary to observation. Similar configurational analysis can be extended to other polymers formed with substituted monomers.

Because of significant advances in catalyst design (67), synthesis of highly ordered polyolefins with fewer defects and improved control of defect distribution has become possible. These advances in chemistry have raised an even greater interest

in the study of polyolefin structure and development of more diverse applications. In a head–tail alternating copolymer, the possibility exists that a head–head or tail–tail defect linkage can occur. Specific spectroscopic features have been identified for analysis of chain–chain configuration in syndiotactic polypropylenes (sPPs) containing varying racemic content (37). The earliest method for characterization of sPP configuration was, in fact, infrared spectroscopy. That study suggested a structural parameter referred to as "syndiotacticity index" (68,69). Raman features sensitive to tacticity distribution were subsequently found. The Raman active skeletal bending modes in the 300–400 cm^{-1} region (Fig. 5) were sufficiently sensitive to differentiate between racemic and meso sequences for characterization of the overall chain configuration (37,70). Based on theoretical normal coordinate analysis, the syndiotacticity content of imperfect polypropylenes can be directly measured using the relative intensity of Raman active bands in the 300 and 400 cm^{-1} region (Fig. 5). The syndiotacticity index, which provides a fast and extremely easy parameter for determination of chain configuration, is shown in Figure 6. It was also demonstrated that those bands are sensitive to differences in chain configuration and insensitive to chain conformation (64).

Chain Conformation—Ordered. For sPP, the number of seemingly stable chain conformations and packing is intriguing. The relative volume fraction of each state is highly dependent on thermal history, time, processing, and, in many cases, type and number of configurational defects. At least three different crystalline forms are associated with sPP. The helical form I, with ggtt chain conformation, is the most common (71,72). Form II with an all-trans sequence can be obtained by quenching the polymer from the melt, followed by stretching (72). Form III, with conformational features of both forms I and II, has also been suggested. This form appears to have the conformation $(g_2t_2g_2t_6)_n$ (73–75). It was recently found that the planar zigzag structure forms spontaneously over an extended length of time by quenching from melt into ice water and storing at or below 0°C (76,77). Form III has also been observed when a drawn sample of form II is exposed to benzene, toluene, or xylene vapor (73,74). Both forms II and III are stable at room temperature, and then revert to form I spontaneously with heating.

Raman spectra obtained from polypropylenes of different conformational distributions can be simulated accurately (37). Identification of specific features such as those centered at 800 and 400 cm^{-1} enabled understanding of the change of polypropylene from a completely disordered state to a more ordered state or states including crystallization. Although the bands found in the 800 cm^{-1} region (Fig. 7) are generally referred to as regularity bands, they have only recently been accurately assigned (37). The bands at approximately 826 and 845 are suggested to be associated with form I and the amorphous chains, respectively (70,78). Based on simulation results, the 830 cm^{-1} band can only be associated with long helical ggtt chain conformations. All extremely short helical segments situated between either conformational or configurational defects contribute to the intensity in the middle 845 cm^{-1} region. The broad band at 845 cm^{-1} is the dominant feature of a polypropylene melt. With increasing configurational disorder, the 826 and 865 cm^{-1} bands decrease in intensity relative to the 845 cm^{-1} peak. The high frequency component is then assigned to an all-trans structure of fairly long length. Based on these experimental and simulated Raman features, it is possible to deduce that sPP crystallizes into a helical structure at crystallization temperatures

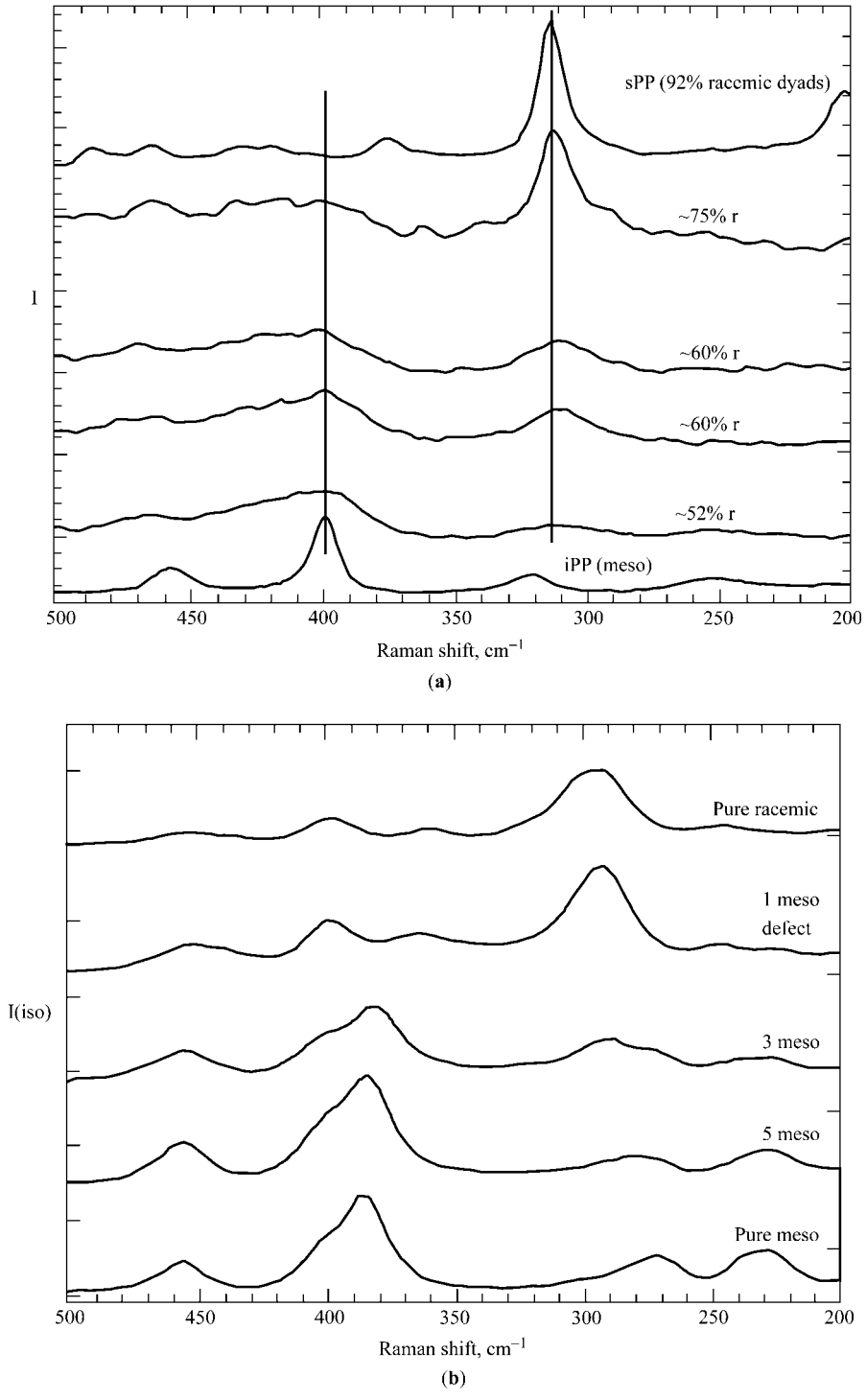

Fig. 5. Fourier transform Raman spectra of various syndiotactic polypropylenes with known configurational defects: (**a**) experimental; (**b**) theoretical.

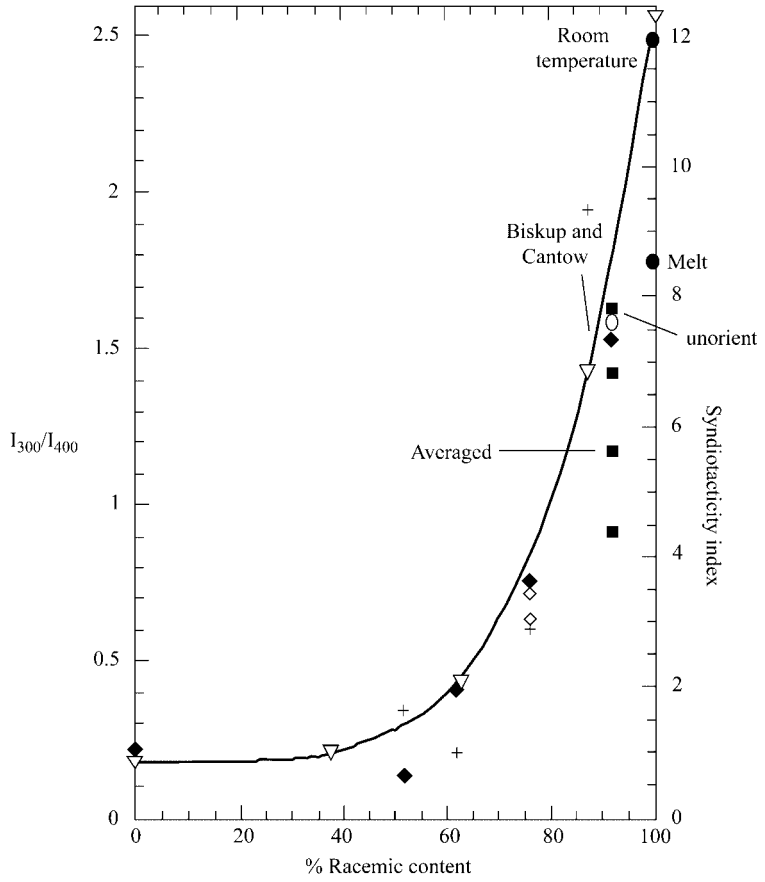

Fig. 6. Syndiotacticity index for syndiotactic polypropylene developed based on the relative intensity of the Raman active 300 and 400 cm^{-1} bands. ♦ Solid; ■ trans SPP–orinted; ◇ 75% racemic–aging time; ● Flory RIS calculations; ○ spp melt; —▽— calculated curve; + syndiotacticity index.

above 0°C (Fig. 7). Conversely, for sPP crystallized at temperatures below 0°C, only all-trans structures are formed. Raman data are clear regarding the structures formed (37,64). The mechanisms responsible for such behavior are still unavailable.

Vibrational spectroscopy can also determine chain packing and associated structural transitions in semicrystalline polymer solids. As mentioned above, intermolecular vibrations, lattice modes characteristic of whole chain segment movements, or delocalized skeletal modes of fully ordered crystalline states, are found in the low frequency region (49,54,55). For polymers with a well-defined crystalline state, the lattice modes are extremely sensitive to changes in the magnitude and specificity of intermolecular interactions (49). For highly crystalline *trans*-1,4-polybutadiene, the vibrations, which were observed below 200 cm^{-1} in the infrared and Raman spectra, can all be assigned to lattice modes (Fig. 8) (49). This is indicated not only by the fact that the single-chain calculation predicts no modes below 200 cm^{-1} (49,79), but also by temperature dependence. When

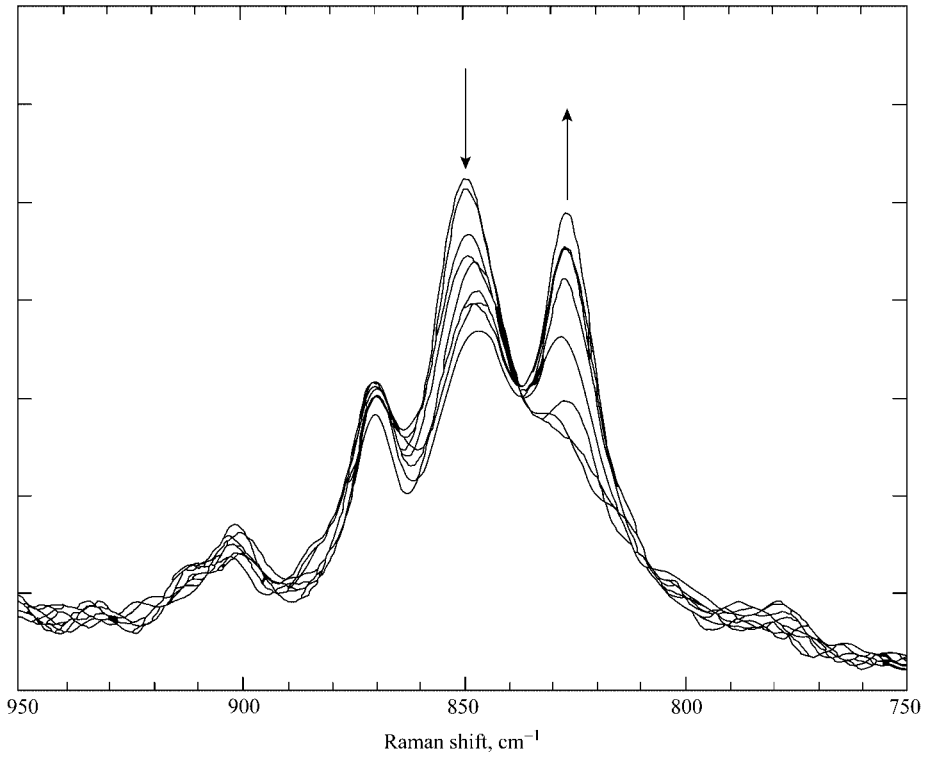

Fig. 7. Raman spectra obtained for syndiotactic polypropylene as a function of time at room temperature. The initial sample is obtained by quenching a molten sample into liquid nitrogen.

the temperature is lowered, the four Raman bands at 48, 70, 104, and 118 cm^{-1} all exhibit large shifts to higher frequencies. This is characteristic of interchain modes, since intermolecular interactions increase in magnitude as the distances diminish in the contracted unit cell. Crystal field splittings should also increase under these circumstances, as seen for the bands near 240 cm^{-1}. In addition, if the TPBD (*trans*-1,4-polybutadiene) sample is heated beyond the crystal phase transition, the four Raman bands disappear. This is as expected, since not only do distances between chains increase but torsional oscillations within the chain increase. Both features diminish the magnitude and specificity of interchain interactions. Several studies have used TPBD as a model to investigate intermolecular forces and their influence on chain conformation. By incorporating intermolecular atom–atom interactions derived by other characterization techniques, these lattice modes and crystal field effects are all satisfactorily accounted for (49,79). By studying TPBD in the highly crystalline state as well as in single crystals, bands associated with noncrystalline conformations were also assigned.

Chain Conformation—Disordered. An area of current interest is application of vibrational spectroscopy, particularly Raman, for analysis of disordered chains which may include polymers in solution, melt, or the solid state. These chains lack long-range order but may contain short ordered sequences. In addition, these disordered chains may adopt a specific conformational distribution,

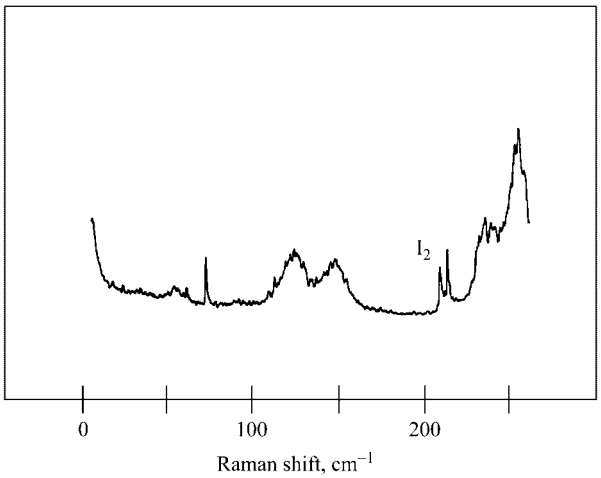

Fig. 8. Low frequency Raman spectrum of TPBD at 110 K, using an iodine absorption cell. Bandpass, 3 cm^{-1}, laser power, 150 mW at 5145.42 Å.

depending on geometric constraints such as surfaces or interfaces. Other constraints may include the presence of junctions such as in networks. Long-range electrostatic forces along the chain may reasonably be expected to further perturb the structure. Polyelectrolytes (qv) or polymeric electrolytes are such examples. Many characterization techniques are capable of measuring ordered structure. Few, however, match the capability of vibrational spectroscopy to quantitatively describe disordered chains. The frequency and relative intensity of observed vibrational bands are dependent on the relative concentration of specific localized structures. For samples involving well-defined structures and dependable band assignments, the method works well. However, when a broad distribution of a large variety of conformations is involved, the method is difficult to apply with confidence. The bands of disordered structures are broad, weak, and often overlap. Vibrational spectroscopy, particularly Raman, is ideal for studies involving disordered structures as polarizability changes associated with different carbon–carbon backbone conformations are directly reflected in the obtained spectra. Because it is a scattering phenomena associated with a tensor, the depolarized data still contain considerable structural information for samples of partial disorder or even in melt or solution.

Based on relative intensity and, particularly, bandshape of skeletal bands, it has become possible to obtain the relative energy difference between various rotational isomeric states. In the first study of this type, Snyder and co-workers analyzed low frequency (0–600 cm^{-1}) Raman spectra of *n*-alkanes in the liquid state (35). The method was subsequently applied to analysis of the low frequency Raman spectrum of molten state isotactic polypropylene. The vibrational spectroscopic analysis was successfully used to differentiate the correct model governing the chain (80) and has been extended to analysis of higher frequency vibrations (0–1500 cm^{-1}) of liquid *n*-alkanes (36).

The utility of Raman spectroscopy has proven useful in the study of poly(ethylene oxide) (PEO) in both aqueous solutions and molten states (38). The

structures of this family of polymers, either homopolymer or part of a copolymer, determine properties in numerous applications including thermoelastomers (81–83), polymeric electrolytes (84–87), and surfactants. Steric considerations alone suggest that the minimum energy conformer is all trans, designated ttt, in a notation that successively references backbone O—C, C—C and C—O bonds. However, the most stable conformation in the crystal includes a gauche conformation and is designated tgt (62). Since the conformation present in the crystal must be the result of the interaction of a number of factors, there is no way to use the crystal structure to predict with certainty the dominant conformation present in the melt or solution.

Chain structure departs from tgt and changes to ttt when PEO is blended with poly(methyl methacrylate) (88). The structure of adsorbed PEO chains in the air–solution interface was found to be very different from the disordered structure expected for the solution state (89–91). In fact, the vibrational bands for these adsorbed chains have characteristics similar to those in the crystalline state (90). Various theoretical studies have led to quite different results for chain conformations of PEO (62,92–98). Because of differences in the local dielectric environment, different sets of rotational isomeric states need be considered.

Several liquid systems of PEO, both molten state and solution, have been investigated using vibrational spectroscopy (99). The Raman spectrum of PEO in the melt as well as chloroform and aqueous solutions reveal that the conformations in an aqueous solution retain the tgt conformation that occurs in the crystalline solid. The Raman spectrum of the chloroform solution, however, more closely resembles that of the melt. The conformational distribution was not deducible due to uncertainty in band assignments.

The isotropic Raman spectra of PEO in the melt and aqueous solution shown in Figure 9 suggest new indicators for characterizing conformational distribution. Considerable differences are evident in band shape for the 850 cm^{-1} band and the region near 365 cm^{-1} (38). Although insignificant in the normal Raman spectrum, the shape and position of features in these two regions differ substantially in the isotropic spectrum. The strong bands in the 850 cm^{-1} region are almost mirror images in the two experiments (Fig. 9). The most intense feature in the 800 cm^{-1} region for the aqueous solution is located at 880 cm^{-1}. In contrast, the intense feature for the melt centers at 830 cm^{-1}. The shapes of the skeletal deformation in the 200 cm^{-1} region are also quite different in frequency and shape. These are to be correlated with differences in conformational distributions in the melt and aqueous solution of PEO (Fig. 9).

The relationship between the global chain conformation for polyelectrolytes, in terms of a persistence length and excluded volume parameter to chain conformation described by a rotational isomeric state model, is untested. Vibrational spectroscopy can partially close the gap by measuring conformational changes as chain stiffness is varied. Most previous solution characterizations of polyelectrolytes employed methods such as viscometry and light scattering which provide only global structural information. These studies were interpreted to show that chain stiffness increases with ionization. It has been suggested that in the extreme case the chain is fully extended. Polarized Raman spectroscopy is ideally suited to address issues of local structure and thus complement previous work (33,34). Information provided by polarization studies, which are sensitive to

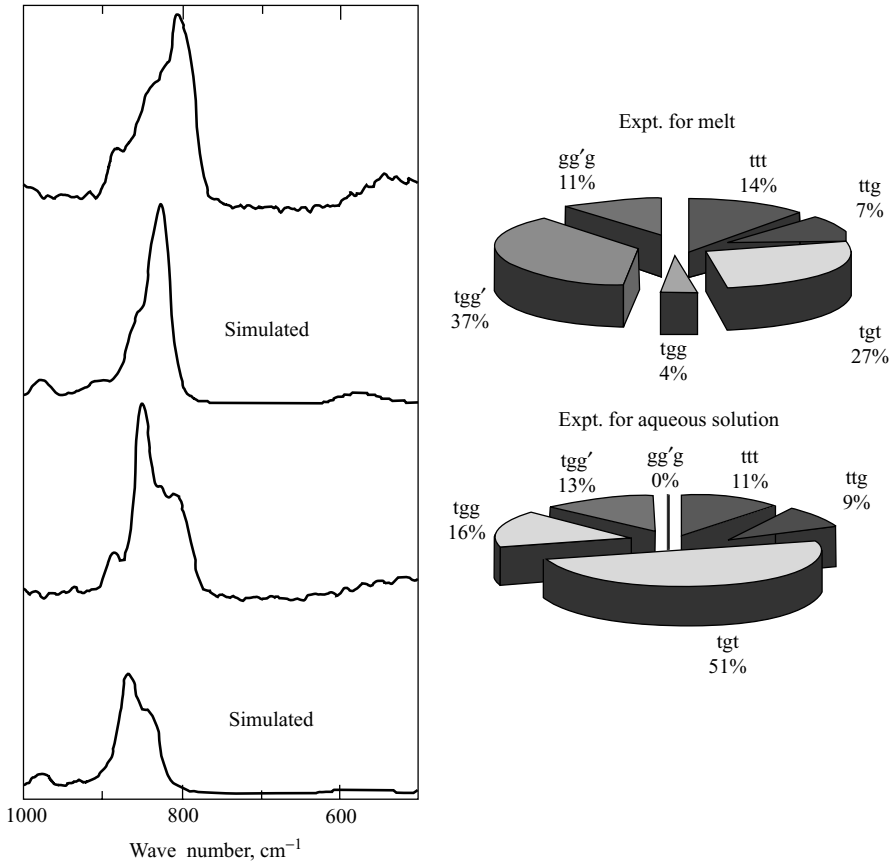

Fig. 9. Simulated and observed isotropic Raman spectra of poly(ethylene oxide). Different conformational distributions for melt and aqueous solution are described in text.

changes in conformational distribution, ie changes in the distribution of torsional angles among the various rotational states permitted in a vinyl chain backbone, can yield substantial structural information. Similar approaches have been pursued to study conformational changes in neutral polymer solutions, for example to identify the θ condition or quantify the enthalpy or entropy of helix formation (28–32). A direct calculation of the persistence length from depolarization data has been hampered by the absence of polarizability derivative values for different conformations, even in small molecules. Other studies (100,101) make it possible, in conjunction with a simplified form of the rotational isomeric state model, to calculate the persistence length using the CH stretching depolarization ratio of poly(acrylic acid) (PAA) (33,34).

Several interesting aspects of ionized structure were revealed by the Raman study (33,34). Based on polarization data, the ΔE, C_∞, and L_t values can be calculated from the depolarization data. The energy difference between isomers grows by a surprisingly low value of approximately 8% as compared to the initial value of 6155 J/mol (1471 cal/mol) for the unionized polymer to 6627 J/mol

(1584 cal/mol) for the fully ionized sample. In comparison, the energy change between the same isomers is 600 cal/mol for polyethylene at room temperature and reportedly 1100–2300 cal/mol for polytetrafluoroethylene (62). The small change in conformer energy upon PAA ionization indicates that the polymer does not stiffen appreciably upon ionization in a salt-free, semidilute solution. The lengths calculated from spectroscopic data fall within the range of persistence lengths determined via small-angle X-ray scattering (SAXS) (102). Such analysis demonstrates the potential for the Raman technique to contribute to the understanding of the interplay of local and nonlocal polyelectrolyte forces.

Analysis of Structural Unit-Size. The strength of vibrational spectroscopy lies in its ability to characterize chemical composition and localized structure of polymers. The observation of the intense longitudinal acoustic mode (LAM) in the extremely low frequency region ($<50\ cm^{-1}$) of the Raman spectra of semicrystalline polymers provides a very different morphological tool for measurement of structural subunits in the order of several hundreds of angstroms.

The earliest observation of a Raman active fundamental mode in *n*-paraffins was made in 1949 (103). The characteristics of this vibration are its extremely strong intensity and the fact that the observed frequency is inversely proportional to the straight chain segment length. This mode was hypothesized to be related to the longitudinal acoustic vibration along the backbone of the entire chain segment. The frequency of vibrations is then related by the expression shown below.

$$\nu = \frac{m}{2cL}\sqrt{\frac{E}{\rho}} \tag{6}$$

where m is the order of the mode (only odd modes are Raman active), c is the speed of light, L is the straight chain segment, E is Young' modulus, and ρ is the single chain density. The origin of this mode was explained by use of dispersion curves calculated for an infinite planar zigzag chain (104).

The first observation of such a vibration in polyethylene single crystals was seen some years later (56). A direct relationship was found between the central frequency of the observed mode and the long period in SAXS. The assumption is that the straight chain segment is the segment within the crystalline region or corresponds to the lamella thickness. It should be emphasized that these two techniques are extremely different in origin. The long period measured by SAXS measures the distance and how individual lamellae stack relative to each other. Thus the measured long period includes the contribution from the amorphous regions. The Raman technique measures the straight chain segment in the lamellae independent of the degree of tilt.

Despite numerous studies, the observation of LAM in other polymers proved elusive for quite some time (105,106). For isotactic polypropylene, LAM was not obtained until ~25 years after the initial observation. The first LAM observation was for an isotactic polypropylene prepared under special conditions of extrusion and orientation (107). Both sample transparency and the preferential reduction in Rayleigh scattering made the observation possible (Fig. 10). LAM has now been observed in a number of polymer systems such as PTFE, polyoxymethylene, PEO,

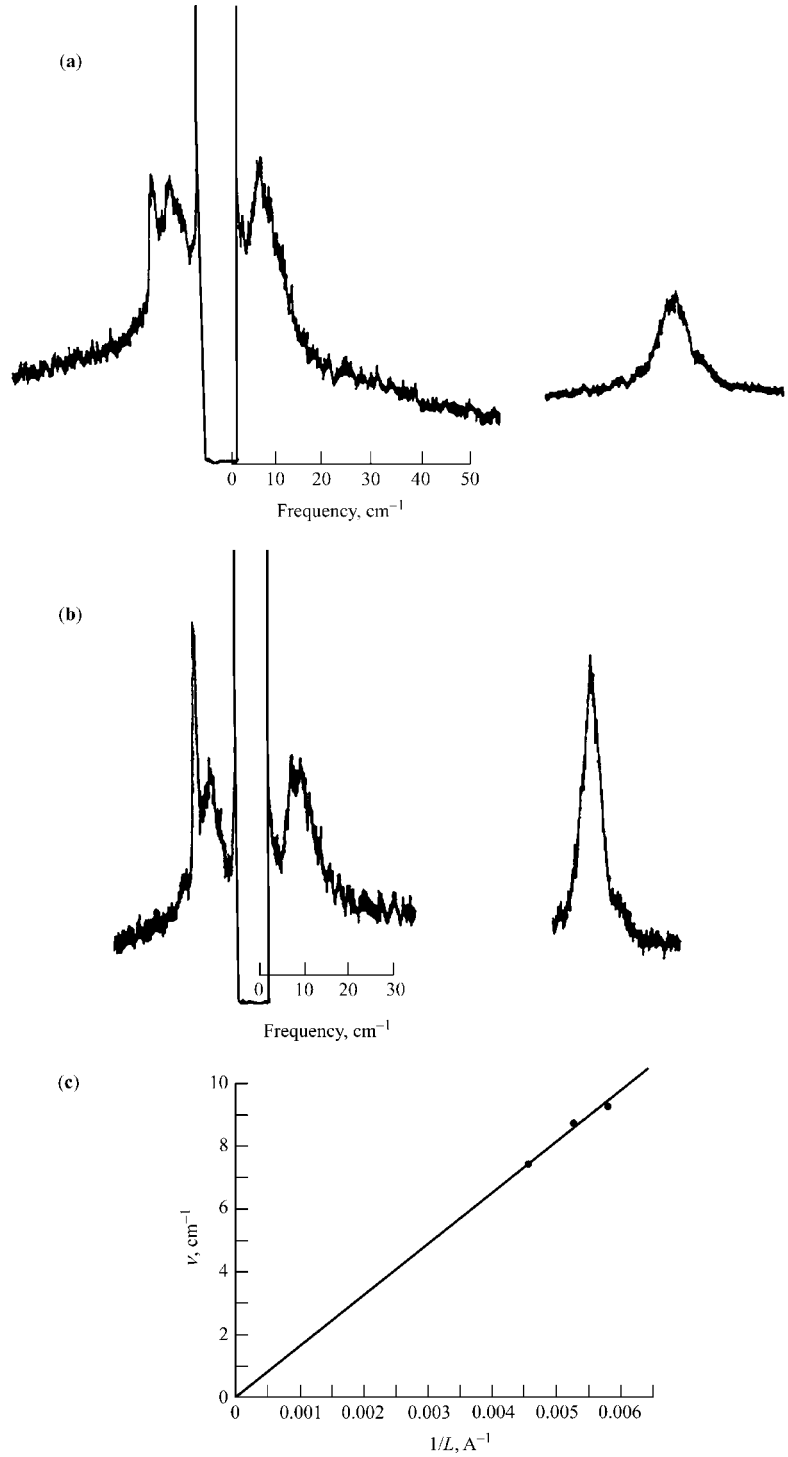

Fig. 10. Characteristics of the LAM found in highly oriented transparent isotactic polypropylene (**a**) at 300 K and (**b**) at 110 K; band at right is at 398 cm^{-1}; (**c**) plot of Raman frequency versus $L - 1$ (L is the Bragg spacing of the X-ray small-angle maximum).

and linear aliphatic polyesters (108–116). LAM has also recently been observed in a biodegradable thermoplastic, poly(β-hydroxybutyrate) (PHB) (117). This LAM observation is especially intriguing since the chemical structure and the equilibrium conformation of PHB differ significantly from those of all polymers known to exhibit LAM bands.

The fact that LAM is not easily found in other polymers can be explained by the fact that force as well as mass perturbations along the chain may lead to coupling of transverse and longitudinal motions (115). The effect of "perturbing" influences within chains such as methyl side-group placement on *n*-alkanes (118), double bond placement in *trans*-alkanes (119) and hydrogen bonds (120) has been studied and shown to affect this mode to varying degrees of intensity and frequency. A LAM-like vibration was also observed for these linear aliphatic polyesters (114–116). Based on a series of normal vibrational analyses, the masses placed off the main chain act as unbalanced mass units, which leads to the presence of several LAM-like modes, each with differing amounts of transverse and longitudinal character (115). With increased structural complexity, these structural perturbations may become more significant, leading eventually to the total disruption of any longitudinal acoustic mode. The presence of an amorphous or loosely folded layer of material at the lamellae surface has also been analyzed in terms of effective frequency and intensity (107,111,121–124).

The effects of intermolecular interactions are interesting to analyze. The earliest studies definitely established that the LAM of a planar zigzag chain conformation is a single chain phenomenon. Because of the planar zigzag structure, LAM in polymethylene systems is necessarily confined to the plane containing the skeletal backbone. The LAM is essentially independent of intermolecular interactions. Previous normal coordinate analysis of crystalline PEO has shown that, in contrast to all-trans polyethylene chains, LAM in helical chains has a significant interchain effect due to the large radial component present in the atomic displacement of LAM for such polymers (113). Unlike the planar symmetry case, the deformation of a helix must necessarily involve winding and unwinding of the entire chain segment. The temperature dependence of the frequency change observed as a function of temperature suggests that the influence of intermolecular interactions may be more important for helical chains of low modulus than those (such as polyethylene) of high modulus.

As mentioned previously, by using relation 6, the single chain elastic modulus within a crystalline lamella for various polymers can be calculated from the slope of the line fitted to the plot of ν versus $1/L$. This estimation requires the single chain density generally obtained from unit cell parameters. For example, the modulus for polyethylene is found to be 300 GPa (124). The fact that the upper limit of the modulus along the chain direction can be measured is particularly valuable when an estimation of processing efficiency is required.

The utility for use of LAM as a morphological technique stems from its ability to provide a different method to measure straight chain segment length. The X-ray technique is clearly sensitive to long-range order. The Raman technique is sensitive to short-range order or disorder. Thus the Raman technique provides very different morphological information by providing the straight chain segment distribution associated with crystalline regions. The central peak position may be related to the most probable chain length. The bandwidth of LAM can be related to the chain length distribution and may yield a chain length distribution when no

other technique is available. The conversion from the frequency space to the chain segment length space (weak broad LAM) may, however, require special attention (125).

Chain folding is perhaps one of the most fundamental concepts associated with polymer crystallization for semicrystalline polymers. From the kinetic theory of crystallization, the lamellar thickness is known to depend on the degree of supercooling (126). The nature of chain folds and end groups may greatly influence the lamellar thickness and folding scheme in formation of morphological subunits. DSC, wide-angle X-ray diffraction scattering, electron microscopy, and vibrational spectroscopy have been used to characterize many facets of the crystalline portion of semicrystalline polymers. LAM exhibits particular advantages in characterization of morphological features. For example, the integer fold scheme in PEO supports the idea first proposed based on X-ray data (127). This scheme indicates that the chain ends are not located within the crystalline lamellae but are rejected into the amorphous layers separating the crystals (127). All stems of a molecule are of the same length with chain ends located at the lamellar surfaces. Subsequent LAM studies of PEO, together with DSC and SAXS data, suggest the existence of lamellae containing a mixture of integer folded structures as well as lamellae composed of chains with simple fractional-integer folds (Fig. 11) (112). Such complex folding schemes are also indicated by results on ultralong *n*-paraffins (112). In this case, Raman contributes to a better understanding of a fundamental aspect of polymer structure.

Annealing of semicrystalline polymers is a difficult process to understand. Both microscopic and macroscopic defects are reduced upon sample exposure to temperatures somewhat below the crystalline temperature. Polymer crystals are metastable, ie the lamellae thickness and lateral size are generally determined by the degree of supercooling balanced by the side and end free energies. Therefore, as a function of time, chain-folded polymer crystals thicken on annealing to minimize the number of folds. Although the exact mechanism has yet to be determined

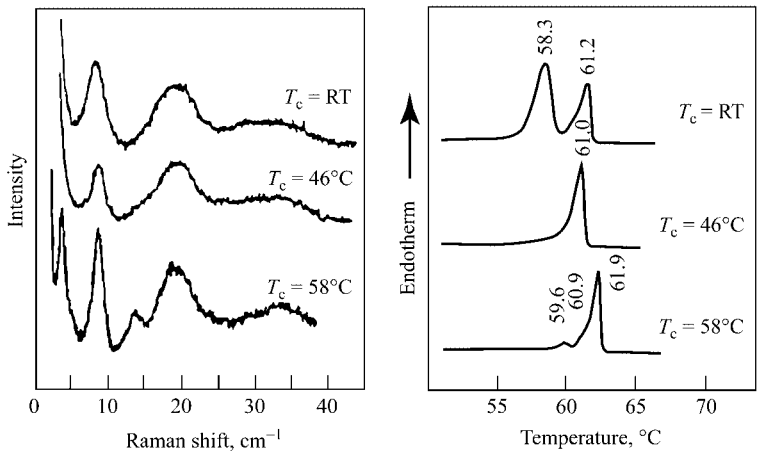

Fig. 11. (**a**) Low frequency Raman spectra and (**b**) DSC melting curves of PEO 3000 crystallized at different crystallization temperatures (T_c) (112).

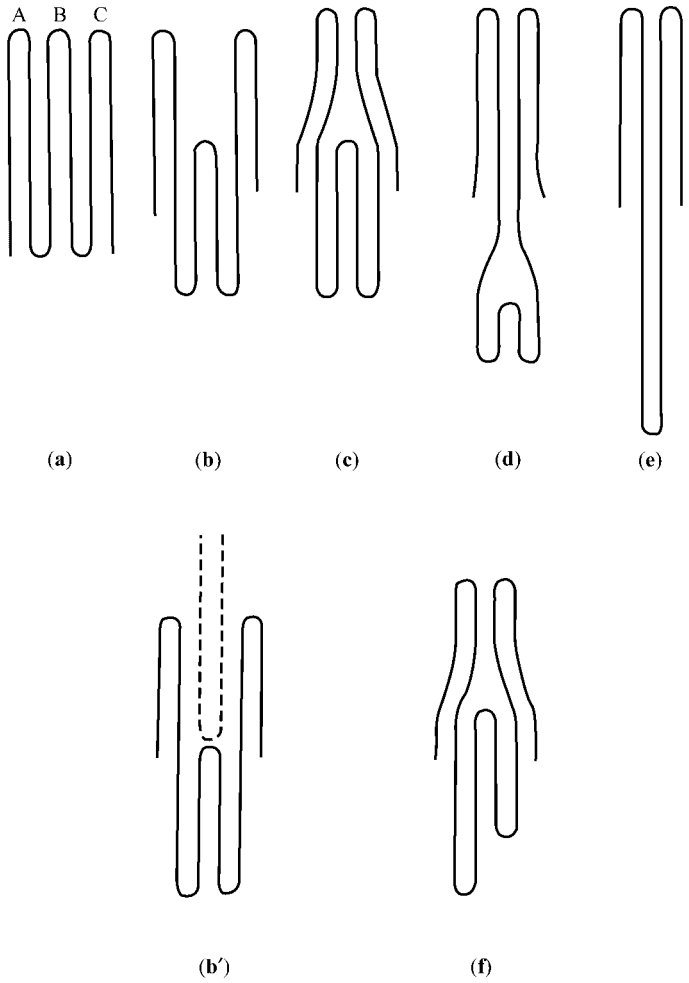

Fig. 12. Schematic representation of various stages of the fold length increase to a doubled fold length by the Dreyfus scheme as described in the text (129).

(128–131), one is shown in Figure 12. Traditionally thermal analysis can be used to follow changes in melting temperature when crystal volume increases. SAXS can be used to measure the long period when crystalline lamellae thicken. Density increases for annealed samples can also be measured. The utility of LAM in this area of study has proven particularly invaluable.

The most detailed study to characterize changes in segment length distribution (Fig. 13) employed the LAM technique (132). Unannealed samples had a most probable chain length of 100 Å with a distribution of less than 20 Å. Samples annealed for a longtime approach the well-defined chain length distribution of the initial material. The measured distributions as a function of time and temperature are extremely interesting in that they are quite asymmetric. For the annealed sample, the band is asymmetric and more intense on the low frequency side of the band maximum. After the sample was annealed at 120°C, the asymmetry was

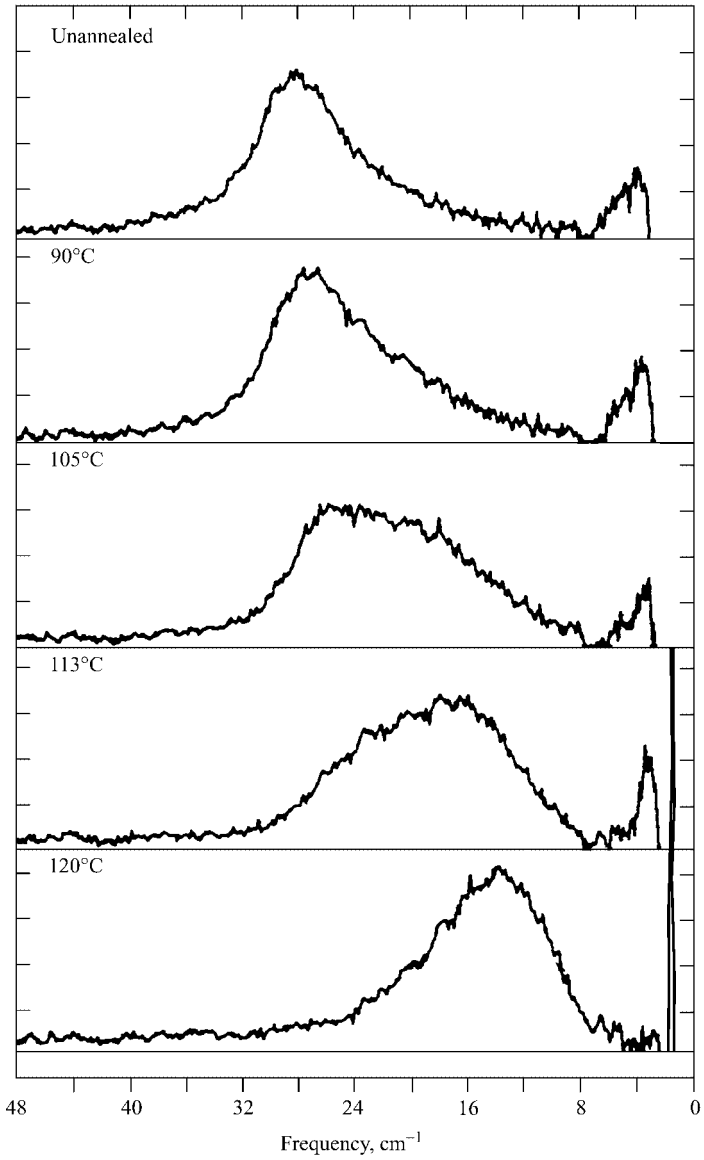

Fig. 13. Low frequency Raman spectra of polyethylene single crystal at 28°C after annealing at successively higher temperatures. Annealing time at each temperature was 6 h (132).

reversed so that the band became more intense on the high frequency side. Bands associated with intermediate annealing temperatures appear to have shoulders. They do not, however, appear to be consistent with the predictions of the model proposed earlier (129).

Because of the strong dipole–dipole interactions, one would expect that the formation and subsequent changes in polyester crystals would be different from polyethylene and possess some characteristics of nylons. LAM observed for various

as-crystallized and annealed linear aliphatic polyesters exhibits a fairly complex pattern. In linear aliphatic polyesters, the changes in Raman or SAXS are highly dependent on temperature and annealing time. In addition, for samples annealed at lower temperature (50°C), there can be changes in either Raman frequency or in periodicity measured by SAXS. Both need not change simultaneously. For long annealing time these data can also be described by a straight line function independent of initial crystallization temperatures. This observation illustrates the complementary nature of the Raman and small-angle X-ray techniques. The differences revealed may be important in structural studies of polyester single crystals.

A number of flexible polymers have been solid-state extruded or drawn to form ultraoriented, high modulus fibers. Information obtained from X-ray scattering, electron microscopy, vibrational spectroscopy, and calorimetric measurements has been used to form structural models, each differing in the description of crystallite size and connectivity. The deformation process involving measurement of LAM positions at various points of drawn polyethylene has been carried out (26,27,133–135). It was particularly interesting to examine the effect of temperature and draw ratio on chain orientation and extended chain length distribution during extrusion by removing a partly extruded billet and examining points within the die region and along the extruded fiber, thereby revealing various stages of deformation (26,27).

Structure analysis based on LAM is quite instructive regarding stability of highly deformed materials. As mentioned above, the most probable chain length and half-width in chain distribution have been established for a series of annealed polyethylenes. Among the most interesting observations for highly deformed materials is that the LAM bands exhibit considerable departure from the relationship found for annealed single crystals of polyethylene. It should be noted that the departure occurs only for samples extruded at low temperatures (Fig. 14). Samples extruded at 130°C follow the same trend as annealed single crystals. Although there is no fundamental reason to relate the half-width, $L_{1/2}$ to L_{MAX}, there appears to be a relationship that occurs for particular processing methods or history (26,27). The reduced half-width $L_{1/2}$ is a useful quantity showing obvious differences in various polyethylene structures. The degree of chain mobility is an important factor in removing structural defects introduced during mechanical deformation. For samples extruded at low temperature, limited chain mobility exists. For samples extruded at high temperature, more defects disappear, forming highly ordered structures which are dimensionally stable. The annealed polyethylene single crystals approach equilibrium and therefore contain fewer structural defects, resulting in smaller $L_{1/2}$ values.

Low Frequency Observations for Amorphous Polymers. Many amorphous materials studied by Raman exhibit an extremely broad band in the low frequency region. This is true for polycarbonate, poly(methyl methacrylate), and polystyrene (58). Low frequency Raman bands can potentially provide much information regarding the density of states (directly related to the intensity distribution of the broad Raman active band) as well as anomalous behavior observed for the specific heat (58). Often the separation of main-chain and side-chain bands is important in modeling of specific heat, making careful band assignment extremely meaningful (136,137). This separation is analogous to inclusion of optical

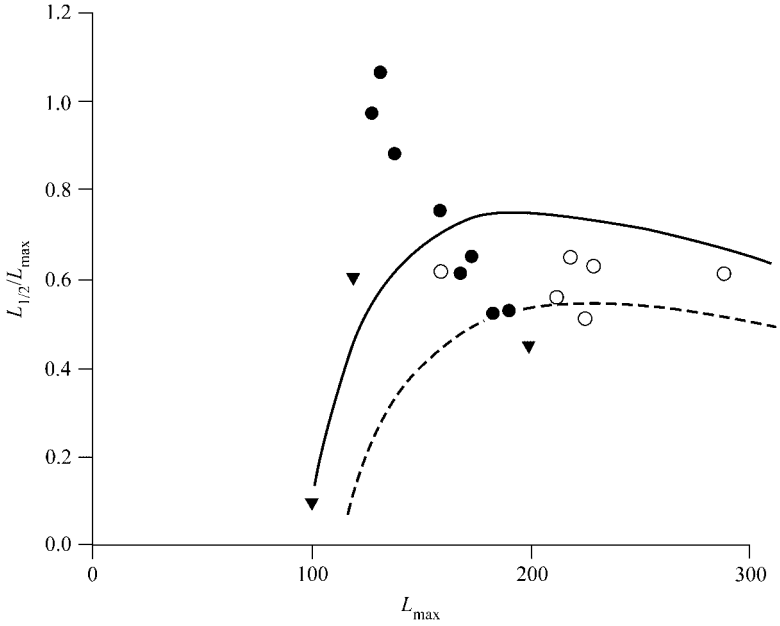

Fig. 14. Relationship for $\Delta L_{1/2}$ and L_{MAX} in variously prepared polyethylene; (●) 80°C sample; (○) 130°C sample; (▼) annealed single crystals (26,27). The solid lines refer to changes observed for annealed single crystals (132).

and acoustic transitions to specific heat calculations (138). The low frequency region is expected to contain both intrachain skeletal bending modes and interchain lattice modes.

The low frequency Raman spectrum can provide information on the density of states $g(\omega)$ in the low frequency region. In the quasi-harmonic approximation the specific heat is given by

$$C_V = k\int_{\omega_{min}}^{\omega_{max}} g(\omega)\left(\frac{\hbar\omega}{kT}\right)\frac{e^{-\hbar\omega/kT}}{(e^{-\hbar\omega/kT}-1)^2}\,d\omega \tag{7}$$

and the scattering intensity is related to the density of states by the following expression:

$$\frac{I}{\omega^2} \propto \sum_i g_i(\omega) \tag{8}$$

Thus the scattered low frequency intensity can be directly related to the specific heat calculation. Such calculations have been carried out satisfactorily for amorphous polycarbonate (58).

These low lying vibrations can be used to examine intermolecular interactions and associated steric hindrance to intrachain motions and thus provide information regarding free volume (139). Nearly 100% sPS has been reported (140). The solid-state structure includes several well-defined crystalline phases with at

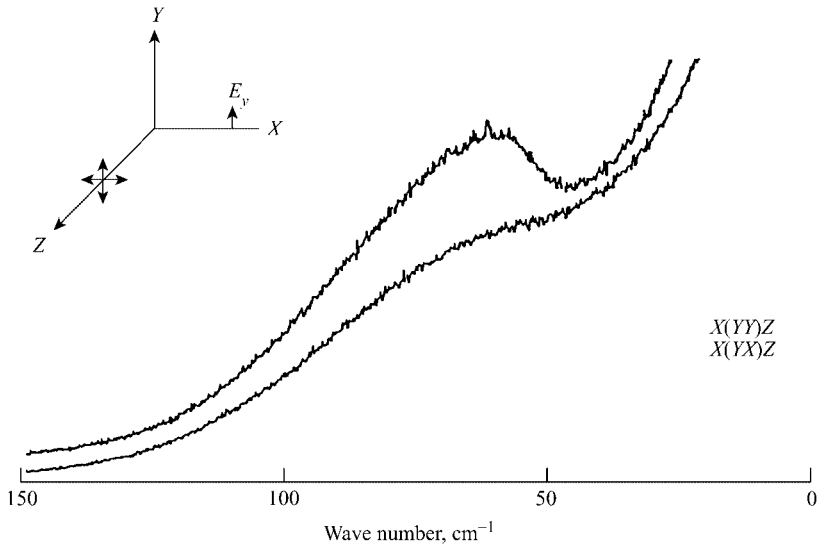

Fig. 15. Low frequency band observed for annealed syndiotactic polystyrene.

least two different chain conformations (141–146). A most striking spectroscopic feature is the extremely intense broad (bandwidth $\sim$100 cm^{-1}) vibration observed in the 20–200 cm^{-1} region for all polystyrene samples (Fig. 15) (139). The intense polarized vibration first observed for sPS is independent of molecular weight, degree of crystallinity, tacticity, or chain conformation (139). Since this band is independent of all polystyrene chemical structure, it is most likely associated with the torsional mode of an aromatic ring (139,147).

The frequency of this vibration is dependent on the exact location of substitution at the ring. A methyl group placed at the para position leaves the frequency unperturbed. Substitution at the ortho position will, however, change the frequency. The intensity of this motion has been reported to be related to the mass of substitution (147). The measured depolarization ratio for this vibration is $\sim$0.22 (Fig. 15). The optical activity is such that the first overtone is responsible for the observed intensity while the fundamental is forbidden (139). The change in polarizability tensor elements has also been predicted using ab initio calculations performed with the GAUSSUN 86 package for the related compound *p*-difluorobenzene to obtain the principal components. A quite strong $2 \rightarrow 0$ phenyl torsion transition has been reported in the 112–128 cm^{-1} region of the Raman spectrum of styrene. This mode has not been observed in the infrared spectrum. Although this vibration is intramolecular in origin, the bandwidth was found to be highly sensitive to the solvent-complexed crystalline state and therefore the intermolecular ring environment.

Phase Transformation. The utility of vibrational spectroscopy in measuring structure at a localized level cannot be overemphasized. TPBD has a first-order crystal–crystal phase transition at 76°C (148). Two crystalline forms are known to exist. One is stable below 76°C and transforms to the other above the phase-transition temperature. The transformation is reversible. The crystal

structure changes from a monoclinic unit cell to pseudohexagonal packing at high temperature. The conformational changes of the chain associated with this phase transition are

(1) There is a change in the —CH—CH_2— ϕ angle from 60–71° to 100°, causing a shortening of the repeat length from 0.0483 to 0.0466 nm;
(2) The molecular chain exists in a considerably distorted state due to torsional disorder about C—C bonds;
(3) The interchain distance in the unit cell increases from 0.0454–0.0460 to 0.0495 nm.

The distortion of the molecular chain may have the following consequences:

(1) Chains may exist with irregular conformations which have lost the inversion symmetry and cause breakdowns of the mutual exclusion principle.
(2) In some chain segments, the CH_2—CH_2 groups may no longer be trans to each other, which may result in observation of trans-gauche amorphous bands.

The similarity between high temperature and room temperature spectra indicates that no additional bands can reasonably be attributed to trans-gauche conformations (79). Although considerable distortions must be associated with the TPBD in the high temperature form, Raman spectra show the molecular chain has a large degree of conformational regularity, consistent with X-ray results. All observed lattice modes disappear when the sample is heated beyond the crystal phase transition. This is as expected since not only does the distance between chains increase but there is an increase of torsional disorder about the C—C bond as well as translational disorder along the chain axis. Close to the transition temperature, the 549 (skeletal angle bend), 1305 (CH_2 twist), 1340 (CH_2 wag), and 1433 (CH_2 bend) cm^{-1} bands all show a doublet in the observed Raman spectra. The two components are representative of the two structures above and below the phase transition. Only one band exists below 70°C or above 80°C. This fact indicates that the two forms coexist, even though this is considered to be a "sharp" crystal–crystal thermodynamic transition. This may not be surprising since X-ray patterns for single crystals indicate the two forms coexist between 55.5 and 69.5°C. This coexistence presents the possibility that the energy minima for TPBD are not as shallow as previously indicated (149).

One of the most interesting observations in vibrational spectroscopy is the effect of accidental degeneracy or Fermi resonance (150). This subject is introduced here to show its utility and stimulate further interest in this subject. Numerous studies have utilized the effects of Fermi resonance to characterize structural transitions in polymeric solids. These transitions can in fact be observed with a higher sensitivity than achieved by any other characterization technique. Fermi resonance may occur if two vibrational levels belonging to different vibrations have nearly the same energy, that is may be accidentally degenerate. As first recognized in the case of CO_2, such a "resonance" leads to a perturbation of energy levels. For example, in the case of CO_2 the fundamental of ν_1 (1337 cm^{-1}) has nearly

the same energy as the second harmonic of ν_2. The ν_2 fundamental is found at 667 cm^{-1} (1). The two vibrational levels having nearly the same energy "repel" each other and the actual level shifts from values expected from a harmonic oscillator model. Thus for CO_2 two vibrations are observed. At the same time a redistribution of band intensity occurs. The second harmonic, generally very weak, borrows intensity from the fundamental and may cause observation of two bands of similar intensity.

The vibrational spectra of polymers provide many opportunities for observation of Fermi resonance. In the 3300 cm^{-1} region of proteins and polypeptides, infrared active amides A and B are assigned to the fundamental NH stretching ($\sim$3300 cm^{-1}) and the second harmonic of the amide II vibration in the 1500 cm^{-1} (61). For synthetic polymers, the region of most interest is the C—H stretching region. To the first-order approximation, C—H stretching modes are highly localized and involve nearly pure hydrogen motion. They are essentially insensitive to the molecular conformation and environment, in sharp contrast to skeletal modes at lower frequencies. This hypothesis appeared intuitively sound and was supported by a half century of evidence from infrared spectroscopy. It is therefore surprising that changes in the C—H stretching region of Raman spectra are the first indications of changes in chain conformation and environment (151,152).

Other polymers exhibit similar changes during structural transformation. In *trans*-1,4-polybutadiene, at least six components are observed for the crystalline state at room temperature (79). Given the inversion symmetry of the chain, at most one =C—H and two CH_2 stretching modes are expected. When these crystals are heated to above 71°C, a solid–solid phase transformation occurs, causing changes in both chain conformation and packing. The changes in the overall infrared and Raman spectra are quite minimal at this transition. Most surprising is the observation that sharp defined features in the C—H stretching region evolve into a profile containing four bands. Similarly in lipid bilayers, the relative intensity of the $\sim$2900 cm^{-1} CH_2 asymmetric stretching to the 2850 cm^{-1} symmetric stretching band proves one of the most sensitive indicators of structural change. Many models are available for arrangement of proteins and lipids in biomembranes. An important difference between these models is the degree to which lipid bilayers, with ordered fatty acid chains, play a role in the structure. Better understanding of structural changes would provide better understanding of membrane functions (152,153).

The complexities observed in the Raman spectra of the C—H stretching region of polymethylene chains result from Fermi resonance interactions involving completely symmetric double excitations of fundamentals at lower frequencies with higher frequency C—H stretching of the symmetry. The sensitivity of C—H stretching vibrations to structural change results from the inherent *amplification* factor. Low lying vibrations are known to be sensitive to both chain conformation and chain packing differences. Because of the coupling between the second harmonics and fundamental at higher frequencies, small changes in the frequency of the lower vibrations may cause significant changes in the overall profile (1). The smaller the difference in the two components, the greater the anharmonicity of the potential well and the greater the mixing of the two modes. Thus small changes in the lower frequency component have the potential to considerably change the overall spectrum.

For polymethylene chains, the origin of these complexities may be described in terms of the appropriate binary combinations involving methylene bending modes interacting with the infrared or Raman-active symmetric stretching fundamental (154,155). Two levels of Fermi resonance interactions, intramolecular and intermolecular, need be distinguished, however. Unexpectedly, the Raman-active bands observed for different intermolecular packings are quite different (Fig. 16).

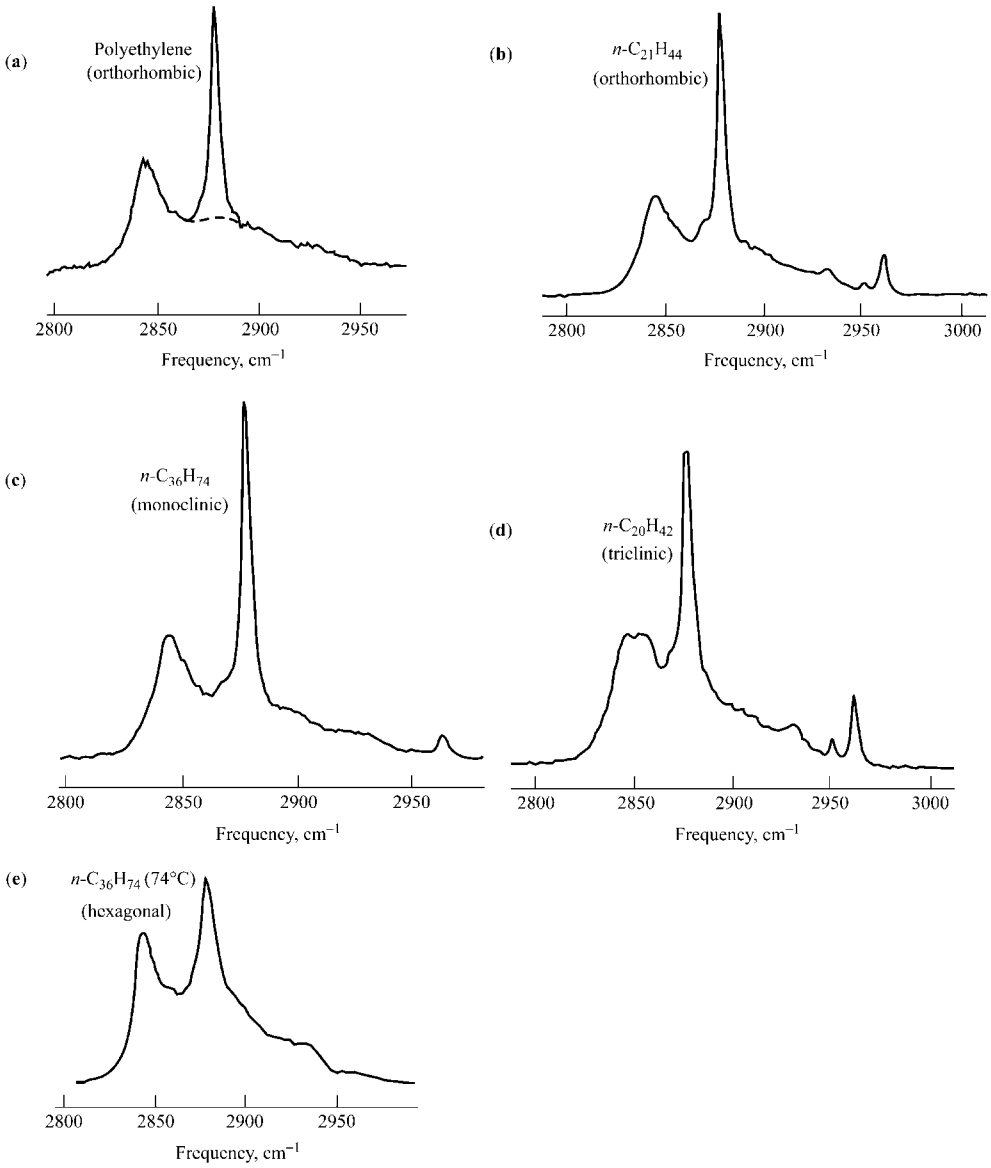

Fig. 16. C—H stretching region of the Raman spectra of (**a**) orthorhombic polyethylene at 110 K, (**b**) orthorhombic n-$C_{21}H_{44}$ at 110 K, (**c**) monoclinic n-$C_{36}H_{74}$ at 110 K, (**d**) triclinic n-$C_{20}H_{42}$ at 110 K, and (**e**) hexagonal n-$C_{36}H_{74}$ at 347.5 K. All Raman spectra were taken with bandpass 1.5 cm^{-1} at 510 nm. Laser power 200 mW at 514.54 nm.

For example, a multiplet exists at the 2850 cm^{-1} region for triclinic packing. It is also clear that upon structural transition, such as when chains disorder as in the hexagonal phase, the relative intensity of the dominant components changes. Thus if the interchain environment changes, Fermi resonance interactions amplify these, resulting in significant changes in relative band intensity.

Spectroscopic Characterization of Heterogeneous Polymers. Polymer physical properties can be altered by blending chemically and physically dissimilar components. Vibrational spectroscopy is often utilized to characterize the thermodynamic parameter governing mixing behavior. The morphology development can also be characterized based on the relative band intensity and frequency of specific features. Even relative chain dynamics can be monitored. The first example shown here involves polyurethanes. The wide-ranging applications of polyurethanes result from their versatile chemistry and attractive physical properties. These are formed from hard segments composed of isocyanates and soft segments such as polyethers. The hard segments phase-separate into domains creating junctions connecting soft polyethers. Polyurethanes therefore have many characteristics associated with elastomers. Both molecular architecture and chemical immiscibility are responsible for the formation of this phase-separated structure. A number of functional groups associated with both hard and soft segments can form interchain hydrogen bonds. Based on characteristics of the measured hydrogen bonds, vibrational spectroscopy yields much information regarding degree of phase separation, kinetics of phase separation, and perfection of hard domains.

Localized vibrations such as N—H or C=O stretching vibrations are strongly perturbed by formation of hydrogen bonds (156). Both frequency shifts and intensity changes are characteristics of the specificity or magnitude of the hydrogen bonds (157). The intensity of each type of hydrogen bonded vibration, if properly assigned, can potentially yield information regarding the degree of polyurethane phase separation (81–83). Infrared spectra of the carbonyl stretching region generally shows two distinct peaks. The higher absorbance observed for the 1700 cm^{-1} peak relative to the 1730 cm^{-1} component is characteristic of a phase-separated polyurethane structure. The peak at 1730 cm^{-1} is assigned to the free carbonyl. The peak clearly distinguishable at 1700 cm^{-1} is assigned to carbonyl groups hydrogen bonded to the N—H group.

Although polyurethane structure has been extensively characterized, experimental studies characterizing phase separation kinetics of segmented polyurethanes are scarce (158,159). Theoretical development of segmented block copolymers is also far from complete. Vibrational spectroscopy can also be of benefit in these studies. As mentioned above, hydrogen bonds form between the N—H and C=O groups of hard segments. A strong hydrogen bond between the N—H group of hard segment dispersed in the soft matrix and the C—O—C group of soft segment is also possible (81–83). A phase mixed state obtained at elevated temperatures can be preserved by rapidly quenching the sample to below the glass-transition temperature of the soft segments (81–83). Isothermal phase separation kinetics can then be studied by measuring changes in the infrared spectrum as a function of time at constant temperature (Fig. 17). Since most hard segments in the homogeneous state are surrounded by soft segments, the carbonyl groups are free of hydrogen bonding as characterized by the high absorbance of the 1730 cm^{-1} peak. During phase separation from a homogeneous single phase to

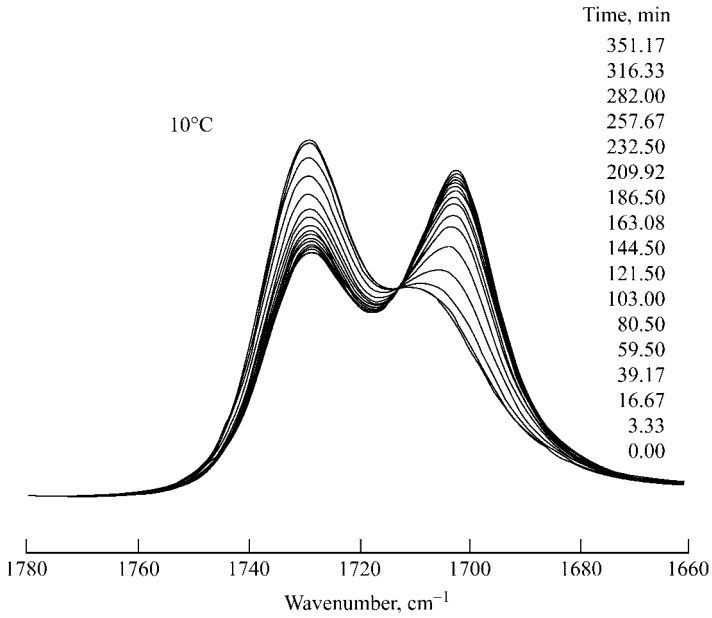

Fig. 17. Infrared spectra obtained for polyurethane undergoing phase separation.

a heterogeneous phase, the carbonyl group of hard segments is transformed from a free state to a hydrogen bonded state with N—H groups. Based on the relative intensity of the hydrogen bonded or free C=O stretching vibrations, the degree of phase separation has been analyzed as a function of time and temperature. The time dependence of the fractional decrease of the free C=O stretching vibration at 1735 cm^{-1} using the intensity of the observed C=O stretching components as a measure of structural change is shown in Figure 18. It is clear that the phase separation mechanism is changing as a function of time. There are no established mechanisms to explain the measured phase separation kinetics. One possibility is spinoidal decomposition which occurs in polymer blends at early stages of phase separation. However, the data obtained is not consistent with the prediction of Cahn–Hilliard expression (160).

In theory, the N—H stretching vibration should yield structural information complementary to the C=O stretching vibration. Generally speaking, the frequency of N—H groups free from hydrogen bonding is at 3450 cm^{-1}. The hydrogen-bonded component is usually measured near 3300 cm^{-1}. This shift is characteristic of the strength of hydrogen bonds formed (156). It is interesting to note that hydrogen bonds between hard and soft segments are stronger than those formed between hard segments. This observation suggests phase separation cannot be due to chemical immiscibility alone. N—H vibration is complicated not only by the two types of hydrogen bonding but also by other second-order spectroscopic effects involving the N—H stretching fundamental and combinations of lower lying amide vibrations. The intensity of these modes is also difficult to analyze because of resonance effects (161).

A most interesting contribution of vibrational spectroscopy is elucidation of the origin of specific interactions. Because of the large molecular size of polymers,

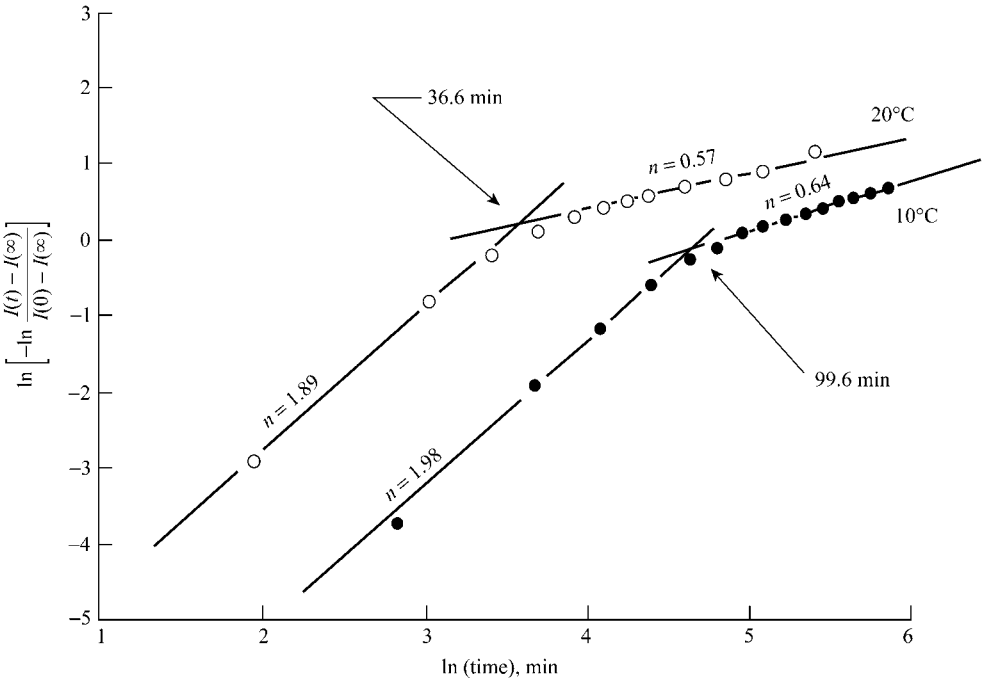

Fig. 18. The time dependence of phase separation kinetics observed for polyurethanes; (○) data obtained at 20°C; (●) data obtained at 10°C.

the entropy of mixing is relatively insignificant as a driving force in the mixing of polymers. Therefore the change in the overall free energy on mixing must arise principally from the term related to the heat of mixing, ie the interaction parameter χ. In some cases, molecular architecture also requires consideration (162). The enthalpic contribution to the free energy depends on the magnitude and specificity of the interaction between components. Spectroscopic features assigned to various functional groups of the polymer components may be affected by changes in intermolecular interactions, including permanent dipole interactions, transition dipole interactions, and, the strongest, hydrogen-bonding interactions. Interpretation of such spectroscopic features is useful in assigning a molecular origin to the thermodynamic parameter.

The most dominant specific interaction is hydrogen bonding. Its role in polyurethanes is documented above. This interaction has been used to obtain very detailed descriptions of polymer phase diagrams with strong interactions (163). These studies serve as valuable predictive tools for formulating miscible polymer blends. In most cases, the evidence of changing interactions is much more subtle and rather small changes in band position are generally observed. The experimental situation has improved since the use of Fourier transform infrared instruments has become relatively common. These instruments make extremely small differences in band position, shape, and intensity easier to detect. Difference spectra can be obtained by subtracting a spectrum of neat component from that of binary mixtures within the computer associated with the instrument. The spectroscopic differences are presumed owing to differences in intermolecular interactions

between neat and mixed states. However, the infrared spectra may show features not related to intermolecular interactions, ie band shape differences. These result from differences in the local index of refraction of the two components, sample thickness, and effects due to the optical properties of the sample substrate (164).

Blends of polystyrene (PS) and poly(vinyl methyl ether) (PVME) can be used to illustrate the use of vibrational spectroscopy to characterize specific interactions. A number of studies have shown that solvent, molecular weight, composition, and temperature can all affect compatibility of these two polymers (165). The nature of the intermolecular interaction between the two components has been established (166,167). Vibrations involving the oxygen atom are known to usually exhibit high sensitivity to blend compatibility. The skeletal vibrations involving oxygen are observed in the 1100 cm^{-1} region. In the infrared spectrum of PVME a strong doublet at 1085 and 1107 cm^{-1} with a shoulder at 1132 cm^{-1} shows the greatest change upon change of the molecular environment. Based on comparison of various blends and neat samples, it can be concluded that the frequency change and relative intensity are sensitive to structural changes and environment and possibly the miscibility of PS/PVME blends. It has been further suggested that the interaction between the components involves partial sharing of the ether lone-pair electrons with the benzene ring of polystyrene (167). Variation in the critical transition temperatures has further confirmed the earlier assignment (168,169). It should be mentioned that the changes in band positions are extremely small, in the order of a few wave numbers.

Among the large number of studies on polymer blends, one very interesting subset consists of binary mixtures with crystallizable components. Familiar examples include blends of chemically dissimilar polymers, eg poly(vinylidene fluoride) (PVF_2) with poly(methyl methacrylate) (PMMA), PVF_2 with poly(ethyl methacrylate), and poly(α-caprolactone) with poly(vinyl chloride) or blends of chemically similar polymers, eg isotactic PMMA with syndiotactic PMMA and PEO with poly(propylene oxide) (PPO) and isotactic polystyrene with poly(styrene-*co*-*p*-methylstyrene). Crystallization of neat polymers is already a complicated process. Crystallization of polymer blends is even more so. Several factors need be considered. The nucleation process depends very much on temperature and, particularly, on the difference between crystallization and melting temperatures. Because the second component, the suppression of the melting temperature can be significant, thus affecting the nucleation rate (170). Furthermore, from qualitative considerations, the crystal growth depends on the local concentration of the crystallizable component and on chain mobility.

The binary mixture of PEO and PMMA is an extremely interesting blend. From relative solubility considerations, it has been predicted and verified that PEO and PMMA are miscible in the melt (171). Few studies, however, have been conducted to better understand the crystallization kinetics, thermodynamic interaction parameters, and microstructures of this specific blend. Because of experimental constraints, the crystallization kinetics and microstructures of PEO/PMMA blends are most conveniently investigated by scattering methods. Therefore, most studies devoted emphasis to samples containing high percentages of PEO (172). It is to be expected that nucleation and subsequent crystallite growth rate are affected by blend composition. Few attempts have been made to characterize the crystallization behavior and microstructures of blends containing

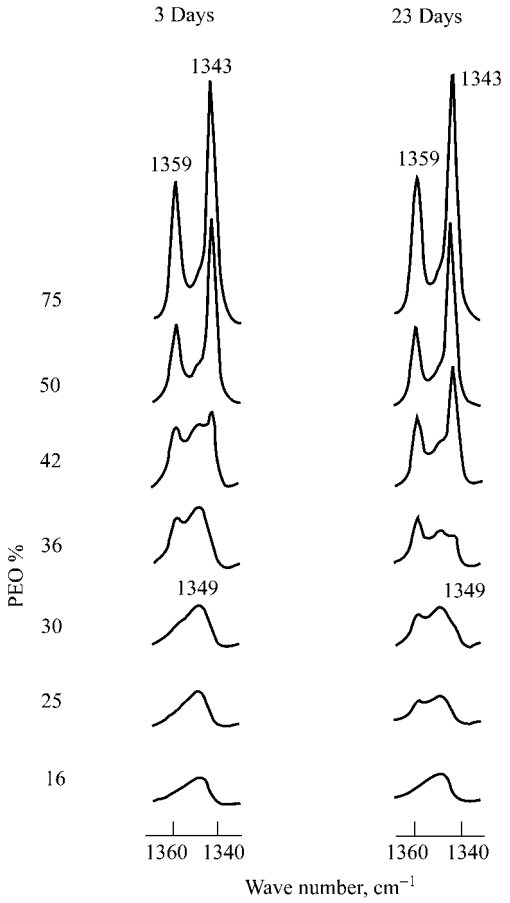

Fig. 19. Infrared spectra obtained as a function of time for PEO/PMMA blends with varying PEO compositions.

low PEO concentrations. Only infrared spectroscopy and now AFM can follow crystallization behavior (Fig. 19) (88,170). In addition based on the skeletal vibration in the 1300 cm^{-1} region, a different chain conformation was observed (88). This is important because the change in chain conformation implies the existence of long-range ordered crystallites. The reason that the gauche state is favored for neat PEO is due to the interaction between oxygen atoms and CH_2 groups (62). Perhaps a specific interaction with PMMA in the melt alters this interaction, causing the relative change in the microstructures.

Imaging Spectroscopy (Heterogeneous Materials: Impurities, Blends, Composites, and Laminates)

A most interesting development in vibrational spectroscopy is the growing use of microspectroscopy for the identification and quantification of very small amounts of polymer sample as well as composition of very small area (13,173). Sample size

or sampling area may be as small as 1–3 μm. By focusing on specific spectroscopic features, a chemical map may be obtained. This is particularly important when other imaging techniques are limited by experimental conditions or lack of contrast between area of interest and surrounding area. In many applications, it is important to have spatial resolution in the lateral direction. Spatial definition is sometimes required for all three dimensions. The depth profile along the propagating optical axis is often needed. Confocal spectroscopy enables such analyses. The signal from the small volume element of study requires better separation from signals arising from the surrounding material. The development of Raman or infrared microspectroscopy complements imaging techniques such as optical or electron microscopies. Applications of infrared or Raman microspectroscopy include contaminant analysis (synthetic and biological samples), identification of sample heterogeneity such as blends, or polymorphic structures introduced during processing. Parameters responsible for the high performance of laminates or composites can also be defined.

The limiting factor of spatial resolution is the wavelength of incident radiation. Infrared spectroscopy employs much longer wavelength radiation than the ones used in Raman spectroscopy. Diffraction effects cannot be overcome. Therefore, the resolution achievable is much less for infrared spectroscopy than Raman spectroscopy. If the sample is freestanding, the diffraction only gives rise to stray light, making quantitative analysis difficult. It does not normally affect sample identification to any great degree. If the small sample is embedded in some second substance, diffraction leads to spectral contamination by the substrate. Although Raman microspectroscopy has a spatial resolution of 1 μm in ideal cases, the spatial resolution in infrared spectroscopy is less easily defined because of difficulties arising with diffraction effects (long wavelength of the incident radiation). In these cases, diffraction effects can be quite important. For infrared, under most optimistic circumstances, the limiting size is approximately 10 μm and down to 3 μm in diameter. Although essentially unimportant in Raman microspectroscopy, sample thickness may be critically important in infrared transmission microspectroscopy. The sample must be about 10 μm thick to give good infrared results. Raman microspectroscopy can be used effectively to study very small samples or small areas within a transparent sample. Generally speaking, diffraction effects can be measured out to 50 μm from the central axis (173). The spectral contamination from material beyond perhaps 10–15 μm is sufficiently low, but not negligible.

Infrared or Raman spectra can be obtained point by point to obtain a chemical map of the sample in two dimensions. The sample can be moved relative to the probing beam. These images are derived from a material's intrinsic vibrational spectroscopic features. Point-by-point or line-by-line scanning techniques may not be practical for many applications, however. The high laser power focused at localized areas may cause sample degradation. A more practical approach is to use the global illumination method (174). Most Raman imaging spectrometers employ CCD detection. By using specific tunable filters to let specific frequencies through (175), it is possible to obtain both the overall images generally obtained by optical microscopy and the Raman images generated with specific Raman-active bands. The images obtained are usually of the quality dictated by the diffraction limit of the employed optics. The experimental conditions to obtain these images are not significantly different from ordinary experimental conditions (176).

Both infrared and Raman microspectroscopy are useful for composite analysis. The commercial value of fiber-glass reinforced composites is undisputed. Incorporation of high performance fibers into low cost matrix material significantly increases overall mechanical properties at moderate cost. Raman is required for study of carbon and silicon carbide fibers, since the former has no infrared spectrum and that in the latter is extremely weak. Raman spectroscopy has contributed significantly to understanding stress distribution in the composites upon application of an macroscopic stress. The imaging capability of the Raman technique is a powerful technique to measure stress at each point along the reinforcement fiber for comparison to theories first developed nearly 50 years ago. One example presented here illustrates the advantages of the Raman microspectroscopic technique. The success of this study was dependent on several aspects:

(1) Several Raman-active bands of polymers exhibit a frequency shift when the sample is stressed.
(2) The Raman technique exhibits high spatial resolution so that Raman spectrum can be obtained from specific locations.
(3) High sensitivity can be obtained if resonance Raman spectrum can be obtained.

The initial study employing polydiacetylene single crystals proved extremely successful (177). This system is quite interesting for several reasons:

(1) The polydiacetylene single crystals are fiber-like with high aspect ratio.
(2) The shape of the fiber can be altered to test some basic assumptions of stress transfer mechanism.
(3) Since these fibers are single crystals, the stress experienced at any particular point is directly related to the strain.
(4) These polydiacetyelenes have an electronic absorption spectrum extending well into the visible range, making resonance Raman spectrum easy to obtain.

This last point is important because imaging optics can be dealt easily with high spatial resolution, using various lasers from 500 to 700 nm.

Because of the resonance conditions achieved, only skeletal stretching vibrations coupled to the electronic transitions are excited. Typical high quality Raman spectra of C=C stretching as a function of stress can be obtained readily. In order to obtain a spectrum from the embedded fiber in the matrix, it is necessary for the incident excitation to be propagated through the matrix and for the scattered Raman radiation back through the matrix to the collection lens. Because the relative intensity of the Raman scattering originates from the matrix versus the fiber, the signal from the fiber can be collected easily without interference from the matrix. Other polymers have been studied with various degrees of success.

This model system has shown the potential of the technique and has been very successful in validation of models developed for composites. The predicted stress distribution along the fiber axis x (shown below) is indeed verified (Fig. 20) (178,179).

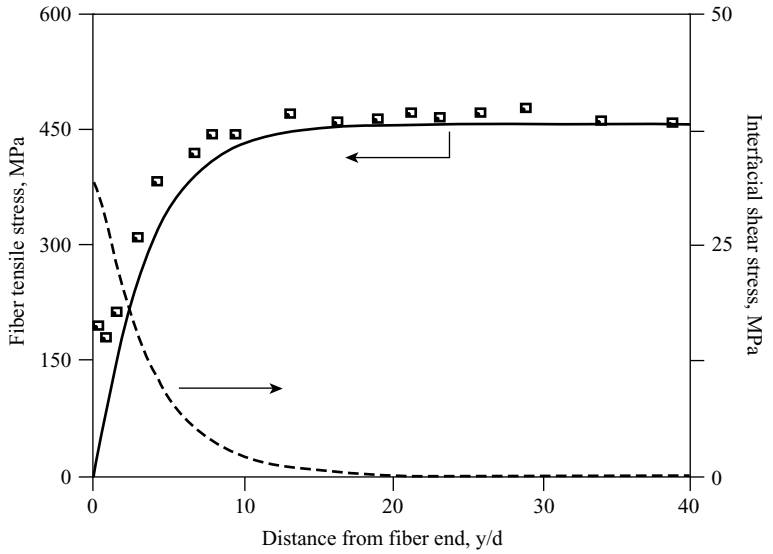

Fig. 20. Stress distribution along polydiacetylene fiber in model composite. Calculated tensile stress distribution from equation 9 (———); Calculated interface shear stress distribution (– – –); and experimental tensile stress distribution (▫).

$$\sigma_f = \frac{(E_f - E_m)\sigma_c}{E_m}\left[1 - \frac{\cosh\,\beta\left(\frac{l}{2} - x\right)}{\cosh\,\beta\frac{l}{2}}\right] \tag{9}$$

where E_f and E_m are the moduli of the fiber and matrix respectively, σ_f and σ_c are the stress along the fiber and applied stress respectively, l is the fiber length longer than the critical length, and β is related to the elastic constants and cross-sectional area. Several other aspects associated with stress transfer composites are of interest and need to be answered (180–183). For example, does fiber–matrix interface matter? The relationship between the magnitude of residual stress and the processing conditions has been analyzed. One interesting study deals with the shape of the reinforcement fiber. In theory, a fiber of tapered end can be an extremely effective reinforcement as shown by the measured stress distribution. Although kink bands associated with failures have often been observed, a direct relationship between this macroscopic observation and the critical compressive stress had been virtually impossible to establish until this spectroscopic technique was established (Fig. 21).

Microspectroscopic infrared spectroscopic studies have emphasized the role of the interphase in fiberglass-reinforced composites (184). Spectral subtraction along with two-dimensional mapping experiments revealed features characteristic of the interfacial region. Different glass fibers were used to observe spectral differences at the interphase. When as-received and heat-cleaned glass fibers were used, certain similarities were observed, although an inhibition of the curing occurred at the interfacial region of epoxy-heat-cleaned glass fibers. When the glass fibers were treated with an aminosilane coupling agent, spectral evidence indicated that the glass surface modified the epoxy-glass fiber interphase.

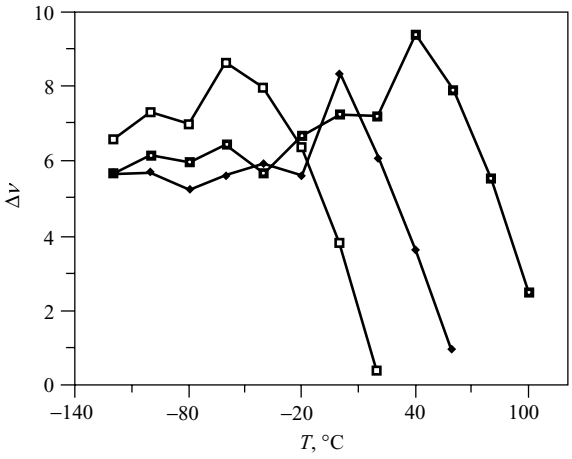

(**a**)

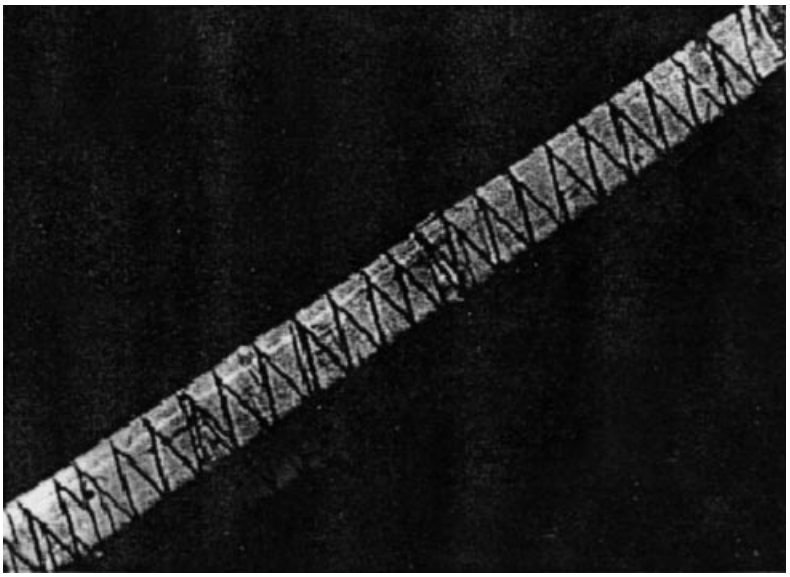

(**b**)

Fig. 21. Kinks measured for fibers in model composites. (**a**) The change in the backbone stretching vibration as a function of temperature for polydiacetylene fiber in model composite. —□— $T_c = 20^\circ$C; —■— $T_c = 60^\circ$C; —□— $T_c = 100^\circ$C. (**b**) Polydiacetylene fiber in model composite examined under cross-polarized light, showing kinks produced when strain is larger than critical value.

Polymers sometimes by design contain substantial impurities or contaminants introduced during processing. These heterogeneities are often very small, but many in number, resulting in degradation of desirable properties. Identification of the material causing the heterogeneity is normally a prerequisite to its removal or control. Microspectroscopy is a very powerful tool in this context.

During the processing of semiconductor silicon by deposition of polyimide insulating layers on silicon wafers, it was noted that small solid particles were present in the polyimide, which caused serious problems during further processing. The composition of these particles was identified by infrared microspectroscopy as dicyclohexylurea. This material is formed by reaction of dicyclocarbodiimide, a reagent used in preparation of polyimide, with water. Apparently excess dicyclocarbodiimide was used in preparation of certain batches of polyimide. This excess material reacted with moisture from the air over a period of time to form an impurity; if an impurty exists, the spectrum obtained for each isolated unit often provides positive identification.

Infrared and Raman spectroscopies have been used for many years to study phase-separated heterogeneous polymers. Most studies focused on thermodynamics and physical properties achievable. Morphological features have been studied with other microscopic techniques. The advent of Raman and infrared microspectroscopic methods has an potentially important effect on this field of study. Chemical mapping provides contrast when other microscopic methods fail. The micro-Raman technique has been used in conjunction with other techniques to characterize the somewhat controversial issue regarding miscibility behavior of linear and branched polyethylenes (185). By using specific Raman features of each component, it is possible to detect crystallinity variations and reveal a biphasic structure in quenched blends that displays a morphological phase structure when examined in the transmission electron microscope. The domains formed for copolymers and polymer blends have also been studied using infrared microspectroscopy. The variation in infrared features corresponds to the relative polymer concentration (186). A more general case is provided by the study of phase structure and composition of polymer blends by Raman microspectroscopy. The technique is illustrated with use of various polymer mixtures (187). A Raman image of rubber-toughened epoxy resin developed using 1665 cm^{-1} band is shown in Figure 22.

In another application, an interfacial profile of polymer gels during phase transition was examined (188). The interface profiles between *N*-isopropylacrylamide (NIPA) hydrogel and water were directly observed using the Raman microimaging technique. As the NIPA hydrogel undergoes the volume phase transition, the interface becomes thicker and smoother. The average interfacial thickness of the NIPA gel at room temperature is about 37 μm, but increases to 65 μm at 37°C, which is above the phase-transition temperature. The thicker interface may be related to a dense shell formation during the gel shrinking process. The repulsive energy between water and polymer is minimized when the total surface of the interface is reduced, a process which results in a smoother surface. Without microspectroscopy, it would be impossible to obtain such structural variation in the presence of water.

A related application requiring a two-phase treatment is that of polymer dispersed liquid crystals. The optical properties of these films may be electrically modulated and their potential for application is quite high (189). By controlled cooling, the size of the liquid crystal droplets in the polymer matrix may be varied between 1 and 30 μm or larger. Three commercial liquid crystals were dispersed in two thermoplastics [poly(vinylpyrrolidone) and poly(methyl methacrylate)] and epoxy. These were studied by infrared microspectroscopy, both polarized

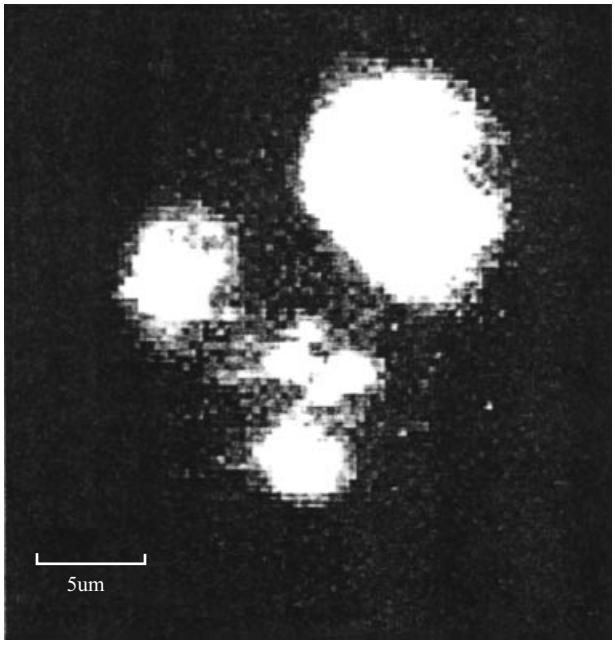

Fig. 22. Raman image at 1665 cm^{-1} (minus 1720 cm^{-1} background) of a thin film of rubber-toughened epoxy resin (187).

and unpolarized. Changes were observed in the droplets as a function of infrared polarization and applied electric field. Indications of partial solubility of the liquid crystal in the polymer matrix were obtained and orientational information about functional groups on the liquid crystal molecules as a function of the presence of the electric field were deduced.

Structural variation also exists as a result of differences in processing conditions. Phase structure, composition, and orientation of polycarbonate/poly(styrene-*co*-acrylonitrile) blends were studied by the Raman imaging technique. The existence of two-phase (PC-rich and PSAN-rich) microdomains was revealed. During drawing the microdomains are significantly deformed. In conjunction with polarized photoacoustic Fourier transform infrared spectroscopy, substantial orientation of the PC chains was revealed. In contrast PSAN chains exhibit only slight orientation. A similar study mapped the transition region in the neck of uniaxially drawn poly(vinylidene fluoride) with regard to crystalline structure as a function of stress (190,191). The morphology change as a function of position is shown in Figure 23. The stress exerted transformed the polymer from structure II (nonplanar, TGTG′ conformation) to structure I (planar, all-trans conformation).

Raman spectroscopy in conjunction with infrared dichroism has been used to characterize the segmental orientation at specific locations within processed polyethylenes (192). The variation of the segmental orientation through sample thickness was investigated for the cylindrical rods and an H-shaped molding produced by extrusion and rolling. The second moment of the segmental distribution

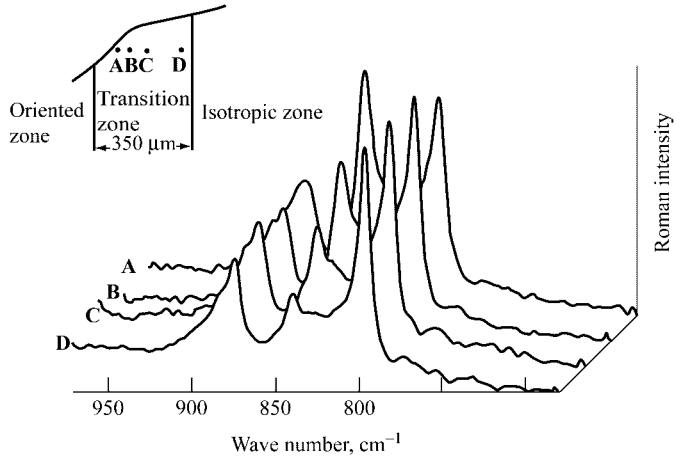

Fig. 23. Micro-Raman spectra of PVF_2 recorded in the transition zone at positions **A**, **B**, **C**, and **D** (191).

function, $\langle P_2 \rangle$, for both crystalline and amorphous regions was measured using a combination of X-ray diffraction, infrared, and Raman measurements. It should be mentioned that bands may be associated with specific chain conformation and not necessarily crystalline units. The fourth-order coefficient $\langle P_4 \rangle$ was also determined from X-ray diffraction and Raman spectroscopy for a series of cylindrical rods of draw ratios ranging from 6 to 20. The Raman spectroscopy results indicate that the all-trans chain conformations located in the amorphous phase are aligned perpendicular to the extrusion direction for the highly deformed rod, and gradually reorient towards the fiber axis for draw ratios up to 20. The $\langle P_2 \rangle$ and $\langle P_4 \rangle$ coefficients calculated for the crystalline phase remain constant for all draw ratios. Minor differences in the degree of molecular orientation were detected between the center and surface of the rods, whereas important variations were measured for the H-shaped sample. These are shown in Figure 24. In some cases, values obtained by Raman spectroscopy are lower than those calculated for the crystal phase from X-ray diffraction and polarized infrared, but are higher than the orientation determined for vinyl end groups. These differences can be explained by the fact that the vibrational bands assignable to the all-trans conformers can be found in both amorphous and crystalline regions.

Another application of microspectroscopy is characterization of laminated polymer films. Multilayer polymer films of different functionality are common in the packaging industry and identification of the different layers is of commercial importance. The layers vary from about 1 μm in thickness (adhesive) to 10–50 μm and there are often several layers. If there are only two layers, attenuated total reflectance (ATR) methods can be used for identification. For films with more than two layers, the normal procedure is to microtome a 10–20 μm cross section for edgewise analysis using microspectroscopy. A comparison of infrared and Raman microspectroscopies for some multilayer films has been published (Fig. 25) (193).

Clarification of the mechanisms of adhesion between two different polymers is an important field of study. Although investigations of the adhesive mechanisms of the polymer-to-polymer interface in painted surfaces have been undertaken, few

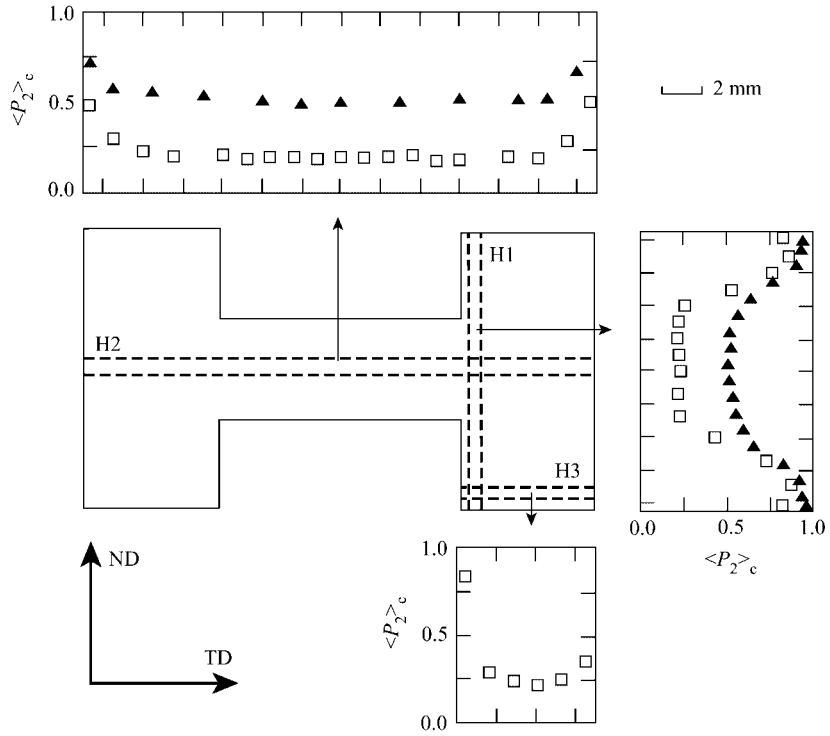

Fig. 24. $\langle P_2 \rangle_c$ coefficients measured by X-ray diffraction (110, 200, and 020 reflections) and Raman spectroscopy at different positions for the H1, H2, and H3 platelets (192) ▲ X ray; □ Roman.

studies are reported for structural changes caused by the adhesion. Fourier transform infrared microspectroscopy was used to analyze the interaction of the coated interface between two different polymers (176). The samples investigated were prepared by coating urethane paint on an ethylene–acrylic acid copolymer (EAA) and on an ethylene–ethyl acrylate copolymer whose ethylester group had been partially hydrolyzed (EAA/EEA). It was demonstrated that a mixed phase was formed along the coated interface between the urethane paint and the EAA and between the paint and the EAA/EEA. The interaction between molecules of the polyurethane and the EAA was observed (176). Using similar techniques, concentration profiles and interdiffusion coefficients of contacting compatible polymers have been established (194).

Assessment of Anisotropy in Polymers: Segmental Orientation

Motivation. Structural anisotropy in all materials, especially polymers, is a readily accepted concept. Physical properties such as thermal conductivity, optical transmission, electrical conduction, piezoelectricity, shrinkage stability, and, particularly, mechanical performance are all highly dependent on the degree of anisotropy. For many polymer applications, high modulus and strength are especially important. These qualities can be obtained by polymers with desired degrees

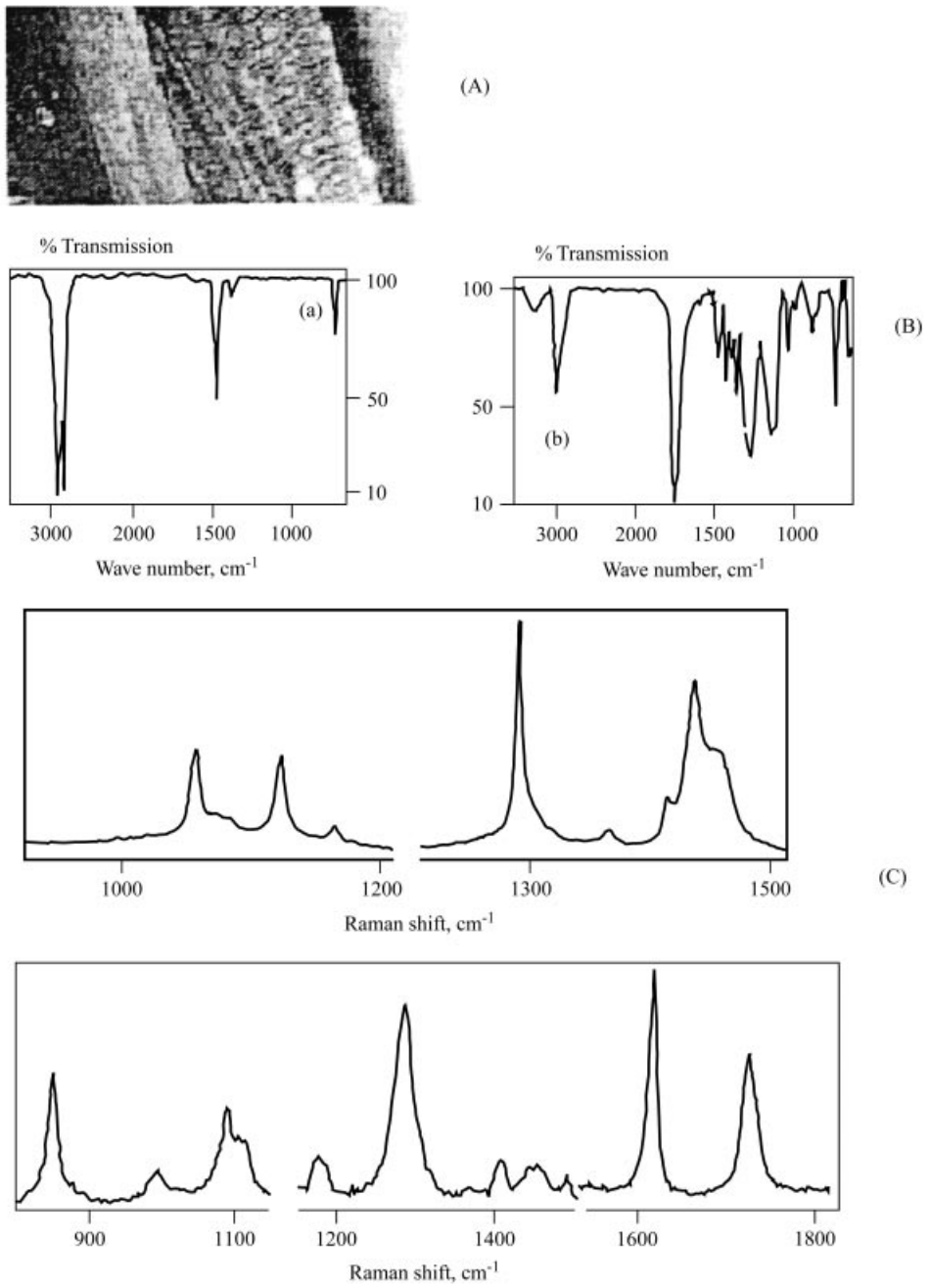

Fig. 25. Microspectroscopic studies of polyethylene and poly(ethylene terephthalate) laminate: (**A**) optical of micrograph; (**B**) micro-infrared spectra of the components obtained (left PE, right PET); (**C**) micro-Raman spectra obtained (top PE, bottom PET) (193).

of anisotropy. The deformation process, whether in the solid state, melt, or solution, induces the alignment of molecular chains along the elongation direction, which results in an increase in strength and modulus of the material in that direction. Uniaxial deformation can be utilized to achieve samples of a fibrous nature. Biaxial orientation along two perpendicular axes has been extremely successful in producing materials of interwoven fibers to yield films or sheets with desirable mechanical performance along the two plane axes. For amorphous samples, understanding the deformation behavior of individual chains is important. For crystalline polymers, the relationship between the overall deformation behavior must be related to the relative motion of amorphous chains and crystalline regions. The deformation process must be correlated to the deformation mechanisms available to the crystalline portion. The crystalline degree, size, perfection, and interconnectivity are all important in the overall consideration of deformation mechanisms. The absence of a well-formed model to describe the deformation process makes experimental studies extremely important in relating every aspect of the structure to the overall applied stress or strain.

A commonly used criterion to assess mechanical performance of processed polymers is modulus measured under extension. In most cases the experimental values generally fall substantially lower than theoretical estimates. The difference is undoubtedly due to both conformation and orientational disorder in the processed samples. The best illustration of the complex processing steps required and the resulting structure is polyethylene. With the tremendous developments in polymer processing methods, materials with controlled, and in some cases nearly perfect, chain segment orientation can be obtained. For example, gel spun polyethylene fibers and biaxially oriented blown films possess properties much higher than the isotropic state. The modulus of as-polymerized material generally is measured in the range of 1 GPa (195). It was shown that the modulus of polyethylene can be increased significantly to a value approaching theory, ~300 GPa (104,124). In processed fibers virtually all chains are perfectly extended and aligned with respect to the deformation axis, thus producing the extremely high modulus value. Generally speaking the force required to deform a backbone bond is approximately 10 times higher than that needed to deform a valence angle, which, in turn, is approximately 10 times higher than that needed to change the torsional angle of bonds along the backbone. If it is possible to orient and extend individual polyethylene chains into a planar zigzag conformation as in these highly deformed fibers, thus eliminating the torsional deformation of disordered chains, the modulus can be increased significantly (196).

Polymers are processed into anisotropic materials to lower the number of structural defects and achieve segmental orientation. Undoubtedly these two properties are correlated, making measurement of sample anisotropy crucial. Different characterization techniques measure segmental orientation of different morphological subunits. Some address overall sample anisotropy. Others address specific structural units, crystalline, amorphous, or interface. Different sample portions may possess different degrees of orientation. For example, the extrudate interior may yield a considerably different degree of orientation in comparison to sample surface. Measurement techniques include X-ray pole figure analysis (192,197), infrared dichroism, polarized Raman scattering, birefringence, NMR, fluorescence. Each technique can potentially yield different information regarding

orientation of morphological subunits, both crystalline and noncrystalline. The increase in sample anisotropy as a function of deformation can be assessed by measuring sample density, degree of crystallinity, birefringence, etc. The importance of vibrational spectroscopy in orientation analysis cannot be overestimated. Because they are capable of extremely high spatial resolution, fibers, films, and sections of large specimens can all be analyzed. On-line analysis is important. Raman with associated fiber optics presents interesting opportunities to obtain orientation data at different stages of deformation. No other technique is available for this purpose.

It is important to model the deformation process as a function of draw ratio. As mentioned above, even for highly deformed material, some imperfection in segmental orientation remains. Knowledge concerning the molecular mechanism and degree of segmental orientation achievable by various drawing, extrusion, or other deformation techniques is, in fact, quite limited. Therefore, two aspects concerning formation of anisotropic polymers are required: (*1*) a quantitative description of segmental orientation achieved; and (*2*) relationship between segmental orientation and draw ratio.

The distribution of chain segments relative to the reference axis yields the fraction of chains in each angular volume element and is expressed as (198)

$$\frac{\mathrm{d}n}{N} = f(\zeta,\phi)\ \mathrm{d}\zeta\ \mathrm{d}\phi$$

where ζ is defined as $\zeta = \cos\theta$, where θ is the angle measured with respect to the reference axis. In the three-dimensional space, the distribution function is often expanded as a series of spherical harmonics (199,200). If the system does not have angular dependence (uniaxially oriented system with a symmetry plane perpendicular to the deformation axis), the distribution function can be written as

$$f(\zeta,\phi) = \sum_{l=0}^{\infty} C_l P_l(\zeta) \tag{10}$$

and then

$$C_l = \int_{-l}^{l} f(\zeta) P_l(\zeta)\ \mathrm{d}\zeta \tag{11}$$

For an axially symmetric system, only even series of Legendre polynomials are retained. A full description of the segmental orientation function requires that the individual component be defined. The coefficients *C*'s, characteristic of the distribution function, represent the contribution from each Legendre polynomials. The second-order coefficient is the well-known *Herman orientation function* (201) and is generally the only one used for structural analysis in polymers.

$$C_2 = \frac{3\cos^2\theta - 1}{2} \tag{12}$$

This expression represents an average taken over all sample orientation. Practically speaking many methods can measure the second moment, which can range from −0.5 to 1.0. One extreme signifies that the segment is oriented perpendicular and parallel with respect to the deformation axis. A zero value is found for the case of random orientation. For infrared spectroscopy, the second moment can usually be given by the expression

$$C_2 = \left(\frac{D-1}{D+2}\right)\left(\frac{D_0+2}{D_0-1}\right) \tag{13}$$

where D is the dichroic ratio defined as the ratio of relative absorptions, $A_\parallel/A_\perp$, $D_0 = 2\cot^2\alpha$, and α is the angle of the transition moment with respect to the chain axis. Because of its sensitivity to short-range order or disorder, vibrational spectroscopy provides detailed information regarding orientation of chain segments, either in the ordered or disordered states, and for a large variety of samples, including fibers or films. Because an extremely fine focus can be achieved, samples such as fine fibers can be studied. In addition, surface versus bulk can be differentiated for larger samples.

Raman can produce higher moment, C_4. In practice, experimental difficulties severely limit applications of the eloquent theoretical expressions derived (202). In theory and practice, only X-ray diffraction is capable of measuring higher moments of the distribution function accurately (192,197). Even then, the high quality diffraction data necessary for determining higher moments in the distribution function are difficult to obtain. For smaller draw ratios, evaluation of the second moment is usually quite sufficient. Obviously, samples deformed to a higher degree require a precise determination of the orientation function.

The expressions presented above contribute to assessment of the segment distribution relative to any axis. From practical considerations, it is often desirable to relate this distribution function to the degree of deformation associated with polymer chain transformation from an isotropic to anisotropic state. This transformation may depend on the size, perfection, and interconnectivity of the morphological units. It is virtually impossible to define polymer structures sufficiently accurately to describe the deformation behavior analytically. The only case that can be determined in a closed form is to imagine the entire polymer sample being deformed to consist of a network of totally flexible chains and each chain to consist of totally flexible chain segments, ie Gaussian chains. Using this model, the calculated orientation of chain segments as a function of draw ratio is surprisingly low (199,200). However, if the number of connecting units between segments is small, or the structural unit is large, the change in orientation function can be seen to increase significantly as a function of strain (203). This model has been used in many infrared-deformation studies.

The specific utility of vibrational spectroscopy in these orientation studies is illustrated below. If a polymer film is oriented by drawing or extrusion, the polarized infrared spectra reveal tremendous differences in absorption for incident radiation polarized parallel or perpendicular to the drawing direction. Polarized infrared spectra of polyethylene are shown in Figure 26. The CH_2 rocking vibrations in the 700 cm^{-1} region, or the CH_2 wagging or CH_2 bending vibrations in the 1300–1400 cm^{-1} regions, exhibit very different polarization behavior.

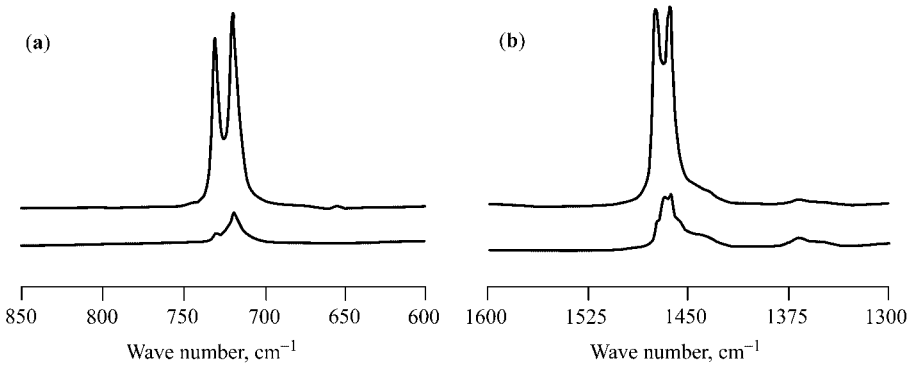

Fig. 26. Polarized infrared spectra of polyethylene: (**a**) CH_2 rocking region; (**b**) CH_2 wagging and bending regions; top is spectra with polarization parallel to the draw direction and bottom with polarization perpendicular to draw direction.

This observation highlights several important features of polarization spectra. First, and most importantly, the polarization measured is associated with the direction of the vibration transition moment. The direction of this transition moment relative to the chain segment must be considered in order to determine the overall chain segmental orientation. For some functional groups and extremely well-defined polymer structures the transition moment can be estimated. In many cases, however, this is difficult to accomplish. Orientation information obtained from spectroscopy is highly selective and can be used to characterize individual chain segmental orientation in both crystalline and amorphous regions. The relative orientation of the amorphous bands to the crystalline bands can provide much information regarding the deformation process in forming highly anisotropic fibrous samples. In a second example, polarized Raman scattering are shown in Figure 27. Isotactic polypropylene exists in a 3_1 helix. Its vibrations can be divided into 25 A modes and 26 degenerate E modes. The optical activity of the two optical active species are quite different and can exhibit quite different polarization characteristics. The classification of various normal vibrations into symmetry classes is greatly facilitated by performing appropriate Raman scattering experiments (22).

Surface Characterization

The importance of polymer interfaces and polymer–external surface interactions cannot be overemphasized. Interface performance to a large extent determines the overall mechanical properties of composites and heterophase polymers including polymer blends. Polymer interaction with external surfaces is also central to a broad range of applications such as corrosion inhibition, adhesive joint strength, fabrication of electronic components, and decorative plating. Several techniques, each with particular advantages or disadvantages, including contact angle, X-ray photon electron spectroscopy (XPS), and radioactive labeling, are available. Contact angle is perhaps one of the easiest to carry out, but the information obtained

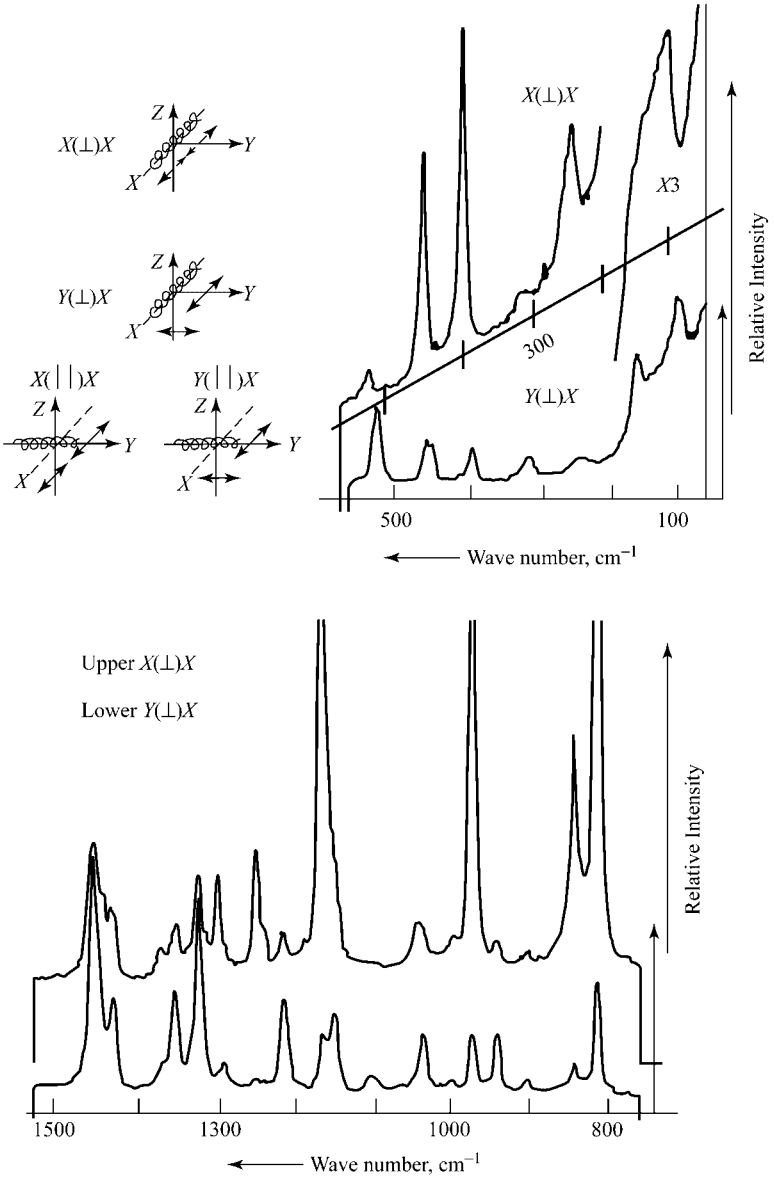

Fig. 27. Polarized Raman spectra of oriented isotactic polypropylene fibers (22).

is somewhat limited. XPS can be used to measure surface composition accurately with high spatial resolution, but the high vacuum requirement may make such experiments difficult to conduct. Vibrational spectroscopy has proven a useful technique in surface analysis, both chemical composition and structure.

Perhaps because of dramatic improvements in instrumentation or changing research perspectives, the study of surfaces has changed dramatically. Spatial resolution of surfaces or interfaces of a few micrometers is no longer sufficient.

Investigation of the mechanical, adhesion, and electrical behavior of ultrathin polymer films requires spatial resolution of the order of 10–100 Å. Specular reflectance spectroscopy is a most convenient technique for probing structures on either metallic or dielectric surfaces. Furthermore, techniques such as polarization modulation spectroscopy have significantly increased sensitivity and the possibility of photoacoustic spectroscopy is also available.

Because of the small amount of sample being probed and necessarily at the surface, transmission spectroscopy does not provide sufficient sensitivity to discriminate differences from samples at the surface from the remainder of the sample. Some type of reflection technique which localizes the probing radiation to the region of interest is desired. The contribution of infrared spectroscopy has perhaps been much more useful than Raman spectroscopy in surface analysis. Almost every laboratory using infrared spectroscopy has some type of reflection cell. These are well designed and sold through spectrometer manufacturers and independent firms making specialized accessories. In contrast, few laboratories with Raman instruments have the capability to measure Raman spectra from surfaces. Many specialized Raman techniques have been developed for surface analysis. The high power laser required, sample degradation, high cost, lack of construction capability have all limited its utility in general surface analysis. The infrared technique is generally the one of choice. It should be emphasized that different infrared techniques probe materials at different depth from surfaces. ATR has a sampling depth of approximately 1–10 μm (10). In contrast, grazing specular reflectance spectroscopy can probe film thickness as thin as 1 nm (204).

The attenuated reflectance technique presents an excellent example of how radiation at sample surface can enhance signal-to-noise ratio. Details of general optics and reflectance techniques can be found in the classic text (10). This technique is used extensively to determine differences between the structure of polymers in surface and bulk phases. Commercial accessories make these spectroscopic experiments easy to perform, although quantitative analysis of the data remains difficult. Examples of ATR applications include chemical composition analysis of polymers, surface orientation resulting from various processing methods, and chemical or thermal degradation of polymers. For samples such as powders or poorly defined surfaces, the diffuse reflectance technique can be used (11). In addition, the photoacoustic technique has been used to probe surface structure and multilayer structure commonly found in polymer laminates (17). In all these cases, optical effects can complicate analysis of infrared spectra. Nevertheless, these data have proven very useful in analytical applications.

The development of the reflectance technique and quantitative analysis of results demand thorough understanding. Knowing how the probing beam is reflected, refracted, or absorbed at the polymer–polymer, air–polymer, or polymer–solvent interface is crucial. This can be understood only if the optical property of the individual medium is carefully defined. The basic consideration for any analysis must consider the real and imaginary parts of the index of refraction for the polymer *films* and substrates being studied. The situation can be particularly complex if the film is highly ordered or oriented. Film thickness can introduce unexpected errors as well. Differences in band frequency, shape, and intensity between the transmission and reflection infrared data arise from optical effects associated with thin films, which may have no correlation with

structural differences (14). Computer algorithms have been developed to appraise these optical effects. In most analyses, the structural information is obtained from interpreting only a few isolated well-assigned infrared bands. Therefore, the exact calculation of optical effects for thin film or substrate need not be undertaken for the entire frequency range but rather a limited range of interest. Knowing film thickness, optical coefficients of the substrate, angle of incidence, and isotropic transmission spectrum, the spectra expected from the reflectance technique can be predicted.

If the substrate used is metallic in nature, the boundary condition for an incident electromagnetic wave is such that only the electric field with polarization in the plane of scattering (defined as the plane containing the incident and reflected rays) has energy at the surface (205). The intensity of the other component polarization is zero near the conducting substrate surface. Hence, only one of the two perpendicularly polarized radiations will be absorbed by the thin polymer film. The use of reflectance infrared spectroscopy to characterize the composition of chemically or physically absorbed layers on external surfaces can be easily appreciated. Only vibrations with components of the transition moments perpendicular to the metallic surface are expected to appear with enhanced intensity. Those having transition moments nearly parallel to the surface are expected to be weak or nonexistent. The most definitive studies undoubtedly involve highly ordered model compounds prepared by the Langmuir–Blodgett technique. When bands are accurately assigned, and particularly when the directions of transition moments are well defined, much information can be derived from the highly polarized reflectance infrared spectroscopy of such films on external surfaces (206).

In most cases, the dynamic range of a Fourier transform instrument is more than adequate to differentiate adsorptions of these two components. However, by using the double modulation technique together with phase-sensitive detection, a far better signal-to-noise ratio can be obtained (207) since the difference between the two components is measured directly. It should be mentioned that double modulation spectroscopy has also been used to elucidate structure of adsorbed films from dielectric surfaces (208).

By definition, most high frequency vibrations are well-defined localized vibrations involving few nuclei, making transition dipoles easy to define and understand. Examples are the C=O and CH_2 stretching vibrations in n-$C_{15}H_{31}CO_2H$ absorbed on Al_2O_3 (Fig. 28) (206). The significant difference between the reflectance and transmission spectra can be accounted for by preferential orientation of the carboxylate groups. Information on the exact orientation of the alkyl tail of the hexadecanoic acid can also be obtained from the high frequency spectra shown in Figure 28.

An example involving stacks of nematic liquid crystalline polymers (benzenehexa-*n*-alkanoates) on substrate is presented. Because of lack of suitable vibrations it is difficult to determine the orientation of the central benzene rings of BHn. Therefore another series of tetrakis(octanoyloxy)*p*-benzoquinone (QTE8), with C=O directly attached to the benzene ring, is prepared. Optical and X-ray diffraction studies reveal that the structure consisting of a rigid aromatic core and flexible side chains can be characterized as forming columns in a hexagonal array. The methylene sequences are nearly extended with an all-trans conformation in the crystalline phase (209). The degree of conformational order varies

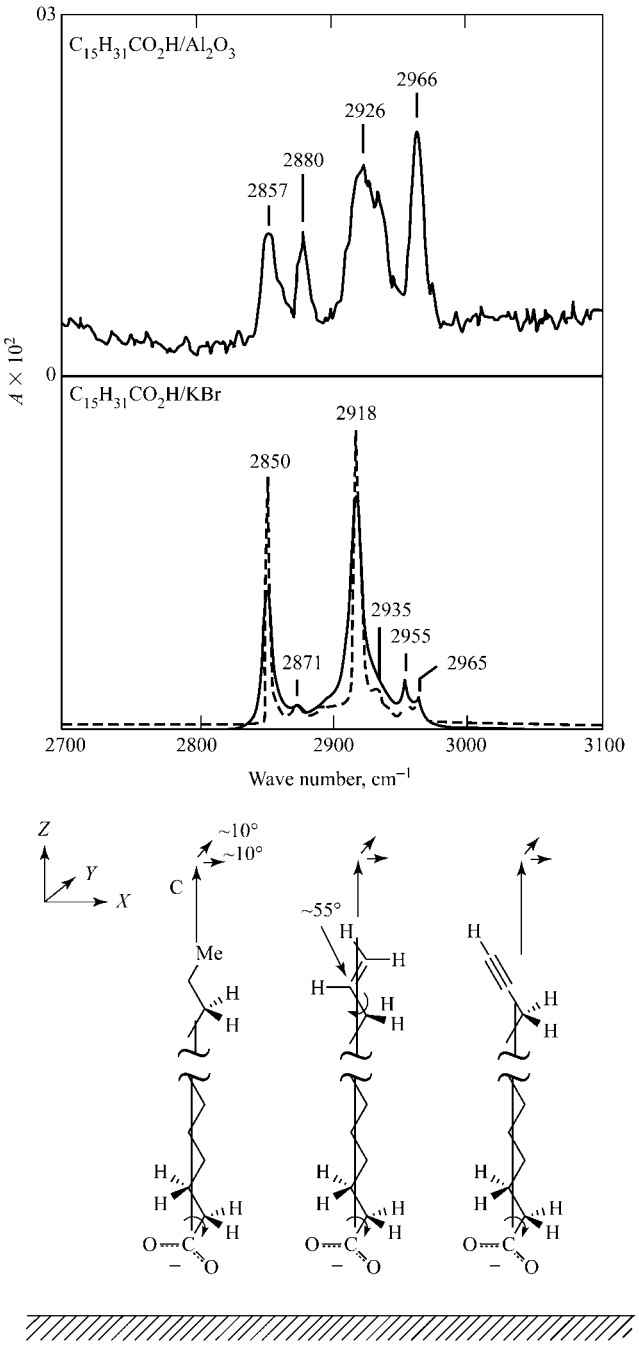

Fig. 28. Spectra and proposed structure of films absorbed onto substrate. (Top) Spectra in the mid-frequency region of n-$C_{15}H_{31}CO_2H$ as a film adsorbed on Al_2O_3 (top) and in a KBr matrix (bottom). The KBr experimental spectrum is accompanied by a deconvoluted spectrum (dashed curve), which represents enhanced resolution. n-$C_{15}H_{31}CO_2H$; (Bottom) Proposed structure of the adsorbed species having fully extended chains. The molecular orientation is defined relative to the surface coordinates (206).

considerably with temperature. Furthermore, conformational isomers are found for the ester groups. By using polarized reflection spectroscopy it is possible to deduce the structural transformation of individual subunits when overall phase transition occurs.

Structural changes corresponding to isotropic–nematic and nematic–crystalline transitions are expected to occur in the temperature range of 56–60°C. Bands assignable to methyl groups (2964 and 2873 cm^{-1} asymmetric and symmetric stretchings respectively) and methylene chains (2928 and 2858 cm^{-1} asymmetric and symmetric stretchings) are well known (Fig. 29). The relative intensities of the bands in this region change significantly as a function of temperature. Based on the relative intensity of the polarized spectra in the isotropic surface phase at 60°C, the methylene chains are mostly oriented at a slight angle relative to the external surface. The orientation of the skeletal plane is identically 0.0, supporting the view that these arms disorder quite quickly and completely in the isotropic phase. On decreasing the temperature from 60 to 56°C the orientation of the plane containing the methylene skeleton increases, indicating a substantial increase in this orientation function to above 0.2. Based on polarization studies of *n*-alkanes, the transition moment of the higher frequency component is parallel to the skeletal plane and that of the lower frequency component is normal to the skeletal plane. Both components contribute nearly equally to the band seen in the reflection spectrum of the isotropic melt at 60°C. As seen in Figure 29, the higher frequency component is much stronger than the lower frequency component in reflection spectra of the liquid crystalline and crystalline phases at temperatures at or below 56°C if the C—C—C skeletal plane is perpendicular to the metallic surface in the crystalline phase.

Furthermore, the relative intensity of the quinone C=O stretching vibration in the reflection spectrum at room temperature is much smaller than its intensity

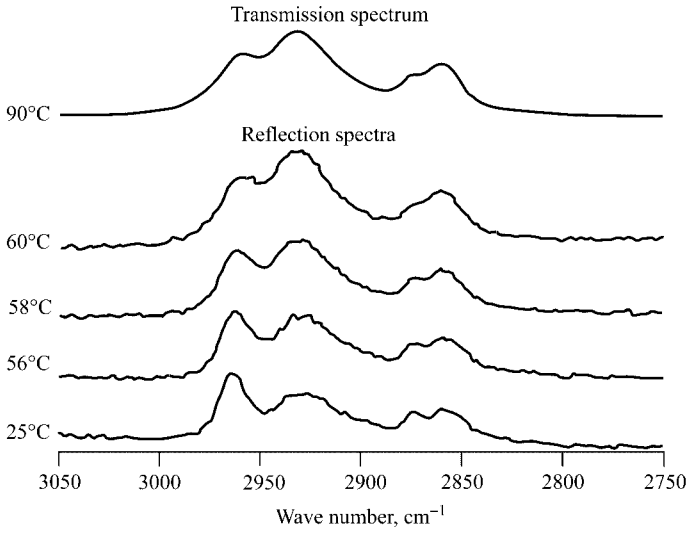

Fig. 29. Transmission spectrum of the isotropic melt and reflection spectra in the CH stretching region of adsorbed films of QTE8 as a function of temperature.

in the transmission spectrum of the isotropic state. This suggests that the transition moment of the in-plane C=O stretching 1690 cm^{-1} vibration tends to be parallel to the metal surface in nematic or crystalline phases. Semiempirical conformational calculations suggest that the transition moment angle of the ester C=O vibrations relative to the normal of the core plane is expected to be in the range of 31–53°. From our intensity data and these theoretical values, the possible range of the orientation function for the aromatic ring can be obtained. Even in the isotropic state (60–80°C), the aromatic core shows a slight tendency toward parallel orientation with respect to the substrate surface.

Potentially important ultrathin Langmuir–Blodgett films have been the focus of numerous studies (210). These are generally divided into two areas, those that concentrate on the film at the air–solution interface or on films which have been transferred to a supporting substrate (211–214). Most studies to date have focused on the second area. The first area is important for several reasons:

(1) The formation of the transferred films is dependent on the initial state at the air–solution interface.
(2) The changes in polymer conformation in constrained geometries is of fundamental importance and can be studied most conveniently at the air–solution interface.
(3) Reflectance spectroscopy developed for the air–solution interface is generally applicable to coatings on dielectric surfaces.
(4) Structural characterization of adsorbed chains is often complicated by substrate roughness.

Force–area relationships suggest the presence of varying structures (chain conformation, packing, and orientation) at the air–water interface, depending on the concentration of the molecules present. Detailed microscopic information such as changes in chain conformation is unavailable. The extremely small number of molecules present at the interface requires sensitive measurement techniques. Developments in the use of external reflection infrared experiments, however, allow spectra of molecules at the air–water interface to be obtained at nearly any concentration (215–217).

In contrast to the metallic substrate usually employed in reflection experiments, the complex boundary conditions that govern electromagnetic waves interacting with dielectric surfaces such as water make interpretation of spectra from the air–water interface more difficult (212). Several variations of computational methods for optical reflections from dielectric media have been reported (89,212,218,219). For a dielectric surface, both *s* and *p* polarized radiation within the film are present. Even though more spectroscopic information is available, the information obtained is more difficult to analyze. Infrared reflection studies of molecules at the air–water interface are most easily analyzed using isolated high frequency ($\sim$3000 cm^{-1}) C—H stretching vibrations. Phase transformations that involve chain packing and/or segmental orientation changes have been analyzed (89,215–217).

Insoluble polypeptide monolayer films at the air–water interface have been used as model compounds for biological systems to investigate chain

folding, molecular orientation, and domain formation (217). Little is known about the conformational state and stability of polypeptides confined at this interface. Poly(β-benzyl-L-aspartate) and poly(β-methyl-L-aspartate) usually form a left-handed 3.6_{13} α-helix (220,221). The relative stability of the left- and right-handed α-helical forms were estimated by molecular mechanics methods. Differences of only a few tenths of a kilocalorie per mole per residue were reported (222). The determining factor in inducing the left-handed helix appears to be the contribution of electrostatic energy that arises in the interaction between dipoles associated with the ester and amide groups. The calculation suggests that the interaction was more repulsive in the right-handed than left-handed form, thus destabilizing the right-handed helix. The similar conformational energies of left- and right-handed helices suggest that these forms may interconvert on heating or on altering the strength of the dipole–dipole interaction. The presence of water has been suggested to weaken interactions between effective charges on the atoms of the ester and amide groups, thereby destabilizing the left-handed helical structure and favoring the right-handed form. The circumstances in which right-handed α-helices form remain undefined.

The presence of different helical forms in polypeptide systems can be detected by infrared measurements of conformationally sensitive vibrational bands of the amide linkage. A correlation exists between the helix screw sense and frequencies of the amide I and amide II bands. The ranges of the amide I and II bands were respectively 1656–1659 and 1552–1555 cm^{-1} for the right-handed α-helix, 1664–1668 and 1555–1561 cm^{-1} for the left-handed α-helix, and 1675 and 1536 cm^{-1} for the ω-helix of poly(β-benzyl-L-aspartate). From external reflectance infrared spectra directly obtained at the air–water interface (Fig. 30), the conformation of poly(β-benzyl-L-aspartate) established that a right-handed α-helix, 4.0_{13} ω-helix, and a left-handed α-helix can all exist simultaneously at such an interface (217). The right-handed α-helix forms immediately when the film is cast on a surface of pure water. These helices persist at all compressions in a Langmuir trough. The helical screw sense can be reversed by lowering polarity of the aqueous phase. In addition, an alternate conformation similar to the ω-helix forms on addition of small amounts of 2-propanol to the aqueous subphase and appears to be an intermediate in the helix–helix transition.

A second example involves reflectance infrared spectroscopic structural analysis of polydimethylsiloxane at the air–water interface. Surface pressure versus surface area or surface concentration isotherms of polydimethylsiloxane on water have been studied since 1947 at least (223). Upon compression, the isotherm begins at zero surface pressure at surface concentrations significantly below 0.75 mg/m^2. Around Γ_1 0.75 mg/m^2, the surface pressure π jumps substantially to about 9 mN/m, where it exhibits a plateau until about Γ_2 1.6 mg/m^2, where a small π jump occurs followed by a smaller rise (Fig. 31). Structural features associated with the various transitions have often been debated. Particular controversy is associated with the π plateau around 9 mN/m between Γ_1 and Γ_2 (224,225). In conjunction with other techniques, such as epifluorescence microscopy, external reflectance infrared spectroscopy was used to study microstructural features (coexistence of two phases) of polydimethylsiloxane CH_3—$[Si(CH_3)_2$—$O]_n$—$Si(CH_3)_3$, spread at the air–water interface in the vicinity of the π plateau at 9 mN/m (226). A broad band containing several components is found in the 1000–1100 cm^{-1}

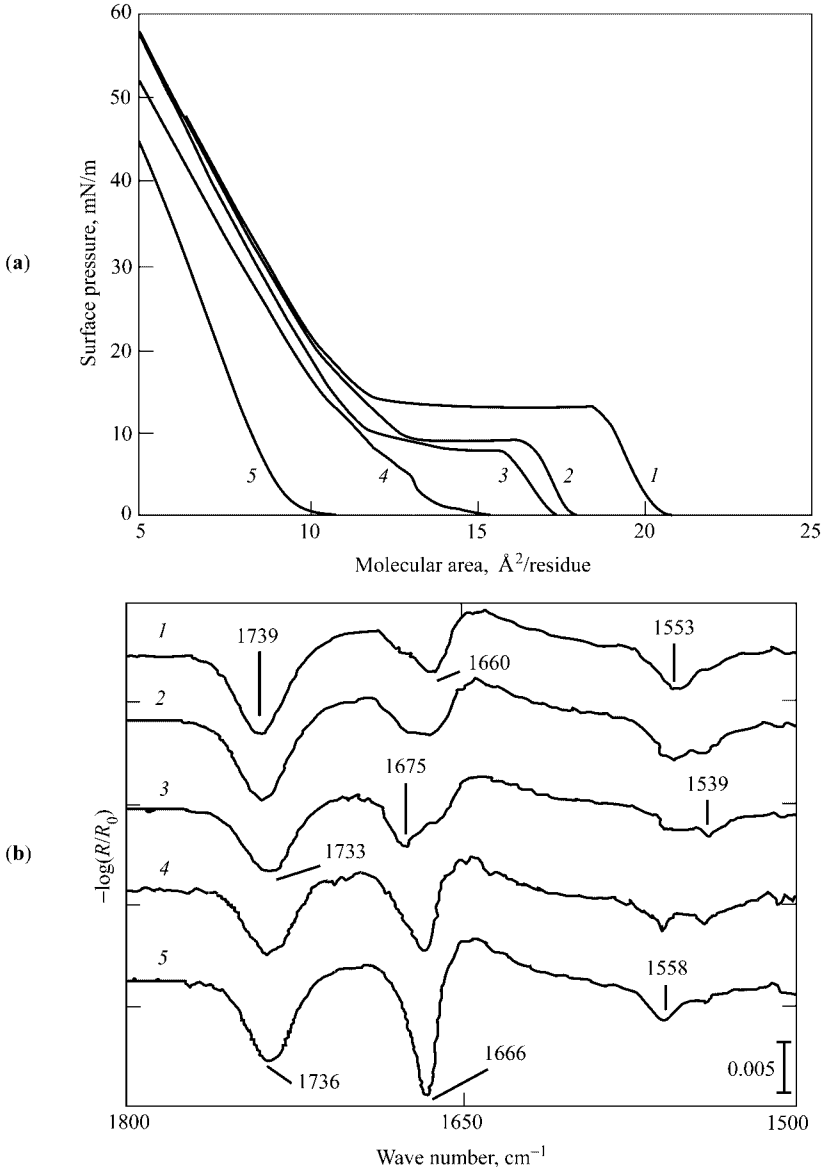

Fig. 30. (Top) Surface pressure–area isotherms for poly(β-benzyl-L-aspartate) films spread on water containing small concentrations of 2-propanol: (*1*) 0 vol%; (*2*) 0.4 vol%; (*3*) 0.5 vol%; (*4*) 0.85 vol%; and (*5*) 1.0 vol%. (Bottom) External reflection infrared spectra obtained at 40 mN/m from these films.

region. The spectra (Fig. 32) change significantly as surface concentration is varied between Γ_1 and Γ_2. At Γ_1 the most intense band is at 1005 cm^{-1}. At Γ_2, the most intense peak occurs at 1020 cm^{-1}. Weaker components are found around 1055 and 1090 cm^{-1}. All components persist to some extent at all concentrations studied. These spectra suggest that the 1020 cm^{-1} band originates in one

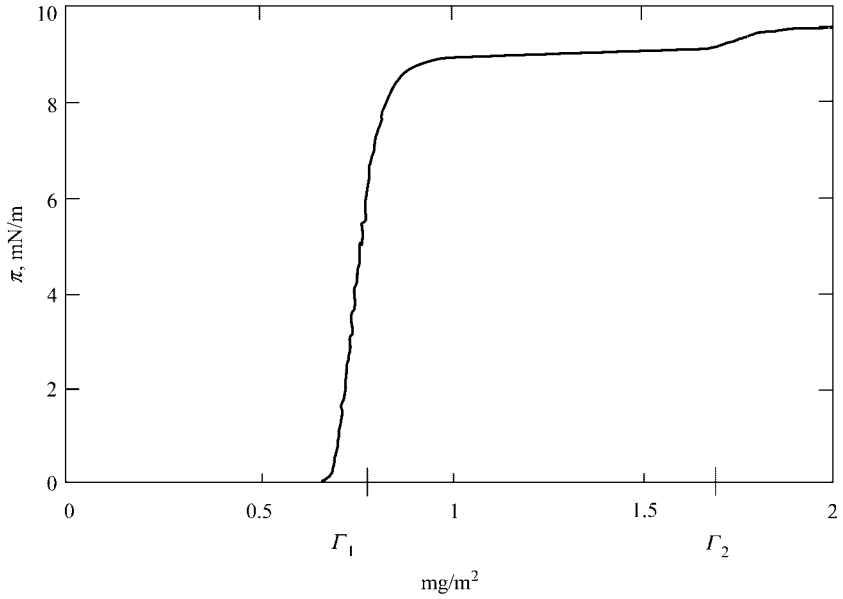

Fig. 31. A typical isotherm observed for polydimethylsiloxane film cast on a water surface.

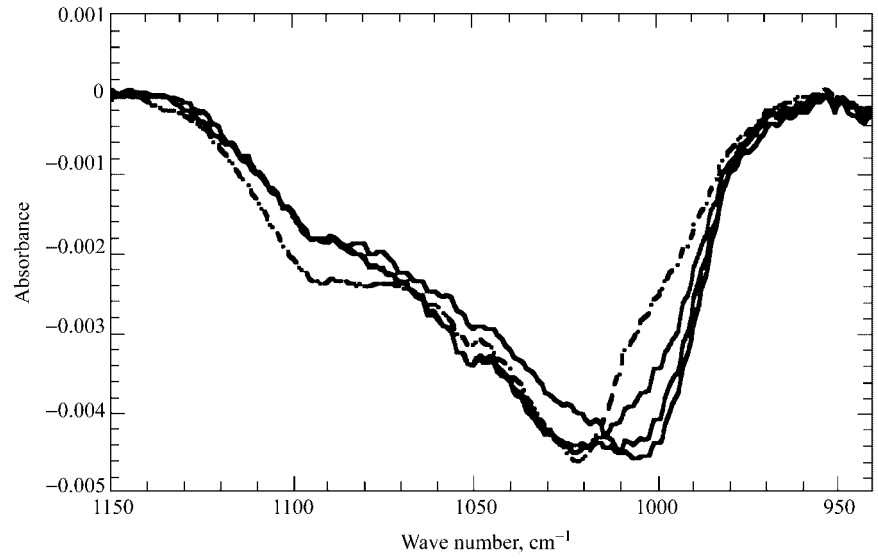

Fig. 32. Scaled external reflectance infrared spectra of the ν_{as} band for polydimethylsiloxane film spread on water at several concentrations between Γ_1 and Γ_2.

structure and the 1005 cm^{-1} band in another. In fact, these structures are consistent with the presence of a caterpillar-like structure at low surface pressure. For this structure, all the oxygen in the water and all the methyl groups point away from the water surface. The structure becomes considerably twisted with an initial jump in surface pressure to a helix with the helix axis parallel to the

water surface. The polarization characteristics of the infrared spectra obtained are consistent with transition moments calculated for these two models.

In a third example, polymer structural transition at interfaces has been demonstrated to significantly differ from that in bulk or solution (227). The polymer (designated poly[$(AG)_3EG$]) consists of 36 repeat units of an octapeptide sequence [$(AG)_3EG$] constituted from glycine (G), alanine (A), and glutamic acid (E) designed to adopt a folded-chain lamellar architecture in the solid state with the oligoalanylglycine segments forming β-strands and the periodic glutamic acid residues positioned in reverse turns at lamellar surfaces. Spectroscopic and X-ray diffraction analyses show that the crystalline polypeptide displays the expected architecture and the folding periodicity is as expected (228). In contrast, based on conformationally sensitive amide vibrations, poly[$(AG)_3EG$] in aqueous solution adopts a random coil conformation. The external infrared reflectance spectrum of poly[$(AG)_3EG$] at the air–water interface of a D_2O solution at pD 5.1 is quite different from the absorption spectrum of the same solution; the amide I′ band in the reflection spectrum appears at 1635 cm^{-1}, characteristic of the β-pleated sheet structure. Thus poly[$(AG)_3EG$] shows β-sheet character at the air–water interface but retains a random conformation in bulk solution. Furthermore, the amide I frequency of the polymer at the air–water interface shows a marked pH dependence. The amide I frequency shifts from about 1650 cm^{-1} at pH 13.6 to 1635 cm^{-1} at pH 5.0. Mild acidification drove a coil-to-sheet transition at the air–water interface. These results demonstrate that the conformational properties and transitions of adsorbed macromolecules can be very different from those in bulk solution. Adsorption of poly[$(AG)_3EG$] at the air–water interface allows a coil-to-sheet transition that is not observed in bulk.

Characterization of Silk Crystallization Behavior on Highly Oriented Substrate. The silk fibers produced by spiders and silkworms exhibit many impressive physical and mechanical properties which have inspired numerous attempts to spin such fibers from silk solutions *in vitro* (229). It is particularly interesting that silk originates from an aqueous solution. In the spinning process water-soluble silk fibroin is converted at room temperature to insoluble high performance fibers by a physical rather than a chemical process. Silk chains form a β-pleated sheet packed in an antiparallel fashion, referred to as silk II structure. The less stable water-soluble form is referred to as silk I. Either silk I or II structures can be obtained from solution, depending on crystallization conditions. In the substantial silk literature dealing with the mechanism of crystallization, parameters such as solvent, concentration, temperature, drying rate, and substrate are found to be important in determining chain conformation (229,230). Mechanical stress accompanying flow of the aqueous silk solution has been found crucial to the crystallization of b-form silk crystals from solutions of silk fibroin.

Orientation of silk molecules can be accomplished by shearing silk fibroin solution (231) or by adsorption to the air–water interface (232). The influence of an oriented substrate on the crystallization of silk from aqueous solution has been investigated by casting a film of silk from solution on a highly oriented poly(tetrafluoroethylene) substrate (233). This substrate is easily obtained by rubbing a poly(tetrafluoroethylene) block on glass slides under pressure at a suitable temperature. Transmission infrared spectroscopy has been used to characterize silk films since the early 1950s. External reflection infrared spectroscopy was

chosen to characterize both the microstructure of the substrate and that of the silk crystals. Silk films cast from either aqueous silk solution or aqueous silk-LiBr solution on the oriented poly(tetrafluoroethylene) surface exhibit more silk II structure than those cast on glass slides or on unoriented poly(tetrafluoroethylene) surfaces under identical conditions. Oriented poly(tetrafluoroethylene) films can therefore be used as templates to control cast film structures.

Double Modulation Spectroscopy

Some of the most interesting recent studies are designed around polarization modulation spectroscopy (16,207,234). Reflectance spectroscopy can be carried out with high sensitivity. Mechanical-vibrational spectroscopy has opened new areas relating polymer macroscopic behavior such as rheology to microstructural responses at the molecular level (235). The technique usually involves analysis of small differences. In the reflection experiment, for example, two different spectra are obtained using *s* and *p* radiations. The amount of energy absorbed by the film is extremely small with an absorbance unit in the third or fourth digit. Measuring the two spectra separately and analyzing their extremely small difference is a challenging task. The dynamic range of many instruments cannot differentiate differences beyond the signal to noise needed. Polarization modulation spectroscopy permits direct measurement of the difference.

The optical experiment setup used in other modulation experiments, shown in Figure 33, is quite similar to that used for vibrational circular dichroism experiments, described in detail elsewhere (234). Perhaps the experiment can best be understood from the following equations. Additional details can be found in the reference provided. The modulated beam is produced by the stress-induced difference in the index of refraction associated with the two perpendicular directions of a photoelastic modulator (PEM), in most cases a ZnSe crystal. Therefore, the

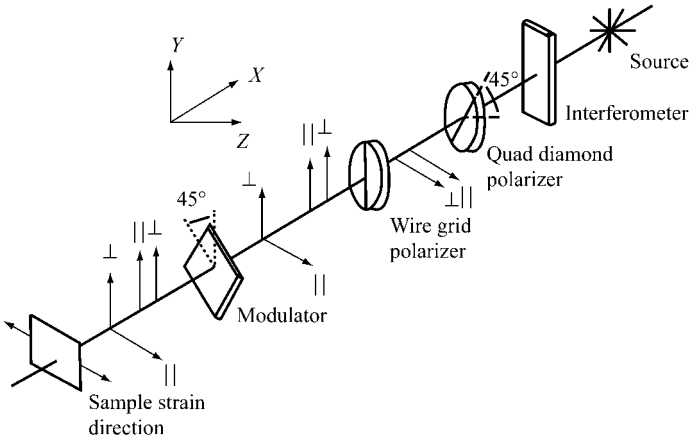

Fig. 33. Optical arrangement of elements in infrared modulation spectroscopy.

electric field E seen at the crystal is

$$E = \begin{pmatrix} \cos\alpha & \sin\alpha \\ -\sin\alpha & \cos\alpha \end{pmatrix} \begin{pmatrix} E_x \\ E_y \end{pmatrix} \tag{14}$$

For propagation along the z direction when only E_y is present, the PEM sees an electric field of

$$E = E_y \begin{pmatrix} \sin\alpha \\ \cos\alpha \end{pmatrix} \tag{15}$$

At any instant, the velocity of light through the PEM crystal with polarization parallel (p) and perpendicular (s) to the strain differ depending on the refractive indices, thus producing a phase difference δ between these two components. This phase difference depends on the wavelength, crystal thickness, and difference in index of refraction (122).

An additional phase $e^{i\delta}$ associated with the electric field along the p direction, leads to

$$E = E_y \begin{pmatrix} e^{i\delta}\sin\alpha \\ \cos\alpha \end{pmatrix} \tag{16}$$

After the crystal, it is necessary to consider radiation back into the laboratory frame, ie

$$E = \begin{pmatrix} \cos\alpha & -\sin\alpha \\ \sin\alpha & \cos\alpha \end{pmatrix} E_y \begin{pmatrix} e^{i\delta}\sin\alpha \\ \cos\alpha \end{pmatrix} = E_y \begin{pmatrix} (e^{i\delta}-1)\cos\alpha\ \sin\alpha \\ e^{i\delta}\ \sin^2\alpha + \cos^2\alpha \end{pmatrix} \tag{17}$$

Passing through the sample, the extinction coefficients for the incident infrared radiation may be quite different for the two axes. The intensity measured at the detector can be approximated by

$$|E|^2 = \frac{E_y^2}{2}(\varepsilon_s + \varepsilon_p) + \frac{E_y^2}{2}(\varepsilon_s - \varepsilon_p)\cos\,\delta \tag{18}$$

where ε_p and ε_s are the relative absorptions between two perpendicular axes in the polymer sample film. The two axes are usually defined as along and perpendicular to the applied strain. Since the crystal is being oscillated continuously at a frequency ω_m, the phase difference d is given as

$$\delta = \delta(t) = \delta_0\,\sin\,\omega_m t \tag{19}$$

and the intensity at the detector is

$$|E|^2 = I = \frac{E_y^2}{2}(\varepsilon_s + \varepsilon_p) + \frac{E_y^2}{2}(\varepsilon_s - \varepsilon_p)\cos\,\delta = I_{DC} + I_{AC}\,\cos(\delta_0 \sin\,\omega_m t) \tag{20}$$

Using the expansion for $\cos(\delta_0 \sin \omega_m t)$ in terms of Bessel functions, the intensity is written as

$$I = J_0(\delta_0) + 2\sum j_n(\delta_0) \cos(n\omega_m t) \tag{21}$$

Thus, it is possible to use a lock-in amplifier to select the time-dependent component and eliminate the -d-c component, and so the entire dynamic range of the infrared instrument is available to measure $\varepsilon_p - \varepsilon_s$ directly.

The power of this technique can be illustrated in the measurement of segmental orientation when polymers are deformed macroscopically. Despite the tremendous improvement of signal-to-noise ratio available with the Fourier transform instrument, it has not been possible to measure extremely small changes in segment orientation as a function of strain. The usual polarization measurements involve two separate measurements, one parallel and one perpendicular, followed by calculation of their difference to obtain the dichroic ratio, and then the calculation of the orientation function (eq. 13). For nearly isotropic materials this type of measurement is of marginal value. However, with the polarization modulation technique it is possible to obtain extremely accurate polarization changes when samples are mechanically deformed. Extremely accurate polarization measurements can be obtained in this way, even for amorphous segments in poly(butylene terephthalate-*co*-tetramethylene oxide) (236).

Other applications of modulation spectroscopy have been developed, ie two-dimensional infrared analysis (16). In this case, a spectrum is generated by a cross-correlation analysis of dynamic fluctuations of infrared signals induced by an external perturbation. The basic concept of two-dimensional infrared is somewhat analogous to that of two-dimensional NMR. The method for generation of a two-dimensional infrared spectrum is based on the ability to detect various relaxation processes occurring at much slower rates than vibrational relaxation. When a perturbation is applied to a system, various chemical constituents of the system are selectively excited. The excitation and subsequent relaxation toward equilibrium can often be monitored with polarized infrared radiation. It is often necessary to measure the relative phase shift between the periodic excitation of the piezoelectric modulator, the periodic excitation of the sample, and the interferometer of the spectrometer. The effect of perturbation-induced changes in a local molecular environment is manifested by time-dependent fluctuations of various spectra representing the system. In infrared spectroscopy, typical changes are the variation of intensities, frequency shift, and change in polarized absorbances. To simplify analysis, the amplitude of perturbation applied to the system is usually very small. Even with very small mechanical deformations, the energy dissipated in the sample may induce irreversible structural changes.

It is often important to correlate changes in polymer chain segments relative to the deformation axis in terms of the dichroic ratio. Typically, relative absorbances are measured for various functional groups. The differences represent the time-dependent reorientational rates of different structural units. The orientation of various functional groups may be dependent on the magnitude and specificity of various inter- and intramolecular interactions. Therefore, the rates of orientation and relaxation provide useful information of the local chemical environment. In polystyrene, a pair of strong cross peaks can be located at the lower left

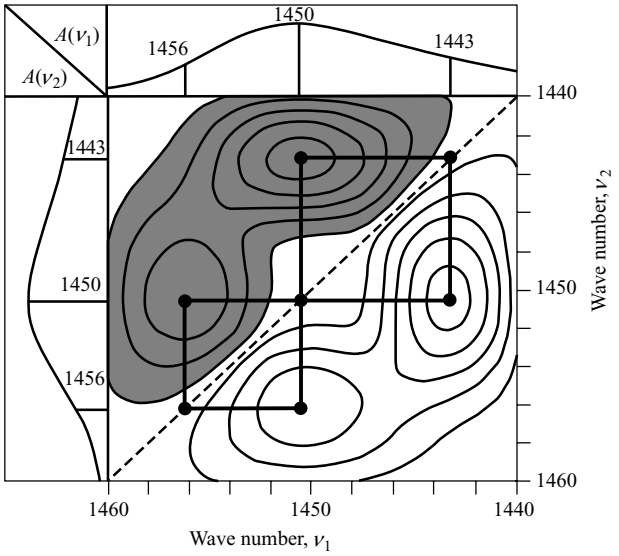

Fig. 34. Contour map of an asynchrous two-dimensional infrared correlation spectrum of atactic polystyrene near 1450 cm^{-1}.

corner of the spectrum (237). The cross peaks indicate the independent reorientation of the electric dipole-transition moments which give rise to the bands at 1490 and 1495 cm^{-1} (1). A similar cross-peak pair is developed at 1450 and 1495 cm^{-1}, suggesting the decoupling of bands. The transition moment giving rise to the band at 1495 cm^{-1} clearly exhibits a reorientation rate substantially different from the rest of the system.

Several peaks are observed (237) around the middle of the asynchronous spectrum between 1440 and 1460 cm^{-1}. The details of this region are more easily discernible in Figure 34. Four well-resolved peaks are located near the diagonal, which establish two correlation squares joined at 1450 cm^{-1}. The corresponding one-dimensional absorbance spectrum shows only a broad single peak. The two-dimensional infrared spectrum clearly resolves at least three distinguishable bands at 1443, 1450, and 1456 cm^{-1} by spreading them over the second dimension. The infrared absorbance peak of atactic polystyrene centered around 1450 cm^{-1} apparently is a triplet with its finer features obscured by the high degree of overlap. These bands have been suggested to originate from similar submolecular groups located in different local molecular environments. Others arise from vibrations of different structures.

Furthermore, at least six major distinguishable infrared bands located at 1443, 1450, 1456, 1465, 1490, and 1495 cm^{-1} have been identified (237). The obscure features of the ordinary spectrum consisting of two broad absorbance peaks with some shoulders can be clearly differentiated by use of the high resolution capability of the two-dimensional infrared spectrum. The six bands are grouped into three pairs of highly correlated bands reorienting at the same rate. For each pair, the cross peaks of the synchronous spectrum indicate reorientation.

When the sample is excited with a dynamic strain, the transition moments at 1443, 1450, and 1456 cm^{-1} reorient in the direction perpendicular to the strain direction; those at 1465, 1490, and 1495 cm^{-1} reorient parallel to strain. The

order of reorientation sequence is such that the coupled band pair at 1443 and 1495 cm^{-1} reorient first, followed by the pair at 1450 and 1490 cm^{-1}. There is approximately a 4 ms time lag between reorientations of the two. The last at 1456 and 1465 cm^{-1} moves about 5 ms behind the first. A detailed step-by-step description of the orientational relaxation processes of the transition moments should provide unique insight into the local molecular environment of the system.

The modulated technique is very general; it does not specify the physical nature or mechanisms through which the perturbation affects the system (15,16). Many different types of external perturbations could be used to stimulate the system of interest. For example, various molecular-level excitations may be induced by electrical, thermal, magnetic, chemical, acoustic, or mechanical excitations. Each perturbation affects the system in a unique and selective way, governed by the specific interaction mechanisms relating the macroscopic stimulus to microscopic or molecular responses of individual system constituents. The type of information contained in a dynamic spectrum is, therefore, determined by the selection of a perturbation method and electromagnetic probe. Recently, such modulation spectroscopy has been applied to Raman spectroscopy in which rheological properties of polymers have been measured. In addition, surface profile using modulated photoacoustic spectroscopy has proved successful. Lastly, it should be mentioned that modulation spectroscopy is not influenced by the purge quality of the instrument. The instrument chamber is often open during our reflectance experiments.

BIBLIOGRAPHY

"Infrared-Absorption Spectroscopy" in *EPST* 1st ed., Vol. 7, pp. 620–643, by I. Kössler, Ustav Fysikalní hemie, Ceskoslovenska Akademie Ved; "Infrared-Absorption Spectroscopy" in *EPST* 2nd ed., Vol. 8, pp. 69–101, by M. M. Coleman and P. C. Painter, The Pennsylvania State University; "Raman Spectroscopy" in *EPST* 2nd ed., Vol. 14, pp. 8–45, by N. E. Schlotter, Bell Communications Research.

1. G. Herzberg, *Infrared and Raman Spectra*, Vol. **2**, D. Van Nostrand Co., Princeton, N.J., 1945.
2. P. Painter, M. Coleman, and J. L. Koenig, *The Theory of Vibrational Spectroscopy and Its Application to Polymeric Materials*, John Wiley & Sons, Inc., New York, 1982.
3. J. L. Koenig, *Spectroscopy of Polymers*, American Chemical Society, Washington, D.C., 1992.
4. G. Zerbi, ed., *Modern Polymer Spectroscopy*, Wiley-VCH, New York, 1999.
5. N. B. Colthup, L. H. Daly, and S. E. Wiberly, *Introduction to Infrared and Raman Spectroscopy*, 3rd ed., Academic Press, Inc., Boston, 1990.
6. H. Tadokoro, *Structure of Crystalline Polymers*, Wiley-Interscience, New York, 1979.
7. R. Zbinden, *Infrared Spectroscopy of High Polymers*, Academic Press, Inc., New York, 1964.
8. S. Krimm, *Fortschr. Hochpolym.—Forsch.* **2**, 51 (1960).
9. L. A. Woodward, *Introduction to the Theory of Molecular Vibrations and Vibrational Spectroscopy*, Oxford University Press, Oxford, 1972, p. 370.
10. N. J. Harrick, *Internal Reflection Spectroscopy*, John Wiley & Sons, Inc., New York, 1967.
11. P. R. Griffiths and J. A. D. Haseth, *Anal. Chem. Appl.* **83**, 457 (1986).
12. R. J. Bell, *Introductory Fourier Transform Spectroscopy*, Academic Press, New York, 1972.
13. J. L. Koenig, *Microspectroscopic Imaging of Polymers*, American Chemical Society, Washington, D.C., 1998.

14. S. L. Hsu, in C. Booth and C. Price, eds., *Comprehensive Polymer Science*, Vol. **1**, Pergamon, Oxford, 1989, p. 429.
15. I. Noda, Y. Liu, and Y. Ozaki, *J. Phys. Chem.* **100**, 8665 (1996).
16. I. Noda, G. M. Story, A. E. Dowrey, R. C. Reeder, and C. Marcott, *Macromol. Symp.* **119**, 1 (1997).
17. M. W. Urban, *Macromol. Symp.* **141**, 15 (1999).
18. C. V. Raman, *Indian J. Phys.* **2**, 387 (1928).
19. C. V. Raman and U. S. Krishnan, *Nature* **121**, 501 (1928).
20. S. P. S. Porto, *J. Opt. Soc. Am.* **56**, 1585 (1966).
21. K. Nakamoto, *Infrared and Raman Spectra of Inorganic and Coordination Compounds*, John Wiley & Sons, Inc., New York, 1986.
22. R. T. Bailey and A. J. Hyde, and J. J. Kim, *Spectrochim Acta* **30A**, 91 (1974).
23. R. G. Snyder, *J. Mol. Struct.* **36**, 222 (1971).
24. R. G. Snyder, *J. Mol. Spectrosc.* **37**, 353 (1971).
25. R. G. Snyder, S. L. Hsu, and S. Krimm, *Spectrochim. Acta, Part A* **34**, 395 (1978).
26. Y. K. Wang, D. A. Waldman, R. S. Stein, and S. L. Hsu, *J. Appl. Phys.* **53**, 6591 (1982).
27. Y. K. Wang, D. A. Waldman, R. S. Stein, and S. L. Hsu, *Macromolecules* **15**, 1452 (1982).
28. I. W. Shepherd, *Biochem. J.* **155**, 543 (1976).
29. P. W. Thornley and I. W. Shepherd, *J. Polym. Sci., Polym. Phys. Ed.* **15**, 97 (1977).
30. P. W. Thornley and I. W. Shepherd, *J. Polym. Sci., Polym. Phys. Ed.* **15**, 1339 (1977).
31. R. Speak and I. W. Shepherd, *J. Polym. Sci., Polym., Symp.* **44**, 209 (1974).
32. A. J. Hartley, Y. K. Leung, J. Mc Mahon, C. Booth, and I. W. Shepherd, *Polymer* **18**, 336 (1977).
33. W. J. Walczak, D. A. Hoagland, and S. L. Hsu, *Macromolecules* **25**, 7317 (1992).
34. W. Walczak, D. A. Hoagland, and S. L. Hsu, *Macromolecules* **29**, 7514 (1996).
35. R. G. Snyder and Y. Kim, *J. Phys. Chem.* **95**, 602 (1991).
36. R. G. Snyder, *J. Chem. Soc., Faraday Trans* **88**, 1823 (1992).
37. T. D. Hahn, *Ph.D. dissertation*, University of Massachusetts, 1998.
38. X. Yang, Z. Su, D. Wu, S. L. Hsu, and H. D. Stidham, *Macromolecules* **30**, 3796 (1997).
39. G. Turrell, *Infrared and Raman Spectra of Crystals*, Academic Press, New York, 1972.
40. E. B. Wilson, J. C. Decius, and P. C. Cross, *Molecular Vibrations: The Theory of Infrared and Raman Vibrational Spectra*, Dover Publications, Inc., New York, 1955.
41. P. W. Higgs, *Proc. Roy. Soc. London, Ser. A* **220**, 472 (1953).
42. R. G. Snyder and J. H. Schachtschneider, *Spectrochim. Acta* **19**, 85 (1963).
43. R. G. Snyder and J. H. Sachtschneider, *Spectrochim. Acta* **20**, 853 (1964).
44. R. G. Snyder and J. H. Schachtschneider, *Spectrochim. Acta* **21**, 169 (1965).
45. C. W. Bunn, *Trans. Faraday Soc.* **35**, 483 (1939).
46. B. Wunderlich, *Macromolecular Physics*, Vol. **1**, Academic Press, Inc., New York, 1973.
47. B. Wunderlich, *Macromolecular Physics*, Vol. **2**, Academic Press, New York, 1976, Chapt. "6".
48. R. G. Snyder, *J. Mol. Spectrosc.* **4**, 411 (1960).
49. S. L. Hsu, W. H. Moore, and S. Krimm, *J. Appl. Phys.* **46**, 4185 (1975).
50. S. Krimm and Y. Abe, *Proc. Natl. Acad. Sci. U.S.A.* **69**, 2788 (1972).
51. T. Miyazawa, *J. Chem. Phys.* **32**, 1647 (1960).
52. S. Kang, X. Yang, S. L. Hsu, H. Stidham, P. B. Smith, and A. Leugers, *Macromolecules* **34**, 4542 (2001).
53. X. Yang, S. Kang, S. L. Hsu, H. D. Stidham, P. B. Smith, and C. Leugers, *Macromolecules* **34**, 4542 (2001).
54. D. E. Williams, *J. Chem. Phys.* **43**, 4424 (1965).
55. D. E. Williams, *J. Chem. Phys.* **45**, 3770 (1966).
56. W. L. Peticolas, G. W. Hibler, J. L. Lippert, A. Peterlin, and H. Olf, *Appl. Phys. Lett.*

18, 87 (1971).
57. C. K. Wu and M. Nicol, *J. Chem. Phys.* **58**, 5150 (1973).
58. F. Viras and T. A. King, *Polymer* **25**, 1411 (1984).
59. J. H. Schachtschneider and R. G. Snyder, *Spectrochim. Acta.* **19**, 117 (1963).
60. J. H. Schachtschneider and R. G. Snyder, *Spectrochim. Acta* **21**, 1527 (1965).
61. W. H. Moore and S. Krimm, *Biopolymers* **15**, 2439 (1976).
62. P. J. Flory, *Statistical Mechanics of Chain Molecules*, Wiley-Interscience, New York, 1969.
63. H. J. Tao, W. J. MacKnight, K. D. Gagnon, R. W. Lenz, and S. L. Hsu, *Macromolecules* **28**, 2016 (1995).
64. T. Hahn, W. Suen, S. Kang, S. L. Hsu, H. D. Stidham, and A. R. Siedle, *Polymer* **42**, 5813 (2001).
65. S. L. Hsu, T. Hahn, W. Suen, S. Kang, H. D. Stidham, and A. R. Siedle, *Macromolecules* **34**, 3376 (2001).
66. S. L. Hsu, J. P. Sibilia, K. P. O'Brien, and R. G. Snyder, *Macromolecules* **11**, 990 (1978).
67. J. A. Ewen, R. L. Jones, A. Razavi, and J. D. Ferrara, *J. Am. Chem. Soc.* **110**, 6255 (1988).
68. M. Peraldo and M. Cambini, *Spectrochimica Acta* **21**, 1509 (1965).
69. A. Zambelli, G. Natta, and I. Pasquon, *J. Polym. Sci., Part C* **4**, 411 (1963).
70. G. Masetti, F. Cabassi, and G. Zerbi, *Polymer* **21**, 143 (1980).
71. G. Natta, P. Corradini, and P. Ganis, *Makromol. Chem.* **39**, 238 (1960).
72. G. Natta, M. Peraldo, and G. Allegra, *Makromol. Chem.* **75**, 215 (1964).
73. T. Asakura, A. T. D. Aoki, M. Demura, and T. Asanuma, *Polym. J.* **28**, 24 (1996).
74. Y. Chatani, H. Maruyama, T. Asanuma, and T. Shiomura, *J. Polym. Sci., Part B: Polym. Phys.* **29**, 1649 (1991).
75. P. Sozzani, R. Simonutti, and A. Comotti, *Magn. Reson. Chem.* **32**, S45 (1994).
76. T. Nakaoki, Y. Ohira, H. Hayashi, and F. Horii, *Macromolecules* **31**, 2705 (1998).
77. Y. Wang, T. D. Hahn, S. L. Hsu, H. D. Stidham, and A. Seidle, manuscript in preparation.
78. J. M. Chalmers, *Polymer* **18**, 681 (1977).
79. S. L. Hsu and S. Krimm, *J. Polym. Sci., Phys. Ed.* **14**, 521 (1976).
80. V. M. Hallmark, S. P. Bohan, H. L. Strauss, and R. G. Snyder, *Macromolecules* **24**, 4025 (1991).
81. H. S. Lee, Y. K. Wang, and S. L. Hsu, *Macromolecules* **20**, 2089 (1987).
82. H. S. Lee and S. L. Hsu, *Macromolecules* **22**, 1100 (1989).
83. H. S. Lee, Y. K. Wang, W. J. MacKnight, and S. L. Hsu, *Macromolecules* **21**, 270 (1988).
84. S. Yoon, K. J. M. W. Ichikawa, and S. L. Hsu, *Macromolecules* **28**, 4278 (1995).
85. S. Yoon, K. Ichikawa, W. J. MacKnight, and S. L. Hsu, *Macromolecules* **28**, 5063 (1995).
86. S. Yoon, W. J. MacKnight, and S. L. Hsu, *J. Appl. Polym. Sci.* **21**, 197 (1997).
87. S. Yoon, PhD Thesis, University of Massachusetts, 1995.
88. X. Li and S. L. Hsu, *J. Polym. Sci., Polym. Phys. Ed.* **22**, 1331 (1984).
89. Y. Ren, C. W. Meuse, S. L. Hsu, and H. D. Stidham, *J. Phys. Chem.* **98**, 8424 (1994).
90. Y. Ren, M. S. Shoichet, T. J. McCarthy, H. D. Stidham, and S. L. Hsu, *Macromolecules* **28**, 358 (1995).
91. Y. Ren, PhD Thesis, University of Massachusetts, 1995.
92. K. Inomata and A. Abe, *J. Phys. Chem.* **96**, 7934 (1992).
93. A. Abe and K. Tasaki, *J. Mol. Struct.* **145**, 309 (1986).
94. G. D. Smith, R. L. Jaffe, and D. Y. Yoon, *J. Am. Chem. Soc.* **117**, 530 (1995).
95. S. Tsuzuki, T. Uchimaru, K. Tanabe, and T. Hirano, *J. Phys. Chem.* **97**, 1346 (1993).
96. G. D. Smith, D. Y. Yoon, R. L. Jaffe, R. H. Colby, R. Krishnamoorti, and L. J. Fetters, *Macromolecules* **29**, 3462 (1996).
97. S. Neyertz and D. Brown, *J. Chem. Phys.* **102**, 9725 (1995).

98. K. Tasaki, *J. Am. Chem. Soc.* **118**, 8459 (1996).
99. J. Koenig and A. C. Angood, *J. Polym. Sci., Part A-2* **8**, 1787 (1970).
100. K. M. Gough, *J. Chem. Phys.* **91**, 2424 (1989).
101. W. F. Murphy, J. M. Fernandez-Sanchez, and K. Raghavachari, *J. Phys. Chem.* **95**, 1124 (1991).
102. Y. Muroga, I. Noda, and M. Nagasawa, *Macromolecules* **18**, 1576 (1985).
103. S. I. Mizushima and T. Shimanouchi, *J. Am. Chem. Soc.* **71**, 1320 (1949).
104. R. F. Schaufele and T. Shimanouchi, *J. Chem. Phys.* **47**, 3605 (1967).
105. P. C. Painter, L. E. Mosher, and C. Rhoads, *Biopolymers* **21**, 1469 (1982).
106. B. Fanconi, *Biopolymers* **12**, 2759 (1973).
107. S. L. Hsu and S. Krimm, *J. Appl. Phys.* **47**, 4265 (1976).
108. J. F. Rabolt and B. Fanconi, *J. Polym. Sci., Polym. Lett. Ed.* **15**, 121 (1977).
109. J. F. Rabolt and B. Fanconi, *Polymer* **18**, 1258 (1977).
110. J. F. Rabolt, *Polymer* **22**, 890 (1981).
111. A. Hartley, Y. K. Leung, C. Booth, and I. W. Shepherd, *Polymer* **17**, 354 (1976).
112. K. Song and S. Krimm, *Macromolecules* **22**, 1505 (1988).
113. K. Song and S. Krimm, *J. Polym. Sci., Polym. Phys. Ed.* **28**, 63 (1990).
114. M. J. Folkes, A. Keller, and J. Stejny, *Colloid Polym. Sci.* **253**, 354 (1975).
115. C. Chang, Y. K. Wang, D. A. Waldman, and S. L. Hsu, *J. Polym. Sci., Polym. Phys. Ed.* **22**, 2185 (1984).
116. Y. K. Wang, P. H. C. Shu, R. S. Stein, and S. L. Hsu, *J. Polym. Sci., Polym. Phys. Ed.* **18**, 2287 (1980).
117. B. Chien, H. D. Stidham, S. L. Hsu, *Macromolecules* **29**, 4247 (1996).
118. B. Fanconi and J. Crissman, *J. Polym. Sci., Polym. Lett. Ed.* **13**, 421 (1975).
119. J. F. Rabolt, R. Twieg, and C. Snyder, *J. Chem. Phys.* **76**, 1646 (1982).
120. J. Rabolt, *J. Polym. Sci., Polym. Phys. Ed.* **17**, 1457 (1979).
121. H. G. Olf, A. Peterlin, and W. L. Peticolas, *J. Polym. Sci., Phys. Ed.* **12**, 359 (1974).
122. A. Peterlin, H. G. Olf, W. L. Peticolas, G. W. Hibler, and J. L. Lippert, *J. Polym. Sci., Part B* **9**, 359 (1971).
123. S. Krimm and S. L. Hsu, *J. Polym. Sci., Phys. Ed.* **16**, 2105 (1978).
124. G. R. Strobl and R. Eckel, *J. Polym. Sci., Phys. Ed.* **14**, 913 (1976).
125. R. G. Snyder, S. J. Krause, and J. R. Scherer, *J. Polym. Sci., Polym. Phys. Ed.* **16**, 1593 (1978).
126. A. Keller, *Rep. Prog. Phys.* **31**, 41 (1968).
127. J. P. Arlie, P. Spegt, and A. Skoulios, *Makromol. Chem.* **104**, 212 (1967).
128. I. Sanchez, *J. Appl. Phys.* **44**, 4332 (1973).
129. P. Dreyfus and A. Keller, *J. Polym. Sci., Part B* **8**, 253 (1970).
130. A. H. Windle, *J. Mater. Sci.* **10**, 252 (1975).
131. A. H. Windle, *J. Mater. Sci.* **10**, 1959 (1975).
132. R. G. Snyder, J. R. Schere, D. H. Reneker, and J. P. Colson, *Polymer* **23**, 1286 (1982).
133. G. V. Fraser, P. J. Hendra, M. E. A. Cudby, and H. A. Willis, *J. Mater. Sci.* **9**, 1270 (1974).
134. G. Capaccio, M. A. Wilding, and I. M. Ward, *J. Polym. Sci., Phys. Ed.* **19**, 1489 (1981).
135. C. J. Farrell and A. Keller, *J. Mater. Sci.* **12**, 966 (1977).
136. V. V. Tarasov, *New Problems in the Physics of Glass*, Oldbourne Press, Jerusalem, 1963.
137. B. Wunderlich, *Pure Appl. Chem.* **67**, 1019 (1995).
138. C. Kittel, *Introduction to Solid State Physics*, 7th ed., John Wiley & Sons, Inc., New York, 1996.
139. J. D. Savage, Y. K. Wang, M. Corbett, H. D. Stidham, and S. L. Hsu, *Macromolecules* **25**, 3164 (1992).
140. N. Ishihara and M. Kuramoto, *Catalyst Design For Tailor-Made Polyolefins*, Elsevier Science B.V., Amsterdam, the Netherlands, Vol. **89**, 1994, p. 339.

141. A. Immirzi, F. de Candia, P. Iannelli, and A. Zambelli, *Makromol. Chem., Rapid Commun.* **9**, 761 (1988).
142. V. Vittoria, F. de Candia, P. Iannelli, and A. Immirzi, *Makromol. Chem., Rapid Commun.* **9**, 765 (1988).
143. N. M. Reynolds, J. D. Savage, and S. L. Hsu, *Macromolecules* **22**, 2867 (1989).
144. M. Kobayashi, T. Nakaoki, and N. Ishihara, *Macromolecules* **22**, 4377 (1989).
145. G. Guerra, V. M. Vitagliano, C. De Rosa, V. Petraccone, and P. Corradini, *Macromolecules* **23**, 1539 (1990).
146. M. Gomez and A. E. Tonelli, *Macromolecules* **23**, 3385 (1990).
147. S. J. Spells, I. W. Shepherd, and C. J. Wright, *Polymer* **18**, 905 (1977).
148. T. Tatusumi, T. Fukushima, K. Imada, and M. Takayanagi, *J. Macromol. Sci., Part B: Phys. Ed.* **1**, 450 (1967).
149. J. M. Stellman, A. E. Woodward, and S. D. Stellman, *Macromolecules* **6**, 330 (1973).
150. E. Z. Fermi, *Physik* **71**, 250 (1931).
151. B. P. Gabor and W. L. Peticolas, *Biochim. Biophys. Acta* **465**, 260 (1977).
152. B. J. Bulkin and A. Krishnamachan, *J. Am. Chem. Soc.* **94**, 1109 (1972).
153. J. Thomas, S. L. Hsu, and D. A. Tirrell, *New J. Chem.* **18**, 407 (1994).
154. R. G. Snyder, S. L. Hsu, and S. Krimm, *Spectrochim. Acta, Part A* **34**, 395 (1978).
155. R. G. Snyder and J. R. Scherer, *J. Chem. Phys.* **71**, 3221 (1979).
156. G. C. Pimentel and C. H. Sederholm, *J. Chem. Phys.* **24**, 639 (1956).
157. G. C. Pimentel, *J. Am. Chem. Soc.* **79**, 3323 (1957).
158. G. L. Wilkes and J. A. Emerson, *J. Appl. Phys.* **47**, 4261 (1976).
159. T. K. Kwei, *J. Appl. Polym. Sci.* **27**, 289 (1982).
160. J. E. Hillard, in H. I. Aaronson, ed., *Spinodal Transformations*, American Society of Metals, Metals Park, Ohio, 1968.
161. H. Tsubomura, *J. Chem. Phys.* **24**, 927 (1956).
162. H.-J. Tao, C. F. Fan, W. J. MacKnight, and S. L. Hsu, *Macromolecules* **27**, 1720 (1994).
163. M. M. Coleman, J. F. Graf, and P. C. Painter, *Specific Interactions and the Miscibility of Polymer Blends*, Technomic Publishing Co., Lancaster, 1991.
164. D. L. Allara, *Appl. Spectrosc.* **33**, 358 (1979).
165. T. K. Kwei, T. Nishi, and R. F. Roberts, *Macromolecules* **7**, 667 (1974).
166. F. J. Lu, E. Benedetti, and S. L. Hsu, *Macromolecules* **16**, 1525 (1983).
167. D. Garcia, *J. Polym. Sci., Polym. Phys.* **22**, 1773 (1984).
168. J. L. Halary, J. M. Ubrich, L. Monnerie, H. Yang, and R. S. Stein, *Polym Commun.* **26**, 73 (1985).
169. F. B. C. Larbi, S. Leloup, J. L. Halary, and L. Monnerie, *Polym. Commun.* **27**, 23 (1986).
170. F. Gornick and L. Mandelkern, *J. Appl. Phys.* **33**, 907 (1962).
171. I. C. Sanchez, in D. R. Paul and S. Newman, eds., *Polymer Blends*, Academic Press, New York, 1978, p. 115.
172. E. Martuscelli, G. Demma, E. Rossi, and A. L. Segre, *Polym. Commun.* **24**, 266 (1983).
173. J. E. Katon, *Vib. Spectrosc.* **7**, 201 (1994).
174. L. Markwort, B. Kip, E. Da Silva, and B. Roussel, *Appl. Spectrosc.* **49**, 1411 (1995).
175. H. R. Morris, C. C. Hoyt, P. Miller, and P. J. Treado, *Appl. Spectrosc.* **50**, 805 (1996).
176. T. Nishioka, T. Nakano, and N. Teramae, *Appl. Spetrosc.* **46**, 1904 (1992).
177. C. Galiotis, R. J. Young, P. H. Yeung, and D. N. Batchelder, *J. Mater. Sci.* **22**, 3640 (1984).
178. H. L. Cox, *Brit. J. Appl. Phys.* **3**, 72 (1952).
179. G. S. Holister and C. Thomas, *Fibre Reinforced Materials*, Elsevier, Amsterdam, 1966.
180. C. F. Fan and S. L. Hsu, *J. Polym. Sci., Polym. Phys. Ed.* **27**, 337 (1989).
181. C. F. Fan and S. L. Hsu, *Macromolecules* **22**, 1474 (1989).
182. C. F. Fan and S. L. Hsu, *J. Polym. Sci., Part B: Polym. Phys.* **27**, 2605 (1989).
183. C. F. Fan and S. L. Hsu, *J. Polym. Sci., Part B: Phys. Ed.* **29**, 235 (1991).
184. C. D. Arvanitopoulos and J. L. Koenig, *Appl. Spectrosc.* **50**, 1 (1996).

185. R. L. Morgan, M. J. Hill, P. J. Barham, A. van der Pol, B. J. Kip, R. Ottjes, and J. van Ruitein, *Polymer* **42**, 2121 (2001).
186. M. A. Harthcock and S. C. Atkin, *Appl. Spectros.* **42**, 449 (1988).
187. A. Garton, D. N. Batchelder, and C. Cheng, *Appl. Spectrosc.* **47**, 922 (1993).
188. R. Appel, T. W. Zerda, C. Wang, and Z. Hu, *Polymer* **42**, 1561 (2001).
189. C. A. McFarland, J. L. Koenig, and J. L. West, *Appl. Spectrosc.* **47**, 321 (1993).
190. T. Jawhari, J. C. Merino, J. C. Rodriguez-Cabello, and J. M. Pastor, *Polymer* **34**, 1613 (1993).
191. T. Jawhari, J. C. Merino, J. C. Rodriguez-Cabello, and J. M. Pastor, *Polymer* **33**, 4199 (1992).
192. C. P. Lafrance, P. Chabot, M. Pigeon, R. E. Prud'homme, and M. Pezolet, *Polymer* **34**, 5029 (1993).
193. T. Jawhari, J. M. Pastor, *J. Mol. Struct.* **266**, 205 (1992).
194. R. Neuber and H. A. Schneider, *Polymer* **42**, 8085 (2001).
195. M. Mackley, *MRS Bull.* **22**, 47 (1997).
196. A. Zwijnenburg and A. J. Pennings, *Colloid Polym. Sci.* **253**, 452 (1975).
197. C. P. Lafrance, M. Pezolet, and R. E. Prudhomme, *Macromolecules* **24**, 4948 (1991).
198. W. Kuhn and F. Grun, *Kolloid Z.* **101**, 248 (1942).
199. R. J. Roe and W. R. Krigbaum, *J. Chem. Phys.* **40**, 2608 (1964).
200. R. J. Roe and W. R. Krigbaum, *J. Appl. Phys.* **35**, 2215 (1964).
201. P. H. Hermans, J. J. Hermans, D. Vermaas, and A. Weidinger, *J. Polym. Sci.* **3**, 1 (1947).
202. D. I. Bower, *J. Polym. Sci., Phys. Ed.* **10**, 2135 (1972).
203. H. J. Marrinan, *J. Polym. Sci.* **39**, 461 (1959).
204. C. W. Meuse, X. Yang, D. Yang, and S. L. Hsu, *Macromolecules* **25**, 925 (1992).
205. R. G. Greenler, *J. Phys. Chem.* **44**, 310 (1966).
206. D. L. Allara and R. G. Nuzzo, *Langmuir* **1**, 52 (1985).
207. A. E. Dowrey and C. Marcott, *Appl. Spectrosc.* **36**, 414 (1982).
208. D. Blaudez, T. Buffeteau, J. C. Cornut, B. Desbat, N. Escafre, M. Pezolet, and J. M. Turlet, *Appl. Spectrosc.* **47**, 869 (1993).
209. X. Yang, M. Kardan, D. Collard, R. B. Heath, C. P. Lillya, and S. L. Hsu, *J. Phys. Chem.* **92**, 196 (1988).
210. A. Ulman, *An Introduction to Ultrathin Organic Films*, Academic Press, Boston, 1991.
211. R. A. Dluhy and D. G. Cornell, *J. Phys. Chem.* **89**, 3195 (1985).
212. R. A. Dluhy, *J. Phys. Chem.* **90**, 1373 (1986).
213. R. Elbert, T. Folda, and H. Ringsdorf, *J. Am. Chem. Soc.* **106**, 7687 (1984).
214. G. L. Gaines, *Langmuir* **7**, 3054 (1991).
215. S. A. Riou, S. L. Hsu, and H. D. Stidham, *J. Polym. Sci, Polym. Phys.* **35**, 2843 (1997).
216. S. A. Riou, S. L. Hsu, and H. D. Stidham, *Biophys. J.* **75**, 2451 (1998).
217. S. A. L. H. S. Riou and H. D. Stidham, *Langmuir* **14**, 3062 (1998).
218. A. Gericke, A. V. Michailov, H. Huhnerfuss, *Vib. Spectrosc.* **4**, 335 (1993).
219. L. J. Fina and Y. Tung, *Appl. Spectrosc.* **45**, 986 (1991).
220. R. H. Karlson, K. S. Norland, G. D. Fasman, and E. R. Blout, *J. Am. Chem. Soc.* **82**, 2268 (1960).
221. E. M. Bradbury, A. R. Downie, A. Elliott, and W. E. Hanby, *Proc. Roy. Soc. London* 1960, 110.
222. M. Goodman, F. Boardman, and I. Listowsky, *J. Am. Chem. Soc.* **85**, 2491 (1963).
223. H. W. Fox, P. W. Taylor, and W. A. Zisman, *Ind. Eng. Chem.* 1947, 1401.
224. L. T. Lee, E. K. Mann, D. Langevin, and B. Farnoux, *Langmuir* **7**, 3076 (1991).
225. E. K. Mann, S. Henon, D. Langevin, and J. Meunier, *J. Phys. II, France* **2**, 1683 (1992).
226. T. D. Hahn, H. D. Stidham, and S. L. Hsu, *Macromolecules* **30**, 87 (1997).
227. H. Chen, S. L. Hsu, D. A. Tirrell, and H. D. Stidham, *Langmuir* **13**, 4775 (1997).

228. M. T. Krejchi, E. D. T. Atkins, A. J. Waddon, M. J. Fourinier, T. L. Mason, and D. A. Tirrell, *Science* **265**, 1427 (1994).
229. J. Magoshi, Y. Magoshi, and S. Nakamura, in W. W. A. D. Kaplan, B. Farmer, and C. Viney, eds., *Silk Polymers*, American Chemical Society, Washington, D.C., 1994, p. 292.
230. M. Ishida, T. Asakura, M. Yokoi, and H. Saito, *Macromolecules* **23**, 88 (1990).
231. K. Yamaura, Y. Okumura, and S. Matsuzawa, *J. Macromol. Sci., B: Phys.* **21**, 49. (1982).
232. W. S. Muller, L. A. Samuelson, S. A. Fossey, and D. Kaplan, *Langmuir* **9**, 1857 (1993).
233. C. C. Chen, S. Riou, S. L. Hsu, and H. D. Stidham, *Langmuir* **12**, 1025 (1995).
234. L. A. Nafie and D. W. Vidrine, in J. R. Ferraro and L. J. Basile, eds., *Fourier Transform Infrared Spectroscopy*, Vol. **3**, Academic Press, New York, 1982, p. 83.
235. L. A. Archer, G. G. Fuller, and L. Nunnelley, *Polymer* **33**, 3574 (1992).
236. E. Dobrovolny-Marand and S. L. Hsu, *Mater. Res. Soc. Symp. Proc.* **79**, 439 (1987).
237. I. Noda, *Appl. Spectrosc.* **44**, 550 (1990).

SHAW LING HSU
University of Massachusetts

VINYL ACETAL POLYMERS

Introduction

Vinyl acetal polymers are made by hydrolyzing poly(vinyl acetate) [9003-20-7] to poly(vinyl alcohol) [9002-89-5] and the reaction of the latter with an aldehyde in the presence of an acid catalyst. These two reactions, hydrolysis and acetalization, can be conducted either sequentially or concurrently (1). The acetalization reaction, shown in Figure 1, strongly favors complete condensation of one molecule of aldehyde with the 1,3-glycol of two vinyl alcohol units of poly(vinyl alcohol) to form the 1,3-dioxane ring of one vinyl acetal unit.

The first reported vinyl acetal polymers were prepared in Germany by W. Haehnel and W. O. Herrmann in the 1920s by acetalization of poly(vinyl alcohol) (2). Commercialization of vinyl acetal polymers began during the 1930s and 1940s following development efforts by a number of companies, including Consortium für Electrochemische Industrie, I.G. Farbenindustrie, Wacker, Canadian Electro Products, Union Carbide, General Electric, DuPont, Shawinigan Chemicals and Monsanto (both now Solutia) (3–11). Poly(vinyl butyral) [63148-65-2] (PVB, R = C_3H_7) from butyraldehyde [123-72-8] is superior over the vinyl acetal polymers from either formaldehyde [50-00-0], acetaldehyde [75-07-0], or propionaldehyde [123-38-6] for laminated safety glass owing to its better cold temperature characteristics (1). PVB provides flexible toughness over a wide range of temperatures and at a lower cost than longer chain aldehydic carbon acetals. PVB and to a lesser extent poly(vinyl formal) [9003-33-2] (PVF, R = H) continue to be made in significant commercial quantities. Where stiffer performance at higher temperatures is required, PVF provides significant property advancement.

Encyclopedia of Polymer Science and Technology. Copyright John Wiley & Sons, Inc. All rights reserved.

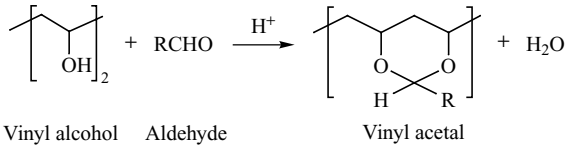

Fig. 1. Acid-catalyzed acetalization of two vinyl alcohol units of poly(vinyl alcohol).

Vinyl acetal polymers form hard, unpliable materials that are difficult to process without using solvents or plasticizers. PVF was developed for use in lacquers and impregnating materials and for wire insulation. PVF is combined with other reactive resins and cured to form tough, chemical- and abrasion-resistant coatings. The impetus for PVB development was the discovery of the greatly improved properties of laminated safety glass made with plasticized PVB interlayer over that offered by plasticized cellulose acetate then in general use. This application was expanded to include the architectural as well as automotive fields, and is today the largest single use of vinyl acetal polymer (12). Small amounts of PVB resin are used for a variety of adhesive, printing, and surface coating applications. Applications for PVF and PVB resins make use of the toughness, resilience, optical clarity, high pigment and filler binding capacity, and high adhesion the resins can provide when appropriately formulated.

Synthesis and Structure

Acetals are formed under conditions of acid catalysis by the reaction of aldehydes with alcohols (Fig. 2). The initial product of nucleophilic addition of alcohol to the carbonyl group is called a hemiacetal. In the net reaction, one molecule of aldehyde reacts with two molecules of alcohol (13).

Similarly, vinyl acetal polymers are manufactured by the reaction of aldehydes with poly(vinyl alcohol) in the presence of an acid catalyst. Reaction of the aldehyde with an alcohol, in this instance the polymeric alcohol poly(vinyl alcohol), yields the unstable hemiacetal. Complete condensation with loss of water is strongly favored to form the cyclic acetal. Poly(vinyl alcohol) used to manufacture vinyl acetal polymers is produced by hydrolysis of poly(vinyl acetate) homopolymer with methanol or ethanol. Both acids and bases catalyze the reaction, but base catalysis is usually done with methanol (14). The catalyst is either acid or base, depending on the process. Poly(vinyl acetate) is polymerized from vinyl

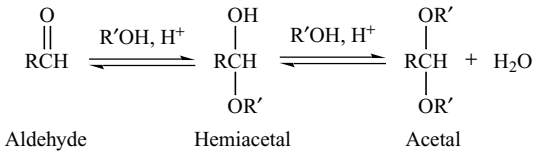

Fig. 2. One molecule of aldehyde reacts with two molecules of alcohol under conditions of acid catalysis to make an acetal.

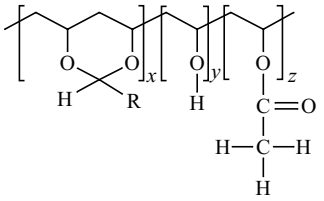

Fig. 3. Generalized terpolymer structure for vinyl acetal polymers, R = C_3H_7 for poly(vinyl butyral) PVB and R = H for poly(vinyl formal) PVF. Ranges for commercial grades of Butvar PVB from Solutia and Pioloform B PVB from Wacker include the following: *x*, vinyl butyral, is 52–74 mol% or 77–90 wt%; *y*, vinyl alcohol, is 26–45 mol% or 10–20 wt%; *z*, vinyl acetate, is 0–4 mol% or 0–3 wt% (19,20). For commercial grades of Vinylec PVF from Chisso: *x*, vinyl formal, is 73–79 mol% or 80–86 wt%; *y*, vinyl alcohol, is 10–14 mol% or 5.0–6.5 wt%; *z*, vinyl acetate, is 10–14 mol% or 9.5–13 wt% (21)

acetate by suspension or solution polymerization. (See VINYL ALCOHOL POLYMERS; VINYL ACETATE POLYMERS.)

Hydrolysis of poly(vinyl acetate) produces a poly(vinyl alcohol) with predominantly 1,3-glycol units. The derived poly(vinyl alcohol) can contain up to 2.3 mol% 1,2-glycol units that come from head-to-head placement of vinyl acetate monomer (15). Lower vinyl acetate polymerization temperature and conversion reduces the irregularities of the polymer, such as branching and the 1,2-glycol structure (16–18). Poly(vinyl acetate) hydrolysis is seldom complete, and for some applications, not desired. Therefore, vinyl acetal polymers are terpolymers, reflecting the three reactions that are used in their manufacture. The class can be represented by the generalized terpolymer structure (Fig. 3), with vinyl acetal, vinyl alcohol, and vinyl acetate units. A five-membered-ring acetal from acetalization of a 1,2-glycol unit is not shown.

A statistical estimate of the maximum degree of acetalization or mole fraction of isolated, unreacted hydroxyl units is 0.1840 for 1,3- and 1,2-glycol containing poly(vinyl alcohol) and 0.1353 for pure 1,3-glycol containing poly(vinyl alcohol) for irreversible acetalization (22). For acetalization with butyraldehyde, assuming no vinyl acetate component, this corresponds to an unreacted vinyl alcohol weight of 12.25% in PVB for the first case and 8.84% in PVB for the second case. As acetalization is reversible, interchange to higher levels of acetalization was also modeled (23). In practice, however, quantitative conversion is accompanied by intermolecular acetalization, which effectively limits higher levels of acetalization in commercial products.

The tacticity of hydroxyls in commercial poly(vinyl alcohol) is nominally atactic. However, an excess of *cis*-1,3-dioxane stereoisomers is formed during acetalization. Acetal formation depends strongly on process kinetics (24,25) and small quantities of other system components (26). During acetalization of poly(vinyl alcohol), for example, cis-acetalization is more rapid than trans-acetalization (27). In addition, the rate of hydrolysis of the trans-acetal is faster than for the more stable cis-acetal conformation (28). Because hydrolysis competes with acetalization during the acetalization process, a high cis/trans ratio is favored. The stereochemistry of PVF and PVB resins has been studied by proton and carbon NMR spectroscopy (29–32).

Manufacture

Although there are a number of potential methods for the manufacture of vinyl acetal polymers, in practice, only two basic processes with variants are used commercially today. By the solution process, formation of the acetal is as a solution in an organic solvent. By the aqueous process, the acetal is precipitated during the reaction of the aldehyde with an aqueous solution of poly(vinyl alcohol). These two reactions, hydrolysis and acetalization, can be conducted either sequentially or concurrently in the solvent process (1).

A solvent process with concurrent hydrolysis and acetalization is used to produce PVF resin (21,33–35). The hydrolysis of poly(vinyl acetate) and acetalization of the resultant poly(vinyl alcohol) to the formal are carried out concurrently in an aqueous acetic acid solution that also contains a strong mineral acid catalyst. Final polymer composition is controlled by the ratio of acetic acid, water, and formaldehyde in the starting mixture. When the reaction is complete, the mineral acid is neutralized. As water is added to the agitated mixture, the PVF resin precipitates. Color can be improved by adding antioxidants (qv) during acetalization (36). The resin is centrifuged and dried after washing with water to remove salt and organic by-products. Figure 4 is a flow diagram for the manufacture of PVF (33).

PVB resin can be produced by either a solvent process (37,38) or an aqueous process (11,39,40). The flow sheets for these processes are shown in Figures 5 and 6. In the aqueous process, poly(vinyl alcohol) is dissolved in water or an aqueous solution that contains acetic acid, then acidified with a mineral acid and reacted with butyraldehyde. During acetalization, PVB precipitates from the aqueous reaction mixture.

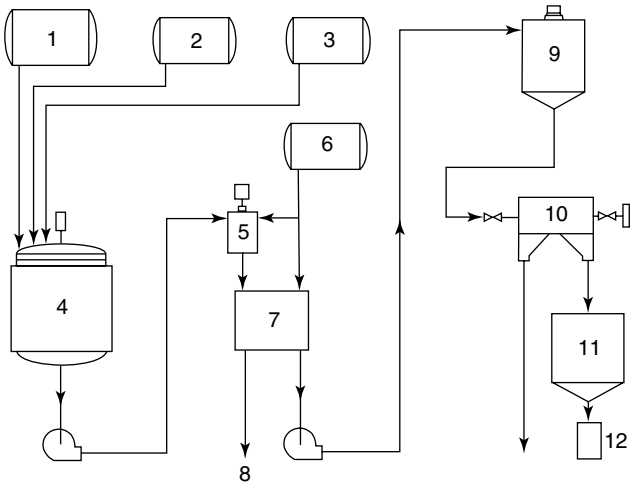

Fig. 4. Flow sheet for the manufacture of poly(vinyl formal) by a concurrent solvent process. 1, Poly(vinyl acetate) solution; 2, sulfuric acid tank; 3, sodium acetate tank; 4, reactor for hydrolysis and acetalization; 5, precipitator; 6, water tank; 7, wash tank; 8, liquor recovery system; 9, hold-up tank; 10, centrifuge; 11, dryer; 12, finished product (33). Courtesy of The Electrochemical Society, Inc.

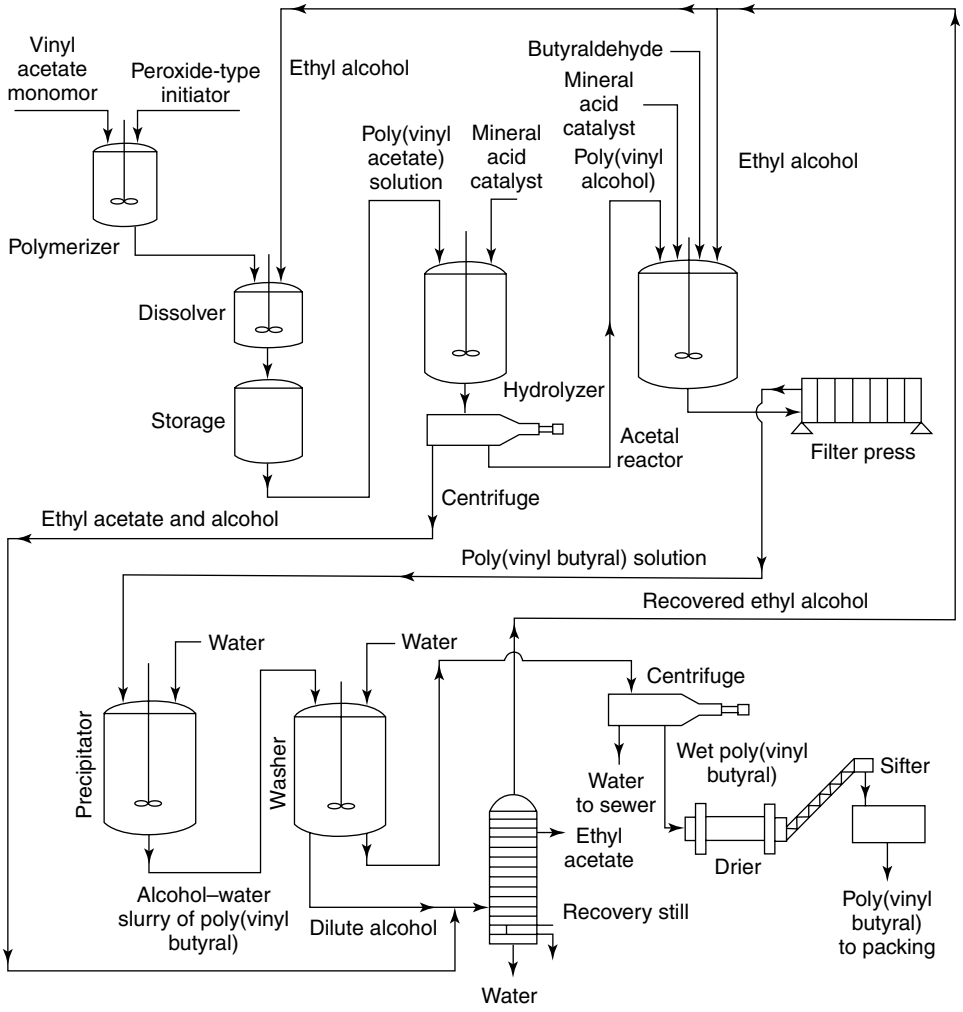

Fig. 5. Flow sheet for the manufacture of poly(vinyl butyral) by a solvent process using sequential hydrolysis and acetalization (38). Courtesy of McGraw-Hill, Inc.

In the solvent process to make PVB (Fig. 5), poly(vinyl acetate) is saponified by transesterification in the presence of ethanol and a mineral acid catalyst to produce poly(vinyl alcohol). The ethanol and ethyl acetate are separated from the precipitated poly(vinyl alcohol) by centrifugation. Because the desired properties of the final PVB require a low poly(vinyl acetate) content, concurrent hydrolysis and acetalization, employed for PVF manufacture, cannot be used. In a separate unit operation, poly(vinyl alcohol) is acetalized after being reslurried with ethanol, and heated with butyraldehyde and the acid catalyst. As the acetalization reaction proceeds in the solvent process, the slurry of poly(vinyl alcohol) dissolves as PVB in the ethanolic reaction mixture.

Upon completion of the acetalization reaction in both solvent and aqueous processes, the acid catalyst is neutralized. PVB is precipitated into water during

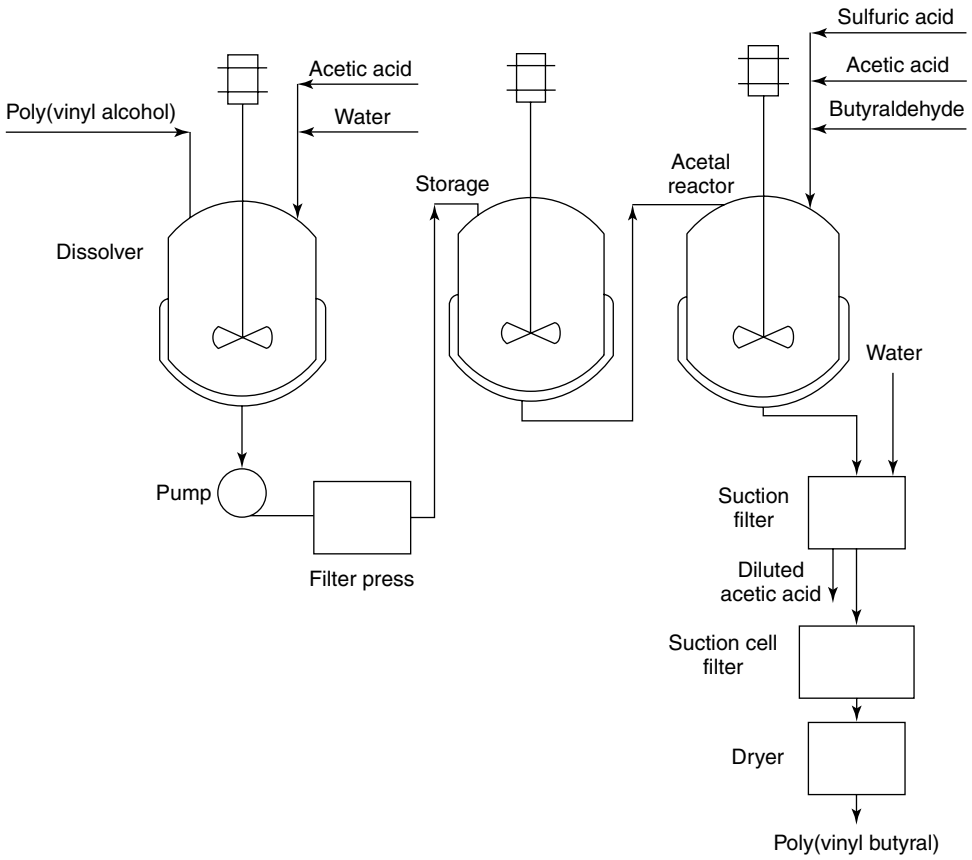

Fig. 6. Flow sheet for the manufacture of poly(vinyl butyral) by an aqueous process (39).

aqueous neutralization in the solvent process. In both aqueous and solvent processes, resin is then separated, washed, and dried. Neutralization, typically with sodium hydroxide or potassium hydroxide, and washing stages are necessary to remove the acid catalyst, salt, and to achieve a more alkaline resin pH for improved resin thermal stability (8,10,37).

For the solvent process, the ethyl acetate by-product can be recovered, refined, and sold as an additional product. This somewhat offsets the cost of sequential polymerization, hydrolysis, acetalization, and solvent recovery unit operations in one manufacturing plant. Because of the low capital investment required to produce PVB with market poly(vinyl alcohol) however, most of the recent published literature has dealt with the aqueous process.

Resin from the solvent acetalization reaction has very low levels of gel from intermolecular acetalization, whereas precipitated resin in the aqueous acetalization reaction has a tendency toward high levels of intermolecular acetalization. Cross-linking can be minimized by adding emulsifiers to control particle size (40–45), or substances like ammonium thiocyanate (46) or urea (47), to improve the solubility of PVB in the aqueous phase. To increase the average molecular weight

and polydispersity of the resin, small quantities of a dialdehyde or trialdehyde can be added during the acetalization step (48).

Properties

The properties of vinyl acetal polymers are a function of the relative amounts of the three randomly distributed units and the molecular weight. As indicated in Figure 3, manufacturers offer a variety of hydroxyl levels. Generally, PVB grades are produced commercially with either high (17–20 wt%) residual vinyl alcohol content or low (10–13 wt%) vinyl alcohol content. The acetate level for commercial PVB resins is usually low (0–3 wt%). However, comparatively higher acetate levels are produced for PVF resin grades to improve solubility at the expense of strength and dimensional stability (33). Residual vinyl acetate and vinyl alcohol contents are 9.5–13 wt% and 5.0–6.5 wt%, respectively, for commercial PVF grades available (21). Weight–average molecular weight ranges from about 25,000 to 100,000 Da for PVF resins and from 30,000 to 350,000 Da for PVB resins, depending on the grade.

Table 1 lists suppliers for PVB resins, commercial trade names, and reported 1999 plant capacities (49). The only major manufacturer of PVF resins is Chisso Corp. in Japan (trade name Vinylec). Chisso purchased Monsanto's PVF Formvar business in 1992. Wacker no longer manufactures PVF Pioloform F resins, only PVB Pioloform B resins. Table 2 lists reported properties of Vinylec PVF resins (21). The physical, mechanical, and thermal properties of various grades of Solutia's Butvar resins are listed in Table 3 (19). In general, resin melt and solution viscosity increase with increasing molecular weight and vinyl alcohol content, whereas the tensile strength of materials made from PVB increases with vinyl alcohol content for a given molecular weight.

The major use of PVB resin is for the manufacture of sheet used as an interlayer in laminated safety glass for automotive and architectural applications. PVB for laminated safety glass contains typically only 1–3 wt% of residual vinyl acetate units and 18–23 wt% vinyl alcohol units (49). The remaining hydroxyl

Table 1. Major PVB Resin Producing Companies

Resin plants	Plant location	Trade name	1999 Annual capacity[a], 10^3t
United States			
Solutia	Trenton, Mich, and Springfield, Mass	Butvar	57
DuPont	Fayetteville, N.C., and Parkersburg, W.Va.	Butacite	41
Europe			
Solutia	Antwerp, Belgium	Butvar	20
Kuraray	Frankfurt, Germany	Mowital	25
Wacker	Burghausen, Germany	PioloformB	[b]
Asia			
Sekisui	Koga-gun, Shiga Prefecture, Japan	S-Lec	30

[a]Ref. 49.
[b]Not available.

Table 2. Properties of Vinylec PVF Resins[a]

	PVF
Vinyl alcohol, wt%	5.0–6.5
Vinyl acetate, wt%	9.5–13
Specific gravity	1.1–1.3
Tensile strength, MPa[b]	49–78
Flexural strength, MPa[b]	108–127
Hardness, shore	70–80
Flow temperature, °C	140–150
Heat distortion temperature, °C	84–93
Dielectric strength, kV/mm	26–39
Dielectric constant, 60 Hz	3.0–3.7
Volume resistivity, Ω·cm	10^{14}–10^{16}
Dissipation factor, 60 Hz	0.006–0.015

[a]Ref. 21.
[b]To convert MPa to psi, multiply by 145.

groups have reacted with butyraldehyde to form acetal units. Hydroxyl level provides the prime leverage on performance in most applications. Unacetalized hydroxyls take part in both intramolecular and intermolecular hydrogen bonding. Intermolecular hydrogen bonding helps bind individual macromolecules together, making it more difficult for chains to untangle and slip by each other. Resin glass-transition temperature (T_g), viscosity, modulus, and tensile strength increase with higher residual hydroxyl levels. Simultaneously, processability and resiliency are reduced. Backbone hydroxyl groups also can form hydrogen and covalent bonds to the surface of polar substrates and are largely responsible for the adhesion. It is postulated that both hydrogen bonds and silyl alkyl ether covalent bonds are formed between resin hydroxyl groups and silanol groups at the PVB interlayer–glass interface (50). Film is made by the addition of plasticizer and other additives to the resin. Resin functionalities as well as plasticizer and moisture level of the formulation are important to PVB's safety glass properties.

A wide range of thermal performance results from the selection of aldehyde in addition to the composition of hydroxyl and acetate units in vinyl acetal polymers. The thermal glass-transition temperature (T_g) of vinyl acetal polymers of aliphatic aldehydes can be estimated from equation 1. VOH and VAC are the weight percent of residual vinyl alcohol and residual vinyl acetate units and C is the number of carbons in the chain derived from the aliphatic aldehyde (51).

$$T_g = 65 + 1.26(\mathrm{VOH} - 19.0) - 0.6(\mathrm{VAC} - 1.5) + 46\ln(4/C) \quad (1)$$

The equation is set up for a typical PVB with 19% residual vinyl alcohol and 1.5% residual vinyl acetate. For this typical PVB ($C = 4$, VOH = 19.0, and VAC = 1.5) the equation reduces to a predicted thermal glass transition of 65°C. Vinyl acetal polymers of any glass-transition temperature between roughly 20 and 120°C can be obtained by formulating with mixed aldehydes. Glass-transition temperatures for mixed aldehyde polymers can be estimated using equation 1 by

Table 3. Properties of Butvar PVB Resins[a]

	Method	B-72	B-74	B-76	B-90	B-98
Vinyl alcohol, wt%		17–20	17–20	11–13	18–20	18–20
Vinyl acetate, wt%		0–2.5	0–2.5	0–1.5	0–1.5	0–2.5
Mol weight ave, 10^3 Da	[b]	170–250	120–150	90–120	70–100	40–70
Viscosity, Pa·s[c]	[d]	7–14	3–7	0.5–1	0.6–1.2	0.2–0.4
Viscosity, Pa·s	[e]	1.6–2.5	0.8–1.3	0.2–0.45	0.2–0.4	0.07–0.2
Ostwald viscosity, cP	[f]	170–260	40–50	18–28	13–17	6–9
Specific gravity at 23°C	ASTM D792-50	1.100	1.100	1.083	1.100	1.100
Refractive index	ASTM D542-50	1.490	1.490	1.485	1.490	1.490
Tensile strength, MPa[g]						
Yield	ASTM D638-58T	47–54	47–54	40–47	43–50	43–50
Break		48–55	48–55	32–39	39–46	39–46
Elongation, %						
Yield	ASTM D638-58T	8	8	8	8	8
Break		70	75	110	100	110
Elastic modulus, GPa[h]		2.30	2.30	1.97	2.10	2.17
Flexural strength, MPa						
Yield	ASTM D790-59T	83–90	83–90	72–79	76–83	76–83
Rockwell hardness						
M	ASTM D785-57	115	115	100	115	110
E		20	20	5	20	20
Impact strength, J/m[i]	ASTM D256-56[j]	58.7	58.7	42.7	48	37.4
Flow temperature, °C	ASTM D569-59	145–155	135–145	110–115	125–130	105–110
Heat distortion temp, °C	ASTM D648-56	56–60	56–60	50–54	52–56	45–55
Heat sealing temp, °C	[k]	220	220	200	205	200
T_g, °C	[l]	72–78	72–78	62–72	72–78	72–78

[a] Ref. 19.
[b] Determined by size exclusion chromatography in tetrahydrofuran with low angle light scattering.
[c] To convert Pa·s to cP, multiply by 100.
[d] 15 wt% measured in 60:40 toluene/ethanol at 25°C using a Brookfield viscometer.
[e] 10 wt% measured in 95 wt% ethanol at 25°C using an Ostwald–Cannon–Fenske viscometer.
[f] B-72 in 7.5 wt% anhydrous methanol at 20°C; B-76 and B-79 in 5.0 wt% SD-29 ethanol at 25°C; B-74, B-90, and B-98 in 6.0 wt% anhydrous methanol at 20°C, all using an Ostwald–Cannon–Fenske viscometer.
[g] To convert MPa to psi, multiply by 145.
[h] To convert GPa to psi, multiply by 145,000.
[i] To convert J/m to (ft·lb)/in., divide by 53.38.
[j] Notched Izod [1.27 × 1.27 cm (0.5 × 0.5 in.)].
[k] Dried film (0.025 mm) on paper cast from 10 wt% resin in 60:40 toluene/ethanol; heat sealer dwell time, 1.5 s at 60 psi.
[l] By differential scanning calorimetry from 30 to 100°C on dried resin.

computing an average chain length weighted by the respective aldehyde mole fractions.

Practical considerations have thus far precluded commercial manufacture of vinyl acetal polymers from higher molecular weight aldehydes or from mixed aldehydes. At an aldehyde chain length of more than four carbon atoms, the aldehyde becomes insoluble in water, with the result that washing and purification of the resin are extremely difficult. T_g drops with increasing aldehyde chain length and

Table 4. Solubility Parameter Ranges of PVF and PVB Resins

Resin[a]	Low hydrogen-bonding solvents	Medium hydrogen-bonding solvents	High hydrogen-bonding solvents
PVF, 9.5–13 wt% vinyl acetate	9.3–10.0	9.7–10.4	9.9–11.8
PVB, 10–13 wt% vinyl alcohol	9.0–9.8	8.4–12.9	9.7–12.9
PVB, 17–20 wt% vinyl alcohol	[b]	9.9–12.9	9.7–14.3

[a]Ref. 52.
[b]Insoluble.

so drying and storage without agglomeration becomes impractical. In general, a reasonable compromise in properties can be reached by selection of a commercially available PVF or PVB resin combined with a suitable plasticizer. A close working relationship with the manufacturer can be helpful for applications development.

Vinyl acetal polymers form hard, unpliable materials that are difficult to process without using solvents or plasticizers. The solubility parameter ranges for commercially available PVF and PVB resins are listed in Table 4. For most applications, T_g is far more practically manipulated with plasticizers. However, acetalization with longer chain aldehydes (53–55) and polyoxyalkylene chains (56) provides a degree of internal plasticization to reduce T_g without relying exclusively on liquid plasticizers.

PVB resins are soluble in alcohols, glycol ethers, and selected mixtures of polar and nonpolar solvents. The low (10–13 wt%) vinyl alcohol content PVB resins are soluble in a wider range of solvents than are the high (17–20 wt%) vinyl alcohol content PVB resins. Solvent blends are commonly used, the exact solvent blend and resin composition dictated by the end use of the solution and the required drying properties (19,20). PVF resins are soluble in a more limited number of solvents and in certain mixtures of alcohols and aromatic hydrocarbons. Table 5 compares solvent compatibilities of PVF and PVB resins.

A wide variety of plasticizers are suitable for PVB and PVF resins. For many years, the universally used plasticizer for PVB was triethylene glycol di(2-ethylbutyrate) [95-08-9] (6). More recently this has been supplanted by triethylene glycol di(2-ethylhexanoate) [94-28-0], tetraethylene glycol diheptanoate [70729-68-9], dihexyl adipate [110-33-8], 2-ethylhexyl diphenyl phosphate [1241-94-7], and a variety of other oligomeric ethylene glycol esters and ethers, and other adipate, phosphate, phthalate, sebacate, and ricinoleate esters (19,20,57–62). For PVF, diethyl, diphenyl, and dicyclohexyl phthalates, as well as tributyl, triphenyl, and tricresyl phosphates are useful plasticizers (21). By proper choice of plasticizer type and level, the physical–mechanical, chemical, and adhesion properties of these resins can be tailored for a wide variety of applications (see PLASTICIZERS).

Vinyl acetal polymers can be formulated with other thermoplastic polymers and with a variety of multifunctional cross-linkers. Examples of polymers that are at least partially compatible with PVF or PVB resins include some types of polyurethanes, some types of celluloses, epoxies, isocyanates, phenolics, silicones, unsaturated polyesters, and melamine– and urea–formaldehyde polymers (19–21). Although vinyl acetal polymers are thermoplastic, hydroxyl groups permit cross-linking reactions with a variety of thermosetting resins, for example,

Table 5. Solvent Compatibilities of PVF and PVB Resins[a,b]

	PVF	PVB	PVB
Vinyl alcohol, wt%	5.0–6.5	10–13	17–20
Vinyl acetate, wt%	9.5–13	0–3	0–3
Acetic acid (glacial)	S	S	S
Acetone	I	S	I
n-Butanol	I	S	S
Butyl acetate	I	S	I
Carbon tetrachloride	I	I	I
Cresylic acid	S	S	S
Cyclohexanone	I	S	S
Diacetone alcohol	I	S	S
Diisobutyl ketone	I	S	I
Dioxane	S	S	S
N,*N*-dimethylacetamide	S	S	S
N,*N*-dimethylformamide	S	S	S
Ethanol, 95 wt%	I	S	S
Ethyl acetate, 99 wt%	I	S	I
Ethyl acetate, 85 wt%	I	S	S
Ethyl "Cellosolve"	I	S	S
Ethylene chloride	S	S	S
Hexane	I	I	I
Isopropanol, 95 wt%	I	S	S
Methyl acetate	I	S	S
Methanol	I	I	S
Methyl "Cellosolve"	I	S	S
Methyl "Cellosolve" acetate	I	S	I
2-Methyl-3-butyn-2-ol	S	S	S
3-Methyl-1-pentyn-3-ol	S	S	S
Methyl ethyl ketone	I	S	I
Methyl isobutyl ketone	I	S	I
N-methyl-2-pyrrolidinone	S	S	S
Nitropropane	I	I	I
2-Propanol, 95 wt%	I	S	S
Toluene	I	S	I
Toluene/ethanol (60:40 wt%)	S	S	S
Xylene	I	I	I
Xylene/*n*-butanol (60:40 wt%)	I	S	S

[a] Ref. 52.
[b] S = completely soluble; I = insoluble or not completely soluble.

thermosets such as phenolics, ureas, melamines, and epoxies and chemicals such as dialdehydes and diisocyanates. In this manner, incorporation of even small amounts of the vinyl acetal polymer into thermosetting compositions markedly improves the toughness, flexibility, and adhesion of the cured composition. Alternatively, incorporation of smaller quantities of thermosets often gives the vinyl acetal polymer a better balance of properties. Illustrations of the mechanisms and formulation recipes for cross-linking vinyl acetal polymers can be found in the product literature (19,20).

Vinyl acetal polymers have adequate thermal stability for many applications. Thermogravimetric analysis indicates significant rate of weight loss, starting about 240°C in air or about 320°C in nitrogen for PVF (63,64) compared to about 280°C in air or up to about 320°C in nitrogen for PVB (65). In air, significant oxidative degradation occurs at lower temperatures with longer thermal exposure as evidenced by loss of solubility, color development, and increasing T_g attributed to the initial formation of unsaturated bonds and cross-linking (64,66). Mechanisms for degradation have also been studied employing combination techniques, including gas chromatography/mass spectrometry and infrared spectroscopy/thermogravimetry (65,67). For both PVF and PVB, the activation energy for degradation is much less in air than in nitrogen, suggestive of a reaction of oxygen resulting in structures more favorable for degradation (64,65). Side-group elimination, begun at about 280°C for PVB, by rupture of the acetal ring is proposed to occur by a free-radical mechanism involving hydroperoxide formation subsequent to an initial attack of molecular oxygen. This leads to the formation of carbonyl (C═O) groups and liberation of small molecules, including the original aldehyde. The first stage of PVB degradation in nitrogen (ranging from 320 to 355°C) is mainly due to the elimination of water from the vinyl alcohol with the formation of small amounts of butyraldehyde. The second stage of PVB thermal degradation (ranging from 355 to 450°C) is associated with side-group elimination and main-chain scission during which most of the polymer is degraded (67).

Health and Safety

The U.S. Food and Drug Administration regulates PVB resins used as indirect food additives (19,20). However, PVB resin is practically nontoxic by single-dose oral ingestion ($LD_{50} > 10.0$ g/kg for rats). Unformulated PVB and PVF resins have flash points above 370°C. The lower explosive limit for PVB dust in air is 20 g/m^3. Details on specific products are available with the manufacturer.

Economic Aspects

During 1998, about 107,000 t of unplasticized PVB was manufactured in the United States, Western Europe, and Japan (49). Of this amount, more than 87% was plasticized and extruded into sheet for use in laminated safety glass for vehicle windshields and laminated architectural glazing. The remainder, less than 13%, was used for noninterlayer applications. The U.S. list price for PVB non-sheet grade, specialty resins was $9.48 per kg in 1998 ($6.11–11.45 per kg in Japan). 2003 PVB specialty resins prices, as surveyed by the author, remain essentially unchanged from $6.50–9.50 per kg depending on grade in the United States and Europe. 2003 PVF resins range from $15.00–20.00 per kg, a significant increase over historical values when PVF resins were available at lower prices than PVB specialty resins. The only producers of PVB non-sheet grade, specialty resins, not captive for interlayer, are Solutia (Butvar) and Wacker (Pioloform B). Major producers of interlayer for laminated glass are Solutia (Saflex), the largest producer,

followed by DuPont (Butacite), Sekisui (S'Lec), and HT-Troplast (Trosifol). The only major manufacturer of PVF resins is Chisso Corp. (trade name Vinylec).

Applications

Laminated Glass. PVB sheet is manufactured by extrusion of an intimate mixture of PVB resin, plasticizer, and trace additives. Commercial PVB sheet is available in thicknesses from 0.038 to 0.152 cm, with 0.076 cm predominant. The sheet must have a surface topography to enable optimal handling and subsequent removal of air from between sheets while laminating at elevated temperature. Laminated to glass, PVB exhibits high adhesion, optical clarity, stability to sunlight, and high tear strength and impact-absorbing characteristics. It adheres to glass fragments after a glass-breaking impact, thereby helping to reduce injury from flying glass. After the glass is broken during an impact, the interlayer's high tear strength and resiliency acts like a safety net by absorbing enough energy to resist penetration by a projectile or a vehicle occupant's head (12). In addition to its safety features, laminated glass in automotive and architectural applications adds sound attenuation (68,69), heat insulation, and break-in security, and also blocks ultraviolet radiation.

For laminated safety glass, the strength of the adhesive bond between the glass and the interlayer is carefully controlled with additives, usually salts, to achieve the desired balance (70–80). Adhesion to clean glass is very high. If adhesion is too high, a projectile can easily penetrate the laminate because cracks made in the glass propagate through the interlayer. Group IA or IIA alkanoate salts as well as moisture are thought to reduce adhesion by competing with resin hydroxyls for bonding sites on the glass surface. If adhesion is too low, glass retention during an impact will be reduced even though the interlayer is not penetrated.

Interlayer with gradient color bands are made for automobile windshields (81–83). The band is printed on the interlayer surface or tinted by coextrusion with pigmented resin. Curvature for a windshield is accomplished by differentially stretching sheet heated at about 85–100°C over a tapered shaping drum. Rolls of sheet or precut interlayer blanks are usually stored or shipped refrigerated at 3–10°C, or shipped at ambient conditions with an interleaved thin sheet of plastic such as polyethylene to prevent blocking.

PVB composites layered with a film of poly(ethylene terephthalate), acrylic, or polycarbonate, or metal fabric, in addition to glass are designed for some specialty uses (84–87). Most laminated safety glazings are a trilayer composite of glass–PVB–glass, but some specialty applications can include a polymer film interlayer in the PVB to achieve decorative designs or solar reflective properties, or even a metal fabric to provide radio frequency shielding from external sources. For security applications, such as bullet- and projectile-resistant laminates, multi-ply PVB interlayer and glass composites are also designed.

Surface Coatings and Primers. The first and most extensive application for PVF resins starting in 1938 was for electrical insulation and this still remains its major application (5). In these applications the PVF resin component helps provide dielectric properties, toughness, as well as abrasion and thermal resistance. PVF is combined with other ingredients, such as phenolic, epoxy,

or melamine resins, to produce a thermoset coating solution for copper or aluminum wire. Coated wire is cured at elevated temperatures to give a cross-linked film coating with excellent uniformity, and electrical and chemical resistance (88–94).

Wash primer formulations with PVB form a good foundation for various types of topcoats (19,95,96). Wash primers provide good adhesion to metal surfaces and stabilize the metal surface by continuously supplying corrosion-inhibiting ions. Phosphoric acid with zinc chromate or chromic acid can be used to make anticorrosive wash primers. However, due to toxicity concerns associated with chromates, alternative anticorrosive formulations, such as with a pigment of zinc molybdate (97) or borate and phosphate pigments (98), have been recommended. Non-solvent-borne wash primer formulations have been obtained with self-emulsifying water-borne PVB dispersions (99). Water-borne PVB dispersions eliminate the need for volatile organic solvents.

The dispersion of plasticized PVB in water, marketed by Solutia as Butvar Dispersion BR, is used as a permanent surface size in textile applications where toughness of the butyral film lends outstanding abrasion resistance to the fabric (100). PVB dispersions can be applied to textiles by spraying, from a dilute bath by impregnation on a padder, or from a thickened dispersion by coating on spreading equipment. The dried dispersion imparts a soft, full-bodied finish to rayon, cotton, or nylon and helps prevent unraveling of filament yarns. PVB has also been used as a component of wash coats and sealers in wood finishing operations. It confers good holdout, intercoat adhesion, moisture resistance, flexibility, impact resistance, and protection against wood discoloration (19,101). Vinyl acetal polymers can also be used in coating formulations for other polymer surfaces (102,103).

Adhesives and Binders. The principal adhesive uses of vinyl acetal resins are in high performance thermosetting adhesives and in thermoplastic hot-melt formulations. PVB binds the glass beads used in retroreflective films for licence plates, decals, and road signs (104–106). PVB resin is formulated with plasticizers, waxes, and other resins to make hot-melt adhesives (107). Vinyl acetal polymers are used for green strength as a fugative binder in ceramic tapes for electronics (108–110), but the largest application is as the binder in the production of ceramic substrates used primarily for electronic devices (111–117).

Printing Inks and Toners. PVB resins have been used in printing ink formulations for many years. PVB resins are soluble in mild solvents, such as alcohols and esters, so can be used in solvent-based flexographic, gravure, screen, and ink-jet printing formulations as a binder to improve flexibility, adhesion, and toughness (19,20,118,119). Flexographic and gravure printing are the dominant processes employed for printing flexible packaging used mainly in the food-processing industry, and to a lesser extent in the pharmaceutical and chemical industries.

PVB is also used in toner formulations as a binder (19,120). PVB is added to the formulations to increase viscosity, to improve film integrity over the fuser roll, and to prevent blocking. The overall toughness of PVB enhances the integrity of the toner during the milling process and extended machine operation. This minimizes the level of fines without detracting from the flow properties.

BIBLIOGRAPHY

"Vinyl Alcohol Polymers, Poly(Vinyl Acetals)" in *EPST* 1st ed., Vol. 14, pp. 208–239, by M. K. Lindemann, Chas. S. Tanner Co.; "Vinyl Acetal Polymers" in *EPSE* 2nd ed., Vol. 17, pp. 136–167, by T. P. Blomstrom, Monsanto Chemical Co.

1. N. Platzer, *Mod. Plast.* **28**, 142 (June 1951).
2. Ger. Pats. 480,866 (July 20, 1924) and 507,962 (Apr. 30, 1927), W. O. Herrmann and W. Haehnel (both to Consortium für Electrochemische Industrie).
3. U.S. Pats. 1,955,068 (Apr. 17, 1934) and Ger. Pat. 683,165 (Oct. 12, 1939), H. Hopff and E. Kuehn (both to I.G. Farbenindustrie).
4. U.S. Pat. 2,036,092 (Mar. 31, 1936), RE20,430 (Reissued June 29, 1937), G. O. Morrison, F. W. Skirrow, and K. G. Blaikie (to Canadian Electro Products Co.).
5. U.S. Pat. 2,114,877 (Apr. 19, 1938), R. W. Hall (to General Electric Co.).
6. U.S. Pats. 2,162,678 (June 13, 1939) and 2,162,680 (June 13, 1939), H. F. Robertson (both to Carbide and Carbon Chemicals Corp.).
7. U.S. Pats. 2,168,827 (Aug. 8, 1939), 2,176,859 (Oct. 17, 1939), and 2,179,051 (Nov. 7, 1939), G. O. Morrison and A. F. Price (all to Shawinigan Chemicals Ltd.).
8. U.S. Pat. 2,258,410 (Oct. 7, 1941), J. Dahle (to Monsanto Chemical Co.).
9. U.S. Pat. 2,265,255 (Dec. 9, 1941), G. S. Stamatoff (to E. I. du Pont de Nemours & Co., Inc.).
10. U.S. Pats. 2,282,026 (May 5, 1942), B. C. Bren, J. H. Hopkins, and G. H. Wilder; 2,282,057 (May 5, 1942), J. H. Hopkins and G. H. Wilder (both to E. I. du Pont de Nemours & Co., Inc.).
11. U.S. Pats. 2,400,957 (May 28, 1946), and 2,422,754 (June 24, 1947), G. S. Stamatoff (both to E. I. du Pont de Nemours & Co., Inc.).
12. R. H. Fariss, *CHEMTECH* **23**, 38 (Sept. 1993).
13. F. A. Carey, *Organic Chemistry*, McGraw-Hill, Inc., New York, 1992, p. 689.
14. G. Odian, *Principles of Polymerization*, John Wiley & Sons, Inc., New York, 1981, p. 675.
15. K. Hayashi and T. Ostu, *Makromol. Chem.* **127**, 54 (1969).
16. W. S. Lyoo, S. M. Lee, K. Koo, J. Lee, H. D. Ghim, J. P. Kim, and J. Lee, *J. Appl. Polym. Sci.* **82**, 1897 (2001).
17. D. B. Britton, F. Heatley, and P. A. Lovell, *Macromolecules* **31**, 2828 (1998).
18. D. B. Britton, F. Heatley, and P. A. Lovell, *Macromolecules* **33**, 5048 (2000).
19. Butvar Polyvinyl Butyral Properties & Uses, On-line Technical Bulletin 2008084D, Solutia, Inc., St. Louis, Mo., 1999.
20. Pioloform B Polyvinyl Butyrals, Technical Bulletin 5567E, Wacker Polymer Systems, Burghausen, Germany, Jan. 2001.
21. Vinylec Polyvinyl Formal Resins, On-line Technical Bulletin, Chisso America Corp., New York, 2002.
22. P. J. Flory, *J. Am. Chem. Soc.* **61**, 1518 (1939).
23. P. J. Flory, *J. Am. Chem. Soc.* **72**, 5052 (1950).
24. Y. Ogata, M. Okano, and T. Ganke, *J. Am. Chem. Soc.* **78**, 2962 (1956).
25. G. Smets and B. Petit, *Makromol. Chem.* **33**, 41 (1959).
26. Eur. Pat. 402,213 (Sept. 21, 1994), D. Dages and D. Klock (to E. I. du Pont de Nemours & Co., Inc.).
27. K. Shibatani, K. Fujii, Y. Ohyanagi, J. Ukida, and M. Matsumoto, *J. Polym. Sci., Part C* **23** (Pt 2), 647 (1968).
28. K. Fujii, J. Ukida, and M. Matsumoto, *Makromol. Chem.* **65**, 86 (1963).
29. K. Fujii, K. Shibatani, Y. Fujiwara, Y. Ohyanagi, J. Ukida, and M. Matsumoto, *J. Polym. Sci., Polym. Lett. Ed.* **4**, 787 (1966).
30. M. D. Bruch and J. K. Bonesteel, *Macromolecules* **19**, 1622 (1986).

31. B. Lebek, K. Schlothauer, A. Krause, and H. Marschner, *Acta Polym.* **40**, 92 (1989).
32. P. A. Berger, E. E. Remsen, G. C. Leo, and D. J. David, *Macromolecules* **24**, 2189 (1991).
33. A. F. Fitzhugh, E. Lavin, and G. O. Morrison, *J. Electrochem. Soc.* **100**, 351 (1953).
34. S. Matsuzawa, T. Imoto, and K. Ogasawara, *Kobunshi Kagaku* **25**, 173 (1968).
35. S. Matsuzawa, *Kobunshi Kako* **18**, 35 (1969).
36. Ger. Pat. 1,071,343 (Dec. 17, 1959), E. Bergmeister, J. Heckmaier, and H. Zoebelein (to Wacker Chemie GmbH).
37. U.S. Pat. 2,496,480 (Feb. 7, 1950), E. Lavin, A. T. Marinaro, and W. R. Richard (to Shawinigan Resins Corp.).
38. *Chem. Eng. (N.Y.)* **61**, 122,123, 346–349 (Feb. 1954).
39. R. D. Dunlop, FIAT Final Report No. 1109, U.S. Government Printing Office, Washington, D.C., 1947.
40. U.S. Pat. 3,153,009 (Oct. 13, 1964), L. H. Rombach (to E. I. du Pont de Nemours & Co., Inc.).
41. Ger. Pat. Appl. 3,526,314 (Feb. 13, 1986), R. Degeilh (to Saint-Gobain Vitrage).
42. Rom. Pat. Appl. 63,627 (Apr. 30, 1978), A. Chifor, V. Dumitrascu, and I. Manu.
43. Ger. Pat. 2,838,025 (Sept. 10, 1992), P. Dauvergne (to Saint-Gobain Industries SA).
44. Jpn. Kokai 58,067,701 (Apr. 22, 1983), 57,195,706 (Dec. 1, 1982), and 57,030,706 (Feb. 19, 1982), S. Nomura, M. Miyagawa, and K. Asahina (all to Sekisui Chemical Co. Ltd.).
45. U.S. Pat. 5,349,014 (Sept. 20, 1994), R. Degeilh (to E. I. du Pont de Nemours & Co., Inc.).
46. Pol. Pat. 96,247 (Dec. 31, 1977), H. Pietkiewicz, M. Knypl, and A. Madeja.
47. L. N. Verkhotina, L. S. Gembitskii, E. N. Gubenkova, L. S. Sev'yants, and A. M. Sarkis'yan, *Plast. Massy* **7**, 35 (1977).
48. U.S. Pats. 4,902,464 (Feb. 20, 1990), 4,874,814 (Oct. 17, 1989), 4,814,529 (Mar. 21, 1989), and 4,654,179 (Mar. 31, 1987), G. E. Cartier and P. H. Farmer (all to Monsanto Co.).
49. W. K. Johnson, G. Humphries, and K. Sakota, *CEH Product Review, Polyvinyl Butyral*, SRI International, Menlo Park, Calif., (Nov. 1999).
50. D. H. David, in Proceedings: Polymer–Solid Interfaces, First International Conference, Namur, Belgium, 1992, p. 133.
51. G. E. Cartier, unpublished data, Solutia, Inc., Springfield, Mass., 1987.
52. Butvar, Poly(vinyl butyral) and Formvar, Poly(vinyl fomal), Technical Bulletin No. 6070E, Monsanto Co., St. Louis, Mo., June 1980.
53. A. F. Fitzhugh and R. N. Crozier, *J. Polym. Sci.* **8**, 225 (1952); *Errata* **9**, 96 (1952).
54. Jpn. Kokai 62,278,148 (Dec. 3, 1987), K. Morita and T. Ii (to Sekisui Chemical Industries).
55. U.S. Pat. 5,137,954 (Aug. 11, 1992), A. M. Das Gupta, D. J. David, and R. J. Tetreault (to Monsanto Co.).
56. Eur. Pat. 394,884 (May 11, 1994), M. Gutweiler, R. K. Driscoll, and E. I. Leupold (to Hoechst AG).
57. U.S. Pat. 3,841,955 (Oct. 15, 1974), A. W. M. Coaker, J. R. Darby, and T. C. Mathis (to Monsanto Co.).
58. U.S. Pats. 3,884,865 (May 20, 1975) and 3,920,878 (Nov. 18, 1975), R. H. Fariss and J. A. Snelgrove (to Monsanto Co.).
59. U.S. Pat. 4,128,694 (Dec. 5, 1978), D. A. Fabel, J. A. Snelgrove, and R. H. Fariss (to Monsanto Co.).

60. U.S. Pat. 4,144,217 (Mar. 13, 1979), J. A. Snelgrove and D. I. Christensen (to Monsanto Co.).
61. U.S. Pat. 4,230,771 (Oct. 28, 1980), T. R. Phillips (to E. I. du Pont de Nemours & Co., Inc.).
62. Eur. Pat. 877,665 (Aug. 23, 2000), J. J. D'Errico, B. A. Jemmott, M. S. Krach, and J. R. Moran (to Monsanto Co.).
63. M. Chandra, W. S. J. Kumar, and P. Raghavendrachar, *J. Polym. Sci.* **23**, 755 (1979).
64. H. Aoki and T. Suzuki, *J. Polym. Sci., Part A: Polym. Chem.* **26**, 31 (1988).
65. L. C. K. Liau, C. K. Thomas, and D. S. Viswanath, *Polym. Eng. Sci.* **36**, 2589 (1996).
66. H. C. Beachell, P. Fotis, and J. Hucks, *J. Polym. Sci.* **7**, 353 (1951).
67. L. C. K. Liau, C. K. Thomas, and D. S. Viswanath, *Appl. Spectrosc.* **50**, 1058 (1996).
68. J. Lu, in International Congress and Exposition on Noise Control Engineering, Internoise 2002, Dearborn, Mich., Apr. 2002, Papers IN_02_581 and IN_2_582.
69. R. A. Esposito and G. E. Freeman, in Proceedings of the 2002 SAE International Body Engineering Conference and Automotive and Transportation Technology Conference, Paris, France, July 2002, Paper 2002-01-1993.
70. U.S. Pat. 3,262,837 (July 26, 1966), E. Lavin, G. E. Mont, and A. F. Price (to Monsanto Co.).
71. U.S. Pat. 3,249,487 (May 3, 1966), F. T. Buckley and J. S. Nelson (to Monsanto Co.).
72. Jpn. Kokai 50,121,311 (Sept. 23, 1975), I. Karasudani, T. Takashima, and Y. Honda (to Sekisui Chem. Co., Ltd.).
73. Ger. Pat. 2,410,153 (Feb. 3, 1977), R. Beckmann and W. Knackstedt (to Dynamit Nobel, AG).
74. U.S. Pats. 3,718,516 (Feb. 27, 1973) and 3,556,890 (Jan. 19, 1971), F. T. Buckley, R. F. Riek, and D. I. Christensen (both to Monsanto Co.).
75. Ger. Pat. 2,904,043 (Nov. 15, 1990), H. K. Inskip (to E. I. du Pont de Nemours & Co., Inc.).
76. Ger. Pat. 2,646,280 (Oct. 10, 1985), H. D. Hermann and J. Ebigt (to Hoechst, AG).
77. Eur. Pat. 617,078 (Feb. 25, 1998), H. Fischer (to Hoechst, AG).
78. Ger. Pat. Appl. 3,417,653 and 3,417,654 (Nov. 14, 1985), H. D. Hermann, K. Fock, K. Fabian, and J. Ebigt (to Hoechst, AG).
79. U.S. Pat. 4,292,372 (Sept. 29, 1981), R. E. Moynihan (to E. I. du Pont de Nemours and Co., Inc.).
80. U.S. Pat. 5,728,472 (Mar. 17, 1998), J. J. D'Errico (to Monsanto Co.).
81. U.S. Pat. 3,982,984 (Sept. 28, 1976), D. B. Baldridge (to Monsanto Co.).
82. U.S. Pat. 3,973,058 (Aug. 3, 1976), J. L. Grover and W. H. Power (to Monsanto Co.).
83. Ger. Pat. 2,841,287 (July 14, 1983), D. S. Postupack (to PPG Industries, Inc.).
84. Jpn. Kokai 6,155,681 (June 3, 1994), H. Yatani (to Asahi Kasei Kogyo).
85. Structural Performance of Laminated Architectural Glass, Technical Bulletin 2458043A, Solutia, Inc., St. Louis, Mo., 1999.
86. Security Glazing Design Guide, Technical Bulletin 2458104B, Solutia, Inc., St. Louis, Mo., 1999.
87. Vancevatm Advanced Solutions for Glass, Technical Bulletin 2459766, Solutia, Inc., St. Louis, Mo., 2002.
88. U.S. Pat. 2,307,588 (Jan. 5, 1943), E. H. Jackson and R. W. Hall (to General Electric Co.).

89. U.S. Pat. 3,069,379 (Dec. 18, 1962), E. Lavin, A. F. Fitzhugh, and R. N. Crozier (to Shawinigan Resins Corp. and Phelps Dodge Copper Products Corp.).
90. U.S. Pat. 3,104,326 (Sept. 17, 1963), E. Lavin, A. H. Markhart, and R. F. Kass (to Shawinigan Resins Corp.).
91. E. Lavin, A. H. Markhart, and R. W. Ross, *Insulation* **8**, 25 (1962).
92. U.S. Pats. 3,516,858 (June 23, 1970), A. F. Fitzhugh and J. A. Snelgrove; 3,639,330 (Feb. 1, 1972), A. F. Fitzhugh and R. M. Huck (both to Monsanto Co.).
93. U.S. Pat. 4,129,678 (Dec. 12, 1978), M. Seki, M. Sato, H. Tsukioka, E. Ohe, and A. Mitsuoka (to Hitachi Ltd.; Hitachi Cable Ltd.).
94. U.S. Pat. 4,254,007 (Mar. 3, 1981), R. G. Flowers and W. A. Fessler (to General Electric Co.).
95. J. D. Scantlebury and F. H. Karman, *Corros. Sci.* **35**, 1305 (1993).
96. Military Specifications: DOD-P-15328D and MIL-C-8514C (ASG), Information Handling Services (HIS), Englewood, Colo.
97. J. L. Nogueira, *Corros. Prot. Mater.* **11**, 11 (1992).
98. T. Foster, G. N. Blenkinsop, P. Blattler, and M. Szandorowski, *J. Coat. Technol.* **63**, 91 (1991).
99. M. Gerlitz and E. Supper, *Surf. Coat. Int., Part A: Coat. J.* **84**, 389 (2001).
100. Butvar Polyvinyl Butyral Resin Dispersion BR Resin Technical Bulletin, Publication No. 2006019F, Solutia, Inc., St. Louis, Mo., 2002.
101. U.S. Pat. 3,320,203 (May 16, 1967), M. D. Kellert (to Monsanto Co.).
102. U.S. Pat. 3,313,651 (Apr. 11, 1967), R. J. Burns (to Union Carbide Corp.).
103. Ger. Pat. 2,144,233 (Mar. 8, 1973), H. Hinrichs, J. Peter, and W. D. Schuessler (to Reichhold-Albert Chemie AG).
104. Eur. Pat. 223,564 (Aug. 28, 1991), T. R. Bailey, R. R. Kult, and L. C. Belisle (to 3M Co.).
105. Eur. Pat. 360,420 (Mar. 27, 1996), B. B. Wilson and R. E. Grunzinger (to 3M Co.).
106. U.S. Pat. 6,221,496 (Apr. 24, 2001), Y. Mori (to 3M Co.).
107. Czech. Pat. 155,587 (Dec. 15, 1974), M. Schatz, K. Salz, and J. Volek.
108. Rus. Pat. 744,741 (June 30, 1980), D. T. Kostin, I. A. Budkin, A. F. Rozov, V. N. Stazhkov, and I. V. Skvortsov.
109. Rus. Pat. 860,142 (Aug. 30, 1981), D. T. Kostin, V. N. Stazhkov, A. G. Yashenkov, I. A. Budkin, and A. F. Rozov.
110. R. E. Mistler, *Am. Ceram. Soc. Bull.* **77**, 82 (1998).
111. Ger. Pat. 2,227,343 (Dec. 24, 1981), L. C. Anderson, R. W. Nufer, and F. G. Pugliese (to IBM Corp.).
112. Jpn. Kokai 62,046,954 (Feb. 28, 1987), K. Hoshi, S. Tosaka, and T. Yoshimi (to Taiyo Yuden Co., Ltd.).
113. Jpn. Kokai 61,266,350 (Nov. 26, 1986), N. Ushifusa, S. Ogiwara, K. Nagayama, K. Shinohara, and A. Toda (to Hitachi, Ltd.).
114. Jpn. Kokai 60,122,767 (July 1, 1985) (to NGK Spark Plug Co., Ltd.).
115. Eur. Pat. 200,484 (Feb. 5, 1992), M. S. H. Chu and C. E. Hodgkins (to TAM Ceramics, Inc.).
116. Jpn. Kokai 57,067,075 (Apr. 23, 1982) (to Nippon Kouatsu Electric Co., Ltd.).
117. U.S. Pat. 4,786,342 (Nov. 22, 1988), J. E. Zellner and R. M. Martin (to Coors Porcelain Co.).
118. U.S. Pat. 3,951,882 (Apr. 20, 1976), A. H. Markhart and D. R. Cahill (to Monsanto Co.).
119. Ger. Pat. Appl. 2,547,862 (May 6, 1976), K. Taubert (to Sandoz-Patent-GmbH).
120. Jpn. Kokai 08,328,303 (Dec. 13, 1996) and 08,292,596 (Nov. 5, 1996), H. Minamino, T. Takahashi, and K. Noguchi (both to Sekisui Chemical Co. Ltd.).

GENERAL REFERENCES

E. Lavin and J. A. Snelgrove, in M. Grayson, ed., *Kirk-Othmer Encyclopedia of Chemical Technology*, 3rd ed., Vol. 23, John Wiley & Sons, Inc., New York, 1983, pp. 798–816.
J. W. Knapczyk, in J. I. Kroschwitz, ed., *Kirk-Othmer Encyclopedia of Chemical Technology*, 4th ed. (On-line), John Wiley & Sons, Inc., New York, 1997.
P. H. Farmer and B. A. Jemmott, in I. Skeist, ed., *Handbook of Adhesives*, 3rd ed., Van Nostrand Reinhold, New York, 1990, pp. 423–436.

BRUCE WADE
Solutia, Inc.

VINYL ALCOHOL POLYMERS

Introduction

Poly(vinyl alcohol) (PVA), a polyhydroxy polymer, is the largest volume, synthetic water-soluble resin produced in the world. It is commercially manufactured by the hydrolysis of poly(vinyl acetate), because monomeric vinyl alcohol cannot be obtained in quantities and purity that makes polymerization to PVA feasible (1–3).

Poly(vinyl alcohol) was discovered by Haehnel and Herrmann who, through the addition of alkali to a clear alcoholic solution of poly(vinyl acetate), were able to obtain the ivory-colored PVA (4). The first scientific reports on PVA were published in 1927 (5,6).

The excellent chemical resistance and physical properties of PVA resins have resulted in broad industrial use. The polymer is an excellent adhesive and possesses solvent, oil, and grease resistance, properties matched by few other polymers. Poly(vinyl alcohol) films exhibit high tensile strength, abrasion resistance, and oxygen barrier properties which under dry conditions are superior to those of most polymers. The polymer's low surface tension provides for excellent emulsification and protective colloid properties.

The main uses of PVA are in textile sizing, adhesives, protective colloids for emulsion polymerization, fibers, production of poly(vinyl butyral), and paper sizing. Significant volumes are also used in the production of concrete additives and joint cements for building construction and water-soluble films for containment bags for hospital laundry, pesticides, herbicides, and fertilizers. Smaller volumes are consumed as emulsifiers for cosmetics, temporary protective film coatings, soil binding to control erosion, and photoprinting plates.

Encyclopedia of Polymer Science and Technology. Copyright John Wiley & Sons, Inc. All rights reserved.

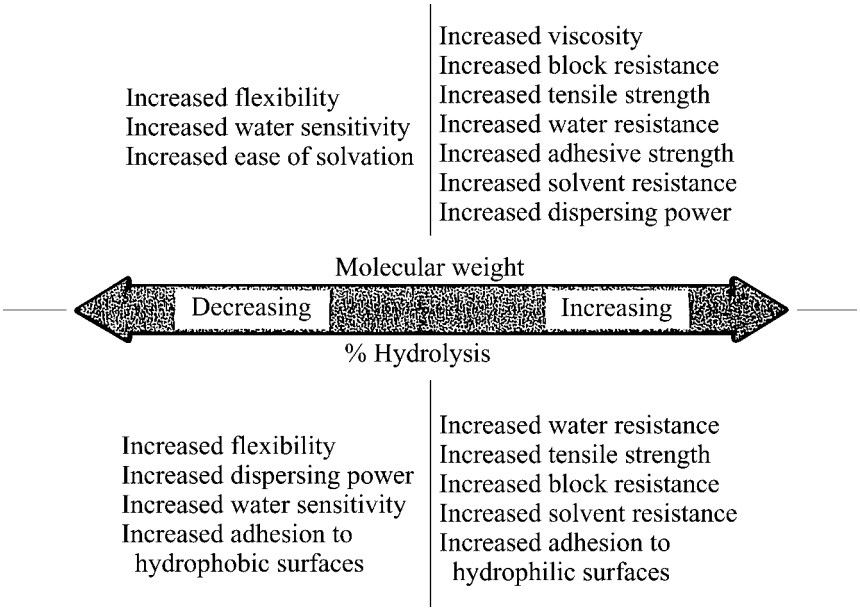

Fig. 1. Effect of molecular weight and hydrolysis on the properties of PVA (7).

Physical Properties

The physical properties of PVA are highly correlated with the method of preparation. The final properties are affected by the polymerization conditions of the parent poly(vinyl acetate), the hydrolysis conditions, drying, and grinding. Further, the term PVA refers to an array of products that can be considered to be copolymers of vinyl acetate and vinyl alcohol.

The effect of hydrolysis and molecular weight is illustrated in Figure 1. The variations in properties with molecular weight are for a constant degree of hydrolysis (mol%) (7), and the effect of hydrolysis is at a constant molecular weight. Representative properties are shown in Table 1.

Crystallization and Melting Point. The ability of PVA to crystallize is the single most important physical property of PVA as it controls water solubility, water sensitivity, tensile strength, oxygen barrier properties, and thermoplastic properties. Thus, this feature has been and continues to be the focal point of academic and industrial research (8–37). The degree of crystallinity as measured by x-ray diffraction can be directly correlated to the products density or the swelling characteristic of the insoluble part (Fig. 2).

The size of the crystals determines the melting point. Reported values for the melting point of PVA range between 220 and 267°C for fully hydrolyzed PVA (38–42). Exact determination of the crystalline melting point using normal data techniques is difficult as decomposition takes place above 140°C. The divergence in melting point may be ascribed to decomposition or prior treatment history. The melting point of PVA containing an appropriate amount of diluent or comonomer is less influenced by decomposition. Thus, the melting point of fully hydrolyzed PVA can be determined by the extrapolation of the measured values to 0% diluent.

Table 1. Physical Properties of Poly(vinyl alcohol)

Property	Value	Remarks
Appearance	White to ivory white granular powder	
Specific gravity	1.27–1.31	Increases with degree of crystallinity
Tensile strength, MPa[a] (98–99% hydrolyzed)	67–110	Increases with degree of crystallinity (heat treatment), and molecular weight, decreases with increasing humidity
Tensile strength, MPa (87–89% hydrolyzed)	24–79	Increases with molecular weight and decreases with increasing humidity
Elongation, %	0–300	Increases with increasing humidity
Thermal coefficient of expansion per °C	$7–12 \times 10^{-5}$	
Specific heat, J/(g·K)[b]	1.67	
Thermal conductivity, W/(m·K)	0.2	
Glass-transition temperature, K	358	98–99% hydrolyzed
	331	87–89% hydrolyzed
Melting point, K	503	98–99% hydrolyzed
	453	87–89% hydrolyzed
Electrical resistivity, Ω·cm	$(3.1–3.8) \times 10^{7}$	
Thermal stability	Gradual discoloration above 100°C; darkens rapidly above 150°C; rapid decomposition above 200°C	
Refractive index n_D(20°C)	1.55	
Degree of crystallinity	0–0.54	Increases with heat treatment and degree of hydrolysis
Storage stability (solid)	Indefinite when protected from moisture	
Flammability	Burns similarly to paper	
Stability in sunlight	Excellent	

[a]To convert MPa to psi, multiply by 145.
[b]To convert J to cal, divide by 4.184.

A more reliable melting point is obtained in this manner. The melting points determined by the diluent method are 255–267°C for commercial superhydrolyzed PVA (greater than 99% hydrolysis). The melting point determined by melting point depression caused by noncrystallizing comonomer units assumes as a first approximation that the vinyl acetate units are randomly distributed. This assumption usually does not apply to commercial PVA. The extrapolated values of

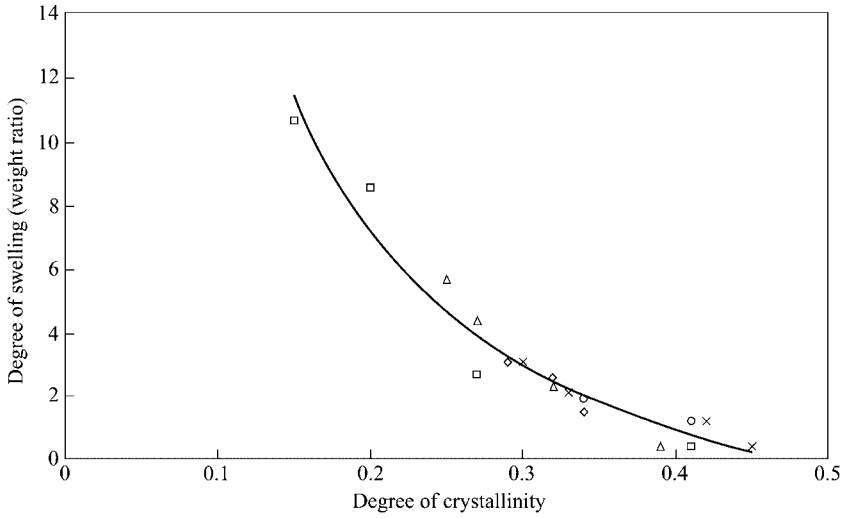

Fig. 2. Relationship between swelling and crystallinity. □, DP 304; △, DP 708; ○, DP 1288; ◇, DP 2317; ×, DP 4570.

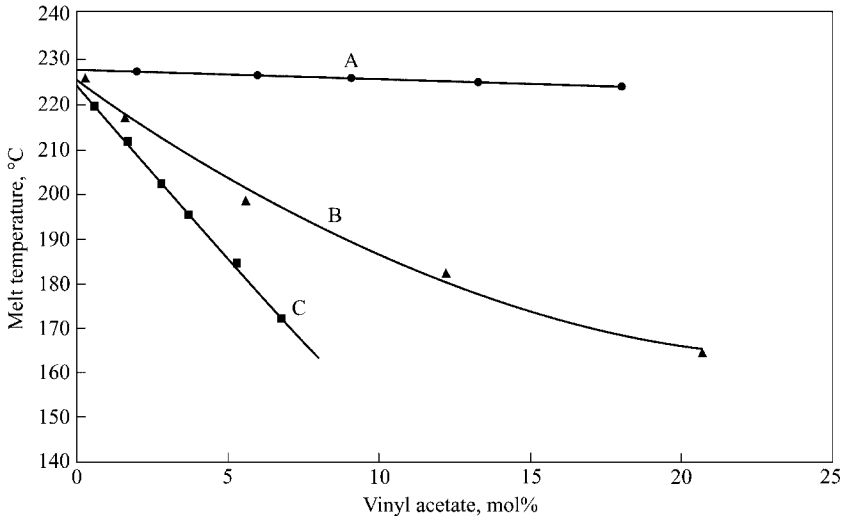

Fig. 3. Influence of vinyl alcohol–vinyl acetate copolymer composition on melting temperature (44), where A represents block copolymers; B, block copolymers; and C, random copolymers.

heat of fusion and melting point obtained with this method are therefore highly dependent on the manufacturing method and the resulting blockiness (Fig. 3). The heat of fusion, determined by either of the above methods, has been calculated as 6.82 ± 2.1 kJ/mol (43–45).

Glass-Transition Temperatures. The glass-transition temperature of fully hydrolyzed PVA has been determined to be 85°C for high molecular weight material. The glass transition in case of 87–89% hydrolyzed PVA varies according to the shown formula (46):

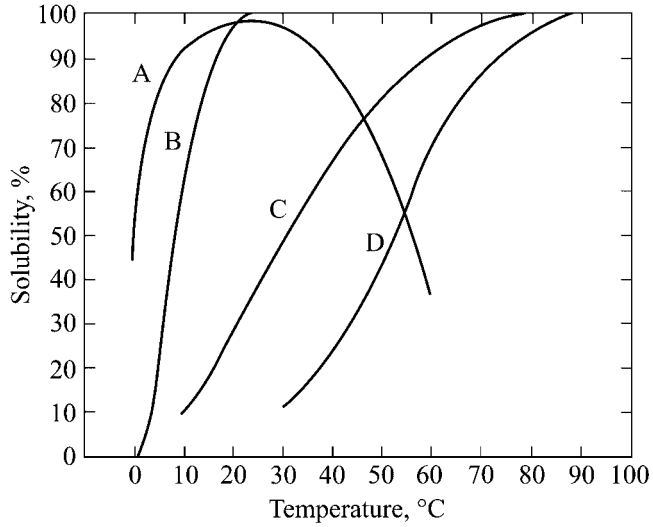

Fig. 4. Water solubility of PVA grades: A, 78–81 mol% hydrolyzed, DP = 2000–2100; B, 87–89 mol% hydrolyzed, DP = 500–600; C, 98–99 mol% hydrolyzed, DP = 500–600; D, 98–99 mol% hydrolyzed, DP = 1700–1800 (47).

$$T_g = 58 - (2.0 \times 10^{-3}/\mathrm{DP})[^\circ\mathrm{C}] \quad (1)$$

Solubility. Poly(vinyl alcohol) is only soluble in highly polar solvents, such as water, dimethyl sulfoxide, acetamide, glycols, and dimethylformamide. The solubility in water is a function of the degree of polymerization (DP) and hydrolysis (Fig. 4). Fully hydrolyzed PVA is only completely soluble in hot to boiling water. Partially hydrolyzed grades are soluble at room temperature, although grades with a hydrolysis of 70–80% are only soluble at water temperatures of 10–40°C. Above 40°C the solution first becomes cloudy (cloud point), followed by precipitation of PVA.

The hydroxyl groups in PVA contribute to strong hydrogen bonding both intra- and intermolecularly, which reduces solubility in water. The presence of residual acetate groups in partially hydrolyzed PVA weakens these hydrogen bonds and allows solubility at lower temperatures.

The hydrophobic nature of the acetate groups results in a negative heat of solution (48–50), which increases as the number of acetate groups is increased. This means that the critical θ temperature is lower, ie, the solubility decreases as the temperature is increased.

Heat treatment or drying of a few minutes increases crystallinity and greatly reduces the solubility and water sensitivity (Fig. 5). Prolonged heat treatment does not further increase crystallinity. The heat treatment melts the smaller crystals, allowing for diffusion and reformation of crystals with a melting point higher than that of the treatment temperature. The presence of acetate groups reduces the extent of crystallinity; thus, heat treatment has little or no influence on low hydrolysis grades. The influence of heat treatment is desirable in some applications such as adhesives and paper coatings where a greater degree of water resistance

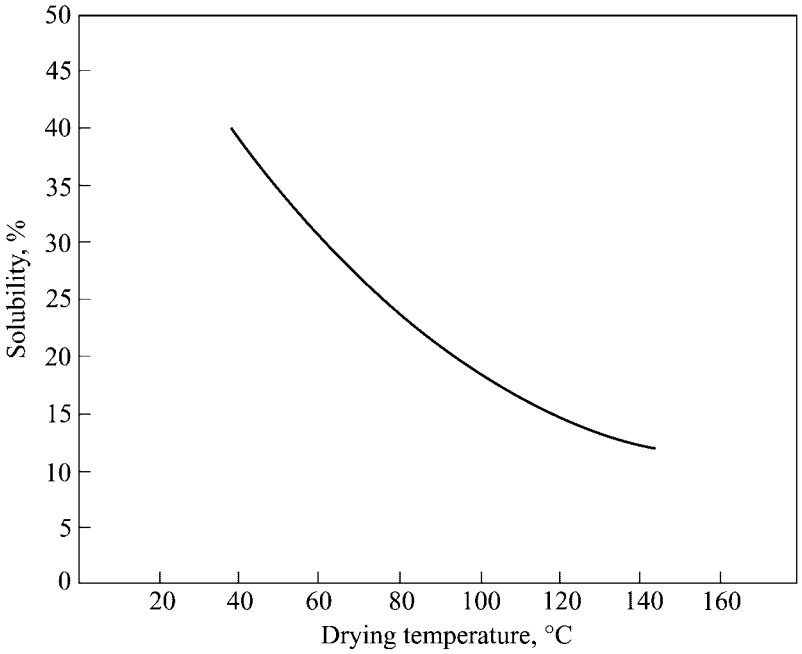

Fig. 5. Influence of heat treatment on solubility at 40°C; DP = 1700, 98–99 mol% hydrolyzed.

is needed, but is highly undesirable in textile warp sizing where the polymer must be removed after a drying cycle.

Poly(vinyl alcohol) solutions also exhibit high tolerance toward many electrolytes (Table 2).

Solution Viscosity. The viscosities of PVA solutions are mainly dependent on molecular weight and solution concentration (Fig. 6). The viscosity increases with increasing degree of hydrolysis and decreases with increasing temperature. Materials with a high degree of hydrolysis tend to show an increase in viscosity on standing and may even gel (47,51–55). The rate of increase depends upon dissolution temperature, concentration, and storage temperature. The lower the storage and dissolution temperatures and the higher the concentration, the higher is the rate of the viscosity increase (Fig. 7). Viscosity can be stabilized to a certain degree by adding small amounts of lower molecular weight aliphatic alcohols (56), urea, or salts such as thiocyanates. The solution viscosity of partially hydrolyzed PVA grades exhibit a greater degree of stability.

Mechanical Properties

The tensile strength of unplasticized PVA depends on degree of hydrolysis, molecular weight, and relative humidity (Fig. 8). Heat treatment and molecular alignment resulting from drawing increase the tensile strength; plasticizers reduce tensile strength disproportionately because of increased water sensitivity.

Tensile elongation of PVA is extremely sensitive to humidity and ranges from <10% when completely dry to 300–400% at 80% rh. Addition of plasticizer

Table 2. Minimum Salt Concentration for Precipitation of a 5% Poly(vinyl alcohol) Solution[a,b]

Salt	Concentration, g/L
$(NH_4)_2SO_4$	66
Na_2SO_4	50
KSO_4	61
$ZnSO_4$	113
$CaSO_4$	112
$Fe_2(SO_4)_3$	105
$MgSO_4$	60
$Al_2(SO_4)_3$	57
$KAl(SO_4)_2$	58
NH_4NO_3	490
$NaNO_3$	324
KNO_3	264
$Al(NO_3)_3$	255
NaCl	210
KCl	194
Na_3PO_4	77
K_2CrO_4	136

[a] Ref. 47.
[b] 98% hydrolyzed, DP = 1700–1800.

can double these values. Elongation is independent of degree of hydrolysis but proportional to the molecular weight. Tear strength increases with increasing relative humidity or with the addition of small amounts of plasticizer.

Solvent Resistance. Poly(vinyl alcohol) is virtually unaffected by hydrocarbons, chlorinated hydrocarbons, carboxylic acid esters, greases, and animal or vegetable oils. Resistance to organic solvents increases with increasing hydrolysis. This resistance has promoted the use of PVA in the manufacture of gloves for use when handling organic solvents (57).

Gas-Barrier Properties. The oxygen-barrier properties of PVA at low humidity are excellent. However, barrier performance deteriorates above 60% rh (Fig. 9). No additives or chemical modifiers are known that can effectively reduce moisture sensitivity. The gas-barrier performance is affected by the degree of hydrolysis and rapidly diminishes as the hydrolysis is decreased below 98% (see BARRIER POLYMERS).

Surface Tension. The surface tension of aqueous solution of PVA varies with concentration (Fig. 10), temperature, degree of hydrolysis, and acetate distribution on the PVA backbone. Random distribution of acetyl groups in the polymer results in solutions having higher surface tension compared to those of polymers in which the blocks of acetyl groups are present (58–61). The surface tension decreases slightly as the molecular weight is reduced (Fig. 11).

Intrinsic Viscosity and Molecular Weights. The relationship between the intrinsic viscosity and molecular weight changes with degree of hydrolysis of the polymer (Table 3). Methods for determining molecular weight and molecular weight distribution using gpc and low angle laser light scattering detection have been developed and utilized (63,64). These methods show a polydispersity of 2.0

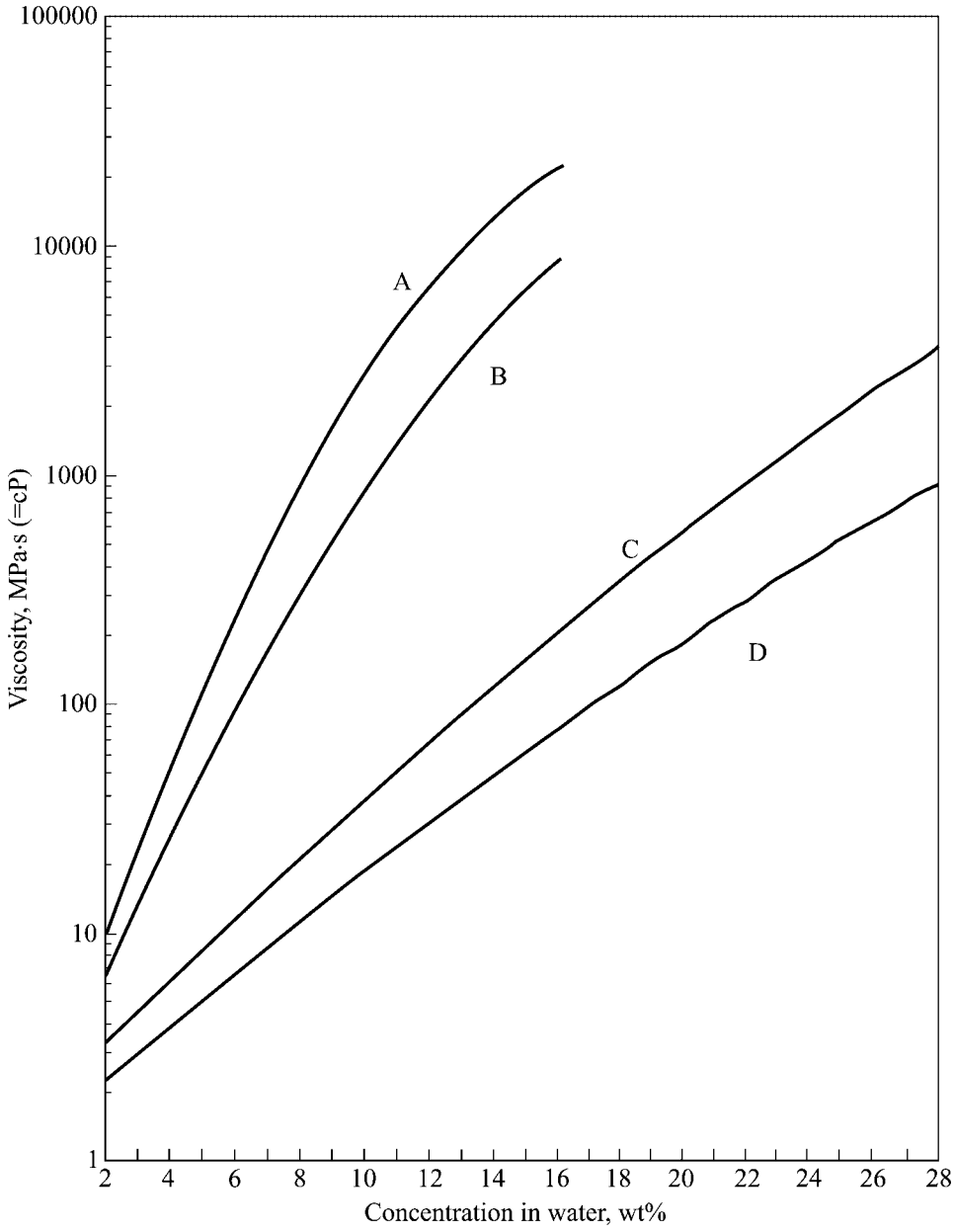

Fig. 6. Solution viscosity of 87–89 mol% hydrolyzed PVA at 20°C. DP: A, 2200; B, 1500; C, 550; D, 220.

or less, which indicates the presence of few long-chain branches. No long-chain branches are found in PVA samples that have a degree of hydrolysis higher than 80 mol%. The number of short-chain branches is identical to the mole percent of short-chain branches generated during the formation of the poly(vinyl acetate) in the range of 0.12–0.17 mol% (65).

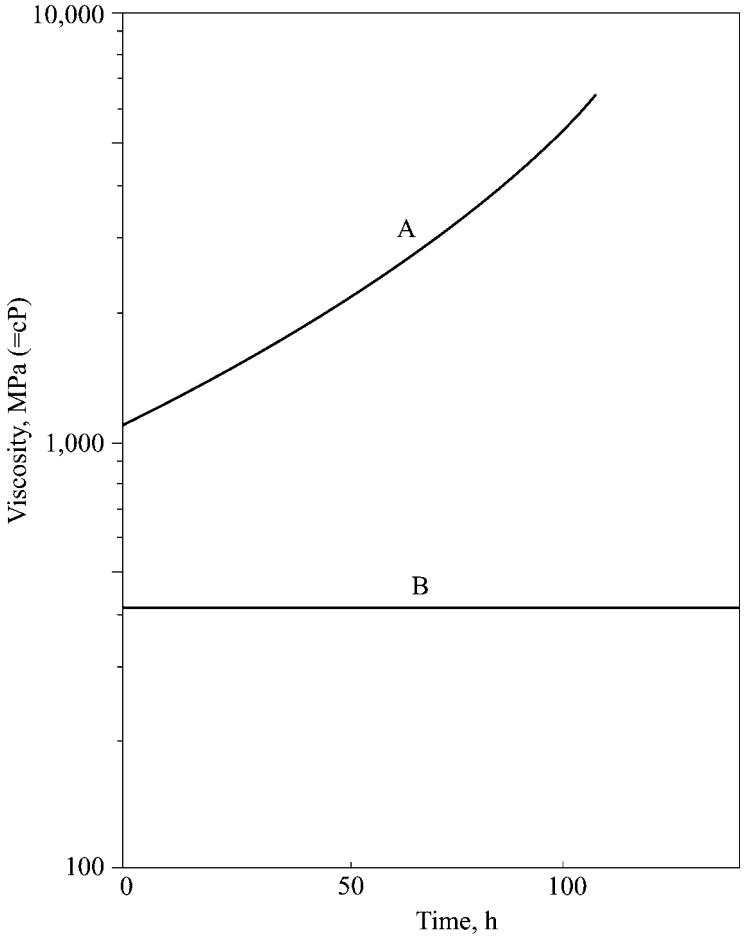

Fig. 7. Effect of aging on solution viscosity of PVA (47): A, DP = 1500, degree of hydrolysis, 98–99 mol%; B, DP = 1500, degree of hydrolysis, 87–89 mol%.

Chemical Properties

Poly(vinyl alcohol) participates in chemical reactions in a manner similar to other secondary polyhydric alcohols (66–68). Of greatest commercial importance are reactions with aldehydes to form acetals, such as poly(vinyl butyral) and poly(vinyl formal) (see VINYL ACETAL POLYMERS).

Table 3. Intrinsic Viscosity–Viscosity-Average Molecular Weight Relationship as a Function of Hydrolysis[a]

Hydrolysis, mol%	$[\eta]$
86.8	$(8.0 \times 10^{-4})\, M_v^{0.58}$
93.5	$(7.4 \times 10^{-4})\, M_v^{0.60}$
96.4	$(6.9 \times 10^{-4})\, M_v^{0.61}$
100.0	$(5.95 \times 10^{-4})\, M_v^{0.63}$

[a] Ref. 62.

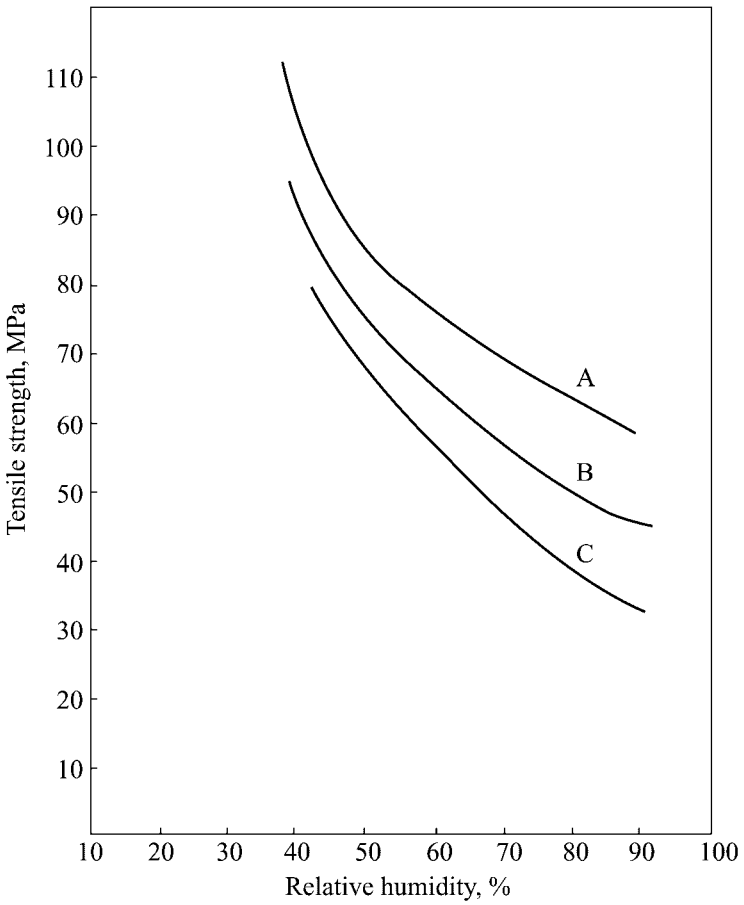

Fig. 8. Tensile strength as a function of relative humidity for fully hydrolyzed PVA films. A, DP = 2400; B, DP = 1700; C, DP = 500 (47). Reproduced by permission of John Wiley & Sons, Ltd. To convert MPa to psi, multiply by 145.

Esterification.

Inorganic Esters. Boric acid and borax form cyclic esters with PVA (69–76). The reaction is markedly sensitive to pH, boric acid concentration, and the cation-to-boron ratio. An insoluble gel is formed at a pH above 4.5–5.0.

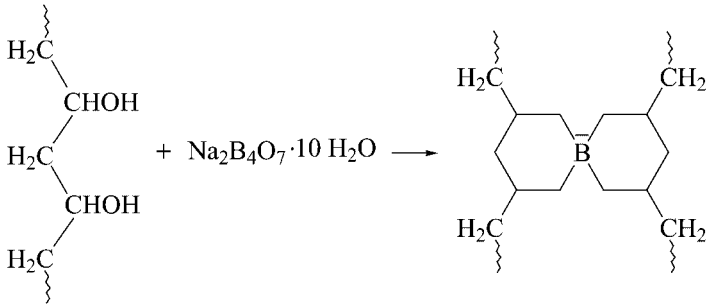

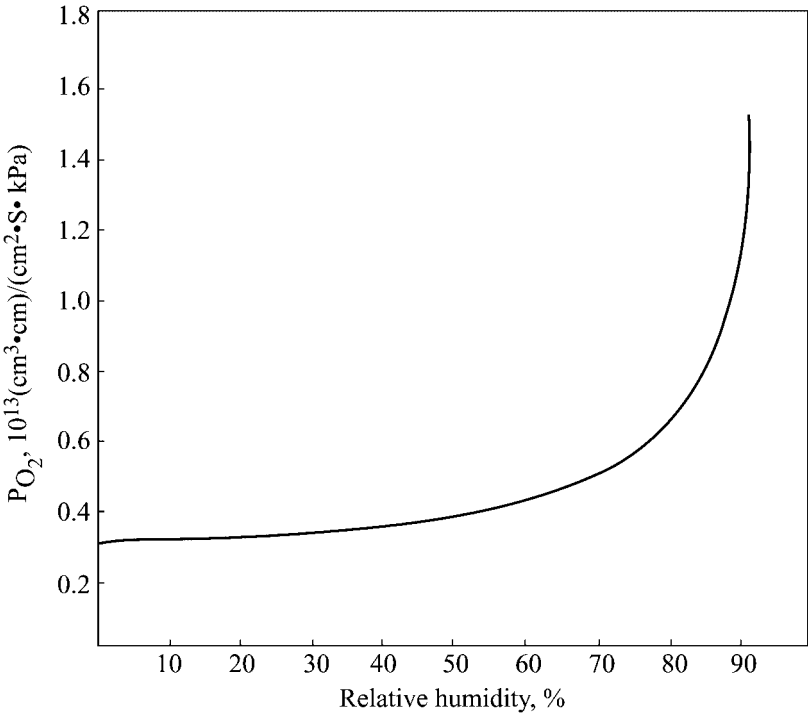

Fig. 9. Oxygen permeability of PVA as a function of humidity; degree of hydrolysis, 99.9 mol%, DP = 1750 (47).

Similar complexes are formed between PVA and titanium lactate (72,77), titanyl sulfate (78), or vanadyl compounds (79).

Poly(vinyl nitrate) has been prepared and studied for use in explosives and rocket fuel (80,81). Poly(vinyl alcohol) and sulfur trioxide react to produce poly(vinyl sulfate) (82–86). Poly(vinyl alkane sulfonate)s have been prepared from PVA and alkanesulfonyl chlorides (87,88). In the presence of urea, PVA and phosphorus pentoxide (89) or phosphoric acid (90) yield poly(vinyl phosphate)s.

Organic Esters. An unlimited number of organic esters can be prepared by reactions of PVA employing standard synthesis (66,68). Chloroformate esters react with PVA to yield poly(vinyl carbonates) (91).

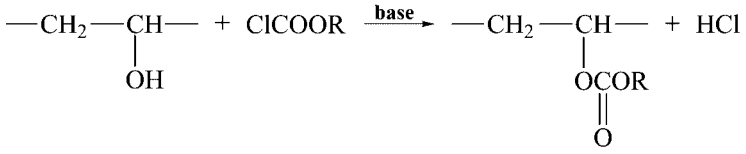

Poly(acrylic acid), poly(methacrylic acid), and maleic anhydride containing polymers react with PVA to form insoluble gels (92–94) useful as absorbents for water, blood, urine, etc.

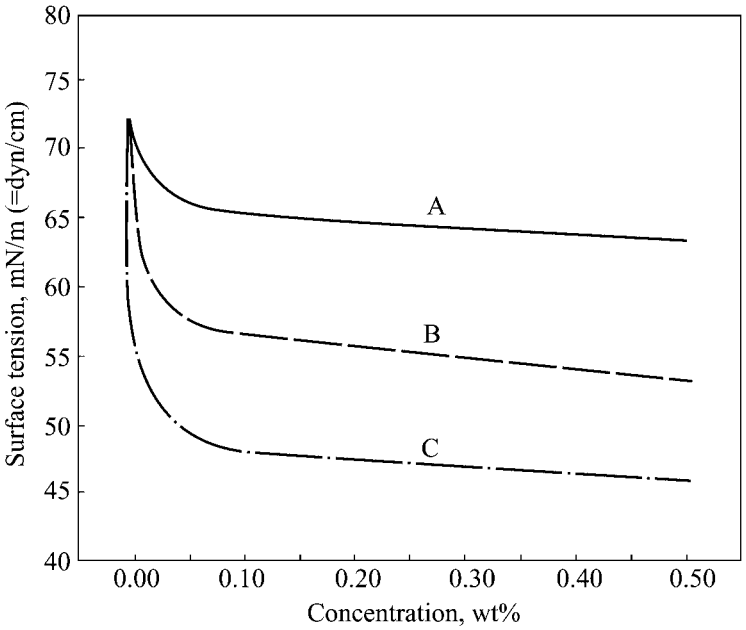

Fig. 10. Surface tension of aqueous PVA solutions at 20°C, DP = 1700. A, 98–99 mol% hydrolyzed; B, 87–89 mol% hydrolyzed; C, 78–81 mol% hydrolyzed.

Urea and PVA form a polymeric carbamate ester (95–98):

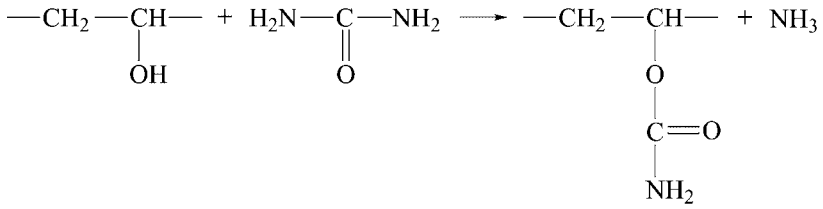

Reaction between PVA and isocyanates yields substituted carbamate esters (99–103):

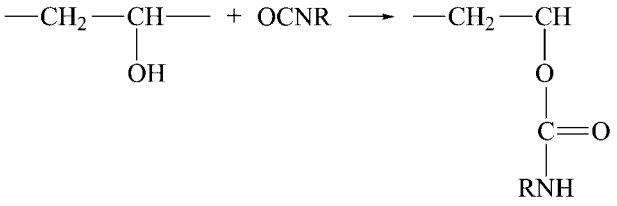

Etherification. Ethers of PVA are easily formed. Insoluble internal ethers are formed by the elimination of water, a reaction catalyzed by mineral acids and alkali.

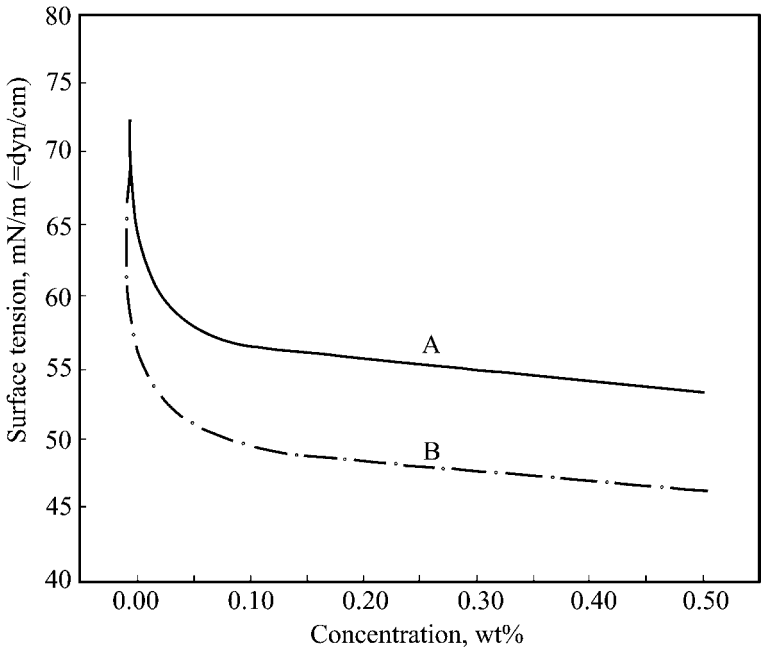

Fig. 11. Surface tension dependence on molecular weight at 20°C, degree of hydrolysis 87–89 mol%. DP: A, 1700; B, 550.

Ethylene oxide reacts with PVA under normal ethoxylation conditions (104–110). The resulting products have properties which make them useful as cold water-soluble films.

Cationic PVA has been prepared by the reaction of *N*-(3-chloro-2-hydroxypropyl)-*N*,*N*,*N*-trimethylammonium chloride and PVA and sodium hydroxide (111). Reactions between alkylidene epoxide and PVA in particulate, free-flowing form in an alkaline environment have been reported (112).

Poly(vinyl alcohol) undergoes Michaels addition with compounds containing activated double bonds, including acrylonitrile (115–117), acrylamide (118–120), *N*-methylolacrylamide (121–123), methyl vinyl ketone (124,125), acrolein (124), and sodium 2-acrylamido-2-methylpropanesulfonate (126). The reactions have been carried out under conditions spanning homogeneous reactions in solvent to heterogeneous reactions in the swollen powder or fiber.

Poly(vinyl alcohol) also reacts with monochloroacetates to yield glycolic acid ethers (127).

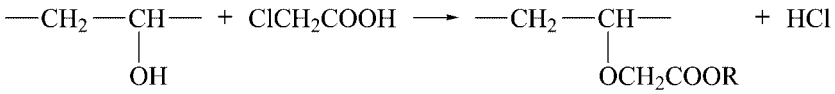

Acetalization. Poly(vinyl alcohol) and aldehydes form compounds of industrial importance.

(1) *Intramolecular acetalization*

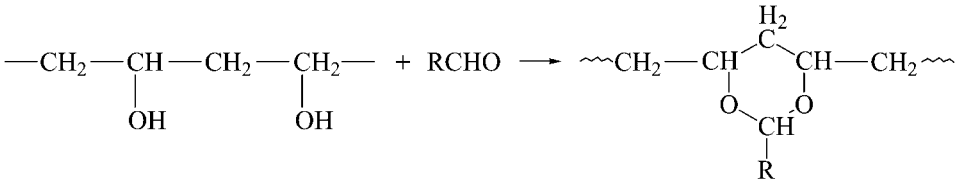

(2) *Intermolecular acetalization*

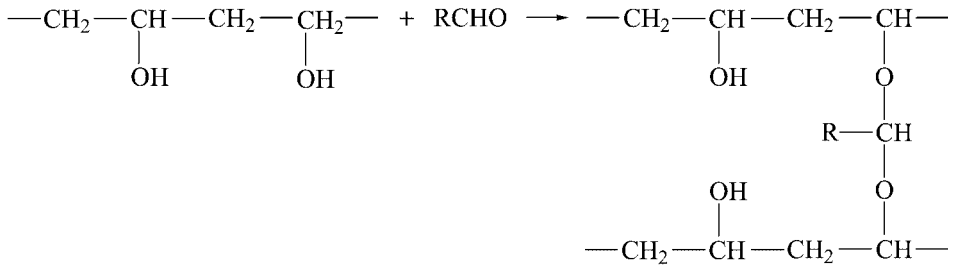

Poly(vinyl butyral) prepared by reacting PVA with *n*-butyraldehyde finds wide application as the interlayer in safety glass and as an adhesive for hydrophilic surfaces (128). Another example is the reaction of PVA with formaldehyde to form poly(vinyl formal), used in the production of synthetic fibers and sponges (129).

Poly(vinyl alcohol) is readily cross-linked with low molecular weight dialdehydes such as glutaraldehyde or glyoxal (130). Alkanol sulfonic acid and PVA yield a sulfonic acid modified product (131).

Other Reactions. Poly(vinyl alcohol) forms complexes with copper in neutral or slightly basic solutions (132). Sodium hydroxide or potassium hydroxide forms an intermolecular complex with PVA (132,133) causing gelation of the aqueous solution.

Certain organic compounds form reversible gels with PVA. Congo red, for example, yields a red gel that melts sharply at about 40°C. Other organic compounds that form a temperature reversible complex with PVA include azo dyes, resorcinol, catechol, and gallic acid (133,134)

Fully hydrolyzed PVA and iodine forms a complex that exhibits a characteristic blue color similar to that formed by iodine and starch (135–137). The color of the complex can be enhanced by the addition of boric acid to the solution consisting of iodine and potassium iodide. This affords a good calorimetric method for the determination of PVA. Color intensity of the complex is effected by molecular weight, degree of hydrolysis, extent of branching, stereoregularity, 1,2-glycol content, and reagent composition. The higher the 1,2-glycol content and the lower the molecular weight, the weaker the color (138–140). Partially hydrolyzed PVA and iodine forms a red complex, which is sensitive to the sequence distribution of the remaining acetate groups. The color intensity increases with increasing blockiness (141–148).

Cross-linking. Poly(vinyl alcohol) can be readily cross-linked using a multifunctional compound that reacts with hydroxyl groups. These types of reactions

are of significant industrial importance as they provide ways to obtain improved water resistance of the PVA or to increase the viscosity rapidly. The most commonly used cross-linking agents include glyoxal, glutaraldehyde, urea–formaldehyde, melamine–formaldehyde, trimethylolmelamine sodium borate or boric acid, and isocyanates. Most of the reactions are either acid- or base-catalyzed.

The study of hydrogel formation and their properties is a field of active academic research (76,149–151). The PVA molecule is loosely cross-linked, using standard cross-linking agents as mentioned above, which prevents solubility but allows for swelling. Application areas of interest range from enhanced oil recovery to drug delivery.

Strongly chelating metal salts of copper and nickel, eg, cupric ammonium complexes, chromium complexes, and organic titanates and dichromates, can be effective insolubilizers for PVA. Heat treatment during drying of the PVA film or coating is generally sufficient to accomplish the cross-linking reaction. The dichromate reaction is catalyzed by ultraviolet light.

Poly(vinyl alcohol), even when insolubilized by cross-linking, swells in water and loses strength on extended exposure. Complete water insensitivity cannot be achieved.

Thermal Decomposition. The thermal decomposition of PVA in the absence of oxygen occurs in two stages. The first stage begins at about 200°C and is mainly dehydration, accompanied by the formation of volatile products (152–158). The residue is predominantly macromolecules of polyene structure (152,159,160). Further heating to 400–500°C yields carbon and hydrocarbons (152,158). The available data on the nature of the decomposition products show some disagreement (152–157). Differences in manufacturing conditions of the PVA can significantly impact the thermal stability of the PVA as both molecular structure and the presence of catalyst residues are known sources for decreased thermal stability. The most common decomposition products of vinyl alcohol – vinyl acetate copolymers are shown in Table 4. The formation rate of volatile vapors from PVA pyrolyzed at 185–350°C can be described using a first-order rate equation (159).

Table 4. Thermal Decomposition Products of Vinyl Alcohol–Vinyl Acetate Copolymers, %[a]

	Hydrolysis, mol%						
Product	0	33	50	68	75	84	98
Water	14.10	16	20.30	43.57	60.24	59.98	73.88
Methanol	1.05	2.0	2.20	7.53	3.80	1.32	0.56
Acetone	4.20	2.1	8.90	4.35	2.62	2.62	0.85
Ethanol	7.00	6	2.30	1.13	0.43	0.61	1.25
n-Propanol	1.10	1.40	1.50	1.0	0.48	1.39	traces
Cotonaldehyde	–	3.05	2.30	traces	traces	0.67	traces
Acetic acid	74.00	79.00	59.03	35.13	26.30	26.68	6.98
Unidentified compounds	–	1.98	3.01	1.6	1.83	traces	8.03
Benzene	5	traces	–	–	–	–	–

[a]Ref. 142.

The thermal degradation of PVA in the presence of oxygen can be described by the same decomposition scheme as in the absence of oxygen with one modification. Oxidation of the unsaturated polymeric residue from the dehydration introduces ketone groups in the polymer chain. These groups promote the dehydration of the neighboring units, producing conjugated unsaturated ketone structures (161). Cross-linking under these conditions has also been observed (162). The first-stage degradation is similar to that obtained during vacuum pyrolysis (160). Above 250°C in the presence of oxygen, induced decomposition with self-ignition may take place (163).

Biodegradation. Poly(vinyl alcohol) is one of the few truly biodegradable synthetic polymers with the degradation products being water and carbon dioxide. At least 55 species or varieties of microorganisms have been shown to degrade or take an active role in the degradation of PVA (164). Poly(vinyl alcohol) degrading organisms consist not only of 20 different genera of bacteria, but molds, yeast, and fungi as well. The microorganisms which degrade PVA exist in most environments including activated sludge, facultative ponds, anaerobic digesters, septic systems, compost, aquatic systems, soil, and landfills. The time period for PVA to degrade is dependent upon the physical properties of the polymer, the form in which the product exists and the environment in which it is degraded. PVA is rapidly degraded by activated sludge especially if the sludge has already been adapted to the PVA molecule (164–168). Many of the microorganisms which degrade PVA can be isolated from soil (169–173).

The mechanism of PVA degradation consists of a random oxidation of a hydroxyl group to a ketone through the influence of a secondary alcohol oxidize. The random oxidation is continued until a β-diketone is formed. This group is cleaved by a extracellular hydrolase, leading to a reduction in molecular weight and the formation of a carboxylic end group and a methyl ketone end group. Continued degradation eventually leads to the formation of acetic acid, which in turn is converted into carbon dioxide and water. The degradation is normally accomplished by means of symbiotic organisms. Symbiotic bacterial pairs known to degrade PVA include, for Type I, *Pseudomonas putida* VM 15A, *P. vesicularas* Va., *P. porolyticus* PH, and *P. alkaligenes*; and for Type II, *P. Sp.* VM15C, *P. vesicularis* XL, *P. vesicularis* XL, and *P. vesicularis* PD. More recent studies have shown that isotactic blocks in PVA molecule are more readily biodegraded than those having an atactic structure (174,175). The biological oxygen demand for degradation of a 0.1% PVA solution is approximately 5 ppm (170).

Manufacture

Poly(vinyl alcohol) can be derived from the hydrolysis of a variety of poly(vinyl esters) such as poly(vinyl acetate), poly(vinyl formate), and poly(vinyl benzoate) and from the hydrolysis of poly(vinyl ethers). However, all commercially produced PVA is manufactured by the hydrolysis of poly(vinyl acetate). The manufacturing process can be viewed as one segment that deals with the polymerization of vinyl acetate and another that handles the hydrolysis of poly(vinyl acetate) to PVA.

Production of Poly(vinyl acetate).

Chemistry. Vinyl acetate is polymerized commercially using free-radical polymerization in either methanol or, in some circumstances, ethanol. Suitable

thermal initiators include organic peroxides such as butyl peroxypivalate, di(2-ethylhexyl) peroxydicarbonate, butyl peroxyneodecanoate, benzoyl peroxide, and lauroyl peroxide, and diazo compounds such as 2,2′-azobisisobutyronitrile (176–179). The temperatures of commercial interest range from 55 to 85°C (176,177).

Propagation of the polymerization occurs nearly exclusively by head-to-tail with only a small fraction of head-to-head reactions. The relative ratio of the two reactions is only a function of temperature and has been found to be independent of molecular weight, polymerization solvent, and method of polymerization. The head-to-head addition yields a 1,2-glycol structure in the resulting PVA, which in turn can influence the degree of crystallinity, strength, solubility, and thermal stability.

Termination reaction with vinyl acetate is nearly exclusively by disproportionation (180), although there are reports that recombination increases in importance at lower temperatures (181). Termination by disproportionation produces a double bond at the end of one molecule and a saturated bond at the other. The presence of the unsaturated bond results in an aldehyde group once the associated acetate group is hydrolyzed (182–184). The resulting aldehyde group decreases the thermal stability of the PVA, because the activation energy for splitting off water is reduced on account of the increased ability for formation of conjugated double bonds. The higher color level, observed in lower molecular weight commercial PVA grades, is a result of this reaction.

Chain transfer to monomer is important during vinyl acetate polymerization (181,185,186). The reaction is an abstraction of the hydrogen on the acetyl group of the vinyl acetate (187–189). The growing radical is transferred to the vinyl acetate monomer, which then reinitiates the polymerization. The reaction results in an unsaturated end group, which is still polymerizable. The inclusion of this terminal end group in a growing chain leads to a trifunctional branch point with the incorporation of the entire polymer molecule as a long-chain branch (185–187,187–192).

Chain transfer to polymer is considerable in vinyl acetate polymerization. The intermolecular transfer of a growing radical to a polymer molecule results in a branch point. Several studies have determined the fraction of branch points through the acetate group compared to those generated directly on the main chain (191,193–197). The results reported in the literature have been highly variable, ranging from over 0.95 to less than 0.5 at 60°C. The main distinction between branches generated through the acetoxy group and those connected directly to the main chain is that the first type is cleavable upon hydrolysis, the latter is not.

It has been shown that intramolecular chain transfer to polymer occurs during the polymerization of vinyl acetate, leading to short-chain branching (65,198–201). The number of short-chain branches has been estimated by nmr to be in the range of 0.12–1.7 mol% (65). The number of short-chain branches increases significantly with decreasing monomer concentration.

Chain transfer to low molecular weight alcohols occurs readily. However, the resulting end groups are not known to affect the physical or chemical properties of the resulting PVA. Chain transfer to acetaldehyde results in the incorporation of a ketone end group. Acetaldehyde is formed as a result of the transesterification between vinyl acetate and the added alcohol solvent. A small amount of an acid

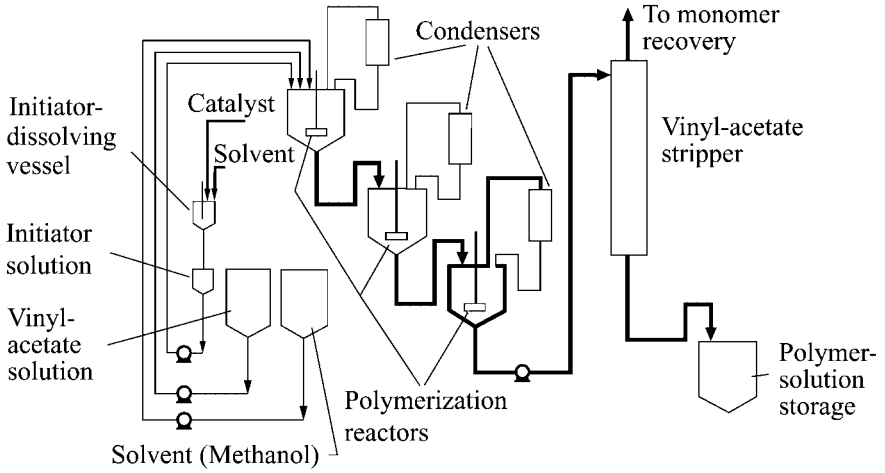

Fig. 12. Typical polymerization flow diagram for the continuous polymerization of vinyl acetate (208).

(2–50 ppm) may be added to the vinyl acetate in order to limit the transesterification (177,202–207). Suitable acids include phosphorous acid, oxalic acid, citric acid, and tartaric acid. The presence of the ketone end group in the resulting PVA facilitates the formation of conjugated double bonds and leads to color.

Commercial Manufacturing Processes.

Continuous Polymerization. A typical continuous flow diagram for the vinyl acetate polymerization is shown in Figure 12. The vinyl acetate is fed to the first reactor vessel, in which the mixture is purged with an inert gas such as nitrogen. Alternatively, the feed may be purged before being introduced to the reactor (176). A methanol solution containing the free-radical initiator is combined with the above stream and passed directly and continuously into the first reactor from which a stream of the polymerization mixture is continuously withdrawn and passed to subsequent reactors. More initiator can be added to these reactors to further increase the conversion.

The polymerization temperatures can range from 45 to 130°C; the preferred range is 55–85°C, which results in operating pressures of 0.1–0.5 MPa (1–5 atm). The heat of reaction is removed by condensing monomer and solvent vapors. Cooling coils show low efficiency because of the low heat transfer coefficient of the highly viscous material. Viscosity during polymerization can range from 10 to 500 P. Molecular weight is controlled by the residence time in the reactors, monomer feed rate, solvent concentration, initiator concentration, and polymerization temperature.

A stripping column is used to remove unpolymerized vinyl acetate from the poly(vinyl acetate) solution leaving the last reactor (Fig. 13). Methanol vapors are used to strip vinyl acetate from the solution (209,210). An inhibitor such as hydrazine, hydroquinone, sulfur, or quinone can be added to poly(vinyl acetate) solution leaving the reactor in order to prevent further polymerization in the stripping column (176). The overhead fraction from the stripping column consisting of solvent and vinyl acetate may be passed to a recovery system, or directly recycled

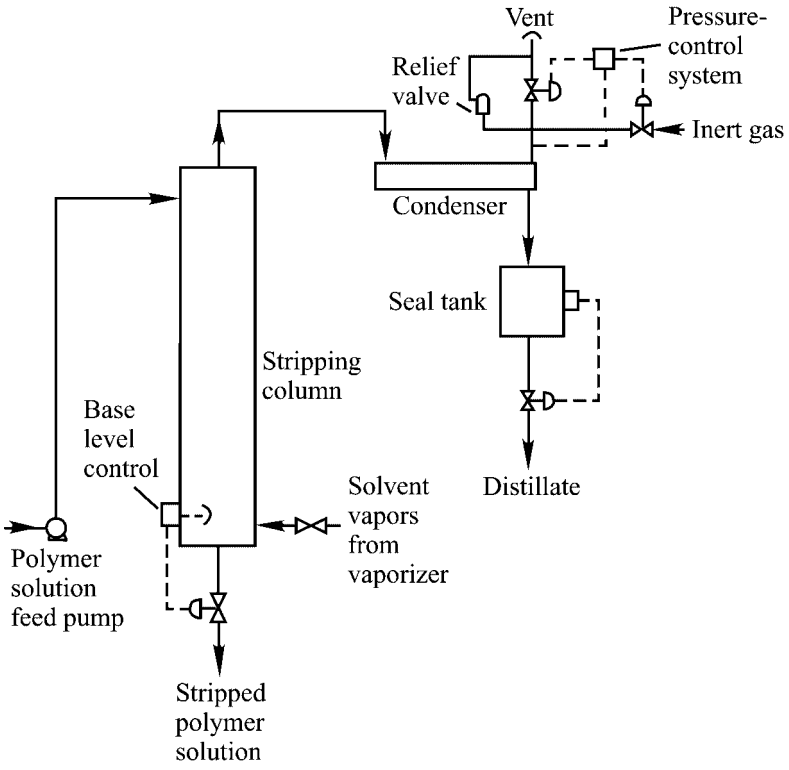

Fig. 13. Typical scheme for monomer stripping (209).

to the reactor. Vinyl acetate and methanol not recycled to the reactor must be separated and purified. Extractive distillation is normally used because methanol and vinyl acetate form an azeotrope. Suitable solvents include water and ethylene glycol.

The vinyl acetate content in the bottom effluent from the stripping column is reduced to less than 0.07 wt%. Higher concentrations of vinyl acetate will lead to yellowing because of acetaldehyde formation and subsequent aldol condensation during the hydrolysis reaction.

Batch and Semibatch Polymerization. The reactor is normally operated in a semicontinuous mode by delaying the addition of vinyl acetate, solvent, and initiator. The same reactor can be used for stripping the poly(vinyl acetate) solution, provided that careful addition of methanol is used in order to prevent the viscosity in the reactor from becoming excessive (211). The disadvantages of batch polymerization are the lack of product consistency and unsatisfactory economics in large-scale production. The true batch reaction, where all the reactants are added to the reactor at time zero, yields a product having a very broad molecular weight distribution of limited commercial value.

Production of PVA.

Chemistry. Poly(vinyl acetate) can be converted to PVA by transesterification, hydrolysis, or aminolysis. Industrially, the most important reaction is that

of transesterification, where a small amount of acid or base is added in catalytic amounts to promote the ester exchange.

The catalysts most often described in the literature (176,177,212) are sodium or potassium hydroxide, methoxide, or ethoxide. The reported ratio of alkali metal hydroxides or metal alcoholates to that of poly(vinyl acetate) needed for conversion ranges from 0.2 to 4.0 wt% (177). Acid catalysts are normally strong mineral acids such as sulfuric or hydrochloric acid (213). Acid-catalyzed hydrolysis is much slower than that of the alkaline-catalyzed reaction, a fact that has limited the commercial use of these catalysts.

The solution of poly(vinyl acetate) generated during the stripping operation is normally passed directly through to the alcoholysis system. This has limited the available solvents to methanol and ethanol (176,177). Substituting the alcohol used as solvent with the generated ester limits the hydrolysis and greatly affects how the remaining acetyl groups are distributed on the PVA chain (214–216). The distribution is often referred to as the blockiness of the PVA. The higher the methyl acetate concentration, the higher the degree of blockiness.

The presence of catalyst residues, such as alkali hydroxide or alkali acetate, a by-product of the hydrolysis reaction, is known to increase the thermal instability of PVA. Transforming these compounds into more inert compounds or removal through washing are both methods that have been pursued. The use of mineral acids such as sulfuric acid (217), phosphoric acid (218), and *ortho*-phosphoric acid (219) has been reported as means for achieving increased thermal stability of the resulting PVA.

Commercial Hydrolysis Process. The process of converting poly(vinyl acetate) to PVA on a commercial scale is complicated on account of the significant physical changes that accompany the conversion. The viscosity of the poly(vinyl acetate) solution increases rapidly and greatly as the conversion proceeds because the resulting PVA is insoluble in the most common solvents used for the polymerization of vinyl acetate. The outcome is the formation of a gel swollen with the resulting acetic acid ester and the alcohol used to effect the transesterification.

Continuous Saponification. There are several types of continuous systems, each with their own benefits and drawbacks. The basic premise is that continuous mixing is not required after the poly(vinyl acetate) and the caustic is mixed (220). Several designs for the high intensity mixing unit have been suggested in order to obtain efficient mixing and little fouling (221,222).

In the belt process, the mixture is cast onto the belt or conveyer (high temperature polyethylene) (223) where the gelling occurs (220,224). The gel is removed from the surface before syneresis, cut into smaller particles, and passed to a holding or washing tank (Fig. 14). The liquid is removed from the precipitate using common chemical deliquefying methods, and the resulting particles are dried in a continuous dryer.

In the slurry process, the hydrolysis is accomplished using two stirred tank reactors in series (225). Solutions of poly(vinyl acetate) and catalyst are continuously added to the first reactor, where 90% of the conversion occurs, and then transferred to the second reactor to reach full conversion. Alkyl acetate and alcohols are continuously distilled off in order to drive the equilibrium of the reaction. The resulting PVA particles tend to be very fine, resulting in a dusty product. The process has been modified to yield a less dusty product through process changes

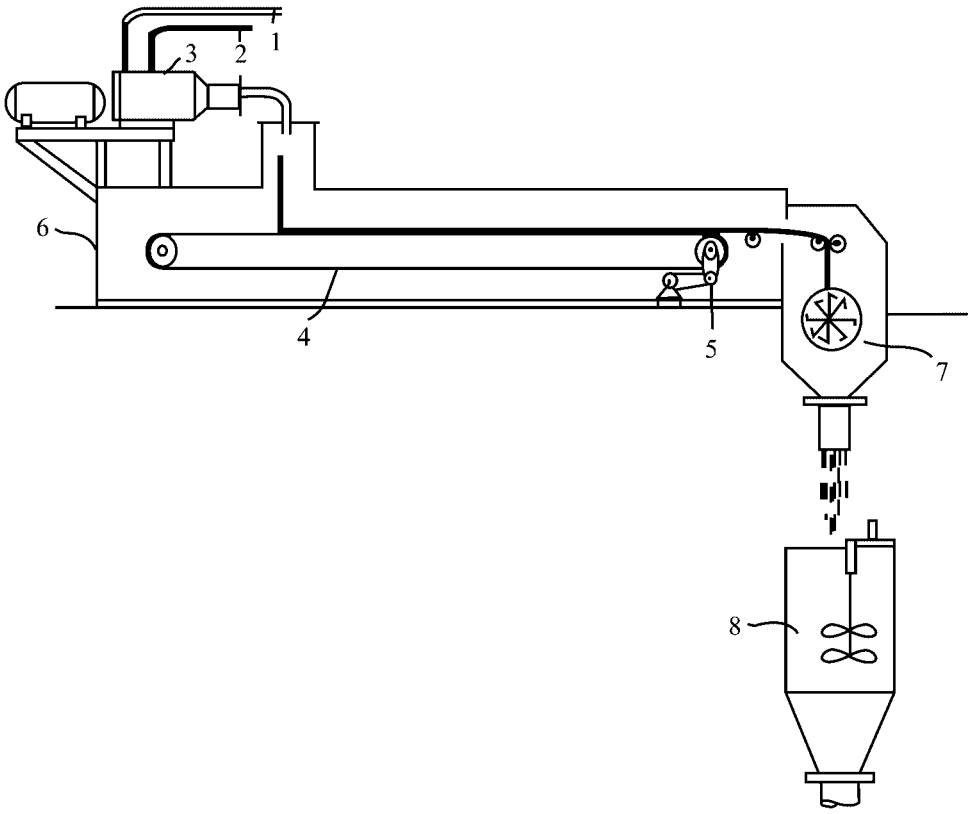

Fig. 14. The belt saponification process as used in the production of PVA (223). 1, Polyvinyl acetate/methanol mixture; 2, catalyst in methanol; 3, mixer; 4, belt; 5, drive; 6, housing; 7, cutter; 8, slurry tank (wash tank).

(226,227) and the use of additives (228). Partially hydrolyzed products having a narrow hydrolysis distribution cannot be prepared by this method.

In the screw conveyer process, solutions of poly(vinyl acetate) and catalyst are mixed in a high intensity mixer and continuously introduced to a screw-type saponification and conveyer system (229). Downstream details are similar to those found in the belt process.

Other methods also exist for handling the reaction mixture. For instance, an intermeshing, self-wiping, twin-screw extruder process has been proposed (230). The advantages described include higher saponification temperature (less catalyst), increased water solubility, and fewer impurities (231).

Batch Saponification. Batch saponification, the oldest PVA manufacturing method (232), is mainly used for the production of specialty products. The process uses a kneader in which the hydrolysis, washing, and drying operations are performed. This is the simplest method of saponification, but the production rates are low, and producing the product quality needed by many end uses is difficult.

Drying/Solids Separation. Separation of the polymer gel from the methanol/methyl acetate liquid is an important step, accomplished by using standard pieces of equipment such as filters, screw presses, or centrifuges.

Drying of the PVA is critical both to the color and solubility of the final product. Excessive drying temperatures result in high product color and an increase in the crystallinity, which in turn reduces the solubility of the product. Drying is initially subjected to a flash regime, where the solvent not contained within the particles is flashed off. This first phase is followed by a period where the rate is controlled by the diffusion rate of solvent from the PVA particles. Because the diffusion rate falls as the material dries, complete drying is not practical. The polymer is, therefore, generally sold at a specification of 95% solids.

Solvent Recovery. A mixture of methanol and methyl acetate is obtained after saponification. The methyl acetate can be sold as a solvent or converted back into acetic acid and methanol using a cationic-exchange resin such as a cross-linked styrene–sulphonic acid gel (233–236). The methyl acetate and methanol mixture is separated by extractive distillation using water or ethylene glycol (237–241). Water is preferred if the methyl acetate is to be hydrolyzed to acetic acid. The resulting acetic acid solution is concentrated by extraction or azeotropic distillation.

Copolymers

Numerous vinyl alcohol copolymers have been prepared (242). Copolymers with ethylene and methyl methacrylate are the only copolymers that have found sizable commercial utility. Ethylene–vinyl alcohol (EVOH) copolymers containing 20–30 mol% ethylene are used as an oxygen barrier in food packaging. However, a five-layer coextruded structure with polyolefins is needed in order to protect the EVOH from moisture. Vinyl alcohol–methyl methacrylate copolymers are used as sizing agents in the textile industry. The presence of the methacrylate unit disrupts the crystallinity making the product easier to remove during the desizing operation. The product is especially useful as an alkaline-resistant textile size.

Economic Aspects

The capacity of PVA in 2001 was greater than 625,000 t. The industry has experienced major changes since 1995, including the sale of the Air Products & Chemicals position to Celanese in September 2000, and the Clariant (formerly Hoechst) position to Kuraray in July 2001. New capacity, 40,000 t, was added by Kuraray and Nippon Gohsei in form of a joint venture, located in Singapore. Incremental expansion projects have also been initiated or completed by several of the current producers.

Approximately two-thirds of capacity is located in Japan, China, and Taiwan, with the remainder in the United States and Europe. Approximately 50,000 t of the Japanese and a large portion of the Chinese production is captively consumed for fiber production. The principal PVA producers in the world (capacity >30,000 t/year) are shown in Table 5.

The PVA process is highly capital-intensive as separate facilities are required for the production of poly(vinyl acetate), its saponification to PVA, the recovery of unreacted monomer, and the production of acetic acid from the ester formed

Table 5. Principal Poly(vinyl alcohol) Producers

Producer	Trade name	Capacity, t/year
Celanese	Celvol	90,000
Chang Chun	CCP	75,000
Chin-Shan Petrochemical		33,000
DuPont	Elvanol	68,000
Kuraray	Poval	194,000
Nippon Goshei	Gohsenol	77,000
Shi-Shan Vinylon		45,000

during alcoholysis. Capital costs are far in excess of those associated with the traditional production of other vinyl resins.

The PVA price has historically reflected the cost of ethylene, acetic acid, and energy. However, recent overcapacity has put strain on the pricing structure and lowered the return on investment. The price rose from $0.77/kg in 1970 to $2.20/kg in 1980, $2.75/kg in 1988, $2.65/kg in 1995, and $2.20/kg in 2001 for medium molecular weight fully hydrolyzed grade.

Specifications and Standards

The important commercial grades of PVA are distinguished by the degree of hydrolysis and molecular weight. The resins are most often categorized by degree of hydrolysis, ie, mole percent of alcohol groups in the resin (Table 6). Poly(vinyl alcohol)s having other degrees of hydrolysis are also produced, but maintain a much smaller market share than those shown in Table 6.

Poly(vinyl alcohol) is produced mainly in five molecular weight ranges expressed as degree of polymerization (DP) (Table 7). Several other molecular weight resins are available, but their market shares are relatively low. Industry practice expresses the molecular weight of a particular grade in terms of the viscosity of a 4% aqueous solution. An unlimited number of viscosities can be generated by blending the available molecular weights. Products having different degrees of hydrolysis can also be blended to obtain a particular performance characteristic. However, blended products have a broad distribution with respect to molecular weight and in some cases hydrolysis, which may be undesirable in some applications.

Table 6. Degree of Hydrolysis of Commercial Poly(vinyl alcohol) Grades

Grade	Hydrolysis, mol%
Super	99.3+
Fully	98.0–98.8
Intermediate	95.9–97.0
Partially	87.0–89.0
Low	79.0–81.0

Table 7. Viscosity and DP[a] of Principal Commercial Poly(vinyl alcohol) Grades[b]

Grade	Nominal DP	Viscosity of 4% solution, mPa·s (=cP)
Low–low	220	3–4
Low	550	5–7
Intermediate	900	13–16
Medium	1500	28–32
High	2200	55–65

[a]DP = Degree of polymergation.
[b]Grade = molecular range.

Table 8. FDA Regulations for Poly(vinyl alcohol) in Food Applications

Regulation	Description
181.30	Manufacture of paper and paperboard products used in packaging of fatty foods
175.105	Adhesives, no limitations
176.170	Components of paper and paperboard in contact with aqueous and fatty food; extractive limitations
176.180	Components of paper and paperboard in contact with dry food; no limitations
177.1200	Cellophane coating; no limitations
177.1670	Poly(vinyl alcohol) film
177.2260	Filters, resin-bonded where fiber is cellulose
177.2600	Filters, extractables must be less than 0.08 mg/cm^2
175.200	Resinous and polymeric coating
175.320	Resinous and polymeric coatings for polyolefin films; net extractable less than 0.08 mg/cm^2
177.2800	Textiles and textile fibers; for dry foods only
178.3910	Surface lubricants in the manufacture of metallic articles

PVA is an innocuous material with unlimited storage stability. It is most commonly supplied in 20-, 22.7- (50-lb), and 25-kg bags equipped with a moisture barrier to prevent caking. Poly(vinyl alcohol) is also available in bulk or in super sacks. The FDA regulations governing the use of PVA are shown in Table 8. Poly(vinyl alcohol) maintains an exemption for tolerance from the EPA.

Analytical and Test Methods

The important analytical test methods are those related to the determination of degree of hydrolysis, pH, viscosity, ash, and volatiles. Percent hydrolysis of the PVA is measured by placing the material in a mixture of water and methanol, adding a predetermined quantity of sodium hydroxide, and boiling under reflux to hydrolyze residual acetate groups. The moles of sodium hydroxide consumed are equivalent to the number of hydrolyzable acetate groups and are determined by back titration with strong acid.

The pH is measured using a 4% aqueous solution. Viscosity is normally measured using a Brookfield viscometer. Alternatively, a capillary viscometer or falling ball such as Hõppler may be employed. The type of viscometer used must always be noted.

Ash is a measure of residual sodium acetate. A simple method consists of dissolving the PVA in water, diluting to a known concentration of about 0.5 wt% and measuring the electrical conductivity of the solution at 30°C. The amount of sodium acetate is established by comparing the result to a calibration curve. A more lengthy method involves the extraction of the PVA with methanol using a Soxhlet extractor. The methanol is evaporated and water is added. The solution is titrated using hydrochloric acid in order to determine the amount of sodium acetate.

Volatiles such as residual methanol, methyl acetate, and water are determined as the loss in mass when the polymer is dried at 105 ± 2°C until constant mass is attained. Higher drying temperatures may cause decomposition and related weight loss.

Health and Safety Factors

Poly(vinyl alcohol) is a nonhazardous material according to the American Standard for Precautionary Labeling of Hazardous Industrial Chemicals (ANSI 2129.1-1976). Extensive tests indicate a very low order of toxicity when it is administered orally to laboratory animals (170). No toxicity was detected by oral administration of the maximum amount of 1500 mg/kg of two types of PVA (DP 1400, 99.5% hydrolyzed; and DP 1700, 86.8% hydrolyzed) or by subcutaneous injection of 3000 mg/kg to mice. PVA injected under the skin or into the lungs is not absorbed by the tissue and remains as a foreign body. The increase in growth and weight of mice given 1000 mg/kg every day during a 3-month chronic toxicity test was about the same as that of the control group animals. No histopathologic tensions were observed.

Poly(vinyl alcohol) has a low oral toxicity rating. The oral LD_{50} is higher than 10,000 mg/kg (rats). Concentrations of up to 10,000 mg/L in water were tested for toxicity to bluegill sunfish. No mortality or response indicative of intoxication was observed (243).

Short-term inhalation of PVA dust has no known health significance but can cause discomfort and should be avoided in accordance with industry standards for exposure to nuisance dust. The dust is mildly irritating to the eyes. There are no known dermal effects arising from short-term exposure to either solid PVA or its aqueous solutions.

During transport and handling, granular PVA may form an explosive mixture with air. However, the severity rating is 0.1 (Bureau of Mines Rating) on a scale in which coal dust has a rating of 1.0 (244). The explosive hazard does depend on particle size, and extremely fine dust has a higher explosive rating of 1.0–2.0. Residual methanol and methyl acetate can accumulate in the air space of bulk storage tanks; this is especially true at elevated temperatures. Precautions should be taken to ventilate the air space in large vessels and eliminate spark-producing equipment in the area. The issue of residual organic volatiles

has been addressed by a few PVA producers who have proactively implemented manufacturing specifications aimed at obtaining less than 1 wt% organic volatiles in the final product.

Processing

Poly(vinyl alcohol) is not considered a thermoplastic polymer because the degradation temperature is below that of the melting point. Thus, industrial applications of PVA are based on and limited by the use of water solutions.

Solution Preparation and Handling. Poly(vinyl alcohol) should be completely dispersed in water at room temperature, or lower, before heating of the water solution is commenced. Good agitation is important to prevent lumping during the addition of solid PVA to water. A large diameter, low speed agitator is preferred for providing good mixing at the surface without excessive air entrainment. Agitation requirements increase with solution concentration and with decreasing hydrolysis; the latter is associated with greater solubility in cold water and a tendency to lump.

The temperature of the slurry must be increased to 70–90°C in order to solubilize the PVA fully. Ways to increase the temperature includes direct steam injection, jet cooking, or heating with jacket or coil. Aqueous solutions of PVA are stable on storage but must be protected from bacterial growth. An increase in viscosity is commonly observed when storing fully hydrolyzed PVA solutions. Stainless steel or plastic containers are recommended for long-term storage. Many biocides are effective including FDA-approved compounds (245).

Prolonged heating of the PVA solution has negligible effect on its properties. However, the addition of strong acid or base to solutions of partially hydrolyzed PVA can increase the degree of hydrolysis.

Extrusion. Several attempts to introduce and produce extrudable PVA products have and continue to be made (246–260). However, these types of products have not achieved any significant commercial success. The main obstacles are thermal stability during extrusion and gels in the final product. A wide variety of high boiling water-soluble organic compounds containing hydroxyl groups have been used as plasticizers in order to lower the melt temperature and avoid decomposition. Glycerol and low molecular weight poly(ethylene glycol)s are most widely used. Water is an excellent plasticizer for PVA, although extrusion temperatures below 100°C are required in order to avoid the formation of foam at the extruder outlet.

Uses

The main applications for PVA are in textile sizing, adhesives, polymerization stabilizers, and paper coating, poly(vinyl butyral), and PVA fibers. In terms of percentage, and omitting the production of PVA not isolated prior to the conversion into poly(vinyl butyral), the principal applications are textile sizes, at 30%; adhesives, including use as a protective colloid, at 25%; fibers, at 15%; paper sizes, at 15%, poly(vinyl butyral), at 10%; and others, at 5%, which includes water-soluble films, nonwoven fabric binders, thickeners, slow release binders for fertilizer, photoprinting plates, sponges for cosmetic, and healthcare applications.

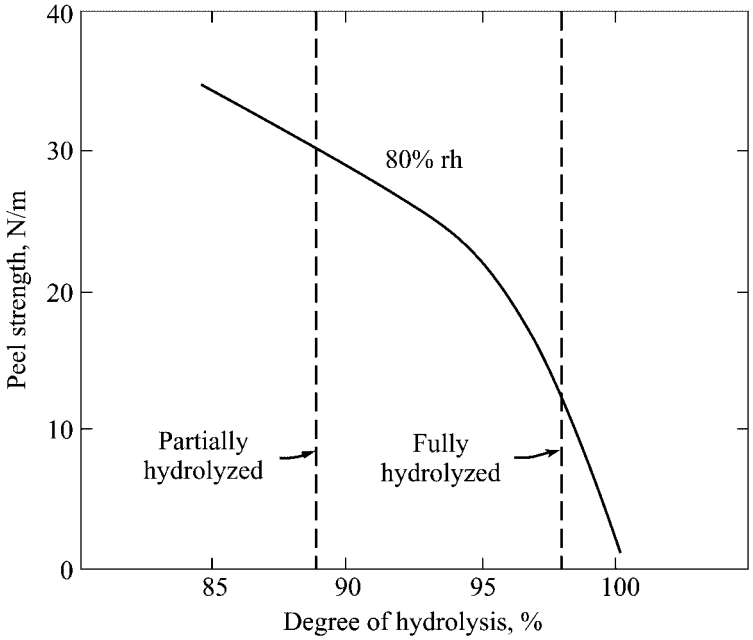

Fig. 15. Adhesion expressed as peel strength of PVA film on polyester film (7). To convert N/m to ppi, divide by 175.

Textile and Warp Sizing. Warps are sized to obtain increased abrasion resistance and strength in order to avoid breakage when passing through the loom. Yarn breakage during the weaving process reduces weaving efficiency and detracts from the quality of the finished cloth. The sizing material must allow for both easy splitting of the warp yarns after sizing and rapid desizing once the weaving process is complete. The typical sizing process consists of a size application box, squeeze rolls to remove excess size, drying drums, yarn-splitting rods, and beam-winding equipment.

Poly(vinyl alcohol) is an excellent textile warp size because of superior strength, adhesion, flexibility, and film-forming properties. The adhesion of PVA to natural or synthetic fibers or fiber blends depends on the degree of hydrolysis. Adhesion to such hydrophobic fibers as polyester is enhanced as the degree of hydrolysis is reduced (Fig. 15). Fully hydrolyzed grades adhere well to cotton and other hydrophilic fibers and impart the highest tensile strength for equivalent amounts added. However, there continues to be a trend away from fully hydrolyzed PVA because of its poor adhesion to synthetic fibers and the difficulty encountered when desizing heat-set fabric (176,261,262). The best hydrolysis grade for warp sizing is specific to each manufacturing operation and is controlled by factors such as yarn quality, yarn construction, and speed and type of loom.

The highest molecular weight grades provide the best protection at equivalent concentration for spun yarns. However, low solids sizing solutions are needed to maintain manageable viscosity; this increases drying cost and limits production. Desizing of the fabric is difficult because of the lower solubility rate of these grades.

Thus, the commonly used warp size grades for spun yarns are the medium to lower molecular weight resins because they provide balance, strength, solution viscosity, and desizing to yield the best possible economics. The best size for filament yarns are those PVA grades that have low degrees of polymerization.

Typical size formulations contain a lubricating wax, starch, and other processing aids. The role of these materials is to provide easy splitting of the yarns after drying, to decrease the sticking tendency of PVA to the drying drums, and to provide lubricity during the weaving process. The additives must to a large degree be incompatible with the dried PVA film to provide the desired function. However, a large degree of incompatibility can result in decreased encapsulation of the yarn and increased shedding during the weaving operation. Poly(vinyl alcohol) is normally used in 3–10-wt% concentrations in the aqueous size solution. Amount of size needed depends on both fabric and loom type, but is usually in the 5–10% range.

The fabric is desized after the weaving operation by passing it through a heated water bath to remove all the size. The rate at which this operation can be accomplished depends to a great degree on solubility rate of the PVA. Difficulties encountered in completely removing the lubricating wax, usually tallow wax, has led to the development of several wax-free size compositions (263–271). The main component contained in these blends is PVA in combination with a small amount of a synthetic water-soluble lubricant.

Poly(vinyl alcohol) can be recovered from the desizing liquid by means of commercial ultrafiltration equipment. Recovery rates and effluent losses are inversely proportional to the PVA solution viscosity and independent of the degree of hydrolysis.

Adhesives. Poly(vinyl alcohol) is used as a component in a wide variety of general- purpose adhesives to bond cellulosic materials, such as paper and paperboard, wood textiles, some metal foils, and porous ceramic surfaces to each other. It is also an effective binder for pigments and other finely divided powders. Both fully and partially hydrolyzed grades are used. Sensitivity to water increases with decreasing degree of hydrolysis and the addition of plasticizer. Poly(vinyl alcohol) in many applications is employed as an additive to other polymer systems to improve the cohesive strength, film flexibility, moisture resistance, and other properties. It is incorporated into a wide variety of adhesives through its use as a protective colloid in emulsion polymerization.

Adhesives for paper tubes, paperboard, corrugated paperboard, and laminated fiberboard are made from dispersions of clays suspended with fully hydrolyzed PVA. Addition of boric acid improves wet tack and reduces penetration into porous surfaces (73,272). The tackified grades have higher solution viscosity than unmodified PVA and must be maintained at pH 4.6–4.9 for optimum wet adhesion.

Poly(vinyl alcohol) is employed as a modifier of thermosetting resins used as adhesives in plywood and particleboard manufacture (273,274). The polymer is added to urea–formaldehyde or urea–melamine–formaldehyde resins to improve initial grab, increase viscosity, and in general to improve the characteristics of the board.

Poly(vinyl alcohol)s are used as components in vinyl acetate emulsions both as a protective colloid and as a means for improving adhesive properties. Addition

of PVA to the resulting emulsions is commonly employed to modify viscosity, flow properties, and the rate of formation of the adhesive bond as well as the quality. High addition rates of partially hydrolyzed PVA can be used to prepare remoistenable adhesive formulations. All PVA grades promote the acceptance of starch and clay fillers into a formulation, which in turn prevents excessive adhesive penetration into porous surfaces. The PVA also offers reactive sites that can be used to cross-link the adhesive and improve the water resistance. Cross-Linking is accomplished by means of either *N*-methylolacrylamide, copolymerized with the vinyl acetate (275,276), or other commonly used cross-linking agents, such as glyoxal. The performance of poly(vinyl acetate)-based wood glues is to a great extent dependent upon the presence of PVA to provide both the cohesive and adhesive properties.

Emulsion Polymerization. Poly(vinyl acetate) and poly(vinyl acetate) copolymer latices prepared in the presence of PVA find wide applications in adhesives, textile finishes, and coatings. The emulsions show excellent stability to mechanical shear and to the addition of electrolytes, and possess excellent machining characteristics.

Partially hydrolyzed PVA grades are preferred because they have a hydrophobic/hydrophilic balance that make them uniquely suited for emulsion polymerization. The compatibility of the residual acetate units with the poly(vinyl acetate) latex particles partly explains the observed stabilization effect. The amount of PVA employed is normally 4–10% on the weight of vinyl acetate monomer. The viscosity of the resulting latex increases with increasing molecular weight and decreasing hydrolysis of the PVA (277).

Paper Coating. The unique binding properties of PVA has made it a primary contributor to the development of higher quality, specialized paper products. Its use spans a great variety of grades, including silicone-coated release liners, grease-proof and glassine packaging papers, food-grade boards, carbonless grades, currency and banknote grades, offset printing papers, high brightness printing and writing grades, offset masters, ink-jet and thermal printing papers, and cigarette filter tip papers.

Poly(vinyl alcohol) is utilized principally as a surface-treating agent, as in clear sizing, pigmented sizing, and pigmented coating. Exceptions include its use as a creping aid in tissue and towel manufacturing, in dye encapsulation for carbonless papers, and in some wet-end addition applications. Poly(vinyl alcohol) imparts exceptional strength and outstanding resistance to oils, greases, and organic solvents, and is widely recognized as the strongest paper binder available (Table 9) (278).

The resistance of the polymer to oils and organic solvents can be directly attributed to the hydroxyl functionality and the film-forming properties of the polymer. Treated paper substrates display a significant amount of oil resistance which make them valuable for packing papers and food-grade paperboard containers. This performance improvement is achieved despite the fact that the 1–3 wt% add-on level, typical of size press applications, is too low to provide a continuous PVA film.

The fully and super-hydrolyzed PVA grades are preferred by the paper industry as they provide superior strength, greater adhesion to cellulose, better water resistance, and low foaming. However, the intermediate and partially hydrolyzed

Table 9. Relative Strength of Paper Binders

Binder	Parts for equal strength
Poly(vinyl alcohol)	1
Styrene–butadiene	2–2.5
Poly(vinyl acetate)	2–3
Soy protein	2.5–3
Casein	2.5–3
Starch	3–4

grades provide better surface-filming characteristics on many paper and paperboard substrates.

Poly(vinyl alcohol) is widely used on release liners for silicone topcoat holdout. The wide diversity in performance requirements of the various release liners has resulted in recommendation for add-on ranging from 1.5–2.0 (279) to 10 g/m^2. Ultimately, the characteristics of the base paper itself, as well as the level of release required of the finished sheet, determine the best add-on level of the PVA.

The role of PVA in ink-jet printing papers is described in numerous patents. The market has shown fast growth in recent years. Most of the technology has been developed in Japan, which by 1985 had filed 75% of the 400 issued patents (280). Requirements call for a hydrophilic, high porosity surface capable of absorbing ink-jet droplets quickly, with little spreading, wicking, or dye penetration. The coating on the base sheet primarily consists of silica powder using PVA as the binder of choice (281).

Building Products. Poly(vinyl alcohol) is widely used in connection with spray-drying of emulsions, in particular ethylene–vinyl acetate copolymer emulsions. The PVA is added both as a protective colloid during the polymerization and as a redispersing aid prior to the actual spray drying for a total amount of 2–15 wt% (282–285). The PVA contained in these products greatly enhances the adhesion to cementitious materials, improves water retention, and increases strength. The powder, when added to tile grouts, joint compounds, textured compounds, and cementitious repair mortars, improves the bond strength, abrasion resistance, and flexibility of the final construction.

Poly(vinyl alcohol) is used as an additive to dry-wall joint cements and stucco-finish compounds. Rapid cold water solubility, which can be achieved with finely ground PVA, is important in many dry mixed products. Partially hydrolyzed grades are commercially available in fine particle size. The main purpose of the PVA is to improve adhesion and to act as a water-retention aid.

Fibers. Poly(vinyl alcohol) fibers possess excellent strength characteristics and provide a pleasant feel in fabrics. The fiber is usually spun by a wet process employing a concentrated aqueous solution of sodium sulfate as the coagulating bath. Water insolubility, even in boiling water, can be obtained by combining stretching, heat treatment, and acetalization with formaldehyde. Super-hydrolyzed PVA is the preferred material for fiber production.

PVA fibers have found widespread industrial use in cement as replacement for asbestos in cement products, reinforcement of rubber material such as conveyer belts, and hydraulic rubber hoses used in cars, ropes, fishing nets, etc. Only a small

amount of fibers is used in the production of textiles. Several patents (286–288) have been issued, claiming processes for production of ultrahigh tensile strength PVA fibers, which have tensile strength comparable to that of Kevlar.

Other Applications. Poly(vinyl alcohol) film can be produced by solution casting or extrusion. Film casting is most common as unplasticized films of all molecular weights and extents of hydrolysis can readily be produced. Water solubility of the film can be controlled by selection of the proper degree of hydrolysis. These films can be made into bags used for packaging of detergents, insecticides, hospital laundry, and numerous other items that are to be placed in water.

Poly(vinyl alcohol) is useful as a temporary protective coating for metals, plastics, and ceramics. The coating reduces damage from mechanical or chemical agents during manufacturing, transport, and storage. The protective film can be removed by peeling or washing with water.

The ultraviolet cross-linking of PVA with dicromates is the basis for its use in photoengraving, screen printing, printed circuit manufacture, and color television tube manufacture.

Partially hydrolyzed grades are used in many cosmetic applications because of their emulsifying, thickening, and film-forming properties. Poly(vinyl alcohol) is also used as a viscosity builder for aqueous solutions and dispersions.

BIBLIOGRAPHY

"Vinyl Alcohol Polymers" in *EPST* 1st ed., Vol. 14, pp. 149–207, by M. K. Lindemann, Chas. S. Tanner Co.; "Vinyl Alcohol Polymers" in *EPSE* 2nd ed., Vol. 17, pp. 167–198, by F. L. Marten, Air Products and Chemicals.

1. J. M. Hay and D. Lyon, *Nature* **216**, 790 (1967).
2. B. Capon, D. S. Watson, and C. Zucco, *J. Am. Chem. Soc.* **103**, 1761 (1987).
3. B. N. Novak and A. K. Cederstav, *J. Am. Chem. Soc.* **116**, 4073 (1994).
4. Ger. Pat. 450,286 (1924), W. Haehnel and W. O. Herrmann (to Consortium für Electrochemie, GmbH).
5. W. O. Hermann and W. Haehnel, *Ber. Dtsch. Chem. Ges.* **60**, 1658 (1927).
6. H. Staudinger, K. Frey, and W. Stark, *Ber. Dtsch. Chem. Ges.* **60**, 1782 (1927).
7. *Airvol Poly(vinyl alcohol) Manual*, Air Product and Chemicals, Inc., Allentown, Pa., 1990.
8. K. Tsuboi and T. Mochizuki, *Kobunshi Kagaku* **23**, 645 (1966).
9. K. Tsuboi and T. Mochizuki, *Kobunshi Kagaku* **24**, 245 (1967).
10. K. Tsuboi, K. Fujii, and T. Mochizuki, *Kobunshi Kagaku* **24**, 361 (1967).
11. K. Tsuboi and T. Mochizuki, *Kobunshi Kagaku* **24**, 366 (1967).
12. K. Monobe and Y. Fujiwara, *Kobunshi Kagaku* **21**, 179 (1964).
13. K. Tsuboi and T. Mochizuki, *J. Polym. Sci., Polym. Lett. Ed.* **1**, 531 (1963).
14. K. Tsuboi and T. Mochizuki, *Kobunshi Kagaku* **24**, 433 (1967).
15. A. Packter and M. S. Nerurkar, *J. Polym. Sci., Polym. Lett. Ed.* **7**, 761 (1969).
16. N. A. Peppas and P. J. Hansen, *J. Appl. Polym. Sci.* **27**, 4787 (1982).
17. N. A. Peppas and E. W. Merrill, *J. Polym. Sci., Polym. Chem. Ed.* **14**, 441 (1976).
18. N. A. Peppas and E. W. Merrill, *J. Appl. Polym. Sci.* **20**, 1457 (1976).
19. N. A. Peppas, *J. Appl. Polym. Sci.* **20**, 1715 (1976).
20. N. A. Peppas, *Eur. Polym. J.* **12**, 495 (1976).
21. K. Fujii, *J. Polym. Sci.* **D1**, 431 (1972).
22. S. Matsuzawa and co-workers, *Makromol. Chem.* **180**, 2009 (1979).

23. J. F. Kenney and G. W. Willcockson, *J. Polym. Sci., Part A* **4**, 679 (1966).
24. I. Sakurada, Y. Nukushina, and Y. Sone, *Kabunshi Kagaku* **12**, 506 (1955).
25. I. Sakurada, Y. Nukushina, and Y. Sone, *Ric. Sci.* **25A**, 715 (1955).
26. Y. Sone and I. Sakurada, *Kobunshi Kagaku* **14**, 92 (1957).
27. Y. Ikada and co-workers, *Radiat. Phys. Chem.* **9**, 633 (1977).
28. A. Packter and M. S. Nerurkar, *Eur. Polym. J.* **4**, 685 (1968).
29. A. Packter and M. S. Nerurkar, *Colloid Polym. Sci.* **253**, 916 (1975).
30. S. H. Hyon, H. D. Chu, and R. Kitamaru, *Bull. Inst. Chem. Res., Kyoto Univ.* **53**, 367 (1975).
31. Y. Nakanishi, *J. Polym. Sci., Polym. Chem. Ed.* **13**, 1223 (1975).
32. A. Booth and J. N. Hay, *Polymer* **12**, 365 (1971).
33. A. Booth and J. N. Hay, *Br. Polym. J.* **4**, 18 (1972).
34. J. N. Hay, *Br. Polym. J.* **9**, 72 (1977).
35. E. Riande and J. M. Fatou, *Polymer* **17**, 795 (1976).
36. N. A. Peppas, *Makromol. Chem.* **178**, 595 (1977).
37. N. A. Peppas and R. E. Benner, *J. Biomaterials* **1**, 158 (1980).
38. T. Osugi, *Man-Made Fibers*, Vol. **3**, Wiley-Interscience, New York, 1968, p. 258.
39. R. K. Tubbs and T. K. Wu, *Polyvinyl Alcohol*, John Wiley & Sons, Inc., London, 1973, p. 169.
40. I. Sakurada, A. Nakajima, and H. Takida, *Kobunshi Kagaku* **12**, 21 (1955).
41. J. Brandrup and E. H. Immergut, *Polymer Handbook*, 2nd ed., John Wiley & Sons, Inc., New York, 1975.
42. F. Hamada and A. Nakajima, *Kobunshi Kagaku* **23**, 395 (1966).
43. R. K. Tubbs, H. K. Inskip, and P. M. Subramanian, *Properties and Applications of Polyvinyl Alcohol* Monograph No. 30, Society of Chemical Industry, London, 1968, p. 88.
44. R. K. Tubbs, *J. Polym. Sci.*, Part A, **3**, 4181 (1965).
45. K. Kikukawa, S. Nozakura, and S. Murahashi, *Kobunshi Kagaku* **25**, 19 (1968).
46. *Unpublished data Air Products & Chemicals*, (1984).
47. K. Toyoshima, in C. A. Finch, ed., *Polyvinyl Alcohol*, John Wiley & Sons, Inc., London, 1973, pp. 17–65, 339–389.
48. I. Sakurada, Y. Sakaguchi, and Y. Ito, *Kobunshi Kagaku* **14**, 141 (1957).
49. S. N. Timasheff, *J. Amer. Chem. Soc.* **73**, 289 (1951).
50. K. Satake, *Kobunshi Kagaku* **12**, 122 (1955).
51. E. Prokopova, P. Stern, and O. Quadrat, *Colloid Polym. Sci.* **263**, 899 (1985).
52. P. Stern, E. Prokopova, and O. Quadrat, *Colloid Polym. Sci.* **265**, 234 (1987).
53. E. Prokopova, P. Stern, and O. Quadrat, *Colloid Polym. Sci.* **265**, 903 (1987).
54. F. F. Vercauteren and co-workers, *Eur. Polym. J.* **23**, 711 (1987).
55. S. Fujishige, *J. Colloid Interface Sci.* **13**, 193 (1958).
56. D. Eagland and co-workers, *Eur. Polym. J.* **22**, 351 (1986).
57. A. D. Schwope and co-workers, *Am. Ind. Hyg. Assoc. J.* **53**, 352 (1992).
58. K. Noro, *Br. Polym. J.* **2**, 128 (1970).
59. S. Hayashi, C. Nakano, and T. Motoyama, *Kobunshi Kagaku* **20**, 303 (1963).
60. S. Hayashi, C. Nakano, and T. Motoyama, *Kobunshi Kagaku* **21**, 300 (1964).
61. M. Matsumoto and Ohyanagi, *J. Polym. Sci.* **31**, 225 (1958).
62. A. Beresniewicz, *J. Polym. Sci.* **39**, 63 (1959).
63. D. J. Nagy, *J. Polym. Sci.*, Part C, **24**, 87 (1986).
64. D. C. Bugada and A. Rudin, *J. Appl. Polym. Sci.* **30**, 4137 (1985).
65. Y. Morishima and S. Nozakura, *J. Polym. Sci., Chem. Ed.* **14**, 1277 (1976).
66. S. Noma, in *First Osaka Symposium, Kobunshi Gakkai*, Tokyo, 1955, pp. 81–103.
67. F. Kainer, *Polyvinylalkohole*, F. Enke, Stuttgart, 1949, pp. 55–92.
68. C. A. Finch, Ref. 39, pp. 183–202.

69. J. P. Lorand and J. O. Edwards, *J. Org. Chem.* **24**, 769 (1959).
70. S. Saito, H. Okayama, H. Kishimoto and Y. Fujiyama, *Kolloid-Z.* **144**, 41 (1955).
71. R. K. Schultz and R. R. Myers, *Macromolecules* **2**, 281 (1969).
72. U.S. Pat. 3,668,166 (1972), T. G. Kane and W. D. Robinson (to E. I. du Pont de Nemours & Co., Inc.).
73. U.S. Pat. 3,135,648 (June 2, 1964), R. L. Hawkins (to Air Products & Chemicals).
74. M. Shibayama and co-workers, *Polymer* **29**, 336 (1988).
75. U.S. Pat. 4,331,781 (May 25, 1982), W. Zimmermann and G. Pospich (to Hoechst Aktiengesellschaft).
76. E. T. Wise and S. G. Weber, *Macromolecules* **28**, 8321 (1995).
77. J. H. Haslam, *Adv. Chem.* **23**, 272 (1950).
78. U.S. Pat. 2,518,193 (Aug. 8, 1950), F. K. Signaigo (to E. I. du Pont de Nemours & Co., Inc.).
79. U.S. Pat. 3,518,242 (June 30, 1970), J. D. Crisp (to E. I. du Pont de Nemours & Co., Inc.).
80. W. Diepold, *Explosivstoffe* **17**, 2 (1970).
81. K. Noma, S. Oya, and K. Nakamura, *Kobunshi Kagaku* **4**, 112 (1947).
82. A. Takahashi, M. Nagasawa, and I. Kagawa, *Kogyo Kagaku Zasshi* **61**, 1614 (1958).
83. R. Asami and W. Tokura, *Kogyo Kagaku Zasshi* **62**, 1593 (1959).
84. U.S. Pat. 2,623,037 (Dec. 23, 1952), R. V. Jones (to Phillips Petroleum Co.).
85. I. M. Finganz and co-workers, *J. Polym. Sci.* **56**, 245 (1962).
86. Jpn. Pat. 12,538 (Aug. 31, 1958), I. Sakurada, Y. Noma, and K. En (to Daiichi Kogyo Seiyaku Co.).
87. D. D. Reynolds and W. O. Kenyon, *J. Am. Chem. Soc.* **72**, 1584 (1950).
88. J. R. Williams and D. G. Borden, *Makromol. Chem.* **73**, 203 (1964).
89. R. E. Ferrel, H. S. Olcott, and H. Frenkel-Conrat, *J. Am. Chem. Soc.* **70**, 2101 (1948).
90. G. C. Daul, J. D. Reid, and R. M. Reinhardt, *Ind. Ing. Chem.* **46**, 1042 (1954).
91. U.S. Pat. 2,592,058 (Apr. 8, 1952), I. E. Muskat and F. Strain (to Columbia-Southern Chemical Co.).
92. Jpn. Pat. 059419 (May 17, 1978) (to Sumitomo Chem. Ind. KK).
93. D. Graiver, S. Hyon, and Y. Ikada, *J. Appl. Polym. Sci.* **57**, 1299 (1995).
94. Eur. Pat. Appl. EP- 366968 (May 9, 1990), G. Haeubl and W. Scheuchenstuhl (to Chemie Linz GmbH).
95. A. M. Paquin, *Z. Naturforsch.* **1**, 518 (1946).
96. U.S. Pat. 3,193,534 (Feb. 26, 1961), K. Matsubayashi and M. Matsumoto (to Kurashiki Rayon Co.).
97. I. Sakurada, A. Nakajima and K. Shibatani, *J. Polym. Sci., Part A* **2**, 3545 (1964).
98. G. O. Yahya and co-workers, *J. Appl. Polym. Sci.* **57**, 343 (1995).
99. U.S. Pat. 4,340,686 (July 20, 1982), R. P. Foss (to E. I. du Pont de Nemours & Co., Inc.).
100. U.S. Pat. 3,776,889 (Dec. 4, 1973), K. C. Pande and S. E. Kallenbach (to Powers Chemco, Inc.).
101. F. Masuo, T. Nakano, and Y. Kimura, *Kogyo Kagaku Zasshi* **57**, 365 (1954).
102. U.S. Pat. 2,728,745 (Dec. 27, 1955), A. C. Smith and C. C. Unruh (to Eastman Kodak).
103. U.S. Pat. 2,887,469 (May 19, 1959), C. C. Unruh and D. A. Smith (to Eastman Kodak).
104. U.S. Pat. 3,125,556 (Jan. 2, 1964), J. C. Lukman (to The Borden Co.).
105. S. G. Cohen, H. C. Haas, and H. Slotnick, *J. Polym. Sci.* **11**, 193 (1953).
106. U.S. Pat. 2,844,570 (July 22, 1958), R. E. Broderick (to Union Carbide).
107. U.S. Pat. 2,990,398 (June 27, 1961), H. K. Inskip and W. Klabunde (to E. I. du Pont de Nemours & Co., Inc.).

108. U.S. Pat. 2,434,179 (Jan. 6, 1948), W. H. Sharkey (to E. I. du Pont de Nemours & Co., Inc.).
109. U.S. Pat. 3,052,652 (Sept. 4, 1962), B. D. Halpern and B. O. Krueger.
110. U.S. Pat. 2,844,571 (July 22, 1958), A. E. Broderick (to Union Carbide).
111. U.S. Pat. 4,775,715 (Oct. 4, 1988), A. Beresniewicz and T. Hassall Jr. (to E. I. du Pont de Nemours & Co., Inc.).
112. U.S. Pat. 4,822,851 (Apr. 18, 1989), R. Stober, E. Kohn, and D. Bischoff (to Degussa Aktiengesellschaft).
113. R. W. Roth, L. J. Patella, and B. L. Williams, *J. Appl. Polym. Sci.* **9**, 1083 (1965).
114. L. Alexandru, M. Opris, and Ciocanel, *J. Polym. Sci.* **59**, 129 (1962).
115. U.S. Pat. 3,194,798 (July 13, 1965), L. W. Frost (to Westinghouse Electric Co.).
116. F. Ide, S. Nakano, and K. Nakatsuka, *Kobunshi Kagaku* **24**, 549 (1967).
117. F. Arranz, M. Sanchez-Chaves, and M. M. Gallego, *Angew. Makromol. Chem.* **218**, 183 (1994).
118. U.S. Pat. 3,505,303 (Apr. 7, 1970), M. K. Lindemann (to Air Reduction Co.).
119. H. Ito, *Kogyo Kagaku Zasshi* **63**, 338 (1960).
120. U.S. Pat. 5,104,933 (Apr. 14, 1992), P. Shu (to Mobil Oil Corp.).
121. Y. Nakamura and M. Negishi, *Kogyo Kagaku Zasshi* **68**, 1762 (1965).
122. Y. Nakamura and M. Negishi, *Kogyo Kagaku Zasshi* **70**, 774 (1967).
123. Y. Nakamura, M. Negishi, and Y. Takekawa, *Kogyo Kagaku Zasshi* **68**, 1766 (1965).
124. Ger. Pat. 738,869 (July 29, 1943), K. Billig (to I. G. Farben).
125. M. Tsunooka and co-workers, *Kobunshi Kagaku* **23**, 451 (1966).
126. U.S. Pat. 5,350,801 (Sept. 27, 1994), A. Famili, L. A. Vratsanos, and F. L. Marten (to Air Products & Chemicals, Inc.).
127. M. Hida, *Kogyo Kagaku Zasshi* **55**, 275 (1952).
128. K. Asahina, in C. A. Finch, ed., *Poly(vinyl alcohol) Developments* John Wiley & Sons, Inc., London, 1992, pp. 673–688.
129. I. Sakurada, *Poly(vinyl alcohol) Fibers*, Marcel Dekker, Inc., New York, 1985.
130. B. Gebben, H. W. A. van den Berg, and D. Bargeman, *Polymer* **26**, 1737 (1985).
131. Ger. Pat. DE 3,316,948 (Nov. 15, 1984), W. Zimmerman and W. Eichhorn (to Hoechst AG).
132. Y. Mori, H. Yokoi, and Y. Fujise, *Polym. J.* **3**, 271 (1995).
133. M. Nagano and Y. Yoshioka, *Kobunshi Kagaku* **9**, 19 (1952).
134. T. Uragami and M. Sugihara, *Angew. Makromol. Chem.* **57**, 123 (1977).
135. C. Dittmar and W. J. Priest, *J. Polym. Sci.* **18**, 275 (1955).
136. R. C. Schulz and J. A. Trisnadi, *Makromol. Chem.* **177**, 1771 (1976).
137. M. Shibayama and co-workers, *Macromolecules* **27**, 1738 (1994).
138. K. Shibatini, M. Nakamura, and Y. Oyanagi, *Kobunshi Kagaku* **26**, 118 (1969).
139. Y. Morishima, K. Fujisawa, and S. Nozakura, *Polym. J.* **10**, 281 (1978).
140. K. Kikukawa, S. Nozakura, and S. Murahashi, *Polym. J.* **2**, 212 (1971).
141. T. Hirai, A. Okazaki, and S. Hayashi, *J. Appl. Polym. Sci.* **32**, 3919 (1986).
142. S. S. Mnatsakanov and co-workers, *Polym. Sci. U.S.S.R.* **14**, 946 (1972).
143. B. J. R. Scholtens and B. H. Bijsterbosch, *J. Polym. Sci., Polym. Phys. Ed.* **17**, 1771 (1979).
144. S. Hayashi, C. Nakano, and T. Moyoyama, *Kobunshi Kagaku* **20**, 303 (1963).
145. S. Hayashi and co-workers, *J. Polym. Sci., Polym. Lett. Ed.* **20**, 69 (1982).
146. S. Hayashi and co-workers, *J. Polym. Sci., Polym. Chem. Ed.* **20**, 839 (1982).
147. S. Hayashi and co-workers, *Makromol. Chem.* **176**, 3221 (1975).
148. T. Hirai and co-workers, *J. Polym. Sci., Polym. Lett. Ed.* **26**, 299 (1988).
149. Y. Zhuang, Z. Zhu, and L. Chen, *J. Appl. Polym. Sci.* **63**, 267 (1997).
150. G. Paradossi and co-workers, *J. Polym. Sci., Polym. Chem. Ed.* **34**, 3417 (1996).
151. N. J. Atkin and co-workers, *J. Polym. Sci., Polym. Phys. Ed.* **39**, 1471, (2001).

152. Y. Tsuchiya and K. Sumi, *J. Polym. Sci.*, Part A 1, **7**, 3151 (1969).
153. C. Vasile, C. N. Cascaval, and P. Barbu, *J. Polym. Sci., Polym. Chem. Ed.* **19**, 907 (1981).
154. C. Vasile, S. F. Patachia, and V. Dumitrascu, *J. Polym. Sci., Polym. Chem. Ed.* **21**, 329 (1983).
155. C. Vasile and co-workers, *J. Polym. Sci., Polym. Chem. Ed.* **23**, 2579 (1985).
156. B. Kaesche-Krischer and H. J. Heinrich, *Z. Physik. Chem.* **23**, 292 (1960).
157. K. Ettre and P. F. Varadi, *Anal. Chem.* **35**, 69 (1963).
158. H. Fischer, *Z. Naturforsch.* **19a**, 866 (1964).
159. H. Futama and H. Tanaka, *J. Phys. Soc. Jpn.* **12**, 433 (1957).
160. T. Yamaguchi and M. Amagasa, *Kobunshi Kagaku* **18**, 645 (1961).
161. A. S. Dunn, R. L. Coley, and B. Duncalf, Ref. 43, p. 208.
162. B. Duncalf and A. S. Dunn, *Properties and Applications of Polyvinyl Alcohol*, Monograph No. 26, Society of Chemical Industry, London, New York, 1967, p. 162.
163. B. Kaesche-Krischer and H. J. Heinrich, *Chem. Ing. Tech.* **32**, 740 (1960).
164. R. J. Axelrod and J. H. Phillips, *Plastic Waste Management Workshop*, New Orleans, La., Dec. 9, 1991.
165. J. P. Casey and D. G. Manley, Proceedings of 3rd International Biodegradation Symposium, Applied Science Publishers, Ltd., London.
166. W. Schefer and K. Romanin, *Z. Wasser-Abwasser-Forsch.* **22**, 157 (1989).
167. K. Fischer, Melliand Textile Reports, 65, 269–274 and 340–345, 1984.
168. U.S. Pat. 3,926,796 (Dec. 16, 1975), Y. Fujita, I. Kawasaki, and H. Nishikawa (to Nippon Gohsei Kagaku Kogyo Kabushiki Kaisha).
169. T. Suzuki and co-workers, *Agric. Biol. Chem.* **37**, 747 (1973).
170. H. Nishikawa and Y. Fujita, *Chem. Econ. Eng. Rev.* **7**, 33 (1975).
171. M. Morita and co-workers, *Agric. Biol. Chem.* **43**, 1225 (1979).
172. K. Sakai and co-workers, *Agric. Biol. Chem.* **45**, 63 (1981).
173. K. Sakai, N. Hamada, and Y. Watanabe, *Agric. Biol. Chem.* **48**, 1093 (1984).
174. R. Fukae and co-workers, *Polym. J.* **26**, 1381 (1994).
175. S. Matsumura, Y. Shimura, and K. Toshima, *Macromol. Chem. Phys.* **196**, 3437 (1995).
176. U.S. Pat. 3,689,469 (Sept. 5, 1972), H. K. Inskip and R. L. Adelman (to E. I. du Pont de Nemours & Co., Inc.).
177. U.S. Pat. 4,618,648 (Oct. 22, 1986), F. L. Marten (to Air Products & Chemicals, Inc.).
178. Jpn. Pat. 63 18,542 (Sept. 17, 1963), K. Noro, G. Morimoto, and E. Uemura (to Nippon Gohsei Co.).
179. W. Baade, H. U. Moritz, and K. H. Reichert, *J. Appl. Polym. Sci.* **27**, 2249 (1982).
180. B. L. Funt and W. Pasika, *Can. J. Chem.* **38**, 1865 (1960).
181. C. H. Bamford, R. W. Dyson, and G. C. Eastmond, *Polymer* **10**, 885 (1969).
182. U.S. Pat. 3,679,648 (July 25, 1972), J. E. Bristol (to E. I. du Pont de Nemours & Co., Inc.).
183. U.S. Pat. 3,679,646 (July 25, 1972), J. E. Bristol (to E. I. du Pont de Nemours & Co., Inc.).
184. Br. Pat. 808,108 (Jan. 28, 1959) (to Celanese Corporation of America).
185. N. Friis and A. E. Hamielec, *J. Appl. Polym. Sci.* **19**, 97 (1975).
186. N. Friis and co-workers, *J. Appl. Polym. Sci.* **18**, 1247 (1974).
187. H. N. Friedlander, H. E. Harris, and J. G. Pritchard, *J. Polym. Sci.* **4**, 649 (1966).
188. S. Nozakura, Y. Morishima, and S. Murahashi, *J. Polym. Sci., Chem. Ed.* **10**, 2853 (1972).
189. J. T. Clarke, R. O. Howard, and W. H. Stockmeyer, *Makromol. Chem.* **44–46**, 427 (1961).
190. W. W. Graessley and H. M. Mittelhauser, *J. Polym. Sci.*, Part A-2, **5**, 431 (1967).

191. W. W. Graessley, R. D. Hartung, and W. C. Uy, *J. Polym. Sci.*, Part A-2, **7**, 1919 (1969).
192. K. Nagasubramanian and W. W. Graessley, *Chem. Eng. Sci.* **25**, 1559 (1970).
193. S. Nozakura, Y. Morishima, and S. Murahashi, *J. Polym. Sci.*, Part A-1, **10**, 2767 (1972).
194. S. Nozakura, Y. Morishima, and S. Murahashi, *J. Polym. Sci.*, Part A-1, **10**, 2781 (1972).
195. S. Nozakura, Y. Morishima, and S. Murahashi, *J. Polym. Sci.*, Part A-1, **10**, 2853 (1972).
196. S. Nozakura, Y. Morishima, and S. Murahashi, *J. Polym. Sci.*, Part A-1, **10**, 2867 (1972).
197. T. J. Markley, R. K. Pinschmidt, and J. W. Vanderhoff, *J. Polym. Sci., Polym. Chem. Ed.* **34**, 2581 (1996).
198. S. Nozakura and co-workers, *J. Polym. Sci., Polym. Chem. Ed.* **14**, 759 (1976).
199. Y. Morishima and co-workers, *J. Polym. Sci., Polym. Chem. Ed.* **14**, 1269 (1976).
200. Y. Morishima and S. Nozakura, *J. Polym. Sci., Polym. Chem. Ed.* **14**, 1277 (1976).
201. Y. Morishima, H. Iimuro, Y. Irie and S. Nozakura, *J. Polym. Sci., Polym. Ed. Lett.* **13**, 157 (1975).
202. Jpn. Pat. 61 16,446 (Sept. 15, 1961), S. Otsuka, Y. Ono, and S. Masuda (to Denki Kagaku Kogyo Co., Ltd.).
203. Jpn. Pat. 63 14,711 (Aug. 13, 1963), Y. Kotani (to Nippon Gohsei Co., Ltd.).
204. Jpn. Pat. 72 24,533 (July 6, 1972), J. Fujitani (to Denki Kagaku Kogyo Co., Ltd.).
205. Jpn. Pat. 71 14,649 (Apr. 20, 1972), T. Wakasugi and I. Niida (to Kurera Co., Ltd.).
206. J. H. Oak and S. N. Park, *Hwahak Kwa Hwahak Kongop* **5**, 239 (1971).
207. U.S. Pat. 4,708,999 (Nov. 24, 1987), F. L. Marten (to Air Products & Chemicals, Inc.).
208. H. Shohata, Ref. 43, pp. 18–45.
209. Br. Pat. 811,535 (1957) (to E. I. du Pont de Nemours & Co., Inc.).
210. U.S. 2,878,168 (Mar. 17, 1959), W. B. Tanner and J. R. Wesel (to E. I. du Pont de Nemours & Co., Inc.).
211. *East Ger. Pat.* (Jan. 28, 1987) (to VEB Chemische Werke Buna).
212. I. Sakurada and Y. Sakaguchi, *Kobunshi Kagaku* **13**, 441 (1956).
213. E. Hackel, Ref. 43, p. 1.
214. K. Noro, *Br. Polym. J.* **2**, 128 (1970).
215. F. Gregor and E. Engel, *Chem. Prumysl.* **10**, 53 (1960).
216. U.S. Pat. 3,156,678 (Nov. 10, 1964), H. Dexheimer and co-workers, (to Farbwerke Hoechst).
217. Jpn. Pat. 52,026,589 (Aug. 27, 1975) (to Electro Chemical Industry KK).
218. U.S. Pat. 3,156,667 (Nov. 10, 1964), J. G. Martins (to Shawinigan Resins Corp.).
219. U.S.S.R. Pat. 211,091 (May 7, 1965), L. E. De-Millo, T. V. Kyazeva, and V. A. Kuznetsova.
220. U.S. Pat. 2,643,994 (June 30, 1953), L. M. Germain (to Shawinigan Chemicals Ltd.).
221. Jpn. Pat. 13,141 (1960) (Nippon Gohsei Co.).
222. S. Yamane, in K. Nagano, S. Yamane, and K. Toyoshima, eds., *Poval Kobunshi Kankokai*, Kyoto, 1981, p. 114.
223. Br. Pat. 1,168,757 (Feb. 2, 1969), H. A. Eilers and co-workers (to Farbwerke Hoechst AG).
224. U.S. Pat. 2,642,419 (June 16, 1953), G. P. Waugh and W. O. Kenyon (to Eastman Kodak Co.).
225. U.S. Pat. 2,734,048 (Feb. 7, 1956), J. E. Bristol and W. B. Tanner (to E. I. du Pont de Nemours & Co., Inc.).

226. U.S. Pat. 3,296,236 (Jan. 3, 1967), W. B. Tanner (to E. I. du Pont de Nemours & Co., Inc.).
227. U.S. Pat. 3,487,060 (Dec. 30, 1969), J. E. Bristol (to E. I. du Pont de Nemours & Co., Inc.).
228. U.S. Pat. 4,389,506 (June 21, 1983), T. Hassall Jr. (to E. I. du Pont de Nemours & Co., Inc.).
229. U.S. Pat. 3,278,505 (Sept. 10, 1966), T. Kominami (to Kurashiki Rayon Co., Ltd.).
230. U.S. Pat. 4,338,405 (July. 6, 1982), R. I. Saxton (to E. I. du Pont de Nemours & Co., Inc.).
231. U.S. Pat. 4,401,790 (Aug. 30, 1983), H. Jung, L. Reihs, and G. Roh (to Hoechst Aktiengesellschaft).
232. E. Hackel, Ref. 43, p. 1.
233. U.S. Pat. 4,352,949 (Oct. 10, 1982), R. L. Adelman and R. Segars (to E. I. du Pont de Nemours & Co., Inc.).
234. L. Alexandru, F. Butaciu, and I. Balint, *J. Prakt. Chem., 4th ser.* **16**, 125 (1962).
235. Ger. Pat. 1,211,622 (Mar. 3, 1966), G. Kuenstle and H. Siegl (to Wacker Chemie AG).
236. A. Nakumura, *Kogyo Kagaku Zasshi* **72**, 626 (1969).
237. U.S. Pat. 2,671052 (Mar. 2, 1954), R. L. Mitchell and J. W. Walker (to Celanese Corp.).
238. U.S. Pat. 2,636,050 (Apr. 21, 1953), R. L. Hoaglin and W. M. Frankenberger (to Union Carbide Corp.).
239. U.S. Pat. 2,650,249 (Mar. 25, 1953), M. Mention and J. Mercier (to Les Usines de Melle).
240. U.S. Pat. 3,011,954 (Dec. 5, 1961), D. B. Halpern and B. O. Kreuger (to Borden Co.).
241. U.S. Pat. 3,239,572 (Mar. 8, 1966), C. A. Zinsstag (to Lonza Ltd.).
242. T. Okaya, in Ref. 128, pp. 79–103.
243. *Elvanol Safe Handling Information*, E. I. du Pont de Nemours & Co., Inc..
244. *Material Safety Data Sheet for Polyvinyl Alcohol*, Air Products & Chemicals, Inc., Allentown, Pa., 1981.
245. *Airvol Product Handbook*, Air Products and Chemicals, Inc., Allentown Pa., 1998.
246. U.S. Pat. 4,611,019 (Sept. 9, 1986), H. H. Lutzmann and G. W. Miller.
247. U.S. Pat. 4,215,169 (July 29, 1980), R. D. Wysong (to E. I. du Pont de Nemours & Co., Inc.).
248. U.S. Pat. 4,206,101 (June 3, 1980), R. D. Wysong (to E. I. du Pont de Nemours & Co., Inc.).
249. U.S. Pat. 4,267,145 (May 12, 1981), R. D. Wysong (to E. I. du Pont de Nemours & Co., Inc.).
250. U.S. Pat. 4,156,047 (May 22, 1979), R. D. Wysong (to E. I. du Pont de Nemours & Co., Inc.).
251. U.S. Pat. 4,155,971 (May 22, 1979), R. D. Wysong (to E. I. du Pont de Nemours & Co., Inc.).
252. U.S. Pat. 4,119,604 (Oct. 10, 1978), R. D. Wysong (to E. I. du Pont de Nemours & Co., Inc.).
253. Jpn. Pat. J 51,089,562 (Aug. 5, 1976) (to Unitika KK).
254. U.S. Pat. 4,672,087 (June 9, 1987), G. W. Miller and H. Lutzmann.
255. U.S. Pat. 4,369,281 (Jan. 18, 1983), W. Zimmerman and A. Harreus (to Hoechst AG).
256. U.S. Pat. 4,529,666 (July 16, 1985), F. Kleiner, K. Reinking, and H. Salzburg (to Bayer AG).
257. U.S. Pat. 3,607,812 (Sept. 9, 1971), T. Hayashi and co-workers (to Denki Kagaku Kogyo).

258. U.S. Pat. 4,469,837 (Sept. 4, 1984), P. Cattaneo.
259. U.S. Pat. 5,051,222 (Sept. 24, 1991), F. L. Marten, A. Famili, and J. F. Nangeroni (to Air Products & Chemicals, Inc.).
260. U.S. Pat. 5,137,969 (Sept. 24, 1991), F. L. Marten, A. Famili, and J. F. Nangeroni (to Air Products & Chemicals, Inc.).
261. J. E. Mooreland, *Text. Chem. Color.* **12**(4), 21 (1980).
262. D. L. Nehrenberg, in *AATCC RA73 Research Committee Warp Size Symposium*, Atlanta, Ga., Mar. 7, 1981, E. I. du Pont de Nemours & Co., Inc., Wilmington, Del.
263. U.S. Pat. 4,844,709 (July 4, 1989), F. L. Marten (to Air Products and Chemicals, Inc.).
264. U.S. Pat. 4,845,140 (July 4, 1989), F. L. Marten (to Air Products and Chemicals, Inc.).
265. Jpn. Pat. 47 45,634 (Nov. 17, 1972), M. Yamamoto and co-workers (to Unichika Co., Ltd.).
266. U.S. Pat. 4,640,946 (Feb. 3, 1987), D. A. Vasallo and D. W. Zunker (to E. I. du Pont de Nemours & Co., Inc.).
267. U.S. Pat. 4,383,063 (May 10, 1983), R. W. Rees (to E. I. du Pont de Nemours & Co., Inc.).
268. U.S. Pat. 4,399,245 (Aug. 16, 1983), R. Kleber and H. Stuhler (to Hoechst Aktiengesellschaft).
269. U.S. Pat. 4,222,922 (Sept. 16, 1980), R. W. Rees (to E. I. du Pont de Nemours & Co., Inc.).
270. U.S. Pat. 4,309,510 (Jan. 5, 1982), R. Kleber (to Hoechst Aktiengesellschaft).
271. U.S. Pat. 4,251,403 (Feb. 17, 1981), R. W. Rees (to E. I. du Pont de Nemours & Co., Inc.).
272. Eur. Pat. Appl. 306,250 (July 15, 1987), R. M. Marshall and P. L. Krankkala (to H. B. Fuller Co.).
273. Jpn. Pat. 49 12,590 (Mar. 23, 1974), M. Kurata, Y. Hase, and J. Ichimura (to Sugiyama Industrial Chemical Institute).
274. Jpn. Pat. 46 27,256 (Aug. 7, 1971), N. Kobakashi, M. Nomura, and Y. Yamitaki (to Dainippon Ink and Chemicals Inc.).
275. U.S. Pat. 3,941,735 (Mar. 2, 1975), M. K. Lindemann (to Chas. S. Tanner Co.).
276. U.S. Pat. 4,001,160 (Jan. 4, 1977), M. K. Lindemann (to Chas. S. Tanner Co.).
277. M. Shiraishi, *Br. Polym. J.* **2**, 135 (1970).
278. *Synthetic Binders in Paper Coatings* (*TAPPI Monograph No. 37*), 1975.
279. D. Wolf, *Kunstharz Nachr.* **17**, 34 (1981).
280. M. B. Lyne and J. S. Aspler, *TAPPI J.* 106 (May 1985).
281. Jpn. Pat. 88 118,286 (May 23, 1988) (to Asahi Glass Co. Ltd.).
282. U.S. Pat. 3,784,648 (Jan. 8, 1974), E. Bergmeister, P. G. Kirst, and H. Winkler (to Wacker Chemie GmbH).
283. U.S. Pat. 5,118,751 (June 2, 1992), J. Schulze, H. Herold, and J. Hinterwinkler (to Wacker Chemie GmbH).
284. U.S. Pat. 3,883,489 (May 13, 1975), K. Matschke and co-workers (to Hoechst Aktiengesellschaft).
285. U.S. Pat. 5,519,084 (May 21, 1996), H. Pak-Harvey and C. L. Mao (to Air Products and Chemicals, Inc.).
286. U.S. Pat. 4,440,711 (Apr. 3, 1984), Y. D. Kwon, S. Kavesh, and D. C. Prevorsek (to Allied Corp.).
287. U.S. Pat. 4,603,083 (July 29, 1986), H. Tanaka and F. Ueda (to Toray Industries, Inc.).
288. U.S. Pat. 4,551,296 (Nov. 5, 1985), S. Kavesh and D. C. Prevorsek (to Allied Corp.).

GENERAL REFERENCES

C. A. Finch, ed., *Polyvinyl Alcohol Developments*, John Wiley and Sons, Ltd., London, 1992.
I. Sakurada, *Poly(vinyl alcohol) Fibers*, Marcel Dekker, Inc., New York, 1985.
C. A. Finch, ed., *Polyvinyl Alcohol*, John Wiley and Sons, Ltd., London, 1973.
Properties and Applications of Poly(vinyl alcohol) (Monograph No. 30), Society of the Chemical Industry, London, 1968.
J. G. Pritchard, *Poly(vinyl alcohol) Basic Properties and Uses*, Gordon and Breach, Inc., New York, 1970.

F. L. MARTEN
Air Products and Chemicals, Inc.

VINYL CHLORIDE POLYMERS

Introduction

Poly(vinyl chloride) (PVC), a polymer prepared from vinyl chloride monomer (VCM),

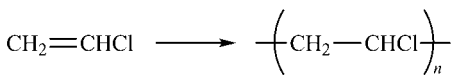

where $n = 700–1500$, holds a unique position among the polymers produced today. It is relatively inexpensive and is used in such a wide range of applications that its versatility is almost unlimited. However, if it were discovered today it would probably be shelved as a somewhat intractable and thermally unstable material. How can this apparent contradiction be explained?

The uniqueness of PVC can be considered under three headings: morphology, versatility, and molecular structure.

Morphology. As made, PVC is particulate in nature and comes in two main sizes depending on the process used. Suspension and mass polymerizations give grains (particles) of 100–180 μm in diameter, whereas the emulsion process affords a latex of particle size 0.1–3.0 μm. The latter is dried to yield friable grain-like structures of 5–50 μm.

Because of this unique particulate structure the most frequently used word in the vocabulary of the PVC technologist is morphology. In no other polymer is it as important as it is in PVC.

In its polymerization, a growing PVC chain becomes insoluble in VCM above a chain length of about 10 units (1) and so PVC is essentially insoluble in its monomer and the process is thus classified as a precipitation suspension

Encyclopedia of Polymer Science and Technology. Copyright John Wiley & Sons, Inc. All rights reserved.

polymerization. However, PVC is heavily swollen and partly solvated by the monomer to the extent of 27 wt% (2) and this has a major influence on the polymerization itself as well as the final properties and end uses of PVC. Hence, the way the PVC separates from the monomer, its future growth mechanism, and the swelling of the polymer by the monomer are critically important in its formation, handling, and subsequent processing.

Versatility. Poly(vinyl chloride) is a generic name. Each producer makes a range of PVC polymers which vary in morphology and in molecular mass, depending on the intended end use. In industry, the K-value and viscosity number are used to represent molecular mass, and producers often reflect these parameters in the grade codes used to define different products (eg, S68/173 refers to a suspension type material with a K-value of 68, and VY110/57 to a resin with a viscosity number of 110). The calculation of the K-value is given in Reference 3 and the relationship between these parameters and molecular mass in Reference 4.

PVC with $K = 66$–68 can be processed in rigid formulations to give pipes, conduit, sheet, and window profiles; $K = 65$–71 in flexible formulations for flexible sheet, flooring, wallpapers, cable coverings, hoses, tubing, and medical products; and PVC with low K-values (55–60) in formulations for injection molding of pipe and conduit fittings, integral electrical plugs, and blow molding of bottles and other containers.

In contrast, poly(methyl methacrylate) of even very high molecular mass is still soluble in its monomer and produces only glass-like solid beads at the end of polymerization which have no internal morphology and as such are limited to a narrow range of end uses (eg, moldings for optical applications such as covers for car lights and illuminated signs).

Molecular Structure. Among the range of polymeric materials produced, PVC is unique because the bulky chlorine atom imparts a strongly polar nature to the PVC polymer chain, and the essentially syndiotactic conformation of the repeat unit in the chain leads to a limited level of crystallinity (5). This results in good mechanical properties, particularly stiffness at low wall thickness, high melt viscosity at relatively low molecular mass, and the ability to maintain good mechanical properties even when highly plasticized. This enables a wide range of softness and flexibility to be achieved and hence leads to an even wider variety of end uses.

Physical and Chemical Properties

Vinyl Chloride Monomer (VCM). Vinyl chloride monomer (VCM), bp -13.4°C, is a gas at room temperature and pressure. Therefore, it is handled as a compressed volatile liquid in all polymerization operations. Its vapor pressure over the typical polymerization temperature range of 50–70°C is 800–1250 kPa. As a result, PVC polymerization reactors are thick-walled jacketed steel vessels with a pressure rating of 1725 kPa. VCM is slightly soluble in water (0.11 wt% at 20°C). This has some influence on the suspension polymerization process and is critically important to the success of the emulsion polymerization process. The

Table 1. Typical Properties of Rigid PVC (UPVC)

Property	Test	Value
Tensile strength at 23°C, MPa[a]	BS 2782:301G ISO R527	55
Tensile modulus (1% strain, 100 s), GPa[b]	BS 4618 ISO R899	2.7–3.0
Tensile modulus (1% strain, 3 years), GPa[b]	ISO R899	1.7
Izod impact, J/m[c]	BS 2782:306A ISO R180	107 (unmodified) 534 (modified)
Specific gravity	ISO R1183	1.38–1.45
Coefficient of linear thermal expansion, K^{-1}	BS 4618:3.1	6×10^{-5}
Coefficient of thermal conductivity, W/mK		0.14
Flammability (oxygen index)	ASTM D2863 (Fenimore Martin)	45
Weathering resistance		Very good (especially white)
Resistance to concentrated mineral acids (at 20°C)		Excellent
Maximum continuous operating temperature	Field experience	60°C

[a]To convert MPa to psi, multiply by 145.
[b]To convert GPa to psi, multiply by 145,000.
[c]To convert J/m to ft·lb/in., divide by 53.38.

polymerization of VCM is strongly exothermic, and its specific heat and heat of evaporation of 1.352 kJ/(kg · K) and 20.6 kJ/mol, respectively, allow the removal of the heat of reaction by the use of a condenser as well as by the more conventional jacketed vessel systems. Its explosive limits in air are 4–22 vol% and plant design, particularly when handling unreacted VCM in the recovery system, must be designed and operated accordingly.

Poly(Vinyl Chloride) (PVC). Poly(vinyl chloride) is never used alone. It is always mixed with heat stabilizers, lubricants, plasticizers, fillers, and other additives to make processing possible, all of which can influence its physical and mechanical properties. Table 1 lists properties of rigid (unplasticized) PVC with a total additives content of <10%. Table 2 lists properties of flexible (plasticized) PVC where the range of physical properties varies widely, depending on the plasticizer content. Plasticizer content can vary between 20 and 100 phr and so as a guide properties typical of a plasticizer content of 50 phr are given.

In addition, the molecular mass of the PVC can also influence properties significantly. Molecular mass is expressed by *K*-values as explained in a later section.

PVC has extremely good chemical resistance to all but low molecular mass chlorinated solvents. Therefore, it is widely used in the construction and lining of chemical plants.

Table 2. Typical Properties of Flexible PVC

Property	Test	Value
Specific gravity	ISO R1183	1.19–1.68
Tensile strength, MPa[a]	BS 2782.320A	7.5–30
Elongation at break, %	BS 2782.320A	140–400
BS softness	BS 2782 365A	5–100
Cold flex temperature, °C	BS 2782 159B	−20 to −60
Volume resistivity at 23°C, Ω·cm	BS 2782 202A	10^{10}–10^{15}
Ageing resistance	Field experience	Excellent
Ozone resistance	Field experience	Very good

[a]To convert MPa to psi, multiply by 145.

Raw Materials and Production

Monomer. VCM is produced industrially by two main reactions: (*1*) hydrochlorination of acetylene and (*2*) thermal cracking of 1,2-dichloroethane produced by direct chlorination or oxychlorination of ethylene in the balanced process. Presently, more than 90% of the VCM produced is based on this route.

In an ideal situation a PVC plant is fully integrated, beginning with ethylene and chlorine (salt), but various levels of integration are employed worldwide. Stand-alone PVC plants, supplied with VCM by sea, road, or rail, are well known as are ones making the bulk of their VCM requirements from scratch on site, with supplementary supplies of 1,2-dichloroethane for cracking to satisfy peak demand. Finally, there are fully integrated plants which have the benefit of uninterrupted supplies of base raw materials (ethylene and salt) and where the monomer is supplied by pipeline at a significant cost benefit. It can cost up to 65 Euro/t to transport VCM within continental Western Europe depending on distance and type of freight used, ie road, rail, or ship.

Polymer Production. There are three main processes used for the commercial production of PVC: suspension (providing 80% of world production), emulsion (12%), and mass, also called bulk (8%).

Suspension Polymerization

The layout of a typical suspension PVC plant is shown in Figure 1.

The suspension polymerization process is essentially a bulk polymerization process carried out in millions of small "reactors" (droplets). Liquid vinyl chloride under its autogeneous vapor pressure is dispersed in water by vigorous stirring in a reactor (autoclave) of 25–150 m^3 capacity, fitted with a jacket and/or condenser for heat removal and baffles for optimum agitation. This results in the formation of droplets of average diameter 30–40 μm, which are stabilized against coalescence by one or more protective colloids (granulating agent). The other essential ingredient is a monomer-soluble free-radical initiator.

The formulations charged to the reactors (otherwise known as autoclaves, kettles, or polymerizers) are normally referred to as recipes. A basic recipe for

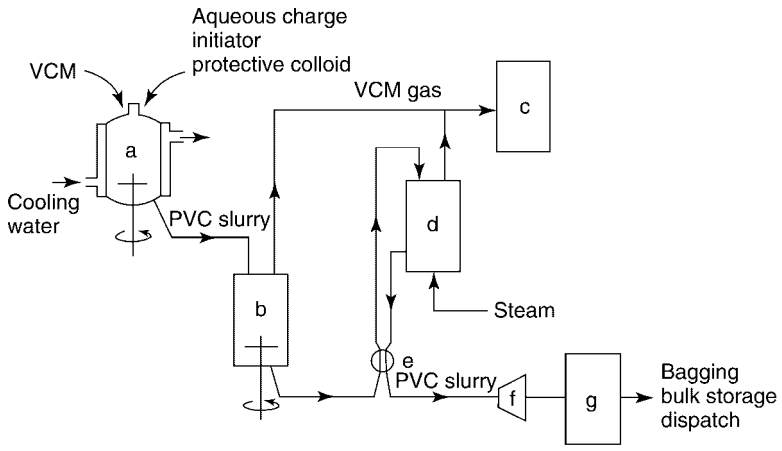

Fig. 1. Suspension PVC plant: a, reactor; b, blowdown vessel; c, VCM recovery plant; d, stripping column; e, heat exchanger; f, centrifuge; and g, driers.

suspension processes can be simply water, VCM, initiator, and suspension agent, for example,

VCM	100 parts
Water	90–130 parts
Protective colloid	0.05–0.15 parts
Initiator	0.03–0.08 parts

These quantities vary depending on the PVC grade, reactor size, plant type, etc.

Although this will produce a particulate PVC, it is unlikely to have the optimum morphology. This will only be achieved if other additives are employed, such as oxygen, buffers, secondary or tertiary granulating agents, chain-transfer or chain-extending agents, comonomers, antioxidants, together with the right level of agitation and homogenization, and the correct charging procedure and timing for each additive addition. A combination of just the right number and degree of the above parameters to achieve the optimum morphology usually determines the quality of a PVC grade.

After charging, the reactor contents are heated to the reaction temperature of 45–75°C. Reactors are 80–95% full at this stage. Heat causes some of the initiator to decompose into free radicals, and the monomer in the droplets begins to polymerize. The strongly exothermic reaction (1540 kJ/kg) is controlled by removing heat via the jacket and/or by boil-off into a condenser from which the condensed monomer is returned to the reactor.

Progress of the reaction in a jacketed reactor can be followed by continuously monitoring the water temperature in the jacket since the flow rate is constant and a constant batch temperature is maintained by progressively reducing the cooling water temperature (see Fig. 2).

Although PVC is insoluble in its monomer, the polymer is swollen by ca 27 wt% VCM to form a coherent gel (2). Therefore, as the conversion increases

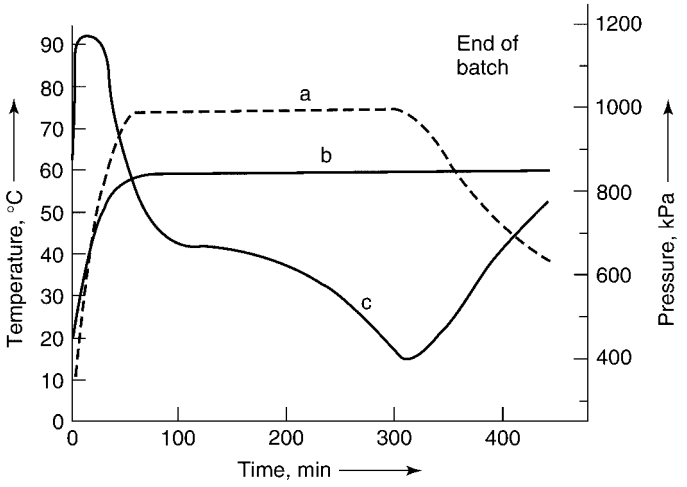

Fig. 2. Reaction profile for a typical suspension polymerization: a, pressure; b, batch temperature; and c, Jacket temperature.

toward 70% and beyond, the pressure in the reactor starts to fall, slowly at first, but then much more rapidly as the last of the free liquid monomer is consumed. Polymerization continues in the gel phase, very rapidly at first since chain termination is hindered by lack of mobility of the growing chain, but, as conversion increases beyond 80–85%, monomer starvation rapidly reduces the rate.

The reaction is terminated at a predetermined pressure by either adding a chain terminator and/or venting off the unreacted monomer to the recovery plant. After venting, the resin in the aqueous slurry can still contain 2–3% of unreacted monomer, which is removed by stripping, either batchwise (as in older plants) or continuously in a column. The batch is discharged from the reactor to a feed vessel and then fed continuously through a stripper column (Fig. 3). The unreacted monomer is recovered, liquified, and reused in later polymerizations. After passing through a heat exchanger the slurry is fed to a continuous centrifuge to give a wet-cake with 20–30% moisture content. The remaining water is then removed by conventional flash and/or fluid-bed drying to give a dry, free-flowing powder with a residual VCM content below 1 ppm.

Additives.

Water. The water used in the process should be demineralized (ie, of low conductivity) since ionic species, especially sodium ions, can affect the performance of other additives such as protective colloids and influence final polymer properties such as volume resistivity.

Protective Colloids (Granulating Agents). The protective colloids used in the suspension polymerization process are of two types: primary and secondary. The main function of the primary granulating agents is to control grain size, but they also affect porosity and other morphological properties. The demand for polymers with reduced residual VCM levels and better plasticizer adsorption led to the need for higher and more uniform porosity within each grain and this is achieved by using a secondary stabilizer in addition to the primary.

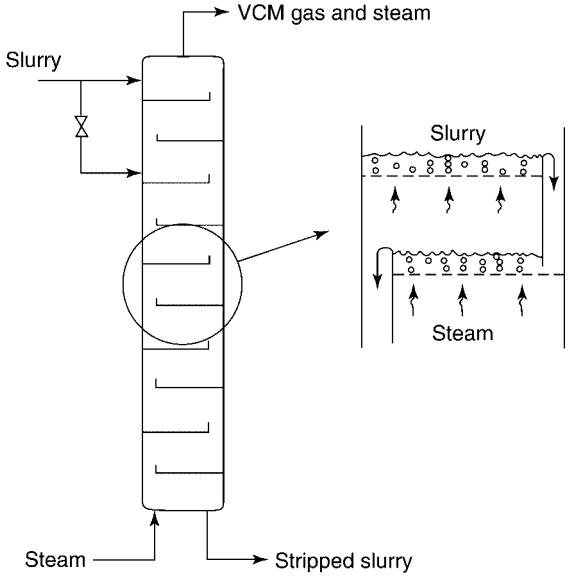

Fig. 3. Stripping column.

Although a wide variety of surface active materials have been or are still used, the substances most commonly used today are cellulose ether derivatives and partially hydrolyzed poly(vinyl acetates) or poly(vinyl alcohols) (PVAs). The latter are usually preferred and are used alone or in combination with the cellulose type, which they are gradually replacing. Typical PVA protective colloids are listed in Table 3.

As PVA primary granulating agents are prepared by alkaline hydrolysis of poly(vinyl acetates), they are complex mixtures containing fractions with different degrees of hydrolysis and molecular mass and having a block distribution of the OH groups (6). Because of this complexity, suspension processes need fine-tuning around the chosen agent since decreasing the average degree of hydrolysis of the PVA increases the porosity of the PVC grains and affects the grain size, as shown in Figure 4. This behavior is used in conjunction with agitation to achieve the optimum size and porosity. Below 70% hydrolysis the PVAs are insoluble in water and lose their ability to stabilize the VCM droplets adequately; so the normal range of PVA granulating agents used are in the range of 70–88%.

Many surfactants of low molecular mass have been claimed as useful secondary stabilizers, but in practice few can be used without adverse side effects. One exception is the nonionic sorbitan monolaurate. Again, PVAs are much more widely used. However, this family is prepared by acid hydrolysis of low molecular mass poly(vinyl acetates) and has a random distribution of acetate groups (6). Initially, these materials, which are insoluble in water, were prepared as methanolic solutions (eg, Polivic S202) but more recently aqueous-based, low hydrolysis PVAs (eg, Alcotex A55 and Polivic S 404W), which are safer to handle and are environmentally more acceptable, have been developed and are now very widely used in the industry. Typical secondary protective colloids are listed in Table 3.

Table 3. Typical Primary and Secondary Protective Colloids Used in the Suspension Polymerization of Vinyl Chloride

Trade name	Manufacturer	Degree of hydrolysis	Viscosity of 4% aqueous solution, mPa · s (=cP)
Primaries			
Alcotex 72.5/B72	Synthomer	71.5–73.5	5.5–7.5
Alcotex 78	Synthomer	76–79	5.5–7.5
Poval L9	Kuraray	70–72	6.0–6.5
Poval L10	Kuraray	71–73	5.5–7.5
Gohsenol KP08	Nippon Gohsei	71–75	6–9
Gohsenol KH17	Nippon Gohsei	78.5–81.5	32–38
Gohsenol KH20	Nippon Gohsei	78.5–81.5	44–52
Gohsenol GH20	Nippon Gohsei	86.5–89	40–46
Secondaries			Solvent base
Alcotex 55-002H/552P	Synthomer	54–57	Aqueous
Polivic S202	3V-Sigma	47	Methanolic
Polivic S404W	3V-Sigma	55	Aqueous
Poval LM10HD	Kuraray	38–42	Solid
Gohsenol LL02	Nippon Gohsei	45–51	Solid
Atlas G72143	ICI	50	Methanolic
Span 20 (sorbitan monolaurate)	ICI		Red-brown liquid, no solvent

The use of secondary granulating agents affects the mean grain size and grain size distribution and so the concentration of the primary ones must be adjusted to compensate. Since each producer uses autoclaves of different size and shape, equipped with different agitation and baffle systems, with or without condensers, and makes many different types of resin, no absolute formula is available which determines the magnitude of this change in primary concentration; this must be developed in-house by the suspension polymerization technologist.

Initiators. A range of initiators have been used, but currently a relative few are widely employed. At one time benzoyl peroxide and azo initiators were typically used, but diacetyl peroxides, peroxydicarbonates (PDC), and alkyl peroxyesters are now preferred (see INITIATORS, FREE-RADICAL). Typical initiators are listed in Table 4.

The half-life $t_{1/2}$ at a particular temperature is the main factor which determines the choice of an initiator for a given PVC grade. The initiator should have a half-life of ca 2 h at reaction temperature to optimize reaction time. Since the best plant output is obtained when the reaction profile (Fig. 2) is as square as possible, two initiators of different activity are often chosen to try to achieve this ideal. The more reactive initiator is used to start the polymerization but then as this exhausts itself the slower one takes over to completion. When preparing K 70–80 resins at temperatures at or below 52°C, a peroxydicarbonate (eg, **6**, **7**, **8**, or **9**) is used as the primary initiator, with an active initiator such as **1** or **12** helping to bolster the slow initial rate which is obtained at these low temperatures. In the intermediate range of K 63–68 a single PDC is usually sufficient, but at or below K 60 the PDC needs the extra radical flux of a slow initiator to prevent exhaustion

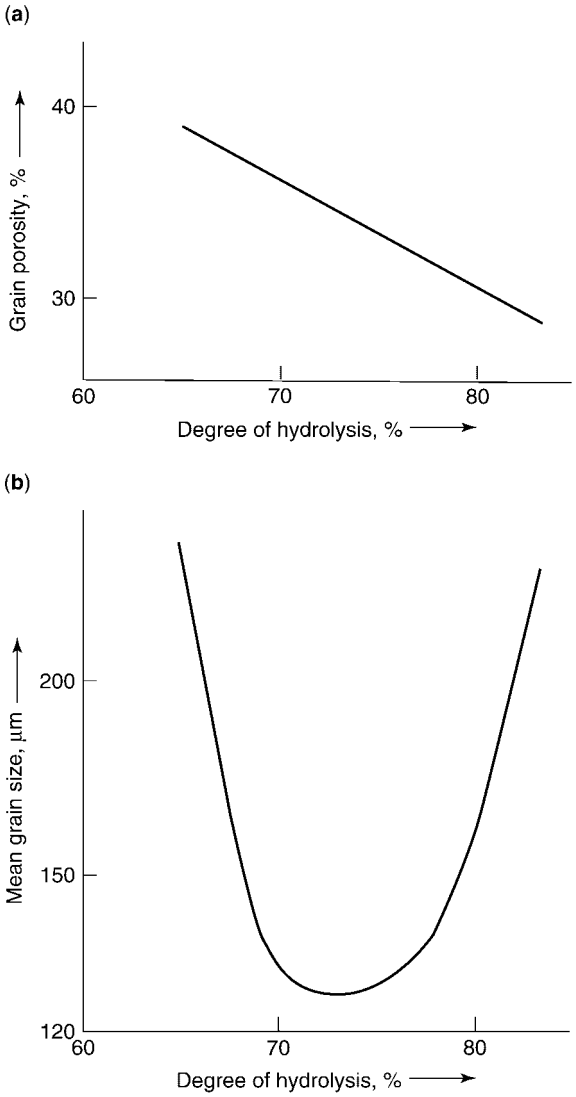

Fig. 4. The effect of the degree of hydrolysis of poly(vinyl acetate) on PVC grain properties. A, grain porosity and B, mean grain size.

of the reaction, and so a less active diacyl peroxide such as **4** or **13** is used as a secondary.

Three other factors are also important: water solubility, storage and handling, and reactor fouling.

The initiators' water solubility can affect their efficiency by making them more susceptible to hydrolysis and can affect their distribution between VCM droplets; the higher the solubility, the more homogeneous the distribution.

The ease of storage and handling has a major influence on the acceptability of an initiator to a PVC producer. In general, the shorter the half-life of the initiator,

Table 4. Initiators for Suspension or Mass Polymerization of VCM

Name	Storage temp.,[a] °C	M_r	Supplied form	$T_{1/2}$, °C[b]			$t_{1/2}$, min[c]		
				10 h	1 h	6 min	50°C	60°C	70°C
Diacyl peroxides									
Acetylcyclohexane sulfonyl peroxide (**1**)	−15	222	Solution	37	51	66	70	15	
Dioctanoyl peroxide (**2**)	10	286	Solid	61	79	100		700	190
Didecanoyl peroxide (**3**)	25	343	Solid	60	79	99		700	190
Dilauroyl peroxide (**4**)	30	398	Solid	62	80	99		850	220
Peroxydicarbonates									
Bis(2-ethylhexyl) peroxydicarbonate (**5**)	−15	346	Solution	44	61	80	250	70	21
Dicyclohexyl peroxydicarbonate (**6**)	10	286	Solid	44	59	76	250	58	16
Dicetyl peroxydicarbonate (**7**)	25	571	Solid or dispersion	45	61	79	320	70	20
Bis(4-*tert*-butyl cyclohexyl) peroxydicarbonate (**8**)	30	398	Solid or dispersion	43	60	78	250	60	18
Dimyristyl peroxydicarbonate (**9**)	20	515	Solid	46	62	79	320	70	20
Alkyl peroxyesters									
tert-Butyl peroxyneodecanoate (**10**)	−5	246	Solution	42	62	84	250	70	25
tert-Amyl peroxyneodecanoate (**11**)	−5	260	Solution	30	59	83	560	180	55
Cumyl peroxyneodecanoate (**12**)	−20	306	Solution	36	54	74	100	30	9
tert-Butyl peroxypivalate (**13**)	−5	174	Solution	51	71	94	700	200	70
Azo initiator									
Azobisisobutyronitrile (AIBN) (**14**)	20	164	Solution	59	79	101		500	170

[a] Maximum.
[b] Temperature at which $t_{1/2}$ = 10 h, 1 h, or 6 min, as indicated.
[c] Approximate.

the more unstable it is, and the lower its self-decomposition temperature. The stability also depends on the radical energy and physical form. Solid crystalline initiators such as **8** (BCHPC) are more stable than their liquid analogues, eg **5** (EHPC). Many of the more active initiators must be stored under refrigeration, which tends to restrict their acceptability. Liquid initiators have the advantage that they can be automatically metered into reactors, which is essential in larger computer-controlled plants. However, the current trend is to use initiators as finely divided aqueous dispersions. This has the advantage of improving their homogeneity of distribution throughout the VCM droplets, allows them to be added at any time or temperature during the charging procedure, and renders them very safe to handle since their heat of decomposition is less than the heat of evaporation of the carrier. Dispersion of 25–40% are typical, and systems must be carefully designed to ensure that complete homogenization of the dispersion is maintained and accurate metering achieved. As the water solubility of the initiator increases so does its tendency to cause reactor fouling. This is of increasing importance as more and more processes switch from the open to the closed mode of operation.

Kinetics. The kinetic profile seen in Figure 2 is typical of many VCM suspension polymerizations conducted at the lower end of the temperature range and exhibits the classical acceleration with conversion as shown by the gradually decreasing jacket temperature. At higher temperatures the reaction rate is more constant and a square-wave profile is obtained. Three different phases in the reaction can be identified:

Low Conversion (<5%). Polymerization occurs largely in the monomer phase because the quantity of polymer produced is so small. It is only this early stage that follows classical kinetics where the rate of polymerization is dependent on the square root of the initiator concentration:

$$\frac{-\mathrm{d[M]}}{\mathrm{d}t} = \frac{k_\mathrm{p}[\mathrm{M}] \cdot k_\mathrm{d}[\mathrm{I}]^{1/2}}{k_\mathrm{t}}$$

where
[M] = monomer concentration
[I] = initiator concentration
k_p = propagation rate constant
k_d = initiator decomposition rate constant
k_t = termination rate constant

As the amount of polymer phase increases with conversion the rate deviates more and more from this equation because of a decrease in k_t. A full description of the models used to explain the deviations from ideality is given in References 7 and 8.

Medium Conversion (5–65%). Polymerization continues in both the free monomer and polymer–monomer gel phases. This region shows the classical acceleration with increasing conversion (9). Since termination occurs primarily by the diffusion together and collision of two bulky macroradicals, it is considerably slower in the viscous polymer phase. As a result the termination rate constant is dramatically reduced and the rate of polymerization in this phase is much faster. As the amount of polymer phase increases, the rate of polymerization accelerates.

High Conversion (>65%). No free monomer is left to maintain the autogeneous pressure (which falls), and polymerization occurs in the polymer gel phase of rapidly increasing viscosity as the remaining VCM is consumed. Hence, the rate of polymerization increases still further to reach a maximum just after pressure drop but then decreases progressively owing to increasing monomer starvation. When the instantaneous polymerization rate falls below the overall rate of reaction the batch is terminated, either by venting off unreacted VCM to the recovery plant or by adding a chain terminator and then venting. Depending on the properties required, a conversion of 70–95% is chosen. It is uneconomic to continue to very high conversion, and as properties such as plasticizer absorption, dry-up rate (ie, the time taken to achieve a free-flowing PVC–plasticizer dry blend), and initial color/heat stability deteriorate rapidly above 85–90% conversion, most flexible resins are stopped at around 85% and rigid resins at around 90% conversion.

Morphology. Control of the morphology of each PVC grain is the main parameter controlling the quality of a PVC resin. This subject covers mean grain size, grain size distribution, and, most important of all, porosity (cold plasticizer absorption) and bulk density, which are closely interrelated.

Control of Grain Size. At the beginning of the batch the bulk vinyl chloride phase is broken down into droplets of 30–40 μm mean size under the influence of agitation and by the presence of the water-soluble protective colloid, which is adsorbed at the monomer–water interface. As polymerization proceeds, graft copolymerization of PVC onto the interfacial layer of protective colloid reduces its mobility and protective ability, and droplet coalescence begins to occur at around 4–5% conversion. As the conversion increases, changes in the surface layer of the droplet as a result of further polymerization suppress the droplet coalescence step, which ceases at 20% conversion, and the grain size remains largely constant for the remainder of the polymerization. Altering the stirrer speed after this point has no further effect on the mean grain size (MGS) (10) of the final product, which is controlled to between 100 and 180 μm, depending on resin type, by a combination of initial agitator speed and protective colloid(s) concentration and type.

Polymerizations with high concentrations of colloid and less agitation give spherical grains of low porosity ($\leq$10%) and very high bulk density ($\geq$700 g/L) and are of little interest, generally because of problems of VCM removal and poor gelation. Flexible resins are made with a low MGS (100–130 μm), rigid polymers with a higher MGS (150–180 μm), and low K resins with intermediate size (130–160 μm).

In extreme cases it is possible to stabilize the droplets to such a degree that no coalescence occurs. Specialized vinyl chloride monomer–vinyl acetate copolymers for gramophone record production fall into this category as do blending resins (30 μm MGS) for use as viscosity depressants in plastisols.

Alongwith achieving the desired MGS it is equally important to control the size distribution. A Gaussian distribution is normally produced and it is important to make this as narrow as possible since a coarse fraction (>250 μm) can give rise to fisheyes (dispersion faults), and make VCM removal difficult as well as result in loss of yield due to screen rejects, while fines (<60 μm) can be lost in aqueous and gaseous effluent or cause powder flow problems.

Control of Porosity and Bulk Density. Porosity in PVC grains is created by a complex series of interrelated steps in the formation and growth of the submicroscopic structure within each droplet and also depends on the unique nature of the VCM–PVC system.

PVC is insoluble in its monomer, and the growing oligomers start to precipitate when the chain length exceeds 10 monomer limits (1). This initial precipitation results in the formation of microdomains of about 15–20 nm in diameter (11). This occurs at as low as 0.001% conversion (12). The microdomains rapidly become unstable and aggregate to form domains (primary particle nuclei) of about 0.1 μm in diameter. After this stage no further domains are formed and the number of primary particles is fixed. All new PVC radicals that are produced in the monomer phase collide with and are precipitated onto the vast existing surface area of primary particles before a new domain can be formed. Since the existing PVC phase is swollen with monomer and contains initiator, initiator radicals, and growing chains undergoing chain transfer, primary particles grow rapidly by accretion of new microradicals and microdomains and by gel-phase polymerization. They in turn become unstable and a final agglomeration step to form 1–2 μm primary particle aggregates takes place. By the end of the polymerization the primary particles have grown to 1 μm within the aggregates, which themselves have grown to 2–5 μm. The whole mechanism is outlined in Table 5 and discussed in detail in Reference 13.

The arrangement of the aggregates of primary particles within each monomer droplet has a major influence on the morphology of the final PVC grain. The conversion of VCM of density 0.85 g/cm^3 at 52°C to PVC of 1.4 g/cm^3 produces a volume contraction of 39%. If the polymerizing droplets contract totally the final grain has no porosity. If, however, the contraction is prevented totally the final grain porosity can be as high as 39%. Therefore, the better the three-dimensional spatial arrangement of the aggregates relative to one another, the higher the porosity that is achieved.

The main aim of the polymer technologist is to create the best possible spatial network of aggregates relative to one another so that a network is formed that is strong enough to resist droplet contraction and hence maximize porosity. The sooner this is achieved in the polymerization the better the porosity attained. In practice 34–35% is easily achievable. At ca 65–70% conversion all of the free monomer is consumed, and the only VCM remaining is that swelling the polymer gel (27%) and in the vapor space and dissolved in the water. At this stage the voids in the grain (the porosity) are filled with batch water so that the quantity of water in interstitial spaces between the grains is reduced and a significant increase in slurry viscosity is observed since less mobilizing water is available to separate the grains.

The control of bulk density or apparent density (AD) is more important than even porosity to the processor. The latter is concerned with charge size and cycle times in high speed mixers, output rates, motor torque and degree of gelation in extruders, and mechanical properties of the article being produced. These parameters are very dependent on AD. The reason for introducing the control of porosity before control of AD is that the latter is very heavily influenced by the former. Apparent density depends on porosity, grain shape, and grain size distribution in order of priority and is best described by examining the packing fraction (PF)

Table 5. The Mechanism of VCM Polymerization[a]

Stage	Species		Conversion, %	Size	
				When formed	Finally
Initiation R1 + VCM →	Coiled macroradicals				
1st aggregation step			<1		
	Microdomain (ca 50 macroradicals)			10–20 nm	?
2nd aggregation step			1–2		
	Domain (primary nucleus) (ca 10^3 microdomains)			0.1–0.2 μm	
Growth (intraprimary)					
	Primary particle				0.6–0.8 μm
3rd aggregation step		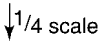	4–10	(primaries now 0.2–0.4 μm)	
	Agglomerate			1–2 μm	
Growth (interprimary)		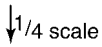			
	Fused agglomerate		90		2–10 μm

[a]From Ref. 13, courtesy of Elsevier Applied Science Publishers.

concept, ie, the ability of the somewhat irregular PVC grains to fill a space to the maximum efficiency.

$$PF = \frac{(1 + 0.014 \cdot CPA)(AD \cdot 0.1)}{1.4}$$

where CPA is cold plasticizer absorption (porosity).

Most extruders used in processing PVC are of the twin screw type and these operate like a simple pump: increasing the feed rate by 10% (10% higher AD) increases the discharge or output rate by 8–9% (see Chapt. 8 in Ref. 9). In practice, controlling porosity is relatively easy since a number of effective secondary stabilizers are available. Maximizing the AD is much more difficult since control of grain shape comes from a complex interaction of both agitation and choice of primary and secondary granulating agents together with in-house expertise of charging techniques and use of other additives. A range of grain shapes which can be produced is shown in Figure 5.

In practice typical property targets for porosity and AD are

(1) For flexible resins (K 70): porosity of ≥30% and AD of ≥500 g/L
(2) For rigid extrusion resins (K 66–68): porosity of 20% and AD of 580 g/L
(3) For bottle resins (K 57–60): porosity of 18–20% and AD of 560 g/L

***K*-Value (Molecular Mass).** PVC is again rather unique in its relationship between reaction temperature and *K*-value. With PVC the rate of polymer formation by chain–chain termination is small because of the influence of gel-phase polymerization described above. Instead, since chain transfer to monomer is a predominant step in the polymerization of VCM, the length of the polymer chain (degree of polymerization, DP) is determined by the ratio of the rate of chain propagation to chain transfer:

$$DP = \frac{\text{Rate of propagation}}{\text{Rate of chain transfer}} = \frac{k_P[R_n][M]}{k_{tr}[R_n][M]} = \frac{k_p}{k_{tr}}$$

where
[M] = monomer concentration
$[R\cdot_n]$ = radical concentration
k_p = propagation rate constant
k_{tr} = chain-transfer rate constant

As k_p and k_{tr} depend only on temperature the molecular mass of PVC is controlled by the reaction temperature (see Fig. 6).

If a particularly low molecular mass polymer is required or if a reactor's pressure rating is too low to operate at very high temperatures, an additional chain-transfer agent can be employed. This reduces the molecular mass by increasing the chain-transfer rate constant above that for monomer alone in the above equation. As a result DP decreases, depending on the quantity of chain transfer agent used.

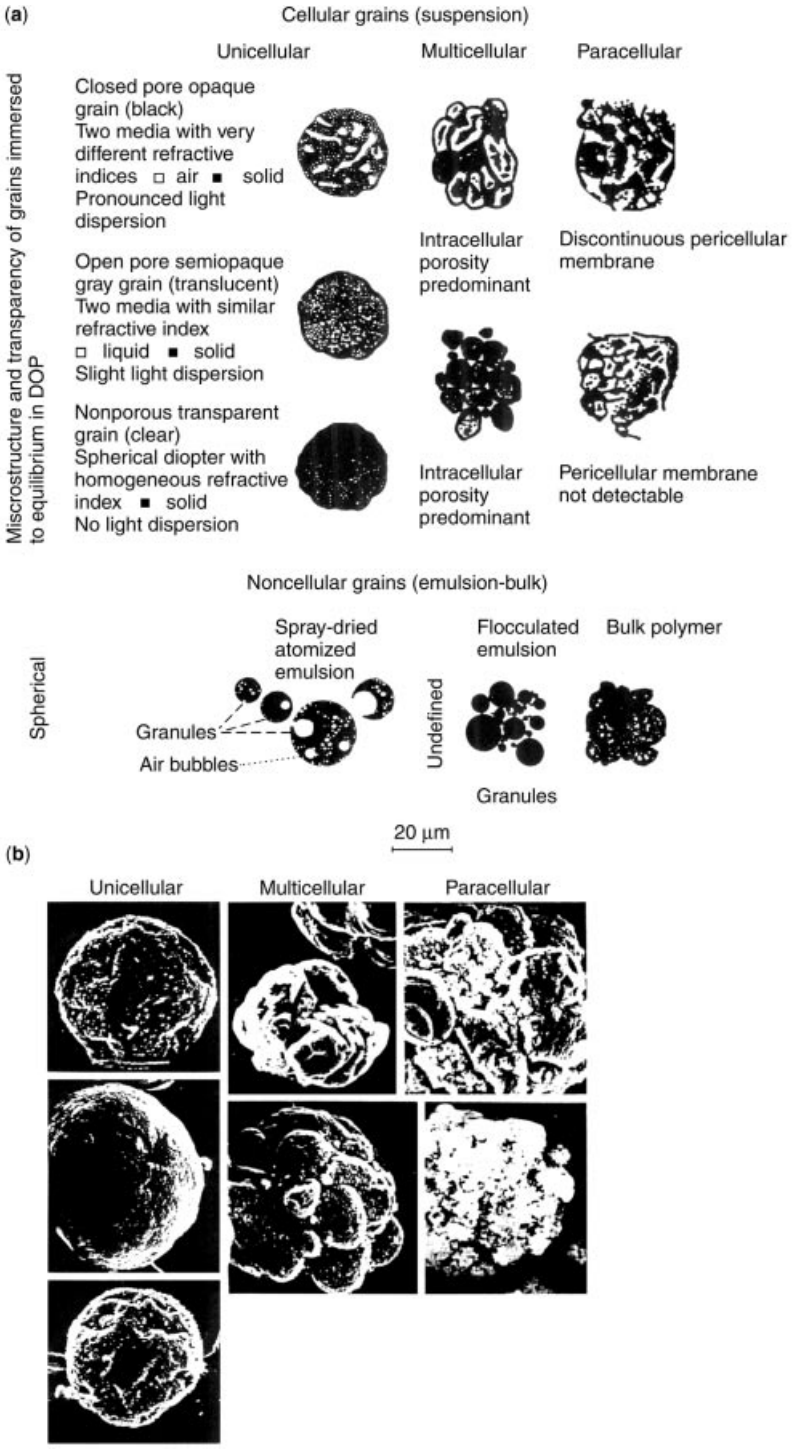

Fig. 5. (**a**) Classification of PVC grains and (**b**) typical cellular PVC grains—layout as in Figure 6a From Ref. 13, courtesy of Elsevier Applied Science Publishers.

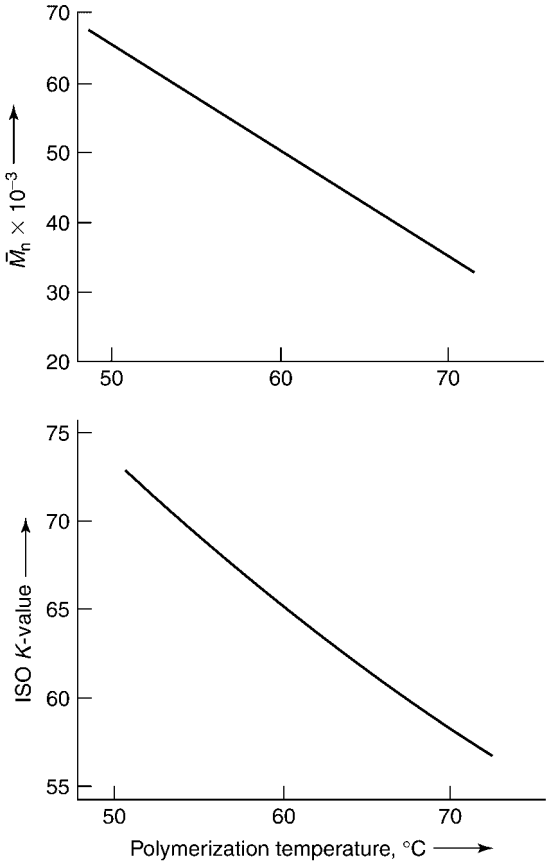

Fig. 6. The effect of temperature on molecular mass and *K*-value.

The general *K*-value range of commercial resins is K 55 to K 75, with a few producers providing speciality resins outside this range to K 50 and K 80 and with just one or two K 90–100 polymers also being available. Despite the relatively narrow *K*-value/molecular mass range of most commercial resins (see Table 6) the polar nature of the PVC chain gives rise to a considerable melt viscosity span. Mechanical properties increase slightly with increasing *K*-value; so wherever possible the highest *K*-value polymer is used. However, the power and mechanical robustness of equipment and the complicated melt-flow pattern requirements in molds often restrict the *K*-value which can be used. For example, most bottles are made from K 57 polymers, some from K 60, but this is the limit for the application because bottles are blow-molded, thus restricting the melt viscosity that can be handled.

Problem Areas. There are relatively few problems in the operation of the suspension polymerization process. However, to obtain the best possible quality and consistency some points need special attention.

In the past, reactor fouling was bad and mechanical cleaning between each batch essential. With the advent of clean-wall technology, high pressure rinse

Table 6. Correlation of Various PVC Molecular Mass (Expressions)[a]

European methods						Japanese method	American methods				
Viscosity number ISO/R 174 (1974)	Specific viscosity 0.5 g/100 mL cyclohexanone at 25°C	*K*-value 0.5 g/100 mL^{-1} cyclohexanone at 25°C	Relative viscosity 0.5 g/100 mL ethylene dichloride at 25°C	Specific viscosity 1.0 g/100 mL cyclohexanone at 25°C	*K*-value 1.0 g/100 mL cyclohexanone at 25°C	Polymerization degree JIS K 6721	Inherent viscosity ASTM D 1243-58T (method A)	Specific viscosity ASTM D 1243-58T (method B)	Specific viscosity 0.2 g/100 mL cyclohexanone at 30°C	Specific viscosity 0.4 g/100 mL nitrobenzene at 25°C	Approximate number average molecular mass
70	0.35	53.9	1.304	0.70	54	560	0.62	0.239	0.13	0.24	36,000
73	0.37	55	1.316	0.74	55	600	0.65	0.25	0.14	0.25	
77	0.38	56.1	1.329	0.77	57	640	0.67	0.264	0.145	0.26	40,000
80	0.40	57.2	1.342	0.80	58	680	0.70	0.275	0.15	0.27	
83	0.42	58.3	1.355	0.83	59	720	0.73	0.285	0.155	0.29	
87	0.44	59.5	1.369	0.86	60	760	0.75	0.3	0.16	0.30	45,500
90	0.45	60.6	1.383	0.87	61	800	0.78	0.31	0.17	0.31	
94	0.47	61.9	1.397	0.92	62	840	0.80	0.32	0.175	0.32	50,000
98	0.49	62.9	1.412	0.95	63	885	0.83	0.33	0.18	0.33	
102	0.51	64	1.427	0.98	64	930	0.85	0.34	0.19	0.34	
105	0.53	65.2	1.443	1.01	65	975	0.83	0.36	0.195	0.35	55,000
109	0.55	66.3	1.458	1.04	66	1025	0.91	0.37	0.20	0.36	
113	0.57	67.4	1.474	1.07	67	1070	0.92	0.38	0.205	0.37	
117	0.59	68.5	1.491	1.10	68	1120	0.95	0.39	0.21	0.39	60,000
121	0.61	69.7	1.508	1.13	69	1175	0.99	0.40	0.22	0.39	
125	0.63	70.5	1.525	1.16	70	1230	1.01	0.41	0.225	0.41	64,000
130	0.65	71.2	1.543	1.19	70.5	1300	1.03	0.43	0.23	0.43	
134	0.67	72.2	1.562	1.22	71	1350	1.06	0.44	0.235	0.44	
138	0.69	73.0	1.581	1.25	72	1420	1.08	0.45	0.24	0.46	70,000
142	0.71	74.0	1.60	1.28	73	1490	1.11	0.46	0.25	0.48	
145	0.73	74.5	1.62	1.31	74	1570	1.13	0.47	0.255	0.49	73,000
149	0.75	75.5	1.64			1650	1.16	0.49	0.26	0.50	
153	0.77	76.3	1.661			1720	1.18	0.50	0.27	0.51	
157	0.79	77.0	1.682			1810	1.21	0.51	0.275	0.52	
161	0.81	77.5	1.704			1900	1.23	0.53	0.28	0.53	80,000
165	0.83	78.5	1.726			1980	1.26	0.54	0.29	0.54	82,000

[a]From Ref. 44, courtesy of Elsevier Applied Science Publishers.

systems, and improved recipes it is now possible to operate in a closed manner, thereby reducing problems of VCM exposure (see Chapt. 5 in Ref. 9). Reactor opening for cleaning is reduced to once in several hundred batches. It is essential to ensure that the reactor is rendered completely free of polymer between batches since this is the most common cause of fisheyes. Equally important is to ensure there is no chance of cross-grade contamination in the downstream operations of slurry handling, stripping, drying, and storage. Contamination of the product by foreign substances is eliminated by good housekeeping and plant management together with the right choice of metals of construction and design. Stainless steel is widely used in many sections of PVC plants.

Bulk or Mass Polymerization

The mass polymerization process is virtually identical to that taking place within each monomer droplet in the suspension process. As such the mechanism and kinetics are very similar to those described previously. The major difference is in the mechanical operation of the process.

About 10% of world PVC production is provided by the mass process. The process was developed by Pechiney St. Gobain (PSG) who are now part of the

French ATO Co. All mass producers are licensees of the PSG technology. The process is carried out in two stages:

(1) In the first stage monomer and initiator are charged and vigorously agitated in a vertical, stainless-steel autoclave (prepolymerizer) of 8–25 m^3 capacity, fitted with a water-cooled jacket and condenser. Rapid polymerization takes place at 62–75°C to give ca 100 μm aggregated spherical flocs composed of 0.1 μm primary particles, which form the basis or seeds of the final PVC grain. Conversion is taken to 7–12% in ca 30 min, by which time the initiator used is exhausted.

(2) The slurry from the prepolymerizer is discharged into the second-stage reactor, which has a volume of 12–50 m^3, with fresh initiator and more VCM. Up to five second-stages can be fed from one prepolymerizer. In the second stage the 0.1 μm primary particles making up each seed grow in size and fuse together to give the final grain of PVC of 130–160 μm diameter. As the conversion increases the physical nature changes from a wet powder at ca 20% to a dry one at 40% conversion. The heat of polymerization is removed from the growing grains by evaporation of the VCM and condensation on the cooled wall of the reactor or in a water-cooled reflex condenser(s). The second stage takes 3–9 h, depending on *K*-value.

Originally, the second-stage reactor was a horizontal jacketed vessel with one or more condensers, agitated by slowly rotating (6–10 rpm) ribbon blenders with some blades set very close to the reactor wall to keep it clean. However, it proved difficult to discharge and clean the reactor to a sufficiently high standard to prevent the formation of fisheyes (dispersion faults) in PVC grades intended for plasticized applications (15). The product can contain up to 10% of coarse material, which must be sieved out and recovered by grinding, milling, and reclassifying.

This led to the development in 1978 of a vertical second-stage reactor of up to 50-m^3 capacity fitted with two independent agitators designed to overcome the above discharge problems. However, there has been little interest in this development and all recent investment in new PVC plants has been in the suspension process. In theory the mass process should be cheaper since it does not need a drying stage. However, it is a two-stage process, it is difficult to remove traces of unreacted monomer, and it gives a significant amount of oversized material, all of which offset its advantages.

Several of the smaller and older mass-polymerization plants have closed in recent years because they find it more and more difficult to meet increasingly stringent environmental standards and are becoming less and less competitive compared to suspension-polymerization plants on the basis of production rate.

The mass process is discussed in more detail in References 15 and 16.

Emulsion Polymerization

The emulsion polymerization process involves the polymerization of monomer in an aqueous medium containing surfactant and a water-soluble initiator, producing PVC lattices. PVC lattices are colloidal dispersions of spherical particles, ranging

Table 7. World Emulsion PVC Production in 1989

Region	Production, 10^3t	Percentage
Western Europe	720	42
United States	292	17
Japan	149	9
Rest of the world	544	32
Total capacity	*1705*	*100*

in size between 0.1 and 3.0 μm. Most PVC lattices are spray-dried and then milled to obtain fine powders, made up of agglomerates of latex particles. When mixed with plasticizers they disperse readily to form stable suspensions. During mixing, most of the agglomerates are broken down into the original latex particles. Such dispersion of fine particles in plasticizers are known as plastisols or pastes, and the powder is called dispersion or paste polymer. The surfactant layer around the particle surface prevents their adsorbing the plasticizer at room temperature and so they can be used as liquids and may then be spread onto fabric or other substrates, poured on molds, or deposited on formers to produce flooring, wall covering, artificial leather, balls, toys, or protective gloves. There are other grades of PVC polymers, produced by emulsion polymerization, that do not form plastisols and that are used as blends with suspension PVC grades for extrusion application or in the manufacture of battery separator plates. These so-called emulsion polymers are of only minor economic interest. Sales in latex form are very limited; lattices are used in water-based paints, printing inks, and impregnated fabrics. The total production capacity of emulsion PVC is given in Table 7.

Emulsion Polymerization Processes. The ways to produce PVC lattices are

(1) The classic emulsion polymerization, in which the particle size and particle size distribution are controlled by a water-soluble initiator and a surfactant (17–21). They are monodisperse with a particle size typically less than 0.1 μm.

(2) Seeded emulsion polymerization, in which the particle size distribution of the final latex depends on the amount and the size of the latex used as seed and on the amount of surfactant and the way in which it is added (22,23). A typical material has 0.2 and 1.2 μm particles (see Fig. 7).

(3) Microsuspension polymerization, in which a monomer-soluble initiator is used. Polymerization takes place within the fine droplets in which the monomer is dispersed by passing a coarse emulsion of monomer, initiator, and surfactant through a mechanical homogenizer (24–26). The resulting particle size distribution is Gaussian between 0.2 and 1.2 μm.

(4) Polymerization of fine emulsions achieved by using a combination of a typical surfactant such as sodium dodecyl sulfate and a long-chain fatty alcohol. This gives rise to spontaneous emulsification of the monomer into very fine droplets. In this case the polymerization can be carried out by using a water-soluble or a monomer-soluble initiator (27). The latex particle size distribution is the same as for microsuspension polymerization.

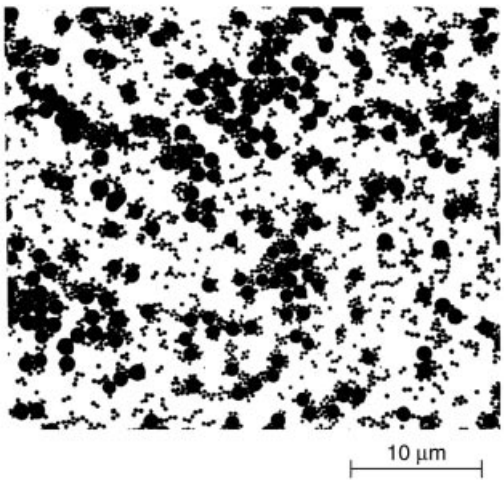

Fig. 7. Electron micrograph of latex particles obtained by seeded emulsion polymerization.

The industrial polymerization techniques used for carrying out these processes are the following:

(1) Batch polymerization where all the monomer is charged at the beginning
(2) Semibatch or semicontinuous polymerization, with the monomer added in stages or continuously as reaction proceeds
(3) Continuous polymerization where monomer and other components are fed continuously into the reactor and the latex is withdrawn from the bottom of the reactor

All these processes are in current use to achieve a wide range of latex characteristics, which are related to the rheological properties of the PVC plastisols (28).

Description of the Batch Process. The emulsion polymerization of PVC consists of the following stages: (*1*) polymerization, (*2*) VCM removal, (*3*) latex storage, (*4*) drying, (*5*) milling, and (*6*) packing and storage. Figure 8 shows a schematic representation of the stages required for a plant which produces all the emulsion, seeded, and microsuspension grades.

A recipe for a simple batch emulsion polymerization (in parts by weight) is as follows:

Demineralized water	110–140
Vinyl chloride	100
Emulsifier	0.1–1
Initiator	0.1–0.2

The polymerization takes place in an autoclave resistant to the VCM vapor pressure. Pressures of 6.4–10.0 bar correspond to polymerization temperatures of 40–60°C, depending on the desired molecular mass. The polymerization reaction

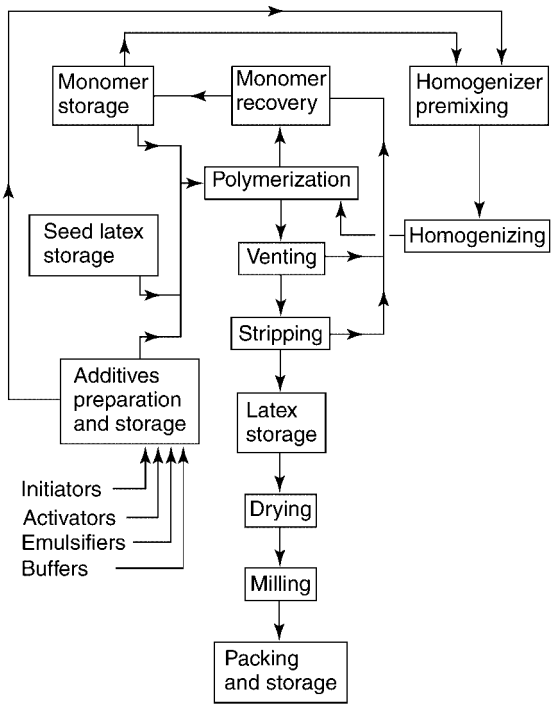

Fig. 8. Schematic representation of the stages required for a plant which produces all emulsion, seeded, and microsuspension grades.

is strongly exothermic with a heat of polymerization of 1534 kJ/kg. Heat removal can be a problem as the size of the autoclave increases because the ratio between surface area and volume becomes less favorable. For this reason industrial plants commonly use water cooling, and external condensers. Modern plants use autoclaves with capacities ranging between 30 and 80 m^3. Large autoclaves can present agitation problems because low shear rates are required to maintain mechanical stability of the latex and to avoid coagulation.

Initiators. Although organic peroxides slightly soluble in water such as methyl ethyl ketone peroxide and 1-hydroperoxy-1′-hydroxydicyclohexyl peroxide can be used, the most widely used initiators are ammonium or potassium peroxosulfate. Their decomposition in aqueous solution is first-order with respect to the peroxosulfate ion concentration (29). The rate may be increased significantly by using a reducing agent. Redox catalysis involves the use of transition-metal ions such as copper or iron (30). The systems widely used in emulsion polymerization of vinyl chloride are potassium peroxosulfate–sodium bisulfate–copper or iron. Redox systems can also be used in microsuspension, an example being dilauroyl peroxide–copper–ascorbic acid (31).

Emulsifiers. Emulsifiers are very important in the emulsion polymerization of vinyl chloride because they determine not only the latex characteristics but also the properties of the final product (32–34). Moreover, the nature and the

concentration of the emulsifier, together with the agitation, are major parameters controlling the mechanical stability of the latex during polymerization and handling, and the major cause of reactor wall encrustation and lump formation. Since the latex is dried by spray drying, the emulsifier remains in the resin and can influence properties of the product such as the flowability of the powder, plastisol formation, the viscosity of the plastisol, and also the properties of the final article such as heat stability, water adsorption, and coat adhesion. For this reason a wide variety of emulsifiers are used. During polymerization anionic types are usually used, while nonionics are generally added to the latex after polymerization. Typical emulsifiers are the sodium salts of alkyl sulfates, alkyl sulfonates, alkylbenzenesulfonates, dialkyl sulfosuccinates, alkyl ethoxysulfates, fatty acid soaps, alkyl phenol ethoxylates, and fatty acid ethoxylates.

Particle Formation. Emulsifiers are characterized by the critical concentration at which their molecules aggregate to form micelles (35,36). In Figure 9 a plot of surface tension versus emulsifier concentration is shown; the point at which the curve exhibits a marked change is known as the critical micelle concentration (CMC). Conventional emulsion polymerization is carried out at a concentration above the CMC. In this way, particle formation is controlled by the micelles, which solubilize the monomer by swelling and become the loci of polymerization. The nucleation phase stops when the micelles disappear, and the emulsifier is absorbed onto the surface of the particles. Depending on the balance between the hydrophilic and hydrophobic part of the molecule, each emulsifier plays a specific role in the emulsion polymerization, as they have different CMC values, surface covering powers, and stabilizing effects.

VCM Removal. The polymerization is terminated at 90% conversion and is followed by the venting of unreacted monomer to a gas holder. After degassing, the latex contains 3% vinyl chloride and further reductions must be made to fulfil legal requirements for environmental protection. The residual VCM is removed by stripping under vacuum in a stripping vessel. Although VCM loss from particles

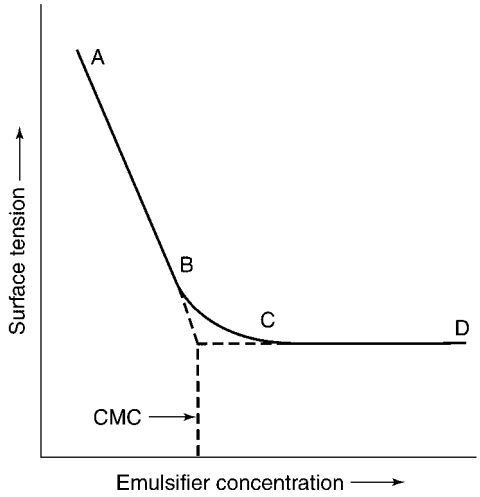

Fig. 9. Dependence of surface tension on emulsifier concentration.

by diffusion is fast, VCM removal from an emulsion is much more difficult than from suspension slurries as the surfactants lead to large amounts of foam formation. Continuous processes using a thin-film evaporator or which spray the latex into an evacuated chamber against a countercurrent stream of gas reduce considerably the problems of foaming and coagulation (37–40). The residual vinyl chloride monomer content of the latex after stripping ranges between 200 and 2000 ppm, depending on the type of latex and the operating conditions.

Drying and Milling. Although there are several different techniques to separate polymer from water, such as freeze drying, drum drying, or coagulation followed by centrifugation, the most widely used is spray drying because this confers a special structure to the dried particle that is important for the production of plastisols. A fine spray of latex is introduced into a hot air stream where evaporation takes place.

The spray is obtained by various types of atomizers, such as

(1) Spinning disks or wheels rotating at 15,000–20,000 rpm
(2) Single pressure nozzles operating at 10–50 MPa (100–500 bar)
(3) Two-fluid pressure nozzles using compressed air up to 0.4 MPa as atomizing fluid (41)

The drying air temperature at the inlet is 150–240°C and at the outlet, 55–80°C, depending on the quality of the required product and the type of latex. By varying the drying conditions it is possible to change the resin characteristics, and hence its use, even from a typical paste grade to a general-purpose emulsion resin, eg for rigid extrusion. The dry powder consists of spherical aggregates, with the size usually ranging from 1 to 100 μm in diameter with an average of 30–40 μm. The aggregates are called secondary particles, to distinguish them from those of the latex, which are known as primary particles. The way the aggregates form is complex and depends on many parameters such as primary particle size, type and amount of emulsifier, mean residence time in the drying chamber, droplet size of the spray, and temperature (42). Figure 10 shows a scanning electron micrograph of spray-dried PVC particles formed from bimodal seeded latex.

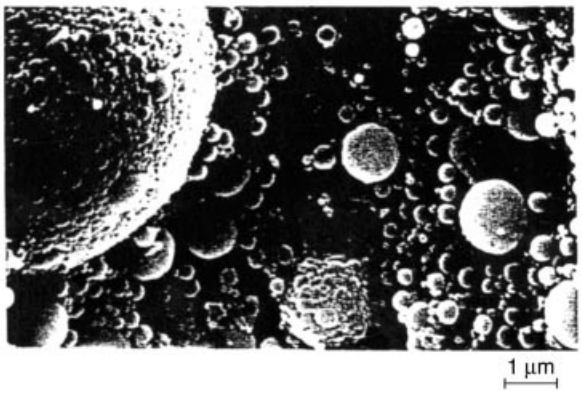

Fig. 10. Scanning electron micrograph of spray-dried PVC particles produced from bimodal seeded latex.

Plastisol-grade resins, usually made from multimodal latex (ie, with a Gaussian particle size distribution), are milled to reduce the size of the coarse fraction, which can cause problems in coating applications of the plastisol. Generally the viscosity of the plastisol increases when the polymer has been milled, and so it is desirable to reduce milling as far as possible and to use air classification to remove the coarse fraction (>65 μm) under control. In industrial production, air classifiers or mills or a combination of both are used. After milling, the average particle size of the resin is in the range of 5–15 μm.

Polymers for rigid extrusion and for manufacturing plate separators in batteries are sold in unmilled form. Resins are characterized by analysis of molecular mass, emulsifier and salt content, pH of aqueous extract, granulometry, and viscosity and rheological behavior of the pastes.

Plastisols. Plastisols, commonly called pastes, are dispersions of PVC powders in plasticizers. A wide range of plasticizers are used in plastisol formulations, but the most widely used are C_4–C_{12} esters such as phthalates, adipates, azelates, sebacates, trimellitates, and phosphates. Chlorinated paraffins are used as secondary plasticizers. A good plasticizer should have low volatility, low color value, neutral reaction, resistance to hydrolysis, insolubility in water, flame resistance, and nontoxicity. As no plasticizer can satisfy all these properties, several plasticizers are mixed to achieve the desired properties of the final product. Table 8 shows the influence of plasticizers on plastisol properties; Table 9, the influence of plasticizers on final product properties; and Table 10, the influence of resin characteristics on plastisol and final product properties.

The amount of plasticizer used in plastisol formulations plays a major role in determining the hardness and flexibility of the end product and can vary from 40

Table 8. Influence of Plasticizers on Plastisol Properties

Plastisol properties	Plasticizers[a]
Low fusion temperature	DBP, BBP, TCP
Low viscosity	DOA, DOS, DIPA
High viscosity	BBP, TCP, polymerics
High fusion temperature	DIDA, DOZ, DTDP, DOS, polymerics

[a]DBP = dibutyl phthalate, BBP = butyl benzyl phthalate, TCP = tricresyl phthalate, DOA = dioctyl adipate, DOS = dioctyl sebacate, DIDA = diisodecyl adipate, DOZ = dioctyl azelate, DTDP = ditridecyl phthalate.

Table 9. Influence of Plasticizers on Final Product Properties

Product properties	Plasticizers
Flame retardancy	Phosphates, chlorinated paraffins
Light and heat resistance	Epoxy plasticizers
Low temperature flexibility	Adipates, azelates, sebacates, straight-chain phthalates
Low volatility	Polymerics, trimellitates, linear phthalates, epoxy plasticizers
Stain resistance	Butyl benzyl phthalate
Low migration	Polymerics, trimellitates

Table 10. Influence of Resin Characteristics on Plastisol and Final Product Properties

	Effect of resin characteristics[a]			
Plastisol and product properties	Molecular mass	Particle size	Particle size distribution	Emulsifier type and quantity
Paste making		S	S	S
Plastisol viscosity		S	S	S
Air release				S
Gelation	M	M	M	S
Fusion	S			
Mechanical properties	S			
Gloss		S	M	
Transparency		S		S
Foaming	S	M		S
Fogging				S
Streaking flow		S		
Water resistance				S

[a] M = moderate effect; S = strong effect.

to 130 phr. In Figure 11 the influence of plasticizer content on plastisol viscosity is shown.

The other essential ingredients in plastisol formulations are as follows:

(1) Heat stabilizers, which generally are the same compounds used for suspension polymers.

(2) Dyes and pigments suitable for coloring plastisols. The most widely used is titanium dioxide.

(3) Fillers, generally inorganic materials such as calcium carbonate, barite, silicate, kaolin, or china clay, are used primarily to lower costs and also to impart special properties such as hardness, abrasion resistance, and no sticking.

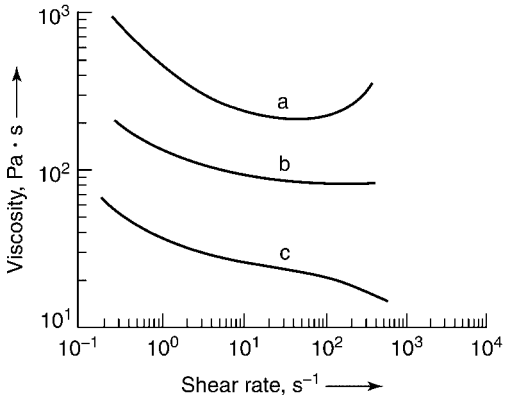

Fig. 11. Influence of plasticizer content on plastisol viscosity: a, PVC/DOP = 100/40; b, PVC/DOP = 100/50; and c, PVC/DOP = 100/60 [DOP = dioctyl phthalate].

Table 11. Influence of Plastisol Ingredients on the Final Product Characteristics[a]

Characteristics	Filler	Pigment	Stabilizers	Quantity of plasticizer	Plasticizer type	Resin
Tensile properties	M			S	M	S
Flexibility	M			S	M	
Hardness	M			S	M	
Low temperature bending resistance	M			S	S	M
Gloss	S	S				S
Volatility				S	S	
Extraction				S	S	
Color	S	S	M			
Light resistance		S	S		M	
Cost	S		M	M	M	

[a] M = moderate effect; S = strong effect.

(4) Blowing agents for foamed PVC production such as azodicarbonamide.
(5) UV adsorbers to prevent the decomposition action of sunlight.
(6) Esters of poly(ethylene glycol), phosphate esters, and fatty acid amines and amides are usually employed as antistatic agents.
(7) Viscosity depressants, such as white spirit, poly(ethylene glycol) monolaurate, alkylphenols, and low molecular mass paraffins.
(8) Extender resin or filler polymer—a PVC grade of spherical form, made by the suspension process and therefore cheaper than dispersion resin, which is used to reduce cost and viscosity of the plastisol (43,44).

In Table 11 the influence of plastisol ingredients on the final product characteristics is shown.

Polymer–Plasticizer Interaction. Figure 12 illustrates the types of dependence of viscosity on shear rate:

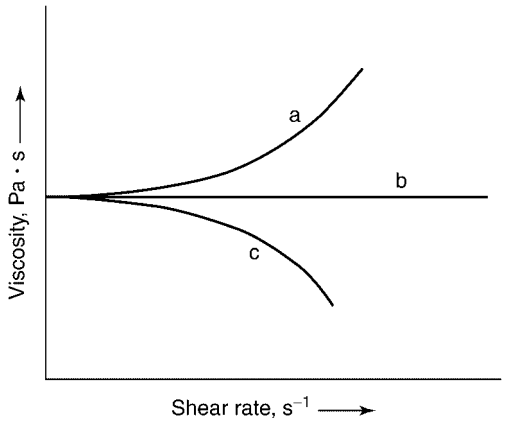

Fig. 12. Effect of shear rate on dilatant: a, Newtonian; b, pseudoplastic, and c, fluids.

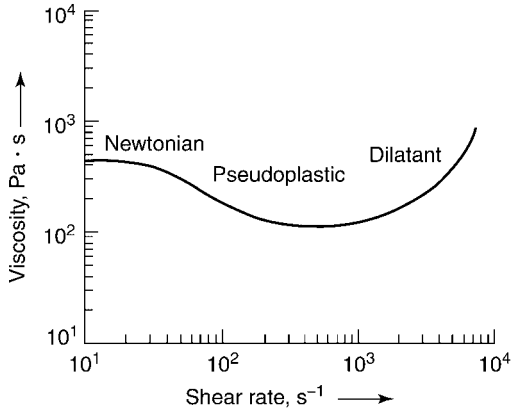

Fig. 13. Effect of shear rate on the PVC plastisol viscosity (DOP/PVC = 100/50 at T = 25°C).

(1) Newtonian (viscosity is independent of shear rate)
(2) Pseudoplastic (viscosity decreases as shear rate increases)
(3) Dilatant (viscosity increases with increasing shear rate)

Over a wide range of shear rate a plastisol may exhibit all three types of behavior since the viscosity of plastisols rarely displays true Newtonian behavior. At low shear rates they are generally pseudoplastic, at intermediate values they show dilatancy, and may sometimes become pseudoplastic again at higher shear rates, as shown in Figure 13. There is no certainty on the exact mechanism as the rheology of PVC plastisols is complex and affected by many factors such as

(1) Polymer/plasticizer mixing ratio
(2) Type of plasticizer and its interaction with polymer
(3) Particle size and their distribution of primary particles
(4) Structure, shape, porosity, and surface of the secondary particles
(5) Surfactants, added during polymerization or in the paste
(6) Molecular mass and molecular mass distribution
(7) Paste-making conditions such as mixing temperature, time, and intensity (45).

Gelation and Fusion. *Gelation* is defined as the change from liquid to semisolid state, and fusion, when a homogeneous phase at molecular level between polymer and plasticizer is reached. These processes have been examined by determining viscosity changes of the liquid system, the tensile strength, and changes in complex viscosity and viscoelastic properties over the temperature range 25–200°C.

At the beginning of heating, plasticizer viscosity decreases, as does the plastisol viscosity. At the same time, polymer particles adsorb plasticizer and swell, reducing the fraction of liquid plasticizer, and the viscosity then increases rapidly. When the liquid phase is completely absorbed by the particles, the system

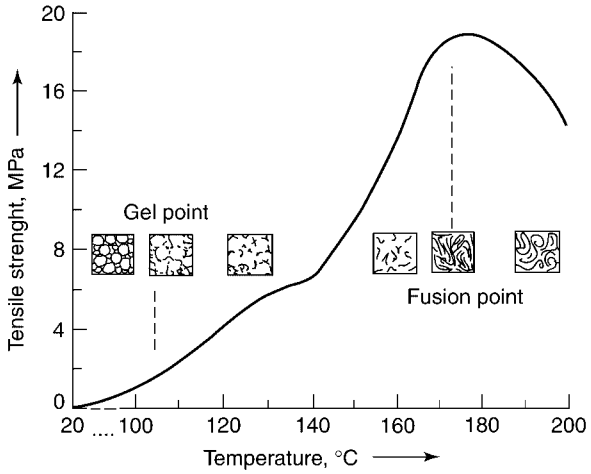

Fig. 14. Changes in morphology and mechanical properties of PVC plastisol during gelation and fusion.

becomes dry. As the process continues the interparticle boundaries disappear and the polymer chains become increasingly entangled and development of the physical properties begins. At this point the gelation stage is complete and the fusion process starts, as illustrated in Figure 14. Further heating of plastisol makes the polymer flow in a continuous mass. The melt viscosity, after having reached a maximum, starts to decrease and the process passes through the fusion stage. Morphology of the particles, particle size, particle size distribution, and molecular mass of the resin affect the viscosity behavior. Low molecular mass resin starts the gelation phase earlier and completes the gelation process at lower temperature. The same result is obtained by using plasticizers with higher solvating action, while larger particle size increases gelation temperature or time because it slows the penetration of the plasticizer into the resin (46).

Applications. Vinyl plastisols can be applied by spread coating, knife coating, roll coating, molding, dipping, and spraying; the most widely used application is coating.

Coating. Vinyl plastisol can be used to coat paper, fabrics, metals, felt, and glass fibers to produce wallpapers, floor coverings, vinyl leather, conveyor belts, and tarpaulins. Each application needs its own formulation, in which the appropriate resin grade and plasticizer must be used to give the required rheological characteristics. In the case of fabric coating where direct spreading is employed, it is important to avoid penetration of plastisol into the fabric; therefore, the viscosity behavior of the paste must be strongly pseudoplastic at low shear rate and have moderate viscosity at high shear rate. In wallpapers, where thin coatings are applied, a low viscosity resin with Newtonian behavior is required. In production of floor coverings, three or even four coatings are applied: an impregnation layer to saturate the fibers, one or two foam coats, and a wear layer with high mechanical strength. Each coat, which needs different grade resin to achieve the required properties, is gelled at 150°C before application of the next layer. When the last coat is applied the entire coating is fused in an oven at 200°C. The foam layer can

be chemically or mechanically foamed (47). Usually mechanical embossing is used to create surface textures and apply colored patterns.

Dipping. The product, mainly work, household, and surgical gloves, is obtained by dipping metal or ceramic molds or an article to be coated into the plastisol and then withdrawing it, draining it, and then curing it in an oven.

Molding. This is used for producing hollow articles such as balls, dolls, and toys. The process requires a plastisol with low viscosity at low shear rate that has a short gelation time and is easy to deaerate. In rotational molding the plastisol is poured into a cold mold that rotates around two perpendicular axes whilst entering an oven where it is heated with air to 200–250°C. After gelation and fusion, the mold is cooled in a waterbath.

Further information is given in References 28,35,36,41,44, and 48–50.

Chlorinated Poly(Vinyl Chloride) (CPVC)

The softening point (heat distortion temperature or T_g) of PVC can be increased by chlorination of the polymer, either in a solvent or as a suspension. The normal chlorine content of 56.7% is raised to 63–68%, depending on type, and this increases the softening point from ca 78–83°C (depending on formulation) to at least 120°C.

The older method involves chlorination of the PVC dissolved in a chlorinated solvent, but the process is expensive because of the need for an extensive solvent recovery system. However, it has the benefit of yielding a homogeneous material. The product is difficult to handle physically because of its very low bulk density.

The most common commercial process in use today disperses the PVC grains in water and swells them with a chlorinated hydrocarbon. The reactor is degassed to remove oxygen and heated to reaction temperature (50–60°C); chlorine is added continuously and the system irradiated with UV light to produce chlorine radicals. Hydrogen chloride is produced as a by-product and is removed at the end by washing with an inorganic base, after which the product is dried (51). The degree of chlorination is variable, with the surface layers of the grains being preferentially treated.

CPVC is less thermally stable than conventional PVC and requires higher temperatures to develop good mechanical properties. Hence, it is difficult to process and quite expensive, but blends with suspension PVC can be used to achieve a specific softening point. CPVC products have not been very successful commercially but have found a specific niche in the market. They are used for hot-water systems in mobile homes in the United States and for the manufacture of fibers, for use in thermal underwear, in France.

Environmental Protection

Potential problem areas associated with the production, handling, and use of PVC are small if a few simple measures to avoid environmental contact and pollution are followed.

Losses of VCM from polymerization plants have been reduced to extremely low levels following conversion to closed-lid operation as a result of toxicological problems (9). Although modern column strippers reduce VCM levels in PVC to less than 10 ppm, a small quantity of VCM is lost from the drier section. The older batch strippers present more of a problem since they cannot achieve such low residual VCM contents.

PVC powder can be lost in centrifuge and scrubber effluent and by overfilling stock tanks and from pipeline leaks. It is important that all plant drains which are likely to contain PVC are directed to settling pits where flocculation treatment can be used so that the final discharge is free of PVC. All wet waste is collected and reclaimed as second- or third-grade material for use in noncritical applications such as one-trip horticultural products and fencing.

Powder losses from drier stacks can be minimized by ensuring that drier cyclones are adequately sized to the air conveying rates used. Some modern plants use bag filter systems to meet current regulations that restrict the amount of PVC dust loss to 50 mg/m^3 air (52).

Compared to other polymers and typical metals PVC requires less energy per unit weight for its production (53). Although plastics in general are blamed for long-lasting litter problems, it is significant that only 12% of PVC is used for consumables, while 64% is incorporated into products with an expected useful life of 15 years or more, probably much more. Disposal is therefore less of an immediate problem than is often thought.

As landfill sites are used up more municipal waste is being incinerated. Though inherently nonflammable, PVC will burn in an existing fire to release hydrogen chloride gas, which can be scrubbed out satisfactorily. Fears about the increased release of dioxins during incineration owing to the presence of PVC in waste have proved to be unfounded (54).

Quality Specifications and Analysis

All PVC producers test a number of parameters on every batch produced as part of routine quality control operation. These include *K*-value, mean grain size and grain size distribution, apparent density, porosity, contamination, dispersion, color and heat stability, and residual VCM content. Most plants use statistical process control techniques to ensure that product consistency from batch to batch meets the stringent requirements of today's customers. It is difficult to give a typical testing regime since every plant makes batches of different size, has slurry blending facilities of differing degrees of sophistication, and has hoppers of different capacity on their drying plants. For a modern plant operating large autoclaves there is considerable testing of each polymerization batch (wet stage) together with additional testing of the dried and blended material as a cross check.

In-house tests have been collected and correlated by national and international standards organizations to make them universally applicable. ISO has defined tests and standards set up by other organizations such as the ASTM and DIN so that ISO methods are now widely accepted worldwide. ASTM D1755 defines a system for classifying general-purpose (mass and suspension) and dispersion (paste) resins (55).

Storage and Transportation

Most plants handle more than 80% of their production in bulk, and storage and supply in 25-kg bags is diminishing all the time as customers convert. After drying, the material is conveyed by blow-eggs (vessels in which the powder is pressurized and fluidized) of 2–15-t capacity via pipeline to the silo farm where it is stored in silos of capacity 100–500 t. PVC is discharged either directly or via a smaller loading hopper into 20-t road tankers, the most popular form of PVC transportation. Sometimes big bags made of woven polypropylene are used for 1-t lots of PVC, and 20-t ISO metal containers are used for long-distance deliveries. PVC is not a difficult material to handle and the logistics side of the operation is straightforward. It is essential to prevent cross-contamination of the PVC by other products and thorough intertrip cleaning is essential, since many operators use their tankers for back carriage of a wide range of products, many nonpolymeric.

Processing and End Uses

Because of its unique combination of properties PVC is never handled on its own. Instead a complex formulation incorporating several additives is used. A typical base formulation contains PVC resin, heat stabilizer(s), internal lubricant(s), external lubricant(s), processing aid, and additionally, impact modifier, filler(s), pigment, UV stabilizer, as well as primary and secondary plasticizers (see HEAT STABILIZERS; PLASTICIZERS; UV STABILIZERS).

PVC is intrinsically unstable because of molecular defects in some of the polymer chains (56,57) and when subjected to heat they initiate a self-accelerating dehydrochlorination reaction. Stabilizers neutralize the HCl produced and introduce nucleophilic substitution reactions that prevent further degradation (56,57) (see DEGRADATION).

The Ca–Zn stabilizer family is becoming increasingly popular as objections to the use of heavy-metal systems are increasing. In Europe withdrawal of cadmium stabilizers was planned for the end of 2001, and although it has been shown that use of the highly effective lead stabilizers is safe, adverse publicity will slowly erode their market position.

Table 12 gives a summary of the heat stabilizers in regular use.

The polar, highly viscous PVC melt sticks easily to metal walls of extruder barrels, calenders, mills, etc, and so an *external lubricant* is employed to assist the smooth passage of the melt. *Internal lubricants* help to reduce melt viscosity and prevent overheating and so help to ensure good color of the final product. *Processing aids* improve the surface appearance of extruded sections and reduce melt defects such as screw memory, where the helical nature of the screw can be seen as regular ripples in the pipe surface. Many other additives can be used, eg, *impact modifiers* for bottles and uv stabilizers and *fillers* (eg, TiO_2) for house sidings and window frames, to ensure the best possible in-service performance or longevity.

In all extrusion and some other conversion processes the PVC grain is not broken down to its constituent primary particles (58), unlike emulsion PVC processing. Instead the suspension grains (150 μm) gradually lose their original form

Table 12. Heat Stabilizers for PVC

Stabilizer	Properties
Lead stabilizers	
Lead soaps	Good heat stability
Lead salts	Sulfur staining
Liquid lead complex	Lead phosphites give good light stability
Lead one-pack systems	Kickers for chemical blown foam
Tin stabilizers	
Organo sulfur tin	Excellent heat stability, good clarity; poor light stability
Organo tin carboxylates	Medium heat stability; excellent light stability
Barium–zinc stabilizers	
Ba–Zn liquid	Good heat and light stability on high quality grades; general-purpose stabilizers.
Calcium–zinc stabilizers	
Ca–Zn soaps	Low toxicity
Ca–Zn liquid	Medium heat and light stability
Organic costabilizers	
Thiourea derivatives	Synergistic effects with epoxy plasticizer and/or Ca–Zn, Ba–Zn
Indol derivatives	
Amino crotonic acid esters	
Diketones	
Organic phosphites	
Antioxidants	
Epoxidized soybean oil (ESBO)	Synergistic effect with Ca–Zn and Ba–Zn
Epoxy esters	

by fusion and elongation under the influence of heat, pressure, and shear so that in badly processed PVC grain memory can be detected by optical microscopy of cross sections of extrudates (58). In practice, converters take great care to ensure that the degree of gelation (ie, lack of grain memory) in the final PVC article is very high. Degree of gelation can be measured by determining the degree of attack by a poor solvent such as acetone or methylene chloride or by measurement of flow pressure to assess the strength and elasticity of partially fused material directly (59).

The enormous subject of processing, including different aspects such as formulations, types of processing equipment, gelation, rheology, and mechanical properties is covered more widely in References 14,58, and 60–63.

Table 13. Typical End Uses for PVC

Application	Rigid PVC	Flexible PVC
Construction	Window frames, gutters, pipes, cars, housesiding, ports, roofing	Waterproof membranes, cable insulation, roof lining, greenhouses
Domestic	Curtain rails, drawer sides, laminates, audio and video tape cases, records	Flooring, wall coverings, shower curtains, leathercloth, hosepipes
Packaging	Bottles, blister packs, transparent packs and punnets	Cling film
Transport	Car seat backs	Underseal, roof linings, leathercloth upholstery, wiring insulation, window seals, decorative trim
Medical		Oxygen tents, bags and tubing for blood transfusions, drips and dialysis liquids
Clothing	Safety equipment	Waterproofs for fishermen and emergency services, life-jackets, shoes, wellington boots, aprons and baby pants
Others	Floppy-disk covers, credit cards	Conveyor belts, inflatables, sports goods, toys

The versatility of PVC can be gauged by the very broad summary of typical end uses given in Table 13.

Economic Aspects

Fear of litigation, the need to handle VCM (a known carcinogen), and reduced funding have all but eliminated fundamental research into VCM polymerization. Work on processing of PVC continues, but at a much reduced level. Many companies have scaled down R&D and process development, and raw material suppliers are now increasingly responsible for technological developments.

Since 1992 the main trend in the PVC industry has been survival by amalgamation. Some well-known companies, including pioneers from the 1940s (eg, B.F Goodrich/GEON, ICI, and Chisso) have disappeared through aquisition, and many others have formed larger conglomerates to survive. The current feeling in the industry is that a minimum capacity of 500,000 t/a is required for a viable operation.

Irresponsible investment in new plant near the peak of the economic cycle has resulted in overcapacity, weakened prices, lower company profits, and economic casualties, just as it did in ca 1990. Even the staid Japanese PVC industry has seen amalgamations and plant closures since ca 1995, and the former 15 companies have been reduced to just five major production groups. Changes in the Western European PVC scene are summarized in Figure 15.

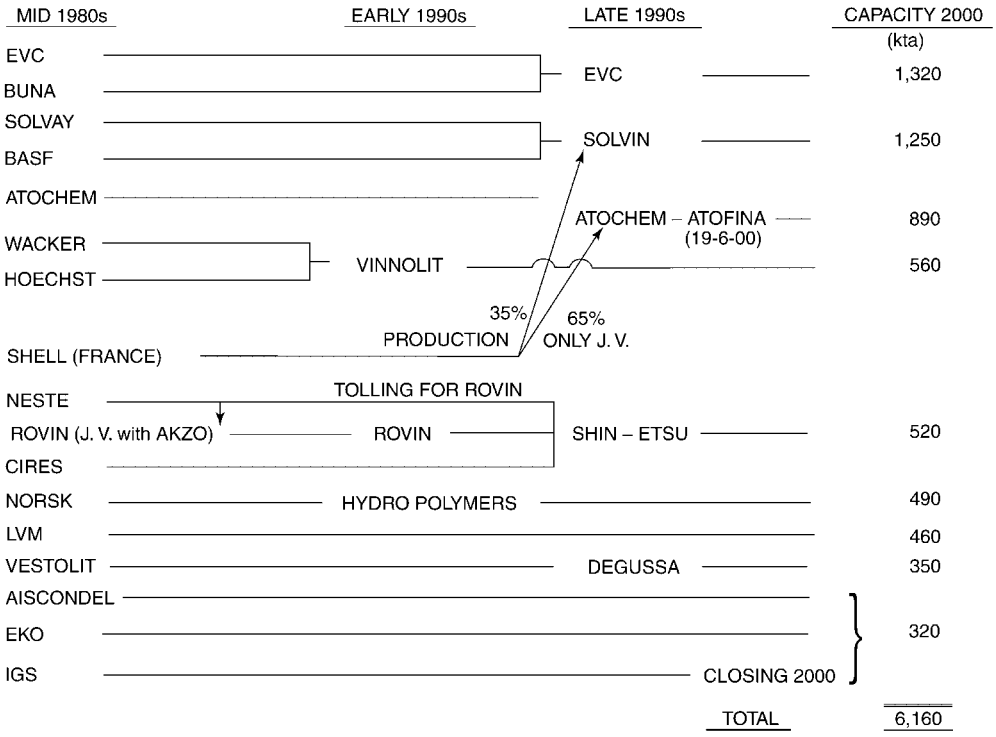

Fig. 15. Evolution of the PVC industry in Western Europe (J.V. = joint venture).

Table 14 lists the regional capacities (in 10^3 t/a) of the top 10 producers, which represent 48% of world capacity of 29.8×10^6 t/a. World production in 2000 was 23.3×10^6 t (78% of capacity).

Since ca 1990 China has emerged as a major force on the global PVC market, and its tremendous import capacity has had a large impact on the world price/consumption relationship. The eight main Chinese producers use

Table 14. Regional Capacities (in 10^3 t/a) of the Top 10 PVC Producers in 2000[a]

Company	S. America	Asia	NAFTA[b]	W. Europe	Total
Shin-Etsu	140	550	1500	520	2710
Formosa		1240	1170		2410
Oxy-Vinyls			2020		2020
Solvay	450	190		1250	1890
EVC				1320	1320
Georgia-Gulf			1270		1270
Atofina				890	890
Borden			690		690
L.G. Chemical		600			600
Taiyo Vinyl		600			600

Table 15. World Consumption of PVC Resin

Consumption of PVC esin (kt/a)		
	1997	2000
Japan	2030 (15 producers)	1750 (15 producer groups)
China	2250	3380
Consumption per Capita (kg) (200)		
"West" Germany	27.1	
North America	15.1	
Western Europe	14.6	
South America	3.6	
East Europe	3.5	
China	3.1	
Asia/Pacific	2.6	
Africa/Middle East	1.9	
India	1.0	

[a]The top 10 producers represent about 48% of world capacity of 29.8 million tons. World production in 2000 was 23.3 million tons (78% occupacity).
[b]NAFTA: North Atlantic Free Trade Area.

ethylene-based VCM and produce 42% of the total output, while about 70% of producers manufacture the remaining 42% using VCM from a calcium carbide based process. The 8 principal producers have plants with capacities $>100 \times 10^3$ t/a. These are 10 plants with capacities between 50 and 100×10^3 t/a and 51 plants with capacity of less than 50×10^3 t/a. Between 1996 and 2000 output of PVC increased on average by 12% per annum, consumption by 15%, and imports by 20% per annum.

The consumption of PVC resion in Japan and China in 1997 and 200 as well as the per given in Table 15.

World PVC production was 23.3×10^6 t/a in 2000, and growth ranged from −3% (Japan) to +8% (China). Overall long-term growth worldwide is estimated at ca 4%. Table 16 summarizes the world supply/demand balance.

Table 16. World Supply/Demand Balance for PVC in 1999 (in 10^3 t/a)

	Capacity	Operating rate, %	Production	Imports	Exports	Consumption
N. America	7480	91	6800	110	370	6540
S. America	1930	81	1560	470	460	1570
W. Europe	6100	89	5410	610	390	5630
Japan	2810	87	2450	10	780	1680
Korea	1150	100	1150	30	380	820
Taiwan	1760	79	1390	160	360	1190
Other Asia	4620	74	3430	1950	450	4930
E. Europe	2290	54	1240	250	760	730
Africa	360	85	310	210	10	510
Middle East	910	88	810	510	340	980
Others	3820	67	2550	1050	1120	2480

Toxicology and Occupational Health

Vinyl Chloride Monomer (VCM). Since vinyl chloride boils at −13°C it is handled as a compressed liquid. It has a vapor density greater than air and so precautions are taken in design not to contain the vapor in restricted areas. Protection of reactors by relief valves or bursting disks and double-valve isolation of all lines containing VCM are basic precautions taken in the design and construction of any PVC plant vessel which contains monomer. The gas is explosive between 3.6 and 25 vol% with air and 12 vol% oxygen is required for ignition (64). Therefore, a special series of working conditions must be satisfied in the working environment and great care is always taken to purge lines, pumps, valves, etc before any maintenance work is started. Thorough documentation (eg, clearance to work certificates) are always used to ensure that proper isolation of plant equipment is carried out before any entry. The whole plant is contained within a "red-fence" area where smoking is not permitted and where all electrical equipment is of a gas-tight and "flame-free" construction.

VCM has a narcotic effect at 8–12 vol% concentration and can cause death at higher concentrations (64). For this reason early VCM and PVC plants were designed to avoid buildup of gas above 1000 ppm in the atmosphere. VCM has a pleasant ethereal smell which is first noticed at concentrations of 500–2000 ppm.

Exposure to VCM has been shown to lead to two distinct problems. In the mid-1960s it became clear that a number of workers involved in reactor cleaning suffered from a bone condition called acroosteolysis (AOL), which affects mainly the hands and feet. Removal of the worker from exposure to VCM leads to an almost complete recovery. Since improvements to ventilating reactors and the introduction of high pressure water cleaning the incidence of AOL has ceased (65). A study of long-term exposure of rats to 30,000 ppm VCM did not reproduce any sign of AOL but they did develop cancers in various sites (66).

Subsequently, an extensive study with a wide range of dose conditions relating to occupational exposure was begun in 1971 at the Institute of Oncology in Bologna (67). This showed that a very rare liver cancer, angiosarcoma, could be formed in rats at levels of 250–500 ppm VCM. The first correlation between exposure to VCM and cancer in humans was made in 1973 when three workers at a plant in Louisville, Kentucky, were shown to have died from angiosarcoma (68). Since then other cases have been identified, all of which involved workers exposed to high concentrations of VCM as reactor cleaners or charging operators. As the period between first exposure to VCM and the appearance of angiosarcoma is 20–25 years it is likely that the incidence of the disease will soon decrease following improvements made to operation of PVC plants since 1973.

The knowledge that VCM is a human carcinogen has led to the introduction of very stringent controls by governmental and regulatory authorities to limit the exposure of workers and the general public to the monomer. In the United States, OSHA has set an 8-h TWA of 1 ppm VCM. During a shift an employee's exposure must not exceed 5 ppm over a period of 15 min or less (69). The European regulations, EC directive 78/610, require an annual average of <3 ppm in the plant's airspace with alarm values of 15 ppm over 1 h, 20 ppm over 20 min, and 30 ppm over 2 min.

Poly(Vinyl Chloride) (PVC). Strict limits have been set for the quantity of residual VCM in processed PVC articles intended for use in food contact applications.

In 1979 the EC set an upper limit of 1.0 ppm in the article and 10 ppb in the food. In 1986 the FDA suggested levels of $\leq$5 ppb in rigid and $\leq$10 ppb in plasticized PVC articles in food contact applications. To ensure these limits are met, PVC producers aim for these concentrations in the polymer grains themselves so that any further loss during processing ensures even greater safety.

There is little evidence that PVC powder itself causes any significant medical problems but steps are always taken to reduce powder emissions because of its nuisance value.

BIBLIOGRAPHY

"Vinyl Chloride Polymers" in *EPST* 1st ed., Vol. 14, pp. 305–483, by C. A. Brighton, J. L. Benton, and C. G. Marks, BP Chemicals International, Ltd., and (Fibers) J. P. Dux, American Viscose Division; "Vinyl Chloride Polymers" in *EPSE* 2nd ed., Suppl. Vol., pp. 822–889, by P. V. Smallwood, ICI Chemicals and Polymers, Ltd., and R. C. Stephenson and M. W. Newman, European Vinyls Corp.; "Vinyl Chloride Polymers, Polymerization" in *EPSE* 2nd ed., Vol. 17, pp. 295–376, by M. J. Bunten, European Vinyl Corp., Ltd.

1. J. D. Cotman, M. F. Gonzales, and G. C. Claver, *J. Polym. Sci. Polym. Chem. Ed.* **5**, 1137–1164 (1967).
2. M. R. Meeks, *Polym. Eng. Sci.* **9**, 141 (1969).
3. H. Fikentscher, *Kolloid Z.* **53**, 34 (1932).
4. G. A. R. Matthews and R. B. Pearson, *Plastics (London)* **28**, 98 (1963).
5. W. F. Maddams, in E. D. Owen, ed., *Degradation and Stabilisation of PVC*, Applied Science Publishers, Barking, 1984.
6. C. A. Finch, ed., *Poly(vinyl alcohol), Properties and Applications*, John Wiley & Sons, Inc., New York, 1973.
7. D. G. Kelsall and G. C. Maitland, in K. H. Reichert and W. Geisseler, eds., *Polymer Reaction Engineering, Influence of Reaction Engineering on Polymer Properties*, Hanser Publishers, München, 1983.
8. G. Wieckert, G. Henschel, and K. D. Weissenborn, *Angew. Makromol. Chem.* **147**, 1 (1987).
9. R. H. Burgess, ed., *Manufacturing and Processing of PVC*, Applied Science Publishers, London, 1982.
10. B. Mariasi, *J. Vinyl Technol.* **8**(1), 20 (1986).
11. M. W. Allsopp, in Ref. 9, p. 152.
12. J. Boissel and N. Fischer, *J. Macromol. Sci. Chem. A* **11**, 1249 (1977).
13. M. W. Allsopp, in Ref. 9, p. 181.
14. G. C. Portingell, in G. Butters, ed., *Particulate Nature of PVC*, Applied Science Publishers, London, 1982, pp. 135–234.
15. N. Fischer, *J. Vinyl Technol.* **6**(1), 35 (1984).
16. M. W. Allsopp, in Ref. 9, Chapt. 2.
17. U.S. Pat. 2068424 (1931), H. Fikentscher (to I. G. Farben).
18. W. D. Harkins, *J. Am. Chem. Soc.* **69**, 1428 (1947).
19. W. V. Smith and R. H. Ewart, *J. Chem. Phys.* **16**, 592 (1948).
20. J. Ulgestad, P. C. Mork, and J. O. Aasen, *J. Polym. Sci., Polym. Chem. Ed.* **5**, 2281 (1967).

21. E. Peggion, F. Testa, and G. Talamini, *Makromol. Chem.* **71**, 173 (1964).
22. G. Gatta, G. Benetta, G. P. Talamini, and G. Vianello, in R. F. Gould, ed., *Addition and Condensation Polymerization* (Advances in Chemistry Series), Vol. **91**, 1969, p. 158.
23. J. Ugelstad, H. Flogstad, F. K. Hansen, and T. Ellingsen, *J. Polym. Sci. Polym. Symp.* **473**, 473 (1973).
24. GB Pat. 978875 (1981), A. Frangou (to ICI).
25. GB Pat. 1435425 (1976), T. Kemp (to Rhône-Progil).
26. GB Pat. 1503247 (1977) (to Rhône-Poulenc).
27. J. Ugelstad, F. K. Hansen, and S. Lange, *Makromol Chem.* **175**, 507 (1974).
28. D. E. M. Evans, in Ref. 9, pp. 67–75.
29. I. M. Koltoff and I. K. Miller, *J. Am. Chem. Soc.* **73**, 3055 (1951).
30. R. G. R. Bacon, *Q. Rev.* **9**, 283 (1955).
31. EP 38634 (1981), (to ICI).
32. P. Rangnes and O. Palmgren, *J. Polym. Sci., Part C* **33**, 181–192 (1970).
33. DE 1964029 (1970) (to Hüls).
34. BE 857235 (1970) (to Hüls).
35. P. Becher, *Emulsion: Theory and Practice*, Reinhold, New York, 1955, p. 173.
36. F. A. Bovey, I. M. Koltoff, A. I. Medalia, and A. J. Meehan, *Emulsion Polymerization*, Interscience Publishers, New York, 1954.
37. DE 2429776 (1980) (to Hoechst).
38. U.S. Pat. 4233437 (1980) (to Hüls).
39. DE-OS 3020237 (1980) (to Montedison).
40. U.S. Pat. 4283526 (1981) (to ICI).
41. K. Masters, *Spray Drying Handbook*, Georg Godwin, London, 1979.
42. U.S. Pat. 4229249 (1980), K. S. Felsvang and O. E. Hansen (to Niro Atomizer).
43. K. Kern Sears and J. R. Darby, *The Technology of Plasticizers*, Wiley-Interscience, New York, 1982.
44. H. A. Sarvetnick, *Plastisols and Organosols*, Van Nostrand Reinhold, New York, 1972.
45. H. Zecha, J. Schneider, and K. Wulf, *Kunststoffe* **76**(1), 51 (1986).
46. N. Nakajima and E. R. Harrel, *Adv. Polym. Technol.* **6**, 409 (1986).
47. U.S. Pat. 3293094 (1966) (to Congoleum-Nairn).
48. F. Candau and R. H. Ottewill, *Scientific Methods for the Study of Polymer Colloids and their Application*, Kluwer, London, 1990.
49. G. Matthews, *Vinyl and Applied Polymers*, Vol. **2**, Iliffe, London, 1972.
50. L. I. Nass, *Encyclopaedia of PVC*, Marcel Dekker, New York, 1976.
51. R. G. Parker and G. Martello, in L. I. Nass and C. A. Heiberger, eds., *Encyclopaedia of PVC*, 2nd ed., Vol. **1**, Marcel Dekker, New York, 1986, p. 619.
52. TA Luft, 1986.
53. *The Energy Content of Plastics Articles*, British Plastics Federation, London, 1986.
54. Company brochure, Solvay et Cie, PVC and The Environment, 1986.
55. D. J. Brandt, R. S. Guise, and B. A. McCoy, in L. I. Naas and C. Heiberger, eds., *Encyclopaedia of PVC*, 2nd ed., Vol. **1**, Marcel Dekker, New York, 1986.
56. T. Hjerberg and E. M. Sörvik, in E. D. Owen, ed., *Degradation and Stabilisation of PVC*, Applied Science Publishers, Barking, 1984.
57. D. Braun and E. Bazdadea, in L. I. Nass and C. A. Heiberger, eds., *Encyclopaedia of PVC*, 2nd ed., Vol. **1**, Marcel Dekker, New York, 1986.
58. M. W. Allsopp, in Ref. 9, Chapt. 8.
59. A. Gonze, *Plastica* **24**(2), 49 (1971).
60. D. A. Tester, in Ref. 9, Chapts. 9 and 10.
61. N. L. Perry, in L. I. Nass and C. A. Heiberger, eds., *Encyclopaedia of PVC*, 1st ed., Vol. 2, 1976, p. 601; 2nd ed., Vol. 2, 1988, p. 1.

62. W. Henschel and P. Franz, in W. V. Titow, ed., *PVC Technology*, 4th ed., Applied Science Publishers, Barking, 1984.
63. E. D. Owen, *Degradation and Stabilisation of PVC*, Applied Science Publishers, Barking, 1984.
64. J. T. Barr, in L. I. Nass and C. A. Heiberger, eds., *Encyclopaedia of PVC*, 2nd ed., Vol. **1**, Marcel Dekker, New York, 1986, Chapt. "5".
65. R. H. Burgess, in Ref. 1, p. 101.
66. P. L. Viola, A. Bigotti, and A. Caputo, *Cancer Res.* **31**, 516 (1971).
67. C. Maltoni, *Vinyl Chloride Carcinogenicity; Available Scientific Evidence and Control Measures*, Association of Plastics Manufacturers in Europe, Brussels, 1986.
68. J. L. Creech and M. N. Johnson, *JOM, J. Occup. Med.* **16**, 150 (1974).
69. *Fed. Regist.* **39**, 35890–35898 (1974).

GENERAL REFERENCES

R. H. Burgess, ed., *Manufacturing and Processing of PVC*, Applied Science Publishers, London, 1982.
G. Butters, ed., *Particulate Nature of PVC*, Applied Science Publishers, London, 1982.
L. I. Nass and C. S. Heiberger, eds., *Encyclopaedia of PVC*, 2nd ed., Vols. **1–3**, Marcel Dekker, New York, 1986.
G. Matthews, *Vinyl and Allied Polymers*, Vol. **2**, Iliffe, London, 1972.
A. Whelan and J. L. Craft, eds., *Development in PVC Production and Processing*, Applied Science Publishers, London, 1977.

MICHAEL W. ALLSOPP
Independent PVC Technology Consultant
GIOVANNI VIANELLO
European Vinyls Corporation (IT) (retired)

VINYL FLUORIDE POLYMERS (PVF). See Volume 4.

VINYLIDENE CHLORIDE POLYMERS. See Volume 4.

VINYLIDENE FLUORIDE POLYMERS. See Volume 4.

VISCOELASTICITY. See Volume 4.

WEATHERING. See Volume 4.

X-RAY MICROSCOPY

Introduction

Various types of microscopy have played a crucial role throughout the history of Polymer Science by elucidating the underlying organization and morphology of multiphasic polymeric materials and systems in real space. In many applications, there is often the need to not only visualize the morphology of a multicomponent system or material, but to also quantify the composition of the various phases in detail. Typically, techniques providing very high quantitative chemical information, such as infra red (ir), Raman, and nuclear magnetic resonance (nmr) spectroscopy, would be ideal for these tasks, but these techniques have very limited spatial resolution and achieve at best a resolution of the order of a micron. In contrast to this, electron microscopy has very high spatial resolution, but relies generally on heavy metal staining or only elemental contrast to provide qualitative compositional information. On surfaces, scanning force microscopy (sfm) has proven to be a very versatile characterization tool, but the compositional information obtained is only qualitative in nature. X-ray microscopy bridges this gap between ir, nmr on the one hand and electron and scanning force microscopy on the other, and fills a need by providing quantitative compositional information at a spatial resolution of presently 40 nm.

This article reviews Near Edge X-ray Absorption Fine Structure (nexafs) spectroscopy, which underlies the ability for quantitation of sample composition in x-ray microscopy. Also covered are state-of-the-art x-ray microscopy instrumentation techniques and a relatively complete overview of nexafs microscopy applications.

Encyclopedia of Polymer Science and Technology. Copyright John Wiley & Sons, Inc. All rights reserved.

Near Edge X-ray Absorption Fine Structure Spectroscopy

The utility of x-ray microscopy is based on the range and subtlety of the spectroscopic and hence compositional information content of nexafs spectroscopy. As is true for all spectroscopies, the higher the chemical speciation capability that can be achieved, the better the compositional quantitation. In nexafs spectroscopy, the photoabsorption cross section for the excitation or photoionization of tightly bound core electrons is measured. NEXAFS spectra are necessarily element specific, as each element has a characteristic core binding energy (ie, carbon 1*s*: ∼290 eV, nitrogen 1*s*: ∼400 eV, oxygen 1*s*: ∼530 eV, etc). The spectral features observed in nexafs spectra correspond to transitions from the ground state to a core excited state. Figure 1 presents a schematic of the x-ray photoabsorption process for the carbon 1*s* nexafs spectrum of poly(styrene-*r*-acrylonitrile) (SAN). The most pronounced spectral features are intense and narrow peaks at the lowest energies in the spectrum. The first transition at ∼285 eV is a C $1s \rightarrow \pi^*$ transition corresponding to carbon atoms of the phenyl functional group. The second transition at ∼287 eV is a C $1s \rightarrow \pi^*$ electronic transition corresponding to the carbon atoms of the acrylonitrile functional groups. The energy of these features is dictated by the combination of initial state effects (core binding energies) and final state effects (energy of the optical orbital in the presence of the core hole). The relative magnitude of initial and final state effects in SAN can be gleamed from the energy diagram on the right-hand side of Figure 1. At higher photon energies in the spectrum, broad C $1s \rightarrow \sigma^*$ transitions are superimposed on the photoionization continuum.

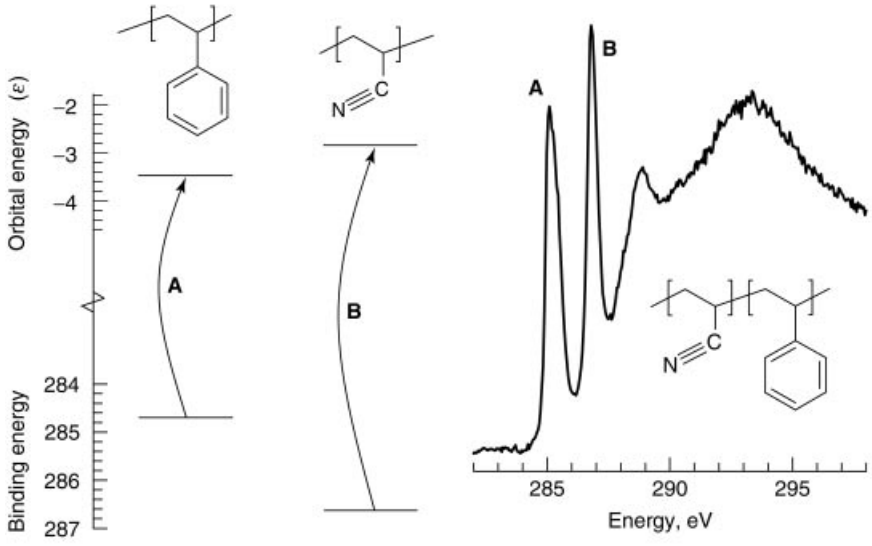

Fig. 1. Electronic schematic for the nexafs photoabsorption spectrum of poly(styrene-*r*-acrylonitrile). The C 1*s* binding energies were obtained from xps. Orbital energies of the C $1s \rightarrow$ LUMO(π^*) transition of the phenyl (A) and acrylonitrile (B) functional groups were obtained from ab initio calculations. Reproduced from Ref. 1.

A more broadly based illustration of the compositional sensitivity of nexafs spectroscopy can be seen in Figure 2 (1), displaying spectra from a number of unsaturated polymers that consist primarily of various aromatic functional groups, C=C bonds in the polymer chain backbone, as well as amide, ester, and carbonyl groups. It is readily apparent that the shape and intensity of the spectral features observed are unique for each polymer. Most nexafs spectra of these polymers are dominated by low energy C 1*s* $\rightarrow \pi^*_{C=C}$ transitions at 285–287 eV. The shape and intensity of this $\pi^*_{C=C}$ band varies with the chemical and hence electronic structure. An example of this chemical sensitivity can be observed in the C 1*s* nexafs spectra of polystyrene (PS) and poly(bromo styrene) (PBrS) (right panel of Fig. 2). In the PBrS spectrum, the core $\rightarrow \pi^*_{C=C}$ (LUMO) transition has two major components, a C 1*s*(C—H) $\rightarrow \pi^*_{C=C}$ component at ~285 eV and a C 1*s*(C—Br) $\rightarrow \pi^*_{C=C}$ component at ~286.2 eV, whereas PS has only one major component at ~285 eV. Note that in this notation, the core level is indicated parenthetically before the arrow (eg C—H), and the nature of the upper level of a given transition is indicated by the final subscript (eg C=C for phenyl). The inductive effect of the bromine shifts the C 1*s* ionization potential of the C—Br carbon atom to lower energy, increasing the energy of the C 1*s*(C—Br) $\rightarrow \pi^*_{C=C}$ transition to the common manifold of π^*(LUMO) states.

A similar situation applies to 4,4′-methylene di-*p*-phenylene isocyanate (MDI) and toluene diisocyanate (TDI) polyurea and polyurethane spectra, where the core $\rightarrow \pi^*_{C=C}$ (LUMO) transition has two major components: a C 1*s*(C—H) $\rightarrow \pi^*_{C=C}$ component at ~285 eV and a C 1*s*(C—R) $\rightarrow \pi^*_{C=C}$ component at ~286.5 eV. In TDI, the main, low energy π^* peak itself is furthermore split into two components. The inductive effect of a heteroatom can also be clearly observed by comparing the spectra of neoprene (NP) and polyisoprene (PI). A complementary series of nexafs spectra is shown in Figure 3, which presents the evolutionary trend of the spectral signature of carbonyl functional groups as the nearest neighbor environment is changed progressively and systematically from a keton to a carbonate (2).

Unfortunately, peaks attributable to different functional groups and specific carbon atoms have the tendency to overlap in a nexafs spectrum. Most of the spectroscopic information is compressed into a 6-eV wide energy window, while lineshapes are about 100 meV wide. Most notably, π^* spectral features corresponding to carbonyl, ester, and carbonate groups generally sit on top of C 1*s* (C—H) $\rightarrow \sigma^*$ transitions or the vacuum continuum.

Sometimes the shifts of slightly inequivalent carbon atoms are small and of the order of the intrinsic line width of a spectral feature (about 80–100 meV) that arises from the finite core-hole lifetime. Small chemical shifts can be found, for example, for the six inequivalent carbon atoms of the phenyl ring of PS. Further complicating matters, these small chemical energy shifts overlap with vibrational effects that have also similar energy shifts. The chemical shifts can thus not be observed in isolation from vibration and are furthermore convolved with the natural line width. The relative contributions of chemical and vibrational effects to the spectrum of PS has been explored (3). The magnitude of the shifts of these six carbon atoms based on calculations ranges from 50 to 400 meV. Figure 4 shows the lowest energy spectral features of PS and deuterated PS (d-PS). Difference of up to 15% in intensity can be observed that can be clearly attributed to vibrations.

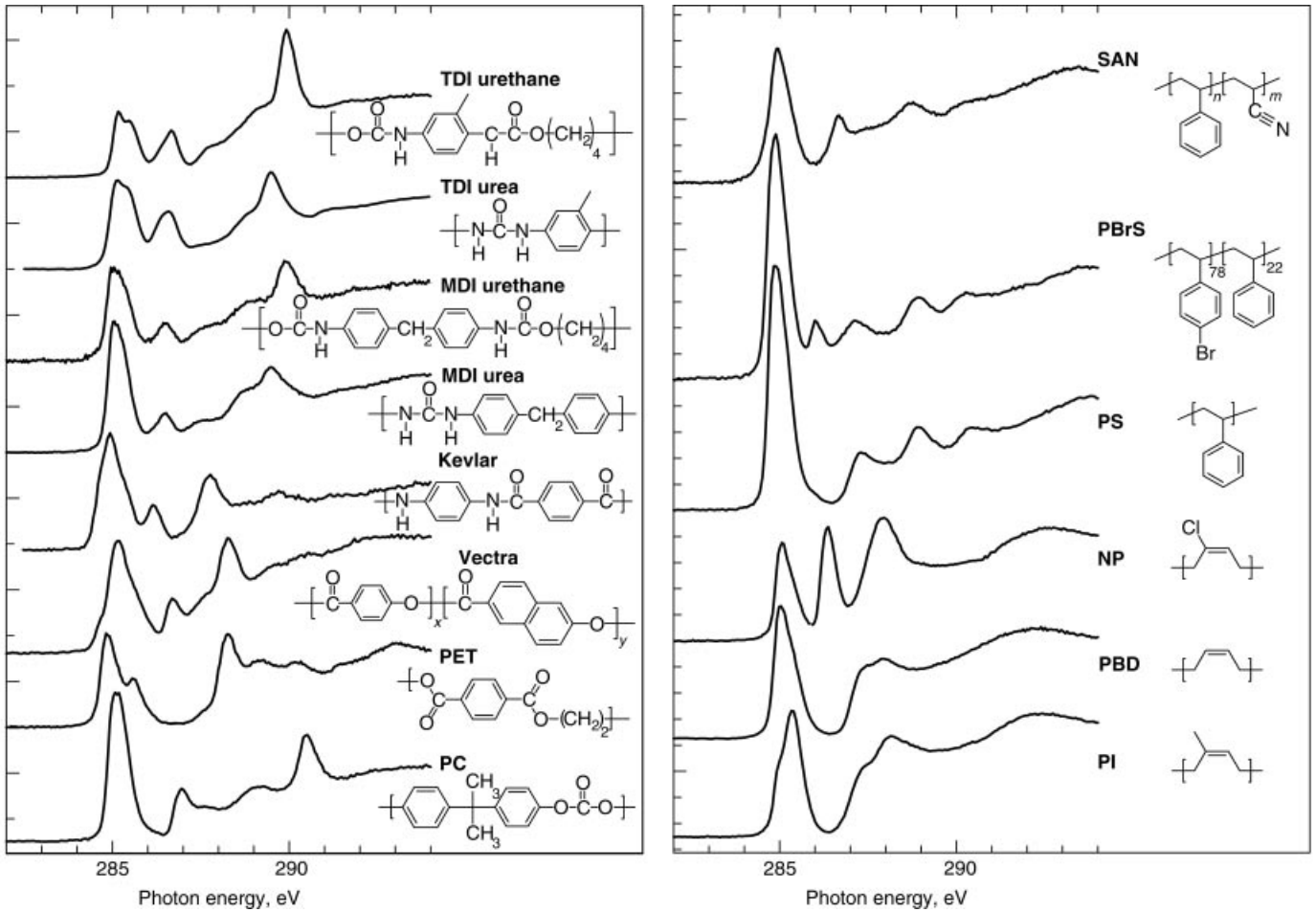

Fig. 2. C 1*s* nexafs spectra for a series of unsaturated polymers, recorded with the Stony Brook STXM. Reproduced from Ref. 1.

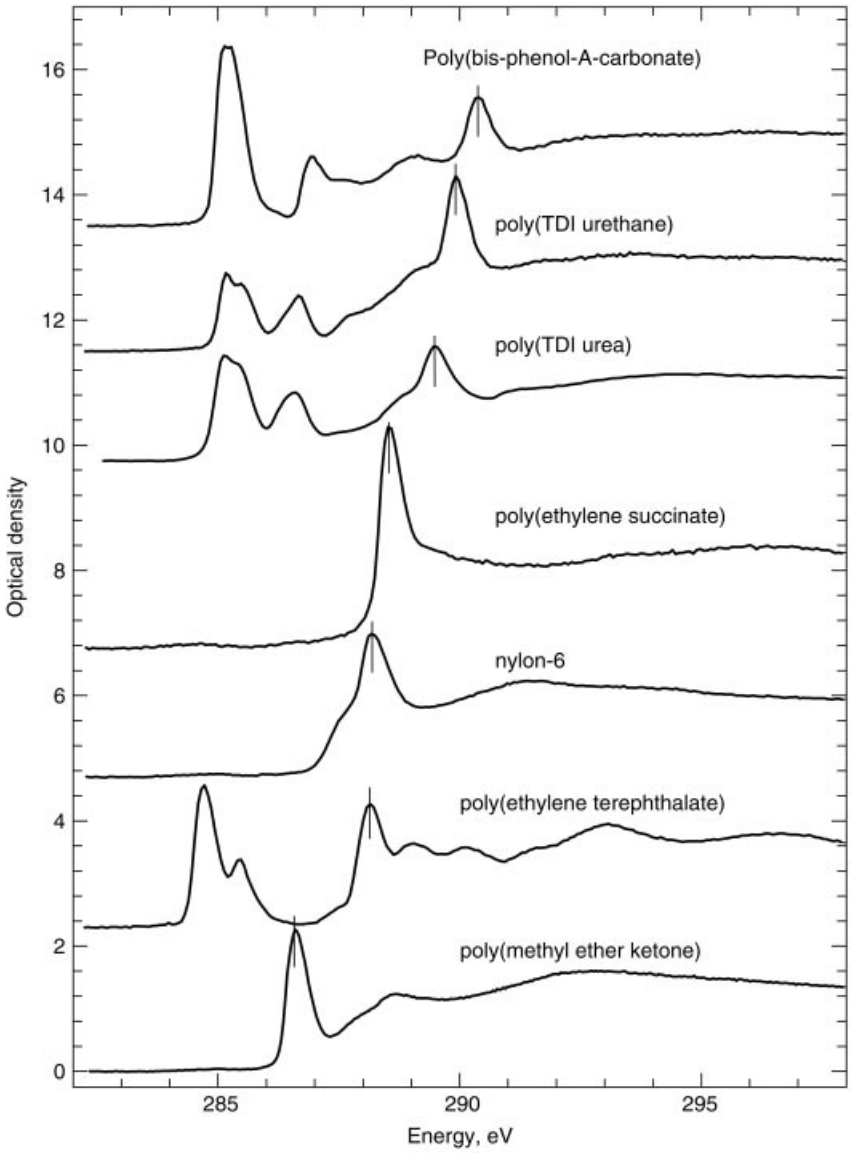

Fig. 3. C 1*s* nexafs spectra for a series of polymers that have carbonyl functional groups in different local electronic environments. (Data recorded with the Stony Brook STXM.) Reproduced from Ref. 2.

NEXAFS spectroscopy is also sensitive to differences in the chemical structure of saturated polymers (polyolefins and polyethers). The nexafs features in spectra of these materials are predominantly core $\rightarrow \sigma^*$ electronic transitions with some Rydberg character (4–6). In general, the spectral differences and variations observed for σ^* transitions as a function of chemical structure are not as great as those for π^* transitions. Only slight, although noticeable, differences in the

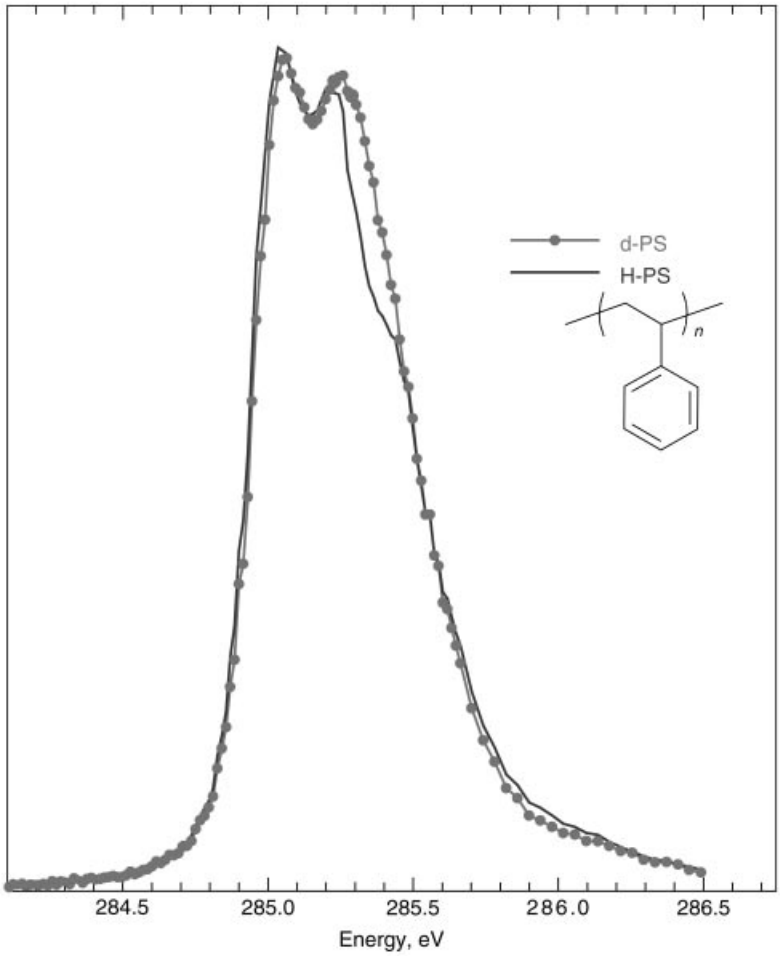

Fig. 4. C 1*s* nexafs spectra of polystyrene (blue line) and deuterated polystyrene (red line) recorded with a resolving power of about 6100. The area of the C $1s \rightarrow \pi^*$ transition is normalized so that absolute differences in the spectral intensity are chemically meaningful. (Data acquired with ALS BL7.0 STXM.) Reproduced from Ref. 3.

nexafs spectra of polyethylene (PE), polypropylene (PP), polyisobutylene (PIB), and ethylene propylene rubber (EPR) have been observed (1). The main chemical structural differences between these polymers are the number and distribution of methyl groups to the $(CH_2)_x$ backbone. The small spectroscopic differences are not surprising, since the structural differences involve bonds of the same C—C and C—H σ-bonded character. Nevertheless, spectroscopic differences have even been observed for PE of different density. These differences have been attributed to a matrix effect that varies between amorphous and crystalline regions of the semicrystalline PE materials (6). The largest spectral differences between the nexafs spectra of saturated polymers are observed when heteroatoms such as oxygen, chlorine, or fluorine are present. Substantial shifts of the corresponding features

of PE toward higher energy are observed in poly(ethylene oxide), polytetrafluoroethylene, polyvinylidine, or poly(vinyl chloride), primarily on account of shifts in the ionization potential because of the heteroatom.

NEXAFS experiments are almost exclusively performed with linearly polarized light from synchrotron radiation facilities. Since the discrete nexafs transitions obey dipole selection rules, oriented samples exhibit linear x-ray dichroism. This can be utilized to explore and measure orientation in polymeric materials. As an example, Figure 5 displays two nexafs spectra of an oriented long-chain hydrocarbon molecule (8). The orientation of the electric field vector with respect to the sample can be changed by rotating the sample relative to the x-ray beam. The spectra shown in Figure 5 correspond to glancing and normal incident radiation. Large spectral differences are observed, even though saturated molecules with only σ bonds tend to give less well-defined spectral features than polymers with π bonds.

The principles and underlying physics of nexafs spectroscopy and x-ray linear dichroism and their applications to small molecules and some polymers have been

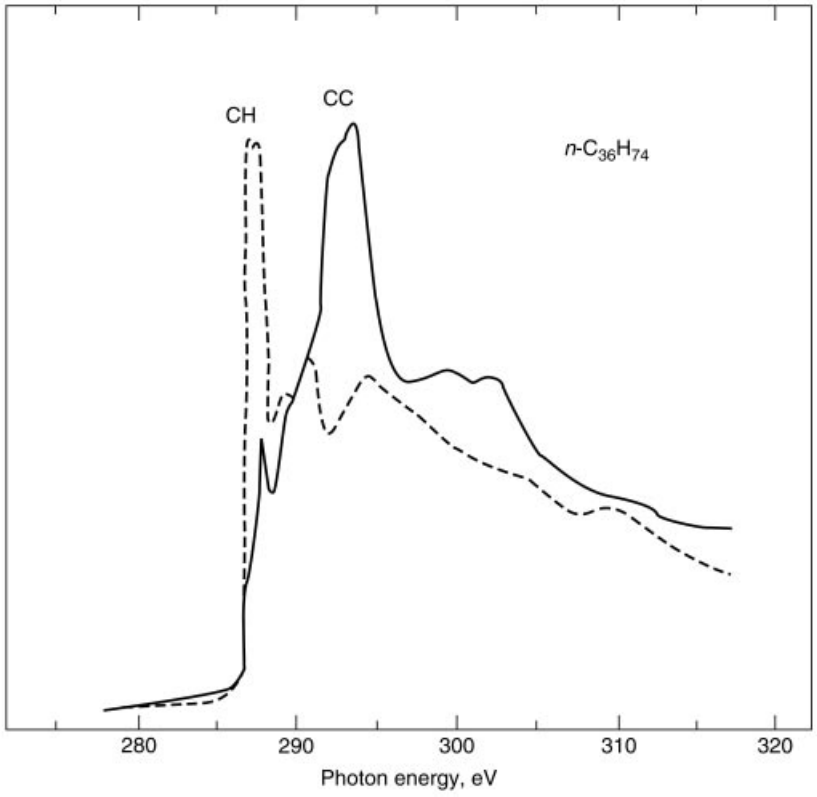

Fig. 5. Angle-dependent C 1*s* nexafs spectra of evaporated hexatriacontane-$CH_3(CH_2)_{34}CH_3$. Although this is not a polymeric substance, it provides a good illustration how large the linear dichroic signal can be even for fully saturated materials. The solid line data has the polarization vector aligned along the molecular axis of the oriented materials, while the dashed line data is for polarization perpendicular to the molecular axis. Reproduced from Ref. 7.

reviewed in a monograph (9). Complementary, but somewhat limited, overviews of polymer nexafs spectra have been presented (10–13). A more detailed "primer" of nexafs spectroscopy of polymers has also been provided (1). A carefully energy-calibrated library of nexafs spectra is presently being compiled by the North Carolina State University nexafs microscopy research group. Energy calibration is accomplished by leaking a small amount of CO_2 gas into the experimental chamber and by recording characteristic polymer features and characteristic features of the CO_2 gas simultaneously, thus reducing any ambiguity about the energy scale (14).

The chemical and orientational sensitivity of nexafs spectroscopy has been used for analysis in a variety of applications. Examples of studies involving nexafs spectroscopy are given below:

(1) Photoactive polymers: poly(phenylene vinylene) (15), poly-*p*-phenylenes and polyacenes (16), photo-oxidation of electroluminescent polymers (17), and uv-polymerized diacetylene (8)
(2) Polyurethanes and model compounds (18,19)
(3) Plasma and radiation damaged polymers: oxygen plasma damaged polypropylene (20) and argon plasma damaged polycarbonate (21). Electron and x-ray beam damaged or decomposing polymers: poly(methy methacrylate) (PMMA) (22–24), several polymers with carbonyl functionality (25).
(4) Metal polymer interfaces: chromium coated poly(ethylene terephthalate) (PET) (26) and metalized polycarbonate (PC)(27)
(5) Surface relaxation of PS (28)
(6) Surface structure of polyimides (29–34)
(7) Surface orientation and grafting density of semifluorinated polymers (35–39)
(8) Organic geochemical polymers: petroleum asphaltenes and coals (40,41) and kerogens and bitumens (42)
(9) Inorganic polymers: polydimethylsilane films (43,44) and poly(di-*N*-hexyldisiloxane) (45).

Additional studies comprise various forms of polyethylene $(CH_2)_x$, such as oriented homopolymer (7,46). Other examples include polytetrafluoroethylene homopolymer and models (7,47–50); poly(ethylene terephthalate) and the related polymers poly(butylene terephthalate) and poly(ethylene naphthalate) (51–53); and electrochemically polymerized thin films such as poly(3-methyl thiophene) (54) and polypyrrole (55). This is not intended to be a comprehensive list, but only an indication of the wide range of applications possible with nexafs spectroscopy.

Energy electron loss spectroscopy (eels) used under dipole approximation conditions is a closely related tool to nexafs spectroscopy as it measures the same electronic transitions (56,57). Indeed, most of the early polymer core excitation spectroscopy, work particularly at the C 1*s* core edge, was performed by eels (58–61). EELS can be performed in a scanning transmission electron microscope (stem) at high spatial resolution (62–64), or by energy filtered tem imaging (65). The relatively poor energy resolution in commercial instruments and higher beam damage (66) limits the use of these eels methods for compositional analysis of complex

polymeric materials. EELS is best used for elemental analysis or semiquantitative low loss spectroscopy (67–69). Specialized tem–eels instruments have demonstrated 0.2–0.4 eV FWHM energy resolution for semiconductors (70) and nickel aluminum intermetallics (71). The development of tem-monochromators capable of reaching 50 meV resolution is in progress (72–74).

NEXAFS Microscopy: Instrumentation and Analysis Tools

Having seen the power (and limitation) of nexafs spectroscopy in the preceding sections, one can readily envision the enhanced utility of nexafs spectroscopy as a characterization tool that would result from the addition of high spatial resolution capabilities. Since the spectroscopic sensitivity to specific moieties and functional groups can in many or even most cases be exceeded by ir, nmr, and Raman spectroscopies, nexafs microscopy will have to exceed the spatial resolution of these other spectroscopy techniques in order to be truly useful. To date, nexafs microscopy has surpassed a spatial resolution of 50 nm both in transmission to measure bulk properties (75–77) and in a reflection geometry to study surfaces (78,79). This level of spatial resolution is at least an order of magnitude better than what can be accomplished with complementary compositional analysis techniques. Future developments in nexafs microscopy might achieve a spatial resolution of a few nanometers (80,81). In addition, nexafs microscopy has exceptional surface sensitivity of about 10 nm, a sensitivity that could be improved to about 1 nm with photoemission electron microscopes (peem's) that incorporate a bandpass filter (80–82).

High spatial resolution nexafs microscopy is generally accomplished in two ways: (*1*) instruments for transmission experiments typically employ high resolution zone plate optics (83), whereas (*2*) surfaces are characterized with peem's (78,79,82). Zone-plate-based microscopes are true x-ray microscopes. PEEM's are essentially electron microscopies in which high spatial resolution is achieved with electrostatic or electromagnetic electron optics. The quality of the optics system is essential in both cases.

For zone-plate-based microscopes, the accuracy of the zone placement and the width of the outermost zone determines the spatial resolution achievable with these elements. The Rayleigh resolution of a perfect zone plate is 1.22 times the outermost zone width. Zone plates with outermost zone widths between 20 and 40 nm are presently in use with experimental spatial resolution in the range of 25–50 nm (77). Two types of instruments have been developed and are being continually refined and improved: (*1*) scanning transmission x-ray microscopes (stxm) and (*2*) full-field conventional transmission x-ray microscopes (txm) (see schematics in Fig. 6). Present stxm's generate a microprobe of about 40–50 nm in size, and the sample is raster scanned through the focus of the x-ray microprobe by mechanical means (84,85). In a txm, a zone plate downstream of the stationary sample magnifies the sample onto a 2-D detector (86–88). NEXAFS microscopy with good chemical sensitivity requires good energy resolution. For a stxm that is operated in the 200–900 eV energy range, this is achieved with a grazing incidence monochromator upstream of the microscope. Near the carbon edge, the most widely used edge for polymeric materials, a resolving power of 2000–5000 is

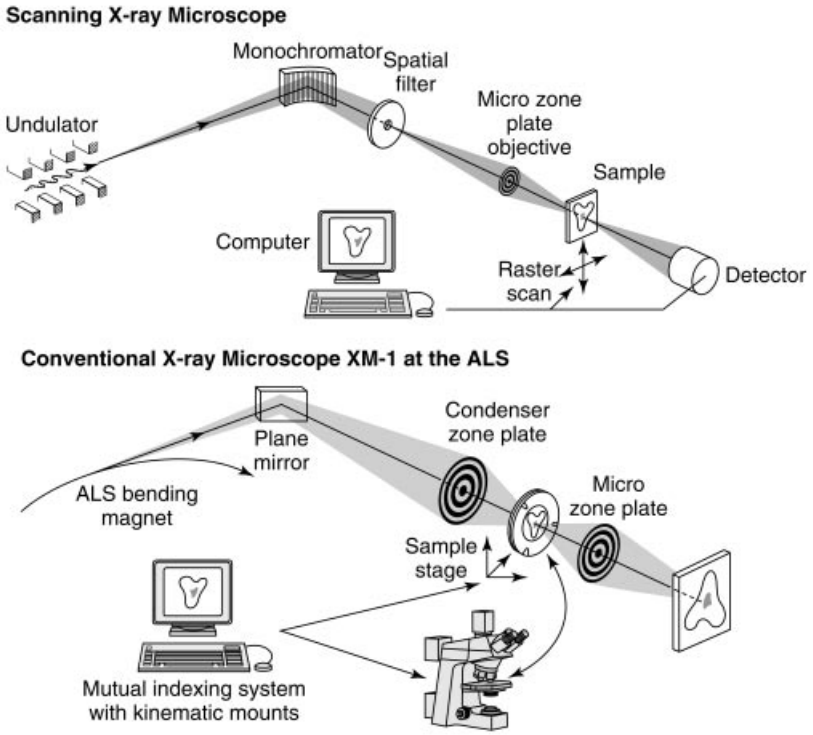

Fig. 6. Schematic of a scanning transmission x-ray microscope (stxm) and a conventional transmission x-ray microscope (txm). Courtesy of W. Meyer-Ilse, CXRO.

routinely available (85,89,90). TXM's presently employ zone plate monochromators in order to match the numerical aperture of the illumination at the sample to the numerical aperture of the objective. Present zone plate monochromators used in a txm have relatively low energy resolution ($\sim$0.5 eV), limiting the utility of txm for nexafs microscopy of polymers. Efforts are underway to improve this shortcoming of txm's.

Zone plates are highly chromatic, with a focal length proportional to the photon energy. As a result, continual refocusing is required during the photon energy change necessary for spectroscopy. This is accomplished by changing the sample to zone plate distance. If a high spatial resolution point spectrum is to be acquired, care and effort must be exercised to control the transverse motion of the scanned element (sample or zone plate) during refocusing to avoid blurring of the region from which the spectrum is acquired. Controlling this "run-out" is a technological challenge, and places severe constraints on the accuracy of the mechanical apparatus. An accuracy, stability, and repeatability consistent with the spatial resolution of the zone plate has not yet been routinely achieved in existing stxms. One way to work around these problems, at least partially, is to acquire image sequences at each photon energy in the spectrum (91). The images in these sequences can then be correlated to each other and shifted to provide the proper alignment. If one is only interested in spectra from a few locations, the image

sequence approach results in a time penalty: image sequences typically require between 0.5 and 3 h, while a few point spectra require a few minutes. Refocusing after a change in energy is also necessary in a txm, with similar requirements to an stxm regarding stability and alignment. In a txm, one has to translate both the zone plate objective and the detector in order to keep the magnification the same.

The first stxm had been operated at a relatively low brightness bending magnet beamline at the National Synchrotron Light Source (NSLS) uv ring (92), but was moved to an undulator beamline as these high brightness sources became available (93). This was motivated by the requirement to illuminate the zone plate coherently to achieve the highest spatial resolution possible. High intensity at high spatial resolution is thus most easily accomplished at the brightest sources available, ie, undulator sources at synchrotron radiation facilities (83,85,90). In order to increase stxm capacity at relatively low cost, an effort is underway to build an stxm at a bending magnet beamline at the Advanced Light Source (ALS) in Berkeley that is about two orders of magnitude brighter than a bending magnet at the NSLS uv ring. In order to achieve the best data rates for the majority of polymer experiments, the ALS bending magnet stxm and beamline has been optimized for C-nexafs (94). The brightness requirement for a txm is less severe than for an stxm. TXM's can be successfully operated with short exposure times at bending magnet beamlines even at second generation synchrotron facilities. Since most laboratory based x-ray sources do not have a continuous and stable emission spectrum, laboratory based nexafs microscopy, with its requirement for photon energy tunability, is an unlikely development in the near future.

To study surfaces, secondary processes, such as fluorescent photons and secondary or primary photoelectrons, that track the absorption cross section as a function of photon energy are utilized. All three of these secondary processes are already extensively employed in nexafs spectroscopy without spatial resolution, in what is called the fluorescent yield (FY), total- (TEY) or partial electron yield (PEY) mode, respectively (9). PEY traditionally refers to experiments that utilize a bias voltage on the channel plate or channeltron detector or an energy window set with an energy analyzer. Both methods strive to accept primarily electrons with kinetic energy in the 100–300 eV range near the minimum of the secondary electron mean free path in order to achieve high surface sensitivity of about 1 nm. In nexafs microscopy, only a modified version of PEY mode is presently available. In a peem, the photoelectrons emitted from the sample surface are accelerated in a cathode lens to high energies, and subsequent electrostatic or electromagnetic lenses magnify the image onto a 2-D detector (see Fig. 7 as an example). The peem instrument itself acts as a low pass energy filter with a bandwidth of a few electro volts near the photoelectron threshold. This energy window is not near the mean free path minimum and has a large sampling depth of about 10 nm associated with it. True energy filtering in a peem would allow operation near the mean free path minimum. However, the one instrument presently available with an energy filter, the spectroscopic low energy electron microscope (SPLEEM) developed by the group of E. Bauer, has not yet been utilized for nexafs experiments (95).

Several contrast mechanisms assert themselves simultaneously in a peem instrument: (*1*) composition, ie, the cross section difference between different materials at a given photon energy, (*2*) topography and (*3*) illumination effects. Topographic contrast arises from the modified collection efficiency in the peem from

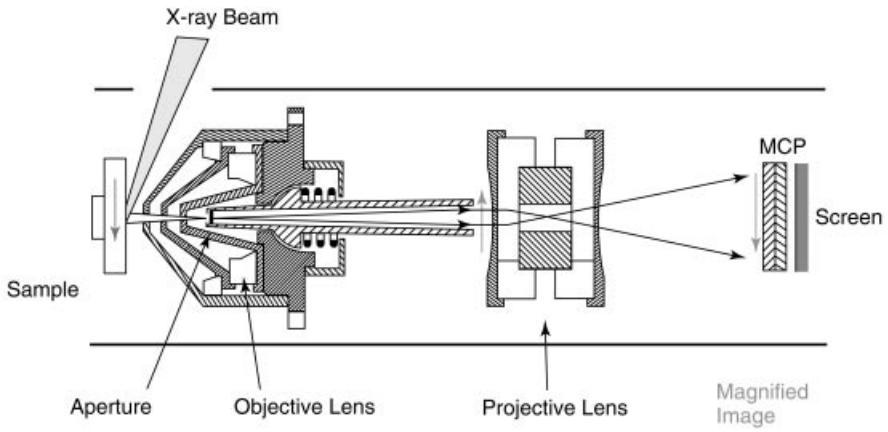

Fig. 7. Schematic of a photoemission electron microscope (peem). Courtesy of S. Anders, ALS, and B. Tonner, University of Central Florida.

sample locations that are not perpendicular to the optical axis. Concave round features tend to have reduced collection efficiency, while convex features are enhanced. Illumination effects arise because the sample is illuminated at a shallow angle of 30° or less. The local photon intensity of the sample depends thus on the topography. Even complete shadowing is possible. Typically, one is interested primarily in the compositional information, and analysis procedures are presently developed to disentangle the spectroscopic, ie, compositional, information from topography and illumination effects. Generally, these methods use pre- and post-edge normalization of the nexafs spectra acquired with the peem and reference spectra acquired with the same instrument (see, for example, Ref. 96)

Since peem's acquire information in parallel from all pixels in the image, and incoherent illumination of the sample is possible, the source requirements are generally not extreme. peem's can be successfully operated at any bending magnet beamline that provides sufficient energy resolution (78,79,97,98). PEEM's also do not require any refocusing during photon energy changes. However, for future ultrahigh spatial resolution (<10 nm) instruments, the necessary flux densities on the sample can only be provided with undulator beamlines.

Quantitative Microanalysis. In transmission nexafs spectroscopy, quantitative analysis can be achieved by inverting Lambert–Beer's law of x-ray absorption:

$$\mathrm{OD} = \mu\rho t = \alpha t = -\ln(I/I_0)$$

where OD is the optical density, μ is the energy-dependent mass absorption coefficient, ρ is the density, t is the sample thickness, and an energy scan from the sample (I) is normalized to another energy scan recorded without a sample (I_0). The product of μ and ρ is the linear absorption coefficient α.

For accurate quantitation, well-characterized nexafs spectra of carefully chosen analytical models of the polymer components are required. The basic and

well-founded assumption is that nexafs spectra of *non-interacting* moieties or components are additive. For a blend of two or more homopolymers, such as PS/PMMA, the analytical models can simply be the individual homopolymers. Even for quantitation of components in a random block copolymer, eg poly(styrene-*r*-acrylonitrile) (SAN), the spectra of the homopolymers PS and polyacrylonitrile (PAN) can be used, provided that the blocks do not interact electronically. Accuracy of a few per cent can presently be obtained for a variety of polymers including polyurethanes (19). In general, care must be exercised to choose models and reference spectra that indeed reflect noninteracting moieties (1). The utility and limitations of quantitative nexafs analysis for polymeric materials has recently been discussed (1).

Quantitative Image Analysis. Two methods are available if the composition of large sample areas is to be analyzed quantitatively: (*1*) singular value decomposition (SVD) of a few images at carefully chosen photon energies (98–101), or (*2*) acquisition of image sequences at many energies that provide nexafs spectra at each point (91). SVD requires prior knowledge about the sample and works only if the overall composition of the sample is known. In addition, the linear absorption coefficients of the components must be accurately known in order to minimize systematic errors in the analysis. The nexafs spectra used as standards must be free of spectral distortions caused by absorption saturation because of the presence of higher order spectral contamination and detector nonlinearity.

The SVD procedure requires a series of images acquired at a number of energies that equal or exceed the number of compositional components. The reference spectra provide crucial guidance for the selection of the photon energy. Usually energy values for images are chosen that correspond to large spectral differences between the constituent components. An example of raw transmission images is shown in Figure 8. Each transmission image is converted to an optical density (OD) image by computing $\mathrm{OD} = -\ln(I/I_0)$, where I is the transmitted intensity and I_0 is the incident intensity. The normalization with I_0 can be most readily and accurately accomplished if the image itself contains an open area (see Fig. 9), but recording a separate I_0 spectrum is also possible. Since $\mathrm{OD} = \alpha t = \mu\rho t$, each pixel in an OD image can be described by a linear combination of the product of the linear absorption coefficient α and the thickness t for each component respectively. This results in a set of linear equations that can be solved for the thickness of each component. Since SVD utilizes only a limited and small number of images, it results in the smallest (and minimum) dose to the sample to extract the desired information. Since $\alpha t = \mu\rho t$, one could alternatively use the mass absorption coefficient as the known quantity and calculate the mass-thickness ρt, rather than the thickness itself. The latter is advantageous if the same component might be present in the sample with different densities, ie, a polymer in an amorphous and crystalline form. The relative contrast and intensities of the images derived from the SVD analysis are not affected by this change in perspective, only their interpretation.

Acquisition of image sequences has the advantage that complete spectroscopic information is acquired from all sample areas (91). Hence the spectra extracted from image sequences can be compared *post facto* to a large number of possible reference spectra, and the existence and identification of unknown species can be more readily accomplished than with SVD (see, for example, Ref. 96).

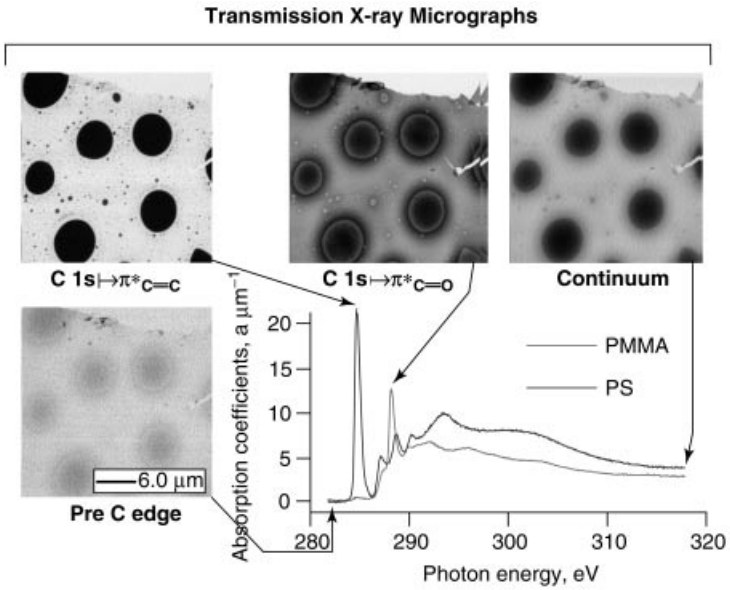

Fig. 8. Basic data set for SVD analysis, with reference spectra of PS and PMMA and transmission images of a PS/PMMA sample at the four energies indicated. Generally, each image has a weighted absorption for each substance present, based on the cross sections at the particular photon energy and the abundance of the substance, even though the absorption in some x-ray micrographs can be dominated by one or the other chemical substance, eg 285.2 eV is dominated by PS absorption. (Data acquired with the Stony Brook STXM.) Courtesy of D. A. Winesett, NCSU.

For C-NEXAFS transmission, optimum signal-to-noise ratios are achieved with sample thicknesses of 50–200 nm. For bulk materials, these sample requirements can usually be met using well-developed electron microscopy (em) preparation techniques such as ultramicrotomy or cryomicrotomy. Alternatively, thin films can be spun-cast to the right thickness and transferred to em grid for x-ray microscopy inspection. Thin samples and section of samples can also be examined in a completely hydrated/solvated state sandwiched between two very thin Si_3N_4 membranes (102). For surface analysis in a peem, polymer thin films typically show the propensity to charge. Generally, only thin polymer films with a thickness of less than 200 nm on top of a conducting substrate can be investigated. Precise temperature control in an stxm and txm is not yet routinely available. PE samples have been melted near 120°C (6), and biological materials have been examined in the frozen state (103). Temperature range in a peem can be from −70 to >1200°C. However, accuracy for near room temperatures is not very good.

NEXAFS Microscopy: Applications

NEXAFS spectroscopy and microscopy provide a new approach to study carbon-based materials. During the last couple of years, nexafs microscopy has been successfully applied to materials characterization in a variety of fields ranging from polymer science and biology to meteoritics (1,83,99). Here, the discussion is focused

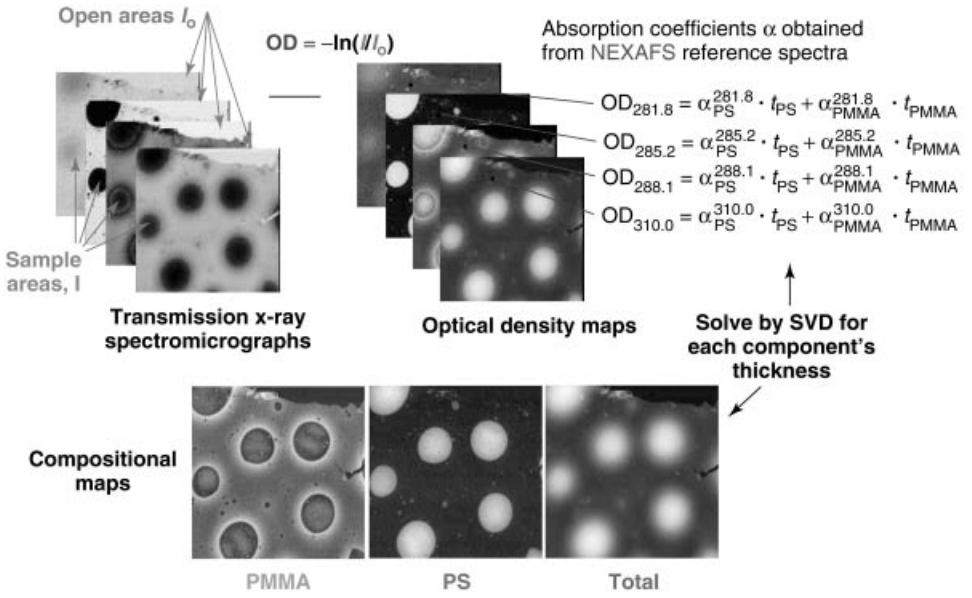

Fig. 9. The transmission images shown in Figure 8 are normalized to optical density (OD) images by inversion of Lambert–Beer's Law. These OD images are now linear in the absorption coefficients α and thickness t. A set of OD images can subsequently be processed via a singular value decomposition (SVD) procedure to yield quantitative composition maps in terms of the thickness t. (Data acquired with the Stony Brook STXM.) Courtesy of D. A. Winesett, NCSU.

on synthetic polymeric materials. Organizing the presentation by separating it into compositional and orientational analysis does not work well, as several studies of one material combine both aspects of nexafs spectroscopy. The discussion progresses thus from the "simple" to the apparently or supposedly "more complex" without regards as to whether compositional or orientational information is sought. The discussion starts with homopolymer surfaces, then progresses to single or multicomponent thin polymer films and structured spheres, followed by bulk properties of multicomponent polymers. The latter might involve formation of "unknown" compounds during processing, presenting a challenge that necessitates careful selection of nexafs reference spectra. These applications will be complemented by a short discussion of research on polymer fibers.

Homopolymer and Polymer Blend Surfaces and Ultrathin Films. Because of the various technological applications of polymer thin films, ranging from multicolor photographic printing to flat panel and liquid crystal displays, it is important to understand thin film and polymer surface characteristics in order to improve performance or to develop entirely new applications or processing methodologies. Polymer and block copolymer thin films and surfaces thus enjoy continued research interest from both a technological and fundamental perspective.

NEXAFS spectroscopy, on account of its excellent surface sensitivity (about 1–10 nm) and its polarization dependence, can and has been utilized to study

a variety of surface properties. Some recent, nonexhaustive examples of nexafs spectroscopy applications are the investigation of the alignment and orientation of polymers and its functional groups in polyimide surfaces after rubbing with a buffing cloth (29–34), the surface relaxation of PS (28), and the orientation of semifluorinated polymers and block copolymers (35–38,104,105). The potential for nexafs characterization of polymer surfaces even without spatial resolution is in fact enormous. A large number of polymer surface characterizations, eg in adhesion science, are currently performed with laboratory x-ray photoemission spectroscopy (xps), even though nexafs spectroscopy might be much more suitable to the task because of increased chemical and surface sensitivity. NEXAFS microscopy has been utilized to investigate the stability and dewetting behavior of bilayers, the phase separation in polymer thin films, and the orientation produced by buffing and rubbing polyimide films. Several examples are provided below.

Polyimide Films and Surfaces. In flat panel displays, polyimide films typically about 0.2-μm thick are coated onto the electrode surfaces. To prepare a surface that aids the alignment of the liquid crystal (LC) molecules in the final device, the polyimide surface is buffed with a velour cloth. Valuable information about the function and the possible improvement of flat panel displays is provided by understanding the conditions and factors that cause LC alignment. Numerous nexafs studies without spatial resolution have investigated the effect of the buffing (29–34). In addition, nexafs microscopy in a peem was utilized to characterize the inhomogeneity of the surface orientation produced by buffing (106). Stripes several microns in width were observed with contrast based entirely on differences in local orientation of polymer chains, chain segments, or moieties. While it was clearly observed that buffing does not orient the surface homogeneously, polyimide films produced under the same rubbing conditions than the samples observed in the peem resulted in LC films with the liquid crystal oriented uniformly over the entire sample surface. The separation distance between the oriented stripes of polymers was less than the correlation length of the liquid crystal and the heterogeneous distribution of the pinning centers is sufficient to align the liquid crystal.

Local stress during buffing is an important parameter that might cause the polymer to orient. However, the local stress cannot be estimated well for buffing with a cloth. Hence, BPDA-PDA polyimide surfaces rubbed with a stylus of well-defined shape and with a known load were also investigated with nexafs microscopy. Stylizing with a radial tip is an ideal model case that produces an ellipsoidal stress profile on the polymer surface. The nexafs micrographs of a track from the stylus are shown in Figure 10, acquired at two different sample orientations relative to the polarization orientation of 285.3 eV x-rays. Spectra from inside the track from the two different sample orientations relative to the polarization orientation of the x-rays are displayed in Figure 11 and clearly demonstrate the dichroic nature of the contrast in Figure 10. By measuring the width of the track that resulted in alignment and comparing it to the expected stress profile, the minimum stress necessary to cause alignment of the BPDA-PDA film was determined to be 45 MPa. This stress is much lower than the bulk yield stress of 200–300 MPa. The low surface value was attributed to a reduction of polymer entanglement at the surface.

Confined Free-Standing Homopolymer Thin Films. Free standing thin polymer films (eg of PS) can form holes when annealed, driven by dispersion

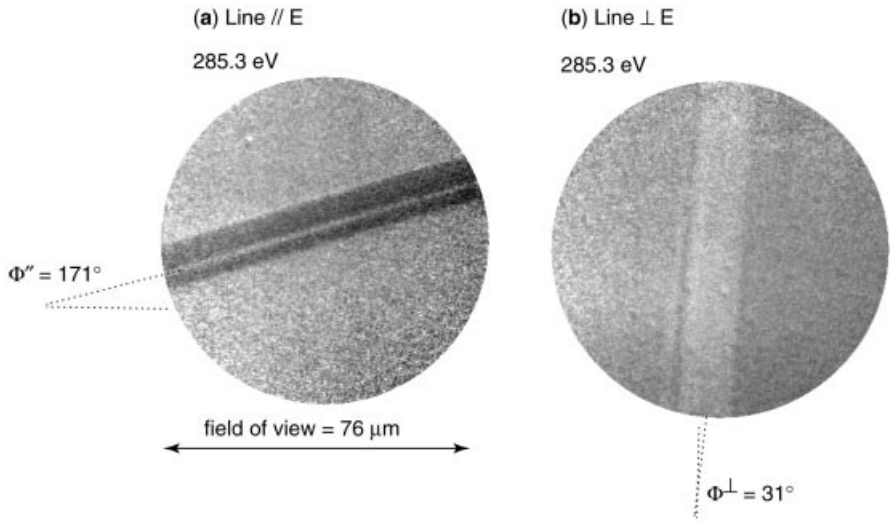

Fig. 10. PEEM images of a stylus track on a polyimide surface at a photon energy of 285.3 eV and two different orientations as indicated. Contrast is based on differences in functional group alignment between the stylus track and the virgin surface. The uniform gray outside the track corresponds to isotropic chains (106). (Data acquired with ALS PEEM-I.) Courtesy of A. Cossey-Favre.

forces that amplify structural instabilities at the film surface. Mechanical confinement offers the possibility to control these instabilities, and raises the possibility to generate unique self-assembled structures. While thin (∼50 nm) PS films confined between continuous layers of silicon oxide (SiO_x) are prevented from hole formation, aggressive annealing at temperatures well above the PS glass-transition temperature generates an in-plane microstructure (107). The formation of the microstructure is driven by the attractive dispersion force between the SiO_x–air surface. To properly model the mechanisms for this spontaneously generated lateral morphology, it is important to measure the thickness of the trapped polymer film throughout the structure. This requires a quantitative tool that can measure the thickness of the polymer inside the trilayer system. While it might be a reasonable assumption that there is almost a complete exclusion of the PS in the thin regions of the pattern, nexafs microscopy indicated ∼30% residual PS in the thinnest parts of the sample (see Fig. 12) (108). This fact can now be incorporated into models of the structure formation.

Superabsorbent Polymers: Lightly Cross-Linked Homopolymers. Third generation superabsorbent polymers (SAP) are a class of highly engineered cross-linked polymers widely used as gels in a variety of fields. SAPs are designed to simultaneously provide high fluid absorption capability, retain the fluid in a weight bearing mode with high gel strength, provide attrition resistance during manufacture, be compatible with other manufacturing materials, and remain safe for hygienic uses (109–111). SAPs are made from partially neutralized polyacrylic acid which is lightly cross-linked throughout small (<0.5 mm) beads to form an insoluble, hydrophilic gel. Several different methods have been developed for surface cross-linking SAP gels as means to improve materials properties (112,113).

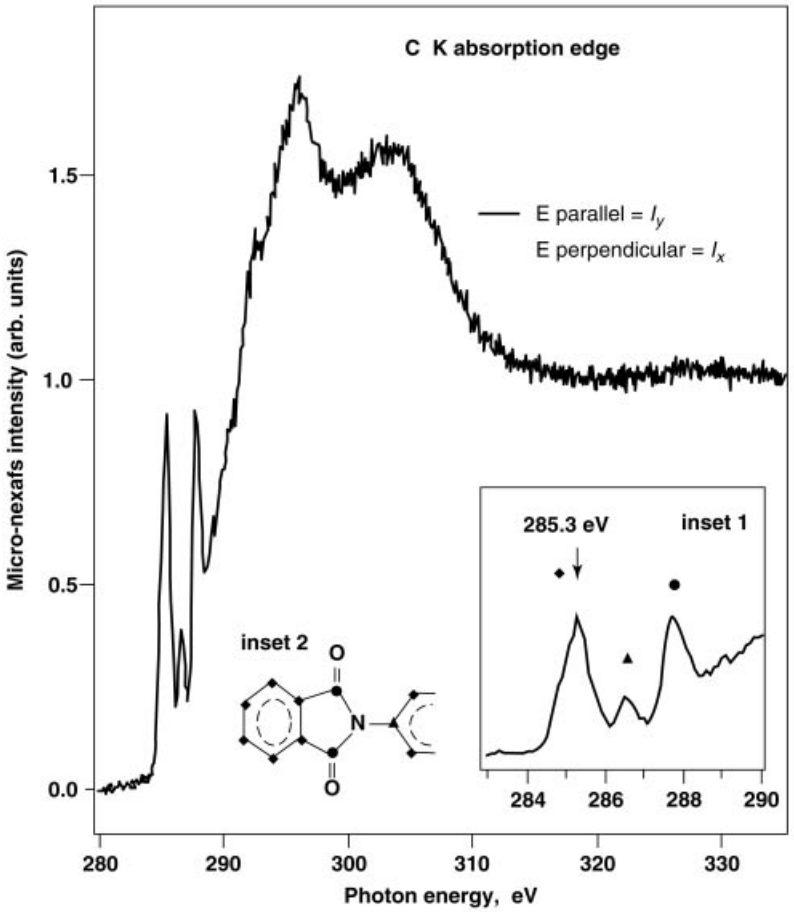

Fig. 11. Linear dichroic nexafs spectra from within the stylus track in Figure 10 at two orientations. Spectral differences are due to differences in orientation and alignment of the polymer functional groups (106). Primary peak assignment is indicated by the symbols. (Data acquired with ALS PEEM-I.) Courtesy of A. Cossey-Favre.

Until now, however, the outcome of these different surface cross-link processes, and the resulting core/shell structure and cross-link density gradient could not be directly visualized and quantitatively assessed.

Crosslinking involves the change in only a very small number of bonds and cannot be monitored directly via spectroscopic differences. A more indirect method, that nonetheless can provide quantitative cross-link density, has to be used. The swelling of SAP beads (polyacrylic acid, sodium salt) and particularly of the more highly cross-linked surface shell depends on the cross-link density of the polymer. Regions or beads with a high cross-link density will expand less in water and therefore will have a higher carbon density when examined in the swollen state. A wet cell was developed and used to characterize cross-link density in thin sections from SAP beads (102,114). NEXAFS resonances were used to provide the highest image contrast possible: The π^* spectral feature of the carboxylic acid

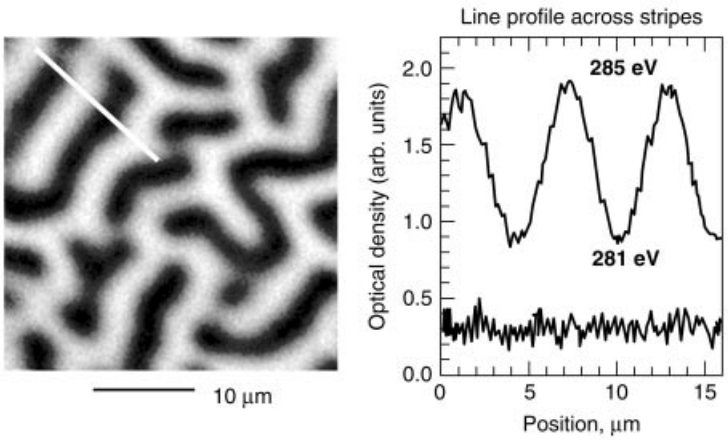

Fig. 12. Image acquired at 285.2 eV of a trilayer structure consisting of a 60-nm thick film of polystyrene (PS) coated on each side with 30 nm of SiO_x. Annealing above the glass-transition temperature of PS results in the observed morphology. Profiles that emphasize PS (top profile labeled 285 eV) and spectra show that significant amounts of PS remain in the thin regions. Note that the preabsorption edge profile at 281 eV is essentially flat. (Data acquired with the ALS BL7.0 STXM.) Courtesy of A. P. Hitchcock, McMaster University, and J. Dutcher, Guelph University.

increased the signal by a factor of 2 with respect to the core edge jump. Core/shell structures in SAP beads prepared by chemically cross-linking the surface of SAP beads were directly visualized, and variations in surface cross-link density resulting from different cross-link protocols were observed and compared on a common, quantitative cross-link density basis. Figures 13 and 14 compare the results of two different processes that resulted in a gradient and abrupt surface cross-link density profile, respectively. The direct observation of these cross-link density profiles can now be used to optimize the manufacturing and development process of these polymers.

Thin-Film Blends and Bilayers. Generally, the properties of polymer blends when they are processed into thin films are not as well understood as those of bulk polymer blends. The constraints imposed by the two close-by interfaces alter the equilibrium morphology as well as the polymer mobility and phase separation dynamics. Numerous studies (115–124) have elucidated some aspects of these effects. Interfacial energies are important since they determine thermodynamic equilibrium structures. The viscosity and diffusion near surfaces and attractive interfaces can be substantially modified (125), which will influence the dynamics, and possibly cause the formation of kinetically trapped morphologies. A number of morphologies that evolve during the phase separation process in polymer thin films have been previously observed (117–123,126). NEXAFS microscopy provides an additional tool to study such systems (100,127–129). The two primary beneficial aspects of nexafs microscopy for these applications are (*1*) quantitative mapping that can be translated into thickness profiles, and (*2*) compositional analysis of surfaces.

The first nexafs microscopy characterization of phase-separated thin-film blends was performed by two groups (127,130,131). The first group observed good

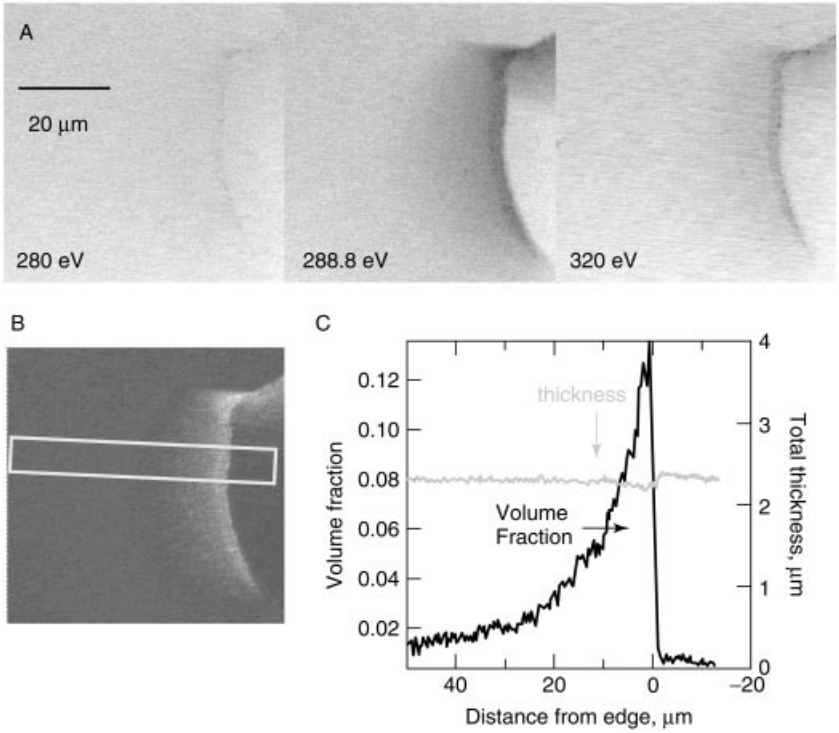

Fig. 13. (**A**) Transmission nexafs images of a saline-swollen microtomed thin section of an SAP bead that was surface cross-linked with ethylene glycol diglycidyl ether. The images were recorded at 280, 288.8, and 320 eV, as indicated; (**B**) Quantitative map of the polymer volume fraction derived via SVD from the three images; (**C**) Profiles of the polymer volume fraction and the total sample thickness (water and polymer) across the edge of the SAP bead, derived from the SVD analysis in the indicated region. (Data acquired with the ALS BL7.0 STXM.) Courtesy of G. Mitchell (102).

chemical contrast between PS and PBrS phases in phase-separating PS/PBrS blends, and made a strong suggestion that the PS encapsulates the PBrS after sufficient annealing (130,131). The second group used a peem to observe chemical surface contrast in annealed, phase-separated PS/PVME (PVME – poly(vinyl methyl ether)) and PS/SAN thin-film blends (127). Additional peem observations concluded that the formation of protrusions in the PS/PVME film are not accompanied by a total dewetting of the polymers from the Si substrate.

PS/PBrS Thin-Film Blends and Bilayers. Initial nexafs microscopy investigations explicitly exploring the time evolution and composition of domains in thin films focused on morphology formation during spin-casting and annealing of PS and PBrS blends. Emphasis was placed on elucidating the late stage morphology after annealing above the glass-transition temperature of both components for samples with different PS/PBrS composition ratios (128). Quantitative nexafs maps derived via SVD composition procedures were compared to atomic force afm topographs and complemented with secondary ion mass spectroscopy (sims) depth profiling. NEXAFS microscopy of annealed samples showed directly that the

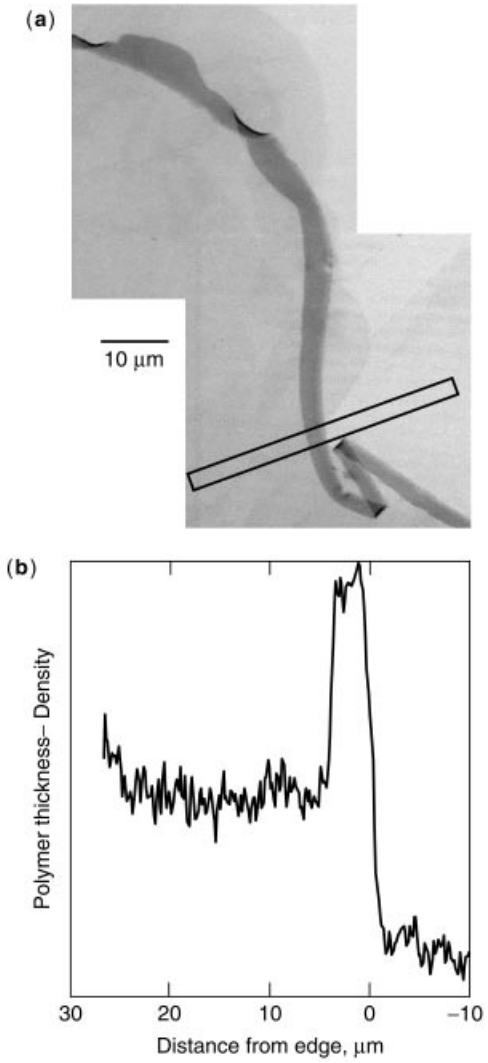

Fig. 14. (**a**) Transmission nexafs image acquired at 288.8 eV of the microstructured shell of an SAP bead surface cross-linked with glycerol. A 5-μm wide band of uniform cross-link density that is twisting back and forth can be observed; (**b**) Profile of polymer density–thickness across the edge of the cross-linked shell in the region indicated on the image. (Data acquired with the ALS BL7.0 STXM.) Courtesy of G. Mitchell (102).

morphology changes from "PS droplets" to "PS surface holes" in a continuous PBrS matrix layer as PBrS becomes the majority phase. SIMS data indicated a continuous PS layer at the substrate and the surface interface. The observed continuous PS layer for all blend compositions explained the observed "droplet" and "hole" structures formed for different PBrS fractions. Although the interfacial energy could have been minimized in the bulk if the PS formed spheroidal domains in the

PBrS-rich phases, the continuity constraint of the PS at the interfaces requires the formation of the hole morphologies at high PBrS volume fraction. From the morphologies formed, constraints for the values of the various interfacial energies could be deduced.

PEEM from surfaces can provide a much more direct and unambiguous means of showing PS encapsulation of PBrS than the combination of area averaged sims, surface afm (atomic force microscopy), and bulk stxm measurements. Direct evidence for encapsulation was observed during the dewetting of a PS/PBrS bilayer consisting of a 50-nm thick PBrS film on top of a 30-nm thick PS film (98). These investigations were the first combination of surface (peem) and quantitative bulk (stxm) characterization of a polymeric system to assess and reconstruct the 3-D morphology. As the PBrS is dewetting the PS sublayer, holes form randomly in the PBrS top layer and subsequently grow to form Veronoi tesselation patterns. These patterns consist of an interconnected network of spines that eventually break up to form droplets. The mass thickness maps of the constituent polymers PBrS and PS, as well as the total thickness maps of the bilayer annealed for 1 week, reveal that these "spines" consist of sharply delineated PBrS, which are at least partially wetted, if not encapsulated, by PS walls. PEEM studies of the same type of sample provided surface nexafs spectra from the top 10 nm of the surface from sample areas that included the spines and droplets. Since the PBrS C 1*s* to π^* characteristic spectral feature at 286 eV was not observed from any sample areas (see Fig. 15), one can conclude that the PBrS spines are completely encapsulated. The time taken for evolution (from 0 to 11 days of annealing) of the dewetting process furthermore revealed the encapsulation pathway and also allowed one to know whether polymer diffusion or viscous flow was the dominant encapsulation process: A sufficient number of holes have to form in the PBrS layer through which the PS can penetrate the PBrS film and subsequently flow along the PBrS/air and PBrS/PS interfaces.

Related studies showed that the apparent contact angle at the polymer/air interface decreases exponentially with the PS film thickness, with a constant that depend upon the radius of gyration R_g. The droplets consist of a PBrS core fully

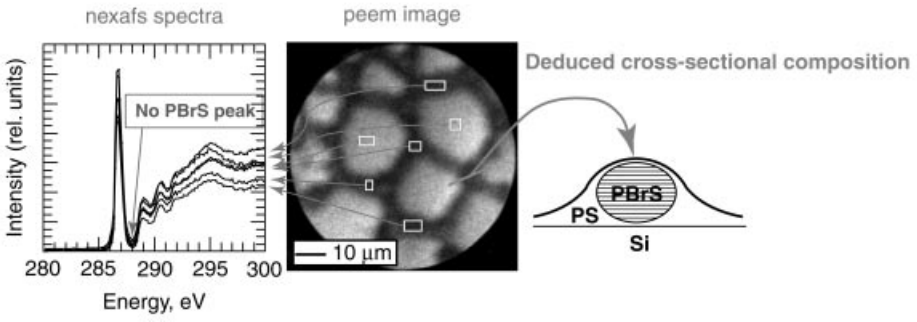

Fig. 15. PEEM images and spectra from a dewetting PBrS/PS bilayer after one week of annealing at 180°C. Spectra from the sample locations are indicated. The combination of stxm and peem characterization allowed the deduction of the 3-D morphology with certainty. (Data acquired with the ALS PEEM-I.) Adapted from Ref. 98.

encapsulated by PS for substrates thicker than R_g while only partial encapsulation is seen with nexafs for substrates with a thickness less than R_g (132).

PS/PMMA Thin-Film Blends. Another excellent model system to investigate the dynamics and the morphologies formed during phase separation in thin films are PS/PMMA blends. A variety of interesting morphologies during both the early and late stages of the phase separation process in PS/PMMA blends have been observed and characterized by a combination of quantitative nexafs mapping and lateral force microscopy (100). Films (143 nm thick) of monodisperse, 50/50 (w/w) PS/PMMA blends spun cast out of toluene solution onto Si substrates were annealed in a vacuum, quenched to room temperature, and subsequently characterized. The composition of the mixed phases resulting from solvent spin casting were determined with quantitative nexafs microscopy. After very short annealing times at 180°, a sudden rearrangement into domains smaller than those originally formed was observed. Subsequently, unique, jagged patterns formed during the early stages of coarsening. These patterns resemble turbulent hydrodynamic mass flow, although they might have an entirely different physical origin. A 50-nm thick 50/50 (w/w) blend of PS/PMMA 27K/27K film on Si annealed at 165°C, and a 50-nm thick 50/50 (w/w) blend of 90k PS and 27K PMMA on Au showed the same kind of ragged morphology, while a 50-nm layer of the 90K/27K blends on Si did not (129). Complicated polymer/polymer interface morphologies persisted in several cases even after extended annealing. These were explained by the dependence of polymer viscosity on film thickness and the constraints imposed by the substrate (100). An example is shown in Figure 16 that shows trapped PMMA spikes inside the PS droplets.

As shown by numerous studies, the initial morphologies from spin casting as well as the final morphologies after annealing depend on the substrate utilized. The dependence of PS/PMMA morphologies and phase separation dynamics on Si, Au, and Co surfaces has been investigated (129). Clearly phase-separated domains are observed on Si and Au surfaces. The morphologies on Co surfaces, however, are more complex. They have a layered appearance and do not evolve much during

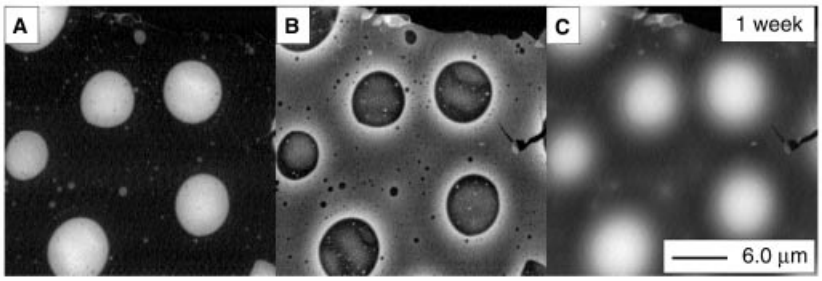

Fig. 16. Quantitative compositional maps derived via an SVD procedure of a nominally 143-nm thick 50/50 (w/w) PS/PMMA blend annealed for 1 week: (**A**) PS mass thickness, (**B**) PMMA mass thickness, and (**C**) total thickness maps, ie, PS plus PMMA maps. All images are individually scaled for good contrast, with Black = 0 and White = maximum mass-thickness. The maximum total thickness of the films increases from the initial 143 nm to 460 nm in Figure 16C due to surface roughening. (Data acquired with the Stony Brook STXM at the National Synchrotron Light Source.) Adapted from Ref. 100.

annealing, presumably because of a lack of either a PS or PMMA wetting layer on the substrate.

PS/PMMA blends spun to different film thickness onto SiO_x surfaces showed that time-temperature superposition is observed. Indirectly, this indicates that the influence of the film thickness on the dynamics is relatively small (133).

While most work on annealed PS/PMMA blends support the formation of phase-separated domains right to the surface, a recent study (134) reports that an encapsulating layer of PS-skin forms over the PMMA domains. The stxm and peem might be a good complementary tool to afm, xps, and nexafs spectroscopy to further elucidate PS/PMMA thin-film blends, their phase separation dynamics, and their surface composition (96).

PS/PMMA with PS-*b*-PMMA Copolymer Thin-Film-Blends and Bilayers. Polymer blends when processed into thin films are typically rough when produced by spin casting on a substrate and roughen even further when annealed. The surface modulation amplitudes of certain spatial frequencies might actually get much larger than the original film thickness. This is due to the phase separation between immiscible polymers, and the effect can be readily observed from Figure 16. This roughening would be a serious problem in many applications and limits the use of polymer blends as materials in ultrathin films. A common strategy to improve miscibility of polymer blends is to add copolymer compatibilizers. The compatibilizer will reduce the interfacial tension if located at the polymer/polymer interface. The tendency of the compatibilizer to form micelles in one of the phases often limits the amount of copolymer that locates at the interface. For relatively strongly segregating systems, formation of a microemulsion has never been achieved. Relying on entropy as a driving mechanism, rather than interfacial energies, it was shown that PS/PMMA thin films can be compatibilized with a PS-*b*-PMMA diblock copolymer (135). Samples of a bottom PMMA layer and a top layer of a blend of PS and 30% of a PS-*b*-PMMA diblock copolymer were annealed. When the top PS/PS-*b*-PMMA layer thickness was comparable to or less than the size of bulk micelles, the film evolves toward a stable 2-D microemulsion. The two-dimensionality of the film was established by showing with nexafs microscopy that the microemulsion phases extended throughout the thin film. It was observed (135) that the loss in configurational entropy as a result of confinement can change the micellar transition for copolymers. Mixing in thin films in the presence of block copolymers can thus be achieved independently of the specific polymer chemistry by making the films thin enough.

The dynamics of the formation of the microemulsion has been assessed (136). The initial growth of the domain size had a growth exponent of 1/3, using the inverse of the wave-vector with maximum amplitude q_{max} derived from Fourier transform analysis as the measure of the domain size. At long annealing times, domain growth slowed dramatically as the block copolymer was forced to the interface, lowering the interfacial energy and thus reducing the driving force for further phase separation. NEXAFS microscopy of the microemulsion thin films that had the PS preferentially washed with cyclohexane revealed directly that the PS-*b*-PMMA diblock copolymer is located at the PS/PMMA interface (see Fig. 17).

Polystyrene/Poly(*n*-butyl methacrylate) Thin-Film Blends. The morphology of polystyrene/poly(*n*-butyl methacrylate) (PS/PnBMA) thin-film blends, and whether encapsulation occurs in this system has been assessed by using SFM,

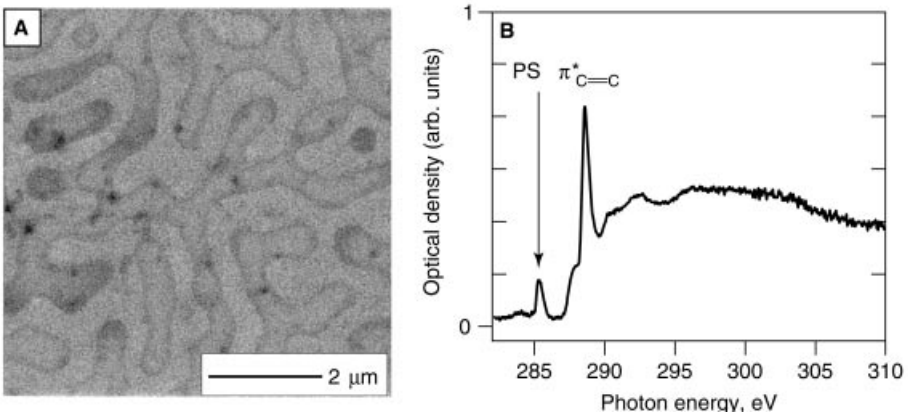

Fig. 17. (**A**) PS $\pi^*_{C=C}$ image acquired at 285.3 eV from a 168-h annealed PS/PMMA/PS-*b*-PMMA microemulsion thin film washed with cyclohexane to remove all PS. At this photon energy, only the aromatic content of styrene will appear dark. Enhanced absorption, although at low contrast, can be detected at the domain interfaces that directly shows that the highest PS-*b*-PMMA block copolymer concentration is located at the PS/PMMA domain interface; (**B**) The nexafs spectrum acquired from 10 μm^2 area of this sample. The PS and PMMA intensities reveal that cyclohexane washing is removing essentially all PS. The remnant 285 eV signal is consistent with expected signal from the PS-*b*-PMMA block copolymer. (Data acquired with the Stony Brook STXM.)

txm, and peem (137). The same droplet-to-hole transition found in the earlier studies by Slep and co-workers (128) with PS/PBrS blends as a function of composition was observed in the PS/PnBMA blends. This strongly suggests that one of the two polymers preferentially segregates to both the substrate and air interface. Investigations of the PS/PnBMA thin films with peem were indeed interpreted to have preferential PnBMA segregation to the surface. Based on the surface composition and morphology observation, one would expect PnBMA to also segregate to the substrate, although no direct measurement regarding preferential segregation to the substrate has been made (137).

Block Copolymer Thin Films. NEXAFS microscopy is also a tool that can provide complementary and unique information for block copolymer organization, which traditionally has been investigated using a wide variety of analytical techniques, including electron microscopy, x-ray scattering, and optical microscopy. These traditional techniques yield considerable information about the morphology and organization of block copolymer materials, but occasionally the information provided is incomplete and provides only "circumstantial" evidence for a conclusion. For example, the novel molecular organization of a high molecular weight rod-coil block copolymer has been investigated (138). This block copolymer has a PS coil block of 9K molecular weight and a main-chain poly(hexyl isocyanate) (PHIC) rod block of 245K molecular weight. Homopolymer PHIC is known to behave as a lyotropic nematic liquid crystal in a wide range of solvents with a persistence length of 50–60 nm. Rotational motion along the backbone of the PHIC is limited by short-range interactions, leading to inherent chain stiffness. The PS behaves as a typical coil polymer with a low persistence length. Combined as a block copolymer, there is competition between the microphase separation of the

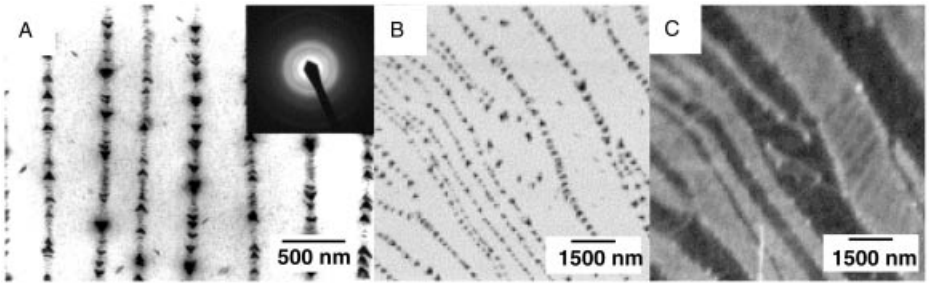

Fig. 18. (**A**) tem image of PS-*b*-PHIC diblock copolymer and small area electron diffraction pattern averaged over several lamellae; (**B**) nexafs image at 285.2 eV (PS dark); and (**C**) nexafs image at 288.5 eV, where the PHIC layers have altering contrast because of differences in orientation. (Data acquired with the Stony Brook STXM.) Courtesy of C. Zimba, NIST, and E. Thomas, MIT.

PS and PHIC blocks into periodic structures and the tendency of the PHIC block to form anisotropically ordered structures, giving rise to new morphologies. A typical tem image from solution cast thin films is shown in Figure 18A and clearly shows a microphase-separated morphology with long-range order over tens of microns. The PS domains, stained with RuO_4, appear as dark regions shaped somewhat like arrowheads while the PHIC regions appear as largely featureless light regions between rows of PS domains. An interesting feature in this image is the orientation of the PS arrowheads which changes direction between adjacent PS-rich layers. On account of radiation damage, the small area electron diffraction (SAED) pattern had to be obtained from a sample area of 10–20 lamellae. The SAED pattern (inset of Fig. 18A) shows a superposition of two distinct single crystal-like PHIC patterns rotated relative to each other by approximately 90°, indicating that the PHIC chain axis alternates between +45° and −45° with respect to the geometric normal of the lamellae layers. While the evidence for the alternating 45° PHIC oriented layers is quite strong, it is only indirect, and the orientation could not be observed directly with tem.

To directly investigate the orientation of the PHIC lamella, thin film samples cast from 0.05% solutions in toluene onto uncoated tem grids were examined with nexafs microscopy (139). Using an x-ray energy corresponding to the phenyl carbon resonance of the PS (285.2 eV), nexafs imaging clearly shows a similar arrowhead morphology as the tem image, albeit at lower spatial resolution (see Fig. 18B). At the carbonyl resonance of the PHIC at 288.5 eV, nexafs images reveal the structure of the PHIC layers in ways not available with tem (Fig. 18C). The PHIC domains appear as layers of alternating intensity separated by the PS domains that appear as white pearls. The intensity variation of the PHIC layers arises from differences in dichroic absorbance of the polarized synchrotron radiation because of orientation of the carbonyl moiety, and thus also the backbone, of the PHIC. In contrast to the average SAED pattern, the nexafs image is able to give detailed information about the orientation of individual PHIC domains. NEXAFS microscopy furthermore reveals previously unsuspected microstructure within the PHIC domains that are clearly not entirely homogeneous, but show striations in a direction across the lamellae.

Multicomponent, Multiphasic Polymers

Many polymeric materials of academic and industrial interest are multicomponent polymers that have multiple phases in the bulk. Control over the composition and size distribution of the domains and their interface properties is often very important in determining the materials properties. A variety of blends and multiphasic polymers have already been investigated with nexafs microscopy. These include studies of

(1) the morphology of PET/PC (140), low density PE/PET/Kraton (141), and PC/(acrylonitrile butadiene styrene) blends (141,142), and macrophase-separated random block copolymer/homopolymer blends (143);
(2) the morphology and composition of mechanically alloyed PET/poly (oxybenzoate-*r*-oxynaphthoate) [Vectra (Celanese Corp.)] blends (144), mechanically alloyed and rubber-toughened PMMA (145), mechanically alloyed poly(ethylene-*alt*-propylene) (PEP)/PMMA and PI/PMMA blends (146–150), and the assessment of recycling of tires by mechanical alloying (151);
(3) the characterization of phase separation during processing, such as the formation of precipitates in polyurethanes (13,19,152) and multiphase liquid crystalline polyesters (141);
(4) single- and multistep synthesized latexes and structured microspheres (153–155); and
(5) various multilayers (156,157).

Included here as examples is a discussion of the characterization of PET/Vectra blends, blends produced by cryogenic mechanical alloying, various polyurethane polymers, multilayers and structured spheres, as well as rubber composites. The discussion of the PET/Vectra blends is particularly instructive, as this study combined chemical and orientational analysis.

NEXAFS Microscopy of Mechanically Alloyed Blends. Mechanical alloying of polymers has the potential of becoming an alternative, novel means of producing and recycling polymer blends (144,146–148,150,151,158). The efficacy of such a new method is best assessed by direct visualization of the morphology of the generated materials.

Since incorporation of liquid crystalline polymers (LCPs) into commodity thermoplastic polymers remains an ongoing challenge in the design of new high performance, low cost polymeric blends, the feasibility of blending of PET and Vectra A950 [73/27 (mol/mol) oxybenzoate/2,6-oxynaphthoate] with mechanical alloying was investigated (144). The morphology and composition of dispersions in PET and Vectra blends are difficult to assess with conventional microscopies, because of a lack of staining agents for electron microscopy, and spatial resolution limitations of optical and ir microscopy. Despite the presence of similar functional groups in each polymer, such as aromatic and carbonyl groups, nexafs microscopy can readily delineate the morphology. After mechanical alloying, the resulting powders were melt-pressed at 285°C (above the melting points of PET and Vectra) for 5 min and cryomicrotomed at −100°C to obtain sufficiently thin sections for nexafs microscopy. Melt-pressed films of PET/Vectra alloyed blends

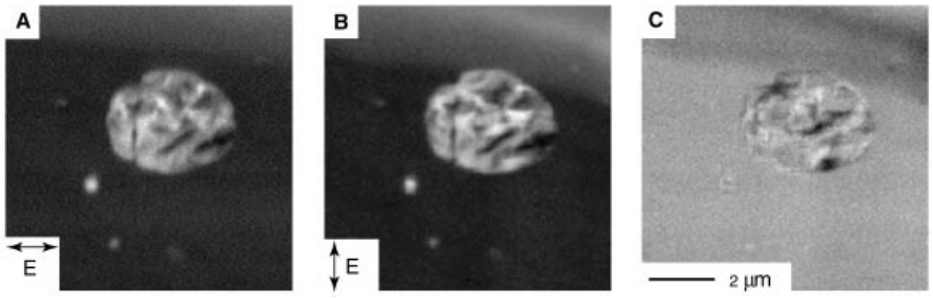

Fig. 19. NEXAFS images acquired at 286.7 eV of a 99/1 (w/w) PET/Vectra blend subjected to post-milling melt pressing. Images (**A**) and (**B**) have been converted to optical density. In images (**A**) and (**B**), the electric polarization vector $\vec{E}$ is rotated by 90° with respect to each other, as indicated. Changes in the relative intensity in these images are primarily due to anisotropic molecular orientation. The ratio of these images (**C**) reveals the linear dichroism of the specimen. Small Vectra domains appear gray and possess no discernible orientation, whereas the large dispersion exhibits a measurable degree of molecular orientation (black and white areas) because of the nematic nature of this liquid crystalline polymer. (Data acquired with the Stony Brook STXM.) Reproduced from Ref. 144.

varying in composition from 75/25 to 99/1 by weight percent were investigated. The frequency and size of the Vectra dispersions increased with increasing Vectra concentration (144). The distribution in size ranged from 100 nm to about 20 μm in diameter. The presence of these small, 100-nm Vectra domains demonstrated that mechanical alloying is capable of pulverizing Vectra. The PET/Vectra blends retained much of the initial degree of mixing during post-processing in the molten state. Point nexafs spectroscopy showed that the Vectra domains contained little, if any PET. Molecular orientation in the Vectra domains was characterized with linear dichroism microscopy. Figure 19 shows x-ray micrographs of the 99/1 (w/w) PET/Vectra blends acquired at 286.7 eV. The image contrast between Vectra dispersions and the PET matrix is based on differences in the nexafs spectra of the two polymers (see Fig. 2). Some of the contrast within the larger Vectra domains arises from molecular orientation and thickness variations. The dichroic ratio image (Fig. 19C), derived from the two orientations displayed in Figures 19A and 19B, cancels thickness and compositional effects: anisotropic orientation inside Vectra domains was only observable in domains larger than about 2 μm.

Other blends produced by mechanical alloying and investigated with nexafs microscopy included blends of poly(ethylene-*alt*-propylene) (PEP), polyisoprene (PI), and PMMA (146–150). PI can be readily differentiated from PMMA with electron microscopy by heavy metal staining of the PI, but PEP and PMMA cannot be differentiated. In the blends investigated, intimate mixing at the nanoscale was accomplished. Since mechanical alloying is a highly nonequilibrium, high energy method with effects that resemble those of high energy radiation (159), it seems likely that bonds are breaking, and radicals, and maybe even new bonds in new chemical configuration, are forming during alloying. It is the detection of these chemical modifications where nexafs microscopy might be particularly useful. However, the extent of any chemical changes occurring has been below the sensitivity limit of nexafs microscopy.

In the PEP/PMMA blends an anomalous phase inversion was observed (148). Phase inversion in polymer blends is typically encountered under conditions of melt flow. However, the unexpected phase inversion occurred upon quiescent annealing in an asymmetric blend of PMMA and PEP prepared by cryogenic mechanical alloying, where there is very little flow. For short milling times, consolidation of the cryomilled powders at temperatures above the glass-transition temperature of PMMA exhibited dispersions of PEP in 75/25 (w/w) PMMA/PEP blends. However, as the milling time increased to 10 h, the consistency of the blends changed from rigid to pliable. nexafs microscopy revealed that for the long milling times the PMMA becomes the dispersed phase upon consolidation, and it directly confirmed that phase inversion occurs during consolidation. The transition from PEP dispersions to a continuous PEP phase as observed with nexafs microscopy is shown in Figure 20.

The strategy of producing highly dispersed blends of thermoplastics and tires was also investigated in an effort to provide a potentially new route by which to recycle discarded tires (151). NEXAFS microscopy showed that cryogenic mechanically alloyed tires can be dispersed in PET and PMMA matrices with submicron domains. The tire and thermoplastic did not appear to interact chemically. For the milling conditions employed, there was also no significant chemical interaction between constituent polymers in PI/tire/PMMA ternary blends. Based on the ability to produce good dispersion of the tire material, the results indicated that

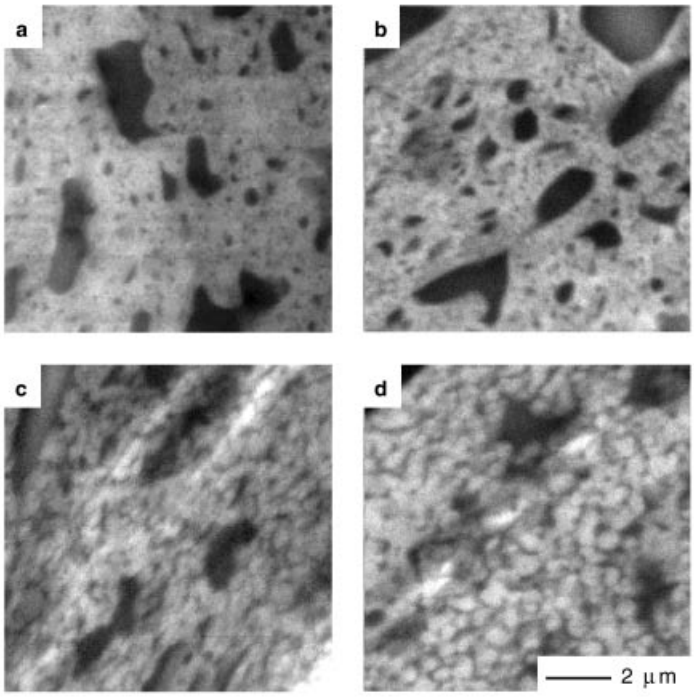

Fig. 20. NEXAFS images at 288 eV (PEP appears dark) of a 25/75 PEP/PMMA blend cryomilled for 10 h and annealed at 150°C for different times (in min): (**a**) 1, (**b**) 2, (**c**) 5, and (**d**) 30. (Data acquired with the Stony Brook STXM.) Adapted from Ref. 148.

cryogenic mechanical alloying constitutes a viable alternative for recycling elastomeric materials.

Engineered Polyurethane and Polyurea Polymers. Polyurethane polymers constitute a versatile class of engineered polymers of great economic value. Despite the ubiquitous utilization and considerable past research, several fundamental aspects of these polymers are not well understood because of the complex chemical reactions and physical processes during production. Over the past few years it has become clear that x-ray spectromicroscopy can uniquely address some complex issues in polyurethane research (19,66,160–163).

The urea distribution in polyurethanes is presumed to have a major influence on the mechanical properties of polyurethane foam (modulus, compression set, load bearing, etc), yet relatively little is known beyond the average size and nanoscale distribution of the so-called hard-segment urea as measured with x-ray and neutron scattering techniques. The mesoscale hard-segment urea distribution in polyurethane materials might be connected to physical properties and is strongly influenced by the relative amounts of urea and carbamate (urethane) present, which in turn is closely linked to formulation and processing. The urea/urethane ratio and its distribution through the material is thus an important quantity. In certain formulations, macrophase separation occurs. Using polymer reference standards with known chemical composition, the spectral signal corresponding to the urea and urethane components (typically only $\sim$20% in systems of interest) can be isolated and quantified (18,19). Based on similar quantitation, the composition and sharpness of precipitates in two high water TDI polyurethane plaques made with different polyols have been assessed at the submicron level (164). The precipitates in both materials were highly enriched in urea. One of the materials had a fuzzy interface to the polyether-rich matrix, while the second material had a more sharply delineated interface. The fuzzy precipitates were more isolated, while the sharper "precipitates" appear to have formed a network of urea-rich domains. These observations will lead to an improved understanding of structure–property–processing relationships in polyurethane polymers.

Another key parameter influencing physical properties in polyurethane foams is the distribution of additive or modifier phases. These modifier phases are typically smaller than a few microns in size. Two compositionally different, common modifier particles, polyurethane-rich, polyisocyanate polyaddition (PIPA) based and styrene-acrylonitrile (SAN) based particles, were dispersed in a TDI-based, polyether-rich polyurethane matrix. Both particles have the same contrast in tem and cannot be distinguished. In contrast, nexafs micrographs of this material show clear differences: at 285 eV, both types of particles are dark dispersions, while at 287 eV, only the SAN particles are highly absorbing relative to the matrix. The uniformity of their composition and the size distribution could thus be determined (165). Discrimination between the two types of particles has also been achieved at the nitrogen absorption edge and, to a lesser extent, the oxygen edge. The chemical composition of the largest SAN particles was found to be independent of particle size. It was furthermore determined that the SAN particles contain about 12 wt% polyether.

Structured walls of complex capsules based on polyurea chemistry have been investigated (166). Polymer capsules are frequently used to encapsulate other chemicals for a variety of purposes, including controlled release of drugs, nutrients,

or pesticides. In these applications, the structure and composition of the capsule wall is of paramount importance. The capsules investigated were produced by a polymerization reaction between amine- and isocyanate-based chemicals at the interface of organic and aqueous phases. In addition to the amine–isocyanate reaction that produces an asymmetric aromatic urea, a competing reaction between the isocyanate and water produces a symmetric diaromatic urea. These competing reactions can lead to the formation of compositional gradients in the submicrometer thick capsule wall. Figure 21 shows reference spectra of model urea compounds, compositional maps, and line profiles of two capsule walls produced by different protocols. The asymmetry of the urea and diurea functionalities can be clearly observed. Comparison of these compositional profiles with diffusion and reaction kinetics will allow the detailed modeling of the capsule wall formation.

Multilayers and Structured Spheres. Multilayer structures are used extensively in photographic applications, such as optical and x-ray photography and xerographic processes, as well as in packaging materials. Several such materials were so far investigated with nexafs microscopy.

The degree of spatial uniformity of a nitrogen containing charge transfer compound present in a protective polycarbonate (PC) capping layer above the image sensing layer of a test photoconductive thin-film structure from Xerox Research Center of Canada has been determined with nexafs microscopy. A simple, 5-min measurement consisting of an image at 407 eV of the film and a nitrogen 1*s* linescan energy sequence showed that the ($\sim$10%) nitrogen content of the PC layer was distributed throughout the PC layer with a relatively uniform ($\pm$20%) distribution, but with some gradient in density toward the exterior of the thin film. By comparison, it was barely possible to detect any nitrogen, and thus impossible to analyze the spatial distribution of the charge transfer component, by either energy loss or x-ray fluorescence spectroscopy in a state-of-the-art JEOL 2010 analytical tem (168).

Several multilayer polymer films used in photography have been characterized with nexafs microscopy. In one structure, consisting of four layers of 0.7–3 μm in thickness coated on a base layer, nexafs images clearly showed each of the layers. The nexafs spectra from closely spaced points showed no significant interpenetration between two layers of interest, poly(styrene acrylonitrile) and a porous carbon black (156). The nexafs microscopy of another laminate consisting of nine layers on a base layer revealed a microstructure of undetermined origin dispersed throughout the fourth layer (169,170). The domains of these microstructures are elongated in the direction parallel to the layer boundary. This microstructure is not observed in the tem, and is likely due to a compositional microphase separation or a preferential orientation of the aromatic groups present in some of the compounds.

A commercially available multilayer used as food container provided a suitable test structure for nexafs microscopy, particularly since this multilayer had been previously characterized with ir microscopy. Because of the spatial resolution limitations of ir microscopy, a special procedure had to be used to analyze the thinnest of the nine layers, about 4 μm thick. The objective of an x-ray microscopy study of this multilayer was to further elucidate the chemical composition of the thinnest layers within the sample, and to provide a basic comparison between ir and nexafs microscopy (157). NEXAFS microscopy could acquire spectra from all

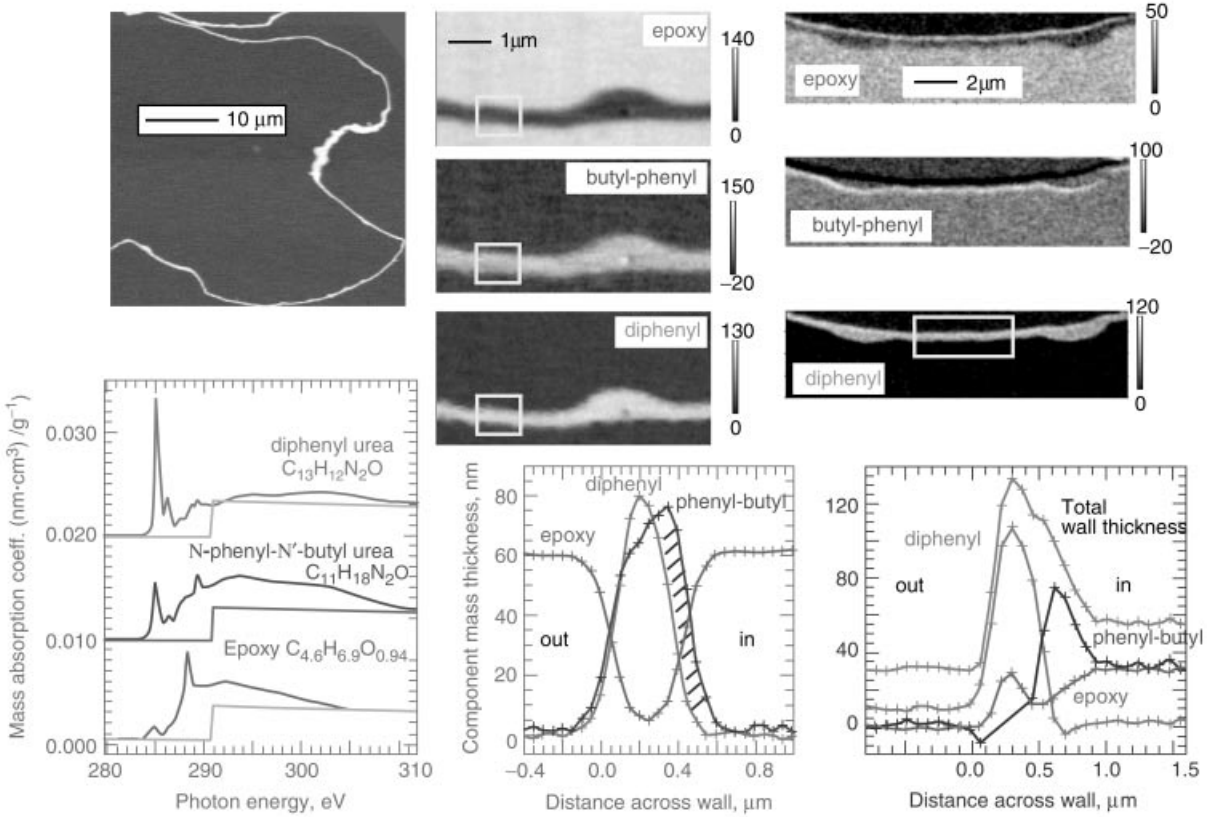

Fig. 21. NEXAFS characterization of polyurea capsules. The upper left shows a low resolution image acquired at 285 eV of a microtomed section containing a nearly complete capsule embedded in epoxy. The lower right shows the C 1*s* spectra of the epoxy, butylphenylurea (asymmetric model) and diphenylurea (symmetric model). The center panel displays (top) component maps derived from image sequences and (bottom) average line profiles of each component across the capsule wall in the indicated region. The right panel shows the corresponding signals for a capsule wall prepared with a longer emulsification step. This process leads to a thick outer skin of symmetric urea. (Data acquired with the ALS BL 7.0 STXM.) Courtesy of A. P. Hitchcock. Adapted from Ref. 166 and 167.

layers without interference from adjacent layers. It established that several of the thin layers had virtually the same composition, a result not obtained from the ir measurements. Unfortunately, the present lack of a comprehensive and accurate nexafs spectroscopy database of polymers prevented the positive identification of some of the layers.

Structured polymer microspheres are attractive for a wide number of applications, including biomedical devices and controlled release reservoirs. Particular morphologies desired for different applications require control over internal porosity and core–shell structures. In order to optimize the internal or core–shell morphologies of such composite materials for particular applications, quantitative compositional analysis is often required. Structured latex spheres have first been analyzed using nexafs microscopy (153). More recently, core–shell microspheres have been investigated (155). In the latter experiment, a two-step precipitation polymerization resulted in 3.2 μm polydivinylbenzene-55 (DVB55) cores coated with $\sim$0.4–0.9 μm wide shells composed of poly(DVB55-*co*-EDMA), a copolymer of DVB55 and ethylene glycol dimethylacrylate (EDMA). Singular value decomposition of images recorded at selected photon energies yielded quantitative maps of the DVB55 and EDMA components. The EDMA concentration in the shell as determined by nexafs microscopy was in good agreement with that predicted from the comonomer composition. It was shown that the precision of compositional quantitation is adequate to be useful in guiding the development of structured polymeric systems for particular applications.

Elastomeric Composites. Blends and composites based on styrene–butadiene rubber (SBR) and butadiene rubber (BR) are widely used throughout the rubber industry in order to get a balance of properties that cannot be achieved through the use of a single elastomer. Typically blends are formed using immiscible elastomers. The vast majority of these blends are heterogeneous on some length scale (171,172), and their mechanical properties are determined, in part, by their phase morphology. Many blends are further complicated by the addition of both fillers and curatives. In addition to determining the polymer phase structure itself, it is desirable to determine the distribution of fillers and curatives in each of the elastomer phases.

Most present automobile and truck tires are made from SBR and BR mixtures. These application requirements are severe and tires are constantly being improved. For example, poly(isobutylene-*co*-4-bromomethylstyrene) can be blended with highly unsaturated general-purpose rubbers to impart unique barrier or dynamic properties and enhanced oxidative stability. The final properties of such a blend are the result of a complex series of compounding, mixing, and curing stages. These stages profoundly impact the homogeneity of the mixed components, which include the polymers, the filler, and the curatives. The characterization of the phase morphology of blends of commercial rubbers like polybutadiene (PB), polyisoprene (PI), poly(butadiene-*co*-styrene), and brominated poly(isobutylene-*co*-4-methylstyrene) (BIMS) continues to represent a problem for conventional techniques, especially in the case of filled rubbers. The utility of nexafs microscopy for these applications have thus been explored and it was found that the phase morphology of various blends and the distribution of silica and carbon black fillers can be determined based on spectroscopic differences (173). However, the size of most filler particles is still below the present spatial resolution of nexafs microscopy.

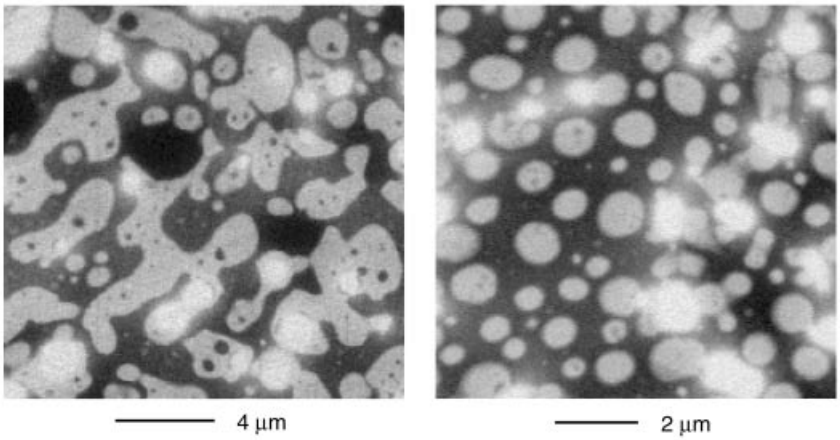

Fig. 22. NEXAFS micrographs of (**A**) d-PB/BIMS-1 [50/50 (w/w)] and (**B**) d-PB/BIMS-1/hSBR [45/45/10 (w/w)] blend supported by a Si_3N_4 membrane. The film was annealed in a vacuum oven for 18 h at 150°C. The dark areas correspond to the dPB phase. (Data acquired with the Stony Brook STXM.) Adapted from Ref. 174.

These kinds of applications will greatly benefit from future technical advances and improvements in spatial resolution.

Similar elastomer blends were also studied (174). The interfacial properties of PB and BIMS blends were determined with a variety of tools including neutron scattering and microscopy. The interfacial width decreased with increasing bromine functionality. The effects of a styrene butadiene random copolymer (SBR) on the miscibility were also investigated. The results show that SBR enhances the compatibilization of the PD/BIMS blends. NEXAFS micrographs of annealed PB/BIMS and PB/BIMS/SBR blends are shown in Figure 22. The smaller BIMS domains in the PB/BIMS/SBR blends indicate that SBR indeed compatibilizes PB/BIMS blends, which is consistent with the observations and conclusions drawn from neutron reflectivity and afm measurements. The effects of carbon black and silica on the interfacial properties of PB/BIMS blends have been investigated with neutron reflectivity, ultra-small angle neutron scattering, spm, and nexafs microscopy (175).

Fibers

NEXAFS microscopy is also well suited to study the composition and structure of fibers. The qualitative orientation of functional groups in poly(*p*-phenylene terephthalamide) [Kevlar (DuPont)] fibers has been investigated and it was found that aromatic groups are, on average, pointing radially outwards (176). Subsequently, the relative quantitative orientational order was characterized in three different grades of Kevlar fibers and it was found that Kevlar 149 is 2.3 and 1.6 times as radially orientated as Kevlar 29 and Kevlar 49, respectively (177). This variation in orientation is relatively large, given that the crystallinity of all fiber grades is above 85%. More recent work on these fibers combined absorption spectroscopy at the carbon, nitrogen, and oxygen edges. This combination, in conjunction with

theoretical calculations, can estimate the absolute degree of radial orientation in these fibers. Preliminary analysis indicated that Kevlar 149 is about 50% radially orientated (178,179).

NEXAFS microscopy has been used to study the effect of heat treatment on polyacrylonitrile fibers (180). In heat-treated fibers, a clear core-rim structure was observed in images at several photon energies. A decrease in the nitrile group concentration was measured in the core of these fibers when compared to the untreated fibers.

Conclusion and Future Outlook

NEXAFS microscopy has moved well beyond proof-of-principle experiments and has evolved into a tool that has been used in a variety of polymer science and technology projects. It is particularly noteworthy to remark that numerous industrial partners have participated over the last few years in nexafs microscopy experiments. Some of these industrial experiments performed, some with high industry internal impact, will remain unpublished, because of proprietary concerns.

While nexafs microscopy capabilities are continually improving, the field has not yet reached any fundamental performance limits. For example, the far-field wavelength-limited spatial resolution for zone-plate-based microscopes is about 3 nm for carbon K-edge energies, about an order of magnitude better than the resolution presently achieved. Similarly, several aberration corrected peem's with a projected spatial resolution of about 2 nm are planned or under construction (80,81), while the best peem's to date have a spatial resolution of 20 nm. Significant technical challenges have to be overcome for both peem and, in particular, zone-plate-based microscopes to achieve these substantial improvements in spatial resolution. Nonetheless, improvements and further technological developments can be confidently anticipated in the next few years.

Several new operating modalities such as tomography (181,182), cryomicroscopy (103,182), and dark-field microscopy (183) have already been implemented in transmission. Because of their limited routine availability, they have not been discussed in detail in this review. These operating modes should prove very beneficial for certain applications in polymer science and technology. In particular, the radiation dose will have to increase as the spatial resolution improves. This might evolve into a relatively serious issue for the study of the more sensitive polymeric materials. Procedural improvements, more efficient detector development, and use of cryomicroscopy might have to be used extensively to minimize damage.

Applications beyond those possible today might be enabled through the use of higher energy resolution that reveals subtle spectral features. Studies on PS and deuterated PS have shown, for example, that nexafs of polymers can be sensitive to vibrations (3). This might serve as an additional contrast mechanism in several applications. The establishment of a nexafs spectroscopy database similar to the spectroscopy database available in the ir community would greatly facilitate quantitation and analysis of materials for which prior knowledge is very limited. In parallel to the development of a spectroscopic database, improved theoretical modeling would expand the ability to interpret nexafs spectra and the chemical structural information that they provide.

Improved and more dedicated facilities are about to be commissioned at the ALS in Berkeley and BESSY-II in Berlin, and are under development at the Canadian Light Source in Saskatoon. While there remain many scientific questions that can be addressed with the present performance of existing nexafs microscopes, improved capabilities and the increasing availability of nexafs microscopy will result in significant growth of applications in polymer science and related fields.

Based on the progress made to date and the improvements that can still be achieved, we are confidently looking forward to continuing growth of the nexafs spectroscopy and microscopy community and to exciting applications that have not yet been conceived.

BIBLIOGRAPHY

1. H. Ade and S. Urquhart, in T. K. Sham, eds., *Chemical Applications of Synchrotron Radiation*, World Scientific Publishing, Singapore, 2002.
2. S. G. Urquhart and H. Ade, *J. Phys. Chem. B* in press.
3. S. G. Urquhart and co-workers, *Chem. Phys. Lett.* **322**, 412 (2000).
4. P. S. Bagus and co-workers, *Chem. Phys. Lett.* **248**, 129 (1996).
5. K. Weiss, P. S. Bagus, and C. Wöll, *J. Chem. Phys.* **111**, 6834 (1999).
6. A. Schöll, R. Fink, E. Umbach, G. Mitchell, S. G. Urquhart, and H. Ade, submitted.
7. T. Ohta, and co-workers, *Phys. Scr.* **41**, 150 (1990).
8. K. Seki and co-workers, *Phys. Scr.* **41**, 172 (1990).
9. J. Stöhr, *NEXAFS Spectroscopy*, Springer-Verlag, Berlin, 1992.
10. J. Kikuma and B. P. Tonner, *J. Electron Spectrocs. Relat. Phenom.* **82**, 53 (1996).
11. W. E. S. Unger and co-workers, *Fresenius' J. Anal. Chem.* **358**, 89 (1997).
12. H. Ade, in J. A. R. Samson and D. L. Ederer, eds., *Experimental Methods in the Physical Science*, Vol. **32**, Academic Press, New York, 1998, p. 225.
13. H. Ade, *Trends Polym. Sci.* **5**, 58 (1997).
14. H. Ade and co-workers, *J. Electron Spectrosc. Relat. Phenom.* **84**, 53 (1997).
15. J.-H. Guo and co-workers, *J. Chem. Phys.* **108**, 5990 (1998).
16. T. Yokoyama, and co-workers, *Phys. Scr.* **41**, 189 (1990).
17. D. G. J. Sutherland and co-workers, *Appl. Phys. Lett.* **68**, 2046 (1996).
18. S. G. Urquhart and co-workers, *J. Phys. Chem. B* **103**, 4603 (1999).
19. S. G. Urquhart and co-workers, *J. Electron Spectrosc. Relat. Phenom.* **100**, 119 (1999).
20. T. Gross and co-workers, *Polymer* **35**, 5590 (1994).
21. M. Keil and co-workers, *Appl. Surf. Sci.* **125**, 273 (1998).
22. M. C. K. Tinone and co-workers, *J. Chem. Phys.* **100**, 5988 (1994).
23. M. C. K. Tinone and co-workers, *Appl. Surf. Sci.* **80**, 89 (1994).
24. X. Zhang and co-workers, *J. Vac. Sci. Technol., B* **13**, 1477 (1995).
25. T. Coffey, S. G. Urquhart, and H. Ade, *J. Electron Spectrosc. Relat. Phenom.* **122**, 65 (2002).
26. I. Koprinarov and co-workers, *Polymer* **38**, 2005 (1997).
27. A. Lippitz and co-workers, *Polymer* **37**, 3157 (1996).
28. Y. Liu and co-workers, *Macromolecules* **30**, 7768 (1997).
29. J. Stöhr and co-workers, *Macromolecules* **31**, 1942 (1998).
30. J. Stöhr and M. G. Samant, *J. Electron Spectrosc. Relat. Phenom.* **99**, 189 (1999).
31. M. G. Samant and co-workers, *Macromolecules* **29**, 8334 (1996).
32. K. Weiss and co-workers, *Macromolecules* **31**, 1930 (1998).
33. K. Weiss, C. Wöll, and D. Johannsmann, *J. Chem. Phys.* **113**, 11297 (2000).
34. I. Mori and co-workers, *J. Electron Spectrosc. Relat. Phenom.* **78**, 371 (1996).

35. J. Genzer and co-workers, *Mater. Res. Soc. Symp. Proc.* **524**, 365 (1998).
36. J. Genzer and co-workers, *Macromolecules* **33**, 1882 (2000).
37. J. Genzer and co-workers, *Langmuir* **16**, 1993 (2000).
38. J. Genzer and co-workers, *Macromolecules* **33**, 6068 (2000).
39. M. L. Xiang and co-workers, *Macromolecules* **33**, 6106 (2000).
40. S. M. Kirtley and co-workers, *Fuel* **72**, 133 (1993).
41. O. C. Mullins and co-workers, *Appl. Spectrocs.* **47**, 1268 (1993).
42. S. Mitra-Kirtley and co-workers, *Energy Fuels* **7**, 1128 (1993).
43. S. Furukawa and T. K., *Solid State Commun.* **87**, 931 (1993).
44. K. Seki and co-workers, *J. Electron Spectrosc. Relat. Phenom.* **78**, 403 (1996).
45. V. R. McCrary and co-workers, *J. Chem. Phys.* **88**, 5925 (1988).
46. J. Stöhr and co-workers, *Phys. Rev. B* **36**, 2976 (1987).
47. H. Ågren and co-workers, *Phys. Rev. B* **51**, 17848 (1995).
48. D. G. Castner and co-workers, *Langmuir* **9**, 537 (1993).
49. K. Nagayama and co-workers, *J. Electron Spectrosc. Relat. Phenom.* **78**, 375 (1996).
50. C. Ziegler and co-workers, *Langmuir* **10**, 4399 (1994).
51. A. Lippitz and co-workers, *Polymer* **37**, 3151 (1996).
52. I. Ouchi and co-workers, *J. Electron Spectrosc. Relat. Phenom.* **78**, 363 (1996).
53. T. Okajima and co-workers, *J. Phys. Chem. A* **102**, 7093 (1998).
54. X. Q. Yang and co-workers, *Synth. Met.* **28**, C329 (1989).
55. G. Appel and co-workers, *Chem. Phys. Lett.* **313**, 411 (1999).
56. A. P. Hitchcock, *Phys. Scr. T* **31**, 159 (1990).
57. P. Rez, in Ref. 62, p. 107.
58. J. Fink and co-workers, *Phys. Rev. B* **34**, 1101 (1986).
59. J. Fink and co-workers, *Synth. Met.* **18**, 163 (1987).
60. J. J. Ritsko and co-workers, *J. Chem. Phys.* **69**, 3931 (1978).
61. J. J. Ritsko and R. W. Bigelow, *J. Chem. Phys.* **69**, 4162 (1978).
62. M. M. Disko, C. C. Ahn, and B. Fultz, eds., *Transmission Electron Energy Loss Spectrometry in Materials Science Minerals*, Metals and Materials Society, Warrendale, Pa. 1992.
63. R. F. Egerton, *Electron Energy Loss Spectroscopy in the Electron Microscope*, Plenum Press, New York, 1986.
64. D. A. Muller and co-workers, *Nature* **366**, 725 (1993).
65. F. P. Ottensmeyer, *J. Ultrastruct. Res.* **88**, 121 (1984).
66. E. G. Rightor and co-workers, *J. Phys. Chem. B* **101**, 1950 (1997).
67. K. Siangchaew and M. Libera, *Macromolecules* **32**, 3051 (1999).
68. G. Kim and M. Libera, *Macromolecules* **31**, 2569 (1998).
69. Y. C. Wang and co-workers, *Microsc. Microanal.* **4**, 146 (1998).
70. P. E. Batson, in Ref. 62, p. 217.
71. D. A. Muller, P. E. Batson, and J. Silcox, *Phys. Rev. B.* **58**, 11970 (1998).
72. H. W. Mook and P. Kruit, *Electron Microsc. Anal.* **153**, 81 (1997).
73. P. Kruit, *Electron Microsc. Anal.* **153**, 269 (1997).
74. P. E. Batson, H. W. Mook, and P. Kruit, *Inst. Phys. Conf. Ser.* **165**, 213 (2000).
75. H. Ade and co-workers, *Science* **258**, 972 (1992).
76. M. Feser and co-workers, *Proc., SPIE.* **3449**, 19 (1998).
77. E. H. Anderson and co-workers, *J. Vac. Sci. Technol. B* **18**, 2970 (2000).
78. S. Anders and co-workers, *Rev. Sci. Instrum.* **70**, 3973 (1999).
79. G. De Stasio and co-workers, *Rev. Sci. Instrum.* **70**, 1740 (1999).
80. R. Fink and co-workers, *J. Electron Spectrosc. Relat. Phenom.* **84**, 231 (1997).
81. R. Wichtendahl and co-workers, *Surf. Rev. Lett.* **5**, 1249 (1998).
82. E. Bauer and co-workers, *J. Electron Spectrosc. Relat. Phenom.* **84**, 201 (1997).
83. J. Kirz, C. Jacobsen, and M. Howells, *Q. Rev. Biophys.* **28**, 33 (1995).

84. C. Jacobsen and co-workers, *Opt. Commun.* **86**, 351 (1991).
85. T. Warwick and co-workers, *Rev. Sci. Instrum.* **69**, 2964 (1998).
86. W. Meyer-Ilse, D. Attwood, and M. Koike, in B. Chance and co-workers, *Synchrotron Radiation in Biosciences*, Clarendon Press, Oxford, 1994, p. 624.
87. B. Nieman, D. Rudolph, and G. Schmahl, *Appl. Opti.* **15**, 1883 (1976).
88. G. Schmahl and co-workers, *Q. Rev. Biophys.* **13**, 297 (1980).
89. B. Winn and co-workers, *Rev. Sci. Instrum.* **67**, A31 (1996).
90. B. Winn and co-workers, *Proc. SPIE* **2856**, 100 (1996).
91. C. Jacobsen and co-workers, *J. Microsco.—Oxford* **197**, 173 (2000).
92. J. Kirz and H. Rarback, *Rev. Sci. Instrum.* **56**, 1 (1985).
93. H. Rarback and co-workers, *J. X-Ray Sci. Technol.* **2**, 274 (1990).
94. T. Warwick, H. W. Padmore, and H. Ade *Proc. SPIE* **3449**, 12 (1998).
95. T. Schmidt and co-workers, *Surf. Rev. Lett.* **5**, 1287 (1998).
96. C. Morin and co-workers, *J. Electron Spectrosc. Relat. Phenom.* **121**, 203 (2001).
97. B. P. Tonner and co-workers, *J. Electron Spectrocs. Relat. Phenom.* **75**, 309 (1995).
98. H. Ade and co-workers, *Appl. Phys. Lett.* **73**, 3775 (1998).
99. X. Zhang and co-workers, *J. Struct. Biol.* **116**, 335 (1996).
100. H. Ade and co-workers, *Europhys. Lett.* **45**, 526 (1999).
101. C. J. Buckley, N. Khaleque, S. J. Bellamy, M. Robbins, and X. Zhang, in J. Thieme, G. Schmahl, E. Umbach, and D. Rudolph, eds., *X-ray Microscopy and Spectromicroscopy*, Springer-Verlag, Berlin, 1997.
102. G. E. Mitchell and co-workers, *Macromolecules* **35**, 1336 (2002).
103. J. Maser and co-workers, *J. Microsc.* **197**, 68 (2000).
104. J. Genzer and K. Efimenko, *Science* **290**, 2130 (2000).
105. T. Hayakawa and co-workers, *Macromolecules* **33**, 8012 (2000).
106. A. Cossy-Favre and co-workers, *Macromolecules* **31**, 4957 (1998).
107. K. Dalnoki-Veress, B. G. Nickel, and J. R. Dutcher, *Phys. Rev. Lett.* **82**, 1486 (1999).
108. A. P. Hitchcock, T. Tyliszczak, I. Koprinarov, H. Stöver, W.-H. Li, Y.-M. Heng, H. W. Ade, J. Dutcher, and K. Dalnoki, *Advanced Light Source Compendium of User Abstracts*, 1999.
109. F. L. Buchholz, in F. L. Buchholz and A. T. Graham, eds., *Modern Superabsorbent Polymer Technology*, Wiley-VCH, New York, 1998, p. 251.
110. T. Shimomura and T. Namba, in F. L. Buchholz and N. A. Peppas, eds., *Superabsorbent Polymers: Science and Technology*, American Chemical Society, Washington, D.C., 1994 p. 112.
111. K. Hogari and F. Ashiya, in Ref. 110, p. 128.
112. T. L. Staples, D. E. Henton, and F. L. Buchholz, in Ref. 109, p. 55.
113. F. L. Buchholz, in Ref. 109, p. 190.
114. G. Mitchell and co-workers, *Inst. Phys. Conf. Ser.* **165**, 113 (2000).
115. S. Reich and Y. Cohen, *J. Polym. Sci. Part B: Polym. Phys.* **19**, 1255 (1981).
116. F. Bruder and R. Brenn, *Phys. Rev. Lett.* **69**, 624 (1992).
117. J. Genzer and E. J. Kramer, *Phys. Rev. Lett.* **78**, 4946 (1997).
118. S. Affrossman and co-workers, *Macromolecules* **29**, 5010 (1996).
119. E. Kumacheva and co-workers, *Langmuir* **13**, 2483 (1997).
120. G. Krausch and co-workers, *Appl. Phys. Lett.* **64**, 2655 (1994).
121. W. Straub and co-workers, *Europhys. Lett.* **29**, 353 (1995).
122. K. Tanaka, A. Takahara, and T. Kajiyama, *Macromolecules* **29**, 3232 (1996).
123. S. Walheim and co-workers, *Macromolecules* **30**, 4995 (1997).
124. A. Karim and co-workers, *Macromolecules* **31**, 857 (1998).
125. X. Zheng and co-workers, *Phys. Rev. Lett.* **74**, 407 (1995).
126. P. Müller-Buschbaum and co-workers, *Macromolecules* **31**, 5003 (1998).
127. A. Cossy-Favre and co-workers, *Acta Phys. Pol. A* **91**, 923 (1997).

128. D. Slep and co-workers, *Langmuir* **14**, 4860 (1998).
129. D. A. Winesett and co-workers, *Polym. Int.* **49**, 458 (2000).
130. A. P. Smith, H. Ade, D. Slep, S. Qu, M. Rafailovich, J. Sokolov, G. Halada, S. A. Schwarz, and Y. Strzhemechny, *Abstracts, MRS 1996 Fall Meeting*, 1996.
131. A. P. Smith, H. Ade, D. Slep, S. Qu, M. Rafailovich, and J. Sokolov, NSLS Activity Report for 1996, Brookhaven National Laboratory, 1997.
132. D. Slep and co-workers, *Langmuir* **16**, 2369 (2000).
133. D. A. Winesett and co-workers, *High Perform. Polym.* **12**, 599 (2000).
134. C. Ton-That and co-workers, *Macromolecules* **33**, 8453 (2000).
135. S. Zhu and co-workers, *Nature* **400**, 49 (1999).
136. D. A. Winesett, H. Ade, D. Gersappe, M. H. Rafailovich, J. Sokolov, and S. Zhu, in preparation.
137. T. Schmitt, P. Guttmann, O. Schmidt, P. Müller-Buschbaum, M. Stamm, G. Schönhense, and G. Schmahl, *X-ray Microscopy, AIP Conf. Proc.* **507**, 245 (1999).
138. J. T. Chen and co-workers, *Science* **273**, 343 (1996).
139. C. Zimba, E. Thomas, and C. Ober, unpublished.
140. H. Ade and co-workers, *Polymer* **36**, 1843 (1995).
141. H. Ade and co-workers, *Mater. Res. Soc. Symp. Proc.* **437**, 99 (1996).
142. C. C. Sloop and co-workers, *J. Polym. Sci. Part B: Polym. Phys.* **39**, 531 (2001).
143. A. P. Smith and co-workers, *Macromolecules* **30**, 663 (1997).
144. A. P. Smith and co-workers, *Macromol. Rapid Commun.* **19**, 557 (1998).
145. A. P. Smith and co-workers, *Microsc. Microanal.* **4 S-2**, 142 (1998).
146. A. P. Smith and co-workers, *Macromolecules* **33**, 2595 (2000).
147. A. P. Smith and co-workers, *Macromolecules* **33**, 1163 (2000).
148. A. P. Smith and co-workers, *Macromolecules* **34**, 1536 (2001).
149. A. P. Smith and co-workers, *Macromol. Mater. Eng.* **274**, 1 (2000).
150. A. P. Smith and co-workers, *Adv. Mater.* **11**, 1277 (1999).
151. A. P. Smith and co-workers, *Polymer* **42**, 4453 (2001).
152. A. P. Hitchcock and co-workers, *Microsc. Microanal.* **4 S-2**, 808 (1998).
153. G. Mitchell, M. Cheatham, Y. Chonde, J. Marshall, H. Ade, and V. Zhuang, 1995 National Synchrotron Light Source Activity Report, 1996.
154. A. P. Hitchcock and co-workers, *AIP Conf. Proc. Ser.* **507**, 235 (2000).
155. I. Koprinarov and co-workers, *Macromolecules* **34**, 4424 (2001).
156. C. G. Zimba, H. W. Ade, and A. P. Smith, "Characterization of the Interfacial Regions in Multilayer Coatings by nexafs Microscopy," presented at the Society of Plastics Engineers, Brookfield, Conn., 2000 (unpublished).
157. A. P. Smith and co-workers, *Appl. Spectrosc.* **55**, 1676 (2001).
158. A. P. Smith and co-workers, *Polymer* **41**, 6271 (2000).
159. A. P. Smith, R. J. Spontak, and H. Ade, *Polym. Degrad. Stab.* **72**, 519 (2001).
160. S. G. Urquhart and co-workers, *J. Polym. Sci., Part B: Polym. Phys.* **33**, 1593 (1995).
161. S. G. Urquhart and co-workers, *J. Polym. Sci., B: Polym. Phys.* **33**, 1603 (1995).
162. S. G. Urquhart and co-workers, *J. Phys. Chem. B* **101**, 2267 (1997).
163. S. G. Urquhart and co-workers, *Mater. Res. Soc. Symp. Proc.* **437**, 243 (1996).
164. E. G. Rightor, S. Urquhart, A. Hitchcock, H. Ade, A. P. Smith, G. Mitchell, R. Priester, and W. Lidy, *Macromolecules*, in press.
165. A. P. Hitchcock and co-workers, *Ultramicroscopy* **88**, 33 (2001).
166. A. P. Hitchcock, *J. Synchr. Radiat.* **8**, 66 (2001).
167. A. P. Hitchcock, I. N. Koprinarov, H. P. Stöver, L. Croll, and E. Kneedler, in preparation.
168. I. N. Koprinarov, A. P. Hitchcock, C. MCCrory, and R. F. Childs, *J. Phys. Chem. B* in press.
169. C. Zimba, A. P. Smith, and H. Ade, unpublished.

170. C. Zimba, A. P. Smith, and H. Ade, NSLS Activity Report for 1996, Brookhaven National Laboratory, 1997.
171. C. M. Roland, *Rubber Chem. Technol.* **62**, 456 (1989).
172. W. M. Hess, C. R. Herd, and P. C. Vegvari, *Rubber Chem. Technol.* **66**, 329 (1993).
173. J. Dias, S. G. Urquhart, H. Ade, and P. Stevens, 155th Meeting of the Rubber Division (Paper no. 30), American Chemical Society, Chicago, 1999.
174. Y. Zhang and co-workers, *Polymer* **42**, 9133 (2001).
175. Y. M. Zhang and co-workers, *Macromolecules* **34**, 7056 (2001).
176. H. Ade and B. Hsiao, *Science* **262**, 1427 (1993).
177. A. P. Smith and H. Ade, *Appl. Phys. Lett.* **69**, 3833 (1996).
178. H. Ade and co-workers, *Bull. Am. Phys. Soc.* **42**, 47 (1997).
179. A. P. Smith, A. Garcia, and H. Ade, *Microsc. Microanal.* **4 S-2**, 812 (1998).
180. J. Kikuma and co-workers, *J. Electron. Spectrosc. Relat. Phenom.* **94**, 271 (1998).
181. Y. Wang and co-workers, *J. Microsc.* **197**, 80 (2000).
182. D. Weiss and co-workers, *Ultramicroscopy* **84**, 185 (2000).
183. H. N. Chapman, C. Jacobsen, and S. Williams, *Ultramicroscopy* **62**, 191 (1996).

H. ADE
North Carolina State University

X-RAY SCATTERING. See SYNCHROTON RADIATION.

ZIEGLER–NATTA CATALYSTS

Introduction

Ziegler–Natta catalysts have had enormous impact on the polymer industry in the past 50 years, with current world production of polyolefins using Ziegler–Natta catalysis amounting to more than 50 million tons per annum. The vast advances made during the past decades stem from breakthrough discoveries made by Karl Ziegler and Giulio Natta in the early 1950s. It was in 1953 that Ziegler and co-workers, at the Max Planck Institute in Mülheim, were investigating the "Aufbau" reaction in which triethylaluminum reacts with ethylene to give higher aluminum trialkyls (1). Unexpectedly, one experiment led not to the oligomerization of ethylene via the Aufbau reaction, but to the formation of 1-butene. It turned out that this dimerization reaction had been catalyzed by traces of nickel present as a contaminant in the reactor. Soon afterwards, a revolutionary breakthrough was achieved when combinations of transition-metal compounds and aluminum alkyls were found that could polymerize ethylene under mild conditions, yielding high density polyethylene (2,3). In 1954 Giulio Natta and co-workers at Milan Polytechnic succeeded not only in polymerizing propylene with the Ziegler catalyst combination $TiCl_4/Al(C_2H_5)_3$, but also in fractionating the resulting polymer to obtain and characterize isotactic polypropylene (4–6). This demonstration of stereoregular polymerization led to an explosive growth of new polymers and industrial applications as the full scope of Ziegler–Natta catalysis was realized (7–9); Ziegler and Natta were jointly awarded the Nobel Prize for Chemistry in 1963.

Ziegler–Natta catalysts for polyethylene and polypropylene have progressed from first-generation titanium trichloride catalysts, used in the manufacturing processes of the late 1950s and the 1960s, to the high activity magnesium chloride supported catalysts used today. Improvements in catalyst performance have

Encyclopedia of Polymer Science and Technology. Copyright John Wiley & Sons, Inc. All rights reserved.

facilitated the development of efficient gas-phase and bulk processes for polyethylene and polypropylene, and at the same time have led to ever-increasing control over polymer composition and properties.

Early Catalysts

Titanium Trichloride. One of the first catalysts found by Ziegler to be effective in ethylene polymerization was the product of the reaction of titanium tetrachloride with triethylaluminum. At low Al/Ti ratios, this reaction yields titanium trichloride as a solid precipitate. $TiCl_3$ exists in four crystalline modifications, the α, β, δ, and γ forms, of which the β-modification has a linear (chain-like) structure and the α, δ, and γ forms have a layered structure (10,11). The reaction product of $TiCl_4$ and AlR_3 is β-$TiCl_3$, which can be converted to the γ form by heating. The latter catalyst has much higher stereoregulating ability in propylene polymerization, while β-$TiCl_3$ is an effective catalyst for the production of *cis*-1,4-polyisoprene. α-$TiCl_3$ can be prepared by reduction of $TiCl_4$ with hydrogen or with aluminum powder. The δ form can be prepared by prolonged grinding of γ- or α-$TiCl_3$ and has a more disordered structure as a result of sliding of Cl–Ti–Cl triple layers during mechanical activation (12).

The first-generation Ziegler–Natta catalysts used in early manufacturing processes for polypropylene (PP) comprised $TiCl_3$ and cocrystallized $AlCl_3$, resulting from reduction of $TiCl_4$ with Al or an aluminum alkyl. The cocatalyst used in the polymerization process was $Al(C_2H_5)_2Cl$ (DEAC). Catalyst activity was relatively low, giving polymer yields of around 1 kg PP/g cat., necessitating removal (deashing) of catalyst residues from the polymer. In many cases, extractive removal of atactic polymer was also required.

Other Early Developments. In addition to the breakthrough by Ziegler, two other discoveries of ethylene polymerization catalysts were made in the early 1950s. A patent by Standard Oil of Indiana, filed in 1951, disclosed reduced molybdenum oxide or cobalt molybdate on alumina (13). At the same time, Phillips discovered supported chromium oxide catalysts, prepared by impregnation of a silica–alumina support with CrO_3 (14–16). Both the Phillips catalyst and titanium chloride based Ziegler catalysts are widely used in the production of high density polyethylene (HDPE).

The various discoveries made independently by different industrial research groups in the early 1950s resulted in intensive patent litigations (8,17,18), which in the case of PP continued up to the 1980s, when a composition of matter patent on PP was awarded in the United States to Phillips, because a fraction of crystalline PP was found to be present in a polymer prepared using a $CrO_3/Al_2O_3/SiO_2$ catalyst (19). However, despite the importance of the Phillips catalyst for HDPE, it was unsuitable for PP, which is produced entirely using Ziegler–Natta catalysts and (to a much smaller extent) metallocene-based catalysts.

Second-Generation Catalysts. In the 1970s, an improved $TiCl_3$ catalyst for PP was developed by Solvay (20). Catalyst preparation involved reduction of $TiCl_4$ using DEAC, followed by treatment with an ether and $TiCl_4$. The ether treatment results in removal of $AlCl_3$ from $TiCl_3 \cdot nAlCl_3$, while treatment with $TiCl_4$ effects a phase transformation from β- to δ-$TiCl_3$ at a relatively mild

temperature (<100°C) (21). Using catalysts of this type, it was possible to obtain PP yields in the range 5–20 kg/g cat. in 1–4 h of polymerization in liquid monomer (22). Commercial implementation of second-generation catalysts was, however, overshadowed by the advent of third- and later-generation magnesium chloride supported catalysts (discussed under Ziegler–Natta Catalysts for Polypropylene).

Polymerization and Particle Growth

Polymer Chain Growth. The essential characteristic of Ziegler–Natta catalysis is the polymerization of an olefin or diene using a combination of a transition-metal compound and a base-metal alkyl cocatalyst, normally an aluminum alkyl. The function of the cocatalyst is to alkylate the transition metal, generating a transition-metal–carbon bond. It is also essential that the active center contains a coordination vacancy. Chain propagation takes place via the Cossee–Arlman mechanism (23), in which coordination of the olefin at the vacant coordination site is followed by chain migratory insertion into the metal–carbon bond, as illustrated in Figure 1.

Regulation of polyolefin molecular weight is effected by the use of hydrogen as chain-transfer agent. Chain transfer can also occur via β-hydrogen transfer from the growing chain to the transition metal or to the monomer, and to a lesser extent via alkyl exchange with the cocatalyst (Fig. 2).

In propylene polymerization using titanium chloride catalysts, chain propagation takes place via primary (1,2-) insertion of the monomer. For isospecific propagation, there must be only one coordination vacancy and the active site must be chiral. Corradini and co-workers have demonstrated that the asymmetric

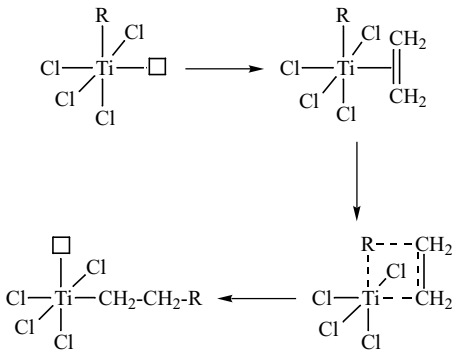

Fig. 1. Cossee–Arlman mechanism for polymerization.

$$\text{Ti-CH}_2\text{-CH}_2\text{-Polymer} + \text{H}_2 \longrightarrow \text{Ti-H} + \text{CH}_3\text{-CH}_2\text{-Polymer}$$

$$\text{Ti-CH}_2\text{-CH}_2\text{-Polymer} + \text{CH}_2{=}\text{CH}_2 \longrightarrow \text{Ti-CH}_2\text{-CH}_3 + \text{CH}_2{=}\text{CH-Polymer}$$

$$\text{Ti-CH}_2\text{-CH}_2\text{-Polymer} + \text{AlR}_3 \longrightarrow \text{Ti-R} + \text{AlR}_2\text{-CH}_2\text{-CH}_2\text{-Polymer}$$

Fig. 2. Chain transfer in ethylene polymerization.

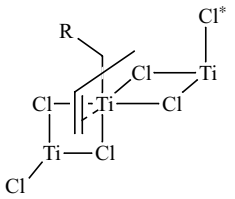

Fig. 3. Model for stereospecific polymerization of propylene. The orientation of the growing chain is influenced by the chlorine atom marked with an asterisk.

environment of the active site forces the growing chain to adopt a particular orientation so as to minimize steric interactions with (chlorine) ligands present on the catalyst surface (24). This in turn leads to one particular prochiral face of the incoming monomer being preferred, as illustrated in Figure 3, leading to isotactic polymer.

An elegant demonstration of the above mechanism has been provided by Zambelli and co-workers (25), who showed that the first insertion of propylene into a Ti—CH_3 bond generated by chain transfer with Al alkyl using the system $TiCl_3/Al(CH_3)_3$ is *not* stereospecific, whereas the second insertion (ie into Ti–isobutyl) *is* stereospecific. The importance of the combined effects of the steric bulk of the Ti–alkyl group and the halide ligand is apparent from the very high stereospecificity observed using TiI_3 (26). Particularly high stereospecificity (but low activity) was also found by Natta when $TiCl_3$ was used in combination with $Al(C_2H_5)_2I$ (27).

In contrast to the isospecific titanium-based catalysts, vanadium-based catalysts give predominantly syndiotactic PP. At very low polymerization temperature (-78°C), living polymerization can be obtained using homogeneous catalysts obtained by reaction of a vanadium compound (eg VCl_4 or a V(III) β-diketonate) with R_2AlCl (28,29). With these catalysts, syndiospecific propagation occurs via secondary (2,1-) insertion of the monomer. The overall stereo- and regioregularity of the polymer is poor, comprising not only syndiotactic blocks resulting from secondary insertions but also short, atactic blocks arising from sequences of primary insertions. This polymer has not been developed commercially, but vanadium catalysts are used in ethylene (co)polymerization (outlined under Ziegler–Natta Catalysts for Ethylene (Co)polymerization). C_s-symmetric metallocene catalysts (30) have been developed for the production of syndiotactic polypropylene having significantly higher chain regularity.

Polymer Particle Growth. A very important feature of any heterogeneous catalyst used in slurry and gas-phase processes for polyolefin production is particle morphology. Heterogeneous Ziegler–Natta catalysts are microporous solids, with particle sizes typically in the range 10–100 μm. Each particle comprises millions of primary crystallites with sizes of up to about 15 nm. On contacting the catalyst components, at the start of polymerization, cocatalyst and monomer diffuse through the catalyst particle and polymerization takes place on the surface of each primary crystallite within the particle. As solid, crystalline polymer is formed, the primary crystallites are pushed apart as the particle grows, analogous to the expanding universe. The particle shape is retained, and this phenomenon

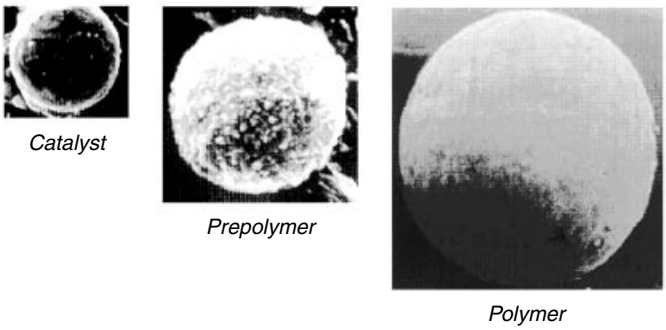

Fig. 4. "Replication" phenomenon during polymerization.

is therefore referred to as replication (Fig. 4). Ideally, the catalyst particle should have spherical morphology and controllable porosity. It is important that the mechanical strength of the catalyst is high enough to prevent disintegration but low enough to allow progressive expansion as polymerization proceeds (31). Further implications of particle morphology and porosity are discussed under Ziegler–Natta Catalysts for Ethylene (Co)polymerization and also under Reactor Granule Technology.

Ziegler–Natta Catalysts for Ethylene (Co)polymerization

Ziegler–Natta catalysts are widely used in the production of high density and linear low density polyethylene (HDPE and LLDPE). More than half the world production of HDPE is based on Ziegler–Natta catalysts, chromium catalysts also being widely used. Less than 1% of HDPE production utilizes metallocene or other single-site catalysts. In LLDPE production, Ziegler–Natta catalysts occupy a dominant position, accounting for more than 90% of the total production. Single-site catalysts currently account for less than 10% of this market, but increased use of such catalysts is expected throughout the next decade.

The most important titanium-based catalysts for HDPE and LLDPE are those comprising a titanium component on magnesium chloride or on a magnesium chloride containing support. Toward the end of the 1960s, catalysts obtained by reaction of $TiCl_4$ or a derivative thereof with a magnesium compound such as Mg(OH)Cl, $Mg(OH)_2$, or $MgCl_2$ were found to give very high activity in ethylene polymerization, eliminating the need for deashing of the polymer (31,32). The most effective support was found to be active magnesium chloride, prepared by co-milling of $MgCl_2$ and titanium halides or by chlorination of organomagnesium compounds (32). Numerous catalyst systems and methods of preparation have been disclosed (33), and the characteristics of magnesium chloride as a support for Ziegler–Natta catalysts are discussed in depth under Ziegler–Natta Catalysts for Polypropylene. Magnesium chloride can also be used in combination with a silica support, for example by impregnation of the porous support with a solution of $MgCl_2$ and $TiCl_4$ in tetrahydrofuran (34).

An important manufacturing process for HDPE that makes use of high mileage catalysts is the cascade process, in which polymerization reactors in series are used to give reactor blends with improved properties for film and pipe applications (35). Broad molecular weight distribution (MWD) can be obtained by the use of different hydrogen concentrations in each reactor. In addition, the process can be designed to give low molecular weight homopolymer in the first reactor and a high molecular weight copolymer in the second. The high molecular weight copolymer chains function as tie molecules linking the crystalline, homopolymer domains, thereby leading to high stress crack resistance of the polymer. This process allows an "inverse" comonomer distribution to be obtained, in the sense that the comonomer is in the high molecular weight fraction, counteracting the general tendency of Ziegler–Natta catalysts to incorporate the comonomer mainly in the low molecular weight chains. The latter feature is an important consideration in Ziegler–Natta catalyst design for LLDPE. Comonomer incorporation is highest at the most open catalytic centers, whereas sterically hindered centers will tend to give polyethylene chains with little or no comonomer. The best catalysts for LLDPE are therefore those that have relatively uniform active center distribution, lacking excessively hindered or unhindered active sites.

Vanadium catalysts have also been developed for polyethylene and ethylene-based copolymers, particularly ethylene–propylene–diene rubbers (EPDM). Homogeneous (soluble) vanadium catalysts produce relatively narrow MWD polyethylene, whereas supported vandium catalysts give broad MWD (36). Polymerization activity is strongly enhanced by the use of a halogenated hydrocarbon as promoter in combination with a vanadium catalyst and aluminum alkyl cocatalyst (36,37).

Ethylene polymerization, in contrast to the polymerization of propylene and other alpha-olefins, is often affected by diffusion limitations, which occur if the monomer reactivity in polymerization is high relative to diffusivity through the catalyst particle. This can result in the formation of an "onion" particle structure as polymerization first takes place at the external surface of the particle, particle growth occurring step by step as the monomer reaches the inner parts of the catalyst particle. This mechanism of particle growth is associated with a kinetic profile in which an initial induction period is followed by an acceleration period, after which, in the absence of chemical deactivation, a stationary rate is obtained.

Ziegler–Natta Catalysts for Polypropylene

Worldwide manufacture of PP, currently around 30 million tons per annum, is dominated by high activity $MgCl_2$-supported Ziegler–Natta catalysts. The first- and second-generation $TiCl_3$ catalysts have all but disappeared, and the recently developed metallocene catalysts still account for less than 1% of all PP produced, although they are likely to grow in importance. The development and implementation of $MgCl_2$-supported catalysts in bulk (liquid monomer) and gas-phase processes has led to the advent of simple, low-cost (nondeashing, nonextracting) manufacturing processes for PP (18).

The basis for the development of the high activity supported catalysts lay in the discovery, in the late 1960s, of "activated" $MgCl_2$ able to support $TiCl_4$ and give

high catalyst activity, and the subsequent discovery, in the mid-1970s, of electron donors (Lewis bases) capable of increasing the stereospecificity of the catalyst so that (highly) isotactic PP could be obtained (32,38,39). A further feature that has contributed greatly to the commercial success of $MgCl_2$-supported catalysts is the development of spherical catalysts with controlled particle size and porosity (40), which not only replicate their morphology during polymerization as the polymer particle grows, but which have now opened the way to a broad range of homo- and copolymers and multiphase polymer alloys via what has been termed Reactor Granule Technology (41).

Catalyst Structure and Composition. In the early stages of $MgCl_2$-supported catalyst development, activated magnesium chloride was prepared by ball milling in the presence of ethyl benzoate, leading to the formation of very small ($\leq$3 nm thick) primary crystallites within each particle (21). Nowadays, however, the activated support is prepared by chemical means such as complex formation of $MgCl_2$ and an alcohol or by reaction of a magnesium alkyl or alkoxide with a chlorinating agent or $TiCl_4$. Many of these approaches are also effective for the preparation of catalysts having controlled particle size and morphology. For example, the cooling of emulsions of molten $MgCl_2 \cdot nC_2H_5OH$ in paraffin oil gives almost perfectly spherical supports, which are then converted into the catalysts (18). A typical catalyst preparation involves reaction of the $MgCl_2 \cdot nC_2H_5OH$ support with excess $TiCl_4$ in the presence of an "internal" electron donor. Temperatures of at least 80°C and at least two $TiCl_4$ treatment steps are normally used, in order to obtain high performance catalysts in which the titanium is mainly present as $TiCl_4$ rather than the $TiCl_3OC_2H_5$ generated in the initial reaction with the support. Catalysts obtained via chemical routes generally have a BET surface area of around 300 m^2/g and pore volumes in the range 0.3–0.4 cm^3/g (18).

High activity Ziegler–Natta catalysts comprising $MgCl_2$, $TiCl_4$, and an internal donor are typically used in combination with an aluminum alkyl cocatalyst such as $Al(C_2H_5)_3$ and an "external" electron donor added in polymerization. The first catalyst systems containing ethyl benzoate as internal donor were used in combination with a second aromatic ester such as methyl *p*-toluate as external donor (39). These were followed by catalysts containing a diester (eg diisobutyl phthalate) as internal donor, used in combination with an alkoxysilane external donor of type $RR'Si(OCH_3)_2$ or $RSi(OCH_3)_3$ (42). The combination $MgCl_2/TiCl_4$/phthalate ester–AlR_3–alkoxysilane is currently the most widely used catalyst system in PP manufacture. The most effective alkoxysilane donors for high isospecificity are methoxysilanes containing relatively bulky alkyl groups branched at the position alpha to the silicon atom (43–46). Typical examples include cyclohexyl(methyl)dimethoxysilane and dicyclopentyldimethoxysilane (47). Of these, the latter gives particularly high stereospecificity (48) and broader MWD (49). High PP stereoregularity and broad MWD have also been obtained by the use of dimethoxysilanes containing polycyclic amino groups (50,51).

The function of the internal donor in $MgCl_2$-supported catalysts is twofold. One function is to stabilize small primary crystallites of magnesium chloride; the other is to control the amount and distribution of $TiCl_4$ in the final catalyst. Activated magnesium chloride has a disordered structure comprising very small lamellae. Giannini (32) has indicated that, on preferential lateral cleavage surfaces, the magnesium atoms are coordinated with four or five chlorine atoms, as

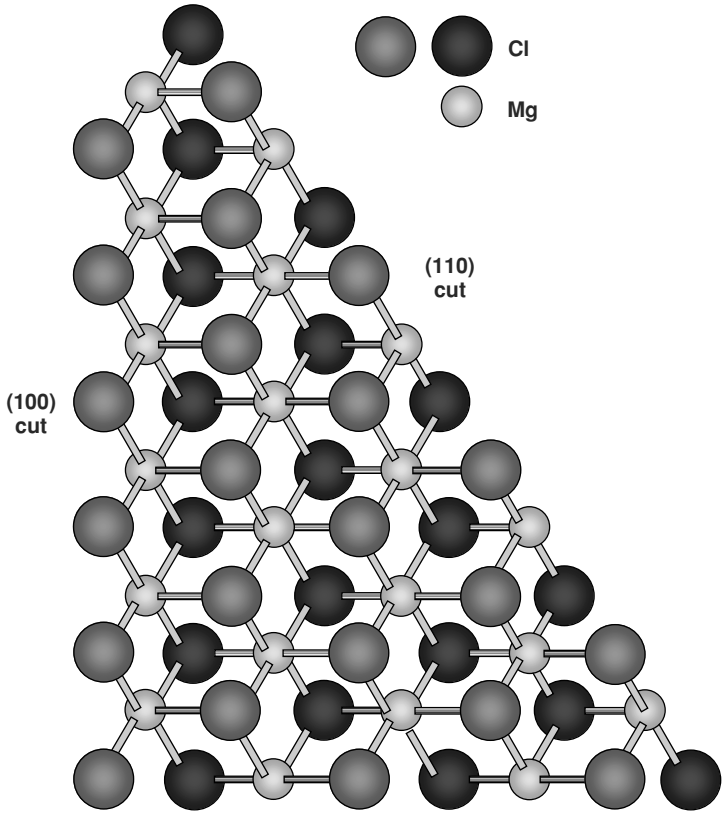

Fig. 5. Model of a $MgCl_2$ layer showing the (100) and (110) lateral cuts. Based on Ref. 31.

opposed to six chlorine atoms in the bulk of the crystal. These lateral cuts correspond to (110) and (100) faces of $MgCl_2$, as shown in Figure 5.

It has been proposed that bridged, dinuclear Ti_2Cl_8 species can coordinate to the (100) face of $MgCl_2$ and give rise to the formation of chiral, isospecific active species (Fig. 6), it being pointed out that Ti_2Cl_6 species formed by reduction on contact with $Al(C_2H_5)_3$ would resemble analogous species in $TiCl_3$ catalysts (52, 53). Accordingly, it has been suggested (18) that a possible function of the internal donor is preferential coordination on the more acidic (110) face of $MgCl_2$, such that this face is prevailingly occupied by donor and the (100) face is prevailingly occupied by Ti_2Cl_8 dimers.

Analytical studies (54) have indicated that a monoester internal donor such as ethyl benzoate is coordinated to $MgCl_2$ and not to $TiCl_4$. In the search for donors giving catalysts having improved performance, it was considered (55) that bidentate donors should be able to form strong chelating complexes with tetracoordinate Mg atoms on the (110) face of $MgCl_2$, or binuclear complexes with two pentacoordinate Mg atoms on the (100) face. This led to the development of the $MgCl_2/TiCl_4$/phthalate ester catalysts, used as indicated above in combination with an alkoxysilane as external donor. The requirement for an external donor when using catalysts containing a benzoate or phthalate ester is due to

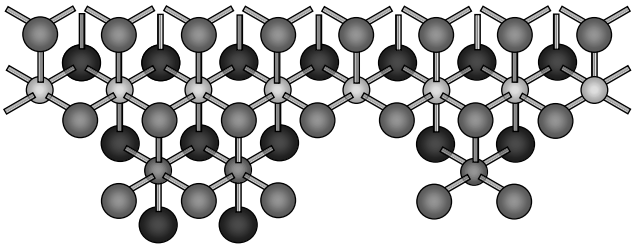

Fig. 6. Model showing dimeric and monomeric Ti species on a (100) lateral cut of $MgCl_2$. Based on Ref. 31.

the fact that, when the catalyst is brought into contact with the cocatalyst, a large proportion of the internal donor is lost as a result of alkylation and/or complexation reactions. In the absence of an external donor, this leads to poor stereospecificity because of increased mobility of the titanium species on the catalyst surface. When the external donor is present, contact of the catalyst components leads to replacement of the internal donor by the external donor, as has been shown (56,57) with $MgCl_2/TiCl_4$/ethyl benzoate–$Al(C_2H_5)_3$–methyl *p*-toluate and with $MgCl_2/TiCl_4$/dibutyl phthalate–$Al(C_2H_5)_3$–$C_6H_5Si(OC_2H_5)_3$. The most active and stereospecific systems were those which allowed the highest incorporation of external donor (58), the effectiveness of a catalyst system depending more on the combination of donors rather than on the individual internal or external donor. For example, the use of a monoester rather than an alkoxysilane as external donor with a phthalate-containing system is ineffective (59), as in this case very little of the external donor is adsorbed (58). Further studies (60,61) showed that a phthalate-containing catalyst adsorbed alkoxysilanes to a greater extent than a catalyst without internal donor.

Recently, research on $MgCl_2$-supported catalysts has led to systems not requiring the use of an external donor. This required the identification of bidentate internal donors that not only had the right oxygen–oxygen distance for effective coordination with $MgCl_2$ but that, unlike phthalate esters, were not removed from the support on contact with $Al(C_2H_5)_3$ and that were unreactive with $TiCl_4$ during catalyst preparation. It was found (55,62–64) that certain 2,2-disubstituted 1,3-dimethoxypropanes met all these criteria. The best performance was obtained when bulky substituents in the 2-position resulted in the diether having a most probable conformation (65) with an oxygen–oxygen distance in the range 2.8–3.2 Å. The successive "generations" of high activity $MgCl_2$-supported catalyst systems for PP are summarized below:

(1) $MgCl_2/TiCl_4$/ethyl benzoate–AlR_3–aromatic ester
(2) $MgCl_2/TiCl_4$/phthalate ester–AlR_3–alkoxysilane
(3) $MgCl_2/TiCl_4$/diether–AlR_3

Catalyst performance has improved considerably with each generation. The PP yield obtained under typical polymerization conditions (liquid monomer, in the presence of hydrogen, 70°C, 1–2 h) has increased from 15–30 kg/g cat. for

the third-generation ethyl benzoate containing catalysts to 30–80 kg/g cat. for the fourth-generation phthalate-based catalysts. With the recently developed fifth-generation catalysts containing a diether as internal donor, yields of 80–160 kg/g cat. can be achieved. These different catalysts also display different kinetic profiles in propylene polymerization. The catalysts containing a diether as internal donor exhibit very stable activities during polymerization. A low rate of catalyst decay during polymerization is also obtained with the catalyst system $MgCl_2/TiCl_4$/phthalate ester–AlR_3–alkoxysilane, whereas the system $MgCl_2/TiCl_4$/ethyl benzoate–AlR_3–aromatic ester has a very high initial polymerization activity but also a high decay rate, limiting the final polymer yield. The rapid decay in activity can at least partially be ascribed to the use of an ester as external as well as internal donor, the ester being able to react with titanium–hydrogen bonds formed in chain transfer with hydrogen, generating Ti—O bonds inactive for chain propagation (66).

Most recently, a further family of $MgCl_2$-supported catalysts has been developed (67,68), in which the internal donor is a succinate rather than a phthalate ester. As is the case with the phthalate-based catalysts, an alkoxysilane is used as external donor. The essential difference between these catalysts is that the succinate-based systems produce PP having much broader MWD (discussed under Catalyst/Polymer Relationship).

Mechanistic Aspects. It is well established that effective external donors not only increase the isotactic index of the polymer (the proportion of polymer insoluble in boiling heptane or in xylene at 25°C), but can also increase in absolute terms the amount of isotactic polymer formed. This has been demonstrated by Kashiwa (69) for the catalyst system $MgCl_2/TiCl_4$–$Al(C_2H_5)_3$. An increase in the molecular weight and stereoregularity of the isotactic fraction was also noted. Similar trends are apparent with catalyst systems of type $MgCl_2/TiCl_4$/phthalate ester–AlR_3–alkoxysilane (70). Kakugo (71) has used elution fractionation to demonstrate that the external donor not only decreases "atactics" formation but also increases the degree of steric control at isospecific sites. Soga has reported that an almost aspecific $MgCl_2/TiCl_3$ catalyst, with a very low content of (probably isolated, monomeric) Ti species, could be rendered isospecific by the addition of ethyl benzoate as external donor (72) or by using $Cp_2Ti(CH_3)_2$ as cocatalyst (73). It was suggested (74) that in both cases aspecific sites having two coordination vacancies could be converted to isospecific sites by blocking one of the two vacancies.

A powerful technique to study the effects of electron donors on site selectivity in Ziegler–Natta catalysts is the determination of the stereoregularity of the first insertion step in propylene polymerization. Sacchi and co-workers (60,75) have investigated the effect of Lewis bases on the first-step stereoregularity resulting from propylene insertion into a Ti—C_2H_5 bond formed via chain transfer with ^{13}C-enriched $Al(C_2H_5)_3$. First-step stereoregularity is particularly sensitive to the steric environment of the active center, because the stereospecificity of the first monomer insertion is always lower than that of the following propagation steps. For example, with a $MgCl_2/TiCl_4$/diisobutyl phthalate catalyst it was found (60) that the mole fraction of erythro (isotactic) placement in the isotactic polymer fraction was 0.67 with no external donor, 0.82 with $CH_3Si(OC_2H_5)_3$, and 0.92 with $C_6H_5(OC_2H_5)_3$. It could be concluded that the alkoxysilane external donor

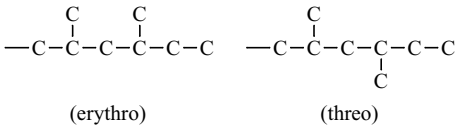

Fig. 7. Erythro (isotactic) and threo (syndiotactic) placement resulting from insertion into a Ti–ethyl unit.

was present in the environment of at least part of the isospecific centers (Fig. 7). Subsequent studies (76,77) indicated that similar considerations apply to diether donors.

Recently, significant advances have been made in understanding the fundamental factors determining the performance of state-of-the-art $MgCl_2$-supported catalysts. Studies by Busico and co-workers (78) have shown that the chain irregularities in isotactic PP prepared using heterogeneous catalysts are not randomly distributed along the chain but are clustered. The chain can therefore contain, in addition to highly isotactic blocks, sequences that can be attributed to weakly isotactic (isotactoid) and to syndiotactic (syndiotactoid) blocks. This implies that the active site can isomerize very rapidly (during the growth time of a single polymer chain, ie in less than a second) between three different propagating species. The same sequences are present, but in different amounts, in both the soluble and the insoluble fractions. The polymer can therefore be considered to have a stereoblock structure in which highly isotactic sequences alternate with defective isotactoid and with syndiotactoid sequences. A mechanistic model has been formulated in which the relative contributions of these sequences can be related to site transformations involving the presence or absence of steric hindrance in the vicinity of the active species. ^{13}C NMR studies have indicated (79) the presence of C_1-symmetric active species in $MgCl_2$-supported catalysts, with a mechanism of isotactic propagation which is analogous to that for certain C_1-symmetric metallocenes, in the sense that propylene insertion at a highly enantioselective site tends to be followed by chain "back-skip" rather than a less regio- and stereoselective insertion when the chain is in the coordination position previously occupied by the monomer. The probability of chain "back-skip" will increase with decreasing monomer concentration, and it has indeed been confirmed that increased polymer isotacticity is obtained at low monomer concentration. It is proposed (78) that a (temporary) loss of steric hindrance from one side of an active species with local C_2-symmetry, giving a C_1-symmetric species, may result in a transition from highly isospecific to moderately isospecific propagation. Loss of steric hindrance on both sides can lead to syndiospecific propagation in which chain-end control becomes operative. The model is illustrated in Figure 8.

If it is considered that the steric hindrance in the vicinity of the active species can result from the presence of a donor molecule, and that the coordination of such a donor is reversible, the above model provides us with an explanation for the fact that strongly coordinating, stereorigid donors typically give stereoregular polymers in which the highly isotactic sequences predominate. Several types of active species in which the presence of a donor in the vicinity of the active Ti atom is necessary for high isospecificity have been proposed (80), although the exact structure of the active species is still by no means resolved. Isospecific active

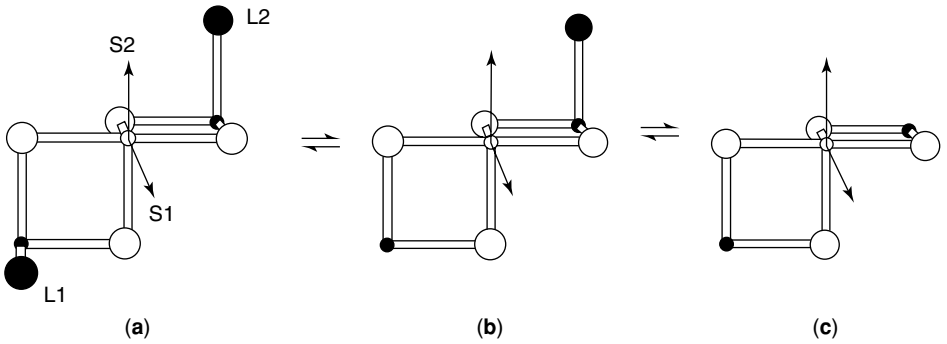

Fig. 8. Model of possible active species for (**a**) highly isotactic, (**b**) isotactoid, and (**c**) syndiotactic propagation (78).

species not requiring the presence of a donor for high stereospecificity have also been proposed (81).

In PP production, hydrogen is used as a chain-transfer agent for polymer molecular weight (melt-flow rate) control. The effect of hydrogen (concentration) on polymer molecular weight is dependent on the catalyst system. An advantage of catalysts containing a diether donor, in addition to very high activity, is high sensitivity to hydrogen, so that relatively little hydrogen is required for molecular weight control. This effect can be ascribed to chain transfer after the occasional secondary (2,1-) rather than the usual primary (1,2-) insertion, a 2,1-insertion slowing down a subsequent monomer insertion and therefore increasing the probability of chain transfer (82). Reactivation of "dormant" (2,1-inserted) species via chain transfer with hydrogen also explains the frequently observed activating effect of hydrogen in propylene polymerization, giving yields which may be around three times those observed in the complete absence of hydrogen. These conclusions have been based on the ^{13}C NMR determination of the relative proportions of *i*-C_4H_9 and *n*-C_4H_9 terminated chains, resulting from chain transfer with hydrogen after primary and secondary insertion respectively:

$$\mathrm{Ti{-}CH_2{-}CH(CH_3){-}[CH_2{-}CH(CH_3)]_nPr + H_2 \rightarrow Ti{-}H + \mathit{i}{-}C_4H_9{-}CH(CH_3)[CH_2(CH_3)]_{n-1}Pr}$$

$$\mathrm{Ti{-}CH(CH_3){-}CH_2{-}[CH_2{-}CH(CH_3)]_nPr + H_2 \rightarrow Ti{-}H + \mathit{n}{-}C_4H_9{-}CH(CH_3)[CH_2(CH_3)]_{n-1}Pr}$$

Other studies have demonstrated that chain transfer is dependent not only on regio- but also on stereoselectivity (48). This is in keeping with the tendency that, with catalyst systems of type $MgCl_2/TiCl_4$/phthalate ester–AlR_3–alkoxysilane, the silanes that give the most stereoregular isotactic polymer also give relatively low hydrogen response.

Catalyst/Polymer Relationship. By varying the catalyst composition, and in particular the nature of the electron donors (esters, silanes, diethers) present in the catalyst system, it is possible to control the PP tacticity, molecular weight, and MWD to produce a range of polymers having the processing and end-use properties required for very different applications. Ziegler–Natta catalysts typically give broader MWDs than are obtained with homogeneous

(metallocene) catalysts. This is because Ziegler–Natta catalysts contain a range of different active centers, each center giving different relative rates of chain propagation and chain transfer. Each individual site produces a Schulz–Flory distribution with $M_w/M_n = 2$ and $M_z/M_w = 1.5$, and the overall polymer MWD represents a combination of these individual distributions. The dominant effect of active center distribution has been demonstrated by the use of stopped-flow polymerization (83), where the polymer MWD was shown to be unaffected by the polymerization time. Stopped-flow polymerization has also been used to determine active site concentration ($C*$) and propagation rate constants, k_p. For $MgCl_2$-supported catalysts, $C*$ values of around 4% (of total Ti present) have been obtained from stopped-flow experiments (84). $C*$ values obtained by other techniques, notably ^{14}CO quenching of propylene polymerization, have ranged from 1% or less (85) to more than 20% (86). Clearly, there are large differences in $C*$ values obtained by different groups, but it is consistently found that the major proportion of the Ti present in Ziegler–Natta catalysts is inactive. The k_p values for isospecific active sites are around an order of magnitude greater than those for weakly specific sites (85,86). The value of k_p increases significantly in the presence of hydrogen (87), in accordance with the reactivation of "dormant" (2,1-inserted) centers by chain transfer.

Recent work by Terano and co-workers (88) has shown that, under stopped-flow conditions, hydrogen is only effective as chain-transfer agent when catalyst and cocatalyst have been precontacted. These and subsequent (89,90) results indicated that effective chain transfer with hydrogen requires the presence of species able to promote the dissociation of H_2 to atomic hydrogen.

The donors present in the catalyst system play an active role in the formation or modification of isospecific sites, and the polymer MWD depends on the relative contribution and hydrogen response (ie sensitivity to chain transfer with hydrogen) of each type of active site. The incorporation of an external donor into the catalyst system generally leads to an increase in molecular weight, the magnitude of the MW increase depending on the nature of the donor. The characteristics of different catalyst systems with regard to PP MWD are as follows (68):

Internal donor	External donor	M_w/M_n
Diether	—	5–5.5
Phthalate	Alkoxysilane	6.5–8
Succinate	Alkoxysilane	10–15

It can be seen that the diether-based catalysts give relatively narrow MWD. A narrow MWD, and relatively low molecular weight, is advantageous in fiber spinning applications. In contrast, extrusion of pipes and thick sheets requires high melt strength, and therefore relatively high molecular weight and broad MWD. A broad MWD, along with high isotactic stereoregularity, is also beneficial for high crystallinity and therefore high rigidity. The new succinate-based catalysts enable very broad MWD PP homopolymers to be produced in a single reactor and are also of interest for the production of heterophasic copolymers having an improved balance of stiffness and impact strength, taking into account that the incorporation

of a rubbery (ethylene/propylene) copolymer phase into a PP homopolymer matrix increases impact strength but leads at the same time to decreased stiffness.

The relatively narrow PP molecular weight distributions obtained using diether-based catalysts can be attributed to the fact that in these systems even the most highly stereospecific active sites are not totally regiospecific. A proportion of approximately one secondary insertion for every 2000 primary insertions at highly isospecific sites has been noted for the system $MgCl_2/TiCl_4$/diether–AlR_3 (82). The probability of chain transfer with hydrogen after a secondary insertion is such that this is sufficient to prevent the formation of very high molecular weight chains, taking into account that the highest molecular weight fraction of the polymer is formed on the active species having the highest isospecificity. The broader MWDs obtained with catalysts containing ester internal donors are likely to be due to the presence of (some) isospecific active sites having very high regiospecificity and therefore lower hydrogen sensitivity. Such results illustrate the profound effect of catalyst regio- and stereospecificity distribution on both molecular weight control and polymer MWD and properties.

Reactor Granule Technology. As indicated in the section Polymer Particle Growth, particle morphology and porosity are very important features of a Ziegler–Natta catalyst used in modern bulk (liquid monomer or gas-phase) polymerization processes. Under appropriate polymerization conditions, polymer particles can be obtained that have an internal morphology that can range from a compact to a porous structure (91). In what is termed Reactor Granule Technology (RGT), porous polymer particles can be produced, which can then function as a microreactor for the polymerization of other monomers within the solid matrix. A polypropylene skin encloses the second polymer phase, thereby preventing coalescence of particles in which the second phase is an amorphous, low-melting material (92). RGT has been defined as "controlled, reproducible polymerization of olefinic monomers on an active $MgCl_2$-supported catalyst, to give a growing, spherical granule that provides a porous reaction bed within which other monomers can be introduced and polymerized to form a polyolefin alloy" (93).

Today, RGT is able to provide products ranging from superstiff, high fluidity PP homopolymers to stiff/impact or clear/impact heterophasic copolymers and supersoft alloys, produced using the *Catalloy* process (31,68). The feasibility of producing heterophasic alloys containing up to 70% of multimonomer copolymers arises from the use of a controlled porosity catalyst and the ability to control the porosity of the growing polymer particle during the early stages of polymerization. Prepolymerization is applied to give the particles sufficient heat capacity to withstand injection into a gas-phase polymerization step.

Several models have been put forward to explain the mechanism of particle growth during polymerization. One of the most popular models is the "multigrain model," put forward by Ray and co-workers (94), in which the monomer diffuses into the catalyst macroparticle and polymerizes on the surface of the microparticles within, causing the macroparticle to expand progressively as polymerization proceeds. An investigation by Kakugo and co-workers (95) of nascent polymer morphology obtained using a $TiCl_3$ catalyst showed that the polymer particle comprised numerous globules, each of which contained some tens of much smaller primary particles. Recently, a model for particle growth with $MgCl_2$-supported catalysts has been proposed by Cecchin (68,96), who has also provided evidence for

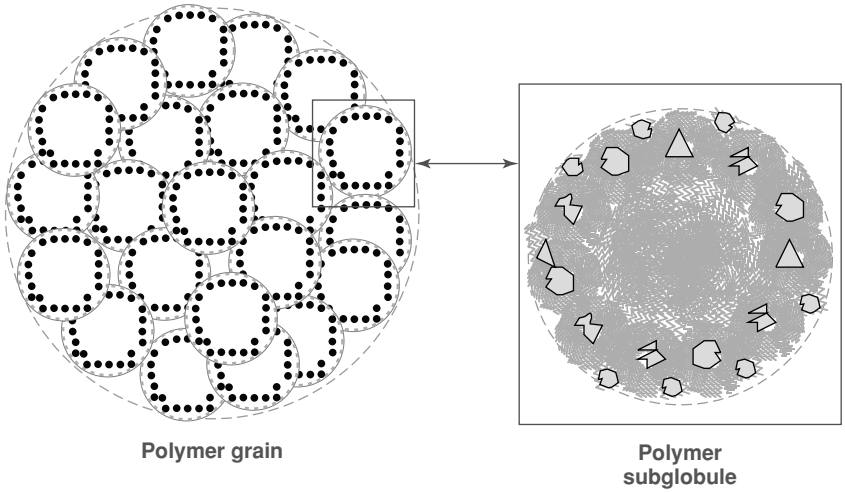

Fig. 9. Particle growth model for propylene polymerization with a $MgCl_2$-supported catalyst (96).

polymer "subglobule" formation within the growing particle. Again, these subglobules originate from clusters of primary crystallites, but the crystallites themselves are pushed to the surface of each subglobule as the polymer forms. This model, illustrated in Figure 9, explains the fact that, in the preparation of heterophasic copolymers via propylene homopolymerization followed by ethylene/propylene copolymerization, the rubbery ethylene/propylene copolymer is formed at the surface of the homopolymer subglobules, gradually filling up the pores within the particle. Clearly, the higher the porosity of the homopolymer matrix, the greater the proportion of (rubbery) copolymer that can be incorporated into the particle without running into problems of stickiness if the rubber phase blooms to the surface. Evidence for drifting of catalyst microparticles to the surface of polymer (sub)globules has been provided by scanning electron microscopy studies of prepolymerized catalyst particles (97).

Polymerization of Other Monomers Using Ziegler–Natta Catalysts

In addition to their widespread use in the production of polyethylene and polypropylene, Ziegler–Natta catalysts play an important role in the production of poly-1-butene and are also widely used in the manufacture of synthetic rubbers such as *cis*-1,4-polybutadiene and *cis*-1,4-polyisoprene, the synthetic equivalent of natural rubber. Ziegler–Natta catalysts for the manufacture of butadiene rubber, based on titanium, cobalt, nickel, or neodymium systems, are described elsewhere (see BUTADIENE POLYMERS). Isoprene rubber is produced using β-$TiCl_3$ (98), typically prepared by reaction of approximately equimolar quantities of $TiCl_4$ and Al-*i*-$(C_4H_9)_3$ in the presence of a small quantity of an ether. Increased catalyst activity can be obtained by incorporation of a sterically hindered phenoxyaluminum cocatalyst component (99). The latter component also gives increased activity in propene polymerization using $TiCl_3$ (100); in both cases the improvement

in catalyst performance can be attributed to selective complexation of the catalyst poison $RAlCl_2$. In addition to aluminum alkyls, poly(*N*-alkylaluminoxanes) have been found to be effective cocatalysts in isoprene polymerization (101). These components have cage structures (eg $[HAlN\text{-}i\text{-}C_3H_7]_6$) in which both Al and N atoms are tetracoordinated (102).

Cis-1,4-polymerization of conjugated dienes requires the presence of two coordination vacancies on the transition-metal atom, allowing bidentate coordination of the diene. β-$TiCl_3$ has a fiber-like structure in which the titanium atoms in the lattice are octahedrally coordinated to six chlorine atoms. The terminal titanium atoms are, however, incompletely coordinated and are linked to four or five chlorine atoms. Alkylation of the tetracoordinated titanium atoms will generate the double-vacancy species active in isoprene polymerization. Stereospecificity in diene polymerization can change dramatically if one of the coordination vacancies is blocked by a Lewis base. An interesting illustration of this (103) is that the addition of an external donor in isoprene polymerization with $TiCl_4$–$Al(C_2H_5)_3$ or $MgCl_2/TiCl_4$–$Al(C_2H_5)_3$ changes the catalyst stereospecificity to give mainly *trans*-1,4- rather than *cis*-1,4-polyisoprene. At the same time, a notable increase in isospecificity in propylene polymerization is observed.

$TiCl_3$-based and $MgCl_2$-supported catalysts have been developed for the production of poly-1-butene. $TiCl_3$ catalysts are used with dialkylaluminum halide cocatalysts, $Al(C_2H_5)_2I$ giving higher isotacticity than $Al(C_2H_5)_2Cl$ (104). Very high isotacticity has been obtained using $TiCl_3$ in combination with $Cp_2Ti(CH_3)_2$ (105). Much higher polymerization activity, as well as high isotacticity and broad MWD, is obtained using $MgCl_2$-supported catalysts, for example the catalyst system $MgCl_2/TiCl_4$/diisobutyl phthalate–$Al(C_2H_5)_3$–alkoxysilane (106).

Ziegler–Natta catalysts have also been developed for the polymerization of 4-methyl-1-pentene (107) and higher alpha-olefins. Polymerization activity decreases with increasing steric bulk of the monomer. For example, with the catalyst system $MgCl_2/TiCl_4$/ethyl benzoate–$Al(C_2H_5)_3$–ethyl benzoate the relative activities in propylene, 1-butene, and 4-methyl-1-pentene polymerization were 100:80:15 (108). For catalyst systems of type $MgCl_2/TiCl_4$/phthalate ester–AlR_3–alkoxysilane, the type of silane required is dependent on the steric bulk of the monomer. An active center having high stereospecificity in propylene polymerization may be too sterically hindered for effective polymerization of a bulkier monomer, propylene/1-butene copolymerization studies having shown (109) that the incorporation of 1-butene into the polymer chain decreases with increasing site stereospecificity. This phenomenon is also illustrated by the fact that nonbulky alkoxysilanes such as $(CH_3)_3SiOCH_3$ are effective donors in 4-methyl-1-pentene polymerization (110), whereas such donors are relatively ineffective in propylene polymerization.

Concluding Remarks

The dominant position of Ziegler–Natta catalysts in the manufacture of polyolefins, in particular PP, is likely to continue for a considerable length of time, despite the many developments taking place in the field of metallocene and other single-site catalysis. Indeed, the range of polymer types and grades is so varied

that there is ample scope for further development and implementation of both Ziegler–Natta and single-site catalysts.

It will be clear that the composition and characteristics of a Ziegler–Natta catalyst must be tailored such that the required polymer molecular structure and properties are obtained. Different catalysts are required for different polymer applications, and the recent development and implementation of $MgCl_2$-supported catalysts containing diether and succinate donors, for the production of narrow and broad MWD PP respectively, illustrates the ongoing activity in Ziegler–Natta catalyst research. The ability to control catalyst particle size, morphology, and porosity has allowed the development of advanced and versatile polymerization process technologies, so that the characteristics of the catalyst can be tuned to both process and product requirements.

Ziegler–Natta catalysts are complex systems and are still by no means fully understood, but significant advances in basic understanding have recently been made. This will continue, with both experimental and molecular modeling studies providing additional mechanistic insight, which in turn can be applied in the further development and implementation of these catalysts.

BIBLIOGRAPHY

1. G. Wilke, in G. Fink, R. Mülhaupt, and H. H. Brintzinger, eds., *Ziegler Catalysts. Recent Scientific Innovations and Technological Improvements*, Springer-Verlag, Berlin, 1995, p. 1.
2. Ger. Pat. 973626 (Filed Nov. 17, 1953), K. Ziegler, H. Breil, E. Holzkamp, and H. Martin; *Chem. Abstr.* **54**, 14794b (1960).
3. K. Ziegler, E. Holzkamp, H. Breil, and H. Martin, *Angew. Chem.* **67**, 541 (1955).
4. Ital. Pat. 535712 (Filed June 8, 1954), G. Natta (to Montecatini).
5. G. Natta, *J. Polym. Sci.* **16**, 143 (1955).
6. G. Natta, P. Pino, P. Corradini, F. Danusso, E. Mantica, E. Mazzanti, and G. Moraglio, *J. Am. Chem. Soc.* **77**, 1708 (1955).
7. P. Pino and R. Mülhaupt, *Angew. Chem., Int. Ed. Engl.* **19**, 857 (1980).
8. P. Pino and G. Moretti, *Polymer* **28**, 683 (1987).
9. P. Corradini, *Macromol. Symp.* **89**, 1 (1995).
10. G. Natta, P. Corradini, and G. Allegra, *J. Polym. Sci.* **51**, 399 (1961).
11. J. Boor, *Ziegler–Natta Catalysts and Polymerizations*, Academic Press, Inc., New York, 1979.
12. G. Guidetti, R. Zannetti, D. Ajo, A. Marigo, and M. Vidali, *Eur. Polym. J.* **16**, 1007 (1980).
13. U. S. Pat. 2692257 (Filed Apr. 28, 1951), A. Zletz (to Standard Oil of Indiana).
14. Belg. Pat. 530617 (Filed Jan. 27, 1953), J. P. Hogan and R. L. Banks (to Phillips Petroleum Co.).
15. H. R. Sailors and J. P. Hogan, *J. Macromol. Sci., Chem. A* **15**, 1377 (1981).
16. M. P. McDaniel, in D. D. Eley, H. Pines, and P. B. Weisz, eds., *Advances in Catalysis*, Vol. **33**, Academic Press, Inc., New York, 1985, p. 47.
17. H. Martin, in G. Fink, R. Mülhaupt, and H. H. Brintzinger, eds., *Ziegler Catalysts. Recent Scientific Innovations and Technological Improvements*, Springer-Verlag, Berlin, 1995, p. 15.
18. E. P. Moore, *Polypropylene Handbook. Polymerization, Characterization, Properties, Processing, Applications*, Hanser Publishers, Munich, 1996.

19. U.S. Pat. 4376851 (Filed Jan. 11, 1956), J. P. Hogan and R. L. Banks (to Phillips Petroleum Co.).
20. U.S. Pat. 4210738 (Filed Mar. 21, 1972), J. P. Hermans and P. Henrioulle (to Solvay).
21. B. L. Goodall and S. van der Vens, *Polypropylene and Other Polyolefins. Polymerization and Characterization*, Elsevier, Amsterdam, 1990, Chapt. "1".
22. A. Bernard and P. Fiasse, in T. Keii and K. Soga, eds., *Catalytic Olefin Polymerization*, Elsevier, Amsterdam, 1990, p. 405.
23. E. J. Arlman and P. Cossee, *J. Catal.* **3**, 99 (1964).
24. P. Corradini, V. Busico, and G. Guerra, *Comprehensive Polymer Science*, Vol. **4**, Pergamon Press, Oxford, U.K., 1988, p. 29.
25. A. Zambelli, M. C. Sacchi, P. Locatelli, and G. Zannoni, *Macromolecules* **15**, 211 (1982).
26. I. Tritto, M. C. Sacchi, and P. Locatelli, *Makromol. Chem.* **187**, 2145 (1986).
27. G. Natta, I. Pasquon, A. Zambelli, and G. Gatti, *J. Polym. Sci.* **51**, 387 (1961).
28. Y. Doi, S. Suzuki, and K. Soga, *Makromol. Chem., Rapid Commun.* **6**, 639 (1985).
29. A. Zambelli, I. Sessa, F. Grisi, R. Fusco, and P. Accomazzi, *Macromol. Rapid Commun.* **22**, 297 (2001).
30. J. A. Ewen, R. L. Jones, A. Razavi, and J. D. Ferrara, *J. Am. Chem. Soc.* **110**, 6255 (1988).
31. T. Simonazzi and U. Giannini, *Gazz. Chim. Ital.* **124**, 533 (1994).
32. U. Giannini, *Makromol. Chem., Suppl.* **5**, 216 (1981).
33. K.-Y. Choi and W. H. Ray, *J. Macromol. Sci., Rev. Macromol. Chem. Phys. C* **25**, 1 (1985).
34. Eur. Pat. 4647 (Filed Mar. 30, 1979), G. L. Goerke, B. E. Wagner, and F. J. Karol (to Union Carbide Corp.).
35. L. L. Böhm, D. Bilda, W. Breuers, H. F. Enderle, and R. Lecht, in G. Fink, R. Mülhaupt, and H. H. Brintzinger, eds., *Ziegler Catalysts. Recent Scientific Innovations and Technological Improvements*, Springer-Verlag, Berlin, 1995, p. 387.
36. F. J. Karol, K. J. Cann, and B. E. Wagner, in W. Kaminsky and H. Sinn, eds., *Transition Metals and Organometallics as Catalysts for Olefin Polymerization*, Springer-Verlag, Berlin, 1988, p. 149.
37. H. L. Hsieh, M. P. McDaniel, J. L. Martin, P. D. Smith, and D. R. Fahey, in R. B. Seymour and T. Cheng, eds., *Advances in Polyolefins*, Plenum Press, New York, 1985, p. 153.
38. P. Galli, L. Luciani, and G. Cecchin, *Angew. Makromol. Chem.* **94**, 63 (1981).
39. P. C. Barbè, G. Cecchin, and L. Noristi, *Adv. Polym. Sci.* **81**, 1 (1987).
40. P. Galli, P. C. Barbè, and L. Noristi, *Angew. Makromol. Chem.* **120**, 73 (1984).
41. P. Galli, *Macromol. Symp.* **78**, 269 (1994); *Macromol. Symp.* **112**, 1 (1996).
42. Eur. Pat 45977 (Filed Aug. 13, 1981), S. Parodi, R. Nocci, U. Giannini, P. C. Barbè, and U. Scatà (to Montedison).
43. J. V. Seppälä, M. Härkönen and L. Luciani, *Makromol. Chem.* **190**, 2535 (1989).
44. M. Härkönen, J. V. Seppälä, and T. Väänänen, in T. Keii and K. Soga, eds., *Catalytic Olefin Polymerization*, Elsevier, Amsterdam, 1990, p. 87.
45. A. Proto, L. Oliva, C. Pellecchia, A. J. Sivak, and L. A. Cullo, *Macromolecules* **23**, 2904 (1990).
46. T. Okano, K. Chida, H. Furuhashi, A. Nakano, and S. Ukei, in T. Keii and K. Soga, eds., *Catalytic Olefin Polymerization*, Elsevier, Amsterdam, 1990, p. 177.
47. Eur. Pat. 350170 (Filed June 13, 1989), N. Ishimaru, M. Kioka, and A. Toyota (to Mitsui).
48. J. C. Chadwick, G. M. M. van Kessel, and O. Sudmeijer, *Macromol. Chem. Phys.* **196**, 1431 (1995).
49. J. C. Chadwick, *Macromol. Symp.* **173**, 21 (2001).

50. Eur. Pat. 841348 (Filed Nov. 3, 1997), S. Ikai, H. Ikeuchi, H. Satoh, T. Inoue, and H. Sano (to Grand Polymer).
51. S. Yao and Y. Tanaka, *Macromol. Theory Simul.* **10**, 850 (2001).
52. P. Corradini, V. Busico, and G. Guerra, in W. Kaminsky and H. Sinn, eds., *Transition Metals and Organometallics as Catalysts for Olefin Polymerization*, Springer-Verlag, Berlin, 1988, p. 337.
53. V. Busico, P. Corradini, L. De Martino, A. Proto, V. Savino, and E. Albizzati, *Makromol. Chem.* **186**, 1279 (1985).
54. M. Terano, T. Kataoka, and T. Keii, *Makromol. Chem.* **188**, 1477 (1987).
55. E. Albizzati, U. Giannini, G. Morini, C. A. Smith, and R. C. Zeigler, in G. Fink, R. Mülhaupt, and H. H. Brintzinger, eds., *Ziegler Catalysts. Recent Scientific Innovations and Technological Improvements*, Springer-Verlag, Berlin, 1995, p. 413.
56. V. Busico, P. Corradini, L. De Martino, A. Proto, and E. Albizzati, *Makromol. Chem.* **187**, 1115 (1986).
57. L. Noristi, P. C. Barbè, and G. Baruzzi, *Makromol. Chem.* **192**, 1115 (1991).
58. M. C. Sacchi, I. Tritto, C. Shan, R. Mendichi, G. Zannoni, and L. Noristi, *Macromolecules* **24**, 6823 (1991).
59. R. Spitz, C. Bobichon, and A. Guyot, *Makromol. Chem.* **190**, 707 (1989).
60. M. C. Sacchi, F. Forlini, I. Tritto, R. Mendichi, G. Zannoni, and L. Noristi, *Macromolecules* **25**, 5914 (1992).
61. M. Kioka and N. Kashiwa, *J. Mol. Catal.* **82**, 11 (1993).
62. Eur. Pat. 361494 (Filed Sept. 29, 1989), E. Albizzati, P. C. Barbè, L. Noristi, R. Scordamaglia, L. Barino, U. Giannini, and G. Morini (to Himont).
63. Eur. Pat. 728724 (Filed Feb. 21, 1996), G. Morini and A. Cristofori (to Montell).
64. E. Albizzati, U. Giannini, G. Morini, M. Galimberti, L. Barino, and R. Scordamaglia, *Macromol. Symp.* **89**, 73 (1995).
65. L. Barino and R. Scordamaglia, *Macromol. Symp.* **89**, 101 (1995).
66. E. Albizzati, M. Galimberti, U. Giannini, and G. Morini, *Makromol. Chem., Macromol. Suppl.* **48/49**, 223 (1991).
67. Int. Pat. WO 00/63261 (Filed Apr. 12, 2000), G. Morini, G. Balbontin, Y. Gulevich, H. Duijghuisen, R. Kelder, P. A. Klusener, and F. Korndorffer (to Basell).
68. G. Cecchin, G. Morini, and A. Pelliconi, *Macromol. Symp.* **173**, 195 (2001).
69. N. Kashiwa, J. Yoshitake, and A. Toyota, *Polym. Bull. (Berlin)* **19**, 333 (1988).
70. J. C. Chadwick, in G. Fink, R. Mülhaupt, and H. H. Brintzinger, eds., *Ziegler Catalysts. Recent Scientific Innovations and Technological Improvements*, Springer-Verlag, Berlin, 1995, p. 427.
71. M. Kakugo, T. Miyatake, Y. Naito, and K. Mizunuma, *Macromolecules* **21**, 314 (1988).
72. K. Soga, J. R. Park, T. Shoino, and N. Kashiwa, *Macromol. Chem., Rapid Commun.* **11**, 117 (1990).
73. K. Soga, J. R. Park, H. Uchino, T. Uozumi, and T. Shiono, *Macromolecules* **22**, 3824 (1989).
74. K. Soga, *Makromol. Chem., Macromol. Symp.* **66**, 43 (1993).
75. M. C. Sacchi, C. Shan, P. Locatelli, and I. Tritto, *Macromolecules* **23**, 383 (1990).
76. M. C. Sacchi, F. Forlini, I. Tritto, P. Locatelli, G. Morini, G. Baruzzi, and E. Albizzati, *Macromol. Symp.* **89**, 91 (1995).
77. G. Morini, E. Albizzati, G. Balbontin, I. Mingozzi, M. C. Sacchi, F. Forlini, and I. Tritto, *Macromolecules* **29**, 5770 (1996).
78. V. Busico, R. Cipullo, G. Monaco, G. Talarico, M. Vacatello, J. C. Chadwick, A. L. Segre, and O. Sudmeijer, *Macromolecules* **32**, 4173 (1999).
79. V. Busico, R. Cipullo, G. Talarico, A. L. Segre, and J. C. Chadwick, *Macromolecules* **30**, 4786 (1997).
80. L. Barino and R. Scordamaglia, *Makromol. Theory Simul.* **7**, 407 (1998).

81. M. Boero, M. Parrinello, S. Hüffer, and H. Weiss, *J. Am. Chem. Soc.* **122**, 501 (2000).
82. J. C. Chadwick, G. Morini, E. Albizzati, G. Balbontin, I. Mingozzi, A. Cristofori, O. Sudmeijer, and G. M. M. van Kessel, *Macromol. Chem. Phys.* **197**, 2501 (1996).
83. T. Keii, M. Terano, K. Kimura, and K. Ishii, *Makromol. Chem., Rapid Commun.* **8**, 583 (1987).
84. B. Liu, H. Matsuoka, and M. Terano, *Macromol. Rapid Commun.* **22**, 1 (2001).
85. G. D. Bukatov and V. A. Zakharov, *Macromol. Chem. Phys.* **202**, 2003 (2001).
86. P. J. Tait, G. H. Zohuri, A. M. Kells, and I. D. McKenzie, in G. Fink, R. Mülhaupt, and H. H. Brintzinger, eds., *Ziegler Catalysts. Recent Scientific Innovations and Technological Improvements*, Springer-Verlag, Berlin, 1995, p. 343.
87. G. D. Bukatov, V. S. Goncharov, and V. A. Zakharov, *Macromol. Chem. Phys.* **196**, 1751 (1995).
88. H. Mori, K. Tashino, and M. Terano, *Macromol. Rapid Commun.* **16**, 651 (1995).
89. H. Mori, K. Tashino, and M. Terano, *Macromol. Chem. Phys.* **197**, 895 (1996).
90. H. Mori, T. Iizuka, K. Tashino, and M. Terano, *Macromol. Chem. Phys.* **198**, 2499 (1997).
91. P. Galli, *Prog. Polym. Sci.* **19**, 959 (1994).
92. J. C. Chadwick, *Encyclopedia of Materials: Science and Technology*, Elsevier, 2001, p. 7703.
93. P. Galli and J. C. Haylock, *Makromol. Chem., Macromol. Symp.* **63**, 19 (1992).
94. R. A. Hutchinson, C. M. Chen, and W. H. Ray, *J. Appl. Polym. Sci.* **44**, 1389 (1992).
95. M. Kakugo, H. Sadatoshi, M. Yokoyama, and K. Kojima, *Macromolecules* **22**, 547 (1989).
96. G. Cecchin, E. Marchetti, and G. Baruzzi, *Macromol. Chem. Phys.* **202**, 1987 (2001).
97. J. T. M. Pater, G. Weickert, J. Loos, and W. P. M. van Swaaij, *Chem. Eng. Sci.* **56**, 1 (2001).
98. E. Schoenberg, H. A. Marsh, S. J. Walters, and W. M. Saltman, *Rubber Chem. Technol.* **52**, 526 (1979).
99. Eur. Pat. 107871 (Filed Sept. 30, 1983), J. C. Chadwick and B. L. Goodall (to Shell).
100. B. L. Goodall, in W. Kaminsky and H. Sinn, eds., *Transition Metals and Organometallics as Catalysts for Olefin Polymerization*, Springer-Verlag, Berlin, 1988, p. 361.
101. A. Mazzei, S. Cucinella, and W. Marconi, *Makromol. Chem.* **122**, 168 (1969).
102. A. Balducci, M. Bruzzone, S. Cucinella, and A. Mazzei, *Rubber Chem. Technol.* **48**, 736 (1975).
103. K. Soga, T. Sano, K. Yamamoto, and T. Shiono, *Chem. Lett. (Japan)* 425 (1982).
104. S. van der Ven, *Polypropylene and other Polyolefins. Polymerization and Characterization*, Elsevier, Amsterdam, 1990, Chapt. 11.
105. K. Soga and H. Yanagihara, *Makromol. Chem.* **189**, 2839 (1988).
106. U. S. Pat. 6306996 (Filed Mar. 4, 1999), G. Cecchin, G. Collina, and M. Covezzi (to Basell).
107. L. C. Lopez, G. L. Wilkes, P. M. Stricklen, and S. A. White, *J. Macromol. Sci., Rev. Macromol. Chem. Phys. C* **32**, 301 (1992).
108. N. Kashiwa and J. Yoshitake, *Polym. Bull. (Berlin)* **11**, 485 (1984).
109. M. C. Sacchi, Z.-Q. Fan, F. Forlini, I. Tritto, and P. Locatelli, *Macromol. Chem. Phys.* **195**, 2805 (1994).
110. U. S. Pat. 4659792 (Filed Dec. 23, 1985), N. Kashiwa and K. Fukui (to Mitsui).

JOHN C. CHADWICK
Dutch Polymer Institute,
Eindhoven University of Technology

ACRYLIC FIBERS

Introduction

The first reported synthesis of acrylonitrile [107-13-1] and polyacrylonitrile (PAN) [25014-41-9] was in the 1890s (1). The polymer received little attention for a number of years, until shortly before World War II, because there were no known solvents and the polymer decomposes before reaching its melting point. The first breakthrough in developing solvents for PAN occurred at I. G. Farben in Germany, where fibers made from the polymer were dissolved in aqueous solutions of quaternary ammonium compounds, such as benzylpyridinium chloride, or of metal salts, such as lithium bromide, ammonium thiocyanate, and zinc

Encyclopedia of Polymer Science and Technology. Copyright John Wiley & Sons, Inc. All rights reserved.

chloride (2). In the United States, DuPont discovered an organic solvent for PAN, *N,N*-dimethylformamide (DMF) (3,4). The same solvent was discovered independently by I. G. Farben at about the same time (5) (see ACRYLONITRILE AND ACRYLONITRILE POLYMERS).

Using DMF as the spinning solvent, DuPont produced the first commercial acrylic fiber under the trade name Orlon® in 1950. Orlon® was spun using a "dry spinning" process at a plant in Camden SC. Shortly afterward, Chemstrand, a joint venture of Monsanto and American Viscose (now Solutia), introduced Acrilan® acrylic, produced using Monsanto polymer technology and American Viscose wet spinning technology with *N,N*-dimethylacetamide (DMAc) solvent. As is common with new technologies, both products got off to rocky starts, Orlon with poor dyeing performance, Acrilan with fibrillation, but by the late 1950s each had solved the initial problems and established viable markets.

Modacrylic fibers (defined in the United States as those with 35–85% by weight acrylonitrile units) can be dissolved by more conventional solvents, such as acetone, and so were earlier on the market. Union Carbide introduced the first flame-resistant modacrylic fiber in 1948 under the trade names Vinyon N and Dynel. Vinyon N was a continuous filament yarn; Dynel was the staple form. Both were based on 60% vinyl chloride – 40% acrylonitrile copolymer.

During the 1950s, at least 18 companies began production of acrylic fibers. Because acrylic fibers require a spinning solvent, and newly discovered solvents received patent protection, the range of technology used commercially is far greater for acrylics than for any other fiber. The most significant were American Cyanamid's aqueous sodium thiocyanate wet spinning process, and Asahi's nitric acid wet spinning process. In the 1950s and 1960s, world production was concentrated in western Europe, Japan, and the United States. By 1960, annual worldwide production had risen to over 100 million kilograms. Once staple processes were developed, acrylic fibers became a significant competitor in markets held primarily by woolen fibers. By 1963 the carpet and sweater markets accounted for almost 50% of the total acrylic production. In the 1970s, the growth rate in the United States and Western Europe decreased sharply. This was due to the maturing of the wool replacement market and loss of market to nylon in carpeting and to polyester in many apparel applications. In the 1970s there was rapid growth of acrylic fiber production capacity in Japan, eastern Europe, and developing countries. By 1981 an estimated overcapacity of approximately 21% had developed. The 1990s saw significant shrinkage of acrylic production in the United States as DuPont and Mann Industries (formerly Badische) exited the business. Significant change has continued into the new century. In 2002, Sterling (formerly Cytec) significantly reduced production of commodity acrylics at their Pace FL plant. These changes have left Solutia as the principal U.S. supplier. In Europe, the changes have been mainly swaps of ownership, with Acordis now having both the Courtaulds and Hoechst businesses, and Fraver, an Italian firm, taking over Bayer's business. Aksa in Turkey, with the world's largest acrylic fiber plant, has become an important supplier to Europe. Explosive industry growth has taken place in the Far East, particularl y China, where plants based on DuPont and Sterling (Cytec) processes have proliferated. China now has 22% of world capacity, versus 9% 10 years earlier. Japan has reduced capacity, with Asahi Chemical being the latest to announce closure (March 2003) of their

business. Modacrylics have all but disappeared from the marketplace, as demand for flame-retardant textiles have been met by treated cotton or other synthetics at lower cost. A few new markets have emerged, such as carbon-fiber precursors and asbestos replacement fibers, but the volume is small compared to that of the markets lost. For acrylic producers, profit will continue to be sparse.

Physical Properties

Acrylic fibers are sold mainly as staple and tow. Staple lengths may vary from 25 to 150 mm, depending on the end use. Fiber fineness may vary from 1.0 to 22 dtex (0.9–20 dpf; dpf = denier per filament), 2.2 dtex (2.0 dpf), and 1.3 dtex (1.2 dpf) are the most common forms. Tow is sold as a bundle of up to 2.2 million kilotex (2.0 million total denier).

The fiber cross-section under microscopic examination is generally one of three shapes (Fig. 1)—round (wet spun, slow coagulation), bean (wet spun, fast coagulation), or dogbone-shaped (dry spun). It is also possible to produce acrylics with special shapes, such as ribbon or mushroom, by use of shaped or bicomponent spinnerettes. The cross-section may show particles such as TiO_2 added to reduce luster or other pigment to provide coloration. The surface of acrylic fibers is fibrillar, with the fibril size dependent on the spinning process (Fig. 2).

The physical properties of these fibers are compared with those of natural fibers and other synthetic fibers in Table 1.

The elastic properties of these fibers can be characterized as wool-like, with high elongation and elastic recovery. The tensile strength of acrylics and modacrylics is about the same, both considerably lower than that of other synthetics but higher than that of wool, of and about the same as that of cotton. These elastic properties rank acrylics and wool as compliant fibers, yielding fabric with a characteristically soft handle. Acrylics with tenacities as high as 80 cN/tex (9 gf/den) can be produced (8), but these are usually from higher molecular weight polymers, with low comonomer content and higher stretch orientation. Specialty products such as carbon-fiber precursor and cement-reinforcing fiber are produced using this technology.

The mechanical properties of acrylic fiber are deficient under hot-wet conditions. This is primarily due to the fact that the wet T_g of acrylonitrile copolymers is lower than the boiling point of water. Textile wet-processing must be carried out in such a way as to minimize yarn or fabric distortion. Shape retention and maintenance of original bulk under the lower temperatures in home laundering cycles are acceptable. Typical stress–strain curves for acrylic fiber in air and in wet conditions are shown in Figure 3.

Moisture regain, a property that has a great effect on wear comfort, at about 2%, is reasonably good though not as high as that of cotton (7%) or wool (14%). This property can be enhanced by adding hydrophilic comonomers or by generating a porous internal structure in the fiber. Dunova, an acrylic formerly marketed by Bayer, achieved moisture absorption and transport by internal porosity. The adequate regain plus their high compliancy make acrylics competitive in the wear-comfort markets. However, acrylics cannot match the wrinkle resistance and crease retention of polyester.

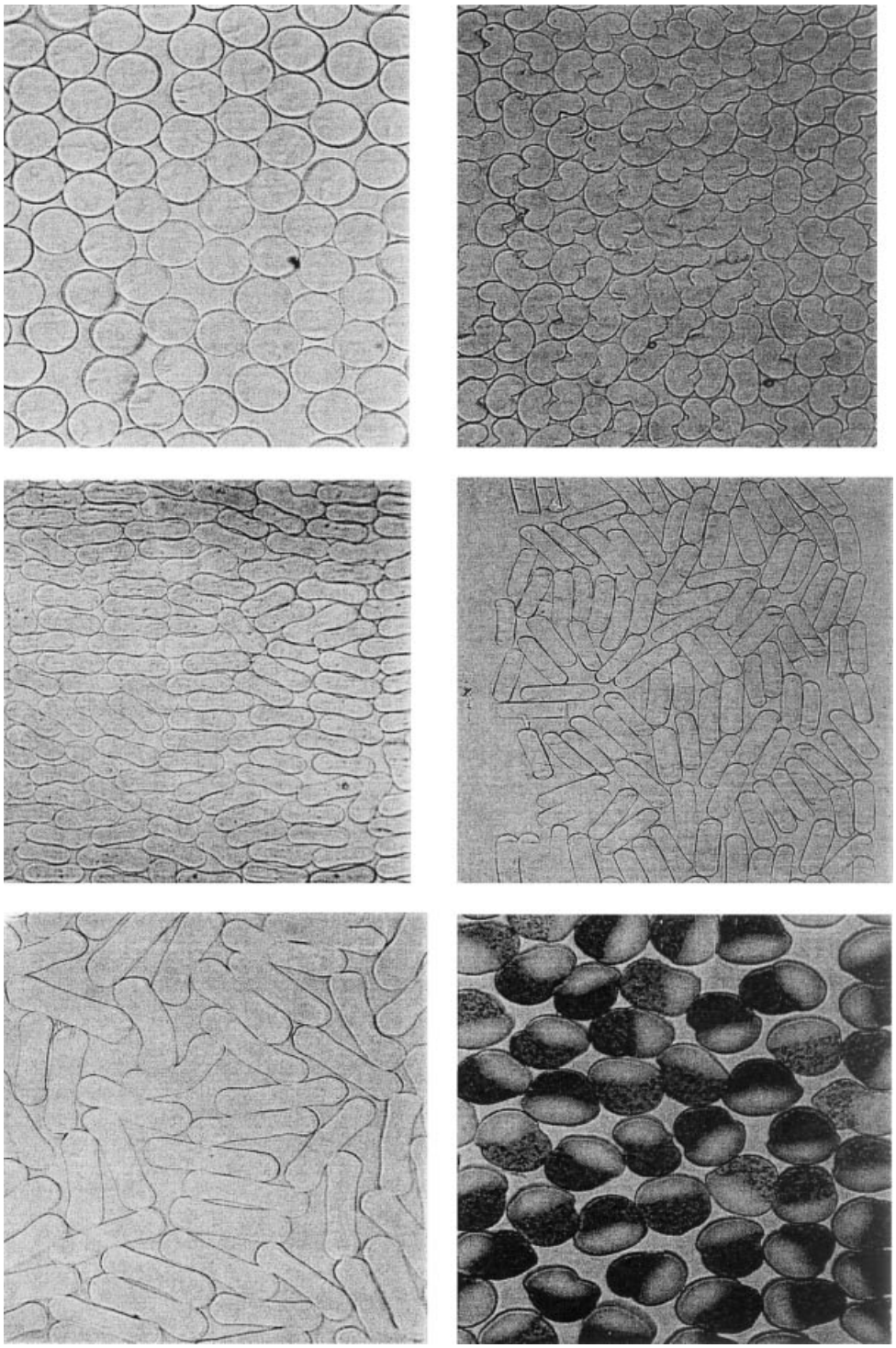

Fig. 1. Acrylic fiber cross sections (Scale: 1 mm = 10 μm).

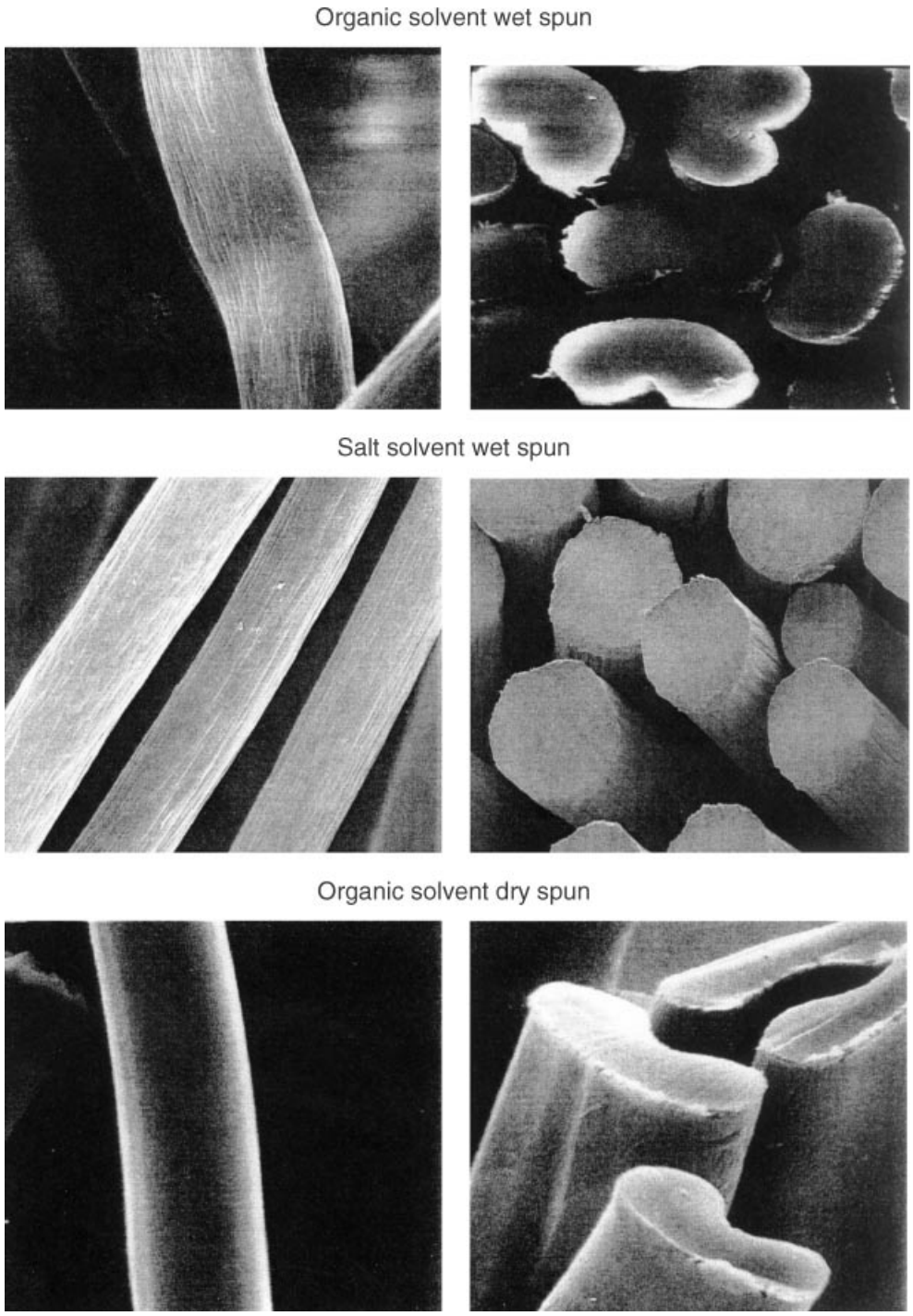

Fig. 2. Acrylic fiber structure comparisons (Scale: 1 mm = 0.5 μm).

Table 1. Physical Properties of Staple Fibers[a]

Property	Acrylic	Modacrylic	Nylon-6,6	Polyester	Polyolefin	Cotton	Wool
Specific gravity	1.14–1.19	1.28–1.37	1.14	1.38	0.90–1.0	1.54	1.28–1.32
Tenacity, N/tex[b]							
Dry	0.09–0.33	0.13–0.25	0.26–0.64	0.31–0.53	0.31–0.40	0.18–0.44	0.09–0.15
Wet	0.14–0.24	0.11–0.23	0.22–0.54	0.31–0.53	0.31–0.40	0.21–0.53	0.07–0.14
Loop/knot tenacity	0.09–0.3	0.11–0.19	0.33–0.52	0.11–0.50	0.27–0.35		
breaking elongation, %							
Dry	35–55	45–60	16–75	18–60	30–150	<10	25–35
Wet	40–60	45–65	18–78	18–60	30–150	25–50	
Average modulus, N/tex[b]	0.44–0.62	0.34	0.88–0.40	0.62–2.75	1.8–2.65		
dry elastic recovery, %							
2% stretch	99	99–100		67–86		74	99
10% stretch		95	99	57–74	96		
20% stretch							65
Electrical resistance	High	High	Very high	High	High	Low	Low
Static buildup	Moderate	Moderate	Very high	High	High	Low	Low
Flammability	Moderate	Low	Self-extinguishing	Moderate	Moderate	Spontaneous ignition at 360°C	Self-extinguishing
Limiting oxygen index	0.18	0.27	0.20	0.21		0.18	0.25
Char/melt	Melts	Melts	Melts, drips	Melts, drips	Melts	Chars	Chars
Resistance to sunlight	Excellent	Excellent	Poor; must be stabilized	Good	Poor; must be stabilized	Fair; degrades	Fair; degrades
Resistance to chemical attack	Excellent	Excellent	Good	Good	Excellent	Attacked by acids	Attacked by alkalies, oxidizing, and reducing agents
Abrasion resistance	Moderate	Moderate	Very good	Very good	Excellent	Good	Moderate
Index of birefringence	0.1		0.6	0.16			0.01
Moisture regain, 65% r.h, 21°C, %	1.5–2.5	1.5–3.5	4–5	0.1–0.2	0	7–8	13–15

[a] Ref. 7.

[b] To convert N/tex to gf/den, multiply by 11.3.

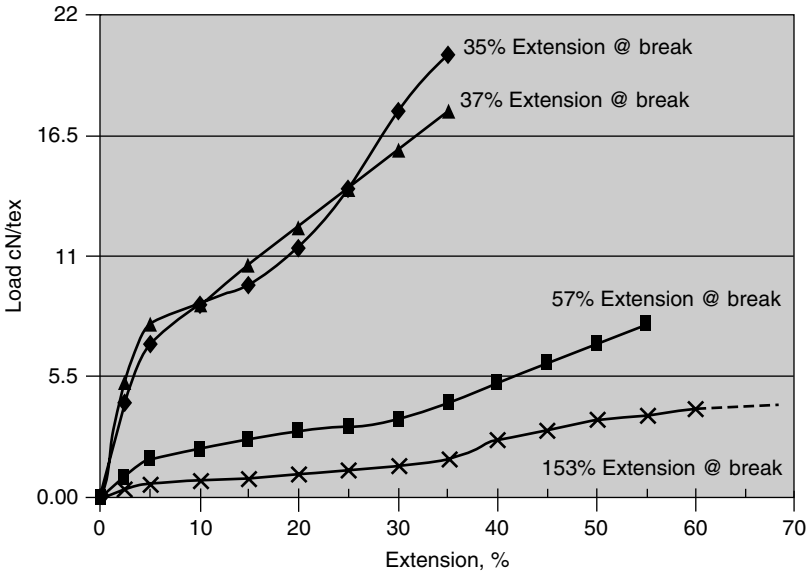

Fig. 3. Acrylic fiber stress–strain behavior at wet and dry conditions. —◆— 30°C dry; —■— 95°C dry; —▲— 25°C wet; —×— 90°C wet. To convert cN/tex to gf/den, multiply by 0.113.

Chemical Properties

Among the outstanding properties of acrylic fibers is their very strong resistance to sunlight. One study (9), found that the acrylic fibers resisted degradation eight times longer than olefin fibers, over five times longer than either cotton or wool, and almost four times longer than nylon. This property makes the acrylics particularly useful for outdoor applications, such as in awnings, tents, and sandbags, as well as for upholstery for autos and outdoor furniture. Pigmented acrylic or modacrylic fibers with lightfast colors are particularly useful for outdoor applications.

Acrylic fibers are also resistant to all biological and most chemical agents. Weak acids or bases, organic solvents, and oxidizing agents affect acrylics very little. They are attacked by strong bases and highly polar organic solvents such as DMAc, DMF, and DMSO (dimethyl sulfoxide). Acrylic fibers tend to be much more susceptible to chemical attack by alkali than by acid. For example, acrylic fibers are stable for up to 24 h at 100°C in 50% sulfuric acid: these same fibers begin degrading with <0.5% sodium hydroxide at the same exposure time and temperature (10).

In resistance of fibers to oxidizing agents, Orlon acrylic (a former DuPont product) was compared to cotton and acetate yarns (10). The acrylic yarn is far superior in strength retention. After 6 h of exposure to bleach, the cotton and acetate yarns had completely deteriorated, whereas the acrylic retained approxmately 92% of its original strength.

The excellent chemical resistance of acrylic fiber stems from its laterally bonded structure. Dipole bonds, formed between nitrile groups of adjacent chains,

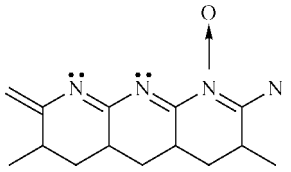

Fig. 4. Structure of air-oxidized PAN.

must be broken before chemical attack, melting, or solvation can occur. In addition, the repulsive forces between adjacent nitriles in one chain result in a very stiff polymer backbone, which yields very little entropy gain when the bonds between adjacent chains are broken in solvation or melting. Therefore, relatively high temperatures are required for solvation and melting.

Acrylic fibers discolor and decompose rather than melt when heated. The discoloration process involves formation of a ladder structure containing conjugated C=N double bonds. Some color formation accompanies fiber production; commercial acrylics often contain low levels of blue dye or pigment to mask the yellow tinge. In comparison to polyester, acrylic fiber whiteness stability in sublimation dyeing is deficient; this limits acrylic utility in fleece and sheeting markets. Extensive heating in air leads to a color progression, ending in a black fiber having the structure shown in Figure 4. This product, termed Panox, is useful as a flame-resistant textile. Conversion of acrylic fiber to Panox is the first step in carbon fiber production.

Flammability. Most apparel uses either do not have any flammability standard, or only a modest one which serves to eliminate "torch" fabrics. More rigorous standards are applied for end uses such as carpet, children's sleepwear, drapery, and bedding. Fibers for these applications must be self-extinguishing after removal from the ignition source. Cotton, rayon, and acrylics burn with the formation of a char. The char acts as a wick that feeds additional fuel to the flame. Nylon and polyester meet some flammability tests by melting away from the ignition source. Modacrylics self-extinguish by generation of chlorine radicals, which interfere with the flame-propogation mechanism. This is generally achieved by incorporating vinylidene chloride or vinyl chloride comonomers. Blends of a char-forming fiber with a meltable one require incorporation of an active fire-retardant to meet any stringent flammability test (see FLAMMABILITY; FIRE RETARDANTS).

A measurement used to compare the flammability of textile fibers is the limiting oxygen index (LOI). This quantity describes the minimum oxygen content (%) in nitrogen necessary to sustain candle-like burning. Values of LOI, considered a measure of the intrinsic flammability of a fiber, are listed in Table 2 in order of decreasing flammability.

Polymer Analysis

Many techniques are available for characterizing acrylic and modacrylic materials in order to establish the dyesite content, molecular weight, and chemical

Table 2. Limiting Oxygen Index of Textile Fibers[a] in Order of Decreasing Flammability

Fiber	LOI	Ignition temperature, °C
Cotton	18.0	400
Acrylic	18.2	560
Rayon	19.7	420
Nylon	20.1	530
Polyester	21.0	450
Wool	25.0	600
Modacrylic	27.0	690
Verel modacrylic	33.0	Self-extinguishing
100% PVC	37.0	Self-extinguishing

[a] Ref. 11.

composition. The dye-site content of the polymer may be determined by dyeing a polymer suspension with a cationic dye of known molecular weight. The dye attached to the polymer dye sites may be measured directly of by difference. The dye sites themselves, in most acrylics and modacrylics, are sulfonate and sulfate end groups derived from the free-radical initiator used in polymerization. Therefore, the dye site content of the polymer can be measured by potentiometric titration of the strong acid groups or by determining the sulfur content of the polymer. The low levels of sulfur normally required for fiber dyeability can be measured accurately by X-ray fluorescence. Some acrylics have added "dye receptors"—acidic monomers such as sodium *p*-vinylbenzene sulfonate (SSS) or itaconic acid (IA). This sulfonate can be determined directly using ultraviolet spectroscopy. Sulfur analysis will yield a total dye-site value including the end groups and the SSS. Potentiometric titration of a polymer containing IA will yield two breaks, one for the sulfonate/sulfate end groups, and a second for one of the IA carboxyls. Dyeing of polymers containing weak-acid dye receptors such as IA does not give an accurate value for total sites, as the dyeing of the IA is incomplete.

The weight-average molecular weight of the polymer can be measured using gel-permeation chromatography with low-angle-light-scattering detection (see CHROMATOGRAPHY, SIZE EXCLUSION). Solvent systems such as DMF–LiCl are employed to eliminate ionic effects (12). Osmometry may be used to obtain number-average molecular weight (13). These methods are useful to provide absolute values and to determine changes in molecular-weight distribution. However, methods based on solution viscosity are the most popular in commercial practice. The simplest method is to measure the viscosity of a solution of the polymer at a specified concentration and temperature. This may be done using a capillary viscometer. For quality assurance purposes, usually a single point ("specific viscosity") determination is sufficient. The viscosity-average molecular weight may be obtained by extrapolating specific viscosities at several concentrations to zero concentration. The intrinsic viscosity thus derived is then used in the Staudinger equation (14) or Cleland–Stockmayer equation (15) to give the viscosity-average molecular weight (see MOLECULAR WEIGHT DETERMINATION).

Typical acrylic polymers have number-average molecular weights in the 30,000–40,000 range, or roughly 700 repeat units. The weight-average

molecular weight is typically in the range 90,000–120,000, with a polydispersity index (M_w/M_n) between 2.0 and 3.5. Fiber producers favor the lowest molecular weight and broadest distribution that is consistent with acceptable fiber physical properties, as that will result in the highest number of sulfate and sulfonate dye sites.

Analytical methods for identifying and quantifying the chemical composition of acrylic and modacrylic materials are numerous. The usual comonomers found in acrylics—vinyl acetate, methyl acrylate, and methyl methacrylate—can be identified using NMR. They may be quantified using infrared (IR) spectroscopy by the absorbance of the carbonyl group; calibration of the method is sometimes accomplished by preparation of C^{14} tagged polymer standards. Sulfonated monomers, such as SSS or sodium *p*-(sulfophenyl) methallyl ether, can be detected by strong ultraviolet absorbance due to the phenyl group. Halogen monomers can be quantitatively measured by pyrolyzing the polymer and analyzing the pyrolysis products by halide titration. X-ray fluorescence may also be used to determine the concentration of specific halogens. Comonomer content may also be quantified by differential scanning calorimetry of a water–polymer slurry. The mole fraction of comonomer depresses the melting point linearly (16).

Fiber Characterization

To establish whether a fiber or fabric is acrylic or a blend containing acrylic, a portion should be separated into the individual filaments and introduced in a density gradient column [ASTM DI505-8ST (density gradient)]. Acrylic fibers have a density of 1.17 ± 0.01. An IR scan of a KBr pellet of ground fiber can be used to identify the presence of nitrile groups. It is more difficult to establish the fiber supplier. A library of cross sections, known comonomer type, and other specific information is required. Since many producers now use almost identical technology, it may not be possible to achieve positive identification unless the fiber contains a marker.

In addition to characterizing the properties introduced by the choice of comonomers and the polymerization process itself, further characterization is required to describe the properties imparted by spinning and subsequent downstream processing. These properties relate to the order and microstructure of the fibers, and the resultant performance characteristics, such as crimp retention, abrasion resistance, and mechanical properties. Mechanical testing, to determine breaking elongation, tenacity, and modulus of elasticity, is carried out using devices such as the Instron. Dry-heat shrinkage and shrinkage in boiling water are measured by determining the difference in the length of a section of fiber after treatment at specified conditions. Other properties important to ease of processing or the end use include finish level, crimp frequency and amplitude, whiteness, and dyeing rate.

Acrylonitrile Polymerization

Virtually all acrylic fibers are made from acrylonitrile combined with at least one other monomer. The comonomers most commonly used are neutral comonomers,

such as methyl acrylate [96-33-3] and vinyl acetate [108-05-4] to increase the solubility of the polymer in spinning solvents, modify the fiber morphology, and improve the rate of diffusion of dyes into the fiber. Sulfonated monomers, such as sodium *p*-(vinylbenzene)sulfonate [27457-28-9] (SSS), sodium methallyl sulfonate [1561-92-8] (SMAS), and sodium *p*-(sulfophenyl) methallyl ether [1208-67-9] (SPME) are used to provide additional dye sites or to provide a hydrophilic component in water-reversible-crimp bicomponent fibers. Halogenated monomers, usually vinylidene chloride [75-35-4] or vinyl chloride [75-01-4], impart flame resistance to fibers used in the home furnishings, awning, and sleepwear markets.

Polymerization Methods. Acrylonitrile and its comonomers can be polymerized by any free-radical method. Bulk polymerization is the most fundamental of these, but its practical use is limited by its autocatalytic nature. Aqueous dispersion polymerization is the most common commercial method; solution polymerization, where the spin solvent serves as the polymerization medium, is the other commercial process. Emulsion polymerization is used for certain modacrylic compositions.

Aqueous Dispersion Polymerization. By far the most widely used method of polymerization in the acrylic fibers industry is aqueous dispersion (also called suspension). When inorganic compounds such as persulfates, chlorates, or hydrogen peroxide are used as radical generators, the initiation and primary radical growth steps occur mainly in the aqueous phase. Chain growth is limited in the aqueous phase, however, because the monomer concentration is normally low and the polymer is insoluble in water. Nucleation occurs when aqueous chains aggregate or collapse after reaching a threshold molecular weight. If many polymer particles are present, as is the case in commercial continuous polymerizations, the dissolved radicals are likely to be captured on the particle surface by a sorption mechanism. The particle surface is swollen with monomer. Therefore, the polymerization continues in the swollen layer and the sorption becomes irreversible as the chain end grows into the particle.

Since polymer swelling is minimal and the aqueous solubility of acrylonitrile is relatively high, the tendency for radical capture is limited. Consequently, the rate of particle nucleation is high throughout the course of the polymerization, and particle growth occurs predominantly by a process of agglomeration of primary particles. Unlike emulsion particles of a readily swollen polymer, such as polystyrene, the acrylonitrile aqueous dispersion polymer particles are massive agglomerates of primary particles which are approximately 100 nm in diameter.

Redox initiation is normally used in commercial production of polymers for acrylic fibers. This type of initiator can generate free radicals in an aqueous medium efficiently at relatively low temperatures. The most common redox system consists of ammonium or potassium persulfate (oxidizer), sodium bisulfite (reducing agent), and ferric or ferrous ion (catalyst). The mechanism is shown in Figure 5. This redox system works at pH 2.0–3.5, where the bisulfite ion predominates and the ferric ion is soluble. The sulfate and sulfonate ion-radicals react with monomer to initiate rapid chain growth. Termination occurs by radical recombination or by chain transfer. Bisulfite ion is both a reducing agent, and a chain-transfer agent; it reacts by transferring a hydrogen radical to terminate the chain, thus producing a bisulfite radical to initiate a new chain. The bisulfite concentration has a pronounced effect on polymer molecular weight with virtually

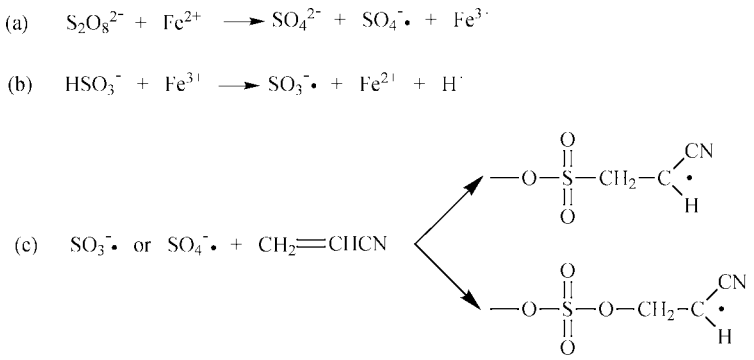

Fig. 5. Persulfate redox initiation mechanism.

no effect on the overall rate of polymerization (17). The ratio of bisulfite to persulfate in the reaction mixture has a strong effect on the dye-site content of the polymer (17,18). Bisulfite chain transfer increases the total dye-site content of the polymer by reducing the polymer molecular weight but at the same time produces chains with just one dyesite. At a given molecular weight the dye-site content of the polymer can, in theory, vary from two per chain at low bisulfite levels to one per chain at very high bisulfite levels.

In commercial practice, excess reducing agent to oxidizing agent ratios are used, for example, molar ratios of bisulfite to persulfate ranging from 5 to 15. These high ratios give narrower molecular weight distributions and, for a given molecular weight, relatively low conversion to polymer. Low conversion is an effective means of minimizing branching and color producing side reactions.

A comprehensive review of aqueous polymerization has been published (19). Many reviews of acrylonitrile polymerization have been published (20–23).

In commercial practice, polymerization is effected in a continuous-stirred-tank reactor (CSTR), a system in which all components are fed continuously and mixed, and the product is continuously discharged. For start-up, the reactor is charged with a certain amount of pH-adjusted water or the reactor is filled with overflow from another reactor already operating at steady state. The reactor feeds are metered in at a constant rate for the entire course of the production run, which normally continues until equipment cleaning or maintenance is needed. A steady state is established by taking an overflow stream at the same mass flow rate as the combined feed streams. The reaction vessel is normally an aluminum alloy; this minimizes scale buildup as the wall provides a sacrificial surface. The reactor is jacketed; steam may be introduced to heat the contents for start-up, but once the polymerization is initiated, water is circulated in the jacket to remove the heat of polymerization and maintain a constant temperature, usually 50–60°C.

An example of a continuous aqueous dispersion process is shown in Figure 6 (24). A monomer mixture composed of acrylonitrile and up to 10% of a neutral comonomer, such as methyl acrylate or vinyl acetate, is fed continuously. Polymerization is initiated by feeding aqueous solutions of potassium persulfate (oxidizer), sulfur dioxide (reducing agent), ferrous iron (promoter), and sodium bicarbonate (buffering agent). Alternately the system may employ a sodium bisulfite/sulfur

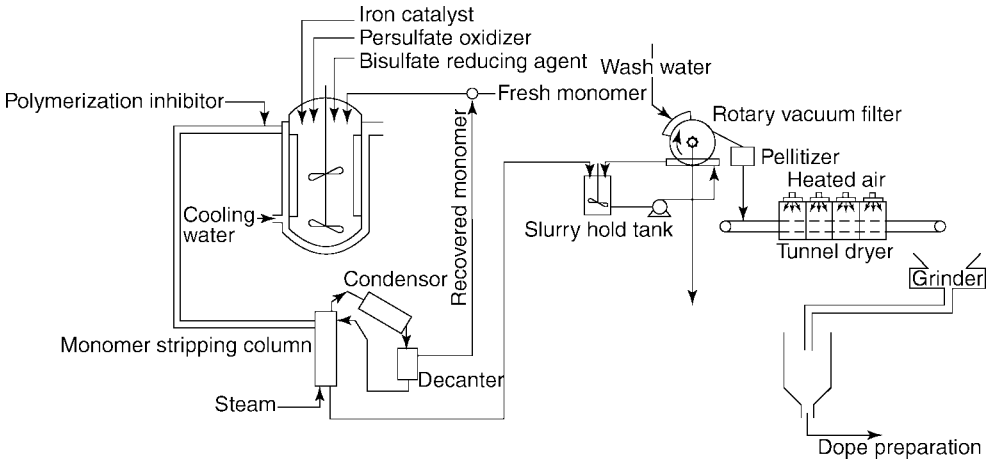

Fig. 6. CSTR Dispersion polymerization process.

dioxide or a sodium bisulfite/sulfuric acid buffer. The aqueous and monomer feed streams are fed at rates that give a reactor dwell time of 40–120 min, and a feed ratio of water to monomer in the range 2–5. The reactor overflow, an aqueous slurry of polymer particles, is mixed with an iron chelating agent, or the pH is raised to stop the polymerization. The slurry is then fed to the top section of a baffled monomer-separation column. The separation of unreacted monomer is effected by contacting the slurry with a countercurrent flow of steam introduced at the bottom of the column. Monomer plus water is condensed from the overheads stream and the monomer separated using a decanter, the water phase being returned to the column. The stripped slurry is taken from the column bottoms stream, and the polymer separated using a continuous vacuum filter. After filtration and washing, the polymer is pelletized, dried, ground, and then stored for later spinning.

A less desirable recovery process is to filter or centrifuge the slurry (with washing) to recover the polymer and then pass the filtrate plus wash water through a conventional distillation tower to recover the monomers. Delaying monomer removal may increase operator exposure, results in monomer in drier emissions, and reduces acrylonitrile yield through emissions and a side reaction. The need for monomer recovery may be minimized by using two-stage filtration with the first stage filtrate recycled to the reactor. Nonvolatile monomers, such as SSS, can be partially recovered in this manner. This makes process control more difficult because some reaction by-products can affect the rate of polymerization and the concentration of the recycle stream may vary.

Cost reduction has been a focus of fiber producers since the overall market for acrylic fibers in developed countries has not grown. A significant savings is realized by operating continuous aqueous dispersion processes at very low water-to-monomer ratios. Mitsubishi Rayon, for example, has reported ratios as low as 1.75 (25,26). This compares to ratios of 4–5 widely used in the 1970s. The low water-to-monomer ratios produce a change in the nucleation and particle growth mechanisms that yields denser polymer particles. The dense particles yield a fluid

reaction mass, so long as conversion is relatively high. Removal of the heat of polymerization is more difficult in low water-to-monomer polymerizations as there is more heat generated per unit volume. The cost reduction comes in the drying step. While conventional water-to-monomer ratios give wet cake moisture levels of 200% (dry basis), the modified process yields wet cake moisture levels of 100% or less. Thus a savings in drying cost is realized. The low water-to-monomer process has the added advantage of increased reactor productivity.

After monomer removal by slurry distillation, salts are removed from the polymer by washing, either on a rotary vacuum filter or centrifuge. In the case where fiber will be produced from aqueous salt spin solvents such as sodium thiocyanate (NaSCN), the polymer cake may be used without drying to make a spin dope. With organic solvents, a drying step is required. Both belt dryers (with a pretreatment of pelletizing the polymer) and cyclone dryers are used; the former is most common. After drying, the pellets are again reduced to a powder and sent to bin storage. To ensure uniformity, the contents of several bins may be fed to the dope preparation area simultaneously.

Solution Polymerization. Solution polymerization is used by a few producers in the acrylic fiber industry. The reaction is carried out in a homogeneous medium by using a solvent for the polymer. Suitable solvents are aqueous NaSCN used by Acordis and dimethyl sulfoxide [67-68-5] (DMSO) used by Toray. The homogeneous solution polymerization of acrylonitrile follows the conventional kinetic scheme developed for vinyl monomers (27–29) (see BULK AND SOLUTION POLYMERIZATIONS REACTORS).

Thermally activated initiators such as azobisisobutyronitrile (AIBN), ammonium persulfate, or benzoyl peroxide can be used in solution polymerization, but these initiators are slow acting at temperatures required for fiber-grade polymer processes. Half-lives for this type of initiator are in the range of 10–20 h at 50–60°C (30). Therefore, these initiators are used mainly in batch processes where the reaction is carried out over an extended time. Redox initiators, such as the ammonium persulfate/sodium bisulfite/copper system, have much higher initiation rates and are reported to be employed in the Acordis NaSCN process. A typical continuous solution polymerization equipment diagram is shown in Figure 7.

Chain transfer is an important consideration in solution polymerization. Chain transfer to solvent may reduce the rate of polymerization as well as the molecular weight of the polymer. Other chain-transfer reactions may introduce dye sites, branching, and structural defects which reduce thermal stability. The organic solvents used for acrylonitrile polymerization are active in chain transfer. DMSO and DMF have chain-transfer constants of $(0.1–0.8) \times 10^{-4}$ and $(2.7–2.8) \times 10^{-4}$ respectively—high when compared to a value of only 0.05×10^{-4} for acrylonitrile itself and 0.006×10^{-4} for aqueous zinc chloride.

Of the two common comonomers incorporated in textile-grade acrylics, methyl acrylate is the least active in chain transfer, whereas vinyl acetate is as active in chain transfer as DMF. Vinyl acetate is also known to participate in the chain transfer-to-polymer reaction (31). This occurs primarily at high conversion, where the concentration of polymer is high and monomer is scarce.

The advantage of solution polymerization is that the polymer solution can be converted directly to spin dope by removing the unreacted monomer.

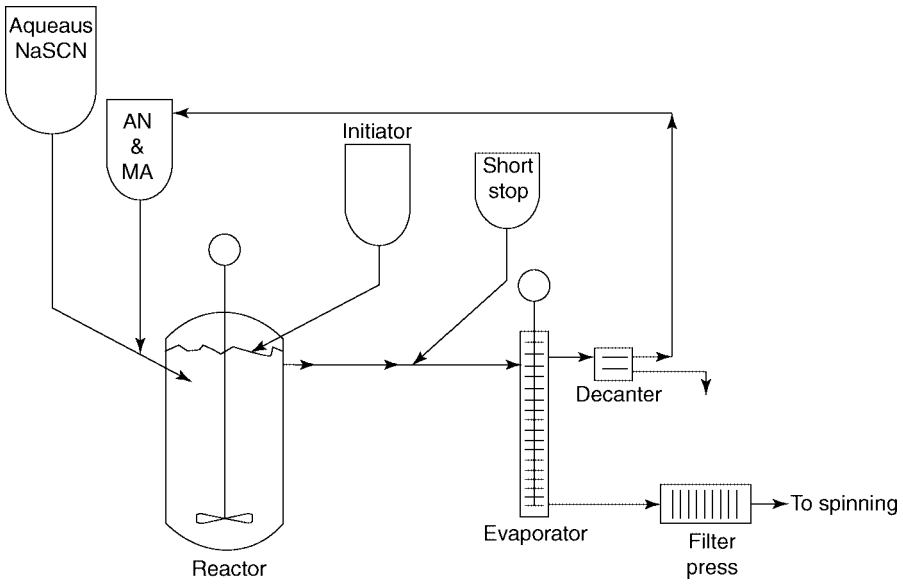

Fig. 7. CSTR NaSCN solution polymerization process. AN = acrylonitrile; MA = methyl acrylate.

Incorporation of nonvolatile monomers, such as the sulfonated monomers, can be a problem. The sulfonated monomers must be converted to a soluble form such as the amine salt. Nonvolatile monomers are difficult to recover or purge from the reaction medium. Monomer recovery systems based on carbon adsorption have been developed. However, the usual practice is to maximize the single-pass conversion of these monomers.

Subsequent to the polymer reactor, acrylonitrile and volatile comonomers are removed in a thin-film evaporator. Additives such as pigments or stabilizers may be incorporated using a static or active mixer before the dope is transferred to the spinning area.

Bulk Polymerization. The idea of bulk polymerization is attractive, since the polymer would not require water removal and the process would not have the low propagation rates and high chain transfer rates of solution processes (see BULK AND SOLUTION POLYMERIZATIONS REACTORS). But bulk polymerization of acrylonitrile is complex. Even after many investigations into the kinetics of the polymerization, it is still not completely understood. The complexity arises because the polymer precipitates from the reaction mixture barely swollen by its monomer. The heterogeneity leads to kinetics that deviate from normal.

When initiator is first added, the reaction medium remains clear while particles 10–20 nm in diameter are formed. As the polymerization proceeds, the particle size increases, giving the reaction medium a white milky appearance. When a thermal initiator, such as AIBN or benzoyl peroxide, is used the reaction is autocatalytic. This contrasts sharply with normal homogeneous polymerizations in which the rate of polymerization decreases monotonically with time. With acrylonitrile bulk polymerization, *three* propagation reactions occur simultaneously,

accounting for the anomalous autoacceleration (32,33). These are chain growth in the continuous monomer phase, chain growth of radicals that have precipitated from solution onto the particle surface, and chain growth of radicals within the polymer particles (30,34).

Bulk polymerization is not used commercially because the autocatalytic nature of the reaction makes control difficult. This, combined with the fact that the heat generated per unit volume is very high, makes commercial operations difficult to engineer. Last, the viscosity of the medium becomes very high at conversion levels above 40–50%. Therefore, commercial operation at low conversion would require an extensive monomer recovery operation. A bulk process was developed (35) by MEF, which limited conversion to ~50%; it reportedly reached pilot-plant stage but was not commercialized.

Emulsion Polymerization. The use of emulsion polymerization in the acrylic fiber industry is limited to the manufacture of modacrylic compositions. One notable example of an emulsion process was the former Union Carbide process for Dynel (36,37). The mechanism of emulsion polymerization was first developed qualitatively (38) and later quantitatively (39,40) (see HETEROPHASE POLYMERIZATION). It was shown that the emulsifier disperses a small portion of the monomer in aggregates of 50–100 molecules approximately 5 nm in diameter called *micelles*. The majority of the monomer stays suspended in droplet form. These droplets are typically 1000 nm in diameter, much larger than the micelles. Since a water-soluble radical initiator is used, polymerization begins in the aqueous phase. The micelle concentration is normally so high that the aqueous radicals are rapidly captured (41). The micelle is essentially a tiny reservoir of monomer; therefore, polymerization proceeds rapidly, converting the micelle to a polymer particle nucleus. Since the halogen-containing monomers have little water solubility, the micelle promotes their ability to react. The ability of emulsion polymerization to segregate radicals from one another is of great importance commercially. The effect is to minimize the rate of radical recombination, allowing high rates of polymerization to be achieved along with high molecular weight. This is important in modacrylic polymerizations where chain-transfer constants of the halogen monomers are high. Comprehensive reviews of emulsion polymerization technology have been published (42–44), and emulsion polymerization reactor modeling has been reviewed (45). The polymer for Kanekaron modacrylic is reported to be prepared by emulsion polymerization.

Copolymerization.

Homogeneous Copolymerization. Virtually all acrylic fibers are made from acrylonitrile copolymers containing one or more additional monomers that modify the properties of the fiber. Thus copolymerization kinetics is a key technical area in the acrylic fiber industry. When carried out in a homogeneous solution, the copolymerization of acrylonitrile follows the normal kinetic rate laws of copolymerization. Comprehensive treatments of this general subject have been published (46–50). The more specific subject of acrylonitrile copolymerization has been reviewed (51). The general subject of the reactivity of polymer radicals has been treated in depth (52).

For textile end- use acrylics, the most common comonomer is vinyl acetate, followed by methyl acrylate. The monomer pair acrylonitrile–methyl acrylate is close to being an ideal monomer pair. Both monomers are similar in resonance,

polarity, and steric characteristics. The acrylonitrile radical shows approximately equal reactivity with both monomers, and the methyl acrylate radical shows only a slight preference for reacting with acrylonitrile monomer. Many acrylonitrile monomer pairs fall into the nonideal category, for example, acrylonitrile–vinyl acetate. This example is of a nonideality, sometimes referred to as kinetic incompatibility. A third type of monomer pair is that which shows an alternating tendency. This tendency is related to the polarity properties of the monomer substituents (53). Monomers that are dissimilar in polarity tend to form alternating monomer sequences in the polymer chain. An example is the monomer pair acrylonitrile–styrene. Styrene, with its pendent phenyl group, has a relatively electronegative double bond whereas acrylonitrile, with its electron-withdrawing nitrile group, tends to be electropositive.

Copolymer composition can be predicted for copolymerizations with two or more components, such as those employing acrylonitrile plus a neutral monomer and an ionic dye receptor. These equations are derived by assuming that the component reactions involve only the terminal monomer unit of the chain radical. The theory of multicomponent polymerization kinetics has been treated (46,47).

Heterogeneous Copolymerization. When copolymer is prepared in a homogeneous solution, kinetic expressions can be used to predict copolymer composition. Bulk and dispersion polymerization are somewhat different, since the reaction medium is heterogeneous and polymerization occurs simultaneously in separate loci. In bulk polymerization, eg, the monomer-swollen polymer particles support polymerization within the particle core as well as on the particle surface. In aqueous dispersion or emulsion polymerization, the monomer is actually dispersed in two or three distinct phases: a continuous aqueous phase, a monomer droplet phase, and a phase consisting of polymer particles swollen at the surface with monomer. This affects the ultimate polymer composition because the monomers are partitioned such that the monomer mixture in the aqueous phase is richer in the more water-soluble monomers than the two organic phases. Where polymerization occurs predominantly in the organic phases, these relatively water-soluble monomers may get incorporated into the copolymer at lower levels than expected. For example, in studies of the emulsion copolymerization of acrylonitrile and styrene, the copolymer was richer in styrene than copolymer made by bulk polymerization, using the same initial monomer composition (54–56). Analysis of the reaction mixtures (57) showed that nearly all of the styrene was concentrated in the droplet and swollen particle phases. The acrylonitrile, on the other hand, was distributed between both the aqueous and organic phases. The monomer compositions in the droplet and particle phase were found to be essentially the same. The effect of monomer partitioning on copolymer composition is strongest with the ionic monomers, since this type of monomer is usually soluble in water and nearly insoluble in the other monomers. Reviews of emulsion copolymerization kinetics and the effects of reaction heterogeneity on reaction locus have been publis hed (58,59).

In a CSTR dispersion process, the percentage of the less reactive monomer increases until steady state is reached. For example, if a reactor is fed monomer composed of 91% acrylonitrile and 9% vinyl acetate and the process is carried to 75% conversion, the polymer will contain 7.4% vinyl acetate. The unreacted monomer composition will be 86.2% acrylonitrile and 13.8% vinyl acetate.

Table 3. Polymer Concentrations Suitable for Solution Spinning

Solvent	Polymer Concentration, %
Dimethylformamide (DMF)	20–32
Dimethylacetamide (DMAc)	20–27
Dimethyl sulfoxide (DMSO)	20–30
Ethylene carbonate (EC)	15–18
Sodium thiocyanate (NaSCN) 45–55% in water	10–15
Zinc chloride ($ZnCl_2$) 55–65% in water	8–12
Nitric acid (HNO_3) 65–75% in water	8–12

Solution Spinning

As the acrylic fiber industry has matured, the wide range of spin solvents that were commercialized in the 1950–1960s has narrowed. DMSO and zinc chloride are each limited to one producer; no processes based on ethylene carbonate solvent remain in operation. Most newer plants are based on either DMAc or NaSCN wet spinning. Table 3 shows commercial solvents and the dissolved polymer concentration range for a spin solution.

For dry polymer, the dope-making process may use chilled solvent to form a slurry and wet out the polymer particles before they begin to dissolve, or may use hot solvent so that the solutioning process occurs immediately. Additives such as thermal stabilizers and delusterant (TiO_2) are added at this time. In both cases, active mixing is required. Subsequently, the suspension is pumped through a shell-tube heat exchanger to complete dissolution. The resulting dope is degassed and filtered (plate and frame) before being pumped to the spin area.

Dry Spinning. This was the process first employed commercially by DuPont in 1950. It is shown schematically in Figure 8. For acrylic fibers, the only dry-spinning solvent used commercially is DMF. The DMF spin dope coming from the dope preparation unit is filtered and then heated to approximately

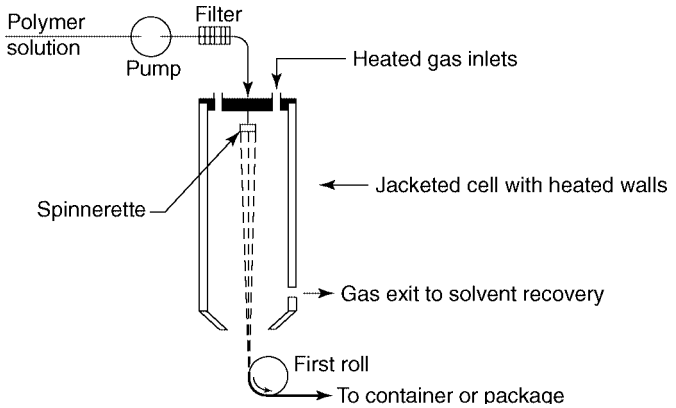

Fig. 8. Schematic of dry-spinning tower.

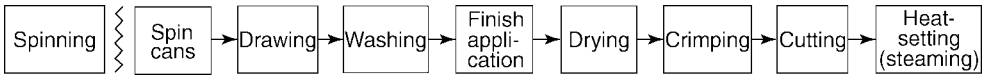

Fig. 9. Conventional wash-draw-dry-relax fiber process.

140°C. It is pumped through spinnerettes of up to 2800 holes placed at the top of a solvent removal tower. The DMF is evaporated by circulating an inert gas through the tower at 300–350°C. The tower walls are also heated to prevent any solvent condensation. With such a high boiling solvent (b.p. 153°C) it is not possible (or desirable) to remove all solvent in the tower. Consequently, the fiber from the bottom of the tower contains 10–25% solvent. In discontinuous processes, the fiber exiting the tower is wet with water and combined with the product from other threadlines into a rope; the rope is plaited into a can. The residual DMF is removed in a second step by passing the rope via roll sets through a series of hot water baths. A more modern process, introduced by Bayer, washes the fiber by sprays while passing on a belt. The as-spun fiber has little orientation, and so it is stretched three- to sixfold either before or concurrent with the washing step. The fiber is crimped to improve bulk and textile processing, then dried by heated air on a moving belt. During drying, the fiber structure collapses to the same density as solid polymer and the length decreases as the structure relaxes. A "finish" comprising an antistatic agent and a lubricant are applied by spray or kiss rolls and the product is either cut to staple or packaged directly as tow. Figure 9 shows the subsequent process steps.

The filament microstructure in dry spinning is derived from gelation exclusively. As evaporation proceeds, the polymer concentration in the filament increases until gelation occurs. This may happen within a few centimeters of the spinneret face. Since no nonsolvent is used, precipitation does not occur during solvent removal. Fiber densities from wet and dry spinning have been compared (60); density of as-spun fiber is much higher in dry-spun fiber. The fiber cross-section shape is typically a "dogbone" (Fig. 2). Very little fibrillar structure, characteristic of wet-spun fibers, is observed in the dry spun filaments. During stretching, however, the dry spun fibers develop a fibrillar network similar to that of the wet spun fibers but finer in diameter. This mode of fiber formation is economical for commodity fibers of 1–5 dtex but has severe limitations for other products:

(1) Solvent removal is not fast enough to produce fibers of 12–20 dtex suitable for the carpet industry.
(2) The limitation on the number of holes per spinneret makes production of fine filaments (<1 dtex) expensive as, unlike the wet-spinning process, the number of holes per spinneret is limited.
(3) The compact structure makes producer dyeing of fiber more difficult.
(4) The gelation process does not work well to produce special-shaped filaments; the dogbone cross-section is not suitable as a carbon fiber precursor; and it is not possible to produce a fibrillated product for the asbestos-replacement market.

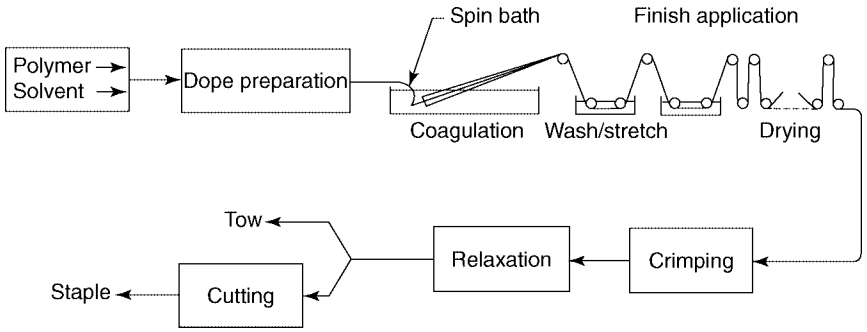

Fig. 10. Wet-spinning organic solvent process.

Wet Spinning. Wet spinning differs from dry spinning primarily in the way solvent is removed from the extruded filaments. Instead of evaporating the solvent in a drying tower, the fiber is spun into a liquid bath containing a solvent/nonsolvent mixture called the coagulant, as shown in Figures 10 and 11. The solvent is the same as the dope solvent and the nonsolvent is usually water. Filament fusion is less of a problem in wet spinning, and so the number of capillaries in wet spinning spinnerettes is much larger than in dry spinning. The spinnerettes in commercial processes may have anywhere from 3000 to 100,000 + capillaries, which may range in diameter from 0.05 to 0.25 mm; it is common to use multiple spinnerettes in a single spinbath.

Because the fiber microstructure is established in the spinbath, the coagulation conditions employed are the result of extensive optimization. The critical part of this process is the transition from a liquid to a solid phase within the

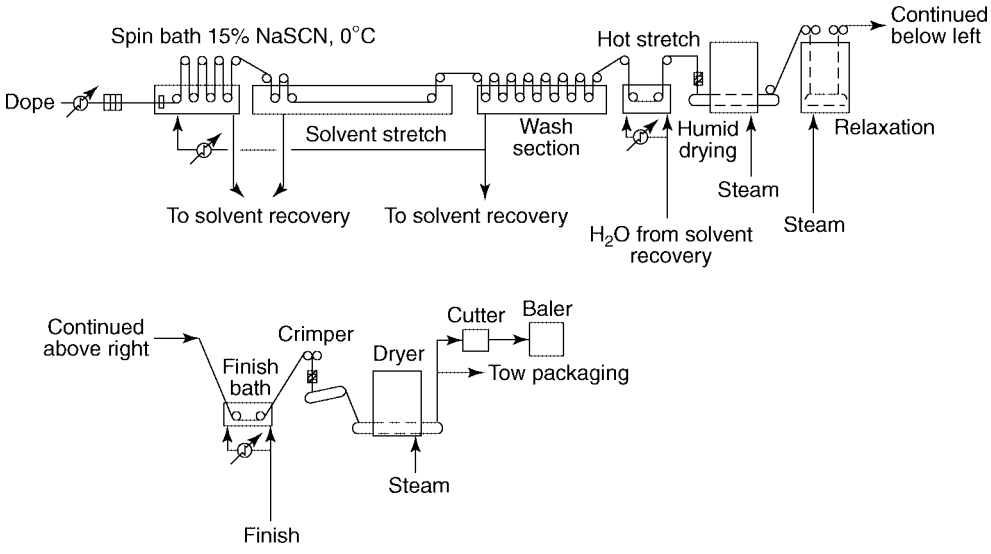

Fig. 11. Wet-spinning NaSCN salt process.

filaments. Two liquid-to-solid phase transitions are possible. The first is precipitation of the polymer to form a microporous solid phase. In extreme cases, precipitation produces a structure with macrovoids which must be "healed" in later processing, or the fiber lateral properties will suffer. Precipitation is favored when the solvent is organic and the nonsolvent is water, as the solubility of polymer decreases abruptly with water concentrations of only a few percent. The second and more desirable solid phase is the gel state, characterized by hydrogen and dipole bonding between the polymer and solvent. The gel state is desirable because it gives rise to a finer microstructure once the solvent is removed. Thus, the conditions in the spinbath should be optimized so that gelation of the polymer precedes precipitation. Studies (61) have shown that gelation occurs more rapidly at high dope solids and lower spinbath temperatures.

Low spinbath solvent concentration promotes initial rapid solvent extraction but also produces a thicker filament skin, that ultimately reduces the rate of solvent extraction and may lead to the formation of macrovoids. High spinbath solvent concentration gives a denser microstructure, but solvent extraction is slow and filament-to-filament fusion may occur. Other spinbath conditions that affect coagulation and microstructure are dope solids, spinbath temperature, jet stretch (the ratio of actual filament speed to theoretical speed in the capillary), and immersion time.

The fiber emerging from the spinbath is a highly swollen gel containing both solvent and nonsolvent from the spinbath. The fibers are essentially unoriented except at the fiber skin. The microstructure consists of a fibrillar network. The spaces between fibrils are called microvoids. Depending on the conditions of coagulation, the filaments may also contain large voids radiating out from the center of the fiber. The best combination of tensile properties, abrasion resistance, and fatigue life is realized when the coagulated fiber has a homogeneous, dense structure with small fibrils and no macrovoids (62).

Fiber cross-sectional shape is determined by the coagulation conditions. A thick skin characteristic of most organic solvent-spun fibers will generate a bean-shaped cross-section as the solvent is removed from the interior. The thinner skin characteristic of inorganic solvent-spun fibers can contract with solvent removal and retain the round shape. It is possible, however, to produce the opposite shape in either system. Examples of these shapes were shown in Figure 1. Special cross-sections, such as rectangular or oval, can be made from nonround capillaries by controlling coagulation conditions. Control of die swell is of critical importance. Die swell occurs because most spin dopes are viscoelasic in nature. After undergoing stretching deformation during extrusion through the small spinnerette hole, the dope partially rebounds to a larger, preextrusion diameter. To maintain a non-round shape, the tension on the filament at the spinnerette face must be great enough to counterbalance die-swell.

After the spin-bath or spin-tower step, the tow processing is similar for both wet- and dry-spun yarns. Wet-spun tows however, may contain 100–300% of solvent/nonsolvent, while dry-spun tows generally hold only 10–30% solvent. Therefore, the initial washing steps differ in their details. The key wet-spinning steps are washing, stretching, finish application, collapse, drying, crimping, and relaxing. The washing step consists of several countercurrent stages, with the effluent being recycled to a solvent recovery process. Various wash units are

employed including baths, sprays, and proprietary devices (63); washing efficiency is a key aspect of cost, as it impacts recovery of solvent from the effluent. The wash step may also be combined with stretching. In one variation of this method, the tow is drawn between sets of godets and passed through a series of solvent extraction baths at the same time.

The washing step may be followed by additional stretching. The porous fibrillar structure of wet-spun fibers increases in density with stretching. In-line dyeing of fiber using cationic dyes is usually carried out after almost all solvent is removed. Because of the open structure of wet-spun fiber, dye penetration and fixation is rapid. An additional wash step removes auxiliaries and unfixed dye. After the fiber is washed, stretched, and optionally dyed, finish may be applied using a bath or similar device. If drying is accomplished on heated rolls (Fig. 10), a predrying finish is required to prevent fiber fusion. In other processes (Fig. 11), finish application may be postponed until the fiber is dried and collapsed.

The collapsing-drying step can be accomplished with the tow held at constant length by contacting the tow on heated rolls or by passing the tow through an in-line oven using a conveyor belt. For fiber that contains a large void structure, roll drying is necessary to effect collapse of the voids. After collapse, boiling water shrinkage is reduced and higher temperatures are required for subsequent relaxation.

After drying/collapsing, the tow is relaxed. Relaxation is essential because it reduces the tendency for fibrillation and increases the dimensional stability of the fiber. Relaxation also increases fiber elongation while reducing strength and increases dye diffusion rate. Relaxation can be done in-line or in batches in an autoclave. For fiber that has been belt dried, relaxation can be accomplished by an atmospheric process (Fig. 11). However, for roll-dried fiber, saturated steam is used because the moisture reduces the process temperatures required. This process can be accomplished in-line, but more commonly it is done batchwise in an autoclave. Fiber shrinkage during relaxation ranges from 10 to 40% depending on the temperature, the polymer composition, and the amount of prior orientation. The amount of relaxation is tailored to the intended application of the product.

Fiber crimping using a stuffer box device may be done before in-line relaxation or before autoclaving. The relaxation process tends to "set" the crimp. In some autoclave processes, a second crimping step is employed subsequent to relaxation. Fiber may be cut to staple at the machine end for in-line relax processes or batchwise for autoclave processes. Tow can be produced from either process type, although large packages of one ton or more are produced more readily from the in-line relax process.

Process speeds for wet spinning vary from 55 to 260 m/min. The limitations are the speed at which the fiber can move through the spinbath without filament breakage and the equipment line length required to complete the washing and drying processes. A single machine may have up to 48 spinnerettes (6 rows of 8) with a total productivity of 50 ton/day.

Air-Gap Spinning. This process, also termed dry-jet wet spinning, is used to provide filament yarn either for textile use or as a carbon fiber precursor. It is suitable for producing the small bundles required for these end uses because the filament has been drawn before it enters the bath, and so drag forces are less likely to cause breakage; thus, much higher line speeds can be achieved. In theory, any

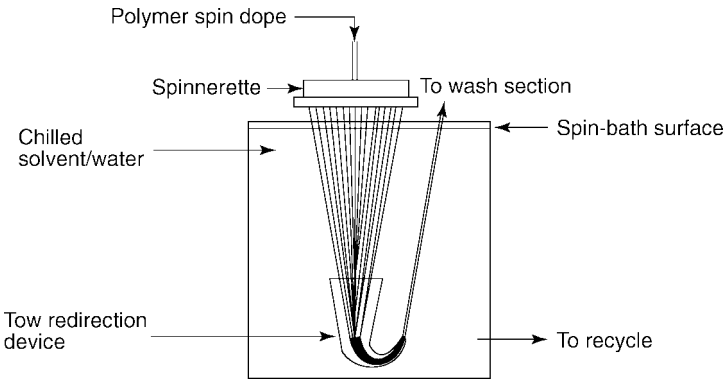

Fig. 12. Air gap coagulation.

acrylic solvent can be used in air gap spinning. Commercial examples are known from DMAc, NaSCN, and DMSO.

The dope solids for air-gap spinning are higher than for wet spinning, the intent being to achieve quick gelation on extrusion. The spinnerette is positioned a short distance above the bath, which is a solvent/nonsolvent mixture, typically at low temperature. The fiber is spun vertically into the bath, and then rerouted out via a tube or pulley as shown in Figure 12. Spinnerettes may be less then 1000 holes for a textile product or as many as 4000 for a carbon fiber precursor. The remainder of the process resembles the wet-spinning process, except that there are many small bundles that must be kept separate and the final product is taken up on bobbins. Final line speeds may be up to 500 m/min, but because of the small bundle size, machine productivity may be only 5 ton/day.

Solvent Recovery. Efficient use of solvent and water are key elements in an economic process. With most spinning processes practiced on a large scale, less than 1% solvent is not recycled, based on fiber produced. Since the ratio of solvent to fiber is in the range of 4:1, this means less than 0.25% of the solvent employed is expended per pass. Solvent loss is of several types: (*1*) solvent remaining in final fiber; (*2*) solvent lost as vapor; (*3*) solvent decomposed; (*4*) solvent lost in reprocessing or maintenance.

The main means of solvent recycling is distillation, either atmospheric or vacuum. With the organic solvents, the water is distilled, perhaps in several steps; then the higher boiling solvent is distilled, leaving behind dissolved salts and low molecular weight polymer. Amide solvents such as DMF and DMAc are subject to hydrolysis and may require a step to remove the acid generated; the recovered water may require removal of dimethylamine before reuse. Figure 13 shows a DMF recovery train (64). Salt solvents such as NaSCN are concentrated by water removal in multieffect evaporators, then may have an ion exchange and/or crystallization step to remove impurities. Recycled water may have the pH adjusted by addition of acid or base to assure neutralization of the fiber in the washing step.

Melt Spinning. Compared to most other synthetic fibers, acrylics have always had the disadvantage of extra process steps and cost incurred because

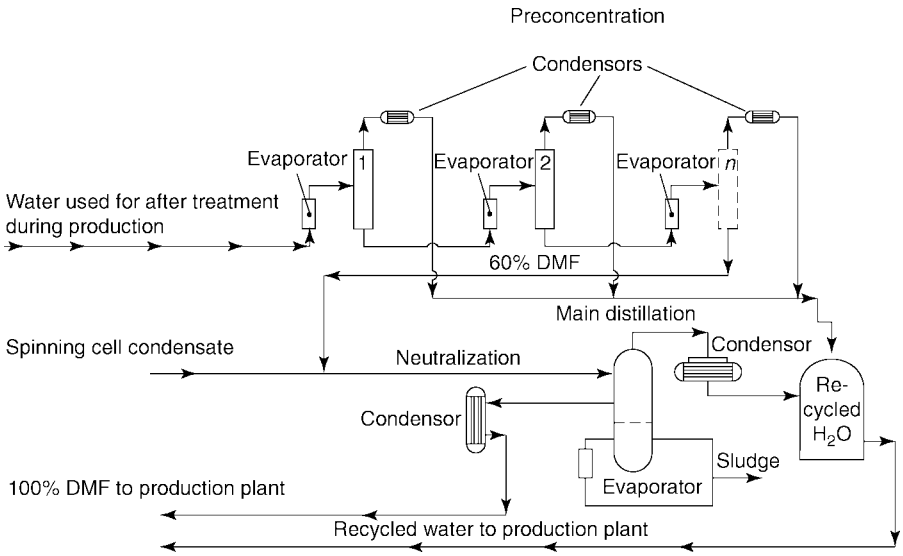

Fig. 13. Diagram of DMF recovery unit.

they could not be melt spun. Several approaches to eliminating this limitation have been proposed. Plasticization of the polymer with DMSO was proposed (65) as this lowered the melting point. This only reduced the amount of solvent to be recovered but did not eliminate the washing and solvent recovery steps. A more promising approach was plastization with water (66). This eliminated the process steps, but it was necessary to heat the plasticized mass to 200°C under pressure. The fiber had to be extruded into a chamber also under pressure, or the result would be a foam structure as the water vapor flashed.

A true melt spinning process has been developed by a group at Standard Oil (67). Their approach was to make a polymer containing substantial comonomer content by a process which minimized "blocking" of acrylonitrile groups. The resultant polymer was melt-processible without degradation. Possible limitations of this approach are that the high comonomer content leads to high relaxation shrinkage as well as lower softening and sticking temperatures. These are disadvantages in modern textile processes. No commercial applications of this technology have appeared.

Modifications of Properties.

Reduced Pilling. Staple fabrics, in general, develop small balls of fiber or pills on the fabric surface as a result of abrasive action on the fabric surface. However, the pills build up more on acrylic fabrics than on comparable woolens. Pilling can be reduced by increasing the likelihood that the pills will break or wear off. Thus, the most effective approaches include reducing fiber strength, incorporating defects in the fiber, increasing fiber brittleness, and reducing shear strength. Using the same polymer base, wet-spinning processes can be modified by using low solvent concentration in the spin-bath and high spin-bath temperature to give more brittle fibers with high void content. Other possible approaches are lower draw ratios, which result in low tensile strength, and less complete relaxation,

which reduces fiber elongation to break. Commercial examples include Dralon L930 (Fraver), Super Camelon (Mitsubishi Rayon), and Acrilan® Pil-Trol™ (Solutia).

Improved Abrasion Resistance. Abrasion resistance is generally improved by reducing the microvoid size and increasing the initial fiber density. Abrasion-resistant fibers have been produced by incorporating hydrophilic comonomers or comonomers with small molar volumes. Sulfonated monomers, acrylamide derivatives, and *N*-vinylpyrolidinone are some of the hydrophilic comonomers that can be used to slow coagulation, thus reducing the void content. Vinylidene chloride, with its relatively small molar volume, is effective in increasing fiber density. The spinning process itself has a significant effect on initial fiber density and abrasion resistance. Dry spinning, for example, produces a denser initial fiber structure than conventional wet spinning. Wet-spinning techniques used to improve abrasion resistance generally do so by promoting gelation. Examples include high spinbath that concentration, low spinbath temperature, and additives to the dope or spinbath that slow coagulation. Spinbath additives include nondiffusing nonsolvents, such as poly(ethylene glycol) or high molecular weight alcohols, such as *tert*-butyl alcohol, in place of water.

Commercial Products

The majority of acrylic fiber production is 1.0–5.6 dtex (0.9–5 den) staple and tow furnished, undyed, in either bright or semidull (~0.5% TiO_2) luster. The principal markets are in apparel and home furnishings. Within the apparel sector these fibers are used in sweaters and in single jersey, double-knit, and warp-knit fabrics for a variety of knitted outerwear garments such as dresses, suits, and children's wear. Other markets for acrylics in the knit goods area are hand-knitting yarns, deep-pile fabrics, circular knits, fleece fabrics, and half-hose. Acrylics also find uses in broadwoven fabric categories such as blankets, drapery, and upholstery. Minor tufted end uses include area rugs and carpets.

Acrylic Tow. A significant proportion of acrylic fiber, perhaps 25% in the United States and more than 50% in Europe, is sold as tow for conversion to yarn through stretch-breaking using the Superba, Seydel, or similar equipment. Tow packages may be as large as 1 ton, with no break in the bundle. The larger the tow package, the higher the tow customer's productivity. Ability to offer a large tow package implies that a producer has a highly stable process, as no knots are allowed. Producers with continuous relaxation have no limit on the package size they can offer; the only limits are those arising in package handling. In Europe, many fiber producers convert tow to "tops"—stretch broken product that is ready for yarn spinning.

Acrylic Filament Yarns. Continuous filament acrylic yarns face stiff competition from nylon and polyester. Since they are more costly, acrylics have penetrated only those markets where they have a clear advantage in a critical property. In Japan, continuous filament yarns in very fine deniers are valued as a silk replacement. In this market, the yarn is a premium product used in high fashion dress fabrics, satins, and poplins, or to produce a cloth suitable for surface raising to give a suede or fine velour effect.

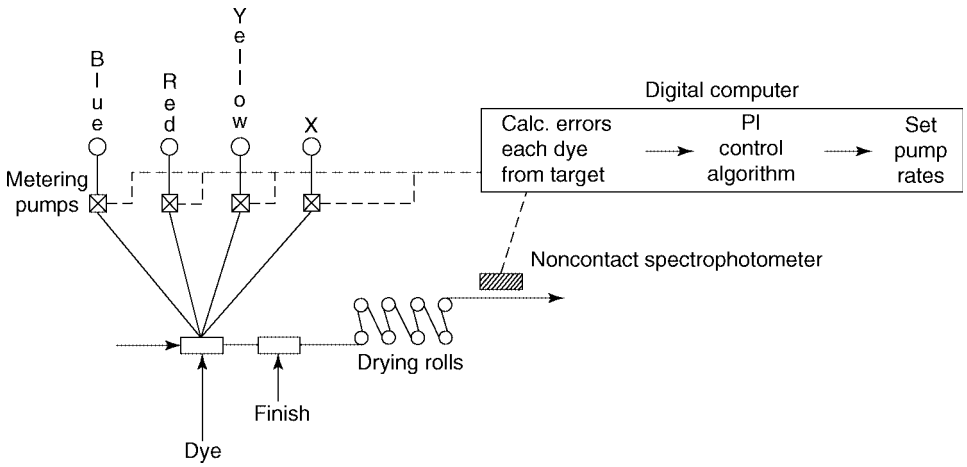

Fig. 14. Color control in a producer-dyed fiber process.

Producer-Dyed Fiber. The largest volume "specialty" product offered by acrylic producers is producer-dyed fiber (PDF). Producer dyeing decreases systems cost by elimination of a process step for the customer, but it complicates the inventory. PDF is usually made in an on-line process as shown in Figure 14 (68). The dye is applied using a device which promotes rapid penetration of the fiber mass, as acrylics have a high strike rate and very poor leveling qualities. The process is automated to maintain constant color (shade and depth) by real-time color analysis and correction. Since the final color is influenced by relaxation and crimp, further monitoring and testing may be required. Alternately, the dyes are premixed and a mixed stream is injected into the dyeing device. If the shade is right, then only depth needs adjustment. PDF fiber spun using this dyeing technology is usually sold as "lots," as color from one production run to the next may not match sufficiently for critical end uses. Dry-spun fibers are difficult to dye in-line as their compact structure makes dyeing too slow to be compatible with the required process speeds. For dry-spun acrylic, the only practical process is dope dyeing. For colors with only a low demand, some producers may use post-production dyeing with a device such as a Serricant Tow-Fix-R. More than 20 producers worldwide offer PDF acrylic.

Pigmented Fiber. Pigmented acrylic and a small amount of modacrylic are used in outdoor applications where outstanding light stability provides a competitive advantage. Pigmentation provides more stable coloration than dyeing through the lifetime of the fabric. End uses include awnings, tents, and lawn furniture. Modacrylic is used where local codes require a flame-retardant fabric. The technology involves mixing of the pigments with the spin dope prior to extrusion. The same feedback mechanism of color control described for PDF may be used with pigmented fiber. About a dozen producers offer pigmented fiber; however, some only sell one color—black. Generally, pigmented fiber commands a higher price than does PDF owing to the high cost of organic pigments. This coupled with the decreased luster of the pigmented products means they do not usually compete in the same end uses.

Fibers with High Bulk and Pile Properties. High-bulk acrylic fibers are commonly made by blending high shrinkage and low shrinkage staple fibers, or by blending relaxed and unrelaxed sliver from tow. The two staple products are made by variation in the fiber stabilization process. When the resulting yarn is allowed to relax, the high shrink component causes the low shrinkage (relaxed) fiber to buckle and add bulk to the yarns.

Another method of producing high bulk yarns is the use of bicomponent fibers. Bicomponent fibers have developed from a desire to match the bulkiness and handle of wool. The three-dimensional crimp of animal fibers in general comes from the presence of two components on the fiber surface. Acrylic bicomponent fibers achieve three-dimensional crimp by spinning two copolymer dopes into a single fiber. If the two streams are present in the same proportion in each spinneretto hole, the process is "true" bicomponent; if the proportion varies from filament to filament, then it is a "random" bicomponent. To generate the spiral crimp, the two polymers must have different responses to heat or moisture. For example, if one polymer is more moisture absorbent than the other, a crimp develops when the fiber is dried. The copolymers for this type of bicomponent may be acrylonitrile–vinyl acetate and acrylonitrile–vinyl acetate–sodium *p*-(vinylbenzene) sulfonate. In this combination, the copolymer containing the sulfonate moiety is the more moisture absorbent and therefore shrinks the most on drying. This type of crimp is reversible because it can be renewed by wetting and redrying. Solutia's A-21 and B-21 are examples of commercial water-reversible-crimp fibers. Crimp can also be imparted by using polymers that react differently to heat. By using copolymers of different compositions, the crimp is imparted permanently when the fiber is heated. The copolymers for this type of bicomponent have a single comonomer, such as vinyl acetate or methyl acrylate, incorporated at two different levels.

True bicomponents require special spinneretters that provide the required dopes to each hole. In random-bicomponent technology, the second component is incorporated through a layering device prior to the spinnerette. This concept is based on the fact that the viscous spinning solutions can be merged without complete mixing (69). When passed through a standard spinnerette, bicomponent fibers are produced ranging in composition from 100% component A to 100% component B. For many years, this was the only bicomponent technology available to wet spinners.

Flame-Resistant Fibers. Acrylics have relatively low flame resistance, comparable to cotton and regenerated cellulose fibers. Additional flame resistance is required for certain end uses, such as children's sleepwear, blankets, carpets, outdoor awnings, and drapery fabrics. The only feasible route is copolymerization of acrylonitrile with halogen-containing monomers such as vinyl chloride, vinyl bromide, or vinylidene chloride. Modacrylics were developed for uses where a high resistance to burning is required. In such fibers, the level of halogen-containing units was up to 60%, as in Dynel, one of the earliest modacrylics. This fiber, no longer produced, was 40–60 acrylonitrile–vinyl chloride copolymer. Tennessee Eastman's Verel, an acrylonitrile–vinylidene chloride copolymer, has also been discontinued. Solutia's SEF modacrylic is the only remaining U.S.-produced modacrylic flame-resistant fiber. It is produced solely in pigmented form as SEF FR for the commercial awning business. Kanekaron, another acrylonitrile–vinyl

chloride composition produced in Japan by Kanegafuchi, finds use in wigs, toys, pile, and industrial filter fabrics.

There have been reviews of flammability (70–74), methods that can be used to enhance the flame resistance of acrylic and modacrylic fibers (75), and the mechanism of flame-retardant additives (76).

High Strength Fibers by Conventional Solution Spinning. As a reinforcing material for ambient-cured cement building products, acrylics offer three key properties: high elastic modulus, good adhesion, and good alkali resistance (77). The high modulus requires an unusually high stretch orientation. This can be accomplished by stretching the fiber 8- to 14-fold above its glass-transition temperature, T_g. Normally this is done in boiling water or steam to give moduli of 8.8–13 N/tex (100–150 gf/den) (78,79). Alternatively, the stretch orientation can be achieved by a combination of wet stretch at 100°C and plastic stretch on hot rolls, or in a heat-transfer fluid such as glycerol. This technique is reported to give moduli as high as 17.6 N/tex (200 gf/den) (80,81). Mitsubishi Rayon Co. reported an acrylic asbestos-replacement fiber with a tensile strength of almost 600 MPa (87,000 psi) (82). Many patents have been obtained for acrylic-reinforcing fibers (83–85). The Acordis fiber, marketed under the trade name Dolanit, is offered in several forms (Table 4).

Acrylic fibers such as Dolanit (86) are blended in ambient-cured cement at a rate of 1–3%, compared with 9–15% by weight for asbestos. The flexural strength of cement sheets of acrylic-reinforced cement is equivalent to asbestos-reinforced cement and nearly double that of untreated cement (87). Two factors limiting the rapid development of acrylic asbestos-replacement fibers are a high manufacturing cost (compared to asbestos) and uncertainty as to the long-term stability of the acrylic fiber. Loss of modulus and chemical degradation may be significant over a period of decades. Other studies of acrylic fibers for concrete reinforcement have been carried out (88).

Table 4. Properties of Dolanite Asbestos Replacement Fibers[a]

	Dolanite Type 10	Dolanite Type 12			
Filament fineness, dtex[b]	1.5	0.7	1.7	2.2	8.2
Staple length, mm	6, 12	40	50	60, 80	80
Tenacity, cN/tex[c]	80–87	65–70	65–70	54–58	43–47
Elongation to break, %	8–12	15–20	15–20	13–16	14–17
Boiling water shrink, %	1.5				
Hot air shrink, % @ 150°C	1–2				
Same, yam form @ 200°C	3–4				
Hydrolysis resistance	Very good—after 350 h @ 130°C—93% tenacity remains				
Resistance to acids	Very good—after 8 weeks @ 20°C in 50% sulfuric acid—85% tenacity remains				
Heat resistance	Good—200 h @ 150°C, 75% tenacity remains	Good—permanent operating temperature up to 125°C, peaks up to 140°C			

[a] Ref. 7.
[b] To convert dtex to den, multiply by 0.9.
[c] To convert cN/tex to gf/den, multiply by 0.113.

Carbon Fiber. Carbon fibers (qv) are valued for their unique combination of extremely high modulus and strength and low specific gravity. Precursors for carbon fiber can be pitch, rayon, or acrylic fiber. Rayon offers a very low yield of carbon fiber and is no longer used as a precursor. Pitch is useful for generating carbon fiber of exceptionally high modulus, but the predominant precursor is acrylic. Precursors are converted into carbon fibers in a two-stage thermal treatment—a medium temperature "oxidation" stage in air that renders the fiber infusible, and a high temperature "carbonization" treatment in an inert atmosphere, where the fiber is converted into nearly pure carbon. The polymer composition generally has about 98% acrylonitrile and 2% of a weak acid such as itaconic or acrylic acid. The function of the acid is to provide a site to initiate the "ladder" formation in the oxidation step, and thus lower the temperature at which the reaction occurs and reduce the exotherm. Acrylic precursors are usually made by air gap spinning, as it allows higher line speed and the small bundle size is not a serious drawback. One exception is the Courtaulds (now Acordis) process, which uses wet spinning to produce a splittable tow; Toray is reported to use both wet- and air-gap processes to produce precursor. Increased stretch orientation is required to generate the high tenacity and modulus required in a precursor. It has been shown that precursor properties translate directly to carbon fiber properties (89). Precursor fiber is roll dried and not relaxed subsequent to drying. Special attention must be paid to the electrolyte content of the fiber and to drying conditions in order to produce a precursor which will perform well in oxidation and carbonization. The use of PAN as a carbon fiber precursor has been reviewed (90,91).

Other Specialty Fibers.

Microdenier. In the late 1980s, producers of polyester introduced "microdenier" products, that offered softer, more luxuriant handle to fabrics. Some acrylic producers have followed. There are no appreciable technical hurdles to producing a fiber with a denier of 0.6–0.9 (0.66–1.00 dtex), but unless commensurate changes are made in line speed or the number of spinneret holes, productivity will suffer. Acrylic microfibers on the market are all staple products, with Sterling in the United States producing a 0.8 dpf acrylic staple product named MicroSupreme and Solutia a 0.95 dpf product called Ginny. Mitsubishi Rayon offers H-129 (1.0 dtex).

Antimicrobial. For certain end uses such as half-hose, the ability to inhibit the growth of bacteria and fungi provides a marketing advantage. Several producers offer acrylics which have this characteristic. The antimicrobial effect is achieved by incorporating an additive such as chitosan (from chitan, a polysaccharide from the exoskeleton of crusteations), metal ions or chlorinated phenols. Commercial examples are New Tafel and Parclean from Mitsubishi Rayon and BioFresh from Sterling.

Fibrillated Fibers. Acrylic fibers are sold in the form of fibrillated pulps for use as highly efficient binders. These fibrillated fibers have a tree-like structure with "limbs" (fibrils) attached to the main "trunk" (fiber). The trunk is 20–50-μ diameter and the limbs range from a few microns to submicron. The product is generated from a special precursor fiber by intense mechanical action. Commercial examples are CCF from Sterling Fibers, Acri-Pulp from Solutia, and Dolanit 10D from Acordis.

Dry pulps are used in dry mix compounding applications such as non-asbestos friction materials. In these applications the product provides green strength for friction material performs. As little as a few percent pulp is required.

Wet pulps are used in specialty paper applications such as speaker cones, filtration, and specialty papers. These pulps have been successfully processed on cylinder, rotoformer, and Fourdrinier paper machines. As little as 15% of a highly fibrillated pulp can interlock other fibers or powders without the need for resin binders.

Conductive Fibers. Acrylic conductive fibers are used in areas where electrostatic discharge is a problem such as electronic device manufacture. Here the applications include dissipative clothing, flooring and work surfaces. Another application is solids/air filtration where discharge has the potential to trigger an explosion. Sterling Fibers manufactures Contructrol, which utilizes a combination of condutive carbon in the fiber and a conductive polymer attached to the fiber surface. Tex-Stat markets Thunderon, which uses a chemically bonded copper sulfide technology.

Economic Aspects

As has been mentioned earlier, the focus of acrylic production has moved to Asia which now accounts for 46% of world capacity. The most recent information on world acrylic capacity is listed in Table 5 (92). China leads in building new acrylic capacity with 16 plants as of 2000 and 19% of world capacity versus 8 plants and 9% of world capacity only 7 years earlier (93). Conversely, Europe, which had 38% of capacity in 1993 now has 29%. The changes in capacity and ownership of the major producers are shown graphically in Figure 15.

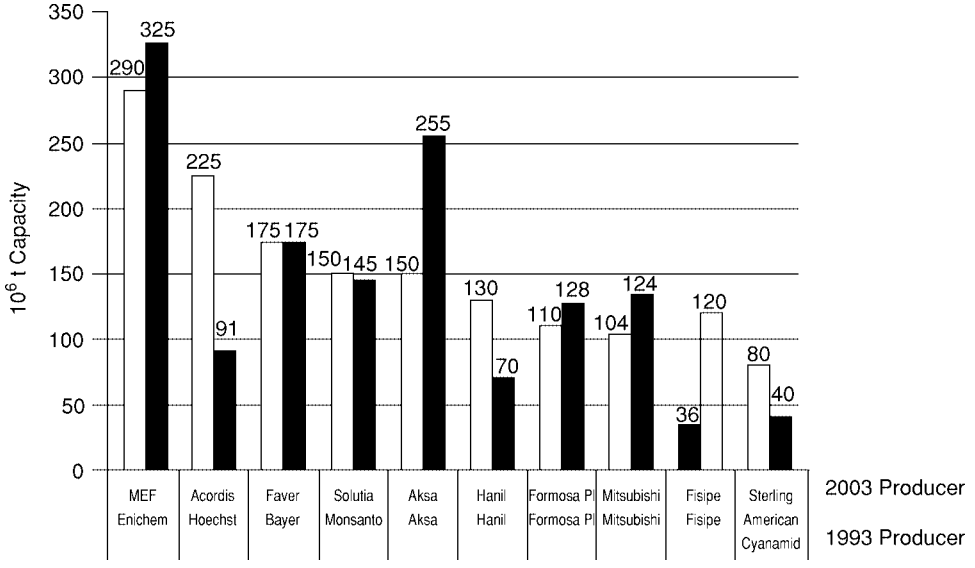

Fig. 15. Leading acrylic producers. □ 1993; ■ 2003.

Table 5. World Acrylic Fiber Production 2003

Country	Company	Location	Process	Capacity, 10^3 t	Comments
Europe					
Belarus	Novepolosk Polimir	Novopolotskoe	Susp. NaSCN wet	25	10 mod. (acetone)
	Novepolosk Polimir	Novopolotskoe	Sol. DMF wet	35	
Bulgaria	Dimitar Dimov	Burgas	Susp. DMF wet	15	
Germany	Fraver	Dormagen	Susp. DMF dry	115	
		Lingen	Susp. DMAc wet	60	
	Acordis	Kelheim	Susp. DMF wet	11	
	Markische Faser	Premnitz	Susp. DMF wet	Shut	Capacity 48
Hungary	Zoltek	Nyergesujfalu	Susp. DMF wet	35	5 Precursor
Italy	Montefibre	Porto Marghera	Susp. DMAc wet	150	
		Ottana	Susp. DMAc wet	90	
Macedonia	OHIS	Skopje	Sol. NaSCN wet	60	Operates intermittently
Portugal	Fisipe	Lisbon	Susp. DMAc wet	50	
Romania	Melana	Savintsa	Emul acetone wet	46	Modacrylic
Spain	Fisipe	Prat de Liobreget	Sol. NaSCN wet	70	
	Montefibre	Miranda del Ebro	Susp. DMAc wet	85	
Russia	JS Nitron	Saratov	Sol. NaSCN wet	23	
Uzbekistan	Navolazot Production Assn.	Navoi	Sol. NaSCN wet	23	
United Kingdom	Acordis	Grimsby	Sol. NaSCN wet	80	
Total Europe				*973*	
America					
Argentina	Noy Valesina	Veradero	Sol. DMF wet	20	
Brazil	Sudamericas de Fibras	Camacari	Susp. DMF dry	Shut	Capacity 25
	Crylor Industria	San Jose Dos Campos	Susp. DMF wet	25	
Mexico	CYDSA	El Salto, Jalisco	Susp. DMF wet	100	
	Fibras Sinteticas	Cotaxla, Veracruz	Susp. HNO_3 wet	28	
	Fibras Nationales de Acrilica	Altamira, Tamaulipa	Sol. DMF wet	50	
Peru	Fibras Sudamericanas	Lima	Susp. DMF dry	36	

Table 5. (continued)

Country	Company	Location	Process	Capacity, 10^3 t	Comments
United States	Hexcel	Decatur AL	Susp. NaSCN air	4	
	Solutia	Decatur AL	Susp. DMAc wet	145	
	Sterling	Pace FL	Susp. NaSCN wet	40	
Total America				*428*	
Japan	Asahi	Fuji	Susp. HNO_3 wet	Shut	Capacity 98
	Japan Exlan	Saidaiji	Susp. NaSCN wet	59	
	Kanebo	Hofu	Susp. DMF wet	38	
	Kanegafuchi	Takasago	Emul acetone wet	55	
	Mitsubishi Rayon	Otake	Susp. DMAc wet	119	
	Mitsubishi Rayon	Otake	Susp. DMF dry	5	
	Toho Rayon	Mishima	Sol. $ZnCl_2$ wet	50	
	Toray	Ehima	Sol. DMSO wet	44	
Total Japan				*370*	
China	Anqing Petrochemical	Anqing, Anhui Prov.	Susp. NaSCN wet	70	
	Daqing Petrochem Acry. Fiber	Daqing, Heilonggijang P.	Susp. NaSCN wet	54	
	Daquing Petrochem Chem Fiber	Daqing, Heilonggijang P.	Susp. NaSCN wet	10	
	Daqing Refin-chem Acry. Fiber	Daqing, Heilonggijang P.	Susp. NaSCN wet	30	
	Fushun Petrochem. Acrylic	Fushun, Liaoning Prov.	Susp. DMF dry	30	
	Fushon Flame-retard. Acry.	Fushun, Liaoning Prov.	Susp. acetone dry	5	
	Gaoglai No. 2 Chemical Plant	Shanghai	Sol. NaSCN wet	7.5	
	Jilin Chemical Fiber	Jilin, Jilin Prov.	Susp. DMAc wet	70	
	Jinyong Acrylic Fiber Co.	Zhejiang Prov.	Susp. DMF dry	30	
	Lanzhou Chemical Fiber Plant	Lanzhou, Gansu Prov.	Susp. NaSCN wet	20	
	Maoming Acrylic Fiber	Maoming, Guangdong P	Susp. DMF dry	30	
	Qinghuangdao Acrylic Fibre	Qinghuangdao, Hebel P.	Susp. DMF wet	50	
	Qilu Petrochem. Acry. Fiber	Zibo, Shandong Prov.	Susp. DMF dry	54	
	Shanghai Petrochemical	Shanghai	Susp. DMF dry	120	
	Xunyin Chemical Fiber Co.	Zibo, Shandong Prov.	Sol. NaSCN wet	28	
Total China				*608.5*	

Other Asia					
Indonesia	Golden Key	Serang	Susp. DMF dry	Shut	Capacity 40
India	Consolidated Fibres	Haldia W. Bengal	Susp. NaSCN wet	Shut	Capacity 12
	Indian Acrylics	Sangrur Punjab	Susp. DMAc wet	36	
	J. K. Synthetics	Kota Rajasthan	Susp. DMAc wet	Shut	
	Indian Petrochemicals	Baroda Gujarat	Susp. HNO_3 wet	15	
	Indian Petrochemicals	Baroda Gujarat	Susp. DMF dry	12	
	Pasupati Acrylon	Thakurdwara, Uttar Pradesh	Susp. DMF wet	20	
	Vardhman	Gujarat	Susp. NaSCN wet	17	
Pakistan	Dewan Saiman	Hattar, North-west Frontier		25	
South Korea	Hanil	Masan, Kyongsangnam-do	Susp. HNO_3 wet	90	
	Tae Kwang Industrial Co.	Ulsan, Kyongsangnam-do	Susp. NaSCN wet	92	
Taiwan	Tong Hwa Synthetic Fiber	Chupel City, Hsinchu Halen	Susp. NaSCN wet	54	
	Formosa Plastic	Jenwu, Kaoshiung Hsien	Susp. HNO_3 wet	95	
Thailand	Thai Acrylic Fiber	Sara Buri	Susp. NaSCN wet	57	
Total Other Asia				*513*	15.9%
Middle East					
Iran	Polyacryl Iran	Isfahan	Susp. DMF dry	39	
South Africa	Sasol Industries	Durban	Sol. NaSCN wet	Shut	Capacity 40
Turkey	Aksa	Yalova	Susp. DMAc wet	255	
	Yalova Elyaf	Yalova	Susp. DMF wet	35	
Total Middle East				*329*	
Total World				*3221.5*	

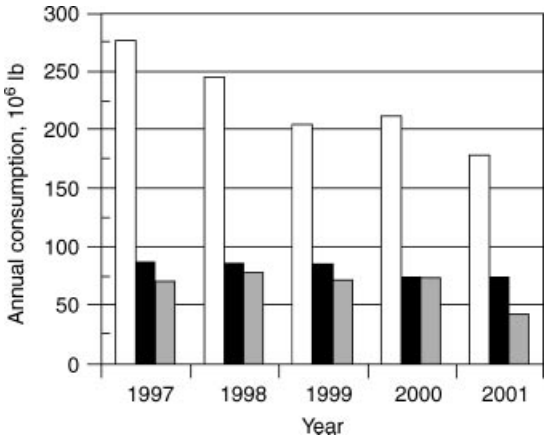

Fig. 16. U.S. acrylic fiber consumption (excluding carbon fibers). □ Apparel; ■ home furnishings; ▭ industrial and nonwovens.

Markets for acrylic fiber in developed countries have been stagnant or declining as shown in the example for the United States in Figure 16. Many acrylic articles such as sweaters come into the United States as finished goods from Asia. The volumes consumed in U.S. apparel markets are shown in Table 6. All developed countries face a similar situation due to the disparity of labor costs. Losses of volume in western Europe in the late 1990s have been less severe than in the United State, but still ominous as shown in Table 7 (94). The next decade will likely continue the exodus of capacity from the United State, Europe, and Japan.

Table 6. U.S. Shipments of Acrylic and Modacrylic for Apparel Markets, 10^3 t

Year	Sweaters	Socks	Craft	Pile	Fleece
1995	24.1	9.5	11.8	6.4	28.6
1996	25.0	9.1	11.8	6.4	33.6
1997	30.0	10.0	10.0	8.2	27.3
1998	22.3	10.5	9.1	8.6	21.8
1999	14.1	8.6	9.1	7.7	15.9

Table 7. Western European Consumption of Acrylic Fiber, 10^3 t

Year	Weaving	Knitting	Carpet	Others	Total
1995	77	201	12	12	302
1996	76	225	10	12	323
1997	52	280	7	7	346
1998	48	248	7	7	310
1999	48	244	11	7	310
2000	43	245	7	7	301

Acknowledgments

The authors wish to thank Dr. Fred Kanel and Dr. Ashesh Agrawal for their many helpful suggestions in the preparation of this article. We also appreciate the assistance of Dr. Raffaele Tedesco and Mr. Shimpei Haratake in constructing the table of plant capacities. Finally we acknowledge a debt to Dr. Ray Knorr, the prior author of this work, whose words and references we have built on.

BIBLIOGRAPHY

"Acrylic Fibers" in *EPST* 1st ed., Vol. 1, pp. 342–373, by C. W. Davis and P. Shapiro, The Dow Chemical Company; "Acrylic Fibers" in *EPSE* 2nd ed., Vol. 1, pp. 334–388. by H. C. Bach and R. S. Knorr, Monsanto Co.

1. C. Moureau, *Ann. Chem. Phys.* **2**(7), 186 (1893).
2. H. Rein, *Angew. Chem.* **60**, 159 (1948).
3. R. C. Houtz, *Tex. Res. J.* **20**, 786 (Nov. 1950).
4. U.S. Pat. 2,404,714; 2,414,717; 2,414,720 (June 17, 1942), R. G. Lathan and R. C. Houtz (all to E. I. du Pont de Nemours & Co. Inc.).
5. DPA 72,024 IVC/39b (Apr. 13, 1942), H. Rein (to I. G. Farbenindustrie).
6. W. E. Morton and J. W. S. Hearle, *Physical Properties of Textile Fibers*, 2nd ed., John Wiley & Sons, Inc., New York, 1975.
7. *Text. World* (Aug. 1992); *Text. World* **152**(11) (Nov. 2002).
8. Acordis Technical Bulletin Dolanit® Type 10 Technological Data, 2003; Acordis Technical Bulletin Dolanit® Type 12 Technological Data, 2003.
9. W. Teige, *Chemiefasern/Textilind.* **33/85**, 636 (1983).
10. J. B. Quig, *Pap. Am. Assoc. Text. Technol.* **4**, 61 (1948); R. S. Knorr, *Can. Text. J.* **66**(1), 42,46 (1949); R. S. Knorr, *Rayon Synth. Text.* **30**(2), 79 (1949); **30**(3), 67 (1949); **30**(4), 91 (1949).
11. R. S. Knorr, Kirk-Othmer Encyclopedia of Science and Technology, John Wiley & Sons, Inc., New York, 1994.
12. F. W. Billmeyer Jr., Textbook of Polymer Science, 3rd ed., John Wiley & Sons, Inc., New York, 1984, Chapt. 8.
13. A. Rudin, *The Elements of Polymer Science and Engineering*, Academic Press, Inc., New York, 1982, Chapt. 3.
14. H. Staudinger and W. Heur, *Chem. Ber.* **63**, 222 (1930).
15. R. L. Cleland and W. H. Stockmayer, *J. Polym. Sci.* **18**, 473 (1955).
16. B. G. Frushour, *Polym. Bull.* **4**, 305 (1981); *Polymer Bull.* **7**, 1 (1982); *Polymer Bull.* **11**, 375 (1984).
17. L. H. Peebles Jr., *J. Appl. Polym. Sci.* **17**, 113 (1973).
18. L. H. Peebles Jr., R. B. Thompson Jr., J. R. Kirby, and M. Gibson, *J. Appl. Polym. Sci.* **16**, 3341 (1972).
19. S. R. Palit, T. Guha, R. Das, and R. S. Konar, in N. M. Bikales, ed., Encyclopedia of Polymer Science and Technology, 1st ed., Vol. 2, John Wiley & Sons, Inc., New York, 1965, p. 229.
20. K. Stueben, in E. C. Leonard, ed., *Vinyl and Diene Monomers*, Part I, High Polymers Series Vol. XXIV, Wiley-Interscience, New York, 1970, Chapt. 1, p. 181.
21. W. M. Thomas, *Adv. Polym. Sci.* **2**, 401 (1961).
22. *The Chemistry of Acrylonitrile*, 2nd ed., American Cyanamid Publisher, New York, 1959.

23. A. D. Jenkins, in G. E. Ham, ed., *Vinyl Polymerization*, Part I, Marcel Dekker, New York, 1967, pp. 369–400.
24. U.S. Pat. 3,454,542 (July 8, 1969), D. W. Cheape and W. R. Eberhardt (to Monsanto Co.).
25. S. Ito, Y. Kawai, and T. Oshita, *Kobunshi Ronbunshu* **43**, 345 (1986).
26. S. Ito, *Sen'i Gakkaishi.* **43**, 236 (1987); S. Ito and C. Okada, *Sen'i Gakkaishi.* **42**, T618–T625 (1986).
27. G. Vidotto, S. Brugnaro, and G. Talamini, *Die Macromol. Chem.* **140**, 263 (1970).
28. J. C. Bevington, *Radical Polymerization*, Academic Press, Inc., New York, 1961.
29. C. H. Bamford, W. C. Barb, A. D. Jenkins, and P. F. Onyon, *The Kinetics of Vinyl Polymerization by Radical Mechanisms*, Academic Press, Inc., New York, 1958.
30. K. E. J. Barret and H. R. Thomas, in K. E. J. Barret, ed., *Dispersion Polymerization in Organic Media*, John Wiley & Sons, Inc., New York, 1975, Chapt. 4.
31. N. Friis, D. Goosney, J. D. Wright, and A. E. Hamielic, *J. Appl. Polym. Sci.* **18**, 1247 (1974).
32. C. H. Bamford and A. D. Jenkins, *Proc. R. Soc. London, Ser. A.* **226**, 216 (1953); *Proc. R. Soc. London, Ser.* **228**, 220 (1920); C. H. Bamford, A. D. Jenkins, M. C. R. Symons, and M. G. Townsend, *J. Polym. Sci.* **34**, 181 (1959).
33. A. D. Jenkins, in G. Ham, ed., *Vinyl Polymerization*, Part I, Marcel Dekker, New York, 1967, Chapt. 6.
34. L. H. Peebles Jr., *Copolymerization*, Wiley-Interscience, New York, 1964, Chapt. 9.
35. Can. Pat. 911,650 (Oct. 3, 1972), P. Melacini, R. Tedesco, L. Patron, and A. Moretti (to Montedison Fibre); U.S. Pat. 3,787,365 (Jan. 22, 1974), U.S. Pat. 3,821,178 (June 28, 1974), U.S. Pat. 3,879,360 (Apr. 22, 1975), P. Melacini, R. Tedesco, L. Patron, and A. Moretti (all to Montefibre).
36. E. W. Rugeley, T. A. Field Jr., and G. H. Fremon, *Ind. Eng. Chem.* **40**, 1724 (1948).
37. U.S. Pat. 2,420,330 (May 13, 1947), L. C. Shriver and G. H. Fremon (to Carbide and Carbon Chemicals Corp.).
38. W. D. Harkins, *J. Am. Chem. Soc.* **69**, 1428 (1947).
39. W. V. Smith and R. H. Ewart, *J. Chem. Phys.* **16**, 592 (1948); W. V. Smith, *J. Am. Chem. Soc.* **70**, 3695 (1948). W. V. Smith, *J. Am. Chem. Soc.* **71**, 4077 (1949).
40. J. L. Gardon, *J. Polym. Sci., Part. A-1* **6**, 643, 665, 687, 2853, 2859 (1968); J. L. Gardon, *Brit. Polym. J.* **2**, 1 (1970).
41. R. M. Fitch and Lih-bin Shih, *Prog. Colloid Polym. Sci.* **56**, 1 (1975).
42. D. C. Blackley, *Emulsion Polymerization Theory and Practice*, John Wiley & Sons, Inc., New York, 1975.
43. D. R. Bassett and A. E. Hamielec, eds., *Emulsion Polymers and Emulsion Polymerization* (ACS Symposium Series, Vol. 165), American Chemical Society, Washington, D.C., 1981.
44. I. Piirma, ed., *Emulsion Polymerization*, Academic Press, Inc., New York, 1982.
45. K. W. Min and W. H. Ray, *J. Macromol. Sci., Part C: Rev. Macromol. Chem.* **11**(2), 177 (1974).
46. G. E. Ham, in Ref. 49, Chapt. 1, pp. 1–64.
47. A. Valvassori and G. Sartori, *Adv. Polym. Sci.* **5**, 28 (1967).
48. T. Alfrey Jr., J. J. Bohrer, and H. Mark, eds., *Copolymerization*, Wiley-Interscience, New York, 1952.
49. G. E. Ham, ed., *Copolymerization*, Wiley-Interscience, New York, 1964.
50. G. E. Ham, in J. I. Kroschwitz, ed., Encyclopedia of Polymer Science and Technology, 2nd ed., Vol. 4, John Wiley & Sons, Inc., New York, 1966, p. 165.
51. L. H. Peebles Jr., in Ref. 49.
52. A. D. Jenkins and A. Ledwith, eds., *Reactivity, Mechanism and Structure in Polymer Chemistry*, Wiley-Interscience, New York, 1974.

53. F. R. Mayo and C. Walling, *Chem. Rev.* **46**, 191 (1950).
54. R. G. Fordyce and E. C. Chapin, *J. Am. Chem. Soc.* **69**, 581 (1947).
55. R. G. Fordyce, *J. Am. Chem. Soc.* **69**, 1903 (1947).
56. R. G. Fordyce and G. E. Ham, *J. Polym. Sci.* **3**(6), 891 (1948).
57. W. V. Smith, *J. Am. Chem. Soc.* **70**, 2177 (1948).
58. D. W. Ley and W. F. Fowler Jr., *J. Polym. Sci., Part A.* **A2**, 1863 (1964).
59. V. I. Eliseeva, S. S. Ivanchev, S. I. Kuchanov, and A. V. Lebedev, *Emulsion Polymerization and Its Applications in Industry*, English Translation Consultants Bureau, New York, 1981.
60. J. P. Craig, J. P. Knudsen, and V. F. Holland, *Text. Res. J.* **33**, 435 (1962).
61. D. R. Paul, *J. Appl. Polym. Sci.* **11**, 439 (1967); *J. Appl. Polym. Sci.* **12**, 383 (1968).
62. J. P. Knudsen, *Text. Res. J.* **33**, 13 (1963).
63. U.S. Pat. 3,353,381 (Nov. 21, 1967); U.S. Pat. 3,791,788 (Feb. 12, 1974) E. A. Taylor Jr. (both to Monsanto Co.).
64. B. von Falkai, in J. C. Masson, ed., *Acrylic Fiber Technology and Applications*, Marcel Dekker, New York, 1995, p. 159.
65. J. C. Masson, *AN Solution Polymerization in DMSO*, Monsanto Corp., Research Tringle Park, N.C., 1969 (internal document).
66. A. A. Armstrong, *Melt Spinning of Acrylic Copolymers*, Monsanto Corp., Research Tringle Park, N.C., 1971, (internal document).
67. U.S. Pat. 6,114,034 (Sept. 5, 2000), R. J. Jorkasky, L. E. Ball, M. M. Wu, and C. E. Uebele (to Standard Oil).
68. J. C. Masson, in J. C. Masson, ed., *Acrylic Fiber Technology and Applications*, Marcel Dekker, New York, 1995, p. 180.
69. W. E. Fitzgerald and J. P. Knudsen, *Text. Res. J.* **37**, 447 (1967).
70. A. A. Vaidya and S. Chattopadhyay, *Text. Dyer Printer.* **10**(8), 37–41 (1977).
71. M. Lewin, in M. Lewin and S. B. Sello, eds., Handbook of Fiber Science and Technology, Vol. II, Part B, Marcel Dekker, Inc., New York, 1985, pp. 1–141.
72. A. A. Kumar, K. V. Vaidya, and K. V. Datye, *Man-Made Text. (India)* **24**(1), 23 (1981).
73. M. M. Gauthier, R. D. Deanin, and C. J. Pope, *Polym. Plast. Technol. Eng.* **16**(1), 39 (1981).
74. C. Hsieh, *Hsin Hsien Wei.* **20**(11), 12 (1979); M. Hatano and H. Ogawa, *Kagaku Keizoi* **27**(7), 77 (1980).
75. R. C. Nametz, *Ind. Eng. Chem.* **62**, 41 (1970).
76. N. A. Khalturinskii, T. V. Popova, and A. A. Berlin, *Russ. Chem. Rev.* **53**(2), 197 (1984).
77. *High Perform. Text.* **8**(11), 7 (1988); *High Perform. Text.* **3**(10), 3 (1983).
78. Br. Pat. 2,018,188A (Nov. 24, 1978) (to American Cyanamid).
79. U.S. Pat. 3,814,739 (June 4, 1974), H. Takeda (to Toray).
80. R. Moreton, *Carbon Fibres: Their Composites and Applications*, (Paper No. 12), The Plastics Institute, London, 1971.
81. Eur. Pat. Appl. 44,534 (Jan. 27, 1982) (to Hoechst AG).
82. *High Perf. Text.* **8**(11), 7 (1988); *High Perf. Text.* **4**(12), 3 (1984).
83. Jpn. Pat. 17,966 (Feb. 20, 1981); Jpn. Pat. 60,051 (May 6, 1980); Jpn. Pat. 98,025 (Feb. 13, 1976) (all to Asahi Chem.).
84. Ger. Pat. DE 3,012,998 (Oct. 15, 1981), A. Wuestfeld and C. Wuestfeld.
85. Pat. 889,260 (Oct. 16, 1981) S. A. Belg (to REDCO).
86. *Hoechst High Chem. Mag.* **1**, 66 (1986).
87. *High Perf. Text.* **3**(10), 3 (1983).
88. J. Wang, S. Backer, and V. C. Li, *J. Mater. Sci.* **22**(12), 4281 (1987).
89. E. Maslowski and A. Urbanska, *Am. Text. Int.* **18**, FW2 (1989).
90. P. Rajalingam and G. Radhakrishnan, *J. Macromol. Sci., Part C: Rev. Macromol. Chem.* **31**(2) (1991).

91. R. Prescott, *Mod. Plast. Ency.* **66**(11), 232 (1989).
92. *Manufactured Fiber Handbook*, SRI International, Menlo Park Calif., 2000.
93. G. J. Capone, in J. C. Masson, ed., *Acrylic Fiber Technology and Applications*, Marcel Dekker, New York, 1995, p. 74.
94. *Fibre Consumption in the Main-Uses*, International Rayon & Synthetic Fibers Committee Tables, 2000.

GARY J. CAPONE
Solutia, Inc.
JAMES C. MASSON
JCM Consulting

ACRYLONITRILE AND ACRYLONITRILE POLYMERS.
See Volume 1.

ACRYLONITRILE–BUTADIENE–STYRENE POLYMERS.
See Volume 1.

ADDITIVES. See Volume 1.

ADHESION. See Volume 1.

ADHESIVE COMPOUNDS. See Volume 1.

ADSORPTION. See Volume 5.

AGING, PHYSICAL. See Volume 1.

ALKYD RESINS. See Volume 1.

ALLYL RESINS. See THERMOSETS.

AMINO RESINS AND PLASTICS. See Volume 1.

AMORPHOUS POLYMERS. See Volume 5.

ANIONIC POLYMERIZATION. See Volume 5.

ANTIFOAMING AGENTS. See Volume 1.

ANTIOXIDANTS. See Volume 5.

ANTIOZONANTS. See RUBBER CHEMICALS.

ATOM TRANSFER RADICAL POLYMERIZATION.

See LIVING RADICAL POLYMERIZATION.

ATOMIC FORCE MICROSCOPY.

See Volume 1.

ATRP.

See LIVING RADICAL POLYMERIZATION.

CARBON BLACK

Introduction

Carbon black is a generic term for an important family of products used principally for the reinforcement of rubber, as a black pigment, and for its electrically conductive properties. It is a fluffy powder of extreme fineness and high surface area, composed essentially of elemental carbon. Carbon black is one of the most stable chemical products. In a general sense, it is the most widely used nanomaterial, with its aggregate dimension ranging from tens of nanometers to a few hundred nanometers, and imparts special properties to composites of which it is a part. Plants for the manufacture of carbon black are strategically located worldwide in order to supply the rubber tire industry, which consumes 70% of carbon black production. About 20% is used for other rubber products and 10% is used for special nonrubber applications (1). World capacity in 2001 was estimated at over eight million metric tons (1). U.S. capacity was approximately 24 million metric tons. Over 42 grades, listed in ASTM 1765-01 (2), are used by the rubber industry. Many additional grades are marketed in the nonrubber markets.

Carbon blacks differ from other forms of bulk carbon such as diamond, graphite, cokes, and charcoal in that they are composed of aggregates having complex configurations, quasigraphitic in structure, and are of colloidal dimensions. They differ from other bulk carbons in being formed from the vapor phase by homogeneous nucleation through the thermal decomposition and the partial combustion of hydrocarbons. Carbon black is the product of a technology incorporating state-of-the-art engineering and process controls. Its purity differentiates it from soots that are impure by-products from the combustion of coal and oils and from the use of diesel fuels. Carbon blacks are essentially free of the

Encyclopedia of Polymer Science and Technology. Copyright John Wiley & Sons, Inc. All rights reserved.

inorganic contaminants and extractable organic residues characteristic of most forms of soot.

A number of processes have been used to produce carbon black including the oil furnace, impingement (channel), lampblack, the thermal decomposition of natural gas, and decomposition of acetylene (3). These processes produce different grades of carbon black and are referred to by the process by which they are made, eg, oil-furnace black, lampblack, thermal black, acetylene black, and channel black. A small amount of by-product carbon from the manufacture of synthesis gas from liquid hydrocarbons has found applications in electrically conductive compositions. The different grades from the various processes have certain unique characteristics, but it is now possible to produce reasonable approximations of most of these grades by the oil-furnace process. Since over 95% of the total output of carbon black is produced by the oil-furnace process, this article emphasizes this process (1).

History of Carbon Black Manufacture

Carbon blacks' use as a pigment dates back to prehistoric times. Wall paintings from Paleolithic caves are the earliest known use. The Egyptians used carbon black to pigment paints and lacquers. In China, about 3000 BC, carbon black for pigment use was made by burning vegetable oils in small lamps and collecting the carbon on a ceramic lid.

Prior to 1870 the dominant carbon black manufacture was by the lampblack process where oil from animal or vegetable sources was burned in a shallow pan with a restricted air supply. Starting in 1870, natural gas began to be used as the feedstock for carbon black manufacture. The resulting blacks were much darker and better covering than lampblacks. Over a couple of decades, the channel process was developed in which small gas flames burning in restricted air supply impinged on iron channels. The black adhered to the cool channel surface and was recovered by scraping it from the channel. Carbon yields were poor—a few percent. In part this was from the inefficiency of methane as a feedstock, but it also reflects the very poor capture efficiency of the early channel black process. Reportedly the smoke plumes from channel black plants could be seen for 50 miles. The last channel black plant in the United States was closed in 1976. Two plants remain in the former Soviet Union, and a related but much evolved process is still operated in Germany.

A critical event in the development of the carbon black industry was the discovery of the benefits of carbon black as a reinforcing agent for rubber in 1904 (4). As the automobile became ubiquitous during the decade of the twenties, the application in pneumatic tires grew rapidly and soon by-passed other applications, causing rapid growth in consumption. During the 1920s, two other processes were introduced, both using natural gas as feedstock, but having better yields and lower emissions than the channel process. One was the thermal black process in which a brick checker-work alternately absorbs heat from a natural gas air flame, and then gives up heat to crack natural gas to carbon and hydrogen. The other process was the gas-furnace process which is no longer practiced.

The oil-furnace process was first introduced by Phillips Petroleum at its plant in Borger, Texas, in 1943. This process rapidly replaced all others for the

production of carbon black for use in rubber. In this process fuel is burned with air in a primary combustion flame which contains excess air. A heavy, highly aromatic oil is then atomized in the hot gases leaving the primary combustion flame. A portion of the oil is burned by the excess oxygen, providing the heat to maintain temperature and pyrolyze the remainder of the oil. In a modern version of the oil-furnace process, carbon yields range from 65% downward, depending on the surface area of the product. Product recovery is essentially 100% as a result of high efficiency bag filters. The overwhelming majority of carbon black reactors today are based on the oil-furnace process.

The wide adoption of radial tires during the decades of the 1970s and 1980s caused a major contraction in demand for blacks for tire use as the expected life of an automobile tire moved from 20,000 miles with bias ply tires to over 40,000 miles with radial tires. This brought about considerable consolidation in the carbon black industry, particularly in North America and Europe.

Properties and Characterization

The structure of carbon black is schematically shown in Figure 1. The primary dispersable unit of carbon black is referred as an "aggregate," which is a discrete,

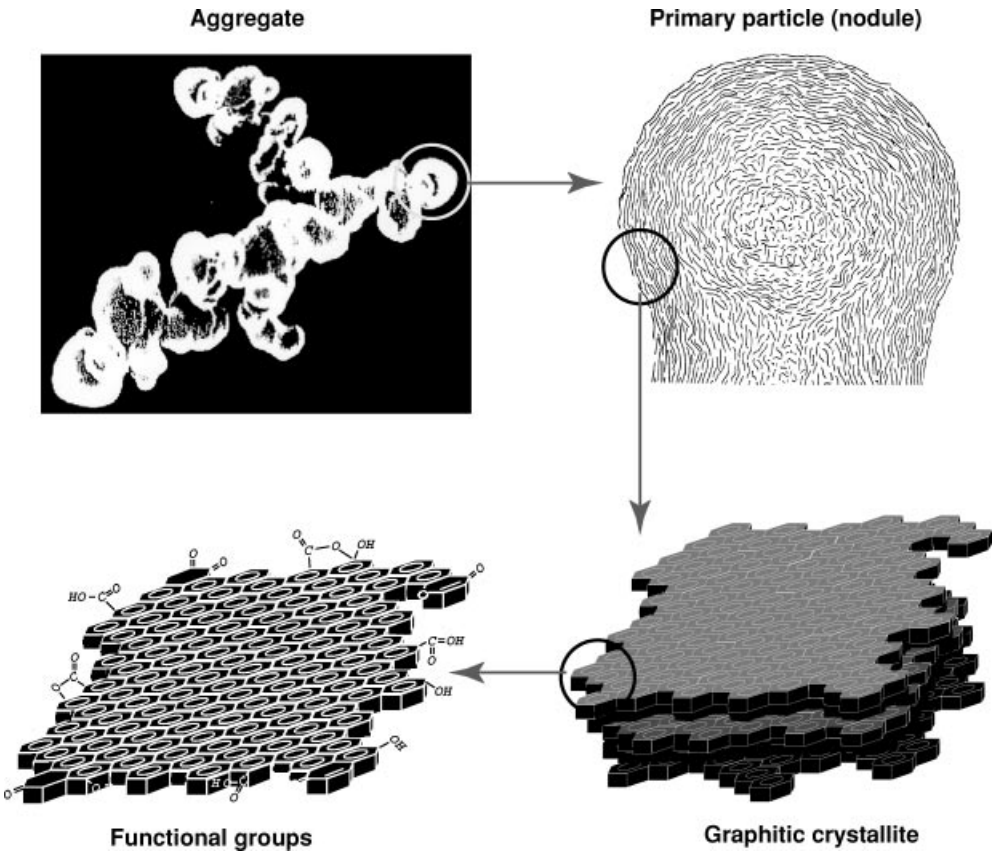

Fig. 1. Structure of carbon black.

rigid colloidal entity. It is the functional unit in well-dispersed systems. The aggregate is composed of spheres that are fused together for most carbon blacks. These spheres are generally termed as primary "particles" or "nodules." These nodules are composed of many tiny graphite-like stacks. Within the nodule the stacks are oriented so that their *c*-axis is normal to the sphere surface, at least near the nodule surface.

The carbon blacks are characterized by their chemical compositions, microstructure, morphologies, and the physical chemistry of the surface. Morphology is a set of properties related to the average magnitude and frequency distribution of the nodule diameter, aggregate diameter, and the way nodules are connected in the aggregates.

Chemical Composition. Oil-furnace blacks used by the rubber industry contain over 97% elemental carbon. Thermal and acetylene black consist of over 99% carbon. The ultimate analysis of rubber-grade blacks is shown in Table 1. The elements other than carbon in furnace black are hydrogen, oxygen, sulfur, and nitrogen. In addition there are mineral oxides, salts, and traces of adsorbed hydrocarbons. The hydrogen and sulfur are distributed on the surface and the interior of the aggregates. The oxygen content is located on the surface of the aggregates as C_xO_y complexes.

Since carbon blacks are produced from hydrocarbon materials, the dangling bonds at the edges of the basal planes of graphitic layers are saturated mostly by hydrogen. The graphitic layers are large polycyclic aromatic ring systems.

Oxygen-containing complexes are by far the most important surface groups. The oxygen content of carbon blacks varies from 0.2–1.5% for furnace blacks to 3–4% for channel blacks. Some speciality blacks used for pigment purposes contain larger quantities of oxygen than normal furnace blacks. These blacks are made by oxidation in a separate process step using nitric acid, ozone, air, or other oxidizing agents. They may contain from 2 to 12% oxygen. The oxygen-containing groups influence the physicochemical properties, such as chemical reactivities, wettability, catalytic, electrical properties, and adsorbability. Oxidation improves dispersion and flow characteristics in pigment vehicle systems such as lithographic inks, paints, and enamels. In rubber-grade blacks surface oxidation reduces pH and changes the kinetics of vulcanization, making the rubber compounds less scorchy and slower curing.

A convenient method for assessing the extent of surface oxidation is the measurement of volatile content. This standard method measures the weight loss of the evolved gases on heating up from 120 to 950°C in an inert atmosphere.

Table 1. Chemical Composition of Carbon Blacks

Type	Carbon, %	Hydrogen, %	Oxygen, %	Sulfur, %	Nitrogen, %	Ash, %	Volatile, %
Furnace rubber-grade	97.3–99.3	0.20–0.80	0.20–1.50	0.20–1.20	0.05–0.30	0.10–1.00	0.60–1.50
Medium thermal	99.4	0.30–0.50	0.00–0.12	0.00–0.25	NA	0.20–0.38	
Acetylene black	99.8	0.05–0.10	0.10–0.15	0.02–0.05	NA	0.00	<0.40

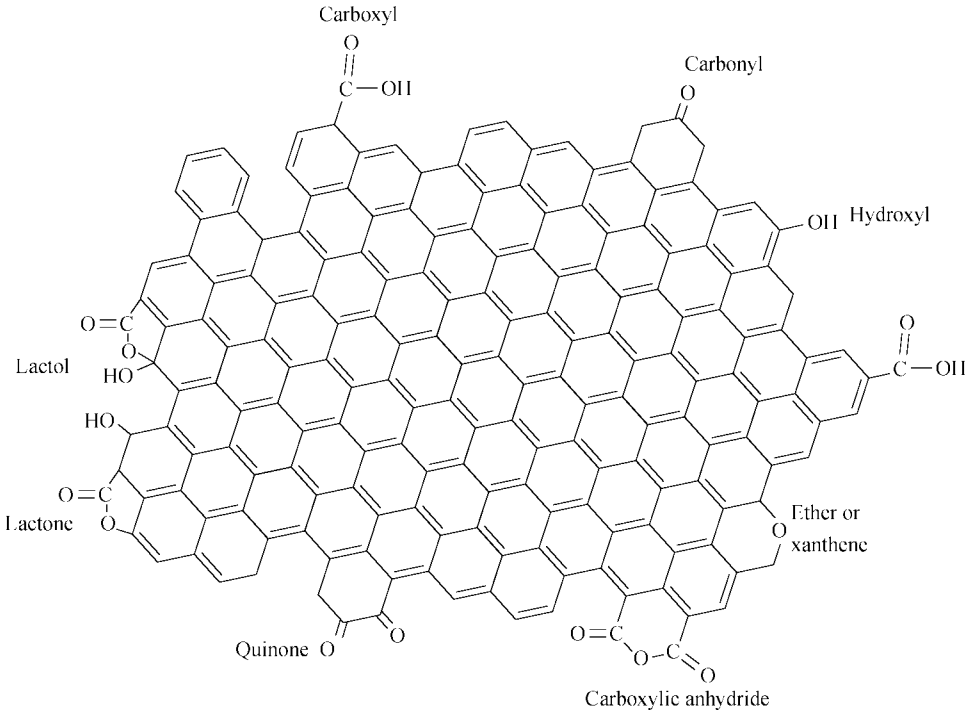

Fig. 2. Aromatic layer plane with functional groups.

The composition of these gases consists of three principal components: hydrogen, carbon monoxide, and carbon dioxide. The volatile content of normal furnace blacks is under 1.5%, and the volatile content of oxidized special grades is 2–22%.

The origin of the volatile gases is the functional groups attached to carbon black, especially those on the surface. Surface oxides bound to the edges of the of carbon layers are phenols, hydroquinones, quinones, neutral groups with one oxygen, carboxylic acids, lactones, and neutral groups containing two oxygens (5). Figure 2 shows an idealized graphite surface layer plane with the various functional groups located at the periphery of the plane. Carbon blacks with few oxygen groups show basic surface properties and anion exchange behavior (6,7).

In addition to combined hydrogen and oxygen, carbon blacks may contain as much as 1.2% combined sulfur resulting from the sulfur content of the aromatic feedstock that contains thiophenes, mercaptans, and sulfides. The majority of the sulfur is not potentially reactive as it is inacessibly bound in the interior of carbon black particle and does not contribute to sulfur cross-linking during the vulcanization of rubber compounds.

The nitrogen in carbon blacks is the residue of nitrogen heterocycles in the feedstocks. Thus carbon blacks derived from coal tars have far more nitrogen than petroleum-derived blacks.

The ash content of furnace blacks is normally a few tenths of a percent but in some products may be as high as 1%. The chief source of ash is the water used to quench the hot black from the reactors during manufacture and for wet-pelletizing the black.

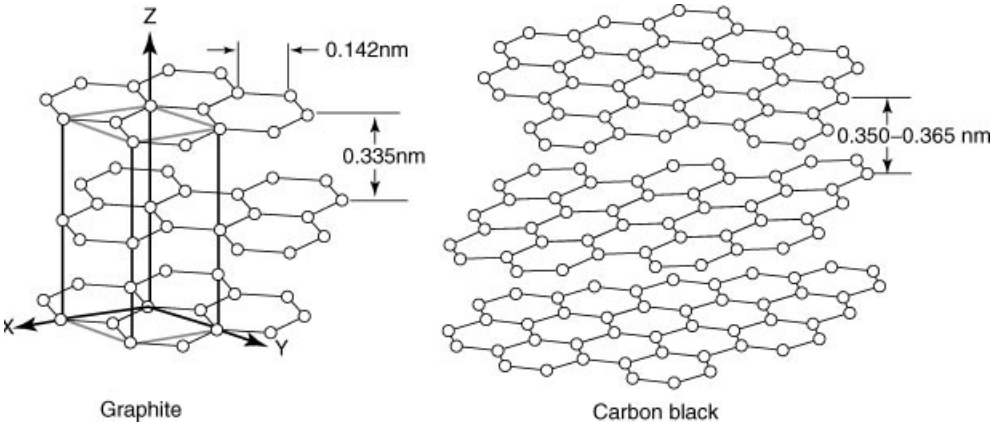

Fig. 3. Atomic structural models of (**a**) graphite and (**b**) carbon black.

Microstructure—Molecular and Crystallite Structure. The arrangement of carbon atoms in carbon black has been well-established by x-ray diffraction methods (8,9). The diffraction patterns show diffuse rings at the same positions as diffraction rings from pure graphite. The suggested relation to graphite is further emphasized as carbon black is heated to 3000°C. The diffuse reflections sharpen, but the pattern never approaches that of true graphite. Carbon black has a degenerated graphitic crystalline structure as defined above. While graphite has three-dimensional order, as seen in the model structures of Figure 3, carbon black has two-dimensional order. The x-ray data indicate that carbon black consists of well-developed graphite platelets stacked roughly parallel to one another but random in orientation with respect to adjacent layers. As shown in Figure 3 the carbon atoms in the graphitic structure of carbon black form large sheets of condensed aromatic ring systems with an interatomic spacing of 0.142 nm within the sheet identical to that found in graphite. However, the interplanar distances are quite different. While graphite interplanar distance is 0.335 nm that results in a relative density of 2.26, the interplanar distance of carbon black is larger, in the range of 0.350–0.365 nm, as a consequence of the random planar orientations or so-called turbostratic arrangement. The relative density of commercial carbon blacks are 1.76–1.90 depending on the grade. About half of the decrement in density is attributed to L_c in the crystallites. X-ray diffraction data provide estimates of crystallite size. For a typical carbon black, the average crystallite diameter L_a is about 1.7 nm and average thickness L_c is 1.5 nm, which corresponds to an average of four layer planes per crystallite containing ca 375 carbon atoms.

It was originally suggested that these discrete crystallites were in random orientation within the particle. This view was later abandoned when electron microscopy of graphitized and oxidized carbon blacks indicated more of a concentric layer plane arrangement which can be described by a paracrystalline model. This structure has been confirmed by the use of high resolution phase-contrast electron microscopy that made possible the direct imaging of graphitic layer planes in carbon black (10). Figure 4 shows a phase-contrast electron micrograph of carbon

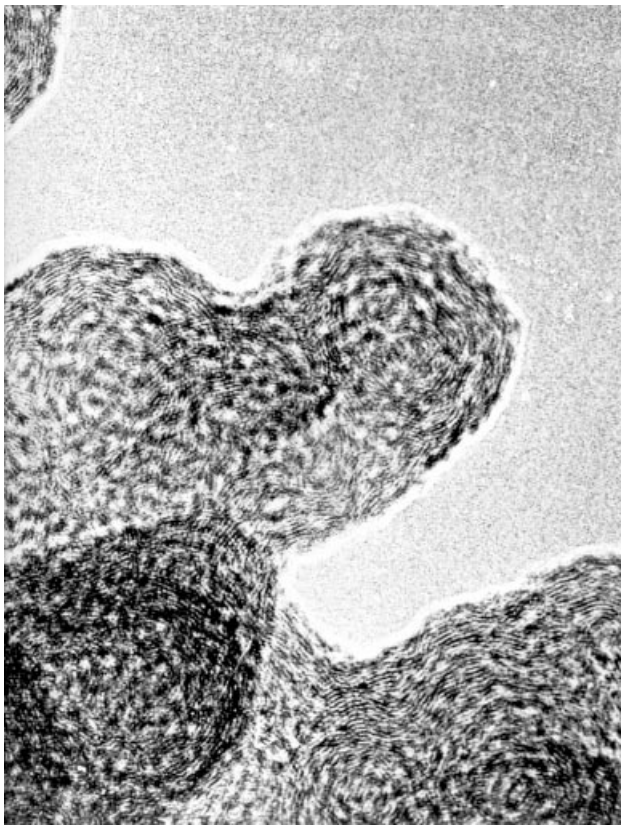

Fig. 4. High resolution (3,000,000×) electron micrograph of N220-grade carbon black. Courtesy of W. M. Hess.

black at high resolution that displays the marked concentric arrangement of the layer planes at the surface and around what appear to be growth centers.

More recently, the microstructure of the carbon black surface has been investigated by means of scanning tunneling microscopy (STM) (11,12). Figure 5 shows the STM images obtained in the current mode for graphite, graphitized carbon black, and normal carbon black N234. Compared to graphite, the structure of carbon blacks graphitized for 24 h at a temperature of 2700°C in an inert atmosphere still remains in a certain imperfect state, shown by different tunneling current partterns in the organized domains. The surface structure of carbon black can be classified into two types: organized domains and unorganized domains. The organized domains occupy the majority of the carbon black surface, and its size generally decreases with decreasing particle size.

Morphology. Morphologically, carbon blacks differ in primary "particle" or nodule size, surface area, aggregate size, aggregate shape, and in the distribution of each of these.

Primary "Particle" (Nodule) Size. Although the smallest discrete entity of carbon black is the aggregate, the particle size, and its distribution is one of the most important morphological parameters with regard to its end-use applications,

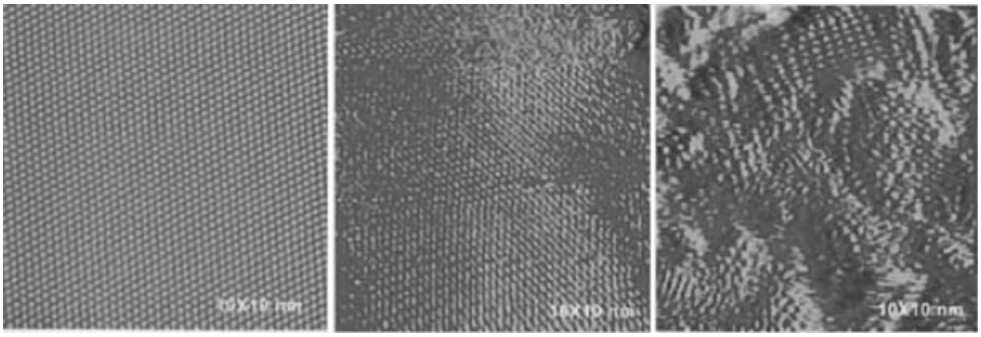

Fig. 5. STM images of graphite, graphitized carbon black and carbon black N234.

even though the particles do not exist as discrete entities except for thermal black. The particle size is of critical importance to the specific surface of the carbon blacks and has been taken as the principal parameter for grade classification of rubber blacks in ASTM. In almost all types of carbon black, the primary particles within a single aggregate are similar. However, the types of blacks can differ in the uniformity of the primary particles of different aggregates. While many types do show a quite narrow range of primary particles, others are clearly quite broad mixtures of aggregates of differing primary particle size or specific surface area. The electron microscope is the universally accepted instrument for measuring particle size, aggregate size, and aggregate morphology. Typical electron micrographs of rubber-grade carbon blacks are shown in Figure 6.

Particle size measurement is based on the visual electron microscope counts for several thousand particles on electromicrographs of known magnification (ASTM D3849). Automated image analyzers provide measurements of a variety of particle parameters.

Surface Area. The surface area is one of the most important features influencing the performance of carbon blacks. It is an extensity factor that determines the interfacial area between carbon black and the medium in which a given volume of black is dispersed.

The surface area can be calculated from particle size measured with transmission electron microscope (TEM) (ASTM D3849). Generally, for rubber grade, the surface areas determined by TEM are in reasonable agreement with surface areas determined by nitrogen adsorption measurements. However, for those carbon blacks that have highly developed micropores such as special pigment blacks and blacks used for electrical conductivity, the surface areas calculated from their particle diameters are smaller than those calculated from gas absorption, as the internal surface area in the micropore is excluded.

While the TEM images contain very detailed statistical information, such images are expensive and time-consuming to obtain. Direct measurement of specific surface area is much faster and cheaper. Such measurements are most easily made by gas- and liquid-phase adsorption techniques that depend on the amount of adsorbate required to form a surface monolayer. If the area occupied by a single-adsorbate molecule is known, a simple calculation will yield the surface area.

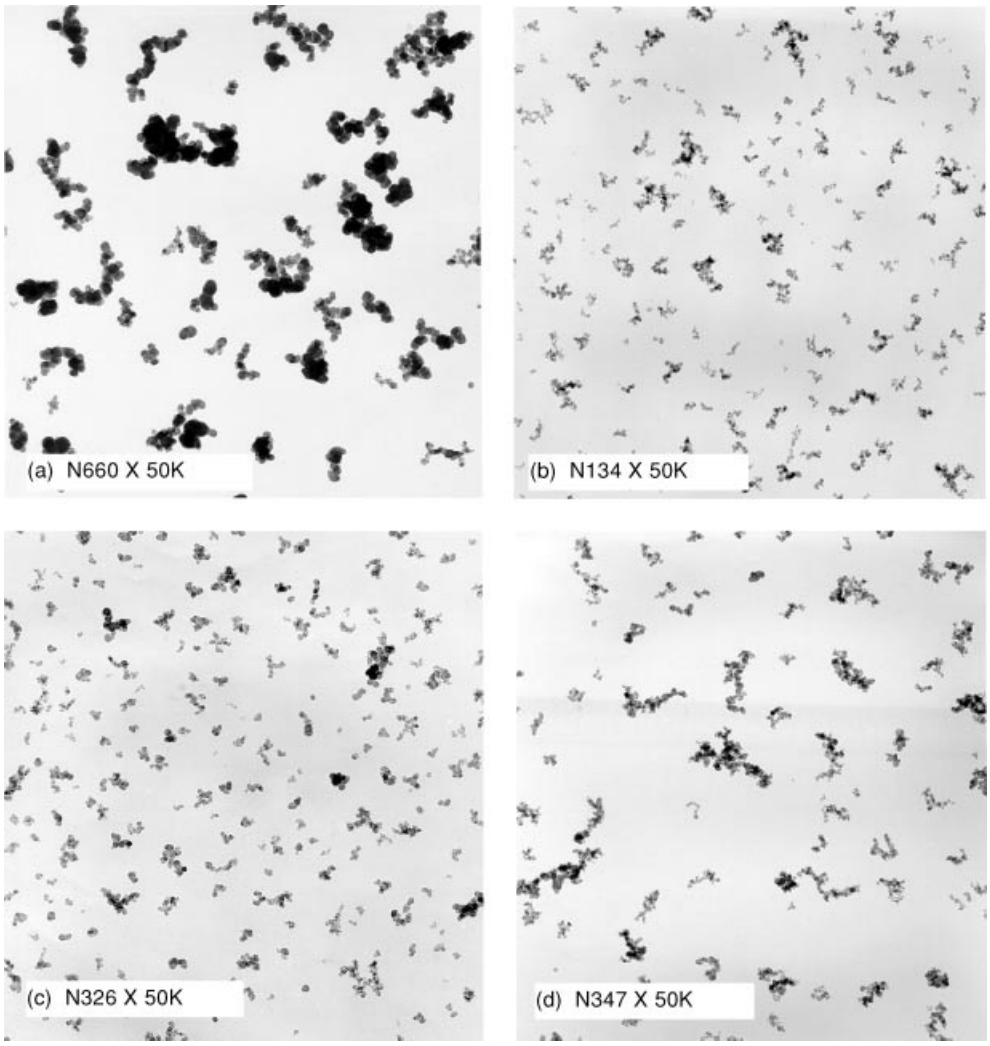

Fig. 6. Electron micrographs of rubber-grade carbon blacks.

A low temperature nitrogen adsorption method, based on the original method of Brunauer, Emmett, and Teller (BET) (13), has been adopted by ASTM as standard method D6556. It is not sensitive to changes in the surface chemistry of carbon black such as those that result from surface oxidation and presence of trace amount of tarry material. With a molecular diameter of less than 0.5 nm, nitrogen is small enough to enter the micropore space so that the surface measured by BET is the total area, inclusive of micropore. For some application, such as rubber reinforcement, the internal surface area in the micropore with less than 2 nm diameter is inaccesible to large rubber molecules, and thus it plays no part or has a negative effect on rubber reinforcement. The specific surface area that is accesible to rubber is defined as "external" surface area. This is conveniently

measured by a multilayer nitrogen adsorption, also defined in ASTM D6556 and known as the statistical thickness surface area (STSA) (14).

Liquid-phase adsorption methods are also widely used. The adsorption of iodine from potassium iodide solution is the standard ASTM method D1510. The surface area is expressed as the iodine number whose units are milligrams of iodine adsorbed per gram of carbon blacks. The test conditions such as adsorbate concentration and the amount of carbon black sample used are specified in such a way that the values of iodine numbers turn out to be about the same as the values for surface areas in square meters per gram that is measured by nitrogen adsorption for nonporous and nonoxidized furnace carbon blacks. The iodine number is raised by porosity and decreased by surface oxygen or adsorbed organics. Still it is the most easily measured surface area estimate and is used extensively, especially for process control.

Another standard industry method for surface area measurement is based on the adsorption of cetyltrimethylammonium bromide (CTAB) from aqueous solution. This is ASTM method D3765 and has largely been replaced by STSA in the last decade.

Aggregate Morphology (Structure). The aggregate morphology is another important characteristic that influences performance. The term "structure" is widely used in the carbon black and rubber industries to describe the aggregate morphology. It was originally introduced in 1944 (15) to describe the ensemble of aggregates that is a stochastic distribution of the number and arrangement of the nodules that make up the aggregates.

Structure comparisons of grades with different surface areas cannot be made. It is now known that the properties associated with structure are associated principally with the bulkiness of individual aggregates. Aggregates of the same mass, surface area, and number of nodules have high structure in the open bulky and filamentous arrangement and a low structure in a more clustered compact arrangement. Therefore, the structure is now used to describe the relative void volume characteristics of grades of black of the same surface area. Structure is determined by aggregate size and shape, and their distribution. They are geometrical factors which affect aggregate packing and the volume of voids in the bulk material. Therefore, in composite systems, it is also a principal feature that determine the performance of carbon black as a reinforcing agent and as a pigment (16). In liquid media structure affects rheological properties such as viscosity and yield point. In rubber, viscosity, extrusion die swell, modulus, abrasion resistance, dynamic properties, and electrical conductivity are affected by structure.

The direct method for structure measurement of carbon black is TEM (ASTM D3849). It is unique in furnishing information about the aggregate size, shape, and the distribution of these. Typical electron micrographs of rubber-grade carbon blacks are shown in Figure 6. There is an enormous range in aggregate size. The size of the aggregates is generally related to the size of the particles. The shapes of the aggregates have infinite variety from tight grape-like clusters to open dendritic or branched arrangements to fibrous configurations.

A useful method for determining relative aggregate sizes and distributions is by centrifugal sedimentation. For a sphere, the diameter can be derived from the sedimentation rates in the gravitational field according to Stokes equation. For the nonspherical particles such as carbon black aggregates, an equvalent Stokes

Table 2. Carbon Black Morphology

ASTM designation	Particle size[a] D_{wm}[b], nm	Aggregate size[a], D_{wm}[b], nm	D_{st}[c], nm	Surface area[a], m^2/g
N110	27	93	76–111	143
N220	32	103	95–117	117
N234	31	109	74–97	120
N326	41	108	98	94
N330	46	146	116–145	80
N339	39	122	96–125	96
N351	50	159	127	75
N375	36	106	91	105
N550	93	240	220–242	41
N660	109	252	227–283	34
N774	124	265	261	30
N990	403	593	436	9

[a] Measured by TEM.
[b] D_{wm} = weight mean diameter = $\sum nd^4/\sum nd^3$.
[c] Stokes diameter by centrifugal sedimentation from various sources.

diameter D_{st} can be obtained as the diameter of a sphere of carbon black having the same settling behavior. A convenient instrument for these measurements is the Joyce Loebl disk centrifuge photosedimentometer (DCP) (17). Large aggregates sediment at a faster rate than smaller ones. The sedimentation rate is also influenced by the bulkiness of the aggregates. At constant volume or mass, a bulky aggregate sediments more slowly than a compact aggregate because of frictional drag. The DCP curve is characteristic of the black structure but the measured diameters need to be viewed with suspicion.

Table 2 lists average D_{st} values and the weight mean diameter D_{wm} for the aggregates calculated from their estimated volumes measured by TEM. There is reasonable agreement between the two diameters. Aggregate size distributions from centrifugal sedimentation analysis are very useful for assessing the differences in this characteristic within a given grade or at constant surface area.

By far the most intensively investigated measure of structure is the maximum packing fraction. In fact the amount of void at the maximum packing has almost become synonymous with carbon black "structure." At least two approaches are widely used. The first determines the amount of liquid that is needed to just fill all the spaces between aggregates when the aggregates are pulled together by the surface tension forces of that liquid. This is done by means of an absorptometer with dibutyl phthalate (DBP) as the liquid (ASTM D2414). This is based on the change in torque during mixing of carbon black and the liquid as there is a sharp increase in viscosity of the mixture, when it changes from free flowing powder to a semiplastic continuous paste. The viscosity, hence the torque, will drop as the liquid is continually added, because of the lubrication effect. The volume of DBP needed for a unit mass of carbon blacks to reach a predetermined level of torque is termed the DBP number. In order to eliminate the effects of pelletizing conditions, the DBP absorption test has been modified to use a sample that has been precompressed at a pressure of 165 MPa (24,000 psi) and then broken up four successive

times (24M4) (ASTM D3493). This procedure causes some aggregate breakdown and is claimed to more closely approximate the actual breakdown that occurs during rubber mixing. The DBP numbers measured for compressed samples are also termed crush DBP (CDBP) number.

The maximum random packing for mono-sized spheres is a volume fraction of 68%. This is equivalent to a DBP number of 25 mL/100 g of carbon black. The types of blacks with the lowest DBP number, and therefore highest packing, have values around 30–35 mL/100 g. The types with the highest structure, and therefore lowest packing, have a DBP number of around 140 mL/100 g. Grades with significantly higher DBP number do not have solid primary particles and the fluid is absorbed both within the primary particles and between the aggregates.

The second way of estimating the maximum packing fraction is mechanical compression. Most commonly this is practiced in uniaxial compression. The test is termed the void volume measurement (ASTM D6086). With both liquid and mechanical compaction, the measured value can be influenced to some degree by either the speed of the compaction, ie, the time the particles have to rearrange, and the final pressure to which they are subjected.

Tinting strength, adopted by ASTM as D3265, is another industry method used for the classification of carbon blacks. In this test a small amount of carbon black is mixed with zinc oxide and an oil vehicle to produce a black or gray paste. The reflectance of this paste is measured and compared to the reflectance of a paste made with a reference black. The ratio of the reference black paste reflectance to the sample black multiplied by 100 is the tint strength. It provides a rough estimate of the reinforcing potential of carbon black in rubber. Tint strength is closely related to carbon black morphology. The carbon blacks with smaller particle size, ie, larger surface area and smaller size of the aggregates (ie, lower structure), show a greater ability to cover the typically larger size zinc oxide particles, giving higher tinting strength. The tinting strength is also related to the aggregate size distribution. The narrower the aggregate size distribution, the higher is the tinting strength.

Surface Activity. Surface activity is also an important factor in performance. This factor can, in a chemical sense, be related to different chemical groups on the carbon black surface. In a physical sense, variations in surface energy determine the adsorptive capacity of the carbon blacks and their energy of adsorption. However, compared with the morphologies, a satisfactory description of surface properties of carbon black is still lacking because only a limited number of tools have been available to assess the carbon black surface in terms of ensemble properties.

With regard to rubber reinforcement, the surface activity of carbon black has traditionally been measured by bound rubber. *Bound rubber*, sometimes termed "*carbon gel*," is defined as the rubber portion in an uncured compound which cannot be extracted by a good solvent of the polymer owing to the adsorption of the rubber molecules onto the filler surface. This phenomenon has been studied extensively and is recognized as a typical feature of carbon black surface activity. For given polymer systems and for the carbon black with comparable surface area, the higher the bound rubber content, the higher is the polymer–filler interaction, and hence the higher is the surface activity of carbon black. Generally speaking, bound rubber is a parameter that is simple to measure, but the factors that influence

the test results are highly complicated. It has been recognized that carbon black – polymer interaction leading to the formation of bound rubber involves physical adsorption, chemisorption, and mechanical interaction.

It is generally found that the surface energy of carbon blacks have a much greater effect on the mechanical properties of filled elastomers than the chemical composition, particularly when general-purpose hydrocarbon rubbers are concerned. The surface energy γ is defined as the work necessary to create a unit new surface of liquid or solid. This energy is caused by different types of cohesive forces, such as dispersive, dipole–dipole, induced dipole–dipole, and hydrogen bond forces. In the case of all these cohesive forces being involved in independent ways, the surface energy can be expressed as the sum of several components, each corresponding to a type of molecular interaction (dispersive, polar, hydrogen bond, etc). Since the effect of the dispersive force is universal, the dispersive component of the surface free energy γ^{d} is particularly important. If a solid substance can have only dispersion interaction with its environment, its surface energy γ_s is identical with its dispersive component $\gamma_s{}^{d}$. For most substances, the surface energy of a solid is the sum of $\gamma_s{}^{d}$ and $\gamma_s{}^{sp}$ that is the sum of the other components of surface energy and is termed "specific component" or "polar" component. The higher the $\gamma_s{}^{d}$ of the carbon black, the stronger is the interaction between carbon black and non- or less-polar polymers such as hydrocarbon rubbers. The higher polar component of the surface energy leads to higher interaction with polar polymer or polar groups in the polymer chains.

Several methods to measure the solid surface energy can be used for carbon black. However, inverse gas chromatography (IGC) has recently been shown to be one of the most sensitive and convenient methods for measuring carbon black surface energy (18). In IGC, the filler to be characterized is used as the stationary phase and the solute injected is called a probe. When the probe is operated at infinite dilution, the adsorption energy of the probe on the carbon black surface and hence the surface energy of the black can be calculated from the net retention volume (18). If, however, the surface is energetically heterogeneous, the values of parameters obtained from IGC measurement are mean values over the whole surface of the fillers, but they are "energy-weighted," ie, the high energy sites play a very important role in the determination of adsorption parameters measured (19). When the probe is operated at finite concentration, the adsorption isotherms of the probes on carbon black surface can be generated from the pressure dependence of the retention volume and, hence, the distribution of free energy of adsorption of the probe chemicals can be derived from the isotherm (19).

Other Methods for Carbon Black Characterization. There are many other test methods used to characterize carbon blacks for quality control and specification purposes. Table 3 lists some of these methods which, with a few exceptions, have been adopted by ASTM.

Classification of Carbon Black

Carbon blacks have been classified by their production process, by their production feedstocks such as acetylene blacks, by their application field, such as rubber blacks, color blacks, electric conductive blacks, and by properties of end-use

Table 3. Special Analytical Test Methods for Carbon Black

Test method	Standard	Comment
Iodine adsorption, mg/g	ASTM D1510	Amount of iodine adsorbed from aqueous solution as a measure for the specific surface area; not applicable for oxidized or highly porous carbon blacks
N_2 surface area and external surface area, m^2/g	ASTM D6556	Determination of the total surface area (NSA) by BET theory of multilayer gas adsorption behavior using multipoint determinations and the external surface area based on the statistical thickness surface area (STSA) method
CTAB surface area, m^2/g	ASTM D3765	Amount of cetytrimethylammonium bromide adsorbed from aqueous solution as measure of specific nonporous (outer) surface area
Aggregate dimension and aggregate size distribution	ASTM D3849	Determination of aggregate dimensions (unit length, width, etc) by electron microscope image analysis.
Aggregate size distribution		Diameters of equivalent solid spheres that sediment at same rate as aggregates during centrifuging
DBP absorption, mL/100 g	ASTM D2414	Determination of the void volume with dibutyl phthalate in a special kneader as measure of structure
24 M4-DBP absorption, mL/100 g	ASTM D3493	Determination of DBP absorption after four repeated compressions at 165 MPa (24,000 psi)
Compressed volume index	ASTM D6086	Determination of compressed volume of carbon black under a specified compression force.
Jetness		Light absorption of a carbon black paste in linseed oil; determination by visual comparison against standard blacks or by measuring the absolute light emission
Tint strength, %	ASTM D3265	Ability of a carbon black to darken a white pigment in an oil paste. The tinting strength is the reflectance of the tested carbon black paste with respect to the reflectance of the reference carbon black paste.
Volatiles, %		Weight loss when calcined at 950°C for 7 min
Heating loss (moisture), %	ASTM D1509	Weight loss on drying at 125°C for 1 h
pH	ASTM D1512	pH of an aqueous slurry of carbon black; pH is mainly influenced by surface oxides
Extractables, %	ASTM D1618	Amount of material which can be extracted by a boiling solvent, usually toluene
Extractables, %	ASTM D4527	Determination of the total material extracted from carbon black by toluene under specified conditions. The procedure is also applicable to other solvents

Table 3. (continued)

Test method	Standard	Comment
Ash content, %	ASTM D1506	Amount of noncombustible material after burning the carbon black at 675°C
Sulfur content, %	ASTM D1619	
Sieve residue, %	ASTM D1514	Amount of coarse impurities that cannot be purged through a testing sieve by water
Pour density, g/L	ASTM D1513	Measure for the densification of carbon black
Tamped density, g/L		Similar to bulk density; however, void volume is reduced by temping
Pellet crush strength	ASTM D5230	Automated individual pellet crush strength
Pellet crush strength	ASTM D3313	Individual pellet crush strength
Pellet mass strength	ASTM D1937	Pellet mass strength
Pellet size distribution	ASTM D1511	Determination by means of sieve shaker
Fines content, %	ASTM D1508	Only for pelletized blacks; percentage passing through a sieve of 125 μm (mesh) width

products such as high abrasion furnace black and fast extrusion furnace black. From their applications, the carbon black is classified into two groups: one used for rubber products, and another for non-rubber applications. They are referred to as special blacks. Generally, special carbon blacks cover a wider range of morphology and surface chemistry than rubber blacks.

The rubber industry is by far the major consumer of carbon black. For rubber grades, a classification system issued by ASTM is based essentially on particle size, structure, and their effect on the cure rate of filled rubber compounds which is related to the degree of surface oxidation (ASTM D1765). It is composed of a letter followed by three numbers. The N series are for the normal-curing furnace and thermal blacks and S for slow-curing blacks with higher degree of oxidation, such as channel black and oxidized furnace blacks that are acidic in nature. The first number of the three-digit suffix identifies particle size and is inversely related to the surface area. The range of particle sizes from 0 to 500 nm has been grouped into 10 categories, covering surface areas from 0 to 150 m^2/g. The remaining two digits are assigned arbitrarily by the carbon black manufacturers. A selected list of typical properties, taken from ASTM D1765 of rubber-grade carbon blacks, is shown in Table 4. In addition to the assigned ASTM N-numbers, the list includes the old letter designations, pour densities, structure, surface areas, and tint data. The structure–area relationships of these grades, called the carbon black spectrum, is illustrated in Figure 7, which shows a diagram of DBP numbers for compressed samples versus the nitrogen surface areas.

Carbon Black Formation

The formation of particulate carbon involves either pyrolysis or incomplete combustion of hydrocarbon materials. Enormous literature has been published

Table 4. Typical Properties of Rubber-Grade Carbon Blacks

ASTM classification	Iodine no., mg/g	DBP no. mL/100 g	CDBP no.[a], mL/100 g	NSA, m^2/g	STSA, m^2/g	Tint strength, %
N110	145	113	97	127	115	123
N115	160	113	97	137	124	123
N120	122	114	99	126	113	129
N121	121	132	111	122	114	119
N125	117	104	89	122	121	125
N134	142	127	103	143	137	131
N135	151	135	117	141		119
S212		85	82	120	107	115
N220	121	114	98	119	106	116
N231	121	92	86	111	107	120
N234	120	125	102	119	112	123
N293	145	100	88	122	111	120
N299	108	124	104	104	97	113
N315		79	77	89	86	117
N326	82	72	68	78	76	111
N330	82	102	88	78	75	104
N335	92	110	94	85	85	110
N339	90	120	99	91	88	111
N343	92	130	104	96	92	112
N347	90	124	99	85	83	105
N351	68	120	95	71	70	100
N356	92	154	112	91	87	106
N358	84	150	108	80	78	98
N375	90	114	96	93	91	114
N539	43	111	81	39	38	
N550	43	121	85	40	39	67
N582	100	180	114	80		
N630	36	78	62	32	32	
N642	36	64	62	39		
N650	36	122	84	36	35	
N660	36	90	74	35	34	
N683	35	133	85	36	34	
N754	24	58	57	25	24	
N762	27	65	59	29	28	
N765	31	115	81	34	32	
N772	30	65	59	32	30	
N774	29	72	63	30	29	
N787	30	80	70	32	32	
N907		34		9	9	
N908		34		9	9	
N990		43	37	8	8	
N991		35	37	8	8	

[a]For compressed samples.

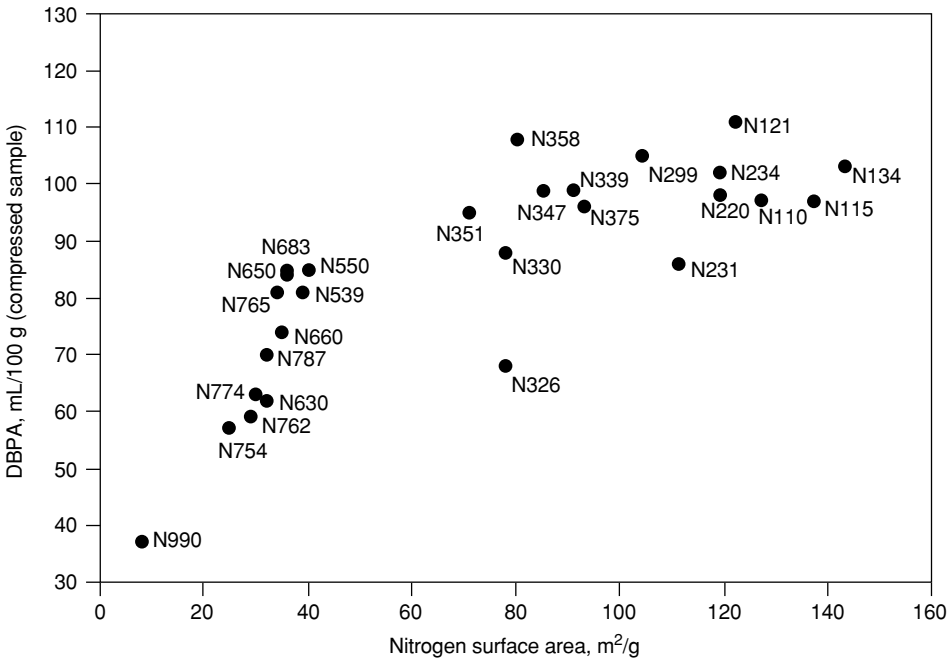

Fig. 7. Rubber-grade carbon black spectrum.

to describe the mechanism of carbon black formation, from a series of lectures by Michael Faraday at the Royal Institution in London in the 1860s (20) to a recent intensive review (21). Since Faraday's time, many theories have been proposed to account for carbon formation, but controversy still exists regarding the mechanism.

Mechanisms of carbon black formation must account for the experimental observations of the unique morphology and microstructure of carbon black. These include the presence of nodules, or particles, multiple growth centers within some nodules, the fusion of nodules into large aggregates, and the paracrystalline or concentric layer plane structure of the aggregates. It is generally accepted that the mechanism of formation involves a series of stages as follows:

(1) Formation of gaseous carbon black precursors at high temperature. This involves dehydrogenation of primary hydrocarbon molecular species to atomic carbon or primary free radical and ions which condense to semisolid carbon precursors (or polynuclear aromatic sheet) and/or formation of large hydrocarbon molecules by polymerization, which then is dehydrogenated to particle precursors.

(2) Nucleation. Because of increasing mass of the carbon particle precursors through collision, the larger fragments are no longer stable and condense out of the vapor phase to form nuclei or growth centers.

(3) Particle growth and aggregation. In the system, three processes go on simultaneously: condensation of more carbon precursors on the existing nuclei,

coalescence of small particles into larger ones, and formation of new nuclei. Coalescence and growth seem to predominate. The products of this stage are "proto-nodules."

(4) Surface growth. Surface growth includes the processes in which the small species attach to or deposit on the surfaces of existing particles or aggregates, forming the nodules and aggregates with their characteristic onion microstructure. The surface growth represents about 90% of total carbon yield. It is responsible for the stability of the aggregates because of the continuous carbon network formation. Aggregates are formed and cemented in this stage.

(5) Agglomeration. Once no more carbon is forming and aggregation ceases, aggregates collide and adhere from van der Waals forces but there is no material to cement them together, hence they form temporary structures.

(6) Aggregate gassification. After its formation and growth, the carbon black surface undergoes reaction with the gas phase, resulting in an etched surface. Species such as CO_2, H_2O, and of course any residual oxygen attack the carbon surface. The oxidation is determined by gas-phase conditions, such as temperature, oxidant concentration, and flow rates.

Practically, the carbon black morphology and surface chemistry can be well controlled by changing the reaction parameters. For furnace carbon blacks, the reaction temperature is the key variable that governs the surface area. The higher the temperature, the higher is the pyrolysis rate and the more nuclei are formed, resulting in an earlier stop of the growth of the particles and aggregates because of the limitation of starting materials at given feedstock. Therefore, with higher reaction temperature, that can be achieved by adjusting air rate, fuel rate, and feedstock rate, the surface area of carbon black can be increased. Addition of alkali metal salts into the reactor can modify the aggregation process, influencing carbon black structure. At the reactor temperature, the salts of alkali metals, such as potassium, are ionized. The positive ions adsorb on the forming carbon black nodules and provide some electrostatic barrier to internodule collisions, resulting in lower structure (22).

The time scale of carbon black formation varies substantially across the range of particle sizes found in commercial furnace blacks. For blacks with surface areas around 120 m^2/g, the carbon black formation process from oil atomization to quench takes less than 10 ms. For blacks with surface areas around 30 m^2/g, formation times are a few tenths of seconds.

Manufacture

Oil-Furnace Process. The oil-furnace process accounts for over 95% of all carbon black produced in the world. It was developed in 1943 and rapidly displaced prior gas-based technologies because of its higher yields and the broader range of blacks that could be produced. It also provides highly effective capture of particulates and has greatly improved the environment around carbon black plants. As indicated in the mechanism discussion, it is based on the partial combustion of

residual aromatic oils. Because residual oils are ubiquitous and are easily transported, the process can be practiced with little geographic limitation. This has allowed construction of carbon black plants all over the world. Plants are typically located in areas of tire and rubber goods manufacture. Because carbon black is of relatively low density, it is far less expensive to transport feedstock than to transport the black.

Over the 50 years since its invention, the oil-furnace process has undergone several cycles of improvement. These improvements have resulted in improved yields, larger process trains, better energy economy, and improved product performance. A simplified flow diagram of a modern furnace black production line is shown in Figure 8 (23). This is intended to be a generic diagram and contains elements from several operators' processes. The principal pieces of equipment are the air blower, process air and oil preheaters, reactors, quench tower, bag filter, pelletizer, and rotary dryer. The basic process consists of atomizing the preheated oil in a combustion gas stream formed by burning fuel in preheated air. The atomization is carried out in a region of intense turbulent mixing. Some of the atomized feedstock is combusted with excess oxidant in the combustion gas. Temperatures in the region of carbon black formation range from 1400 to over 1800°C. The details of reactor construction vary from manufacturer to manufacturer and are confidential to each manufacturer. Leaving the formation zone, the carbon black containing gases are quenched by spraying water into the stream. The partially cooled smoke is then passed through a heat exchanger where incoming air is preheated. Additional quench water is used to cool the smoke to a temperature consistent with the life of the bag material used in the bag filter. The bag filter separates the unagglomerated carbon black from the by-product tail gas which contains nitrogen, hydrogen, carbon monoxide, carbon dioxide, and water vapor. It is mainly nitrogen and water vapor. The tail gas is frequently used to fuel the dryers in the plant, to provide other process heat, and sometimes is burned to manufacture steam and electric power either for internal plant use or for sale.

The fluffy black from the bag filter is mixed with water, typically in a pin mixer, to form wet granules. These are dried in a rotary dryer, and the dried product is conveyed to bulk storage tanks. For special purposes, dry pelletization in rotary drums is also practiced. Most carbon black is shipped by rail or in bulk trucks. Various semibulk containers are also used including IBC's and large semibulk bags. Some special-purpose blacks are packed in paper or plastic bags.

While the reactor and its associated air-moving and heat-exchange equipment are where the properties of the black are determined, they tend to be dwarfed by the bag collectors, the dryers, and particularly the storage tanks.

Feedstocks. Feedstocks for the oil-furnace process are heavy fuel oils. Preferred oils have high aromaticity, are free of suspended solids, and have a minimum of asphaltenes. Suitable oils are catalytic cracker residue (once residual catalyst has been removed), ethylene cracker residues, and distilled heavy coal tar fractions. Other specifications of importance are freedom from solid materials, moderate to low sulfur, and low alkali metals. The ability to handle such oils in tanks, pumps, transfer lines, and spray nozzles is also a primary requirement.

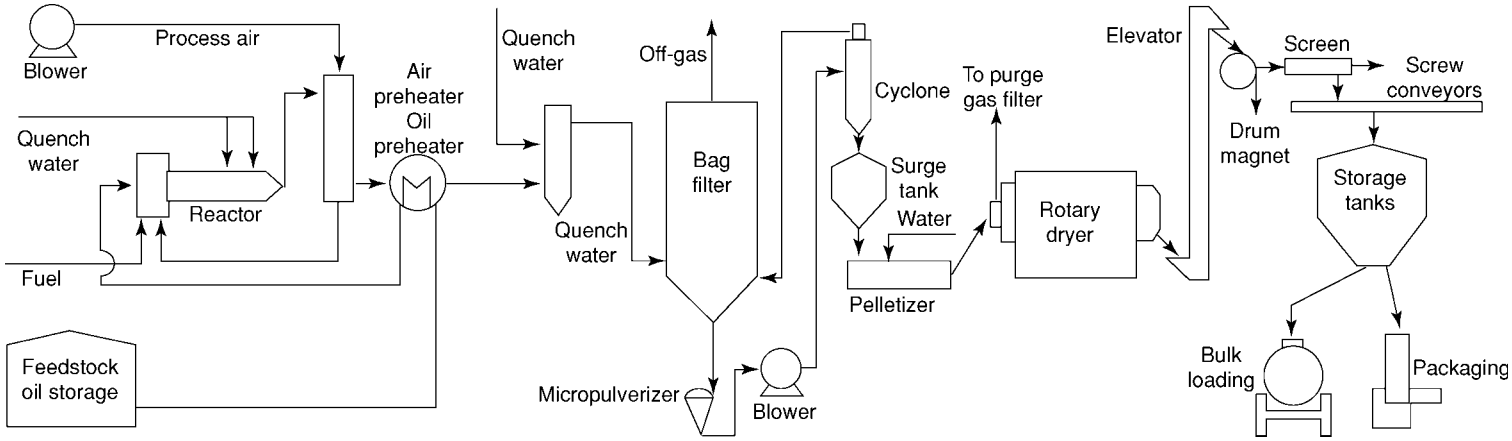

Fig. 8. Flow diagram of oil-furnace black process.

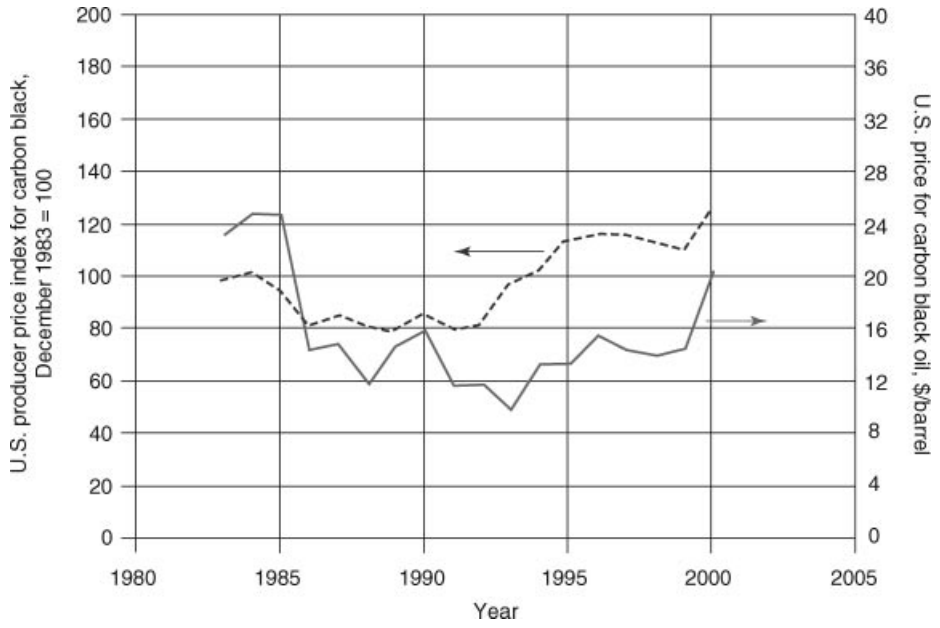

Fig. 9. Carbon black price and raw material cost in the United States (1983–2000) (1).

The pricing of carbon black feedstocks depends on their alternate market as residual fuel oil, especially that of high sulfur No. 6 fuel oil. The actual price is determined by the supply/demand relationships for these two markets. Feedstock cost contributes about 60% of the total manufacturing cost. The market price of carbon black is strongly dependent on the feedstock cost, as shown in Figure 9.

Reactor. The heart of a furnace black plant is the furnace or reactor where carbon black formation takes place under high temperature, partial combustion conditions. The reactors are designed and constructed to be as trouble-free as possible over long periods of operation under extremely aggressive conditions. They are monitored constantly for signs of deterioration in order to ensure constant product quality. The wide variety of furnace black grades for rubber and pigment applications requires different reactor designs and sizes to cover the complete range, though closely related grades can be made in the same reactor by adjusting input variables. Reactors for higher surface area and reinforcing grades operate under high gas velocities, temperatures, and turbulence to ensure rapid mixing of reactant gases and feedstock. Lower surface area and less reinforcing grades are produced in larger reactors at lower temperatures, lower velocities, and longer residence time. Table 5 lists carbon formation temperatures and residence times for the various grades of rubber blacks.

A key development in the carbon black reactor technology was the development of the zoned axial flow reactor for reinforcing blacks in the early 1960s (22). The reactor consists of three zones. The first zone is a combustion zone in which fuel and air are completely burned to produce combustion gases with excess oxygen. This gas flow is accelerated to high velocity in a throat zone with intense turbulent mixing. The feedstock is injected either into this throat zone or just

Table 5. Reactor Conditions for Various Grades of Carbon Blacks

Carbon black	Surface area, m^2/g	Temperature, °C	Residence time, s	Maximum velocity, m/s
N100 series	145	1800	0.008	
N200 series	120		0.010	180–400
N300 series	80	1550	0.031	
N500 series	42		1	30–80
N700 series	25	1400	1.5	0.5–1.5
N990 thermal	8	1200–1350	10	10

ahead thereof. The reacting gases issue from the throat into a second cylindrical zone as a turbulent diffusion jet. Depending on the desired black, the jet may be allowed to expand freely, or may be confined by bricking. Downstream of the reaction zone is a water quench zone. The throughput of a single reactor train varies from manufacturer to manufacturer and with grade of black. The largest reactors in operation have capacities of over 30,000 t/year. Many producers operate smaller reactors in parallel. Reactors are typically designed to make a series of related blacks. Air and gas may be introduced to the primary combustion zone either axially, tangentially, or radially. The feedstock can be introduced into the primary fire either axially or radially in the high velocity section of the mixing zone. The high velocity section may be venturi-shaped or consist of a narrow diameter choke. Plants may have from one to several operating trains.

Carbon black reactors are made of carbon steel shells lined with several courses of refractory. The most severe services are in the combustor and in the throat zone. Different manufacturers take different approaches to these elements, some using exotic materials or selected water-cooled metal surfaces, others using conventional materials and limiting temperatures to what their materials can stand. Most manufacturers achieve refractory life of one to several years. For the rubber-grade carbon blacks, at least three different reactor designs must be used to make this range of furnace blacks. Figures 10 and 11 show the designs of commercial reactors based on the patent literature.

The quality and yield of carbon black depend on the quality and carbon content of the feedstock, the reactor design, and the input variables. Surface area in particular is controlled by adjusting the temperature in the reaction zone. Structure is adjusted by introducing potassium into the combustion gas. This may be done in any of a variety of ways.

The energy utilization in the production of 1 kg of oil-furnace carbon black is in the range of $(9–16) \times 10^7$ J, and the yields are 300–660 kg/m^3 depending on the grade. The energy inputs to the reactor are the heat of combustion of the preheated feedstock, heat of combustion of natural gas, and the thermal energy of the preheated air. The energy output consists of the heat of combustion of the carbon black product, the heat of combustion and the sensible heat of the tail gas, the heat loss from the water quench, heat loss by radiation to atmosphere, and the heat transferred to preheat the primary combustion air.

The Thermal Black Process. Thermal black is a large particle size, low structure carbon black made by the thermal decomposition of natural gas, coke

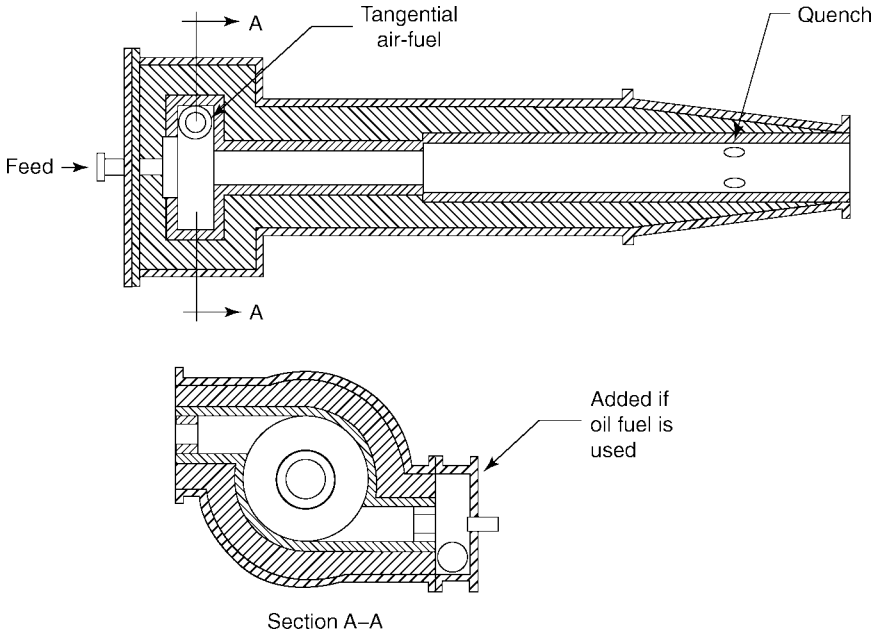

Fig. 10. Reactor for N300–N200 carbon blacks (24).

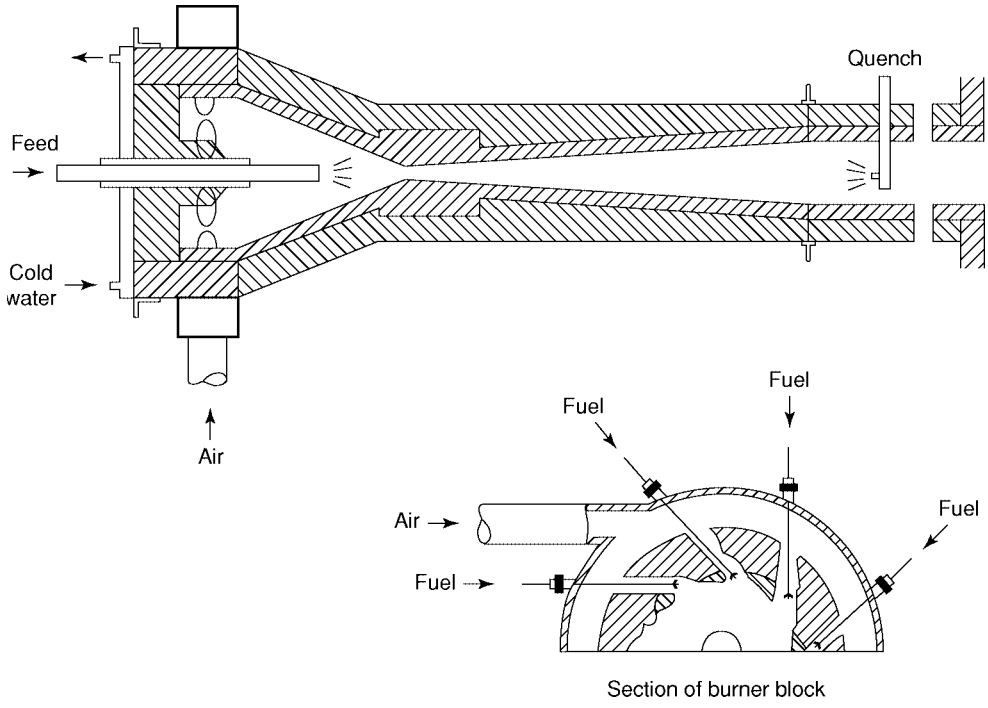

Fig. 11. Reactor for tread blacks (25).

oven gas, or liquid hydrocarbons in the absence of air or flames. Its economic production requires inexpensive natural gas. Today it is among the most expensive of the blacks regularly used in rubber goods. It is used in rubber and plastics applications for its unique properties of low hardness, high extensibility, low compression set, low hysteresis, and excellent processability. Its main uses are in O-rings and seals, hose, tire innerliners, V-belts, other mechanical goods, and in cross-linked polyethylene for electrical cables.

The thermal black process dates from 1922. The process is cyclic using two refractory-lined cylindrical furnaces or generators about 4 m in diameter and 10 m high. During operation, one generator is being heated with a near stoichiometric ratio of air and off-gas from the make generation, whereas the other generator, heated to an average temperature of 1300°C, is fed with natural gas. The cycle between black production and heating is 5 min alternating between generators, resulting in a reasonably continuous flow of product and off-gases to downstream equipment. The effluent gas from the make cycle, which is about 90% hydrogen, carries the black to a quench tower where water sprays lower the temperature before it enters the bag filter. The effluent gas is cooled and dehumidified in a water scrubber for use as fuel in the heating cycle. The collected black from the filters is conveyed to a magnetic separator, screened, and hammermilled. It is then bagged or pelletized. The pelletized form is bagged or sent to bulk loading facilities.

There are thermal black plants in Canada, the United States, the United Kingdom (1), and Russia. Two common grades are manufactured. These are Medium Thermal Black N990 and Fine Thermal Black N880.

Acetylene Black Process. The high carbon content of acetylene (92%) and its property of decomposing exothermically to carbon and hydrogen make it an attractive raw material for conversion to carbon black. Acetylene black is made by a continuous decomposition process at an atmospheric pressure of 800–1000°C in water-cooled metal retorts lined with refractory. The process consists of feeding acetylene into the hot reactors. The exothermic reaction is self-sustaining and requires water cooling to maintain a constant reaction temperature. The carbon-black-laden hydrogen stream is then cooled followed by separation of the carbon from the hydrogen tail gas. The tail gas is either flared or used as fuel. After separation from the gas stream, acetylene black is very fluffy with a bulk density of only 19 kg/m^3. It is difficult to compact and resists pelletization. Commercial grades are compressed to various bulk densities up to 200 kg/m^3.

Acetylene black is very pure with a carbon content of 99.7%. It has a surface area of about 65 m^2/g, an average particle diameter of 40 nm, and a very high but rather weak structure with a DBP number of 250 mL/100 g. It is the most crystalline or graphitic of the commercial blacks. These unique features result in high electrical and thermal conductivity, low moisture adsorption, and high liquid absorption.

A significant use of acetylene black is in dry cell batteries where it contributes low electrical resistance and high capacity. In rubber it gives electrically conductive properties to heater pads, tapes, antistatic belt drives, conveyor belts, and shoe soles. It is also useful in electrically conductive plastics such as electrical magnetic interference (EMI) shielding enclosures. Its contribution to thermal conductivity has been useful in rubber curing bags for tire manufacture.

Lampblack Process. The lampblack process has the distinction of being the oldest and most primitive carbon black process still being practiced. The ancient Egyptians and Chinese employed techniques similar to modern methods, collecting the lampblack by deposition on cool surfaces. Basically, the process consists of burning various liquid or molten raw materials in large, open, shallow pans 0.5–2 m in diameter and 16 cm deep under brick-lined flue enclosures with a restricted air supply. The smoke from the burning pans passes through low velocity settling chambers from which the carbon black is cleared by motor-driven ploughs. In more modern installations the black is separated by cyclones and filters. By varying the size of the burner pans and the amount of combustion air, the particle size and surface area can be controlled within narrow limits. Lampblacks have similar properties to the low surface area oil-furnace blacks. A typical lampblack has an average particle diameter of 65 nm, a surface area of 22 m^2/g, and a DBP number of 130 mL/100 g. Production is small, mostly in Western and Eastern Europe. Its main use is in paints, as a tinting pigment where blue tone is desired. In the rubber industry lampblack finds some special applications.

Impingement (Channel, Roller) Black Process. From World War I to World War II the channel black process made most of the carbon black used worldwide for rubber and pigment applications. The last channel black plant in the United States was closed in 1976. Operations still exist and are even being expanded in Europe. The demise of channel black was caused by environmental problems, cost, smoke pollution, and the rapid development of oil-furnace process grades that were equal or superior to channel black products particularly for use in synthetic rubber tires.

The name channel black came from the steel channel irons used to collect carbon black deposited by small natural gas flames impinging on their surface iron channels. Today tar fractions are used as raw material in addition to natural gas. In modern installations channels have been replaced by water-cooled rollers. The black is scraped off the rollers, and the off-gases from the steel-box-enclosed rollers are passed through bag filters where additional black is collected. The purified exhaust gases are vented to the atmosphere. The oils used in this process must be vaporized and conveyed to the large number of small burners by means of a combustible carrier gas. Yield of rubber-grade black is 60% and 10–30% for high quality color grades.

The characteristics of roller process impingement blacks are basically similar to those of channel blacks. They have an acidic pH, a volatile content of about 5%, surface area of about 100 m^2/g, and an average particle diameter of 10–30 nm. The smaller particle-size grades are used as color (pigment) blacks, and the 30-nm grade is used in rubber.

Recycle Blacks. The pyrolysis of carbon black containing rubber goods has been promoted as a solution to the accumulation of waste tires. In the processes in question, tires are pyrolyzed in the absence of oxygen, usually in indirect fired rotary kiln-type units. The rubber and extender oils are cracked to hydrocarbons which are collected and sold as fuels or petrochemical feedstocks. The gaseous pyrolysis products are burned as fuel for the process. Steel tire cord is removed magnetically and the remainder of the residue is milled into a “pyrolysis black.” This contains the carbon black, silica, and other metal oxides from the rubber and some newly created char. Typically these materials have 8–10% ash, and contain

a lot of coarse residue. Most are difficult to pelletize. They have, on average, the reinforcing properties of a N300 black but because they are a mixture of N600 and 700 blacks with N100 and N200 blacks, they are not particularly suitable for either reinforcing or semireinforcing applications. To date they find application in relatively nondemanding uses such as playground and floor mats.

Surface Modification of Carbon Blacks

For most of its long history, the carbon black industry had concentrated on the morphology as the key factor controlling product performance and grade differentiation. Recently the importance of the composition of the interface between the carbon blacks and the medium in the composite in which the carbon black is used has been recognized.

The early stages of surface modification can be traced back to 1940s and 1950s. The approaches include physical adsorption of some chemicals on carbon black surface, heat treatment, and frequently oxidation. During 1980s and 1990s, some work on plasma treatment was reported. For chemical and polymer grafting modifications, a great deal of academic work was done in 1950s and 1960s in France, United States, and Japan, using surface oxygen groups as functional groups. However, because of rapid development applications of carbon black in different areas and the challenge from other reinforcing particles in its traditional applications, the surface modification technology for carbon black has been developing very rapidly over the last decade. These include surfactant-treated surfaces, chemically modified surfaces, and deposition of other phases during or after black formation. Today there is active commercial development and new product introduction in all areas.

Attachments of the Aromatic Ring Nucleus to Carbon Black. Two approaches characterize this area. A number of patents have been issued to Cabot Corp. (26,27), which describe that the decomposition of a diazonium compound derived from a substituted aromatic or aliphatic amine results in the attachment of a substituted aromatic ring or chain onto the surface of the carbon black. This results in a stable attachment which is not sensitive to moisture. Examples show attachment of amines, anionic and cationic moieties, polysulfide moieties that can be attached into an elastomer network, and alkyl, polyethoxyl, and vinyl groups. Practically, the surface chemistry and physical chemistry can be tailored according to the applications of carbon blacks. Some applications are claimed in aqueous media for dispersion (28), in oil-based coatings and inks for dispersion (29), and in rubbers for reduction of hysteresis and wear-resistance improvement (30). The initially attached groups can also function as sites for further chemical substitution. Another approach has been developed by Xerox Corp. in which oligomers of the polymer of one's choice are prepared using stable free-radical polymerization and these are attached to the carbon black surface by reaction of the stable radical (31).

Attachments to the Aromatic Ring Structure Through Oxidized Groups. The acidic surface groups that result from surface oxidation of carbon black are natural synthons for the attachment of functionality. Generally, chemistry is done through either phenolic or carboxylic acid groups on the surface. Some

of these groups are present in most blacks, but their density can be increased by treating with various oxidants such as ozone, nitric acid, or hypochlorite (32–34). Compared to the previous class, these C—O attachments are somewhat more labile, being particularly susceptible to hydrolysis. The concept of using phenolic groups as points of attachment for conventional silane treating agents has been described in several patents with the particular aim of attaching polysulfide moieties that can be vulcanized into elastomer networks for hysteresis reduction (35). Recently, patents have been issued on using the acidic sites on carbon black surfaces as points of reaction of amines. In the particular case in point, the attachment was used to improve compound stability and dispersion in conductive plastics applications (36).

Metal Oxide Treatments. The carbon black industry has worked on ways to respond to the challenge of silica in tire treads for low rolling resistance (replacing all or some of the carbon black). Cabot has filed on and widely published a class of dual-phase fillers in which silica or other metal oxides and carbon are coformed in a carbon-black-like reactor (37). In the particular product they describe, the carbon black and silica are intimately intermixed on a scale that is about the same size as the carbon black crystallite. In more recent variants, materials where the silica location is more on the exterior of the particle are described (38). In these materials, the silica is the minor constituent. The main characteristics of these carbon blacks are their lower filler-filler interactions. Filler-polymer interactions are also increased, but by incorporating coupling agents these interactions can be adjusted as required. These materials are used as fillers for low rolling resistance, higher wet skid resistance, and improved wear resistance in tire treads when used with conventional sulfide–silane coupling agents (39,40), or as fillers for silicone rubber when used with alkyl silane and vinyl silane agents (41). The patent literature suggests that other applications have been considered as well (42). Patents have also been issued on coated carbon black by depositing silica on the black surface in an aqueous solution of sodium silicate by adjusting pH with acid (43,44).

Applications

U.S. consumption of carbon black in 2000 by various market sectors is shown in Table 6. About 89% of total consumption is in the rubber industry and 70% for tires. About 10% is consumed for other automotive products and 9% for rubber products

Table 6. U.S. End-Use Consumption of Carbon Black in 2000[a]

	Millions of metric tons	Percent of total
Automotive rubber uses tire and tire products	1.17	70
Belts, hoses, and other automotive products	0.17	10
Industrial rubber products	0.16	9
Nonrubber uses	0.18	11
Total	*1.67*	*100*

[a] From Ref. 1.

unrelated to the automotive industry. The automotive industry accounts for 80% of consumption. Eleven percent of the blacks is for nonrubber uses and its main applications are related to pigmentation, ultraviolet absorption, and electrical conductivity of other products such as plastics, coating, and inks. These carbon blacks are also termed special blacks (1).

Rubber-Grade Carbon Blacks. Carbon black is a major component in the manufacture of rubber products, with a consumption second only to rubber itself. It is by far the most active rubber-reinforcing agent owing to its unique ability to enhance the physical properties of rubbers. Table 7 lists the principal rubber grades by their N-number classification, general rubber properties, and typical uses.

The consumption of the various carbon black grades can be divided into tread grades for tire reinforcement and nontread grades for nontread tire use and other rubber applications. Table 8 shows the distribution of production of types for these uses. A typical passenger tire has several compounds and uses five to seven different carbon black grades.

The behavior of different grades in rubber is dominated mainly by surface area, structure (DBPA), and surface activity. All these parameters play a role in rubber reinforcement through different mechanisms, such as interfacial interaction between rubber and carbon black, occlusion of the polymer in the internal voids of the aggregate, and the agglomeration of carbon black aggregates in the polymer matrix.

Table 7. Application of Principal Rubber-Grade Carbon Blacks

Designation	General rubber properties	Typical uses
N110, N121	Very high abrasion resistance	Special tire treads, airplane, off-the-road racing
N220, N299, N234	Very high abrasion resistance, good processing	Passenger, off-the-road, special service tire treads
N339, N347, N375, N330	High abrasion resistance, easy processing, good abrasion resistance	Standard tire treads, rail pads, solid wheels, mats, tire belt sidewall, carcass retread compounds
N326	Low modulus, good tear strength, good fatigue, good flex cracking resistance	Tire belt, carcass, sidewall compounds, bushings, weather strips, hoses
N550	High modulus, high hardness, low die swell, smooth extrusion	Tier inner liners, carcass, sidewall, inner tubes, hose, extruded goods, V-belts
N650	High modulus, high hardness, low die swell, smooth extrusion	Tire innerliners, carcass, belt, sidewall compounds, seals, friction compounds, sheeting
N660	Medium modulus, good flex fatigue resistance, low heat buildup	Carcass, sidewall, bead compounds, innerliners, seals, cable jackets, hose, soling, EPDM compounds
N762	High elongation and resilience, low compression set	Mechanical goods, footwear, innertubes, innerliners, mats

Table 8. Carbon Black Production (10^3 t) by Grade in the United States for 2000[a]

N330 high abrasion	0.623
N550 fast extruding	0.138
N762 semireinforcing	0.129
N660 general-purpose	0.356
N110 super abrasion	0.061
N220 intermediate super abrasion	0.170
N990 thermal	0.014
Total	*1.493*

[a] From Ref. 1.

One of the consequences of the incorporation of carbon blacks into a polymer is the creation of an interface between a rigid solid phase and a soft elastomer phase. For rubber-grade carbon blacks, whose surfaces exhibit very little porosity, the total area of the interface depends on both filler loading and the specific surface area of the filler. Owing to the interaction between rubber and filler, two phenomena are well documented: the formation of bound rubber and a rubber shell on the carbon black surface. Both are related to the restriction of the segmental movement of polymer molecules.

The effect of filler structure on the rubber properties of filled rubber has been explained by the occlusion of rubber by filler aggregates (45). When structured carbon blacks are dispersed in rubber, the polymer portion filling the internal void of the carbon black aggregates, or the polymer portion located within the irregular contours of the aggregates, is unable to participate fully in the macrodeformation. The partial immobilization in the form of occluded rubber causes this portion of rubber to behave like the filler rather than like the polymer matrix. As a result of this phenomenon, the effective volume of the filler, with regard to the stress–strain behavior and viscoelastic properties of the filled rubber, is increased considerably.

The filler aggregates in the polymer matrix have a tendency to associate to agglomerates, especially at high loadings, leading to chain-like filler structures or clusters. These are generally termed secondary structure or, in some cases, filler network, even though the latter is not comparable to the continuous polymer network structure. The formation of filler network is dependent on the intensity of interaggregate attractive potential, the distance between aggregates and polymer–filler interaction (46).

From the point of view of carbon black morphology, high surface area produces high reinforcement as reflected in high tensile and tear strengths, high resistance to abrasive wear, higher hysteresis, and poorer dynamic performance, while high structure leads to higher viscosity, lower die swell, and high modules. Listed in Table 9 are the effects of surface area and structure which can be a guideline for choice of carbon blacks according to the processability and property requirements of rubber products.

A present day challenge to carbon black technologists is to optimize the balance between tire wear, tire hysteresis that determines the rolling resistance, and wet skid resistance. It is now recognized that besides the morphology, while the wear resistance is closely related to the polymer-filler interaction and dispersion

Table 9. Effect of Carbon Black Morphologies on the Properties of Filled Compounds

Surface area increase	Rubber properties	Structure increase
Higher	Abrasion resistance	Depend on severity
Higher	Hardness	Higher
Higher	Tensile strength	Lower
Not main factor	Modulus	Higher
Lower	Elongation	Lower
Lower	Rebound	Not main factor
Higher	Viscosity	Higher
Lower	Dispersibility	Higher
Not main factor	Dimensional stability	Higher

of the carbon blacks, the hysteresis is mainly deterimined by filler networking or agglomeration. For tread compounds of tire, depression of filler networking results in lower hysteresis at the temperatures from 50 to 80°C, leading to low rolling resistance, and in higher hysteresis at lower temperature which is in favor of wet skid resistance. Some progress on this problem has been made by using new furnace designs and other process variables that broaden the aggregate size distributions and lower the tint strength while maintaining surface area, and structure (47,48). A substantial improvement in global tire performance can be achieved through surface modification of carbon blacks, such as carbon-silica dual phase fillers (39,40,49).

Special-Grade Carbon Blacks

Besides reinforcement for rubber, the principal functions that carbon black imparts to a compound material are color, ultraviolet damage resistance, electrical conductivity, nondegradation of polymer physical properties, and ease of dispersion. The carbon blacks used for these purposes are classified as special-grade blacks. Smaller volume applications exploit other principal attributes, such as chemical inertness, thermal stability, and an open porous structure. The secondary attributes include chemical and physical purity, low affinity for water adsorption, and ease of transportation and handling.

In 2000, 11% of U.S. consumption of carbon black was special blacks. About 51% of special blacks are used in plastics, 32% in printing inks, 5% in paint, 3% in paper, and 9% in miscellaneous applications (1).

Dispersion. The ability to disperse the special grades is an important consideration in almost all applications. The customer's milling costs can be comparable to the purchase price of the carbon black. In other cases, the inability to achieve an excellent dispersion impairs the ability to realize the full performance of the blacks or it creates other undesirable characteristics. For example, a black plastic part will not appear as dark nor have a smooth surface if the black cannot be fully dispersed.

The term "dispersion" is used in several ways in actual applications. It may refer to the amount of work required to achieve a specified level of imperfections or it may refer to the level of imperfections per se. When a black is referred to as "easily dispersed" it can mean that relatively low shear mixers can achieve a compound that is relatively free of imperfections. Or it may mean that with a given mixing protocol the compound achieves an imperfection count below a specified level.

The "level of imperfections" is most often assessed in one of two ways. Most often it refers to the size distribution of surface imperfections on an extruded or injection-molded part. It may also refer to the rate of pressure buildup on an extrusion screen pack.

Undispersed material is one of three types. The first is non-carbon contaminants that come either in the feedstock or the result of corrosion of the manufacturing train. The second are carbon contaminants that occur when the feedstock droplets fail to evaporate. If the residual material in the droplet fails to evaporate, but is pyrolyzed in place, the contaminant is referred to as a coke ball. If the droplet reaches the wall before it is completely pyrolyzed, the resulting buildup is termed wall coke and it can flake off and contaminate the carbon black product. Finally the aggregates of carbon black can remain agglomerated or undispersed. Too often the concepts of contaminant-free and the difficulty of separating agglomerates into aggregates are not clearly distinguished. Detailed microscopy is required to determine the nature of defects and therefore resolve if the problem is contamination or true difficulty in dispersion.

In most cases the properties of special carbon black aggregates that engender performance are antagonistic to achieving a good dispersion. High pigmenting strength for both light and ultraviolet radiation implies high surface area. High surface area increases the difficulty of dispersion. Achieving an electrically conductive network at low concentration implies a black with high structure. High structure, per se, is an asset in dispersion. However, most carbon black formation technologies will not make high structure blacks unless the surface area is also high and the trade-off means that the best conducting grades are difficult to disperse.

Pigmentation. Carbon black is an excellent pigment. It is considerably more effective in absorbing light than any other material on either a weight or a cost basis. It is also environmentally stable.

Black pigments are used both alone and with other pigments. In the first the measure of performance is termed mass tone and is simply the ability to prevent the transmission or reflection of light. The second is called tint tone and it is the ability to soften or darken other colors.

How black is black? Two aspects can be important. The first is the total amount of white light that is either transmitted or reflected by a black material. The second is variation in these values with the frequency or color of the light. In almost all cases, relatively higher red light adsorption is valued as it gives the material a blue "undertone." Various measures are used to equate blue tone with overall absorption. These color metrics are based on subjective judgments and are most highly developed for automotive paints.

Surface area and structure, or aggregate size, play a role in determining color strength. Pigmenting carbon blacks are used at quite low concentrations. Single

particle Mie scattering theory is reasonably applicable. In applying the theory, an aggregate of carbon black is viewed as a composite of carbon and the resin or polymer. The refractive index of the carbon is taken as 1.84(1-0.46i) (50). And the index of refraction of the composite particle is the volume average of the carbon black and polymer values. The difficulty in using single- particle scattering theory is in evaluating the size and carbon content of the "scattering particle." Various methods are used to estimate aggregate size and to divide the CDBP value into "intra" and "inter" aggregate parts. The "intra-aggregate" part is considered to form part of the composite scattering particle.

Because aggregate and primary particle size cannot be controlled independently in carbon black reactors, and because the ability to achieve complete dispersion depends upon morphology, the coloring properties of carbon blacks are often treated empirically.

The theory works best when carbon black is used with other pigments, ie, in tinting applications. In these applications, both theory and experiments indicate that smaller primary particles and aggregates absorb more light and have a bluer tone.

Table 10 shows the entire range of properties of blacks sold for color applications. Blacks with large primary particle sizes are used in news inks and other nondemanding applications. The extremely fine blacks are used in high performance enamels and automotive paints.

An emerging application is as the colorant in jet printer inks. The requirement of extremely high quality dispersion meant that the original black inks were dyes. The image permanence of carbon blacks lead to the displacement of dyes when techniques were developed that assured the stability of excellent, water-based dispersion.

The blacks used for UV protection of polymers have very small primary particle sizes. The industry standard for UV protection is primary particle sizes of less than 20 nm.

Conductivity. Carbon black is added to polymer or resin compounds to achieve electrical conductivity. If their concentrations are high enough, carbon black aggregates will form interconnected paths through the compound material. These networks can have resistivities in the range of 1–10 $\Omega \cdot$ cm.

Concentrations that are too low will not form percolation networks. The Jansen equation (51) predicts that the critical concentration occurs when volume of polymer equals four times the volume of the CDBP value. The compounds are continuous when the amount of polymer is the CDBP value or greater and contain continuous carbon networks when the volume of polymer is between the CDBP value and four times that amount.

In general it is desirable to achieve percolation at low loading to reduce the negative effects of the presence of the carbon black on the physical properties of the compound. Therefore blacks with high CDBP values are used in conducting application. Figure 12 shows the percolation threshold of a number of carbon blacks with widely varying CDBP values.

One of the most demanding applications for conducting compounds is as a layer around the center conductor of a high voltage cable. The purpose of the compound is to smooth any surface imperfection that would otherwise result in high electric field gradients and the breakdown of the insulating layers. These

Table 10. Types and Applications of Special Pigment Grades of Carbon Blacks

Type	Surface area, m^2/g	DBP number, mL/100 g	Volatile, %	Uses
Normal grades				
High color	230–560	50–120	2	High jetness for alkyl and acrylic enamels, lacquers, and plastics
Medium color	220–220	70–120	1–1.5	Medium jetness and good dispersion for paints and plastics; ultraviolet and weathering protection for plastics
Regular color	80–140	60–114	1–1.5	For general pigment applications in inks, paints, plastics, and paper; gives ultraviolet protection in plastics, high tint, jetness, gloss, and dispersibility in inks and paints
	46	60	1.0	Good tinting strength, blue tone, low viscosity; used in gravure and carbon paper inks, paints, and plastics
	45–85	73–100	1.0	Main use is in inks; standard and offset news inks
Low color	25–42	64–120	1.0	Excellent tinting black–blue tone; used for inks-gravure, one-time carbon paper inks; also for paints, sealants, plastics, and cements
Thermal blacks	7–15	30–35	<0.5	Tinting-blue tone; plastics and utility paints
Lamp blacks	20–95	100–160	0.4–0.9	Paints for tinting-blue tone
Surface oxidized grades				
High color	400–600	105–121	8.0–9.5	Used for maximum jetness in lacquers, coatings, plastics, fibers, record disks
Medium color, long flow	138	55–60	5	Used in lithographic, letterpress, carbon paper, and typewriter ribbon inks; high jetness, excellent flow, low viscosity, high tinting strength, gloss, and good dispersability
Medium color, long flow	96	70	2.5	Used for gloss printing and carbon paper inks; excellent jetness, dispersibility; tinting strength, and gloss in paints
Low color	30–40	48–93	3.5	Used for tinting where flooding is a problem; easy dispersion

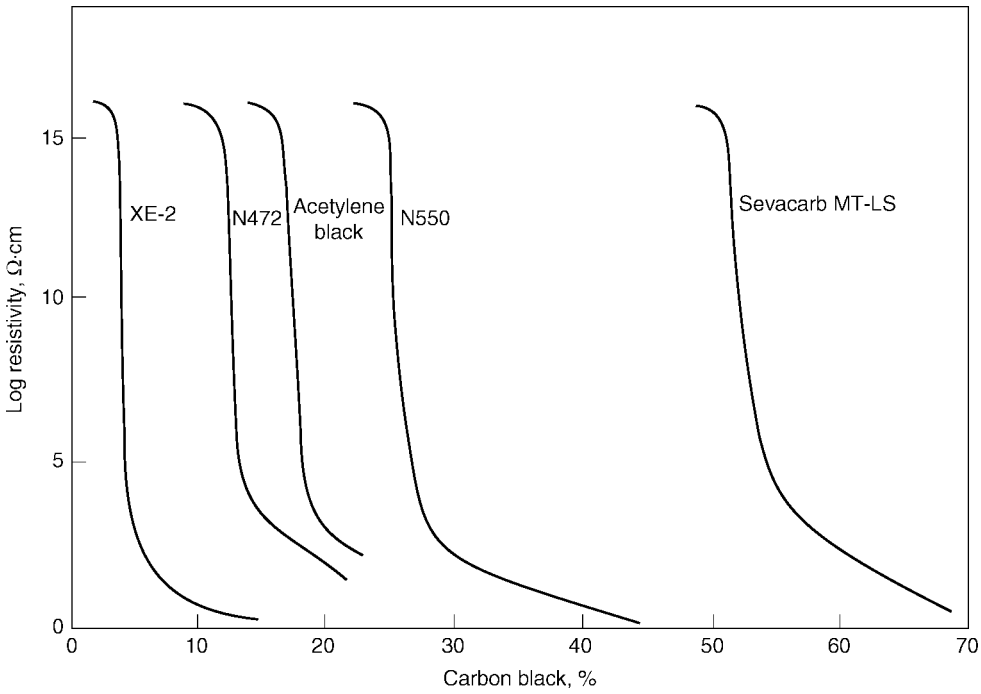

Fig. 12. Electrical resistivity–concentration curves for various carbon blacks (52).

compounds have the highest loading of carbon blacks to achieve the lowest possible resistance. Two very important secondary requirements are that the black is quite hydrophobic, free of inorganic salts, and has extremely low contaminant levels.

Other applications of carbon-black-filled polymers do not require as low a level of conductivity. The purpose is the dissipation of static electricity. These types of compounds are used in carrying containers for microelectronic components and in containers and pipes for combustible liquids such as gasoline. The newest application is adding enough conductivity to automobile panels to enable coatings of electrostatically charged paint particles.

Other Uses. Carbon blacks are used to make highly porous structures for catalyst supports. Most supports are metal oxides rather than carbon, but in certain circumstances a chemically inert support is required. The open structure of the carbon black aggregates allows control of the pore size distribution within the consolidated carbon body.

Fuel cell electrodes are a particularly interesting catalyst application. The active layers of the proton conducting membrane fuel cells must have the ability to transport both gases and hydrogen ions to the catalyst as well as conducting water away. Mixtures of carbon blacks with special polymers create the desired hydrophilic and hydrophobic pore structures.

The so-called boundary layer capacitors are also electrochemical devices that rely carbon blacks to achieve the appropriate pore structures.

Special carbon blacks are also used in batteries, with the largest use in old technology nonrechargeable cells.

Table 11. U.S. Production of Carbon Black (1971–2000)[a]

Year	Production (millions of metric tons)
1971	1.380
1976	1.415
1981	1.285
1986	1.200
1991	1.230
1994	1.475
1997	1.660
2000	1.665

[a]From Ref. 1.

Manufacturers and Production

Starting with the oil crisis of 1973, consumption of carbon black in the United States decreased to 1.2 million tons in 1986 (1). A number of events had contributed to decreased consumption by the rubber and tire industries including tire radialization, increased tire mileage, downsizing of tires, and increased imports of foreign cars. The negative influence of these events have pretty much run their course, and during the last two decades there has been a modest growth in carbon black production. Production for the period 1971–2000 is shown in Table 11.

The shrinkage in demand has resulted in a restructuring of the carbon black industry. Several of the principal multinational oil companies have left the business including Ashland, Cities Service Co., Phillips, and Conoco. Some plants have changed ownership. Decreased margins, rising feedstock, and environmental compliance costs have led to further restructuring in the late 1990s and early 2000 time period. ECI and Degussa consolidated their operations in 2002. Today's U.S. industry consists of five principal producers. Rated capacities of the six U.S. manufacturers is shown in Table 12. Cabot Corp., ECI–Degussa, and Columbian Chemicals are the leading producers, followed by Continental Carbon Co. and Sid Richardson.

Table 12. U.S. Carbon Black Manufacturers and Capacities, 2000[a]

	Furnace black		Total carbon black	
	Millions of metric tons	% of Capacity	Millions of metric tons	% of Capacity
Cabot Corp.	0.451	24	0.451	24
Columbian Chemicals Co.	0.361	19	0.361	19
Continental Carbon Co.	0.254	14	0.254	13
Degussa-ECI	0.463	25	0.484	25
Sid Richardson Carbon Co.	0.340	18	0.340	18
Others	0.000		0.014	1
Total	*1.869*	*100*	*1.903*	*100*

[a]From Ref. 1.

Table 13. World Carbon Black Capacities of July 1, 2001[a]

	Capacity (millions of metric tons)	% of Total
North America[b]	2.4	28
South America	0.5	6
Western Europe	1.5	17
Japan	0.8	9
Other Asia	2.0	24
Other[c]	1.3	16
Total	*8.5*	*100*

[a] From Ref. 1.
[b] Including Mexico.
[c] Including Eastern Europe, Africa and the Middle East.

World carbon-black-rated capacities are shown in Table 13. North America has the largest capacity, and Africa and the Middle East have only a small production. The growth areas are predicted to be the Asian and Eastern European markets.

Health, Safety and Environmental

Health. There is a long history of health studies, many of them sponsored by the carbon black manufacturing industry and a number of authoritative publications on carbon black SH&E aspects. In particular, Patty's Handbook chapter on Industrial Hygiene and Toxicology of carbon black is a recent authoritative reference (53). Mortality and worker health have been extensively studied, often in studies sponsored by the carbon black industry. These studies have included mortality (54,55) and health (55–57) in workers in the carbon black industry against unexposed controls in the same industry as well as those in nonindustry populations. The North American mortality studies (54) have logged about 55,000 worker exposure years since the first studies were first undertaken in 1939. They show no elevation in death rate among carbon black workers and no elevation in cancers of the respiratory organs because of occupational exposure to carbon black. In the United kingdom a study of workers in five carbon black plants (55) shows that among this population there is an elevation of the death rate from cancers of the respiratory organs which is significant versus the U.K. population, but the study indicated clearly that there was no correlation of the incidence of disease with exposure to carbon black. In other words, some other factor rather than carbon black exposure appeared to be the source of the excess cancers. Studies of worker health among both U.S. and European workers have been completed in the last decade and publications of the results of these studies continue to appear. These show no evidence of clinically significant health effects due to occupational exposure to carbon black. While there are some differences in the exposure metric between the North American Studies and the European studies, they show very similar effects. Over the course of time covered by these various studies, there has been a marked improvement in the workplace air quality.

In 1995, IARC (International Agency for Research on Cancer) revised its evaluation of carbon black from category 3, "not classifiable as to its carcinogenicity to

humans" to category 2B, "possibly carcinogenic to humans" based on lung tumor formation in two long-term inhalation studies in rats (58–60). Comparable studies in mice and golden hamsters have failed to find any elevation of tumor incidence of lung or any other tissue (61). Other insoluble respirable materials have shown similar positive responses in rats, but not in other rodent species.

There are two major areas of carcinogenic concern with carbon black. Of these, the one that has historically attracted the most attention is the few tens to hundreds of ppms of polynuclear aromatic hydrocarbons (PAH) that are adsorbed on the surface of most blacks. An extract made by exhaustive extraction of these materials with aromatic solvent has been shown to cause skin tumors in rodents. The PAH on carbon black is very tightly adsorbed and is not liberated by biological fluids. Hence this material is believed to have little or no bioavailability (62). This is supported in the companion studies to those referenced by IARC (59,63). Attempts were made to get a dose response to PAH by using PAH-free black and doping it with high levels of PAH. There was no statistically significant difference in the tumor incidence or type between the two groups.

The second carcinogenic mechanism seems to be common to all inert respirable insoluble particles. Positive carcinogenic responses have been shown with TiO_2, talc, carbon black, and diesel soot in the female rat (64). There is evidence that a common mechanism is at work in all these cases involving a process of damage to the lung epithelium, inflammatory response, saturation of the body's defense mechanisms, proliferation of new epithelial cells, recruitment of activated polymorphonuclear (PMN) cells, secretion of radical-forming species by the PMN cells, and damage to the DNA in the dividing epithelial cells. Studies by Driscoll and co-workers are building a strong case for this mechanism and are ongoing (65). These data indicate that the distinction between the rat and other rodents is the nature of the inflammatory response which appears quite intense in the rat compared to other species. If indeed this proves to be the explanation, a strong case can be made for a threshold and establishment of a no observed adverse effect level (NOAEL). It is also clear that in the rat, an overload mechanism is at work in which above a certain critical loading, the mechanisms which normally clear dust particles from the lung lose effectiveness. Again this suggests a threshold and a NOAEL.

Carbon black inhalation is currently regulated by Occupational Safety and Health Administration (OSHA) in the United States at 3.5 mg/m^3 (total dust), by the Health and Safety Executive (HSE) in the United Kingdom at 3.5 mg/m^3 (inhalable dust), by the MAK Commission in Germany at 6.0 mg/m^3 (inhalable dust) for an 8-h time-weighted average (53). Reviews of these occupational exposure levels are currently underway by the MAK Commission, the HSE, and the American Conference of Governmental Industrial Hygienists (ACGIH). It is unlikely that any of these reviews will be completed before 2005.

Safety. Carbon blacks will burn in air if ignited and once ignited, are difficult to extinguish. In bulk storage, local hot spots can exist for very long periods. Great care needs to be exercised where a smoldering fire is suspected as there can be accumulations of carbon monoxide in enclosed spaces.

Carbon black dust clouds in air are not considered flammable. Carbon blacks have a high ignition energy requirement, and entrained dust clouds do not propagate flame, nor exhibit substantial overpressures. This is presumably because

they have essentially no combustible volatile matter. Carbon black in air can be incinerated but only with difficulty, requiring long burnout times.

Environmental. The carbon black industry takes extreme efforts to confine the product during all stages of manufacturing and transport. Highly efficient bag filters are used to collect the product. After collection the fluffy carbon black is densified and pelletized to minimize dusting during shipment and use by customers. The process gas leaving the bag filter contains primarily water, nitrogen, carbon monoxide, carbon dioxide, and hydrogen. There are also traces of hydrogen sulfide, carbon disulfide, carbonyl sulfide, and various nitrogen-containing species. A portion of these gases is burned for internal plant fuel, and the residual gas is generally burned in a flare or incinerator. Where local conditions warrant, the remaining gas may be used to generate power or steam, either for the plant itself, or for merchant sale.

Like all other operators of combustion equipment, carbon black plants are subject to the usual pressures for reduced sulfur and nitrogen oxide emissions. It appears that the use of lower sulfur feedstock is the most economic way of reducing sulfur emissions. Redesign of combustion equipment for nitrogen oxide reduction is showing some promise. The primary NO_X issues arise from the combustion of tail gas since the carbon black production process is exceedingly fuel-rich.

BIBLIOGRAPHY

"Carbon" in *EPST* 1st ed., Vol. 2, PP. 820–836, by K. A. Burgess, F. Lyon, and W. S. Stoy, Columbian Carbon Co.; "Carbon" in *EPSE* 2nd ed., Vol. 2, pp. 623–640, by F. Lyon and K. A. Burgess, Columbian Chemicals Co.

1. J. F. Aucher, T. Kälin, and Y. Sakuma, CEH Marketing Research Report, Carbon Black, *Chemical Economic Handbook*, SRI International, Menlo Park, Calif., Jan. 2002.
2. *2001 Annual Book of ASTM Standard.*, Vol. 9, American Society for Testing and Materials, Philadelphia, Pa., 2001.
3. G. Kühner and M. Voll, in J.-B. Donnet, R. C. Bansal, and M.-J. Wang, eds., *Carbon Black, Science and Technology*, Marcel Dekker, Inc., New York, 1993, Chapt. 1.
4. E. M. Dannenberg, The Carbon Black Industry: Over a Century of Progress, *Rubber World Mag. Spec. Pub.—Rubber Div. 75th Anniv.*, 1907–1984.
5. J. Janzen, *Rubber Chem. Technol.* **56**, 669 (1982).
6. H. P. Boehm, *Farbe und Lack* **79**, 419 (1973).
7. C. A. Leon, J. M. Solar, V. Calemma, and L. R. Radovic, *Carbon* **30**, 797 (1992).
8. C. R. Houska and B. E. Warren, *J. Appl. Phys.* **25**, 1503 (1954).
9. B. E. Warren, *Phys. Rev.* **59**, 693 (1941).
10. L. L. Ban and W. M. Hess, In *Abstr. 9th Bienn. Conf. Carbon*, 1969, p. 162.
11. J.-B. Donnet and E. Custodero, *Carbon* **30**, 813 (1992).
12. M.-J. Wang, S. Wolff, and B. Freund, *Rubber Chem. Technol.* **67**, 27 (1994).
13. S. Brunauer, P. H. E. Emmett, and J. Teller, *J. Am. Chem. Soc.* **60**, 310 (1938).
14. B. C. Lippens and J. H. de Boer, *J. Catal.* **4**, 319 (1965); R. W. Magee, *Rubber Chem. Technol.* **68**, 590 (1995).
15. C. W. Sweitzer and W. C. Goodrich, *Rubber Age* **55**, 169 (1944).
16. A. I. Medalia, in E. K. Sichel, ed., *Carbon Black—Polymer Composites*, Marcel Dekker, Inc., New York, 1982, Chapt. 1.
17. E. Redman, F. A. Heckman, and J. E. Connelly, In *ACS Meeting*, Paper No. 14, Rubber Division, American Chemical Society, Chicago, Ill., 1977.

18. M.-J. Wang, S. Wolff, and J.-B. Donnet, *Rubber Chem. Technol.* **64**, 714 (1991).
19. M.-J. Wang and S. Wolff, *Rubber Chem. Technol.* **65**, 890 (1992).
20. M. Faraday, in W. Crooker, ed., *The Chemical History of a Candle*, Viking Press, New York, 1960.
21. R. C. Bansal and J.-B. Donnet, in J.-B. Donnet, R. C. Bansal, and M.-J. Wang, eds., *Carbon Black, Science and Technology*, Marcel Dekker, Inc., New York, 1993, Chapt. 2.
22. U.S. Pat. 3,010,794 (1961), G. F. Frianf and B. Thorley (to Cabot Corp.).
23. D. Rivin, *Rubber Chem. Technol.* **56**, 709 (1982).
24. U.S. Pat. 2,564,700 (1951), J. C. Krejci (to Phillips Petroleum Co.).
25. U.S. Pat. 3,490,869 (1970), G. L. Heller (to Columbia Carbon Co.).
26. U.S. Pat. 5,554,739 (1996), J. A. Belmont (to Cabot Corp.).
27. U.S. Pat. 5,851,280 (1998), J. A. Belmont, R. M. Amici, and C. P. Galloway (to Cabot Corp.).
28. U.S. Pat. 5,672,198 (1997), J. A. Belmont (to Cabot Corp.).
29. U.S. Pat. 5,713,988 (1998), J. A. Belmont and C. E. Adams (to Cabot Corp.).
30. U.S. Pat. 6,494,946 (2002), J. A. Belmont, R. M. Amici, and C. P. Galloway (to Cabot Corp.).
31. U.S. Pat. 5,545,504 (1996), B. Keoshkerian, M. K. Georges, and S. V. Drappel (to Xerox).
32. R. C. Bansal and J.-B. Donnet, in J.-B. Donnet, R. C. Bansal, and M.-J. Wang, eds., *Carbon Black, Science and Technology*, Marcel Dekker, Inc., New York, 1993, Chapt. 4.
33. U.S. Pat. 4,366,138 (1982), E. Eisenmenger, R. Engel, G. Kuehner, R. Reck, H. Schaefer, and M. Voll (to Degussa AG).
34. U.S. Pat. 2,439,442 (1948), F. H. Amon and F. S. Thornhill (to Cabot Corp.).
35. U.S. Pat. 5,159,009 (1992), S. Wolff and U. Gorl (to Degussa AG).
36. U.S. Pat. 5,708,055 (1998), G. A. Joyce and E. L. Little (to Columbian Chemical Co.).
37. U.S. Pats. 5,830,930 (1998) and 5,877,238 (1999), K. Mahmud, M.-J. Wang, and R. A. Francis (both to Cabot Corp.); U.S. Pats. 5,904,762 (1999) and 6,211,279 (2001), K. Mahmud and M.-J. Wang (both to Cabot Corp.).
38. U.S. Pat. 6,364,944 (2002), K. Mahmud, M.-J. Wang, and Y. Kutsovsky (to Cabot Corp.).
39. M.-J. Wang, K. Mahmud, L. J. Murphy, and W. J. Patterson, *Kauts Gummi Kunsts.* **51**, 348 (1998).
40. M.-J. Wang, Y. Kutsovsky, P. Zhang, L. J. Murphy, S. Laube, and K. Mahmud, *Rubber Chem. Technol.* **75**, 247 (2002).
41. U.S. Pat. 6,020,402 (2000), J. N. Anand, J. E. Mills, and S. R. Reznek (to Cabot Corp.).
42. U.S. Pat. 5,919,855 (1999), T. Reed and K. Mahmud (to Cabot Corp.).
43. U.S. Pat. 5,679,728 (1997), T. Kawazura, H. Kaido, K. Ikai, F. Yatsuyanagi, and M. Kawazoe (to Yokohama Rubber Co.).
44. U.S. Pats. 5,916,934 (1999) and 6,197,274 (2001), K. Mahmud, M.-J. Wang, S. R. Reznek, and J. A. Belmont (to Cabot Corp.).
45. A. I. Medalia, *J. Colloid Interface Sci.* **32**, 115 (1970).
46. M.-J. Wang, *Rubber Chem. Technol.* **71**, 520 (1998).
47. U.S. Pats. 4,071,496 (1978), 4,241,022 (1980), and 4,267,160 (1982), G. Kraus and H. R. Hunt (both to Phillips Petroleum Co.).
48. U.S. Pat. 4,478,973 (1984), S. Misono and H. Suzuki (to Tokai Carbon Co.).
49. Eur. Pats. EP 0 877 047 A1 (1998) and EP 0 890 607 A1 (1999), G. Labouze and S. Cohen (both to Michelin); Eur Pat. EP 0 997 490 A1 (2000), Y. Mizuno and M. Uchida (to Sumitomo Rubber Industries); Eur. Pat. EP 1 254 786 A1 (2002), C. E. Drvol, S. L. Taylor, T. D. Linster, M. B. Rodger, and F. Ozel (to Goodyear).
50. A. I. Medalia and L. W. Richards, *J. Colloid and Interface Sci.* **40**, 233 (1972).
51. J. Jansen, *J. Applied Phys.* **46**, 966 (1975).
52. N. Probst, European Rubber J. 25 (Nov. 1984).

53. R. J. McCunney, H. J. Muranko, and P. A. Valberg, in E. Bingham, B. Cohrssen, and C. H. Powell, eds., *Patty's Toxicology*, 5th ed., John Wiley and Sons, Inc., New York, 2001, Vol. 8.
54. J. Robertson and K. J. Inman, *J. Occup. Environ. Med.* **38**, 569 (1996).
55. K. Gardiner, W. N. Trethowan, J. M. Harrington, I. A. Calvert, and D. C. Glass, *Ann. Occup. Hyg* **36**, 447 (1992).
56. P. Harber, H. Muranko, S. Solis, A. Torosian, and B. Merz, *J. Occup. Environ. Med.* **45**, 144 (2003).
57. K. Gardiner, M. Van Tongeren, and J. M. Harrington, *Occup Environ. Med.* **58**, 496 (2001).
58. IARC Monograph 65, IARC, Lyon, France, 1996, pp. 149–262.
59. U. Heinrich, L. Peters, O. Creutzenberg, C. Dasenbrock, and H. G. Hoymann, in U. Mohr, D. L. Dugworth, J. L. Mauderly, and G. Oberdorster, eds., *Toxic and Carcinogenic Effects of Solid Particles in the Respiratory Tract*, ILSI Press, Washington, D.C., 1994, pp. 433–441.
60. J. L. Mauderly, M. B. Snipes, E. B. Barr, S. A. Belinsky, J. A. Bond, A. L. Brooks, I.-Y. Chang, Y. S. Cheng, N. A. Gillett, W. C. Griffith, R. F. Henderson, C. E. Mitchell, K. J. Nikula, and D. G. Thomassen, HEI Research Report Number 68, Health Effects Institute, Cambridge, Mass., 1994.
61. K. J. Nikula, M. B. Snipes, E. B. Barr, W. C. Griffith, R. F. Henderson, and J. L. Mauderly, in U. Mohr, D. L. Dungworth, L. L. Mauderly, and G. Oberdorster, eds., *Toxic and Carcinogenic Effects of Solid Particles in the Respiratory Tract*, ILSI Press, Washington, D.C., 1994, pp. 566–568.
62. D. Rivin and J. H. Atkins, *Carbon* **25**, 135 (1987).
63. U. Heinrich, R. Fuhst, S. Rittinghausen, O. Creutzenberg, B. Bellman, W. Koch, and K. Levsen, *Inhal. Toxicol.* **7**, 533 (1995).
64. G. Oberdorster, *Regulatory Toxicol. Pharmacol.* **27**, 123 (1998).
65. K. E. Driscoll, J. M. Carter, B. W. Howard, D.G. Hassenbein, W. Papelko, R. B. Baggs, and G. Oberdorster, *Toxicol. Appl. Pharmacol.* **136**, 372 (1996).

MENG-JIAO WANG
CHARLES A. GRAY
STEVE R. REZNEK
KHALED MAHMUD
YAKOV KUTSOVSKY
Cabot Corporation

CARBON FIBERS

Introduction

Carbon fibers continue to be the main reinforcement materials in advanced composites (qv). The ability to manipulate their physical, chemical, electrical, and thermal properties makes carbon fibers suitable across a wide range of commercial applications, including military [aircraft and missiles (1)], structural [concrete reinforcement (2,3) and automobile body panels], sports equipment (golf

Encyclopedia of Polymer Science and Technology. Copyright John Wiley & Sons, Inc. All rights reserved.

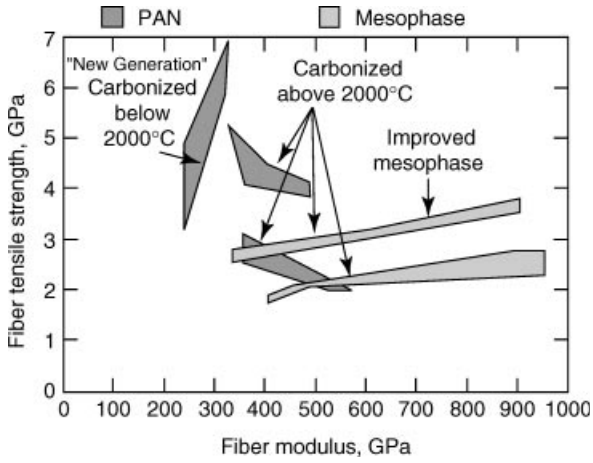

Fig. 1. Tensile strength versus modulus for some commercial carbon fibers. From Ref. 8. To convert GPa to psi, multiply by 145,000.

clubs, skis, surfboards, and softball bats), energy storage [batteries and capacitors (4,5)], and activated carbons (catalysis, gas storage, and purification) (6,7). The ultimate properties of the carbon fiber directly depend on the selection and processing of the precursor materials, the formation of the fiber, and subsequent processing of the fiber. Figure 1 shows a comparison of carbon fiber strengths and moduli as a function of precursor selection and treatment temperature.

Carbon fibers are defined by the International Union of Pure and Applied Chemistry (IUPAC) as "fibers (filaments, tows, yarns, rovings) consisting of at least 92% (mass fraction) carbon, usually in a non-graphitic state (9)." Carbon fibers are produced either through carbonization (the controlled pyrolysis of a fiber precursor in an inert atmosphere) or through growth from gaseous hydrocarbons. The carbonization process is preceded by a stabilization step in which precursor fibers are converted to thermally stable forms that will not melt during carbonization. During the carbonization process, inorganics and aliphatic carbons are driven off, leaving a fiber consisting of graphene layer planes. An idealized carbon fiber is shown in Figure 2.

Real carbon fibers cannot achieve the graphitic ideal. Instead the graphene planes are uneven and wavy, with a mean interplanar spacing significantly greater than the 0.335 nm of graphite. This turbostratic structure of carbon fibers is shown in Figure 3.

The carbon fiber production process involves a series of steps including spinning of the precursor fiber, stabilization, carbonization, and post-carbonization treatments that include sizing and surface treatments. The specifics of these steps vary greatly, depending on the precursor material and the desired properties of the carbon fiber. Figure 4 shows a schematic of the carbon fiber production process.

In the United States, carbon fibers are classified into two broad categories: high performance (HP) and general performance (GP) (12). High performance fibers are further classified into high tensile (HT) and high modulus (HM). Table 1 summarizes the tensile properties of HT and HM fibers.

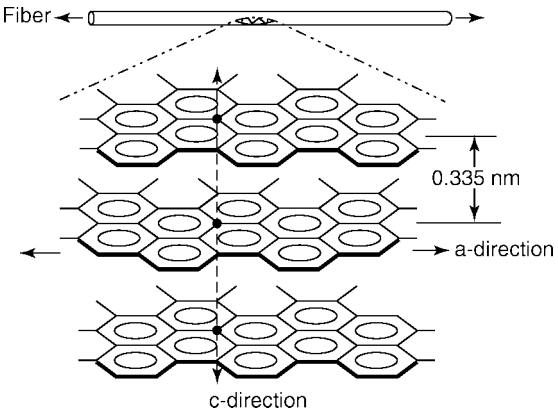

Fig. 2. Idealized carbon fiber structure. Adapted from Ref. 10.

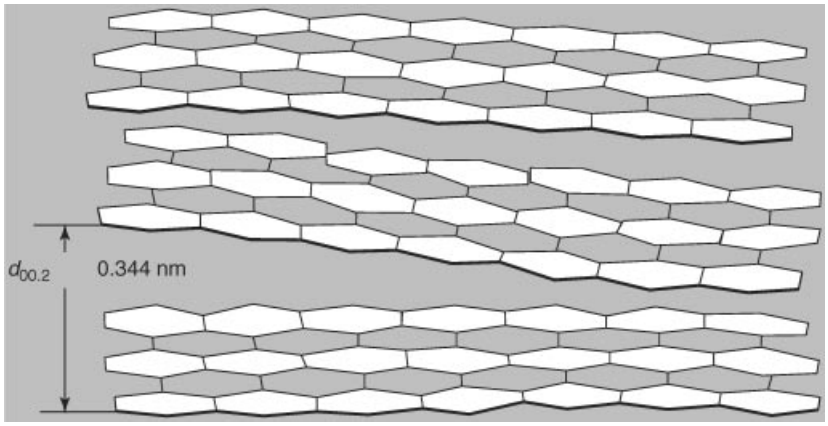

Fig. 3. The turbostratic structure of carbon fibers. Adapted from Ref. 11.

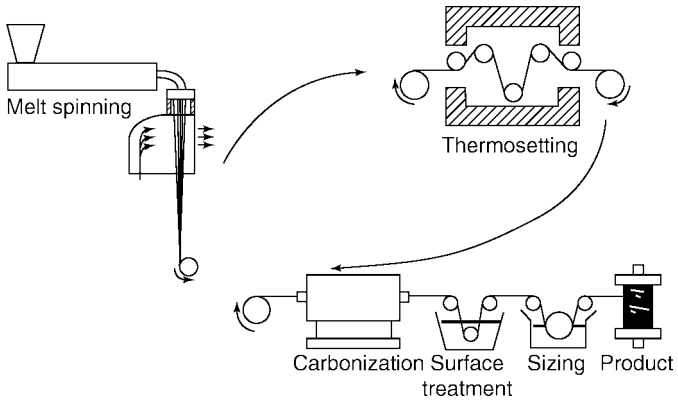

Fig. 4. Schematic of carbon fiber production. Adapted from Ref. 11.

Table 1. Properties of High Performance Carbon Fibers[a]

Fiber type	Tensile strength, GPa	Young's modulus, GPa
High tensile (HT)	3.0–7.1	150–300
High modulus (HM)	0.2–3.0	400–900

[a] Ref. 12.

This categorization of carbon fibers is not uniform. In the United Kingdom, the fiber categories are Type I (HM), Type II (HS), and Type III (GP) (13). Some researchers refer to fibers at the higher end of the Young's modulus range as ultra-high modulus (UHM) fibers (14). Fibers are also distinguished as being graphitizable or nongraphitizable. Graphitizable fibers can, upon heat treatment, be converted to graphene layer planes with a mean interlayer spacing of less than 0.34 nm (9), compared to the 0.335-nm spacing for pure graphite. Although there is an objective standard for graphitizable fibers, many researchers incorrectly use the term to describe any carbon fiber that develops measurable three-dimensional order. The Inorganic Chemistry Division Commission on High Temperature and Solid State Chemistry Subcommittee has developed recommended terminology to alleviate the confusion in nomenclature (9), but the multiple terminologies remain embedded in the culture of carbon fiber research.

The majority of commercial carbon fibers are produced from polyacrylonitrile (PAN) fibers. In fact, HTA-12K PAN-based carbon fibers are the most commonly used commercial carbon fiber (15). PAN-based fibers are the strongest commercially available carbon fibers and dominate structural applications. Mesophase pitch-based carbon fibers represent a smaller but significant market niche. These fibers develop exceptional moduli and excel in lattice-based properties, including stiffness and thermal conductivity (1). Rayon-based fibers are used in heat shielding and in missile nosecones (16). Carbon fibers made from high performance polymers (17–19) or from chemical vapor deposition of hydrocarbons, such as benzene or methane, display unique properties that make them potentially attractive future alternatives (20–22).

PAN-Based Carbon Fibers

PAN-based carbon fibers develop exceptional tensile strength [in excess of 7000 MPa (23)] and are more resistant to compressive failure than high performance polymers (24). These factors combine to make PAN-based carbon fibers the ideal choice for applications requiring significant fiber strength. However, PAN-based fibers are less appropriate than mesophase pitch-based fibers for applications in which molecular order-dependent properties are key.

Commercial PAN is actually a copolymer of acrylonitrile and another monomer (vinyl acetate, methyl acrylate, or acrylic acid) that is added to lower the glass-transition temperature of the material and control its oxidation resistance (see ACRYLONITRILE AND ACRYLONITRILE POLYMERS). The repeat unit of PAN is shown in Figure 5. The copolymer is formed through a wet-spinning process in which the polymer solution is extruded directly into a liquid bath. A blend of

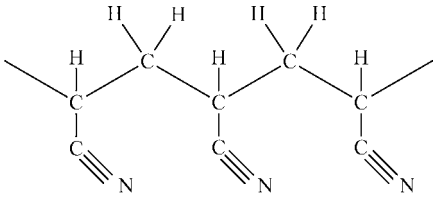

Fig. 5. The molecular structure of PAN.

phase separation and chemical reaction in the liquid results in solidification of the polymer. A concentrated copolymer solution containing 93–95 wt% acrylonitrile is dissolved in a solvent (typically dimethylacetamide) to form a concentrated polymer solution that is fed to a storage tank (25). The solution is filtered to minimize impurities and passed through a spinnerette.

The fibers emerge through the small capillary holes directly into a coagulation bath containing ethylene glycol that extracts the solvent from the fiber. The solvent extraction rate is governed by complex thermodynamic and kinetic relationships but can be influenced by the selection of coagulation liquid, temperature, and the circulation rate of the fluid within the bath. Figure 6 shows a schematic representation of the wet spinning of PAN fibers.

The development of internal voids or flaws in the fiber as well as the shape and texture of the fiber are controlled by the solvent removal rate. Concentration gradients can occur during the solvent extraction process, resulting in a warping of the fiber. For example, dog-bone–shaped fibers result from removing the solvent too rapidly (23). The fiber that emerges from the coagulation bath undergoes a series of post-spinning steps including washing, drawing, and drying during which the fiber solidifies into its final form. These processes play a crucial role in developing the internal morphology of the fibers (26).

Before the acrylic fibers (qv) produced in the wet-spinning process can be subjected to the elevated temperatures of carbonization, they must be converted to a thermally stable form that will not melt through oxidative stabilization. Stabilization is usually performed in air at temperatures between 200 and 300°C (27) and under tension to prevent fiber shrinkage (28).

During the stabilization process, dehydrogenation, oxidation, and nitrile cyclization reactions result in the formation of a condensed pyridine ring "ladder" structure that is suitable for subsequent carbonization (29). The general mechanism is shown in Figure 7. The details of the stabilization mechanism are highly

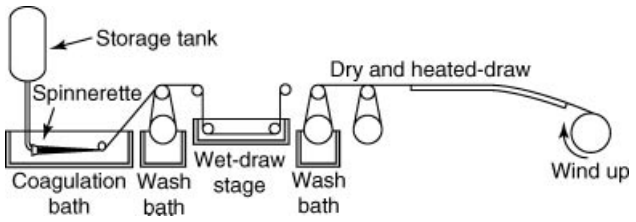

Fig. 6. Wet spinning of PAN fibers. Adapted from Ref. 24.

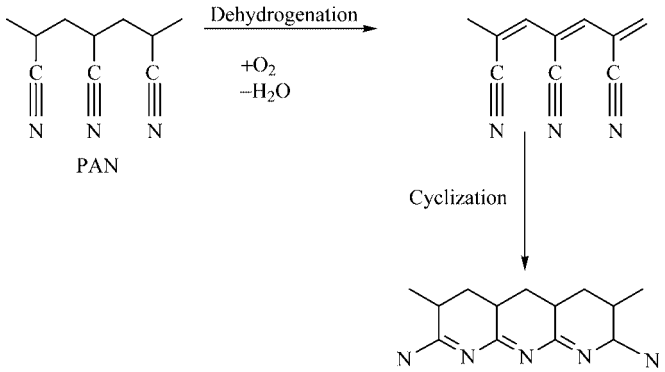

Fig. 7. General mechanism for the stabilization of PAN. Adapted from Ref. 12.

complex and have been the subject of many studies (30–33). All studies agree that control of the heating rate is essential because the reaction is highly exothermic. The stabilization time varies greatly with the size of the fiber bundle, the temperature, and the oxidizing environment. Studies of stabilization at elevated temperatures (350–400°C) show the development of additional intermolecular crosslinking, resulting in improved strengths (34,35). The stabilized fiber is carbonized in an inert atmosphere at temperatures ranging from 1000 to 3000°C, depending on the desired properties. During the pyrolysis, nearly all inorganic and nonaromatic carbons are driven off. Primary off-gases include hydrogen cyanide, carbon dioxide, water, ammonia, methane, and hydrogen (35). The carbon yield during the process is generally in the range of 40–45% (36).

Heating rate plays a major role in controlling the release of gases. A decrease in tensile strength is generally observed at temperatures above 1500°C (37), which corresponds to the final major release of nitrogen (38). As a result, many of the highest strength PAN-based carbon fibers contain residual nitrogen. Although heat treatments of PAN-based carbon fibers above 1700°C are often referred to as graphitization, these fibers are not graphitizable and do not develop highly ordered graphene planes.

Because PAN-based carbon fibers are commonly used in applications requiring high tensile strength, great care must be taken to preserve the potential for high tensile strength during the spinning of the precursor fibers. A fiber is often viewed as a chain consisting of interlocking links. If there were no misalignments or flaws, each link would fail at essentially the same tensile load. However, flaws in the fiber act as weak links in the chain, lowering the observed tensile strength of the fiber (39). As a result, the actual strength at which a given fiber will fail depends on both the frequency and severity of these flaws (40,41). Macroscopic flaws can result from inclusions, large voids, or damage from handling. Microscopic flaws can also lead to premature failure but are more difficult to quantify. Johnson (42) attributed many flaws to the misalignment of crystallites that interlink and result in voids. Highly ordered fibers are far more sensitive to these crystallite misalignments. As a result, fibers with high moduli tend to have lower tensile strengths than less-ordered, less–flaw-sensitive lower modulus fibers.

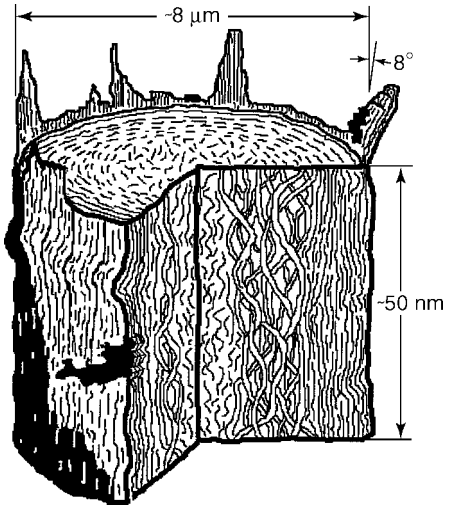

Fig. 8. Schematic representation of a carbonized PAN fiber. Adapted from Ref. 43.

Diefendorf and Tokarsky (43) showed that carbonized PAN fibers have a fibrillar microstructure as shown in Figure 8. This microstructure may be viewed as undulating ribbons and is highly resistant to premature tensile failure because of its flexibility. Therefore, PAN-based carbon fibers are well suited to developing high tensile strengths, but are not likely to develop the high level of three-dimensional order associated with high modulus precursor materials such as mesophase pitch. As such, PAN-based carbon fibers are considered nongraphitizing and maintain a highly turbostratic organization of the graphene layer planes, even when exposed to very high treatment temperatures (42).

Recent research in Poland is helping PAN-based carbon fibers find new applications as biological implants. Low temperature carbonized fibers have found use in ligament and tendon prostheses and in surgical sutures (44,45). These fibers are heat treated to temperatures below 1300°C and are far less crystalline than traditional carbonized PAN fibers (46,47). Despite the promise of these studies, low temperature carbonized PAN fibers do not share the commercial success of their high performance cousins.

Mesophase Pitch-Based Carbon Fibers

Pitch consists of a heavy fraction of predominantly aromatic hydrocarbons that is the residue of petroleum or coal tar distillation following the removal of creosote oil and anthracene (48). Table 2 provides a list of the major components in coal-tar fractions. The pitch consists of hundreds of thousands of different species with an average molecular weight of several hundreds. Many of the species are heterocyclic and are formed by a complex variety of chemical reactions, including thermal decompositions, hydrogen transfers, and oligomerization reactions (49). Pitch is a glassy solid at room temperature, but softens upon heating to form a

Table 2. Major Components in Coal-Tar Fractions[a]

Boiling Temperature, °C				
<200	200–250	250–300	300–350	>350
Benzene	Tar acids	Methyl-naphthalene	Phenathracene	Chrysene
Toluene	Tar bases	Acenapthene	Anthracene	Fluoranthene
Xylene	Naphthalene	Fluorene	Carbazole	Pyrene
Tar acids		Diphenylene oxide		
Tar bases				
Solvent				
Naphtha				

[a]Ref. 50.

viscous liquid. Pitches are often characterized by determining their solubility in different organic solvents. Solvent fractionation also serves as a critical method of altering the composition of pitches prior to fiber spinning (48).

Certain pitches can be spun directly into isotropic pitch fibers with only minor devolitization. Carbonized isotropic pitch fibers cannot be graphitized and develop mechanical and thermal properties that are substantially inferior to those produced by other precursors. However, isotropic pitch fibers are very inexpensive and have found commercial applications in areas that do not require the exceptional mechanical and thermal properties of mesophase pitch-based carbon fibers. Isotropic pitch-based carbon fibers are used in filters, brake pads, activated carbons, and as substrates for chemical vapor deposition (23). Table 3 summarizes properties of isotropic pitch-based carbon fibers.

The physical explanation for why some precursors produced graphitizable carbons while others did not was developed by Brooks and Taylor (51). During thermal treatment of aromatic hydrocarbons between 400 and 550°C, an intermediate liquid crystalline phase (mesophase) of spheroids with a mosaic structure formed within the continuous isotropic phase. Selected-area electron diffraction patterns show that each mesophase sphere has a single direction of preferred orientation as shown in Figure 9. As the pyrolysis progresses, the spherules grow and coalesce. Ultimately, a phase inversion occurs and the mesophase becomes the continuous phase (52). There are no grain boundaries in the mesophase, though disclinations do exist. The composition of each phase changes continuously during the pyrolysis and when the entire material is mesophase, polymerization continues with the release of volatiles (48). The formation of the mesophase can be

Table 3. Properties of Isotropic Pitch-Based Carbon Fibers[a]

Fiber type	Carbon wt%	Density, g/cm^3	Tensile strength, MPa	Young's modulus, GPa
T-101F	>95	1.65	790	33
T-101S	>95	1.65	720	32
T-201F	>99	1.57	690	33
T-201S	>99	1.57	590	30

[a]Ref. 12.

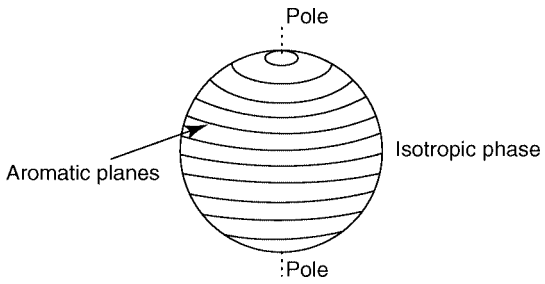

Fig. 9. Lamellar structure of mesophase spherule

influenced by numerous factors including the presence of insoluble particles, the presence of oxygen or sulfur, the applied pressure, the nature of the pitch itself, and the temperature of the heat-soak treatment. Partial oxidation of the pitch is particularly troubling because it results in the presence of inclusions of isotropic pitch which persist in the carbonized product and will not convert to mesophase at any treatment temperature (51).

The two main processes for producing mesophase from pitch are heat soaking and solvent extraction. The first heat-soaking process was developed at Union Carbide in 1977 to convert 50 wt% of low cost Ashland 240 isotropic pitch into a spinnable mesophase by heating the pitch for approximately 40 hours at 400–410°C (53). During this process, the higher density of the mesophase fraction caused it to collect on the bottom of the vessel. Agitating the pitch during pyrolysis led to a homogeneous emulsion of the mesophase and isotropic fraction that resulted in a more uniform and spinnable product (54). Chwastiak and Lewis (55) produced 100% bulk mesophase by using an inert gas to agitate the mixture and remove volatile components. Subsequent research by Otani and Oya (56) produced a mesophase pitch with a lower softening temperature by adding a hydrogenation step either before or after the production of the mesophase. Figure 10 shows a typical molecule of mesophase pitch formed during the heat-soaking process.

Mesophase is also produced through a solvent extraction technique. A portion of an isotropic pitch is extracted with an organic solvent such as benzene, hexane, or toluene. The remaining insoluble fraction is pyrolized for 10 min (as opposed to 40 h in the Lewis heat-soaking process) in a temperature range from 230°C to 400°C, yielding a 75–100 wt% mesophase product (57). Both production strategies convert inexpensive pitch feedstocks to spinnable mesophases, but neither can overcome some fundamental limitations of the feedstocks themselves. Pitch is a mixture of components refined through a complex process of feedstocks that are inherently variable, making batch-to-batch consistency extremely difficult. Further, during every step of pitch production and pyrolysis, impurities are concentrated in the retained fraction. These problems have spurred interest in alternative mesophase production strategies.

Mochida (58) developed a process in which a synthetic mesophase is produced from the HF/BF_3 catalyzed polymerization of naphthalene or methyl naphthalene. HF/BF_3 is a Bronsted acid that has been used to catalyze coal liquifaction and aromatic condensation. The aromatic resin (AR)-mesophase produced through this process is both more spinnable and more easily oxidized than that produced from

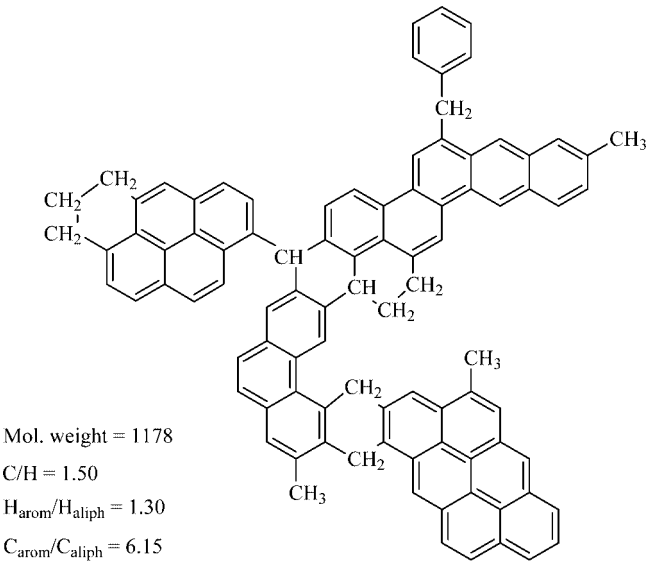

Fig. 10. A typical heat-soaked mesophase molecule. Adapted from Ref. 55.

traditional pitch precursors. Mochida (59) reports that the thermal and mechanical properties of the carbonized AR-mesophase fibers are comparable with those of the best commercial fibers. AR-mesophase has a much narrower molecular weight distribution than a mesophase formed from natural pitch and is free from sulfur and other impurities that present problems in traditional pitches. Figure 11 shows representative benzene-soluble fractions of AR-mesophase.

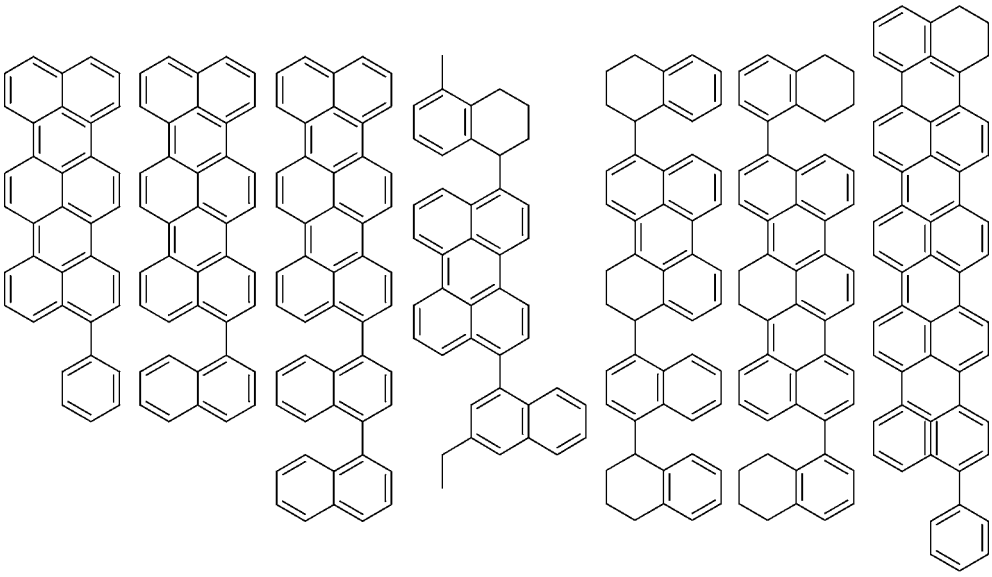

Fig. 11. Representative benzene-soluble fractions from AR-mesophase. Adapted from Ref. 12.

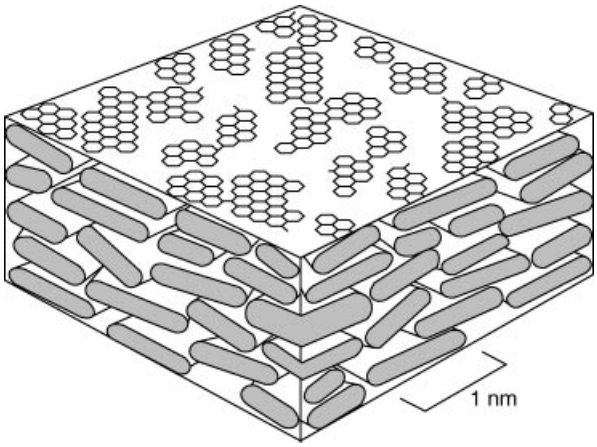

Fig. 12. The stacking behavior of mesophase pitch. Adapted from Ref. 64.

Another approach to improving the quality of the mesophase precursor involves supercritical fluid extraction, which has been shown to fractionate isotropic petroleum pitches into fractions of different compositions, some of which contain 100% mesophase (60). When using supercritical fluids, both temperature and pressure can be used to alter the strength of the solvent (61). Continuously varying the temperature and pressure allows selective fractions of relatively narrow molecular weight distributions to be isolated (62). Supercritical fluid extraction offers several advantages in mesophase preparation including lower solvent requirements and the ability to use a single, cost-effective solvent to produce a variety of pitch fractions (63).

Once the mesophase pitch has been prepared, the next step in processing is spinning it into fibers. This process is particularly important because when mesophase pitch is carbonized, the morphology of the pitch is the dominant factor in determining the microstructure of the resulting graphitic fiber. This results from the stacking behavior of the mesophase molecules (64), as shown in Figure 12.

Mesophase pitch fibers are produced through melt spinning that is essentially the same as that used to spin commercial polymers. Figure 13 shows this process in which an extruder melts pitch particles and pumps the molten pitch through a multiholed spinnerette. The high extensional shear orients the liquid crystalline mesophase molecules as it approaches and flows through the spinnerette. The fibers emerging from the spinnerette are drawn by a windup spool.

Although there are considerable similarities between melt spinning pitch and polymers, the rheological behavior of mesophase pitch is far more complex than that of most polymers. First, the viscosity of mesophase pitch displays an extreme sensitivity to temperature (65–67). This has direct impact on fiber spinning because pitch fibers achieve their final diameter within a few millimeters of exiting the spinnerette, unlike most polymeric materials. These data provide no insight into the texture in the developing fibers, but provide a basis for determining appropriate spinning temperatures for pitches. Mesophase pitch exhibits shear-thinning behavior at low shear rates and becomes increasingly Newtonian

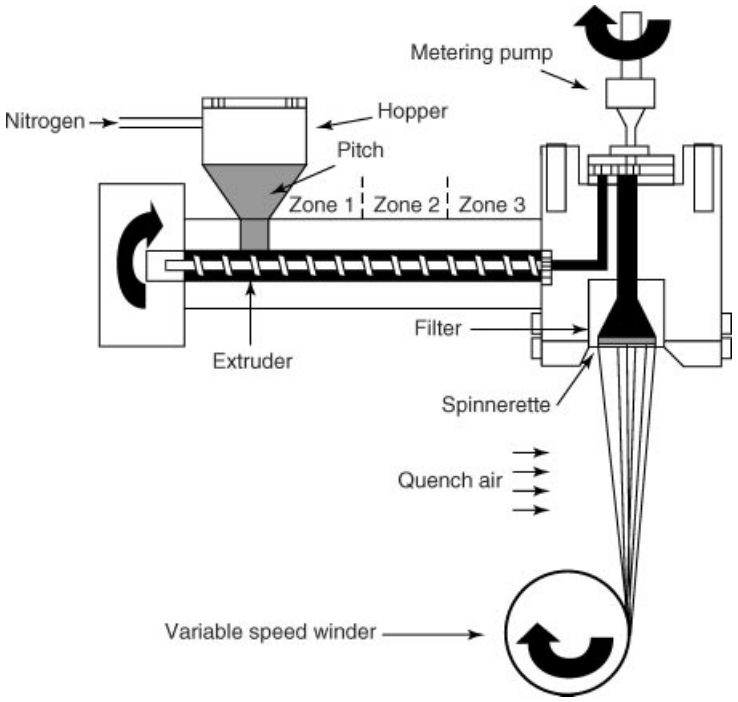

Fig. 13. Melt spinning of mesophase pitch fibers.

as shear rate increases (65). The pseudoplasticity of the mesophase likely relates to the alignment of the liquid crystalline mesophase domains at elevated shear (67). Mesophase pitch has been reported to display thixotropic behavior, but no clear basis for this behavior has been developed (68,69).

McHugh and Edie (68) demonstrated that the microstructure of carbonized mesophase pitch-based carbon fibers can be predicted through the application of continuum theory. Leslie (69) and Ericksen (70) proposed a continuum theory that applies to the flow of nematics. In addition to the standard conservation equations (continuity and the equation of motion), a conservation of angular momentum equation (known as the balance of torques) is also considered. Unfortunately, the shear stress is not proportional to the shear rate. Instead, the viscous stress tensor is the sum of six terms, each with its own unique viscosity coefficient. Although these equations are quite complex, they can be solved for a unique analytical solution for a given geometry. When applied to fiber spinning, the Leslie and Ericksen model can predict the flow-induced orientation of the aromatic planes in the as-spun fiber. For example, the equations predict and explain the development of the radial texture observed for fully developed flow of discotic mesophase through a circular capillary (ie, a spinnerette hole). The balance of torques requires the mesophase to flow with a radial orientation as shown in Figure 14.

As a result of the ability to predict fiber texture as a function of geometry, improved spinning geometries can be evaluated. McHugh and Edie (68) showed that a capillary with a tapered entry forms a more ordered fiber as a result of

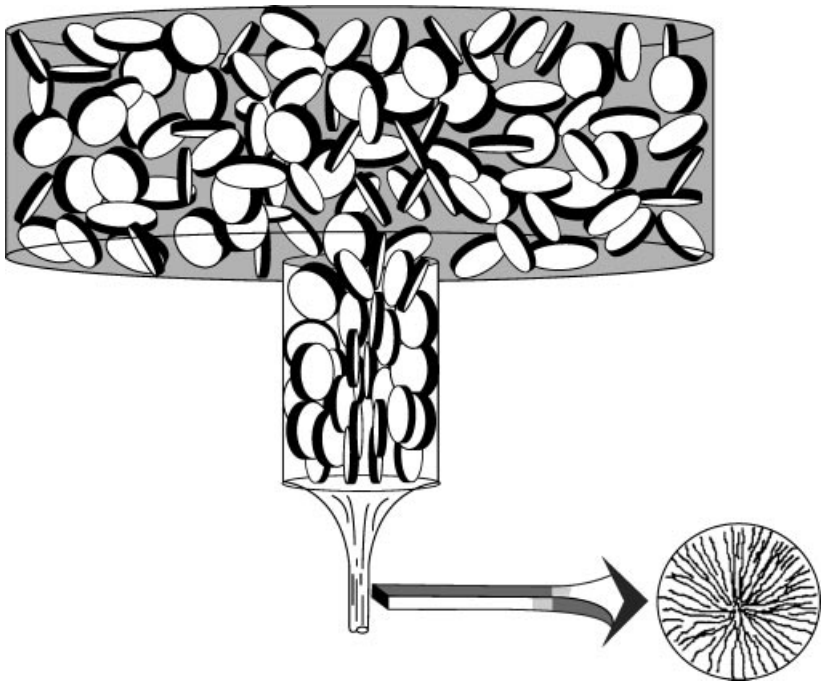

Fig. 14. Origin of radial structure in mesophase pitch fibers. From Ref. 23.

creating less disruption to the fully organized flow assumed by the Leslie and Ericksen model. Spinning fibers through a rectangular capillary generates fiber with a highly linear texture that results in fibers with higher thermal conductivity (71). The line-origin texture of these "ribbon fibers" is shown in Figure 15. Figure 16 shows the Leslie and Ericksen model solution to flow of discotic mesophase flowing through a rectangular channel. The edges within the channel represent the edges of the aromatic planes (68).

Regardless of the shape and texture, the as-spun fibers must be stabilized prior to carbonization. During this process, oxygen reacts with side groups in the pitch fiber, creating cross-linkages and adding weight. Typically, a 6% weight gain is needed to completely stabilize mesophase pitch fibers (72), while an 8% weight gain is more typical for PAN (73). Lower heating rates and lower temperatures

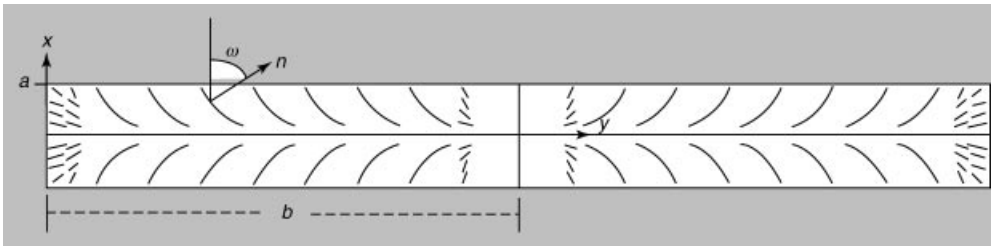

Fig. 15. The line-origin texture of ribbon fibers.

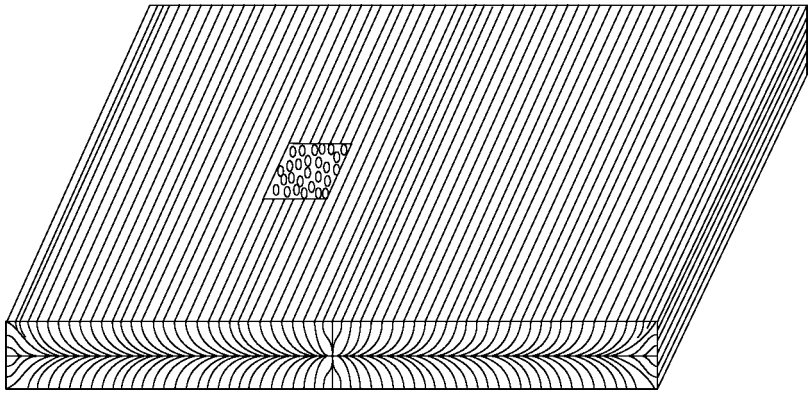

Fig. 16. Orientation developed in discotic mesophase flow through a rectangular channel. Adapted from Ref. 68.

during stabilization result in a more uniform stabilization, but also add to processing time (74).

The carbonization of mesophase pitch-based fibers closely resembles that which is previously described for PAN, but occurs in two stages. Typically, fibers are heated to approximately 1000°C and held there allowing for the evolution of off-gases. The rate-limiting step in this low temperature carbonization is the free-radical breaking of carbon–hydrogen bonds. Following the release of gases, the fibers are heated to their final treatment temperature, which may be as high as 3000°C.

Unlike PAN-based carbon fibers, mesophase pitch-based fibers experience significant graphitization during which dislocations in the turbostratic carbon stacks are gradually annealed, resulting in the formation of a three-dimensional lattice. Fischbach (75) presented a detailed study of graphitization which characterizes the process as a combination of atomic diffusion and crystallite growth. Table 4 provides a comparison of properties for some commercial pitch- and PAN-based carbon fibers.

Table 4. Properties of Commercial Carbon Fibers[a]

Fiber type	Precursor material	Tensile strength, GPa	Young's modulus, GPa
T-300	PAN	3.66	231
T-650/35	PAN	4.28	241
T-650/42	Pitch	4.62	290
P-25	Pitch	1.38	159
P-30X	Pitch	2.76	201
P-55S	Pitch	1.90	379
P-75S	Pitch	2.07	517
P-100S	Pitch	2.41	759
P-120S	Pitch	2.41	828
K-1100	Pitch	3.10	931

[a] Ref. 76.

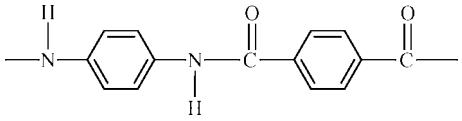

Fig. 17. The repeat unit of Kevlar.

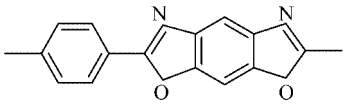

Fig. 18. The repeat unit of PBO.

Carbon Fibers from High Performance Polymers

The primary factor limiting the increased commercial application of carbon fibers is their high production cost, a significant portion of which is directly attributable to the lengthy stabilization process required by both pitch and PAN (77). The rigid-rod structure and high degree of aromaticity allow Kevlar (poly *p*-phenylene terephthalamide) and PBO (poly *p*-phenylene benzobisoxazole) fibers to be converted directly to carbon fiber without any stabilization (17–19). The repeat units of Kevlar and PBO are shown in Figures 17 and 18 (see POLYAMIDES, AROMATIC; RIGID-ROD POLYMERS). Surprisingly, PBO-based carbon fibers also show some capacity to graphitize (19). However, the commercial development of high performance polymer-based carbon fibers is impeded by their comparatively poor tensile strength. Table 5 compares the properties of PBO- and Kevlar-based carbon fibers with typical pitch- and PAN-based fibers.

In spite of the relatively poor tensile strengths of the fibers, carbonized Kevlar possesses characteristics that make it an ideal candidate as a substrate for chemical vapor deposition of silicon carbide including a compatible coefficient of thermal expansion, sufficient tensile strength to survive the coating process, availability from a reliable domestic supplier, and a smooth, even diameter of less than 7 μm (78).

Table 5. Properties of High Performance Polymer Based Carbon Fibers[a]

Precursor material	Product designation	Tensile strength, GPa	Young's modulus, GPa	Electrical Resistivity, $\mu\Omega$-m
PBO	Batch, 1800°C	0.52	245	13
PBO	Continuous, 1800°C	0.85	183	10
Kevlar-29	1600°C	0.94	143	23
PAN	T-300	3.66	231	18
Pitch	P-55	1.90	415	9

[a]Refs. 18,78.

Rayon-Based Carbon Fibers

The first carbonization of cellulose-based fibers dates back to Thomas Edison, who carbonized a natural cellulose filament for use as an incandescent lamp filament. In the mid-1950s, the Carbon Wool Corporation introduced the first commercial carbonized rayon fibers (79). PAN- and pitch-based carbon fibers have replaced rayon-based fibers in most high performance applications; however, they continue to find use as ablative materials in missile nosecones and heat shielding (16). Additionally, the combination of low cost, ease of handling, and high natural porosity makes rayon an attractive precursor for activated carbon fibers (see CELLULOSE FIBERS, REGENERATED).

Activated carbon fiber (ACF) offers several advantages over traditional granular and powdered carbons as an absorbent material. Rayon-based ACFs (80) possess

(1) smaller fiber diameters, which encourages rapid adsorption and desorption by minimizing diffusion limitation;
(2) more concentrated and controllable pore size distributions; and
(3) excellent adsorption capacity at low adsorbate concentrations.

Rayon-based ACFs are used in the adsorption of many volatile organic compounds including formaldehyde (80), methyl ethyl ketones (81), and benzene (81). ACFs are also finding uses in natural gas storage (82), electrodes for batteries (83), catalyst supports (84), and NO_x removal (85). Stabilized rayon fibers are carbonized and then activated with air (80), steam (86), or carbon dioxide (87), much as in granular carbon activation. The extent of pyrolysis governs the pore structure, carbon yield, and surface area of the fiber, while activation impacts the presence of functional groups on the pore surface (12). Properties of some commercial ACFs are summarized in Table 6.

ACFs develop a pore structure with micropores (<60 nm) open directly to the surface, unlike granular carbons where extensive surface oxidation results in macropores on the surface (88) with microporosity only in inner zone, as shown in Figure 19. The presence of extensive surface microporosity has a significant impact on the adsorption of volatile organic compounds. The overlap of attractive forces on opposite micropore walls are primarily responsible for the adsorption of gases at low concentrations (89).

Carbonized rayon fibers present one drawback as an ACF precursor. Nearly 82% of the mass of the original fiber is evolved during pyrolysis, resulting in a

Table 6. Properties of Commercial Active Carbon Fibers[a]

Fiber	Precursor	Surface area, m^2/g	Mean pore size, nm	Benzene adsorption, wt%	Tensile strength, MPa
Toyobo KF Series	Rayon	1000–1600	0.5–10	30–60	60–130
Toho Finegard	PAN	500–1200	2–4	20–50	196–490
Adol A Series	Pitch	1000–2000	1–2.5	20–45	60–130

[a] Ref. 12.

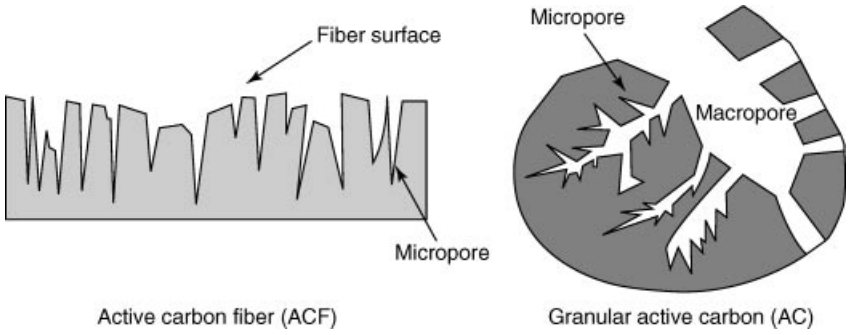

Fig. 19. Pore models for ACFs and granular carbon. Adapted from Ref. 88.

loss of both strength and flexibility (90). Rayon carbonization consists of a blend of depolymerization and dehydration reactions. The depolymerization involves the formation of *l*-glucosan and volatile products, while the dehydration reaction inhibits *l*-glucosan and volatile production, resulting in a higher carbon yield (91–93). The inclusion of Lewis acids such as $AlCl_3$ and $ZnCl_2$, during low temperature carbonization enhances the carbon yield by favoring the dehydration reactions (94).

Vapor-Grown Carbon Fibers

Vapor-grown carbon fibers (VGCFs) have been produced by decomposing benzene or methane over transition metal catalyst particles within a temperature range of 1000–1300°C (95–97). Fibers produced in this manner develop an annular ring texture (often referred to as a tree trunk structure) with graphene planes running parallel to the fiber axis (98), as shown in Figure 20. This microtexture facilitates graphitization and leads to excellent electrical, thermal, and mechanical properties (99,100).

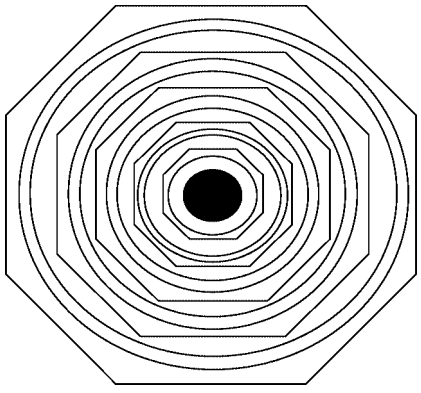

Fig. 20. Cross-section of VGCFs with octagons representing graphene planes and circular lines representing circular carbon layers. Adapted from Ref. 98.

Table 7. Properties of Submicrometer Vapor-Grown Carbon Fibers[a]

Property	Carbonized s-VCGFs	Graphitized s-VCGFs	Measurement method
Lattice parameter, nm	0.6900	0.6775	XRD[b]
Diameter, μm	0.2	0.2	SEM[c]
Length of fiber, μm	10–20	10–20	SEM[c]
Volume Density, g/cm^3	0.02–0.07	0.02–0.07	Tapping
Real Density, g/cm^3	1.9	2.1	Pycnometer
BET surface area, m^2/g	37	15	Nitrogen adsorption
Ash content, %	1.5	0.03	SDK[d]
pH	5	7	JIS K 6621[e]
Starting temp. of oxidation, °C	550	650	TGA[f]

[a] Ref. 101.
[b] X-ray diffraction.
[c] Scanning electron microscopy.
[d] Scintillation detection.
[e] Japan Industrial Standard.
[f] Thermogravimetric analysis.

The production strategy with the greatest potential for scale-up into mass production may be the "floating reactant method." This technique disperses catalyst particles with the reactive hydrocarbon in a reaction chamber, resulting in a high yield of relatively uniform diameter fibers of 0.1 to 0.2 μm (101). Fibers produced in this fashion are considered submicrometer VGCFs (s-VGCFs) and are much smaller than VGCFs produced by the traditional seeding techniques. Typical diameters range from 10 to 20 μm, about the size of carbonized PAN fibers. The high surface-to-volume ratio and electrical conductivity make the submicrometer fibers exceptional candidates to be anode materials in lithium batteries. Table 7 summarizes the properties of s-VGCFs.

The development of soot as an unwanted byproduct is a problem in the "floating reactant method" of producing s-VCGFs (102). The addition of gaseous ammonia to the hydrocarbon feed along with hydrogen sulfide and iron particles improves the length and uniformity of the fibers while reducing soot production (103).

While substantial research has focused on developing submicron VGCFs, significant interest also exists in developing large, rapidly-produced, inexpensive VCGFs for use as filler materials in carbon composites. Koyama and co-workers (104) first reported achieving vapor grown carbon fibers of 25 cm in length from the thermal decomposition of benzene in a hydrogren atmosphere in 1972. More recently, Masuda and co-workers (105,106) have developed a liquid pulse injection technique that produces VCGFs with lengths of up to 5 cm in less than 30 s. By adding phenyl silane to the benzene feedstock, the oxidation resistance of the resultant fibers increased without reducing the mechanical or electrical properties of the fibers (107).

During heat treatment, VCGFs (both traditional and submicrometer) undergo significant topological changes. During the growth process, the hydrocarbon feed molecules decompose and the carbon would diffuse into the catalyst particle. This diffusion of atomic carbon into the metal particle is generally considered to

be the rate-limiting step of the process (108). In fact, fiber yield has been shown to increase greatly near the melting point of the metal catalyst (108). Once the carbon has diffused to the active site, the central core growth of the new fiber would occur in the first seconds, terminate, and then the fiber would begin thickening (109). This thickening process is primarily responsible for determining the surface texture of VGCFs. When heat-treated to 2000°C, the smooth surface containing small pores transforms into a rope-like texture as a result of the sudden density increase in the material corresponding to the decrease in mean interlayer spacing. As the graphitizing fiber becomes less turbostratic, the contraction results in an anisotropic shrinkage. By 2800°C, well-developed microdomains form throughout the fiber and appear to be limited primarily by the diameter of the fiber (109).

Summary

Carbon fibers have advanced greatly from Edison's early experiments with carbonizing cellulose as an iridescent light bulb fiber. PAN-based carbon fibers dominate commercial high performance applications where the tensile strength of the fiber is paramount, but the same fibrillar microtexture that enables carbonized PAN to achieve exceptional tensile strengths limits its long-range order. For applications requiring exceptional molecular-order–dependent properties such as stiffness and thermal conductivity, mesophase pitch-based fibers are preferred. Pitch-based fibers are made from the high molecular weight remains of petroleum or coal-tar distillation, though synthetic aromatic resins have been developed that can be converted to graphitized fibers while avoiding the problems inherent in conventional pitches. Application of transport phenomena principles to the liquid crystalline flow of mesophase have enabled researchers to explain the development of structure in the fiber and to suggest improved spinnerette designs.

For applications that do not require exceptional mechanical properties, carbon fibers made from high performance aramid polymers show considerable potential. These aramid fibers do not require stabilization prior to carbonization, which substantially simplifies the production process. Rayon-based carbon fibers continue to appear in some composite applications, but have become key substrates for the development of activated carbon fibers. These ACFs develop a microporous surface structure that is ideal for adsorption of low levels of volatile organic compounds.

Carbon fibers are also produced from the catalytic decomposition of hydrocarbon gases. These vapor-grown fibers can be produced at submicrometer diameters and show great potential in battery applications. Larger vapor-grown fibers can be produced rapidly by pulse injection and show promise as filler material in composites.

Despite the continued commercial dominance of pitch- and PAN-based fibers, the carbon fiber field is continuously changing. Significant current research is focused on the production of carbon nanotubes. Other researchers continue to enhance the understanding of the processes and mechanisms governing the fiber production today. As researchers are better able to understand and manipulate fiber microstructures, the commercial applications for carbon fibers will continue to expand.

BIBLIOGRAPHY

"Carbon Fibers" in *EPSE* 2nd ed., Vol. 2, pp. 640–685, by John P. Riggs, Calanese Corp.

1. A. Cato and D. D. Edie, *Carbon* **41**, 1411 (2003).
2. X. Fu, W. Lu, and D. D. L. Chung, *Carbon* **36**, 1337 (1998).
3. Y. Xu and D. D. L. Chung, *Carbon* **39**, 1995 (2001).
4. T. Momma, X. J. Liu, T. Osaka, and T. Sawada, *J. Power Sources* **60**, 249 (1996).
5. E. Mora, C. Blanco, V. Prada, R. Santamaria, M. Granda, and R. Menendez, *Carbon* **40**, 2719 (2002).
6. T. J. Mays, in T. D. Burchell, ed., *Carbon Materials for Advanced Technologies*, Pergamon, New York, 1999.
7. I. Mochida, S. Kawano, N. Shirahama, T. Enjoji, S. H. Moon, K. Sakanishi, Y. Korai, Y. Yasutake, and M. Yoshikawa, *Fuel* **80**, 2227 (2001).
8. E. Fitzer, K. H. Kochling, H. P. Boehm, and H. Marsh, *Pure Appl. Chem.* **67**(3), 473 (1995).
9. R. Bacon, unpublished data, Amoco Performance Products, Inc., Alpharetta, Ga., 1990.
10. D. D. Edie, in J. L. Figuerido, ed., *Carbon Fibers, Filaments, and Composites*, Kluwer Academic Publishing, Dordrecht, the Netherlands, 1990.
11. D. D. Edie and J. J. McHugh, in T. Burchell, ed., *Carbon Materials for Advanced Technologies*, Pergamon Press, New York, 1999.
12. S. H. Yoon, Y. Korai, and I. Mochida, in H. Marsh and F. R. Reinoso, eds., *Sciences of Carbon Materials*, Universidad de Alicante Publicaciones, Alicante, Spain, 2000.
13. E. Pamula and P. Rouxhet, *Carbon* **41**, 1905 (2003).
14. D. Schulz, *SAMPE J.* **23**(2), 27 (1987).
15. HTA Fiber Data Sheet, Toho Tenax Corp., Mishima, Japan, 2003.
16. F. T. Traceski, *Acquisition Rev. Q.* 179 (Spring 1999).
17. J. A. Newell, D. K. Rogers, D. D. Edie, and C. C. Fain, *Carbon* **32**, 651 (1994).
18. J. A. Newell and D. D. Edie, *Carbon* **34**, 551 (1996).
19. J. A. Newell, D. D. Edie, and E. L. Fuller Jr., *J. Appl. Polym. Sci.* **60**, 825 (1996).
20. M. Endo, *CHEMTECH* **18**, 568 (1988).
21. G. G. Tibbetts, *Carbon* **30**, 399 (1992).
22. M. Jayasankar, R. Chand, S. Gupta, and D. Kunzru, *Carbon* **33**, 253 (1995).
23. D. D. Edie, J. J. McHugh, and J. A. Newell, in H. Marsh and F. R. Reinoso, eds., *Sciences of Carbon Materials*, Universidad de Alicante Publicaciones, Alicante, Spain, 2000.
24. Toray Product Catalog, Mitsui Plastics, Inc., White Plains, N.Y., 1998.
25. M. K. Jain and M. S. Abhiraman, *J. Mater. Sci.* **22**, 278 (1990).
26. G. J. Capone, in J. C. Masson, ed., *Acrylic Fiber Technology and Applications*, Marcel Dekker, Inc., New York, 1995.
27. L. H. Peebles, *Carbon Fibers: Formation, Structures, and Properties*, CRC Press, Boca Raton, Fla., 1995.
28. W. Johnson and W. Watt, *Nature* **215**, 384 (1967).
29. E. Fitzer, W. Frohs, and M. Heine, *Carbon* **24**, 387 (1986).
30. A. Deurbergue and A. Oberlin, *Carbon* **29**, 621 (1991).
31. W. Pinghua, L. Jie, Y. Zhongren, and L. Rengyuan, *Carbon* **30**(1), 113 (1992).
32. M. G. Dunham and D. D. Edie, *Carbon* **30**, 435 (1992).
33. R. R. Mathur, O. P. Bahl, and J. Mittal, *Carbon* **30**, 657 (1992).
34. J. Mittal, O. P. Bahl, R. R. Mathur, and N. K. Sandle, *Carbon* **32**, 1113 (1994).
35. W. Watt, *Nature* **222**, 265 (1969).
36. D. M. Riggs, R. J. Shuford, and R. W. Lewis, in G. Lubin, ed., *Handbook of Composites*, Van Nostrand Reinhold Co., New York, 1982.
37. T. Matsumoto, *Pure Appl. Chem.* **57**, 1553 (1985).

38. E. Fitzer, *Carbon* **27**, 621 (1989).
39. S. Chwastiak and I. C. Lewis, *Carbon* **16**, 156 (1978).
40. E. G. Stoner, D. D. Edie, and S. D. Durham, *J. Mater. Sci.* **29**, 6561 (1994).
41. J. A. Newell and M. T. Sagendorf, *High Perform. Polym.* **11**, 297 (1999).
42. D. J. Johnson, *Chem. Phys. Carbon* **20**, 1 (1987).
43. R. J. Diefendorf and E. Tokarsky, *Polym. Eng. Sci.* **15**(3), 150 (1975).
44. M. Blazewicz, S. Blazewicz, and C. Wajler, *Ceram. Int.* **20**(2), 99 (1994).
45. S. Blazewicz, C. Wajler, and J. Chlopek, *J. Biomed. Mater. Res.* **32**, 215 (1996).
46. M. R. Alexander and F. R. Jones, *Carbon* **34**, 1093 (1996).
47. E. Pamula and P. Rouxhet, *Carbon* **41**, 1905 (2003).
48. B. Rand, in W. Watt and B. V. Perov, eds., *Handbook of Composites*, Elsevier Science Publishers, New York, 1985.
49. L. S. Singer, *Faraday Discuss. Chem. Soc.* **79**, 265 (1985).
50. F. A. Smith, T. F. Eckle, R. J. Osterholm, and R. M. Stichel, in A. J. Hoiberg, ed., *Bituminous Materials*, Vol. III, R. E. Kreiger, Huntington, New York, 1966.
51. J. D. Brooks and G. H. Taylor, *Chem. Phys. Carbon* **4**, 243 (1968).
52. G. W. Collett and B. Rand, *Carbon* **16**, 477 (1978).
53. U.S. Pat. 4,005,183 (1977), L. S. Singer (to Union Carbide).
54. U.S. Pat. 4,032,430 (1977), I. C. Lewis (to Union Carbide).
55. S. Chwastiak and I. C. Lewis, *Carbon* **16**, 156 (1978).
56. S. Otani and A. Oya, *ACS Symp. Ser.* **303**, 323 (1986).
57. U.S. Pat. 4,208,267 (1980), R. J. Diefendorf and D. M. Riggs (to Union Carbide).
58. I. Mochida, K. Shimizu, Y. Korai, H. Otsuka, and S. Fujiyama, *Carbon* **26**, 843 (1988).
59. Y. Korai, S. Ishida, S. H. Yoon, Y. G. Wang, I. Mochida, Y. Nakagawa, Y. Matsumara, Y. Sakai, and M. Komatu, *Carbon* **34**, 1569 (1996).
60. G. Bolanos, G. Z. Liu, T. Hochgeschurtz, and M. C. Thies, *Fluid Phase Equilib.* **82**, 303 (1993).
61. M. McHugh and V. Krukonis, *Supercritical Fluid Extraction*, 2nd ed., Butterworth Heinemann, Stoneham, Mass., 1994.
62. K. W. Hutchenson, J. R. Roebers, and M. C. Thies, *Carbon* **29**, 215 (1991).
63. F. M. Dauche, G. Bolanos, A. Blasig, and M. C. Thies, *Carbon* **36**, 953 (1998).
64. J. E. Zimmer and J. L. White, in H. G. Brown, ed., *Advances in Liquid Crystals*, Vol. 5, Academic Press, New York, 1982.
65. F. F. Nazem, *Carbon* **20**(4), 345 (1982).
66. D. D. Edie and M. G. Dunham, *Carbon* **27**, 647 (1989).
67. J. J. McHugh and D. D. Edie, *Carbon* **34**, 1915 (1996).
68. J. J. McHugh and D. D. Edie, *Liq. Cryst.* **18**, 327 (1995).
69. F. M. Leslie, *Q. J. Mech. Appl. Math.* **19**, 357 (1966).
70. J. L. Ericksen, *Trans. Soc. Rheol.* **5**, 23 (1961).
71. D. D. Edie, C. C. Fain, K. E. Robinson, A. M. Harper, and D. K. Rogers, *Carbon* **31**, 941 (1993).
72. W. C. Stevens and R. J. Diefendorf, in *Carbon '86, Proceedings of the International Conference on Carbon*, Baden-Baden, Germany, 1986.
73. E. Fitzer, in J. L. Figuerido, ed., *Carbon Fibers, Filaments, and Composites*, Kluwer Academic Publishing, Dordrecht, the Netherlands, 1990.
74. T. Matsumoto and I. Mochida, *Carbon* **31**, 143 (1993).
75. D. B. Fischbach, *Chem. Phys. Carbon* **7**, 1 (1971).
76. Thornel Carbon Fiber Data Sheet, BP Amoco Chemicals, U.K., 2003.
77. J. R. Glatz, M. A. Kinna, and W. C. Riley, *DOD Metal Matrix Compos. Inf. Anal. Center Curr. Highlights* **8**, 1 (1988).
78. J. A. Newell and A. A. Puzianowski, *High Perform. Polym.* **11**, 197 (1999).
79. R. Bacon, *Chem. Phys. Carbon* **9**, 1 (1973).

80. H. Rong, Z. Ryu, J. Zheng, and Y. Zhang, *Carbon* **40**, 2291 (2002).
81. Z. H. Huang, F. Kang, Y. P. Zheng, J. B. Yang, and K. M. Liang, *Carbon* **40**(8), 1363 (2002).
82. J. Alcaniz-Monge, M. A. de la Casa-Lillo, D. Cazorla-Amoros, and A. Linares-Solano, *Carbon* **35**, 291 (1997).
83. M. Endo, Y. Nishimura, T. Takahashi, A. Takamuku, and T. Tamaki, *Carbon* **34**, 1165 (1996).
84. K. Otsuka, H. Ogihara, and S. Takenaka, *Carbon* **41**(2), 223 (2003).
85. N. Shirahama, S. H. Moon, K. H. Choi, T. Enjoji, S. Kawano, Y. Korai, M. Tanoura, and I. Mochida, *Carbon* **40**, 2605 (2002).
86. J. B. Tomlinson and C. R. Theocharis, *Carbon* **30**, 907 (1992).
87. Y. Ko, U. S. Choi, J. S. Kim, and Y. S. Park, *Carbon* **40**, 2261 (2002).
88. Y. Sanada, M. Suzuki, and K. Fujimoto, *Active Carbon*, Koudansha, Tokyo, 1992.
89. R. H. Bradley and B. Rand, *J. Colloid Interface Sci.* **169**, 168 (1995).
90. A. C. Pastor, F. Rodriguez-Reinoso, H. Marsh, and M. A. Martinez, *Carbon* **37**, 1275 (1999).
91. M. M. Tang and R. Bacon, *Carbon* **2**, 211 (1964).
92. K. Gurudatt and V. S. Tripathi, *Carbon* **36**, 1371 (1998).
93. F. Caturla, M. Molina-Sabio, and F. Rodriguez-Reinoso, *Carbon* **29**, 1999 (1991).
94. A. Huidobro, A. C. Pastor, and F. Rodriguez-Reinoso, *Carbon* **39**, 389 (2001).
95. G. G. Tibbetts, D. W. Gorkiewicz, and R. L. Alig, *Carbon* **31**, 809 (1993)
96. M. Endo, *CHEMTECH* **18**, 568 (1988).
97. M. Jayasankar, R. Chand, S. Gupta, and D. Kunzru, *Carbon* **33**(3), 253 (1995).
98. T. Hashishin, H. Iwanaga, M. Ichihara, and S. R. Mukai, *Carbon* **41**(2), 343 (2003).
99. G. G. Tibbetts, *Appl. Phys. Lett.* **42**, 666 (1983).
100. J. S. Speck, M. Endo, and M. S. Dresselhaus, *J. Cryst. Growth* **94**, 834 (1989).
101. M. Endo, Y. A. Kim, T. Hayashi, K. Nishimura, T. Matusita, K. Miyashita, and M. S. Dresselhaus, *Carbon* **39**, 1287 (2001).
102. G. G. Tibbetts, *Carbon* **27**, 745 (1989).
103. S. Collins, R. Brydson, and B. Rand, *Carbon* **40**, 1089 (2002).
104. T. Koyama, *Carbon* **10**, 757 (1972).
105. T. Masuda, S. R. Mukai, and K. Hashimoto, *Carbon* **31**, 783 (1993).
106. T. Masuda, S. R. Mukai, H. Fujikata, Y. Fujikata, and K. Hashimoto, *Mater. Manufacturing Process.* **9**, 237 (1994).
107. S. R. Mukai, T. Masuda, T. Harada, and K. Hashimoto, *Carbon* **38**, 1801 (2000).
108. G. G. Tibbetts and M. P. Balogh, *Carbon* **37**, 241 (1999).
109. Y. A. Kim, T. Matusita, T. Hayashi, M. Endo, and M. S. Dresselhaus, *Carbon* **39**, 1747 (2001).

JAMES A. NEWELL
Rowan University

CASTING. See PLASTICS, PROCESSING.

CELLULAR MATERIALS. See Volume 5.

CELLULOSE. See Volume 5.

CELLULOSE ESTERS, INORGANIC

Introduction

Cellulose (qv) plays an extremely important structural role in nature. Cellulose is a linear polysaccharide comprised of β-1,4-linked cellobiose repeat units (Fig. 1). The three free hydroxyls present on each anhydroglucose unit provide the biopolymer with the ability to form strong structures through hydrogen bonding. This vast network of hydrogen bonds that link the individual polymer chains into more complex structures greatly reduces the solubility of cellulose in conventional organic and aqueous solvents. Derivatization of cellulose as esters and/or ethers modifies the solubility profile of the cellulosic while maintaining many of the polymeric properties of the molecule. Cellulose esters have found numerous commercial applications, including plastics, coatings, and ion-exchange applications. Esters of cellulose can be either inorganic or organic. The focus of this article is on inorganic esters of cellulose. This report covers both the synthesis and the use of inorganic esters of cellulose.

Inorganic esters of cellulose have been known for well over 100 years and are still commercially viable products. Cellulose nitrate, commonly called

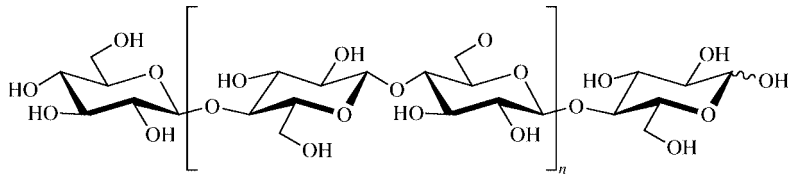

1

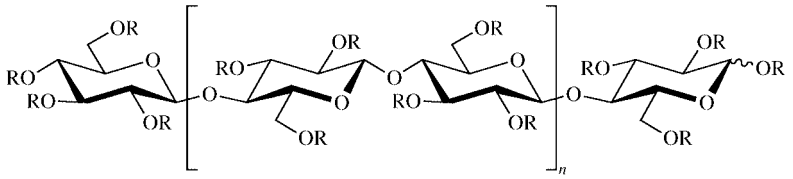

2

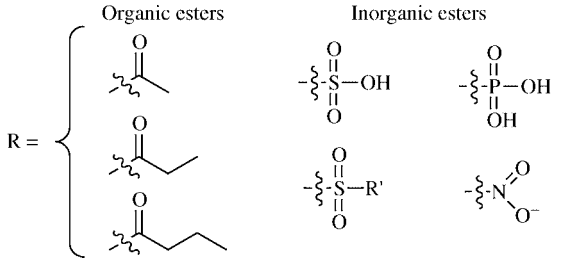

Fig. 1. General structures of cellulose **1** and cellulose esters **2**.

Encyclopedia of Polymer Science and Technology. Copyright John Wiley & Sons, Inc. All rights reserved.

nitrocellulose, is the ester with the most significant historical importance. Cellulose nitrate led to the birth of the plastics industry, the film and motion picture industry, and major improvements in explosives and coatings applications. Additionally, cellulose nitrate played a prominent role in numerous biochemical discoveries, including elucidation of the genetic code.

Because of its historical importance cellulose nitrate has traditionally dominated the content of articles devoted to inorganic esters of cellulose. While not understating the importance of cellulose nitrate, this report emphasizes the value of other inorganic esters of cellulose, including cellulose phosphate, cellulose sulfate, and cellulose sulfonates.

Preparation of Inorganic Esters of Cellulose

Inorganic esters of cellulose include all esters where the atoms linked directly to the cellulosic oxygens are non-carbon, for examples, cellulose nitrate, cellulose sulfate, cellulose sulfonate, and cellulose phosphate.

Nitrogen-Containing Esters of Cellulose.

Cellulose Nitrate. Cellulose nitrate, without question the most commercially important inorganic ester of cellulose, was first prepared in 1833 (1). Schonbein prepared the first stable form of cellulose nitrate in 1846 (2). The preparation of cellulose nitrate, most commonly called nitrocellulose, has been reviewed in the literature numerous times (3,4). Several nitration techniques have been reported for the preparation of cellulose nitrate, including $HNO_3/H_2SO_4/H_2O$, HNO_3 (>75%), N_2O_4 (g), HNO_3/H_3PO_4, $HNO_3/H_3PO_4/P_2O_5$, $HNO_3/Mg(NO_3)_2$, HNO_3/CH_2Cl_2, and $HNO_3/HOAc/Ac_2O$ (5–11). Cellulose nitrate is still manufactured using a mixture of nitric acid, sulfuric acid, and water.

A number of versions of cellulose nitrate are commercially available. Variations in nitrogen content and viscosity are the main differences between nitrocellulose product lines. The amount of water present during the preparation of cellulose nitrate directly influences the final nitrogen content of the product (Fig. 2). The viscosity of the final product is determined by selecting a starting material with the appropriate degree of polymerization and/or by performing a viscosity reduction step following nitration. Cellulose trinitrate has a degree of substitution (DS) of 3 and a nitrogen content of 14.15%. Cellulose dinitrate (DS = 2) and cellulose mononitrate (DS = 1) have nitrogen contents of 11.11 and 6.76%, respectively (12). The maximum DS_N of commercial nitrocellulose is approximately 2.9 (about 13.8% N). The hydroxyl group at C6 is nitrated much faster than those at C2 and C3. The relative rates of nitration of the hydroxyl groups on cellulose are as follows: C6 = 5.8, C2 = 1.8, C3 = 1.0 (13).

Sulfur-Containing Esters of Cellulose. Cellulose sulfate and cellulose sulfonates are examples of sulfur-containing esters of cellulose. The sulfur is linked directly to an oxygen atom contained within an anhydroglucose unit of cellulose (see Fig. 3).

Cellulose Sulfate. Sulfation of cellulose has been accomplished via a number of procedures. Three forms of cellulose sulfate have been described in the literature: surface modified cotton fabric or fibers, water-swellable cellulose sulfate, and

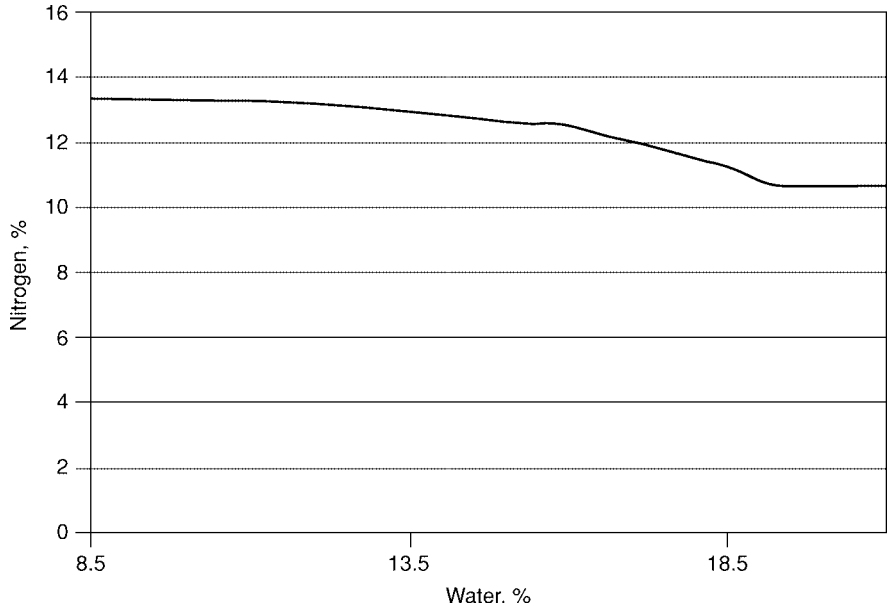

Fig. 2. Influence of water on degree of nitration of cellulose.

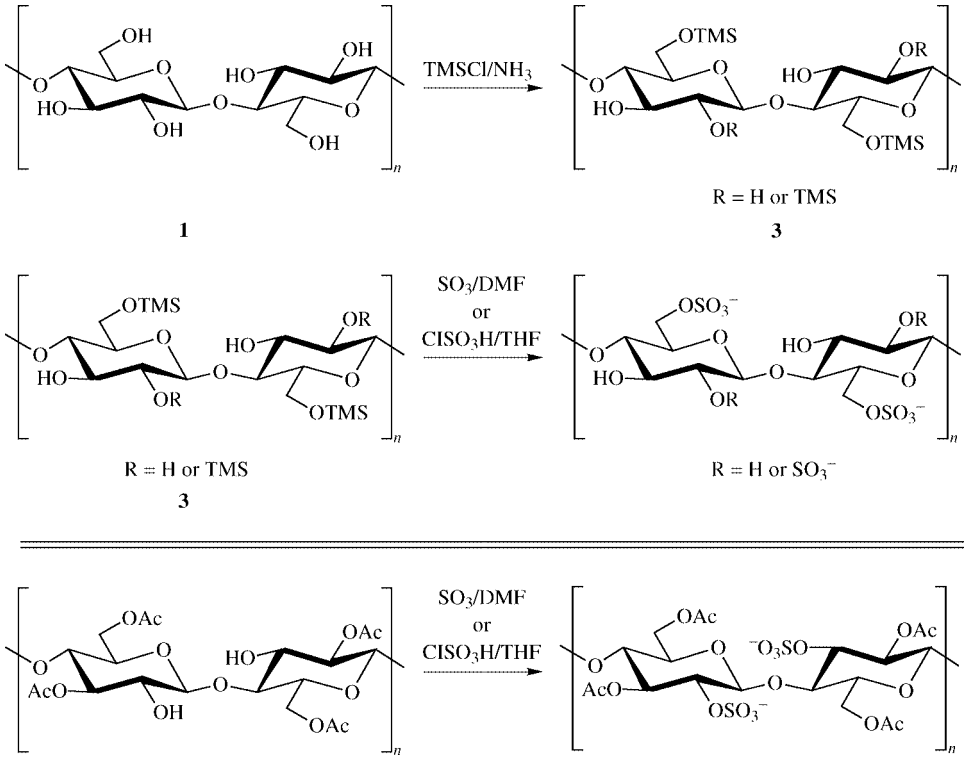

Fig. 3. Synthesis of cellulose sulfate from silylated and acetylated cellulose.

Table 1. Preparation of Cellulose Sulfate Using H_2SO_4

Sulfation system	DS
H_2SO_4	1.0–2
$H_2SO_4 + SO_2$	0.9
H_2SO_4 + chlorinated hydrocarbon	0.3
H_2SO_4 + diethyl ether	0.2–0.4
H_2SO_4 + low aliphatic alcohol	0.05–1
H_2SO_4 + low aliphatic alcohol + inert solvent	0.35–0.7
H_2SO_4 + chlorinated aliphatic alcohol	0.5
$H_2SO_4 + Ac_2O$	0.6–2.8
$H_2SO_4 + Ac_2O$ + HOAc + salt	0.1–0.5
$H_2SO_4 + Ac_2O$ + HOAc + inert solvent	0.3–1.0
$H_2SO_4 + Ac_2O$ + pyridine + dioxane	2
H_2SO_4 + aliphatic carboxylic acid C3-C4	
H_2SO_4 + HOAc + salt	0.3
H_2SO_4 + HOAc + benzene	0.6

water-soluble cellulose sulfate. Sulfation of cellulose is commonly accomplished using sulfuric acid, chlorosulfonic acid, or sulfur trioxide/pyridine (eq. 1).

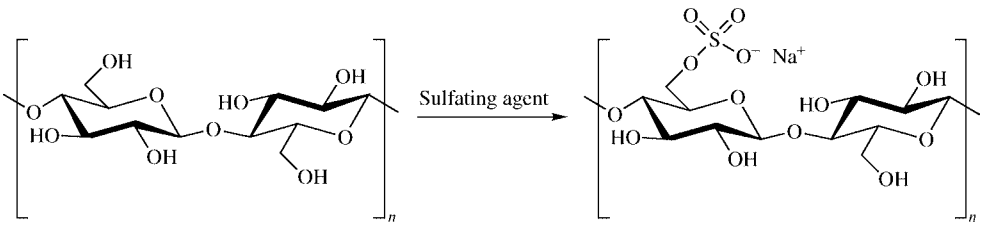

1 3 (1)

Philipp and Wagenknecht compiled a list of 50 sulfation strategies for the preparation of cellulose sulfate (Tables 1–5) (14). The methods described in Tables 1–5 produce cellulose sulfate with various degrees of substitution. A common theme in the synthesis of cellulose esters (both inorganic and organic) is the trade-off between esterification and polymer degradation. Preparation of cellulose sulfate is no exception to this rule. Increasing the temperature during the sulfation

Table 2. Preparation of Cellulose Sulfate Using $ClSO_3H$

Sulfation system	DS
$ClSO_3H$	
$ClSO_3H + SO_2$	1.8
$ClSO_3H$ + chlorinated hydrocarbon	
$ClSO_3H$ + pyridine	1.9–2.8
$ClSO_3H$ + pyridine propanolamine	1.6
$ClSO_3H$ + pyridine + toluene	2.8
$ClSO_3H$ + formamide	2

Table 3. Preparation of Cellulose Sulfate Using SO_3

Sulfation system	DS
SO_3	3
$SO_3 + SO_2$	2.2
$SO_3 + CS_2$	3
SO_3 + chlorinated hydrocarbon	0.5–0.9
SO_3 + diethyl ether	1.3–2.1
SO_3 + DMSO	1.3–2.0
SO_3 + DMF	1.5–2.6
SO_3 + pyridine	
SO_3 + pyridine + various solvents	0.1–2.2
SO_3 + aliphatic amine + DMF + chlorinated hydrocarbon	0.4–2.0
SO_3 + aliphatic amine + pyridine	1.5
SO_3 + triethylphosphate	3
$SO_3 + N_2O_4$ + DMF	0.3–1.1
$SO_3 + N_2O_4$ + DMF + various solvents	<2.0

Table 4. Preparation of Cellulose Sulfate Using SO_2Cl_2

Sulfation system	DS
SO_2Cl_2 + alkali cellulose	
SO_2Cl_2 + benzene + alkali cellulose	
$SO_2Cl_2 + ClCH_2COOH$ + alkali cellulose	
SO_2Cl_2 + DMF, formamide	0.2–0.5
$SO_2Cl_2 + N_2O_4$ + DMF	0.4–0.8

reaction produces a more homogeneous mixture and thus more complete sulfation, but the rate of polysaccharide chain degradation is also rapidly increased. The rate of sulfation for the following sulfating agents is as follows: $H_2SO_4 < SO_3 < SO_2Cl_2 < HSO_3Cl$, with SO_2Cl_2 generating the most chain degradation during sulfation (14). Chlorosulfonic acid is generally considered the most effective sulfation agent with regard to both sulfation and retention of chain length. Excess sulfuric acid

Table 5. Preparation of Cellulose Sulfate Using Miscellaneous Reagents

Sulfation system	DS
$NaSO_3Cl$ + HOAc	
$NaSO_3Cl + Ac_2O$ + HOAc	
$NaSO_3Cl$ + pyridine	
$EtSO_3H$ + pyridine + nitrobenzene	2.8
NH_2SO_3H + urea	
FSO_3H + pyridine	
FSO_3Na + benzene + EtOH + alkali cellulose	
FSO_3NH_4 + benzene + EtOH + alkali cellulose	
Na-acetylsulfate	
$NOSO_4H$ + DMF, DMSO, DMAc	0.7–1.2
$NOSO_4H$ + diethyl ether, various solvents	0.02–0.4

is typically used during sulfation reactions; however, stoichiometric amounts of acetylsulfuric acid can be used to prepare cellulose sulfate (15).

Cellulose sulfates with a wide range of degree of substitution can be water-soluble, for example, cellulose sulfates with DS_S as low as 0.25 can be water-soluble. The solubility of the final product is influenced by the method of preparation. The regioselectivity of sulfation can affect the properties and end uses of cellulose sulfate. A heterogeneous process, a homogeneous process, or a protection–deprotection strategy can be used to regioselectively derivatize cellulose (16). Generally, a bulky substituent is required to achieve reasonable regioselectivity in a heterogeneous process, and so either a homogeneous process or a protection–deprotection strategy is preferred for the preparation of regioselectively substituted cellulose sulfate. Cellulose sulfates can be prepared under homogeneous conditions by first converting cellulose to the trimethylsilyl ethers (17) (Fig. 3). Water-soluble cellulose sulfates were obtained by applying this strategy. The TMS ethers apparently act as reactive intermediates resulting in SO_3-induced sulfation only at sites previously silylated. The free hydroxyls present in the TMS cellulose ($DS_{Si} = 1.5–2.5$) are unreactive during sulfation. When a similar sulfation strategy is applied to cellulose acetates ($DS_{Ac} = 1.8–2.5$), the free hydroxyls are readily sulfated. It has been suggested that the TMS groups effectively shield the unreacted hydroxyl groups, thus preventing sulfation (18). Sulfation of TMS cellulose derivatives with SO_3 or HSO_3Cl in DMF possibly occurs via insertion of SO_3 into the Si—O bond with the sulfate generated by subsequent hydrolysis and neutralization (17,19). Wagenknecht (20) and Mischnick (21) have developed routes to evaluate the substitution pattern of cellulose sulfates.

There are numerous synthetic strategies available for preparing cellulose sulfates with a wide range of properties.

Cellulose Sulfonates. Cellulose sulfonates are inorganic esters of cellulose and sulfonic acids in which there is a sulfur–oxygen bond formed to link the cellulose and sulfonic acid moieties. Figure 4 depicts the three most common cellulose sulfonates described in the literature, cellulose methanesulfonate (mesylate) (**4**), cellulose toluenesulfonate (tosylate) (**5**), and cellulose dansylate (**6**) (22–25). Cellulose tosylate is the most commonly described cellulose sulfonate in the literature. Cellulose sulfonates are typically prepared in a homogeneous process by dissolving cellulose in a dimethylacetamide/lithium chloride (DMAc/LiCl) mixture and reacting the cellulose with sulfonylchloride in the presence of triethylamine (Fig. 5) (25). Cellulose sulfonates can also be prepared *in situ* for use as reactive intermediates (26,27). The use of cellulose tosylate as a reactive intermediate is be discussed in more detail later in this report.

Cellulose deoxysulfonates have been described in the literature, but is not be discussed further in this report (28).

Phosphorus-Containing Esters of Cellulose.

Cellulose Phosphates. There are a number of strategies for preparing cellulose phosphate. Reaction of cellulose with tetrapolyphosphoric acid in the presence of triethylamine produced cellulose phosphate with $DS_P \leq 1.75$ (29). Treatment of cellulose with $POCl_3$ resulted in cellulose phosphate with low DS_P, but also resulted in introduction of chloride to the cellulosic backbone (Table 6) (30). Phosphorylations of cellulose with *N*-phosphoryl-*N*′-methylimidazole and a

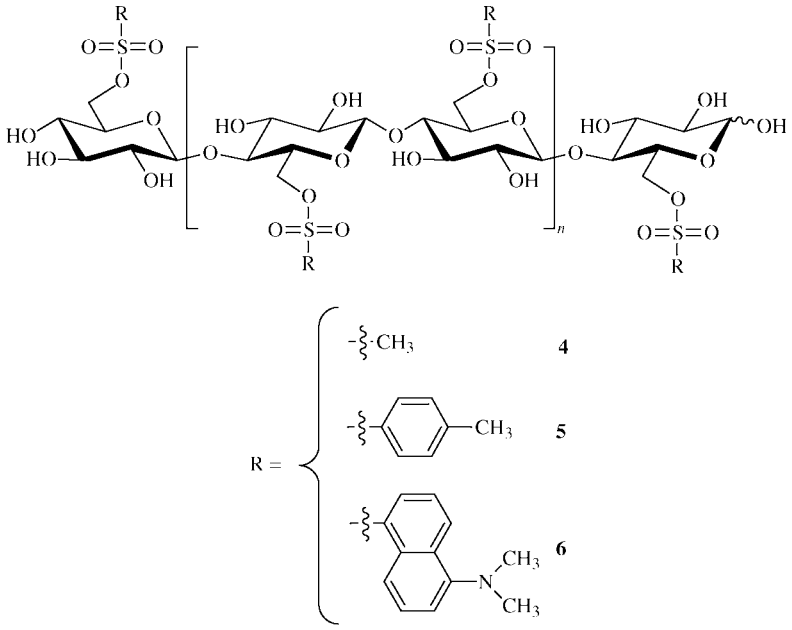

Fig. 4. Structures of cellulose sulfonates.

mixture of phosphorus pentoxide, triethyl phosphate, and phosphoric acid have been reported (Fig. 6) (31,32).

Properties of Inorganic Esters of Cellulose

In general, inorganic esters of cellulose have significantly different solubility profiles than native cellulose. Cellulose has poor solubility in most organic or aqueous systems, while inorganic esters of cellulose are typically more soluble. Inorganic esters of cellulose that are soluble in organic or aqueous solvents are available.

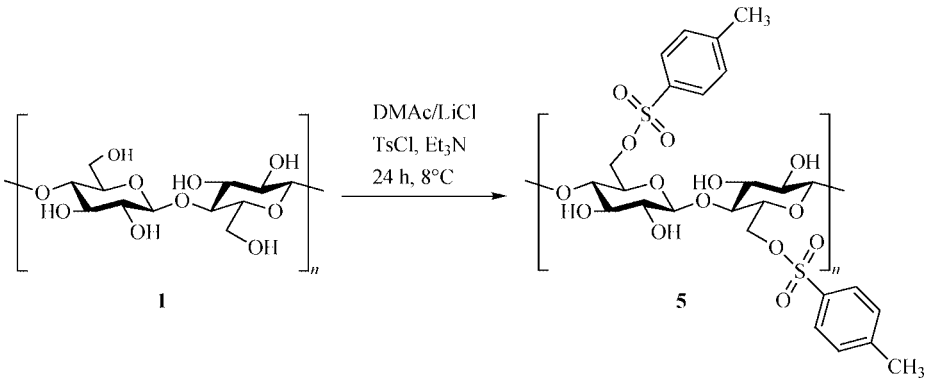

Fig. 5. Homogeneous synthesis of cellulose-6-tosylate.

Table 6. Phosphorylation and Chlorination of Cellulose with $POCl_3$

Reaction Temp.	$POCl_3$, %	DS_P	DS_{Cl}
50	2	0.09	0.02
	4	0.08	0.03
	8	0.03	0.03
75	2	0.19	0.04
	4	0.08	0.08
	8	0.06	0.47
	10	0.08	0.52
	12	0.07	0.55
100	2	0.22	0.04
	4	0.18	0.12
	8	0.20	0.37

The solubility of inorganic esters of cellulose is dependent upon the identity and degree of substitution of the substituents, the number of unreacted free hydroxyls, and the degree of polymerization of the cellulose backbone.

Solubility. Cellulose sulfate and cellulose phosphate can be either water-soluble or water-swellable depending on the conditions used during preparation (*vide supra*). Cellulose nitrate and some cellulose sulfonates are generally more hydrophobic and are typically soluble in organic solvents. In general, the level of esterification of cellulose directly impacts the solubility of the product in various solvents and solvent blends.

Film Formation and Rheology. The ability to form films is the most important property of cellulose nitrate. When cellulose nitrate is dissolved in an organic solvent and then applied to a substrate (eg, wood, metal, glass), a clear

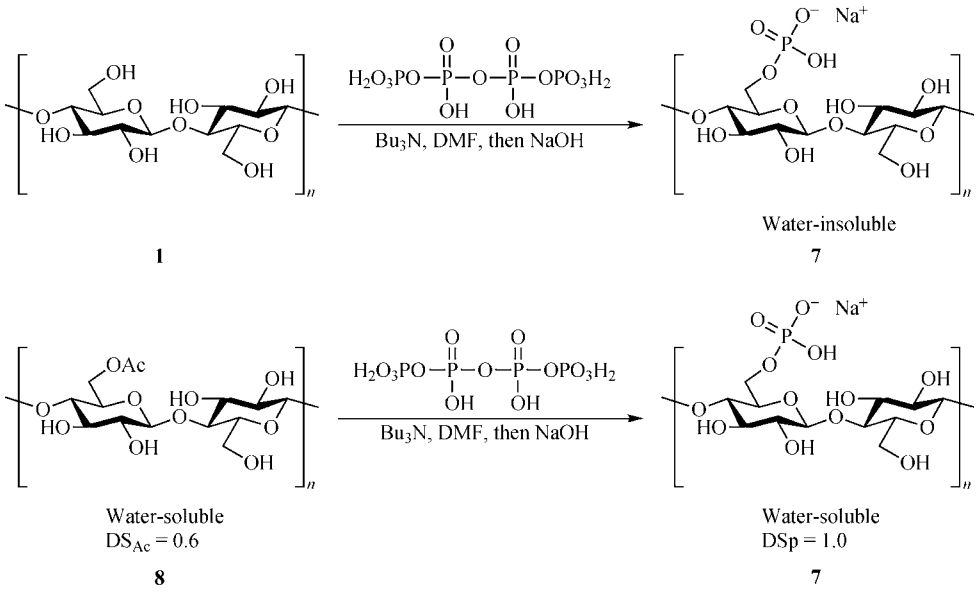

Fig. 6. Synthesis of water-insoluble and water-soluble cellulose phosphate.

film is formed on the substrate once the solvent evaporates. Coatings of this nature are referred to as lacquers. Coatings applications are the largest commercial applications for cellulose nitrate and will be discussed further in the applications section.

Applications of Inorganic Esters of Cellulose

Nitrocellulose is the most commercially important inorganic ester of cellulose. The use of nitrocellulose led to development of the plastics industry, the motion picture industry, and powderless ammunition. In most cases nitrocellulose has been replaced over the years by less expensive or less flammable materials. Although considerable market share for nitrocellulose has been lost to alternate products, nitrocellulose remains a commercially viable product and should be for many years.

Coatings, Adhesives, and Inks. The largest market for cellulose nitrate is in the coatings industry. Relatively clear and workable (ie, sandable or removable) lacquers are generated when cellulose nitrate is used in a coatings application. Cellulose nitrate lacquers dry rapidly, have excellent flow properties, and the final coating has excellent appearance, with reasonable strength and durability. Cellulose nitrate became a commercially viable product in the 1920s and rapidly replaced slower drying varnishes that were used in both automotive and wood coatings (33). Cellulose nitrate has played such a significant role in lacquer coatings applications that cellulose nitrate based lacquers are simply referred to as lacquers and it is assumed that a lacquer is cellulose nitrate based unless stated otherwise. Over time, cellulose nitrate was replaced in automotive topcoats by more durable acrylic lacquers. Cellulose nitrate maintained much of its market share in applications where high temperature curing is not acceptable, for example in wood coatings (33). Cellulose nitrate is still used in some automotive primer refinish applications, but currently its primary use is in wood coatings. Cellulose nitrate provides enhanced wood grain appearance, rapid drying, and easy damage repair to wood coatings. Cellulose nitrate has also been used as an additive to improve the performance, appearance, and drying time of coatings based on other resins, such as acrylics, vinyls, polyamides, epoxies, and polyesters (34). Cellulose nitrate aids in pigment dispersion and acts as a binder following solvent evaporation.

Cellulose nitrate used in coatings applications is commercially available in three general forms based on nitrogen content: SS (10.7–11.3% N), AS (11.3–11.7% N), and RS (11.7–12.2% N) (33). Additionally, each product type is available in low, medium, and high viscosity grades. According to product literature from ICI Nobel Enterprises (Scotland, UK), low and medium nitrogen grades are typically used in ink applications. Medium nitrogen content is used for film coatings. High nitrogen content cellulose nitrate is commonly used in wood coatings, general-purpose lacquers, and automotive refinish applications. Cellulose nitrate-based lacquers have many advantages over other coatings. They are easily applied, have good adhesion, good solvent release properties, and excellent pigment dispersion. The problems with nitrocellulose lacquers include yellowing, flammability, and that they must be sprayed at low solids levels. Nitrocellulose based lacquers found

use in cloth book bindings (34). Nitrocellulose is also used in adhesives and inks (34,35).

Explosives. Cellulose nitrate with a nitrogen content of 12.3–13.5% N ($DS_N = 2.25–2.5$) is used in explosive and propellant applications. Cellulose nitrate was initially developed for use in explosives and propellants and this remains one of the largest markets for cellulose nitrate today.

Plastics. In 1847 it was discovered that cellulose nitrate could be dissolved in a mixture of ether and alcohol to produce a solution called collodion. Collodion is still in use today in pharmaceutical applications. Combination of nitrocellulose with castor oil and eventually camphor by Parkes (1862) and Hyatt (1870) led to the production of celluloid and ultimately the birth of the plastics industry.

Flame Retardants. Flame-retardant cotton fibers are prepared by surface modification of cotton cellulose via phosphorylation or phosphorylation/halogenation, producing cellulose phosphate and deoxychlorocellulose phosphate, respectively. Surface modification of cotton fibers generates flame-retardant fabrics by increasing the char content of the fiber. This in turn produces a lower percentage of flammable volatiles. Since the phosphorylated/halogenated fibers break down to produce acidic products, the overall thermal stability of the fabric is greatly reduced, and the material breaks down at a lower temperature and ultimately reduces the potential of the fabric bursting into flames (36).

Ion-Exchange Separations. Inorganic esters of cellulose have been used in ion-exchange applications and as chromatographic adsorbents since the late 1950s (37). Cellulose sulfate and cellulose phosphate are excellent ion exchangers. Exposure of the ester to a salt of a metal ion (eg NaCl, KCl) or neutralization of the acid with a base (eg NaOH, KOH) will result in exchange of the metal ion from the salt or base onto the sulfate or phosphate attached to the cellulose backbone (Fig. 7).

Cellulose phosphate is the most widely used cellulose inorganic ester for ion exchange. Cellulose phosphate is an effective cation-exchanger used in the bioprocessing industry (38). Cellulose phosphate and cellulose polyphosphate effectively remove Al^{3+} contamination from ATP (39). A number of products are commercially available, most notably from Whatman, for use as stationary phases in column chromatography and filtration applications. Whatman P1, P11, and P81 are examples of commercially available cellulose phosphate based ion exchangers.

The ion exchange nature of cellulose sulfate resulted in its use to concentrate viruses (40).

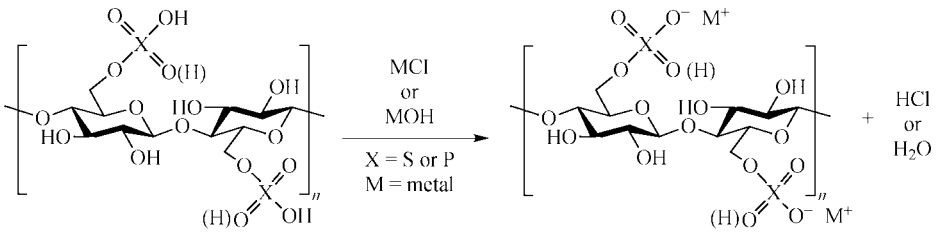

Fig. 7. Use of cellulose phosphate and cellulose sulfate as ion exchangers.

Membrane Applications. Cellulose esters are effective in membrane applications. Ultrafiltration membranes based on cellulose nitrate were first described by Collander in 1924 (41). Cellulose nitrate films cast from mixtures of methyl acetate or acetone with glycerol and mixtures of ether and ethanol produce microfiltration and ultrafiltration membranes, respectively (42). Cellulose nitrate microfiltration membranes typically have 0.02–10 μm diameter pores and 4×10^{-3} – 15 $cm^3/cm^2 \cdot s \cdot atm$ permeability. Cellulose nitrate ultrafiltration membranes typically have 0.003–0.03 μm diameter pores and $(1–100) \times 10^{-4}$ $cm^3/cm^2 \cdot s \cdot atm$ permeability (42). Nitrocellulose membranes are used in numerous biochemical and diagnostic applications and is discussed later.

Cellulose sulfate, in particular C6 sulfates, can be used for preparing polyanion–polycation complexes for pervaporation membranes (43–45).

Synthetic Intermediates. Cellulose sulfonates have been evaluated as synthetic intermediates (27,46–49). Cellulose tosylate activates the C6 hydroxyl for substitution with various nucleophiles (eq. 2 where Nu = Cl^-, N_3^-, $NH_2{-}(CH_2)_m{-}NH_2$, or other nucleophiles).

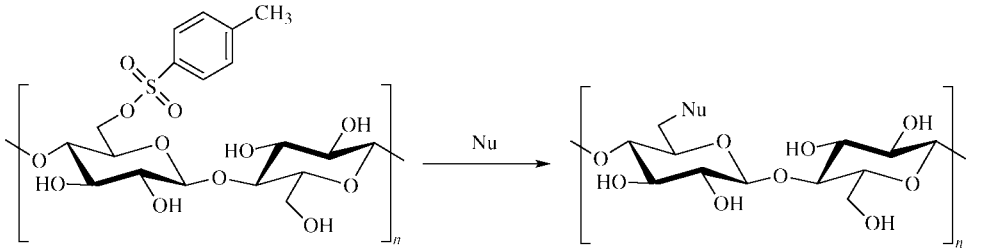

(2)

Additionally, cellulose sulfonates can also function as a protecting group to prevent reaction of the C6 hydroxyl during esterification reactions (Fig. 8). Cellulose tosylates with degrees of substitution from 0.38 to 2.30 have been reported. Although an effective synthetic tool, the expense of organic solvents utilized and the cost and corrosive nature of tosyl chloride have limited the use of this methodology on a commercial scale.

Medical Applications. Inorganic esters of cellulose have been evaluated in a number of medical/pharmaceutical applications. A few examples include treatment of hypercalciura, use as antiviral agents, reduction of cholesterol levels, orthopedic applications, and blood stabilization.

Sodium cellulose phosphate is used in the treatment of adsorptive hypercalciura and nephrocalcinosis (both a common cause of kidney stones). The ability of inorganic esters of cellulose to function as ion exchangers, described previously, is the key to the use of sodium cellulose phosphate in the treatment of adsorptive hypercalciuria. Hypercalciuria is an increased level of calcium in a patient's urine. This disorder commonly results in painful kidney stones. Sodium cellulose phosphate has been used to complex the calcium ions and thus remove them from the patient and minimize the risk of stone formation (50–54).

It is well established that sulfated polysaccharides play important biological roles (55–63). Cellulose sulfate displays heparin-like activity and to a lesser

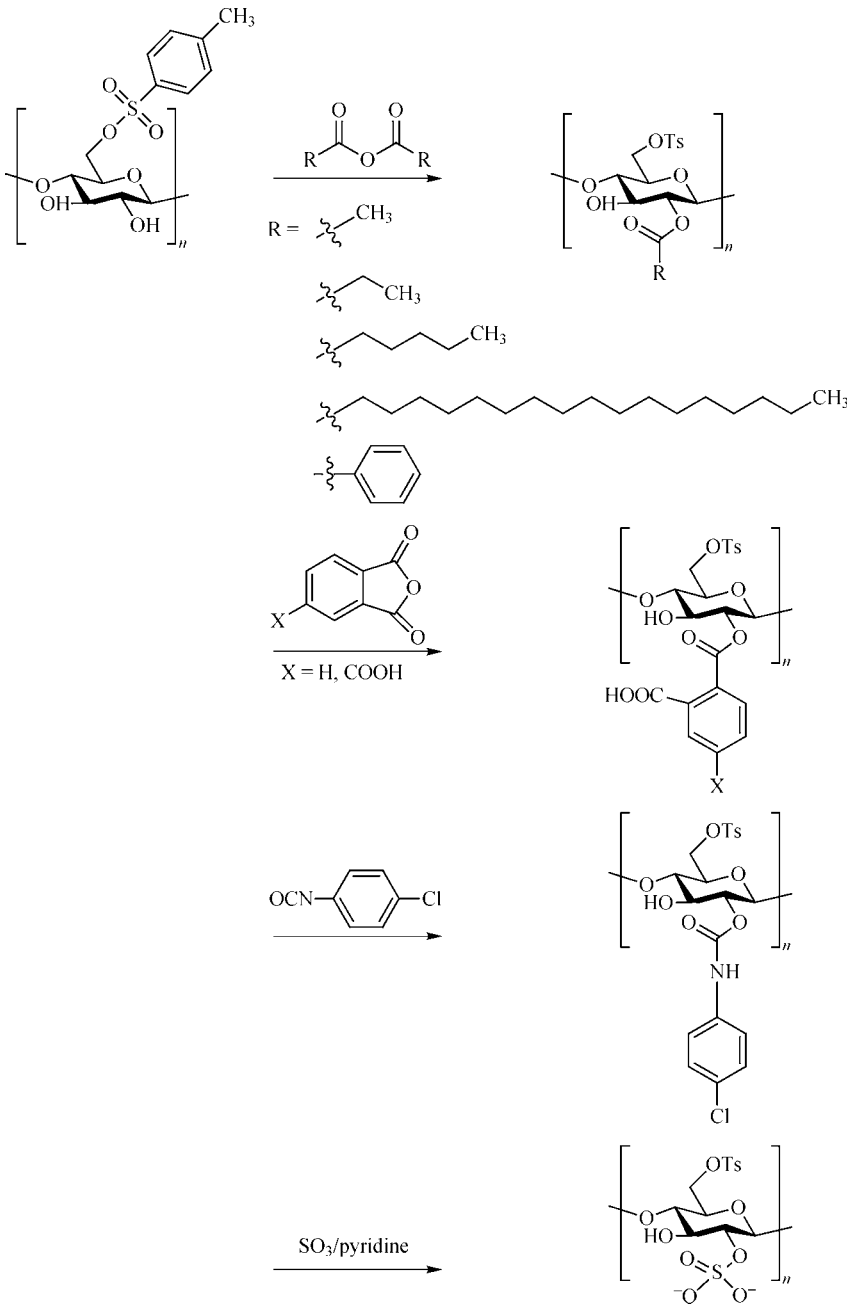

Fig. 8. Subsequent chemical modification of cellulose tosylate.

extent antiviral activity (64). More specifically, cellulose sulfates with a medium to high degree of sulfation at the C2 and C6 positions of the anhydroglucose units are the most active forms of the ester. High molecular weight cellulose sulfate lowers cholesterol levels in humans by inhibiting pancreatic cholesterol esterase

(65,66). Contamination of high molecular weight cellulose sulfate with its low molecular weight counterpart results in a toxic, unusable product. A method to prepare and isolate high molecular weight cellulose sulfate without contamination with low molecular weight cellulose sulfate has been developed (65). Ushercell (a commercial form of sodium cellulose sulfate marketed by Polydex Pharmaceuticals) has been evaluated in the treatment of papilloma virus infection (67). Usher and co-workers have also investigated the use of sodium cellulose sulfate as an antimicrobial agent and a contraceptive (68). Cellulose sulfate with a DS $>$ 1.0 and sodium cellulose sulfate when complexed with (β-hydroxy-γ-trimethylaminopropyl)hydroxyethyl cellulose chloride show excellent anticoagulative property (69,70).

Encapsulation of microorganisms, enzymes, plant cells, and animal cells (including mammalian cells) has been accomplished using a mixture of sodium cellulose sulfate with polydiallyldimethyl ammonium chloride (71,72). Encapsulation of hydridoma cells with cellulose sulfate has provided a means of subcutaneous delivery of monoclonal antibodies. The implant vascularized as early as 15 days after implantation and the "neoorgan" remained an active source of antibodies in mice for several months (73).

Cellulose phosphate has been evaluated in femoral implants to improve the mineralization of biomaterials used in orthopedic applications (74). Cellulose phosphate (with or without bound antimicrobial agents) and cellulose phosphate borate effectively stabilize blood for over 4 years (75).

Biochemical Applications. Cellulose phosphate paper (P81), also called phosphocellulose paper, has been used for enzyme assay applications (76). As with many other applications of cellulose phosphate, the ability of the material to act as an ion exchanger is the key property that leads to its use in enzyme assays. Cellulose phosphate paper quantitatively binds small peptides that contain at least two basic residues and a free amino terminus. This allows for protein kinase assays to be performed and ^{32}P-labeled cofactors [γ-^{32}P]ATP and nonpeptidic byproducts [^{32}P]Pi to be washed away (77).

Even though a number of applications have been demonstrated for cellulose phosphate in the biotechnology laboratory, the use of cellulose nitrate dominates the field. Cellulose nitrate filters and membranes have played key roles in numerous biochemistry and molecular biology discoveries and still play important roles in these laboratories today. Protein and glycoprotein immobilization, absorption of single-stranded DNA (Southern blotting), absorption of single-stranded RNA (Northern blotting), binding of transfer RNA linked to ribosomes, tissue printing, and dialysis are common practices accomplished through the use of nitrocellulose membranes or filters (78–83). The binding of ribosomes and tRNAs to nitrocellulose was used to elucidate the genetic code. Cellulose nitrate is an efficient binder of antibodies and can be used as a solid support for immunoaffinity chromatography (84).

Diagnostic Applications. The binding characteristics of cellulose nitrate membranes have led to their use in numerous biosensor applications, such as in an electrochemical microbial biosensor for EtOH (85) and in glucose oxidase based glucose sensors (86). Cellulose nitrate continues to play an important role in the development of new biosensors as both a solid support and a method for removal of unbound reagents (87–93).

Additionally, cellulose nitrate has been utilized in nonbiological detectors including an indoor radon gas detector. The cellulose nitrate portion of the film-based detector is the active portion for the detection of α-particles (94).

Conclusion

Inorganic esters of cellulose have a valuable place in history, from the birth of the plastics industry to elucidation of the genetic code. It is important not to forget the large number of applications in which these materials have played a role: coatings, explosives, pharmaceuticals, membranes, and synthetic intermediates. Although inorganic esters of cellulose have been around for over 100 years, these materials remain important tools for coatings scientists, explosives experts, and biochemists.

BIBLIOGRAPHY

"Cellulose Esters, Inorganic" in *EPST* 1st ed., Vol. 3, pp. 307–325, by G. N. Bruxelles and V. R. Grassie, Hercules Powder Co.; "Cellulose Esters, Inorganic" in *EPSE* 2nd ed., Vol. 3, pp. 139–157, by R. J. Brewer and R. T. Brogan, Eastman Kodak Co.

1. H. Braconnot, *Ann. Pharm.* **7**, 242 (1833).
2. C. F. Schönbein, *Philos. Mag.* **31**, 7 (1847).
3. R. T. Bogan, C. M. Kuo, and R. J. Brewer, *Kirk-Othmer Encyclopedia of Chemical Technology*, John Wiley & Sons, Inc., New York, 1979, p. 118.
4. R. J. Brewer and R. T. Bogan, *Encyclopedia of Polymer Science and Engineering*, Vol. 2, Wiley-Interscience, New York, 1998, p. 139.
5. Can. Pat. 536,191 (Jan. 22, 1957), W. C. Ramsey (to Olin Mathieson Chemical Corp.).
6. U.S. Pat. 2,776,965 (Jan. 8, 1957), J. L. Bennett, R. M. Brooks, J. G. McMillan, and W. L. Plunkett (to Hercules Powder Co.).
7. U.S. Pat. 3,063,981 (Nov. 13, 1962), J. D. Cochrane III and D. S. Wilt (to Hercules Powder Co.).
8. C. Bennett and T. Timell, *Svensk Paperstidn.* **58**, 281 (1955).
9. D. Goring and T. Timell, *Tappi* **45**, 454 (1962).
10. K. Thinius and W. Tummler, *Makromol. Chem.* **99**, 117 (1966).
11. M. Marx-Figini, *Makromol. Chem.* **50**, 196 (1961).
12. C. W. Saunders and L. T. Taylor, *J. Energ. Mater.* **8**(3), 149 (1990).
13. T. K. Wu, *Macromolecules* **13**, 74 (1980).
14. B. Philipp and W. Wagenknecht, *Cellul. Chem. Technol.* **17**, 443 (1983).
15. U.S. Pat. 4,480,091 (Oct. 30, 1984), R. J. Brewer (to Eastman Kodak Co.).
16. B. Philipp, W. Wagenknecht, I. Nehls, D. Klemm, A. Stein, and T. Heinze, *Polym. News* **21**, 155 (1996).
17. W. Wageknecht, I. Nehls, A. Stein, D. Klemm, and B. Philipp, *Acta Polym.* **43**, 266 (1992).
18. B. Philipp, D. Klemm, and U. Heinze, *Polym. News* **24**, 305 (1999).
19. D. Klemm, T. Heinze, B. Philipp, and W. Wagenknecht, *Acta Polym.* **48**, 277 (1997).
20. B. Saake and W. Wagenknecht, *Carbohydr. Polym.* **48**, 7 (2002).
21. M. Gohdes and P. Mischnick, *Carbohydr. Res.* **309**, 109 (1998).
22. T. Heinze and K. Rahn, *Macromol. Symp.* **120**, 103 (1997).
23. M. Sakamoto, Y. Yamada, N. Ojima, and H. Tonami, *J. Appl. Polym. Sci.* **16**, 1495 (1972).
24. K. Rahn, M. Diamantoglou, D. Klemm, H. Berghmans, and T. Heinze, *Angew. Makromol. Chem.* **238**, 143 (1996).

25. T. Heinze and K. Rahn, *J. Pulp. Pap. Sci.* **25**(4), 136 (1999).
26. T. Heinze, K. Rahn, M. Jaspers, and H. Berghmans, *Macromol. Chem. Phys.* **197**, 4207 (1996).
27. A. Koschella and T. Heinze, *Macromol. Biosci.* **1**, 178 (2001).
28. K. I. Furuhata and H. Ikeda, *React. Funct. Polym.* **42**, 103 (1999).
29. G. A. Towle and R. L. Whistler, *Methods Carbohydr. Chem.* **6**, 408 (1972).
30. T. L. Vigo and C. M. Welch, *Carbohydr. Res.* **32**, 331 (1974).
31. H. Takaku, Y. Shimada, and K. Aoshima, *Chem. Pharm. Bull.* **21**, 2068 (1973).
32. P. L. Granja, L. Pouysegu, M. Petraud, B. De Jeso, C. Baquey, and M. A. Barbosa, *J. Appl. Polym. Sci.* **82**, 3341 (2001).
33. E. C. Hamilton and L. W. Early, *Federation Series on Coatings Technology* **Unit 21**, 3 (1973).
34. R. A. Weidener, *Treatise Adhes. Adhesn.* **2**, 429 (1969).
35. PCT Int. Appl. WO 01/90221 (Nov. 29, 2001), G. E. Miller Jr. (to Arizona Chemical Co.).
36. R. K. Jain, K. Lal, and H. L. Bhatnagar, *J. Appl. Polym. Sci.* **33**, 247 (1987).
37. N. Kabay, M. Demircioglu, S. Yayli, M. Yuksel, M. Saglam, and P. R. Levison, *Sep. Sci. Technol.* **34**, 41 (1999).
38. J. M. Ward, L. J. Wallace, D. Cowan, P. Shadbolt, and P. R. Levison, *Anal. Chim. Acta* **249**, 195 (1991).
39. J. V. Schloss, G. Smith, A. Aulabaugh, and W. W. Cleland, *Anal. Biochem.* **120**, 176 (1982).
40. K. Tamayose, Y. Hirai, and T. Shimada, *Hum. Gene Ther.* **7**, 507 (1996).
41. R. Collander, *Soc. Sci. Fennica, Commentationes Biol.* **2**, 1 (1926).
42. W. Pusch, *Wood Cellul.* 475 (1987).
43. DE 4229530 (Sept. 08, 1992), M. Aderhold, R. D. Behling, K. V. Peinemann, N. Scharnagel, H. H. Schwarz, D. Paul, K. Richau, R. Apostel, and G. Frigge (to GKSS-Forschungszentrum Geesthacht GmbH).
44. DE 4435180 (Sept. 30, 1994), W. Wagenknecht and H. H. Schwarz (to Fraunhofer-Gesellschaft zur Foerderung der Angewenten Forschung e.V. and GKSS-Forschungszentrum Geesthacht GmbH).
45. DE 4437869 (May 02, 1995), H. H. Schwarz, K. Richau, R. Apostel, and G. Frigge (to GKSS-Forschungszentrum Geesthacht GmbH).
46. T. Heinze, *J. Appl. Polym. Sci.* **60**, 1891 (1996).
47. T. Heinze and K. Rahn, *Papier (Darmstadt)* **50**, 721 (1996).
48. G. Siegmund, and D. Klemm, *Polym. News* **27**(3), 84 (2002).
49. P. Berlin, D. Klemm, J. Tiller, and R. Rieseler, *Macromol. Chem. Phys.* **201**, 2070 (2000).
50. R. Hautmann, R. J. Hering, and W. Lutzeyer, *J. Urol.* **120**, 712 (1978).
51. C. Y. Pak, *J. Clin. Pharm.* **9**, 451 (1979).
52. A. Dwarakanathan and W. G. Ryan, *Bone Miner.* **2**, 333 (1987).
53. Y. Mizusawa and J. R. Burke, *J. Ped. Child Health* **32**, 350 (1996).
54. U. Backman, B. G. Danielson, G. Johansson, S. Ljunghall, and B. Wilkstrom, *J. Urol.* **123**, 9 (1980).
55. R. Sasisekharan, Z. Shriver, G. Venkataraman, and U. Narayanasami, *Nat. Rev. Cancer* **2**, 521 (2002).
56. PCT Int. Appl. WO 02/41901 (May 30, 2002), D. Cullis-Hill (to Arthropharm Pty Ltd. and Cullis-Hill, David).
57. A. Chaidedgumjorn, H. Toyoda, E. R. Woo, K. B. Lee, Y. S. Kim, J. Toida, and T. Imanari, *Carbohydr. Res.* **337**, 925 (2002).
58. C. Fukuda, O. Kollmar, T. Schafer, Y. H. Tian, and M. K. Schilling, *Transpl. Int.* **15**(1), 17 (2002).
59. U.S. Pat. 6,372,794 (Apr. 16, 2002), M. E. Nimni.

60. PCT Int. Appl. WO 02/08295 (Jan. 31, 2002), J. Diaz, C. Pecquet, E. Perrin, and C. Viskov (to Aventis Pharma SA).
61. PCT Int. Appl. WO 02/02189 (Jan. 10, 2002), T. C. Usher, R. A. Anderson, and L. J. D. Zaneveld (to Polydex Pharmaceuticals Ltd. and Rush-Presbyterian-St. Luke's Medical Center).
62. K. Moelling, T. Schulze, and H. Diringer, *J. Virol.* **63**, 5489 (1989).
63. PCT Int. Appl. WO 9630027 (Oct. 3, 1996), S. N. Anderson, J. P. Schaller, T. B. Mazer, and S. J. Kirchner (to Abbott Laboratories).
64. I. Yamamoto, K. Takayama, K. Honma, T. Gonda, K. Matsuzaki, K. Hatanaka, T. Uryu, O. Yoshida, H. Nakeshima, N. Yamamoto, Y. Kaneko, and T. Mimura, *Carbohydr. Polym.* **14**, 53 (1991).
65. Eur. Pat. 0 712 864 (Oct. 13, 1996), L. G. Lange III, C. A. Spilburg, and D. T. Rearden (to CV Therapeutics, Inc.).
66. U.S. Pat. 5,378,828 (Sept. 2, 1993), T. C. Usher, N. Patel, and C. G. Tele (to Dextran Products Ltd.).
67. WO 02/02189 (Jan. 10, 2002), T. C. Usher, R. A. Anderson, and L. J. D. Zaneveld (to Polydex Pharmaceuticals Ltd. and Rush-Presbyterian-St. Luke's Medical Center).
68. WO 9712621 (Sept. 27, 1997), R. A. Anderson, L. J. D. Zaneveld, N. Patel, and T. C. Usher (to Novadex Pharmaceuticals and Rush-Presbyterian-St. Luke's Medical Center).
69. T. Groth and W. Wagneknecht, *Biomaterials* **22**, 2719 (2001).
70. U.S. Pat. 4,708,951 (Nov. 24, 1987), H. Inagaki, T. Miyamoto, H. Ito, and T. Shibata (to Daicel Chemical Industries, Ltd.).
71. H. Dautzenberg, U. Schuldt, G. Grasnick, P. Karle, P. Muller, M. Lohr, M. Pelegrin, M. Piechaczyk, K. V. Rombs, W. H. Gunzburg, B. Salmons, and R. M. Saller, *Ann. N.Y. Acad. Sci.* **875**, 46 (1999).
72. S. Yao, *Chem. Eng. J.* **78**, 199 (2000).
73. M. Pelegrin, M. Marin, D. Noel, M. del Rio, R. Saller, J. Stange, S. Mitzner, W. H. Gunzburg, and M. Piechaczyk, *Gene Ther.* **5**, 828 (1998).
74. P. L. Granja, M. A. Barbosa, C. Pouysegu, B. De Jeso, F. Rouais, and C. Bacquey, *J. Mater. Sci.* **36**, 2163 (2001).
75. T. J. M. Sinha and P. Vasudevan, *Biomater. Med. Devices Artif. Organs* **12**, 273 (1985).
76. M. J. King and R. K. Sharma, *Anal. Biochem.* **199**, 149 (1991).
77. J. E. Casnellie, *Methods Enzymol.* **200**, 115 (1991).
78. M. Schärfke, H. Baumeister, and W. Meyerhof, *BioTechniques* **30**, 266 (2001).
79. D. J. Thornton, I. Carlstedt, and J. K. Sheehan, *Methods Mol. Biol.* **32**, 119 (1994).
80. A. P. Nygaard and B. D. Hall, *Biochem. Biophys. Res. Commun.* **12**, 98 (1963).
81. B. D. Hall, L. Haarr, and K. Kleppe, *Trends Biochem. Sci.* **28**, 254 (1980).
82. D. Voet and J. G. Voet, *Biochemistry*, 2nd ed., John Wiley & Sons, Inc., New York, 1995.
83. R. Taylor, *Methods Plant Electron Microsc. Cytochem.* 101 (2000).
84. J. Thalhamer, P. Hammerl, and A. Hartl, *Methods Mol. Biol.* **147**, 89 (2000).
85. S. Subrahmanyam, K. Shanmugam, T. V. Subramanian, M. Murugesan, V. M. Madhar, and D. Jeyakumar, *Electoroanalysis* **13**, 944 (2001).
86. G. Cui, J. H. Yoo, J. Yoo, S. W. Lee, H. Nam, and G. S. Cha, *Electroanalysis* **13**, 224 (2001).
87. R. Graf and P. Friedl, *Electrophoresis* **22**, 890 (2001).
88. WO 01/03721 (Jan. 18, 2001), G. Cullen (to Merlin Biomedical & Pharmaceutical, Ltd.).
89. WO 01/11363 (Feb. 15, 2001), J. Carlsson and M. Lonnberg (to Pharmacia Diagnostics AB).
90. WO 01/46464 (June 28, 2001), M. Huber, W. Schmidt, M. Muller, and R. Hiller (to Lion Bioscience AG).
91. WO 01/44813 (June 21, 2001), R. M. Kaylor, A. B. Choi, M. H. H. Grunze, and C. D. Chidebelu-Eze (to Kimberly-Clark Worldwide, Inc.).

92. WO 01/81921 (Nov. 1, 2001), R. M. Kaylor, C. D. Chidebelu-Eze, and A. B. Choi (to Kimberly-Clark Worldwide, Inc.).
93. U.S. Pat. 6,221,678 (April 24, 2001), H. M. Chandler.
94. G. Jonsson, *Nucl. Tracks Radiat. Meas.* **13**(1), 85 (1987).

MICHAEL C. SHELTON
Eastman Chemical Company

CELLULOSE ESTERS, ORGANIC

Introduction

Cellulose (qv) is one of nature's most abundant structural materials, providing the primary framework of most plants. For industrial purposes cellulose is derived from two primary sources, cotton linters and wood pulp. Linters are derived from the machine by the same name used for removing the short fibers adhering to cotton seeds after ginning and consist essentially of pure cellulose (see COTTON). Wood, on the other hand, contains 40–60% cellulose, which must be extracted by the chemical degradation of the wood structure.

The chemical structure of cellulose is relatively simple (Fig. 1). The simplicity lies in the repetitive utilization of the anhydroglucose unit $C_6H_{10}O_5$ as the building block for chain structure. The term *cellulose* does not designate a specific chemical or homogeneous substance but serves to characterize the homologous series of compounds having specifically a (1→4) β (diequatorial) linkage between each anhydroglucose unit. Many other polyglucoside structural isomers exist (Fig. 2), but few have achieved the widespread commercial applications of cellulose. Thus two samples of cellulose contain the same relative amounts of carbon, hydrogen, and oxygen, but may vary considerably in chemical reactivity and physical properties. Molecular weight and, consequently, the number of anhydroglucose units per molecule or degree of polymerization (DP) vary as a function of the type of cellulose. Molecular weight determinations by the ultracentrifuge method have assigned a molecular weight average of 570,000 to native cellulose. In the synthesis of cellulose derivatives, however, chain cleavage determines the molecular weight of the product and, hence, many of the observed physical properties.

Cellulose esters are commonly derived from natural cellulose by reaction with organic acids, anhydrides, or acid chlorides. Cellulose esters of almost any organic acid can be prepared, but because of practical limitations esters of acids containing more than four carbon atoms have not achieved commercial significance.

Cellulose acetate [9004-35-7] is the most important organic ester because of its broad application in fibers and plastics; it is prepared in multi-ton quantities with degrees of substitution (DS) ranging from that of hydrolyzed, water-soluble

Encyclopedia of Polymer Science and Technology. Copyright John Wiley & Sons, Inc. All rights reserved.

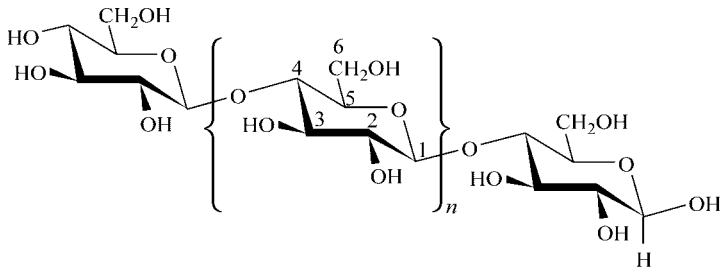

Fig. 1. Structure of natural cellulose $C_6H_{12}O_6$.

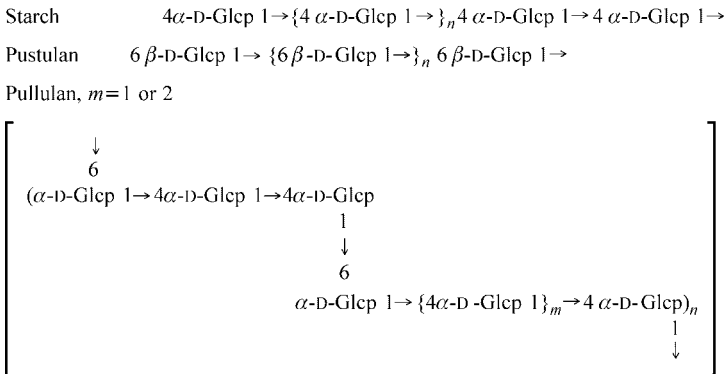

Fig. 2. Structural isomers of cellulose.

monoacetates to those of fully substituted triacetate (Table 1). Soluble cellulose acetate was first prepared in 1865 by heating cotton and acetic anhydride at 180°C (1). Using sulfuric acid as a catalyst permitted preparation at lower temperatures (2), and later, partial hydrolysis of the triacetate gave an acetone-soluble cellulose acetate (3). The solubility of partially hydrolyzed (secondary) cellulose acetate in

Table 1. Relationship of Cellulose Acetate DS to Acetyl Content and Combined Acetic Acid

DS[a]	Acetyl, wt%[b]	Combined acetic acid, wt%[c]
0.5	11.7	16.3
0.75	16.7	23.2
1.0	21.1	29.4
1.5	28.7	40.0
2.0	35.0	48.8
2.5	40.3	56.2
3.0	44.8	62.5

[a] Defined as the average number of acetyl groups in the anhydroglucose unit of cellulose.
[b] Unit molecular weight of acetyl group CH_3CO is 43.
[c] Degree of acetylation is often expressed as percent combined acetic acid.

less expensive and less toxic solvents, such as acetone, aided substantially in its subsequent commercial development.

During World War I, cellulose acetate replaced the highly flammable cellulose nitrate coating on airplane wings and the fuselage fabrics. After World War I, it found extensive use in photographic and X-ray films, spun fibers, and molding plastics.

Although cellulose acetate remains the most widely used organic ester of cellulose, its usefulness is restricted by its moisture sensitivity, limited compatibility with other synthetic resins, and relatively high processing temperature. Cellulose esters of higher aliphatic acids, C_3 and C_4, circumvent these shortcomings with varying degrees of success. They can be prepared relatively easily with procedures similar to those used for cellulose acetate. Mixed cellulose esters containing acetate and either the propionate or butyrate moieties are produced commercially in large quantities by Eastman Chemical Co. in the United States. In mid-1987, Bayer AG discontinued the production of mixed esters at Leverkusen in Germany, citing poor economics as the reason for the closing.

Cellulose esters of aromatic acids, aliphatic acids containing more than four carbon atoms, and aliphatic diacids are difficult and expensive to prepare because of the poor reactivity of the corresponding anhydrides with cellulose; little commercial interest has been shown in these esters. Of notable exception, however, is the interest in the mixed esters of cellulose succinates, prepared by the sodium acetate catalyzed reaction of cellulose with succinic anhydride. The additional expense incurred in manufacturing succinate esters is compensated by the improved film properties observed in waterborne coatings (4).

Mixed cellulose esters containing the dicarboxylate moiety, eg, cellulose acetate phthalate, have commercially useful properties such as alkaline solubility and excellent film-forming characteristics. These esters can be prepared by the reaction of hydrolyzed cellulose acetate with a dicarboxylic anhydride in a pyridine or, preferably, an acetic acid solvent with sodium acetate catalyst. Cellulose acetate phthalate [9004-38-0] for pharmaceutical and photographic uses is produced commercially via the acetic acid–sodium acetate method.

Properties

The properties of cellulose esters are affected by the number of acyl groups per anhydroglucose unit, acyl chain length, and the degree of polymerization (DP) (molecular weight). The properties of some typical cellulose triesters are given in Table 2. In this series, with increasing acyl chain length from C_2 to C_6, the melting point, tensile strength, mechanical strength, and density generally decrease, whereas solubilities in nonpolar solvents and resistance to moisture increase. Fewer acyl groups per anhydroglucose unit, ie, increased hydroxyl content, increase the solubility in polar solvents and decrease moisture resistance. The physical and chemical properties of mixed esters vary according to the ratio of the esters used, eg, acetyl to butyl or acetyl to propionyl. General trends of the properties of mixed esters, such as cellulose acetate butyrate [9004-36-8] (CAB), as a function of composition are illustrated in Figure 3, in which increasing butyryl (decreasing

Table 2. Properties of Cellulose Triesters[a]

Cellulose ester	Shrinking point, °C	mp[b], °C	Water tolerance value[c]	Moisture regain[d],%			Density, g/mL	Tensile strength, MPa[e]
				50% rh	75% rh	95% rh		
Cellulose[f]				10.8	15.5	30.5	1.52	
Acetate		306	54.4	2.0	3.8	7.8	1.28	71.6
Propionate	229	234	26.9	0.5	1.5	2.4	1.23	48.0
Butyrate	178	183	16.1	0.2	0.7	1.0	1.17	30.4
Valerate	119	112	10.2	0.2	0.3	0.6	1.13	18.6
Caproate	84	94	5.88	0.1	0.2	0.4	1.10	13.7
Heptylate[g]	82	88	3.39	0.1	0.2	0.4	1.07	10.8
Caprate	82	86	1.14	0.1	0.1	0.2	1.05	8.8
Caprate[h]	87	88		0.1	0.2	0.5	1.02	6.9
Laurate	89	91		0.1	0.1	0.3	1.00	5.9
Myristate	87	106		0.1	0.1	0.2	0.99	5.9
Palmitate	90	106		0.1	0.1	0.2	0.99	4.9

[a] Ref. 5. Courtesy of the American Chemical Society.
[b] Char point is 315°C or higher unless otherwise noted.
[c] Milliliters of water required to start precipitation of the ester from 125 mL of an acetone solution of 0.1% concentration.
[d] At 25% rh, moisture regain for cellulose is 5.4%; for the acetate, 0.6%; for the propionate and butyrate, 0.1%; all others are zero.
[e] To convert MPa to psi, multiply by 145.
[f] Starting cellulose, prepared by deacetylation of commercial, medium viscosity cellulose acetate (40.4% acetyl content).
[g] Char point = 290°C.
[h] Char point = 301°C.

acetyl) content increases flexibility, moisture resistance, and nonpolar solubility, and decreases melting point and density.

The common commercial products are the primary (triacetate) and the secondary (acetone-soluble, ca 39.5% acetyl, 2.45 DS) acetates; they are odorless, tasteless, and nontoxic. Their properties depend on the combined acetic acid content (acetyl, see Table 1 and Fig. 4) and molecular weight. Solubility characteristics of cellulose acetates with various acetyl contents are given in Table 3.

Cellulose triacetate [9012-09-3] has the highest melting point (ca 300°C) of the triesters; CA melting points generally decrease to a minimum of ca 230°C as the acetyl content decreases to 38–39% (secondary acetate).

Table 3. Solubility Characteristics of Cellulose Acetates

Acetyl, %	Soluble in	Insoluble in
43.0–44.8	dichloromethane	acetone
37–42	acetone	dichloromethane
24–32	2-methoxymethanol	acetone
15–20	water	2-methoxymethanol
≤13	none of the above	all of the above

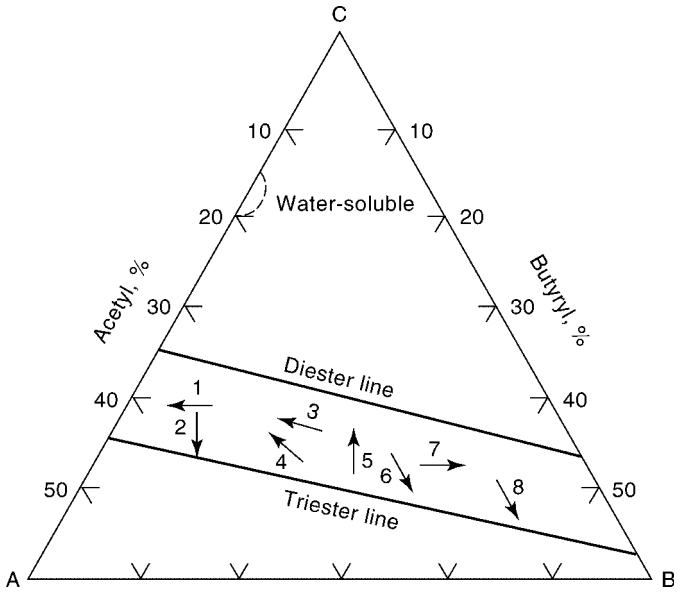

Fig. 3. Effects of composition on physical properties. A, acetyl; B, butyryl; C, cellulose. 1, increased tensile strength, stiffness; 2, decreased moisture sorption; 3, increased melting point; 4, increased plasticizer compatibility; 5, increased solubilities in polar solvents; 6, increased solubilities in nonpolar solvents; 7, increased flexibility; 8, decreased density (6).

Moisture sensitivity and vapor-permeability rate of cellulose acetate increase with decreasing acetyl (increasing hydroxyl) content. Thermoplastic characteristics are greatly improved as the acetyl content is increased from ca 20% [DS (acetyl) = 1] to ca 39% [DS (acetyl) = 2.4] (8).

The bulk density of cellulose acetate varies with physical form from 160 kg/m^3 (10 lb/ft^3) for soft flakes to 481 kg/m^3 (30 lb/ft^3) for hammer-milled powder, whereas the specific gravity (1.29–1.30), refractive index (1.48), and dielectric constant of most commercial cellulose acetates are similar.

In fibers, plastics, and films prepared from cellulose esters, mechanical properties, such as tensile strength, impact strength, elongation, and flexural strength, are greatly affected by the degree of polymerization and the degree of substitution. Mechanical properties significantly improve as the DP is increased from ca 100 to 250 repeat units.

Liquid Crystalline Solutions. Cellulose esters, when dissolved in the appropriate solvents at the proper concentration, show liquid crystalline characteristics similar to those of other rigid chain polymers (9) because of an ordered arrangement of the polymer molecules in solution. Cellulose triacetate dissolved at 30–40 wt% in trifluoroacetic acid, dichloroacetic acid, and mixtures of trifluoroacetic acid and dichloromethane exhibits brilliant iridescence, high optical rotation, and viscosity–temperature profiles characteristic of typical aniostropic phase-containing liquid crystalline solutions (10). Similar observations have been made for cellulose acetate butyrate (11), cellulose diacetate (12), and other cellulose derivatives (13,14). Wet spinning of these liquid crystalline solutions yields fibers

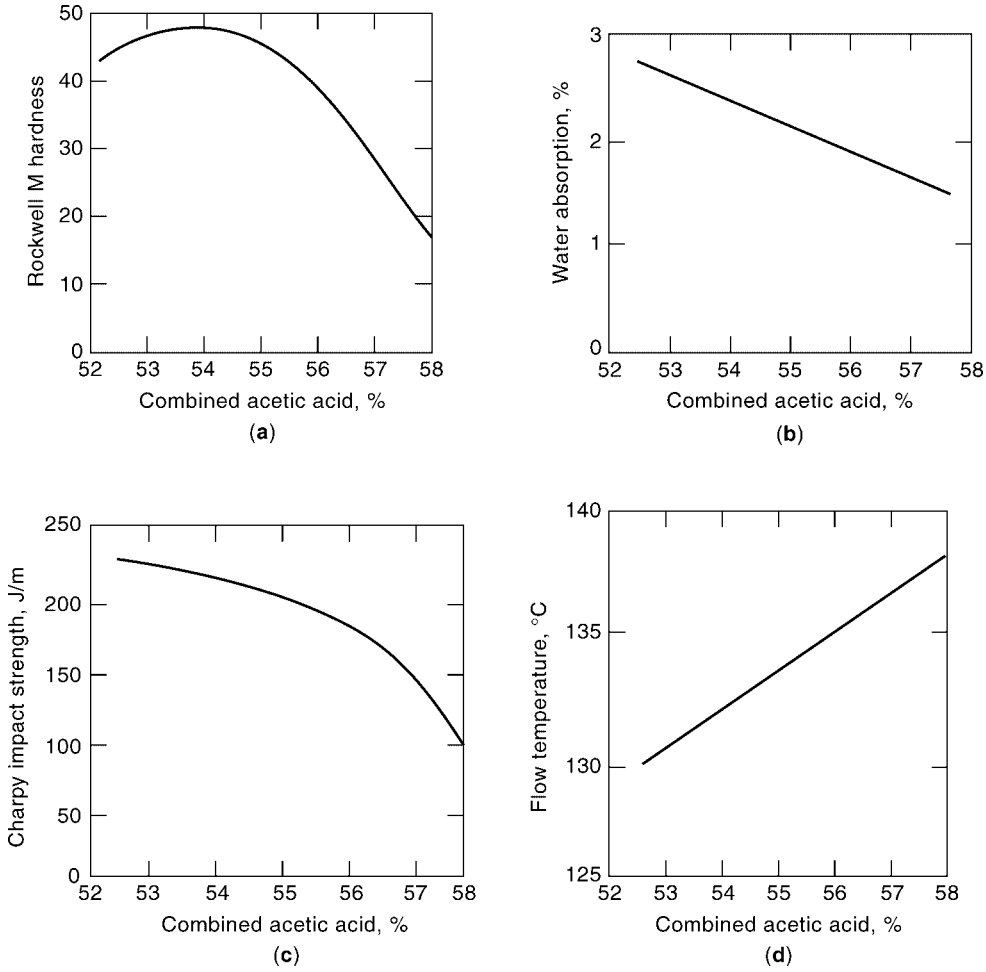

Fig. 4. Effect of combined acetic acid content on (**a**) hardness, (**b**) absorption, (**c**) impact strength, and (**d**) temperature of cellulose acetate (7). To convert J/m to ft·lb/in., divide by 53.38.

with much higher strength properties than fibers normally obtained from cellulose esters (15,16).

Manufacture and Processing

Simple triesters such as cellulose formate [9036-95-7] (6), cellulose propionate [9004-48-2] (8,17), and cellulose butyrate [9015-12-7] (18) have been prepared and their properties studied; none of these triesters is produced in large quantities. Cellulose formate esters, prepared by reaction of cellulose with formic acid, are thermally (19) and hydrolytically (6) unstable. Cellulose propionate and cellulose butyrate triesters are synthesized by methods similar to those used in the preparation of cellulose acetate with propionic or butyric anhydride in the presence of

an acid catalyst (20). These anhydrides, especially butyric, react more slowly with cellulose than acetic anhydride. Therefore, the cellulose must be activated and the temperature must be controlled to avoid degradation. Esterification rates decrease with increasing acyl chain length, and degradation becomes more severe in the following order: acetic < propionic < butyric < isobutyric anhydride. Esterification with isobutyric anhydride is normally so slow that highly activated cellulose must be used and the sulfuric acid catalyst must be distributed uniformly. Swelling agents, eg, water, containing dissolved acid catalyst are used to ensure uniform catalyst distribution for the preparation of isobutyrate esters. The swelling agent is removed by solvent exchange, leaving sorbed acid uniformly distributed in the activated cellulose (21).

Cellulose activated with ethylenediamine [107-15-3] is used to prepare high molecular weight cellulose butyrate (22). Cellulose so activated has a larger measured surface area (120 m^3/g) than cellulose activated with acetic acid (4.8 m^3/g). The diamine is removed with water, followed by solvent exchange with acetic acid and butyric acid before esterification.

More recently, however, a process for the manufacture of ultrahigh molecular weight cellulose esters has been developed by reaction of nonactivated, secondary cellulose with trifluoroacetic acid, trifluoroacetic anhydride, and either an organic acid or acid chloride (23). This process is amenable to a larger variety of organic esters not normally available through conventional means. The technique requires less reaction time and less excess solvent, and it is easier to control the extent of the reaction than conventional sulfuric acid activation. Unfortunately, the handling and toxic nature of trifluoroacetic acid and the anhydride currently limit its utility.

Cellulose valerates have been synthesized by conventional methods using valeric anhydride and sulfuric acid catalyst (24,25). Alternatively, the cellulose is activated by soaking in water, which is then displaced by methylene chloride or valeric acid; the temperature is maintained at $<38^\circ C$ to minimize degradation.

Cellulose esters from aromatic acids are usually prepared from highly reactive regenerated cellulose, and their physical properties do not differ markedly from cellulose esters prepared from the more readily available aliphatic acids. Benzoate esters have been prepared from regenerated cellulose with benzoyl chloride in pyridine–nitrobenzene (26) or benzene (27). These benzoate esters are soluble in common organic solvents such as acetone or chloroform. Benzoate esters, as well as the nitrochloro- and methoxy-substituted benzoates, have been prepared from cellulose with the appropriate aromatic acid and chloroacetic anhydride as the impelling agent and magnesium perchlorate as the catalyst (28).

Cellulose chloroacetates (29) and aminoacetates (29,30), acetate sorbates (31), and acetate maleates (32) have been prepared but are not commercially important. These esters are made from hydrolyzed cellulose acetate with the appropriate anhydride or acid chloride in pyridine.

Cellulose esters of unsaturated acids, such as the acetate methacrylate, acetate maleate (33), and propionate crotonate (34), have been prepared. They are made by treating the hydrolyzed acetate or propionate with the corresponding acyl chloride in a pyridine solvent. Cellulose esters of unsaturated acids are crosslinkable by heat or UV light; solvent-resistant films and coatings can be prepared from such esters.

Amine-containing cellulose esters, eg, the acetate *N,N*-diethylaminoacetate (35) and propionate morpholinobutyrate (34), are of interest because of their unique solubility in dilute acid. Such esters are prepared by the addition of the appropriate amine to the cellulose acrylate crotonate esters or by replacement of the chlorine on cellulose acrylate chloroacetate esters with amines. This type of ester has been suggested for use in controlled release, rumen-protected feed supplements for ruminants (35,36).

Mixed esters, such as cellulose acetate propionate and cellulose acetate butyrate, have desirable properties not exhibited by the acetate or the high acyl triesters. These mixed esters are produced commercially in multi-ton quantities by methods similar to those for cellulose acetate; they are prepared over a wide range of acyl substitutions and viscosities. The ratio of acetyl to higher acyl in the product is proportional to the concentration of components in the esterification solution (Figs. 5 and 6). Thus it is possible to esterify cellulose with propionic or butyric anhydride in the presence of acetic acid to produce the mixed esters. In a similar manner, acetic anhydride can be used in the esterification with either propionic or butyric acid to produce a cellulose ester containing both acyl moieties. The commercial production of cellulose acetate butyrate has been described (37), and the different reactivities of lower anhydrides toward cellulose have been investigated in detail. Cellulose butyrate has been prepared in homogenous solution by the reaction of cellulose in dimethyl sulfoxide (DMSO)–paraformaldehyde with butyric anhydride and pyridine catalyst (38). The maximum degree of substitution is ca 1.8, and the products are soluble in common organic solvents. Dichloromethane has been used in the preparation of cellulose acetate butyrate to prevent excessive degradation and provide an ester with higher molecular weight (39).

Mixed esters containing the dicarboxylate moiety, eg, cellulose acetate phthalate, are usually prepared from the partially hydrolyzed lower aliphatic acid

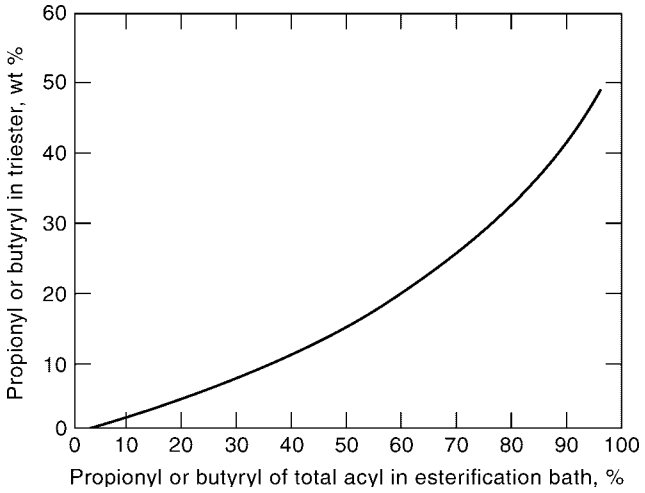

Fig. 5. Composition of cellulose acetate butyrate (propionate) as a function of butyryl (propionyl) content of esterification bath.

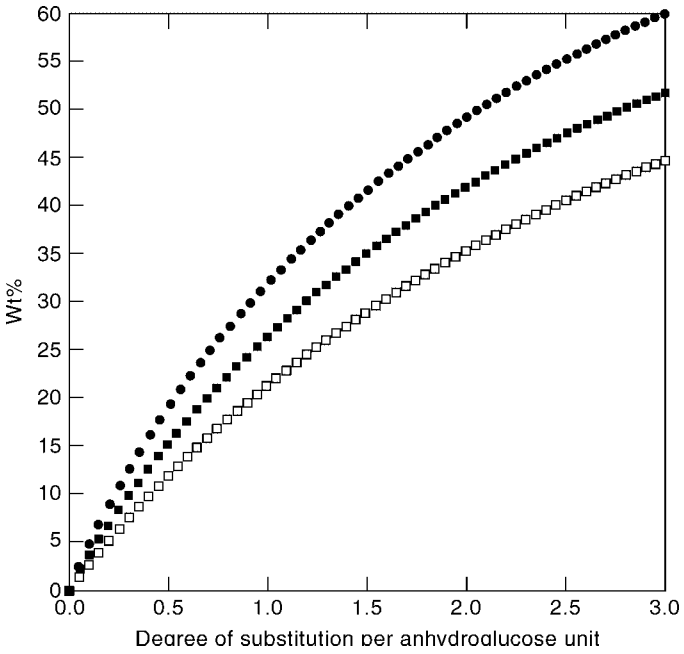

Fig. 6. Conversion of weight percent to degree of substitution per anhydroglucose unit (max. = 3.0), where • is butyryl, ♦ is propionyl, and ◊ is acetyl.

ester of cellulose in acetic acid solvent by using the corresponding dicarboxylic acid anhydride and a basic catalyst such as sodium acetate (40,41). Cellulose acetate succinate and cellulose acetate butyrate succinate are manufactured by similar methods as described in Reference (42).

Other mixed esters, eg, cellulose acetate valerate [55962-79-3], cellulose propionate valerate [67351-41-1], and cellulose butyrate valerate [53568-56-2], have been prepared by the conventional anhydride sulfuric acid methods (24). Cellulose acetate isobutyrate [67351-38-6] (43) and cellulose propionate isobutyrate [67351-40-0] (44) have been prepared with a zinc chloride catalyst. Large amounts of catalyst and anhydride are required to provide a soluble product, and special methods of delayed anhydride addition are necessary to produce mixed esters containing the acetate moiety. Mixtures of sulfuric acid and perchloric acid are claimed to be effective catalysts for the preparation of cellulose acetate propionate in dichloromethane solution at relatively low temperatures (45); however, such acid mixtures are considered too corrosive for large-scale productions.

Mixed esters are hydrolyzed by methods similar to those used for hydrolyzing cellulose triacetate. The hydrolysis eliminates small amounts of the combined sulfate ester, which, if not removed, affects thermal stability. Sulfuric acid is the preferred catalyst for hydrolysis since it is already present in the esterification mixture. On a large scale, partial neutralization of the catalyst may be necessary before hydrolysis. Increasing the amount of water during hydrolysis reduces the rates of viscosity reduction and acyl hydrolysis of cellulose acetate propionate and acetate butyrate esters (46). Several methods of hydrolyzing cellulose esters

of higher aliphatic acids are described (47,48). Acetate phthalate mixed esters preferentially lose acetyl groups when hydrolyzed in aqueous acetic acid media with sulfuric acid catalyst. On the other hand, hydrolysis with a basic catalyst such as sodium or potassium acetate in aqueous acetic acid results in preferential loss of the phthaloyl moiety (49). Ester properties can be modified by changing the DS, ie, by removing acyl groups.

Stabilization. After hydrolysis, precipitation, and thorough washing of the cellulose esters to remove residual acids, the esters must be stabilized against thermal degradation and color development, which may occur during processing, such as extrusion or injection molding. Thermal instability is caused by the presence of oxidizable substances and small amounts of free and combined sulfuric acid (50). The sulfuric acid combines with the cellulose almost quantitatively and most of it is removed during the latter stages of hydrolysis. The remaining sulfuric acid can be neutralized with alkali metal salts, such as sodium, calcium, or magnesium acetate, to improve ester stability. The combined sulfate ester may also be removed by treatment in boiling water or at steam temperatures in an autoclave. Treatment with aqueous potassium or calcium iodide reportedly stabilizes the cellulose acetate against thermal degradation (51).

Dialkyl esters of 3,3′-thiodipropionic acid (52), cyclic phosphonites such as neopentylphenyl phosphite, derivatives of phosphaphenathrene-10-oxide (53), secondary aromatic amines such as diphenylamine (54), and epoxidized soybean oils (55) are effective stabilizers for preventing discoloration of cellulose esters during thermal processing.

Chemical cellulose esters are relatively stable to UV radiation since they lack aromatic chromophores. Even so, exposure to UV radiation may cause some chain scission and loss of physical properties in cellulose esters exposed to outdoor environments; esters formulated for such use must be stabilized accordingly. Some resorcinol and benzophenone derivatives, such as resorcinol monobenzoate and 2-hydroxy-4-methoxybenzophenone, are reportedly excellent UV-light stabilizers for cellulose esters (56,57). Other stabilizers include piperidine derivatives (58) and substituted triazole compounds alone (59) and in combination with resorcinol monobenzoate (60).

Cellulose Acetate. Almost all cellulose acetate, with the exception of fibrous triacetate, is prepared by a solution process employing sulfuric acid as the catalyst with acetic anhydride in an acetic acid solvent. The acetylation reaction is heterogeneous and topochemical wherein successive layers of the cellulose fibers react and are solubilized in the medium, thus exposing new surfaces for reaction. The reaction course is controlled by the rates of diffusion of the reagents into the cellulose fibers, and therefore the cellulose must be swollen or activated before acetylation to achieve uniform reaction and avoid unreacted fibers in the solution (61).

Cellulose dissolved in suitable solvents, however, can be acetylated in a totally homogeneous manner, and several such methods have been suggested. Treatment in dimethyl sulfoxide (DMSO) with paraformaldehyde gives a soluble methylol derivative that reacts with glacial acetic acid, acetic anhydride, or acetyl chloride to form the acetate (62). The maximum degree of substitution obtained by this method is 2.0; some oxidation also occurs. Similarly, cellulose can be acetylated in solution with dimethylacetamide–paraformaldehyde and

dimethylformamide–paraformaldehyde with a potassium acetate catalyst (63) to provide an almost quantitative yield of hydroxymethylcellulose acetate.

Several derivatives of cellulose, including cellulose acetate, can be prepared in solution in dimethylacetamide–lithium chloride (64). Reportedly, this combination does not react with the hydroxy groups, thus leaving them free for esterification or etherification reactions. In another homogeneous-solution method, cellulose is treated with dinitrogen tetroxide in dimethylformamide (DMF) to form the soluble cellulose nitrite ester; this is then ester-interchanged with acetic anhydride (65). With pyridine as the catalyst, this method yields cellulose acetate with DS $\leq$ 2.0.

In the fibrous acetylation process, part or all of the acetic acid solvent is replaced with an inert diluent, such as toluene, benzene, or hexane, to maintain the fibrous structure of cellulose throughout the reaction. Perchloric acid is often the catalyst of choice because of its high activity and because it does not react with cellulose to form acid esters. Fibrous acetylation also occurs upon treatment with acetic anhydride vapors after fiber impregnation with a suitable catalyst such as zinc chloride (66).

An apparatus for the continuous fibrous acetylation of cellulose in benzene has been described (67,68). The process involves continuous activation, acetylation, partial saponification of the resulting triacetate, and drying of the product.

Activation of Cellulose. The activation required depends on the source of cellulose (cotton linter or wood pulp), purity, and drying history. Typical specifications for an acetylation-grade cellulose are given in Table 4. Cellulose that has never been dried or has been mildly dried to ca 5% moisture requires little, if any, further activation.

Normally, water or aqueous acetic acid is the activating agent; glacial acetic acid may also be used. Water is more effective because it swells the fibers more than other agents and alters the hydrogen bonding between the polymer chains to provide a greater surface area for reaction. When water or aqueous acids are used, the cellulose must be dehydrated by displacing the water with acetic acid

Table 4. Typical Specifications for Acetylation-Grade Pulp[a]

Property	Value
α-Cellulose, min. %	95.6
Moisture, %	5.8[b]
Pentosans, max. %	2.1
Cuprammonium viscosity[c], mPa·s (= cP)	1100–4000
Intrinsic viscosity, dL/g	5.5–7.5
Ether extractable, max. %	0.15
Ash, max. %	0.08
Iron, max. ppm	10
Trial acetylation	
Haze, max. ppm	100
Color, max. ppm	600

[a] Ref. 61.
[b] Off supplier's dryer.
[c] 2.5% solution.

before the start of acetylation. Commercially, it is not unusual to activate cellulose with glacial acetic acid containing a small part of the total required sulfuric acid catalyst; this reduces the molecular weight of the cellulose as needed to obtain a satisfactory product. The efficiency of activation is increased by increased temperature, time, amount of catalyst, and lower acetic acid–cellulose ratio. Several other swelling agents and methods for cellulose activation have been reported but have little commercial value because of cost and performance considerations.

Ethylenediamine (69,70), benzyl alcohol and acetone (71), ethylene glycol (72), and C_2–C_{18} carboxylic acids (73) are claimed to increase the reactivity of cellulose toward acetylation. Sodium hydroxide and liquid ammonia (70) are excellent swelling agents and have been used to activate cellulose before esterification. Ultrasonic treatment of cellulose slurries (74) reportedly swells the fibers and improves reactivity.

In one process to produce highly activated cellulose for acetylation, cellulose is treated with NaOH (mercerization) followed by a hydroxyalkylating agent, eg, ethylene oxide or propylene oxide, to give a cellulose hydroxyalkyl ether with a DS of 0.05–0.3 (75). The resulting water-insoluble material is highly reactive to conventional acetic anhydride–sulfuric acid acetylation.

Catalysts for Acetylation. Sulfuric acid is a convenient catalyst for esterifying cellulose. The role of sulfuric acid during acetylation has been discussed (76,77). In the presence of acetic anhydride, sulfuric acid rapidly and almost quantitatively forms the cellulose sulfate acid ester (76). Even in the absence of anhydride, the sulfuric acid is physically or mechanically retained (sorbed) on the cellulose. The degree of absorption is a measure of the reactivity or accessibility of different celluloses.

Sulfuric acid reacts with acetic anhydride to form acetylsulfuric acid (78). This reaction is favored by low temperature and high anhydride concentration. In cellulose acetylation, probably both sulfuric acid and acetylsulfuric acid exist and react with cellulose to form cellulose sulfate acid ester.

Perchloric acid is a well-known acetylation catalyst, especially in the fibrous method of preparing cellulose triacetate. Unlike sulfuric acid, perchloric acid does not combine with cellulose (79), ie, it does not form esters, and therefore virtually complete acetylation (DS 3.0, 44.8% acetyl) occurs. However, the extremely corrosive nature of perchloric acid and explosive nature of its salts have precluded its use industrially as an acetylation catalyst.

Zinc chloride is a Lewis acid catalyst that promotes cellulose esterification. However, because of the large quantities required, this type of catalyst would be uneconomical for commercial use. Other compounds such as titanium alkoxides, eg, tetrabutoxytitanium (79), sulfate salts containing cadmium, aluminum, and ammonium ions (80), sulfamic acid, and ammonium sulfate (81) have been reported as catalysts for cellulose acetate production. In general, they require reaction temperatures above 50°C for complete esterification. Relatively small amounts ($\leq$ 0.5%) of sulfuric acid combined with phosphoric acid (82), sulfonic acids (eg, methanesulfonic), or alkyl phosphites (83) have been reported as good acetylation catalysts, especially at reaction temperatures above 90°C.

Hydrolysis. The primary functions of hydrolysis are to remove some of the acetyl groups from the cellulose triester and to reduce or remove the combined acid sulfate ester to improve the thermal stability of the acetate.

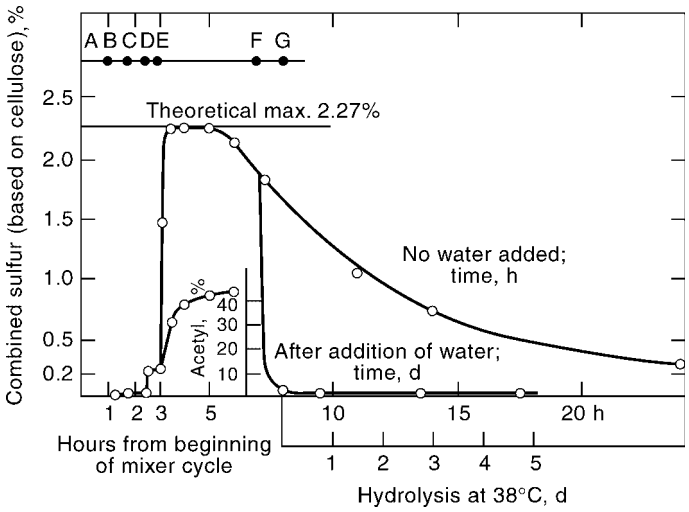

Fig. 7. Combined sulfur during preparation of cellulose acetate; hydrolysis of sulfate and esters (5). Acetylation schedule: **A**, mixer charged with linters and acetic acid; **B**, minor portion of catalyst added; **C**, began cooling to 18°**C**; **D**, acetic anhydride added and continued cooling to 16°**C**; **E**, significant portion of catalyst added; **F**–**G**, water added during 1 h.

The acetylation reaction is stopped by the addition of water to destroy the excess anhydride, causing rapid hydrolysis of the combined sulfate acid ester (Fig. 7). This is followed by a much slower rate of hydrolysis of the acetyl ester groups. The rate of hydrolysis is controlled by temperature, catalyst concentration, and, to a lesser extent, by the amount of water. Higher temperatures and catalyst concentrations increase the rate of hydrolysis. Higher water content slightly increases the hydrolysis rate and helps minimize degradation (84). The amount of water also influences the ratio of primary to secondary hydroxy groups in the hydrolyzed cellulose acetate; high water content favors primary hydroxyl formation (85).

In commercial processes, the water content during hydrolysis ranges from 5 to 20 wt% based on total liquids and depends on the temperature and the final product desired. Hydrolysis reactions can be performed at temperatures ranging from ca 38°C to pressurized reactions at 229°C (86). In a continuous process at 129°C, a triacetate solution is passed vertically upward through three consecutive chambers containing rotating disks to maximize plug flow of the solution (87). Kinetics of cellulose triacetate hydrolysis have been investigated (88) and, with sulfuric acid as the catalyst, the rate constant was found to be linear for both catalyst concentration and water content.

The rate of hydrolysis of cellulose acetate can be monitored by removing samples at intervals during hydrolysis and determining the solubility of the hydrolyzed acetate. When the desired DS is reached, the hydrolysis is stopped by neutralizing the catalyst with magnesium, calcium, or sodium salts dissolved in aqueous acetic acid.

Precipitation and Purification. During the hydrolysis, control tests are made by turbidimetric titration of samples taken intermittently. When the desired degree of hydrolysis is reached, the ester is precipitated from the reaction

solution into water. It is important for the precipitate to have the proper texture for subsequent washing to remove acid and salts for thermal stabilization. Before precipitation, the reaction solution is usually diluted with additional aqueous acetic acid to reduce the viscosity. If a flake texture is desired, the solution is poured into a vigorously stirred, 10–15% aqueous acetic acid. To precipitate the acetate in powder form, dilute acetic acid is added to the stirred reaction solution. In both cases, the precipitated ester is suspended in 25–30% aqueous acid solutions and finally washed with deionized water. The dilution, precipitation temperature, agitation, and strength of the acid media must be controlled to ensure uniform texture.

Another method for direct precipitation of cellulose acetate powder suitable for extrusion into plastics is described (89). The reaction solution is precipitated with dilute aqueous acetic acid at 80–85°C in the presence of a coagulant such as isopropyl acetate. The resulting powder particles have a higher bulk density and absorb plasticizers more readily than powders obtained by the usual methods.

Granules can be precipitated and formed by extruding the viscous reaction mixture through a circular die containing several holes over which a knife blade rotates to cut the strands into granules (90). The granules are simultaneously slurried in dilute acetic acid to harden the particles for further washing.

Solution Process. With the exception of fibrous triacetate, practically all cellulose acetate is manufactured by a solution process using sulfuric acid as the catalyst with acetic anhydride in an acetic acid solvent. An excellent description of this process is given (84). In the process (Fig. 8), cellulose (ca 400 kg) is treated with ca 1200 kg acetic anhydride in 1600 kg acetic acid solvent and 28–40 kg sulfuric acid (7–10% based on cellulose) as catalyst. During the exothermic reaction, the temperature is controlled at 40–45°C to minimize cellulose degradation. After the reaction solution becomes clear and fiber-free and the desired viscosity has been achieved, sufficient aqueous acetic acid (60–70% acid) is added to destroy the excess anhydride and provide 10–15% free water for hydrolysis. At this point, the sulfuric acid catalyst may be partially neutralized with calcium, magnesium, or sodium salts for better control of product molecular weight.

The cellulose acetate is hydrolyzed in solution at 40–50°C for varying lengths of time (4–20 h) until the desired DS is obtained; at this point, the ester is precipitated with dilute aqueous acetic acid. The precipitate is hardened in 25–30% aqueous acetic acid, which is drained off and recovered.

The ester is washed thoroughly in iron-free water to remove acid and salts; these wash liquids are sent for acid recovery. The final wash may contain some sodium, calcium, or magnesium ions to stabilize traces of sulfate esters remaining on the cellulose acetate.

Recent Developments. A considerable amount of cellulose acetate is manufactured by the batch process, as described previously. In order to reduce production costs, efforts have been made to develop a continuous process that includes continuous activation, acetylation, hydrolysis, and precipitation. In this process, the reaction mixture (ie, cellulose, anhydride, catalyst, and solvent) passes continuously through a number of successive reaction zones, each of which is agitated (91,92). In a similar process, the reaction mass is passed through tubular zones in which the mixture is forced through screens of successively small openings to homogenize the mixture effectively (93). Other similar methods for continuous acetylation of cellulose have been described (94,95).

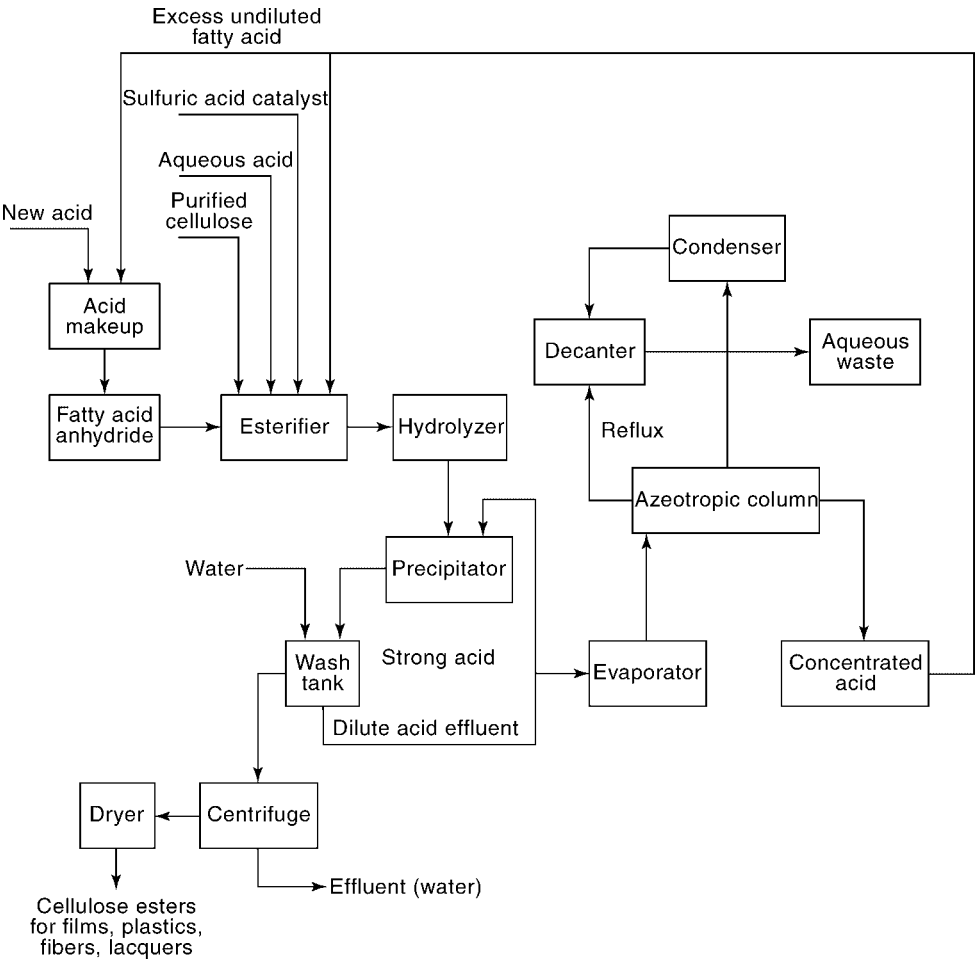

Fig. 8. Process flow sheet for cellulose esters.

Cellulose acetate with improved solubility properties can be prepared from low quality wood pulps by multistage addition of the components (96) or by interrupting the reaction in the early stages, filtering, and continuing the acetylation with fresh reactants (97,98).

In an integrated continuous process, cellulose reacts with acetic anhydride prepared from the carbonylation of methyl acetate with carbon monoxide. The acetic acid liberated reacts further with methanol to give methyl acetate, which is then carbonylated to give additional acetic anhydride (99,100).

High temperature acetylation of cellulose above 50°C produces cellulose acetate from low purity wood pulp cellulose in shorter reaction times. In a high temperature method recently disclosed (101), cellulose reacts with 200–400% acetic anhydride in the presence of <5% acid catalyst at 68–85°C for 3–20 min. After the acid catalyst is neutralized with magnesium acetate, the cellulose acetate is

hydrolyzed at 120°C for 2 h (102). Several modified catalyst systems have been developed for acetylation of cellulose above 90°C (88,89).

Economic Aspects

The principal use of cellulose acetate flake is in the production of filter tow. Other uses include the manufacture of textile fibers and in compounding to produce sheet, molded products, film, and LCD displays.

In 2001, the global cellulose acetate fiber industry was valued at $2.8 billion. Cigarette filter applications accounted for $2.2 billion, and textile yarns accounted for $0.6 billion (103). In 2002, the total consumption of cellulose acetate flake in the United States, Western Europe, Japan, and China was 655×10^3 t (104).

Cellulose acetate is a mature product and growth has declined in many areas of the world except China. In 1987, the Chinese government decided to produce filtered cigarettes. Production of filtered cigarettes in China grew from almost 0% in 1987 to 97.3% on 2000. Per capita cigarette use is growing in Eastern Europe and other Asian countries. China's demand for cellulose acetate tow is only partially supplied by domestic product. Increased manufacture in China is expected, but will just replace imports since the market is now mature (103).

The global supply of cellulose acetate fibers is controlled by a few companies. These companies produce both tow and textile fibers. Celanese Acetate holds 29% of the world supply. Voridian, a division of the Eastman Chemical Co., follows with a 24% share. The remaining 32% of supply is manufactured by Rhodia, Daicel, Mitsubishi Rayon, and Acordis. There has been a recent trend of these companies closing down their smaller flake-production units and getting their product from larger and more efficient locations (104).

The oversupply of polyester fibers and the trend toward casual dress has had a negative impact on the cellulose acetate textile market. Use in plastics applications has also declined. Worldwide demand for fiber declined at the rate of 9% per year for the period 1996–2001. It is estimated that the decline will continue at the rate of 3% per year during the period 2001–2006.

Analytical and Test Methods

Standardized test methods for analyzing the chemical composition, viscosity, and physical properties of cellulose esters have been adopted by the ASTM and are described in substantial detail (105).

Degree of Substitution and DS Distribution. For cellulose esters, the substitution level is usually expressed in terms of degree of substitution (DS); that is, the average number of substituents per anhydroglucose unit (AGU). Cellulose contains three hydroxyl groups in each AGU unit that can be substituted; therefore DS can have a value between 0 and 3. Because DS is a statistical mean value, a value of 1 does not assure that every AGU has a single substituent. Any given cellulose ester molecule is a mixture of tri-, di-, mono-, and unsubstituted monomers. The physical properties commonly associated with commercial cellulose acetates,

cellulose acetate butyrates, and cellulose acetate propionates are, in many cases, directly related to the degree of substitution as well as the overall substitution pattern. The degree of substitution or acetyl content of cellulose acetate has traditionally been determined by saponifying a known amount of the ester with an excess of standard sodium hydroxide solution in the presence of swelling agent or solvent. The excess sodium hydroxide is back-titrated with a standard solution of hydrochloric acid to determine the total acetyl content. The relative amounts of acetyl, propionyl, and butyryl in cellulose mixed esters, however, are determined by partition analysis in butyl acetate–water mixtures. The esters are saponified in sodium hydroxide, and phosphoric acid is added to liberate the organic acids from their sodium salts. The acids are partitioned between butyl acetate and water and their mole ratios are determined by comparison to carefully prepared control standards.

The acetyl content of cellulose acetate may be calculated by difference from the hydroxyl content, which is usually determined by carbanilation of the ester hydroxy groups in pyridine solvent with phenyl isocyanate [103-71-9], followed by measurement of UV absorption of the combined carbanilate. Methods for determining cellulose ester hydroxyl content by near-infrared spectroscopy (106) and acid content by NMR spectroscopy (107) and pyrolysis gas chromatography (108) have been reported.

With the advent of high resolution proton and carbon nuclear magnetic resonance spectroscopy, however, determining the DS and the DS distribution of mixed ester systems by aqueous saponification has become obsolete. Numerous studies have shown NMR to be a fundamental tool for probing the microscopic behavior of a wide variety of synthetic polymers and biomacromolecules (109,110). In the past, however, most spectral assignments required laboriously prepared derivatives containing a trideuterioacetyl or trideuteriomethyl group at a predetermined position or by comparison to spectra of mono- or oligosaccharides (111). These methods proved to be limited in detail because of line broadening and small differences in chemical shifts. Understanding the basic relationships between macroscopic properties and the microstructure of these biopolymer derivatives through NMR is the direction of much cellulose esters research.

Determining the degree of substitution using standard proton NMR relies on the integral ratio between the cellulosic ring protons ($\sim$5.0–2.9δ) and the ester alkyl protons ($\sim$ 1.2 δ for butyryl and propionyl and $\sim$2.0δ for acetyl methyl groups). This simple procedure is used extensively to determine the extent of esterification and is currently the fastest, easiest way for determining the DS of mixed cellulose esters.

Standard proton NMR techniques provide information on the degree of substitution and ester ratios in mixed ester systems, but it has been the development of two-dimensional techniques that has allowed the greatest insight into the microstructure of the cellulosic polymer (112–115). The combination of ^{1}H and ^{13}C NMR spectroscopy has, for example, been applied to cellulose triacetate for determination of its configuration (116), identification of the chemical shifts of ring protons and carbons (113), and determination of the distribution of acetyl groups over C_2, C_3, and C_6 (114,117). More complex experiments such as insensitive nuclei assigned by polarization transfer (INAPT) and nuclear Overhauser exchange

spectroscopy (NOESY) have been successfully applied toward the spectral assignments of most common triesters, the results of which are listed in Table 5. With INAPT, the lack of sensitivity that is commonly associated with two-dimensional NMR techniques is generally avoided. This increased sensitivity circumvents the need for ^{13}C enrichment and decreases the demand on instrument time.

Other two-dimensional techniques, such as correlation spectroscopy (COSY) (118), DEPT (119), Homonuclear Hartmann–Hahn (HOHAHA), solid state (120), etc, give varying degrees of success when applied to the structure-property relationship of cellulose triesters. The recent application of $^{1}H—^{13}C$ multiple-bond correlation (HMBC) spectroscopy for the unambiguous assignment of cellulose mixed esters has successfully demonstrated the utility of NMR for the structure elucidation of complex cellulose esters (121). It is this unique ability to provide detailed information on intermolecular interactions of cellulose esters in coatings (115) or in polymeric blends that continues to put NMR spectroscopy well ahead of other analytical techniques.

Viscosity. The viscosity of cellulose esters, a measure of the degree of polymerization, is determined by the falling-ball method. The time in Saybolt units (SU) required for an aluminum or stainless-steel ball of specified diameter to go through a specified distance in a solution of the cellulose ester is determined. The choice of solvents used to prepare the solutions for viscosity determination depends on the DS of the cellulose ester; the concentration of ester in the solution is normally 20wt%. Dilute-solution viscosity (intrinsic viscosity) is determined by using a solution of 0.25-g ester dissolved in 100 mL of solvent. The flow time of the solution through a specially designed capillary viscometer is compared to that of the pure solvent. Methods of calculating molecular weight from intrinsic viscosity of cellulose esters have been reported (122,123).

Thermal Properties. The thermal stability of cellulose esters is determined by heating a known amount of ester in a test tube at a specific temperature for a specified length of time, after which the sample is dissolved in a given amount of solvent and its intrinsic viscosity and solution color are determined. Solution color is determined spectroscopically and is compared to platinum–cobalt standards. Differential thermal analysis (DTA) has also been reported as a method for determining the relative heat stability of cellulose esters (124).

The thermal transitions of a cellulose ester such as the glass-transition temperature and the melting point are usually determined by differential scanning calorimetry (DSC) (Fig. 9), which measures the flow of heat into and out of a sample. Generally a first heating run is necessary in order to erase any previous thermal processing characteristics, ie, regions of crystallinity. A slow cool followed by a reheat above the melt temperature provides information on the glass-transition temperature, crystallization temperature (exothermic), and the melting temperature (endothermic). This information is essential for the development of new thermoplastics.

Similar information can be obtained from analysis by dynamic mechanical thermal analysis (DMTA). DMTA measures the deformation of a material in response to vibrational forces. The dynamic modulus, the loss modulus, and mechanical damping are determined from such measurements. Detailed information on the theory of DMTA is given (125).

Table 5. ^{1}H and ^{13}C NMR Chemical Shifts, ppm, and Coupling Constants, J,[a] for Cellulose Triacetate, Cellulose Tripropionate, and Cellulose Tributyrate[b]

	CTA			CTP	CTB
	DMSO-d_6, 25°C	DMSO-d_6[c]	CDX_3,[d] 25°C	CDX_3,[d] 25°C	CDX_3,[d] 25°C
^{1}H Values					
H-1	4.65 (d, $J_{1,2} = 7.9$ Hz)	4.65 (d, $J_{1,2} = 7.9$ Hz)	4.42 (d, $J_{1,2} = 7.9$ Hz)	4.35 (d, $J_{1,2} = 7.9$ Hz)	4.65 (d, $J_{1,2} = 7.9$ Hz)
H-2	4.52 (t, $J = 7.3$ Hz)	4.55 (t, $J = 8.6$ Hz)	4.79 (t, $J = 8.6$ Hz)	4.77 (t, $J = 8.6$ Hz)	4.76 (t, $J = 8.6$ Hz)
H-3	5.06 (t, $J = 9.2$ Hz)	5.04 (t, $J = 9.2$ Hz)	5.07 (t, $J = 9.0$ Hz)	5.07 (t, $J = 9.1$ Hz)	5.06 (t, $J = 9.2$ Hz)
H-4	3.65 (t, $J = 9.2$ Hz)	3.68 (t, $J = 9.2$ Hz)	3.71 (t, $J = 9.2$ Hz)	3.66 (t, $J = 9.1$ Hz)	3.61 (t, $J = 9.2$ Hz)
H-5	3.81 (m)	3.77 (m)	3.53 (m)	3.47 (m)	3.48 (m)
H-6_s	4.22 (d, $J_{6s,6r} = 10$ Hz)	4.26 (d, $J_{6s,6r} = 10$ Hz)	[e]	[e]	[e]
H-6_r	3.98 (m)	4.04 (m)	4.06 (m)	4.03 (m)	4.03 (m)
^{13}C Values					
C-1		99.8 (d, $J = 167$ Hz)	100.4 (d, $J = 165$ Hz)	100.3 (d, $J = 163$ Hz)	100.1 (d, $J = 163$ Hz)
C-2		72.2 (d, $J = 152$ Hz)	71.7 (d, $J = 153$ Hz)	71.7 (d, $J = 150$ Hz)	71.4 (d, $J = 150$ Hz)
C-3		72.9 (d, $J = 151$ Hz)	72.5 (d, $J = 148$ Hz)	72.2 (d, $J = 148$ Hz)	71.8 (d, $J = 147$ Hz)
C-4		76.4 (d, $J = 151$ Hz)	76.0[f]	75.8 (d, $J = 153$ Hz)	75.8[f]
C-5		72.5 (d, $J = 146$ Hz)	72.7 (d, $J = 139$ Hz)	73.0 (d, $J = 138$ Hz)	73.1 (d, $J = 143$ Hz)
C-6		62.8 (t, $J = 151$ Hz)	61.9 (t, $J = 151$ Hz)	61.9 (t, $J = 147$ Hz)	61.9 (t, $J = 145$ Hz)
C-2 acetyl			169.1[g]		
C-3 acetyl			169.6[g]		
C-6 acetyl			170.7[g]		

[a] Digital resolution for ^{1}H was 0.20–0.26 Hz; For additional information see Ref. 112. For ^{13}C the digital resolution was 0.52 Hz.
[b] All solutions are 30 mg/mL.
[c] At 80°C for ^{1}H, and 90°C for ^{13}C.
[d] X = Cl for ^{1}H; X = I for ^{13}C, 25°C.
[e] H-6_r overlaps with H-1.
[f] The coupled resonance overlaps with the solvent peaks. For additional information see Refs. 112 and 113.
[g] Doublet, coupling constant unavailable.

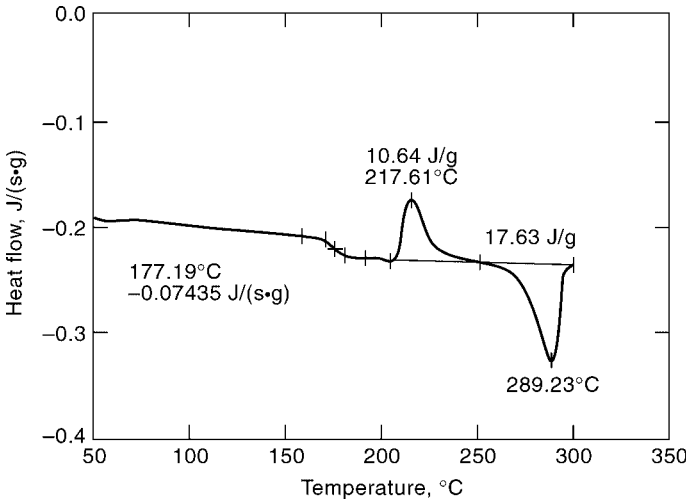

Fig. 9. Differential scanning calorimetry of cellulose triacetate. Second heating at 20°C/min.; glass-transition (T_g) temperature = 177°C; crystallization on heating (T_{ch}) = 217°C; melting temperature (T_m) = 289°C. To convert J to cal, divide by 4.184.

Determination of the thermal decomposition temperature by thermal gravimetric analysis (TGA) defines the upper limits of processing. The TGA for cellulose triacetate is shown in Figure 10. Comparing the melt temperature (289°C) from the DSC in Figure 9 to the onset of decomposition in Figure 10 defines the processing temperature window at which the material can successfully be melt extruded or blended.

Molecular Weight. The molecular weight distribution of cellulose esters is normally determined by gel-permeation chromatography (GPC) (126) in which the ester, dissolved in a suitable solvent, is eluted through a column of porous crosslinked polystyrene. The elution profiles are compared to narrow molecular weight polystyrene standards to obtain the molecular weight or DP distribution. Other

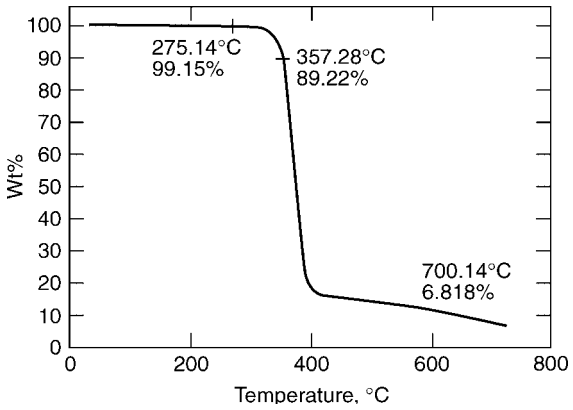

Fig. 10. Thermogravimetric analysis of cellulose triacetate. Method: 20°C/min to 700°C, in (N_2), at a purging rate of 40 mL/min.

methods, such as fractional precipitation and fractional extraction, although considerably more laborious, may be used to determine DP and DS distribution of cellulose esters (127). The DP of cellulose triacetate has been determined by GPC using a styrene–divinylbenzene copolymer column with an assigned peak molecular weight of approximately 60,000. Other solvents such as tetrahydrofuran (THF) and NMP have also been shown to solvate secondary cellulose acetates and mixed esters for GPC analysis (128).

Health and Safety Factors

The vapors of the organic solvents used in the preparation of cellulose ester solutions represent a potential fire, explosion, or health hazard. Care should be taken to provide adequate ventilation to keep solvent vapor concentrations below the explosive limits. Mixing equipment should be designed to ensure that solvent temperatures do not approach their flash point during the mixing cycle. All equipment must be electrically grounded to prevent static discharge, and appropriate precautions should be followed as recommended by the manufacturer of the solvents.

Mixing cellulose esters in nonpolar hydrocarbons, such as toluene or xylene, may result in static electricity buildup that can cause a flash fire or explosion. When adding cellulose esters to any flammable liquid, an inert gas atmosphere should be maintained within the vessel (129). This risk may be reduced by the use of conductive solvents in combination with the hydrocarbon or by use of an antistatic additive. Protective clothing and devices should be provided.

Cellulose esters, like most dry organic materials in powder form, are capable of creating dust explosions (130). The explosion at Bayer's cellulose acetate plant at Dormagen, Germany, in 1976 can attest to the explosive potential of dust. Damage to the plant was estimated at between DM 5–10 million (131).

Cellulose esters are considered nontoxic and may be used in food-contact applications. However, since cellulose esters normally are not used alone, formulators of coatings and films for use in food packaging should ensure that all ingredients in their formulations are cleared by the United States Food and Drug Administration for such use.

Uses

The cellulose esters with the largest commercial consumption are cellulose acetate, including cellulose triacetate, cellulose acetate butyrate, and cellulose acetate propionate. Cellulose acetate is used in textile fibers, plastics, film, LCD displays, sheeting, and lacquers. The cellulose acetate used for photographic film base is almost exclusively triacetate; some triacetate is also used for textile fibers because of its crystalline and heat-setting characteristics. The critical properties of cellulose acetate as related to application are given in Table 6.

Large quantities of secondary cellulose acetate are used worldwide in the manufacture of filter material for cigarettes. Because of its excellent clarity and ease of processing, cellulose acetate film is widely used in display packaging and

Table 6. Uses and Critical Properties of Cellulose Acetate[a]

	Use[b]			
Property	Yarn	Photographic film	Plastics	Lacquers
Color, absence of haze	I		C	I
			I	I
False viscosity[c]	I	I		I
Filterability	C	I	I	I
Adhesion		C		
Radioactive contamination				

[a] Ref. 61.
[b] I = important; C = critical.
[c] Concentrated solution viscosity higher than predicted for the intrinsic viscosity.

extruded plastic film for decorative signs. Injection-molded plastics of cellulose acetate are used in toothbrush handles, computer brushes, and a large variety of other applications (6).

Low viscosity cellulose acetate is used in lacquers and protective coatings for paper, metal, glass, and other substrates and as an adhesive for cellulose photographic film because of its quick bonding rate and excellent bond peel strength (132) (see COATINGS). Heat-sensitive adhesives for textiles have also been prepared from cellulose acetate (133). Extruded cellulose acetate film makes an excellent base for transparent pressure-sensitive tape (134) (see ADDITIVES).

Cellulose acetate films, specially cast to have a dense surface and a porous substructure, are used in reverse osmosis to purify brackish water (135–138) in hollow fibers for purification of blood (artificial kidney) (139), and for purifying fruit juices (140,141) (see MEMBRANE TECHNOLOGY).

Compaction of cellulose acetate desalination membranes, causing reduction in throughput and performance with time, can be significantly reduced by irrigation grafting of styrene onto the membrane (142).

Eyeglass frames made of cellulose acetate plasticized with diglycerol esters do not exhibit opaqueness at the frame–lens junction with polycarbonate plastic lenses (143,144).

Biodegradable film (145), foam-molding compositions (eg, sponges) (146), tobacco substitutes (147), and microencapsulated drug-delivery systems (148) are potentially new and useful applications for cellulose acetate esters.

With the renewed interest in environmentally friendly products, cellulose esters are being reevaluated as a natural source of biodegradable thermoplastics. Cellulose acetates are biodegradable, with the rate of biodegradation increasing with decreasing DS (149). Films prepared from a cellulose acetate with a DS of 2.5 were shown to require only a 10–12 day incubation period for extensive degradation in an *in vitro* enrichment assay. Similarly, films prepared from a cellulose acetate with a DS of 1.7 saw 70% degradation in 27 days in a wastewater treatment facility, whereas films prepared from a cellulose acetate with a DS of 2.5 required approximately 10 weeks for similar degradation to occur. The results of this work demonstrate that cellulose acetate fibers and films can be designed to be environmentally nonpersistant.

Table 7. Application and Characteristics of Commercial-Grade Cellulose Acetate Butyrate[a]

			Degree of esterification[b]			
Acetyl, %	Butyryl, %	Hydroxyl, %	Acetate	Butyrate	Hydroxyl	Application
29.5	17	1	2.1	0.7	0.2	lacquers
20.5	26	2.5	1.4	1.1	0.5	lacquers
13	37	2	0.95	1.65	0.4	plastics, lacquers
6	48	1	0.5	2.3	0.2	melt coatings

[a] Ref. 150.
[b] Ratio of ester groups to glucose residues (see Fig. 6).

Cellulose acetate propionate and butyrate esters have numerous applications, such as sheeting, molding plastics, film products, lacquer coatings, and melt dip coatings. The properties of propionate and acetate propionate esters ordinarily lie between those of cellulose acetate and acetate butyrate. The acetate propionate mixed esters have traditionally covered a narrow composition range compared to the range of acetate butyrate esters. Table 7 shows uses and a range of commercial compositions of cellulose acetate butyrate esters. Through proper variation of acetyl and butyryl contents, the esters can be adapted to a broad range of applications. Cellulose acetate propionate and acetate butyrate are thermoplastic; properly formulated, these esters are processible by methods such as injection molding and extrusion, and can be dissolved and cast into films from a variety of solvents (see FILMS, MANUFACTURE). The mixed esters are generally more compatible with various plasticizers (qv) and synthetic resins than the acetates, and their films possess excellent clarity and toughness. For example, cellulose acetate butyrate is compatible with polyester, acrylic, vinyl, and alkyd resins (qv), depending on the amount of butyryl substitution and the degree of hydrolysis of the esters.

Cellulose acetate butyrates with high butyryl content and low viscosity are soluble in inexpensive lacquer solvents. They are widely used in lacquers for protective and decorative coatings applied to automobiles and wood furniture.

Higher butyryl esters, formulated with acrylic polymers, provide coatings with excellent weather resistance, good colorfastness and dispersibility, and good flow properties (151). Formulations for a typical automotive refinishing lacquer and a wood furniture lacquer are given in Tables 8 and 9, respectively. Low viscosity, high butyryl cellulose esters tolerate substantial amounts of alcohol solvent without appreciable increase in solution viscosity. An alcohol-soluble cellulose acetate butyrate containing ca 50% butyryl and ca 4.5% hydroxy is available commercially.

Low viscosity cellulose propionate butyrate esters containing 3–5% butyryl, 40–50% propionyl, and 2–3% hydroxyl groups have excellent compatibility with oil-modified alkyd resins (qv) and are used in wood furniture coatings (152). Acetate butyrate esters have been used in such varied applications as hot-melt adhesive formulations (153), electrostatically spray-coated powders for fusible, noncratering coatings on metal surfaces (154–156), contact lenses with improved oxygen

Table 8. CAB–Polyester Automotive Refinishing Lacquer[a]

Components	Wt%
Polyester	11.5
CAB 381-20[b]	11.4
CAB 381-0.5[b]	5.7
Phosphoric acid, 85%	0.3
TiO_2 pigment	4.2
Toluene	34.4
Xylene	6.1
MIBK	5.0
Isopropyl alcohol	9.3
Acetone	7.5
n-Butyl alcohol	3.2
Ektasolve EB acetate[c]	1.4
Total	*100.0*

[a]Ref. 151.
[b]CAB = cellulose acetate butyrate.
[c]Eastman Kodak Co.

permeability and excellent wear characteristics (157–159), and as reverse-osmosis membranes for desalination of water (160).

In a relatively new decorative-coating technique called wet-on-wet coatings, cellulose acetate butyrate ester as the pigmented basecoat provides good pigment and metal-flake control before applications of the clear topcoat (161,162). Such coatings provide good appearance and excellent resistance to weathering and are expected to find broad use in automotive decorative coatings.

Because of certain properties, such as a high melting point, high tolerance for alcohol solvents, low odor, and excellent surface hardness, cellulose acetate propionates are used in printing inks (flexographic and gravure) (163) (Table 10). Alcohol-soluble cellulose acetate propionate ester tolerates substantial quantities of water in the solvent blend and thus provides an environmentally desirable system for flexographic ink coatings (164).

Table 9. CAB-Based Clear Topcoat Formulation for Wood Furniture

Components	Wt%
CAB ester[a]	16.1
Unirez 7003 maleic resin[b]	17.4
DOP[c]	4.0
Toluene	35.3
Isopropyl alcohol	14.0
Acetone	4.5
Xylene	7.7
SF-69[d]	1.0
Total	*100.0*

[a]CAB = cellulose acetate butyrate.
[b]Union Camp Corp.
[c]DOP = dioctyl phthalate.
[d]Slip aid; 1% xylene (General Electric Co.).

Table 10. Flexographic Ink Formulation Containing Alcohol-Soluble Cellulose Acetate Propionate

Components	Wt%
Cellulose acetate propionate[a]	6.1
Sucrose acetate isobutryate (SAIB)	1.5
Kodaflex DOP plasticizer[b]	4.1
Uni-Rez 710 maleic resin[c]	8.2
Pigment	5.1
Isopropyl alcohol, 99%[a]	56.3
Water	18.7
Total	*100.0*

[a]Alcohol-soluble propionate (ASP) CAP 504-0.2.
[b]DOP = dioctyl phthalate (Eastman Kodak Co.).
[c]Union Camp Corp.

Acetate propionate esters are nontoxic, exhibit excellent clarity and high tensile strength, and can be formulated into hot-melt dip coatings for food (165). Alternatively, they may be dissolved in volatile solvents and applied to foods in the form of a lacquer coating (166).

Desalination membranes with improved, rigid, and stable surfaces have been prepared from cellulose acetate propionate (167). These films are generally more resistant to hydrolysis than those from cellulose acetate.

Cellulose esters, especially acetate propionate and acetate butyrate mixed esters, have found limited use in a wide variety of specialty applications such as in nonfogging optical sheeting (168), low profile additives to improve the surface characteristics of sheet-molding compounds (SMC) and bulk-molding compounds (BMC) (169,170), and controlled drug release via encapsulation (171).

BIBLIOGRAPHY

"Cellulose Esters, Organic" in *EPST* 1st ed., Vol. 3, pp. 325–354, by Roy O. Hill, Jr., Eastman Chemical Products, Inc., and B. P. Rouse, Jr., Tennessee Eastman Co.; in *EPSE* 2nd ed., Vol. 3, pp. 158–181, by R. T. Bogan and R. J. Brewer, Eastman Kodak Co.

1. P. Schutzenberger, *Compt. Rend.* **61**, 485 (1865).
2. A. Franchimont, *Compt. Rend.* **89**, 711 (1879).
3. U.S. Pat. 835,350 (Dec. 11, 1906), G. W. Miles.
4. *Publication No. X-309*, Eastman Chemical Products, Inc., Eastman Kodak Co., Kingsport, Tenn., Aug. 1990.
5. C. J. Malm and co-workers, *Ind. Eng. Chem.* **43**, 688 (1951).
6. C. J. Malm and G. D. Hiatt, in E. Ott and co-eds., *High Polymers*, 2nd ed., Vol. 5, John Wiley & Sons, Inc., New York, 1954, p. 766.
7. J. A. Brydson, *Plastic Materials*, D. Van Nostrand Co., Inc., New York, 1966, pp. 369–371.
8. J. J. Creely and co-workers, *J. Appl. Polym. Sci.* **19**, 1533 (1965).
9. D. L. Patel and R. D. Gilbert, *J. Polym. Sci., Polym. Phys. Ed.* **19**, 1449 (1981); B. Yu. Yunusov and co-workers, *Vysokomol. Soedin. Ser. B* **24**, 414 (1982).
10. D. G. Gray and co-workers, *Makromol. Chem.* **184**, 1727 (1983).
11. S. Suto and co-workers, *Rheol. Acta* **21**, 62 (1982).

12. E. D. T. Atkins and co-workers, *TAPPI International Dissolving Pulps Conference*, 5th Conference Paper, Technical Association of the Pulp and Paper Industry, Atlanta, Ga., 1980, pp. 208–213.
13. J. Bheda and co-workers, *Colloid Polym. Sci.* **258**, 1335 (1980).
14. J. Bheda and co-workers, Technical Paper, *Regional Technical Conference of the SPE*, May 5–8, 1980, *The Society of Plastics Engineers, Brookfield Center, Conn.*, 1980, p. 321.
15. Jpn. Kokai Tokkyo Koho JP 82 57729 (Apr. 7, 1982) (to Asahi Chemical Industry Co., Ltd.).
16. J. Bheda and co-workers, *J. Appl. Polym. Sci.* **26**, 3955 (1981).
17. C. J. Malm, *Sven. Kem. Tidskr.* **73**, 523 (1961).
18. C. J. Malm and co-workers, *Ind. Eng. Chem.* **50**, 1961 (1958).
19. G. Tocco, *G. Chim. Ind. Appl.* **13**, 325 (1931).
20. U.S. Pat. 2,208,569 (July 23, 1940), L. W. Blanchard Jr. (to Eastman Kodak Co.).
21. U.S. Pat. 2,790,794 (Apr. 30, 1957), C. J. Malm and co-workers (to Eastman Kodak Co.).
22. N. I. Klenhova, *Zh. Prikl. Khim. (Leningrad)* **49**, 2701 (1976).
23. U.S. Pat. Appl. No. 495,186 (June 1989), C. M. Buchanan (to Eastman Kodak Co.).
24. J. W. Mench and co-workers, *Ind. Eng. Chem.* **5**, 110 (1966).
25. U.S. Pat. 3,103,506 (Sept. 10, 1963), C. J. Malm and co-workers (to Eastman Kodak Co.).
26. A. Wohl, *Z. Agnew. Chem.* **26**, 437 (1913).
27. K. Atsuji and K. Shimoyama, *Cellul. Ind. Tokyo* **2**, 336 (1926).
28. U.S. Pat. 1,70,4283 (Mar. 25, 1929), H. T. Clarke and C. J. Malm (to Eastman Kodak Co.).
29. H. A. Khidoyatov and Z. A. Rogovin, *Polym. Sci. USSR* **11**, 2123 (1969).
30. G. D. Hiatt and co-workers, *Ind. Eng. Chem.* **3**, 295 (1964).
31. E. I. Berenshtein and co-workers, *Strukt. Modif. Khlopk. Tsellyul.* **4**, 91 (1969).
32. Russ. Pat. 659,574 (Apr. 30, 1979), Kh. U. Usmanov and co-workers.
33. R. S. Alimardanov and co-workers, *Azerb. Khim. Zh.* **6**, 105 (1980).
34. J. W. Mench and B. Fulkerson, *Ind. Eng. Chem.* **7**, 2 (1968).
35. S. H. Wu and co-workers, in D. H. Lewis, ed., *Controlled Release Pesticides and Pharmaceuticals, Proceedings of 7th International Symposium (1980)*, Plenum Publishing Corp., New York, 1981, pp. 319–331.
36. Def. Publ. U.S. Pat. Off. T100,404 (Mar. 3, 1981), S. H. Wu (to Eastman Kodak Co.).
37. U.S. Pat. 2,824,098 (Feb. 18, 1958), F. M. Volberg and M. D. Martin (to Eastman Kodak Co.).
38. K. Kenichiro and Y. Ogiwara, *Sen-i Gakkaishi* **36**, 82 (1980).
39. E. P. Grishin and co-workers, *Khim. Tekhnol. Proizvod. Tsellyul*. **98** (1971).
40. U.S. Pat. 2,759,925 (Aug. 21, 1956), G. D. Hiatt and co-workers (to Eastman Kodak Co.).
41. C. J. Malm and co-workers, *Ind. Eng. Chem.* **49**, 84 (1957).
42. V. N. Kryazhev and co-workers, *Plast. Massy* **10**, 12 (1970).
43. U.S. Pat. 2,828,303 (Mar. 25, 1958), C. J. Malm and L. W. Blanchard, Jr. (to Eastman Kodak Co.).
44. U.S. Pat. 2,828,304 (Mar. 25, 1958), C. J. Malm and L. W. Blanchard, Jr. (to Eastman Kodak Co.).
45. L. V. Gurkovskoya and co-workers, *Khim. Tekhnol. Proizvod. Tsellyul*. **93** (1971).
46. C. J. Malm and co-workers, *Ind. Eng. Chem.* **5**, 81 (1966).
47. U.S. Pat. 2,801,240 (July 30, 1957), C. J. Malm and L. J. Tanghe (to Eastman Kodak Co.).

48. U.S. Pat. 2,816,106 (Dec. 10, 1957), C. J. Malm and co-workers (to Eastman Kodak Co.).
49. V. N. Kryazhev and co-workers, *Khim. Tekhnol. Vysokomol. Soedin*. 42 (1969).
50. B. P. Smirnov and co-workers, *Sov. Plast.* **1**, 71 (1972).
51. Russ. Pat. 458,560 (Jan. 30, 1975), A. Maciulis and co-workers.
52. U.S. Pat. 3,723,147 (Mar. 27, 1973), E. L. Wood and R. E. Gibson (to Eastman Kodak Co.).
53. U.S. Pat. 4,137,201 (Jan. 30, 1979), C. M. Kuo and co-workers (to Eastman Kodak Co.).
54. A. Z. Tatarnova and co-workers, *Sov. Plast.* **9**, 11 (1969).
55. U.S. Pat. 4,325,997 (Apr. 20, 1982), R. T. Bogan and R. J. Brewer (to Eastman Kodak Co.).
56. L. M. Malinin and K. F. Yakunina, *Plast. Massy* **47** (1966).
57. V. Shlyapintokh and co-workers, *Kunstst. Fortschrittsberg* **1**, 25 (1976).
58. D. Kho Khalikov and co-workers, *Vysokomol. Soedin.* **19**, 1132 (1977).
59. U.S. Pat. 4,269,629 (May 16, 1981), J. S. Zannucci (to Eastman Kodak Co.).
60. Ger. Offen. 3,007,797 (Sept. 25, 1980), R. J. Brewer and R. T. Bogan (to Eastman Kodak Co.).
61. G. D. Hiatt and W. J. Rebel, in N. M. Bikales and L. Segal, eds., *High Polymers*, 2nd ed., Vol. 5, Wiley-Interscience, New York, p. 749.
62. R. B. Seymour and E. L. Johnson, *J. Polym. Sci. Polym. Chem. Ed.* **16**, 1 (1978).
63. R. Leoni and A. Baldini, *Carbohydr. Polym.* **2**(4), 298 (1982).
64. C. L. McCormick and T. S. Chen, in R. Seymour and co-eds., *Macromolecular Solutions: Solvent-Property Related Polymers*, Pergamon Press, Inc., Elmsford, N.Y., 1982, p. 10.
65. P. Mansson and L. Westfelt, *Cellul. Chem. Technol.* **14**(1), 13 (1980).
66. Ref. 59, p. 748.
67. Russ. Pat. 319,227 (Dec. 5, 1975), F. M. Mikhal'skii and co-workers.
68. Ger. Offen. 2,135,735 (Jan. 25, 1973), F. M. Mikhal'skii and co-workers.
69. L. Makova and co-workers, *Zh. Prikl. Khim (Leningrad)* **47**, 610 (1974).
70. A. Koura, G. Faserforsch. *Textiltech.* **29**(6), 414 (1978).
71. Russ. Pat. 479,780 (Aug. 5, 1975), V. J. Sharkov and M. I. Perminova.
72. S. A. Kadyrova and co-workers, *Dokl. Akad. Nauk Uzb. USSR* **26**(10), 29 (1969).
73. U.S. Pat. 4,336,370 (June 22, 1982), V. M. Yasnovaky and D. M. MacDonald (to Inter. Paper Co.).
74. V. V. Safonova and N. I. Klenkova, *Zh. Prikl. Khim. (Leningrad)* **42**, 2636 (1969).
75. K. D. Sears and co-workers, *J. Appl. Polym. Sci.* **27**, 4599 (1982).
76. C. J. Malm and co-workers, *Ind. Eng. Chem.* **38**, 77 (1946).
77. A. J. Rosenthal, *Pure Appl. Chem.* **14**, 535 (1967).
78. L. J. Tanghe and R. J. Brewer, *Anal. Chem.* **40**, 350 (1968).
79. Jpn. Kokai Tokkyo Koho 78 101,083 (Feb. 16, 1978), M. Mishino and co-workers (to Chemical Industry Co., Ltd.).
80. A. Takahashi and S. Takarashi, *Kobunshi Kagaku* **27**, 394 (1970).
81. A. Takahashi and S. Takarashi, *Kobunshi Kagaku* **26**, 485 (1969).
82. U.S. Pat. 4,314,056 (Feb. 2, 1982), R. J. Brewer and B. S. Wininger (to Eastman Kodak Co.).
83. U.S. Pat. 4,329,447 (May 11, 1982), R. J. Brewer and B. S. Wininger (to Eastman Kodak Co.).
84. Ref. 62, p. 756.
85. C. J. Malm and co-workers, *J. Am. Chem. Soc.* **72**, 2674 (1950).
86. U.S. Pat. 2,836,590 (May 27, 1958), H. W. Turner (to Hercules Co.).
87. U.S. Pat. 2,790,796 (Apr. 30, 1957), J. Robin and R. Clevy (to Société Rhodiaceta).
88. V. E. Sabinin and co-workers, *Zh. Prikl. Khim. (Leningrad)* **42**, 1638 (1969).

89. U.S. Pat. 4,228,276 (Oct. 14, 1980), C. M. Kuo and R. T. Bogan (to Eastman Kodak Co.).
90. U.S. Pat. 3,414,640 (Dec. 3, 1968), G. Giuseppe and co-workers (to Rhodiatoce SpA).
91. U.S. Pat. 2,996,485 (Aug. 15, 1961), K. C. Laughlin and co-workers (to Celanese Corp.).
92. Can. Pat. 609,900 (1960), K. C. Laughlin and co-workers (to Celanese Corp.).
93. U.S. Pat. 3,040,027 (Aug. 15, 1961), H. Bates and co-workers (to British Celanese, Ltd.).
94. H. Genevray and J. Robin, *Pure Appl. Chem.* **14**, 489 (1967).
95. U.S. Pat. 3,767,642 (Oct. 23, 1973), K. C. Campbell and co-workers (to Celanese Corp.).
96. Can. Pat. 973,174 (Aug. 19, 1975), K. B. Gibney and co-workers (to Canadian Cellulose Co., Ltd.).
97. Can. Pat. 975,764 (Oct. 7, 1975), K. B. Gibney and co-workers (to Canadian Cellulose Co., Ltd.).
98. U.S. Pat. 3,870,703 (Mar. 11, 1975), K. B. Gibney and co-workers (to Canadian Cellulose Co., Ltd.).
99. U.S. Pat. 4,234,719 (Nov. 18, 1980), C. G. Wan (to Halcon Research and Development Corp.).
100. U.S. Pat. 4,234,718 (Nov. 18, 1980), D. Brown (to Halcon Research and Development Corp.).
101. Jpn. Kokai Tokkyo Koho 81 59,901 (May 23, 1981), I. Yoshiyuki (to Daicel Chemical Industries, Ltd.).
102. U.S. Pat. 4,306,060 (Dec. 15, 1981), I. Yoshiyuki (to Daicel Chemical Industries, Ltd.).
103. F. Hajduk, S. Mueller, and T. Sasano, *Chemical Economics Handbook*, SRI International, Menlo Park, Calif., July 2002.
104. W. Johnson and T. Sasan, *Chemical Economics Handbook*, SRI International, Menlo Park, Calif., July 2003.
105. *ASTM D817-72, Annual Book of ASTM Standards, Pt. 06.02*, American Society of Testing and Materials, Easton, Md., 1983, 198–217.
106. R. L. Jackson, *Tappi* **51**, 560 (1968).
107. V. W. Goodlett and co-workers, *J. Polym. Sci. Part A-1* **9**, 155 (1971).
108. E. Isobe and T. Nakajima, *Sen'i Gakkaishi* **31**, T-101 (1975).
109. F. A. Bowey, *High Resolution NMR of Macromolecules*, Academic Press, Inc., New York, 1972.
110. K. Wutherich, *NMR in Biological Research: Peptides and Proteins*, American Elsevier Publishing, New York, 1976.
111. D. Horton and J. H. Lauterbach, *Carbohyd. Res.* **43**, 9–33 (1975).
112. C. M. Buchanan, J. A. Hyatt, and D. W. Lowman, *J. Am. Chem. Soc.* **111**, 7312–7319 (1989).
113. C. M. Buchanan, J. A. Hyatt, and D. W. Lowman, *Macromolecules* **20**, 2750–2754 (1987).
114. C. M. Buchanan, J. A. Hyatt, and D. W. Lowman, *Carbohydr. Res.* **177**, 228–234 (1988).
115. K. Kamide, K. Okajima, and M. Saito, *Polym. J.* **13**, 115–125 (1981); K. Kamide, K. Okajima, K. Kowsaka, and M. Saito, *Polym. J.* **19**, 1337–1383 (1987); K. Kamide, K. Okajima, and M. Saito, *Polym. J.* **20**, 1091–1099 (1988).
116. R. U. Lemiux and J. D. Steven, *Can. J. Chem.* **43**, 1059 (1965).
117. D. Gagnaire and M. Vincendon, *Bull. Soc. Chim. Fr*. 204 (1966); V. W. Goodlett, J. T. Dougherty, and H. W. Patton, *J. Polym. Sci. A-1* **9**, 155 (1971).
118. R. A. Newmark, *Appl. Spectrosc.* **39**, 507–512 (1985).
119. M. Takai, K. Fukuda, and J. Hayashi, *J. Polym. Soc., Part C: Polym. Lett.* **25**, 121–126 (1987).
120. S. Doyle and co-workers, *Polymer* **27**, 19–24 (1986).

121. T. Iwata, J. I. Azuma, K. Okamura, M. Muraoto, and B. Chun, *Carbohydr. Res.* **224**, 277–283 (1992).
122. L. J. Tanghe and co-workers, in R. L. Whistler, ed., *Methods in Carbohydrate Chemistry*, Vol. III, Academic Press, Inc., New York, 1963, p. 210.
123. L. B. Genung, *Anal. Chem.* **36**, 1817 (1964).
124. A. S. Buntyakov and co-workers, *Plast. Massy* **3**, 71 (1969).
125. T. Murayama, *Dynamic Mechanical Analysis of Polymeric Materials*, Elsevier Scientific Publishing Co., New York, 1978.
126. R. J. Brewer and co-workers, *J. Polym. Sci. Part A-1* **6**, 1697 (1968).
127. R. E. Glegg and co-workers, in Ref. 62, pp. 491–517.
128. J. F. Kennedy, G. O. Phillips, and P. A. Williams, eds., *Wood Cellulose*, Horwood, Chichester, U.K., 1987, pp. 203–210.
129. *Standard on Explosion Prevention Systems, NFPA 69, and Static Electricity, NFPA 77*, National Fire Protection Association, Quincy, Me., 1984.
130. *Prevention of Fire and Dust Explosions in the Chemical, Dye, Pharmaceutical, and Plastics Industry, NFPA 654*, National Fire Protection Association, Quincy, Me., 1982.
131. *Chem. Age (London)* 4 (Oct. 1, 1976); *Eur. Chem. News* **10**, 4 (Sept. 1976).
132. Ger. Offen. 2,104,032 (Aug. 5, 1971), W. Ueno and N. Minagaiwa (to Fuji Photo Film, Ltd.); Brit. Pat. 1,352,605 (May 9, 1974) (to Fuji Photo Film, Ltd.).
133. Brit. Pat. 1,197,570 (July 8, 1970), J. A. Smith and co-workers (to Courtaulds, Ltd.).
134. B. Wright, *Adhes. Age* **14**, 25 (1971).
135. P. Aptel and I. Cabasso, *Desalination* **36**, 25 (1981).
136. R. E. Kesting and co-workers, *Proc. Int. Symp. Fresh Water Sea* **4**, 73 (1976).
137. R. D. Ammons, *Gov. Rep. Announce. U.S.* **79**, 93 (1978).
138. U.S. Pat. 4,145,295 (Mar. 20, 1979), S. Sourirajan and co-workers (to Canadian Patents and Development, Ltd.).
139. Jpn. Kokai Tokkyo Koho JP 82 119,809 (July 26, 1982) (to Daicel Chemical Industries, Ltd.); Ger. Offen. 2,619,250 (Nov. 11, 1976), R. E. Kesting (to Chemical Systems, Inc.).
140. R. L. Merson and co-workers, *Polym. Sci. Technol.* **13**, 405 (1980).
141. A. G. Baxter and co-workers, *Chem. Eng. Commun.* **4**, 471 (1980).
142. H. B. Hopfenberg and co-workers, *Appl. Polym. Symp.* **13**, 139 (1970).
143. Jpn. Kokai 78 58,559 (May 26, 1978), K. Wanatabe and co-workers (to Daicel, Ltd.).
144. Jpn. Kokai Tokkyo Koho 79 08,654 (Jan. 23, 1979), M. Hirotake and co-workers (to Daicel Chemical Industries, Ltd.).
145. V. T. Stannett and co-workers, *J. Macromol. Sci. Chem.* **16**, 473 (1981); *J. Polym. Sci. Polym., Lett. Ed.* **11**, 731 (1973).
146. Fr. Demande 2,140,454 (Feb. 23, 1973), W. Fischer (to Bayer AG).
147. Jpn. Kokai 77 79,096 (July 2, 1977), T. Yokota and co-workers (to Daicel Chemical Industries, Ltd.).
148. M. Singh and co-workers, *Makromol. Chem.* **183**, 1897 (1982).
149. C. M. Buchanan and R. M. Gardner, *Cellulose '91*, New Orleans, 1991, p. 228.
150. K. J. Saunders, *Organic Polymer Chemistry*, Chapman and Hall, London, 1973, p. 265.
151. R. L. Smith, *Paint Varn. Prod. Mngr.* **59**, 53 (1969).
152. U.S. Pat. 4,166,809 (Sept. 4, 1979), R. J. Brewer and W. C. Wooten (to Eastman Kodak Co.).
153. Def. Publ. U.S. Pat. Off. T944,005 (Mar. 2, 1976), R. J. Brewer and co-workers (to Eastman Kodak Co.).
154. R. W. Buchanan, SME Technical Paper FC74-576, Sept. 17–19, 1974.
155. D. Russell, *Met. Finish.* **74**, 32 (1976).
156. U.S. Pat. 4,133,783 (Jan. 9, 1979), R. J. Brewer and co-workers (to Eastman Kodak Co.).

157. Ger. Offen. 2,856,891 (July 17, 1980), F. Wingler and co-workers (to Farbenfabriken Bayer AG).
158. U.S. Pat. 4,116,549 (Jan. 12, 1976), J. E. Harris and B. D. Parish (to Continuous Curve Contact Lenses, Inc.).
159. Brit. Pat. Appl. 1,593,553 (July 15, 1981), S. Loshack and C. M. Shen (to Wesley-J Inc.).
160. H. Ohya and co-workers, *J. Appl. Polym. Sci.* **24**, 663 (1979).
161. K. Walker, *Farbe Lack* **87**, 198 (1981).
162. K. Walker, *Double Liaison-Chim. Print.* **27**, 258 (1980).
163. C. H. Coney and G. B. Bowen, *Am. Inkmaker* **51**(20), 24 (1973).
164. R. L. Baticle and co-workers, *FATIPEC Fed. Assoc. Techn. Ind. Peint Vernis Emaux Impr. Eur. Cont. Congr.* **12**, 437 (1974).
165. U.S. Pat. 3,313,639 (Apr. 11, 1967), F. M. Ball and J. H. Davis (to Eastman Kodak Co.).
166. Ger. Offen. 2,412,426 (Sept. 18, 1975), M. Stemmler and H. Stemmler (to M&H Stemmler G).
167. S. Sourirajan and co-workers, *Can. J. Chem. Eng.* **54**, 364 (1976).
168. Ger. Offen. 3,148,008 (Apr. 5, 1973), K. Landt and P. Neuber (to Winter-Optik GmbH).
169. W. W. Blount, *Mod. Plast.* **49**, 68 (1972).
170. W. W. Blount and co-workers, *SPI Reinforced Plastics Composites Institute, Proceedings of the 27th Annual Conference*, Feb. 8–11, 1972, Society of the Plastic Industry, New York, 1972, Pt. 12-C.
171. D. L. Gardner and co-workers, *Am. Chem. Soc. Div. Org. Coat. Plast. Chem. Pap.* **36**, 362 (1976).

GENERAL REFERENCES

R. T. Bogan and R. J. Brewer, in J. I. Kroschwitz, ed., *Encyclopedia of Polymer Science and Engineering*, 2nd ed., Vol. 3, John Wiley & Sons, Inc., New York, 1985, pp. 158–181.
For a review of cellulose and wood chemistry, see J. F. Kennedy, G. O. Phillips, and P. A. Williams, eds., *Cellulose: Structure and Functional Aspects*, John Wiley & Sons, Inc., New York, 1989.
J. F. Kennedy, G. O. Phillips, and P. A. Williams, eds., *Wood and Cellulose: Industrial Utilizations, Biotechnology, Structure, and Properties*, Ellis Horwood Limited, Chichester, U.K., 1987.
R. A. Young and R. M. Rowell, *Cellulose: Structure, Modifications, and Hydrolysis*, Wiley-Interscience, New York, 1986.
M. Yalpani, *Studies in Organic Chemistry 36: Polysaccharides: Synthesis, Modification, and Structure/Property Relations*, Elsevier, New York, 1988.
E. Sjöström, *Wood Chemistry: Fundamentals and Applications*, Academic Press, Inc., New York, 1981.
J. F. Kennedy, *Carbohydrate Chemistry*, Oxford Science Publication, New York, 1988.

KEVIN J. EDGAR
Eastman Chemical Company

CELLULOSE ETHERS. See Volume 5.

CELLULOSE FIBERS, REGENERATED. See Volume 5.

CHARACTERIZATION OF POLYMERS

Introduction

Over the last 50 years, systematic investigation has established a number of structure–property relationships for polymeric materials, which allow prediction of their physical properties from a knowledge of the chemical structure of the repeat units and molar mass of the material. All polymeric materials can be divided into a series of subclasses, reflecting either their method of synthesis or some particular characteristic of the material. Using this classification, it is possible to quickly identify how the material will respond to external factors such as change of temperature, pressure, stress, impact, etc.

The term *polymer* (*poly*–many, and monomer–low molar mass unit) reflects the simplicity of the high molecular weight macromolecular structure. *Natural polymers*, although they may have complex sequences of repeat units, can exhibit physical properties that obey the same physical laws as their equivalent *synthetic polymers*. The increased use of polymers in everyday life has come with the discovery of simple synthetic routes to the raw materials and the ability to tailor their physical properties to particular applications. Despite the wide range of methods available for their synthesis, the physical characteristics of many polymers can be predicted by recognizing certain generic features in their structure.

Many polymers are created from the reaction of monomers that contain an unsaturated carbon (ene/vinyl) bond. For example, polyethylene [$-(CH_2{=}CH_2)_n-$], where n is the degree of polymerization and indicates the number of the repeat units in the chain. Synthesis of the polymer can be achieved using either free-radical processes, ionic (anionic or cationic initiation), or using a coordination polymerization route that uses an *addition reaction*. These synthetic routes produce macromolecular chains that have similar chain lengths and well-defined physical properties. Polymers with heteroatoms in the polymer backbone are frequently produced by a step-growth method that may either involve ring opening or elimination of a low molecular weight molecular species; eg, poly(ethylene oxide) produced by ring opening of ethylene oxide and poly(ethylene adipate) produced by the condensation of ethylene diol and adipic acid with the elimination of a molecule of water. *Step-growth* methods produce materials with a broad spread of lengths, and consequently a range of physical properties. The distribution of chain lengths is reflected in a range in the physical properties.

Knowledge of the chemical structure of the monomer and the distribution of chain lengths allows prediction of the method used for the production of that polymer. If the monomer is effectively difunctional, then the polymer will have a linear backbone structure and is a *thermoplastic*. Such polymers can be heated to an elevated temperature and shaped. If the monomer has functionality greater than two, then a cross-linked three-dimensional matrix can be created and the material is a *thermoset*, which cannot be reshaped by heating to an elevated temperature. Thermoplastics and thermosets (qv) can be created using similar chemistry, the only difference being the number of functions associated with the primary monomer unit.

Encyclopedia of Polymer Science and Technology. Copyright John Wiley & Sons, Inc. All rights reserved.

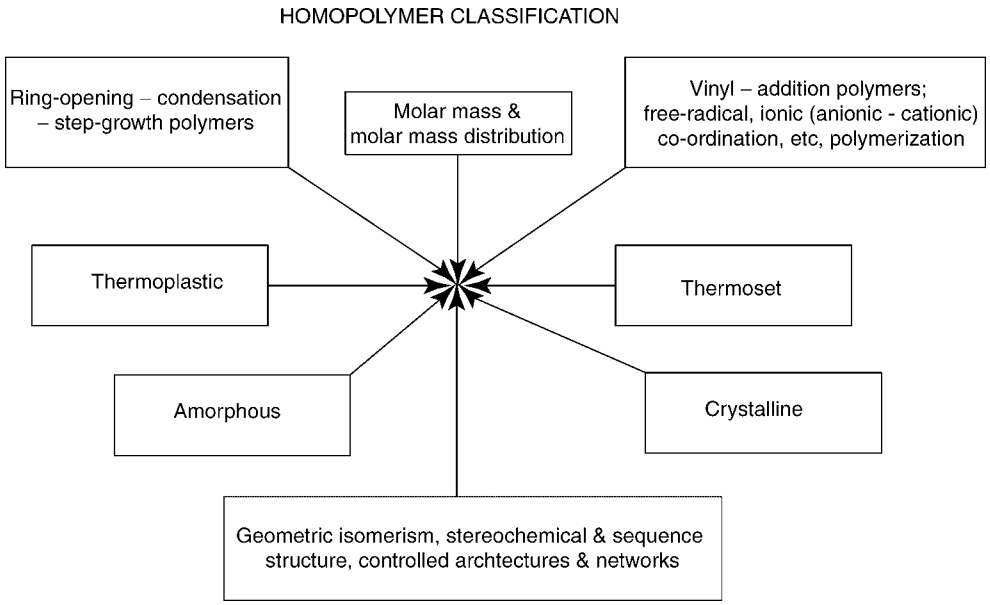

Fig. 1. Classification of homopolymer types.

The chemical structure of the repeat unit has a dominant effect on the ability of the polymer chains to pack together to form an ordered structure. If there is either a high level of symmetry or relative simplicity of the polymer backbone, then packing is encouraged and a *crystalline* structure generated (see SEMICRYSTALLINE POLYMERS). If the monomer structure is asymmetric and/or contains bulky pendant groups, packing may be inhibited and the solid structure is disordered and *amorphous* (see AMORPHOUS POLYMERS). Being able to differentiate between these different types of organization can help with prediction of the physical properties of the solid.

A useful classification of the polymers is presented in Figure 1.

Blending together two different types of compatible polymer material will create physical properties that are different from those of the individual materials (see POLYMER BLENDS). Polymeric materials may be formed using more than one repeat unit, and these are classified as *copolymers*. In real polymeric materials, there may be present a range of additives (qv): plasticizers (qv), antioxidants (qv), processing aids, fillers (qv), reinforcement (qv), antistatic modifiers, pigments, dyes, etc. These additives will influence the physical properties of the material, and understanding their influence is critical to understanding the properties of the material.

The questions that need to be asked in order to fully characterize a polymeric material include the following:

(1) What is the chemical structure of the repeat units from which the polymer is constructed? Does the polymer have a specific geometrical isomeric structure, particular sequence or branched-chain structures?

(2) Is the sample a thermoplastic or a thermoset?
(3) What is the average length of the polymer chains present? Are these chains of the same length or is there a broad distribution of lengths present?
(4) Is the solid a crystalline or an amorphous material?

In addition, knowledge of a number of physical properties is required to determine whether the polymer is suitable for a particular application.

Sample Preparation

All methods used by organic chemists for the determination of molecular structure are appropriate for the characterization of polymers. However, the simple analysis may not be able to differentiate between a homopolymer, a copolymer, or a blend of polymers. Even with a homopolymer, such as a commercial polypropylene, the solid may contain varying amounts of polymers with different molar masses and stereochemical and block sequence structure. Therefore it is desirable to be able to dissolve the polymer in selective solvents and extract species on the basis of solubility.

To obtain an unambiguous characterization of a particular material, it is often essential to fractionate a material (1–3). Synthetic polymers are rarely homogeneous chemical species, but have multivariate distributions in molecular weight, chemical composition, chain architecture, and functionality (4). For a precise characterization of a synthetic polymer, all the distributions need to be determined, which is a difficult, if not virtually impossible, task. Traditionally, fractionation has allowed separation of polymers on the basis of molecular mass or chemical composition (2). With proper techniques it is often possible to separate and characterize complex homo- and copolymer species on the basis of chemical heterogeneity and molar mass.

Separation by Solubility. Fractionation (qv) of a polymer has traditionally been based on solubility using precipitation, fractional dissolution (extraction), coacervate extraction, thin-layer chromatography, counter current distribution, and turbidimetry (5).

Two methods have been developed that are in common usage and aid the fractionation of polymer materials. These are temperature rising elution fractionation (TREF) (6–8) and Field Flow Fractionation (FFF) (9).

TREF was developed to separate semicrystalline polymers according to differences in molecular structure or composition that influence the crystallinity and solubility. TREF can be divided into crystallization and elution stages. In the crystallization stage, the polymer is dissolved in a good solvent, and then allowed to crystallize under controlled conditions by slowly decreasing the temperature. Crystallization may take place on an inert support or the support may be added later. In the elution step, solvent is pumped through a column packed with the polymer-support mixture, while the temperature is increased. Polymer elutes in the reverse order that it was crystallized, with less crystalline material eluting at lower temperatures followed by more crystalline polymer at higher temperatures and has been used for polyalkenes (6,8). In preparative TREF (P-TREF) polymer

fractions are collected at predetermined but different elution temperature intervals from those used in the crystallization (8). Critical, isobaric temperature rising elution fractionation (CITREF) is carried out using supercritical fluids, such as propylene and propane, in a column containing a high surface area stainless steel mesh packing in a manner analogous to P-TREF (10,11).

FFF is based on the simultaneous action of the effect of field forces and the carrier liquid flow on the fractionated species inside a belt-shaped fractionation channel (9,12). FFF is used to fractionate polymers or mixtures. Separation is based on the use of intensive properties, such as chemical composition and structure of the polymer chains, electrical charge, density, etc. Separation is influenced by application of a temperature gradient (ThFFF) (13) or an electrical field (EFFF) (14), and separation is aided by flow. In ThFFF, a temperature difference between the walls of the channel produces a flux, known as the Soret effect, usually towards the cold wall. In the EFFF, an electric potential across the channel generates a transverse flux of charged macromolecules or particles (14). In preparative FFF, a lower dilution of the separated species during the elution occurs as compared with flow FFF, due to partial depletion of the liquid due to the cross-flow. Two-dimensional thermal field-flow fractionation (2D-ThFFF) is devised for continuous fractionation of macromolecules (15). The sample introduced into a disc-shaped channel undergoes radial and tangential flow. Random copolymers of styrene and acrylonitrile (SAN) in toluene have been fractionated. (16). Polymer Brushes (qv) with poly(methyl methacrylate) (PMMA) backbone and polystyrene side chains have been separated using continuous counter-current extraction (17). FFF is applicable for the separation of polymers with molar mass in the range 10^3–10^8 and variants include sedimentation as an applied field (18–20). For small-scale analysis, components are sometimes quickly and conveniently separated by thin-layer chromatography (TLC), (21).

Molecular Size. Separation of soluble macromolecules can be achieved in size-exclusion chromatography (SEC) or gel-permeation chromatography (GPC) as a consequence of the differential permeation of the molecules into the porous solid column packing (see CHROMATOGRAPHY, SIZE EXCLUSION). Small molecules will penetrate more effectively and are eluted last from the column; the large species are eluted first. The separation is based on the size of the polymer molecule in solution—*hydrodynamic volume* that is directly related to molar mass of the polymer molecule. Since the hydrodynamic volume takes into account the polymer–solvent interactions, it is possible to create a universal calibration that takes into account variations in size due to change in polymer–solvent interaction. Care must be taken to ensure that size exclusion is the only separation mechanism operating in the column and to avoid errors arising because of Adsorption (qv) and aggregation (22). The SEC/GPC technique is used for the determination of the molar mass relative to some calibration standards, but can also be used for the separation of the mixtures into narrow molar mass fractions.

Molecular Structure Characterization

The first step in any analysis is determination of the elemental composition of the polymer. Combustion analysis can establish the presence of carbon, hydrogen,

halogen, sulfur, and the Kjeldahl oxidation for nitrogen and, occasionally, phosphorus. The structure of the polymer will then usually be determined by a combination of spectroscopic and mass spectroscopic analysis of degradation products.

Infrared and Raman Spectroscopy. Identification of the type of functional groups present in a polymer is effectively achieved by infrared and Raman analysis (23–28). The spectroscopic selection rules for infrared and Raman activity are respectively a dipole moment or polarizability change during interaction of electromagnetic radiation with the atomic grouping (see VIBRATIONAL SPECTROSCOPY). A vibration that gives a strong infrared signature may be weak in the Raman spectrum and vice versa. It is relatively easy to identify the occurrence of carbonyl, ethers, aromatic functions, hydroxyl groups, epoxy rings, carbon–halogen, and carbon–hydrogen bonds. The techniques are applicable to the study of solids (usually as very thin films), powders, and solutions. Raman spectroscopy is particularly useful when studying aqueous solutions, wet samples, or where differentiation between polymers with similar structures is necessary. Using laser sources, depolarization data associated with the Raman spectra can be obtained and conformational differences in molecular structure determined. At low frequencies, ca 100 cm^{-1}, the longitudinal acoustic mode (LAM) is observed in the Raman and is characteristic of the all trans structure of the polymer backbone and used to study the lamellar structure in crystalline polymers, such as polyethylene (29–32). Shifts in the Raman spectra have been used to indicate how local stresses are distributed within a sample (29,33).

Application of stress can induce changes in the infrared spectrum (34,35). Fourier transform infrared (FTIR) spectroscopy, in which rapid multiple scanning of the sample is possible (22,29), has allowed real-time observation of changes in the spectra. Studies have been reported of materials subjected to an applied external stress or used to follow the cure reaction of a thermoset. Computer libraries allow assignment of the spectra and identification of various functional groups within the polymer. Attenuated total reflection (ATR) attachments allow the surface of films to be explored (36). The ATR technique uses a glancing angle and total internal reflection of the infrared beam to collect information on the groups that lie close to the surface of the film (5–10 μm). Data manipulation techniques such as difference spectroscopy (spectral subtraction), factor analysis, spectral deconvolution, and least squares fitting of calibration plots allow quantitative determination of the species present.

Nuclear Magnetic Resonance Analysis. Nuclear Magnetic Resonance (qv) (NMR) provides both qualitative and quantitative analysis with respect to monomer composition and the average configuration of the polymer chain (22,37, 38). Both solid-state and conventional NMR techniques provide information on molecular structure, dynamics of the chain, crystallinity, network formation, and chain entanglement (39–41). Many types of nuclei may be observed; but proton (^{1}H) and carbon-13 (^{13}C) are usually investigated. Other useful nuclei studied include silicon (^{29}Si), nitrogen (^{15}N), fluorine (^{19}F), and phosphorus (^{31}P). The use of FTNMR with superconducting magnets and wide bore magnets has allowed a wide range of materials to be studied.

Proton (^{1}H) NMR, initially, was used for structural characterization, and use of the Karplus equation has allowed conformational and configurational analysis to be carried out on a wide range of polymers in solution (42). The advent of

various pulse sequences has enhanced the signal sensitivity and consequently the popularity of carbon-13 NMR spectroscopy. The natural abundance of ^{13}C is 1.1% and although there are problems of sensitivity, the spectra are simplified because carbon–carbon coupling is rarely observed in naturally-occurring materials. ^{1}H decoupling leads to spectra that consist of a series of single lines indicative of the types of chemical environment present. The inherent spectral separation of carbon chemical shifts is generally greater than for protons, ie, 0–220 ppm for ^{13}C compared with 0–10 ppm for ^{1}H, making assignment relatively easy. The ^{1}H decoupled line width is typically about 2–10 Hz for solution spectra. Grant and Paul (43) established that since the shifts are dependent on the s-orbital density, the observed shifts can be used to characterize the sequence structure of the polymer backbone. (22,44–50). Many molecular modeling packages contain software which will predict the ^{13}C spectrum. Subtle differences in both configuration and conformation of the polymer chain and changes in the dynamics of the chain backbone as a consequence of substitution can be observed (22,45).

Use of various pulse sequences has allowed solid-state NMR to be used to explore morphological features in solids. Studies of diblock copolymers of poly(styrene)–poly(methyl methacrylate) indicate domain sizes from 1 to 100 nm (51). Studies of the morphology and dynamics in poly(ethylene terephthalate) (52) and polyethylene (53) indicate the presence of a number of different phases. Motional heterogeneities within the phases of core shell particles composed of poly(*n*-butyl acrylate) (PBuA) and poly(methyl methacrylate) (PMMA) have also been demonstrated (54). The scope of the technique is continuing to develop and provide insight into the way in which chain–chain interactions influence the polymer morphology (55).

Detailed analysis of ^{1}H and ^{13}C NMR coupling constants obtained from solution spectra has allowed characterization of the chemical composition and conformation of racemic and meso dyads in glassy polystyrenes (56), and the stereoregularity in poly(methyl methacrylates) (57). With sufficient resolution, detection of tacticity at a pentad and higher level is possible, allowing validation of Bernouillian, Markov, or other statistical models for the description of polymerization processes and the tendency for block formation in copolymers. Geometric isomerism is readily detected in polybutadiene or polyisoprene, which form cis and trans double bonds in the polymer backbone as well as undergoing 1,4 or 1,2 addition. Imaging has allowed the mapping of the diffusion of labeled species in solids (58,59).

Pyrolysis. Spectroscopic methods can provide an identification of the monomeric species present; however, pyrolytic degradation plays an important role in the final assignment of the structure. Pyrolysis-gas chromatography is used extensively for the analysis of synthetic (60–63) and natural polymers (64). Application of heat to a sample leads to degradation (qv) and release of low molecular mass fragments. The composition and relative abundance of the pyrolysis products are characteristic of a given polymer. The technique is used in conjunction with other analytical methods, such as mass spectroscopy, infrared, and combinations such as pyrolysis-gas chromatography-mass spectroscopy. Pyrolysis can be carried out either in a continuous or a pulse mode; the latter has the advantage of minimizing the effects of secondary reactions on the fragmentation products. Small samples, in the microgram to milligram range, are rapidly heated either

directly in the inlet of a gas chromatograph or separately in an attached unit. For pyrolysis-mass spectroscopy, the pyrolysis is carried out in vacuum in the mass spectrometer. In a pulse mode pyrolyzer, the sample is frequently heated by resistive heating of a filament or by radio frequency inductive heating of a ferromagnetic metal (Curie-point pyrolyzer). The sample may be deposited as a thin film obtained by drying a solution or a small sample placed on the filament.

Pyrolysis of poly(methyl methacrylate) at low temperature produces monomer, whereas other acrylics fragment with loss of side chains, scission of the chain backbone, elimination or rearrangement of the products. Knowledge of the degradation pathways for particular polymer sequences is required to interpret the fragmentation patterns obtained from pyrolysis (65–70).

UV Spectroscopy. UV spectroscopy is appropriate for characterization of aromatic or conjugated systems (22). The high sensitivity allows study of species at high dilution and is useful for intrinsically conducting polymers and light-emitting species (71,72). The absorption is characteristic of the π–π^* transition; fluorescence and phosphorescence lifetimes are influenced by the state of aggregation and the matrix structure in which the absorbing species is localized. Many pigments and dyes have characteristic absorption and emission spectra. Luminescence techniques are valuable for the study of degradation and aging in polymers. Rotation and local motion of groups in dilute solution on the order of 10^{-10}–10^{-8} s in amorphous polymers and orientated films may be studied by fluorescence depolarization. Doped polymer films excited with polarized light will exhibit fluorescence depolarization, which is characteristic of the motion in the system.

Luminescence may be suppressed by the presence of antioxidants, light stabilizers, and pigments, which are able to transfer energy form the excited state to other nonfluorescing electronic states. Quenching of excited states also occurs when either oxygen or moisture is present.

Mass Spectrometry. Direct observation of polymers by means of mass spectrometry (qv) has traditionally been limited to molecules with molar mass of about 5000 or less. However, the advent of matrix-assisted laser desorption/ionization (MALDI) (73) has allowed accurate analysis of high molecular mass species to bed one (22). A high powered pulsed laser is used to transfer into the vapor phase the polymeric species which has been dispersed in a low molar mass matrix. The matrix, present in large excess (molar ratio 1:2000), is chosen for its ability to absorb the laser energy and protect the analyte, transferring energy to it in a way that allows desorption and ionization of molecules without significant fragmentation. Surprisingly, this simple change in handling technique has allowed species of up to 10^6 to be studied. Delayed extraction techniques enhance resolution (74,75). Calibration is necessary to quantify the intensities, lighter molecules are preferentially desorbed and ionized with respect to those having higher mass, and correction to the data is necessary. The resolution achievable has been enhanced by the use of time-of-flight mass spectroscopy to give TOF-MALDI (76,77). TOF-MALDI has also been applied successfully to biopolymer systems with precise molecular weight determination being possible up to 400,000 Da (78).

Electrospray mass spectroscopy (ESMS) is used for the study of biological macromolar species (79,80). Spraying produces droplets of the polymer solution which are ionized in an applied electric field and the charged species measured using a mass spectrometer.

Molar Mass and Molar Mass Distribution Determination

The GPC/SEC approach can be used for the determination of the molar mass or the distribution of molar masses. Traditionally, refractive index detection has been used and allows concentration of polymer to be measured as a function of elution volume. Using this approach, and calibration with narrow molar mass distribution samples, it is possible to determine the *relative* molar mass. Use of more complex detector arrays allows internal calibration of the system to be achieved and *absolute* molar mass determination (22,81). The usual triple detector combination uses refractive index, capillary viscometry, and light scattering (82–88). The latter provides an *absolute* calibration of the instrument; the capillary viscometry data gives through the intrinsic viscosity and hydrodynamic volume, information on the polymer–solvent interactions. Using this approach, studies have been carried out on multibranched star-shaped polyethers having poly(ethylene oxide)s (PEO) arms (82) which illustrate how the method can provide information on the architecture as well as molar mass. Due attention must be given to validating the accuracy of the theory for the particular type of polymer being studied (82–88). The multidetector systems are able to provide information on the size of the polymer molecule in solution (89).

Average Molar Mass. The molar mass of a polymer is usually described by an average molar mass. If the chains are counted by number it is the number-average molar mass $\bar{M}_n$, whereas if it is counted by weight it is the weight-average $\bar{M}_w$; higher averages, $\bar{M}_z$, etc, can also be calculated. The parameter M_w/M_n, known as the molar mass distribution, is characteristic of the method of synthesis. Ionic and coordination polymerization will have an M_w/M_n approaching 1.05, whereas a polymer produced using a radical initiated reaction has values between 1.5 and 4.5. Insertion polymerization, eg Ziegler–Natta olefin polymerization, yields values between 5 and 20. With condensation and ring opening step growth polymers, the value of M_w/M_n will be between 3 and 20. The distribution parameter can indicate whether the material is a blend of polymers or is a single material.

Three types of polymer distribution are typically observed in samples obtained from polymerization: logarithmic normal, Poisson, and Schulz–Flory distributions. The Poisson distribution can be very narrow and occurs when a constant number of polymer chains grow simultaneously and addition of the next monomeric unit is independent of previous units and is found in anionic polymerization (qv). The Schulz–Flory distribution, typical of radical polymerization (qv), arises when a constant number of chains growing ends exist and when termination and chain initiation processes are also active. This is in contrast to the Poisson distribution. A logarithmic-normal distribution is found for the polymerization of polyethylene and polypropylene (90,91).

For simple quality assurance, GPC/SEC with a simple refractive index detector is used, as the shape of the trace indicates directly the distribution of molar masses. Comparison of the distribution that is obtained from GPC/SEC with MALDI-TOF has helped clarify the validity of both techniques, especially in the case of low molar mass calibration samples. Simpler traditional methods are often more appropriate where a specific average is required to correlate variations in a polymer material with a physical property. Solution viscosity measurements

Table 1. Methods for Determination of Average Molar Mass

Method	Absolute or relative	Average measured	Molar mass range, g/mol	Characteristics
Ebulliometry	A	M_n	Up to 10^4	Low sensitivity
Cryoscopy	A	M_n	Up to 10^4	Small samples size, fast
Membrane osmometry	A	M_n	5×10^3–10^6	Suitable membranes required
Vapor phase osmometry	R	M_n	$<3 \times 10^4$	Suitable standards for accurate calibration required
End group analysis	A	M_n	$10^2 \sim 3 \times 10^4$	Low sensitivity at higher molar masses
Light scattering	A	M_w	$3 \times 10^4 \sim 10^7$	Low sensitivity at low molar mass
Ultracentrifugation	A	M_n/M_w	$2 \times 10^2 \sim 10^7$	Small samples, time-consuming, difficult technique
Dilute solution viscometry	R	M_v	$10^2 \sim 10^7$	Fast, low cost small samples
SEC/GPC	R	M_n/M_w	$10^2 \sim 10^7$	Popular, small samples, requires calibration samples
SEC/GPC–triple detection	A	M_n/M_w	$10^2 \sim 10^7$	Requires skill and care to obtain reliable results, expensive
MALDI-TOF	A	M_n	$10 \sim 10^7$	Sensitivity varies with molar mass

provide a method of monitoring the effects of degradation (qv) caused by polymer processing and the assessment of physical aging (qv) when polymers are exposed to extreme environments.

Some of the traditional methods are listed in Table 1.

In order to obtain accurate data it is essential that care be taken in the sample preparation. Because M_n is more sensitive to low molar mass components, removal of residual solvents, monomers, salts, catalysts, etc, from a sample before measurement is essential. M_w is more sensitive to the higher molar mass components, as are the higher averages M_z. Incomplete dissolution of a sample often leads to meaningless results. Similarly, polymer degradation during solution preparation or in the process of molar mass measurement must be prevented. Use of ultrasound to aid production of a solution is strongly discouraged. The issues associated with the measurements are discussed in detail elsewhere (22,92–94). Analysis of complex structures, branched chains, dendritic molecules, and regular copolymers has been successfully undertaken by combining data from a series of different methods (95–100). MALDI-TOF, in conjunction with other approaches, is allowing considerable detail to be obtained on copolymer composition changes

during reaction, probability of branching reactions, sequence structure within polymers with more than one reaction mechanistic possibility, etc (101,102).

The importance of knowing the molar mass of a polymer and its distribution of molar masses cannot be overemphasized. Commercially, many polymers, such as polystyrene, are available in different grades. Often the difference between these grades is their molar mass and/or molar mass distribution. One grade will be ideal for injection molding, another for compression molding. Incorrect selection of the grade of polymer would lead to selection of a material that is unsuitable for the application for which it is intended.

Solution Characteristics of Polymers. The molar mass characterization techniques often provide additional information on the nature of the polymer species in solution. In most cases, the solutions used are sufficiently dilute so that the properties being measured are those of the "isolated" molecule. At infinite dilution the size of the polymer coil is dictated by both inter- and intramolecular interactions, the nature of the solvent used, and the temperature. In a viscosity or GPC/SEC experiment the properties being observed can be related to the hydrodynamic volume of the polymer coil. This hydrodynamic volume is the "effective volume" which the polymer occupies in solution. The hydrodynamic volume is implicit in the Mark-Houwink relationship, which describes the value of the limiting infinitely dilute increment to the viscosity—the intrinsic viscosity $[\eta]$ to the molar mass:

$$[\eta] = K.\bar{M}_{\eta}^{\alpha}$$

where K and α are constants valid over a limited molar mass range and specific to a particular temperature–solvent combination. Generally, the value of α is between 0.5 and 1.0, and depends on the conformation of the polymer in solution. For random coil conformations, obtained at theta conditions, α is around 0.5, and extended conformations resulting in rod-like molecules give values approaching 1.0. Because α usually falls somewhere between 0.6 and 0.8, the viscosity average molar mass $\bar{M}_{\eta_v}$ is always somewhere between $\bar{M}_{\mathrm{n}}$ and $\bar{M}_{\mathrm{w}}$. The value of $\bar{M}_{\eta_v}$ is often closer to $\bar{M}_{\mathrm{w}}$ than $\bar{M}_{\mathrm{n}}$. The value of K is typically 1×10^{-4} dL/g, and values of the constant are to be found in the *Polymer Handbook* (103). Because the values of α and K reflect the *hydrodynamic volume* and are sensitive to changes in the polymer architecture, long-chain branching will lower the values in comparison to an equivalent linear polymer.

The concentration dependence of many physical properties indicates the quality of the polymer–solvent interactions, through the second virial coefficients. Study of the concentration and temperature dependence of these parameters provides information on the theta temperature, radius of gyration, and the mean square end-to-end distance for a polymer coil. The *radius of gyration* is defined as the root mean square distance from the center of mass of a polymer chain to a given mass element. The characteristic ratio is a measure of the ratio of the square of the average random-flight end-to-end distance to the product of a number of backbone units times the interactions along the polymer chain. These parameters provide useful information on the validity of a particular theoretical model and its ability to describe the architecture and conformation of a polymer (104).

Molecular Organization and Dynamic Behavior of a Polymer

The ability to produce fractions of polymers has allowed their true physical properties to be determined. Polymer chain interactions are determined by the local interactions and longer range effects that scale with the molar mass of the species. The former will dictate whether it is possible to achieve sufficient favourable interactions for *crystallization* to occur or whether local interactions are sufficiently strong to inhibit ordering and an *amorphous* material is generated. Relatively small changes in the size and distribution of these ordered regions can be responsible for dramatic differences in the physical and mechanical properties of ostensibly the same polymer. The degree of ordering depends on the local organization; hence it is not uncommon to find that an isotactic form of a polymer may be very different to that observed in a syndiotactic molecule. In polypropylene the isotactic form of the polymer has a helical structure that crystallizes, whereas the syndio or atatic forms are unable to pack and have rubbery characteristics (105,106).

The ability of a material to absorb energy reflects the mobility of the chemical entities it contains and the types of interaction that are broken as the temperature is increased. In crystallizable polymers, the interactions between chains depend on the chemical structure and range from the relatively weak van der Waals interactions found in polyethylene to the strong dipole and hydrogen bonding interactions found in nylon and polyurethanes. In between these extremes lie a range of materials with interactions of a dipole–dipole nature and associated with ester, amide, nitro, chloro, and ether groups which may or may not form crystalline phases, depending on the ability of the chains to form a regular packed structure. Hydrogen bonding is the strongest of the interactions and has a dominant effect on the structures formed. In the case of aromatic containing polymers, significant contributions can arise from dipole–induced dipole and higher order interactions associated with the delocalized electronic structure of the molecules. Typically the organized regions, even for the most crystalline of polymers, will be disrupted by conformational (*gauche*) defects. The clustering of these defects will allow the chains to loop or deviate from the lower energy (trans) extended structure that is incorporated into the ordered regions. As a consequence of the defect structure, the size of the crystalline domains will be typically of the order of a few tens of nanometers. Higher order structures are created by organization of these primary lamellae structures. Because of the possibility of chains folding back on one another, the number of chains bridging from one crystallite to another will be fewer than those reentering the structure from which they originate. These bridging chains form a disordered structure that is *amorphous*. The geometry (spherulitic or row-nucleated), size, and distribution of crystalline regions are complex and affect physical properties in a complex way.

In other polymer systems, such as polystyrene, the steric constraints associated with the group pendant to the chain backbone inhibit packing and create a disordered, *amorphous*, structure. Chain–chain interactions, however, can achieve a level of packing density that leads to motion of the backbone being inhibited. In this state, the polymer has properties of a glass. Increasing the temperature leads to expansion, increased chain separation, and a decrease in the strength of the interactions, and the solid exhibits flexible-rubbery characteristics. This

transformation is associated with the inclusion of volume for the chains to move and is known as the glass–rubber transition T_g (see GLASS TRANSITION). The relationship between supermolecular order/disorder and physical or mechanical properties depends on the thermal and mechanical history of a polymer (107).

Thermal Methods. Heating a polymer sample allows observation of the changes in physical properties, associated with changes in the degree of packing and chain–chain interaction. In thermal analysis, the properties are measured as a function of temperature or time at constant temperature. Methods include differential thermal analysis (DTA), differential scanning calorimetry (DSC), thermogravimetric analysis (TGA), evolved gas analysis (EGA), adiabatic calorimetry (AC), and a recent variant of DSC: modulated DSC (MDSC) (108–121). Use of sophisticated mathematical techniques and adaptation of the microscanning techniques have allowed mapping of thermal properties at the micron level. These techniques are not yet widely available, but will make a significant impact on our understanding of the way in which one aspect of morphology influences another in phase-separated materials and apparently homogeneous materials.

Amorphous Materials. The characteristic feature of amorphous polymers (qv) is the observation of a glass–rubber transition temperature (T_g). The glass transition (qv) temperature is associated with cooperative motion of the backbone chain of a polymer and involves the collective motion of between six and 12 chemical bonds on average. (122). The important difference between the T_g and other transitions that are observed below this temperature is that the T_g process requires *free volume* in the region into which the chains are going to move. The free volume is produced by the expansion of the solid as a consequence of the increase in chain–chain separation. As a consequence, the T_g is sensitive to pressure; increasing the pressure to which a material is subjected leads to an increase in Tg. In contrast, the motion of groups attached to the backbone via a flexible linkage exhibits simple Arrhenius/thermal activation behavior, the rate of the motion varying linearly with temperature. The rate of chain motion associated with the T_g does not vary linearly with temperature, usually showing a marked temperature dependence that reflects the limitations imposed by the free volume. The T_g process reflects a dramatic change in physical properties of the material, changing from being a rigid glass to a flexible rubber. The T_g is usually reported as a single value; however, the nature of the processes and its kinetic nature dictates that it occurs over a broad temperature range. The process is complex, and hence different methods of observation lead to a slightly different value being reported for the same material (22,122). In addition, the length of the polymer chains can have an influence on the value observed. The chain ends will require less free volume than the motion of the center of a long chain. As a consequence, it is observed that for many amorphous polymers, the value of T_g varies with molar mass according to the relationship

$$T_g(M) = T_g^{\infty} - \frac{K}{\bar{M}_n}$$

where $T_g(M)$ is the value for that material, K is a constant characteristic of that material, $T_g{}^{\infty}$ is the limiting value observed for a very high molar mass polymer, and M_n is the molar mass of the sample being studied. Recognition of the

sensitivity to the molar mass is very important in understanding how commercial polymers with the same chemical structure have apparently different physical properties. Low molar mass fractions will lower the glass transition temperature and soften the material.

Sub-T_g processes are very important in defining the physical properties of a polymer. The side chain motions can occur below the T_g and absorb energy, helping to dissipate the energy associated with impact and allowing the material to demonstrate ductile fracture behavior. The ability of a polymer to resist impact can be designed into the chemical structure by changing the nature of the side groups, their ability to move, and the efficiency with which they absorb energy. Backbone elements, such as aromatic entities, rotate about the backbone axis without being involved in the collective T_g process and impart high impact resistance to the material, eg, polycarbonate. Backbone and side-chain motions can become closely coupled on certain time–temperature scales, eg, poly(methyl methacrylate). The value of T_g is sensitive to changes in the chemical structure of the backbone and varies between ~160 to ~570 K. Because it is a kinetic process, the T_g is sensitive to the thermal history of the sample. The fabrication process will usually involve the freezing in of a level of entropy reflecting the processing temperature. Heating the sample up close to the T_g will allow slow reorganization of the chain conformations, leading to changes in the bulk physical properties. The time dependence of the physical properties has been extensively studied and is called *physical aging* (107). The side-chain relaxation, designated T_β, often occurs at a temperature of about $0.75T_g$. This correlation reflects the connectivity of the nature of the potential functions responsible for the processes that are taking place. Cross-linking of the polymer structure leads to an increase in the T_g and the introduction of certain fillers can also increase the value of T_g. The presence of low molar mass additives will have the reverse effect and swell the matrix lowering the value of the T_g.

Crystalline Materials. Polymers do not form perfect crystalline structures; however, many polymers, eg polyethylene, exhibit the characteristics of materials in which large elements of the material are regularly packed (see SEMICRYSTALLINE POLYMERS). As in the case of low molecular weight materials, it is possible to observe alignment of the polymer chains that lead to optical characteristics of typical *nematic* or *smectic* liquid crystal phases. The extreme degree of organization is the crystalline phase. Only in solution-grown, low molar mass polymers are nearly perfect crystalline phases observed. In the typical polymer sample, there will be frozen in, at the freezing point, a certain amount of disorder. Order in the crystalline phase is usually associated with the all trans conformation of the backbone, whereas disorder is associated with the gauche conformation. A coincidence of gauche conformations will loop the chain back in its original direction and develop a folded crystalline structure. The loops form a disordered-amorphous interface between the crystalline regions, which are packed into lamellae. The lamellae will in turn organize themselves into spherulite structures. The morphology of crystalline materials is varied and reflects the nature of the nucleation process and the thermal history. As in the case of amorphous polymers, post-thermal treatment can lead to changes in the size of the crystalline content with subsequent variation in the physical properties. The mechanical properties of polyethylene are thus dictated by the ratio of the crystalline to amorphous content. Just below and

above the melting point T_m, the polymer chains can undergo extensive translational movement or flow. The melting of semicrystalline polymers (qv) as observed by DSC indicates that the melting process often occurs over a range of temperatures. The breadth of the distribution is a reflection of the distribution of sizes of the crystallites in the material. The value of T_m is a function of a number of properties that include molar mass, molar mass distribution, percent crystallinity, and dimensions of the polymer crystallites.

An empirical rule which has been observed for many polymers is that $T_g \sim 2/3T_m$, where the temperatures are in Kelvin. This rule is applicable to most vinyl, vinylidene, and condensation polymers. This ratio is lower for polymers with unsubstituted backbones and higher for poly(α-olefins) with long alkyl side groups. $T_{\alpha c}$ occurs in crystalline and semicrystalline polymers and is ascribed to an oscillation about the chain axes within the chain-folded crystals or a translation along the axis. $T_{\alpha c}$ is related to T_m by

$$\frac{T_{\alpha c}}{T_m} = 0.85 + \frac{25}{T_m}$$

where all the temperatures are in Kelvin (123–125). The introduction of branches and bulky side chains into linear polymers can inhibit crystallization and in the case of polytetrafluorethylene aids the processing of the polymer by introducing amorphous structure.

The usual approach to the study of the transitions is by the use of thermal methods (see THERMAL ANALYSIS). The instruments for DTA and DSC are different in construction. In DTA, the temperature difference between a sample and a reference chamber is measured as a function of time or temperature as heat is supplied to both chambers. In DSC, the heat flow into or from a sample chamber compared to a reference chamber is measured as a function of time or temperatures. Modern instrumentation is capable of measuring the heat input or output of samples in the 0.2–30-mg range with high accuracy. The information obtained from DSC and DTA with proper and suitable calibration is in many cases similar, if not identical. Modulated DSC (113–116) is an adaptation of the DSC method in which the heating, instead of being carried out in a linear manner, is applied in an increasing sigmoidal fashion. Fourier transformation of the heat flux against the heat flow allows separation of real and imaginary components. The real part of the transform function is a direct measure of the heat capacity, whereas the imaginary component is a measure of nonreversible heat flow. The latter can be associated with crystallization, cure in the case of a not completely cured thermoset resin, polymer degradation, and other similar types of process. The curves can be used to directly measure the energy associated with the T_m, or the entropy associated with the T_g or parameters characterizing other transitions. The melting behavior can strongly influence the physical properties, and DSC and DTA studies allow quantitative investigation of phase structure in a polymer sample.

Plasticizer efficiency may be evaluated by studying the effects of plasticizers on T_g using thermal methods. The effects of the addition of nucleating agents on the rate and extent of crystallite formation can similarly be quantified. Current

instrumentation can approach the temperatures which materials approach during processing and allow modeling of the processes that occur at a microscopic level.

Thermal stability can be determined in DSC by measuring the temperature of reaction or degradation under isothermal or scanned temperature conditions. Other conditions include an inert or an oxidative atmosphere at ambient or elevated temperature. It is also possible to study the effects of increased pressure using pressurized DSC cells. By varying the conditions, thermooxidative processes can be separated from thermodegradative processes. The induction time before reaction begins is taken as a measure of the stability. The effect of antioxidants and stabilizers on this time may be readily studied.

Mechanical Properties. The measurement of mechanical properties is concerned with load–deformation or stress–strain relationships. Forces may be applied as tension, shear, torsion, and compression and bending. *Stress* is the force divided by the cross-sectional area of the sample. *Strain* is the change in a physical dimension of the sample divided by the original dimension. The ratio of the stress to strain is referred to the *modulus*. Stress may be applied continuously or periodically at varying rates for different tests. The characteristic stress–strain curve, stress relaxation, or impact behavior is very important in determining the applications and limitations of a polymer.

The condition, size, and history of a sample are of great importance in performing mechanical measurements. Samples should be uniform and free of imperfections that can act as stress concentrators. Mechanical properties depend on production techniques. For example, an injection-molded test specimen may be strongly influenced by the molecular orientation resulting from flow in the mold. Sample size should be controlled and is often set for a given test. The thermal history of a sample is very important because aging often produces change; eg, crystallinity may develop in a supercooled polymer over time, or oxidation may produce an alteration of the polymer structure. It is usual with mechanical tests to measure a number of samples and average the results. Even taking the average of a set of data must be carried out intelligently as sometimes there are good reasons; eg, differences in morphology within a sample which are reflected in the measurements. Samples may be subjected to equilibration prior to measurement at some set humidity and temperature; however, this process in itself may be inducing changes in the structure. A myriad of mechanical tests are available, some standardized (126) and some not. A comprehensive list of standards is available on the Web site www.astm.org. It is important to select a test which is applicable to the conditions in the material is going to be used (see MECHANICAL PERFORMANCE).

Stress–Strain Tests. The steady application of a stress (force per unit area) to a material will lead to a measured strain (change in length). The initial slope for many materials is linear, and with reduction in the stress there is also a reduction in the strain. The material is behaving as a simple linear Hookian solid. However, application of higher levels of stress will ultimately lead to the material breaking, and for a hard material this occurs rapidly at a limiting value of the strain. The failure of such a material is designated as being brittle. Some polymers may exhibit curvature in their stress–strain plots at high stresses and this nonlinear behavior is often indicative of ductile behavior (see YIELD AND CRAZING). A further characteristic of a ductile material is the observation of uniform extension or a yield point where the stress remains constant or even decreases

as the strain (elongation) increases. This type of behavior is typical of a necking-down or reduction of sample cross-section at the yield point due to cold drawing of the specimen. A levelling of stress may often occur after the yield point until the break point is reached. As the material takes on a more rubbery characteristic, the length of the region over which the stress remains constant is increased. The initial slope of the stress–strain curve allows measurement of the modulus of the material. The area under the curve indicates the energy required to fracture the sample and is directly related to the toughness of the material. A good elastomer is capable of exhibiting ultimate elongations before failure approaching 1000%.

As the temperature of a sample is raised, the polymer will be transformed from exhibiting brittle to ductile and eventually rubbery characteristics, provided the material is of sufficiently high molar mass. A material that shows tough ductile behavior when stress is applied slowly often behaves as if it were brittle when a large stress is applied rapidly. This observation reflects the ease with which the polymer chains are able to reorganize to redistribute the stress. Similarly, when the temperature is lowered, the tough ductile specimen often becomes brittle even if the stress is applied slowly. The mechanical properties are a direct reflection of the mobility of the chains and can be described by the Williams–Landel–Ferry (WLF) equation. The WLF equation relates through a shift factor a_T, the ratio of the time constant τ of a particular response at a temperature T to a corresponding time constant τ_0 at a reference temperature T_0. Because of the relevance of T_g to defining large-scale molecular motion, this is often selected as the reference temperature. The WLF equation is

$$a_T = \frac{-A(T - T_g)}{B + (T - T_g)}$$

where A and B are constants specific for a given polymer. The constants obtained are typically 17.4 for A and 51.6 for B (127). In practice, slight variations in the values of the constants are observed which reflect the differences in the processes that are responsible for the shift factors.

Dynamic Mechanical Thermal Analysis. Dynamic mechanical thermal analysis (DMTA) subjects the sample to a low amplitude cyclic stress and observes the corresponding strain induced (see DYNAMIC MECHANICAL ANALYSIS). By comparison of the amplitude and the phase of the response, it is possible with suitable calibration to deduce the dynamic modulus, storage modulus (energy dissipated per cyclic of the stress), and tan δ, the ratio of storage to the dynamic modulus for a particular form of deformation. In the typical apparatus it is possible to subject samples to bending, shear, or torsion. Mapping these values of the physical parameters obtained as a function of the temperature allows identification of the major transitions and quantification of the modulus of the glass and rubbery states. The technique is ideally suited for the detection of phase separation in polymers, where two values may be observed for the T_g. These tests are highly sensitive to crystallinity, orientation, morphology, dependence on molar mass in thermoplastics, degree of cure in thermosets, and miscibility of multiphase systems including composites and polymer blends (22,110).

Creep Tests. Creep tests measure deformation upon the application of constant stress such as that obtained by hanging a weight on a sample and noting the change in elongation as a function of time. Creep tests may be performed by applying stress in tension, compression, flexural bending, shear, or torsion (twisting) modes in such a way that the deformation increases with time. Dimensional stability under static loads can be estimated in this manner and this information is very useful to designers, fabricators, and engineers using plastics. Creep results are often reported as the inverse of modulus or compliance (strain divided by the applied stress), which for the reasons outlined above will be a time-dependent quantity. If the level of stress is small it is possible to observe recovery of the original dimensions, creep recovery.

Stress Relaxation Tests. Stress relaxation involves measurement of the stress required to hold a given deformation as a function of time. The deformation is initially applied as rapidly as possible to strain the sample to a certain degree. The modulus calculated from such an experiment decreases with increasing time, reflecting the polymer structure ability to redistribute the stress.

Both creep and stress relaxation is modeled using computer simulation software based on simple spring (elastic deformation) and dashpot (viscous flow) models. Many polymers, when they approach the T_g, will exhibit *viscoelastic* behavior in which the physical characteristics are best described by considering the material as having both solid- and liquid-like properties. Viscoelasticity is an important property to be found in polymeric materials (see VISCOELASTICITY).

Impact Testing. Although not a fundamental materials property, the impact strength is a very valuable parameter when attempting to determine the suitability of a material for a particular application (128). Impact tests usually involve striking a sample of a specified geometry with an object that is travelling at high velocity. The most common tests are the Izod, Charpy, and falling weight. The Izod and Charpy tests both employ a weighted pendulum. In the Izod test, a bar of the polymer is suitably notched to act as a stress concentrator. The notched bar is held vertical while clamped at one end. Charpy test has the specimen clamped at both ends. The falling weight test is usually conducted with a weighted dart or ball striking either a sheet or plate of material (see IMPACT RESISTANCE).

The underlying theme that emerges from the mechanical testing is the requirement to characterize the molecular organization at various levels (129). This organization–morphology is a function of the thermal history and various chemical and molar mass parameters implicit in the material being studied.

Visualization of the Morphology of Polymer Materials

Amorphous materials are defined by a lack of organized structure, but crystalline materials exhibit a range of levels of organization (22,130–133). Visualization of the structure of the polymer is therefore an important component of the characterization of any material that is capable of showing order.

X-Ray Diffraction. Improvements in diffraction methods have allowed the rapid characterization of the order within polymer solids. Synchrotron Radiation (qv) has allowed real-time examination of the creation of order as polymers are

cooled from the melt (134). The X-ray diffraction techniques can be subdivided, depending on the range over which the scattered electrons are collected. The major structural types that are of interest are single crystals, polycrystalline aggregates with crystals, randomly orientated "powder samples," and polycrystalline aggregates in which the crystals show a preferred orientation. The typical distances that are responsible for diffraction can be anywhere between 1 and 20 nm, which requires measurement of very small angles (5°–15°) close to the incident beam. With synchrotron sources it is possible to measure such small angles, whereas with conventional sources this is difficult. The technique is referred to as *small-angle X-ray scattering* (SAXS). Studies of aromatic polyesters indicate that even with these relatively complex molecules, regions of crystalline order can exist and have a profound effect on their physical properties. The extension of the technique, which scans a broader range of angles (∼10°–40°), is designated *wide-angle X-ray scattering* (WAXS) and provides information on spacing between 0.1 and 1 nm. This technique can provide valuable information on the crystalline packing within the crystallites. Whereas in single crystals diffraction spots can be observed, in many polymers halos are observed and these may have bright spots which reflect the preferred orientation of the crystallites within the sample (see X-RAY MICROSCOPY).

Neutron Diffraction and Inelastic Scattering. Use of neutron scattering (qv) can, in principle, allow observation of the location of hydrogen atoms in a lattice (135). The contrast between the scattering cross-section of hydrogen and deuterium allows the distribution of a single labeled chain within a low scattering matrix. Although in principle deuteration leaves the structure of the polymer essentially unchanged, there are distinct thermodynamic differences between the protonated and deuterated polymer raising the question whether the structure may have been changed by the insertion of the labeled polymer (136). Although publications have been produced on neutron diffraction from polymeric single crystals, most of the research has been carried out on inelastic scattering measurements. The latter are concerned with energy transfer processes between the neutron and the matrix and are ideal for the study of dynamic processes, but are less easily interpreted in terms of the structure of the polymer. The one application where neutron scattering has proved to be useful is for the determination of the size of a labeled polymer coil in a nonlabeled matrix. It has been shown that the dimensions of an amorphous polymer in the solid state approximate to those of the ideal random coil dimensions that would be predicted to occur in near-ideal interaction conditions. Low energy or long-wavelength neutrons (0.4–2.0 nm), unlike X-rays, produce little damage and can penetrate samples of up to 1-cm thickness, which is thicker than those used for X-ray analysis.

Electron Scattering and Electron Microscopy Techniques. High energy electrons can be scattered by the molecule in the polymer structure and the diffraction patterns will resemble those obtained from X-rays. Electron diffraction is only really possible on very highly crystalline materials. If the sample is sufficiently thin, then the analogue of the optical microscope can be used in which the electron beam is passed through the sample and imaged on a sensitive photographic, or now an image, plane. The resolution of such a system can be at the 0.1-nm level and provides useful information that is below the resolution limit of the conventional optical microscope. A problem with this method is that the high

energy electron beam (100–200 kV) can produce degradation of the sample, and resolution that is usually associated with high acceleration voltages has to be balanced against the time required to produce an satisfactory image. Transmission electron microscopy (TEM) method has allowed visualization of the chain packing in polyethylene-type of polymer (137). The TEM method requires that the sample be thinned to dimensions which allow the electron beam to pass through the material which is typically below 100 nm. This requirement usually necessitates that the section be prepared using a cold working microtome which generates wafers that are of the order of a few tens of nanometers thick. The TEM method can be used to provide electron diffraction data that can be used to calculate the molecular spacing in crystalline phases in the polymer material. This type of information is very complementary to that obtained from X-ray diffraction, and with the use of computer models of the order structure it is impossible to obtain quite a precise definition of the chain-packing dimensions and orientation (138). The alternative and slightly lower resolution approach to electron microscopy is scanning electron microscopy (SEM) (139). In SEM, the back-scattering of electrons used to provide information on the structure of polymers has resolution limits and cannot normally provide molecular resolution data. The back-scattered electron has an energy which is characteristic of the atoms that produce the scattering, and imaging selective on a particular atomic distribution is possible (140). However, for polymers this is, not usually used as the resolution of light atoms such as carbon and oxygen is very difficult and the method is only useful for heavy atoms. It is, however, possible to identify the segregation of metal catalyst residues in polyolefins. Electron microscopic techniques usually require that the sample be coated with conducting media to avoid loss of resolution as a consequence of the buildup of trapped charge, and hence sample preparation can be problematic.

Supermolecular Organization. Both in biological and synthetic polymer systems, the local order at the nanometer scale very rarely extends to the micro level (140). Interruption of the chain packing occurs by either chain folding or conformational defects leading to major disruption in the perfection of the chain packing. A variety of models have been formulated to assist visualization of these structures, an example of which is the so-called fringe micelle model. Much of our knowledge of the organization at this lengthy scale is obtained from either TEM or SEM studies combined with X-ray diffraction measurements. The SEM technique is ideally suited for the study of polymers allowing the magnification to be changed from relatively low values, where the object can be imaged at optical resolution, to length scales which are submicron to those where the resolution approaches the subnanometer scale. The organization of the polymer chains observed at this scale reflects the packing of smaller scale crystallites and allows visualization of liquid crystalline order within extended domains of the polymer. The discussion of this level of organization is often referred to under the general heading of textured polymer and may, in the case of a polymer such as cellulose, be constrained to the microfibrils. In polyethylene, the organization of the crystalline lamellar structures within domains leads to the creation of microcrystallites that can have micron-size dimensions or larger (130,131) but from the point of view of their mechanical properties are distinct entities. The dimensions of the range of the structure at this level are defined by the extent to which the entity can be considered to have identifiable physical properties. In polyethylene, the cool deformation

of the substrate can lead to significant alignment of the crystallites and enhancement of the modulus in the direction of the applied stress. The alignment of the crystallites, however, has a negative effect: enhancement of the modulus in one direction leads to a reduction in the strength in the direction transverse to the draw direction (130). The development of anisotropy in a crystalline solid can be visualized from examination of the angular dependence of the X-ray scattering plots. The "pole" diagrams (131), which is a plot of scattering intensity as a function of the direction of the draw axis to the X-ray beam axis, allow the extent of the anisotropy to be determined.

Optical Microscopy. Traditionally, light microscopy has played an important role in the visualization of ordered polymers, and a range of different approaches can be adopted to enhance the contrast, phase contrast, polarized light microscopy, orientation birefringence, strain birefringence, modulated contrast, interference microscopy, etc (132,141–144). Light microscopy rarely provides resolution better than several micrometers but can give a quick and easy assessment of the extent of order in the polymer material.

Scanning Atomic Force Microscopy and Related Methods. Whereas the characterization of the structure of the bulk solid is of relevance to the mechanical properties, a knowledge of the surface structure may be important in understanding adsorption (qv), tribology, friction, adhesion, and other surface-dominated phenomena (145,146) (see SURFACE PROPERTIES). The development of atomic force microscopy (qv) (AFM) has allowed imaging at better than a nanometer resolution of phase-separated and similar structure (147) (see also SCANNING FORCE, MICROSCOPY). The surface analytical techniques will not be included in this review but do provide a very important part of the characterization of atomic composition and alignment and segregation of the polymer chains in the surfaces (22) (see SURFACE ANALYSIS).

Positron Annihilation Lifetime Spectroscopy (PALS). A positive electron of very high energy can penetrate matter and through inelastic collisions be slowed down until it has thermal energies. The inelastic collisions will often produce damage resulting in the emission of electrons. The combination of a positron (+ve electron) with an electron forms positronium. Positronium is only stable if thermalized within a void of molecular dimensions. The para-positronium can undergo spin allowed annihilate with the generation of energy. The ortho-positronoium does not have the correct spin and will usually annihilate through spin exchange with the electrons that form the walls of the cavity in which it resides. The process allows determination of the size of the molecular cavity through the lifetime of the ortho-positronium annihilation and the intensity is directly proportional to the number density of the events. The voids measured by this method are essentially those associated with the free volume in an amorphous polymer. Study of PALS can indicate the mechanisms of aging, plasticization, gas diffusion, and other processes that are morphologically controlled in a disordered material (148).

Molecular Dynamics of Polymer Systems

Physical properties are a reflection of the degree and extent of the freedom of the polymer molecule to undergo spatial rearrangement as a consequence of thermal

or an applied perturbation. A variety of methods exist which allow the direct probing of these molecular motions.

Nuclear Magnetic Resonance—Relaxation Time Measurements. The NMR method is usually used in solution for the determination of the structure of a polymer; however, when used in the Fourier transform model it can also probe the rate at which nuclei reorientate within the applied magnetic field (22,122). The relaxation of a particular nucleus can be used to characterize the motion of a specific group. ^{1}H NMR signals are usually not sufficiently decoupled from one another to allow the motion of individual groups to be characterized, and it is usual to limit the discussion to gross differences as between aliphatic and aromatic protons. The low natural abundance of the ^{13}C nucleus allows separation of the resonance of individual groups, and hence the relative rates of the motion between individual atoms can be probe (122). In practice, this level of detailed information can only be obtained for polymer molecules dispersed in solution; the equivalent solid-state spectrum reflects a more highly coupled state in which motions are not resolved. Solid state is sensitive to short-range interactions and has been used to study crystallinity, rotational transitions, relative orientations of polymer chains, solid glassy polymers, compatibility of solid polymer blends, and cross-linking and entanglement (149,155).

Dielectric Relaxation Spectroscopy. Many polymers contain polar groups and the internal motions of these groups lead to fluctuations in the local dielectric permittivity. Measurement of the dielectric relaxation (qv) spectrum over a broad frequency range (10^{-3}–10^{10} Hz) can provide valuable information on the dynamic nature of a polymer at any given temperature (156–162). As with other relaxation measurements, it is conventional to combine temperature and frequency to allow calculation of activation energies and map the dynamics of the polymer system. Because of the breadth of most relaxation processes, it is desirable to explore the influence of factors such as molar mass and morphology on the distribution parameter describing the motion of the dipoles. Various approaches have been used to describe the distribution parameter; however, the most adaptable is that of Havriliak and Negami (163,164). The parameters obtained have no molecular significance, but provide a method of characterizing the influence of various factors on the process being investigated. In amorphous polymers, DRS has been extensively used for the study of sub-T_g processes and, in particular, the effects of physical aging on the nature of these relaxation processes. In the case of thermosets, DRS can be used to monitor the cure process (165,166). In solution, DRS has the capability of probing the backbone local dynamics, and studies as a function of molar mass allow an understanding of the development of cooperative motion as the chain length is increased.

Electron Spin Resonance Spectroscopy. Through the use of stable free-radical species, it has been possible to follow the relaxation processes of these labels and infer the nature of the motion of the elements of the polymer chain to which they are attached. This technique is limited, in that it does not see the actual motion of the linkage to which the probe is attached to the polymer but can provide important information on the nature of the effects of the matrix on the motion of the probe (167–175) (see ELECTRON SPIN RESONANCE).

Luminescence. Many polymer groups, eg naphthalene, are able to exhibit fluorescence, or even phosphorescence, when exposed to light of a suitable

excitation frequency. If the excitation is polarized, it is possible to follow the subsequent motion of the probe during the fluorescence or phosphorescence lifetime. The technique has been successfully applied to the study of a range of polymer systems.

Combining the data obtained from a range of dynamic observations of polymers, it is possible to develop an understanding of the factors that influence the physical properties of these materials. It is clear that short-range forces can control both side-chain and local motion of the polymer backbone. However, in an amorphous solid, provided the motions of the backbone are thermally labile, it is free volume which dictates the temperature at which the T_g occurs (176–180).

Rheology and Melt Flow Behavior. In many applications the ability of the polymer to undergo flow under the influence of an applied force is critical in understanding whether or not that material can be processed using a particular technology. A variety of different types of equipment exist for the measurement of flow under particular constraints: constant shear stress, constant strain, elongation flow, normal force measurements, oscillatory stress, capillary flow, etc. A typical polymer when subjected to oscillatory shear will exhibit a viscosity that reflects the ease with which it can move. Low molar mass polymers exhibit flow characteristics which are similar to simple liquids and are said to be Newtonian. However, as the chain length increases, cooperative motions of the chain become possible leading to the so-called *normal mode* relaxation processes. These collective motions of a flexible polymer chain are a function of the length of the chain and molar mass. These motions will contribute to the flow resistance at low rates of shear but, as the frequency is increased, cease to be able to contribute and lead to the observation of a lower effective viscosity-shear thinning. This phenomenon is observed in many polymer systems and is molar mass dependent. If the chain is sufficiently long, then entanglement is possible and additional constraints are imposed on the flow, and a marked increase in viscosity is observed. For low molar masses the viscosity (η) varies as $\eta \propto M_n$ whereas for polymers above a certain critical molar mass M_c, the viscosity varies as $\eta \propto M_n^{3.5}$. Many applications of polymers in the melt phase require knowledge of M_c that typically has a value of 1.5×10^4 to 6×10^4 for most materials (181–184) (see RHEOLOGICAL MEASUREMENTS).

Thermosetting Polymer Systems

An important group of polymers are classified as being thermosetting materials (165) (see THERMOSETS). The chemistry associated with their formation is often the same as that used for thermoplastic materials, except that in the case of these polymers the monomers used have more than two functions per monomer unit. It is therefore possible to have two materials that ostensibly look chemically similar, but one is a thermoplastic and the other a thermoset. This situation is to be found in Polyurethanes (qv) where, depending on the functionality of the isocyanate or soft block used, the resulting material may be a thermoplastic or a thermoset. In most cases it is desirable to monitor the cure process to avoid either too slow a formation of the three-dimensional network, and hence poor production efficiency, or too quick a cure with the possibility of excessive exotherms and possible degradation of the material. The formation of a network for a material that has a T_g above

the cure temperature can also lead to trapped stresses, and these will usually have to be relieved by post-thermal treatment. A number of rheological, thermal, dielectric relaxation, and spectroscopic methods exist for the monitoring of the cure processes. The techniques used for the study of thermoplastics are generally appropriate for the study of thermosets, provided flow is not required to make the observation.

Other Important Characteristics of Polymers

In terms of application, polymers are used in a variety of different ways that lead to the requirement to measure specific physical properties.

Electrical Characteristics. Although polymers have been traditionally used as insulators, in recent years the ability to achieve intrinsic conductivity has been demonstrated and is associated with systems in which the backbone has developed an extended delocalized electronic structure, eg polyacetylene. Other materials such as poly(vinyl chloride) or polyethylene are used in electric insulation applications. In the latter it is their ability to inhibit electron migration that is the important characteristic. A range of tests exists to help measure such features as the electric breakdown resistance. Other specific types of property observed in polymers include semiconductivity, photoconductivity, piezoelectricity, pyroelectricity, and static electrical charging (triboelectricity). Each of these features is a direct consequence of a combination of chemical and specific morphological feature in the polymer or composite material. These properties have been used to specific effect in microphones, load speakers, photocopying, display technology, etc (185–188) (see ELECTRICALLY ACTIVE POLYMERS; PIEZOELECTRIC POLYMERS).

Stability. Polymers are used in a wide range of environments and their ability to resist environmental factors is often a determining factor in their application. The factors which will lead to degradation include mechanical stresses due to handling, radiation, light, X-rays, and gamma rays; exposure to various gases including oxygen, ozone, sulfur dioxide, nitrogen dioxide and to solvents and corrosive chemicals; and strong acids and strong bases. A variety of different specific tests exist for the study of these features and relate to specific problems. The most commonly encountered problem is thermal degradation associated with injection molding and similar methods and directly related to the relative stability of particular bonds forming the backbone and side chains (189) (see DEGRADATION; STABILIZATION).

Permeability. Many polymers are used in packaging and, in particular, for food. In this latter case the permeability to gases and vapors is of prime importance. The permeation or transmission of a gas or vapor is a function of the solubility of a gas or vapor in the polymer and the rate of diffusion through the matrix. The permeability coefficient, diffusion constant, and solubility coefficients can all be measured and are influenced by the chemical structure and morphology. In order to achieve the required permeability characteristics it is common to co-extrude a series of polymers to form a laminated structure. Such materials allow selective permeation of a specific species and enhance the life of the product (190,191) (see TRANSPORT PROPERTIES).

Flammability. The ability to withstand exposure to fire is often a critically important feature when selecting a specific plastic for a particular application. The *oxygen index*, defined as the percentage of oxygen in an oxygen/nitrogen mixture required to sustain combustion, is often used to rank plastics. The higher the value the better the material's ability to withstand exposure to heat. TGA data is often used to assess the degradation characteristics of a polymer; however, specific simulation tests are required to determine how factors such as heat flow, thermal conductivity, drip, etc, in reality influence the burning characteristics of a material (192) (see FLAMMABILITY; FIRE RETARDANTS).

Solubility. Solubility of a polymer will reflect the compatibility with the solvent. For a polymer to be dissolved there is a requirement for the forces between the solvent to match those between the elements of the polymer itself. If the match is close, then it is possible to create a situation in which the dissolved polymer is in a collapsed state corresponding to the thermodynamic requirements of the theta condition. At this point the forces between the segments balance the forces between the segments and the solvent. If the strength of the interaction is increased, the quality of the solvent is improved and the effective size of the polymer increases; it swells. Thermoplastic polymers can be completely dissolved in a good solvent, whereas thermoset materials are only able to swell to a size that reflects the cross-link density of the matrix. It is possible for two nonsolvents to combine to form a solvating mixture, and this phenomenon is termed co-solvency (see MISCIBILITY).

Density. The ability to achieve a particular level of packing is critical in determining the density of a material and is directly related to the morphology of the polymer. The density may be measured directly or alternatively by determination of the composition of a liquid in which the material is just buoyant (193).

A comprehensive survey of test methods is to be found in the *Handbook of Polymer Testing* (194).

BIBLIOGRAPHY

"Characterization of Polymers" in *EPST* 1st ed., Vol. 3, pp. 611–631, by W. R. Sorenson, Continental Oil Co.; in *EPSE* 2nd ed., Vol. 3, pp. 290–327, by W. J. Freeman, Hercules, Inc.

1. R. Koningsveld, *Adv. Polym. Sci.* **7**, 1 (1970).
2. L. H. Tung, ed., *Fractionation of Synthetic Polymers: Principles and Practices*, Marcel Dekker, Inc., New York, 1977.
3. L. H. Tung, ed., *J. Macromol. Sci. Rev. Makromol. Chem.* **6**(1), 58 (1971).
4. T. Y. Chang, *Adv. Polym. Sci.* **163**, 1 (2003).
5. G. Reiss and P. Callot, in L. H. Tung, ed., *Fractionation of Synthetic Polymers: Principles and Practices*, Marcel Dekker, Inc., New York, 1977.
6. C. A. Fonseca and I. R. Harrison, in R. A. Pethrick and J. V. Dawkins, eds., *Modern Techniques for Polymer Characterization*, John Wiley & Sons, Inc., New York, 2003, pp. 1–13.
7. P. Vastamaki, M. Jussila, and M. L. Riekkola, *Analyst* **128**, 1243 (2003).
8. J. B. P. Soares and A. E. Hamielec, in R. A. Pethrick and J. V. Dawkins, eds., *Modern Techniques for Polymer Characterization*, John Wiley & Sons, Inc., New York, 2003, pp. 1–13.

9. J. Janca, in R. A. Pethrick and J. V. Dawkins, eds., *Modern Techniques for Polymer Characterization*, John Wiley & Sons, Inc., New York, 2003. pp. 1–13,
10. B. Folie, M. Keltchtermans, J. R. Shutt, H. Schoneman, and V. J. Krukonis, *J. Appl. Polym. Sci.* **64**, 2015 (1997).
11. J. J. Watkins, V. J. Krukonis, P. D. Condo, D. Pradham, and P. Ehrlich, *J. Supercrit. Fluids* **4**, 24 (1991).
12. J. C. Giddings, *Sep. Sci.* **1**, 123 (1966).
13. G. H. Thompson, M. N. Myers, J. C. Giddings, *Sep. Sci.* **2**, 797 (1967).
14. K. D. Caldwell, L. K. Kesner, M. N. Myer, and J. C. Giddings, *Science* **176**, 296 (1972).
15. S. Loske, A. Schneider, and B. A. Wolf, *Macromolecules* **36**, 5008 (2003).
16. G. E. Kassalainen and S. K. R. Williams, *J. Chromatogr. A* **988**, 285 (2003).
17. N. Hugenberg, S. Loske, A. H. E. Muller, W. Schartl, M. Schmidt, P. F. W. Simon, A. Strack, and B. A. Wolf, *J. Non-Cryst. Solids* **307**, 765 (2002).
18. J. C. Giddings, *J. Chem. Educ.* **50**, 667 (1973).
19. J. C. Giddings, M. N. Meyers, F. J. F. Yang, and J. K. Smith, in M. Kerker, ed., *Colloid and Interfacial Science*, Vol. 4, Academic Press, Inc., New York, 1976, pp. 381–398.
20. J. C. Giddings, K. A. Graff, K. D. Caldwell, and M. N. Meyers, *Adv. Chem. Ser.* **203**, 257 (1983).
21. H. Inagaki, *Adv. Polymer Sci.* **24**, 189 (1977).
22. D. Campbell, R. A. Pethrick, and J. R. White, *Polymer Characterization: Physical Techniques*, Stanley Thornes (Publishers) Ltd., Cheltenham, U.K., 2000, p. 38.
23. P. C. Painter, M. M. Coleman, and J. L. Koenig, *The Theory of Vibrational Spectroscopy and Its Application to Polymeric Materials*, John Wiley & Sons, Inc., New York, 1982.
24. J. Haslam, H. A. Willis, and D. C. M. Squirell, *Identification and Analysis of Plastics*, 2nd ed., Butterworth Publishers Ltd., London, 1972.
25. P. J. Hendra, *Adv. Polym. Sci.* **6**, 151 (1969).
26. B. Jasse, in J. V. Dawkins, ed., *Developments in Polymer Characterization*, Vol. 4, Elsevier Applied Science Publishers, Ltd., Barking, U.K., 1983.
27. D. J. Cutler, P. J. Hendra, and G. Fraser, *Laser Raman Spectroscopy of Synthetic Polymers*, Vol. 2, Elsevier Applied Science Publishers, Ltd., Barking, U.K., 1980, p. 121.
28. R. S. McDonald, *Anal. Chem.* **54**, 1250 (1982).
29. W. Y. Yeh and R. J. Young, *J. Macromol. Sci., Phys. B* **37**, 83–118 (1998).
30. V. Galitsyn, S. Khizhnyak, P. Pakhomov, and A. Tshmel, *J. Macromol. Sci., Phys. B* **42**, 1085–1095 (2003).
31. S. Webster and D. I. Bower, *Polymer* **36**, 4351–4353 (1995).
32. T. Achibat, A. Boukenter, E. Duval, A. Mermet, M. Aboulfaraj, S. Etienne, and C. Gsell, *Polymer* **36**, 251–257 (1995).
33. J. L. Koenig, *Spectroscopy of Polymers*, American Chemical Society, Washington, D.C., 1992. ACS Professional Reference Book.
34. J. M. Chalmers, M. W. Mackenzie, H. A. Willis, H. G. M. Edwards, J. S. Lees, and D. A. Long, *Spectrochim. Acta, Part A: Mol. Biomol. Spectrsc.* **47**, 1677–1683 (1991).
35. R. P. Wool, *Bull. Am. Phys. Soc.* **26**, 327 (1981).
36. R. J. Jakobsen, in J. R. Ferraro and L. J. Basile, eds., *Fourier Transform Infrared Spectroscopy: Applications to Chemical Systems*, Vol. 1, Academic Press, Inc., New York, 1978, pp. 61–97.
37. F. A. Bovey, *High Resolution NMR of Macromolecules*, Academic Press, Inc., New York, 1972.
38. K. J. Ivin, *Pure Appl. Chem.* **55**, 1529 (1983).
39. V. J. McBrierty and D. C. Douglass, *J. Polym. Sci., Macromol. Rev.* **16**, 195 (1981).
40. B. C. Gerstein, *Anal. Chem.* **55**, 781A, 899A (1983).

41. J. R. Havens and J. L. Koenig, *Applications of High Resolution Carbon -13 NMR Method*, Academic Press, Inc., New York, 1977.
42. K. Wuthrich, *NMR of Proteins and Nucleic Acids*, John Wiley & Sons, Inc., New York, 1986.
43. D. M. Grant and E. G. Paul, *J. Am. Chem. Soc.* **86**, 2984 (1964).
44. C. Delides, R. A. Pethrick, A. V. Cunliffe, and P. G. Klein, *Polymer* **22**, 1205 (1981).
45. A. V. Cunliffe and R. A. Pethrick, *Polymer* **21**, 1026 (1980).
46. J. C. Randall, *Polymer Sequence Determination, Carbon-13 NMR Method*, Academic Press, Inc., New York, 1977.
47. R. A. Pethrick and B. Thomson, *Br. Polym. J.* **18**(3), 171–180 (1986).
48. R. A. Pethrick and B. Thomson, *Br. Polym. J.* **18**, 380–386 (1986).
49. J. B. Stothers, *Carbon-13 NMR Spectroscopy*, Academic Press, Inc., New York, 1972.
50. R. J. Abraham, J. Fisher, and P. Loftus, *Introduction to NMR Spectroscopy*, John Wiley & Sons, Inc., Chichester, U.K., 1988.
51. J. Clauss, K. Schmidtrohr, and H. W. Spiess, *Acta Polym.* **44**(1), 1–17 (1993).
52. J. B. Miller, *J. Therm. Anal.* **49**, 521–524 (1997).
53. F. Horii, H. Kaji, H. Ishida, K. Kuwabara, K. Masuda, and T. Tai, *J. Mol. Struct.* **441**, 303–311 (1998).
54. K. Landfester and H. W. Spiess, *Acta Polym.* **49**, 451–464 (1998).
55. H. N. Cheng and A. D. English, *ACS Symp. Series* **834**, 3–20 (2003).
56. P. Robyr, Z. Gan, and U. W. Suter, *Macromolecules* **31**, 8918–8923 (1998).
57. E. Klesper, in D. O. Huummel, ed., *Polymer Spectroscopy*, Verlag Chemie, Weinheim, Germany, 1974, Chapt. 1
58. S. Hafner, D. E. Demco, and R. Kimmich, *Solid State Nucl. Magn. Reson.* **6**, 275–293 (1996).
59. B. Blumich and P. Blumler, *Makromol. Chem., Macromol. Chem. Phys.* **194**, 2133–2161 (1993).
60. W. J. Irwin, *Analytical Pyrolysis: A Comprehensive Guide, Vol. 22, Chromatographic Science Series*, Marcel Dekker, Inc., New York, 1982.
61. C. J. Wolf, M. A. Grayson, and D. L. Fanter, *Anal. Chem.* **52**, 348A (1980).
62. S. A. Liebman and E. J. Levy, *Adv. Chem. Ser.* **203**, 617 (1983).
63. E. Reiner and T. F. Mason, *Adv. Chem. Ser.* **203**, 703 (1983).
64. F. L. Bayer, *Adv. Chem. Ser.* **203**, 693 (1983).
65. C. G. Smith, *J. Anal. Appl. Pyrolysis* **15**, 209–216 (1989).
66. J. K. Haken and P. I. Iddamalgoda, *J. Chromatogr. A* **756**, 1–20 (1996).
67. J. K. Haken, *J. Chromatogr. A* **825**, 171–187 (1998).
68. F. C. Y. Wang, *J. Chromatogr. A* **843**, 413–423 (1999).
69. J. W. Lyons, D. Poche, F. C. Y. Wang, and P. B. Smith, *Adv. Mater.* **12**, 1847–1854 (2000).
70. S. S. Choi, *J. Anal. Appl. Pyrolysis* **57**, 249–259 (2001).
71. N. N. Barashkov, and O. A. S. Gunder, *Fluorescent Polymers, Polymer Science and Technology, Ellis Horwood Series*, Chichester, U.K., 1994.
72. M. Freemantle, *Chem. Eng. News* **81**(8), 6 (2003).
73. E. Scamporrino and D. Vitalini, in R. A. Pethrick and J. V. Dawkins, eds., *Modern Techniques for Polymer Characterization*, John Wiley & Sons, Inc., New York, 2003, p. 233.
74. R. J. Cotter, *Anal. Chem.* **64**, 1027A (1992).
75. R. S. Brown and J. J. Lennon, *Anal. Chem.* **67**, 1998 (1995).
76. G. Montaudo, *Polym. Prepr*. 290 (1996).
77. E. Scamporrrino, D. Vitalini, and P. Mineo, *Macromolecules* **29**, 5520 (1996).
78. M. Karas, U. Bahr, A. Deppe, B. Stahl, F. Hillenkamp, and U. Giessmann, *Makromol. Chem. Macromol. Symp.* **61**, 397–404 (1992).

79. S. D. Hanton, *Chem. Rev.* **101**, 527–569 (2001).
80. L. Q. Muang, A. Paiva, R. Bhat, and M. Wong, *J. Am. Soc. Mass Spectrosc.* **7**, 1219 (1996).
81. N. Aust, I. Beytollahi-Amtmann, and K. Lederer, *Int. J. Polym. Anal. Charact.* **1**, 245–258 (1995).
82. G. Lapienis and S. Penczek, *Macromol. Symp.* **195**, 317 (2003).
83. Y. Brun, *J. Liq. Chromatogr. Relat. Technol.* **21**, 1979–2015 (1998).
84. W. S. Bahary, M. P. Hogan, M. Jilani, and M. P. Aronson, *Adv. Chem. Ser.* **247**, 151–166 (1995).
85. M. Netopilik, *J. Chromatogr. A* **915**, 15–24 (2001).
86. M. Netopilik, *Polymer* **35**, 4799–4803 (1994).
87. B. Trathnigg, S. Feichtenhofer, and M. Kollroser, *J. Chromatogr. A* **786**, 75–84 (1997).
88. M. Helmstedt and J. Stejskal, *Int. J. Polym. Anal. Charact.* **4**, 219–230 (1998).
89. M. Andersson, B. Wittgren, and K. G. Wahlund, *Anal. Chem.* **75**, 4279–4291 (2003).
90. U. Zucchi and G. Cecchin, *Adv. Polym. Sci.* **51**, 108 (1983).
91. H. G. Ellias, *Macromolecules*, Vols. 1 and 2, Plenum Press, New York, 1977.
92. T. C. Ward, *J. Chem Educ.* **58**, 867 (1981).
93. W. Burchard, *Adv. Polym. Sci.* **48**, 1 (1983).
94. P. Kratochvil, *Pure Appl. Chem.* **54**, 379 (1982).
95. H. Pasch, *Macromol. Symp.* **178**, 25–37 (2002).
96. H. Pasch, *Macromol. Symp.* **174**, 403–412 (2001).
97. H. Pasch, *Adv. Polym. Sci.* **150**, 1–66 (2000).
98. H. Pasch, *Phys. Chem. Chem. Phys.* **1**, 3879–3890 (1999).
99. W. Burchard, *Adv. Polym. Sci.* **143**, 113–194 (1999).
100. H. Pasch, *Adv. Polym. Sci.* **128**, 1–45 (1997).
101. A. Jacobs and O. Dahlman, *Nord. Pulp Paper Res. J.* **15**, 120–127 (2000).
102. J. Spickermann, H. J. Rader, K. Mullen, B. Muller, M. Gerle, K. Fischer, and M. Schmidt, *Macromol. Rapid Commun.* **17**, 885–896 (1996).
103. J. Brandrup, E. H. Immergut, E. A. Grulke, and D. Bloch, eds., *Polymer Handbook*, 4th ed., John Wiley & Sons, Inc., New York, 1999.
104. W. L. Mattice and U. W. Suter, *Conformational Theory of Large Molecules: The Rotational Isomeric State Model in Macromolecular Systems*, John Wiley & Sons, Inc., New York, 1994.
105. P. Blumler and B. Blumich, *Rubber Chem. Technol.* **70**, 468–518 (1997).
106. P. B. Smith, A. J. Pasztor, M. L. McKelvy, D. M. Meunier, S. W. Froelicher, and F. C. Y. Wang, *Anal. Chem*. R95–R121 (1997).
107. L. C. E. Struick, *Internal Stresses, Dimensional Instabilities and Molecular Orientation in Plastics*, John Wiley & Sons, Inc., New York, 1990.
108. R. H. Still, *Br. Polym. J.* **11**(3), 101 (1979).
109. J. R. Freid, in J. V. Dawkins, ed., *Developments in Polymer Characterization*, Vol. 4, 1983, pp. 39–90.
110. J. N. Hay, in L. S. Bark and N. S. Allan, eds., *Analysis of Polymer Systems*, Applied Science Publishers, London, 1982, pp. 103–154.
111. M. J. Richardson, in J. V. Dawkins, ed., *Developments in Polymer Characterization*, Vol. 1, 1978, pp. 205–244.
112. D. M. Price, M. Reading, T. J. Lever, A. Hammiche, and H. M. Pollock, *Thermochim. Acta* **376**, 95–97, (2001).
113. M. Reading, D. M. Price, D. B. Grandy, R. M. Smith, L. Bozec, M. Conroy, A. Hammiche, and H. M. Pollock, *Macromol. Symp.* **167**, 45–62 (2001).
114. M. Reading, *J. Therm. Anal. Calorim.* **64**(1), 7–14 (2001).

115. F. Oulevey, N. A. Burnham, G. Gremaud, A. J. Kulik, H. M. Pollock, A. Hammiche, M. Reading, M. Song, and D. J. Hourston, *Polymer* **41**, 3087–3092 (2000).
116. D. M. Price, M. Reading, and T. J. Lever, *J. Therm. Anal.* **56**, 673–679 (1999).
117. X. Ramis, A. Cadenato, J. M. Morancho, and J. M. Salla, *Polymer* **44**, 2067–2079 (2003).
118. I. R. Harrison, *Thermochim. Acta* **367**, 85–92 (2001).
119. J. Rieger, *Polym. Test.* **20**(2), 199–204 (2001).
120. J. Wolfrum, G. W. Ehrenstein, and M. A. Avondet, *J. Compos. Mater.* **34**, 1788–1807 (2000).
121. I. Lacik, I. Krupa, M. Stach, A. Kucma, J. Jurciova, and I. Chodak, *Polym. Test.* **19**, 755–771 (2000).
122. R. T. Bailey, A. M. North, and R. A. Pethrick, *Molecular Motion in High Polymers*, Oxford University Press, New York, 1981.
123. R. G. Beaman, *J. Polym. Sci.* **9**, 470 (1952).
124. R. F. Boyer, *J. Appl. Phys.* **25**, 825 (1954).
125. R. F. Boyer, *Polym. Yearbook* **2**, 233–344 (1985).
126. ASTM Standards, American Society for Testing and Materials, Philadelphia Pa., 1984. Web site: www.astm.org.
127. M. L. Williams, R. F. Landel, and J. D. Ferry, *J. Am. Chem. Soc.* **77**, 3701 (1955).
128. A. J. Kinloch and R. J. Young, *Fracture Behavior of Polymers*, Applied Sciences Publishers, New York, 1983, pp. 182–225.
129. R. Brown, *Handbook of Polymer Testing*, Marcel Dekker, Inc., New York, 1999.
130. I. M. Ward, in I. M. Ward, ed., *Structure and Properties of Orientated Polymers*, Applied Science Publishers, London, 1975.
131. B. W. Cherry, *Polymer Surfaces, Cambridge Solid State Science Series*, Cambridge University Press, London, 1981, p. 31.
132. R. A. Pethrick, in R. A. Pethrick and C. Viney, eds., *Techniques for Polymer organization and Morphology Characterization*, John Wiley & Sons, Inc., Chichester, U.K., 2003, pp. 1–30.
133. M. E. Vickers, in R. A. Pethrick and C. Viney, eds., *Techniques for Polymer Organization and Morphology Characterization*, John Wiley & Sons, Inc., Chichester, U.K., 2003, pp. 35–69.
134. A. J. Ryan, J. Stanford, W. Bras, and T. M. W. Nye, *Polymer* **38**, 759 (1997).
135. D. M. Sadler, in I. H. Hall, ed., *Structure of Crystalline Polymers*, Elsevier Applied Science Publishers, New York, 1984, Chapt. 4, p. 125.
136. V. Arrighi, D. C. Bucknall, and A. Triolo, in R. A. Pethrick, and C. Viney, eds., *Techniques for Polymer Organization and Morphology Characterization*, John Wiley & Sons, Inc., Chichester, U.K., 2003, pp. 169–197.
137. E. L. Thomas, in I. H. Hall, ed., *Structure of Crystalline Polymers*, Elsevier Applied Science Publishers, New York, 1984, Chapt. 3, p. 79.
138. R. Vialluzzi, in R. A. Pethrick and C. Viney, eds., *Techniques for Polymer Organization and Morphology Characterization*, John Wiley & Sons, Inc., Chichester, U.K., 2003, pp. 145–163.
139. H. Assender, in R. A. Pethrick and C. Viney, eds., *Techniques for Polymer Organization and Morphology Characterization*, John Wiley & Sons, Inc., Chichester, U.K., 2003, pp. 201–218.
140. D. C. Bassett, *Principles of Polymer Morphology, Cambridge Solid State Science Series*, Cambridge University Press, London, 1981, p. 19.
141. A. D. Curson, in D. A. Hemsley, ed., *Applied Polymer Light Microscopy*, Elsevier Applied Science, Barking, U.K., 1989, p. 19.
142. B. P. Saville, in D. A. Hemsley, ed., *Applied Polymer Light Microscopy*, Elsevier Applied Science, Barking, U.K., 1989, p. 73.

143. R. Hoffman, in D. A. Hemsley, ed., *Applied Polymer Light Microscopy*, Elsevier Applied Science, Barking, U.K., 1989, p. 151.
144. D. A. Hemsley, in D. A. Hemsley, ed., *Applied Polymer Light Microscopy*, Elsevier Applied Science, Barking, U.K., 1989, p. 151.
145. R. A. L. Jones and R. W. Richards, *Polymers at Surfaces and Interfaces*, Cambridge University Press, U.K., 1999, p. 94.
146. D. Sarid, *Scanning Force Microscopy*, Oxford University Press, Oxford, 1994.
147. S. Affrossman, G. Henn, S. A. O'Neil, R. A. Pethrick, and M. Stamm, *Macromolecules* **29**, 5010–5016 (1996).
148. R. A. Pethrick, *Prog. Polym. Sci.* **22**, 1–47 (1997).
149. W. P. Slichter and D. W. McCall, *J. Polym. Sci.* **25**, 230 (1957).
150. M. J. Richardson, *Br. Polym. J.* **1**(3), 132 (1969).
151. J. Schafer, E. O. Stejskal, and R. Buchdal, *Macromolecules* **10**, 384 (1977).
152. K. R. Doolan, *J. Polym. Sci., Part B: Polym. Phys.* **40**, 572–584 (2002).
153. B. C. Min and J. W. Lee, *J. Mol. Liq.* **80**(1), 33–51 (1999).
154. M. Laviolette, M. Auger, and S. Desilets, *Macromolecules* **32**, 1602–1610 (1999).
155. M. Geppi, R. K. Harris, A. M. Kenwright, and B. J. Say, *Solid State Nucl. Magn. Reson.* **12**(1), 15–20 (1999).
156. J. F. Mano, *J. Macromol. Sci., Phys. B* **42**, 1169–1182 (2003).
157. J. F. Mano and J. L. G. Ribelles, *Macromolecules* **36**, 2816–2824 (2003).
158. J. P. Eloundou, J. F. Gerard, J. P. Pascault, and D. Kranbuehl, *Macromol. Chem. Phys.* **203**, 1974–1982 (2002).
159. J. Mijovic and J. W. Sy, *Macromolecules* **35**, 6370–6376 (2002).
160. J. Mijovic, M. Y. Sun, and Y. F. Han, *Macromolecules* **35**, 6417–6425 (2002).
161. G. Williams, I. K. Smith, G. A. Aldridge, P. A. Holmes, and S. Varma, *Macromolecules* **34**, 7197–7209 (2001).
162. F. Kremer and A. Schonhals, *Broadband Dielectric Spectroscopy*, Springer, Berlin, 2003.
163. S. Havriliak and J. Havriliak, *Dielectric and Mechanical Relaxation in Materials*, Hanser Publishers, Munich, 1997.
164. C. C. Ku, and R. Liepins, *Electrical Properties of Polymers-Chemical Principles*, Hanser Publishers, Munich, 1987.
165. R. A. Pethrick, in A. K. Kulshreshtha and C. Vasile, eds., *Handbook of Polymer Blends and Composites*, Vol. 1, RAPRA Technology, Shrewsbury, U.K., 2002, Chapt. 10, p. 393.
166. R. A. Pethrick and D. Hayward, *Prog. Polym. Sci.* **27**, 1983–2017 (2002).
167. F. Lembicz, *Polimery* **48**, 557–560 (2003).
168. Y. Miwa, T. Tanase, K. Yamamoto, M. Sakaguchi, M. Sakai, and S. Shimada, *Macromolecules* **36**, 3235–3239 (2003).
169. K. Kruczala, B. Varghese, B. G. Bokria, and S. Schlick, *Macromolecules* **36**, 1899–1908 (2003).
170. M. Lucarini, G. F. Pedulli, and M. V. Motyakin, and S. Schlick, *Prog. Polym. Sci.* **28**, 331–340 (2003).
171. Z. Veksli, M. Andreis, and B. Rakvin, *Prog. Polym. Sci.* **25**, 949–986 (2000).
172. E. J. Harbron, V. P. McCaffrey, R. X. Xu, and M. D. E. Forbes, *J. Am. Chem. Soc.* **122**, 9182–9188 (2000).
173. G. G. Cameron, M. Y. Qureshi, and S. C. Tavern, *Eur. Polym. J.* **32**, 587–591 (1996).
174. G. G. Cameron, D. Stewart, R. Buscall, and J. Nemcek, *Polymer* **35**, 3384–3388 (1994).
175. G. G. Cameron, I. S. Miles, and A. T. Bullock, *Br. Polym. J.* **19**(2), 129–134 (1987).
176. M. Danko, P. Hrdlovic, and E. Borsig, *Chem. Listy* **97**, 1052–1060 (2003).

177. S. Kimata, D. L. Jiang, and T. Aida, *J. Polym. Sci., Polym. Chem.* **41**, 3524–3530 (2003).
178. J. Duhamel, S. Kanagalingam, T. J. O'Brien, and M. W. Ingratta, *J. Am. Chem. Soc.* **125**, 12810–12822 (2003).
179. R. A. L. Vallee, M. Cotlet, J. Hotkens, and F. C. De Schryver, *Macromolecules* **36**, 7752–7758 (2003).
180. R. A. L. Vallee, N. Tomczak, L. Kuipers, G. J. Vancso, and N. F. van Hulst, *Phys. Rev. Lett.* **91**, 38301 (2003).
181. M. Doi and S. F. Edwards, *The Theory of Polymer Dynamics*, Oxford Science Publications, Oxford, 1986.
182. J. D. Ferry, *Viscoelastic Properties of Polymers*, John Wiley & Sons, Inc., New York, 1970.
183. R. Byron Bird, R. C. Armstrong, and O. Hassager, *Dynamic of Polymeric Liquids*, Vol. 1; with C. F. Curtis, Vol. 2, John Wiley & Sons, Inc., New York, 1987.
184. A. A. Collyer, *Techniques in Rheological Measurement*, Chapman and Hall, London, 1993.
185. J. I. Kroschwitz, *Electrical and Electronic Properties of Polymers: A State of the Art Compendium*, John Wiley & Sons, Inc., New York, 1988.
186. H. Kuzmany, M. Mehring, and S. Roth, *Electronic Properties of Conjugated Polymers Solid State Sciences*, Vol. 76, Springer-Verlag, Berlin, 1987.
187. H. Kuzmany, M. Mehring, and S. Roth, *Electronic Properties of Conjugated Polymers Solid State Sciences*, Vol. 63, Springer-Verlag, Berlin, 1985.
188. G. Zerbi, *Polyconjugated Materials*, European Materials Research Society, Amsterdam, 1992.
189. D. Kockott, in R. Brown, ed., *Polymer Testing*, Marcel Dekker, Inc., New York, 1999, p. 697.
190. D. Hands, in R. Brown, ed., *Polymer Testing*, Marcel Dekker, Inc., New York, 1999, p. 747.
191. J. Crank, *The Mathematics of Diffusion*, Oxford Science Publications, Oxford, 1985.
192. K. Paul, in R. Brown, ed., *Handbook of Polymer Testing*, Marcel Dekker, Inc., New York, 1999, p. 659.
193. R. Brown, in R. Brown, ed., *Handbook of Polymer Testing*, Marcel Dekker, Inc., New York, 1999, p. 157.
194. R. Brown, ed., *Handbook of Polymer Testing*, Marcel Dekker, Inc., New York, 1999.

RICHARD A. PETHRICK
University of Strathclyde

CHITIN AND CHITOSAN. See Volume 1.

CHLOROPRENE POLYMERS

Introduction

Polychloroprene [9010-98-4] was discovered in 1930 at E. I. DuPont de Nemours & Co. in Wilmington Delaware. The discovery grew out of a need to develop a synthetic substitute for natural rubber. DuPont first marketed this first commercially successful synthetic elastomer as DuPrene in 1933. In response to new technology development that significantly improved the product and manufacturing process, the name was changed to Neoprene in 1936. The current commercially acceptable generic name for this class of chlorinated elastomers is CR or chloroprene rubber.

Since the time of its introduction to the marketplace, Neoprene has been more than a simple replacement for natural rubber. Like natural rubber, Neoprene is rubbery, resilient, and has high tensile properties. However, Neoprene has better heat stability, better resistance to varying environmental weathering conditions, superior flex life, excellent solvent and oil resistance, and reasonable electrical properties when compared to natural rubber. This unique combination of properties poised Neoprene for solving many of the potential problems besetting the automotive, construction, footwear, specialty apparel, transportation, and wire and cable industry throughout the twentieth century and beyond. The good balance of properties has made the polymer useful in a large divergent list of applications including aircraft, appliance, automotive, bridge pad, chemical-resistant clothing, home furnishings, machinery, mining and oil field belting, underground and undersea cables, recreation, and tires. Current worldwide consumption of polychloroprene approximates 239,239 ton with a value of more than $1.5 billion.

Polymerization Processes

Chloroprene, 2-chloro-1,3-butadiene [126-99-8] monomer undergoes dimerization and autopolymerization when stored at ordinary temperatures. These reactions occur simultaneously by different mechanisms. Free-radical processes normally initiate autopolymerizations. The dimerization reactions are thermally initiated.

Dimerization. The dimerization reactions follow second-order kinetics and involve 2 + 2 and 4 + 2 concerted and nonconcerted cycloaddition reactions. Alternate mechanisms involving Cope rearrangements account for the formation of dichlorocyclooctadiene. The rate of dimer formation is affected both by the temperature and the monomer concentration. Owing to the high (20.9–24 kcal mol^{-1}) activation energy, storage tank temperature is a powerful tool for controlling rates of dimerization (1,2). Free-radical inhibitors do not inhibit chloroprene and dichlorobutadiene dimerization (3–6). As dimerization is one of the major sources of the exothermic heat of reaction, storage vessel temperature control is of primary concern in avoiding uncontrollable runaway reaction during commercial monomer synthesis and storage of chloroprene and dichlorobutadiene.

Encyclopedia of Polymer Science and Technology. Copyright John Wiley & Sons, Inc. All rights reserved.

Dilution of monomer with inert solvents aids the safe shipment of these reactive monomers.

Free-Radical Polymerization. Autopolymerization of chloroprene monomer occurs readily under free-radical and photochemical conditions (see RADICAL POLYMERIZATION). The electron-rich and electronegative chlorine atom facilitates the high reactivity of this monomer. Over the temperature range 20–80°C, the initiation depends on the formation of di-radicals or the added free radical that initiates polymerization (see INITIATORS, FREE-RADICAL). Polymerization proceeds at a rate that follows first-order kinetics with an activation energy of 82 kJ mol^{-1} (19.6 kcal mol^{-1}) and a heat of polymerization of 68–75 kJ mol^{-1} (16–18 kcal mol^{-1}) (1,3,7,8).

$$k(p) = 4.8 \times 10^{-8} s^{-1}$$

Bulk Polymerization. Bulk polymerization is strongly catalyzed by peroxides such as cumene hydroperoxide or chloroprene peroxides. Chloroprene peroxides are formed either by deliberate or adventitious exposure of monomer to oxygen (4,9). Maynard showed that less than 0.1% polymer was formed when specially purified chloroprene monomer was allowed to age in the dark at ambient temperatures for 8 weeks. When chloroprene monomer was exposed to 0.1 mol% oxygen and aged in a similar manner, 19% polymer was formed in only 3 days. Thus, oxygen absorption leading to peroxide formation is a major safety concern in the large-scale manufacture and storage of chloroprene and dichlorobutadiene. Thiodiphenylamine (0.05%) mitigates the problem by reducing the oxygen absorption rate at 25°C by more than four orders of magnitude.

Emulsion Polymerization. Commercial polymers are made by aqueous batch, semicontinuous (semibatch), or continuous free-radical emulsion polymerization. The emulsion system is composed of five components: monomer, surfactant, water, chain-transfer agent, and initiator (2) (see HETEROPHASE POLYMERIZATION). Organic fatty acid salts, sulfonic acid salts, or substituted diterpene salts (sodium abietate) derived from synthetic or natural (eg pine trees) sources constitute the surfactants most commonly employed to stabilize the colloid for emulsion polymerization. Water forms the continuous phase that provides low emulsion viscosity, aids in heat transfer, and compartmentalizes polymerization to allow the rapid formation of high molecular weight polymer where branching can be effectively controlled. Emulsion polymerizations are faster than bulk, solution, or suspension and yield polymers having a much higher molecular weight (10). When used at 0.01–1.5 wt% concentrations, dodecylmercaptan, iodoform, or dialkyl xanthogen disulfides are efficient chain-transfer agents. The molecular weight of chloroprene sulfur copolymers is controlled by a different strategy. Copolymerization of chloroprene with 0.1–2% sulfur followed by cleavage and capping thionyl ends with a combination of 1.0–5.0% tetraethyl thiuram disulfide and 0.25–2.0% sodium dibutyl dithiocarbamate yields a polymer having number-average molecular weights that range up to 500,000 a.m.u. (11).

Polychloroprene emulsion polymerization follows the Smith–Ewert kinetics, developed initially for polystyrene (2). On mixing the monomer, water, and surfactant under high shear, the surfactant molecules will cluster into monomer

swollen micelles and monomer droplets. The micelles number 10^{17}–10^{18} micelles dm^{-3} having diameters ranging from 50 to150 Å. The bulk of the monomer resides in the surfactant-stabilized monomer droplets that number 10^{9}–10^{11} dm^{-3}, with particle diameter ranging from 1 to10 μm. The initiators are generally formed *in situ* by redox reactions of oxidants such as alkali persulfates or peroxides and reducing agents such as alkali sulfites, reducing carbohydrates, or reducing acids. Upon addition of the initiator to the emulsion, free radicals are formed in the emulsion aqueous phase at a rate of 10^{16}–10^{18} radicals dm^{-3} s^{-1}.

Harkins's theory suggests that emulsion polymerization occurs in three intervals. During interval I, or the particle formation phase, the free radicals from initiators either react with monomer in the aqueous phase to propagate oligomeric chains (homogeneous nucleation), enter the micelles to initiate polymerization (micellular nucleation), or less frequently initate polymerization in the much larger and sparser monomer droplets (droplet nucleation). As polymerization continues all micelles continue to grow and are ultimately converted into polymer particles, signaling the start of interval II. During interval II, the polymer particles continue to grow as more monomer diffuses from the droplets to the locus of polymerization. When all monomer has diffused from the droplets to the particles, the monomer droplets disappear, signaling the beginning of interval III. During interval III, polymerization rates initially decrease as the concentration of the monomer has been reduced significantly. At the latter stages of interval III, polymerization rates increase again (Tromsdorff gel effect) because of decreased termination frequency of growing radicals resulting from high internal viscosity (12). At a desired conversion of the monomer, the polymerizations of mercaptan, iodoform, and xanthogen disulfide modified polymerizations or chloroprene–sulfur copolymerizations are quenched with the aid of hindered phenols, alkyl hydroxylamines, or thiodiphenylamine. Typically, an emulsion will contain 30–60% solids at the end of polymerization.

In addition to electrostatic colloid stabilization generated by anionic surfactants, liquid dispersions are also made from nonionic surfactants. Stabilization of the emulsion is achieved by electrosteric stabilization or by pure steric stabilization (2,13). Polyoxyethylene dodecyl ethers, polyoxyethylene nonyl phenyl ethers, and polyoxyethylene nonyl phenol ethers are a few surfactants typically used in emulsion polymerization with nonionic surfactants (14–16). Non-ionic emulsion polymerizations are characterized by lower critical micelle concentration than their ionic counterparts. Thus, the emulsion particle sizes are generally much larger than in the ionic polymerizations. The mechanism of radical entry and exit in polymeric surfactant stabilizer systems are different than in anionic systems. With water-soluble initiators, the kinetics depends on initiator concentration.

Chain-Transfer. In emulsion polymerization, polymer chains grow rapidly to achieve a very high molecular weight. The ultimate polymer molecular weight can, however, be conveniently controlled by chain-transfer agents (AX). A chain-transfer agent, AX, intercepts a growing polymer radical.

$$\mathrm{Rn}\cdot + \mathrm{AX} \xrightarrow{k_{\mathrm{tr,\,AX}}} \mathrm{RnX} + \mathrm{A}\cdot$$

$$\mathrm{A}\cdot + \mathrm{M} \xrightarrow[\text{fast}]{k_{\mathrm{p,\,A}}} \mathrm{R_1}\cdot$$

The active center of the chain-transfer agent reacts with the growing chain to stop further chain propagation. A new free radical, A, is formed from the chain-transfer agent. The new free radical initiates a second polymer chain by reacting with more monomer, M. Thus, the ultimate polymer molecular weight depends on the concentration of the chain-transfer agent (17).

There are at least two conditions that define a chain-transfer agent. A compound becomes a chain-transfer agent if the rate of polymer chain propagation exceeds the rate of chain-transfer.

$$k_p[M] \gg k_{tr,AX}[AX]$$

This condition allows the polymer chain to propagate to a high molecular weight. Secondly, the rate constant for polymer chain propagation, k_p, must be of similar magnitude to the rate constant for re-initiation of the polymer chains by the chain-transfer agent (17). In instances where one or the other condition is not satisfied, the agent could be considered an inhibitor.

$$k_p \geq k_{pA}$$

Thios (eg dodecyl mercaptan), halogenated compounds (eg CBr_4, CCl_4), and activated disulfides such as xanthogen disulfides are normally employed in commercial polychloroprene polymerization.

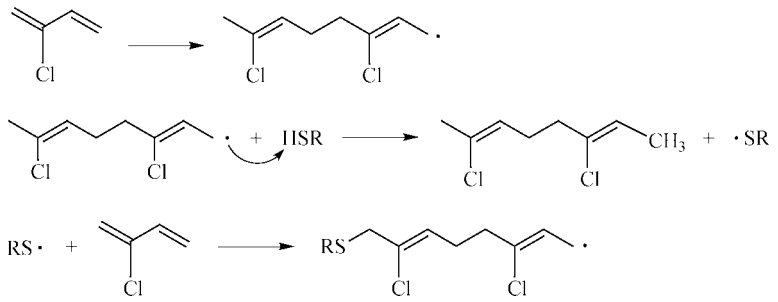

The mechanism of this series of reactions involving dodecyl mercaptan chain-transfer during a high pH polymerization was elucidated using radio-sulfur-tagged dodecylmercaptan (18). The use of multiple chain-transfer agents of different reactivities yielded polymer of more uniform structures (19).

The chain-transfer rate constants, k_{tr}, are determined from the average molecular weight in a polymerizing system. The intercept of a Mayo plot of number-average molecular weight against $[I]/R_p$ where [I] is the initiator concentration and R_p is the polymerization rate (20). Extensive compilations of k_{tr} values are found in the open literature (21). Dodecyl mercaptan is used in the manufacture of commercial Neoprene W. The chain-transfer rate constant for dodecyl mercaptan with chloroprene was determined using the Mayo plot technique (22) as follows:

$$k_{tr,DDM} = 368 \text{ dm}^3/(\text{mol} \cdot s) \text{ at } 40^\circ\text{C}$$

The choice of chain-transfer agents can have an impact on vulcanizate properties. Mercaptan chain-transfer agents yield polymer having nonreactive and dangling end groups. Xanthogen disulfide chain-transfer agents produce polymers having reactive end groups that participate in the vulcanization reaction, contribute to the network structure, and thereby contribute to high modulus of the polymer.

Copolymerization. In free-radical copolymerization (qv), the composition of the copolymer is controlled by the comonomer reactivity ratios (23). The monomer reactivity ratio is defined as the quotient of the rate constants for chain homopropagation to the rate constant for chain cross-propagation.

$$r_A = k_{AA}/k_{AB} \quad r_B = k_{BB}/k_{BA}$$

The expressions are an outcome of the "terminal model" theory with several steady-state assumptions related to free-radical flux (14,23). Based on copolymerization studies and reactivity ratios, chloroprene monomer is much more reactive than most vinyl and diene monomers (Table 1). 2,3-Dichloro-1,3-butadiene is the only commercially important monomer that is competitive with chloroprene in the free-radical copolymerization rate. 2,3-Dichlorobutadiene or "ACR" is used commercially to give crystallization resistance to the finished raw polymer or polymer vulcanizates. α-Cyanoprene (1-cyano-1,3-butadiene) and β-cyanoprene (2-cyano-1,3-butadiene) are also effective in copolymerization with chloroprene but are difficult to manage safely on a commercial scale. Acrylonitrile and methacrylic acid comonomers have been used in limited commercial quantities. Chloroprene–isoprene and chloroprene–styrene copolymers were marketed in low volumes during the 1950s and 1960s. Methyl methacrylate has been utilized in graft polymerization particularly for vinyl adhesive applications. A myriad of other comonomers have been studied in chloroprene copolymerizations but those copolymers have not been used with much commercial success.

Table 1. Chloroprene (M1) Reactivity Ratios

Comonomer M2	r_1	r_2
Acrylonitrile	5.38	0.056
Butadiene	3.41	0.06
2,3-Dichloro-1,3-butadiene	0.31	1.98
1-(2-Hydroxyethylthio)-1,3-butadiene	1.00	0.20
2-Fluoro-1,3-butadiene	3.70	0.22
2-Cyano-1,3-butadiene	0.14	2.8
Diethyl fumarate	6.51	0.02
Isoprene	2.82	0.06
Methacrylic acid	2.7	0.15
Methyl acrylate	10.40	0.06
Methyl methacrylate	6.33	0.08
2,3,3-Trifluoro-1-vinyl cyclobutane	2.71	0.64
Styrene	5.98	0.025
Sulfur	2–4	0.18

Chloroprene–Sulfur Copolymerization. The high reactivities of chloroprene and dichlorobutadiene permit copolymerization with sulfur to yield toluene-insoluble and partially gelled copolymers of high molecular weight. Gelled polymers are highly cross-linked polymers that are insoluble in toluene. In solution or aqueous emulsion polymerization, a growing polychloroprene radical reacts with rhombic (nonpolymeric) sulfur (24) or suitable sulfur donors such as 1,2,3,4-tetrasulfocyclohexane (25) or polysulfides (26) to yield a copolymer. Reaction with elemental sulfur involves cleavage of the eight-membered sulfur in a ring-opening reaction to yield a thionyl-terminated radical.

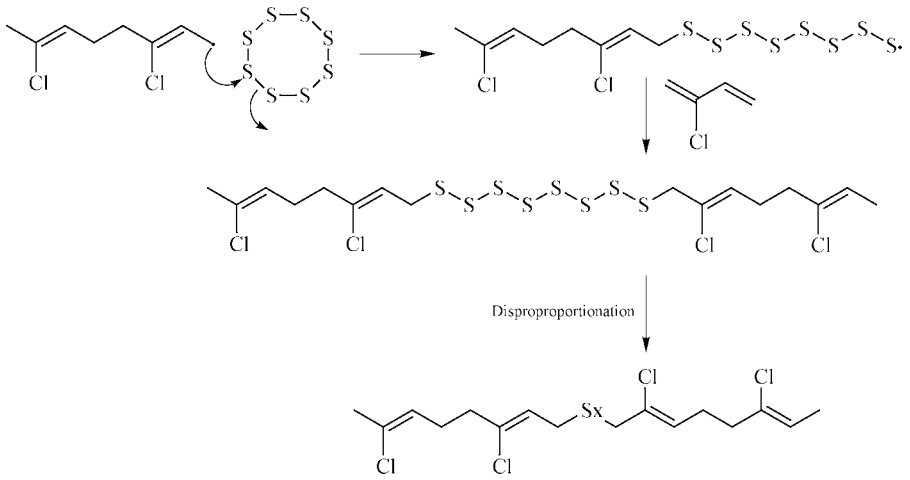

The radical will initiate another homopolymer chain by reaction with more monomer. Finally disproportionation occurs and the sulfur rank is reduced to 3–6 sulfur atoms per block unit. The average number of sulfur atoms between polychloroprene chains or sulfur rank has been explored by ^{1}H NMR. The chemical shift of the methylene hydrogen atoms adjacent to the polythionyl linkages vary from 3.45 to 3.9 ppm (27). It is believed that the sulfur rank for a typical chloroprene–sulfur copolymer contains a predominance of S_3 to S_6 units. The assignment is consistent with ease of reaction of dialkyl polysulfides ($S_x > 2$) with the chemicals normally used in the peptization reactions that follow.

In order for the chloroprene-sulfur copolymer to be useful for rubber processing and curing, the molecular weight or Mooney viscosity must be reduced to approximately 500,000 a.m.u. This molecular weight corresponds to approximately 45 Mooney viscosity, where Mooney viscosity was determined according to ASTM D-1646-96A with a large rotor at 100°C test temperature for 5 min total test time. Molecular weight reduction is achieved by cleaving the sulfur–sulfur bonds of the copolymer through a process termed peptization.

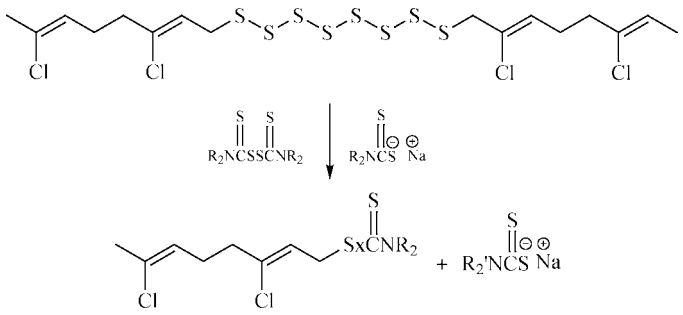

In solution or at the end of emulsion polymerization, tetraalkyl thiuram disulfides are added to the emulsion. Very little reaction occurs at this point. Alkali metal salts of dithiocarbamates, secondary amines, or alkali salts of mercaptobenzothiazole (28) are added to initiate the peptization reaction through sulfur–sulfur bond cleavage. The polychloroprene sulfide ion reacts with the tetraalkyl thiuram disulfide to cap the end of the polymer and generate a second dithiocarbamate salt. The second dithiocarbamate salt propagates the peptization reaction. Thus, the final polymer molecular weight and bulk Mooney viscosity will depend on initial sulfur concentration in the copolymerization and the concentration of tetraalkyl thiuram disulfide and dithiocarbamate salt added during the peptization step.

Interpenetrating Polymer Networks (IPN). Polymerization of vinyl and diene monomers over an already formed molecule held in a polymer particle represents a special case of copolymerization. The interpenetrating polymer networks (qv) thus formed overcome many of the miscibility and other problems associated with physical blends of individual copolymers and leads to new compositions that are useful for coatings, adhesives, and caulks (14). Polychloroprene IPNs have been made by co-curing copolymers of 1-chloro-1,3-butadiene [627-22-5]. The 1-chloro-1,3-butadiene comonomer polymerizes in a fashion to increase the allylic chloride concentration in the copolymer backbone. The butadiene copolymer with 1-chloro-1,3-butadiene (29) and octyl acrylate copolymer (30) improved the low temperature brittleness, oil resistance, and heat resistance of polychloroprene.

Block Copolymers. Block copolymers (qv) have been made in two-step processes. First a mixture of chloroprene and *p*-xylene-bis-*N*,*N*′-diethyl dithiocarbamate was photopolymerized to form a dithiocarbamate-terminated polymer which was then photopolymerized with styrene to give the block copolymer. The block copolymer had the expected morphology of spherical polystyrene domains within the polychloroprene matrix (31). Other routes to block copolymers involved hydrolysis of xanthate or thiocarbamyl end-capped polymers followed by oxidative coupling of the two different homopolymers. Core–shell technology is another potential route to block copolymers.

Graft Polymerization. Graft polymerization is related to block copolymerization. A block copolymer contains long sequences of two monomers (ie AAA monomer blocks followed by BBB monomer blocks) along the copolymer chain. Graft copolymers (qv) consist of long chains of one monomer with occasional branches consisting of long chains of a second (grafted) comonomer. The branched points are normally formed by allylic atom (typically hydrogen) abstraction by free-radical initiators (eg peroxides) to yield a resonance-stabilized free-radical.

The free radical initiates the addition polymerization of a second monomer beginning at the locus of the free radical. Generally grafting is performed to significantly modify polymer properties. In the production of emulsion-polymerized acrylonitrile–butadiene–styrene tripolymer, styrene and acrylonitrile are grafted onto rubbery polybutadiene to improve compatibility between the thermoplastic and rubber matrix used in impact modification (12). Methyl acrylate, acrylonitrile, alkyl methacrylates (eg methyl, octyl, lauryl), fumaronitrile, methacrylic acid, and dichlorobutadiene have been employed in solution and emulsion graft polymerization with polychloroprene. In general, solvent resistance, heat resistance, and hydrolytic resistance were improved. Solution graft polymerization of methyl methacrylate to polychloroprene is a commercially important process for making adhesives finding utility for bonding to vinyl-containing plasticizers that migrate to the surface of the substrate with time.

Other Modes of Polymerizations.

Popcorn Polymerization. ω-Polymerization frequently referred to as popcorn polymerization owing to the physical appearance of the polymer, can be a dangerous side reaction for monomer storage vessels. The polymerization appears to proceed without external initiation (32–34), and is catalyzed by the tightly gelled polymer seeds that are a product of the polymerization. Once seeds are present and immersed either in the liquid or vapor phase of monomer, their weight increases exponentially with time.

Fresh radicals are formed continuously by mechanical rupture of the polymer chains that are swollen by dissolved monomer (32,35). Termination of polymer radicals, in turn, is inhibited by the rigidity of the polymer network. The reaction is temperature sensitive, and can be minimized with adequate cooling (32). On the other hand, heat transfer may be impaired as the mass of material grows. Polymerization continues until the available monomer is consumed or gross amounts of inhibitor are added to the system. A number of inhibitors such as organic nitrites, nitroso compounds (32), oxides of nitrogen (36), alkali metal mercaptides (37), or nitrogen tetroxide adducts with unsaturates (78,79) have been recommended. The best control, however, is routine inspection and clean up of equipment to eliminate seeds.

Non-Free-Radical Polymerization. Nonradical polymerizations have not produced commercially useful products, although a large variety of polymerization systems have been studied. The structural factors that activate chloroprene toward radical polymerization often retard polymerization by other mechanisms.

Cationic polymerization with Lewis acids yields resinous homopolymers containing cyclic structures and reduced unsaturation (41,42,171) (see CARBOCATIONIC POLYMERIZATION). Polymerization with triethylaluminum and titanium tetrachloride gave a product thought to have a cyclic ladder structure (43). Anionic polymerization with lithium metal initiators gave a low yield of a rubber product. The material had good freeze resistance compared with conventional polychloroprene (44). Alternating copolymers of chloroprene have been prepared from a number of donor–acceptor complexes in the presence of metal halides. Frequently this enables preparation of copolymers from monomers having unfavorable reactivity ratios in radical polymerization. Triethylaluminum sesquichloride with a vanadium oxychloride cocatalyst yielded alternating copolymers of chloroprene with acrylonitrile, methyl acrylate, and methyl methacrylate when equimolar amounts

of the two monomers were used (45). Polymer composition tended to follow the composition of the monomer mixture (46). The chloroprene units were shown to be in the trans-1,4-configuration (46) on the basis of infrared spectra. Variables affecting the acrylonitrile copolymerization were studied in detail (47) by infrared spectra. The alternating copolymer of acrylonitrile and chloroprene is resinous. A copolymer containing 35 mol% acrylonitrile was a soft, oil-resistant elastomer (47). Stability constants have been determined for complexes of acrylic monomers with ethylaluminum sesquichloride, and related to the kinetics of copolymerization with chloroprene (48). Kinetic data have been determined for polymerization in the presence of a manganese cocatalyst (49).

A series of graft polymers on polychloroprene were made with isobutylene, iso-butyl vinyl ether, and α-methylstyrene by cationic polymerization in solution. The efficiency of the grafting reaction was improved by use of a proton trap, 2,6-di-tertiarybutyl pyridine (50).

Polymer Microstructure

Unsymmetrical diene monomers such as chloroprene polymerize by four reaction pathways: 1,4-head-to-head, 1,4-head-to-tail, 1,2-and 3,4-polymerization (Fig. 1). The concentrations of microstructure vary with polymerization temperature (51) (Table 2). The (Z)- or trans-configuration predominates at conventional polymerizations carried out in the range of 10–45°C.

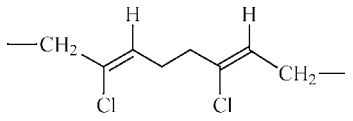

Zusammen, *Z* (or trans)

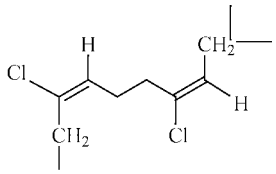

Entgegan, *E* (or cis)

Table 2. Microstructure of Polychloroprene by ^{13}C NMR[a]

Polymerization temperature, °C	1,4-Addition			1,2-Addition tertiary allylic chloride	1,2-Addition isomerized primary allylic chloride	3,4-Addition
	Z or trans	Head to tail (inverted)	*E*- or cis			
+90	85.4	10.3	7.8	2.3	4.1	0.6
+40	90.8	9.2	5.2	1.7	1.4	0.8
+20	92.7	8.0	3.3	1.5	0.9	0.9
0	95.9	5.5	1.8	1.2	0.5	1.0
−20	97.1	4.3	0.8	0.9	0.5	0.6
−40	97.4	4.2	0.7	0.8	0.5	0.6
−150	∼100	2.0	<0.2	<0.2	>0.2	<0.2

[a]Refs. 51,64.

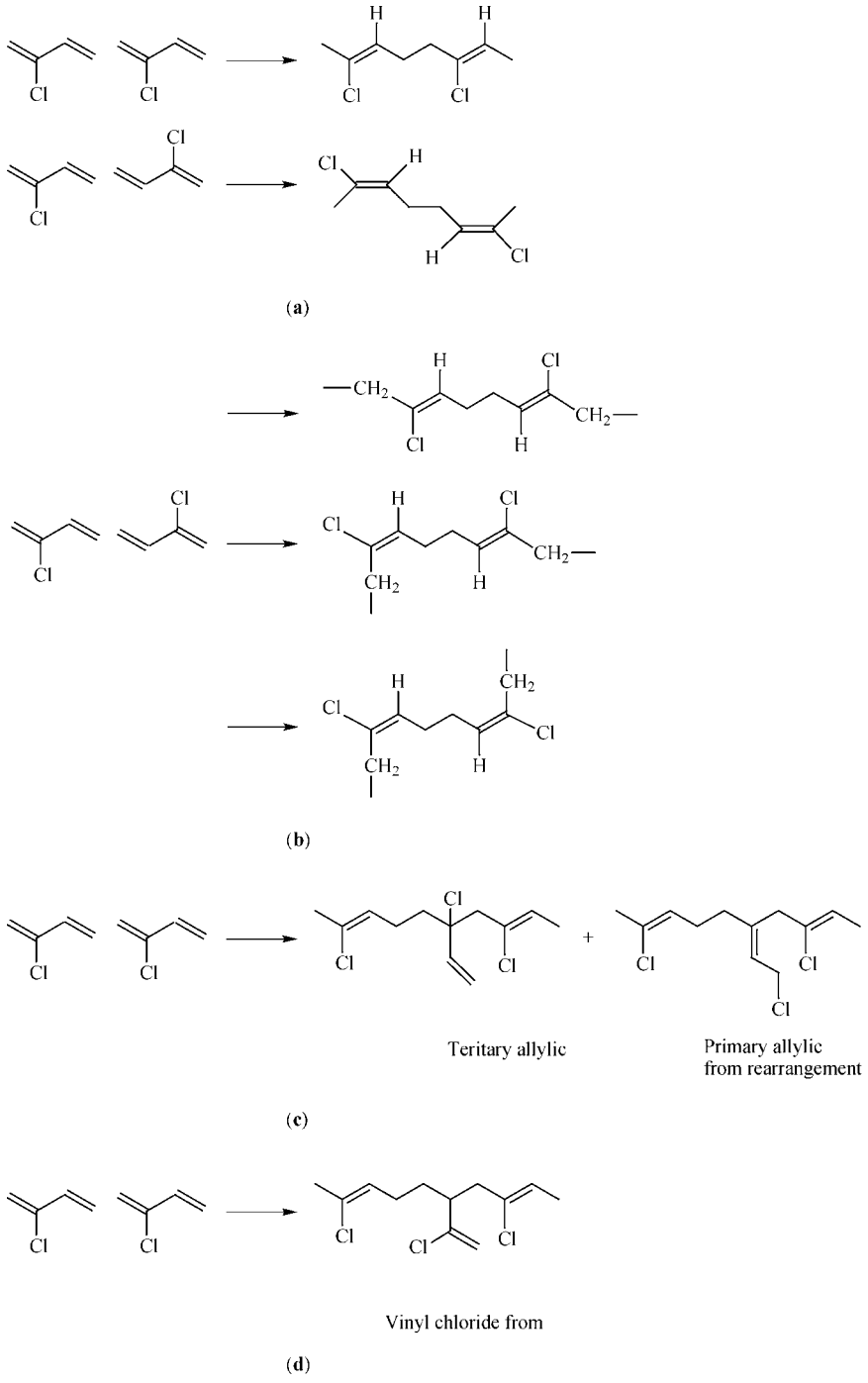

Fig. 1. Four modes of addition resulting in different microstructures. (**a**) 1,4-head-to-head polymerization leading to (*Z*) and (*E*) vinyl chlorides along the main chain; (**b**) 1,4-head-to-tail polymerization leading to (*Z*) and (*E*) vinyl chloride along the main chain; (**c**) 1,2-polymerization leading to allylic chloride; and (**d**) 3,4-polymerization leading to vinyl chloride.

The concentration of (Z)-configuration varies indirectly proportional with the polymerization temperature whereas the other three configurations vary directly proportional with the polymerization temperature. The total amount of *E*-, 1,2-, and 3,4- configurations vary from 5% at −40°C to 30% of the total polymer backbone at 100°C polymerization temperatures. Other structural studies have involved 2,3-dichloro- butadiene homopolymer (52), the free-radical random copolymer with methyl methacrylate (53) with chloroprene, and the alternating copolymer of sulfur dioxide with chloroprene (54). Petiaud and Pham studied the thermodynamics of the various modes of unit addition (55).

The four modes of polymerization result in microstructures that have profound effects on polymer properties and processability. The increased proportion of (Z)-configuration at low temperature leads to more stereoregular polymer chains that crystallize rapidly. This rapid crystallization rate results in a polymer of almost thermoplastic behavior. The polymer hardens rapidly at 25°C and has utility for fast bond-developing adhesive applications. At intermediate and high polymerization temperatures, the higher concentrations of the allylic chloride, pendant vinyl chloride, and head-to-head and head-to-tail moieties provide a degree of crystallization resistance. As the (Z)-configuration is always in high concentration, polychloroprene polymers will crystallize under stress (eg stretching) and providing increased strength to vulcanizates used as mechanical goods.

The allylic chloride moiety is the cure site for polychloroprene polymers (Fig. 2). The reaction of the labile allylic chlorides with bifunctional nucleophiles, metal oxides, or thioureas covalently joins interpolymer chains into a polymer network. The polymer cross-link density is proportional to the concentration of allylic chlorides on the polymer backbone. Thus mechanical goods with high modulus are made from polymers of high allylic chloride concentration. On the other hand, high levels of allylic chlorides decrease the thermal stability of polychloroprene polymers per mechanism described for thermal degradation of unsaturated diene polymer (56,57)

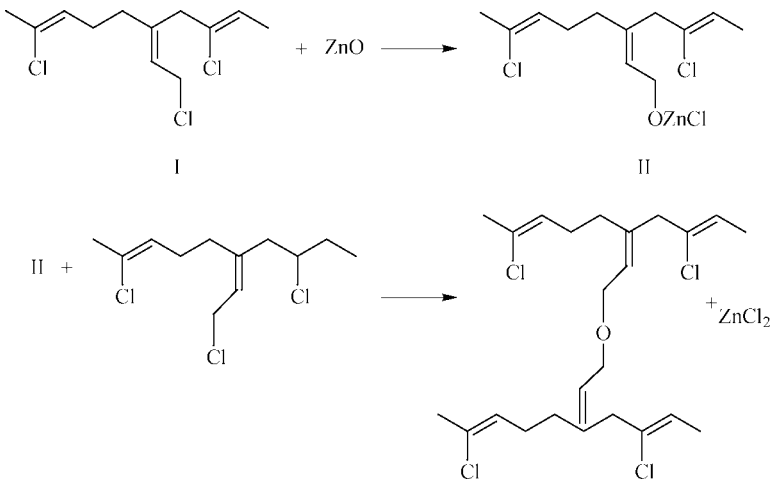

Fig. 2. Function of the allylic chloride in polychloroprene curing.

In 1964, Ferguson and co-workers conducted one of the first studies of microstructure by ^{1}H NMR (15). Ferguson and co-workers determined the relative proportion of head-to-head vs head-to-tail structures. The use of 350 MHz ^{1}H NMR in $CDCl_3$ and C_6D_6 enabled quantitative analysis of head-to-head configurations along with the *E*-configuration (58). With the advent of ^{13}C NMR, a number of additional microstructures were observed. There was good agreement between earlier ^{1}H NMR and ^{13}C NMR techniques (51,55,59–61). Other studies of microstructure have been conducted with the aid of infrared and Raman spectroscopy (62,63)

Copolymerization Microstructure. Dichlorobutadiene is the effective comonomer for polychloroprene copolymerization. The comonomer polymerizes in a 1,4-fashion leading to disruption of the trans chloroprene segments in the polymer chain. Crystallization becomes difficult as polymer chains find it difficult to fit into crystalline lattices. Thus polymers containing dichlorobutadiene are very slow crystallizing. In fact, dichlorobutadiene is frequently referred to as ACR, meaning additive for crystallization resistance.

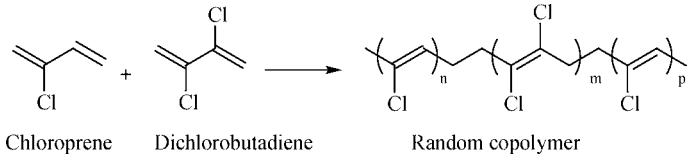

Branching. Branching is a special case of chain-transfer. Instead of free-radical atom extraction from agents such as dodecyl mercaptan (DDM) or xanthogen disulfides, the extraction is from a preformed polymer chain. For polychloroprene, the chain-transfer is to the allylic hydrogen atoms near the double bond. Upon free-radical extraction of the allylic hydrogen a new resonancestabilized free-radical is formed. This new free-radical initiates the growth of a new polymer chain that originates at the locus of the free-radical formation.

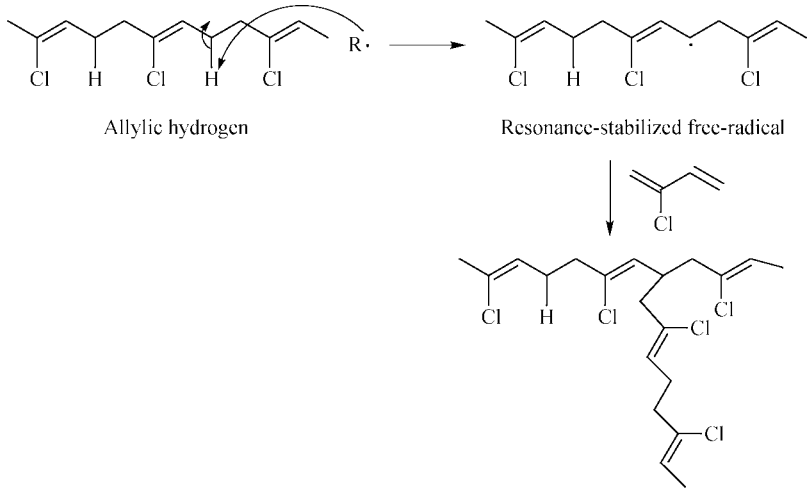

The formation of branched polymer originating at a resonance-stabilized free radical has precedence in the well-understood branching mechanism for vinyl acetate polymerization (65,67). Reaction of polymerizing chloroprene and vinyl acetate with ^{14}C-labeled model compounds was used to determine the relative kinetics of chain-transfer and double bond addition reactions with polymer. Chain-transfer to allylic hydrogens or chlorine atoms on the polymer chain leads to long-chain branching. Addition of the growing chain across a polymer double bond can lead directly to gel formation. Either reaction affects polymer rheology and processability. Vinyl acetate radicals, as a model for initiator fragments, were found to be 570–2427 times faster in chain-transfer reactions than chloroprene radicals. In all cases studied, the rate of double bond addition reactions were significantly faster than transfer reactions. Alternately, rate of chain-transfer can be determined by the method of Mayo (68).

The rates of chain-transfer to polymer and radical addition to double bonds of preformed polymers increase as a function of three variables: (*1*) temperature, (*2*) absence of chain-transfer agent, and (*3*) monomer conversion. Mochel (69) showed that in the absence of a chain-transfer agent, up to 90% of the polymer formed at 30% monomer conversion was gelled.

There are several procedures for determining the extent of long-chain branching.

Long-chain branching is accompanied by increased weight-average molecular weight (M_w) as determined by gel permeation chromatography (GPC)–size-exclusion chromatography (SEC) or ultracentrifugation (22,23). The polydispersity (M_w/M_n) increases as branching increases. Branching has been quantitatively determined using ^1H NMR (16,70).

The effect of branching on the zero-shear-rate intrinsic viscosity is often expressed in terms of branching index, g', defined as the ratio of the zero-shear-rate intrinsic viscosities of a branched to a linear polymer of the same composition and molecular weight.

$$g' = \left[\eta_0^{\mathrm{br}} / \eta_0^{\mathrm{linear}}\right]M \leq 1$$

The zero-shear viscosity of a linear polymer is determined from the Mark–Houwick equation (71,72).

$$\mathrm{IV} = KM^{\alpha}$$

where IV is the intrinsic viscosity, K is the Mark–Houwick coefficient, and α is the Mark–Houwick parameter.

The equation with pertinent constants for polychloroprene is used in determining the extent of branching. Thus, several linear polymers were made under extreme control conditions. The molecular weight distribution and intrinsic viscosities were determined for each polymer. A plot of ln (IV) vs molecular weight yielded α and K values:

$$IV = 1.95 \times 10^{-3} \times M^{0.542}$$

The universal calibration method was then used with the GPC–IV method that involves dual detector measurement of both polymer concentrations by refractive index and the solution intrinsic viscosity by capillary viscometry. The measurements provided full molecular weight distribution and branching distribution of the polymer. Polychloroprene polymers showed branching indices varying from 0.5 to near unity. Polymers designed for different end use applications had different branching parameters, which has been useful in predicting processability (73,74).

Chain-transfer agents such as dodecyl mercaptan or ethyl xanthogen disulfide inhibit long-chain branching and prevent any gel formation up to 60–70% monomer conversion (74). A bis-nonconjugated olefin such as ethylene glycol dimethacrylate is capable of network formation (insoluble gel) during free-radical polymerization with chloroprene monomer (75). The branching index of such a copolymer would be near zero.

The extent of long-chain branching of a series of ethyl xanthogen disulfide modified polymers made at 40°C and varying monomer conversion showed that long-chain branching started near 56% conversion (74). As monomer conversion increased, branching and polydispersity increased. Finally near 82% conversion, the polymer gelled.

Commercial Polymer Manufacture

Commercial polychloroprene rubber is manufactured by aqueous free-radical emulsion polymerization followed by isolation of the solid polymer by one of several processes: freeze roll isolation, drum drying (76), extruder isolation (77), precipitation and drying or spray drying (78,79). Isolation of powdered polychloroprene has been reviewed (80). Of the methods cited, freeze roll and drum drying isolation are commercially important (Fig. 3).

The large-scale commercial manufacture of polychloroprene consists of eight or nine unit operations:

(1) Monomer solution makeup Water solution makeup
(2) Emulsification
(3) Polymerization
(4) Stripping of residual monomer
(5) Peptization for chloroprene–sulfur copolymers
(6) Freeze roll isolation Drum drying
(7) Drying of freeze-rolled film
(8) Roping
(9) Cutting and packaging (25kg)

Manufacture of Chloroprene–Sulfur Copolymer. The process for manufacture of a chloroprene–sulfur copolymer taken from the patent literature will illustrate the batch process (82,83).

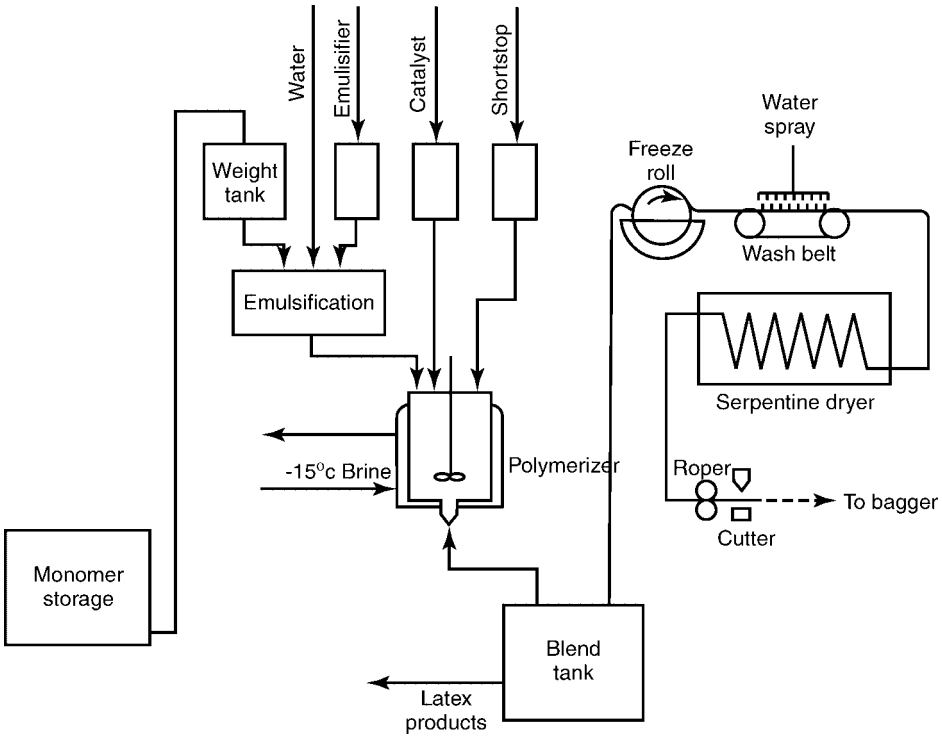

Fig. 3. Commercial manufacturing scheme (81).

The monomer solution makeup involves addition and solubilization of elemental sulfur and rosin (substituted diterpenes) in the chloroprene monomer. The water solution is made in a second vessel. Deionized water, sodium hydroxide, and a dispersant are mixed to form the water solution. The dispersant is a condensation product of naphthalene–sulfonic acid and formaldehyde. The monomer and water solutions are mixed with centrifugal pumps to form an oil-in-water emulsion. The emulsion formed by virtue of formation of the sodium salt of rosin and resin components (abietic and dehydroabietic acids) having hydrophobic and hydrophilic ends. The large carbon-bearing portion of sodium abietate is hydrophobic and thereby solubilizes the monomer. The sodium carboxylate portion of sodium abietate is the hydrophilic end that extends into the aqueous phase and forms the electronic double layer that is critical to emulsion stability (84,85). In the patent example, the emulsion was added to the reactor and the temperature was increased to 40°C polymerization temperature (Table 3).

The reactors in modern commercial processes are brine-jacketed, glass-lined, and fitted with a glass-lined agitator. Glass-lined construction is important to prevent multivalent cations from contaminating the system, and precipitating polymer as coagulum.

Polymerization was initiated by addition of an aqueous potassium persulfate solution to the reactor. The emulsion temperature was maintained near 40°C by control of a combination of three variables: (*1*) reactor jacket temperature, (*2*) agitator speed, and (*3*) catalyst addition rate. The progress of polymerization (86) was

Table 3. Polychloroprene Branching[a]

Parameter	Value					
Conversion, %	11.7	33.6	55.9	62.8	71.9	82.3
$M_n \times 10^{-5}$	1.44	1.44	1.19	1.07	1.05	1.26
M_w/M_n	2.3	2.3	3.4	4.2	5.2	4.9
Branches/100,000 mol. wt			0.15	0.23	0.36	0.52
Branching parameter	0	0	0.38	0.50	0.66	0.76

[a]Emulsion polymerization at 40°C using xanthate modification (74).

measured by specific gravity, which is continually monitored by computer in modern commercial processes. In the patent example, the initial monomer emulsion had 0.95 specific gravity. During polymerization, the specific gravity increased to a goal value owing to continue formation of polymer having nominal 1.23 specific gravity. The free-radical polymerization was quenched at 91% monomer conversion (1.069 specific gravity) by the addition of a xylene solution of tetraethyl thiuram disulfide.

The emulsion was cooled to 20°C. A dithiocarbamate salt or secondary amine was added and the emulsion aged for 8 h to peptize the polymer. The bulk Mooney viscosity of the polymer was thus reduced to levels suitable for rubber processing.

The emulsion or polymer dispersion containing flammable and toxic chloroprene monomer was next steam stripped with the aid of a turbannular stripper (87). The stripped emulsion contained less than 0.1% residual chloroprene monomer. At this point in the process, the emulsion can be further processed into a dry polymer or sold as a liquid dispersion.

Conversion to the dry polymer involved destabilization of the active surfactant, freeze coagulation, and drying. Thus, the stripped emulsion was acidified to pH 5.5–5.8 with 10% acetic acid solution. The surface-active behavior of the sodium rosinate surfactant was thereby effectively destroyed. The marginal colloidal stability of the emulsion was controlled exclusively by the naphthalene sulfonic acid condensate. Since the sulfonate is a salt of a strong acid it cannot be acidified by acetic acid. Acidified emulsion was contacted with the surface of a rotating chilled (−15°C) stainless steel drum (ie the freeze roll) thereby causing the polymer to plate or freeze out onto the drum. The coagulated film was skived from the roll by a stationary knife and conveyed to a woven stainless steel belt where it was thoroughly washed with water sprays to remove electrolytes and other impurities added or formed during polymerization. After washing, approximately 25% of the excess water and serum is squeezed from the film with the use of a squeeze roll. The film was then conveyed onto cloth-covered aluminum girts where it was carried through an air-circulating serpentine dryer having heating compartments with temperatures that start from 120°C. The final dryer compartment operated near 50°C to cool the dried film. The film was cooled further at the exit of the dryer by contacting a rotating cooling roll. In a modern commercial process, the film is gathered into a rope and then conveyed to cutters, where it is cut into small chips. The product is then packaged into bags weighing 25 kg each.

In the patent examples, there were five key features that permitted freeze-roll isolation. The emulsion was of sufficient colloidal stability to prevent spontaneous coagulation before contacting the rotating freeze roll. The sulfonic acid salt

was critical in that connection. The polymer had sufficiently low glass-transition temperature to prevent cracking from the freeze roll at typical (−15°C) freeze-roll operating conditions. The film maintained sufficient strength to be conveyed along the wash belt and through the dryer. In that connection, freeze-roll isolation of very low Mooney viscosity polymers or fluid polymers is difficult or virtually impossible. The dryer cooling temperature and cooling-roll temperature were controlled to prevent polymer cold flow leading to massing after the polymer has been packaged.

Continuous polymerization is a second process practiced on a large commercial scale (88). An illustrative example taken from the patent literature illustrates the continuous polymerization process. Thus a mixture of chloroprene, 2,3-dichloro-1,3-butadiene, dodecyl mercaptan, and phenothiazine (15 ppm) was fed to the first of a cascade of seven reactors. Water solution containing disproportionated potassium abietate, potassium hydroxide, and formamidine sulfonic acid catalyst were fed with the monomer solution to the first reactor. Polymerization initiated immediately. The emulsion was then cascaded to the second reactor and the process continued. The residence time in each reactor was 25 min at 45°C. The emulsion exited the reaction train at 66% monomer conversion. In a second similar process, the catalyst was fed to each reactor along the reaction train.

The descriptions presented above are intended as an overview of polychloroprene technology as practiced over the commercial life of polychloroprene. Product and processes have changed since 1930 to meet changing consumer needs, to upgrade product quality, to improve the quality of the workplace and environment, to improve efficiency of operation, and to meet the demands of a changing global economy. The commercial chloroprene–sulfur copolymers were commercialized in 1937 (89). Low temperature polymerizations for adhesive applications were discovered in the late 1940s. The mercaptan-modified chloroprene homopolymers were commercialized in 1950. The crystallization-resistant chloroprene–dichlorobutadiene copolymers were introduced in 1951. The fluid polychloroprene polymers were commercialized in the late 1950s. The sol–gel blends or "pre-crosslinked" grades were introduced in the 1960s for improved processability. Modifications to these basic types have continued into the twenty-first century.

Commercial Polychloroprene Polymers

At one time, 10 worldwide producers manufactured 160 dry polychloroprene types and 66 liquid dispersions or latex types. More recently six major producers produce 93 dry types. The polymers offered globally fall into five categories: (*1*) standard general-purpose grades, (*2*) crystallization-resistant grades, (*3*) adhesive grades, (*4*) specialty grades, and (*5*) liquid dispersions or latex grades (Table 4). The chloroprene–sulfur copolymers, mercaptan-modified homopolymers, and mercaptan-modified sol–gel blend polymers constitute the standard general-purpose grades. Crystallization resistant grades are made by two commercial processes. Copolymerization of chloroprene with 2,3-dichloro-1,3-butadiene is the method adopted by most producers. High temperature and high pressure emulsion polymerization is a second process used. Adhesive grades are generally made by low temperature polymerizations. The specialty grades are based on xanthogen disulfide chain-transfer during either homopolymerization or copolymerization

Table 4. Polychloroprene Grades—Advantages and Limitations

Polymer Description	Advantages	Limitations
(*1*) Standard general purpose grades		
Chloroprene–sulfur copolymers	Peptizable Good building tack Good tear strength Good flex resistance Low tan delta	Poor heat resistance High compression set Poor shelf stability
Mercaptan-modified homopolymers	Easy molecular weight control Good heat stability Low compression set Good shelf stability	Not peptizable Requires accelerator Low flex resistance
Sol–Gel blends	Improved rheology Low nerve Fast extrusion Low die swell Smooth extrudate surface Collapse resistance Better calendering	Low tensile strength
(*2*) Crystallization resistant grades		
Copolymers of 2,3-dichloro-1,3-butadiene, styrene	Low crystallization rates	Slightly higher T_g
High temperature and high pressure polymerization	Low crystallization rates	Poorer heat resistance
(*3*) Adhesive grades		
Low temperature	Rapid crystallization	Thermal stability
Polymerization	Rapid solubility in organics Adheres to wide variety of substrates	Cannot be used if gelled
(*4*) Specialty grades		
Xanthogen disulfide modified homopolymers and copolymers	High stress–strain Faster cure rate Low tan delta Low compression set	Poorer heat resistance than mercaptan modified types
(*5*) Latex		
Emulsion polymerization	High solids Good film former Gelled polymer for adhesives Environmentally desirable for solvent-free adhesives	Freezes Poor thermal stability Sensitive colloid system

with conventional comonomers or sulfur. Finally, the latex grades are made by the same emulsion polymerization techniques as the dry types but generally with additional surfactants. The latexes are sold as aqueous dispersions. Customers convert the liquid dispersions to dry product according to specific end uses.

Thus, wide ranges of choices are available for a diverse range of properties.

Global Polychloroprene Grades

The six major global producers manufacture all major classes of commercial polychloroprene dry types (90): DuPont Dow Elastomers L.L.C. manufactures Neoprene, Bayer manufactures Baypren, Enichem makes Butachlor, Denki Kagaku makes Denki chloroprene, Tosoh makes Skyprene, and Showa makes Showapren.

Xanthogen disulfide modification has been used in the manufacture of all dry and latex types including chloroprene–sulfur copolymers. The chain-transfer agents have been used in combination with all conventional comonomers. In contrast to dodecylmercaptan modifiers, xanthogen disulfide modification has the advantage that it can be used with chloroprene–sulfur copolymerizations without concerns with reaction with sulfur.

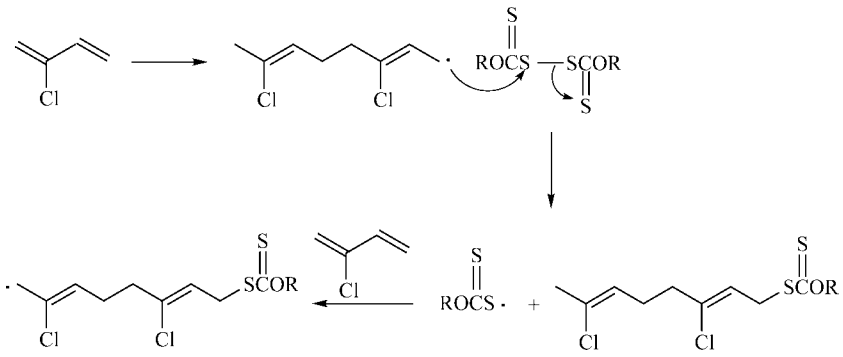

The xanthate-terminated polymers undergo reaction at the end group during vulcanization (91,92). The molecular weight distribution can be wide, leading to better-processing polymers (92,93). In concert with predictions from the Boltzmann's equation, the reactive ends lead to a polymer of greater tensile strength and reduced hysteresis loss and creep.

The sol–gel blend or pre-crosslinked grades of polychloroprene such as the T Type polychloroprenes available from DuPont Dow contain a highly cross-linked network, which that acts as an internal processing aid (94,95). The blend has many of the same characteristics as the sol component, but different compound rheology properties. This composition results in faster extrusion with extrudates having smoother surfaces. Extrudates also retain their shape better with good definition until vulcanized.

Commercial Conversion of Raw Polymers to Final Vulcanizates

Polychloroprene is a multipurpose elastomer that has a good balance or properties that include outstanding physical toughness and wider short-term/long-term

operating temperature range than most general-purpose hydrocarbon elastomers such as EPDM or natural rubber. Polychloroprene has better resistance to hydrocarbon oils, ozone, sun, weather, and heat per ASTM D2000/SAE J2000 categories BC/BE. Finally, it demonstrates flame retardency and self-extinguishing characteristics that purely hydrocarbon-based elastomers lack (96).

As with all elastomers, the properties of the raw polymer can be enhanced by careful choice of rubber compounding formulation (97). Handling precautions, polymer selection guide, compounding guide for specific application, processing guides, and representative formularies are discussed in the *Guide to Grades, Compounding and Processing of Neoprene Rubber* compiled initially by J. C. Bament (98). Future mentions of this document will simply be referenced as the Bament guide published by DuPont Dow (98).

The critical links between the raw polymer and finished vulcanized product used by the global consumer involve the compounding, processing, and curing or vulcanization. There are several major considerations in designing a rubber composition based on polychloroprene dry polymers (Table 5).

Table 5. General Vulcanizate Properties[a,b]

Property	EPDM	CR	NBR
Density	0.86	1.23	1.0
Hardness, shore A	40-95	40-90	45-100
Tensile strength, MPa[c]			
Gum stock	VL	21	VL
Black stock	>21	21	17
Service temperature, °C	−50 to +150	−40 to +120	−20 to +120
Heat resistance	H	FH	M
Cold resistance	M	FH	L–M
T_{10}, °C	−45	−45	−20
Tan delta at 20°C		0.09	0.1–0.18
Set resistance	VH	FH	M–FH
Tear resistance	M	H	M
Aging general	VH	H	M
Ozone/corona resistance	VH	FH–H	M
Aliphatic oil resistance	L	M–H	H
Electrical resistance	H	M	M
Bonding to substrates	M	VH	VH
Useful properties	Excellent aging, medium strength	Low damping; high weather, heat, and flame resistance; moderate oil resistance; good flex & tack	Resists oils chemicals; moderate heat aging
Limiting properties	Self-tack, poor building of composites	Moderate tensile strength	Poor cold resistance

[a] Ref. 97.
[b] VH, very high; H, high; FH, fairly high; M, moderate; L, low; VL, very low.
[c] To convert MPa to psi, multiply by 145.

(1) Selection of a CR or polychloroprene type
(2) Choice of a compound formulary for a specific end use
    a. Acid acceptors
    b. Vulcanizing agent
    c. Vulcanizing accelerators and retarders
    d. Antioxidant and antiozonant
    e. Reinforcing and extending fillers
    f. Plasticizers
    g. Processing aids
(3) Modification of the basic formulary to choose critical ingredients necessary to achieve critical end use properties

Compounding and Processing of Polychloroprene. Typically, dry polymers are mixed with compounding ingredients on a rotating two-roll mill or Banbury mixer.

Polychloroprene	100
Magnesia	4
Stearic Acid	0.5
Antioxidants	2
Antiozonants	2
Fillers, Processing Aids, Plasticizers	As required
Accelerators	0.5
Zinc Oxide	5

Typical Dry Type Compound (99)

Owing to the propensity of the unsaturated polymer to degrade and liberate HCl on long-term in-service use, a special grade of magnesium oxide (Maglite D), from Marine Magnesium Co.) is added as an acid acceptor. Because metal oxides can also function as vulcanizing agents, particularly for chloroprene–sulfur copolymers, an optimum level of MgO is used. An antioxidant is required to attenuate the aging process. Antiozonants are added in addition to antioxidants to prevent ozone-induced stress cracking, particularly in dynamic applications. Plasticizers and oils enhance the rheological properties and also improve vulcanizate properties. Fillers are of paramount importance for all polychloroprene compounds. Of all fillers, carbon black is most important. Carbon black reinforces the rubber leading to higher tensile strength, greater resistance to oil swell, weather resistance, and abrasion and tear resistance. Plasticizers aid in the mixing of ingredients. Depending on the plasticizers selected, stress–strain properties may be increased or low temperature stiffness resistance improved without affecting crystallization rates. Finally, zinc oxide and accelerators function both as acid acceptors and curatives that initiate the cross-linking reaction. Retarders such as sodium acetate or salicylic acid are used to balance the cure rate or scorch thereby improving the curing process safety. In this connection, scorch is defined as cure rate measured on compounded rubber (ASTM D3190-95) as Mooney Scorch with small rotor at

121°C (ASTM D1646-96A) or MDR scorch measured with a moving-die rheometer at 160°C (ASTM D5289-95).

Curing Mechanism. Chloroprene–sulfur copolymers can be cured for some applications with zinc oxide alone. All other polychloroprene types will usually require an organic accelerator to cure. Typically thioureas are used in combination with zinc oxide to effect cure. The accepted mechanism for curing involves reaction of thioureas and zinc oxide at the primary allylic chloride moiety that was formed by sn_i' rearrangement during polymerization or curing (100,101) (Fig. 4).

Thioureas such as ethylene thiourea (ETU, NA22) initially react with the primary allylic chloride to yield the thioether. Zinc oxide then reacts at the thiocarbonyl atom. Further reaction at the curing temperature of 160°C eliminates the ethylene urea and leaves the polymer as the zinc sulfide salt. The sulfide salt reacts with the allylic chloride moiety of a second polymer molecule to generate the thioether-cross-linked polymer (102).

Wide ranges of organic accelerators, which are capable of nucleophilic substitution at the allylic chloride atoms, have been used in polychloroprene curing. Polyhydric phenols (103,104), hydroxyphenyl mercapto-substituted triazoles (105), thiolactams (106), thiazolidine and thiones, Vulkacite (Bayer Chemical Co.). CRV (107,108), alkyl thioamides, formaldehyde amine reaction products, amines, guanidines, dithiocarbamates, thiurams, and sulfenamides have all been used as accelerators.

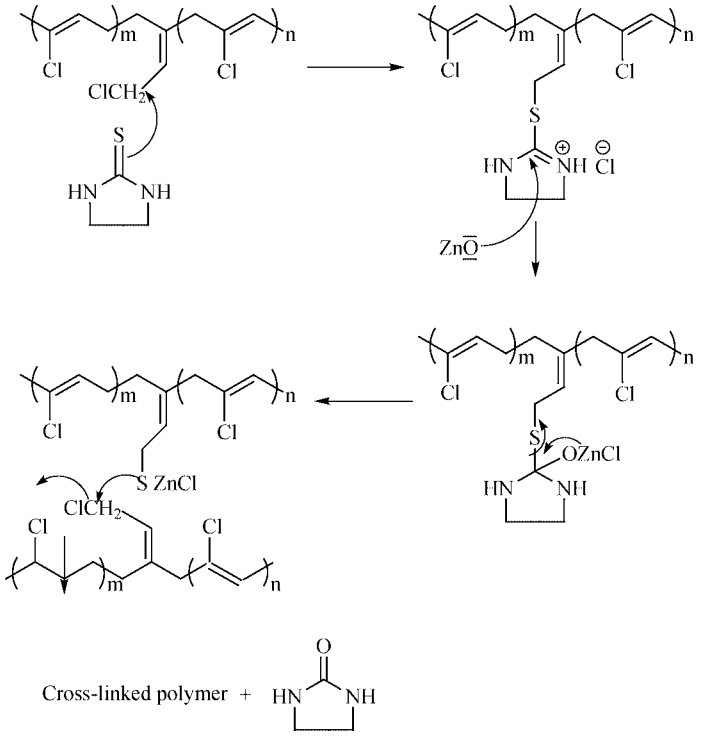

Fig. 4. Curing of chloroprene polymers.

Antioxidants. The sensitivity of polychloroprene to oxidative attack has been discussed (57,109,111). Antioxidants are required for good long-term service. Amines and hindered phenols, and bisphenols are generally the antioxidants of choice. Octylated diphenylamine is frequently used owing to its effectiveness, its nonstraining characteristics, and its noninterfere with the curing reaction (112). Organic monosulfides and phosphates enhance the activity of octylated diphenylamines. *Para*-phenylene-diamines are used but are lightly staining antioxidants. Of the bisphenols, 2,2′-methylene-bis-4-methyl-6-tertiary butyl phenol, 4,4′-thio-bis(2-methyl,6-tertiary butyl phenol) are important. Neozones (ie phenyl-naphthalamines) are staining antioxidants (qv) that have found utility in some applications. When used at levels of 3–5 parts per 100 parts rubber, Neozones are good antioxidants and good antiozonants (99) (see RUBBER CHEMICALS).

Antiozonants. The reaction of atmospheric ozone with olefins is a known organic chemical reaction. Primary and secondary ozonides are formed (113).

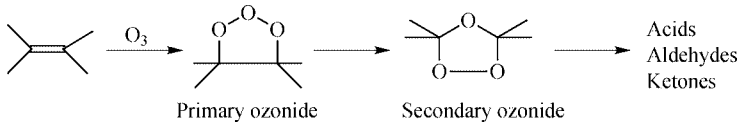

Ozonolysis is most pronounced when vulcanizates are tested under stress-cracking conditions in an atmosphere containing ozone. Owing to the presence of the polar chlorine moieties, polychloroprene resists cracking to a much greater extent than natural rubber or polybutadiene. The long-established use of polychloroprene as telephone wire coatings attests to the high ozone resistance of the polymer. Early on, rubber processors considered ozone cracking as a surface phenomenon. Thus, waxes that would bloom to the vulcanizate surface were used for ozone protection (114). The use of waxes was, however, not a panacea for all problems involving ozone cracking. W. F. Tully noted as early as 1939 that *p*-phenylenediamines were effective antiozonants (115). The choice of *p*-phenylenediamine was critical, however because of the bin instability precipitated by reaction of the bifunctional amine with polychloroprene cure sites, leading to increased viscosity (109). The best balance of bin stability and ozone resistance in a dynamic test at 40°C was achieved by use of a diaryl-hindered *p*-phenylenediamine antiozonant (Table 6).

N-(1,3-Dimethyl butyl)-*N*′-phenyl-*p*-phenylene-diamine and phenyl/tolyl-*p*-phenylene diamine showed best balance of properties.

Table 6. Antiozonant Performance

N, *N*′ Group	Viscosity increase as 121°C	Dynamic test: 3 ppm ozone, 40°C (hours to rating of 4)
Hindered diaryls	10	118
Diaryl	24	110
Alkyl-aryl	>200	84
Alicyclic-aryl	103	81
Dialkyl	73	49

Table 7. Plasticizer Properties for Polychloroprene

Desired property	Preferred plasticizers
Low cost	Petroleum oils, naphthenic and aromatic
Light-colored or nonstaining stocks (including black stock)	Ester plasticizers, chlorinated paraffins, or selected petroleum oils
Low temperature service	Ester plasticizers or *cis*-polybutadiene
Heat resistance	Polymeric plasticizers, chlorinated paraffins, polyester plasticizers, and low volatility petroleum oils
Low flammability	Chlorinated paraffins and organic phosphate esters
Fungus resistance	A polyether-[di(butoxy-ethoxy ethyl) formal]
Use with peroxide cure systems	Ester, chlorinated paraffins, or polymeric plasticizers

Of auxiliary agents, linseed oil, unsaturated vegetable oils, rapeseed oil, and hydrocarbon waxes enhance the efficiency of an antiozonant in a dynamic ozone test as they bloom to the surface of the polymer. Ester plasticizers such as dioctyl sebacate impair ozone resistance presumably because of enhanced solubility of polar esters in the polar polychloroprene network polymer. Finally, the mechanism for ozone attack differs appreciably from oxygen attack at allylic atoms. Thus, an antioxidant is generally used in combination with an antiozonant for polychloroprene.

Plasticizers. Plasticizers (qv) are used in polychloroprene to improve compound processability, to modify vulcanizate properties, and to reduce cost (Table 7).

There are five classes of plasticizers normally employed for polychloroprene vulcanization: (*1*) organic esters, (*2*) petroleum oils, (*3*) vegetable oils, (*4*) chlorinated paraffins, and (*5*) polymeric plasticizers (Table 8). Some attributes of the different classes follow:

Mixing. The ability to be mixed in existing equipment used in natural Rubber Compounding (qv) was one factor that contributed to the easy acceptance of polychloroprene after its discovery (Table 9). Mixing of compounds of various sizes can be performed on two-roll mills or in an internal Banbury mixer. A typical 20-min procedure follows:

Several variations of the basic scheme are used in the industry: (*1*) upside-down mixing, (*2*) sandwich mixing, (*3*) straight mixing, (*4*) optimum dispersion mixing, (*5*) masterbatch mixing. In Upside-down mixing all the filler and oil are loaded first into the mixer and then the rubber added on top. The ram is lowered and the mixing starts. This gives cold rubber, which gives more shear on the black at the critical initial stage and you can therefore get shorter mixing times with better dispersion. The downside temperature develops much faster.

The accelerators and zinc oxide are best added on a second mill or in a second operation just before the stock is needed for curing (96,119). Bin stability is thus enhanced.

Calendering and Extrusion. Friction compounds are used to build up composite structures of fabric and rubber. The surface of the calendered fabric must have good green strength or "building" tack. Thus calendered stocks are usually made from slow-crystallizing polychloroprene types. Polychloroprene

Table 8. Classes of Plasticizers for Polychloroprene

Advantages	Disadvantages
Organic esters (eg dioctyl sebacate, butyl oleate): (refs. 83,116,117)	
Best low temperature brittle point	Higher cost
Nonstaining, nondiscoloring	Volatile, leading to poor heat resistance
Useful for nonblack compounds	May craze plastics
Good compatibility	Decreases stress–strain and tear
	Increases crystallization rates (116,117)
Petroleum oils:	
Low cost	Aromatic oil stain and interfere with peroxide cure Paraffinic oils have low compatibility
General purpose	
Aromatic oils have good compatibility	
Naphthenic oils have moderate compatibility	
Chlorinated paraffins (eg chlorowax, chloroflo)	
Better flame resistance than hydrocarbon rubber	Low plasticizer efficiency
	Increased smoke emissions
Good low temperature properties	
Can be used in nonblack stock	
Good heat resistance	
Moderate compatibility	
Vegetable Unsaturated Oils (linseed and rapeseed)	
Good antiozonant properties	Encourages fungus growth
Good heat resistance	
Retards sunlight-induced discoloration	
Polymeric ester plasticizers (hexa-oxypropylene glycol monomethacrylate) (118)	
Good heat resistance and low volatility	Low plasticizer efficiency
Resins (eg coumarone–indene resins)	
Improved building tack	Reduced resilience
Improved heat resistance	Reduced low temperature properties
Improved tear strength	
High vulcanizate hardness	
Improved abrasion resistance	
Improved crystallization resistance	

compounds can be formulated to process well in the four basic calendering operations, which include unsupported sheet, fractioning, plying-up, and skim coating (120). Unsupported sheet calenders use smooth compounds based on sol/gel blend or pre-crosslinked types. These polymers of very low nerve will calender smoothly and rapidly. Plying up is done when smooth sheets are required in a thickness which cannot be calendered in one operation. Plying up gives a better sheet since pin holes and other flaws do not extend through the full thickness of the sheet. Frictioning stocks are very soft and tacky. They permit penetration and adherence

Table 9. Compounding Polychloroprene

Step	Minutes	Cumulative time
Set mill for 6 mm sheet and turn on cooling water		
Mass polychloroprene containing no accelerator	5	5
Add high activity magnesia, retarders, and antioxidants	2	7
Add hard fillers (fine furnace blacks or silicas)	2–5	9–12
Add soft fillers (large furnace and thermal carbon blacks, and mineral fillers and oils)	4–9	13–21
Add wax, petrolatum, stearic acid	2	15–23
Add zinc oxide and accelerators; cut, batch off, dip, and hang to cool	6	21–29

to the interstices of the fabric. Slow-crystallizing polymers are used for this application. Skim coating is similar to plying up with the fractioned fabric as one ply.

Extrusion. Polychloroprene has been employed in a wide variety of extrusion (qv) processes. Intricate cross-sections such as highway compression seals, bulb weather-stripping, and hose represent a few examples. As with calendering, extrusion is very sensitive to nerve. The DuPont Dow neoprene sol/gel blend types are best suited for extrusion applications. Use of low levels of highly structured furnace carbon blacks, stearic acid, petroleum, paraffin wax, triethanolamine benzoic acid, and calcium stearate are particularly effective extrusion aids. The screw of the extruder should have a constant diameter root with increasing pitch. Heat history of the compound should be minimized, with only a brief warm-up before extrusion begins. The barrel and screw should be run cool, 50°C, and the die hot, 95°C (96,119).

Molding. Molding is used widely for fabricating CR into belts, hose, sponge, and a variety of industrial products. All of the standard molding techniques have been used successfully with commercially available equipment. Molding methods include compression molding, transfer molding, injection molding, blow molding, vacuum molding, and tubing mandrel wrap. An optimum cure cycle-time–temperature relationship must be selected based on the curing characteristics of the compound and the suitability of existing equipment. Mold design must take into consideration the easy rapid removal of the cured part without damage (121). The Bament guide contains specific recommendations on cure condition for specific end use applications (81).

Properties of Polychloroprene Polymers

Crystallization. Some elastomers crystallize at temperatures that can significantly impact processing and vulcanizate behavior. Thus it is necessary to account for these behaviors when developing rubber compound formulations and processes. Crystallization is manifested by stiffening and hardening of the raw polymer, uncured compounded polymer, and the vulcanized polymer. Elastomers that crystallize will do so on stretching and thereby exhibit increased tensile strength. Those elastomers (eg polychloroprene and natural rubber) will

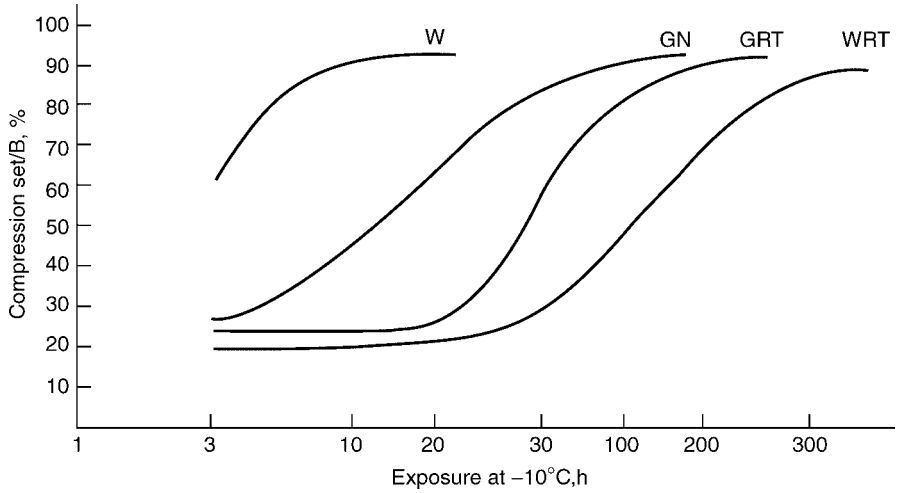

Fig. 5. Profile of low temperature compression set.

require less reinforcing fillers to develop strength than types that do not stress-crystallize (122). Crystallization is also enhanced by compression. Frequently the profile describing the low temperature compression set as a function of time is S shaped, indicating an initial period of nucleation followed by stress-induced rapid crystallization (Fig. 5). The rates of crystallization of some polychloroprene commercial types follow a general trend: homopolymer > chloroprene–sulfur copolymer > chloroprene–sulfur–dichlorobutadiene tripolymer > chloroprene–dichlorobutadiene copolymer having higher levels of dichlorobutadiene (123). Finally, in addition to promoting stress-induced crystallization, polyester plasticizers will also increase crystallization rates. Presumably, the ester plasticizers provide a medium for increased chain mobility that permits polymer chains to migrate to the preferred crystalline cells. Hydrocarbon oil plasticizers and co-blends with hydrocarbon rubbers will retard crystallization rates but may improve low temperature brittleness resistance.

Crystallization is important for some hose manufacturing applications as it imparts some stiffness for braiding. The rapid crystallization of some polychloroprene polymers is fully exploited in adhesive manufacture and use (64).

Crystallization of amorphous polymers is a time-dependent phenomenon. Polychloroprene crystallizes fastest at $-12^{\circ}C$ (123,124). Below this temperature, thermal stiffening commences and restrains molecular motion and alignment. Crystallization rates and degree of crystallization are heavily impacted by several phenomena, of which polymer polymerization temperature and thermal history of the polymer sample before measurements are most important.

Hardness increase, differential scanning calorimetry (DSC), differential thermal analysis (125–127), low temperature compression set, and Gehman torsional stiffness are tests normally employed to measure crystallization properties. The heat of fusion of the crystalline phase of polychloroprene homopolymer is approximately 96 kJ/kg (23 kcal mol^{-1}) and the activation energy for crystallization is 104 kJ/mol (25 kcal mol^{-1}). The extent of crystallization can be calculated from

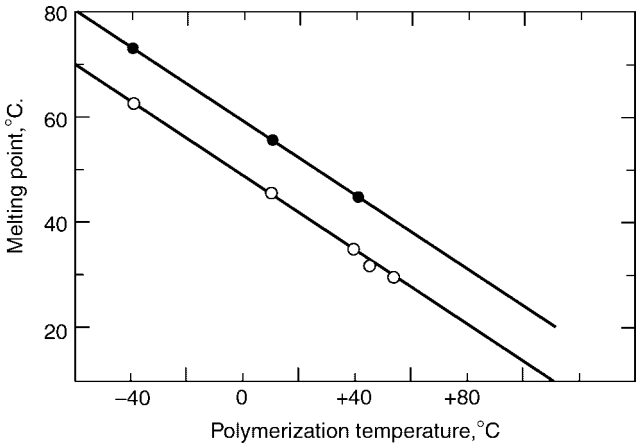

Fig. 6. Effect of polymerization temperature on the crystalline melting point of chloroprene rubbers produced by emulsion polymerization: ●, highest observed value; ○, lowest observed value. From Ref. 124.

the density of amorphous polymer ($\rho = 1.23$) and the crystalline density ($\rho = 1.35$). Thus, a polymer that is polymerized at -40°C melts at 73°C and is 38% crystalline. A polymer polymerized at $+40^{\circ}$C melts at 45°C and is approximately 12% crystalline (Fig. 6).

X-ray diffraction has also been used to measure crystallinity. X-ray diffraction analysis showed that the polychloroprene unit cell is orthorhombic, $a = 0.88$ nm, $b = 1.02$ nm, and $c = 0.48$ nm (128).

Heat Aging and Degradation. The weather and ozone resistance of polychloroprene vulcanizates are enhanced by the presence of chlorine atoms in the molecule. Thus, polychloroprene is more resistant to environmental elements than natural rubber. In comparison to saturated elastomers, polychloroprene is less heat and oxidation resistant. H. C. Bailey studied the degradation of a mercaptan-modified polychloroprene homopolymer and model compound (chlorooctene) under controlled temperature (90–120°C), environmental chamber gas composition, and gas flow rates (124,127,129). Bailey concluded that as the polymer was oxidized hydrogen chloride evolved at a rate that closely matched oxidation or oxygen uptake. Oxidation brought about both scission and cross-linking of the polymer and decreased the proportion of the polymer that was capable of crystallizing. In the early stages of oxidation, cross-linking occurred mainly through the formation of intermolecular peroxides. The activation energies for oxidation and accompanying dehydrochlorination were found to be 17.6 and 25.8 kcal mol^{-1}, respectively, for polychloroprene. Molecular weight determination showed that at low degree of oxidation, scission of polymer molecules predominated over cross-linking. Chain scission resulted from the decomposition of intramolecular peroxides and hydroperoxides, with concomitant evolution of hydrochloride, ketones, and acid chloride moieties. At higher degrees of oxidation, polychloroprene gradually increases in modulus and loses elongation, leading to increased hardness and brittleness.

Oxidation initiates at the allylic hydrogen or chlorine atoms, particularly atoms residing in tertiary positions that are formed during 1,2- or

3,4-polymerization (130–132). After an initial induction period, rapid autoxidation increases with temperature (133). At the low monomer conversion characteristic of mercaptan-modified polymers, the concentration of microstructures arising from 1,2- and 3,4-polymerization is lower than that found in higher conversion types. Thus, polymers made at low polymerization temperatures with mercaptan modification are the most heat-resistant polychloroprene types (93).

Hydrogen chloride evolution with polymer degradation did not occur readily at 120°C in a nitrogen atmosphere (96). At much higher temperatures (eg 275°C), the polychloroprene polymer was carbonized with HCl liberated by a non-free-radical mechanism (134). Polymer polymerized at low temperatures showed better thermal stability (93).

The practical ceiling service temperature in air for conventional polychloroprene polymers used in dynamic applications is approximately 120°C. To reach this high service temperature, antioxidants and antidegradants are added during rubber compounding. Alternately, theory predicts that elimination of tertiary hydrogens and tertiary chlorine atoms would improve heat resistance. Several studies have supported the theory. Thus, post-reaction of polychloroprene with dodecyl mercaptan (135), use of high levels of ethylene thiourea during curing (136), and inclusion of reactive thios such as mercaptobenzimidazole in the cure systems (137) all react away the labile chlorine atoms, thereby improving heat resistance. The latter technique is particularly important in improving the heat resistance of mercaptan-modified polychloroprene.

Commercial Dry Type Applications

The *Guide to Grades, Compounding and Processing of Neoprene Rubber* compiled initially by J. C. Bament lists the major dry type applications and starting formularies for compounds to meet the specific end uses (98).

Formularies for the following applications are included:

Adhesives, automotive, bridge bearing pads, cable jackets, cellular products, coated fabrics, conveyor belts, footwear, hose, power transmission belts, profiles, roll covers, sheeting, and tank lining.

Latex or Liquid Dispersions

Polychloroprene latexes are aqueous dispersions of synthetic polychloroprene polymers with surfactants. The surfactants of choice are markedly different than the protein-based surfactants contained in natural rubber latex that is reportedly at the root of human hypoallergenic reactions associated with the use of natural rubber latex.

Latex products are manufactured in an identical fashion as the dry polymers described earlier. One major exception is that the primary and auxiliary surfactants used in latex manufacture are not destroyed prior to shipment to the end user. Molecular weight control is identical with mercaptan, organic halides, and xanthogen disulfides chain-transfer agents typically used. Copolymerizations are conducted with the same variety of comonomers that include

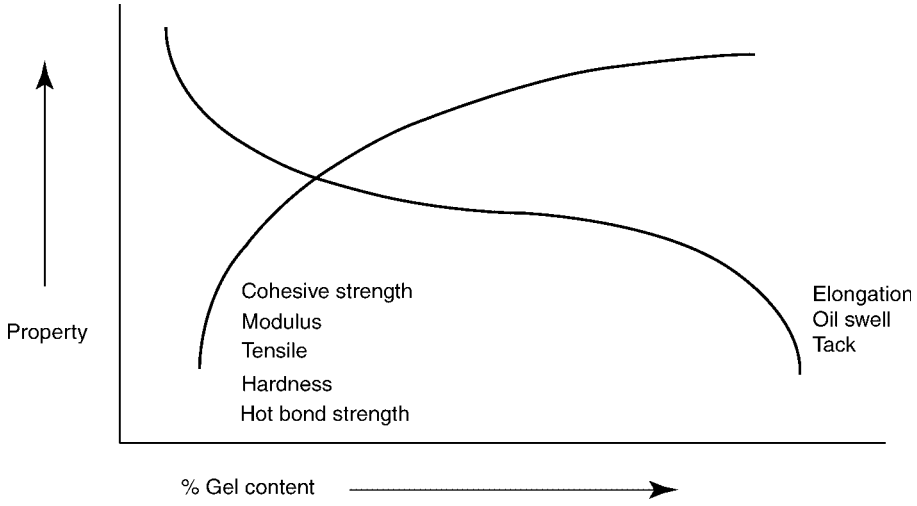

Fig. 7. Properties as a function of gel content.

2,3-dichloro-1,3-butadiene, sulfur, and acrylic acids and esters. Polymerization temperatures are varied from 5° to 50°C at atmospheric pressures to control polymer microstructure and crystallinity. The choice of surfactant package for latex products is much more critical than for dry types, since the latex must remain colloidally stable for time periods measured in weeks or months instead of hours as required in dry-type manufacture.

Since the latexes contain discrete stabilized polymer particles that are dispersed in the aqueous medium, the latex displays good rheological properties. The latex polymer structures can differ appreciably from dry types. Long-chain branching and gelled structures are more tolerable in latex, since the polymer does not need to be isolated by freeze roll. The branched and gelled structures offer advantages to the end users who fabricate adhesives having a high cohesive strength, good stress–strain characteristics, and high bond strength at elevated temperatures (Fig. 7).

Low temperature polymerization yields crystalline polymers having high room-temperature bond strength, high cohesive strength, and good stress–strain characteristics (Fig. 8).

These two phenomena form the basis for propagating the global adhesives product line of which the following is indicative.

Global Latex Product Line. There are three general classes of polychloroprene latexes: anionic, cationic, and nonionic. By far, the anionic latex class constitutes the largest commercial volumes for general use. Cationic latexes are usually made with quaternary ammonium salts and are made in the smallest volume types. The nonionic latexes differ appreciably from ionic lattices in several important aspects, of which chemical and mechanical stability are the most different (Table 10).

The Theoretical Basis of Latex Stabilization. The colloidal stability of each class of latex is primarily dependent on the effectiveness of the surfactant. In the high permittivity of water, most polymer colloid particles carry an electric

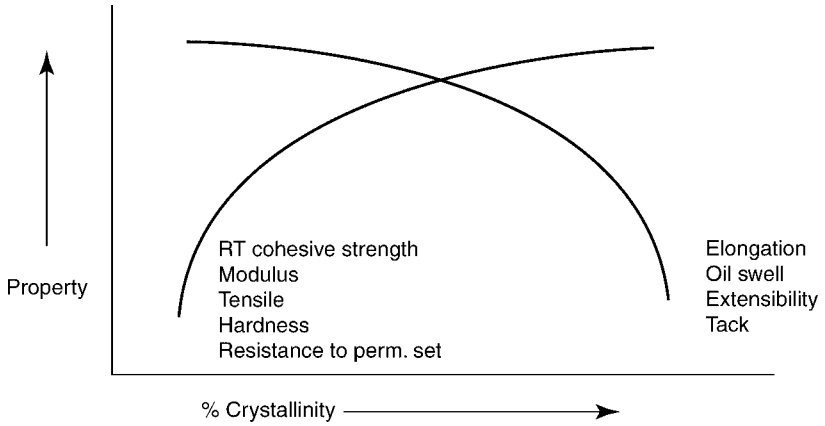

Fig. 8. Properties as a function of crystallinity.

charge. These electric charges arise from the ionization of groups at the polymer surface. In ionic polychloroprene emulsions, the electric charges are formed by the neutralization of substituted carboxylated diterpenes (rosins and resins) with caustic during the emulsification process.

The surface of the polymer particle is smooth and charges are uniformly distributed over the surface. To satisfy the condition of electroneutrality, the sodium carboxylate moiety resides at the interphase with sodium counterions solubilized in the aqueous phase near the carboxylate coions. The spatial distribution of coions and counterions form the electronic "double layer" of $1/\kappa$ thickness. This boundary layer stabilizes the colloid (139). In the 1940s Derjagin, Landau, Verway, and Overbeek suggested that the electrostatic stability (84,85) of latexes could be explained on the basis of three potential energy terms that include repulsive potential

Table 10. Comparison of Anionic and Nonionic Latexes

Comparisons (138)	Anionic	Nonionic
Surfactant type	Sodium or potassium resinates	Poly(vinyl alcohol)
Colloidal stabilization mechanism	Electrostatic	Steric
Stability		
Mechanical	Good	Exceptional
Electrolytic to ionic contaminants	Good	Excellent
Storage	Poor–fair	Excellent
	Good	Gel increases
pH	12 +	7–8
% Solids	38–60	47
Surface tension, mN/m	39	58
Brookfield viscosity, mPa·s (= cP)	5–500	500
Average weight of average particle size, nm	100	300

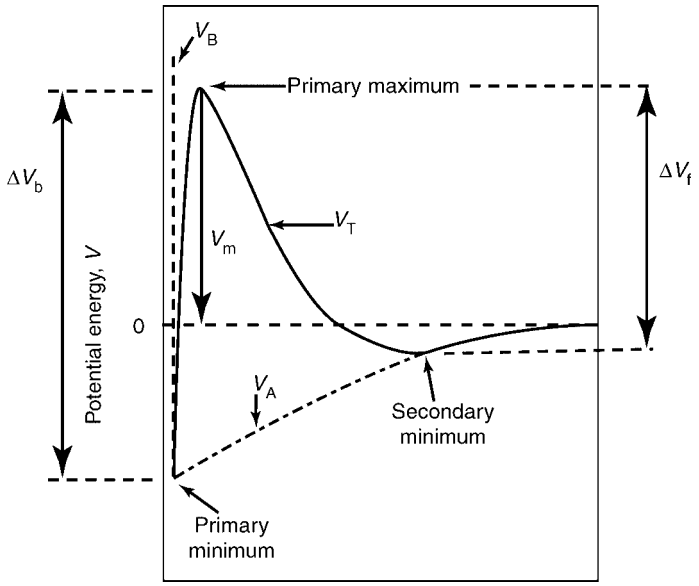

Fig. 9.

energy (V_R), van der Waals attraction (V_A) and the Born potential (V_B). This theory became widely known as the DLVO theory.

$$V_{Total} = V_R + V_A + V_B$$

Latex stability is achieved when the electrostatic repulsion term, V_R, dominates attractive forces at the interparticle distance near $4/\kappa$. At very close interparticle distances, a potential energy barrier is encountered. If particles are forced over the potential energy barrier to the primary minimum, permanent coagulation occurs (Fig. 9).

Thus, stability is heavily dependent on repulsive energies, which are functions of at least three variables: (*1*) boundary layer thickness, (*2*) valence of the counterion and ionic contaminants, and (*3*) concentrations of electrolyte. As electrolyte concentration is increased, the electronic double layer thickness decreases, the particles move toward the primary maximum, and coagulation occurs. Multivalent counterions are important adjuvant for dipped goods manufacture where chemical coagulation is required (Table 11).

In the latex end use applications, DLVO stabilization must be considered in designing a latex compound.

Latex Compounding. Polychloroprene latexes are used in six general applications: adhesives, binders, coatings, dipped goods, elasticizers, and foam. The conversion of the raw latex to a tough finished product depends on compounding and curing. Latex compounding has one complication not present for dry types. The colloid chemical and mechanical stabilities of the aqueous dispersion containing added compounding ingredients must be considered. Masterbatching vs individual dispersion make-up will minimize introduction of electrolytes,

Table 11. Double Layer Thickness with changing Electrolyte Concentration

Electrolyte concentration moles/d^3	$1/\kappa$, nm	$1/\kappa$, nm (high counterion valence)	$1/\kappa$, nm (higher counterion valence)
10^{-5}	96.3	55.6	39.3
10^{-4}	30.4	17.6	12.4
10^{-3}	9.63	5.00	3.93
10^{-2}	3.04	1.76	1.24
10^{-1}	0.96	0.56	0.39

facilitate dispersion of difficult materials, minimize processing mistakes, lower cost, increase production rates, and generally generate less waste. Mechanical stability during compounding is enhanced by control of seven variables:

(1) Use of tanks and pipes having smooth interiors.
(2) Use of low shear and low speed agitators with no dead spots.
(3) Use of gravity flow where possible.
(4) Where gravity flow is not possible, use of positive displacement pumps—no gear or pinch pumps.
(5) Use of air pressure only to transfer but not to store latex.
(6) Use of areas of high humidity to decrease evaporation rates.
(7) Filtration of the compound if viscosity permits.

Depending on the application, a latex compound may contain up to nine compounding ingredients: (*1*) deionized water, (*2*) antifoam, (*3*) colloidal stabilizers, (*4*) polymer stabilizers, (*5*) curatives, (*6*) tackifiers, (*7*) fillers, and (*8*) thickeners. All have specific functions that contribute to the outcome of the finished part (see LATEX TECHNOLOGY).

Polychloroprene Latex

The latex can be chosen from a wide variety of liquid dispersions available on the basis of the crystallization and gel properties desired (Fig 10). For example, Neoprene water-based polychloroprene latexes available from DuPont Dow have the following properties (96,140,141) (Table 12).

Additives.

Antifoam. It is best to prevent foam from forming in the latex than to eliminate foam by use of defoamer. To prevent foam formation,we need to avoid free fall of latex or any dispersion and emulsion, which contains surfactants that will facilitate foam formation. When mixing latex with other ingredients, the agitator impeller should be turned off until the blade is covered with latex. Any fillers, which may have absorbed air on the particles, should be prewetted and foam allowed to subside before adding the fillers to the latex compound.

Colloidal Stabilizers. Colloidal stabilizers are normally added to increase shear stability of anionic latexes, improve chemical stability of nonionic latexes,

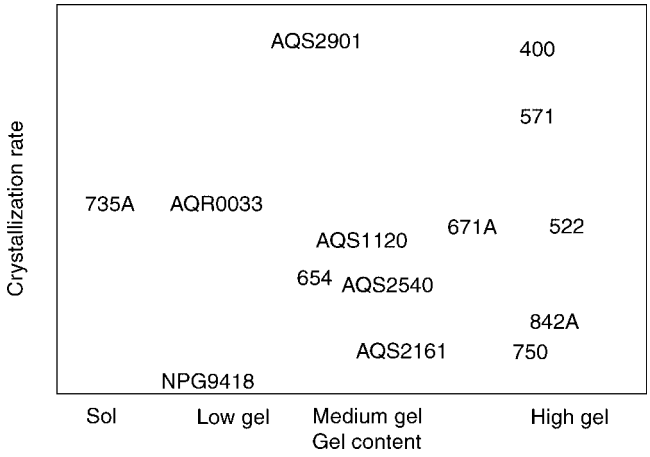

Fig. 10. Crystallization rate vs gel content of water-based polychloroprene latexes.

and to sequester cations. The surfactants are also used to wet-water insoluble additives. Anionic stabilizers such as potassium resinates, potassium caseinate or Darvan WAQ (R. T. Vanderbilt Co.) are used with anionic latexes to improve the mechanical stability in coating and binders. Darvan SMO, sodium sulfated methyloleate, is specifically recommended for use in dipping compounds to improve smoothness and to eliminate striations. Tritons (Dow Chemical Co.), Igepals (Rhodia Chemical Co.), Tergitols (Dow Chemical Co.) are added to nonionic latexes to improve chemical stability. Cationic latexes require cationic or nonionic surfactants (Darvan NS). Cations are normally sequestered with Calgon (Calgon Corporation), sodium silicate, or trisodium phosphate.

Polymer Stabilizers or Antioxidants. No polychloroprene latex compound is complete without additives that give adequate protection against polymer oxidation. The oxidation studies for dry types also apply to polymers contained in latexes. Hindered phenols are used in many applications. When used at 1-phr,

Table 12. Polychloroprene Latex Compound

Neoprene latex	100 Dry weight
Deionized water	Wherever needed
Antifoam	0.05–0.10
Darvan WAQ (R. T. Vanderbilt)	0–1.0
Potassium caseinate	0–1.0
Triton X-100 (Dow Chemical Co.)	0–1.0
Sodium silicate	0.25
Wingstay L (Goodyear Tire and Rubber Co., Chemical Division)	2.0
Zinc oxide	5.0
Sulfur	0–1.0
Thiocarbanilide	0–1.0
Hi/Lo MP tackifiers	As needed
Fillers	As needed
Polyacrylate	As needed

Wingstay L (butyrated-*p*-cresol-bicyclopentadiene) (Goodyear Tire and Rubber Co.) provides adequate protection in most adhesive applications. The bisphenols are nonstaining and generally nondiscoloring.

Curatives. Consistent with dry type technology, metal oxides have three functions in a latex compound. Zinc oxide participates in the curing reaction. Zinc oxide is an effective acid scavenger. In applications where the substrate is not acidic, zinc oxide is not needed. Such substrates include chrysoltile asbestos gaskets or the hydraulic cement in elasticized concrete.

Sulfur is occasionally added to polychloroprene latexes to achieve a higher state of cure. Added sulfur is not effective for chloroprene–sulfur copolymer latexes. Films containing 1-phr sulfur darken considerably upon curing. Retention of elasticity of such films decreases further on continued exposure to heat.

Accelerators. Accelerators catalyze the cross-linking of the polymers by a similar mechanism described for dry types. The latex version has some advantage over dry types in that many of the crosslinks for latex types were formed during polymerization. The use of Thiocarbanilide (*N*,*N*′-thiourea) yields products of higher modulus, lower tensile strength, and best oil swell resistance. Butyl Zimate (zinc dibutyl dithiocarbamate) (R. T. Vanderbilt Co.) is practically equivalent to Thiocarbanilide cures but imparts less color change. Tepidone (sodium dibutyl dithiocarbamate) and tetraethyl thiuram disulfide (TETD) give products of lower modulus, higher tensile strength, higher elongation, and less color.

Ultraviolet Ray Screeners. Carbon black and red iron oxide provide additional resistance to degradation from exposure to sunlight. They are used only sparingly, however, because of discoloration at the adhesive line.

Fillers. Fillers are used in compounds to increase viscosity, increase solids, and to lower cost. Most fillers used in latex do not exhibit the reinforcing effect that is characteristic of their use in dry-type polychloroprene. Water-washed whiting (calcium carbonate) can be added directly to the latex. Most clays are acids and must be neutralized and slurred before adding to the latex. When used at levels ranging from 10- to 20-phr, fine clays such as DIXIE Clay (R. T. Vanderbilt Co.) can add some degree of reinforcement. Hard clays have much smaller particle size than soft clays. Feldspar can be added directly to the latex but will tend to settle quickly. Hydrated alumina is used primarily to improve flame retardancy and improve water resistance. Large-particle-size hydrated alumina can be added directly to the latex.

Thickeners. Thickeners are always the last ingredients to be added. Polyacrylates are the preferred thickeners for polychloroprene latex. They are usually diluted with equal parts of water to generate a pourable fluid, which can be added directly to the compound. Algums have higher viscosity stability than polyacrylates at high pH. Cellulose derivatives are effective thickeners but are much more difficult to handle, usually requiring backmixing with a small amount of latex before adding it to the compound. Bentonite clay is a favorite thickener for very high viscosity adhesives such as mastics. Fumed silica is a good choice for latex formulations having a pH of 7–10.

Biocides. Waterborne systems of pH < 10- are prone to bacterial attack. The phenomenon is normally not a problem with solvent-borne systems. Bacterial infestation normally manifests itself by malodor, discoloration, and gas evolution. Nuosept 95 (Creanova Co.) is an effective biocide.

Latex Applications

A good way to remember the applications for latex is to follow the first six letters of the alphabet: A, adhesives; B, binders; C, coatings; D, dipped goods; E, elasticizers; and F, foam.

Adhesives. An adhesive is a continuous film sandwiched between two substrates. Polychloroprene latexes are used as waterborne contact bond adhesives where a latex-based adhesive compound is placed on both substrates to be bonded. Immediately before the two coated surfaces dry, the two substrates are placed together and bonded. Many of the environmental, personnel exposure and potential fire hazards associated with the use of aromatic-hydrocarbon–solvent adhesives are avoided by the use of latex adhesives. Both anionic and nonionic latexes are used in adhesive applications. The high uncured strength, high cohesive strength, high internal strength, and good contactibility of polychloroprene with a variety of substrates are attributes that make polychloroprene useful in this application. The high uncured strength of the adhesive arises from the crosslinks made in the latex during polymerization.

Binders. A binder is a mixture of discrete polymer particles distributed throughout a matrix. The particulates can be cellulosic, ground leather, or ground rubber. The high internal bond strength of polychloroprene makes the latexes useful for binding cellulosic fibers in sandpaper. Up to 17,000,000 lb/year of polychloroprene latex have been used for shoeboard applications. Regenerated leather made by use of polychloroprene latex to bind ground leather scraps is a prominent example of use as a binder. Wet-web saturation with polychloroprene is used in shoeboard applications requiring a flexible polymer of high binder efficiency, adhesive solvent resistance, and moisture and chemical resistance. The high durability, resistance to weather, and resilience without curing are polychloroprene properties that find utility in fabrication of resilient surfaces such as tennis courts and athletic tracks.

Coatings. Coatings are continuous films adhering to one substrate. The substrate can be fiber glass, fiber glass bats, fabrics, composite laminates, or carpet. Polychloroprene has been used in all of these applications due to its erosion resistance, chemical resistance, abrasion resistance, weather resistance, sound dampening characteristics, thermal insulation properties and the inability of properly formulated polychloroprene to support combustion. Fiber glass and fiber glass bats used in construction ducts are coated with polychloroprene latex to prevent fiber glass particles from contaminating air that passes through the ducts. Polychloroprene-coated fiber glass provides good thermal insulation and sound dampening. Polychloroprene-coated fiber glass is used under automotive hoods to provide a degree of flame retardancy and sound dampening.

Woven fabrics used for printer blankets are coated with polychloroprene to provide resistance to solvent and inks. Polychloroprene composite laminates for industrial suits (eg firefighter's suits) are coated with polychloroprene to provide chemical resistance, weather/abrasion resistance, durability, and a degree of flame retardancy.

Rugs and upholstery can be coated with polychloroprene latex, particularly those used in aircraft. Flame retardancy is a key property highlighted.

There are advantages and disadvantages to using polychloroprene latexes in these applications. The gelled polymer from polymerization provides high uncured strength, particularly in applications where post curing is not practical. The disadvantage lies in the high pound/volume cost. Thus, latexes that permit high filler loading reduced cost without much sacrifice of properties are successful in these applications.

Dipped Goods. Dipped goods have continuous films (supported or unsupported) that are usually formed by chemical coagulation of latex compounds. Polychloroprene latexes are used in a variety of dipped goods applications including automotive, tractor shift controls, convoluted parts, windshield wiper blades, supported and unsupported gloves, and meteorological balloons. The major advantages of polychloroprene are ozone resistance in objects having sharp contours, durability, chemical resistance, flexibility, feel, tear strength, oil/chemical/abrasion resistance and resistance to ultraviolet rays. Generally the latexes are sold to a latex compounder who formulates the latex for the end use fabricators. Polychloroprene latexes have many advantages over natural rubber in terms of resistance to household and industrial detergents and chemicals. Gloves made from polychloroprene have 100% chemical resistance, oil resistance, ozone resistance, and heat resistance.

A unique application involves meteorological balloons. Balloons made from polychloroprene are used to convey sensors up to 150,000 feet into the atmosphere for purposes of determining the direction of weather currents. A special combination of stress–strain properties, resistance to ozone, and ultraviolet sunrays are important for optimum functioning of the balloon.

Elasticizers. Elasticizers are composites of small particles of near molecular size that are distributed throughout some medium. Latexes are formulated into elasticized concrete to minimize stress cracking that is precipitated by concrete expansion and contraction. The application is extremely important for decks on ships, decks in high rise garages, hospital floors, kitchens, and gym floors. Latex-modified concrete provide vibration dampening in the workplace that reduce fatigue to personnel (eg operating rooms) who need to stand for extended periods of time while working.

Latex-modified asphalt and bitumen represent other elasticizers. Latex modification not only reduces stress cracking but also provides adhesion for rocks and chip asphalt fillers. The adhesion prevents chips from flying out of the asphalt on highways and breaking windshields. Many states in the United States require latex-modified asphalt in road construction. All classes of latexes can be used in concrete and asphalt modification.

Foam. Foam is a continuous open-celled matrix produced from froth or coagulation onto a preformed cellular matrix. Over the years, polychloroprene latexes have been used in nursing homes, in mattresses, in journal boxes, in seagoing vessels, and in cushioning and seating. Properly formulated froth and parts made from polychloroprene latexes are water resistant and have a high degree of flame retardency. The journal box application for locomotive lubricants depends on the oil resistance of polychloroprene to deliver oil from the reservoir to the axle of the train. Polychloroprene suffers from two major disadvantages in foam applications: costs and weight. Both limit full utility of these foams in aircraft applications.

Two processes have been used to make foams from froth. For thin foams, dry coagulation is an effective procedure. For thicker foams, chemical coagulation, and chemical and heat gelation are used.

Quality Management. For major polychloroprene producers the quality management systems are described by the international ISO9001-2000 protocol.

Health, Safety, and Environment

Since chloroprene and dichlorobutadiene monomer will undergo runaway reaction, the successful producers of polychloroprene polymers have learned how to safely handle the hazardous monomers and monomer intermediates in large-scale quantities. Monomer synthesis and storages represent the largest concentration of monomers during commercial manufacture. Polymerization, albeit in aqueous media, present safety challenges owing to the presence of free radicals.

Prevention of runaway reactions involving these highly reactive monomers involve strict adherence to six fundamental principles for monomer handling: (*1*) keeping it cold, (*2*) keeping it free of air and oxygen by storage in a nitrogen atmosphere, (*3*) keeping it inhibited where possible, (*4*) keeping it moving, (*5*) keeping it free of contaminants such as popcorn polymer and iron, and (*6*) keeping it diluted where possible.

Residual monomer remaining after polymerization pose a lesser degree of hazard owing to low concentration and the engineering measures implemented in the workplace to prevent personnel exposure to the monomer. Neoprene liquid dispersions contain less than 0.1% residual chloroprene monomer.

The amount of excess caustic in Neoprene polychloroprene liquid dispersions is approximately 0.1%. The liquid dispersions are, however, very basic having pH near 12. While not corrosive in animal tests, eye protection and skin protection are essential in areas where personnel exposure is possible because of possible irritation.

Some dry polychloroprene types have been shown to have low oral toxicity rates. Human patch test for several dry types showed no skin reactions (142). The FDA status of Neoprene polychloroprene is described in the literature (143).

BIBLIOGRAPHY

"2-Chlorobutadiene Polymers" in *EPST* 1st ed., Vol. 3, pp. 705–730, by C. A. Hargreaves II and D. C. Thompson, E. I. du Pont de Nemours & Co., Inc.; in *EPSE* 2nd ed., Vol 3, pp. 441–462, by C. A. Stewart Jr., T. Takeshita, and M. L. Coleman, E. I. du Pont de Nemour & Co., Inc.

1. W. R. Remington and J. S. Lann, JLR-29-5, No. 26.
2. P. A. Lovell and M. S. El-Aasser, *Emulsion Polymerization and Emulsion Polymers*, John Wiley & Sons, Inc., New York, p. 28.
3. L. J. Op, P. J. Hwan, and B. H. On, *Hwahak Kwa Hwahak Kongop* **20**, 119 (1977).
4. W. Kern and co-workers, *Macromol. Chem.* **3**, 223–246 (1950).
5. C. A. Stewart Jr., *Am. Chem. Soc.* **93**, 4815 (1971); **94**, 635 (1972).
6. F. Hrabak and J. Webr, *J. Macromol. Chem.* **104**, 275 (1967).

7. I. Williams, *Ind. Eng. Chem.* **31**, 1204 (1939).
8. S. Ekegren and co-workers, *Acta Chem. Scand.* **4**, 126 (1950).
9. K. A. Nersesyan, R. O. Chaltykyan, and N. M. Beileryan, *Arm. Khim. Zh.* **40**(2), 92–95 (1987).
10. R. N. Haward, *J. Polym. Sci.* **4**, 273 (1949).
11. U.S. 3,925,294 to E. I. Du Pont de Nemours, A. M. Doyle, Controlling Viscosity of Chloroprene–Sulfur Copolymers, 1975.
12. Ref. 13, p. 41.
13. D. H. Napper, *Polymeric Stabilization of Colloidal Dispersions*, Academic Press Inc., New York, p. 38, 1983.
14. Ref. 13, p. 667.
15. R. C. Ferguson, *J. Pol. Sci. Part A* **2**, 4735 (1964)
16. P. A. Lovell, T. H. Shah, and F. Heatley, *Polym. Commun.* **32**, 98–103 (1991).
17. R. G. Gilbert, *Emulsion Polymerization. A Mechanistic Approach*, Academic Press, New York, pp. 189–190.
18. W. E. Mochel, *J. Am. Chem. Soc.* **71**, 1426 (1949).
19. Fr. Demand FP 2,556,730 (June 21, 1985), P. Branlard and F. Sauterey (to Distugil SA).
20. H. G. Elias, *Macaromolecules, Structure and Properties*, Plenum, New York, 1977.
21. M. Buback, L. a. Garcia-Rubio, R. G. Gilbert, D. H. Napper, J. Guillot, A. E. Hamielec, D. Hill, K. F. O'Driscoll, O. F. Olah, J. Shen, D. Soomon, G. Mood, M. Sticlan, M. Tirrell, and M. A. Winnik, *J. Polym. Sci. Lett. Ed.* **26**, 293, (1988).
22. R. A. Hutchinson, M. T. Aronson, and J. R. Richards, *Macromolecules* **26**, 6410–6415 (1993).
23. Ref. 13, p. 28.
24. F. A. Cotton & G. Wilkinson, *Advanced Inorganic Chemistry*, Interscience Publishers, New York, 1988, p. 522.
25. Eur Pat. Appl 146,131 (June 26, 1985), N. Emura, T. Ariyoshi, and T. Kato (to Toyo Soda Mfg. Co., Ltd.).
26. Jpn. Kokai Tokkyo Koho JP 61,238,808 (Oct. 24, 1986), M. Kamezawa, T. Ariyoshi, and Y. Sakanaka (to Toyo Soda Mfg. Co., Ltd.).
27. Y. Miyata and M. Sawoda, *Polymer* **29**, 1495 (1988)
28. Ger. Offen. DE 3,344,065 (June 7, 1984), E. M. Banta and K. D. Fitzgerald (to Denka Chemical Corp.).
29. Jpn. Kokai Tokkyo Koho JP 59 056,440 (Mar. 31, 1984) (to Toyo Soda Mfg. Co., Ltd.).
30. Jpn. Kokai Tokkyo Koho JP 61 118,440 (June 5, 1986), Kato and co-workers (to Toyo Soda Co., Ltd.).
31. Eur Pat. Appl EP 421,149 (Apr. 10, 1991), S. Ozoe and H. Yamakawa (to Tosoh Corp.).
32. L. J. Op, P. J. Hwan, and B. H. On, *Hwahak Kwa Hwahak Kongop* **20**, 299 (1977).
33. H. K. Banock, R. S. Lehrle, and J. C. Robb, *J. Polym. Sci., Part C* **4**, 1165 (1964).
34. G. H. Miller, G. P. Chock, and E. P. Chock, *J. Polym. Sci., Part A* **3**, 3353 (1965).
35. A. N. Pravednikov and S. S. Medvedev, *Dokl. Akad. Nauk., USSR* **109**, 579 (1956).
36. M. F. Margantova and M. P. Zverev, *Ukr. Khim. Zh.* **23**, 734 (1957).
37. U.S. Pat. 2,942,037 and 2,942,038 (June 21, 1960), P. A. Jenkins (to Distillers Co., Ltd.).
38. U.S. Pat. 2,770,657 (Nov. 13, 1956), J. R. Hively (to E. I. du Pont de Nemours & Co., Inc.).
39. U. S. Pat. 3,175,012 (Mar. 23, 1965), G. P. Colbert (to E. I. du Pont de Nemours & Co., Inc.).
40. R. R. Garrett, C. A. Hargeaves II, and D. N. Robinson, *J. Macromol. Sci., Chem. A* **4**, 1979 (1970); T. Okada and T. Ikushige, *J. Polym. Sci., Polym. Chem. Ed*. 2059 (1976).

41. C. A. Aufdermarsh, *J. Org. Chem.* **29**, 194 (1964); C. A. Aufdermarsh and R. Pariser, *J. Polym. Sci. A* **2**, 4727 (1964); R. C. Ferguson, *J. Polym. Sci. A* **2**, 3969 (1966).
42. N. G. Gaylord and co-workers, *J. Polym. Sci. A* **2**, 3969 (1966).
43. N. G. Gaylord and co-workers, *J. Am. Chem. Soc.* **85**, 641 (1963).
44. U.S. Pat. 3,004,011 (Feb. 5, 1958), H. L. Jackson (to E. I. du Pont de Nemours & Co., Inc.); U.S. Pat. 3,004,012 (Feb. 5, 1958), K. L. Seligman and H. L. Jackson (to E. I. du Pont de Nemours & Co., Inc.).
45. N. G. Gaylord and B. K. Patnik, *J. Polym. Sci.* **13**, 837 (1975); A. Masaki, M. Yasui, and I. Yamashita, *J. Macromol. Sci.-Chem. A* **6**, 1285 (1972).
46. T. Okada and M. Oysuru, *J. Appl. Polym. Sci.* **23**, 2215 (1979).
47. K. Irako and co-workers, *Nippon Kagaku Kaishi* **4**, 670 (1967); K. Irako, H. Koyama, and A. Shisra, *Kogyo Kagaku Zasshi* **74**, 2210 (1971).
48. X. Han, F. Guo, and D. Wang, *Yingyong Huaxue* **1**(3), 41 (1984).
49. X. Han and E. Chen, *Gaofenzi Tongxum* (6), 435j (1985).
50. J. P. Kennedy and S. C. Guhaniyogi, *J. Macromol. Sci., Chem. A* **18**(1), 103 (1982).
51. M. M. Coleman, D. L. Tabb, and E. G. Brame, *Rubber Chem. Technol.* **51**, 49 (1978); M. M. Coleman and E. G. Brame, *Rubber Chem. Technol.* **51**, 668 (1978).
52. R. J. Petcavich and M. M. Coleman, *J. Macromol. Sci.,Phys. B* **18**, 47–71 (1980).
53. J. R. Ebdon, *Polymer* **15**, 782 (1974); D. J. T. Hill, J. H. O'Donnell, and P. W. O'Sullivan, *Polymer* **25**, 569 (1984); A. A. Kahn and E. G. Brame Jr., *Rubber Chem. Technol.* **50**, 272 (1977).
54. R. E. Cais and G. J. Stuk, *Macromolecules* **13**, 415 (1980).
55. R. Petiaud and Q. R. Pham, *J. Polym. Sci., Polym. Ed.* **23**, 1333–1334 (1985).
56. J. Brandrup and E. H. Immergut, eds., *Polymer Handbook*, 3rd ed., John Wiley & Sons, Inc., New York, 1989.
57. H. C. Bailey, *Revue Generale du Caoutchou Plastique* **44**(12), 1495–1502 (1967).
58. R. R. Garrett, C. A. Hargraves, and D. V. Robinson, *J. Macromol. Sci. Chem. A* **4**, 1679 (1970).
59. T. A. Babushkina, L. N. Gvozdeva, and G. K. Semin, *J. Mol. Struct.* **73**, 215 (1981).
60. T. A. Babushkina and co-workers, *Vysokomol. Soedin. Ser. A* **23**, 1810 (1981).
61. R. Petiaud, Q. T. Pham, *J. Polym. Sci., Polym. Chem. Ed.* **23**, 1343 (1985).
62. M. M. Coleman and co-workers, *J. Polym. Sci. Polym. Lett. Ed.* **12**, 577 (1974); D. L. Tabb, J. L. Koenig, and M. M. Coleman, *J. Polym. Sci. Phys. Ed.* **13**, 1145 (1975).
63. M. M. Coleman, P. C. Painter, and J. L. Koenig, *J. Raman Spect.* **5**, 417 (1976); M. M. Coleman, R. J. Petacvich, and P. C. Painter, *Polymer* **19**, 1243 (1978).
64. F. Riva, A. Porte, and C. D. Monica, *Colloid Polym Sci.* **259**, 606 (1981); C. Della Monica and co-workers, *Conv. Ital. Sci. Macromol. [Atti]* **2**(6) 179 (1983); A. Forte and co-workers, *Conv. Ital. Sci. Macromol. [Atti]* (5) 381.
65. T. T. Okaya, T. Tanaka, and K. Yuki, *J. Appl. Polym. Sci.* **50**, 745 (1993).
66. G. V. Schulz and L. Roberts-Nowakowsha, *Makromol. Chem.* **80**, 36 (1964).
67. D. Stein, *Makromol. Chem.* **76**, 170 (1964).
68. F. R. Mayo, *J. Am. Chem Soc.* **65**, 2324 (1943).
69. W. E. Mochel, *J. Polym. Sci.* **8**, 583 (1949).
70. P. A. Lovell, T. H. Shah, and F. Heatley, in E. S. Daniels, E. D. Sudol, and M. El Asser, eds., *Correlationof the extent of chain branching with reactor conditions for emulsion polymerization of n-butyl acrylate ACS Symposium Series, k Polymer Latexes-Preparation, Characterization and Applications*, Vol. 492 ACS Washington, D.C., 1992, pp. 188–202
71. H. Mark Der feste Korper, Hirzel, Leipzig, 1938, p. 103.
72. F. Rodriguez, *Principles of Polymer Systems*, Hemisphere Publishing Corporation, New York, 1989, p. 185.

73. E. E. Drott and R. A. Mendelson, *J. Polym. Sci., A-2* **8**, 1361 (1970); G. Kraus and C. J. Stacy, *J. Polym. Sci., Polym. Phys. Ed.* **10**, 657 (1972); *J. Polym. Sci. Polym. Symp.* **43**, 329 (1973).
74. M. M. Coleman and R. E. Fuller, *Macromol. Sci., Phys.* **11**, 419 (1975).
75. Ger. Offen. DE 3,105,339 (Feb. 13, 1981), U. Eisele and co-workers (to Bayer AG).
76. U.S. Pat. 2,914,497 (Nov. 24, 1959), W. J. Keller (to E. I. du Pont de Nemours & Co., Inc.).
77. Eur Pat. Appl. EP 426,023 (May 8, 1991), F. Y. Kafka, A. R. Bice, and D. K. Burchett (to E. I.du Pont de Nemours & Co., Inc.).
78. Jpn. Kokai Tokkyo Koho JP 58,180,501 (Oct. 22, 1983) (to Kenki Kagaku Kogyo); Jpn. Kokai Tokkyo Koho JP 58,189,202 (Nov. 4, 1983) (to Denki Kagaku Kogyo).
79. *Toyo Soda Kenkya Hokoku* **26**(2), 93 (1982).
80. *Toyo Soda Kenkyu Hokoku* **24**, 83 (1979).
81. P. R. Johnson, *Rubber Chem. Technol.* **49**, 650–702 (1976).
82. U. S. Pat. 2,264,173 (Nov. 25, 1941), A. M. Collins (to E. I. du Pont de Nemours & Co., Inc.).
83. C. A. Hargreaves II in J. P. Kennedy and E. G. Tornqvist, eds., *Polymer Chemistry of Synthetic Elastomers*, Wiley-Interscience, New York, 1968, pp. 227–252.
84. D. V. Derjagin and L. Landau, *Acta Physicochim., USSR* **14**, 633 (1941).
85. E. J. W. Verway and J. Th. G. Overbeek, *Theory of Stability of Lyophobic Colloids*, Elsevier, Amsterdam, 1948.
86. R. S. Barrows and G. W. Scott, *Ind. Eng. Chem.* **40**, 2193 (1948).
87. G. E. Alves, *Chem. Eng. Progr.* **66**(7), pp. 50–67 (1970).
88. U.S. Pat. 2,831,842 (Apr. 22, 1958), C. E. Aho (to E. I. DuPont de Neumours & Co., Inc.).
89. L. M. White and co-workers, *Ind. Eng. Chem.* **37**, 770 (1943).
90. *Correlator for Baypren Polychloroprene*, Miles Inc. Technical Literature, 1992.
91. Ger. Pat. 1,186,215 (Jan. 28, 1965), K. L. Miller (to E. I. duPont de Nemours & Co., Inc.); U.S. Pat. 3655,827 (Apr. 11, 1972), J. B. Finlay (to E. I. duPont de Nemours & Co., Inc.).
92. R. Musch and U. Eisle, *Preprints of the ACS Rubber Division Meeting*, Detroit, 1989, The American Chemical Society, Washington, D.C., 1989.
93. U.S. Pat. 3,988,506 (Oct 26, 1976), M. Dohi, T. Sumida, and K. Yokobori (to Denki Kagaku Kabushiki); Eur. Pat. Appl. EP 223,149 (May 27, 1987), T. Takeshita (to E. I.duPont de Nemours & Co., Inc.); Eur. Pat Appl. EP 175,245 (Mar. 26, 1986), T. Takeshita (to E.I. du Pont de Nemours & Co., Inc.).
94. U.S. Pat. 3,042,652 (July 3, 1962), R. Pariser and R. D. Soufie (to E. I.duPont de Nemours & Co., Inc.).
95. S. W. Schmidt, *The Neoprene T. Family*, Du Pont Technical Bulletin NP-240.1, E. I. du Pont de Nemours & Co., Inc., Wilmington, Del., 1977.
96. AquaStik™ is a trademark for DuPont Dow Elastomers L.L.C. liquid dispersions.
97. P. K. Freakley and A. R. Payne, *Theory and Practice of Engineering with Rubber*, Applied Science Publishers, Ltd., London, 1978.
98. L. Outzs, ed., *Neoprene Polychloroprene, A Guide to Grades Compounding & Processing of Neoprene Rubber*, DuPont Dow Elastomers (2002) original Guide was compiled by J. C. Bament of E. I. DuPont de Nemours and is currently known as the "Bament Guide".
99. N. L. Catton, *The Neoprenes*, The Rubber Chemical Division, E. E. DuPont de Nemours & Co., 1953, p. 5.
100. N. Kawasaki and T. Hashimoto, *J. Polym. Sci., Polym. Chem. Ed.* **11**, 671 (1973).
101. Y. Miyata and M. Atsumi, *Rubber Chem. Technol.* **62**, 1 (1989).
102. R. Pariser, *Kunstst*. **50**, 623 (1960).

103. H. Kato and H. Fujita, *Rubber Chem. Technol.* **55**, 949 (1981).
104. Jpn. Kokai Tokkyo Koho JP 02,28,532 (Dec. 10, 1990), N. Yamamoto and co-workers (to Ouchi Shinko Chem. Ind. Co., Ltd.); N. Yamamoto and co-workers, *Nippon Gomu Kyokaishi* **64**, 48 (1991).
105. W. Schunk and co-workers, *Gummi, Fasern, Kunstst.* **43**, 617 (1990); F. M. Helay and co-workers, *Elastomerics* **121**(9), 26 (1989).
106. Y. Sakuramoto and co-workers, *Nippon Gomu Kyokaishi* **56**, 218 (1983).
107. U. Eholzer and T. Kempermann, *Rubber Plast News* **49** (May 25, 1981).
108. W. Warrach and Don Tsou, *Elastomerics* **116**, 26 (1984).
109. W. Schmidt, *Curing Systems for Neoprene*, Du Pont Bulletin NP-330.1, 1982; J. C. Bament, *Neoprene Compounding and Procesing Guide Plus Formulary*, E. I. du Pont de Nemours & Co., Inc., 1987; R. M. Murray and D. C. Thompson, *The Neoprenes*, E. I. du Pont de Nemours & Co., Inc., Wilmington, Del., 1963.
110. R. M. Murray and D. C. Thompson, *The Neoprenes*, E. I. du Pont de Nemours & C., Inc., Wilmington, Del., 1963.
111. Fr. Demande FR 2,459,266 (Jan. 9, 1981), J. E. Vostovich (to General Electric Co.).
112. D. C. H. Brown and J. Thompson, *Rubber World* **185**(2), 32–35 (1981).
113. P. S. Bailey, *Ozonization in Organic Chemistry*, Vol. 1, Academic Press, New York, 1978.
114. B. S. Biggs, *Rubber Chem. Technol.* **31**, 1015 (1958).
115. W. F. Tully, *Industry Eng. Chem.* **31**, 714 (1939).
116. E. Ronde, H. Bechen, and M. Metzger, *Kautsch. Gummi, Kunstst.* **42**, 1121 (1989).
117. E. Ronde, H. Bechen, and M. Mezger, *Polychloroprene Grades and Compounding for Long Term Flexibility at Low Environmental Temperatures*, Scandinavian Rubber Conference SCR/1989, Tampere, Finland, Jan. 30. 1989.
118. *UK Res. Discl.* **211**, 403 (DuPont (U.K.) Ltd.).
119. S. W. Schmidt, *Extrusion of Neoprene*, DuPont Elastomers Bulletin NP-430.1, E. I. du Pont de Nemours & Co., Inc., Wilmington, Del., 1987.
120. S. W. Schmidt, *Calendering Compounds of Neoprene*, Du Pont Elastomers Bulletin NP-440.1, E. I. du Pont de Nemours & Co., Inc., Wilmington, Del., 1987.
121. S. W. Schmidt, *Molding Neoprene*, Du Pont Elastomers Bulletin NP-450.1, E. I. du Pont de Nemours & Co., Inc., Wilmington, Del., 1987.
122. W. R. Krigbaum and R. J. Roe, *J. Polym. Sci., Part A* **2**, 4391 (1964); W. R. Krigbaum, Y. I. Bata, and G. H. Via, *Polymer* **7**, 61 (1966); A. K. Bhowmick and A. K. Gent, *Rubber Chem. Technol.* **56**, 845 (1983).
123. R. M. Murray and J. D. Detenber, *Rubber Chem. Technol.* **34**, 668 (1961).
124. J. T. Maynard and W. E. Mochel, *Polym. Sci.* **13**, 242 (1954).
125. G. I. Tsereteli, I. V. Sochava, and A. Buka, *Vesta Leningr. Univ., Fiz. Khim.* **1975**, 67 (1975).
126. M. M. Coleman, R. J. Petcavich, and P. C. Painter, *Polymer* **19**, 1253 (1978).
127. B. Y. Teitelbaum and N. P. Anoshina, *Vysokol. Soedin.* **7**, 978 (1965); B. Y. Teitlebaum and co-workers, *Dokl. USSR Phys. Chem. Sec. (English)* **150**, 463 (1963).
128. C. W. Bunn, *Proc. R. Soc. London, Ser. A* **180**, 40 (1942).
129. A. S. Kuzminskii and R. Ya. Peschanskaya, *Dokl. Akad. Nauk. SSSR* **85**, 1317 (1952).
130. R. J. Petcavich, P. C. Painter, and M. M. Coleman, *Polymer* **19**, 1249 (1978).
131. V. S. Davtyan and co-workers *Arm. Khin. Zh.* **42**, 7 (1989).
132. K. Itoyama and S. Mastunaga, *Preprints of the ACS 122nd Rubber Division Meeting*, Chicago, Oct. 4, 1982, American Chemical Society, Washington, D.C.
133. H. C. Bailey, *Rev. Gen. Caoutch. Plast.* **44**, 1495 (1971).
134. D. L. Gardner and I. C. McNeill, *Eur. Polym. J.* **7**, 569, 593, and 603 (1971).
135. K. L. Seligman and P. A. Roussel, *Rubber Chem. Technol.* **34**, 869 (1961).

136. T. E. Schroer, *Approaches to Improved Heat Resistance for Dynamic Applications*, Du Pont Elastomers Bulletin C-NP-510.0584, E. I. du Pont de Nemours & Co., Inc., Wilmington, Del., 1984.
137. *The Synthetic Rubber Manual*, 11th ed., Int. Institute of Synthetic Rubber Producers, Inc., Houston, Tex., 1989.
138. D. G. Coe, *Neoprene Latex Based Adhesives*, du Pont de Nemours Int., A Geneva, 1991.
139. T. Fukuda, K. Kudo, and Y. D. Ma, *Prog. Polym. Sci.* **17**, 875 (1992).
140. DuPont Dow Elastomers L.L.C., *Neoprene Waterbase Polychloroprene, Liquid Dispersion Selection Guide*, Rev. 4, 10/ 2003.
141. DuPont Dow Elastomers L.L.C. Aquastik™ Technical Bulletin, *Waterbase Polychloroprene*, Rev. 10/2003.
142. C. W. Stewart Sr., R. L. Dawson, and P. R. Johnson, *Effect of Compounding Variables on the Rate of Heat and Smoke Release from Polychloroprene Foam*, Du Pont Elastomer Bulletin C-NL-550.871, 1974.
143. *FDA Status of Du Pont Neoprene Solid Polymers and Latexes*, Bulletin NP-120.1, E. I. du Pont de Nemours & Co., Inc., Wilmington, Del., 1984.
144. A. M. Collins, *Rubber Chem. Technol.* **46**, G48 (1978).
145. *Worldwide Rubber Statistics 1991*, Int. Institute of Synthetic Rubber Producers, Houston, Tex., 1991.
146. F. Hrabak and M. Bezdek, *Collet. Czech. Chem. Commun.* **33**, 278–285 (1968).
147. E. S. Voskanyan, L. E. Gasparyan, and S. M. Gasparyan, *Arm. Khim. Zh.* **36**(7), 467–476 (1983).
148. Ya. Kh. Bieshev and co-workers, *Dokl. Akad. Nauk. USSR* **301**(2), 362 (1988).
149. W. V. Smith, *J. Am. Chem. Soc.* **70**, 3695 (1948); W. V. Smith and R. H. Ewart, *J. Chem. Phys.* **16**, 592 (1968); W. D. Harkins, *J. Polym. Sci.* **5**, 217 (1950).
150. F. Hrabak and Ya. Zachoval, *J. Polym. Sci.* **52**, 134 (1961); F. Hrabak, V. Hynkova, and M. Bezdec, *J. Polym. Sci., A-1* **7**, 111 (1969); F. Hrabak and co-workers, *J. Polymer Sci., Part C* **16**, 1345 (1967); F. Hrabak and M. Bezdec, *Collect. Czech. Chem. Commun.* **33**, 278 (1968).
151. K. Itoyama and co-workers, *Polym. J. (Tokyo)* **23**, 859 (1991).
152. F. Hrabak and M. Bezdec, *Makromol. Chem.* **115**, 43–55 (1968); M. Bezdec and co-workers, *Makromol. Chem.* **147**, 1 (1971).
153. O. F. Kodenko and co-workers, *Tr. Mosk. Inst. Tonkoi Khim. Technol.* **5**(2), 99 (1975); *Tr. Mosk. Inst. Tonkoi Khim. Technol.* **5**, 78 (1975).
154. R. C. Jordan and M. L. McConnell, *ACS Symp. Ser.* **138**, 107 (1980).
155. H. Lange, *Colloid Polym. Sci.* **264**, 488–493 (1986).
156. Eur. Pat. Appl. EP 53,319 (June 9, 1982), G. Aren and co-workers (to Bayer AG).
157. U.S. Pat. 2,481,044 (Aug. 15, 1950), G. w. Scott (to E. I. du Pont de Nemours & Co., Inc.).
158. Eur. Pat. Appl. EP 336,824 (Mar. 31, 1989), F. Sauterey, P. Branlard, and P. Poullet (to Societe Distugil).
159. Y. Miyata and S. Matsunaga, *Polymer* **28**, 2233 (1987); Y. Miyata and M. Sawada, *Polymer* **29**, 1495 and 1683 (1988).
160. Ger. Offen. 2,755,074 (June 15, 1978), K. L. Miller (to E. I. du Pont de Nemours & Co., Inc.).
161. Ger. Offen DE 3,246,748 (June 20, 1984), R. Musch and co-workers (to Bayer AG).
162. Ger. Offen. 2,924,660 (Jan. 15, 1981), R. Musch and co-workers (to Bayer AG).
163. J. F. Smith, *Adhesives Age* **13**, 21 (1970).
164. M. M. Coleman, R. J. Petcavich, and P. C. Painter, *Polymer* **19**, 1243 (1978).
165. Jpn. Pat. Appl. 60 65,011 (Apr. 1, 1985) (to Toyo Soda Mfg. Co., Ltd.); Jpn. Kokai Tokkyo Koho JP 01 185,309 (July 24, 1989), Y. Masuka and M. Akimoto (to Denki Kagaku Kogyo).

166. Jpn. Kokai Tokkyo Koho 81 20,010 (Feb. 25, 1981) (to Denki Kagaku Kogyo).
167. C. R. Cuervo and A. J. Maldonado, *Solution Adhesives Based on Graft Polymers of Neoprene and Methyl Methacrylate*, DuPont Informal Bulletin, Wilmington, Del., Oct. 1984; K. Itoyama, M. Dohi, and K. Ichikawa, *Nippon Setchaku Kyokaishi* **20**, 268 (1984).
168. K. S. V. Srinivasan, N. Radhakrishnan, and M. K. Pillai, *J. Appl. Polym. Sci.* **37**, 1551 (1989).
169. Jpn. Kokai Tokkyo Koho 01 284,544 (Nov. 15, 1989), S. Takayoshi, Y. Denda, and K. Ichikawa (to Denki Kagaku Kogyo).
170. R. C. Ferguson, *J. Polym. Sci. A* **2**, 4735 (1964).
171. N. G. Gaylord and co-workers, *J. Polym. Sci. A-1* **4**, 2493 (1966).
172. M. A. Youker, *Chem. Eng. Prog.* **41**, 391 (1947).
173. U.S. Pat. 2,187,146 (Jan. 16, 1940), W. S. Calcott and H. W. Starkweather (to E. I. du Pont de Nemours & Co., Inc.).
174. Ger. Offen. 3,002,711 (July 30, 1981), R. Musch and co-workers (to Bayer AG); Ger. Offen. DE 3,605,331 (Aug. 20 1987), R. Musch and co-workers (to Bayer AG).
175. M. Hanok and I. N. Cooperman, *Proceedings of the International Rubber Conference, Preprints Paper*, Washington, D.C., 1952, p. 582.
176. E. Rhode, H. Bechon, and M. Mezger, *Scandinavian Rubber Conference, SCR/89*, Tampere, Finland, 1989.
177. O. F. Belyaev, V. Z. Aloev, and Yu. V. Zelenev, *Vysokomol. Soedin. Ser. A* **30**, 2382 (1988); O. F. Belyaev, V. Z. Aloev, and Yu. V. Zelenev, *Acta Polym.* **39**, 590 (1988).
178. H. W. Siesler, *Makromol. Chem., Rapid Commun.* **6**, 699 (1985).
179. A. M. Mashuryan, K. A. Gasparyan, and G. T. Ovanesov, *Vysokomol. Soedin., Serv. A* **27**, 1660 (1985); G. T. Ovanesov and co-workers, *Vysokomol. Soedin., Ser. A* **28**, 1052 (1986).
180. Y. Miyata and M. Atsumi, *J. Polym. Sci., Part A* **26**, 2561 (1988).
181. Jpn. Kokai Tokkyo Koho JP 58,091,737 (May 31, 1983) (Ouchi Shinko Chemical Industrial Co., Ltd.).
182. U.S. Pat. 4,829,115 (May 9, 1989), K. S. Cottman (to Goodyear Tire and Rubber Co.); Jpn. Kokai Tokkyo Koho JP 62,205,142 (Sept. 9, 1987) (to NOK Corp.).
183. M. S. Al-Mehdawe and J. E. Stucky, *Rubber Chem. Technol.* **62**, 13 (1989); M. S. Al-Mehdawe and co-workers, *J. Pet. Chem. Res.* **7**(2), 99 (1988).
184. Jpn. Kokai Tokkyo Koho, JP 56,125,440 (Mar. 10, 1980) (to Toyoda Gosei Co., Ltd.).
185. E. A. Abdel-Razik, *J. Polym. Sci., Part A: Polym. Chem.* **26**, 2359 (1988).
186. R. L. Clough and K. T. Gillen, *Polym. Degrad. Stab.* **30**, 309 (1990); M. Ito, S. Ohada, and I Kuriyama. *J. Mater. Sci.* **16**, 10 (1981).
187. J. W. Graham, *Selecting a Plasticizer*, Du Pont Bulletin NP-320.1, E. I. du Pont de Nemours & Co., Inc., Wilmington, Del., 1981.
188. Jpn. Kokai Tokkyo Koho, JP 56,106,934 (Jan. 25, 1981) (to Dainichi Nippon Cables, Ltd.).
189. J. W. Graham, *Neoprene: An Overview of Properties, Mixing and Compounding*, Du Pont Elastomers Informal Bulletin, C-NP-050.044, E. I. du Pont de Nemours & Co., Inc., Wilmington, Del., 1982.
190. S. W. Schmidt, *The W. Family*, Du Pont Technical Bulletin NP-230.1, 1977.
191. Y. Miyasita, S. Matsunaga, and M. Mitani, *International Rubber Conference Kyoto*, 16A-12.217, 1985.
192. Ger. Offen. DE 2,755,047 (June 15, 1978), K. L. Miller (to E. I. du Pont de Nemours & Co., Inc.).
193. G. Herzog and E. Rohde, *Advantages of New Baypren Grades, Kaukuk Deregi, 1st Rubber Fair*, Istanbul, June 7–11, 1989.

194. S. W. Schmidt and J. P. Dowd II, *The Neoprene G. Family*, Du Pont Technical Bulletin NP-220, E. I. du Pont deNemours & Co., Inc., Wilmington, Del., 1983.
195. P. Mueller, U. Eisele, and G. Pampus, *Angew. Makromol. Chem.* **98**, 97 (1981).
196. U.S. Pat. 3,655,827 (Feb. 28, 1969), J. B. Finlay and J. F. Hagman (to E. I. du Pont de Nemours & Co., Inc.).
197. Eur. Pat. Appl. EP 65,718 (Dec. 1, 1981), R. Musch and co-workers (to Bayer AG); Ger. Offen. DE 3,105,339 (Sept. 2, 1981), U. Eisele and co-workers (Bayer AG).
198. Jpn. Kokai 73 102,149 (Dec. 22, 1973), T. Kadowaki, K. Takahashi, and M. Dohi (to Denki Kagaku Kogyo.).
199. K. Sandow and H. Murato, *Nippon Gomu Kyokaishi* **63**, 331–340 (1990).
200. S. K. Guggenberger in I. Skiest, ed., *Handbook of Adhesives*, 3rd ed., Van Nostrand Rheinhold Co., Inc., New York, 1990.
201. A. J. Maldonado, *Adhesives Based on Neoprene*, Du Pont Elastomers Informal Bulletin C-ADH-101.0584, 1984.
202. P. Branlard, F. Sauterey, and P. Poullet, *New Chloroprene Rubber Types for Solvent-Based Adhesives, Butaclor Symposium*, Societe Distugil, Paris, 1988.
203. C. M. Matulewicz and A. M. Snow Jr., *Adhes. Age* **24**(3), 40 (1980).
204. *Neoprene Latex Pressure Sensitive Adhesives*, Tape Council (June 16, 1980), E. I. du Pont de Nemours & Co., Inc., 1980.
205. U.S. Pat. 4,342,843 (Aug. 3, 1982), W. Perlinski, I. J. Davis, and J. F. Romanick (to National Starch and Chemical Corp.).
206. C. H. Gelbert, *Selection Guide for Neoprene Latexes*, Du Pont Elastomers Bulletin NL-020.1, 1985, J. C. Carl, *Neoprene Latex*, E. I. du Pont de Nemours & Co., Inc., Wilmington, Del., 1962.
207. Ger. Offen. DE 2,944,152 (May 14, 1981), W. Nolte, W. Keller, and H. Esser (to Bayer AG).
208. Ger. Offen. DE 3,111,138 (Sept. 30, 1982), W. Nolte and H. Esser (to Bayer AG).
209. Ger. Offen. 2,047,449 (Apr. 8, 1971), A. M. Snow Jr. (to E. I. du Pont de Nemours & Co., Inc.); Ger. Offen. 2,047,450 (Apr. 1, 1971), A. M. Snow Jr. (to E. I. du Pont de Nemours & Co., Inc.).
210. F. L. McMillian, *Neoprene Latexes and Their Applications*, Du Pont Elastomers Informal Bulletin, E. I. du Pont de Nemours & Co., Inc., Wilmington, Del., 1991.
211. C. H. Gelbert and H. E. Berkheimer, *Neoprene Latex and Its Applications with Emphasis on Manufacture of Dipped Goods*, Du Pont Elastomers Information Literature, E. I. du Pont de Nemours & Co., Inc., Wilmington, Del., 1987.
212. S. S. Tremelin, *Neoprene Modified Asphalt*, Du Pont Elastomers Bulletin C-NL-541.055, E. I. du Pont de Nemours & Co., Inc., Wilmington, Del., 1982.
213. Can. Pat. Appl. Ca 2,020,179 (Dec. 31, 1990), L. A. Christel (to E. I. du Pont de Nemours & C., Inc.).
214. American Society for Quality, *Quality Management Systems—Guidelines for Performance Improvements*, p. 2, 2000.
215. *Toxicity and Safe Handling of Neoprene Latexes*, E. I. du Pont de Nemours & Co., Inc., Bulletin NL-110.1, 1984.
216. U.S. Pat. 4,283,510 (Aug. 11, 1981) N. L. Turner (to Denka Chemical Corp.).
217. Fr. Demande FR 2,437,348 (Apr. 25, 1980), A. C. Adam (E. I. du Pont de Nemours & Co., Inc.).
218. F. J. Stark Jr., *Polychloroprene as an Extender for Recycled Rubber, Preprints of the ACS Rubber Division Meeting*, 1983, The American Chemical Society, Washington, D.C., 1989.
219. C. A. Stewart Jr., T. Takeshita, and M. L. Coleman in J. I. Kroschwitz, ed., *Encyclopedia of Polymer Science and Engineering*, Vol. 3, 3rd ed., John Wiley & Sons, Inc., New York, 1985, pp. 441–462.

220. I. Piirma, V. R. Kamath, and M. Morton, *J. Polym. Sci, Polym. Chem.* **13**, 2087 (1975)
221. J. M. Kuster, D. H. Napper, D. H. Gilbert, R. G. Gilbert, and A. L. German, *Macromolecules* **25**, 7043 (1992).
222. P. Kovaic, *Industry Eng. Chem.* **5** and **47**, 1090 (1955).
223. R. T. Vanderbilt, *The Rubber Handbook*, 13th ed., R. T. Vanderbilt & Co. (1990)
224. R. Criegie, *Peroxide Reaction Mechanism*, Interscience Publication, New York **29**, 1962.
225. R. H. Otterwill, in P. A. Lovell and M. S. El-Asser, eds., *Stabilization of Polymer Colloids*, Chapt. 3 in *Emulsion Polymerization and Emulsion Polymers*, John Wiley & Sons, Inc., New York, 1997.

FURMAN E. GLENN
DuPont Dow Elastomers L.L.C.

CHLOROSULFONATED POLYETHYLENE.

See ETHYLENE POLYMERS, CHLOROSULFONATED.

CHLOROTRIFLUOROETHYLENE POLYMERS.

See FLUOROCARBON ELASTOMERS.

CHROMATOGRAPHY, AFFINITY.

See Volume 1.

CHROMATOGRAPHY, HPLC.

See Volume 1.

CHROMATOGRAPHY, SIZE EXCLUSION.

See Volume 1.

CHROMOGENIC POLYMERS.

See ELECTROCHROMIC POLYMERS; THERMOCHROMIC POLYMERS.

COATING METHODS, POWDER TECHNOLOGY.

See Volume 5.

COATING METHODS, SURVEY.

See Volume 1.

COATINGS.

See Volume 1.

COEXTRUSION.

See Volume 2.

COLLAGEN.

See Volume 5.

COLLOIDS

Introduction

Matter of colloidal size, just above atomic dimensions, exhibits physicochemical properties that differ from those of the constituent atoms or molecules yet are also different from macroscopic material. The atoms and molecules of classical chemistry are extremely small, usually having molar masses <1000 g/mol and measurable by freezing point depression. Macroscopic particles fall into the realm of classical physics and can be understood in terms of physical mechanics. Residing between these extremes is the colloidal size range of particles whose small sizes and high surface area-to-volume ratios make the properties of their surfaces very important and lead to some unique physical properties. Their solutions may have undetectable freezing point depressions, and their dispersions, even if very dilute, may sediment out very slowly, and not be well described by Stokes' law. Whereas the particles of classical chemistry may have one or a few electrical charges, colloidal particles may carry thousands of charges. With such strong electrical forces, complete dissociation is the rule rather than the exception. In addition, the electric fields can strongly influence the actions of neighboring particles. In industrial practice it is very common to encounter problems associated with colloidal sized particles, droplets, or bubbles.

The field began to acquire its own identity when Graham coined the term colloid in 1861 (1–3). Since that time the language of colloid science has evolved considerably (4–6) and makes two principal distinctions: lyophobic (thermodynamically unstable) and lyophilic (thermodynamically stable) colloidal dispersions. Examples of lyophobic and lyophilic colloidal dispersions are suspensions of gold particles and surfactant micelles in solution, respectively. Colloidal particles (or droplets or bubbles) are defined as those having at least one dimension between $\sim$1 nm and 1 μm. In dealing with practical applications, the upper size limit is frequently extended to tens or even hundreds of micrometers. For example, the principles of colloid science can be usefully applied to emulsions whose droplets exceed the 1-μm size limit by several orders of magnitude (ie, in cases for which the surface properties of the dispersed phase dominate). Simple colloidal dispersions are two-phase systems, comprising a dispersed phase of small particles, droplets, or bubbles, and a dispersion medium (or dispersing phase) surrounding them. In modern practice, the terms lyophilic and lyophobic (especially hydrophilic and hydrophobic) are often used to characterize surfaces in addition to colloidal dispersions. This sometimes leads to confusing usage. For example, a clay dispersion in water could be classified as a lyophobic colloid with hydrophilic surfaces.

Various types of colloidal dispersions occur, as illustrated in Table 1. In practice, many colloidal dispersions are more complex and are characterized by the nature of the continuous phase and a primary dispersed phase, according to the designations in Table 1.

One reason for the importance of colloidal systems is that they appear in a wide variety of practical disciplines, products, and processes. The colloidal involvement in a process may be desirable, as in the stabilizing of emulsions in mayonnaise preparation, or undesirable, as in the tendency of very finely divided and highly charged particles to resist settling and filtration in water treatment

Encyclopedia of Polymer Science and Technology. Copyright John Wiley & Sons, Inc. All rights reserved.

Table 1. Types of Colloidal Dispersion

Dispersed phase	Dispersion medium	Name	Examples
Liquid	Gas	Liquid aerosol	Fog, mist
Solid	Gas	Solid aerosol	Smoke, dust
Gas	Liquid	Foam	Soap suds
Liquid	Liquid	Emulsion	Milk, mayonnaise
Solid	Liquid	Sol, suspension	Ink, paint, gel
Gas	Solid	Solid foam	Polystyrene foam, pumice stone
Liquid	Solid	Solid emulsion	Opal, pearl
Solid	Solid	Solid suspension	Alloy, ruby-stained glass

plants. Examples of the variety of practical problems in colloid chemistry include control of filtration operations, breaking of emulsions, regulating foams, preparing catalysts, managing fluid flow, and cleaning surfaces (see Table 2).

The variety of systems represented or suggested by Tables 1 and 2 underscores the fact that the problems associated with colloids are usually interdisciplinary in nature and that a broad scientific base is required to understand them completely. A wealth of literature exists on the topic of colloidal dispersions, including a range of basic reference texts (7–11), dictionaries (4–6,12), and treatises on the myriad of applied aspects, of which only a few are cited here (13–24).

Preparation and Stability of Dispersions

Preparation. Colloidal dispersions can be formed either by nucleation with subsequent growth or by subdivision processes (7,8,11,25,26). The nucleation process requires a phase change, such as condensation of vapor to yield liquid or solid, or precipitation from solution. Some mechanisms of such colloid formation are listed in Table 3.

The subdivision process refers to the comminution of particles, droplets, or bubbles into smaller sizes by applying high shearing forces, using devices such as a propeller-style mixer, colloid mill, or ultrasound generator. A complex technology has developed to conduct and to control comminution and size-fractionation processes. Mathematical models are available to describe changes in particle size distribution during comminution, but these are generally restricted to specific processes. Comprehensive reviews of the developments in preparing colloidal solids by subdivision should be consulted for further details (27,28). A wide range of techniques is now available, including, eg, atomizers and nebulizers of various designs used, to produce colloidal liquid or solid aerosols, and emulsions having relatively narrow size distributions. Monosized powders and monodispersed colloidal sols are frequently used in many products, eg, pigments, coatings, and pharmaceuticals.

Colloidal suspensions of uniform chemical and phase composition, particle size, and shape are now available for many elements (including sulfur, gold, selenium, and silver, carbon, cobalt, and nickel), many inorganic compounds

Table 2. Some Occurrences of Colloids

Field	Liquid aerosol	Solid aerosol	Foam	Emulsion	Suspension	Solid foam	Solid emulsion	Solid suspension
Environment and meteorology	Fog, mist, cloud, smog	Volcanic smoke, dust, smog	Polluted river foams	Water/sewage treatment emulsions, oil spill emulsions	River water, glacial runoff			
Foods			Champagne, soda and beer heads, whipped cream, meringue	Milk, butter, mayonnaise, cheese, cream liqueurs	Jellies	Leavened breads		
Geology, agriculture, and soil science	Crop sprays		Foam fumigant, insecticide and herbicide blankets	Insecticides and herbicides	Quicksand, clay soil suspensions	Pumice stone, zeolites	Opal, pearl	Pearl
Manufacturing and materials science	Paint sprays	Sand blasting	Foam fractionation, pulping black liquor foam	Polishes	Ink, gel, paints, fiber suspensions	Polystyrene foam, polyurethane foam	High impact plastics, alkaline battery fill	Stained glass, ceramics, cement, plastics, catalysts, alloys, composites
Biology and medicine	Nasal sprays	Airborne pollen, inhalant drugs	Vacuoles, insect excretions, contraceptive foam	Soluble vitamin and hormone products, biological membranes, blood	Liniment suspensions, proteins, viruses	Loofah plant		Wood, bone

Table 2. (Continued)

Field	Liquid aerosol	Solid aerosol	Foam	Emulsion	Suspension	Solid foam	Solid emulsion	Solid suspension
Petroleum production and mineral processing			Refinery foams, flotation froths, fire extinguishing foams, explosion suppressant foam	Oilfield emulsions, asphalt emulsion	Drilling fluids, drill cuttings, mineral slurries, process tailings		Oil reservoir	
Home and personal care products	Hair spray		Shampoo suds, shaving cream, contraceptive foams, bubble bath foam	Hair and skin creams and lotions		Sponges, carpet underlay, cellular foam insulation		Bakelite products

Table 3. Industrially Produced Colloidal Materials and Related Processes

Mechanism	Examples[a]
Vapor → liquid → solid ↓→→→↑	Oxides, carbides via high intensity arc; metallic powders via vaccum or catalytic reactions
Vapor + vapor → solid	Chemical vapor deposition, radio-frequency-induced plasma, laser-induced precipitation
Liquid → solid	Ferrites, titanates, aluminates, zirconates, molybdates via precipitation
Solid → solid	Oxides, carbides via thermal decomposition

[a] Refs. 27 and 28.

(including halide salts, sulfates, oxides, hydroxides, and sulfides), and many organic compounds [including, poly(vinyl acetate), polystyrene, poly(vinyl chloride), styrene–butadiene rubber, poly(acrylic acid), polyurea, poly-styrene–poly(acrylate), and poly(methacrylate)–poly(acrylate)]. (see VINYL ACETATE POLYMERS; STYRENE POLYMERS; VINYL CHLORIDE POLYMERS; STYRENE-BUTADIENE COPOLYMERS; ACRYLIC ESTER POLYMERS; METHACRYLIC ESTER POLYMERS; ACRYLIC (AND METHACRYLIC) ACID POLYMERS).

Stability. A complete characterization of colloid stability requires consideration of the different processes through which dispersed species can encounter each other: sedimentation (creaming), aggregation, and coalescence. Sedimentation results from a density difference between the dispersed and continuous phases and produces two separate layers of dispersion that have different dispersed-phase concentrations. One of the layers will contain an enhanced concentration of dispersed phase, which may promote aggregation. Aggregation is when two or more dispersed species clump together under the influence of Brownian motion, sedimentation, or stirring, possibly touching at some points, and with virtually no change in total surface area. Aggregation is sometimes referred to as flocculation or coagulation (although in specific situations these latter terms can have slightly different meanings). In aggregation, the species retain their identity but lose their kinetic independence since the aggregate moves as a single unit. Aggregation of droplets may lead to coalescence and the formation of larger droplets until the phases become separated. In coalescence thin film drainage occurs, leading to rupture of the separating film, and two or more particles, droplets, or bubbles fuse together to form a single larger unit, reducing the total surface area. In this case the original species lose their identity and become part of a new species. In emulsions, inversion can take place, in which the emulsion suddenly changes form, from oil-in-water (O/W) to water-in-oil (W/O), or vice versa. For example, butter results from the creaming, breaking, and inversion of emulsified fat droplets in milk. Kinetic stability can thus have different meanings. A colloidal dispersion can be kinetically stable with respect to coalescence but unstable with respect to aggregation. Or, a system could be kinetically stable with respect to aggregation but unstable with respect to sedimentation. In summary, lyophobic colloids are

thermodynamically unstable, but may be relatively stable in a kinetic sense, and it is crucial that stability be understood in terms of a clearly defined process.

Dispersed Species Characterization and Sedimentation

The characterization of colloids depends on the purposes for which the information is sought, because a complete description would be an enormous task. Among the properties to be considered are the nature and/or distributions of purity, crystallinity, defects, size, shape, surface area, pores, adsorbed surface films, internal and surface stresses, stability, and state of agglomeration (27,28).

Surface Area, Porosity, and Permeability. Some very interesting and important phenomena involve small particles and their surfaces. For example, SO_2 produced from mining and smelting operations that extract metals such as Cu and Pb from heavy metal sulfide ores can be oxidized to SO_3 in the atmosphere, thus contributing to acid rain problems. The reaction rate depends not only on the concentration of the SO_2 but also on the surface area of any catalyst available, such as airborne dust particles. The efficiency of a catalyst depends on its specific surface area, defined as the ratio of surface area to mass (17). The specific surface area depends on both the size and shape, and is distinctively high for colloidal-sized species. This is important in the catalytic processes used in many industries for which the rates of reactions occurring at the catalyst surface depend not only on the concentrations of the feed stream reactants but also on the surface area of catalyst available. Since practical catalysts frequently are supported catalysts, some of the surface area is more important than the rest. Since the supporting phase is usually porous the size and shapes of the pores may influence the reaction rates as well. The final rate expressions for a catalytic process may contain all of these factors: surface area, porosity, and permeability.

The total surface area can be estimated by measuring the amount of gas needed to form an adsorbed monolayer by physical adsorption (29,30), in which case the number of molecules adsorbed divided by the area per molecule yields the surface area. The classic models for physical adsorption are those of Langmuir (monomolecular adsorption and constant ΔH_{ads}, independent of the extent of surface coverage) and Brunauer, Emmett, and Teller (BET, multilayer adsorption and several ΔH_{ads} components); while many other models are available as well (8,10,17). These models require a knowledge of the area each molecule occupies on the surface. Chemisorption can be studied in the same fashion as described for nitrogen adsorption but using a gas that is chemisorbed, ie, that bonds chemically. This yields a specific chemisorption surface area. In evaluating supported catalyst samples, both kinds of surface area may need to be measured since particle size changes would be reflected in the specific surface area while site deactivation might change only the specific chemisorption area.

The Langmuir and BET equations work well with nonporous solids, but not as well for porous solids because the pores influence the local numbers of adsorption layers formed. By using adsorption gases of different molecular size or by varying the temperature, pores of different size will be accessible to the adsorbing molecule. Coupling this with the appropriate mathematical interpretation allows for the determination of solid porosity using BET analysis. The porosity of a solid

(pore volume divided by bulk volume) is most easily determined by the imbibition method, frequently used in the petroleum industry. A sample of solid is dried and weighed, then saturated with a wetting liquid (often water or heptane) under vacuum. The pore volume accessible is calculated by a material balance. In prepared catalysts, the pore sizes may be quite uniform. However, in most naturally occurring materials there is a wide range of pore sizes. The actual pore size distribution can be obtained from methods such as porosimetry, in which a nonwetting liquid (usually mercury) is pumped into a solid sample (7,8,10,17,29,31). According to the Laplace equation each increment of applied pressure will cause only pores down to a certain size to be filled, and employing a series of pressure increments allows the pore size distribution to be obtained.

The ease with which a fluid can flow through a porous medium, permeability, can be determined through the measurement of pressure drop (Δp) across the porous medium under steady flow. The intrinsic permeability (k) is defined by Darcy's law and is given by $k = (Q/A)(\eta L/\Delta p)$, where Q is the discharge flow rate, A is the cross-sectional area normal to the main flow direction, η is the flowing fluid viscosity, L is the length of the flow path (sample), and Δp is the pressure gradient along the medium (15). Mercury porosimetry can also be used to assess permeability (17,29).

Size and Size Distribution. If the sizes of particles, droplets, bubbles, or their aggregates in a colloidal dispersion are large enough, then optical microscopy can be used to determine the shape, size, and size distribution, but if they are smaller than $\sim$0.5 μm they will not be resolved in a typical optical microscope. Confocal scanning laser microscopes can extend this resolution up to $\sim$0.1 μm. For dispersions of such smaller-size species, the most direct methods include scanning and transmission electron microscopy. Adaptations, such as cryogenic-stage scanning electron microscopy, can be used for emulsions and foams (32,33).

Small, dispersed particles or droplets cause the "cloudy" or "milky" appearance of such diverse colloids as dust clouds, rain clouds, suspended sediment in a river, and milk. This appearance is due to light scattering. When a beam of light enters a colloidal dispersion some light is absorbed, some is scattered, and some is transmitted. The intensity of the scattered light depends largely on the size and shape of the colloidal species, and on the difference in refractive index between the phases. Light scattering analysis is very powerful because it can yield the complete dispersed-phase size distribution. This is important in emulsions that are commonly, but generally incorrectly, characterized in terms of a specified droplet size whereas there is inevitably a size distribution. The theory underlying the determination of size distribution for a colloidal dispersion is quite involved (8,34). Rayleigh theory predicts that larger particles scatter more light than do smaller ones. Since the scattering intensity is proportional to $1/\lambda^4$, blue light ($\lambda = 450$ nm) is scattered much more than red light ($\lambda = 650$ nm). With incident white light a scattering material will, therefore, tend to appear blue when viewed at right angles to the incident light beam, and red when viewed end-on. Thus the sky can appear blue overhead while the sun appears yellowish red when viewed across the horizon as it is rising or setting. When a test tube containing a dilute suspension of particles so small that they would be invisible under the light microscope is held up to the light, it may appear to have a blue colour due to Rayleigh scattering. This

phenomenon provides a way to indirectly observe particles that would otherwise be invisible. In the dark-field microscope, or ultramicroscope, the light scattered by small particles is viewed against a dark background. This method is applied in observing the electrophoretic motions of colloidal particles (35).

Other indirect techniques for determining colloidal species' size or size distribution include sedimentation–centrifugation, conductometric techniques, X-ray diffraction, gas and solute adsorption, ultrafiltration, diffusiometric, and ultrasonic methods (7,8,31,36). Care must be taken in selecting an indirect method since these require assumptions about either the real size distribution, the shape, or the process on which the analysis is based. For example, conductometric "sensing zone" equipment relies on the assumption of sphericity, which is reasonable for emulsion droplets but may not hold for particles in a suspension. Similarly, light-scattering techniques are reliable only if the particle shape and refractive index is known or assumed, and adsorption analyses rely on model adsorption isotherms, the uniformity of particle size and porosity, and the orientation of adsorbed species. In all cases, one must be careful that sample preparation techniques do not change the size distribution (32). Typically, more than one method is needed to characterize size and/or size distribution properly.

Nearly all colloidal systems undergo some aggregation leading to a distribution of aggregate sizes. Ultramicroscopy is the preferred method for measuring the rate and/or extent of aggregation because it is direct. The indirect methods listed above can also be used when tailored to suit the specific colloidal system in hand. More than one technique is required to assess the state of aggregation when a wide range of colloidal dimensions exists. If aggregates larger than approximately 5 μm are present, the aggregate-size distribution can be evaluated using classical techniques such as sieving (27,28,37), as long as such methods do not themselves induce or break aggregates.

Sedimentation. Whereas the use of light scattering to determine a complete size range distribution is quite involved, if the particles or droplets are not too small, a simpler approach can be used that yields an approximate average size. This is done by measuring settling velocities. Consider the small particles in a dust cloud, or suspended sediment in a river. It is principally the small size that keeps these particles from rapidly settling out. If a particle or droplet is placed in a fluid it will fall, or sediment out, if its density is greater than that of the fluid. The driving force is that of gravity. In the Stokes model, the terminal settling velocity is proportional to gravity and the square of particle size and inversely proportional to the fluid viscosity (7,8,31). This assumes that the species is uncharged and spherical, the situation being more complicated for charged and/or asymmetric particles. Further, if the particle concentration is high then the particles do not sediment independently but are influenced by the motions of surrounding particles, producing slower, hindered, settling. Sedimentation under gravity is only practical down to $\sim$1 μm diameter, but the centrifuge or ultracentrifuge can be used to study sedimentation of colloidal systems since the added centrifugal forces can be employed to overcome the mixing tendencies of diffusion and convection. Centrifugal force, like gravitational force, is proportional to the mass but the coefficient is not the acceleration due to gravity (g) but rather the square of the angular velocity (ω) times the distance of the particle from the axis of rotation (x). Since

$\omega^2 x$ is substituted for g in the governing equation, one speaks of multiples of g in a centrifuge. For example, using a conventional laboratory bench-top centrifuge capable of applying thousands of "gs" one can reduce the time needed to sediment out 0.2 μm particles, from an aqueous suspension, to ~20 min compared with the 16 days that would be needed to achieve the same sedimentation from a standing column. In an ultracentrifuge, even greater centrifugal forces (~40,000g) can be employed.

Rheology

For calculations involving pumping and mass transfer, industrial process streams can sometimes be treated as simple, "single phase" fluids that obey Newton's law of viscosity, $\tau = \eta\ \dot{\gamma}$, in which the shear stress, τ, is given as a linear function of the shear rate, $\dot{\gamma}$, with the proportionality constant being the viscosity, η. In fact many industrial process streams occur as colloidal dispersions, introducing the complication that in many cases viscosity is not expressed by a single number at constant temperature and pressure, but also depends on whether the material is flowing, and even its recent history (see RHEOLOGICAL MEASUREMENTS). Because of polydispersity, high dispersed phase content, mutual orienting, and/or structure formation of the dispersed species under flow a non-Newtonian dispersion exhibits a viscosity that is not constant, but is itself a function of the shear rate, [ie, $\tau = \eta\ (\dot{\gamma})\dot{\gamma}$]. The function itself can take many forms (38–43). Many different terms are used to express specific kinds of viscosities, including absolute, apparent, differential, intrinsic, reduced, relative, and inherent viscosity. These are defined elsewhere, as is an entire lexicon of terms used to describe the different rheological classifications of colloidal dispersions (4–6,39,42). Typical rheological classifications are listed in Table 4. Some descriptions appropriate to different yield stresses and some approximate values of shear rate appropriate to various industrial processes are given in Reference 44.

A colloidal system can exhibit several of these characteristics at once. For example, paint must be plastic and thixotropic so that it will flow when brushed on and (only) immediately after brushing (for a smooth finish); a further benefit is that vigorous mixing readily disperses the pigments, which then stay dispersed for some time when standing (high yield stress). Finally, shortly after brushing on, the paint should cease to flow so that it doesn't "run."

A range of methods are available for making rheological measurements (qv) (39–42). A frequently encountered problem involves knowing the particle/droplet/bubble size and concentration in a dispersion and the need to predict the suspension, emulsion, or foam viscosity. Many equations have been advanced for this purpose. In the simplest case, a colloidal system can be considered Einsteinian. Here, the viscosity of the colloidal system depends on that of the continuous phase, η_0, and the volume fraction of colloid, ϕ, according to the Einstein equation, which was derived for a dilute suspension of noninteracting spheres:

$$\eta = \eta_0(1 + 2.5\ \phi)$$

Table 4. Typical Rheological Classifications

Rheological classification	Description	Examples
Pseudoplastic (shear-thinning)	As shear rate increases viscosity decreases.	In paint, a suspension of pigment particles in a liquid, irregular particles can align to match the induced flow, lowering the viscosity.
Dilatant (shear-thickening)	As shear rate increases viscosity increases	In the "drying" of wet beach sand when walked on, a dense packing of particles occurs. Under low shear the particles can move past each other, whereas under high shear the particles wedge together such that the fluid cannot fill the increased void volume.
Pseudoplastic with yield stress (plastic)	Pseudoplastic or Newtonian flow begins only after a threshold shear stress, the yield stress, is exceeded.	In an oil well drilling mud the interparticle network offers resistance to any positional changes. Flow only occurs when these forces are overcome.
Thixotropic	Time-dependent pseudoplastic flow. At constant applied shear rate, viscosity decreases. In a flow curve hysteresis occurs.	In bentonite clay "gels" which "liquefy" on shaking and "solidify" on standing there is a time-dependent aligning to match the induced flow. After the shear rate is reduced it takes some time for the original alignments to be restored.
Rheopectic	Time-dependent dilatant flow. At constant applied shear rate viscosity increases. In a flow curve hysteresis occurs.	A suspension that sets slowly on standing but quickly when gently agitated due to time-dependent particle interference under flow.
Rheomalaxic	Time-dependent behavior in which shear-rate changes cause irreversible changes in viscosity.	An emulsion that when sheared inverts to a higher (or lower) viscosity emulsion, and does not reinvert when the shear is removed.

This relationship forms the basis for the use of volume fraction as the theoretically favored concentration unit in rheology. In practice once ϕ reaches between 0.1 and 0.5 dispersion viscosity increases and can also become non-Newtonian (due to particle/droplet/bubble "crowding," or structural viscosity). The maximum volume fraction possible for an internal phase made up of uniform, incompressible spheres is 0.74, although emulsions and foams with an internal volume fraction of >0.99 can exist as a consequence of droplet/bubble distortion.

Many empirical and theoretical modifications have been made to Einstein's equations. A useful extension to dilute suspensions of anisotropic particles, such as clays, is given by the Simha Equation, which is approximately

$$\eta = \eta_0(1 + a\phi/1.47b)$$

where a is the major particle dimension and b the minor particle dimension. Many of the other viscosity equations are empirical extensions of Einstein's equation for a dilute suspension of spheres, including virial expansions such as

$$\eta = \eta_0\left(1 + \alpha_0\phi + \alpha_1\phi^2 + \alpha_2\phi^3 + \cdots\right)$$

These equations usually apply if the particles or droplets are not too large, and if there are no strong electrostatic interactions. Additional equations are tabulated elsewhere (6,45).

Size distribution also has an important influence on viscosity. For electrostatically or sterically interacting drops, emulsion viscosity will be higher when droplets are smaller. The viscosity will also be higher when the droplet sizes are relatively homogeneous, ie, when the drop size distribution is narrow rather than wide. The rheological properties also depend on any specific interactions among the colloidal species, the dispersing medium, and the solute additives, ie, salts, surfactants, and polymers.

There are many important influences of rheology in industrial practice. From Stokes' law the terminal settling velocity is inversely proportional to the viscosity of a colloidal dispersion, which has a direct impact on sedimentation in, eg, treatment of waste water and on mineral fractionation and/or flotation (46,47). Another major application area is transport behavior, involving the pumping of fluid systems containing colloids, such as in extrusion in the polymer industry, the processing of gelatinous foods and cosmetic items, the fabrication of high performance materials in the ceramic and metallurgical industries, transportation in the petroleum industry, and the preparation and handling of pigment slurries in the paint industry. The prediction and control of suspension, emulsion, and foam rheology, especially the thixotropic and dilatant tendencies, is primarily important for these and other uses.

Interfacial Energetics

In colloidal dispersions, a thin intermediate region or boundary, known as the interface, lies between the dispersed and dispersing phases. Each interface has a certain free energy per unit area that has a great influence on the stability and structure of the colloidal dispersion, and that has a great influence in practical areas such as mineral flotation, detergency, and waterproofing.

Surface and Interfacial Tensions. For a liquid exposed to a gas the attractive van der Waals forces between molecules are felt equally by all molecules except those in the interfacial region. This makes the latter molecules tend to move to the interior and causes the interface to contract spontaneously. This is the reason droplets of liquid and bubbles of gas tend to adopt a spherical shape.

For two immiscible liquids a similar situation applies, except it may not be so immediately obvious how the interface will tend to curve but there will still be an imbalance of intermolecular forces and a configuration that minimizes the interfacial free energy, or interfacial tension. Surface tension can be thought of as either the contracting force around the perimeter of a surface, or as the surface free energy associated with area change. Emulsions and foams represent colloidal systems in which interfacial properties are very important because emulsified droplets and dispersed gas bubbles have large interfacial areas, so that even a modest interfacial energy per unit area can become a considerable total interfacial energy. There are many methods available for the measurement of surface and interfacial tensions (48–51).

Pressure and Curved Surfaces. Interfacial tension causes a pressure difference to exist across a curved surface such that the pressure inside a bubble or drop exceeds that outside. The pressure difference is given, in terms of the principal radii of curvature and surface or interfacial tension, by the Young–Laplace equation (8,10). For spherical droplets of liquid in a gas, $\Delta p = 2\gamma/R$, ie, the pressure difference, Δp, varies inversely with the radius, R. Thus the vapor pressure of a drop should become higher as the drop becomes smaller. This is shown by the Kelvin equation (8,31), which gives the pressure, at equilibrium, above a spherical surface of given radius, r, and surface tension, γ, as $RT \ln(p/p_0) = 2V_L\gamma/r$, where p_0 is the normal vapor pressure and V_L is the molar volume of the liquid. By replacing pressure with activity of dissolved solute and relating activity, in turn, to molar solubility the Kelvin equation can be used to describe a number of supersaturation phenomena, including supercooled vapors and supersaturated solutions.

Contact Angle and Wettability. When a drop of liquid is placed on a solid surface the liquid may form a bead on the surface, or it may spread to form a film. A liquid having a strong affinity for the solid will seek to maximize its contact (interfacial area) and form a film. A liquid with much weaker affinity may form into a bead. This affinity is termed the wettability (10,25,26). To account for the degree of spreading, the contact angle, θ, is defined as the angle, measured through the liquid, that is formed at the junction of the three phases, eg, at the solid–liquid–gas (S-L-G) junction. Whereas interfacial tension is defined for the boundary between two phases, contact angle is defined for a three-phase junction. If the interfacial forces acting along the perimeter of the drop are represented by the interfacial tensions, then an equilibrium force balance is given by Young's equation as $\gamma_{L/G} \cos\theta = \gamma_{S/G} - \gamma_{S/L}$. The solid is completely wetted if $\theta = 0$ and only partially wetted otherwise. Although in theory complete nonwetting would be at $\theta = 180^\circ$, this is not seen in practice and values of $\theta > 90^\circ$ are considered to represent "nonwetting" whereas values $< 90^\circ$ are often considered to represent "wetting." This rather arbitrary assignment is based on correlation with the visual appearance of drops on surfaces.

An example is provided in enhanced oil recovery. In an oil-bearing reservoir the relative oil and water saturations depend on the distribution of pore sizes in the rock, the pressure in a pore, the interfacial tension, and the contact angle according to the Young–Laplace and Young equations. The same relationships determine how water or other fluids can be injected to change pressure, interfacial tension,

and/or contact angle and thereby change the liquid saturations and increase oil recovery (13,52).

Some compounds, like short-chain fatty acids, can be soluble in both water and oil because one part of the molecule has an affinity for oil (the nonpolar hydrocarbon chain) and one part has an affinity for water (the polar group). The energetically most favorable orientation for these molecules is at an interface so that each part of the molecule can reside in the solvent medium for which it has the greatest affinity. These molecules that form oriented monolayers at interfaces show surface activity and are termed surfactants. Some consequences of surfactant adsorption at a surface are that it causes a reduction in surface tension and an alteration in the wettability of the surface. Surfactant molar masses range from a few hundreds up to several thousands of grams per mole.

Surfactants can be used to selectively alter wettability. For example, in mineral flotation surfactant can be added to adsorb on metal ore particles increasing the contact angle, so they attach to gas bubbles. The surfactant is chosen so that it will not adsorb much on silicates, so the latter do not attach to gas bubbles. The surfactant may also stabilize a foam containing the desired particles, thereby facilitating their recovery as a particle-rich froth that can be skimmed. Flotation processes thus involve careful modification of surface tension and wettability.

Another problem in colloids is detergency, which involves the action of surfactants (originally soaps were used) to alter interfacial properties so as to promote dirt or oil removal from solid surfaces. The detergent's role is to alter interfacial tensions in order to reduce the amount of mechanical energy required to dislodge the dirt. If the dirt is solid then it is a simple matter of wettability alteration.

Surfactants play an important role in the formation and stability of emulsions and foams. Surfactant adsorption at fluid interfaces can, eg, lower interfacial tension, increase surface elasticity, increase electric double-layer repulsion (ionic surfactants), lower the effective Hamaker constant, and sometimes increase surface viscosity. For emulsions, the nature of the surfactant can also determine the arrangement of the phases (ie, which phase will form the dispersed vs continuous phase). Several empirical rules and scales have been developed for categorizing emulsifying agents, including the oriented wedge and Bancroft theories, the hydrophile–lipophile balance, HLB, and the phase inversion temperature, PIT (13,26,45). Although there are exceptions to each of these rules, they remain useful for making initial predictions.

Lyophilic Colloids. Another key feature of surfactants is that above a certain solution concentration they form organized aggregates called micelles (19, 26) in which the lipophilic parts of the surfactants associate in the interior of the aggregate, leaving hydrophilic parts to face the aqueous medium. A solution of micelles is a good example of a thermodynamically stable lyophilic colloidal dispersion. The concentration at which micelle formation becomes significant is called the critical micelle concentration (CMC). The CMC is a property of the surfactant and several other factors, since micellization is opposed by thermal and electrostatic forces. A low CMC is favored by increasing the lipophilic part of the molecule, lowering the temperature, and adding electrolyte. Compilations of CMC values are given in References 19 and 53.

The ability of biological amphiphilic molecules to aggregate into spherical and nonspherical clusters, ie, vesicles, may have been important for the development of early living cells (54). Cellular biological membranes in plants and animals share features with these colloidal systems, although the molecular and hierarchical membrane structures, their hydration, and their dynamic properties are complex (54–57). The macroscopic nature of concentrated gels, such as lubricating greases formed by dispersing short-chain surfactants, eg, lithium 12-hydroxystearate, in mineral oil (58), is akin to the behavior of biological amphiphiles, being also dependent on self-assembly mechanisms. The associations between fibrous clusters, the length of threadlike surfactant strands, and the density of their contact points (cross-links) govern the grease's shear resistance (58).

Microemulsions, like micelles, are considered to be lyophilic, stable, colloidal dispersions. In some systems, the addition of a fourth component, a cosurfactant, to an oil–water–surfactant system can cause the interfacial tension to drop to near-zero values, easily on the order of $10^{-3} - 10^{-4}$ mN/m, allowing spontaneous or nearly spontaneous emulsification to very small drop sizes, ~10 nm or smaller. The droplets can be so small that they scatter little light, and the emulsions appear to be transparent and do not break on standing or centrifuging. Unlike coarse emulsions, microemulsions are thought to be thermodynamically stable. The thermodynamic stability is frequently attributed to transient negative interfacial tensions, but this, and the question of whether microemulsions are really lyophilic or lyophobic dispersions are areas of some discussion in the literature. As a practical matter, microemulsions can be formed, have some special qualities, and can have important applications in areas such as enhanced oil recovery, soil and aquifer remediation, foods, pharmaceuticals, cosmetics, herbicides, and pesticides (13,16,45,59–61).

Electrokinetics

Charged Interfaces. Most substances acquire a surface electric charge when brought into contact with a polar medium such as water. The origin of the charge can be ionization, as when carboxyl and/or amino functionalities ionize when proteins are put into water; ion adsorption, as when surfactant ions adsorb onto a solid surface; ion dissolution, as when Ag^+ and I^- dissolve unequally when AgI is placed in water; or ion diffusion, as when a clay particle is placed in water and the counterions diffuse out to form an electric double layer. In the AgI example, the ions Ag^+ and I^- will be potential-determining because either may adsorb at the interface and change the surface potential. Conversely, indifferent ions, such as Na^+ and NO_3^-, will not change the surface potential.

Surface charge influences the distribution of nearby ions in a polar medium: ions of opposite charge (counterions) are attracted to the surface while those of like charge (coions) are repelled. Together with mixing caused by thermal motion a diffuse electric double layer is formed. The electric double layer (EDL) can be viewed as being composed of two layers: an inner layer that may include adsorbed ions, and a diffuse layer, where ions are distributed according to the influence of electrical forces and thermal motion. Gouy and Chapman proposed a simple

quantitative model for the diffuse double layer assuming an infinite, flat, uniformly charged surface, and ions that can be regarded as point charges (also that solvent effects arise only through a uniform dielectric constant, and that the electrolyte is symmetrical [*z*-*z*]). The surface potential is designated as Ψ^0 and the potential at a distance x as Ψ. The Poisson–Boltzmann equation comes from a combination of the Boltzmann distribution of concentrations of ions (in terms of potential), the charge density at each potential (in terms of the concentration of ions), and the Poisson equation (describing the variation in potential with distance). Given the physical boundary conditions, assuming low surface potentials, and using the Debye–Hückel approximation yields,

$$d^2\Psi/dx^2 = [e^2\Psi/(\varepsilon\ \kappa T)]\sum\nolimits_i c_i z_i^2$$

If we now define the cluster of constants as $\kappa^2 = (e^2/\epsilon kT)\ \sum_i\ c_i\ z_i{}^2$ (having units of distance^{-2}) then this can be simplified to

$$d^2\Psi/dx^2 = \kappa^2\Psi \quad \text{or} \quad \Psi = \Psi^0\ \exp(-\kappa x)$$

This is the Debye–Hückel expression for the potential at a distance from a charged surface. The parameter $1/\kappa$ is called the double layer thickness and is given for water at 25°C by $\kappa = 3.288\ \sqrt{I}\ (\text{nm}^{-1})$, where $I = (1/2)\ \sum_i\ c_i\ z_i{}^2$. For 1-1 electrolyte $1/\kappa$ is 1 nm for $I = 10^{-1}\ M$, and 10 nm for $I = 10^{-3}\ M$.

There remain some problems. In order to handle higher (more practical) potentials, the Gouy–Chapman theory can be applied, but with a more complicated result. One such result is

$$\Upsilon = \Upsilon^0\ \exp(-\kappa x)$$

where Υ is a complex ratio involving Ψ given by

$$\Upsilon = \frac{\exp[ze\Psi/2kT] - 1}{\exp[ze\Psi/2kT] + 1}$$

At low surface potentials this equation reduces to the Debye–Hückel expression above. Second, an inner layer exists because ions are not really point charges and an ion can only approach a surface to the extent allowed by its hydration sphere. The Stern model incorporates a layer of specifically adsorbed ions bounded by a plane, the Stern plane. In this case, the potential changes from Ψ^0 at the surface, to $\Psi\ (\delta)$ at the Stern plane, to $\Psi = 0$ in bulk solution.

Electrokinetic Phenomena. Electrokinetic motion occurs when the mobile part of the electric double layer is sheared away from the inner layer (charged surface). There are several types of electrokinetic measurements, electrophoresis, electroosmosis, streaming potential, sedimentation potential, and two electroacoustical methods. The first four methods are described in References 35 and 62. Of these the first finds the most use in industrial practice. The electroacoustical methods involve detection of the sound waves generated when dispersed species are made to move by an imposed alternating electric field, or vice versa (63). In all of the electrokinetic measurements either the liquid is made to move across a

solid surface or vice the versa. Thus the results can only be interpreted in terms of charge density (σ) or potential (zeta potential, ζ) at the plane of shear. The location of the shear plane is generally not exactly known and is usually taken to be approximately equal to the potential at the Stern plane, $\zeta \approx \Psi(\delta)$. Several methods can be used to calculate zeta potentials (11,35,62).

Colloid Stability

A consequence of the small size and large surface area in colloids is that quite stable dispersions of these species can be made. That is, suspended particles may not settle out rapidly and droplets in an emulsion or bubbles in a foam may not coalesce quickly. Charged species, when sedimenting, present a challenge to Stokes' law because the smaller counterions sediment at a slower rate than the larger colloidal particles. This creates an electrical potential that tends to speed up the counterions and slow down the particles. At high enough electrolyte concentrations the electric potentials are quickly dissipated and this effect vanishes.

Although some lyophobic colloidal dispersions can be stable enough to persist for days, months, or even years, they are not thermodynamically stable. Rather, they possess some degree of kinetic stability, and one must consider the degree of change and the timescale in the definition of stability. Having distinguished coalescence and aggregation as processes in which particles, droplets, or bubbles are brought together with and without large changes, respectively, in surface area it is clear that there can be different kinds of kinetic stability. Finally, stability depends upon how the particles interact when this happens, since encounters between particles in a dispersion can occur frequently due to diffusion (as in Brownian motion), sedimentation, or stirring.

Electrostatic and Dispersion Forces. Several repulsive and attractive forces operate between colloidal species and determine their stability (7,8,10,25, 31,54). In the simplest example of colloid stability, particles would be stabilized entirely by the repulsive forces created when two charged surfaces approach each other and their electric double layers overlap. The overlap causes a Coulombic repulsive force acting against each surface, and that will act in opposition to any attempt to decrease the separation distance. One can thus express the Coulombic repulsive force between plates as a potential energy of repulsion. There is another important repulsive force causing a strong repulsion at very small separation distances where the atomic electron clouds overlap, called the Born repulsion.

There also exist dispersion, or London–van der Waals, forces that molecules exert towards each other. These forces are usually attractive in nature and result from the orientation of dipoles, whether dipole–dipole (Keesom dispersion forces), dipole–induced dipole (Debye dispersion forces), or induced dipole–induced dipole (London dispersion forces). Except for quite polar materials the London dispersion forces are the more significant of the three. For molecules, the force varies inversely with the sixth power of the intermolecular distance, whereas for particles, etc, the force varies approximately inversely with interparticle distance.

DLVO Theory. Derjaguin and Landau (64,65) and Verwey and Overbeek (66) developed a quantitative theory for the stability of lyophobic colloids, referred to as DLVO theory. It was known from experiment that classical colloids (AgI, Au)

coagulated quickly at high electrolyte concentrations and slowly at low concentrations, with a very narrow electrolyte concentration range over which the transition from kinetically stable to kinetically unstable occurred. Thus a critical coagulation concentration (CCC) could be defined. Using DLVO theory one can calculate the energy changes that take place when two particles approach each other by estimating the potential energies of attraction (London–van der Waals dispersion, V_A) and repulsion (electrostatic including Born, V_R) versus interparticle distance. These are then added together to yield the total interaction energy, V_T. The theory has been developed for two special cases, the interaction between parallel plates of infinite area and thickness, and the interaction between two spheres. The original calculations of dispersion forces employed a model due to Hamaker although more precise treatments now exist (54).

The parameter V_R decreases exponentially with separation distance, having a range about equal to κ^{-1}, while V_A decreases inversely with separation distance. Figure 1 shows how van der Waals forces can predominate at small and large interparticle distances. Repulsive forces can predominate at extremely

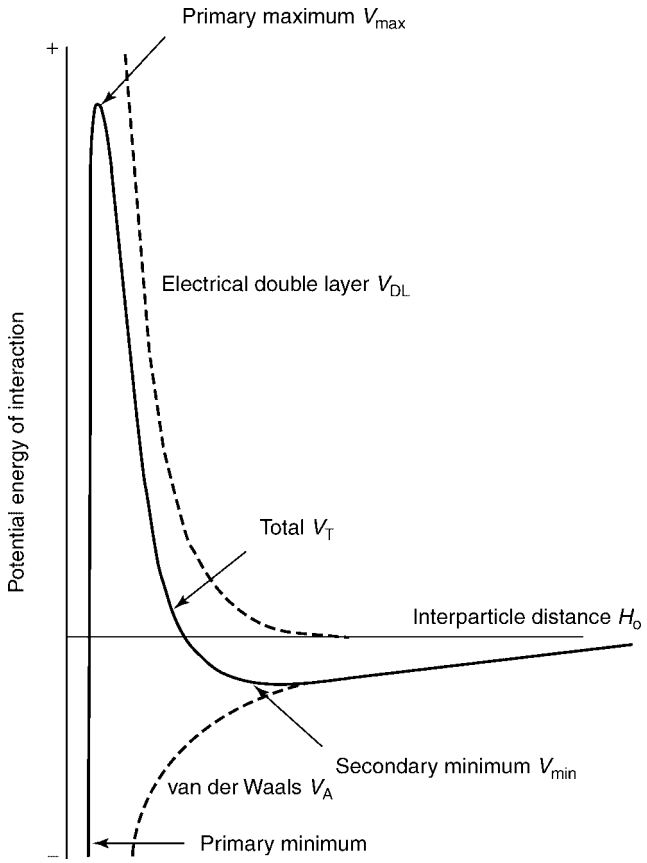

Fig. 1. Potential energies of interaction between two colloidal particles as a function of their distance of separation, for electrical double layers due to surface charge (V_{DL}), London–van der Waals dispersion forces (V_A), and the total interaction (V_T).

small (Born) and intermediate (electric double layer) separation distances. If the colloidal species are charged and have an interfacial potential of ~25–50 mV, the DLVO model predicts for binary particle interactions that a substantial repulsive potential energy barrier will inhibit the close approach of the particles, thereby stabilizing them against aggregation (V_{max} in Fig. 1). The primary maximum usually ensures stability, if its magnitude (V_{max}) exceeds the range 10–15 kT; smaller barriers lead to irreversible aggregation in the primary minimum (7,8,11,31,35,64–66). The secondary minimum (V_{min}) can promote a loose, easily reversible aggregation of particles, if its magnitude is on the order of 10 kT or more (54). In clay colloids, this is part of the explanation for flocculation as distinguished from coagulation. The overall energy barrier to coagulation in the primary minimum is given by $V_{barrier} = V_{max} - V_{min}$, where the primary minimum represents the potential energy at contact. Stability ensues if the magnitude of $V_{barrier}$ exceeds 10–15 kT and is therefore large compared to the thermal energy of the particles. Note that the primary minimum is a finite number because of the contributions that come into play for very small particle separations, ie, the Born repulsion (54).

The classic DLVO models are for flat planes and spheres, but more complex shapes arise in practice. For example, there will be some distortion of originally spherical emulsion droplets as they approach each other and begin to seriously interact, causing a flattening. The model has been extended to systems with particles that differ in size, shape, and chemical composition (64,65), and to those with particles that have an adsorbed layer of ions (7,8,10,11,31,35,64–66), as depicted in Figure 2.

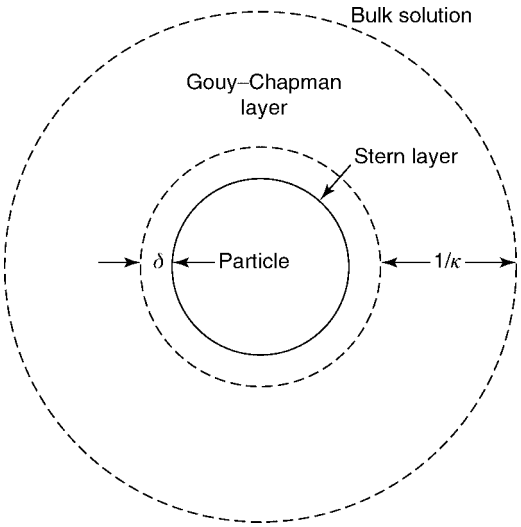

Fig. 2. Schematic diagram of a suspended colloidal particle, showing relative locations of the Stern layer (thickness, δ) that consists of adsorbed ions and the Gouy–Chapman layer ($1/\kappa$), which dissipates the excess charge, not screened by the Stern layer, to zero in the bulk solution (67). In the absence of a Stern layer, the Gouy–Chapman layer dissipates the surface charge.

The role of electrostatic repulsion in the stability of suspensions of particles in nonaqueous media is not entirely clear. In attempting to apply DLVO theory it can be difficult to judge the electrical potential at the surface, the appropriate Hamaker constant, and the ionic strength to be used for the nonaqueous medium. The ionic strength will be low so the electric double layer will be thick, the electric potential will vary slowly with separation distance, and so will the net electric potential as the double layers overlap. As a result the repulsion between particles can be expected to be weak (68).

Returning to aqueous systems, it will be apparent that the DLVO calculations can become quite involved, requiring considerable foreknowledge about the systems of interest. There are empirical "rules of thumb" that can be used to give a first estimate of the degree of colloidal stability a system is likely to have if the Zeta potential is known. For example, in the case of colloids dispersed in aqueous solutions, one such rule stems from observations that the colloidal particles are quite stable when the Zeta potential is $\sim$30 mV (positive or negative) or more, and quite unstable due to aggregation when the Zeta potential is between $+5$ and -5 mV. The transition from stable dispersion to aggregation usually occurs over a fairly small range of electrolyte concentration. This makes it possible to determine aggregation concentrations, often referred to as critical coagulation concentrations (CCC). The Schulze–Hardy rule summarizes the general tendency of the CCC to vary inversely with the sixth power of the counterion charge number (for indifferent electrolyte). The ability to predict CCCs was the first success of DLVO theory.

Steric and Hydrodynamic Effects. Additional influences on dispersion stability beyond those accounted for by the DLVO theory, like steric, surface hydration, and hydrodynamic effects have received considerable attention over the past several decades (54). More generally, the stability of a dispersion can be enhanced (protection) or reduced (sensitization) by the addition of material that adsorbs onto particle surfaces. Protective agents can act in several ways. They can increase double layer repulsion if they have ionisable groups. The adsorbed layers can lower the effective Hamaker constant. An adsorbed film may necessitate desorption before particles can approach close enough for van der Waals forces to cause attraction.

Long-chain surfactants and natural and synthetic high molecular weight polymers can be adsorbed at the surfaces of dispersed species such that a significant amount of adsorbate extends out from the surfaces. In this situation, an entropy decrease can accompany particle approach, providing a short-range stabilization mechanism referred to as steric stabilization. Molecular structure and solvation, adsorption layer thickness and hydrodynamic volume, and temperature determine the effectiveness of steric stabilization (69–73). Finally, the adsorbed material may form such a rigid film that it poses a mechanical barrier to droplet coalescence. Sensitizing agents are the opposite of protective agents. Again there are several possible mechanisms of action. If the additive is oppositely charged to the dispersed particles then decreased double layer repulsion will result. In some kinds of protecting adsorption a bilayer is formed, with the outer layer having lyophilic groups exposed outward; the addition of enough additive to form only the single layer will have lyophobic groups oriented outward, with a sensitizing effect. If the additive is of long chain length, sometimes a bridging between

particles occurs. Colloidal destabilization by electrolytes and bridging flocculation by polymers have been addressed both experimentally and theoretically. Comprehensive reviews on the relevant phenomena that derive from soluble and adsorbed polymers are available (69–73).

Oilfield W/O emulsions may be stabilized by the presence of a protective film around the water droplets. Such a film can be formed from the asphaltene and resin fractions of the crude oil. When drops approach each other during the process of aggregation, the rate of oil film drainage will be determined initially by the bulk oil viscosity, but within a certain distance of approach the interfacial viscosity becomes important. A high interfacial viscosity will significantly retard the final stage of film drainage and promote kinetic emulsion stability. If the films are viscoelastic, then a mechanical barrier to coalescence will be provided, yielding a high degree of emulsion stability (74,75).

Another example can be found in the field of water and wastewater treatment. Water treatment, whether for drinking water or for disposal of industrial wastes, involves the removal of suspended solids usually silt, clay, and organic matter. The electric charge on the solids is often sufficiently negative to yield a stable dispersion that settles slowly and is difficult to filter. The solution to this problem is to reduce the Zeta potential to values that permit rapid coagulation increasing both sedimentation and filterability. A first step toward coagulating the suspension might be to add aluminum sulfate (alum), from which the trivalent aluminum ions will have a powerful effect on the Zeta potential (according to the Schulze–Hardy rule). Figure 3**a** shows an example of this effect. In practice, however, the alum required to reduce the Zeta potential to below about −10 mV or so reduces the solution pH too much (unreacted alum becomes carried to other parts of the plant and forms undesirable precipitates). A second step can be introduced, in which a cationic polyelectrolyte is added to reduce the Zeta potential to about zero without changing the pH. As a final step a high molecular weight anionic polymer may be added (MW 500,000–1,000,000, or more) whose molecules can bridge between agglomerates yielding very large, rapid-settling flocs. Figure 3**b** shows how two New York water samples were treated in this way.

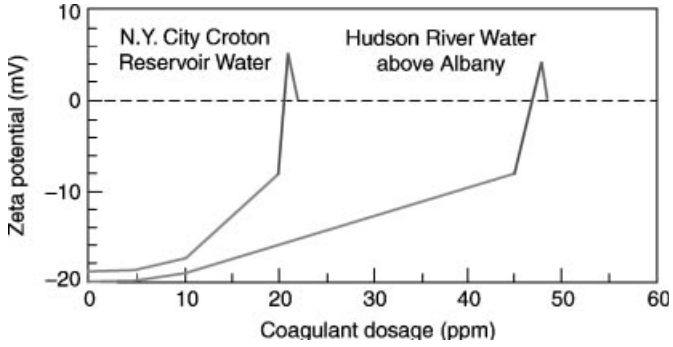

Fig. 3. Illustration of Zeta potentials and coagulation of solids in New York City water treatment through sequential additions of aluminum sulfate (alum), cationic polyelectrolyte, and anionic polymer. Alum ▬▬ Cationic polyelectrolyte ▬▬ Long-chain anionic ▬▬. [Adapted from Ref. 76. Used with permission, L.A. Ravina, Zeta-Meter, Inc., Staunton, Va.]

Kinetic Properties

The best experimental technique for monitoring colloid stability is usually dictated by the nature of the specific colloidal material and the dispersing medium. In principle, any distinctive physical property of the colloidal system in question can be used, at least empirically, to monitor changes in the dispersed state. The more complex a system is (chemically or with respect to its particulate heterogeneity), the less likely it is that a single property uniquely and completely describes changes in the colloidal state. Aggregation and/or coalescence of colloidal material can be monitored by a wide variety of techniques including light scattering, neutron scattering, microscopy, rheology, conductivity, filtration, sedimentation, and electrokinetics.

Encounters between colloidal species can occur frequently due to any of Brownian motion, sedimentation, or stirring. If velocity or shear gradients are present and are sufficiently large, the frequency of collisions depends on the volume fraction of solids and the mean velocity gradient. Assuming that sedimentation is slow compared to other collision mechanisms, the overall aggregation rate, $-\mathrm{d}N/\mathrm{d}t$, is

$$-\mathrm{d}N/\mathrm{d}t = k_\mathrm{d}N^2 + k_sN$$

where N is the number concentration of dispersed species, k_d and k_s are the respective rate constants corresponding to diffusion-controlled and shear-induced collision processes, and the minus sign denotes that the number concentration decreases with time t. The constants k_d and k_s depend on particle/droplet/bubble properties such as chemical composition of the bulk and surface phases, dielectric constant, dipole moment, size, size distribution, shape, surface charge, solid-phase distribution within particles, and particle anisotropy. Properties of the liquid-dispersing medium that contribute significantly to the values of these rate constants are the dielectric constant, the dipole moment, and the ability to dissolve electrolytes and polymers, in addition to the properties cited earlier. The k_d term usually dominates in quiescent systems containing submicrometer particles. The full expression for $(-\mathrm{d}N/\mathrm{d}t)$ and its use are treated in more detail elsewhere (7,8,31,77).

Chemical reactions can also affect the k_d and k_s terms and thereby influence or control colloidal stability (78). Pertinent examples are dissolution, precipitation, hydrolysis, precipitation, and chemical complexing. The last reaction may involve either simple species, eg,

$$\mathrm{Al}^{3+} + \mathrm{SO_4}^{2-} \rightleftarrows \mathrm{AlSO_4}^{+}$$

or complicated solutes such as $\mathrm{Al_8(OH)_{20}}^{4+}$, chelated metals (75), synthetic and natural polymers (25,69–73), or a variety of surfactants and dispersants (19,79). Many of the possible bulk solution chemical reactions that influence colloidal stability, along with specific sample reactions and their general interfacial analogues, are listed in Table 5.

Table 5. Representative Solution and Surface Equilibria Influencing Colloidal Stability

Solution	Surface analogue
Hydrolysis	
$CH_3(CO)OCH_3 + H_2O \rightleftarrows CH_3(CO)OH + CH_3OH$	$M_2O + H_2O \rightleftarrows 2\,MOH$
$PO_4^{3-} + H_2O \rightleftarrows HPO_4^{2-} + OH^-$	$MOH + H_2O \rightleftarrows MOH_2^+ + OH^-$
Dissociation	
$Al(OH)_3 \rightleftarrows Al^{3+} + 3\,OH^-$	$MOH_2^+ \rightleftarrows MO^- + 2\,H^+$
$C_6H_5(CO)OH \rightleftarrows C_6H_5(CO)O^- + H^+$	$MOH \rightleftarrows MO^- + H^+$
Dissolution	
$ZnC_2O_4\,(S) \rightleftarrows Zn^{2+} + C_2O_4^{2-}$	
$Al(OH)_3(S) + OH^- \rightleftarrows AlO_2^- + 2\,H_2O$	
Complexation	
$Cu^{2+} + 4\,OH^- \rightleftarrows Cu(OH)_4^{2-}$	$MO^- + Na^+ \rightleftarrows MO^-Na^+$
$n\text{–}C_{12}H_{25}N(CH_3)_2 + HCl \rightleftarrows n\text{–}C_{12}H_{25}NH^+(CH_3)_2Cl^-$	$MOH + HCl \rightleftarrows MOH_2^+\,Cl^-$

Applications

General Uses. Diffusion, Brownian motion, sedimentation, electrophoresis, osmosis, rheology, mechanics, interfacial energetics, and optical and electrical properties are among the general physical properties and phenomena that are primarily important in colloidal systems (7,8,27,28,31). Chemical reactivity and adsorption often play important, if not dominant, roles. Any physical and chemical feature may ultimately govern a specific industrial process and determine final product characteristics and colloids are deemed either desirable or undesirable on the basis of their unique physiochemical properties.

Although colloids may be undesirable components in industrial systems, particularly as waste or by-products and, in nature, in the forms of fog and mist, they are desirable in many technologically important processes such as mineral beneficiation and the preparation of ceramics, polymers, composite materials, paper, foods, textiles, photographic materials, drugs, cosmetics, and detergents. The remainder of this section specifies some applications for colloidal solids, liquids, and gases and illustrates how colloids affect many technologically important systems in a positive manner.

Colloidal Solids. Some uses of solid colloids include reinforcement aids in metals, ceramics, and plastics; as adhesion promoters in paints and thermoplastics; as nucleating agents in cloud seeding; as activated powder catalysts; as thickening agents in gels and slurries; and as abrasives in toothpastes (7,8,27,28,31,37,80–83). When used as reinforcement agents, the colloidal particles may be spherical, angular, fibrillar, or flake-shaped. Alumina and thoria are used to reinforce aluminum and nickel, respectively, by providing obstacles to the movement of dislocations in the metals, and zirconia and silicon carbide to reinforce a variety of ceramics (eg, alumina, silicon nitride, and glass, by inhibiting the propagation and opening of cracks in the matrix). (See COMPOSITE MATERIALS; REINFORCEMENT). Stable but ordered suspensions can be regarded as precursory systems for ordered, prefired, ceramic components; outlets for such systems include various processing techniques such as slip, tape, freeze, pressure,

centrifugal, and ultrasonic casting, as well as isostatic, and hot pressing (84,85). Asbestos, crystalline silicas, and organic solids are added to concrete to improve its strength by providing an interlocking particulate structure within the concrete matrix (81); asbestos, various oxides, and carbon black are added to reinforce polymers by inducing a stiffened or high yield matrix (27,28,78–81).

The magnitude of the strengthening often depends on particle shape. Fibrillar fillers are used as discontinuous fibers in metals and plastics, eg, in epoxy resin (78–80) and as whiskers in ceramics (86). Glass and aluminum oxide are common fillers that are occasionally pretreated with a polymeric or metallic coating; silica and various clays are also used. The mechanism by which ceramics and metals are reinforced often involves precipitation of colloidal material during thermal treatment of the matrix composition, eg, TiO_2 in borosilicate glasses designed for enamels (87). Strengthening mechanisms (27,28) include precipitation and dispersion when the reinforcing phase is metallic and the toughened materials are metals or ceramics. When inorganic, nonmetallic ceramics strengthen metals or polymers (45), the mechanism may be dispersion or reinforcement, eg, by cross-linking. Reinforcement implies a higher volume fraction than in dispersion hardening. Fillers can be added not only to improve mechanical properties such as impact strength, fracture toughness, and tensile strength of structural ceramics, but also to enhance optical properties, as is done for colored glasses containing colloidal gold or crystalline, chromium-based oxides.

Particle suspensions have long been of great practical interest because of their widespread occurrence in everyday life. Some important kinds of familiar suspensions include those occurring in foods (batters, puddings, sauces), pharmaceuticals (cough syrups, laxative suspensions), household products (inks, paints, "liquid" waxes) and the environment (suspended lake and river sediments, sewage). In the petroleum industry alone, suspensions may be encountered throughout each of the stages of petroleum recovery and processing, including migrating fine solid suspensions during secondary and enhanced oil recovery, dispersions of asphaltenes in crude oils, produced (well-head) solids in oil recovery, drilling muds, well stimulation and fracturing suspensions, well cementing slurries, and oilfield surface treatment facility sludges.

Other applications of colloidal solids include the preparation of rigid, elastic, and thixotropic gels (78–80), aerogel-based thermal insulators (79), and surface coatings (25,27,28,79). Commercial uses of silica gel and sol–gel processing (88) often focus on rigid gels having 20–30 vol% SiO_2. The principal interparticulate forces in a rigid gel are chemical and irreversible, and the colloid improves the gel's mechanical strength. Elastic gels are commonly associated with cellophane, rubber, cellulosic fibers, leather, and certain soaps. Many thixotropic gels and surface coatings contain colloidal solids, eg, clays, alumina, ferric oxide, titania, silica, and zinc oxide. Consumer and industrial pastes belong to this category; putty, dough, lubricating grease, toothpaste, and paint are some examples.

Colloidal Liquids. These fluids are commonly used in the form of emulsions by many industries. Permanent and transient antifoams consisting of an organic material, eg, polyglycol, oils, fatty materials, or silicone oil dispersed in water, is one application (10,89,90) that is important to a variety of products and processes: foods, cosmetics, pharmaceuticals, pulp and paper, water treatment,

and minerals beneficiation. Other emulsion products (see Table 2) include foods, insecticides and herbicides, polishes, drugs, biological systems, asphalt paving emulsions, personal care creams and lotions, paints, lacquers, varnishes, and electrically and thermally insulating materials.

Emulsions may be encountered throughout all stages of the process industries. For example, in the petroleum industry both desirable and undesirable emulsions permeate the entire production cycle, including emulsion drilling fluid, injected or *in situ* emulsions used in enhanced oil recovery processes, well-head production emulsions, pipeline transportation emulsions, and refinery process emulsions (13). Such emulsions may contain not just oil and water, but also solid particles and even gas, as occur in the large Canadian oil sands mining and processing operations (13–15).

Some emulsions are made to reduce viscosity so that an oil can be made to flow. Emulsions of asphalt, a semisolid variety of bitumen dispersed in water, are formulated to be both less viscous than the original asphalt and stable so that they can be transported and handled. In application, the emulsion should shear thin and break to form a suitable water-repelling roadway coating material. Another example of emulsions that are formulated for lower viscosity with good stability are those made from heavy oils and intended for economic pipeline transportation over large distances. Here again the emulsions should be stable for transport but will need to be broken at the end of the pipeline.

Some special problems arise at sea: when crude oil is spilled on the ocean a slick is formed that spreads out from the source with a rate that depends on the oil viscosity. With sufficient energy an O/W emulsion may be formed, which helps disperse oil into the water column and away from sensitive shorelines. Otherwise, the oil may pick up water to form a W/O emulsion, or mousse ("chocolate mousse"). These mousse emulsions can have high water contents and have very high viscosities and, with weathering, they can become semisolid and considerably more difficult to handle. The presence of mechanically strong films makes it hard to get demulsifiers into these emulsions, so they are hard to break.

Demulsification, ie, the breaking of emulsions, is an important process, with the oil industry being a common one in which the process is often critical. The stability of emulsions is often a problem. Demulsification involves two steps. First, there must be agglomeration or coagulation of droplets. Then, the agglomerated droplets must coalesce. Chemical and particulate agents that displace the surfactant and permit an unstabilized interface to form are used for this purpose. Only after these two steps can complete phase separation occur. It should be realised that either step can be rate-determining for the demulsification process. This is a large subject in its own right; see References 13,16 and 89–91.

Other common applications of colloidal liquids include liquid aerosols, such as those occurring in the areas of environment (fog, mist, cloud, smog), agriculture (crop sprays), manufacturing (paint sprays), medicine (nasal sprays), and personal care (hair spray).

Colloidal Gases. Fluid foams are commonplace in foods, shaving cream, fire-fighting foam, mineral flotation, and detergents (10,92–95). Thus, in view of the fact that the concentration of bubbles greatly affects the properties of foams, the production, dispersion, and maintenance of colloidal gas bubbles are basic to foams and related materials. Often, natural and synthetic soaps and surfactants

are used to make fluid foams containing colloidal gas bubbles. These agents reduce the interfacial tension and, perhaps, increase the viscosity at the gas–liquid interface, making the foam stable. Also, some soluble proteins that denature upon adsorption or with agitation of the liquid phase can stabilize foams by forming insoluble, rigid layers at the gas–liquid interface (89).

A class of enhanced oil recovery processes involves injecting a gas in the form of a foam. Suitable foams can be formulated for injection with air–nitrogen, natural gas, carbon dioxide, or steam (14,16). In a thermal process, when a steam foam contacts residual crude oil, there is a tendency to condense and create W/O emulsions. On the other hand, in a nonthermal process, the foam may emulsify the oil itself (now as an O/W emulsion), which is then drawn up into the foam structure; the oil droplets eventually penetrate the lamella surfaces, destroying the foam (14).

Microfoams (also termed colloidal gas aphrons) comprise a dispersion of aggregates of very small foam bubbles in aqueous solution. They can be created by dispersing gas into surfactant solution under conditions of very high shear. The concept is that, under the right conditions of turbulent wave breakup, one can create a dispersion of very small gas bubbles, each surrounded by a bimolecular film of stabilizing surfactant molecules. Under ambient conditions the bubble diameters are typically in the range 50–300 μm. There is some evidence that such microfoams tend to be more stable than comparable foams that do not contain the bimolecular film structure (96–98). Some interesting potential applications have been reported: soil remediation (97,99–102) and reservoir oil recovery (94,103,104), but the literature for these applications is sometimes inconsistent; more work needs to be done in this area.

Some agents will act to reduce the foam stability of a system (termed foam breakers or defoamers) while others can prevent foam formation in the first place (foam preventatives, foam inhibitors). There are many such agents, Kerner (92) describes several hundred different formulations for foam inhibitors and foam breakers. In all cases, the cause of the reduced foam stability can be traced to changes in the nature of the interface, but the changes can be of various kinds. The addition to a foaming system of any soluble substance that can become incorporated into the interface may decrease dynamic foam stability if the substance acts in any combination of increased surface tension, decreased surface elasticity, decreased surface viscosity or decreased surface potential. Such effects may be caused by a cosolubilization effect in the interface or by a partial or even complete replacement of the original surfactants in the interface. Some branched, reasonably high molecular mass alcohols can be used for this purpose. Not being very soluble in water they tend to be adsorbed at the gas–liquid interface, displacing foam-promoting surfactant and breaking or inhibiting foam. Alternatively, a foam can be destroyed by adding a chemical that actually reacts with the foam-promoting agent(s). Foams may also be destroyed or inhibited by the addition of certain insoluble substances such as a second liquid or solid phase. Antifoaming and defoaming represent a large subject on their own (see References 105 and 106).

Other common applications of colloidal gases include solid foams, such as those occurring in the areas of food (leavened breads), geology (pumice stone, zeolites), manufacturing (polystyrene foam, polyurethane foam), and personal care

(synthetic sponges). Solid foams such as polyurethane foam contain dispersed gas bubbles that are often produced via viscoelastic polymer melts within which gas, eg, carbon dioxide, bubbles are nucleated (107).

Chemical and Surface Analysis

Any classical wet-chemical analyses or instrumental techniques that are routinely used to analyze the bulk composition of solids and liquids are, in principle, also suitable for colloids. The available instrumental methods range, eg, from spectrographic analysis for chemical composition, which is limited to crude estimates for impurities, to Raman spectroscopic identification of chemical functionalities, which can be very accurate (see VIBRATIONAL SPECTROSCOPY). These techniques can also be used to analyze adsorbed layers if they can be quantitatively desorbed and collected for study. Surface-chemical analyses that cannot be conducted using conventional methods designed for bulk materials are usually accomplished by optical, diffraction, and spectroscopic techniques; these are often applied under conditions of an ultrahigh vacuum. The spectroscopies measure the responses of solid surfaces to beams of electrons, ions, neutral species, and photons (see SURFACE ANALYSIS). Each spectroscopy has unique attributes (10), making it suitable for certain colloids but unsuitable for others. Although too numerous to list here, descriptions and tabulations of surface techniques and their synonyms and acronyms are given in References 6,10,108, and 109. A wide range of information can be obtained including surface and adsorbed layer compositions (including heterogeneity); surface morphology, atom packing, and structure; and surface reactions and their kinetics. Advances in these fields continue at a significant rate (see SURFACE PROPERTIES).

Hazards of Colloidal Systems

The occurrence of some materials in the form of a colloidal dispersion can introduce or enhance safety hazards. Considering that the dispersion of a material down to colloidal size results in a high specific surface area, colloidal chemical reactivity may differ considerably from that of the identical macroscopic material with less surface area. This is particularly important if the colloidal surface is easily and rapidly oxidized. Dust explosions and spontaneous combustion are potential dangers whenever certain materials exist as finely divided dry matter exposed to oxidizing environments (67,110) (see COATING METHODS, POWDER TECHNOLOGY). Dispersions of charged colloidal particles in nonaqueous media occur throughout the petroleum industry. The flow of petroleum fluids in tanks or pipelines, combined with the low conductivity of the petroleum fluids themselves, can allow the buildup of large potential gradients and a separation of charges. Sufficient charging for there to be an electrostatic discharge can cause an explosion (68).

Health problems can be caused by solids and liquids suspended in air or water. Specific potential hazards have been associated with a diverse spectrum of colloidal materials, including chemicals, coal, minerals, metals, pharmaceuticals, plastics, and wood pulp. Limits for human exposure for many particulate,

hazardous materials are published (108,109). The effects of the colloidal solids and liquids that comprise smog are widespread and well known. Liquid droplets may also constitute a hazard; eg, smog can contain sulfuric acid aerosols. Elements such as lead, zinc, and vanadium that are released into the atmosphere as vapors can subsequently condense or be removed as solid particulates by rain (111,112). Similarly, exposure to airborne pollutants found indoors and in confined spaces, many of which are particulates or microbes of colloidal size, can lead to complex physiological responses. This hazard ranges from short-term allergic reactions (eg, pollen and household dust causing asthma and hay fever) to long-term, possibly fatal effects (eg, silicosis, asbestosis, and black lung disease).

There is a need to understand the environmental properties and risks associated with any large-volume chemicals. The mass of surfactants that could ultimately be released into the environment, for example, is significant. A 1995 estimate of the global use of linear alkylbenzenesulfonates, alcohol ethoxylates, alkylphenol ethoxylates, alcohol sulfates, and alcohol ether sulfates totaled 3 million ton (113). Surfactant usage in industry will probably increase as new applications are found. The toxicity and persistence of surfactants is now fairly predictable for a variety of environmental situations (111,114,115), and although surfactants are not generally viewed as a serious threat to the environment (111) they can exhibit considerable toxicity to aquatic organisms. In addition to products, many industries produce waste containing significant amounts of suspended matter for which treatment incurs significant technological challenges and costs (116–118). Trace metals that are commonly found as suspended matter in the chemical form of hydrous oxides and other insoluble matter are tabulated elsewhere (67,110). Large fractions of readily hydrolyzable metals exist as adsorbed species on suspended (colloidal) solids in fresh and marine water systems and can also be anticipated to exist in industrial wastewater. Continued research is needed to understand the health hazards linked to colloidal pollutants.

Emerging Areas in Colloid Science

Advances on the theoretical front continue to be aided by advances in bulk and surface analytical technology (composition) and in physical surface characterization technology (topology, structure, and forces). Applications of atomic force microscopy in particular continue to expand into diverse areas, including magnetic force microscopy (119).

Much is known about colloids, their formation, properties, and applications, but considerably more surely remains unknown. In particular, the full potential to control colloids is not presently realized. There are several types of mixed colloids that are only poorly understood. For example, the properties of colloids in which more than one type of colloidal particle is dispersed may be dominated by the behavior of the minor dispersed-phase component. The nature and properties of colloids within colloids, such as suspended solids in the dispersed phase of an emulsion, or emulsified oil within the aqueous lamellae of a foam, are only beginning to be understood (13–15).

Nanotechnology refers to the production of materials and structures in the 0.1–100 nm range by any of a variety of nanoscale physical and chemical methods.

This is a rapidly growing area of materials science. As the size range indicates, there is an overlap between nanotechnology and colloid science since they share some similarity of scale, both dealing with matter having dimensions of tens and hundreds of nanometers. Although many areas of nanotechnology do not directly deal with colloidal dispersions, such as nanotubes and nanoelectronic devices, other areas do, eg, the use of colloidal ink dispersions in robocasting to build near-nanometer-scale three-dimensional structures. Examples of work at the interface between these fields is provided by current research aimed at controlling the solubility of nanotubes (120), and in the fabrication of nanoengineered films on colloidal particles (121).

Smart colloids are colloidal dispersions for which certain properties, such as size and structure, can be altered by changing an external influence, such as temperature, eg, cross-linked polymer gels of poly(*N*-isoproplyacrylamide). Such polymer systems can swell or shrink in response to temperature changes, and are also termed "thermo-shrinking polymers." (see References 122–124).

BIBLIOGRAPHY

"Colloids" in *EPST* 1st ed., Vol. 4, pp. 16–73, by Dewey K. Carpenter, Georgia Institute of Technology; "Colloids" in *EPSE* 2nd ed., Vol. 3, pp. 727–746, by Robert M. Fitch, Louis Laboratories, Johnson Wax Co.

1. M. Kerker, *J. Colloid Interface Sci.* **116**, 296 (1987).
2. I. Asimov, *Words of Science and the History Behind Them*, Riverside Press, Cambridge, Mass., 1959.
3. H. Freundlich, *Colloid and Capillary Chemistry*, 3rd. ed., English translation, Methuen, London, 1926.
4. P. Becher, *Dictionary of Colloid and Surface Science*, Dekker, New York, 1990.
5. L. L. Schramm, *The Language of Colloid and Interface Science*, American Chemical Society, Washington, and Oxford University Press, New York, 1993.
6. L. L. Schramm, *Dictionary of Colloid and Interface Science*, John Wiley & Sons, Inc., New York, 2001.
7. D. J. Shaw, *Introduction to Colloid and Surface Chemistry*, 3rd ed., Butterworths, London, 1980.
8. P. Hiemenz and R. Rajagopalan, *Principles of Colloid and Surface Chemistry*, 3rd. ed., Dekker, New York, 1997.
9. D. Myers, *Surfaces, Interfaces, and Colloids*, 2nd ed., Wiley-VCH, New York, 1999.
10. A. W. Adamson, *Physical Chemistry of Surfaces*, 5th ed., John Wiley & Sons, Inc., New York, 1990.
11. H. R. Kruyt, *Colloid Science, Vol. I: Irreversible Systems*, Elsevier, Amsterdam, the Netherlands, 1952.
12. S. P. Parker, ed., *McGraw-Hill Dictionary of Scientific and Technical Terms*, 3rd ed., McGraw-Hill, New York, 1984.
13. L. L. Schramm, ed., *Emulsions: Fundamentals and Applications in the Petroleum Industry*, American Chemical Society, Washington, and Oxford University Press, New York, 1992.
14. L. L. Schramm, ed., *Foams: Fundamentals and Applications in the Petroleum Industry*, American Chemical Society, Washington, and Oxford University Press, New York, 1994.

15. L. L. Schramm, ed., *Suspensions: Fundamentals and Applications in the Petroleum Industry*, American Chemical Society, Washington, and Oxford University Press, New York, 1996.
16. L. L. Schramm, ed., *Surfactants: Fundamentals and Applications in the Petroleum Industry*, Cambridge University Press, Cambridge, U.K., 2000.
17. S. Lowell and J. E. Shields, *Powder Surface Area and Porosity*, Chapman and Hall, London, 1991.
18. D. Myers, *Surfactant Science and Technology*, VCH, New York, 1988.
19. M. J. Rosen, *Surfactants and Interfacial Phenomena*, 2nd ed., John Wiley & Sons, Inc., New York, 1989.
20. M. El-Nokaly and D. Cornell, eds., *Microemulsions and Emulsions in Foods*, American Chemical Society, Washington, D.C., 1991.
21. R. Beckett, ed., *Surface and Colloid Chemistry in Natural Waters and Water Treatment*, Plenum Press, New York, 1990.
22. H. van Olphen, *An Introduction to Clay Colloid Chemistry*, 2nd ed., Wiley-Interscience, New York, 1977.
23. M. M. Rieger and L. D. Rhein, eds., *Surfactants in Cosmetics*, 2nd ed., Dekker, New York, 1997.
24. E. Dickinson, *An Introduction to Food Colloids*, Oxford University Press, New York, 1992.
25. G. D. Parfitt, ed., *Dispersion of Powders in Liquids*, 3rd ed., Applied Science, London, 1981.
26. S. Ross and I. D. Morrison, *Colloidal Systems and Interfaces*, John Wiley & Sons, Inc., New York, 1988.
27. C. R. Veale, *Fine Powders*, John Wiley & Sons, Inc., New York, 1972.
28. J. K. Beddow, *Particulate Science and Technology*, Chemical Publishing, New York, 1980.
29. M. J. Jaycock and G. D. Parfitt, *Chemistry of Interfaces*, Ellis Horwood, Chichester, U.K., 1981.
30. G. D. Parfitt and K. S. W. Sing, eds., *Characterization of Powder Surfaces*, Academic Press, New York, 1976.
31. R. D. Vold and M. J. Vold, *Colloid and Interface Chemistry*, Addison-Wesley, Reading, Mass., 1983.
32. R. J. Mikula and V. A. Munoz, in L. L. Schramm, ed., *Surfactants: Fundamentals and Applications in the Petroleum Industry*, Cambridge University Press, Cambridge, U.K., 2000, pp. 51–77.
33. L. L. Schramm, S. M. Kutay, R. J. Mikula, and V. A. Munoz, *J. Petrol. Sci. Eng.* **23**, 117 (1999).
34. M. Kerker, *The Scattering of Light and Other Electromagnetic Radiation*, Academic Press, New York, 1969.
35. R. J. Hunter, *Zeta Potential in Colloid Science*, Academic Press, New York, 1981.
36. A. J. Babchin, R. S. Chow, and R. P. Sawatzky, *Adv. Colloid Interface Sci.* **30**, 111 (1989).
37. C. Orr, *Particulate Technology*, Macmillan, New York, 1966.
38. Th. G. M. van de Ven, *Colloidal Hydrodynamics*, Academic Press, Inc., London, 1989.
39. R. W. Whorlow, *Rheological Techniques*, Ellis Horwood, Chichester, U.K., 1980.
40. J. R. Van Wazer, J. W. Lyons, K. Y. Kim, and R. E. Colwell, *Viscosity and Flow Measurement*, John Wiley & Sons, Inc., New York, 1963.
41. C. C. Mill, ed., *Rheology of Disperse Systems*, Pergamon Press, Inc., Elmsford, New York, 1959.
42. A. G. Fredrickson, *Principles and Applications of Rheology*, Prentice-Hall, Englewood Cliffs, N.J., 1964.

43. K. Walters, *Rheometry: Industrial Applications*, Research Studies Press, New York, 1980.
44. H. A. Barnes and S. A. Holbrook, in P. Ayazi Shamlou, ed., *Processing of Solid–Liquid Suspensions*, Butterworth Heinemann, Oxford, U.K., 1993, pp. 222–245.
45. L. E. Murr, *Interfacial Phenomena in Metals and Alloys*, Addison Wesley, London, 1975.
46. J. Leja, *Surface Chemistry of Froth Flotation*, Plenum Press, New York, 1982.
47. L. L. Schramm, *J. Can. Petrol. Technol.* **28**, 73 (1989).
48. W. D. Harkins and A. E. Alexander, in A. Weissberger, ed., *Physical Methods of Organic Chemistry*, Interscience, New York, 1959, pp. 757–814.
49. J. F. Padday, in E. Matijevic, ed., *Surface and Colloid Science*, Vol. 1, Wiley-Interscience, New York, 1969, pp. 101–149.
50. C. A. Miller and P. Neogi, *Interfacial Phenomena Equilibrium and Dynamic Effects*, Dekker, New York, 1985.
51. A. I. Rusanov and V. A. Prokhorov, *Interfacial Tensiometry*, Elsevier, Amsterdam, the Netherlands, 1996.
52. L. W. Lake, *Enhanced Oil Recovery*, Prentice Hall, Englewood Cliffs, N.J., 1989.
53. P. Mukerjee and K. J. Mysels, *Critical Micelle Concentrations of Aqueous Surfactant Systems*, NSRDS-NBS 36, National Bureau of Standards, Washington, D.C., 1971.
54. J. N. Israelachvili, *Intermolecular and Surface Forces*, 2nd ed., Academic Press, New York, 1992.
55. G. Cevc and D. Marsh, *Phospholipid Bilayers*, John Wiley & Sons, Inc., New York, 1987.
56. D. Marsh, *Handbook of Lipid Bilayers*, CRC Press, Boca Raton, Fla., 1990.
57. R. Miller and G. Kretzschmar, *Adv. Colloid Interface Sci.* **37**, 97 (1991).
58. J. Prost and F. Rondelez, *Nature (London)* **350**, 11 (1991).
59. D. O. Shah, ed., *Macro- and Microemulsions: Theory and Applications*, American Chemical Society, Washington, D.C., 1985.
60. D. A. Sabatini, R. C. Knoz, and J. H. Harwell, eds., *Surfactant-Enhanced Subsurface Remediation Emerging Technologies*, American Chemical Society, Washington, D.C., 1995.
61. M. El-Nokaly and D. Cornell, eds., *Microemulsions and Emulsions in Foods*, American Chemical Society, Washington, D.C., 1991.
62. A. M. James, in R. J. Good and R. R. Stromberg, eds., *Surface and Colloid Science*, Vol. 11, Plenum, 1979, pp. 121–186.
63. A. J. Babchin, R. S. Chow, and R. P. Sawatzky, *Adv. Colloid Interface Sci.* **30**, 111 (1989).
64. B. V. Derjaguin and L. D. Landau, *Acta Physiochem. URSS* **14**, 633 (1941).
65. B. V. Derjaguin, N. V. Churaev, and V. M. Miller, *Surface Forces*, Consultants Bureau, New York, 1987.
66. E. J. Verwey and J. Th. G. Overbeek, *Theory of the Stability of Lyophobic Colloids*, Elsevier, Amsterdam, the Netherlands, 1948.
67. S. Budavari, M. J. O'Neil, A. Smith, P. E. Heckelman, and J. F. Kinneary, *The Merck Index*, 11th ed., Merck, Rahway, N.J., 1989, p. MISC-53.
68. I. D. Morrison, *Colloids Surfaces* **71**, 1 (1993).
69. T. Sato and R. Ruch, *Stabilization of Colloidal Dispersions by Polymer Adsorption*, Marcel Dekker, New York, 1980.
70. Th. F. Tadros, ed., *The Effect of Polymers on Dispersion Properties*, Academic Press, London, 1982.
71. Y. S. Lipatov and L. M. Sergeeva, *Adsorption of Polymers*, Halsted, New York, 1974.
72. C. A. Finch, ed., *Chemistry and Technology of Water-Soluble Polymers*, Plenum Press, New York, 1983.

73. B. Vincent, in Th. F. Tadros, ed., *Solid / Liquid Dispersions*, Academic Press, Inc., 1987, pp. 147–162.
74. R. J. R. Cairns, D. M. Grist, and E. L. Neustadter, in A. L. Smith, ed., *Theory and Practice of Emulsion Technology*, Academic Press, New York, 1976, pp. 135–151.
75. T. J. Jones, E. L. Neustadter, and K. P. Whittingham, *J. Can. Petrol. Technol.* **17**, 100–108 (1978).
76. *Zeta-Meter Applications Brochures*, Zeta-Meter Inc., New York, 1982.
77. W. Stumm and J. J. Morgan, *Aquatic Chemistry*, 2nd ed., John Wiley & Sons, Inc., New York, 1981.
78. E. Matijević, in K. J. Mysels, C. M. Samour, and J. H. Hollister, eds., *Twenty Years of Colloid and Surface Chemistry*, American Chemical Society, Washington, D.C., 1973, p. 283.
79. *McCutcheon's Detergents and Emulsifiers*, MC Publ. Co., Glen Rock, N.J., 1980.
80. Z. D. Jastrzebski, *The Nature and Properties of Engineering Materials*, 2nd ed., John Wiley & Sons, Inc., New York, 1977.
81. J. E. Gordon, *The New Science of Strong Materials*, 2nd ed., Princeton University Press, Princeton, N.J., 1976.
82. A. G. Guy, *Essentials of Materials Science*, McGraw-Hill Book Co., Inc., New York, 1976.
83. S. J. Lefond, ed., *Industrial Minerals and Rocks*, 4th ed., American Institute of Mineralogy and Metallurgy, Petroleum Engineering, Inc., New York, 1975.
84. F. Y. Wang, *Ceramic Fabrication Processes*, Academic Press, Inc., New York, 1976.
85. J. S. Reed, *Introduction to the Principles of Ceramic Processing*, Wiley-Interscience, New York, 1988.
86. A. Kelly and R. B. Nicholson, eds., *Strengthening Methods in Crystals*, Applied Science Publishing, London, 1971.
87. W. D. Kingery, H. K. Bowen, and D. R. Uhlmann, *Introduction to Ceramics*, 2nd ed., Wiley-Interscience, New York, 1976.
88. C. J. Brinker and G. W. Sherer, *Sol–Gel Science: The Physics and Chemistry of Sol–Gel Processing*, Academic Press, San Diego, Calif., 1990.
89. C. G. Sumner, *Clayton's The Theory of Emulsions and Their Technical Treatment*, 5th ed., Blakiston, New York, 1954.
90. K. J. Lissant, *Demulsification. Industrial Applications*, Dekker, New York, 1983.
91. P. Becher, *Emulsions: Theory and Practice*, 3rd ed., American Chemical Society and Oxford University Press, New York, 2001.
92. H. T. Kerner, *Foam Control Agents*, Noyes Data Corp., Park Ridge, N.J., 1976.
93. D. H. Everett, *Basic Principles of Colloid Science*, Royal Society of Chemistry, London, 1988.
94. A. K. Mirzadjanzade, I. M. Ametov, A. A. Bokserman, and V. P. Filippov, in *Proceedings, 7th European IOR Symposium*, Moscow, Russia, 1993, pp. 27–29.
95. E. Dickinson, ed., *Food Emulsions and Foams*, Royal Society of Chemistry, London, 1987.
96. F. Sebba, *J. Colloid Interface Sci.* **35**, 643 (1971).
97. F. Sebba, *Foams and Biliquid Foams-Aphrons*, John Wiley & Sons, Inc., New York, 1987.
98. F. Sebba, *Chem. Ind.* **4**, 91 (1985).
99. D. Roy, K. T. Valsaraj, and A. Tamayo, *Sep. Sci. Technol.* **27**, 1555 (1992).
100. D. Roy, K. T. Valsaraj, W. D. Constant, and M. Darji, *J. Hazard. Mater.* **38**, 127 (1994).
101. D. Roy, R. R. Kommalapati, K. T. Valsaraj, and W. D. Constant, *Water Res.* **29**, 589 (1995).
102. D. Roy, S. Kongara, and K. T. Valsaraj, *J. Hazard. Mater.* **42**, 247 (1995).

103. M. V. Enzien, D. L. Michelsen, R. W. Peters, J. X. Bouillard, and J. R. Frank, in *Proceedings, 3rd International Symposium on In-Situ and On-Site Reclamation*, San Diego, Calif., 1995, pp. 503–509.
104. A. K. Mirzadjanzade, I. M. Ametov, A. O. Bogopolsky, R. Kristensen, U. N. Anziryaev, S. V. Klyshnikov, A. M. Mamedzade, and T. S. Salatov, in *Proceedings, 7th European IOR Symposium*, Moscow, Russia, 1993, pp. 469–473.
105. J. J. Bikerman, *Foams*, Springer-Verlag, New York, 1973.
106. J. J. Bikerman, *Foams, Theory and Industrial Applications*, Reinhold, New York, 1953.
107. F. W. Billmeyer Jr., *Textbook of Polymer Science*, 2nd ed., Wiley-Interscience, New York, 1971.
108. D. P. Woodruff and T. A. Delchar, *Modern Techniques of Surface Science*, Cambridge University Press, New York, 1986.
109. G. A. Somorjai, *Introduction to Surface Chemistry and Catalysis*, Wiley-Interscience, New York, 1994.
110. R. C. Weast and M. J. Astle, eds., *Handbook of Chemistry and Physics*, 62nd ed., Chemical Rubber Co., Boca Raton, Fla., 1981, p. D-101.
111. A. E. Martell, *Pure Appl. Chem.* **44**, 81 (1975).
112. F. T. Mackenzie and R. Wollast, in E. D. Goldberg, ed., *The Sea*, Vol. 6, Wiley-Interscience, New York, 1977, p. 739.
113. L. N. Britton, *J. Surf. Det.* **1**, 109–117 (1998).
114. L. N. Britton, in L. L. Schramm, ed., *Surfactants, Fundamentals and Applications in the Petroleum Industry*, Cambridge University Press, Cambridge, U.K., 2000, pp. 541–565.
115. C. M. Maddin, In *International Conference on Health, Safety and Environment*, (Preprint) SPE paper 23354, Society of Petroleum Engineers, Richardson, Tex., 1991.
116. J. Wei, T. W. F. Russel, and M. W. Swartzlander, *The Structure of the Chemical Processing Industries*, McGraw-Hill, New York, 1979.
117. M. P. Freeman and J. A. Fitzpatrick, eds., *Physical Separations*, Engineering Foundation, New York, 1980.
118. A. J. Rubin, ed., *Chemistry of Wastewater Technology*, Ann Arbor Sci., Ann Arbor, Mich., 1978.
119. M. Rasa, B. W. M. Kuipers, and A. P. Philipse, *J. Colloid Interface Sci.* **250**, 303–315 (2002).
120. R. Dagani, *Chem. Eng. News* **80**(28), 38 (2002).
121. G. B. Sukhorukov, in D. Möbius and R. Miller, eds., *Novel Methods to Study Interfacial Layers*, Elsevier, New York, 2001, pp. 383–414.
122. E. S. Matsuo and T. Tanaka, *Nature (London)* **358**, 482 (1992).
123. M. Snowden, *Science Spectra* **6**, 32 (1996).
124. M. Snowden, M. J. Murray, and B. Z. Chowdry, *Chem. Ind.*, 15 July, 531 (1996).

LAURIER L. SCHRAMM
Saskatchewan Research Council

COLORANTS.

See Volume 2.

COLORING PROCESSES.

See Volume 2.

COMBINATORIAL METHODS FOR POLYMER SCIENCE.

See Volume 5.

COMPOSITE FOAMS

Introduction

Foams or cellular materials are materials that have a regular arrangement of cells and solid struts as shown in the schematic in Figure 1. *Composite polymer foams* are materials defined as a polymer phase with voids and an additional solid or hollow phase distributed throughout the polymer. They can be thought of as conventional single-phase polymer foams with an additional dispersed solid phase. Thus, the term *composite foam* excludes conventional, single-phase foams made by expanding polymers such as polystyrene, polyurethane, or polypropylene (see CELLULAR MATERIALS; MICROCELLULAR PLASTICS). Also excluded are structures with single-phase core materials and covered with a solid skin because the second phase, the skin, is not dispersed throughout the polymer phase. The fact that voids are engineered into the material results in the most attractive feature of foams, namely low density leading to high specific properties.

Composite foams can be categorized as follws: syntactic foam, particle-reinforced foam, and fiber-reinforced foam. The additional solid constituents are incorporated to enhance certain properties important to the function of the composite foam part such as stiffness, strength, electrical or thermal conductivity, etc. Examples of foams containing particles or fibers are shown in Figures 2**a** and 2**b**. Figure 2**a** shows tungsten particles in polystyrene foam (1), while Figure 2**b** shows Kevlar fibers in a poly(vinyl chloride) foam (2). A syntactic foam is a special type of particle-reinforced foam where the reinforcing particle is hollow. In this case, the additional dispersed solid phase also contains void. Figure 3 is a photograph of Lockheed's Deep Quest submarine, which shows extensive use of a composite foam; a syntactic foam material made from micrometer-sized, hollow glass microballoons (MB) in an epoxy matrix (3). The deep submersible vehicle Deep Quest was designed, built, and operated by Lockheed Missiles & Space Co. Its broad program of research was available to both commercial activities and the U.S. Navy. Deep Quest was launched in June 1967, and it operated from Lockheed's laboratory in San Diego. Deep Quest held the record, for a time, of diving to 2700 m. The submersible was designed and equipped for a variety of missions, including salvage, seafloor survey and inspection, and other special assignments. Deep Quest made its last dive on 9 September 1980.

In this article, we review the processing, characterization, properties, and applications of composite foams and highlight the advantages they have over traditional single-phase foams.

General Characteristics of Foams. Foams, in general, and composite foams, in particular, can provide interesting combination of physical and mechanical properties. Among these are the following characteristics:

(1) Very low density: the density is significantly decreased by the presence of cells containing gas
(2) High specific stiffness and compressive strength, ie, stiffness and strength divided by density: these can be further improved via sandwich construction (two dense faces and a foam core)

Encyclopedia of Polymer Science and Technology. Copyright John Wiley & Sons, Inc. All rights reserved.

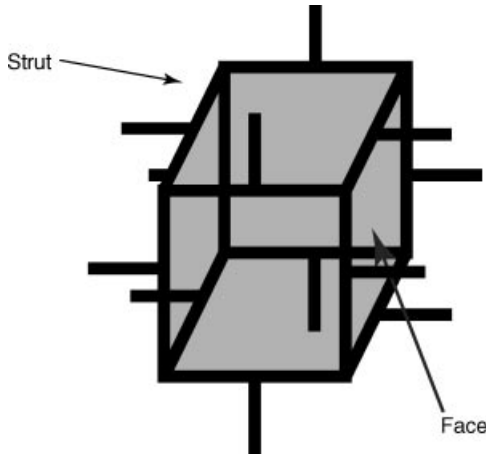

Fig. 1. Construction of a single cell making up a foam.

(3) Excellent energy absorption characteristics
(4) Noise and vibration control

Processing and Microstructure

The processing of composite foams is done in much the same way as the processing of single-phase foams and can be classified under the broad categories of

(1) Introduction of a gas
   a. Physical blowing agent
   b. Chemical blowing agent
   c. Mixing

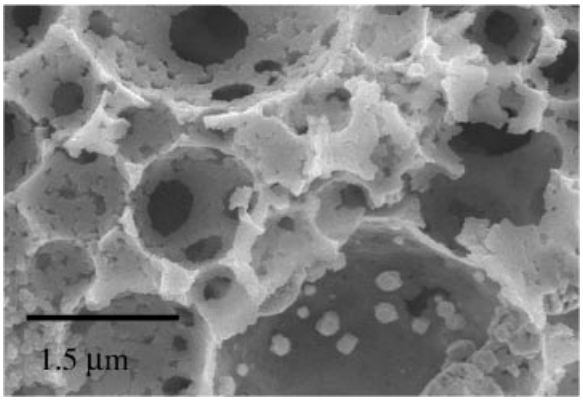

Fig. 2. SEM image of tungsten particle reinforced polystyrene.

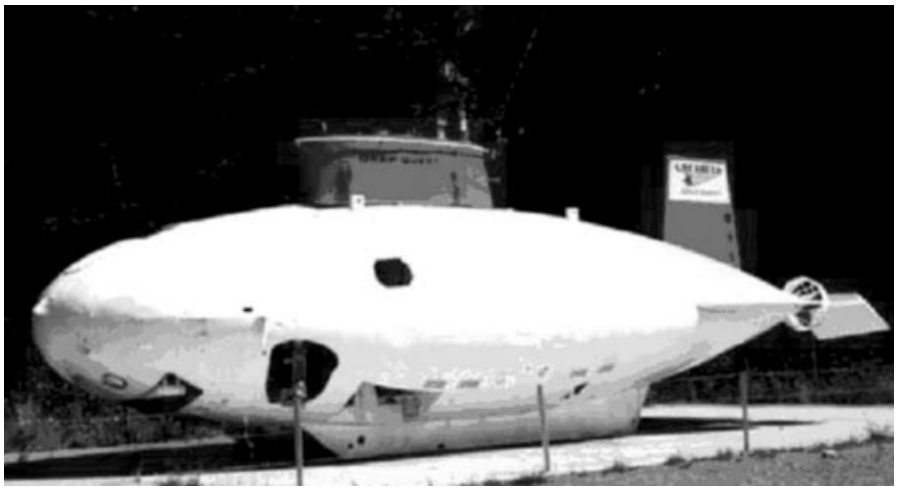

Fig. 3. The Deep Quest submersible made by Lockhead for U.S. Navy made extensive use of hollow glass microspheres/epoxy syntactic foam. Courtesy of Naval Undersea Museum, Keyport, Wash.

(2) Removal of sacrificial cell-forming material
(3) Bonding together of spheres, powders, fibers, etc

It is important to remember that the objective of processing a material into foam material is to intentionally introduce voids in the finished material. The size and distribution of the voids will vary depending on the process chosen, which in turn will control the material properties. Below, we provide highlights of each of the three processing methods with examples, advantages, and disadvantages.

The first method is to introduce gas into the composite material while the material is solidifying or curing. In case of the starting polymer matrix material being a thermoset, one should be able to control the degree of cure, while in the case of a thermoplastic there must be careful control of the temperature during the foaming process.

A *physical blowing agent* is a material that undergoes vaporization during processing. Examples of this are hydrochlorofluorocarbons and pentane. Also included in this category are gases such as nitrogen and carbon dioxide, which dissolve into the polymer material under high pressure. When the pressure is released, the dissolved gas comes out of the solution, blowing the polymer into a foam.

Chemical blowing occurs through (*1*) decomposition of a chemical additive to the polymer or (*2*) when using a thermosetting matrix, one of the reaction products is in the gaseous phase. A well-known example is a "hydrogen-blown" polydimethylsiloxane (PDMS) reinforced with silica as shown in Figure 4, and the simplified chemistry of which is shown in Figure 5.

The actual chemistry involved in making the foams is very complex and involves several molecular weight PDMS reactants in addition to cross-linking agents and tin octoate catalyst. Another example of a chemically blown foam

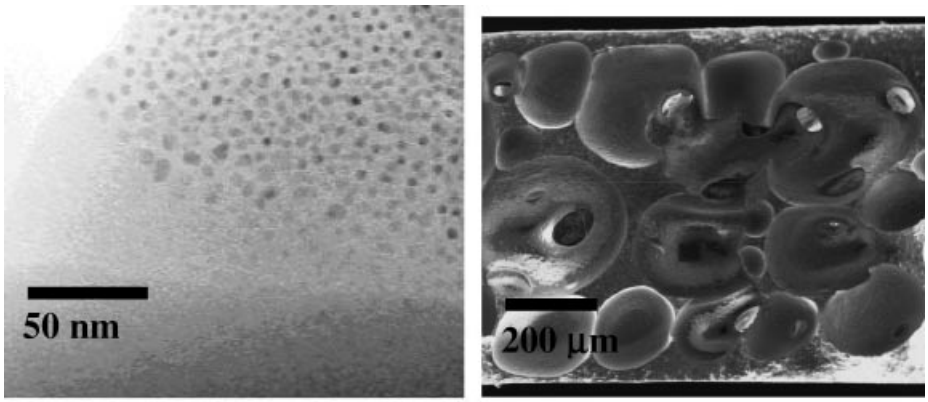

Fig. 4. (**a**) TEM micrograph showing the silica reinforcement in a PDMS matrix; (**b**) SEM micrograph of the structure obtained from a silica-reinforced PDMS hydrogen-blown foam.

occurs in the polyurethane material which can generate CO_2 as a product of the curing reaction. Another interesting chemically blown material occurs in manufacturing hollow phenolic microspheres, a material extensively used as a component in syntactic foams. The patent (4) identifies many examples of chemical blowing agents that decompose and blow individual polymer droplets into hollow structures. Included are carbonates, sulfites, nitrates, and bicarbonates.

When a chemical blowing agent evolves from a cross-linking reaction, careful control is required of the rheological properties of the polymer and kinetics of the reaction generating the blowing agent. If the gas evolves and the resin does not have a high enough viscosity, the foam will be overblown and collapse. The interplay among the reinforcement, viscosity, and gas generation also has direct effect on the cell size in the finished structure.

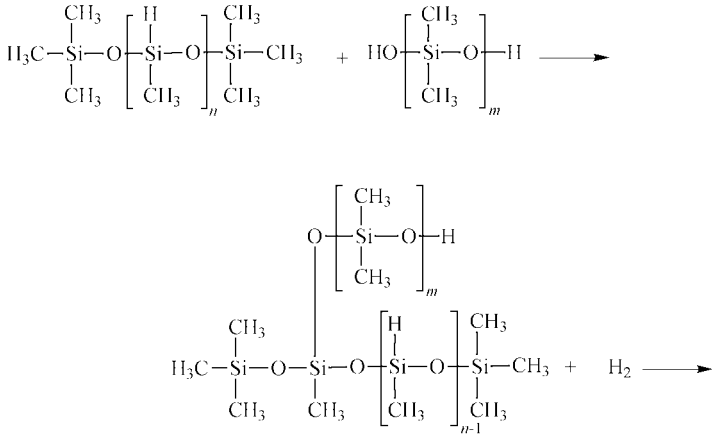

Fig. 5. Chemical reaction illustrating the chemistry involved in a hydrogen-blown PDMS foam.

Mechanical mixing or stirring is another way of introducing voids into a material. It is easy to achieve, but very difficult to control, the type, size, distribution, and volume fraction of voids. The procedure involves vigorously stirring the polymer melt, thus entraining air.

Removal of sacrificial material is an excellent method of ensuring cell size uniformity; however, in order that the method be suitable for manufacturing, a very high volume of sacrificial material must be introduced into the material so that the porosity approaches 100% open-celled. This allows for removal of the sacrificial material in a reasonable time period. A common foam prepared by this method is silica-reinforced PDMS. The PDMS in this case starts out as a gum (high viscosity polymer), and urea prills with dimensions of the desired cell size are introduced by milling. Once a high enough loading of the urea prills is achieved to ensure an open cell structure, the material is molded into the desirable geometry and cured. At this point the composite foam contains the cross-linked PDMS polymer matrix, silica reinforcement, and the sacrificial urea prills. Urea, being soluble in water, is then leached out by placing the part in a water bath. The leaching process can be accelerated if the bath is agitated. A drawback of this method is that the leaching process is efficient only for thin cross sections. Figure 6 shows a silica/PDMS foam from which the urea particles have been leached out.

The last category is the bonding together of spheres, powders, and fibers. This is a broad category that encompasses syntactic foams and frit-type material.

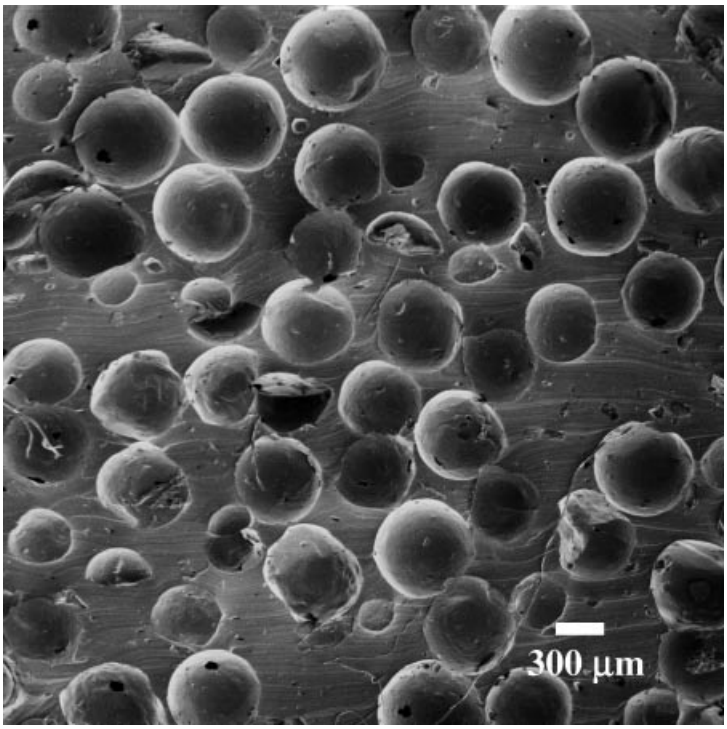

Fig. 6. TEM micrograph showing a silica/PDMS foam from which the urea particles have been leached out.

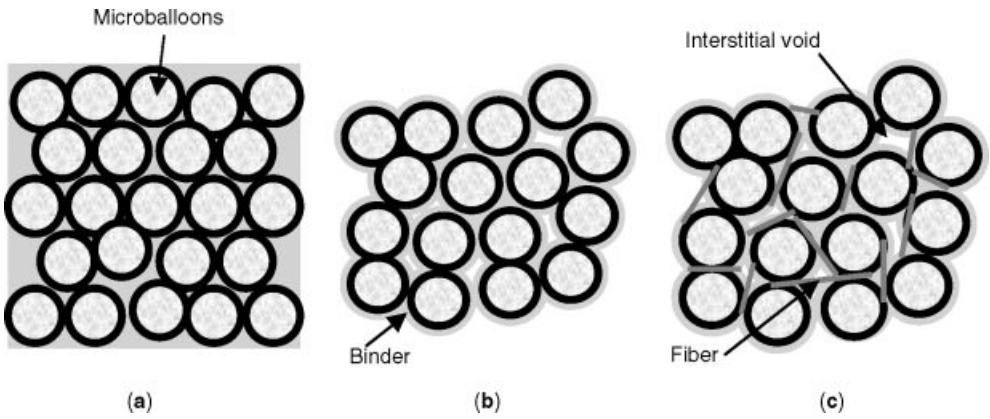

Fig. 7. Schematic structures of different syntactic foams: (**a**) two-phase foam, (**b**) three-phase foam, and (**c**) four-phase foam.

Syntactic foams consisting of hollow spheres distributed in a matrix have become quite important. The word *syntactic* comes from Greek, meaning "to arrange parts together in a unit." Typically, the resin matrix phase in syntactic foam has a large amount of open, interstitial voids. Strictly speaking, the matrix can be a polymer, metal, or ceramic. The polymer matrix can be epoxy, phenolic, ester cyanate, bismalemide (BMI), etc. Hollow spheres range in size from hundreds of nanometers to a few millimeters. When the hollow spheres are in the micrometer-size range, they are commonly referred to as *microballoons*. They may consist of glass, carbon, metal, polymer, or ceramic materials, although most commonly hollow glass microspheres (20–200 μm) are used. The microballoons can be mixed in a polymer either in a liquid or in a solid powder form. By far, the most common syntactic foam is the glass microballoon/epoxy matrix material.

Syntactic foams can be further subdivided into two-, three- or four-phase foams. The microstructure of a two-phase foam has only the polymer binder and hollow microspheres (see Fig. 7**a**). Note that there is enough binder phase to fill the volume between microspheres. In contrast, in a three-phase material there is not enough binder volume to fill the spaces between microspheres (Fig. 7**b**). The voids in the binder constitute the third phases. Of course, fibers can be added to make the fourth constituent in the composite foam (Fig. 7**c**).

A schematic of the processing of a syntactic foam by mixing carbon microballoons in a BMI polymer binder is shown in Figure 8. Short fibers can be added along with the microspheres. The addition of fibers can lead to an increase in mechanical properties, but good dispersion in the binder can be difficult (5–13). Figure 9**a** shows an optical micrograph of syntactic foam consisting of carbon microballoons and a small amount of BMI resin, while Figure 9**b** shows a higher magnification SEM micrograph wherein individual microballoons can be distinguished. The volume fraction of resin in this syntactic foam is about 8%.

Syntactic foams are an attractive design option because they are relatively simple to make. Since the microballoons are hollow, the voids are inherently present and all that is required is to mix the microballoons into the desired polymer matrix. Phenolic microballoons, produced by Asia Pacific Microspheres, and Glass

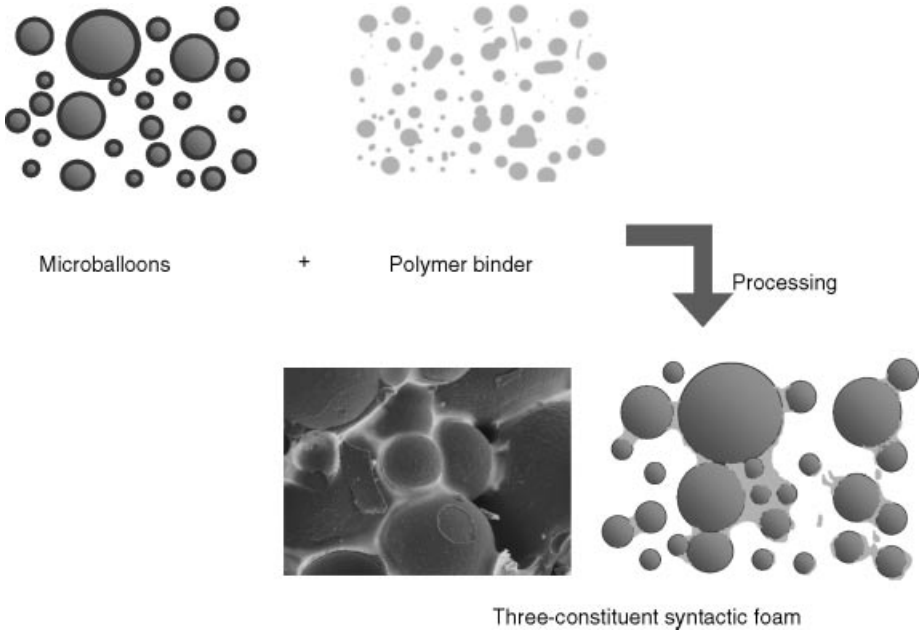

Fig. 8. Schematic of the construction of a three-phase syntactic foam (14).

Microbubbles, produced by 3M, are examples of microballoons that are readily available commercially.

Cell Size. The cell size is an important microstructural parameter. Properties of composite foam depend on the cell size. Typically, one examines the cell structure in two-dimensional micrographs. The average diameter of a circular segment, d, can be obtained by taking the average of nominal cell diameters in a given micrograph. It is important to recognize that the average spherical diameter D is greater than the average circular segment diameter d obtained from a

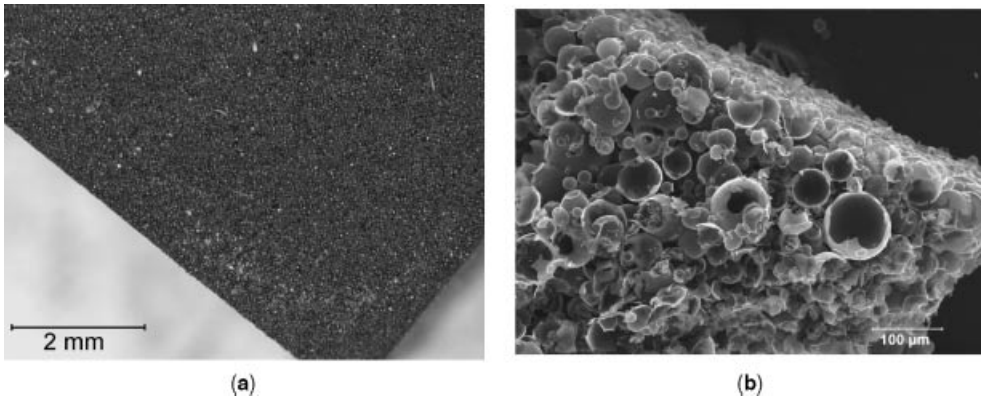

Fig. 9. (**a**) Low magnification optical micrograph showing bulk structure; (**b**) SEM micrograph showing individual carbon microballoons/BMI syntactic foam (14).

two-dimensional micrograph. This is because the cells are randomly truncated along the depth. The ASTM standard D3576 gives the following expression relating d to D:

$$D = \frac{4d}{\pi}$$

It should be pointed out that three-dimensional images can be obtained by computer-tomography technique, which provides cell size and distribution in three dimensions.

Properties

Some foam characteristics are present in both a single-phase foam and a composite foam. For example, both can be classified as either closed-celled or open-celled. If there is material forming the cell wall then it is classified as a closed-cell foam, while an open-celled foam has a discontinuous cell face as shown in Figure 1. They can be rigid or flexible and come in a wide range of densities.

Density. The density of a composite foam material, ρ_f, can be related to the density of the constituents and the void volume fraction by a simple rule of mixtures equation:

$$\rho_f = \frac{m_1 + m_2 + m_3 + \cdots + m_i}{V_f}$$

where m is the mass of constituent 1, 2, 3 ... i, respectively, and V_f is the bulk volume of foam that can usually be measured directly or calculated by the following equation:

$$V_f = V_v + V_1 + V_2 + V_3 + \cdots + V_i$$

where the subscript "v" indicates void and the other symbols are as indicated above.

Because, in a syntactic foam, the reinforcing microballoons can have a wall thickness that varies from batch-to-batch, one can achieve a fixed density foam with various volume fractions of microballoons. The tap density of microballoons that have been made from the same material is an indirect measure of the wall thickness. Assuming that the particles arrange into the same packing factor (settle to the same volume fraction), the wall thickness increases as the tap density increases. Additionally, average dimension of microballoons and ratios of wall thickness to radius can be inferred. Despite the comparative nature of the tap density test, it is an important technique to characterize microballoons and using it can provide an extra degree of freedom in designing syntactic foams. It is the authors' observation that phenolic microballoon manufacturers can control the tap density to ± 0.002 g/cm^3.

Relative Density. One very important parameter in regard to any kind of foam is its *relative density* ρ_r, which is defined as the ratio of the foam density ρ_f

to the theoretical density of the solid material, ρ_s:

$$\rho_r = \frac{\rho_f}{\rho_s}$$

As the relative density ρ_r of the foam increases, its cell walls become thicker. According to Gibson and Ashby (15), above a relative density of about 0.3, there occurs a transition from an open-cell foam to a closed-cell foam. In engineering practice, the parameter relative density, ρ_r, becomes very useful because it is easy to determine:

$$\rho_r = \frac{\rho_f}{\rho_s} = C\frac{t}{D}$$

where ρ_f is the density of the foam, ρ_s is the density of cell wall material, C is a constant, t is the cell wall thickness, and D is the cell diameter. Almost all properties of foam are affected by and are a function of its relative density. Typically, the stiffness and strength increase with increasing relative density.

In the case of a syntactic foam, at a constant volume of fraction of microballoons, a higher relative density implies a higher aspect ratio (wall thickness/diameter) of the microsphere.

Dielectric Constant. The dielectric constant of a syntactic foam generally decreases linearly with decreasing relative density. Some silica microspheres have very low dissipation factors, which makes them suitable for low loss syntactic foams suitable for applications in radomes. Radomes require minimum absorption of electromagnetic energy (16).

Elastic Constants. A number of expressions are available in the literature giving the elastic constants of the foam in terms of the elastic constants and volume fractions of the constituents. Following expressions are due to Nielsen (17):

Shear modulus of the foam,

$$G_F = \left(\frac{1 + AB\phi_2}{1 - B\psi\phi_2}\right)G_1$$

where

$$A = \frac{(7 - 5\nu_1)}{(8 - 10\nu_1)} \quad B = \frac{\left(\frac{G_H}{G_1} - 1\right)}{\left(\frac{G_H}{G_1} + A\right)} \quad \psi \approx 1 + \left(\frac{(1 - \phi_2)}{\phi_M^2}\right)\phi_2$$

In these expressions, G is shear modulus, a and b are respectively the inner and outer radii of the microballoon, ν is Poisson's ratio, ϕ_m is the maximum packing factor that can be achieved, and ϕ_2 is the volume fraction of microballoons. The maximum packing factor, ϕ_m, is about 62.5% (18). The subscript H, S, F, and 1 indicate the hollow sphere, the solid sphere, the foam, and the polymer matrix, respectively. The shear modulus can be converted to Young's modulus by

the following equation valid for isotropic materials:

$$E = 2G(1 - \nu)$$

In general, such equations due to Nielsen or others show a decrease in the modulus or stiffness of the foam with increasing amount of microspheres, assuming a constant wall thickness of the microspheres.

The above analytical model will give a reasonable approximation when designing a syntactic foam material. There are examples of more complicated numerical models available throughout literature if more detailed analysis is desired. We refer the reader to Gibson and Ashby (15) for analytical relationships for elastic properties for both open- and closed-celled foam that are based on the properties of the unfoamed material and relative density of the foam.

Stress–Strain Behavior in Compression. A representative schematic of the compressive stress–strain behavior of an elastic–plastic foam under uniaxial compression is shown in Figure 10. The curve shows a series of regimes. The first regime occurs at small strains and is characterized by elastic bending of struts. The long plateau region at medium strains is plastic yielding of the material. The final regime is densification, where the slope of the stress-strain curve increases rapidly. In this region, cells are collapsing, ie the top of the cell is touching the bottom. In this type of foam (eg polyurethane) full densification can occur and the slope of the stress–strain curve will approach the modulus of the unfoamed material. In practice, mechanical response of such a part in service depends on the amount of compression the part undergoes when installed.

When a brittle composite foam is deformed in compression, the following common features are observed:

(1) Density changes when a cellular material is deformed.
(2) Plastic deformation occurs, which involves successive collapse of cells in localized bands.

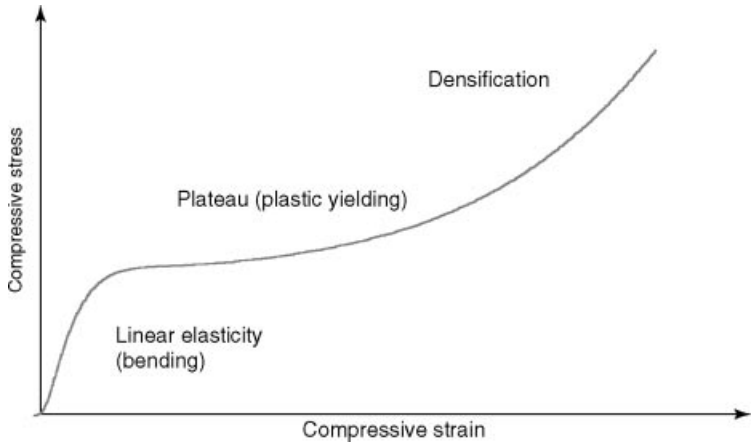

Fig. 10. Generalized compressive response of an elastic–plastic foam.

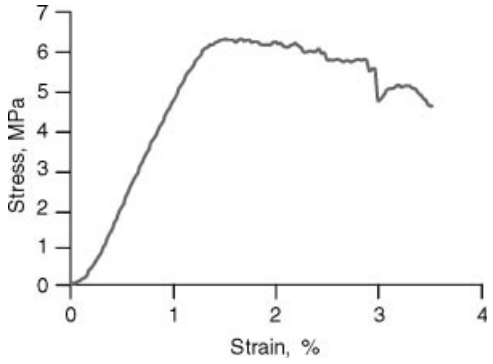

Fig. 11. Compressive behavior of a crushable carbon microballoons/BMI syntactic foam (14).

(3) Stress drops and becomes almost constant when only few noncollapsed cells are left.

An example of crushable syntactic three-phase foam (microballoons undergo crushing) compressive stress versus apparent strain of a carbon microballoon/BMI, is shown in Figure 11. After an initial elastic compression, the microspheres in the foam start fracturing and the stress–strain curve starts to decrease and shows characteristic dips corresponding to isolated crushing of microballoons. Eventually, enough microballoons are broken along a section so that exfoliation or spalling occurs, which is indicated by the large dip in the curve. Continued loading in compression leads to a gradual decrease in the curve and loading of the fractured material that formed the walls of the microballoons.

The behavior of the same syntactic three-phase foam as above under compressive cyclic loading is shown in Figure 12. In the elastic regime, the loading and unloading curves coincide, as expected, and no permanent set or damage results. This figure also shows that when unloaded after attaining the crushing strength

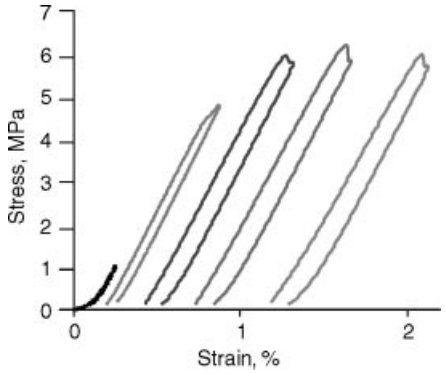

Fig. 12. Mechanical response of a crushable syntactic foam under compressive cyclic loading showing permanent damage on (——) cycle 1,770 MPa; (▬▬) cycle 6,700 Mpa; (▬▬) cycle 11,626 MPa; (▬▬) cycle 13,612 MPa; (▬▬) cycle 17,597 MPa.

of some microballoons, there results a permanent damage. The magnitude of this permanent damage stabilizes with continued cycling.

The strength of two-phase syntactic foam composites will decrease with decreasing content of hollow microspheres. This is due to two factors: a decreased load bearing cross-sectional area and a stress concentration effect of the microporosity. One can combine these effects in the following form (19):

$$\sigma_1 = k \cdot \sigma_m(1 - V_v) \tag{1}$$

where σ_1 is the strength of the foam, σ_m is the strength of the matrix, V_v is the volume fraction of the porosity or voids, and $1/k$ is the stress concentration factor. This expression should give a reasonable approximation when the strength of the microballoon is negligible compared to the matrix surrounding it and applies to two-constituent syntactic foams. The reinforcing effect of these microballoons can be expressed as

$$\sigma_2 = (V_{mb} - V_v)\sigma_{mb} \tag{2}$$

where σ_2 is the strength contribution due to the microballoons, V_{mb} is the volume fraction of the material that forms the microballoons, V_v in the volume fraction of the voids, σ_{mb} is the strength contributed by the material that forms the microballoons. Combining equations 1 and 2, we can write

$$\begin{aligned} \sigma_c &= \sigma_1 + \sigma_2 = k \cdot \sigma_m(1 - V_v) + (V_{mb} - V_v)\sigma_{mb} \\ \sigma_c/\sigma_m &= k(1 - V_v) + (V_{mb} - V_v)\sigma_{mb}/\sigma_m \\ &= k - (k - V_{mb}\sigma_{mb}/\sigma_m)V_v \end{aligned}$$

This expression indicates the expected trend of decreasing strength with increasing void volume fraction in the composite foam. Okuno and Woodhams observed reasonably good agreement with experimental results when an appropriate choice was made of the stress concentration factor k.

In three-phase composite foams, shown in Figure 9**b**, the compressive strength and modulus increase with increasing content of microballoons. In three-phase syntactic foams, where very little polymer binder is present, the strength of the microballoon can contribute to the syntactic foam strength. This is in contrast to a two-phase syntactic foam, where increasing microballoon content results in a decrease in density by the addition of microballoons. Unlike the two-phase foam, in a three-phase syntactic foam an increase in the volume fraction of microballoons will result in a decrease in the interstitial voids and increase in mass because of the increase in total cell walls.

Flammability, Smoke Density, and Toxicity. Along with the conventional mechanical and physical characteristics (stiffness, strength, toughness, density, thermal conductivity, etc), one needs to consider flammability, smoke density, and toxicity of the foam. This set of characteristics is commonly referred to as FST. By far, one of the most important applications of syntactic foams is for building material in deep-sea vehicles (see Fig. 3). Before the introduction of syntactic foams in subsea applications, liquid paraffins lighter than water, such as gasoline, were used to provide the needed buoyancy. Fire hazards, poor

compressive strength, and thermal contraction are the main disadvantages of such materials (20).

Today, using syntactic foams can result in significant improvement in mechanical performance while retaining FST properties comparable to conventional polyurethane foam.

Applications

An important point to recognize is that in most cellular materials, there is always a trade-off between the requirement of a low density and strength required to bear a certain load. This is particularly true for applications involving buoyancy where syntactic foams have been in use since the 1970s. With increasing depth in water, the hydrostatic pressure increases. This requires a syntactic foam with higher strength. The additional strength is obtained by increasing the density of the foam, which means a loss in buoyancy. Below, we give some examples of applications of composite foams.

Buoyancy-Related Subsea Applications. Offshore exploration of oil and gas requires insulated pipelines in order to prevent formation of waxes and hydrates (21). If the temperature of the pipeline drops too low, the heavy fractions in the crude oil can turn waxy. Natural gas can form hydrates. Both of these products can result in the clogging of the pipeline. Syntactic foams are suitable insulating materials for such buoyancy-related applications in deep water because of their higher compressive strength compared to that of conventional foam. Examples of such applications include buoys and floats, and submarine void filler for encapsulating instruments.

Two characteristics that make syntactic foam an efficient buoyancy material are high compressive strength and low density. The low density of the syntactic foam allows buoyant lift to be designed into the insulation system. As an example, Cuming Microwave Corporation makes a series of syntactic foams (low loss dielectric as well as treated lossy materials), which are ultralight and high strength and can be adjusted to specifications. These materials are available in different forms: uncured, pack-in-place, cured sheet, and molded to shape. The pack-in-place variety has the consistency of a snowball, which can be readily packed into complex shapes.

Elastic Compression. Any syntactic foam under hydrostatic pressure will undergo some elastic compressive strain. This will result in a loss of some of its buoyancy. We can write the following relationship from the theory of elasticity:

$$\sigma_{\mathrm{p}} = K \frac{\Delta V}{V}$$

where σ_{p} is the hydrostatic pressure, K is the bulk modulus, and $\Delta V/V$ is the change in volume per unit volume, ie the volumetric strain of the material (in the present case, it is the syntactic foam). For an isotropic material, there exists the following relationship among the bulk modulus K, Young's modulus E, and

Poisson's ratio ν:

$$E = K/[3(1-2\nu)]$$

A typical value of Poisson's ratio for a syntactic foam is 0.15, which would give the Young's modulus to be about $2K$, or K is about $E/2$. Typically, the upper limit on volumetric strain under service conditions is between 1 and 2%, which corresponds to about 65–70% of the critical stress corresponding to the onset of collapse or crushing of foam. This loss of buoyancy will be instantaneous upon the application of hydrostatic pressure.

Water Absorption. Typically, the surface of syntactic foam has microscopic cracks and voids. When immersed in water, they will absorb water because of hydrostatic pressure. Of course, even ambient moisture will get absorbed. The weight gain due to moisture absorption will result in a long-term loss of buoyancy. Typical damage to syntactic foam material is similar to that in fiber-reinforced polymers composites: swelling and debonding accompanied by a degradation in mechanical properties (11,22).

Insulation. Micrometer-sized pores in composite foams, together with their extremely low density, minimize conductive heat transfer. Addition of a small amount of fibers provides some rigidity to the foam. It is easy to visualize that a structure containing billions of cells will block convection and reflect heat energy back to its source. Excellent thermal insulating properties make such composite foams very useful in civil construction as well as in refractory applications.

EMI Shielding. Syntactic foams based on carbon microballoons or silver-coated ceramic microballoons can be used for shielding against electromagnetic interference (EMI) (23). Such syntactic foams can provide the requisite electrical conductivity at very low density, thus avoiding the weight penalty imposed by conventional EMI shielding techniques.

Biomedical Applications. Although applications of composite foams in biomedical area are not commercialized as yet, there is very active research into these materials as porous bioresorbable composite foams for applications as scaffolds in tissue engineering. A thermally induced phase separation technique was used to prepare foams of poly(lactide-*co*-glycolide) (PLGA) that contained up to 50 wt% bioactive glass particles. These composite foams showed well-defined, oriented, and interconnected porosity. An interesting result of this work was that they could control the *in vitro* degradation behavior of PLGA foam composite scaffolds by tailoring the concentration of bioactive glass (24).

Conclusions

(1) Composite foams, a whole new class of materials, are natural extensions of conventional foams.

(2) Additional constituents are incorporated in the formulation of composite foams to improve their overall performance/properties.

(3) Syntactic foams with appropriate control of the size, morphology, and distribution of microballoons can provide a wide range of properties.

(4) Addition of particles or fibers (long or short) provides another microstructural parameter to improve strength and damage tolerance of composite foams.

(5) Composite foams find a wide range of applications: offshore exploration of oil and gas, shielding against electromagnetic interference (EMI), thermal and acoustic insulation, damping, cores in sandwich construction, etc.

BIBLIOGRAPHY

1. W. Steckle and A. Nobile, *Fusion Sci. Technol.* **43**, 301–306 (2003).
2. L. Vaikhanski and S. Nutt, *Comp. Part A, Appl. Sci. Manuf.* **34A**, 1245–1253 (2003).
3. J. J. A. DeRuntz, *J. Appl. Mech.* 23–29 (Mar. 1971).
4. U.S. Pat. (1957), to F. Veatch and R. W. Burhans.
5. C. Karthikeyan, Kishore, and S. Sankaran, *J. Reinforced Plast. Comp.* **19**, 732–742 (2000).
6. N. Gupta, C. Karthikeyan, S. Sankaran, and Kishore, *Mater. Characterization* **43**, 271–277 (1999).
7. C. Karthikeyan, S. Sankaran, and Kishore, *Mater. Lett.* **58**, 995–999 (2004).
8. E. Papa, A. Corigliano, and E. Rizzi, *Struct. Eng. Mech.* **12**(2), 169–188 (2001).
9. C. Karthikeyan and Kishore, *58th Annual Technical Conference of the Society of Plastics Engineers*, Technomic Publishing Co., Inc., Orlando, Fla, 2000.
10. C. Karthikeyan, Kishore, and S. Sankaran, *J. Reinforced Plast. Comp.* **20**, 982–993 (2001).
11. A. Corigliano, E. Rizzi, and E. Papa, *Comp. Sci. Technol.* **60**, 2169–2180 (2000).
12. M. Palumbo and E. Tempesti, *Appl. Comp. Mater.* **8**, 343–359 (2001).
13. H. Kim and C. Mtichell, *J. Appl. Polym. Sci.* **89**, 2306–2310 (2003).
14. K. Carlisle and co-workers, in *14th International Conference on Composite Materials*, San Diego, Calif., 2003.
15. L. J. Gibson and M. F. Ashby, *Cellular Solids: Structure and Properties*, 2nd ed., Cambridge University Press, Cambridge, 1997.
16. M. Puterman, M. Narkis, and S. Kenig, *J. Cellul. Plast.* 223–229 (July/Aug. 1980).
17. L. E. Neilson, *J. Polym. Sci.: Polym. Phys. Ed.* **21**, 1567–1568 (1983).
18. R. K. McKeary, *J. Am. Ceram. Soc.* **44**(10), 513–522 (1961).
19. K. Okuno and R. T. Woodhams, *Cellul. Plast.* 237–244 (Sept./Oct. 1974).
20. A. Winer, *Cellul. Plast.* **2**, 157 (1966).
21. T. Fine, H. Sautereau, and V. Sauvant-Moynot, *J. Mater. Sci.* **38**, 2709–2716 (2003).
22. V. A. Kochetkov and R. D. Maksimov, *Mech. Comp. Mater.* **32**(1), 61–70 (1996).
23. D. W. Radford and B. C. Chang, *SAMPE Q.* **24**(4), 54–61 (1993).
24. A. Boccaccini, I. Notingher, V. Maquet, and R. Jerome, *J. Mater. Sci.: Mater. Med.* **14**, 443–450 (2003).

GARY M. GLADYSZ
Los Alamos National Laboratory
K. K. CHAWLA
University of Alabama at Birmingham

COMPOSITE MATERIALS

Introduction

Composite materials are made by combining two or more materials to give a unique combination of properties. Many common materials are indeed "composites," including wood, concrete, and metals alloys. However, fiber-reinforced composite materials differ from these common materials in that the constituent materials of the composite (eg the two or more phases) are macroscopically distinguishable and eventually mechanically separable. In other words, the constituent materials work together but remain essentially in their original bulk form (apart from the thin hybrid interface between the phases).

The main component of a composite is the matrix material. The reinforcement (qv) can be fibers, particulates, or whiskers. The fibers can be continuous, long, or short. In advanced composites, the fibers (ie the reinforcing phase) are present as unidirectional strands or woven fabric and provide strength and stiffness to the composite. The matrix acts as a load transfer medium assuring rigidity and protects the fibers and the whole composite from environmental attack. Short chopped fibers and mat are used in nonstructural polymer matrix composites. In these cases the fibers provide comparatively less strength and stiffness to the composite.

Fiber-reinforced polymer matrix composites are the most common advanced composites. Early glass-fiber-reinforced composites resins were used in the 1930s to build parts of boats and aircraft. Since the 1970s, application of composites has widely increased owing to the development of new fibers such as carbon, boron, and aramids (see HIGH PERFORMANCE FIBERS). Thermosetting polymers such as epoxy, polyester, and urethane resins are, among the others, the most widely used matrices of advanced composites. (see THERMOSETS). In the 1980s the development of new, cost-effective thermoplastic polymers such as PEEK (poly-ether-ether-ketone) and PEI (Poly-ether-imides) allowed the development of a new class of high performance composites (see ENGINEERING THERMOPLASTICS, OVERVIEW; POLYIMIDES).

Thermosetting and thermoplastic matrix composites are in many ways superior materials compared to common metals and ceramic materials. Their reliability is confirmed by their large use in the aerospace industry. Mechanical advantages of polymer composites are expressed in terms of two main parameters (ie specific modulus and strength) reflecting the key role of density on the selection of high performance materials. The specific modulus E_s is defined as the ratio between the Young's modulus E and density ρ of the material. The other parameter, the specific strength (σ_s), is defined as the ratio of the ultimate strength σ_{ult} and the density

$$E_s = \frac{E}{\rho} \tag{1}$$

$$\sigma_s = \frac{\sigma_{ult}}{\rho} \tag{2}$$

Encyclopedia of Polymer Science and Technology. Copyright John Wiley & Sons, Inc. All rights reserved.

The coefficient of thermal expansion (CTE) of composite structures can be made close to zero by selecting suitable materials and lay-up sequence. Dimensional stability is, in fact, one of the key requirements that many metals cannot satisfy (owing to their higher CTE) in aerospace applications. A CTE that can be tailored for a specific application gives rise to an increased amount of design flexibility with respect to common metals. In Table 1 the relevant thermomechanical properties of common and fiber-reinforced composite materials are reported. The last three columns of Table 1 explain why specific stiffness, strength, and CTE are, among the others, the key parameters in the selection of composite materials in aerospace applications where both performance and cost are a concern. High specific performance of composite materials allows weight saving, with consequent increase in payload and fuel savings. Composite materials can be highly fatigue- and corrosion-resistant, with enhanced life and reduced maintenance costs. The following drawbacks represent limits in using polymer-based composites:

(1) The high cost of fabrication of composites for aerospace applications is still a critical issue. Today most of the effort and investment in this area is devoted toward improving processing and manufacturing techniques in order to lower costs. Medium performance composites, on the contrary, can be made using manufacturing techniques such as sheet molding compound (SMC), structural reinforced injection molding (SRIM), and resin transfer molding (RTM), in which both the cost and the production time have been consistently optimized to compete within the automotive industry.

(2) Unlike metals, fiber-reinforced composites are anisotropic, that is, their properties depend on both the fiber orientation and the lay-up sequence in the laminate. In-plane quasi-isotropic materials can, however, be made by opportune selection of a lay-up sequence (eg a $[0/\pm 45/90]_{2s}$ lamination sequence realizes in-plane equivalent properties from an engineering point of view) or when continuous random mats of fibers are utilized as the reinforcing system (this is the case in parts obtained by SRIM or RTM). In both cases, however, the fibers remain perpendicular to the third direction, and it is this drawback that renders the design procedures far more complicated and intensive than those normally utilized for isotropic materials. In other words, while monolithic materials such as aluminum require only two elastic constants to establish the stress–strain relationship in each body point for a given system of forces acting on it, composite materials require many more elastic constants. For example, in unidirectional composites (where all the fibers lay in one direction) under plane stress conditions (no out-of-plane loads) four elastic constants are required. In addition, the mechanical characterization of a composite structure is far more complex than that of a metal structure if one considers that the techniques for the evaluation and measurement of some composite properties, such as fracture toughness and compressive strength, are still debatable.

(3) The reinforcing fibers in composites offer unique properties but create complications in recycling. Thermoplastic composites have the potential of primary and secondary recycling since the reprocessing of waste can result in a product with the same or comparable properties, whereas thermoset

Table 1. Specific Modulus, Strength, and CTE of Typical Fibers and Bulk Materials.

Material	Density, mg/m^3	Young's modulus, GPa	Specific modulus, $(GPa \cdot m^3)mg$	Ultimate strength, GPa	Specific strength, $(GPa \cdot m^3)/mg$	CTE, $10^{-6}/^{\circ}C^{-1}$
Steel	7.85	200	25.5	0.38–1.79	0.048–0.23	30–51
Aluminum	2.7	70	25.9	0.09–0.572	0.033–0.21	64–71
Titanium	4.5	110	24.4	0.24–1.17	0.053–0.26	25–38
Aramid	1.44	131	91	3.6–4.1	2.5–2.85	Id:−6.0, td:180[a]
Graphite	1.78–2.15	228–724	106–407	1.5–4.8	0.70–2.70	Id:−1.8, td:30
Glass	2.58	72.5	28.1	3.45	1.34	15
Alumina	3.95	379	96	1.38	0.35	22
Unidirectional AS4 graphite–epoxy ($V_f = 70\%$)	1.64	161	98.2	2.77	1.68	Id:-3.84×10^{-2}, td:26
Unidirectional E-glass–epoxy ($V_f = 50\%$)	1.93	38.34	19.86	0.93	0.48	Id: 7.37, td: 28.62
Cross-ply AS4 graphite–epoxy ($V_f = 58\%$)	1.57	77.45	48.98	–	–	1.56
Cross-ply E-glass–epoxy ($V_f = 40\%$)	1.8	21.05	11.69	–	6	

[a] Id = longitudinal direction, td = transverse direction.

composite scraps usually are tertiary recycled (in order to recover the fibers so they can be reused in molding compounds) or essentially burned off.

(4) Repairing composite parts is a very complex process and not always accessible.

(5) Most of the effectiveness of nondestructive techniques for the inspection of metal parts (such as eddy currents, X-ray) is lost when it comes to detection of flaws and cracks in composite structures, unless appropriate modifications are made to the instrumentation hardware or the inspection procedure. Ultrasound, laser (shearography), and acoustic emission techniques are usually preferred for inspecting the crack initialization (see NONDESTRUCTIVE TESTING).

Many of the above drawbacks forced the composite industry to focus significant effort on the development of manufacturing procedures in which the fabrication process is controlled with the highest level of real-time monitoring tools. It is well established that the quality of a composite structure depends almost completely on the process quality. Controlling the manufacturing process depends, first of all, on a deep knowledge of the overall physical and chemical changes occurring within the part. Mathematical modeling then provides estimates of optimum process parameters for a given manufacturing process to produce a high quality product.

Composite Manufacturing Techniques

Composite parts are made using either thermoset or thermoplastic resins with some form of reinforcements. Techniques for manufacturing polymer matrix composites are covered in Composites, Fabrication (qv). Filament winding and robotic winding are used for making pipes and tanks. Pultrusion is used for low cost high volume productions. Autoclave processing is used when high quality panels and structures sometimes having complex shapes are required. RTM is used extensively to make small and large complex structural parts in a cost-effective manner using low cost tooling. Compression molding processes are widely used in the automotive industry for high volume production capabilities and injection molding (qv) is adopted when the production rate is a critical issue, mainly for consumer and automotive applications.

Filament winding consists of drawing resin-impregnated fibers that are wound over a mandrel. Winding patterns are decided at the design stage depending on the desired properties of the product. The winding process of a high quality pressure vessel is shown in Fig. 1.

Pultrusion is a simple, continuous process in which resin-impregnated fibers are pulled through a die to make a part. During passage through the heated die resin-impregnated yarns consolidate due to the incoming cross-linking reaction. Objects with constant cross-section and smooth finish can be obtained.

Autoclave processing is used with prepregs with lay-up realized by automated means or by hand. The assembly is vacuum-bagged in order to minimize the presence of volatile substances (responsible for void/defect growth during the

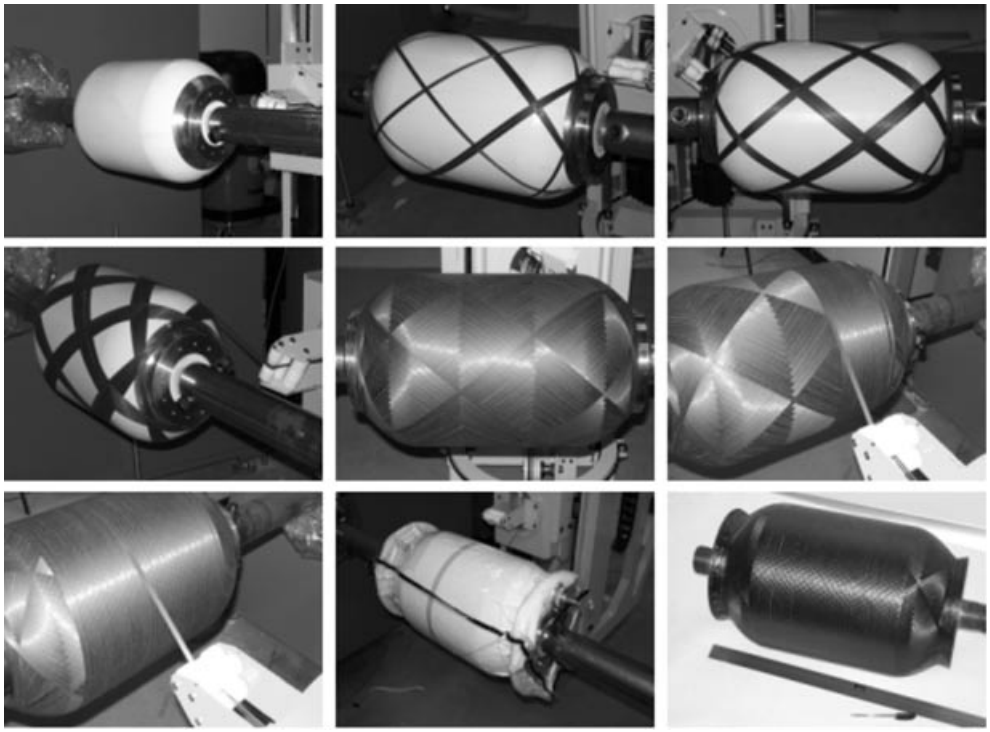

Fig. 1. Filament winding process of high composite pressure vessel. By courtesy of CIRA.

process) and placed inside an autoclave. After the process cycle, consisting, generally, of a sequence of heat and pressure inputs, the part is removed from the tool. It takes several hours generally to complete the process.

In RTM a low viscosity resin is injected under low pressure into a closed mold which contains the fiber preforms or fabrics used as reinforcements. RTM has gained increasing importance, because of its potential for making structural components (due to the use of continuous fibers) in a cost-effective manner.

Compression molding of sheet molding compounds (SMCs) or bulk molding compounds (BMCs) is typically used in the auto industry mainly because of the similarity to stamping technology. In the compression molding operation, the SMC is cut into rectangular shapes and "charged" on the bottom half of a preheated mold. The SMC covers only a part of the mold (between 30 and 90%) while the remaining surface is filled by forcing flow of the "charge" by pressure. When the mold is closed, lying down, and has a constant displacement rate (ie 40 mm/s) the upper half of the mold, the SMC, starts to flow inside the mold, filling the cavity. The molds are generally preheated to about 140–150°C.

Injection Molding (qv) has been generally used for thermoplastic materials for many years. Only during the last decade, because of the increasing demanding has it been considered and successfully applied in the thermoset industry. The mold injection, the subsequent cross-linking of the system, and the final demolding and expulsion of the part takes between 30 and 60 s; therefore this process is

particularly considered when very high volume production is requested. In some cases, using multiple-cavity molds for the consolidation of different element parts at the same time can further increase the production rate.

Many other techniques have been developed over the years. However, each manufacturing process consists of four basic steps, wetting/impregnation, lay-up, consolidation, and solidification, which in case of composites require low energy compared with those for traditional materials. In fact, composites do not have high pressure and temperature requirements for part processing as compared with metal. This is the reason why composite processing techniques such as those described above have the potential of producing complex, high strength, high stiffness, and near-net-shape structures. Therefore the applications of polymer matrix composites range from the aerospace industry to the sporting goods. Composites are the material of choice in space applications owing essentially to two factors: high specific modulus and strength, and dimensional stability. Graphite–epoxy composites are increasingly used in bicycles, sometimes allowing frames to consist of one lightweight piece, or in golf club shafts, using the saved weight in the head. Tennis and racquetball rackets with graphite–epoxy frames are now commonplace. The military aircraft industry has mainly led the use of polymer composites in structural applications while in commercial airlines the use of composites has been conservative because of safety concerns. The graphite–epoxy and aramid honeycomb tail fin of Airbus A310-300 is an example of using composites in the primary structure in commercial airlines. The weight of the tail fin was reduced by 300 kg, together with the number of parts, which decreased from 2000 to 100. Infrastructure applications of polymer composites include bridges—due to low weight, corrosion resistance, longer life cycles, and limited earthquake damage. The application of fiber glass in boats is well known even when hybrids of Kevlar–glass/epoxy are now receiving attention because of the improved weight savings, vibration damping, and impact resistance.

Today's automobile industry uses low amounts of composite parts owing to the unavailability of cost-effective manufacturing techniques. Nowadays about 8% of automobile parts are made of composites.

Process Modeling

During the fabrication process (eg RTM, autoclave, filament winding) a combination of pressure–temperature steps are applied with given histories in order to assure well-consolidated parts with minimum defects. The solidification or curing process involves a number of physical, chemical, and mechanical phenomena in the composite materials. Generally speaking, the formation of a structure due to cross-linking reactions or to the melting and consolidation of thermoplastic polymers is the macroscopic effect of heat and pressure inputs: in real terms continuous changes in degree of cure or crystallinity, gelation (the formation of an infinite polymer network as a consequence of chemical reaction) and vitrification (the passage from a molten/rubbery to a glassy state) occur. As a consequence of the above phenomena, the evolving chemical and thermal shrinkage give rise to the development of stress and strain within the part, whereas the presence

of volatiles in the form of residual plasticizing agents or unreacted resins can eventually induce void growth and resin–fiber debonding.

In all, thermal shrinkage, chemical shrinkage, time–temperature–degree of cure dependent resin properties, viscosity, and structural relaxation shrinkage are the matrix properties to control. Therefore, since the evolution of polymer properties is strongly influenced by processing history, each parameter has to be investigated at each stage of the manufacturing process. Moreover considering that the level of temperature reached during the manufacturing of composite parts does not affect the fiber content, investigations are almost always carried out on the polymer system matrix. Significant progress has been made in quantitatively evaluating process-related parameters such as mold shape, mold material and surface, void content, fiber volume fraction, lay-up sequence. However, considerable work remains to be done to account for constituent resin-related properties. In particular, when new resins are developed a number of experimental tests are necessary to completely characterize the resin (such as toughened epoxies) so as to perform a general analysis of the physical and chemical phenomena and to code it by mathematical tools.

Mathematical modeling of a manufacturing process provides a tool for the process control with minimum costs and high quality production. Typical aerospace manufacturing processes for composites are characterized by a two-step cure cycle. In such a cycle the temperature of the material is increased from room temperature to the first dwell temperature and this temperature is held constant for the first dwell period (~1 h); during this stage the material reaches the minimum value of viscosity to fill the mould and/or compact the whole system. The temperature is then increased again to the second dwell temperature and held constant for the second dwell period (~2–8 h). Post-cure reaction takes place during this second stage. Following this second dwell period the part is cooled down to room temperature at a constant rate or by air to allow the extraction from the mould. It is during the polymerization reaction that the strength and related mechanical properties of the composite are developed, together with incipient flaws (eg voids, resin–fiber debonding) and residual stresses.

The transient heat transfer phenomena induce peculiar property changes at each body point. In this respect, the temperature profiles and the chemorheological functions (viscosity, degree of cure/crystallinity) need to be included within the energy balance equation:

$$\rho C_{\mathrm{P}} \frac{\partial T}{\partial t} = \nabla(K \nabla T) + \rho \dot{Q} \tag{3}$$

where ρ is the density, C_{p} is the specific heat, t is the time, K is the thermal conductivity, and $\dot{Q}$ is the rate of heat generated either by the exothermic polymerization reaction in the case of a thermosetting matrix system or by the crystallization process for thermoplastic matrix.

From the micro-mechanical point of view, the process modeling strategies must consider simultaneous interplay of the following "intrinsic" factors: initial and boundary conditions in terms of pressure and temperature, fiber content and stacking, sequence of layers (ie ply-to-ply orientation), thermal shrinkage, chemical shrinkage, time–temperature–degree of cure dependent resin properties, and

structural relaxation shrinkage. The above factors can play a different role when an even more complex scenario arises for thick composite parts. Therefore a detailed analysis of temperature distribution during the process is crucial for the determination of the complex evolution of the properties at each material point of the composite part. A simple analogy could be made with metals in order to understand this complex scenario. The evolution of the structure for metals inevitably leads to a distribution of grain size as a result of the different temperature profiles experienced during the forming process. In the case of polymeric matrices, the same assumption can be reasonably made considering that each material point will undergo a completely different temperature profile, owing to the relative position occupied in respect to the heat source. For this reason, a thermosetting system matrix necessarily presents a distribution of polymerization reactions at each body point, according to the experienced thermal histories; in the case of thermoplastic systems, because of the strong dependency of the crystallization process upon the temperature profile, a distribution of grain size through the thickness (ie skin–core fine to coarse structure) is obtained. The temperature distribution can be suitably determined using finite element analysis (FEA) software; the temperature at a given point in the structure depends on the boundary and initial conditions, as well as the materials' properties evolution. In fact, as the evolution of the structure is highly dependent on the thermal history, within a thick composite different material properties arise at each material point.

The correct analysis then would be an investigation of the temperature distribution with appropriate boundary conditions for the determination of real temperature profile as a function of the material point. This analysis would be coupled with a structural analysis, which takes into account the whole set of constraint conditions imposed by the mould, as in the case of RTM, or any other tool for a different manufacturing process. Figure 2 illustrates the flow-chart of a generic process modeling procedure.

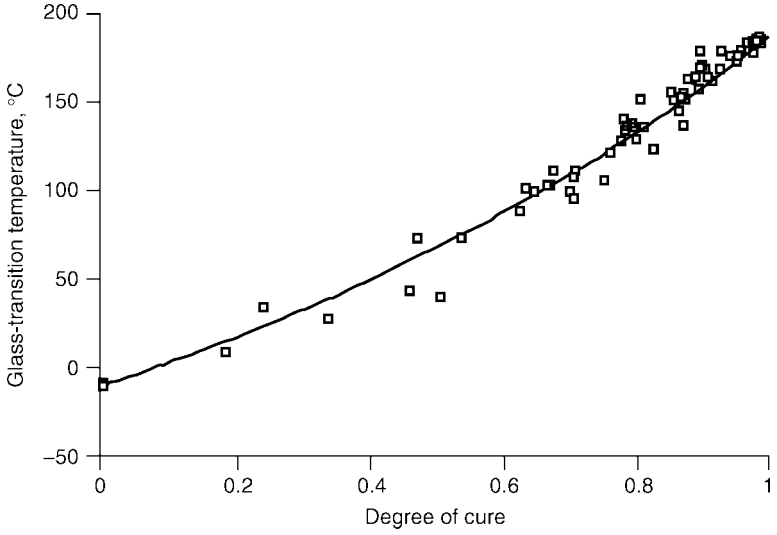

Fig. 2. Experimental data for glass-transition temperature and DiBenedetto model predictions: □, experimental data; ———, fitting model.

Different material parameters need to be quantified to be able to perform the thermostructural analysis. The complex interactions of the different phenomena occurring during the manufacturing process could be schematized as follows.

(1) Both crystallization and polymerization reactions are temperature-activated phenomena, allowing the transformation of the system from a liquid-like to an almost solid-like material. The structure evolution can be suitably monitored by a degree of conversion parameter, which follows an analytical kinetics model.
(2) Thermal (specific heat, thermal conductivity) and viscoelastic properties of the material change during the process owing to both temperature variations (as for traditional materials) and level of conversion.
(3) Variation of the specific volume can be originated by three different phenomena:
   a. thermal expansion (or contraction) due to positive (negative) temperature change,
   b. chemical/physical shrinkage due to the densification (polymerization/crystallization) of the material according to the conversion level, and/or
   c. contraction due to the thermodynamic instability associated with the nonequilibrium kinetics of glass transition (structural relaxation).

The experimental evaluation and the modeling of each contribution still represent a difficult task for many researchers, and at the same time it is the main issue for the correct prediction of

(1) the residual stress formation and warpage effect in thick composite parts
(2) voids and flaw formation, and
(3) resin flow behavior dependent compaction and consolidation feature.

Coupled with the energy equation along with the specific initial and boundary conditions, the mathematical description of the above factors (through the use of suitable submodels for a given manufacturing process) allows the complete analysis of a generic manufacturing process, providing at the same time a fundamental "tool" for the production of high quality parts.

Cure Kinetics and Glass-Transition Model

As stated above, during the cure, at each level of conversion, a thermosetting material could be assimilated to a completely new material with specific thermomechanical properties. Then, the possibility of following with a monitoring variable the level of conversion reached by the system during the manufacturing process represents an important issue.

Thermal analysis provides useful information upon which to construct an adequate kinetics model under both isothermal and dynamic temperature

conditions. The mathematical model selected on the basis of the experimental data generally represents the primary component in studies on the optimization of thermoset molding processes (resin transfer molding, reaction injection molding, prepreg cure, etc). Reliable methods are required to predict the degree of conversion and to control the evolution of the exothermic heat of reaction. Correct kinetics models are also essential to predict the evolution of the structure under more complicated temperature profiles; or to correlate the changes in thermal and mechanical properties of the neat resin through all the manufacturing processes. Thus, the knowledge of the level of conversion of the polymer matrix is fundamental information to monitor the evolution of properties. Curing raw data needed to implement the kinetics models can be obtained, by nearly standardized procedures, through isothermal and dynamic differential scanning calorimetry (DSC) tests.

There are essentially two kinetic models used to describe thermoset-curing reactions.

(1) *Phenomenological Models* (macroscopic level) assume that there is an overall order of reaction and fit this model to the experimental kinetic data. This type of model provides no information about the kinetic mechanism of the reaction and is predominantly used to provide models for industrial applications.
(2) *Mechanistic models* (microscopic level) are derived from a rather complex analysis of the individual reactions occurring during the cure, and require detailed measurements of the concentrations of reactants, intermediates, and products. Mechanistic models are much more complex than empirical models, but are not restricted by changes in the composition of the system.

Despite the efforts that have been made in recent years, in the exploitation of kinetic models for polymerization of thermosetting resin systems (see Table 1), two main problems still arise:

(1) no general model for the cure mechanisms of all systems is available (although many authors in the past have already searched for a generalized model), and
(2) in many cases, for a given resin system, different models are needed to describe isothermal and nonisothermal experimental condition.

The first problem still represents a severe limitation on the industrial application of any monitoring or control system that requires significant prior knowledge of the cure kinetics, which will affect either the time or cost of production. Acquired thermal data are generally fitted with chose kinetics equation to establish the best set of kinetics parameters to predict the conversion evolution for a generic temperature history at every location.

In Table 2, the most used kinetic equations are reported. Advances in the description of cure kinetics were recently used to model the cure of an RTM epoxy

Table 2. Mathematical Models for Cure of Resins

Kinetic model	Expression	Notes
First Order (1)	$\frac{d\alpha}{dt} = A \exp\left(\frac{E_a}{RT}\right)(1-\alpha)$ $k = A \exp\left(\frac{E_a}{RT}\right)$	k = Rate constant E_a = Activation energy A = Rate coefficient
nth order (2–4)	$\frac{d\alpha}{dt} = k(1-\alpha)^n$	n = Reaction order
Polynomial (5)	$\frac{d\alpha}{dt} = k(a_0 + a_1\alpha + a_2\alpha^2)$	a_0, a_1, a_2 = Constant
Autocatal. −1 (6,7)	$\frac{d\alpha}{dt} = (k_1 + k_2\alpha^m)(1-\alpha)^n$	n, m = Reaction orders k_1, k_2 = Rate constants
Autocatal −2 (8)	$\frac{d\alpha}{dt} = (k_1 + k_2\alpha)(1-\alpha)(B-\alpha)$	n, m = Reaction orders k_1, k_2 = Rate constants B = Stoichiometry factor
Mechanistic (9)	$\frac{\alpha}{\alpha_{gel}} = f(\text{concentration})$	α_{gel} = Conversion at gelation
Self-acceleration (10)	$\frac{d\alpha}{dt} = k(1-\alpha)(1-C\alpha)$	C = Constant

resin system by Karkans (11). The kinetics equation used can be stated as

$$\frac{d\alpha}{dt} = k_1(1-\alpha)^{n_1} + k_1\alpha^{n_2}(1-\alpha)^{n_1} \tag{4}$$

where k_1 and k_2 are kinetic reaction rate constants, having an Arrhenius temperature dependence.

$$K_{iT}(T) = k_i \exp\left(-\frac{E_i}{RT}\right) \tag{5}$$

and n_1, m, and n_2 are the model parameters and E_i ($i = 1, 2$) the activation energy.

According to the Rabinowitch theory (12) the reaction is driven by two parallel phenomena, the chemical mechanism and the diffusion-controlled mechanism, as

$$\frac{1}{k_i} = \frac{1}{k_c(T_c)} + \frac{1}{k_d(\alpha, T_c)} \tag{6}$$

where T_c is the curing temperature and k_d is the rate of the diffusion-controlled mechanism based on free volume models as proposed by Simon and Gillham (13)

in the following from:

$$k_d(T) = k_{d0} \exp\left(-\frac{b}{f}\right) \tag{7}$$

In the above equation b is an adjustable parameter to achieve a suitable fit, while the parameter f encapsulates the driving force of the diffusion-controlled mechanism by means of the Doolittle (14) equation, to model the free volume as follows:

$$f(\alpha) = (4.8 \times 10^{-4})\,[T_c - T_g(\alpha)] + 2.5 \times 10^{-3} \tag{8}$$

The diffusion-controlled mechanism occurs during vitrification in the latter stage of the reaction. It is obvious that for a chemical reaction to occur, reactive groups are required to be close to each other and also to be orientated so that eventually the cross-link can be formed. In the early stages of the cure, when the material is very much in a liquid state, the rate of cure is predominantly controlled by chemical kinetics; this essentially means that in the "reaction zone" the temperature of the system is capable of activating a reaction between monomers. Since these processes are very fast owing to the short characteristic times of the liquid state compared to the time of experimental observations, the rate coefficient for the reaction is constant at constant temperature, hence the validity of Arrhenius-type analysis. Theoretical models of this stage of the cure have been extensively discussed by Mita and Horrie (15) using a reptation theory model, and by Rozenberg (16), who also tried to determine the topological area of the reaction associated with reactive groups that are isolated within the gelled structure. Experiments have demonstrated that analytical methods are not sensitive enough to detect these unreacted groups and for this reason it is not possible to evaluate their concentration during the final stages of the curing process. It is clear then, that the overall reaction rate cannot be a function of the temperature alone, but that a dependency on a structural parameter has to be included, which at certain isothermal temperatures will lower the reaction rate, limiting the extent of the reaction.

The glass-transition temperature can be regarded as a suitable structural parameter for following the progressive evolution of the cross-linked system in case of diffusion-controlled mechanism; therefore, a suitable model is needed. The evolution of the glass-transition temperature is modeled according to a widely accepted DiBenedetto equation (17), stated as follows:

$$T_g(\alpha) = \frac{(1-\alpha)T_{g0} + \lambda\alpha T_{g\infty}}{(1-\alpha) + \lambda\alpha} \tag{9}$$

where T_{g0} and $T_{g\infty}$ are the glass-transition temperatures for the uncured and fully cured resin, respectively; λ is the adjustable parameter for a given resin system. Figure 3 reports the experimental determinate values of the glass-transition temperature along with the found model predictions.

Most of the time, the complete kinetics model can result in a multiparameter model characterized by nonunique set of best parameters. Therefore, reliable

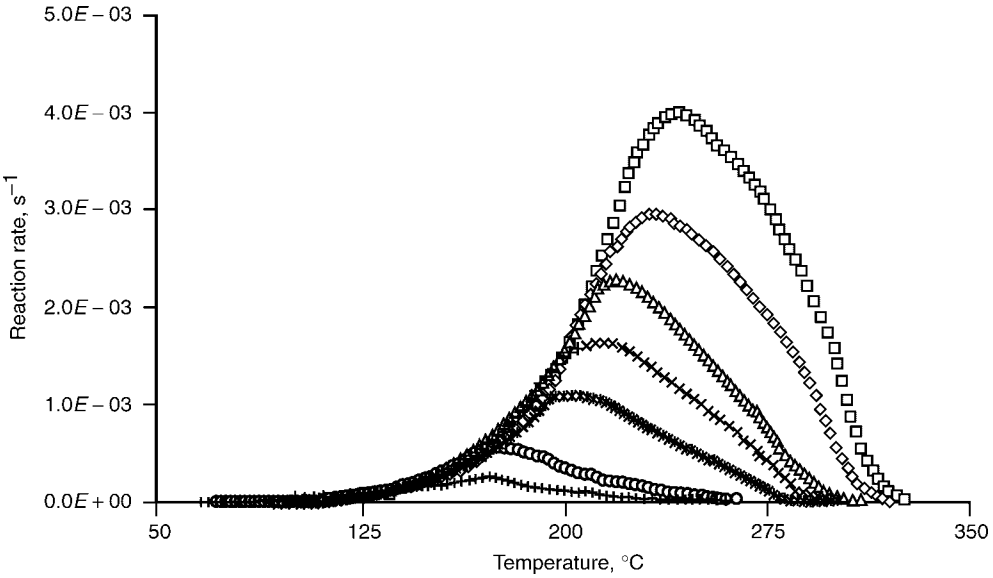

Fig. 3. Experimental reaction rate profiles obtained by DSC scans at different heating rates: □, 20°C/min; ◇, 15°C/min; △, 10°C/min; ×, 7.5°C/min; —×—, 5°C/min; ○, 2°C/min; +, 1°C/min.

fitting techniques based on nonlinear least square fitting algorithms are generally required to determine a suitable set of kinetic parameters. Along with traditional techniques, novel programming algorithm techniques, recently widely used to solve complex problems of optimization in the area of industrial engineering, are being used for kinetics model definition. Appreciable results have been achieved using a hybrid algorithm in the case of a complex empirical model characterized by 14 fitting parameters. This two-stage fitting procedure was implemented considering an "evolutionary type" algorithm (genetic algorithm) to identify the most probable region of the minimum for the least square function followed by a traditional non-linear least square method (ie Lavenber–Marquardt) to determine the precise value of each fitting parameter.

Experimental reaction rate profiles as obtained by thermal analysis tests are reported in Figure 4 for different temperature rates. Cure conversion profiles along with kinetics model predictions, respectively, for dynamic and isothermal conditions are given in Figures 5 and 6.

Shrinkage

Thermal Shrinkage. As for traditional materials, temperature variations during the manufacturing process are associated with local thermal expansion or contraction depending on the sign of the change. For thermosetting systems, it is reasonable to assume that the lower degree of cure leads to a higher mobility of the evolving cross-link structure compared with the fully cured state. Moreover, the content of free volume frozen within the structure will necessarily affect the dimensional stability of the system because of the temperature variation during

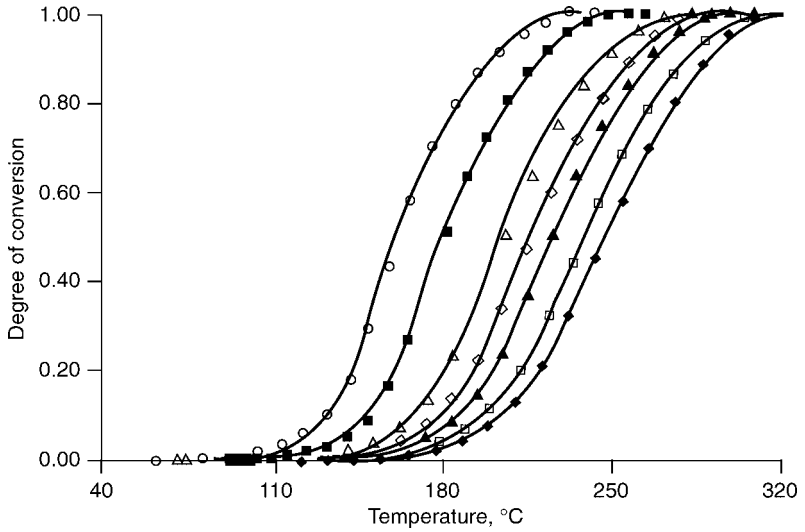

Fig. 4. Experimental matrix conversion profile and model predictions at different dynamic heating rates: ◆, 20°C · min (Exp); □, 15°C · min (Exp); ▲, 10°C · min (Exp); ◇, 7.5°C · min (Exp); △, 5°C · min (Exp); ■, 2°C · min (Exp); ○, 1°C · min (Exp) ———, fitting.

the processing. The effects of volume variation related only to temperature change are known as *thermal shrinkage*.

The evolving structure of the polymeric system can be considered as a "novel" material at each degree of cure as different thermo-mechanical properties are identified. Therefore, coefficients of thermal expansion are necessarily varying with

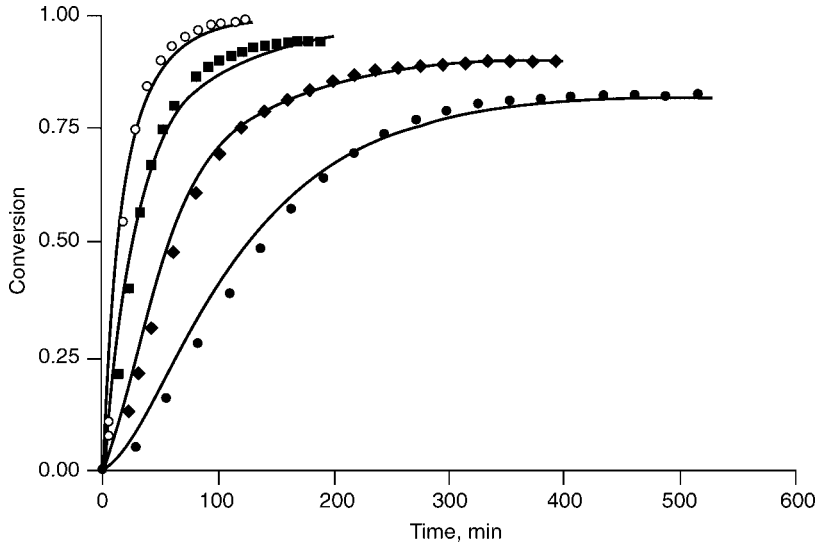

Fig. 5. Experimental matrix conversion profiles at different isothermal temperatures: ———, fitting; ○, 180°C (Exp) ■, 160°C (Exp) ◆, 140°C (Exp); ●, 120°C (Exp).

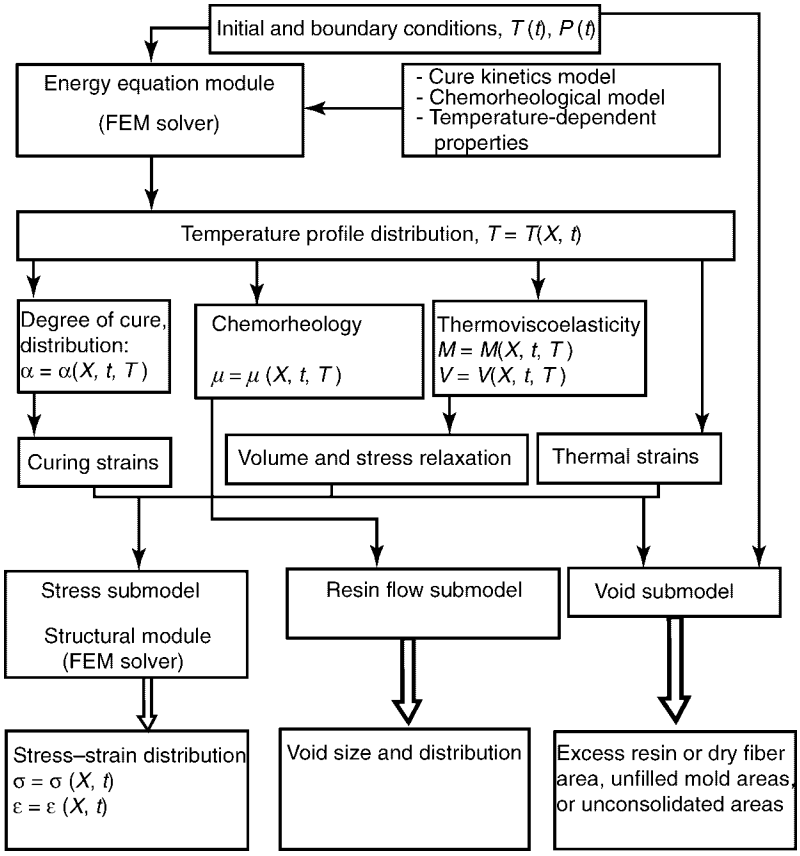

Fig. 6. Schematic flow chart for a generic process modelling sequence.

the degree of cure. A traditional technique which can be used to evaluate the coefficient of thermal expansion at various degrees of conversion is thermomechanical analysis (TMA). Two problems arise when using the TMA procedure:

(1) no test can be performed if the specimen is not solid, and
(2) post-cure reactions will affect the result above the glass-transition temperature.

Since the equipment to measure the temperature-induced dimension variation employs an LVDT displacement sensor, the requirement of a solid sample is mandatory. The effects of post-cure reaction on the measurement, instead, need much more detail and discussion. For a partially cured thermosetting resin, a post-cure reaction is expected when the actual temperature rises above the corresponding glass-transition temperature, T_g. Above this temperature, the volume variation due to post-cure reactions is superimposed upon thermal expansion (18). For this reason, TMA is a technique for measuring the CTE of the partially cured sample that is suitable only within the glassy region ($T < T_g$), while for a fully cured sample useful information can also be obtained for the CTE in the rubbery

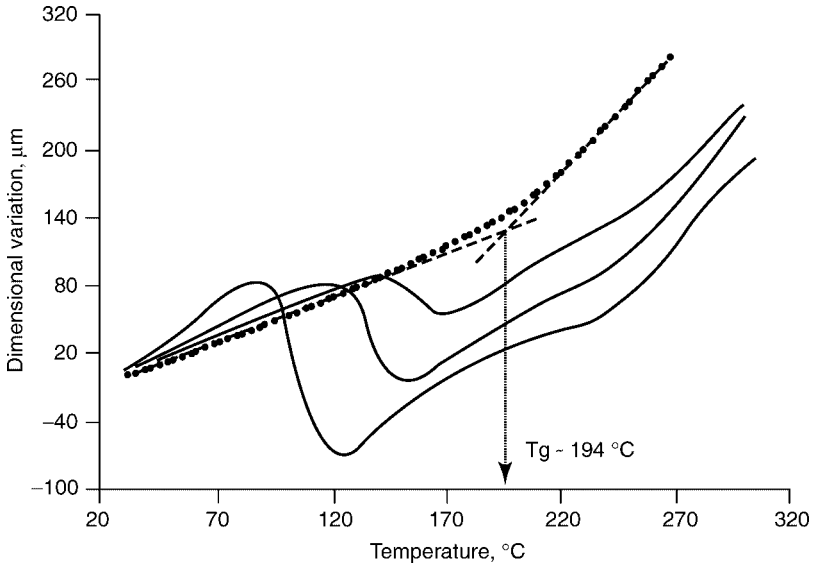

Fig. 7. Thermomechanical curve of data obtained for partially cured samples: ———, sample A; ———, sample B;——, sample C; •, sample E.

region. Figure 7 shows TMA curves for partially cured samples A, B, C, and E. In the case of sample A, when the resin approaches the glass-transition region (110°C) it softens and the measured linear dimensional change drops owing to the static holding force applied by the probe to the specimen during the test. To verify that the characteristic inflections shown by the thermomechanical curves for the partially cured samples are respectively due to the glass transition and the simultaneous effects of temperature and post-cure reaction, it seems appropriate to compare DSC and TMA curves for the same sample (see Fig. 8).

Above the glass transition, the material starts to undergo post-cure reactions, so that the linear thermal expansion is attenuated by the contemporaneous chemical shrinkage effect until the post-cure reaction is completed. At the end of the post-cure reaction, the now fully-cured system expands, only because of temperature changes. Penetration of the probe into the top of the resin specimens cannot be excluded. This further condition will be limiting for any further possible analysis of the curves at $T \geq T_g$.

The glassy coefficients of thermal expansion can then be evaluated as the slopes of the thermal volumetric strain vs. temperature curves below the glass-transition temperature (see Fig. 9), defined at the onset of the first step for each curve. For these curves, in fact, the following relationship can be written:

$$\varepsilon_V(T, \alpha) = \frac{(l - l_o)}{l} = \gamma^{CTE}(\alpha)\Delta T \tag{10}$$

where ε_V is the thermal volumetric strain, l and l_0 are respectively the final and initial sample length; $\gamma^{CTE}(\alpha)$ and ΔT are the coefficient of thermal expansion and the temperature variation. Experimental value determined for the partially cured

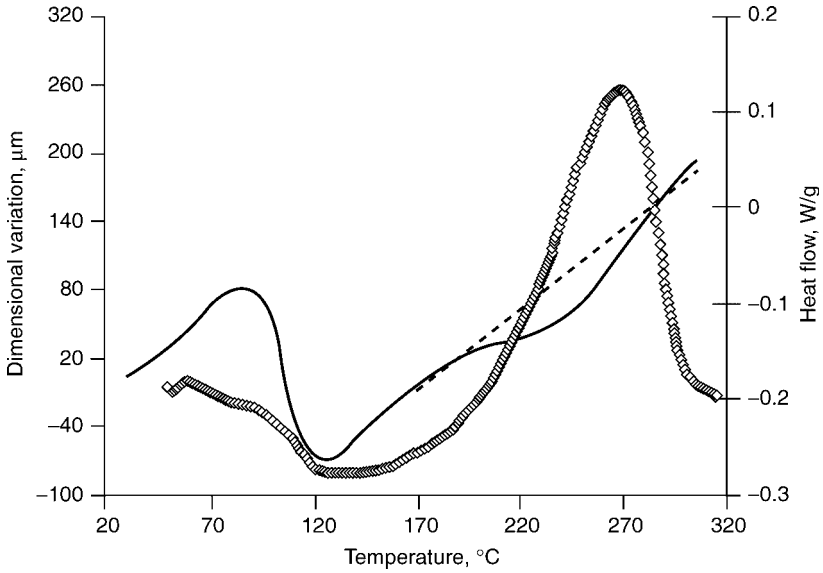

Fig. 8. DSC and TMA thermogram comparison for post-cure effects on dimensional variation: ———, sample A (TMA); ◇, sample A (DSC).

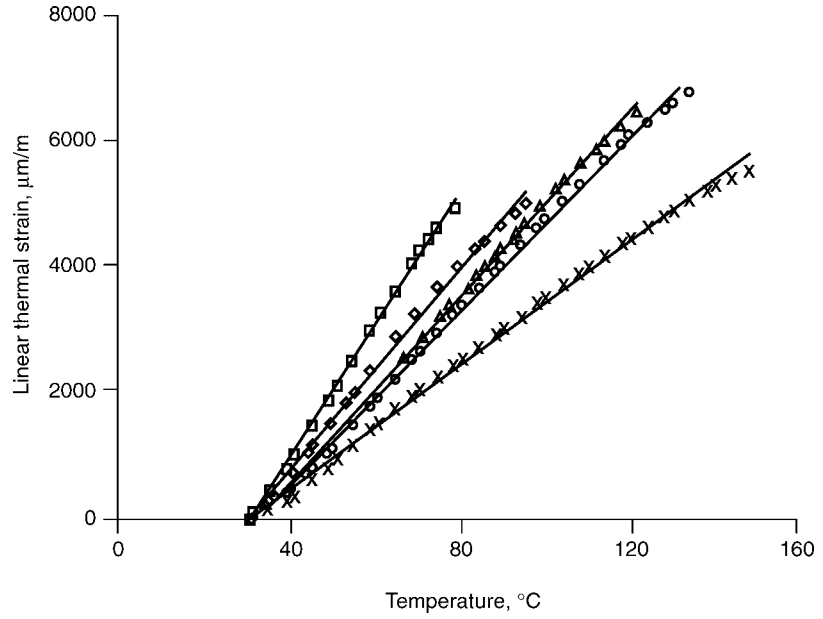

Fig. 9. Glassy CTE values vs. conversion: □, sample A; ◇, sample B; △, sample C; ○, sample D; ×, sample E.

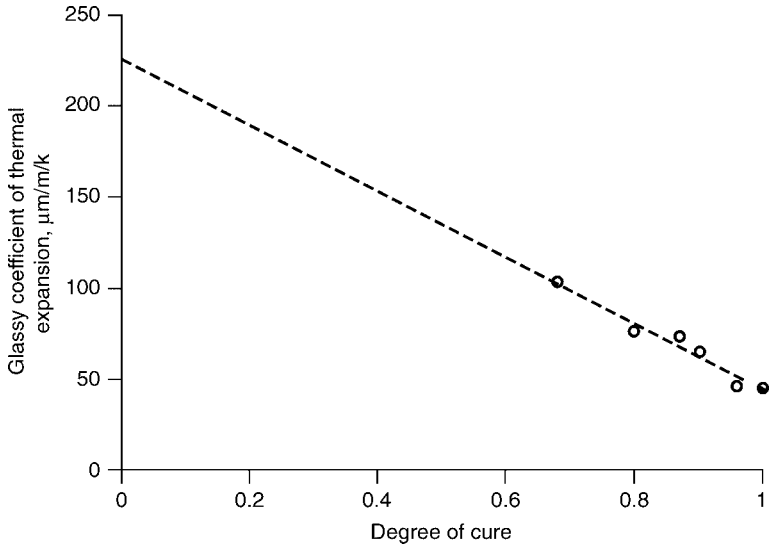

Fig. 10. Experimental values obtained for glassy coefficient of thermal expansion with linear model predictions: ○, experimental; – –, linear interpolation.

samples, $\alpha \in [0.6;1]$, are reported in Figure 10 along with a linear interpolation model.

Chemical Shrinkage. Chemical shrinkage is the result of a progressive matter densification due to the advancement of the reaction. For the resin matrix, volume variations are measured during cure for different isothermal temperatures. The results compared with experimentally determined degree-of-cure profile allow to evaluate the chemical shrinkage coefficient of the matrix system.

Thermal shrinkage is the most obvious source of the residual stresses generated during the manufacturing process of composite laminates or component parts with a polymeric matrix (19). However, other important factors contribute to setting up of residual stresses, or the warpage or poor quality of the manufactured composite part and so need to be investigated. With special reference to composites with a thermosetting matrix, chemical shrinkage comes up as one of the most important factors that need to be taken into account. In fact, organic thermosetting polymers, of the type currently used as a matrix for polymer composites, undergo volumetric changes as a result of the polymerization reaction. Typical values of volumetric shrinkage during cure are 1–5% for epoxy (20) resin and 7–10% for polyester resins (21); however, some thermoplastic polymers may exhibit some degree of crystallization as the matrix cools down from the forming temperature to room temperature, resulting in a volumetric shrinkage of 2 to 36% (22).

Table 3 reports reproducible data for volumetric shrinkage obtained from dilatometric experiments (21,22,24). Modelling of chemical shrinkage, therefore, is of particular relevance for a correct analysis. The absolute volumetric change in a cubic element can be modeled as follows: Considering the dimensions of the cube to be l_1, l_2, l_3 and their relative finite changes as Δl_1, Δl_2, Δl_3, the absolute

Table 3. Shrinkage Measurements on Epon 828 Cured with Different Curing Agents, TETA and DTA[a]

System	Gel time, min	Volume shrinkage after gelation %	Total volume shrinkage
20 phr Triethylenetetramine	116	2.31	5.72%/24 hr.
(TETA), cure at 65°C	112	2.29	5.72%/24 hr.
	110	2.34	5.79%/24 hr.
Diethylenetriamine	130	2.08	4.33 %/48 hr.
	130	2.00	4.33 %/48 hr.
	130	1.96	4.21 %/48 hr.

[a]From Ref. 23.

volume change is

$$|\Delta V^{\mathrm{r}}| = V_{\mathrm{final}} - V_{\mathrm{initial}} = [(l_1 + \Delta l_1)(l_2 + \Delta l_2)(l_3 + \Delta l_3)] - (l_1 l_2 l_3) \tag{11}$$

On dividing by the total unit volume of the element, equation 11 can be expressed in terms of the strain components as follows:

$$\frac{\Delta V^{\mathrm{r}}}{V^{\mathrm{r}}} = \varepsilon_1 + \varepsilon_2 + \varepsilon_3 + \varepsilon_1\varepsilon_2 + \varepsilon_2\varepsilon_3 + \varepsilon_1\varepsilon_3 + \varepsilon_1\varepsilon_2\varepsilon_3 \tag{12}$$

where ε_i for $i = 1, 2, 3$ represents the general strain component in the principal direction.

Assuming that the volumetric shrinkage is isotropic, and neglecting all higher order terms, the strain, $\Delta\varepsilon^{\mathrm{r}}$ corresponding to volume resin shrinkage, $|\Delta V^{\mathrm{r}}|$, can be written as

$$\Delta\varepsilon^{\mathrm{r}} = \frac{1}{2}\left(-1 + \sqrt{\left(1 + \frac{3}{4}\Delta V^{\mathrm{r}}\right)}\right) \tag{13}$$

Although dimensional changes are important in such operations as designing tooling for processing plastics or achieving the tolerances required in electronic and computing applications, and in encapsulating and laminating processes, these dimensional changes are not as important in themselves as they are in determining the stresses set up in the cured resin as a result of chemical shrinkage. When these aspects of polymerization shrinkage are considered, it becomes apparent that from the practical point of view the most important phase of the shrinkage to predict (and, hopefully, to control) is that occurring after gelation. If it is possible to locate on the shrinkage/time curve the point of gelation, then data on shrinkage after gelation become directly available. Shrinkage after gelation is minimized when gelation occurs late in the curing reaction, since constrained conditions arise just at the end of the curing process, thereby reducing the length of the crucial stage during which residual stresses can be set up. Lascoe (25) has reported a very comprehensive study on the volume and linear shrinkage of an epoxy resin system.

Interpolated dilatometric curves obtained during isothermal cure at different temperatures, $T = 120, 130, 140, 150$, and 160°C, are reported in Figure 11. Results

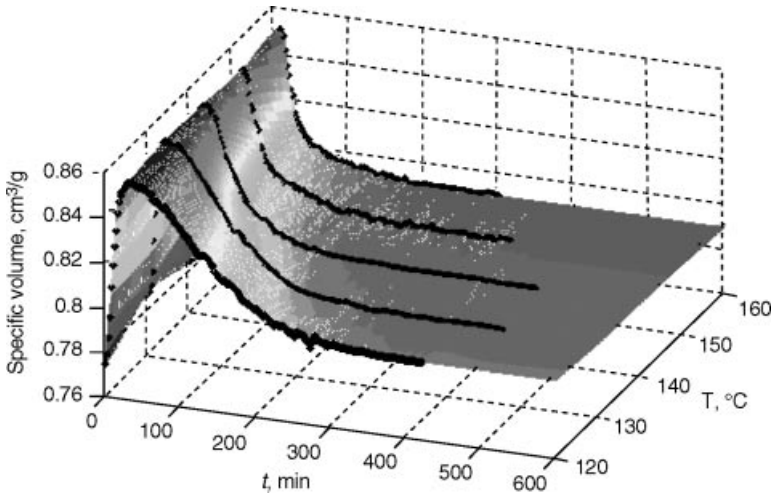

Fig. 11. Linear interpolation of acquired data of specific volume variation during cure at different isothermal temperatures.

have shown that the densification due to polymerization reaction (see Fig. 12) is a linearly dependent phenomena, by a factor of 0.054.

Thermomechanical Properties

The evolution of conversion, α, gives rise to a progressively stiffer material. The passage from a liquid-like to a solid-like material can be suitably described by relaxation modulus as a function of the degree of conversion and temperature.

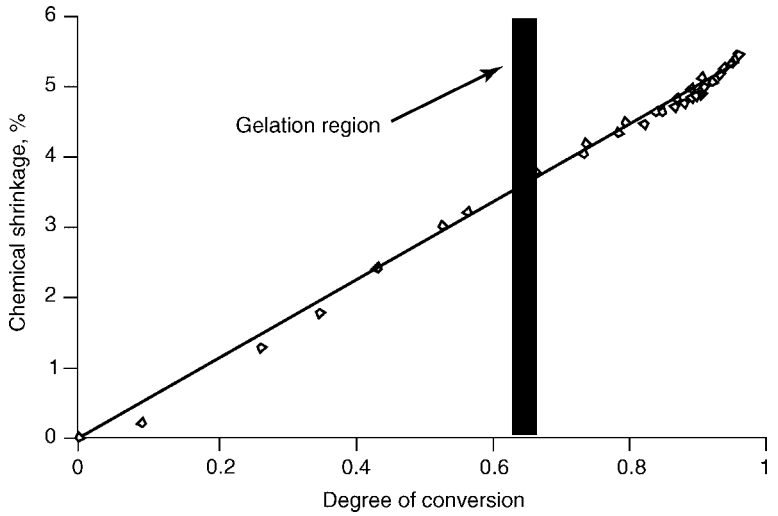

Fig. 12. Linear profile of specific volume change vs. degree of cure.

Mapping the relaxation modulus in each body point then requires the experimental evaluation of such quantity.

The data can be obtained from dynamic mechanical analysis (DMA) tests used to construct the stress relaxation master curves at different levels of conversion, within the frame of time-temperature superposition principle. Curves of stress relaxation modulus can be modeled using the stretched Kohlrausch–William–Watts (KWW) exponential function at each level of conversion, as follows:

$$E(t,\ T,\ \alpha) = E\infty(\alpha)\ \exp\left[-\left(\frac{\xi(t,\ T,\ \alpha)}{\tau_{\mathrm{p}}(\alpha)}\right)^{\beta(\alpha)}\right] \tag{14}$$

where $E\infty$ indicates the fully relaxed modulus and τ_{p} and β are the KWW model parameters. The functionality of the ultimate modulus and the KWW parameters over the degree of conversion is related to the physical assumption to consider as a "new material" the system at each level of conversion. A liner function was found satisfactory to model the nonexponential parameter β vs. conversion; Mijovic and co-workers (26) established the same linear dependency applied to dielectric constant decay function. Assuming that the molecular mobility influences the glass transition through the same mechanism that controls the stress relaxation function, then the behavior of the glass-transition temperature at a fixed degree of cure can be normalized with respect of its value for a given conversion. This normalization will lead to the definition of a potential function, which is identical to that obtained by normalizing in the same way the characteristic relaxation times with respect to the relaxation time at the same fixed conversion. From the mathematical point of view, it can be stated that

$$\frac{T_{\mathrm{g}}(\alpha)}{T_{\mathrm{g}}(\alpha_{\mathrm{ref}})} = g_{T_{\mathrm{g}}}(\alpha) \tag{15}$$

where $T_{\mathrm{g}}(\alpha)$ is the glass-transition temperature as a function of the degree of cure, and $T_{\mathrm{g}}(\alpha_{\mathrm{ref}})$ is the particular value for the fixed conversion. If the same mechanism drives the change in normalized relaxation time, then it follows that

$$\frac{\tau_{\mathrm{p}}(\alpha)}{\tau_{\mathrm{p}}(\alpha_{\mathrm{ref}})} = g_{\tau_{\mathrm{p}}}(\alpha) \tag{16}$$

and therefore,

$$g_{T_{\mathrm{g}}}(\alpha) = g_{\tau_{\mathrm{p}}}(\alpha) \tag{17}$$

where $\tau_{\mathrm{p}}(\alpha)$ is the relaxation time expressed as a function of the degree of cure, and $\tau_{\mathrm{p}}(\alpha_{\mathrm{ref}})$ is the value for the fixed conversion α_{ref}. Figure 13 shows good correlation between the normalized principal stress relaxation time and the normalized value of the glass-transition temperature. Using the transformed KWW model, stress relaxation modulus can be predicted over the whole range of conversion according to the kinetics model at each material point. Figure 14 reports the KWW model prediction for different levels of conversion.

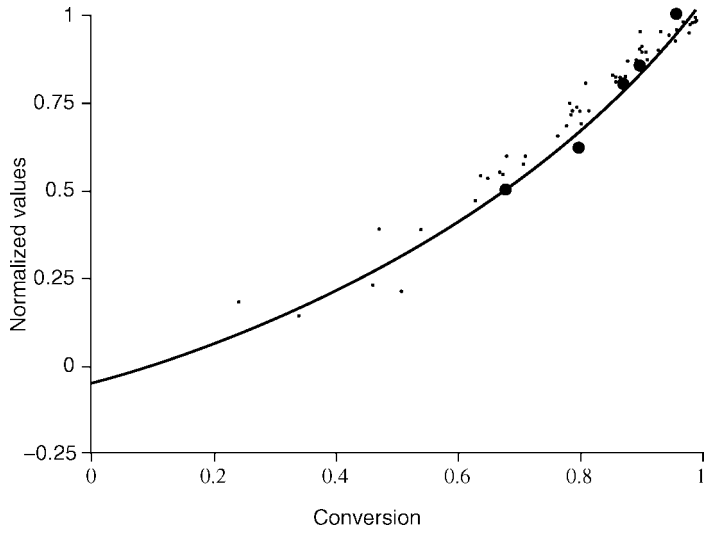

Fig. 13. Normalized values of single relaxation time vs. conversion, compared with normalized values of glass-transition temperature obtained experimentally by thermal analysis as well as torsional rheometry. Predictions of DiBenedetto-type model are also shown (solid line): ———, DiBenedetto model; •, log [tau]/log [tau (0.96)]; •, DSC T_g measurements.

Structural Relaxation

When a material is cooled from above to below T_g, the resulting glass is unstable and its density will gradually increase with time. This process toward thermodynamic equilibrium (called *structural relaxation* or generally *physical aging*)

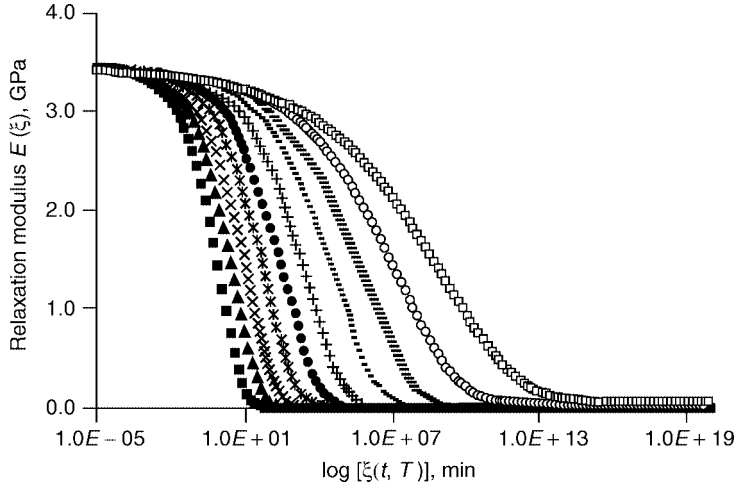

Fig. 14. KWW model prediction for the whole range of conversion: ■, 0.1; ▲, 0.2; ×, 0.3; —×—. 0.4; •, 0.5; +, 0.6; –, 0.7;—, 0.8; ○, 0.9; □, fully cured.

occurs more rapidly at temperatures close to T_g, being an activated phenomenon, and manifests itself through a continuous change of a large number of properties including but not restricted to density, enthalpy, entropy, and consequently all the related viscoelastic functions. The structural relaxation cannot be avoided; it occurs in all glasses even when cooling is performed such that the temperature gradients over the material are small and the resulting thermal stresses are negligible.

The structural relaxation is a direct consequence of the considerably longer time scale of molecular relaxations within and below the glass-transition region compared to the experimental time scale of the applied signal. In other words, even the slowest experimentally attainable cooling rate is much too fast for the polymer chains to relax to equilibrium. The nonequilibrium structure first experiences an abrupt contraction and then undergoes a time-dependent rearrangement toward the equilibrium state. Monitoring the kinetics of any structure-sensitive property changes such as enthalpy or specific volume can follow the gradual rearrangement of the non-equilibrium structure. The multi-parameter phenomenological model for structural relaxation based on the Tool–Narayanaswamy–Mohinyan (TNM) theory was largely utilized in the literature for a number of organic and inorganic glasses.

In principle, the knowledge of TNM model parameters allows the prediction of volume as well as enthalpy relaxation under arbitrary thermal histories. As such, the volume as well as enthalpy fluctuations, which arise when polymers are cooled from the molten rubbery state, can be calculated at each body point provided the local thermal history is known.

Typical experimental volumetric and calorimetric data obtained under different thermal histories are shown in Figures 15 and 16 for given thermal histories (details of the numerical procedure are given in Reference 27). The key parameter of the modeling procedure based on TNM phenomenological approach, is the fictive temperature, T_f. As discussed in the above-cited references, T_f can be conveniently

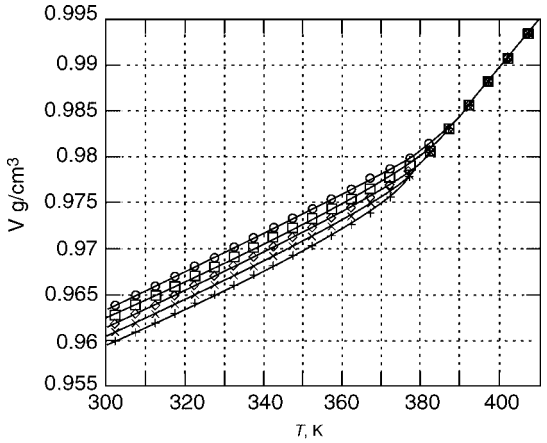

Fig. 15. Experimental specific volume (V) vs. Temperature (T) data during a cooling scan at 1°C/min (open circles) and the corresponding model predictions (full lines) at different cooling rates: ○, 10000°C/min; □, 1000°C/min; ◇ 100°C/min; ×, 10°C/min; +, 1°C/min.

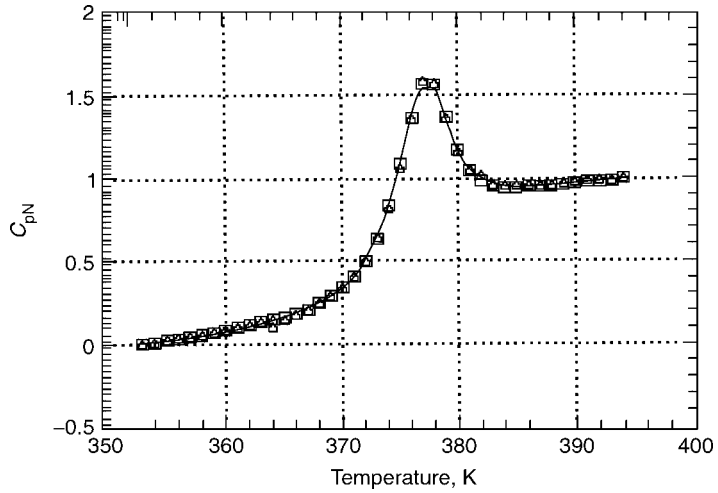

Fig. 16. Normalized specific heat for 1-h-aged sample at $T = 90^{\circ}$C. Heating rate 10°C/min: △, calculated; □, experimental.

regarded as a measure of the actual structural state. Mathematically it is defined as

$$\int_{T}^{T_r} \frac{\partial(P - P_g)}{\partial T}\, dT = \int_{T_f}^{T_r} \frac{\partial(P_e - P_g)}{\partial T}\, dT \tag{18}$$

If P represents the specific volume V, then taking the derivatives of both sides of equation 8 it can be written,

$$\frac{dT_f}{dT} = \frac{\alpha_v - \alpha_{vg}}{\alpha_{vl} - \alpha_{vg}} = \frac{dV^N}{dT} \tag{19}$$

where subscripts l and g stand for liquid and glassy state, respectively and α_v represents the temperature derivative of specific volume. The variation of the normalized functions are described by a relaxation function $\phi(t)$. The most widely used relaxation function is the so-called stretched exponential equation, which is related to the structural sensitive property P according to the following equation

$$\phi(t) = \frac{P - P_e}{P_o - P_e} = \exp\left[-\left(\int_{t_0}^{t} dt'/\tau\right)^{\beta}\right] \tag{20}$$

In equation 16, t' is the time when the change in temperature occurs, β is the exponent, and τ is the characteristic relaxation time. Nonexponentiality (*memory effect*) is reflected in the value of $\beta < 1$. When treating nonisothermal situations (*arbitrary thermal history*) the relaxation function can be represented by the superposition of responses to a series of temperature jumps constituting the actual thermal history. The fictive temperature is defined as the actual

non-equilibrium parameter and takes on the following form:

$$T_f(T) = T_0 + \int_{T_0}^{T} \left\{ 1 - \exp\left[-\left(\int_{t(T)}^{t(T)} \mathrm{d}t/\tau \right) \right] \right\} \mathrm{d}T' \tag{21}$$

with T_0 being the initial temperature. The next input needed by the model is an expression for the structural relaxation time τ, which appears in equation 6. Following Tool's original work, various expressions for the structural relaxation time have been proposed, all in exponential form and containing temperature and fictive temperature as variables.

The Narayanaswamy–Moynihan (NM) expression has the following form:

$$\tau = A \exp\left[x\frac{\Delta h^*}{RT} + (1-x)\frac{\Delta h^*}{RT_\mathrm{f}} \right] \tag{22}$$

where τ is the structural relaxation time, A is a constant (preexponential factor), Δh^* is the characteristic activation energy, and x the partitioning parameter ($0 < x < 1$) that defines the degree of nonlinearity.

The experimental data of Figures 15 and 16 can be utilized to find the optimum set of parameters (A, Δh^*, x, β) that best describes the behavior of the material functions in the glass-transition region. From Figure 17 the coefficient of thermal expansions for a given temperature history (and, therefore, for a given body point during the cooling process) can be obtained.

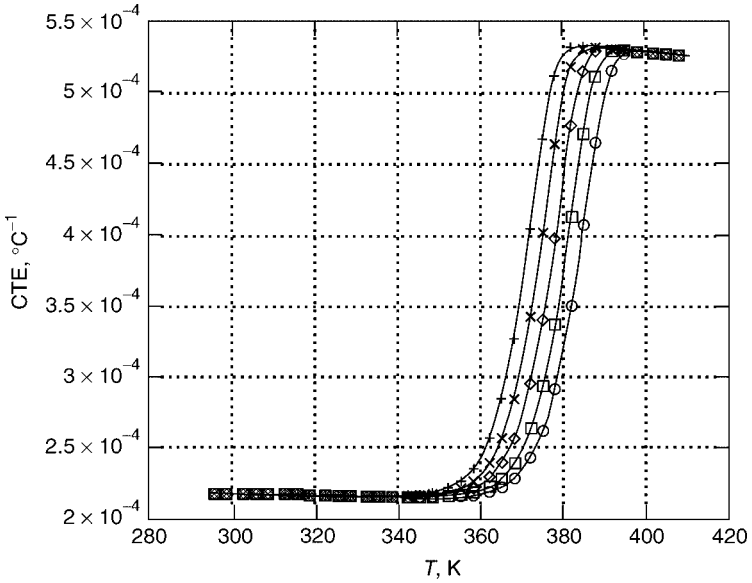

Fig. 17. Model prediction of coefficient of thermal expansion (CTE) as a function of temperature (T) at different cooling rates: ○, α-10000°C/min; □, 1000°C/min; ◇, 100°C/min; ×, 10°C/min; +, 1°C/min.

Submodels

Resin Flow Submodel. Resin flow analysis in a manufacturing process provides estimates of resin flow, and fiber and resin distribution and compaction. In the early stage of the autoclave process, after the prepregs are staked and vacuum bagged, the system is pressurized while the temperature is increased in order to minimize the resin viscosity. In this way the resin flow removes the excess resin from adjacent plies and makes uniform the fiber distribution. In the RTM process the dry fibers inside the mold can be considered as a porous medium through which the resin is injected from a single or multiple inlets: Darcy's law can be used to perform a two-dimensional flow analysis. Darcy's law can be written as

$$\begin{bmatrix} u(x,y) \\ v(x,y) \end{bmatrix} = -\frac{1}{\mu} \begin{bmatrix} k_{xx} & k_{xy} \\ k_{yx} & k_{yy} \end{bmatrix} \begin{bmatrix} \dfrac{\partial P(x,y)}{\partial x} \\ \dfrac{\partial P(x,y)}{\partial y} \end{bmatrix} \tag{23}$$

where k_{ij} is the generic component of the permeability tensor, μ is the viscosity, P is the pressure, and v and u are the components of the velocity in the x- and the y-directions, respectively. If the resin is considered to be an incompressible fluid then the continuity equation can be reduced to the following form:

$$\frac{\partial u}{\partial x} + \frac{\partial v}{\partial y} = 0 \tag{24}$$

and the mass balance in an RTM process assumes the following form, provided the directions x and y coincide with the principal directions of the fiber perform/mat (28).

$$\frac{\partial}{\partial x}\left(\frac{k_{xx}}{\mu}\frac{\partial P}{\partial x}\right) + \frac{\partial}{\partial y}\left(\frac{k_{yy}}{\mu}\frac{\partial P}{\partial y}\right) = 0 \tag{25}$$

In autoclave forming the main resin flow is normal to the tool surface and Darcy's law is again used but in its one-dimensional form:

$$V = -\frac{S}{\mu}\frac{\mathrm{d}P}{\mathrm{d}z} \tag{26}$$

where S is the apparent permeability and z is the direction normal to the tool.

Resin flow parallel to the tool plate takes place along the parallel and perpendicular fiber directions. Between the two mechanisms, the resin flow along the fibers is the most prominent as, in fact, the flow perpendicular to the fibers is small because of the resistance created by the fibers.

The flow along the fiber direction can be modeled as a channel flow (the viscous flow between two parallel plates). Loss and Springer (29) validated thermomechanical models, including the chemorheological behavior of resin and resin flow models.

Void Growth Model. The resin flow during composite processing inevitably leads to the formation and growth of voids. Although all the manufacturing processes of composite materials are based on solid engineering principles, current technologies cannot assure a part-by-part reliability required by the production and assembly of the parts for a complex and larger composite structure. For thick composite parts (30) the occurrence of voids has been widely verified and their detrimental effects proved. The void formation necessarily occurs during the fabrication process and involves the different concurrent phenomenology of heat, mass, and momentum transfer. An even more complex scenario comes out considering that polymerization reaction occurs for the matrix while thermomechanical properties are varying with time, temperature, and degree of conversion. In some cases the system can be considered multiphase.

The correct mechanism of void formation is related to the system being used and to the specific manufacturing process. Even when a part appears to be fully impregnated by the resin and the resin matrix has been previously degassed at the prescribed temperature, in order to eliminate mechanically entrapped air bubbles, void formation still occurs. During a general manufacturing process the voids can be formed either by the mechanical entrapping of air or by a nucleation process. In the first case, it can be related to gas bubbles associated with the mixing operation of the resin bulk, by bridging of particles of additives, by air and wrinkles when the lay-up sequence is built, or by the resin flow during tow impregnation. Particularly important for injection type processes (like RTM, injection molding, or resin film infusion) this latter mechanism leads to the formation of microvoids and consequently dry spots within the low-permeability area of the perform. Schematically, the voids formation associated with the resin flow can be divided in to four stages, as follows:

(1) the flow reaches the tow to be impregnated,
(2) the flow front comes around the tow or bundle and it passes,
(3) still the resin has to penetrate and fill the space inside the tow among the different fibers, and
(4) air voids remain inside the tow and eventually move in the resin between tows owing to the high pressure acting on the tow.

Modeling of void formation is intimately related with cure kinetics and viscosity profiles of the resin system. For modeling purposes it can be conveniently divided into three different phases:

(1) formation and stability of the forming voids,
(2) void growth and/or dissolution by diffusion, and
(3) void transport process.

A nucleation process is generally described assuming the initial formation of the voids to be in accordance with the classical nucleation theory. It can be assumed that nucleation occurs between resin and fiber or resin and added particle (heterogeneous nucleation) or within the resin itself (homogeneous nucleation).

Application of classical nucleation theory (31) leads to favorable results, especially for the case of homogeneous nucleation, for which critical size nuclei can be formed at rate N, given by the following equation:

$$\dot{N} = \left[\frac{P^T}{\sqrt{2\pi MkT}}\right] 4\pi^2 \exp\left(-\frac{\Delta F}{kT}\right) \tag{27}$$

where P stands for the total water plus air pressure, M is the molecular weight of the vapor phase, n the molecular density in the formed nuclei, ΔF the maximum free energy for the nucleation process, and k and T are respectively the Boltzmann constant and the absolute temperature. When the nuclei are formed, several factors determine the stability and the growth of the voids. Changes in temperature and pressure cause an increase in the solubility in the resin leading to the dissolution of the voids. Generally, a void becomes stable when its inner pressure equals or exceeds the surrounding resin hydrostatic pressure plus the surface tension forces. This condition can be stated as follows:

$$P_v - P_{sr} = \frac{\gamma_{r-v}}{R_{v-a}} \tag{28}$$

where P_{v} and P_{sr} are respectively the void and resin pressure, $\lambda_{\mathrm{r-v}}$ is the resin–void surface tension, and $R_{\mathrm{v-a}}$ is the ratio of the volume and surface of the voids. As the temperature and pressure change with time, from a product-quality point of view it is most important to model the time-dependent growth process.

This phenomenon, however, would require the solution of many time-dependent and coupled partial differential equations, which would result in too difficult an approach. To overcome the intrinsic difficulties related to changes physical properties and the excessive computational time of the equation solver, two "equivalent" physical schemes are generally studied assuming that the void growth perpendicular to the ply (critical capillary scheme) or through an isotropic pseudo-homogeneous medium where the growth occurs not preferentially perpendicular to the plies. This latter approach seems to be more realistic considering the physical possibility of pure water vapor growing for diffusion into the surrounding resin or into a void initially consisted of entrapped air and it become equivalent to bubble growth in a liquid medium.

The main assumptions in building a general void growth model are

(1) the voids remain between two plies and move with respect to the fixed coordinates system in the laminate;
(2) the voids are considered spherical and their characteristic dimension is calculated based on an equivalent sphere;
(3) no interactions between two voids are considered;
(4) during the lay-up process and at the beginning of the cure process, void nucleation occurs almost instantaneously;
(5) temperature and moisture concentration are time independent; and
(6) the void growth is limited by the flow rate of arrival of the diffusing species.

Structural Analysis

The complex interactions between material property evolution and the manufacturing stages represent a critical issue for correct part design and for controlling the entire production process. In order to evaluate the integrity of the manufactured part, a structural analysis needs to be performed to simulate the effects of mechanical, nonmechanical, and geometric part constraints due to the manufacturing tools utilized during the specific process.

Modeling of the coupled transfer phenomena (mass, heat, and momentum) need to be solved considering appropriate constitutive equations for the evolving properties in order to optimize the integrity of the final material system and at the same time to control the final shape of produced composite element.

If, as we can recognize, the curing process involves thermal variations from room temperature to cure temperature, then thermal expansion is a necessary part of that process. A common hypothesis has been proposed in past papers (32–36) to simplify the complex phenomenology, that is, no stresses develop prior to completion of the curing process.

Even if it is possible to obtain good results using a simulation model, in which it is assumed that the crucial stage for formation of residual stresses is the period of cooling from cure to ambient temperature, recent work has demonstrated that the residual stress formation mechanism is strongly influenced by the overall curing process (37–43). Moreover, using this approach, the phenomenon of structural relaxation, which occurs near the glass-transition region of the developing structure, is not considered at all. The above phenomena needs much more effort in order to be well quantified and eventually taken into account. In fact, these chemical/physical changes cause more deformation in the transverse directions than in the longitudinal direction since resin-dominant properties are experienced within the ply in that direction.

Mechanical Tests: Review

Mechanical tests for advanced composite materials conform in many respects to the conventional test typology used for traditional isotropic materials. Despite the complication associated with the heterogeneity of composite systems, the interface between fiber and matrix, and the anisotropy at the micro- and macroscopic levels, the same characteristic property definitions generally used for conventional materials can be identified for these novel materials. In some cases additional constants are required and some differences in nomenclature are introduced especially when no isotropic counterpart exists.

Mechanical characterization of composite materials is a complex scenario to deal with, either because of the infinite number of combinations of fiber and matrix that can be used, or because of the enormous variety of spatial arrangements of the fibers and their volume content. The foundation of the testing methods for the measurement of mechanical properties is the classical lamination theory; this theory was developed during the nineteenth century for homogeneous isotropic materials and only later extended to accommodate features enhanced by

fiber-reinforced material, such as inhomogeneity, anisotropy, and anelasticity. Two basic approaches are proposed to determine the mechanical properties of composite materials: *constituent testing and composite sample testing*.

Academically, composite constituents could be tested separately and then composite properties evaluated by simple or more complex mixture rules according to the wanted level of accuracy. Many references can be found in the literature for this approach. Mechanical properties of composites are generally assumed to be dependent on the following variables:

(1) properties of the fiber,
(2) properties of the matrix,
(3) properties of any other additive or phase constituting the composite,
(4) volume fraction of the fiber,
(5) spatial distribution of the fiber (or a third phase), and
(6) nature of interface.

From a strictly theoretical point of view, the so-called constituent testing approach or micromechanics approach is the most valuable. Tests performed on composite constituents supply the required material constants of each phase of the composite material—namely for long-fiber-reinforced composite—for the fiber and the matrix, to use in appropriate mixture rules. These rules obtained by physical and mechanical considerations are the basic relationships between the composite constituents, and they leads to a complete characterization of the final composite.

Fibers can be tested in the form of single fiber, tow, or fabric; all tests can be grouped into three main categories:

(1) Chemical Tests. They are generally used for elemental analysis and surface investigation. Following is a list of the most important chemical tests:
   a. X-ray photoelectron spectroscopy (XPS)
   b. Low-energy electron diffraction (LEED)
   c. Scanning Electron Microscopy (SEM)
   d. Carbon assay (CA)
   e. Fourier transform infrared spectroscopy (FTIS)
   f. Sizing Content (SC)
   g. Thermal desorption mass spectrometry (TDMS)
   h. Auger electron spectroscopy (AES)
(2) Physical tests. They are generally performed to measure different physical properties for fiber and for fabric. Properties of interest required for specific application design are
   a. Density (ASTM D792 using displacement, ASTM D3800 based on Archimedes principle and ASTM D1505 by means of density gradient column)
   b. Weight per length, typically in g/μm
   c. Weight per unit area or aerial weight, reported in g/m^2

d. Filament diameter measured by microscopy image according to the standard ASTM D578
e. Electrical conductivity
f. Thermal expansion
g. Number of twists
h. Tensile strength (ASTM D579)

(3) Mechanical test. It is important to point out that these mechanical tests are chosen based on whether the fiber sample is single fiber, tow, or fabric. For this reason, it is extremely important to define the specific fiber sample typology used during the tests when a mechanical test campaign is started. The main mechanical tests generally performed are

a. Single-filament tensile test [ASTM D3379 (44)]
b. Tensile test for tow [ASTM D4018 (45)]
c. Tensile test for dry fabric [ASTM D579 (46)]

For resin matrix, several tests (chemical, physical, and mechanical) are generally performed by the supplier; their results are used not only for design but also for processing control and optimization. Along with traditional tests, some specific procedures, such as stress relaxation or creep, are considered if viscoelastic effects are investigated. The experimental setup for the stress relaxation test is shown in Figure 18; while stress relaxation raw data, for an epoxy-toughened resin matrix used for aerospace structural composite materials, are reported in Figure 19. Despite the fact that testing of a single constituent could eliminate inherent difficulties related with material handling, this approach is not representative of composite performance; in fact, many factors associated with the manufacturing process and the realistic arrangement of the fiber into the composite system are not taken into account as modeling assumptions are necessary even in the case of more complex schematization.

The second approach, which determines the mechanical properties of the composites by directly testing a composite laminate, is a much more straightforward procedure, widely implemented to determine composite properties required for analysis and design. The whole philosophy of testing a laminate of composite material is essentially based on the classical laminate theory. CLT employs elasticity theory to derive the basic relationships between stress and strain and, therefore, to identify material properties. These relationships are quite simple for traditional homogeneous and isotropic materials, however, for composites they can be either extremely complex or, in some case, these equations are imperfect "tools" for modeling (ie it is not possible to estimate the stress state at the tip of a crack by classical laminate theory). Static and fatigue tests are generally performed on composite laminates as well as on traditional systems; for these novel materials, however, some new test typologies need to be introduced to evaluate specific properties or to describe particular failure modes not shown by traditional materials. Despite inherent imperfections and simplifications, the existing formal framework contains justification for the various constraints and stipulations that have been imposed on test configurations and procedures for long-fiber composites.

Fig. 18. Stress relaxation test in 3-point bending mode for a typical aerospace toughened epoxy composite matrix.

The principal features and precautions arising from the testing of long-fiber composites are in relation to

(1) generation of uniform stress in the critical reference volume,
(2) avoidance of overwhelming "end-effects,"
(3) tension-shear coupling effects,
(4) adequate loading levels to avoid failure or damage at loading points, and
(5) appropriate sample dimensions compared to the scale of structural inhomogeneity.

Even though the inhomogeneity and anisotropy of composite materials give rise to various additional configurations, the above precautions apply similarly to the testing of homogeneous isotropic materials.

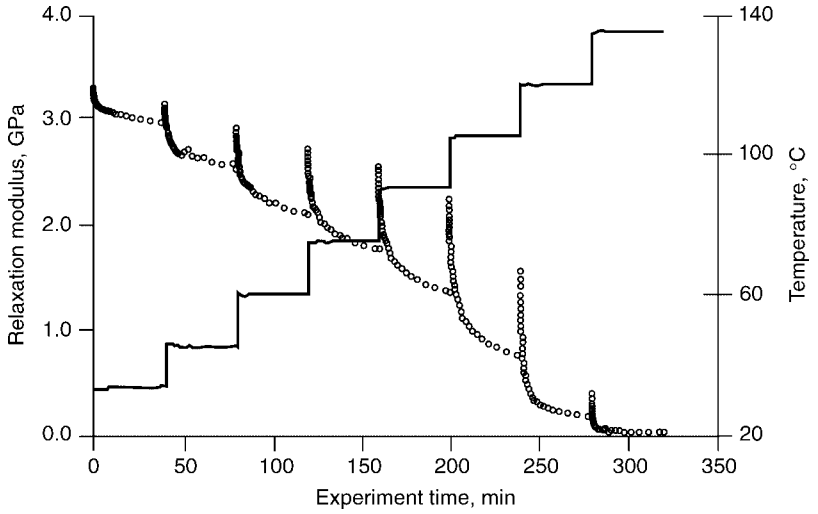

Fig. 19. Typical data obtained from a stress relaxation experiment in 3-point bending mode performed on a toughened epoxy resin system used for aerospace structural composite material: ○, relaxation modulus (resin plate B); ———, temperature (resin plate B).

Specimens for mechanical tests on composites are usually taken in three different forms: pultrusion, filament-would tubes, and flat sheet. For each form, tests can be performed on the entire sample or on coupons of given fixed dimensions. It is extremely important to notice that the first two forms are generally considered for their convenience of fabrication and also because for composite materials, the specific manufacturing process employed strongly influences the final performance of the material in its final application. Therefore, testing on the "realistic" configuration leads to more reliable results in terms of mechanical characterization. Commercially available flat sheets are in the form of randomly oriented fiber, various sequences of UD or woven laminate and sandwich structures. The mechanical properties of these items as well as of the extracted coupons vary with the stacking sequence, the alignment of the specimen's axis in relation to the pattern of the fiber and with the in-plane position of the specimen.

To evaluate the performance of a composite or for a general characterization of a composite system, the following mechanical properties are generally investigated:

(1) Uniaxial tensile modulus
(2) Tensile strength
(3) Uniaxial compression modulus
(4) Compressive strength
(5) Flexural modulus
(6) Flexural strength
(7) In-plane shear modulus
(8) Lateral contraction ratios

Table 4. Mechanical Testing Plan for Mechanical Characterization of Composite for Aeronautical Applications

Tensile strength at room temperature
Uniaxial compression at room temperature
Interlaminar shear at room temperature
Open hole tension at room temperature (see Fig. 19)
Open hole compression at 93°C
Hot/wet compression strength
Edge-plate compression strength after impact, at room temperature

(9) Apparent interlaminar shear strength
(10) Facture toughness

With time, an extensive variety of test methods and procedures have been introduced to develop new applications of composite materials and more in general to sustain the diffusion in various fields of these novel materials. However, the complexity of the properties, the great variety of their applications, and the diversity of their features compared with traditional materials have resulted in the developments, often arbitrary and in some cases more specific, to satisfy particular sectors of the industry.

No single organization or industry is likely to carry out a general investigation program to identify a general routine procedure for mechanical characterization of composite materials, supported by solid theoretical considerations. In order to satisfy the various downstream requirements, which vary from company to company, different test programs have been stipulated. In USA, a large commercial airplane has proposed the test program reported in Table 4 as fundamental for the "initial" evaluation phase of composites, which differs from the test plan identified by U.S. automotive industries, whose test plan is reported in Table 5.

For composite materials, the exposure to critical environment is also an important issue; therefore while selecting an appropriate test method for evaluating composite mechanical properties the extreme conditions experienced during service for a particular application must be taken into account. Environmental exposure can be "accidental" during the specimen preparation and instrumentation, or "planned" to investigate the moisture effect, chemical attack, or cycling

Table 5. Mechanical Test Program Agreed by Important Automotive Manufacturers

Elastic and strength properties at temperature in the range 40–150°C
Effect of loading rate on tensile and compressive properties in the range 0.00167–16.7 s^{-1}
Creep
Creep and stress relaxation
Residual strength after fatigue
Fatigue
Effects of notches and holes
Energy absorption after impact
Manufacturing effects
Joints and fastener characterization

temperature. In both cases, extensive and very expensive tests are performed to assess the performances of the composite material during service at these extreme conditions.

In 1987, a survey (47) of currently available mechanical standardized tests concluded that the existing standardized, semistandardized, or available procedure were deficient in respect to three main aspects:

(1) too many variants were used for a single test and there was no evidence of the effects of the variation of generated data on reliability,
(2) some tests were not fit for their intended purpose, and
(3) some important phenomena were neglected either because they were not properly understood or because they were too time-consuming to assess.

The above-mentioned report has attributed this state of the art to poor interactions between academy and industry and to the failure to establish an adequate common infrastructure among composite experts and manufacturers. In the last few years, many laboratories in the area of composite materials have launched inter-laboratory testing programs to establish common procedures for investigation of mechanical properties by various techniques. Many round-robin test programs (48–54) are still running in the area of interlaminar fracture mechanism on composite laminate fracture toughness of new 3-D-reinforced-fiber materials, dynamic mechanical analysis, through thickness crack propagation test, and fatigue tests. These research programs aim either to harmonize or to build a common framework for parameters acquisition to be used for the analysis and design of high quality composite structure.

Following is a list of the main testing mode adopted to characterize advanced composite materials along with reference standards:

(1) Tension: ASTM D3039, BS 2782-320, CRAG 300-301, CRAG 302, and ISO 572
(2) Compression: ASTM D695M, ASTM 3400, and CRAG 400
(3) Shear: ± 45 tension test, 10° off-axis test, rail shear test, V-notched beam test, plane-twist test, and torsion of thin-walled sample
(4) Flexure: ASTM D790M-93, CRAG report 88012, BS2782-1005, and ISO 14125
(5) Through-thickness testing: BS EN ISO 14 and 130, ASTM D3846, and ASTM D 5379
(6) Interlaminar fracture toughness
(7) Impact: BS 2782, ASTM D3029-FA, ASTM 2930-FB, ISO/DIS 6603/2
(8) Fatigue

Structural tests on real-scale elements are also performed to validate the design criteria and manufacturing settings as a final verification of the desired components. In Figure 20, a typical test is shown for a real-scale composite panel for aeronautical applications. The panel is loaded in shear mode under both static and dynamic conditions.

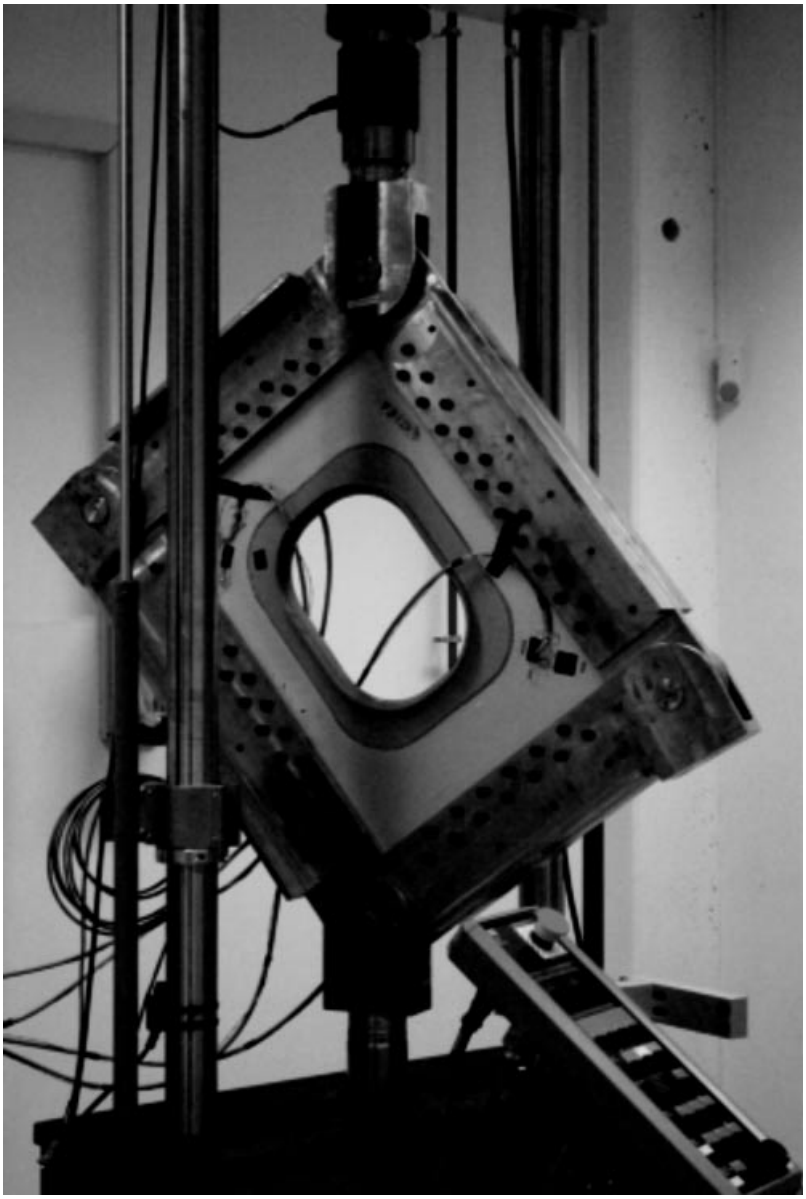

Fig. 20. Structural mechnical test on real scale composite panel for aeronautical application.

BIBLIOGRAPHY

"Composites" in *EPSE* 2nd ed., Vol. 3, pp. 776–820, by Frank P. Gerstle Jr., Sandia National Laboratories.

1. G. C. Martin, A. V. Tungare, B. W. Fuller, and J. T. Gorto, in *SPE ANTEC Technical Papers*, No. 35, 1989, p. 838.

2. E. Knauder, C. Kubla, and D. Poll, *Kunstoffe German Plastics* **81**, 39 (1991).
3. P. L. Chiou and A. Letton, *Polymer* **33**, 3925 (1992).
4. M. E. Ryan, M. Eng. Thesis, McGill University, Montreal, Canada, 1973.
5. T. H. Hsieh and A. C. Su, *J. Appl. Polym. Sci.* **44**, 165 (1992).
6. C. D. Han and K. W. Lem, *Polym. Eng. Sci.* **24**, 473 (1984).
7. A. Hale, M. Gaircia, C. W. Macosko, and L. T. Manzione, in *SPE ANTEC Technical Papers*, No. 35, 1989, p. 796.
8. J. W. Lane and R. K. Khattacj, in *SPE ANTEC Technical Papers*, No. 33, 1987, p. 982.
9. Y. S. Yang and L. Suspene, *Polym. Eng. Sci.* **31**, 321 (1991).
10. A. Ya Malkin and S. G. Kulichikin, *Adv. Polym. Sci.* **101**, 218 (1989).
11. P. I. Karkanas, in Cure Modelling and Monitoring of Epoxy/Amine Resin Systems, PhD Thesis, Cranfield University, United Kingdom, 1997.
12. E. Rabinowitch, *Trans. Faraday Soc.* **33**, 1225 (1937).
13. S. L. Simon and J. K Gillham, *J. Appl. Polym. Sci.* **47**, 461 (1993).
14. J. D. Ferry, *Viscoelastic Properties of Polymers*, John Wiley & Sons, Inc., New York, 1976.
15. Mita and K. Horie, *J. Macromol. Sci. Rev. Macromol. Chem. Phys. C* **27**, 91 (1987).
16. B. A. Rozenberg, *Adv. Polym. Sci.* **75**, 113 (1988).
17. A. T. DiBenedetto, *J. Appl. Polym. Sci., Part B: Polym. Phys.* **25**, 1949 (1987).
18. L. S. Penn, R. C. T. Chou, A. S. D. Wang, and W. K. Binienda, *J. Comp. Mater.* **23**, 570 (1989).
19. L. Di Palma, M. Bellucci, A. Apicella, P. Casone, M. Amato, and S. Rengo, in *32nd International SAMPE Technical Conference*, November 5–9, Boston, USA, 2000.
20. C. T. Chou and L. S. Penn, *J. Comp. Mater.* **26**(2), 171 (1992).
21. E. J. Bartkus and C. H. Kroekel, *Appl. Polym. Symp.* **15**, 113 (1970).
22. T. J. Chapman, J. W. Gillespie, R. B. Pipes, J.-A. E. Manson, and J. C. Seferis, *J. Comp. Mater.* **24**, 616 (1990).
23. H. L. Parry and H. A. Mackay, *SPE J.* **22** (1958).
24. S. R. White and H. T. Hahn, *J. Comp. Mater.* **27**, 1352 (1992).
25. O. D. Lascoe, *Eng. Tool* **1**, 32 (1958).
26. M. Sun, Y. Han, and J. Mijovic, in *Book of Abstracts of the International Conference on "Time of Polymer" (TOP2002)*, Ischia, Italy, October 20–23, 2002.
27. J. Mijovic, A. D'Amore, J. M. Kenny, and L. Nicolais, *Polym. Eng. Sci.* 34–35 (1994).
28. S. K. Mazumdar, *Composites Manufacturing: Materials Product and Process Engineering*, CRC Press, Inc., Boca Raton, Fla., 2002.
29. A. C. Loos and G. S. Springer, *J. Comp. Mater.* **17**, 135 (1983).
30. J. L. Kardos, M. P. Dudukovic, E. L. McKague, and M. W. Lehman, C. E. Browing, ed., *Composite Materials: Quality Assurance and Processing*, ASTM STP 797, American Society for Testing and Materials, Philadelphia, 1983.
31. W. D. Kingery, *Introduction to Ceramics*, John Wiley & Sons, Inc., New York, 1960.
32. H. T. Hahn, *J. Comp. Mater.* **10**, 266 (1976).
33. H. Kau and L. A. Petrusha, Technical Report GMR-6359, G. M. Research Lab., Warren, Mich., 1988.
34. D. R. Doner and R. C. Novak, in *24th Annual Technical Conference* (Paper No. 2), The Society of Plastic Industry, 1969.
35. O. H. Griffin, *J. Comp. Mater.* **17**, 449 (1984).
36. R. J. Stango and S. S. Wang, *J. Eng. Ind.* **106**, 48 (1984).
37. S. R. White and H. T. Hahn, *J. Comp. Mater.* **26**, 2402 (1992).
38. S. R. White and H. T. Hahn, *J. Comp. Mater.* **26**, 2423 (1992).
39. S.-Y. Lee and G. Springer, *J. Comp. Mater.* **22**, 243 (1998).
40. S. Y. Pusatcioglu and H. A. McGee Jr., *J. Appl. Polym. Sci.* **25**, 381 (1980).
41. T. A. Bogetti and J. W. Gillespie, *J. Comp. Mater.* **26**, 262 (1992).

42. S. R. White and Y. K. Kim, *Mech. Comp. Mater. Struct.* **5**, 153 (1998).
43. K. S. Kim and H. T. Hahn, *Comp. Sci. Technol.* **36**, 121 (1989).
44. D3379, *Annual Book of ASTM Standard*, American Society for Testing and Materials, Philadelphia.
45. D4018, *Annual Book of ASTM Standard*, American Society for Testing and Materials, Philadelphia.
46. D579, *Annual Book of ASTM Standard*, American Society for Testing and Materials, Philadelphia.
47. P. J. Hoggs and S. Turner, "The mechanical testing of long-fibre composites: Harmonization and standardization in U. K.", Report of the Department of Trade and Industry, United Kingdom, January 1988.
48. G. D. Sims, "Standards for Polymer Matrix Composites. Part I: Assessment of CRAG Test Methods Data," NPL Report DMM(M)6, 1990.
49. G. D. Sims, "International Standardisation of Coupon and Structural Element Test Methods," in *ECCM-Composites: Testing and Standardisation 2*, Hamburg, 1994.
50. G. D. Sims and W. Nimmo, "A Review of Test Methods for Polymer Matrix Composites at Non-Ambient Temperatures," NPL Report DMM(A)155, 1994. (Summary available)
51. G. D. Sims, "Progress in Mechanical Behaviour and Testing Methods in Composite Materials," in *5th Portuguese Congress on Fracture*, Lisbon, 11–12 April 1994.
52. G. D. Sims, "Developments in Harmonisation of Standards for Polymer Matrix Composites," in *ECCM-Composites: Testing and Standardisation*, Amsterdam, 1992.
53. G. D. Sims, *Composites* **22**, 267–274 (1991).
54. G. D. Sims, "Development of Standards for Advanced Polymer Matrix Composites—A BPF/ACG Overview", NPL Report DMM(A)8, (1990).

ALBERTO D'AMORE
The Second University of Naples—SUN
MAURO ZARRELLI
Italian Aerospace Research Center

COMPOSITES, FABRICATION. See Volume 2.

COMPUTATIONAL QUANTUM CHEMISTRY FOR FREE-RADICAL POLYMERIZATION

Introduction

Chemistry is traditionally thought of as an experimental science, but recent rapid and continuing advances in computer power, together with the development of

Encyclopedia of Polymer Science and Technology. Copyright John Wiley & Sons, Inc. All rights reserved.

efficient algorithms, have made it possible to study the mechanism and kinetics of chemical reactions via computer. In computational quantum chemistry, one can calculate *from first principles* the barriers, enthalpies, and rates of a given chemical reaction, together with the geometries of the reactants, products, and transition structures. It also provides access to useful related quantities such as the ionization energies, electron affinities, radical stabilization energies, and singlet–triplet gaps of the reactants, and the distribution of electrons within the molecule or transition structure. Quantum chemistry can provide a "window" on the reaction mechanism, and assumes only the nonrelativistic Schrödinger equation and values for the fundamental physical constants.

Quantum chemistry is particularly useful for studying complex processes such as free-radical polymerization (see RADICAL POLYMERIZATION). In free-radical polymerization, a variety of competing reactions occur and the observable quantities that are accessible by experiment (such as the overall reaction rate, the overall molecular weight distribution of the polymer, and the overall monomer, polymer, and radical concentrations) are a complicated function of the rates of these individual steps. In order to infer the rates of individual reactions from such measurable quantities, one has to assume both a kinetic mechanism and often some additional empirical parameters. Not surprisingly then, depending upon the assumptions, enormous discrepancies in the so-called "measured" values can sometimes arise. Quantum chemistry is able to address this problem by providing direct access to the rates and thermochemistry of the individual steps in the process, without recourse to such model-based assumptions.

Of course, quantum chemistry is not without limitations. Since the multielectron Schrödinger equation has no analytical solution, numerical approximations must instead be made. In principle, these approximations can be extremely accurate, but in practice the most accurate methods require inordinate amounts of computing power. Furthermore, the amount of computer power required scales exponentially with the size of the system. The challenge for quantum chemists is thus to design small model reactions that are able to capture the main chemical features of the polymerization systems. It is also necessary to perform careful assessment studies, in order to identify suitable procedures that offer a reasonable compromise between accuracy and computational expense. Nonetheless, with recent advances in computational power, and the development of improved algorithms, accurate studies using reasonable chemical models of free-radical polymerization are now feasible.

Quantum chemistry thus provides an invaluable tool for studying the mechanism and kinetics of free-radical polymerization, and should be seen as an important complement to experimental procedures. Already quantum chemical studies have made major contributions to our understanding of free-radical copolymerization kinetics, where they have provided direct evidence for the importance of penultimate unit effects (1,2). They have also helped in our understanding of substituent and chain-length effects on the frequency factors of propagation and transfer reactions (2–5). More recently, quantum chemical calculations have been used to provide an insight into the kinetics of the reversible addition fragmentation chain transfer (RAFT) polymerization process (6,7). For a more detailed introduction to quantum chemistry, the interested reader is referred to several excellent textbooks (8–16).

Basic Principles of Quantum Chemistry

Ab initio molecular orbital theory is based on the laws of quantum mechanics, under which the energy (E) and wave function (Ψ) for some arrangement of atoms can be obtained by solving the Schrödinger equation 1 (17).

$$\hat{H}\Psi = E\Psi \tag{1}$$

This is an eigenvalue problem for which multiple solutions or "states" are possible, each state having its own wave function and associated energy. The lowest energy solution is known as the "ground state," while the other higher energy solutions are referred to as "excited states." The wave function is an eigenfunction that depends upon the spatial coordinates of all the particles and also the spin coordinates. Its physical meaning is best interpreted by noting that its square modulus is a measure of the electron probability distribution. The term ($\hat{H}$) in equation 1 is called the Hamiltonian operator and corresponds to the total kinetic ($\hat{T}$) and potential energy ($\hat{V}$) of the system.

$$\hat{H} = \hat{T} + \hat{V} \tag{2}$$

$$\hat{T} = -\frac{h^2}{8\pi^2}\sum_i \frac{1}{m_i}\left(\frac{\partial^2}{\partial x_i^2} + \frac{\partial^2}{\partial y_i^2} + \frac{\partial^2}{\partial z_i^2}\right) \tag{3}$$

$$\hat{V} = \sum_{i<}\sum_j \left(\frac{e_i e_j}{r_{ij}}\right) \tag{4}$$

In these equations, the kinetic and potential terms are summed over all particles in the system (nuclei and electrons), and each particle is characterized by its Cartesian coordinates, its mass (m) and its electric charge (e). In addition, h is Planck's constant and r_{ij} is the distance separating particles i and j. It can thus be seen that the only empirical information required to solve the Schrödinger equation are the masses and charges of the nucleus and the electrons, and the values of some fundamental physical constants. For this reason, quantum-chemical calculations are referred to as "ab initio" ("without assumptions") procedures.

In applying the Schrödinger equation to problems of chemical interest, two major simplifications can be made. Firstly, the Hamiltonian described by equations 2–4 above is nonrelativistic, and it is valid provided that the velocities of the particles do not approach the speed of light. This is generally reasonable except for the inner shell electrons of heavy atoms, and in these cases corrections for relativistic effects can be made (18). Secondly, the Hamiltonian is further simplified by neglecting the kinetic energy contribution of the nuclei. This is known as the Born–Oppenheimer approximation (19), and amounts to assuming that, since nuclear motion is much slower than electronic motion, the electron distribution depends only upon the positions of the nuclei and not on their motions. Thus, the Schrödinger equation can be rewritten as an electronic Schrödinger equation, as

follows:

$$\hat{H}^{\text{elec}}\Psi^{\text{elec}}(\boldsymbol{r}, \boldsymbol{R}) = E^{\text{eff}}(\boldsymbol{R})\Psi^{\text{elec}}(\boldsymbol{r}, \boldsymbol{R}) \quad (5)$$

In this equation, Ψ^{elec} is the electronic wave function (which depends on the electronic coordinates $\boldsymbol{r}$, as well as the nuclear coordinates $\boldsymbol{R}$) and $\hat{H}^{\text{elec}}$ is the electronic Hamiltonian in which the total kinetic energy is summed over all electrons only. The Born–Oppenheimer approximation is valid provided that the ratio of electron mass to nuclear mass is sufficiently small.

The objective of computational quantum chemistry is to solve this nonrelativistic, electronic Schrödinger equation for $E^{\text{eff}}(\boldsymbol{R})$, that is, the energy corresponding to a given arrangement of nuclei. If the Schrödinger equation is solved for all possible arrangements of nuclei in a system, one obtains the *potential energy surface*. (In fact, one yields the ground-state potential energy surface and any number of excited-state surfaces; however, for the remainder of this chapter we will focus largely on the ground states.) This contains the information required for the quantitative description of chemical structures and processes. For example, by identifying the nuclear coordinates corresponding to local minima in the potential energy surface, one can determine the equilibrium geometries of chemical species. By comparing the energies of alternative local minima, one can determine the relative energies of alternative conformers and isomers, and thus identify the preferred (ie, global minimum energy) structure. Alternative local minima on a potential energy surface may correspond to the reactant(s) and product(s) in a chemical reaction, and by comparing their total energies (including zero-point vibrational energy) one can calculate the reaction enthalpy at 0 K. The transition structure for a chemical reaction can also be identified from the potential energy surface as a first-order saddle point, that is, a stationary point in which the energy is a local maximum in one dimension (corresponding to the reaction coordinate), and a local minimum in all other dimensions. By comparing the total energies at the transition structure and the reactants, one can calculate the energy barrier for the chemical reaction. Having identified the equilibrium geometry of a molecule, one can calculate the second derivative of the energy at that point in the potential energy surface, and this yields the vibrational frequencies of the molecule (ie, the peak positions in its IR and Raman spectra) (see VIBRATIONAL SPECTROSCOPY). The vibrational frequencies can be used to calculate the total zero-point vibrational energy, and also the vibrational contribution to the enthalpy and entropy of a molecule at any temperature. Finally, the potential energy surface provides the information required to calculate the rates of chemical reactions.

Solving the Schrödinger equation also yields the ground-state wave function for the given arrangement of nuclei. Since the square modulus of the wave function is related to the electron probability density, quantum-chemical calculations thus enable us to determine the distribution of electrons within a molecule, and hence the charge distribution. In fact, assigning charges to specific atoms within a molecule raises a number of philosophical problems, as under quantum mechanics electrons do not "belong" to any specific nucleus but are distributed throughout the molecule in *molecular* orbitals. To determine the charge on a specific atom within a molecule, it is necessary to define a scheme for dividing the molecular volume into atomic subspaces. A number of such schemes exist, and the main

ones include the Mulliken population analysis (8), the natural bond orbital analysis (20), and Atoms in Molecules (AIM) theory (21). In very broad terms, the former two schemes assign electrons to a nucleus if they are located in orbitals centered on that nucleus, but differ in the manner in which those "orbitals" are defined. By contrast, AIM theory uses a spatial definition for the atom, and generally provides the most rigorous and the most physically meaningful charges, though it is also the most computationally expensive method. A detailed discussion of wave function analysis methods is provided in Reference (9).

In summary, by solving the Schrödinger equation, one has direct access to electronic-structure information and can calculate from first principles the mechanism, kinetics, and thermodynamics of chemical reactions. In principle, such calculations can be extremely accurate, relying only upon the validity of quantum mechanics, and values for the fundamental physical constants. However, in practice, the multi-electron Schrödinger equation has no analytical solution and numerical approximations must instead be made. These approximations are a potential source of error in the calculations, and it is thus important to understand their underlying assumptions. This article is primarily concerned with ab initio molecular orbital theory, which is one of the principal approaches to solving the electronic Schrödinger equation. In this section, the main principles of ab initio molecular orbital theory are detailed. Other approaches to solving the Schrödinger equation include density functional theory and semiempirical methods, and these are also briefly outlined. Finally, the additional theoretical calculations required in order to use the output of quantum-chemical calculations to obtain the rate coefficients for chemical reactions are described. The method of molecular mechanics (MM)—which is an empirical procedure that is *not* based on solving the Schrödinger equation—is described elsewhere (22–24).

Ab Initio Molecular Orbital Theory

In ab initio molecular orbital theory, the wave function is approximated using one-electron functions or "spin orbitals" (χ). Each spin orbital is a product of a molecular orbital, $\psi(x, y, z)$, which depends on the Cartesian coordinates of the electron, and a spin function, α or β, which corresponds to the spin angular momentum of the electron being aligned along the positive or negative z-axes, respectively. The molecular orbitals (ψ_i) are represented mathematically as a linear combination of a set of N one-electron functions called *basis functions* (ϕ_μ).

$$\psi_i = \sum_{\mu=1}^{N} c_{\mu i}\phi_\mu \tag{6}$$

In this equation, the coefficients $c_{\mu i}$ are called the molecular orbital expansion coefficients, and are optimized during the computational procedure. In chemical terms, one can think of the basis functions as the sets of constituent atomic orbitals, which mix to form the molecular orbitals of the molecule. In order to approach the exact solution to the Schrödinger equation, an infinite set of basis functions would be required, as this would introduce sufficient mathematical

flexibility to allow for a complete description of the molecular orbitals. Of course, in practice a finite set of basis functions must be chosen, and this introduces a potential source of error to the calculations.

Having formed a set of N linearly independent molecular orbitals, these orbitals must then be occupied to form the wave function. In ab initio molecular orbital theory the wave function is formed as the determinant of a matrix, which for an n-electron closed-shell system [ie, n is even (If n were odd, and the system was a doublet species (having one unpaired electron), we could instead form $(n+1)/2$ orbitals, one of which would be singly occupied. The treatment of open-shell systems is discussed in more detail below.)] might be written as follows.

$$\Psi = (n!)^{-1/2} \begin{vmatrix} \psi_1(1)\alpha(1) & \psi_1(1)\beta(1) & \psi_2(1)\alpha(1) & \psi_2(1)\beta(1) & \cdots & \psi_{n/2}(1)\alpha(1) & \psi_{n/2}(1)\beta(1) \\ \psi_1(2)\alpha(2) & \psi_1(2)\beta(2) & \psi_2(2)\alpha(2) & \psi_2(2)\beta(2) & \cdots & \psi_{n/2}(2)\alpha(2) & \psi_{n/2}(2)\beta(2) \\ \vdots & \vdots & \vdots & \vdots & \vdots & \vdots & \vdots \\ \psi_1(n)\alpha(n) & \psi_1(n)\beta(n) & \psi_2(n)\alpha(n) & \psi_2(n)\beta(n) & \cdots & \psi_{n/2}(n)\alpha(n) & \psi_{n/2}(n)\beta(n) \end{vmatrix} \tag{7}$$

This is usually abbreviated as follows.

$$\Psi = |\chi_1(1)\chi_2(2)\ldots\chi_n(n)| \tag{8}$$

In this determinant, which is known as the Slater determinant (25), the first row corresponds to all possible assignments of electron 1 to all of the spin orbitals, the second to all possible assignments of electron 2, and so on. The factor of $(n!)^{-1/2}$ ensures that the total probability of finding an electron anywhere in space is 1.

We have already seen that, from our set of N basis functions (where N should approach infinity), we can form N linearly independent molecular orbitals. However, in an n-electron system, we choose only $n/2$ of these orbitals (if n is even) to occupy in our Slater determinant. Clearly the most appropriate orbitals to occupy should be the $n/2$ lowest energy orbitals, and this is the basis of the well-known *Hartree–Fock theory* (26). While Hartree–Fock theory performs adequately in many cases, its use of a single determinant wave function can also frequently lead to considerable error. The problem is that this approach fails to account for Coulombic electron correlation. That is, it is assumed that each electron "sees" the other electrons as an average electric field and thus no instantaneous electron–electron interactions are included. To approach the exact solution to the Schrödinger equation, the wave function must instead be represented as a linear combination of (an infinite number of) Slater determinants. In each of the additional determinants, one or more of the lowest energy orbitals are substituted with the (previously unoccupied) higher energy orbitals. In chemical terms, one might think of this as allowing for contributions to the wave function from the various possible excited configurations. This approach is known as *configuration interaction* (CI), and when all possible excited configurations are included the method is known as *Full CI*.

Under ab initio molecular orbital theory, the exact solution to the Schrödinger equation could be obtained using the Full CI method in conjunction with an infinite basis set. Since this is impractical, computational methods must place restrictions

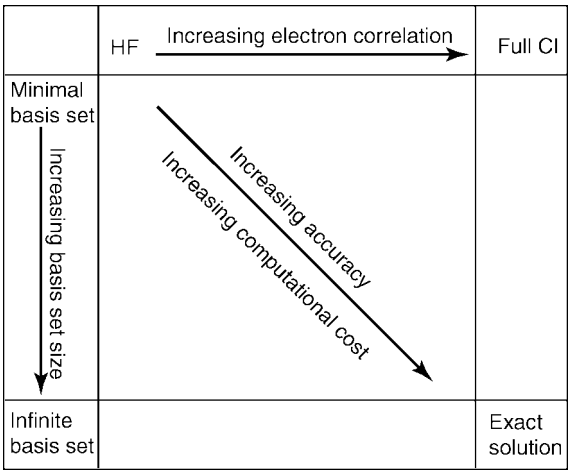

Fig. 1. Pople diagram (8) illustrating the dependence of the accuracy of a computational method on the basis set and the treatment of correlation.

on the number of basis functions included in the calculation, and (in general) simplify the method for treating correlation. The combination of method and basis set chosen for a calculation forms the "level of theory," and by convention is written as "*method*/*basis set*" (using the standard abbreviations for the particular method and basis set chosen). By increasing the size of the basis set and/or improving the method, one can improve the accuracy of the calculation but also its computational cost (see Fig. 1). Furthermore, the performance of a given level of theory can vary considerably depending upon the chemistry of the system, and the type of properties being calculated. The choice of level of theory is therefore very important, and a qualitative understanding of the approximations made at the various levels of theory is thus helpful in choosing appropriate theoretical procedures. For the remainder of the present section, the main qualitative features of commonly used methods and basis sets are described. The accuracy and applicability of these methods for studying the reactions of relevance to free-radical polymerization is discussed in a following section.

Basis Sets.

LCAO Scheme. A basis set is a set of one-electron functions, which are combined to form the molecular orbitals of the chemical species. This is known as the Linear Combination of Atomic Orbitals (LCAO) scheme. To approach the exact solution to the Schrödinger equation, an infinite set of basis functions would be required, as this would introduce sufficient mathematical flexibility to allow for a complete description of the molecular orbitals. In practical calculations, we must use a finite number of basis functions, and it is thus important to choose basis functions that allow for the most likely distribution of electrons within the system. This is achieved using basis functions that are based on the atomic orbitals of the constituent atoms of the molecule. For example, if a chemical system contained an oxygen atom, the chosen basis set would include functions describing each of the 1*s*, 2*s*, and three 2*p* orbitals of an oxygen atom.

The basis functions that are typically used in practice are called Gaussian-type orbitals, and examples of their functional form for s-type and p_y-type orbitals are shown below.

$$g_s(\alpha, r) = \left(\frac{2\alpha}{\pi}\right)^{3/4} e^{-\alpha r^2} \tag{9}$$

$$g_y(\alpha, \boldsymbol{r}) = \left(\frac{128\alpha^5}{\pi^3}\right)^{1/4} y\, e^{-\alpha r^2} \tag{10}$$

The exponent α determines the size of the orbital, and standard values have been determined for the different orbitals on the different atoms. Gaussian-type orbitals such as those shown in equations 9 and 10 are called *primitive Gaussians*. *Contracted Gaussians* are also used, and these consist of linear combinations of primitive Gaussians:

$$\phi_\mu = \sum_p d_{\mu p} g_p \tag{11}$$

The coefficients in this expression ($d_{\mu p}$) are fixed for the basis set of a given atom, and should not be confused with the molecular orbital expansion coefficients ($C_{\mu i}$) of equation 6, which are determined for a given system during the ab initio calculation.

Basis sets thus contain sets of primitive or contracted Gaussians, which correspond to the atomic orbitals of the constituent atoms. *Minimal basis sets* typically contain exactly the number of functions required to accommodate the electrons in the system while maintaining the overall spherical symmetry. For example, a minimal basis set would contain a 1s function for each hydrogen atom, 1s, 2s, and three 2p functions for each carbon atom, and so on. However, in cases where the low lying unoccupied orbitals are frequently involved in bonding (eg, the 2p orbitals of Li or Be), popular minimal basis sets (such as STO-3G) include these additional functions as well.

The problem with minimal basis sets is that the size and shape of the atomic orbitals are fixed, and all that can be varied in the quantum chemical calculation is their contribution to the overall molecular orbitals. However, in reality, the size and shape of the atomic orbitals (and especially the valence orbitals) can depend heavily upon the molecular environment. For example, in polar environments, we might expect a greater degree of asymmetry in the 2p orbitals of oxygen, compared with the same orbitals in nonpolar environments. One way of resolving this problem would be to create individual basis sets for each atom in each conceivable molecular environment, but this would not only be impractical, it would also defeat the purpose of performing ab initio calculations. Instead, a practical solution to this problem is to include additional basis functions of varying sizes and shapes. By varying their individual contribution to the overall molecular orbitals, one effectively introduces flexibility to the size and shape of the constituent atomic orbitals. Some of the main extensions to a minimal basis set are outlined in the following.

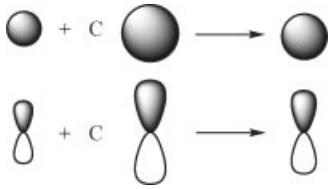

Fig. 2. Demonstration of how the mixing of two basis functions of different size is equivalent to introducing a single basis function with variable size. The basis functions are represented schematically as the boundary surface within which there is a 90% probability of finding the electron. In the first example, two *s*-type basis functions are mixed, while in the second example two *p*-type functions are mixed.

(1) *Double zeta, triple zeta, and quadruple zeta basis sets* include additional sets of each basis function (2, 3, or 4 sets respectively), with each additional set having a different size. By varying the relative contribution of the alternative sizes to the overall molecular orbital, one effectively introduces a single function with a variable size (see Fig. 2).

(2) *Split-valence basis sets* are a simplification to the double, triple, and quadruple zeta basis sets described above. Since the inner shell orbitals are not usually involved in bonding, and their energies are reasonably independent of their molecular environment, it is usually only necessary to include the extra basis functions for the valence orbitals. Basis sets that include different numbers of basis functions for the inner shell and valence electrons are known as split-valence basis sets.

(3) *Polarization functions* are typically included in basis sets to allow for asymmetry in the electron distribution (see Fig. 3). They also allow for the participation of the low lying unfilled atomic orbitals in bonding. Polarization functions typically consist of basis functions corresponding to the low lying unfilled atomic orbitals. For example, the basis set for an oxygen atom might typically include a set of *d*-type orbitals, while those for hydrogen might include a set of *p*-type orbitals. Larger basis sets often include additional polarization functions of higher angular momentum. For example, the 6-311 + G(3df,2pd) basis set includes a set of *f*-type functions and three sets of *d*-type functions for each first row atom, as well as two sets of *p*-type functions and a set of *d*-type functions for each hydrogen atom.

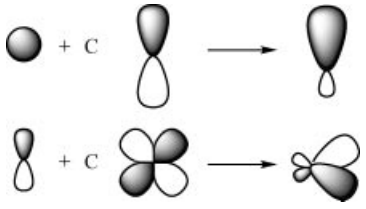

Fig. 3. Demonstration of the effect of polarization functions. In the first example an *s*-type and a *p*-type function are mixed, while in the second case a *p*-type and a *d*-type function are mixed. The mixing of higher angular momentum basis functions allows for an asymmetric distribution of electrons.

(4) *Diffuse functions* are basis functions that have very large amplitudes, far from the atomic nucleus. Sets of diffuse functions are typically added to the basis set when describing species (such as anions) where the electrons are not held very tightly to the nucleus.

(5) *Effective core potentials* (ECPs) are typically used to replace the basis functions of the inner shell electrons for atoms beyond the third row. This reduces the computational cost of the calculations, and is possible because the inner shell electrons on such heavy atoms are relatively unaffected by the molecular environment. Effective core potentials also include corrections for relativistic effects, which are significant for the inner shell electrons of heavy atoms. One of the most commonly used ECPs is called LANL2DZ.

Two commonly used families of extended basis sets are the Pople basis sets (8) and the Dunning basis sets (27). It is worth making a few brief comments on their notation.

(1) *Pople basis sets* have names such as "6-311 + G(3df,2p)." The "6-311" part refers to the fact that it is a split valence set with one copy of each basis function on the inner shell electrons, and three copies on the valence electrons. The "6" refers to the fact that the basis functions on the inner shell electrons consist of a contracted Gaussian-type orbital formed from 6 primitive Gaussians. The "311" part refers to the fact that one set of basis functions on the valence electrons are contracted Gaussians, each formed from 3 primitive Gaussians, while the other two sets of basis functions are primitive Gaussians. The "+" part refers to the fact that one set of *s*-type and *p*-type diffuse functions have been included for each heavy (ie, bigger than hydrogen) atom. The 6-311 ++ G basis set includes an additional set of *s*-type diffuse functions on hydrogen atoms as well. The functions in the bracketed part of the expression (3df,2p) are the polarization functions. The "3df" part refers to the fact that 3 sets of *d*-type functions and one set of *f*-type functions are included for each heavy atom, and "2p" implies that two sets of *p*-type functions are included for each hydrogen atom. Finally, the notations 6-31G* and 6-31G** are also frequently used. The first "*" is an abbreviation for (d) and indicates that a set of *d*-type functions are included for each non-hydrogen atom, while "**" stands for (d,p) and indicates that in addition to the d-type functions for the non-hydrogen atoms, a set of *p*-type functions are included for each hydrogen atom.

(2) *Dunning basis sets* have names such as "cc-pV*n*Z." This notation stands for "correlation-consistent polarized valence *n*-zeta." For a double zeta basis set, *n* is replaced by a "D," for a triple zeta basis set, *n* is replaced by a "T," for a quadruple zeta basis set, *n* is replaced by a "Q," for a quintuple basis set we use a "5," and for a sextuple basis set we use a "6." When diffuse functions are included, an "aug" prefix is included in the name, as in "aug-cc-pVTZ." The cc-pVTZ basis set generally has a performance similar to 6-311G(2df,p). A special feature of the Dunning basis sets is that they have been designed so the series DZ, TZ, QZ, 5Z, 6Z... *systematically* converges on the infinite basis set limit (27). This feature has been exploited in the

infinite basis set extrapolation procedure of Martin and Parthiban (28) (see below).

Plane Waves. While standard ab initio calculations use the LCAO scheme almost exclusively, density functional theory (DFT) calculations (discussed later) sometimes use *plane wave* basis sets. These are solutions of the Schrödinger equation for a free particle and take the general form,

$$g^{PW} = \exp[i\vec{\boldsymbol{k}}\vec{\boldsymbol{r}}] \tag{12}$$

where the vector $\vec{\boldsymbol{k}}$ is related to the momentum $\vec{\boldsymbol{p}}$ of the wave through $\vec{\boldsymbol{p}} = \hbar\vec{\boldsymbol{k}}$. One of the advantages of plane wave basis sets is that they can handle calculations with periodic boundary conditions, and they are thus used widely in solid-state physics. However, a disadvantage is that large basis sets are normally required to achieve acceptable accuracy and, as a result, plane waves are rarely used in calculations of molecular systems. For a detailed discussion of plane wave basis sets, and their application to Car–Parrinello (29) ab initio direct dynamics techniques, the reader is referred to a review by Blöchl and co-workers (30).

Methods.

Hartree–Fock (HF). The foundation of ab initio molecular orbital theory is the Hartree–Fock (HF) method. As we saw above, it is based on a single-determinant wave function (eq. 7) in which the electrons are assigned to the lowest energy orbitals. In fact the Slater determinant of equation 7 applies to *closed-shell systems*, that is, the n electrons occupy the $n/2$ orbitals in pairs of opposite spin. This method is known more specifically as restricted Hartree–Fock (RHF). For *open-shell systems* (that is, those having one or more unpaired electrons), two approaches are possible. In restricted-open-shell Hartree–Fock (ROHF), the determinant is formed from a set of molecular orbitals, which are either doubly or singly occupied, according to the multiplicity of the species. For example, for a radical (doublet) species, the determinant would be formed from $(n + 1)/2$ orbitals, and one of these would be singly occupied. This ensures that there is exactly one unpaired spin in the system, and the species is indeed a pure doublet. In unrestricted Hartree–Fock (UHF), the α and β spin orbitals are defined and optimized separately. Thus there would be $(n + 1)/2$ occupied α spin orbitals, and $(n - 1)/2$ occupied β spin orbitals. The principal differences between the RHF, ROHF, and UHF theory are illustrated in Figure 4.

The UHF method offers some advantages over the ROHF method. In particular, the additional freedom in the wave function (with the provision for noninteger natural orbital occupation numbers) allows it to account in part for nondynamic electron correlation, and leads to lower energies and a better qualitative description of bond dissociation (9). Through its introduction of spin polarization effects, the UHF method can also provide a better (though by no means perfect) qualitative treatment of hyperfine coupling constants (31). However, a disadvantage of UHF is that the independent optimization of the α and β spin orbitals can result in nominally equivalent α and β orbitals having slightly different eigenvalues. In other words, a doublet species could have effectively more than one unpaired electron in the system. This physically unrealistic phenomenon is known as *spin*

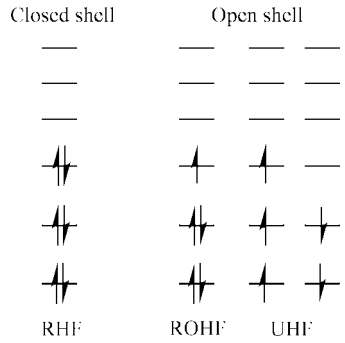

Fig. 4. Electron configuration diagrams highlighting the differences between restricted Hartree–Fock theory (RHF), restricted open-shell Hartree–Fock theory (ROHF), and unrestricted Hartree–Fock theory (UHF).

contamination, and can be a particular problem for the transition structures in the propagation steps of free-radical polymerization. Assessment studies (32,33) for such reactions have revealed that spin-contaminated UHF wave functions make poor starting points for Möller–Plesset (MP) perturbation theory calculations (see below). By contrast, MP calculations based on ROHF wave functions (such as ROMP2) show improved agreement with higher level values. Interestingly, it has been found that for high level methods such as coupled cluster theory (see below), the choice of the starting wave function (ie, UHF vs ROHF) makes little difference to the final calculated energies and geometries for radical reactions (34).

Having constructed a wave function, the remaining unknown parameters in the Schrödinger equation are the molecular orbital expansion coefficients ($c_{\mu i}$), as defined in equation 6. Determining the optimum values of these coefficients is thus the principal task of an ab initio calculation. It is beyond the scope of this chapter to outline the mathematical equations and numerical algorithms used to achieve this, but it is worth describing the general approach in qualitative terms. The basis of this procedure is the *variational principle*. It merely states that for any antisymmetric normalized function of the electronic coordinates (eg, a Slater determinant), the energy of this function is always greater than the expectation value of the exact wave function for the ground state. In other words, the exact wave function serves as a lower bound to the energies calculated from our approximate wave function, and the optimal coefficients $c_{\mu i}$ are merely those that minimize the energy. This principle leads to the Roothaan–Hall equations (35), which are solved iteratively until the $c_{\mu i}$ coefficients converge. At convergence the coefficients are "self-consistent," and hence the HF theory is also known as self-consistent field (SCF) theory.

Configuration Interaction (CI). The description of the wave function using a single determinant (as in HF theory) fails to take electron correlation into account. To obtain the exact solution to the Schrödinger equation we instead need to construct the wave function as a linear combination of determinants, with each additional determinant corresponding to one of the various possible excited configurations obtained when electrons are promoted to the previously unoccupied higher energy orbitals (see Fig. 5). The resulting wave function is written as follows.

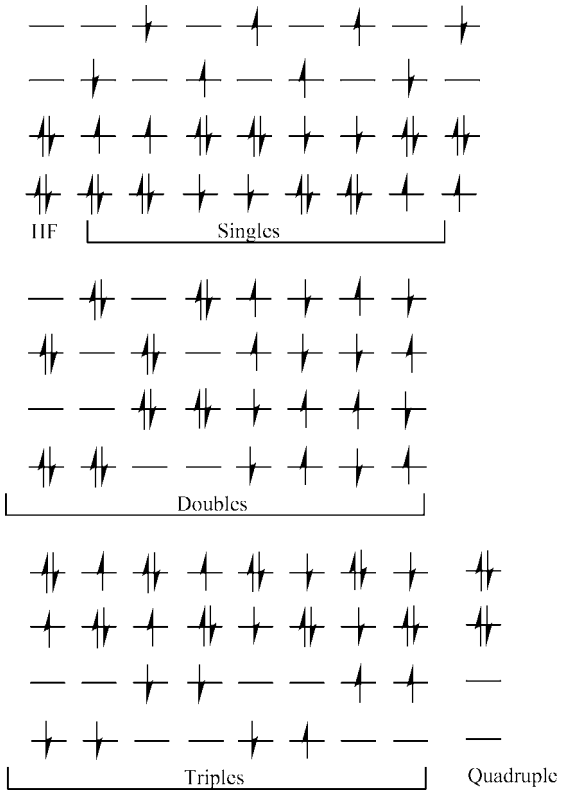

Fig. 5. Electron configuration diagrams showing the configurations corresponding to the HF wave function, and the various possible excited configurations. For this 4-electron system, the combination of single, double, triple, and quadruple excitations constitutes full CI. However, with an infinite basis set, there would be an infinite number of unoccupied orbitals (instead of the two shown here) to promote the electrons into, and thus an infinite number of determinants would be required to obtain the exact solution to the Schrödinger equation.

$$\Psi = a_0\Psi_0 + \sum_{s>0} a_s\Psi_s \tag{13}$$

The Ψ_0 wave function is the HF wave function, while the various Ψ_s determinants correspond to the various excited configurations. The CI method introduces a further set of unknown parameters into the calculation, the coefficients (a_s). These coefficients are optimized as part of the ab initio calculation in order to minimize the energy, in line with the variational principle. CI methods can be based on an RHF wave function (RCI), a UHF wave function (UCI), or an ROHF wave function (URCI).

Full CI is impractical with an infinite basis set (and hence an infinite number of virtual orbitals), or indeed with a finite basis set and a reasonably small number of electrons. For example, even for water with the small 6-31G(d) basis set, the full CI treatment would involve nearly 5×10^8 configurations. For this

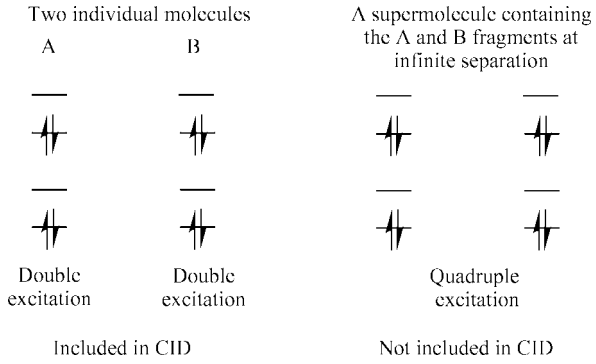

Fig. 6. Electron configuration diagrams illustrating the lack of size consistency in truncated CI. In the first case, A and B are treated separately by CID, and the treatment thus considers the double excitations of electrons in each molecule. In the second case, A and B are calculated as a supermolecule having the A and B fragments at (effectively) infinite separation. Now the simultaneous excitation of two electrons from each of the A-type and B-type orbitals constitutes a quadruple excitation, which is not included in the CID method.

reason, methods based on a truncated CI procedure are generally used in practice. These methods consider a limited number of excited determinants, such as all possible single excitations (CIS) or all possible single and double excitations (CISD). Restricting the CI procedure to single, double, and possibly triple excitations is usually a reasonable approximation, since excitations involving one, two, or three electrons have a considerably higher probability of occurring, and thus contributing to the wave function, compared with excitations of several electrons simultaneously.

However, simple truncated CI methods suffer from a lack of *size consistency*. That is, the error incurred in calculating molecules A and B separately is different from that incurred in calculating a single species, which contains A and B separated by a large (effectively infinite) distance. This can be seen quite clearly in the example shown in Figure 6. The lack of size consistency can be a major problem as it introduces an additional error to calculations of barriers and enthalpies in nonunimolecular reactions. This problem is addressed by including additional terms in the wave function, and the methods based on this approach include *quadratic configuration interaction* (QCI) and *coupled cluster theory* (CC). These methods are typically applied with single and double excitations (QCISD or CCSD), and the triple excitations are often included perturbatively, leading to methods such as QCISD(T) and CCSD(T). When applied with an appropriately large basis set, these methods usually provide excellent approximations to the exact solution to the Schrödinger equation. However, these methods are still very computationally expensive.

Möller–Plesset (MP) Perturbation Theory. By convention, the correlation energy is simply the difference between the Hartree–Fock energy and the exact solution to the Schrödinger equation. Rather than approximate the exact solution to the Schrödinger equation by attempting to build the exact wave function through configuration interaction, an alternative (and considerably less expensive approach) is to estimate the correlation energy as a perturbation on the

Hartree–Fock energy. In other words, the exact wave function and energy are expanded as a perturbation power series in a perturbation parameter λ as follows.

$$\Psi_\lambda = \Psi^{(0)} + \lambda\Psi^{(1)} + \lambda^2\Psi^{(2)} + \lambda^3\Psi^{(3)} + \cdots \quad (14)$$

$$E_\lambda = E^{(0)} + \lambda E^{(1)} + \lambda^2 E^{(2)} + \lambda^3 E^{(3)} + \cdots \quad (15)$$

Expressions relating terms of successively higher orders of perturbation are obtained by substituting equations 14 and 15 into the Schrödinger equation, and then equating terms on either side of the equation. Having obtained these expressions, it simply remains to evaluate the first terms in the series, and this is achieved by taking the $\Phi^{(0)}$ term as the Hartree–Fock wave function. In practice, the MP series must be truncated at some finite order. Truncation at the first order (ie, $E^{(1)}$) corresponds to the Hartree–Fock energy, truncation at the second order is known as MP2 theory, truncation at the third order as MP3 theory, and so on. MP methods based on an RHF, UHF, or ROHF wave function are referred to as RMP, UMP, or ROMP respectively.

When truncated at the second, third, or possibly fourth orders, the MP methods offer a very cost-effective method for estimating the correlation energy. They are also size-consistent methods. However, the validity of truncating the series at some finite order depends on the speed of convergence of the series, and this will vary considerably depending on how closely the Hartree–Fock energy approximates the exact energy. Indeed in some cases, the MP series can actually diverge, and the application of MP methods can in such cases increase rather than decrease the errors in the calculation. As noted above, a relevant example of this problem occurs in the transition structures for radical addition to alkenes for which UMP2 calculations (based on the spin-contaminated UHF wave function) are frequently subject to large errors (32,33). Furthermore, when truncated at some finite order, the MP methods are not variational, and may thus overestimate the correction to the energy. Hence, although MP procedures frequently provide excellent cost-effective performance, they must be applied with caution.

Composite Procedures. The use of CCSD(T) or QCISD(T) methods with a suitably large basis set generally provides excellent approximations to the exact solution of the Schrödinger equation. However, such methods are computationally expensive, and in practical calculations smaller basis sets and/or lower cost methods must be adopted. A major advance in recent years has been the development of high level composite procedures, which approximate high level calculations through a series of lower level calculations. Some of the main strategies that are used are described in the following.

Firstly, it has long been realized that geometry optimizations and frequency calculations are generally less sensitive to the level of theory than are energy calculations. For example, as will be discussed in a following section, detailed assessment studies (36,37) have shown that even HF/6-31G(d) can provide reasonable approximations to the considerably more expensive CCSD(T)/6-311 + G(d,p) level of theory, for the geometries and frequencies of the species in radical addition to multiple bonds (such as C=C, C≡C, and C=S). By contrast, very high levels of

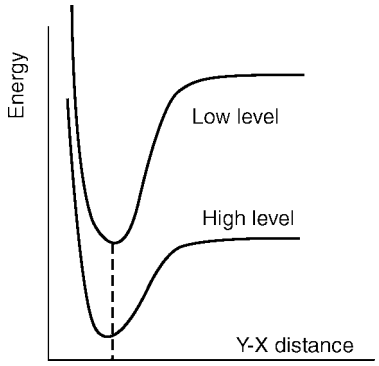

Fig. 7. Illustration of the relative performance of the high and low levels of theory for geometry optimizations and energy calculations. The low level of theory shows a very large error for the absolute energy of structure, a smaller error for the Y—X bond dissociation energy (ie, the well depth), and a very small error for the optimum geometry of the Y—X bond. This reflects the increasing possibility for cancelation of error. In the bond dissociation energy, errors in the absolute energies of the isolated $Y^{\bullet}$ and $X^{\bullet}$ species are canceled to some extent by errors in the Y—X energies. In the geometry optimizations, further cancelation is possible because the position of the minimum energy structure depends on the relative energies of Y—X compounds having very similar Y—X bond lengths.

theory are required to describe the barriers and enthalpies of these reactions. The improved performance of low levels of theory in geometry optimizations and frequency calculations can be understood in terms of the increased opportunity for the cancelation of error, as such quantities depend only upon the *relative* energies of very similar structures (see Fig. 7). In contrast, reaction barriers and enthalpies depend upon the relative energies of the reactants and transition structures or products, and these can have quite different structures, with different types of chemical bonds. It is thus possible to optimize the geometry of a compound at a relatively low level of theory, and then improve the accuracy of its energy using a single higher level calculation (called a "single point"). Since geometry optimizations and frequency calculations are more computationally intensive than single-point energy calculations, this approach leads to an enormous saving in computational cost. By convention, the final composite level of theory is written as "energy method/energy basis set//geometry method/geometry basis set."

Secondly, an extension to the above strategy is known as the *IRCmax* (intrinsic reaction coordinate) *procedure*. It was developed (38) for improving the geometries of transition structures, though techniques based on the same principle have also been used to calculate improved imaginary frequencies and tunneling coefficients (39–41). While low levels of theory are generally suitable for optimizing the geometries of stable species, the geometries of transition structures are sometimes subject to greater error at these low levels of theory. To address this problem, the minimum energy path (MEP) for a reaction is first calculated at a low level of theory, and then improved via single-point energy calculations at a higher level of theory. Now, the transition structure is simply the maximum energy structure along the MEP for the reaction. By identifying the transition structure from the high level MEP (rather than the original low level MEP), one effectively optimizes the reaction coordinate at the high level of theory (see Fig. 8).

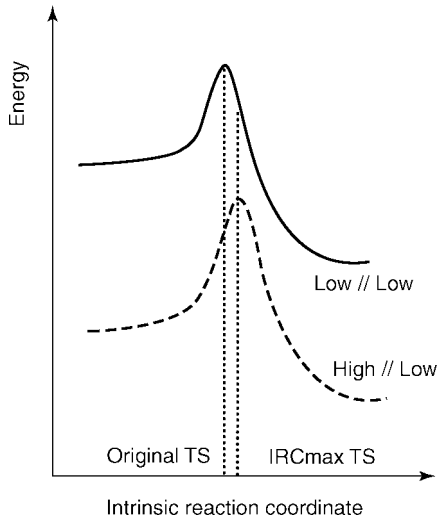

Fig. 8. Illustration of the IRCmax procedure. The minimum energy path (MEP, also known as the intrinsic reaction coordinate or IRC) is optimized at a low level of theory, and then improved using high level single-point energy calculations. The improved transition structure is then identified as the maximum in the high level MEP. This effectively optimizes the reaction coordinate (often the most sensitive part of the geometry optimization) at a high level of theory.

Thirdly, one can improve the single-point energy calculations themselves using additivity and/or extrapolation procedures. In the former case, the energy is first calculated with a high level method (such as CCSD(T)) and a small basis set. The effect of increasing to a large basis set is then evaluated at a lower level of theory (such as MP2). The resulting basis set correction is then added to the high level result, thereby approximating the high level method with a large basis set. The calculation may be summarized as follows.

$$\begin{array}{l} \text{High Method/Small Basis Set} \\ +\text{Low Method/Large Basis Set} \\ -\text{Low Method/Small Basis Set} \\ \hline \approx\text{High Method/Large Basis Set} \end{array} \qquad (16)$$

Procedures for extrapolating the energies obtained at a specific level of theory to the corresponding infinite basis set limit have also been devised. The two main procedures are the extrapolation routine of Martin and Parthiban (18), which takes advantage of the systematic convergence properties of the Dunning DZ, TZ, QZ, 5Z, ... basis sets, and the procedure of Petersson and co-workers (42), which is based on the asymptotic convergence of MP2 pair energies. For the mathematical details of these extrapolation routines, the reader is referred to the original references. The Martin extrapolation procedure is easily implemented on a spreadsheet, while the Petersson extrapolation procedure has been coded into the GAUSSIAN (43) computational chemistry software package.

Building on these strategies, several composite procedures for approximating CCSD(T) or QCISD(T) energies with a large or infinite basis set have been devised. The main families of procedures in current use are the G3 (44), Wn (28), and CBS (42) families of methods. These are described in the following.

(1) In the G3 methods, the CCSD(T) or QCISD(T) calculations are performed with a relatively small basis set, such as 6-31G(d), and these are then corrected to a large triple zeta basis set via additivity corrections, carried out at the MP2 and/or MP3 or MP4 levels of theory (44). There are many variants of the G3 methods, depending upon the level of theory prescribed for the geometry and frequency calculations, the methods used for the basis set correction, and depending on whether CCSD(T) or QCISD(T) is used at the high level of theory. Of particular note are the RAD variants (45) of G3 (such as G3-RAD and G3(MP2)-RAD), which have been designed for the study of radical reactions. G3 methods include an empirical correction term, which has been estimated against a large test set of experimental data, and spin-orbit corrections (for atoms). The G3 methods have been extensively assessed against test sets of experimental data (including heats of formation, ionization energies, and electron affinities) and are generally found to be very accurate, typically showing mean absolute deviations from experiment of approximately 4 $kJ \cdot mol^{-1}$.

(2) In the Wn methods, high level CCSD(T) calculations are extrapolated to the infinite basis set limit using the extrapolation routine of Martin and Parthiban (28). Additional corrections are included for scalar relativistic effects, core-correlation, and spin-orbit coupling in atoms. No additional empirical corrections are included in this method. The Wn methods are very high level procedures, and have been demonstrated to display chemical accuracy. For example, the W1 procedure was found to have a mean absolute deviation from experiment of only 2.5 $kJ \cdot mol^{-1}$ for the heats of formation of 55 stable molecules. For the (more expensive) W2 theory, the corresponding deviation was less than 1 $kJ \cdot mol^{-1}$.

(3) In the CBS procedures, the complete basis extrapolation procedure of Petersson and co-workers is used (42). This calculates the infinite basis set limit at the MP2 level of theory. This is then corrected to the CCSD(T) level of theory using additivity procedures, as in the G3 methods. The CBS procedures also incorporate an empirical correction, and an additional (empirically determined) correction for spin contamination. The accuracy of this latter term for the transition structures of radical addition reactions has recently been questioned (36,37). Nonetheless, the CBS procedures also show similar (excellent) performance to the G3 methods, when assessed against the same experimental data for stable molecules (42).

In summary, using composite procedures, high level calculations can now be performed at a reasonable computational cost. With continuing rapid increases in computer power, details on the computational speeds of the various methods would be rapidly outdated. However, it is worth noting that, at the time of writing, the most cost-effective G3 procedures can be routinely applied to molecules as big

as $CH_3SC^{\bullet}(CH_2Ph)SCH_3$, while the state-of-the-art Wn methods are restricted to smaller molecules, such as $CH_3CH_2CH(CH_3)^{\bullet}$. However, in the near future one can look forward to applying these methods to yet larger systems. In general, the composite procedures described above offer "chemical accuracy" (usually defined as uncertainties of 4–8 $kJ \cdot mol^{-1}$), with the best methods offering accuracy in the kJ range. However, careful assessment studies are nonetheless recommended when applying methods to new chemical systems. A brief discussion of the performance of computational methods for the reactions of relevance to free-radical polymerization is provided in a following section.

Multireference Methods. The post-SCF methods discussed above are all based on a HF or single configuration starting wave function. At the impractical limit of performing full CI (or summing all terms in the MP series) with an infinite basis set, these methods will yield the exact solution to the nonrelativistic Schrödinger equation. However, when truncated to finite order, the use of a single reference wave function can sometimes lead to significant errors. This is particularly the case in the calculation of diradical species (such as the transition structures for the termination reactions in free-radical polymerization), excited states, and unsaturated transition metals. In such situations, the starting wave function itself should be represented as a linear combination of two or more configurations, as follows.

$$\Psi = \sum_j a_j \Psi_j \tag{17}$$

In this equation, the individual wave functions are formed from the lowest energy configuration, and various excited configurations of the Slater determinants, and the a_j coefficients are optimized variationally. While this method, which is known as multireference self-consistent field (MCSCF), may seem analogous to the single-reference CI methods discussed above, there is an important difference between them. In MCSCF, the molecular orbital coefficients (the $c_{\mu i}$ in eq. 6) are optimized for all of the contributing configurations. In contrast, in single-reference methods, the molecular orbital coefficients are optimized for the Hartree–Fock wave function, and are then held fixed at their HF values.

The optimization of both the orbital coefficients and the contribution of the various configurations to the overall wave function can be very computationally demanding. As a result, MCSCF methods typically only consider a small number of configurations, and one of the key problems is choosing which configurations to include. In complete active space self-consistent field (CASSCF), the molecular orbitals are divided into three groups: the inactive space, the active space, and the virtual space (see Fig. 9). The wave function is then formed from all possible configurations that arise from distributing the electrons among the active orbitals (ie, full CI is performed within the active space). It then remains to decide which occupied and virtual orbitals should be included in the active space. Where possible, it is advisable to include all valence orbitals in the active space, together with an equivalent number of virtual orbitals. However, as with any full CI calculation, the computational cost rapidly increases with the number of electrons and orbitals included, and CASSCF calculations are currently limited to active spaces of approximately 16 electrons in 16 molecular orbitals. Thus, for large chemical

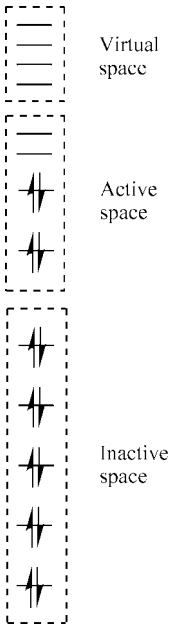

Fig. 9. The partitioning of orbitals between the inactive, active, and virtual spaces in a CASSCF calculation.

systems, full valence active spaces are not as yet possible, and instead a restricted number of orbitals must be chosen.

In non-full valence CASSCF, the active space is typically selected on the basis of "chemical intuition," and might include orbitals that are directly involved in the chemical reaction, or are interacting strongly with the reacting orbitals. For example, in the case of radical–radical reactions, a simplified multireference approach would be a CAS(2,2) method, in which the active space would consist of the two singly occupied molecular orbitals. However, such restricted methods must be used cautiously as they recover correlation in the active space, but not in the inactive space or between the active and inactive spaces. As a result, such procedures can sometimes introduce a bias, which, for example, might lead to an overestimation of the biradical character in systems with nearly degenerate singlet and triplet states (9).

Multireference methods primarily account for nondynamic electron correlation, which arises from long-range interactions involving nearly degenerate states. It is still necessary to correct for dynamic correlation, which arises from short-range electron–electron interactions, and which is primarily addressed in the single-reference post-SCF methods, such as QCISD or MP2. For example, in the case of CI-based methods, it would be necessary to consider excitations from the inactive (as well as active) space orbitals, into all of the virtual orbitals. Multireference versions of post-SCF methods have been derived, including multireference CI (eg, MR(SD)CI, which includes all single and double excitations) and multireference perturbation theory (eg CASPT2, which is a multireference analogue of MP2). The former of these methods is generally more accurate but

also more computationally demanding. For more information on multireference methods, the reader is referred to an excellent review by Schmidt and Gordon (46).

Semiempirical Methods

Semiempirical methods are often used to study large systems for which ab initio calculations are not feasible. A number of different procedures are available, with the main methods being CNDO, INDO, MNDO, MINDO/3, AM1, and PM3. The latter two procedures are generally the best performing of the current available methods, and are thus the most popular in current use. Semiempirical methods are based on ab initio molecular orbital theory, but neglect several of the computationally intensive integrals that are required in Hartree–Fock theory. Depending on the procedure, certain interactions between orbitals are either completely neglected or replaced by parameters that are either derived from experimental data for the isolated atoms or obtained by fitting the calculated properties of molecules to experimental data. This greatly reduces the computational cost of the calculations; however, it can also introduce enormous errors. For more detailed information on the principles and limitations of semiempirical methods, the reader is referred to an article by Stewart (47).

In general, the semiempirical methods perform reasonably well, provided that the species (and properties) being calculated are very similar to those for which the method was parameterized. However, there are many situations in which these methods fail dramatically, and hence such methods should be applied with caution and their accuracy should always be checked against high level calculations for prototypical reactions. In this context it should be noted that such testing has already been performed for the case of radical addition to C=C bonds (32). In this work, semiempirical methods were shown to fail dramatically, and hence (current) semiempirical methods are not generally recommended for studying the kinetics and thermodynamics of the propagation step in free-radical polymerization.

Density Functional Theory

Density functional theory (DFT) is a different quantum chemical approach to obtaining electronic-structure information. The basis of DFT is the Hohenberg–Kohn theorem (48), which demonstrates the existence of a unique functional for determining the ground-state energy and electron density exactly. In the ab initio methods described above, we recall that their objective was to determine the wave function (an eigenfunction) of a system, which thereby enables the energy (the eigenvalue) and electron density (the square modulus of the wave function) to be evaluated. The Hohenberg–Kohn theorem implies that the electronic energy can be calculated from the electron density and there is thus no need to evaluate the wave function. This represents an enormous simplification to the calculation since, in an n-electron system, the wave function is a function of $3n$ variables, whereas the electron density is a function of just 3 variables. Unfortunately, the

Hohenberg–Kohn theorem is merely an existence proof, rather than a constructive proof, and thus the exact functional for connecting the energy and electron density is not known. Hence, although in principle DFT can provide the exact solution to the Schrödinger equation, in practice an approximate functional must be used, and this introduces error to the calculations.

The DFT methods used in practice are based on the equations of Kohn and Sham (49). They partitioned the total electronic energy into the following terms.

$$E = E^{\mathrm{T}} + E^{\mathrm{V}} + E^{\mathrm{J}} + E^{\mathrm{X}} + E^{\mathrm{C}} \tag{18}$$

In this equation, E^{T} is the kinetic energy term (arising from the motions of the electrons), E^{V} is the potential term (arising from the nuclear–electron attraction and the nuclear–nuclear repulsion), E^{J} is the electron–electron repulsion term, E^{X} is the exchange term (arising from the antisymmetry of the wave function), and E^{C} is the dynamical correlation energy of the individual electrons. The sum of the E^{T}, E^{V}, and E^{J} terms corresponds to the classical energy of the charge distribution, while the exchange and correlation terms account for the remaining electronic energy. The task of DFT methods is thus to provide functionals for the exchange and correlation terms. As a matter of notation, DFT methods are typically named as *exchange functional–correlation functional*, using standard abbreviations for the various functionals.

Before discussing the functionals themselves, it is worth making a few comments on *unrestricted Kohn–Sham theory* (50). The effective potential of the Kohn–Sham equations contains no reference to the spin of the electrons, and the energy is simply a functional of the total electron density. (It will only become a functional of the individual spin densities if the potential itself contains spin-dependent parts, such as it would in the presence of an external magnetic field.). Hence, if the exact functional were available, there would normally be no need to consider the α and β spin densities individually, even for open-shell systems. However, in practice we must use approximate functionals, and (for open-shell systems) these are generally more flexible if they explicitly depend on the α and β spin densities. In an analogous manner to UHF, unrestricted Kohn–Sham theory allows the α and β spin densities to optimize independently, and this allows for a better qualitative description of bond-breaking processes but leads to physically unrealistic spin densities and symmetry breaking problems. A more detailed discussion of the advantages and disadvantages of the unrestricted and spin-restricted theories may be found in the excellent textbook by Koch and Holthausen (11), while an example of a practical application of unrestricted Kohn–Sham theory to reactions with biradical transition structures may be found in a paper by Goddard and Orlova (51). On balance, the unrestricted Kohn–Sham theory is normally preferred for open-shell systems; however, as always, careful assessment studies are recommended in order to establish the suitability of any computational method for a specific chemical problem.

Since the exact functional relating the energy to the electron (or spin) density is unknown, it is necessary to design approximate functionals, and the accuracy of a DFT method depends on the suitability of the functionals employed. Many different functionals for exchange and correlation have been proposed, and it is beyond the scope of this article to outline their mathematical forms (these may

be found in textbooks such as Refs. 10 and 11), but it is worth mentioning their main assumptions. Pure DFT methods may be loosely classified into "local" methods and "gradient-corrected" methods. The local DFT methods are based on the local density approximation (LDA, also known as the local spin density approximation, LSDA), in which it is assumed that the electron density may be treated as that of a "uniform electron gas." From this assumption, functionals describing the exchange (called the "Slater" functional, S) (52) and correlation (Vosko–Wilk–Nusair, VWN) (53) can be derived, and the resulting method is known as S-VWN. The treatment of electron density as that of a uniform electron gas is of course an oversimplification of the real situation, and, while it can often provide reasonable molecular structures and frequencies, the LDA model fails to provide accurate predictions of thermochemical properties such as bond energies (for which errors of over 100 $kJ \cdot mol^{-1}$ are typical) (54).

Gradient-corrected DFT methods (also sometimes referred to as nonlocal or semilocal DFT) attempt to deal with the shortcomings of the LDA model through the generalized gradient approximation (GGA). This corrects the uniform gas model through the introduction of the gradient of the electron density. In introducing the gradient, empirical parameters are often incorporated. For example, the Becke-88 exchange functional (55) was parameterized against the known exchange energies of inert gas atoms. This is commonly used in combination with the "LYP" gradient-corrected correlation functional (56), to give the B-LYP method. Another example of a gradient-corrected functional is the Perdew-Wang 91 (PW91) functional, which has both an exchange and a correlation component (57). The GGA methods show improved performance over the LDA model, especially with respect to thermochemical properties. In this regard, the errors generally obtained in standard thermochemical tests of these methods are of the order of 25 $kJ \cdot mol^{-1}$ (54). However, the GGA methods (as well as the LDA methods) perform poorly for weakly bound systems (such as those in which Van der Waal's interactions are important), and they also perform poorly for reaction barriers (54).

The DFT methods described above are pure DFT methods. Another important class of methods is called *hybrid DFT*. In these methods the exchange functional is replaced by a linear combination of the Hartree–Fock exchange term and a DFT exchange functional. In addition, the various exchange and correlation functionals may themselves be constructed as linear combinations of the various available methods. For example, the popular hybrid DFT method, B3-LYP, is defined as follows (58).

$$E_{\mathrm{B3LYP}}^{\mathrm{XC}} = E_{\mathrm{LDA}}^{\mathrm{X}} + c_0\left(E_{\mathrm{HF}}^{\mathrm{X}} - E_{\mathrm{LDA}}^{\mathrm{X}}\right) + c_{\mathrm{X}}\left(E_{\mathrm{B88}}^{\mathrm{X}} - E_{\mathrm{LDA}}^{\mathrm{X}}\right) + E_{\mathrm{VWN}}^{\mathrm{C}} + c_{\mathrm{C}}\left(E_{\mathrm{LYP}}^{\mathrm{C}} - E_{\mathrm{VWN}}^{\mathrm{C}}\right) \tag{19}$$

The coefficients in this expression, $c_0 = 0.20$, $c_{\mathrm{X}} = 0.72$ and $c_{\mathrm{C}} = 0.81$, were obtained by fitting the results of B3-LYP calculations to a test set of experimental atomization energies, electron affinities, and ionization potentials.

Hybrid DFT methods frequently provide excellent descriptions of the geometries, frequencies, and even reaction barriers and enthalpies for many chemical systems. However, owing to their empirical parameters, such methods are increasingly becoming semiempirical in nature and as such can frequently fail when applied to systems other than those for which they were parameterized. A good example of this is the hybrid DFT method MPW1K (59). This was fitted to

a test set of hydrogen abstraction barriers, and performs very well for these reactions. However, the same method has recently been shown to have large errors when applied to the problem of predicting the enthalpies for radical addition to multiple bonds (36,37). Nonetheless, hybrid DFT methods currently present the most cost-effective option for studying larger chemical systems but, as always, the performance of such methods should be carefully assessed for each new chemical problem.

Calculation of Reaction Rates from Quantum-Chemical Data

Quantum and Classical Reaction Dynamics. In the quantum-chemical calculations described above, we solve the *electronic* Schrödinger equation to determine the energy corresponding to a fixed arrangement of nuclei. If such calculations are performed for all possible nuclear coordinates in a chemical system, this yields the *potential energy surface*. However, as we saw above, in constructing this potential energy surface we made the Born–Oppenheimer approximation, and thus ignored the contribution of the motions of the nuclei to the total kinetic energy. This approximation was appropriate for calculating the electronic energy at a specific geometry, but is clearly not very useful for studying the motions of the atoms in chemical reactions. In order to calculate reaction rates, we must construct a new Hamiltonian in which the kinetic energy of the nuclei is taken into account. In this Hamiltonian, the potential energy is simply the total electronic energy, which we obtain from our quantum-chemical calculations. Once we have formed our new Hamiltonian we can then solve the Schrödinger equation again, this time to follow the motion of the nuclei. This procedure is known as *quantum dynamics*, and can in principle yield the exact reaction rates for a chemical system (within the Born–Oppenheimer approximation).

However, there are several practical limitations to quantum dynamics. Firstly, we have already seen that, for all but the simplest chemical systems, obtaining accurate solutions to the electronic Schrödinger equation for a single set of nuclear coordinates is very computationally intensive. Secondly, to construct a potential energy surface, these expensive calculations must be repeated for "every" possible arrangement of nuclei. Efficient algorithms are available for choosing only those geometries necessary for an adequate description of the chemical system (60). However, even using these algorithms, large numbers of quantum-chemical calculations are nonetheless required. For example, approximately 1000 quantum-chemical calculations were required to construct a reliable potential energy surface for the $OH + H_2$ system (61). Furthermore, the number of data points required increases substantially with the number of atoms in the system (due to the increasing dimensionality). Finally, we have the problem of solving the nuclear Schrödinger equation. In practice, this is intractable for all but the simplest systems, as atoms (being heavier) require even more basis functions than are needed to solve the electronic Schrödinger equation. With current available computing power, quantum dynamics calculations are thus restricted to very small systems, such as $OH + H_2$ (61). In this (state-of-the-art) 4-atom calculation, the energies at approximately 10^7 different points on the potential energy surface were required

in order to solve the nuclear Schrödinger equation, and this requirement scales exponentially with the number of atoms in the system.

Classical reaction dynamics provides a strategy for calculating the rate coefficients of larger chemical systems. Having used quantum-chemical techniques to calculate the potential energy surface, the motions of the nuclei are studied by solving the laws of classical or Newtonian dynamics. This is often a reasonable approximation, since the atoms (being heavier) are considerably less subject to quantum effects than the electrons. Nonetheless, standard classical reaction dynamics calculations are still limited by the need to calculate a full potential energy surface (including the first and second derivatives at each point). As a result, standard classical dynamics calculations *involving accurate ab initio potential energy surfaces* are also currently restricted to relatively small chemical systems, such as $H_3C_3N_3$ (62).

An alternative approach to constructing the entire potential energy surface for a chemical system is provided by *direct dynamics*. In both standard classical reaction dynamics and direct dynamics, the basic principle is the same. A starting arrangement of atoms is adjusted (by a small amount) according to the forces acting on them during a small "step" in time, using the laws of classical mechanics. This "time step" is then repeated using the force corresponding to the new geometry, and so on. The process is repeated for many thousands of time steps, until a complete trajectory is mapped out. The process is then repeated for many trajectories until the reaction probability (and other related information) is established to within an acceptable level of statistical error. As we saw above, in standard classical reaction dynamics, the force acting on the molecule as a function of geometry is obtained from the potential energy surface. In direct dynamics, also known as on-the-fly ab-initio dynamics, this force is calculated (using quantum-chemical calculations) at each new position (63). The latter approach is simpler, but less computationally efficient, and is still restricted to relatively small systems (if accurate levels of theory are used to calculate the forces).

It should be noted that the classical reaction dynamics of much larger systems can be studied using approximate potential energy surfaces, constructed using empirical or semiempirical procedures. In particular, the method of molecular mechanics (MM), which is described elsewhere in this *Encyclopedia*, is commonly used to simulate the motion of polymers and proteins. However, the accuracy of MM simulations are limited by the accuracy of the "force field," which is the set of potential functions that are used to govern relative motions of the constituent atoms. Force fields are typically derived on the basis of empirical and semiempirical information, and are typically only accurate for the type of system for which they were parameterized. Recently, much effort has been directed at deriving accurate force fields for reacting systems, and prominent examples include ReaxFF (64) and MMVB (65). However, such force fields are nonetheless approximate, and only suitable for the types of reactions for which they were designed. Accurate force fields for studying the kinetics of free-radical polymerization do not currently exist, and instead high level ab initio calculations are necessary in order to model these reactions accurately.

Transition-State Theory. To study reactions in larger chemical systems using accurate ab initio calculations we need a much simpler approach, and this is provided by *transition-state theory* (66). In its simplest form, it assumes that, in

the space represented by the coordinates and momenta of the reacting particles, it is possible to define a dividing surface such that all reactants crossing this plane go on to form products, and do not recross the dividing surface. The minimum energy structure on this dividing plane is referred to as the transition structure of the reaction. Transition-state theory also assumes there is an internal statistical equilibrium between the degrees of freedom of each type of system (reactant, product, or transition structure), and that the transition state is in statistical equilibrium with the reactants. In addition, it assumes that motion through the transition state can be treated as a classical translation. From these assumptions, the following simple equation relating the rate coefficient at a specific temperature, $k(T)$, to the properties of the reactant(s) and transition state can be derived (66).

$$k(T) = \kappa (c^{\circ})^{1-m} \frac{k_{\mathrm{B}} T}{h} \frac{Q_{\ddagger}^{\ddagger}}{\prod_{\text{reactants}} Q_{\mathrm{i}}} \mathrm{e}^{-E_0/RT} \tag{20}$$

In this equation κ is called the transmission coefficient and is taken to be equal to unity in simple transition-state theory calculations, but is greater than unity when tunneling is important (see below), c° is the inverse of the reference volume assumed in calculating the translational partition function (see below), m is the molecularity of the reaction (ie, $m = 1$ for unimolecular, 2 for bimolecular, and so on), k_{B} is Boltzmann's constant (1.380658×10^{-23} J · molecule^{-1} · K^{-1}), h is Planck's constant ($6.6260755 \times 10^{-34}$ J·s), E_0 (commonly referred to as the reaction barrier) is the energy difference between the transition structure and the reactants (in their respective equilibrium geometries), $Q_{\ddagger}$ is the molecular partition function of the transition state, and Q_{i} is the molecular partition function of reactant i.

Transition-state theory thus reduces the problem of calculating the potential energy surface for "every" possible geometric arrangement of nuclei, to the consideration of a very small number of "special" geometries; namely, the transition structure and the reactant(s). The transition structure is the minimum energy structure on the dividing surface between the reactants and products, and must be located so as to make the "no re-crossing" assumption as valid as possible. In simple transition-state theory, the transition structure is located as the maximum energy structure, along the minimum energy path connecting the reactants and products. This is generally a good approximation for reactions having barriers that are large compared to $k_{\mathrm{B}}T$. However, for reactions with low or zero barriers, a more accurate approach is required. To this end, in *variational transition-state theory*, the transition structure is located as the structure (on the minimum energy path) that yields the lowest reaction rate. In thermodynamic terms, this may be thought of as the maximum in the Gibb's free energy of activation, rather than the maximum internal energy of activation.

In order to calculate reaction rates via transition-state theory, one needs to identify the equilibrium geometries of the reactants, and also the transition structure, and calculate their energies. This information is of course accessible from quantum-chemical calculations. The molecular partition functions for these

species are also required. These serve as a bridge between the quantum mechanical states of a system and its thermodynamic properties, and are given by

$$Q = \sum_i g_i \exp\left(-\frac{\varepsilon_i}{k_B T}\right) \tag{21}$$

The values ε_i are the energy levels of a system, each having a number of degenerate states g_i, and are obtained by solving the Schrödinger equation. In theory, this equation should be solved for all active modes but in practice the calculations can be greatly simplified by separating the partition function into the product of the translational, rotational, vibrational, and electronic terms, as follows.

$$Q = Q_{\text{trans}} \times Q_{\text{rot}} \times Q_{\text{vibr}} \times Q_{\text{elec}} \tag{22}$$

This is generally a reasonable assumption, provided that the reaction occurs on a single electronic surface. Finally, if we assume that reacting species are ideal gas molecules, analytical expressions for the partition functions are as follows:

$$Q_{\text{trans}} = V\left(\frac{2\pi M k_B T}{h^2}\right)^{3/2} = \frac{RT}{P}\left(\frac{2\pi M k_B T}{h^2}\right)^{3/2} \tag{23}$$

$$Q_{\text{vib}} = \prod_i \exp\left(-\frac{1}{2}\frac{h\nu_i}{kT}\right) \times \prod_i \frac{1}{1-\exp\left(-\frac{h\nu_i}{kT}\right)} \tag{24}$$

$$Q_{\text{rot, linear}} = \frac{1}{\sigma_r}\left(\frac{T}{\Theta_r}\right) \quad \text{where} \quad \Theta_r = \frac{h^2}{8\pi^2 I k_B} \tag{25}$$

$$Q_{\text{rot, nonlinear}} = \frac{\pi^{1/2}}{\sigma_r}\left(\frac{T^{3/2}}{(\Theta_{r,x}\Theta_{r,y}\Theta_{r,z})^{1/2}}\right) \quad \text{where} \quad \Theta_{r,i} = \frac{h^2}{8\pi^2 I_i k_B} \tag{26}$$

$$Q_{\text{elec}} = \omega_0 \tag{27}$$

In equations 23–27 R is the universal gas constant ($8.314\ \text{J}\cdot\text{mol}^{-1}\cdot\text{K}^{-1}$); M is the molecular mass of the species; V is the reference volume, and T and P the corresponding reference temperature and pressure: ν_i are the vibrational frequencies of the molecule; I is the principal moment of inertia of a linear molecule, while for the nonlinear case I_x, I_y, and I_z are the principal moments of inertia about axes x, y, and z respectively; σ_r is the symmetry number of the molecule which counts its number of symmetry equivalent forms (67); and ω_0 is the electronic spin multiplicity of the molecule (ie, $\omega_0 = 1$ for singlet species, 2 for doublet species, etc). The information required to evaluate these partition functions is routinely accessible from quantum-chemical calculations: the moments of inertia and symmetry numbers depend on the geometry of the molecule, while the vibrational frequencies are obtained from the second derivative of the energy with respect to the geometry.

A number of additional comments need to be made concerning the use of equations 23–27. Firstly, in the calculation of the translational partition function (eq. 23), a reference volume (or equivalently, a temperature and pressure) is assumed. This is needed for the calculation of thermodynamic quantities such as enthalpy and entropy, but the assumption has no bearing on the calculated rate coefficient, as the reference volume is removed from equation 20 through the parameter $c^\circ (= 1/V)$. Secondly, the vibrational partition function (eq. 24) has been written as the product of two terms. The first of these corresponds to the zero-point vibrational energy of the molecule, while the latter corresponds to its additional vibrational energy at some nonzero temperature T. The zero-point vibrational energy is often included in the calculated reaction barrier E_0. When this is the case, this first term must be removed from equation 24, so as not to count this energy twice. Thirdly, the external rotational partition function is calculated using equation 25 if the molecule is linear, and equation 26 if it is not.

It is also worth noting that there is an entirely equivalent thermodynamic formulation of transition-state theory.

$$k(T) = \kappa \frac{k_B T}{h} (c^\circ)^{1-m} \, e^{\Delta S^\ddagger / R} \, e^{-\Delta H^\ddagger / RT} \tag{28}$$

A derivation of this expression, which is obtained by noting the relationship between the thermodynamic properties of a system (eg enthalpy, H, and entropy, S) and the partition functions, can be found in textbooks on statistical thermodynamics (12–16). The enthalpy of activation ($\Delta H^\ddagger$) for this expression can be written as the sum of the barrier (E_o), the zero-point vibrational energy (ZPVE), and the temperature correction ($\Delta\Delta H^\ddagger$).

$$\Delta H^\ddagger = \Delta E_0 + \mathrm{ZPVE} + \Delta\Delta H^\ddagger \tag{29}$$

The temperature correction ($\Delta\Delta H$) and ZPVE for an *individual* species can be calculated from the vibrational frequencies as follows.

$$\mathrm{ZPVE} = R \frac{1}{2} \sum_i h\nu_i / k_B \tag{30}$$

$$\Delta\Delta H = R \sum_i \frac{h\nu_i / k_B}{\exp(h\nu_i / k_B / T) - 1} + \frac{5}{2} RT + \frac{3}{2} RT \tag{31}$$

In equation 31, the first term is the vibrational contribution to the enthalpy, the second term is the translational contribution, and the third term is the rotational contribution. The entropy of activation ($\Delta S^\ddagger$) is calculated from the vibrational (S_v), translational (S_t), rotational (S_r), and electronic (S_e) contributions to the entropies of the individual species, in turn expressed as follows.

$$S_v = R \sum_i \left(\frac{h\nu_i / k_B T}{\exp(h\nu_i / k_B T) - 1} - \ln(1 - \exp(-h\nu_i / k_B T)) \right) \tag{32}$$

$$S_{\mathrm{t}} = R\left(\ln\left(\left(\frac{2\pi M k_{\mathrm{B}} T}{h^2}\right)^{3/2} \frac{k_{\mathrm{B}} T}{P}\right) + 1 + 3/2\right) \tag{33}$$

$$S_{\mathrm{r,\ linear}} = R\left(\ln\left(\frac{1}{\sigma_r}\left(\frac{T}{\Theta_r}\right)\right) + 1\right) \tag{34}$$

$$S_{\mathrm{r,\ nonlinear}} = R\left(\ln\left(\frac{\pi^{1/2}}{\sigma_r}\left(\frac{T^{3/2}}{(\Theta_{r,x}\Theta_{r,y}\Theta_{r,z})^{1/2}}\right)\right) + 3/2\right) \tag{35}$$

$$S_e = R\ \ln(\omega_0) \tag{36}$$

The parameters required to evaluate these expressions are the same as those used in evaluating the partition functions, as described above.

Finally, by evaluating the derivative of (28) with respect to temperature, it is possible to derive a relationship between the above thermodynamic quantities and the empirical Arrhenius expression for reaction rate coefficients (15):

$$k(T) = Ae^{-Ea/RT} \tag{37}$$

The frequency factor (A) in this expression is related to the entropy of the system, as follows.

$$A = (c^{\circ})^{1-m} e^m \frac{k_{\mathrm{B}} T}{h}\ \exp\left(\frac{\Delta S^{\ddagger}}{R}\right) \tag{38}$$

The Arrhenius activation energy is related to the reaction barrier, as follows.

$$E_{\mathrm{a}} = E_0 + \mathrm{ZPVE} + \Delta\Delta H^{\ddagger} + mRT \tag{39}$$

From these expressions it can be seen that the so-called temperature-independent parameters of the Arrhenius expression are in fact functions of temperature, which is why the Arrhenius expression is only valid over relatively small temperature ranges. It should also be clear that the ZPVE-corrected barrier (E_0 + ZPVE), the enthalpy of activation ($\Delta H^{\ddagger}$), and the Arrhenius activation energy (E_{a}) are only equal to each other at 0 K. At nonzero temperatures, these quantities are nonequivalent and thus should not be used interchangeably.

Extensions to Transition-State Theory. Many variants of transition-state theory have been derived, and a comprehensive review of these recent developments has been provided by Truhlar and co-workers (68). As already noted, one of the main extensions to transition-state theory is variational transition-state theory which, in its simplest form, locates the transition structure as that having the maximum Gibb's free energy (rather than internal energy). Other variations of transition-state theory arise through making different assumptions as to the statistical distribution of the available energy throughout the different molecular modes, and through deriving expressions for the partition functions for cases other than ideal gases. In addition, two simple extensions to the transition-state theory

equations are the inclusion of corrections for quantum-mechanical tunneling, and the improved treatment of the low frequency torsional modes. Since these are of importance in treating certain polymerization-related systems, these are briefly described below.

Tunneling Corrections. One of the assumptions inherent in simple transition-state theory is that motion along the reaction coordinate can be considered as a classical translation. In general, this assumption is reasonably valid since the reacting species, being atoms or molecules, are relatively large and thus their wavelengths are relatively small compared to the barrier width. However, in the case of hydrogen (and to a lesser extent deuterium) transfer reactions, the molecular mass of the atom (or ion) being transferred is relatively small, and thus quantum effects can be very important. Corrections for quantum-mechanical tunneling are incorporated into the κ coefficient of equation 20, and are known as tunneling coefficients.

There is an enormous variety of expressions available for calculating tunneling coefficients. The most accurate tunneling methods, such as *small curvature tunneling* (69), *large curvature tunneling* (70), and *microcanonical optimized multidimensional tunneling* (71), involve solving the multidimensional Schrödinger equation describing motion of the molecules at every position along the reaction coordinate. To calculate such tunneling coefficients, specialized software (such as POLYRATE (72)) is used, and additional quantum-chemical data (such as the geometries, energies, and frequencies along the entire minimum energy path) are required. As a result, simpler (and hence less accurate) expressions are often adopted. These are derived by treating motion along the reaction coordinate as a function of one variable, the intrinsic reaction coordinate, and hence solving a one-dimensional Schrödinger equation. When this is done using the calculated energies along the reaction path, the procedure is known as *zero-curvature tunneling* (73). However, this procedure still entails the numerical solution of the Schrödinger equation, and hence an additional simplification is also often made. Instead of using the calculated energies along this path, some assumed functional form for the potential energy is used instead. This is chosen so that the Schrödinger equation has an analytical solution, and thus a closed expression for the tunneling coefficient can be derived. The derivation of these simple tunneling coefficients is described by Bell (74), and the main expressions used in practice are as follows.

The simplest tunneling coefficients are based on the assumption that the change in energy along the minimum energy path can be described by a truncated parabola. This functional form provides a good description of the energies near the transition structure (where tunneling is most significant), but a very poor description elsewhere. The equation for the tunneling coefficient is given as the following infinite series, which is frequently truncated after the first few terms.

$$\kappa = \frac{\frac{1}{2}u_{\ddagger}}{\sin\left(\frac{1}{2}u_{\ddagger}\right)} - u_{\ddagger}y^{-u_{\ddagger}/2\pi}\left\{\frac{y}{2\pi - u_{\ddagger}} - \frac{y^2}{4\pi - u_{\ddagger}} + \frac{y^3}{6\pi - u_{\ddagger}} - \cdots\right\} \tag{40}$$

where

$$u_{\ddagger} = \frac{h\nu_{\ddagger}}{kT} \quad \text{and} \quad y = \exp\left(-\frac{2\pi V}{u_{\ddagger}kT}\right)$$

Equation 40 is called a *Bell tunneling* correction (74), and in this expression V is the reaction barrier and $\nu_{\ddagger}$ is the imaginary frequency (as obtained from the frequency calculation at the transition structure). By taking the first term of equation 40, expanding it as an infinite series, and then truncating at an early order, the (even simpler) *Wigner* (75) *tunneling* expression is obtained (74).

$$\kappa \approx \frac{\frac{1}{2}u_{\ddagger}}{\sin\left(\frac{1}{2}u_{\ddagger}\right)} \approx 1 + \frac{u_{\ddagger}^2}{24} + \frac{u_{\ddagger}^4}{5760} + \cdots \approx 1 + \frac{u_{\ddagger}^2}{24} \tag{41}$$

A slightly more realistic description of the change in potential energy along the minimum energy path is provided by the following *Eckart* function (76):

$$V(x) = \frac{Ay}{(1+y)^2} + \frac{By}{(1+y)} \quad \text{where} \quad y = e^{x/\Delta} \tag{42}$$

To ensure that the function passes through the reactants, products and transition structures, the parameters A and B are defined as the following functions of the forward (V_{f}) and reverse (V_{r}) reaction barriers (where the reaction is taken in the exothermic direction).

$$A = (\sqrt{V_{\mathrm{f}}} + \sqrt{V_{\mathrm{r}}})^2 \quad \text{and} \quad B = V_{\mathrm{f}} - V_{\mathrm{r}} \tag{43}$$

The remaining parameter Δ is chosen so as to give the most appropriate fit to the minimum energy path. If this fit is biased toward the points near the transition structure (where tunneling is most important), it can be calculated as the following function of the imaginary frequency $\nu_{\ddagger}$ (where c is the speed of light) (39,41):

$$\Delta = \frac{i}{2\pi c \nu_{\ddagger}} \sqrt{\frac{1}{8} \frac{(B^2 - A^2)^2}{A^3}} \tag{44}$$

The Δ value obtained from this expression is in mass-weighted coordinates, which enables the reduced mass to be dropped from the standard (76) Eckart formulae (41), resulting in the following expression for the permeability of the reaction barrier $G(W)$ as a function of the energy W:

$$G(W) = 1 - \frac{\cosh(\alpha - \beta) + \cosh(\delta)}{\cosh(\alpha + \beta) + \cosh(\delta)} \tag{45}$$

where

$$\alpha = \frac{4\Delta\pi^2}{h}\sqrt{2W},\ \beta = \frac{4\Delta\pi^2}{h}\sqrt{2(W-B)},\ \delta = \frac{4\Delta\pi^2}{h}\sqrt{2A - \frac{h^2}{16\pi^2\Delta^2}}$$

The Eckart tunneling correction (κ) is then obtained by numerically integrating $G(W)$ over a Boltzmann distribution of energies, via the formula (74):

$$\kappa = \frac{\exp(V_F/k_BT)}{k_BT}\int_0^\infty G(W)\exp(-W/k_BT)\,dW \tag{46}$$

Although this expression requires numerical integration, it does not require sophisticated software and can be easily implemented on a spreadsheet.

Finally, it is worth making a few comments on the use of the tunneling procedures. Firstly in very general terms, tunneling is important for reactions involving the transfer of a hydrogen or deuterium atom or ion. The importance of tunneling can also be established through examination of the parameter $u_\ddagger$ in equation 40, a value of $u_\ddagger < 1.5$ *usually* indicating negligible tunneling effects (74). Secondly, in principle, the more accurate multidimensional tunneling coefficient expressions should always be used. However, in practice, the more convenient one-dimensional expressions are often adopted. Of these expressions, the Eckart tunneling coefficient is significantly more accurate and should be preferred. For example, the small curvature tunneling method gives a tunneling coefficient (κ) of approximately 10^2 at 300 K, for the hydrogen abstraction reaction between $^{\bullet}NH_2$ and C_2H_6 (77). At the same level of theory, the corresponding κ values for the Wigner, Bell, and Eckart corrections are approximately 5, 10^3, and 10^2 respectively, and hence only the Eckart method yields a tunneling coefficient of the right order of magnitude for this (typical) reaction. The success of the Eckart tunneling method has also been noted by Duncan and co-workers (78), who rationalized it in terms of a favorable cancelation of errors.

Treatment of Low Frequency Torsional Modes. In the vibrational partition function (eq. 24), all modes are treated under the *harmonic oscillator approximation*. That is, it is assumed that the potential field associated with their distortion from the equilibrium geometry is a parabolic well, as in a vibrating spring (see Fig. 10**a**). This is a reasonable assumption for bond stretching motions, but not for hindered internal rotations (see Fig. 10**b**). For high frequency modes ($\nu >$ 200–300 cm^{-1}), the contribution of these motions to the overall partition function is negligible at room temperature (ie $Q_{vib,i} \approx 1$) and thus the error incurred in treating these modes as harmonic oscillators is not significant. However, for the low frequency torsional modes, these errors can be significant and a more rigorous treatment is often necessary, and this is especially the case for the reactions of relevance to free-radical polymerization (3–5,79).

The simplest method for treating the hindered internal rotations is to regard them as one-dimensional rigid rotors. An appropriate rotation angle θ is identified, and then the potential $V(\theta)$ is calculated as a function of this angle (eg from 0 to 360° in steps of 10°) via quantum chemistry. In general, it is recommended that these potentials be obtained as relaxed scans; that is, in calculating the energy at a specific angle, all geometric parameters other than the rotational angle are optimized (79). If the rotational potential can be described as a simple cosine function, the enthalpy and entropy associated with the mode can be obtained directly from the tables of Pitzer and co-workers (80). In order to use these tables,

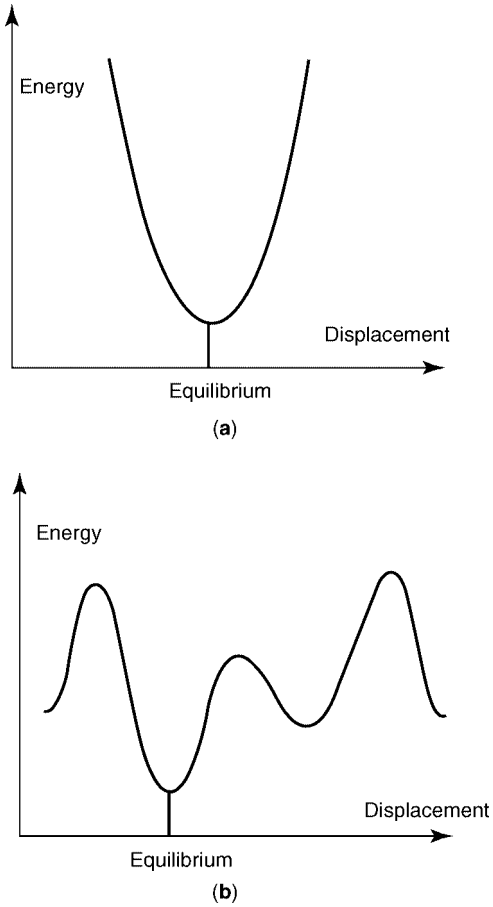

Fig. 10. Typical potentials associated with (**a**) a harmonic oscillator and (**b**) a hindered internal rotation.

one calculates two dimensionless quantities:

$$x = \frac{V}{k_B T} \quad \text{and} \quad y = \frac{\sigma_{int} h}{\sqrt{8\pi^3 I_m k_B T}} \tag{47}$$

In these equations, V is the barrier to rotation, σ_{int} is the symmetry number associated with the rotation (which counts the number of equivalent minima in the potential energy curve), and I_m is the reduced moment of inertia associated with the rotation. This latter parameter is given by the following formula:

$$I_m = A_m \left(1 - \sum_{i=x,y,z} A_m \lambda_{mi}^2 / I_i\right) \tag{48}$$

In this equation, A_m is the moment of inertia of the torsional coordinate itself, I_i is the principal moment of inertia of the whole molecule about axis i, and

λ_{mi} is the direction cosine between the axis of the top and the principal axis of the whole molecule. More information on the calculation of reduced moments of inertia can be found in Reference (81). When the rotational potential cannot be fitted with a simple cosine function (as in Fig. 10**b**), the partition function (and hence the enthalpy and entropy) is obtained instead by (numerically) solving the one-dimensional Schrödinger equation.

$$-\frac{h^2}{8\pi I_m}\frac{\partial^2\Psi}{\partial\theta^2} + V(\theta)\Psi = \varepsilon\Psi \tag{49}$$

This yields the energy levels of the system (ε_i), which are then used to evaluate the partition function via the following equation.

$$Q_{\text{int rot}} = \frac{1}{\sigma_{\text{int}}}\sum_i \exp\left(-\frac{\varepsilon_i}{k_B T}\right) \tag{50}$$

Having obtained the partition function (or equivalently, the enthalpy and entropy) associated with a low frequency torsional mode, this is used in place of the corresponding harmonic oscillator contribution for that mode.

The above treatment of hindered rotors assumes that a given mode can be approximated as a one-dimensional rigid rotor, and studies for small systems have shown that this is generally a reasonable assumption in those cases (82). However, for larger molecules, the various motions become increasingly coupled, and a (considerably more complex) multidimensional treatment may be needed in those cases. When coupling is significant, the use of a one-dimensional hindered rotor model may actually introduce more error than the (fully decoupled) harmonic oscillator treatment. Hence, in these cases, the one-dimensional hindered rotor model should be used cautiously.

Software

There are a large number of software packages available for performing computational chemistry calculations. Some of the programs available include ACES II (83), GAMESS (84), GAUSSIAN (43), MOLPRO (85), and QCHEM (86). Other programs, such as POLYRATE, (72), have been designed to use the output of quantum-chemistry programs to calculate reaction rates and tunneling coefficients. Whereas computational chemistry software has traditionally been operated on large supercomputers, versions for desktop personal computers are increasingly becoming available. In addition, programs for visualizing the output of computational chemistry calculations such as Spartan (87), Molden (88), CS Chem3D (89), Molecule (90), Jmol (91), Gauss View (43), and MacMolPlt (92) are also available. These programs allow one to visualize the geometry and electronic structure of the resulting molecule, and animate its vibrational frequencies. Many of these programs also have built-in computation engines. Computational chemistry is thus increasingly becoming accessible to the nonspecialist user, which brings with it its own problems (see also MOLECULAR MODELING).

Accuracy and Applicability of Theoretical Procedures

By solving the Schrödinger equation exactly, quantum chemistry can, in principle, provide accurate electronic-structure data. However, in practice, approximate numerical methods must be adopted, and these can introduce error to the calculations. As we have already seen, an enormous number of approximate methods are available, and these range from the accurate but computationally expensive to the cheap but potentially nasty. Furthermore, the performance of a particular method varies considerably depending upon the chemical system and the property being calculated. It is therefore very important that computational chemistry studies are accompanied by rigorous assessments of theoretical procedures. In such "calibration" studies, prototypical systems are calculated at a range of levels of theory, and the results are compared both internally (against the highest level procedures) and externally (against reliable experimental data) in order to identify those methods which offer the best compromise between accuracy and expense.

In the present section, the main conclusions from recent assessment studies for the reactions of importance to free-radical polymerization are outlined. In presenting such studies, it must be acknowledged that, with continuing rapid increases in computer power, some of these results will soon be outdated. In particular, as computer power increases, the need to rely upon lower levels of theory for large polymer-related systems will diminish. Instead, the higher levels of theory outlined below will be able to be used routinely. Nonetheless, with increasing computer power, the temptation to apply existing levels of theory to yet larger systems will no doubt ensure that the main conclusions of these studies retain some relevance into the near future.

Radical Addition to C=C Bonds. Radical addition to C=C bonds are of importance for free-radical polymerization as this reaction forms the propagation step, and thus influences the reaction rate and molecular weight distribution in both conventional and controlled free-radical polymerization, and the copolymer composition and sequence distribution in free-radical copolymerization. Numerous studies have examined the applicability of high level theoretical methods for studying radical addition to C=C bonds in small radical systems (32,33,37,93,94). The most recent study (37) included W1 barriers and enthalpies, and geometries and frequencies at the CCSD(T)/6-311G(d,p) level of theory, and is the highest level study to date. The main conclusions from this study, and (where still relevant) the previous lower level studies, are outlined below.

Geometry optimizations are generally not very sensitive to the level of theory, with even the low cost HF/6-31G(d) and B3-LYP/6-31G(d) methods providing reasonable approximations to the higher level calculations (37). In the latter case, there is a small error arising from the tendency of B3-LYP to overestimate the forming bond length in the transition structures, and this can be reduced using an IRCmax technique (94). Alternatively, the error in the B3-LYP transition structures is also reduced when the larger 6-311 + G(3df,2p) basis set is used (37). In addition, the UMP2 method should generally be avoided for these reactions, as they are subject to spin-contamination problems (32,33,37). *Frequency calculations* are also relatively insensitive to the level of theory, especially when the frequencies are scaled by their appropriate scale factors. (Scale-factors for the most commonly used levels of theory may be found in Reference (95). In particular,

the B3-LYP/6-31G(d) level of theory provides excellent performance for frequency factors, temperature corrections, and zero-point vibrational energy calculations, and would be a suitable low cost method for studying larger systems (37).

Barriers and enthalpies are very sensitive to the level of theory. Where possible, high level composite procedures should be used for the prediction of absolute reaction barriers and enthalpies, and of these methods the "RAD" variants of G3 provide the best approximations to the higher level Wn methods (when the latter cannot be afforded) (37). It should also be noted that the (empirically based) spin-correction term in the CBS-type methods appears to be introducing a considerable error to the predicted reaction barriers for these reactions and, until this is revised, these methods should perhaps be avoided for these reactions (37).

When composite methods cannot be afforded, the use of RMP2/6-311 + G(3df,2p) single points provides reasonable absolute values and excellent relative values for the barriers and enthalpies of these reactions (37). In contrast, the hybrid DFT methods such as B3-LYP and MPW1K show considerable error in the reaction enthalpies, even when applied with large basis sets. However, they do provide reasonable addition barriers, owing to the cancelation of errors in the early transition structures for these reactions (37). Interestingly, for the closely related radical addition to C≡C bonds, the situation is reversed and the B3-LYP methods perform well and the RMP2 methods perform poorly (37), and this highlights the importance of performing assessment studies before tackling new chemical problems. Finally, it should be stressed that semiempirical methods do not provide an adequate description of the barriers and enthalpies in these reactions (32).

For *rate coefficients*, the importance of treating the low frequency torsional modes in radical addition reactions as hindered internal rotations has been investigated in a number of assessment studies (37,79,93). For small systems such as methyl addition to ethylene and propylene, the errors are relatively minor (less than a factor of 2) (37). However, for reactions of substituted radicals (such as *n*-alkyl radicals (93) and the ethyl benzyl radical (79)), the errors are somewhat larger (as much as a factor of 6), as there are additional low frequency torsional modes to consider. Nonetheless, the errors are still relatively small, and the harmonic oscillator approximation might be expected to provide reasonable "order-of-magnitude" estimates of rate coefficients.

Radical Addition to C═S Bonds. Radical addition to C═S bonds, and the reverse β-scission reaction, forms the key addition and fragmentation steps of the RAFT polymerization process (96). Ab initio calculations have a role to play in elucidating the effects of substituents on this process, and in providing an understanding of the causes of rate retardation (6,7). A detailed assessment of theoretical procedures has been recently carried out for this class of reactions (36), and the main conclusions are similar to those for addition to C═C bonds (37), as outlined above. In general, low levels of theory, such as B3-LYP/6-31G(d), are suitable for geometry optimizations and frequency calculations, provided an IRCmax procedure is used to correct the transition structures. However, high level composite methods are required to obtain reliable absolute barriers and enthalpies, though reasonable relative quantities can be obtained at the RMP2/6-311 + G(3df,2p) level. As in the case of addition to C═C bonds, the spin correction term in the CBS-type methods appears to require adjustment, and the RAD variants of G3 should be preferred when the higher level Wn calculations are impractical.

Hydrogen Abstraction. Hydrogen abstraction reactions are important chain-transfer processes in free-radical polymerization. In particular, hydrogen abstraction by the propagating polymer radical from transfer agents (such as thiols), monomer, dead polymer, or itself (ie intramolecular abstraction) can affect the molecular weight distribution, the chemical structure of the chain ends, and the degree of branching in the polymer. The accuracy of computational procedures for studying hydrogen abstraction reactions has received considerable attention, and the results of some of the most recent and extensive studies (59,94,97–99) are summarized below.

Geometry optimizations are relatively insensitive to the level of theory; however, there are some important exceptions. In particular, the HF and MP2 methods should be avoided for spin-contaminated systems (99). Moreover, the B3-LYP method does not describe the transition structures very well for a number of hydrogen abstraction reactions (59,97). However, improved performance is obtained using newer hybrid DFT methods such as MPW1K (59) and KMLYP (97), and these methods are suitable as low cost methods, when high level procedures cannot be afforded.

Barriers and enthalpies are more sensitive to the level of the theory, and, where possible, high level composite procedures should be used. In particular, the "RAD" variants of G3 provide an excellent approximation to the higher level Wn methods, and would provide an excellent benchmark level of theory when the latter could not be afforded (99). As in the case of the addition reactions, the spin contamination correction term in the CBS-type methods appears to be introducing a systematic error to the predicted reaction barriers and enthalpies and, until this is revised, this method should perhaps be avoided for spin-contaminated reactions (99). When composite methods cannot be afforded, methods such as RMP2, MPW1K, or KMLYP have been shown to provide good agreement with the high level values (59,97,99), with a procedure such as MPW1K/6-311 + G(3df,2p) providing the best overall performance. By contrast, the popular B3-LYP method performs particularly poorly for reaction barriers and enthalpies (59,94,97–99), and should thus be generally avoided for abstraction reactions. Interestingly, it has been noted that the errors in B3-LYP increase with the increasing polarity of the reactants (98), which suggests that assessment studies based entirely on relatively nonpolar reactions (such as $CH_3^{\bullet} + CH_4$) may lead to the wrong conclusions.

As noted in the previous section, *tunneling* is significant in hydrogen abstraction reactions, and hence accurate quantum-chemical studies of these systems require the calculation of tunneling coefficients. The accuracy of tunneling coefficients is profoundly affected by both the tunneling method and the level of theory at which it is applied. A systematic comparison of the various tunneling methods for the hydrogen abstraction reactions of relevance to free-radical polymerization does not appear to have been performed. However, in the example provided in the previous section, it was seen that the Eckart method was capable of providing the tunneling coefficients of the right order of magnitude (when compared with the more accurate multidimensional methods), while the Wigner and Bell methods respectively underestimated and overestimated the tunneling coefficients by an order of magnitude. Hence, when multidimensional tunneling methods are not convenient, the Eckart tunneling method should be preferred as the best low cost method. An assessment of the effects of level of theory on the tunneling

coefficients, as calculated using this Eckart method, has recently been published (41). It was found that errors in the imaginary frequency at the HF level (with a range of basis sets) leads to errors in the calculated tunneling coefficients of several orders of magnitude (compared to high level CCSD(T)/6-311G(d,p) calculations). The B3-LYP and MP2 methods performed significantly better, showing errors of a factor of 2–3. However, even better performance could be obtained by correcting the HF values to the CCSD(T)/6-311G(d,p) level via an IRCmax procedure.

Applicability of Chemical Models

Assuming high levels of theory are used, quantum-chemical calculations might be expected to yield very accurate values of the rate coefficients for the specific chemical system being studied. With current available computing power, this would in all likelihood consist of a small model reaction in the gas phase. If, for example, this information is then to be used to deduce something about solution-phase polymerization kinetics, the effects of the solvent and (in most cases) the effects of chain length need to be considered. Unfortunately, the treatment of these effects at a high level of theory is not generally feasible with current available computing power, and hence the neglect of these effects (or their treatment at a crude level of theory) remains a potential source of error in quantum-chemical calculations. In this section, these additional sources of error are briefly discussed.

Solvent Effects. The presence of solvent molecules may affect the polymerization process in a variety of ways (100). For example, if polar interactions are significant in the transition structure of the reaction, the presence of a high dielectric constant solvent may stabilize the transition structure and lower the reaction barrier. Solvents may also affect the reactivity of the reacting radicals, and even the mechanism of the addition or transfer reaction, through some specific interaction such as hydrogen bonding or complex formation. In addition, the preferential sorption of the monomer or solvent around the reacting polymer radical may lead to the effective concentrations available for reaction being different to those in the bulk solution, resulting in a difference between the observed and predicted rate coefficients. Solvent effects such as these result in the experimentally measured rate coefficients for a free-radical polymerization varying according to the solvent type.

Over and above these system-specific solvent effects, there is a more general "entropically based" difference between the rate coefficients for gas-phase and solution-phase systems. Whereas in the gas-phase an isolated molecule might be expected to have translational, rotational, and vibrational degrees of freedom, in the solvent phase the translational and rotational degrees of freedom are effectively "lost" in collisions with the solvent molecules. In their place, it is necessary to consider additional vibrational degrees of freedom involving a solute-solvent "supermolecule" (101). Since the vibrational, translational, and rotational modes make different quantitative contributions to the enthalpy and entropy of activation, significant differences might be expected between the gas and solution phases. For bimolecular reactions this effect can be considerable, because the main contribution to the entropy of activation is the six rotational and translational

degrees of freedom in the reactants, which are converted to internal vibrations in the transition structure. In contrast, for unimolecular reactions, the entropically based gas-phase/solution-phase difference is generally much smaller, as the rotational and translational modes are similar for the transition structure and reactant molecule, and thus their contribution largely cancels from the reaction rate.

The treatment of solvent effects varies according to their origin. The influence of the dielectric constant on polar reactions can be dealt with routinely using various continuum models (102), implemented using standard computational software, such as GAUSSIAN (43). However, it should be stressed that these models do not account for the entropically based gas-phase/solvent-phase difference, nor do they deal with direct solvent interactions in the transition structure. When direct interactions involving the solvent are important, it is necessary to include solvent molecules in the quantum-chemical calculation. In theory, one should include many hundreds of solvent molecules but in practice one includes a small number of molecules, and combines this with a continuum model (102). However, even with this simplification, the additional solvent molecules increase the computational cost of the calculations, and it is not currently feasible to apply these methods (at any reasonable level of theory) for polymer-related systems. Even when additional solvent molecules are included in the ab initio calculations, various extensions to transition-state theory are required in order to model the rates of solution-phase reactions (68,101). Unfortunately, the existing models are complicated to use and require additional parameters which are not readily accessible for polymerization-related systems. The development of simplified yet accurate models for dealing with solvent effects is an on-going field of research.

While strategies for calculating solution-phase rate coefficients exist, with the current available computing power these methods are not generally feasible for polymer-related systems. Instead, the following practical guidelines for dealing with solvent effects are suggested. Firstly, when the solvent participates directly in the reaction, the inclusion of the interacting solvent molecule in the gas-phase calculation is essential for gaining a mechanistic understanding of the reaction. Secondly, when polar interactions are expected to be important, the use of a continuum model is recommended, especially if the results are to be used to interpret the polymerization process in polar solvents. Thirdly, for bimolecular reactions, if the a priori prediction of *absolute* rate coefficients is required, a consideration of the entropically based gas-phase/solution-phase difference is necessary. This "entropic" solvent effect might be estimated by comparing corresponding experimental solution- and gas-phase rate coefficients for that class of reaction. For example, solution-phase experimental values for radical addition reactions generally exceed the corresponding gas-phase values by approximately one order of magnitude (103). One might also benchmark the gas-phase calculations by calculating the rate coefficient for a similar reaction, and comparing the calculated result with reliable experimental data. Fourthly, provided that specific interactions are not important, one might expect that solvent effects should largely cancel from *relative* rate coefficients, and hence the gas-phase values should generally be suitable for studying substituent effects and solving mechanistic problems. Finally, when specific interactions are important, simple gas-phase calculations are still useful, as they can provide complementary information about the underlying influences on the mechanism in the absence of the solvent.

Chain-Length Effects. The other simplification that is necessary in order to use high level ab initio calculations on polymer-related systems is to approximate the propagating polymer radical (which may be hundreds or thousands of units long) as a short-chain alkyl radical. Provided that the reaction is chemically controlled, this is not an unreasonable assumption. In chemical terms, the effects of substituents decrease dramatically as they are located at positions that are increasingly remote from the reaction center. For example, the terminal and penultimate units of a propagating polymer radical are known to affect its reactivity and selectivity in the propagation reaction (104); however, substituent effects beyond the penultimate position are rarely invoked in copolymerization models. In order to include the most important substituent effects, it is generally recommended that propagating radicals be represented as γ-substituted propyl radicals (as a minimum chain length). For some systems this is not currently possible without resorting to a low (and thus inaccurate) level of theory. In those cases, the possible influence of penultimate unit effects must be taken into account when interpreting the results of the calculations.

The entropic influence of the chain length on the reaction rates extends slightly beyond the penultimate unit. For example, Deady and co-workers (105) showed experimentally that there was a chain-length effect on the propagation rate coefficient of styrene, which converged at the tetramer stage (ie an octyl radical). Heuts and co-workers (3) have explored this chain-length dependence theoretically, and suggested that it arises predominantly in the translational and rotational partition functions. More specifically, they suggest that there is a small effect of mass that can be modeled by including an unrealistically heavy isotope of hydrogen at the remote chain end. For example, in the propagation of ethylene, a model such as $X{-}(CH_2)_n{-}CH_2^{\bullet}$ could be used, and in this model X is set as a hydrogen atom that happens to have a molecular mass of 9999 amu! They also noted that there is an effect of chain length on the rotational entropy (and especially the hindered internal rotations), which required the more subtle modeling strategy of using slightly longer alkyl chains (ie $n > 1$). Nonetheless, using their "heavy hydrogen" approach, their calculated frequency factors converged to within a factor of 2 of the long chain limit at even the propyl radical stage (ie $n = 2$). More recently it was shown that the consideration of the propagating radical as a substituted hexyl radical (without a heavy hydrogen at the remote chain end) was also sufficient to reproduce experimental values for the frequency factors of propagation reactions (106). For short-chain branching reactions, it has been shown that inclusion of just one methyl group beyond the reaction center is sufficient for modeling the long-chain reactions, provided that the additional methyl group is substituted with a heavy (ie 9999 amu) hydrogen atom (5). Thus, in general, it appears that small model alkyl radicals are capable of providing a reasonable description of polymeric radicals in chemically controlled reactions.

Finally, it is worth noting that the chain-length effects on the propagation steps amount to approximately an order of magnitude difference between the first propagation step and the long chain limit, with the small radical additions having faster rate coefficients. This chain-length error is of the same magnitude and acts in the opposite direction to the gas-phase/solvent-phase difference in bimolecular reactions, and hence substantial cancelation of error might be expected in these cases. Indeed an (unpublished) high level G3(MP2)-RAD calculation of the

propagation rate coefficient for methyl acrylate at 298 K produced the value of $2.0 \times 10^4\ L \cdot mol^{-1} \cdot s^{-1}$, which is in remarkable agreement with the corresponding experimental value (also $2.0 \times 10^4\ L \cdot mol^{-1} \cdot s^{-1}$ at ambient pressure) (107), despite the fact that both the medium and chain-length effects were ignored in the calculation. Hence, careful efforts to correct for chain-length effects but not solvent effects (or vice versa) may actually introduce greater errors to calculated rate coefficients.

Applications of Quantum Chemistry in Free-Radical Polymerization

Quantum chemistry provides a powerful tool for studying kinetic and mechanistic problems in free-radical polymerization. Provided a high level of theory is used, ab initio calculations can provide direct access to accurate values of the barriers, enthalpies, and rates of the individual reactions in the process, and also provide useful related information (such as transition structures and radical stabilization energies) to help in understanding the reaction mechanism. In the following, some of the applications of quantum chemistry are outlined. This is not intended to be a review of the main contributions to this field, nor is it intended to provide a theoretical account of reactivity in free-radical polymerization (108). Instead, some of the types of problems that quantum chemistry can tackle are described, with a view to highlighting the potential of quantum-chemical calculations as a tool for studying free-radical polymerization (see RADICAL POLYMERIZATION).

A Priori Prediction of Absolute Rate Coefficients. The a priori prediction of accurate *absolute* rate coefficients is perhaps the most demanding task in computational chemistry. For example, high level ab initio calculations (at the G3(MP2)-RAD level as a minimum) are required for the calculation of accurate reaction barriers (and enthalpies) in radical addition reactions and, with current available computing power, these can be performed routinely on systems of up to 12–14 non-hydrogen atoms. This allows for the most common polymerization substituents to be included, and often allows for penultimate unit effects to be taken into account. However, it does not allow for the accurate treatment of solvent or chain-length effects. Of course, with continuing rapid increases in computer power, these problems should soon be overcome. In addition, as was noted above, for a bimolecular reaction, the chain-length effects and solvent effects act in opposite directions and may in fact largely cancel, leading to surprisingly accurate results. Certainly, with current available computing power, the prediction of rate coefficients to within 1–2 orders of magnitude (or better) is possible for most chemically controlled polymerization-related reactions, and further increases in accuracy should be attainable in the near future.

The prediction of absolute rate coefficients via quantum chemistry is particularly useful when direct experimental measurements are not possible. A good example of this is in the RAFT polymerization process (96), in which the experimentally observable quantities (such as the overall polymerization rate, the overall molecular weight distribution, and the concentrations of the various species) are a complicated function of the rates of the various individual reactions. In order to measure the rates of these individual steps, it is necessary to relate their rate coefficients to the observable quantities via some kinetic-model-based assumptions. Depending upon the assumptions, enormous discrepancies arise in the estimated

rate coefficients. For example, alternative experimental measurements for the fragmentation rate in cumyl dithiobenzoate mediated polymerization of styrene at 60°C differ by six orders of magnitude (109,110), and this difference arises, at least in part, in the model-based assumptions of the alternative experimental techniques (For a discussion of problems measuring fragmentation rate coefficients, the reader is referred to Reference 111). Recent ab initio calculations of the fragmentation rate coefficient for a model of this system were able to provide direct evidence in support of one measurement (and hence one set of assumptions) over the other, and in doing so provide an insight into the causes of rate retardation in the RAFT process (6).

As accurate calculations become routine, there will be many other applications for the a priori prediction of absolute rate coefficients. The calculation of propagation rate coefficients (which can be measured experimentally via pulsed laser polymerization or PLP (112)) is currently used to benchmark theoretical procedures, but accurate calculations may also be helpful as a stand-alone technique for toxic and hazardous monomers, and in other cases where PLP is difficult (due to problems such as the monomer absorbing at the wavelength of the laser or reactions such as chain transfer broadening the molecular weight distribution). It has also been noted that ab initio calculations may provide the best means of studying long- and short-chain branching in free-radical polymerization (5). Quantum chemistry will also be helpful in extracting the rate coefficients of the individual reactions in other complicated reaction schemes, such as free-radical copolymerization, and the various types of controlled radical polymerization systems.

Prediction of Relative Rate Coefficients: Discriminating Models and Mechanisms. High level ab initio calculations can already predict *relative* rate coefficients with remarkable accuracy. This is because accurate relative values of quantities such as barriers and enthalpies can generally be obtained at lower levels of theory than corresponding absolute values, because of substantial cancellation of error. In addition, one might generally expect that chain-length effects and solvent effects should be reasonably consistent for a series of similar reactions, and thus cancel from the comparative values. The prediction of relative rate coefficients is important for modeling and hence optimizing various aspects of the polymerization process, and some of these applications are outlined below. The prediction of relative rate coefficients is also important for understanding the effects of substituents on the various individual reactions, and these applications are discussed in the following section.

Copolymerization. In free-radical copolymerization (qv), the relative rates of addition of the various types of radical to the alternative monomers are called reactivity ratios, and are the key parameters governing the composition and sequence distribution of the resulting copolymer. Experimentally, these parameters are "measured" for a given system by treating them as adjustable parameters in a least-squares fit of some assumed kinetic model to experimental values of the composition, sequence distribution, and/or propagation rate coefficients. However, there are two important problems with this approach (104). Firstly, it is not always (if ever) clear which copolymerization model (eg the terminal model, the implicit or explicit penultimate model, etc) is appropriate for a given system. If a physically incorrect model is chosen, then the estimated parameters will lack their assumed physical meaning, and will thus be unsuitable for mechanistic studies,

or for predicting other copolymerization properties. Secondly, even if the correct model is chosen, there are often more adjustable parameters than are numerically needed to fit the data, and this can result in large and highly correlated uncertainties in the estimated parameters. The problems in the experimental estimation of reactivity ratios are discussed in more detail in the article on copolymerization (qv).

Quantum chemistry is able to address these problems, as it allows the reactivity ratios to be calculated directly from the rate coefficients for the various types of reaction, without making kinetic-model-based assumptions. Furthermore, quantum chemistry can assist in determining which kinetic model is most appropriate for a given system. For example, by measuring the effects of substituents at the penultimate position of the propagating radical, quantum chemistry can be used to determine whether a terminal or penultimate model is appropriate for a given system. In this respect, quantum chemistry has already made an important contribution to this field by providing evidence for penultimate unit effects in the barriers (1,106) and frequency (2,106) factors of a variety of different systems. Such calculations can thus simplify the model discrimination process by ruling out either the terminal- or penultimate-based models for a given system, and by providing estimates for the main model parameters (ie the reactivity ratios). In addition, quantum chemistry can provide a simple and cost-effective method for screening the reactivity ratios for a wide variety of monomer pairs (including hazardous and yet-to-be synthesized monomers). This may allow the identification of monomer pairs with suitable reactivity ratios for a given application.

Chain Transfer. The relative rate of abstraction to propagation for a specific propagating radical is known as the chain-transfer constant, and is a key parameter governing the molecular weight of the resulting polymer. High level ab initio calculations allow chain-transfer constants to be predicted for a given propagating radical and transfer agent, and thus provide an effective means of screening large numbers of transfer agents. This in turn may assist in the selection of suitable transfer agents for a given polymerization system, and can also aid in our understanding of reactivity in the chain-transfer processes. Already ab initio calculations have been used to study intramolecular chain-transfer processes in free-radical polymerization (5,106), in order to provide estimates of the short-chain branching ratios. Another study investigated the kinetics and thermodynamics of the hydrogen abstraction *by* and *from* the monomer in ethylene polymerization (113), and demonstrated that abstraction from the monomer was the kinetically (but not thermodynamically) preferred process. There is also an enormous body of literature concerning ab initio calculations of hydrogen abstraction reactions in general, and in applications of relevance to other fields such as biochemistry (114,119).

Controlled Radical Polymerization. In recent years, the field of free-radical polymerization has been revolutionalized by the development of techniques for controlling the molecular weight and architecture of the resulting polymer, including nitroxide-mediated polymerization (NMP) (120), atom-transfer polymerization (ATRP) (121), and reversible addition fragmentation chain transfer (RAFT) polymerization (96) (see LIVING RADICAL POLYMERIZATION). In order to control polymerization, these processes aim to minimize the influence of bimolecular

termination processes via a delicate balance of the relative rates of two or more competing reactions. Quantum chemistry can assist in optimizing these processes by providing reliable values for the rate coefficients of the competing reactions, across a wide range of systems. More generally, quantum chemistry can help to provide a detailed understanding of the kinetics and mechanisms of the individual reactions, which can in turn allow for the design of improved control agents.

Quantum chemistry has already been used to study the RAFT process (6,7). As noted above, high level ab initio molecular orbital calculations have been used to obtain direct measurements of the rates of addition and fragmentation in model dithiobenozate-mediated systems, which in turn provided evidence that slow fragmentation is responsible for rate retardation in these systems (6). More recently, ab initio calculations have revealed a new and unexpected side reaction (β-scission of the alkoxy group) in certain xanthate-mediated systems, which may provide an explanation for the experimentally observed inhibition in those systems (7). The ab initio calculations also indicated that fragmentation was considerably faster in the xanthate-mediated systems (compared with other dithioester systems), because of the stabilizing influence of the alkoxy group on the thiocarbonyl product (7). In addition to these ab initio calculations, semiempirical methods have been used to survey the transfer enthalpies for a series of RAFT agents in styrene, methyl methacrylate, and butyl acrylate polymerization (122). Despite the low level of theory used, and the limited accuracy of the quantitative predictions at this level, the calculations were nonetheless shown to have some qualitative value in determining which transfer agents would show the best molecular weight control in RAFT polymerization.

Understanding Reactivity via the Curve-Crossing Model. We have already seen that quantum chemistry can be used to calculate the absolute (and hence relative) rate coefficients for the individual reactions in free-radical polymerization, and is well suited to compiling systematic surveys of the rate coefficients for homologous series of reactions. When such calculations are combined with qualitative theoretical models, quantum chemistry can help to provide an understanding of trends in reactivity. It is beyond the scope of this chapter to provide an account of the main qualitative models and concepts in general theoretical chemistry. However, it is worth introducing one such model—the *curve-crossing model* (123)—as this model has been used extensively to provide a qualitative rationalization of the effects of substituents in some of the key radical reactions that occur in free-radical polymerization, including radical addition to alkenes (103) (ie the propagation step), and hydrogen abstraction (115,116,124) (ie, chain-transfer processes). The main qualitative features of the model and its application to free-radical polymerization are described below; for a more detailed description, the reader is referred to the original references 123, and also the excellent book by Pross (125).

The curve-crossing model (also referred to as the valence-bond state correlation model, the configuration mixing model, or the state correlation diagram) was developed by Pross and Shaik (123) as a unifying theoretical framework for explaining barrier formation in chemical reactions. It is largely based on valence bond (VB) theory (126,127), but also incorporates insights from qualitative molecular orbital theory (128). To understand the curve-crossing model, it is helpful to think of a chemical reaction as being composed of a rearrangement of electrons,

accompanied by a rearrangement of nuclei (ie a geometric rearrangement). We can then imagine holding the arrangement of electrons constant in its initial configuration (which we call the reactant VB configuration), and examining how the energy changes as a function of the geometry. Likewise, we could hold the electronic configuration constant in its final form (the product VB configuration), and again examine the variation in energy as a function of the geometry. If these two curves (energy vs geometry) are plotted, we form a "state correlation diagram." The overall energy profile for the reaction, which is also plotted, is formed by the resonance interaction between the reactant and product configurations (and any other low lying configurations). State correlation diagrams allow for a qualitative explanation for how the overall energy profile of the reaction arises, and can then be used to provide a graphical illustration of how variations in the relative energies of the alternative VB configurations affect the barrier height. This in turn allows us to rationalize the effects of substituents on reaction barriers, and to predict when simple qualitative rules (such as the Evans–Polanyi rule (129)) should break down.

This procedure is best illustrated by way of an example, such as the case of radical addition to alkenes. For this type of reaction, the principal VB configurations that may contribute to the ground-state wave function are the four lowest doublet configurations of the three-electron–three-center system formed by the initially unpaired electron at the radical carbon (R) and the electron pair of the attacked π bond in the alkene (A) (103).

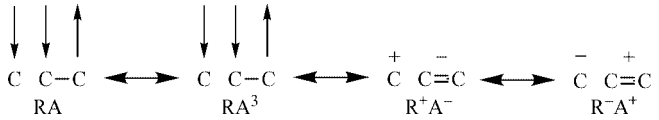

The first configuration (RA) corresponds to the arrangement of electrons in the reactants, the second (RA^3) to that in the products, and the others (R^+A^- and R^-A^+) to possible charge-transfer configurations. The state correlation diagram showing (qualitatively) how the energies of these configurations vary as a function of the reaction coordinate is provided in Figure 11 (103). Let us now examine how this plot could be made for a specific system.

The anchor points on these diagrams are generally accessible from quantum-chemical calculations. For example, the energy difference between the RA configuration at the reactant geometry, and the RA^3 configuration at the product geometry, is simply the energy change of the reaction. The energy difference between the RA and RA^3 configurations at the reactant geometry is simply the vertical singlet-triplet gap of the alkene. At the product geometry, the RA $-$ RA^3 energy difference is also an excitation energy, but this time between the ground state of the doublet product and an excited doublet state (In fact, studies of radical addition to alkenes have ignored the influence of this excitation gap, without detriment to the predictive value of the results (103). This is probably due to the fact that the transition structure is very early in these reactions. However, in studies of hydrogen abstraction reactions, the RA and RA^3 gaps at both the reactant and product geometries can be important. These are calculated as the singlet-triplet gap of the closed-shell substrate in each case.) The charge-transfer configurations can be anchored at the reactant geometry, where they are given as the energy for

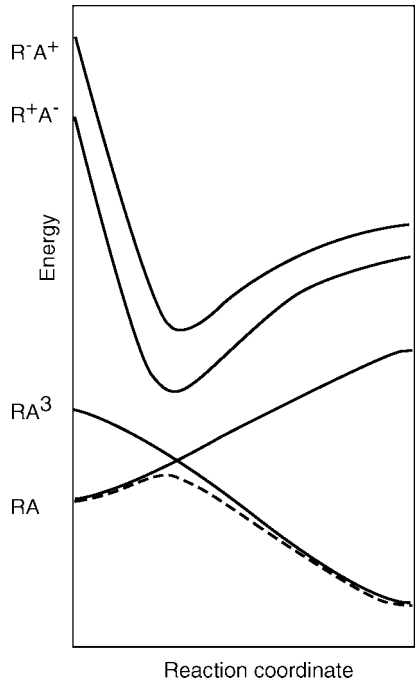

Fig. 11. State correlation diagram for radical addition to alkenes showing the variation in energy of the reactant (RA), the product (RA^3), and the charge-transfer configurations (R^+A^- and R^-A^+) as a function of the reaction coordinate. The dashed line represents the overall energy profile of the reaction.

complete charge transfer between the isolated reactants. For example, the energy difference between the R^+A^- and the RA configuration at the reactant geometry would be given as the energy change of the reaction $R + A \rightarrow R^+ + A^-$. It can be seen that the energy change of this reaction is simply the difference between the ionization energy ($R \rightarrow R^+ + e-$) of the donor species and electron affinity ($A^- \rightarrow A + e-$) of the acceptor.

Although the anchor points in the diagram are obtained quantitatively, we generally interpolate the intervening points on the VB configuration curves qualitatively, on the basis of spin pairing schemes and VB arguments (123). At this point it should be stressed that the overall energy profile for the reaction is of course quantitatively accessible from our quantum-chemical calculations. The objective of the curve-crossing model analysis is not to generate the overall reaction profile but to understand how it arises—and a qualitative approach to generating the VB configuration curves is generally adequate for this purpose. If we consider first the product configuration, its energy is lowered during the course of the reaction because of bond formation between the radical and attacked carbon. At the same time, the relative energy of the reactant configuration increases because the π bond on the attacked alkene is stretched, and this is not compensated for by bond formation with the attacking radical. The energies of the charge-transfer

configurations are initially very high in energy, but are stabilized by Coloumb attraction as the reactants approach one another.

The overall energy profile for the reaction can be formed from the resonance interaction of these contributing configurations. In the early stages of the reaction, the reactant configuration is significantly lower in energy than the others and dominates the ground-state wave function. However, in the vicinity of the transition structure, the reactant and product configurations have similar energies, and thus significant mixing is possible. This stabilizes the wave function, with the strength of the stabilizing interaction increasing with the decreasing energy difference between the alternate configurations. It is this mixing of the reactant and product configurations which leads to the avoided crossing, and accounts for barrier formation. Beyond the transition structure, the product configuration is lower in energy and dominates the wave function. The charge-transfer configurations generally lie significantly above the ground-state wave function for most of the reaction. However, in the vicinity of the transition structure, they can sometimes be sufficiently low in energy to interact. In those cases, the transition structure is further stabilized, and (if one of the charge transfer configurations is lower than the other) the mixing is reflected in a degree of partial charge transfer between the reactants. Since the charge distribution within the transition structure is accessible from quantum-chemical calculations, this provides a testable prediction for the model.

Using this state-correlation diagram, in conjunction with simple VB arguments, the curve-crossing model can be used to predict the influence of various energy parameters on the reaction barrier. For radical addition to alkenes (103), the barrier depends mainly on the reaction exothermicity (which measures the energy difference between the reactant and product configurations at their optimal geometries), the singlet-triplet gap in the alkene (which measures the energy difference between the reactant and product configurations at the reactant geometry), and the relative energies of the possible charge-transfer configurations. The effects of individual variations in these quantities are illustrated graphically in Figure 12. It can be seen that the barrier height is lowered by an increase in the reaction exothermicity, a decrease in the singlet-triplet gap, or a decrease in the relative energy of one or both of the charge-transfer configurations (provided that these are sufficiently low in energy to contribute to the ground-state wave function).

A strategy for understanding the effects substituents in the barriers of radical reactions, such as addition, is to calculate these key quantities [ie, the reaction exothermicity, the singlet-triplet excitation gap of the closed-shell substrate(s), and the energy for charge transfer between the reactants], and look for relationships between these quantities and the barrier heights. In this way, one could establish, for example, the extent of polar interactions in a particular class of reactions. As noted at the beginning of this section, a number of such studies have already been performed for the key reactions in free-radical polymerization. The curve-crossing analysis of radical addition reactions, which is reviewed in detail elsewhere (94,99), indicate that, in the absence of polar interactions, the barrier height depends on the reaction exothermicity, in accordance with the Evans–Polanyi rule (129). However, for combinations of electron-withdrawing and electron-donating reactants, polar interactions are significant,

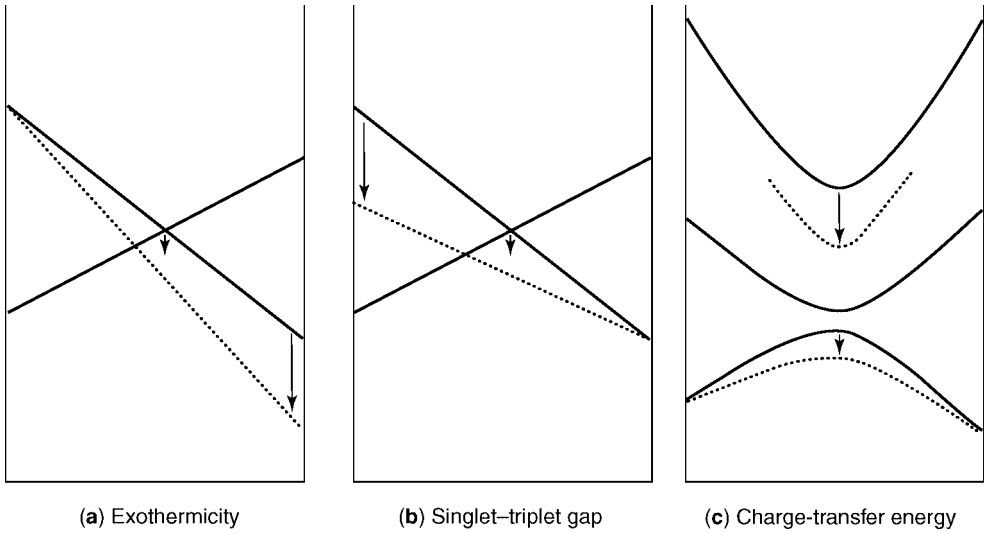

Fig. 12. State correlation diagrams showing separately the qualitative effects of (**a**) increasing the reaction exothermicity, (**b**) decreasing the singlet–triplet gap, and (**c**) decreasing the energy of the charge-transfer configuration. For the sake of clarity the adiabatic minimum energy path showing the avoided crossing, as in Figure 9, is omitted from (**a**) and (**b**).

and cause substantial deviation from Evans–Polanyi behavior. More recently, the curve-crossing model has been used to explain the relative reactivity of the C=C, C=O, and C=S bonds (which is of relevance to RAFT polymerization) (130), and to examine why alkynes are less reactive to addition than alkenes (131). In these cases the differing singlet-triplet gaps of the alternative substrates are also important in governing their relative reactivities. Curve-crossing studies have also been applied to various types of hydrogen abstraction reactions (115,116,124), and, depending upon the substituents, the singlet-triplet gaps (in this case of *both* the reactant and product substrates), exothermicities, and polar interactions have all been found to be important in governing reactivity in these reactions.

The Future

There are many more potential applications for quantum chemistry in free-radical polymerization. As computer power increases, one will be able to calculate rate coefficients for yet larger systems, and at much greater accuracy. In this way, quantum chemistry has a role to play in modeling the kinetics and mechanism of polymerization processes, and predicting the properties of the resulting polymer (such as the molecular weight distribution, the copolymer composition, and the degree of branching). Quantum chemistry may also help in designing improved agents or processes for controlling polymerization, and in identifying their mechanisms. Of course, quantum chemistry may also be used effectively to study other types of polymerization processes, such as ring-opening processes. Provided care

is taken to ensure the accuracy of the methods used, quantum-chemical methods provide a powerful tool for studying free-radical polymerization, and should be seen as a valuable complement to experimental approaches.

BIBLIOGRAPHY

1. M. L. Coote, T. P. Davis, and L. Radom, *Theochem* **461/462**, 91–96 (1999); *Macromolecules* **32**, 2935–2940 (1999); *Macromolecules* **32**, 5270–5276 (1999).
2. J. P. A. Heuts, R. G. Gilbert, and I. A. Maxwell, *Macromolecules* **30**, 726 (1997).
3. J. P. A. Heuts, R. G. Gilbert, and L. Radom, *Macromolecules* **28**, 8771–8781 (1995).
4. D. M. Huang, M. J. Monteiro, and R. G. Gilbert, *Macromolecules* **31**, 5175 (1998).
5. J. S.-S. Toh, D. M. Huang, P. A. Lovell, and R. G. Gilbert, *Polymer* **42**, 1915–1920 (2001).
6. M. L. Coote and L. Radom, *J. Am. Chem. Soc.* **125**, 1490 (2003).
7. M. L. Coote and L. Radom, *Macromolecules* **37**, 590 (2004).
8. W. J. Hehre, L. Radom, P. v. R. Schleyer, and J. A. Pople, *Ab Initio Molecular Orbital Theory*, John Wiley & Sons, Inc., New York, 1986.
9. F. Jensen, *Introduction to Computational Chemistry*, John Wiley & Sons, Inc., New York, 1999.
10. R. G. Parr and W. Yang, *Density Functional Theory of Atoms and Molecules*, Oxford University Press, New York, 1989.
11. W. Koch and M. C. Holthausen, *A Chemist's Guide to Density Functional Theory*, Wiley-VCH, Weinheim, 2000.
12. S. W. Benson, *Thermochemical Kinetics*, John Wiley & Sons, Inc., New York, 1976.
13. D. A. McQuarrie, *Statistical Mechanics*, Harper & Row, New York, 1976.
14. R. G. Gilbert and S. C Smith, *Theory of Unimolecular and Recombination Reactions*, Blackwell Scientific, Oxford, 1990.
15. J. I. Steinfeld, J. S. Francisco, and W. L. Hase, *Chemical Kinetics and Dynamics*, 2nd ed., Prentice-Hall, Englewood Cliffs, N.J., 1999.
16. P. W. Atkins, *Physical Chemistry*, 6th ed., W. H. Freeman and Co., San Francisco, 2000.
17. E. Schrödinger, *Ann. Physik* **79**, 361 (1926).
18. P. Pyykkö, *Chem. Rev.* **88**, 563–594 (1988).
19. M. Born and J. R. Oppenheimer, *Ann. Physik* **84**, 457 (1927).
20. A. E. Reed, L. A. Curtiss, and F. Weinhold, *Chem Rev.* **88**, 899 (1988).
21. R. F. W. Bader, *Atoms in Molecules: A Quantum Theory*, Clarendon Press, Oxford, 1990.
22. C. J. Cramer, *Essentials of Computational Chemistry: Theories and Models*, John Wiley and Sons, Inc., New York, 2002.
23. E. G. Lewars, *Computational Chemistry: Introduction to the Theory and Applications of Molecular and Quantum Mechanics*, Kluwer Academic Publishers, Dordrecht, the Netherlands, 2003.
24. A. K. Rappe and C. J. Casewit, *Molecular Mechanics Across Chemistry*, University Science Books, Herndon, Va., 1997.
25. J. C. Slater, *Phys. Rev.* **34**, 1293 (1929); J. C. Slater, *Phys. Rev.* **35**, 509 (1930).
26. D. R. Hartree, *Proc. Cambridge Philos. Soc.* **26**, 376 (1928); V. Fock, *Z. Phys.* **61**, 126 (1930).
27. A. K. Wilson, T. van Mourik, and T. H. Dunning Jr., *J. Mol. Struct. (Theochem)* **388**, 339–349 (1996), and references cited therein.

28. J. M. L. Martin and S. Parthiban, in J. Cioslowski, ed., *Quantum Mechanical Prediction of Thermochemical Data*, Kluwer Academic Publishers, Dordrecht, the Netherlands, 2001, pp. 31–65, and references cited therein.
29. R. Car and M. Parrinello, *Phys. Rev. Lett.* **55**, 2471 (1985).
30. P. E. Blöchl, P. Margl, and K. Schwarz, in B. B. Laird, R. B. Ross, and T. Ziegler, eds., *Chemical Applications of Density Functional Theory*, American Chemical Society, Washington, D.C., 1996, pp. 54–69.
31. D. M. Chipman, *Theor. Chim. Acta* **82**, 93–115 (1992).
32. M. W. Wong and L. Radom, *J. Phys. Chem.* **99**, 8582–8588 (1995).
33. M. W. Wong and L. Radom, *J. Phys. Chem.* **102**, 2237–2245 (1998).
34. Y. Y. Chuang, E. L. Coitino, and D. G. Truhlar, *J. Phys. Chem. A* **104**, 446 (2000).
35. C. C. J. Roothaan, *Rev. Mod. Phys.* **23**, 69 (1951); G. G. Hall, *Proc. R. Soc. (London)* **A 205**, 541 (1951).
36. M. L. Coote, G. P. F. Wood, and L. Radom, *J. Phys. Chem. A* **106**, 12124–12138 (2002).
37. R. Gómez-Balderas, M. L. Coote, D. J. Henry, and L. Radom, *J. Phys. Chem. A* **108**, 2874–2883 (2004).
38. D. K. Malick, G. A. Petersson, and J. A. Montgomery, *J. Chem. Phys.* **108**, 5704–5713 (1998).
39. V. D. Knyazev and I. R. Slagle, *J. Phys. Chem.* **100**, 16899–16911 (1996); V. D. Knyazev, A. Bencsura, S. I Stoliarov, and I. R. Slagle, *J. Phys. Chem.* **100**, 11346–11354 (1996).
40. M. Schwartz, P. Marshall, R. J. Berry, C. J. Ehlers, and G. A. Petersson, *J. Phys. Chem. A* **102**, 10074–10081 (1998).
41. M. L. Coote, M. A. Collins, and L. Radom, *Mol. Phys.* **101**, 1329–1338 (2003).
42. J. A. Montgomery Jr., M. J. Frisch, J. W. Ochterski, and G. A. Petersson, *J. Chem. Phys.* **112**, 6532–6542 (2000), and references cited therein.
43. M. J. Frisch, G. W. Trucks, H. B. Schlegel, G. E. Scuseria, M. A. Robb, J. R. Cheeseman, J. A. Montgomery Jr., T. Vreven, K. N. Kudin, J. C. Burant, J. M. Millam, S. S. Iyengar, J. Tomasi, V. Barone, B. Mennucci, M. Cossi, G. Scalmani, N. Rega, G. A. Petersson, H. Nakatsuji, M. Hada, M. Ehara, K. Toyota, R. Fukuda, J. Hasegawa, M. Ishida, T. Nakajima, Y. Honda, O. Kitao, H. Nakai, M. Klene, X. Li, J. E. Knox, H. P. Hratchian, J. B. Cross, C. Adamo, J. Jaramillo, R. Gomperts, R. E. Stratmann, O. Yazyev, A. J. Austin, R. Cammi, C. Pomelli, J. W. Ochterski, P. Y. Ayala, K. Morokuma, G. A. Voth, P. Salvador, J. J. Dannenberg, V. G. Zakrzewski, S. Dapprich, A. D. Daniels, M. C. Strain, O. Farkas, D. K. Malick, A. D. Rabuck, K. Raghavachari, J. B. Foresman, J. V. Ortiz, Q. Cui, A. G. Baboul, S. Clifford, J. Cioslowski, B. B. Stefanov, G. Liu, A. Liashenko, P. Piskorz, I. Komaromi, R. L. Martin, D. J. Fox, T. Keith, M. A. Al-Laham, C. Y. Peng, A. Nanayakkara, M. Challacombe, P. M. W. Gill, B. Johnson, W. Chen, M. W. Wong, C. Gonzalez, and J. A. Pople, Gaussian 03, Revision B.03, Gaussian, Inc., Pittsburgh Pa., 2003. Available at http://www.gaussian.com/
44. L. A. Curtiss and K. Raghavachari, *Theor. Chem. Acc.* **108**, 61–70 (2002), and references cited therein.
45. D. J. Henry, M. B. Sullivan, and L. Radom, *J. Chem. Phys.* **118**, 4849–4860 (2003).
46. M. W. Schmidt and M. S. Gordon, *Annu. Rev. Phys. Chem.* **49**, 233–266 (1998).
47. J. J. P Stewart, *J. Compu. Aided Mol. Des.* **4**, 1–105 (1990).
48. P. Hohenberg and W. Kohn, *Phys. Rev. B* **136**, 864 (1964).
49. W. Kohn and L. J. Sham, *Phys. Rev. A* **140**, 1133 (1965).
50. J. P. Perdew, A. Savin, and K. Burke, *Phys. Rev. A* **51**, 4531–4540 (1995).
51. J. D. Goddard and G. Orlova, *J. Chem. Phys.* **111**, 7705–7712 (1999).
52. J. C. Slater, *Quantum Theory of Molecular Solids, Vol. 4: The Self-Consistent Field for Molecular Solids*, McGraw-Hill, Inc., New York, 1974.
53. S. H. Vosko, L. Wilk, and M. Nusair, *Can. J. Phys.* **58**, 1200 (1980).

54. W. Kohn, A. D. Becke, and R. G. Parr, *J. Phys. Chem.* **100**, 12974–12980 (1996).
55. A. D. Becke, *Phys. Rev. A* **38**, 3098 (1988).
56. C. Lee, W. Yang, and R. G. Parr, *Phys. Rev. B* **37**, 785 (1988); B. Miehlich, A. Savin, H. Stoll, and H. Preuss, *Chem. Phys. Lett.* **157**, 200 (1989).
57. J. P. Perdew, K. Burke, and Y. Wang, *Phys. Rev. B* **54**, 16533 (1996), and references cited therein.
58. A. D. Becke, *J. Chem. Phys.* **98**, 5648 (1993).
59. B. J. Lynch, P. L. Fast, M. Harris, and D. G. Truhlar, *J. Phys. Chem. A* **104**, 4811–4815 (2000); B. J. Lynch and D. G. Truhlar, *J. Phys. Chem. A* **105**, 2936–2941 (2001); B. J. Lynch and D. G. Truhlar, *J. Phys. Chem. A* **106**, 842–846 (2002).
60. M. A. Collins, *Theor. Chem. Acc.* **108**, 313–324 (2002).
61. D. H. Zhang, M. A. Collins, and S.-Y. Lee, *Science* **290**, 961–963 (2000).
62. K. Song and M. A. Collins, *Chem. Phys. Lett.* **335**, 481 (2001).
63. A. Sanchez-Galvez, P. Hunt, M. A. Robb, M. Olivucci, T. Vreven, and H. B. Schlegel, *J. Am. Chem. Soc.* **122**, 2911–2924 (2000); M. Sharma, Y. Wu, and R. Car, *J. Chem. Phys.* **95**, 821–829 (2003).
64. A. C. T. van Duin, S. Dasgupta, F. Lorant, and W. A. Goddard III, *J. Phys. Chem. A* **105**, 9396–9409 (2001).
65. M. Garavelli, F. Ruggeri, F. Ogliaro, M. J. Bearpark, F. Bernardi, M. Olivucci, and M. A. Robb, *J. Comput. Chem.* **24**, 1357–1363 (2003).
66. H. Eyring, *J. Chem. Phys.* **3**, 107 (1935).
67. For a more detailed definition of this term, see for example: A. J. Karas, R. G. Gilbert, and M. A. Collins, *Chem. Phys. Lett.* **193**, 181–184 (1992).
68. D. G. Truhlar, B. C. Garrett, and S. J. Klippenstein, *J. Phys. Chem.* **100**, 12771 (1996).
69. R. T. Skodje, D. G. Truhlar, and B. C. Garrett, *J. Phys. Chem.* **85**, 3019 (1981).
70. B. C. Garrett, D. G. Truhlar, A. F. Wagner, and T. H. Dunning Jr., *J. Chem. Phys.* **78**, 4400 (1983).
71. Y. P. Liu, D. H. Lu, A. Gonzalez-Lafont, D. G. Truhlar, and B. C. Garrett, *J. Am. Chem. Soc.* **115**, 7806 (1993).
72. J. C. Corchado, Y.-Y. Chuang, P. L. Fast, J. Villà, W.-P. Hu, Y.-P. Liu, G. C. Lynch, K. A. Nguyen, C. F. Jackels, V. S. Melissas, B. J. Lynch, I. Rossi, E. L. Coitiño, A. Fernandez-Ramos, J. Pu, T. V. Albu, R. Steckler, B. C Garrett, A. D. Isaacson, and D. G. Truhlar, POLYRATE 9.1, University of Minnesota, Minneapolis, Minn., 2002. Available at http://comp.chem.umn.edu/polyrate/
73. A. Kuppermann and D. G. Truhlar, *J. Am. Chem. Soc.* **93**, 1840 (1971); B. C. Garrett, D. G. Truhlar, R. S. Grev, and A. W. Magnuson, *J. Phys. Chem.* **84**, 1730 (1980).
74. R. P. Bell, *The Tunnel Effect in Chemistry*, Chapman and Hall, London, 1980.
75. E. Wigner, *J. Chem. Phys.* **5**, 720 (1937).
76. C. Eckart, *Phys. Rev.* **35**, 1303 (1930).
77. Y.-X. Yu, S.-M. Li, Z.-F. Xu, Z.-S. Li, and C.-C. Sun, *Chem. Phys. Lett.* **302**, 281 (1999).
78. W. T. Duncan, R. L. Bell, and T. N. Truong, *J. Comput. Chem.* **19**, 1039 (1998).
79. V. Van Speybroeck, D. Van Neck, M. Waroquier, S. Wauters, M. Saeys, and G. B. Martin, *J. Phys. Chem. A* **104** 10939–10950 (2000).
80. K. S. Pitzer and W. D. Gwinn, *J. Chem. Phys.* **10**, 428–440 (1942); J. C. M. Li and K. S. Pitzer, *J. Phys. Chem.* **60**, 466–474 (1956).
81. A. L. L. East and L. Radom, *J. Chem. Phys.* **106**, 6655 (1997).
82. V. Van Speybroeck, D. Van Neck, and M. Waroquier, *J. Phys. Chem. A* **106**, 8945–8950 (2002).
83. J. F. Stanton, J. Gauss, J. D. Watts, M. Nooijen, N. Oliphant, S. A. Perera, P. G. Szalay, W. J. Lauderdale, S. A. Kucharski, S. R. Gwaltney, S. Beck, A. Balkovà, D. E. Bernholdt, K. K. Baeck, P. Rozyczko, H. Sekino, C. Hober, and R. J. Bartlett. Integral packages included are VMOL (J. Almlöf and P. R. Taylor), VPROPS (P. Taylor), ABACUS

(T. Helgaker, H. J. Aa. Jensen, P. Jørgensen, J. Olsen, and P. R. Taylor); Quantum Theory Project, University of Florida, Available at http://www.qtp.ufl.edu/Aces2/
84. M. W. Schmidt, K. K. Baldridge, J. A. Boatz, S. T. Elbert, M. S. Gordon, J. H. Jensen, S. Koseki, N. Matsunaga, K. A. Nguyen, S. J. Su, T. L. Windus, M. Dupuis, and J. A. Montgomery, *J. Comput. Chem.* **14**, 1347–1363 (1993). Available at http://www.msg.ameslab.gov/GAMESS/GAMESS.html
85. R. D. Amos, A. Bernhardsson, A. Berning, P. Celani, D. L. Cooper, M. J. O. Deegan, A. J. Dobbyn, F. Eckert, C. Hampel, G. Hetzer, P. J. Knowles, T. Korona, R. Lindh, A. W. Lloyd, S. J. McNicholas, F. R. Manby, W. Meyer, M. E. Mura, A. Nicklaβ, P. Palmieri, R. Pitzer, G. Rauhut, M. Schütz, U. Schumann, H. Stoll, A. J. Stone, R. Tarroni, T. Thorsteinsson, and H.-J. Werner, Available at http://www.molpro.net/
86. J. Kong, C. A. White, A. I. Krylov, C. D. Sherrill, R. D. Adamson, T. R. Furlani, M. S. Lee, A. M. Lee, S. R. Gwaltney, T. R. Adams, C. Ochsenfeld, A. T. B. Gilbert, G. S. Kedziora, V. A. Rassolov, D. R. Maurice, N. Nair, Y. Shao, N. A. Besley, P. E. Maslen, J. P. Dombroski, H. Daschel, W. Zhang, P. P. Korambath, J. Baker, E. F. C. Byrd, T. Van Voorhis, M. Oumi, S. Hirata, C.-P. Hsu, N. Ishikawa, J. Florian, A. Warshel, B. G. Johnson, P. M. W. Gill, M. Head-Gordon, and J. A. Pople, *J. Comput. Chem.* **21**, 1532–1548 (2000). Available at http://www.q-chem.com/
87. Wavefunction, Inc., Available at http://www.wavefun.com/
88. G. Schaftenaar, Available at http://www.cmbi.kun.nl/~schaft/molden/molden.html
89. Cambridgesoft, Available at http://www.cambridgesoft.com/
90. N. J. R. van Eikema Hommes, Available at http://www.ccc.uni-erlangen.de/molecule/
91. Free Open Source Software, Available at http://jmol.sourceforge.net/
92. B. M. Bode and M. S. Gordon, *J. Mol. Graphics Mod.* **16**, 133–138 (1998). Available at http://www.msg.ameslab.gov/GAMESS/GAMESS.html
93. J. P. A. Heuts, R. G. Gilbert, and L. Radom, *J. Phys. Chem.* **100**, 18997–19006 (1996).
94. M. Saeys, M.-F. Reyniers, G. B. Marin, V. van Speybroeck, and M. Waroquier, *J. Phys. Chem. A* **107**, 9147–9159 (2003).
95. A. P. Scott and L. Radom, *J. Phys. Chem.* **100**, 16502–16513 (1996).
96. J. Chiefari, Y. K. B. Chong, F. Ercole, J. Krstina, J. Jeffery, T. P. T. Le, R. T. A. Mayadunne, G. F. Meijs, C. L. Moad, G. Moad, E. Rizzardo, and S. H. Thang, *Macromolecules* **31**, 5559 (1998).
97. J. K. Kang and C. B. Musgrave, *J. Chem. Phys.* **115**, 11040 (2001).
98. H. Basch and S. Hoz, *J. Phys. Chem. A* **101**, 4416 (1997).
99. M. L. Coote, *J. Phys. Chem. A* **108**, 3865–3872 (2004).
100. M. L. Coote, T. P. Davis, B. Klumperman, and M. J. Monteiro, *J. Macromol. Sci., Rev. Macromol. Chem. Phys. C* **38**, 567 (1998), and references cited therein.
101. M. Ben-Nun and R. D. Levine, *Int. Rev. Phys. Chem.* **14**, 215–270 (1995); G. A. Voth and R. M. Hochstrasser, *J. Phys. Chem.* **100**, 13034–13049 (1996).
102. J. R. Pliego Jr. and J. M. Riveros, *J. Phys. Chem. A* **105**, 7241–7247 (2001).
103. H. Fischer and L. Radom, *Angew. Chem., Int. Ed. Engl.* **40**, 1340–1371 (2001).
104. M. L. Coote and T. P. Davis, *Prog. Polym. Sci.* **24**, 1217 (1999), and references cited therein.
105. M. Deady, A. W. H. Mau, G. Moad, and T. H. Spurling, *Makromol. Chem.* **194**, 1691 (1993).
106. J. Filley, T. McKinnon, D. T. Wu, and G. H. Ko, *Macromolecules* **35**, 3731–3738 (2002).
107. M. Buback, C. H. Kurz, and C. Schmaltz, *Macromol. Chem. Phys.* **199**, 1721–1727 (1998).
108. J. P. A. Heuts, in K. Matyjaszewski and T. P. Davis, eds., *Handbook of Radical Polymerization*, John Wiley & Sons, Inc., New York, 2002, pp. 1–76.
109. C. Barner-Kowollik, J. F. Quinn, D. R. Morsley, and T. P. Davis, *J. Polym. Sci., Part A: Polym. Chem.* **39**, 1353 (2001).

110. Y. Kwak, A. Goto, Y. Tsuji, Y. Murata, K. Komatsu, and T. Fukuda, *Macromolecules* **35**, 3026 (2002).
111. C. Barner-Kowollik, M. L. Coote, T. P. Davis, L. Radom, and P. Vana, *J. Polym. Sci., Part A: Polym. Chem.* **41**, 2828–2832 (2003), and references cited therein.
112. M. L. Coote, M. D. Zammit, and T. P. Davis, *Trends Polym. Sci. (Cambridge, U.K.)* **4**, 189 (1996).
113. J. P. A. Heuts, A. Pross, and L. Radom, *J. Phys. Chem.* **100**, 17087–17089 (1996).
114. D. L. Reid, D. A. Armstrong, A. Rauk, and C. von Sonntag, *Phys. Chem. Chem. Phys.* **5**, 3994–3999 (2003).
115. L. Song, W. Wu, K. Dong, P. C. Hibberty, and S. Shaik, *J. Phys. Chem. A* **106**, 11361–11370 (2002).
116. S. Shaik, W. Wu, K. Dong, L. Song, and P. C. Hiberty, *J. Phys. Chem. A* **105**, 8226 (2001).
117. S. L. Boyd and R. J. Boyd, *J. Phys. Chem. A* **105**, 7096 (2001).
118. R. Sumathi, H. H. Carstensen, and W. H. Green Jr., *J. Phys. Chem. A* **105**, 8969–8984 (2001).
119. R. Sumathi, H. H. Carstensen, and W. H. Green Jr., *J. Phys. Chem. A* **105**, 6910–6925 (2001).
120. C. J. Hawker, A. W. Bosman, and E. Harth, *Chem. Rev.* **101**, 3661–88 (2001).
121. J. S. Wang and K. Matyjaszewski, *J. Am. Chem. Soc.* **117**, 5614–5615 (1995).
122. S. C. Farmer and T. E. Patten, *J. Polym. Sci., Part A: Polym. Chem.* **40**, 555 (2002).
123. A. Pross and S. S. Shaik, *Acc. Chem. Res.* **16**, 363 (1983); A. Pross, *Adv. Phys. Org. Chem.* **21**, 99–196 (1985); S. S. Shaik, *Prog. Phys. Org. Chem.* **15**, 197–337 (1985).
124. A. Pross, H. Yamataka, and S. Nagase, *J. Phys. Org. Chem.* **4**, 135 (1991).
125. A. Pross, *Theoretical and Physical Principles of Organic Reactivity*, John Wiley & Sons, Inc., New York, 1995.
126. W. Heitler and F. London, *Z. Phys.* **44**, 455 (1927).
127. L. Pauling, *The Nature of the Chemical Bond*, Cornell University Press, Ithaca, N.Y., 1939.
128. R. B. Woodward and R. Hoffman, *Angew Chem.* **81**, 797 (1969); R. B. Woodward and R. Hoffman, *Angew Chem. Int. Ed. Engl.* **8**, 781 (1969).
129. M. G. Evans, *Disc. Faraday Soc.* **2**, 271–279 (1947); M. G. Evans, J. Gergely, and E. C. Seaman,
J. Polym. Sci. **3**, 866–879 (1948).
130. D. J. Henry, M. L. Coote, R. Gómez-Balderas, and L. Radom, *J. Am. Chem. Soc.* **126**, 1732–1740 (2004).
131. R. Gómez-Balderas, M. L. Coote, D. J. Henry, H. Fischer, and L. Radom, *J. Phys. Chem. A* **107**, 6082–6090 (2003).

MICHELLE L. COOTE
Australian National University

CONDUCTIVE POLYMER COMPOSITES. See Volume 5.

CONFORMATION AND CONFIGURATION. See Volume 2.

CONTACT LENSES. See HYDROGELS.

CONTROLLED MICROSTRUCTURE. See SINGLE SITE CATALYSTS.

CONTROLLED RADICAL POLYMERIZATION.
See LIVING RADICAL POLYMERIZATION.

CONTROLLED RELEASE FORMULATION, AGRICULTURAL

Introduction

Most controlled release formulations (CRF) are based upon macromolecules (usually polymers) as the inert components (sometimes combined with clays, salts, etc). This is because large molecules tend not to move in the environment (being often water-insoluble and nonvolatile) and they can entrap small and large molecules such as pesticides. Thus, formulation with polymers provides the construct needed to entrap the pesticide and to build into the resulting depot device the mechanism for reliable release rates. Such polymers are best degradable so as to remove them from the environment following their use. In selecting polymers for formulation cost is of great importance in agriculture, when compared to medical drug delivery systems where benefits are considered more commercially valuable (see CONTROLLED RELEASE TECHNOLOGY).

CRF aim to make available pesticides at rates appropriate for efficient control of pests under field conditions. These formulations are combinations of the pesticidal active agent with inert materials that protect, and release, the active agent according to the pest control needs. A depot or reservoir of active agent, within the releasing device or particle, is released at a defined rate, or variable rate, into the environment over a specified period. The releasing systems are usually solid and can vary in size from microparticles to large devices several centimeters across. However, the aspect which differentiates CRF from conventional formulations such as emulsifiable concentrates, wettable powders, soluble liquids, and water-dispersible granules is time, and the kinetics of release are central to CRF. In contrast, in the case of conventional formulations, complete availability of the active agent is usually considered to be immediate or rapid following deployment.

CRF can be used with a wide range of pesticides, including inorganic substances, conventional low molecular weight organic substances, high molecular weight substances such as peptides or proteins, microbials (such as mycopesticides), and semiochemicals (which, eg pheromones, modify pest behavior). Applications may be in agriculture, veterinary, and public health sectors and may be aimed at controlling a variety of pest organisms such as insects, mites, rodents, nematodes, weeds, and microorganisms as well as at improving crop production with plant growth regulators. Within the term of "controlled release" there exists a variety of release types such as extended, slow, fast, delayed, programmed, sustained, and pulsed.

Encyclopedia of Polymer Science and Technology. Copyright John Wiley & Sons, Inc. All rights reserved.

As for all pesticide formulations, CRF need to be applied, or placed, in the field appropriately for targeting the pests. In crop protection, this usually means application to the crop, or crop area, by means that achieve good distribution. Such distribution depends on how the pesticide moves to the target organism following application and often needs small particle size to provide this. Thus, the standard application methods of spraying and granules are important in agricultural pesticide delivery, which in turn limits the device size of the controlled release systems deployed. Greatest advances in CRF in agriculture have thus been found with sprayable, and to a lesser extent, granular methods. More specialized methods, eg, based on pheromones or baits, have been commercially possible using larger devices (1).

Controlled release technology aims to manipulate the bioavailability of the pesticide in the local environment following application (2). This approach has many benefits compared to conventional formulations which include increased safety to the environment, workers, and consumers. Lower concentrations of released pesticide in the environment lead to reduced losses, such as leaching, evaporation, degradation, and binding. Reduced losses may mean better pest control, less nontarget impacts, reduced crop phytotoxicity, and safer formulations. Numerous benefits have been given on behalf of CRF, including

(1) protection of active ingredients from environmental degradation,
(2) manipulation of bioavailability and persistence,
(3) reduction of toxicity and operator hazards,
(4) reduction of phytotoxicity to seeds and crops,
(5) improved selectivity between target and nontarget organisms and usage in IPM (integrated pest management),
(6) reduction in repellency (also reduction in odors),
(7) allowing coformulation, especially of incompatible pesticides (eg, of chemical and microbial pesticides),
(8) permitting elimination of solvents,
(9) improving formulation of actives with phase changes near ambient temperatures,
(10) improving handling qualities of formulations and ease of cleaning sprayers, possible reduced application rates.

However, these advantages have been known for some decades (in fact an early publication on a site-specific release formulation of an insecticide dates back to 1948 (3)) but their exploitation has been slow to develop in commercial practice. The first microcapsule formulation came on the market in 1974 (4); since then, uptake represents only a small portion of total pesticide formulations. This is in contrast to the drug sector where controlled release and delivery has been rapidly expanding.

This slow uptake in the pesticide market may be related to the increased costs of the new technology on a product basis (but not on an “effect” basis) and there is a need for a change in attitude to pest control. However, there are also

technical problems involved in active agent delivery in the open environment which may restrict extensive uptake. Renewed interest in good pesticide delivery could be prompted by the inexorable increase in limitations on pesticide numbers and their use as the Environmental Protection Agency (EPA), and other organizations, phases out more pesticides. New active ingredients coming to the market are currently fewer and registration is slow and expensive. In this situation the commercial benefits of new safer CRF may be starting to outweigh the perceived disadvantages and the usual route of new molecule introduction.

Principles of CRF for Use in the Environment

Pesticide Delivery. As with all treatments, based on biologically active molecules, targeting is fundamental to its success. If the substances do not reach the pest, then logically no control will be achieved. Delivery to the target pest is considered both in time and place; sometimes the pesticide moves toward the target (eg, with foliar herbicides (5)) and sometimes the target moves toward the pesticide (residual insecticides (6)). Thus, the efficiency of this delivery process can be defined as the ratio of the amount of pesticide reaching the pest divided by the amount applied, per unit cropping area. For many pest organisms the amount of pesticide needed for control can be ascertained, thus giving some idea of the efficiency of the delivery process. This delivery process is the sum of the placement methods, ie, spraying, granules, bait, etc, and the subsequent movement of the pesticide combined with the movement and growth of the pest itself. Sometimes, the pesticide is activated following application, in which it is chemically transformed into a more pesticidal substance. Transfer of the pesticide occurs through contact and also in mobile phases such as air and water.

Losses and Half Life. During delivery the pesticide is lost by a multitude of processes. The most rapid loss mechanisms cause the greatest amount of loss in which the pesticide is removed from the cropping location. These include spray drift, evaporation, leaching, run-off, sorption, dispersal, and dilution below active concentrations. Slower loss mechanisms include degradation of the pesticide caused by light (photodegradation), by biological processes (especially by microorganisms in soil), and by chemical processes (such as hydrolysis and oxidation) (7). Degradation produces breakdown products (metabolites) that may be more or less toxic than the parent molecule and may be more or less prone to moving away from the application site. The environmental hazard of the metabolites may be greater than the pesticide but usually degradation represents a reduction of the pesticidal activity and overall toxicity. Alternatively, the pesticide, and its metabolites, may be bound into plants or into the organic matter (or clay) of soil.

The tendency for any pesticide to be degraded is characteristic of its molecular properties and can be expressed in the DT_{50} (time for 50% disappearance) or $t_{1/2}$ (half-life), typical values for agricultural soils. This value is based on a pseudo-first-order kinetic for loss. Pesticides with long half-lives, which persist for long periods, are more effective in pest control, and are thus more efficient in contacting the pest, than those with short half-lives. However, such pesticides are less desirable environmentally, as long persistence can allow the substance to migrate, or otherwise cause detrimental impacts, such as by entering the food chain if having a high partition coefficient. In contrast, other bioactives may have short

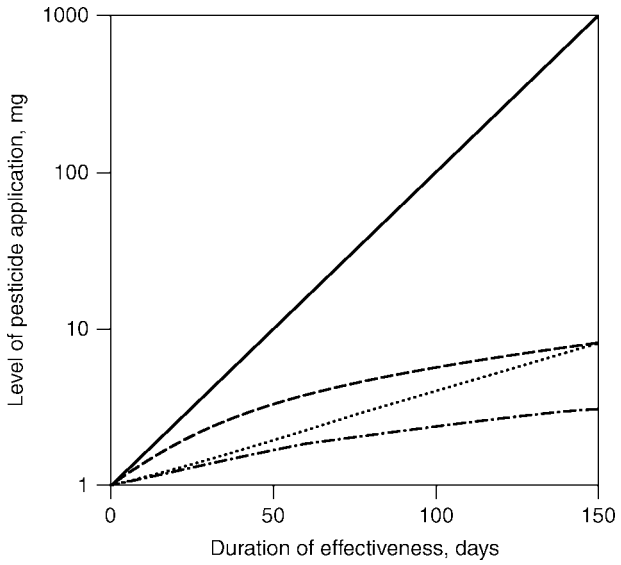

Fig. 1. Relationships between the level of application and the duration of action of two pesticides, P-1 and P-2, with differing half-lives, for conventional (A) and controlled release (B) formulations. _____ P-1 (A); _ _ _ _ P-1 (B); ..... P-2 (A); _.-._.-. P-2 (B).

half-lives, thus requiring large application rates to provide an adequate period of effective control. This is demonstrated in Figure 1 where the durations of control provided by two pesticides, P-1 with a half-life of 15 days and P-2 with a half-life of 50 days, are shown. Both require a minimum active level of 1 mg to provide control, and the two plots "A" compare the periods of control, on a logarithmic basis. It can be seen that the faster degrading pesticide P-1 requires an initial application of 1000 mg whereas the slower degrading P-2 only needs 8 mg to be effective up to 150 days. In this case, the high initial concentration in the environment forms a reservoir or depot albeit exposed to degradation and losses, which is available above the level required for control (ie, 1 mg) for the duration of the control period. Thus, the proportion of pesticide which is lost (ie, wasted) increases as the half-life decreases.

Controlled Delivery. As pesticide loss is concentration-dependent, reducing environmental concentrations will reduce losses. If the concentration at the target pest could be kept at the minimum (or just above) for effective pest control by continuous supplementing for that portion lost or dissipated, then the overall losses could be minimized (8). Keeping this minimum for the duration of control needed would represent the ideal approach with highest possible level of efficiency of delivery.

To maintain the concentration at the target, pesticide needs to be supplied at the same rate at which it is dissipated. Thus, the supply can be set equal to the loss, as in the following equation:

$$(\text{Rate of supply})\ \frac{dS}{dt} = \frac{dM}{dt}(\text{Rate of loss}) \qquad (1)$$

Approximating the loss processes occurring in the environment, the rate of loss at any time is directly proportional to the amount of the pesticide

$$\text{The rate loss } \frac{\mathrm{d}M_t}{\mathrm{d}t} = -kM_t \tag{2}$$

where M_t is the amount of the pesticide at time t and k is the loss coefficient. After integration this gives the relationship:

$$\ln \frac{M_t}{M_0} = -kt \tag{3}$$

and M_0 is the amount of pesticide applied.

The time taken for the initial pesticide application M_0 to dissipate and fall to the minimum level required at the pest for control t_m is

$$t_\mathrm{m} = \frac{1}{k} \ln \frac{M_0}{M_\mathrm{m}} \tag{4}$$

which is used to plot the logarithmic lines in Figure 1 (lines "A").

If the pesticide is delivered from a formulation at a continuous rate to replace that which is lost in the environment

$$\frac{\mathrm{d}S}{\mathrm{d}t} = kM_t \tag{5}$$

$$\mathrm{d}S = kM_t\mathrm{d}_t \tag{6}$$

The incremental change is thus given by

$$\frac{M_0 - M_\mathrm{m}}{M_m} = kt_\mathrm{m} \tag{7}$$

Using this relationship the amount released from the formulation to replace that lost and to prevent the environmental amount from falling below 1 mg can be calculated (8). This provides the curves "B" in Figure 1 for each of the two pesticides. It can be seen that the amount needed to give 150 days control has now fallen to 7.9 mg for P-1 (from 1000 mg) and to 3.1 mg for P-2 (from 8 mg). The areas between the two sets of curves represent logarithmically the pesticide that is lost and that only serves the purpose of a degradable reservoir. The amounts saved at shorter periods are less than for 150 days. Comparing the two sets of curves the potential for saving is substantially greater for the pesticide with the short half-life. In fact, using an ideal controlled delivery system for this pesticide produces an efficiency over the 150 days equivalent of using the second pesticide with the longer half-life.

CRF, combined with other aspects of pesticide application, thus offer the feasibility of improving pesticide delivery, reducing losses, and benefittng the environment. The above model is based on many assumptions, including a constant and uniform environment. The agricultural situation is characterized by continual fluctuation and thus the theoretical objective can only be partially realized.

However, it does demonstrate that compounds of short persistence (such as insect pheromones) may be used effectively in place of long-persistent compounds when appropriately formulated. Loss kinetics for any individual pesticide vary depending on the environmental location considered; for example, loss by evaporation or photodegradation at the surface of plants may be much more rapid than published data giving half-life values for soils (7).

Types of Formulation: Physical, Chemical, Biological

Physical Systems, Matrix, and Reservoir. The role of delivery of pesticides is becoming more recognized as it has been a much neglected part of pest management; in fact, the position of delivery places second only to the discovery of new biologically active molecules. Indeed, with the widespread advent of proteinaceous pesticides the ability to deliver these to the crop plant using genetically modified varieties has reached the level of 100% efficiency, but not with 100% bioavailability or delivery to the pest organism. However, this ability does not apply to all pest problems and situations and it is desirable to maintain a multiplicity of pest management methods (including conventional pesticides), and CRF as described here have an important role in good delivery. In terms of integrated pest management (IPM) controlled delivery has a major contribution to the combination of pesticides with biocontrol methods when compared to conventional formulations.

For environmental application of pesticide delivery, CRF have been traditionally divided into chemical and physical types (9). More recently, a third approach the biological approach, has appeared, partly in response to delivery requirements for genetically engineered pesticides. The types of CRF described to date can be categorized as follows:

Chemical	Physical	Biological
Backbone linking Side-chain bonding Matrix degradation Carrier molecules such as cyclodextrins	Reservoir with membrane (micro- and macroencapsulation, coated solids, laminates, and large devices) Reservoir without membrane (hollow fibers, porous solids and foams, gels, osmotic pumps) Monolith or matrix (films, paint, sheets, slabs, pellets, strips, granules, microparticles, powders, and microspheres)	Living, or dead, cells (microorganisms) as delivery mechanisms

All formulation types have been prepared and tested but not all have reached commercial practice. The more important types are described in the following but this description is not comprehensive and the opportunities are only limited by innovation and development of new approaches (10). The basic configurations of CRF are given in Figure 2.

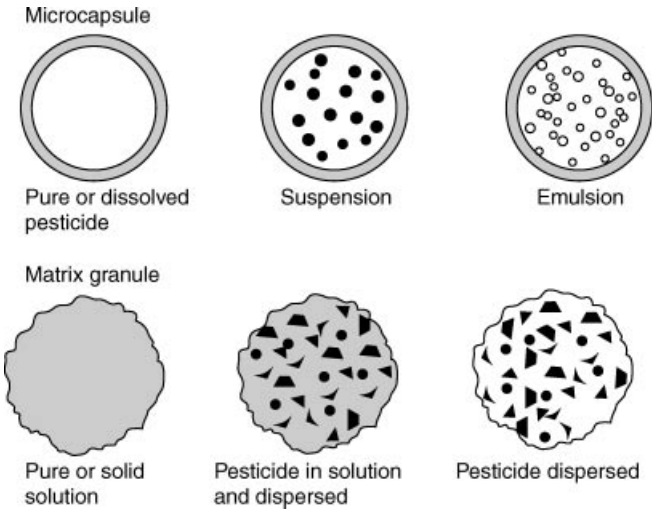

Fig. 2. Various configurations of capsule and matrix formulations.

Kinetics and Characteristics. There is a great deal of variation in the release kinetics of pesticides from the various formulation types described above. However, on the basis of mathematical treatment, the main types of release kinetics are represented in Figure 3. In order to discern the kinetics the rate-controlling step needs to be identified (11). This should be done under controlled conditions ie, in the laboratory, but it does not necessarily follow that this will be true in

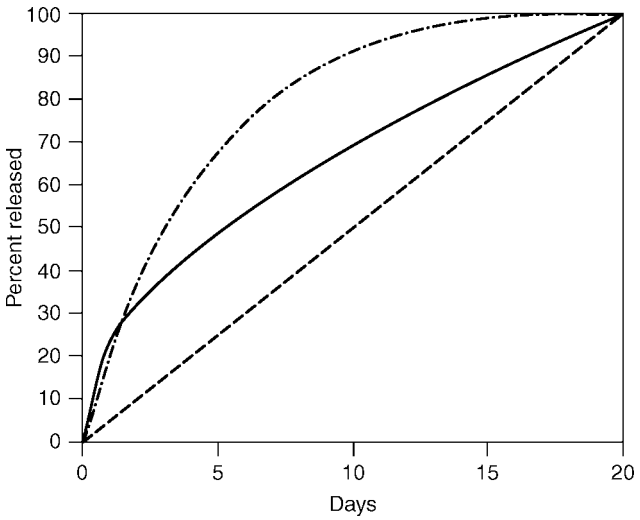

Fig. 3. Cumulative release provided by various release kinetics. A, Constant release, independent of time (zero order), such as that possible from a membrane reservoir device free of lag time or initial burst effects. B, Matrix or monolithic sphere with square root time release. C, First-order release. ---- A-zero order; -.-.-. C-first order; ——— B-square root.

the environment where the formulation is to be used. To study the basic kinetics, ie, those independent of the environment, the formulation has to be placed under "sink" conditions. These prevent the released pesticide from accumulating in the immediate vicinity of the surface of the formulation and the slowing of the release rate. The type of test environment will depend on the interfacial transport mechanism, especially movement into aqueous media or into the vapor phase or uptake by a biological system (12). Ideally, release kinetics ought to be determined under field conditions but this often presents insurmountable problems (especially those resulting from the variability of the open environment) and instead the biological response to the released pesticide is observed over time to validate the performance of any formulation.

Mechanisms of Release. In Figure 3, Line A represents release from a reservoir system with a large core relative to the wall mass. This could be a microcapsule releasing by steady-state diffusion through a uniform nonerodible wall. Transport through the polymer membrane (or matrix) occurs by a dissolution–diffusion process, where the active ingredient first dissolves in the polymer and then diffuses across the polymer to the external surface where the concentration is lower. The diffusion is in accordance with Fick's first law:

$$J = -D\mathrm{d}c_\mathrm{m}/\mathrm{d}x \tag{8}$$

where J is the flux of pesticide, D is the diffusivity, and dc_m/dx is the concentration gradient of the active ingredient. The rate remains constant as long as the internal and external concentrations of the pesticide and the concentration gradient are constant. A lag phase may occur while the system reaches this steady state (7).

Release by Erosion. The rate is independent of the concentration of pesticide remaining in the device. This zero order is also typical of certain surface erodible devices but their geometry is important and only laminar shapes produce a true constant rate as the device is eroded from one or both faces (2). Cylindrical, spherical, and irregular granular shapes provide a decreasing rate (as these particles lose surface area as erosion proceeds) and the overall release rate can be sustained only if hollow (concave) surfaces are available. These erodible systems have not been substantially exploited in pesticide delivery, mainly because of cost. Erosion can occur by dissolution of surface polymer or by degradation of the matrix, the best examples of which are the many polyesters such as d,l-polylactic acid or polyhydroxybutyrate (see POLY(3-HYDROXYALKANOATES); POLYLACTIDES). In this case, erosion may be through bulk hydrolysis of the polymer (13).

Release from Reservoir Systems. Most controlled release systems, including microcapsules, are positively rate-dependent on temperature, which makes effective delivery during cool night periods when interspersed with hot days (such as that required for pheromone release for control of nocturnally mating insect pests) problematic. For microcapsules, if the activity of the pesticide within the reservoir decreases then the release rate will also decrease; this effect will vary according to the capsule dimensions. This leads to a consideration of the polydispersity, or the range of sizes in a given number of microparticles (14). Although the release rate from individual particles may be constant, the duration of this release will varying according to the size of each particle. Thus, small particles become depleted before large particles and the overall release from a population

of particles will decrease with time. This has been shown in laboratory and field tests where overall first-order rates from microcapsules (Penncap-M; 20–40 μm) have been observed (15).

Release from Polymeric Matrices. In nonsurface erodible matrix systems diffusion of the active ingredient occurs from the interior of the particle to the surface. This gives rise to a declining rate of release according to the square root of time ($t^{-1/2}$) as shown by curve B in Figure 3. In practice, the approximate Higuchi model (16) applies and is true up to 60–70% of release, typically from a sphere or microsphere. The pesticide may be dissolved or dispersed in the polymer; for dissolved pesticide the second phase of release is by first-order kinetics. For dispersed pesticide the $t^{-1/2}$ kinetics last for almost all the release. These kinetics are a special case of the generalized description (17) of proportional release (at time t) from matrix or monolithic devices, as follows:

$$\frac{M_t}{M_\infty} = kt^n \tag{9}$$

where k is a constant incorporating characteristics of the polymer and the pesticide, and n is the diffusional exponent and indicative of the transport mechanism. In these cases $n = 0.5$ and indicates Fickian diffusion as the rate-controlling step in release.

Swellable Matrices. In matrix systems where water uptake or swelling can occur, such as may be possible in moist soil or water, the rate-controlling step may be solid-state diffusion or relaxation of the polymer by incoming water or a combination (18). Thus, the time exponent of the equation characterizing the release rate (19) may vary from 0.5 (square root of time) for Fickian diffusion to 1.0 (zero order) for swelling according to the nature of the matrix and the pesticide. Generally, the higher the water solubility of the pesticide the faster will be its rate of release. Less polar molecules with high partition coefficients tend to transport slower. In the case of irregular particles, such as granules, and where polydispersity exists, the overall time exponent will typically be less than the corresponding value for microspheres. For diffusion-controlled systems a typical low value is $n = 0.43$ (19).

First-Order Release. Finally, in situations where a chemical reaction liberates the active species, or where boundary conditions are rate-limiting, the rate of release depends on the concentration in the solid phase (20), and first-order kinetics are seen as in Figure 3 as curve C. Where more than one mechanism (including also diffusion) operates, complex release patterns occur.

Design and Preparation of CRF

Chemical Methods. Chemical methods involve the formation of a chemical bond with the pesticide and another molecule; this bond is then broken in the field to allow the release of the pesticide. The bond energy relates to the ease of breaking and thus the rate of release of the pesticide (21). Where the structure of the pesticide permits, it can be homopolymerized through a condensation reaction and the pesticide forms the backbone of a resulting high molecular weight polymer, which is in effect a polymeric propesticide. In the environment this polymer

depolymerizes to release the original pesticide, usually from each end of the chain (unzipping). Often breakdown of such homopolymers is slow and there is need for copolymerization with another appropriately functional monomer. Pesticides capable of homo- or copolymerization are few and include those containing functional groups such as amino, hydroxyl, and carboxyl groups.

A second approach to chemical-based formulations is where the pesticide is attached to a side chain of a high molecular weight polymer or macromolecule. This polymer may be either preformed, and the pesticide is then bound to appropriate side-chain functional groups, or the pesticide is first attached to a polymerizable monomer which is subsequently polymerized to yield the pesticide-bound polymer (22). Again, the release rate will depend on the energy of the bond holding the pesticide to the polymer which then undergoes scission to release the pesticide moiety (21).

The third approach to chemical-based release of pesticides is where the active is trapped in a network of a cross-linked polymer. Chemical breakdown of this polymer then allows the release of the pesticide. This mechanism incorporates physical processes of diffusion within the release mechanism.

The first two of the chemical release mechanisms usually involve covalent bonding of the pesticide and the formation of a molecular species different to the original structure. As a result of the registration requirements of new pesticide molecules, this approach implies considerable additional costs which outweigh the putative formulation benefits. Thus, true chemical approaches are often proscribed in favor of physical methods.

Physical Methods. Physical methods are divided into two general approaches. The pesticide is entrapped within a physical structure either at a molecular or micro-domain level or the pesticide in the form of a reservoir is enclosed within a polymeric envelope (2). In the first approach, the pesticide is mixed with the polymer (or other material with high energy density) to form a monolithic structure or matrix. Release is normally through diffusion through the matrix or dissolution and erosion of the matrix. In the second approach, structures are based upon a reservoir of the pesticide enclosed by the polymer, from nano-scale up to centimeter-sized devices. The shapes of these devices are varied and include spherical, such as microcapsules, and laminar or layered structures with the reservoir bounded by permeable membranes. These membranes provide a permeable barrier which controls the release rate. Other mechanisms of release include capsule rupture and erosion of the membrane.

As these "physical" methods provide the most important technologies for CRF of pesticides, they will be presented in more detail in the following sections.

Reservoir-Based Formulations with Membrane

In this method a reservoir or depot of the pesticide is bounded by a polymeric membrane, which protects (and separates) it from the environment and also provides a mechanism for its release. Thus, the specifications for the chemical nature and structure of this membrane are critical in the performance of such formulations. This makes for exacting requirements in the manufacturing processes if the desired release rates are to be consistently obtained in the field.

The method most suitable for use for pesticides is microencapsulation, where particle sizes are of the order of 10–100 μm and can be delivered by standard agricultural spraying. Microencapsulation has been defined (23) as the placing of a layer on the surface of a single *liquid* droplet. Conversely, coating refers to the covering of a single *solid* particle, whereas a matrix particle contains the *solid* or liquid active agent dispersed throughout a binding material. Even though these matrix particles are usually granular (they can be similar in size to microcapsules and are also intended for spraying as suspensions), they should be considered as matrices, and are described below.

Microencapsulation. Microencapsulation (qv) has now been commercially practiced for more than 30 years, following the first application of the technology to carbonless copying paper. Pesticide formulations based on microcapsules appeared in 1974 with the product Penncap-M containing the insecticide methyl parathion (4). Since then many microcapsule suspension formulations have been introduced and form the major group of CRF.

Production of microcapsules is based on three main methods (24,25). The oldest, that of phase separation or coacervation, uses emulsification to produce core droplets containing the pesticide dispersed in an immiscible phase in which the wall material is dissolved but then precipitates around the core droplets. Interfacial encapsulation is done by emulsifying or dispersing the pesticide solution in a continuous phase and a polymerization reaction takes place at the interface. Finally, in the physical methods the wall material is spread around the pesticide containing core to make the microcapsule.

Microcapsule Preparation by Interfacial Polymerization. The polymer forming the wall of the microcapsule can be made by addition or condensation polymerization or by *in situ* condensation polymerization. Addition polymerization using unsaturated monomers and free-radical-generating catalysts may start with the monomer in the pesticide-containing dispersed oil phase and the water-soluble catalyst in the aqueous phase. Other combinations of monomer and catalyst distributed between the two phases are possible but less practical. Pesticide impurities can interfere with the polymerization producing unsatisfactory capsules (26).

The condensation route to wall polymers is the best method for pesticide encapsulation. In this process the two reactive monomers, one dissolved in each of the two phases (of the emulsified oil/pesticide in water), polymerize at the interface and generate the wall material. Typically, the oil-phase monomers are polyfunctional isocyanates (A) or acid chlorides (B) and the water-phase reactants are polyalcohols or amines. Compounds sufficiently reactive are chosen such that when they meet at the interface the condensation polymer forms the capsule wall (Fig. 4). Alternatively, the two reactants (a diol and a diisocyanate) and a low boiling solvent make up the oil phase of the emulsion along with the pesticide. When heated the solvent evaporates bringing the monomers together at the droplet surface to form the capsule wall (27).

The resulting polyamide wall tends to be weak and soft, but the polyurea and polyester produce tough and strong materials (28). Other combinations of reactants give tough and strong polyurethane walls (polyamine and bis-haloformate or polyol and polyisocyanate) or epoxy walls (amine and epoxide) (see POLYURETHANES; EPOXY RESINS).

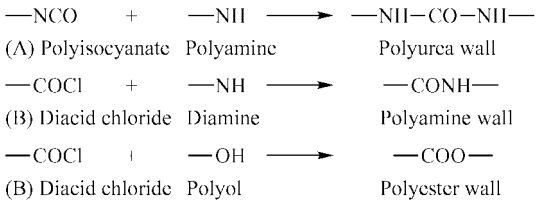

Fig. 4. Various routes to capsule wall formation through condensation polymerization.

For *in situ* condensation polymerization only the oil-phase isocyanate reactant is used (29). When the emulsion is heated, the isocyanate reacts with water at the interface to form an amine which then reacts in turn with the remaining isocyanate. The resulting polyurea wall material formed is thin and strong, providing good release properties for environmental applications. The permeability (the product of the diffusion coefficient and the solubility coefficient) of the wall can be varied by incorporating cross-linking monomers into the oil phase. A typical monomeric system is toluenediisocyanate and polymethylene-polyphenylisocyanate, a multifunctional monomer which causes cross-linking of the wall polymer (see Fig. 5). Both isocyanate monomers react with water at their own rates (see ISOCYANATE-DERIVED POLYMERS).

Forming the wall is only part of the successful microcapsule formulation. Recombination during microcapsule formation or subsequent storage to give large irregular shapes is a problem. Protective colloids offset this and reduce loss of the active ingredient into the continuous phase. Commercial colloids used include poly(methyl vinyl ether/maleic anhydride) cross-linked with poly(vinyl alcohol), styrene/maleic anhydride coplymers, vinylpyrrolidinone/vinyl acetate copolymers, vinylpyrrolidinone/styrene copolymer, and lignin sulfonate. A typical capsule suspension formulation made in this way may have up to 60% of the active ingredient, solvent (up to 20%), polymer (5–10%), protective colloids (1–20%), emulsifiers (1–5%), UV-protectant (0–5%), buffer (5%), viscosity/structure modifiers (2–10%), and water to make up the bulk (26).

Microcapsule Preparation by Phase Separation Methods. The earlier methods used for pesticide microencapsulation were based on phase separation.

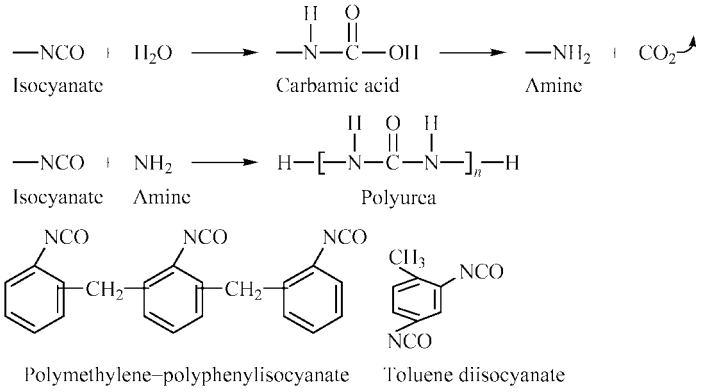

Fig. 5. Monomers and polymer forming reaction for *in situ* microcapsule wall formation.

There are two main approaches to coacervation, based on phase separation. Simple coacervation is when an aqueous solution of a hydrophilic polymer separates into two phases (solid and liquid) on addition of salt, alcohol, or other water-miscible solvents (29). An example would be the phase separation from an aqueous solution of poly(vinyl alcohol) by a nonsolvent such as propyl alcohol or by a salt solution, such as sodium sulfate. Complex coacervation occurs when polymers in solution with opposite electric charge come together and separate from the water. The most common example of complex coacervation is based on gelatin and gum arabic, two natural hydrophilic colloids. The process involves gelatin solution mixed with the core material in oil which is emulsified and the gum arabic added. The emulsion is heated and the phase separation is induced by dilution, reducing pH or cooling. If the pH is reduced below 4.5, the gelatin is then below its isoelectric point (pH 4.5) and its charge becomes positive; it then reacts with the gum arabic which has a residual negative charge and coats the oil droplets. Alternatively phase separation can be caused by dilution. The emulsion would then be cooled and treated with formaldehyde to cross-link and strengthen the capsule wall.

Phase separation can also be produced from solutions of polymers in organic solvents. By addition of a nonsolvent for the polymer to the solution containing the core material the polymer will precipitate around the emulsified core to form microcapsules (30). This can allow for the encapsulation of aqueous solutions or suspensions of pesticides. For example, such an aqueous solution can be emulsified in oil containing the dissolved polymer. Addition of the nonsolvent to the oil phase separates out the polymer, which can then form the wall around the water droplets.

Microcapsule Preparation by Physical Methods. These microcapsules are prepared by passing the two phases, core and wall material, through a small opening such that the wall material coats the core (31). This can be achieved using biliquid extrusion nozzles or with centrifugation in which the two liquids pass through many orifices. These allow the wall material to be cooled or dried after leaving the nozzle, thus forming a rigid wall structure. These processes generally give high wall-to-core ratios and cannot be used to prepare very small microcapsules ($<100\,\mu$m).

Coating of Solid Particles. Covering a solid particle with a polymeric wall is usually referred to as coating although the product may be termed a microcapsule. Various methods may be used with degrees of uniformity of the wall structure (32). Pan coating is well established in which the core particles (>1–2 mm) are tumbled in a rotating drum while the coating solution is sprayed slowly; warm air circulates to remove the solvent. For smaller particles a fluidized bed is needed. The core particles (down to 100–150 μm) are fluidized in a rising air current and the coating solution slowly sprayed into the bed. Spray drying in which the core material and the coating solution is atomized and the droplets dried rapidly in hot air gives poorer quality of encapsulation. There are numerous other methods for encapsulation, many specialized for specific applications.

Laminate Formulations. The laminate system comprises a reservoir layer of pesticide-containing polymer sealed between two other plastic layers (33). The two outer layers of this multilaminate structure protect and release the active ingredient by diffusion driven by the concentration gradient. Often one of the layers is impermeable and functions as a support for adhesion to suitable surfaces. At the surface the pesticide is continually removed by evaporation, degradation,

leaching, or by mechanical contact by humans, insects, moisture, wind, dust, or other agents.

The form and structure of the laminate varies according to the active agent and the intended application. The laminate may be used as a sheet for covering surfaces or may be cut into strips, ribbons, wafers, flakes, confetti, or even into granules or sprayable powders. Laminate strips (2.5×10 cm) consisting of a reservoir of an insecticide in PVC on a base of impermeable Mylar sheet and covered with a 0.127-mm layer of PVC have been developed for indoor cockroach control (Hercon Insectape). The insecticides include chlorpyrifos, diazinon, and propoxur. The tape is intended to be affixed to surfaces frequented by cockroaches and provide control for up to 3–5 months, especially valuable in areas where spraying is not desirable.

The laminate tape may also be used in its strip form as part of a collar for control of ticks and fleas on pet animals. Durations of control of these pests have been demonstrated to be up to 8 months for tick control.

An important application is for release of insect pheromones and attractants for insect control. A combination of the insecticide propoxur with the cockroach attractant periplanone-B provides 1 month of control in a laminate bait strip. Delivery of volatile compounds to the atmosphere surrounding crops is a crucial part of the mating disruption technique for many insect pests (34). The number and disposition of devices releasing the volatile pheromones depends on the pest, crop, and other environmental factors. Laminates can thus be dispersed in the crop as individual large devices (adhesive strips) or as small flakes or confetti applied by aircraft (applied with adhesive to ensure retention toward the top of the crop canopy) according to the control requirements. Among a number of crop pests an important use has been for pink bollworm in cotton. The use of a plastic film for controlling release of pheromones can take the form of the laminate, or film enclosing a reservoir of the active agent on a porous substrate, or even in the form of polyethylene bags, vials, tubes, and caps.

Applications of Microcapsule Formulations

Even though the first microcapsule formulation (using phase separation technology) was introduced into commerce in 1960 for the purpose of releasing ink in carbonless copying, it was not until 1974 that the first pesticide microcapsule appeared (15). This was Penncap-M (Pennwalt), methyl parathion encapsulated within a polyamide/polyurea wall material, prepared from the reaction of sebacoyl chloride and polymethylene polyphenylisocyanate with ethylenediamine and diethylenetetramine, suspended in water (240 g/L). This product showed reduced toxicity and extended insect control. This was followed by a similar formulation based on diazinon for indoor control of cockroaches. Superior and extended pest control was achieved, compared to conventional formulations. Mammalian toxicity was reduced as can be seen for these microcapsule formulations in Table 1. These pioneering formulations were followed by similar types using other insecticides such as ethyl parathion, permethrin, cypermethrin, and chlorpyriphos.

Microcapsule formulations have been made, based on pesticides, for control on crops and soils, on timber and other surfaces for structural and indoor

Table 1. Acute Mammalian Toxicities for Encapsulated and EC Formulations of Methyl Parathion and Diazinon[a]

Formulation	Rat oral LD_{50} mg/kg	Rabbit dermal LD_{50} mg/kg
Diazinon	350	600
Knox Out 2FM	>21,000	>10,000
Methyl parathion	25	400
Penncap-M	600	>5,450

[a]Ref. 35.

pests, and on seeds and livestock. A few examples of microcapsule formulations available worldwide are given in Table 2. Electron micrographs of a pesticide microcapsule formulation are shown in Figure 6. Each particular formulation is designed for its specific application and method of use. Variables that can be exploited for this purpose include capsule size and size range, wall thickness, wall permeability and strength (provided by degree of cross-linking), nature of wall material, adjuvants, and other formulation constituents. Release is usually through diffusion of the active agent through the capsule wall but other mechanisms can be used, such as rupture triggered by mechanical, erosion or degradation, thermal processes, or by osmotic swelling. An example of how encapsulation variables can influence release has been provided by Tsuji for a fenvalerate formulation (36). This polyurethane microcapsule was prepared by interfacial polymerization of polyisocyanate and ethylene glycol and was to have various wall thicknesses and mass median diameters.

Efficacy against the important brassica pest, diamond-back moth (*Plutella xylostella*), was assessed and it was found that the LC_{50} value decreased for the larger capsules (diameter D) when wall thickness (T) was constant and for the thinner wall when the diameter was kept constant. For any batch of microcapsules the ratio of diameter (expressed as the mass median diameter in μm) to the wall thickness (in μm) can be determined. The value D/T can be interpreted as relating to the strength of the capsules. As the ratio D/T increased, the 48-h LD_{50} value decreased. This means that the rupture of the capsules, by insects or other factors, is the important factor in biological efficacy. The availability of the insecticide depends on the strength of the capsule, and thus the persistence

Table 2. Selection of Some of the Microcapsule Formulations

Trade name	Active ingredient	Wall material	Company
Penncap-M	Methyl parathion	Polyamide/polyurea	Atochem
Knox out 2FM	Diazinon	Polyamide/polyurea	Atochem
Micro-Sect	Pyrethrin/synergist	Polyurea	3M
Kareit MC	Fenitrothion	Polyurethane	Sumitomo
Sumithion MC	Fenitrothion	Polyurethane	Sumitomo
Lumbert	Fenitrothion	Polyurethane	Sumitomo
Icon	Lambda-cyhalothrin	Polyurea	Syngenta
Karate Zeon	Lambda-cyhalothrin	Polyurea (thin wall, low cross-linking)	Syngenta

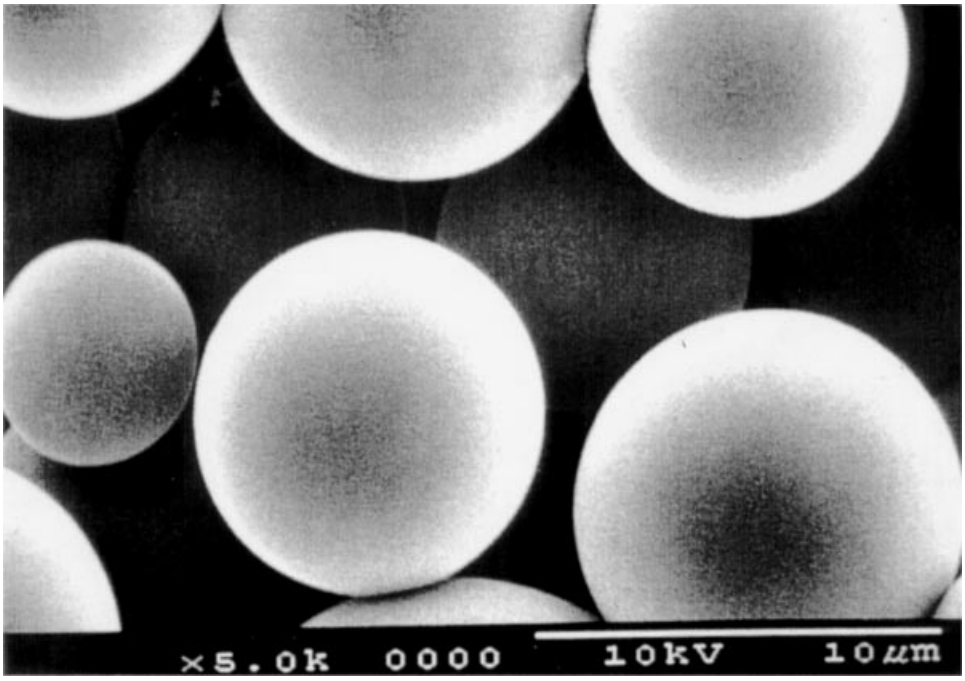

Fig. 6. Electron micrograph of a pesticide microcapsule fomulation.

of action of such microcapsule formulations will depend on having an optimum diameter-to-wall ratio with the wall thickness, neither too thin nor too thick. Other similar microcapsule formulations for use in agriculture have been made based on insecticides fenitrothion and fenpropathrin, which also showed better safety to sensitive crops and also to nontarget organisms such as fish. In extending this technology, formulations based on permethrin were developed for use in transplanted rice, and on fenitrothion and fenobcarb for aerial application in rice for bug and planthopper control.

The mechanism of release for these capsules, ie, by rupture or breakage, is suitable for controlling insect pests on surfaces. Formulations were developed for the control of cockroaches (based on fenitrothion or cyphenothrin), for termites (based on fenitrothion either applied to surfaces or incorporated into the glue of plywood), and for mosquitoes and flies on aggressive surfaces such as cement (based on fenitrothion and lambda-cyhalothrin). In the case of cockroach control the pickup of microcapsules and the efficient delivery (often by grooming and ingestion of dust plus capsules) can give control of individuals resistant to diazinon or fenitrothion.

Formation of microcapsules by *in situ* interfacial polymerization (where the monomers are entirely in the oil phase of the capsule core) yields microcapsules with a high core-to-wall ratio and a bilayer wall with an outer layer (about 0.05 μm) and an inner reinforcing spongy layer (0.5 μm). This method has been used to encapsulate a range of insecticides, pheromones, and herbicides, many of which have been available commercially (37). The capsule size may be varied from submicrometer to 100 μm diameter and the permeability selected for rapid or slow release of

the pesticide. Release is by diffusion through the wall rather than rupture. For an effective formulation the capsule suspension formed after polymerization needs protective stabilizers, dispersants, flow, etc. to provide a high active ingredient content with good shelf life and acceptable handling at dilution.

Applications for MC formulations include seed treatment (especially where an insecticide may be phytotoxic at dosages required), soil treatment of insecticides and herbicides, and treatment of surfaces for cockroach and mosquito control.

Reservoir-Based Formulations without Membrane

Reservoir systems that lack a bounding membrane to protect and regulate the release are usually designed for liquid actives that are volatile. The liquid is held in place through capillary forces and is released in the vapor phase. The rate of evaporation is regulated by diffusion of the vapor through the static air phase above the liquid surface. The simplest example is the hollow fiber, which is a fine polymeric capillary closed at one end and filled (or partially filled) with the liquid active (38). This diffuses through the air column to the opening from where it disperses. This method has been mostly developed to deliver many of the volatile sex pheromones for insect pest control to maintain a minimum concentration in the air surrounding the crop to be protected.

Operating by a similar process are the porous and foam polymers. The active is held in the pores of the structure and released by diffusion through the pores to the surface where it moves away from the particle. The diffusion is driven by evaporation or by dissolution in environmental water which penetrates the porous particle. Highly absorbent polymers such as Culigel (Stockhausen Inc.) have been developed for delivery in water bodies for mosquito control (39).

Matrix Formulations. These formulations, also known as monolithic, consist of a uniform continuous phase with the pesticide dissolved or dispersed throughout. Their preparation is generally easier, requiring less process control but can exhibit a rich variety of release types according to the material and structure of the matrix. An almost endless selection of materials is available for the matrix. Elastomers (rubbers) as well as thermoplastics and thermosets can be used and many applications for pesticides have been developed using the technologies of the rubber and plastics industries (9). Generally, a range of additives such as plasticizers, light protectants, pigments, antioxidants, processing aids, etc are usually included (40). The products can be produced in a number of forms or shapes, especially sheets, ropes, extruded cylinders, slabs, and granules. As release is inversely related to device size, the production of simple powders involves difficulty in uniformity as well as minimal reduction in release kinetics compared to conventional formulations. Many of these large formulation types are, or have been, popular for aquatic applications, such as for insect and mollusc vectors of human disease causing organisms, with few applications in agriculture. Examples have been larvicidal sheets containing temephos, malathion, or chlorpyrifos using polyamide, PVC, polyethylene, and polyurethane. Current survivors of this approach are thermoplastic formulations of chlorpyrifos (Dursban 10CR), of dichlorvos (No Pest PVC strips), and of tributyltin fluoride (Ecopro 1330) for controlling freshwater snails (*Biomphalaria glabrata*), the vector of *Schistosoma*

mansoni, and the causal agent of bilharzia (35). Monolithic systems such as these require appropriate plasticizers to promote migration of the pesticide to the surface, even so a substantial proportion will still remain entrapped when the rate of release declines below effective levels. This is less of a problem with elastomers where diffusion is faster (because of lower intermolecular forces) at similar temperatures.

Pesticide-Containing Films. In the agricultural field the use of plastic mulch and plastic films for plant growing has become widespread, as it advances and enhances cropping when temperatures are low. It also encourages pests, particularly weeds and disease-causing agents. The use of pesticides in these conditions can cause problems (eg, crop phytotoxicity), not least a result of the need for reapplication after the film has been laid. Incorporation of the pesticide into the film obviates both of these problems. Release of the pesticide can occur predominantly on the underside of the film and this pesticide is transported away (to the soil/crop) by condensation (41). Pesticides can be incorporated into agricultural films prior to their being formed by blown extrusion or into other forms such as sheets, tapes, cords, and ropes and chopped pieces such as confetti. Herbicides incorporated into EVA films are said to reduce by two to four times the amounts needed in covering early season vegetables such as cabbage, sweet corn, and celery. Using coating processes films may be applied to seeds (42), which provides a very effective means of controlled delivery of pesticides to the seed region and to the emerging seedling.

Matrix Particles. Small particles based on a matrix can range in size from powders (microparticles) to granules (fine to macrogranules) to pellets (43). Microspheres can be considered as the matrix equivalent to microcapsules. Most controlled release granules are matrix-based, although some have a solid core or reservoir of pesticide (with a coating).

Microparticles. Size matters; release rates depend on surface area, ie, a function of the square of the radius of a spherical particle, and thus larger particles release for longer and are able to manipulate the external availability of the pesticide. Small microparticles are therefore limited in their scope for controlling release but can be used in traditional spraying of dispersions onto soils and crops as well as for seed dressing. Suspension concentrate formulations of matrix microparticles have been developed based on various rosins, phenolic resins, waxes, and bitumens. These have focused on lipophilic pesticides such as trifluralin and chlorpyrifos and reductions in volatility have been demonstrated (43).

Granules. While microparticles refer to sizes up to 100 μm, granules are typically 0.5–2.0 mm (fine granules 0.3–1.0 mm, microgranules 0.1–0.6 mm, macrogranules 2–6 mm). Granular CRF can be achieved by coating as well as from matrices. Although controlled release granules have not been as popular as microcapsules, there have been significant developments for applications to soil especially where extended control is required.

Cane grubs are a widespread pest problem in sugarcane growing and attack the roots of the plant over long periods. Conventional control has used persistent organochlorine insecticides applied at or soon after planting to optimize placement and residual protection. The introduction of long release granule formulations of short-lived insecticides such as chlorpyrifos (suSCon Blue) allowed the phase out of the organochlorines whilst giving good protection to the sugarcane (44). The

Table 3. Acute Oral Toxicities (as LD_{50} Values) of Controlled Release (suSCon) Granules Compared to Technical-Grade Pesticides[a]

Product	Acute oral rat LD_{50}, mg/kg
suSCon Blue (140 g/kg chlorpyrifos)	>1000
Technical chlorpyrifos	135–165
Marshal suSCon (100 g/kg carbosulfan)	>1000
Technical carbosulfan	185–250
suSCon Fu Ming (100 g/kg phorate)	319
Technical carbosulfan	1.6–3.7
G22001 (140 g/kg parathion)	578 (male)
Technical parathion	3.6 (female), 13 (male)

[a] Ref. 44.

formulation is a 2-mm diameter extruded cylindrical granule of polyethylene containing 140 g of active ingredient per kilogram with an additive that sustains release by pore formation, through leaching by soil moisture. Single applications at planting can provide up to 3 years protection through the first harvesting and to several follow-on ratoon crops. This approach to pest control has since been further extended to other problems, especially of concealed insects where systemic insecticides can be used effectively. Shoot borers in sugarcane and forestry, termites and weevils in forestry and ornamentals, and borers and nematodes in a number of crops are examples of potential targets.

In addition to improved delivery and replacing persistent organochlorine pesticides with nonpersistent compounds, controlled release granules also provide reduced toxicity of the product. For example, the acute oral toxicities of these granules are much reduced (giving higher LD_{50} values) compared to unformulated or conventional sprayable formulations, as shown in Table 3.

Other granule formulations are based on biodegradable polymers (qv) which also offer the possibility of using wastes and by-products from biological industries such as farming and forestry. New uses for cornstarch developed by the USDA included processes for the formulation of pesticides based on cross-linking of starch (45). The method involves the use of a corotating twin-screw extruder for mixing and gelatinizing starch with water (90–95°C), introducing the pesticide and providing the extrudate, which is then cut and dried to give the pelleted product. Hydrogen bonding occurs between the starch molecules (a process called *retrogradation*) to give a water-insoluble matrix entrapping the pesticide. Release occurs following soil placement by swelling. Evaluation of this granule formulation, especially of herbicides, has shown good efficacy at the same time, reducing environmental losses and detrimental effects on surface and groundwater quality (46). In field experiments significant reductions in herbicide volatility, surface run-off losses, and leaching have been observed compared to commercial formulations. These effects are particularly noticeable very shortly after application, when commercial formulations make the herbicide rapidly available at high concentrations.

Another natural polymer type abundantly available is the polyphenolic lignin. This aromatic macromolecule which occurs in terrestrial plants is obtained

as a water-insoluble waste or by-product from the pulping of wood. Its natural protective attributes that it contributes to the success of plants can be exploited to protect, and deliver, pesticides (47). It can be melt-processed with compatible pesticides (similar polarity) by blending or screw extrusion to provide granules or powders. Release of pesticides from the granules declines with time, depending on diffusion kinetics according to a swelling-diffusion model (48). Formulations based on a wide range of soil-applied pesticides have been evaluated and field trialed extensively. For example, carbofuran-containing lignin-based granules in tropical flooded rice gave good control of virus disease (through controlling the insect vector of the virus) but using one third of the amount of pesticide compared to conventional formulations (49). This approach afforded safe handling to applicators and reduced risks (to bare feet) during the transplanting of the rice seedlings. A wide range of pesticides have been controlled release formulated by this method.

Other matrix methods for the preparation of granules can use gelating polymers such as alginic acid and other polyelectrolytes (qv). This approach effectively entraps pesticides through cross-linking with polyvalent ions such as Ca^{2+}; combined with adsorbents useful release profiles can be obtained (50). This method of preparation, using mild conditions in aqueous media at ambient temperatures, is used for formulating microbial pesticides to protect and extend the active lives and release of propagules of such living pesticidal agents (51). A wide range of bacteria, fungi, viruses, protozoa, and nematodes have been formulated by this method, and related methods, to provide effective sustained formulations.

Biological Methods

Finally, the use of living cells (such as yeasts) as encapsulating materials has been under investigation for many years. The problems associated with the encapsulation of pesticides within preformed cells have been overcome by using proteinaceous pesticides such as the toxin from *Bacillus thuringiensis* (Bt). The genes for the production of the toxin have been introduced into the soil bacterium *Pseudomonas fluorescens*; the toxin is expressed and is seen as a crystalline inclusion. Following production by fermentation the cells are killed and fixed to provide the capsule formulation which is registered for use on brassicas (52).

BIBLIOGRAPHY

1. B. A. Leonhardt, in R. M. Wilkins, ed., *Controlled Delivery of Crop-Protection Agents*, Taylor and Francis, London, 1990, pp. 169–190.
2. D. H. Lewis and D. R. Cowsar, in H. B. Scher, ed., *Controlled Release Pesticides*, American Chemical Society, Washington, D.C., 1980, pp. 1–16.
3. W. E. Ripper, R. M. Greenslade, J. Heath, and K. Barker, *Nature* **161**, 484 (1948).
4. D. DeSavigny and E. E. Ivy, in Ref. 24.
5. F. R. Hall, in R. M. Wilkins, ed., *Controlled Delivery of Crop-Protection Agents*, Taylor and Francis, London, 1990, pp. 3–22.

6. D. I. Gustafson, in R. M. Wilkins, ed., *Controlled Delivery of Crop-Protection Agents*, Taylor and Francis, London, 1990, pp. 23–42.
7. C. S. Hartley and B. J. Graham-Bryce, *Physical Principles of Pesticide Behaviour*, Vols. 1 and 2, Academic Press, New York, 1980.
8. G. G. Allan, C. S. Chopra, J. F. Friedhoff, R. I. Gara, M. W. Maggi, A. N. Neogi, S. C. Roberts, and R. M. Wilkins, *Chem. Tech.* **3**, 171–178 (1973).
9. A. F. Kydonieus, ed., *Controlled Release Technologies: Methods, Theory and Applications*, Vols. 1 and 2, CRC Press, Boca Raton, Fla., 1980.
10. H. B. Scher, ed., *Controlled-Release Delivery Systems for Pesticides*, Marcel Dekker, Inc., New York, 1999.
11. R. W. Baker and H. K. Lonsdale, in A. C. Tanquary and R. E. Lacy, eds., *Controlled Release of Biologically Active Agents*, Plenum Press, New York, 1974, pp. 15–71.
12. G. Pfister and M. Bahadir, in R. M. Wilkins, ed., *Controlled Delivery of Crop-Protection Agents*, Taylor and Francis, London, 1990, pp. 279–309.
13. A. Gopferich, *Macromolecules* **30**, 2598–2604 (1997).
14. K. L. Smith, in Ref. 10, pp. 137–149.
15. J. R. Lowell, W. H. Culver, and C. B. Savigny, in H. B. Scher, ed., *Controlled Release Pesticides*, American Chemical Society, Washington, D.C., 1980, pp. 145–151.
16. T. Higuchi, *J. Pharm. Sci.* **50**, 874–883 (1961).
17. P. L. Ritger and N. A. Peppas, *J. Controlled Release* **5**, 23–26 (1987).
18. L. R. Sherman, *J. Appl. Polym. Sci.* **27**, 997–1005 (1983).
19. P. L. Ritger and N. A. Peppas, *J. Controlled Release* **5**, 37–42 (1987).
20. A. N. Neogi and G. G. Allan, in A. C. Tanquary and R. E. Lacy, eds., *Controlled Release of Biologically Active Agents*, Plenum Press, New York, 1974, pp. 195–223.
21. G. G. Allan, C. S. Chopra, A. N. Neogi, and R. M. Wilkins, *Nature* **234**, 349–351 (1971).
22. A. Akelah, *Mater. Sci. Eng. C* **4**, 83–98 (1996).
23. R. E. Sparks and I. C. Jacobs, in Ref. 10, pp. 3–29.
24. J. E. Vandegaer, ed., *Microencapsulation Processes and Applications*, Plenum Press, New York, 1974.
25. A. Kondo, *Microcapsule Processing and Technology*, Marcel Dekker, Inc., New York, 1979.
26. M. Gimeno, *J. Environ. Sci. Health B* **31**, 407–420 (1996).
27. H. B. Scher, in H. B. Scher, ed., *Controlled Release Pesticides*, American Chemical Society, Washington, D.C., 1980, pp. 126–144.
28. P. Chamberlain and K. C. Symes, in D. R. Karsa and R. A. Stephenson, eds., *Encapsulation and Controlled Release*, Royal Society of Chemistry, Cambridge, U.K., 1993, pp. 131–140.
29. G. J. Marrs and H. B. Scher, in R. M. Wilkins, ed., *Controlled Delivery of Crop-Protection Agents*, Taylor and Francis, London, 1990, pp. 65–90.
30. U.S. Pat. 3,173,878 (1965), Z. Reyes.
31. J. T. Goodin and G. R. Somerville, in Ref. 24, pp. 155–163.
32. G. B. Beestman, in H. B. Scher, ed., *Controlled Release Pesticides*, American Chemical Society, Washington, D.C., 1980, pp. 31–54.
33. A. G. Kydonieus, in H. B. Scher, ed., *Controlled Release Pesticides*, American Chemical Society, Washington, D.C., 1980, pp. 152–167.
34. C. C. Doane, in Ref. 10, pp. 295–317.
35. A. R. Quisumbing and A. F. Kydonieus, in R. M. Wilkins, ed., *Controlled Delivery of Crop-Protection Agents*, Taylor and Francis, London, 1990, pp. 43–61.
36. K. Tsuji, in Ref. 10, pp. 55–85.
37. H. B. Scher, M. Rodson, and K.-S. Lee, *Pestic. Sci.* **54**, 394–400 (1998).
38. T. W. Brooks, in A. E. Kydonieus, ed., *Controlled Release Technologies: Methods, Theory and Applications*, Vol. 2, CRC Press, Boca Raton, Fla., 1980, pp. 165–193.

39. R. Levy, N. A. Nichols, and T. W. Miller, *Proc. Int. Symp. Control. Rel. Bioact. Mater.* **20**, 212–213 (1993).
40. N. F. Cardarelli, in A. E. Kydonieus, ed., *Controlled Release Technologies: Methods, Theory and Applications*, Vol. 1, CRC Press, Boca Raton, Fla., 1980, pp. 73–128.
41. N. F. Cardarelli and S. V. Kanakkanatt, in H. B. Scher, ed., *Controlled Release Pesticides*, American Chemical Society, Washington, D.C., 1980, pp. 60–73.
42. M. Bahadir and G. Pfister, *Controlled Release, Biochemical Effects of Pesticides, Inhibition of Plant Pathogenic Fungi*, Springer-Verlag, Berlin, 1990, pp. 1–64.
43. D. J. Park, W. R. Jackson, I. R. Mckinnon, and M. Marshall, in Ref. 10, pp. 89–136.
44. N. Boehm and T. P. Anderson, in R. M. Wilkins, ed., *Controlled Delivery of Crop-Protection Agents*, Taylor and Francis, London, 1990, pp. 125–147.
45. M. E. Carr, R. E. Wing, and W. M. Doane, *Cereal Chem.* **68**, 262–266 (1991).
46. G. D. Vail, M. V. Hickman, and M. M. Schreiber, *Weed Sci.* **45**, 842–847 (1997).
47. R. M. Wilkins, in Ref. 10, pp. 195–222.
48. A. Ferraz, J. A. Souza, F. T. Silva, A. R. Contrim, A. R. Gonçalves, R. E. Bruns, and R. M. Wilkins, *J. Agric. Food Chem.* **45**, 1001–1005 (1997).
49. R. M. Wilkins, E. A. Batterby, G. B. Aquino, and J. Valencia, *Econom. Entomol.* **77**, 495–499 (1984).
50. A. B. Pepperman and J.-C. W. Kuan, *J. Controlled Release* **26**, 21–30 (1993).
51. W. J. Connick Jr., in B. Cross and H. B. Scher, eds., *Pesticide Formulations: Innovations and Developments* (ACS Symposium Series, Vol. 371), American Chemical Society, Washington, D.C., 1988, pp. 241–250.
52. F. H. Gaertner and L. Kim, *Trends Biotechnol.* **3**, 4–7 (1988).

GENERAL REFERENCES

A. F. Kydonieus, ed., *Controlled Release Technologies: Methods, Theory and Applications*, CRS Press, Boca Raton, Fla., 1980.

H. B. Scher, ed., *Controlled-Release Delivery Systems for Pesticides*, Marcel Dekker, Inc., New York, 1999.

R. M. Wilkins, ed., *Controlled Delivery of Crop-Protection Agents*, Taylor and Francis, London, 1990.

The Proceedings of the International Symposium on the Controlled Release of Bioactive Materials published annually since 1973 (Controlled Release Society, Deerplain, Ill.), and the Volumes on Pesticide Formulations and Application Systems (eg, Vol. 13, ASTM STP 1183, 1993; American Society for Testing and Materials, Philadelphia, Pa.) are useful sources, as are some issues of the following journals: Journal of Controlled Release; Journal of Microencapsulation; Journal of Agricultural and Food Chemistry; Chemosphere; and Pest Management Science.

RICHARD WILKINS
University of Newcastle

CONTROLLED RELEASE TECHNOLOGY. See Volume 5.

COORDINATION POLYMERS. See METAL-CONTAINING POLYMERS.

COPOLYMERIZATION

Introduction

This article is primarily concerned with chain copolymerization. Chain copolymerization is important as it allows a wide array of functional molecules to be designed and incorporated into polymeric materials. In addition, fundamental studies on copolymerization allow the mapping out of monomer structure–reactivity relationships that underpin our knowledge of polymerization reaction mechanisms.

In recent years it has become evident that the reaction mechanism involved in free-radical copolymerization propagation is appreciably more complicated than originally postulated in the terminal model developed back in the 1940s. There is still some reluctance to acknowledge this fact as it is often more convenient to simplify the mechanism. In some instances this may be appropriate; however, in many cases where specific information about radical reactivity is garnered from the data reduction, significant problems may arise if the interpretation is oversimplified. In an attempt to clarify the position, we would like to draw an analogy with the development of understanding in the study of a human cell. As experimental techniques (particularly the electron microscope) have become more sophisticated for studying cells, our recognition of the complexity of cellular processes has been enhanced and new theories and ideas have been advanced to accompany the increased appreciation of cellular processes, leading to an understanding of the importance and role of apoptosis in designing new cancer treatments. In a similar way as experimental methods have improved to study free-radical copolymerization (most notably, size-exclusion chromatography, pulsed-laser polymerization, soft ionization mass spectrometry and ab initio calculations) our understanding of the complexity of radical copolymerization has improved and it would be a mistake if all these new experimental data were ignored, leaving theory restricted to the basic terminal model developed in the 1940s on the basis of fairly rudimentary experimental data. The complexity of radical processes should be recognized while allowing for the fact that by using carefully designed synthetic methods where some kinetic pathways are suppressed (ie, controlled/living radical polymerization) we can largely overcome many of the side reactions to generate bespoke polymer structures. In 1985–1987 the implicit copolymerization model was developed by Professor Fukuda, when his team discovered that the terminal model failed in the prediction of average propagation rate coefficients. In subsequent years it has become clear, mainly through advanced quantum calculations, that the cause of failure of the terminal model can be ascribed to a combination of radical stabilization, entropic interactions, and partial charge transfer in the transition state (so-called polarity effects), which are all significantly influenced by penultimate units. This leads to a conclusion that the physical chemistry underpinning copolymerization can be best described by an explicit modelling approach. This complexity causes some problems in the data reduction of copolymerization experiments. However, for the simple prediction of composition the terminal model, although fairly crude, provides an adequate method in many instances. The problems only arise when it is used to study absolute rate coefficients (cross-propagation rate coefficients) or when it is used to predict other quantities such as average propagation rates or sequence distribution. Therefore it is imperative that the limitations of the terminal

Encyclopedia of Polymer Science and Technology. Copyright John Wiley & Sons, Inc. All rights reserved.

model are recognized particularly when adding layers of experimental complexity (controlled/living radical copolymerization). Very similar arguments can be made for the area of termination in free-radical copolymerization with the recent development of SP-laser experiments, enabling the study of the reaction with greater precision and accuracy than was previously possible. A continuous development of knowledge via copolymerization research should result from a simultaneous progression in both experimental techniques and modified theory.

This article progresses to discuss the newly emerging field of controlled/living radical copolymerization, and the novel materials that can be made using these highly versatile synthetic methods. Finally we cover in brief ionic chain copolymerization and cross-linking copolymerization.

Propagation Kinetics and Copolymerization Models

Copolymerization propagation kinetics have perhaps the most significant impact on copolymer properties. The rates of the individual propagation reactions in a free-radical copolymerization not only affect the overall rate of polymerization and the molecular weight distribution of the resulting polymer, but also directly govern the copolymer composition and microstructure (ie, whether the monomers form block, alternating, or random copolymers), and the chain-end composition of the living radicals (which in turn affects the chain-end composition of the dead polymer). Furthermore, it is the geometry of the transition structure in the propagation reaction that governs the stereochemistry of the resulting polymer. The ability to understand the fundamental influences on the propagation reaction (both from a kinetic and mechanistic point of view) thus enables these important properties to be modeled, and hence controlled, simply by manipulating the reaction conditions (such as solvent type, monomer feed composition, and temperature).

There are an enormous number of different copolymerization models available in the literature. The simplest kinetic model, the terminal model, was derived in the 1940s and, while it continues to receive widespread use, 60 years of experimental and theoretical studies have revealed serious deficiencies in this model for a wide range of systems. In response to these problems, numerous alternative copolymerization models have been derived. These models differ primarily in their assumptions as to what factors affect the rate of the propagation step. For example, in the terminal model it is assumed that the composition of the terminal unit of the propagating radical (ie, the α- and β-substituents) and the monomer affect the propagation rate, while in the penultimate model it is assumed that the penultimate unit of the propagating radical (ie, the γ- and possibly δ-substituents) is also important. Other models incorporate possible side reactions that might affect the overall propagation rate, such as depropagation or various types of solvent effect.

In what follows we briefly outline the assumptions and equations corresponding to the most important copolymerization models. To keep this as a compact and accessible summary, we do not present derivations for the equations. Neither do we present the lengthy equations needed to predict the various triad and pentad fractions under specific models. For more detailed information of this nature, the reader is referred to the original references. In addition, a general account of the main steps in deriving a copolymerization model is found in Reference 1.

For the sake of simplicity, we present equations for each of the types of models in their low-conversion, "instantaneous" forms, but conclude with a brief discussion of the extension of the models to their conversion-dependent "integrated" form. Having outlined all of the models, we then discuss the main experimental evidence for or against them, and make some general suggestions concerning their applicability to specific types of system. We then conclude with a short discussion of reactivity in free-radical copolymerization. More fundamental aspects of this topic are addressed in a separate article (see COMPUTATIONAL QUANTUM CHEMISTRY FOR FREE-RADICAL POLYMERIZATION).

Terminal Model

In the terminal model it is assumed that the terminal unit of a propagating polymer radical is the only factor influencing its reactivity, and that side reactions are not significant. As a result, there are only four types of propagation reaction in the free-radical copolymerization of any two given monomers (M_1 and M_2):

$$RM_i\cdot + M_j \xrightarrow{k_{ij}} RM_iM_j\cdot \quad i,j = 1 \text{ or } 2$$

From this assumption, Jenkel (2), Mayo and Lewis (3), and Alfrey and Goldfinger (4) all independently derived an expression for the copolymer composition (F_1/F_2) as a function of the monomer feed fractions (f_1 and f_2) and the reactivity ratios (r_1 and r_2) of the monomers:

$$\frac{F_1}{F_2} = \frac{f_1}{f_2}\cdot\frac{r_1 f_1 + f_2}{r_2 f_2 + f_1} \quad \text{where} \quad r_i = \frac{k_{ii}}{k_{ij}}\ i \neq j \quad \text{and} \quad i,j = 1 \text{ or } 2 \tag{1}$$

Alfrey and Goldfinger (4) also derived expressions for the sequence distribution and the number-average degree of polymerization expected for a copolymerization obeying the terminal model. They later extended the terminal model to describe polymerizations involving three or more monomers (5,6). Fukuda and co-workers (7) derived the following expression for the copolymerization propagation rate constant $\langle k_p \rangle$ under the terminal model:

$$\langle k_p \rangle = \frac{r_1 f_1^2 + 2 f_1 f_2 + r_2 f_2^2}{[r_1 f_1 / k_{11}] + [r_2 f_2 / k_{22}]} \tag{2}$$

This equation follows from the kinetic analysis of copolymerization by Melville and co-workers (8) and Walling (9), who arrived at an expression for the overall rate of copolymerization assuming a terminal model for both propagation and termination.

Explicit and Implicit Penultimate Models

In the *explicit penultimate model*, it is assumed that both the terminal and penultimate units of a polymer radical may affect the rate of the propagation reaction. As in the terminal model, side reactions are considered to be insignificant. The explicit penultimate model was first suggested in 1946 by Merz and co-workers (10), who derived equations for predicting the composition and sequence distribution under this model. A full description of the model—including an expression for $\langle k_p \rangle$—has since been provided by Fukuda and co-workers (11), and it is their notation that is used below. In addition, penultimate model equations for the case of terpolymerization have been published by Coote and Davis (12).

In the presence of a penultimate unit effect, there are eight different types of propagation reactions:

$$RM_iM_j\cdot + M_k \xrightarrow{k_{ijk}} RM_iM_jM_k\cdot \quad i,j,k = 1 \text{ or } 2$$

From their eight different propagation rate constants, four different monomer reactivity ratios (r_i and r_i') and two radical reactivity ratios (s_i) can be defined as follows.

$$r_i = \frac{k_{iii}}{k_{iij}} \quad r_i' = \frac{k_{jii}}{k_{jij}} \quad s_i = \frac{k_{jii}}{k_{iii}} \quad \text{where} \quad i \neq j \quad \text{and} \quad i,j = 1 \text{ or } 2$$

These are used to calculate the adjusted parameters $\bar{r}_i$ and $\bar{k}_{ii}$:

$$\bar{r}_i = r_i'\left(\frac{f_i r_i + f_j}{f_i r_i' + f_j}\right) \quad \text{where} \quad i,j = 1 \text{ or } 2 \quad \text{and} \quad i \neq j \tag{3}$$

$$\bar{k}_{ii} = k_{iii}\left(\frac{r_i f_i + f_j}{r_i f_i + f_j/s_i}\right) \quad \text{where} \quad i,j = 1 \text{ or } 2 \quad \text{and} \quad i \neq j \tag{4}$$

These are used in place of r_i and k_{ii}, in the terminal model expressions for composition and $\langle k_p \rangle$ (ie, eqs. 1 and 2 above).

The *implicit penultimate model* was first suggested by Fukuda and coworkers (7) in 1985, in order to describe their observation that the terminal model could be fitted to the composition data for the copolymerization of styrene with methyl methacrylate, though it could not simultaneously describe the propagation rate coefficients. In this model, the following restriction is placed on the explicit penultimate model.

$$r_i\left(=\frac{k_{iii}}{k_{iij}}\right) = r_i''\left(=\frac{k_{jii}}{k_{jij}}\right) = \frac{k_{ii}}{k_{ij}} \quad \text{where} \quad i \neq j \quad \text{and} \quad i,j = 1 \text{ or } 2 \tag{5}$$

The penultimate unit effect is thus assumed to be absent from the monomer reactivity ratios, which are equivalent to their terminal model forms, and only to

exist in the radical reactivity ratios (ie, through values of $s_i \neq 1$). This amounts to assuming that the magnitude of the penultimate unit effect on reactivity is independent of the type of monomer with which it is reacting (since the equality $k_{jii}/k_{iii} = k_{iij}/k_{iij}$ follows directly from the assumption that $r_i = r_i'$). In other words, it assumed that there is a penultimate unit effect on reactivity but not selectivity. On the basis of this assumption (ie, eq. 5), equation 3 collapses into

$$\bar{r}_i = r_i''\left(=\frac{k_{jii}}{k_{iij}}\right) = r_i\left(=\frac{k_{iii}}{k_{iij}}\right) = \frac{k_{ii}}{k_{ij}} \quad \text{where} \quad i \neq j \quad \text{and} \quad i,j = 1 \text{ or } 2 \qquad (6)$$

Thus the adjusted monomer reactivity ratios of the penultimate model are replaced simply by their corresponding terminal model values. However, since the penultimate unit effect can remain in the radical reactivity ratios (ie, through values of $s_i \neq 1$), equation 4 does not collapse to its equivalent terminal model form (ie, $\bar{k}_{ii} \neq k_{iii}$). Since the composition and triad/pentad fraction equations contain only $\bar{r}_i$ terms, they collapse to the corresponding terminal model equations. However, since it contains both $\bar{r}_i$ and $\bar{k}_{ii}$ terms, the propagation rate equation, though simpler than that of the explicit penultimate model, continues to differ from that of the terminal model. There is thus an implicit penultimate unit effect—that is, a penultimate unit effect on the propagation rate but not the composition or sequence distribution.

Solvent Effects

Solvent Polarity Effects. When polar interactions are important in the transition structure of the propagation reaction, the polarity of the solvent may affect the propagation rate. This may be explained as follows. Polar interactions are said to occur when the transition structure is stabilized by charge transfer between the reacting species (13). The amount of charge transfer, and hence the amount of stabilization, is inversely proportional to the energy difference between the charge transfer configuration and the product and reactant configurations that combine to make up the ground-state wave function of the transition structure. Now it is known that polar solvents can stabilize charged species, as seen in the favorable effect of polar solvents on both the thermodynamics and kinetics of reactions in which charge is generated (13). Thus, when charge transfer in the transition structure is important, the relative stability of the charge-transfer configuration, and thus of the transition structure, will be affected by the polarity of the solvent. Hence, when polar interactions are important in a propagation reaction, a polar solvent can stabilize the transition structure and hence lower the reaction barrier.

When such effects are important, the polarity of the solvent affects radical selectivity as well as radical reactivity. This is because the extent to which charge-transfer stabilization can occur, and hence the extent to which polar solvents can further enhance these effects, depends on both reacting species. For instance, in a free-radical copolymerization, it is likely that polar interactions would be more important in the cross-propagations (when the monomer and radical bear different substituents and thus have different electronic properties) than in the

homopropagations (when the monomer and radical bear the same substituents). Hence the effect of solvent polarity on the stability of the transition structure (and thus the propagation rate) would generally be expected to be greater in the cross- than in the homopropagation reactions. Thus, there would be a net effect of solvent polarity on the reactivity ratios of the copolymerization (regardless of whether or not these polar interactions are influenced by the penultimate unit, or merely by the terminal unit).

There are two cases to consider when predicting the effect of solvent polarity on copolymerization propagation kinetics:

(1) the solvent polarity is constant as a function of the monomer feed composition for the given copolymerization system, as would be the case if the solvent polarity is dominated by an added diluent, or if the comonomers have similar dielectric constants, such as in the bulk copolymerization of styrene with methyl methacrylate

(2) the solvent polarity varies with the comonomer feed mixture for the given system, as would be the case in a bulk copolymerization of monomers with significantly different dielectric constants, such as styrene and acrylonitrile

In case (*1*), the effect on copolymerization kinetics is simple. The various reactivity ratios would vary from solvent to solvent, but, for a given copolymerization system, they would be constant as a function of the monomer feed ratios. The copolymerization kinetics would simply follow the appropriate base model for that system (according to which side reactions were assumed to be important, and which units were assumed to affect radical reactivity).

In case (*2*), the effect of the solvent on the copolymerization kinetics is more complicated since the various reactivity ratios would not be constant as a function of the monomer feed. To model such behavior, it would first be necessary to select an appropriate base model for the copolymerization (based on the usual assumptions). It would then be necessary to replace the various reactivity ratios (included in the base model as constants) by functions of the composition of the comonomer feed mixture. These functions would need to relate the reactivity ratios to the solvent polarity, and then relate the solvent polarity to the comonomer feed composition, and would thus vary depending upon the particular chemical properties of the monomers. It is therefore difficult to suggest a general kinetic model to describe these systems, but it is clear that such effects would result in deviations from the behavior predicted by their appropriate base model.

Radical Complexes. Solvents can also interfere with the propagation step via the formation of radical–solvent complexes. When complexation occurs, the complexed radicals are generally more stable than their corresponding uncomplexed radicals as it is this stabilization that drives the complexation reaction. Thus, in general, one might expect complexed radicals to propagate more slowly than their corresponding uncomplexed radicals, if indeed they propagate at all. However, in the special case that one of the comonomers is the complexing agent, the propagation rate of the complexed radical may instead be enhanced if propagation through the complex offers an alternative less-energetic reaction pathway. In any case, the complexed radicals would be expected to propagate at a rate

different from their corresponding free radicals; thus, the formation of radical–solvent complexes would affect the copolymerization propagation kinetics.

A terminal radical–complex model for copolymerization was formulated by Kamachi (14). He proposed that a complex is formed between the propagating radical and the solvent (which may be the monomer) and that this complexed radical propagates at a different rate compared with the corresponding uncomplexed radical. Under these conditions (and assuming that the terminal unit is the only unit affecting radical reactivity), there are eight different propagation reactions to characterize in a binary copolymerization. These are as follows:

$$\mathrm{RM}_i\cdot + \mathrm{M}_j \xrightarrow{k_{ij}} \mathrm{RM}_i\mathrm{M}_j\cdot \text{ or } \mathrm{RM}_i\mathrm{M}_j\cdot\ \mathrm{S} \quad \text{where} \quad i, j \quad 1 \text{ or } 2$$

$$\mathrm{RM}_i\cdot\mathrm{S} + \mathrm{M}_j \xrightarrow{k_{cij}} \mathrm{RM}_i\mathrm{M}_j\cdot \text{ or } \mathrm{RM}_i\mathrm{M}_j\cdot\ \mathrm{S} \quad \text{where} \quad i, j = 1 \text{ or } 2$$

There are also two equilibrium reactions for the formation of the complex (assuming that there is only one complexing agent which can complex with either radical):

$$\mathrm{RM}_i\cdot + \mathrm{S} \xleftrightarrow{K_i} \mathrm{RM}_i\cdot\ \mathrm{S} \quad \text{where} \quad i, j \quad 1 \text{ or } 2$$

On the basis of these reactions, Kamachi (14) derived expressions for the copolymer composition under this model. Fukuda and co-workers (15) later provided expressions for the composition, triad/pentad fractions, and propagation rate by deriving expressions for $\bar{r}_i$ and $\bar{k}_{ii}$, which could be used in place of r_i and k_{ii} in the terminal model equations (ie, eqs. 1 and 2 above). These are as follows:

$$\bar{k}_{ii} = k_{ii}\frac{1+\bar{s}_{ci}K_i[\mathrm{S}]}{1+K_i[\mathrm{S}]} \tag{7}$$

$$\bar{r}_i = r_i\frac{1+\bar{s}_{ci}K_i[\mathrm{S}]}{1+(r_i/\bar{r}_{ci})\bar{s}_{ci}K_i[\mathrm{S}]} \tag{8}$$

$$\text{where} \quad r_i = \frac{k_{ii}}{k_{ij}}, \quad \bar{r}_{ci} = \frac{k_{cii}}{k_{cij}}, \quad \bar{s}_{ci} = \frac{k_{cii}}{k_{ii}}, \quad i, j = 1 \text{ or } 2 \quad \text{and} \quad i \neq j$$

Variants of this model may be derived by assuming an alternative basis model (such as the implicit or explicit penultimate model) or by making further assumptions as to the nature of the complexation reaction. For instance, in the special case that the complexed radicals do not propagate (ie, $\bar{s}_{ci} = 0$ for all i), the reactivity ratios are not affected (ie, $\bar{r}_i = r_i$ for all i), and the complex formation serves only to remove radicals (and monomer, if monomer is the complexing agent) from the reaction, resulting in a solvent effect that is analogous to a bootstrap effect (see below).

Monomer Complexes. A solvent may also interfere in the propagation step via complexation with the monomer. As was the case with radical–solvent complexes, complexed monomer might be expected to propagate at a rate different from that of free monomer, since complexation might stabilize the monomer, alter its steric properties, and/or provide an alternative pathway for propagation. In

examining the effect of such complexation on copolymerization kinetics, there are a number of different mechanisms to consider. In the case that the complex is formed between the comonomers, there are three alternatives:

(1) The monomer–monomer complex propagates as a single unit, competing with the propagation of free monomer.
(2) The monomer–monomer complex propagates as a single unit, competing with the propagation of free monomer, but the complex dissociates during the propagation step and only one of the monomers is incorporated into the growing polymer radical.
(3) The monomer–monomer complex does not propagate, and complexation serves only to alter the free monomer concentrations.

In the case that the complex is formed between one of the monomers and an added solvent, there are two further mechanisms to consider:

(4) The complexed monomer propagates, but at a different rate to that of the free monomer.
(5) The complexed monomer does not propagate. Models based on mechanisms (*1*) and (*2*) are known respectively as the monomer–monomer complex participation (MCP) and dissociation (MCD) models. Mechanisms (*3*) and (*5*) would result in a solvent effect analogous to a bootstrap effect (see below), while mechanism (*4*) would result in a model similar to the MCD model, though it would be based on a slightly different equilibrium expression. The MCP and MCD models are outlined in the following paragraphs.

The *Monomer–Monomer Complex Participation (MCP) Model* was first suggested by Bartlett and Nozaki (16), later developed by Seiner and Litt (17), and refined by Cais and co-workers (18). In this model, it is assumed that the two monomers can form a 1:1 donor–acceptor complex and add to the propagating chain as a single unit in either direction. Assuming that the terminal unit is the only unit affecting radical reactivity, eight addition reactions and an equilibrium constant are required to describe the system.

$$RM_i\cdot + M_j^0 \xrightarrow{k_{ij}} RM_iM_j\cdot \quad \text{where} \quad i, j \quad 1 \text{ or } 2$$

$$RM_i\cdot + M_iM_j \xrightarrow{k_{iij}} RM_iM_iM_j\cdot \quad \text{where} \quad i, j = 1 \text{ or } 2 \quad \text{and} \quad i \neq j$$

$$RM_i\cdot + M_jM_i \xrightarrow{k_{iij}} RM_iM_jM_i\cdot \quad \text{where} \quad i, j \quad 1 \text{ or } 2 \quad \text{and} \quad i \neq j$$

$$M_1^0 + M_2^0 \xleftrightarrow{K} M_1M_2$$

The composition and propagation rate can be expressed in terms of the following parameters (15).

$$\frac{F_1}{F_2} = \frac{f_1^\circ}{f_2^\circ} \frac{(A_2B_1)r_1f_1^\circ + (A_1C_2)f_2^\circ}{(A_1B_2)r_2f_2^\circ + (A_2C_1)f_1^\circ} \tag{9}$$

$$\langle k_p \rangle = \frac{(A_2B_1)r_1(f_1^\circ)^2 + (A_1B_2)r_2(f_2^\circ)^2 + (A_1C_2 + A_2C_1)f_1^\circ f_2^\circ}{(A_2r_1f_1^\circ/k_{11}) + (A_1r_2f_2^\circ/k_{22})} \tag{10}$$

where

$$\begin{array}{cccc} A_1 = 1 + r_1 s_{1c} Q f_1^\circ & \text{and} & A_2 = 1 + r_2 s_{2c} Q f_2^\circ \\ B_1 = 1 + s_{1c}(1 + r_{1c}^{-1}) Q f_2^\circ & \text{and} & B_2 = 1 + s_{2c}(1 + r_{2c}^{-1}) Q f_1^\circ \\ C_1 = 1 + r_1 s_{1c}(1 + r_{1c}^{-1}) Q f_1^\circ & \text{and} & C_2 = 1 + r_2 s_{2c}(1 + r_{2c}^{-1}) Q f_2^\circ \end{array}$$

$$2Qf_i^\circ = \left\{[Q(f_j - f_i) + 1]^2 + 4Qf_i\right\}^{1/2} - [Q(f_i - f_j) + 1] \quad \text{and} \quad Q = K[\mathrm{M}]$$

f_i = feed composition of M_i and $f_i^0 = [M_i^0]/[M]$

where [M] is the total monomer feed and $[M_i^\circ]$ the uncomplexed M_i

$$r_i = \frac{k_{ii}}{k_{ij}}, \quad r_{ic} = \frac{k_{iij}}{k_{ijj}}, \quad s_{ic} = \frac{k_{iij}}{k_{ii}} \quad \text{where} \quad i, j = 1 \text{ or } 2 \quad \text{and} \quad i \neq j$$

As with all of the models, variations are possible by making a different assumption as to which units can affect radical reactivity. For instance, Brown and Fujimori (19) have derived expressions for composition and sequence distribution for the "Comppen" model, a complex-participation model that is based on the penultimate model.

In the *Monomer–Complex Dissociation (MCD) Model* it is assumed that the monomer–monomer complex described in the MCP model dissociates upon addition to the chain, with only one unit adding (20). A model based on this mechanism was first formulated by Karad and Schneider (21), and later generalized by Hill and co-workers (22). Assuming that only the terminal unit of the radical affects the propagation step, eight rate constants and two equilibrium constants are required to describe the system.

$$\mathrm{RM}_i\cdot + \mathrm{M}_j \xrightarrow{k_{ij}} \mathrm{RM}_i\mathrm{M}_j\cdot \quad \text{where} \quad i, j = 1 \text{ or } 2$$

$$\mathrm{RM}_i\cdot + \mathrm{M}_j\mathrm{C} \xrightarrow{k_{ijc}} \mathrm{RM}_i\mathrm{M}_j\cdot \quad \text{where} \quad i, j = 1 \text{ or } 2$$

$$\mathrm{M}_i + \mathrm{C} \underset{}{\overset{K_i}{\rightleftharpoons}} \mathrm{M}_i\mathrm{C} \quad \text{where} \quad i = 1 \text{ or } 2$$

As with the penultimate and radical–complex models, it is possible to express the model in terms of equations for $\bar{r}_i$ and $\bar{k}_{ii}$, which could be used in place of r_i and k_{ii} in the terminal model equations 1 and 2. These are as follows (15):

$$\bar{k}_{ii} = k_{ii}\,\frac{1 + s_{ic}K_i[\mathrm{C}]}{1 + K_i[\mathrm{C}]} \tag{11}$$

$$\bar{r}_i = r_i\,\frac{1 + s_{ic}K_i[\mathrm{C}]}{1 + (r_i/r_{ic})s_{ic}K_i[\mathrm{C}]} \tag{12}$$

$$\text{where} \quad r_i = \frac{k_{ii}}{k_{ij}}, \quad r_{ic} = \frac{k_{iic}}{k_{ijc}}, \quad s_{ic} = \frac{k_{iic}}{k_{ii}}, \quad i,j = 1 \text{ or } 2 \quad \text{and} \quad i \neq j$$

This form of the model is for monomer–solvent complexes generally. Under the MCD model, the complexing agent C is the other monomer (M_j). As with all of the solvent effects models, variations are possible by making a different assumption as to which units can affect radical reactivity.

Monomer Partitioning: The Bootstrap Effect. In the bootstrap model, solvent effects on the propagation rate are attributed to solvent partitioning and the resulting difference between bulk and local monomer concentrations. In this way, a solvent could affect the measured propagation rate coefficient without changing the reactivity of the propagation step. Bootstrap effects may arise from a number of different causes. As noted above, when radical–solvent or monomer–solvent complexes form and the complexes do not propagate, the effect of complexation is to alter the effective radical or monomer concentrations, thereby causing a bootstrap effect. Alternatively, a bootstrap effect may arise from some bulk preferential sorption of one of the comonomers around the growing (and dead) polymer chains. This might be expected to occur if one of the monomers is a poor solvent for its resulting polymer. A bootstrap effect may also arise from a more localized form of preferential sorption in which one of the comonomers preferentially solvates the active chain end rather than the entire polymer chain. In all cases, the result is the same: the effective free-monomer and/or radical concentrations differ from those calculated from the monomer feed ratios, leading to a discrepancy between the predicted and actual propagation rates.

Copolymerization models based upon a bootstrap effect were first proposed by Harwood (23) and Semchikov (24). Harwood suggested that the terminal model could be extended by the incorporation of an additional equilibrium constant relating the effective and "bulk" monomer feed ratios. Different versions of this so-called bootstrap model may be derived depending upon the baseline model assumed (such as the terminal model or the implicit or explicit penultimate models) and the form of equilibrium expression used to represent the bootstrap effect. In the simplest case, it is assumed that the magnitude of the bootstrap effect is independent of the comonomer feed ratios. Hence in a bulk copolymerization, the monomer partitioning may be represented by the following equilibrium expression:

$$\frac{f_1}{f_2} = K\left(\frac{f_{1\,\text{bulk}}}{f_{2\,\text{bulk}}}\right) \tag{13}$$

The equilibrium constant K may be considered as a measure of the bootstrap effect. Using equation 13 to eliminate the effective monomer fractions (f_1 and f_2) from the terminal model (ie, eqs. 1 and 2 above), replacing them with the measurable "bulk" fractions (f_1 bulk and f_2 bulk), the following equations for composition (25) and $\langle k_p \rangle$ may be derived (26).

$$\frac{F_1}{F_2} = \left(\frac{K f_{1\,\text{bulk}}}{f_{2\,\text{bulk}}}\right)\left(\frac{r_1 K f_{1\,\text{bulk}} + f_{2\,\text{bulk}}}{r_2 f_{2\,\text{bulk}} + K f_{1\,\text{bulk}}}\right) \tag{14}$$

$$\langle k_p \rangle = \left(\frac{1}{f_{2\,\text{bulk}} + K f_{1\,\text{bulk}}} \right) \left(\frac{r_1 K^2 f_{1\,\text{bulk}}^2 + 2K f_{1\,\text{bulk}} f_{2\,\text{bulk}} + r_2 f_{2\,\text{bulk}}^2}{r_1 K f_{1\,\text{bulk}} / k_{11} + r_2 f_{2\,\text{bulk}} / k_{22}} \right) \quad (15)$$

It should be noted that the above equations are applicable to a bulk copolymerization. When modeling solution copolymerizations under the same conditions, the same equations may be used for predicting copolymer composition since it is only the relationship between bulk and local monomer feed ratios that determines the effect on the composition and microstructure of the resulting polymer. However, some additional information about the net partitioning of monomer and solvent between the bulk and local phases is required before the propagation rate can be modeled. Modeling of the propagation rate in a solution copolymerization could be achieved by rewriting the above equilibrium expression in terms of molar concentrations (rather than comonomer feed ratios), and including the solvent concentration in this expression.

The bootstrap model may also be extended by assuming an alternative model (such as the explicit penultimate model) as the baseline model, and also by allowing the bootstrap effect to vary as a function of monomer feed ratios. Closed expressions for composition and sequence distribution under some of these extended bootstrap models may be found in papers by Klumperman and co-workers (25,27).

Depropagation

All of the models discussed thus far have assumed that the propagation steps are irreversible. However, while this is usually a reasonable assumption, at high temperatures (and, for some bulky or exceptionally stable monomers, even at low temperatures) the depropagation reaction is significant. Consideration of the depropagation reactions leads to kinetic models that are quite different from the terminal model and thus some deviations from the terminal model may be caused by the reversibility of one or more of the propagation steps. A large number of depropagation models are possible, depending upon both the basis model assumed and the assumptions that are made as to the nature of the depropagation reaction (such as which units can depropagate, and which units of the polymer radical can affect the depropagation rate). Early depropagation models were derived by Barb (28) (who incorporated depropagation into a simplified terminal MCP model), and Walling (29) (who incorporated depropagation into a simplified penultimate model). Lowry (30) and later Wittmer (31,32) derived composition equations for a number of different sets of assumptions concerning the depropagation reaction, assuming the terminal model for propagation. Howell and co-workers (33) generalized these equations, and provided corresponding expressions for the sequence distribution. Expressions for the propagation rate coefficient for some of these cases have recently been published by Martinet and Guillot (34) and by Kukulj and co-workers (35). Given the large number of possible depropagation models, the various equations will not be reproduced here but can be found in the original papers.

Conversion-Dependent Models

The equations for copolymer composition presented thus far are "instantaneous" or low-conversion equations, relating the copolymer composition to the exact monomer feed present in the reactor. However, during the course of copolymerization, monomers with differing reactivities tend to be incorporated into copolymers at different rates. As a result, in a batch reaction, this leads to a drift in the comonomer feed composition, which in turn leads to a drift in the copolymer composition. To model this behavior it is necessary to integrate the copolymer composition equation. This is achieved by noting that the copolymer composition, given as F_1/F_2 in the instantaneous equations, is in its more general form actually the derivative $d[M_1]/d[M_2]$ which can be integrated. Let us consider, as an example, the following integrated equation for the terminal model, published by Mayo and Lewis (3):

$$\log\left(\frac{[M_2]}{[M_2^0]}\right) = \frac{r_2}{1-r_2}\log\left(\frac{[M_1][M_2^0]}{[M_2][M_1^0]}\right) - \frac{(1-r_1r_2)}{(1-r_1)(1-r_2)}\log\left(\frac{1-r_2+(r_1-1)\frac{[M_1]}{[M_2]}}{1-r_2+(r_1-1)\frac{[M_1^0]}{[M_2^0]}}\right) \tag{16}$$

In this equation, $[M_1]$ and $[M_2]$ refer to the instantaneous monomer concentrations and $[M_1{}^0]$ and $[M_2{}^0]$ to the initial concentrations. An alternative form (expressed in terms of total molar conversion of monomer) was later published by Meyer and Lowry (36):

$$\frac{[M]}{[M^0]} = \left(\frac{f_1}{f_1^0}\right)^{\alpha}\left(\frac{f_2}{f_2^0}\right)^{\beta}\left(\frac{f_1^0-\delta}{f_1-\delta}\right)^{\gamma} \tag{17}$$

$$\text{where} \quad \alpha = \frac{r_2}{1-r_2}, \quad \beta = \frac{r_1}{1-r_1}, \quad \gamma = \frac{1-r_1r_2}{(1-r_1)(1-r_2)}, \quad \delta = \frac{1-r_2}{2-r_1-r_2}$$

Using either form of the equation, one can calculate the instantaneous comonomer feed composition as a function of the conversion, knowing the initial feed composition. This can then be used to calculate the copolymer composition, sequence distribution, and propagation rate using the corresponding instantaneous equations.

Model Discrimination: Which Model to Use for a Given System?

The choice of copolymerization model for any given system is often one of great debate in the polymer literature. This, to a large extent, is caused by the fact that all of the alternative models contain a number of characteristic constants (such as monomer and radical reactivity ratios). Since these are difficult to measure directly, they are usually (if not always) estimated by treating them as adjustable parameters and fitting the copolymerization model to the available data. As a result, many different models can often be made to fit the same experimental data. If the sole purpose of the model is merely to provide a shorthand version of the existing experimental data, provided the model provides a good fit to that data, any of the fitted models are appropriate to use. If however the estimated parameters are then to be used to make other model predictions or to deduce something about

the reaction mechanism, it is necessary to select the copolymerization model with the correct assumptions.

In what follows we examine which assumptions are likely to be valid for different types of copolymerization systems. In doing this, we make a distinction between what we refer to as a "basis model," a model containing the set of assumptions likely to be applicable to most of the copolymerization systems, and models for "exceptional systems," in which additional system-specific influences are likely to be operating in conjunction with those accounted for by the basis model. We have recently reviewed and assessed the experimental evidence for the different copolymerization models both for basis systems (37) and exceptional systems (38) and will not attempt to reproduce these reviews here. Instead we merely outline the main conclusions of this work and make some general comments concerning the applicability of the alternative models.

Basis Model. For many years, people believed that the terminal model was the basis of copolymerization propagation kinetics because it could be fitted to the composition data for most systems tested. However, in 1985 Fukuda and coworkers (7) demonstrated that the terminal model failed to predict the propagation rate coefficients for the copolymerization of styrene with methyl methacrylate—a system for which the composition data had been widely fitted by the terminal model (see Fig. 1). These results were later confirmed by several independent groups, both for the styrene–methyl methacrylate system (under a wide range of different conditions), and also several other copolymerizations—indeed for almost all systems so far tested (37). It now appears likely that the failure of the terminal model to describe simultaneously the composition and propagation rate coefficients of ordinary free-radical copolymerization systems is general, with the terminal model being applicable only to those exceptional systems in which the comonomers have very similar reactivities.

Although there is strong evidence against the terminal model, there has been much reluctance to abandon this model since this would undermine the 50

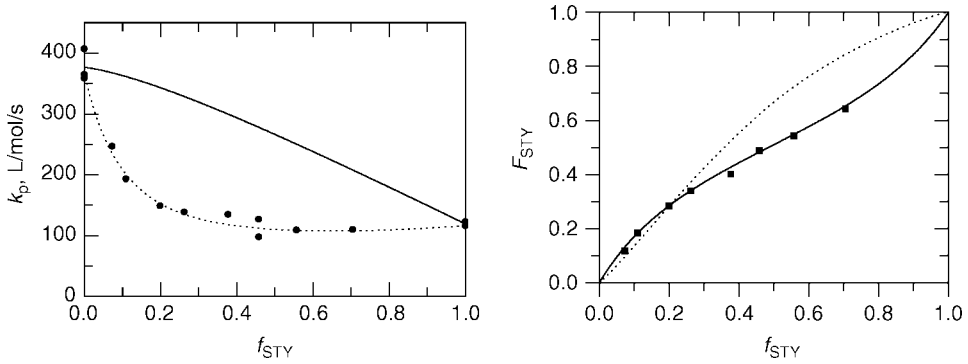

Fig. 1. Shown here is Fukuda's 40°C $\langle k_p \rangle$ data (**a**) and composition data (**b**) (7). The solid line on each graph is the terminal model predictions using the reactivity ratios that provide the best fit to the composition data ($r_{STY} = 0.523$ and $r_{MMA} = 0.460$) while the dotted line in each graph is the terminal model predictions using the reactivity ratios that provide the best fit to the $\langle k_p \rangle$ data ($r_{STY} = 2.5724$ and $r_{MMA} = 0.7973$). Clearly the terminal model can fit the composition or the $\langle k_p \rangle$ data but not both simultaneously.

years of terminal model reactivity ratios that have been and continue to be published (see, eg, the large listing of terminal model reactivity ratios in the *Polymer Handbook* (39), and the various empirical schemes, such as the Patterns (40) and *Q*–*e* schemes (41), that have been developed for predicting these parameters). The implicit penultimate model was proposed as a solution to this problem. As seen above, by assuming that the penultimate unit affected only the reactivity but not the selectivity of the propagating radical, it is possible to obtain a copolymerization model that retains the terminal model composition equation but includes a non-terminal model $\langle k_p \rangle$ equation. This thus enabled the failure of the terminal model $\langle k_p \rangle$ equation to be accounted for without abandoning the terminal model composition equation and the accompanying large database of reactivity ratios.

However, recent experimental and theoretical work has shown that the *assumptions* of the implicit penultimate model are unlikely to be applicable to the majority of copolymerization systems. We have recently published a review of this evidence (37,42), which draws on direct experimental and theoretical measures of reactivity ratios, model testing in a range of copolymerization systems, and other tests of the mechanism of the propagation step via, for example, the examination of solvent effects on reactivity ratios. These studies provide strong evidence for penultimate unit effects but, in all cases where penultimate unit effects have been measured directly, effects on radical selectivity have been shown to be significant. In other words all available evidence contradicts the assumption of the implicit penultimate model that the penultimate unit affects reactivity but not selectivity.

Furthermore, recent theoretical studies have provided a rationalization for this result that suggests it is likely to be a general feature of free-radical polymerization. As noted earlier, for a penultimate unit effect in the reaction barrier to be *implicit*, it is necessary for this penultimate unit effect to occur in the absence of polar, steric, or other forms of direct interaction that, by their very nature, are dependent on and will thus vary with the chemical structure of the reacting monomer. Fukuda proposed (11) that an implicit effect could occur if the penultimate unit affected *only* the radical stability. A radical stabilization penultimate unit effect would affect the reaction enthalpy, and the reaction barrier (via the Evans–Polanyi rule). Provided there are no other types of penultimate unit effect operating (eg, steric or polar effects), such a penultimate unit effect would be implicit. However, high-level ab initio molecular orbital calculations of a representative range of model propagation reactions have shown that, although penultimate unit effects in radical stability are significant, these effects largely cancel from the reaction barrier—owing to the early transition structure in these exothermic reactions (43). As a result, for such a penultimate unit effect in the barrier to be significant, the corresponding effect on radical stability has to be enormous and thus requires substituents with very strong electron-withdrawing or -donating properties. The theoretical calculations demonstrated that large penultimate unit effects of this nature simultaneously affected the charge-transfer configurations of transition structure, leading to explicit polar penultimate unit effects. Given that the majority of copolymerization systems have highly exothermic propagation steps and thus early-transition structures, it would seem that, in general, implicit radical stabilization penultimate unit effects are unlikely to occur in the absence of explicit polar effects.

In addition, steric penultimate unit effects should also lead to explicit (rather than implicit) penultimate unit effects, as they would obviously be sensitive to the steric properties of the monomer with which they were reacting. Recently, experimental evidence for significant entropic penultimate unit effects has been published (44), confirming predictions made in an earlier theoretical study (45). These studies further confirm that, if there are penultimate unit effects in free-radical copolymerization, then they are most likely to be explicit effects.

To summarize, we know firstly from simple model-testing studies spanning the last 20 years that for almost all systems tested, the terminal model can be fitted to $\langle k_p \rangle$ or composition data for a copolymerization system, but not both simultaneously. Secondly, more recent experimental and theoretical studies have demonstrated that the assumption of the implicit penultimate model—that the penultimate unit affects radical reactivity but not selectivity—cannot be justified. Therefore, on the basis of existing evidence, the explicit penultimate model should replace the terminal model as the basis of free-radical copolymerization propagation kinetics, and hence *the failure of the terminal model* $\langle k_p \rangle$ *equation must be taken as a failure of the terminal model and hence of the terminal model composition equation*. This means that the terminal model composition equation is not *physically valid* for the majority of systems to which it has been applied.

Exceptional Systems. It is likely that side reactions are also important in a large number of copolymerization systems. As seen above, their presence further complicates the copolymerization kinetics by adding extra parameters to the copolymerization models, thereby making model discrimination even more difficult. Indeed (with the possible exception of those few systems that have been shown to obey the terminal model in all respects) it is very difficult to find any copolymerization system for which there is consensus about the type of copolymerization model that should be applied. There is, however, strong independent evidence for the various types of side reactions in specific copolymerization systems, and hence for these systems such side reactions need to be incorporated into copolymerization models and taken into account when studying the propagation reaction. Indeed, for some systems, the presence of side reactions such as complexation may provide a means of controlling the composition and microstructure of the copolymer and, in some cases, even its stereochemistry. In what follows, we make a few general comments about the types of systems in which the various side reactions are likely to be occurring.

Depropagation is known to become significant with increasing polymerization temperature, and most polymerizations are known to have a ceiling temperature beyond which polymerization will not proceed. This arises because of the exothermic and exentropic nature of the propagation step for most polymerization reactions (ie, since $\Delta G = \Delta H - T\Delta S$ and both ΔH and ΔS are negative, there will exist a temperature T_c such that for all $T > T_c$, $\Delta G > 0$). For most polymerization systems, these ceiling temperatures are well above ordinary operating conditions; however, for polymerizations involving exceptionally stable or bulky monomers such as CO, SO_2, and α-methylstyrene, depropagation is significant at much lower temperatures and thus needs to be incorporated into copolymerization models. The importance of depropagation in a particular system can be determined directly from measurements of the entropy and enthalpy of the propagation reaction, or indirectly by measuring the ceiling temperature of each of

the comonomers. The use of monomers such as α-methylstyrene to assist in the control of molecular weight by exploiting their slow propagation kinetics is often used in industry as a facile method of reaction control (46,47).

Monomer–monomer complexes are known to form in solutions containing an electron donor monomer with an electron acceptor monomer. Many such complexes have been detected spectroscopically (48) and one of the most well-known examples is that between maleic anhydride and styrene. There has been much dispute over the role these complexes play in the reaction mechanism, concerning, for example, whether they can propagate via an MCP or MCD mechanism, or whether they are unreactive and merely result in a bootstrap effect. For some complexes, the heat of formation is less than the heat of propagation and hence it seems unlikely that the MCP model could be appropriate for these systems, as the complex should be disrupted during the propagation step. In other systems, however, this is not the case and there is reasonable circumstantial evidence that these complexes could be propagating as a single unit. For instance, it has been observed that in the copolymerization of *N*-phenylmaleimide with chloroethyl vinyl ether, the stereochemistry at succinimide units is predominately cis (as it would be in the complex) and random elsewhere, and further that the proportion of cis linkages was correlated with the variables with which the concentration of the complex was also correlated (49). It seems likely that, depending on factors such as the strength of the complex, the role of monomer–monomer complexes in free-radical copolymerization will vary and model discrimination should be on a case-by-case basis. However, where there is (spectroscopic) evidence for their existence, they must always be taken into account when deriving copolymerization models.

Radical–solvent complexes are more difficult to detect spectroscopically; however, they do provide a plausible explanation for many of the solvent effects observed in free-radical homopolymerization—particularly those involving unstable radical intermediates (such as vinyl acetate) where complexation can lead to stabilization. For instance, Kamachi (50) observed that the homopropagation rate of vinyl acetate in a variety of aromatic solvents was correlated with the calculated delocalization stabilization energy for complexes between the radical and solvent. If such solvent effects are detected in the homopolymerization of one or both of the comonomers, then they are likely to be present in the copolymerization systems as well. Indeed, radical–complex models have been invoked to explain solvent effects in the copolymerization of vinyl acetate with acrylic acid (51). Radical–solvent complexes are probably not restricted merely to systems with highly unstable propagating radicals. In fact, radical–solvent complexes have even been proposed to explain the effects of some solvents (such as benzyl alcohol, *N*,*N*-dimethyl formamide, and acetonitrile) on the homo- and/or copolymerizations of styrene and methyl methacrylate (52–54). Certainly, radical–solvent complexes should be considered in systems where there is a demonstrable solvent effect in the copolymerizations and/or in the respective homopolymerizations.

Polarity effects can also result in solvent effects in free-radical copolymerization. Recent theoretical studies (43,55–57) of small-radical addition reactions suggest that in a wide range of cross-propagation reactions, the transition structure is stabilized by the contribution of charge-transfer configurations. When this is the case, the extent of stabilization (and hence the propagation rate) will be

influenced by the dielectric constant of the reaction medium. Solvent effects on reactivity ratios have been known for a long time and at least some of these [for instance those for styrene-methyl methacrylate copolymerization (58–60) and styrene–acrylonitrile copolymerization (61,62) in a variety of solvents] have been shown to correlate with the dielectric constant of the reaction medium. Furthermore, it is possible that solvent effects in other systems may in part be attributable to polarity effects, although additional effects (such as radical–solvent complexes or monomer partitioning) obscure a direct correlation. As noted above, polarity effects need only be explicitly considered in a copolymerization model if the polarity of the reaction medium varies significantly as a function of the monomer feed fraction (as it would in a bulk copolymerization of two monomers with widely differing dielectric constants). However, it is worth noting that polarity effects are likely to be operating at least to some extent in copolymerizations of monomers with even moderately different electronegativities and, where such effects do occur, the reactivity ratios (and hence composition and sequence distribution) can be manipulated by varying the solvent polarity.

Bootstrap effects arise from a number of different causes. For instance, a bootstrap effect can be expected if there is preferential sorption of one of the monomers around the growing polymer chain—as might be expected if one of the monomers is a poor or nonsolvent for the resulting polymer. This can sometimes be established by examining the appropriate polymer–solvent interaction parameters. Nonideal mixing of the comonomers can also be independently established via measurements of solution thermodynamics. Indirect evidence for bootstrap effects arising from preferential solvation of the polymer chain can be obtained by examining the copolymer composition as a function of molecular weight, since it would be expected that this type of bootstrap effect would lead to chain length effects on copolymer composition, even for nonoligomeric systems that would normally be expected to satisfy the long-chain assumption. On the basis of this method and measurements of solution thermodynamics, Semchikov (24,63) has shown that such bootstrap effects do indeed operate in a number of bulk copolymerization systems including AN–STY, STY–MA, VAC–STY and VAc–NVP, but not in the system STY–MMA (at 298–343K). Bootstrap effects can also be expected if unreactive monomer–monomer, monomer–solvent, radical–solvent, or radical–monomer complexes form. As noted above, there is evidence for many of these complexes in certain types of system, though there is frequently dispute as to the role these complexes play in the reaction mechanism. Bootstrap effects should certainly be considered when attempting to model systems for which there is demonstrable evidence for the existence of such complexes.

Which Model to Use and When: Practical Recommendations

It is clear from the above discussion that any physically realistic model for free-radical copolymerization kinetics should be based on the penultimate model and, depending on the system, should also incorporate various types of solvent effects and/or depropagation. The resulting model would not only be very complex, but would also contain numerous characteristic constants (ie, reactivity ratios, equilibrium constants). This poses a major problem as such parameters are difficult to

measure directly, and are therefore usually treated as adjustable parameters, and estimated as part of the model-fitting process. As we have argued elsewhere (1), even in oversimplified models there are usually more adjustable parameters than are mathematically required to fit data. This results in large and highly correlated uncertainties in the parameter estimates, with multiple parameter sets providing excellent fits to the experimental data. Hence, the use of physically realistic models may not be practical for most copolymerization systems, unless they are accompanied by independent measurements of the model-parameters.

As a solution to this problem, we recommend that, provided they can be fitted to the data, simplified models such as the implicit penultimate model (and hence the terminal model composition equation) continue to be used for descriptive purposes. However, it is important to recognize that the resulting parameter estimates will at best convey qualitative information about radical reactivity and should not be used to make quantitative predictions of quantities other than those to which they were fitted. When physically meaningful information is required, more direct approaches should be adopted. For example, substituent effects on radical reactivity and selectivity in small-radical models can be studied directly via a host of experimental approaches, and also via high-level ab initio molecular orbital calculations. Various spectroscopic techniques can be used to study radical and monomer complexes, and indeed ab initio molecular orbital calculations could also be used to tackle this problem. Information on possible monomer partitioning can be accessed from polymer–solvent interaction parameters, and other measurements of solution thermodynamics. Likewise, thermodynamic measurements (and ab initio calculations) can assist in the study of depropagation. These direct approaches not only help to identify the physically realistic model for a given system, but can also provide independent measurements of the corresponding reactivity ratios and equilibrium constants (thereby reducing the number of adjustable parameters in the model).

Measurement of Reactivity Ratios

Reactivity ratios are typically measured by fitting the terminal model composition equation to experimental composition data. Depending on the chemical structure of the comonomers, a variety of methods can be used to measure copolymer composition, including ^{1}H NMR, uv–visible spectroscopy, elemental microanalysis, and Fourier transform infrared (FTIR) spectroscopy. For information on these procedures, the reader is referred to Reference 64. In order to fit the model to the data, it is necessary to measure the copolymer composition for multiple initial values of the comonomer feed ratios. As always, choosing an appropriate experimental design is important for minimizing the statistical uncertainties in the parameter estimates. It is worth noting that the common practice of choosing comonomer feed ratios at regular intervals between $f_1 = 0$ and 1 is not the optimum design for measuring terminal model reactivity ratios. Instead, Tidwell and Mortimer (65) recommended multiple determinations at the following two feed ratios:

$$f_1 = \frac{2}{2 + r_1} \quad \text{and} \quad f_1 = \frac{r_2}{2 + r_2} \tag{18}$$

Of course, the implementation of such a design presupposes knowledge of the reactivity ratios we are trying to measure. However, one can normally obtain a useful design using approximate reactivity ratios, as obtained from preliminary experiments or literature values for related systems.

Having obtained the composition data it is then necessary to fit it with the terminal model, using the two reactivity ratios as adjustable parameters. For many years, the standard method for fitting the data was first to linearize the composition equation, as described by Fineman and Ross (66), thereby allowing linear regression or indeed a simple graphical procedure. However, it is now generally accepted that this method transforms error structure in such a way that linear regression is no longer valid (67), and instead nonlinear regression using the original composition equation should be adopted. Nowadays linearization of the equation is in fact unnecessary, as modern mathematical software packages routinely perform nonlinear regression. In particular, a free program called *Contour* (68,69) has been provided specifically for the estimation of reactivity ratios. In implementing the nonlinear regression procedure, it is important to weight the residuals according to the expected error structure in the data (70).

Finally, it should be noted that the above discussion refers to low-conversion copolymerizations, for which composition drift is not significant. For conversion-dependent data, the appropriate integrated composition equation should instead be fitted to the data using an error-in-variables procedure (71) to deal with the statistical uncertainties in the multiple independent variables.

Reactivity in Free-Radical Copolymerization

It is clear from the above discussion that reactivity in free-radical copolymerization depends on a rich array of factors. There is strong evidence that the reactivity of the propagating radical is governed by the nature of both its terminal and penultimate units. Depending on the system, these substituent effects in turn arise from both steric and electronic factors, with the latter itself being a complex result of sigma- and/or pi-effects on the stability of the propagating radical and the monomer, as well as the possible stabilization of the transition structure through partial charge transfer. A consequence of this latter effect is that the reactivity of the propagation reaction can be dependent on the dielectric constant of the reaction medium. The solvent (which may be the monomer) can also affect the propagation reaction by forming a complex with the propagating radical or comonomer, thereby altering its reactivity. In some cases this may result in an altogether different propagation mechanism. In addition, monomer partitioning can at times affect the apparent reactivity of the propagation step, as can depropagation. This complex nature of propagation in free-radical copolymerization offers huge potential for controlling the copolymer composition and microstructure (by, eg, manipulating the feed composition, temperature or solvent type), and even perhaps the stereochemistry (through the manipulation of radical or monomer complexes). An understanding of substituent effects on the reactivity of the propagation step is important for exploiting this potential for control.

The earliest attempts to describe substituent effects on reactivity were empirical schemes, based on the terminal model. The most widely used of these are

the Q–e (41) and Patterns (40) schemes, and as an example we will briefly outline the former. In the Q–e scheme, the rate coefficient for attack of radical i on monomer j is given by the following equation:

$$k_{ij} = P_i Q_j \mathrm{e}^{-e_i e_j} \tag{19}$$

Hence the terminal model reactivity ratios are given by

$$r_i = \frac{Q_i}{Q_j}\ \mathrm{e}^{-e_i(e_i - e_j)} \tag{20}$$

In order to apply this equation, each monomer i is assigned empirically derived Q_i and e_i values, as obtained by fitting equation 20 to sets of experimental reactivity ratios. In this way, provided the Q and e values of the individual monomers are known, reactivity ratios can be predicted for previously unmeasured combinations of monomers. An extensive listing of Q and e values has been provided by Greenley (72).

There are a number of shortcomings in the scheme. As noted above, the terminal model does not provide a physically realistic description of copolymerization kinetics and, as such, predictions (in this case of other reactivity ratios) based on terminal model reactivity ratios may be subject to considerable error. Even in the context of the terminal model, the assignment of independent Q and e values for a "monomer," regardless of whether it is acting as the monomer or radical and regardless of what it is reacting with, is a major oversimplification. In addition, the experimental database of terminal model reactivity ratios used to obtain the Q and e values was largely compiled nearly 50 years ago, using somewhat limited analytical methods. As a result of these problems, the predictions of the Q–e scheme are at best qualitative, and are generally most successful for combinations of monomers that are not subject to strong polar or steric effects.

More modern descriptions of reactivity in copolymerization have arisen from the quantum chemical study of the addition of small radicals to alkenes. Such small-radical models are applicable to propagation because the propagation reaction is chemically controlled, and not generally influenced by substituents beyond the penultimate unit. On the basis of a large collection of both theoretical and experimental studies of substituent effects in radical addition reactions, Fischer and Radom (57) have recently presented a theoretical account of reactivity framed in terms of the curve-crossing model (13). Under this model, the barrier for an addition reaction is dependent on the exothermicity of the reaction, the singlet–triplet gap of the double-bonded substrate and the possibility for low-lying charge-transfer configurations in the transition structure, in turn estimated by a consideration of the ionization energies and electron affinities of the reactants. These quantities are easily accessible from both experiment and high-level ab initio molecular orbital calculations, and the model thus offers a powerful approach for predicting and understanding reactivity in free-radical copolymerization. For more details of the curve-crossing model, and more fundamental aspects of reactivity in radical addition reactions, the reader is referred to References 13 and 57 (also see COMPUTATIONAL QUANTUM CHEMISTRY FOR FREE-RADICAL POLYMERIZATION).

Termination in Free-Radical Copolymerizations

Detailed knowledge of free-radical copolymerization termination rate coefficients is of technical as well as fundamental importance. The radical–radical termination reaction in free-radical polymerization is the most complex reaction in the polymerization process (73,74). Its termination rate coefficient, k_t, is influenced by a multitude of different factors, which are not easily separated. Only within the last 15 years have new methods become available that allow for an accurate measurement of this rate coefficient. The scatter of the termination rate coefficients given in the *Polymer Handbook* (75) reported for the same monomer at the same reaction temperature is a direct manifestation of the influence of these various parameters on k_t. While the advanced techniques available to study termination processes in homopolymerizations and the current theoretical models describing the termination process are discussed in the chapter "Free Radical Polymerization," the present section focuses on the use of kinetic data from free-radical binary and ternary copolymerizations to clarify the termination process as well as on giving practical guidelines for the estimation of termination rate coefficients in copolymerization.

Theoretical Background. Modeling of the (average) termination rate coefficient, $k_{t,copo}$, at low monomer conversions as a function of the initial monomer feed in the reaction mixture has been thoroughly reviewed by Fukuda and co-workers (76). The present chapter considers the most important models presented in Reference 76.

Model A, which has been proposed by Fukuda and co-workers, assumes diffusion-controlled termination to be related to the composition of the generated copolymer according to equation 21

$$k_{t,copo}^{-1} = k_{t\ 11}^{-1} F_1 + k_{t\ 22}^{-1} F_2 \tag{21}$$

where F_i is the mole fraction of comomoner i segments within the copolymer.

Similar in its underlying idea is one of the earliest models for the description of the termination rate coefficient introduced by Atherton and North (77):

$$k_{t,copo} = k_{t\ 11} F_1 + k_{t\ 22} F_2 \tag{22}$$

In *Model B*, two types of free radicals, one carrying a monomeric unit 1, the other with a monomeric unit 2 at the chain end, are considered to sufficiently account for copolymerization k_t according to

$$k_{t,copo} = k_{t\ 11} P_1^{\ 2} + 2k_{t\ 12} P_1 P_2 + k_{t\ 22} P_2^{\ 2} \tag{23}$$

where the k_{tii}'s are the homotermination rate coefficients and the P_i's are the relative populations of the two types of the terminal free radicals ($P_1 = 1 - P_2$). Φ, which is referred to as Walling factor (9), describes the size of the cross-termination rate coefficient ($k_{t12} = k_{t21}$) relative to the geometric mean of the homopolymerization rate coefficients:

$$\Phi = \frac{k_{t\ 12}}{(k_{t\ 11} k_{t\ 22})^{0.5}} \tag{24}$$

It should be noted that a so-called geometric mean rule, which is formally identical to equation 24 has been frequently used in free-radical gas kinetics to estimate cross-recombination rate coefficients k_{AB} from the associated homo-recombination rate coefficients k_{AA} and k_{AB} (78). Two other models given in Fukuda's review (76), C and D, in addition to the terminal unit also consider the penultimate unit at the free-radical chain end as has first been tried by Russo and Munari (79,80). These models are associated with a greater number of individual termination rate coefficients. Given in equation 27 is the expression for $k_{t,copo}$ of a binary copolymerization, for which 10 termination rate coefficients, $k_{tij,kl}$, need to be considered. $k_{tij,kl}$ refers to the reaction of (two) radicals terminating in the monomer units ij and kl, respectively. The P_{ij}'s and P_{kl}'s indicate relative populations of the four types of "penultimate" free radicals (with chains ending in units 11, 12, 21, and 22, respectively). These populations are available from the propagation rate coefficients and reactivity ratios as given below in equations 25 and 26 (15):

$$P_1 = 1 - P_2 = \frac{\bar{r_1} f_1 / \bar{k_{11}}}{(\bar{r_1} f_1 / \bar{k_{11}}) + (\bar{r_2} f_2 / \bar{k_{22}})} \tag{25}$$

and

$$P_{11} = P_1 - P_{21} = \frac{r_{11} f_1 P_1}{r_{11} f_1 + f_2 / s_1} \tag{26}$$

The population P_{22} is calculated analogously to P_{11}.

$$k_{t,copo} = \sum_{l=1}^{2} \sum_{k=1}^{2} \sum_{i=1}^{2} \sum_{j=1}^{2} P_{ij} P_{kl} k_{t\ ij,kl} \tag{27}$$

To reduce the relatively large number of termination rate coefficients, *Model C* replaces rate coefficients for reactions between "unlike" free radicals, $k_{tij,kl}$ (with ij being different from kl), by the corresponding coefficients for termination of the "like" radicals, $k_{tij,ij}$ and $k_{tkl,kl}$, via the arithmetic mean approximation in equation 28 (76):

$$k_{t\ ij,kl} = 0.5(k_{t\ ij,ij} + k_{t\ kl,kl}) \tag{28}$$

Using equation 28 to eliminate all "unlike" termination rate coefficients turns equation 27 into equation 29, which contains only the four "like" (penultimate) termination coefficients:

$$k_{t,copo} = k_{t\ 11,11} P_{11} + k_{t\ 21,21} P_{21} + k_{t\ 22,22} P_{22} + k_{t\ 12,12} P_{12} \tag{29}$$

Model D differs from Model C in that a geometric mean approximation (eq. 30) is applied to reduce the number of penultimate termination rate coefficients from 10 to 4:

$$k_{t\ ij,kl} = (k_{t\ ij,ij} k_{t\ kl,kl})^{0.5} \tag{30}$$

Equation 30 is the expression used by Fukuda and co-workers (76). Russo and Munari in their pioneering study had an additional factor of 2 on the r.h.s. of equation 30, with this formulation being identical to what is used in gas kinetics to estimate cross-termination (78).

Substituting equation 30 into equation 27 yields the expression (eq. 31) for $k_{t,copo}$ according to Model D:

$$k_{t,copo}^{0.5} = k_{t\ 11,11}^{0.5} P_{11} + k_{t\ 21,21}^{0.5} P_{21} + k_{t\ 22,22}^{0.5} P_{22} + k_{t\ 12,12}^{0.5} P_{12} \tag{31}$$

Fukuda and co-workers (76) presented Model D in a slightly different way (eq. 32), with the two penultimate rate coefficients, $k_{t12,12}$ and $k_{t21,21}$, being replaced by two parameters δ_1 and δ_2:

$$k_{t,copo}^{0.5} = k_{t11,11}^{0.5}(P_{11} + \delta_1 P_{21}) + k_{t21,21}^{0.5}(P_{22} + \delta_2 P_{12}) \tag{32}$$

δ_1^2 is defined as

$$\delta_i^2 \equiv \frac{k_{t\,ji,ji}}{k_{t\,ii,ii}} \tag{33}$$

Models A through D have been extensively tested toward their ability to describe the termination rate coefficients in various copolymerization systems.

Binary Copolymerization. A large body of work has been carried out to test the applicability of the Models A to D to copolymerizations of acrylate, methacrylates, and styrenic monomers (76,77,79–82). It has proven advantageous to study the copolymerization termination rate coefficient in related monomer families (eg within the acrylate or methacrylates families). For example, Buback and Kowollik investigated dodecyl acrylate (DA) and methyl acrylate (MA) copolymerizations via the single-pulse pulsed-laser polymerization (SP-PLP) technique. MA and DA have homotermination rate coefficients that differ by orders of magnitude [ie, log (k_t)(L/mol/s) (1000 bar, 40°C, conv. < 0.1, DA) = 6.38 and log (k_t)(L/mol/s) (1000 bar, 40°C, conv. < 0.1, MA) = 8.13]. The ability of the above-mentioned models to describe the experimentally obtained copolymerization termination rate coefficients can be tested by plotting log $k_{t,copo}$ versus the comonomer mixture composition, f^0. Such a plot—together with the corresponding model descriptions—is given in Figure 2.

Models A and B, which both consider only two types of terminating free radicals, seriously fail to represent the experimental $k_{t,copo}$ data. The line referring to Model B has been calculated under the assumption that equation 24 holds with $\Phi = 1$. Even major changes in Φ do not result in a significantly improved quality of representing the experimental data by Model B. Also Model C, which assumes diffusion control with four kinds of penultimate free-radical species, fails to provide an adequate fit of the measured $k_{t,copo}$ data. Model D, on the other hand, allows for an excellent representation of the experimental data. It should be noted that the straight line through the DA–MA data in Figure 2 is not obtained just from a linear least-squares procedure, but is derived from a fit to Model D. The almost linear change of log $k_{t,copo}$ with monomer feed composition f should be particularly

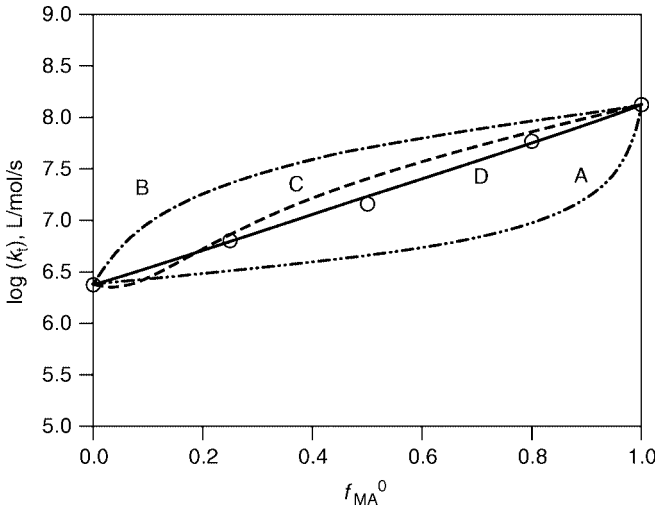

Fig. 2. Copolymerization termination rate coefficients at low conversions in MA/DA copolymerizations at 40°C and 1000 bar plotted against the mole fraction of MA. The lines A through D correspond to the copolymerization k_t models given in the text.

noted. This result bears important mechanistic information. Moreover, this linear correlation may be useful for predicting or estimating copolymerization k_t even in situations where more than two monomers from the same family are polymerized (see below).

The close-to-linear correlation that is seen in acrylate–acrylate copolymerization systems is also found in intrafamily methacrylates copolymerizations. Studies on such systems have been carried out in the past by Ito and O'Driscoll (83) by rotating sector experiments at 30°C and ambient pressure. The data given in their pioneering study differ in the format in which they are presented: In the case of the methyl methacrylates (MMA)–butyl methacrylates (BMA) system k_p and k_t values for the copolymerizations are given, whereas in the case of the MMA–dodecyl methacrylates (DMA) system the termination rate coefficients are given relative to the homotermination rate coefficient of MMA (ie, $k_{t,copo}/k_{t,homo}$). The k_t values given for the homopolymerization of MMA and BMA are not in agreement with the nowadays accepted values. (84) However, the difference of both values is close to the difference which can be deduced from the more recent numbers. The same observation holds true for the propagation rate coefficients presented by these authors. This observation indicates that their measurements are reliable in a relative way, but their absolute numbers are shifted. The data presented by Ito and O'Driscoll are also best represented by Model D (see Fig. 3), which was found to fit the experimental data excellently, with the "like" termination rate coefficient being in between the homopolymerization rate coefficients and very similar in value.

The data for intrafamily copolymerization of acrylate- and methacrylates-type monomers suggest that $k_{t,copo}$ might be generally accessible from homotermination data by employing equation 34, which has been termed the *general*

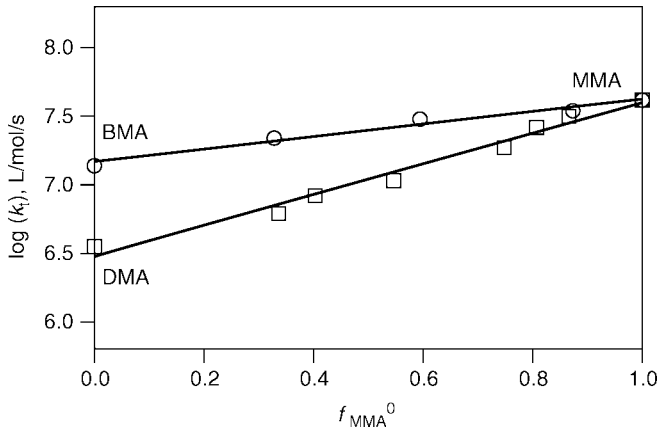

Fig. 3. Termination rate coefficients from Ito and O'Driscoll (83) for dodecyl methacrylate (DMA)–methyl methacrylate (MMA) (at 40°C and 1000 bar, rescaled) and butyl methacrylate (BMA)–methyl methacrylate (MMA) (at 30°C and ambient pressure) copolymerizations. The data in Ref. 83 for the MMA–DMA system are given as relative rate coefficients $k_{t,copo}/k_{t,homo}$. The $k_{t,copo}$ values were calculated using $k_{t,homo}$ from Ref. 84. The lines are best fit representations of Model D.

geometric mean rule (GGM) (79–81):

$$\log k_{t,copo} = f_1^0 \log k_{t,11} + f_2^0 \log k_{t,22} \tag{34}$$

This, however, must not be generally true for two main reasons: (*1*) The linear log $k_{t,copo}$ versus f correlation seen for the above systems will certainly be restricted to situations where the same mechanism controls termination behavior. Under conditions where $k_{t,homo}$ varies with monomer conversion (which indicates a change in the mode of termination rate control), the linear log $k_{t,copo}$ versus f correlation is no longer valid. At total monomer conversion between 20 and 35%, the log $k_{t,copo}$ values for $f_{MA}{}^0 = 1.00$ and 0.80 are almost the same (81), and linear plots as depicted in Figures 2 and 3 can no longer be drawn at this stage of the reaction. (*2*) The theoretical concepts on which equation 34 is based (85) focus on the idea of a purely diffusional controlled reaction. Cullinan and co-workers derived that the composition dependence of the binary mutual diffusion coefficient D_{ij} tends to be linear between the infinitely dilute extremes (85). These authors demonstrated (and found agreement with the existing experimental data) that a modification of absolute rate theory based on thermodynamic aspects yields an expression which predicts the concentration dependence of the binary mutual diffusion coefficient in terms of equation 35:

$$D_{ij} = D_j^{f_j^0} D_i^{f_i^0} \tag{35}$$

which can be easily rearranged into equation 36

$$\log D_{ij} = f_j^0 \log D_j + f_i^0 \log D_i \tag{36}$$

The formal similarity with equation 34 is quite obvious. Understanding termination rate coefficients at low conversions in purely translational diffusion terms may lead to equation 34. However, this concept is not in agreement with the ideas pioneered by Russo and Munari (79,80). These authors assume chemical (most likely steric) effects to be important in the termination reaction. They suggested the penultimate unit effect model (eq. 27). If the termination process was governed by the same translational diffusion mechanism in the initial plateau region for all monomers considered in this work, no curved dependencies of log k_t versus f should be obtained, since equation 34 (and eq. 36) always predicts straight lines. If, however, the termination reaction is to some extent controlled by chemical effects (Model D), curved dependencies may occur, depending on the individual radical populations P_{ij} (which directly go into the modeling procedure). Thus, copolymer systems with a pronounced curvature in the log $k_{t,copo}$ versus f plots provide the best argument against any oversimplification of $k_{t,copo}$ behavior. Indeed, Fukuda and co-workers reported such dependencies for different copolymerizations, eg styrene and ethyl acrylate at 40°C and ambient pressure (76). More recently, Buback and Feldermann (82) reported curved dependencies in the interfamily copolymerizations of MMA–DA and DMA–MA.

Ternary Copolymerization. As technical polymerization processes with more than two monomers are frequently met, it is an interesting question whether a correlation corresponding to equation 34 will hold for terpolymerizations. The resulting expression for terpolymerization k_t would read

$$\log k_t = f_1 \log k_{t,1} + f_2 \log k_{t,2} + f_3 \log k_{t,3} \tag{37}$$

where the monomer mole fractions f_i add up to $f_1 + f_2 + f_3 = 1$ and where $k_{t,3}$ is the homotermination rate coefficient of monomer 3. Buback and Kowollik test equation (eq. 37) for the intrafamily terpolymerizations of MA–BA–DA and MMA–BMA–DMA (86). Remarkably, these two terpolymerization systems adhered strictly to equation 37. It is worthwhile to plot binary low conversion copolymerization data for the systems MA–BA, BA–DA, and MA–DA, together with low conversion data on the MA–BA–DA terpolymerization system. Inspection of Figure 4 shows that all ternary copolymerization k_t values are located on a surface area that is indicated by the triangle (full lines) within the figure. The termination rate surface is restricted to a certain set of initial mole fractions, as they have to add up to 1; eg it is not possible to conduct a terpolymerization at the mole fractions of 0.8 for MA and 0.5 for DA. This (quite obvious) restriction is the reason for the triangular form of the termination rate surface.

The success of equation 37 in describing intrafamily terpolymerization termination rate coefficients provides considerable temptation to propose an expression (eq. 38) that may be useful (or even must be used because of missing alternatives) for modeling k_t of monomer mixtures that contain i monomeric species:

$$\langle k_t \rangle = \prod_{1}^{i} k_{t,i}^{f_i} \tag{38}$$

with the sum over f_i adding up to 1.

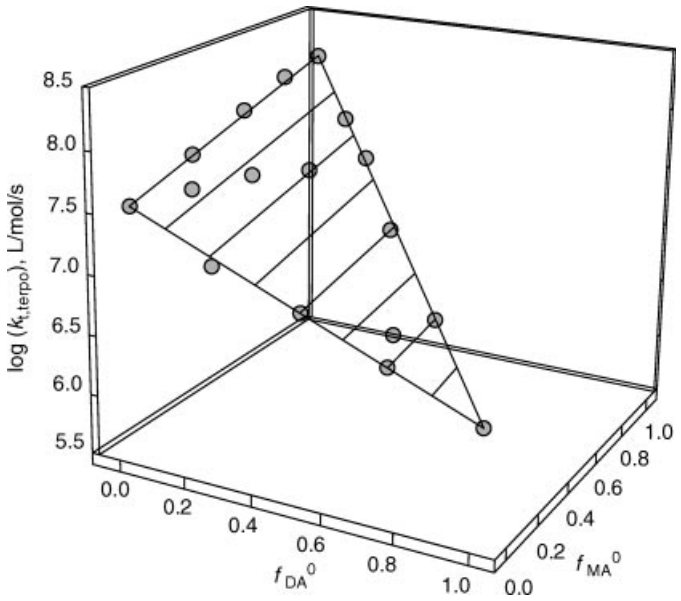

Fig. 4. Low conversion termination rate coefficients, $k_{t,terpo}$, for a MA–BA–DA terpolymerization at 40°C and 1000 bar plotted vs the mole fraction of DA and MA in the initial composition of the reaction mixture (86). The triangle indicates the surface on which the termination rate coefficients are located.

Equation 38 represents the generalized formulation of equations 34 and 37 in nonlogarithmic terms. $\langle k_t \rangle$ refers to the termination rate coefficient of a multimonomer copolymerization in the initial plateau region (at low and moderate conversions, with this range depending on the particular type and concentration of the monomers). $k_{t,i}$ is the homotermination rate coefficient of monomer i in this inital plateau region and f_i is the mole fraction of monomer i in the reaction mixture.

Controlled/Living Radical Copolymerization

Controlled/living radical polymerization (CRP) has been successfully applied to many different radically polymerizable monomers. A recent book has summarized this very rapidly developing field, at least till 2001 (87). Because of limited space available, only the most important issues will be discussed here.

Currently three systems seem to be the most efficient processes for conducting a CRP: nitroxide mediated polymerization (NMP) (eq. 1 in Fig. 5), atom transfer radical polymerization (ATRP) (eq. 2 in Fig. 5) and degenerative transfer systems (eq. 3 in Fig. 5) such as reversible addition–fragmentation transfer (RAFT) or iodine degenerative transfer (IDT) processes (88–90). The key feature of all CRPs is the dynamic equilibration between active radicals and various types of dormant species.

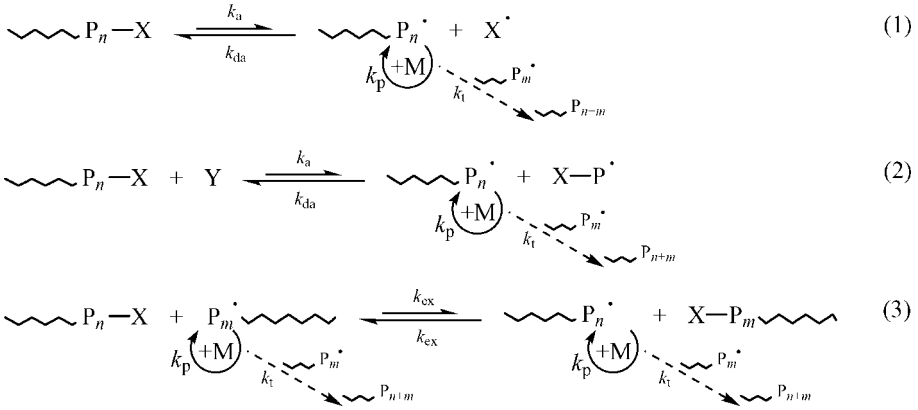

Fig. 5. Three most common mechanisms of exchange between active and dormant species in CRP.

The activation process (k_a) for the dormant species (P_n—X) to form propagating radicals ($P_n^{\bullet}$) may be spontaneous, ie, thermal (alkoxyamines in NMP) (91) or catalytic (activation of alkyl (pseudo)halides by redox active transition-metal complexes (92–94), Y, in ATRP). It may be also bimolecular [dithioesters in RAFT (95) and alkyl iodides in IDT (96)]. The degenerative transfer process may proceed through the addition–fragmentation chemistry or through hypervalent radical intermediates of very short or sometimes longer lifetime. In the latter case some retardation may occur. In all of these systems only radicals propagate (k_p). The conditions for the reaction are selected so that the reversible activation or reversible transfer reaction provides a small steady concentration of growing radicals, at concentrations similar to or smaller than in conventional radical polymerization (RP). Although termination (k_t) does occur in all CRPs, the proportion of dead chains is relatively small (typically between 1 and 10%) in comparison with all living chains. The latter constitutes tiny amounts of growing species (ppm) and a dominating proportion of dormant chains which are potentially active. In NMP and ATRP, the formation of active radicals is accompanied by the generation of a persistent radical species, such as a nitroxide or a higher oxidation state transition-metal complex, which can deactivate growing radicals reversibly. Both processes follow persistent radical effect kinetics (97,98).

In all of these systems, propagation involves radical species, and therefore chemoselectivities (reactivity ratios and transfer coefficients), regioselectivities (head-to-head units), and stereoselectivities (tacticity) determined for CRPs are similar to those in conventional RP.

Developments in CRP were also applied to copolymerizations (99–102). Since CRP is a living system, for the first time segmented copolymers (block and graft copolymers) were prepared in high yield via radical mechanisms. Simultaneous copolymerization results in preparation of statistical copolymers, with comonomers displaying reactivity ratios similar to those in RP. However, since nearly all chains start growing at the same time and continue till the end of the reaction, drift in comonomer feed is reflected in composition variation along the backbone of all chains and results in the preparation of tapered or gradient copolymers. This is in contrast to RP, in which copolymers formed at the early stage of

the copolymerization are rich in one comonomer and at the later stages are rich in another comonomer.

In this section, some peculiarities of copolymerization conducted in CRP systems will initially be discussed and then examples of various types of copolymers will be provided. They will include statistical, gradient, and alternating copolymers, as well as block and graft copolymers. Some special systems will be also presented and they will include preparation of stereoblock copolymers, and various hybrid materials formed by either mechanistic transformation or by growing well-defined polymers from flat, colloidal, or irregular surfaces.

Reactivity Ratios. In CRP, monomer is consumed only in the reaction with growing radicals. Therefore, in the first approximation, composition of copolymers in CRP and RP should be the same and in many cases the simplest four-reaction copolymerization scheme should be applied, with all restrictions discussed earlier in this article (103). The relative rates of comonomer consumption and consequently apparent reactivity ratios in CRP should be the same as in RP. However, some small discrepancies are expected, and indeed have been observed, in the values of reactivity ratios from ATRP and conventional radical polymerizations (104–107). There are a number of reasons for these discrepancies, sometimes as obvious as conducting the copolymerization at different reaction temperatures and in the presence of solvents. Additionally, differences in the rate of chain growth can also alter the observed reactivity ratios. In a controlled polymerization, polymer is slowly formed throughout the reaction and there is a continuous increase in the molecular weight of the polymer, whereas in a conventional system high molecular weight polymer is formed at the beginning of the reaction and the composition of the polymer can be established at low conversion. This difference in the rate of chain growth may also amplify the bootstrap effect (23). The presence of a transition-metal catalyst in ATRP may further complicate the picture by introducing the possibility of complexation of some monomers with the Lewis acidic transition-metal catalysts (108–110). The final, and perhaps most important, cause of discrepancies in reactivity ratios observed in ATRP, are the differences in methodologies of measuring reactivity ratios in controlled and conventional radical polymerizations (106). In a conventional process the monomer reactivity ratios are measured at low conversion with different monomer feeds. However, in the ATRP, measurements at low conversions could be affected by the structure of the initiator, which may preferentially react with one comonomer. For this reason it is necessary to measure the cumulative composition of the copolymers at a conversion higher than in a conventional process. However, as the cumulative composition of a copolymer will always be equal to the monomer feed at 100% monomer conversion, the closer the reaction gets to 100% conversion, the less precise the information that can be obtained on reactivity ratios.

In CRP, the classic copolymerization scheme (Fig. 6) should be supplemented by the reversible activation steps for both initiation and propagation steps:

The values of the individual equilibrium constants should have an effect on the total radical concentration, ie, the overall polymerization rate. However, the reversible activation processes should not affect the relative rates of comonomer consumption, once the steady state between radicals is established. Nevertheless, during the initial stage of the reaction, cross-propagation reactions may not be fully equilibrated and therefore concentration of both growing species in CRP may

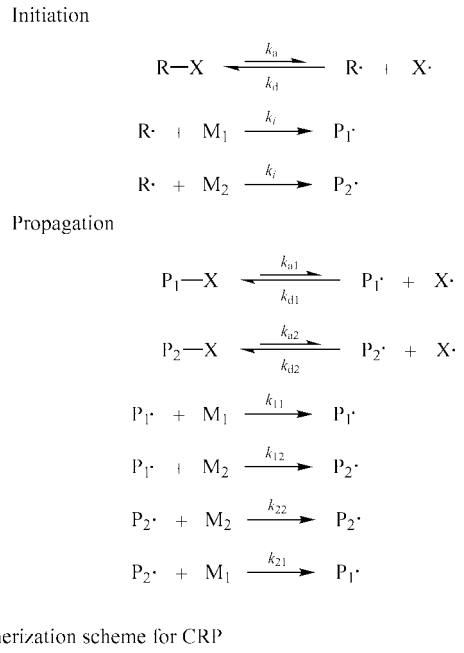

Fig. 6. Simplified copolymerization scheme for CRP.

be different than in conventional RP. Thus, some discrepancies between CRP and RP can be observed (107,111). In addition, diffusion phenomena may play some role, especially in copolymerization of macromonomers (112–115). Nevertheless, in a large majority of CRP systems examined the reported reactivity ratios are very similar to those in conventional RP.

The penultimate effect on the kinetics of the activation/deactivation processes may be quite significant. For example, model studies of activation of various dimers in ATRP copolymerization of methyl acrylate (MA) and methyl methacrylate (MMA) showed the following relative values of k_{act} for dimeric species: H–MA–MA–Br, H–MMA–MA–Br, H–MA–MMA–Br, and H–MMA–MMA–Br to be 1, 4.6, 19, and 96, respectively. The back-strain effect resulting from the presence of a MMA penultimate unit, and formation of a thermodynamically more stable radical from a MMA–Br terminal unit, increased the values of k_{act} by ∼5 and ∼20 times, respectively, in comparison to MA penultimate/terminal units. The combined effects resulted in a ∼100-fold increase of k_{act} for H–MMA–MMA–Br relative to H–MA–MA–Br (116).

Statistical and Gradient Copolymer. As shown in Figure 7, composition along the chain varies in different ways for block, gradient, and random copolymers. The composition does not vary in a block copolymer until after the crossover point between blocks where there is an instantaneous composition change, a random copolymer shows no continuous change in composition, and gradient copolymers are copolymers in which the instantaneous composition varies continuously along the chain contour (117–119).

In order to achieve this continuous change in instantaneous composition, all chains must be initiated simultaneously, and must survive until the end of the

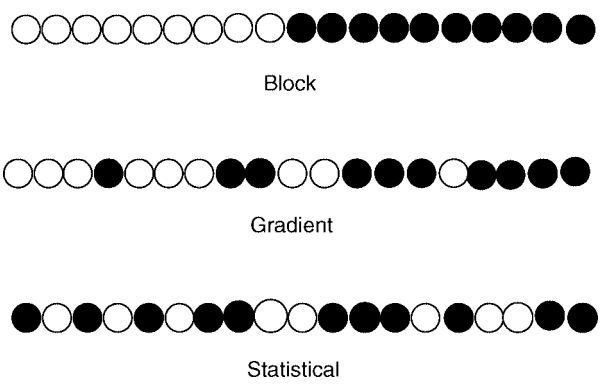

Fig. 7. Schematic representation of block, gradient, and statistical copolymers.

polymerization. Therefore, a living (ionic) or controlled/living radical polymerization technique must be employed, as the significant presence of chain-breaking reactions would lead to heterogeneity in composition as well as in molecular weight.

Because of facile cross-propagation, statistical (or nearly random) copolymerization is very easily achieved in free-radical systems, in contrast to ionic reactions. The reactivity of many comonomers are relatively similar. For example, in RP, methacrylates have similar reactivity to styrene and are ∼3 times more reactive than acrylates. However, in anionic polymerization acrylates are 100 times more reactive than methacrylates and the latter much more reactive than styrene. In cationic polymerization the opposite reactivity order is observed. The copolymerization of monomers with similar reactivity should result in statistical copolymers with no compositional variation during the polymerization. This has been observed for copolymerization of the same type of monomers such as various styrenes, various methacrylates, and various acrylates. This is the case for both CRP and conventional RP. However, in batch copolymerizations of different classes of comonomers there is a continuous change of residual monomer composition in the reaction because one comonomer reacts faster than the other one.

The slow rate of initiation relative to propagation in conventional RP composed of two or more classes of monomers leads to chains which have differing compositions depending on when they were grown. This difference in reactivity results in compositional variation *among the chains* and, in the extreme cases, may result in a mixture of two homopolymers. In CRP, all the chains are initiated early in the reaction and, under proper conditions, retain activity over the entire course of the reaction. Therefore, changes in the instantaneous composition arising from variations in the relative concentrations of monomers are reflected *along all chains*. In the extreme case of very different reactivity ratios, this may lead to formation of block copolymers. At the end of the reaction, the cumulative compositions of the conventional and controlled reactions should be the same but in the conventional case, a variety of compositions will be observed between the chains while in CRP all chains will have a similar structure, a gradient of composition along the chain (118,119). Such gradient (or tapered) copolymers have properties different to either block or random copolymers, making them candidates for

applications such as blend compatibilizers, vibration-dampening materials, and pressure-sensitive adhesives (117,119,120).

The shape of the gradient depends on the reactivity ratios, on the composition of the monomer feed and on whether a mono- or multi-functional initiator was employed. Forced gradient copolymers can also be prepared by CRP processes. In the latter system, one monomer is fed into a reactor already containing another monomer in a semibatch mode. In such a case gradient copolymers can also be obtained from comonomers with the same reactivity ratios.

Because of the relative infancy of CRP, only a limited number of gradient copolymers have been reported (102,119). Spontaneous gradient copolymers were formed in ATRP copolymerization of styrene with *n*-butyl acrylate (nBA) (121,122), and with MMA and nBA (123). Both systems had reactivity ratios similar to those in conventional RP. Preparation of a forced gradient copolymerization was studied for styrene and MMA (99). The molecular weight of the copolymer was controlled, polydispersity was low, $M_w/M_n < 1.25$, and the instantaneous composition of styrene relative to MMA in the backbone decreased as MMA was added. In another study examining the forced gradient copolymerization of methyl acrylate (MA) and styrene, changes in the feed rate of MA (0.085 vs. 0.050 mL/min) resulted in differences in the instantaneous composition of MA in the copolymer. At a higher feed rate, there was more MA incorporated into the chains at a given fractional chain length (conversion) (119). The DSC and dynamic mechanical analysis indicated that gradient copolymers have significantly different properties than block copolymers. The DSC traces showed that the forced gradient copolymer behavior depends on the thermal history. The lower modulus (G′) of the forced gradient copolymer compared to the statistical gradient copolymer demonstrates that materials with different properties were produced. The synthesis of forced gradient copolymers of styrene and acrylonitrile as well as spontaneous gradients of styrene and *n*-butyl acrylate were also reported (119,121,122).

Alternating Copolymers. Alternating copolymers can be formed when reactivity ratios for both comonomers are very low, approaching zero (109). Another option is to use large excess of one comonomer with $r \sim 0$. Both of these systems have been used in CRP. The first successful attempts were based on copolymerization of methyl acrylate and acrylonitrile with a large excess of isobutene using ATRP. Well-defined but low molecular weight alternating copolymers were prepared. Subsequently, well defined alternating structures of styrene with either maleic anhydride or maleimides were prepared by NMP, RAFT, and ATRP (124–126).

A more challenging synthetic task was to force monomers such as styrene and MMA to form alternating copolymers. This was successfully accomplished by complexing MMA, BMA, or MA with Lewis acids such as aluminumalkylchlorides (108). Complexation significantly increased the rate of cross-propagation. By using RAFT as the CRP process, it was possible to prepare not only alternating copolymers but also block copolymers containing segments of both alternating and homopolymer structures (126–128).

Block Copolymers. CRP, as any controlled/living polymerization, can be used for the preparation of well-defined segmented copolymers, ie, block and graft copolymers (qv) with various architectures (101). Block copolymers (qv) can be formed by simple chain extension through the addition of the second monomer

at the end of the polymerization of the first one. They have been synthesized from the isolated macroinitiators and have been also made by the transformation of the chain ends of macroinitiators prepared by another technique, eg ionic, coordination, ring-opening polymerization, step growth, etc. (129–135). By using multifunctional initiators, star-block copolymers have been made (136) (see also BLOCK COPOLYMERS, TERNARY TRIBLOCKS).

Many block copolymers have been prepared by ATRP, NMP, and RAFT (99). Since NMP can not yet be successfully used for the synthesis of polymethacrylates only block copolymers with styrenes, acrylates, and acrylamide segments have been made. RAFT and ATRP can incorporate a broader range of monomers into block copolymers. Efficient blocking requires cross-propagation to be fast relative to the rate of polymerization of the second block. Since the rate of propagation in NMP and ATRP depends on the product of the equilibrium constant and true radical propagation constants, certain rules apply for successful block copolymerization. The same is true for RAFT, which requires fast fragmentation of the first segment to achieve efficient crosspropagation (137,138). In general, more stabilized radicals, such as methacrylates, propagate via RP slower than those forming less stabilized radicals (acrylates). However, equilibrium constants and rates of fragmentation are much higher for stabilized radicals and therefore they dominate the overall rate control. This means that blocking from polymethacrylates to polyacrylates is efficient for both ATRP and RAFT, but the opposite is not true. Similar observations were reported for NMP and ATRP during preparation of block copolymers that required blocking from polyacrylonitrile to poly(butyl acrylate) (139) .

ATRP offers one synthetic setup to overcome this deficiency, via the halogen exchange technique, which allows an approach to combat the crossover problem. This technique utilizes a mixed-halogen system, ie, a bromo-containing initiator and a Cu(I)Cl catalyst, to afford better control over initiation from the macroinitiator and subsequent polymerization of the second methacrylates block, which is particularly useful for preparing acrylate–methacrylate block copolymers (140,141). Halogen exchange provides a method for adjusting the equilibrium when moving from a less reactive macroinitiator (A), with an apparently smaller equilibrium constant, to successfully initiate polymerization of a monomer that has a larger equilibrium constant (B in Fig. 8). Since ATRP equilibrium constants under comparable conditions for methacrylates are ∼1000 times higher than for acrylates (142–144), cross-propagation from polyacrylates to polymethacrylates is inefficient in spite of ∼100 times higher propagation rate constants for the latter (145). However, since alkyl bromides are ∼100 times more active than structurally similar alkyl chlorides (146), the cross-propagation becomes successful.

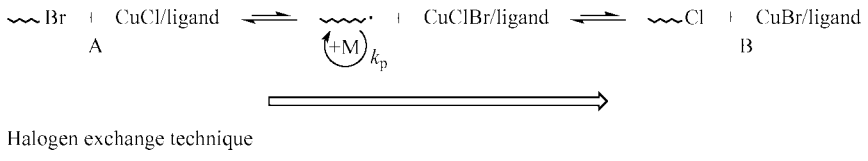

Fig. 8. Halogen exchange technique.

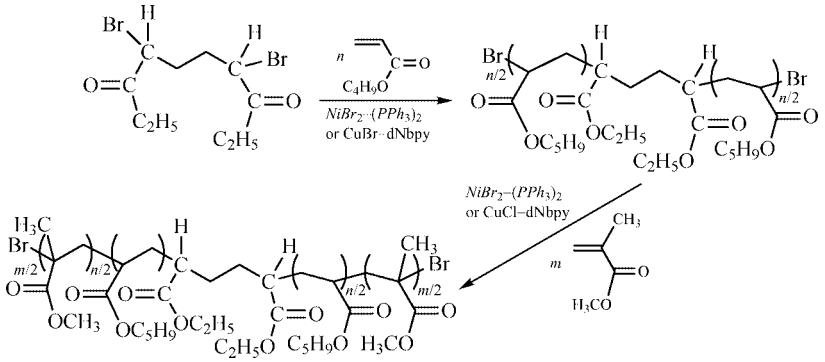

Fig. 9. Preparation of triblock copolymers with poly(butyl acrylate) central and poly(methyl methacrylate) outer segments by ATRP.

When difunctional pnBA was used to prepare ABA block copolymers with MMA using a Ni system, without halogen exchange, it was reported that the mechanical properties of the resulting copolymers were poor compared to those of the copolymers prepared by ionic methods, presumably because of the broad polydispersity of the outer pMMA blocks (see Fig. 9) (147). Complete incorporation of the macroinitiator did not occur until >30% monomer conversion. The block copolymers did, however, microphase separate into ordered structures (148).

In comparison, block copolymers prepared using a copper catalyst employing the halogen exchange technique had predictable molecular weights and narrower molecular weight distributions (141). There was no evidence of slow initiation and the outer pMMA blocks were more uniform. When Moineau and co-workers used this system, the mechanical properties were greatly improved relative to the copolymers prepared with the Ni catalyst (149). It has been also reported that the proper choice of solvent also improves block copolymerization (150).

Another approach to form similar materials is to add MMA to the growing pBA chains before complete consumption of the BA to form gradient A segments. The properties of these triblocks were different than those observed for "clean" ABA blocks, with lowered glass-transition temperatures (T_g) for the mostly hard outer blocks as well as increased tensile strength and elongation, as shown in Figure 10 (120).

The stress–strain curves recorded for the two triblock copolymer samples during cold drawing of films with a constant rate of 1 mm/min are shown in Figure 11. The gradient copolymer has much higher tensile elongation (1000% vs. 300%) but much lower tensile strength (4.5 MPa vs. 7.3 MPa) than the copolymer with pure homopolymeric blocks.

The ABA-isolated sample was a clean triblock, with a pnBA central block of $M_n = 65{,}200$, two blocks of MMA with an $M_n = 13{,}150$, and an overall $M_w/M_n = 1.34$. The ABA-sequential copolymer contained a clean central block of nBA of $M_n = 67{,}500$, and two gradient end block copolymers containing 13 mol% nBA and 87 mol% MMA, with an $M_n = 10{,}600$, and an overall $M_w/M_n = 1.24$ (120). The insert shows the small-angle X-ray scattering intensities for these samples, which correspond to cylindrical morphology of pMMA hard segments. Since both types

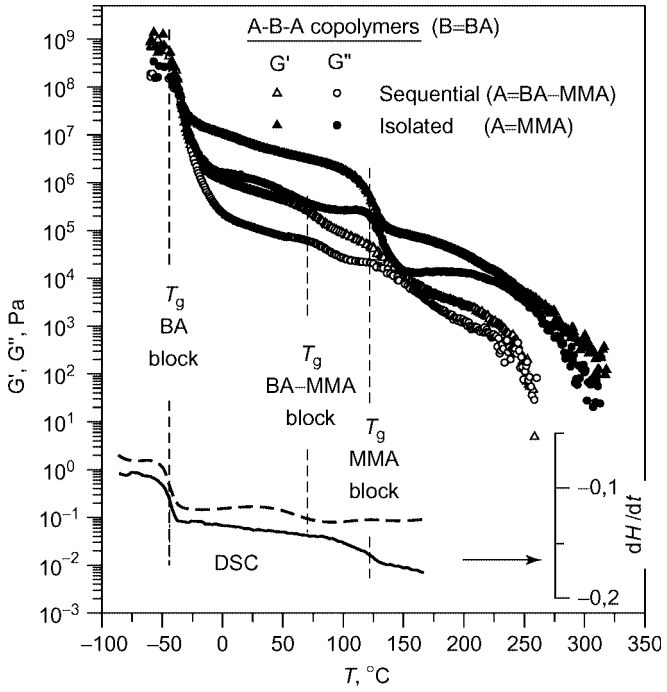

Fig. 10. Temperature dependencies of the real (G′) and imaginary (G″) component of the shear modulus measured at the deformation frequency of 10 rad/s. for the pure and tapered triblock copolymers pMMA-*b*-pBA-*b*-pMMA and p(MMA-*grad*-BA)-*b*-pBA-*b*- p(MMA-*grad*-BA) of approximately the same overall composition, MW and polydispersity. For comparison DSC traces are shown, which help to localize the glass-transition temperatures (T_g) of the microphases.

of block copolymers had similar compositions and only varied in the sequence distribution of the monomers, this type of structural control provides yet another route to tailor make polymers with specific properties by CRP methods.

Graft Copolymers. Graft copolymers can be prepared by three different techniques: grafting from the backbone, grafting through by using macromonomers, and grafting onto the backbone.

CRP has been applied to the synthesis of each segment in the either entire graft system or exclusively to the preparation of specific segments such as backbone, macromonomer, macroinitiator, or the grafting process. For example, NH_2-terminated dendrons were grafted onto backbones made by CRP containing *N*-oxysuccinimide 4-vinylbenzoate (151). Alternatively macromonomers were made by either ATRP or other process (coordination, or conventional RP) and they were subsequently used for grafting through (152,153). In another approach, macromonomers were made by group transfer polymerization, or other controlled polymerization processes, but ATRP was used for the grafting through copolymerization (112,114). Perhaps the simplest is the grafting-from process, which can involve CRP for the synthesis of the backbone, for the grafting-from reaction, or both (Fig. 12).

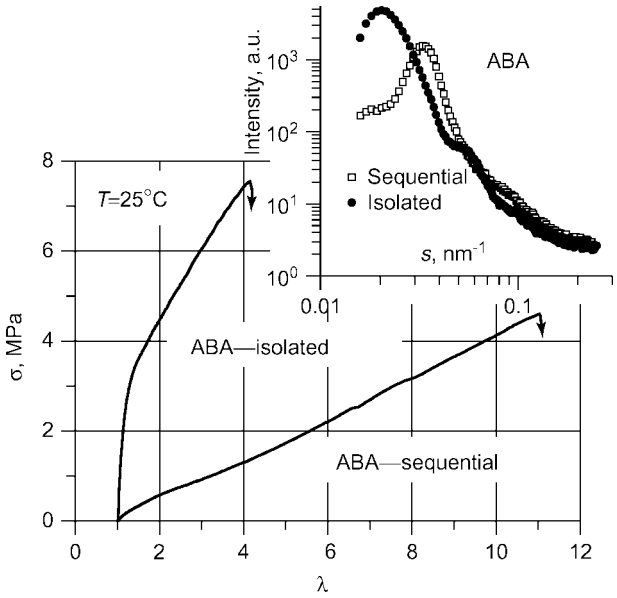

Fig. 11. The stress–strain curves recorded for the two triblock copolymer samples during cold drawing of films with a constant rate of 1 mm/min. ABA-isolated sample was a pure triblock but ABA-sequential contained a pure central block of *n*-butyl acrylate of M_n = 67,500, and two end gradient blocks containing 13 mol% *n*-butyl acrylate and 87 mol% methyl methacrylate, with an $M_n = 10600$, and an overall polydispersity of $M_w/M_n = 1.24$. The insert shows the small angle X-ray scattering intensities for these samples.

Grafting-From Technique. Graft copolymers were among the first materials prepared by CRP. After establishing that a unimolecular TEMPO-based initiator successfully controlled the polymerization of styrene (154), the grafting-from approach was used to demonstrate that graft copolymers were possible using CRP techniques (155). The multifunctional macroinitiator was prepared by free-radical copolymerization of styrene with a vinyl benzyl TEMPO derivative using AIBN at 60°C. The macroinitiator was heated to 130 °C in the presence of more styrene, which led to the preparation of a graft copolymer. The molecular weight of the polymer increased from $M_n = 12{,}000$ ($M_w/M_n = 1.86$) to $M_n = 86{,}000$ ($M_w/M_n = 2.01$). After cleavage of the grafted side chains, analysis of the graft units gave $M_n = 23{,}000$ with $M_w/M_n = 1.26$, in good agreement with the expected value of 21,000 (155).

Expanding on this idea, an alkene-functionalized TEMPO derivative was copolymerized with propylene or 4-methylpentene using a cationic metallocene compound to prepare an α-olefin-based macroinitiator for graft copolymerization [$M_n = 28{,}000$ ($M_w/M_n = 1.80$) or $M_n = 6080$ ($M_w/M_n = 1.65$)] (Fig. 13) (156). Heating the propylene-based copolymer to 123 °C in the presence of 200 equiv St increased its molecular weight to $M_n = 210{,}000$, with $M_w/M_n = 2.0$. The final molecular weights of the graft copolymers were dependent on the concentration of St added to the reaction.

The grafting-from technique can also provide a route to graft copolymers via ATRP. A poly[(vinyl chloride)-*co*-(vinyl chloroacetate)] copolymer, containing

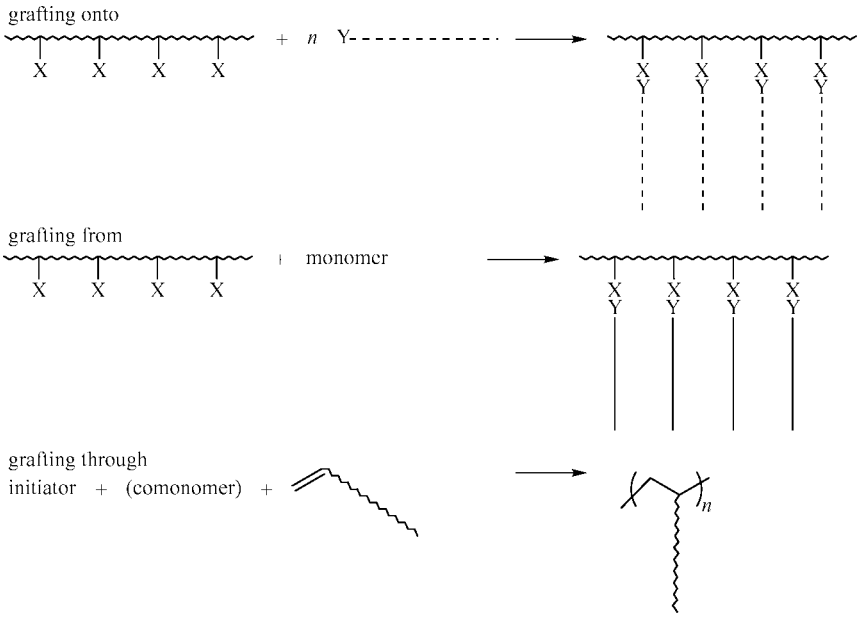

Fig. 12. Three approaches to prepare graft copolymers.

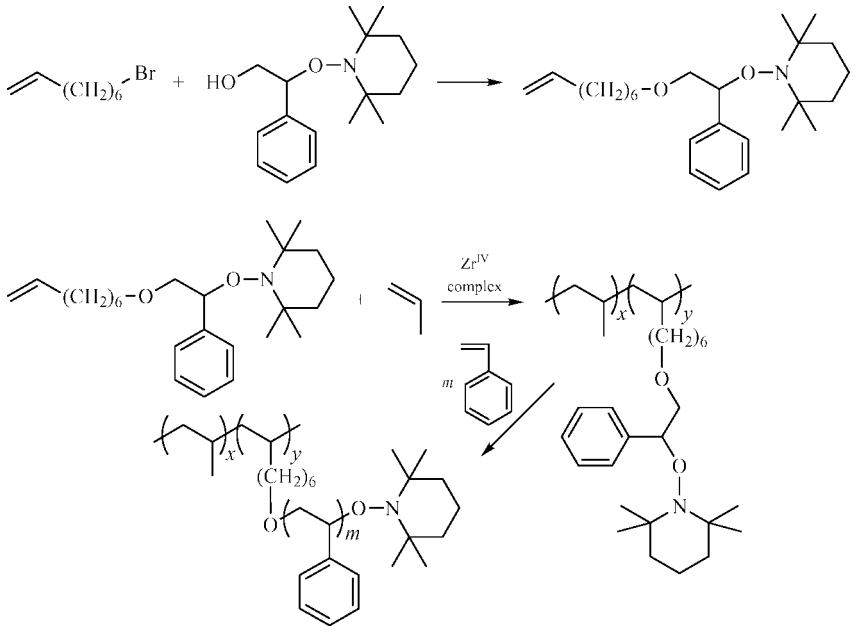

Graft copolymerization of styrene with olefins

Fig. 13. Graft copolymerization of styrene with olefins.

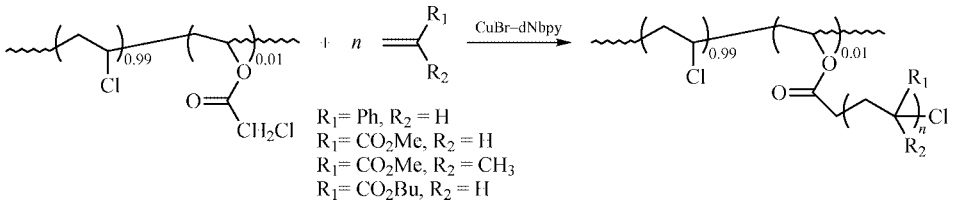

Fig. 14. Grafting from poly(vinyl chloride) by ATRP.

about 1% of the chloroacetate groups, was used to initiate the ATRP of St, MA, nBA, and MMA, resulting in graft copolymers with well-defined graft units (Fig. 14) (157).

^{1}H NMR analysis showed that the molecular weight of the macroinitiator increased substantially after the ATRP graft copolymerization (M_n = 47,400 to M_n = 112,700–363,000). The mole percent of the grafted monomer ranged from 50 to 80% in the copolymer, but GPC analysis was not useful for determining the molecular weight of the copolymers (157). A detailed analysis of the ATRP of nBA using ^{1}H NMR and FT-IR spectroscopy showed that with increasing reaction time, the mole percent of nBA in the copolymer increased and the T_g decreased. This work demonstrated that commercially available macroinitiators can be used to prepare graft copolymers via ATRP. In a similar way grafting was performed from the defects in pVC (158).

Brominated polyethylene or ethylene styrene copolymers were also used as initiators in the presence of a CuBr–PMDETA catalyst for the subsequent ATRP grafting from copolymerization of acrylic monomers. In similar studies, syndiotactic pSt-*g*-pMMA, syndiotactic pSt-*g*-pMA, and syndiotactic pSt-*g*-atactic pSt were synthesized by ATRP using brominated syndiotactic pSt as the initiator and a CuBr–PMDETA catalyst. Both the graft density and the MW of the graft segments were controlled by changing the bromine content of syndiotactic pSt and the amount of monomer used in the grafting-from reaction. The ATRP mechanism for grafting was supported by NMR analysis of the end groups. The thermal properties of the graft copolymers depended on both the graft density and the graft length (159).

Another commercially available polymer, poly(isobutylene-*co*-*p*-methylstyrene-*co*-*p*-bromomethylstyrene), was used as a macroinitiator for the ATRP of St to produce a graft copolymer (160). After 23 h at 100°C, with 1 equivalent of catalyst relative to the number of moles of initiator, monomer conversion was 81%; however, increasing the concentration of catalyst fivefold resulted in the same efficiency after only 11 h. No evidence of unreacted macroinitiator was found in the GPC analysis, indicating that nearly all of the chains contained some grafted sites. Results from mechanical analysis showed that when the wt% of St was high (28%), the graft copolymer exhibited no special properties; however, with only 6 wt% pSt, the polymer was elastomeric and could be reversibly stretched to 500% of its initial dimension (160).

It was demonstrated that the grafting of St and MMA using a similar backbone is better controlled by applying the halogen exchange method (161,162). Mechanical and viscoelastic properties depend strongly on the morphologies of

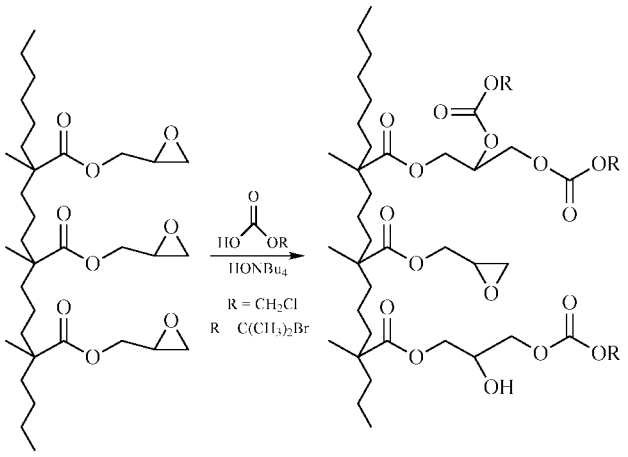

ATRP grafting from poly(ethylene-*co*-glycidyl methacrylate)

Fig. 15. ATRP grafting from poly(ethylene-*co*-glycidyl methacrylate).

the samples, which are defined by the proportion of the hard and soft segments as well as by the uniformity of the hard pMMA grafts (161).

A commercially available poly(ethylene-*co*-glycidyl methacrylate) [p(E-*co*-GMA)] polymer was transformed into an ATRP macroinitiator (163) by reacting the p(E-*co*-GMA) with either 2-bromoisobutyric acid or chloroacetic acid to prepare a backbone with multiple initiator sites. The resulting polymer was used as a macroinitator for ATRP of St and MMA (Fig. 15). The consumption of both monomers increased with time, as did the weight percent of the side chains in the copolymer. GPC analysis of the cleaved pSt side chains showed a linear increase of molecular weight with monomer conversion, and $M_w/M_n < 1.4$ (163).

ATRP has been also used in the grafting-through process using hyperbranched polyethylene macromonomers with methacrylate functionality prepared by the living Pd-mediated process (164).

Inorganic macroinitiators can also be used for graft copolymerizations. Pendant vinyl functional pDMS was subjected to hydrosilation with 2-(4-chloromethylphenyl)ethyldimethylsilane to prepare a multifunctional ATRP macroinitiator (133,165). The ATRP of St was carried out using a pDMS macroinitiator with an $M_n = 6600$ and an $M_w/M_n = 1.76$ to yield a graft copolymer with an $M_n = 14{,}800$ and an $M_w/M_n = 2.10$. The increased polydispersity was attributed to the variation in the number of initiating sites on the pDMS backbone. ^{1}H NMR analysis showed that less than 5% of the total number of benzyl chloride moieties were left unreacted and that the weight ratio of pSt/pDMS was 1.18 (133).

The field of densely grafted copolymers has received considerable attention in recent years. The materials (also called bottle-brush copolymers) contain a grafted chain at each repeat unit of the polymer backbone. As a result, the macromolecules adopt a more elongated conformation. Examples of brush copolymers have been provided within the context of defining the level of control available through ATRP (152,166,167). Synthesis of the macroinitiator involved the ATRP of 2-trimethylsilyloxyethyl methacrylate followed by esterification of the protected

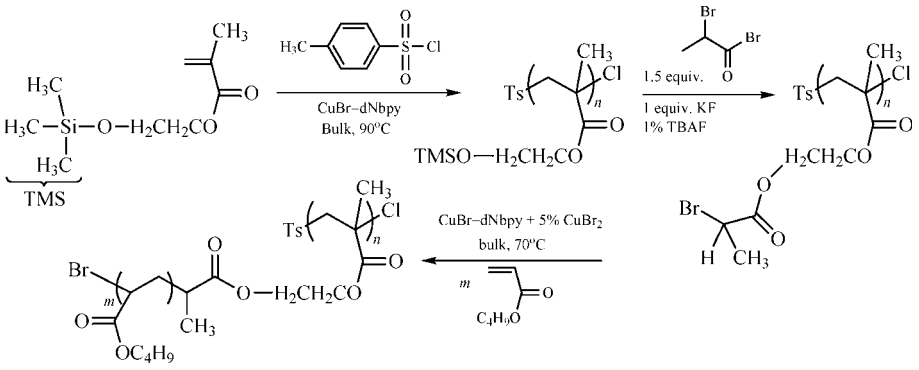

Fig. 16. Synthesis of densely grafted brushes by ATRP.

alcohol with 2-bromopropionyl bromide provided a macroinitiator of well-defined structure ($M_n = 55{,}500$, $M_w/M_n = 1.3$) leading to a brush synthesized entirely by a controlled process (Fig. 16). The macroinitiator was used for either the ATRP of St or nBA, leading to the desired densely grafted structures. The grafting reactions were found to be very sensitive to reaction conditions; the presence of additional deactivator, high concentrations of monomer, and reduced temperatures were all necessary to produce the desired materials without occurrence of any coupling reactions.

Since the aspect ratio and size of the macromolecules were so large, individual chains were capable of being observed by atomic force microscopy (AFM) (153). The brushes with pSt side chains form elongated structures on a mica surface with an average length of 100 nm, a width of 10 nm, and a height of 3 nm. pnBA absorbs well onto the mica surface and forms spectacular single-molecule brushes in which the backbone and side chains can be visualized using tapping mode AFM.

Similarly, core-shell cylindrical brushes were prepared by conducting a block copolymerization. A well-defined backbone with a degree of polymerization of ~500 was initially prepared by ATRP, which was followed by a transesterification and the subsequent grafting of pnBA chains using ATRP. A final chain extension with St produced the block copolymers. The final structure consisted of a macromolecule with a soft pnBA core and a hard pSt shell (167). High resolution AFM micrographs of the block copolymer [pBPEM-*g*-(pnBA-*b*-pSt)] brushes show a necklace morphology. The synthesis of well-defined brush block copolymers demonstrates the synthetic power of ATRP.

Other Systems. CRP has been recently applied to grafting from many surfaces, including colloidal particles, flat wafer surfaces, and delaminated clay nanolayers, in addition to irregular surfaces such as cellulose (filter paper), silica (glass frits), and many other solid substrates (168). All of them can be considered as copolymers of biopolymers, inorganics, and well-defined organic polymers. Some of the advantages of using CRP for the synthesis include large range of polymerizable monomers, undemanding reaction conditions, and simple functionalization of surfaces. For example, hydroxy groups on the surface of cellulose, or

essentially any oxidized polymer surface, can be esterified with α-bromoesters to provide ATRP initiating sites. In the same way silanol groups on glass or oxidized silicon surface can be condensed with chloro- and alkoxysilanes containing similar bromoesters (169). Then any polymer can be grown with a high precision from these functionalized surfaces. In this approach to material synthesis not only density of grafting and chain length can be controlled but also composition, yielding responsive block, gradients, or statistical copolymers.

A special case of control over the structure of copolymers may include the first stereoblock copolymers made by CRP. By applying either RAFT or ATRP to polymerization of acrylamides in the presence of rare-earth triflates such as $Y(OTf)_3$ and $Yb(OTf)_3$, it was possible to enhance isotacticity of *N*,*N*-dmiethylacrylamide (DMA) from ∼50% meso to ∼90% meso dyads (170). At the same time control of molecular weights and polydispersity was preserved. Similar results were obtained for RAFT of *N*-ispropylacrylamide (171). The ATRP and RAFT of DMA was applied to the first one-pot stereoblock synthesis by radical mechanism. RAFT or ATRP of DMA were started without Lewis acid to produce the first atactic block. Subsequently, the complexing agent was added at the desired conversion to continue the chain growth with the preferential isotactic placement (170).

Ionic Copolymerization

The copolymerization proceeding via an ionic mechanism is markedly different from the free radical copolymerization (172). The reaction of ions with a vinylic monomer molecule is generally governed by the polarity of the double bond and is therefore much more selective than the radical addition reaction, in which radical stability is the controlling factor. The reactivity ratios are significantly different from that measured in free-radical copolymerization (see Table 1) and cover a much wider range. (Tabulated values of reactivity ratios in anionic and cationic copolymerization can for instance be found in References 173 and 174.) The number of monomer pairs that undergo ionic copolymerizations is hence limited. In most cases one of the reactivity ratios is larger than 1; the resulting copolymerization favors the incorporation of one monomer into the polymeric chain leading to extensive blocks. Because of the inverse polarity of anions and cations the reactivity ratios exhibit an inverse behavior, that is, if $r_1 > r_2$ in an anionic copolymerization, $r_1 < r_2$ will hold in a cationic copolymerization (see Table 1). There is a tendency that the product $r_1 \cdot r_2$ is close to one when two resonance

Table 1. Monomer Reactivity Ratios of Selected Comonomer Pairs for Different Polymerization Mechanisms

Monomer		Free radical		Cationic		Anionic	
1	2	r_1	r_2	r_1	r_2	r_1	r_2
Styrene	Vinyl acetate	55	0.01	8.3	0.015	0.01	0.1
Styrene	Chloropren	0.005	6.3	15.6	0.24	–	–
Styrene	Methyl methacrylate	0.52	0.46	10.5	0.1	0.12	6.4
Acrylonitrile	Methyl methacrylate	0.18	1.35	–	–	7.9	0.25

stabilized monomers are involved. In such an ideal copolymerization the relative reactivities of the two propagating ionic species toward the two different monomers are approximately the same. The product is, however, often found to be much larger with one comonomer not stabilized, leading to block-copolymer behavior. This characteristic is for instance observed in the copolymerization of dimethyltrimethylene carbonate and pivalolactone in toluene initiated with K-naphtalene, which proceeds via an anionic ring-opening polymerization (175). The ^{13}C NMR analysis of the generated block copolymer only reveals signals corresponding to homodiads (176), demonstrating a well-defined crossover reaction. Less pronounced block copolymerization behavior in living ionic polymerization, however, will lead to a gradient composition profile along the chain (177). In the organolithium-initiated anionic copolymerization of isoprene (or butadiene) and styrene in hydrocarbon solvents, for instance, isoprene is polymerized almost exclusively in the first phase of the process, followed by polymerization of styrene, producing a terminal polystyrene block. The products formed by such a process are so-called tapered block copolymers, which are characterized by a fuzzy border between the two blocks. If the fuzzy border region reaches the length of the whole macromolecule, the polymeric material is called a gradient copolymer (see above). To obtain block copolymers with a distinct border, one of the monomers is first polymerized in the presence of an initiator to give an active homopolymer, which is then put into the medium of another monomer, the polymerization of which results in the formation of the second block (178). This sequential block copolymerization has been utilized in living ionic polymerizations to synthesize a wide variety of linear, and star-branched block copolymers [eg, carbocationic copolymerization of isobutylene (yielding a rubbery block) with styrene (179), α-methylstyrene (180), or indene (181) (generating a plastic segment)]. Block copolymers containing crystallizable blocks have improved properties since the interplay of crystallization and microphase segregation of crystalline–amorphous block copolymers greatly influences the final equilibrium ordered states and results in a diverse morphological complexity. Because of the lack of suitable vinyl monomers that give rise to a crystallizable segment by cationic polymerization, living cationic sequential block copolymerization is unsuitable for the synthesis of these types of block copolymers. An active-site transformation technique can be used to synthesize block copolymers consisting of two monomers that are polymerizable only by two different mechanisms (182,183). In this method, the propagating active center is transformed into a different kind of active center, and a second monomer is subsequently polymerized by a mechanism different from the first one. The key process in this method is the diligent control of end functionality, capable of initiating the second monomer. Following this idea, poly(isobutylene-*block*-pivalolactone) diblock and poly(pivalolactone-*block*-isobutylene-*block*-pivalolactone) triblock copolymers were synthesized using first cationic polymerization followed by anionic ring-opening polymerization (182) and polyisobutylene-*block*-poly(*tert*-butyl methacrylate) block copolymers were produced employing cationic polymerization followed by anionic polymerization after quenching with thiophene and subsequent metallization, yielding an anionic macroinitiator (184).

The preparation of triblock copolymers can be conducted either via subsequent addition of two different monomers or synthesizing a bifunctional growing chain. The success of any block copolymerization is always dependent on the ability

Table 2. Reactivity Ratios in the Anionic Copolymerization of Styrene and Isoprene in Different Solvents at Room Temperature, Using C_2H_5Li as the Initiator (186,187)

Solvent	Styrene r_1	Isoprene r_2
Toluene	0.25	9.5
Triethylamine	0.8	1.0
Tetrahydrofuran	9.0	0.1

of the active center to attack the next monomer. This general problem can, however, be circumvented via end group alterations of the generated polymer blocks in order to generate block copolymers of monomers that usually do not homopolymerize [eg producing amphiphilic poly(*tert*-butyl acrylate)-*block*-polystyrene-*block*-poly(4-vinylpyridine) (185)]. Ionic copolymerizations were throughout a long period of time the major technique to generate block copolymers. However, they seem to be superceded nowadays by the new living free-radical polymerizations, because of their versatility and robustness (see above).

Another characteristic feature of ionic copolymerization is the sensitivity of the reactivity ratios toward changes in the initiator, solvent, and temperature. The reaction conditions have in general a dramatic effect on the r values, as illustrated in Table 2 for the anionic copolymerization of styrene and isoprene in different solvents (186,187).

The usage of different counterions also significantly changes the copolymerization behavior: employing an organosodium initiator in the copolymerization of styrene and butadiene in toluene instead of an organolithium initiator leads to a change of the reactivity ratios from $r_1 = 0.004$ and $r_2 = 12.925$ to $r_1 = 0.42$ and $r_2 = 0.30$ (188), whereas usage of an organopotassium initiator yields the values $r_1 = 3.3$ and $r_2 = 0.12$ (189). The reactivity ratios may also be influenced by the presence of polar substances like ethers or amines in the reaction system. An indisputable advantage of ionic copolymerization over free-radical copolymerization is hence the possibility to control efficiently the reactivity ratios by varying the polymerization conditions.

These findings imply that the reactivity ratios are in general not only governed by the relative reactivities of the free ionic species, but additionally by the equilibrium between free ions and ion pairs. The conventionally determined reactivity ratios will therefore describe average reactivities. Considering an equilibrium that precedes the actual propagation step (see eqs. 39 and 40)

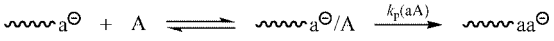

(39)

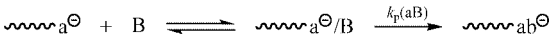

(40)

the rate-determining steps are the propagation reactions of the intermediate products with the rate coefficient k_p. The conventionally determined monomer

reactivity ratios are hence not measures for the reactivities of the macro-ions but rather for the concentration of the intermediates and the related rate coefficients. The different reactivity ratios in different solvent systems cannot solely be explained by macroscopic polar or electrostatic effects (190). The concept of preferential solvation of the growing ion by either the solvent or the comonomer is helpful (191); however, the whole process is still far from being understood in depth and additional effects (eg, complexation) have to be taken into account (192). The effect of solvents on monomer reactivity ratios cannot be considered independent of the counterion used. Whereas some comonomer systems show altered reactivity ratios for different initiator systems, others exhibit no significant effect.

Temperature has a greater influence on the r_1 and r_2 values of ionic copolymerizations than in free-radical copolymerization because of the greater spread of activation energies for the propagation reactions involving ions. There is no general trend observable and the monomer reactivity ratios may increase or decrease with temperature: in the isobutylene–styrene copolymerization r_1 increases by a factor of 1.5 and r_2 increases by a factor of 3 when going from -94°C to -30°C (193), whereas in acenaphtylene-α-methyl styrene r_1 increases from 0.075 to 1.49 and r_2 decreases from 8.3 to 0.1 when going from -70°C to 20°C (194).

In contrast to the free-radical copolymerization, the lack of termination in living ionic copolymerization enables the direct determination of the rate coefficients of the cross-propagation step. The reaction rate of monomer B with the living chain end a^- is directly accessible via the concentration decrease of a^-, which may be traced via a suitable spectroscopic method. Alternatively, the concentration of B can be determined as a function of time with the concentration of a^- being held constant. The latter experimental technique requires extrapolation of time toward zero, because the cross-propagation step is immediately followed by homopropagation of B.

Alternatively, the propagation step in ionic polymerization can be described using model reactions, arriving at an estimate of reactivity ratios. Mayr and coworkers, for instance, have developed a reactivity scale for the electrophilic attack of carbocations on nucleophiles (195–197). Employing (i) photometric and/or conductometric measurements of the consumption of persistent carbocations, (ii) photometric detection of laser flash photolysis generated carbocations, and (iii) competitive experiments yielding relative reactivities of different electrophiles toward nucleophiles, they obtained consistent results and established a general scale which assigns to all electrophiles and nucleophiles an electrophilicity parameter E (describing the carbocation) and a nucleophilicity parameter N (describing the monomer), respectively. It could be shown via correlation analysis that the reaction rate coefficient k follows the linear free-energy relationship

$$\log k(20^\circ\text{C}) = s(N + E) \tag{41}$$

with s being a slope parameter (198). For most π-nucleophiles the s parameter ranges between 0.8 and 1.1 and can therefore be generally neglected. It has been shown that copolymerization in the cationic polymerization can only be expected between monomers for which $N \approx -E$ holds (196).

The copolymerization behavior of heterocyclic monomers following an ionic mechanism (ie, ring-opening polymerization) is even more complex than that of vinylic monomers (199). In cationic ring-opening polymerization, for instance, there are often effects present which complicate the kinetic investigations: exchange reactions, macrocyclization, reversibility of polymerization (eg the homopolymerization step of the monomer with the smaller strain is often reversible) and multiplicity of active species. The concept of describing the whole process via the simple four-parameter equation for the calculation of the reactivity ratios is hence not applicable. The reactivity of the monomer in cationic ring-opening polymerization is increasing with its basicity, but it is not influenced by the ring strain. On the other hand, the active species (eg the onium ions) decrease their reactivity with increasing basicity and an enhanced ring strain leads to an increased reactivity. Further details of the ionic ring-opening polymerization may be found in References 200–202.

The different homo- and cross-propagation steps within one ionic copolymerization system generally exhibit significantly different rate coefficients. The resulting polymers therefore consist mainly of one comonomer species, constituting almost homopolymers. The industrial applications of ionic copolymerization are therefore limited. One of the few examples is the anionic copolymerization of butadiene and styrene in solution for the production of the so-called SBR (styrene–butadiene rubber) (203).The copolymer consists approximately of equal amounts of styrene, *cis*-1,4-butadiene, *trans*-1,4-butadiene, and 1,2-butadiene units. Stereoregularity, polymer composition, molecular weight, and branching can be determined via the process control which governs the concentration and nature of the active ionic species. Another industrially significant process is the cationic copolymerization of isobutylene with ∼2% isoprene using $AlCl_3/CH_3Cl$ at $-90^\circ C$ in boiling ethene (203–206). The incorporated double bonds may subsequently be vulcanized to give an elastomer with good impermeability to water and gas, weather stability, ozone resistance, and heat stability (207).

Cross-Linking

Monomers exhibiting two vinylic double bonds are often used as comonomers in order to achieve a cross-linked structure of the final polymeric chains (208,209). The cross-linking reaction occurs during the reaction or subsequently, depending on the reactivity of the second double bond. The bifunctional comonomer is generally employed in low concentrations, because a high concentration of dienes leads to a significant amount of unreacted double bonds in the final polymeric product, which lower the resistance toward outside physical and chemical influences. However, the extent of cross-linking is dependent on the amount of bifunctional monomer BB (with B indicating the double bonds of the diene comonomer). The critical reaction extent at which cross-linking occurs during a copolymerization with dienes can easily be derived mathematically for the case of equally reactive double bonds both in A and BB. The copolymerization of styrene and divinylbenzene (210), vinyl acetate with divinyl adipate (211), and methyl methacrylate with ethylene glycol dimethacrylate (212) are examples of such a behavior. At the double bond conversion c there are c[A] reacted monomer units A, c[B] reacted double bonds of the

monomer B and c^2[BB] reacted monomer units BB (with [B]=2[BB]). The number of crosslinks is simply the number of BB monomer molecules in which both B double bonds are reacted, that is c^2[BB]. The number of polymer chains is the total number of A and B double bonds reacted divided by the average degree of polymerization *DP*. The critical double bond conversion c_{crit} at which cross-linking occurs is reached when the number of crosslinks per chain is 1/2 and is therefore described by

$$c_{crit} = \frac{[A] + [B]}{[B] \cdot DP} \tag{42}$$

for long chains. *DP* is the mass-average degree of polymerization (for details see Ref. 213) that would be observed in the absence of any bifunctional comonomer. Equation 42—denoted as Flory–Stockmayer equation (213)—has been found useful for the prediction of the onset of the cross-linking, also denoted as the gel-point, for equally reactive double bonds, especially when low concentrations of dienes are employed (mole fraction of BB below 0.05). With increasing diene concentration, equation 42 predicts smaller critical conversions than found experimentally (214). This effect is called "delayed gelation." The primary factor for this observation is the significance of the thermodynamic excluded volume effect on the intermolecular cross-linking reaction between the growing radical and the preformed polymer, especially at higher molecular weights. Beyond the theoretical critical conversion, a secondary factor is related to the intramolecular cyclization (215) which becomes progressively important with conversion. The latter leads to the restriction of segmental motion of the preformed polymer and causes steric hindrance.

The critical conversion in the copolymerization process in which the double bond in comonomer A and the first double bond in comonomer BC has the same reactivity, but the second double bond in BC is less reactive, can be described by equation 43:

$$c_{crit} = 1 - \exp\left(\frac{-1}{2 \cdot x_{BC} \cdot DP \cdot r_{BC}}\right) \tag{43}$$

with x_{BC} being the mole fraction of BC and r_{BC} being the reactivity ratio between the B and C double bond. The copolymerization of methyl methacrylate and allyl methacrylate would be an example for such a behavior (216). The resulting copolymer will consist of copolymerized A and B double bonds. The relatively unreactive C double bonds start to react, ie, crosslink, in the later stage of the copolymerization.

BIBLIOGRAPHY

"Copolymerization" in *EPST* 1st ed., Vol. 4, pp. 165–244, by George E. Ham, Gulf Oil Corporation; "Copolymerization" in *EPST* 2nd ed., Vol. 4, pp. 192–233, by David A. Tirrell, University of Massachusetts.

1. M. L. Coote and T. P. Davis, in K. Matyjaszewski and T. P. Davis, ed., *Handbook of Radical Polymerization*, John Wiley & Sons, Inc., New York, 2002, pp. 263–300.

2. E. Jenkel, *Z. Phys. Chem. Abt. A* **190**, 24 (1942).
3. F. R. Mayo and F. M. Lewis, *J. Am. Chem. Soc.* **66**, 1594 (1944).
4. T. Alfrey and G. Goldfinger, *J. Chem. Phys.* **12**, 205 (1944).
5. T. Alfrey and G. Goldfinger, *J. Chem. Phys.* **12**, 322 (1944).
6. T. Alfrey and G. Goldfinger, *J. Chem. Phys.* **14**, 115 (1946).
7. T. Fukuda, Y.-D. Ma, and H. Inagaki, *Macromolecules* **18**, 17 (1985).
8. H. W. Melville, B. Noble, and W. F. Watson, *J. Polym. Sci.* **2**, 229 (1947).
9. C. J. Walling, *J. Am. Chem. Soc.* **71**, 1930 (1949).
10. E. Merz, T. Alfrey Jr., and G. Goldfinger, *J. Polym. Sci.* **1**, 75 (1946).
11. T. Fukuda, K. Kubo, Y.-D. Ma, and H. Inagaki, *Polym. J. (Tokyo)* **19**, 523 (1987).
12. M. L. Coote and T. P. Davis, *Polym. React. Eng.* **7**, 347 (1999).
13. A. Pross, *Theoretical and Physical Principles of Organic Reactivity*, John Wiley & Sons, Inc., New York, 1995.
14. M. Kamachi, *Adv. Polym. Sci.* **38**, 56 (1981).
15. T. Fukuda, K. Kubo, and Y.-D. Ma, *Prog. Polym. Sci.* **17**, 875 (1992).
16. P. D. Bartlett and K. Nozaki, *J. Am. Chem. Soc.* **68**, 1495 (1946).
17. J. A. Seiner and M. Litt, *Macromolecules* **4**, 308 (1971).
18. R. E. Cais, R. G. Farmer, D. J. T. Hill, and J. H. O'Donnell, *Macromolecules* **12**, 835 (1979).
19. P. G. Brown and K. Fujimori, *J. Polym. Sci., Part A: Polym. Chem.* **A32**, 2971 (1994).
20. E. Tsuchida and H. Tomono, *Makromol. Chem.* **141**, 265 (1971).
21. P. Karad and C. Schneider, *J. Polym. Sci., Part A: Polym. Chem.* **16**, 1295 (1983).
22. D. J. T. Hill, J. H. O'Donnell, and P. W. O'Sullivan, *Macromolecules* **16**, 1295 (1983).
23. H. J. Harwood, *Makromol. Chem., Macromol. Symp.* **10/11**, 331 (1987).
24. Y. D. Semchikov, *Macromol. Symp.* **111**, 317 (1996).
25. B. Klumperman and K. F. O'Driscoll, *Polymer* **34**, 1032 (1993).
26. M. L. Coote, L. P. M. Johnston, and T. P. Davis, *Macromolecules* **30**, 8191 (1997).
27. B. Klumperman and I. R. Kraeger, *Macromolecules* **27**, 1529 (1994).
28. W. G. Barb, *J. Polym. Sci.* **10**, 49 (1952).
29. C. Walling, *J. Polym. Sci.* **16**, 315 (1955).
30. G. G. Lowry, *J. Polym. Sci.* **42**, 463 (1960).
31. P. Wittmer, *Adv. Chem. Ser.* **99**, 140 (1971).
32. P. Wittmer, *Makromol. Chem.* **177**, 997 (1976).
33. J. A. Howell, M. Izu, and K. F. O'Driscoll, *J. Polym. Sci., Part A-1* **8**, 699 (1970).
34. F. Martinet and J. Guillot, *J. Appl. Polym. Sci.* **65**, 2297 (1997).
35. D. Kukulj, T. P. Davis, and R. G. Gilbert, *Macromolecules* **31**, 994 (1998).
36. V. E. Meyer and G. G. Lowry, *J. Polym. Sci. A* **3**, 2843 (1965).
37. M. L. Coote and T. P. Davis, *Prog. Polym. Sci.* **24**, 1217 (1999).
38. M. L. Coote, T. P. Davis, B. Klumperman, and M. J. Monteiro, *J. Macromol. Sci., Rev. Macromol. Chem. Phys.* **C38**, 567 (1998).
39. J. Brandrup and E. H. Immergut, eds., *Polymer Handbook*, Wilely Interscience, New York (1989), p II/181.
40. C. H. Bamford, A. D. Jenkins, and R. Johnston, *Trans. Faraday. Soc.* **55**, 418 (1959).
41. T. Alfrey and C. C. Price, *J. Polym. Sci.* **2**, 101 (1947).
42. M. L. Coote, T. P. Davis, and L. Radom, *ACS Symp. Ser.* **768**, 82 (2000).
43. M. L. Coote, T. P. Davis, and L. Radom, *Macromolecules* **32**, 2935 (1999).
44. L. H. Yee, T. P. Davis, and J. P. A. Heuts, *Macromolecules* **34**, 3581 (2001).
45. J. P. A. Heuts, R. G. Gilbert, and I. A. Maxwell, *Macromolecules* **30**, 726 (1997).
46. D. Kukulj, J. P. A. Heuts, and T. P. Davis, *Macromolecuels* **31**, 6034 (1998).
47. C. Barner-Kowollik and T. P. Davis, *Macromol. Theory Simul.* **10**, 255 (2001).
48. D. J. T. Hill, J. J. O'Donnell, and P. W. O'Sullivan, *Prog. Polym. Sci.* **8**, 215 (1982).
49. K. G. Olson and G. B. Butler, *Macromolecules* **16**, 707 (1983).

50. M. Kamachi, J. Satoh and S.-I. Nozakura, *J. Polym. Sci., Polym. Chem. Ed.* **16**, 1789 (1978).
51. B. Heublein and G. Heublein, *Acta Polym.* **39**, 324 (1988).
52. K. F. O'Driscoll, M. J. Monteiro, and B. Klumperman, *J. Polym. Sci., Part A: Polym. Chem.* **35**, 515 (1997).
53. M. D. Zammit, T. P. Davis, G. D. Willett, and K. F. O'Driscoll, *J. Polym. Sci., Part A: Polym. Chem.* **A35**, 2311 (1997).
54. M. L. Coote and T. P. Davis, *Eur. Polym. J.* **36**, 2423 (2000).
55. M. L. Coote, T. P. Davis, and L. Radom, *Theochem* **91**, 461–462 (1999).
56. M. W. Wong, A. Pross, and L. Radom, *J. Am. Chem. Soc.* **116**, 6284 (1994).
57. H. Fischer and L. Radom, *Angew. Chem., Int. Ed. Engl.* **40**, 1340 (2001).
58. G. Bonta, B. Gallo and S. Russo, *Polymer* **16**, 429 (1975).
59. T. Ito and T. Otsu, *J. Macromol. Sci., Chem.* **A3**, 197 (1969).
60. H. Fujihara, K. Yamazaki, Y. Matsubara, M. Yoshihara and T. Maeshima, *J. Macromol. Sci., Chem.* **A13**, 1081 (1979).
61. B. Sandner and E. Loth, *Faserforschung Textiltechnik* **27**, 571 (1976).
62. B. Sandner and E. Loth, *Faserforschung Textiltechnik* **27**, 633 (1976).
63. G. A. Egorochkin, Y. D. Semchikov, L. A. Smirnova, N. V. Karyakin, and A. M. Kut'in, *Eur. Polym. J.* **28**, 681 (1992).
64. J. F. Rabek, *Experimental Methods in Polymer Chemistry*, Wiley-Interscience, New York, 1980.
65. P. W. Tidwell and G. A. Mortimer, *J. Polym. Sci., Part A: Polym. Chem.* **3**, 369 (1965).
66. M. Fineman and S. D. Ross, *J. Polym. Sci.* **5**, 269 (1965).
67. P. W. Tidwell and G. A. Mortimer, *J. Macromol. Sci., Rev. Macromol. Chem.* **4**, 281 (1970).
68. A. M. van Herk, *Contour*, available from the author: Laboratory of Polymer Chemistry, Eindhoven University of Technology, PO Box 513, 5600 MB Eindhoven.
69. A. M. van Herk, *J. Chem. Educ.* **72**, 13 (1995).
70. J. P. A. Heuts, M. L. Coote, T. P. Davis, and L. P. M. Johnston, *ACS Symp. Ser.* **685**, 120 (1998).
71. H. L. Britt and R. H. Luecke, *Technometrics* **15**, 223 (1973).
72. R. Z. Greenley, *J. Macromol. Sci., Chem.* **A14**, 427 (1980).
73. M. Buback, M. Egorov, R. G. Gilbert, V. Kaminsky, O. F. Olaj, G. T. Russell, P. Vana, and G. Zifferer, *Macromol. Chem. Phys.* **203**, 2570 (2003).
74. E. L. Madruga, *Revista de Plasticos Modernos* **74**, 151 (1997).
75. A. Brandrup, E. H. Immergut, and E. A. Grulke, *Polymer Handbook*, 4th ed., John Wiley & Sons, Inc., New York, 1999, pp. II/77.
76. T. Fukuda, N. Ide, and Y.-D. Ma, *Macromol. Symp.* **111**, 305 (1996).
77. N. Atherton and A. M. North, *Trans. Faraday Soc.* **58**, 2049 (1962).
78. K. D. Bayes and L. J. Garland, *J. Phys. Chem.* **94**, 4941 (1990).
79. S. Russo and S. Munari, *J. Macromol. Sci. Chem.* **2**, 1321 (1968).
80. G. Bonta, B. M. Gallo, and S. Russo, *J. Chem. Soc., Faraday Trans. 1* **71**, 1727 (1975).
81. M. Buback and C. Kowollik, *Macromolecules* **32**, 1445 (1999).
82. M. Buback and A. Feldermann, *Aust. J. Chem.* **55**, 475 (2002).
83. K. F. O'Driscoll and K. Ito, *J. Polym. Sci.* **17**, 3913 (1979).
84. M. Buback and C. Kowollik, *Macromolecules* **31**, 3221 (1998).
85. H. T. Cullinan Jr., *Ind. Eng. Chem. Fundam.* **5**, 281 (1966).
86. M. Buback and C. Kowollik, *Macromol. Chem. Phys.* **200**, 1764 (1999).
87. K. Matyjaszewski and T. P. Davis, *Handbook of Radical Polymerization*, Wiley-Interscience, Hoboken, 2002.
88. K. Matyjaszewski, ed., *Controlled Radical Polymerization*, Vol. **685**, American Chemical Society, Washington, DC, 1998.

89. K. Matyjaszewski, ed., *Controlled/Living Radical Polymerization: Progress in ATRP, NMP, and RAFT*, Vol. **768**, American Chemical Society, Washington, DC, 2000.
90. K. Matyjaszewski, ed., *Advances in Controlled/Living Radical Polymerization*, Vol. **854**, American Chemical Society, Washington, DC, 2003.
91. C. J. Hawker, A. W. Bosman, and E. Harth, *Chem. Rev.* **101**, 3661 (2001).
92. K. Matyjaszewski and J. Xia, *Chem. Rev.* **101**, 2921 (2001).
93. J. S. Wang and K. Matyjaszewski, *J. Am. Chem. Soc.* **117**, 5614 (1995).
94. M. Kamigaito, T. Ando and M. Sawamoto, *Chem. Rev.* **101**, 3689 (2001).
95. J. Chiefari, Y. K. B. Chong, F. Ercole, J. Krstina, J. Jeffery, T. P. T. Le, R. T. A. Mayadunne, G. F. Meijs, C. L. Moad, G. Moad, E. Rizzardo, and S. H. Thang, *Macromolecules* **31**, 5559 (1998).
96. K. Matyjaszewski, S. G. Gaynor, and J.-S. Wang, *Macromolecules* **28**, 2093 (1995).
97. H. Fischer, *J. Polym. Sci., Part A: Polym. Chem.* **37**, 1885 (1999).
98. C. Yoshikawa, A. Goto, and T. Fukuda, *Macromolecules* **36**, 908 (2003).
99. J.-S. Wang, D. Greszta and K. Matyjaszewski, *Polym. Mater. Sci. Eng.* **73**, 416 (1995).
100. T. E. Patten and K. Matyjaszewski, *Adv. Mater.* **10**, 901 (1998).
101. K. A. Davis and K. Matyjaszewski, *Advances in Polymer Science* **159**, 2 (2002).
102. E. L. Madruga, *Prog. Polym. Sci.* **27**, 1879 (2002).
103. J. P. A. Heuts and T. P. Davis, *Macromol. Rapid Commun.* **19**, 371 (1998).
104. D. M. Haddleton, M. C. Crossman, K. H. Hunt, C. Topping, C. Waterson, and K. G. Suddaby, *Macromolecules* **30**, 3992 (1997).
105. K. Matyjaszewski, *J. Macromol. Sci., Pure Appl. Chem.* **A34**, 1785 (1997).
106. K. Matyjaszewski, *Macromolecules* **31**, 4710 (1998).
107. K. Matyjaszewski, *Macromolecules* **35**, 6773 (2002).
108. H. Hirai, *J. Polym. Sci., Macromol. Rev.* **11**, 47 (1976).
109. J. M. G. Cowie, ed., *Alternating Copolymers*, Plenum Press, New York, 1985.
110. J. Afchar-Momtaz, A. Polton, M. Tardi and P. Sigwalt, *Eur. Polym. J.* **21**, 583 (1985).
111. B. Klumperman, G. Chambard, and R. H. G. Brinkhuis, *ACS Symp. Ser.* **854**, 180 (2003).
112. S. G. Roos, A. H. E. Mueller, and K. Matyjaszewski, *Macromolecules* **32**, 8331 (1999).
113. H. Shinoda and K. Matyjaszewski, *Macromol. Rapid Commun.* **22**, 1176 (2001).
114. H. Shinoda and K. Matyjaszewski, *Macromolecules* **34**, 6243 (2001).
115. H. Shinoda, K. Matyjaszewski, L. Okrasa, M. Mierzwa, and T. Pakula, *Macromolecules* **36**, 4772 (2003).
116. A. K. Nanda and K. Matyjaszewski, *Macromolecules* **36**, 8222 (2003).
117. T. Pakula and K. Matyjaszewski, *Macromol. Theory Simul.* **5**, 987 (1996).
118. D. Greszta and K. Matyjaszewski, *Polym. Prep. (Am. Chem. Soc., Polym. Div.)* **37**, 569 (1996).
119. K. Matyjaszewski, M. J. Ziegler, S. V. Arehart, D. Greszta, and T. Pakula, *J. Phys. Org. Chem.* **13**, 775 (2000).
120. K. Matyjaszewski, D. A. Shipp, G. P. McMurtry, S. G. Gaynor, and T. Pakula, *J. Polym. Sci., Part A: Polym. Chem.* **38**, 2023 (2000).
121. S. V. Arehart, D. Greszta, and K. Matyjaszewski, *Polym. Prepr. (Am. Chem. Soc., Div. Polym. Chem.).* **38**(1), 705 (1997).
122. G. Chambard and B. Klumperman, *ACS Symp. Ser.* **768**, 197 (2000).
123. M. J. Ziegler and K. Matyjaszewski, *Macromolecules* **34**, 415 (2001).
124. H. De Brouwer, M. A. J. Schellekens, B. Klumperman, M. J. Monteiro, and A. L. German, *J. Polym. Sci., Part A: Polym. Chem.* **38**, 3596 (2000).
125. F.-M. Li, G.-Q. Chen, M.-Q. Zhu, P. Zhou, F.-S. Du, and Z.-C. Li, *ACS Symp. Ser.* **768**, 384 (2000).
126. D. Benoit, C. J. Hawker, E. E. Huang, Z. Lin, and T. P. Russell, *Macromolecules* **33**, 1505 (2000).

127. B. Kirci, J. F. Lutz, and K. Matyjaszewski, *Macromolecules* **35**, 2448 (2002).
128. J.-F. Lutz, B. Kirci, and K. Matyjaszewski, *Macromolecules* **36**, 3136 (2003).
129. S. Coca and K. Matyjaszewski, *J. Polym. Sci., Part A: Polym. Chem.* **35**, 3595 (1997).
130. S. Coca and K. Matyjaszewski, *Macromolecules* **30**, 2808 (1997).
131. S. Coca, H.-J. Paik, and K. Matyjaszewski, *Macromolecules* **30**, 6513 (1997
132. S. G. Gaynor, and K. Matyjaszewski, *Macromolecules* **30**, 4241 (1997).
133. P. J. Miller and K. Matyjaszewski, *Macromolecules* **32**, 8760 (1999).
134. H.-J. Paik, M. Teodorescu, J. Xia, and K. Matyjaszewski, *Macromolecules* **32**, 7023 (1999).
135. K. Jankova, X. Chen, J. Kops, and W. Batsberg, *Macromolecules* **31**, 538 (1998).
136. K. Matyjaszewski, P. J. Miller, E. Fossum, and Y. Nakagawa, *Appl. Organomet. Chem.* **12**, 667 (1998).
137. J. Chiefari, R. T. A. Mayadunne, C. L. Moad, G. Moad, E. Rizzardo, A. Postma, M. A. Skidmore, and S. H. Thang, *Macromolecules* **36**, 2273 (2003).
138. Y. K. Chong, J. Krstina, T. P. T. Le, G. Moad, A. Postma, E. Rizzardo, and S. H. Thang, *Macromolecules* **36**, 2256 (2003).
139. C. Tang, T. Kowalewski, and K. Matyjaszewski, *Macromolecules* **36**, 1465 (2003).
140. K. Matyjaszewski, D. A. Shipp, J.-L. Wang, T. Grimaud, and T. E. Patten, *Macromolecules* **31**, 6836 (1998).
141. D. A. Shipp, J.-L. Wang, and K. Matyjaszewski, *Macromolecules* **31**, 8005 (1998).
142. K. Davis, H.-J. Paik, and K. Matyjaszewski, *Macromolecules* **32**, 1767 (1999).
143. J.-L. Wang, T. Grimaud, and K. Matyjaszewski, *Macromolecules* **30**, 6507 (1997).
144. J. Pyun, S. Jia, T. Kowalewski, G. D. Patterson, and K. Matyjaszewski, *Macromolecules* **36**, 5094 (2003).
145. S. Beuermann and M. Buback, *Prog. Polym. Sci.* **27**, 191 (2002).
146. K. Matyjaszewski, H.-J. Paik, P. Zhou, and S. J. Diamanti, *Macromolecules* **34**, 5125 (2001).
147. C. Moineau, M. Minet, P. Teyssie, and R. Jerome, *Macromolecules* **32**, 8277 (1999).
148. P. Leclere, G. Moineau, M. Minet, P. Dubois, R. Jerome, J. L. Bredas, and R. Lazzaroni, *Langmuir* **15**, 3915 (1999).
149. G. Moineau, M. Minet, P. Teyssie, and R. Jerome, *Macromol. Chem. Phys.* **201**, 1108 (2000).
150. M. F. Garcia, J. L. de la Fuente, M. Fernandez-Sanz, and E. L. Madruga, *Polymer* **42**, 9405 (2001).
151. A. Desai, N. Atkinson, F. Rivera Jr., W. Devonport, I. Rees, S. E. Branz, and C. J. Hawker, *J. Polym. Sci., Part A: Polym. Chem.* **38**, 1033 (2000).
152. K. Yamada, M. Miyazaki, K. Ohno, T. Fukuda, and M. Minoda, *Macromolecules* **32**, 290 (1999).
153. K. Matyjaszewski, K. L. Beers, A. Kern, and S. G. Gaynor, *J. Polym. Sci., Part A: Polym. Chem.* **36**, 823 (1998).
154. C. J. Hawker and J. L. Hedrick, *Macromolecules* **28**, 2993 (1995).
155. C. J. Hawker, J. M. J. Frechet, R. B. Grubbs, and J. Dao, *J. Am. Chem. Soc.* **117**, 10763 (1995).
156. U. M. Stehling, E. Malmstroem, R. M. Waymouth, and C. J. Hawker, *Macromolecules* **31**, 4396 (1998).
157. H.-J. Paik, S. G. Gaynor, and K. Matyjaszewski, *Macromol. Rapid Commun.* **19**, 47 (1998).
158. V. Percec and F. Asgarzadeh, *J. Polym. Sci., Part A: Polym. Chem.* **39**, 1120 (2001).
159. S. Liu and A. Sen, *Macromolecules* **33**, 5106 (2000).
160. T. Fonagy, B. Ivan, and M. Szesztay, *Macromol. Rapid Commun.* **19**, 479 (1998).
161. S. C. Hong, T. Pakula, and K. Matyjaszewski, *Macromol. Chem. Phys.* **202**, 3392 (2001).

162. S. G. Gaynor and K. Matyjaszewski, *ACS Symp. Series* **685**, 396 (1998).
163. K. Matyjaszewski, M. Teodorescu, P. J. Miller, and M. L. Peterson, *J. Polym. Sci., Part A: Polym. Chem.* **38**, 2440 (2000).
164. S. C. Hong, K. Matyjaszewski, A. Gottfried, and M. Brookhart, *J. Polym. Sci., Part A: Polym. Chem.* **40**, 2736 (2001).
165. Y. Nakagawa, P. J. Miller, and K. Matyjaszewski, *Polymer* **39**, 5163 (1998).
166. K. L. Beers, S. G. Gaynor, K. Matyjaszewski, S. S. Sheiko, and M. Moeller, *Macromolecules* **31**, 9413 (1998).
167. H. G. Boerner, K. Beers, K. Matyjaszewski, S. S. Sheiko, and M. Moeller, *Macromolecules* **34**, 4375 (2001).
168. J. Pyun and K. Matyjaszewski, *Chem. Mater.* **13**, 3436 (2001).
169. J. Pyun, K. Matyjaszewski, T. Kowalewski, D. Savin, G. Patterson, G. Kickelbick, and N. Huesing, *J. Am. Chem. Soc.* **123**, 9445 (2001).
170. J.-F. Lutz, D. Neugebauer, and K. Matyjaszewski, *J. Am. Chem. Soc.* **125**, 6986–6993 (2003).
171. B. Ray, Y. Isobe, K. Morioka, S. Habaue, Y. Okamoto, M. Kamigaito, and M. Sawamoto, *Macromolecules* **36**, 543 (2003).
172. M. Szwarc, *Ionic Polymerization Fundamentals*, Hanser Gardner Publications, New York, 1996.
173. G. E. Ham, ed., *Copolymerization*, Wiley-Interscience, New York, 1964, pp. 296 ff, 430 f.
174. Y. Yamashita, *Kobunshi* **15**, 167149 (1966).
175. H. Keul and H. Höcker, *Macromol. Rapid. Commun.* **21**, 869 (2000).
176. H. Keul, P. Schmidt, B. Robertz, and H. Höcker, *Macromol. Symp.* **95**, 243 (1995).
177. T. Hashimoto, Y. Tsukahara, K. Tachi, and H. Kawai, *Macromolecules* **16**, 648 (1983).
178. L. Sipos, Y. Cao, and R. Faust, *Macromolecules* **34**, 456 (2001).
179. M Gyor, Z. Fodor, H.-C. Wang, and R. Faust, *J. Macromol. Sci.* **A31**, 2055 (1994).
180. D. Li and R. Faust, *Macromolecules* **28**, 4893 (1995).
181. Z. Fodor and R. Faust, *J. Macromol. Sci.* **A31**, 1985 (1994).
182. Y. Kwon and R. Faust, *Macromolecules* **35**, 3348 (2002).
183. Y. Kwon, R. Faust, C. X. Chen, and E. L. Thomas, *Polym. Mater. Sci. Eng.* **84**, 843 (2001).
184. N. Martinez-Castro, M. G. Lanzendoerfer, A. H. E. Mueller, J. C. Cho, M. H. Acar, and R. Faust, *Macromolecules* **36**, 6985 (2003).
185. F. Liu and A. Eisenberg, *Angew. Chem., Int. Ed.* **42**, 1404 (2003).
186. Y. L. Spirin, D. K. Polyakov, A. R. Gantmakher, and S. S. Medvedev, *J. Polym. Sci.* **53**, 233 (1961).
187. Y. L. Spirin, A. A. Arest-Yakubovich, D. K. Polyakov, A. R. Gantmakher, and S. S. Medvedev, *J. Polym. Sci.* **58**, 1181 (1962).
188. A. A. Arest-Yakubovich, G. I. Litvinenko, and R. V. Basova, *Polym. Prepr. (Am. Chem. Soc., Div. Polym. Chem.)* **35**, 544 (1994).
189. B. I. Nakhmanovich, A. A. Arest-Yakubovich, T. N. Prudskova, and G. I. Litvinenko, *Macromol. Rapid Commun.* **17**, 31 (1996).
190. M. Boelke, G. Knoeppel, P. Hallpap, D. Stadermann, and G. Heublein, *Makromol. Chem., Rapid Commun.* **10**, 157 (1989).
191. K. Matyjaszewski, *Macromolecules* **21**, 519 (1988).
192. C. Zune, C. Archambeau, P. Dubois, and R. Jerome, *J. Polym. Sci., Part A: Polym. Chem.* **39**(10), 1774 (2001).
193. J. Rehner, Jr., R. L. Zapp and W. J. Sparks, *J. Polym. Sci.* **11**, 21 (1953).
194. C. G. Overberger, D. Tanner and E. M. Pearce, *J. Am. Chem. Soc.* **80**, 4566 (1958).
195. H. Mayr, M. Roth, and G. Lang, *ACS Symp. Series* **665**, 25 (1997).
196. H. Mayr, and M. Patz, *Makromol. Chem., Macromol. Symp.* **107**, 99 (1996).

197. H. Mayr, T. Bug, M. F. Gotta, N. Hering, B. Irrgang, B. Janker, B. Kempf, R. Loos, A. R. Ofial, G. Remennikov, and H. Schimmel, *J. Am. Chem. Soc.* **123**, 9500 (2001).
198. H. Mayr and M. Patz, *Angew. Chem.* **106**, 990 (1994).
199. K. Matyjaszewski, *J. Macromol. Sci., Rev. Macromol. Chem.* **C26**(1), 1 (1986).
200. D. J. Brunelle, ed. *Ring-Opening Polymerization*, Hanser, Munich, 1993.
201. S. Penczek, P. Kubisa, and K Matyjaszewski, *Advances in Polymer Science, Vol. 68/69: Cationic Ring-Opening Polymerization, Part 2: Synthetic Applications*, Springer-Verlag, Berlin, 1985, p. 317.
202. H. Höcker and H. Keul, *Macromol. Symp.* **157**, 71 (2000).
203. M. L. Senyek, *Encycl. Polym. Sci. Eng.* **8**, 487 (1987).
204. J. E. Puskas, *Plast. Eng.* **61**, 817 (2001).
205. P. L. Ku, *Adv. Polym. Techn.* **8**, 201 (1988).
206. G. Holden and C. R. Wilder, *Plast. Eng.* **61**, 321 (2001).
207. R. N. Datta, *Gummi, Fasern, Kunststoffe* **56**, 94 (2003).
208. A. Matsumoto, *Adv. Polym. Sci.* **123**, 41 (1995).
209. G. V. Korolev and M. L. Bubnova, *e-Polymers* [online computer file], Paper No. 30 (2002).
210. R. H. Wiley, *Pure Appl. Chem.* **43**, 57 (1975).
211. J. W. Breitenbach and G. Gleixner, *Monatsh. Chem.* **107**, 1315 (1976).
212. S. Zhu and A. Hamielec, *Makromol. Chem., Macromol. Symp.* **63**, 135 (1992).
213. W. H. Stockmayer, *J. Chem. Phys.* **12**, 125 (1944).
214. A. Matsumoto, Y. Kitaguchi, and O. Sonoda, *Macromolecules* **32**, 8336 (1999).
215. O. Okay, M. Kurz, K. Lutz, and W. Funke, *Macromolecules* **28**, 2728 (1995).
216. Y. Liu, R. Mao, M. B. Huglin and P. A. Holmes, *Polymer* **37**, 1437 (1996).

CHRISTOPHER BARNER-KOWOLLIK
THOMAS P. DAVIS
The University of New South Wales
MICHELLE L. COOTE
Australian National University
KRZYSZTOF MATYJASZEWSKI
Carnegie Mellon University
PHILIPP VANA
Georg-August-Universität Göttingen

COTTON. See Volume 5.

CRAZING. See YIELD AND CRAZING.

CREEP. See VISCOELASTICITY.

CRITICAL PHASE POLYMERIZATIONS. See Volume 2.

CRYSTALLINE POLYMERS. See SEMICRYSTALLINE POLYMERS.

CRYSTALLINITY DETERMINATION

Introduction

A variety of natural and synthetic polymers are well known to crystallize on cooling from the melt or from solution. In fact, roughly 1/2 to 2/3 of useful polymers are crystalline or crystallizable. Unlike many low molecular weight organic compounds and inorganic crystals, polymeric materials are semicrystalline and the extent of crystallinity formation is critically important in determining ultimate physical properties, and hence suitability for particular applications (see SEMICRYSTALLINE POLYMERS). Degrees of crystallinity vary over a wide range between crystallizable polymers, as well as within a given polymer system. The crystallinity developed is dependent on average molecular weight and distribution (which influence crystallization kinetics), crystallization/processing conditions (and its relationship to the glass-transition temperature, T_g, of the polymer), and the chemical structure of the chains [flexible like polyethylene (PE) and poly(ethylene oxide) (PEO), or more rigid like poly(ethylene terephthalate) (PET) and poly(ether ether ketone)]. Structural regularity of the chain is also of paramount importance: ie, whether the chains contain comonomer units, stereoirregularity, etc.

This article provides an overview of common methods for determining degrees of crystallinity in polymer systems, focusing on isotropic materials.

X-ray Diffraction

Traditional Approaches. For many purposes, relative degrees of crystallinity (sometimes referred to as the *crystallinity index*) are sufficient and a number of approximate wide-angle X-ray diffraction (WAXD) methods have been reported and utilized. Before the advent of modern computational tools, WAXD patterns were simply resolved into contributions from crystalline and amorphous reflections, and a "polynomial" background (1). The degree of crystallinity was then calculated as $I_c/(I_c + I_a)$, where I_c is the diffracted intensity from all resolved crystalline reflections, I_a the diffraction intensity under the amorphous halo, and $(I_c + I_a)$ the total intensity. This was an improvement over older work where peak separation was carried out arbitrarily (eg, by simply constructing a line between intensity minima; this results in lower determined crystallinity).

Similar approaches are used today to obtain relative degrees of crystallinity from WAXD experiments, but modern curve resolving routines are frequently employed. Of course, the "raw" WAXD data must be of sufficiently high quality, having low signal-to-noise ratio (ie, the data must be obtained at sufficiently slow angular scan speeds or for sufficiently long count times), to permit reliable curve fitting. If one is interested in absolute values of the crystallinty, it is important to multiply (ie, correct) the observed diffraction peaks by Lorentz and polarization factors to obtain a more accurate estimate of the total intensity diffracted by the crystalline phase (2).

Encyclopedia of Polymer Science and Technology. Copyright John Wiley & Sons, Inc. All rights reserved.

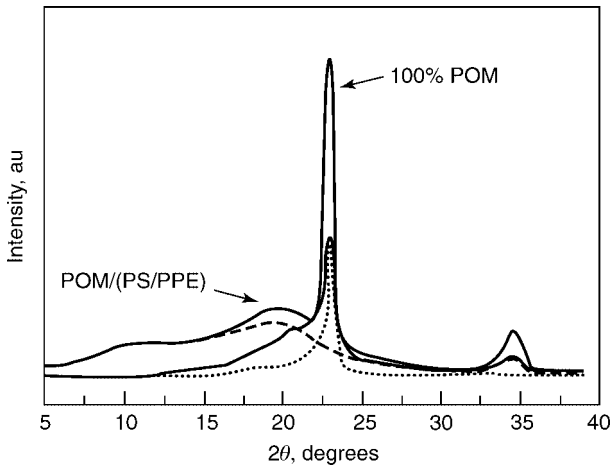

Fig. 1. Resolution of the WAXD pattern of a multiphase POM/PS/PPO blend. The experimental WAXD pattern of the ternary blend is represented by the full bold line and that of the amorphous component by the dashed line. The result after subtraction is given by the dotted line and this can be considered as the WAXD pattern of the POM phase alone. The full fine line represents normalization to 100% POM. From Ref. 3

As an example, determination of the crystallinity index of polyoxymethylene (POM) in a ternary blend with polystyrene (PS) and poly(phenylene oxide) (PPO) is presented (3). Although the latter polymer in this mixture is crystallizable, it does not do so under the processing conditions used in Reference 3. Degrees of crystallinity were estimated as the ratio of the integrated areas under the POM (100) and (105) diffraction peaks (A_{110} and A_{105}, respectively) to the total integrated diffracted intensity, ie, $X_{c,WAXD} = (A_{110} + A_{105})/(A_{110} + A_{105} + A_a)$, where A_a is the area under the amorphous halo (see Fig. 1). In this case, the amorphous halo was fit using a Lorentzian function and the crystalline reflections with a Pearson function, using commercial peak fitting software.

As another example, see the WAXD pattern for a monoclinic isotactic polypropylene (PP) in Figure 2. In this case, the amorphous halo of the semicrystalline material was obtained by scaling the diffraction pattern of noncrystalline atactic PP to obtain the best fit to the experimental spectrum. The authors of Reference 2 demonstrated that the WAXD pattern of isotactic PP at a temperature (T) greater than the melting point (T_m, 180°C in this case) was the same as that from atactic PP at the same temperature. The entire diffracted intensity from the crystalline reflections (I_c) was determined, and the crystallinity determined from $I_c/(I_c + I_a)$.

The use of traditional WAXD in the determination of degrees of crystallinity for some other semicrystalline polymers can be found in References 4–8.

As a result of the high X-ray flux available at synchrotron X-ray sources such as that at the National Synchrotron Light Source at Brookhaven National Labs, WAXD patterns (and hence degrees of crystallinity) can be determined during the course of crystallization at a specific temperature, or at programmed heating or cooling rates (see SYNCHROTRON RADIATION). Data is typically acquired over

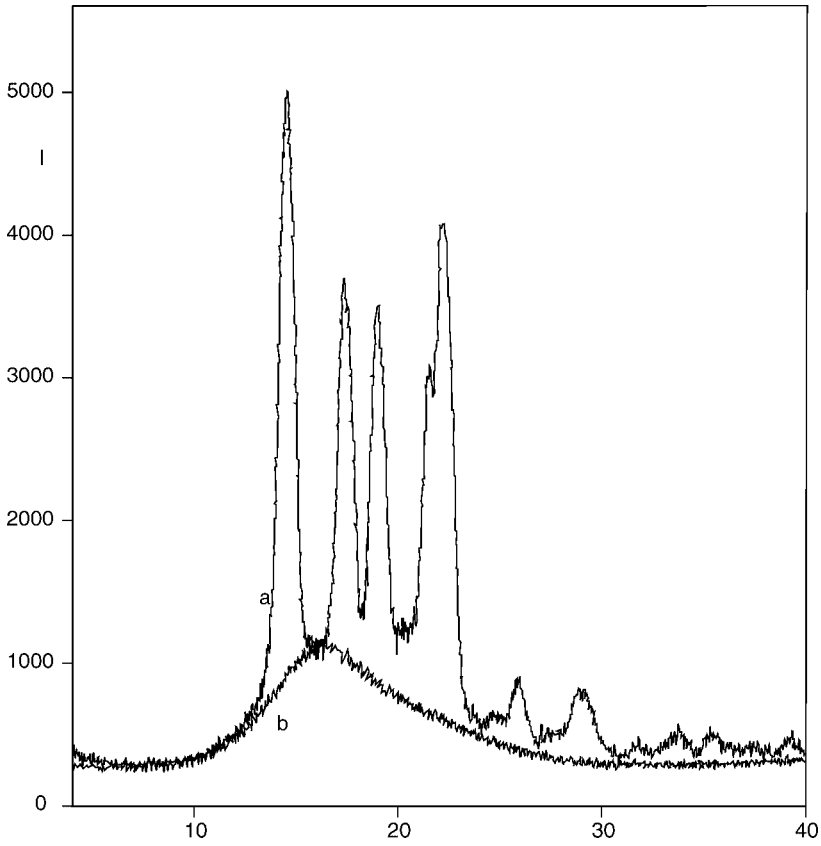

Fig. 2. X-ray diffraction patterns taken at room temperature: (**a**) isotactic polypropylene crystallized at 145°C and (**b**) a sample of atactic polypropylene. From Ref. 2.

a limited angular range in such experiments, and a crystallinity index or relatively crystallinity is generally the best one can do. In addition, such capabilities are often linked with small-angle X-ray scattering (SAXS) instrumentation allowing one to follow the development of the lamellar microstructure in real time, along with crystallinity development. References 9–13, and the references therein, provide details of such experiments on a variety of crystallizing polymer systems.

As an example, Figure 3 shows the sequence of WAXD patterns acquired (one every 30 s) during isothermal crystallization of high molecular weight PEO using a specially designed sample holder to allow for a rapid jump between the melt temperature and selected crystallization temperatures (T_c) (14). Degrees of crystallinity were determined using a curve-fitting program where the diffraction profile was separated into three crystalline PEO reflections and an amorphous halo (10). The apparent degree of crystallinity was defined as the ratio of the area under the resolved crystalline peaks to the total unresolved area. The first several patterns in Figure 3 originate from amorphous PEO. Crystallization begins subsequently and is largely complete at a time <900 s. No changes in the

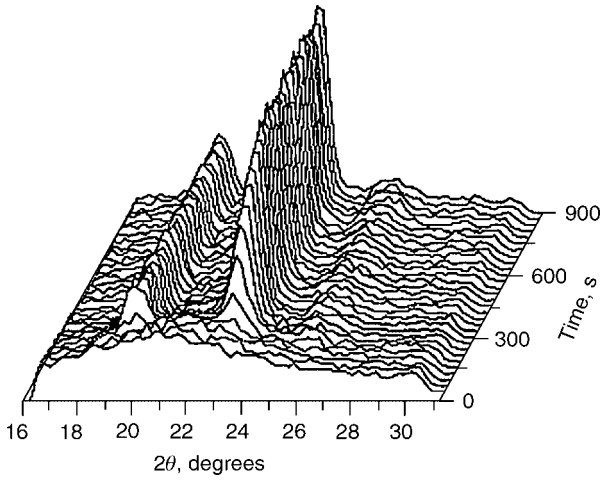

Fig. 3. Development of WAXD diffraction profiles as a function of crystallization time for PEO during crystallization at 45°C. 2θ is relative to $\lambda = 0.154$ nm. From Ref. 10.

positions of the WAXD crystalline reflections (indicative of changes in the crystalline unit cell or unit cell parameters) or the widths at half peak height (indicative of "crystallite size") were noted during the crystallization of PEO at this temperature.

Absolute Degrees of Crystallinity. Determination of the absolute degree of crystallinity from WAXD requires diffraction data over a wide angular range and correction for air scattering, incoherent scattering, and diffuse scattering arising from thermal fluctuations and paracrystalline disorder. Only a brief summary of this approach is presented here. The interested reader is directed to the original Ruland and Vonk References 15–17 as well as several more recent publications (18–20).

This approach (often referred to as the *Ruland method*) is based on the conservation of the total scattered intensity by a set of atoms, independent of their state of structural order. The experimental X-ray diffraction pattern is first acquired over a broad angular range [or equivantly, a broad s range: the reciprocal space parameter s is used here for consistency with References 16–21, where $s = (2\sin\theta)/\lambda$ and λ is the X-ray wavelength] and corrected for air and incoherent scattering. It was recognized that even completely crystalline solids exhibit diffuse scattering with corresponding loss of intensity in the crystalline reflections, as a result of thermal vibrations and imperfections in the crystalline lattice (ie, paracrystalline disorder). The absolute degree of crystallinity ($X_{\mathrm{abs,WAXD}}$) is then determined as

$$X_{\mathrm{abs,WAXD}} = \frac{\int_{s_1}^{s_2} s^2 I_c(s)\ ds}{\int_{s_1}^{s_2} s^2 I(s)\ ds} \cdot K \qquad (1)$$

where s_1 are s_2 are indicative of the angular limits of the experiment, and

$$K = \frac{\int_{s_1}^{s_2} s^2 \bar{f}^2 \; ds}{\int_{s_1}^{s_2} s^2 \bar{f}^2 D \; ds} \tag{2}$$

where $\bar{f}^2$ is the mean-square atomic scattering factor for the polymer. *D(s)* is the generalized Debye–Waller factor that takes into account thermal atomic vibrations as well as paracrystalline disorder, both of which result in crystalline peak intensities decreasing as θ (or s) increases. As for other methods discussed above, a critical feature of this procedure is the accurate separation of crystalline reflections from the overall background scattering.

Small-Angle X-ray Scattering. SAXS is an X-ray scattering method that is used frequently to investigate the lamellar microstructure of semicrystalline polymer systems; that is, to characterize structural periodicities on the order of 5–50 nm. For melt-crystallized systems, one typically observes a maximum in the scattered intensity at low angles associated with the so-called long period (L), which is associated with the mean center-to-center between lamellae. Figure 4 illustrates the room temperature SAXS profiles of a poly(L-lactide/D-lactide) random copolymer crystallized isothermally at selected temperatures. The parameter q in Figure 5 is the scattering vector [$q = \frac{4\pi}{\lambda}\sin(\theta/2)$ and θ is the scattering angle]. The

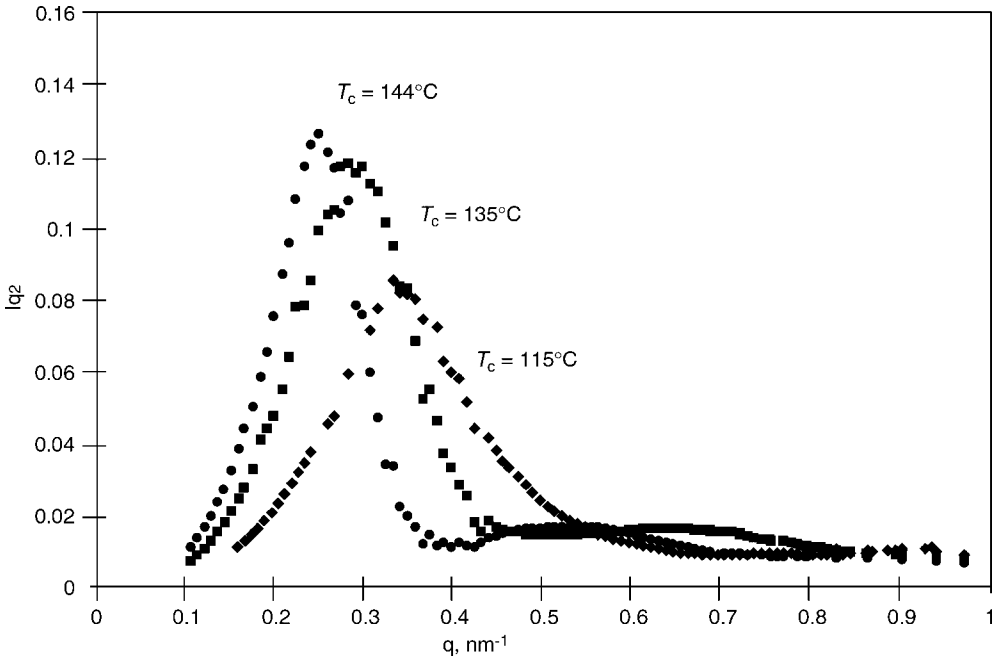

Fig. 4. Room temperature small-angle X-ray scattering patterns of a poly(L-lactide/D-lactide) random copolymer containing 1.5% D-lactide crystallized at the T_cs shown in the figure. The scattered intensities have been Lorentz-corrected (by q^2). From Ref. 22.

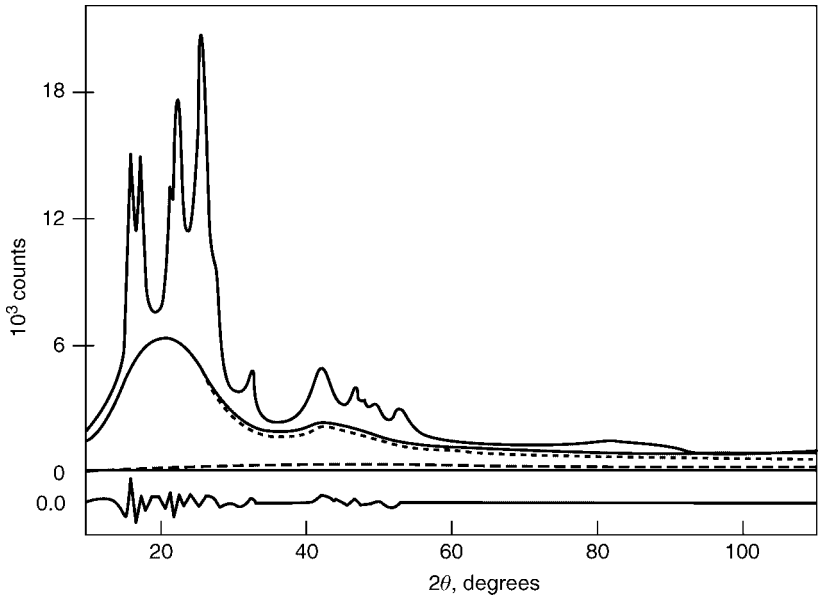

Fig. 5. Schematic of components in absolute crystallinity determination of an unoriented sample of PET. The dashed line represents the incoherent scattering and the dotted line represents the sum of the incoherent scattering and the scattering due to the amorphous component. The solid line (not bold) represents the global background scattering. The solid line at the bottom of the figure represents the residuals. The absolute crystallinity of this sample was determined to be 51%. From Ref. 18.

long periods ($L = 2\pi/q_{max}$) increase progressively with T_c, as is normally observed for crystalline polymers. Weak second-order reflections are also observed for several of these samples, particularly at higher T_c, indicating relatively well-ordered lamellar stacks.

It is sometimes assumed that the bulk degree of crystallinity is same as the SAXS "linear crystallinity." The linear crystallinity (w_c) is defined on the basis of a one-dimensional view of a lamellar stack morphology. For a stack of lamellae, the linear crystallinity is defined simply as l_c/L, where l_c is the crystalline thickness ($L = l_c + l_a$, where l_a is the amorphous layer thickness between lamellae). In the case of volume-filling lamellar stacks (the so-called "infinite stack" model), as might be anticipated for polymers exhibiting relatively high degrees of crystallinity like linear PE and PEO, the bulk crystallinity measured by another method such as WAXD or differential scanning calorimetry (DSC) would be expected to be near w_c. This has been shown to be the case in a number of instances (21). Therefore, to a first approximation, one can estimate the mean lamellar thickness for a given polymer that exhibits an infinite stack morphology from $l_c = L \cdot \phi_c$, where ϕ_c is the volume fraction crystallinity determined from DSC, WAXD, or another method.

However, this simple model is not generally valid, particularly for lower crystallinity materials. In the latter, the (linear) crystallinity of lamellar stacks can be relatively high, but the bulk crystallinity low. In this case $\phi_c = V_s \times w_c$ (where V_s is the volume fraction of lamellar stacks) and $V_s < 1$ and $w_c > \phi_c$.

Thermal Analysis

Probably the most widely used technique for determining degrees of crystallinity is differential scanning calorimetry (see THERMAL ANALYSIS). This is due to the ready availability of such instrumentation, rapid turn around time, and apparent simplicity. The heat of fusion is measured experimentally and the weight-fraction degree of crystallinity defined as:

$$X_{c,DSC} = \Delta H_f / \Delta H_f^0 \tag{3}$$

where ΔH_f is the measured heat of fusion (strictly, referred to temperature T) and $\Delta H_f{}^0$ is the heat of fusion of the 100% crystalline polymer (again, strictly, determined at T). Since ΔH_f is measure at the melting point and $\Delta H_f{}^0$ is estimated at comparable temperatures, it is important to recognize that $X_{c,DSC}$ is therefore defined near T_m, not at ambient temperature where values from other analytical methods are usually determined.

The main experimental problem encountered in measuring heats of fusion is the construction of an appropriate baseline delineating the melting endotherm from the underlying heat capacity contribution. The general equation relating measured heat capacity to thermal measurement is (23)

$$H = X_c \cdot H_c + (1 - X_c)H_a + (dX_c/dT)\Delta H_f \tag{4}$$

where H is the measured heat capacity and the subscripts c and a refer to the crystalline and amorphous states, respectively. In the melting region, the last term in equation 4 dominates and in the vast majority of the cases in the literature, a straight line is used to connect the onset to the last trace of melting. For relatively sharp-melting materials, the error involved in using a flat baseline is typically small. Some polymers, on the other hand, may melt over a wide temperature range, and it can be difficult to determine where melting actually begins. In addition, appreciable baseline curvature can arise from instrumental factors or changes in heat capacity with temperature. As a result, the simple linear baseline construction is not necessarily correct.

To avoid potential inconsistencies and uncertainties noted above, three similar methods have been proposed in literature. A brief summary of these approaches is provided below, and the interested reader is encouraged to consult the original publications. Although by all accounts these are preferred methods, they are not routinely applied in the literature.

The first of these is now often referred to as the *total enthalpy method* (24,25). In one version, the crystallinty is determined as follows (25). At a temperature T_1 below where melting begins, the total heat capacity can be written simply as

$$H_1 = X_{c,1} \cdot H_{c,1} + (1 - X_{c,1})H_{a,1} \tag{5}$$

where $X_{c,1}$ is the crystallinity at T_1 and $H_{c,1}$ and $H_{a,1}$ are the heat-capacity contributions from the crystalline and amorphous components, respectively, at T_1. At a temperature T_2 where the sample is completely molten: $C_{p,2} = C_{p,a,2}$. By

difference,

$$\Delta H_{2,1} = H_2 - H_1 = \Delta H_{a(2,1)} + \Delta H_{f,1}^0 \cdot X_{c,1} \quad (6)$$

where $H_{a(2,1)} = H_{a,2} - H_{a,1}$ and $\Delta H_{f,1}{}^0$ is the enthalpy required to convert 1 g of completely crystalline material into 1 g of completely amorphous material at T_1. Solving for $X_{c,1}$ leads to

$$X_{c,1} = m \cdot \Delta H_{2,1} - b \quad (7)$$

where $m = (\Delta H_{f,1}{}^0)^{-1}$ and $b = \Delta H_{a(2,1)}/\Delta H_{f,1}{}^0$. Equation 7 demonstrates that the degree of crystallinity at T_1 is related to the *total enthalpy* absorbed between T_1 and T_2 (measured from the DSC trace). The advantage of this method is that it provides the correct crystallinity at T_1 regardless of the path the polymer takes to T_2. However, the disadvantage is that $\Delta H_{a(2,1)}$ and $\Delta H_{f,1}{}^0$ must be known to calculate $X_{c,1}$.

A similar approach for determining $X_{c,1}$ has been proposed by Mathot and Pijpers (26,27). Finally, the so-called "First Law method" has been proposed by Hay and co-workers (28,29). This involves two measurements: (*1*) a DSC experiment that determines the enthalpy change on heating from T_1 to T_2 ($>T_m$) and (*2*) a virtual experiment determining the enthalpy change on cooling from T_2 to T_1 without crystallization taking place. The difference between steps 1 and 2 leads to a residual enthalpy; ie, the heat of fusion of the sample at $T_1 \cdot \Delta H_f{}^0$ reported in the literature is normally determined near the equilibrium melting point ($T_m{}^0$) but to determine $X_{c,1}$, $\Delta H_{f,1}{}^0$ is needed. It has been shown that the latter can be obtained from the experiments as

$$\Delta H_{f,1}^0 = \Delta H_f^0 - \int_{T_1}^{Tm^0} (H_a - H_c)\ dT \quad (8)$$

where H_a and H_c are the heat capacities of the completely amorphous and crystalline states, respectively. Once $\Delta H_{f,1}{}^0$ is determined from equation 8, $X_{c,1}$ can be calculated readily.

References 23 and 30 remain the best sources of a collection of $\Delta H_f{}^0$ values, but there has been considerable work on a variety of polymers since their publication and it is recommended to verify particular values by reference to more recent literature. Since perfectly crystalline materials are rarely available, $\Delta H_f{}^0$ values must be estimated, typically by an "extrapolation" method. For example, a series of samples of a particular polymer can be crystallized to varying degrees, and the experimental ΔH_f measured along with the sample densities. The measured ΔH_f values are then plotted vs density (or equivalently, specific volume) and the data linearly extrapolated to the density of the perfectly crystalline version of the polymer in question (19) [a value which is generally well established (see a following section)]. This extrapolation can be rather lengthy, especially for polymers of low crystallinity. In a similar fashion, measured ΔH_f values are plotted vs $l_c{}^{-1}$ and $\Delta H_f{}^0$ is obtained by extrapolating to $l_c{}^{-1} \rightarrow 0$ (31). Crystalline lamellar thicknesses are typically determined from SAXS experiments, although other

methods like the Raman longitudinal acoustic mode or microscopic techniques (ie, transmission electron or atomic force) are sometimes used. For polymers for which a series of analogs of various low molecular weights are available (eg *n*-alkane analogs for linear PE), measured heats of melting of the analogs can be plotted vs n^{-1} (where n = number of C atoms in an *n*-alkane) and ΔH_f^0 for the polymer obtained by extrapolation of the measured heats to $n^{-1} \rightarrow 0$ (32). Finally, ΔH_f^0 has been estimated from the melting point (dissolution temperature) depression observed in the presence of a miscible diluent (33). Particularly care must be exercised when using this latter approach to use equilibrium dissolution temperatures (ie, extrapolated values representing the dissolution of a perfect crystal of the polymer at a particular diluent concentration), not simply experimentally measured quantities.

Readers interested in additional background on Thermal Analysis (qv) techniques applied to polymeric materials, may see, for example, References 34–36.

Vibrational Spectroscopy

Infrared (IR) and Raman spectroscopies have been used for decades to routinely characterize polymeric and other materials. Vibrational Spectroscopy (qv), particularly Fourier transform IR (FTIR), has been used extensively to probe crystalline and amorphous conformations in a wide variety of polymers, as well as to determine a measure of the crystallinity of such materials. In the FTIR spectra of crystalline polymers, one or more absorption bands are often observed that disappear when crystallization is inhibited. Provided these bands can be genuinely assigned to 3-D crystalline order, and if the absorbance of this band in the specimen under examination is in the range for which the Beer–Lambert Law is applicable, then

$$A = \log(I_0/I) = a_c \cdot X_{c,ir} \cdot \rho \cdot t \tag{9}$$

where A is the absorbance or optical density, I_0 and I the incident and transmitted intensities, respectively, t the specimen thickness, ρ the overall density, and a_c the absorption coefficient of the 100% crystalline material. Since fully crystalline specimens are rarely available, a_c must be estimated, as will be discussed shortly. If the spectrum contains bands indicative of noncrystalline material, an expression similar to equation 9 can be written for the amorphous component.

Infrared bands should only be designated as crystalline bands if they disappear on melting, are predicted from group theory, and X-ray or other data proves the polymer to be crystalline. Only in a few rare cases have true crystalline bands been observed; for example, the 720–730 cm^{-1} CH_2 rocking doublet of crystalline PE is a reflection of a genuine crystallinity effect, as the splitting results from intermolecular interaction of segments in the orthorhombic unit cell (37). More frequently, reported "crystalline" bands are associated with a preferred crystalline conformation that may also be present (in lower concentration) in the noncrystalline phase.

As an example of crystallinity determination by FTIR, the procedure used in Reference 38 for polyethylene is summarized here. The infrared spectrum of a solution-crystallized sample of polyethylene in the region of its CH_2 rocking (and

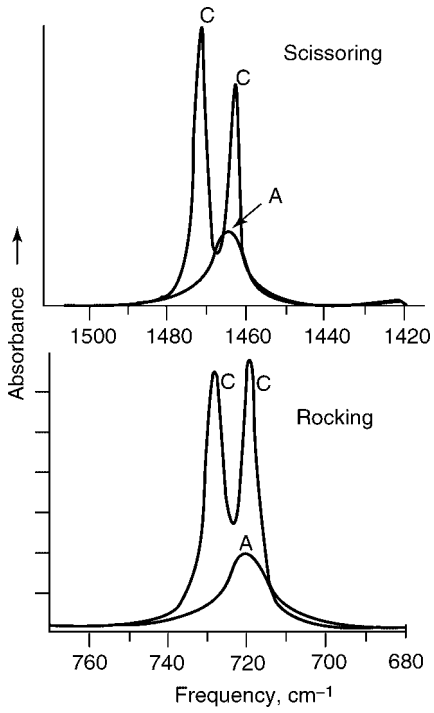

Fig. 6. FTIR spectrum of a solution-crystallized polyethylene (NIST standard SMR 1482, $M_w = 1.36 \times 10^4$) in the CH_2 rocking and bending (scissoring) regions. Pictured are the crystalline and amorphous components in each of these regions, as resolved using a band fitting procedure. From Ref. 38.

bending) modes is shown in Figure 6. The crystallinity was calculated from the ratio of the integrated intensities (absorbances) of the crystalline component in the CH_2 rocking region ($I_{722} + I_{730}$) to the total absorbance in this region. The latter is determined by $I_{722} + I_{730} + \gamma I_{723}$, where I_{723} is the contribution from the amorphous component, and γ is included to account for the fact that intrinsic intensities of the crystalline and amorphous bands are not equal ($\gamma = a_c/a_a$, where a_a is the absorption coefficient of the amorphous component). The value of γ was determined to be $\sim$1.2 in this case. Degrees of crystallinity were determined for a variety of polyethylene samples using this method and found to be the same within experimental uncertainty as those derived from DSC experiments on the same samples. This result led these authors to conclude that this FTIR method measures the "core crystallinity," as does DSC (38).

A similar approach has been used to determine the crystallinity of poly(ε-caprolactone) by FTIR, in which γ was measured by monitoring changes in the absorbances of the amorphous and crystalline components of the carbonyl band during isothermal crystallization (39). In many cases in the literature a "crystallinity index" is effectively determined, either because true crystalline or amorphous IR bands are rarely available and/or γ is assumed to be equal to 1. However, such an index may prove to be suitable for a variety of purposes.

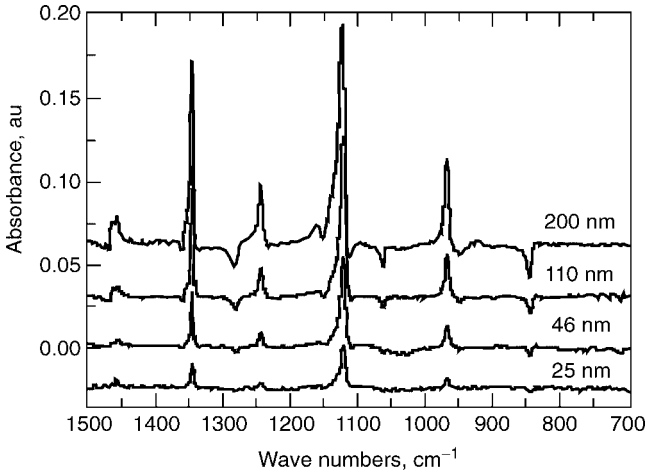

Fig. 7. Grazing incidence reflection FTIR spectra (p-polarized) of PEO (pyrene end-labeled) ultrathin films on oxidized silicon with different thicknesses (crystallized isothermally at 40°C). The negative bands are typical of grazing incidence reflection spectra on nonmetallic surfaces. From Ref. 42.

There is widespread interest in thin and ultrathin (thickness <100 nm) polymer films for use in packaging, electronics and other applications, and infrared spectroscopy is a particularly useful tool for characterizing the crystallinity in such systems. For example, attenuated total reflectance FTIR has been used to provide qualitative information on crystallinity and molecular orientation as a function of depth into drawn films of PET (40). Crystallinity measurements on ultrathin films are clearly difficult by conventional methods, but can be accomplished using FTIR spectroscopy in reflection mode (41,42). For example, grazing incidence reflection FTIR has been used to provide insight on molecular orientation as well as a qualitative measure of conformational order in ultrathin films of PEO on an oxidized silicon surface (42). Figure 7 shows grazing incidence reflection spectra of PEO films with different thicknesses. The absorbance near 1120 cm^{-1} is not sensitive to conformational order (ie, is an "internal thickness" band), and all spectra are therefore normalized to A_{1120} to permit evaluation of the relative crystallinity (conformational order) as a function of film thickness. The crystallinity was found to decrease significantly with decreasing film thickness, in keeping with the usual observation of slowing of crystallization for films with thicknesses below ca 100 nm (43,44). It has been postulated that a reduction in molecular mobility occurs in ultrathin films, resulting from the onset of diffusion control of crystallization (45,46).

Volumetric Methods

Measurement of sample densities also provides an effective way of determining degrees of crystallinity, (47–50), although this approach is not used as commonly as in the past because of the availability and ease of utilizing DSC, FTIR, and WAXD. The weight fraction degree of crystallinty can be determined from the

measured density by

$$X_{c,d} = \left(\rho_a^{-1} - \rho^{-1}\right) / \left(\rho_a^{-1} - \rho_c^{-1}\right) = (\bar{V}_a - \bar{V})/(\bar{V}_a - \bar{V}_c) \quad (10)$$

where ρ_a and ρ_c are the densities of completely amorphous and crystalline versions of the polymer in question, and $\overline{V}$ are the comparable specific volumes. The relationship between the weight fraction crystallinty and volume fraction crystallinty (ϕ_c), regardless of method used, is simply: $\phi_c = X_c\,(\rho/\rho_c)$. Values of ρ and ρ_c are generally such that ϕ_c and X_c are within several percent of each other.

Sample density can be measured using a variety of methods: density-gradient column, dilatometry, pycnometry, and flotation or buoyancy. The density-gradient column approach is probably used most frequently to determine sample densities for crystallinity measurements. When thermostated and appropriately calibrated with floats, this approach permits measurements to accuracies of 0.2 mg/cm^3 or better. Dilatometers are well suited for measuring specific volumes and following crystallization, as a function of temperature.

Although the above-mentioned techniques are routine, a number of problems can lead to errors in measured densities. For example, the solvent used must completely wet the specimen but not cause swelling, and the sample must be free of closed porosity. Solvents that induce further crystallization should be avoided.

Even in the absence of reliable ρ_a and ρ_c values, density measurements can be used for qualitative ranking of specimens of a given polymer on the basis of degree of crystallinity. Values for ρ_c are generally known reasonably well since they can be calculated from the dimensions of the appropriate unit cell for the polymer in question. The lattice parameters are determined from WAXD experiments, as discussed elsewhere in this edition. Estimation of ρ_a is generally more difficult. Some polymers can be prevented from crystallizing by quenching from above T_m to below T_g (eg isotactic polystyrene and PET) and their amorphous density can therefore be measured directly at ambient temperature. In other cases, ρ_a has been estimated by extrapolating specific volume data (from dilatometry) in the melt to ambient temperature. This extrapolation can be lengthy and introduces a degree of uncertainty in ρ_a.

It has been found in a number of cases that X_c from density and WAXD measurements is equivalent within experimental error, but is higher than that from DSC (19,47). These observations have led to the conclusion that DSC provides a measure of the core crystallinity only, while the crystallinity from density and WAXD is a measure of the core crystallinity along with the crystal–amorphous interphase.

Solid-State Nuclear Magnetic Resonance

This section provides a broad overview of the application of NMR spectroscopy to crystallinity determination in polymers. The approaches illustrated are certainly not exhaustive of those available for the powerful NMR technique and the interested reader is encouraged to consult one or more of the reference books on NMR spectroscopic investigations of polymeric materials (51–53) (see NUCLEAR MAGNETIC RESONANCE).

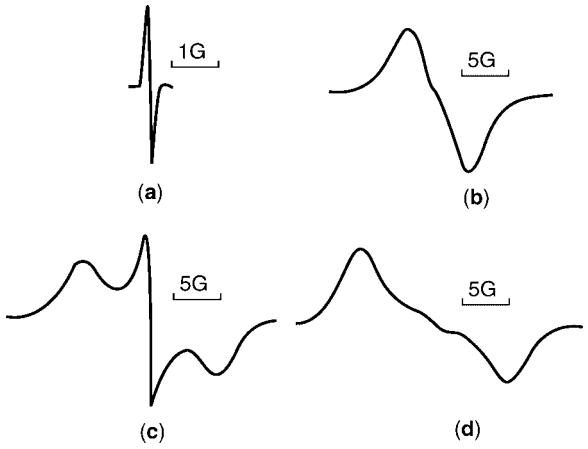

Fig. 8. Broadline ^{1}H NMR spectra: (**a**) polybutadiene at 20°C; (**b**) poly(ethylene terephthalate) at 20°C; (**c**) polyethylene at 20°C; and (**d**) polyethylene at −150°C. From Ref. 54.

Clasic Broadline ^{1}H NMR. This technique has been utilized for many decades. Broadline ^{1}H NMR spectra, the first derivatives of the NMR absorption spectra, of several polymers are shown in Figure 8.

At temperatures above their T_g, the resonance spectrum of noncrystalline polybutadiene (PB) (Fig. 8**a**) is clearly different from that of the semicrystalline polyethylene (Fig. 8**c**). Amorphous PB exhibits a narrow Lorentzian line shape with a width of ∼0.2 G. In contrast, the PE spectrum comprises two components, ie, narrow and broad line shapes. When the spectra of semicrystalline polymers are recorded in the glassy state (Figs. 8**b** and 8**d**), only a broad component is observed. This indicates that the line shape corresponds to molecular mobility and the line width reflects a correlation (or relaxation) time. Therefore, the broad and narrow components of semicrystalline PE (Fig. 8**c**) are related to protons of methylene groups in rigid and mobile (amorphous) environments, respectively. On the basis of this, it was proposed that the degree of crystallinity could be determined by resolving the area of the broad component (rigid phase) from the spectrum.

For many polymers, however, the degree of crystallinity estimated from the two-component analysis was found to be appreciably larger than that obtained from WAXD or density measurements on the same materials. In addition, although the crystallinity of PE determined by density methods remains constant below room temperature (∼60%), the broadline NMR "crystallinity" increases continuously to 100% at temperatures approaching T_g (55). Thus the area under the broad portion of the derivative curve is proportional to the number of immobile protons in both crystalline and rigid noncrystalline phases. As a result, methods to decompose such spectra into three components were developed (56,57).

Broadline NMR spectra can be expressed as

$$y(H) = w_b y_b(H, b_b) + w_m y_m(H, b_m) + w_n y_n(H, b_n) \tag{11}$$

where y_b, y_m, and y_n are the elementary spectra of the broad, medium, and narrow components, respectively, and w_b, w_m and w_n are the weight fractions of these

components ($w_b + w_m + w_n = 1$). The line widths of the broad, medium, and narrow components are b_b, b_m, and b_n, respectively. The calculated spectra of these components can be obtained as described in References 56 and 57. In the fitting process, the line widths and weight fractions of all elementary spectra are modified so as to minimize the difference between the calculated and experimental spectra. A detailed discussion and examples of the broadline H^1 NMR technique can be found in Reference 54.

Fourier Transform NMR. In Fourier transform NMR (FTNMR), a repetitive radio frequency (RF) pulse is applied in order to excite all of the nuclei of the particular nuclear species being studied. The sum of the free induction decay (FID) curves from each pulse is analyzed by a Fourier transform method in order to generate the familiar frequency domain spectra. Fundamentally, parameters such as the frequency, intensity, application time of the appropriate RF pulse, and time intervals between these pulses are important variables when using this technique. The principle of the pulsed Fourier transform technique can be found in books covering the fundamental concepts of NMR spectroscopy (58,59).

The application of a properly timed rf pulse disturbs the net equilibrium magnetization aligned parallel to the magnetic field H_0. The return of nuclear magnetization to equilibrium for solid polymers depends on the chain mobility and is monitored by the FID. The crystalline phase content can be extracted by deconvoluting the decay curve into portions corresponding to crystalline and noncrystalline components. Crystallinity determination of various polyethylene samples by FID ^{1}H NMR based on two- and three-component approaches, as well as

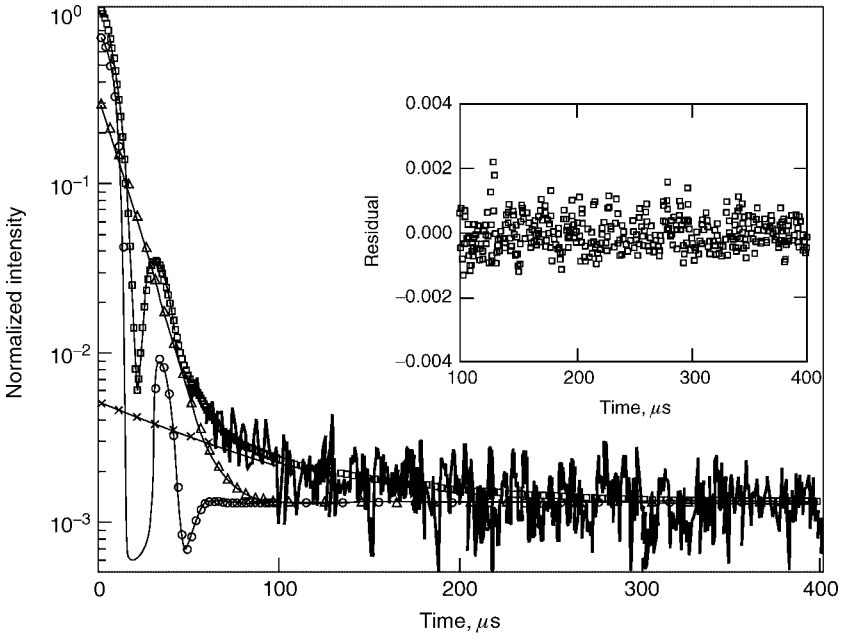

Fig. 9. FID resolution into three components for ultrahigh molecular weight PE reactor powder. The inset figure shows residuals between the observed and fitted data in the long decay region (100–400 μs). ——— Observed, □ fitted, ○ crystalline, △ intermediate, × mobile. From Ref. 62.

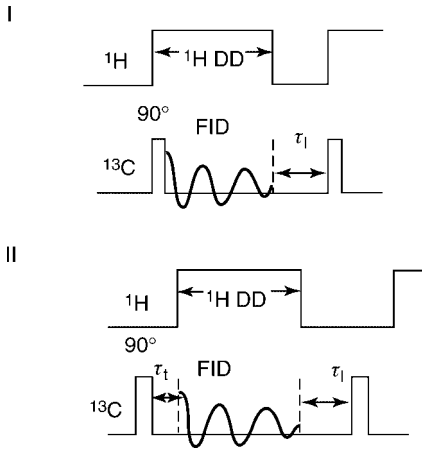

Fig. 10. Pulse sequences for DD/MAS ^{13}C NMR (without CP). From Ref. 65.

comparison of these crystallinities with those determined from other methods, is discussed in References 60–62. Figure 9 presents a summary of the FID ^{1}H NMR spectral analysis of PE, based on a three-component method (62). The crystallinity is determined by the initial normalized magnetization (zero time) of the calculated decay of the crystalline component.

The degree of crystallinity can be determined via FT ^{1}H NMR spectra as well (60,61) Similar to broadline ^{1}H NMR line shapes for the various components are fit to the experiment spectrum in order to extract that of the crystalline component, and the ratio of the area under the resolved crystalline spectrum divided by the total area represents the weight fraction of the crystalline phase. The use of this approach to determine the crystallinity of polyethylene, ethylene–vinyl alcohol copolymers and polypropylene can be found in References 60, 63 and 64, respectively.

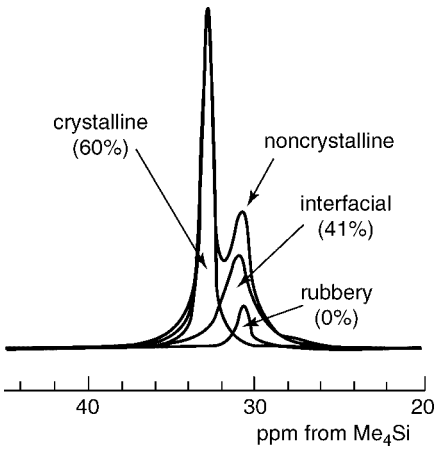

Fig. 11. Fully relaxed DD/MAS ^{13}C NMR spectrum of metallocene-catalyzed lineer low density polyethylene. From Ref. 67.

Solid-State High Resolution C^{13} NMR. C^{13} NMR with dipolar decoupling (DD), magic angle spinning (MAS), and cross-polarization (CP) can distinguish phases in semicrystalline polymers by differentiating their chemical shifts and relaxation times. Useful pulse sequences utilized to obtain NMR spectra are presented in Figure 10. Spectra with partial or total contribution from the respective components (phases) can be obtained by appropriate choice of the waiting times, τ_l and τ_t. The spectrum acquired from pulse sequences I and II depends on the material relaxation times, ie spin-lattice relaxation time (T_{1C}) and spin–spin lattice relaxation time (T_{2C}). With pulse sequence I (Fig. 10), if τ_l is longer than 5 times the longest spin-lattice relaxation time, the spectrum

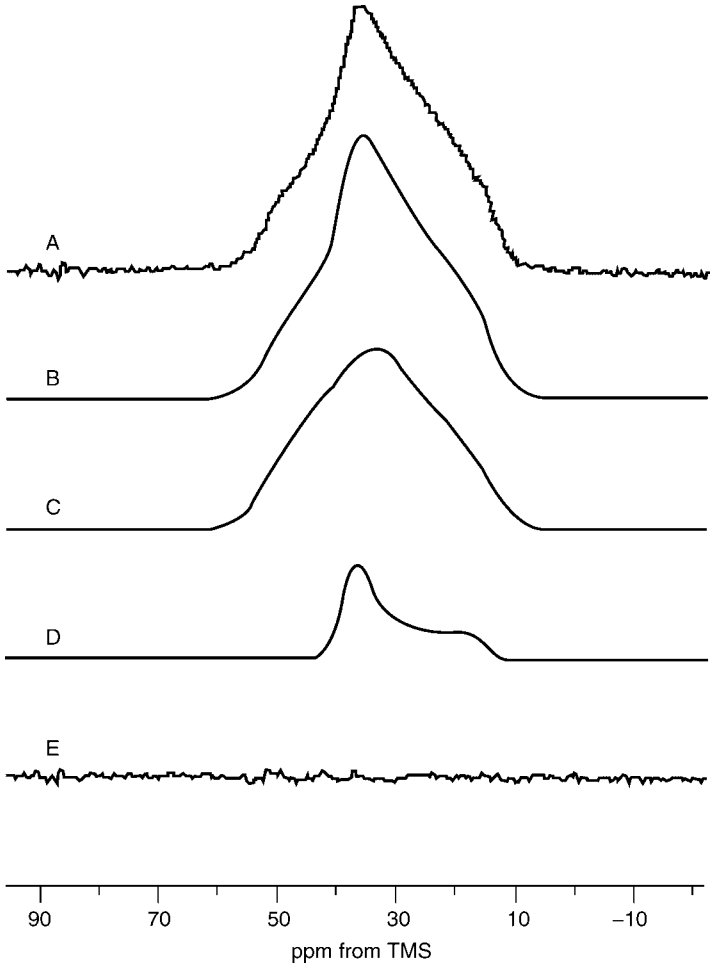

Fig. 12. A: Cross-polarized, ^1H-decoupled, static 25.152 MKz ^{13}C NMR spectrum of Phillips 6050 polyethylene. The spectral window was 5 KHz, no line broadening, 24150 transients. B: Calculated "best-fit" spectrum, the sum of the crystalline and the amorphous tensor components. C: The crystalline tensor. D: The amorphous tensor. E: Residual spectrum (A-B). The chemical shifts are relative to the methyl resonance of hexamethylbenzene (17.6 ppm from TMS). From Ref. 68.

(see Fig. 11) contains contributions from all structural phases. In order to extract the crystalline content, the location and shape of the resonance lines of each component and proper composition model are required.

For PE, it has been shown by many research groups (65–67) that the resonance line at 33, 31.3, and 31 ppm arise from the orthorhombic crystalline, the crystalline-amorphous interfacial, and the amorphous (rubbery) components, respectively. Detailed studies using different pulse sequences (varying τ_l and τ_t to extract the information of individual component from the partial relaxed NMR spectrum can be found in References 65–67. On the basis of chemical shifts of all components, the experimental spectrum is analyzed using three calculated Lorentzian curves centered at 33, 31.3, and 31 ppm, by least-squares fitting, as seen in Figure 11. In the NMR study of PE in Reference 66, the monoclinic crystal form (with the resonance line centered at 34.3 ppm) was observed in addition to the resonance of the usual orthorhombic form. Spectra were therefore analyzed using four components, using the same principles as described above.

In addition to DD/MAS ^{13}C NMR, the crystallnity of PE can be determined from the ^{1}H-decoupled/CP ^{13}C NMR. Spectra consist of contributions from the different phases, which are differentiated by their shielding tensors (anisotropic chemical shift), as seen in Figure 12 (68). The crystalline fraction is estimated from the ratio of the area under the crystalline tensor to the total area.

In summary, the key feature of these approaches is the deconvolution of the spectrum of interest, which is sensitive to the presence of the different phases, into spectra corresponding to each component. Although the above discussion focused on semicrystalline polyethylene, detailed discussion of crystallinity measurements by ^{13}C NMR for other selected polymers can be found in the following references: poly(vinyl chloride) (69), polypropylene (70), and polylactides (71).

Finally, in addition to ^{1}H and ^{13}C NMR, ^{19}F NMR has proven to be very useful for determining the degree of crystallinity of fluoropolymers such as polytetrafluoroethylene (72,73).

BIBLIOGRAPHY

"Crystallinity" in *EPST* 1st ed., Vol. 4, pp. 449–528, by Robert L. Miller, Chemstrand Research Center, Inc.; "Crystallinity Determination" in *EPSE* 2nd ed., Vol. 4, pp. 482–519, by James Runt, Pennsylvania State University."

1. A. M. Hindeleh and D. Johnson, *Polymer* **19**, 27 (1978).
2. J. R. Isasi, L. Mandelken, M. J. Galante, and R. G. Alamo, *J. Polym. Sci., Polym. Phys.* **37**, 323 (1999).
3. V. Everaert, G. Groeninckx, M. H. J. Koch, and H. Reynaers, *Polymer* **44**, 3491 (2003).
4. N. S. Murthy, Y. P. Khanna, and A. J. Signorelli, *Polym. Eng. Sci.* **36**, 1254 (1994).
5. H. Sato, S. Sasao, K. Matsukawa, Y. Kita, H. Yamaguchi, H. Siesler, and Y. Ozaki, *Macromol. Chem. Phys.* **204**, 1351 (2003).
6. S. Murakami, K. Ueda, T. Kitade, Y. Ikeda, and S. Kohjiya, *Solid State Ionics* **154**, 399 (2002).
7. E. Walenta, H. Fink, P. Weigel, and J. Ganster, *Macromol. Mater. Eng.* **286**, 456 (2001).
8. K. J. Wright and A. J. Lesser, *Macromolecules* **34**, 3626 (2001).

9. Z. G. Wang, X. Wang, B. S. Hsiao, S. Andjelic, D. Jamiolkowski, J. McDivitt, J. Fischer, J. Zhou, and C. C. Han, *Polymer* **42**, 8965 (2001).
10. M. S. Lisowski, Q. Liu, J. Cho, J. Runt, F. Yeh, and B. S. Hsiao, *Macromolecules* **33**, 4842 (2000).
11. F. Yeh, B. S. Hsiao, B. Chu, B. B. Sauer, and E. A. Flexman, *J. Polym. Sci., Polym. Phys.* **37**, 3115 (1999).
12. J. D. Cho, S. Baratian, J. Kim, F. Yeh, B. S. Hsiao, and J. Runt, *Polymer* **44**, 2711 (2003).
13. P. D. Olmsted, W. C. K. Poon, T. C. B. McLeish, N. J. Terrill, and A. J. Ryan, *Phys. Rev. Lett.* **81**, 373 (1998).
14. B. S. Hsiao, and R. K. Verma, *J. Synchrontron Rad.* **5**, 23, (1998).
15. W. Ruland, *Acta Crystallogr.* **14**, 1180 (1961).
16. W. Ruland, *Polymer* **5**, 89 (1964).
17. C. G. Vonk, *J. Appl. Crystallogr.* **6**, 148 (1973).
18. P. Riello, G. Fagherazzi, P. Canton, D. Clemente, and M. Signoretto, *J. Appl. Cryst.* **28**, 121 (1995).
19. Z. Mo and H. Zhang, *J. Macromol. Sci.—Rev., Macromol. Chem. Phys.* **C35**, 555 (1995).
20. S. Rabiej, *Eur. Polym. J.* **9**, 947 (1991).
21. S. Talibuddin, L. Wu, J. Runt, and J. S. Lin, *Macromolecules* **29**, 7527 (1996).
22. S. Baratian, E. S. Hall, R. Xu, J. S. Lin, and J. Runt, *Macromolecules*, **34**, 4857 (2001).
23. B. Wunderlich, *Macromolecular Physics*, Vol. **1**, Academic Press, New York, 1973.
24. M. J. Richardson, *J. Polym. Sci., Polym. Symp.* **38**, 251 (1968).
25. A. P. Gray, *Thermochim. Acta* **1**, 563 (1970).
26. V. B. F. Mathot, and M. F. J. Pijpers, *J. Therm. Anal.* **28**, 349 (1983).
27. V. B. F. Mathot, and M. F. J. Pijpers, *Thermochim. Acta* **151**, 241 (1989).
28. Y. Kong, and J. N. Hay, *Polymer* **43**, 3873 (2002).
29. A. A. Mehmet-Alkan, and J. N. Hay, *J. Therm. Anal.* **40**, 791 (1993).
30. B. Wunderlich, *Macromolecular Physics*, Vol. **3**, Academic Press, New York, 1980.
31. L. Mandelkern, A. L. Allou, and M. Gopalan, *J. Phys. Chem.* **72**, 309 (1968).
32. C. M. L. Atkinson and M. J. Richardson, *Trans. Faraday Soc.* **65**, 1749 (1969).
33. R. Chiang and P. J. Flory, *J. Am. Chem. Soc.* **83**, 2857 (1961).
34. S. Z. D. Cheng, ed. Handbook of Thermal Analysis and Calorimetry. Vol 3:, *Applications to Polymers and Plastics*, P. K. Gallagher, series ed., Elsevier, Amsterdam, (2002).
35. T. Hatakeyama and F. X. Quinn, *Thermal Analysis: Fundamentals and Applications to Polymer Science*, 2nd ed., John Wiley & Sons, Inc., New York, 1999.
36. E. A. Turi, ed., *Thermal Characterization of Polymeric Materials*, 2nd ed., Academic Press, San Diego, 1997.
37. P. C. Painter, M. M. Coleman, and J. L. Koenig, *The Theory of Vibrational Spectroscopy and Its Application to Polymeric Materials*, John Wiley & Sons, Inc., New York, 1982.
38. H. Hagemann, R. G. Snyder, A. J. Peacock, and L. Mandelkern, *Macromolecules* **22**, 3600 (1989).
39. Y. He and Y. Inoue, *Polym Int.* **49**, 623 (2000).
40. D. J. Walls and J. C. Coburn, *J. Polym. Sci., Polym. Phys.* **30**, 887 (1992).
41. T. Elzein, M. Brogly, and J. Schultz, *Polymer* **43**, 4811 (2002).
42. H. Schönherr and C. W. Frank, *Macromolecules* **36**, 1188 (2003).
43. G. Reiter and J. U. Sommer, *J. Chem. Phys.* **112**, 4376 (2000).
44. K. Dalnoki, J. A. Forrest, M. V. Massa, A. Pratt, and A. Williams, *J. Polym. Sci., Polym. Phys.* **39**, 2615 (2001).
45. Y. Kikkawa, H. Abe, T. Iwata, Y. Inoue, and Y. Doi, *Biomacromolecules* **3**, 350 (2002).

46. O. Melling, S. Kihlman Oiseth, A. Krozer, J. Lausmaa, and T. Hjertberg, *Macromolecules* **34**, 7496 (2001).
47. J. R. Isasi, L. Mandelken, M. J. Galante, and R. G. Alamo, *J. Polym. Sci., Polym. Phys.* **37**, 323 (1999).
48. A. M. Voice, D. I. Bower, and I. M. Ward, *Polymer* **34** 1154 (1993).
49. B. Crist and P. R. Howard, *Macromolecules* **32**, 3057 (1999).
50. S. H. Hong, R. Kim, C. N. Choi, H. Choi, W. E. Lee, and S. Y. Cho, *Polymer-Korea* **2**, 106 (2003).
51. A. E. Tonelli, *NMR Spectroscopy and Polymer Microstructure: The Conformational Connection*, VCH, New York, 1989.
52. H. N. Cheng and A. D. English, eds., *NMR Spectroscopy of Polymers in Solution and in the Solid State*, ACS Symposium Series 834, American Chemical Society, Washington, D.C., 2003.
53. F. A. Bovey and P. A. Mirau, *NMR of Polymers*, Academic Press, San Diego, 1996.
54. R. Kitamura and F. Horii, *Adv. Polym. Sci.* **26**, 137 (1978).
55. N. Fuschillo, E. Rhian, and J. A. Sauer, *J. Polym. Sci.* **25**, 381 (1957).
56. K. Bergmann and K. Nawotki, *Colloid Polym. Sci.* **250**, 1094 (1972).
57. K. Bergmann, *Colloid Polym. Sci.* **251**, 962 (1973).
58. M. Mehring, *Principles of High Resolution NMR in Solids*, 2nd ed., Springer-Verlag, New York, 1983.
59. W. W. Paudler, *Nuclear Magnetic Resonance General Concepts and Application*, John Wiley & Sons, Inc., New York, 1987.
60. R. R. Eckman, P. M. Henrichs, and A. J. Peacock, *Macromolecules* **30**, 2474 (1997).
61. E. W. Hansen, P. E. Kristiansen, and B. Pedersen, *J. Phys. Chem. B* **102**, 5444 (1998).
62. H. Uehara, T. Aoike, T. Yamanobe, and T. Komoto, *Macromolecules* **35**, 2640 (2002).
63. E. Perez, M. L. Cerrada, and D. L. Vanderhart, *J. Polym. Sci., Polym Phys.* **36**, 2103 (1998).
64. D. Dadayli, R. K. Harris, A. M. Kenwright, B. J. Say, M. M. Sunnetcioglu, *Polymer* **35**, 4083 (1994).
65. R. Kitamazu, F. Horii, and K. Murayama, *Macromolecules* **19**, 636 (1986).
66. Y. Shimizu, Y. Harashina, Y. Sugiura, and M. Matsuo, *Macromolecules* **28**, 6889 (1995).
67. K. Kuwabara, K. Hironori, F. Horii, D. C. Bassett, and R. H. Olley, *Macromolecules* **30**, 7516 (1997).
68. C. D. Hughes, N. K. Sethi, J. H. Baltisberger, and D. M. Grant, *Macromolecules* **22**, 5 (1989).
69. W. Barendswaard, V. M. Litvinov, F. Souren, R. L. Scherrenberg, C. Gondard, and C. Colemonts, *Macromolecules* **32**, 167 (1999).
70. Y. Ohira, F. Horii, and T. Nakaoki, *Macromolecules* **33**, 1801 (2000).
71. K. Thakur, R. T. Kean, J. M. Zupfer, N. U. Buehler, M. A. Doscotch, and E. J. Munson, *Macromolecules* **29**, 8844 (1996).
72. A. J. Vega and A. D. English, *Macromolecules* **13**, 1635 (1980).
73. R. J. Lehnert, P. J. Hendra, N. Everall, and N. J. Clayden, *Polymer* **38**, 1521 (1997).

JAMES RUNT
MANTANA KANCHANASOPA
The Pennsylvania State University

CRYSTALLIZATION KINETICS

Introduction

Crystallizable polymers form semicrystalline materials containing chains or fractions of chains that are trapped in nonequilibrium, amorphous states. Because of this semicrystalline nature, the crystal morphology, rather than the underlying crystal structure, often controls the final properties of a polymer article (see SEMICRYSTALLINE POLYMERS; MORPHOLOGY). Simply by changing the processing conditions, the mechanical properties, for example, Young's modulus, of a typical polymer such as polyethylene can be altered by several orders of magnitude.

Because polymers crystallize so far from equilibrium conditions, a simple examination of the phase diagram gives us little insight into the crystal morphology that is formed or the route that is taken to its formation. To understand, and ultimately control, such behavior, it is necessary to gain an understanding of the kinetics of crystallization, as it is the kinetics of the process that define the structure and properties of the material.

The above insight, gained soon after the discovery of polymer single crystals, and the subsequent discovery of chain folding (1–3), has mapped out the route taken by much of the research into polymer crystallization over the subsequent decades. It soon became clear that the thickness of polymer lamellae was controlled by the supercooling at which they were crystallized and defined by the kinetics of crystallization. The crystal thickness, or alternatively the thickness of each new crystalline layer in a growing crystal, is the one that grows the fastest (4,5) rather than the one that is at equilibrium (6). There is now a wealth of information available on the crystallization of many polymers, as well as several theories that aim to predict the crystallization rates, crystal shapes, and lamellar thickness.

Crystallization kinetics is the area of polymer science that deals with the rate at which randomly ordered chains transform into highly ordered crystals, and includes every aspect of the resultant structure that is dependent on the route that was taken between those different states. It is a broad and mature area of scientific research, given an uncommon diversity when compared to the crystallization of small molecules because of the wide range of different chemistries and chain topologies that are available to macromolecules. These add layers of complexity that can make it difficult to find generalizing principles. For the sake of brevity, this article, therefore, concentrates on areas that are of particular interest to the author, and to principles and observations that have, in the author's opinion, the widest applicability.

As in any transformation, it is possible to measure bulk rates of polymer crystallization and to characterize the process in terms of the shape of these transformation curves. Because of limitations on space the interested reader is pointed toward the relevant literature (7–12), as this approach, although useful for quantifying experimental observations, does not attempt to provide an insight into what is happening at the molecular scale. Polymer crystallization, like many phase transitions, occurs through a process of nucleation and growth, and it is often more revealing to look at the rates of these two processes independently, and to try to gain an understanding of the factors affecting each. Although of fundamental importance, the nucleation step is still poorly understood and only

Encyclopedia of Polymer Science and Technology. Copyright John Wiley & Sons, Inc. All rights reserved.

occasionally studied. The next section outlines the key experimental data and the theories that have been developed to explain this data. A brief look at some more recent approaches is also given. The majority of this article considers the growth process itself, concentrating on linear, flexible polymers as this is where the most complete data set is available, but also touching on more complex materials. An outline of the theories that have been developed to explain and predict crystallization behavior is also given, concentrating on their fundamental assumptions and predictions rather than their mathematical intricacies.

Nucleation

Any supercooled or supersaturated system contains local fluctuations in order and density, which will, at times, correspond to crystallographic order. These crystalline regions are known as embryos and offer the chance, but not the certainty, of starting the process of phase transformation. Most of these embryos are short-lived, but there is a small probability (depending on the supercooling or supersaturation) of any particular fluctuation reaching a critical size. This critical size is the size at which it is in unstable equilibrium with the surrounding phase—it has formed a critical nucleus, and there is a high probability of it continuing to grow to macroscopic size.

Nucleation can be divided into homogeneous nucleation and heterogeneous nucleation, the former being the sporadic formation of critical nuclei from the pure phase, the latter occurring at the surface of impurities within the system. In high polymers heterogeneous nucleation dominates in most cases (13). Heterogeneous nucleation can be divided into different classes; epitaxy, in which there is a lattice match [usually within 10% (14,15)] between a crystal plane in the polymer and a free surface in the "impurity", and nonspecific surface nucleation, in which the presence of the impurity surface leads to a chain conformation closer to that in the crystal. A final class of nucleation is self-nucleation, in which during the melting of the polymer the temperature was too low, or the time at that temperature too short, to allow the whole sample to melt. This is particularly common in polymers and is caused by the broad range of melting temperatures typically present in any sample because of a combination of factors including the range of crystal sizes, molecular weight, chain perfection, and local environment. Small crystalline "seeds" are left in the sample, which then act as epitaxial sites for nucleation on cooling (16,17), leading to the name "self-seeding" being applied to this form of nucleation.

Experiments on Nucleation. The most commonly observed crystal morphology when polymers are crystallized from the quiescent melt is the spherulite (see SEMICRYSTALLINE POLYMERS) (18). Figure 1 shows a typical polarized light micrograph of the growth and intersection of a spherulitic sample, from which it can be seen that the individual spherulites intersect with each other to form polygons with straight sides. It is immediately apparent that, assuming the growth rate is constant across the sample, all of the nucleation sites must have become active at the same time, that is, the growth of all the spherulites started at the same time. If the same sample is melted and then recrystallized at the same temperature, the spherulites grow back in the same place. Nucleation is heterogeneous under these most common circumstances, occurring on impurities or added nucleating

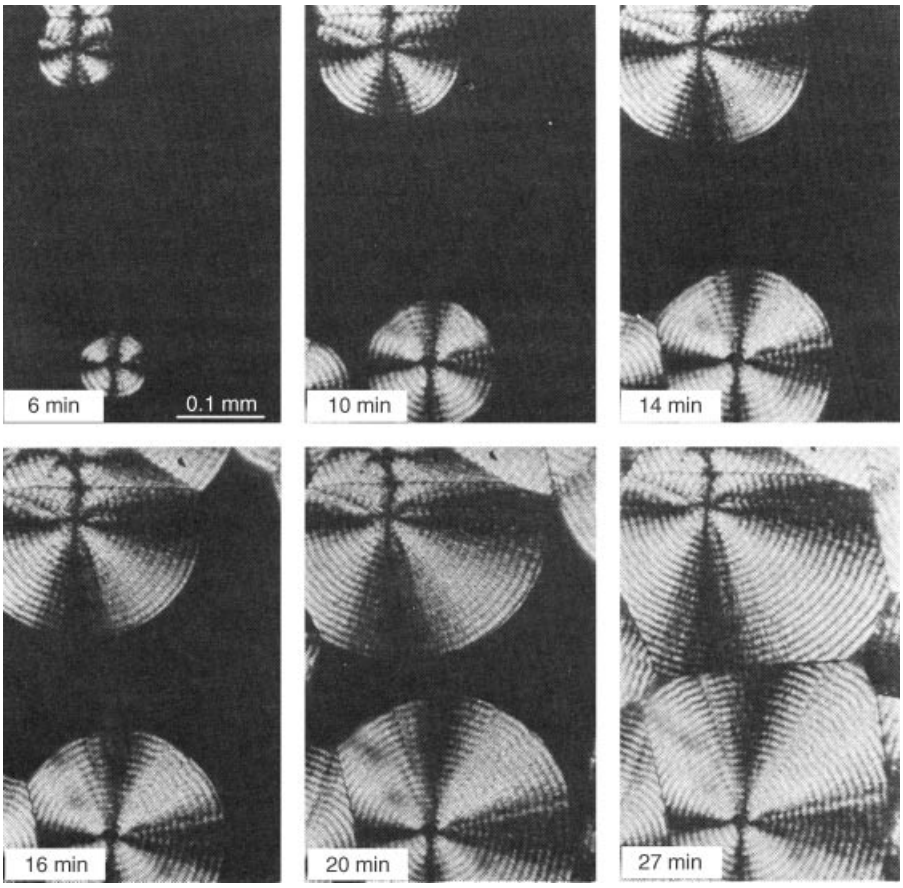

Fig. 1. A series of images showing the growth of spherulites of polyethylene. The uniformity of spherulite size, and the linear intersection of the spherulites once crystallization is complete, can be clearly seen. Exposures taken after the marked times. Optical micrographs with the sample between crossed polars. Reprinted from Ref. 19. Copyright (1982), with permission from John Wiley & Sons, Inc.

agents. Measurement of the size of the spherulites gives a measure of the number of nuclei per unit volume, and the variation of this with temperature can be simply obtained (20). Some polymers behave differently, nucleation occurring more sporadically, giving a measurable nucleation rate as a function of crystallizable volume at a particular temperature (21,22). An example of this behavior is shown in Figure 2 for polyethylene succinate, with the variation with molecular weight also included. Whether this nucleation is actually homogeneous, or if the number of heterogeneities and their relative activity is just low, is unclear.

Great lengths have been gone to in order to obtain truly homogeneous nucleation rates. Initially, one of the driving factors for this work was to obtain a figure for the side surface free energy for use in secondary nucleation crystal growth theory. In systems such as polyethylene, where nucleation rates are high and purity is low, it is necessary to divide the sample up into a large number of droplets

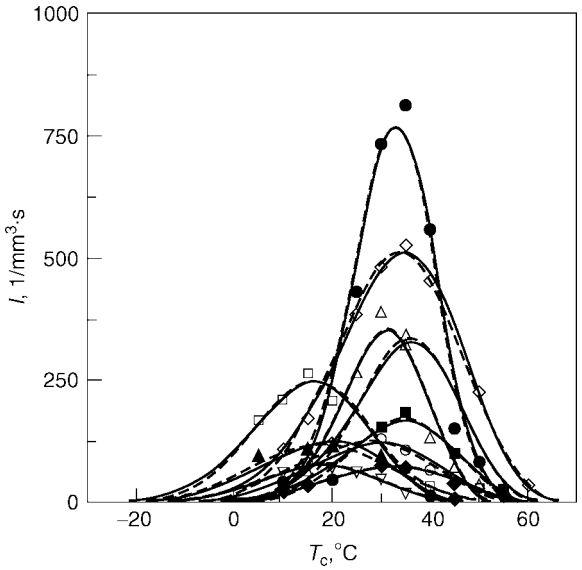

Fig. 2. A graph showing the temperature dependence of the nucleation rate for a series of different molecular weight fractions of polyethylene succinate. The molecular weight shown is the peak molecular weight as measured by GPC. mp: □ 1,160, ▲ 2,060, ▽ 3,380, ◆ 4,660, ○ 6,670, ■ 8,770, △ 10,980, ▼ 13,660, ◇ 18,340, ● 21,210. Reprinted from Ref. 23. Copyright (2002), with permission from Marcel Dekker, Inc.

(19,24–27). Many of the droplets will contain impurities and nucleate relatively early in the experiment; however, some will remain amorphous for long times, and, if the rate of nucleation in these droplets is measured, the variation of nucleation rate with temperature can be obtained. If the nucleation is truly homogeneous, and the droplet size is monodisperse, the nucleation rate should, at a particular temperature, depend only on the sample volume. Recently, similar experiments have been carried out on phase-separated block copolymers, in which the crystallizable domains are isolated spheres in the hard (or semihard) segregation limit (28,29). An example of data obtained by these two different methods is shown in Figures 3 and 4.

Nucleation Theory. Classical theories for nucleation in small molecules balance the reduction in free energy that occurs because the solid is more stable than the supercooled liquid against a surface term that accounts for the free-energy cost of creating a solid–liquid interface. For a spherical crystallite this is given by

$$\Delta G = \frac{4}{3}\pi r^3 \Delta G_v + 4\pi r^2 \sigma \tag{1}$$

Where ΔG is the Gibbs free energy, r is the radius of the sphere, ΔG_v is the difference in free energy between the bulk fluid and bulk crystalline phase, and σ is the surface free energy of the crystal fluid interface. The function ΔG goes through a maximum at the critical nucleus size, resulting in a nucleation barrier—the maximum in the increase in free energy necessary to form the critical

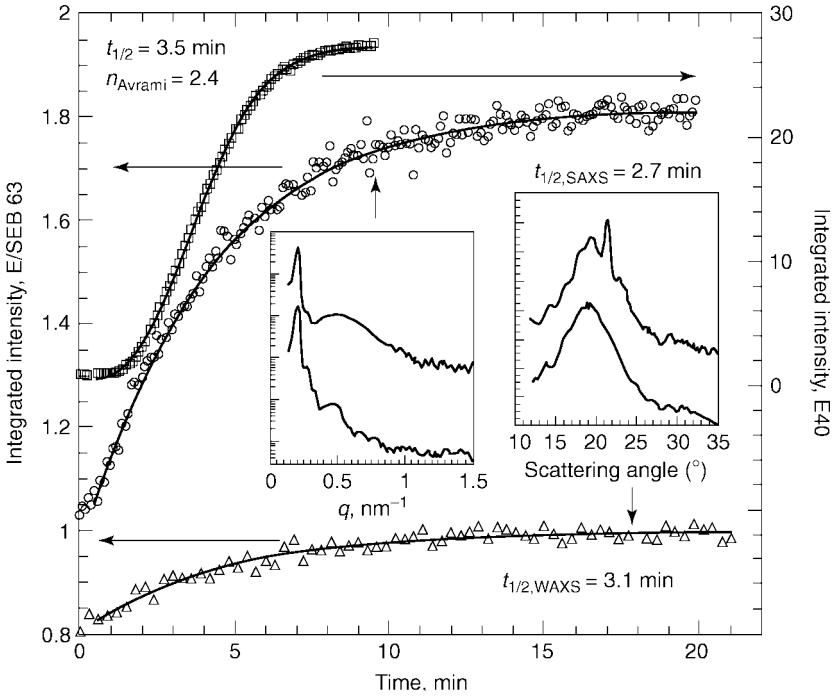

Fig. 3. A composite graph showing the crystallization of micro phase-separated spheres of E/SEB63 (polyethylene block styrene–ethylene–butene). The polyethylene block exists in spherical domains with a radius of 12.7 nm in a matrix of rubbery material. At sufficiently high supercoolings the polyethylene nucleates separately in each domain. The graph shows the time course of the integrated small-angle X-ray scattering (middle curve) and wide-angle X-ray scattering (bottom curve) intensities for E/SEB63 crystallized at 67°C (the insets show the regions of integration). The SAXS intensity for the polyethylene (E40) homopolymer, which shows a sigmoidal time evolution, is shown for comparison (top curve, 95°C, similar half-time). Reprinted from Ref. 28. Copyright (2000), with permission from the American Physical Society.

nucleus—given by

$$\Delta G^* = \frac{16\pi\sigma^3}{3(\Delta G_\upsilon)^2} \tag{2}$$

For polymers the situation is changed by two factors. Firstly, the connectivity along the chain of identical crystallizing units means that the nucleus is unlikely to be spherical, and a better first approximation is a cuboid. Secondly, the end surface (the surface perpendicular to the chains) has a very different energy from the side surface. These lead to a slightly different equation, allowing for the different geometry, given by

$$\Delta G = -\upsilon\mu l a_0 b_0 \Delta G_\upsilon + 2\mu\upsilon a_0 b_0 \sigma_e + 2\sigma l(\mu b_0 + \upsilon a_0) \tag{3}$$

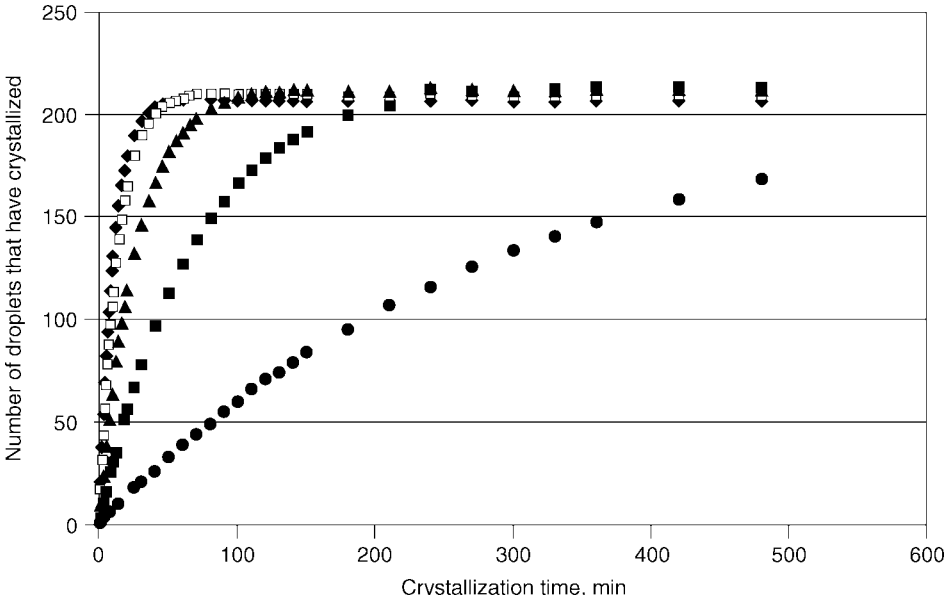

Fig. 4. A graph showing the rate of nucleation of droplets of polyethylene. Isolated droplets are produced by spraying from solution. As the droplets are only ~1 μm in size, most of them do not contain large heterogeneous nucleating agents so high supercoolings can be reached. The nucleation rate can be measured directly by counting the number of droplets that have crystallized as a function of time. The data were all collected from the same preparation of droplets, which could not be cooled below 87°C without all the droplets crystallizing. ◆ 87.5°C, □ 88.4°C, ▲ 89.6°C, ■ 90.1°, ● 90.8°C. Reprinted from Ref. 27. Copyright (2000), with permission from Kluwer Academic Publishers.

Where ν and μ are the number of stems in the length and breadth of the lamella, a_0 and b_0 are the cross-sectional dimensions of a stem, l is the thickness of the lamella, ΔG_v is the difference in bulk free energy between the crystalline and liquid phases, σ_e is the fold surface free energy, and σ is the side surface free energy. This then leads to the rate of formation I of folded chain nuclei given by

$$I = I_0 \exp\left[\frac{-\Delta F_D}{kT}\right] \exp\left[\frac{32\sigma^2\sigma_e(T_m^0)^2}{kT(\Delta T)^2(\Delta H_v)^2}\right] \tag{4}$$

which is equivalent to the well-known Turnbull–Fisher equation (30). The factor ΔF_D here corresponds to the energy barrier affecting transport of material across the crystal–liquid interface, and, under the assumption that this is an activated process, leads to the first exponential term. I_0 is essentially temperature-independent and depends on molecular parameters, ΔH_v is the enthalpy of fusion per unit volume, T_m^0 is the equilibrium melting temperature, and k is the Boltzmann constant. Heterogeneous nucleation is introduced simply by altering one of the side surface energies to allow for the relatively low energy penalty associated with the formation of a polymer-nucleating surface interface (13). Experimental studies (19,24–27) are broadly in agreement with the predicted behavior for the

supercooling dependence of nucleation rate under conditions of homogeneous nucleation.

Equations 3 and 4 apply to nucleation with chain folding, and so for a high molecular weight polymer only one or a few molecules might be involved in a single nucleus. This situation could occur in dilute solutions, but seems unlikely as the concentration is increased, or in the melt. An alternative is to assume that the nucleation is of a bundle of stems, each stem coming from a different polymer chain, forming a ciliated or "fringed-micelle" nucleus. Now, in addition to the unfavorable entropy contribution from demixing the polymer from solution, there is an unfavorable contribution from the restrictions on the conformations accessible to the noncrystalline portion of the polymer molecules imposed by their incorporation into the nucleus. Flory (31) [and later Mandelkern (32)] considered these contributions in his original work on polymer crystallization, and, although some of the initial assumptions have proven to be in disagreement with experiment, the resulting formalism is still relevant under certain situations such as the crystallization of parts of chains confined between lamellae. This approach leads to the following expression for the free energy of formation of a ciliated crystal, in the limit of high dilution (polymer volume fraction tends to zero):

$$\Delta G = -\upsilon\mu l a_0 b_0 \Delta G_\upsilon + 2\mu\upsilon a_0 b_0 \left(\sigma_e - \frac{kT \ln \nu_2}{2a_0 b_0}\right) + 2\sigma l(\mu b_0 + \upsilon a_0) \qquad (5)$$

where ν_2 is the volume fraction of polymer.

Testing the above theories, which are in essence just classical nucleation theory applied to polymers, has proved problematic because, as already mentioned, under most circumstances nucleation is heterogeneous and often virtually instantaneous. In the case of polyethylene, it is necessary to divide the polymer into such small volumes in order to observe something that might be homogeneous nucleation that the effect of the surfaces of the droplet might well start to play a significant role (33,34). Studies using block copolymers, although of great value, are studying nucleation in a different polymer, and the effect of connectivity to an uncrystallizable unit is complex (35).

Recently, several groups have reported data collected in the early stages of crystal growth that they have interpreted as being evidence of spinodal decomposition in the melt prior to nucleation and growth (36–38). These follow from similar suggestions made in the 1980s (39–41). The interpretations are based around the observation of small-angle X-ray scattering (SAXS), usually associated with the formation of lamellae, prior to the wide-angle signal that comes from crystallographic order. The evolution of the SAXS signal in this initial stage is characterized by first-order kinetics (Avrami exponent of one), and identified with a spinodal-like transformation. This is a difficult area, as identifying the point at which an increasing signal rises above the background noise is not clear-cut (38,42), and there are many problems associated with comparing wide- and small-angle data (38). It has been proposed that the components of the melt that are phase-separating are segments of the chain that are closer to, and further from, their crystalline conformation. This separation is driven by a coupling between density and order in the chain, in that by aligning, for instance, similarly helical chains they are able to pack more closely and increase the local density

(43). Thus the melt separates into regions of higher order/density and lower order/density, and nucleation is more likely to occur in the already more ordered regions. The "phase" separation drives a change in order into a state that is still far from crystalline, but has a higher probability of crystallizing than the initially supercooled melt. If the transformation occurs under conditions of constant pressure, as is usually the case, it will eventually result in an overall densification of the melt. The theory is internally consistent, but there is still an active debate as to whether or not it actually applies to the experimental situation. A priori, it seems more likely that it is of relevance to polymers with more rigid chains, and crystallization at high supercoolings.

Crystal Growth

In this section an overview of key experimental results on the growth of polymer crystals is given, concentrating on linear molecules with simple chemistry and moderate molecular weight. Although these molecules are the most commonly used in industrial applications, there are many other types of behavior that are markedly different, and some indication of these perturbing effects is given. This will provide the data against which any theory should be tested, and it is the basis of the different theories that are discussed in the next section. Finally, over the last 10 years, there has been a spate of new ideas, due both to the data provided by new experimental techniques such as synchrotron x rays and scanning probe microscopy and to the increasing power of computer simulation. These new approaches are covered in the last section.

Key Experimental Results. Polymer crystals grow in the form of lamellae in which the chain axis is oriented approximately perpendicular to the basal plane (1). As these lamellae are typically between 5 and 50 nm in thickness, the chains must fold back on themselves, reentering the same crystal many times. The extent to which chains reenter the crystal on average at the adjacent lattice site, or elsewhere, has been a subject of argument for 40 years (44). Although the exact nature of this "chain-folding" is still not agreed upon it is this morphological characteristic that signals most clearly the importance of kinetics in polymer crystallization. It has been widely accepted since the early 1960s that the equilibrium polymer crystal contains chains that are extended. The lamellae that are commonly observed are thinner than this, as the most rapid way that the available free energy can be consumed is by the formation of fast-growing thin crystals rather than slow-growing thick crystals.

Figure 5 shows a plot of crystal thickness vs supercooling, showing the increase in crystal thickness that occurs as the melting temperature is approached (45,46). The graph includes data for both solution and melt crystallization, showing that it is not the absolute temperature that is the controlling factor on crystal thickness, but rather the supercooling (or supersaturation) at which crystallization occurred. Supercooling is here defined as the equilibrium melting temperature (T_m^0) minus the crystallization temperature, where the equilibrium melting temperature is the temperature at which an equilibrium, infinite, extended chain crystal would melt. These data were collected for polyethylene, but similar data exist for a range of other polymers. The supercooling controls the crystal thickness,

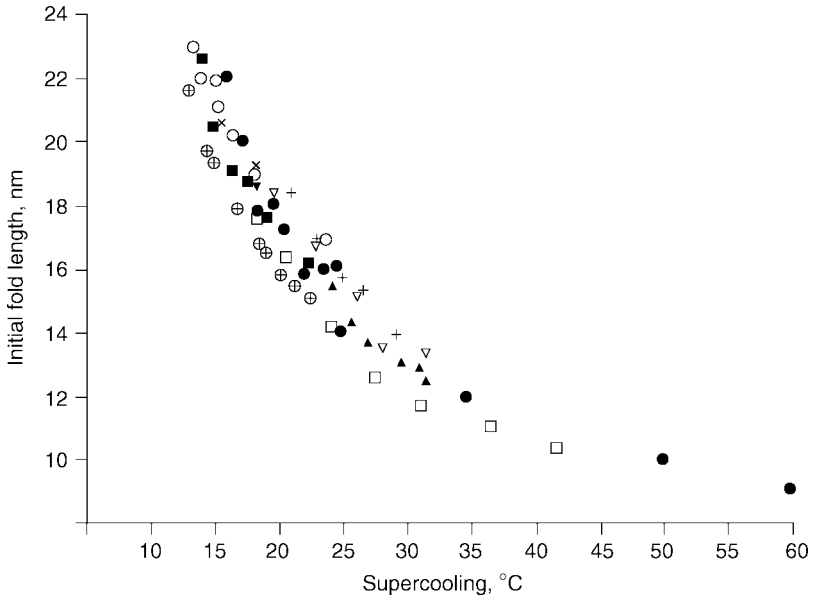

Fig. 5. A graph showing the variation of the fold length (l) with supercooling (ΔT) for polyethylene crystallized from a variety of solvents and from the melt. In the case of solvent crystallization, supercooling is taken with respect to the so-called equilibrium dissolution temperature. For the melt-crystallized data set the equilibrium melting temperature is used. The remarkable coincidence between the curves, despite the wide range of absolute temperatures to which each supercooling corresponds, is strong evidence in favor of the kinetic origin of crystal thickness selection. Solvents: □ xylene, ■ hexyl acetate, ⊕ ethyl esters, ○ dodecanol, ▽ dodecane, ▲ octane, × tetradecanol, + hexadecane, ● melt crystallized. Reprinted from Ref. 44. Copyright (1985), with permission from Kluwer Academic Publishers.

and the thickness that grows is just thicker than the minimum stable thickness at that temperature. This minimum stable thickness comes from the balancing of the increase in energy due to the presence of the crystal melt interface, with the reduction in free energy due to the bulk free energy of the crystal—that is, the Gibbs–Thomson equation. In the case of lamellae with large lateral dimensions this can be simplified to give

$$l_{\min} = \frac{2\sigma_e}{\Delta F} \tag{6}$$

where $l_{\min}$ is the minimum stable thickness, σ_e is the fold-surface free energy, and ΔF is the bulk free energy of crystallization per unit volume.

Interestingly, despite this clear evidence of the influence of kinetics on morphology, the crystal structure itself, and in many cases even the topology of the noncrystalline fold surface, seem to be controlled by equilibrium considerations (47). Recent computer simulations (48), in which a random polyethylene fold surface was allowed to relax, resulted in a 201 crystallographic fold plane, in agreement with experimental observations of crystallization (49).

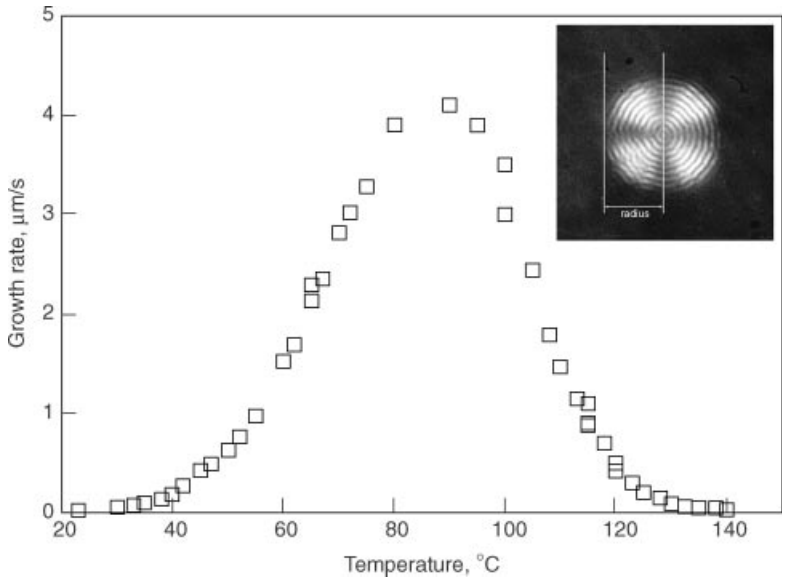

Fig. 6. A graph of the variation in growth rate with temperature for poly(hydroxybutyrate), showing the typically observed bell-shaped temperature dependence, with the crystallization rate reducing to zero well before the equilibrium melting temperature (∼198°C for this polymer) and, after passing through a maximum, again reducing to zero before the glass-transition temperature (∼0°C). (Unpublished data of the author.)

As detailed in the article on semicrystalline polymers, polymer lamellae, when crystallized from the melt, typically form aggregates. The most common of these aggregates, if the melt is unperturbed, is the spherulite. The growth rates of spherulites have been measured as a function of crystallization temperature for a wide range of different polymers. These rates are found to be approximately constant at a particular temperature for a particular polymer sample. An example of the variation in growth rate with temperature of polyhydroxybutyrate, a biodegradable thermoplastic, is shown in Figure 6. A bell-shaped relationship is apparent, typical of glass-forming liquids. Similar data have been obtained for many other polymers, the lower limit of the growth depending on the glass-transition temperature of the material, the upper limit depending on the melting temperature, and the peak rate varying from only a few nanometers per second to hundreds of micrometers per second, depending on the polymer. The inset shows an optical micrograph of a growing spherulite from which rate measurements can be made. The rate that is measured in a typical experiment is the average growth rate of many lamellae as they grow over a distance of several microns. It is not the growth rate of an individual lamella, and is certainly not measured over length scales comparable with either the size of the unit cell, or even the thickness of a lamella. This is simply a result of using diffraction-limited optics to measure rate.

It is common practice to replot ln(growth rate) against $1/T\Delta T$, so as to linearize the data and to allow its analysis in the context of secondary nucleation theory (see section under Secondary Nucleation Theory). A large body of data

exists in which these essentially linear plots contain one or two changes in slope, and the different linear portions are associated with different "regimes" of growth (50–58). This is a difficult area, and has been the subject of debate for many years (58,60). There certainly are instances when a true change in the temperature dependence of growth rate occurs, in many cases accompanied by a change in the crystal morphology. A systematic survey of the effect of varying the additional transport term that is often included in the y-axis of the plot, or of the often imprecisely defined value of $T_m{}^0$, is not available. However, growth rate is clearly exponentially dependent on $1/T\Delta T$ at small supercoolings.

The rate of growth is influenced not only by molecular architecture and temperature, but also by molecular weight (61). Figure 7 shows the effect of molecular weight on growth rate for a series of different molecular weight fractions of polyethylene succinate (62). The variation in growth rate with molecular weight leads to complex effects during polymer crystallization, as in all high polymer

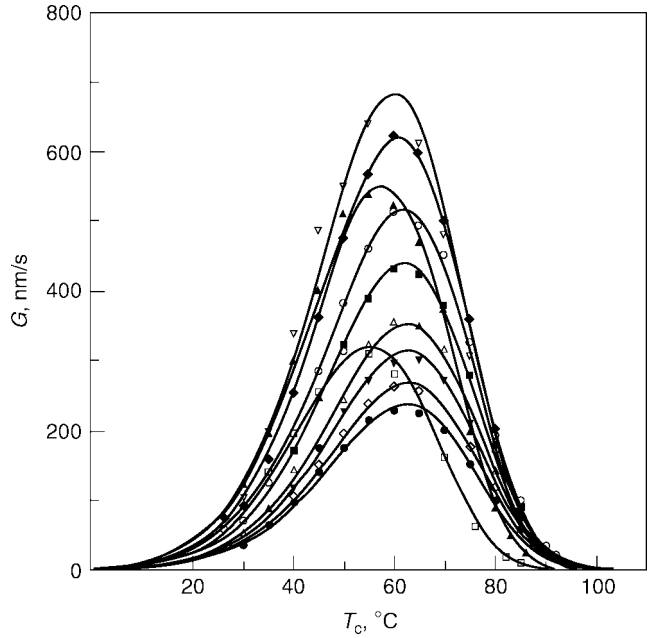

Fig. 7. A graph showing the variation in linear crystal growth rate with temperature for a series of different molecular weight fractions of polyethylene succinate, showing the typically observed behavior. Again, the molecular weight shown is the peak molecular weight as measured by GPC. In Ref. 61 the authors obtain a "master curve" for polymer growth rate by plotting the reduced growth rate G/G_{max} (where G is the growth rate and G_{max} is the fastest growth rate exhibited by the particular polymer sharp fraction) against the reduced temperature T/T_{cmax} (where T is the crystallization temperature and T_{cmax} is the temperature at which the maximum growth rate occurs). This leads to the intriguing possibility of a universal relationship between growth rate and molecular weight. In particular, it is found that the molecular weight dependence of G_{max} can be expressed as a power law, G_{max} proportional to MW^{α} where α depends on the adsorption mechanism for polymer molecules on the growth front and is equal to -0.5 for folded chain growth. MP: □ 1,130, ▲ 2,080, ▽ 3,220, ◆ 4,590, ○ 6,570, ■ 9,150, △ 10,900, ▼ 13,700, ◇ 17,900, ● 21,600. Reprinted from Ref. 62. Copyright (2002), with permission from Elsevier Science Ltd.

samples there is a distribution of chains with different molecular lengths. Careful studies of the molecular weight distribution within the crystallized and uncrystallized portions of a sample at different stages of growth have shown a remarkable degree of fractionation (63,64). At high temperatures the longest chains crystallize most readily and so fractionation occurs during growth, leaving the shorter molecules to either crystallize more slowly later, or on cooling if the distribution of lengths is very broad. At lower temperatures, the shorter chains are able to crystallize more rapidly, due to their shorter relaxation times, and thus they will have a stronger influence on the measured growth rate. The extent of fractionation, particularly apparent during solution crystallization, has lead to the suggestion that there must be a process of "molecular nucleation" (65), in which each molecule nucleates on the growth front as a separate object rather than the important step being the nucleation of parts of a chain or chains. This provides a mechanism by which the growth process can "feel" the molecular length of each chain that attaches to the growth front. A fuller discussion is given in Reference 65.

Crystallization studies carried out in dilute solution have frequently been used to gain additional insights into the process of growth, as the crystallizing lamellae can be more straight forwardly examined by electron microscopy after their growth (66,67). Figure 8 shows an atomic force microscope (AFM) topography image of a typical single crystal of polyethylene, from which the very regular crystal thickness can be seen. The well-defined crystallographic shape is typical of solution-grown crystals of many (but not all) polymers, their exact shape depending on the underlying crystallography and the interplay of growth rates of the different crystal faces, which also varies with crystallization temperature (see SEMICRYSTALLINE POLYMERS for more detail on crystal shape). Crystal thickness is typically plotted against the equilibrium dissolution temperature, a temperature that has an ill-defined meaning (68,69), but these plots give a remarkably similar temperature dependence of thickness to that seen for melt crystallization, in the case of polyethylene. Despite technical difficulties, growth rates as a function of temperature can be measured by careful experimentation (70–75), and can be plotted to give an approximately linear relationship with $1/T\Delta T$. An example is shown in Figure 9. The additional complexity that the effect of polymer concentration adds to the story has been studied in some detail (71–75), but is beyond the scope of this review.

There are many factors that can affect the way crystallization occurs, and lead to differences from the above outlined pattern of behavior. Linear homopolymers consist of repeating units, all of which can crystallize. Even in this simple case, the end groups are chemically different from the rest of the chain, and this can lead to some perturbations in behavior. End groups are usually excluded to the surface of crystals (76). For low molecular weight polymers ($M_w < 10{,}000$), the presence of end groups starts to play a role in the rate of crystallization (77–79). In polymers of very uniform molecular weight, such as the monodisperse alkanes (78), and sharp fractions of low molecular weight poly(ethylene oxide) (77,79), local minima in the variation in free energy with crystal thickness exist, such that the formation of crystals that are an integer fraction of the extended chain crystal thickness is strongly favored. In this case, steps and even minima in growth rate are observed in the region where the crystallization temperature allows thinner crystals to become stable (80). An example of these local minima in growth

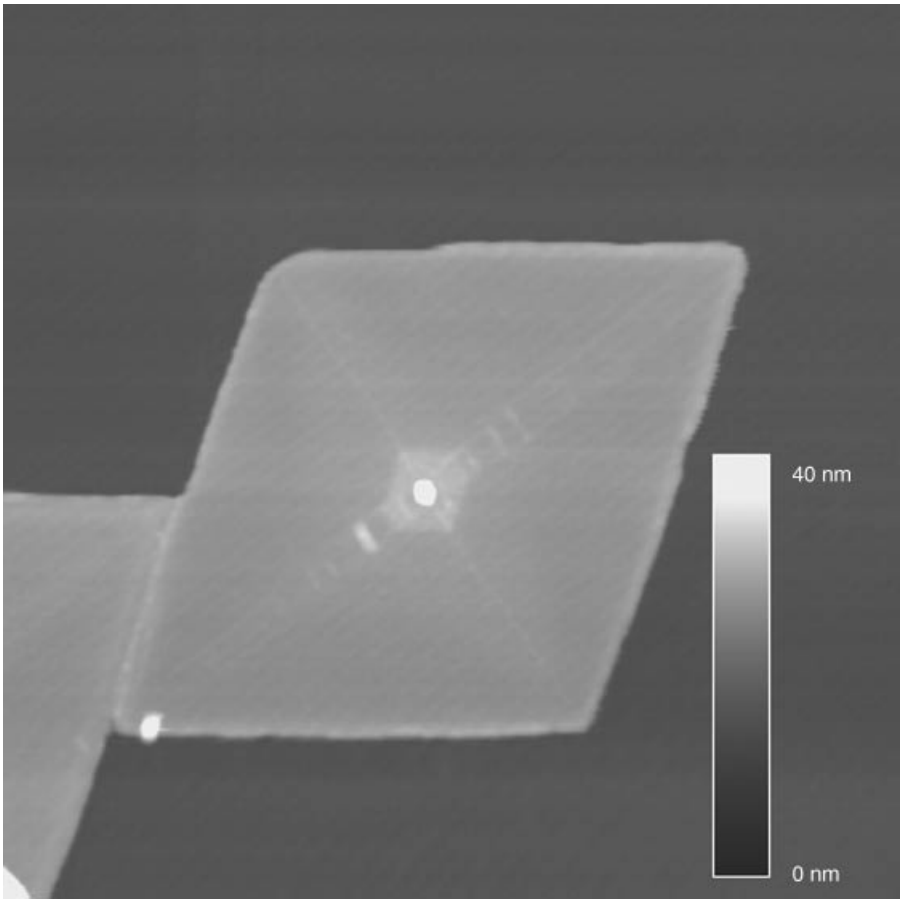

Fig. 8. An AFM topographic image showing a group of single crystals of polyethylene crystallized from xylene at 70°C. The grey scale shows the variation in height, from which the very uniform thickness of the crystal can be clearly seen. (Unpublished data; image courtesy of Dr. A. K. Winkel).

rate is shown in Figure 10 (81). These minima occur because of competition at the growth front between different metastable "phases"—for example once-folded and twice-folded crystals (82).

If copolymers are crystallized, it is necessary to consider the cocrystallizability of the different chemical species (31), the length and distribution of sequences, the miscibility of the melt (ie, do the comonomers mix) (83), and many other factors (84). These areas have all been extensively studied, and are still the subject of active debate. However, the recent advent of more controlled techniques for polymerization offers hope of reaching a greater understanding. In most cases, one of the copolymer species will crystallize, excluding the other from its lattice. Crystals can only form if sequence lengths are sufficiently long to span the thickness of the crystal, and so an additional control on crystal thickness, on top of kinetics, is added. It is now necessary to sort the molecules at the growth front so as to access the crystallizable sequences, and this additional step slows the growth

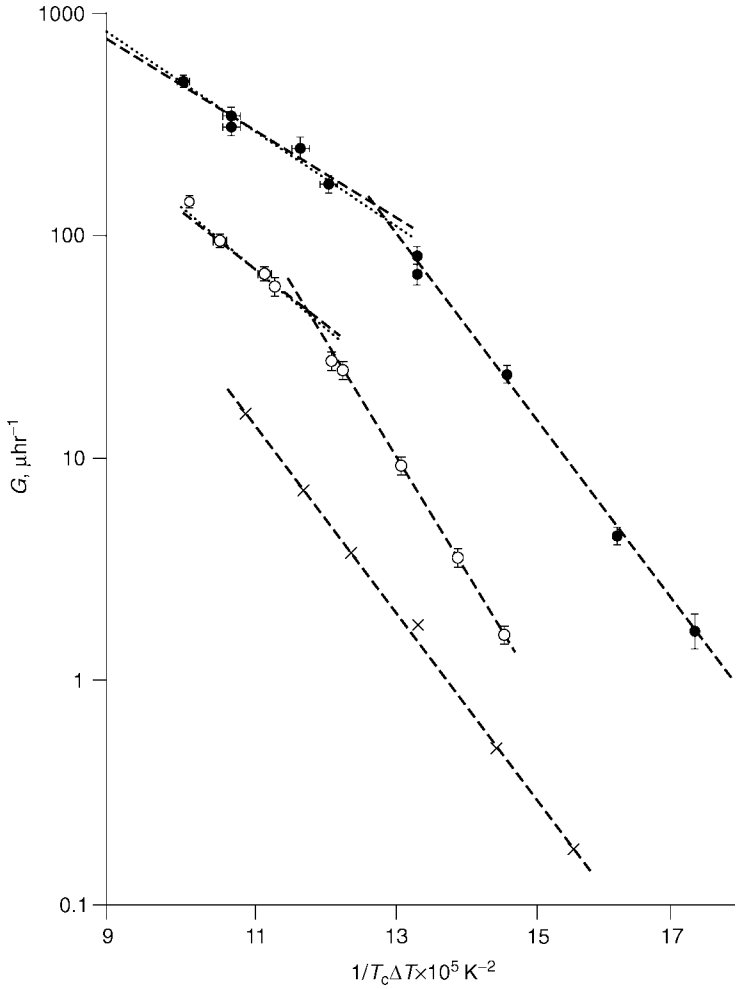

Fig. 9. A graph showing the variation in growth rate with $1/T\Delta T$ for single crystals of polyethylene grown from different solvents. The top data set is for 0.05% Rigidex 50 in tetradecanol, the middle one of 0.05% Rigidex 50 in hexadecane, and the bottom one for 0.l% Marlex 6009 in xylene. The best fit lines (dashed) show an approximate linear dependence, while the dotted lines in the top two data sets are lines in which the ratio of the slopes to the higher temperature lines is exactly 2, as predicted by theory (see section under Secondary Nucleation Theory). Reprinted from Ref. 74. Copyright (1986), with permission from John Wiley & Sons, Inc.

rate. Also, at a particular temperature, some sequences will be too short to crystallize (crystals of a thickness commensurate with the length of the sequence are not stable at that temperature), and so will be unable to crystallize until a lower temperature is reached. Lower total crystallinities are usually obtained, because it is not always possible for all of the sequences that are potentially crystallizable at a particular temperature to find a crystal into which to crystallize, considering the constraints due to the crystallization of other sequences in the same chain. A very similar behavior is observed with branched polymers, as longer branches

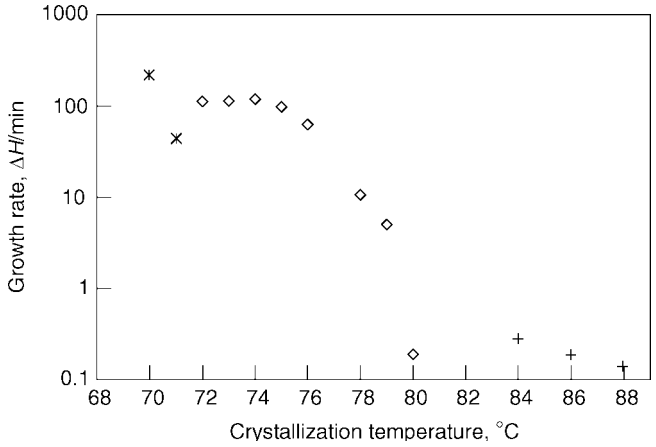

Fig. 10. A graph showing the variation in crystallization rate with temperature for the ultralong alkane $C_{246}H_{494}$. + extended chain growth, ◇ integer once-folded chain growth, ∗ twice-folded chain growth. A minimum in crystallization rate can be seen at the temperature where the transition from primary growth in different folded forms occurs. This is believed to be caused by competition at the growth front between the more stable thicker crystal and the now just stable, thinner form. Reprinted from ref. 81. Copyright (2000), with permission from Elsevier Science Ltd.

are excluded from the lattice (85). The distance between branch points defines the maximum crystal thickness into which a particular chain segment can crystallize. If this is thinner than the minimum stable thickness for a crystal, the chain segment cannot crystallize at that temperature. Again, this leads to a slowing of the overall growth rate, a reduction in the achieved crystallinity, and a widening of the temperature over which crystallization occurs. In the case of polyethylene, which has been extensively studied because of the commercial importance of low density polyethylene, some material is believed to not crystallize until temperatures below $-20^{\circ}C$ are reached. If high pressure is added, it has been shown (86) that it is even possible for the side branches to crystallize, albeit into a hexagonal phase.

As well as chain chemistry and chain length, different behaviors from the above outlined "typical behavior" can also be found because of differences in the crystallization conditions of an otherwise "typical" flexible linear polymer. Crystallization under flow leads to a change in morphology (87–89). Initially, oriented nuclei are formed with a largely extended chain character. These nuclei consist of the high molecular weight tail of the molecular weight distribution, both high molecular weight and polydispersity apparently being required (89–91). From these oriented backbones, plate-like lamellae then grow, largely perpendicular to the backbone, as shown in Figure 11 (92). These lamellae grow in a manner similar to that seen in the absence of flow, and have been used as model geometries for the study of lamellar growth (93). However, the growth of the backbone itself is very difficult to follow, due both to its size—although up to several microns in length, their width is typically less than 10 nm—and the very rapid rate of its formation.

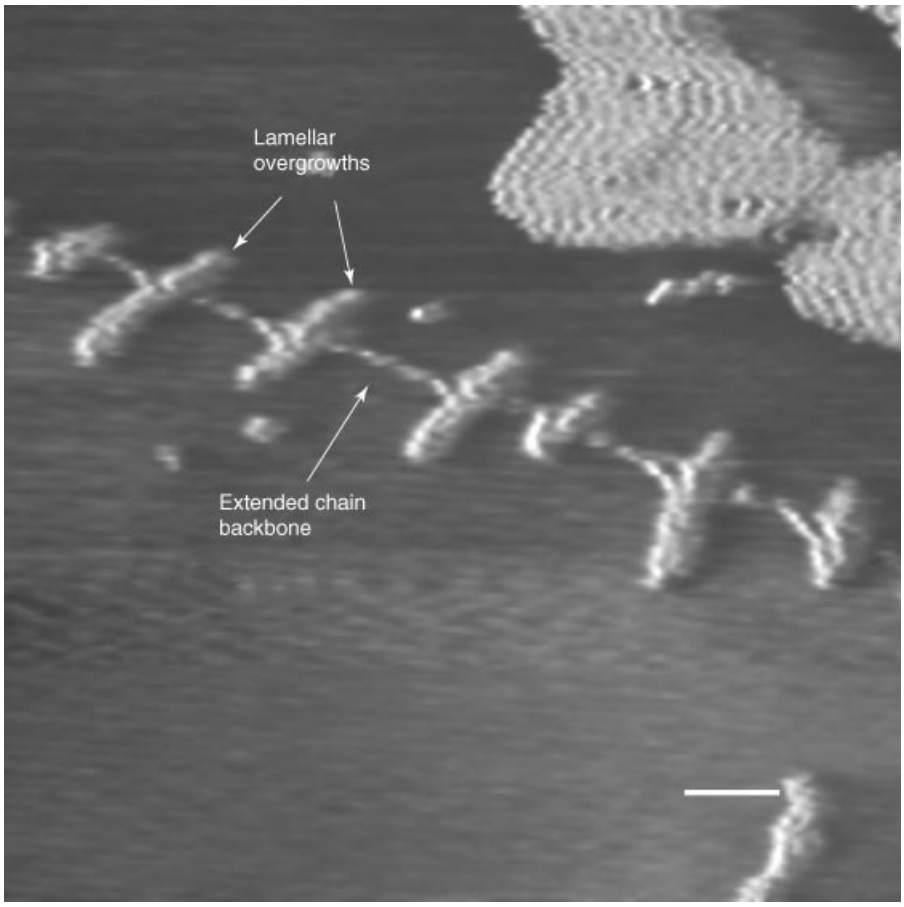

Fig. 11. An AFM micrograph (phase image) showing a shish-kebab crystal of polyethylene in a matrix of molten polymer. Image collected at 135°C. The bright area in the top right of the image is the glass substrate. The extended chain backbone and lamellar overgrowths can be clearly seen. The scale bar represents 100 nm. Reprinted from Ref. 92. Copyright (2001), with permission from the American Chemical Society.

In many commercial applications, polymers are now being used to add value through the use of very thin coatings whether protective, lubricating, or with some other purpose (94). This, combined with new techniques such as AFM, has led to an increased interest in crystallization in thin films (95–98). Once film thickness becomes comparable with the size (eg, radius of gyration) of the polymer molecule, both the morphology and kinetics of crystallization start to change. In very thin films, where the film thickness is thinner than the thinnest stable crystal thickness, it is clear that material transport dominates the morphology, leading to morphological instabilities [such as the Mullins–Sekerker instability (99)], and dendritic structures (100). An example of such a structure in poly(ethylene oxide), in which the morphology is dominated by material transport, is shown in Figure 12. Figure 13 shows the variation in growth rate, with film thickness at a constant temperature in isotactic polystyrene (98), in which a change in the

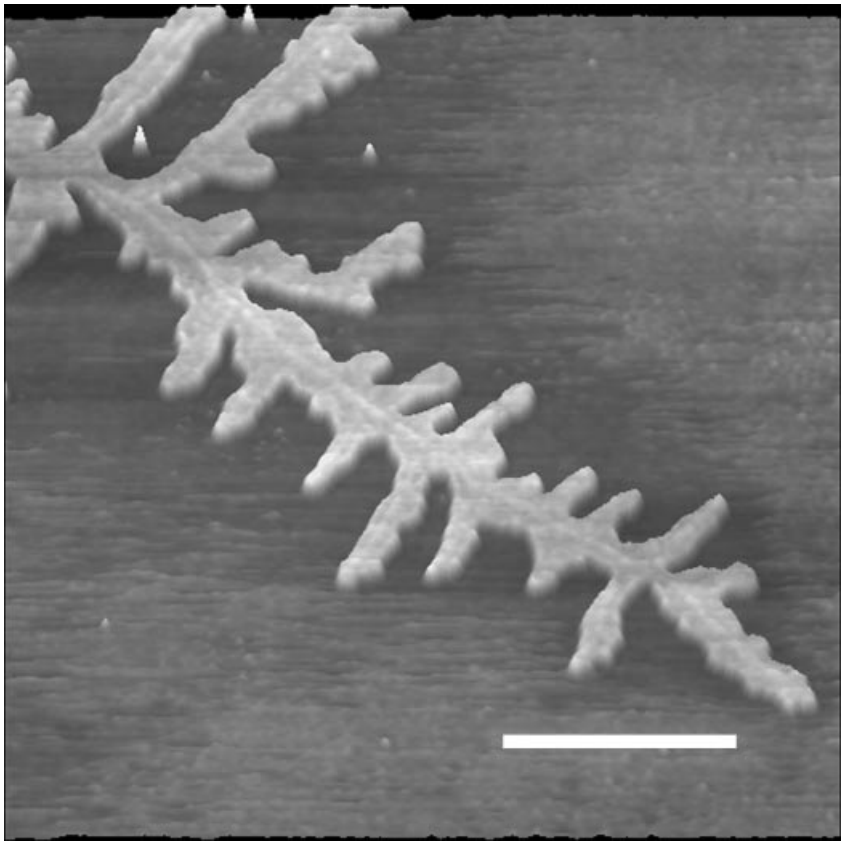

Fig. 12. An AFM image showing part of a growing poly(ethylene oxide) dendrite in an ultrathin film on a glass substrate. A topography image, black to white represents 20 nm, is presented in pseudo 3-D. The scale bar represents 1 μm. (Unpublished data of the author).

growth rate dependence once the film is thinner than the crystal thickness can be seen. Polymers can provide model systems for the study of diffusion-limited growth structures because of the tunability of the crystallization conditions, and the relatively slow rates of growth compared to small molecules (101,102).

It is worth noting that under industrial processing conditions, the behavior outlined above cannot be simply applied. Typical industrial grade polymers have wide molecular weight distributions, poorly characterized degrees of branching, and possibly copolymer content. Crystallization is often carried out during a rapid quench, and so the temperature varies during crystallization and across the sample. Also, crystallization often occurs at high supercoolings where, in polyethylene for instance, accurate growth rate data have not been obtained. The general assumption has been that the behavior during growth under these conditions is a simple superposition of the effects that have been studied under more controlled environments. However, this may not be the case, and predictive phenomenological models are only now starting to be produced for these complex but commercially important situations.

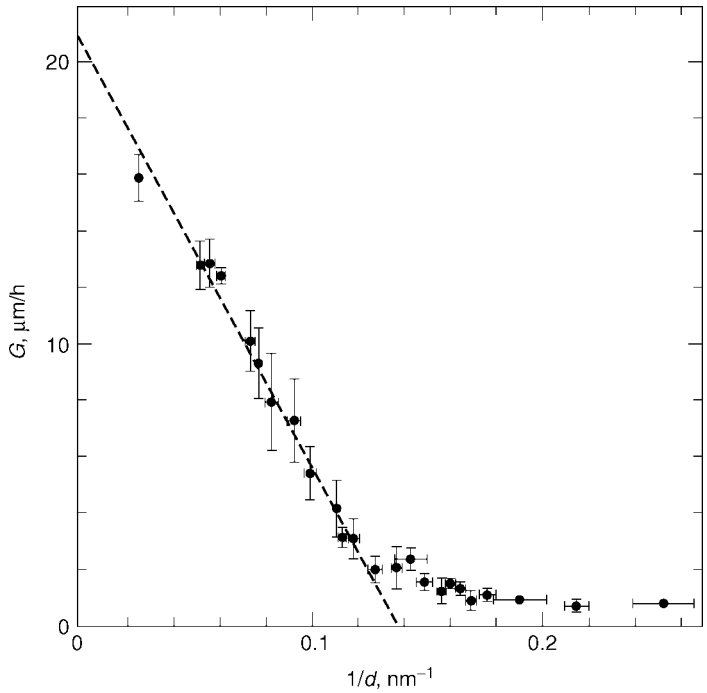

Fig. 13. A graph showing the variation of growth rate with the inverse of film thickness ($1/d$) for isotactic polystyrene crystals grown at 180°C in ultrathin films. A step in the behavior can be seen at a thickness of ~8 nm. At this temperature, this corresponds to the thickness of the single lamella, showing a change in thickness dependence once the film is thinner than the growing crystal. Reprinted from Ref. 98. Copyright (2002), with permission from Marcel Dekker, Inc.

Growth Theories

Polymer crystallization theory is a mature area, and there are several review articles available that present and discuss the different theories in great detail (eg, 103,104). Having said that, over the last 5 years or so there has been a flurry of new interest because of the increase in computational power, which has the potential to decisively enter the debate in some areas. In the following the underlying themes of the two principle theories of polymer crystallization, secondary nucleation theory and rough-surface or entropic barrier theory, are outlined. The results of more recent simulations are then briefly discussed, in which the constraints of the above theories, introduced to provide analytical solutions, have been relaxed. Finally, some of the more fundamentally different ideas that have recently appeared are discussed.

Out of the above overview of experimental data, crystallization theories have aimed primarily to explain three observations: the dependence of crystal thickness on supercooling, the dependence of crystal growth rate on supercooling, and the shape of single crystals grown from dilute solution.

In all systems, crystallization occurs because of the lower free energy, over a certain temperature range, of the crystalline phase compared to the disordered

melt, solution, or vapor phase. The processes that occur as the material transforms from one state to another are very complicated and diverse. However, they can be categorized into interface and diffusion-controlled growth. In diffusion-controlled growth it is the rate of transport of something—heat, mass, etc—either to or from the growth front that limits the rate of growth. In interface-controlled growth it is the actual process of attaching and detaching molecules at the surface that controls the growth rate. In some situations both processes can have a strong influence on the observed crystal morphology (100) and so it is not always simple to determine which is the rate-determining factor. In the case of polymer crystallization most activity has concentrated on the development of theories in which it is assumed that interface-controlled growth dominates. This is most likely a reasonable assumption in dilute solution and possibly also at small supercoolings during melt growth where faceted crystals are sometimes obtained. In both these situations it is intuitive that the physical process of attaching a long polymer molecule in register with a lattice is difficult when compared to small molecule growth. However, it is certainly not clear that it should always be the case as is often assumed. A more detailed discussion of this issue is contained in Reference 103, but suffice it to say that such theories can only be applied with confidence to solution crystallization.

Secondary Nucleation Theory. Polymer secondary nucleation theory is an extension of nucleation theory in small molecules, but allowing for the connectivity of the units that constitute the crystal (ie, the polymer chain). In all crystal growth theories there is a driving force for crystal growth that comes from the lower free energy of the crystalline phase when compared to the liquid phase (be that melt or solution). In nucleation theory the barrier to growth is provided by an increase in surface energy that is postulated to occur when a crystallizing unit attaches in crystallographic register onto the growth front. This energy increase is due to the formation of a new crystal–liquid interface. The attachment of a single unit does not release sufficient energy to make up for the increase in free energy associated with the formation of a new surface, and so several units must form together, through random fluctuations, to provide a "nucleus." This nucleus is a crystal patch of sufficient size that the addition of further units leads to a reduction in free energy rather than to an increase. The most probable process is then for the patch to continue to grow, rather than to dissolve. The process is termed *secondary nucleation* because it considers the nucleation of a new patch onto an existing crystal, in contrast to *primary nucleation* that deals with the formation of the first nucleation event.

The various nucleation theories differ in the exact way in which the attachment process is envisaged to occur, and in what nucleation process is presumed to be the most important (105–108). Figure 14 shows the situation that is usually considered and the definition of the different surfaces. In most nucleation theories, for instance Lauritzen–Hoffmann theory (105), the nucleation process is the attachment of the first stem. This occurs in a single step [more generalized cases where it occurs in multiple steps have been considered (109–111)], and the addition of further stems leads to a reduction in the total free energy of the crystal. Some justification and discussion of reducing the complex process of depositing an entire stem to a single step is given by Frank (4). Once the first stem has deposited, further increases in free energy only occur when a new fold is formed, and this has

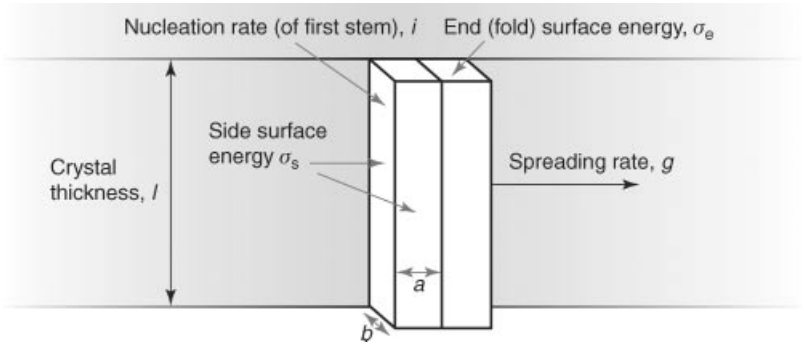

Fig. 14. A schematic diagram representing the growth front of a polymer lamella. The polymer chain is represented by a series of boxes (stems) with defined surface energies.

a high energy associated with it that can be approximated by the loss in energy that occurs from the exclusion of the fold monomers from the crystal lattice. Most forms of secondary nucleation theory assume that the chain folds back on itself into the adjacent lattice site, and so the deposition of each new stem leads to an additional fold surface energy.

The rate at which stable patches nucleate on an existing crystal substrate, i, and the rate at which stable patches grow, g, controls the overall rate of crystal growth. At a particular temperature, crystals with a thickness below a certain critical value (usually denoted $l_{\min}$) are unstable as, however many stems are added, the surface energy is always greater than the bulk free energy of the crystal (this is simply the Gibbs–Thomson melting point depression due to limited phase size). This minimum stable crystal thickness decreases with decreasing temperature, and gives a lower limit to the possible thickness that can grow at a particular temperature. Conversely, the rate of nucleation of stable patches, i, decreases as the thickness of the patch increases because of the increasing free-energy cost of creating the two new lateral surfaces on either side of the first stem. That is, the longer the stem the more side surface it will have and hence a higher barrier to growth. The competition between these two factors leads to a maximum in growth rate at a thickness that is slightly greater than $l_{\min}$.

From the above model of growth three different regimes can be defined, depending on the relative values of i and g.

(1) The rate of nucleation i is considerably smaller than the rate of spreading. Each new patch grows to fill the entire available substrate before a second patch is nucleated. In this case the overall growth rate will be proportional to i.

(2) The rate of nucleation i is sufficiently high that more than one growing patch exists on each substrate. Each patch is also able to support new nucleation events, and so the growth occurs in several layers. In this case the growth rate will be proportional to $\sqrt{(ig)}$

(3) A third situation can also be identified in which the rate of stem nucleation is greater than the rate of spreading, in which case the rate of growth is again proportional to i. Here the growth front has been kinetically roughened.

These three different situations have been termed regime I, II, and III respectively, and a large body of supporting experimental evidence on growth rates has been obtained, largely from melt crystallization, as detailed under Key Experimental Results.

To obtain actual values for the crystal thickness and growth rates, expressions for i and g need to be obtained. Here a brief outline is given, following the approach due to Lauritzen and Hoffmann (105).

The change in free energy ΔG for the formation of a patch with υ stems is given by

$$\Delta G = -abl\Delta F + 2bl\sigma_s + (\upsilon - 1)(-abl\Delta F + 2ab\sigma_e) \tag{7}$$

Where σ_s is the side surface free energy, σ_e is the end surface free energy, l is the thickness of the crystal, a and b are the width and thickness of the stem (as marked in Fig. 14), and ΔF is the bulk free energy of crystallization per unit volume. The term $2bl\sigma_s$ is due to the formation of the side surfaces, $(\upsilon - 1)(2ab\sigma_e)$ is due to the end surfaces, and the terms in ΔF are due to the reduction in free energy because of the lower energy of the bulk crystal compared to the bulk melt. In all cases it is assumed that the "known" macroscopic energies can be simply used. Four rate constants are defined:

(1) A_0: the rate constant for adding a new stem to the substrate
(2) B_0: the rate constant for removing an isolated stem from the substrate
(3) A_1: the rate constant for adding a stem next to an existing stem of the same length (ie, without the formation of any new side surface)
(4) B_1: the rate constant for removing a stem such as that added in A_1.

The excess energy that comes from adding the fold is not included in the initial stem deposition (ie, process A_0), but rather with the deposition of the adjacent stem. A choice is then made about how to apportion the different changes in free energy in view of the physical process of crystallization. This requires the introduction of an additional factor Ψ which defines the proportion of the bulk free energy that is released during the initial deposition of the stem and hence reduces the barrier to deposition that comes from the increase in surface free energies.

From here, the steady-state flux of stems over the barrier can be determined—that is, the net rate of transition of a patch with n stems to a patch with $n + 1$ stems assuming that the total number of patches with n stems in the ensemble remains constant. This flux will depend on the thickness of the crystal. At a particular temperature it is assumed that there is a range of different crystal thicknesses that will grow, and the probability of obtaining a particular thickness is proportional to the steady-state flux for that crystal thickness. This leads to the average thickness of an ensemble of crystals given by

$$\langle l \rangle_{av} = \frac{2\sigma_e}{\Delta F} + \delta l \tag{8}$$

where δl is a small additional thickness beyond the minimum stable thickness, an exact form for which can be straightforwardly obtained (105). Thus the observed crystal thickness is slightly greater than the minimum that would be stable at the crystallization temperature, and follows the experimentally observed dependence on $1/\Delta T$. Expressions for the growth rates in the different regimes of growth can be determined by finding the values of i and g (103,105). For example, in regime I, the growth rate is given by

$$G_{\mathrm{I}} = \frac{b}{a}\beta L_{\mathrm{p}} \exp\left(\frac{2ab\sigma_{\mathrm{e}}\Psi}{kT}\right) \exp\left(\frac{-4b\sigma_{\mathrm{s}}\sigma_{\mathrm{e}}}{\Delta FkT}\right) \tag{9}$$

where L_{p} is the persistence length of the crystal (the effective size of the crystal face onto which nucleation is occurring, usually equated with the distance between defects, rather than the total length of the crystal surface). These expressions exhibit the experimentally observed dependence of $\ln G$ on $1/T\Delta T$, although an additional front factor β, which governs the rate of transport of polymer to the crystal surface, is also included. When fitting experimental data to the theory, great care needs to be taken when deciding on the form to be used for β and on the range of other behaviors that could be obtained if a different form was used. In several cases it is possible to introduce or remove multiple kinks in the growth rate curve by the choice of β, and hence to introduce types of behavior, such as growth regime changes, when none may truly exist.

Secondary nucleation theory has had a great deal of success in fitting experimental data, and by so doing obtaining best values for the parameters of the model. It is a highly flexible model and has been adapted to agree with most of the new experimental observations as they have been made. It does, however, suffer from several internal flaws of varying importance (see, for example, References 102 and 111 for a discussion of these) as well as, arguably, an unacceptable level of disagreement with an increasing body of experimental evidence. Whether this can be rectified within the context of a model in which the barrier to growth is nucleation, is currently unclear.

Entropic Barrier Model. Although secondary nucleation theories have been very successful in fitting experimental data on growth rates and crystal thicknesses, there are several areas where, as initially formulated, they have failed. Solution-grown single crystals of polyethylene formed at low temperatures (crystallized from solvents in which there is a high entropy of mixing) have flat, crystallographic surfaces. However, if crystals are grown at higher temperatures, either from solution or in the melt, they have curved edges (113–115). If these surfaces are rough on a molecular scale, then there will be no obvious barrier to nucleation—there will always be a niche available into which a stem can deposit without having to create new side surfaces, so the initial stage of the nucleation of the first stem will never occur. It was also observed that when single crystals formed certain sorts of twins, a niche or reentrant corner exists at the twin boundary where a newly deposited stem would create no new side surfaces and the nucleation barrier would be removed (116). Thus, if the secondary nucleation model is correct, such twin crystals would be expected to grow very rapidly along the axis of the twin boundary. Such enhanced growth at twin boundaries is not generally observed in high polymers. These observations led Sadler and Gilmer

to reject the idea that polymer crystal growth was governed by a nucleation step, and instead to adopt a new approach, dependent on the assumption that polymer crystallization often occurred at sufficiently high temperatures to be above a roughening transition (117).

In simple terms, the roughening transition is the temperature above which the energy cost of forming a step on the surface is less than the entropy gained by its formation. The surface then becomes rough on a macroscopic and often molecular scale. The formation of curved crystal surfaces at high temperatures is immediately explained. However, above the roughening transition, the growth rate is expected to be proportional to ΔT, rather than the experimentally observed form $\ln G \propto 1/T\Delta T$. A new barrier to growth needed to be found, and the then recently developed tool of computer simulation was utilized to do this (118–121).

The thinking behind the computer simulations is as follows. Polymer units are continuously attaching and detaching from the crystal face. Growth occurs through the net accumulation of material onto the crystal face, but the possible positions in which a unit can attach are limited because of the connectivity of the polymer chain. If a stem has folded over, the stem cannot lengthen by the attachment of further units above the fold surface. If the stem is shorter than the minimum thickness it must first unfold (that is, undo the "incorrect" unit depositions) before it can lengthen so as to become stable. Similarly, if a chain forms stems at two sites that are well separated, it might not be possible for them to lengthen without the detachment of one of the stems, due to the length of the connection between the two stems. Through the process of random attachment and detachment a stable crystal will grow, but its growth will be hindered by the necessity to undo, or reject, unviable unit attachments. These fluctuations that occur in and out of unviable states therefore create a barrier to growth that is entropic in origin because it arises from the consideration of all of the pathways available to the system. As the thickness of the crystal increases, the number of possible unfavorable states will increase, giving a barrier to growth that increases with thickness. Models and approximate solutions to the problem show that the barrier increases exponentially with thickness, as required by experimental observation. Through Monte Carlo simulations growth rates and crystal profiles could be obtained, and these could, under certain conditions, agree with experimental observation. Analytical solutions of very simplified models could also be obtained.

The principle objection to the above theory lies in its assumption of a roughening transition, for which little evidence exists. However, as will be seen below, the insight that a nucleation barrier is not required to explain the experimental data is an important one.

New Approaches to Crystallization Kinetics

Over the past decade or so there have been several significant advances both in experimental techniques, and in the power of computer simulation, that have led to an ongoing reappraisal of our understanding of polymer crystallization. In the following, some attempt is made to outline the most significant features of these new ideas and to point the interested reader toward the literature.

Computer simulation has been used as a tool to study the predictions of existing theories, as well as to try to gain an insight into the controlling physics of crystal growth through direct or simplified simulation of the phase transition but with less constraint on how the process occurs (122–127). In a series of papers Doye and Frenkel (128–130) have simulated both secondary nucleation and Sadler's models but with the constraints removed that had previously been imposed either to give analytic tractability, or sufficiently short computation time. In the simulation of the secondary nucleation model the chain is allowed to deposit unit by unit, rather than in a single step, with both attachments and detachments being allowed. This work shows that the proposed nucleation step, that is the deposition of the first stem, does not exist if the first two stems are deposited together—as had been previously suggested by Point (131). The peak in free energy that has to be overcome for nucleation to occur is no longer seen. It is argued that this observation alone invalidates secondary nucleation theory.

In simulations that are not attached to any particular theory the same authors have suggested a new mechanism for the selection of crystal thickness. By carrying out simulations of the deposition of new crystal layers but without any constraint that the new layer must be the same thickness as the previous layer, or indeed that each stem must have the same length as its neighbors, it was found that the growing crystal quickly adopted an average stem length that was slightly thicker than the minimum stable thickness. The mechanism behind this was quite simple. As the chain deposits, there is always a finite probability of it turning back on itself and starting to form a new, adjacent stem. If it does this before the currently depositing stem has reached a stable length, it will most probably detach, and so stem lengths smaller than $l_{\min}$ are disallowed. However, once it is longer than $l_{\min}$, the probability of growing thicker becomes decreasingly small, as there is always the same fixed probability at each new segment attachment that it will fold back to make a new stem. Crucially, the probability of a new stem being longer than the stem in the previous layer is very small as it would no longer be part of a well-defined lattice. Thus there is a particular crystal thickness at every temperature where the most probable thickness of a new layer is the same as the thickness of the previous layer, and this is the crystal thickness that will grow. In other words, there is a fixed-point attractor at a crystal thickness that is slightly thicker than the minimum stable thickness at that temperature—that is, in agreement with the experimental data. Figure 15 shows an example of a growth front formed during a simulation, and a graph showing the most probable stem length of a new stem given the length of the neighboring stem. Perhaps most interestingly, however, is the conclusion that the thickness that grows is not in fact the fastest growing at that temperature but rather the most probable. The same group reanalyzed the Sadler–Gilmer model and concluded that it was predicting a similar type of behavior. The mechanism of thickness selection in that model was also the presence of a fixed-point attractor.

Simulations by Muthukumar and co-workers (133–135) have also thrown considerable doubt on some of the underlying premises of secondary nucleation theory, and also on some of the constraints that are in place in the Sadler–Gilmer model. Specifically, the assumption is generally made that each layer as formed has a particular thickness that is the final thickness of the crystal, the reorganization of the chain within the crystal is not allowed for. The simulations find that

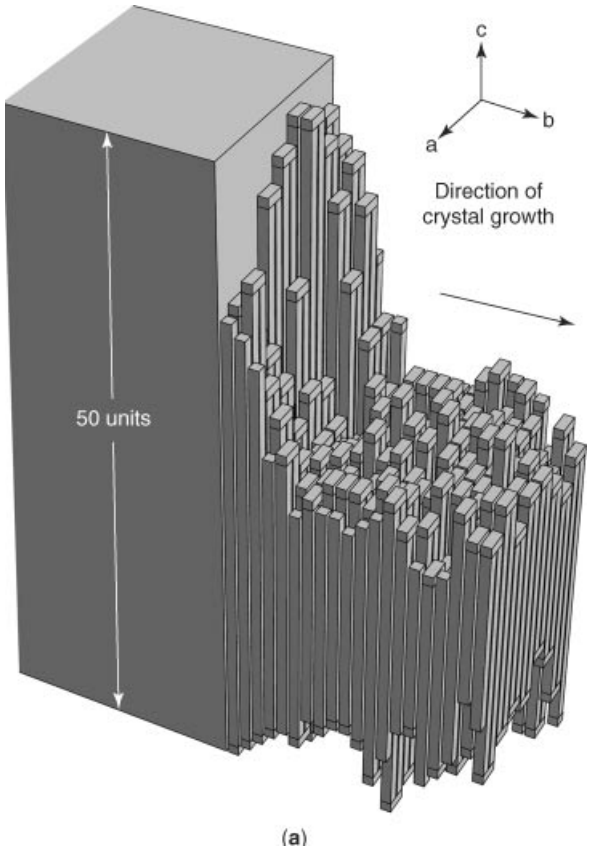

Fig. 15. (**a**) A cut through a polymer crystal grown in the simulation of Doye and coworkers. The crystal was produced by the growth of 20 successive layers on a surface with a uniform thickness of 50 units. The stems are represented by vertical cuboids. The cut is 16 stems wide. (**b**) A graph showing the dependence of the stem length on the length of the previous stem for growth of a single layer on a surface 50 units thick. There is a thickness, in this case 36 units, for which the average length of the next stem is the same as for the previous one, and this corresponds to the average thickness of the layer. This shows the way in which a new layer will converge to a particular thickness dependent on the thickness of the previous layer. Reprinted from Ref. 132. Copyright (1999), with permission from American Institute of Physics.

the process of reorganization is a key part of the crystallization process, and of the selection of the final crystal thickness. The barrier to crystal growth is again found to be entropic in origin.

All of these simulations apply to crystallization from solution but are still constrained by computing power to only a relatively limited extent of crystal growth. Some of the supporting evidence in favor of secondary nucleation theory, such as the crystallographic shape, has not been dealt with explicitly. However, there clearly is considerable conflict between the existing theories and these new data, and the acceptance of a model for polymer crystal growth from solution or under similar conditions (136), in which the barrier to growth is entropic in origin, is perhaps emerging.

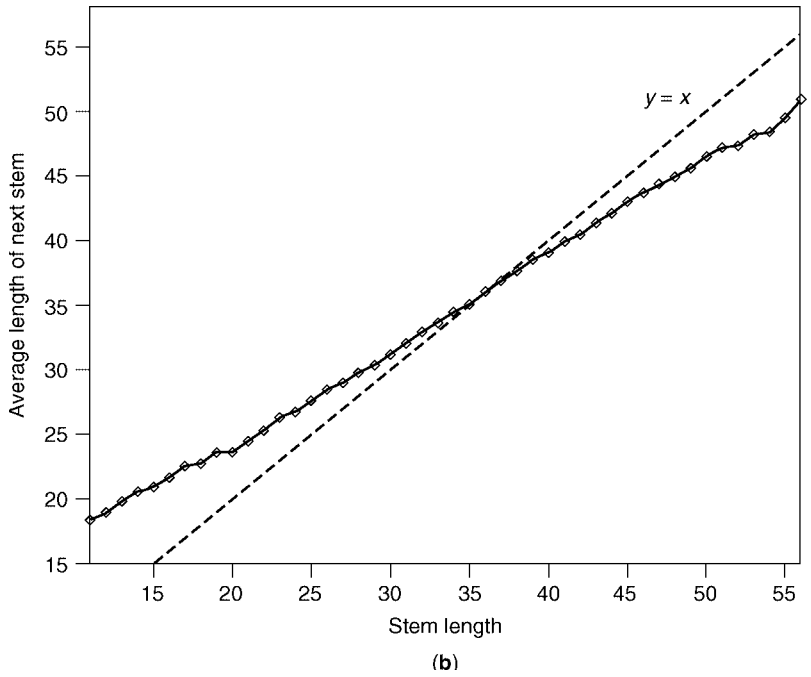

(b)

Fig. 15. (continued)

In addition to new insights gained from computer simulation, new experimental techniques have led to some reassessments of previously accepted wisdom. The suggestion that spinodal decomposition of the melt could exist as a precursor to polymer nucleation has already been mentioned. Several groups have suggested that crystallization occurs through a series of intermediate stages and that the final crystal structure is not a reflection of the structure that initially formed from the supercooled melt (137–141).

The ideas of the Bristol group (137,138) were based on the observation that polyethylene has a stable hexagonal phase at high temperature and pressure, with a hexagonal–orthorhombic–liquid triple point at a temperature of $\sim$215°C and a pressure of $\sim$3.6 kbar. If the polymer was crystallized at slightly lower temperatures and pressures than the triple point, the initial crystal form was still clearly hexagonal, although at a later time a transformation into the more stable orthorhombic form sometimes occurred. This led to the suggestion that, even under ambient conditions, when polymer chains attach to the growth front they initially form a crystal with hexagonal symmetry, which rapidly thickens in the chain direction and transforms into the orthorhombic phase when a critical thickness is reached. It was suggested that the hexagonal phase is in fact more stable than the orthorhombic phase if the crystal thickness is sufficiently small, due to the difference in the ratio of surface energy to bulk free energy. This introduced the idea of a size-dependent phase transition. On a broader basis, Ostwald's Stage Rule (142) has been used to justify the suggestion that crystallization will occur through intermediate states if such states exist. As the material transforms from the high free-energy liquid state to the minimum free-energy

crystalline state (never reached in the case of polymers because of the kinetic trap of chain folding), it will pass through any intermediate states where local minima in free energy exist. In the case of polyethylene, the hexagonal phase in which the still mobile chains pack like parallel rods, is clearly a possible intermediate state. Direct experimental evidence of an intermediate hexagonal phase during the crystallization of polyethylene under ambient pressure has not been forthcoming. Some evidence from simulations of small molecule systems supporting the existence (and persistence) of a higher symmetry intermediate phase during nucleation has been published (143), but the complexity of polymeric systems puts similar studies beyond current computer power.

A very similar set of arguments to the above has been made by Strobl and co-workers (140,141) although coming from a somewhat different set of initial assumptions. In this case it is proposed that crystallization occurs through a partially ordered mesophase, which then transforms into crystalline blocks and these blocks in turn heal together to form the final lamellae. Experimentally this is justified by a series of observations both direct and indirect, although the primary data are a body of measurements on melting behavior and crystal thicknesses. In particular, the existence of a continuous distribution of melting temperatures for crystals of the same thickness is clear evidence of a variation in crystal perfection that is not accounted for in the traditional theories.

Although these new ideas are internally consistent and supported by some experimental evidence, it has been suggested that they are contradicted strongly by the behavior of several well-studied systems. In particular, the selection of chain chirality during crystallization has been used as an argument against the possibility of a loosely packed intermediate structure, both in achiral molecules where the chain can adopt helical conformations of either handedness, and in enantiomorphic mixtures of optically pure materials. For instance, in α-iPP, where left- and right-handed helices pack in a well-ordered antiparallel fashion dictated by the stable unit-cell structure, it is hard to envisage the existence of an essentially randomly packed intermediate state that could then sort itself out into the correct packing through a solid-state crystal–crystal transformation, considering the interconnectivity of the stems that make up the crystal. This argument is made very strongly in Reference 144 and is yet to be convincingly answered.

Clearly there still exists considerable controversy over the factors controlling polymer crystallization. New experimental techniques are, however, starting to become available that might lead to a resolution of some of these issues. Scanning probe microscopy offers the opportunity to follow crystal growth at a surface in real-time, with nanometer resolution, and hence to quantify the kinetics by direct observation at length scales that are close to those of the fundamental crystallizing unit, and to the size scale of the polymer chain (92,145–152). Several groups (145–147,149) have reported that lamella crystallization from the melt, at least where several lamellae are growing adjacently, does not occur at a constant temperature-controlled rate. Instead, growth rates are sporadic over length scales of several tens of nanometers, with lamellae or parts of lamellae spurting forwards briefly, then slowing down and being overtaken by their neighbors (146). Although this does not contradict the mean rates previously measured optically, because of the different length scale of the measurement, it does contradict the predictions of secondary nucleation theory, if it is applied to melt crystallization

(which is commonly the case; see above). Figure 16 shows a series of images of lamella crystallization, from which the growth rates can be measured. Currently it is only possible to use this technique to study crystallization at very slow rates, at the lower limits of those traditionally measured optically. However, with the advent of faster scanning techniques, it should be possible to obtain real-time growth rate measurements with nanometer resolution under more usual crystallization conditions, and provide a definitive test of theory.

A complimentary technique is the development of very fine beam micro-focus X-ray sources, in which submicron beams are starting to become available (153). This technique has not yet been applied to polymer crystallization, but is capable of providing spatially resolved scattering data from growth fronts that is of great

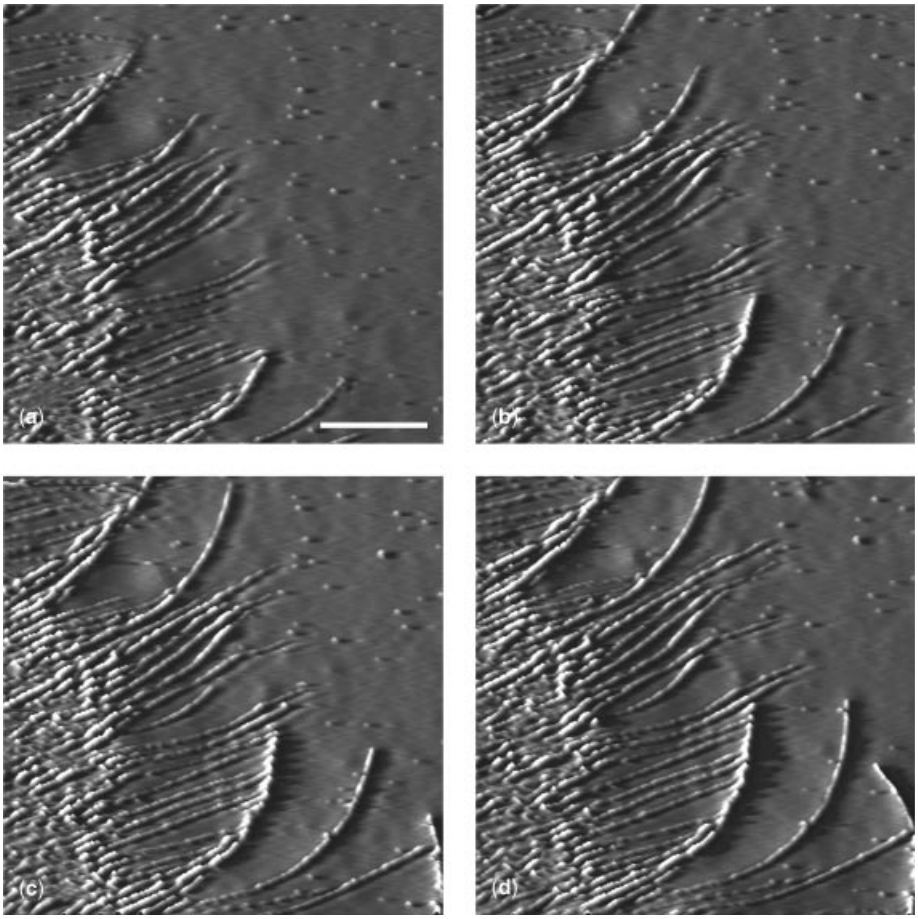

Fig. 16. A series of AFM amplitude images showing the growth of an oriented polyethylene structure. The individual lamellae can be resolved as they grow into the melt. The growth rates of lamellae can be measured and it is seen that they vary both from lamella to lamella, and with time for each lamella. The local environment of a growing lamella is also seen to have a profound effect on its growth. (**a**) taken at 0 s, (**b**) at 181 s, (**c**) at 344 s, (**d**) at 591 s. The scale bar represents 1 μm. Reprinted from Ref. 146. Copyright (2001), with permission from the American Chemical Society.

potential value. Similarly, advances in instrumentation in other techniques such as NMR, Raman microscopy, and electron microscopy toward higher spatial and temporal resolution, as well as new methods for materials synthesis that can produce cleaner, better-defined polymers, promise to have a significant impact on our understanding of polymer crystallization kinetics at the molecular level.

Conclusions

The complexity of polymeric systems has made the development of a full understanding of the crystallization process difficult. A wealth of experimental evidence has been gathered, but interpretation has often been problematic because of the ambiguities frequently found in such complex systems. The capabilities of new experimental techniques to obtain both time and spatially resolved information during the phase transformation is improving rapidly and may prove to be decisive.

Although secondary nucleation theory was, for a period, widely accepted, it is now coming under increasing pressure, from experimental data, from computer simulation, and from new approaches to the fundamental process of crystallization. It is not clear at this stage whether all that is required is a few adjustments to the theory, or whether the idea of a nucleation barrier is flawed, or even if the idea that the crystal thickness seen is the fastest growing is correct. With the development of new theoretical tools, and the increased integration of theory with computer simulation, it is hoped that a more complete model for polymer crystallization can be developed.

A full understanding of crystallization from the melt still seems elusive, with very little work being carried out to confront the issues of mass transport, of transient stresses caused by the volume reduction that accompanies crystallization [known to be sufficiently high to cause cavitation (154,155), or even to fracture the growing crystal (156)], or of the relationship between modes of growth and morphologies seen in polymers but also seen in other systems. The extent and importance of the role played by intermediate phases is also unclear, although this is an area that, with the development of new experimental techniques, and the pushing of the spatial resolution of existing techniques down toward the nanometer level, should be resolvable.

Despite these questions, the body of knowledge on crystallization kinetics is very extensive. As new theories are developed, it is clearly of paramount importance that they use as an input all of the available information. The wide variety of different chemistries and behaviors that are observed can lead to a temptation to discard generalizing principles, but it is the author's opinion that this temptation should be avoided. At a phenomenological level, polymer crystallization is well characterized, and the kinetics of growth can be controlled in a precise manner, at least on a macroscopic scale. It is hoped that, over the next few years, newly available experimental data can be married to the vast store of existing knowledge and assimilated, through the help of the growing power of computer simulation, to provide a new model for crystal growth that will provide the fundamental understanding necessary if crystallizable polymers are to meet the demands placed on them by the emerging fields of nanotechnology and nanoscience.

BIBLIOGRAPHY

"Kinetics of Crystallization" in *EPST* 1st ed., Vol. 8, pp. 63–83, by F. P. Price, General Electric Co.; "Crystallization Kinetics" in *EPSE* 2nd ed., Suppl. Vol., pp. 231–296, by J. G. Fatou, C.S.I.C., Madrid, Spain.

1. A. Keller, *Phil. Mag.* **2**, 1171 (1957).
2. E. W. Fischer, *Z. Naturf.* **12a**, 753 (1957).
3. P. H. Till, *J. Polym. Sci.* **24**, 30 (1957).
4. F. C. Frank and M. Tosi, *Proc. R. Soc. A* **263**, 323 (1961).
5. J. J. Weeks, *J. Res. Natl. Bur. Stand. (U.S.)* **67A**, 441 (1963).
6. A. Peterlin, *J. Appl. Phys.* **31**, 1934 (1960).
7. M. Avrami, *J. Chem. Phys.* **7**, 1103 (1939).
8. M. Avrami, *J. Chem. Phys.* **8**, 212 (1940).
9. M. Avrami, *J. Chem. Phys.* **9**, 177 (1941).
10. A. N. Kolmogoroff, *Isv. Akad. Nauk SSSR, Ser. Math.* **1**, 355 (1937).
11. G. Eder, *Nonlin. Anal., Theory, Meth. Appl.* **30**, 3807 (1997).
12. U. W. Gedde, *Polymer Physics*, Chapman & Hall, London, 1995, pp. 175–178.
13. F. P. Price, in A. C. Zettlemoyer, ed., *Nucleation*, Marcel Dekker, Inc., New York, Chapt. 8, 1969, p. 405.
14. C. Mathi, J. A. Thierry, and J. C. Wittmann, and B. Lotz, *J. Polym. Sci., Polym. Phys.* **40**, 2504 (2002).
15. J. C. Wittmann and B. Lotz, *Prog. Polym. Sci.* **15**, 909 (1990).
16. D. J. Blundell and A. Keller, *J. Macromol. Sci. Phys. B* **2**, 301 (1968).
17. D. J. Blundell, A. Keller, and A. J. Kovacs, *Polym. Lett.* **4**, 481 (1966).
18. D. C. Bassett, *Principles of Polymer Morphology*, Cambridge University Press, Cambridge, 1981.
19. P. J. Barham, D. A. Jarvis, and A. Keller, *J. Polym. Sci., Polym. Phys. Ed.* **20**, 1733 (1982).
20. A. Sharples, *Polymer* **3**, 250 (1962).
21. P. J. Barham, *J. Mater. Sci.* **19**, 3826 (1984).
22. N. Okui, *J. Macromol. Sci*. (in press).
23. S. Umemoto, N. Kobayashi, and N. Okui, *J. Macromol. Sci., Phys. B* **41**, 923 (2002).
24. D. Turnbull and R. L. Cormia, *J. Chem. Phys.* **34**, 820, (1961).
25. R. L. Cormia, F. P. Price, and D. Turnbull, *J. Chem. Phys.* **37**, 1333 (1962).
26. G. S. Ross and L. J. Frolen, *J. Res. Nat. Bur. Stands* **79A**, 701 (1975).
27. P. J. Barham, *J. Mater. Sci* **35**, 5139 (2000).
28. Y. L. Loo, R. A. Register, and A. J. Ryan, *Phys. Rev. Lett.* **84**, 4120 (2000).
29. A. Rottele, T. Thurn-Albrecht, J. U. Sommer, and G. Reiter, *Macromolecules* **36**, 1257 (2003).
30. D. Turnbull, and J. C. Fisher, *J. Chem. Phys.* **17**, 71 (1949).
31. P. J. Flory, *J. Chem. Phys.* **17**, 223 (1949).
32. L. Mandelkern, *J. Appl. Phys.* **26**, 443 (1955).
33. J. L. Keddie, R. A. L. Jones, and R. A. Cory, *Europhys. Lett.* **27**, 59 (1994).
34. M. Durell, J. E. MacDonald, D. Trolley, A. Wehrum, P. C. Jukes, R. A. L. Jones, C. J. Walker, and S. Brown, *Europhys. Lett.* **58**, 844 (2002).
35. J. P. A. Fairclough, S. M. Mai, M. W. Matsen, W. Bras, L. Messe, S. C. Turner, A. J. Gleeson, C. Booth, I. W. Hamley, and A. J. Ryan, *J. Chem. Phys.* **114**, 5425 (2001).
36. M. Imai, K. Mori, T. Mizukami, K. Kaji, and T. Kanaya, *Polymer* **33**, 4451 (1992).
37. N. J. Terrill, P. A. Fairclough, E. Towns-Andrews, B. U. Komanschek, R. J. Young, and A. J. Ryan, *Polymer* **39**, 238 (1998).
38. *Faraday Discuss*. (112), 64–75 (1999).
39. J. Petermann, *Macromol. Chem. Phys.* **182**, 613 (1981).

40. J. Petermann, R. M. Gohil, J. M. Schultz, R. W. Hendricks, and J. S. Lin, *J. Polym. Sci. B, Polym. Phys. Ed.* **20**, 523 (1982).
41. P. Meakin and D. J. Scalapino, *J. Polym. Sci., Part B: Polym. Phys. Ed.* **23**(1), 179 (1985).
42. Z. G. Wang, B. S. Hsiao, E. B. Sirota, and S. Srinivas, *Polymer* **41**, 8825 (2000).
43. P. D. Olmsted, W. C. K. Poon, T. C. B. McLeish, N. J. Terrill, and A. J. Ryan, *Phys. Rev. Lett.* **81**, 373 (1998).
44. *Faraday Discuss. R. Soc. Chem.* **68** (1979).
45. P. J. Barham, R. A. Chivers, A. Keller, J. Martinez-Salazar, and S. J. Organ, *J. Mater. Sci.* **20**, 1625 (1985).
46. S. J. Organ and A. Keller, *J. Mater. Sci.* **20**, 1602 (1985).
47. H. Tadokoro, *Structure of Crystalline Polymers*, John Wiley & Sons, Inc., New York, 1979.
48. S. Gautam, A. Balijepalli, and G. C. Rutledge, *Macromolecules* **33**, 9136 (2000).
49. D. C. Bassett and A. M. Hodge, *Proc. R. Soc. London, A* **377**, 25 (1981).
50. J. D. Hoffman, L. J. Frolen, G. S. Ross, and J. I. Lauritzen, *J. Res. Natl. Bur. Stand. A: Phys. Chem.* **79A**, 671 (1975).
51. P. J. Phillips, in D. T. J. Hurle, ed., *Handbook of Crystal Growth, Vol. 2: Bulk Crystal Growth. Part b: Growth Mechanisms and Dynamics*, North-Holland, Amsterdam, 1994.
52. R. Allen and L. Mandelkern, *Polym. Bull.* **17**, 473 (1987).
53. R. Vasanthakumari and A. Pennings, *Polymer* **24**, 175 (1983).
54. P. J. Phillips and N. Vantansever, *Macromolecules* **20**, 2138 (1987).
55. S. Lazcano, J. G. Fatou, C. Marco, and A. Bello, *Polymer* **29**, 2076 (1988).
56. P. J. Barham, A. Keller, E. L. Otun, and P. A. Holmes, *J. Mater. Sci.* **19**, 2781 (1984).
57. A. J. Lovinger, D. D. Davis, and F. J. Padden Jr., *Polymer* **26**, 1595 (1985).
58. D. B. Roitman, H. Marand, R. L. Miller, and J. D. Hoffman, *J. Phys. Chem.* **93**, 6919 (1989).
59. J. J. Point and M. Dosiere, *Macromolecules* **22**, 3501 (1989).
60. J. D. Hoffman and R. L. Miller, *Macromolecules* **22**, 3502 (1989).
61. J. H. Magill, *J. Appl. Phys.* **35**, 3249 (1964).
62. S. Umemoto and N. Okui, *Polymer* **43**, 1423 (2002).
63. D. M. Sadler, *J. Polym. Sci. A* **2**, 779 (1971).
64. R. B. Prime and R. Wunderlich, *J. Polym. Sci. A* **2**, 2061 (1969).
65. B. Wunderlich, *Macromolecular Physics, Vol. 2: Crystal Nucleation, Growth, Annealing*, Academic Press, New York, 1976.
66. P. H. Geil, *Polymer Single Crystals*, John Wiley & Sons, Inc., New York, 1963.
67. A. Keller, *Kolloid-Zeit. Zeit. Polym.* **231**, 386 (1969).
68. T. Kawai, *Polym. Lett.* **2**, 965 (1964).
69. J. K. Hobbs, M. J. Hill, A. Keller, and P. J. Barham, *J. Polym. Sci., Polym. Phys.* **37**, 3188 (1999).
70. D. J. Blundell and A. Keller, *Polym. Lett.* **6**, 433 (1968).
71. A. Keller and E. Pedemonte, *J. Cryst. Growth* **18**, 111 (1973).
72. M. Cooper and R. St. J. Manley, *Macromolecules* **8**, 219 (1975).
73. J. J. Point, M. Ch. Colet, and M. Dosiere, *J. Polym. Sci., Polym. Phys.* **24**, 357 (1986).
74. S. J. Organ and A. Keller, *J. Polym. Sci., Part B: Polym. Phys.* **24**, 2319 (1986).
75. A. Toda, *J. Chem. Soc., Faraday Trans.* **91**, 2581 (1995).
76. A. Keller and D. J. Priest, *J. Macromol. Sci. Phys., B* **2**, 479 (1968).
77. C. P. Buckley and A. J. Kovacs, in I. H. Hall, ed. *Structure of Crystalline Polymers*, Elsevier Applied Science, London, 1984, p. 261.
78. G. Ungar, J. Steyny, A. Keller, I. Bidd, and M. C. Whiting, *Science* **229**, 386 (1985).
79. S. Z. D. Cheng and J. Chen, *J. Polym. Sci., Part B: Polym. Phys.* **29**, 311 (1991).

80. G. Ungar and A. Keller, *Polymer* **28**, 1899 (1987).
81. J. K. Hobbs, M. J. Hill, and P. J. Barham, *Polymer* **41**, 8761 (2000).
82. G. Ungar and K. B. Zeng, *Chem. Rev.* **101**, 4157 (2001).
83. I. W. Hamley, *The Physics of Block Copolymers*, Oxford University Press, Oxford, 1998.
84. P. J. Flory, *Trans. Faraday Soc.* **51**, 848 (1955).
85. B. Wunderlich, *Macromolecular Physics, Vol. 3: Crystal Melting*, Academic Press, New York, 1980.
86. A. Rastogi, J. K. Hobbs, and S. Rastogi, *Macromolecules* **35**, 5861 (2002).
87. P. J. Lemstra, N. A. J. M. van Aerle, and C. W. M. Bastiaansen, *Polym. J.* **19**(1), 85 (1987).
88. A. J. McHugh, *Polym. Eng. Sci.* **22**, 15 (1982).
89. J. A. Odell, A. Keller, and M. J. Miles, *Colloid Polym. Sci.* **262**, 683 (1984).
90. M. Seki, D. W. Thurman, J. P. Oberhauser, and J. A. Kornfield, *Macromolecules* **35**, 2583 (2002).
91. A. Liedauer, G. Eder, H. Janeschitzkriegl, P. Jerschow, W. Geymayer, and E. Ingolic, *Int. Polym. Proc.* **8**, 236 (1993).
92. J. K. Hobbs and M. J. Miles, *Macromolecules* **34**, 353 (2001).
93. A. W. Monks, H. M. White, and D. C. Bassett, *Polymer* **37**, 5933 (1996).
94. U. Durig, G. Cross, M. Despont, U. Drechsler, W. Haberle, M. I. Lutwyche, H. Toghuizen, R. Stutz, R. Widmer, P. Vettiger, G. K. Binnig, W. P. King, and K. E. Goodson, *Tribology Lett.* **9**(1/2), 25 (2000).
95. H. D. Keith, F. J. Padden, B. Lotz, and J. C. Wittmann, *Macromolecules* **22**, 2230 (1989).
96. G. Reiter, and J.-U. Sommer, *Phys. Rev. Lett.* **80**, 3771 (1998).
97. K. Taguchi, H. Miyaji, K. Izumi, A. Hoshino, Y. Miyamoto, and R. Kokawa, *Polymer* **42**, 7443 (2001).
98. K. Taguchi, H. Miyaji, K. Izumi, A. Hoshino, Y. Miyamoto, and R. Kokawa, *J. Macromol. Sci. Phys. B* **41**, 1033 (2002).
99. W. W. Mullins and R. W. Sekerka, *J. Appl. Phys.* **34**, 323 (1963).
100. J. S. Langer, *Science* **243**, 1150 (1989).
101. V. Ferreiro, J. F. Douglas, J. Warren, and A. Karim, *Phys. Rev. E* **65**, 051606 (2002).
102. V. Ferreiro, J. F. Douglas, J. Warren, and A. Karim, *Phys. Rev. E* **65**, 042802 (2002).
103. K. A. Armistead and G. Goldbeck-Wood, *Adv. Polym. Sci.* **100**, 219 (1992).
104. J. D. Hoffman and R. L. Miller, *Polymer* **38**, 3151 (1997).
105. J. D. Hoffman, J. I. Lauritzen, and G. T. Davis, in N. B. Hannay, ed., *Treatise on Solid State Chemistry*, Plenum Press, New York, 1976, Vol. 3.
106. M. Hikosaka, *Polymer* **28**, 1257 (1987).
107. J. D. Hoffman and J. I. Lauritzen, *J. Natl. Bur. Stand. A* **64**, 73 (1960).
108. E. A. DiMarzio, *J. Chem. Phys* **47**, 3451 (1967).
109. F. C. Frank, *J. Cryst. Growth* **22**, 233 (1974).
110. J. J. Point, *Macromolecules* **12**, 770 (1979).
111. E. A. DiMarzio and C. M. Guttman, *J. Appl. Phys.* **53**, 6581 (1982).
112. J. J. Point and A. J. Kovacs, *Macromolecules* **13**, 399 (1980).
113. S. J. Organ and A. Keller, *J. Mater. Sci.* **20**, 157 (1985).
114. A. Toda and A. Keller, *Colloid Polym. Sci.* **271**, 328 (1993).
115. D. C. Bassett, R. H. Olley, and I. A. M. Raheil, *Polymer* **29**, 1539 (1988).
116. D. M. Sadler, *Polyum. Commun.* **25**, 196 (1984).
117. D. M. Sadler and G. H. Gilmer, *Polymer* **25**, 1446 (1984).
118. D. M. Sadler, *Nature* **326**, 174 (1987).
119. D. M. Sadler, *J. Chem. Phys.* **87**, 1771 (1987).
120. D. M. Sadler, *Polymer* **28**, 1440 (1987).
121. D. M. Sadler and G. H. Gilmer, *Phys. Rev. B* **38**, 5684 (1988).

122. G. L. Liang, D. W. Noid, B. G. Sumpter, and B. Wunderlich, *J. Polym. Sci., Part B: Polym. Phys.* **31**, 1909 (1993).
123. T. Yamamoto, *J. Chem. Phys.* **107**, 2653 (1997).
124. T. Yamamoto, *J. Chem. Phys.* **109**, 4638 (1998).
125. M. S. Lavine, N. Waheed, and G. C. Rutledge, *Polymer* **44**, 1771 (2003).
126. W. B. Hu, D. Frenkel, and V. B. F. Mathot, *Macromolecules* **35**, 7172 (2002).
127. W. Hu, *J. Chem. Phys.* **115**, 4395 (2001).
128. J. P. K. Doye and D. Frenkel, *J. Chem. Phys.* **109**, 10033 (1998).
129. J. P. K. Doye and D. Frenkel, *J. Chem. Phys.* **110**, 7073 (1999).
130. J. P. K. Doye and D. Frenkel, *Polymer* **41**, 1519 (2000).
131. J. J. Point, *Faraday Discuss. Chem. Soc.* **68**, 365 (1979).
132. J. P. K. Doye and D. Frenkel, *J. Chem. Phys.* **110**, 2692 (1999).
133. P. Welch and M. Muthukumar, *Phys. Rev. Lett.* **87**, 218302 (2001).
134. C. Lui and M. Muthukumar, *J. Chem. Phys.* **109**, 2536 (1998).
135. M. Muthukumar and P. Welch, *Polymer* **41**, 8833 (2000).
136. J. U. Sommer and G. Reiter, *J. Chem. Phys.* **112**, 4384 (2000).
137. A. Keller, M. Hikosaka, S. Rastogi, A. Toda, P. J. Barham, and G. Goldbeckwood, *J. Mater. Sci.* **29**, 2579 (1994).
138. A. Keller, M. Hikosaka, and S. Rastogi, *Physica Scripta* **T66**, 243 (1996).
139. S. Z. D. Cheng and A. Keller, *Annu. Rev. Mater. Sci.* **28**, 533 (1998).
140. G. Strobl, *Eur. Phys. J., E* **3**, 165 (2000).
141. T. Hugel, G. Strobl, and R. Thomann, *Acta Polymerica* **50**, 214 (1999).
142. W. Ostwald, *Z. Physik. Chem.* **22**, 286 (1897).
143. S. Auer and D. Frenkel, *Nature* **409**, 1020 (2001).
144. B. Lotz, *Eur. Phys. J., E* **3**, 185 (2000).
145. J. K. Hobbs, T. J. McMaster, M. J. Miles, and P. J. Barham, *Polymer* **39**, 2437 (1998).
146. J. K. Hobbs, A. D. L. Humphris, and M. J. Miles, *Macromolecules* **34**, 5508 (2001).
147. R. Pearce and G. J. Vancso, *Polymer* **39**, 1237 (1998).
148. R. Pearce and G. J. Vancso, *J. Polym. Sci. B* **36**, 2643 (1998).
149. L. Li, C.-M. Chan, J.-X. Li, K.-M. Ng, K.-L. Yeung, and L.-T. Weng, *Macromolecules* **32**, 8240 (1999).
150. J. M. Schultz and M. J. Miles, *J. Polym. Sci. B* **36**, 2311 (1998).
151. D. A. Ivanov, T. Pop, D. Y. Yoon, and A. M. Jonas, *Macromolecules* **35**, 9813 (2002).
152. L. G. M. Beekmans, R. Vallee, and G. J. Vancso, *Macromolecules* **35**, 9383 (2002).
153. R. Kolb, C. Wutz, N. Stribeck, G. von Krosigk, and C. Riekel, *Polymer* **42**, 5257 (2001).
154. A. Galeski and E. Piorkowska, *J. Polym. Sci., Polym. Phys.* **21**, 1299 (1983).
155. A. Galeski, L. Koenczoel, E. Piorkowska, and E. Baer, *Nature* **325**(6099), 40 (1987).
156. J. K. Hobbs, T. McMaster, M. J. Miles, and P. J. Barham, *Polymer* **37**, 3241 (1996).

JAMIE K. HOBBS
University of Bristol

CURING.

See THERMOSETS.

CYANOACRYLIC ESTER POLYMERS.

See POLYCYANOACRYLATES.

CYCLIC OLEFIN POLYMERS.

See ETHYLENE-NORBORNENE COPOLYMERS.

CYCLODEXTRINS

Introduction

A wide area of supramolecular chemistry focuses on host–guest interactions between two or more molecules that are not covalently bonded (1). A special part of this chemistry deals with cyclodextrins and their derivatives (2). It is well known that cyclodextrins tend to include several types of hydrophobic guest molecules into their cavity. Accordingly, a large number of applications have been found in many areas, eg, in food chemistry as well as in the pharmaceutical (3) and cosmetic industries. Furthermore, cyclodextrins may be used in organic chemistry and also in polymer chemistry.

Cyclodextrins (CDs) are produced in technical plants by enzymatically catalyzed degradation of starch. The naturally occurring products of cyclodextrin are cyclic oligosaccharides built up of 6 (α), 7 (β), or 8 (γ) glucopyranose units, which are connected with $\alpha(1\rightarrow4)$-glycosidic linkages, forming a torus-shaped ring structure with a hydrophobic cavity and a hydrophilic exterior. The primary hydroxy groups in the 6-position are located at the narrow side of the torus, whereas the secondary glucopyranose hydroxy groups are located at the wider side of the torus (Fig. 1). β-CD shows a water solubility about 1.85 g/L at 20°C. Intramolecular hydrogen bonding between the C2-OH group of one with the C3-OH of a neighboring glucose unit is probably responsible for the poor water solubility of β-cyclodextrin. Because of the high water solubility of randomly methylated β-cyclodextrin (RAMEB) with an average degree of methylation around 1.8 per glucose unit, it may be used in consumer products, and in industrially synthesized on a large scale.

Because of their polar hydrophilic outer shell and relatively hydrophobic cavity, cyclodextrins are able to form inclusion complexes with a wide variety of suitable hydrophobic molecules (4) eg, nonpolar hydrocarbons, polar carboxylic acid, and amine derivatives (Fig. 2, Table 2). This phenomenon leads to significant changes of the solubility and reactivity of the guest molecules without any chemical modification. Water-insoluble molecules become completely water-soluble by treatment with aqueous solution of native cyclodextrins or their derivatives, eg, methylated or hydroxypropylated cyclodextrins.

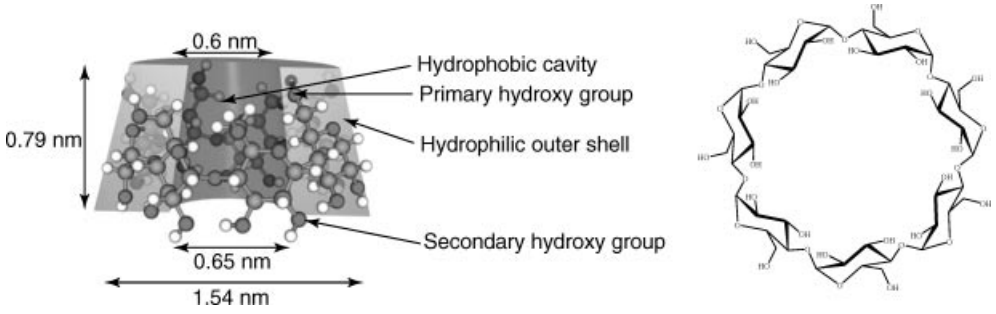

Fig. 1. 3-Dimensional and molecular structure of β-cyclodextrin.

Encyclopedia of Polymer Science and Technology. Copyright John Wiley & Sons, Inc. All rights reserved.

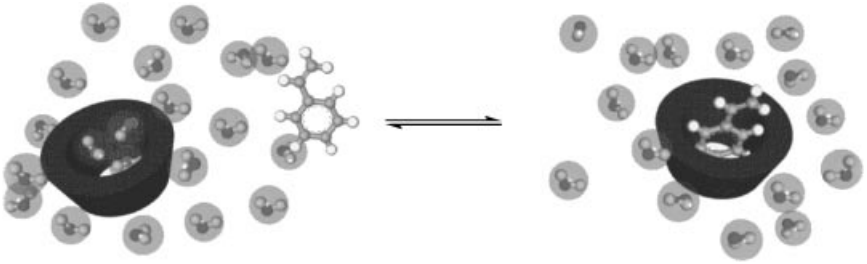

Fig. 2. Scheme of formation of styrene–cyclodextrin host–guest complex

In this article, the synthesis of new monomers, their inclusion in cyclodextrin derivatives, and polymerization in aqueous medium are described.

Complexation with Cyclodextrins

Water-soluble cyclodextrin complexes of water-insoluble monomers were achieved by stirring a slight excess of cyclodextrin derivatives, in most cases RAMEB, and different monomers in water. Several methods were applied to the characterizations of the host–guest complexes. The most important behavior of the complexes is that the hydrophobic guest monomers become water-soluble by being included into cyclodextrin. Reaction control by thin-layer chromatography (TLC) with methanol as mobile phase, followed by UV detection and iodine development, shows complete conversion to the corresponding cyclodextrin complexes. The R_f values of the complexes are significantly different from the value of uncomplexed monomers and cyclodextrin (Table 1).

Table 1. R_f Values of Uncomplexed Monomers and Their RAMEB Complexes in Comparison to 2,6-Dimethylated Cyclodextrin

Monomer	$R_{f(monomer)}$	$R_{f(monomer/RAMEB)}$
Styrene	0.85	0.57
Methyl methacrylate (**1a**)	0.89	0.57
n-Butyl methacrylate (**1b**)	0.94	0.50
tert-Butyl methacrylate (**1c**)	0.92	0.54
Cyclohexyl methacrylate (**1d**)	0.80	0.54
Phenyl methacrylate (**1e**)	0.92	0.54
n-Propyl acrylate (**1f**)	0.78	0.54
n-Butyl acrylate (**1g**)	0.90	0.45
n-Pentyl acrylate (**1h**)	0.88	0.55
n-Hexylacrylate (**1i**)	0.85	0.77
Cyclohexyl acrylate (**1j**)	0.87	053
N-Methacroyl-L-tyrosin methylester (**2a**)	0.85	0.50
N-Methacroyl-L-tyrosin ethylester (**2b**)	0.78	0.42
Isobornyl acrylate (**3a**)	0.86	0.51
Isobornyl methacrylate (**3b**)	0.82	0.53
2,3-Ethylenedioxythiophen (**EDT**)	088	0.38
(2,6-Dimethyl)-β-cyclofextrin	0.66	

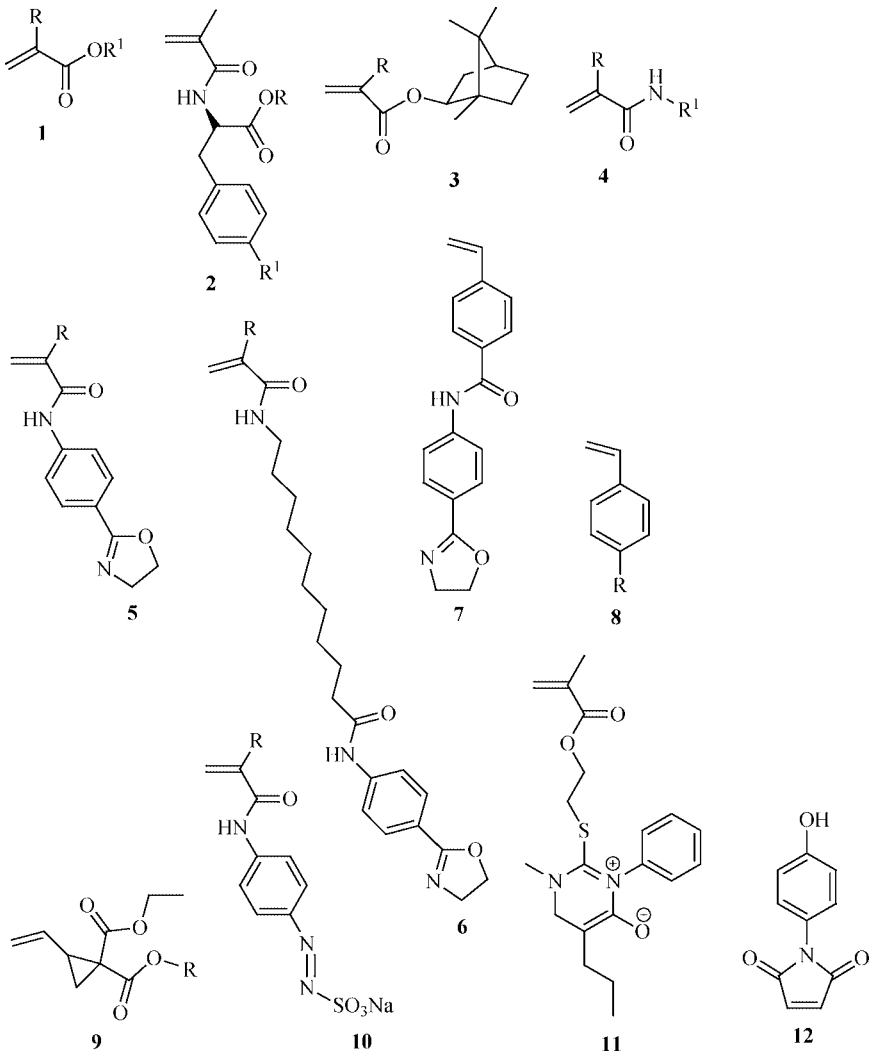

The formation of the complexes can also be verified by ^{1}H NMR spectroscopy and 2D-ROESY NMR analyses. For example, the ^{1}H NMR spectrum of *N*-methacroyl-L-tyrosin methylester (**2a**) in comparison to its complex with heptakis(2,6-di-*O*-methyl)-β-cyclodextrin (DIMEB) shows that in complex the signals of the aromatic protons in ortho position to OH group as well as the signals of the methacryl group are shifted to the lower magnetic field, whereas no changes occurred for the aliphatic protons and the ester groups (Fig. 3). The 2D-ROESY NMR spectrum of the RAMEB-complexed *N*-metacroyl-L-tyrosin ethylester (**2b**) shows strong interactions between the aromatic protons of the monomer with the H(3), H(5), and the methoxy groups of cyclodextrin (Fig. 4.)

The structure analysis of the RAMEB-complexed monomers by X-ray diffraction confirmed the results of the above-mentioned methods. As an example, the X-ray structure of DIMEB complexed isobornyl acrylate (**3a**) and *n*-butyl acrylate

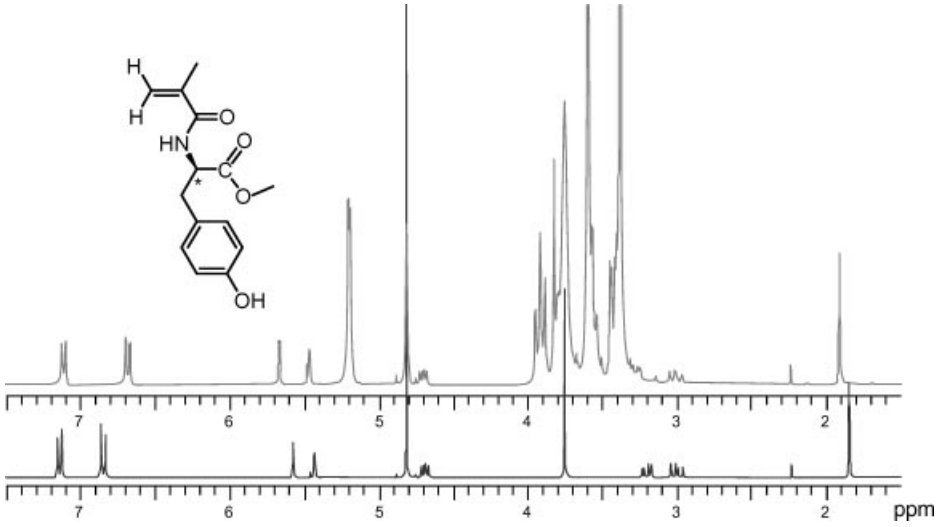

Fig. 3. 300 MHz ^{1}H NMR spectra of *N*-methacryoyl-L-tyrosine methylester (**2a**) and their DIMEB complex in D_2O[5].

(**1g**) show that the monomeric guest molecules are completely included within the cavity of β-cyclodextrin and the double bonds of acrylic groups are located at the narrow side of the host molecule bearing the primary methoxy groups (Figs. 5**a** and 5**b**). Surprisingly, the X-ray analysis of 3,4-diethylendioxythiophene (EDT)/α-cyclodextrin shows that the monomer does not fit into the cavity of α-cyclodextrin, but a 1:1 noninclusion channel-type packed supramolecular complex based on multiple hydrogen bonds (Fig. 5**c**). When DIMEB was used as a host molecule for EDT, it was observed that the complex crystallized out of the aqueous solution at higher temperatures, whereas upon cooling it was dissolved again. Additionally, the photophysical properties of inclusion complexes γ-cyclodextrin as host and 2,2′:5,2″-terthiophen (αT) as guest have been investigated. α-T is believed to form 1:2 or 2:2 complexes with γ-cyclodextrin.[6]

Polymerization of the Cyclodextrin Complexed Monomers

In recent years, much attention has been directed toward the use of cyclodextrin derivatives in polymer chemistry. The emulsion polymerization of vinyl monomers, eg, methacrylates in the presence of β-cyclodextrin using anionic surfactant, has been described (9,10). However, this type of polymerization leads often to polymer particles having a heterogeneous particle-size distribution (PSD).

In our group, different types of vinyl monomers showing low solubility towards water (Table 2) were complexed with cyclodextrin and the obtained water-soluble complexes were subjected to free-radical polymerizations and copolymerizations in aqueous phase. The optically clear solution of the complex becomes turbid because of the precipitating polymeric powder. It was shown in nearly all cases that higher monomer conversions were obtained as compared with polymerization

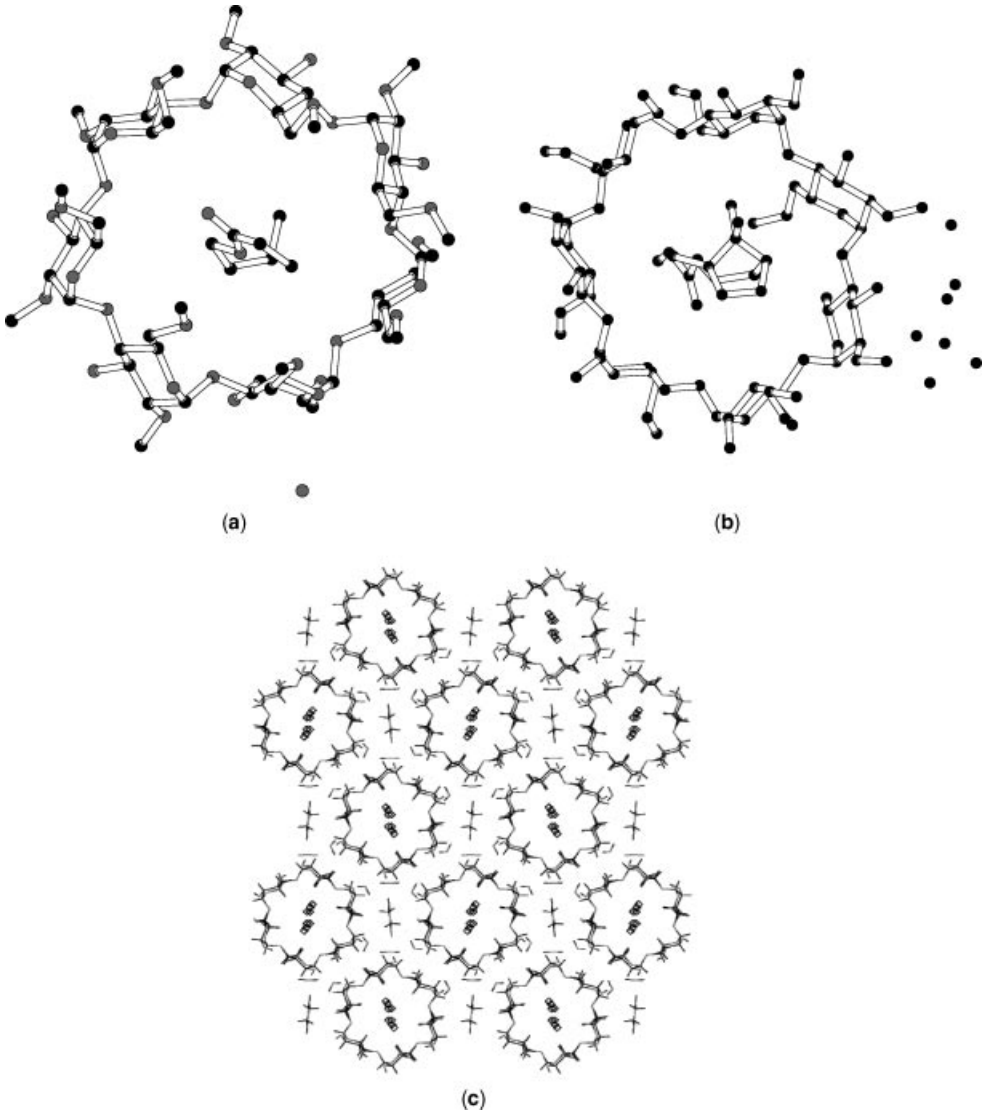

Fig. 4. 600 MHz ^{1}H, ^{1}H ROESY NMR spectrum of *N*-methacryoyl-L-tyrosine ethylester (**2b**) in D_2O[5].

of uncomplexed monomers. During polymerization, the cyclodextrin generally slips off from the guest monomer and remains nearly quantitatively in the aqueous phase owing to its high water solubility (Fig. 6). The received polymers contain only a trace of cyclodextrin (about <5 mol%). Furthermore, cyclodextrin solution can be reused to enclose new monomers. The surfactant free polymerization technique is a new alternative method to emulsion polymerization, which has been established as industrial processes since decades.

At the beginning of our research the interest was focused on commercial standard vinyl monomers, eg, styrene (**8a**) and methyl methacrylate (**1a**). An

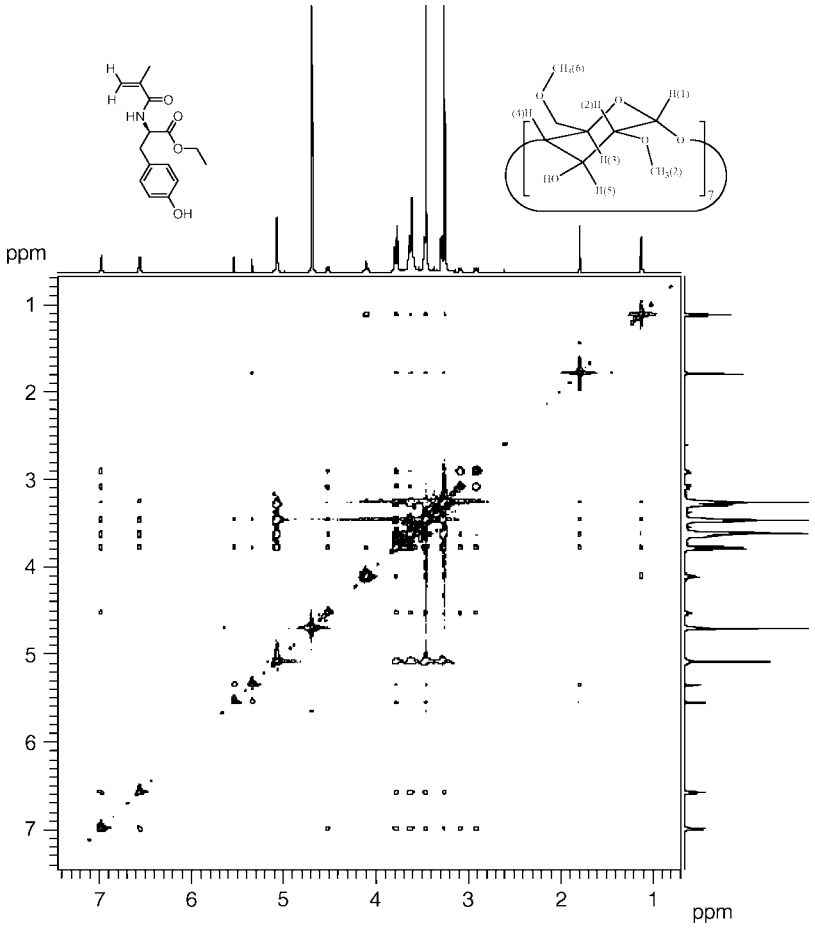

Fig. 5. X-ray structure of (**a**) *n*-butyl acrylate (**1g**)/DIMEB, (**b**) isobornyl acrylate (**3a**)/DIMEB (7), and (**c**) EDT/α-cyclodextrin (8).

equimolar of styrene or **1a** was dispersed in an aqueous solution of RAMEB and stirred at room temperature to give a clear homogenous solution of the complexed monomers. The complex stability of styrene with RAMEB in water is much higher (500 M^{-1}) than the complex stability of **1a** (25 M^{-1}) at room temperature. The aqueous solution of water-soluble complex was homopolymerized radically in water using a free-radical redox initiator $K_2S_2O_8/NaHSO_3$ at 60°C. In both cases, it was shown that polymerization in the presence of cyclodextrin is faster and ends up with higher yields, higher molecular weights, and higher polydispersity (PD) of polymers than polymerization in homogeneous organic solution (11). This observation was also in good agreement with the previous results obtained with RAMEB-complexed and uncomplexed cyclohexyl methacrylate (**1d**) and phenyl methacrylate (**1e**) (12).

Stereoregular polystyrene was prepared using various molar equivalents of β-cyclodextrin (13). A mixture of styrene and β-cyclodextrin was stirred for 30 min,

Table 2. Suitable Guest Monomers for the Complexation with Methylated β-Cyclodextrin

Monomer	R	R^1
1a	Me	Me
1b	Me	-*n*-butyl
1c	Me	-*tert*-butyl
1d	Me	-cyclohexyl
1e	Me	-phenyl
1f	H	-*n*-propyl
1g	H	-*n*-butyl
1h	H	-*n*-pentyl
1i	H	-*n*-hexyl
1j	H	-cyclohexyl
1k	Me	—$CH_2CF_2CF_3$
1l	Me	—$CH_2CH_2(CH_2)_5CF_3$
1m	Me	—$CH_2CH_2(CH_2)_7CF_3$
1n	H	—$CH_2CH_2(CH_2)_7CF_3$
1o	Me	—$(CH_2)_{17}CH_3$
2a	Me	—OH
2b	Et	—OH
2c	Me	—$OC(O)CH_3$
2d	Et	—$OC(O)CH_3$
2e	Me	—H
3a	H	
3b	Me	
4a	Me	—$(CH_2)_{10}COOH$
4b	Me	—$(CH_2)_8CH_3$
4c	Me	—C_6H_4OH
4d	Me	—$(CH_2)_{10}C(O)NHC_6H_4OH$
5a	H	
5b	Me	
6a	H	
6b	Me	
8a		—H
8b		—CHO
9a		—O-*n*hexyl
9b		—O-cyclohexyl
9c		—$OCH_2CH_2(CF_2)gCF_3$
9d		—NHC_6H_4OH

and polymerized with potassium peroxodisulfate as initiator, sodium lauryl sulfate as an emulsifying agent, and sodium hydrogen phosphate as buffer in water at 60–80°C. It was observed that the molecular weights of the polymers obtained in the presence of β-cyclodextrin were lower than that of the control experiments. Thus, an increase in the styrene/β-cyclodextrin ratios 20:1 caused an increase in the percentage of syndiotacticity. Also, the glass-transition temperature (T_g) of the polymers increased analogous to higher melting temperature at higher styrene/β-cyclodextrin ratios.

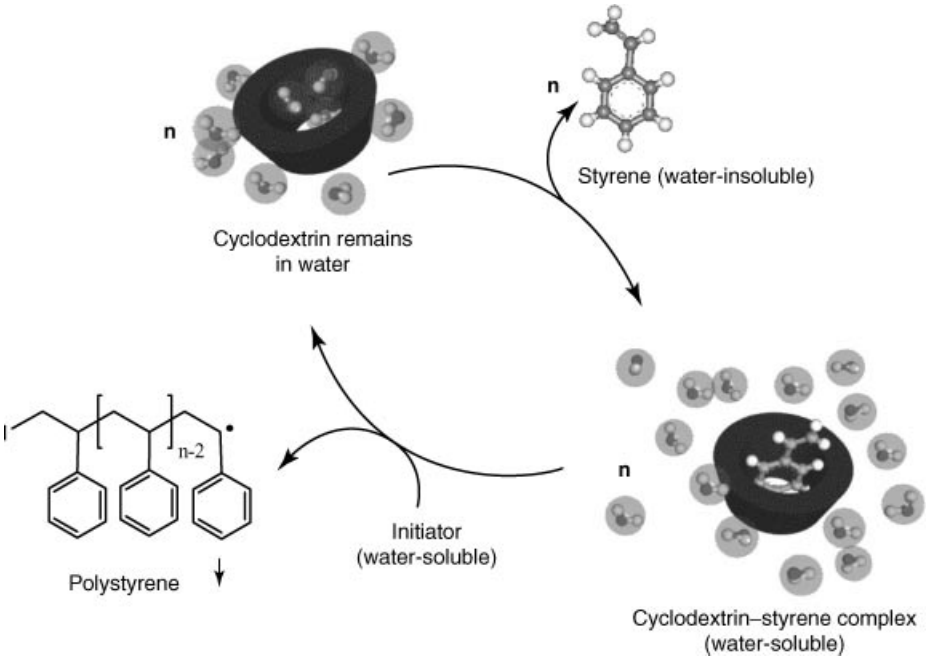

Fig. 6. Schematic presentation of complexation and polymerization of cyclodextrin complexed styrene.

Polystyrene (PS) and polymethyl methacrylate (PMMA) with a narrow particle-size distribution were synthesized under semicontinuous conditions in the presence of different amounts of RAMEB in water using potassium peroxodisulfate (14). The monomers were constantly added to a mixture of RAMEB/initiator solution at 80°C over a period of 2 h. Using these conditions, very stable latices of PS was obtained. It was observed that the polydispersities of PS latex particles prepared in the presence of cyclodextrin were much smaller than in the latices prepared without cyclodextrin. The average particle size decreased with increase in RAMEB concentration from 403 nm (0 wt% of RAMEB) to 267 nm (11 wt% of RAMEB) and increased again to 318 nm (22 wt% of RAMEB) (Fig. 7). The polydispersities of a PMMA latex, prepared in the presence of cyclodextrin, were in the same order as the polymer synthesized without RAMEB. The average particle size increased with increasing amount of RAMEB in the reaction mixture and the particle-size distributions were narrow. However, SEM images of PMMA particles (Fig. 8) showed that the use of cyclodextrin has no influence on the particle-size distribution. It turned out that all the latices contained no aggregates.

Butyl Methacrylate. The role of β-cyclodextrin in the emulsion polymerization of vinyl monomers has been investigated (9). Surfactant free polymerization of *n*-butyl methacrylate in the presence of β-cyclodextrin yielded stable lattices in a formulation which give a grossly coagulated product without cyclodextrin (15). The free-radical polymerization of cyclodextrin complexed *tert*-butyl methacrylate (**1c**) in aqueous phase has been described (10) The influence

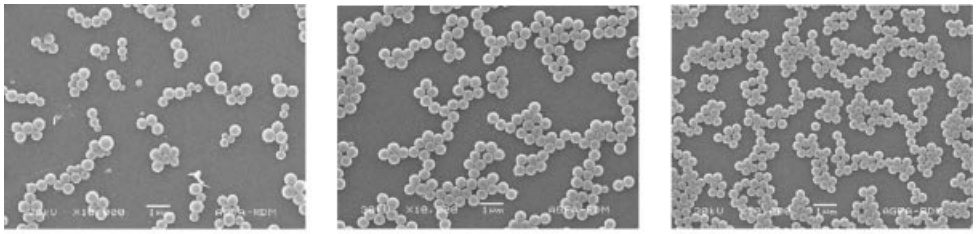

Fig. 7. SEM image of PS particles. (**a**) Polymer was obtained without cyclodextrin. Polymer synthesis in the presence of (**b**) 5.6 wt%, cyclodextrin (**c**) 11.1 wt% cyclodextrin (14).

of sodium nitrite and ascorbic acid on the free-radical polymerization of **1c** has been reported (16) in water at 80°C.

More recent, the free-radical polymerization of water-soluble *tert*-butyl methacrylate (**1c**) (water solubility $\sim 1.69 \times 10^{-3}$ mol/L) and its RAMEB complex at different temperatures has been studied (17). RAMEB and the hydrophobic **1c** were mixed in water in a molar ratio of 1.5:1 yielding the water-soluble complex with the binding constant $K = 65\ M^{-1}$. The homopolymerization reactions were carried out in the presence of water-soluble initiator 2,2′-azobis(amidinopropane)-dihydrochloride (VA044) or $K_2S_2O_8/Na_2S_2O_5$. The polymerization of the complexed monomer or free monomer at 80°C leads to poly(*tert*-butyl methacrylate) with molecular weights in the range of 16,000–41,000 g/mol. In contrast to these results the polymerization without cyclodextrin showed significantly lower yields. It was observed that no polymerization of free monomer occurred at 20°C, whereas, under the same condition, the homopolymerization of the RAMEB-complexed monomer leads to polymer in a high yield (∼75%) with high molecular weight (38,600–64,000 g/mol).

Fluorinated Methacrylates. Fluorinated polymers are very important materials because of their water- and oil-repellent properties. The synthesis of fluoropolymers is one case in which special polymerization techniques are required; eg, emulsion polymerization with added fluorinated surfactant, and

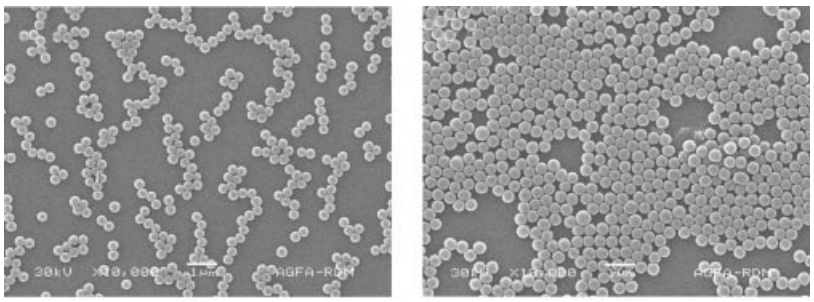

Fig. 8. SEM image of PMMA. Polymer was obtained (**a**) without RAMEB, (**b**) with 5.3 wt% RAMEB (14).

polymerization in organic solvents or solvent mixtures containing CFCs. On the other hand, because of hydrophobic and lipophobic nature of fluorinated monomers, the copolymerization with lipophilic or hydrophilic monomers has been carried out in organic solvents, in mixtures of different solvents, or in emulsion. The low solubility of the fluorinated monomers prohibits the copolymerization in water without addition of fluorinated surfactants or cosolvents. But the cyclodextrin-mediated polymerization in aqueous solution opens up new possibilities to the synthesis of fluorinated polymers without using surfactants or cosolvents. Therefore, fluorinated methacrylates (1*H*,1*H*-pentafluoropropyl) methacrylate (**1k**), (1*H*,1*H*,2*H*,2*H*-tridecafluorooctyl) methacrylate (**1l**) and (1*H*,1*H*,2*H*,2*H*-heptadecafluorodecyl) methacrylate (**1m**) were homopolymerized in the presence of 1 mol equivalent of RAMEB in water at 50°C using water-soluble azo initiator or the redox initiator. This concept was also applied to free-radical copolymerization of the monomers **1k, 1l**, and **1m** with styrene (**8a**) in complexed form. The copolymers were isolated via filtration, whereby in all cases almost quantitative yields of the "statistical copolymers" were achieved. The homopolymers poly(**1k**), poly(**1l**), and poly(**1m**) show glass-transition temperatures (T_g's) of 69.5°C, 39°C, and 71°C, respectively. Whereas the copolymers poly(**1k**-*co*-**8a**), poly(**1l**-*co*-**8a**), and poly(**1m**-*co*-**8a**) show higher T_g's at 79.9°C, 60°C, and 85°C.

An additional poly[(1*H*,1*H*,2*H*,2*H*-heptadecafluorodecyl acrylate (**1n**))-*co*-(stearyl methacrylate (**1o**))] was successfully obtained in water in the presence of RAMEB. The copolymer shows two broad endothermic transitions at 32°C and 50°C, which indicates a liquid-crystalline behavior. The results of X-ray diffraction of the copolymer poly(**1n**-*co*-**1o**) at 20°C indicate highly ordered lamella structure (18).

Polymerization of Methyl Methacrylate (1a) Using Atom-Transfer Radical Polymerization. Living Radical Polymerization (qv) (19) is the most significant and useful procedure to synthesize polymers with well-defined structure, controlled molecular weight, and narrow molecular weight distribution. Metal-catalyzed atom-transfer radical polymerization (ATRP) (20), nitroxide-mediated polymerization (21), and reversible addition–fragmentation chain transfer (RAFT) polymerization (22) have been widely used for this purpose. We have investigated for the first time the polymerization of host-guest complexe of methyl methacrylate (**1a**) and RAMEB in aqueous medium using atom-transfer radical polymerization ATRP (23). 4,4′-Di-(5-nonyl)-2,2′-bipyridyl (dNbpy) was used as a very effective ligand in the ATRP of **1a**, which was complexed with large (approximately 4-fold molar) excess of RAMEB in water. The polymerization of **1a**/RAMEB complex was initiated by ethyl 2-bromoisobutyrate (EBIB) in the presence of copper(I)bromide as catalyst. It was found that the polymerization of **1a** under this condition has a "living character." The obtained polymer shows much lower polydispersity (PD = 1.3–1.8) than those obtained from conventional free-radical polymerizations. Additionally, it was observed that a higher conversion of **1a** could be achieved using dNbpy/RAMEB as ligand compared to bipyridine (bipy). Furthermore, the block copolymerization of poly(methyl methacrylate) bearing a bromoester end-group with RAMEB-complexed styrene was also carried out under ATRP conditions in aqueous medium.

Synthesis and Polymerization of New (Meth)acrylic Derivatives

***N*-Methacryloyl Amino Derivatives.** *N*-methacryloyl-11-aminoundecanoic acid (**4a**) and *N*-methacryloyl-1-aminononane (**4b**) were easily prepared by the reaction of methacrylic anhydride with 11-aminoundecanoic acid and aminononane in dichlormethane. The relatively hydrophobic monomers were incorporated into the cavity of RAMEB. The homopolymerization of the complexed monomers was investigated in water or in mixture water:dimethyl sulfoxide (1:4 vol%) initiated by the redox initiator system potassium peroxodisulfate and potassium hydrogensulfite. The kinetics of the polymerization reactions in water/dimethyl sulfoxide measured by the use of ^{1}H NMR spectroscopy showed relatively high polymerization rates for the RAMEB-complexed monomers compared to the polymerization rates of the water-insoluble guest (Fig. 9) (24).

Furthermore, the water-soluble complex consisting of *N*-methacryloyl-11-aminoundecanoic acid (**4a**) and unmodified β-cyclodextrin was obtained at 65°C in water and polymerized in an aqueous medium using the water-soluble azoinitiator 2,2′-azobis(*N*,*N*′-dimethyleneisobutyramidine). The polymer with relatively high molecular weights was isolated in 93% yield after 24 h at 70°C (25).

Oxazoline Derivatives. Oxazolines are of great interest because of their ability to undergo cationic ring-opening polymerization. In this connection, the functionalized monomers *N*-[4-(4′,5′-dihydrooxazol-2-yl)phenyl]acryl amide (**5a**), *N*-[4-(4′,5′-dihydrooxazol-2-yl)phenyl]-2-methacryl amide (**5b**), *N*-{10-[4-(4′,5′-dihydrooxazol-2-yl)phenylcarbamoyl]decyl}-2-acryl amide (**6a**),

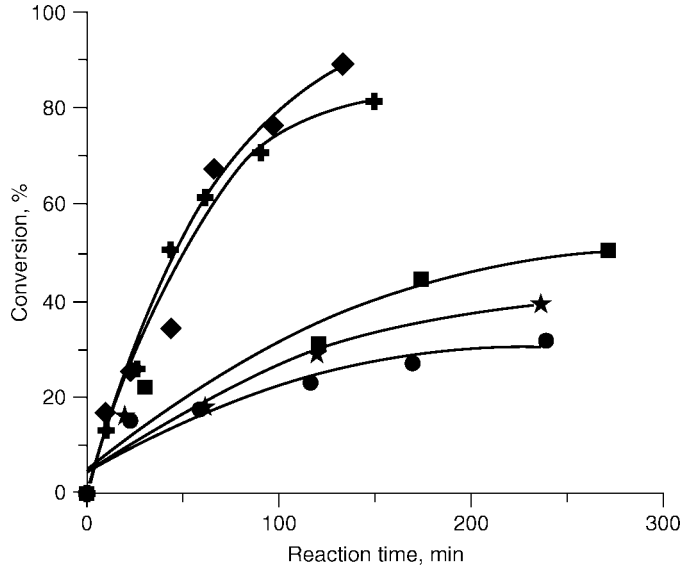

Fig. 9. The influence of methylated β-cyclodextrin on the polymerization rates: + *N*-methacryloyl-11-aminoundecanoic acid (**4a**)/CD complex in water; ◆ *N*-methacryloyl-11-aminononane (**4b**)/CD complex in water; ■ *N*-methacryloyl-11-aminoundecanoic acid (**4a**)/CD complex in water/DMSO; ★ *N*-methacryloyl-11-aminoundecanoic acid (**4a**) in water/DMSO; ● *N*-methacryloyl-11-aminononane (**4b**) in water/DMSO.

N-{10-[4-(4′,5′-dihydrooxazol-2-yl)phenylcarbamoyl]decyl}-2-methacryl amide (**6b**) and *N*-[4-(4′,5′-dihydrooxazol-2-yl)phenyl]-4-vinylbenz amide (**7**) were prepared by condensation of *p*-aminophenyl-2-oxazoline with corresponding acrylic monomers in the presence of 1-ethoxycarbonyl-2-ethoxy-1,2-dihydroquinolin (EEDQ) in dioxane. Oxazoline derivatives were completely incorporated into the RAMEB at room temperature using methanol. As expected, after evaporating the organic solvent, the complexes were completely water-soluble. Their polymerization was carried out in water at 60°C in the presence of 2,2′-azobis(2-amidinopropane) dihydrochloride (AAP) as initiator. ^{1}H NMR and IR spectra of the polymers clearly showed the presence of oxazoline ring as a functional group, which offers possibilities of further modification of the polymers, eg, ionic grafting of alkyloxazoline (26).

Vinylcyclopropane Derivatives. Vinylcyclopropyl acrylates have a potential in the preparation of materials with low shrinkage. 1,1-disubstituted 2-vinylcyclopropane (**9**) containing electron-withdrawing and radical-stabilizing groups are known to undergo radical ring-opening polymerization leading to polymers that consist predominantly of 1,5-linear olefin structure (27, 28) and also isomer cyclobutane-ring structures probably formed by recyclization of the propagating ring-opened radical (29). According to these results, 1-ethoxycarbonyl-1-hexyloxycarbonyl-2-vinylcyclopropane (**9a**) and 1-ethoxycarbonyl-1-cyclohexyloxycarbonyl-2-vinylcyclopropane (**9b**) were synthesized by condensation of 1-ethoxycarbonyl-2-vinylcyclopropane-1-carboxylic acid in the presence of dicyclohexylcarbodiimide (DCC) and 4-dimethylaminopyridine (DMAP) or pyrrolidinylpyridine (PPy). It was found that the radical polymerization of the RAMEB-complexed monomers leads to polymers with higher yields and molecular weights compared to the corresponding values obtained from uncomplexed monomers (30,31).

1-Ethoxycarbonyl-1-[(1*H*,1*H*,2*H*,2*H*)perfluorodecyl]oxycarbonyl-2-vinylcyclopropane (**9c**) was prepared and complexed with RAMEB according to the above-mentioned procedure. Its copolymerization with different ratio of hexyl-substituted vinylcyclopropane **9a** was performed via their respective RAMEB complexes in aqueous solution. In all cases, upon polymerization the water insoluble polymers were isolated by filtration. The prepared polymers exhibited liquid crystalline behavior. The SEC analysis of soluble copolymer (eg, 29 mol% of fluorinated monomer) shows, in fact, monomodal curves with a molar mass of M_n = 68,000 g/mol and polydispersity of PD = 1.62. ^{1}H NMR spectrum of corresponding copolymers shows that the amount of olefin repeating units increased with decreasing content of fluorinated monomer (31).

Mesoionic 6-Oxo-1,6-dihydropyrimidin-3-ium-4-olates. Mesoionic 6-oxo-1,6-dihydropyrimidin-3-ium-4-olates are six-membered heterocycles. Their pharmacological activities are of certain interest, and it was found that irradiation of the mesoionic monomers leads irreversibly to the bis(β-lactame) (32). Up to now, different approaches toward preparing polymers containing mesoionic groups in the main chain in organic solution were attempted (33). Referring to the above results, we have synthesized high melting crystalline methacrylic esters containing mesoionic 6-oxo-1,6-dihydropyrimidin-3-ium-4-olates and then prepared their RAMEB complexes in aqueous medium.

For example, mesoionic 2-[2-(isopropenylcarbonyloxy)ethylthio]-1-methyl-6-oxo-3-phenyl-5-propyl-1,6-dihydro-pyrimidin-3-ium-4-olate (**11**) (34) was stirred in equimolar amount with a solution of RAMEB for 5 days at ambient temperature. The 2:1 host–guest complex **11**/RAMEB was isolated in 71% yield relative to the guest monomer. The water solubility of complex was about 800 mg in 1-ml water at ambient temperature. The radical polymerization of RAMEB-complexed monomer was carried out with 3.3 mol% of redox initiator potassium peroxodisulfate and sodium hydrogensulfite. According to the results of the gel-permeation chromatography (GPC) obtained for the polymer prepared from the uncomplexed monomer, 85% of **11** was unreacted after 1 h. Additionally, the molecular weight distribution of the polymer synthesized without RAMEB is bimodal with M_w = 11,000 g/mol and polydispersity of 4.5 (35).

***N*-Isopropyl Acrylamide.** Homopolymers from *N*-isopropyl acrylamide (NIPAAm) are well known and have been of great interest because of their low critical solution temperature (LCST) behavior in water-solution. The polymer is soluble at low temperatures in water and precipitates above the LCST upon heating. Those kinds of polymers are potentially useful in the pharmaceutical or medical area. The homo- and copolymerization with water-soluble comonomers such as 2-hydroxyethyl methacrylate and characterization of the corresponding polymers of NIPAAm are described in some papers. In the case of copolymerization with hydrophobic comonomers, the use of an organic solvent is necessary, otherwise the polymerization has to be carried out in emulsion. But the different solubilities of the monomers in water often make the copolymerization of water-soluble and water-insoluble monomers by classical emulsion polymerization difficult. Because of the above discussed property of cyclodextrin derivatives, these problems can be avoided if the copolymerization reactions are performed in the presence of cyclodextrin derivatives.

Regarding our current work on the polymerization using cyclodextrins, the copolymerization of RAMEB-complexed *n*-butyl methacrylate (**1b**), cyclohexyl methacrylate (**1d**), isobornyl acrylate (**3a**), isobornyl methacrylate (**3b**), and styrene (**8a**) with the water-soluble *N*-isopropyl acrylamide (NIPAAm) was examined. The RAMEB complexes of **1b, 1d, 3a, 3b**, and **8a** were copolymerized with NIPAAm in water in molar ratios of 1:9 (90 mol% NIPAAm) and 1:4 (80 mol% NIPAAm), respectively for 12 h at 80°C using 5.5 mol% of AAP. For comparison, the copolymerization of styrene (**8a**) with NIPAAm at the same initial concentrations at molar ratios of 1:2 (67 mol% of NIPAAm) and 1:1 (50 mol% of NIPAAm), respectively, were also carried out under similar reaction conditions, in a mixture of *N*,*N*′-dimethylformamide (DMF) and water (9:1, vol%), without RAMEB. Surprisingly, it was found by means of SEC data that for all molar ratios of the incorporated monomer units, the average weight M_w of the copolymers obtained from complexed styrene (**8a**) and NIPAAm is about 3 to 7 times higher than that corresponding to the copolymers obtained from uncomplexed styrene and NIPAAm in DMF/water solution. In all cases, UV signal and RI signal of SEC elution of the monomodalic SEC curves deviated only slightly by about 10% of the maximum (36).

The concept has been applied to the free-radical copolymerization of a water-soluble azo monomer with a water-insoluble monomer, eg, styrene. The RAMEB-complexed styrene was copolymerized in various molar ratios with sodium-4-(acrylamido)-phenyldiazosulfonate (**10**) at 40°C using 1.5 mol% of water-soluble

free-radical initiator 2,2′-azobis-(*N*,*N*′-dimethyleneisobutyramidine) dihydrochloride (VA 044) (37). Depending on the amount of styrene in the copolymer, water- or DMF-soluble copolymers with high molecular weights were obtained. In all cases, the azo content of the polymer was below that of the monomer feed, as was determined by elemental analysis and UV spectroscopy. These results indicate that the diazosulfonate monomer is less reactive than the complexed styrene (**4a**). The molecular weight of the polymers were in the range of M_n = 14,000-24,000 g/mol, with an unexpected low polydispersity (PD = 2.4–2.5). Because of the high absorption coefficient [above 15 000 $(mol \cdot cm)^{-1}$] of the diazosulfonates, rapid photochemical decomposition was observed upon irradiation with suitable wavelength of the UV light. The rapid degradation of the azochromophores during irradiation of the polymers in DMSO solution was observed by UV–visible analysis.

Finally, it was thus interesting to investigate the possibility to use a suitable cyclodextrin complexed photoinitiator for initiation of polymerization in aqueous medium. In comparison to the thermal polymerization, the main advantage of the photoinitiated radical polymerization is the high efficiency and the reduced energy consumption.

Thus, a mixture of photoinitiator 2-hydroxy-2-methyl-1-phenylpropan-1-one (Ciba) and RAMEB in water was sonificated for 5 min yielding a clear solution of the complexed initiator. To evaluate the influence of cyclodextrin, the polymerization of NIPAAm in aqueous solution initiated with complexed and uncomplexed photoinitiator Ciba was performed. After the addition of 2 mol% of RAMEB-complexed Ciba, the mixture was irradiated with a high pressure mercury lamp at 20°C. UV spectroscopic measurements (Fig. 10) revealed that the polymerization reaction initiated with the RAMEB-complexed initiator is faster and ends up with higher yield than the polymerization in the absence of cyclodextrin (38).

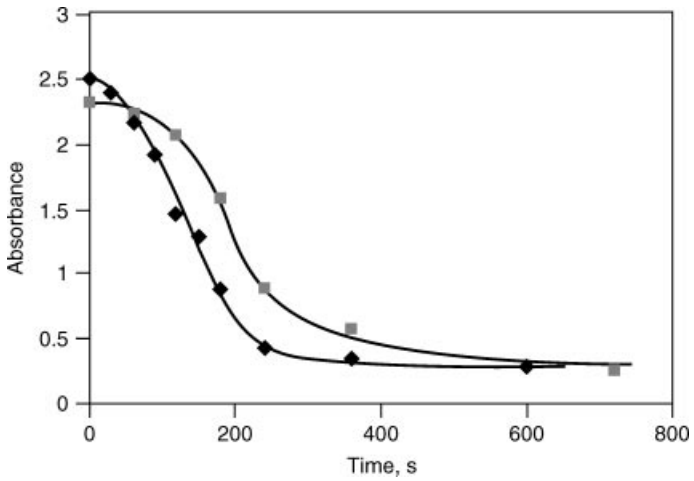

Fig. 10. UV absorbance of nonreacted NIPAAm during polymerization reactions initiated with 2-hydroxy-2-methyl-1-phenylpropan-1-one (Ciba) in the presence of cyclodextrin (■) without cyclodextrin (◆).

Unsaturated Polyester. Commercially available unsaturated polyester (39) has found a large number of applications in many areas, eg, auto industries and coating materials. A water-soluble unsaturated polymer with the molecular weights of 11,000–13,000 g/mol was cross-linked with the RAMEB-complexed styrene at 25°C using 4 mol% of the water-soluble redox initiator. A comparative experiment with uncomplexed comonomer styrene showed that higher yield and a higher content of polystyrene in the copolymer was achieved in the presence of RAMEB (40).

***N*-Methacryloyl-D,L-phenylalanine Methyl Ester.** The enantiodiscriminating influence of cyclodextrin in the free-radical polymerization of the racemic monomer *N*-methacryloyl-D,L-phenylalanine methyl ester (**2e**) (41) was investigated for the first time. **2e** was synthesized in 99% yield by the reaction of phenylalanine methyl ester hydrochlorides with methacryloyl chloride in the presence of triethylamine. The racemic monomer was subsequently added to an aqueous solution of RAMEB yielding a clear colorless solution of complexed monomer. Homopolymerizations were carried out in the presence of redox initiator at various temperatures. It was showed that the L-enantiomer is enriched in the residual monomer mixture. This observation confirms that complexed D-enantiomer polymerizes faster than the complexed L-enantiomer. No polymerization of **2e** was observed without cyclodextrin under the same conditions.

Cyclodextrin as Thermosensitive Stabilizer and Retardant

Cyclodextrin is not only used for improving the solubility of several water-insoluble hydrophobic monomers in aqueous medium, but also to stabilize some special monomers and to reduce the reactivity in the radical polymerization at room temperature. Because of the position of the vinyl group in the cyclodextrin cavity or strong interactions with the complexed monomer, cyclodextrin may act as thermosensitive stabilizer and also retard the free-radical polymerization process. For example, in the case of *N*-methacryloyl-L-tyrosine derivatives, no polymerization reactions were observed at room temperature in the presence of cyclodextrin (8).

4-Vinylbenzaldehyde. 4-Vinylbenzaldehyde (**8b**) was synthesized by Heck reaction of 4-bromobenzaldehyde with ethylene in the presence of palladium(II)acetate, tri(*o*-toluoyl)phosphine and triethylamine in dimethyl formamide (42), and then complexed with RAMEB to obtain a clear homogenous solution of the host–guest complex. The complex of **8b** was polymerized in water, and for comparison the uncomplexed monomer was polymerized in water and also in organic solution (43). The polymers obtained in the presence of cyclodextrin precipitated in lower yields and the molecular weights were higher than those of the polymers obtained in benzene. The lower yield of the polymer indicates that the spatial structure of the complex reduces the probability of chain radicals to react with the vinyl groups located in the center of the cyclodextrin cavity. However, at higher temperature (70°C), the mobility of 4-vinylbenzaldehyde in complexed form is strongly increased, which leads to a higher yield of polymer. The higher yields and slightly higher molecular weights of the polymers obtained from the uncomplexed **8b** under identical reaction conditions demonstrates the

ability of the cyclodextrin to act as spatial protection group for the vinyl double bond.

***N*-Methacryloyl-L-tyrosine Derivatives.** *N*-Methacryloyl-L-tyrosine methyl ester (**2a**) and *N*-methacryloyl-L-tyrosine ethyl ester (**2b**) were prepared by the reaction of trimethysilyl-protected L-tyrosine esters with methacryloyl chloride. The synthesis of acetyl derivatives **2c** and **2d** was carried out by reaction of *N*-methacryloyl-L-tyrosine esters **2a** and **2b** with acetyl chloride in the presence of triethylamine. The cyclodextrin complexes of the monomers were prepared by stirring an equimolar amount of RAMEB and the corresponding monomers **2a–2d** in water. The clear aqueous solution of the host–guest complexes was initiated with free-radical redox initiator $K_2S_2O_8/NaHSO_3$ at room temperature. The reaction mixture remained clear for up to five days, which suggests the existence of stable host–guest complexes at ambient temperature. At higher temperature ($>40^\circ$C) the mobility of the guest monomer increases, which leads to rapid polymerization of the RAMEB-complexed monomers **2a–2d** in aqueous medium. However, the polymerization of the monomers **2a–2d** in the presence of RAMEB at 60°C ends up with higher molecular weights and higher polydispersities (PD) than in the case of polymerization of uncomplexed monomers in water and also in organic solvents (8).

Oxidative Polymerization in the Presence of Cyclodextrin Derivatives

Enzyme-Catalyzed Polymerization. Horseradish peroxidase (HRP) has been used for the oxidation of a wide variety of compounds, eg, phenol derivatives in the presence of hydroperoxide (44). HRP is a kind of heme glycoprotein that catalyzes the oxidation of phenol to phenoxy radicals. Subsequently, the resulting phenoxy radicals couple each other to oligo or polyphenol derivatives step by step (see OXIDATIVE POLYMERIZATION).

The enzyme-catalyzed polymerization of phenol is an alternative to the production of conventional Phenolic Resins (qv), without use of toxic formaldehyde and under milder conditions. Because of the poor solubility of phenol derivatives and detrimental effect of excess of organic solvent on enzyme activity, the reactions catalyzed by HRP are often carried out in a mixture of water-miscible organic solvents, eg, dioxane and an aqueous buffer. To overcome the above limitations, the oligomerization process in the presence of cyclodextrin derivatives has been combined with the HRP-catalyzed oxidative coupling. Water-soluble complexes of para-substituted phenol derivatives *N*-(4-hydroxyphenyl)-maleimide (**12**), 4′-hydroxymethylacrylanilide (**4c**), *N*-methacryloyl-11-aminoundecanoyl-4-hydroxyanilide (**4d**), 1-[(4-hydroxyphenyl)aminocarbonyl)]-2-vinylcyclopropane carboxylate (**9d**), and RAMEB were formed in water and polymerized oxidative using HRP/H_2O_2 (45,46). The HRP-catalyzed oligomerization chemoselectively produced a polymer containing a reactive unsaturated group in the side chain.

The oligormer obtained from complexed *N*-(4-hydroxyphenyl)-maleimide had a high molecular weight fraction up to 3000 Da and was soluble in tetrahydrofuran. FT–IR spectrum of the oligomer showed no phenoxy ether linkages. It was found that the oligomerization rate of complexed monomer was about 10%

faster than that of the uncomplexed monomer. This indicates that the cyclodextrin molecules did not block the reactive sites of the phenoxy radical. Free-radical copolymerization of the corresponding oligomer obtained from monomer **12** with styrene and AIBN as initiator in tetrahydrofuran leaded to three-dimensional network. The powdery material was insoluble in common organic solvents, eg, methanol, dimethylformamide, or dimethylsulfoxide, and showed no glass transition or melting point below 300°C.

Also, free-radical ring-opening polymerization of oligomer obtained from complexed **9d** with AIBN in tetrahydrofuran at 65°C formed a network.

Oxidative Polymerizable Monomers. A further successful example of a cyclodextrin-mediated polymerization reaction is the oxidative oligomerization of heterocyclic aromatic compounds such as pyrrole or 3,4-substituted dioxythiophene EDT. Electrochemical and chemical polymerization [Fe(III)chloride or potassium peroxodisulfate] of homogenous aqueous solution of cyclodextrin-complexed monomers resulted in precipitation of the corresponding polypyrrole and PEDT. Conductivity measurements of the polymers showed identical electrical properties (10–100 S/cm) as a conventionally prepared polymer (7). Because of the substantial π-electron delocalization along their backbones, these polymers show interesting (nonlinear) optical properties and become good electric conductors when being oxidized or reduced (see ELECTRICALLY ACTIVE POLYMERS). Conducting polymers open up a variety of potential practical applications in industrial terms, eg, information storge, optical signal processing, recharged batteries, light-emitting diodes, field effect transistors, printed circuit boards, sensors, antistatic materials, electromagnetic interference (EMI) shielding, and solar energy conversion (47,48). Electropolymerization (qv) of aromatic and heteroaromatic compounds is one of the most valuable techniques for the synthesis of electrically conducting organic polymers (49). Because of the low water solubility of the monomers and the high reactivity of the initially formed radical cations towards water molecules, most conducting polymers are synthesized in organic solution. However, water is the ideal solvent for practical use and industrial applications. The high water solubility of the host–guest complex has led to considerable interest in usage of the cyclodextrin derivatives in the synthesis of conducting polymers.

Electrochemical properties of polypyrrole films grown in $LiClO_4$ acetonitrile solution (2% water) at gold electrodes modified with thiolated β-cyclodextrin self-assembled monolayers have been investigated. Scanning electron microscopic results show that thiolated β-cyclodextrin acts as a molecular template to restrict the growth sites within the β-cyclodextrin cavities (50).

Inclusion compounds using hydroxypropyl-β-cyclodextrin as host molecules have been used to electropolymerize bithiophene for the first time in aqueous medium (51). Thin films of polybiothiophene were produced by electrooxidation of an aqueous solution of bithiophene, cyclodextrin, and $LiClO_4$ at platinum electrodes, using cyclic voltametry and galvanostatic method.

The chemical synthesis and electrosynthesis of polypyrrole in the presence of sulfonated cyclodextrin as a dopant has been reported (52). In this case, cyclodextrin seems to play an important role in forming polymer with ordered structure.

Influence of Methylated β-Cyclodextrin as Host Molecule on the Kinetics of the Free-Radical Copolymerization

Reactivity Ratios. The new cyclodextrin-mediated polymerization method of hydrophilic monomers differs strongly from classical methods such as emulsion polymerization. For example, because of the inclusion of the monomers into the cyclodextrin cavities, the copolymerization parameters may be influenced significantly (see COPOLYMERIZATION). As an interesting observation, it was found that the reactivity ratios of the RAMEB-complexed monomers isobornyl acrylate (**3a**) and *n*-butyl acrylate (**1g**) ($r_{\mathbf{3a}/\mathrm{RAMEB}} = 0.3 \pm 0.1$), ($r_{\mathbf{1g}/\mathrm{RAMEB}} = 1.7 \pm 0.1$) differ significantly from the *r* values of the corresponding uncomplexed monomers in dimethyl formamide ($r_{\mathbf{3a}} = 1.3 \pm 0.1$) and ($r_{\mathbf{1g}} = 1{,}0 \pm 0.1$). Analogous to the above-described homopolymerization reactions, the molecular weights (M_n) of the copolymers obtained from the complexed monomer were about five times higher than those corresponding to the copolymers obtained from organic solution (53).

Additionally, copolymerization of RAMEB-complexed monomers *n*-butyl acrylate (**1g**), *n*-hexyl acrylate (**1i**) and cyclohexyl acrylate (**1j**) led to the following arithmeric averages of the reactivity ratios: copolymerization of **1g**/RAMEB and **1i**/RAMEB: ($r_{\mathbf{1g}/\mathrm{RAMEB}} = 1.01 \pm 0.01$, $r_{\mathbf{1i}/\mathrm{RAMEB}} = 1.04 \pm 0.01$); copolymerization of **1j**/RAMEB and **1i**/RAMEB: ($r_{\mathbf{1j}/\mathrm{RAMEB}} = 0.74 \pm 0.01$, $r_{\mathbf{1i}/\mathrm{RAMEB}} = 1.28 \pm 0.01$); copolymerization of **1j**/RAMEB and **1g**/RAMEB: ($r_{\mathbf{1j}/\mathrm{RAMEB}} = 0.75 \pm 0.04$, $r_{\mathbf{1g}/\mathrm{RAMEB}} = 1.13 \pm 0.01$). Only the copolymerization of water-soluble cyclodextrin-complexed **1g** with cyclodextrin-complexed **1i** leads to a nearly ideal statistical copolymer. The copolymerization in the absence of cyclodextrin in DMF/H_2O solution resulted to nearly ideal statistical copolymers in all cases: **1g** and **1i**: ($r_{\mathbf{1g}} = 1.01 \pm 0.01$, $r_{\mathbf{1i}} = 0.91 \pm 0.03$); **1j** and **1i**: ($r_{\mathbf{1j}} = 1.04 \pm 0.04$, $r_{\mathbf{1i}} = 1.04 \pm 0.08$); **1j** and **1g**: ($r_{\mathbf{1j}} = 0.95 \pm 0.02$, $r_{\mathbf{1g}} = 1.24 \pm 0.04$) (54). It can be concluded that the interactions between monomer and cyclodextrin are liable substantially for the control of copolymerization reactivity ratio. According to these experiments, it can be postulated that the stronger the interaction between host and guest, the lower the *r* value.

Initial Rate v_0. The influence of the hydrophilic character of acrylate side groups on the initial polymerization rate v_0 in the presence of cyclodextrin has also been investigated. For kinetic studies, the RAMEB-complexed monomers *n*-propyl, butyl, pentyl, hexyl, and cyclohexy acrylate **1f–1j** were polymerized in water by free-radical mechanism, using the water-soluble initiator 2,2′-azobis(2-amidinopropane) dihydrochloride (AAP). The concentration of nonreacted monomer in the reaction mixture was deteminated using UV spectroscopy or high performance liquid chromatography (HPLC). The initial reaction rate v_0 increases from RAMEB-complexed monomer **1f** (12.5 ± 1.18) via **1g** (27.5 ± 0.83) to **1h** (44.2 ± 3.54) to **1j** (49.4 ± 1.18) up to **1i** (75.8 ± 2.55) $\times 10^{-6}$ mol/L·s. However, the water solubility of uncomplexed monomer increases in the following order: *n*-hexyl acrylate > *n*-pentyl acrylate > cyclohexyl acrylate > *n*-butyl acrylate > *n*-propyl acrylate. The increasing hydrophobic character of the side group causes the reduced water solubility of the monomers **1f–1i**. Moreover, the stability of the host–guest complex generally increases with geometrical fit of the guest in the cyclodextrin cavity. Also, the complex and dynamic stabilities, which

are influenced by the sterical demands of the guest monomers, have an influence on the overall rate of polymerization. But the increase of the initial rate v_0 with the increasing hydrophobic character of the complexed monomers seems to be the most important factor for the involved monomers **1f–1i**. It was postulated that the more hydrophobic the monomer, the higher the local concentration of complexes close to the active radical chain end of the phase-separated polymer. This leads to higher values of the initial rate v_0 (55).

Chain-Transfer Agents. Radical chain-transfer agents, eg, various thiols, have been applied over several decades to control the molecular weight of the polymerization or to terminate the growing polymer chain, eg, in the case of telomerization (38). Recently, we have observed that the chain-transfer constants of the water-soluble *N*-acetyl-L-cystein to RAMEB-complexed monomers, eg, methyl methacrylate and styrene, are three times higher in water than in the case of a mixture of *N*,*N*′-dimethylformamide and water.

Also, for the determination of the chain-transfer constants the RAMEB-complexed monomers methyl methacrylate **1a** and styrene **8a** were polymerized for 4 h at 80°C using 0.3% (wt/wt) of the water-soluble free-radical initiator AAP in the presence of different amounts of the water-soluble chain-transfer agent *N*-acetyl-L-cystein from 0 to 3.0 mol%. Relatively high chain-transfer constants of *N*-acetyl-L-cysteine were found in the case of the complexed monomers **1a** and **8a** in water ($Cs_{\mathbf{1a}/\mathrm{RAMEB}} = 1.7 \pm 0.3$ and $Cs_{\mathbf{8a}/\mathrm{RAMEB}} = 2.6 \pm 0.3$). In contrast, the chain-transfer constants in DMF/water mixture are significantly lower for uncomplexed monomers **1a** and **8a** ($Cs_{\mathbf{1a}} = 0.7 \pm 0.1$ and $Cs_{\mathbf{8a}} = 0.7 \pm 0.1$). From these results, it can be concluded that the molecular weight of the polymer obtained from complexed monomers can be controlled more effectively using hydrophilic thiol-containing chain-transfer agents than in the case of a polymerization of the respective uncomplexed monomers in an organic medium (56). Furthermore, the chain-transfer constants of RAMEB-complexed dodecanethiol for **1a**/RAMEB ($Cs_{\mathbf{1a}/\mathrm{RAMEB}} = 0.5 \pm 0.2$) and for **4a**/RAMEB ($Cs_{\mathbf{8a}/\mathrm{RAMEB}} = 2.2 \pm 0.3$) were observed in water. They also differ significantly from the corresponding values obtained from the polymerization experiments with uncomplexed monomers in the presence of uncomplexed dodecanethiol in an organic solution ($Cs_{\mathbf{1a}} = 3.1 \pm 0.3$ and $Cs_{\mathbf{8a}} = 3.4 \pm 0.3$). In this case, the molecular weight of the polymers obtained from organic solution can be controlled more effectively by the uncomplexed hydrophobic thiol as the chain-transfer agent (57).

BIBLIOGRAPHY

1. J. M. Lehn, J. L. Atwood, J. E. D. Davies, D. D. Macnicol, and F. Vogtle, *Comprehensive Supramolekular Chemistry*, Vols. **1–11**, Pergamon, Oxford, 1996.
2. J. Szejtli, *J. Mater. Chem.* **7**, 575 (1997).
3. G. Piel, B. Evrard, M. Fillet, G. Llabres, and L. Delattre, *Int. J. Pharm.* **169**(1), 15 (1998).
4. S. Li, and W. C. Purdy, *Chem. Rev.* **92**, 1457 (1992).
5. M. Tabatabai, H. Ritter, and M. Schmelzer, *e-Polymers* 39 (2002).
6. S. De Feyter, J. Van Stam, F. Imans, L. Viaene, F. C. De Schryver, and C. H. Evans, *Chem. Phys. Lett.* **277**, 44 (1997).

7. P. Glöckner, D. Schollmeyer, and H. Ritter, *Designed Monom. Polym.* Vol. **5**, 163 (2002).
8. J. Storsberg, H. Ritter, H. Pielartzik, and L. Groenendaal, *Adv. Mater.* **12**, 567 (2000).
9. S. Rimmer and P. I. Tattersall, *Polymer* **40**, 6673 (1999).
10. P. E. Madison and T. E. Long, *Biomacromolecules* **1**, 615 (2000).
11. J. Storsberg and H. Ritter, *Macromol. Rapid Commun.* **21**, 236 (2000).
12. J. Jeromin and H. Ritter, *Macromol. Rapid Commun.* **19**, 377 (1998).
13. P. Ravi, K. Udayasankar, and S. Divakar, *J. Incl. Phenom. Macromol. Chem.* **38**, 99 (2000).
14. J. Storsberg, H. Van Aert, C. von Roost, and H. Ritter, *Macromolecules* **36**, 50 (2003).
15. S. Rimmer, *Macromol. Symp.* **150**, 149 (2000).
16. C. Determbleur, A. Mouithys-Mickalda, P. Teyssie, and R. Jerome, *e-Polymers* 4 (2000).
17. S. Schwarz-Barać and H. Ritter, *J. Macromol. Sci. Part A: Pure Appl. Chem. A* **40**, 437 (2003).
18. J. Storsberg and H. Ritter, *Macromol. Rapid Commun.* **203**, 812 (2002).
19. K. Matyjaszewski, ed., *Controlled/Living Radical Polymerization*, Progress in ATRP, NMP, and RAFT; ACS Symposium Series, 2000, p. 668.
20. K. Matyjaszewski and J. Xia, *Chem. Rev.* **101**, 2921 (2001).
21. S. G. Gaynor, J. Qiu, and K. Matyjaszewski, *Macromolecules* **31**, 5951 (1998).
22. A. Goto, K. Sato, Y. Tsujii, T. Fukuda, G. Moad, E. Rizzardo, and S. H. Thang, *Macromolecules* **34**, 402 (2001).
23. J. Storsberg, M. Hartenstein, A. H. E. Müller, and H. Ritter, *Macromol. Rapid Commun.* **21**, 1342 (2000).
24. J. Jeromin, O. Noll, and H. Ritter, *Macromol. Chem. Phys.* **199**, 2641 (1998).
25. J. Jeromin and H. Ritter, *Macromolecules* **32**, 5236 (1999).
26. M. Fischer and H. Ritter, *Macromol. Rapid Commun.* **21**, 142 (2000).
27. N. Mosner, T. Völkel, U. K. Fisher, and V. Rheinberger, *Macromol. Rapid Commun.* **20**, 33 (1998).
28. N. Mosner, F. Yeuner, T. Völkel, and V. Rheinberger, *Macromol. Chem. Phys.* **200**, 2173 (1999).
29. J. Sugiyama, N. Kayamori, and S. Shimada, *Macromolecules* **29**, 1943 (1996).
30. V. Alupei and H. Ritter, *Macromol. Rapid Commun.* **22**, 1349 (2001).
31. S. W. Choi, O. Kretschman, H. Ritter, M. Ragnoli, and G. Galli, *Macromol. Chem. Phys.* **204**, 1475 (2003).
32. M. Hellberg, J. F. Stubbins, and R. A. Glennon, *Bioorg. Med. Chem.* **8**, 1917 (2000).
33. A. Theis, H. Ritter, F. Böhme, C. Klinger, B. Menges, and S. Mittler, *Chem. Mater.* **14**, 2109 (2002).
34. A. Theis and H. Ritter, *Des. Monom. Polym.* **4**, 177 (2001).
35. A. Theis and H. Ritter, *Macromol. Chem. Phys.* **204**, 1279 (2003).
36. P. Casper, P. Glöckner, and H. Ritter, *Macromolecules* **33**, 4361 (2000).
37. J. Storsberg, P. Glöckner, M. Eigner, U. Schnöller, H. Ritter, B. Voit, and O. Nuyken, *Des. Monom. Polym.* **4**, 9 (2001).
38. I. C. Alupei, V. Alupei, and H. Ritter, *Macromol. Rapid Commun.* **23**, 55 (2002).
39. D. Braun, H. Cherdron, and H. Ritter, *Polymer Synthesis: Theory and Practice*, 3rd ed., Springer, Berlin, 2001.
40. I. C. Alupei, V. Alupei, and H. Ritter, *Macromol. Rapid Commun.* **24**, 527 (2003).
41. S. Schwarz-Barać, H. Ritter, and D. Schollmeyer, *Macromol. Rapid Commun.* **24**, 325 (2003).
42. H. Detert and E. Sugiono, *J. Prakt. Chem.* **34**, 358 (1999).
43. M. Heineberg and H. Ritter, *Macromol. Chem. Phys.* **203**, 1804 (2002).
44. S. Kobayashi, H. Uyama, and S. Kimura, *Chem. Rev.* **101**, 3793 (2001).
45. M. H. Reihmann and H. Ritter, *Macromol. Chem. Phys.* **201**, 798 (2000).

46. Y. Pang, H. Ritter, and M. Tabatabai, *Macromolecules* **36**, 7090 (2003).
47. H. S. Nalwa., ed., *Handbook of Organic Conductive Molecules and Polymers, Vol. 4: Conductive Polymers: Transport, Photophysics, and Application*, John Wiley & Sons Ltd., Chichester, U.K., 1997.
48. T. A. Skotheim, R. L. Elsenbaumer, J. R. Reynolds, eds., *Handbook of Conducting Polymers*, 2nd ed., Marcel Dekker, New York, 1998.
49. H. S. Nalwa., ed., *Handbook of Organic Conductive Molecules and Polymers, Vol. 2: Conductive Polymers: Synthesis and Electrical Properties*, John Wiley & Sons Ltd., Chichester, U.K., 1997.
50. J.-Y. Lee and S.-M. Park, *J. Electrochem. Soc.* **147**, 4189 (2000).
51. C. Largrost, J. C. Lacroix, S. Aeiyach, M. Jouini, K. I. Chane-Ching, P. C. Lacaze, *Chem. Commun.* 489 (1998).
52. W. Chen, X. Wan, N. Zu, and G. Zue, *Macromolecules* **36**, 276 (2003).
53. P. Glöckner and H. Ritter, *Macromol. Rapid Commun.* **20**, 602 (1999).
54. S. Bernhardt, P. Glöckner, and H. Ritter, *Polym. Bull.* **46**, 153 (2001).
55. S. Bernhardt, P. Glöckner, A. Theis, and H. Ritter, *Macromolecules* **34**, 1647 (2001).
56. P. Glöckner, N. Metz, and H. Ritter, *Macromolecules* **33**, 4288 (2000).
57. P. Glöckner, N. Metz, and H. Ritter, *Macromol. Chem. Phys.* **201**, 2455 (2000).

HELMUT RITTER
MONIR TABATABAI
Heinrich-Heine-Universität

CYCLOHEXANEDIMETHANOL POLYESTERS.

See Volume 2.

CYCLOPENTADIENE AND DICYCLOPENTADIENE.

See Volume 5.

BIODEGRADABLE POLYMERS AND PLASTICS IN LANDFILL SITES

Introduction

Today, landfill may be regarded as a last resort for the waste management of plastics. Recycle through the reuse of plastic waste in fabrication, incineration for energy generation, and recycle through the natural cycle of biodegradation in compost or soil are much preferred disposal methods. However, considerable quantities of plastics (millions of tons annually), particularly packaging plastics, are still being dumped into landfills, where they occupy large volumes and contribute to capacity shortages.

Modern landfills are generally classified in several ways. One classification is by the types of waste that they receive, such as hazardous waste or municipal waste. In practice, these are not exclusive classifications since inevitably there is always some crossover because of source separation problems. An alternative classification is based on the functional mode of the landfill. Total containment landfills are designed to prevent any exchange with the surrounding environment and are particularly desirable for hazardous waste disposal. Leachate recycle landfills are designed to capture and recycle aqueous leachate to prevent or reduce environmental leakage of potentially harmful waste or degradation residues. Controlled contaminant release landfills allow for gradual migration of leachate into the environment under closely monitored conditions to ensure that no harmful events happen. Unrestricted contaminant release landfills, which are older waste dumps, are particularly prevalent in poorer nations, and have no controls of leachate or environmental contamination.

Plastics entering any of these landfill types may or may not degrade and/or biodegrade depending on their composition and the particular landfill environmental conditions to which they are exposed. By their nature, landfill

Encyclopedia of Polymer Science and Technology. Copyright John Wiley & Sons, Inc. All rights reserved.

environments are initially aerobic and undergo transition into anaerobic environments at a rate dependent on the utilization of oxygen by the microorganisms present to degrade waste and on the depth of the landfill. This article reviews what is known regarding the fate of common plastics placed into landfill sites for disposal or for a specific application such as a landfill daily cover. Degradations in both aerobic and anaerobic environments are discussed for a variety of packaging plastics and other polymers commonly found in landfill sites.

Polyolefins, particularly polyethylene, have been studied extensively in the real-world environment of landfills, where evidence of degradation and some potential for biodegradation is becoming apparent, though not yet conclusive. For most other plastics, anaerobic testing in laboratory simulation of landfills has been the focus with mixed results. Some polymers, such as the naturally produced polyhydroxyalkanoates, are biodegradable in aerobic and anaerobic environments, whereas most others are not at all biodegradable in anaerobic environments. Clearly, much work remains to be done to understand degradation and biodegradation in landfills, both in the laboratory and in the real world. The results will be important and will have great impact on the future directions for polymer and plastics waste management.

Composition of Trash in Landfill Sites

William L. Rathje, Professor of Archeology at the University of Arizona, is one of the most experienced and articulate "garbage pickers" in the world today. As the founder of the Garbage Project, he, his colleagues, and his students have been investigating the contents of landfills for about 30 years. His published analyses include landfills in and around Chicago, the San Francisco Bay area, Tuscon, Phoenix, Toronto, and New York City (1). As well as providing an historical context [garbage through the ages, as it were (2)], Prof. Rathje relates differences in social patterns and life styles to what he finds in landfills, sanitary, or otherwise. He has also noted that there are common misperceptions about what materials are actually discarded, collected, and deposited in landfills.

In 1991, Rathje estimated that every person in the continental United States generated an average of 1.8 kg (4 lb) of trash per day. The Fresh Kills Landfill (on Staten Island, now closed) received 15,500 t of garbage daily from New York City, 6 days a week. Prof. Rathje's assessment of the content by wt% is as follows: paper 50%, plastic 10%, metal 6%, glass 1%, and organic 13% (including yard waste, food waste, wood). The remaining 20% is a mixture that includes construction debris, disposable diapers, rubber, textiles, and tires. Rather more detail is available (3) about the composition of refuse from the Mallard North Landfill site (Chicago). Mean weight percent values are as follows: paper 32.7%, ash 22.2%, wood 12.3%, fines 8.6%, ferrous metal 7.4%, plastic 5.6%, glass 4.5%, textiles 3.8%, garden waste 1.9%, and rubber 1.0%; food, nonferrous metals, foamed polystyrene and cigarettes were each less than 1%. The waste, dated by means of discarded newspapers, was excavated in 1988, when it was about 20 years old.

The data derived from Prof. Rathje's excavations during October 1991 in the metropolitan Toronto area (4) are consistent with those obtained by his team of "garbologists" from analogous investigations throughout the United States.

Omitting the construction and demolition debris from the calculations, the composition (by volume this time) is as follows: paper and paperboard 50%, plastics 14%, metals 12%, glass 4%, organics 6%, and miscellaneous 14%. All plastic packaging (post-consumer, industrial, commercial, and institutional) represented about 8% of the overall refuse. It is a reasonable assumption that the composition of plastics discarded in landfills is a reflection of the quantities produced for packaging applications; the commodity plastics polyethylene, polypropylene, polystyrene, and poly(vinyl chloride) should be well represented (see ETHYLENE POLYMERS; PROPYLENE POLYMERS (PP); STYRENE POLYMERS; VINYL CHLORIDE POLYMERS).

Degradation Processes in Landfills

The fate of polymers and plastics in landfill can be represented schematically as shown below:

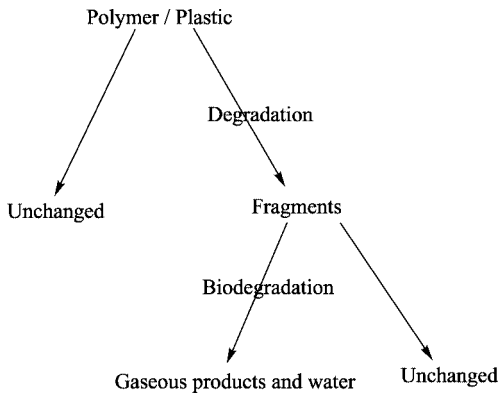

They may remain unchanged, or they may degrade by some biotic or abiotic process to fragments that either remain or biodegrade to gaseous products and water. The gaseous products are carbon dioxide in an aerobic environment and a mixture of carbon dioxide and methane in an anaerobic environment. The pathways obviously play a strong role in the subsequent stability and volume usage of the landfill, and there needs to be a thorough understanding of the chemistries involved with the particular polymer or plastic.

Biodegradation of organic materials is the result of activities of microorganisms, such microflora as fungi, yeasts, actinomycetes, and bacteria. Focusing on the first and last of these, the two main groups represent an enormous array of possibilities. Fungi operate primarily under aerobic, moist conditions, and proliferate by sporulation. Their spores and hyphal fragments are found universally and will generate new colonies whenever and wherever favorable conditions exist or arise. The environment "selects" which of the 80,000 or so species will germinate and grow. Bacteria, like fungi, are distributed universally throughout the surface of the earth and in the atmosphere. Around 2000 species of bacteria are known, but there are almost certainly many more species that are not known. Bacteria proliferate by cell division and require the presence of liquid water.

Biodegradation is nature's way of returning nonliving organic material to the carbon cycle. Commonly, microorganisms generate and secrete aqueous solutions of enzymes that chemically degrade and dissolve

supporting material (the substrate), which is then absorbed back into the organism through the cell walls, as food for growth and energy generation. Moisture is essential and the organic substrates should be hydrophilic and easily "wettable" to provide sites for enzyme activity. Under the right conditions, the proliferation of microorganisms can occur to a phenomenal extent. It has been calculated, for example, that the weight of microorganisms in arable land is 3 to 5 ton in an area of 4.05×10^3 m^2 (1 acre) to a depth of 30 cm (1 foot), and that 1 g of microorganisms may contain 10^{10} individuals. In soil, bacteria are found at greater depths than are fungi since many of them, the anaerobes, are able to survive without free oxygen in the reducing conditions that kill all other forms of life. This fact is relevant to microbial activity at the lower levels in landfills.

There is much evidence of extensive microbial activity in landfills, which is not surprising in view of the large organic content of waste, and the ubiquitous occurrence of fungi and bacteria, The heat generated by the microbes as they convert carbon into usable intermediates is significant, even at only moderate depths below the active face of the landfill. For some time (months, a year, or even longer) following the dumping of waste at the active face of a landfill, there will be enough oxygen present to allow for vigorous aerobic biodegradation of the susceptible refuse by fungi, bacteria, and the like. At some later stage, after a time period that will vary with conditions and operating procedures, a shortage of oxygen is likely to develop, and at the deeper levels of the landfill, anaerobic biodegradation largely by bacteria will begin and eventually dominate. It may be argued that it is entirely preferable to encourage as much biodegradation as possible during the aerobic period, for these reasons:

(1) The ultimate conversion product of the organic carbon in the waste from aerobic biodegradation is carbon dioxide, CO_2, whereas the major product from anaerobic biodegradation is methane, CH_4. The latter gas is 24.5 times more potent than carbon dioxide (5) as a greenhouse gas.
(2) The commodity of value in the operation of a landfill is space, and the more rapidly abiotic degradation and biodegradation occur, the longer the space will last before a new site is required.
(3) The more rapidly the biodegradation occurs, the shorter and less expensive will be the after-care period, and the sooner the site can be used safely for another purpose.

The Resource Conservation and Recovery Act, the US Federal Government, defines the criteria for the operation of Municipal Solid Waste Landfills (MSWLF), effective October 1993. Daily and alternative daily cover (ADC) requirements are described under Subtitle D, as follows:

(1) the owner or operator of all MSWLF must cover disposed solid waste with 150 mm (6 in.) of earthen material at the end of each operating day, or at more frequent intervals if necessary, in order to control disease vectors, fires, odor, blowing litter, and scavenging;
(2) alternative materials of a thickness other than 150 mm earthen material may be approved...if the owner or operator demonstrates that the alternative material performs the same functions as the 150 mm of soil.

In addition this ADC must not present a threat to human health and the environment.

A comprehensive investigation carried out (6) at the District of Chilliwack's Bailey Sanitary Landfill (approximately 60 km east of Vancouver, B.C.) based on the merits of ADC material evaluated technology developed by EPI Environmental Products Inc. as a landfill cover. This 76-μm (3 mil) polyethylene film contained an additive formulation (totally degradable plastic additives or TDPA) that results in a much higher than normal rate of oxidation. The heat generated by the activity of microorganisms in the landfill initiated the thermal oxidation of the polyethylene film, and the prodegradant in the additive dramatically increased the rate of oxidative degradation of the plastic. After burial for 98 days (December 18, 1995 to March 21, 1996) at a mean monthly air temperature between 1 and 5°C and a cumulative rainfall of about 700 mm, the film no longer existed as an intact layer but was punctured by numerous holes, and mixed up with the waste. The melt index of the plastic had increased, and the tensile breaking strength and elongation to break had decreased significantly. Fourier transform infrared (FTIR) spectroscopy of the recovered material indicated extensive film oxidation and degradation, as a result of thermal initiation. Similar observations were made (6) on the oxidation of a polyethylene ADC film used at the Shenzehu Xiapin landfill in China during the period October to December 1998. In this case, analysis of a sample exposed on the surface indicated that the EPI film, prepared using a TDPA formulation, is also susceptible to photochemically induced oxidation. Analogous results were obtained (7) in a study conducted by M. J. Carter Associates at the Edwin Richards Quarry landfill site located near Birmingham, England. A controlled trial showed that polyethylene containing a TDPA formulation undergoes significant chemical and mechanical degradation over a period of several months (2001–2002) in a landfill environment. Heavy rainfall and low ambient temperatures kept the average temperature in the waste below 30°C for the first seven months after the film samples were placed. After a further seven months, however, molar mass reduction of the polyethylene film that incorporated EPI's TDPA prodegradant formulation was from M_w 115,000 to 4250, well below the threshold for significant biodegradability. In contrast, the control film (containing no TDPA) had a final M_w of 107,000. The report by M. J. Carter Associates reached the conclusion that the results of this trial "confirm the benefits of using degradable plastic materials in a landfill environment." Simply stated these are as follows.

(1) "Refuse sacks that degrade will expose the enclosed refuse to water and micro-organisms and accelerate biodegradation of the waste."
(2) "Using degradable plastic sheets as cover for landfills will reduce the need for conventional imported cover materials and maximize void in the site for waste."

Degradation of Plastics

Standard laboratory testing methods have been developed by ASTM and others to measure degradation and biodegradation in landfill sites in both the initial

aerobic or oxygen-containing phase and in the later anaerobic or oxygen-deficient phase of this environment.

These laboratory simulation tests generally are used for estimating the degradation of condensation polymers, which hydrolytically degrade and then biodegrade in aerobic environments. In anaerobic environments, degradation and biodegradation are generally very slow. Poly(3-hydroxyalkanoates) (qv) produced naturally by bacteria, are an exception to this anaerobic rule as they are readily biodegradable in such environments.

Addition polymers, such as polyolefins, on the other hand, have had limited testing in the laboratory and extensive testing in the real world in working landfill sites. They degrade initially by oxidation and subsequently by biodegradation.

Degradation of Addition Polymers.

Conventional Polyolefins. Among the most versatile of all plastics, the polyolefins (all varieties of polyethylene, and polypropylene) are widely used in a very large number of applications. A partial list of their properties provides the explanation: inexpensive, light, strong, tough, stretchy, low glass-transition temperatures, easy to fabricate, excellent barrier properties and wet strength, and biologically inert. The last three items in particular contribute to the usefulness in food packaging applications, which are characterized by a relatively short use life followed by disposal in a landfill.

It has been recognized for many years that polyolefins are susceptible to oxidative degradation, and a great deal of research has been done to determine why and how, and what to do about it. The reader is encouraged to consult monographs and review articles (8–13) in order to acquire some of the details and complexities of polyolefin oxidation (see also DEGRADATION; STABILIZATION). In essence, oxidative degradation can be summarized as follows.

Even in the presence of a processing antioxidant, the heat and mechanical shear stress of extrusion will give rise to low levels of hydroperoxide group formation, by reactions 1, 2, and 3 where RH is a polyolefin. There is always a trace of oxygen present in extrusion equipment. It is the inevitable presence of hydroperoxide groups that renders polyolefins susceptible to oxidative degradation (frequently called peroxidation). Indeed polyolefins, if pure, would not absorb any radiation from terrestrial sunlight and would be inherently photostable. Such is not the case, however. The major difference between the oxidative degradation of polyolefins initiated by heat (thermal oxidation) and by near-UV light (photooxidation) is that ketone groups are stable to heat but are unstable to UV light, and this adds to the rate of photodegradation.

Oxidative Degradation

$$\mathrm{RH} \xrightarrow[\text{conditions}]{\text{Processing}} \mathrm{R}\cdot + \cdot\mathrm{H} \qquad (1)$$

$$\mathrm{R}^{\bullet} + \mathrm{O}_2 \Rightarrow \mathrm{ROO}^{\bullet} \qquad (2)$$

$$\mathrm{ROO}^{\bullet} + \mathrm{RH} \Rightarrow \mathrm{ROOH} + {}^{\bullet}\mathrm{R} \qquad (3)$$

$$\mathrm{ROOH} \xrightarrow[\text{UV light}]{\text{Heat or}} \mathrm{RO}\cdot + \cdot\mathrm{OH} \tag{4}$$

$$\mathrm{RO}\cdot \xrightarrow[\text{rapidly}]{\text{Very}} \text{Ketones (by } \beta\text{-scission)} \Downarrow \text{Acids, esters, etc} \tag{5}$$

or

$$\mathrm{RO}^{\bullet} \Rightarrow \text{Alcohols (by hydrogen abstraction)} \tag{6}$$

It should be noted that reaction 6 does not lead to polymer chain scission; ie, there is no molar mass reduction here, in contrast to reaction 5 where there is a molar mass reduction. It should also be noted that the formation and reaction of hydroperoxide groups attached to polymer molecules (reactions 3 and 4) are much slower, ie, rate determining, than the other processes shown. It will be apparent from the free-radical products formed in reactions 1 through 4 that this whole peroxidation procedure is a branching chain reaction. Additive chemistry is required to provide polyolefins with any sort of prolonged service life, and such chemistry is well known and entirely effective.

Polyolefins are semicrystalline materials in which oxidation is initially focused in the less-ordered (amorphous) zones. These zones are where impurities, oxygen, stabilizers, and virtually all other additives (if present) are located. In the absence of stabilizing additives, or after the depletion of them, chain scission will occur, tensile elongation values will decrease markedly, and the polyolefin will become brittle. It is generally accepted that at values of elongation at break below 10%, the material breaks into fragments very readily.

Differences in the rates at which various polyolefins undergo oxidative degradation are related primarily (but not entirely) to their molecular structures. There is a significant correlation, for example, between relatively high levels of susceptibility to oxidation and number of tertiary C—H bonds since these bonds have lower bond-dissociation energies than secondary C—H bonds. If this were the only relevant criterion, then the order of increasing susceptibility to oxidation would be HDPE < LDPE < LLDPE < PP. The actual situation is not that simple, but the important point is that there are differences.

As noted above, the primary products of the oxidative degradation (the peroxidation chain reaction) of polyolefins are hydroperoxides, which are unstable and undergo thermolysis or photolysis with chain scission. The products are lower molar mass materials including carboxylic acids, alcohols, aldehydes, and ketones (14,15). Depending on the amounts of antioxidant and other stabilizers that are present, and on the nature of the environment in which they are discarded, it may take a few years or even decades before conventional polyolefins undergo sufficient oxidative degradation to become brittle and disintegrate.

Activated Polyolefins. There are a number of ways of rendering polyolefins unusually photosensitive, the more effective of which involve copolymerizing

ethylene, for example, with other monomers such that ketone groups are introduced into the polymer chains. Such plastics photodegrade readily, but this is not a particularly useful characteristic for materials that will be disposed of in landfill sites. In this context, an activated polyolefin is one which incorporates an additive that will significantly increase the rate of oxidative degradation of the plastic that occurs in warm environments. The mechanism and products of the oxidation that is initiated thermally will normally be the same as for conventional polyolefins not containing the additive. In other words, this is the same situation that was described in the previous section for conventional polyolefins. The same chemistry occurs for activated polyolefins (only it all happens very much faster) at a rate controlled by the level of prodegradant additive. As was indicated above, the slowest part of the oxidation chain reaction is the decomposition of the hydroperoxide groups attached to the polyolefin molecules, and it is the thermolysis of these groups that will lead (much of the time, as shown) to molar mass reduction of polyolefins that are buried in landfills. It has been known for many years that traces of transition metals accelerate the thermal oxidation of polyethylene (and other hydrocarbons) by inducing hydroperoxide decomposition. The relevant mechanism is usually a redox reaction that is genuinely catalytic.

$$M^n + ROOH \Rightarrow M^{n+1} + RO^{\bullet} + OH^- \quad (7)$$

$$M^{n+1} + ROOH \Rightarrow M^n + ROO^{\bullet} + H^+ \quad (8)$$

Hydroperoxide decomposition by this pair of processes is essentially equivalent to the lowering of the activation energy of the bimolecular peroxide decomposition reaction. It is a major factor in both heat- and light-induced oxidation of activated polyolefins. In view of the mandatory requirement for a shelf life and a use life, even when these total only months rather than years, it is important to note that prodegradant additives for polyolefins that are based on transition metals are not oxidizing agents. In other words, the presence of these prodegradants does not render the plastic instantly unstable. They simply increase, typically by two or three orders of magnitude, the rate of polyolefin oxidation after it has been initiated by heat, UV light, mechanical stress, or some combination of these.

An early manifestation of the use of metal-containing prodegradants to convert polyolefin film products to oxo-biodegradable materials was the Scott/Gilead system (16,17, and references therein). In its simplest form, the additive here contains a metal ion complexed to sulfur (for example, a ferric dithiocarbamate) such that the metal complex is an antioxidant until exposed outdoors where it undergoes photolysis. The metal ion then acts as a prodegradant, as indicated in reactions 7 and 8. Products based on this and related clever chemistries have been used for many years with great success as agricultural mulch films, and the like. The relevance of that technology here is that Scott/Gilead systems can act as thermal pro-oxidants as well.

The prodegradant systems for polyolefins and polystyrene developed by EPI Environmental Products Inc. involve additives that also impart sensitivity to heat and/or UV light. The composition and quantity of their TDPA formulations added to conventional polyolefin resins provide performance that features a controlled

lifetime (storage, use) followed by rates of oxidation/biodegradation commensurate with the disposal environment. This combination of controlled but adjustable service life and a variety of degradation rates has been demonstrated (18–22) for a number of applications, such as agricultural mulch films, litter control, and compost bags. It should be noted, however, that the emphasis in the landfill disposal environment for the polyolefin products incorporating TDPA is for packaging plastics, shopping bags, ADC materials, and numerous other plastics that are disposed of in landfill. In this case, the activated materials become brittle and disintegrate in a matter of 6 to 18 months, much more rapidly than the corresponding products made from ordinary polyolefins.

Other Addition Polymers. There are few studies on other reported polymer and plastic components of landfills. Poly(vinyl chloride) seems to be inert in landfill showing no degradation in real-world tests (23,24) and laboratory simulations (25). In the latter study, plasticizer migration occurred with its subsequent biodegradation.

In an evaluation of cross-linked poly(acrylate) superabsorbents (26), little or no changes were seen and migration was not observed.

Condensation Polymers. The degradation pathways for condensation polymers are shown schematically below for both aerobic and anaerobic environments.

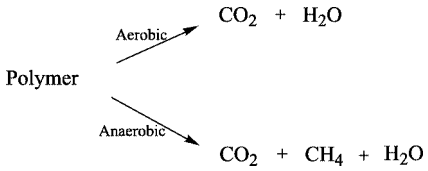

Testing for degradation in aerobic landfill environments is typified by an ASTM standard method for soil burial (27), by changing the environment, where measurements of carbon dioxide are related to rate and degree of biodegradation.

Notwithstanding the difficulties of testing in anaerobic environments, several laboratory methods, as indicated earlier, have been developed. These measure carbon dioxide and methane evolution. The ASTM standard was developed on the basis of work from Europe (28) and is widely used for these polymers (29). Several variants on this method reported for example by Barlaz and co-workers (30) for a variety of polymers including polyesters, acrylates, cellulosics, and others are used. Similarly, the earlier pioneering work of McCarthy and co-workers is also useful (31).

Polyhydroxyalkanoates, which are produced by bacterial synthesis, are well known to biodegrade (32) under anaerobic conditions, and several studies have been reported and compared with synthetic polyesters such as polycaprolactone (33). Radiolabeled C_{14} polyesters give credence to biodegradation by allowing methane and carbon dioxide to be readily quantified. R.-J. Mueller and co-workers (34) reported similar results in a comparative laboratory test with synthetic and natural polyesters. Work in Asia is also consistent with the anaerobic biodegradation of polyhydroxyalkanoates (35) in contrast with other condensation polymers including poly(lactic acid), and aromatic and aliphatic polyesters, which, apparently, do not biodegrade in the absence of oxygen.

Summary

Discarded plastics, especially packaging plastics, represent a significant part of the solid waste that is disposed of in landfills. They can persist for many years in this environment and thereby contribute to the premature filling of the sites. Activated polyolefins, such as those containing EPI's TDPA prodegradants, degrade and disintegrate as a result of the heat generated by microorganisms in landfills, and this permits much more rapid aerobic biodegradation of the other organic waste, thus prolonging the useful life of landfills. Little evidence has been acquired to date about the biodegradation of addition polymers in landfills. A number of hydrolyzable condensation polymers will biodegrade aerobically, but only the polyhydroxyalkanoates have been shown to biodegrade under anaerobic conditions.

BIBLIOGRAPHY

"Microbiological Degradation" in *EPST* 1st ed., Vol. 4, pp. 716–725, by Walter M. Bejuki, BioSciences Information Service of Biological Abstracts; "Biodegradable Polymers" in *EPSE* 2nd ed., Vol. 2, pp. 220–243, by Samuel J. Huang, The University of Connecticut; "Disposal and Reuse of Plastics" in *EPSE* 2nd ed., Vol. 5, pp. 103–128, by Harvey Alter, U.S. Chamber of Commerce."

1. W. L. Rathje, *Natl. Geogr.* **179**, 116 (1991).
2. W. L. Rathje, *Atlantic Monthly* **264**, 99 (1989).
3. R. V. Kinman, D. L. Nutini, and W. L. Rathje, Paper presented at the 44th Annual Purdue Industrial Waste Conference, May 9, 1989.
4. News and Views for the Environment and Plastics Institute of Canada (Spring 1992).
5. G. Scott, *Polymers and the Environment*, The Royal Society of Chemistry, Cambridge, 1999.
6. G. Scott and D. M. Wiles, in G. Scott, ed., *Degradable Polymers: Principles and Applications*, 2nd ed., Kluwer Academic Publishers, Dordrecht, The Netherlands, 2002, pp. 456–457.
7. Joseph G. Gho, personal communication, Dec. 2002.
8. G. Scott, *Atmospheric Oxidation and Antioxidants*, Elsevier, Amsterdam, 1965.
9. G. Geuskens, ed., *Degradation and Stabilisation of Polymers*, Applied Science, London, 1975.
10. N. S. Allen, ed., *Degradation and Stabilisation of Polyolefins*, Applied Science, London, 1983.
11. N. Grassie and G. Scott, *Polymer Degradation and Stabilisation*, Cambridge University Press, Cambridge, 1985.
12. D. J. Carlsson and D. M. Wiles, *Encyclopedia of Polymer Science and Engineering*, 2nd ed., Vol. 4, John Wiley & Sons, Inc., New York, 1986, pp. 631–696.
13. G. Scott, ed., *Atmospheric Oxidation and Antioxidants*, Vol. II, Elsevier, Amsterdam, 1993.
14. A.-C. Albertsson, C. Barenstadt, S. Karlsson, and T. Lindberg, *Polymer* **36**, 3075 (1995).
15. S. Karlsson and A.-C. Albertsson, *Polym. Eng. Sci.* **38**, 1251 (1998).
16. G. Scott, *Polym. News* **14**, 168 (1989).
17. G. Scott, *Polym. Deg. Stab.* **29**, 135 (1990).
18. D. M. Wiles, B. E. Cermak, J. G. Gho, and C. W. J. Hare, *Environews* **8**, 6 (1998).

19. J.-F. Tung, D. M. Wiles, B. E. Cermak, J. G. Gho, and C. W. J. Hare, in *Proceedings of the Fifth International Plastics Additives and Modifiers Conference*, Prague, Oct. 27–28, 1999, Paper 17.
20. D. M. Wiles, J.-F. Tung, B. E. Cermak, C. W. J. Hare, and J. G. Gho, in *Proceedings of the Biodegradable Plastics 2000 Conference*, Frankfurt, June 6–7, 2000.
21. B. Raninger, G. Steiner, D. M. Wiles, and C. W. J. Hare, in H. Insam, S. Klammer, and N. Riddich, eds., *Microbiology of Composting*, Springer-Verlag, Berlin, 2002, pp. 299–308.
22. N. C. Billingham, M. Bonora, and D. De Corte, in *Proceedings of the 7th World Conference on Biodegradable Polymers and Plastics*, Pisa, Italy, June 4–8, 2002.
23. I. Mersiowsky and R. Stegmann, in *6th International Landfill Conference*, October 13–17, 1997, Vol. 1, Monograph, pp. 220–235.
24. I. Mersiowsky, J. Ejlertsson, and M. Weller, *ACS Abstr.* 222 (Aug. 2001).
25. I. Mersiowsky, M. Weller, and J. Ejlertsson, *Water Res.* **35**, 13, 3063–3070, (2001).
26. R. Stegmann, S. Lotter, L. King, and W. D. Hopping, *Waste Manage Res.* **11**, 2, 155–170, (1993).
27. ASTM D5988-96, Standard Method for Determining the Aerobic Biodegradation of Plastic Materials in Soil Burial.
28. ASTM D5526-94, Standard Test Method for Determining the Anaerobic Biodegradation of Plastic Materials under Accelerated Landfill Conditions.
29. *Mededelingen van de Faculteit Landbouwwetenschappen* **58**(4a), 1621–1628 (1993).
30. M. A. Barlaz, B. B. Rees, P. P. Calvert, and C. A. Pettigrew, *Environ. Sci. Technol.* **32**, 6, 821–827 (1998).
31. D. S. McCarthy, D. Kaplan, J. Mayer, D. Eberiel, R. Gross, and co-workers, *Polym. Prepr. Am. Chem. Soc., Div. Polym. Chem.* **31**, 1, 439–440, 443 (1990).
32. B. Schink, P. H. Janssen, and J. Frings, *FEMS Microbiol. Rev.* **103**, 2–4, 311–316 (1992).
33. T. W. Federle, *Biomarcomolecules* **3**(4), 813–822 (2002).
34. R.-J. Mueller, D.-M. Abou-Zeid, and W.-D. Deckwer, *J. Biotechnol.* **86**, 2, 113–126 (2001).
35. K. S. Pyong, H. K. Myung, M. K. Jong, P. K. Shin, M. H. Kim, and J. M. Kim, *J. Environ. Polym. Degrad.* **5**, 33–39, 1997.

GRAHAM SWIFT
GS Polymer Consultants
DAVID M. WILES
Plastichem Consulting

BIODEGRADABLE POLYMERS, MEDICAL APPLICATIONS.

See Volume 5.

BIOMOLECULES AT INTERFACES.

See Volume 5.

BIOTECHNOLOGY APPLICATIONS.

See Volume 1.

BLOCK COPOLYMERS.

See Volume 1.

BLOCK COPOLYMERS, TERNARY TRIBLOCK.

See Volume 1.

BLOWING AGENTS. See CELLULAR MATERIALS.

BLOW MOLDING. See Volume 1.

BULK AND SOLUTION POLYMERIZATIONS REACTORS. See Volume 5.

BUTADIENE POLYMERS. See Volume 5.

BUTYL RUBBER. See Volume 5.

DRAG REDUCTION

Introduction

The main objective of drag reduction is to reduce the fluid mechanical force known as "drag," which is exerted on an engineering system improving its efficiency. There are passive and active techniques to reduce the drag (1). The passive techniques do not require any energy input to flow; only installation and maintenance costs are involved. The riblets and large eddy breakup devices fall into this category. However, the maximum drag reduction is limited up to 10%. The active techniques require certain energy input. However, level of drag reduction achieved is up to 80%. Among all the techniques, additions of minute amount of high molecular weight polymers and surfactants have been very active area of research ever since Toms reported it in 1949 (2).

The discovery of turbulent drag reduction due to particle suspensions goes back to the 1930s. Forest and Grierson (3) reported the turbulent drag reduction in pipe flow of wood-pulp fiber suspensions of water. Vanoni (4) observed that water with suspended sand flowed more rapidly in an open channel. Toms (5) and Mysels (6) independently observed the striking reduction in turbulent drag in pipe flows

Encyclopedia of Polymer Science and Technology. Copyright John Wiley & Sons, Inc. All rights reserved.

of solutions of high molecular weight poly(methyl methacrylate) (5–10 ppm by weight) in monochlorobenzene and of aluminum disoaps in hydrocarbon liquids, respectively. Since Toms (2,5) was the first to publish his results, the phenomenon of turbulent drag reduction is also known as Toms effect. Ever since the reporting of these results, there has been extensive research activity in this fascinating field of fluid mechanics and polymer science. Nadolink and Haigh (7) compiled an exhaustive bibliography on the subject containing over 4900 references dating from 1931 to 1994.

The soluble polymers are the most potential drag-reducing agents of all the additives mainly because drag reduction of up to 80% can be obtained with the addition of a few tens of ppm by weight in a particular solvent. The polymer solution drag reduction has been investigated in aqueous and hydrocarbon liquids, and a number of excellent reviews have been written by a number of experts (8–25). Many state-of-the-art papers have also appeared in number of conference proceedings (26–31).

Drag-reducing polymers have been successfully applied for potential benefits in various industrial processes and operations, such as long-distance transportation of liquids, oil-well operations, sewage and flood water disposal, fire fighting, transport of suspensions and slurries, irrigation, water-heating and [cooling circuits, jet cutting, and marine and biomedical operations. The developments in the above] cited fields are reviewed in the 1990s by Singh (20), Morgan and McCormick (21), Den Toonder (22), Gyr and Bewersdorff (23), Moussa (24), and Gad-El-Hak (25).

The most successful application of drag-reduction phenomenon has been in reducing the drag in crude oil transport through Trans Alaskan Pipelines (TAPS) and other pipelines in several countries. The first large-scale use of hydrocarbon-soluble drag reducer addition (DRA) in TAPS was accomplished in 1979. The technology made spectacular advancement since then. Within 10 years, the effectiveness of additives increased 12 times (32). Because of the effectiveness of the polymer injection technique, the need of building two delayed pumping stations disappeared. The 1 ppm of the drag reducer used in the pipeline increased the flow rate by 33%. Several important pipelines such as Tukey-Iraq, Bas Strait (Australia), Bombay Off Shore (India), etc, have used drag-reducing additive injection for saving considerable energy. Newer areas are being explored (23,25,33).

High molecular weight polymers ($>10^5$) are very effective drag reducers, but get degraded in turbulent flows and lose their effectiveness after a short interval of time or flow. Aluminum diasops and other surfactants form aggregates or micelles at a critical micellar concentration (CMC). These micelles are responsible for drag reduction. These micelles also degrade after critical shear stress though anionic soaps are found to be good and mechanically stable drag reducers (34). But when shear stress becomes lower than the critical shear stress, the micelles are reformed and restore the drag reduction effectiveness. Because of their repairability and the capability to withstand higher temperatures, the research activity in surfactant drag reduction has increased appreciably. The anionic, cationic, nonionic, and zwitterionic surfactants have been investigated for their drag-reduction effectiveness (DRE). Though anionic soaps are found to be good and mechanically stable drag reducers (34), their use is not favoured because of their vulnerability

to calcium and magnesium ions normally present in tap and sea water, and their foam-forming characteristics (35). Nonionic surfactants have narrow temperature window of applicability around their cloud points (36). Cationic surfactants show much broader effective temperature window of applicability, and thus have larger potential for practical applications (37). The drag-reducing characteristics of zwitterionic surfactants are being studied (38–40).

The potential application of surfactants exists in district heating and cooling systems. The characteristics of surfactant drag reducers differ from polymeric drag reducers in several aspects particularly having higher level of drag reduction crossing the Virk's maximum drag reduction asymptote (41,42).

Several attempts have been made to enhance the DRE and mechanical stability of polymer drag reducers. In general, homopolymers, alternate copolymers, graft polymers, and polyelectrolytes and polysaccharides from natural and microbial resources are efficient drag reducers in water, organic solvents, and crude oil (23,25,43). The extent of drag reduction increases with the molecular weight and length of the polymers, and so does their susceptibility to flow-induced degradation.

Recently, three approaches have been put forward to enhance the DRE and shear stability of polymers. The DRE of polysaccharides can be enhanced by grafting synthetic polyacrylamide branches onto their main chains; the resulting graft polymers combine efficiency of synthetic polymers and robustness of polysaccharide chains (44,45). The reversible intermolecular associations in solution increase the molecular weight of polymer associates and provide mechanical stability (46–49).

The third approach is by using cross-linking among the polymer molecules. The drag-reducing polymers such as guar gum can be cross-linked with concentration below those required for gel formation. The presence of intermolecular cross-links leads to increased dimensions of the macromolecules resulting in enhanced drag reduction though the induced degradation of the polymers is not appreciably affected by the addition of cross-linking agents (50). The first and third approaches have been pursued for water-soluble systems. It has been observed that in the first approach, the level of DRE is higher, that too at low concentrations ($<$100 ppm) of graft copolymers, and that cross-linking is not effective in shear degradation.

Rheology of polymers and surfactants solutions plays an important part in drag reduction. Though very dilute drag-reducing solutions have rheological behaviors similar to Newtonian solvents except for the anionic polyacrylamide solutions having shear-thinning behaviors at drag-reducing concentration of 50 ppm (51), their extensional effects may be important. Efforts are still in progress to measure and correlate the extensional effects to drag reduction (52–60). The degradation of polymers in turbulent flow needs to be investigated in order to enhance the effectiveness of polymers by modeling degradation mechanism (43,61–65).

There are three ways of introducing a polymer solution in the water flow. In the first case of homogeneous drag reduction, the polymer is allowed to mix homogeneously into the solvent. In the second case of heterogeneous drag reduction, a highly concentrated polymer solution is injected in the center or at the wall of the pipe, which disperses completely by turbulent diffusion to yield homogenous

solution some distance downstream the injector. In the third case, a concentrated polymer solution is injected into the center line of a turbulent flow at a high enough concentration that a single coherent unbroken polymer thread forms at the injector and continuous downstream for several hundred pipe diameters. The polymer threads have also been injected at the wall or buffer zone of the flow by Frings (66), who attained highly heterogeneous mixtures downstream. In some cases (67–69), high concentration strings of polymer develop rather than a single coherent thread.

All the above forms of drag reduction have been studied in the case of surfactant drag reduction as well. The origin of drag reduction in all cases has been indicated to be similar (70,71). The origin of drag reduction has been extensively investigated from the very beginning. With the advent of laser Doppler anemometry (LDA) (72), and later on with the phase laser anemometry (73), it was possible to measure and investigate velocity characteristics of flows with precision without interfering with them. LDA has been extensively used to study various aspects of drag reduction, particularly in channel flows (74).

Dodge and Metzner (75) developed a correlation between friction factor and Reynolds number for turbulent pipe flow of purely viscous shear-thinning liquids based upon a power-law model of shear viscosity. Metzner and Park (76) correlated the degree of drag reduction in turbulent flow of viscoelastic polymer solutions with the ratio of elastic to viscous stress, ie with N_i/τ_s, where N_i is the first normal stress difference for a given wall shear–strain rate γ, and τ_s the corresponding shear stress. Though the role of extensional viscosity in causing turbulent suppression or drag reduction is being debated till date, there is a persistent view that the elongational viscosity, possibly in combination with viscoelasticity, is responsible for drag reduction.

Gadd (77) was among the first to point out that the damping of the turbulence by polymer additives is due to their resistance to elongational strain, which suppresses shear formation and bursting in near-wall region. Lumley (78,79) suggested that the uncoiling of polymer molecules under fluctuating shear rate in the buffer region of turbulent flow causes drag reduction because of increase of extensional viscosity. Gyr (80), Durst and co-workers (81), and Bewersdorff and Berman (82) provided the extensional viscosity model of drag reduction. Vlassopoulos and Schowalter (51,52) suggested that the origin of DRE is due to the fluid elasticity inferred from oscillation-induced streaming. Matthys (83) pointed out the common origin of the extensional viscosity and viscoelasticity. de Gennes (84) hypothesized that the polymer drag reduction is due to the elastic, rather than the viscous, phenomenon. Several direct numerical simulations by Orlandi (85), Den Toonder and co-workers (64,86), and Massah and Hanratty (87) examined the role of viscoelasticity, extensional viscosity, and stress anisotropy in drag reduction. Direct numerical simulation (DNS) investigation of Den Toonder and co-workers (86) points out that drag increases rather than decreases when the elastic contributions are taken into account.

For the case of viscous anisotropic polymer model, almost all turbulence statistics and power spectra calculated agree in qualitative sense with experimental results. Dimitropolous and co-workers (88) did DNS for fully turbulent channel flow of a polymer solution using the finitely extensible nonlinear elastic head spring dumbbell model with Peterlin approximation (FENE-P) and the Giesekus

model. They demonstrated that the solution extensional viscosity plays the primary role in turbulent drag reduction. Comparing the mean velocity profiles and statistical features of the turbulent flow showed agreement with well-established experimental observations, such as enhanced buffer zone, increase in the spacing of the streamwise streaks, decrease in the streamwise vorticity fluctuations, and increase in the streamwise velocity fluctuations. This demonstrated the onset of drag reduction in a turbulent flow at a sufficiently high level of viscoelasticity in the flow and reinforced previously held hypothesis that one of the prerequisites for the phenomenon of drag reduction is sufficiently enhanced extensional viscosity.

However, Sreenivasan and White (89) point out that the connection between fluctuating strain rates and large extensional viscosity is circumstantial. Further polymer coils can only be partially stretched in a random field of strain rate. Sreenivasan and White (89) point out that the elastic theory proposed by de Gennes (84) is compatible with at least two experimental observations; ie, the dependence of drag reduction onset on polymer concentration and maximum drag reduction asymptote.

On the other hand, DNS of turbulence in channel flow based on FENE-P bead-spring chains in the presence of large-enough velocity gradients by Massah and Hanratty (87) indicates that polymers cause drag reduction by selectively changing the structures of eddies that produce Reynolds stresses. Their calculations (87) support the suggestions by Lumley (78) that the polymers can become unravelled by the turbulence in the buffer region. The calculated unravelling of a bead-spring chain in the viscous sublayer could explain the increased viscosity observed by Vismann and Bewersdorff (90) and by James and co-workers (91) in elongational flow when the solution is presheared in laminar Couette or channel flow. Thus these investigations point out the basis of further research on the origin of drag reduction and explanation of its various manifestations in both polymeric and surfactant drag reduction. A large number of reviews are available in literature till 1990. In this review, emphasis will be given on the researches reported since then, with comprehensive accounts of materials, mechanisms, and applications in the field of turbulent drag reduction in liquids.

Characteristics of Turbulent Drag Reduction

Mathematical Description. Lumley's (92) definition of drag reduction, "drag reduction is the reduction of skin friction in turbulent flow below that of the solvent," will be followed in this review. Most of the studies on drag reduction have been confined to hydraulically smooth pipe flows or channels; hence various physical parameters will be described in terms of smooth pipe flows.

Reynolds was the first to find out that transition from laminar to turbulent flow takes place in cylindrical-pipe flows of water at a particular value (=2300) of a dimensionless parameter known as the Reynolds number (R_e), where R_e is given by the following relation:

$$R_e = \frac{\bar{u}D}{\upsilon} \tag{1}$$

where $\bar{u}$ is the mean flow velocity, D is the pipe diameter, and $\upsilon(=\frac{\eta}{\rho})$ is the kinematic viscosity. υ is equal to the ratio of viscosity η and the density of the liquid, ρ.

The pressure loss in pipe is due to fluid friction resistance. The friction factor f may be derived as

$$f = \frac{\Delta p D}{2\rho \bar{u}^2 L} \tag{2}$$

where $\Delta\, p$ is the pressure drop and L is the pipe length. The wall shear stress, τ_{w}, in a fully developed pipe flow is related to the pressure drop by the following equation:

$$\tau_{\mathrm{w}} = \frac{\Delta p D}{4L} \tag{3}$$

Hence the Fanning friction factor:

$$f = \frac{\tau_w}{\frac{1}{2}\ \rho \bar{u}^2} \tag{4}$$

The friction velocity u_{T} can also be evaluated as

$$u_{\mathrm{T}} = \left(\frac{\tau_{\mathrm{w}}}{\rho}\right)^{1/2} \tag{5}$$

Prandtl–Karman coordinates ($f^{-1/2}$ vs $R_{\mathrm{e}}\ f^{1/2}$) are, in general, used to present the drag reduction data because in these coordinates Prandtl–van Karman law for Newtonian turbulent pipe flow appears as a straight line in a semilogarithmic diagram (see Fig. 1).

$$f^{-1/2} = \frac{u}{\sqrt{2}u_{\mathrm{T}}} \text{ as ordinate}$$

and

$$R_{\mathrm{e}} f^{1/2} = \sqrt{2}\frac{D u_{\mathrm{T}}}{\upsilon} \text{ as abscissa}$$

represent ratios of bulk to turbulent velocities and pipe to turbulent length scales respectively (10).

The drag-reducing polymers, such as poly(ethylene oxide) or polyacrylamide, exhibit drag reduction at such low concentrations that the solution viscosity is close to solvent viscosity. In laminar flows, the majority of drag-reducing polymer solutions obey Poisseulli's law, ie

$$f^{-1/2} = \frac{R_{\mathrm{e}} f^{1/2}}{16} \quad \text{or} \quad f = \frac{16}{R_{\mathrm{e}}} \tag{6}$$

In case there is no drag reduction, the friction factor is given by the Prandtl–van Karman law for Newtonian turbulent pipe flow, ie

$$\frac{1}{f^{1/2}} = 4.0\ \log_{10}\left(R_{\mathrm{e}} f^{1/2}\right) - 0.4 \tag{7}$$

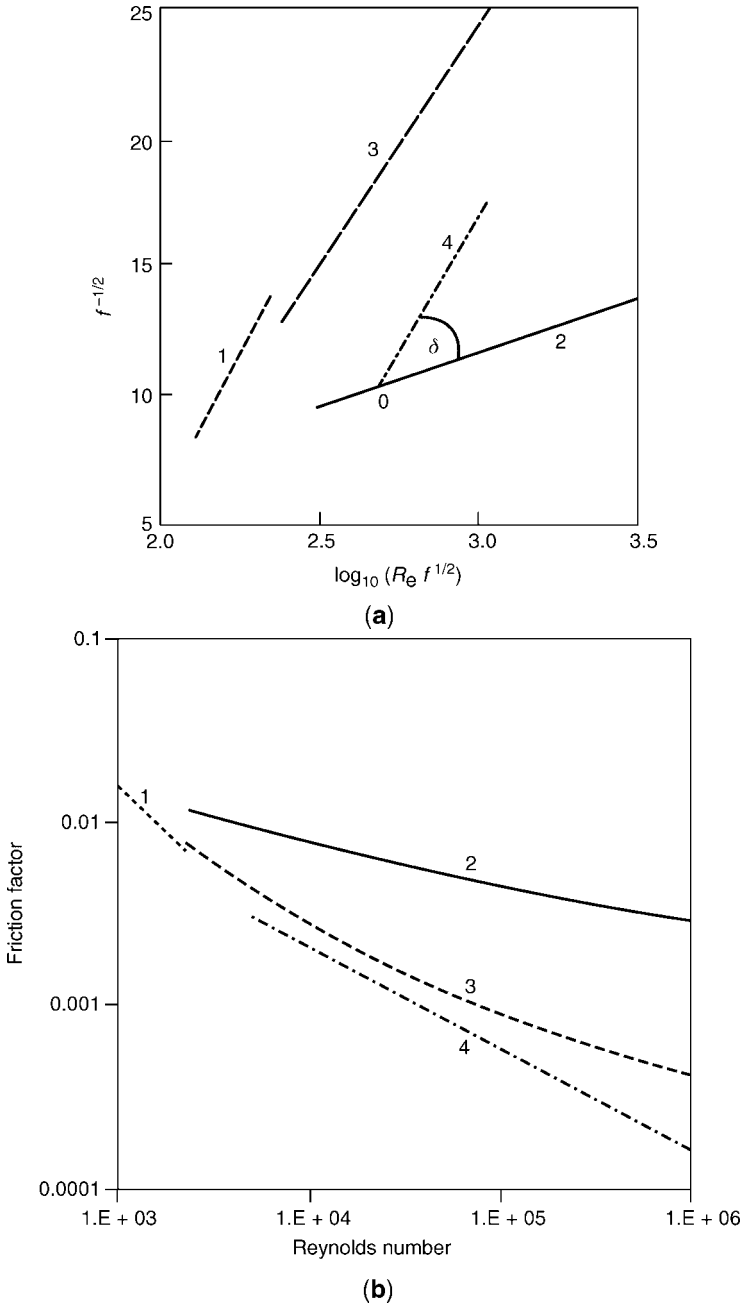

Fig. 1. (**a**) The variation of $f^{-1/2}$ with $\log_{10}(R_e f^{1/2})$ in case of dilute drag-reducing polymer solutions. The various regimes are depicted as follows: 1 by the Newtonian laminar region; 2 by the Prandtl–Karman curve for Newtonian fluids in a smooth pipe; 3 by Virk's maximum drag reduction asymptote; 4 by a typical curve for polymer solutions. δ is the slope increment. Adapted from Figure 1.3 of the Ref. 23. (**b**) The variation of friction factor with Reynolds number in case of drag-reducing surfactant solutions. 1, Laminar; 2, von Karman Linc; 3, Virk asymptote; 4, Zakin and co-workers asymptote. Adapted from Figure 2 of the Ref. 42.

Virk (10) observed that the maximum possible drag reduction asymptote (MDRA) is given by the following equation, where the drag reduction is insensitive to polymer properties:

$$\frac{1}{f^{1/2}} = 19 \log_{10}\left(R_e f^{1/2}\right) - 32.4 \tag{8}$$

In the regime below the maximum drag reduction asymptote, the friction factor varies with polymer properties and flow variables:

$$f^{1/2} = [4.0 + \delta] \log_{10}\left(R_e f^{1/2}\right) - 4.0 - \delta \log_{10}\left(\sqrt{2}D\right) w \tag{9}$$

where δ and w are polymer solution parameters.

In case of surfactant solutions, friction factors significantly lower than the predicted by MDRA for high polymer solutions are predicted. Zakin and coworkers (93) provided an equation given below for maximum drag reduction asymptote for surfactant solutions

$$f \approx 0.32\, R_e^{0.55} \tag{10}$$

The velocity profiles in terms of universal dimensionless coordinates [$u^+ = \frac{u}{u_T}$ and $y^+ = \frac{y\, u_T}{\upsilon}$] offer an alternative representation of drag reduction behavior. The local velocity u varies with y, the distance from the wall. There are three distinct regions that can be represented by the following equations:

Close to the wall, the flow in the viscous sublayer and in the buffer layer are represented by equations 11 and 12 respectively.

$$u^+ = y^+ \ (0 < y^+ < 5) \text{ (viscous sublayer)} \tag{11}$$

$$u^+ = y^+ \ (0 < y^+ \leq 30) \text{ (buffer layer)} \tag{12}$$

The logarithmic layer is given by

$$u^+ = 2.5 \ln y^+ + 5.5 \ (y^+ > 30) \tag{13}$$

The velocity profiles of drag-reducing flows in many cases show a peculiarity. A logarithmic profile starts at the intersection with a steeper slope and describes the velocity at maximum drag reduction. Virk's (10) maximum drag reduction profile is given by

$$u^+ = 11.7 \ln y^+ - 17 \tag{14}$$

For drag-reducing polymers, the velocity profile is parallel to the Newtonian profile and is separated by a factor ΔB depending on the polymer, and on pipe and flow characteristics (see Fig. 2).

$$u^+ = 2.5 \ln y^+ + 5.5 + \Delta B \tag{15}$$

The first region (viscous sublayer) extends to about $y^+ = 5$. The drag-reducing flows intersect the maximum drag reduction line instead of $u^+ = y^+$. The region between the viscous sublayer and Newtonian plug is known as the elastic sublayer

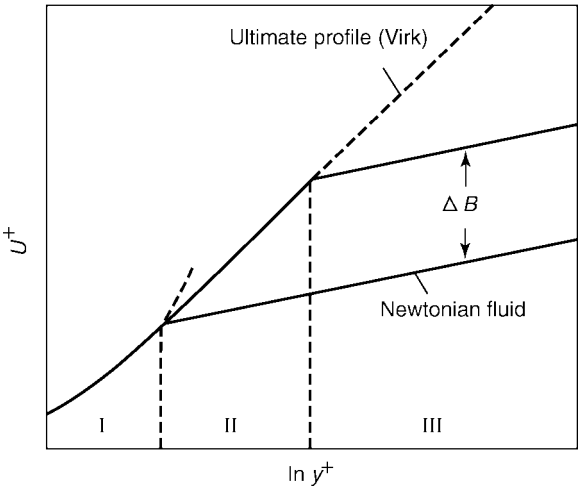

Fig. 2. Main stream velocity profile for drag-reducing fluids according to Virk's model: 1, viscous sublayer; 2, elastic buffer layer; 3, turbulent core.

since the solution in this zone exhibits an elastic flow behavior. In case of maximum drag reduction, the elastic region extends to the center of the pipe and the Newtonian region disappears. By integrating the equations, we obtain the total volumetric flow rate and friction factor:

$$\frac{1}{f^{1/2}} = 4\log_{10}(Rf^{1/2}) - 0.4 - \frac{\Delta B}{\sqrt{2}} \tag{16}$$

In the 19th century, Reynolds established the basic approach to analyze the turbulent flow. He introduced in the momentum equations the time fluctuating velocity whose average value over a period of time is zero but whose time-averaged squares and products are not zero. The relation for velocity components and pressure can be written as follows:

$$u = \bar{u} + u' \tag{17}$$

$$v = \bar{v} + v' \tag{18}$$

$$w = \bar{w} + w' \tag{19}$$

$$p = \bar{p} + p' \tag{20}$$

where u', v', and w' are fluctuating velocity components in turbulence in x, y, and z directions, respectively, and p' is the fluctuating pressure component in turbulence. The time average at a fixed point in space can be given as

$$\bar{u} = \frac{1}{t'}\int_{t_0}^{t_0+t'} u\, dt \tag{21}$$

u can be further split into time average mean and a phase-locked average (91), where $\tilde{u}$ is thought to be an oscillatory part of the velocity field and u' is the remaining turbulent fluctuation.

$$u = \bar{u} + \tilde{u} + u' \tag{22}$$

The components of stress tensor due to the turbulent velocity components of the flow are given by

$$\begin{vmatrix} \sigma'_{xx} & \sigma'_{xy} & \sigma'_{xz} \\ \sigma'_{xy} & \sigma'_{yy} & \sigma'_{yz} \\ \sigma'_{xz} & \sigma'_{yz} & \sigma'_{zz} \end{vmatrix} = -\rho \begin{vmatrix} \overline{u'^2} & \overline{u'v'} & \overline{u'w} \\ \overline{u'v'} & \overline{u'^2} & \overline{u'w'} \\ \overline{u'w'} & \overline{v'w'} & \overline{w'^2} \end{vmatrix} \tag{23}$$

The diagonal components $\overline{u'^2}$, $\overline{v'^2}$, and $\overline{w'^2}$ denote twice the average kinetic energy per unit mass of the respective velocity components. The nondiagonal terms $\overline{u'v'}$, $\overline{u'w'}$, and $\overline{v'w'}$ denote negative components of turbulent and Reynolds shear stress.

The correlation coefficient Ψ between the longitudinal and transverse fluctuations at the same point is defined as

$$\Psi = \frac{\overline{u'v'}}{\sqrt{\overline{v'^2}}\sqrt{\overline{u'^2}}} \tag{24}$$

Taylor (95) pointed out that in order to quantify special structure of turbulence, the velocity fluctuations at two neighbouring points, 1 and 2, in flow fields have to be observed. This will define correlation function $\bar{R}$ as

$$\bar{R} = \frac{\overline{u'_1}\,\overline{u'_2}}{\sqrt{\overline{u'^2_1}\,\overline{u'^2_2}}} \tag{25}$$

The integral of the correlation function $\bar{R}$ is known as scale of turbulence.

$$\bar{L} = \int_0^{1/2\,D} \bar{R}(r)\,dr \tag{26}$$

If the second quantity u_2' is measured at the same location but at a different instant of time (u_1' at instant t_1 and u_2' at instant $t_2 = t_1 + \tau$), we obtain the auto-correlation function κ. The x component of κ, ie κ_x, can be written as

$$\kappa_x = \overline{u'_1(x,t)u'_2(x,t+\tau)} \tag{27}$$

These functions are equivalent to a spectral decomposition of the kinetic energy of the fluctuations, K.

The alternate description of the structure of turbulence is obtained when a frequency analysis of the motion is provided instead of a correlation function.

These functions are equivalent to a spectral decomposition of the kinetic energy of the fluctuations in the respective directions, eg

$$\bar{u}_1^2 = \frac{1}{\pi} \int_0^\infty E_x(x,\omega)\, du \tag{28}$$

into components for each frequency ω, the so-called power spectrum. It follows from this definition that

$$K_x(\chi,\omega) = \frac{1}{2\pi} \int_{-\infty}^{\infty} E_x(x,\omega)\, e^{-i\omega\tau}\, d\omega \tag{29}$$

and vice versa:

$$E_x(\chi,\omega) = \int_{-\infty}^{\infty} K_x(\chi,\tau) e^{-i\omega\tau}\, d\tau \tag{30}$$

A complete insight into the statistical turbulence and turbulence process not only requires the study of the axial and transverse fluctuations but also to measure space and time correlation functions.

Experimental Results: Investigations of Drag Reduction and Turbulence Parameters. In the last decade, a large number of experimental articles have appeared on polymer drag reduction in pipe and channel flows, where LDA and 2D LDA have been used to measure various velocity components and Reynolds stresses. Pinho and Whitelaw (96), Harder and Tiederman (97), Wei and Willmarth (98), Walker and Tiedermann (99), Tong and co-workers (100), Codot and co-workers (101), Den Toonder and co-workers (86), Dimitropoulos and co-workers (88), Hoyer and co-workers (102), Fortaine and co-workers (103), Nieder Schulte and co-workers (104), Bewersdorff and co-workers (105), and Massah and Hanratty (87) reported various measurements on velocity components and Reynolds stresses. The most important findings reported in these articles are that the polymers not only suppress the turbulent motion but also increase the streamwise turbulent intensity, while the normal turbulence intensity is decreased. Wei and Willmarth (98) reported that the energy in the normal turbulence intensity is drastically suppressed over all frequencies while there is redistribution of energy from high frequencies to low frequencies for the streamwise component.

The drag reduction (DR) for pipe flow of an incompressible fluid additive system (20,23) is defined as

$$\mathrm{DR} = (1 - \Delta P_\mathrm{f}/\Delta P_\mathrm{s}) \tag{31}$$

where ΔP_f is the pressure drop with a fluid additive system, and ΔP_s is the pressure drop with a pure fluid, measured at constant flow rate. It may be assumed

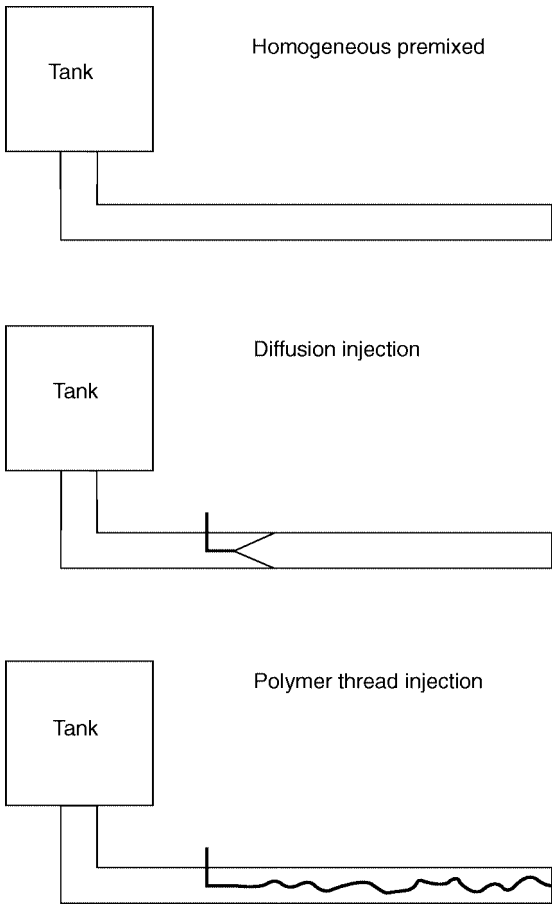

Fig. 3. Various methods of polymer addition for manifestation of the turbulent drag reduction phenomenon (63).

that small additions (at the ppm level) of the additives do not change the fluid density and shear viscosity. The fluid additive system is called drag-reducing if DR is positive.

Methods of Drag Reduction. There have been three basic methods for adding a polymer to the turbulent flow, and consequently three types of drag-reduction methods (70) (see Fig. 3). In homogeneous drag reduction, the polymer is mixed into the solvent and it disperses uniformly before it is allowed to flow in the pipe, and measurements are taken for various parameters of drag reduction. In another form of homogeneous drag reduction, the diffusive flow of the polymers takes place. Here the polymer is injected into the centre or at the wall of a pipe at a concentration which disperses completely by turbulent diffusion to yield a homogeneous solution some distance downstream the injector. In the second case, known as heterogeneous drag reduction, concentrated drag-reducing polymer solution is injected into the centerline of a turbulent flow so that a single coherent unbroken polymer thread forms at the injector and continues downstream for several hundred pipe diameters. The third type of drag reduction takes place (67)

when the injection is such that many high concentration strings of the polymer develop, rather than a single coherent thread from the centerline injector. Frings (66) used very high polymer concentrations in a wall injector and obtained highly heterogeneous mixtures downstream. Most of the wall injector studies yield flows similar to the second case, and the first case describes majority of the drag reduction studies.

Two other type of drag reduction (10,106) within the polymeric regime have been observed. In type A drag reduction, a family of additive solutions yield friction factor segments fanning outwards from a common "onset" point on the Pradtl–Karman line, their slopes increasing with increasing concentrations and drag reduction increasing with increasing $R_e f^{1/2}$. This is characteristic of random coiling macromolecules. In type B drag reduction, a family of additive solutions yield segments that are roughly parallel to that displaced upwards from the P-K line, with drag reduction essentially independent of $R_e f^{1/2}$ but increasing with increasing concentration. This behavior is exhibited by a variety of additives including extended polyelectrolytes, fibers, soaps, and clays. This drag reduction occurs without any discernible onset effect where the macromolecules causing the effect are already in the extended state and do not need to be stretched by a strong flow.

The various investigations on heterogeneous drag reduction carried out up to 1987 have been discussed by Singh (20) and Gyr and Bewersdorff (23). Hoyer and Gyr (71) have provided the critical analysis of heterogeneous drag reduction. Usui and co-workers (68,107,108) have investigated the velocity profile of the injected polymer phase and the surrounding water phase separately by seeding both liquids with tracer particles. They monitored the flow using a video camera, which was moved with flow velocity (see Fig. 4). On the basis of their results (68, 107,108), Usui and co-workers (108) suggested that the main interaction between polymer thread and the turbulence which results in drag reduction takes place in the central part of the flow and suppresses the large-scale motions of the flow in agreement with earlier results by Vleggar and Tells (109,110) and Bewersdorff (23,69,105). Gyr and Bewersdorff (23) showed that by varying the ratio of polymer injection velocity to the bulk velocity and by mounting contractions in pipe, the drag reduction increases with the elongation of the polymer thread as long as the thread stays intact and is not broken into pieces. Hoyt and Sellin (111) investigated the thread injection techniques using various viscoelastic solutions ranging from water-soluble polyacrylamide (PAM) and PEO and surfactant tetradecyltrimethyl ammonium bromide +2% sodium salycilate (C_{16}TASal) and hexadecyl trimethyl ammonium bromide +2% sodium salycilate (C_{16}TASal), as well as water-insoluble FLO (commercial pipeline drag reducer), polyisobutene, and PEO dissolved in dichloromethane. They attributed that the drag reduction effect is due to dissolved molecules removed from the thread at high Reynolds numbers, whereas at low Reynolds number an interaction of the thread with large-scale eddies should be responsible for the observed drag reduction.

A number of very precise measurements by Smith and Tiederman (70) and Hoyer and co-workers (71,102) reveal that the mechanism of polymer thread drag reduction is caused by a modification at or near wall, or by modification in the central portion of the flow. The drag reduction is ascribed to minute quantity of polymers removed from the thread and dispersed into the bulk of the fluid. Smith

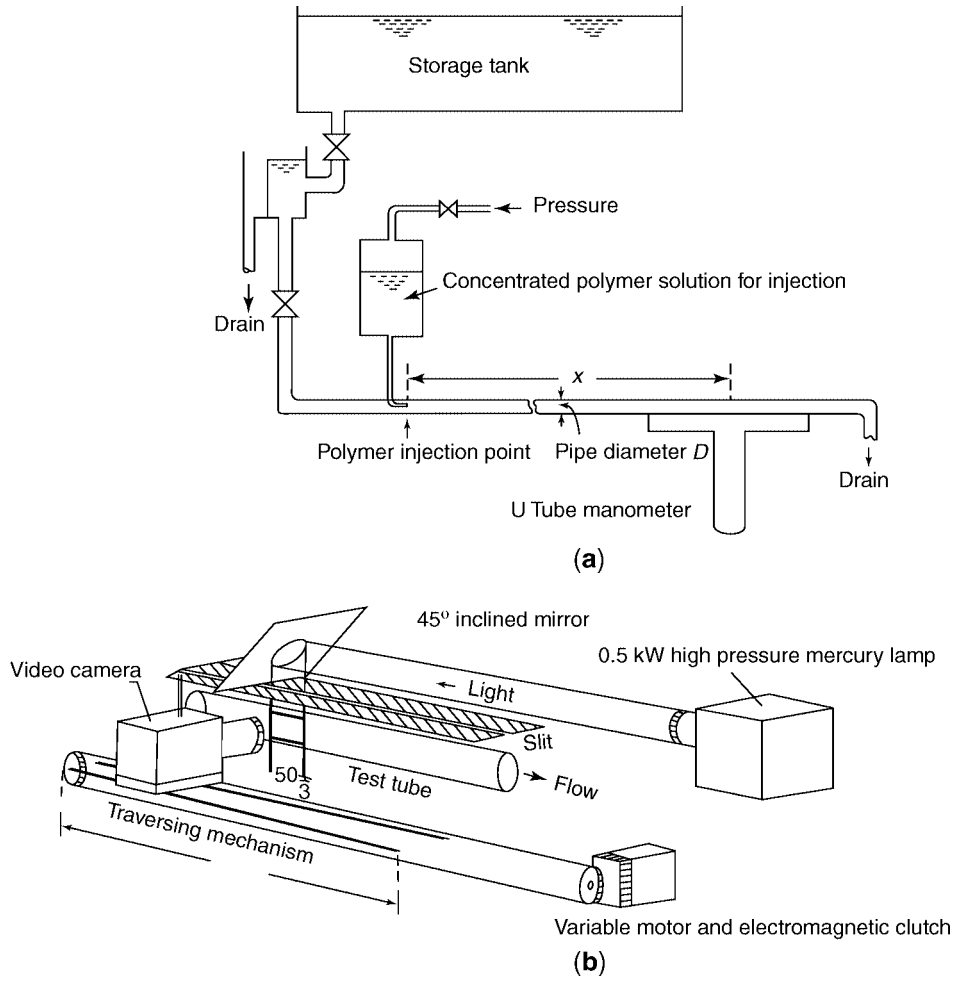

Fig. 4. Experimental setup for measurement of (**a**) drag reduction and (**b**) tracer particle trajectories; (**c**) profiles of turbulent intensity in the longitudinal direction: △, Water; ○, polymer injection (water phase); ●, polymer injection (polymer thread);□, premixed flow; ——— Pennel and co-workers (Newtonian fluid, $R_e = 11400$); —— —— McComb–Rabie (injection); – – – – Reishman–Tiederman (premix, 100-ppm Separan AP-273, $R_e = 44500$, DR = 39%).

and Tiderman (70) measured drag reduction, radial location of thread, and the polymer concentration in the near-wall region. The concentration was measured by laser-induced fluorescence utilizing fluorescin dye as tracer. In their experiment, the polymer injected was 500 ppm by weight of Separan AP273 dyed by 8.8 ppm by weight of fluorescin; the unbroken threads existed for more than 200 pipe diameters downstream the injector and produced drag reduction of the order of 40%. They found that the thread did not appear in the region $y^+ < 100$. When there was no polymer at $y^+ = 50$, there was no drag reduction. As soon as measurable amount of polymer was found at $y^+ = 50$, there was drag reduction. The major conclusion arrived at by Smith and Tiderman (70) was that low concentrations of

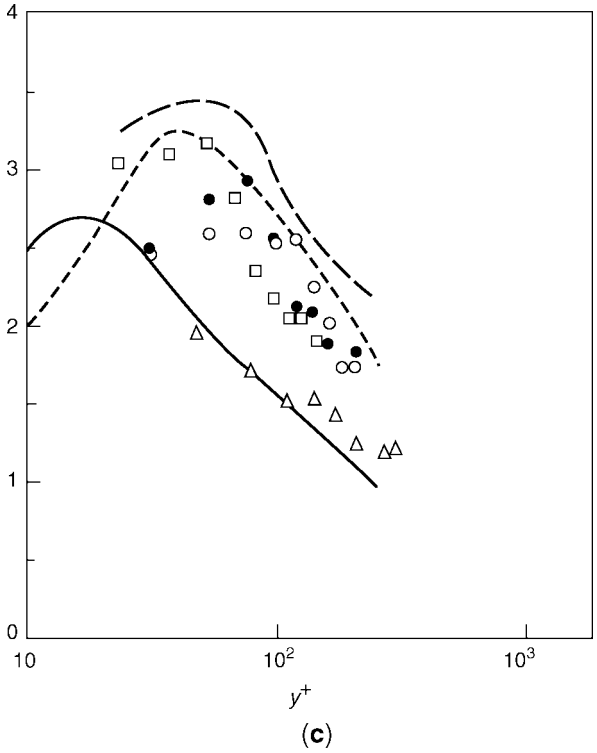

Fig. 4. (Continued).

polymer in the near-wall region are sufficient to cause drag reduction measured in the polymer thread experiments. The polymer that is diffused from the thread is the major cause of the drag reduction.

In the experiment of Hoyer and co-workers (102), the thread was sucked out and drag reduction downstream of the withdrawl point was measured, and in a second series of measurements near wall, the fluid was withdrawn and the drag reduction of that fluid in a bypass was measured (see Fig. 5). The thread trapping and bypass experiments indicate that the heterogeneous drag reduction is at least partly due to minute amounts of polymers removed from the thread and dispersed in the bulk of the fluid. It was found that the effect decreases if the thread ruptures into pieces instead of being enhanced as expected for a diffusion process. With decreasing u^*, the effect increases and the onset point is lowered. This suggests that diffusion is not the mechanism by which the polymer enters the bulk of the fluid. Further, it was observed that the drag reduction occurred whenever the thread started forming loops. In these loops, the thread unravelled locally into various strands which unified again when the thread was stretched. Hoyer in further experiments (71,102) collected near-wall fluid from 30-mm inner diameter circular pipe (D_1) using a slit suction device of height 0.25 mm and integrated in a 4-mm pipe for drag-reduction capability. The average thickness of collected wall layer never exceeded 22 viscous units and thus ensured that no part of the concentrated polymer thread was sampled. He observed the following:

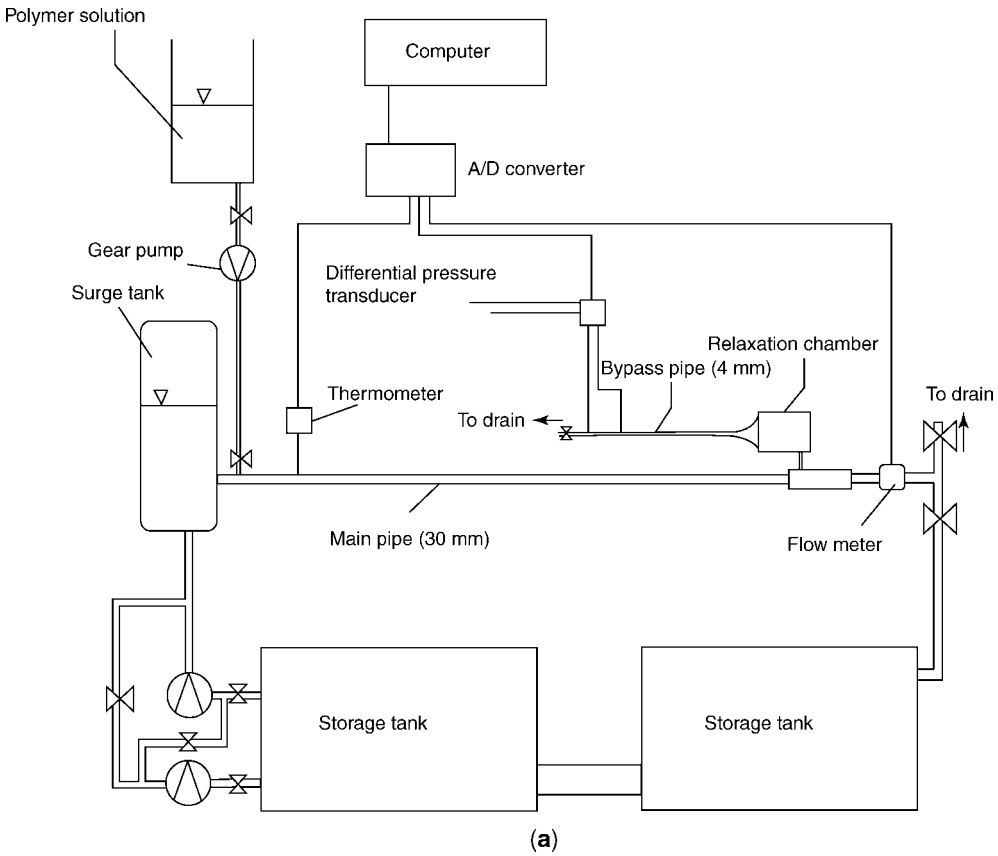

Fig. 5. (**a**) A typical experimental setup for measuring drag reduction using a bypass pipe; (**b**) influence of the injection ratio u^* on the friction behavior in round pipe with $c_P = 0.8\%$ and $c_R = 5$ ppm: ○, Commercial guar gum; ●, purified guar gum; △ GM_3. Adapted from Ref. 102.

(1) The near-wall fluid collected just before the onset in the main pipe showed no drag reduction.
(2) The fluid collected within increasing levels of drag reduction in the main pipe showed increasing drag reduction capabilities in the small pipe.

Polymeric Drag Reduction. The following macromolecular parameters seem to influence the drag-reduction characteristics, ie chemical and physical structure, molecular weight, length, extension, flexibility, and elasticity. Both synthetic and natural linear polymers having molecular weight of 5×10^5 or more have been found to be good drag reducers (19–24,112).

The lower molecular weight polymers capable of forming higher molecular weight aggregates have also been found to be effective drag reducers (46–48). Lodes and Macho (113) reported that the aqueous solutions of a 19000 kg/mol partially sponified poly(vinyl acetate) with various degrees of hydrolysis exhibited drag reductions close to the MDRA. In case of still lower molecular weight

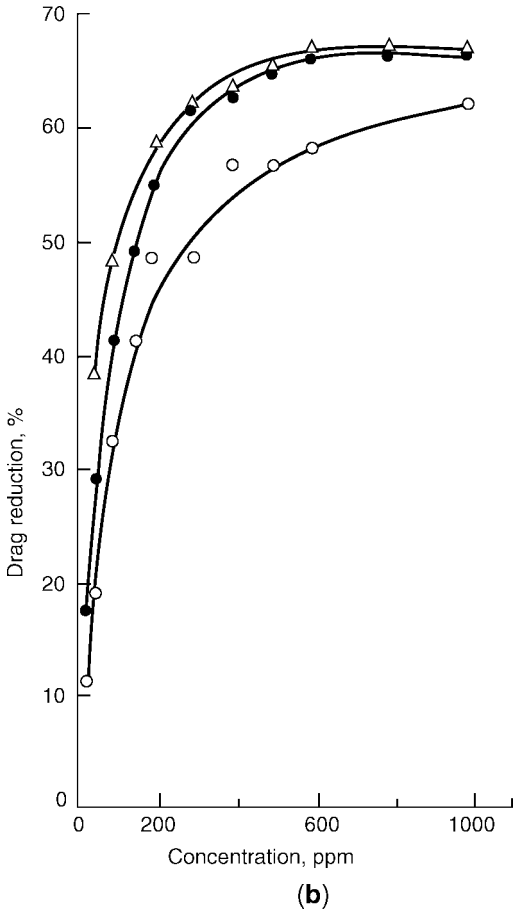

Fig. 5. (Continued).

(=6000), 0.4 and 0.6% by weight aqueous solutions of Tylose, a methylhydroxy cellulose from Hoechst, Pereira and Pinho (114) showed drag reductions (=25–35%) of the half that reported to occur with other low elasticity, shear-thinning, high molecular weight aqueous solution of CMC (molecular weight 300000 kg/mol) (96). The drag reduction caused by Tylose may be either due to the high molecular weight fractions present in its sample or associated complexes, which may be present at such high concentrations as tens of ppm (by weight) of polymers. On the other hand, rigid shear stable polymers such as polysaccharides (ie, guar gum, carboxymethylcellulose, and xanthan gum in the form of natural gum or formed by algae and bacteria) cause maximum drag reduction of up to 60% at the concentrations of a few hundred ppm by weight (20,23,115).

Among the synthetic polymers, poly(ethylene oxide) is the most efficient but relatively lesser shear stable than polyacrylamide. Molecular weight, length, and coil dimensions are the chief attributes of polymers to drag reduction (21). It has been shown by Olivier and Bakhtiyarov (116) that polyacrylamide of very high molecular weight, ie $M_w = 20–25 \times 10^6$, causes drag reduction in as low as

0.02-ppm solution. Gampert and Wagner (117) have prepared highly fractionated samples of polyacrylamide. They have shown that drag reduction increases with molecular weight. In mixtures of various fractions, it is the highest fraction that contributes the most in drag reduction.

Drag reduction is shown by polysaccharides, which are linear in nature. Highly branched materials such as gum arabic and dextran do not seem to reduce drag (17). Polyelectrolytes, such as partially hydrolyzed polyacrylamide (64,106), polyacrylic acid (118), acrylamide sodium acrylate copolymer (119), and sodium alginate (120), show higher drag reduction when the chain is extended or there is increment in coil dimensions. The coil expansion takes place because of coulombian repulsion and solvent steric hindrance of side group and main chain (119).

Virk and Wagger (106) reported that drag reduction results in case of partially hydrolyzed polyacrylamides (PAMH) of molecular weight $M_a = 15 \times 10^6$. When the charge neutralization was obtained by adding 0.1 M NaCl, the additive solutions yield friction factor segments fanning out from a common "onset" point on Prandtl–Karman line, their slopes increasing with increasing concentrations and drag reduction increasing with increasing $R_e f^{1/2}$. This is the characteristic of random coiling macromolecules. Virk designated it as type A drag reduction. In B type of drag reduction, obtained without adding any NaCl or adding up to 0.001 M NaCl to 0.0003 M NaCl (practically no or very little charge neutralizations took place), a family of additive solutions yield segments that are roughly parallel to, but displaced upwards from, the P-K line, with drag reduction essentially independent of $R_e f^{1/2}$ but increasing with increasing concentration. This type of behavior is exhibited by additives such as extended polyelectrolytes (PAMH), fibers, and soaps, and clays such as asbestos, xanthan, asbestos, paper-making fibers, and nylon fibers.

Among the polymers that show drag reduction in nonaqueous solvent and crude oil, polyisobutylenes, polyisoprene, polystyrene, homo and copolymers of alkylstyrene, acrylates, methacrylates, and FLO are the prominent ones. A detailed catalog of drag-reducing polymers has been given by Singh (20) and Gyr and Bewersdorff (23). The recently studied drag-reducing polymers are listed in Table 1.

In search for better drag-reduction efficiency and shear stability at low cost, a systematic investigation has been made in the author's laboratory by grafting efficient drag reducer such as polyacrylamide chains onto robust polysaccharide backbones to develop graft polymers having drag-reduction efficiency of synthetic polymers and shear stability of polysaccharides main chains (121–128). The maximum in drag reduction is also obtainable at the concentrations ranging from 50 to 100 ppm (see Fig. 6). As the grafting alters the regularity of the molecular structures, it inhibits the enzyme attack on main chain, thus enhancing the biodegradation resistance of graft copolymers and increasing the shelf life (44). Starch and low molecular weight (125000) poly(vinyl alcohol) are not drag-reducing. However, on grafting polyacrylamide branches, the graft copolymers show drag reduction efficiency and shear stability. A large number of graft polymers of amylose/amylopectin/CMC/guar gum/poly(vinyl alcohol)/starch/xanthan gum) have been synthesized. The graft polymers having longer and fewer polyacrylamide branches have been found to be more drag-reduction effective and shear stable. It has also been observed that purification of guar gum and xanthan

Table 1. Recently Investigated Drag-Reducing Additives

The reducing polymers	Molecular weight	Reference
Carboxy methylcellulose (CMC)	High viscosity grade OSA Co.	115
Xanthan gum (XG)	A food grade applied by Kelco Div of Merck and Co., Inc.	115
Polyacrylamide	Floerger/Dow Chemicals	99,115
Separan AP273	$6–8 \times 10^6$ g/mol	22,65,86
Superfloc A110, partially hydrolyzed polyacrylamide	Cytec Co.	
Anionic polyacrylamide	$13 \times 10^6 – 17 \times 10^6$ g/mol	51
Acrylamide-*co*-acrylic acid		
Cyanatol-750		
Poly(ethylene oxide)	Union Carbide Corp.	51,53,65,80, 151,152
Nonionic polymer	7×10^6 g/mol	
Poly OX WSR-303	4×10^6 g/mol	
Poly OX WSR-301	2×10^6 g/mol	
Xanthan gum (XG)	Sigma Chemical Co.	
Hydroxy propyl	Dowell Schlumberger 2.5×10^6 g/mol	50,52
Guar gum HPG	Alliburton	
Guar gum		
Polyisolutylene	Aldrich Chemical Co. 3.79×10^6 g/mol	43
Polyacrylamide/separan AP-30, AP-302	Dow Chemical Co.	43
Commercial drag reducer (CDR)	Esso Australia	43
Magnafloc 866A 50% hydrolyzed PAM	$16 \times 10^6 – 19 \times 10^6$ g/mol American Cynamid	51
PAM-Nonionic	$5 \times 10^6 – 6 \times 10^6$ g/mol Polysciences	51
Poly OX WSR-301	4×10^6 g/mol Union Carbide	51
Cetyl trimethyl ammonium bromide (CTAB) and sodium silicate	BDH Ltd.	
Poly OX WSR-303	Union Carbide 7×10^6 g/mol	51
Anionic PAM (acrylamide-*co*-acrylic acid 30%) Cyanatrol 750	American Cynamid Co. 14.25×10^6 gm/mol	

gum enhances their drag-reduction efficiency as removal of low molecular weight ingredients like fats and proteins increases the fraction of high molecular weight polymers, and hence improves their drag-reduction ability. The drag-reduction ability of grafted polymers is not affected by the salts present in seawater. These graft copolymers also have synergetic flocculation characteristics (44,45).

Bello and co-workers (50) have recently reported the effect of cross-linking agents on the drag-reduction efficiency of hydroxylpropyl guar and guar gum solutions in turbulent flow through a horizontal pipe. The results show that the addition of cross-linking agent (borax) to solution with concentrations below those required for gel formation enhances the drag reduction due to increased dimensions of the macromolecules in the presence of intermolecular cross-links. The

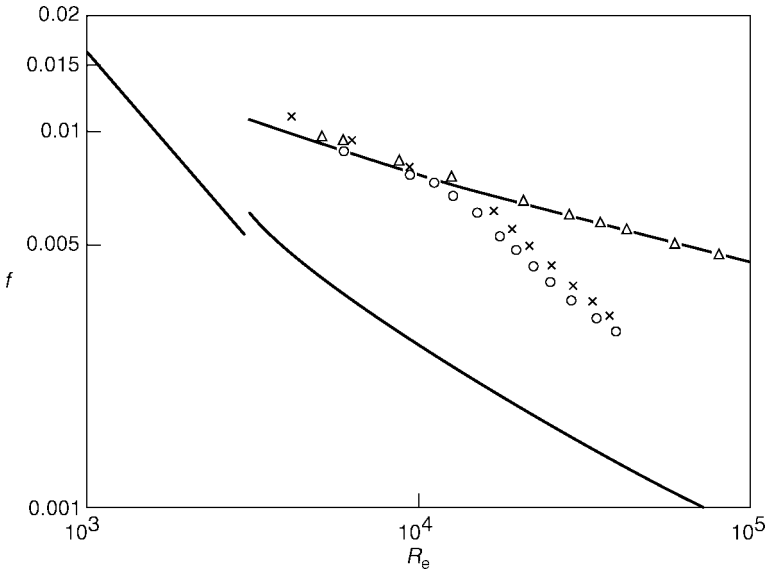

Fig. 6. The variation of drag reduction percentage with concentration in commercial, purified, and polyacrylamide grafted guar gum (GM_3) at R_e-14000: △ Water; × diameter = 1 mm, $u^* = 0.57$; ○ diameter = 3 mm, $u^* = 0.06$ (116,118).

flow-induced degradation of the polymers is not appreciably affected by the addition of cross-linking agent. The intermolecular bonds are stable to flow-induced degradation since their presence does not significantly alter the degradation rate. The enhancement of drag reduction also takes place at concentration of the macromolecules above 500 ppm. The enhanced drag reduction is up to 35%. On the other hand, grafting and purification enhance the drag reduction up to 68%, that too at concentrations below 100 ppm (121,123,128,129). Hence, it is worth investigating the effect of cross-linking of graft copolymers for further enhancement of drag-reduction efficiency.

McCormic and co-workers (130–136) have investigated the DRE of polyacrylamide copolymers. The various copolymers studied by this group include polyelectrolytes [(PAM-*co*-sodium-2-acrylamido-2-methylpropane sulphonate (NaAMPS); PAM-*co*-sodium-3-acrylomido-2-methylbutenoate (NaAMB)]; polyamphotytes [(poly-2-acrylimido-2-methyl propyl) dimethyl ammonium chloride-*co*-NaAMPS (ADAS); poly(acrylimide-*co*-2-acrylimido-methylpropenedimethyl ammonium chloride-*co*-sodium-2-acrylimido-methyl-propane sulfonate (ADASAM)]; and hydrophohically modified acrylamides [(PAM-*co*-diacetone acrylamide) (DAAM); PAM-*co*-*N*-*n*-decrylamide; PAMCO; (PAM-C_{10}), *N*-isopropylacrylamide-*co*-acrylamide (1PAM) copolymers]. Several of these copolymers showed better drag-reduction efficiency than PAM.

Kowalik and co-workers (46) and Malik and co-workers (47–49) presented a new approach in development of shear stable and efficient drag reducers based on intermolecular associations and intermolecular complexes based on secondary interactions. These systems displayed higher drag-reduction efficiency and shear stability. The associations may be caused by electrostatic, hydrogen-bonding, or

hydrophobic interactions. The increased shear stability was attributed to the reversible breakage of secondary bonds in preference to cleavage of polymer backbone. Malik and co-workers (47–49) introduced chemical moieties with interacting functionalities on the backbone of a polymer to cause association effects. These interpolymer complexes were based on a copolymer of 97 wt% dodecyl acrylate and 3 wt% methacrylic acid (proton-donating polymer), and a terpolymer is constituted by 50 wt% dodecylacrylate, 46 wt% styrene, and 4 wt% 4-vinyl pyridine (proton-accepting polymer). These hydrogen bonding mediated interpolymer complexes exhibited higher drag reduction and shear stability; though low molecular weight donor polymer is more shear stable than proton-accepting polymer, it is not an effective drag reducer. The shear stability has been discussed in terms of mechanistic considerations. It is apparent from the above discussion that though a lot of experimental results based on commercially available polymer drag reducers have been reported, the development of new drag-reducing agents with higher drag-reducing efficiency and shear stability is limited.

Mechanism of Drag Reduction

The effect of polymers on turbulence has been discussed by Singh (20), Gyr and Bewersdorff (23), and Gad-El-Hak (25), and several research articles have been published in 1990s. The gist of the past and present researches is being provided below and is the status of still eluding origin of drag reduction.

(1) The turbulent intensity of streamwise components has been reported for drag-reducing flows. All experiments indicated that the position of the maximum is further away from the wall than for Newtonian fluids and is generally found at $y^+ \cong 30$–60.

(2) For transverse intensity component in the presence of drag-reducing additives, the radial fluctuations are strongly damped in the buffer region and $(\overline{v}')^2$ maximum is shifted to $y^+ \cong 200$ or even to the centre of the pipe if large drag reduction is there. In the core region, the intensity is the same as for the solvent. The *xy* component of Reynolds shear stress is the measure of intensity of turbulence transport. In the pipe flow of Newtonian fluid, it starts growing from zero at the wall to a maximum at $y^+ \cong .05d^+$ and decreases nearly to zero at the pipe axis. In drag-reducing flow, the intensity is reduced and the maximum is shifted further from the wall.

(3) The frequency spectra of wall shear stress fluctuations for drag-reducing flows show the relative attenuation of high frequency components. The decrease in high frequency content and increase in low frequency are observed in the frequency spectra of axial as well as transverse fluctuations for drag-reducing flows.

(4) As streak spacing is a measure of the size of coherent eddies in viscous and buffer layers, the drag-reducing polymers change the structure of the flow. There is an increase in the nondimensional streak spacing as the drag reduction increases.

(5) The bursting period is an indication of time between occurrences of secondary instabilities. The burst produces extensive Reynolds stresses. The bursting is more energetic and its frequencies decrease as the drag reduction increases. In the maximum drag reduction region, the bursting period becomes two to three times as large as that of the Newtonian fluid at the same Reynolds number.

(6) In homogeneous drag reduction, only in the buffer region, the Reynolds stresses are produced in contrast to the case of heterogeneous drag reduction where there is a much larger region where the Reynolds and viscous shear stresses are of the same order of magnitude. The characteristic time of big eddies is of the same order as that of relaxation times of injected polymer solutions for shear rates of $10–10^3\ s^{-1}$, indicating an interaction between big eddies and polymer threads.

(7) The polymer threads influence the large-scale structures; it appears that highly elastic polymer threads restrict their motion leading to reduced transport of momentum from this region to the dissipating small eddies, and thus causing the observed drag reduction.

(8) According to the Lumley (78,79,92,137), the large eddies are formed in the viscous sublayer and are extended into the buffer layer. The polymer molecules are extended when subjected to fluctuating strain rate outside the viscous sublayer. This causes an increase in the extensional viscosity. This high extensional viscosity damps the small dissipating eddies. Because of the decreased intensity of small eddies, stress in the buffer layer delays the reduction in the mean profile slope, resulting in the thickening of the buffer layer. As the molecules are not extended in the viscous sublayer, it is not affected by polymer.

(9) The change in mean velocity profile causes the expansion of large eddies. The expanded large eddies produce an increased streamwise fluctuating velocity, primarily in the buffer layer. In the maximum drag reduction region, only large eddies are supposed to remain. According to the Lumley (78,79,92,137) hypothesis, the eddies in the buffer layer that are primarily responsible for Reynolds stress production are those associated with secondary instability on inflectional profile. These eddies are presumably damped.

(10) Luchik and Tiderman (138) postulated that turbulence and the polymer molecules in dilute polymer flows reach statistical equilibrium, where the remaining turbulent stretching keeps the molecule extended so that lower threshold motions can be damped by the viscoelastic properties of the dilute polymer solution. Gyr (80) was more specific and attributed the required molecular extension to a wall-layer structure of vortices.

(11) It seems that the high shear rates of a turbulent flow in the near-wall region are necessary to deform the spherical polymer molecule to an ellipsoid which becomes aligned with its long axis in flow direction. These deformed and aligned molecules are able to exhibit an increased resistance against vortex stretching and, therefore, can interact with turbulent structures.

(12) In the drag reduction by the surfactant solutions when a critical shear gradient is exceeded, the shear viscosity suddenly increases because of the formation of the so-called shear induced state (SIS). In SIS, the micelles become aligned in flow direction. Furthermore, in the SIS, the micelles have to build up larger, super-order structures. The critical shear rate for the occurrence of the SIS can be related with the onset of drag reduction (139), and it seems that drag-reducing surfactant solutions appear to exhibit an increased shear viscosity in the buffer zone of a turbulent velocity profile.

(13) The various theories explaining drag reduction may be divided into three categories: first, an explanation in which the increase in extensional viscosity for the polymer solution is the main ingredient; second, a theory that stresses the importance of anisotropic effects introduced by the extended polymer molecules; and third, a proposed explanation in which elastic effects are responsible for drag reduction.

(14) On the basis of DNS, a large number of investigations have been undertaken to explain the drag-reduction. Den Toonder (22,54,65,86) has proposed the following mechanism for the drag reduction by polymer additives. The polymers become extended by the flow at a certain Reynolds number, depending on the time scale of the polymer molecules in relation to the time scale of the turbulence. Hence, this "onset" phenomenon is determined by elastic properties of the fluid. When the polymers are extended, viscous anisotropic effects introduced by the extended polymers in the relation between the stress and the deformation cause a change in turbulent structure and the anisotropy production leading to a reduction in drag. At this stage, elasticity plays a counterproductive role in the drag-reduction process.

(15) Dimitropolous and co-workers (88) pointed out that previous work on numerical simulation on drag reduction has focused on the investigation of the role of elongational viscosity through the use of generalized Newtonian models. They used the nonlinear elastic model with the Peterlin approximation (FENE-P) and the Giesekus model (140) of viscoelasticity for the solution at high extensional rates. In both the cases, comparing the mean velocity profiles and the statistical features of the turbulent flow showed agreement with well-established experimental observations, such as the increase in the spacing of the streamwise streaks and the increase in the streamwise vorticity fluctuations. In addition, the hypothesis that drag reduction is primarily an effect of the extension of the polymer chains, where the increase in the extensional viscosity leads to the inhibition of turbulence-generating events, was once again reinforced.

(16) Sreenivasan and White (89) recently invoked the theory based on the elastic behavior of stretched polymers of de Gennes (84), who states that coil-stretch transition does not occur in turbulent flows in randomly fluctuating strain rates and that, if moderately stretched, the polymers produce no measurable change in viscosity. Sreenivasan and White (89) were able to explain the onset of drag reduction and maximum drag reduction asymptote on the basis of the elastic theory, and their results qualitatively explain the existing experiments.

Degradation and Shear Stability Mechanisms

Though the DRE of polymers is very high at extremely low dose, the practical problem in widespread applications of polymer additives is the degradation of polymers in turbulent flow. The degradation leads to a marked loss of the drag-reducing capability of the polymer.

There are two types of degradation, chemical degradation and mechanical degradation (65). Chemical degradation causes change in the structure of polymers by chemical reactions. It can occur, for example, by the presence of metal or any free-radical initiators when oxygen is present. The high salinity or calcium concentrations in solvent can also cause chemical degradation (141).

Mechanical degradation is caused by mechanical energy input to the polymers in solutions, which means passing the solution through pumps or pipes or both. Mechanical degradation has long been associated with shear flow. To some extent, the shear flow causes the degradation of dilute poly(enthylene oxide) solutions (14). Bueche (142) showed in his pioneering work that the elongational stresses which exist in some regions of turbulent pipe flow are more severe and cause scission of polymer molecules. A molecule in a shear flow is subjected to both rotation due to the presence of vorticity and to stretching and compressive stresses. Bueche (142) showed that in simple shear flows, the molecule is rotated past principle axes much too fast to allow the flow to stretch it to a large extent. On the other hand, in elongational type of flows, the vorticity is much less relative to the stretching and aligning action of the strain than in shear flows. A large number of investigations have been reported, which convincingly indicate that the molecules are fully extended followed by mid-chain scission under elongational flow field (143–147).

Mechanical degradation of polymers in turbulent flow has been extensively investigated and reviewed by Pollert and Sellin (148), Singh (20), Moussa and co-workers (149), Moussa and Tiu (43), Gyr and Bewersdorff (23), Den Toonder and co-workers (65), Nguyen and Kausch (146), Brostow and co-workers (62–64), Choi and co-workers (141), Rho and co-workers (150), Kim and co-workers (151–155), and Choi and co-workers (156–159).

It is well established that the extent of drag reduction increases with the molecular weight and length of polymers, and so does their susceptibility to flow-induced degradation (20). The rate of mechanical degradation increases with the increasing molecular weight. In most of the cases, it is possible to represent degradation by an exponential expression using flow time or number of passes as an independent variable. In turbulent flow, the degradation is more in poor solvent at low Reynolds number, whereas the opposite was observed at high Reynolds number. For constant wall shear stress and pipe diameter, the degradation rate was found to be directly proportional to the molecular weight of polymers. For constant wall shear stress and polymer concentration, the degradation rate was found to be inversely related to pipe diameter. For constant wall shear stress and pipe diameter, the degradation rate was found to be inversely propotional to polymer concentration. For constant polymer concentration and pipe diameter, the degradation rate was found to increase with wall shear stress. In general, the shear stability increased with solvation number. The higher the ratio of total length to the width of the polymer molecule, the faster will be the degradation. In

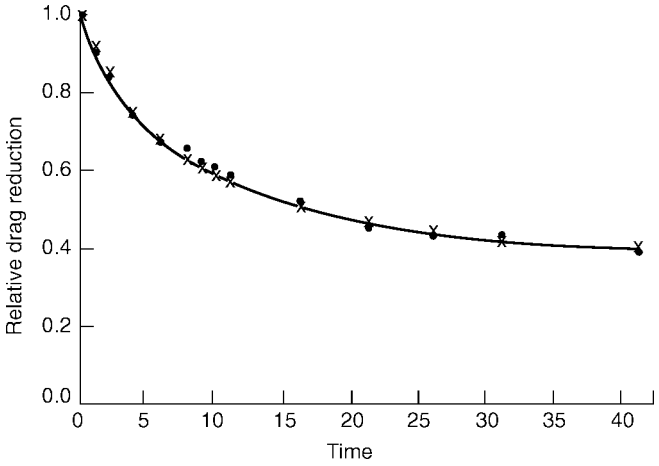

Fig. 7. The variation of relative drag reduction with time for mixtures of pure xanthan gum (10 ppm) and polyacrylamide (10 ppm): ×, Theoretical (Brostow Polymer Flow Model); ●, experimental (59).

high turbulent flow, the degradation is not caused not only by scission of polymer chains, but also by a radical propagation reaction initiated by scission of polymer chains.

The critical Reynolds number $R_e{}^*$ or apparent shear/extension rate $(v/d)^*$ was found to increase with polymer concentration and molecular weight as represented by the dimensionless concentration $c[\eta]$. Most of the degradation takes place at the entrance region because of high extensional straining of polymers.

The molecular degradation in turbulent flow is also explainable by the theoretical model of Brostow (62–64) (see Fig. 7). The mid chain scission in turbulent flow has been experimentally and theoretically explained (143–145,147). Recently, Kim and co-workers (153) studied the mechanical degradation of high molecular weight polystyrene under turbulent flow using a rotating disk apparatus for three various solvent systems. They found that the extent of the degradation depended on the solubility parameter of the solvents. Their experimental data for molecular degradation in turbulent flow gave an excellent fit with the Brostow model (62–64). Brostow (62) obtained the following relation:

$$\frac{\mathrm{DR}(t)}{\mathrm{DR}_0} = \frac{1}{1 + w\,(1 - \mathrm{e}^{ht})} \tag{32}$$

where $\mathrm{DR}(t)$ and DR_0 are the percentage drag reductions at times t and $t = 0$, respectively. A large value of h indicates fast degradation, and a large value of w implies a low shear stability. Their data give excellent fit to the equation.

Choi and co-workers (158) observed the following correlation between time-dependent drag reduction and mechanical degradation:

$$\frac{\mathrm{DR}(t)}{\mathrm{DR}_0} = \exp(-t/\lambda_0) \tag{33}$$

where DR(t) and DR_0 are the percentage drag reductions at times t and $t = 0$ respectively, and λ_0 is an adjustable parameter. $1/\lambda_0$ measures the rate of degradation. It describes the degradation mode very well for shear-resistant polymers such as various CMC and CMC-based graft copolymers (125) and xanthan gum (160).

However, the exponential equation deviates from the experimental data for drag reducers such as flexible PEO. Recently Sohn and co-workers (161) and Kim and co-workers (155) have studied the drag-reduction characteristics of polysaccharides such as xanthan gum and guar gum respectively. They are found to be reasonably shear-stable drag-reducing agents (123,162,163). They are highly susceptible to biodegradation. To overcome this disadvantage these polysaccharides have been grafted by flexible polyacrylamide branches (122,123). The solutions of both polymers conform to the empirical relationship between drag-reduction efficiency and polymer solution properties (156) at a fixed Reynolds number, ie

$$\frac{C}{\mathrm{DR}} = \frac{K[C]}{\mathrm{DR}_{\max}} + \frac{C}{\mathrm{DR}_{\max}} \tag{34}$$

where DR_{max} is the maximum drag reduction, K is the characteristic parameter which depends on the polymer solvent system, and C is the intrinsic concentration (W_{ppm}) defined by

$$[C] = \frac{\mathrm{DR}_{\max}}{\mathrm{Lim}_{C\to 0}\left(\frac{\mathrm{DR}}{C}\right)} \tag{35}$$

and the universal curve for drag reduction when normalized by the hydrodynamic volume fraction of the polymer solution (% DR/$[\eta]C$ vs $[\eta]C$) is due to McCormic and co-workers (130–137).

They reported that volume fraction normalization allows the comparison of drag-reduction efficiencies of polymers of widely differing structures. Xanthan gum molecules in deionized water exhibit higher drag reduction in the range of 50–60°C than at room temperature because of conversion to individual xanthan gum molecules from aggregated helics. In case of guar gum, it was confirmed that K is a characteristic constant of a particular polymer/solvent system and does not depend on molecular weight.

The turbulent drag reduction and drag reduction of DNA has been recently investigated by Choi and co-workers (164). Double-stranded DNA is found to be a good drag reducer when compared with the other normal linear polymers. However, the drag-reducing power of DNA disappears when DNA denatures into two single-stranded molecules. DNA is always cut in half by the turbulence. Its degradation is different from that of the normal flexible long-chain polymers.

In a number of graft copolymers (122,124,165,166), it has been found that the grafting increases the shear stability. However, in some cases, the grafting has been found to reduce the shear stability of graft copolymers (123,125,126), which supports the mechanistic analysis of Agrawal and Mashelkar (167).

A highly branched polymer of high molecular weight amylopectin and its graft copolymer with polyacrylamide have been investigated by subjecting the solutions by intensive turbulent flow in turbulent rheometer at Reynolds number

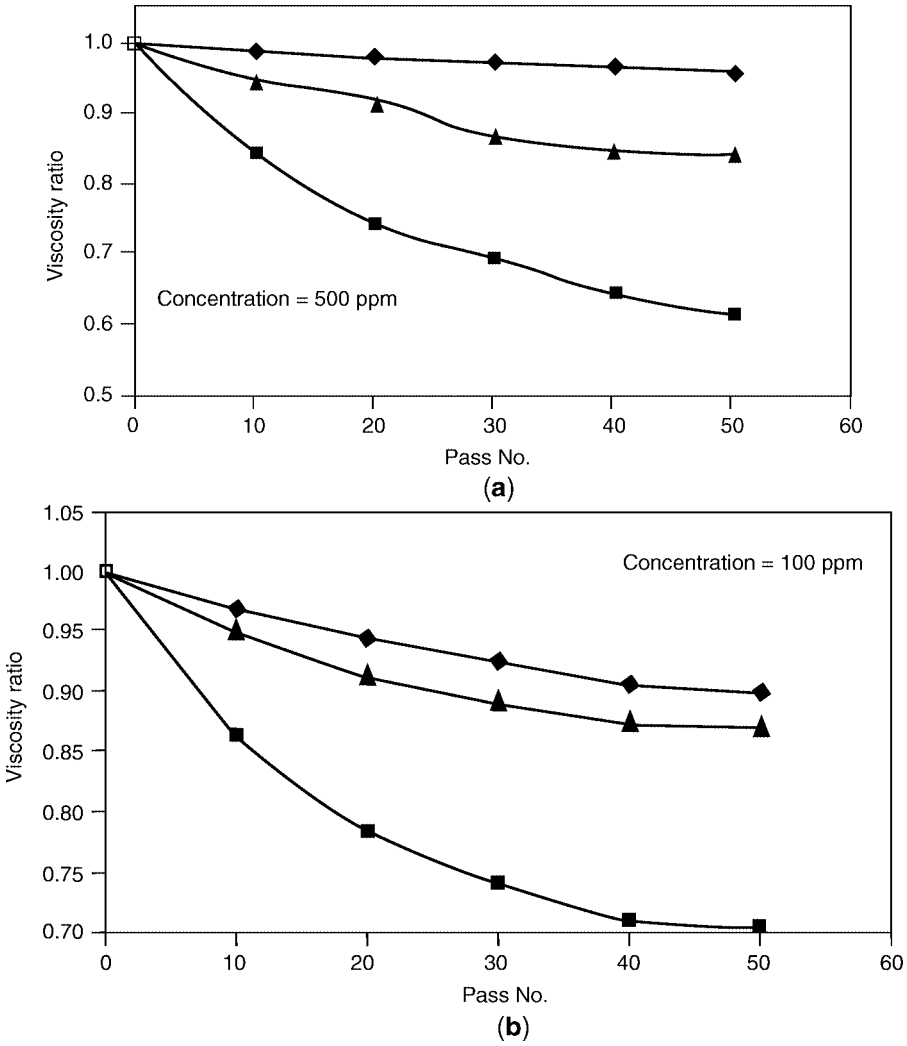

Fig. 8. The variation of viscosity ratio versus pass number at concentrations of 500 ppm (**a**) and 100 ppm (**b**) respectively in case of solutions of polyacrylamide grafted amylopectin (◆), amylopectin (▲) and polyacrylamide (■) ($R_e = 14000$), and at 50 ppm (**c**) for polyacrylamide (◇) experimental and (□) theoretical according to Brostow model ($R_e = 14000$). (161).

of 14,000 (168) (see Fig. 8). The solutions were investigated in the concentration range of 50–500 ppm, and mechanical degradation was monitored by measuring absolute viscosities of sheared solutions from 10 to 50 pass numbers in turbulent flow rheometer. As is evident from Figure 8, the results contradict the Agrawal and Mashelkar theory (167) and support the Brostow polymer model (62–64). Apart from grafting, two other approaches have been put forward to enhance the shear stability. The reversible intermolecular association in solution increases the molecular weight of polymer and provides enhanced shear stability (46–49). The drag-reducing polymers can be cross-linked to enhance drag reduction; the flow

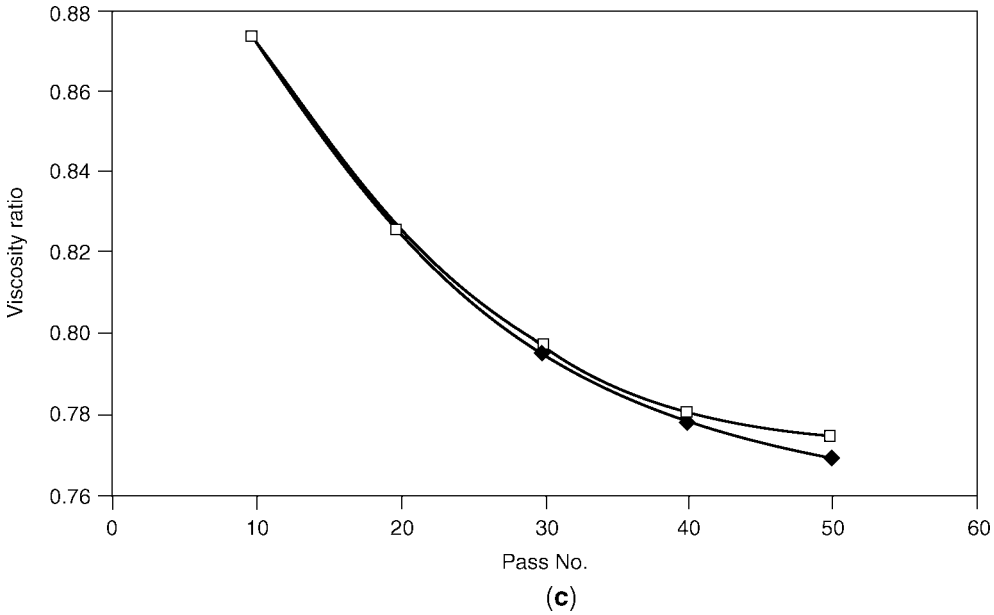

Fig. 8. (Continued).

induced degradation of the polymers is not appreciably affected by the addition of cross-linking agents (50).

Drag Reduction by Mixed Systems

The earlier work on drag reduction by fibers, polymer/polymer, polymer/fiber, and polymer/soap mixtures has been reviewed by Singh (20) and Gyr and Bewersdorff (23). It has been noticed that fibers with high aspect ratio (l/d), flexibility, and surface roughness show good drag-reduction effectiveness. At equal aspect ratio, fibers with smaller diameter cause more drag reduction. This can be attributed to the improved flexibility due to decrease in diameter of the fibers. The fibers of nylon, wood pulp, acrylic, glass, and asbestos have been reported to cause drag reduction in suspensions.

Both positive and negative deviations from the linear additive line have been observed in drag reduction caused by polymer/polymer mixtures depending upon their composition, flow rate, and polymer species. The maximum synergism is obtained at a specific composition. The random coil size, rigidity, and salvation of polymer molecules appear to be responsible for the synergism in drag reduction by polymer/polymer mixtures (169).

The maximum drag reduction caused by polymer/fiber mixtures is more than predicted by Virk's maximum drag reduction asymptote (170). Kale and Metzner (171,172) explained the reasons for synergism in drag reduction by high extensional effects on polymers along with fibers and consequent high extensional viscosities of polymer solutions. Reddy and Singh (169) found strong synergistic effect

with both guar gum and xanthan gums in combination with asbestos fibers. A 50:50 mixture by weight gave the maximum in both cases. As observed by Hoyt (17), both mass and length are responsible for suppression of turbulence by these systems.

Recently, Inaba and co-workers (173) pointed out that it is possible to reduce the pumping power, to downsize the transport system, and to decrease the heat loss to environment by using surfactant water solution as a thermal energy transport medium. The environmental pollution caused by discarding the used surfactant solution has become a serious problem. It is required that the new additive have the same flow drag reduction effect as surfactant solution, and also that little environment load be used. They used pulp fiber as the new type of flow drag reduction additive in a circular pipe. The pulp fiber consists of a vegetative fiber that forms paper. Therefore, pulp fiber does not have harmful effects on the environment. The fibers were of the diameter range 6.45–29 μm and had an aspect ratio of 50:1. The flow resistance and heat-transfer characteristics of water suspensions with pulp fibers were measured. The velocity distribution of the pulp fiber suspension was similar to the plug flow in the laminar flow. The flow drag reduction effect was observed. The enhancement effect of heat transfer in the laminar flow and the heat-transfer reduction effect in the turbulence were observed. The nondimensional correlation equations of pipe flow resistance and heat-transfer resistance were derived in terms of various nondimensional parameters in the above study (see Fig. 9).

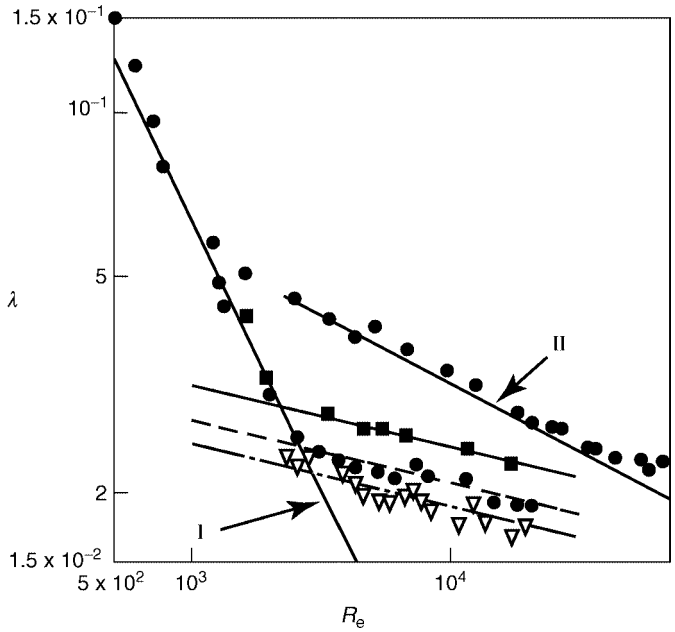

Fig. 9. Relationship between pipe friction coefficient λ and Reynolds number for various pulp water suspensions. I depicts the theoretical equation of the flow resistance in laminar flow in pipe and II depicts the Blasius resistance formula of turbulent flow. C_p, %: ●, 0 (Water); ■, 0.30 ———; ●, 0.55 —— ——; ▽, 0.72—-—. Adapted from Figure 9 of Ref. 166.

Drag reduction caused by passive devices such as riblets has been confirmed for various boundary layers and pipe flows (174–178). However, riblets have a narrow range of the effective flow rates, and if the flow rate is higher than this effective range, the riblets increase the friction drag just like normal rough wall (179). Walsh and co-workers (175–177) found that the triangular grooves of roughly equal height and azimuthal spacing, ie h/s ≈ 1, provided the optimal drag reduction performance. They further found that relative to a smooth wall, riblets with $h/s \approx 1$ exhibited two general flow regimes:

(1) For nondimensional riblet height $h^+ < 25$, the riblets reduced drag with the largest reduction of the order of 10% at $h^+ \approx 15$.
(2) For nondimensional riblet height $h^+ > 25$, the riblets enhanced the drag by as much as 30% at $h^+ \approx 50$.

It has been established that interflows of air and water in riblet-lined pipes (180–183) show the same behavior as the external flows over riblets. According to Walsh (175,176), riblets act as fences to isolate the low speed streaks that exist near the wall (184), and thus retard their bursting.

Bechert and co-workers (185) and Choi (186) have proposed that the riblets impede spanwise motions of streamwise vortex pairs associated with sublayer streaks, resulting in weakened bursts and lower shear stress. Choi and co-workers (187) and Pullese and co-workers (188) conducted measurements of three rms turbulence intensities and turbulence shear stress over riblet surfaces in their drag-reducing regimes. These physical entities were reduced relative to their respective magnitudes over smooth surfaces at the same force stream velocity. However, axial to transverse correlations near the riblets surface remain much the same as those near a smooth surface. This is in contrast to polymer drag reduction, where significant reductions in the axial to transverse velocity correlations relative to solvent are observed (10). The drag enhancement by riblets at high h^+ was attributed by Walsh (175,176) to adverse effects of the increased riblet wetted surface area overwhelming the riblet-induced drag reduction. However, Tani (189) observed the riblet drag enhancement as being akin to that by sand-roughened pipes and estimated the equivalent sand roughness of riblets to be about a quarter of their actual height.

Choi and co-workers (190) have carried out direct numerical simulation of turbulent flow over riblets at $h^+ \approx 20$ and 40, respectively, in drag-reducing and drag-enhancing regimes. Interpreting their calculations in terms of coherent structures, they pointed out that riblets reduce drag when the streamwise vortices above them are aligned such that only a small portion of a riblet, near the tip, is exposed to their downwash at higher h^+; the streamwise vortices become smaller relative to the riblets; and their downwash affects a greater fraction of the riblet surface, enhancing drag.

The combined polymer additives and riblets are expected to cancel out the drawbacks associated with applying each of these systems and to produce a positive synergistic effect. The effect of combined experiment would also elucidate the respective drag-reduction mechanism. Choi and co-workers (190) experimented on a ship model with riblets and then coated the model with polymer. The

measured drag of the model revealed that the combined system caused 2% higher drag reduction than the additives of each systems effect. Rohr and co-workers (191) measured the friction factor for dilute PEO in a pipe lined with 0.076-mm, V-groove riblets (3MCO). He found that the combined system produced the same drag reduction ratio as the polymer additive alone. Christodoulou and co-workers (192) and Anderson and co-workers (180) carried out similar experiments. In both experiments, results obtained for combined systems using PEO solutions showed that the drag-reduction rates were less than the sum of two systems. In contrast, Anderson and co-workers (180) observed for combined system using guar gum that the drag rate was greater than the sum of the drag-reduction rates of the individual systems and that the critical shear stress of the additive was lowered. Koury and co-workers (178) carried out a systematic experiment for a combined system of polyox and a riblet pipe. The positive synergistic effect was observed to occur.

Recently, Mijunuma and co-workers (179) investigated the drag reduction for combined system of polymer additives and riblet pipe. The riblet groups were V-shaped, the spacing of which was 1.3 mm and the height 1.01 mm. For higher h^+, a triangular riblet system including other geometries increases the drag to levels similar to those of normal transient roughness. The polymer additives were Aronfloc N-110 and separan AP-31. The critical shear stress, τ^*, at which N-110 started the drag reduction was approximately eight times higher than τ^* for AP-30. In the combined system, the synergistic drag reduction for higher h^* was discussed under the assumption that additives suppressed the drag increase resulting from riblets. Since additives thicken a wall layer covering the region from a viscous sublayer to a buffer layer, the relative height h to this wall layer thickness is lowered. Another cause of the synergistic effect is the flow enhancement due to additives, which suppresses the riblet-induced drag increase. Hence the combined effects almost cancel out the drag increase due to riblets. This synergistic effect exceeds 10%. The analysis based on velocity profiles indicated that these effects can produce synergistic drag reduction for higher h^*.

Drag reduction can be achieved by direct injection of microbubbles through slots or porous skin (193–196) or the generation of hydrogen by electrolysis at the wall (197). The primary parameters, independent of gas type and Reynolds number, appear to be the actual gas flow rate referenced to injector conditions of temperature and pressure (198–200) and the location of the bubbles in the turbulent boundary layer (198,199,201–203). Merkle and Deutsch (196) have provided a comprehensive review on skin friction reduction by microbubble injection. Mahadevan and co-workers (204) postulated that microbubbles like polymer solution destroy turbulence production by selectively increasing the viscosity near the buffer region. They increase the local dynamic viscosity. Pal and co-workers (205) demonstrated that microbubble and polymer solution shear stress statistics as measured by flush mounted hot film sensors are similar at equivalent value of drag reduction.

Fontaine and co-workers (206), on the basis of these similarities, envisaged that high levels of drag reduction can be achieved by combining low concentrations of polymer and surfactants with microbubble injection at low injection rates. The influence of homogeneous surfactant (Aerosol OT) and homogeneous polymer (PEO) solutions on the performance of microbubble skin friction reduction

was investigated on an axisymmetric body. Carbon dioxide was injected in water, homogeneous surfactant solution, and homogeneous polymer solutions. The integrated skin friction measurements were obtained at two free-stream velocities as a function of gas injection rate and PEO concentration. At similar gas injection rates, microbubble injection exhibited more drag reduction. At low gas injection rates, the results of this investigation indicate that the combination of microbubble injection with polymer additives can yield drag reduction levels exceeding those of the individual systems. Maximum drag reduction in the combined system was greater than 80% for 20-ppm polymer concentration and higher gas injection rates. This level of drag reduction is higher than the levels obtained with either polymer or microbubbles separately at these concentrations or injection rates. In this study, synergism between microbubble and polymers was not obtained. Reducing the bubble size through addition of surfactant did not affect the characteristics of microbubble drag reduction. The resulting size of microbubble is still large compared to turbulent scales and, thus, may explain the lack of effect on drag-reduction characteristics of microbubbles with and without surfactant.

Watanabe and co-workers (207–210) reported drag-reduction phenomena in different geometries having highly water-repellent walls in laminar region. The basic material of the highly repellent wall is fluorine alkane modified acrylic resin with added hydrophobic silica, and the contact angle of the wall is about 150°. Watanabe and co-workers (207) reported for the first time the laminar drag reduction of Newtonian fluids flowing in a channel with square and rectangular ducts with highly water-repellent walls. The maximum drag reduction ratio of water was 22% for the square duct. The drag-reduction phenomena were also observed for the frictional resistance of an enclosed rotating disk with highly water-repellent walls. The maximum drag reduction ratio for tap water was about 25% at the Reynolds number of 2×10^5. In their recent investigation (208–210), the drag-reduction phenomenon in which 14% drag reduction of tap water flowing in a 16-mm diameter pipe occurring in a laminar region has been explained. This phenomenon occurred because of the presence of fluid slip at the wall. The measured velocity profile gives the slip velocity at the pipe wall, and it was shown that the shear stress is directly proportional to the slip velocity. The friction factor formula for a pipe flow with fluid slip at the wall has been obtained analytically from the exact solution of the Navier Stokes equation, and it well agrees qualitatively with the experimental data. The main reasons for the fluid slip have been pointed out. In these cases, the molecular attraction between the liquid and the solid surface is reduced because the free energy of the solid is very low, and the contact area of the liquid is decreased compared with conventional smooth surface because the solid surface has many fine grooves. A liquid cannot flow into the fine grooves owing to surface tension. These concepts are supported by the experimental result that the drag reduction does not occur in the case of surfactant solutions.

Turbulent Drag Reduction by Surfactants

Recently, turbulent drag reduction by surfactants has been extensively reviewed by Gyr and Bewersdorff (23), Zakin and co-workers (42), and Myska and Zakin

(41). The main features of the surfactant drag reduction and their industrial applications are summarized here.

The polymer solutions are strongly affected by mechanical degradation during turbulent flow which limits the lifetime of their DRE. The surfactants have been found to reduce the frictional drag by 70–80%. At high stress, the surfactants also suffer temporary mechanical degradation of their microstructure, but they have the ability to repair themselves in the order of seconds (42).

The drag-reducing surfactant solutions are characterized by the presence of rod-like micelles which are formed by single surfactant molecules above a certain characteristic concentration (139). This critical concentration depends strongly on temperature and electrolyte concentration. As mentioned earlier, critical wall shear stress, a shear induced state (SIS), is achieved when the micelles are coalesced to form larger structure aligned in flow direction. This is also the onset stress of drag reduction by surfactant. The observed loss of drag reduction beyond this critical wall shear stress is reversible. The drag reduction is caused by anionic, cationic, nonionic, and zwitterionic surfactants. Nonionic surfactants are chemically stable, endowed with low toxicity, and biodegradable. However, their effective temperature range is limited. Zwitterionic surfactants are more useful as they have a larger effective temperature range. As they have both positive and negative charges in single surfactant molecule they may be sensitive to ions existing in water. The cationic surfactants with the organic counterions are excellent drag reducers in aqueous system. They have fairly wide temperature ranges and are not sensitive to calcium or magnesium ions present in water. Because of their potential for practical applications, they have been extensively investigated in the 1990s.

The DRE of cationic surfactant is greatly dependent on their chemical structures, surfactants, and counterion concentrations. Surfactants with short alkyl chains are effective at low temperatures, while those with long alkyl chains are effective at high temperatures. The dramatic effect of the counterion to surfactant concentration ratio on fluid characteristics of surfactant solutions has been found recently. The proper combination of both can extend the effective range widely.

The surfactant drag reducers may exhibit strong viscoelasticity and high extensional viscosity. Excess counterions in cationic surfactant may make the solution still nonviscoelastic with distinct extensional viscosity. This suggests the correlation between drag reduction and extensional viscosity.

The surfactant drag reduction may exceed Virk's drag reduction asymptote for high polymers, and velocity profiles may be steeper than his elastic sublayer. The turbulence in radial and tangential directions is suppressed by surfactants. The zero Reynolds stress profiles have been observed for surfactants. Though the drag reduction mechanism is not established for surfactant drag reduction like polymer drag reduction, its mechanism may be different.

Along with the reduction in momentum transport, drag-reducing fluids have also been found to reduce the heat-transfer coefficients particularly in tube-in-tube heat exchangers. The heat-transfer reduction accompanying drag reduction may be caused by the thickening of the viscous boundary near the wall, which increases the thermal resistance between wall and bulk fluid and reduces the radial turbulence intensity. Heat exchangers with flow channels which disturb the fluid more, such as plate exchangers, show less heat-transfer reduction. Despite

several successful fields tests in district heating and district cooling systems, no commercial scale applications of surfactant drag reduction have been undertaken so far (23,31,42).

Applications of Drag Reduction

Introduction. Ever since the discovery of the drag-reduction phenomenon, efforts have been made for its industrial applications. In the last five decades, the range of applications of drag reduction has increased tremendously. The possible areas include oil-well fracturing operations, crude oil and refined petroleum product transport through pipelines, fire fighting, sewerage and flood water disposal, irrigation, hydrotransport of solids, water-heating circuits, jet cutting, hydraulic machinery, and marine and biomedical applications. The detailed progress made in these areas has been reported in various reviews (14,15,17,20,23,42,44,112,211, 212).

In crude oil transport and storm sewers, because of the economic benefits, the drag-reducing polymers have been put into practice in Trans Alaska Pipeline and other 100 pipeline sites, as well as in other pipelines transporting refined petroleum products (213,214). Similarly, drag-reducing polymers in storm sewers for Knowle and Dallas sewers (15) have been put to practice. Exigency requirements are in favour of applications of the drag-reducing polymers in fire fighting. Hence the practice has been accepted by New York City Council and the City of Hamburg. Large-scale field experiments have shown the efficacy of using drag-reducing polymers in hydrotransport of fly ash and sludge, heating circuits, water power stations, and irrigation from Czechoslovakia (211). Use of drag-reducing polymers has been made in short diversion tunnels and culverts in Yugoslovakia (215). Drag-reducing polymers have been used in energy requirements of sprinkler irrigation, reduction of percolation losses, and development of slow-release urea in India (33,44).

The efficacy of drag-reducing polymers in reducing the drag, hull of a 42.7-m long HMS Highbortor has been reported from the United Kingdom (216). In other cases, laboratory scale experiments have been performed, indicating beneficial use of drag reduction. Large-scale applications are inhibited in many cases because of the high cost of polymers and their degradation. Large-scale laboratory experiments as well as field trials have been reported indicating efficacy of cationic surfactants in district heating circuits (42). Economically feasible applications are described in some important cases.

Crude Oil Transport and Refined Petroleum Products. The most spectacular success of the application of drag-reducing polymers has been in the Trans Alaskan Pipeline (TAPS) in 1979, where the throughput capacity has been above 2 million barrels of oil per day (BPD) from pipeline capacity of 1.5 million BPD without the use of polymeric drag reducers (DRA) at present. The pioneering use in TAPS was to increase throughput while pump stations were being constructed and commissioned. As the effectiveness of the DRAs improved in the period 1979–1984, the need to build pumping station nos. 5 and 11 of the 12 disappeared. Present day DRAs are 12 times as effective as the initial materials used in TAPS in 1979.

In the Iraq-Turkey pipeline, DRA is injected downstream from each of the 15 pump stations. The injections of 40–50 ppm of DRA at each pump station allowed for an increase in throughput to 1 million BPD from a base flow of 0.7 million BPD.

A similar application of DRA has been undertaken to oil being pumped from the offshore platforms to shore facilities (217). Since 1983, some pipelines have used DRA for pipeline transportation of refined petroleum products (213). Treated fluids include gasoline, diesel, heating oil, and C_4 carbon. Today, approximately 100 pipeline sites use DRA for increased throughput (213,214). Typical dose rates for 10–30% flow improvement in these pipelines are no more than 1–2 ppm polymer per injection. Tests indicate excellent drag reduction without adverse effect on engine (218). In 1994, DRAs were 14 times more effective than the initial material used in TAPS in 1980.

The rapid and completely dissolving formulation will increase DRA effectiveness and improve application predictability. In addition, the incorporation of DRA into the design status of new pipeline construction deserves consideration for either downsizing pipes or reducing the number of pumping facilities.

Applications of Drag-Reducing Agents in Agriculture. Drag-reducing polymers reduce the drag in a turbulent flow and increase the drag in laminar flow because of an increase in shear viscosity. This feature of drag-reducing polymers has been utilized in reducing the energy requirement of sprinkler irrigation system in which the flow is in turbulent region in laterals, risers, and jets. Their use also increases the throughput and the area of coverage of sprinkler irrigation system (33,44,219–226). Water containing the drag-reducing polymers percolates slowly in the soil. This is due to increased shear and elongation viscosities of aqueous polymer solutions. The increased elongational viscosity produces a higher resistance in the porous media flow in the soil. Utilizing this aspect, a slow-release urea has been developed by blending urea with guar gum (33,223), which has boosted yields of wheat and paddy by 20–25% in field trials at IIT Kharagpur. It also increased the yield of vegetables such as cauliflower and brinjal in another field trial done in IHRI, Ranchi, India (227).

As guar gum is biodegradable, it does not affect the soil adversely. As a matter of fact the residual positive effects in yield in subsequent crops have been observed by Kar and Sahoo (228). There have been considerable developments in materials and polymer solution injection systems in sprinkler irrigation system.

Singh and co-workers (229,230) have developed a series of polyacrylamide grafted polysaccharides as drag reducers which are biodegradable and shear stable. Of these, polyacrylamide grafted amylopectin has been found to be the most effective drag reducer, and it reduces percolation losses most effectively by 50% at a concentration of 100 ppm.

In most of the reported investigations on sprinkler irrigation system, homogeneous drag reduction has been used in which the drag-reducing polymers are dissolved in the inlet source itself. In field conditions, the main water source for sprinkler irrigation can be tubewell, open well, reservoir, or a running stream or canal. In case of such sources, the polymer solution is required to be injected either at the inlet or outlet of the main pump. As evident from Figure 10, outlet injection is most effective as the drag-reducing polymers are not

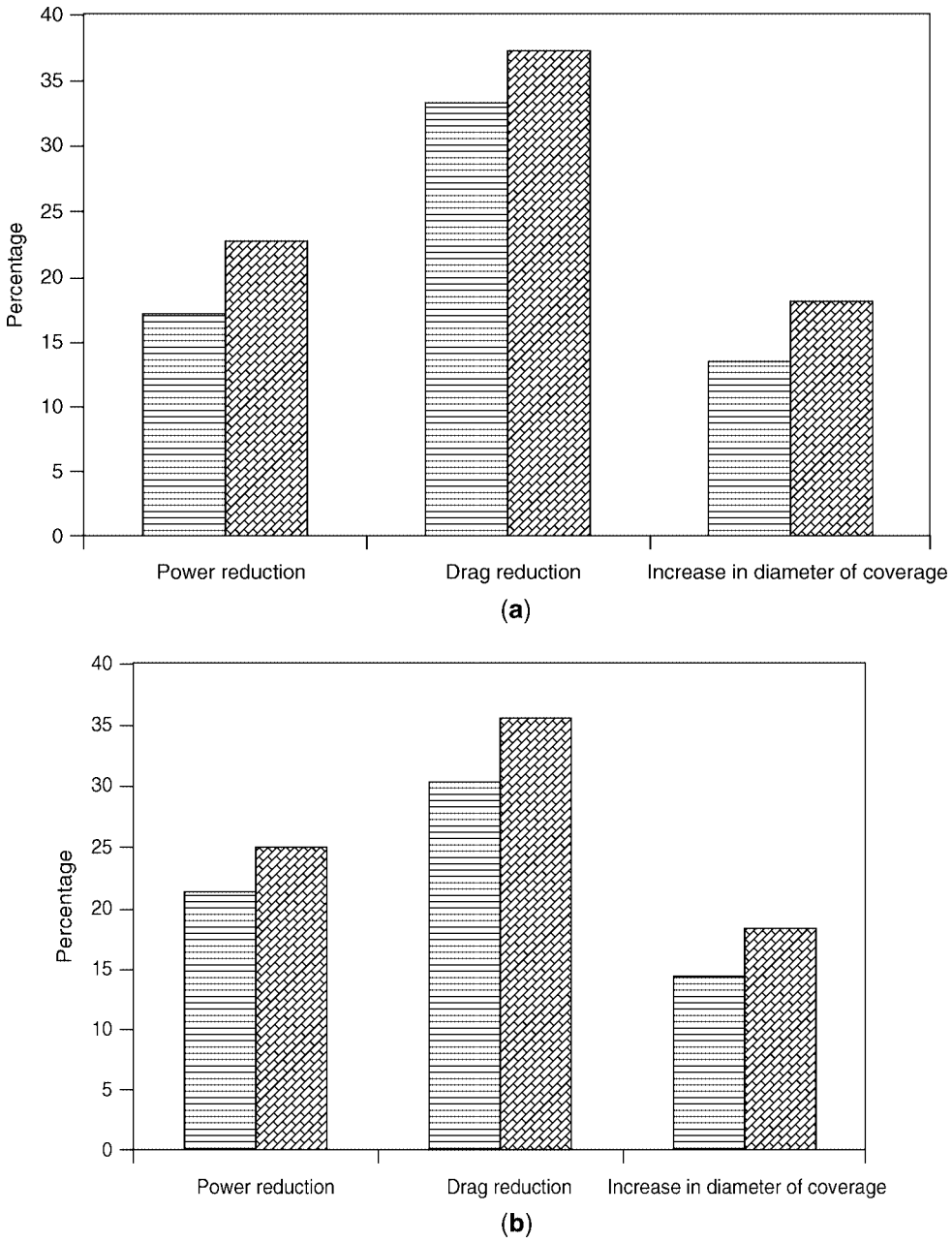

Fig. 10. Effect of injection method on drag-reduction characteristics of 50 ppm of polyacrylamide grafted amylopectin (AP-g-PAM) and 100 ppm of AP-g-PAM ▭ Inlet; ▨ Ventury (224).

degraded by the centrifugal pump (231). The cost benefit analysis shows that using drag-reducing polymers in sprinkler irrigation allows reduction in the pipe diameter and the power of centrifugal pump, which reduces the installation costs as well as the energy required. The reduction in the percolation losses

brings down the amount of water needed. This integrated technology is important for all those countries in the world which suffer from a shortage of water (23).

Storm Sewer Augmentation. Many sewers face overloading for a short duration during storms or heavy rains or because of increase in catchment area over the years owing to continued development. The capacity of sewers can be increased by drag-reducing polymer dosing. It has been shown by Sellin and coworkers (15) that the capital cost of dosing installations, recurring cost of polymers and maintenance, etc, are much lower than the capital cost involved in laying down a new sewer of 381-mm diameter in place of the existing 305-mm diameter sewer (in the rate of 1:15 according to prices in 1979). Fully automatic polymer dosing stations have already been installed in Buchman Creek (Dallas, Tex.) and Knowle (Bristol, U.K.). In these installations, drag-reducing polymer powder poly(ethylene oxide) water slurry is injected in the sewer. Bewersdorff and co-workers (232,233) showed that polyacrylamide suspensions (SEDIPUR AL436 containing 25% active material PAM by weight) can be injected economically to enhance the output of a sewer in Dortmund (Hohensyburg Sewer). During storms, 20–30 ppm of poly(ethylene oxide) or polyacrylamide can augment the flow capacity by 20–30%; economic feasibility studies together with 5-year data from an automatic dosing station (234) demonstrate that this is a viable and practical solution to many flooding situations.

Conclusions and Future Scope

The origin of drag-reducing polymers still remains enigmatic though considerable progress has been made in understanding it at the molecular level. Now it is possible to measure the extensional viscosity and other rheological properties of drag-reducing polymers at drag-reducing concentrations. The numerical simulations are also revealing other facets of the turbulent drag reduction phenomenon. Various molecular models such as FENE-P are being tested. As has been pointed out by Zhou and Akhavan (235), the most promising approach to accurate computation of polymer drag reduction at present is through stochastic simulations. However, on the application side, drag-reducing polymers are being used, as a routine practice, in crude oil and other petroleum product transport. The most prominent application seems to be yet realized in agriculture (236). On the materials side, the hydrolyzed and nonhydrolyzed grafted polysaccharides seem to have a bright future, because these materials have not only distinguished drag-reducing characteristics in turbulent flow of water but also distinguished flocculation and viscosifying attributes. Cationic surfactants seem to offer a shear- and heat-resistant material for district heating and cooling systems (31,34). Further research to identify a stable, low toxicity, and rapid biodegrading surfactant drag-reducing system is being focused for the coming decades (31,42,237–241). Biomedical applications of drag-reducing polymers also have a very bright future. In the years to come, turbulent drag reduction would remain an exotic field of research and applications.

BIBLIOGRAPHY

"Friction Reduction" in *EPST* 1st ed., Vol. 15, pp. 224–253, by G. E. Gadd, National Physical Laboratory, U.K.; "Drag Reduction" in *EPSE* 2nd ed., Vol. 5, pp. 129–151, by J. W. Hoyt, San Diego State University.

1. K. S. Choi, K. K. Prasad, and T. V. Truong, *Emerging Techniques in Drag Reduction*, Mechanical Engineering Publications Ltd., London, U.K., 1996.
2. B. A. Toms, *Proceedings of the 1st International Rheological Congress*, Part 2, North Holland Publishing Co., the Netherlands, 1949, pp. 135–142.
3. F. Forest and G. A. Grierson, *Paper Trade J.* **92**(22) 39–41 (1931).
4. V. A. Vanoni, *Trans. Am. Geophys. Union, Pt III* 621–668 (1941).
5. B. A. Toms, *J. Colloid Sci.* **4**, 511 (1949).
6. U.S. Pat. 249,2173 (Dec. 27, 1949), K. J. Mysels.
7. R. H. Nadolink and W. W. Haigh, *Appl. Mech. Rev.* **48**, 351–459 (1995). ASME Reprint No. A AMR 168562.
8. J. L. Lumley, *Ann. Rev. Fluid Mech.* **1**, 367–384 (1969).
9. G. K. Patterson, J. L. Zakin, and J. M. Rodriguez, *Ind. Eng. Chem.* **61**, 22–30 (1969).
10. P. S. Virk, *AIChE J.* **2**, 625–656 (1975).
11. A. White and J. A. G. Hemmings, *Drag Reduction by Additives. Review and Bibliography*, BHRA Fluid Engineering, Cranfield, U.K., 1976, pp. 182.
12. H. Block, in A. M. North and A. Ledwith, eds., *Molecular Behavior and Development of Polymeric Materials*, Chapmann and Hall Ltd., London, 1975, pp. 492–527.
13. N. S. Berman, *Ann. Rev. Fluid Mech.* **10**, 47–64 (1978).
14. R. H. J. Sellin, J. W. Hoyt, and O. Scrivener, *J. Hydraulic. Res.* **20**, 29–68 (1982).
15. R. H. J. Sellin, J. W. Hoyt, J. W. Pollert, and O. Scrivener, *J. Hydraulic. Res.* **20**, 235–292 (1982).
16. H. Giesekus, H. W. Bewersdorff, B. Frings, M. Hibberd, K. Kleinecke, M. Kwade, D. Moller, and R. Schroder, *Fortschritte der Verfahrenstechnik* **23**, 3–40 (1985).
17. J. W. Hoyt, in Y. Rabin, ed., *AIP Conference Proceedings Series, Polymer Flow Interaction*, American Institute of Physics, New York, 1985, pp. 95–115.
18. H. Giesekus and M. F. Hibberd, in A. S. Majumdar and R. A. Mashelkar, eds., *Advances in Transport Process, Vol. 5: Turbulence Phenomena in Drag Reduction*, Wiley Eastern Ltd., New Delhi, India, 1987, pp. 229–284.
19. W. M. Kulicke, H. Kotter, and H. Grager, *Adv. Polym. Sci.* **89**, 1–68 (1989).
20. R. P. Singh, *Encyclopedia of Fluid Mechanics*, Vol. 9, Gulf Publishing Co., Houston, Tex., 1990, Chapt. 14, pp. 425–480.
21. S. E. Morgan and C. L. McCormick, *Prog. Polym. Sci.* **15**, 103–145 (1990).
22. J. M. J. Den Toonder, Ph.D. dissertation, Technische Universiteit Delft, the Netherlands, 1995.
23. A. Gyr and H. W. Bewersdorff, *Drag Reduction of Turbulent Flows by Additives*, Kluwer Academic Publishers, Dordrecht, the Netherlands, 1995.
24. T. Moussa, Ph.D. dissertation, Monash University, Melbourne, Australia, 1992.
25. M. Gad-El-Hak, *Flow Control*, Cambridge University Press, Cambridge, U.K., 2000.
26. R. H. J. Sellin and R. T. Moses, eds., in *Proceedings Third International Conference on Drag Reduction*, University of Bristol, 1984.
27. B. Gampert, ed., in *IUTAM Symposium*, Essen, 1984, Springer Verlag, Berlin, 1985.
28. Y. Rabin ed., in *AIP Conference Proceedings Series*, American Institute of Physics, New York, 1985.
29. R. H. J. Sellin and M. T. Moses, eds., *Drag Reduction in Fluid Flows*, Ellis Horwood, Chichester, England U.K., 1989.
30. A. Gyr, ed., in *Proceedings of the IUTAM Symposium*, Zurich, 1989, Springer, Berlin, 1990.

31. ASME, *Proceedings of the ASME Fluids Engineering Division Summer Meeting*, FED-Vol. 237, 1996.
32. J. F. Motier and A. M. Carrier, in Ref. 29, pp. 197–204 (1989).
33. R. P. Singh, J. Singh, S. R. Deshmukh, D. Kumar, and A. Kumar, *Curr. Sci.* **68**, 631–641 (1995).
34. J. G. Savins, *Rheol. Acta* **6**, 323–330 (1967).
35. J. L. Zakin, M. Poreh, A. Brosh, and M. Warshavsky, *Chem. Eng. Prog. Sym. Ser.* **67**, 85–89 (1971).
36. J. L. Zakin and H. L. Liu, *Chem. Eng. Comm.* **23**, 77–80 (1983).
37. L. C. Chou, Ph.D. dissertation, The Ohio State University, Columbus, Ohio, 1991.
38. I. Harwigsson, Ph.D. dissertation, Lund University, Sweden, 1995.
39. I. Harwigsson and M. Hellsten, *J. Am. Oil Chem. Soc.* **73**, 921–928 (1996).
40. M. Hellsten, I. Harwigsson, C. Blais, and J. Wollerstrand, *Proceedings of the ASME Fluids Engineering Division Summer Meeting*, ASME Publ. FED-Vol. 237, 1996, pp. 37–46.
41. J. Myska and J. L. Zakin, *Ind. Eng. Chem. Res.* **36**, 5483–5487 (1997).
42. J. L. Zakin, B. Lu, and H. W. Bewersdorff, in N. R. Amundson, D. Luss, and A. Marmur, eds., *Reviews in Chemical Engineering, Vol. 14: Surfactant Drag Reduction*, Freund Publishing House Ltd., London, England, 1998, pp. 253–320.
43. T. Mousa and C. Tiu, *Chem. Eng. Sci.* **49**, 1681–1692 (1994).
44. R. P. Singh, in P. N. Prasad, J. E. Mark and T. J. Fai, eds., *Polymer and other Advanced Materials: Emerging Technologies and Business Opportunities*, Plenum Press, New York, Vol. 1, 1995, pp. 227–250.
45. R. P. Singh, G. P. Karmakar, S. K. Rath, N. C. Karmakar, S. R. Pandey, T. Tripathy, J. Panda, K. Kannan, S. K. Jain, and N. T. Lan, *Polym. Eng. Sci.* **40**, 46–60 (2000).
46. R. M. Kowalik, I. Duvdoani, D. G. Peerffei, R. D. Lundeberg, K. Katano, and D. N. Schultz, *J. Non-Newtonian Fluid Mech.* **24**, 1–10 (1987).
47. S. Malik, S. N. Shantre, and R. A. Mashelkar, *Macromolecules* **26**, 55–59 (1993).
48. S. Malik, Ph.D. dissertation, IIT Kharagpur, India, 1993.
49. S. Malik and R. A. Mashelkar, *Chem. Eng. Sci.* **50**, 105–116 (1995).
50. J. B. Bello, A. J. Muller, and A. E. Saez, *Polym. Bull.* **36**, 111–118 (1996).
51. D. Vlassopoulos and W. R. Schowalter, *J. Non-Newtonian Fluid Mech.* **49**, 205–230 (1993); *J. Rheol.* **38**, 1427–1446 (1994).
52. J. P. Tathan, S. Carrington, J. A. Odell, A. C. Gamboa, A. J. Muller, and A. E. Salz, *J. Rheol.* **39**, 961–986 (1995).
53. M. A. Zirnsk, D. V. Boger, and V. Tirtaamadja, *J. Rheol.* **43**, 627–650 (1999).
54. J. M. J. Den Toonder, F. T. M. Nieuwstadt, and G. D. C. Kuiken, *Appl. Sci. Res.* **54**, 95–123 (1995).
55. M. Stelter, G. Brenn, A. L. Yarin, R. P. Singh, and F. Durst, *J. Rheol.* **44**, 595–616 (2000); M. Stetler, *J. Rheol.* **46**, 507–527 (2002).
56. M. Stelter, T. Wunderlich, S. K. Rath, G. Brenn, A. L. Yarin, R. P. Singh, and F. Durst, *J. Appl. Polym. Sci.* **74**, 2773–2782 (1999).
57. T. Wunderlich, M. Stelter, T. Tripathy, B. R. Nayak, G. Brenn, A. L. Yarin, R. P. Singh, P. O. Brunn, and F. Durst, *J. Appl. Polym. Sci.* **77**, 3200–3209 (2000).
58. B. Lu, Ph.D. dissertation, The Ohio State University, Columbus, Ohio, 1997.
59. B. Lu, X. Li, L. E. Scriven, H. T. Davis, Y. Talmon, and J. L. Zakin, *Langmuir* **14**, 8–16 (1998).
60. J. R. Eastman, J. W. Goodwin, and A. M. Howe, *Colloids Surf. A* **161**, 329–338 (2000).
61. J. Pollert and R. H. J. Sellin, in R. H. J. Sellin and R. T. Moses, eds., *Drag Reduction in Fluid Flows*, Ellis Horwood, Chichester, U.K., 1989, pp. 179–188.
62. W. Brostow, *Polymer* **24**, 631–638 (1983).

63. W. Brostow, H. Ertipinar, and R. P. Singh, *Macromolecules* **231**, 5109–5118 (1990).
64. W. Brostow, S. Majumdar, and R. P. Singh, *Macromol. Rapid Commun.* **20**, 144–147 (1999)
65. J. M. J. Den Toonder, A. A. Draad, G. D. C. Kiuken, and F. T. M. Nieuwstadt, *Appl. Sci. Res.* **55**, 63–82 (1995).
66. F. Frings, Ph.D. dissertation, University of Dortmund, Germany, 1985.
67. N. S. Berman, in P. Cherimisinoff, ed., *Encyclopedia of Fluid Mechanics*, Vol. 1, Gulf Publishing Co., Houston, Tex., 1986, pp. 1060–1081.
68. H. Usui, in A. Gyr, ed., *IUTAM Symposium*, Zurich 1989, Springer-Verlag, New York, 1990, pp. 257–274.
69. H. W. Bewersdorff, in B. Gampert, ed., *Proceedings of the IUTAM Symposium*, Essen, 1984 Springer Verlag, New York, 1985, pp. 337–348.
70. R. E. Smith and W. G. Tiederman, *Rheol. Acta* **30**, 103–113 (1991).
71. K. W. Hoyer and A. Gyr, *Trans. ASME* **120**, 818–823 (1998).
72. F. Durst, A. Melling, and J. H. Whitelaw, *Principles and Practice of Laser Doppler Anemometry*, 2nd ed., Academic Press, New York, 1981.
73. F. Durst, G. Brenn, and T. H. Xu, *Meas. Sci. Technol.* **8**, 1203–1221 (1997).
74. W. G. Tiederman, in A. Gyr, ed., *Structure of Turbulence and Drag Reduction*, IUTAM Symposium, Zurich, Switzerland, Springer-Verlag, Berlin, 1990.
75. D. W. Dodge and A. B. Metzner, *AIChE J.* **5**, 189–204 (1959).
76. A. B. Metzner and M. G. Park, *J. Fluid Mech.* **20**, 291–303 (1964).
77. G. E. Gadd, *Encyclopedia of Polymer Science and Technology*, Vol. 15, Wiley-Interscience, New York, 1971, pp. 224–253.
78. J. L. Lumley, *Phys. Fluids* **20**, S64–S71 (1977).
79. J. L. Lumley, *J. Polym. Sci. Macromol. Rev.* **7**, 283–290 (1973).
80. A. Gyr, in Ref. 26, pp. B.10-1–B.10-7; in Ref. 69, pp. 233–247.
81. F. Durst, R. Hass, and W. Interthal, *Rheol. Acta* **21**, 572–577 (1982).
82. H. W. Bewersdorff and N. S. Berman, *Rheol. Acta* **27**, 130–136 (1988).
83. E. F. Matthys, *J. Non-Newtonian Fluid Mech.* **38**, 313–342 (1991).
84. P. G. de Gennes, *Introduction to Polymer Dynamics*, Cambridge University Press, New York, 1990, pp. 1–16.
85. P. Orlandi, *J. Non-Newtonian Fluid Mech.* **60**, 277–301 (1996).
86. J. M. J. Den Toonder, M. A. Hulsen, G. D. C. Kuiken, and F. T. M. Nieuwstadt, *J. Fluid Mech.* **337**, 193–232 (1997).
87. H. Massah and T. J. Hanratty, *J. Fluid Mech.* **337**, 67–111 (1997).
88. C. D. Dimitropolous, R. Suresh Kumar, and A. N. Beris, *J. Non-Newtonian Fluid Mech.* **79**, 433–468 (1998).
89. K. R. Sreenivasan and C. M. White, *J. Fluid Mech.* **409**, 149–164 (2000).
90. K. Vissmann and H. W. Bewersdorff, *J. Non-Newtonian Fluid Mech.* **34**, 289–317 (1990).
91. D. F. James, B. D. McLean, and J. H. Saringer, *J. Rheol.* **31**, 453–481 (1987).
92. J. L. Lumley, *Ann. Rev. Fluid Mech.* **1**, 367–384 (1969).
93. Z. L. Zakin, J. Myska, and Z. Chara, *AIChE J.* **42**, 3544–3546 (1996).
94. A. K. M. F. Hussain and R. C. Reynolds, *J. Fluid. Mech.* **41**, 241–258 (1970).
95. I. G. Taylor, *Proc. R. Soc. London, Ser. A* **151**, 421–478 (1935).
96. F. T. Pinho and J. H. Whitelaw, *J. Fluid Mech.* **226**, 475–496 (1991).
97. K. J. Harder and W. G. Tiederman, *Philos. Trans. R. Soc. London, Ser. A* **336**, 19–34 (1991).
98. T. Wei and W. W. Willmarth, *J. Fluid Mech.* **245**, 619–641 (1992).
99. D. T. Walker and W. G. Tiederman, *J. Fluid Mech.* **218**, 377–403 (1990).
100. P. Tong, W. J. Goldburg, and J. S. Huang, *Phys. Rev. A* **45**, 7231–7241 (1992).
101. O. Codot, D. Bonn, and S. Doudy, *Phys. Fluids* **10**, 426–435 (1998).

102. K. Hoyer, H. W. Bewersdorff, A. Gyr, and A. Tsinober, in P. Moldenaers, and R. Keunings, eds., *Proceedings of the XIth International Congress Rheology*, Brussels, Belgium, August 17–21, 1992, Elsevier Science Publishers, pp. 183–185.
103. A. A. Fortaine, H. L. Petrie, and T. A. Brungart, *J. Fluid Mech.* **238**, 435–466 (1992).
104. M. A. Nieder Schulte, R. J. Andrian, and T. J. Hanratty, *Exp. Fluids* **9**, 222–231 (1990).
105. H. W. Bewersdorff, A. Gyr, K. Hoyer, and A. Tsinober, *Rheol. Acta* **32**(2) 140–149 (1993).
106. P. S. Virk and D. L. Wagger, in *IUTAM Symposium*, Zurich, Switzerland, 1989, pp. 201–213.
107. H. Usui, Y. Sakuma, and T. Saeky, in *Proceedings of the 9th Symposium on Turbulent Shear Flow*, Kyoto, 1993, pp. 1–6, 20–23.
108. H. Usui, K. Malguchi, and Y. Sans, *Phys. Fluids* **31**, 2518–2533 (1988).
109. J. Vleggar, Ph.D. dissertation, Universiteit van Amsterdam, 1973.
110. J. Vleggar and M. Tells, *Chem. Eng. Sci.* **28**, 965–968 (1973).
111. J. W. Hoyt and R. H. J. Sellin, *Rheol. Acta* **30**, 307–315 (1991).
112. J. W. Hoyt, *Encyclopedia of Polymer Science and Engineering*, 2nd ed., Vol. 5, 1986, pp. 129–157.
113. A. Lodes and V. Macho, *Exp. Fluids* **11**, 7 (1989).
114. A. S. Pereira and F. T. Pinho, *J. Non-Newtonian Fluid Mech.* **55**, 321–344 (1994).
115. M. P. Escudier, F. Presti, and S. Smith, *J. Non-Newtonian Fluid Mech.* **81**, 197–213 (1999).
116. D. R. Olivier and S. I. Bakhtiyarov, *J. Non-Newtonian Fluid Mech.* **12**, 113–118 (1983).
117. B. Gampert and P. Wagner, in *IUTAM Symposium*, Essen, 1984, Springer-Verlag, Berlin, 1985, pp. 71–85.
118. M. Walsh, *Int. Shipbuild. Prog.* **14**, 134–139, 152, (1967).
119. W. M. Kulicke and J. Klein, in Essen B. Gampert, ed., *IUTAM Symposium*, Springer Verlag, Berlin, 1985, pp. 43–60.
120. J. W. Hoyt, *Solution Properties of Natural Polymers*, The Chemical Society, London, 1968, pp. 207–215. Special Pub. No. 23.
121. S. R. Deshmukh, P. N. Chaturvedi, and R. P. Singh, *J. Appl. Polym. Sci.* **30**, 4013–4020 (1985).
122. S. R. Deshmukh and R. P. Singh, *J. Appl. Polym. Sci.* **32**, 6133–6177 (1986).
123. S. R. Deshmukh and R. P. Singh, *J. Appl. Polym. Sci*. 1963–1975 (1987).
124. S. Ungeheur, H. W. Bewersdorff, and R. P. Singh, *J. Appl. Polym. Sci.* **37**, 2933–2948 (1989).
125. S. R. Deshmukh, K. Sudhakar, and R. P. Singh, *J. Appl. Polym. Sci.* **48**, 1091–1101 (1991).
126. R. P. Singh, S. R. Deshmukh, and S. K. Majumdar, in *Xth Proceedings of the International Congress on Rheology*, Sydney, Plenum Press, New York, Vol. II, 1988, pp. 278–281.
127. R. P. Singh, J. Singh, S. R. Deshmukh, and A. Kumar, in B. Gampert, ed., *IUTAM Symposium*, Essen, Springer-Verlag, Berlin, 1985, pp. 113–139.
128. R. P. Singh, in *Proceedings of the Workshop on Use of Polymers in Oil Field Operations*, K DMIPE, ONGC, Dehradun, India, 1999.
129. R. P. Singh, B. R. Nayak, D. R. Biswal, T. Tripathi, and K. Banik, *Mater. Res. Innovt.* **7**, 331–340 (2003).
130. P. S. Mumick, S. E. Morgan, and C. L. McCormic, *Polym. Prepr. (Am. Chem. Soc., Div. Polym. Chem.)* **30**, 256 (1989).
131. C. L. McCormic, R. D. Hester, S. E. Morgan, and A. M. Safiedine, *Molecules* **23**, 2132 (1990).
132. A. M. Safiedine, Ph.D. dissertation, University of South Mississippi, Hattiesburg, Mass., 1990.

133. P. S. Mumick and C. L. McCormic, *SPE ANTEC Tech. Papers* **38**, 2095 (1992).
134. P. S. Mumick, P. M. Welch, R. D. Hester, and C. L. McCormic, *Polym. Prepr. (Am. Chem. Soc., Div. Polym. Chem.)* **33**(2) 337 (1992).
135. P. S. Mumick and C. L. McCormic, *Polym. Eng. Sci.* **38**, 1419 (1994); P. S. Mumick, R. D. Hester, and C. L. McCormic, *Polym. Eng. Sci.* **34**, 1429–1439 (1994).
136. M. E. Cowan, C. Garner, R. D. Hester, and C. L. McCormic, *J. Appl. Polym. Sci.* **82**, 1222–1231 (2001).
137. J. Lumley, in G. Gampert, ed., *IUTAM Symposium*, Essen, 1984, Springer-Verlag, Berlin, 1985, pp. 4–21.
138. T. S. Luchik and W. G. Tiederman, *J. Fluid Mech.* **190**, 241–263 (1988).
139. H. W. Bewersdorff, in A. Gyr, ed., *Structure of Turbulence and Drag Reduction*, Springer, Berlin, 1990, pp. 293–312.
140. H. Giesekus, *J. Non-Newtonian Fluid Mech.* **11**, 69–109 (1982).
141. S. U. S. Choi, Y. I. Cho, and E. Kasza, *J. Non-Newtonian Fluid Mech.* **41**, 189–307 (1992).
142. F. Bueche, *J. Appl. Polym. Sci.* **4**, 101–106 (1960).
143. A. F. Horn and K. W. Merrill, *Nature* **312**, 140–141 (8 Nov. 1984).
144. E. W. Merrill and A. F. Horn, *Polym. Commun.* **25**, 144–146 (1984).
145. A. F. Horn and E. W. Merrill, *Polym. Commun.* **28**, 172–173 (1987).
146. T. R. Nguyen and H. H. Kausch, *Colloid Polym. Sci.* **264**, 764–772 (1986).
147. A. Keller and J. A. Odell, *Colloid Polym. Sci.* **263**, 181–201 (1985).
148. J. Pollert and R. H. J. Sellin, in R. H. J. Sellin and R. T. Moses, eds., *Drag Reduction in Fluid Flows*, Ellis Horwood, Chichester, U.K., 1989, pp. 179–188.
149. T. Moussa, C. Tiu, and T. Sridhar, *J. Non-Newtonian Fluid Mech.* **48**, 21–284 (1993).
150. T. Rho, J. Park, C. Kim , H. K. Yoon, H.-S. Suh, *Polym. Degrad. Stab.* **51**, 287–293 (1996).
151. C. A. Kim, H. J. Choi, C. B. Kim, and M. S. John, *Macromol. Rapid Commun.* **19**, 419–422 (1998).
152. C. A. Kim, J. H. Sung, H. J. Choi, C. B. Kim, W. Chun, and M. S. John, *J. Chem. Eng. Jpn.* **32**, 803–811 (1999).
153. C. A. Kim, J. T. Kim, K. Lee, H. J. Choi, and M. S. John, *Polymer* 7611–7615 (2000).
154. C. A. Kim, D. S. Choi, C. B. Kim, and M. S. John, *Polym. Testing* **20**, 43–48 (2001)
155. C. A. Kim, S. T. Lim, H. J. Choi, J.-I. Sohn, and M. S. John, *J. Appl. Polym. Sci.* **83**, 2938–2944 (2002).
156. H. J. Choi and M. S. John, *Ind. Eng. Chem. Res.* **35**, 2993–2998 (1996).
157. H. J. Choi, C. A. Kim, and M. S. John, *Polymer* **40**, 4527–4530 (1999).
158. H. J. Choi, C. A. Kim, J.-I. Sohn, and M. S. John, *Polym. Degrad. Stab.* **69**, 341–346 (2000).
159. H. J. Choi, C. A. Kim, J. H. Sung, C. B. Kim, W. Chun, and M. S. John, *Colloid Polym. Sci.* **278**, 701–705 (2000).
160. P. R. Kenis, *J. Appl. Polym. Sci.* **15**, 607–618 (1971).
161. J.-I. Sohn, C. A. Kim, H. J. Choi, and M. S. John, *Carbohydr. Polym.* **45**, 61–68 (2001).
162. S. Chakraborti, B. Seidl, J. Vorwerk, and P. O. Brunn, *Rheol. Acta* **30**, 114–130 (1991).
163. S. Chakraborti, B. Seidl, J. Vorwerk, and P. O. Brunn, *Rheol. Acta* **30**, 124–130 (1991).
164. H. J. Choi, S. T. Lim, P.-Y. Lai, and C. K. Chan, *Phys. Rev. Lett.* **89**, 1–4 (2002).
165. O. K. Kim, R. C. Little, R. L. Patterson, and Y. R. Ting, *Nature* **250**, 408 (1974).
166. S. H. Agrawal, R. F. Jenkins, and R. S. Porter, *J. Appl. Polym. Sci.* **27**, 113 (1982).
167. U. S. Agrawal and R. A. Mashelkar, *J. Non-Newtonian Fluid Mech.* **54**, 1–10 (1994).
168. T. Reddy and R. P. Singh, *Polychar* **9**, 41 (2001).
169. G. V. Reddy and R. P. Singh, *Rheol. Acta* **24**, 296–311 (1985).
170. W. K. Lee, R. C. Vaselski, and A. B. Metzner, *AIChE J.* **20**, 128–33 (1974).
171. D. D. Kale and A. B. Metzner, *AIChE J.* **20**, 1218–1219 (1974).

172. A. B. Metzner, *Phys. Fluids* **20**, S145 (1977).
173. H. Inaba, N. Haruki, and A. Horibe, *Int. J. Therm. Sci.* **39**, 18–29 (2000).
174. A. M. Savill, in A. Gyr, ed., *IUTAM Symposium*, Zurich, Switzerland, 1989, Springer-Verlag, Berlin, 1990, pp. 429–465.
175. M. J. Walsh, in G. R. Hough, ed., *Viscous Flow Drag Reduction*, AIAA, New York, 1979, pp. 168–184.
176. M. J. Walsh, Riblets, in D. M. Bushnell and J. N. Hefner, eds., *Viscous Drag Reduction in Boundary Layers*, AIAA, Washington, D.C. 1990, pp. 203–262.
177. M. J. Walsh and A. M. Linemann, AIAA paper, pp. 84–347, 1984.
178. E. Koury and P. S. Virk, *Appl. Sci. Res.* **54**, 323–347 (1995).
179. H. Mijunuma, K. Veda, and Y. Yokouchi, *J. Fluids Eng. (ASME)* **121**, 533–547 (1999).
180. G. W. Anderson, J. J. Rohr, and S. D. Stanley, *J. Fluids Eng.* **115**, 213–221 (1993).
181. K. Liu, C. Christodoulou, O. Riccius, D. D. Joseph, in A. Gyr, ed., *Structure of Turbulence and Drag Reduction*, Springer-Verlag, Berlin, 1989, pp. 542–552.
182. S.-I. Nakao, *J. Fluids Eng.* **113**, 587–590 (1990).
183. P. Nitschke, NASA TM No. 77480, 1989.
184. S. J. Kline, W. C. Reynolds, F. A. Schraub, and P. W. Runstadler, *J. Fluid Mech.* **30**, 741 (1967).
185. D. W. Bechert, M. Bertenwerfer, G. Hoppe, and W.-E. Reif, ICAS paper, pp. 86–183, 1986.
186. K.-S. Choi, in A. Gyr, ed., *Structure of Turbulence and Drag Reduction*, Springer-Verlag, Berlin, 1989, pp. 553–560.
187. K. S. Choi, H. H. Pearcey, A. M. Savill, and S. Svensson, in R. H. J. Sellin and M. T. Moses, eds., *Drag Reduction in Fluid Flows*, Ellis Horwood, Chichester, U.K., 1989, pp. 271–277.
188. C. J. A. Pullese, K. Krishnaprasad, F. T. M. Nieuwstadt, *Appl. Sci. Res.* **46**, 197–208 (1989).
189. I. Tani, *Proc. Jpn. Acad. B* **64**, 21–24 (1988).
190. H. Choi, P. Moin, and J. Kim, *J. Fluid Mech.* **235**, 503–539 (1993).
191. J. Rohr, G. W. Anderson, and L. W. Reidy, in R. H. J. Sellin and M. T. Moses, eds., *Drag Reduction in Fluid Flows*, Ellis Horwood, Chichester, U.K., 1990, pp. 263–270.
192. C. Christodoulou, K. N. Liu, and D. D. Joseph, *Phys. Fluids A* **3**(5) 995–996 (1991).
193. G. S. Migirenko and A. R. Erseev, *Problem of Thermophysics and Physical Hydrodynamics*, Novosibirska, Nauka, Russia, 1974.
194. V. G. Bogdevich and A. G. Maluga, *Investigation of Boundary Layer Control*, Thermophysics Institute Publishing, Novosibirsk, Siberia, 1976, p. 62.
195. V. G. Bogdevich and A. R. Erseev, in S. S. Kutateladgze and G. S. Migirenko, eds., *Investigation of Boundary Layer Control*, Thermophysics Institute Publishing, Nobosibirsk, Siberia, 1976, p. 49.
196. C. L. Merkle and S. Deutsch, in M. Gad-El-Hak, ed., *Frontiers in Experimental Fluid Mechanics*, Springer, Berlin, 1989, pp. 291–335.
197. M. E. McCormic and R. Bhattacharya, *Nav. Eng. J.* **85**, 11–16 (1973).
198. N. K. Mahadevan, S. Deutsch, and C. L. Merkle, *J. Fluid Mech.* **156**, 237–256 (1985).
199. N. K. Mahadevan, S. Deutsch, and C. L. Merkle, *J. Fluids Eng.* **107**, 370–377 (1985).
200. A. A. Fontaine and S. Deutsch, *Exp. Fluids* **13**, 128–136 (1992).
201. S. Pal, S. Deutsch, and C. L. Merkle, *Phys. Fluids* **31**, 744–751 (1988).
202. H. H. Legner, *Phys. Fluids* **27**, 2788–2790 (1984).
203. J. L. Marie, *J. Phys. Chem. Hydrodynamics* **13**, 213–220 (1987).

204. N. K. Mahadevan, S. Deutsch, and C. L. Merkle, *Phys. Fluids* **27**, 356–363 (1984).
205. S. Pal, S. Deutsch, and C. L. Merkle, *Phys. Fluids* **31**, 1360–1362 (1989).
206. A. A. Fontaine, S. Deutsch, T. A. Brungart, H. L. Petric, and Fenstermacker, *Exp. Fluids* **26**, 397–403 (1999).
207. K. Watanabe, O. Yanuar, and H. Mizunuma, in *Proceedings of the ASME FED Summer Meeting*, FED-237, Vol. 2. 1996, pp. 115–119.
208. K. Watanabe, O. Yanuar, and H. Gadagawa, *J. Fluid Mech.* **381**, 225–238 (1999).
209. K. Watanabe and T. Akino, *J. Fluids Eng. (ASME)* **121**, 541–547 (1999).
210. S. Ogata and K. Watanabe, in *Proceedings of the Symposium on Flow Control of Wall Boundary and Free Shear Flows*, Joint ASME/JSME Fluid Eng. (FEDS M-99-6936) Conf., San Francisco, Calif., June 18–22, 1999, pp. 1–6.
211. J. Pollert, in G. Gampert, ed., *IUTAM Symposium*, Essen, Germany, 1984, Springer-Verlag, Berlin, 1985, pp. 371–395.
212. J. W. Hoyt, in R. H. J. Sellin and R. T. Moses, eds., *Drag Reduction*, University of Bristol, 1984, pp. I.1-1–I.1-8.
213. J. F. Motier, L. Chou, and Nages Kommareddi, in *Proceedings of the Fluids Engineering Division Summer Meeting*, FED-237, Vol. 2, 1996, pp. 229–234.
214. J. F. Motier and A. M. Carrier, in R. H. J. Sellin and M. T. Moses, eds., *Drag Reduction in Fluid Flows*, Ellis Horwood, Chichester, U.K., 1989, pp. 197–204.
215. C. Maksimovic, *Water Power Dam Constr.* 53–58 (June 1978).
216. H. J. S. Cunham, J. P. Catchpole, R. F. Long, *Nav. Archit. J. RINA* **2**, 187 (1971).
217. D. Hall, *Pipeline Gas J.* **211**(7) 17 (1984).
218. W. R. Carradine, G. J. Hanna, G. F. Pace, and R. N. Grabois, *Oil Gas J.* **81**, 92–98 (1983).
219. V. Elias and J. Vocel, Communication of the Institute of Hydrodynamics 8, Prague, 1978.
220. V. Elias and J. Vocel, in *International Commission on Irrigation and Drainage 11th Congress*, 1980, pp. 227–230.
221. V. Elias and J. Vocel, Communications of the Institute of Hydrodynamics 10, Prague, 1980.
222. R. P. Singh, J. Singh, and S. H. Holey, *J. Agric. Eng.* **16**, 53–59 (1978).
223. R. P. Singh, J. Singh, D. Kumar, and S. R. Deshmukh, in R. H. J. Sellin and R. T. Moses, eds., *Drag Reduction in Fluid Flows*, Ellis Horwood, Chichester, U.K. 1989, pp. 240–246.
224. G. Sanker, R. P. Singh, and J. Singh, *J. Agric. Eng.* **19**, 9–14 (1982).
225. N. B. Nagdeve, K. N. Tiwari, and R. P. Singh, *J. Agric. Eng. Ind.* **23**, 310–317 (1986).
226. S. Phukan, P. Kumar, J. Panda, B. R. Nayak, K. N. Tiwari, and R. P. Singh, *Agric. Water Manage.* **47**, 101–108; **51**, 79–86 (2001).
227. S. C. Kottur, *Indian J. Agric. Sci.* **63**, 436–439 (1993)
228. S. Kar and S. Sahoo, private communication, 2002.
229. Pat. Appl. 187/Cal/2001 (Mar. 29, 2001), R. P. Singh, J. Panda, and K. N. Tiwari.
230. Pat. Appl. 196/KOL/03 (Apr. 1, 2003), R. P. Singh and D. Biswal.
231. J. Panda, Ph.D. dissertation, IIT Kharagpur, India, 2003.
232. H. W. Bewersdorff , V. Oles, and F. D. Martischius, Kurzfristige Kapazitatser- ho hung von Alwasserkanalen, gwf-wasser/abwasser Vol. 127, H.12, 1986, pp. 633–636.
233. H. W. Bewersdorff, in *Proceedings of the Fourth International Conference on Urban Drainage*, Lausanne, 1987.
234. Datasheet DR/10684, Russel Fluid Control Ltd., Lydney, Gloucester, U.K., 1984.
235. Q. Zhou and R. Akhavan, *J. Non-Newtonian Fluid Mech.* **109**, 115–155 (2003).
236. K. S. Jayaraman, ed., *Nature Newsindia* 12 (Aug. 2002).
237. P. Li, Y. Kawaguchi, and A. Yabe, in *Proceedings of the Symposium on Energy Engineering in the 21st Century*, Hong Kong, Jan. 9–13, 2000, pp. 716–722.

238. Z. Lin, Y. Zheng, H. T. Davis, L. E. Scriven, Y. Talman, and J. L. Zakin, *J. Non-Newtonian Fluid Mech.* **93**, 363–373 (2000).
239. Y. Qi, Y. Kawaguchi, Z. Lin, M. Ewing, R. N. Christensen, and J. L. Zakin, *Int. Heat Mass Transfer* **42**, 1495–1505 (2001).
240. P. Li, Y. Kawaguchi, H. Daisaka, A. Yabe, K. Hishida, and M. Maeda, *J. Heat Transfer* **123**, 779–789 (2001).
241. Y. Kawaguchi, T. Segawa, Z. Feng, and P. Li, *Int. J. Heat Fluid Flow* **23**, 700–709 (2002).

RAM PRAKASH SINGH
Indian Institute of Technology

DYNAMIC MECHANICAL ANALYSIS

Introduction

Dynamic mechanical analysis (DMA) is the technique of applying a stress or strain to a sample and analyzing the response to obtain phase angle and deformation data. The data collected allow the calculation of dynamic mechanical properties like the damping or tan delta (δ) as well as complex modulus and viscosity data. Modulus data in the form of the storage modulus is conceptually equivalent to that collected from traditional mechanical tests and gives a measurement of the strength and stiffness of the material. Viscosity information on how the material flows under stress can be obtained from the complex viscosity. The ratio of the storage to loss modulus is called damping or tan δ and is calculated directly from the phase angle δ. Damping is a measure of the internal friction of the material and indicates the amount of energy loss in the material as dissipated heat. This allows DMA to be used to predict how good a material is at acoustical or vibrational damping. Normally, DMA data for solids is displayed as storage modulus and damping versus temperature, with multicurve used to show frequency effects. Melt data is often shown against frequency like classical rheological data. Two approaches are used: (*1*) forced frequency, where the signal is applied at a set frequency and (*2*) free resonance, where the material is perturbed and allowed to exhibit free resonance decay. Most DMAs are of the former type while the torsional braid analyzer (TBA) is of the latter. In both approaches, the technique is very sensitive to the motions of the polymer chains and it is a powerful tool for measuring transitions in polymers. It is estimated to be 100 times more sensitive to the glass transition than differential scanning calorimetry (DSC) and it resolves other more localized transitions not detected in DSC. In addition, the technique

Encyclopedia of Polymer Science and Technology. Copyright John Wiley & Sons, Inc. All rights reserved.

allows the rapid scanning of a material's modulus and viscosity as a function of temperature or frequency.

Theory and Operation of DMA

Forced Frequency Analyzers. If a constant load applied to a sample begins to oscillate sinusoidally (Fig. 1a), the sample will deform sinusoidally. This will be reproducible if the material is deformed within its linear viscoelastic region. For any one point on the curve, the stress applied is described in equation 1

$$\sigma = \sigma_0 \sin \omega t \tag{1}$$

where σ is the stress at time t, σ_0 is the maximum stress, ω is the frequency of oscillation, and t is the time. The resulting strain wave shape will depend on how much viscous as well as elastic behavior the sample has. In addition, the rate of stress can be determined by taking the derivative of the above equation in terms of time:

$$d\sigma/dt = \omega\sigma_0 \cos \omega t \tag{2}$$

The two extremes of the material's behavior, elastic and viscous, provide the limiting extremes that will sum to give the strain wave (see VISCOELASTICITY). The

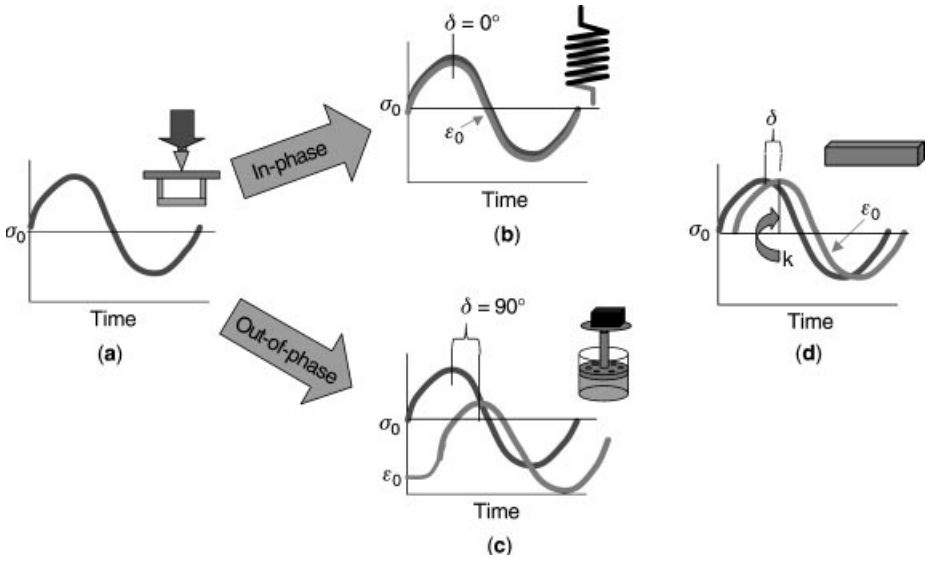

Fig. 1. (**a**) When a sample is subjected to a sinusoidal oscillating stress, it responds in a similar strain wave, provided the material stays within its elastic limits. When the material responds to the applied wave perfectly elastically, an in-phase, storage, or elastic response is seen (**b**), while a viscous response gives an out-of-phase, loss, or viscous response (**c**). Viscoelastic materials fall in between these two extremes as shown in (**d**). For the real sample in (**d**), the phase angle δ and the amplitude at peak k are the values used for the calculation of modulus, viscosity, damping, and other properties.

behavior can be understood by evaluating each of the two extremes. The material at the spring-like or Hookean limit will respond elastically with the oscillating stress. The strain at any time can be written as

$$\varepsilon(t) = E\sigma_0 \sin(\omega t) \tag{3}$$

where $\varepsilon(t)$ is the strain at any time t, E is the modulus, σ_0 is the maximum stress at the peak of the sine wave, and ω is the frequency. Since in the linear region σ and ε are linearly related by E, the relationship is

$$\varepsilon(t) = \varepsilon_0 \sin(\omega t) \tag{4}$$

where ε_0 is the strain at the maximum stress. This curve shown in Figure 1b has no phase lag (or no time difference from the stress curve) and is called the in-phase portion of the curve.

The viscous limit was expressed as the stress being proportional to the strain rate, which is the first derivative of the strain. This is best modeled by a dashpot, and for that element, the term for the viscous response in terms of strain rate is described as

$$\varepsilon(t) = \eta \, \mathrm{d}\sigma_0/\mathrm{d}t = \eta\omega\sigma_0 \cos(\omega t) \tag{5}$$

or

$$\varepsilon(t) = \eta\omega\sigma_0 \sin(\omega t + \pi/2) \tag{6}$$

where the terms are as above and η is the viscosity. Substituting terms as above makes the equation

$$\varepsilon(t) = \omega\sigma_0 \cos(\omega t) = \omega\sigma_0 \sin(\omega t + \pi/2) \tag{7}$$

This curve is shown in Figure 1c. Now, take the behavior of the material that lies between these two limits. The difference between the applied stress and the resultant strain is an angle δ, and this must be added to equations. So the elastic response at any time can now be written as

$$\varepsilon(t) = \varepsilon_0 \sin(\omega t + \delta) \tag{8}$$

Using trigonometry this can be rewritten as

$$\varepsilon(t) = \varepsilon_0[\sin(\omega t)\cos\,\delta + \cos(\omega t)\,\sin\,\delta] \tag{9}$$

This equation, corresponding to the curve in Figure 1d, can be separated into the in-phase and out-of-phase strains that correspond to curves like those in

Figure1b and 1c, respectively. These are the in-phase and out-phase moduli and are

$$\varepsilon' = \varepsilon_0 \sin(\delta) \tag{10}$$

$$\varepsilon'' = \varepsilon_0 \cos(\delta) \tag{11}$$

and the vector sum of these two components gives the overall or complex strain on the sample:

$$\varepsilon^* = \varepsilon'' + i\varepsilon'' \tag{12}$$

Free Resonance Analyzers. If a suspended sample is allowed to swing freely, it will oscillate like a harp string as the oscillations gradually come to a stop. The naturally occurring damping of the material controls the decay of the oscillations. This produces a wave, shown in Figure 2, which is a series of sine waves decreasing in amplitude and frequency. Several methods exist to analyze these waves and are covered in the review by Gillham (2,3). These methods have also been successfully applied to the recovery portion of a creep-recovery curve where the sample goes into free resonance on removal of the creep force (4). From the decay curve, the period T and the logarithmic decrement Λ can be calculated. Both manual and digital processing methods have been reported (2,3,5). Fuller details of the following may be found in References 2,3, and 5. The decay of the amplitude is evaluated over as many swings as possible to reduce error References:

$$\Lambda = 1/j \ln(A_n/A_{n+j}) \tag{13}$$

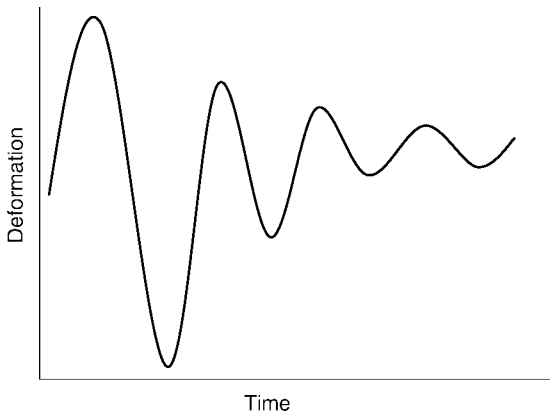

Fig. 2. The decay wave from a free resonance analyzer shows the decreasing amplitude of signal with time. Reprinted with permission from Ref. 1. Copyright (1999) CRC Press.

where j is the number of swings and A_n is the amplitude of the nth swing. For one swing, where $j = 1$, the equation becomes

$$\Lambda = \ln(A_n/A_{n+j}) \tag{14}$$

For a low value of Λ where A_n/A_{n+1} is approximately 1, the equation can be rewritten as

$$\Lambda \approx \tfrac{1}{2}\{(A_n^2 - A_{n+1}^2)/A_n^2\} \tag{15}$$

From this, since the square of the amplitude is proportional to the stored energy $\Delta W/W_{st}$ and the stored energy can be expressed as $2\pi \tan \delta$, the equation becomes

$$\Lambda \approx \tfrac{1}{2}(\Delta W/W_{st}) = \pi \tan \delta \tag{16}$$

which gives us the phase angle δ. The time of the oscillations, the period T, can be found using the following equation:

$$T = 2\pi\sqrt{\frac{M}{\Gamma_1}}\sqrt{\frac{1+\Lambda^2}{4\pi^2}} \tag{17}$$

where Γ_1 is the torque for one cycle and M is the moment of inertia around the central axis. Alternatively, T can be calculated directly from the plotted decay curve as

$$T = (2/n)(t_n - t_0) \tag{18}$$

where n is the number of cycles and t is time. From this, the shear modulus G can be calculated, which for a rod of length L and radius r is

$$G = \left(\frac{4\pi^2 ML}{NT^2}\right)\left(1 + \frac{\Lambda^2}{4\pi^2}\right) - \left(\frac{mgr}{12N}\right) \tag{19}$$

where m is the mass of the sample, g the gravitational constant, and N is a geometric factor. In the same system, the storage modulus G' can be calculated as

$$G' = (I/T^2)(8\pi ML/r^4) \tag{20}$$

where I is the moment of inertia for the system. Having the storage modulus and the tangent of the phase angle, the remaining dynamic properties can be calculated.

Free resonance analyzers normally are limited to rod or rectangular samples or materials that can be impregnated onto a braid. This last approach is how the curing studies on epoxy and other resin systems were done in torsion and gives these instruments the name of torsional braid analyzers (TBA).

Instrumentation. One of the biggest choices made in selecting a DMA is to decide whether to choose stress (force) or strain (displacement) control for applying the deforming load to the sample. Strain-controlled analyzers, whether for simple static testing or for DMA, move the probe a set distance and use a force balance transducer or load cell to measure the stress. These parts are typically located on different shafts. The simplest version of this is a screw-driven tester, where the sample is pulled one turn. This requires very large motors so that the available force always exceeds what is needed. They normally have better short-time response for low viscosity materials and can normally perform stress relaxation experiments easily. They also usually can measure normal forces if they are arranged in torsion. A major disadvantage is their transducers may drift at long times or with low signals.

Stress-controlled analyzers are cheaper to make because there is only one shaft, but somewhat trickier to use. Many of the difficulties have been alleviated by software and many strain-controlled analyzers on the market are really stress-controlled instruments with feedback loops making them act as if they were strain-controlled. In stress control, a set force is applied to the sample. As temperature, time, or frequency varies, the applied force remains the same. This may or may not be the same stress: in extension for example, the stretching and necking of a sample will change the applied stress seen during the run. However, this constant stress is a more natural situation in many cases and it may be more sensitive to material changes. Good low force control means they are less likely to destroy any structure in the sample. Long relaxation times or long creep studies are more easily performed on these instruments. Their biggest disadvantage is that their short-time responses are limited by inertia with low viscosity samples.

Since most DMA experiments are run at very low strains ($\sim$0.5% maximum) to stay well within a polymer's linear region, it has been reported that both the analyzers give the same results. However, when one gets to the nonlinear region, the difference becomes significant, as stress and strain are no longer linearly related. Stress control can be said to duplicate real-life conditions more accurately since most applications of polymers involve resisting a load.

DMA analyzers are normally built to apply the stress or strain in two ways (Fig. 3). One can apply force in a twisting motion so that one can test the sample in torsion. This type of instrument is the dynamic analog of the constant shear spinning disk rheometers. While mainly used for liquids and melts, solid samples may also be tested by twisting a bar of the material. Torsional analyzers normally also permit continuous shear and normal force measurements. Most of these analyzers can also do creep-recovery, stress-relaxation, and stress–strain experiments. Axial analyzers are normally designed for solid and semisolid materials and apply a linear force to the sample. These analyzers are usually associated with flexure, tensile, and compression testing, but they can be adapted to do shear and liquid specimens by proper choice of fixtures. Sometimes the instrument's design makes this inadvisable however. (For example, working with a very fluid material in a system where the motor is underneath the sample has the potential for damage to the instrument if the sample spills into the motor.) These analyzers can normally test higher modulus materials than torsional analyzers and can run TMA studies in addition to creep-recovery, stress-relaxation, and stress–strain experiments.

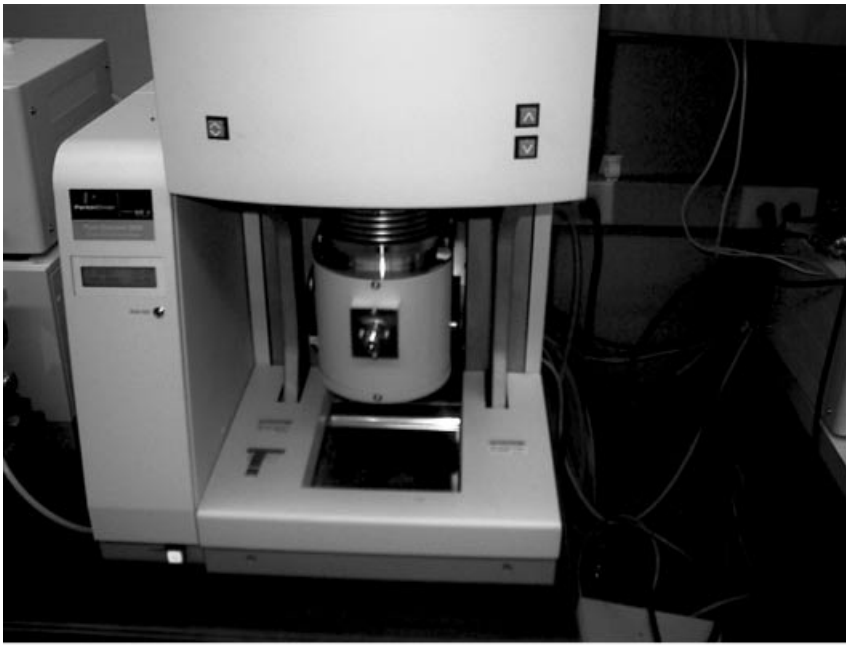

(a)

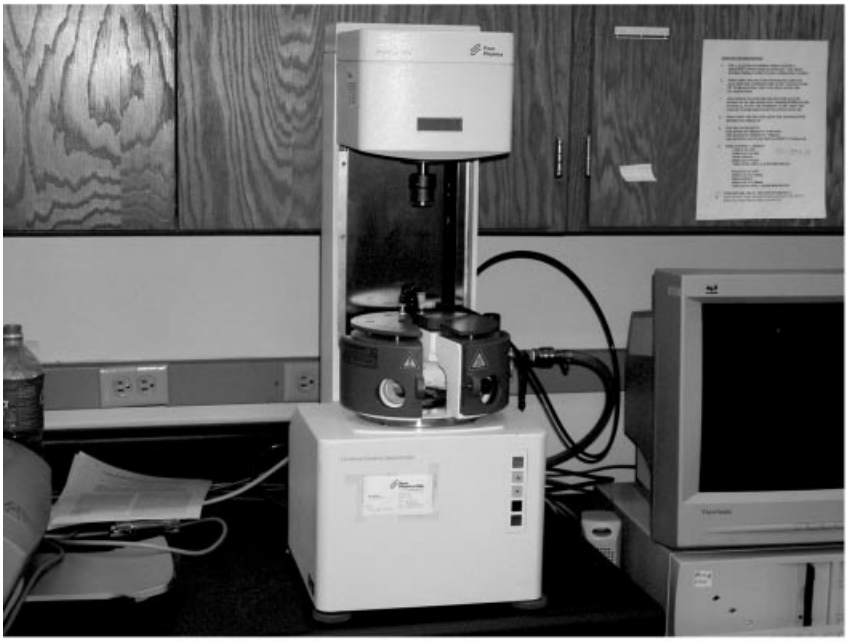

(b)

Fig. 3. Modern DMAs are shown. The PerkinElmer Diamond DMA (**a**) is an axial instrument while the Parr Physica (**b**) and the ATS Rheo (**c**) are torsional DMAs. (**d**) shows a TBA. Photos of the equipment were taken by the author at the University of North Texas' Materials Science and Engineering Department. (**d**) is used with the permission of Dr. John Enns, Polymer Network Characterizations, Inc., Jacksonville, Fla.

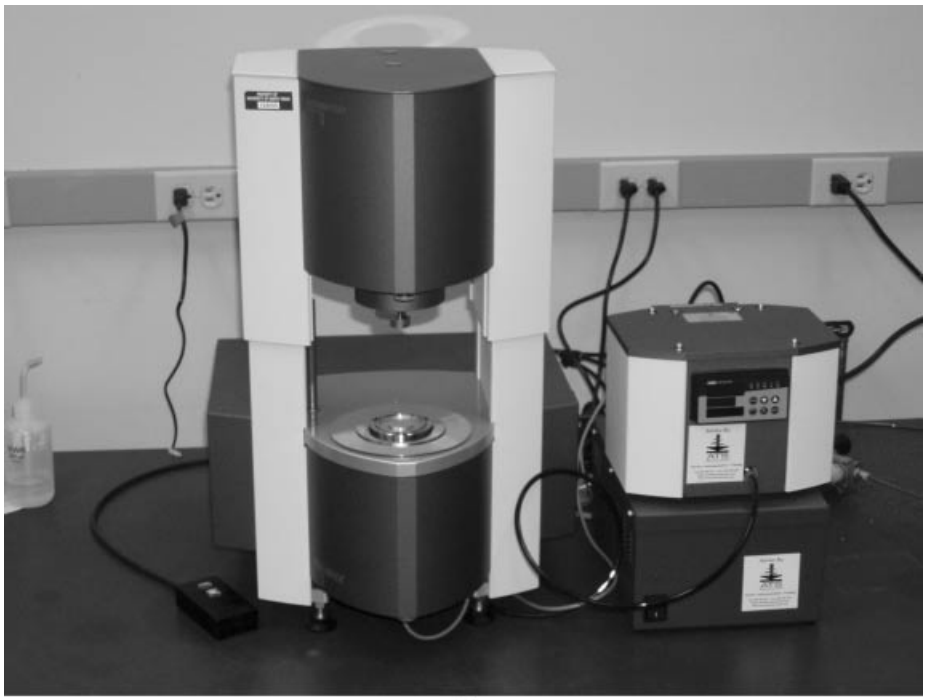

(c)

(d)

Fig. 3. (Continued)

There is considerable overlap between the type of samples run by axial and torsional instruments. With the proper choice of sample geometry and good fixtures, both types can handle similar samples, as shown by the extensive use of both types to study the curing of neat resins. Normally, axial analyzers cannot handle fluid samples below about 500 Pa · s.

Applications for Thermoplastic Solids and Cured Thermosets

As mentioned above, the thermal transitions in polymers can be described in terms of either free volume changes (6) or relaxation times. A simple approach to looking at free volume, which is popular in explaining DMA responses, is the crankshaft mechanism, where the molecule is imagined as a series of jointed segments. From this model, it is possible to simply describe the various transitions seen in a polymer. Other models exist that allow for more precision in describing behavior; the best seems to be the Doi–Edwards model (7). Aklonis and Knight (8) give a good summary of the available models, as does Rohn (9).

The crankshaft model treats the molecule as a collection of mobile segments that have some degree of free movement. This is a very simplistic approach, yet very useful for explaining behavior (Fig. 4). As the free volume of the chain segment increases, its ability to move in various directions also increases. This increased mobility in either side chains or small groups of adjacent backbone atoms results in a greater compliance (lower modulus) of the molecule. These movements have been studied and Heijboer (10) classified β- and γ-transitions by their type of motions. The specific temperature and frequency of this softening help drive the end use of the material.

Moving from very low temperature, where the molecule is tightly compressed, to higher temperatures, the first changes are the solid-state transitions. This process is shown in Figure 5. As the material warms and expands, the free volume increases so that localized bond movements (bending and stretching) and

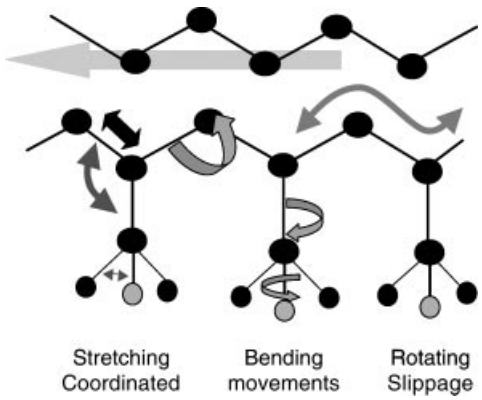

Fig. 4. The crankshaft mechanism is a simple way of considering the motions of a polymer chain permitted by increases in free volume. The molecule is visualized as a series of balls and rods and these move as the free volume increases.

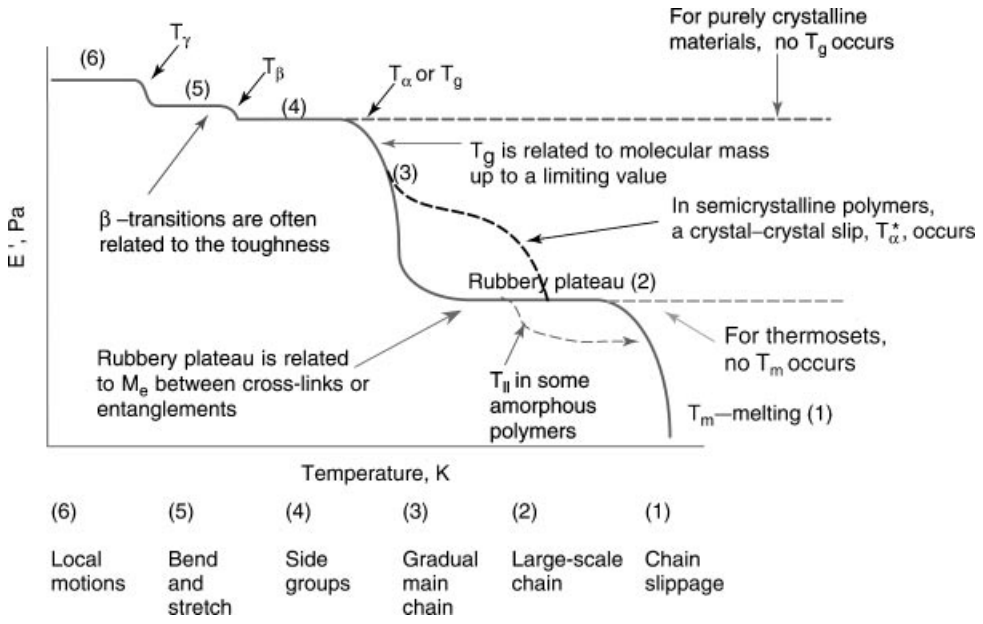

Fig. 5. Idealized temperature scan of a polymer: Starting at low temperature the modulus decreases as the molecules gain more free volume resulting in more molecular motion. This shows the main curve divided into six regions which correspond to local motions (6), bond bending and stretching (5), movements in the side chain or adjacent atoms in the main chain (4), the region of the T_g (3), coordinated movements in the amorphous portion of the chain (2), and the melting region (1). Transitions are marked as described in the text. Reprinted with permission from Ref. 1. Copyright (1999) CRC Press.

side-chain movements can occur. This is the gamma transition, T_γ, which may also involve associations with water. As the temperature and the free volume continue to increase, the whole side chains and localized groups of four to eight backbone atoms begin to have enough space to move and the material starts to develop some toughness (11). This transition, called the beta transition (T_β), is not as clearly defined as described here. Often it is the T_g of a secondary component in a blend or of a specific block in a block copolymer. However, a correlation with toughness is seen empirically (12).

As heating continues, the T_g or glass transition appears when the chains in the amorphous regions begin to coordinate large scale motions. One classical description of this region is that the amorphous regions have begun to melt. Since the T_g only occurs in amorphous material, in a 100% crystalline material there would not be a T_g. Continued heating drives the material through the $T_\alpha{}^*$ and T_{ll}. The former occurs in crystalline or semi-crystalline polymer and is a slippage of the crystallites past each other. The latter is a movement of coordinated segments in the amorphous phase that relates to reduced viscosity. These two transitions are not universally accepted. Finally the melt is reached where large-scale chain slippage occurs and the material flows. This is the melting temperature T_m. For a cured thermoset, nothing happens after the T_g until the sample begins to burn and degrade because the cross-links prevent the chains from slipping past each other.

This quick overview provides an idea of how an idealized polymer responds. Now a more detailed description of these transitions can be provided with some examples of their applications. The best general collection of this information is still McCrum's 1967 text.

Sub T_g Transitions. The area of sub-T_g or higher order transitions has been heavily studied (10,13–19) as these transitions have been associated with mechanical properties. These transitions can sometimes be seen by DSC and TMA, but they are normally too weak or too broad for determination by these methods. DMA, DEA (dielectric analysis), and similar techniques are usually required (20). Some authors have also called these types of transitions (9,10) second order transitions to differentiate them from the primary transitions of T_m and T_g, which involve large sections of the main chains. Boyer reviewed the T_β in 1968 (11) and pointed out that while a correlation often exists, the T_β is not always an indicator of toughness. Bershtein (21) has reported that this transition can be considered the "activation barrier" for solid-phase reactions, deformation, flow or creep, acoustic damping, physical aging changes, and gas diffusion into polymers as the activation energies for the transition and these processes are usually similar. The strength of these transitions is related to how strongly a polymer responses to those processes. These sub-T_g transitions are associated with the materials properties in the glassy state. In paints, for example, peel strength (adhesion) can be estimated from the strength and frequency dependence of the sub-ambient beta transition (22). For example, nylon-6,6 shows a decreasing toughness, measured as impact resistance, with declining area under the T_β peak in the tan δ curve. It has been shown, particularly in cured thermosets, that increased freedom of movement in side chains increases the strength of the transition. Cheng (15) reports in rigid rod polyimides that the beta transition is caused by the non-coordinated movement of the diamine groups although the link to physical properties was not investigated. Johari has reported in both mechanical (14) and dielectric studies (13) that both the β- and γ-transitions in bisphenol A based thermosets depend on the side chains and unreacted ends, and that both are affected by physical aging and postcure. Nelson (23) has reported that these transitions can be related to vibration damping. This is also true for acoustical damping (24). In both of this cases, the strength of the beta transition is taken as a measurement of how effectively a polymer will absorb vibrations. There is a frequency dependence in this transitions and this is discussed below.

Heijober (10) and Boyer (11) showed that this information needs to be considered with care as not all beta transitions correlate with toughness or other properties. This can be due to misidentification of the transition or that the transition does sufficiently disperse energy. A working rule of thumb (10,16,25,26) is that the beta transition must be related to either localized movement in the main chain or very large side chain movement to sufficiently absorb enough energy. The relationship of large side chain movement and toughness has been extensively studied in polycarbonate by Yee (27) as well as in many other tough glassy polymers (28).

Less use is made of the T_γ transitions and they are mainly studied to understand the movements occurring in polymers. Wendorff (29) reports that this transition in polyarylates is limited to inter- and intramolecular motions within the scale of a single repeat unit. Both McCrum (5) and Boyd (18) similarly limited

the T_γ and T_δ to very small motions either within the molecule or with bound water. The use of what is called two-dimensional IR, which couples at FTIR and a DMA to study these motions, is a topic of current interest (30,31).

The Glass Transition (T_g or T_α). As the free volume continues to increase with increasing temperature, the glass transition T_g occurs where large segments of the chain start moving. This transition is also called the α- transition, T_α. The T_g is very dependent on the degree of polymerization up to a value known as the critical T_g or the critical molecular weight. Above this value, the T_g typically becomes independent of molecular weight (32). The T_g represents a major transition for many polymers, as physical properties change drastically as the material goes from a hard glassy to a rubbery state. It defines one end of the temperature range over which the polymer can be used, often called the operating range of the polymer. For where strength and stiffness are needed, it is normally the upper limit for use. In rubbers and some semicrystalline materials like polyethylene and polypropylene, it is the lower operating temperature. Changes in the temperature of the T_g are commonly used to monitor changes in the polymer such as plasticizing by environmental solvents and increased crosslinking from thermal or UV aging (see GLASS TRANSITION).

The T_g of cured materials or thin coatings is often difficult to measure by other methods, and more often than not the initial cost justification for a DMA is measuring a hard-to-find T_g. While estimates of the relative sensitivity of DMA to DSC or DTA (differential thermal analysis) vary, it appears that DMA is 10–100 times more sensitive to the changes occurring at the T_g. The T_g in highly crosslinked materials can easily be seen long after the T_g has become too flat and broad to be seen in DSC. This is also a problem with certain materials like medical grade urethanes and very highly crystalline polyethylenes.

The method of determining the T_g in DMA can be a manner for disagreement as at least five ways are in current use (Fig. 6). Depending on the industry

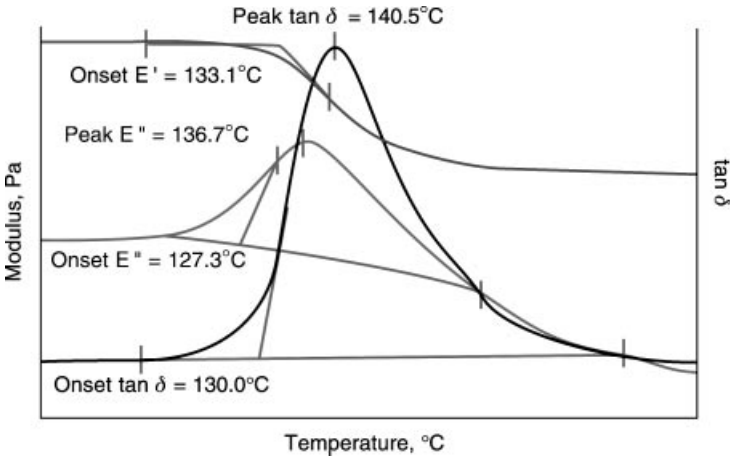

Fig. 6. Methods of determining the T_g are shown for DMA. The temperature of the T_g varies by as much as 10°C in this example depending on the value chosen. Differences as great as 25°C have been reported. Reprinted with permission from Ref. 1. Copyright (1999) CRC Press.

standards or background of the operator, the peak or onset of the tan δ curve, the onset of the E′ drop, or the onset or peak of the E″ curve may be used. The values obtained from these methods can differ up to 25°C from each other on the same run. In addition, a 10–20°C difference from the DSC is also seen in many materials. In practice, it is important to specify exactly how the T_g should be determined. For DMA, this means defining the heating rate, applied stresses (or strains), the frequency used, and the method of determining the T_g. For example, the sample will be run at 10°C° min^{-1} under 0.05% strain at 1 Hz in nitrogen purge (20 $\text{cc} \cdot \text{min}^{-1}$) and the T_g determined from the peak of the tan δ curve.

It is not unusual to see a peak or hump on the storage modulus directly preceding the drop that corresponds to the T_g. This is also seen in DSC and DTA and corresponds to a rearrangement in the material to relieve stresses frozen in below the T_g by the processing method. These stresses are trapped in the material until enough mobility is obtained at the T_g to allow the chains to move to a lower energy state. Often a material will be annealed by heating it above the T_g and then slowly cooling it to remove this effect. For similar reasons, some experimenters will run a material twice or use a heat–cool–heat cycle to eliminate processing effects.

The Rubbery Plateau, $T_\alpha{}^*$ and T_{ll}. The area above the T_g and below the melt is known as the rubbery plateau and its length as well as viscosity are dependent on the molecular weight between entanglements (M_e) (33) or cross-links. The molecular weight between entanglements is normally calculated during a stress-relaxation experiment but similar behavior is observed in DMA. The modulus in the plateau region is proportional to either the number of cross-links or the chain length between entanglements. This is often expressed in shear as

$$G' \cong (\rho RT)/\mathrm{M_e} \tag{21}$$

where G' is the shear storage modulus of the plateau region at a specific temperature, ρ is the polymer density, and M_e is the molecular weight between entanglements. In practice, the relative modulus of the plateau region shows the relative changes in M_e or the number of cross-links compared to a standard material.

The rubbery plateau is also related to the degree of crystallinity in a material, although DSC is a better method for characterizing crystallinity than DMA (34, 35). Also as in the DSC, there is evidence of cold crystallization in the temperature range above the T_g (Fig. 7). That is one of several transitions that can be seen in the rubbery plateau region. This crystallization occurs when the polymer chains have been quenched (quickly cooled) into a highly disordered state. On heating above the T_g, these chains gain enough mobility to rearrange into crystallites, which causes a sometimes-dramatic increase in modulus. DSC or its temperature-modulated variant, StepScan™ Differential Scanning Calorimetry, can be used to confirm this (36). The alpha star transition $T_\alpha{}^*$, the liquid–liquid transition T_{ll}, the heat-set temperature, and the cold crystallization peak are all transitions that can appear on the rubbery plateau. In some crystalline and semicrystalline polymer, a transition is seen here called the $T_\alpha{}^*$ (18,37). The alpha star transition is associated with the slippage between crystallites and helps extend the operating range of a material above the T_g. This transition is very susceptible to processing induced changes and can be enlarged or decreased by the applied heat history,

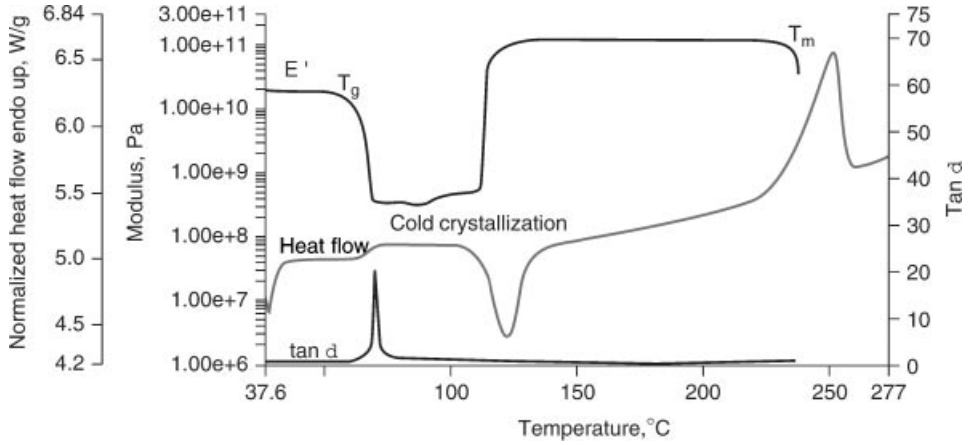

Fig. 7. Cold crystallization in PET caused a large increase in the storage modulus E' above the T_g. A DSC scan of the same material is included. Reprinted with permission from Ref. 1. Copyright (1999) CRC Press.

processing conditions, and physical aging (38,39). Hence, the $T_\alpha{}^*$ has been used by fiber manufacturers to optimize properties in their materials.

In amorphous polymers, the T_{ll} transition is seen instead, which is a liquid–liquid transition associated with increased chain mobility and segment–segment associations (40). This order is lost when the T_{ll} is exceeded and regained on cooling from the melt. Boyer (41,42) reports that, like the T_g, the appearance of the T_{ll} is affected by the heat history. The T_{ll} is also dependent on the number-average molecular weight M_n, but not on the weight-average molecular weight, M_w. Bershtein (19) suggests that this may be considered as quasi-melting on heating or the formation of stable associates of segments on cooling. While this transition is reversible, it is not always easy to see, and Boyer (43) spent many years trying to prove it was real. It is still not totally accepted. Following this transition, a material enters the terminal or melting region.

Depending on its strength, the heat-set temperature can also be seen in DMA. While it is normally seen in a TMA experiment, it will sometimes appear as either a sharp drop in storage modulus (E') or an abrupt change in probe position. Heat set is the temperature at which some strain or distortion is induced into polymeric fibers to change its properties, such as to prevent a nylon rug from feeling like fishing line. Since heating above this temperature will erase the texture, and polyesters must be heated above the T_g to dye them, it is of critical importance to the fabric industry. Many final properties of polymeric products depend on changes induced in processing (44,45).

The Terminal Region. On continued heating, the melting point T_m is reached. The melting point is where the free volume has increased so the chains can slide past each other and the material flows. This is also called the terminal region. In the molten state, this ability to flow is dependent on the molecular weight of the polymer (Fig. 5). The melt of a polymer material will often show changes in temperature of melting, width of the melting peak, and enthalpy as the material changes (46,47) resulting from changes in the polymer molecular weight and crystallinity.

Degradation, polymer structure, and environmental effects all influence what changes occur. Polymers that degrade by cross-linking will look very different from those that exhibit chain scission. Very highly cross-linked polymers will not melt as they are unable to flow.

The study of polymer melts and especially their elasticity was one of the areas that drove the development of commercial DMAs. Although a decrease in the melt viscosity is seen with temperature increases, the DMA is most commonly used to measure the frequency dependence of the molten polymer as well as its elasticity. The latter property, especially when expressed as the normal forces, is very important in polymer processing.

Frequency Dependencies in Transition Studies. The choice of a testing frequency or its effect on the resulting data must be addressed. A short discussion of how frequencies are chosen and how they affect the measurement of transitions is in order. Considering that higher frequencies induce more elastic-like behavior, there is some concern that a material will act stiffer than it really is if the test frequency is chosen to be too high. Frequencies for testing are normally chosen by one of three methods. The most scientific method would be to use the frequency of the stress or strain that the material is exposed to in the real world. However, this is often outside of the range of the available instrumentation. In some cases, the test method or the industry standard sets a certain frequency and this frequency is used. Ideally a standard method like this is chosen so that the data collected on various commercial instruments can be shown to be compatible. Some of the ASTM methods for TMA (thermomechanical analysis) and DMA are listed in Table 1. Many industries have their own standards so it is important to

Table 1. ASTM test for DMA

D3386	CTE of electrical insulating materials by TMA
D4065	Determining DMA properties terminology[a]
D4092	Terminology for DMA tests
D4440	Measurement of polymer melts
D4473	Cure of thermosetting resins
D5023	DMA in three-point bending tests
D5024	DMA in compression
D5026	DMA in tension
D5279	DMA of plastics in tension
D5418	DMA in dual cantilever
D5934	DMA tensile modulus under constant loading
D6382	DMA testing on waterproof roffing materials
D228-95	CTE by TMA with silica dilatometer
E473-94	Terminology for thermal analyusis
E831-93	CTE of solids by TMA
E1363-97	Temperature calibration for TMA
E1545-95(a)	T_g by TMA
E1640-99	T_g by DMA
E1824-96	T_g by TMA in tension
E1867-01	Temperature calibration for DMA
E2254-03	Storage moldulus calibration for DMA

[a]This standard qualifies a DMA as a acceptable for all ASTM DMA standards.

know whether the data is expected to match a Mil-spec, an ASTM standard, or a specific industrial test. Finally, one can arbitrarily pick a frequency. This is done more often than not, so that 1 Hz and 10 $rad \cdot s^{-1}$ are often used. As long as the data are run under the proper conditions, they can be compared to highlight material differences. This requires that frequency, stresses, and the thermal program be the same for all samples in the data set.

Lowering the frequency shifts the temperature of a transition to a lower temperature (Fig. 8). At one time, it was suggested that multiple frequencies could be used and the T_g should then be determined by extrapolation to 0 Hz. This was never really accepted as it represented a fairly large increase in testing time for a small improvement in accuracy. For most polymer systems, for very precise measurements, one uses a DSC. Different types of transitions also have different frequency dependencies and McCrum and co-workers listed many of these. If one looks at the slope of the temperature dependence of transitions against frequency, one sees that in many cases the primary transitions like T_m and T_g have a different dependence on frequency than the lower temperature transitions. In fact, the activation energies are different for α-, β-, and γ- transitions because of the different motions required, and the transitions can be sorted by this approach.

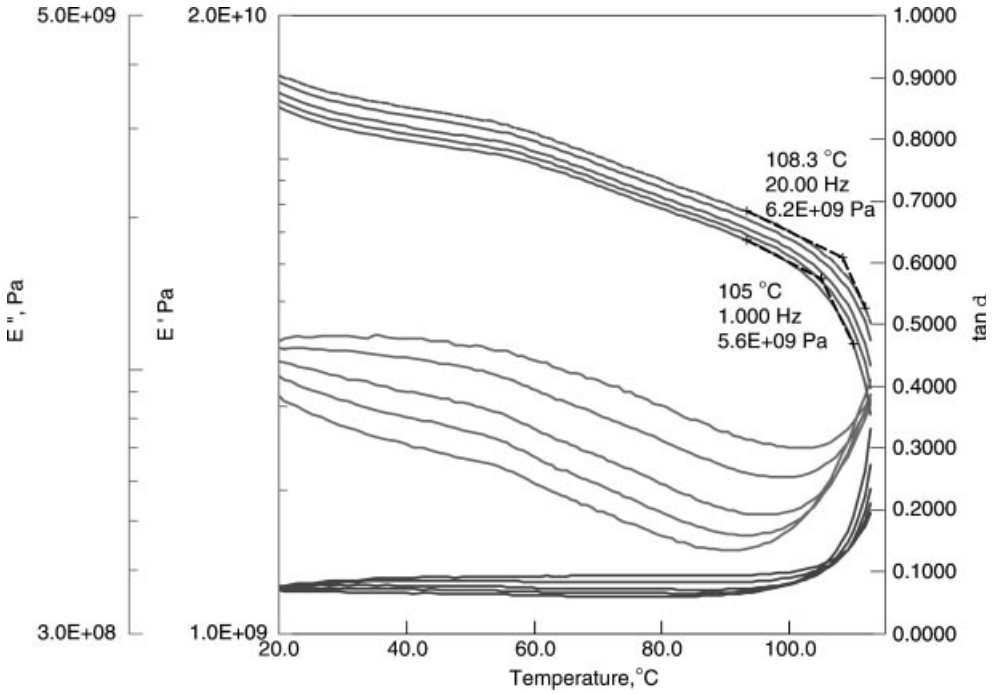

Fig. 8. Effect of frequency on transitions: the dependence of the T_g in polycarbonate on frequency. Data generated on a Perkin-Elmer Diamond DMA by the author.

Polymer Melts and Solutions, Applications

A fluid or polymer melt responds to strain rate rather than to the amount of stress applied. The viscosity is one of the main reasons why people run frequency scans. As the stress–strain curves and the creep recovery runs show, viscoelastic materials exhibit some degree of flow or unrecoverable deformation. The effect is the strongest in melts and liquids where frequency versus viscosity plots are the major application of DMA. Figure 9 shows a frequency scan on a viscoelastic material. In this example, the sample is a rubber above the T_g in three-point bending, but the trends and principles apply to both solids and melts. The storage modulus and complex viscosity are plotted on log scales against the log of frequency. In analyzing the frequency scans, trends in the data are more significant than specific peaks or transitions.

On the viscosity curve η^*, a fairly flat region appears at low frequency, called the zero shear plateau (9). This is where the polymer exhibits Newtonian behavior and its viscosity is dependent on molecular weight, not the strain rate. The viscosity of this plateau has been shown to experimentally relate to the molecular weight for Newtonian fluid

$$\eta \propto cM_v^1 \tag{22}$$

for cases where the molecular weight M_v is less than the entanglement molecular weight M_e, and for cases where M_v, is greater than M_e:

$$\eta_0 \propto cM_v^{3.4} \tag{23}$$

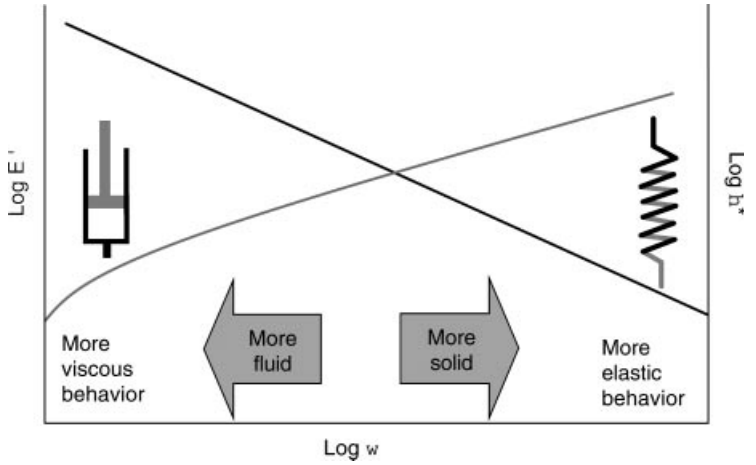

Fig. 9. An example of a frequency scan showing the change in a material's behavior as frequency varies. Low frequencies allow the material time to relax and respond, hence, flow dominates. High frequencies do not, and elastic behavior dominates. Reprinted with permission from Ref. 1. Copyright (1999) CRC Press.

where η_0 is the viscosity of the initial Newtonian plateau, c is a material constant, and M_v the viscosity average molecular weight. This relationship can be written in general terms, replacing the exponential term with the Mark-Houwink constant a. Equation 23 can be used as a method of approximating the molecular weight of a polymer. The value obtained is closest to the viscosity-average molecular weight obtained by osmometry (48). In comparison with the weight-average data obtained by gel permeation chromatography, the viscosity-average molecular weight would be between the number-average and weight-average molecular weights, but closer to the latter (49). This was originally developed for steady shear viscosity but applies to complex viscosity as well. The relationship between steady shear and complex viscosity is fairly well established. Cox and Merz (50) found that an empirical relationship exists between complex viscosity and steady shear viscosity when the shear rates are the same. The Cox–Merz rule is stated below:

$$|\eta(\omega)| = \eta(\dot{\gamma})|_{\dot{\gamma}=\omega} \tag{24}$$

where η is the constant shear viscosity, η^* is the complex viscosity, ω the frequency of the dynamic test, and $d\gamma/dt$ the shear rate of the constant shear test. This rule of thumb seems to hold for most materials to within about $\pm 10\%$. Another approach is the Gleissile (51) Mirror Relationship that states the following:

$$\eta\dot{\gamma} = \eta^+(t)|_{t=1/\dot{\gamma}} \tag{25}$$

when $\eta^+(t)$ is the limiting value of the viscosity as the shear rate $\dot{\gamma}$ approaches zero.

The low frequency range is where viscous or liquid-like behavior predominates. If a material is stressed over long enough times, some flow occurs. As time is the inverse of frequency, this means materials are expected to flow more at low frequency. As the frequency increases, the material will act in a more and more elastic fashion. Silly Putty (Billy and Smith, Inc.), the children's toy, shows this clearly. At low frequency, Silly Putty flows like a liquid, while at high frequency it bounces like a rubber ball. This behavior is also similar to what happens with temperature changes. A polymer becomes softer and more fluid as it is heated and it goes through transitions that increase the available space for molecular motions. Over long enough time periods, or small enough frequencies, similar changes occur. So one can move a polymer across a transition by changing the frequency. This relationship is also expressed as the idea of time–temperature equivalence (52). Often stated, as low temperature is equivalent to short times or high frequency, it is a fundamental rule of thumb in understanding polymer behavior.

As the frequency is increased in a frequency scan, the Newtonian region is exceeded and a new relationship develops between the rate of strain, or the frequency, and the viscosity of the material. This region is often called the power law zone and can be modeled by

$$\eta^* \cong \eta(\dot{\gamma}) = c\dot{\gamma}^{n-1} \tag{26}$$

where η^* is the complex viscosity, $\dot{\gamma}$ is the shear rate, and the exponent term n is determined by the fit of the data. This can also be written as

$$\sigma \cong \eta(\dot{\gamma}) = c\dot{\gamma}^n \tag{27}$$

where σ is the stress and η is the viscosity. The exponential relationship is why the viscosity versus frequency plot is traditionally plotted on a log scale. With modern curve fitting programs, the use of log–log plots has declined and is a bit anachronistic. The power law region of polymers shows shear thickening or thinning behavior. This is also the region in which the E'–η^* or the E'–E'' crossover point is found. As frequency increases and shear thinning occurs, the viscosity (η^*) decreases. At the same time, increasing the frequency increases the elasticity (E'). This is shown in Figure 9. The E'–η^* crossover point is used an indicator of the molecular weight and molecular weight distribution (53). Changes in its position are used as a quick method of detecting changes in the molecular weight and distribution of a material. After the power law region, another plateau is seen, the infinite shear plateau.

This second Newtonian region corresponds to where the shear rate is so high that the polymer no longer shows a response to increases in the shear rate. At the very high shear rates associated with this region, the polymer chains are no longer entangled. This region is seldom seen in DMA experiments and usually avoided in use because of the damage done to the chains. It can be reached in commercial extruders and can cause degradation of the polymer, which causes the poorer properties associated with regrind.

As the curve in Figure 9 shows, the modulus also varies as a function of the frequency. A material exhibits more elastic-like behavior as the testing frequency increases, and the storage modulus tends to slope upwards toward higher frequency. The storage modulus' change with frequency depends on the transitions involved. Above the T_g, the storage modulus tends to be fairly flat, with a slight increase with increasing frequency as it is on the rubbery plateau. The change in the region of a transition is greater. If one can generate a modulus scan over a wide enough frequency range, the plot of storage modulus versus frequency appears like the reverse of a temperature scan. The same time–temperature equivalence discussed above also applies to modulus, as well as compliance, tan δ, and other properties.

The frequency scan is used for several purposes that will be discussed in this section. One very important use, that is very straightforward, is to survey the material's response over various shear rates. This is important because many materials are used under different conditions. For example adhesives, whether tape, Band-Aids, or hot melts, are normally applied under conditions of low frequency and this property is referred to as tack. When they are removed, the removal often occurs under conditions of high frequency called peel. Different properties are required at these regimes and to optimize one property may require chemical changes that harm the other. Similarly, changes in polymer structure can show these kinds of differences in the frequency scan. For example, branching affects different frequencies (9).

In a tape adhesive, for example, sufficient flow under pressure at low frequency is desired to fill the pores of the material to obtain a good mechanical

bond. When the laminate is later subjected to peel, the material needs to be very elastic so that it will not pull out of the pores (54,55). The frequency scan allows measurement of these properties in one scan thus ensuring that tuning one property does not degrade another. This type of testing is not limited to adhesives as many materials see multiple frequencies in the actual use. Viscosity versus frequency plots are used extensively to study how changes in polymer structure or formulations affect the behavior of the melt. Often changes in materials, especially in uncured thermosetting resins and molten materials, effect a limited frequency range and testing at a specific frequency can miss the problem.

It should be noted that since the material is scanned across a frequency range, there are some conditions where the material–instrument system acts like a guitar string and begins to resonate when certain frequencies are reached. These frequencies are either the natural resonance frequency of the sample–instrument system or one of its harmonics. When the harmonics occur, the sample–instrument system oscillates like a guitar string and the desired information about the sample is obscured. Since there is no way to change this resonance behavior (and in a free resonance analyzer, this effect is necessary to obtain data), it is required to redesign the experiment by changing sample dimensions or geometry to escape the problem. Using a sample with much different dimensions, which change the mass, or changing from extension to three-point bending geometry changes the natural oscillation frequency of the sample and hopefully solves this problem.

Thermosets, Applications

The DMA's ability to give viscosity and modulus values for each point in a temperature scan allows the estimation of kinetic behavior as a function of viscosity. This has the advantage of describing how viscous the material is at any given time, so as to determine the best time to apply pressure, what design of tooling to use, and when the material can be removed from the mold. Recent reviews have summarized this approach for epoxy systems (56).

Curing. The simplest way to analyze a resin system is to run a plain temperature ramp from ambient to some elevated temperature (57,58). This "cure profile" allows collection of several vital pieces of information as shown in Figure 10. Samples may be run "neat" or impregnated into fabrics in techniques that are referred to as torsional braid. There are some problems with this technique, as temperature increases will cause an apparent curing of nondrying oils as thermal expansion increases friction. However, the "soaking of resin into a shoelace," as this technique has been called, allows one to handle difficult specimens under conditions where the pure resin is impossible to run in bulk (due to viscosity or evolved volatiles). Composite materials like graphite–epoxy composites are sometimes studied in industrial situations as the composite rather than the "neat" or pure resin because of the concern that the kinetics may be significantly different. In terms of ease of handling and sample, the composite is a better sample. Another area of concern is paints and coatings (59) where the material is used in a thin layer. This can be addressed experimentally by either a braid as above or coating the material on a thin sheet of metal. The metal is often run first and its scan

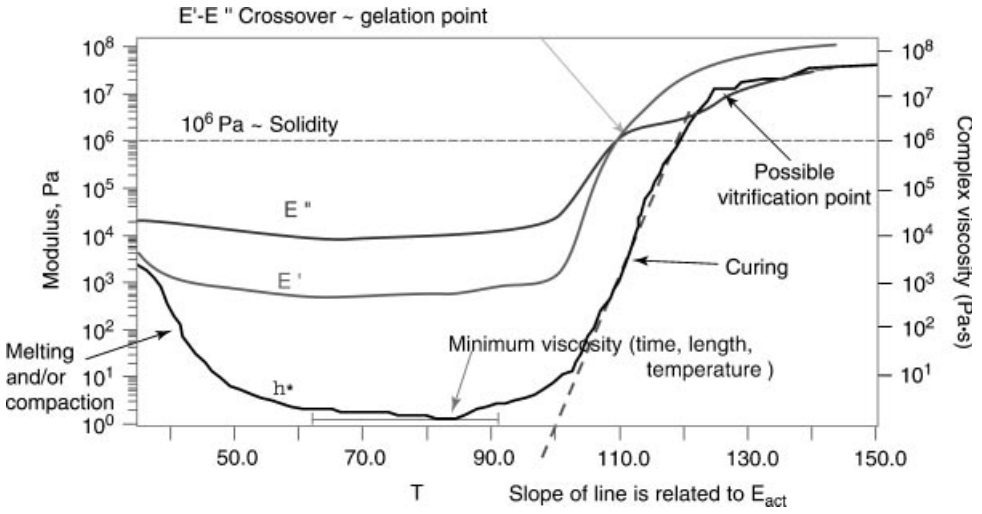

Fig. 10. The DMA cure profile of a two-part epoxy showing the typical analysis for minimum viscosity, gel time, vitrification time, and estimation of the action energy (see discussion in text). Reprinted with permission from Ref. 1. Copyright (1999) CRC Press.

subtracted from the coated sheet's scan to leave only the scan of the coating. This is also done with thin films and adhesive coatings.

From the cure profile seen in Figure 10, it is possible to determine the minimum viscosity ($\eta^*_{\min}$), the time to $\eta^*_{\min}$ and the length of time it stays there, the onset of cure, the point of gelation where the material changes from a viscous liquid to a viscoelastic solid, and the beginning of vitrification. The minimum viscosity is seen in the complex viscosity curve and is where the resin viscosity is the lowest. A given resin's minimum viscosity is determined by the resin's chemistry, the previous heat history of the resin, the rate at which the temperature is increased, and the amount for stress or strain applied. Increasing the rate of the temperature ramp is known to decrease the $\eta^*_{\min}$, the time to $\eta^*_{\min}$, and the gel time. The resin gets softer faster, but also cures faster. The degree of flow limits the type of mold design and when as well as how much pressure can be applied to the sample. The time spent at the minimum viscosity plateau is the result of a competitive relationship between the material's softening or melting as it heats and its rate of curing. At some point, the material begins curing faster than it softens, and that is where the viscosity starts to increase.

As the viscosity begins to climb, an inversion is seen of the E'' and E' values as the material becomes more solid-like. This crossover point also corresponds to where the tan δ equals 1 (since $E' = E''$ at the crossover). This is taken to be the gel point, (60) where the cross-links have progressed to forming an "infinitely" long network across the specimen. At this point, the sample will no longer dissolve in solvent. While the gel point correlates fairly often with this crossover, it doesn't always. For example, for low initiator levels in chain addition thermosets, the gel point precedes the modulus crossover (61). A temperature dependence for the presence of the crossover has also been reported (57,58). In some cases, where powder compacts and melts before curing, there may be several crossovers (62).

Then, the one following the $\eta^*_{\min}$ is usually the one of interest. Some researchers (63,64) believe that the true gel point is best detected by measuring the frequency dependence of the crossover point. This is done either by multiple runs at different frequencies or by multiplexing frequencies during the cure. At the gel point, the frequency dependence disappears (64). This value is usually only a few degrees different from the one obtained in a normal scan and in most cases not worth the additional time. During this rapid climb of viscosity in the cure, the slope for η^* increase can be used to calculate an estimated E_a (activation energy) (65). This will be discussed below, but the fact that the slope of the curve here is a function of E_a is important. Above the gel temperature, some workers estimate the molecular weight, M_c, between cross-links as

$$G' = RT\rho/\mathrm{M_c} \tag{28}$$

where R is the gas constant, T is the temperature in Kelvin, and ρ is the density. At some point the curve begins to level off and this is often taken as the vitrification point, T_{vf}.

The vitrification point is where the cure rate slows because the material has become so viscous that the bulk reaction has stopped. At this point, the rate of cure slows significantly. The apparent T_{vf} however is not always real: any analyzer in the world has an upper force limit. When that force limit is reached, the "topping out" of the analyzer can pass as the T_{vf}. Use of a combined technique like DMA–DEA DEA is dielectric analysis, where an oscillating electrical signal is applied to a sample. From this signal, the ion mobility can be calculated, which is then converted to a viscosity (see Ref. 5 for details). DEA will measure to significantly higher viscosities than DMA to see the higher viscosities or the removal of a sample from parallel plate and sectioning it into a flexure beam is often necessary to see the true vitrification point. Vitrification may also be seen in the DSC if a modulated temperature technique like StepScan is used (66). A reaction can also completely cure without vitrifying and will level off the same way. One should be aware that reaching vitrification or complete cure too quickly could be as bad as too slowly. Often an overly aggressive cure cycle will cause a weaker material as it does not allow for as much network development, but gives a series of hard (highly cross-linked) areas among softer (lightly cross-linked) areas. On the way to vitrification, an important value is 10^6 Pa · s. This is the viscosity of bitumen (67) and is often used as a rule of thumb for where a material is stiff enough to support its own weight. This is a rather arbitrary point, but is chosen to allow the removal of materials from a mold and the cure is then continued as a post-cure step. The cure profile is both a good predictor of performance as well as a sensitive probe of processing conditions. As discussed above under TMA applications, a volume change occurs during the cure (68). This shrinkage of the resin is important and can be studied by monitoring the probe position of some DMA's as well as by TMA and dilatometry.

The above is based on using a simple temperature ramp to see how a material responds to heating. In actual use, many thermosets are actually cured using more complex cure cycles to optimize the tradeoff between the processing

time and the final product's properties (69). The use of two-stage cure cycles is known to develop stronger laminates in the aerospace industry. Exceptionally thick laminates often also require multiple stage cycles in order to develop strength without porosity. As thermosets shrink on curing, careful development of a proper cure cycle to prevent or minimize internal voids is necessary. One reason for the use of multistage cures is to drive reactions to completion. Another is to extend the minimum viscosity range to allow greater control in forming or shaping of the material. The development of a cure cycle with multiple ramps and holds would be very expensive if done with full-sized parts in production facilities. The use of the DMA gives a faster and cheaper way of optimizing the cure cycle to generate the most efficient and tolerant processing conditions.

Because of the limits of industrial equipment and cost constraints, curing is done at a constant temperature for a period of time. This can be done both to initially cure the material or to "post-cure" it. (The kinetic models discussed in the next section also require data collected under isothermal conditions.) It is also how rubber samples are cross-linked, how initiated reactions are run, and how bulk polymerizations are performed. Industrially, continuous processes, as opposed to batch, often require an isothermal approach. UV light and other forms of nonthermal initiation also use isothermal studies for examining the cure at a constant temperature.

Photocuring. A photocure in the DMA is run by applying a UV light source to a sample (held a specific temperature or subjected to a specific thermal cycle) (70). Photocuring is done for dental resin, contact adhesives, and contact lenses. UV-exposure studies are also run on cured and thermoplastic samples by the same techniques as photocuring to study UV degradation. The cure profile of a photocure is very similar to that of a cake or epoxy cement. The same analysis is used and the same types of kinetics developed as is done for thermal curing studies.

The major practical difficulty in running photocures in the DMA is the current lack of a commercially available photocuring accessory, comparable to the photocalorimeters on the market. One normally has to adapt a commercial DMA to run these experiments. The Perkin-Elmer DMA-7e has been successfully adapted (71) to use quartz fixtures and commercial UV source from EFOS, triggered from the DMA's software. This is a fairly easy process and other instruments like the RheoSci^{TM} DMTA (dynamic mechanical thermal analyzer) Mark 5 have also been adapted.

Curing Kinetics by DMA. Several approaches have been developed to studying the chemorheology of thermosetting systems. MacKay and Halley (72) reviewed chemorheology and the more common kinetic models. A fundamental method is the Williams–Landel–Ferry (WLF) model, (73) which looks at the variation of T_g with degree of cure. This has been used and modified extensively (74). A common empirical model for curing has been proposed by Roller (75,76). In the latter approach, samples of the thermoset are run isothermally as described above and the viscosity versus time data collected. This is plotted as log (versus time in seconds, where a change in slope is apparent in the curve. This break in the data indicates the sample is approaching the gel time. From these curves, the initial viscosity, η_0 and the apparent kinetic factor k can be determined. By plotting the

log viscosity versus time for each isothermal run, the slope k, and the viscosity at $t = 0$ are apparent. The initial viscosity and k can be expressed ase

$$\eta_0 = \eta_\infty \, \mathrm{e}^{\Delta E_\eta / RT} \tag{29}$$

$$k = k_\infty \, \mathrm{e}^{\Delta E_k / RT} \tag{30}$$

Combining these allows setup of the equation for viscosity under isothermal conditions as

$$\ln \, \eta(\mathrm{t}) = \ln \, \eta_\infty + \Delta E_k / RT + t k_\infty \mathrm{e}^{\Delta E_k / RT} \tag{31}$$

By replacing the last term with an expression that treats temperature as a function of time, the equation becomes

$$\ln \, \eta(T, \, \mathrm{t}) = \ln \, \eta_\infty + \Delta E_\eta / RT + \int_0^t k_\infty \, \mathrm{e}^{\Delta E_k / RT} \, \mathrm{d}t \tag{32}$$

This equation can be used to describe viscosity–time profiles for any run where the temperature can be expressed as a function of time. The activation energies can now be calculated. The plots of the natural log of the initial viscosity (determined above) versus $1/T$ and the natural log of the apparent rate constant k versus $1/T$ are used to give us the activation energies ΔE_η and ΔE_k. Comparison of these values to the k and ΔE to those calculated by DSC shows that this model gives larger values (59). The DSC data is faster to obtain, but it does not include the needed viscosity information. Several corrections have been proposed, addressing different orders of reaction (77) (the above assumes first order) and modifications to the equations (78,79). Many of these adjustments are reported in Roller's 1986 review (76) of curing kinetics. It is noted that these equations do not work well above the gel temperature. This same equation has been used to predict the degradation of properties in thermoplastics successfully (80).

The Gillham–Enns Diagram. The most complete approach to studying the behavior of a thermoset was developed by Gillham (81,82) and is analogous to the phase diagrams used by metallurgists. The time–temperature–transformation diagram (TTT) or the Gillham–Enns diagram (after its creators) is used to track the effects of temperature and time on the physical state of a thermosetting material. Figure 11 shows an example. Running isothermal studies of a resin at various temperatures and recording the changes as a function of time can do this. One has to choose values for the various regions and Gillham has done an excellent job of detailing how one picks the T_g, the glass, the gel, the rubbery, and the charring regions (3,83). These diagrams are also generated from DSC data (84), and several variants, (85) like the continuous heating transformation and conversion–temperature–property diagrams, have been reported. While easy to develop and use, TTT diagrams have not yet been accepted in industry despite their obvious utility. This may be due to the fact that they take some time to generate. A recent review (3) will hopefully increase the use of this approach.

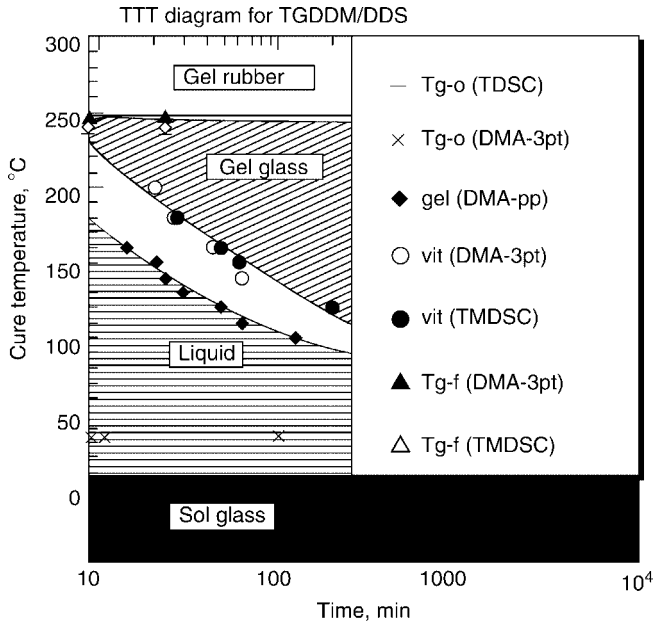

Fig. 11. An example of the Gillham–Enns diagram generated by the author on a commercial epoxy resin system. The lines of gelation and vitrification are marked.

BIBLIOGRAPHY

"Dynamic Mechanical Properties" in *EPSE* 2nd ed., Vol. 5, pp. 299–329, by T. Murayama, Monsanto Co.

1. K. Menard, *Dynamic Mechanical Analysis: A Practical Introduction*, CRC Press, Boca Raton, Fla., 1999.
2. J. Gillham, in J. Dworkins, ed., *Developments in Polymer Characterizations*, Vol. 3, Applied Science Publishers, Princeton, N.J., 1982, pp. 159–227.
3. J. Gillham and J. Enns, *Trends Polym. Sci.* **2**, 406 (1994).
4. U. Zolzer and H.-F. Eicke, *Rheol. Acta* **32**, 104 (1993).
5. N. McCrum, B. E. Read, and G. Williams, *Anelastic and Dielectric Properties of Polymeric Solids*, Dover, New York, 1991, pp. 192–200.
6. P. Flory, *Principles of Polymer Chemistry*, Cornell University Press, Ithaca, N.Y., 1953.
7. M. Doi and S. Edwards, *The Dynamics of Polymer Chains*, Oxford University Press, New York, 1986.
8. J. J. Aklonis and W. J. MacKnight, *Introduction to Viscoelasticity*, John Wiley & Sons, Inc., New York, 1983.
9. C. L. Rohn, *Analytical Polymer Rheology*, Hanser-Gardener, New York, 1995.
10. J. Heijboer, *Int. J. Polym. Mater.* **6**, 11 (1977).
11. R. F. Boyer, *Polym. Eng. Sci.* **8**(3), 161, (1968).
12. Ref. 9, pp. 279–283.
13. M. Mangion and G. Johari, *J. Polym. Sci., Part B: Polym. Phys.* **29**, 437 (1991).
14. G. Johari and G. Mikoljaczak, *J. Cavaille, Polym.* **28**, 2023 (1987).
15. F. Arnold, M. Eashoo, D. Shen, C. Lee, K. Bruno, and S. Cheng, *Polym. Sci. Eng.* **33**, 373 (1993).
16. G. Johari, *Lect. Notes Phys.* **277**, 90 (1987).

17. R. Daiz-Calleja and E. Riande, *Rheol. Acta* **34**, 58 (1995).
18. R. Boyd, *Polym.* **26**, 323 (1985).
19. V. Bershtien, V. Egorov, L. Egorova, and V. Ryzhov, *Thermochim. Acta* **238**, 41 (1994).
20. B. Twombly, *Proc. NATAS* **20**, 63 (1991).
21. V. Bershtien and V. Egorov, *Differential Scanning Calorimetery in the Physical Chemistry of Polymers*, Ellis Horwood, Chichester, U.K., 1993.
22. B. Coxton, private communication, 1996.
23. F. C. Nelson, Shock, and Vibration, *Digest* **26**(2), 11 & 24 (1994).
24. W. Brostow, private communication, 1998.
25. J. Heijboer, in J. Prins, ed., *Physics of Non-Crystalline Solids*, Wiley-Interscience, New York, 1965.
26. J. Heijboer, *J. Polym. Sci., Part C 1* **6**, 3755 (1968); L. Nielsen and R. Landel, *J. Macromol. Sci., Phys.* **9**, 239 (1974); S. Wu, *J. Appl. Polym. Sci.* **46**, 619 (1986).
27. A. Yee and S. Smith, *Macromolecules* **14**, 54 (1981).
28. G. Gordon, *J. Polym. Sci., Part A* **2**, 9, 1693 (1984).
29. J. Wendorff and B. Schartel, *Polym.* **36**, 899 (1995).
30. I. Noda, *Appl. Spectrosc.* **44**, 550 (1990).
31. V. Kien, in *Proc. 6th Sympos. Radiation Chem.*, Vol. 6, Issue 2, 1987, p. 463.
32. L. H. Sperling, *Introduction to Physical Polym. Science*, 2nd ed., John Wiley & Sons, Inc., New York, 1992.
33. C. Macosko, *Rheology*, VCH Publishers, New York, 1994.
34. T. Hatakeyama and F. Quinn, *Thermal Analysis*, John Wiley & Sons, Inc., New York, 1994.
35. B. Wunderlich, *Thermal Analysis*, Academic Press, New York, 1990.
36. J. Schawe, *Thermochim. Acta* **261**, 183 (1995); J. Schawe, *Thermochim. Acta* **260**, 1 (1995); J. Schawe, *Thermochim. Acta* **271**, 1 (1995); B. Wunderlich, A. Boller, and Y. Jin, *J. Therm. Anal.* **42**, 949 (1994).
37. R. H. Boyd, *Polym.* **26**, 1123 (1985).
38. S. Godber, private communication.
39. M. Ahmed, *Polypropylene Fiber—Science and Technology*, Elsevier, New York, 1982.
40. A. Lobanov, *Polym. Sci. (U.S.S.R.)* **22**, 1150 (1980).
41. R. Boyer, *J. Polym. Sci., Part B: Polym. Phys.* **30**, 1177 (1992); J. K. Gillham, R. Boyer, and S. Standnicki, *J. Appl. Polym. Sci.* **20**, 1245 (1976).
42. J. B. Enns and R. Boyer, *Encyclopedia of Polym. Science*, Vol. 17, 1989, pp. 23–47.
43. C. M. Warner, Evaluation of the DSC for Observation of the Liquid–Liquid Transition, Master thesis, Central Michigan State University, 1988.
44. J. Dealy and K. Wissbrun, *Melt Rheology and Its Role in Plastic Processing*, Van Nostrand Reinhold Co., Toronto, 1990.
45. N. Chereminsinoff, *An Introduction to Polym. Rheology and Processing*, CRC Press, Boca Raton, Fla., 1993.
46. E. Turi, ed., *Thermal Characterization of Polymeric Materials*, Academic Press, Boston, 1981.
47. E. Turi, ed., *Thermal Analysis in Polymer Characterization*, Heydon, London, 1981.
48. M. Miller, *The Structure of Polymers*, Reinhold, New York, 1966, pp. 611–612.
49. S. Rosen, *Fundamantal Principles of Polymeric Materials*, Wiley-Interscience, New York, 1993, pp. 53–77 and 258–259.
50. W. Cox and E. Merz, *J. Polym. Sci.* **28**, 619 (1958); P. Leblans, H. Booij, J. Palmen, and G. Tiemersma-Thone, *J. Polym. Sci.* **21**, 1703 (1983).
51. W. Gleissele, in G. Astarita and E. Astarita, eds., *Rheology*, Vol. 2, Plenum Press, New York, 1980, p. 457.
52. D. W. Van Krevelin, *Properties of Polymers*, Elsevier, New York, 1987, p. 289.

53. C. Macosko, *Rheology*, VCH Publishers, New York, 1994, pp. 120–127.
54. L.-H. Lee, ed., *Adhesive Bonding*, Plenum Press, New York, 1991.
55. L.-H. Lee, ed., *Fundamentals of Adhesion*, Plenum Press, New York, 1991.
56. W. Brostow, B. Bilyeu, and K. Menard, *J. Mater. Educ.* **21**, 281 (1999); **22**, 107 (2000); **23**, 189 (2001).
57. G. Martin, A. Tungare, and J. Gotro, in C. Craver and T. Provder, eds., *Polymer Characterization*, American Chemical Society, Washington, D.C., 1990.
58. M. Ryan, *ANTEC Proc.* **32**, 187 (1973); C. Gramelt, *Am. Lab. Jan*. 26 (1984); S. Etoh, *SAMPE J.* **3**, 6 (1985); F. Hurwitz, *Polym. Composites* **4**(2), 89 (1983).
59. M. Roller, *Polym. Eng. Sci.* **19**, 692 (1979); M. Roller, *J. Coating Technol.* **50**, 57 (1978).
60. G. Martin, M. Heise, and J. Gotro, *Polym. Eng. Sci.* **30**, 83 (1990); K. O'Driscoll, J. Dionisio, H. Mahabad, E. Abuir, and A. Lissi, *J. Polym. Sci.: Polym. Chem.* **17**, 1891 (1979); O. Okay, *Polym.* **35**, 2613 (1994).
61. M. Heise, G. Martin, and J. Gotro, *Polym. Eng. Sci.* **30**(2), 83 (1990).
62. K. Wissbrun and K. DeKee, *J. Coating Technol* **48**, 42 (1976).
63. F. Champon, *J. Rheol.* **31**, 683 (1987); H. Winter, *Polym. Eng. Sci.* **27**, 1698 (1987).
64. C. Michon, *Rheol. Acta* **32**, 94 (1993).
65. I. Kalnin, in C. Mays, ed., *Epoxy Resins*, Marcel Dekker, New York, 1987.
66. B. Bilyeu, W. Brostow, and K. Menard, in A. T. Riga and L. H. Judovits, eds., *Materials Characterization by Dynamic and Modulated Thermal Analytical Techniques, ASTM STP 1402*, American Society for Testing and Materials, West Conshohocken, Pa., 2001.
67. H. Banes, K. Walters, and J. Hutton, *An Introduction to Rheology*, Elsevier, New York, 1989.
68. A. W. Snow and J. Armistead, *J. Appl. Polym. Sci.* **52**, 401 (1994).
69. R. Geimer, G. Meyers, A. Christiansen, J. Koutsky, and R. Follenbee, *J. Appl. Polym. Sci.* **47**, 1481 (1993); R. Roberts, *SAMPE J.* **5**, 28 (1987).
70. T. Renault, *NATAS Notes* **25**, 44 (1994); H. L. Xuan and C. Decker, *J. Polym. Sci., Part A* **31**, 769 (1993); W. Shi and B. Ranby, *J. Appl. Polym. Sci.* **51**, 1129 (1994).
71. J. Enns, private communication, 1999.
72. P. J. Halley and M. E. MacKay, *Polym. Eng. Sci.* **36**, 593 (1996).
73. J. Ferry, *Viscoelastic Properties of Polymers*, 3rd ed., John Wiley & Sons, Inc., New York, 1980.
74. J. Mijovic and A. Koutsky, *J. Comp. Met.* **23**, 163 (1989); J. Mijovic and A. Koutsky, *SAMPE J.* **23**, 51 (1990).
75. M. Roller, *Met. Finishing* **78**, 28 (1980); M. Roller, *ANTEC Proc.* **24**, 9 (1978); J. Gilham, *ACS Symp. Ser.* **78**, 53 (1978); M. Roller, *ANTEC Proc.* **21**, 212 (1975); M. Roller, *Polym. Eng. Sci.* **15**, 406 (1975).
76. M. Roller, *Polym. Eng. Sci.* **26**, 432 (1986).
77. C. Rohn, *Problem Solving for Thermosetting Plastics*, Rheometrics, Austin, 1989.
78. J. Seferis, in C. May, ed., *Chemorheology of Thermosetting Polymers*, American Chemical Society, Washington, D.C., 1983, p. 201.
79. P. R. Patel, W. Pinnello, and Y. Li, *J. Therm. Anal.* **39**, 229 (1993).
80. M. Roller, private communication, 1998.
81. J. Gillham and J. Enns, *Polym. Composites* **1**, 97 (1980); J. Gillham and J. Enns, *J. Appl. Polym. Sci.* **28**, 2567 (1983); L. C. Chan, H. Nae, and J. Gillham, *J. Appl. Polym. Sci.* **29**, 3307 (1984); J. Gillham and G. Palmese, *Polym. Eng. Sci.* **26**, 1429 (1986); S. Simon and J. Gillham, *J. Appl. Polym. Sci.* **51**, 1741 (1994); G. Palmese and J. Gillham, *J. Appl. Polym. Sci.* **34**, 1925 (1987).
82. J. Gillham and J. Enns, in C. Craver, ed., *Polymer Characterization*, American Chemical Society, Washington, D.C., 1983.
83. J. Gillham and S. Simon, *J. Appl. Polym. Sci.* **53**, 709 (1994).

84. A. Otereo, N. Clavaguera, M. Clavaguera-Mora, S. Surinach, and M. Baro, *Thermochim. Acta* **203**, 379 (1992).
85. J. Gillham and G. Wisanrakkitt, *J. Appl. Polym. Sci.* **42**, 2453 (1991); B. Osinski, *Polymers* **34**, 752 (1993).

KEVIN P. MENARD
University of North Texas Materials Science Department

Nomenclature

δ	phase angle
$\tan\delta$	tangent of the phase angle, also called the damping
σ	stress
γ	shear strain
ε	tensile strains
$\dot{\gamma}$	shear strain rate
$\dot{\varepsilon}$	strain rate
η	viscosity
η^*	complex viscosity
η'	storage viscosity
η''	loss viscosity
E^*	complex Modulus
E'	storage Modulus
E''	loss Modulus
J	compliance
k	deformation
T	period
ρ	density
G	shear modulus
M_e	entanglement molecular weight
M_c	molecular weight between cross-links
M_w	molecular weight
f	frequency
ω	frequency in Hertz
k	Rate constant
E_a	Activation Energy
v^f	free volume
$T_{\alpha\beta,\gamma}$	transition (subscript type)
Λ	logarithmic decrement
Γ	torque

ELECTROCHROMIC POLYMERS

Introduction to Electrochromism

Color changes in an object give visual signals that can be used to convey useful information to an observer (1). Furthermore, by selective absorption or transmission of light by a material, the light energy impinging upon an observer can be modulated (1). Where a chemical or physical external stimulus causes a reversible color change or variation in light transmission, the possible applications are considerable. For such systems, color change phenomena are classified after the stimulus that causes the change, such as electrochromism, photochromism, thermochromism and gasochromism (1). An *electrochromic material* is one where a reversible color change takes place upon reduction (gain of electrons) or oxidation (loss of electrons), on passage of electrical current after the application of an appropriate electrode potential (2–10).

Many chemical species can be switched between redox states that have distinct electronic absorption spectra. Such spectra arise from either a moderate-energy internal electronic excitation or an intervalence optical charge transfer where the chemical species has two centers of differing valence or oxidation state (2–10). While materials are considered to be electrochromic when marked visible color changes are shown under illumination, recent interest in electrochromic devices (ECDs) for multispectral energy modulation by reflectance and absorbance has extended the definition (11). Chemical species are now being studied for modulation of radiation in the near infrared (NIR) (10,12), thermal infrared and microwave regions, and "color" can mean response of detectors to these electromagnetic regions, not just the human eye (11).

Encyclopedia of Polymer Science and Technology. Copyright John Wiley & Sons, Inc. All rights reserved.

Types of Electrochromic Materials. Electrochromic materials are of three basic types (2). In a given electrolyte solution, type I materials are soluble in both the reduced and oxidized (redox) states. Type II materials are soluble in one redox state, but form a solid film on the surface of an electrode following electron transfer. Electrochromic polymers are examples of type III materials, where both redox states are solids, generally studied as thin films on electrode surfaces. For types II and III, once the redox state has been switched, no further charge injection is needed to retain the new electrochromic state, and such systems are said to have "optical memory". In contrast, for type I electrochromic materials, diffusion of the soluble electrochemically-generated product material away from the electrode occurs and it is necessary to keep current flowing until the whole solution has been electrolyzed.

Where more than two redox states are electrochemically accessible in a given electrolyte solution, the electrochromic material may exhibit several colors and be termed polyelectrochromic, a frequent property of electrochromic polymers (2).

Applications of Electrochromic Materials. Commercial applications of electrochromic materials in devices include antiglare car rearview mirrors (4,8), electrochromic strips as battery state-of-charge indicators, and electrochromic sunglasses. Proposed applications include "smart windows" (based on modulation of either the transmitted or reflected solar radiation) for use in cars and in buildings (8), reusable price labels, protective eyewear, controllable aircraft canopies, glare-reduction systems for offices, devices for frozen-food monitoring (13), camouflage materials, spacecraft thermal control, and controllable light-reflective or light-transmissive devices for optical information and storage. In the case of long-term data displays, "paper-quality" railway termini information displays are now close to commercialization, using a new type of nanostructured electrochromic organic-inorganic hybrid system, where electrochromic groups such as phosphonated viologens and phenothiazine molecules are attached to the rough surface of a very high surface area porous oxide film (14,15). Typically, such films consist of networks of interconnected semiconducting or conducting metal oxide nanocrystals, deposited onto an optically transparent conducting glass electrode. On applying a negative potential, electrons are injected into the conduction band of the semiconductor and the absorbed molecule is reduced and changes color. Applying a positive potential reverses the process.

Chemical Classes of Electrochromic Material. There is a vast number of chemical species that show electrochromic properties (2), including both metal coordination complexes in solution and as polymer films (10), metal oxides (2,3) (especially tungsten oxide), viologens (4,4′-bipyridylium salts) (2,16), and conducting polymers (2,17–21) such as polypyrrole, polythiophene, and polyaniline. Other classes of electrochromic material include metal deposition/stripping systems (2) and Y, La, and Y/La alloys, which switch from a reflecting-mirror metallic state to a transparent semiconducting phase on hydride formation (8,22). It is important, however, to realize that whilst many types of chemical species exhibit electrochromism, only those with favorable electrochromic performance parameters (2) are potentially useful in commercial applications. Thus, most applications require electrochromic materials with a high contrast ratio, coloration efficiency, cycle life, and write-erase efficiency (2). Some performance parameters are application dependent; displays need low response times, whereas smart windows can tolerate response times of up to several minutes.

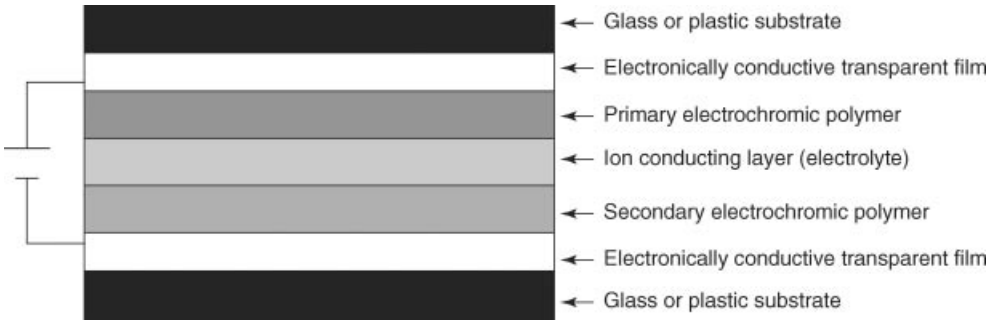

Fig. 1. Schematic design of an electrochromic device (ECD), suitable for a transmissive light-modulation application. In this case, a secondary electrochromic polymer is shown, the color change of which would need to be complementary to that of the primary electrochromic polymer.

Experimental Methods for Studying Electrochromic Materials. Redox systems which are likely to show promise as electrochromic materials are first studied, either as an electroactive surface film or an electroactive solute, at an electrochemically inert "working" electrode, under potentiostatic or galvanostatic control (2). Traditional electrochemical techniques (23), such as cyclic voltammetry (CV), coulometry, and chronoamperometry, all partnered by *in situ* spectroscopic measurements as appropriate (24,25), are employed for characterization. Three-electrode circuitry is generally employed, with "counter" and "reference" electrodes completing the electrical circuit (2).

For ECD investigations, a simple two-electrode circuit is used, with a solid (often polymeric), gel, or liquid electrolyte being sandwiched between the "primary" electrochromic electrode and a charge-balancing "secondary" electrode, in what is essentially a rechargeable electrochemical cell (Fig. 1). The electrode substrates are typically of glass or flexible plastic [generally of poly(ethylene terephthalate) (PET) such as Mylar] sheet, coated with an optically transparent electrically conducting film such as tin-doped indium oxide (ITO), antimony-doped tin oxide, or F-doped tin oxide. ECDs are designed to operate in either transmissive or, with one electrode substrate having a silvered backing, reflective modes. For type I and II systems, the electrochromic material is dissolved in the electrolyte solution. For type III systems, the electrochromic material is first deposited onto the electrode substrate (Fig. 1). Color switching of an ECD takes place on charge/discharge by application of an appropriate electrical potential.

The secondary electrode redox reaction is chosen to be a system where there is little perceptible visible color change or as an electrochromic system where the color change is complementary to that of the color change at the primary electrochromic electrode.

Electrochromic Polymers based on Transition Metal Coordination Complexes

Transition metal coordination complexes are potentially useful as electrochromic materials because of their intense coloration and redox reactivity (10,26).

Chromophoric properties arise from low energy metal-to-ligand charge transfer (MLCT), intervalence CT, intraligand excitation, and related visible-region electronic transitions. Because these transitions involve valence electrons, chromophoric characteristics are altered or eliminated upon oxidation or reduction of the complex. Any colored transition metal coordination complex that is redox-switchable will undergo an accompanying color change, and will therefore be electrochromic at least to some extent. While these spectroscopic and redox properties alone would be sufficient for direct use of transition metal coordination complexes in solution-phase ECDs, polymeric systems based on coordination complex monomer units, which have potential use in all-solid-state systems, are frequently investigated.

Electrochemical polymerization is often used to prepare redox active polymer films on electrode surfaces (27). This technique has the advantage that a wide variety of conducting substrates can be used, and that film thickness can be directly controlled by the electrochemical potential scan rate, the potential range, polymerization time, and the choice of monomer concentration and electrolyte solution.

Reductive Electropolymerization of Polypyridyl Complexes. Good examples of transition-metal coordination complexes that could have potential use in ECDs include the $[M^{II}(bipy)_3]^{2+}$ (M = iron, ruthenium, osmium; bipy = 2,2′-bipyridine) series which are respectively red, orange, and green in the M(II) redox state, due to the presence of an intense MLCT absorption band (26). Electrochromicity results from loss of the MLCT absorption band on switching to the M(III) redox state.

Reductive electropolymerization of suitably substituted $[M^{II}(bipy)_3]^{2+}$ complexes allows the preparation of electrochromic redox active polymer films (28). This technique relies on the ligand-centered nature of the three sequential reductions of complexes such as $[Ru(L^1)_3]^{2+}$ (L^1 = 4-vinyl-4′-methyl-2,2′-bipyridine **2**), combined with the anionic polymerizability of suitable ligands (28). Vinyl-substituted pyridyl ligands such as (**1-3**), are generally employed, although metallopolymers have also been formed from complexes of halo-substituted pyridyl ligands such as 4-(bromomethyl)-4′-methyl-2,2′-bipyridine, via electrochemically initiated carbon–halide bond cleavage (29).

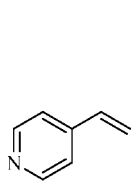

1

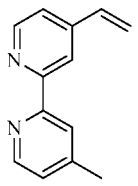

2

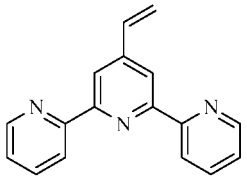

3

In either case, electrochemical reduction generates radicals which lead to carbon-carbon bond formation and oligomerization. Oligomers above a critical size are insoluble and thus thin films of the electroactive metallopolymer are produced on the electrode surface. As noted above, the color of such metallopolymer films in the M(II) redox state may be selected by suitable choice of the metal.

In a novel approach, spatial electrochromism has been demonstrated in metallopolymeric films based on polymeric polypyridyl complexes (30). Photolysis of

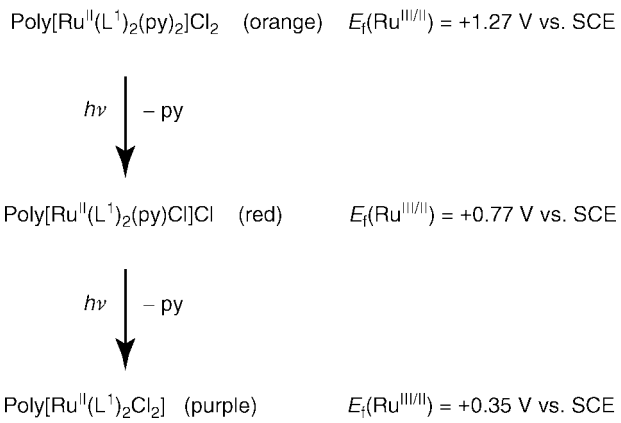

Fig. 2. Spatial electrochromism in metallopolymeric films using photolabile pyridine ligands.

poly[$Ru^{II}(L^1)_2(py)_2$]Cl_2 thin films on ITO glass in the presence of chloride ions leads to photochemical loss of the photolabile pyridine (py) ligands, and sequential formation of poly-[$Ru^{II}(L^1)_2$(py)Cl]Cl and poly-[$Ru^{II}(L^1)_2Cl_2$]. Contact lithography can be used to spatially control the photosubstitution process to form laterally resolved bicomponent films with image resolution below 10 μm. Dramatic changes occur in the colors and redox potentials of such ruthenium(II) complexes upon substitution of chloride for the pyridine ligands (Fig. 2). Striped patterns of variable colors are observed on addressing such films with a sequence of potentials.

Oxidative Electropolymerization of Polypyridyl Complexes. Oxidative electropolymerization of suitably substituted $[M^{II}(bipy)_3]^{2+}$ complexes offers an alternative approach to the preparation of electrochromic redox active polymer films. Oxidative electropolymerization has been described for iron(II) and ruthenium(II) complexes containing amino-substituted (31) and pendant aniline-substituted (32) 2,2′-bipyridyl ligands, and amino- and hydroxy-substituted 2,2′:6′,2″-terpyridinyl ligands (33) [ligand structures (**4**) and (**5**)]. Analysis of IR spectra suggests that the electropolymerization of $[Ru(L^4)_2]^{2+}$ [L^4 = (**4**)], via the pendant aminophenyl substituent, proceeds by a reaction mechanism similar to that of aniline (33). The resulting metallopolymer film reversibly switches from purple to pale pink on oxidation of Fe(II) to Fe(III). For polymeric films formed from $[Ru(L^5)_2]^{2+}$ [L^5 = (**5**)], via polymerization of the pendant hydroxyphenyl group, the color switch is from brown to dark yellow (see ELECTROPOLYMERIZATION).

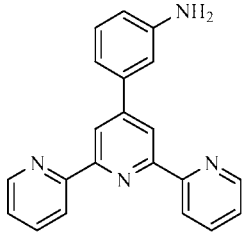

4

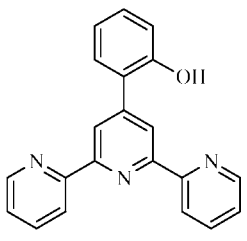

5

The dark yellow color is attributed to an absorption band at 455 nm, probably due to quinone moieties in the polymer formed during electropolymerization. IR spectra confirm the absence of hydroxyl groups in the initially deposited brown films.

Metallopolymer films have also been prepared by oxidative polymerization of complexes of the type $[M(phen)_2(4,4'\text{-bipy})_2]^{2+}$ (M = Fe, Ru, or Os; phen = 1,10-phenanthroline; 4,4′-bipy = 4,4′-bipyridine) (34). Such films are both oxidatively and reductively electrochromic; reversible film-based reduction at potentials below −1.00 V leads to dark purple films (34), the color and potential region being consistent with the viologen dication/radical cation electrochromic response. A purple state at high negative potentials has also been observed for polymeric films prepared from $[Ru(L^6)_3]^{2+}$ [L^6 = (**6**)] (35).

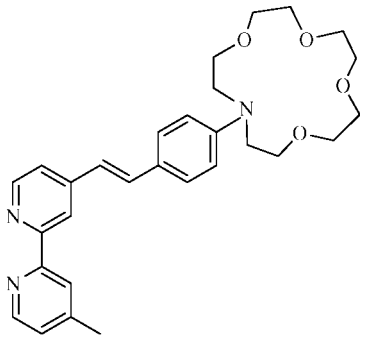

6

Electropolymerized films prepared from the complexes $[Ru(L^7)(bipy)_2][PF_6]_2$ (36) and $[Ru(L^8)_3][PF_6]_2$ (37,38) exhibit reversible orange/transparent electrochromic behaviour associated with the Ru(II)/Ru(III) interconversion [L^7 = (**7**); L^8 = (**8**)].

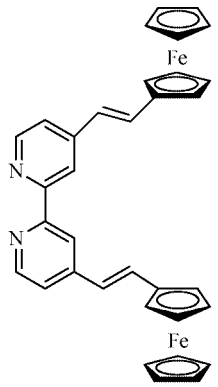

7

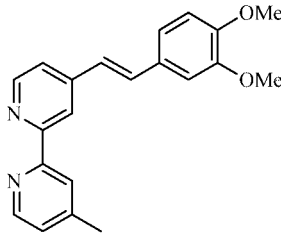

8

Electrochemical Routes to Polymeric Metallophthalocyanine Electrochromic Films. The porphyrins are a group of highly colored, naturally occurring pigments containing a tetrapyrrole porphine nucleus (Fig. 3) with substituents at the eight β-positions of the pyrroles, and/or the four

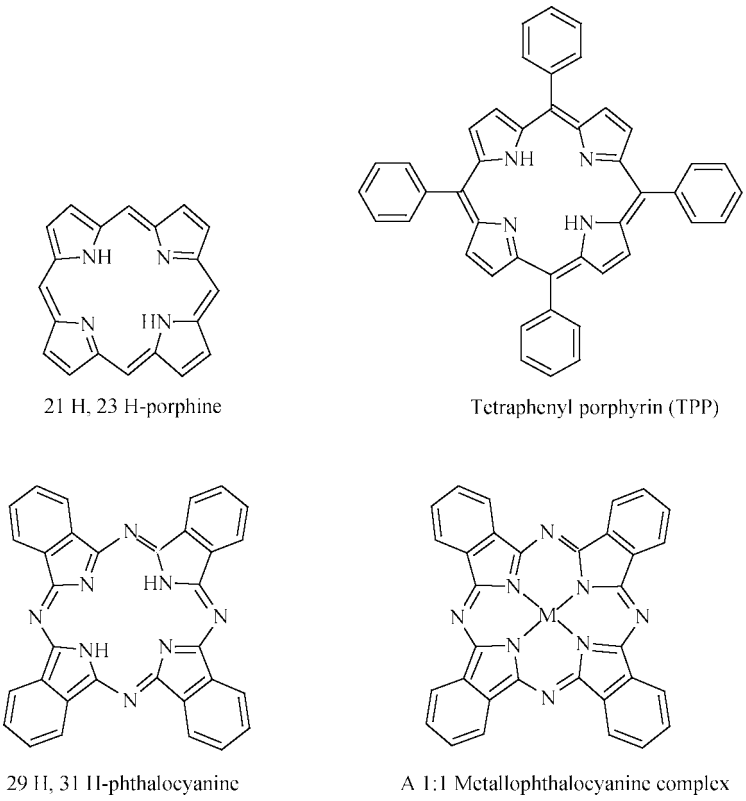

Fig. 3. Structures of a selection of porphyrins and phthalocyanines.

meso-positions between the pyrrole rings (39). The natural pigments are metal chelate complexes of the porphyrins. Phthalocyanines (Fig. 3) are tetraazatetrabenzo derivatives of porphyrins with highly delocalised π-electron systems.

The metal ion in metallophthalocyanines lies either at the center of a single phthalocyanine ligand (Pc = dianion of phthalocyanine) (Fig. 3), or between two rings in a sandwich-type complex (40). Phthalocyanine complexes of transition metals usually contain only a single Pc ring while lanthanide-containing species usually form bis(phthalocyanines), where the π-systems interact strongly with each other.

Since the discovery of the electrochromism of lutetium bis(phthalocyanine) [$Lu(Pc)_2$] thin films (2), the electrochromic properties of numerous (mainly rare-earth) metallophthalocyanines have been investigated. Lutetium bis(phthalocyanine) thin films are in fact polyelectrochromic, the initially deposited vivid green films being oxidized through a yellow-tan form, to a red form. Upon reduction, the green state can be switched first to a blue redox form, and then to a violet-blue form (2). Although, as described, [$Lu(Pc)_2$] films can exhibit five colors, only the blue-green transition is used in most prototype electrochromic devices. There are mechanical problems associated with the use of [$Lu(Pc)_2$]-based films, but in spite of such difficulties, electrochromic displays with good reversibility, fast response times, and little degradation over 5×10^6 cycles have been described.

The electrochromic properties of metallophthalocyanine films are generally investigated using low molecular weight sublimed (physical vapor deposition) films (40), although studies have also been carried out on films prepared using the Langmuir–Blodgett technique (40). More recently, methods for preparing thin films of polymeric phthalocyanines have been investigated. Such materials are attractive because of their rigidity, high stability, and strong, well-defined coupling of the electronic π-systems. Because polymeric phthalocyanines are not soluble and cannot be vaporized, new methods of thin-film formation have been developed.

For complexes with pendant aniline and hydroxy-substituted ligands, oxidative electropolymerization is a useful route to the preparation of metallophthalocyanine electrochromic films. Although polymer films prepared from $[Lu(L^9)_2]$ (L^9 = 4,4′,4″,4‴-tetraaminophthalocyanine) monomer show loss of electroactivity on cycling to positive potentials, in dimethyl sulfoxide (DMSO) the electrochemical response at negative potentials is stable, with the observation of two broad quasi-reversible one-electron redox couples (41). Spectroelectrochemical measurements reveal switching times of <2 s for the observed green-grey-blue color transitions in this region. The oxidative electropolymerization technique using pendant aniline substituents has also been applied to monophthalocyaninato transition-metal complexes (42); the redox reactions and color changes of two of the examples studied are given in equations (1–4).

$$\underset{\text{(blue-green)}}{\text{poly}-[Co^{II}(L^9)]} + ne^- \rightarrow \underset{\text{(yello-brown)}}{\text{poly}-[Co^{I}(L^9)]^-} \quad (1)$$

$$\underset{\text{(yellow-brown)}}{\text{poly}-[Co^{I}(L^9)]^-} + ne^- \rightarrow \underset{\text{[red-brown (thickfilms), deeppink (thinfilms)]}}{\text{poly}-[Co^{I}(L^9)]^{2-}} \quad (2)$$

$$\underset{\text{(green)}}{\text{poly}-[Ni^{II}(L^9)]} + ne^- \rightarrow \underset{\text{(blue)}}{\text{poly}-[Ni^{II}(L^9)]^-} \quad (3)$$

$$\underset{\text{(blue)}}{\text{poly}-[Ni^{II}(L^9)]^-} + ne^- \rightarrow \underset{\text{(purple)}}{\text{poly}-[Ni^{II}(L^9)]^{2-}} \quad (4)$$

The first reduction in the cobalt-based polymer is metal-centered, resulting in the appearance of a new MLCT transition, with the second reduction being ligand-centered. For the nickel-based polymer in contrast, both redox processes are ligand-based.

Electrochromic polymer films have been prepared by oxidative electropolymerization of the monomer tetrakis(2-hydroxyphenoxy)phthalocyaninato cobalt(II) (43). The technique involved voltammetric cycling at 100 $mV \cdot s^{-1}$ from -0.2 to $+1.2$ V vs SCE in dry acetonitrile, resulting in the formation of a fine green polymer. Cyclic voltammograms during polymer growth showed the irreversible

phenol oxidation peak at +0.58 V and a reversible phthalocyanine ring oxidation peak at +0.70 V. Polymer-modified electrodes gave two distinct redox processes with half-wave potentials at −0.35 [Co(II)/Co(I)] and −0.87 V (reduction of the ring). Color switching was from transparent light green [Co(II) state] to yellowish green [Co(I) state] to dark yellow (reduced ring).

The synthesis and electropolymerization of two tetrakis(2-pyrrol-1-ylalkoxy)phthalocyanines has been reported, and the electrical and optical properties discussed (44). This is the first example of the electropolymerization of a phthalocyanine where the electropolymerizable group (pyrrole) is electronically isolated from the phthalocyanine.

A complementary ECD using plasma-polymerized ytterbium bis(phthalocyanine) [PP-Yb($Pc)_2$] and thin films of the mixed-valence inorganic complex Prussian blue (PB) iron(III) hexacyanoferrate(II) films on ITO with an aqueous solution of 4 *M* KCl as electrolyte has been fabricated (45). Blue-to-green electrochromicity was achieved in a two-electrode cell by complementing the green-to-blue color transition (on reduction) of the PP-Yb($Pc)_2$ film with the blue (PB)-to-colorless (PW, Prussian white) transition (oxidation) of the PB. A three-color display (blue, green, and red) was fabricated in a three-electrode cell in which a third electrode (ITO) was electrically connected to the PB electrode. A reduction reaction at the third electrode, as an additional counter electrode, provided adequate oxidation of the PP-Yb($Pc)_2$ electrode, resulting in the red coloration of the PP-Yb($Pc)_2$ film.

Viologen Electrochromism and Polymeric Viologen Systems

Salts of quaternised 4,4′-bipyridine are herbicides and are manufactured on a large scale (16). The ready availability of 4,4′-bipyridine and the ease of varying the nature of the quaternizing agent have allowed intensive research into the electrochromic properties of such "viologens" (16). The prototype viologen, 1,1′-di-methyl-4,4′-bipyridilium, is known as methyl viologen (MV), with other simple symmetrical bipyridilium species being named "substituent" viologen. Of the three common viologen redox states (Fig. 4), the dication is the most stable and is colorless when pure unless optical charge transfer with the counter anion occurs. Reductive electron transfer to the viologen dication forms the radical cation, the stability of which is attributable to the delocalisation of the radical electron

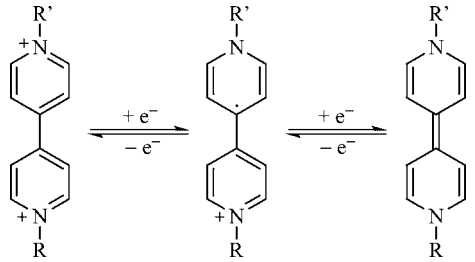

Fig. 4. The three common redox states of viologens, showing the two successive electron transfer reactions.

throughout the π-framework of the bipyridyl nucleus, the 1 and 1′ substituents commonly bearing some of the charge.

The viologen radical cations are intensely colored, with high molar absorption coefficients, owing to optical charge transfer between the (formally) +1 and zero valent nitrogens. Suitable choice of nitrogen substituents in viologens to attain the appropriate molecular orbital energy levels can, in principle, allow color choice of the radical cation. Simple alkyl groups, for example, promote a blue/violet color whereas aryl groups such as 4-cyanophenyl in 1,1′-bis(4-cyanophenyl)-4,4′-bipyridilium generally impart a green hue to the radical cation. The intensity of the color exhibited by di-reduced viologens (Fig. 4) is low since no optical charge transfer or internal transition corresponding to visible wavelengths is accessible.

Polymeric Viologen Systems. The write-erase efficiency of an ECD using for example aqueous MV would be low since both the dicationic and radical-cation states are very soluble. Improved MV-based systems may be made by retarding the rate at which the radical-cation product of electron transfer diffuses away from the electrode by use of an anionic polyelectrolyte such as poly(2-acrylamido-2-methylpropane-sulfonic acid) (polyAMPS) (46,47) or the sulfonated perfluorinated polyether, Nafion (48). An alternative approach is the surface modification of an electrode using silanization methodology (49), a preformed polymeric viologen salt (50) or oxidative electropolymerization of a pyrrole-substituted viologen (51) (Fig. 5).

In a more recent approach, polyelectrolyte multilayers of poly(butanyl viologen) dibromide (PBV) and poly(styrene sulfonate) sodium salt (PSS) have been prepared (52) using an alternating polyion solution deposition technique. In this technique, the ITO substrate is alternatively exposed to positive and negative polyelectrolytes, with spontaneous polymer deposition via coulombic interactions between surface and polyion of opposite charge. In this "layer-by-layer" deposition technique, all redox material is electrochemically addressable, with good electrochromic performance characteristics.

Conducting Electrochromic Polymers

Chemical or electrochemical oxidation of numerous resonance-stabilised aromatic molecules, such as pyrrole (**9**), thiophene (**10**), aniline (**11**), furan (**12**), carbazole (**13**), azulene (**14**) and indole (**15**), produces electronically conducting polymers (2,17–21,53–55) (see ELECTRICALLY ACTIVE POLYMERS).

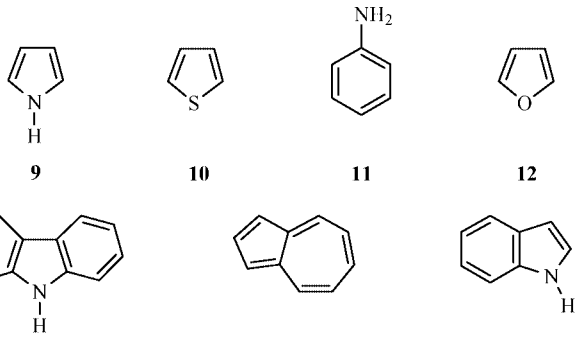

9 **10** **11** **12**

13 **14** **15**

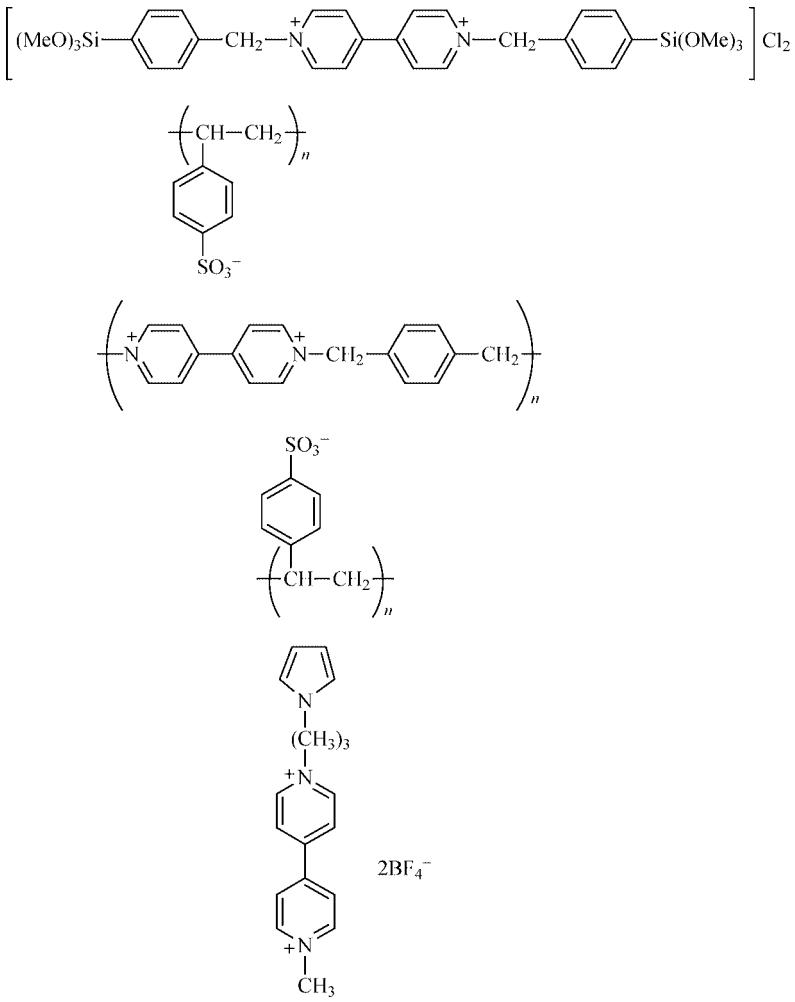

Fig. 5. Modified viologens used for surface modification.

Polymerization is initiated by monomer oxidation to yield the radical cation. The mechanism (55) is believed then to involve either radical-cation/radical-cation coupling or reaction of a radical-cation with a neutral monomer. The mechanism of electropolymerization of five-membered heterocycles with radical-cation/radical-cation coupling is shown in Fig. 6.

After loss of two protons and rearomatization, the dimer forms from the di-hydro dimer dication. The dimer (and succeeding oligomers) is more easily oxidized than the monomer and the resulting dimer radical cation undergoes further coupling reactions, proton loss, and rearomatization. Electropolymerization (qv) proceeds through successive electrochemical and chemical steps according to a general E(CE)n scheme, until the oligomer becomes insoluble in the electrolyte solution and precipitates onto the electrode surface (55).

In the oxidized state, conducting polymers are "doped" with counter anions ("p-doping") and have a delocalised π-electron band structure (55). The fairly large

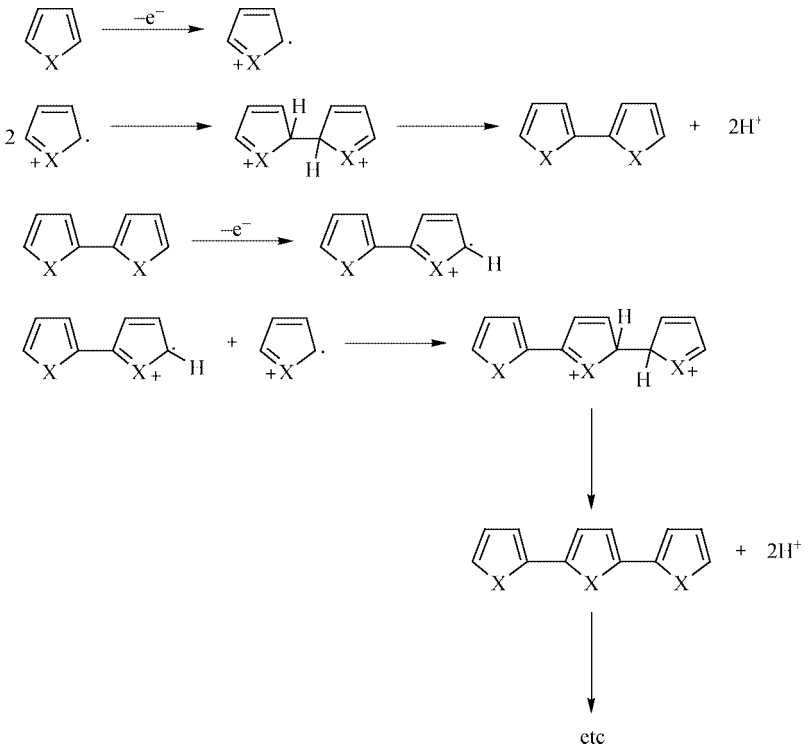

Fig. 6. Proposed mechanism of electropolymerization of five-membered heterocycles. The case of radical-cation/radical-cation coupling is shown.

energy bandgap (E_g) between the highest occupied π-electron band (valence band) and the lowest unoccupied band (the conduction band) determines the intrinsic optical properties of these materials. Reduction of p-doped conducting polymers, with concurrent counter anion exit, removes the electronic conjugation to give the "undoped" (neutral) electrically insulating form. On further reduction, the undoped neutral state can also undergo cathodic doping, with cation insertion ("n-doping") to balance the injected charge. However, the stability of the negatively charged polymer state is rather limited and n-doping is generally more difficult to achieve. It is to be noted that the p-doping and n-doping nomenclature comes from classical extrinsic semiconductor theory. The supposed similarity between conducting polymers and doped semiconductors arises from the way that redox changes in the polymer causes the incorporation (and hence doping) of counter ions into the polymer. In fact, the suitability of the terms *doping* and *dopant* has been criticised when referring to the movement of counter ions and electronic charge through these polymers because true doping involves such tiny (classically sub ppm) amounts of dopant. However, terms such as doping are now so widely used that additional, new terminology might confuse.

All conducting polymers are potentially electrochromic in thin-film form, redox switching giving rise to new optical absorption bands in accompaniment with simultaneous transport of electronic charge and counter ions in the polymer matrix. p-doping shifts the optical absorption band towards the lower energy

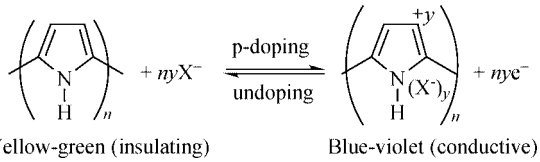

Fig. 7. Electrochromism in polypyrrole thin films. The yellow-green (undoped) form undergoes reversible oxidation to the blue-violet (conductive) form, with insertion of charge-compensating anions (X^-).

part of the spectrum. The color contrast between doped and undoped forms of the polymer depends on the magnitude of the bandgap of the undoped polymer. The final doped conducting state is characterized by the presence of positive charges along the polymer chains associated with charge-compensating anions. Thin films of conducting polymers with E_g greater than 3 eV (~400 nm) are transparent or slightly colored in the undoped form, and in the doped form are generally highly absorbant in the visible region. Those with small E_g [1.5 (~800 nm)–2 eV (~600 nm)] are highly absorbant in the undoped form but, after doping, the free carrier absorption is relatively weak in the visible region.

An early reported example of an electrochromic conducting polymer is polypyrrole (56), which in the undoped (reduced) insulating state is yellow/green, with a peak maximum characteristic of a π–π^* interband transition. The interband transition energy decreases upon doping to yield the blue/violet doped (oxidized) conductive state (Fig. 7).

The electrochromism of polypyrrole is unlikely to be exploited, because of the degradation of the film on repetitive color switching. Electrochromic conducting polymers based on thiophene and aniline have received greater attention.

Polythiophenes as Electrochromic Materials. Polythiophenes (55) are of interest as electrochromic materials due to their ease of chemical and electrochemical synthesis, environmental stability, and processability. A huge number of substituted thiophenes has been synthesized, and this has led to the study of numerous novel polythiophene(s), with particular emphasis on poly(3-substituted thiophenes) and poly(3,4-disubstituted thiophenes) (55).

Thin polymeric films of the parent thiophene are blue ($\lambda_{max} = 730$ nm) in the doped (oxidized) state and red ($\lambda_{max} = 470$ nm) in the undoped form. However, because of its lower oxidation potential, the electropolymerization of 3-methyl thiophene has been more intensively studied than the parent thiophene. Furthermore, the introduction of a methyl group at the β-position of the thiophene ring leads to a significant increase of the polymer conjugation length and hence electronic conductivity (55). This effect has been attributed to the statistical decrease in the number of α–β' couplings and to the decrease of the oxidation potential caused by the inductive effect of the methyl group (55). Poly(3-methylthiophene) is purple when neutral and turns pale blue on oxidation.

The evolution of the electronic band structure during electrochemical p-doping of poly(3-methylthiophene) has been followed by recording *in situ* visible and NIR spectra (55). The undoped polymer's strong absorption band, with a maximum at 530 nm (2.34 eV), is characteristic of a π–π^* interband transition. Upon doping, the interband transition decreases, and two new optical transitions (at

$\sim$1.5 and $\sim$0.5 eV) appear at lower energy, corresponding to the presence of two bipolaron (a double-charged spinless defect) bands. A pair of polarons (each single charged of spin $\frac{1}{2}$) is unstable with respect to the formation of a bipolaron, and in thiophene-based polymers the bipolaron states appear even at low doping levels. The characteristic absorption pattern of the free carrier of the metallic-like state then appears when the bipolaron bands finally merge with the valence and conduction bands.

Tuning of color states is possible by suitable choice of thiophene monomer, and this represents a major advantage of using conducting polymers for electrochromic applications. Subtle modifications to the monomer can significantly alter spectral properties. For example, the colors available with polymer films prepared from 3-methylthiophene–based oligomers are strongly dependent on the relative positions of methyl groups on the polymer backbone (57,58). Colors available include pale blue, blue, and violet in the oxidized form, and purple, yellow, red, and orange in the reduced form. The color variations have been ascribed to changes in the effective conjugation length of the polymer chain.

In research directed to using the same electrochromic material for both the primary and secondary electrodes, a series of conducting polymer films based on 3-(*p*-X-phenyl)thiophene monomers (X = —CMe_3, —Me, —OMe, —H, —F, —Cl, —Br, —CF_3, —SO_2Me) has been investigated (59). In this case the presence of electron-withdrawing groups on the phenyl ring serve to assist the stabilization of the n-doped state and these materials can be both reversibly reduced and oxidized (n- and p-doped). A model ECD using poly(cyclopenta[2,1-*b*; 4,3-*b*′]dithiophene-4-(cyano, nonafluorobutylsulfonyl)-methylidene), a low bandgap conducting polymer which is both p- and n-dopable, as both the anode and the cathode material has been reported (60).

Study of the effects of steric factors is provided by the electronic properties of polythiophenes with 3,4-dialkyl substituents. In principle, disubstitution at the β, β' positions should provide the synthetic basis to perfectly stereoregular polymers. However, this approach is severely limited by the steric interactions between substituents, which leads to a decrease in polymer conjugation length. In fact, poly(3,4-dialkylthiophenes) have higher oxidation potentials, higher optical bandgaps, and lower conductivities than poly(3-alkylthiophenes) (55). Cyclization between the 3 and 4 positions relieves steric hindrance in thiophenes, but many are harder to electropolymerize than, say, 3-methylthiophene. The electron-donating effect of alkoxy groups offers a solution here, and alkoxy-substituted polythiophenes are intensively investigated for their electrochromic properties (61,62). Materials based on poly(3,4-(ethylenedioxy)thiophene) (PEDOT) have a bandgap lower than polythiophene and alkyl-substituted polythiophenes, owing to the presence of the two electron-donating oxygen atoms adjacent to the thiophene unit.

The bandgap of PEDOT ($E_g = 1.6 - 1.7$ eV) itself is 0.5 eV lower than polythiophene, which results in an absorbance maximum in the NIR region. Compared to other substituted polythiophenes, these materials exhibit excellent stability in the doped state which is associated with high conductivity. Doped PEDOT is almost transparent in the visible region (with a sky-blue tint) and the neutral polymer is deep blue. Because PEDOT and its alkyl derivatives are cathodically-coloring electrochromic materials, they are suitable for use with "anodically-coloring" conducting polymers in the construction of dual polymer ECDs (63).

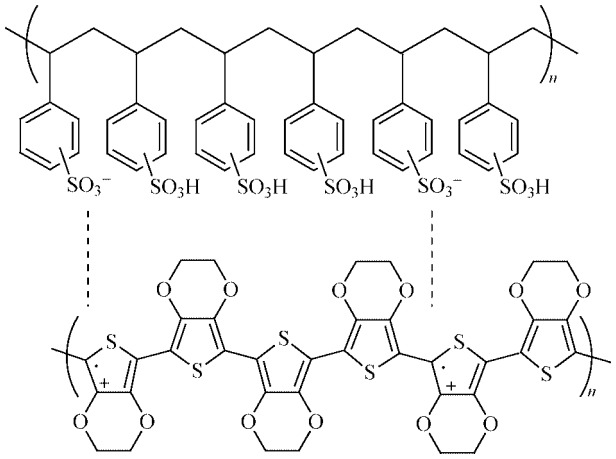

Fig. 8. Structure of the PEDOT:PSS blend (BAYTRON P).

PEDOT was first developed by Bayer AG research laboratories in Germany in an attempt to produce an easily oxidized and stable conducting polymer (64,65). By blocking the β-positions of the heterocyclic ring, the formation of α–β linkages during polymerization is prevented, resulting in a more regiochemically defined material. To aid processing, the insolubility of PEDOT can be overcome by the incorporation of a water-soluble polyelectrolyte [poly(styrene sulfonate), PSS] as the counter ion in the doped state, to yield the commercially available product PEDOT:PSS (BAYTRON P) (Fig. 8), which forms a dispersion in water. [Bayer AG now produce the EDOT monomer 3,4-(ethylenedioxy)thiophene, on a multiton scale and it is available commercially as BAYTRON M.]

As for thiophene, many substituted EDOT monomers have been synthesized, and this has led to the study of a range of variable-bandgap PEDOT-based materials (61,62). The bandgap of such conjugated polymers is controlled by varying the degree of π-overlap along the backbone via steric interactions, and by controlling the electronic character of the π-system with electron-donating or-accepting substituents. The latter is accomplished by using substituents and co-repeat units that adjust the highest occupied molecular orbital (HOMO) and lowest unoccupied molecular orbital (LUMO) energy levels of the α-system (61,62). An interesting set of materials is the family of EDOT-based polymers that has been prepared with higher energy gaps than the parent PEDOT. Using a series of oxidatively polymerizable bis-arylene EDOT monomers (Fig. 9), polymers with bandgaps ranging from 1.4 – 2.5 eV have been prepared (61,62). In the neutral polymers, a full "rainbow" of colors is available, from blue through purple, red, orange, green, and yellow. A few examples include bis-arylene EDOT-based polymers, with spacers of vinylene ($E_g = 1.4$ eV); 2,5-dialkoxyphenylene ($E_g = 1.75 - 2.0$ eV); biphenyl ($E_g = 2.3$ eV); dialkylfluorene ($E_g = 2.3$ eV); and carbazole ($E_g = 2.5$ eV).

Following earlier work (52) with polyviologen systems, the layer-by-layer deposition of PEDOT:PSS (as the polyanion) with linear poly(ethylene imine) (LPEI) (as the polycation) has recently been reported (66). The PEDOT:PSS/LPEI (cathodically coloring) electrode was then combined with a polyaniline/polyAMPS

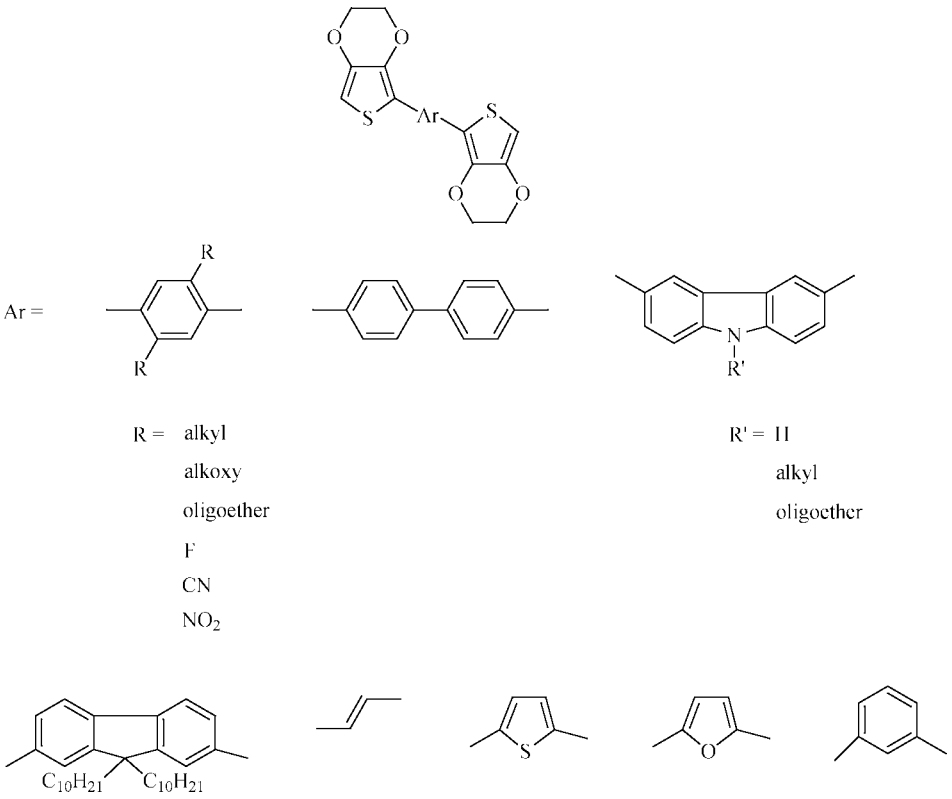

Fig. 9. Bis-EDOT-arylene co-oligomers.

(anodically coloring) layered system to give a blue-green to yellow electrochromic device. More recently, the redox and electrochromic properties of films prepared by the layer-by-layer deposition of fully water-soluble, self-doped poly(4-(2,3-dihydrothieno [3,4-*b*]-[1,4]dioxin-2-yl-methoxy))-1-butanesulfonic acid, sodium salt (PEDOT-S) and poly(allylamine hydrochloride) (PAH) onto unmodified ITO-coated glass have been studied (67). For this system, both the film preparation and redox switching is carried out in an aqueous medium. [PEDOT-S is a self-doping polymer where oxidation and reduction of the polymer backbone is coupled with cation movement out of (oxidized) and back into (reduced) the polymer film]. The PEDOT-S/PAH film was found to switch from light blue in the oxidized form to pink/purple in the reduced form.

A new organic/inorganic complementary ECD has recently been described (68) on the basis of the assembly of PEDOT/ITO glass and Prussian blue [PB, iron(III) hexacyanoferrate(II)]/ITO glass substrates with a poly(methyl methacrylate) (PMMA)-based gel polymer electrolyte (GPE: 1 *M* $LiClO_4$/propylene carbonate/10wt% PMMA). The color states of the PEDOT (blue/colorless) and PB (colorless/blue) films fulfill the complementary requirement.

"Star" conducting polymers, which have a central core with multiple branching points and linear conjugated polymeric arms radiating outward, are currently being investigated for electrochromic applications (69,70). Examples include star

conducting polymers in which the centrosymmetric cores include hyperbranched poly(1,3,5-phenylene) (PP) and poly(triphenylamine) (PTPA), and the radiating arms are regioregular poly(3-hexylthiophene), poly(3,4-ethylenedioxythiophene-didodecyloxybenzene) and poly(dibutyl-3,4-propylenedioxythiophene). These polymers have the advantage that they are all castable by spin coating from a carrier solvent such as tetrahydrofuran (THF), and several can be doped in solution, so that thin films of both doped and undoped forms can be prepared. Despite the branched structure, star polymers self-assemble into thin films with morphological, electrical, and optical properties that reveal a surprisingly high degree of structural order. The polymers, which are smooth and reflective, all have spectral features that produce a strong band in the visible region for the reduced state and a broad band extending into the NIR for the oxidized state. The color of the polymers ranges from red to violet to deep blue in the reduced state, and blue to very pale blue in the oxidized state.

Polyanilines as Electrochromic Materials. Polyaniline films are polyelectrochromic (transparent yellow-green-dark blue-black) (71), the yellow-green transition being durable to repetitive color switching (72). Several redox mechanisms involving protonation–deprotonation and/or anion ingress/egress have been proposed (73–75), with Figure 10 giving the composition of the various redox states.

The two low wavelength spectral bands observed in films of polyanilines are assigned to an aromatic π–π^* transition ($\leq$330 nm) related to the extent of conjugation between the adjacent rings in the polymer chain, and to radical cations formed in the polymer matrix ($\leq$440 nm) (76,77). With increase in applied potential, the $\leq$330 nm band absorbance decreases and the $\leq$440 nm increases. Beyond +0.30 V the conducting region is entered; the $\leq$440 nm band decreases as a broad free carrier electron band $\sim$800 nm is introduced.

Of the numerous conducting polymers based on substituted anilines that have been investigated, those with alkyl substituents have received much attention. Poly(*o*-toluidine) and poly(*m*-toluidine) films have been found to offer enhanced stability of polyelectrochromic response in comparison with polyaniline (78). Absorption maxima and redox potentials shift from values found for polyaniline because of the lower conjugation length in polytoluidines. Response times, τ, for the yellow-green electrochromic transition in the films correlate with the likely differences in the conjugation length implied from the spectroelectrochemical data. τ values for polyaniline are found to be lower than for poly(*o*-toluidine), which in turn has lower values than poly(*m*-toluidine). As for polyaniline, response times indicate that the reduction process is faster than the oxidation. Electrochemical quartz crystal microbalance (EQCM) studies have demonstrated the complexity of redox switching in poly(*o*-toluidine) films in aqueous perchloric acid solutions which occurs in two stages and is accompanied by nonmonotonic mass changes that are the result of perchlorate counterion, proton co-ion, and solvent transfers (79). The extent and rate of each of these transfers are dependent upon electrolyte concentration, experimental time scale, and the switching potential, so that observations in a single electrolyte on a fixed time scale cannot be unambiguously interpreted.

Although electropolymerization is a suitable method for the preparation of relatively low surface area electrochromic conducting polymer films, it may not

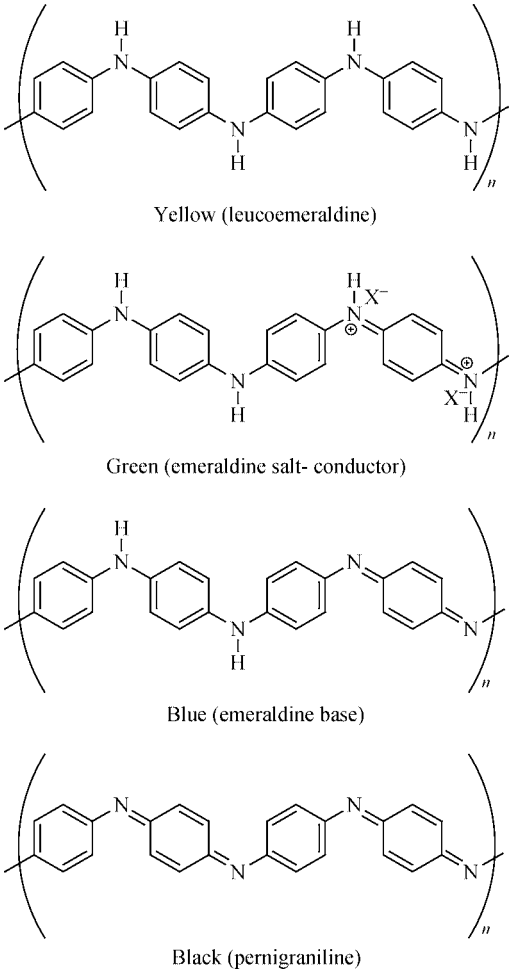

Fig. 10. Proposed composition of some of the redox states of polyaniline, from the fully reduced (leucoemeraldine) through to the fully oxidised (pernigraniline) forms. X^- is a charge-balancing anion.

be suitable for fabricating large-area coatings. Significant effort therefore goes into the synthesis of soluble conducting polymers such as poly(*o*-methoxyaniline) which can then be deposited as thin films by casting from solution. In a novel approach, large-area electrochromic coatings have been prepared by incorporating polyaniline into polyacrylate-silica hybrid sol–gel networks using suspended particles or solutions and then spray or brush-coating onto ITO surfaces (80). Silane functional groups on the polyacrylate chain act as coupling and cross-linking agents to improve surface adhesion and mechanical properties of the resulting composite coatings.

Similarly to the PEDOT/PB system noted above, numerous workers (81–88) have combined Prussian blue with polyaniline in complementary ECDs that exhibit deep-blue to light-green electrochromism. Electrochromic compatibility is

obtained by combining the colored oxidized state of the polymer with the blue PB, and the "bleached" reduced state of the polymer with Prussian green (PG) (eq. 5):

$$\underset{\text{(colored)}}{\text{Oxidizedpolyaniline}} + \text{PB} \rightarrow \underset{\text{(bleached)}}{\text{Emeraldinepolyaniline}} + \text{PG} \tag{5}$$

An electrochromic window for solar modulation using PB, polyaniline, and WO_3 has been developed (84,85,87,88), where the symbiotic relationship between polyaniline and PB, and incorporated PB together with polyaniline and WO_3, was exploited in a complete solid-state electrochromic window. The total device comprised

glass|ITO|polyaniline|PB|polyAMPS|WO_3|ITO|glass

Compared to earlier results with a polyaniline/WO_3 window, much more light was blocked off by inclusion of PB within the polyaniline matrix, while still regaining about the same transparency during the bleaching of the window. Other polyaniline-based ECDs include a device that exhibits yellow–transparent electrochromicity using electropolymerized 1,1′-bis[[p-phenylamino(phenyl)]amido-]ferrocene (89).

Composite Conducting Polymer Electrochromic Materials. The electropolymerization of monomers in the presence of other electrochromic additives which may have electrochromic or other properties has been a popular approach to the preparation of materials with tailored properties (2). A water-soluble poly(styrenesulfonic acid)-doped polyaniline has been prepared both by persulfate oxidative coupling and anodic oxidation of aniline in aqueous dialysed poly(styrenesulfonic acid) solution (90). Composites of polyaniline and cellulose acetate have been prepared both by casting of films from a suspension of polyaniline in a cellulose acetate solution and deposition of cellulose acetate films onto electrochemically prepared polyaniline films (91). The electrochromic properties of the latter films were studied by spectroelectrochemistry and the presence of the cellulose acetate was found not to impede the redox processes of the polyaniline. The electroactivity and electrochromism of the graft copolymer of polyaniline and nitrilic rubber have been studied using stress–strain measurements, cyclic voltammetry, frequency response analysis, and visible range spectroelectrochemistry (92). Results indicated that the graft copolymer exhibits mechanical properties similar to a cross-linked elastomer with the electrochromic and electrochemical properties typical of polyaniline.

An example of a case where the additive itself is electrochromic is the encapsulation of the redox indicator dye indigo carmine within a polypyrrole matrix (93,94). More recently, 3-D graphs have been constructed from absorbance data acquired during cyclic voltammetry. The enhancement and modulation of the color change on indigo carmine insertion into polypyrrole or polypyrrole/dodecylsulfonate films was shown (95). As expected, the use of indigo carmine as dopant improves the films' electrochromic contrast ratio.

Conclusions

The field of electrochromism is rapidly expanding both in terms of the range of electrochromic systems that has been reported and the novel commercial applications that are being proposed. In the case of electrochromic polymers, a number of representative examples of both redox and conductive polymers have been described in this article. Tailoring the color of electrochromic polymers remains an area of active research. Although not described here, in addition to the synthesis of novel functionalized monomers and use of composites, other chemical and physical methods are investigated for the control of the perceived color of electrochromic polymers. Methods include the use of copolymers, polymer blends, laminates and patterning using screen and ink-jet printing (96). Analysis of ECD color changes are now routinely measured by spectrocolorimetry using Commission Internationale de l'Eclairage (CIE) (x,y)-chromaticity coordinates. This method is useful for the comparison of the electrochemical and optical properties of conjugated polymers, and for gaining control of the color of dual polymer electrochromic devices (97). By controlling the electron density and steric interactions along conjugated polymer backbones, a set of electrochromic polymers that provide colors through the full range of color space have been developed through the study of twelve electrochromic polymers (97).

In addition to possible roles as the active electrochromic material, it should be recognized that polymers may also be used in electrochromic devices as electrolyte solution thickeners, as plasticizers, as the matrix or solid phase of gels, as solid polymer electrolytes, and even as sealants to insulate a glass unit configuration (98).

Further developments in the field of electrochromic polymers seem limited only by the skills, resources, and imagination of synthetic organic chemists, polymer chemists, and material scientists. However, the ultimate usefulness of such fascinating materials hinges on a detailed understanding of their fundamental redox operation and the accompanying physicochemical–structural changes, and therefore the field is truly interdisciplinary.

For comprehensive surveys of the field of electrochromism, readers should scan the now compendious review (2-10) and primary literature, proceedings of conferences (99–107), the extensive patent literature (quite neglected here), and the Internet. Electrochromism research conferences regularly take place under the auspices of the Electrochemical Society (ECS) (99–103). Other sponsors also participate, for example the American Institute of Chemical Engineers at the Annual Meeting held in Chicago, 11–16 November 1990 ("Fundamentals of Electrochromic Devices"), also published (104), and many, often under the "Displays" heading, in the United Kingdom and Europe. Since the first meeting in Venice in 1994, the International Meeting on Electrochromism (IME) series has established itself as a leading conference for the dissemination of scientific and technical information in the field of electrochromics. The Second International Meeting on Electrochromism (IME-2) in 1996 in San Diego, U.S., was reported in a special (and belated) issue of *Solar Energy Materials and Solar Cells* (105). IME-3 in 1998 in London, U.K., and IME-4 in 2000 in Uppsala, Sweden, appeared in special issues of *Electrochimica Acta* (106,107). The proceedings of IME-5 in 2002 in

Golden, Colorado, U.S., will be published in a special issue of *Solid State Ionics*. IME-6 (28 August – 2 September 2004) will take place in the Czech Republic.

BIBLIOGRAPHY

1. P. Bamfield, *Chromic Phenomena: Technological Applications of Colour Chemistry*, Royal Society of Chemistry, Cambridge, 2001.
2. P. M. S. Monk, R. J. Mortimer, and D. R. Rosseinsky, *Electrochromism: Fundamentals and Applications*, VCH, Weinheim, Germany, 1995.
3. C. G. Granqvist, *Handbook of Inorganic Electrochromic Materials*, Elsevier, Amsterdam, 1995.
4. M. Green, *Chem. Ind.* 641–644 (1996).
5. N. Leventis, in *McGraw-Hill Encyclopedia of Science and Technology*, Vol. 6, 9th ed., McGraw-Hill, New York, 2002, pp. 254–257.
6. R. J. Mortimer, *Chem. Soc. Rev.* **26**, 147–156 (1997).
7. R. J. Mortimer, *Electrochim. Acta* **44**, 2971–2981 (1999).
8. D. R. Rosseinsky and R. J. Mortimer, *Adv. Mater.* **13**, 783–793 (2001).
9. N. M. Rowley and R. J. Mortimer, *Sci. Prog.* **85**, 243–262 (2002).
10. R. J. Mortimer and N. M. Rowley, in J. A. McCleverty and T. J. Meyer, eds., *Comprehensive Coordination Chemistry–II: From Biology to Nanotechnology*, Elsevier, Oxford. M. D. Ward, ed., Vol. 9.2 (in press).
11. R. D. Rauh, *Electrochim. Acta* **44**, 3165–3176 (1999).
12. M. D. Ward and J. A. McCleverty, *J. Chem. Soc., Dalton Trans.* 275–288 (2002).
13. R. A. Colley, P. M. Budd, J. R. Owen, and S. Balderson, *Polym. Int.* **49**, 371–376 (2000).
14. M. Grätzel, *Nature* **409**, 575–576 (2001).
15. D. Cummins, G. Boschloo, M. Ryan, D. Corr, S. Nagaraja Rao, and D. Fitzmaurice, *J. Phys. Chem. B* **104**, 11449–11459 (2000).
16. P. M. S. Monk, *The Viologens: Physicochemical Properties, Synthesis and Applications of the Salts of 4,4′-Bipyridine*, John Wiley & Sons, Inc., Chichester, U.K., 1998.
17. T. A. Skotheim, R. L. Elsenbaumer, and J. R. Reynolds, eds., *Handbook of Conducting Polymers*, 2nd ed., Marcel Dekker, New York, 1998.
18. J. Heinze, *Top. Curr. Chem.* **152**, 1–47 (1990).
19. S. J. Higgins, *Chem. Soc. Rev.* **26**, 247–257 (1997).
20. M. Mastragostino, in B. Scrosati, ed., *Applications of Electroactive Polymers*, Chapman and Hall, London, 1993, Chapt. 7, pp. 223–249.
21. B. Scrosati, in Ref. 20, Chapt. 8, pp. 250–282.
22. J. N. Huiberts, R. Griessen, J. H. Rector, R. J. Wijngarden, J. P. Decker, D. G. de Groot, and N. J. Koeman, *Nature* **380**, 231–234 (1996).
23. A. J. Bard and L. R. Faulkner, *Electrochemical Methods: Fundamentals and Applications*, 2nd ed., John Wiley & Sons, Inc., New York, 2001.
24. R. J. Mortimer, in J. C. Lindon, G. E. Tranter, and J. L. Holmes, eds., *Encyclopedia of Spectroscopy and Spectrometry*, Vol. 3, Academic Press, London, 1999, pp. 2161–2174.
25. R. J. Mortimer, in J. C. Lindon, G. E. Tranter, and J. L. Holmes, eds., *Encyclopedia of Spectroscopy and Spectrometry*, Vol. 3, Academic Press, London, 1999, pp. 2174–2181.
26. A. Juris, V. Balzani, F. Barigelletti, S. Campagna, P. Belser, and A. von Zelewsky, *Coord. Chem. Rev.* **84**, 85–277 (1988).
27. R. J. Mortimer, in R. G. Compton and G. Hancock, eds., *Research in Chemical Kinetics*, Vol. 2, Elsevier, Amsterdam, 1994 pp. 261–311.
28. H. D. Abruña, P. Denisevich, M. Umaña, T. J. Meyer, and R. W. Murray, *J. Am. Chem. Soc.* **103**, 1–5 (1981).

29. S. Gould, G. F. Strouse, T. J. Meyer, and B. P. Sullivan, *Inorg. Chem.* **30**, 2942–2949 (1991).
30. R. M. Leasure, W. Ou, J. A. Moss, R. W. Linton, and T. J. Meyer, *Chem. Mater.* **8**, 264–273 (1996).
31. C. D. Ellis, L. D. Margerum, R. W. Murray, and T. J. Meyer, *Inorg. Chem.* **22**, 1283–1291 (1983).
32. C. P. Horwitz and Q. Zuo, *Inorg. Chem.* **31**, 1607–1613 (1992).
33. K. Hanabusa, A. Nakamura, T. Koyama, and H. Shirai, *Polym. Int.* **35**, 231–238 (1994).
34. H.-T. Zhang, P. Subramanian, O. Fussa-Rydal, J. C. Bebel, and J. T. Hupp, *Sol. Energy Mater. Sol. Cells* **25**, 315–325 (1992).
35. P. D. Beer, O. Kocian, R. J. Mortimer, C. Ridgway, and N. R. Stradiotto, *J. Electroanal. Chem.* **408**, 61–66 (1996).
36. P. D. Beer, O. Kocian, and R. J. Mortimer, *J. Chem. Soc., Dalton Trans.* 3283–3288 (1990).
37. P. D. Beer, O. Kocian, R. J. Mortimer, and C. Ridgway, *J. Chem. Soc. Faraday Trans.* **89**, 333–338 (1993).
38. P. D. Beer, O. Kocian, R. J. Mortimer, and C. Ridgway, *J. Chem. Soc. Dalton Trans.* 2629–2638 (1993).
39. T. Mashiko and D. Dolphin, in G. Wilkinson, R. D. Gillard, and J. A. McCleverty, eds., *Comprehensive Coordination Chemistry*, Vol. 2, Pergamon, Oxford, 1987, Chapt. 21.1.
40. C. C. Leznoff and A. B. P. Lever, eds., *Phthalocyanines: Properties and Applications*, John Wiley & Sons, Inc., New York, Vol. 1, 1989; Vol. 2, 1993; Vol. 3, 1993; Vol. 4, 1996.
41. D. J. Moore and T. F. Guarr, *J. Electroanal. Chem.* **314**, 313–321 (1991).
42. H. F. Li and T. F. Guarr, *J. Electroanal. Chem.* **297**, 169–183 (1991).
43. M. Kimura, T. Horai, K. Hanabusa, and H. Shirai, *Chem. Lett.* **7**, 653–654 (1997).
44. N. Trombach, O. Hild, D. Schlettwein, and D. Wöhrle, *J. Mater. Chem.* **12**, 879–885 (2002).
45. N. Kashiwazaki, *Sol. Energy Mater. Sol. Cells* **25**, 349–359 (1992).
46. J. M. Calvert, T. J. Manuccia, and R. J. Nowak, *J. Electrochem. Soc.* **133**, 951–953 (1986).
47. A. F. Sammells and N. U. Pujare, *J. Electrochem. Soc.* **133**, 1270–1271 (1986).
48. R. J. Mortimer and J. L. Dillingham, *J. Electrochem. Soc.* **144**, 1549–1553 (1997).
49. R. N. Dominey, T. J. Lewis, and M. S. Wrighton, *J. Phys. Chem.* **87**, 5345–5354 (1983).
50. H. Akahoshi, S. Toshima, and K. Itaya, *J. Phys. Chem.* **85**, 818–822 (1981).
51. G. Bidan, A. Deronzier, and J.-C. Moutet, *J. Chem. Soc., Chem. Commun.* 1185–1186 (1984).
52. J. Stepp and J. B. Schlenoff, *J. Electrochem. Soc.* **144**, L155–L157 (1997).
53. G. P. Evans, in H. Gerischer and C. W. Tobias, eds., *Advances in Electrochemical Science and Engineering*, Vol. 1, VCH, Weinheim, Germany, 1990, pp. 1–74.
54. K. Hyodo, *Electrochim. Acta* **39**, 265–272 (1994).
55. J. Roncali, *Chem. Rev.* **92**, 711–738 (1992).
56. E. M. Genies, G. Bidan, and A. F. Diaz, *J. Electroanal. Chem.* **149**, 101–113 (1983).
57. M. Mastragostino, C. Arbizzani, A. Bongini, G. Barbarella, and M. Zambianchi, *Electrochim. Acta* **38**, 135–140 (1993).
58. M. Mastragostino, C. Arbizzani, P. Ferloni, and A. Marinangeli, *Solid State Ionics* **53–56**, 471–478 (1992).
59. D. J. Guerrero, X. M. Ren, and J. P. Ferraris, *Chem. Mater.* **6**, 1437–1443 (1994).
60. J. P. Ferraris, C. Henderson, D. Torres, and D. Meeker, *Synth. Met.* **72**, 147–152 (1995).
61. L. Groenendaal, F. Jonas, D. Freitag, H. Pielartzik, and J. R. Reynolds, *Adv. Mater.* **12**, 481–494 (2000).
62. L. Groenendaal, G. Zotti, P.-H. Aubert, S. M. Waybright, and J. R. Reynolds, *Adv. Mater.* **15**, 855–879 (2003).

63. S. A. Sapp, G. A. Sotzing, and J. R. Reynolds, *Chem. Mater.* **10**, 2101–2108 (1998).
64. F. Jonas and L. Schrader, *Synth. Met.* **41–43**, 831–836 (1991).
65. G. Heywang and F. Jonas, *Adv. Mater.* **4**, 116–118 (1992).
66. D. DeLongchamp and P. T. Hammond, *Adv. Mater.* **13**, 1455–1459 (2001).
67. C. A. Cutler, M. Bouguettaya, and J. R. Reynolds, *Adv. Mater.* **14**, 684–688 (2002).
68. T.-S. Tung and K.-C. Ho, in *Electrochromics Materials and Applications Symposium*, 203rd Electrochemical Society Meeting, Paris, France, 27 April–2 May 2003. Meeting Abstracts, Vol. 2003–01, Abstract No. 1313 (Symposium Organisers: A. Rougier, D. Rauh, G. A. Nazri, and G. Hunter).
69. R. D. Rauh, D. Peramunage and F. Wang, in *Electrochromics Materials and Applications Symposium*, 203rd Electrochemical Society Meeting, Paris, France, 27 April–2 May 2003. Meeting Abstracts, Vol. 2003–01, Abstract No. 1330 (Symposium Organisers: A. Rougier, D. Rauh, G. A. Nazri, and G. Hunter).
70. R. D. Rauh, F. Wang, J. R. Reynolds, and D. L. Meeker, *Electrochim. Acta* **46**, 2023–2029 (2001).
71. A. F. Diaz and J. A. Logan, *J. Electroanal. Chem.* **111**, 111–114 (1980).
72. T. Kobayashi, H. Yoneyama, and H. Tamura, *J. Electroanal. Chem.* **161**, 419–423 (1984).
73. A. G. MacDiarmid and A. J. Epstein, *Faraday Discuss. Chem. Soc.* **88**, 317–332 (1989).
74. A. Ray, A. F. Richter, A. G. MacDiarmid, and A. J. Epstein, *Synth. Met.* **29**, 151–156 (1989).
75. F. Rourke and J. A. Crayston, *J. Chem. Soc., Faraday Trans.* **89**, 295–302 (1993).
76. D. E. Stilwell and S.-M. Park, *J. Electrochem. Soc.* **136**, 427–433 (1989).
77. Y. Wei, W. W. Focke, G. E. Wnek, A. Ray, and A. G. MacDiarmid, *J. Phys. Chem.* **93**, 495–499 (1989).
78. R. J. Mortimer, *J. Mater. Chem.* **5**, 969–973 (1995).
79. S. Ramirez and A. R. Hillman, *J. Electrochem. Soc.* **145**, 2640–2647 (1998).
80. G.-W. Jang, C. C. Chen, R. W. Gumbs, Y. Wei, and J.-M. Yeh, *J. Electrochem. Soc.* **143**, 2591–2596 (1996).
81. E. A. R. Duek, M.-A. De Paoli, and M. Mastragostino, *Adv. Mater.* **4**, 287–291 (1992).
82. E. A. R. Duek, M.-A. De Paoli, and M. Mastragostino, *Adv. Mater.* **5**, 650–652 (1993).
83. M. Morita, *J. Appl. Polym. Sci.* **52**, 711–719 (1994).
84. B. P. Jelle, G. Hagen, and S. Nodland, *Electrochim. Acta* **38**, 1497–1500 (1993).
85. B. P. Jelle, and G. Hagen, *J. Electrochem. Soc.* **140**, 3560–3564 (1993).
86. N. Leventis and Y. C. Chung, *J. Electrochem. Soc.* **137**, 3321–3322 (1990).
87. B. P. Jelle and G. Hagen, *J. Appl. Electrochem.* **29**, 1103–1110 (1999).
88. B. P. Jelle and G. Hagen, *Sol. Energy Mater. Sol. Cells* **58**, 277–286 (1999).
89. L. Wang, Q. Q. Wang, and V. Cammarata, *J. Electrochem. Soc.* **145**, 2648–2654 (1998).
90. K. Shannon and J. E. Fernandez, *J. Chem. Soc., Chem. Commun.* 643–644 (1994).
91. M. A. De Paoli, E. R. Duek, and M. A. Rodrigues, *Synth. Met.* **41**, 973–978 (1991).
92. E. L. Tassi, M. A. De Paoli, S. Panero, and B. Scrosati, *Polymer* **35**, 565–572 (1994).
93. Z. Gao, J. Bobacka, A. Lewenstam, and A. Ivaska, *Electrochim. Acta* **39**, 755–762 (1994).
94. Y. Li and S. Dong, *J. Electroanal. Chem.* **348**, 181–188 (1993).
95. E. M. Girotto and M. A. De Paoli, *Adv. Mater.* **10**, 790–793 (1998).
96. J. P. Ferraris, D. S. K. Mudiginda, D. L. Meeker, J. Boehme, D. C. Loveday, T. H. Dam, and I. D. Brotherston, in *Electrochromics Materials and Applications Symposium*, 203rd Electrochemical Society Meeting, Paris, France, 27 April – 2 May 2003. Meeting Abstracts, Vol. 2003–01, Abstract No. 1329 (Symposium Organisers: A. Rougier, D. Rauh, G. A. Nazri, and G. Hunter).
97. B. C. Thompson, P. Schottland, K. Zong, and J. R. Reynolds, *Chem. Mater.* **12**, 1563–1571 (2000).

98. H. J. Byker, *Electrochim. Acta* **46**, 2015–2022 (2001).
99. M. K. Carpenter and D. A. Corrigan, eds., *Proceedings of the First Symposium on Electrochromic Materials*, Vol. 90-2, The Electrochemical Society, Pennington, N.J., 1990.
100. K.-C. Ho and D. A. MacArthur, eds., *Proceedings of the Second Symposium on Electrochromic Materials*, Vol. 94-2, The Electrochemical Society, Pennington, N.J., 1994.
101. K.-C. Ho, C. B. Greenberg, and D. M. MacArthur, eds., *Proceedings of the Third Symposium on Electrochromic Materials*, Vol. 96-24, The Electrochemical Society, Pennington, N.J., 1996.
102. *Electrochromics Materials and Applications Symposium*, 203rd Electrochemical Society Meeting, Paris, France, 27 April–2 May 2003. Meeting Abstracts, Vol. 2003–01 (Symposium Organisers: A. Rougier, D. Rauh, G. A. Nazri, and G. Hunter).
103. A. Rougier, D. Rauh, and G. A. Nazri, eds., *Proceedings of the Symposium on Electrochromic Materials, Vol. IV*, The Electrochemical Society, Pennington, N.J. (in press).
104. *Sol. Energy Mater. Sol. Cells* **25**, 195–381 (1992).
105. *Sol. Energy Mater. Sol. Cells* **56**, 193–493 (1999).
106. *Electrochim. Acta* **44**, 2969–3258 (1999).
107. *Electrochim. Acta* **46**, 1919–2292 (2001).

ROGER J. MORTIMER
Department of Chemistry, Loughborough University

ELECTRON SPIN RESONANCE

Introduction

Electron spin resonance (ESR) is a spectroscopic technique that detects the transitions induced by electromagnetic radiation between the energy levels of electron spins in the presence of a static magnetic field. The method can be applied to the study of species containing one or more unpaired electron spins; examples include organic and inorganic radicals, triplet states, and complexes of paramagnetic ions. Electron paramagnetic resonance (EPR) and EPR imaging (EPRI) are often used in the literature instead of ESR and ESRI. Spectral features such as resonance frequencies, splittings, line shapes, and line widths are sensitive to the electronic distribution, molecular orientations, nature of the environment, and molecular motions. Theoretical and experimental aspects of ESR have been covered in a number of books (1–8), and reviewed periodically (9–11).

The great sensitivity and specificity of ESR methods have been utilized to advantage in order to investigate and clarify important questions in polymeric systems (12). The most obvious candidates for initial studies were chain-growth and depolymerization reactions; in both cases radical intermediates are the driving force for reaction and can be detected by ESR (12–15). Analyses of radicals produced by high-energy irradiation (γ, electron beams) contributed to a better

Encyclopedia of Polymer Science and Technology. Copyright John Wiley & Sons, Inc. All rights reserved.

understanding of the reaction mechanism, and to the determination of reaction rate constants; the most detailed studies were performed on polystyrene (PS) and poly(methyl methacrylate) (PMMA).

But even in systems that lack species with unpaired electrons, doping of the system with stable radicals as "spin probes," or attachment of radicals to polymeric chains as "spin labels," have extended the use of ESR methods to a large number of polymer types and self-assembled polymeric systems (9,16–21).

Since the last edition of *EPST*, ESR methods have undergone great advances in experimental techniques and in the simulation of ESR spectra. Examples include, but are not limited to, high-field ESR at frequencies up to 250 GHz, time domain (pulsed) ESR techniques, double resonance methods, and ESR imaging. Some of these important advances have extended the range and capabilities of ESR spectroscopy and have made possible the deduction of quantitative information on the structure, dynamics, transport, and distribution of paramagnetic species. The development of advanced methods for spectra simulations has made possible the deduction of detailed motional mechanisms. These novel ESR methods have been applied to polymeric systems: experimental results together with computer simulation of the line shapes have added important details concerning microphase separation and ion clustering in ionomers, chain aggregation in solutions of amphiphilic polymers, interaction of polyelectrolytes with their counterions, and structure of polyelectrolyte–surfactant complexes. In recent years ESR imaging (ESRI) methods have been developed and applied for measurements of diffusion coefficients, and for nondestructive spectral profiling of degradation processes in polymeric materials. For these reasons, this article will focus on the application and significance of recent advanced ESR methods to polymeric systems.

Fundamentals of Electron Spin Resonance (ESR) Spectroscopy

Basic Principles. The Hamiltonian energy operator $\mathcal{H}_{\text{spin}}$ for an electron spin is given by equation 1 (operators, vectors, and tensors are in bold),

$$\mathcal{H}_{\text{spin}} = g_{\text{e}}\beta_{\text{e}}\boldsymbol{S}\cdot\boldsymbol{H} \tag{1}$$

where $\boldsymbol{S}$ is the spin angular momentum, $\boldsymbol{H}$ is the magnetic field vector in gauss (G) or tesla (1 T $= 10^4$ G), β_{e} is the Bohr magneton equal to 9.274×10^{-21} erg/G (or 9.274×10^{-24} J/T), and g_{e} (equal to 2.0023 for a free electron) is the g factor or spectroscopic splitting factor (dimensionless). This spin Hamiltonian operates only on the spin wave functions α and β, whose spin angular momenta are $+1/2$ and $-1/2$ in units of $h/2\pi$; h is the Planck's constant. For a magnetic field oriented along the z direction equation 1 becomes

$$\mathcal{H}_{\text{spin}} = g_{\text{e}}\beta_{\text{e}}S_zH \tag{1a}$$

The energy difference between the two levels is $\Delta E = h\nu = g_{\text{e}}\beta_{\text{e}}H$. Typically ESR is carried out in a magnetic field of about 3500 G (or 0.35 T). The corresponding absorption frequency is ≈9.5 GHz, in the microwave frequency range known

as the X band. ESR measurements at other frequencies are also carried out, and will be described below.

The real power of electron spin resonance spectroscopy for structural studies is based on the interaction of the unpaired electron spin with nuclear spins. This interaction splits the energy levels and often allows determination of the atomic or molecular structure of species containing unpaired electrons, and of the ligation scheme around paramagnetic transition-metal ions. The more complete Hamiltonian is given in equation 2 for a species containing *one* unpaired electron, where the summations are over all the nuclei, n, interacting with the electron spin.

$$\mathcal{H}_{\text{spin}} = \beta_e \boldsymbol{H} \cdot g_e \cdot \boldsymbol{S} - \sum g_n \beta_n \boldsymbol{H} \cdot \boldsymbol{I}_n + h \sum \boldsymbol{S} \cdot \boldsymbol{A}_n \cdot \boldsymbol{I}_n + h \sum \boldsymbol{I}_n \cdot Q_n \cdot \boldsymbol{I}_n \tag{2}$$

In equation 2 $\boldsymbol{g}_e$ is the electronic g tensor, g_n is the nuclear g factor (dimensionless), β_n is the nuclear magneton in erg/G (or J/T), $\boldsymbol{I}_n$ is the nuclear spin angular momentum operator, $\boldsymbol{A}_n$ is the electron–nucleus hyperfine tensor in Hz, and $\boldsymbol{Q}_n$ (nonzero for $\boldsymbol{I}_n \geq 1$) is the quadrupole interaction tensor in Hz. The first two terms in the Hamiltonian are the electron and nuclear Zeeman interactions, respectively; the third term is the electron–nuclear hyperfine interaction; and the last term is the nuclear quadrupole interaction. For the usually investigated Kramers systems with an odd number of unpaired electrons, the transition moment is finite only for a magnetic dipole moment operator oriented perpendicular to the static magnetic field direction. In an ESR resonator in which the sample is placed, the microwave magnetic field must be therefore perpendicular to the external static magnetic field. The selection rules for the electron spin transitions are given in equation 3,

$$\Delta m_S = \pm 1 \text{ and } \Delta m_I = 0 \tag{3}$$

where m_S and m_I refer to the electron and nuclear spin quantum numbers, respectively. Transitions correspond therefore to a *change* in the electron spin orientation, and a *fixed* nuclear spin orientation. The energy difference between two adjacent transitions associated with the same type of nucleus is defined as the hyperfine constant, usually symbolized by A in frequency units (MHz). Since $\Delta m_I = 0$, the effect of the nuclear Zeeman term (second term on the right-hand side of eq. 2) and of the nuclear quadrupole term (last term on the right-hand side of eq. 2) in the spin Hamiltonian cancel out to first order. In the solid state the selection rules are not strictly obeyed when the hyperfine coupling and nuclear Zeeman interaction are of the same order of magnitude. Forbidden transitions with $\Delta m_S = \pm 1$ and $\Delta m_I = \pm 1$ then have a finite transition probability and can be used for measuring nuclear frequencies by time-domain techniques. In this situation ESR line shapes are slightly influenced by the nuclear Zeeman and nuclear quadrupole interactions.

Anisotropic g and Hyperfine Interaction. The hyperfine tensor $\boldsymbol{A}$ for each nucleus is a real 3×3 matrix that can always be diagonalized. The components of the diagonalized hyperfine tensor consist of an isotropic part, a_o, and a purely anisotropic part, $\boldsymbol{a}'$, whose orientational average is zero. Thus, the $\boldsymbol{a}'$ components are averaged out in fluid media and can only be determined in the solid state or in the case of highly restricted molecular motion. The diagonal elements

of a diagonalized hyperfine tensor are called the principal values. The *complete* hyperfine tensor (including anisotropic and isotropic contributions) is determined from single-crystal spectra, or by analysis of ESR spectra in disordered ("powder") samples, which consist of a superposition of all possible orientations.

The physical interpretation of the anisotropic principal values is based on the classical magnetic dipole interaction between the electron and nuclear spin angular momenta, and depends on the electron–nuclear distance, r_n. Assuming that both spins can be described as point dipoles, the interaction energy is given by equation 4, where θ is the angle between the external magnetic field and the direction of r_n.

$$\mathcal{H}_{spin}(\text{aniso}) = -g_e\beta_e g_n\beta_n\left[(1-3\cos^2\theta)/r_n^3\right]\boldsymbol{I}\cdot\boldsymbol{S} \tag{4}$$

Thus, for the general case of a delocalized electron spin, the anisotropic hyperfine components depend upon the orientation-weighted spatial average of ${r_n}^{-3}$ over the electronic orbital of the unpaired electron in a paramagnetic species. The number of spectral lines associated with a given interacting nucleus is $2\boldsymbol{I}_n + 1$ and the lines are of equal intensity. Often an anisotropic hyperfine interaction is accompanied by g anisotropy, and the components of the g tensor can be determined in a similar way, from ESR spectra measured in single crystals or disordered systems. Single crystal studies also allow the determination of the orientation between the principal directions of the g- and hyperfine tensors, and the crystal symmetry axes.

Analysis of the complete anisotropy (rhombic symmetry) allows the determination of the x, y, and z components of the $\boldsymbol{g}$ and $\boldsymbol{A}$ tensors. For point symmetries or pseudosymmetries that include a rotation axis C_n with $n \geq 3$, the tensors have axial symmetry; an example is seen in Figure 1**a**, for paramagnetic VO^{2+} in polyacrylamide gels swollen by water and measured at 253 K (23). The hyperfine interaction is between the electron spin and the ^{51}V nucleus ($I = 7/2$). In this case we measure the hyperfine interaction and the g value parallel to the symmetry axis of the $VO(H_2O)_5{}^{2+}$ complex ($A_\parallel$ and $g_\parallel$, respectively), and in the axial plane ($A_\perp$ and $g_\perp$), as indicated in the "stick" diagrams of Figure 1**a**.

Isotropic Hyperfine Analysis. The special case of isotropic g and hyperfine interaction will now be considered. This simplification is valid when the anisotropic interactions are averaged by rapid tumbling. The quadrupole interaction will be omitted because it is purely anisotropic. The resulting simplified spin Hamiltonian is given in equation 5.

$$\mathcal{H}_{spin}(\text{iso}) = g_e\beta_e\boldsymbol{H}\cdot S - \sum g_n\beta_n\boldsymbol{H}\cdot\boldsymbol{I}_n + h\sum A_n\boldsymbol{S}\cdot\boldsymbol{I}_n \tag{5}$$

In some systems, when an anisotropic spectrum is detected at low temperatures, increasing the temperature leads to averaging of the principal components of the hyperfine and g tensors, and therefore to isotropic spectra. As an example, we show in Figure 1**b** the ESR spectrum at 278 K of VO^{2+} in polyacrylamide networks swollen by a water/acetone mixture (80:20 v/v), which consists of eight equally spaced lines of equal intensity (22,23). The height of each line is different, because the dynamical process gives lines with different widths. The experimental spectrum is well reproduced (broken lines) using a theoretical expression for the

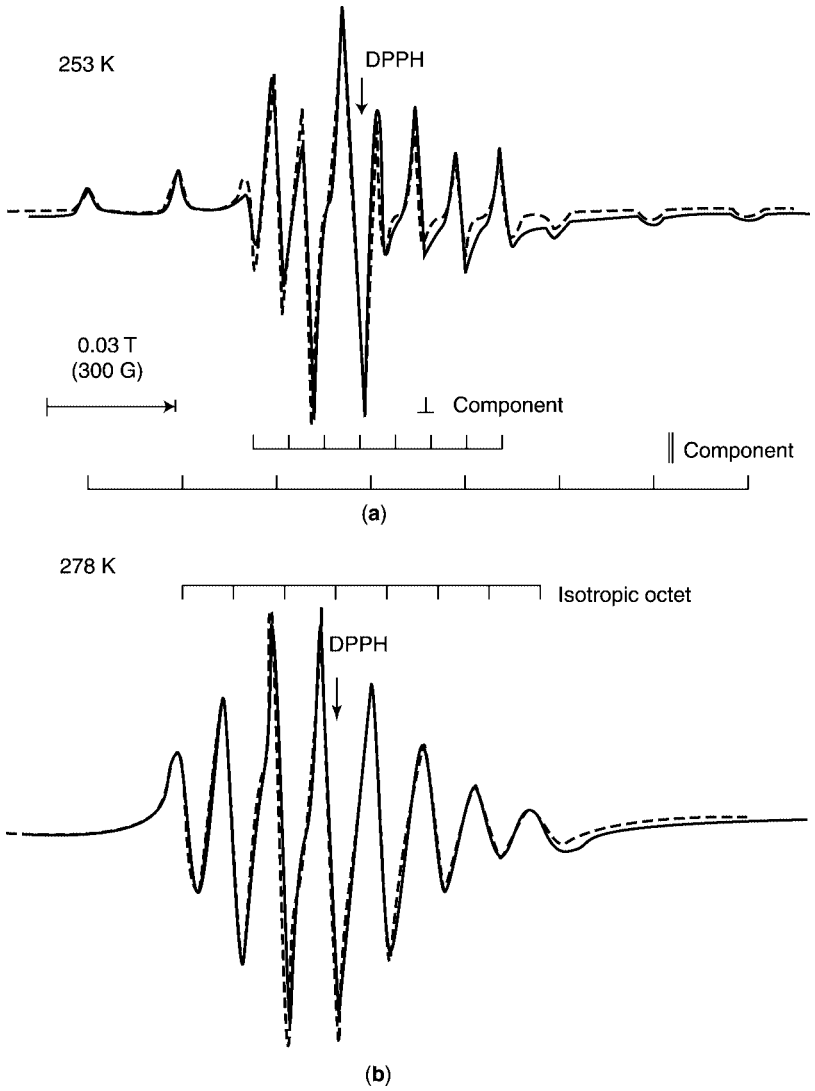

Fig. 1. X-band ESR spectra of VO^{2+} (—): (**a**) at 253 K, in chemically cross-linked polyacrylamide gels swollen by water; (**b**) at 278 K, in chemically cross-linked polyacrylamide gels swollen by water/acetone mixture (80:20 v/v). Simulated spectra (----) based on the rigid limit model in (**a**) and motionally narrowed model in (**b**). "Stick" diagrams show the positions of signals for the parallel and perpendicular components (**a**) and isotropic component (**b**). DPPH is used as a g-marker, $g = 2.0036$.

line width variation that is based on relaxation theory. The stick diagram above the spectrum shows the line positions.

Line Shape Analysis for Nitroxide Spin Probes. Nitroxide radicals as spin probes and labels are useful for the determination of the motional mechanism, rotational correlation time, τ_c, and local polarity. Figure 2**a** demonstrates that the relative line widths and line heights depend on the rotational correlation time τ_c, which is inversely proportional to the diffusion constant of rotational diffusion,

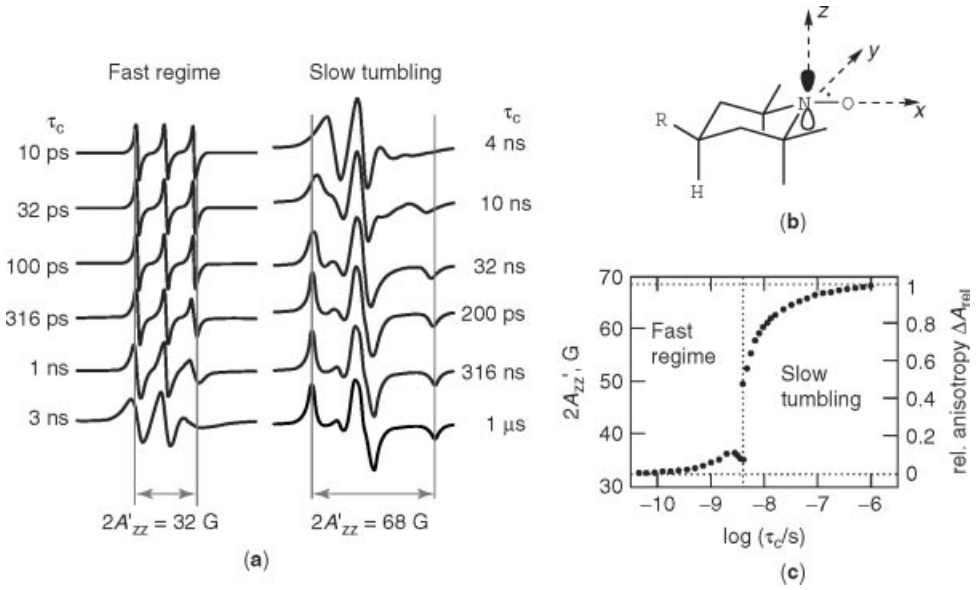

Fig. 2. (**a**) Dependence of nitroxide spectra on the rotational correlation time, τ_c, for isotropic rotational diffusion. (**b**) molecular axes system of a nitroxide radical. R is a hydrogen atom for TEMPO or a functional group in other nitroxides. (**c**) Dependence of the extreme separation, $2A'_{zz}$, and the relative anisotropy, ΔA_{rel}, on the rotational correlation time.

and can be deduced from simulating the ESR spectra. Qualitatively, τ_c can be interpreted as a typical time during which the paramagnetic species maintains its spatial orientation. The molecular axes system of a nitroxide radical is presented in Figure 2**b** (24). The motionally narrowed ESR spectrum of a nitroxide radical, corresponding to $\tau_c < 10$ ps, consists of three equally spaced signals separated by $\approx$16 G due to hyperfine splitting of ^{14}N nuclei ($a_N = 16$ G), top trace in the left panel of Figure 2**a**. The separation between the outer extrema of the spectrum in this limit is $2A_{zz,fast} \approx 32$ G. A dramatically different spectrum is observed in the rigid limit corresponding to $\tau_c > 1$ μs, where the extreme separation measured in the powder spectrum becomes $2A_{zz,slow} \approx 68$–70 G, depending on the local polarity.

In polymeric materials the rigid limit can be obtained at ambient temperatures if the polymer is below the glass-transition temperature, T_g; otherwise the sample must be cooled. For rotational correlation times between the two limits, the line shape depends strongly on τ_c. For unrestricted, isotropic tumbling, rotational correlation times can be determined from the extreme separation $2A'_{zz}$ (Fig. 2**c**). On the basis of the relative anisotropy defined in equation 6,

$$\Delta A_{rel} = (2A'_{zz} - 2A_{zz,fast})/(2A_{zz,slow} - 2A_{zz,fast}) \quad (6)$$

the line shape analysis becomes independent of the isotropic and anisotropic hyperfine coupling of the particular nitroxide.

The dynamics of spin probes in polymers is often characterized by T_{50G}, the temperature for which the extreme separation is 50 G, corresponding to $\Delta A_{rel} = 0.5$ and $\tau_c \approx 3.5$ ns. Below T_{50G} the nitroxide is in the slow tumbling regime and

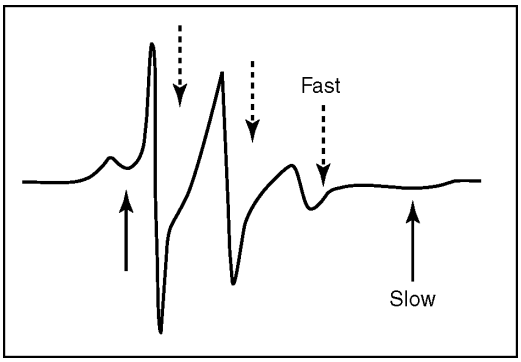

Fig. 3. X-band ESR spectrum at 300 K of a nitroxide radical derived from Tinuvin 770, a hindered amine stabilizer, in heterophasic poly(acrylonitrile–butadiene–styrene) (ABS). Fast and slow components are indicated (see text).

the spectra are anisotropic; above T_{50G} the fast regime is reached. The relation between T_{50G} (measured by ESR) and T_g (measured by DSC, for instance) depends, however, on the type of spin probe or label and its interaction with the polymer matrix.

In microphase-separated systems, ESR spectra may consist of two contributions, from nitroxides in both fast and slow tumbling regimes, thus providing evidence for the presence of two types of domains with different dynamics and transition temperatures. This case is illustrated in Figure 3 for a nitroxide radical in heterophasic poly(acrylonitrile–butadiene–styrene) (ABS); the fast and slow components in the ESR spectrum measured at 300 K are indicated, and represent radicals in butadiene-rich and acrylonitrile/styrene-rich domains, respectively (25).

Advanced ESR Methods

Multifrequency (MF) and High Field (HF) ESR. ESR spectra are often measured at a frequency of ≈9.4 GHz (X band), because of convenient sample size and availability of commercial spectrometers. Multifrequency ESR has been proven beneficial for both the quality and quantity of information that can be obtained. The optimal frequencies are system dependent: spectra at 35 GHz (Q band) are used to increase the separation (in G) when species differing in g values are present. The corresponding magnetic field at Q band is ≈12,000 G. Because large g anisotropies are detected for transition-metal ions, ESR spectra at Q band are useful for discriminating between ions in different environments. In recent years, however, it has become evident that microwave frequencies *lower* than 9 GHz are sometimes the best choice, especially in disordered systems, where local heterogeneities ("strain") lead to a distribution of ESR parameters and to considerable line broadening. This conclusion emerged from a study of $^{63}Cu^{2+}$ in Nafion perfluorinated ionomers swollen by acetonitrile: the line width of the parallel component, $\Delta H_{\parallel}$, in the ESR spectrum was studied at four microwave frequencies, in the range 1.2–9.4 GHz (26). The narrowest line widths for the $m_I = -3/2$ and $-1/2$ signals (the two low-field lines of the parallel quartet) were

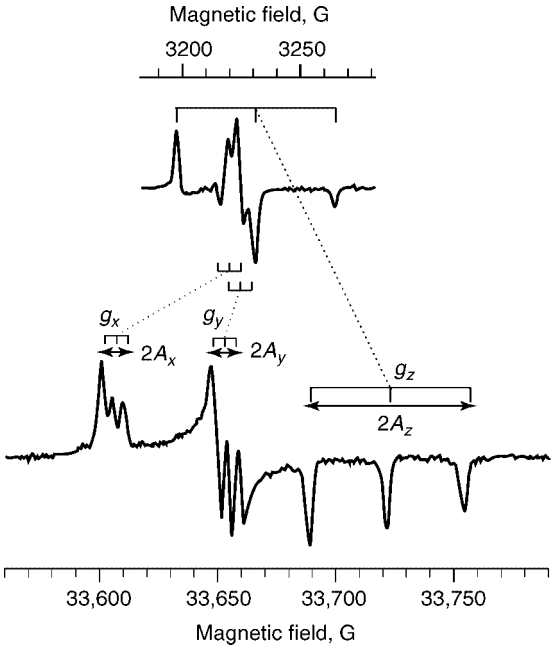

Fig. 4. ESR spectra of aqueous solution of a perdeuterated nitroxide PDTEMPONE in toluene-d_8 at 130 K (at or close to the rigid limit). Top: at 9 GHz. Bottom: at 94.4 GHz. Principal values of the g and A tensors are shown respectively by vertical bars and horizontal arrows. To convert G to T, multiply by 1×10^{-4}. Redrawn from Ref. 11, with permission.

detected at C band (4.7 GHz) and L band (1.2 GHz), respectively. Signals at Q band and higher frequencies are excessively broadened by strain.

HF ESR has been utilized to advantage for increasing the resolution in terms of the g tensor components; Figure 4 presents a comparison of ESR spectra of a nitroxide radical at 9 GHz (top) and at 94.4 GHz (bottom) (11). Major advantages of HF ESR are: improved accuracy in the determination of the principal values of the g tensor, the ability to measure splittings in the x and y directions that are not resolved at X band, and increased ability to resolve species with different magnetic parameters.

Time-Domain ESR Methods. Performing ESR experiments with pulsed instead of continuous irradiation provides great flexibility for designing experiments that can be adapted to specific problems. In general, such time-domain experiments can be used to distinguish between different types of spin relaxation and to separate the various interactions in the spin Hamiltonian (8). Separation of interactions corresponds to an increase in resolution and allows precise measurement of small contributions to the spin Hamiltonian in the presence of line broadening due to larger contributions. Such techniques are therefore most useful for solid materials or soft matter, where ESR spectra are usually poorly resolved.

Solid-state time-domain ESR is usually based on echo experiments. The transverse magnetization is excited by a pulse with a flip angle of $\pi/2$ and decays within the deadtime t_d of the spectrometer following the high-power pulse. In the two-pulse echo experiment this transverse magnetization is refocused by a second pulse with a flip angle of π, which is applied after a delay $\tau > t_d$ with respect

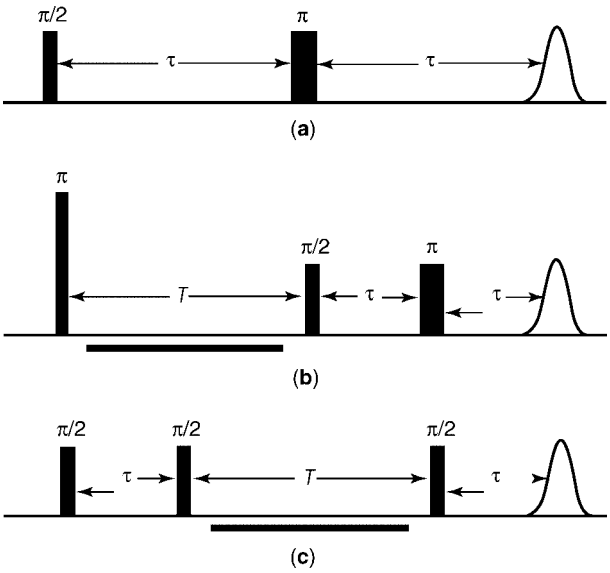

Fig. 5. Pulse sequences for basic time-domain ESR and pulsed ENDOR experiments. (**a**) Primary echo experiment. (**b**) Inversion recovery experiment (variation of T) or Davies ENDOR. (**c**) Stimulated echo experiment or Mims ENDOR. For ENDOR experiments, the horizontal bar in (**b**) and (**c**) indicates a radiofrequency pulse, whose frequency is varied while all interpulse delays are fixed.

to the first pulse (Fig. 5**a**). The integral of the echo signal centered at time 2τ is measured either as a function of the static field H at constant τ (echo-detected ESR spectroscopy), or as a function of τ at constant H. In the latter experiment we observe the echo decay due to transverse relaxation with time constant T_2. Combining the variations of the two parameters in a two-dimensional experiment allows the characterization of the anisotropy of T_2, which is in turn related to the specific motion of the paramagnetic center in the material.

To measure the longitudinal relaxation time T_1, an inversion or saturation pulse is applied, followed, after a variable time T, by a two-pulse echo experiment for detection (Fig. 5**b**). The inversion or saturation pulse induces a large change of the echo amplitude for $T \ll T_1$. With increasing T, the echo amplitude recovers to its equilibrium value with time constant T_1. The echo amplitude of the stimulated echo (Fig. 5**c**) decays with time constant T_2 when the interpulse delay τ is incremented, and with the stimulated-echo decay time constant $T_{SE} \leq T_1$ when the interpulse delay T is incremented. A faster decay, compared to inversion or saturation recovery experiments, can arise from spectral diffusion, because of a change of the resonance frequency for the observed spins, of the order of $\Delta\nu = 1/\tau$ on the time scale of T. Quantitative analysis of spectral diffusion can provide information on the reorientation dynamics of the paramagnetic centers.

Double Resonance Methods. Electron nuclear double resonance (ENDOR) is the effect of applying a radiofrequency that induces nuclear spin flips, in addition to the microwave frequency that induces electron spin flips. In the CW version of the experiment, the ENDOR effect is an *increase* in the intensity of

a partially saturated ESR signal when the applied radiofrequency field partially desaturates the transition (27,28).

Experimentally, ENDOR is carried out by fixing the external magnetic field on a hyperfine line, and sweeping the radiofrequency from 1 to ≈100 MHz. ENDOR lines are observed, corresponding to the different nuclei coupled with the electron spin in the paramagnetic system. ENDOR lines are centered on *either* the free nuclear frequency ν_n, *or* half the hyperfine constant $A/2$, depending on the relative magnitudes of these two frequencies. If $\nu_n > A/2$, as is common for small *proton* hyperfine couplings, the ENDOR lines are centered around ν_n; for spin 1/2 nuclei two ENDOR transitions, at $\nu_n \pm A/2$ for each chemically distinct nucleus, are observed. If $A/2 > \nu_n$, the ENDOR lines appear at $A/2 \pm \nu_n$ for each ESR line observed. In both cases the coupled nucleus can be identified from the value of ν_n.

Matrix ENDOR. Structural information can be obtained from an analysis of *matrix* ENDOR signals, from nuclei situated at large distances from the paramagnetic centers (usually >5Å); these nuclei interact with the electron only through dipolar interaction. By interpreting the matrix ENDOR signal, it is possible to measure distances between the paramagnetic center and the nuclei (for instance ^{19}F), even if the electron–nuclear interaction is too small to be measured directly by ESR. In liquids the matrix ENDOR line is averaged to zero by rapid tumbling of the radical. In disordered systems such as powders and glasses, the matrix ENDOR line dominates the spectrum and masks small splittings. In order to extract these small interactions, the matrix line must be simulated using a suitable theoretical model (29). The line width of the matrix ENDOR signal has been used to estimate the distance between the interacting nuclei and the electron spins in Nafion ionomers (30,31).

Pulsed ENDOR. In both the inversion recovery (Fig. 5**b**) and stimulated echo experiment (Fig. 5**c**), the echo amplitude is influenced by a radiofrequency pulse applied during the interpulse delay of length T, if this pulse is on-resonance with a nuclear transition. In the former experiment, such a pulse exchanges magnetization between inverted and noninverted transitions, so that echo recovery is enhanced (Davies ENDOR) (32). In the latter experiment the on-resonance radiofrequency pulse induces artificial spectral diffusion, so that the echo amplitude decreases (Mims ENDOR) (33). These pulsed ENDOR experiments exhibit less baseline artifacts and are easier to set up compared with CW ENDOR experiments, as the required mean radiofrequency power is smaller and the ENDOR effect does not depend on a certain balance of relaxation times. Davies ENDOR is better suited for couplings exceeding 1–2 MHz, while Mims ENDOR is better suited for small couplings, for instance matrix ENDOR measurements.

Pulsed ELDOR. Distances between electron spins can be measured by double electron–electron resonance (DEER) experiments such as the four-pulse experiment illustrated in Figure 6 (34). Similar to measurements of electron-nucleus distances, this technique is based on the r^{-3} dependence of the magnetic dipole interaction between electron spins and can determine larger distances, in the range 1.5–5 nm. One of two spins (color-coded green, observer) is observed by a refocused primary echo with fixed interpulse delays τ_1 and τ_2, so that relaxation does not induce variations in the echo amplitude during the experiment. The second spin (color-coded red, pumped) imposes a local dipole field at the site of the first spin, with a magnitude that depends on the distance. At a variable delay t with respect

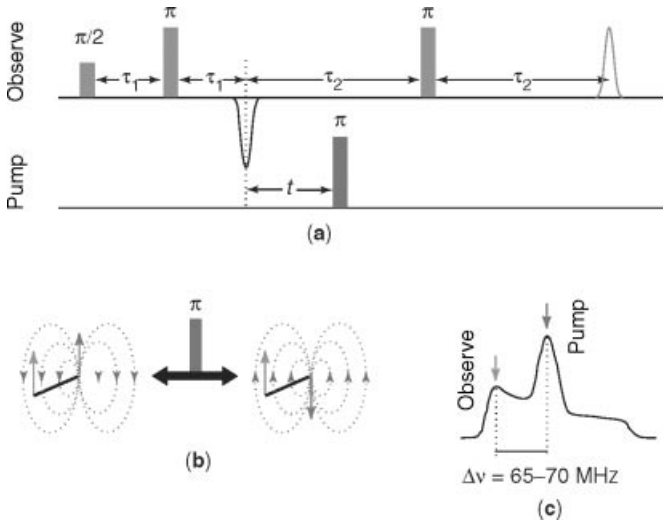

Fig. 6. The four-pulse DEER experiment. (**a**) Pulse sequence consisting of a refocused primary echo subsequence with fixed interpulse delays for the observer spins (top) and a pump pulse at variable delay t with respect to the first primary echo (bottom). (**b**) The pump pulse inverts the local field at the site of the observer spin (left arrow in each panel) imposed by a pumped electron spin (right arrow in each panel). (**c**) Observer and pump positions in an echo-detected EPR spectrum of a nitroxide.

to the first primary echo, a pump pulse inverts this local field (Fig. 6**b**). In this way the resonance frequency of the first spin is changed and the second echo refocusing is perturbed. As a result, the echo amplitude is modulated by the dipolar frequency

$$\nu_{\mathrm{dip}} = (g\beta_{\mathrm{e}})^2/h[(1-3\cos^2\theta)/r^3] \tag{7}$$

By analyzing the dependence of the echo amplitude on the delay t, it is possible to determine the spin–spin pair correlation function, which corresponds to the distribution of electron spins in the vicinity of the observed spin (35,36). Such spatial distributions of spin probes or spin labels can be interpreted by a model-free approach if they are reasonably narrow, or by simple models for the geometry of the system under investigation, if they are broad (37–39). The experiment requires that observer and pumped spins be excited separately, a condition that is easily achieved for nitroxide spin probes and labels by setting the difference of the two excitation frequencies to 65–70 MHz (Fig. 6**c**).

ESR Imaging

Paul Lauterbur was the first to propose, in his notebook entry of 2 September 1971, the use of magnetic field gradients in order to "tell exactly where a nuclear magnetic resonance (NMR) signal came from"; his first proton density map appeared soon afterwards (40). The name he coined for the technique, *zeugmatography*, comes from the Greek word for "joining together," meaning to join the magnetic field gradient and the corresponding radiofrequency in an NMR experiment. This connection allowed to encode spatial information in the NMR spectra. The use

of magnetic field gradients to separate the resonant frequencies corresponding to different spatial elements led to the development of NMR imaging (NMRI) or, in current language, magnetic resonance imaging (MRI). In the last 20 years, NMRI has blossomed into an essential diagnostic procedure in medicine that provides an image of previously hidden anatomic parts. Applications of NMRI to materials science and other important disciplines, although not as dramatic as the medical applications, are steadily developing (41). The wonderful story on the discovery of NMR imaging has been told recently (42).

Imaging based on magnetic field gradients can also be applied to imaging of unpaired electron spins via electron spin resonance (ESR) spectroscopy. The advantages of ESR imaging (ESRI) are the specificity for the detection of paramagnetic species, and the high sensitivity. Papers describing the feasibility of ESRI started to appear in the late 1970s and continue to this day. The early instrumentation, software, and applications of ESRI have been described in a 1991 monograph (43). The challenges in the application of the Lauterbur method to ESRI are numerous: First, higher gradients are needed compared to NMRI, usually 100–1000 times larger. Second, the ESR spectra are often complex and contain hyperfine splittings that complicate the ESRI experiments. Third, most systems do not contain stable paramagnetic species on which imaging is based; ESR imaging is usually performed on radicals produced by irradiation, paramagnetic transition-metal ions, or stable nitroxide radicals as dopants.

As seen in the 1991 monograph, the early efforts laid the foundation for the hardware necessary for ESRI and developed the software necessary for image reconstruction in 1-D (spatial) and 2-D (spectral–spatial and spatial–spatial). These studies also investigated the feasibility of ESRI experiments in a variety of "phantom" samples, and discussed and estimated the spatial resolution. The resolution in most ESRI experiments is of the order of 50–100 μm, but can vary widely, depending on the ESR line shapes and line widths.

Information on the spatial distribution of paramagnetic molecules deduced from ESRI experiments has been used successfully for measurement of the translational diffusion. Diffusion coefficients of paramagnetic diffusants can be deduced from an analysis of the time dependence of the concentration profiles along a selected axis of the sample. The determination of diffusion coefficients for spin probes in liquid crystals and model membranes, and the effect of polymer and probe polydispersity, have been described in a series of papers by Freed and co-workers (44). These papers represent an effort to move beyond phantoms, and to extract quantitative information from ESRI experiments.

The ability to perform ESRI is restricted to a small number of groups worldwide. While most groups study biological applications of ESRI (45–48), a small number of studies on polymeric materials have appeared: Diffusion coefficients of guests in ion-containing polymers, polymer solutions, cross-linked polymers swollen by solvents, and in self-assembled polymeric surfactants have been determined by 1-D ESRI (49–52). Lucarini and co-workers have determined by 1-D ESRI the distribution of the nitroxide radicals in UV-irradiated polypropylene (PP) containing a hindered amine stabilizer (HAS) (53–55). Ahn and co-workers have deduced the concentration profile of heat-induced radicals in a polyimide resin (56). *In vitro* degradation of poly(ortho esters) containing 30 mol% lactic acid has been studied by 1-D and 2-D spectral–spatial ESRI, based on pH-sensitive nitroxide spin probes (57). Spatially resolved degradation in heterophasic

polymer systems, such as poly(acrylonitrile-butadiene-styrene) (ABS) and ethylene–propylene copolymers (HPEC), has been described in a series of recent papers (19,25,55,58–64).

ESR Spectra in the Presence of Field Gradients. ESR spectroscopy can be transformed into an imaging method for samples containing unpaired electron spins, if the spectra are measured in the presence of magnetic field gradients. In an ESR imaging experiment the microwave power is absorbed by the unpaired electrons located at point x when the resonance condition, equation 8, is fulfilled.

$$\nu = (g\beta_e/h)(H_{\text{res}} + xG_x) \tag{8}$$

In equation 8 G_x is the linear magnetic field gradient (in G/cm) at x. As in NMR imaging, the field gradients produce a correspondence between the location x and the resonant magnetic field H_{res}. If the sample consists of two point samples, for example, the distance between the samples along the gradient direction can be deduced if the field gradient is known (65). An example is shown in Figure 7, for a "phantom" consisting of two parallel capillary tubes (55).

The spatial resolution, Δx, is an important parameter in imaging, and can de defined in various ways, as discussed recently (66); the resolution depends on the line width and line shape. Most commonly Δx is expressed as the ratio of the line width to the field gradient, $\Delta H/G_x$; this definition implies that two signals separated by one line width due to the field gradient can be resolved.

An ESR imaging system can be built with small modifications of commercial spectrometers: gradient coils fixed on the poles of the spectrometer magnet, regulated DC power supplies, and required computer connections. In most systems

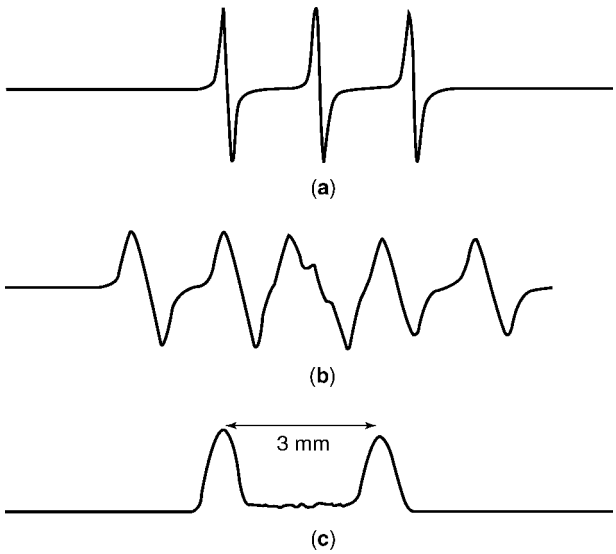

Fig. 7. 1-D ESRI at 298 K of a phantom consisting of two parallel capillary tubes separated by 3 mm and filled with a solution of TEMPO in benzene. (**a**) X-band ESR spectrum recorded in the absence, and (**b**) in the presence of the magnetic field gradient (100 G/cm). The radical distribution is shown in (**c**). Redrawn from Ref. 55, with permission.

the software for image reconstruction in 1D and 2D ESRI experiments must be developed on site.

Intensity Profiling from 1-D ESRI. In the general case, the sample contains a distribution of paramagnetic centers along a given direction, for example x. The ESR spectrum in the presence of the magnetic field gradient is a superposition of signals from paramagnetic centers located at different positions. In 1-D ESRI experiments, the intensity profile is obtained from two ESR spectra: $F_0(H)$ measured in the absence of magnetic field gradient, and $F(H)$ measured in the presence of the gradient.

Mathematically, $F(H)$ is a convolution of $F_0(H)$ with the distribution function of the paramagnetic centers (43,67), equation 9,

$$F(H) = \int_{-\infty}^{\infty} F_0(H - H^*)C(H^*)\mathrm{d}H^* \tag{9}$$

where $H^* = H_0 - xG, H_0 = h\nu/g\beta_e$, and $C(H^*)$ is the intensity distribution (profile) of the paramagnetic centers along the gradient direction. It is essential to note that the convolution expressed in equation 9 is correct only if the ESR line shape *has no spatial dependence.* As will be seen below, this requirement has dictated the conditions for data acquisition in the 1-D ESRI study of degradation processes.

Various optimization methods are viable alternatives to the deconvolution method. The process starts by assuming an initial distribution, which can be described by some parameters. In diffusion studies, for example, the initial distribution is calculated as a function of the diffusion coefficient, diffusion time, and other parameters that define the sample configuration (49,50). Optimization methods use the convolution of this initial distribution function with the experimental spectrum in the absence of magnetic field gradient in order to calculate the spectrum in the presence of the gradient. The deviation between the calculated and the experimental spectra is then minimized by an optimization procedure. In our initial ESRI studies, the concentration profiles of the radicals were deduced by Fourier transform followed by optimization with the Monte Carlo (MC) procedure (53–55). The disadvantage of this method is the high frequency noise present in the optimized profiles. In more recent publications, the intensity profile was fitted by analytical functions and convoluted with the ESR spectrum measured in the absence of the field gradient in order to simulate the 1-D image. The best fit was obtained by variation of the type and parameters of the analytical functions chosen (Gauss or Boltzmann, for example) in order to obtain good agreement with the 1-D image, and selected by visual inspection (62,63).

Lately the genetic algorithm for minimization of the difference between simulated and experimental 1-D images was implemented; this procedure allowed the best fit to be chosen automatically (64). A typical genetic algorithm (GA) consists of creation of the initial population, calculation of the fit to experimental data, selection of the couples, crossover (reproduction), and mutation. The approach and terminology are adopted from biology and resemble fundamental steps in evolution.

Line Shape Profiling from 2-D Spectral–Spatial ESRI. Each 2-D image is reconstructed from a complete set of projections, collected as a function of the magnetic field gradient, using a convoluted back-projection algorithm (58).

The number of points for each projection (1024) is kept constant. The maximum experimentally accessible projection angle, α_{max}, depends on the maximum gradient G_{max} according to $\tan \alpha_{max} = (L/\Delta H)G_{max}$, where L is the sample length, and ΔH is the spectral width. The maximum sweep width is $SW_{max} = \sqrt{2}\Delta H/\cos\alpha_{max}$. For a width $\Delta H \approx 65$ G (which is typical for the slow-motional spectral component of a nitroxide radical present in irradiated polymers), a sample length of 4 mm, and a maximum field gradient of 250 G/cm along the vertical axis, we obtain $\alpha_{max} = 57^\circ$ and $SW_{max} = 169$ G. A complete set of data for one image consists of 64–128 projections, taken for gradients corresponding to equally spaced increments of α in the range -90° to $+90^\circ$; for a total of 64 projections, typically 41 or 43 are experimentally accessible projections and the rest are projections at missing angles (for α in the intervals 60° to 90°, and -60° to -90°). The projections at the missing angles can be assumed to be the same as those at the maximum experimentally accessible angle α_{max}, or determined by the projection slice algorithm (PSA) with several iterations (43,63,64).

Spin Probes in Ion-Containing Polymers

Ionomers (qv) are polymers that contain a small fraction of ionic groups, typically less than 15 mol%. The percentage is calculated from the number of backbone atoms or repeat units to which the ionic groups are attached. This definition is not completely specific, because the ionic groups are often at the end of pendant chains of varying lengths or part of different structures. For this reason, the equivalent weight (EW), which is the amount of ionomer (in g) containing one mole of ionic groups, is also an indication of the ionic content. The definition in terms of ion content or EW is of course useful for comparison of ionomers with the same, or very similar, backbone and pendant groups (68–70).

The ionic groups, although present in small amounts, dominate the viscoelastic behavior of ionomers, their transport properties and their ability to sorb a variety of solvents; moreover, the ion effect is specific. In terms of morphology, the presence of ions leads to microphase separation into ionic and nonpolar domains. Increasing interest in structural aspects of ionomers is closely related to their numerous applications as bulk materials, in various devices, as catalysts, in controlled release systems, and as proton exchange membranes (PEM) in fuel cells (71).

Small-angle X-ray and neutron scattering, SAXS and SANS, respectively are important methods for the study of ionomer morphology, because an extra peak (the "ionic peak") is detected in ionomers and is absent in the polymers that consist of the organic backbone alone. The value of the scattering vector corresponding to maximum scattering intensity has been used to deduce a characteristic size of the ionic domains. The appearance of the ionic peak is a function of temperature, solvent structure and content, and degree of neutralization. The absence of the ionic peak is sometimes explained by a fortuitous cancellation of electron densities (72–75).

Spectroscopic data offer a more local view of the ionomer structure, and can be considered complementary to the small-angle scattering methods. Binding of paramagnetic cations in Nafion ionomers has been studied by multifrequency ESR and simulations (76). Self-assembling of ion-containing polymers, as swollen

membranes and in solutions, was extensively studied in recent years by ESR spectroscopy of nitroxide radicals as spin probes (76–83). The most important nitroxide spin probes used were the amphiphilic *n*-doxylstearic acids [*n*DSA (**1**, X = H, Na; $n = 5, 7, 10, 16$] and their corresponding methyl esters [*n*DSE (**1**), X = CH_3; $n = 5, 7$]; hydrophobic doxyl-substituted hydrocarbons such as 5-doxyldecane (5DD)(**2**) and 10-doxylnonadecane (10DND) (**3**); and cationic probes with different lengths of the alkyl substituents CAT1 (**4**) and CAT16 (**5**). The spin probe method is based on the exceptional sensitivity of the nitroxide ESR line shapes to the local environment, and of the ^{14}N hyperfine splittings to the polarity of the medium. Depending on probe hydrophobicity, charge, length of the alkyl chain, and, in the case of amphiphilic probes, position of the nitroxide group with respect to the polar head group, different regions of self-assembled systems can be identified and studied. The ESR spectra of the probes are a rich source of information on local properties such as viscosity, molecular packing and ordering, polarity, and the presence of ions in the probe vicinity, on a nanoscale range, typically 0.5–5 nm.

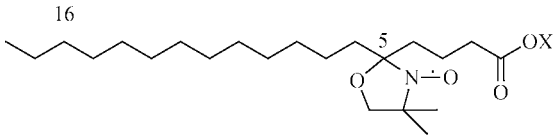

1

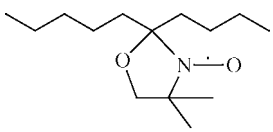

2

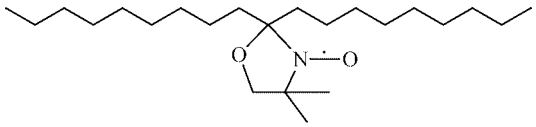

3

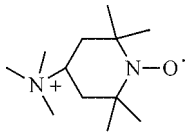

4

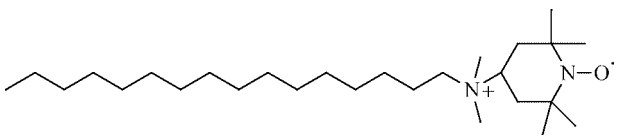

5

Some of the probes mentioned above have been used for a comparative study of Nafion perfluorinated ionomer (**6**) neutralized by Li^+, and the protiated ionomer

poly(ethylene-*co*-methacrylic acid) (EMAA) (**7**) neutralized by Na^+ and K^+, as dry or water-swollen membranes and in aqueous solutions.

Both materials at ambient conditions are insoluble in water. They can be dissolved, however, at high temperatures in an autoclave, using ethanol/water mixture as a solvent for Nafion, and alkaline water for EMAA. Aqueous solutions of Nafion can be obtained by dialysis of alcoholic solutions against water. Recent SAXS and SANS experiments on a range of Nafion concentrations, for volume fractions in the range 0.16–0.95 measured in a wide range of scattering vectors introduced the novel idea of Nafion organization, based on aggregation of ionomer chains into elongated polymer bundles surrounded by the electrolyte solution (74,75). Aggregation into spherical or elipsoidal micelles in EMAA has been demonstrated by SAXS experiments (72,73).

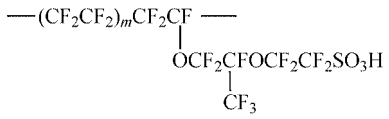

6

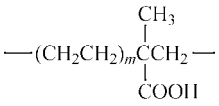

7

The ESR spectra of the nitroxide probes in Nafion and EMAA have been in agreement with the scattering results, and have provided additional local details on the aggregates. In addition, the spectra have revealed important differences between EMAA and Nafion systems. In the case of EMAA micelles, probes based on doxylstearic acid have exhibited the "dipstick effect": their dynamics became slower as the probe penetrated deeper inside the aggregate, from the hydrophilic *n*DSA to the hydrophobic *n*DSE, and from 5DSA or 5DSE to 10DSA or 10DSE, respectively. The ^{14}N hyperfine splitting, a_N, decreased in the same order, indicating a polarity gradient from the polar interface to the nonpolar aggregate interior (79,80,82).

In the case of Nafion micelles, the mobility also decreased in the order 5DSA > 10DSA > 10DSE, but all three probes reported a polar environment. The decreased mobility was explained by assuming that the probes intercalate between perfluorinated polymer chains; the high polarity at the probe site was thought to be a result of the water present inside the micelles. This explanation was supported by the results of a fluorescence study using pyrene (P) as a polarity probe (84). Results obtained for the cationic probes CAT*n* have also indicated the penetration of the protiated segments of the probe inside the perfluorinated host aggregates, and have suggested that the amount of water in Nafion micelles increases in more dilute ionomer solutions (81).

On the basis of the ESR study a structural model of internal structure of EMAA aggregates was proposed, as seen in Figure 8 (right panel). According to the model, the EMAA micelle consists of three regions: the hydrophobic core of polyethylene chains, an intermediate layer which contains both ionomer chains

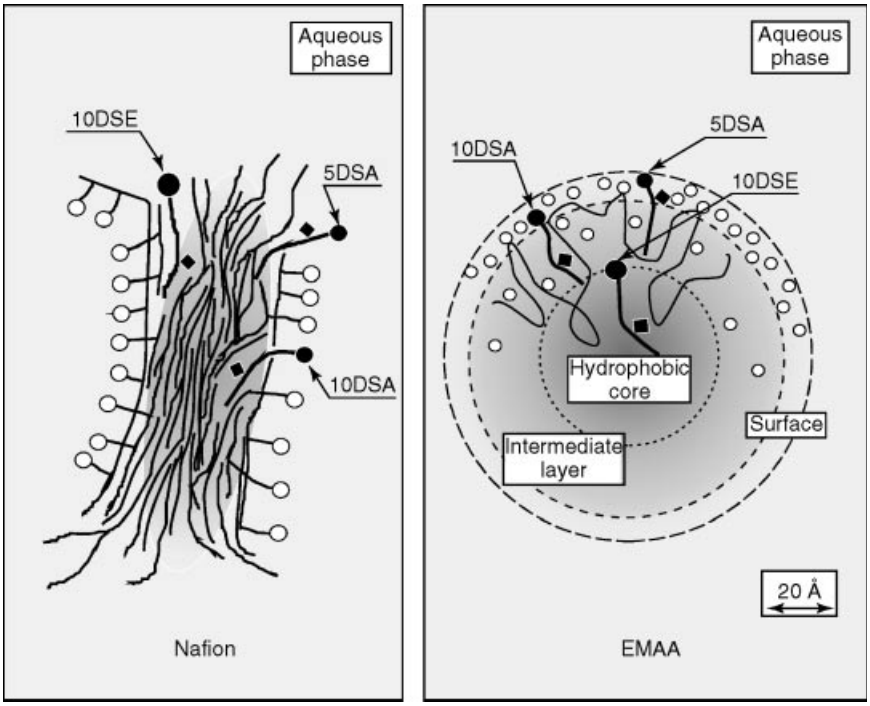

Fig. 8. Structural models of large aggregates in ionomer solutions, and suggested locations for doxyl spin probes based on ESR results: ●, probe head groups; ◆, nitroxide groups; ○, ionomer head groups.

and some ions, and a hydrophilic surface layer where most of the ions are located. The carboxylic groups of *n*DSA probes are anchored in this layer, while the heads of esters are located at the interphase between the core and intermediate layer (79,80). In Nafion micelles, as in EMAA micelles, the nitroxide group of 5DSA is located closer to the surface than that of 10DSA, and 10DSE radical is most deeply buried in the aggregate (Fig. 8, left panel). In the case of 10DSE the preferred chain orientation is parallel to the long axis of the rod, as suggested by the value of the parallel component of the rotational diffusion tensor, which was deduced from simulations (78).

The local structure in and near the ionic aggregates in EMAA ionomer membranes neutralized by Na^+ was investigated as a function of the degree of membrane neutralization, x, by spin probe ESR using 5DSA, 7DSA, 10DSA, 7DSE, and 10DND as spin probes (82). The ESR studies revealed that the five spin probes used are position-selective, and provide local information on different regions in the self-assembled ionomers. Three hydrophilic doxylstearic acid probes (*n*DSA) are anchored to the ionic aggregates, two (5DSA and 7DSA) are located in the ionic core and one (10DSA) is in the hydrocarbon shell; the two hydrophobic probes (7DSE and 10DND) report on the amorphous region. The extreme separation (ES) of the probes is sensitive to the local environment, as seen in Figure 9; ES is also sensitive to the degree of neutralization (82).

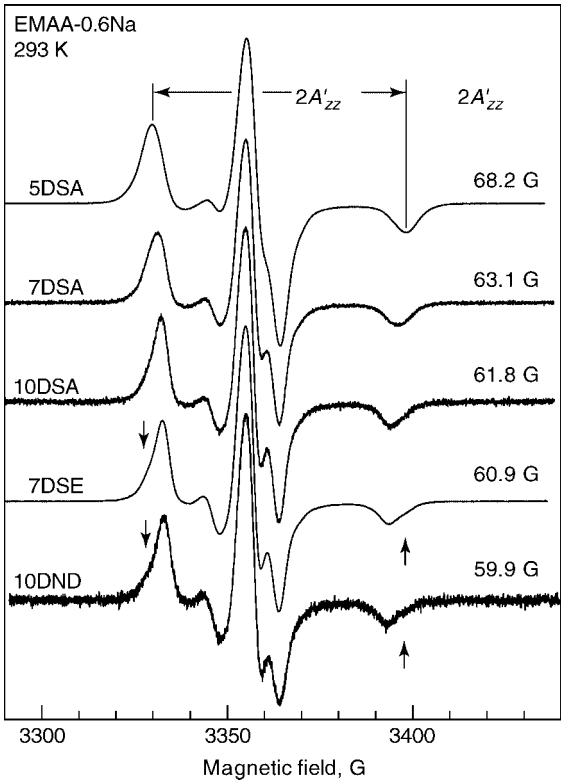

Fig. 9. X-band ESR spectra at 293 K for the indicated spin probes in EMAA-0.6Na. Spectra are normalized to a common microwave frequency (9.43 GHz). Microwave power, 1 mW; modulation amplitude, 1 G. (To convert G to T, multiply by 1×10^{-4}.) The corresponding extreme separation, $2A'_{zz}$, is shown on the right. Downward and upward arrows point to the incipient shoulders in the low field and high field signals for 7DSE and 10DND, respectively; these shoulders are more pronounced for higher degrees of neutralization. From Ref. 82, with permission.

The local polarity was expressed in terms of the polarity index $\Delta A_o = a_N$ (ionomer) $-a_N$ (np), where a_N (ionomer) is the isotropic ^{14}N hyperfine splitting in the ionomer, and a_N (np) is the corresponding value in a nonpolar medium; this definition implies a higher polarity index, ΔA_o, in a more polar environment, as seen in Figure 10**a**. The variation of the polarity indices of these position-selective probes as a function of the degree of neutralization indicated the presence of an ion-depleted zone (hydrocarbon shell) surrounding the ionic core, and also the presence of a small amount of isolated ionic groups in the amorphous regions. Suggested locations of the different probes in the membranes are shown in Figure 10**b**. The structural features deduced by spin probe ESR were in support of the SAXS profile analysis based on a depleted-zone core–shell structure of the aggregate. The SAXS studies provided additional information on the geometrical shape and size of the aggregate, and the number of ionic groups in each aggregate. Thus, microstructural insights into the ionic aggregate from both approaches, polarity from ESR and electron density from SAXS, are consistent and complementary.

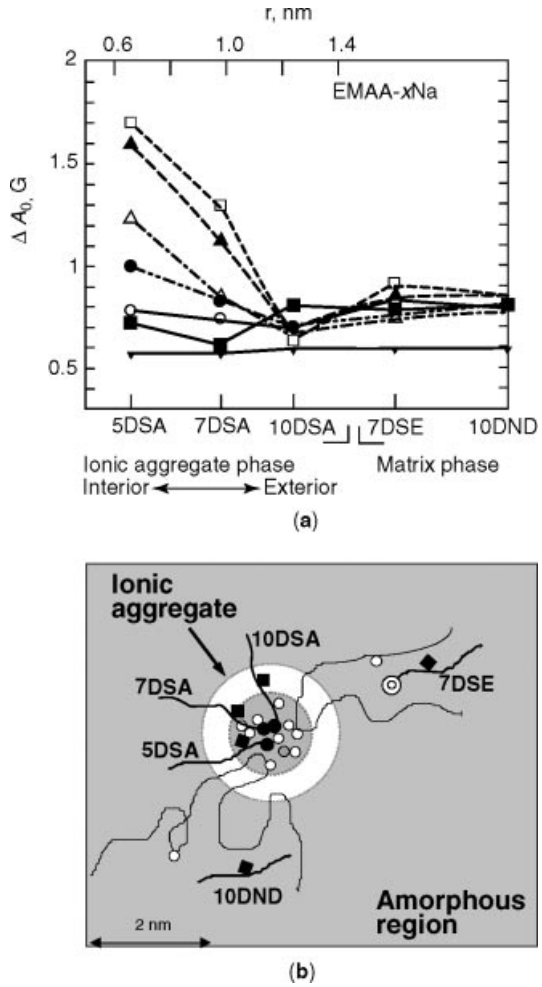

Fig. 10. (**a**) Variation of the polarity index, ΔA_0 in G, for the five spin probes in EMAA-xNa (x in the range 0–0.9) with the distance from the center of the ionic aggregate, r, together with the data for low density polyethylene (LDPE). The r values were assumed identical to the distance of the nitroxide group from the carboxylic group in the nDSA probes. —□— $x = 0.9$, —▲— $x = 0.8$,—△—$x = 0.6$, —●— $x = 0.4$, —○— $x = 0.2$, —■— $x = 0$ —▼— LDPE. (**b**) Suggested locations of 5DSA, 7DSA, 10DSA, 7DSE, and 10DND probes in dry EMAA ionomers, based on the analysis of the ESR results: ○ the carboxylate and carboxylic acid groups of the ionomer; ●, and the acid groups; ◎, the methyl ester group; and ■, the nitroxide groups of the probes are indicated. Dark shaded, white, and grey-shaded regions represent, respectively, the ionic core and hydrocarbon shell (ion-depleted zone) of the aggregate, and the amorphous region. From Ref. 82, with permission.

Pulsed ESR Studies in Ionically End-Functionalized Block Copolymers

Telechelic ionomers are a special class of ionic polymers in which the charged groups are situated exclusively at the chain ends (see TELECHELIC POLYMERS (85,86)) Accordingly, their solid-state structure is characterized by self-assembly of the chain ends into ion multiplets or ionic clusters. Because of this defined

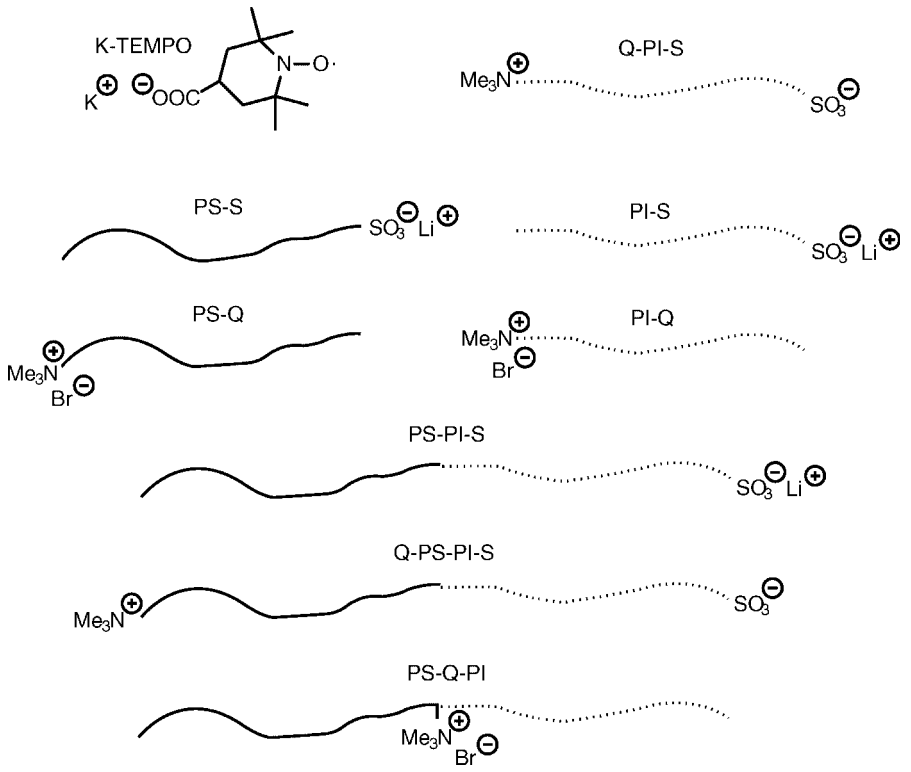

Fig. 11. Structure of the anionic spin probe K-TEMPO and schematic structures of telechelic ionomers. Solid lines denote polystyrene blocks, while dotted lines denote polyisoprene blocks.

topology, telechelic ionomers form less complex structures compared with random ionomers, and can be used as a point of departure for studying the balance between electrostatic self-assembly and self-assembly induced by microphase separation of diblock copolymers (87). For such a study it is advantageous to include reference samples that carry one ionic group at the chain junction (Fig. 11) in which ionic clusters are situated in the interface between the microphases. As in the case of random ionomers, the properties of the ionic clusters in such systems were interrogated by ionic spin probes (86,87), as initially established by the CW ESR techniques discussed in the previous section. With respect to its size and ion site, the anionic nitroxide probe K-TEMPO (Fig. 11) used with the telechelic ionomers resembles the cationic CAT1 probe and is thus expected to be located at the cluster surface or even inside the cluster.

Interestingly, K-TEMPO probes in monoionic block copolymers of type polystyrene–polyisoprene (notation PS-PI-S, where S stands for the spin probe) exhibited homogeneous dynamics, ie, a relatively narrow, monomodal distribution of rotational correlation times; by contrast, the same probes in zwitterionic block copolymers of type Q-PS-PI-S (where Q stands for a quaternary ammonium group) exhibited heterogeneous dynamics, ie, a bimodal distribution of rotational correlation times (87). By comparison of results for telechelic homopolymeric

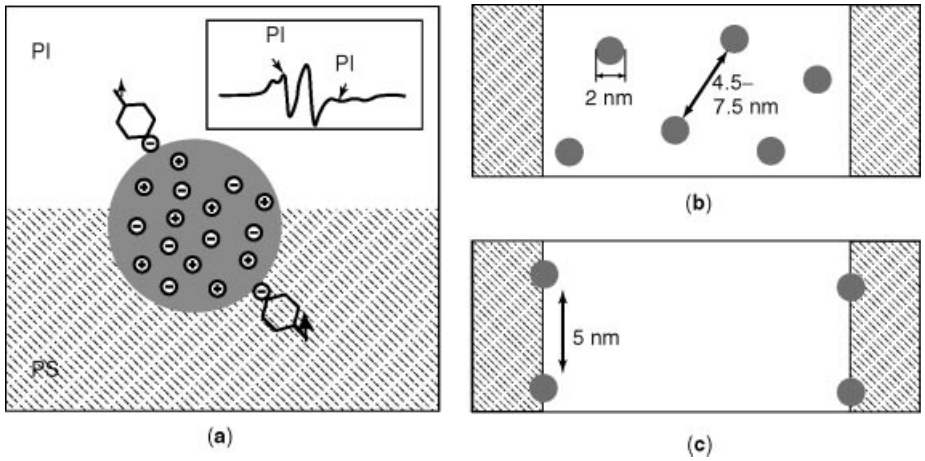

Fig. 12. Ionic clusters in telechelic ionomers based on diblock copolymers (see also Fig. 11). (**a**) Spin probes attached to ionic clusters located at the interface between the polystyrene (PS) and polyisoprene (PI) microphases. The inset shows the CW ESR spectrum for PS-Q-PI, where Q is a quaternary ammonium group. The fast component (arrows) was assigned to probes in the PI microphase. (**b**) The distribution of ionic clusters in monoionic diblock copolymers suggested by DEER experiments. (**c**) The distribution of ionic clusters in zwitterionic diblock copolymers suggested by DEER experiments.

ionomers PS-S, PS-Q, PI-S, and PI-Q, the fast component could be assigned to probes in a PI matrix, and the slow component to probes in a PS matrix. For both components, T_{50G} was significantly higher than for similarly sized spin probes in unfunctionalized PI and PS, respectively. Taken together, these results suggested that the probes are located at the surface of the ionic cluster, which in the zwitterionic case is situated at the interface between the PS and PI microphases (Fig. 12**a**). If the probes were located mainly inside the clusters or if the clusters would have a preference for one of the microphases, a monomodal distribution of rotational correlation times would be expected. The interpretation of clusters at the interface was supported by three additional results: the fractions of the two components are rather similar for the zwitterionic case, the same type of behavior is observed for the monoionic diblock copolymer with an ionic group at the chain junction (PS-Q-PI), and the fractions depend on the morphology of the diblock copolymer and thus on the curvature of the interface (87,88).

Characterization of cluster sizes and cluster distribution by SAXS was not successful, as the electron density contrast between PS and PI leads to SAXS curves that are strongly dominated by features due to block copolymer morphology. Therefore, the ionic peaks could not be detected. As the K-TEMPO spin probes are attached to the clusters and both cluster sizes and intercluster distances are expected to fall in the sensitive range of DEER experiments (1.5–8 nm), this problem was addressed by pulsed ELDOR distance measurements (37,88). For such studies, a ratio of 2:15 between the spin probe and chain end concentrations was chosen. Assuming that on the average 12–20 chain ends assemble into a cluster (89), the spin pairs have similar probabilities of being located on the same cluster and on directly neighboring clusters. Accordingly, the DEER signal is the product

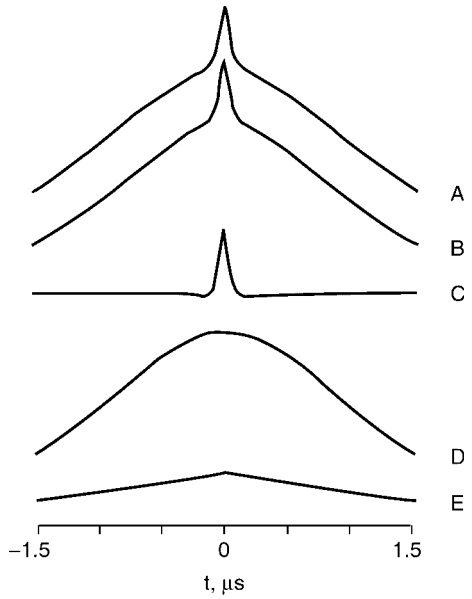

Fig. 13. Experimental four-pulse DEER signal for ionomer PI-Q and deconvolution into its components. (A) Experimental data. (B) Best fit. (C) Fast decaying component due to spin probes located in the same cluster, with a characteristic distance of 2.2 nm. (D) Slow modulation due to spin probes in vicinal clusters, with a characteristic distance of 6.6 nm. (E) Exponential background due to spin probes in remote clusters.

of three contributions: a fast decaying oscillatory part corresponding to spin probes located on the same cluster, a slowly decaying modulation corresponding to spin probes located on directly neighboring clusters, and a very slow exponential background decay due to spin probes located on remote clusters (Fig. 13). Mean distances and distance variations for the first two components were determined by fitting a distance distribution consisting of two Gaussian peaks and a constant background contribution to the data. The mean distance of the first peak (spin probes on the same cluster) roughly corresponds to the radius of the cluster, while the mean distance of the second peak corresponds to the intercluster distance for direct neighbors (37).

In general, we find that cluster radii vary only slightly (r_{cluster} = 1.8–2.2 nm); the only exception was a PS-S sample with a low molecular weight, M_{n} = 4.8 kg/mol, for which the radius was 1.4 nm. No significant correlation between cluster size and polymer chain length was found when varying the molecular weight of diblock copolymer samples between 10 and 50 kg/mol (see solid circles in Fig. 14**a**). This result agrees with earlier work on α, ω-dicarboxylatopoly(butadienes) and α,ω-dicarboxylatopolyisoprenes, in which the size of the clusters (or multiplets) also appeared to be independent of chain length (90). Analysis of SAXS data for ion domain radii was not attempted for the homopolymers or the diblock copolymers, but had been performed for the α, ω-dicarboxylatopoly(butadienes) and α, ω-dicarboxylatopolyisoprenes (90). In these cases r_{cluster} ranged from 0.6 to 1.1 nm, which is somewhat surprising given the fact that clusters of both quaternary ammonium end groups and sulfonate

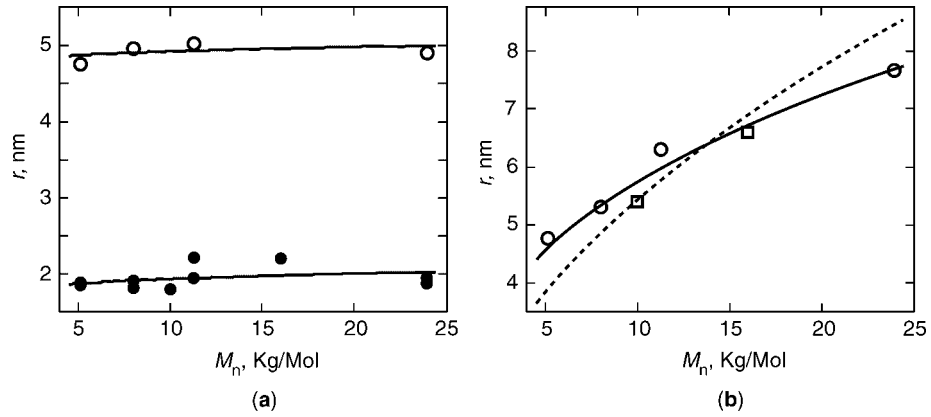

Fig. 14. Scaling of characteristic distances between anionic K-TEMPO spin probes in ionomers based on diblock copolymers. (**a**) Direct neighbor distance between clusters in zwitterionic diblock copolymers Q-PS-PI-S (○), cluster radii of all samples (●). Solid lines are best-fit scaling laws (see text). (**b**) Direct neighbor distance in monoionic diblock copolymers PS-PI-S (○) and in monoionic homopolymers PI-S (□). The solid line is the best fit for a scaling law with exponent 1/3, and the dashed line is the best fit for a scaling law with exponent 1/2.

end groups are apparently twice as large. Molecular modeling suggests that the cluster size for aggregates of 10–12 chain ends should be closer to the DEER values than to the SAXS values. In the latter case, radii were calculated from the surface-to-volume ratio S/V, which is measured, by assuming spherical objects. While for such spherical objects S/V scales with r^{-1}, slight deviations from a spherical shape lead to a large increase in S/V, which in turn corresponds to an underestimate of the mean radius (37).

Direct-neighbor distances between clusters obtained by SAXS and DEER could be compared to each other for the three homopolymeric ionomers PI-Q, PI-S, and Q-PI-S with molecular weights of the polymer chain of 10 kg/mol (37). Distances determined by DEER were found to be 1–1.5 nm shorter than distances obtained by SAXS, but showed the same trend, a decrease in the sequence PI-Q, PI-S, Q-PI-S. The difference may be due to the fact that the spin probes are attached to the cluster surface and the r^{-3} averaging inherent in DEER data overemphasizes shorter distances, so that DEER actually measures the surface-to-surface distance of the clusters while SAXS measures the distance between the centers of clusters. We note however that the Bragg equation underlying the analysis of SAXS data is not expected to be strictly valid for systems lacking long-range order, so that part of the deviation might also be attributed to a systematic error in the SAXS measurements.

Significantly, DEER measurements also provided intercluster distances for the homopolymers, for which the ionic peak cannot be detected reliably in SAXS curves, and for the diblock copolymers, where it cannot be detected at all. The scaling coefficient x in $r = AM_n^x$ for the intercluster distances r with molecular weight M_n provides information on the spatial distribution of the clusters. In earlier work on α, ω-dicarboxylatopolybutadienes and α, ω-dicarboxylatopolyisoprenes, the range of molecular weights was too narrow for a definite conclusion about

this scaling, but extrapolation of the SAXS data to $M_n = 0$ suggested a scaling coefficient of $x \approx 1/2$ (90). This result is somewhat surprising, as any deviation from $x = 1/3$ implies a nonuniform distribution of clusters in the matrix. A nonuniform distribution can be expected for the diblock copolymers if the clusters were either attracted or repelled by the interface between the two blocks, but cannot be easily understood for the homopolymers. Indeed, DEER data provided $x = 0.311$, ie, a scaling exponent very close to 1/3 even for monoionic diblock copolymers PS-PI-S with lamellar morphology (Fig. 14**b**). The M_n range of the PI block, 5.1–24 kg/mol, is broad enough to exclude a scaling coefficient of 1/2, which corresponds to a fit with a root-mean-square error that is 3 times larger than for the fit with scaling coefficient 1/3. This result indicates that the ionic clusters are distributed throughout the PI microphase, ie, they are neither repelled nor attracted by the interface region. Hence, electrostatic self-assembly and block copolymer morphology are apparently independent of each other for the *monoionic* telechelic ionomers.

A different cluster distribution was detected for the zwitterionic case, as seen by comparing the open circles in Figure 14**a** and 14**b**. For the zwitterionic samples Q-PS-PI-S the best fit $r = AM_n^x$ provided a scaling coefficient of 0.016, which does not significantly differ from zero. Indeed a scaling coefficient $x = 0$ is expected for a two-dimensional distribution of clusters that are strictly confined to the interface between the PS and PI microphases, as the number of clusters per unit interface area does not depend on M_n, as long as the number of chain ends per cluster does not depend on M_n. The latter assumption is strongly suggested by the constant size of the clusters. Nevertheless, the absence of any significant changes is somewhat suprising, given the fact that a solid-state NMR study of related nonionic diblock copolymers indicated a thickness of the interfacial region of several nanometers as far as chain ordering is concerned (91). Taken together the data may then suggest that the interactions that govern ion cluster distribution dominate over the interactions that govern this chain ordering close to the interface. This poses the question whether in monoionic diblock copolymers changes in chain dynamics imposed by the interface are still detectable close to the ion clusters, which reside exclusively in one of the microphases.

Comparison of T_{50G} values from CW ESR experiments on monoionic homopolymers (86) and diblock copolymers (87) does not indicate significant differences in the dynamics of the ionic spin probes. However, the CW ESR experiments may not be very suitable for answering this question, as they are most sensitive to differences in dynamics at 330 K, which is significantly higher than the T_g of the PI microphase (270–280 K). Dynamics at temperatures below T_g can be characterized by relaxation measurements in high field ESR echo experiments (92). Comparison of echo decay time constants for PI-S and PS-PI-S at 260 K revealed that only the longitudinal relaxation times T_1 obtained by saturation recovery are the same for both cases, while both T_2 and the decay time constant of the stimulated echo T_{SE} differ between the homopolymer and diblock copolymer. For an M_n of PI of approximately 10 kg/mol, T_2 values are up to 20% and T_{SE} values up to 50% longer than for the diblock copolymer. Hence, anchoring of PI chains to the more rigid PS blocks leads to a change of chain dynamics that is sufficient to influence small-angle reorientation of the ionic spin probe K-TEMPO. This probe is attached to the ionic clusters, ie, it resides in the vicinity of the other end of the PI chain. We note however that this result does not necessarily imply that

the changes in dynamics are transmitted by a single PI chain over its full length; the slight immobilization may be caused by the collective behavior of the PI microphase in the vicinity of the block copolymer interface.

A more detailed analysis of dynamics of the ionic spin probe for the monoionic homopolymer PI-S revealed hierarchical processes on different time scales (93). Fast *intramolecular* libration on a time scale of a few picoseconds is the dominating contribution to longitudinal relaxation (T_1), which explains why T_1 is rather insensitive to changes in the environment of the spin probe. This environment can be considered as a cage of the spin probe that consists of the polymer chains and, on one side, of the surface of the ionic cluster. Reorientation of this cage on a time scale of a few hundred nanoseconds is the main contribution to transverse relaxation, so that T_2 is sensitive to polymer chain dynamics. The anisotropy of this reorientation motion can be characterized in detail by performing the experiments at W-band frequencies of ~94 GHz, where the x, y, and z directions of the molecular frame of the nitroxide molecule (Fig. 2**b**) are resolved (Fig. 4). Using this information on anisotropy and the constraints on dynamics derived from the CW ESR line shape and stimulated echo decay, it can be shown that the local rearrangement has to be described as anisotropic free rotational diffusion that covers an angular range of only 3–4°. This process does not couple strongly to the glass transition.

Finally, stimulated echo decay is sensitive to spin probe reorientation on a time scale of several microseconds. It can be demonstrated that the process governing T_2 is not sufficient to explain this decay, as is also suggested by the qualitatively different temperature dependence of T_2 and T_{SE} in the range $0.64 < T/T_g < 1.05$. Stimulated echo decay is almost independent of temperature below T_g but becomes much faster as the glass-transition temperature is approached, because stimulated echo decay requires jump reorientation, which becomes much more likely when cooperative dynamics sets in at T_g. Although DSC does not detect a significant change in T_g between PI matrices in homopolymeric and copolymeric ionomers, such changes are highly significant in the stimulated echo decay. Again this appears to be a matter of different time scales, on the time scale of DSC of a few seconds the subtle differences between the two polymers are lost.

Spatially Resolved Degradation from 1-D and 2-D Spectral–Spatial ESRI Experiments

During degradation (qv) processes polymers lose some of their most important properties: strength, flexibility, and the ability to withstand extreme temperatures and chemicals. Oxygen, sunlight, and heat are the major factors in the degradation process. The oxidative degradation of polymeric materials can be viewed on the molecular level as a cascade of events triggered by chemically reactive molecules such as free radicals ($R^\bullet$, $RO^\bullet$ and $ROO^\bullet$), and hydroperoxides (ROOH). The modification of the polymer properties due to exposure to environmental factors is both on the molecular and macroscopic levels: change of the chemical structure (double bond formation, chain scission, and cross-linking), and of the elastic moduli. Accelerated degradation is often performed in the laboratory, and the results are interpreted in terms of polymer lifetimes in actual applications (94–97).

Recent advances in the understanding of degradation processes are anchored on the finding that polymer degradation is often spatially heterogeneous. When the rate of oxygen diffusion is not sufficient to supply all the oxygen that can be consumed, only outside layers in contact with oxygen are degraded, whereas the sample interior is protected: this is the diffusion-limited oxidation (DLO) regime (98–100). The DLO concept implies that in order to understand degradation and predict lifetimes of polymeric materials in different environments, it is necessary to develop profiling methods that determine the variation of the extent of degradation within the sample depth.

In this article the focus will be on the application of one-dimensional (1-D) and two-dimensional (2-D) spectral–spatial ESRI to the photo- and thermal degradation of poly(acrylonitrile-butadiene-styrene) (ABS) (19–55,58–63). The ESRI approach was applied to ABS because it represents a polymer that is exceptionally important in technological applications, yet is also vulnerable to photo- and thermal degradation, and can be used only in the presence of protective additives. Hindered amine stabilizers (HAS), for instance bis(2,2,6,6-tetramethyl-4-piperidinyl) sebacate (Tinuvin 770, (**8**)), are added for stabilization of polymeric materials (101,102).

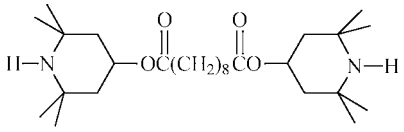

8

The HAS-derived nitroxides are thermally stable, but can react with free radicals (as scavengers) to yield diamagnetic species; the hydroxylamines can regenerate the original amine, thus resulting in an efficient protective effect. Equation 10 presents some of the chemical processes involving HAS during exposure to radiation and oxygen. The presence of nitroxide radicals in HAS-stabilized polymers makes possible the ESRI experiments, with the radicals providing the imaging contrast.

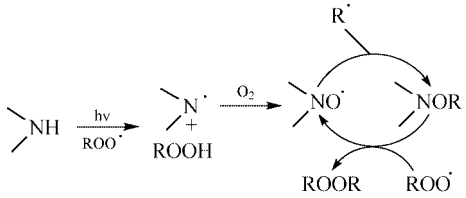

10 (10)

The HAS-derived nitroxides in the ABS and in the heterophasic ethylene–propylene copolymers (HPEC) also studied (64) by ESRI perform a triple role. First, they provide the contrast necessary in imaging experiments; second, they probe the morphology of the system, in terms of glass-transition characteristics and dynamics; and third, they reflect the degradation process. Once ESRI data were collected, and transformed into intensity profile (from 1-D ESRI) and spectra

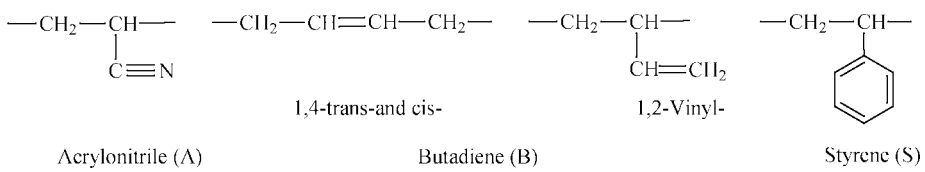

Fig. 15. Repeat units in ABS polymer.

as a function of sample depth (from 2-D ESRI), the remaining challenge is to translate information extracted from ESRI experiments into details on degradation kinetics and mechanism.

As will become clear from the results presented below, the spatial heterogeneity in the distribution of nitroxide radicals deduced by 1-D ESRI as a result of photo- and thermal degradation has been taken as an indicator of heterogeneous degradation Moreover, nitroxide radicals reflect not only the spatial extent of degradation, but also events that occur in different morphological domains: In recent studies of ABS polymers, 1-D and 2-D spectral–spatial ESRI images have enabled the visualization of the selective damage, along the sample depth, in butadiene (B)-rich domains, compared to styrene/acrylonitrile (SAN)-rich domains.

ABS polymers are complex, multiphase materials consisting of a butadiene (B) core to which a copolymer of styrene (S) and acrylonitrile (AN) has been grafted (Figure 15) (103). The SAN-rich phase is normally continuous, and the size of the B-rich ("rubber") domains is ≤ 1 μm in emulsion polymerization, and 0.5–5 μm in mass polymerization. The properties of ABS polymers can be modified by variation of the grafting conditions and monomer ratio, to produce a polymer suitable for specific applications (104). Most ESRI experiments were performed on ABS containing $\approx$10% B (Magnum 342 EZ, from Dow Chemical Co.), doped with 2 wt% Tinuvin 770 (**8**). The notation is ABS2H. For the ESRI experiments, cylindrical samples 4 mm in diameter were cut from the plaques; the samples were placed vertically in the ESR resonator, with the symmetry axis along the field gradient.

X-band ESR spectra at 300 K of the HAS-NO in UV-irradiated ABS for the indicated irradiation time in the weathering chamber are presented in Figure 16**a**. All spectra, except that corresponding to the longest irradiation time ($t = 2425$ h), consist of a superposition of two components, from nitroxide radicals differing in their mobility: a "fast" component (F, width $\approx$32 G), and a "slow" component (S, width $\approx$64 G). These spectra indicated the presence of HAS-NO radicals in two different environments, and were assigned to nitroxides located respectively in low T_g domains dominated by B sequences ($T_g \approx 200$ K), and in high T_g domains dominated by S ($T_g \approx 370$ K) or AN sequences ($T_g \approx 360$ K), as also seen in Figure 3. The relative intensity of the F component decreased with increasing irradiation time, and was negligible for $t = 2425$ h. Subtraction of the spectrum of the slow component (upper spectrum in Fig. 14**a**) from composite spectra gave the fast component; by superimposing the two components, it was possible to reproduce all composite spectra and to determine the relative concentration of each component. The decrease of the relative intensity of F with irradiation time was explained by the consumption of the HAS-derived nitroxide radicals located in B-rich domains of the polymer, as the B component is expected to be more vulnerable to degradation compared with the other repeat units in ABS (33).

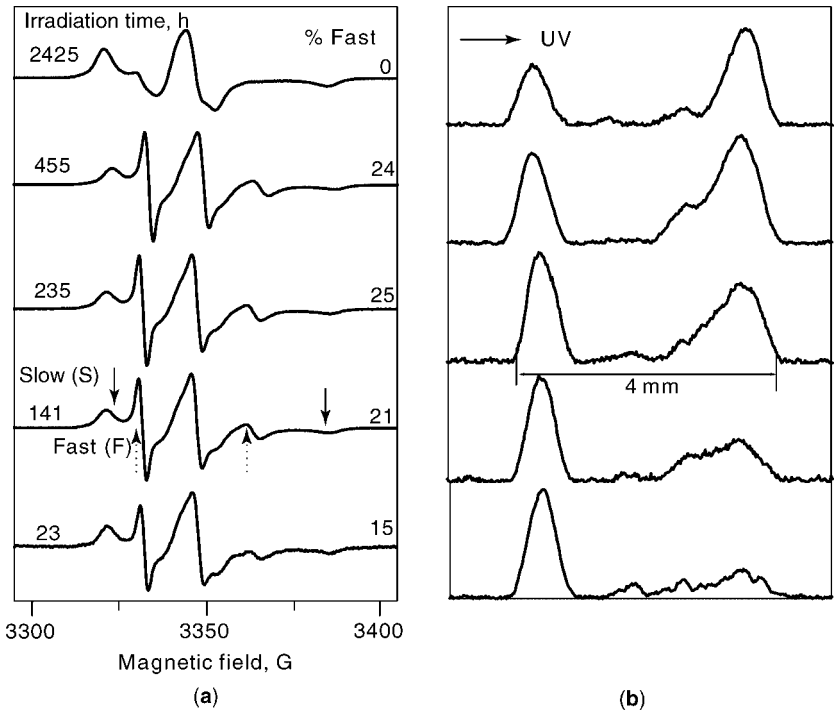

Fig. 16. (**a**) X-band ESR spectra at 300 K of ABS containing Tinuvin 770 for the indicated irradiation times. Vertical arrows point to the extreme low and high field features of the "slow" (S) and "fast" (F) spectral components, respectively. The percentage of the fast component, %F, in each spectrum is indicated. (**b**) Concentration profiles for the indicated irradiation times in the weathering chamber. The horizontal arrow indicates the irradiated side of the sample. From Ref. 55, with permission.

The presence of the two spectral components, F and S, is due to the heterophasic nature of ABS. The variation of the F/S ratio with irradiation time is, however, due to chemical reactions; in this way a connection was established between the concentration and ESR line shapes of the nitroxides, and the degradation process.

Figure 16**b** shows nitroxide profiles along the irradiation depth, deduced by deconvolution of 1D ESR images measured at 240 K; this temperature was chosen in order to avoid spatial variation of the line shapes. The larger nitroxide concentration near the outer planes of the sample and the gradual increase of the nitroxide concentration at the nonirradiated side clearly indicated the combined effects of oxygen and UV radiation, and the onset of DLO conditions. We note that the signal on the nonirradiated side appeared also in samples whose back was covered with aluminum foil, indicating that the radicals present on this side are not formed by direct irradiation, for instance, by scattered light. The mechanism responsible for the appearance of radicals on the nonirradiated side is currently under investigation in our laboratory.

Figure 17 presents 2-D spectral–spatial perspective and contour images of nitroxide radicals in ABS UV-irradiated for 70 h (in A) and for 643 h (in B) in the weathering chamber. The ESR intensity is presented in absorption mode.

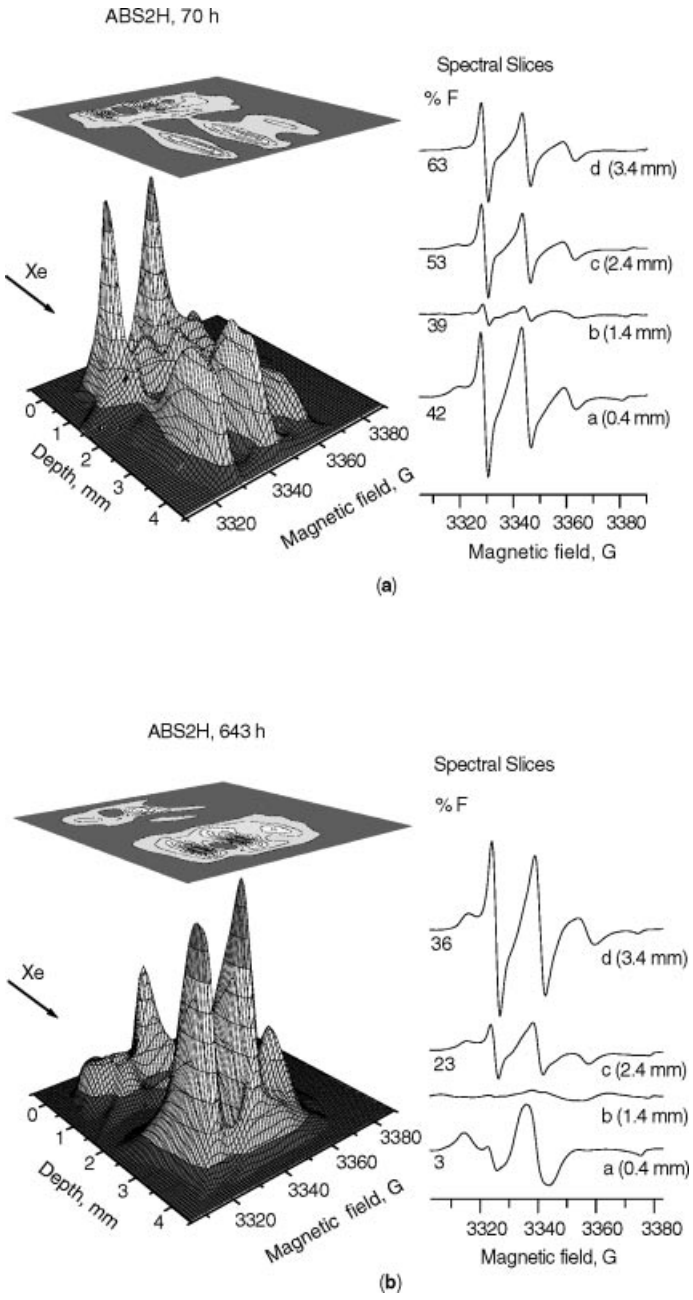

Fig. 17. 2-D spectral-spatial ESRI contour (top) and perspective (bottom) plots of HAS-derived nitroxides in ABS2H after 70 h (**a**) and 643 h (**b**) of irradiation by the Xe arc in the weathering chamber, presented in absorption. The spectral slices a, b, c, and d for the indicated depths are presented in the derivative mode; these slices were obtained from digital (nondestructive) sections of the 2-D image. %F is shown for a, b, c, and d slices in (**a**) and for a, c, and d slices in (**b**). Both 2-D images were reconstructed from 83 real projections, Hamming filter, 2 PSA iterations, $L = 4.5$ mm, $\Delta H = 70$ G, and were plotted on a 256×256 grid.

To the right we also present the corresponding "virtual" spectral slices (in the derivative mode) obtained nondestructively at the indicated depths of the sample (slices a–d). The perspective plot and the spectral slices indicate the line shape variation and the relative intensity of each spectral component as a function of depth. For the short irradiation time ($t = 70$ h) the ESR spectrum of the directly irradiated part of the sample exhibits two spectral components with $\%F \approx 42$; near the nonirradiated side $\%F = 63$. After 643 h of irradiation, the irradiated side contains no fast component, and %F is significantly lower at and near the nonirradiated side. Section b in Figure 17**b** represents a very weak signal and %F was not calculated for this section. The major conclusion from the 2-D images presented in Figure 17 is that the nitroxides in the B-rich domains are consumed rapidly on the irradiated side, and their concentration decreased to zero after 643 h of irradiation. On the nonirradiated side the degradation is less pronounced, but even on this side a decrease of %F is detected when the irradiation time increases from 70 to 643 h.

Spectral profiles can be deduced from 2-D spectral–spatial ESRI, as shown in Figure 18: the evolution of %F along the sample depth as a function of irradiation time ($t = 70$ and 643 h). The plots do not include data at depth range 0.5–1.7 mm because the intensity of the signal is too low and the margin for error in %F is too large. As the %F reflects the nitroxide radicals located in the B-rich domains, the profiles presented in Figure 18 can also be considered as *elastomer profiles*: a look into spatial changes in the elastomeric properties of ABS as degradation progresses.

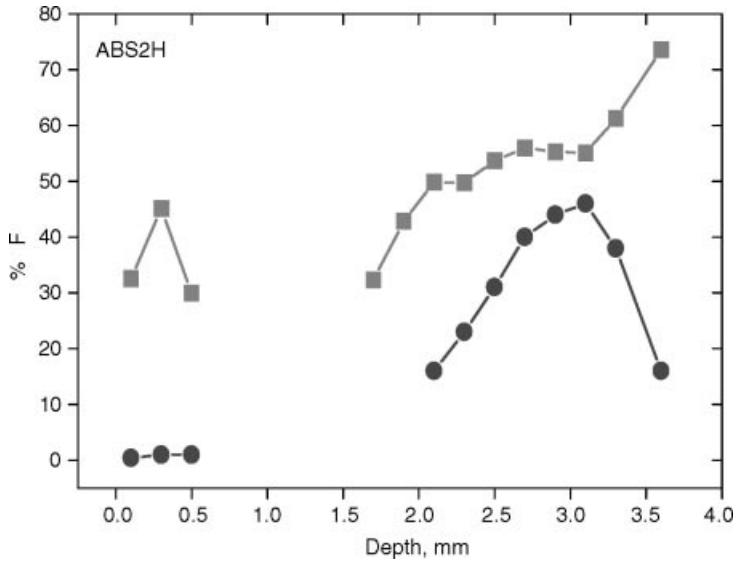

Fig. 18. Percentage of the fast component of HAS-derived nitroxides (%F) as a function of depth in ABS2H for the indicated irradiation times by the Xe arc in the weathering chamber: ■, 70 h Xe; ●, 643 h Xe. 834 h. Data were deduced from digital (nondestructive) sectioning of the 2-D spectral-spatial ESR images, such as those presented in Figure 17; see text. From Ref. 60, with permission.

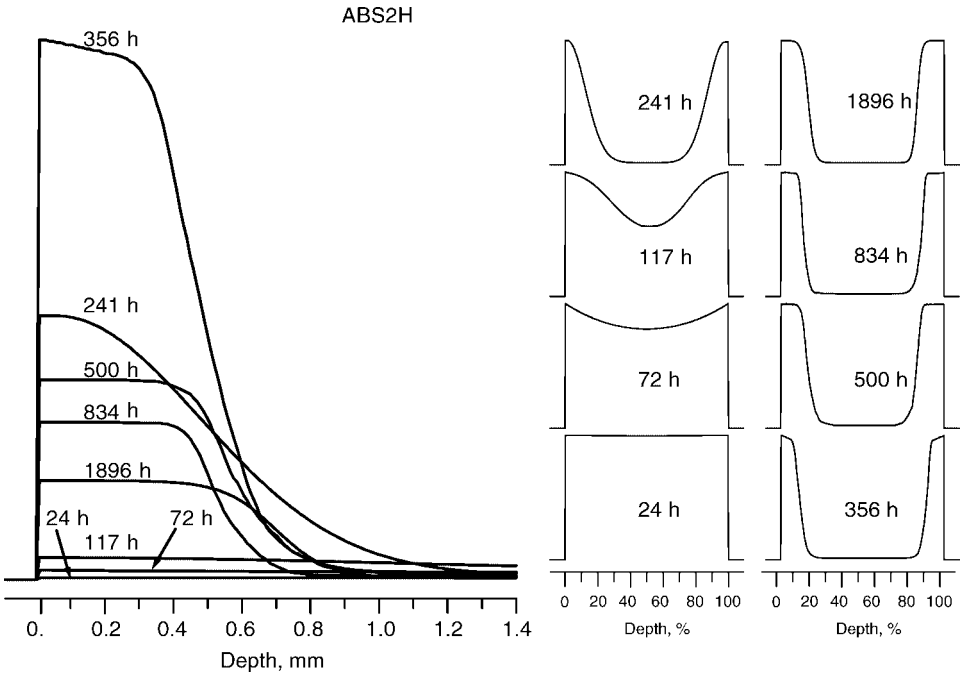

Fig. 19. Right: 1-D concentration profiles for ABS2H for the indicated time of thermal treatment at 393 K, Left: 1-D concentration profiles normalized to the corresponding nitroxide concentration. Only one side of each (symmetrical) profile is shown. From Ref. 62, with permission.

The concentration profiles for the indicated thermal treatment at 393 K are shown in Fig 19; the profiles were deduced by simulation of 1-D ESR images measured at 240 K. All profiles on the right side are presented with the same maximum height; the profiles on the left are given for one side of the samples (because of symmetry), and normalized by the nitroxide concentration measured in whole samples. The evolution from flat profiles in the initial stages of thermal ageing to spatially heterogeneous profiles due to DLO is clearly seen in Figure 19. The 1-D profiles indicate that the HAS-derived nitroxides are located at the two sample extremities, in regions of widths it is 500–600 μm in ABS2H. Figure 20 presents *spectral profiles* as a result of thermal treatment of ABS2H at 393 K for $t = 72$, 241, and 834 h. As in the data shown in Figure 18, the F component was assigned to nitroxides located in PB (elastomeric) domains. Conclusions from the ESRI experiments were substantiated by attenuated total reflectance (ATR) FTIR spectroscopy of microtomed samples of the polymer (60–63,105).

In conclusion, results from ESR imaging, together with the determination of the nitroxide concentration, allowed the mapping of the temporal and spatial variation of the nitroxides, depending on the irradiation source, and the time and temperature of treatment. Moreover, the nondestructive ESRI method is sensitive to early stages in the degradation process, and is expected to be complementary to existing profiling methods, for instance FTIR, which are normally applied to more advanced stages of degradation. Finally, the ESRI is of special interest for

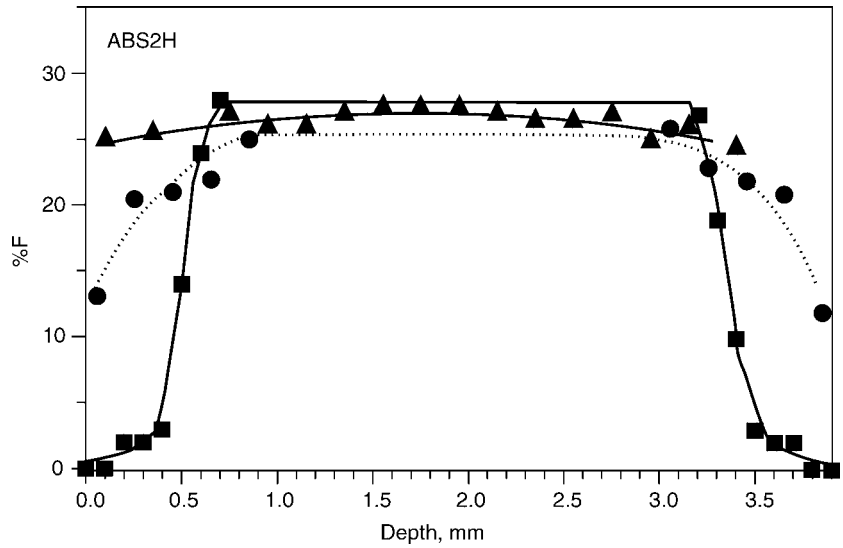

Fig. 20. Spectral profiling as a function of sample depth for ABS2H for the indicated time of thermal treatment at 393 K: ▲, 72 h; ●, 241 h; ■, 834 h. Data points were deduced from 200-μm-thick virtual slices in the corresponding 2-D spectral-spatial ESR images.

the study of polymers with phase-separated morphologies. In ABS and HPEC systems, ESRI studies have demonstrated a hierarchical variation of the HAS-derived nitroxide concentration: within the sample depth on the scale of millimeters, and within morphological domains on the scale of a few micrometers. As a result, it has become possible to establish an elastomer profile, which tracks the evolution of the elastomer properties as a function of sample depth, type and length of treatment, and temperature.

Conclusions and Prospects

The CW and pulsed ESR methods described above are exceptionally sensitive and specific to the presence of species with unpaired electron spins, such as organic and inorganic radicals, paramagnetic ions, and triplet states. Organic radicals are present in important polymerization processes, or are introduced deliberately as dopants, and report on the properties of the system in terms of dynamics, degree of order, and local polarity. In most cases the reporters are nitroxide radicals, which are available in a large range of structures, and can be selected for the specific system that is investigated and research goals.

Recent work has demonstrated that spin probes can be incorporated into complex materials and used as local reporters of the polymer host. By a judicious choice of the polarity, size, and chemical structure of the probe, it is possible to explore specific regions of microphase-separated or self-assembled system, thus by-passing the often difficult synthetic procedures of preparing covalently bound spin labels. The site selected by the probes is based on the very same weak intermolecular interactions (electrostatic, hydrogen bonding, metal coordination) that

govern supramolecular self-assembly. Basic CW ESR experiments can provide a wealth of information on spin probe dynamics and polarity of the local environment. Quantitative results can be deduced, based on line shape simulations. This is meaningful in particular if the spin probe can be regarded as a tracer for a specific component of a complex material, or if a set of probes with systematically varied structure is used, for example a series of *n*DSA or CAT*n* probes.

Once the attachment site of a spin probe is established by CW ESR, advanced ESR experiments can be used to characterize the spatial distribution of probes and the structure of the material in the vicinity of the probe. Such approaches are just emerging and have not yet reached their full potential. The spatial distribution of probes can be determined on macroscopic-length scales by ESR imaging (ESRI) and on microscopic-length scales in the nanometer range by DEER measurements. These two techniques complement each other but have not yet been applied simultaneously to the same system.

Polarity indices are a helpful tool for characterizing heterogeneous materials in general, including polymers. Separating the effects of matrix polarity and hydrogen bonding on the magnetic parameters of a spin probe is possible with high field ESR (106), but has not yet been utilized in materials science applications.

Matrix ENDOR of spin probes that reside in an internal interface has the potential to provide detailed information on the microscopic structure of this interface, but measurement techniques and data analysis are still in their infancy, so that only semiquantitative information can be obtained to date. Development of more precise and sensitivity-optimized measurement techniques and better quantification of the spectra are now in progress.

In recent years, advanced methods of polymerization such as living radical polymerization have been developed; the major advantages are the ability to synthesize polymers with narrow distributions of molecular weights, and tailor-made block copolymers of high purity (107,108). Some of these methods depend on the presence of nitroxide radicals in order to control the reactivity of growing chains via the equilibrium between alkoxy amine chain ends and active free-radical chain ends. ESR methods can be used to provide mechanistic details that are hard to obtain by other methods, for instance the electronic and steric effects of the penultimate unit in the propagating radical (109). It is expected that ESR methods will figure prominently in the field of living radical polymerization, for the detection and analysis of signals from free radicals (polymer-derived or nitroxides), and from transition-metal cations.

BIBLIOGRAPHY

"Electron Spin Resonance" in *EPST* 1st ed., Vol. 5, pp. 669–692, by S. E. Bresler and E. N. Kazbekov, Institut Vysokomolekulyarnykh Soedineii Akademii Nauk SSSR; "Electron Spin Resonance" in *EPSE* 2nd ed., Vol. 5, pp. 687–724, by Kenneth DeVries, University of Utah, and David Roylance, Massachusetts Institute of Technology.

1. A. Carrington and A. D. McLachlan, *Introduction to Magnetic Resonance, with Applications to Chemistry and Chemical Physics*, Harper & Row, New York, 1967.
2. R. S. Alger, *Electron Paramagnetic Resonance: Techniques and Applications*, Wiley-Interscience, New York, 1968.

3. A. Abragam and B. Bleaney, *Electron Paramagnetic Resonance of Transition Ions*, Clarendon, Oxford, U.K., 1970.
4. C. P. Poole, Jr, *Electron Spin Resonance: A Comprehensive Treatise on Experimental Techniques*, John Wiley & Sons, Inc., New York, 2nd ed., 1983.
5. J. R. Pilbrow, *Transition Ion Electron Paramagnetic Resonance*, Clarendon, Oxford, UK, 1990.
6. L. Kevan and M. K. Bowman, eds., *Modern Pulsed and Continuous-Wave Electron Spin Resonance*, Wiley, New York, 1990.
7. J. A. Weil, J. R. Bolton, and J. E. Wertz, *Electron Paramagnetic Resonance: Elementary Theory and Practical Applications*, John Wiley & Sons, Inc., New York, 1994.
8. A. Schweiger and G. Jeschke, *Principles of Pulse Electron Paramagnetic Resonance*, Clarendon, Oxford, U.K., 2001.
9. A. M. Wasserman, in *Electron Spin Resonance, Specialist Periodical Reports*, Vol. 15, Royal Society of Chemistry, London, 1996, pp 115–152.
10. D. Goldfarb, in *Electron Spin Resonance, Specialist Periodical Reports*, Vol. 15, Royal Society of Chemistry, London, 1996, pp 186–243.
11. A. Smirnov, in *Electron Spin Resonance, Specialist Periodical Reports*, Vol. 18, Royal Society of Chemistry, London, 2002, pp 109–136.
12. B. Rånby and J. F. Rabek, *ESR Spectroscopy in Polymer Research*, Springer-Verlag: Berlin, 1977.
13. E. Reichmanis and J. H. O'Donnell, eds., *The Effects of Radiation on High-Technology Polymers*, American Chemical Society, Washington, D.C., 1989.
14. D. J. T. Hill, T. T. Le, J. H. O'Donnell, M. C. S. Perera, and P. J. Pomery, in E. Reichmanis, C. W. Frank, and J. H. O'Donnell, eds., *Irradiation of Polymeric Materials: Processes, Mechanisms, and Application*, American Chemical Society, Washington, D.C., 1993.
15. T. G. Carswell, R. W. Garrett, D. J. T. Hill, J. H. O'Donnell, P. J. Pomery, and C. L. Winzor, in A. H. Fawcett, ed., *Polymer Spectroscopy*, John Wiley & Sons, Inc., Chichester, U.K., 1996, Chapt. 10, pp. 253–274.
16. L. J. Berliner, ed., *Spin Labeling, Theory and Applications*, Academic Press, New York, 1976.
17. L. J. Berliner, ed., *Spin Labeling II, Theory and Applications*, Academic Press, New York, 1979.
18. L. J. Berliner and J. Reuben, eds., *Biological Magnetic Resonance. Spin Labeling*, Vol. 8, Plenum, New York, 1989.
19. M. V. Motyakin and S. Schlick, in C. J. Bender, and L. J. Berliner, eds., *Instrumental Methods in Electron Magnetic Resonance, Biological Magnetic Resonance*, Vol. 21, Kluwer Academic/Plenum Publishing Corp., New York, 2004, pp 349–384.
20. R. F. Boyer and S. E. Keineth, eds., *Molecular Motions in Polymers* by E.S.R., Symposium Series Vol. 1, MMI Press: Harwood, Chur, 1980.
21. G. G. Cameron and I. G. Davidson, in A. H. Fawcett, ed., *Polymer Spectroscopy*, John Wiley & Sons, Inc., Chichester, U.K., 1996, Chapt. 9, pp. 231–252.
22. G. C. Rex, Ph. D. Dissertation, University of Detroit, 1989.
23. G. C. Rex and S. Schlick, *Polymer* **33**, 2036–2042 (1992).
24. P. L. Nordio, in Chapt. 2, Ref. 16, pp. 5–52.
25. M. V. Motyakin, J. L. Gerlock, and S. Schlick, *Macromolecules* **32**, 5463–5467 (1999).
26. J. Bednarek and S. Schlick, *J. Am. Chem. Soc.* **113**, 3303–3309 (1991).
27. L. Kevan and L. D. Kispert, *ENDOR Spectroscopy*, John Wiley & Sons, Inc., New York, 1976.
28. H. Kurreck, B. Kirste, and W. Lubitz, *ENDOR Spectroscopy of Radicals in Solution*, VCH Publishers, New York, 1988.

29. S. Schlick and L. Kevan, in J. Kershaw, ed., *Spectroscopic Analysis of Coal Liquids*, Elsevier, Amsterdam, 1989, Chapt. 9, pp. 267–305.
30. S. Schlick, L. Sjoqvist, and A. Lund, *Macromolecules* **21**, 535–537 (1988).
31. S. Schlick, G. Gebel, M. Pineri, G. Rius, and F. Volino, *Colloids Surf. A: Physicochem. Eng. Aspects* **78**, 181–188 (1993).
32. E. R. Davies, *Phys. Lett.* **A47**, 1–2 (1974).
33. W. B. Mims, *Proc. R. Soc. London* **283**, 452–457 (1965).
34. M. Pannier, S. Veit, A. Godt, G. Jeschke, and H. W. Spiess, *J. Magn. Reson.* **142**, 331–340 (2000).
35. G. Jeschke, A. Koch, U. Jonas, and A. Godt, *J. Magn. Reson.* **155**, 72–82 (2002).
36. G. Jeschke, *Chem. Phys. Chem.* **3**, 927–932 (2002).
37. M. Pannier, V. Schädler, M. Schöps, U. Wiesner, G. Jeschke, and H. W. Spiess, *Macromolecules* **33**, 7812–7818 (2000).
38. G. Jeschke and A. Godt, *Chem. Phys. Chem.* **4**, 1328–1334 (2003).
39. D. Hinderberger, H. W. Spiess, and G. Jeschke, *J. Phys. Chem. B*, **108**, 3698–3714 (2004).
40. P. Lauterbur, *Nature* **242**, 190–191 (1973).
41. P. Blümler, B. Blümich, R. Botto, and E. Fukushima, eds., *Spatially Resolved Magnetic Resonance: Methods, Materials, Medicine, Biology, Rheology, Ecology, Hardware*, Wiley-VCH, Weinheim, Germany, 1998.
42. B. H. Kevles, *Naked to the Bone: Medical Imaging in the Twentieth Century*, Rutgers University Press, New Brunswick, N.J., 1997, Chapt. 8, pp. 173–200.
43. G. R. Eaton, S. S. Eaton, and K. Ohno, eds., *EPR Imaging and in Vivo EPR*, CRC Press, Boca Raton, Fla., 1991.
44. D. Xu, E. Hall, C. K. Ober, J. K. Moscicki, and J. H. Freed, *J. Phys. Chem.* **100**, 15856–15866 (1996), and references therein.
45. H. J. Halpern, C. Yu, M. Peric, E. Barth, D. J. Grdina, and B. Teicher, *Proc. Natl. Acad. Sci. U.S.A.*, **91**, 13047–13051 (1994).
46. H. J. Halpern, G. V. R. Chandramouli, E. D. Barth, B. B. Williams, and V. E. Galtsev, *Curr. Top. Biophys.* **23**, 5–10 (1999).
47. J. L. Zweier and P. Kuppusamy, in Ref. 41, Chapt. 34, pp. 373–388.
48. K. Oikawa, T. Ogata, H. Togashi, H. Yokoyama, H. Ohya-Nishiguchi, and H. Kamada, *Appl. Radiat. Isot.* **47**, 1605–1609 (1996).
49. E. N. Degtyarev and S. Schlick, *Langmuir* **15**, 5040–5047 (1999).
50. J. Pilar, J. Labsky, A. Marek, C. Konak, and S. Schlick, *Macromolecules* **32**, 8230–8233 (1999).
51. S. Schlick, P. Eagle, K. Kruczala, and J. Pilar, in Ref. 41, Chapt. 17, pp. 221–234.
52. A. Marek, J. Labsky, C. Konak, J. Pilar, and S. Schlick, *Macromolecules* **35**, 5517–5528 (2002).
53. M. Lucarini, G. F. Pedulli, V. Borzatta, and N. Lelli, *Res. Chem. Intermed.* **22**, 581–591 (1996); *Polym. Degrad. Stab.* **53**, 9–17 (1996).
54. M. Lucarini, and G. F. Pedulli, *Angew. Makromol. Chem.* **252**, 179–193 (1997).
55. M. Lucarini, G. F. Pedulli, M. V. Motyakin, and S. Schlick, *Prog. Polym. Sci.* **28**, 331–340 (2003).
56. M. K. Ahn, S. S. Eaton, G. R. Eaton, and M. A. B. Meador, *Macromolecules* **30**, 8318–8321 (1997).
57. S. Capancioni, K. S. Abdellaoui, W. Kloeti, W. Herrmann, H. Brosig, H.-H. Borchert, J. Heller, and R. Gurny, *Macromolecules* **36**, 6135–6141 (2003).
58. S.-C. Kweon, M.Sc. Thesis, University of Detroit Mercy, 1993.
59. K. Kruczala, M. V. Motyakin, and S. Schlick, *J. Phys. Chem. B* **104**, 3387–3392 (2000).
60. M. V. Motyakin and S. Schlick, *Macromolecules* **34**, 2854–2864 (2001).

61. S. Schlick, K. Kruczala, M. V. Motyakin, and J. L. Gerlock, *Polym. Degrad. Stab.* **73/3**, 471–475 (2001).
62. M. V. Motyakin and S. Schlick, *Polym. Degrad. Stab.* **76**, 25–36 (2002).
63. M. V. Motyakin and S. Schlick, *Macromolecules* **35**, 3984–3992 (2002).
64. K. Kruczala, J. G. Bokria, and S. Schlick, *Macromolecules* **36**, 1909–1919 (2003).
65. L. J. Berliner and H. Fujii, *Science* **227**, 517–519 (1985).
66. M. Van Kienlin and R. Pohmann, in Ref. 41, Chapt. 1, pp. 3–20.
67. O. E. Yakimchenko, E. N. Degtyarev, V. N. Parmon, and Ya. S. Lebedev, *J. Phys. Chem.* **99**, 2038–2041 (1995).
68. S. Schlick, ed., *Ionomers: Characterization, Theory, and Applications*, CRC Press, Boca Raton, Fla., 1996.
69. M. R. Tant, K. A. Mauritz, and G. L. Wilkes, eds., *Ionomers: Synthesis, Structure, Properties and Applications*. Blackie Academic and Professional, London, UK, 1997.
70. A. Eisenberg and J.-S. Kim, *Introduction to Ionomers*, John Wiley & Sons, Inc., New York, 1998.
71. W. M. Risen, in Ref. 68, Chapt. 12, pp. 281–300.
72. G. Gebel, B. Loppinet, in Ref. 68, Chapt. 5, pp. 83–106.
73. B. Loppinet, G. Gebel, and C. E. Williams, *J. Phys. Chem. B* **101**, 1884–1892 (1997).
74. A.-L. Rollet, O. Diat, and G. Gebel, *J. Phys. Chem. B* **106**, 3033–3036 (2002)
75. L. Rubatat, A.-L. Rollet, G. Gebel, and O. Diat, *Macromolecules* **35**, 4050–4055 (2002).
76. E. Szajdzinska-Pietek and S. Schlick, in Ref. 68, Chapt. 7, pp. 135–163.
77. G. Martini, S. Ristori, and M. Visca, in Ref. 68, Chapt. 10, pp. 219–250, and references therein.
78. E. Szajdzinska-Pietek, J. Pilar, and S. Schlick, *J. Phys. Chem.* **99**, 313–319 (1995).
79. S. Kutsumizu, H. Hara, and S. Schlick, *Macromolecules* **30**, 2320–2328 (1997).
80. S. Kutsumizu and S. Schlick, *Macromolecules* **30**, 2329–2336 (1997).
81. E. Szajdzinska-Pietek, T. S. Pillars, S. Schlick, and A. Plonka, *Macromolecules* **31**, 4586–4594 (1998).
82. S. Kutsumizu, M. Goto, S. Yano, and S. Schlick, *Macromolecules* **35**, 6298–6305 (2002).
83. I. Dragutan, J. G. Bokria, B. Varghese, E. Szajdzinska-Pietek, and S. Schlick, *J. Phys. Chem. B* 11397–11403 (2003).
84. E. Szajdzinska-Pietek, M. Wolszczak, A. Plonka, and S. Schlick, *J. Am. Chem. Soc.* **120**, 4215–4221 (1998).
85. V. Schädler, V. Spickermann, H.-J. Räder, and U. Wiesner, *Macromolecules* **29**, 4865–4870 (1996).
86. V. Schädler, A. Franck, U. Wiesner, and H. W. Spiess, *Macromolecules* **30**, 3832–3838 (1997).
87. V. Schädler, V. Kniese, T. Thurn-Albrecht, U. Wiesner, and H. W. Spiess, *Macromolecules* **31**, 4828–4837 (1998).
88. M. Pannier, M. Schöps, V. Schädler, U. Wiesner, G. Jeschke, and H. W. Spiess, *Macromolecules* **34**, 5555–5560 (2001).
89. P. Vanhoorne and R. Jérôme, in Ref. 68, Chapt. 11, pp. 187–217.
90. C. E. Williams, T. P. Russell, R. Jérôme, and J. Horrion, *Macromolecules* **19**, 2877–2884 (1986).
91. T. Dollase, R. Graf, A. Heuer, and H. W. Spiess, *Macromolecules* **34**, 298–309 (2001).
92. D. Leporini, V. Schädler, U. Wiesner, H. W. Spiess, and G. Jeschke, *J. Non-Cryst. Solids* **307–310**, 510–516 (2002).
93. D. Leporini, V. Schädler, U. Wiesner, H. W. Spiess, and G. Jeschke, *J. Chem. Phys.* **119**, 11829–11846 (2003).
94. J. H. O'Donnell, in E. Reichmanis and J. H. O'Donnell, eds., *The Effects of Radiation on High-Technology Polymers*, American Chemical Society, Washington, D.C., 1989, Chapt. 1, pp. 1–13.

95. S. H. Hamid, M. B. Amin, and A. G. Maadhah, eds., *Handbook of Polymer Degradation*, Marcel Dekker, New York, 1992.
96. E. Reichmanis, C. W. Frank, and J. H. O'Donnell, eds., *Irradiation of Polymeric Materials: Processes, Mechanisms, and Applications*, American Chemical Society, Washington, D.C., 1993.
97. R. L. Clough, N. C. Billingham, and K. T. Gillen, eds., *Polymer Durability: Degradation, Stabilization and Lifetime Prediction*, Adv. Chem. Series 249, American Chemical Society, Washington, D.C., 1996.
98. K. T. Gillen and R. L. Clough, *Polymer* **33**, 4359–4365 (1992).
99. J. Wise, K. T. Gillen, and R. L. Clough, *Radiat. Phys. Chem.* **49**, 565–573 (1997).
100. N. C. Billingham, in G. Scott, ed., *Atmospheric Oxidation and Antioxidants*, Vol. II, Elsevier, Amsterdam, 1993, Chapt. 4, pp. 219–277.
101. J. Pospisil, *Adv. Polym. Sci.* **124**, 87–189 (1995).
102. J. L. Gerlock, D. R. Bauer, and L. M. Briggs, *Polym. Degrad. Stab.* **14**, 53–71 (1986); J. L. Gerlock, T. Riley, and D. R. Bauer, *Polym. Degrad. Stab*. 73–84; J. L. Gerlock and D. R. Bauer, *Polym. Degrad. Stab*. 97–112; J. L. Gerlock, A. V. Kucherov, and C. A. Smith, *Polym. Degrad. Stab.* **73**, 201–210 (2001), and references therein.
103. D. M. Kulich and S. K. Gagger, in Ref. 97, Chapt. 31, pp. 483–501.
104. Y. Aoki, A. Hatano, T. Tanaka, and H. Watanabe, *Macromolecules* **34**, 3100–3107 (2001).
105. J. G. Bokria and S. Schlick, *Polymer* **43**, 3239–3246 (2003).
106. H. J. Steinhoff, A. Savitsky, C. Wegener, M. Pfeiffer, M. Plato, and K. Möbius, *Biochim. Biophys. Acta* **1457**, 253–262 (2000).
107. G. Moad and D. H. Solomon, *The Chemistry of Free Radical Polymerization*, 1st ed., Elsevier, Oxford, 1995.
108. T. E. Patten, J. Xia, T. Abernathy, and K. Matyjaszewski, *Science* **272**, 866–868 (1996).
109. A. Kajiwara, A. K. Nanda, and K. Matyjaszewski, *Macromolecules* **37**, 1378–1385 (2004).

SHULAMITH SCHLICK
University of Detroit Mercy
GUNNAR JESCHKE
Max Planck Institute for Polymer Research

ELECTRONIC PACKAGING. See Volume 2.

ELECTROOPTICAL APPLICATIONS. See Volume 2.

EPOXY RESINS

Introduction

Epoxy resins are an important class of polymeric materials, characterized by the presence of more than one three-membered ring known as the epoxy, epoxide, oxirane, or ethoxyline group.

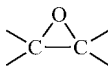

The word "epoxy" is derived from the Greek prefix "ep," which means over and between, and "oxy," the combining form of oxygen (1). By strict definition, epoxy resins refer only to uncross-linked monomers or oligomers containing epoxy groups. However, in practice, the term *epoxy resins* is loosely used to include cured epoxy systems. It should be noted that very high molecular weight epoxy resins and cured epoxy resins contain very little or no epoxide groups. The vast majority of industrially important epoxy resins are bi- or multifunctional epoxides. The monofunctional epoxides are primarily used as reactive diluents, viscosity modifiers, or adhesion promoters, but they are included here because of their relevance in the field of epoxy polymers.

Epoxies are one of the most versatile classes of polymers with diverse applications such as metal can coatings, automotive primer, printed circuit boards, semiconductor encapsulants, adhesives, and aerospace composites. Most cured epoxy resins provide amorphous thermosets with excellent mechanical strength and toughness; outstanding chemical, moisture, and corrosion resistance; good thermal, adhesive, and electrical properties; no volatiles emission and low shrinkage upon cure; and dimensional stability—a unique combination of properties generally not found in any other plastic material. These superior performance characteristics, coupled with outstanding formulating versatility and reasonable costs, have gained epoxy resins wide acceptance as materials of choice for a multitude of bonding, structural, and protective coatings applications.

Commercial epoxy resins contain aliphatic, cycloaliphatic, or aromatic backbones and are available in a wide range of molecular weights from several hundreds to tens of thousands. The most widely used epoxies are the glycidyl ether derivatives of bisphenol A (>75% of resin sales volume). The capability of the highly strained epoxy ring to react with a wide variety of curing agents under diverse conditions and temperatures imparts additional versatility to the epoxies. The major industrial utility of epoxy resins is in thermosetting applications. Treatment with curing agents gives insoluble and intractable thermoset polymers. In order to facilitate processing and to modify cured resin properties, other constituents may be included in the compositions: fillers, solvents, diluents, plasticizers, catalysts, accelerators, and tougheners.

Epoxy resins were first offered commercially in the late 1940s and are now used in a number of industries, often in demanding applications where their performance attributes are needed and their modestly high prices are justified. However, aromatic epoxies find limited uses in exterior applications because of their

Encyclopedia of Polymer Science and Technology. Copyright John Wiley & Sons, Inc. All rights reserved.

poor ultraviolet (UV) light resistance. Highly cross-linked epoxy thermosets sometimes suffer from brittleness and are often modified with tougheners for improved impact resistance.

The largest use of epoxy resins is in protective coatings (>50%), with the remainder being in structural applications such as printed circuit board (PCB) laminates, semiconductor encapsulants, and structural composites; tooling, molding, and casting; flooring; and adhesives. New, growing applications include lithographic inks and photoresists for the electronics industry.

History

The patent literature indicates that the synthesis of epoxy compounds was discovered as early as the late 1890s (2). In 1934, Schlack of I.G. Farbenindustrie AG in Germany filed a patent application for the preparation of reaction products of amines with epoxies, including one epoxy based on bisphenol A and epichlorohydrin (3). However, the commercial possibilities for epoxy resins were only recognized a few years later, simultaneously and independently, by the DeTrey Fréres Co. in Switzerland (4) and by the DeVoe and Raynolds Co. (5) in the United States.

In 1936, Pierre Castan of DeTrey Fréres Co. produced a low melting epoxy resin from bisphenol A and epichlorohydrin that gave a thermoset composition with phthalic anhydride. Application of the hardened composition was foreseen in dental products, but initial attempts to market the resin were unsuccessful. The patents were licensed to Ciba AG of Basel, Switzerland, and in 1946 the first epoxy adhesive was shown at the Swiss Industries Fair, and samples of casting resin were offered to the electrical industry.

Immediately after World War II, Sylvan Greenlee of DeVoe and Raynolds Co. patented a series of high molecular weight (MW) epoxy resin compositions for coating applications. These resins were based on the reaction of bisphenol A and epichlorohydrin, and were marketed through the subsidiary Jones-Dabney Co. as polyhydroxy ethers used for esterification with drying oil fatty acids to produce alkyd-type epoxy ester coatings. Protective surface coatings were the first major commercial application of epoxy resins, and they remain a major outlet for epoxy resin consumption today. Concurrently, epoxidation of polyolefins with peroxy acids was studied by Daniel Swern as an alternative route to epoxy resins (6). Meanwhile, Ciba AG, under license from DeTrey Frères, further developed epoxy resins for casting, laminating, and adhesive applications, and the Ciba Products Co. was established in the United States.

In the late 1940s, two U.S. companies, Shell Chemical Co. and Union Carbide Corp. (then Bakelite Co.), began research on bisphenol A based epoxy resins. At that time, Shell was the only supplier of epichlorohydrin, and Bakelite was a leading supplier of phenolic resins and bisphenol A. In 1955, the four U.S. epoxy resin manufacturers entered into a cross-licensing agreement. Subsequently, The Dow Chemical Co. and Reichhold Chemicals, Inc. joined the patent pool and began manufacturing epoxy resins.

In the 1960s, a number of multifunctional epoxy resins were developed for higher temperature applications. Ciba Products Co. manufactured and marketed *o*-cresol epoxy novolac resins, which had been developed by Koppers Co.

Dow developed the phenol novolac epoxy resins, Shell introduced polyglycidyl ethers of tetrafunctional phenols, and Union Carbide developed a triglycidyl *p*-aminophenol resin. These products continue to find uses today in highly demanding applications such as semiconductor encapsulants and aerospace composites where their performance justifies their higher costs relative to bisphenol A based epoxies.

The peracetic acid epoxidation of olefins was developed in the 1950s by Union Carbide in the United States and by Ciba AG in Europe for cycloaliphatic structures. Ciba Products marketed cycloaliphatic epoxy resins in 1963 and licensed several multifunctional resins from Union Carbide in 1965. The ensuing years witnessed the development of general-purpose epoxy resins with improved weathering characteristics based on the five-membered hydantoin ring and also on hydrogenated bisphenol A, but their commercial success has been limited because of their higher costs. Flame-retardant epoxy resins based on tetrabromobisphenol A were developed and commercialized by Dow Chemical for electrical laminate and composite applications in the late 1960s.

In the 1970s, the development of two breakthrough waterborne coating technologies based on epoxy resins helped establish the dominant position of epoxies in these markets: PPG's cathodic electrodeposition automotive primer and ICI-Glidden's epoxy acrylic interior can coatings.

While epoxy resins are known for excellent chemical resistance properties, the development and commercialization of epoxy vinyl ester resins in the 1970s by Shell and Dow offered enhanced resistance properties for hard-to-hold, corrosive chemicals such as acids, bases, and organic solvents. In conjunction with the development of the structural composites industry, epoxy vinyl ester resin composites found applications in demanding environments such as tanks, pipes and ancillary equipment for petrochemical plants and oil refineries, automotive valve covers, and oil pans. More recently, epoxy and vinyl esters are used in the construction of windmill blades for wind energy farms. Increasing requirements in the composite industries for aerospace and defense applications in the 1980s led to the development of new, high performance multifunctional epoxy resins based on complex amine and phenolic structures. Examples of those products are the trisphenol epoxy novolacs developed by Dow Chemical and now marketed by Huntsman (formerly Ciba).

The development of the electronics and computer industries in the 1980s demanded higher performance epoxy resins. Faster speeds and more densely packed semiconductors required epoxy encapsulants with higher thermal stability, better moisture resistance, and higher device reliability. Significant advancees in the manufacturing processes of epoxy resins led to the development of electronic-grade materials with lower ionic and chloride impurities and improved electrical properties. Dow Chemical introduced a number of new, high performance products such as hydrocarbon epoxy novolacs based on dicyclopentadiene. The 1980s also witnessed the development of the Japanese epoxy resin industry with focus on specialty, high performing and high purity resins for the electronics industry. These include the commercialization of crystalline resins such as biphenol diglycidyl ether.

More recently, in order to comply with more stringent environmental regulations, there has been increased attention to the development of epoxy resins

for high solids, powder, and waterborne and radiation-curable coatings. Powder coatings based on epoxy–polyester and epoxy–acrylate hybrids have continued to grow in the global markets, including new applications such as primer-surfacer and topcoats for automotive coatings. Radiation-curable epoxy–acrylates and cycloaliphatic epoxies showed tremendous growth in the 1990s in radiation-curable applications. These include important and new uses of epoxy resins such as the photoresists and lithographic inks for the electronics industry. Waterborne epoxy coatings are projected to grow substantially.

The continuing trend of device miniaturization in the computer industry, and the explosive growth of portable electronics and communications devices such as wireless cellular telephones in the 1990s demanded new, high performance resins for the PCB market. This has led to the development of new epoxies and epoxy hybrid systems having lower dielectric constants (D_k), higher glass-transition temperatures (T_g), and higher thermal decomposition temperatures (T_d) for electrical laminates. Environmental pressures in the PCB industry have fueled the development of a number of new bromine-free resin systems, but their commercialization is limited because of higher costs.

Significant efforts have been directed toward performance enhancements of epoxy structural composites. Advances have been made in the epoxy-toughening area. Epoxy nanocomposites and nanotube systems have been studied and are claimed to bring exceptional thermal, chemical, and mechanical property improvements. However, commercialization has not yet materialized.

In 1999, Dow Chemical introduced a new epoxy-based thermoplastic resin, BLOX*, for gas barrier, adhesives, and coatings applications.

Industry Overview

From the first commercial introduction of diglycidyl ether of bisphenol A (DGEBA) resins in the 1940s, epoxy resins have gradually established their position as an important class of industrial polymers. Epoxy resin sales increased rapidly in the 1970s and continued to rise into the 1980s as new applications were developed (annual growth rate >10% in the U.S. market, Table 1). More recently, the slower growth rates (3–4%) of the U.S., Japanese, and European markets in the 1990s were made up for by the higher growth rate (5–10%) in the Asia-Pacific markets outside of Japan, particularly in Taiwan and China. Epoxy resin growth has historically tracked well with economic developments and demands for durable goods, and so the growth of the epoxy markets in Asia-Pacific is expected to continue into the next decade.

The global market for epoxy resins is estimated at approximately 1.15 million metric tons (MT) for the year 2000 (8). This is an increase of 5% over 1999 demands. The North American market consumed over 330,000 MT of epoxy resins, the European market is estimated at more than 370,000 MT, and the Asian market has surpassed both the North American and European markets by consuming 400,000 MT of epoxy resins. About 50,000 MT of epoxies were consumed in the South American markets. Imports of epoxy resins from Asia into North America has steadily grown to about 120,000 MT in 2000. Epoxy resins were used with over

Table 1. History of U.S. Epoxy Resin Annual Production[a]

Year	Production, 10^3 MT
1955	10
1960	30
1965	55
1970	79
1975	100
1980	201
1985	347
1990	475
1994	433

[a] Data from U.S. International Trade Commission, *Synthetic Organic Chemicals*. Data include modified and unmodified epoxy resins. Modified epoxy resins include solid epoxy resin (SER), vinyl ester resins, epoxy acrylates, etc. There appear to be some discrepancies in epoxy resin production and market data as reported by different publications and organizations (7). This is primarily due to the fact that some epoxy resins such as liquid DGEBA resins and epoxy novolacs are used as raw materials to produce modified or advanced epoxy resins, which may be further converted to end-use products. Some publications report only unmodified epoxies.

400,000 MT of curing agents to produce an estimated 3 million MT of formulated compounds, worth over $20 billion.

Up until the mid-1990s, the major worldwide producers of epoxy resins were Dow Chemical, Shell, and Ciba-Geigy. However, both Shell and Ciba-Geigy have recently divested their epoxy resins businesses. Shell sold their epoxy business to Apollo Management LP (based in New York City) in the year 2000 and the company was renamed Resolution Performance Products. Similarly, Ciba's epoxy business was sold in 2000 to Morgan Grenfell, a London (U.K.)-based private equity firm, and the new company name was Vantico. More recently, in June 2003, the Vantico group of companies joined Huntsman. The Vantico business units are now named Huntsman Advanced Materials. The cycloaliphatic epoxy business of Union Carbide became part of The Dow Chemical Company after their merger in the year 2001. Together, these three producers continue to dominate the world market for epoxy resins, accounting for almost 65% of the global market. However, this is a reduction from over 70% of market shares owned by the three largest producers in the 1980s. Smaller producers of epoxy resins for the North American markets are Reichhold (owned by Dainippon Ink and Chemicals), CVC Specialty Chemicals, Pacific Epoxy Polymers, and InChem (phenoxy thermoplastic resins). Suppliers of epoxy derivatives include Ashland Specialty Chemical, UCB Chemicals (Radcure), AOC LLC, Eastman Chemical, and Interplastic Corp.

The market in Europe is similarly dominated by the three big producers: Dow, Resolution, and Huntsman and their affiliated joint ventures. Other smaller epoxy producers include Bakelite AG, LEUNA-Harze, Solutia, SIR Industriale, and EMS-CHEMIE. Imports from Asia have become significant in recent years.

The last two decades marked the emergence of the Asian epoxy industry. In the 1980s, the Japanese epoxy industry was transformed from a number of joint venture companies with Dow, Shell, and Ciba into independent producers and the emergence of a high number of new producers. This coincides with the development of Japan as a world-class manufacturing base. The Japanese epoxy industry is known for their special focus on high performance, high purity resins for the electronics industry. According to data from the Japan Epoxy Resin Manufacturers Association, the total Japanese market demand is estimated at approximately 200,000 MT for the year 2000. The production capacity is estimated at 240,000 MT annually. Exports accounted for an estimated 40,000 MT in 2000. Major Japanese epoxy resin producers are Tohto Kasei, Japan Epoxy Resins Corp. (formerly Yuka-Shell), Asahi Kasei, Dai Nippon Ink and Chemicals, Dow Chemical Japan, Mitsui Chemicals, Nihon Kayaku, Sumitomo Chemical, and Asahi Denka Kogyo. In Japan, Tohto Kasei is a leading resin producer, with epoxy technology licensing arrangements with numerous resin producers in Asia.

Outside of Japan, there have been significant increases in epoxy market demands and capacity in the 1990s. This is due to the migration of many PCB, electronic, computer, and durable goods manufacturing plants into the region, which has considerably lower manufacturing costs. Nan Ya, a subsidiary of the Formosa Plastics Group based in Taiwan, is emerging as a major epoxy resin producer with some import presence in North America and Europe. Similarly, Kukdo of Korea also exports to the North American and European markets. The output of these two companies now account for an estimated 15% of the world market. In China, there are numerous (more than 200) small domestic producers of epoxy resins. Recently, a number of major epoxy producers have announced joint ventures or plans to build manufacturing plants in China. These include a number of companies with integrated capacity into electrical laminates and PCB manufacturing, following the business model pioneered by the Formosa Plastics Group. Other notable Asian producers include Asia Pacific Resins, Chang Chun, and Eternal Chemical of Taiwan; Thai Epoxy of Thailand; Kumho, LG Chemical, and Pacific Epoxy Resins of Korea; and Guangdong Ciba Polymers, Sinopec Baling Petrochemical, Jiangsu Sanmu, and Wuxi DIC Epoxy Resin of China. The LG Chemical epoxy business was purchased by Bakelite in late 2002. A significant amount of resin produced in Taiwan and China is directed toward electrical laminates applications. The aggressive buildup of epoxy capacity in Asia has put significant pressures on resin prices, particularly the high volume products such as liquid epoxy resins based on bisphenol A (Table 2). But as of January 2004, the epoxy market demand in China alone has increased to more than 500,000 MT (Chinese Epoxy Industry Web site).

Estimated average prices for epoxy resin products in North America are given in Table 3. As with other petrochemical-based products, they depend on crude-oil prices. Prices of multifunctional resins are typically higher. They are based on more expensive raw materials than DGEBA resins and involve more complex manufacturing procedures. A listing of some major epoxy resin producers and the trade names of their products is shown in Table 4.

There are numerous suppliers of epoxy curing agents. Some of the major producers are Air Products and Chemicals, Cognis, Degussa, DSM, Huntsman, and Resolution.

Table 2. Epoxy Production Capacity in Asia-Pacific[a] (2001)

Country	Existing capacity, 1000 MT/year	Announced capacity, 1000 MT/year
Japan	240	
Taiwan	239	70
China	100	255
Korea	180	
Thailand	30	
Malaysia	10	
Philippines	10	
Total	*809*	*325*

[a] Compilation of published data by Dow Chemical.

Classes of Epoxy Resins and Manufacturing Processes

Most commercially important epoxy resins are prepared by the coupling reaction of compounds containing at least two active hydrogen atoms with epichlorohydrin followed by dehydrohalogenation:

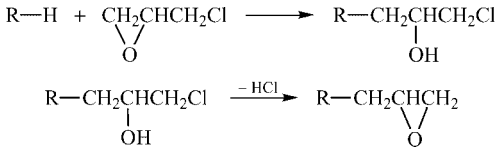

Table 3. U.S. Average Epoxy Resin Prices and Applications (2000)

Resin	$/kg	Applications
Liquid epoxy resins (Diglycidyl ether of bisphenol A, DGEBA)	2.2	Coatings, castings, tooling, flooring, adhesives, composites
Solid epoxy resins (SER)	2.4	Powder coating; epoxy esters for coatings; can, drum, and maintenance coatings
Bisphenol F epoxy	4.4	Coatings
Multifunctional		
Phenol epoxy novolac	4.8	Castings, coatings, laminates
Cresol epoxy novolac	8.8	Electronics encapsulants, powder coatings, laminates
Other multifunctional epoxies	11–44	Composites, adhesives, laminates, electronics
Cycloaliphatic epoxies	6.6	Electrical castings, coatings, electronics
Brominated epoxies	3.3–5.5	Printed wiring boards, composites
Epoxy vinyl esters	3.3	Composites
Phenoxy resins	11–17	Coatings, laminates, glass sizing
Epoxy diluents	4–11	

Table 4. List of Some Epoxy Resin Producers and Their Product Trade Names

Company	Trade name
Resolution Performance Products	Epon, Eponol, Eponex, Epi-Cure, Epikote
Dow Chemical	D.E.R., D.E.N., D.E.H., Derakane, E.R.L
Hunstman Advanced Materials (formerly Ciba, Vantico)	Araldite, Aralcast
Reichhold Chemical	Epotuf
Nan Ya	NPEL, NPES
Kukdo Chemical	YD
Dainippon Ink & Chemical (DIC)	Epiclon
Tohto Kasei	Epotohto
Japan Epoxy Resin (JER)	Epikote
Asahi Kasei	A.E.R.
Mitsui Chemical	Eponik
Sumitomo Chemical	Sumiepoxy
Thai Epoxy	Epotec
Chang Chun	
InChem	Paphen
Pacific Epoxy Polymers	PEP
CVC Specialty Chemicals	Erysis, Epalloy

These included polyphenolic compounds, mono and diamines, amino phenols, heterocyclic imides and amides, aliphatic diols and polyols, and dimeric fatty acids. Epoxy resins derived from epichlorohydrin are termed *glycidyl-based resins*.

Alternatively, epoxy resins based on epoxidized aliphatic or cycloaliphatic dienes are produced by direct epoxidation of olefins by peracids:

Approximately 75% of the epoxy resins currently used worldwide are derived from DGEBA. This market dominance of bisphenol A based epoxy resins is a result of a combination of their relatively low cost and adequate-to-superior performance in many applications. Figure 1 shows U.S. consumption of major epoxy resin types for the year 2000.

Liquid Epoxy Resins (DGEBA)

The most important intermediate in epoxy resin technology is the reaction product of epichlorohydrin and bisphenol A. It is often referred to in the industry as *liquid epoxy resin* (LER), which can be described as the crude DGEBA where the degree

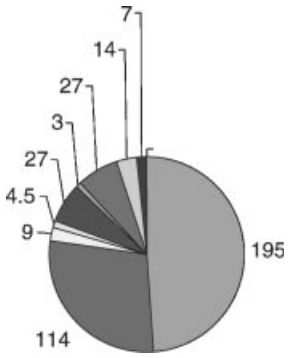

Fig. 1. Major epoxy resin and derivatives markets (10^3 MT). LER; SER; epoxy novolacs; other multifunctional epoxies; brominated epoxies; cycloaliphatic; vinyl esters; and epoxy acrylates.

of polymerization, n, is very low ($n \cong 0.2$):

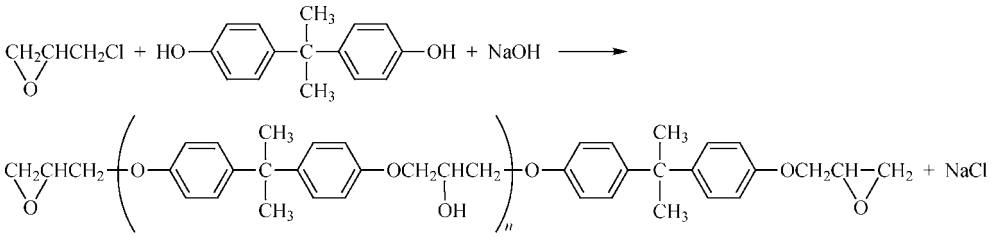

DGEBA

Pure DGEBA is a crystalline solid (mp 43°C) with an epoxide equivalent weight (EEW) of 170. The typical commercial unmodified liquid resins are viscous liquids with viscosities of 11,000–16,000 MPa·s (= cP) at 25°C, and an *epoxide equivalent weight* of ca 188.

EEW is the weight of resin required to obtain one equivalent of epoxy functional group. It is widely used to calculate reactant stoichiometric ratios for reacting or curing epoxy resins. It is related to the epoxide content (%) of the epoxy resin through the following relationship:

$$\mathrm{EEW} = \frac{43.05}{\%\mathrm{Epoxide}} \times 100$$

where 43.05 is the molecular mass of the epoxide group, $-C_2H_3O$. Other equivalent terminologies common in the industry include *weight per epoxide* (Wpe) or *epoxide equivalent mass* (EEM).

The outstanding performance characteristics of the resins are conveyed by the bisphenol A moiety (toughness, rigidity, and elevated temperature performance), the ether linkages (chemical resistance), and the hydroxyl and epoxy groups (adhesive properties and formulation latitude; reactivity with a wide variety of chemical curing agents).

LERs are used in coatings, flooring and composites formulations where their low viscosity facilitates processing. A large majority of LERs are used as starting materials to produce higher molecular weight (MW) solid epoxy resins (SER) and brominated epoxy resins, and to convert to epoxy derivatives such as epoxy vinyl esters, epoxy acrylates, etc. The bisphenol A derived epoxy resins are most frequently cured with anhydrides, aliphatic amines, phenolics, or polyamides, depending on desired end properties. Some of the outstanding properties are superior electrical properties, chemical resistance, heat resistance, and adhesion. Cured LERs give tight cross-linked networks having good strength and hardness but have limited flexibility and toughness.

Epichlorohydrin, or 3-chloro-1,2-epoxy propane (bp 115°C), is more commonly prepared from propylene by chlorination to allyl chloride, followed by treatment with hypochlorous acid. This yields glycerol dichlorohydrin, which is dehydrochlorinated by sodium hydroxide or calcium hydroxide (9).

In industrial practices, epichlorohydrin is produced by direct chlorohydroxylation of allyl chloride in chlorine and water (10–13). Alternatively, a new epichlorohydrin process has been developed and commercialized by Showa Denko (14) in Japan in 1985. It involves the chlorination of allyl alcohol as the precursor and is claimed to be more efficient in chlorine usage.

Bisphenol A (mp 153°C), or 2,2-bis(*p*-hydroxyphenyl)propane, is prepared from 2 *M* of phenol and 1 *M* of acetone (15,16)

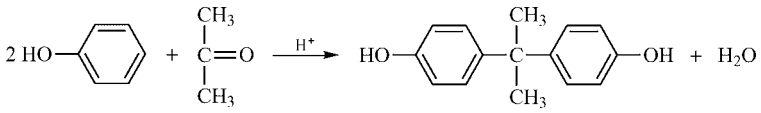

Bisphenol A based liquid epoxy resins are prepared in a two-step reaction sequence from epichlorohydrin and bisphenol A. The first step is the base-catalyzed *coupling* of bisphenol A and epichlorohydrin to yield a chlorohydrin.

Bases that may be used to catalyze this step include sodium hydroxide, lithium salts, and quaternary ammonium salts. Dehydrohalogenation of the chlorohydrin intermediate with a stoichiometric amount of base affords the glycidyl ether. Manufacturing processes can be divided into two broad categories according to the type of catalyst used to couple epichlorohydrin and bisphenol A (17,18).

Caustic Coupling Process. In this process, caustic is used as a catalyst for the nucleophilic ring-opening (coupling reaction) of the epoxide group on the primary carbon atom of epichlorohydrin by the phenolic hydroxyl group and as a

dehydrochlorinating agent for conversion of the chlorohydrin to the epoxide group:

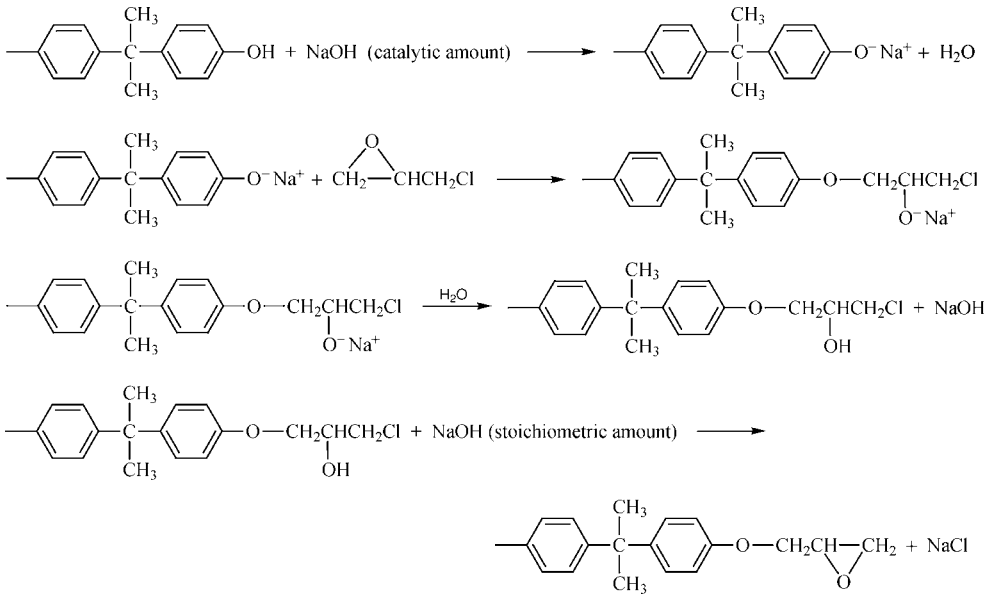

In caustic coupling processes, caustic (20–50% sodium hydroxide in water) is slowly added to an agitated mixture of epichlorohydrin and bisphenol A. The highly exothermic coupling reaction proceeds during the initial stages. As the coupling reaction nears completion, dehydrochlorination becomes the predominant reaction. A high ratio (usually 10:1) of epichlorohydrin/bisphenol A is charged to the reactor to maximize the yield of monomeric ($n = 0$) DGEBA. At a 10:1 level of epichlorohydrin/bisphenol A, the $n = 0$ monomer comprises >85% of the reaction product mixture.

Phase-Transfer Catalyst Process. Alternatively, the coupling reaction and dehydrochlorination can be performed separately by using phase-transfer coupling catalysts, such as quaternary ammonium salts (19), which are not strong enough bases to promote dehydrochlorination. Once the coupling reaction is completed, caustic is added to carry out the dehydrochlorination step. Higher yields of the $n = 0$ monomer (>90%) are readily available via this method.

Many variations of these two basic processes are described in process patents (20,21), including the use of co-solvents and azeotropic removal of water to facilitate the reactions and to minimize undesirable by-products such as insoluble polymers. The original batch methods have been modified to allow for continuous or semicontinuous production. New developments have been focused on improving manufacturing yield and resin purity.

The description of liquid DGEBA resins presented so far is oversimplified. In reality, *side reactions* result in the formation of low levels of impurities that both decrease the epoxide content from the theoretical amount of 2 per molecule and affect the resins properties, both before and after curing (22). The five common side reactions are as follows:

(1) *Hydrolysis of epoxy groups.* Unavoidable hydrolysis of the epoxide ring gives a small amount (0.1–5%) of monohydrolyzed resin (MHR) or α-glycol. It has been reported that dispersability of pigments are enhanced and rates of epoxy resin curing with diamines can be dramatically increased by higher levels of MHR (23).

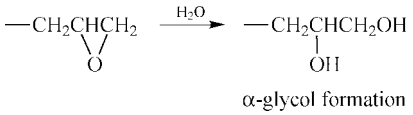

α-glycol formation

(2) *Incomplete dehydrochlorination* results in residual saponifiable or hydrolyzable chloride:

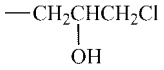

Incomplete dehydrochlorination increases the level of hydrolyzable chloride in the resin, which affects its suitablity for applications requiring superior electrical properties. In addition, hydrolyzable chlorides can affect reactivity by neutralizing basic catalysts such as tertiary amines. Many formulators adjust their formulations according to resin hydrolyzable chloride content. Typical hydrolyzable chloride contents of LERs range from <100 ppm for electronic grade resin to 200–1000 ppm for standard grade resins.

(3) *Abnormal addition of epichlorohydrin,* ie, abnormal phenoxide attack at the central carbon of epichlorohydrin results in an end group that is more difficult to dehydrochlorinate:

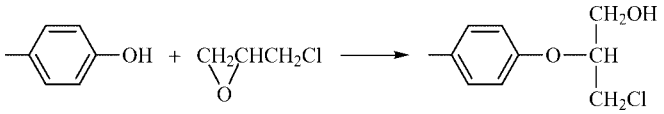

(4) *Formation of bound chlorides* by reaction of epichlorohydrin with hydroxy groups in the polymer backbones:

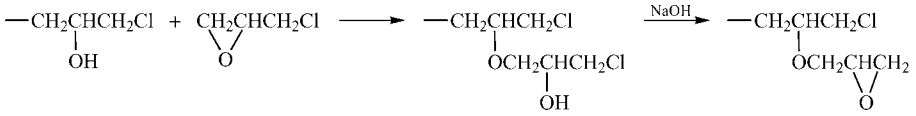

The bound chloride is not readily saponified with metal hydroxide solutions and is analyzed as part of the total chloride of the resin. Typical total chlorides values are 1000–2000 ppm.

(5) *Higher oligomer formation.* Reaction of a phenolic terminal group with another epoxy resin molecule instead of an epichlorohydrin molecule gives epoxy resins with broader oligomer distribution and increased viscosity ($n = 1$ and higher oligomers). Typical LERs contain 5–15% of the higher oligomers, mostly $n = 1$ and $n = 2$ compounds.

Pure DGEBA is a solid melting at 43°C. The unmodified commercial liquid resins are supercooled liquids with the potential for crystallization, depending on purity and storage conditions. This causes handling problems, particularly for ambient cure applications. Addition of certain reactive diluents and fillers can either accelerate or retard crystallization. Crystallization-resistant, modified resins are available. A crystallized resin can be restored to its liquid form by warming.

Solid Epoxy Resins Based on DGEBA

High molecular weight (MW) SERs based on DGEBA are characterized by a repeat unit containing a secondary hydroxyl group with degrees of polymerization, ie, n values ranging from 2 to about 35 in commercial resins; two terminal epoxy groups are theoretically present.

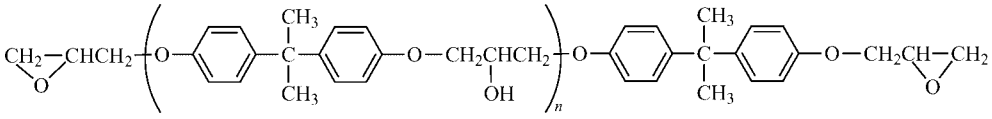

The epoxy industry has adopted a common nomenclature to describe the SERs. They are called type "1," "2" up to type "10" resins, which correspond to the increased values of n, the degree of polymerization, EEW, MW, and viscosity. Examples of SERs are D.E.R. 661, 662, 664, 667, 669 resins from Dow Chemical, and Epon 1001 to 1009 series from Resolution. A comparison of some key properties of LERs and SERs is shown in Table 5.

SERs based on DGEBA are widely used in the coatings industry. The longer backbones give more distance between cross-links when cross-linked through the terminal epoxy groups, resulting in improved flexibility and toughness. Furthermore, the resins can also be cured through the multiple hydroxyl groups along the backbones using cross-linkers such as phenol–formaldehyde resoles or isocyanates to create different network structures and performance.

SERs are prepared by two processes: the *taffy* process and the *advancement* or *fusion* process. The first is directly from epichlorohydrin, bisphenol A, and a stoichiometric amount of NaOH. This process is very similar to the *caustic coupling* process used to prepare liquid epoxy resins. Lower epichlorohydrin to bisphenol A ratios are used to promote formation of high MW resins. The term *taffy* is derived from the appearance of the advanced epoxy resin prior to its separation from water and precipitated salts.

Table 5. DGEBA-Based Epoxy Resins

Resin type	n value[a]	EEW	Mettler softening point, °C	Molecular weight (M_w)[b]	Viscosity at 25°C, MPa·s (= cP)
Low viscosity LER	<0.1	172–176		~350	4,000–6,000
Medium viscosity LER	~0.1	176–185		~370	7,000–10,000
Standard grade LER	~0.2	185–195		~380	11,000–16,000
Type 1 SER	~2	450–560	70–85	~1,500	160 – 250[c]
Type 4 SER	~5	800–950	95–110	~3,000	450 – 600[c]
Type 7 SER	~15	1,600–2,500	120–140	~10,000	1,500–3,000[c]
Type 9 SER	~25	2,500–4,000	145–160	~15,000	3,500–10,000[c]
Type 10 SER	~35	4,000–6,000	150–180	~20,000	10,000–40,000[c]
Phenoxy resin	~100	>20,000	>200	>40,000	

[a] n value is the number-average degree of polymerization which approximates the repeating units and the hydroxyl functionality of the resin.
[b] Molecular weight is weight average (M_w) measured by gel-permeation chromatography (GPC) using polystyrene standard.
[c] Viscosity of SERs is determined by kinematic method using 40% solids in diethylene glycol monobutyl ether solution.

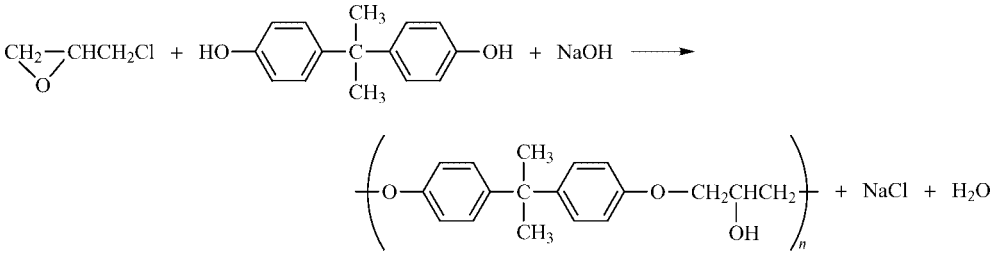

In the taffy process, a calculated excess of epichlorohydrin governs the degree of polymerization. However, preparation of the higher molecular weight species is subject to practical limitations of handling and agitation of highly viscous materials. The effect of epichlorohydrin–bisphenol A (ECH–BPA) ratio for a series of solid resins is shown in Table 6.

In commercial practice, the *taffy* method is used to prepare lower MW solid resins, ie, those with maximum EEW values of about 1000 (type "4"). Upon completion of the polymerization, the mixture consists of an alkaline brine solution and a water–resin emulsion. The product is recovered by separating the phases, washing the taffy resin with water, and removing the water under vacuum. One disadvantage of the taffy process is the formation of insoluble polymers, which create handling and disposal problems. Only a few epoxy producers currently manufacture SERs using the taffy process. A detailed description of a taffy procedure follows (24).

Table 6. Effect of Epichlorohydrin–Bisphenol A Ratio on Resin Properties of Taffy SERs

Mole ratio ECH/BPA	EEW	Softening point, °C
1.57:1.0	450–525	65–75
1.22:1.0	870–1025	95–105
1.15:1.0	1650–2050	125–135
1.11:1.0	2400–4000	145–155

A mixture of bisphenol A (228 parts by weight) and 10% aqueous sodium hydroxide solution (75 parts by weight) is introduced into a reactor equipped with a powerful agitator. The mixture is heated to ca 45°C and epichlorohydrin (145 parts by weight) is added rapidly with agitation, giving off heat. The temperature is allowed to rise to 95°C, where it is maintained about 80 min for completion of the reaction. Agitation is stopped, and the mixture separates into two layers. The heavier aqueous layer is drawn off and the molten, taffy-like product is washed with hot water until the wash water is neutral. The taffy-like product is dried at 130°C, giving a solid resin with a softening point of 70°C and an EEW of ca 500.

Alternatively, epichlorohydrin and water are removed by distillation at temperatures up to 180°C under vacuum. The crude resin/salt mixture is then dissolved in a secondary solvent to facilitate water washing and salt removal. The secondary solvent is then removed via vacuum distillation to obtain the taffy–resin product.

Resins produced by this process exhibit relatively high α-glycol values, ie, ca 0.5 eq/kg, attributable to hydrolysis of epoxy groups in the aqueous phase. Although detracting from epoxide functionality, such groups act as accelerators for amine curing. Resins produced by the taffy process exhibit n values of 0, 1, 2, 3, etc, whereas resins produced by the *advancement* process (described below) exhibit mostly even-numbered n values because a difunctional phenol is added to a diglycidyl ether of a difunctional phenol.

An alternative method is the chain-extension reaction of liquid epoxy resin (crude DGEBA) with bisphenol A, often referred to as the *advancement* or *fusion process* (25) which requires an advancement catalyst:

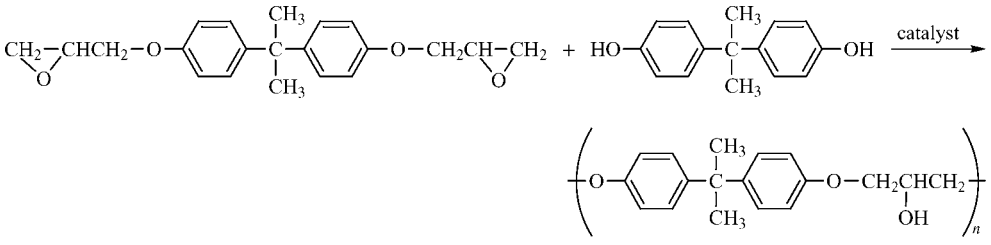

The advancement process is more widely used in commercial practice. Isolation of the polymerized product is simpler, since removal of copious amounts of NaCl is unnecessary. The reaction can be carried out with or without solvents.

Solution advancement is widely practiced by coatings producers to facilitate handling of the high MW, high viscosity epoxy resins used in many coating formulations. The degree of polymerization is dictated by the ratio of LER to bisphenol A; an excess of the former provides epoxy terminal groups. The actual MW attained depends on the purity of the starting materials, the type of solvents used, and the catalyst. Reactive monofunctional groups can be used as chain terminators to control MW and viscosity build.

The following formula can be used to calculate the relative amount of bisphenol A that must be reacted with epoxy resin to give an advanced epoxy resin of predetermined EEW:

$$\text{Bis A} = \frac{\text{EEW}_i^{-1} - \text{EEW}_f^{-1}}{\text{EEW}_i^{-1} + \text{PEW}^{-1}}$$

where Bis A is the mass fraction of bisphenol A in the mixture prior to advancement, EEW_i is the EEW of the epoxy resin that is to be advanced, EEW_f is the EEW of the advanced epoxy resin, and PEW is the phenol equivalent mass of the bisphenol, which is 115.1 g per equivalent for bisphenol A.

In a typical advancement process, bisphenol A and a liquid DGEBA resin (175–185 EEW) are heated to ca 150–190°C in the presence of a catalyst and reacted (ie, advanced) to form a high MW resin. The oligomerization is exothermic and proceeds rapidly to near completion. The exotherm temperatures are dependent upon the targeted EEW and the reaction mass. In the cases of higher MW resins such as type "7" and higher, exotherm temperatures of >200°C are routinely encountered.

Advancement reaction catalysts facilitate the rapid preparation of medium and high MW linear resins and control prominent side reactions inherent in epoxy resin preparations, eg, chain branching due to addition of the secondary alcohol group generated in the chain-lengthening process to the epoxy group (26,27). Nuclear Magnetic Resonance (NMR) spectroscopy can be used to determine the extent of branching (28).

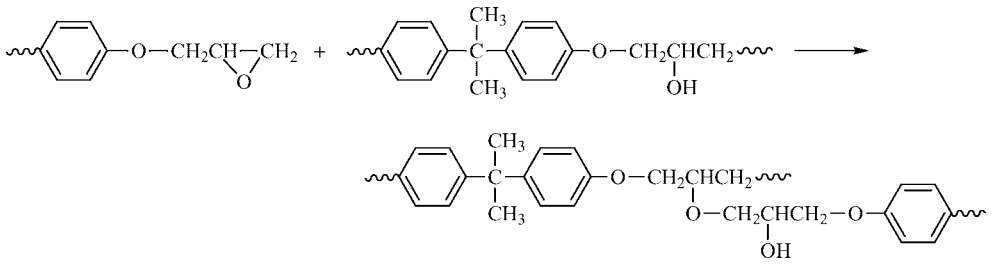

Conventional advancement catalysts include basic inorganic reagents, eg, NaOH, KOH, Na_2CO_3, or LiOH, and amines and quaternary ammonium salts. One mechanism proposed for the basic catalysts involves proton abstraction of

the phenolic compound as the initiation step:

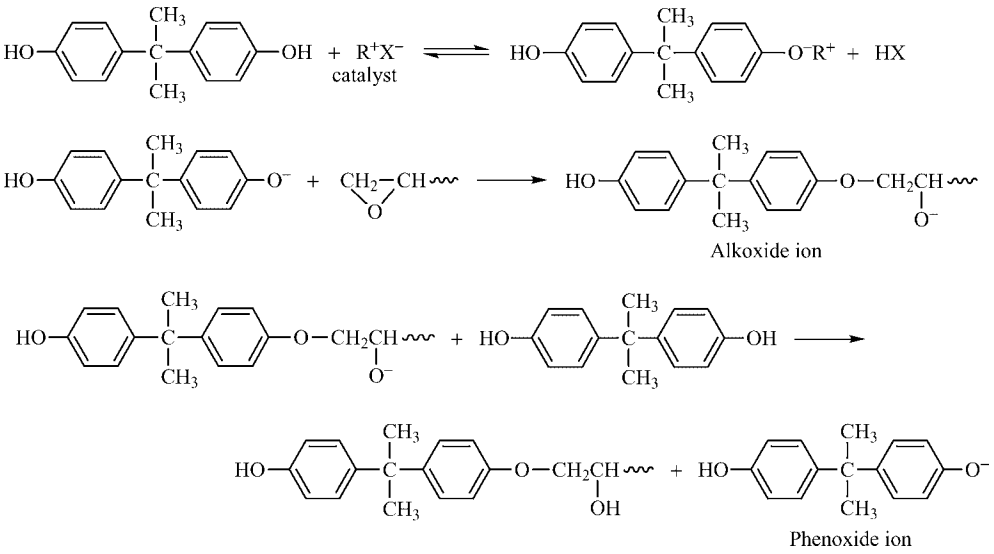

The phenoxide ion then attacks the epoxy ring, generating an alkoxide, which immediately abstracts a proton from another phenolic OH group. This is called the propagation step. Regeneration of the phenoxide ion repeats the cycle. The potential for side reactions increases after the phenolic OH groups have been consumed, particularly in melt (ie, fusion) polymerization reactions.

One key disadvantage of catalysts based on inorganic bases and salts is the increased ionic impurities added to the resin, which is not desirable in certain applications.

Imidazoles, substituted imidazoles, and triethanolamine have been patented as advancement catalysts (29). However, most of the inorganic bases, salts, and amines produce resins with broad MW distribution and viscosity instability. This is due to poor catalyst selectivity and the continuing activity of the catalyst after completion of the advancement reaction.

Alternatively, a broad class of catalysts derived from aryl or alkyl phosphonium compounds were developed. Extensive patent literature claims a high order of selectivity (30,31). Selections of the phosphonium cation and counter ion have been shown to affect initiation rate, catalyst selectivity, catalyst lifetime, and, consequently, product quality and consistency. Some of the phosphonium salts are deactivated at high temperatures by the reaction exotherm, and are claimed to give better resin stability in terms of viscosity, EEW, and MW during the subsequent finishing steps (32–35).

Few mechanistic studies have been published on the selectivity of phosphonium compounds, but one publication describes the role of triphenylphosphine in advancement catalysis (36). Nucleophilic attack by triphenylphosphine opens the

epoxy ring, producing a betaine:

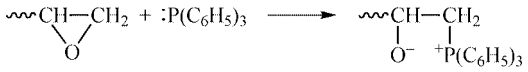

Proton abstraction from bisphenol A yields the phenoxide anion, forming a phosphonium salt. The phenoxide reacts with the electrophilic carbon attached to the positive phosphorus regenerating the catalyst:

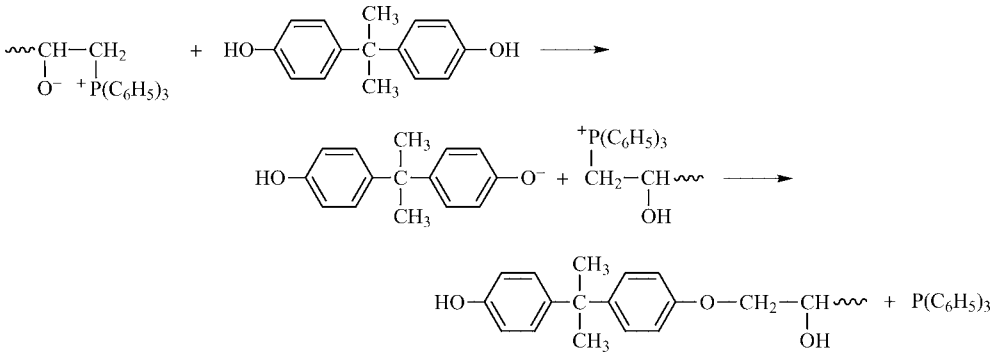

When the bisphenol A is consumed, the betaine decomposes into a terminal olefin and triphenylphosphine oxide:

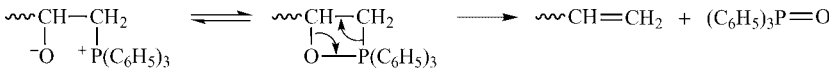

Branched epoxies (37) are prepared by advancing LER with bisphenol A in the presence of epoxy novolac resins. Such compositions exhibit enhanced thermal and solvent resistance.

SERs are available commercially in solid form or in solution. MW distributions of SERs have been examined by means of theoretical models and compared with experimental results (38). Taffy-processed resins were compared with advancement-processed resins by gel-permeation chromatography (GPC) and high performance liquid chromatography (HPLC) (39) in conjunction with statistical calculations. The major differences are in the higher α-glycol content and the repeating units of oligomers. Resin viscosity and softening points are also lower with taffy resins. In addition, certain formulations based on taffy resins exhibit different behavior in pigment loading, formulation rheology, reactivity, and mechanical properties compared to those based on advancement resins.

SER Continuous Advancement Process. The recent literature review indicates efforts to develop continuous advancement processes to produce SERs. Companies seek to improve process efficiencies and product quality. One of the major deficiencies of the traditional batch advancement process is the long reaction time, resulting in EEW and viscosity drift, variable product quality, and gel formation. In addition, it is difficult to batch process higher MW, higher viscosity SERs such as types "9" and "10" resins. Shell patented several versions of the

continuous resin advancement processes using modified reactor designs (40). Dow Chemical received patents covering the uses of reactive extrusion (41) (REX) to produce SERs and other epoxy thermoplastic resins (42). The latter process makes use of a self-wiping twin-screw extruder. LER, bisphenol A, and catalyst are fed directly to the extruder to complete the resin advancement reaction in several minutes compared to the traditional several hours in a batch process. The process is claimed to be very efficient and is particularly suitable for the production of high molecular weight SERs, phenoxy resins, and epoxy thermoplastic resins. Compared to the traditional taffy processes used to produce phenoxy resins, the chemistry is salt-free, and the resins made via the REX process are fully converted in a matter of minutes, significantly reducing manufacturing costs. Additional benefits include reduced lot-to-lot variations in MW distribution, the flexibility to make small lots of varying molecular weights with minimal waste, and the ability to make custom resins with a variety of additives such as pigments and flow modifiers.

Phenoxy Resins. *Phenoxy resins* are thermoplastic polymers derived from bisphenol A and epichlorohydrin. Their weight-average molecular weights (M_w) are higher (ie, >30,000) than those of conventional SERs (ie, 25,000 maximum). They lack terminal epoxides but have the same repeat unit as SERs and are classified as polyols or polyhydroxy ethers:

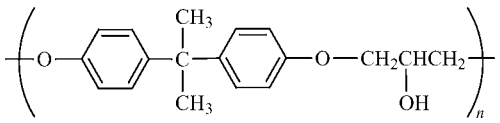

Phenoxy resins were originally developed and produced by Union Carbide (trade names PKHH, PKHC, PKHJ) using the taffy process. The process involves reaction of high purity bisphenol A with epichlorohydrin in a 1:1 mole ratio. Alternatively, phenoxy resins can be produced by the fusion process which uses high purity LER and bisphenol A in a 1:1 mole ratio. High purity monomers and high conversions are both needed to produce high MW phenoxy resins. The effects of monomer purity on phenoxy resin production are significant: monofunctional components limit MW, and functionality >2 causes excess branching and increased polydispersity. Solution polymerization may be employed to achieve the MW and processability needed (43). This, however, adds to the high costs of manufacturing of phenoxy resins, limiting their commercial applications.

The phenoxies are offered as solids, solutions, and waterborne dispersions. The majority of phenoxy resins are used as thermoplastics, but some are used as additives in thermoset formulations. Their high MW provide improved flexibility and abrasion resistance. Their primary uses are in automotive zinc-rich primers, metal can/drum coatings, magnet wire enamels, and magnetic tape coatings. However, the zinc-rich primers are being phased out in favor of galvanized steel by the automotive industry. Smaller volumes of phenoxy resins are used as flexibility or rheology modifiers in composites and electrical laminate applications, and as composite honeycomb impregnating resins. A new, emerging application is fiber sizing, which utilizes waterborne phenoxies. Literature references indicate

their potential uses as compatiblizers for thermoplastic resins such as polyesters, nylons, and polycarbonates because of their high hydroxyl contents.

Current producers of phenoxy resins include the Phenoxy Specialties division of InChem Corp., Resolution, Huntsman, Tohto Kasei, and DIC.

Epoxy-Based Thermoplastics. Some of the new epoxy products developed in the past few years are the thermoplastic resins based on epoxy monomers. Polyhydroxy amino ether (44,45) (PHAE) was commercialized by Dow Chemical in 1999 and trade named BLOX*. It is produced by the reaction of DGEBA with monoethanol amine using the reactive extrusion process. The high cohesive energy density of the resin gives it excellent gas-barrier properties against oxygen and carbon dioxide. It also possesses excellent adhesion to many substrates, optical clarity, excellent melt strength, and good mechanical properties. The product has been evaluated as a barrier resin for beer and beverage plastic bottles, as thermoplastic powder coatings, and as a toughener for starch-based foam (46). Another epoxy thermoplastic resin under development by Dow is the polyhydroxy ester ether (PHEE). It is a reaction product of DGEBA with difunctional acids. The ester linkage makes it suitable for biodegradable applications (47).

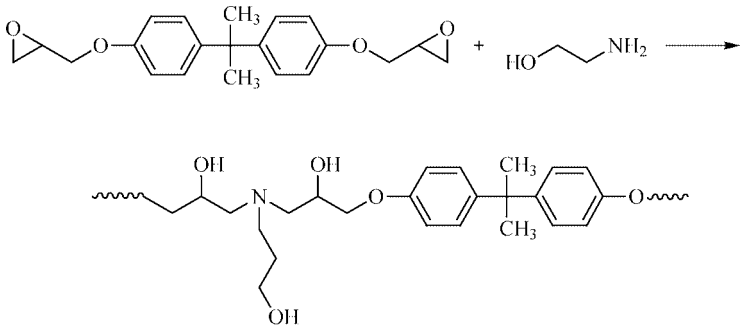

Polyhydroxy amino ether (PHAE) resin

Halogenated Epoxy Resins

A number of halogenated epoxy resins have been developed and commercialized to meet specific application requirements. Chlorinated and brominated epoxies were evaluated for flame retardancy properties. The brominated epoxy resins were found to have the best combination of cost/performance and were commercialized by Dow Chemical in the late 1960s.

Brominated Bisphenol A Based Epoxy Resins. Many applications of epoxy resins require the system to be ignition-resistant, eg, electrical laminates for PCBs and certain structural composites. A common method of imparting this ignition resistance is the incorporation of tetrabromobisphenol A (TBBA), 2,2-bis(3,5-dibromophenyl)propane, or the diglycidyl ether of TBBA, 2,2-bis[3,5-dibromo-4-(2,3-epoxypropoxy)phenyl]propane, into the resin formulation. The diglycidyl ether of TBBA is produced via conventional liquid epoxy resin processes. Higher MW resins can be produced by advancing LERs or diglycidyl ether of TBBA with TBBA. The lower cost, advanced brominated epoxies based on LERs

and TBBA containing ca 20 wt% Br are extensively employed in the PCB industry. The diglycidyl ether of TBBA (ca 50 wt% Br) is used for critical electrical/electronic encapsulation where high flame retardancy is required. Brominated epoxies are also used to produce epoxy vinyl esters for structural applications. Very high MW versions of brominated epoxies are used as flame-retardant additives to engineering thermoplastics used in computer housings.

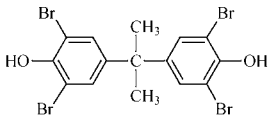

Tetrabromo bisphenol A

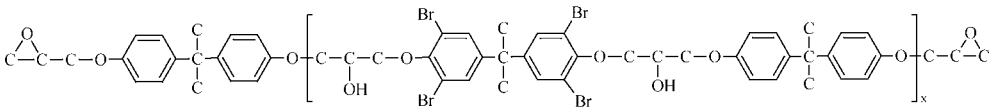

Advanced brominated epoxy resin

In order to meet increased requirements of the PCB industry for higher glass-transition temperature (T_g), higher thermal decomposition temperature (T_d), and lower dielectric constant (D_k) products, a number of new epoxy resins have been developed (48,49).

Fluorinated Epoxy Resins. Fluorinated epoxy resins have been researched for a number of years for high performance end-use applications (50). Fluorinated epoxies are highly resistant to chemical and physical abuse and should prove useful in high performance applications, including specialty coatings and composites, where their high cost may be offset by their special properties and long service life. The following fluorinated diglycidyl ether, 5-heptafluoropropyl-1,3-bis[2-(2,3-epoxypropoxy) hexafluoro-2-propyl] benzene, illustrates an example of fluoroepoxy resins (51) under development.

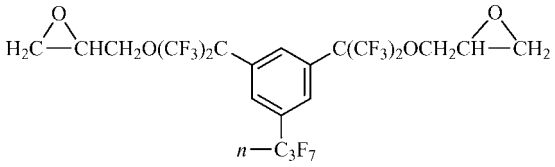

This resin is a viscous, colorless liquid (bp 118°C at 20 Pa · s) that contains 52 wt% fluorine. It has a low surface tension, which makes it a superior wetting agent for glass fibers. The reactivity of this resin with amine or anhydride curing agents is comparable to epoxy resins based on bisphenol A and results in a thermoset that has a low affinity for water and excellent chemical resistance. Another fluorinated epoxy resin derived from hexafluorobisphenol A was introduced to the marketplace aiming at the anticorrosion coatings market for industrial vessels and pipes. The key disadvantages of fluorinated epoxies are their relatively high costs and low T_g, which limit their commercialization (52).

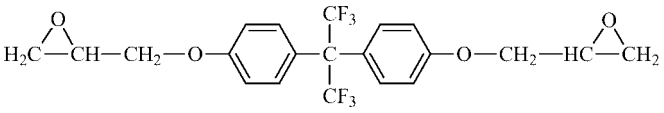

Multifunctional Epoxy Resins

The multifunctionality of these resins provides higher cross-linking density, leading to improved thermal and chemical resistance properties over bisphenol A epoxies.

Epoxy Novolac Resins. Epoxy novolacs are multifunctional epoxies based on phenolic formaldehyde novolacs. Both epoxy phenol novolac resins (EPN) and epoxy cresol novolac resins (ECN) have attained commercial importance (53). The former is made by epoxidation of the phenol–formaldehyde condensates (novolacs) obtained from acid-catalyzed condensation of phenol and formaldehyde (see PHENOLIC RESINS). This produces random *ortho*- and *para*-methylene bridges.

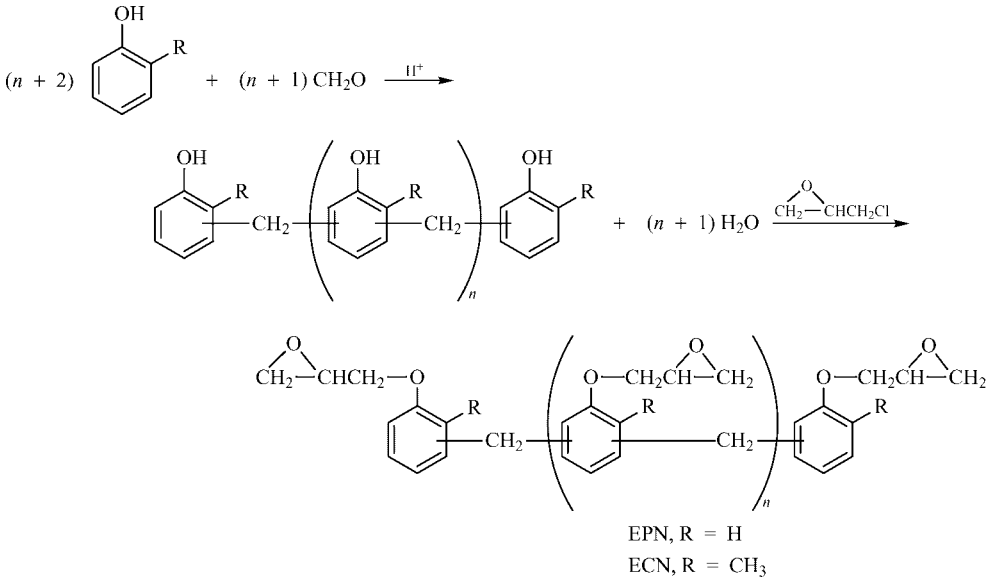

An increase in the molecular weight of the novolac increases the functionality of the resin. This is accomplished by changing the phenol or cresol to formaldehyde ratio. Epoxidation with an excess of epichlorohydrin minimizes the reaction of the phenolic OH groups with epoxidized phenolic groups and prevents branching. The epoxidation is similar to the procedure described for bisphenol A. EPN resins range from a high viscosity liquid of $n = 0.2$ to a solid of $n > 3$. The epoxy functionality is between 2.2 and 3.8. Properties of epoxy phenol novolacs are given in Table 7. When cured with aromatic amines such as methylenedianiline, the heat distortion temperatures (HDT) of EPN-based thermosets range from 150°C to 200°C, depending on cure and post-cure schedules.

Table 7. Typical Properties of Epoxy Phenol Novolacs

Property	D.E.N. 431,[a] EPN 1139[b]	D.E.N. 438,[a] EPN 1138[b]	D.E.N. 439[a]
n	0.2	1.6	1.8
EEW[c]	175	178	200
Viscosity, MPa·s (= cP)	1,400[d]	35,000[d]	3,000[e]
Softening point[f]			53
Color, Gardner	1	2	2

[a]The Dow Chemical Co.
[b]Huntsman.
[c]Epoxide equivalent weight.
[d]Temperature of measurement = 52°C.
[e]Temperature of measurement = 100°C.
[f]Durran's mercury method.

Curing agents that give the optimum in elevated temperature properties for epoxy novolacs are those with good high temperature performance, such as aromatic amines, catalytic curing agents, phenolics, and some anhydrides. When cured with polyamide or aliphatic polyamines and their adducts, epoxy novolacs show improvement over bisphenol A epoxies, but the critical performance of each cure is limited by the performance of the curing agent.

The improved thermal stability of EPN-based thermosets is useful in elevated temperature services, such as aerospace composites. Filament-wound pipe and storage tanks, liners for pumps and other chemical process equipment, and corrosion-resistant coatings are typical applications which take advantage of the chemical resistant properties of EPN resins. However, the high cross-link density of EPN-based thermosets can result in increased brittleness and reduced toughness.

Bisphenol F Epoxy Resin. The lowest MW member of the phenol novolacs is bisphenol F, which is prepared with a large excess of phenol to formaldehyde; a mixture of *o*,*o*′, *o*,*p*′, and *p*,*p*′ isomers is obtained:

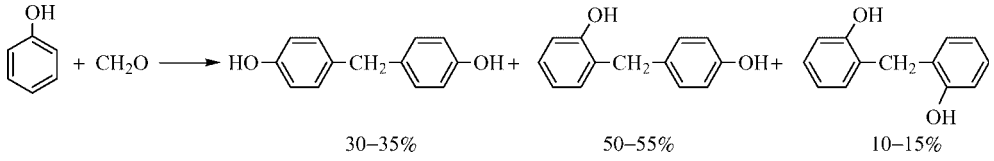

Epoxidation yields a liquid bisphenol F epoxy resin with a viscosity of 4000–6000 MPa·s (= cP), an EEW of 165, and $n \cong 0.15$.

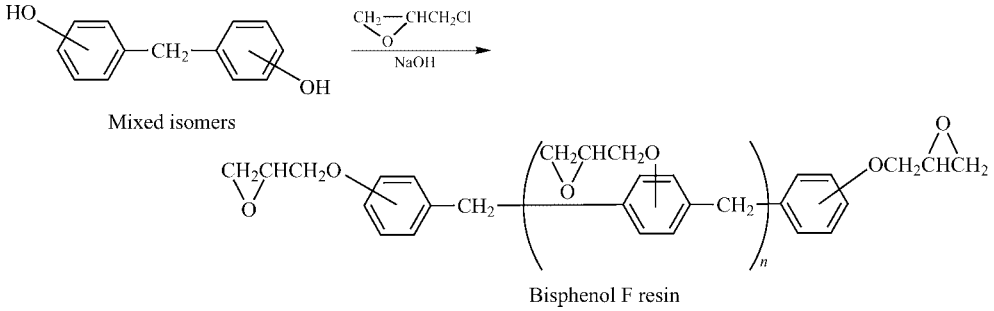

Bisphenol F resin

This unmodified, low viscosity liquid resin exhibits slightly higher functionality than unmodified bisphenol A liquid resins. Crystallization, often a problem with liquid bisphenol A resins, is reduced with bisphenol F resin. Consequently, noncrystallizing LERs which are blends of DGEBA and bisphenol F epoxy are available. Epoxy resins based on bisphenol F are used primarily as functional diluents in applications requiring a low viscosity, high performance resin system (eg, solvent-free coatings). Higher filler levels and faster bubble release are possible because of the low viscosity. The higher epoxy content and functionality of bisphenol F epoxy resins provide improved chemical resistance compared to conventional bisphenol A epoxies. Bisphenol F epoxy resins are used in high solids, high build systems such as tank and pipe linings, industrial floors, road and bridge deck toppings, structural adhesives, grouts, coatings, and electrical varnishes.

Cresol Epoxy Novolacs. The *o*-cresol novolac epoxy resins (ECN) are analogous to phenol novolac resins. ECNs exhibit better formulated stability and lower moisture adsorption than EPNs, but have higher costs. ECN resins are widely used as base components in high performance electronic (semiconductors) and structural molding compounds, high temperature adhesives, castings and laminating systems, tooling, and powder coatings. Increasing demands by the semiconductor industry has led to significant advances in ECN resin manufacturing technologies to reduce impurities, mainly the ionic content, hydrolyzable chlorides, and total chlorides. The use of polar, aprotic solvents, such as dimethyl sulfoxide (DMSO), as a co-solvent to facilitate chloride reduction has been patented (54). Typical high purity ECN resins contain $<$1000 ppm total chlorides and $<$50 ppm hydrolyzable chlorides.

The melt viscosity of these resins, which are solids at room temperature, decreases sharply with increasing temperature (Table 8). This affords the formulator an excellent tool for controlling the flow of molding compounds and facilitating the incorporation of ECN resins into other epoxies, eg, for powder coatings. While Ciba-Geigy was the first producer of ECN resins, many Japanese companies (Nippon Kayaku, Sumitomo Chemical, DIC, and Tohto Kasei) supply the majority of high purity ECN resins for the semiconductor industry today. Other suppliers are based in Korea and Taiwan.

Glycidyl Ethers of Hydrocarbon Epoxy Novolacs. In response to the increased performance demands of the semiconductor industry, hydrocarbon epoxy novolacs (HENs) were developed by Dow Chemical in the 1980s. HENs exhibit a much lower affinity for water compared to cresol or phenol epoxy novolacs. This translates directly into increased electrical property retention, which is important

Table 8. Typical Properties of Epoxy Cresol Novolac Resins[a]

Property	ECN 1235	ECN 1273	ECN 1280	ECN 1299
Molecular weight	540	1080	1170	1270
EEW[b]	200	225	229	235
Softening point, °C	35	73	80	99
Epoxide functionality	2.7	4.8	5.1	5.4

[a] Huntsman.
[b] Epoxide equivalent weight.

in the reliability of an electronic device encapsulated in the resin. An epoxy resin that is typical of this class is based on the alkylation product of phenol and dicyclopentadiene (55) ($n = 0.1$), 2,5-bis[(2,3-epoxypropoxy) phenyl]octahydro-4,7-methano-5*H*-indene (272 EEW; softening point 85°C; η at 150°C 0.4 Pa · s). The product is available from Huntsman as TACTIX∗ 556. Similar products based on *o*-cresol are commercialized in Japan by DIC (EPICLON HP-7200L).

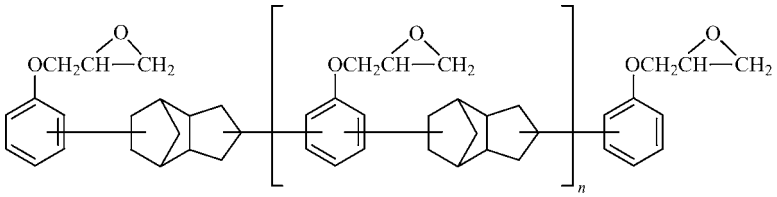

Bisphenol A Epoxy Novolacs. Bisphenol A novolacs are produced by reacting bisphenol A and formaldehyde with acid catalysts. Epoxidation of the bisphenol A novolacs gives bisphenol A epoxy novolac (BPAN) with improved thermal properties such as T_g, T_d of the epoxy-based electrical laminates.

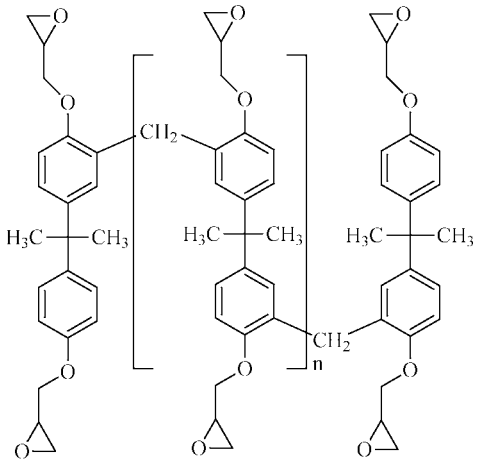

Bisphenol A epoxy novolac

Other Polynuclear Phenol Glycidyl Ether Derived Resins. In addition to the epoxy novolacs, there are other epoxy resins derived from

phenol–aldehyde condensation products. New applications that require increased performance from the epoxy resin, particularly in the electronics, aerospace, and military industries, have made these types of resins more attractive despite their relatively high cost.

Glycidyl Ether of Tetrakis(4-hydroxyphenyl)ethane. One of the first polyfunctional resins to be marketed (by Shell) is based on 1,1,2,2-tetrakis[4-(2,3-epoxypropoxy)phenyl]ethane (56). It is used primarily as additives in standard epoxy resin formulations for electrical laminates, molding compounds, and adhesives in which increased heat distortion temperature and improved chemical resistance are desired. Tetrakis(4-hydroxyphenyl)ethane is prepared by reaction of glyoxal with phenol in the presence of HCl. The tetraglycidyl ether (mp ca 80°C, and an EEW of 185–208) possesses a theoretical epoxide functionality of 4.

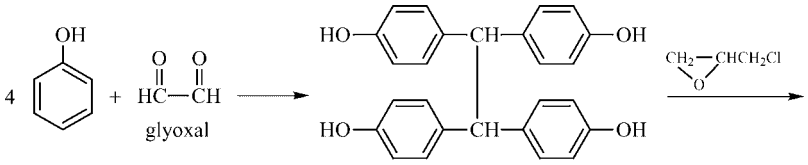

Tetrakis(4-hydroxyphenyl)ethane

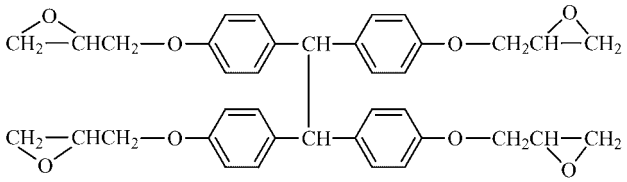

Tetraglycidyl ether of tetrakis(4-hydroxyphenyl)ethane

The commercial products Araldite 0163 (Huntsman) and Epon 1031 (Resolution) are tan-colored solids. They are widely used in high temperature resistance electrical laminates for high density PCBs and military applications. Their costs are typically higher than those of phenol and cresol epoxy novolacs.

Trisphenol Epoxy Novolacs. In the 1980s, new trifunctional epoxy resins based on tris[4-(2,3-epoxypropoxy)phenyl]methane isomers were introduced by Dow Chemical to help close the performance gap between phenol and cresol epoxy novolacs and high performance engineering thermoplastics (57). These products were later sold to Ciba-Geigy and continued to be marketed under the TACTIX* 740 and XD 9053 trade names by Huntsman.

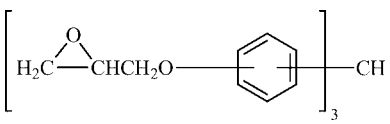

The resins are prepared via acid-catalyzed condensation of phenol and a hydroxybenzaldehyde, eg, salicylaldehyde, to afford the trifunctional phenol, which is epoxidized with epichlorohydrin. These resins range from semisolids (162 EEW;

Durran softening point 55°C; η at 60°C 11.5 Pa · s, at 150°C 0.055 Pa · s) to nonsintering solids (220 EEW; Durran softening point 85°C; η at 150°C 0.45 Pa · s).

The semisolid resins are used in advanced composites and adhesives where toughness, hot-wet strength, and resistance to high temperature oxidation are required. Their purity, formulated stability, fast reactivity, and retention of electrical properties over a broad temperature range make the solid resins suitable for use in the semiconductor molding powders industry. The trisphenol-based epoxies command significant high prices ($28–48/kg), limiting their uses.

Aromatic Glycidyl Amine Resins. Among the multifunctional epoxy resins containing an aromatic amine backbone, only a few have attained commercial significance. Their higher costs limit their uses to critical applications where their costs are justified. Glycidyl amines contain internal tertiary amines in the resin backbone, hence their high reactivity. Epoxy resins with such built-in curing catalysts are less thermally stable than nitrogen-free multifunctional epoxy resins.

Triglycidyl Ether of p-Aminophenol. The triglycidyl derivative of *p*-aminophenol was originally developed by Union Carbide (58) and is currently marketed by Huntsman under the designation MY 0500 and 0510. Epoxidation of *p*-aminophenol is carried out with a large excess of epichlorohydrin under carefully controlled conditions, since the triglycidylated resin exhibits limited thermal stability and polymerizes vigorously under the influence of its tertiary amine moiety.

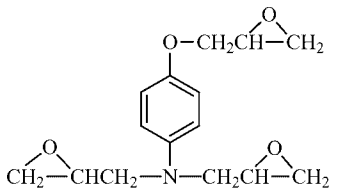

Triglycidyl-*p*-aminophenol

The resin exhibits a low viscosity, 2500–5000 MPa·s (= cP) at 25°C, and an EEW of 105–114; a molecularly distilled version (0510) has a viscosity of 550–850 MPa·s (= cP) at 25°C and an EEW of 95–107. It is considerably more reactive toward amines than standard bisphenol A resins. The trifunctional resin permits curing at low temperatures, ie, 70°C, and rapidly develops excellent elevated-temperature properties. Used as additives to increase cure speed, heat resistance, and T_g of bisphenol A epoxy resins, it has utility in such diverse applications as high temperatures adhesives, tooling compounds, and laminating systems.

Tetraglycidyl Methylenedianiline (MDA). These resins are used as binders in graphite-reinforced composites and are the binders of choice for many military applications. Epoxidation of MDA is carried out with stoichiometric excess of epichlorohydrin and under carefully controlled conditions to avoid rapid polymerization side reactions.

The tetrafunctional glycidylated MDA resins range in viscosity from 5000 to 25,000 MPa·s (= cP) at 50°C and have an EEW of 117–133; they are commercially available as Araldite MY 720 (Huntsman) and Epiclon 430 (DIC). When used in combination with the curing agent 4,4′-diaminodiphenylsulfone (DADS), it is the

first system to meet the performance requirements set by the aerospace industry and is the standard against which other resin systems are judged (59). Because of its outstanding properties, this resin is often used as the primary resin in high heat resistance formulations for military applications, despite its high costs (~$22/kg). Among its attributes are excellent mechanical strength, high T_g, good chemical resistance, and radiation stability.

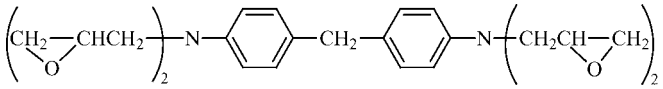

N,N,N′,N′-Tetraglycidyl-4,4′-diaminodiphenylmethane

Another commercially important aromatic glycidyl amine resin is triglycidyl isocyanurate (TGIC), which is discussed in the "Weatherable Epoxy Resins" section.

Specialty Epoxy Resins

Crystalline Epoxy Resins Development. A number of new epoxy resins used in epoxy molding compounds (EMC) have been developed by Japanese resin producers in response to the increased performance requirements of the semiconductor industry. Most notable are the commercialization of crystalline epoxies based on biphenol by Yuka-Shell (60):

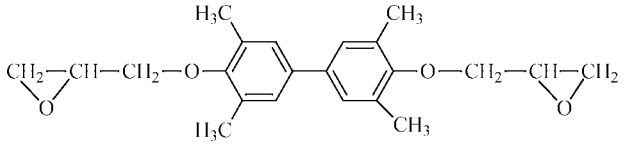

Diglycidyl ether of tetramethyl biphenol

The very low viscosity of these crystalline, solid epoxies when molten allows very high filler loading (up to 90 wt%) for molding compounds. The high filler loading reduces the coefficient of thermal expansion (CET) and helps manage thermal shock and moisture and crack resistance of molding compounds used in new, demanding semiconductor manufacturing processes such as Surface Mount Technology (SMT). It should be noted that cured thermosets derived from these crystalline resins do not retain crystallinity. Recently, a number of capacity expansions were announced for biphenol epoxies (sold as YX-4000 resin by Japan Epoxy Resins Corporation, formerly Yuka-Shell). DIC has developed dihydroxy naphthalene based epoxies (61) as the next generation product for this high performance market. Prices for crystalline epoxies are generally high ($22–26/kg), limiting their uses to high end applications.

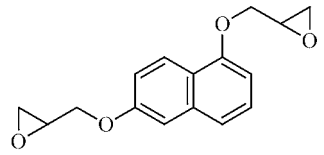

Diglycidyl ether of 1,5-dihydroxy naphthalene

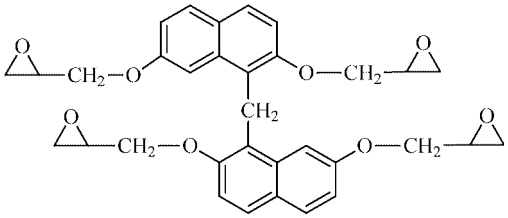

Tetraglycidyl ether based on dihydroxy napthalene

Dow Chemical developed liquid crystalline polymers (LCP) based on diglycidyl ether of 4-4′-dihydroxy-α-methylstilbene in the 1980s (62,63). Liquid crystal thermoplastics and thermosets based on this novel chemistry showed excellent combinations of thermal, mechanical, and chemical properties, unachievable with traditional epoxies. However, commercialization of these products has not materialized.

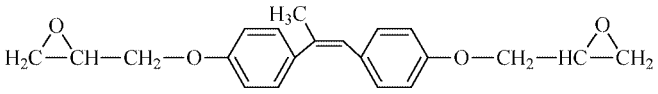

Diglycidyl ether of 4-4' -dihydroxy-α-methylstilbene

Weatherable Epoxy Resins. One of the major deficiencies of the aromatic epoxies is their poor weatherability, attributable to the aromatic ether segment of the backbone, which is highly susceptible to photoinitiated free-radical degradation. The aromatic ether of bisphenol A absorbs UV lights up to about 310 nm and undergoes photocleavage directly. This in turn produces free radicals that lead to oxidative degradation of bisphenol A epoxies, resulting in chalking. Numerous efforts have been devoted to remedy this issue, resulting in a number of new weatherable epoxy products. However, their commercial success has been limited, primarily because of higher resin costs and the fact that end users can topcoat epoxy primers with weatherable coatings based on other chemistries such as polyesters, polyurethanes, or acrylics. The following epoxy products when formulated with appropriate reactants can provide certain outdoor weatherability.

Hydrogenated DGEBA. In 1976, Shell Chemical Co. introduced epoxy resins based on the diglycidyl ether of hydrogenated bisphenol A, 2,2-bis[4-(2,3-epoxypropoxy)cyclohexyl]propane (232–238 EEW; η at 25°C 2–2.5 Pa · s).

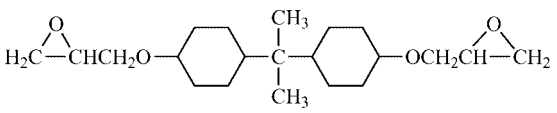

These resins resist yellowing and chalking because of their aliphatic structure. Epoxy resins based on hydrogenated bisphenol A are made by the epoxidation of the saturated diol, 2,2-bis(4-hydroxycyclohexyl)propane or 2,2-bis(4-hydroxycyclohexyl)propane with epichlorohydrin, or by the hydrogenation of a low molecular weight DGEBA resin (64). Commercially available products include an Epalloy 5000 resin from CVC. One disadvantage is their much higher costs, and consequently, the products have not found broad acceptance in the industry. Furthermore, cross-linked networks based on hydrogenated bisphenol A epoxies lose some of the characteristic temperature and chemical resistances inherent with the bisphenol A backbone.

Heterocyclic Glycidyl Imides and Amides. In the 1960s, considerable work was devoted to preparing triglycidyl isocyanurate, 1,3,5-tris(2,3-epoxypropyl)-1,3,5-perhydrotriazine-2,4,6-trione (65). The epoxidation of cyanuric acid with epichlorohydrin gives triglycidyl isocyanurate (TGIC), marketed as PT 810 by Huntsman. It is a crystalline compound (mp 85–110°C) with an EEW of ca 108. Miscibility with organic compounds is limited. Because of its excellent weatherability, TGIC is widely used in outdoor powder coatings with polyesters (66), despite its higher cost (~$12/kg).

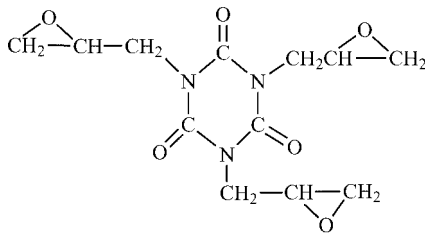

Triglycidyl isocyanurate

Hydantoin-Based Epoxy Resins. These resins were commercialized by Ciba-Geigy. Hydantoins are prepared from carbon dioxide, ammonia, hydrogen cyanide, and ketones via the Bucherer reaction and can be epoxidized with epichlorohydrin (67). Cured and uncured resin properties depend greatly on the nature of the substituents R and R′. The hydantoin derived from acetone furnishes a low viscosity, water-dispersable epoxy resin, 5,5-dimethyl-1,3-bis(2,3-epoxypropyl)-2,4-imidazolidinedione ($R = R' = CH_3$; 145 EEM; η at 25°C 2.5 Pa · s). A nonsintering solid epoxy resin is obtained if $R = R' = -(CH_2)_5-$.

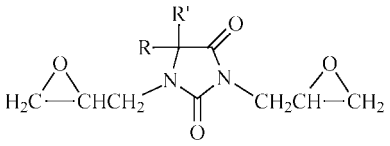

When cured with aromatic amines or anhydrides, these resins show high heat distortion temperatures and excellent adhesion and weatherability. A variety of applications are suggested for these new resins, particularly in applications in which a non-yellowing epoxy resin is desirable.

Elastomer-Modified Epoxies. Epoxy thermosets derive their thermal, chemical, and mechanical properties from the highly cross-linked networks. Consequently, toughness deficiency is an issue in certain applications. To improve the impact resistance and toughness of epoxy systems, elastomers such as BF Goodrich's CTBN rubbers (carboxyl-terminated butadiene nitrile) are often used as additives or pre-reacted with epoxy resins (68). Most commonly used products are reaction adducts of liquid epoxy resins (DGEBA) with CTBN in concentrations ranging from 5 wt% to 50 wt%. They have been shown to give improved toughness, peel adhesion, and low temperature flexibility over unmodified epoxies. Primary applications are adhesives for aerospace and automotive and as additives to epoxy vinyl esters for structural composites. Formation of adducts of epoxy resins and carboxylated butadiene–acrylonitrile copolymers (CTBN) is promoted by triphenylphosphine or alkyl phosphonium salts. Other elastomers used to modify epoxies include amine-terminated butadiene nitrile (ATBN), maleated polybutadiene and butadiene–styrene, epoxy-terminated urethane prepolymers, epoxy-terminated polysulfide, epoxy–acrylated urethane, and epoxidized polybutadiene.

Monofunctional Glycidyl Ethers and Aliphatic Glycidyl Ethers

A number of low MW monofunctional, difunctional, and mutifunctional epoxies are used as reactive diluents, viscosity reducers, flexiblizers, and adhesion promoters. Recent trends toward lower VOC, higher solids and 100% solids epoxy formulations have resulted in increased utilization of these products. Most of these epoxies are derived from relatively compact hydroxyl-containing compounds, such as alcohols, glycols, phenols, and epichlorohydrin. Epoxidized vegetable oils, such as epoxidized linseed oils, are also used as reactive diluents. They are produced using a peroxidation process and are discussed in more detail in the cycloaliphatic epoxies and epoxidized vegetable oils section. Typically, these products have very low viscosity (1–70 cP at 20°C) relative to LERs (11,000–16,000 cP). They are often used in the range of 7–20 wt% to reduce viscosity of the diluted system to 1000 cP. However, the uses of reactive diluents, especially at high levels, often result in decreased chemical resistance and thermal and mechanical properties of the cured epoxies.

Important products include butyl glycidyl ether (BGE), alkyl glycidyl ethers of C8–C10 (Epoxide 7) and C12–C14 (Epoxide 8), *o*-cresol glycidyl ether (CGE), *p-tert*-butyl glycidyl ether, resorcinol diglycidyl ether (RDGE), and neopentyl glycol diglycidyl ether (Table 9). While BGE is the most efficient viscosity reducer and has been widely used in the industry for many years, it has been losing market share because of its volatility and obnoxiousness. Phenyl glicidyl ether (PGE) is no longer used by many formulators because of its toxicity. The industry trend is moving toward longer chain epoxies such as Epoxide 8 or neopentyl glycol diglycidyl ether.

Major suppliers of these products are Resolution, Air Products, Ciba Specialty Chemicals, Huntsman, CVC Specialty Chemicals, Pacific Epoxy Polymers, and Exxon.

An example of multifunctional aliphatic epoxies is the triglycidyl ether of propoxylated glycerine (Heloxy 84) from Resolution. A similar product is based on

Table 9. Some Common Commercial Glycidyl Ether Reactive Diluents

Name	Structure
n-Butyl glycidyl ether	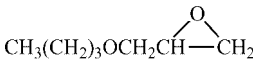
C12–C14 Aliphatic glycidyl ether	
o-Cresol glycidyl ether	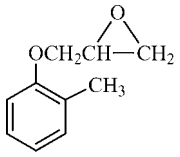
Neopentylglycol diglycidyl ether	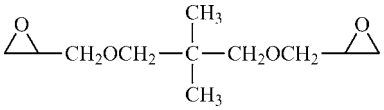
Butanediol diglycidyl ether	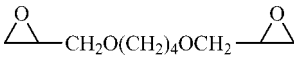

epoxidized castor oil (Heloxy 505). These products are used primarily as viscosity reducers while increasing functionality and cross-linking density of the cured systems.

Epoxy resins based on long-chain diols, such as the diglycidyl ether of polypropylene glycol [α,ω-bis(2,3-epoxypropoxy)poly(oxypropylene)] (305–335 EEW; η at 25°C 0.055–0.10 Pa · s), are used as flexibilizing agents to increase a thermoset's elongation and impact resistance. Because of the low reactivity of the aliphatic diols toward epichlorohydrin, these epoxies are produced by first coupling the diols with epichlorohydrin using phase-transfer catalysts such as ammonium salts or Lewis acid catalysts (boron trifluoride, stannic chloride), followed by epoxidation with caustic (69,70). A prominent side-reaction is the conversion of aliphatic hydroxyl groups formed by the initial reaction into chloromethyl groups by epichlorohydrin. The resultant epoxy resins are known to have lower reactivity toward conventional amine curing agents relative to bisphenol A epoxies. Dow Chemical manufactures D.E.R. 732 and D.E.R. 736 aliphatic epoxy resins. They are derived from polyglycols with different chain lengths.

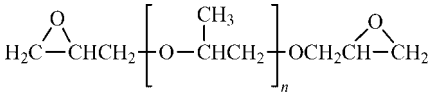

Polyglycidyl ethers of sorbitol, glycerol, and pentaerythritol are used as adhesion promoters for polyester tire cords. Their high chloride content improves adhesion to rubber.

Cycloaliphatic Epoxy Resins and Epoxidized Vegetable Oils

Resins based on the diepoxides of cycloaliphatic dienes were first commercialized in the 1950s by Union Carbide Corp. The combination of aliphatic backbone, high oxirane content, and no halogens gives resins with low viscosity, weatherability, low dielectric constant, and high cured T_g. This class of epoxy is popular for diverse end uses including auto topcoats, weatherable high voltage insulators, UV coatings, acid scavengers, and encapsulants for both electronics and optoelectronics. A comparison of some properties of two common aliphatic epoxies with those of LER (DGEBA) is shown in Table 10.

The preferred industrial route to cycloaliphatic epoxy resins is based on the epoxidation of cycloolefins with peracids, particularly peracetic acid (71). Few side reactions are encountered. Some properties of various commercial products are given in Table 11. The peracid cannot be made *in situ* because the cyclic olefins are sensitive to impurities generated in this process.

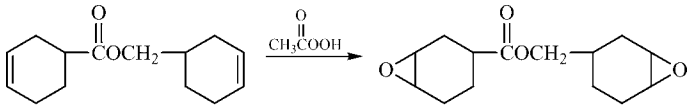

3′-Cyclohexenylmethyl 3-Cyclohexenecarboxylate

3′,4′-Epoxycyclohexylmethyl 3,4-Epoxycyclohexanecarboxylate

An important secondary reaction is the acid-catalyzed hydrolysis of the epoxide groups. The reaction is minimized at low temperatures and strongly depends on the constituents and the reaction medium.

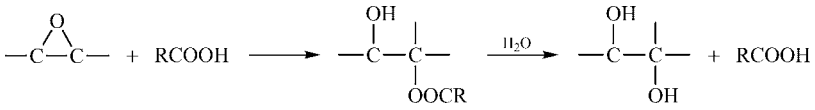

The cycloaliphatic epoxides are more susceptible to electrophilic attack because of the lower electronegativity of the cycloaliphatic ring relative to the bisphenol A aromatic ether group in DGEBA resins. Consequently, cycloaliphatic epoxies do not react well with conventional anionic epoxy curing agents such as amines. They are commonly cured via thermal or UV-initiated cationic cures. In addition,

Table 10. Comparative Viscosities of Cycloaliphatic Epoxies, Epoxidized Oils, and DGEBA

Epoxy type	Viscosity, MPa·s (= cP)	EEW
Cyclo Diepoxy ERL-4221[a] (3′,4′-epoxycyclohexylmethyl-3,4-epoxycyclohexanecarboxylate)	400	135
DGEBA	11000	190
Linseed Oil Epoxy	730	168

[a]Trademark of the Dow Chemical Co.

Table 11. Cycloaliphatic Epoxy Resins

Chemical name	Structure	Commercial products	EEW[a]	Viscosity, MPa·s (= cP) at 25°C[b]
3′,4′-Epoxycyclohexylmethyl-3,4-epoxycyclohexanecarboxylate	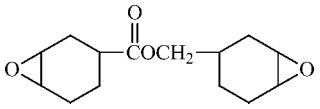	ERL-4221[c] UVR-6110	131–143	350–450
3,4-Epoxycyclohexyloxirane	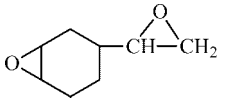	CY-179[d] ERL-4206[c]	70–74	15
2–(3′,4′-Epoxycyclohexyl)-5,1″-spiro-3″,4″-epoxycyclohexane-1,3-dioxane	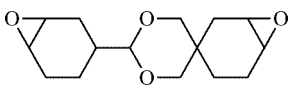	ERL-4234[c]	133–154	7,000–17,000[e]
Vinyl cyclohexene monoxide	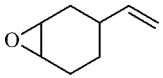	VCMX	124	5
3,4-Epoxycyclohexanecarboxylate methyl ester	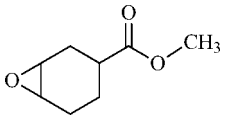	ERL-4140	156	6
Bis(3,4-epoxycyclohexylmethyl) adipate	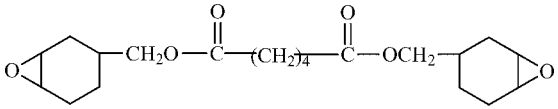	ERL-4299[c] UVR-6128	180–210	550–750

[a] Epoxide equivalent weight.
[b] Unless otherwise stated.
[c] Union Carbide, division of The Dow Chemical Co.
[d] Huntsman.
[e] At 38°C.

cycloaliphatic epoxy resins are low viscosity liquids that can be thermally cured with anhydrides to yield thermosets having a high heat distortion temperature. They are often used as additives to improve performance of bisphenol A epoxies. Their higher prices ($6.60–8.80/kg) have limited their commercial applications to high end products.

The largest end uses of cycloaliphatic epoxies in order of volume are electrical, electronic components encapsulation, and radiation-curable inks and coatings. A potentially large volume application is UV-curable metal can coatings for beer can exterior and ends, but the market has not been growing significantly in recent years. Other uses include acid scavengers for vinyl-based transformer fluids and lubricating oils; filament winding for aerial booms and antennas; and as viscosity modifier for bisphenol A LERs in tooling compounds. An epoxy silicone containing cycloaliphatic epoxy end groups and a silicone backbone is used as radiation-curable release coatings for pressure-sensitive products. Dow Chemical is the largest producer of cycloaliphatic epoxies. Daicel of Japan has entered the cycloaliphatic epoxy resin market.

Epoxidation of α-olefins, unsaturated fatty acid esters, and glycerol esters is affected readily by peracids including *in situ* peracids generated from hydrogen peroxide and carboxylic acids.

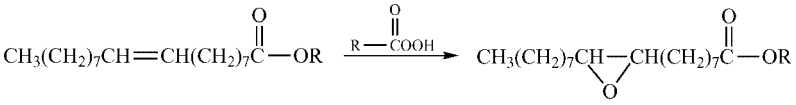

α-Olefin epoxies find utility as reactive diluents for coatings and as chemical intermediates for lubrication fluids. Larger volume epoxidized soybean and linseed oils are most frequently used as *secondary* plasticizers and co-stabilizers for PVC.

Epoxy Esters and Derivatives

Epoxy Esters. The esterification of epoxy resins with commercial fatty acids is a well-known process that has been employed for industrial coatings for many years. The carboxylic acids are esterified with the terminal epoxy groups or the pendant hydroxyls on the polymer chain.

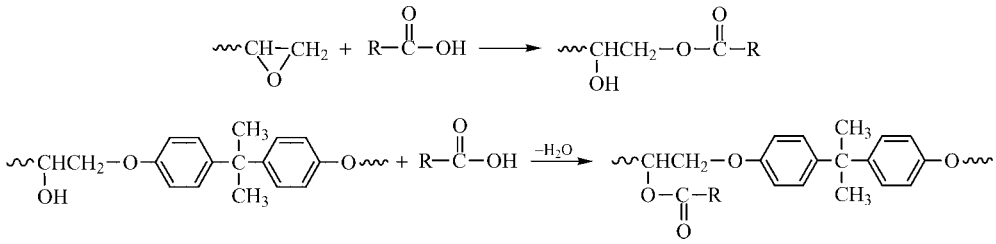

A wide variety of saturated and unsaturated fatty acids are utilized to confer properties useful in air-dried, protective, and decorative coatings. Typical fatty

acids include tall oil fatty acids, linseed oil fatty acid, soya oil fatty acid and castor oil fatty acid. A medium molecular weight SER, a so-called 4-type, is commonly used. Catalysts such as alkaline metal salts (Na_2CO_3) or ammonium salts are essential to prevent chain branching and gelation caused by etherification of the epoxy groups.

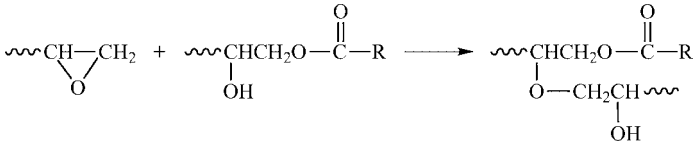

Esterification is generally conducted in an inert atmosphere at 225–260°C, with sparging to remove by-product water. The course of the reaction is monitored by acid number to a specified end point and by viscosity. The product is then dissolved in a solvent (72).

Metallic driers are incorporated in unsaturated ester solutions to promote cure via air-drying, ie, oxidative polymerization of the double bonds of the fatty acids. Chemical resistance is generally lower than that of unmodified epoxy resins cured at ambient temperatures with amine hardeners. Epoxy esters are also used to produce anodic electrodeposition (AED) coatings by further reaction with maleic anhydride followed by neutralization with amines to produce water-dispersable coatings. Epoxy esters were widely used as automotive primer-surfacer and metal can ends coatings for many years, but are being replaced by other technologies. Their high viscosity limited their uses in low solids, solvent-borne coatings. Waterborne epoxy esters are now available and are used in flexographic inks for milk cartons.

Glycidyl Esters. Glycidyl esters are prepared by the reaction of carboxylic acids with epichlorohydrin followed by dehydrochlorination with caustic:

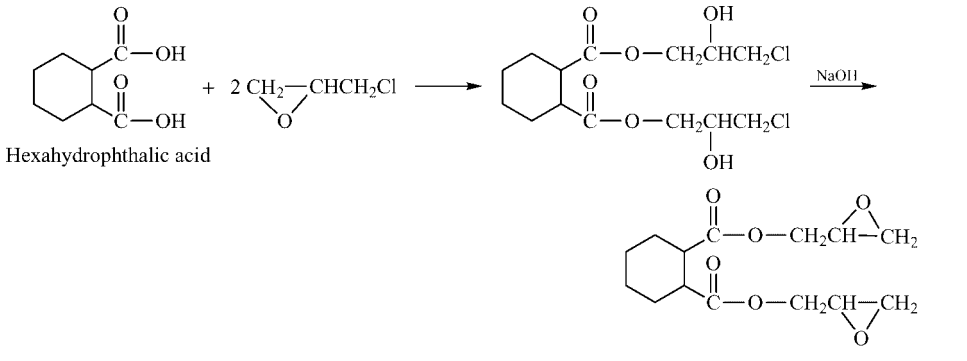

Hexahydrophthalic acid

Diglycidyl ester of hexahydrophthalic acid

The viscosity of these esters is low, ie, ca 500 MPa·s (= cP), and their reactivity resembles that of bisphenol A resins. Similar epoxy resin derived from dimerized linoleic acid is also commercially available. They are often used as flexiblizing agents instead of epoxidized long-chain diols.

The *glycidyl ester of versatic acid* or neodecanoic acid is an example of high MW monoglycidyl aliphatic epoxy. The molecule is highly branched, thus providing steric effects to protect it from hydrolysis, resulting in good weatherability and water resistance. On the other hand, it suffers from high viscosity, and therefore it is not an effective diluent. It is often used to improve scrubability, chemical resistance, and weatherability of coatings. The product is commercially available from Resolution (Cardura E-10) and Exxon (Glydexx N-10).

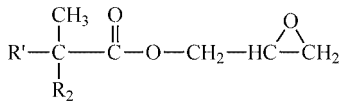

Where R's = alkyl or substituted alkyls

Glycidyl ester of versatic acid

A commercially important glycidyl ester is *glycidyl methacrylate (GMA)*, a dual functionality monomer, containing both a terminal epoxy and an acrylic C=C bond. It is produced by the reaction of methacrylic acid with epichlorohydrin. The dual functionality of GMA brings together desirable properties of both epoxies and acrylics, eg, the weatherability of acrylics and chemical resistance of epoxies, in one product. GMA is useful as a comonomer in the synthesis of epoxy-containing polymers via free-radical polymerization. The resultant epoxy-containing polymers can be further cross-linked. An example of such polymers is GMA acrylic, which is an acrylic copolymer, containing about 10–35% by weight of GMA. Cure is by reaction with dodecanedioic acid. Its primary uses are in automotive powder coatings. GMA-containing polymers are also used as compatiblizers for engineering thermoplastics, in adhesives and latexes, and as rubber and asphalt modifiers (73). Dow Chemical and Nippon Oils & Fats are two major producers of GMA.

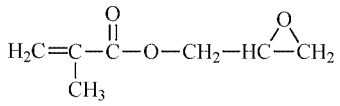

Glycidyl methacrylate (GMA)

Epoxy Acrylates. Epoxy resins are reacted with acrylic acid to form epoxy acrylate oligomers, curable via free-radical polymerization of the acrylate C=C bonds initiated by light (74). UV lights are most commonly used, but electron beam (EB) curing is becoming more common because of its decreasing equipment costs. This is a fast-growing market segment for epoxy resins because of the environmental benefits of the UV cure technology: low to zero VOC, low energy requirements. Major applications include coatings for overprint varnishes, wood substrates, and plastics. Radiation-cured epoxy acrylates are also growing in importance in inks, adhesives, and photoresists applications. The 2001 global market for epoxy acrylates was estimated at 40,000 MT with an annual growth rate projected to be 8–10%.

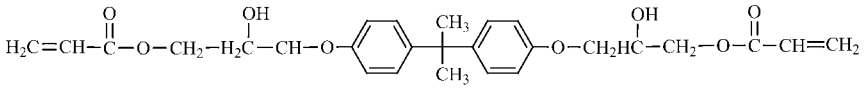

Epoxy acrylate based on DGEBA

Liquid epoxy resins such as DGEBA are most commonly used to produce epoxy acrylates. When higher thermal performance is required, multifunctional epoxies such as epoxy novolacs are used. Epoxy acrylates from epoxidized soybean oil and linseed oil are often used as blends with aromatic epoxy acrylates to reduce viscosity of the formulations. Major producers of UV-curable epoxy acrylates are UCB, Radcure, Dow Chemical, Sartomer, and Henkel.

Epoxy Vinyl Esters. A major derivative of epoxy resins is the epoxy vinyl ester resin. Originally developed by Dow Chemical (75,76) and Shell Chemical in the 1970s, it is considered a high performance resin used in glass-reinforced structural composites, particularly for its outstanding chemical resistance and mechanical properties. The resins are made by reacting epoxy resins with methacrylic acid and diluted with styrene to 35–40% solvent by weight. Liquid epoxy resins (DGEBA) are commonly used. Epoxy novolacs are used where higher thermal or solvent resistance is needed. Brominated epoxies are also used to impart flame retardancy for certain applications. In the final formulation, peroxide initiators are added to initiate the free-radical cure reactions of the methacrylic C=C bonds and styrene to form a random copolymer thermoset network.

The vinyl ester functionality of the epoxy vinyl esters provides outstanding hydrolysis and chemical resistance properties, in addition to the inherent thermal resistance and toughness properties of the epoxy backbone. These attributes have made epoxy vinyl esters a material of choice in demanding structural composite applications such as corrosive chemicals storage tanks, pipes, and ancillary equipment for chemical processing. Other applications include automotive valve covers and oil pans, boats, and pultruded construction parts. Significant efforts have been devoted to improve toughness and to reduce levels of styrene in epoxy vinyl ester formulations because of environmental concerns. In addition to Dow Chemical, other major suppliers of epoxy vinyl esters include Ashland, AOC, DSM, Interplastic, and Reichhold (DIC).

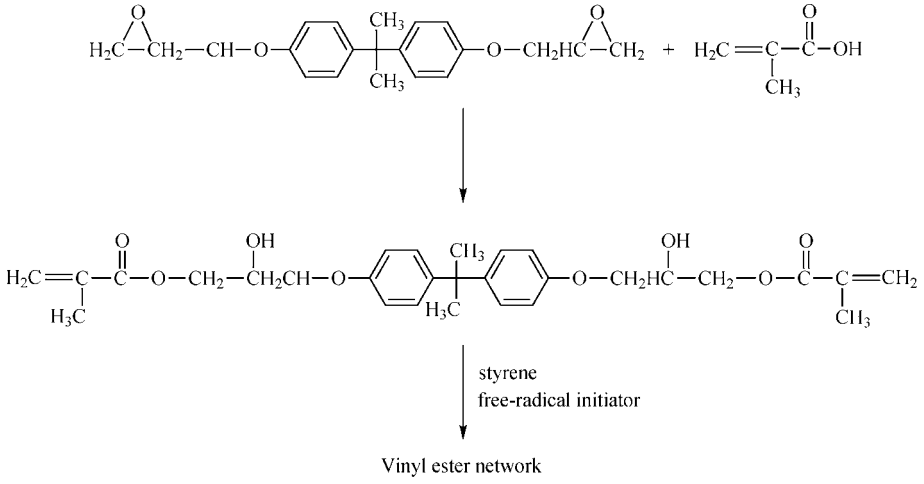

Epoxy Phosphate Esters. Dow Chemical developed the epoxy phosphate ester technology in the 1980s (77). Epoxy phosphate esters are reaction products of epoxy resins with phosphoric acid. Depending on the stoichiometric ratio and

reaction conditions, a mixture of mono-, di- and triesters of phosphoric acid are obtained. Subsequent hydrolysis of the esters is used as a way to control the esters distribution and product viscosity. Epoxy phosphate esters can be made to disperse in water to produce waterborne coatings. They are used primarily as modifiers to improve the adhesion property of nonepoxy binders in both solvent-borne and waterborne systems for container and coil coatings.

Characterization of Uncured Epoxies

Most industrial chemicals and polymers are not the 100% pure, single chemicals as described in their general chemical structures. In the case of epoxy resins, they often contain isomers, oligomers, and other minor constituents. As a first requirement, one would need to know the epoxy content or EEW of the epoxy resin so the proper stoichiometric amount of cross-linker(s) can be calculated. However, a successful thermoset formulation must also have the proper reactivity, flow, and performance. Consequently, other epoxy resin properties are required by the formulators and supplied by the resin producers.

Liquid epoxy resins are mainly characterized by epoxy content, viscosity, color, density, hydrolyzable chloride, and volatile content (78). Less often analyzed are α-glycol content, total chloride content, ionic chloride, and sodium. Solid epoxy resins are characterized by epoxy content, solution viscosity, melting point, color, and volatile content. Less often quoted are phenolic hydroxyl content, hydrolyzable chloride, ionic chloride, sodium, and esterification equivalent. Table 12 lists analytical methods adopted by ASTM (79) as standard testing methods for epoxy resins.

In addition, gel-permeation chromatography (GPC), high performance liquid chromatography (HPLC) (39,80), and other analytical procedures such as nuclear magnetic resonance (NMR) (28) and infrared spectroscopy (IR) (81) are performed to determine MW, MW distribution, oligomer composition, functional groups, and impurities.

Table 12. Uncured Epoxy Resin Test Methods

Test Item	Unit	Condition	ASTM method
EEW			D1652-97
Viscosity, neat	cP[a]	25°C	D445-01
Viscosity, solution	cSt[b]	25°C	D445-01
Viscosity, melt	cSt[b]	150°C	D445-01
Viscosity, ICI Cone and Plate	Pa · s		D4287-00
Viscosity, Gardner–Holdt			D1545-98
Color, Co-Pt			D1209-00
Color, Gardner			D1544-98
Color, Gardner in solution			D1544-98
Moisture	ppm		E203-01
Softening point	°C		D3104-99

[a] cP = MPa·s.
[b] cSt = mm^2/s.

Resin components such as α-glycol content and chloride types and levels are known to influence certain formulation reactivity and rheology, depending on their interactions with the system composition such as basic catalysts (tertiary amines) and/or amine curing agents. Knowing the types and levels of chlorides guides formulators in the adjustment of their formulations for proper reactivity and flow.

Epoxide Equivalent Weight. The epoxy content of liquid resins is frequently expressed as *epoxide equivalent weight (EEW)* or *weight per epoxide (WPE)*, which is defined as the weight in grams that contains 1 g equivalent of epoxide. A common chemical method of analysis for epoxy content of liquid resins and solid resins is titration of the epoxide ring by hydrogen bromide in acetic acid (82). Direct titration to a crystal violet indicator end point gives excellent results with glycidyl ethers and cycloaliphatic epoxy resins. The epoxy content of glycidyl amines is determined by differential titration with perchloric acid. The amine content is first determined with perchloric acid. Addition of tetrabutylammonium iodide and additional perchloric acid generates hydrogen iodide, which reacts with the epoxy ring. The epoxy content is obtained by the second perchloric acid titration to a crystal violet end point.

In another procedure, a halogen acid is generated by the reaction of an ionic halide salt, eg, tetraethylammonium bromide in acetic acid with perchloric acid with subsequent formation of a halohydrin; the epoxy group is determined by back-titration with perchloric acid using crystal violet indicator (83). The end point can be determined visually or potentiometrically. A monograph on epoxide determinations was published in 1969 (84). This is the method adopted by ASTM and is currently used by most resin producers.

Viscosity of epoxy resins is an important characteristic affecting handling, processing, and application of the formulations. For example, high viscosity LERs impede good mixing with curing agents, resulting in inhomogeneous mixtures, incomplete network formation, and poor performance. On the other hand, too low viscosity would affect application characteristics such as coverage and appearance.

Viscosities of liquid resins are typically determined with a Cannon–Fenske capillary viscometer at 25°C, or a Brookfield viscometer. The viscosity depends on the temperature, as illustrated in Figure 2. Viscosities of solid epoxy resins are determined in butyl carbitol (diethylene glycol monobutyl ether) solutions (40% solids content) and by comparison with standard bubble tubes (Gardner–Holdt bubble viscosity). The Gardner color of the same resin solution is determined by comparison with a standard color disk. Recently, data have been reported for solid epoxy resins using the ICI Cone and Plate viscometers, which are much more time-efficient because they do not require sample dissolution.

Hydrolyzable chloride (HyCl) content of liquid and solid epoxy resins is determined by dehydrochlorination with potassium hydroxide solution under reflux conditions and potentiometric titration of the chloride liberated by silver nitrate. The solvent(s) employed and reflux conditions can influence the extent of dehydrochlorination and give different results. The "easily hydrolyzable" HyCl content, which reflects the degree of completion of the dehydrochlorination step in the epoxy resin manufacturing process, is routinely determined by a method using methanol and toluene as solvents. This is the method most commonly used to characterize LER and SER.

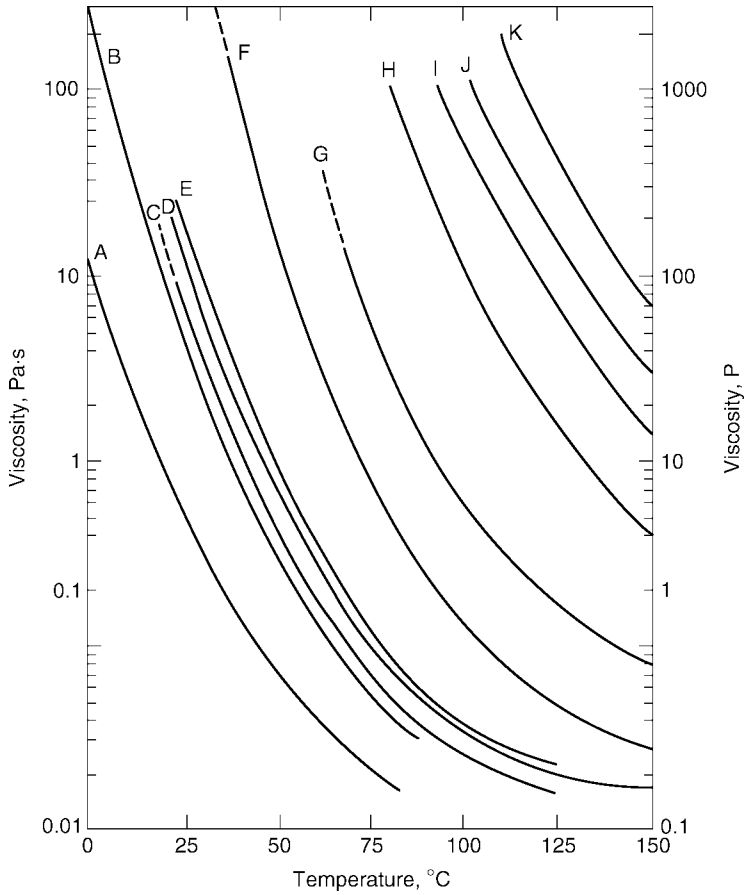

Fig. 2. Viscosity–temperature profiles for bisphenol A epoxy resins with the following EEW (epoxide equivalent weight): A, 175–195 and 195–215 diluted resins; B, 172–178; C, 178–186; D, 185–192; E, 190–198; F, 230–280; G, 290–335; H, 450–550; I, 600–700; J, 675–760; K, 800–975.

For epoxy resins used in electronic applications, such as cresol epoxy novolacs, more powerful polar aprotic solvents such as dioxane or dimethyl formamide (DMF) have been used to hydrolyze the difficult-to-hydrolyze HyCls, such as the abnormal chlorohydrins and the organically "bound" chlorides. The issue here is the inconsistency in results obtained by different methods (78). The presence of ionic hydrolyzable chlorides and total chlorides has been shown to affect electrical properties of epoxy molding compounds used in semiconductor encapsulation (85). For these applications, producers offer high purity grade epoxy resins with low ionic, hydrolyzable and total chloride contents.

Total chloride content of epoxy resins can be determined by the classical Parr bomb method in which the sample is oxidized in a Parr bomb, followed by titration with silver nitrate (78). The major disadvantage of this method is that it is time-consuming. Alternatively, X-ray fluorescence has been used successfully as a simple, nondestructive method to determine total chloride of epoxy resins.

The method, originally developed by Dow Chemical, has been under consideration for adoption by ASTM.

The "ball and ring" and Durran's methods traditionally measure the softening point of SERs, which is important in applications such as powder coatings. The Durran's method involves heating a resin sample topped with a certain weight of mercury in a test tube until the resin reaches its softening point and flows, allowing the mercury to drop to the bottom of the test tube. The method is accurate but involves handling of highly hazardous mercury at elevated temperatures. The Mettlers' softening point method is more widely used recently because of its simplicity.

The esterification equivalent of solid resins is defined as the weight in grams esterified by one mole of monobasic acid. This value includes both the epoxy and hydroxyl groups of the solid resin. It is determined by esterification of the sample with acetic anhydride in the presence of pyridinium chloride, followed by titration with sodium methoxide to a thymol blue–phenolphthalein end point.

Molecular structure of epoxy resins. Infrared spectroscopy (IR) is used to determine the epoxide content of resins as well as their structure. A compilation of IR spectra of uncured resins has been published (86) and their use in quality control and identification of components of resin blends has been described. Recently, near IR (NIR) has emerged as a useful tool to characterize epoxy resins (87).

NMR has been utilized to characterize epoxy resins, formulations and cured networks. It has been shown to be useful in determining the level of branching in epoxy resins and isomers distribution in epoxy novolacs (88,89).

GPC and HPLC are utilized to characterize both liquid and solid epoxy resins (90). MW and MW distributions are obtained from GPC measurements, but differences in chemical composition of resin samples are more apparent from HPLC chromatograms because of better resolution (91).

HPLC has proven to be a good fingerprinting tool to characterize LERs and SERs. Chromatograms of liquid epoxy resins (crude DGEBA) indicate a homologue distribution of $n = 0$, 85%, and, in a specific case, $n = 1$, 11.5%, although the values obtained depend on the source of the liquid resin. HPLC analysis of both liquid and solid epoxy resins has been studied in some detail using normal-phase and reversed-phase columns, respectively (39).

The difference between taffy-processed and fusion advancement solid resin can be noted in HPLC chromatograms. In the advancement process, the even-membered oligomers predominate, whereas taffy-produced resins exhibit both even- and odd-numbered oligomers. Compounds that contribute to hydrolyzable chloride and α-glycol content can be quantified by HPLC. The presence of branched chain components is detectable in studies using an improved reversed-phase gradient HPLC method (92,93). Excellent reviews of applications of chromatographic techniques to the analysis of epoxy resins are available (94).

Curing of Epoxy Resins

With the exception of the very high MW phenoxy resins and epoxy-based thermoplastic resins, almost all epoxy resins are converted into solid, infusible, and insoluble three-dimensional thermoset networks for their uses by curing with

cross-linkers. Optimum performance properties are obtained by cross-linking (qv) the right epoxy resins with the proper cross-linkers, often called hardeners or curing agents. Selecting the proper curing agent is dependent on the requirements of the application process techniques, pot life, cure conditions, and ultimate physical properties. Besides affecting viscosity and reactivity of the formulation, curing agents determine both the types of chemical bonds formed and the degree of cross-linking that will occur. These, in turn, affect the chemical resistance, electrical properties, mechanical properties, and heat resistance of the cured thermosets.

Epoxy resins contain two chemically reactive functional groups: epoxy and hydroxy. Low MW epoxy resins such as LERs are considered difunctional epoxy monomers or prepolymers and are mostly cured via the epoxy group. However, as the MW of SERs increases, the epoxy content decreases, whereas the hydroxyl content increases. High molecular weight SERs can cross-link via reactions with both the epoxy and hydroxyl functionalities, depending on the choice of curing agents and curing conditions. Reaction of the epoxy groups involves opening of the oxirane ring and formation of longer, linear C—O bonds. This feature accounts for the low shrinkage and good dimensional stability of cured epoxies. The polycondensation curing is accompanied by generation of volatile by-products, such as water or alcohol, requiring heat for proper cure and volatiles removal.

It is the unique ability of the strained epoxy ring to react with a wide variety of reactants under many diverse conditions that gives epoxies their versatility (95). Detailed discussions on the probable electronic configurations, molecular orbitals, bond angles, and reactivity of the epoxy ring are available in the literature (96).

Compared to noncyclic and other cyclic ethers, the epoxy ring is abnormally reactive. It has been postulated that the highly strained bond angles, along with the polarization of the C—C and C—O bonds account for the high reactivity of the epoxide. The electron-deficient carbon can undergo nucleophilic reactions, whereas the electron-rich oxygen can react with electrophiles. It is customary in the epoxy industry to refer to these reactions in terms of anionic and cationic mechanisms. The terminology was attributed to the fact that an anionic intermediate or transition state is involved in a nucleophilic attack of the epoxy while a cationic intermediate or transition state is formed by an electrophilic curing agent (97). For the sake of clarity, the nucleophilic and electrophilic mechanism terminology is used in this article.

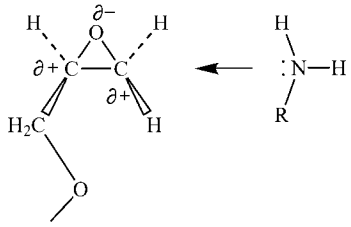

Curing agents are either catalytic or coreactive. A catalytic curing agent functions as an initiator for epoxy resin homopolymerization or as an accelerator for other curing agents, whereas the coreactive curing agent acts as a comonomer in the polymerization process. The majority of epoxy curing occurs by nucleophilic

mechanisms. The most important groups of coreactive curing agents are those with active hydrogen atoms, eg, primary and secondary amines, phenols, thiols, and carboxylic acids (and their anhydride derivatives). Lewis acids, eg, boron trihalides, and Lewis bases, eg, tertiary amines, initiate catalytic cures.

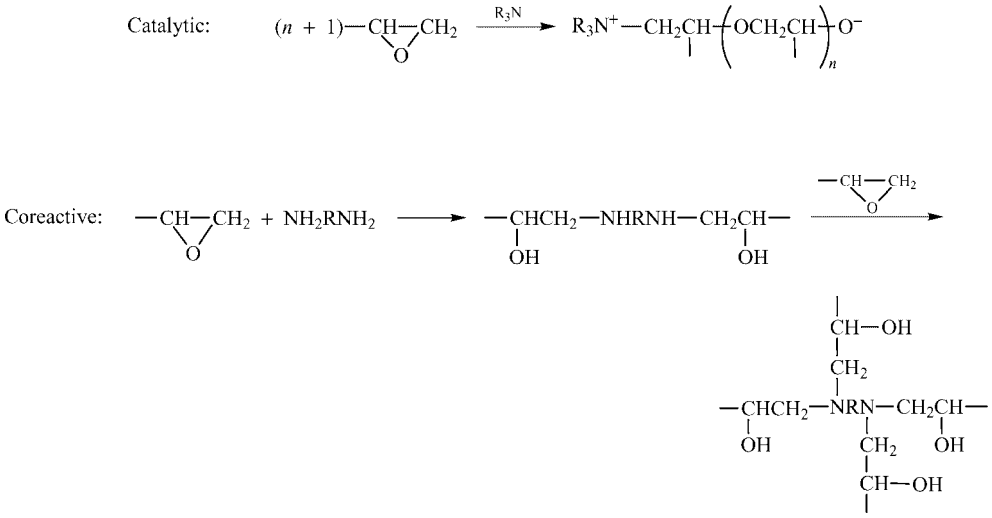

The functional groups surrounding the epoxide resin also affect the curing process. Steric factors (98,99) can influence ease of cure. Electron-withdrawing groups adjacent to the epoxide ring often enhance the reactivity of the epoxy resin to nucleophilic reagents, while retarding its reactivity toward electrophilic reagents (98,100,101). In general, aromatic and brominated aromatic epoxy resins react quite readily with nucleophilic reagents, whereas aliphatic and cycloaliphatic epoxies react sluggishly toward nucleophiles (102).

Figure 3 shows the pseudo first-order kinetic response for the disappearance of the epoxy in buffered methanol solutions (lines are for clarity only).

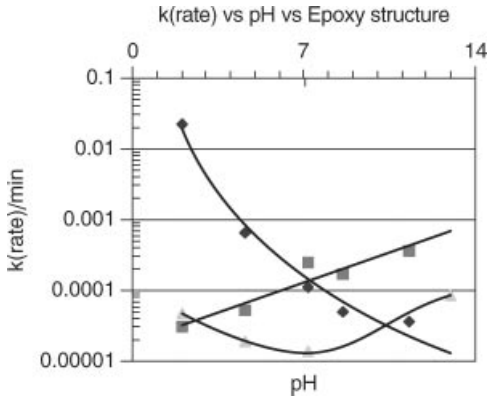

Fig. 3. Efects of pH on reaction rates of epoxies. ◆ Cyclohexene oxide; ■ phenylglycidyl ether; ▲ vinyl cyclohexane oxide.

Table 13. U.S. Consumption of Curing Agents for Epoxy Resins (2001)

Curing agents	Consumption, 10^3 MT	Market percentage
Amine functional compounds	50	48
Aliphatic amines and adducts	16	
Polyamides	14	
Amidoamines	9	
Cycloaliphatic amines	6.8	
Phenalkamines	1.8	
Dicyandiamide (DICY)	1.8	
Aromatic polyamines	0.9	
Carboxylics	37	36
Polycarboxylic polyesters	22	
Anhydrides	15	
Resole resins	9	9
Amino formaldehydes	4.5	
Phenol formaldehyde	4.5	
Novolacs and other phenolics	2.7	2.6
Polysulfides and polymercaptans	14	1.3
Catalysts	3.2	3
Anionic	3.1	
Cationic	0.1	
Others	0.9	<1

Clearly the epoxy structure dramatically influences the cure response of the epoxy as a function of pH. Cycloaliphatic epoxies are fast-reacting under low pH conditions. Aromatic glycidyl ethers are faster under high pH conditions. These results generally agree with "practical" cures: aromatic epoxies are easily cured with amines and amidoamines. Cycloaliphatics (102) are cured with acids and superacids. The behavior of the aliphatic epoxies is more complex but on balance is similar to that of cycloaliphatics.

In 2001, the U.S. market for epoxy curing agents was estimated at 165×10^3 MT (see Table 13), while approximately 318×10^3 MT of epoxy resins was consumed. The most commonly used curing agents are amines, followed by carboxylic-functional polyesters and anhydrides.

A description of advantages, disadvantages and major applications of typical curing agents is given in Table 14.

Coreactive Curing Agents

Commercially, epoxy resins are predominantly cured with coreactive curing agents. Following are important classes of epoxy coreactive curing agents.

Amine Functional Curing Agents. This section describes one of the most important classes of epoxy coreactive curing agents.

Primary and Secondary Amines. Primary and secondary amines and their adducts are the most widely used curing agents for epoxy resins, accounting for close to 50% of all the epoxy curing agents used in the United States in 2001.

Table 14. Curing Agents for Epoxy Resins

Type	Advantages	Disadvantages	Major applications
Aliphatic amines and adducts	Low viscosity; ambient cure temperature; little color; low cost	Short pot life; rapid heat evolution; critical mix ratio; some are moderately toxic; high moisture absorption; blush; carbonation; limited high temperature performance (<100°C)	Flooring; civil engineering; marine and industrial coatings; adhesives; small castings
Cycloaliphatic amines	Low viscosity; long pot-life; room temperature (RT) cure and heat-curable; adhesion to wet cement; good color; low toxicity; good electrical, mechanical, thermal properties (high T_g)	Slower reactivity; high costs	Flooring; paving; aggregate; industrial coatings; adhesives; tooling; composites; castings
Aromatic amines	Excellent elevated temperature performance (150°C); good chemical resistance; long pot life; low moisture absorption	Solids; incompatibility with resins; long cure cycles at high temperature (150°C); toxicity	High performance composites and coatings; adhesives; electrical encapsulation
Amidoamines	Low viscosity; reduced volatility; good pot life; ambient cure temperature; convenient mix ratios; good toughness	Poor performance at high temperature (<65°C); some incompatibility with epoxies	High solids, solvent-free coatings; floorings; concrete bonding; troweling compounds
Polyamides	Good mix ratios; pot life; RT cure; good concrete wetting; flexibility; low volatility and toxicity	High viscosity; low temperature performance; poor color; higher cost	Marine and maintenance coatings; civil engineering; castings; adhesives
Anhydrides	Low exotherm; good thermal (high T_g), mechanical,	Long cure cycles at high temperature (200°C)	Composites; castings; potting; encapsulation

Table 14. (Continued)

Type	Advantages	Disadvantages	Major applications
	electrical properties; low shrinkage and viscosity; long pot life; little color		
Catalytic	Long pot life; high temperature resistance	Brittle; moisture-sensitive	Adhesives; prepregs; electrical encapsulation; powder coatings
Dicyandiamide	Good electrical properties; high temperature resistance; latent systems	Incompatibility with epoxy resins	Electrical laminates; powder coatings; single-package adhesives
Carboxylic-terminated polyesters	Good weatherability, corrosion resistance, and mechanical properties; low cost	Poor chemical resistance	Powder coatings
Isocyanates	Fast cure at low temperature; good flexibility and solvent resistance	Moisture-sensitive; toxic	Powder coatings; maintenance coatings
Phenol–formaldehyde, novolacs	Good chemical resistance, electrical properties, shelf stability, and compatibility with epoxies; high temperature resistance	High melting solids; high temperature cure; poor UV stability	Molding compounds; powder coatings; electrical laminates
Polysulfides and polymercaptans	RT rapid cure times; flexible systems; moisture insensitive	Poor performance at high temperature; odorous	Consumer adhesives; sealants; traffic paints
Melamine–formaldehyde	Good color and hardness; stable one-component systems	High temperature cure	Stove paints; can coatings
Urea–formaldehyde	Stable one-component systems; little color; low cost	High temperature cure; formaldehyde emission	Fast-bake enamels; stove primers; can and drum coatings
Phenol–formaldehyde resoles	Stable one-component systems; excellent chemical resistance	High temperature cure; brittle; gold color	Baked enamels; can, drum and pail coatings; high temperature service coatings

The number of amine hydrogen atoms present on the molecule determines the functionality of an amine. A primary amine group, one which has two hydrogens bound to it, will react with two epoxy groups while a secondary amine will react with only one epoxy group. A tertiary amine group, which has no active hydrogen, will not react readily with the epoxy group, but will act as a catalyst to accelerate epoxy reactions. Reactions of a primary amine with an oxirane group or an epoxy resin are shown in the following (103).

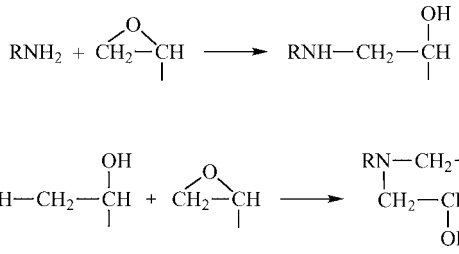

It has been reported that primary amines react much faster than secondary amines (101,104). Reaction of an epoxy group with a primary amine initially produces a secondary alcohol and a secondary amine. The secondary amine, in turn, reacts with an epoxy group to give a tertiary amine and two secondary hydroxyl groups. Little competitive reaction is detectable between a secondary hydroxyl group in the backbone and an epoxy group to afford an ether (100), provided a stoichiometric equivalent or excess amine is maintained. However, with excess epoxy, the secondary hydroxyl groups formed gradually add to the epoxide groups (105). This reaction can be catalyzed by tertiary amines.

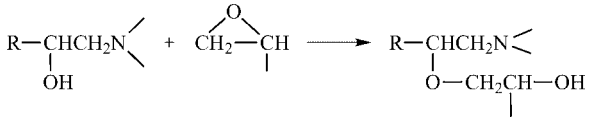

Hydroxyl compounds accelerate the rate of amine curing. A mechanism has been proposed (100) in which the hydrogen atom of the hydroxyl group partially protonates the oxygen atom on the epoxy group, rendering the methylene group more susceptible to attack by the nucleophilic amine. Reactivity is proportional to the hydroxyl acidity and functionality; phenolics, aryl alcohols, and polyfunctional alcohols afford the best results.

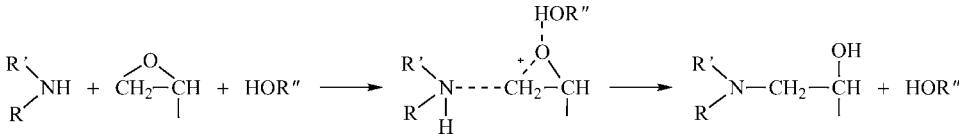

In general, reactivity of amines toward aromatic glycidyl ethers follows their nucleophilicity: aliphatic amines > cycloaliphatic amines > aromatic amines. Aliphatic amines cure aromatic glycidyl ether resins at room temperature (RT) without accelerators, whereas aromatic amines require elevated temperatures.

However, with the help of accelerators, the cure rates of aromatic amines can approach those of some aliphatic amines. In general, the steric and electronic effects of substituents of the epoxy and the amine influence the reaction rate of an amine with an epoxy resin.

Aliphatic Amines. The liquid aliphatic polyamines such as polyethylene polyamines (PEPAs) were some of the first curing agents used with epoxies. They give good RT cures with DGEBA-type resins. The low equivalent weights of the ethylene amines give tightly cross-linked networks with good physical properties, including excellent chemical and solvent resistance but limited flexibility and toughness. Good long-term retention of properties is possible at temperatures up to 100°C. Short-term exposure to higher temperatures can be tolerated. Certain aliphatic amines cured epoxies will blush (or bloom) under humid conditions. This undesirable property has been attributed to the incompatibility of some amine curing agents with epoxy resins. Incompatible amines can exude to the surface during cure and react with atmospheric carbon dioxide and moisture to form undesirable carbamates (carbonation). This, in turn, leads to gloss reduction and intercoat adhesion and recoatability problems in coating applications (106).

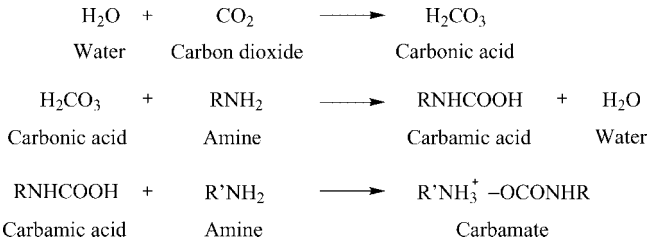

Mixing ratios with epoxy resin are very critical, and working pot lives are too short for some applications. Aliphatic polyamines are hygroscopic and volatile, have bad odor, and cause dermatitis if improperly handled. Another disadvantage is high exotherm in thick sections or large mass parts that can lead to thermal decomposition. Consequently, significant efforts have been devoted toward remedying these shortcomings by modifications of the polyethylene polyamines. Adducts with epoxy resins (resin adducts), carboxylic acids (polyamides, amidoamines), ketones (ketimines), and phenols/formaldehyde (Mannich bases) (107) are widely used commercially. Longer chain alkylenediamines such as hexamethylenediamine (HMD) and polyetheramines (polyglycol-based polyamines) have also been developed. Currently, very small amounts of unmodified polyamines are used as curing agents for epoxies. They are primarily used to produce epoxy adducts (up to 90%). Chemical modification by reaction with epoxy groups to yield epoxy adducts affords products with better handling properties, lower vapor pressure, reduced tendency to blush, and less critical mix ratio. For example, diethylenetriamine (DETA) readily reacts with ethylene oxide in the presence of water to give a mixture of mono- and dihydroxyethyl diethylenetriamine with a longer pot life and fewer dermatitic effects than free DETA.

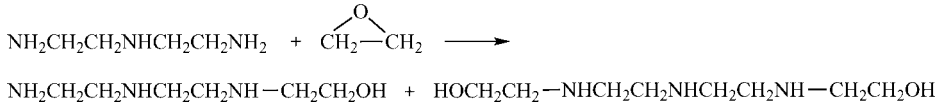

Resinous adducts are produced by reaction of excess diamine with epoxy resins.

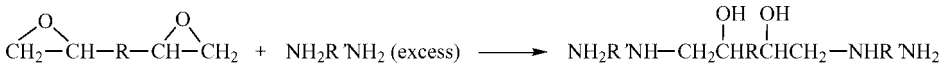

The higher molecular weight of the adduct affords a more desirable, forgiving ratio of resin to curing agent, lower water absorption, and better resin compatibility.

Ketimines. Ketimines are the reaction products of ketones and primary aliphatic amines. In the absence of reactive hydrogens, they do not react with epoxy resins. They can be considered blocked amines or latent hardeners, since they are readily hydrolyzed to regenerate the amines. They have low viscosity, cure rapidly when exposed to atmospheric humidity, and are useful in high solids coatings. Similar products have been obtained with acrylonitrile.

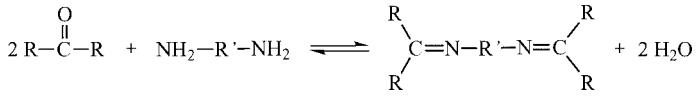

Mannich Base Adducts. Mannich base adduct is the reaction product of an amine with phenol and formaldehyde.

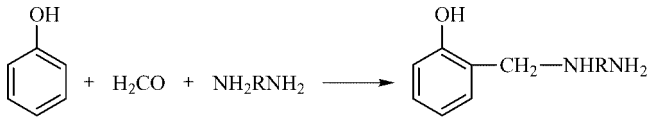

Mannich base

The resultant product has an internal phenolic accelerator. Compared to unmodified amines Mannich base adducts have lower volatility, less blushing and carbonation, and, despite their higher MW, faster reactivity.

Polyetheramines. Polyetheramines are produced by reacting polyols derived from ethylene oxide or propylene oxide with amines. The more commercially successful adducts are based on propylene oxide and are available in different MWs (JEFFAMINE* from Huntsman). The longer chain backbone provides improved flexibility but slower cure rate. Chemical and thermal resistance properties are also reduced. Polyetheramines are often used in combination with other amines in flooring, and adhesive and electrical potting applications.

Cycloaliphatic Amines. Cycloaliphatic amines were originally developed in Europe, where their use as epoxy curing agents is well established. Compared to aliphatic amines, cycloaliphatic amines produce cured resins having improved thermal resistance and toughness. Glass-transition temperatures (T_g) approach those of aromatic amines (>150°C), while percent elongation can be doubled.

However, chemical resistance is inferior to that of aromatic amines. Because cycloaliphatic amines are less reactive than acyclic aliphatic amines, their use results in a longer pot life and in the ability to cast larger masses. Unmodified cycloaliphatic amines require elevated temperature cure, but modified systems are RT-curable. Properly formulated, they can give an excellent balance of properties: fast cure, low viscosity, low toxicity, good adhesion to damp concrete, and excellent color stability. They are, however, more expensive than other types of curing agents.

Isophorone diamine (IPDA), bis(4-aminocyclohexyl)methane (PACM), and 1,2-diaminocyclohexane (1,2-DACH) are the principal commercial cycloaliphatic polyamine curing agents. IPDA is the largest volume cycloaliphatic amine. Commercial cycloaliphatic amines are formulated products. In addition to the cycloaliphatic amines, other components such as aliphatic amines and plasticizers are also included to improve RT cure speed and end-use properties. One popular formulation consists of IPDA used in combination with trimethylhexamethylenediamines (TMDA) or *meta*-xylenediamine (MXDA), and plasticizers/accelerators such as nonyl phenol or benzyl alcohol. In some ambient cure coating applications, cycloaliphatic amines can be reacted with phenol and formaldehyde to form the Mannich base products, which have an internal phenol accelerator and cure readily at ambient temperatures.

The largest market for cycloaliphatic amines is in flooring, followed by high solids coatings, composites, adhesives, castings, and tooling. Cycloaliphatic amines experienced significant growth in the early 1990s as replacements for more toxic aromatic amines such as MDA. However, anhydrides have been more successful at replacing aromatic amines in composite applications.

Aromatic Amines. Because of conjugation, aromatic amines have lower electron density on nitrogen than do the aliphatic and cycloaliphatic amines. Consequently, they are much less reactive toward aromatic epoxies. They have longer pot-lives and usually require elevated temperature cures. Aromatic amines are usually solid at room temperature. These hardeners are routinely melted at elevated temperatures and blended with warmed resins to improve solubility. Eutectic mixtures of *meta*-phenylenediamine (MPD) and methylenedianiline (MDA or DDM) exhibit a depressed melting point resulting in an aromatic hardener that remains a liquid over a short period of time. MDA or 4,4′-diaminodiphenylmethane (DDM), 4,4′-diaminodiphenyl sulfone (DDS or DADPS), and MPD are the principal commercial aromatic amines. A new aromatic amine, diethyltoluenediamine (DETDA) has gained more significant uses in recent years.

Epoxies cured with aromatic amines typically have better chemical resistance and higher thermal resistance properties than products cured with aliphatic and cycloaliphatic amines. Their best attribute is their retention of mechanical properties at long exposures to elevated temperatures (up to 150°C). Consequently, they are widely used in demanding structural composite applications such as aerospace, PCB laminates, and electronic encapsulation. 4,4′-DDS is the standard curing agent used with a multifunctional amine epoxy (MY 720) for high performance aerospace and military composite application. 3,3′-DDS is used in aerospace honeycomb for its excellent peel strength. MDA, which has excellent mechanical and electrical properties, is the most widely used aromatic curing agent, but recently has been classified as a potential human carcinogen and its

volume has been declining. Alkyl-substituted MDAs such as tetraethyl-MDA have been developed with lower toxicity and improved performance (108,109). However, none of the replacement products has the performance/cost combination of MDA. Anhydrides and cycloaliphatic amines have been used to replace aromatic amines in a number of composite applications. Efforts have been made to develop ambient-curable aromatic amines by adding accelerators such as phenols to MDA.

Arylyl Amines. These amines have cycloaliphatic or aromatic backbones, but the amine functional groups are separated from the backbone by methylene groups (benzylic amines). Consequently, arylyl amines are much more reactive toward epoxies than aromatic amines while having improved thermal and chemical resistance over aliphatic amines. Fast cures at ambient and sub-ambient are possible with arylyl amines. These amines are more widely used in Japan and Europe than in North America. Meta-Xylylene diamine (MXDA) and its hydrogenated product, 1,3-bis(aminomethyl cyclohexane) (1,3-BAC) are popular arylyl amines.

The commercial polyamine curing agents are given in Table 15.

The stoichiometric quantity of polyamine used to cure an epoxy resin is a function of the molecular weight and the number of active hydrogens of the polyamine (amine equivalent weight, AEW) and the EEW or equivalent weight of epoxy resin; it is expressed as follows:

$$\left(\frac{\text{AEW}}{\text{EEW}}\right) \times 100 = \text{parts by weight polyamine per 100 parts by weight epoxy resin}$$

Polyamides. Polyamides are one of the largest volume epoxy curing agents used. They are prepared by the reaction of dimerized and trimerized vegetable-oil fatty acids with polyamines. Dimer acid is made by a Diels–Alder reaction between 9,12- and 9,11-linoleic acids. Subsequent reaction with diethylenetriamine or other suitable multifunctional amines yields the amine-terminated polyamides. They are available in a range of molecular weights and compositions.

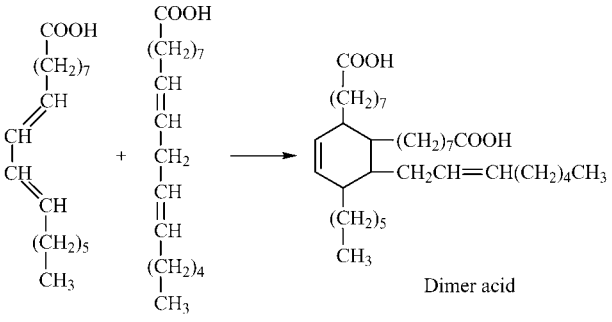

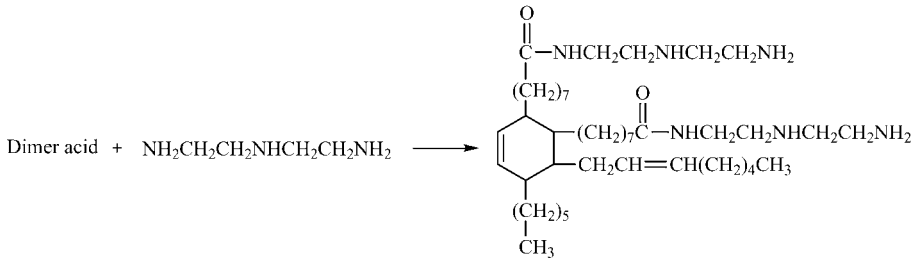

Table 15. Commercial Amine Curing Agents

Formula	Name	Abbreviation
Aliphatic		
$NH_2CH_2CH_2NHCH_2CH_2NH_2$	Diethylenetriamine	DETA
$NH_2CH_2CH_2NHCH_2CH_2NHCH_2CH_2NH_2$	Triethylenetetramine	TETA
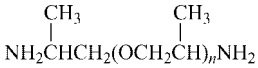	Poly(oxypropylene diamine)	
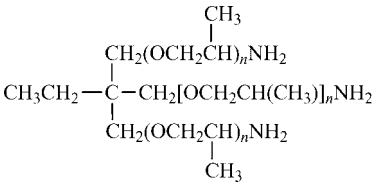	Poly(oxypropylene triamine)	
$NH_2(CH_2)_3O(CH_2)_2O(CH_2)_3NH_2$	Poly(glycol amine)	
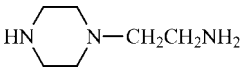	*N*-Aminoethylpiperazine	AEP
Cycloaliphatic		
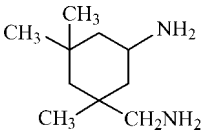	Isophorone diamine	IPDA
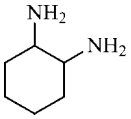	1,2-Diaminocyclohexane	DACH
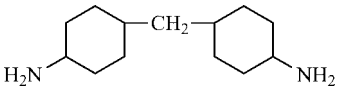	Bis(4-aminocyclohexyl) methane	PACM
Aromatic		
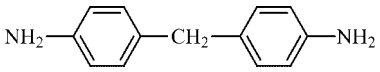	4,4′-Diamino-diphenylmethane	MDA, DDM
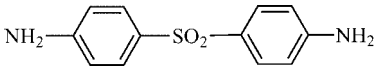	4,4′-Diaminodiphenyl sulfone	4,4′-DDS
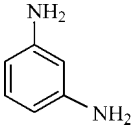	*m*-Phenylenediamine	MPD
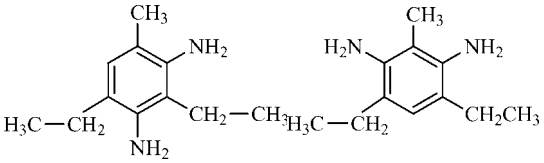	Diethyltoluenediamine	DETDA

Table 15. (Continued)

Formula	Name	Abbreviation
Arylyl amines		
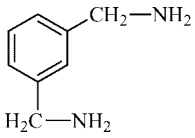	*meta*-Xylene diamine	MXDA
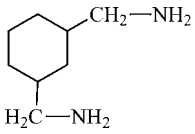	1,3-Bis(aminomethyl cyclohexane)	1,3-BAC

Polyamides are extremely versatile curing agents. The polyamides react with the epoxide group through the amine functionality in the polyamide backbone. The unreacted amide NH groups in the backbone provide good intercoat adhesion and the fatty acid structures provide good moisture resistance and mechanical properties. Wetting of cement surfaces is excellent. As a result of their relatively higher molecular weight, the ratio of polyamide to epoxy is more forgiving than with low MW polyamines. They are inexpensive, less toxic to handle; give no blushing; exhibit readily workable pot lives; and cure under mild conditions. Polyamides are mainly used in coating and adhesive formulations, mostly in industrial maintenance and civil engineering applications. The various MW polyamides exhibit different degrees of compatibility with epoxy resins. To ensure optimum properties, the polyamide/epoxy mixture must be allowed to react partly before being cured. This partial reaction assures compatibility and is known as the *induction period*.

Disadvantages of polyamides include slower cure speeds and darker color than polyamine-cured epoxies. Polyamide-cured epoxies lose structural strength rapidly with increasing temperature. This limits their use to applications not subjected to temperatures above 65°C. Formulations with tertiary amines, phenolic amines, or co-curing agents help to speed up cures at low temperatures. Alternatively, polyamides derived from polyamines with phenolic-containing carboxylic acids are called *phenalkamines* (110). These curing agents have low viscosity and fast ambient cure speed and are widely used in on-site marine coatings and concrete deck applications.

The high viscosity of polyamides limits their uses primarily to low solids coatings, which have been losing ground to higher solids coatings. Waterborne polyamides have been developed for use with waterborne epoxies, but their growth has been modest over the past decade because the conversion to waterborne epoxy coatings has been slower than expected. Commercial polyamides include

the Versamid resins from Cognis, Ancamide resins from Air Products, and Epicure resins from Resolution.

Amidoamines. Amidoamines have all the properties of polyamides, except for a significantly lower viscosity, which make them useful in high solids and solvent-free coating formulations. They are prepared by the reaction of a monofunctional acid like tall-oil fatty acid with a multifunctional amine such as DETA, resulting in a mixture of amidoamines and imidazolines.

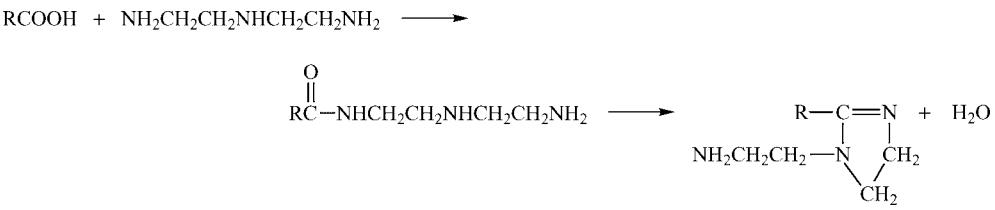

Imidazoline is formed by intramolecular condensation at high reaction temperatures. Commercial amidoamines are produced with different imidazoline contents to regulate reactivity and cured product performance. The pot life/reactivity of amidoamines varies with imidazoline content. High imidazoline contents offer longer pot life and semi-latent curing system activated by moisture. They are useful in wet concrete applications. Like the polyamides, amidoamines can be used over a range of additive levels to enhance a specific property. However, amidoamines offer several advantages over aliphatic amines and polyamides. They offer more convenient mix ratios, increased flexibility, and better moisture resistance than aliphatic polyamines, and they offer lower color and viscosity than polyamides. Consequently, the volume of amidoamines has grown significantly in the past decade.

Dicyandiamide. Dicyandiamide (DICY) is a solid latent hardener (mp 208°C). Its latent nature is due to its insolubility in epoxy resins at RT. DICY can be mixed in with epoxy resins to provide a one-package formulation with good stability up to 6 months at ambient temperatures. Cure of epoxies with DICY occurs with heating to 150°C. It is often used with imidazoles as catalysts. DICY offers the advantage of being latent (reacts with epoxy resin upon heating and stops reacting temporarily when the heat is removed). This partially cured or "B-staged" state is ideal for prepreg applications. Typically, DICY is used at levels of 5–7 parts per 100 parts of liquid epoxy resins and 3–4 parts per 100 parts of solid epoxy resins.

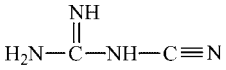

DICY

DICY is one of the first curing agents to be used with epoxy resins. It cures with epoxies to give a highly cross-linked thermoset with good mechanical strength, thermal properties, and chemical resistance, and excellent electrical properties. Because of its latency, low quantity requirements and excellent balance of properties, DICY is a widely used curing agent in powder coating and

electrical laminate applications. These two applications account for 85% of DICY consumption as epoxy curing agent.

The curing mechanism is rather complex, involving several simultaneous reactions. There are a number of conflicting proposed mechanisms in the literature. One study proposed the initial reaction of all four active hydrogens with epoxy resin catalyzed by tertiary amine catalysts followed by epoxy homopolymerization. The last step involves reactions between the hydroxyl groups of the epoxy resin with the cyano group (108,109). One of the more recent and plausible mechanism of DICY cure with epoxies is that of Gilbert and co-workers (111). The Gilbert mechanism is summarized in Figure 4. Gilbert and co-workers investigated the reaction of DICY with methyl glycidyl ether of bisphenol A (MGEBA). Products were analyzed using HPLC, NMR, and FTIR. On the basis of products that were isolated and characterized, Gilbert and co-workers proposed the mechanism shown in Figure 4.

The first step in the mechanism is the reaction of DICY with epoxy to form the alkylated DICY. This was confirmed by the imide IR peak at 1570 cm^{-1}. The second step involves further alkylation of the nitrogen that reacted in step 1, to form the *N*,*N*-dialkyldicyandiamide. No alkylation of the other amino group was suggested. The third step is the intramolecular cyclization step to form a zwitterionic five-membered intermediate. This involves the intramolecular reaction of the secondary alcohol formed in step 2 with the imide functionality (—C=N—). This is in contrast with the Zahir mechanism (112) where the intramolecular cyclization involves the hydroxy and the nitrile groups. The fourth step involves the elimination of ammonia and the formation of 2-cyanimidooxazolidine. The formation of this heterocycle is consistent with the observed bathocromic IR shift from 1570 cm^{-1} to 1650 cm^{-1}. The ammonia that is eliminated can then react with epoxy to form a trifunctional cross-link. The last step involves the hydrolysis of the oxazolidine to form the oxazolidone and cyanamide. The hydrolysis step accounts for the formation of the carbonyl group.

Carboxylic Functional Polyester and Anhydride Curing Agents. Carboxylic polyesters and anhydrides are the second most important class of epoxy curing agent. Together, they constitute 36% of the total curing agent volume used in the U.S. market (2001 data). Polyesters have been growing rapidly in powder coatings formulations with epoxy resins, consuming the highest tonnage of epoxy curing agents. This is driven in part by the conversion to the more environmentally friendly powder coating technologies, and in part by the versatility and cost efficiency of polyester–epoxy hybrid powder coatings. Anhydrides have been successfully replacing more toxic aromatic amines in composites. They account for 70% of the volume of curing agents used in structural composite applications. Both polyesters and anhydrides are used in heat-cured applications only.

Carboxylic Functional Polyesters. The reaction of polyacids with polyalcohols produces polyesters. The terminal functionality is dictated by the ratio of the reactants. By virtue of their relatively cheap, widely available raw materials and good flexibility and weatherability, acid functional polyesters are used in hybrid epoxy powder coatings for a wide range of applications. For applications requiring good weatherability, triglycidyl isocyanurate (TGIC) is often used as curing agent for acid functional polyesters.

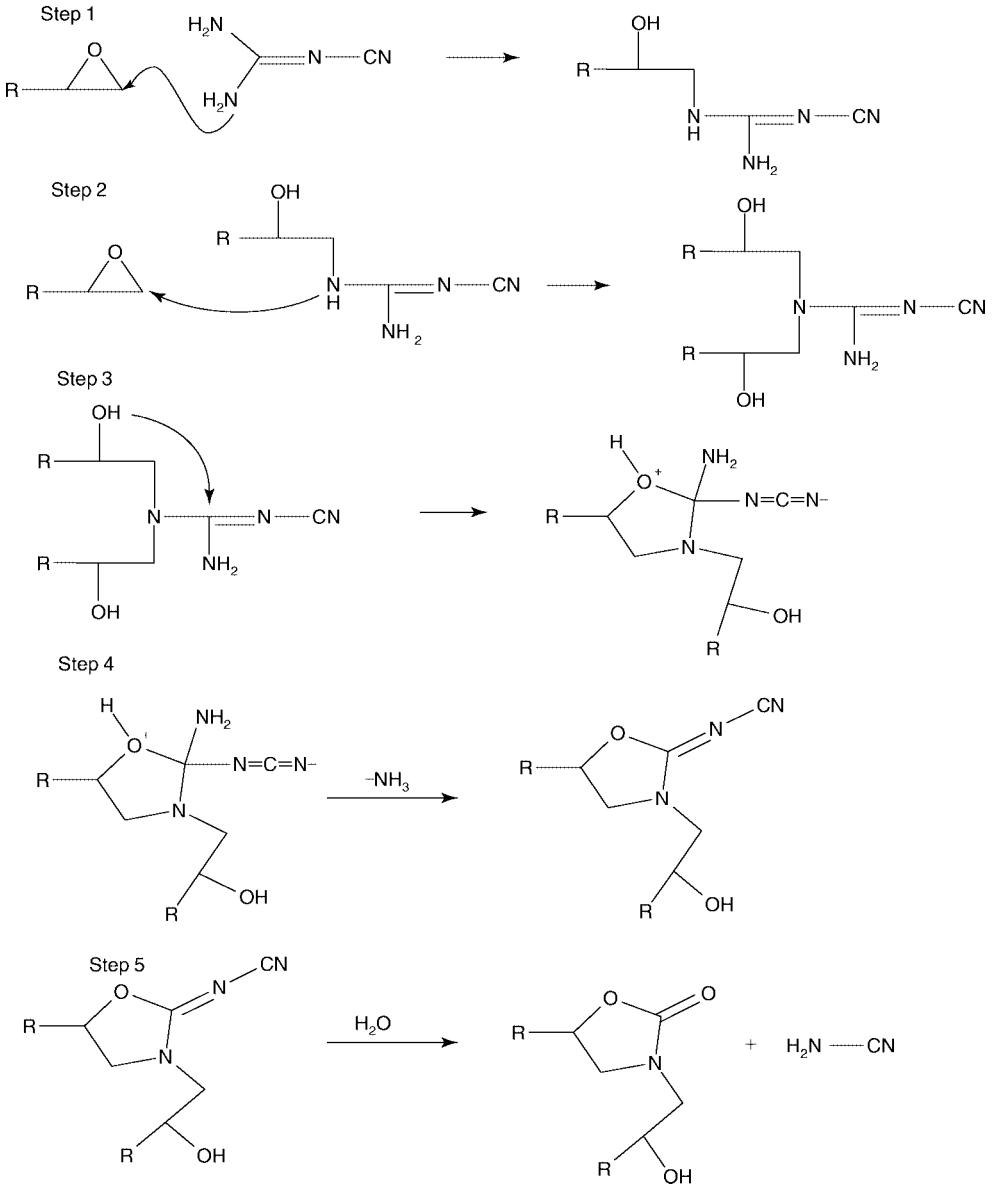

Fig. 4. The Gilbert mechanism for the DICY curing of epoxy. From Ref. 111.

Terephthalic acid, trimellitic anhydride, and neopentyl glycol are commonly used raw materials to produce polyesters. Other acids, anhydrides, and glycols can also be used to modify functionality, MW, viscosity, and mechanical properties (after curing) of the polyesters. This versatility of the polyester building blocks allows many useful combinations of epoxy–polyester hybrid systems to be developed for a wide range of applications (113). Major applications include coatings for metal furniture, general metal finishing, appliances, machinery and equipment,

automotive, and wood. Automotive is a new, large, and fast growing market with many car makers converting to primer-surfacer based on epoxy–polyester powder coatings. Wood coatings are a new, emerging market.

The curing mechanism of epoxy–polyester thermosets involves reaction of the acid functionality with epoxy followed by esterification of the epoxy hydroxyl groups with the acids (114). Compounds such as amines and phosphonium salts catalyze these reactions. Water is a condensation reaction by-product that must be allowed to escape during the curing process to avoid coating defects.

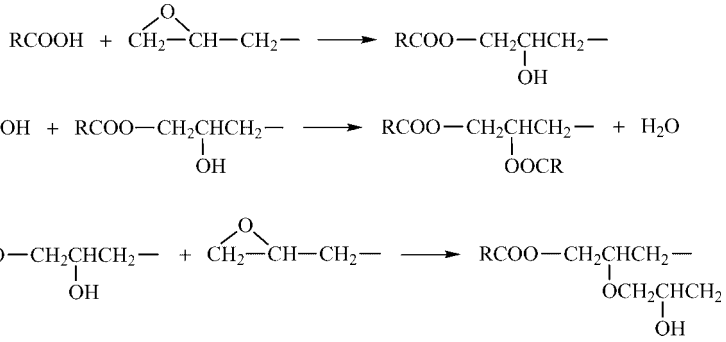

The first product is a β-hydroxypropyl ester, which reacts with a second mole of carboxylic acid to yield a diester. The hydroxyl ester can also undergo polymerization by reaction of its secondary hydroxyl group with an epoxy group.

Acid Anhydrides. Anhydrides are some of the very first epoxy curing agents used, and they remain a major class of curing agents used in heat-cured structural composites and electrical encapsulation. Their consumption volume equals that of all aliphatic amines and adducts in 2001 in the United States. While the carboxylic-terminated polyesters find widespread uses in coatings, anhydride use in coatings is minimal.

Epoxy–anhydride systems exhibit low viscosity and long pot life, low exothermic heats of reaction, and little shrinkage when cured at elevated temperatures. The low exotherm heat generation is a unique attribute of anhydrides, making them suitable for uses in large mass epoxy cures. Curing is slow at temperatures below 200°C and is often catalyzed by Lewis bases or acids. Post-cure is often needed to develop optimum properties. Tertiary amines such as benzyldimethylamine, dimethylaminomethylphenol, tris(dimethylaminomethyl)phenol, boron trihalide amine complexes, stannic chloride, ammonium salts, phosphonium salts, and substituted imidazoles are effective catalysts. Proper catalyst concentration (0.5–2.5% of resin weight) is critical, depending on the types of anhydrides and resins used and the cure schedules, and is known to affect high temperature performance.

Cured epoxy–anhydride systems exhibit excellent thermal, mechanical, and electrical properties, and are used in filament-wound epoxy pipe, PCB laminates, mineral-filled composites, and electrical casting and encapsulation applications. Anhydride-cured epoxies also have better aqueous acid resistance than similar amine-cured systems. Anhydrides are the principal curing agents for cycloaliphatic and epoxidized olefin resins in electrical casting and potting. Some

key physical properties of exemplary epoxy resins cured with hexahydrophthalic anhydride are shown in Table 16.

The mechanism of anhydride cure is complex and controversial because of the possibility of several competing reactions. The uncatalyzed reaction of epoxy resins with acid anhydrides proceeds slowly even at 200°C; both esterification and etherification occur. Secondary alcohols from the epoxy backbone react with the anhydride to give a half ester, which in turn reacts with an epoxy group to give the diester. A competing reaction is etherification of an epoxy with a secondary alcohol, either on the resin backbone or that formed during the esterification, resulting in a β-hydroxy ether. It has been reported that etherification is a probable reaction since only 0.85 equivalents of anhydrides are required to obtain optimum cross-linked density and cured properties (103).

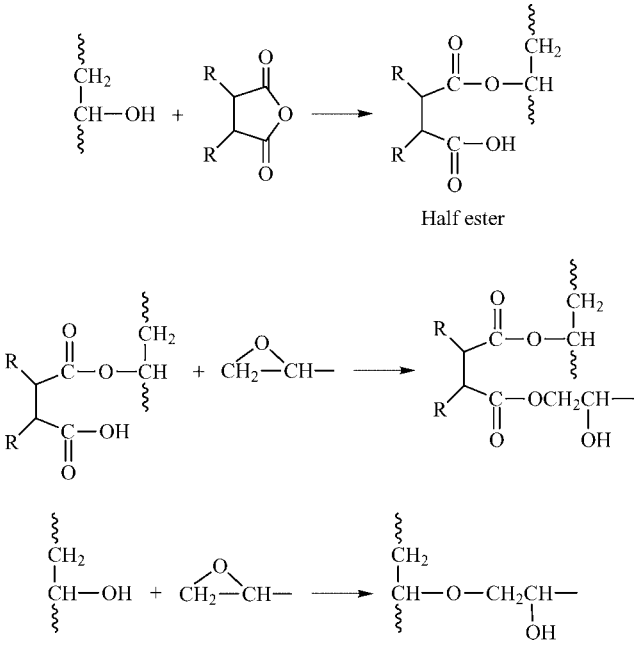

Lewis bases such as tertiary amines and imidazoles are widely used as epoxy–anhydride catalysts. Conflicting mechanisms have been reported for these catalyzed reactions (115). The more widely accepted mechanism (103) involves the reaction of the basic catalyst with the anhydride in the initiation step to form a betain (internal salt). The propagation step involves the reaction of the carboxylate anion with the epoxy group, generating an alkoxide. The alkoxide then further reacts with another anhydride, propagating the cycle by generating another carboxylate which reacts with another epoxy group. The end result is the formation of polyester-type linkages. In practice, it has been observed that optimum properties are obtained when stoichiometric equivalents of epoxy and anhydride are used with high temperature cures, which is consistent with this mechanism and does not involve etherification reactions. At lower anhydride/epoxy ratios (0.5:1)

Table 16. Formulation and Properties of Epoxy Resins Cured With Hexahydrophthalic Anhydride

	DGEBA	3′,4′-Epoxycyclohexylmethyl 3,4-epoxycyclohexanecarboxylate	Hexahydrophthalic acid diglycidyl ester
Formulation			
Resin, pbw[a]	100	100	100
Hexahydrophthalic anhydride, pbw[a]	85	105	100
Accelerator type	Tertiary amine	Metal alkoxide salt	Quaternary ammonium salt
pbw[a]	3	12	4
Cure schedule, h at °C	2 at 100 1 at 150	4 at 120	4 at 80 4 at 140
Typical cured properties at 25°C			
Tensile strength, MPa[b]	65	r68	83
Tensile modulus, MPa[b]	3400	3300	3000
Flexural strength, MPa[b]	131	89	127
Flexural modulus, MPa[b]	3400	3000	3000
Elongation, %	5.0	2.7	3.5
Compressive strength, MPa[b]	124	151	124
Heat-deflection temperature, °C	120	150	105
Water absorption, % weight gain[c]	0.5	0.4	0.4
Dielectric constant at 60 Hz	3.4	3.3	3.5
Dissipation factor at 60 Hz	0.006	0.005	0.007
Volume resistivity, $\Omega \cdot cm \times 10^{16}$	2.0	10.0	3.0

[a] Parts by weight.
[b] To convert MPa to psi, multiply by 145.
[c] After boiling for 1 h.

and lower cure temperatures, some etherifications can take place by reaction of the alkoxide with an epoxy group.

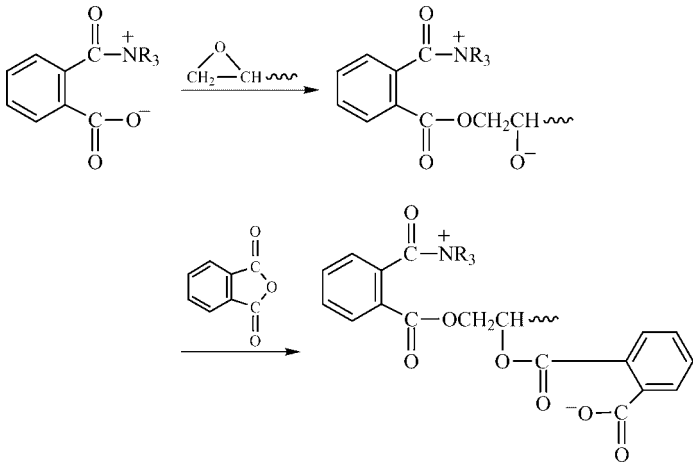

Numerous structurally different anhydrides can be used as epoxy curing agents, but the most widely used are liquids for ease of handling. The most important commercial anhydrides are listed in Table 17. Methyltetrahydrophathalic anhydride (MTHPA) is the largest volume anhydride, used in filament-winding composites. Phthalic anhydride (PA) is the next largest volume and is inexpensive; so it is used widely in mineral-filled laboratory bench top manufacturing, which requires low exotherm heat generation to avoid cracking. Dodecylsuccinic anhydride (DDSA) has a long aliphatic chain in the backbone and is used as blends to improve flexibility. Benzophenonetetracarboxylic dianhydride (BTDA) is a relatively new, multifunctional anhydride developed for high temperature applications, capable of achieving a high cross-linking density with a heat distortion temperature (HDT) of 280°C. It has been used as a replacement for more toxic aromatic amines. Tetrachlorophthalic anhydride (TCPA) is used in epoxy powder coatings for small electronic components with flame-retardancy requirements.

Phenolic-Terminated Curing Agents. Phenolics form a general class of epoxy curing agents containing phenolic hydroxyls capable of reacting with the epoxy groups. They include phenol-, cresol-, and bisphenol A terminated epoxy resin hardener. More recent additions include bisphenol A based novolacs. Cure takes place at elevated temperatures (150–200°C) and amine catalysts are often used.

The bisphenol A terminated hardeners are produced using liquid epoxy resins and excess bisphenol A in the resin advancement process. They are essentially epoxy resins terminated with bisphenol A. They are popular in epoxy powder coating applications for rebar and pipe, providing more flexible epoxy coatings than the novolacs.

The novolacs are produced via the condensation reaction of phenolic compounds with formaldehyde using acid catalysts. They are essentially precursors to epoxy novolacs. Novolacs are multifunctional curing agents and can impart higher cross-link density, higher T_g, and better thermal and chemical resistance

Table 17. Commercially Important Anhydride Curing Agents

Name	Structure
Phthalic anhydride (PA)	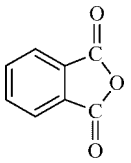
Tetrahydrophthalic anhydride (THPA)	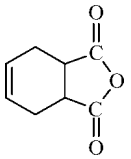
Methyltetrahydrophthalic anhydride (MTHPA)	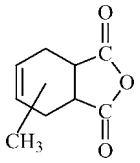
Methyl hexahydrophthalic anhydride (MHHPA)	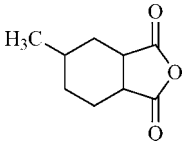
Hexahydrophthalic anhydride (HHPA)	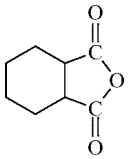
Nadic methyl anhydride or methyl himic anhydride (MHA)	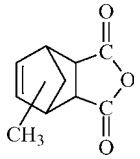
Benzophenonetetracarboxylic dianhydride (BTDA)	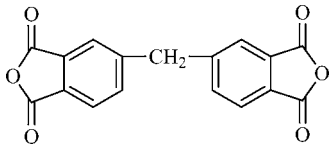
Tetrachlorophthalic anhydride (TCPA)	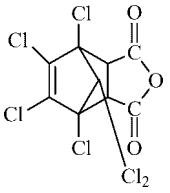

than other phenolics. Cresol novolacs provide higher solvent and moisture resistance, but are more brittle than their phenol novolac counterparts. Recently, bisphenol A based novolacs have been used in electrical laminate formulations to improve thermal performance (T_g and T_d) (116). Novolacs are widely used in composites, PCB laminates, and electronic encapsulation applications. Their uses in coatings are limited to high temperature applications such as powder coatings for down-hole oil-field pipe coatings.

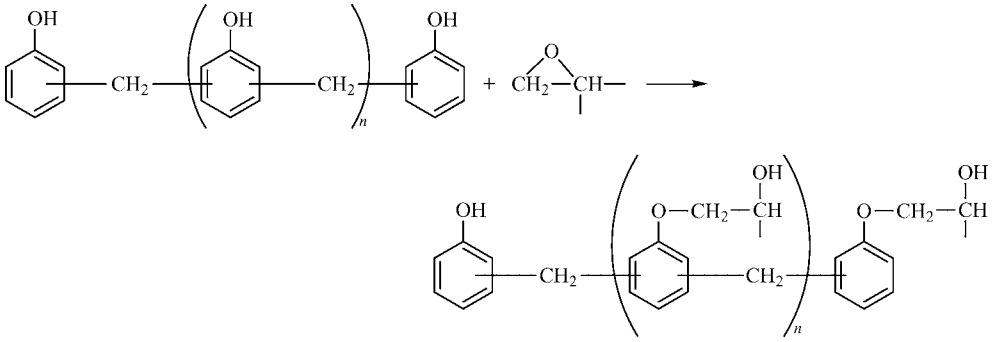

Melamine–, Urea–, and Phenol–Formaldehyde Resins. Melamine–formaldehyde, urea–formaldehyde, and phenol–formaldehyde resins react with hydroxyl groups of high MW epoxy resins to afford cross-linked networks (72).

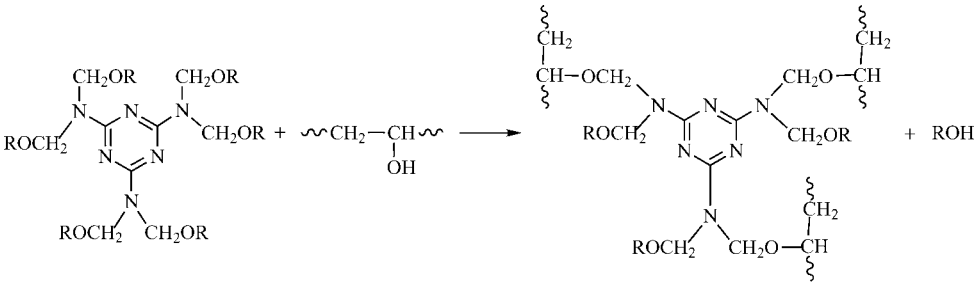

Melamine–formaldehyde resin

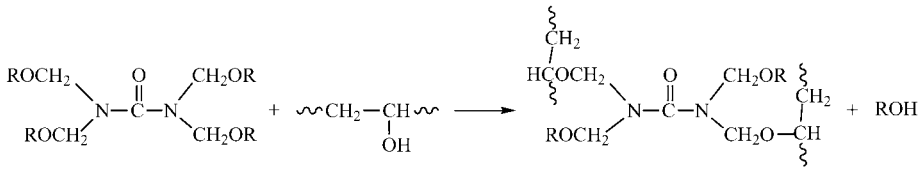

Urea–formaldehyde resin

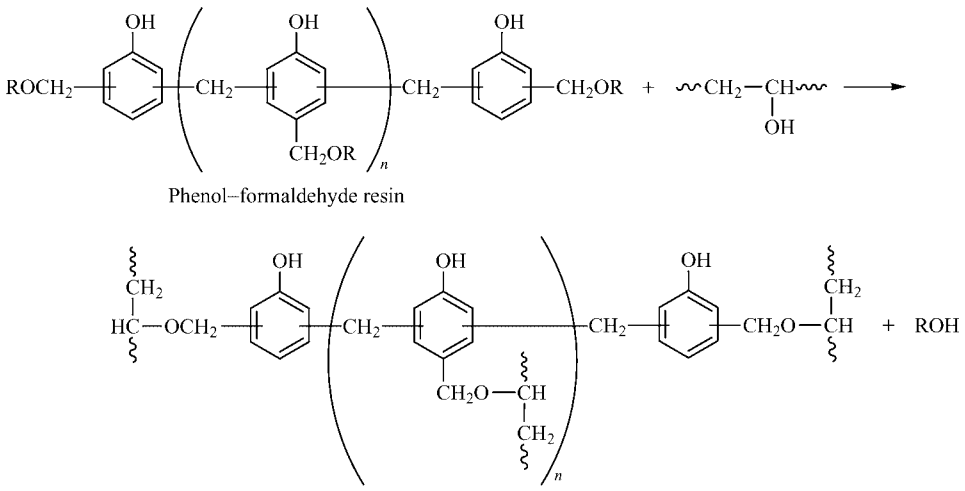

The condensation reaction occurs primarily between the methylol or alkylated methylol group of the formaldehyde resin and the secondary hydroxyl group on the epoxy resin backbone. The high bake temperatures used in these applications drive off the condensation by-products (alcohol or water). Acids such as phosphoric acid and sulfonic acids are often used as catalysts.

There are two types of phenol–formaldehyde condensation polymers: resoles and novolacs (117). Phenol–formaldehyde polymers prepared from the base-catalyzed condensation of phenol and excess formaldehyde are called resoles. In most phenolic resins commonly used with epoxies, the phenolic group is converted into an ether to give improved alkali resistance. At elevated temperatures (>150°C), resole resins react with the hydroxyl groups of the epoxy resins to provide highly cross-linked polymers.

The melamine- and urea–formaldehyde resins are also called amino resins (118). The phenol–formaldehyde resoles are often called phenolic resins, which is rather easily confused with phenolic-terminated cross-linkers such as novolacs and bisphenol A terminated resins.

These formaldehyde-based resins are widely used to cure high MW solid epoxy resins at elevated temperatures (up to 200°C) for metal can, drum, and coil coatings applications. The resultant coatings have excellent chemical resistance, good mechanical properties, and no effects on taste (adding or taking away taste from packaged foods or drinks). The vast majority of the food and beverage cans produced in the world today are coated internally with epoxy–formaldehyde resin coatings. The phenol–formaldehyde resoles are also used with epoxies in coatings for high temperature service pipes and to protect against hot, corrosive liquids.

Mercaptans (Polysulfides and Polymercaptans) Curing Agents. The mercaptan group of curing agents includes polysulfide and polymercaptan compounds which contain terminal thiols.

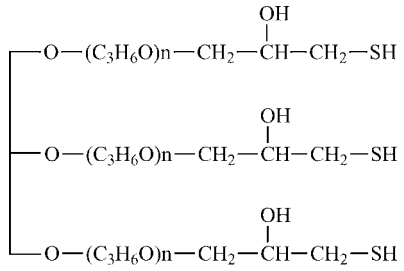

Polymercaptans

In the language commonly used in this industry, "polysulfides" typically have a functionality of 2, while "polymercaptans" have an average functionality of 3. By itself, the thiol or mercaptan group (SH) reacts very slowly with epoxy resins at ambient temperature. However, when converted by a tertiary amine to a mercaptide ion, they are extremely reactive (119).

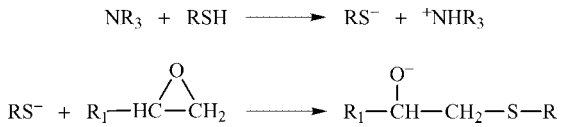

Increasing the basic strength of the amine increases the reaction rate. Polar solvents are also known to speed up these reactions. Fast curing at ambient conditions is the primary attribute of this class of curing agent, lending themselves to applications such as the "5-minutes" consumer adhesives, concrete road repairs, and traffic marker adhesives. In practice, they are often formulated with co-curing agents such as amines or polyamides to achieve a balance of fast cure with improved mechanical properties. The tertiary amine accelerated polymercaptan/epoxy systems exhibit good flexibility and tensile strength at ambient temperature. They are used in high lap-shear adhesion applications such as concrete patch repair adhesives. One disadvantage of polymercatans is their strong odor. Aliphatic amine/polysulfide co-curing agent systems yield improved initial elevated temperature performance and are widely used as building adhesives for their excellent adhesion to both glass and concrete. However, both systems lose some flexibility on aging.

Cyclic Amidines Curing Agents. Cyclic amidine curing agents are typically used in epoxy powder coating formulations and in decorative epoxy–polyester hybrid powder coatings to produce matte surface for furniture and appliance finishes. 2-Phenyl imidazoline has been used successfully to produce low gloss epoxy powder coatings. It is highly reactive, capable of curing at relatively low temperatures (140°C) and is suitable for curing of coatings on temperature-sensitive substrates such as wood and plastics. Other curing agents in this group include salts of polycarboxylic acids and cyclic amidines. Their volume is currently small but is expected to grow as the markets for low gloss and low temperature cure

powder coatings develop. They can also be used as tertiary amine catalysts similar to imidazoles.

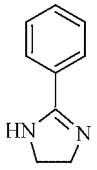

2-Phenyl imidazoline

Isocyanate Curing Agents. Isocyanates react with epoxy resins via the epoxy group to produce an oxazolidone structure (120,121) or with a hydroxyl group to yield a urethane linkage. The urethane linkage provides improved flexibility, impact, and abrasion resistance. The oxazolidone products have been successfully commercialized in high temperature resistance coating and composite applications. Blocked isocyanates are used as cross-linkers for epoxy in PPG's cathodic electrodeposition (CED) coatings. Isocyanates are also used to cure epoxies in some powder coatings, but their toxicity has limited their use.

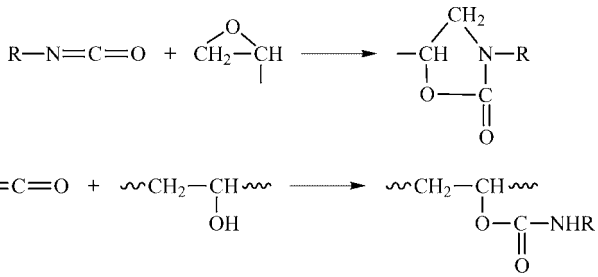

Cyanate Ester Curing Agents. Cyanate esters can be used to cure epoxy resins to produce highly cross-linked thermosets with high modulus and excellent thermal, electrical, and chemical resistance properties. They are used in high performance electrical laminate and composite applications. Cure involves oxazoline formation catalyzed by metal carboxylates in addition to homopolymerization of both cyanate ester and epoxy (122). The high costs of cyanate esters however limit their uses.

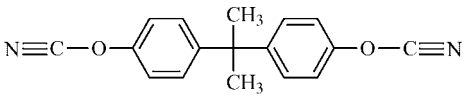

Bisphenol A based dicyanate ester

Catalytic Cure

The catalytic curing agents are a group of compounds that promote epoxy reactions without being consumed in the process. In some of the epoxy literature, catalysts

are referred to as "accelerators"; the distinction of these two types of additives is discussed in later sections.

Lewis Bases. Lewis bases contain an unshared pair of electrons in an outer orbital and seek reaction with areas of low electron density. They can function as nucleophilic catalytic curing agents for epoxy homopolymerization; as co-curing agents for primary amines, polyamides, and amidoamines; and as catalysts for anhydrides. Tertiary amines and imidazoles are the most commonly used nucleophilic catalysts. Several different mechanisms are possible:

(1) The catalytic curing reactions of tertiary amines with epoxy resins follow two different pathways, depending on the presence or absence of hydrogen donors, such as hydroxyl groups. In the absence of hydrogen donors (123), tertiary amines react with the electron-poor methylene carbon of the epoxy group to form an intermediate zwitterion. The zwitterion then attacks another epoxy group to continue homopolymerization via an anionic mechanism. In the presence of hydrogen donors such as alcohols, the zwitterion abstracts the proton from the alcohol to generate an alkoxide,

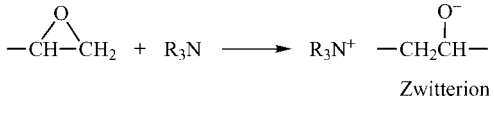

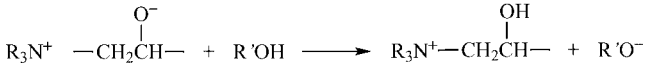

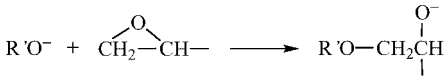

which further reacts with an epoxide group. Chain propagation continues by way of a polymeric anion mechanism.

(2) With more acidic hydrogen donors such as benzyl alcohol, phenols, or mercaptans, the tertiary amine acts as a co-curing agent by first abstracting the proton from the hydrogen donor:

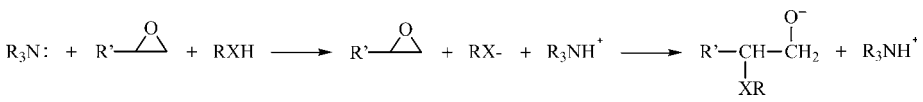

(3) With anhydrides, the catalyst facilitates the anhydride ring opening:

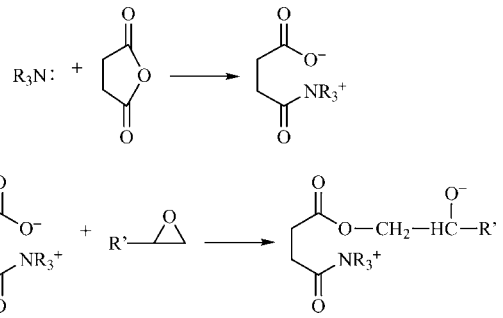

Commonly used tertiary amines include 2-dimethylaminomethylphenol (DMAMP) and 2,4,6-tris(dimethylaminomethyl)phenol (TDMAMP, trade name DMP-30 of Rohm and Haas), which contain built-in phenolic hydroxyl groups and can be used as a good catalysts and co-curing agents for room temperature cure of epoxies.

The rate of cure of epoxy resins with tertiary amines depends primarily upon the extent to which the nitrogen is sterically blocked. The homopolymerization reaction depends on the temperature as well as the concentration and type of tertiary amine. Benzyldimethylamine (BDMA) and TDMAMP are mainly used as accelerators for other curing agents, in the curing of anhydride- and dicyandiamide-based systems. Other tertiary amine catalysts include 1,4-diazabicyclo(2,2,2)octane (DABCO) and diazabicycloundecene (DBU).

Imidazoles such as 2-methylimidazole (2-MI) and 2-phenylimidazole (2-PI) contain both a cyclic secondary and a tertiary amine functional groups and are used as catalysts, catalytic curing agents, and accelerators (124,125). They are widely used as catalysts for DICY-cured epoxies in electrical laminates. For powder coatings, 2-MI adducts of LER are often used to facilitate dispersion of the components in powder coating formulations and to enhance shelf-life. Other modified imidazoles are also commercially available. The main advantage of imidazoles is the excellent balance of pot life and fast cure. 2-PI is used to increase T_g and thermal resistance.

Cyclic amidines such as 2-phenylimidazoline have also been used as a catalyst and co-curing agent in epoxy–polyester and epoxy powder coatings.

Substituted ureas are another group of epoxy nucleophilic catalytic curing agent, derived by blocking of isocyanates with dimethylamine. They are commonly used as catalysts for DICY cure of epoxies in adhesives, prepregs, and structural laminates. The ureas exhibit outstanding latency at room temperature and are widely used in one-pack adhesives. The catalytic mechanism of ureas is not well understood, but it has been postulated that DICY assists in deblocking of the urea to generate a tertiary amine, which in turns acts as epoxy curing catalyst. Commercially important substituted ureas are 3-phenyl-1,1-dimethyl urea (Amicure UR by Air Products), a reaction product of phenyl isocyanate with dimethylamine; and Amicure UR 2T, a reaction product of toluene diisocyanate (TDI) with dimethylamine.

Quaternary phosphonium salts such as the tetraalkyl and alkyltriphenylphosphonium halides have been used as fast catalysts for curing of phenolics, carboxylic acid-terminated polyesters, or anhydrides with epoxies (126). Used in powder coatings, they showed good latency and fast cure rates at moderate temperatures.

Air Products is a major epoxy catalyst supplier. Others include Huntsman, Cognis, and SKW Chemicals.

Lewis Acids. Lewis acids, eg, boron trihalides, contain an empty outer orbital and therefore seek reaction with areas of high electron density. Boron trifluoride, BF_3, a corrosive gas, reacts easily with epoxy resins, causing gelation within a few minutes. Complexation of boron trihalides with amines enhances the curing action. Reasonable pot lives using these complexes can be achieved because elevated temperatures are required for cure. Reactivity is controlled by the choices of the halide and the amine. The amine choice also affects other properties such as solubility in resin and moisture-sensitivity. Boron trifluoride monoethylamine ($BF_3 \cdot NH_2C_2H_5$), a crystalline material which is a commonly used catalyst, cures epoxy resins at 80–100°C. A chloride version is also commercially available. Other Lewis acids used in epoxy curing include stannic chloride and tin octanate.

Different mechanisms have been proposed for curing epoxy resins with BF_3 complexes or salts. In general, it is assumed that complexation with the oxirane oxygen is involved, facilitating proton transfer and ether formation. Thermal dissociation of the BF_3–amine complex may form a proton that further reacts with the epoxy group to initiate the curing process (127). Another mechanism assumes an amine adduct or salt is solvated by the epoxy groups, resulting in an oxonium ion (128). The curing reaction is initiated and propagated by attack of other epoxy groups on the oxonium ion.

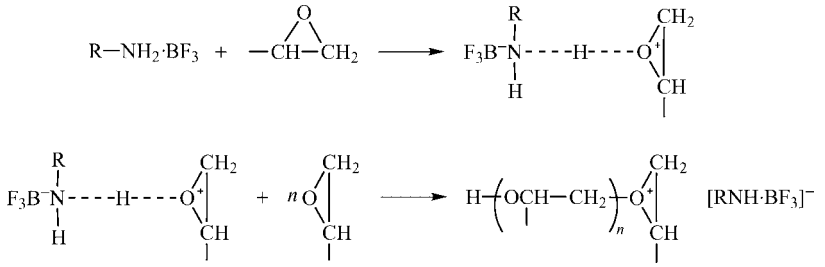

Photoinitiated Cationic Cure. Photoinitiated cationic curing of epoxy resins is a rapidly growing method for the application of coatings from solvent-free or high solids systems. This technology allows the formulation of epoxy coatings and adhesives with essentially "infinite" shelf life, but almost "instantaneous" cure rates. Cycloaliphatic epoxies are widely cured using photoinitiated cationic initiators.

Photoinitiators used for epoxy curing include aryldiazonium salts ($ArN_2^+X^-$), diaryliodonium salts ($Ar_2I^+X^-$), and onium salts of Group VIa elements, especially salts of positively charged sulfur ($Ar_3S^+X^-$). The anions must be of low nucleophilicity, such as tetrafluoroborates or hexafluorophosphates, to promote polymer chain growth rather than chain termination. Upon UV irradiation,

photoinitiators yield a "super" acid, which polymerizes the epoxy resins by a conventional electrophilic mechanism.

The photolysis of diaryliodonium and triarylsulfonium salts may proceed via formation of a radical cation, which abstracts a hydrogen atom from a suitable donor.

$$Ar_3S^+\ PF_6^- \xrightarrow{UV} Ar_2S^{+\cdot} + Ar\cdot + PF_6^-$$

$$Ar_2S^{+\cdot} + R{-}H \longrightarrow Ar_2SH^+ + R\cdot$$

$$Ar_2SH^+ + PF_6^- \rightleftharpoons Ar_2S + HPF_6$$

Subsequent loss of a proton yields the Brønsted acid HPF_6. Catalytic curing of the epoxy resin proceeds through an onium intermediate:

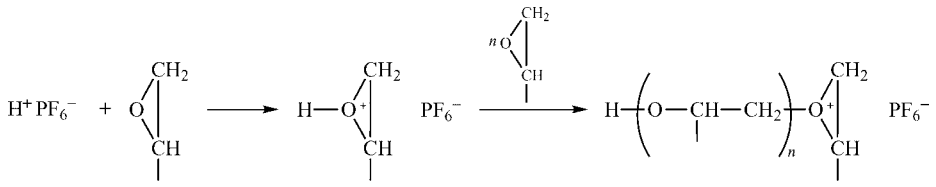

In the presence of triarylsulfonium and diaryliodonium salts, polymerization continues even if UV irradiation is terminated. This phenomenon is called "dark cure" and is due to the "living" nature of the "superacid" generated cation. The cure regime can be thought of as UV-initiated but "thermally cured." Thermally initiated cationic catalysts are also available (129).

In contrast, dialkylphenacyl sulfonium salts undergo reversible dissociation upon photolysis with formation of an ylid and a Brønsted acid. Cessation of UV activation results in termination of epoxy homopolymerization, since the acid is consumed in a reverse reaction with the ylid.

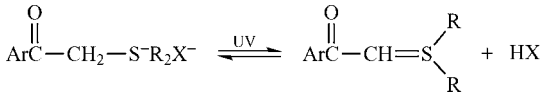

This type of behavior provides a means of controlling the degree of cure. Dialkylphenacyl sulfonium salts are thermally stable in epoxy resins at room temperature and up to 150°C for 1–2 h. Significant interest in thermal cationic cure of epoxies, especially cycloaliphatic epoxies, has developed (130).

Formulation Development With Epoxy Resins

The most important step in using epoxy resins is to develop the appropriate epoxy formulation since most are used as precursors to a three-dimensional cross-linked network. With the exception of the very high MW phenoxy resins and the epoxy-based thermoplastics, epoxy resin is rarely used by itself. It is usually formulated with modifiers such as fillers and used in composite structures with glass fiber or

metal substrates (coatings). To design a successful epoxy formulation that will give optimum *processability* and *performance*, the following factors must be carefully considered:

(1) Selection of the proper combination of epoxy resin(s) and curing agent(s) structures
(2) Epoxy/Curing agent stoichiometric ratio
(3) Selection of catalyst/accelerator
(4) Curing/post-curing processes and conditions
(5) Formulation modifiers such as fillers, diluents, toughening agents, etc
(6) Interactions among the formulation ingredients and with the composite materials (fibers, metals, etc) on the system chemistry, adhesion, rheology, morphology, and performance

The development of an epoxy formulation containing a high number of components can be very resource and time-consuming. Techniques such as design of experiments (DOE) are useful tools to facilitate the formulation development process and to obtain optimum performance (131,132). Future developments should include application of high throughput techniques to epoxy formulation development and optimization.

Relationship Between Cured Epoxy Resin Structure and Properties. The following diagram illustrates the formation of cured epoxy networks using different ratios of a difunctional epoxy and a tetrafunctional hardener. The structures formed are significantly different, depending on the ratio used. Consequently, it is expected that performance of these networks will be quite different despite the fact that they are derived from identical building blocks (Fig. 5).

The structure between the cross-linking position and the distance between any two of these points are important characteristics. *Molecular weight between cross-links* (M_c) and *cross-link* density are terms developed to describe "distance" between cross-link points. The concept originated with the rubber elasticity theory developed for the lightly cross-linked elastomers and has been adopted for use with epoxy thermosets with mixed success (133,134). The cured epoxy system derives its properties mostly from a combination of cross-link density, monomer structure and the curing process. The two-dimensional schematic network structures do not represent spatial reality but have been devised to help understand the nature of the various structures (135). A good understanding of the structure/property relationship is critical in designing the appropriate epoxy/curing agent combination. For example, cross-linking with dicarboxylic anhydrides yields polyesters that are resistant to oxidation, but less so to moisture, especially in the presence of basic components. Amine cross-linked systems are resistant to saponification but not to oxidation. There is a large body of specific structure/property relationship knowledge in the epoxy industry and literature, but only a few systematic treatments are available (136–138).

Cross-link density increases with degree of cure up to its limit at full conversion of the (limiting) functional groups. The curing temperature and process strongly influence cross-link density, molecular architecture, network morphology, residual stress, and the ultimate performance. The effects of degree of cure

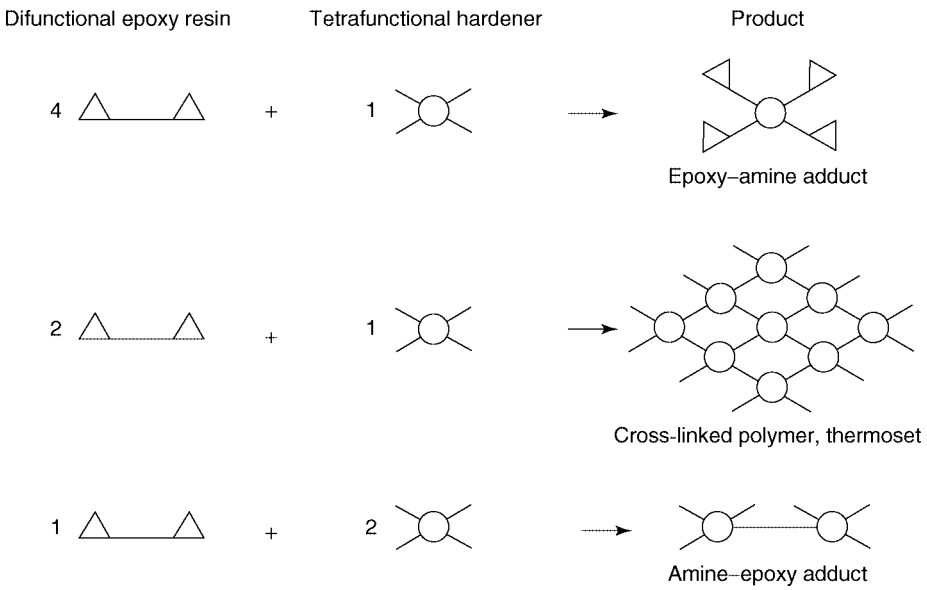

Fig. 5. Formation of resin–hardener networks.

and subsequent cross-link density on the chemical resistance of a cured DGEBA–aromatic polyamine adduct system are depicted in Figure 6. The increase in chemical resistance properties after post-cure also demonstrates the effects of increased cross-link density. The cross-link density of a cured epoxy system can be estimated by a number of different techniques as described in the characterization of cured epoxy section.

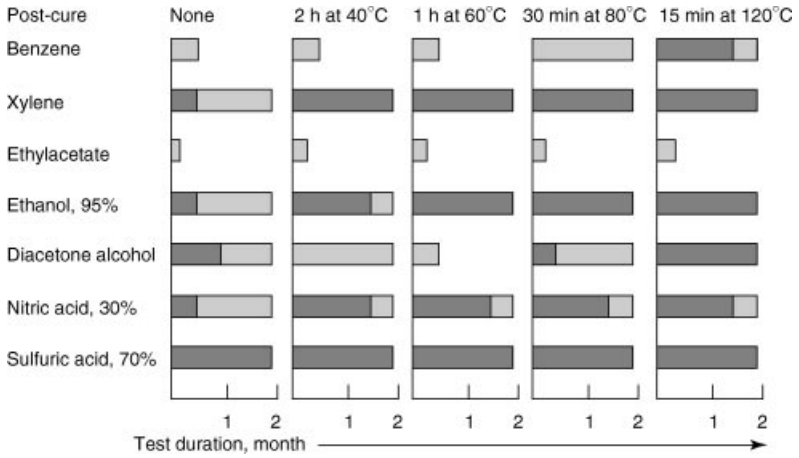

Fig. 6. Chemical resistance of a DGEBA–aromatic polyamine adduct. Post-cured substrate: sandblasted mild steel; film thickness: 300–350 μm; cure: 7 d at 20°C. ▭ Degraded; ■ resistant.

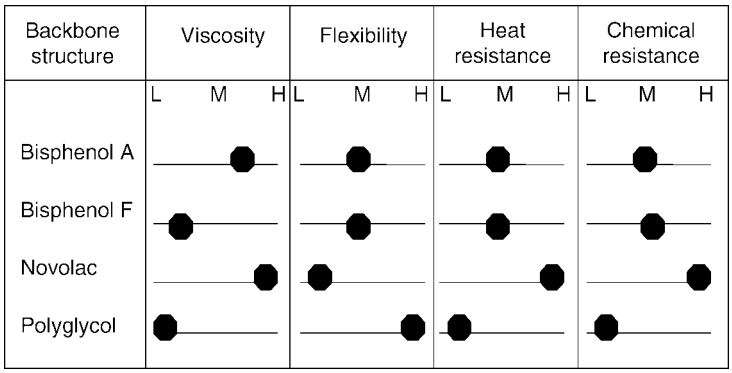

Fig. 7. Comparison of relative properties of common epoxy resins. L, low; M, medium; H, high.

Selection of Epoxy Resins. Successful performance of epoxy-based systems depends on proper selection and formulation of components. The components that have the most significant influences are the epoxy resins and the curing agents. As discussed in earlier sections, there are numerous choices of epoxy resins and curing agents presenting a wide variety of structure and functionality. Figure 7 shows the general attributes of common types of epoxy resins.

Epoxy resins can be used separately or in combination, such that formulations can be designed to take advantage of the desirable characteristics of several components. Because combining resins from different families can result in certain trade-offs, a careful balance of components should be investigated to produce optimal performance for specific applications. Table 18 shows effects of different resin backbones on cured properties with formulations based on hexahydrophthalic anhydride as curing agent.

The difunctional DGEBA resins are offered commercially in a wide range of molecular weights. As the molecular weight increases, so does the chain length between the epoxy end groups. Table 5 shows the effects of increasing EEW and MW of bisphenol A based epoxy resins on resin properties. The cross-link density of a difunctional resin cured by way of the epoxy group decreases as the resin molecular weight increases. High molecular weight resins are frequently cured via the secondary hydroxyl group, chemistry that results in a different set of structure–property relationships.

Multifunctional epoxy resins are available with functionalities ranging from above 2 to about 5. When cured to the same degree using a given curing agent at stoichiometric ratios, they produce a higher cross-link density, higher glass-transition temperature, better thermal and chemical resistances compared with difunctional epoxy resins.

Selection of Curing Agents. The selection of curing agents is just as critical as the selection of resins. As discussed in the Curing Agents section, there are numerous types of chemical reagents that can react with epoxy resins. Since coreactive curing agents become part of the network structure, careful consideration must be paid to their contributions. Besides affecting viscosity and reactivity of

the formulation, curing agents determine both the types of chemical bonds formed and the functionality of the cross-link junctions that are formed. Table 18 show performance examples of a liquid epoxy resin cured with different curing agents. Several authors have attempted to rationalize the curing agent selection process for different applications (106,139).

The effect of hardener structure on heat resistance of a cross-linked DGEBA resin is shown in Table 19 (140). Thermal stability is affected by the structure of the hardener. The heat resistance of aliphatic amine cured epoxy is low as measured by TGA. The nitrogen atoms are oxidized by atmospheric oxygen to amine oxides, which attack the polymer backbone. Anhydride systems tend to split off the anhydride at temperatures well below their decomposition point at about 390°C. The ether segments formed by 2-MI and phenolic cured epoxies have the highest thermal stability.

Epoxy/Curing Agent Stoichiometric Ratios. In addition to the choices of epoxy resins and curing agents, the stoichiometric ratio of epoxy/curing agent is another factor that has significant effects on the network structure and performance. A variety of products are obtained from different ratios. Network formations for a difunctional epoxy resin and a tetrafunctional amine are illustrated in Figure 5. The products range from an epoxy–amine adduct with excess epoxy to an amine–epoxy adduct with excess amine.

Theoretically, a cross-linked thermoset polymer structure is obtained when equimolar quantities of resin and hardener are combined. However, in practical applications, epoxy formulations are optimized for *performance* rather than to complete stoichiometric cures. This is especially true when curing of high MW epoxy resins through the hydroxyl groups.

In primary and secondary amines cured systems, normally the hardener is used in near stoichiometric ratio. Because the tertiary amine formed in the reaction has a catalytic effect on reactions of epoxy with co-produced secondary alcohols, slightly less than the theoretical amounts should be used. However, if substantially less than the theoretical amount of amine is used, the epoxy resin will not cure completely unless heat is applied (post-cure). The use of excess amine will result in unreacted amine terminated dangling chain ends and reduced cross-linking, yielding a polymer that can be somewhat tougher but which is considerably more susceptible to attack by moisture and chemicals. In formulations containing anhydrides, less than stoichiometric ratios of curing agents normally are used (0.50 to 0.85 of anhydride to 1 epoxy stoichiometric ratio) because of significant epoxy homopolymerization.

Ladder studies are often conducted varying the stoichiometric ratios and other factors to determine the optimum formulations. Statistical design of experiment (DOE) methodology has been used to efficiently carry out ladder studies (141). Information concerning network structures can be obtained using dynamic mechanical analysis (DMA) (142,143) and chemorheology to guide formulation development (144,145).

Catalysts. The choice of a catalyst and of its amount is important. As discussed in previous sections, some tertiary amine catalysts can play multiple roles in the curing reaction. Anhydride cure in particular is highly sensitive to catalyst amount. Nucleophilic catalysts, used with acidic curing agents such as

Table 18. Typical Properties, Chemical Resistance, and Thermal Degradation of Liquid DGEBA Resin (185 EEW) Cured With Common Hardeners (Dow Chemical Data)

	Curing agent				
	TETA[a]	MDA[b]	Polyamide[c]	Anhydride[d]	BF_3–MEA[e]
Property					
phr[f]	13	26	43	87.5	3
Formulation viscosity, Pa · s[g] (°C)	2.25 (25)	0.110 (70)	1.25 (50)	0.038 (80)	0.040 (100)
Cure schedule, h (°C)	16 (25) 3 (100)	16 (55) 2 (125) 2 (175)	16 (25) 3 (100)	4 (100) 4 (165) 16 (200)	4 (100) 16 (150)
Heat distortion temperature, °C	111	160	101	156	168
Strength, MPa[h]					
Compression	112	116	85.6	126	114
Flexural	96	93	67	97	100
Tensile	79	70.4	57.3	69	39.4
Modulus, GPa[i]					
Compression	3.05	2.6	2.6	3.04	2.3
Flexural	3.05	2.7	2.14	3.05	3.1
Textile elongation,%	4.4	4.4	3.9	2.5	1.6
Dielectric constant at 10^3 Hz	3.90	4.06	3.19	3.14	3.45
Dissipation factor at 10^3 Hz	0.020	0.015	0.0070	0.0054	0.0053
Resistivity at 25°C, 10^{-17} Ω · m					
Volume	6.1	12.2	12.2	6.1	8.6
Surface	7.8	>7.9	5.5	>7.3	>7.9
Chemical resistance					
% Weight gain after 28 d					
50% NaOH	0.04	−0.05	0.07	−0.12	−0.02
30% H_2SO_4	1.8	1.6	1.9	0.83	1.1
Acetone	2.1	4.6	7.3	15.0	1.2
Toluene	0.07	0.13	3.7	0.09	0.17
Water	0.86	1.1	1.3	0.82	1.2
Thermal degradation					
% Weight loss after 300 h at 210°C	6.8	5.5	5.0	1.5	4.9

[a] Triethylenetetramine.
[b] 4,4′-Methylenedianiline.
[c] Versamide 140 (Henkel Corp.).
[d] Methylbicyclo[2.2.1]heptene-2,3-dicarboxylic anhydride catalyzed with 1.5 phr benzyldimethylamine.
[e] Methylethylamine.
[f] Parts per hundred epoxy resin.
[g] To convert Pa · s to P, multiply by 10.
[h] To convert MPa to psi multiply by 145.
[i] To convert GPa to psi, multiply by 145,000.

Table 19. Effect of Hardener Structure on Reactivity and Heat Resistance of a Cross-Linked Bisphenol A Diglycidyl Ether

Curing agent	T_{rmax}, °C	E_a, J/mol[a]	TGA, 4°C/min: Weight loss before decomposition	TGA, 4°C/min: T_{dec}, °C
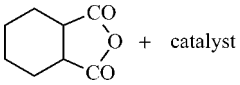	125	92	12	392
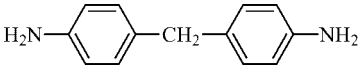	154	50	0	390
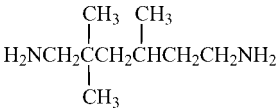	90	58		320
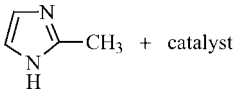	126	67	3.2	420
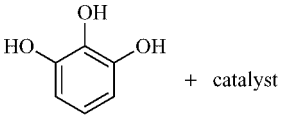	185	54	2.9	400
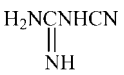	207	125	0	373

[a] To convert J to cal, divide by 4.184.

anhydrides and novolacs, can greatly reduce the gel time. In the case of anhydrides, a nucleophilic catalyst attacks the anhydride ring, causing the ring to open and promote bonding to the epoxy ring. Figure 8 shows the effect of BDMA and 1-propylimidazole levels on the pot life of a system combining D.E.R. 331 resin and nadic methyl anhydride at 90°C (194°F) (146). Imidazoles are more efficient accelerators than tertiary amines; only half the concentration is required to produce the same catalytic effect.

Accelerators. Accelerators are commonly added to epoxy systems to speed up curing. This term should be used to describe compounds which increase the rate of catalyzed reactions but which by themselves are not catalysts. However, the term *accelerator* is often used synonymously with *catalyst* in some of the literature. Hydrogen donors such as hydroxyl groups facilitate epoxy reactions via hydrogen bonding or reaction with the oxygen on the epoxide ring. More acidic donors such as phenols and benzyl alcohols increase the rate of acceleration. However, very strong acids can interfere with amine curing agents by protonation of the amine to form an amine salt, resulting in increased pot life. Figure 9 shows the effects of different accelerators on the rate of a DGEBA/triethylenetriamine formulation.

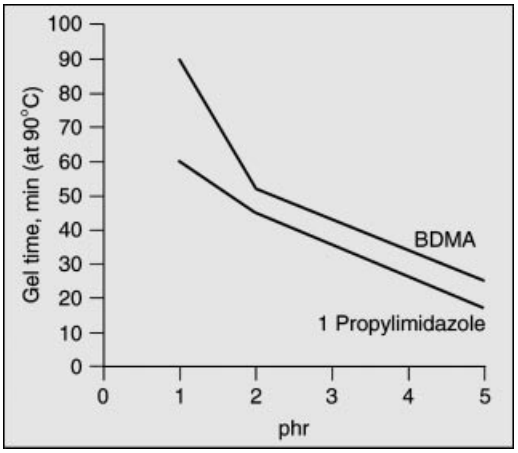

Fig. 8. Effects of accelerator on epoxy/nadic methyl anhydride cure.

Epoxy Curing Process

The epoxy curing process is an important factor affecting the cured epoxy performance. Consequently, it is imperative to understand the curing process and its kinetics to design the proper cure schedule to obtain optimum network structure and performance. Excellent reviews on this topic are available in the literature (147,148).

The curing of a thermoset epoxy resin can be expressed in terms of a time–temperature-transformation (TTT) diagram (Fig. 10) (149,150). Later, a CTP (cure-temperature–property) diagram was proposed as a modification of the TTT diagram (151). For nonisothermal cure, the conversion-temperature-transformation (CTT) diagram has been shown to be quite useful (152). In the TTT diagram, the time to gellation and vitrification is plotted as a function of

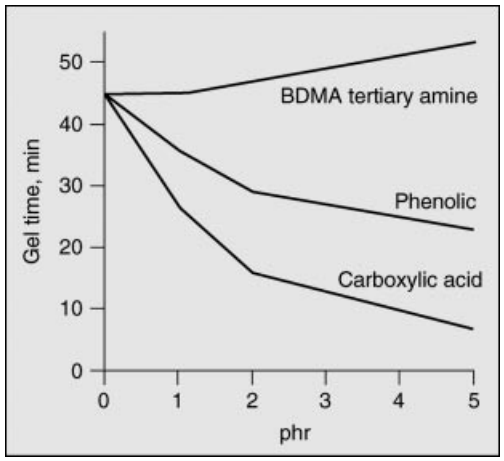

Fig. 9. Effects of accelerator on epoxy/triethylene triamine cure.

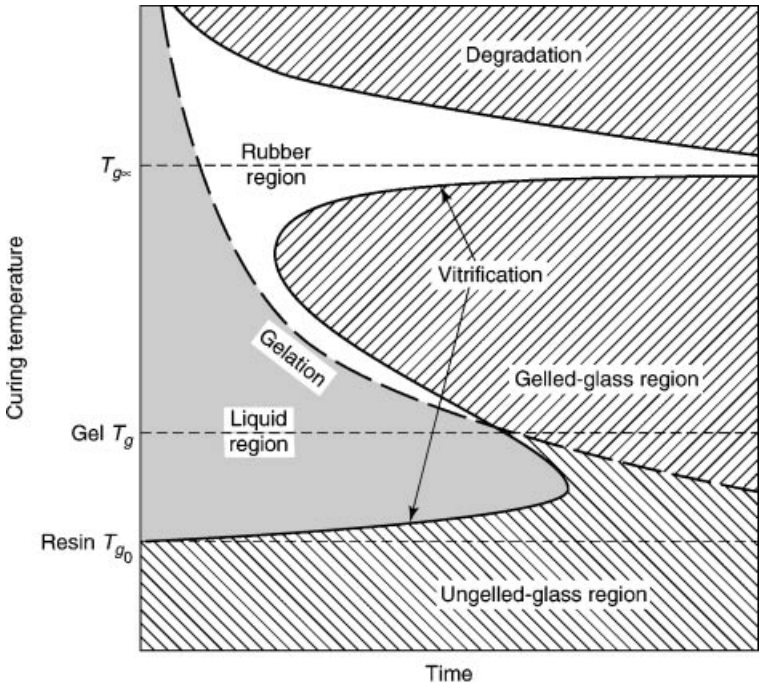

Fig. 10. Time–temperature-transformation diagram.

isothermal cure temperature. Important features are the gel point and the onset of vitrification. The gel point (qv) is defined as the onset of the formation of insoluble, cross-linked polymer (gel fraction) in the reaction mixture. However, a portion of the sample may still be soluble (sol fraction). The onset of vitrification is when the glass-transition temperature (T_g) of the curing sample approaches the curing temperature T_c. Ideally, a useful structural thermoset would cure until all monomers are built into the network, resulting in no soluble fraction.

The S-shaped vitrification curve and the gelation curve divide the time–temperature plot into four distinct states of the thermosetting-cure process: liquid, gelled rubber, ungelled glass, and gelled glass. T_{g0} is the glass-transition temperature of the unreacted resin mixture; $T_{g\infty}$ the glass-transition temperature of the fully cured resin; and gel T_g the point where the vitrification and gellation curves intersect.

In the early stages of cure prior to gelation or vitrification, the epoxy curing reactions are kinetically controlled. When vitrification occurs the reaction is diffusion controlled, and the reaction rate is orders of magnitude below that in the liquid region. With further cross-linking of the glass, the reaction rate continues to decrease and is eventually quenched. In the region between gelation and vitrification (rubber region) the reaction can range from kinetic to diffusion control. This competition causes the minimum in vitrification temperature seen in the TTT diagram between gel T_g and $T_{g\infty}$. As the cure temperature is raised the reaction rate increases and the time to vitrification decreases until the decrease in diffusion begins to overcome the increased kinetic reaction rate. Eventually,

slower diffusion in the rubbery region decreases the overall reaction rate and thus the increase in time to vitrify is seen. Below $T_{g\infty}$, the reaction does not go to completion. As curing proceeds, the viscosity of the system increases as a result of increasing molecular weight, and the reaction becomes diffusion-controlled and eventually is quenched as the material vitrifies (153). After quenching, the cure conversion can be increased by raising the temperature. This is often practiced as post-cure for certain epoxy systems to achieve maximum cure and performance. Post-cure is only effective at temperatures higher than $T_{g\infty}$. However, it must be noted that at temperatures sufficiently above $T_{g\infty}$, onset of network degradation can also be seen if sufficient time is involved. Thus one must be careful about potential "over-curing."

The TTT diagram is useful in understanding the cure kinetics, conversion, gelation, and vitrification of the curing thermoset. Gelation and vitrification times can be determined from the intersections of the storage and loss moduli and the maxima in the loss modulus of an isothermal dynamic mechanical spectrum, respectively. Recently, techniques have been developed using rheological and dynamic mechanical analysis instruments to determine the gel point and vitrification (154). Understanding the gelation and vitrification characteristics of an epoxy/curing agent system is critical in developing the proper cure schedule/process to achieve optimum performance.

One important application is the management of cure temperatures (T_c) and heating rate: if T is too low, vitrification may occur before gelation and further reactions may not be completed, resulting in an incomplete network structure and poor performance. This is of particular relevance in ambient cures and radiation cures (155). Furthermore, attention must be paid to the relationship between mixing of reactants and gel point. Epoxy resins and curing agents must be thoroughly mixed prior to the gel point since the rapid viscosity buildup at gel point inhibits homogeneous mixing of reactants, resulting in potential network and morphological inhomogeneities and defects (156).

Curing and quenching processes of epoxies have been reported to affect performance of certain epoxy coatings and composites. These effects have been attributed to phenomena known as internal or residual stress and physical aging of cured epoxies (147).

Internal stresses arise mainly because of the diminishing capacity of the cross-linked polymer to expand or contract to the same extent (volume) with the solid substrate to which it is adhered. This phenomenon is caused by mismatches of coefficients of thermal expansion (CTE) of the substrates (metal, glass, etc) and the cross-linked epoxies during nonisothermal cures; and cure shrinkage (solvent loss, cross-linking). The effect often contributes to adhesion failures and is more prominent in metal coatings and large composite parts manufacturing, especially when the T_g of the cross-linking polymer approaches T_c. As discussed previously, while curing of epoxy functional groups via polycondensation reaction results in relatively low shrinkage, failures attributable to internal stresses such as delamination have been observed in certain epoxy coatings of metal substrates, epoxy encapsulants for electronic devices and glass-fiber-reinforced composites (157). The effect can be very severe in the case of photoinitiated curing of epoxy acrylates as well as free-radical curing of epoxy vinyl esters. Shorter bonds are formed during these free-radical curing processes, which result in significant shrinkage.

Post-cure with heat is often required to release some of the internal stresses and to improve adhesion. Efforts have been focused on understanding the mechanism of stress development, and stress minimization by modifications of the cure and post-cure cycles (158).

Physical aging is a well-known phenomenon in glassy polymers and has been studied quite extensively in amorphous thermoplastics (see AGING, PHYSICAL; AMORPHOUS POLYMERS) (159). The term *physical aging* refers to the gradual changes in polymer physical properties with time after a glassy polymer is heated above its T_g and rapidly cooled (quenching) to temperatures below T_g. The physical aging process differs from chemical aging processes, in which breakage or formation of chemical bonds are involved such as continuing cure, hydrolytic aging, and photochemical and thermal degradation. The phenomenon has been attributed to the nonequlibrium state of the glassy polymer at temperatures below its T_g, in which the polymer contains excessive free volume as it is quenched. As the polymer recovers gradually over time to approach equilibrium, a reduction in free volume and an increase in density results. Consequently, the term *densification* is sometimes used to describe physical aging. For certain epoxy systems, physical aging has been reported to cause increases in stiffness and decreases of toughness (160,161). Hardening of certain baked epoxy coatings with time and failures of the coatings due to loss of ductility have been observed. However, physical aging has been reported to be reversible (erasable) by post-heating above polymer T_g. Proper selection of the cure and post-cure schedules including quenching cycle is important to minimize the potential detrimental effects of physical aging (162). In some epoxy systems, it is difficult to distinguish physical aging from the effects of residual solvent loss and/or continuing cross-linking. They all can contribute to increases in stiffness of the system.

To develop a proper curing process, it is important to understand the reactivity of different curing agents toward the epoxy structure of interest. The effect of hardener structure on reactivity of a cross-linked DGEBA resin (determined by DSC) is shown in Table 19. Aliphatic amines show a maximum reaction rate, called T, at 90°C (heating rate 10°C/min). The same epoxy resin is somewhat less reactive ($T_{rmax} = 126$°C) when homopolymerized via initiators. Aromatic amines and phenols cure considerably more slowly, requiring higher curing temperatures. The highest temperatures are required for dicyandiamide curing, which can, however, be accelerated by basic components.

Relative reaction rates are often expressed in terms of the activation energy E_a (Arrhenius type relationship). E_a allows comparisons of reaction rates at different temperatures and is influenced by the type of chemical reactions involved in the cure. Curing of epoxy resins with phenols or aromatic and aliphatic amines proceeds with a fairly low activation energy of 50–58.5 kJ/mol (12–14 kcal/mol). Activation energies are higher when epoxy compounds having low hydroxyl content are cured alone in the presence of catalysts (92 kJ/mol = 22 kcal/mol) or with dicyandiamide (125.5 kJ/mol = 30 kcal/mol).

Characterization of Epoxy Curing and Cured Networks. Cured thermoset polymers are more difficult to analyze than thermoplastics since they are insoluble and generally intractable. Their properties are influenced by factors at the molecular level, such as backbone structures of epoxy resin and curing agent; nature of the covalent bond developed between the epoxy resin and the curing

agent during cross-linking; and density and extent of cross-linking, ie, degree of cure.

Epoxy resin formulators are concerned with formulation reactivity and flow during application. Reactivity tests or gel time tests are used to determine the proper reactivity of the formulations. Formulators also developed flow tests to check for the formulation rheology profile. The coatings industry widely uses MEK (methyl ethyl ketone) double rubs as an indication of cure. While the test does give a relative indication of cure for a certain system, caution must be exercised when comparing different systems, which may have very different inherent resistance against MEK. In general, these end-use tests do not provide insights on the structure–property relationship of the system.

Epoxy curing process can be monitored by a number of different techniques:

(1) Analysis of the disappearance and/or formation of functional groups
(2) Indirect estimation of cure conversion
(3) Measurements of changes in thermal, physical, and mechanical properties of the system

Comprehensive reviews of different techniques for epoxy cure monitoring are available (86,94). Wet chemical or physical analysis methods, such as solvent swell (163), titration of functional groups, IR, near IR (164), or NMR spectroscopy, are commonly used to monitor epoxy cure.

The thermal properties of the system reflect the degree of cure, and Thermal Analysis (qv) (DSC, DMA, TGA) has been used extensively in studies of epoxy resins (156). Correlation between T_g and degree of cure has been well established for many systems.

Viscosity build is observed with increased reaction conversion in epoxy curing. More recently, chemorheology, which utilizes rheological measurement (qv) and thermal analysis such as DSC, has been applied to study epoxy cure (166,167).

Since epoxy curing involves epoxy ring opening and the generation of polar groups, which have a high dipole moment, dielectric measurements have been applied to monitor cures. Dielectric methods (168,169) encompass both macroscopic and microscopic features: the dipoles being oriented during dielectric measurements are on a microscopic scale, whereas the degree and rate of orientation may depend on macroscopic properties such as viscosity and density.

The mechanical properties of a resin system can also be used to estimate the degree of cure (170). The methods range from hardness (qv) evaluation to complex static measurements or sensitive dynamic mechanical analysis (qv) (DMA). Table 20 gives ASTM standard procedures for measuring the properties of cured or partially cured epoxy resin systems.

Direct measurement of the cross-link density of thermoset polymers including those from epoxy resins remains one of the most difficult analytical challenges in the field. A far too common approach simply relates the rubbery modulus (G_r), the thermoset modulus above T_g, to the molecular weight between cross-links (M_c) using the theory of rubbery elasticity (133,134). Unfortunately thermoset networks have much more complex features than do true elastomers, including non-Gaussian chain behavior, interchain interactions, and entanglements (172).

Table 20. ASTM[a] Procedures for Cured or Partially Cured Epoxy Resin Systems

Test	ASTM standard
Chemical	
Density by displacement	D792
Water absorption in plastics	D570
Moisture absorption properties in composites	D5229
Void content in composites	D2734
Electrical	
Volume resistivity	D257
Surface resistivity	D257
Dielectric strength	D149
Dielectric constant and dissipation factor	D150
Insulation resistance	D257
Thermal	
Heat-deflection temperature	D648
Glass-transition temperature	D696
Dynamic mechanical properties of plastics	D4065
Coefficient of thermal linear expansion	D296
Coefficient of linear thermal expansion by thermomechanical analysis	E831
Coefficient of thermal conductivity	C177
Mechanical	
Tensile strength	D638
Compressive strength (plastic)	D695
Compressive testing (composite)	D3410
Flexural strength	D790
Impact strength	D256
Fracture strength in cleavage of adhesives in bonded metal joints	D3433
Fracture strength in "T" peel of adhesives in bonded joints	903
Fracture testing in 180° peel of adhesives	D5528
Mode I interlaminar fracture toughness of composites	D2344
Apparent interlaminar shear strength of composites	D5045
Plane strain fracture toughness of plastics	D4255
On-plane shear response of composites	
Hardness, Barcol	D2583
Hardness, Rockwell M	D785

[a]From Ref. 171.

These factors render rubbery elasticity theory inadequate as an absolute measure of M_c from G_r, and doing so can lead to totally erroneous conclusions on the network structure (173). In a given family of thermosets, changes in G_r can be considered to reflect *relative* changes in M_c. Estimates of the expected M_c can be calculated from monomer MW and functionality for stochiometric systems (174). More extensive network structure calculations including M_c are done using statistical relations developed by Miller and Makosco (175).

In many applications, epoxy systems derive their high thermal and mechanical performance (qv) of plastics characteristics from highly cross-linked network structures. However, this often results in brittleness of the epoxy thermosets and loss of end-use properties such as impact resistance. Elongation at break (% elongation) has been a popular test used in the industry for many years to measure *toughness*, ability to resist failure under tensile stress. While useful in certain applications, good correlations between elongation at break and end-use properties of cured epoxies are not always possible. The failure envelope concept has been useful in looking at the entire time–temperature failure spectrum of epoxies (176). More recently, progress in the field of fracture mechanics (177,178) has led to advanced fracture toughness tests that are more useful in characterizing cured epoxy performance. Examples of such tests are critical elastic strain release rate (G_{IC}) and critical stress intensity factor (K_{IC}) (179).

Dynamic mechanical analysis (DMA) of cross-linked epoxy resins typically shows, in order of decreasing temperature, an α transition corresponding to T_g, a β transition associated with relaxation of the glyceryl groups, and a γ transition due to methylene group motions (180). Both the β and the γ transitions, which are typically observed at -30 to $-70^{\circ}C$ and at about $-140^{\circ}C$, respectively, are attributed to crankshaft motions of the polymer chain segments. The appearance of transitions between the α and β transitions is highly variable and has been attributed to segmental motions due to particular curing agents (181). No definitive correlations between the appearance of sub-T_g relaxations and mechanical properties have been observed (182). Like many other plastics, cross-linked epoxy resins undergo a change in fracture mechanism from brittle to ductile (T_b) with increasing temperature. The window between T_g and T_b has been shown to correlate well with the formability of epoxy can coatings in the draw-redraw (DRD) process (183,184).

Adhesion (qv) is an important issue in epoxy applications since epoxy is almost always used as part of a composite system. Examples are epoxy coatings on metal substrates, epoxy adhesives for metal surfaces, and matrix resin in fiber-reinforced composites such as PCB laminates and aerospace composites. Consequently, optimum epoxy adhesion to the substrate is a prerequisite for good system performance in terms of static and dynamic mechanical properties and environmental durability. In rubber-toughened composite systems, it has been reported that a threshold of interfacial adhesion between both phases (rubber and resin matrix) is needed for maximum toughening by promoting the cavitation mechanism and by activating the crack-bridging mechanism (185). Excellent review papers are available on the issue of adhesion of epoxy in composites (186), coatings, and adhesives (187). Effects of internal stresses on coating adhesion failures including the role of coating defects and pigments as potential stress concentrators have been reported (188).

Surface analysis such as dynamic contact angle and surface tension are used to ensure proper wetting of epoxy and the substrate. Microscopic techniques, such as scanning electron microscopy (SEM), transmission electron microscopy (TEM), and atomic force microscopy (AFM), are widely used to study morphology, fracture, and adhesion issues of cured epoxy systems. Chemical analysis techniques, such as micro-IR, X-ray photoelectron spectrometry (XPS), and secondary ion mass

spectrometry (SIMS), are useful in providing functional group analysis at the interfaces.

Consumers of products which use epoxy resins have developed increasing expectations for longer and more reliable performance. In automobiles, for example, the coating is expected to maintain its initial "Class A" finish for 10 years and the composite leaf spring is designed to last for the life of the vehicle. To meet these expectations, the long-term durability of epoxy thermosets is a key material-specific and application-specific consideration. The durability of polymeric materials in general depends on phenomena such as physical aging, environmental exposure (such as weathering), and mechanical experience (such as impact and load). A detailed discussion of this topic is beyond the scope of this review; interested readers are referred to a leading reference (189).

In addition, the processing of epoxy formulations into their final thermoset structure and form has a major effect on ultimate performance. Material properties such as rheology and reaction kinetics interplay with processing variables such as temperature and shear rate to affect key properties of extent of cure, orientation, and residual stress. Design of the final form of the material also should incorporate fundamental thermoset properties using finite element analysis methods. Optimization of any given epoxy thermoset application is therefore very specific to formulation, processing conditions, and final form and use of the material, and involves the contributions from chemistry, engineering, and material science disciplines to be fully successful.

Formulation Modifiers

The processing behavior (mainly viscosity and substrate wetting) and other properties of an epoxy system can be modified by diluents, fillers, toughening agents, thixotropic agents, etc. Most commercial epoxy resin systems contain modifying agents.

Diluents. Diluents affect the properties of the cured resin system and, in particular, lower the viscosity in order to improve handling and wetting characteristics. They are often used in the range of 2–20 wt% based on the epoxy resin. Diluents can be classified into *reactive* and *nonreactive* types.

The *reactive* diluents are products with low viscosity (1–500 cP at 25°C) used to lower the viscosity of standard epoxy formulations. The effect of reactive diluents on DGEBA viscosity is illustrated in Figure 10. Lower viscosity allows higher filler loading, lower costs, and/or improved processability. Because of the epoxy functionality, the diluents become part of the cured networks. However, the reactive diluents can negatively impact properties, and so balancing of viscosity reduction and property loss is an important consideration. Decreases in tensile strength, glass-transition temperature, chemical resistance, and electrical properties are usually observed. Toxicity is another concern, particularly the aromatic mono glycidyl ethers such as phenyl glycidyl ether (PGE) and *o*-cresol glycidyl ether (CGE). *n*-Butyl glycidyl ether (BGE) is one of the most efficient viscosity reducers, but it has been losing favor because of its volatility and noxiousness. Longer chain alkyls, polyfunctional or aromatic glycidyl ethers such as bisphenol F epoxy, neopentylglycol diglycidyl ether, and triglycidyl ether of propoxylated

glycerine are gaining popularity as epoxy reactive diluents. Cycloaliphatic epoxies and glycidyl esters of acids such as neodecanoic acid are also used as reactive diluents.

Acrylics such as 1,6-hexanediol diacrylate and trimethylolpropane triacrylate are nonepoxy multifunctional diluents, which react readily with primary and secondary amines by means of Michael addition of the the amine to the acrylic double bond (190). They have been used to increase cure speed or to lower cure temperature of epoxy–amine systems. Caprolactone acrylates have also been used for this application (191).

Solvents and plasticizers are *nonreactive* diluents. The most common nonreactive diluents are nonyl phenol, furfuryl alcohol, benzyl alcohol, and dibutyl phthalate. These materials have the advantage of being able to add to the amine side of the system to better balance mix ratios. Nonyl phenol and furfuryl alcohol also improve wet-out and accelerate cure slightly. They are also capable of reacting with the epoxy group under high temperature cure conditions. Benzyl alcohol is a popular diluent used with amine-cured systems. In addition to viscosity reduction, it is also known to increase cure speed. Benzyl alcohol can be used up to 10 wt% level without significant effects on cured properties. Dibutyl phthalate is widely used as a nonreactive diluent for liquid resins. However, performance properties will drop off more quickly with increasing levels of nonreactive diluents than with increasing levels of reactive diluents.

Aromatic hydrocarbons, such as toluene or xylene, significantly reduce the viscosity of liquid DGEBA resins, but their use can be accompanied by a 15–25% decrease in compressive yield strength and a 10–20% reduction in compressive modulus (Fig. 11). If the solvent is trapped in the cured system, solvent resistance is reduced and cracks develop if the resin is used in heat-cured castings. The use of solvents and reactive diluents in epoxy systems is reviewed in References 192 and 193.

Thixotropic Agents. *Thixotropy* is the tendency of certain colloidal gels to flow when subjected to shear, and then to return to a gel when at rest. A thixotropic gel can be produced through the addition of either high surface area fillers such as colloidal silicas and bentonite clays or of chemical additives. Thixotropy is desirable in applications such as encapsulation where the coating is applied by dipping. The resin will wet out and coat the object being dipped, but will not run off when the object is removed from the dipping bath.

Fillers. Fillers (qv) are incorporated in epoxy formulations to enhance or obtain specific desired properties in a system. The type and amount of filler used are determined by the specific properties desired. Fillers can also reduce the cost of epoxy formulations. Inert commercial fillers (qv) can be organic or inorganic, and spheroidal, granular, fibrous, or lamellar in shape. The properties of commercial fillers are given in Table 21, and some effects on epoxy resins are shown in Tables 22 and 23. Some formulations contain up to 90 wt% fillers. For certain applications, fillers can have significant effects on thermoset morphology, adhesion, and the resulting performance.

Filler loading is often limited for a given application by the maximum viscosity allowable and/or the reduction in some mechanical properties such as tensile and flexural strength in the cured material. Viscosity can be modified by heat or by addition of a reactive diluent; heating is preferred since diluents affect overall

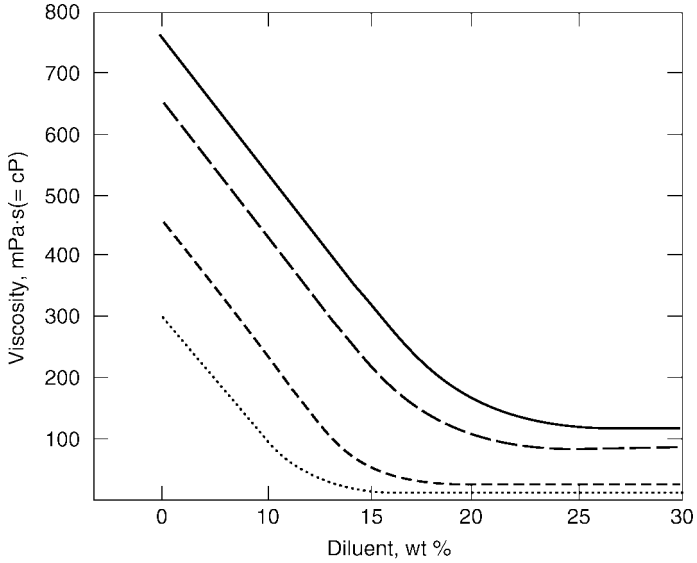

Fig. 11. Reduction of DGEBA viscosity by reactive diluents:——, *o*-cresol glycidyl ether; – – –, butanediol diglycidyl ether; ----------, C_{12}–C_{14} aliphatic glycidyl ether (Epoxide 8); ·····, *n*-butyl glycidyl ether.

system properties. Some of the major property enhancements affected by fillers are described below.

Pot life and exotherm. Fillers can increase pot life and lower exotherm of epoxy systems. Fillers reduce the reactant concentration in the formulation and act as a heat sink. Generally, they have higher heat capacities than the epoxy resins. They are also better heat conductors than the resins, and thus help to dissipate exotherm heat more readily. Commonly used fillers are silica, calcium carbonate, alumina, lithium aluminum silicate, and powdered metals.

Thermal shock resistance. Fillers help to increase thermal shock resistance and to decrease the thermal expansion coefficient of an epoxy system by replacing part of the resin with a material that does not change its volume as significantly with temperature variations. Such fillers are clay, alumina, wood flour, sawdust, silica, and mica. Epoxy molding compounds (EMC) can contain up to 90% of fused silica to manage the thermal stress experienced by the encapsulated semiconductors. Powdered metals are used when bonding metals together to better match the coefficient of thermal expansion of the bond with that of the metal, thus minimizing thermal stress.

Shrinkage. Using fillers as a partial replacement for a reactive resin that shrinks on curing can reduce shrinkage of the system. Any inert filler will decrease shrinkage, but the most commonly used are silica, calcium carbonate, alumina talc, powdered metals, and lithium aluminum silicate.

Machinability and abrasion resistance. The addition of fillers can increase the machinability and abrasion resistance of an epoxy resin system by

Table 21. Typical Properties of Fillers

Name	Composition	Particle shape	Surface area volume	Bulk density, kg/m^3	Characteristics and main use
Marble flour, dolomitic	Magnesium–calcium carbonate	Granular	Medium	1120–1300	General-purpose fillers, particularly recommended for castings requiring machining
Chalk powder	Precipitated calcium carbonate	Crystalline	High	800–880	
Sand	Quartz, feldspar, and subsidiary minerals	Spheroidal	Low	1500–1700	Bulk filler giving high compressive strength and abrasion resistance; difficult to machine
Silica flour	Ground quartz	Granular	Medium	1100–1150	Standard filler for large electrical castings; high abrasion resistance; difficult to machine
Mica flour	Muscovite[a]	Lamellar	High	300–400	Filler giving high crack resistance to castings exposed to mechanical and thermal shock
Slate powder	Slatea	Mainly lamellar	Medium	700–900	General-purpose filler giving high abrasion resistance; difficult to machine
Vermiculite[b]	Vermiculite[a]	Exfolidated laminae	High	100–150	Fillers giving lightweight bulk in cores or thick backing to increase the rigidity of thin sections
Phenolic microballoons	Phenolic resins	Hollow spheres	Medium	100–150	
Zircon flour	Zircon[a]	Granular	Medium	1700–1900	Filler giving high abrasion resistance; difficult to machine

Aluminum powder	Metallic aluminum	Granular	Medium	1000–1100	Filler imparting thermal conductivity, eg, to prevent excessive temperature buildup in electrical components or in tools for hot-forming plastics
Chopped glass strand[c]	Low alkali glass	Fibrous	Medium	100–250	Fillers improving the mechanical strength of prominent edges and thin sections
Hydrated aluminum oxide	Alumina trihydrate	Granular	Medium	700–1300	Filler improving wet and dry arc-track resistance and flame retardance

[a] Silicate.
[b] Grain size = 0.15–0.32 cm.
[c] Length = 0.60 cm.

Table 22. Effect of Fillers

Advantages	Disadvantages
Lower cost of product	Increased weight[a]
Reduced shrinkage upon curing	Loss of transparency
Decreased exothermic temperature rise on curing[a]	Tendency to entrap air
Increased thermal conductivity[a]	Difficulty of machining hard fillers
Reduced expansion and contraction with temperature change	Decreased impact and tensile strengths
Higher deflection temperature	Increased dielectric constanta and power factor[a]
Improved heat-aging properties[a]	
Reduced water absorption[a]	
Improved abrasion resistance[a]	
Increased surface hardness[a]	
Increased compressive strength[a] and Young's modulus[a]	
Increased electric strength[a]	

[a] Certain fillers, such as vermiculite and phenolic microballoons, have the reverse effect.

increasing the hardness of the thermoset. Greater hardness leads to a higher energy required to scratch but cleaner cuts upon machining. Fillers used for this purpose are powdered metals, wood flour, calcium carbonate, sawdust, clay, and talc.

Electrical conductivity. In certain applications, conducting fillers are added to epoxy formulations to reduce the good insulating properties of the epoxy systems. The most commonly used fillers are graphite and powdered metals.

Other properties that can be affected with the proper choice of fillers for a specific application include compressive strength, adhesion, arc and tracking resistance, density, and self-lubricating properties.

Epoxy Nanocomposites. Significant recent developments in polymer property enhancement involve polymer nanocomposites. This is a special class of fillers (mostly clay derivatives) in which the nanoscale, highly oriented particles are formed in the polymer matrix through monomer intercalation and particle aggregate exfoliation (see NANOCOMPOSITES, POLYMER-CLAY) (194,195). The objective is to combine the performance attributes of both hard inorganic and plastic materials. Significant efforts have been dedicated to develop epoxy nanocomposites in the past decade. Improvements in electrical and mechanical properties, chemical resistance, high temperature performance, and flame retardancy have been reported. Other silica-based organic hybrids have been developed (196) for military and aerospace applications.

The emerging field of nanotechnology has produced new materials such as the carbon nanotubes, which are filaments of carbon with atomic dimensions. Recent publications claimed exceptional property enhancement from nanotube-laced

Table 23 Influence of Filler on Epoxy Resin Properties[a]

Filler	Ease of dispersion	Antisettlin	Cost	Shrinkage	Exotherm	Thermal conductivity	Coefficient of expansion	Deflection	Weight	Machinability	Abrasion resistance	Impact strength	Tensile strength	Flexural strength	Compressive strength	Thixotropy	Dielectric constant	Power factor	Protection against		
																			Electric strength	Mineral acids	Caustic alkalies
Marble flour, dolomitic	P	N	–	–	–	+	–	+	+	O	O	–	–	–	+	O	+	O	O	– –	–
Chalk powder	N	·	–	–	–	+	–	O	+	O	O	– –	–	–	O	O	+	O	O	– –	–
Sand	P	N	– –	–	–	+	– –	+	+	–	+ +	–	O	O	+	O	+	+	+	O	O
Silica flour	·	N	–	–	–	+	– –	+	+	–	+ +	–	O	O	+ +	O	+	+	+	O	O
Mica flour	N	·	–	–	–	+	–	+	+	–	+	+	O	–	O	O	+	+	+	O	O
Slate powder	P	N	–	–	–	+	–	+	+	–	+ +	–	O	O	+	O	+	+	+	O	O
Vermiculite	N	P	– –	O	+	–	O	O	– –	+	– –	– –	– –	– –	– –	O	–	–	– –	[b]	[b]
Phenolic microballoons	P	P	– –	O	+	–	O	O	– –	+ +	– –	– –	– –	– –	– –	O	–	–	– –	[b]	[b]
Zircon flour	P	N	–	–	–	+	– –	+	– +	– –	+ +	–	O	O	+	O	+	+	O	O	O
Aluminum powder	P	N	O	–	–	+ +	–	+	+	+	–	–	O	O	+	O	+ +	O	– –	–	–
Chopped glass strand	N	P	O	–	–	+	–	+	+	–	+	+	+	+	+	O	+	+	O	O	O
Hydrated aluminum oxide	N	P	–	–	–	+	–	+	+	O	O	– –	–	–	+	O	+	+	O	O	O

[a] Key: P = positive effect; N = negative effect; – = no significant effect; - = significant decrease; - - = large decrease; + = significant increase; + + = large increase; · = fillers taken for arbitrary standard for comparison of dispersibility and setting.

[b] Porosity of filler reduces protection provided by resin.

epoxy (hardness, electrical and heat-conducting properties) (197). However, cost remains a barrier for commercialization.

Toughening Agents and Flexiblizers. Some cross-linked, unmodified epoxy systems exhibit brittleness, poor flexibility, and low impact strength and fracture resistance. Modifiers can be used to remedy these shortcomings. However, there usually will be some sacrifices of properties. In general, there are two approaches used to modify epoxies to improve these features.

(1) *Flexiblization.* Aliphatic diepoxide reactive diluents enhance the flexibility or elongation by providing chain segments with greater free rotation between cross-links. Polyaminoamide hardeners, based on aliphatic polyamines and dimerized fatty acids, perform similarly. Liquid polysulfide polymers possessing terminal mercaptan functionality improve impact properties in conjunction with polyamine hardeners.
Flexible chain segments are incorporated in an epoxy resin by many means (189). One approach is the incorporation of oligomeric aliphatic polyesters containing carboxylic acid end groups, forming an epoxy resin adduct. This is one of the reasons that epoxy–polyester hybrid powder coatings have become very popular. The effects of flexiblizers are shown in Table 24. Flexiblization can enhance elongation of the system but is often accompanied by a reduction of glass-transition temperature, yield stress, and elastic modulus. Other properties (eg, water absorption and thermal and chemical resistance) may also be affected.

(2) *Toughening* refers to the ability to increase resistance to failure under mechanical stress. Epoxies derive their modulus, chemical, and thermal resistance properties from cross-link density and chain rigidity. Increasing cross-link density to meet higher thermal requirements (T_g) often comes

Table 24. Effect of Flexiblizers

Flexiblizers	Concentration, %	Advantages	Disadvantages
Poly(propylene glycol) diglycidyl ether	10–60	Low viscosity, good flexibility	Poor water resistance fair impact resistance
Polyaminoamides	30–70	Good abrasion resistance, good flexibility	Fair chemical resistance
Liquid polysulfides	10–50	Good corrosion resistance, excellent flexibility	Odor Poor heat resistance tendency to cold flow
Aliphatic polyester adducts	10–30	Good water resistance Fair flexibility over a range of temperatures	High viscosity

at the expense of toughness. Toughening approaches for epoxies (199–202) include the dispersion of preformed elastomer particles into the epoxy matrix and reaction-induced phase separation of elastomers or thermoplastic particles during cure.

Elastomers such as carboxyl-terminated poly(butadiene-*co*-acrylonitrile)s (CTBN) have been popular tougheners for epoxies. Toughening by elastomers can be attributed to the incorporation of a small amount of elastic material as a discrete phase of microscopic particles embedded in the continuous rigid resin matrix. The rubbery particles promote absorption of strain energy by interactions involving craze formation and shear deformation. Craze formation is promoted by particles of 1–5-μm size, and shear deformation by particles >0.5 μm. Systems possessing both small and large particles, ie, bimodal distribution, provide maximum toughness (203). The rubber is incorporated in the epoxy resin in a ratio of 1:8 in the presence of an esterification catalyst. The product is an epoxy ester capped with epoxy groups. The adduct is then formulated with unmodified resin and cured with standard hardeners and accelerators. Phase separation, of the adduct occurs during the curing process, resulting in the formation of segregated domains of elastomer-like particles covalently bound to the epoxy resin matrix. Optimum particle size and particle-size distribution, phase separation, and phase morphology are crucial for the development of desirable properties of the system. If the elastomer remains soluble in the epoxy matrix, it serves as a flexiblizer and reduces the glass-transition temperature significantly. Some reductions in T_g and modulus are typical of CTBN-modified epoxies. Amine-terminated poly(butadiene-*co*-acrylonitrile)s (ATBN) are also available (68).

Elastomer-modified epoxy resins are used in composites and structural adhesives, coatings, and electronic applications. Similar approach to toughen epoxy vinyl esters using other elastomeric materials has been reported (204). Other elastomer-modified epoxies include epoxy-terminated urethane prepolymers, epoxy-terminated polysulfide, epoxy–acrylated urethane, and epoxidized polybutadiene. Preformed dispersions of epoxy-insoluble elastomers have been developed and reported to achieve toughening without T_g reduction (205,206).

Other epoxy toughening approaches include chemical modifications of the system either through the epoxy backbone and/or crosss-linker. Dow Chemical developed a cross-linkable epoxy thermoplastic system (CET) (207). The concept involves introducing stiffer polymer segments into the network structure to maintain the glass-transition temperature while allowing cross-link density reduction to improve toughness. Thermoplastics, core-shell rubbers (CSR), and liquid crystal polymers (LCP) have also been used. Semi-interpenetrating network (IPN) approaches involve formation of a dispersed, cross-linked epoxy second phase in a thermoplastic matrix. The systems were reported to have good combinations of toughness, high T_g, high modulus, and processability.

Incorporation of block copolymers (qv) has been shown to improve toughness of certain epoxy systems (208). More recently, nanocomposites and self-healing epoxy systems (209) represent new approaches to develop more damage-tolerant epoxies.

Through the proper selection of resin, curing agent, and modifiers, the cured epoxy resin system can be tailored to specific performance characteristics. The choice depends on cost, processing and performance requirements. Cure is possible at ambient and elevated temperatures. Cured epoxies exhibit good combinations of outstanding properties and versatility at moderate cost: excellent adhesion to a variety of substrates; outstanding chemical and corrosion resistance; excellent electrical insulation; high tensile, flexural, and compressive strengths; good thermal stability; relatively low moisture absorption; and low shrinkage upon cure. Consequently, epoxies are used in diverse applications.

Coatings Applications

Commercial uses of epoxy resins can be generally divided into two major categories: protective coatings and structural applications. U.S. consumption of epoxy resins is given in Figure 12. The largest single use is in coatings (>50%), followed by structural composites. Among the structural composite applications, electrical laminates contribute the largest epoxy consumption. A similar trend is observed for the European market, but the Asian consumption is heavily tilted toward electrical laminate and electronic encapsulant applications (210). Electrical and electronic applications account for the largest consumption of epoxy resins in Japan (>40%). In 2000, it is estimated that the Asia-Pacific region consumed up to 70% of all epoxies used in electrical laminate production worldwide. While the overall epoxy markets continue to grow at a steady pace over the past two decades, more rapid growth has occurred in powder coatings, electrical laminates, electronic encapsulants, adhesives, and radiation-curable epoxies.

The majority of epoxy coatings are based on DGEBA or modifications of DGEBA. Chemical and corrosion-resistant films are obtained by curing at ambient

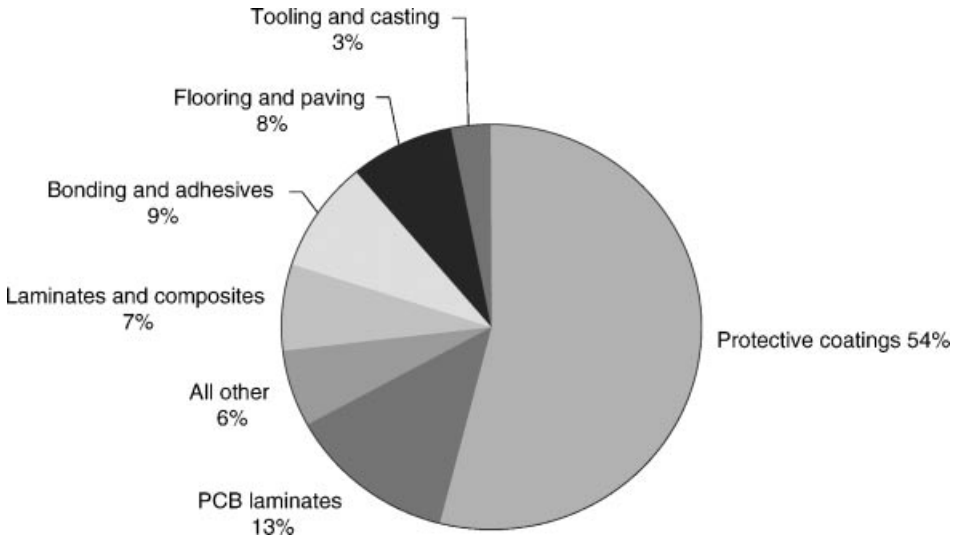

Fig. 12. End-use markets of epoxy resins (U.S. data, 2000).

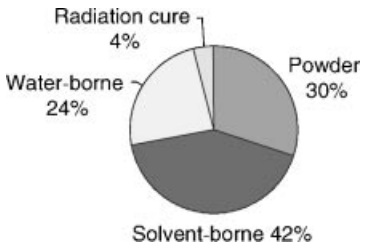

Fig. 13. Global epoxy coating application technologies (211).

and/or elevated temperatures. Ambient temperature cured coatings primarily involve cross-linking of the epoxy groups in mostly two-package systems, while elevated temperature cured coatings in one-package systems take advantage of the reactivity of both the epoxy and the secondary hydroxyl groups. As a class, epoxy coatings exhibit superior adhesion (both to substrates and to other coatings), chemical and corrosion resistance, and toughness. However, epoxy coatings have been employed mainly as primers or undercoats because of their tendency to yellow and chalk on exposure to sunlight.

Epoxy-based coatings are the preferred and dominant choices for cathodic electrodeposition of automotive primers, marine and industrial maintenance coatings, and metal container interior coatings. Use of epoxy flooring for institutions and industrial buildings has been growing at a steady rate as the industry becomes more aware of its benefits.

Solvents are commonly used to facilitate dissolution of resins, cross-linkers, and other components, and for ease of handling and application. Although most of the epoxy coatings sold in the 1970s were solvent-borne types, they made up only 40% of epoxy coating consumption in 2001 (211). Economic and ecological pressures to lower the volatile organic content (VOC) of solvent-borne coatings have stimulated the development of high solids, solvent-free systems (powder and liquid), and waterborne and radiation-curable epoxy coatings technologies (212). These environmentally friendly coating technologies have experienced rapid growth in the past decade. For example, epoxy powder coatings have been growing at rates exceeding those of other coating technologies as new applications such as automotive primer-surfacer and low temperature cure coatings for heat-sensitive substrates are developed. Radiation-curable liquid coatings based on epoxy acrylates and cycloaliphatic epoxies have also been growing significantly over the last decade. The current distribution of coating technologies is summarized in Figure 13.

Coatings Application Technologies.

Low Solids Solvent-Borne Coatings. These traditional low solids coatings contain less than 60% solids by volume (typically 40%). Their advantages include established application equipment and experience, fast drying and cure at ambient temperatures and excellent film formation at extremely fast cure conditions like those used in coil coatings (<30 s, $>200^{\circ}$C). However, because of stricter VOC regulations, solvent-based coatings have been losing market share steadily to more environmentally friendly technologies.

High Solids Solvent-Borne Coatings. High solids coatings contain 60–85% by volume of solids. They are mostly based on standard LERs or low molecular weight SERs modified by reactive diluents, low viscosity multifunctional aliphatic epoxies, or bisphenol F epoxy resins. High film build is one key advantage of high solids coatings. Examples include the coal-tar epoxy coatings that contain up to 85% solids used in industrial protective coatings.

Solvent-Free Coatings (100% Solids). Ecological concerns have led to increasing uses of these materials. Low viscosity LERs based on bisphenol A and bisphenol F epoxies are often used in combination with reactive diluents. The advantages include high buildup in a single application, minimization of surface defects owing to the absence of solvents, excellent heat and chemical resistance, and lower overall application costs. Disadvantages include high viscosity, difficulties to apply and produce thin films, poor impact resistance and flexiblity, short pot life, and increased sensitivity to humidity. Weatherable cycloaliphatic epoxies can be used to formulate solvent-free thermally curable coatings because of their low viscosities (213).

Waterborne Coatings. In the switch from solvent-borne to waterborne systems, epoxies are successfully bridging the gap largely by adaptation of conventional resins. Waterborne coatings accounted for almost 25% of epoxy coating consumption in 2001.

In addition to the waterborne epoxy dispersions which are typically supplied by epoxy resin producers, significant advances in waterborne coatings have been made by coatings producers such as PPG Industries, ICI Paint, and others utilizing modified epoxies. PPG coatings are used in cathodic electrodeposition systems that are widely accepted for automobile primers. Many patents have been issued for this important technology (214). The Glidden Co. (now ICI Paint) developed a waterborne system for container coatings based on a graft copolymerization of an advanced epoxy resin and acrylic monomers (215). These two waterborne epoxy coatings were significant breakthroughs in the coatings industry in the 1970s and are still widely used today.

For ambient temperature cure applications such as industrial maintenance and marine coatings, LERs or low molecular weight SERs (type 1 resin) are dispersed in water with a surfactant package and small amounts of co-solvents (216). Some producers offer waterborne curing agents that, typically, are salts of polyamines or polyamides. Key disadvantages include higher costs, slow cure at ambient and humid conditions, and tendency to cause flash rush. In addition, expensive stainless steel equipment are required for application. Recent developments include the elimination of co-solvents in some epoxy dispersions (217). Custom synthesized acrylic latexes have shown promise when thermally cured with cycloaliphatic epoxies (218). While the overall volume is still relatively modest (estimated at <20,000 MT in 2000 for the global market), it is expected that future growth rate for this segment will be much higher than standard epoxy resins, particularly in Europe where environmental pressures are stronger.

Powder Coatings. Epoxy-based powder coatings exhibit useful properties such as excellent adhesion, abrasion resistance, hardness, and corrosion and chemical resistance. The application possibilities are diverse, including metal finishing, appliances, structural rebars, pipes, machinery and equipment, furnitures,

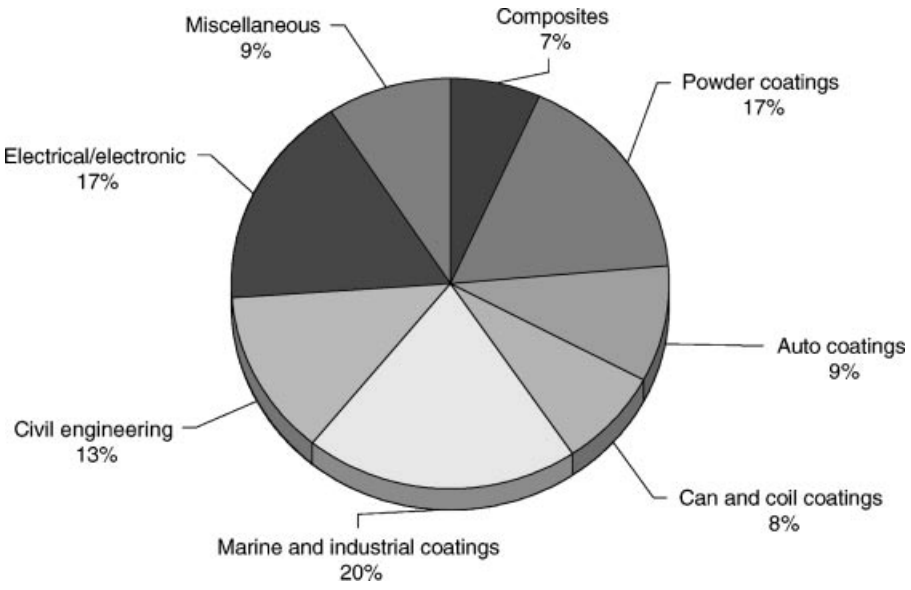

Fig. 14. Major global epoxy resin markets (Dow Chemical data, 2001).

and automotive coatings. Together, these applications accounted for 30% of epoxy coatings (Fig. 13) and 17% of epoxy resin consumption globally in 2001 (Fig. 14). This is a high growth segment of epoxy coatings (see COATING METHODS, POWDER TECHNOLOGY).

The development of highly reactive powder systems which cure using low energy (150°C) and the possibility of economical thin films (30–40 μm) have made powder coatings competitive with waterborne and high solids systems. Powder coatings can be applied by fluidized-bed (thick films, 50–150 μm) or electrostatic spray (thin films, 30–40 μm).

In powder coatings, epoxies are continuing to grow at rates exceeding other technology segments mainly because of the 100% solids feature, improved coverage, and recyclability of overspray materials. Pipeline projects, important because of worldwide energy problems, are significant consumers of epoxy powder coatings. The value of improved service life is being increasingly accepted even at the somewhat higher material cost of epoxy systems. Four types of epoxy resin systems are commonly used as powder coatings.

(1) *Epoxy powder coatings* are based on SERs of intermediate molecular weight (800–2000 EEW). They provide good flow and reactive terminal epoxy functionality. The properties of these thermoset coatings depend on the curing agents, which are friable solids such as dicyandiamide (DICY), phenol-terminated epoxy hardener, and anhydrides. Epoxy powder coatings are generally employed for interior or undercoat uses. Functional epoxy powder coatings are thick films (0.1–0.5 mm, 5–20 mil) used to protect automotive and truck parts, pipe, and concrete reinforcing bars. Fusion-bonded-epoxies (FBE), first developed by 3M Co., are epoxy powder coatings used

to protect oil and gas pipelines where long-term corrosion protection under adverse conditions (for example, the Alaska oil and North Sea underwater pipelines) is critical. The performance requirements for FBEs are challenging as the hard, cross-linked coatings are expected to survive the pipe bending/unwinding processes and handling abuses in the field. FBEs are also used to protect rebars embedded in critical concrete structures such as bridges, tunnels, and highways. Their primary function is to extend the lifetime of the concrete structures (5–10 years when built with uncoated rebars) to 20–30 years, reducing maintenance and repair costs. Epoxy powder coatings also serve as electrical insulation for bus bars, motor armatures, and similar articles. Decorative epoxy coatings are applied as a thin film (0.02–0.1 mm, 1–5 mil) and used mainly in appliance and general metal product applications. Coating for heat-sensitive substrates is an emerging market for epoxy powders.

(2) *Epoxy–polyester hybrids* are mixtures of solid epoxy resins based on bisphenol A and acid-terminated polyester solid resin (25–85 acid equivalent weight). These hybrids are typically less expensive than the epoxy-based powder coatings and offer improved weatherability, and better resistance to overbake yellowing while retaining many of the properties of the standard epoxies. Corrosion resistance is equivalent to epoxy powders in most cases, although solvent and alkali resistance is inferior. One significant new application of the epoxy–polyester hybrids is the primer-surfacer coating for automobiles. Primer-surfacer coatings based on epoxy–polyester hybrid is applied in between the epoxy primer and the topcoats. Its functions are to provide intercoat adhesion and to improve the chip resistance properties of the coatings. Automakers have also found that the epoxy–polyester hybrid primer-surfacer give a smoother surface under the top coats, resulting in a better quality appearance (219). Epoxy–polyester hybrids have experienced exceptional growth in the global market in the past decade.

(3) *Polyester–TGIC*, a third type of epoxy powder coating, is based on a mixture of polyester polycarboxylic acids (18–37 acid equivalent mass) and triglycidyl isocyanurate (TGIC). The TGIC-cured powder coatings have excellent UV resistance, good gloss and color retention, as well as good adhesion and mechanical properties. They were originally developed in Europe for coating metal window frames and buildings, exterior siding, outdoor hardware, high quality outdoor furniture, and other articles requiring superior outdoor durability. These polyester–TGIC powder coatings have gained popularity worldwide. In recent years, there have been concerns over toxicity of TGIC, and a number of potential replacement compounds have been developed. Among these, β- hydroxyalkylamide (HAA), trade named Primid by EMS-Chemie is gaining in popularity, particularly in Northern Europe.

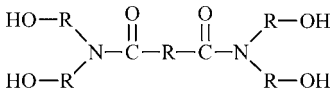

Hydroxy alkylamide (HAA)

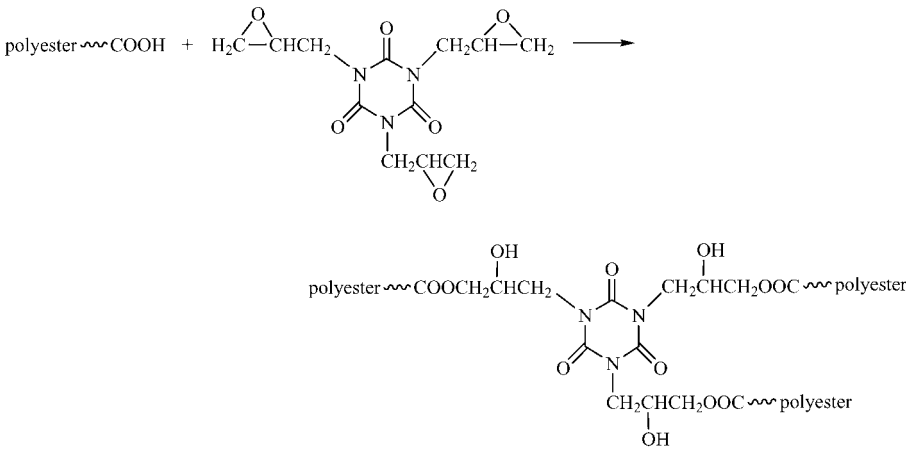

Reaction scheme of TGIC with carboxylic-terminated polyesters

(4) *Glycidyl methacrylate–acrylic.* These powder coatings are based on copolymers of glycidyl methacrylate (GMA) and acrylic monomers. They are often thermally cured with dodecanedioic acid (DDDA) and are used in automotive primer-surfacer and clear coats of luxury automobiles such as BMW (220,221).

Recent developments in powder coatings based on epoxy include UV-curable GMA–acrylic coating for automotive parts; lower temperature cure coatings for heat-sensitive substrates such as wood (222,223) and plastics; and dual cure (thermal/UV) systems.

Radiation-Curable Coatings. UV and electron beam (EB) radiation curable coatings (74) is a fast-growing segment of epoxy coatings, increasing at 8–10% annual growth rate. The technology is environmental-friendly. No solvent is used, and volatile emission is essentially eliminated. Cure is highly effective and energy-efficient at ambient temperatures, lending the technology highly applicable to heat-sensitive substrates such as wood, plastics, and paper. Capital cost requirements are low especially when compared to new thermal ovens for solvent-borne and waterborne coatings. EB cure is a relatively new technology which initiates cure via highly energetic electron beams, and unlike UV cure no photoinitiator is needed. However, EB capital cost is higher.

Epoxy acrylates are widely used as the base resin in many UV-initiated free-radical cure varnish formulations. Epoxy acrylates provide varnishes with excellent scuff resistance, high gloss, and good adhesion. Major markets are overprint varnishes for papers (books, magazines, cards, labels, etc) and exterior can coatings. Wood furniture and particle board are new but growing markets for this technology. Alternatively, cycloaliphatic epoxies can be UV-cured via a photo-initiated cationic mechanism. They are used in metal container exterior overprint varnish and inks, and high performance electronic applications. While cycloaliphatic epoxies are more expensive than epoxy acrylates, they offer several advantages: better adhesion to metals, fewer hazards in handling, and continued curing in the dark (which is important in certain applications). A related and high value market is

inks and resists, where radiation and heat-curable epoxies and epoxy acrylates are used. As discussed in the powder coatings section, radiation-curable epoxy powder coatings are being developed for a number of applications.

Epoxy Coatings Markets. The major global market segments of epoxies are represented in Figure 14. The marine and industrial protective coating is the largest market for epoxy coatings, followed by powder coatings, automotive, and container coatings.

Marine and Industrial Maintenance Coatings. The combined marine and industrial maintenance coatings application constitutes the largest epoxy coating market segment globally. While the end-use markets and application requirements are different, the basic epoxy systems utilized in these two markets are quite similar. The basic function of these coatings is to protect metal and concrete structures from degradation in aggressive environments for extended periods of time. The long service life of the coating and/or extended intervals between repairs are critical requirements, especially for marine applications, because of the high costs of dry-docking of ships for re-painting. The excellent corrosion, abrasion, and chemical resistance properties of epoxy coatings allow their dominant position in these markets. They are used in new construction as well as in maintenance and repair works. Examples are corrosion-resistant coatings for ships, shipping containers, offshore oil rigs and platforms, transportation infrastructures such as bridges, rail car coatings, coatings for industrial storage tanks, and primers for light industrial and agricultural equipment.

Most coatings used in these markets are two-component systems applied and cured at ambient conditions. LERs and low molecular weight SERs based on bisphenol A and bisphenol F epoxies are commonly used (224). Aliphatic polyamines, adducts of epoxy resins with aliphatic and aromatic amines, ketimines, phenalkamines, amidoamide, and polyamide resins are employed as curing agents. The working pot life of the amine–epoxy resin systems depends on the curing agent, solvents, catalysts, and temperature. High solids solvent-borne coatings are most popular. Tighter VOC regulations have facilitated the development of lower VOC, 100% solids, and waterborne epoxy coating systems. Important types of epoxy coatings in this segment include the following.

(1) *Two-component epoxy–amine coatings* are used primarily as a primer or mid-coat over the inorganic zinc-rich primer coating. High solids epoxy mastics can be applied over contaminated substrates and form thick, good barrier coatings. These coatings account for the majority of epoxies used in marine and industrial protective coatings markets.

(2) *Organic (epoxy) zinc-rich primers* are used in place or to repair imperfections of the inorganic zinc-rich primer. Their advantages over inorganic zincs include improved adhesion to the epoxy primer coating and better tolerance to poor surface cleaning.

(3) *Coal-tar epoxies* are historically some of the most popular high solids epoxy coatings, having excellent water barrier, chemical resistance properties, and low costs. They are typically cured with polyamides and are used as ship bottom or primer coatings for tanks, pipes, and steel pilings. However, their use has been declining or banned in certain countries because of concerns and regulations over the toxicity of coal-tar as a suspected carcinogen.

(4) *Epoxy esters* are used as primers in less demanding applications. Their performance is inferior to epoxy–amine systems but their costs are lower.

(5) *Waterborne coatings.* These are based on two-component epoxy–polyamine/polyamidoamine or epoxy–acrylic latex hybrids. One limitation of the water-borne systems is their poor cure in high humidity conditions. They have made some penetration in industrial maintenance coatings and are expected to grow more significantly in the future.

Epoxy coatings are known to have poor weatherability and often chalk when exposed to sunlight for long periods of time. Over the years, significant efforts have been dedicated to develop weatherable epoxy resin systems such as hydrogenated bisphenol A epoxy cured with siloxane-modified epoxy curing agent (225), but higher costs and compromises in curing characteristics and performance limited their commercialization. Today, most industrial structures are only coated with epoxy coatings which can last up to 10–15 years. When appearance is critical, epoxy primers are often top-coated with aliphatic isocyanate based polyurethane coatings. Marine coatings have very diverse requirements depending on the specific functions of the parts of the ship being coated. For example, ship decks are coated with antislip, abrasion- and corrosion-resistant epoxy coatings; the cargo tanks require highly chemical-resistant coatings; ship exteriors above the water line are coated with epoxy primers followed by urethane top coats for appearance; underwater ship bottoms are coated with multilayer coatings including a zinc-rich or epoxy primer, epoxy intermediate coats and antifouling top coats based on vinyls or acrylates.

Concerns over the safety of large tankers have led to regulations and construction of double-hull ships, increasing epoxy coatings consumption. While Japan was the center of the ship-building industry since the 1980s, Korea and China have emerged as major players in this market because of their low cost advantages. According to data from the Japanese Ship Building Industry Association, Korea has overtaken Japan as the global leader in ship building in the year 2000. The combined market shares of these three Asian countries now account for more than 80% of the global ship-building business. In addition, China already owns 80% of the world shipping container construction business.

The migration of ship building yards to Korea and China has led to significant increases in marine epoxy coatings consumption in that region, and has resulted in increased demands for lower temperature cure (LTC) epoxy systems. Traditional ambient-cure epoxy coatings do not cure well at temperatures below 10°C (50° F). They often require excessive cure time, affecting productivity and performance, and shorten the painting season in colder climates such as in Korea. A number of LTC epoxy coating technologies have been developed. Uses of accelerators such as tertiary amines, organic acids or alkyl-substituted phenols have allowed cures at 4.45°C (40° F) temperature range. However, shorter pot-life is a limitation of these systems. Newer epoxy coatings utilizing cycloaliphatic amines, phenalkamines as curing agents can cure at temperatures of about 30°F (0°C). For industrial protective coatings, systems developed by Ameron International (Amerlock 400) and ICI-Devoe (Bar-Rust 235) are claimed to achieve LTC down to 0°F (−18°C).

Other new technology developments in this market segment include surface-tolerant epoxy coatings for aged or marginally-prepared surfaces, interval-free

epoxy coatings to extend coating service life, mineral spirit-soluble epoxy coatings for shipping containers repairs, and styrene-free coatings to replace foul-smelling and regulated organic solvents such as toluene and xylene in coatings for new shipping containers.

Metal Container and Coil Coatings. Metal container and coil coatings represent a major outlet for epoxy resins considering there are more than 100 billion beverage cans and 30 billion food cans produced annually in the United States. Globally, the metal can market is estimated at over 300 billion cans. While the majority of metal containers coated with epoxy coatings are aluminum and steel food and beverage cans, coatings for drums, pails, and aerosol spray cans are included in this market segment. Coil coating is a highly efficient, automated coating process used to produce precoated metal coils, which are subsequently stamped and fabricated to parts. The majority of epoxy coil coatings are used to produce metal can ends and can bodies with smaller amounts going to building products, appliance panels, transportation, and metal furniture applications.

Higher molecular weight SERs (EEW = 2000–4000), which contain predominantly secondary hydroxyl groups, are used in these coatings where maximum resistance, to chemicals, good flexibility, freedom from taste, good thermal stability, blush (hydrolysis) resistance, and the ability to hold corrosive foods and beverages are needed. In addition, compliance with food regulations such as the Food and Drugs Administration (FDA) rules is required for food and beverage interior can coatings. This application is where the unique combination of properties of epoxy resins stand out.

The can and coil coatings, generally, are cross-linked with phenol, melamine, or urea–formaldehyde condensation products at elevated temperatures (150–200°C) with acid catalysts. Normal epoxy–amino resin weight ratios are epoxy–urea, 70:30; epoxy–benzoguanamine, 70:30; epoxy–melamine, 80:20, and 90:10. Increasing cross-linker levels give improved thermal and chemical resistance at the sacrifice of coating flexibility and adhesion.

Phenol–formaldehyde resole cured epoxies have excellent chemical resistance and hardness and are the popular choices for drum coatings. Their golden color is affecting their uses in food can coatings because of the increasing popularity of the water-white coatings based on melamine–formaldehyde resins, which are perceived to be "cleaner" by the consumers and the food industry. Melamine–formaldehyde resins are the primary cross-linker for beer and beverage interior can coatings. Urea–formaldehyde resins can be cured at lower temperatures and faster speed than phenol and melamine–formaldehyde resins and are widely used in the coil coatings industry where cure schedules are extremely short. However, their use has been declining because of concerns over the release of formaldehyde fumes. Recently, there have been regulatory issues in the can industry concerning worker exposure to volatile formaldehyde emission from the formaldehyde resins. A number of new, formaldehyde-free coating formulations have been introduced by coating suppliers (226).

High solids binders for metal can coatings have been developed on the basis of dimer acid modification of epoxy resins, whereby a flexible C_{34} difunctional acid is used to esterify a conventional diepoxide resin (227). The resultant epoxy ester possesses a sufficiently lower viscosity to provide binders with solids contents >70

vol%. Curing is accomplished by a melamine–formaldehyde resin (Cymel 303, from Cytec) in conjunction with phosphoric acid catalyst.

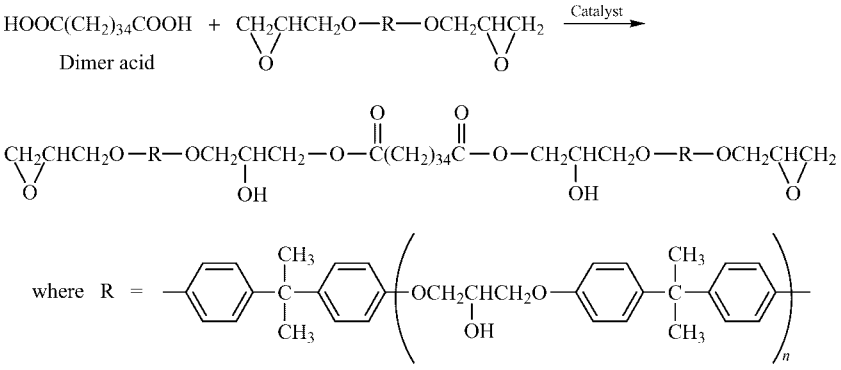

In the 1970s, a waterborne coating system for aluminum beverage can coatings was developed by the Glidden Company (ICI Packaging Coatings) on the basis of a graft copolymerization of an advanced epoxy resin and acrylic monomers (228,229). The acrylic–vinyl monomers are grafted onto preformed epoxy resins in the presence of a free-radical initiator; grafting occurs mainly at the methylene group of the aliphatic backbone on the epoxy resin:

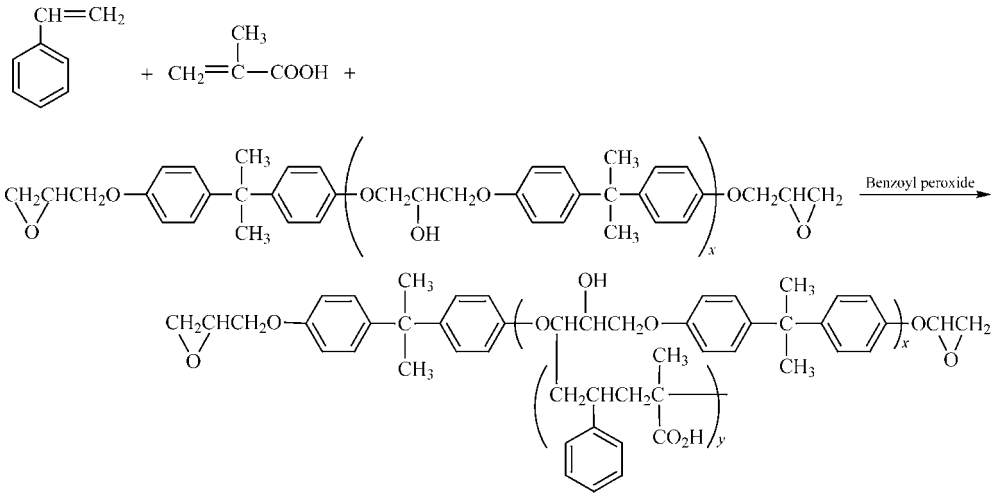

The polymeric product is a mixture of methacrylic acid–styrene copolymer, SER, and graft copolymer of the unsaturated monomers onto the epoxy resin backbone. It is dispersible in water upon neutralization with an amine, and cured with an amino–formaldehyde resin. The technology revolutionized the can coatings industry in the 1970s which was primarily based on low solids, solvent-borne coatings. This waterborne epoxy coating system and its variations continue to be the dominant choices for interior beer and beverage can coatings globally today.

They are also formulated with phenol–formaldehyde resole and used as interior coatings in the new two-piece food can plants in the United States.

UV-curable coatings based on cycloaliphatic epoxies are used on the exterior of some beer, beverage, and food cans, as well as food and composite can ends. The technology is environmentally friendly and energy-efficient.

Coil coatings have been gaining in the appliance market. More OEMs have turned to precoated metal coils as an efficient manufacturing alternative to produce appliance panels, eliminating the needs for post-formed coating processes. PVC organosol (copolymers of vinyl chloride and vinyl acetate) coatings for coil-coated can ends and bodies have been under environmental pressures and epoxy has been gaining as PVC coatings are replaced (230).

The growth of can coatings has been steady globally because of the expansion of new can plants in Asia-Pacific and South America in the 1980s and early 1990s, which made up for the stagnant growth of the U.S. market. However, growth of plastic bottles based on PET [poly(ethylene terphthalate)] has recently eroded the metal can position in beverage packaging, affecting epoxy can coatings growth. In addition, new can fabrication technologies utilizing other polymers are being developed which may challenge the dominant position of epoxy coatings in metal cans.

In the 1980s, Toyo Seikan Co. of Japan successfully developed and commercialized TULC (Toyo Ultimate Laminate Cans), a revolutionary technology in which cans are fabricated using a deep draw process from metal coils laminated with thermoplastic polyester films (231,232). No epoxy coating is used in this technology. Special polyester film combinations were used (in a much higher thickness than typical epoxy coatings) to facilitate the demanding deep draw process while maintaining all of the other requirements of can coatings. This technology is a significant breakthrough with claimed benefits such as no solvent emission, lower energy and water usage, and excellent quality cans. The costs however are significantly higher than those of conventional cans, and the technology has found widespread application only in Japan where higher packaging costs are acceptable. Other companies such as British Steel have been actively promoting laminated cans as a way to produce differentiable packaging like shaped cans with very limited success. Higher cost is the biggest barrier to their broad commercialization. Recent developments include attempts to fabricate can ends and bodies from extrusion-coated metals by companies such as Alcoa. Thermoplastics like modified polyesters are providing challenges to epoxies in these new technologies due to their excellent formability. However, their resistance against aggressive drinks, foods, and retort are inferior to those of epoxies.

More recently in the United States, Campbell Soup Co. has successfully launched a new line of microwaveable, ready-to-eat plastic cans. These cans are constructed from a molded thermoplastic can body (polypropylene, high density polyethylene) and an easy-open-end (EOE) of coated metal. In addition, flexible pouches have made inroad as an alternative for metal cans in certain markets such as packaged tuna fish.

Recently, there have been debates in the can coatings industry concerning the potential health effects of residual bisphenol A and DGEBA in epoxy can coatings. The resin suppliers, can coatings producers, and can makers have jointly formed an industry group to coordinate a number of studies on this issue. Results

indicated that epoxy can coatings, when properly formulated and cured, are safe and in compliance with global food contact regulations. Current regulatory guidelines such as the Specific Migration Levels for Europe set extractable limits of 1 mg/kg for DGEBA and 3 mg/kg for bisphenol A. Additional information is available in the references (233,234). Some polyester coatings have been developed as epoxy coating alternatives, but high costs and inferior pasteurization-resistance limit their uses (235).

Automotive Coatings. Automotive coatings are another major application for epoxy resins. The excellent adhesion and corrosion resistance properties of epoxies make them the overwhelming choice for automotive primers. One new, growing application is the use of epoxy–polyester or acrylic–GMA powders in primer-surfacer coatings. In addition, glycidyl methacrylate (GMA) is used as a comonomer in etch-resistant liquid top coats containing acrylic acid/anhydride (236) and in GMA-acrylic powder coatings for clear coats and automotive parts (220). Epoxy powder coatings for automobiles are expected to grow significantly in the near future.

Electrodeposition processes using epoxy-based automotive primers were developed for anodic and cathodic systems. Anodic systems (AED) employ carboxylated epoxy resins neutralized with an amine. A typical binder is prepared by the esterification of the terminal epoxy groups of a solid resin (EEW = 500) with stoichiometric quantities of dimethylolpropionic acid to form a hydroxyl-rich resin. This intermediate is subsequently treated with a cyclic anhydride to form an acid functionalised polymer, which is then neutralized with the amine.

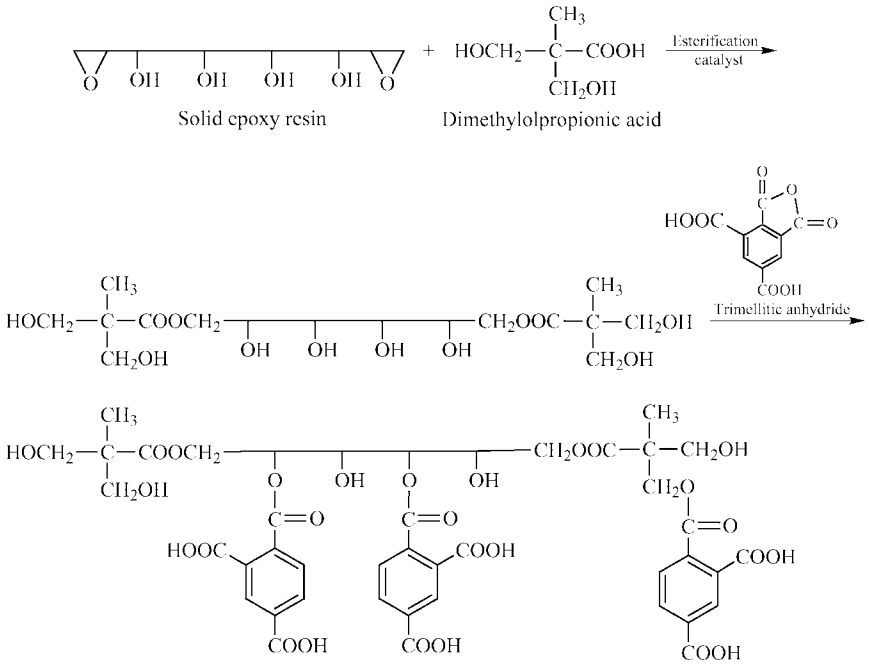

Significant advances in waterborne automotive coatings have been made by PPG Industries and others utilizing epoxies as co-resins in the 1970s. These

coatings are used in cathodic electrodeposited (CED) systems, which are widely accepted for automobile primers. Many patents have been issued for this important technology (214). Cathodic systems, which have superior corrosion resistance, have replaced anodic systems. A typical epoxy binder for cathodic electrodeposition is prepared by first forming a tertiary amine adduct from an epoxy resin and a secondary amine, followed by neutralization with an acid to form a water-soluble salt:

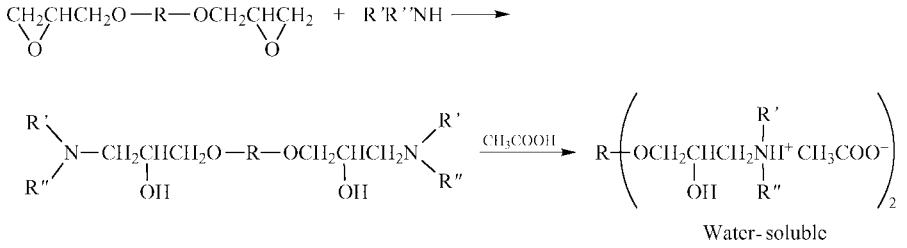

Cross-linking is achieved by reaction of the hydroxyl groups with a blocked isocyanate, which is stable at ambient temperature.

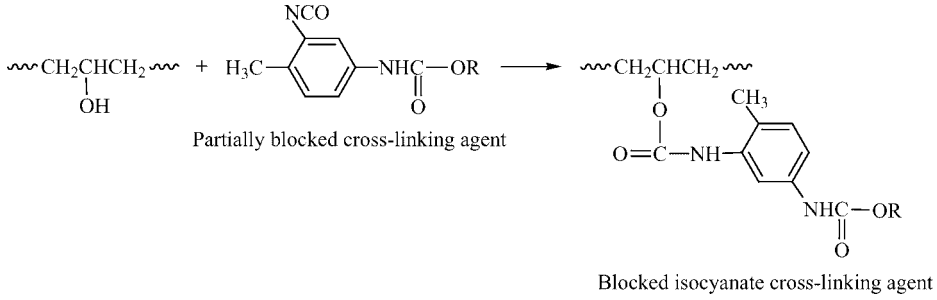

where R = 2-ethylhexanol

The ability of the CED coating system to thoroughly coat all metal surfaces of the car and the resultant superior corrosion resistance was a significant breakthrough, enabling its dominant position in the global automotive industry.

PPG has continued to develop new generations of improved CED epoxy coatings (237). Dupont, BASF, and a number of Japanese coating companies such as Nippon Paint and Kansai Paint have contributed to the epoxy primer coating technology by developing advanced coating systems to meet higher performance and regulatory requirements of the automotive industry (238–240). The popular pigment systems based on heavy metals such as lead and chromium in primer coatings have been recently banned in certain countries, leading to efforts to develop new formulations with improved corrosion resistance. Nippon Paint has proposed pigment-free CED systems (241).

Epoxy–polyester and acrylic–GMA powder coatings have made significant advances recently in the area of primer-surfacer coatings. They offer better adhesion to topcoats and significantly improve chip resistance compared to the traditional liquid polyester and epoxy ester coatings. This translates to warranty cost reductions, leading many car manufacturers to convert to the powder coating technologies.

While epoxy coatings based on DGEBA and other aromatic epoxies are limited to undercoats and under-the-hood applications because of their poor UV resistance, GMA-based coatings have been developed for improved acid-etch performance automotive top coats. They compete with traditional acrylic polyol–melamine topcoats that are highly susceptible to acid rain-induced hydrolysis, and offer better mar resistance and less worker exposures than isocyanate-based topcoats (242,243). BMW has coverted to a GMA–acrylic powder clear coat developed by PPG.

Inks and Resists. Inks and resists comprise a relatively small but high value and growing market for epoxies and epoxy derivatives. In 2001, there were an estimated of 6800 MT of epoxies and epoxy derivatives used in this market to produce ink and resist formulations worth almost $400 million in the U.S. market. Epoxies are often used with other resins such as polyester acrylates and urethane acrylates in these formulations. The largest applications are lithographic and flexographic inks followed by electronic inks and resists.

Resist technology is widely used in the electronics industry to manufacture printed circuits (see Lithographic Resists). The resist (a coating or ink) is applied over a conducting substrate such as copper in a pattern to protect its surface during etching, plating, or soldering. Cure is either by radiation or heat. The uncured coating (or ink) is removed later by solvents. Solder masks perform similar functions in the manufacturing of printed circuit boards. The growth of the computer and electronics industries has fueled growth of epoxy-based inks and resists. The market is projected to grow at 10% annually.

The primary resins used in this market are the radiation-curable epoxy acrylates, accounting for 60% of the resins used. A small amount of cycloaliphatic epoxies are also used in UV-curable inks and resists. Phenol and cresol epoxy novolacs, and bisphenol A based epoxies are used in thermally cured formulations. The epoxy novolacs are used where higher heat resistance is needed such as in solder masks. Both free-radical and cationic-curable UV inks and colored base coats have grown rapidly because of the needs for higher line speeds, faster cleanup or line turnaround, less energy consumption, less capital for a new line, and fewer emissions.

A unique epoxy (epoxy chalcone) produced by Huntsman can be used for dual cure (244):

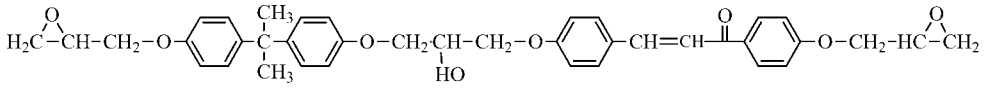

Radiation-initiated free-radical cure is possible via the double bonds, while the epoxy groups are available for thermal cure. Epoxy chalcone is used as a photopolymerizable solder mask and in photoresists.

Structural Applications

Next to coatings, structural applications account for the second largest share of epoxy resin consumption (~40%). Epoxy resins in structural applications can be

divided into three major areas: fiber-reinforced composites and electrical laminates; casting, encapsulation, and tooling; and adhesives. Within this segment, the largest applications are electrical laminates for PCB and composites made of epoxy and epoxy vinyl ester for structural applications.

Structural Composites. Epoxy resins and epoxy vinyl ester resins are well suited as fiber-reinforcing materials because they exhibit excellent adhesion to reinforcement (qv), cure with low shrinkage, provide good dimensional stability, and possess good mechanical, electrical, thermal, chemical, fatigue, and moisture-resistance properties. Epoxy composites are formed by aligning strong, continuous fibers in an epoxy resin-curing agent matrix. Processes currently used to fabricate epoxy composites include hand lay-up, spray-up, compression molding, vacuum bag compression molding, filament winding, resin transfer molding reaction, injection molding, and pultrusion (see COMPOSITES, FABRICATION).

Important fiber materials are surface-treated glass, boron, graphite (carbon), and aromatic polyaramides (eg, DuPont's Kevlar). In most composites the reinforcement constitutes ca 65% of the final mass. Orientation of the fibers is important in establishing the properties of the laminate. Unidirectional, bidirectional, and random orientations are possible. The characteristics of the cured resin system are extremely important since it must transmit the applied stresses to each fiber. A critical region in a composite is the resin–fiber interface. The adhesive properties of epoxy resins make them especially suited for composite applications.

The most important market for epoxy composites is for corrosion-resistant equipment where epoxy vinyl esters is the dominant material of choice. Other smaller markets are automotive, aerospace, sports/recreation, construction, and marine. Because of their higher costs, epoxy and epoxy vinyl esters composites found applications where their higher mechanical strength and chemical and corrosion resistance properties are advantageous.

Epoxy Composites. Composites made with glass fibers usually have a bisphenol A based epoxy resin–diamine matrix and are used in a variety of applications including automotive leaf springs and drive shafts, where mechanical strength is a key requirement. A large and important application is for filament-wound glass-reinforced pipes used in oil fields, chemical plants, water distribution, and as electrical conduits. Low viscosity liquid systems having good mechanical properties when cured are preferred. These are usually cured with liquid anhydride or aromatic–amine hardeners. Similar systems are used for filament-winding pressure bottles and rocket motor casings. Other applications that use fiber-reinforced epoxy composites include sporting equipment, such as tennis racquet frames, fishing rods, and golf clubs, as well as industrial equipment. The wind energy field is emerging as a potential high growth area for epoxy composites, particularly in Europe where a number of new wind energy farms are planned. With windmill blades increasing in lengths (up to 50 m), the strength and fatigue properties of epoxy composites provide benefits over competitive chemistries.

In the aerospace industry, particularly in military aircraft construction, the use of graphite fiber-reinforced composites has been growing because of high strength-to-weight ratios. Some newer commercial airliners now contain up to 10% by weight of composite materials. High performance polyfunctional resins, such as the tetraglycidyl derivative of methylenedianiline in combination with

diaminodiphenylsulfone or nadic methyl anhydride, are used to provide good elevated temperature properties and humidity resistance. Handling characteristics are well suited to the autoclave molding technique primarily used in the manufacture of such components. The low viscosity and high T_g of cycloaliphatic epoxies has led to their use in certain aerospace applications. Newer resins such as diglycidyl ether of 9,9′-bis(4-hydroxyphenylfluorene) have been developed.

While the overall growth of composites in the aerospace industry is continuing, epoxy has been facing stiff competition from other materials and the growth rate has been relatively small (2% annually). While epoxies are still used in many exterior aircraft parts, carbon fiber composites based on bismaleimide and cyanate esters have shown better temperature and moisture resistance than epoxies in military aircaft applications. In the commercial aircraft arena, phenolic composites are now preferred for interior applications because of their lower heat release and smoke generation properties during fires. High performance thermoplastics, such as polysulfone, polyimides, and polyetherether ketone (PEEK), have also found some uses in aerospace composites.

Epoxy Vinyl Ester Composites. Epoxy vinyl ester composites are widely used to produce chemically resistant glass-reinforced pipes, stacks, and tanks by contact molding and filament-winding processes. Epoxy vinyl ester resins provide outstanding chemical resistance against aggressive chemicals such as aqueous acids and bases and are materials of choice for demanding applications in petrochemical plants, oil refineries, and paper mills. Epoxy vinyl ester composites are also used in demanding automotive applications such as engine and oil pan covers where high temperature performance is required. Exterior panels and truck boxes are also growth automotive applications for vinyl esters. However, in less demanding automotive applications, cheaper thermoplastics and thermosets such as unsaturated polyesters or furan resins are often used. In general, epoxy vinyl ester is considered to be a premium polyester resin with higher temperature and corrosion resistance properties at higher costs. It is used where the cheaper unsaturated polyesters cannot meet performance requirements. For the same reason, epoxy vinyl ester has not grown significantly in less demanding civil engineering applications. Other uses of epoxy vinyl ester composites include boat hulls, swimming pools, saunas, and hot tubs.

Improved versions of the high performance resin systems continue to be developed (245,246). Toughening of epoxies and epoxy vinyl esters has emerged as an area for investigation (247). Lower styrene content vinyl esters have been developed to reduce worker exposure. Performance enhancements with epoxy and vinyl ester nanocomposites have been reported in the literature, but commercialization has not been yet realized.

Mineral-Filled Composites. Epoxy mineral-filled composites are widely used to manufacture laboratory equipment such as lab bench tops, sinks, hoods, and other laboratory accessories. The excellent chemical and thermal resistance properties of epoxy thermosets make them ideal choices for this application. Typically, liquid epoxy resins of bisphenol A are cured with anhydrides such as phthalic anhydride, which provide good exotherm management and excellent thermal performance. The systems are highly filled with fillers such as silica or sand (up to 70 wt%). Multifunctional epoxy novolacs can be added when higher chemical and thermal performance is needed.

Civil Engineering, Flooring, and Construction. Civil engineering is another large application for epoxies, accounting for up to 13% of total global epoxy consumption. This application includes flooring, decorative aggregate, paving, and construction (248). Key attributes of epoxies such as ease of installation, fast ambient cure, good adhesion to many substrates, excellent chemical resistance, low shrinkage, good mechanical strength, and durability make them suitable for this market. In the United States an estimated 20,000 MT of resins were used for flooring applications in 2000. The building boom in China has provided significant growth for this market during the past decade. Epoxy flooring compounds are expected to grow well as the construction industry becomes more aware of their benefits.

Epoxy resins are used for both functional and decorative purposes in monolithic flooring and in factory-produced building panel applications. Products include floor paints, self-leveling floors, trowelable floors, and pebble-finished floors. Epoxy floorings provide wear-resistant and chemical-resistant surfaces for dairies and food processing and chemical plants where acids normally attack concrete. Epoxies are also used in flooring for walk-in freezers, coolers, kitchens, and restaurants because of good thermal properties, slip resistance, and ease of cleanup. In commercial building applications, such as offices and lobbies, terrazzo-like surfaces can be applied in thin layers. Continuous seamless epoxy floors are competitive with ceramic tiles. They are usually applied by trowel over a prepared subfloor. Semiconductive epoxy/carbon black floorings are used in electronics manufacturing plants because of their ability to dissipate electrical charges. Decorative slip-resistant coatings are available for outdoor stair treads, balconies, patios, walkways, and swimming-pool decks. Epoxy aggregates are highly filled systems, containing up to 90% of stones or minerals. They are used for decorative walls, floors, and decks.

Usually, two-component systems consisting of liquid epoxy resin, diluents, fillers (eg, sands, stones, aggregates), pigments, thickening agents, and polyamine or polyamide curing agents are employed. Cycloaliphatic amines and their adducts are used when either better low temperature cure or adhesion to wet concrete is desired. The other components of the flooring formulation are as critical as the resin and hardener. Typical filler and pigment levels are 10% for paving, 30% for flooring, and 40% or higher for decorative aggregates. Self-leveling floors consist of resin-hardener mixtures with low filler content or unfilled compositions with high gloss. In epoxy terrazzo floors, an epoxy binder replaces the cement matrix in a marble aggregate flooring, providing impact resistance, mechanical strength, and adhesion.

Epoxy systems for roads, tunnels and bridges are effective barriers to moisture, chemicals, oils, and grease. They are used in new construction as well as in repair and maintenance applications. Typical formulations consist of liquid epoxy resins extended with coal tar and diethylenetriamine curing agent. Epoxy resins are widely used in bridge expansion joints and to repair concrete cracks in adhesive and grouting (injectable mortar) systems. Epoxy pavings are used to cover concrete bridge decks and parking structures. Formulations of epoxy resins and polysulfide polymers in conjunction with polyamine curing agents are used for bonding concrete to concrete. After cleaning the old surface, the epoxy

adhesive is applied and good adhesion between the old and the new concrete is obtained.

Recent developments in the construction and civil engineering industry include the development of "intelligent concrete" with self-healing capability in Japan (249). Some of the systems are based on epoxy resins encapsulated in concrete which when triggered by cracks open and cure to repair the concrete.

Electrical Laminates. Printed wiring boards (PWB) or printed circuit boards (PCB) are used in all types of electronic equipment. In noncritical applications such as inexpensive consumer electronics, these components are made from paper-reinforced phenolic, melamine, or polyester resins. For more critical applications such as high end consumer electronics, computers, complex telecommunication equipment, etc, higher performance materials are required and epoxy resin based glass fiber laminates fulfill the requirements at reasonable costs. This application constitutes the single largest volume of epoxies used in structural composites. In 2000, an estimated 200,000 MT of epoxy resins were used globally to manufacture PCB laminates.

Systems are available that meet the National Electrical Manufacturers Association (NEMA) G10, G11, FR3, FR4, FR5, CEM-1, and CEM-3 specifications. Both low viscosity liquid (EEW = 180–200) and high melting solid (EEW = 450–500) epoxy resins are used in printed circuit prepreg manufacture. Currently, the most widely used boards (>85%) are manufactured to the flame-retardant FR4 specification using epoxy thermosets. Flame retardance is achieved by advancing the liquid DGEBA epoxy resin with tetrabromobisphenol A (TBBA). This relatively low cost resin which contains about 20 wt% bromine is the workhorse of the PCB industry. Epoxy resins based on diglycidyl ether of TBBA are also available, which allow the preparation of resins with even higher bromine content, up to 50 wt%. Multifunctional epoxy resins such as epoxy novolacs based on phenol, bisphenol A, and cresol novolacs or the tetraglycidyl ether of tetrakis(4-hydroxyphenyl)ethane are used as modifiers to increase the glass-transition temperature ($T_g > 150^\circ C$), thermal decomposition temperature (T_d), and chemical resistance.

The most commonly used curing agent for PWBs is dicyandiamide (DICY) catalyzed with imidazoles such as 2-methylimidazole (2-MI), followed by phenolic novolacs and anhydrides.

The epoxy–DICY systems offer the following advantages:

(1) Cost effectiveness (DICY is a low equivalent weight, multifunctional curing agent)
(2) Stable formulations
(3) Excellent adhesion to copper and glass
(4) Good moisture and solder resistance
(5) Good processability

The primary disadvantage of the standard epoxy–DICY systems is their relatively low thermal performance ($T_g < 140^\circ C$, $T_d = 300^\circ C$), which limits their uses in more demanding applications such as the FR-5 boards and other high density circuit boards. Specialty epoxy–DICY systems are available with T_g approaching

190°C but at higher costs. Alternatively, high temperature epoxy systems are obtained using diaminodiphenyl sulfone (DDS) as curing agent and boron trifluoride monoethylamine (BF_3/MEA) complex, benzyldimethylamine (BDMA), or various imidazoles as catalysts. However, concerns over the toxicity of DDS have led to significant decrease of its use. More recently, higher thermally resistant laminates using novolac curing agents, including bisphenol A based novolacs, have become popular in the industry. However, brittleness is a significant disadvantage of these systems.

Prepreg is commonly prepared by passing the glass cloth through a formulated resin bath followed by heat treatment in a tower to evaporate the solvent and partially cure the resin to an intermediate or B stage. Prepreg sheets are stacked with outer layers of copper foil followed by exposure to heat and high pressure in a laminating press. This structure is cured (C-staged) at high temperature (150–180°C) and pressure for 30–90 min. Attempts to develop continuous prepreg and laminating processes have only achieved limited commercialization. Laminate boards may be single-sided (circuitry printed on only one side), double-sided, or multilayered (3 to 50 layers) for high density circuitry boards. Electrical connections for mounted components are obtained via drilled holes which are plated with copper.

The 1990s witnessed the explosive growth of the personal computer, consumer electronics, and wireless telecommunication industries, resulting in significant demands for PWB based on epoxy resins. The PWB industry trends toward device miniaturization, multilayer laminates, high density circuitries, lead-free solder, and faster signal transmission speeds have resulted in increased performance requirements. For example, lead-free legislation which bans electronics containing lead in the European Union became law in 2003 with an implementation date of 2006. This legislation is expected to speed up the phase-out of lead-based solders globally, forcing the industry to use alternatives such as tin alloys which have much higher soldering temperatures, and thereby drives the need for epoxy systems with higher thermal performance.

The end-use industries' demands for PCB boards with better heat resistance (250,251), higher glass-transition temperature (T_g), higher thermal decomposition temperatures (T_d), lower water absorption, lower coefficient of thermal expansion (CTE), and better electrical properties (dielectric constant D_k and dissipation factor D_f) have led to the development of new, high performance epoxies and cross-linker systems (252). Toughness is also becoming an issue as electrical connection holes are drilled in the highly cross-linked, high T_g laminates.

Since reinforcing materials make up from 40 to 60 wt% of the PCB laminates, their contributions to the laminate dielectric properties are significant. The standard reinforcing glass–cloth compositions in electrical laminates are designated E (electrical) glass. Woven E glass is most commonly used, but other reinforcing materials such as nonwoven glass mat, aramid fiber, S-2 glass, and quartz are available. In recent years, the PCB industry has been evaluating materials with better dielectric properties, but they are much more expensive than standard E glass (Table 25).

In recent years, environmental concerns over toxic smoke generation during fire and end-of-life incineration of electronic equipment containing brominated

Table 25. Reinforcing Material Comparison[a]

Reinforcing material	D_k (at 1MHz)	D_f (at 1MHz)	Relative cost
E glass	6.5	0.003	1
S-2 glass	5.3	0.002	4
D glass	3.8	0.0005	10
Quartz	3.8	0.0002	30
Aramid	3.8	0.012	10

[a]From Ref. 253.

products, particularly in Europe and Japan, have driven development efforts on halogen-free resins. This has resulted in a number of alternative products such as phosphorous additives and phosphor-containing epoxies (254–256). Some examples of these phosphorous compounds are as follows:

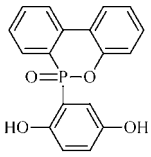

9,10-Dihydro-9-oxa-10-phosphathenanthrene-10-oxide

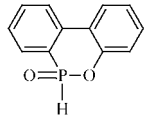

6*H*-dibenz(*C*,*H*)(1,2)oxaphosphorin,6-oxide

However, commercialization of phosphor-containing epoxies has been limited because of higher costs and other disadvantages such as poorer moisture resistance and lower thermal performance. In addition, concerns over phosphine gas emission during fires and potential leakage of phosphorous compounds in landfills have raised questions about their long-term viability. Alternatively, the industry has been researching new epoxy resins based on nitrogen, silicon, sulfur-containing compounds, and new phenolic resins as potential halogen-free, phosphor-free replacements. Inorganic fillers such as alumina trihydrate, magnesium hydroxide, and zinc borate have also been evaluated as flame-retardant alternatives in epoxy systems.

While brominated epoxy resin remains the workhorse of the PCB industry (FR-4 boards) because of its good combination of properties and cost, it is facing competition from other thermoset and thermoplastic materials as industry performance requirements increase. Thermosets with higher temperature performance ($>180^\circ$C T_g) and lower dielectric properties include polyimides, cyanate esters, and bismaleimide–triazine (BT) resins. They are used alone or as blends with epoxies in high performance chip-packaging boards and military applications. GE's GETEK system is an interpenetrating network of polyphenylene oxide (PPO) in epoxy and has lower dielectric constant than standard epoxies. Polytetrafluoroethylene (PTFE) has a very low dielectric constant (Table 26) and is

Table 26. Base Resin Systems Used in PCB Laminates

Resin system	T_g, °C	D_k (at 1MHz)	D_f (at 1MHz)	Estimated relative resin cost	Laminate cost
Standard Epoxies	135–140	4.6–4.8	0.015–0.020	1	1
High performance Epoxy	170–180	4.6–4.8	0.015–0.020	1.5–2	1.5
PPO/Epoxy	175–185	3.6–4.2	0.009–0.015	4–6	2–3
BT/Epoxy	170–220	3.9–4.2	0.008–0.013	8–15	2–5
Polyimide	260	3.9–4.4	0.012–0.014	5–16	3–6
Cyanate ester	230–260	3.5–3.7[a]	0.005–0.011[a]	5–16	4–8
Polyester	135–140	3.1–3.2[b]	0.004–0.014[b]	—	7–10
PTFE	NA	2.1–2.5[b]	0.0006–0.0022[b]	40	15–50

[a]Measured at 1GHz.
[b]Measured at 10 GHz.

used primarily in high performance PCBs for military and high frequency (eg, radars) applications. While these alternative materials offer certain performance advantages over standard epoxies, they are generally more expensive and more difficult to process. Thermosets such as polyimides, cyanate ester, and BT resins are very brittle and have higher water absorption than epoxies. PTFE has very poor adhesion to substrates, requiring special treatments. Consequently, they are limited to niche, high performance applications (250).

In flexible printed circuits, polyimide and polyester films are the preferred choices over epoxies. Molded interconnects based on heat-resistant thermoplastics such as polyether sulfone, polyether imide, and polyarylate have been developed to replace epoxy-based PCBs in certain applications. However, their uses are limited to special applications.

There has been a significant migration of the PCB laminate manufacturing capacity to Asia (mainly Taiwan and China) in the late 1990s. In 2001, 70% of epoxy resins used in PCB laminates was consumed in the region and the trend is expected to continue in the near future.

Other Electrical and Electronic Applications.

Casting, Potting, and Encapsulation. Since the mid-1950s, electrical-equipment manufacturers have taken advantage of the good electrical properties of epoxy and the design freedom afforded by casting techniques to produce switchgear components, transformers, insulators, high voltage cable accessories, and similar devices.

In casting, a resin-curing agent system is charged into a specially designed mold containing the electrical component to be insulated. After cure, the insulated part retains the shape of the mold. In encapsulation, a mounted electronic component such as a transistor or semiconductor in a mold is encased in an epoxy resin based system. Coil windings, laminates, lead wires, etc, are impregnated with the epoxy system. Potting is the same procedure as encapsulation except that the mold is a part of the finished unit. When a component is simply dropped into a

resin-curing agent system and cured without a mold, the process is referred to as *dipping*. It provides little or no impregnation and is used mainly for protective coatings.

The choice of epoxy resin, curing agent, fillers, and other ancillary materials depends on factors such as cost, processing conditions, and the environment to which the insulated electrical or electronic component will be exposed.

The type and amount of filler that can be incorporated into the system are very important and depend on the viscosity of the resin at the processing temperature. Filler loading reduces costs, increases pot life, improves heat dissipation, lowers exotherms, increases thermal shock resistance, reduces shrinkage, and improves dimensional stability.

The exotherm generated during the resin cure must be controlled to prevent damage to the electrical or electronic component. The exotherm is easily controlled during the production of small castings, pottings, and encapsulations. In the production of large castings, the excess heat of reaction must be dissipated in order to prevent locked-in thermal stresses. During the 1970s, the pressure gelation casting process was developed (257); this method provides better temperature control and reduces cycle times. The heat generated by polymerization is used to heat the resin mass and is not dissipated in the mold.

Both DGEBA and cycloaliphatic epoxy resins are used in casting systems. Most systems are based on DGEBA resins cured with anhydride hardeners and contain 60–65 wt% inert fillers. The cycloaliphatic resin systems exhibit good tracking properties and better UV resistance than DGEBA resins, the latter of which causes crazing (qv) and surface breakdown. An electrical current is more likely to form a carbonized track in aromatic-based resins than in nonaromatic ones. Their lower viscosity also facilitates device impregnation. The cycloaliphatic epoxies are often used as modifiers for DGEBA resin systems. This application represents a significant outlet for cycloaliphatic epoxies.

Amine curing agents are used in small castings, and anhydrides are used in large castings. Anhydrides are less reactive and have lower exotherms than amines. In addition, their viscosity and shrinkage are low and pot lives are longer.

Transfer Molding. Epoxy molding compounds (EMC) are solid mixtures of epoxy resin, curing agent(s) and catalyst, mold-release compounds, fillers, and other additives. These systems can be formulated by dry mixing or by melt mixing and are relatively stable when stored below room temperature. Molding compounds become fluid at relatively low temperatures (150–200°C) and can be molded at relatively low pressures (3.5–7.0 MPa) by compression, transfer, or injection molding. Advantages of molding over casting are elimination of the mixing step immediately before use, improved handling and measuring procedures, and suitability for high production quantities. A typical standard EMC formulatio gn contains approximately 30% epoxies, 60% filler, and 10% of curing agents and other additives such as release agent.

An important application of epoxy molding compounds is the encapsulation of electronic components such as semiconductor chips, passive devices, and integrated circuits by transfer molding. Transfer molding is a highly automated, efficient method of encapsulation. High purity phenol and cresol epoxy novolacs and phenol and cresol novolacs and/or anhydride curing agents are used most often in semiconductor applications. For passive device encapsulation, standard

epoxy novolacs can be used as blends with bisphenol A based solid resins. The ECN or EPN molding powders can be processed at relatively low pressures and provide insulation for the electronic components. Ionic impurities, ie, NaCl or KCl, must be kept to a minimum, since trace quantities can cause corrosion and device failure. In addition, residual stress and thermal and mechanical shock resistances are issues that must be managed properly (258).

Efforts have been made to improve the high temperature performance of these systems by replacing the epoxy novolacs with other multifunctional epoxy resins. Hydrocarbon based epoxy novolacs (HEN) were developed to improve the moisture resistance of molding compounds. Crystalline epoxy resins derived from biphenol and dihydroxy naphthalenes were developed for high end semiconductor encapsulants using Surface Mount Technology (SMT). The emergence of SMT as a key semiconductor manufacturing technology requires epoxy molding compounds with a high filler loading capacity (up to 90 wt%) to enhance solder crack resistance. SMT uses new solder alloys to attach components to the PCB board at high temperatures (215–260°C). Solder reflow, delamination, and package cracks are problems often encountered with conventional molding compounds based on cresol epoxy novolacs. The high filler content helps lower costs, reduces moisture absorption, and decreases the thermal expansion coefficient of the system. Crystalline products with very low melt viscosity such as biphenyl epoxies facilitate the processing of the high silica filler formulations while maintaining other critical requirements: moisture resistance and electrical, thermal, and mechanical properties (61). The majority of high purity epoxies used in epoxy molding compounds (EMC) for semiconductor encapsulations are supplied by Japanese producers and a few Asian companies.

Adhesives. Epoxy-based adhesives provide powerful bonds between similar and dissimilar materials such as metals, glass, ceramics, wood, cloth, and many types of plastics. In addition, epoxies offer low shrinkage, low creep, high performance over a wide range of usage temperatures and no by-products (such as water) release during cure. The epoxy adhesives were originally developed for use in metal bonding in the aircraft industry (259,260). In aircraft wing assemblies, high strength epoxy adhesives are used in place of metal fasteners to avoid corrosion problems inherent with metal fasteners, to reduce weight, and to eliminate "point" distribution by spreading the load over a large area. Today, epoxy is the most versatile engineering/structural adhesive, widely used in many industries including aerospace, electrical/electronic, automotive, construction, transportation, dental, and consumer. The market is of high value, consuming 25,000 MT of epoxies in North America in 2001 worth almost $500 million.

The broad range of epoxy resins and curing agents on the market allows a wide selection of system components to satisfy a particular application. Although the majority of epoxy adhesives are two-pack systems, heat activated one-pack adhesives are also available. Low molecular weight DGEBA liquid resins are the most commonly used. Higher molecular weight (EEW = 250–500) DGEBA epoxy resins improve adhesive strength because of the increased number of hydroxyl groups in the resin backbone. For applications requiring high temperature or improved chemical performance, the multifunctional epoxy phenol novolac and triglycidyl-*p*-aminophenol resins are employed. More recent products include vinyl epoxies. Adhesive systems modified with reactive diluents facilitate wetting of the

Table 27. Epoxy Adhesive Lap-Shear Strengths

Hardener	Lap-shear strength,[a] MPa[b]
Aliphatic polyamine	19
Polythiol cohardener	18
Aromatic diamine	24

[a]Adhesive strength.
[b]To convert MPa to psi, multiply by 145.

substrate, allowing more filler to be added and modifying handling characteristics; however, adhesive strength is reduced. Toughened epoxy adhesives are available.

Polyamines or polyamides are the curing agents for ambient, or slightly elevated, temperature cures, and aromatic polyamines or anhydride hardeners are used for hot cures. These systems provide exceptional bonding strength but slower cure time. Boron trifluoride amine complexes and dicyandiamide are used in one-component adhesives. Polythiols (polysulfides, polymercaptans) are the fast-curing hardeners in "5-min" consumer epoxy formulations. The lap-shear strengths of a DGEBA epoxy cured with different hardeners are given in Table 27.

Cationically cured UV laminating adhesives based on cycloaliphatic epoxies are emerging as an alternative to solvent-based adhesives. The "dark cure" of cationics allows UV exposure and post lamination in line. This process does not require UV exposure "through" the plastic barrier material.

Epoxy adhesives are expected to grow at GDP (3–4%) over the next decade. Increased usage in the automotive and recreational markets, and replacement of mechanical fasteners help offset the slowdown in the aerospace industry (see also Adhesive Compositions).

Tooling. Tools made with epoxy are used for producing prototypes, master models, molds and other parts for aerospace, automotive, foundry, boat building, and various industrial molded items (261). Epoxy tools are less expensive than metal ones and can be modified quickly and cheaply. Epoxy resins are preferred over unsaturated polyesters and other free-radical cured resins because of lower shrinkage, greater interlaminar bond strength and superior dimensional stability.

Most epoxy-based tooling formulations are based on liquid DGEBA resins. Aliphatic polyamines, amidoamines, or modified cycloaliphatic amines are used for ambient temperature cure, and modified aromatic diamines and anhydrides are used for high temperature cure. When high heat resistance is required ($>350^{\circ}$F), epoxy novolac resins can be employed. Reactive diluents such as aliphatic glycidyl ethers are often employed to permit higher filler load or to reduce the system viscosity for proper application. Fillers, reinforcing fibers, toughening agents, thixotropic agents, and other additives are often used depending on the desired application and final properties.

Tooling production uses four major processing methods: lamination, surface cast, splining, and casting. Lamination is made by alternating layers of glass cloth or fabric and formulated resin, usually on a framework of metal or plastic. Surface cast utilizes a filled resin compound that is applied onto the surface of a mold,

which is later filled with a core material that adheres to the casting compound. Splining employs heavily filled formulations that are directly applied to a surface and manually molded or leveled to the desired shape, before or after curing, with the help of proper tools. Lastly, casting compounds are filled formulations that are directly poured or compressed into a mold coated with a release agent.

Health and Safety Factors

There have been many investigations of the toxicity of various classes of epoxy-containing materials (glycidyloxy compounds). The use and interpretation of the vast amount of data available has been obscured by two factors: (*1*) proper identification of the epoxy systems in question and (*2*) lack of meaningful classification of the epoxy materials. In general, the toxicity of many of the glycidyloxy derivatives is low, but the diversity of compounds found within this group does not permit broad generalizations for the class. Information on toxicity and safe handling of epoxy compounds are summarized in References 262,263, and 264.

Diglycidyl ether of bisphenol A. Bisphenol A based epoxies are the most commonly used resins. Although unmodified bisphenol A epoxy resins have a very low order of acute toxicity, they should be handled carefully and personal contact should be avoided. Prolonged or repeated skin contact with liquid epoxy resins may lead to skin irritation or sensitization. Susceptibility to skin irritation and sensitization varies from person to person. Skin sensitization decreases with an increase in MW, but the presence of low MW fractions in the advanced resins may present a hazard to skin sensitization. Inhalation toxicity does not present a hazard because of low vapor pressure. DGEBA-based resins have been reported to cause minimal eye irritation. Toxicological studies support the conclusion that bisphenol A based epoxy resins do not present a carcinogenic or mutagenic hazard. Because of the solvents used, solution of epoxy resins are more hazardous to handle than solid resins alone. Depending on the solvents used, such solutions may cause irritation to the skin and eyes, are more likely to cause sensitization responses, and are hazardous if inhaled.

Epoxy phenol novolac resins. Acute oral studies indicate low toxicity for these resins. Eye studies indicate only minor irritation in animals. The EPN resins have shown weak skin sensitizing potential in humans.

Low MW epoxy diluents, particularly the aromatic monoepoxides such as phenyl glycidyl ether (PGE) are known to have high toxicity and should be handled with care. They are capable of causing skin and eye irritation and sensitization responses in people. They may also present a significant hazard from inhalation.

Curing agents. In general, amine curing agents are much more hazardous to handle than the epoxy resins, particularly at elevated temperatures. Aliphatic amines and anhydrides are capable of serious skin or eye irritation, sensitization, and even burns. Other curing agents possess consideration

variation in the degree of health hazards because of the variety of their chemical structures and it is impossible to generalize.

All suppliers provide material safety data sheets (MSDS), which contain the most recent toxicity data. These are the best sources of information and should be consulted before handling the materials.

Acknowledgments

The authors would like to acknowledge the contributions of Robert F. Eaton of the Dow Chemical Co. in Bound Brook, N.J., who contributed to the sections on cycloaliphatic epoxies and epoxidized vegetable oils and the cationic curing mechanism. We also would like to thank Timothy Takas of Reichhold who kindly reviewed the article. We are indebted to many colleagues in the Epoxy Products and Intermediates business at Dow Chemical for their assistance in many ways to make this article possible.

BIBLIOGRAPHY

"Epoxy Resins" in *EPST* 1st ed., Vol. 6, pp. 209–271, by H. Lee and K. Neville, The Epoxylite Corp.; in *EPSE* 2nd ed., Vol. 6, pp. 322–382, by Louis V. McAdams and John A. Gannon, CIBA-GEIGY Corp.

1. S. J. Hartman, *The Epoxy Resin Formulators Training Manual*, The Society of the Plastics Industry, Inc., New York, 1984, p. 1.
2. H. Lee and K. Neville, *Handbook of Epoxy Resins*, McGraw-Hill, Inc., New York, 1967, reprinted 1982.
3. Ger. Pat. 676,117 (1938) and U.S. Pat. 2,136,928 (Nov. 15, 1938), P. Schlack (to I. G. Farbenindustrie).
4. U.S. Pat. 2,324,483 (July 20, 1943), P. Castan (to Ciba-Geigy Corp.).
5. U.S. Pat. 2,456,408 (Dec. 14, 1948), S. O. Greenlee (to DeVoe & Raynolds).
6. D. Swern, *Chem. Rev.* **45**, 1 (1949).
7. E. O. C. Greiner, F. Dubois, and M. Yoneyama, *Epoxy Resins, Chemical Economics Handbook (CEH) Marketing Research Report*, Stanford Research Institute (SRI) International, Menlo Park, Calif., 2001.
8. Dow Chemical data, the Dow Chemical Co., Midland, Mich.
9. W. L. Faith, D. B. Keyes, and R. L. Clark, *Industrial Chemistry*, 3rd ed., John Wiley & Sons, Inc., New York, 1965, p. 404.
10. H. H. Szmant, *Organic Building Blocks of the Chemical Industry*, John Wiley & Sons, Inc., New York, 1989, p. 281.
11. P. H. Williams, *Encyclopedia of Chemical Technology*, 1st ed., Vol. 3, John Wiley & Sons, Inc., New York, 1965, pp. 857, 865.
12. W. F. Richey, *Encyclopedia of Chemical Technology*, 4th ed., Vol. 6, John Wiley & Sons, Inc., New York, 1993, pp. 140, 155.
13. U.S. Pat. 2,714,123 (July 26, 1955), G. F. Johnson (to Shell Oil Co.); Belgian Pat. 517,463 (Nov. 6, 1959) (to Solvay & CIE).
14. Jpn. Pat. 88 290,835 (Nov. 28, 1988), N. Nagato, H. Mori, and R. Ishioka (to Showa Denko K. K.); U.S. Pat. 4,634,784 (Jan. 6,1987), N. Nagato, H. Mori, K. Maki, and R. Ishioka (to Showa Denko K. K.).

15. Bisphenol A, Chem Systems Report, Sept. 2002.
16. U.S. Pat. 4,400,555 (Aug. 23, 1983), Mendiretta (to General Electric Co.); WO 00/35847 (June 22, 2000), G. M. Kissinger and R. Sato (to General Electric Co.).
17. W. G. Potter, *Epoxide Resins*, Springer-Verlag, New York, 1970.
18. U.S. Pat. 2,575,558 (Nov. 20, 1951), H. A. Newley and E. C. Shokal (to Shell Oil Co.).
19. U.S. Pat. 2,943,095 (June 28, 1960), N. H. Reinking (to Union Carbide Corp.).
20. U.S. Pat. 2,848,435 (Aug. 18, 1958), L. H. Griffin and J. H. Long (to Shell Development); U.S. Pat. 2,921,049 (Jan. 12, 1960), H. L. Moroson (to Reichhold Chemicals, Inc.); U.S. Pat. 3,069,434 (Dec. 18, 1962), S. P. Spence, A. R. Grover, F. P. Klosek, and R. E. Nicolson (to Union Carbide Corp.).
21. U.S. Pat. 4,499,255 (Feb. 12, 1985), C. S. Wang, H. Q. Pham, and J. L. Bertram (to the Dow Chemical Co.); Jpn. Pat. 61/195111A (Aug. 29, 1986), T. Ogata, H. Nakanishi, and M. Aritomi (to Tohto Kasei K. K.).
22. N. S. Enikolopyan, M. A. Markevitch, L. S. Sakhonenko, S. Z. Rogovina, and V. G. Oshmyan, *J. Polym. Sci., Chem. Ed.* **20**, 1231–1245 (1982).
23. D. O. Bowen and R. C. Whiteside, in R. F. Gould, ed., *Epoxy Resins*, Advances in Chemistry Series 92, American Chemical Society, Washington, D.C., 1970, p. 48.
24. U.S. Pat. 2643239 (June 23, 1953), E. C. Shokal, H. A. Newley, and T. E. Bradley (to Shell Oil Co.); U.S. Pat. 2,879,259 (Mar. 24, 1959), R. W. H. Tess (to Shell Development Co.).
25. U.S. Pat. 2,456,408 (Sept. 14, 1943), S. O. Greenlee (to Devoe & Raynolds Co., Inc.).
26. H. Batzer and S. A. Zahir, *J. Appl. Polym. Sci.* **19**, 601 (1975).
27. W. Burchard, S. Bantle, and S. A. Zahir, *Makromol. Chem.* **182**, 145 (1981).
28. U. Fuchslueger, H. Stephan, H.-J. Grether, and M. Grasserbauer, *Polymer* **40**, 661–673 (1999).
29. U.S. Pat. 3,634,323 (Jan. 11, 1972), R. M. Moran (to Ciba-Geigy Corp.).
30. U.S. Pat. 3,477,990 (Nov. 11, 1969), M. F. Dante and H. L. Parry (to Shell Oil Co.).
31. U.S. Pat. 3,948,855 (Apr. 6, 1976), W. O. Perry (to the Dow Chemical Co.).
32. U.S. Pat. 4,302,574 (Nov. 24, 1981), G. A. Doorakian and J. L. Bertram (to the Dow Chemical Co.).
33. U.S. Pat. 4,358,578 (Nov. 9, 1982), T. F. Brownscombe (to Shell Oil Co.).
34. U.S. Pat. 4,366,295 (Dec 28, 1982), M. C. Tyler, Jr. and A. L. McCrary (to the Dow Chemical Co.).
35. U.S. Pat. 4,808,692 (Feb. 28, 1989), H. Q. Pham and L. A. Ho (to the Dow Chemical Co.).
36. W. A. Romanchick and J. F. Geibel, *Org. Coat. Appl. Polym. Sci. Proc.* **46**, 410 (1982).
37. J. F. Geibel, *Org. Coat. Plast. Chem.* **43**, 545 (1980).
38. H. Batzer and S. A. Zahir, *J. Appl. Polym. Sci.* **21**, 1843 (1977).
39. D. P. Sheih and D. E. Benton, ASTM Special Technical Publication STP 1119, Analysis of Paints and Related Materials: Current Techniques for Solving Coatings Problems, 1992, pp. 41–56.
40. WO 01/16204 A1 (Mar. 8, 2001), S. MK. Li (to Shell International Research); WO Appl. 01/46287 A1 (June 28, 2001), R. R. Dominquez, H. Frank, and S. MK. Li (to Resolution Research Nederland B. V.).
41. U.S. Pat. 4,612,156 (Sept. 16, 1986), B. W. Heinemeyer and S. D. Tatum (to the Dow Chemical Co.).
42. J. E. White, H. C. Silvis, M. S. Winkler, T. W. Glass, and D. E. Kirkpatrick, *Adv. Mater.* **12**, 1791, 1800 (Dec. 2000).
43. Br. Pat. 980,509 (Jan. 13, 1965) (to Shell Oil Co.).
44. U.S. Pat. 5,275,853 (Jan. 4, 1994), H. C. Silvis and J. E. White (to the Dow Chemical Co.).

45. H. C. Silvis, C. N. Brown, S. L. Kram, and J. E. White, *Polym. Prepr.* **36**(2), 178–179 (1995).
46. T. Glass, H. Pham, and M. Winkler, in *Proceedings of the 58th SPE Annual Technical Conference and Exhibits (ANTEC 2000)*, Lauderdale, Fla., 2000.
47. U.S. Pat. 5,134,201 (July 28, 1992), M. N. Mang and J. E. White (to the Dow Chemical Co.).
48. U.S. Pat. 6,512,075 (Jan. 28, 2003), M. J. Tzou (to Nan Ya Plastics Corp. Taiwan).
49. Jpn. Pat. 08198949 A (Aug. 6, 1996), K. Ishihara, T. Sato, K. Aida, and T. Hoshono (to Tohto Kasei K.K.).
50. J. R. Griffith, *CHEMTECH* **12**, 290–293 (1982).
51. U.S. Pat. 3,879,430 (Apr. 22, 1975), J. R. Griffith and J. G. O'Rear (to the United States of America).
52. T. E. Twardowski and P. H. Geil, *J. Appl. Polym. Sci.* **42**, 69 (1991).
53. U.S. Pat. 2,521,912 (Sept. 12, 1950), S. O. Greenlee (to Devoe & Raynolds).
54. U.S. Pat. 4,785,061 (Nov. 15, 1988), C. S. Wang and Z. K. Liao (to the Dow Chemical Co.); Jpn. Pat. 200239346 (Sept. 5, 2000), Y. Murata and B. Shigeki (to Yuka Shell Epoxy Co.).
55. U.S. Pat. 4,394,497 (July 19, 1983), D. L. Nelson and B. A. Naderhoff (to the Dow Chemical Co.).
56. U.S. Pat. 2,806,016 (Sept. 10, 1957), C. G. Schwartzer (to Shell Development Co.).
57. K. L. Hawthorne and F. C. Henson, in R. S. Bauer, ed., *Epoxy Resin Chemistry II*, ACS Symposium Series 221, American Chemical Society, Washington, D.C., 1983, Chapt. 7, pp. 135–151.
58. U.S. Pat. 2,951,825 (Sept. 6, 1960), N. H. Reinking, B. P. Barth, and F. J. Castner (to the Union Carbide Corp.).
59. T. J. Galvin, M. A. Chaudhari, and J. J. King, *Chem. Eng. Prog.* **81**(1), 45–48 (1985).
60. Jpn. Pat. 3,315,436 (Aug. 19, 2002), Y. Murata, Y. Nakanishi, and M. Yosumura (to Shell Internationale Research B. V.).
61. I. Ogura and T. Imada, Dai Nippon Inks & Chemical (DIC) Technical Review No. 5, 1999.
62. U.S. Pat. 5,463,091 (Oct. 31, 1995), J. D. Earls, R. E. Hefner Jr., and P. M. Puckett (to the Dow Chemical Co.); U.S. Pat. 5,266,660 (Nov. 30, 1993), R. E. Hefner Jr., J. D. Earls, and P. M. Puckett (to the Dow Chemical Co.).
63. H.-J. Sue, J. D. Earls, R. E. Hefner Jr., M. I. Villarreal, E. I. Garcia-Meitin, P. C. Yang, C. H. Cheatham, and C. J. G. Plummer, *Polymer* **39**, 4707–4714 (1998).
64. R. S. Bauer, in G. D. Parfitt and A. V. Patsis, eds., *Organic Coatings, Science and Technology*, Vol. 5, Marcel Dekker, New York, 1983, pp. 1–33.
65. U.S. Pat. 3,288,789 (Nov. 29, 1966), M. Budnowski and M. Dohr (to Henkel & Cie. GmbH).
66. Br. Pat. 1,381,262 (1975); U.S. Pat. 4,147,737 (April 3, 1979), A. J. Sein, J. Reitberg, and J. M. Schouten (both to Internationale Octrool Maatschappij Octropa).
67. E. H. Catsiff, R. E. Coulehan, J. F. Diprima, D. A. Gordan, and R. Seltzer, in R. S. Bauer, ed., *Epoxy Resin Chemistry*, ACS Symposium Series 114, American Chemical Society, Washington, D.C., 1979, Chapt. 10, pp. 115–156.
68. R. Y. Ting, in C. A. May and Y. Tanaka, eds., *Epoxy Resins Chemistry and Technology*, 2nd ed., Marcel Dekker, Inc., New York, 1988, p. 551, 601.
69. H. Jahn, *J. Polym. Sci., Part C* **16**, 1829, 1841 (1967).
70. U.S. Pat. 4,273,921 (Apr. 21, 1980), J. L. Bertram and P. S. Sheih (to the Dow Chemical Co.).
71. U.S. Pat. 2,716,123 (Aug. 23, 1953), B. Phillips and F. Frostick Jr. (to Union Carbide Corp.).

72. P. K. T. Ording, *Waterborne and Solvent Based Epoxies and Their End User Applications*, John Wiley & Sons, Inc., New York, 1996, pp. 57, 100.
73. J. C. Kenny, T. Ueno, and K. Tsutsui, *J. Coat. Technol.* **68**, 855 (1996); T. Agawa and E. D. Dumain, *Proc. Waterborne High-Solids Powder Coat. Symp.* **24**, 342–353 (1997); B. V. Gregorovich and I. Hazan, *Prog. Org. Coat.* **24**, 131 (1994).
74. G. Webster, *Chemistry & Technology of UV & EB Formulation for Coatings, Inks & Paints*, Vol. 2, John Wiley & Sons, Inc., New York, 1997, pp. 41, 73.
75. U.S. Pat. 3,367,992 (Feb. 6, 1968), C. Bearden (to the Dow Chemical Co.); U.S. Pat. 3,524,901 (Aug. 18, 1970), D. J. Najvar (to the Dow Chemical Co.).
76. T. F. Anderson and V. B. Messick, in G. Pritchard, ed., *Developments in Reinforced Platics 1*, Allied Science Publishers Ltd., London, 1980, pp. 29, 58.
77. U.S. Pat. 4,397,970 (Aug. 9, 1983), K. D. Campbell, H. G. Langer, and P. H. Martin (to the Dow Chemical Co.).
78. H. Jahn and P. Goetzky, in C. A. May and Y. Tanaka, eds., *Epoxy Resins Chemistry and Technology*, 2nd ed., Marcel Dekker, Inc., New York, 1988, pp. 1049, 1087.
79. Annu. Book ASTM Stand. Section 8 (Plastics). Web site: http://www.astm.org.
80. H. Pasch, R. Unvericht, and M. Resch, *Angew. Makromol. Chem.* **212**, 191–200 (1993); H. Pasch, J. Adrian, and D. Braun, *GIT Spezial Separation* **21**(2), 104–108 (2001).
81. D. Crozier, G. Morse, and Y. Tajima, *SAMPE J.* **18**(5), 17–22 (1982).
82. A. Durbetaki, *Anal. Chem.* **28**, 2000 (1956).
83. R. Jay, *Anal. Chem.* **36**, 667 (1964).
84. B. Dobinson, W. Hofmann, and B. Stark, *The Determination of Epoxide Groups*, Pergamon Press, Elmsford, N.Y., 1969.
85. G. H. Schneer, W. van Gilder, V. E. Hauser, and P. E. Schmidt, *IEEE Trans. Electron. Devices* ED–15 (1969).
86. H. Lee and K. Neville, *Handbook of Epoxy Resins*, McGraw-Hill, Inc., New York, 1967, reprinted 1982.
87. M. C. Paputa Peck, R. O. Carter III, and S. B. A. Qaderi, *J. Appl. Polym. Sci.* **33**(1), 77–86 (1987); G. Lachenal and Y. Ozaki, *Macromol. Symp.* **141** 283–292 (1999). 13th European Symposium on Polymer Spectroscopy, 1998.
88. W. B. Moniz and C. F. Poranski Jr., *Org. Coat. Plast. Chem.* **39**, 99–102 (1978).
89. E. Mertzel and J. L. Koenig, in K. Dusek, ed., *Epoxy Resins and Composites III, Advances in Polymer Science 75*, Springer-Verlag, Berlin, 1986, pp. 73, 112.
90. W. A. Dark, E. C. Conrad, and L. W. Crossman Jr., *J. Chromatogr.* **91**, 247–60 (1974).
91. D. J. Crabtree and D. B. Hewitt, *Liq. Chromatogr. Polym. Relat. Mater.* **8**, 63–77 (1977), Chromatographic Science Series.
92. G. Eppert and G. Liebscher, *J. Chromatogr.* **238**, 399 (1982).
93. S. A. Zahir and S. Bantle, in R. S. Bauer, ed., *Epoxy Resin Chemistry II*, ACS Symposium Series 221. American Chemical Society, Washington, D.C., 1983, pp. 245, 262.
94. D. K. Hadad, in C. A. May and Y. Tanaka, eds., *Epoxy Resins Chemistry and Technology*, 2nd ed., Marcel Dekker, Inc., New York, 1988, pp. 1089, 1172.
95. W. Lwowski, in A. R. Katritsky and C. W. Rees, eds., *Comprehensive Heterocyclic Chemistry*, Vol. 7, Pergamon Press, Oxford, 1984, pp. 1, 16.
96. R. E. Parker and N. S. Isaacs, *Chem. Rev.* **59**, 737, 799 (1959).
97. Y. Tanaka and R. S. Bauer, in C. A. May and Y. Tanaka, eds., *Epoxy Resins Chemistry and Technology*, 2nd ed., Marcel Dekker, Inc., New York, 1988, pp. 465, 550.
98. L. Shechter and J. Wynstra, *Ind. Eng. Chem.* **48**, 86 (1956)
99. I. T. Smith, *Polymer* **2**, 95 (1961).
100. N. B. Chapman, R. E. Parker, and N. S. Issacs, *J. Chem. Soc.* **2**, 1925 (1959).
101. N. G. Rondan, M. J. Marks, S. Hoyles, and H. Pham, paper presented at the *225th ACS National Meeting*, New Orleans, La., March 2003.
102. R. F. Eaton, *Paint Coat. Ind*. 76–80 (June 1999).

103. L. Shechter, J. Wynstra, and R. P. Kurkjy, *Ind. Eng. Chem.* **48**, 94 (1956).
104. K. Horie, H. Hiura, M. Sawada, I. Mita, and H. Kambe, *J. Polym. Sci., A–1* **8**, 1357 (1970).
105. K. Dusek, M. Ilavsky, and S. Lunak, *J. Polym. Sci., Polym. Symp.* **53**, 29 (1975).
106. C. V. Hare, *Protective Coatings: Fundamentals of Chemistry and Composition*, Technology Publishing Co., Pittsburg, Pa., 1994, pp. 187, 238.
107. Br. Pat. 886, 767 (Jan. 10, 1962), P. Halewood [to CIBA (A.R.L) Ltd.].
108. W. R. Ashcroft, in B. Ellis, ed., *Chemistry and Technology of Epoxy Resins*, 1st ed., Blackie Academic & Professional, Glasgow, U.K., 1993, pp. 37, 71.
109. M. Fedtke, F. Domaratius, and A. Pfitzmann, *Polym. Bull.* **23**, 381, 388 (1990).
110. U.S. Pat. 3,390,124 (June 25, 1968), J. B. Kittridge and A. L. Michelli (to Minnesota Mining & Manufacturing Co.).
111. M. D. Gilbert, N. S. Schneider, and W. J. McKnight, *Macromolecules* **24**, 360 (1991).
112. S. A. Zahir, in G. D. Parfitt and A. V. Patsis, eds., *Advances in Organic Coatings Science and Technology, Vol. IV: Sixth International Conference in Organic Coatings Science and Technology*, Technomic Publishing Co., Inc., Lancaster, Pa., 1982, p. 83.
113. M. J. Husband, in P. Oldring and G. Haywood, eds., *Resins for Surface Coatings, SITA Technology*, John Wiley & Sons Ltd., London, 1987, pp. 63, 167.
114. P. J. Madec and E. Marechal, *Makromol. Chem.* **184**, 323 (1983).
115. L. Matejka, J. Lovy, S. Pokorny, K. Bouchal, and K. Dusek, *J. Polym. Sci., Polym. Chem. Ed.* **21**, 2873 (1983).
116. H. Kunitomo, in *Proceedings of the 26th Technical Conference of the Japan Society of Epoxy Resin Technology*, Tokyo, Japan, July 2002, pp. 19, 33.
117. A. Gardziella, L. A. Pilato, and A. Knop, *Phenolic Resins Chemistry, Applications, Standardization, Safety and Ecology*, 2nd ed., Springer, Berlin, 1999.
118. A. J. Kirsch, *50 Years of Amino Coatings*, American Cyanamid Co., Wayne, N.J., 1986.
119. T. M. Rees, *J. Oil Color Chem. Assoc.* **71**(2), 39, 41 (Feb. 1988).
120. U.S. Pat. 3,020,262 (Feb. 6, 1962), G. P. Speranza (to Jefferson Chemical); U.S. Pat. 4,658,007 (14 Apr. 1987), M. J. Marks and R. A. Plepys (to the Dow Chemical Co.).
121. M. J. Marks, *Polym. Mater. Sci. Eng. (Am. Chem. Soc., Div. Polym. Sci. Eng.)* **58**, 864 (1988).
122. D. A. Shimp, F. A. Hudock, and S. J. Ising, paper presented at 33rd SAMPE, Anaheim, Calif, March 7–10, 1988.
123. B. A. Rozenberg, in K. Dusek, ed., *Epoxy Resins and Composites II*, Advances in Polymer Science 75, Springer-Verlag, Berlin, 1986, pp. 146, 156.
124. F. Ricciardi, W. A. Romanchick, and M. M. Joullie, *J. Polym. Sci., Polym, Chem. Ed.* **21**, 1475 (1983).
125. M. S. Heise and G. C. Martin, *Macromolecules* **22**, 99 (1989).
126. J. D. B. Smith, *Org. Coat. Plast. Chem.* **39**, 42–46 (1978).
127. R. J. Arnold, *Mod. Plast.* **41**(4), 149 (1964).
128. J. J. Harris and S. C. Temin, *J. Appl. Polym. Sci.* **10**, 523 (1966).
129. J. V. Crivello and J. H. W. Lam, *Macromolecules* **10**, 1307 (1977); *ACS Symp. Ser.* **114**, 1 (1979).
130. R. F. Eaton and K. T. Lamb, paper presented at the *23th International Waterborne, Higher Solids and Powder Coatings Symposium*, New Orleans, La., Feb. 1996.
131. J. M. Land, A. Aubuchon, C. Pundmann, W. L. Dechent, and J. O. Stoffer, *Book of Abstracts, 211th ACS National Meeting*, New Orleans, La., March 24–28, 1996, *PMSE-181*, American Chemical Society, Washington, D.C., 1996.
132. D. W. Brooker, G. R. Edwards, and A. McIntosh, *J. Oil Color Chem. Assoc.* **52**, 989–1034 (1969); G. K. Noren, *J. Coat. Technol.* **72**(905), 53–59 (2000).
133. J. E. Mark and B. Erman, *Rubber Elasticity: A Molecular Primer*, John Wiley & Sons, New York, 1988.

134. T. I. Smith, *J. Polym. Sci., Polym. Symp.* **46**, 97 (1974).
135. F. Lohse and R. Schmid, paper presented at the Fifth International Conference in Organic Coatings Science and Technology, Athens, FATIPEC, Liége, Belgium, 1979.
136. I. Ogura, Dainippon Ink & Chemicals (DIC) Technical Review No. 7, 2001. Paper written in Japanese.
137. T. Kamon and H. Furukawa, in K. Dusek, ed., *Epoxy Resins and Composites IV*, Advances in Polymer Science 80, Springer-Verlag, Berlin, 1986, pp. 173, 202.
138. E. F. Oleinik, in Ref. 137, pp. 50, 99.
139. W. R. Ascroft, *Eur. Coat. J.* **4**, 229, 241 (1991).
140. R. S. Bauer, *CHEMTECH* **10**, 692 (Nov. 1980).
141. C. Rooney, *Mod. Paint Coat.* **81**(5), 44–50 (1991).
142. J. K. Gillham and C. A. Grandt, in S. S. Labana, ed., *Chemistry and Properties of Cross-Linked Polymers*, Academic Press, Inc., Orlando, Fla., 1977, pp. 491, 520.
143. J. D. Keenan, *J. Appl. Polym. Sci.* **24**, 2375, 2387 (1979).
144. C. A. May, ed., *Chemorheology of Thermosetting Polymers*, ACS Symposium Series 227, American Chemical Society, Washington, D.C., 1983.
145. D. Adolf and J. E. Martin, *Macromolecules* **23**, 3700, 3704 (1990).
146. *General Guide to Formulating with Dow Epoxy Resins*, the Dow Chemical Co., Midland, Mich., 1983.
147. B. Ellis, in B. Ellis, ed., *Chemistry and Technology of Epoxy Resins*, 1st ed., Blackie Academic & Professional, Glasgow, U.K., 1993, pp. 72, 116.
148. J. P. Pascault, H. Sautereau, J. Verdu, and R. J. J. Williams, *Thermosetting Polymers*, Marcel Dekker, Inc., New York, 2001.
149. J. C. Seferis and L. Nicolais, eds., *The Role of Polymer Matrix in Processing and Structural Properties of Composites*, Plenum Press, New York, 1983, pp. 127–145.
150. J. K. Gillham, *Encyclopedia of Polymer Science and Engineering*, 2nd ed., John Wiley & Sons, Inc., New York, 1986, pp. 519, 524.
151. X. Wang and J. K. Gilham, *J. Coat. Technol.* **64**, 37, 45 (1992).
152. H. E. Adabbo and R. J. J. Williams, *J. Appl. Polym. Sci.* **27**, 1327, 1334 (1982).
153. J. B. Enns and J. K. Gillham, *J. Appl. Polym. Sci.* **28**, 2567 (1983).
154. C. M. Tung and J. P. Dynes, *J. Appl. Polym. Sci.* **27**, 569, 574 (1982); M. E. Smith and H. Ishida, *J. Appl. Polym. Sci.* **73**, 593, 600 (1999).
155. T. Glauser, M. Johansson, and A. Hult, *Polymer* **40**, 5297, 5302 (1999).
156. K. Dusek, in K. Dusek, ed., *Epoxy Resins and Composites III*, Advances in Polymer Science 78, Springer-Verlag, Berlin, 1986, pp. 1, 59.
157. S. G. Croll, in K. L. Mittal, ed., *Adhesion Aspects of Polymeric Coatings*, Plenum Press, New York 1983.
158. D. B. Adolf and J. E. Martin, *J. Comp. Mater.* **30**(1) 13–34 (1996).
159. J. C. Arnold, *Polym. Eng. Sci.* **35**(2), 165–169 (1995).
160. E. S.-W. Kong, in K. Dusek, ed., *Epoxy Resins and Composites IV*, Advances in Polymer Science 80, Springer-Verlag, Berlin, 1986, pp. 125, 172.
161. R. S. Durran, *J. Non-Cryst. Solids* **131–133**, 497–504 (1990); D. J. Plazek and Z. N. Frund, *J. Polym. Sci., Bert. Polym. Phys.* **28**, 431–448 (1990).
162. S. L. Maddox and J. K. Gillham, *J. Appl. Polym. Sci.* **64**, 55–67 (1997).
163. L. W. Hill, *J. Coat. Technol.* **64**(808), 29 (1992).
164. C. Billaud, M. Vandeuren, R. Legras, and V. Carlier, *Appl. Spectr.* **56**, 1413–1421 (2002).
165. G. Wisanrakkit and J. K. Gilham, *J. Appl. Polym. Sci.* **41**, 2885, 2929 (1990).
166. C. W. Macosko and D. R. Miller, *Macromolecules* **9**, 199, 206 (1976); J. Mijovic and C. H. Lee, *J. Appl. Polym. Sci.* **29**, 2155, 2170 (1989).
167. C. A. May, ed., *Chemorheology of Themosetting Polymers*, ACS Symposium Series 227, American Chemical. Society, Washington, D.C., 1983.

168. S. D. Senturia and N. F. Sheppard Jr., in K. Dusek, ed., *Epoxy Resins and Composites IV*, Advances in Polymer Science 80, Springer-Verlag, Berlin, 1986, pp. 1, 47.
169. G. P. Johari and D. A. Wasylyshyn, *J. Polym. Sci., Polym. Phys.* **38**, 122–126 (2000).
170. J. H. Flynn, in H. F. Mark, N. M. Bikales, C. G. Overberger, G. Menges, eds. *Encyclopedia Polymer Science and Engineering*, 2nd ed., Suppl. Vol., John Wiley & Sons, New York, 1989, pp. 715, 723.
171. Annu. Book ASTM Stand. Web site: http://www.astm.org
172. J. M. Charlesworth, *Polym. Eng. Sci.* **28**, 230 (1988).
173. M. J. Marks, *Polym. Mater. Sci. Eng.* **66**, 365 (1992).
174. A. J. Lesser and E. Crawford, *J. Appl. Polym. Sci.* **66**, 387, 395 (1997); E. Crawford and A. J. Lesser, *J. Appl. Polym. Sci., Part B: Polym. Phys.* **36**, 1371, 1382 (1998).
175. C. W. Macosko and D. R. Miller, *Macromolecules* **9**, 206, 211 (1976); D. R. Miller, E. M. Valles, and C. W. Macosko, *Polym. Eng. Sci.* **19**, 272, 283 (1979).
176. E. D. Crawford and A. J. Lesser, *Polym. Eng. Sci.* **39**, 385, 392 (Feb. 1999).
177. J. G. Williams, *Fracture Mechanics of Polymers*, Ellis Horwood, Chichester, U.K., 1984.
178. A. J. Kinloch, in K. Dusek, ed., *Epoxy Resins and Composites 1*, Advances in Polymer Science 72, Springer-Verlag, Berlin, 1986, pp. 1, 59.
179. W. J. Cantwell and H. N. Kausch, in B. Ellis, ed., *Chemistry and Technology of Epoxy Resins*, 1st ed., Blackie Academic & Professional, Glasgow, U.K., 1993, pp. 144, 174.
180. J. M. Charlesworth, *Polym. Eng. Sci.* **28**, 221 (1988).
181. E. Urbaczweski-Espuche, J. Galy, J. Ferard, J. Pascault, and H. Sautereau, *Polym. Eng. Sci.* **31**, 1572 (1991).
182. J. Galy, J. Gerard, H. Sautereau, R. Frassine, and A. Pavan, *Polym. Networks Blends* **4**, 105 (1994).
183. R. A. Dubois, D. S. Wang, and D. Sheih, in C. B. Arends, ed., *Polymer Toughening*, Marcel Dekker, Inc., New York, 1996, pp. 381, 409.
184. R. A. Dubois and D. S. Wang, *Prog. Org. Coat.* **22**, 161 (1993).
185. J. P. Pascault, H. Sautereau, J. Verdu, and R. J. J. Williams, *Thermosetting Polymers*, Marcel Dekker, Inc., New York, 2001, p. 400.
186. L. T. Drzal, in K. Dusek, ed., *Epoxy Resins and Composites II*, Advances in Polymer Science 75, Springer-Verlag, Berlin, 1986, pp. 3, 32.
187. R. G. Schmidt and J. P. Bell, in K. Dusek, ed., *Epoxy Resins and Composites II*, Advances in Polymer Science 75, Springer-Verlag, Berlin, 1986, pp. 33, 71.
188. Z. W. Wicks Jr., F. N. Jones, and S. P. Pappas, *Organic Coatings Science and Technology*, 2nd ed., Wiley-Interscience, New York, 1999, pp. 77, 111.
189. W. Brostow and R. D. Corneliussen, eds., *Failure of Plastics*, Hanser, Munich, 1989.
190. U.S. Pat. 4,051,195 (Sept. 27, 1977), M. F. McWhorter (to Celanese Corp.).
191. R. F. Eaton and K. T. Lamb, in *SPE Proceedings*, Epoxy Resin Formulators Division of the Society of Plastic Industry, Inc., Aspen Co., May 1996 (Paper 7).
192. M. DiBenedetto, *Mod. Paint. Coat*. 39 (Jul. 1980).
193. J. Melloan, paper presented at the *Epoxy Resins Formulators Division of SPI Meeting*, Atlanta, Ga., Nov. 1983, The Society of Plastics Industry, New York.
194. Z. Wang, J. Massam, and T. J. Pinnavaia, in T. J. Pinnavaia and G. W. Beall, eds., *Polymer-Clay Nanocomposites*, John Wiley & Sons, New York, 2000, pp. 127, 149.
195. J. H. Park and S. C. Jana, *Macromolecules* **36**, 2758–2768 (2003).
196. *Proceedings of POSS (Hybrid Plastics, Inc.) Nanotechnology Conference*, Huntington Beach, Calif., Sept. 2002.
197. M. J. Biercuk, M. C. Llaguno, M. Radosavljevic, J. K. Hyun, A. T. Johnson, and J. E. Fischer, *J. Appl. Phys. Lett.* **80**, 2767, 2769, (2002).
198. R. A. Dubois and P. S. Sheih, *J. Coat. Technol.* **64**, 51 (1992).
199. B. L. Burton and J. L. Bertram, in C. B. Arends, ed., *Polymer Toughening*, Marcel Dekker, Inc., New York, 1996, pp. 339, 379.

200. H. S. Sue, E. I. Garcia-Meitin, and D. M. Pickleman, in N. P. Cheremisinoff, ed., *Rubber-Modified High Performance Epoxies*, CRC Press, Boca Raton Fla., 1993, Chapt. 18, pp. 661, 700.
201. A. F. Yee, J. Du, and M. D. Thouless, in D. R. Paul and C. R. Bucknall, eds., *Polymer Blends*, Vol. 2, John Wiley & Sons, Inc., New York, 2000, pp. 226, 267.
202. Y. Huang, D. L. Hunston, A. J. Kinloch, and C. K. Riew, in C. K. Riew and A. J. Kinloch, eds., *Toughened Plastics 1*, Advances in Chemistry Series 233, American Chemical Society, Washington, D.C., 1993, pp. 1, 35.
203. C. K. Riew, E. H. Rowe, and A. R. Siefert, *ACS Adv. Chem. Ser.* **154**, 326 (1976).
204. H. Chen, N. Verghese, H. Pham, and N. Jivraj, paper presented at the 9th Annual International Conference on Composites Engineering, San Diego, Calif., July 2002.
205. U.S. Pat. 4,708,996 (Nov. 24, 1987), D. K. Hoffman and C. B. Arends (to the Dow Chemical Co.).
206. H. J. Sue, *Polym. Eng. Sci.* **31**, 275 (1991).
207. U.S. Pat. 4,594,291 (June 10, 1986); U.S. Pat. 4,725,652 (Feb. 16, 1988), J. L. Bertram, L. L. Walker, and V. I. W. Stuart (both to the Dow Chemical Co.).
208. J. M. Dean, P. M. Lipic, R. B. Grubbs, R. F. Cook, and F. S. Bates, *J. Polym. Sci., Part B: Polym. Phys.* **39**, 2996, 3010 (2001); S. Ritzenthaler, F. Court, and L. David, *Macromolecules* **35**, 6245, 6254 (2002).
209. S. R. White, N. K. Sottos, P. H. Geubelle, J. S. Moore, M. R. Kessler, S. R. Sriram, E. N. Brown, and S. Viswanathan, *Nature* **409**, 794, 797 (2001).
210. E. O. C. Greiner, F. Dubois, and M. Yoneyama, *Epoxy Resins*, Chemical Economics Handbook (CEH) Marketing Research Report, Stanford Research Institute (SRI) International, Menlo Park, Calif., 2001.
211. E. Linak, F. Dubois, and M. Yoneyama, *Epoxy Surface Coatings*, Chemical Economics Handbook (CEH) Marketing Research Report, Stanford Research Institute (SRI) International, Menlo Park, Calif., 2001.
212. E. W. Flick, *Contemporary Industrial Coatings, Enviromentally Safe Formulations*, Noyes Publishers, Park Ridge, N.J., 1985.
213. R. F. Eaton and K. T. Lamb, *J. Coat. Technol.* **68**, 49 (1996).
214. U.S. Pat. 3,984,299 (Oct. 5, 1976), R. D. Jerabek (to PPG Industries, Inc.); U.S. Pat. 4,009,133 (Feb. 22, 1977), J. E. Jones (to PPG Industries, Inc.).
215. U.S. Pat. 4,212,781 (July 15, 1980), J. M. Evans and V. W. Ting (to SCM Corp.).
216. E. C. Galgoci and P. C. Komar, *Paints Coat. Ind*. 50 (Aug. 1994).
217. D. S. Kincaid, P. Komar, and J. R. Hite, paper presented at the 24th International Waterborne, High Solids and Powder Coatings Symposium, New Orleans, La., 2002.
218. M. D. Soucek, G. Teng, and S. Wu, *J. Coat. Technol.* **73**, 117, 125 (Oct. 2001).
219. E. Linak and A. Kishi, *Thermoset Powder Coatings*, Chemical Economics Handbook (CEH) Marketing Research Report, Stanford Research Institute (SRI) International, Menlo Park, Calif., 2002.
220. R. Amey and R. Farabaugh, *Mod. Paint Coat*. 28, 30 (June 1997).
221. H. Nowack, *Proc. PCE 2000* 365, 375 (2000).
222. P. Horinka, *Powder Coating Magazine* 33, 48 (Aug. 2002).
223. K. Buysens and K. Jacques, *Eur. Coat. J.* 22, 26 (Sept. 2001).
224. D. L. Steele, *Surface Coat. Aus.* 6, 12 (Oct. 1992); W. Wood, *J. Protective Coat. Linings* 32, 38 (Apr. 1987).
225. U.S. Pat. 5,275,645 (Jan. 4, 1994), L. R. Ternoir, R. E. Foscante, and R. L. Gasmens; U.S. Pat. 5,618,860 (Apr. 8, 1997), N. R. Mowrer, R. E. Foscante, and J. L. Rojas (to Ameron International Corp.).
226. U.S. Pat. 5,508,325 (Apr. 16, 1996), G. P. Craun, D. J. Telford, and H. J. DeGraaf (to the Glidden Co.).
227. U.S. Pat. 4,119,595 (Oct. 10, 1978), R. S. Bauer and J. A. Lopez (to Shell Oil Co.).

228. J. T. K. Woo, V. Ting, J. Evans, C. Ortiz, G. Carlson, and R. Marcinko, in R. S. Bauer, ed., *Epoxy Resin Chemistry 2*, American Chemical Society, Washington, D.C., 1983, pp. 283, 300.
229. U.S. Pat. 5,532,297 (Jul. 2, 1996), J. T. K. Woo, G. C. Pompighano, D. E. Awarski, and K. A. Packard (to the Glidden Co.).
230. P. Newman, *The Canmaker* 57 (Apr. 2001).
231. D. Hayes, *The Canmaker* 37, 40 (Nov. 1998).
232. Eur. Pat. Appl. EP 493133 A2 (1992), N. Sato, and K. Imazu (to Toyo Seikan Kaisha Ltd., Japan).
233. Bisphenol A: Information Sheet from the Global Industry Group, Safety of Epoxy Can Coatings (Oct. 2002) at http://www.bisphenol-a.org; Statement from CEPE (European Confederation of Paints, Printing Inks and Artists Colours Manufacturers), Feb. 2000.
234. P. Hitchin, *The Canmaker* 43, 46 (Oct. 2001).
235. U.S. Pat. 6,472,480 (Oct. 29, 2002), R. L. Anderson (to BP Corp. North America Inc.); U.S. Pat. 6,235,102 B1 (May 22, 2002), G. G. Parekh and L. P. Seibel (to the Valspar Corp.).
236. U.S. Pat. 4,650,718 (Mar. 17, 1987), D. A. Simpson, D. L. Singer, R. Dobenko, W. P. Blackburn, and C. M. Kania (to PPG Industries).
237. L. Mauro, *25th FATIPEC Congr.* **4**, 1, 10 (2000).
238. Eur. Pat. Appl. 581175 A2 (1994), K. Huemke and C. Sinn (BASF).
239. Jpn. Pat. 08003483 A2 (1996), H. Haishi, M. Kume, H. Ishiiand, and K. Myawaki (to Kansai Paint Co. Ltd; Nippon Packaging K.K.).
240. U.S. Pat. Appl. 2002139673 A1 (2002), Y. Kojima and M. Yamada (to Nippon Paint).
241. Eur. Pat. Appl. 0974623 A2 (2000), H. Sakamoto, T. Kawanami, I. Kawakami, T. Kokubun, T. Saito, and S. Yoshimatsu (to Nippon Paint Co., Ltd., Japan).
242. G. Mauer and D. Singer, *PPG Technol. J*. 63, 72. (1999).
243. Y. Okude and S. Ishikura, *Prog. Org. Coat.* **26**, 197, 205 (1995).
244. G. E. Green, B. P. Stark, and S. A. Zahir, *J. Macromol. Sci. Revs. Macromol. Chem.* **21**, 187 (1981/1982).
245. P. Kelly, G. Pritchard, eds., *Reinforced Plastics Durability*, CRC Press, Boca Raton, Fla., 1999, pp. 282–321.
246. M. R. Thoseby, B. Dobinson, and C. H. Bull, *Br. Polym. J.* **18**, 286 (1986).
247. U. Helrold, J. Mason, N. Verghese, H. Chen, and H. Reddy, in *Proceedings of NACE Corossion 2003 Conference*, Houston, Tex., March 16–20, 2003.
248. D. Kriegh, ed., *Epoxies with Concrete*, American Concrete Institute, Detroit, Mich., 1968; R. L. McGown, in *Proceedings of the 1991 Steel, Structures, Painting Council (SSPC) National Conference and Exhibition*, Long Beach, Calif.
249. H. Mihashi and Y. Kaneko, *Transactions Mater. Res. Soc. Japan* **25**, 557, 560 (2000).
250. S. Ehrler, *PC Fab* 32, 38 (Apr. 2002); Part 2, PC Fab 32, 36 (May 2002).
251. W. Christiansen, D. Shirrell, B. Aguirre, and J. Wilkins, in *Proceedings of the Technical Conference*, IPC Printed Circuits Expo 2001, Anaheim, Calif., Apr. 2001, pp. SO3-1-1, SO3-1-7.
252. J. Sharma, M. Choate, and S. Peters, in *Proceedings of the Technical Conference*, IPC Printed Circuits Expo 2002, Long Beach, Calif., Mar. 2002, pp. SO5-1-1, SO5-1-8.
253. D. Sober, in Base Material Basics, *IPC Printed Circuits Expo 2002*, Long Beach, Ca.
254. U.S. Pat. 5,506,313 (Apr. 9, 1996), P. Flury, C. W. Mayer, W. Scharf, and E. Vanoli (to Ciba-Geigy Corp.).
255. C. S. Cho, L. W. Chen, and Y. S. Chiu, *Polym. Bull.* **41**(1), 45, 52 (1998).
256. D. K. Luttrull and F. E. Hickman III, Future Circuits International, Mar. 2001.
257. U.S. Pat. 3,754,071 (Aug. 21, 1973), O. Ernst, E. Kusenberg, E. Hubler, and H. R. Aus Der Au (to Ciba-Geigy AG).
258. K. Ito and Y. Nakamura, *IEEE Electrical Insulation Mag.* **6**(4), 25, 32 (1990).

259. T. M. Goulding, in A. Pizzi and K. L. Mittal, eds., *Handbook of Adhesive Technology*, 2nd ed., Marcel Dekker, Inc., New York, 2003, pp. 823, 838.
260. A. F. Lewis, in C. A. May and Y. Tanaka, eds., *Epoxy Resins Chemistry and Technology*, 2nd ed., Marcel Dekker, Inc., New York, 1988, pp. 653, 718.
261. J. Sheehan, *the Epoxy Resin Formulators Training Manual*, The Society of the Plastics Industry, Inc., New York, 1984, Chapt. XV, p. 175.
262. J. Waechter, *Patty's Industrial Hygiene and Toxicology*, 5th ed., Vol. 6, John Wiley & Sons, Inc., New York, 2001, Chapts. 82 and 83, pp. 993, 1145.
263. *Epoxy Resin Systems Safe Handling Guide*, the Society of Plastics Industry (SPI), Inc., New York, Sept. 1997. Publication No. AE-155. Web site: http://www.plasticsindustry.org/about/epoxy/epoxy_guide.htm.
264. Epoxy Resins and Curing Agents, prepared by the Epoxy Resins Committee of the Association of Plastics Manufacturers in Europe (APME), Jan. 1996. Web site: http://www.apme.org/dashboard/presentation_layer_htm/dashboard.asp.

GENERAL REFERENCES

B. Ellis, ed., *Chemistry and Technology of Epoxy Resins*, 1st ed., Blackie Academic & Professional, Glasgow, U.K., 1993.
H. Lee and K. Neville, *Handbook of Epoxy Resins*, McGraw-Hill, Inc., New York, 1967. Reprinted 1982.
C. A. May and Y. Tanaka, eds., *Epoxy Resins Chemistry and Technology*, 2nd ed., Marcel Dekker, Inc., New York, 1988.
B. Sedlacek and J. Kahovec, eds., *Crosslinked Epoxies*, Walter de Gruyter, Berlin, 1987.
K. Dusek, ed., *Epoxy Resins and Composites I–IV*, Advances in Polymer Science 72, 75, 78, 80, Springer-Verlag, Berlin, 1986.
Epoxy Resins, Advances in Chemistry Series 92, American Chemical Society, Washington, D.C., 1970.
Epoxy Resin Chemistry, ACS Symposium Series 114, American Chemical Society, Washington, D.C., 1979.
Epoxy Resin Chemistry II, ACS Symposium Series 221, American Chemical Society, Washington, D.C., 1983.
The Epoxy Resin Formulators Training Manual, the Society of Plastics Industry, Inc., New York, 1984.
E. O. C. Greiner, F. Dubois, and M. Yoneyama, *Epoxy Resins*, Chemical Economics Handbook (CEH) Marketing Research Report, Stanford Research Institute (SRI) International, Menlo Park, Calif., 2001.
J. W. Muskopf and S. B. McCollister, *Ullman's Encyclopedia of Industrial Chemistry*, 5th ed., Vol. A9, 1987, pp. 547–563.

HA. Q. PHAM
MAURICE J. MARKS
Dow Chemical

ETHYLENE COPOLYMERS. See Volume 6.

ETHYLENE OXIDE POLYMERS

Introduction

Poly(ethylene oxide) [25322-68-3] (PEO) is a water-soluble, thermoplastic polymer produced by the heterogeneous polymerization of ethylene oxide. The white, free-flowing resins are characterized by the following structural formula:

$$-(CH_2CH_2O)_n-$$

The resins are available in a broad range of molecular weight grades, from as low as 100,000 to over 7×10^6. Although most commonly known as poly(ethylene oxide) resins, they are occasionally referred to as poly(ethylene glycol) or poly-oxyethylene resins. The CAS Registry Number of these resins is also used for low molecular weight oligomers of ethylene oxide, eg, tetraethylene glycol.

Physical Properties

Crystallinity. At molecular weights of 105–107, poly(ethylene oxide) forms a highly ordered structure. This has been confirmed by NMR and X-ray diffraction patterns and by the sharpness of the crystalline melting point (62–67°C). However, the highest degree of crystallinity (ca 95%) is obtained at a molecular weight of 6000. The polymer chain contains seven structural units per fiber identity period (1.93 nm) (1). The diffraction pattern of the monoclinic unit cell of poly(ethylene oxide) contains four molecular chains, in which $a = 0.796$ nm, $b = 1.311$ nm, $c = 1.939$ nm, and $\beta = 124°48'$. Infrared studies show that the oxygen atoms of the crystalline polymer are in the gauche configuration. Because of this arrangement, the intermolecular dipole forces are oriented along the axis of the helix and ca 15 monomer units are involved within a single repeat unit. The heat of fusion of the polymer is 8.3 kJ (1980 cal) per structural unit (2). The high molecular weight poly(ethylene oxide) resins are of the spherulitic structure (3). Proper annealing of a melt-cast film produces a distinct lamellar structure. The molecular conformation of poly(ethylene oxide), as determined by the use of X-ray diffraction, IR, and Raman spectroscopic methods, is shown in Figure 1.

Density. Although the polymer unit cell dimensions imply a calculated density of 1.33 g/cm^3 at 20°C, and extrapolation of melt density data indicates a density of 1.13 g/cm^3 at 20°C for the amorphous phase, the density actually measured is 1.15–1.26 g/cm^3, which indicates the presence of numerous voids in the structure.

Glass-Transition Temperature. The glass transition (qv) temperature, T_g, of poly(ethylene oxide) has been measured over the molecular weight range of 10^2–10^7 (4,5). The T_g–molecular weight relationship is shown in Figure 2. These data indicate a rapid rise in the transition temperature to a maximum of −17°C for a molecular weight of 6000. The highest percentage of crystalline character

Encyclopedia of Polymer Science and Technology. Copyright John Wiley & Sons, Inc. All rights reserved.

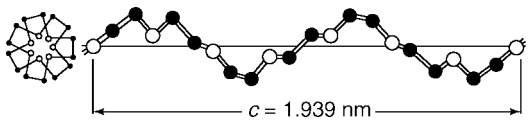

Fig. 1. Molecular conformation of poly(ethylene oxide).

develops at that molecular weight, and it is at that point that T_g is the highest. Beyond this point, chain entanglement reduces crystallinity.

Solubility. Poly(ethylene oxide) is completely soluble in water at room temperature. However, at elevated temperatures (>98°C) the solubility decreases. It is also soluble in several organic solvents, particularly chlorinated hydrocarbons. Aromatic hydrocarbons are better solvents for poly(ethylene oxide) at elevated temperatures. Solubility characteristics are listed in Table 1.

Aqueous poly(ethylene oxide) solutions of higher molecular weight (ca 10^6) become stringy at polymer concentrations less than 1 wt%. At concentrations of 20 wt%, solutions become nontacky elastic gels; above this concentration, the solutions appear to be hard, tough, water-plasticized polymers.

Concentration and Molecular Weight Effects. The viscosity of aqueous solutions of poly(ethylene oxide) depends on the concentration of the polymer solute, the molecular weight, the solution temperature, the concentration of dissolved inorganic salts, and the shear rate. Viscosity increases with concentration and this dependence becomes more pronounced with increasing molecular weight. This

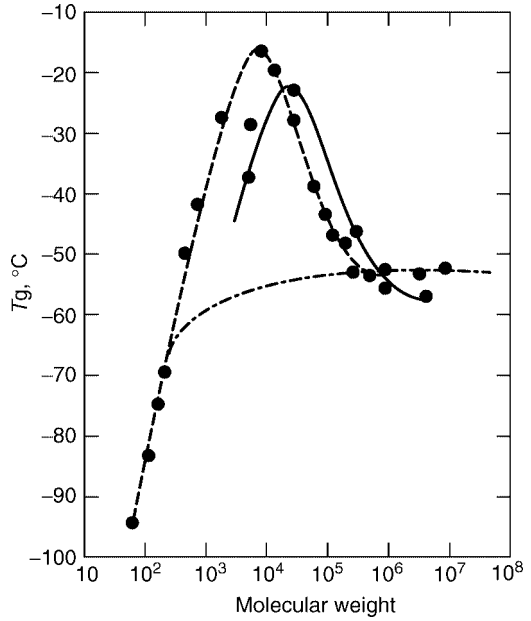

Fig. 2. Glass-transition temperature–molecular weight relationship for poly(ethylene oxide): (——) represents classical T_g–mol wt relationship; (- —), data from Ref. 6; and (– –), data from Ref. 4.

Table 1. Solubility of Poly(ethylene oxide)[a] in Several Solvents[b]

Solvent[c,d]	Temperature: Resin dissolves on heating >25°C, °C	Temperature: Resin precipitates on cooling, °C
Dissolves at room temperature in		
water		<0
carbon tetrachloride		<0
acetonitrile		<0
ethylene dichloride		<0
trichloroethylene		<0
methylene dichloride		<0
benzene		2
2-propanol (91%)		2
dimethylformamide		14
methanol		20
methyl ethyl ketone		20
Dissolves with heating in[e]		
toluene	30	20
xylene	30	20
acetone	35	20
Cellosolve[f] acetate	35	25
anisole	40	0
1,4-dioxane	40	4
ethyl acetate	40	25
ethylenediamine	40	26
dimethyl Cellosolve[f]	40	27
Cellosolve[f] solvent	45	28
ethanol (dry)	45	31
Carbitol[f] solvent	50	32
n-butanol	50	33
butyl Cellosolve[f]	50	33
n-butyl acetate	50	34
2-propanol (dry)	50	36
methyl Cellosolve[f]	50	46

[a] Mol. wt. = (1–50) × 10^5.
[b] Ref. 6.
[c] Solution concentration = ca 1 wt%.
[d] All solvents except 2-propanol (91%) were carefully dried before testing.
[e] The polymer was insoluble in 1,3-butanediol, ethylene glycol, and glycerol at all temperatures.
[f] Registered trademark of Union Carbide Corp.

combined effect is shown in Figure 3, in which solution viscosity is presented as a function of concentration for various molecular weight polymers.

The dependence of the intrinsic viscosity $[\eta]$ on molecular weight M for these polymers can be expressed by the Mark-Houwink relationship:

$$[\eta] = KM^a$$

The constants K and a for high molecular weight poly(ethylene oxide) in several solvents at various temperatures are summarized in Table 2.

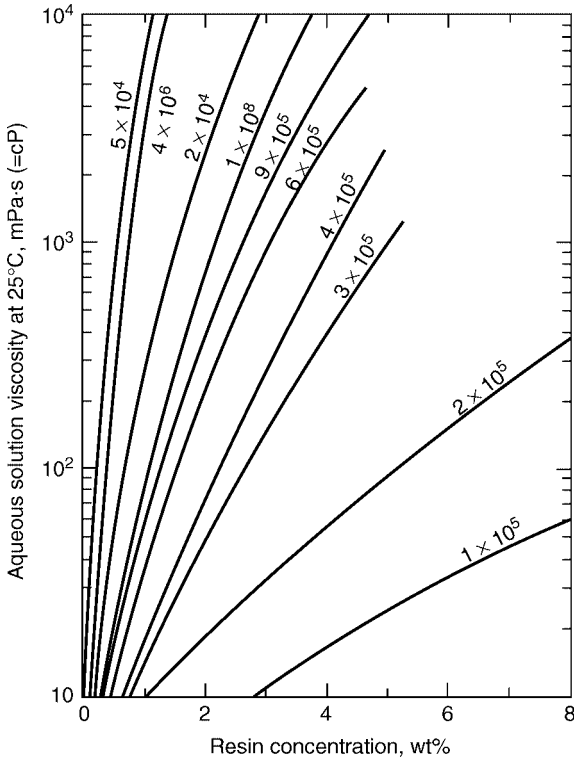

Fig. 3. Solution viscosity vs concentration for ethylene oxide polymers (7). The molecular weight of the polymer is indicated on each curve.

Temperature Effect. Near the boiling point of water, the solubility–temperature relationship undergoes an abrupt inversion. Over a narrow temperature range, solutions become cloudy and the polymer precipitates; the polymer cannot dissolve in water above this precipitation temperature. In Figure 4, this limit or cloud point is shown as a function of polymer concentration for poly(ethylene oxide) of 2×10^6 molecular weight.

The viscosity of the aqueous solution is also significantly affected by temperature. In polymers of molecular weights $(1–50) \times 10^5$ the solution viscosity

Table 2. Mark–Houwink Constants for Poly(ethylene oxide)

Solvent	Temperature, °C	$K \times 10^5$	a	Approx. M	Ref.
Water	25	11.92	0.76	$(5–40) \times 10^5$	8
	35	6.4	0.82	10^4–10^7	9
	45	6.9	0.91	10^4–10^7	9
0.45 M $K2SO_4$ (aq)	35	130	0.5	10^4–10^7	9
0.39 M $MgSO_4$ (aq)	45	100	0.5	10^4–10^7	9
Benzene	25	39.7	0.686	$(8–500) \times 10^4$	10
	30	61.4	0.64	$(3–20) \times 10^5$	7

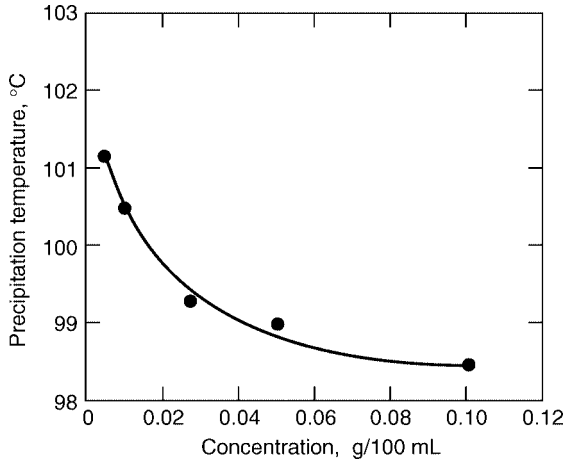

Fig. 4. Upper temperature limit for solubility of poly(ethylene oxide) in water. Molecular weight is 2×10^6 (3).

may decrease by one order of magnitude as the temperature of measurement is increased from 10 to 90°C. Figure 5 shows this effect.

Effects of Salts. The presence of inorganic salts in aqueous solutions of poly(ethylene oxide) reduces the upper temperature limit of solubility and viscosity. The upper temperature limit of solubility decreases in proportion to the concentration and valence of the ionic species present. The size of the ions is also important; eg, smaller hydrated ions have the greatest effect. The effect of a number of inorganic salts on the upper temperature limit of solubility of poly(ethylene oxide) in water is illustrated in Figure 6. The decrease in temperature is nearly

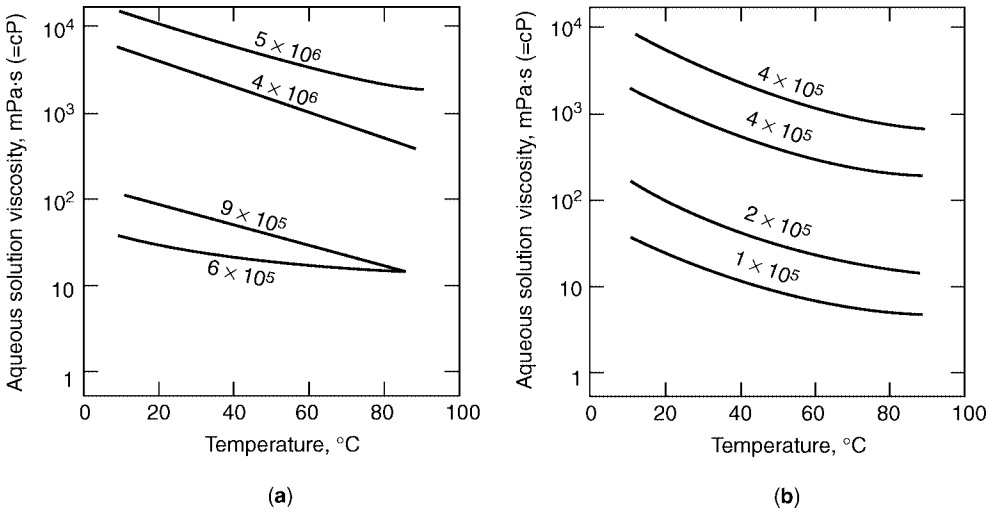

Fig. 5. Solution viscosity vs temperature: (**a**) 1.0 wt% solution and (**b**) 5.0 wt% solution (11) for polymers of various molecular weights, indicated on the curves.

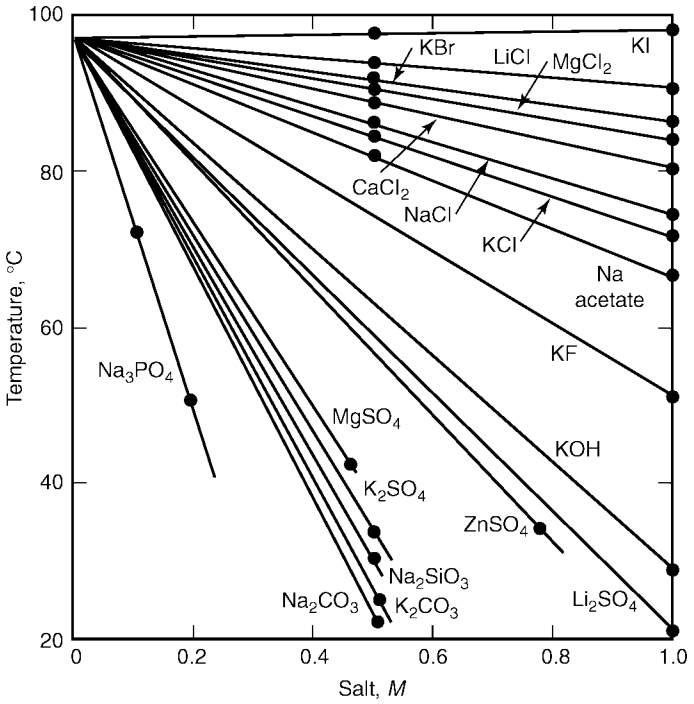

Fig. 6. Upper temperature limit of solubility in salt solution. Resin concentration is 5.0 wt% (7).

a linear function of salt concentration. However, this salting-out effect cannot always be correlated with the ionic strength principle. For example, potassium and magnesium sulfate have approximately the same effect, but potassium halides are widely different. Thus, it appears that the anion has the greater effect on the upper temperature limit of solubility. The effectiveness of anions to reduce the Θ temperature of aqueous poly(ethylene oxide) solution decreases in the following order: $PO_4^{3-} > HPO_4^{2-} > S_2O_3^{2-} > H_2PO_4^{-} > F^{-} > HCO_2^{-} > CH_3CO_2^{-} > Br^{-} > I^{-}$. The order for cations was found to be $K^{+} \approx$; $Rb^{+} \approx$; $Na^{+} \approx$; $Cs^{+} > Sr^{2+} > Ba^{2+} \approx$; $Ca^{2+} > NH^{+}_4 > Li^{+}$ (12). The presence of inorganic salts in solutions of poly(ethylene oxide) also can reduce the hydrodynamic volume of the polymer, with attendant reduction in intrinsic viscosity; this effect is shown in Figure 7.

Effect of Shear. Concentrated aqueous solutions of poly(ethylene oxide) are pseudoplastic. The degree of pseudoplasticity increases as the molecular weight increases. Therefore, the viscosity of a given aqueous solution is a function of the shear rate used for the measurement. This relationship between viscosity and shear rate for solutions of various molecular weight poly(ethylene oxide) resins is presented in Figure 8.

Thermoplasticity. High molecular weight poly(ethylene oxide) can be molded, extruded, or calendered by means of conventional thermoplastic processing equipment (13). Films of poly(ethylene oxide) can be produced by the blown-film extrusion process and, in addition to complete water solubility, have

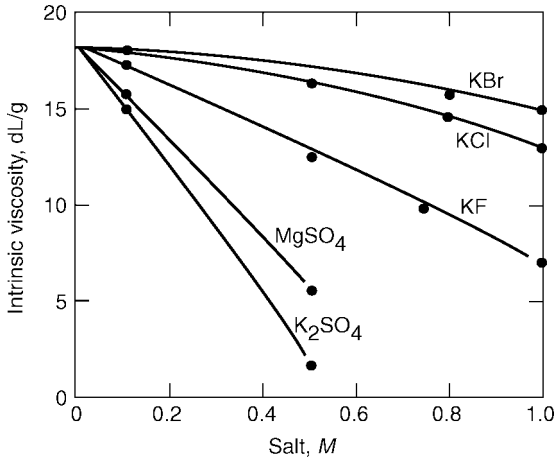

Fig. 7. Effects of salts on the intrinsic viscosity of poly(ethylene oxide) at 30°C. Molecular weight is 5.5×10^6 (3).

the typical physical properties shown in Table 3. Films of poly(ethylene oxide) tend to orient under stress, resulting in high strength in the draw direction. The physical properties, melting behavior, and crystallinity of drawn films have been studied by several researchers (14–17).

At 100–150°C above the melting point, the melt viscosities of these polymers may exceed 10 kPa·s (10^5 P) (Fig. 9). These high melt viscosities indicate extremely high molecular weight. Melt viscosities are relatively unaffected by temperature changes but are directly proportional to the molecular weight of the polymer. Thus, polymers with molecular weights of $(1–3) \times 10^5$ are usually used for applications involving thermoplastic forming processes.

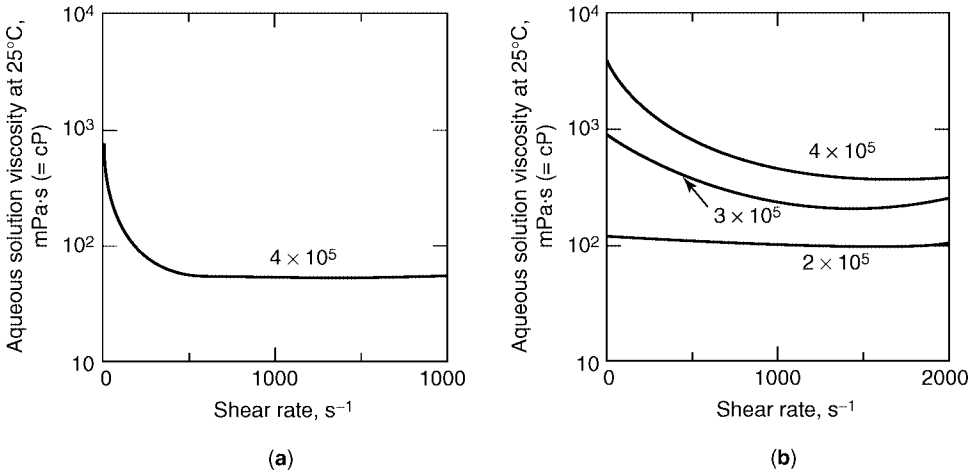

Fig. 8. Effect of shear on aqueous solution viscosities of poly(ethylene oxide) resins: (**a**) 1.0 wt% solution; (b) 5.0 wt% solution (7). Each curve represents a different molecular weight.

Table 3. Typical Physical Properties of Poly(ethylene oxide) Film

Property	Value
Specific gravity	1.2
Tensile strength, MP[a]	
Machine direction	16
Transverse direction	13
Secant modulus, MP[a]	
Machine direction	290
Transverse direction	480
Elongation, %	
Machine direction	550
Transverse direction	650
Tear strength, kN/m[b]	
Machine direction	100
Transverse direction	240
Dart Impact at 50% failure, kN/m[b]	80
Release time in water, s	15
O_2 transmission, μmol/(m·s·GPa)[c]	85.8
Melting point, °C	67
Heat-sealing temperture, °C	71–107
Cold-crack resistance, °C	−46

[a] To convert MPa to psi, multiply by 145.
[b] To convert kN/m to lbf/in., multiply by 57.14.
[c] To convert μmol/(m · s · GPa) to $cm^3 \cdot mil/(in.^2 \cdot d \cdot atm)$, multiply by 5.

Polymer Blends. The miscibility (qv) of poly(ethylene oxide) with a number of other polymers has been studied, eg, with poly(methyl methacrylate) (18–23), poly(vinyl acetate) (24–27), polyvinylpyrrolidinone (28), nylon (29), poly(vinyl alcohol) (30), phenoxy resins (31), cellulose (32), cellulose ethers

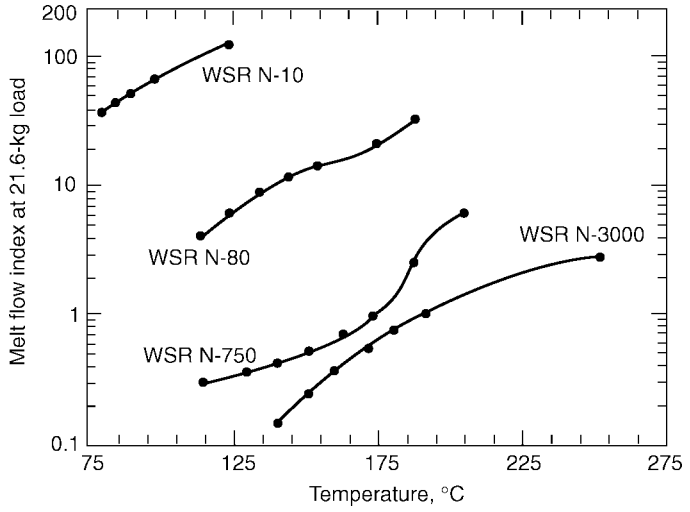

Fig. 9. Melt flow index as a function of temperature for varying molecular weights of poly(ethylene oxide). WSR = Polyox water-soluble resins.

(33), poly(vinyl chloride) (34), poly(lactic acid) (35), polyhydroxybutyrate (36), poly(acrylic acid) (37), polypropylene (38), polyethylene (39) , and poly(styrene-*co*-maleic anhydride) (40). The crystallization behavior of representive PEO blends have been studied using time-resolved wide- and small-angle X-ray scattering (41).

Chemical Properties

Association Complexes. The unshared electron pairs of the ether oxygens, which give the polymer strong hydrogen bonding affinity, can also take part in association reactions with a variety of monomeric and polymeric electron acceptors (42,43). These include poly(acrylic acid), poly(methacrylic acid), copolymers of maleic and acrylic acids, tannic acid, naphtholic and phenolic compounds, as well as urea and thiourea (44–49).

When equal amounts of solutions of poly(ethylene oxide) and poly(acrylic acid) are mixed, a precipitate, which appears to be an association product of the two polymers, forms immediately. This association reaction is influenced by hydrogen-ion concentration. Below ca pH 4, the complex precipitates from solution. Above ca pH 12, precipitation also occurs, but probably only poly(ethylene oxide) precipitates. If solution viscosity is used as an indication of the degree of association, it appears that association becomes more pronounced as the pH is reduced toward a lower limit of about 4. The highest yield of insoluble complex usually occurs at an equimolar ratio of ether and carboxyl groups. Studies of the poly(ethylene oxide)–poly(methacrylic acid) complexes indicate a stoichiometric ratio of three monomeric units of ethylene oxide for each methacrylic acid unit.

These association reactions can be controlled. Acetone or acetonylacetone added to the solution of the polymeric electron acceptor prevents insolubilization, which takes place immediately upon the removal of the ketone. A second method of insolubilization control consists of blocking the carboxyl groups with inorganic cations, ie, the formation of the sodium or ammonium salt of poly(acrylic acid). Mixtures of poly(ethylene oxide) solutions with solutions of such salts can be precipitated by acidification.

Poly(ethylene oxide) associates in solution with certain electrolytes (50–54). For example, high molecular weight species of poly(ethylene oxide) readily dissolve in methanol that contains 0.5 wt% KI, although the resin does not remain in methanol solution at room temperature. This salting-in effect has been attributed to ion binding, which prevents coagulation in the nonsolvent. Complexes with electrolytes, in particular lithium salts, have received widespread attention on account of the potential for using these materials in a polymeric battery. Variable temperature IR studies have been used to explain the structural changes in these systems (55). The use of complexes of poly(ethylene oxide) in analytical chemistry has also been reviewed (56).

Oxidation. Because of the presence of weak C—O bonds in the backbone, high molecular weight polymers of ethylene oxide are susceptible to oxidative degradation in bulk, during thermoplastic processing, or in solution. The mechanistic aspects of poly(ethylene oxide) oxidation have been reviewed (57). During thermoplastic processing at elevated temperature, oxidative degradation

is manifested by a rapid decrease in melt viscosity with time. In aqueous solution at ambient temperatures, the decay of solution viscosity also is an indication of oxidative degradation, and the rate of decay is increased by the presence of traces of chlorine, peroxides, permanganate, or persulfate and certain transition-metal ions such as Cu^{+}, Cu^{2+}, Cu^{3+}, Fe^{3+}, and Ni^{2+}. A combination of these agents can lead to severe viscosity losses.

Several stabilizers are useful in minimizing oxidative degradation during thermoplastic processing or in the bulk solid. Phenothiazine, hindered phenolic antioxidants such as butylated hydroxytoluene , butylated hydroxyanisole, and secondary aromatic amines in concentrations of 0.01–0.5% based on the weight of polymer, are effective.

Aqueous solutions can be stabilized against viscosity loss by addition of 5–10 wt% anhydrous isopropyl alcohol, ethanol, ethylene glycol, or propylene glycol. The manganous ion (Mn^{2+}) also is an effective stabilizer at concentrations of 10^{-5}–10^{-2} wt% of the solution.

Manufacture and Processing

Heterogeneous Catalytic Polymerization. The preparation of polymers of ethylene oxide with molecular weights greater than 100,000 was first reported in 1933. The polymer was produced by placing ethylene oxide in contact with an alkaline-earth oxide for extended periods (58). In the 1950s, the low yield and low polymerization rates of the early work were improved upon by the use of alkaline-earth carbonates as the catalysts (59). Further improvements in reaction rates and polymerization control have led to the commercial availability of poly(ethylene oxide) of varying molecular weights.

The polymerization of ethylene oxide to produce high molecular weight polymer involves heterogeneous reaction with propagation at the catalyst surface. The polymerization can involve anionic or cationic reactions of ethylene oxide that generally produce lower molecular weight products. The mechanism for production of extremely high molecular weight polymers is thought to involve a coordinate anionic reaction where ethylene oxide is coordinated with a metal atom of the catalyst and is then attacked by an anion. The various polymerization mechanisms have been described (60).

Catalysts capable of polymerizing ethylene oxide to high molecular weight polymers include many metal compounds. Among those reported are alkaline-earth carbonates and oxides (61), alkyl zinc compounds (62–64), alkyl aluminum compounds and alkoxides (65–67), and hydrates of ferric chloride, bromide, and acetate (68,69). Other catalysts include various alkyls and alkoxides of aluminum, zinc, magnesium, and calcium, and mixtures of these materials with various other inorganic salts. The preparation and utilization of the various catalysts have also been described (70,71). The molecular weight of the polymer appears to be controlled by the catalyst systems as well as by polymerization conditions. Rigid control of catalyst preparation and raw material quality appear to be mandatory for successful laboratory preparation of high molecular weight poly(ethylene oxide).

Polymer Suspensions. Poly(ethylene oxide) resins are commercially available as fine granular solids. However, the polymer can be dispersed in a nonsolvent to provide better metering into various systems. Production processes involve the use of high shear mixers to disperse the solids in a nonsolvent vehicle (72–74).

Thermoplastic Processing. Poly(ethylene oxide) resins can be thermoplastically formed into solid products, eg, films, tapes, plugs, retainers, and fillers (qv). Through the use of plasticizers (qv), poly(ethylene oxide) can be extruded, molded, and calendered on conventional thermoplastic processing equipment. Sheets and films of this resin are heat sealable (75,76).

Irradiation and Cross-Linking. Exposure of poly(ethylene oxide) to ionizable radiation (gamma irradiation, electron beam, or ultraviolet light) can result in molecular weight breakdown or cross-linking, depending on the environmental conditions. If oxygen is present, hydroperoxides are formed and chain scission leads to an overall decrease in molecular weight (77). However, in the absence of oxygen, cross-linking becomes the preferred reaction (78,79,90). The resulting polymer network exhibits hydrogel properties of high water capacity (81,82).

Studies of the cross-linking mechanism and structure of the cross-linked polymer indicate that a complex network of cross-linked chains of varying lengths is present (83–86). When the cross-linking is performed in solution, the cross-links can be both intermolecular and intramolecular; the overall structure of the cross-linked polymer is the combined result of chain scission, intramolecular bonding, and intermolecular bonding. Under conditions of high aggregation in solution, for example, high concentration, intermolecular cross-linking is preferred and a continuous gel is formed. When the polymer is not aggregated in solution, intramolecular cross-linking predominates, and microgels, rather than a cohesive gel network, are formed. Detailed positron annihilation studies have been used to reveal the evolution of small pore structure for semicrystalline PEO under gamma irradiation (87).

Economic Aspects

Only Japan and the United States have significant commercial facilities for the production of poly(ethylene oxide) resins. In Japan, Meisei Chemical Works Ltd. produces Alkox and Sumitomo Seika Kagaky Co., Ltd. produces PEO. In the United States, The Dow Chemical Corp. produces Polyox. Precise figures have not been released on capacities or annual production.

Specifications, Standards, and Quality Control

The primary quality control measure for these resins is the concentrated aqueous solution viscosity, which is related to molecular weight. Specifications for Polyox are summarized in Table 4. Additional product specifications frequently include moisture content, particle-size distribution, and residual catalyst by-product level.

Table 4. Aqueous Solution Viscosity Specifications for Polyox Resins[a]

Grade	Approximate M_w	Concentration wt%	Brookfield Viscometer Spindle Number	Speed, rmp	Viscosity at 25°C, Pa · s[b]
WSR-308	8×10^6	1.0	2	2	10,000–15,000
WSR-303	7×10^6	1.0	2	2	7,500–10,000
COAG	5×10^6	1.0	2	2	5,500–7,500
WSR-301	4×10^6	1.0	1	2	1,650–5,500
WSRN-60K	2×10^6	2.0	3	10	2,000–4,000
WSRN-12K	1×10^6	2.0	1	10	400–800
WSR-1105	9×10^5	5.0	2	2	8,800–17,600
WSR-205	6×10^5	5.0	2	2	4,500–8,800
WSRN-3000	4×10^5	5.0	1	2	2,250–4,500
WSRN-750	3×10^5	5.0	1	10	600–1000
WSRN-80	2×10^5	5.0	1	50	65–115
WSRN-10	1×10^5	5.0	1	50	12–50

[a] Ref. 88.
[b] To convert Pa · s to Poise, multiply by 10.

Analytical and Test Methods

Molecular Weight. Measurement of intrinsic viscosity in water is the most commonly used method to determine the molecular weight of poly(ethylene oxide) resins. However, there are several problems associated with these measurements (89,90). The dissolved polymer is susceptible to oxidative and shear degradation, which is accelerated by filtration or dialysis. If the solution is purified by centrifugation, precipitation of the highest molecular weight polymers can occur and the presence of residual catalyst by-products, which remain as dispersed, insoluble solids, further complicates purification.

A number of techniques, including static and dynamic light scattering (91), viscometry (92), and gel-permeation chromatography (GPC) with low angle laser light-scattering detection (93), have been used to study the behavior of poly(ethylene oxide) in solution. Dynamic light scattering (94,95) has also been used to determine the molecular weight distribution of poly(ethylene oxide) and to study crystallization from dilute solutions (96,97).

Attempts to measure average molecular weight and molecular weight distribution of poly(ethylene oxide) for molecular weights above 1 million, using GPC, are extremely difficult because of the effect of shear on the high molecular weight polymer molecules in the GPC column and the lack of adequate standards for calibration of the columns. However, one group has been successful in using high speed gel filtration to fractionate high molecular weight poly(ethylene oxide) and provide materials with narrow molecular weight distributions suitable for use as standards for GPC (98). An alternative method for average molecular weight determination is cloud point titration (99) (see MOLECULAR WEIGHT DETERMINATION).

Aqueous Solution Viscosity. A special solution preparation method is used for one type of measurement of aqueous solution viscosity (100). The appropriate amount of poly(ethylene oxide) resin is dispersed in 125 mL of anhydrous isopropyl alcohol by vigorous stirring. Because the resin is insoluble in anhydrous

isopropyl alcohol, a slurry forms and the alcohol wets the resin particles. An appropriate amount of water is added and stirring is slowed to about 100 rpm to avoid shear degradation of the polymer. In Table 4, the nominal resin concentration reported is based on the amount of water present and ignores the isopropyl alcohol.

Analysis for Poly(ethylene oxide). Another special analytical method takes advantage of the fact that poly(ethylene oxide) forms a water-insoluble association compound with poly(acrylic acid). This reaction can be used in the analysis of the concentration of poly(ethylene oxide) in a dilute aqueous solution. Freshly prepared poly(acrylic acid) is added to a solution of unknown poly(ethylene oxide) concentration. A precipitate forms, and its concentration can be measured turbidimetrically. Using appropriate calibration standards, the precipitate concentration can then be converted to concentration of poly(ethylene oxide). The optimum resin concentration in the unknown sample is 0.2–0.4 ppm. Therefore, it is necessary to dilute more concentrated solutions to this range before analysis (101). Low concentrations of poly(ethylene oxide) in water may also be determined by viscometry (102) or by complexation with KI_3 and then titration with $Na_2S_2O_3$ (103).

Health and Safety Factors: Toxicology

Poly(ethylene oxide) resins are safely used in numerous pharmaceutical and personal care applications. Poly(ethylene oxide) resins show a low order toxicity in animal studies by all routes of exposure. Because of their high molecular weight, they are poorly adsorbed from the gastrointestinal tract and are completely and rapidly eliminated (104). The resins are not skin irritants or sensitizers, nor do they cause eye irritation.

Considerable interest has been shown in poly(ethylene oxide) for diverse applications in food, drug, and cosmetic products. Such uses fall within the scope of the Federal Food, Drug, and Cosmetic Act. The U.S. Food and Drug Administration (FDA) has recognized and approved the use of poly(ethylene oxide) for specific food and food packaging uses. USP/NF grades of Polyox water-soluble resins (The Dow Chemical Co.) that meet all requirments of the United States Pharmacopeia/National Formulary (USP/NF) are available for pharmaceutical applications (105).

Uses

Significant use properties of poly(ethylene oxide) are complete water solubility, low toxicity, unique solution rheology, complexation with organic acids, low ash content, and thermoplasticity.

Pharmaceutical and Biomedical Applications. On account of its low toxicity and unique properties, poly(ethylene oxide) is utilized in a variety of pharmaceutical and biomedical applications.

Denture Adhesives. Fast hydration and gel-forming properties are ideally mated to produce a thick, cushioning fluid between the dentures and gums (106).

The biologically inert nature of poly(ethylene oxide) helps reduce unpleasant odors and taste in this type of personal care product. The use of PEO blends has also been shown as a means to optimize denture adhesive properties (107).

Mucoadhesives. Poly(ethylene oxide) has good adhesive properties to mucosal surfaces because of its high molecular weight, linear molecules, and fast hydration properties. *In vivo* results have shown that the duration of adhesion increases with molecular weight up to 400,000. Further increase in molecular weight results in a concomitant decrease in adhesive properties, most likely because of the swelling of the resulting hydrogel (108). The mucoadhesive properties have been utilized in the design of buccal-sustained drug delivery systems (109,110) and occular delivery systems (111).

Ophthalmic Solutions. The viscoelastic properties of poly(ethylene oxide) produce unique benefits for vitreous fluid substitution for ophthalmic surgery. Solutions of high molecular weight poly(ethylene oxide) have been used as vehicles for therapeutics for the eye (112) and as a contact lens fluid for hard or gel-type lenses (113). A treated lens appears to have a high viscosity layer at the low shear rates that occur on the inside surface. This provides a thick, comfortable cushioning layer. At high shear rates caused by the blinking eyelid, the apparent viscosity is much lower. This allows the lid to move smoothly and effortlessly over the outside surface of the lens. Unlike the cellulosics, poly(ethylene oxide) does not support bacterial growth. Lens solutions are easier to keep sterile.

Wound Dressings. Cross-linked poly(ethylene oxide) solutions form hydrogels which contain about 90–97% of water. These hydrogels (qv) are clear, transparent, permeable to gases, and absorb 5–100 times their weight in water. Such characteristics make these hydrogels interesting materials for wound dressings. Compared to other occlusive dressings, these hydrogels have shown the promotion of rapid healing (114) . Release of therapeutic substances from these dressings has been demonstrated (115,116).

Oral Drug Release. The dissolution rate of tableted poly(ethylene oxide) depends on the molecular weight and particle-size distribution. High molecular weight resin provides an excellent tablet binder for sustained drug release from matrix tablets (117–119) (see CONTROLLED RELEASE TECHNOLOGY). The good flow properties and compressibility of poly(ethylene oxide) powder can be advantageously exploited in preparing tablets by direct compression. The high swelling capacity of high molecular weight poly(ethylene oxide) tablets when exposed to intestinal fluids has been successfully used in osmotic delivery systems for water-insoluble drugs (120–123). A detailed review of these osmotic systems is available (124). A zero-order drug release has been reported from films produced from poly(ethylene oxide) and polycaprolactone. The change in drug release profile with respect to film composition, thickness, and morphology has been described (125). Novel PEO matrix systems aimed at gastric delivery and chewable forms have been described (126,127). The thermoplastic properties of PEO lend themselves to the use of extrusion methods in the preparation of oral delivery systems (128,129).

Biomaterials with Low Thrombogenicity. Poly(ethylene oxide) exhibits extraordinary inertness toward most proteins and biological macromolecules. The polymer is therefore used in bulk and surface modification of biomaterials to develop antithrombogenic surfaces for blood contacting materials. Such modified

surfaces result in reduced concentrations of cell adhesion and protein adsorption when compared to the nonmodified surfaces (130,131).

Lubricious Coatings for Biomaterials. Coatings of poly(ethylene oxide) when dry are tactile. If brought into contact with water, the poly(ethylene oxide) hydates rapidly and forms a lubricious coating. This type of technology is of great interest for biomedical devices introduced into the human body, such as catheters and endotracheal tubes, and for sutures (132–135).

Industrial Applications. Poly(ethylene oxide)s also have numerous industrial uses.

Flocculation. Poly(ethylene oxide)s of molecular weights greater than 4 million have been used as specialty flocculants. The ability of the PEO molecule to hydrogen-bond with the surface hydroxyl layers of silica, kaolinites, and other mineral oxides leads to adsorption of the polymer on the substrate. The balance between the hydrophilicity of the ether oxygen moiety and the hydrogen-bonding forces on the solid substrate results in a loop-tail conformation essential to flocculation. Some of the end uses for PEO as a flocculant are as a fines retention aid in the paper industry, a low pH flocculant of silica in beryllium, uranium, and copper mines that use acid leaching, and as a dewatering aid in industrial waste treatment. In the paper industry, PEO is widely used as a retention aid and pitch control agent in the newsprint industry (136–157). Typically, a phenol formaldehyde-type resin is added to the substrate before the addition of PEO. The chemical that is added before PEO has been referred to as an *enhancer*. Recent publications on designing enhancers that work with PEO have resulted in expanding the use of PEO in flocculation of several substrates (146,147,158,159).

Several technical articles suggest that the use of PEO increases the dewatering efficiency of mineral sludges significantly (160–176). In the mining industry, PEO is used to flocculate siliceous substrates at pH <2 during the acid leaching operations. The low pH stability provides PEO polymers with unique advantages in this application.

Drag Reduction. The addition of 0.03% of high molecular weight PEO (greater than 4 million) to aqueous solutions has resulted in a 100% increase in the flow rate at fixed pump pressures (177). The significant reduction in friction as a result of the addition of PEO has been attributed to supermolecular structure formation of PEO (178) and to expansion and orientation of the polymer in rotation-free draining flow (179,180). Drag reduction (qv) properties have been demonstrated by trials using fire hoses, which show that water travels 50% further because of the addition of small quantities of PEO. Investigations on the effect of Reynold's number, orifice size of the pumping device, and polymer blends have led to a better understanding for suitable drag-reducing systems that may use PEO (177–191). Degradation of PEO and point of addition of the polymer appear to play a significant role in successful manipulation of this property in end uses (192,193). Some references also suggest the use of this property in reducing arterial pressure in medical applications (190) and in ocean transport (194–197).

Binders in Ceramics, Powder Metallurgy, and Water-Based Coatings for Fluorescent Lamps. In coatings and ceramics applications, the suspension rheology needs to be modified to obtain a uniform dispersion of fine particles in the

finished product. When PEO is used as a binder in aqueous suspensions, it is possible to remove PEO completely in less than 5 min by baking at temperatures of 400°C. This property has been successfully commercialized in several ceramic applications, in powder metallurgy, and in water-based coatings of fluorescent lamps (198–201).

Personal Care. The addition of PEO provides a silky feel to solid and liquid products. This unique lubricious property has been successfully exploited in formulation of razor strips (202,203) and in shampoos, detergents, and other personal care applications. The combination of water solubility and the ability to produce films and other devices by thermoplastic processing enables the use of the PEO in flushable articles (204–207). PEO has also been used as an antimisting agent in personal care and cleaning formulations (208) and has been shown to enhance the deposition of active ingredients to the hair and skin, as well as to act as a foam enhancer (209). Fundamental investigations have examined the interaction of PEO and surfactants in aqueous solutions (210–213).

Adhesives. High concentration (>10%) solutions of poly(ethylene oxide) exhibit wet tack properties that are used in several adhesive applications (214). The tackiness disappears when the polymer dries, and this property can be successfully utilized in applications that require adhesion only in moist conditions. PEO is also known to form solution complexes with several phenolic and phenoxy resins. Solution blends of PEO and phenoxy resins are known to exhibit synergistic effects, leading to high adhesion strength on aluminum surfaces.

Acid Cleaners. The addition of PEO can significantly increase the viscosity of acid solutions. Highly viscous acid solutions are used in cleaning formulations for glass, ceramic, and metal surfaces. The increase in viscosity increases the contact time of the cleaning solution when it is sprayed on vertical surfaces. Some acids that can be thickened by using PEO are hydrochloric, sulfuric, phosphoric, and oxalic . The order of addition of the polymer and oxidative stabilizers appears to play an important role in formulating highly viscous acid solutions. The manufacturers provide several formulations to thicken different acids.

Drift and Mist Control. The pseudoplastic properties of PEO solutions reduce mist formation during spraying of aqueous solutions that contain PEO. This property is used in metal-working fluids to lower worker exposure to mists from the cutting and grinding aids. PEO may also be used to focus the spraying area of herbicides and water-based coatings.

Construction. The addition of PEO to concrete has been a subject of several investigations (215). Research studies and patent literature suggests that PEO can be used as a pumping aid to concrete, where the lubricity of PEO allows concrete to be pumped to longer distances (216–219). In addition, PEO is also used to disperse the water more uniformly in the concrete mixture, which promotes better uniformity of the concrete mixture. Formulations in the construction industry are proprietary and not easily available.

Batteries. Polymer electrolytes based on PEO have been widely reviewed (220,221). The prospect of using a thin-layer, flexible battery for applications ranging from cellular phones to electric vehicles has led to several patents (222,223) and research papers in this field. Typically, a salt such as potassium iodide, lithium triflate, or lithium perchlorate is complexed with PEO in a methylene chloride solvent. The solution complex is cast into thin films and the solvent

is evaporated. The complex has been characterized; it is believed that the 7C2 helical structure of PEO allows an ideal structure for ion transport and leads to effective use as a battery. The dissociation of the anion–cation pair in the PEO salt complex has been attributed to the oxygen atoms, which form a cage around the cation and lead to ionic conductivity. The crystallinity of PEO at room temperature has limited the use of this technology to batteries that are used at temperatures higher than 65°C, the melting point of PEO. Research in the 1990s focuses on modifying the complex or the PEO molecule to overcome the crystallinity problem and in understanding the interaction of PEO with lithium salts (224–235).

Other Applications. PEO has also been used as an antistat additive (236,237), a water-soluble packaging material of seeds and fertilizers (238), and a rheology modifier in aqueous flexographic printing inks (239), and for the production of nanofibers containing multiwalled carbon nanotubes (240).

BIBLIOGRAPHY

"Ethylene Oxide Polymers under 1,2 Epoxide Polymers" in *EPST* 1st ed., Vol. 6, pp. 103–145, by F. W. Stone and J. J. Stratta, Union Carbide Corp.; in *EPSE* 2nd ed., Vol. 6, pp. 225–273, by Nye Clinton and Paul Matlack, Union Carbide Corp.

1. F. E. Bailey Jr. and J. V. Koleske, *Poly(Ethylene Oxide)*, Academic Press, Inc., New York, 1976, p. 105.
2. P. J. Flory, *Principles of Polymer Chemistry*, Cornell University Press, Ithaca, N.Y., 1953, pp. 266–313.
3. S. Z. Cheng, J. S. Barley, and E. D. Von Meerwall, *J. Polym. Sci., Part B: Polym. Phys.* **29**, 515–525 (1991).
4. B. E. Read, *Polymer* **3**, 529 (1962).
5. J. A. Faucher and co-workers, *J. Appl. Phys.* **37**, 3962 (1966).
6. F. W. Stone and J. J. Stratta, in N. Bikales, ed., *Encyclopedia of Polymer Science and Technology*, Vol. **6**, Wiley-Interscience, New York, 1967, pp. 103–145.
7. T. A. Ritscher and H. G. Elias, *Makromol. Chem.* **30**, 48 (1959).
8. G. Nabi, *J. Sci.* **20**(3), 136 (1968).
9. F. E. Bailey Jr. and R. W. Callard, *J. Appl. Polym. Sci.* **1**, 56 (1959).
10. G. Allen and co-workers, *Polymer* **8**, 391 (1967).
11. Union Carbide Technical Bulletin, F44029C, 1981.
12. M. Ataman, *Colloid Polym. Sci.* **265**(1), 19–25 (1987).
13. Union Carbide Technical Bulletin, UC-420, 1994.
14. B. Kim and R. Porter, *Macromolecules* **18**, 1214 (1985).
15. D. Mitchell and R. Porter, *Macromolecules* **18**, 1218 (1985).
16. B. Bogdanov and M. Mikhailov, *J. Therm. Anal.* **30**, 551 (1985).
17. B. Bogdanov and M. Mikhailov, *Acta Polym.* **35**, 469 (1984).
18. C. Marco and co-workers, *Macromolecules* **23**, 2183 (1990).
19. G. Weill, *J. Macromol. Sci. Chem. A* **27**, 1769, (1990).
20. S. Liberman, A. Gomes, and E. Macchi, *J. Polym. Sci., Polym. Chem. Ed.* **22**, 2809, (1984).
21. E. Martuscelli and co-workers, *Makromol. Chem.* **187**, 1557 (1986).
22. S. Cimmino, *Makromol. Chem.* **191**, 2447 (1990).
23. S. Cimmino, E. Martuscelli, and C. Silvestre, *J. Calorim. Anal. Therm. Thermodyn. Chim.* **17**, 188 (1986).
24. E. Munoz and co-workers, *Polym. Bull. (Berlin)* **7**, 295 (1982).

25. E. Martuscelli, C. Silvestre, and C. Gismondi, *Makromol. Chem.* **186**, 2161 (1985).
26. E. Martuscelli, L. Vicini, and A. Seves, *Makromol. Chem.* **188**, 607 (1987).
27. C. Han, H. Chung, and J. Kim, *Polymer* **33**, 546 (1992).
28. J. Horrion, R. Jerome, and P. Teyssie, *J. Polym. Sci., Part A: Polym. Chem.* **28**, 153 (1990).
29. M. Coleman, J. H. C. Serman, and P. Painter, *Polym. Mater. Sci. Eng.* **59**, 321 (1988).
30. J. Quintana and co-workers, *Polymer* **32**, 2793 (1991).
31. M. Iriarte and co-workers, *Macromolecules* **24**, 5546 (1991).
32. Y. Nishio, N. Hirose, and T. Takahashi, *Polym. J. (Tokyo)* **21**, 347 (1989).
33. P. Sundararajan, P. Bluhm, and Y. Piche, *Polym. Bull. (Berlin)* **27**, 345 (1991).
34. Margaritia and N. Kalfoglou, *J. Polym. Sci., Part B: Polym. Phys.* **26**, 1595 (1988).
35. Nakafuku and M. Sakoda, *Polym. J. (Tokyo)* **25**, 909 (1993).
36. M. Avella and E. Martuscelli, *Polymer* **29**, 1731 (1988).
37. P. Sanjay and E. Goethals, *New Polym. Mater.* **4**, 1 (1993).
38. T. Tang and B. Huang, *J. Polym. Sci., Part B: Polym. Phys.* **32**, 1991 (1994).
39. Pukanszky and F. Tudos, *Makromol. Chem. Macromol. Symp.* **38**, 205 (1990).
40. H. Al-Salah, *J. Appl. Polym. Sci.* **77**, 1, (2000).
41. B. S. Hsiao, *Macromolecules* **33**, 4842, (2000).
42. Ref. 1, p. 87.
43. Union Carbide Technical Bulletin, SC-1170, 1991.
44. M. Pradip and co-workers, *Langmuir* **7**, 2108 (1991).
45. K. L. Smith, A. E. Winslow, and D. E. Peterson, *Ind. Eng. Chem.* **51**, 1361 (1959).
46. Guner and O. Guven, *Makromol. Chem.* **179**, 2789 (1978).
47. G. E. Baker and H. J. Ronsanto, *J. Am. Oil Chem. Soc.* **32**, 249 (1955).
48. E. Bailey Jr. and H. G. Brance, *J. Polym. Sci.* **49**, 397 (1961).
49. Chenite and F. Brisse, *Macromolecules* **24**, 2221 (1991).
50. H. Daoust and B. Cloutier, *Makromol. Chem. Macromol. Symp.* **20/21**, 221 (1988).
51. P. Wright, *Polymer* **30**, 1179 (1989).
52. H. Honda and K. Ono, *Macomolecules* **23**, 4950 (1990).
53. R. Sartori and co-workers, *Macromelecules* **23**, 3878 (1990).
54. K. Ono, H. Honda, and K. Murakami, *Macromol. Sci. Chem. A* **26**, 567 (1989).
55. B. Bogdanov, C. Uzov, and G. Gavrailova, *Acta Polym.* **45**, 381 (1994).
56. T. Okada, *Analyst* **118**, 959, (1993).
57. M. Donbrow, *Surf. Sci. Ser.* **23**, 1011 (1987).
58. H. Staudinger and H. Lohmann, *Ann. Chemie* **505**, 41 (1933).
59. N. Hill, F. E. Bailey Jr., and J. T. Fitzpatrick, *Ind. Eng. Chem.* **50**, 5 (1958).
60. Ref. 1, p. 20.
61. N. Hill, F. E. Bailey Jr., and J. T. Fitzpatrick, *Ind. Eng. Chem.* **50**, 5 (1958).
62. F. E. Bailey Jr., G. M. Powell III, and K. L. Smith, *Ind. Eng. Chem.* **50**, 8 (1958).
63. Jpn. Pat. JP 05017566 (Jan. 26, 1993) (to Sumitomo Seika KK, Japan).
64. Eur. Pat. Appl. EP 239973 (Oct. 7, 1987) (to Union Carbide Corp.).
65. R. A. Miller and C. C. Price, *J. Polym. Sci.* **34**, 161 (1959).
66. Y. Zhang, X. Chen, and Z. Shen, *Inorg. Chim. Acta* **155**(2), 263, (1989).
67. PCT Int. Appl. WO 2002098559 (Dec. 12, 2002) (to Union Carbide Corp.).
68. U.S. Pat. 2,706,181 (Apr. 12, 1955), M. E. Pruitt and J. M. Baggett (to Dow Chemical Co.).
69. U.S. Pat. 2,706,189 (Apr. 12, 1955), M. E. Pruitt and J. M. Baggett (to Dow Chemical Co.).
70. W. R. Sorenson and T. W. Cambell, *Preparative Methods of Polymer Chemistry*, Interscience Publishers, New York, 1961.
71. U.S. Pat. 3,470,078 (Sept. 30, 1969), P. A. King (to Union Carbide Corp.).

72. U.S. Pat. 3,736,288 (May 29, 1973), J. J. Stratta, C. W. Frank, and J. A. Barrere (to Union Carbide Corp.).
73. U.S. Pat. 3,843,589 (Oct. 22, 1974), L. H. Wartman (to Union Carbide Corp.).
74. U.S. Pat. 3,900,043 (Aug. 19, 1975), J. H. Bowen and K. J. Sollman (to Union Carbide Corp.).
75. R. Ramachandran, *Annu. Tech. Conf.—Soc. Plast. Eng., 53rd* **2**, 2154, (1995).
76. PCT Int. Appl. WO 9933899 (July, 8, 1999) (to Kimberly-Clark Worldwide, Inc.).
77. U.S. Pat. 3,470,078 (Sept. 30, 1969), P. A. King (to Union Carbide Corp.).
78. U.S. Pat. 3,336,129 (Aug. 15, 1967), R. A. Herrett and P. A. King (to Union Carbide Corp.).
79. U.S. Pat. 3,734,876 (May 22, 1973), N. S. Chu (to Union Carbide Corp.).
80. U.S. Pat. 3,900,378 (Aug. 19, 1975), S. N. Yen and F. D. Osterholtz (to Union Carbide Corp.).
81. E. Nedkov and S. Tsvetkova, *Radiat. Phys. Chem.* **44**, 257 (1994).
82. E. Merrill, K. Dennison, and C. Sung, *Biomaterials* **14**, 1117 (1993).
83. E. Nedkov and S. Tsvetkova, *Radiat. Phys. Chem.* **44**, 251 (1994).
84. L. Minkova and co-workers, *J. Polym. Sci.* **27**, 621 (1989).
85. L. Zhang and co-workers, *Radiat. Phys. Chem.* **40**, 501 (1992).
86. E. Nedkov and S. Tsvetkova, *Radiat. Phys. Chem.* **43**, 397 (1994).
87. M. Misheva and N. Djourelov, *Radiat. Phys. Chem.* **62**, 379 (2001).
88. Union Carbide Technical Bulletin, F44029C, 1981.
89. E. Bartel and A. Kochanowski, *Makromol. Chem. Rapid Commun.* **1**, 205 (1980).
90. Wolfe, *Can. J. Chem. Eng.* **58**, 634 (1980).
91. K. Devanand and J. C. Selser, *Macromolecules* **24**, 5943 (1991).
92. Woodley and co-workers, *Macromolecules* **25**, 5283 (1992).
93. Eshuis and P. F. Mijnlieff, *Polymer* **27**, 1951 (1986).
94. M. Mettille and R. Hester, *ACS Symp. Ser.* **467**, 276 (1991).
95. M. T. Kezirian, Ph.D. dissertation, Massachusetts Institute of Technology, 1996, p. 91.
96. N. Ding and co-workers, *Polymer* **29**, 2121 (1988).
97. N. Ding, R. Salovey, and E. Amis, *Polym. Prepr. (Am. Chem. Soc., Div. Polym. Chem.)* **29**, 385 (1988).
98. Y. Kato and co-workers, *J. Chromatogr.* **190**, 297 (1980).
99. Bortel and A. Kochanowski, *J. Appl. Polym. Sci.* **28**, 2445 (1983).
100. *Union Carbide Technical Bulletin*, SC-1169A, Apr. 1993.
101. *Union Carbide Technical Bulletin*, F44029C, 1981.
102. Moudgil, B. Shah, and S. Jayanti, *Colloids Surf.* **20**, 101 (1986).
103. Perina and co-workers, *Khim. Tekhnol. Svoista Primen. Plastmass* **159** (1990).
104. H. Leung, B. Ballantyne, S. Hermansky, S. Frantz, *Int. J. Toxicol.* **19**, 305 (2000).
105. US Pharmacopeia, USP 26/NF20, 2599-2600, United States Pharmacopeial Convention, Inc., Rockville, Md.
106. U.S. Pat. 2,978,812 (Apr. 11, 1961), M. W. Rosenthal and H. A. Cohen (to Block Drug Co., Inc.).
107. U.S. Pat. 5302628 (1994) (to Block Drug Co., Inc.).
108. P. Bottenberg and co-workers, *J. Pharm. Pharmacol.* **43**, 457–464 (1991).
109. U.S. Pat. 4,713,243 (Dec. 15, 1987), M. Shiraldi and co-workers (to Johnson and Johnson Products).
110. U.S. Pat. 4,764,378 A. Keith and W. Snipes (to Zetachron, Inc.).
111. G. Di Colo and co-workers, *Int. J. Pharm.* **220**, 169 (2001).
112. Dimitrova and co-workers, *Int. J. Pharm.* **93**, 21–26 (1993).
113. Brit. Pat. 1,340,516 (Dec. 12, 1973), B. F. Rankin (to Burton Parsons Chemicals, Inc.).
114. S. Mandy, *J. Dermatol. Surg. Oncol.* **9**(2), 153–155 (1983).

115. P. Mertz and co-workers, *Arch. Dermatol.* **122**, 1133–1138 (1983).
116. Fulton Jr., *J. Dermatol. Surg. Oncol.* **16**, 460–467 (1990).
117. M. Dimitrov and N. Lambov, *Int. J. Pharm.* **189**, 105 (1999).
118. Int. Pat. WO 9937302 (date) (to Abbott Laboratories, USA).
119. C. Kim, *J. Pharm. Sci.* **84**, 303 (1995).
120. Apicella and co-workers, *Biomaterials* **14**(2) (1993).
121. U.S. Pat. 4,859,470 (Aug. 22, 1989), R. Cortese and co-workers (to Alza Corp.).
122. U.S. Pat. 5,330,762 (July 19, 1994), A. Ayer and D. Ridzon (to Alza Corp.).
123. U.S. Pat. 4,404,183 (Sept. 13, 1983), K. Hiroitsu and co-workers (to Yamanouchi Pharmaceutical Co.).
124. G. Santus and R. Baker, *J. Controlled Release* **35**, 1 (1995).
125. C. Yoo and C. Y. Chung, *Pollimo* **18**(1), 103–112 (1994).
126. Int. Pat. WO 9855107 (Dec. 10, 1998) (to Depomed, Inc.).
127. U.S. Pat. Appl. 20031755336 (Sept. 18, 2003) (to J. Luber and F. Bunick).
128. Int. Pat. WO 9749384 (1998) (to Univ. Texas System).
129. R. Schmitt and H. Huang, *Proc. Int. Symp. Controlled Release Bioactive Mater.* **27**, 1252 (2000).
130. C. Espadas-Torre and M. Meyerhoff, *Anal. Chem.* **67**, 3108 (1995).
131. D. Holt, R. Eberhart, and M. Prager, *ASAIO J.* **40**, M858 (1994).
132. U.S. Pat. 5,077,352 (Dec. 31, 1991), R. Elton (to C. R. Bard Co.).
133. U.S. Pat. 5,041,100 (Aug. 20, 1991), S. Rowland and R. Wright (to Cordis Corp.).
134. U.S. Pat. 4,487,808 (Dec. 11, 1984), H. Lambert (to Astra Meditec Aktiebolag).
135. U.S. Pat. 4,649,920 (Mar. 17, 1987), J. Rhum (to Pfizer Hospital Products Group, Inc.).
136. Koppelman and I. K. Migliorini, *Tappi J.* **69**(11), 74–78 (1986).
137. R. Waagberg and T. Lindstroem, *Colloids Surf.* **27**(1–3), 29–42 (1987).
138. P. K. Leung and E. D. Goddard, *Tappi J.* **70**(7), 115–118 (1987).
139. A. Stack and K. Noel, *Appita J.* **43**(2), 125–129 (1990).
140. Coghill, *Appita J.* **42**, 373–375; (1989).
141. WO Pat. 9322243-A1 (Nov. 11, 1993), A. O. P. Anderson and co-workers (to Eka Nobel AB).
142. WO Pat. 9315271-A1 (Aug. 5, 1993), M. Owens (to Kemba Kemi AB).
143. Brine, R. M. Brauer, and N. Wiseman, *Appita J.* **45**(2), 118–120 (1992).
144. Jpn. Pat. 04240296-A (Jan. 22, 1991), S. Owari (to OJI Paper Co.).
145. Can. Pat. 2042907-A (Nov. 1, 1992) (to Radu G.).
146. Can. Pat. 2040967-A (Oct. 24, 1992) (to Radu G.).
147. A. Stack and N. K. Roberts, *J. Wood Chem. Technol.* **13**, 283–308; (1993).
148. A. Braun and K. Ehms, *Tappi J.* **67**(9), 110–114 (1984).
149. Bokstroem and L. Oedberg, *Res. Discl.* **237**, 5 (1984).
150. Lindstroem and Glad-Nordmark, *J. Colloid Interface Sci.* **97**(1), 62–67, (1984).
151. Lindstroem and Glad-Nordmark, *J. Colloid Interface Sci.* **4**, 404–411 (1983).
152. S. Tay and T. A. Cauley, *Papermakers Conf.* 205–210 (1982).
153. Furusawa and Y. Watanabe, *Kobunshi Ronbunshu* **41**, 727–732 (1984).
154. R. Pelton, *Can. Chem. News* **50**, 14 (1998).
155. Can. Pat. Appl. CA 2194205 (Jun. 30, 1998) .
156. A. Gibbs, R. Pelton, and R. Cong, *Colloids Surf. A: Physicochem. Eng. Aspects* **159**, 31 (1999).
157. A. Gibbs, R. Pelton, and R. Cong, *TAPPI Papermakers Conf. Trade Fair* **2**, 445 (2000).
158. L. Chen and R. Pelton, *J. Colloid Interface Sci.* **254**, 101 (2002).
159. R. Cong and R. Pelton, *J. Colloid Interface Sci.* **261**, 64 (2003).
160. R. H. Shen and co-workers, *Trans. Soc. Min. Metall. Explor.* **286**, (1989).
161. T. Tadros, *Polym. J.* **23**(5), 683–696 (1991).

162. Liu and R. Audebert, *Colloid Polym. Sci.* **272**(2), 196–203 (1994).
163. M. A. Cohen-Stuart and G. J. Fleer, *ACS Symp. Ser.* **532**, 14–22 (1993).
164. S. Behl and B. Moudgil, *J. Colloid Interface Sci.* **161**(2), 422–429 (1993).
165. S. Behl and B. Moudgil, *J. Colloid Interface Sci.* **161**(2), 443–449 (1993).
166. Moudgil and S. Behl, *Miner. Metall. Process* **10**(2), 62–65 (1993).
167. J. Scheiner and G. M. Wilemon, *Process Technol. Proc.*, 175–185 (1987).
168. M. Brown, D. A. Stanley, and B. J. Scheiner, *Miner. Metall. Process* **6**(4), 196–200 (1989).
169. J. Scheiner and D. A. Stanley, *Miner. Metall. Process* **6**, 206–210 (1989).
170. A. Stanley, B. J. Scheiner, and P. M. Brown, *Miner. Metall. Process* **7**(2), 114–117 (1990).
171. J. Scheiner, *Coal Sci. Technol.* **9**, 135 (1985).
172. J. Scheiner and A. G. Smelley, *Rep. Invest. 9131 U.S. Bur. Mines* (1982).
173. J. Scheiner, A. G. Smelley, and D. R. Brooks, *Proceedings of the Flocculation and Dewatering Symposium*, New York, 1988, pp. 272–277.
174. J. Scheiner and A. G. Smelley, *Report Gov. Rep. Announce. Index (U.S.)* **93**(8) (1993).
175. Koksal and co-workers, *Powder Technol.* **62**(3), 253–259 (1990).
176. M. Pawlik and J. S. Laskowski, *3rd Proc. UBC-McGill Bi-Annu. Int. Symp. Fundam. Miner. Process.* **541** (1999).
177. Union Carbide Technical Bulletin, UC-728, 1995.
178. K. Kazimierz and G. Piotr, *Chem. Inz. Chem.* **16**, 29–39, (1986).
179. Usui, K. Matsuru, S. Yuji, *J. Chem. Eng. (Japan)* **21**(2), 132–140, (1988).
180. M. E. Cowan, C. Garner, R. D. Hester, and C. L. McCormick, *J. Appl. Polym. Sci.* **82**, 1222 (2001).
181. V. N. Kalshnikov and M. G. Tsiklauri, *Inzh.Fiz. Zh.* **58**(1), (1990.
182. K. Kim, L. S. Choi, T. D. Long, and T. H. Yoon, *Polym. Prepr. (Am. Chem. Soc. Div. Polym. Chem.)* **28**(2), 68–69 (1987).
183. Abdelhak, J. Patrice and G. Etienne *Acad. Sci. Ser. 2* **303**, 1161–1164 (1986).
184. H. Sedahmed and M. A. Fawzy, *Br. Cooros. J.* **21**, 225–227, (1986).
185. R. Phillips, *SPE Reservoir Eng.* **5**, 481–486 (1990).
186. L. Ralph and co-workers, *Ind. Eng. Chem. Res.* **30**, 403–407, (1991).
187. S. Golub and co-workers, *Dokl. Acad. Nauk. SSSR* **295**(4), 813–816, (1987).
188. I. Polimeni and B. T. Ottenbreit, *J. Cardiovasc. Pharmacol.* **14**, 374–380 (1989).
189. U.S. Pat. 5,045,588 (Sept. 3, 1991), B. A. Alexander and S. Madre (to U.S. Sec. of Navy).
190. V. N. Kalashinikov, *J. Non-Newtonian Fluid Mech.* **75**, 209 (1998).
191. E. Sabadini and M. I. Alkschibirs, *J. Phys. Chem. B* **108**, 1183 (2004).
192. H. J. Choi, C. A. Chul, J. Sohn, and M. S. Jhon, *Polym. Degrad. Stab.* **69**, 341 (2000).
193. M. W. Liberatore, E. J. Pollauf, and A. J. McHugh, *J. Non-Newtonian Fluid Mech.* **113**, 193 (2003).
194. U.S. Pat. 5571314 (Nov. 5, 1996), R. F. Supcoe and I. M. Felsen (to U.S. Dept. of Navy).
195. U.S. Pat. 5565133 (Oct. 15, 1996), R. F. Supcoe and A. P. Evans (to U.S. Dept. of Navy).
196. U.S. Pat. 5488076 (Jan. 30, 1996), R. F. Supcoe and F. J. Moran Jr. (to U.S. Dept. of Navy).
197. U.S. Pat. 5521242 (May 28, 1996), R. F. Supcoe and A. P. Evans (to U.S. Dept. of Navy).
198. Jpn. Pat. JP 63199043 and JP 92029451 (Aug. 17, 1988 and May 19, 1992), H. Uba and co-workers (to UBE Industries KK).
199. Jpn. Pat. JO 3083-805 (Sept. 4, 1991), K. Saida and S. Fujiwara (to Sumitomo Chem.).
200. Jpn. Pat. JP 62226874 (May 10, 1987) (to Tagaitt.).
201. Jpn. Pat. 63317581 (Dec. 26, 1988), M. Magai (to Hitachi KK).

202. Eur. Pat. 276-094-A (July 27, 1988), D. B. Braun and co-workers (to Warner-Lambert Co.).
203. Int. Pat. WO 9205929 (Apr. 16, 1992), M. Tseng (to Gillette Com.).
204. Int. Pat. WO 9933920 (July 8, 1999), D. Soerens and J. H. Wang (to Kimberly-Clark Workdwide Inc.).
205. PCT Int. Appl. WO 9718082 (May 5, 1997), B. Cohen, L. Jameson, L. Gipson, and J. Faass (to Kimberly-Clark Worldwide, Inc.).
206. PCT Int. Appl. WO 2002074352 (Sept. 26, 2002), J. Zhao and co-workers (to The Procter & Gamble Co.).
207. U.S. Pat. Appl. US 2003040695 (Feb. 27, 2003), J. Zhao and co-workers (to The Procter & Gamble Co.).
208. PCT Int. Appl. WO 2004010930 (Feb 5, 2004), N. Becher, H. Scher, and D. Winetzky (to Genencor International, Inc.).
209. W. Li, S. Jordan, X. Zhang, J. Amos, and C. Davis, *Cosmetic Toiletries Manuf.* (in-press).
210. E. Feitosa, W. Brown, and M. Swanson-Vethamuth, *Langmuir* **12**, 5985 (1996).
211. A. Muller and co-workers, *Prog. Colloid Polym. Sci.* **122**, 73 (2003).
212. L. M. Smitter, J. F. Guedez, A. J. Mueller, and A. E. Saez, *J. Colloid Interface Sci.* **236**, 343 (2001).
213. L. M. Smitter, M. E. Torres, A. J. Mueller, and A. E. Saez, *J. Colloid Interface Sci.* **244**, 164 (2001).
214. E. Feitosa, W. Brown, M. Vasilescu, and M. Swanson-Vethamuth, *Macromolecules* **29**, 6837 (1996).
215. D. Saucier, *Concrete Int. Design Construct.* **9**(5), 42–47, (1987).
216. Jpn. Pat. J6 3050-356-A (Aug. 21, 1986), O. Hatakeyama (to Hazama Gumi).
217. Jpn. Pat. J6 3288 934-A (Nov. 15, 1988), T. Kidda (to Denki Kagaku Kogyo KK).
218. U.S. Pat. GB2211-183-A (Oct. 18, 1988) (to Courtaulds Pls.).
219. Jpn. Pat. JO 1160-853-A (Dec. 18, 1987) (to Tokyo Kensetsu KK).
220. B. Scrosati, ed., *Second International Symposium on Polymer Electrolytes*, Elsevier Science Publishing Co., Inc., New York, 1990.
221. F. M. Gray, *Polymer Electrolytes, RSC Material Science Monograph*, The Royal Society of Chemistry, 1997, p. 20.
222. Ger. Pat. DE 19527741 (Mar. 7, 1996), A. Vallee, M. Duval, F. Brochu, M. Kono, E. Hayashi, and T. Sada (to Hydro-Quebec, Can. and Dai-Ichi Kogyo Seiyaku Co., Ltd.).
223. U.S. Pat. US 5755985 (May 26, 1998), A. Vallee, M. Duval, F. Brochu, M. Kono, E. Hayashi, and T. Sada (to Hydro-Quebec, Can. and Dai-Ichi Kogyo Seihyaku Co., Ltd.).
224. J. Fan and C. A. Angell, *Electrochim. Acta* **40**, 2397 (1995).
225. D. Fauteux and P. McCabe, *Polym. Adv. Technol.* **6**, 83 (1995).
226. M. Dissanayake and R. Frech, *Macromolecules* **28**, 5312 (1995).
227. R. Frech, W. Huang, and M. Dissanayke, *Mater. Res. Soc. Symp. Proc. (Solid State Ionics IV)* **369**, 523 (1995).
228. R. Frech and W. Huang, *Macromolecules* **28**, 1246 (1995).
229. S. Chintapalli, C. Quinton, R. Frech, and C. Vincent, *Macromolecules* **30**, 7472 (1997).
230. S. Chintapalli and R. Frech, *Electrochim. Acta* **43**, 1395 (1998).
231. J. R. MacCallum and S. Seth, *Eur. Polym. J.* **36**, 2337 (2000).
232. C. P. Rhodes and R. Frech, *Macromolecules* **34**, 2660 (2001).
233. S. Kohjiya and Y. Ikeda, *Recent Res. Dev. Electrochem.* **4**, 99 (2001).
234. S. Passerini and co-workers, *Proc. Electrochem. Soc.* **21**, 529 (2001).
235. J. Kang, W. Li, X. Wang, Y. Lin, X. Xiao, and S. Fang, *Electrochim. Acta* **48**, 2487 (2003).
236. U.S. Pat. 3425981 (Feb. 12, 1965) (to Union Carbide Corp.).
237. Jpn. Pat. JO 3188-142-A (Dec. 15, 1989) (to Mitsui Toatsu Chem, Inc.).
238. U.S. Pat. 5206278 (Apr. 27, 1993) (to Air Products & Chemicals, Inc.).

239. U.S. Pat. 4014833 (Mar. 29, 1977) (to Owens-Illinois, Inc.).
240. P. J. Yoon, D. L. Hunter, and D. R. Paul, *Polymer* **44**, 5323 (2003).

DARLENE M. BACK
ROBERT L. SCHMITT
The Dow Chemical Company

ETHYLENE POLYMERS, CHLOROSULFONATED.
See Volume 2.

ETHYLENE POLYMERS, HDPE. See Volume 2.

ETHYLENE POLYMERS, LDPE. See Volume 2.

ETHYLENE POLYMERS, LLDPE. See Volume 2.

ETHYLENE–ACRYLIC ELASTOMERS. See Volume 2.

ETHYLENE–NORBORNENE COPOLYMERS. See Volume 2.

ETHYLENE–PROPYLENE ELASTOMERS. See Volume 6.

EXTRUSION. See Volume 2.

FILLERS

Introduction

By definition, fillers are used to extend a material and to reduce its cost. However, few inexpensive fillers, such as walnut shells, fly ash, wood flour, and wood cellulose, are still being used purely for filling purposes; nearly all fillers employed provide more than space filling. Considering their relative higher stiffness compared to the material matrix, they will always modify the mechanical properties of the final filled products, or composites. Fillers can constitute either a major or a minor part of a composite. The structure of filler particles ranges from precise geometrical forms, such as spheres, hexagonal plates, or short fibers, to irregular masses. Fillers are generally used for nondecorative purposes in contrast to pigments, although they may incidentally impart color or opacity to a material. Additives that supply bulk to drugs, cosmetics, and detergents, often referred to as fillers, are actually applied as diluents because their primary purpose is to adjust the dose or concentration of a product, rather than modify its properties or reduce cost. Fibers and whiskers are not discussed here because they are generally regarded as reinforcements, not fillers, although a majority of the fillers discussed here have reinforcing effects (see REINFORCEMENT). Also, fillers and additives that primarily modify or impart electromagnetic properties, such as electrical conductivity, are not discussed (see CONDUCTIVE POLYMER COMPOSITES).

The first manmade composites appeared in ∼5000 BC in the Middle East region, where pitch was used as a binder for reeds in building boats. Although

Encyclopedia of Polymer Science and Technology. Copyright John Wiley & Sons, Inc. All rights reserved.

glass fiber was known to be used by Phoenicians for bottle making, the use of fillers to modify the properties of a material started in early Roman times, when artisans used ground marble in lime plaster, frescoes, and pozzolanic mortar. It was not until the establishment of the modern polymer industry in the mid-nineteenth century that the rapid development of commercial fillers occurred. The first polyester resin was prepared by the Swedish chemist Berzelius in 1847, although the first commercial plastic was not forthcoming until 1862 when Parkes introduced a cellulose nitrate plastic. With the marketing of Bakelite resin in 1909, a phenol–formaldehyde plastic filled with paper or cloth, along with the usage of Carbon Black (qv) fillers by B. F. Goodrich in natural rubbers, the modern age of filled polymers was ushered in.

Fillers can be classified according to their source, function, composition, and/or morphology. No single classification scheme is entirely adequate due to the overlap and ambiguity of these categories. Considering some examples of fillers used in modern polymers listed in Table 1 (1), the emphasis of this article is on particulate fillers. Extensive usage of particulate fillers in many commerical polymers is for the enhancement in stiffness, strength, dimensional stability, toughness, heat distortion temperature, damping, impermeability, and cost reduction, although not all of these desirable features are found in any single filled polymer. The properties of particulate-filled polymers are determined by the properties of the components, by the shape of the filler phase, by the morphology of the system, and by the polymer-filler interfacial interactions.

Table 1. Fillers Used in Commercial Polymers

Particulate		Fibrous	
Organic	Inorganic	Organic	Inorganic
Wood flour	Glass	Cellulose	Whiskers
Cork	Calcium carbonate	Wool	Asbestos
Nutshell	Beryllium oxide	Carbon/graphite	Glass
Starch	Iron oxide	Aramid fiber	Mineral wool
Polymers	Magnesia	Nylons	Calcium sulphate
Carbon	Magnesium carbonate	Polyesters	Potassium titanate
Proteins	Titanium dioxide		Boron
Carbon nanotube	Zinc oxide		Alumina
	Zirconia		Metals
	Hydrated alumina		
	Antimony oxide		
	Metal powder		
	Silica		
	Silicates		
	Organo-nanoclays		
	Clays		
	Barium ferrite		
	Silicon carbide		
	Potassium titanate		

Physical Properties of Fillers

The overall value of a filler is a complex function of intrinsic material characteristics, such as average particle size, particle shape, intrinsic strength, and chemical composition; of process-dependent factors, such as particle-size distribution, surface chemistry, particle agglomeration, and bulk density; and of cost. Abrasion and hardness properties are also important for their impact on the wear and maintenance of processing and molding equipment.

Particle Morphology, Shape, Size, and Distribution. Filler particles come in a variety of shapes and sizes. In general, for most polymer applications, the filler size required is <40 μm. Finer particles, <3 μm, provide stronger enhancements in properties. Nanoparticles, with dimensions ranging up to 100 nm, deliver the strongest enhancements when they all are properly dispersed. Due to increases in both the surface area and the corresponding surface area to volume ratio with a reduction in filler particle size, finer particles are prone to agglomerate for the conservation of internal energy (2) and are more difficult to be dispersed.

The shape of an individual particle has great impact on the flexural modulus (3), permeability (4), and flow behavior (5) of a filled polymer. Although there are many ways to measure the shape (6) of a filler particle, the aspect ratio, or the ratio of the longest length of particle to its thickness, is most commonly used. A sphere, regardless of its size, has the lowest aspect ratio equal to 1.0. As a filler's shape progresses from a sphere to a block, to a plate, or to a flake, the aspect ratio increases. The aspect ratio of a filler affects its packing and, hence, its loading level in a polymer. Theoretically, percolation, or filler networking, occurs when the volume fraction of monodispersed spherical particles reaches 0.156 (7). The increase in the filler's aspect ratio lowers the percolation threshold and this reduction, in turn, is of critical importance in loading electrical conductive fillers in a material to achieve electrical conductivity (8).

Almost all fillers do not exist as the discrete individual particles of their primary structure. They form aggregates, ie, secondary structure, which can agglomerate into tertiary structures in the material to be filled. An aggregate is a collection of primary particles that are chemically bonded together. The surface area of an aggregate is less than the sum of surface areas of all primary particles in that aggregate. In general, aggregates are extremely difficult to be broken down into individual primary particles by physical methods such as mechanical mixing. The union of aggregates, although weakly associated through nonbonded physical interactions, leads to an agglomerate. Filler materials often exist as agglomerates in their natural state. The total surface area of an agglomerate is similar to the sum of individual surface areas of aggregates in that agglomerate. The mixing and dispersion of fillers in a material involves primarily the incorporation and distribution of filler pellets or powders, and breakdown into agglomerates, and then into aggregate structures.

In any commercial filler grade, there exists a collection of multiple shapes and sizes. The particle size and shape distributions of fillers can be best measured by direct microscopic inspection together with image processing although there are other methods to determine particle sizes and shapes. The size distribution of fillers that are >40 μm and are also moderately spherical in shape could

be determined conveniently by sieving in accordance to the ASTM E-11-70 sieve designation. The Coulter technique could be used to measure fillers in sizes ranging form 4–40 μm. Filler particle-size distributions <4 μm could be obtained by sedimentation, permeametry, or light-scattering methods (9,10). Laser light-scattering method can now analyze particles ranging from 0.05 to 2000 μm. Most descriptions of particulate fillers are given in terms of equivalent spherical diameter, ie, the diameter of a sphere having the same volume as the particle. Although microscopy can provide direct observation of filler particles, two-dimensional (2D), instead of the true three-dimensional (3D), size and shape distributions are acquired in most cases. Statistical transformation of a 2D size distribution into a 3D size distribution for near-spherical, randomly distributed, particles can be performed (11).

Intrinsic Strength, Hardness, and Abrasivity. The intrinsic strengths and moduli of some crystalline fillers can be calculated along the crystallographic axes using molecular simulation (12,13). For these crystalline fillers, such as talc and mica, the common fracture results from the delamination between the crystalline planes. As for the hardness, the primary measure is based on the Mohs hardness scale, which is an empirical hardness measure according to the ability of one material to scratch another (14) (see HARDNESS). The Mohs hardness goes from 1, such as for talc, to 3, such as for calcite, to 7, such as for quartz, to 10, such as for diamond, on a nonlinear scale. Abrasivity of a filler particle depends on its hardness, but also on its size and shape. Particles with sharp edges or rod shapes are more abrasive than those of smooth and round particles, and large particles are more abrasive than smaller particles of the same shape. Additionally, the coefficient of friction, surface treatment, surface energy, and purity of a filler all affect its abrasivity. Purity is important since one of the most common contaminants in natural fillers is the highly abrasive sand.

Surface Area, Chemistry, Wetting, and Coupling. Available surface areas of fillers include surfaces of filler aggregates and agglomerates and surfaces in their pores, crevices, and cracks. Measured values of surface area of fillers vary depending on the measurement methods. The direct method of surface area summation from microscopic imaging of filler particle size distribution typically yields a lower surface area value because of the inability to measure surfaces in pores and crevices by microscopy. In practice, surface area is determined from the measured nitrogen adsorption assuming monolayer coverage on the filler particle surface (15) according to the BET theory (16) and is expressed in square meters per gram (m^2/g).

The chemical compatibility between the filler surface and a polymer to be filled is critically important in both the wetting and dispersion of this filler by the polymer and the final physical performance of the resulting filled polymer. Filler surfaces are commonly defined, according to water affinity, as hydrophilic, which has a high affinity for water, to hydrophobic. Many commercial fillers, especially mineral types, are surface coated or chemically treated with hydrophobic wetting agents to modify their surface chemistry, to alter wetting characteristics, and to aid their dispersion in organic polymers, particularly in nonpolar polymers. These wetting agents also assist in deagglomerating filler particles which, in turn, allow for higher filler loadings with lower viscosities during filler incorporation. A filler particle's oil or water absorption value provides an indirect measurement of filler

relative wetting properties. The wettability can also be estimated by the contact angle (17) measured between a drop of water or oil and the filler surface. Commercial wetting agents typically include polymeric esters, stearates, fatty-acid esters, and organosilanes, among which the organosilanes, are the most widely used.

Organosilane wetting agents are also called silane coupling agents (qv) and, in general, consist of a trialkoxy group and a functional group having a $(RO)_3$—Si—R^* structure. The trialkoxy [$(RO)_3$ group provides chemical interactions or reactions with functional groups on the filler surface, and the R^* functional group delivers compatibility with the polymer matrix across the silane coupling bridge. This functional group can be selected from various chemical groups, such as isobutyl, mercapto, aminopropyl, methacryl, vinyl, epoxy, or haloalkyl, in accordance to the desirable interactions required with the polymer matrix (3). However, the extent and uniformity of the alkoxide reaction with a filler particle's surfaces vary depending on the treatment method. The pretreatment of fillers generally results in a more uniform reaction with a coupling agent than that obtained by mixing all ingredients in an internal mixer, particularly under low shear conditions.

Loading and Density. The amount of filler in a filled polymer is termed the *loading* and is always expressed quantitatively although the quantitative measures vary from industry to industry. In plastics and rubber industries, filler loading is formulated according to parts of filler used per 100 parts of polymer (phr), weight percent (wt%), or volume percent (vol%). In the paint industry, volume percent pigment (filler) in the dry paint film or the volume ratio of filler to binder is commonly used. In the paper industry, filler weight percent of sheet weight or percent ash based on a loss-on-ignition method is applied.

The optimal loading of fillers in a polymer is a balance between physical property enhancement and trade-off, and processing and material cost over the filler loading range. A theoretical maximum filler loading based on packing efficiency of monodispersed particles sets the upper limit of filler loading. The maximum volume fraction of spherical fillers in a hexagonal close packing is 0.74, whereas the maximum volume fractions achievable in a random close packing and in a cubic packing are 0.64 and 0.52, respectively (18). In practice, the maximum packing varies with particle shape, particle size distribution, and state of particle agglomeration. Agglomerates and nonspherical particles generally have smaller maximum packing than that of spheres (19). It is possible to achieve maximum packing with minimum void volumes by having very wide particle-size distribution (20). Except in a few cases, it is difficult to predict the maximum volume fraction from theory.

The average mass per unit volume of the individual particle is the true density or specific gravity of the filler. It is used to calculate the volume fraction of fillers and is determined by a simple liquid displacement method for large, nonporous, and spherical particles. Densities of finely divided, porous, and irregular fillers are typically measured by a gas pycnometer that ensures all pores and crevices of filler agglomerates are penetrated. Apparent, or bulk, filler density refers to the total amount of volume occupied by a given mass of dry fillers and it includes the void volumes in the filler aggregates and agglomerates. Bulk density is used in weighting fillers during filler purchasing, shipping, and storage.

Filled Polymers

It is probably true that all polymers contain some form of additive, ranging from small fractions of catalyst residue to large-scale incorporation of fillers. Fillers commonly used in plastics and rubbers and their primary functions have been extensively discussed (21,22). Fillers such as clay, kaolin, talc, calcium carbonate, or silica, and pigments such as titanium dioxide, are typically added in paper in a pulp slurry prior to its deposition onto the wire for paper making. Similarly, these types of fillers along with pigments are incorporated into paint formulations prior to paint application. All fillers are employed for such reasons as processing improvements, mechanical reinforcements, thermal stability, optical properties, permeability reduction, or cost saving.

Rheology and Processability. The presence of fillers affects the flow characteristics of the filled polymers. The immediate effect of a filler is to increase viscosity, interfere with the polymer flow pattern in a given process, produce thixotropy, and give rise to machine wear. The relevant properties of the filler are concentration, size, aspect ratio, stiffness, strength, and specific interaction between filler and the polymer matrix. Within these are the special cases of easily deformable fillers that could easily be broken down or shaped during flow.

In a simplest case with nondeformable, or rigid, spherical fillers in a very diluted concentration, the viscosity of the filled Newtonian polymer melt can be predicted by a simple Einstein equation (23).

$$\eta = \eta_s(1 + 2.5\ \varphi) \tag{1}$$

Here, the viscosity of the filled polymer, η, is related to the viscosity of the polymer, η_s, and the filler volume fraction, φ. At higher filler concentrations where the particles start to physically interact with one another, the Einstein equation is no longer applicable.

When filler spheres are close enough, hydrodynamic interactions between particles need to be considered. By factoring in the effects of two-body interactions, a modified equation was derived that is applicable up to $\varphi = 0.1$ (24).

$$\eta/\eta_s = 1 + 2.5\varphi + 6.2\varphi^2 \tag{2}$$

For filled Newtonian polymer melts of even higher filler volume fractions, a general empirical expression can be used to calculate shear viscosity of the composite (25).

$$\eta/\eta_s = (1 - \varphi/\varphi_m)^{-[\eta]\varphi_m} \tag{3}$$

Here, φ_m is the maximum packing volume fraction and its value and $[\eta]$ have been tabulated (26) for a variety of particles from spheres to glass fibers. It needs to be emphasized that at high filler loading the particle size distribution has a strong effect on viscosity.

With an increase in filler concentration that exceeds the filler percolation threshold, a loose filler network is formed that would show elastic behavior and,

in particular, a yield stress or thixotropy (5,27,28). This non-Newtonian behavior is not limited to filled polymers with high filler concentrations. Many polymer melts are viscoelastic and non-Newtonian. In these filled polymer melts, flow behavior is governed by viscoelastic properties of polymer compounded by the diverse properties of densely packed fillers and cannot be modeled and predicted theoretically. However, fine and particulate fillers are known to suppress elasticity of viscoleastic gum rubbers and render them better processability, such as less die swell, less shrinkage, and less melt fracture.

Mixing and Dispersion. In preparation of filled polymers, the process of uniformly distributing fillers without forming any filler composition gradients is most important. The process of mixing consists of three basic elements: incorporation, distribution, and dispersion. These elements occur simultaneously throughout the mixing cycle. Incorporation, which predominates the early stage of mixing, involves blending of separate ingredients into a coherent, although still inhomogenous, mass. In the distribution step, homogenizing occurs in which the ingredient becomes randomly distributed throughout the polymer matrix.

Dispersion is specifically concerned with the breakdown of filler agglomeration or physical association. It consists of three stages: initial wetting, breakdown of agglomerates, and intimate wetting of particles to displace air pockets. Dispersion becomes increasingly more difficult as particle size decreases and as processing continues. The actual choice of mixing and dispersion process and equipment depends on cost and polymer-filler system. Typically, it involves the high viscosity shear mixing, such as internal mixing, blade mixing, and single-or twin-screw extrusion.

The lower the filler loading, the more physical mixing is required to attain a suitable distribution. It is for this reason that the technique of masterbatching a concentrated mix of polymer and filler is commonly used in polymer compounding for adding smaller amounts of filler in a polymer by diluting the masterbatch with the polymer. The acceptable level of mixing depends on the particular filled polymer system and its property requirements. Not all filled polymers require fillers to be completely randomized.

Mechanical Properties. In addition to the hydrodynamic effects of particulate fillers on polymer flow behavior, an enhanced stiffening effect is observed in filled polymers. For soft polymers, such as elastomers, with diluted filler loading, effects of filler on modulus are proportional to that on viscosity and can be represented by the Einstein equation, equation 1, with viscosity terms replaced by modulus terms. However, this viscosity to modulus relationship only holds when the polymer is incompressible, such as elastomers with Poisson's ratio of 0.5, and when the rigidity of the filler is very much greater than that of the polymer.

The Guth–Gold model (29) is an extension of the Einstein model, whereby interactions of neighboring particles are incorporated. Normalized initial moduli, normalized against the polymer modulus, of filled polymers are related to the filler volume fraction by a polynomial series as follows:

$$E/E_s = (1 + 2.5\ \varphi + 14.1\varphi^2) \tag{4}$$

Here, E_s is the modulus of the polymer and φ is the filler volume fraction. Further modification of the Guth-Gold model leads to the Guth model (30) in which a geometric factor, g, was introduced. The Guth model is shown below.

$$E/E_s = [1 + 0.67\, g\varphi + 1.62(g\varphi)^2] \tag{5}$$

This geometric factor is applied to account for the fact that the filler aggregate structure could affect the stiffness strongly at high filler loading and represent initially the ratio of the length to the width of the filler aggregate. Typically, g is used as a fitting parameter and has a value between 4 and 10. According to 3D finite element simulations with randomly placed filler particles in polymers, the modulus enhancement of filled polymers can be well modeled by amplification of the first stretch invariant (31,32). The polynomial amplification factor employed for the stretch invariant is similar to the Guth-Gold model but with different prefactor for φ^2 term.

Although the modulus increases for polymers upon filler addition, the tensile strength and elongation to break values do not follow the same relationship. Tensile strengths of rigid polymers filled with rigid fillers, in general, decrease with increasing filler loading due to stress concentration effects. However, for some filled soft elastomers, tensile strength increases with an increase in filler concentration, up to an optimal concentration (33). Other factors that could affect the ultimate tensile properties are interfacial adhesion, particle size, and geometric shape. Large particles give rise to higher stress concentration, and thus lower tensile strength, than do smaller particles. It is for this reason that fillers used especially in elastomers are preferred to be smaller than micron size.

Rigid fillers, in general, cause a decrease in elongation to break since, proportionally, more of the experimental strain is being sustained by intrinsically less polymer. Additionally, the actual strain experienced by the polymer matrix is much higher than the applied strain around rigid fillers (34). For filler particles that have good adhesion with the polymer matrix, it was found that the elongation to break of the filled polymers, ε, follows (34,35)

$$\varepsilon = \varepsilon_s(1 - \varphi^{1/3}) \tag{6}$$

where ε_S is the elongation to break of the unfilled polymer. If there is poor adhesion between fillers and the polymer matrix, the decrease in elongation to break with increasing filler loading is more gradual than that calculated from equation 6. However, there are cases where fillers promote craze formation that give rise to an increase in elongation to break with filler addition (36).

Rigid fillers in a rigid polymer generally decrease the impact strength of a polymer (37). Impact strength in a filled polymer is largely determined by the dewetting and crazing phenomena. Typically, dewetting and cavitation at the poles of spherical particles during tensile loading of polymers occur first, followed by crack–craze formation at the equators of filler particles (38). Although debonding and crack formation lower the strengths in filled polymers, there are cases in which the actual fracture energy of brittle plastics, such as polyesters and epoxies, increase in the presence of fillers. It is believed that, in these cases, fillers can

impede crack growth (1). Additionally, rigid polymers filled with elastomeric particles could have high impact strengths if good interfacial adhesion exists between fillers and polymers (39).

Thermal Properties. Since polymers generally have a much larger thermal expansion coefficient than most rigid fillers, there is a significant mismatch in thermal expansion in a filled polymer. This mismatch could lead to generation of thermal stresses around filler particles during fabrication and, most severely, induce microcracks at the filler interface that could lead to premature failure of the filled polymer. As for the thermal expansion coefficient of a filled polymer, it generally falls below the value calculated from the simple rule of mixtures but follows the Kerner equation (40) for nearly spherical particles.

$$\alpha = \alpha_1\varphi_1 + \alpha_2\alpha_2 - (\alpha_1 - \alpha_2)\varphi_1\varphi_2(1/B_1 - 1/B_2)/(\varphi_1/B_2 + \varphi_2/B_1 + 3/4G) \tag{7}$$

The volume coefficients of thermal expansion of the composite, polymer, and filler are α, α_1, and α_2 respectively. The bulk moduli of the components are B_1 and B_2, respectively. The parameter G is the shear modulus of the polymer. The more the filler particles deviate from spherical, the greater the divergence of the thermal expansion coefficient from this equation. In such cases, the Thomas equation (41), or the logarithmic rule of mixtures, provides a better estimate.

$$\log \alpha = \varphi_1 \log \alpha_1 + \varphi_2 \log \alpha_2 \tag{8}$$

Polymers have lower thermal conductivity compared to metals and many inorganic materials (1). By the incorporation of metal or carbon fillers, a substantial increase in thermal conductivity can be obtained. Considering that thermal conductivities of filled polymers typically lie in between the limits set by rule of mixtures, Ziebland (42) proposed the use of the arbitrary relationship:

$$\log k = \varphi_1 \log k_1 + \varphi_2 \log k_2 \tag{9}$$

where k and k_1 are the thermal conductivities of the composite and polymer, respectively. The parameter k_2 is the hypothetical thermal conductivity of the particulate filler and it is determined from a one-point solution based on a single reading on the filled polymer of known composition. It is noted that this equation is similar to that of the Thomas equation for thermal expansion coefficient.

The melting temperature of a crystalline polymer is largely unaffected by the presence of fillers, whereas the glass transition temperature of a polymer is slightly raised by fillers. But the increase in heat distortion temperature in the presence of fillers could be quite substantial, often by as much as 10–20°C or more. In general, fillers raise the heat distortion temperature of a material by the increase in modulus and the reduction in high temperature creep of a material in the presence of fillers (43–45).

Optical Properties. The use of fillers has indirect effect, or direct in the case of pigments, on the optical properties of polymers. The light transmissivity in a filled polymer is controlled primarily by light scattering, which in turn depends on the differences in refractive indexes between the polymer and filler. A filler with a refractive index near to that of the polymer, such as silica in polyester, can

provide a translucent filled polymer. If the filler is optically anisotropic, such as calcite and talc, the corresponding filled polymers may appear in color under the polarized light or by optical interference. When the filler particle size is smaller than the wavelength of the light, $<0.4\ \mu$m, the filled polymer becomes transparent, which is one reason for the interest in using nanofillers.

Permeability. High aspect-ratio plate-like fillers can drastically lower the diffusivity or permeability of gases in solid polymers. Experimentally, it has been demonstrated that the barrier properties of a polymer could be significantly improved with just a few percent of exfoliated high aspect-ratio silicate fillers (46–49). Without considering the possible changes in the local permeability values due to molecular-level transformation by the presence of silicates, this permeability reduction simply arises from the increase in diffusion path lengths. Since molecules are now required to make long detours around the platelets, Nielsen (4) developed a simple model to determine the reduction in permeability in a polymer by accounting for the increase in torturosity with impermeable and planarly oriented platy fillers.

$$P/P_s = (1-\varphi)/(1+a\varphi/2) \tag{10}$$

Here, P is the permeability, P_s is the permeability of the polymer without fillers, φ is the filler volume fraction, and a is the aspect ratio. Cussler and coworkers (50) and Fredrickson and Bicerano (51) provided further refinements of the model by removing the position order but with perfect orientation. Recently, Gusev and Lusti (52) conducted direct 3D finite-element permeability calculations with a multiinclusion computer model comprising of randomly dispersed, perfectly oriented, and nonoverlapping platelets. They found all their numerical simulated permeability values could be well represented with a stretched exponential function as

$$P/P_s = \exp[-(a\varphi/3.47)^{0.71}] \tag{11}$$

This Gusev and Lusti equation, despite its empirical nature, has been demonstrated to model excellently the literature data for nylon-layered silicate nanocomposites.

Filler Types

Mineral Fillers. Mineral fillers (21,53) are naturally occurring materials that are mined and are ground to a specified particle size. Grinding may be done dry using mechanical mills. For a finer product the ore is ground wet. Wet grinding may be autogenous where the ore grinds by attrition with itself or a grinding media may be employed. Additional processing may include a combination of steps. They include (*1*) separation of fine and coarse particles by use of screens, by air- or water flotation, or by centrifugal filtration; (*2*) removal of impurities by washing, heat treatment, magnetic separation, or chemical treatment; and/or (*3*) surface treatment with a variety of chemicals to improve the compatibility with the polymer matrix.

Calcium carbonate ($CaCO_3$), also known as whiting, limestone, marble, chalk, or calcite, that has been ground is added to polymer compounds to reduce cost and to impart hardness and opacity to polymer articles. Particle sizes range from 2 to 80 μm for dry-ground product and from 0.5 to 11 μm for wet-ground product. The chemical composition and crystalline nature depend on the limestone deposit that is mined, eg, chalk or marble, and the color of the deposit. The most important applications of calcium carbonate by the polymer industry are uses in electrical wire and cable insulation, where the low moisture content and natural insulating properties make it a preferred filler in the production of articles, where low cost and smooth surface appearance are desired, such as footwear; and in extruded hoses and automotive sealing parts. Typical calcium carbonate levels used in polymer compounds range from 20 to 300 phr.

Baryte is predominately barium sulfate ($BaSO_4$) that is available in particle sizes from 1 to 20 μm. It is used as a filler when a high specific gravity is required of the polymer article. Typical polymer loading levels are 25–100 phr for articles such as stoppers and seals.

Crystalline silica (SiO_2) from sand or quartz can be ground and used as a degrading or extending filler for low cost polymer articles. To minimize the health hazards of exposure to airborne crystalline silica, particle sizes are large, normally ranging from 2 to 20 μm. Naturally occurring silica (SiO_2) or dolomite is often referred to as diatomaceous earth since the primary deposits are the exoskeletons formed by diatoms that have extracted silicic acid from sea water and formed amorphous silica shells. Diatomaceous earth is usually very high in surface area because the shells retain the radial and/or rod-like structures of the living creature. The largest deposits are several million years old and have been partially converted to crystalline silica over time. Diatomaceous earth obtained from sedimentary rocks often contains up to 30% organic matter and inorganic impurities such as sand, clay, and soluble salts (54) requiring separation or treatment to remove crystalline content, which could represent a health hazard. Biogenic silica is used as a semireinforcing filler or as a solid carrier for liquid compounding ingredients.

Kaolin clay (55,56), also called kaolinite or China clay, is hydrous aluminum silicate [$Al_2Si_2O_5(OH)_4$] consisting of platelets with alternating layers of silica and alumina in the structure. The fine particles of clay are formed by the weathering of granite. Clay deposits are classified as primary, secondary, and tertiary. Primary deposits are mixtures of clay and granite that are found where the clay was originally weathered. They contain only 40–50% particles <2 μm in diameter. Secondary deposits are formed when fine particles from primary deposits are carried by water flow and are deposited in a new location. Tertiary deposits are the most important commercial deposits because of their fine particle size with $>80\%$ of the particles being <2 μm in diameter. Their high purity results when water carries the fine particles of a secondary deposit to a new location. The most significant deposits of tertiary clay in the world are found in the southeastern United States, Cornwall, United Kingdom, the Amazon region of Brazil, and Australia. Clay is broadly divided into soft and hard clay in that they produce softer and harder polymer compounds, respectively, at a given loading level. Because clay is mined as a fine particle-size material, it does not require significant grinding for use in polymers. There are five basic processes for producing clay for polymer

reinforcement from the mined form. (*1*) Air-floated clay, in which the ore is milled to break up lumps and air classified, is the least expensive form of clay and imparts moderate reinforcement. (*2*) Water-washed clay involves gravity separation of impurities, bleaching, magnetic separation to improve color properties, and centrifuging to produce the desired particle-size range to impart higher reinforcement by the control of pH, color, and particle size. (*3*) Delaminated kaolin uses chemical and/or mechanical means to break apart the platelet structure of the clay, which further increases the available surface area and reinforcement properties. (*4*) Metakaolin is partially calcined by heat treating to 600°C. (*5*) Calcined clay is formed by heating to 1000°C, which produces a very white, high surface area mineral with an inert surface.

Clay is a widely used filler for polymer compounds of all types including components of tires such as fiber adhesive compounds, and the entire range of nontire polymer applications where good reinforcement, moderate cost, and good processability is desired. Clays are usually added to polymer compounds at levels of 20–150 phr. The aspect ratio of clay is between 4 and 12, with average particle size ranging from 0.5 to 2.3 μm.

Talc [$Mg_3Si_4O_{10}(OH)_2$] is a platelet form of magnesium silicate with a high aspect ratio, 5–20. Because the platelets can orient in the extrusion process, it provides polymer extrudates with smooth surfaces that can be extruded at high rates. It is commonly used in compounds, which have critical surface appearance such as exterior automotive components or consumer goods. Talc is used in tires in white sidewall compounds to provide a smooth appearance to the buffed sidewall. The large platelets of talc provide a barrier to gas and moisture permeability in compounds which allows talc to be used in applications such as hydraulic and automotive hoses, barrier films, and tire innerliners. Talc is usually used in addition to other fillers with total filler content of 30–150 phr. The average particle size of talc ranges from 5 to 8 μm.

Mica is a generic name given to a family of hydrous potassium aluminum silicates having similar physical properties. Mica is a common rock-forming mineral and is found around the world. Muscovite and phlogopite micas are most commonly used. Muscovite mica, $K_2Al_4(Al_2Si_6O_{20})(OH)_4$, has a layer structure composing of three planes and has an average particle size of 5 μm. The center is a pseudo-octahedral gibbsite plane that is chemically bonded to two tetrahedra silica planes. Phlogopite mica, $K_2(Mg, Fe)_6(Al_2Si_6O_{20})(OH,F)_4$, with the same structure as that for Muscovite mica, is opaque to ultraviolet (UV) radiation. Phlogopite mica has a particle size of 20 μm and has an aspect ratio from 30 to 100 similar to that of muscovite mica. The largest usage of mica is in polyolefins. The high aspect ratio of mica could provide enhancements in properties as stiffness, tensile strength, dimensional stability, and heat deflection temperature.

Nanoclays. Nanocomposites are materials that contain nanofillers, or fillers of nanometer dimensions. The successful synthesis of nylon–clay nanocomposites (57–59) ushered in nylon nanocomposites that could attain high modulus, heat distortion temperature, dimensional stability, impermeability, and strength with only a few percent modified clay nanofillers. Although it has been long known that polymers could be mixed with appropriately modified clay minerals and synthetic clays, the field of polymer-layered silicate nanocomposites has gained

tremendous momentum since the initial publications. The nylon–clay nanocomposites have since been commercialized and were utilized for automotive timing-belt covers and packaging barrier films (see NANOCOMPOSITES, POLYMER CLAY).

The layered silicates used in nylon–clay nanocomposites are 2:1 phyllosilicates with layers made up by fusing two silica tetrahedra to an edge-shared octahedral sheet of aluminum hydroxide. Isomorphic substitution within the layers, such as Al^{3+} replaced by Mg^{2+}, generates negative charges defined by the charge exchange capacity (CEC). Stacking of the layers leads to a gap between layers called the interlayer or gallery that is pristinely filled with exchangeable hydrated alkali metal cations to counterbalance these negative charges. Ion exchange of these alkali metal cations with various organic cations, such as alkyl ammonium cationic surfactants, could render the normally hydrophilic silicate surface hydrophobic. These layered silicates, or phyllosilicates, intercalated by organic cations are called organosilicates.

Commonly used 2:1 phyllosilicates include hectrite, saponite, montmorillonite, and synthetic mica. These silicates are stacks of layers of 1 nm in thickness and about 50 nm (hectrite), 170 nm (saponite), 200 nm (montmorillonite), and 1230 nm (synthetic mica) in length (60). In particular, naturally occurring montmorillonite with CEC ranging from 0.9 to 1.2 mequiv/g, depending on the mineral origin, is most frequently used and was the type employed in the initial nylon–clay nanocomposites. Organosilicates consisting of alkyl ammonium-exchanged montmorillonites are also commercial.

The nylon–clay nanocomposites were prepared by *in situ* polymerization in the presence of organically modified, with aminolauric acid, montmorillonite. The reaction between nylon monomer and modified montmorillonite rendered nylon chains end-tethered though aminolauric acid to the silicate surface leading to exfoliated silicates (61). However, not all polymer nanocomposite systems could be produced via *in situ* polymerization processes because of the chemical sensitivity of polymerization catalysts. Direct melt blending of hydrophilic polymers with montmorillonite in its pristine state or polymers with surfactant-intercalated montmorillonite was found to be possible to deliver polymer intercalated or exfoliated nanocomposites (62,63).

Commercial organosilicates based on montmorillonites are effective agglomerates of smaller, primary particles consisting of 10–20 layers in a coplanar orientation. Those primary particles are usually referred to as the tactoids. The first step of melt mixing is to break up the agglomerates of organosilicates to their primary particles through diffusion of polymer chains into the agglomerates. This, in turn, will provide fillers from micron in size with aspect ratios of about 1 to fillers of submicron, 0.1–0.2 μm, with aspect ratios of $\sim$20. The ultimate goal in melt mixing is to diffuse polymers into the silicate galleries to completely exfoliate organosilicates leading to fillers 1 nm thick with aspect ratios of $\sim$200.

Synthetic Fillers. Synthetic fillers are generally manufactured by precipitation of soluble materials under carefully controlled conditions to provide tailored properties. They may be found as colloidal particles that may be spherical, ellipsoid, rod, or tube-shaped; as aggregates which are covalently bonded groupings of individual particles; or as agglomerates that are loosely held associations of aggregates physically interacting. Reinforcement properties are a function of the colloidal particle size and shape, the aggregate dimensions and morphology,

and the ability of agglomerates to break down during mixing. Additionally, the composition and surface chemistry of the filler plays a significant role.

Precipitated calcium carbonate is formed by dissolving limestone and precipitating $CaCO_3$ as very fine particles using carbon dioxide (Aroganite Process) or sodium carbonate (Solvay Process). Typical particle sizes range from 0.02 to 2 μm. Most commercially available precipitated calcium carbonate is spherical colloidal particles or aggregates consisting of a few spherical particles. Additional shapes and aggregates of varying morphology are possible and provide increased reinforcement. Precipitated calcium carbonate is used as a semireinforcing filler in shoe products and industrial polymer goods, particularly when resistance to alkali solutions is needed. The low moisture content and good reinforcement allow precipitated calcium carbonate to be used in wire and cable insulation applications.

Zinc oxide, which is formed from the burning of zinc metal, was the first nonblack filler used for reinforcement of rubber compounds. Although zinc oxide and magnesium oxide are still used as reinforcing fillers in some specialty compounds, particularly those that require heat resistance, their role in rubber compounding in the last several decades is that of an activator for the sulfur cure system or as curatives for chloroprene rubber compounds.

The rutile form of titanium dioxide (TiO_2) is an important filler for white and colored polymer articles. The ability of the titanium dioxide particle to scatter light provides high whiteness and opacity to polymer, which gives the filler particle the ability to cover background colors. The anatase crystalline form of titanium dioxide is also used.

Alumina trihydrate ($Al_2O_3{\cdot}3H_2O$), ATH, is an intermediate mineral that is formed in the conversion of bauxite to aluminum. The major types of ATH are ground and precipitated. Alumina trihydrate is ground and classified using the same procedures as other minerals, and is available in particle sizes from <1 μm to several micrometers in diameter. Alumina trihydrate is used to provide flame-retardant properties to polymer articles and to suppress smoke formation. The water of hydration of the ATH crystal is released beginning at 230°C, which absorbs heat and provides water vapor to cool the polymer article and disperse smoke.

Amorphous silica (64) consists of ultimate particles of the inorganic polymer $(SiO_2)_n$ where a silicon atom is covalently bonded in a tetrahedral arrangement to four oxygen atoms. Each of the four oxygen atoms is covalently bonded to at least one silicon atom to form either a siloxane (—Si—O—Si—) or a silanol (—Si—O—H) functionality. Surface silanol groups can be isolated from one another such that hydrogen bonding between the silanols cannot occur, vicinal to one another promoting the formation of intramolecular hydrogen bonding, or geminal to one another where two silanol groups are bonded to the same silicon atom. Particulate silicas are made by precipitation from aqueous solution. The physical and chemical properties of precipitated silicas can vary according to the manufacturing process. Reinforcement and control of suspension pH, temperature, and salt content can vary the ultimate particle and aggregate sizes of silicas precipitated from solution. The surface area, as determined by nitrogen (16) or cetyltrimethylammonium bromide (CTAB) adsorption (65) is a function of the ultimate particle size. Ultimate particles can range from 5 to 50 nm in diameter. Aggregates are 3D clusters of ultimate particles covalently bonded to one another via siloxane bonds, and range in size up to 500 nm in diameter. Aggregates can physically

agglomerate through intermolecular hydrogen bonding of surface silanol groups of one aggregate to a silanol group of another aggregate affording structures up to ~100 μm in diameter. The median agglomerate particle size is generally 20–50 μm in diameter, but can be reduced in size by milling to ~1 μm. Precipitated silica is prepared from an alkaline metal silicate solution, such as sodium silicate in a ratio of ~2.5–3.3 SiO_2:Na, but using lower concentrations of silicate than is used in silica gel preparation (66). In the absence of a coagulant, silica is not precipitated from solution at any pH value (66). Silica is precipitated by adding acid to sodium silicate to reduce the pH value of the hot suspension to a pH value of 9 to 10, where the concentration of sodium ion exceeds approximately 0.3 *N*. Sulfuric acid is normally used to neutralize sodium silicate and precipitate silica.

Because of its small particle size and complex aggregate structure, precipitated silica imparts the highest degree of reinforcement to elastomer compounds among all of the nonblack particulate fillers. This superior reinforcement is employed in a variety of polymer compounds for shoe soles, industrial polymer goods, and tires (67–69). Precipitated silica is used in shoe soles for its resistance to wear and to tearing, its nonscuffing characteristics, and in order to obtain compounds with light color, or even a transparent material. Precipitated silica is used to improve the tear strength and resistance to flex fatigue (cracking, cut-growth) and heat aging in a wide variety of manufactured rubber goods including conveyor and power transmission belts, hoses, motor and dock mounts, and bumper pads. Rubber rolls that utilize the abrasion resistance, stiffness, and nonmarking characteristics of precipitated silica are important for use in paper processing and the dehulling of grains, particularly rice (70).

Amorphous pyrogenic or fumed silicas are generally less dense and of higher purity than silicas precipitated from solution. They are much less hydrated and are sometimes completely anhydrous, with the surface silanol group density ranging from 2 to 4/nm^2 of surface area. The $SiCl_4$ can be burned with methane (CH_4) or hydrogen (H_2) gases to produce SiO_2, H_2O, and HCl, an important commercial method (71). Particle size is controlled by combustion conditions during the flame hydrolysis. Pyrogenic silicas with surface areas <300 m^2/g are essentially nonporous, while those with higher surface areas can have some porosity. They generally contain a few hundred ultimate particles fused into branched-chain, 3D aggregates (71). Pyrogenic silicas in the 100–2000-nm particle size range are common (72). Pyrogenic silica is used in applications which require a low level of surface water per unit surface area of the silica, primarily as a reinforcement in adhesives, sealants (73), and elastomer compounds based on silicone polymers (74,75). They are used as a thixotropic agent, free flow, antistatic agent, carrier, coating additive, and antifoaming agent (76).

Amorphous silicates (77) are precipitated from aqueous blends of soluble silicate, typically sodium silicate, and soluble salts of other metals. The most important types for reinforcement of elastomers are aluminosilicates with mixed Al_2O_2 and SiO_2 structures, magnesium aluminosilicates, and calcium silicates. The silicates have surface areas and resultant reinforcement that span the range from the highest surface area clays (~30 m^2/g) to the lower end of the precipitated silicas (~100 m^2/g).

Nanoscale Oxides and Metals. Using vapor-phase plasma-based techniques, precipitation sol–gel reaction, or simple grinding, nanoscale metal oxides

are being produced in competition with existing fumed oxide products (78). On the basis of physical vapor synthesis methods developed in the 1980s, zinc oxide nanoparticles are produced for use as a sunscreen and fungicide in personal care and cosmetics products. Using a pulsed plasma process, nanometals, such as aluminum and silver nanoparticles, and nanoscale oxides, are being produced. Potential commerical markets for nanometals include aluminum nanoparticles in explosives and pyrotechnics and sliver nanoparticles in electronics and medicines.

Carbon Fillers. The application of carbon black (qv) in rubber compounds is over a hundred years old. Unlike the well-known crystalline forms of carbon, such as diamond and graphite, carbon black is amorphous and is a manufactured product (79,80). Carbon blacks are prepared by incomplete combustion of hydrocarbons or by thermal cracking. Presently, almost all rubber-reinforcing blacks are manufactured by the oil furnace process. A fuel is burned in an excess of air to produce finely divided carbon. Furnace blacks have low oxygen contents with neutral or alkaline surfaces. In the thermal process, oil or natural gas is cracked in an absence of oxygen to produce unoxidized blacks of small surface areas, or thermal blacks.

Many grades of carbon blacks are manufactured for various applications. These include blacks of higher surface area, different internal porosity, and higher surface oxidation. There are also electrical conductive blacks, such as acetylene black. The American Society of Testing Materials (ASTM) has established a carbon black classification system based on particle size and surface oxidation, ASTM D1765. The degree of surface oxidation affects the cure time of carbon-black–filled rubber compounds. The "N" denotes normal curing blacks and the "S" refers to slow curing blacks. After N or S, the first number of the three-digit suffix identifies the particle size and the remaining two digits are assigned arbitrarily. Specifications are given both in terms of analytical processes of characterizing the black and of resulting physical properties of carbon-black–filled rubbers prepared in standard recipes. In accordance to the designation, N550 black, for example, denotes a normal-curing carbon black with particle size in the range of 40–48 nm.

Carbon black owes its reinforcing character to the size, shape, and surface chemistry of the aggregate structures that consists of primary particles essentially spherical in shape that are chemically bonded to one another (80). The two most important properties of carbon black are surface area and structure. Surface area depends inversely upon the size of the primary particles and is one measure of the area available for physical interaction with the polymer. Surface area ranges from 10–140 m^2/g with thermal blacks having the lowest values based on nitrogen adsorption via ASTM D4820. The structure of carbon black depends on the size and grouping of these primary particles in the aggregate. The more primary particles in the aggregate, the higher structure of the carbon black due to the more complex shape and void volume (porosity). Structure varies from 35 to 130 $cm^{-3}/100$ g as measured by dibutylphthalate oil absorption via ASTM D2414. Surface activity refers to the strength of the carbon black/polymer interaction either from physical adsorption or chemisorption. The small (2–3%) but significant amount of noncarbon heteroatoms, such as hydrogen, oxygen, and sulfur, that are present on the carbon black surface results in surface activity differences. During mechanical mixing with polymers, it is desirable to minimize the presence of agglomerates.

Aggregate structures are not thought to be broken down into primary particles by simple mechanical processes.

Carbon blacks are extensively used in rubbers and elastomers, in loading from 10 to 150 phr, and for improvements in stiffness, strength, processability, and abrasion resistance (79). Particle size and concentration are optimized on the basis of balances in mixing–compounding, heat buildup, property improvement, and cost. Carbon black fillers, without considering the electrical conductive blacks, are used in plastics, predominantly as pigment or colorant.

Carbon Nanotubes. Carbon nanotubes are graphene cylinders end-capped with pentagonal rings. They were discovered in 1991 (81) during the arc-evaporation synthesis of fullerenes. The arc-evaporation method produces only multilayered tubes. Multiwalled nanotubes were first produced in 1983 before their structure was fully understood. These multiwalled nanotubes are sold in commercial quantities for electrostatic discharge control in polymers for electronic and automobile applications. Addition of metals to the graphite electrodes was found in 1993 (82) to synthesize single-layer–wall carbon nanotubes. An alternative method of preparing single-walled nanotubes was developed in 1996 (83) leading to the commercialization of single-walled carbon nanotubes, or buckytubes. Single-walled nanotubes have fewer defects and much improved performance compared to multiwalled tubes. The use of single-walled tubes in flat panel displays, conductive plastics, and high performance fibers are recent application developments.

Economic Aspects

Sales of fillers worldwide were estimated to be on the order of 10^6 t and $9 billion for 1990, with paint (42%), paper (21%), and plastics (16%) as the principal consumers on a dollar basis. When viewed on a volume basis, paint and paper are even at 37% each, plastics use 21%, and rubber 6%. Titanium dioxide represented 67% of the dollar volume, with 60% of its use in paint. The filler industry appeared to approach market saturation in 1998 (84) before the introduction of nanofillers. The nanomaterials business, at the present time, consists of three lines: nanoclays, nanoscale oxides and metals, and carbon nanotubes. The most established market now is nanoclays. The nanomaterials market is expected to increase by 12.8%/year, to $900 million by 2005 (85). The global market for coupling agents used in plastics grew at about 7% in 2001 and was expected to reach $300 million (86). The coupling agent market has three major categories: silanes, which make up ~85% of demand; organometallics acount for 10%; and maleated polyolefins have 5%.

Health and Safety

The principal hazard involved in the handling and use of many fillers is inhalation of airborne particles (dusts) in the respirable size range, ie, 10 μm and below. Filler dusts may be classified as nuisance particulates, fibrogens, and carcinogens. Nuisance particulates are dusts that have a long history of little adverse effect

on the lungs and do not produce significant organic disease or toxic effect when exposures are kept under reasonable control. The American Conference of Governmental and Industrial Hygienists (AC-GIH) establishes threshold limit values for the airborne concentration of many fillers in workroom air (87). A new manner of occupational and environmental legislation is aimed at the hazards of ultrafine particles, and OSHA regulations effective in 1992 regulate the total workplace, including nonproduction areas (88). In addition, concern for the toxicity of many metals and their compounds is limiting the use of many fillers, eg, Pb, Co, Cr, and Ba compounds, and possibly the use of certain organometallic surface coatings. Suppliers have information on proper usage and handling of their products. The use of National Institute for Occupational Safety and Health – Occupational Safety and Health Administration (NIOSH–OSHA)-approved dust masks or respirators is required when dust concentrations exceed permissable exposure limits. It has been reported that because of concerns by some international agencies over the possibility that crystalline silica might be a carcinogen, a 0.1% max silica (crystalline) specification has been mandated in mineral fillers (89).

BIBLIOGRAPHY

"Fillers" in *EPST* 1st ed., Vol. 6, pp. 740–763, by W. J. Frissell, Rohm & Haas Co.; in *EPSE* 2nd ed., Vol. 7, pp. 53–73, by W. S. Stoy and F. J. Washabaugh, Engelhard Corp.

1. R. P. Sheldon, *Composite Polymeric Materials*, Applied Science publisher, New York, 1982.
2. E. Matijevic, *MRS Bull.* **14**, 18 (1989).
3. D. Sekutowski, in J. Ededbaum, ed., *Plastics Additives and Modifiers Handbook*, revised ed., Chapman & Hall, London, 1996, Chapt. 35, p. 493.
4. L. E. Nielsen, *J. Macromol. Sci. (Chem.) A* **1**, 929 (1967).
5. R. G. Larson, *The Structure and Rheology of Complex Fluids*, Oxford University Press, New York, 1999, p. 279.
6. J. C. Russ, *The Image Processing Handbook*, 2nd ed., CRC Press, Boca Raton, Fla., 1995, p. 523.
7. D. Stauffer, *Introduction to Percolation Theory*, Taylor & Francis, London, 1985.
8. D. S. McLachlan, M. Blaszkiewicz, and R. E. Newnham, *J. Am. Ceram. Soc.* **73**, 2187 (1990).
9. T. Allen, *Particle Size Measurement*, Chapman and Hall, London, 1974, p. 93.
10. R. R. Irani and C. F. Callis, *Particle Size: Measurement, Interpretation, and Application*, John Wiley & Sons, Inc., New York, 1963.
11. E. E. Underwood, *Quantitative Stereology*, Addison-Wesley, Reading, Mass., 1969.
12. J. B. Wachtman, Jr., *Mechanical and Thermal Properties of Ceramics*, John Wiley & Sons, Inc., New York, 1996.
13. A. U. McNeil, L. E. Grimsditch, and M. Ti, *J. Phys. Condens. Matter* **5**, 1681 (1993).
14. F. Mohs, *The Characteristics of the Natural History System of Mineralogy*, W. & C. Tait, Edinburgh, 1820.
15. R. W. Camp and H. D. Stanley, *Am. Lab.* **23**, 34 (1991).
16. S. Brunauer, P. H. Emmett, and E. Teller, *J. Am. Chem. Soc.* **60**, 309 (1938).
17. A. W. Adamson, *Physical Chemistry of Surfaces*, 4th ed., John Wiley & Sons, Inc., New York, Chap. X, p. 332.
18. R. K. McGeary, *J. Am. Ceram. Soc.* **44**, 513 (1961).
19. T. B. Lewis and L. E. Nielsen, *Trans. Soc. Rheol.* **12**, 421 (1968).

20. C. C. Furnas, *Ind. Eng. Chem.* **23**, 1052 (1931).
21. H. S. Katz and J. V. Milewski, eds., *Handbook of Fillers for Plastics*, Van Nostrand Reinhold Co., Inc., New York, 1987.
22. W. Hofmann, *Rubber Technology Handbook*, Hanser publisher, Munich, 1989.
23. A. Einstein, *Ann. Phys.* **34**, 591 (1911).
24. G. K. Batchelor, *J. Fluid Mech.* **46**, 813 (1971).
25. I. M. Krieger and T. J. Dougherty, *Trans. Soc. Rheol.* **3**, 137 (1959).
26. H. A. Barnes, J. F. Hutton, and K. Walters, *An Introduction to Rheology*, Elsevier, New York, 1989.
27. C. D. Han, *Rheology in Polymer Processing*, Academic Press, New York, 1976, p. 182.
28. K. Yurekli, R. Krishnamoorti, M. F. Tse, K. O. McElrath, A. H. Tsou, and H.-C. Wang, *J. Polym. Sci.: Polym. Phys.* **39**, 256 (2001).
29. E. Guth and O. Gold, *Phys. Rev.* **53**, 322 (1938).
30. E. Guth, *J. Appl. Phys.* **16**, 20 (1945).
31. J. S. Bergstrom and M. C. Boyce, *Mech. Mater.* **32**, 627 (2000).
32. J. S. Bergstrom and M. C. Boyce, *Rubber Chem. Technol.* **72**, 633 (1999).
33. J. T. Byers, in M. Morton, ed., *Rubber Technology*, 3rd ed., Kluwer Academic publisher, Dordrecht, Netherlands, 1999, Chapt. 3, p. 59.
34. L. E. Nielsen, *J. Appl. Polym. Sci.* **10**, 97 (1966).
35. T. L. Smith, *Trans. Soc. Rheol.* **3**, 113 (1959).
36. L. Nicolais and M. Narkis, *Polym. Eng. Sci.* **11**, 194 (1971).
37. G. P. Larson, *Mod. Plast.* **35**, 157 (1958).
38. A. E. Oberth and R. S. Bruenner, *Trans. Soc. Rheol* **9**, 165 (1965).
39. L. E. Nielsen, *Mechanical Properties of Polymers and Composites*, Vol. 2, Marcel Dekker, New York, 1974, Chapter 7, p. 379.
40. E. H. Kerner, *Proc. Phys. Soc. B* **B 69**, 808 (1956).
41. J. P. Thomas, U.S. Dept. Commerce Rept. AD 287826, Kluwer, Dordrecht, the Netherlands.
42. H. Ziebland, *Reinforced Plastics* **25**, 110 (1981).
43. I. E. Neimark, A. A. Chuiko, and I. B. Slinyakova, *SPE Trans.* **2**, 135 (1962).
44. E. A. Noga and R. T. Woodhams, *SPE J.* **26**, 23 (1970).
45. F. G. Krautz, *SPE J.* **27**, 74 (1971).
46. K. Yano, A. Usuki, and A. Okada, *J. Polym. Sci., Part A: Polym. Chem.* **35**, 2289 (1997).
47. T. Lan, P. D. Kaviratna, and T. J. Pinnavaia, *Chem. Mater.* **6**, 573 (1994).
48. E. P. Giannelis, *Adv. Mater.* **8**, 29 (1996).
49. R. J. Xu, E. Manias, A. J. Snyder, and J. Runt, *Macromolecules* **34**, 337 (2001).
50. E. L. Cussler, S. E. Hughes, W. J. Ward, III, and R. Aris, *J. Membr. Sci.* **38**, 161 (1988).
51. G. J. Fredrickson and J. Bicerano, *J. Chem. Phys.* **110**, 2181 (1999).
52. A. A. Gusev and H. R. Lusti, *Adv. Mater.* **13**, 1641 (2001).
53. R. A. Baker, *An Overview of Hidden Minerals of Polymer Applications*, J. M. Huber Corp., Engineered Materials Division, Atlanta, 1993.
54. W. S. Stoy and F. J. Washabaugh, in J. I. Kroschwitz, ed., Encyclopedia of Polymer Science and Engineering, 2nd ed., Vol. 7, John Wiley & Sons, Inc., New York, 1988, p. 53.
55. *Kaolin Clays and Their Industrial Uses*, J. M. Huber Corp., Engineered Minerals Division, Atlanta, 1955.
56. T. G. Florea, *Elastomerics* **118**, 22 (1986).
57. A. Okada, M. Kawasumi, T. Kurauchi, and O. Kamigaito, *Polym. Prepr.* **28**, 447 (1987).
58. Y. Kojima, A. Usuki, M. Kawasumi, A. Okada, Y. Fukushima, T. Kurauchi, and O. Kamigaito, *J. Mater. Res.* **8**, 1185 (1993).

59. K. Yano, A. Usuki, A. Okada, T. Kurauchi, and O. Kamigaito, *J. Polym. Sci., Part A: Polym. Chem.* **33**, 2493 (1993).
60. R. A. Vaia, S. Vasudevan, W. Krawiec, L. G. Scanlon, and E. P. Giannelis, *Adv. Mater.* **7**, 154 (1995).
61. A. Usuki, Y. Kojima, M. Kawasumi, A. Okada, Y. Fukushima, T. Kurauchi, and O. Kamigaito, *J. Mater. Res.* **8**, 1179 (1993).
62. R. A. Vaia, H. Ishii, and E. P. Giannelis, *Chem. Mater.* **5**, 1694 (1993).
63. K. Yano, A. Usuki, and A. Okada, *J. Polym. Sci., Part A: Polym. Chem.* **35**, 2289 (1997).
64. W. H. Waddell and L. R. Evans, in *Encyclopedia of Chemical Technology*, 4th ed., Vol. 21, John Wiley & Sons, Inc., New York, 1997.
65. National French Test Method, T 45-007 (1987).
66. R. K. Iler, *The Chemistry of Silica*, John Wiley & Sons, Inc., New York, 1979.
67. M. P. Wagner, *Rubber Chem. Technol.* **49**, 703 (1976).
68. W. H. Waddell and L. R. Evans, *Rubber Chem. Technol.* **69**, 377 (1996).
69. W. H. Waddell and L. R. Evans, in John Dick, ed., *Rubber Compounding and Testing for Performance*, Hanser publisherNames, Munich, 2000.
70. R. F. Wolf and C. Stueber, *Rubber Age* **87**, 1001 (1960).
71. P. Kleinschmit, *Spec. Inorg. Chem.* **40**, 196 (1981).
72. R. D. Kulkarni, E. D. Goddard, and B. Kanner, *Ind. Eng. Chem. Fundam.* **16** (1977).
73. H. Cochrane and C. S. Lin, *Rubber World* **192**, 29 (1985).
74. B. B. Boonstra, H. Cochrane, and E. M. Dannenberg, *Rubber Chem. Technol.* **48**, 558 (1975).
75. J. C. Saam, *Mater. Res. Soc. Symp. Proc.* **274**, 91 (1992).
76. Chemical Economics Handbook Marketing Research Report, *Silicas and Silicates*, SRI International, Menlo Park, Calif., Dec. 1993.
77. J. W. Maisel, W. E. Seeley, and R. J. Woodruff, Unique Sodium Aluminosilicate (SSAS) Pigments as TiO2 Extenders in Rubber Compounds, Presentation to the Rubber Division, ACS, Mexico City, 1989.
78. A. M. Thayer, *Chem. Eng. News*, Oct. 16, 2000.
79. M. Morton, ed., *Rubber Technology*, 3rd ed., Kluwer Academic Publishers, Boston, 1999.
80. S. Laube, S. Monthey, and M.-J. Wang, in John Dick, ed., *Rubber Compounding and Testing for Performance*, Hanser publisherNames, Munich, 2000.
81. S. Iijima, *Nature (London)* **354**, 56 (1991).
82. S. Iijima and T. Ichihashi, *Nature (London)* **363**, 603 (1993).
83. A. Thess, R. Lee, P. Nikolaev, H. J. Dai, P. Petit, J. Robert, C. H. Xu, Y. H. Lee, S. G. Kim, A. G. Rinzler, D. T. Colbert, G. E. Scuseria, D. Tomanek, J. E. Fischer, and R. E. Smalley, *Science* **273**, 483 (1996).
84. *Chemical Week*, Feb. 18, 1998.
85. *Chemical Week*, Oct. 16, 2002, p. 17.
86. *Chemical Week*, July 18, 2001.
87. *TLV and Biological Exposure Indices, 1987–1988*, ACGIH, Cincinnati, Ohio, 1988.
88. W. Gregg and J. W. Griffin, *Poll. Eng.* **80** (Apr. 1991).
89. *Mod. Plast*. (Feb. 1992).

ANDY H. TSOU
WALTER H. WADDELL
ExxonMobil Chemical Co.

FILMS, MANUFACTURE. See Volume 6.

FILMS, MULTILAYER. See COEXTRUSION.

FILMS, ORIENTATION. See Volume 2.

FLAME RETARDANCY

Introduction

The retardants discussed herein are those believed to be in actual use or in advanced stage of development. Where no reference is cited, the information is principally from the manufacturers' literature.

The global usage of flame retardants was estimated in 2003 to be almost 1 million metric tons/year valued at $2.2 billion. On the basis of value, brominated materials comprise about 35–37%, chlorine (and chlorine–phosphorus) about 5%, nonhalogenated phosphorus about 25%, antimony oxide about 16%, alumina trihydrate about 11%, and others (melamines, magnesium hydroxide, borates, etc) about 6%. Both the entire industry and the brominated segment are growing at about 4% annually (1,2).

In terms of usage, the main applications are construction, electrical equipment, and motor vehicles. Other important areas are textiles, paper, and wood products.

Inorganic Flame Retardants

Inorganic phosphorus compounds are described in the section, commercial Phosphorus-Based Flame Retardants.

Oxides.

Alumina Trihydrate (Aluminum Hydroxide, Aluminum Trihydroxide, ATH)[21645-51-2]. On a weight basis, ATH is the largest flame retardant in current use http://www.manufacturing.net/pur/article/CA147910 (Nov. 1999). A review of ATH and other metal hydroxides and hydroxycarbonates is available (3). Much proprietary technology, involving either grinding (generally less costly) or precipitation achieves the desired particle size distribution, morphology, surface properties, and consistency (4–6). There are various surface-treated versions where the treatment (such as silanation) improves the miscibility or the mechanical properties of the final composition.

Major applications are vinyl and polyolefin cable jacket, unsaturated polyester resin (sanitary ware, counter tops), cast artificial stone, elastomers such as conveyer belts, and carpet backing. ATH tends to suppress smoke as well as flame. The mode of action is believed to be attributable mainly to endothermic dehydration at about 230°C with 34.5% weight loss of water by 350°C, consuming

Encyclopedia of Polymer Science and Technology. Copyright John Wiley & Sons, Inc. All rights reserved.

1190 J/g of heat. This water loss acts to withdraw heat, which would otherwise serve to pyrolyze the polymer, and the resultant emission of water vapor also dilutes and cools combustible volatile fragments emitted from breakdown of the polymer. The residual anhydrous alumina also serves as a thermal barrier. Typical levels of addition are at least 50 parts by weight per 100 parts of polymer.

Magnesium Hydroxide[1309-42-8]. An estimated 8000 ton (value about $15 million) was used as flame and smoke suppressant in 2003. Its use appears to be growing more rapidly than ATH despite higher cost per pound (3,7,8). In contrast to ATH, magnesium hydroxide can be used in polymers with processing temperatures up to about 340°C, for example, in polypropylene or polyamides. It is also less abrasive than ATH.

The largest-volume uses are wire and cable, and increasingly in thermoplastic polyolefin roofing membranes (9). Grades in use range from the natural mineral brucite to tailored particle morphologies such as Kyowa's KISUMA. A typical less-specialized and inexpensive grade is Martin Marietta's MAGSHIELD, which can be used at up to about 330–340°C (8).

The mode of action is endothermic water release as in the case of ATH, but not starting until about 340°C completing itself with 30.9% weight loss and consuming 1300 J/g of heat by about 450°C. The residual MgO serves as a highly reflective thermal barrier. In some polymers, magnesium hydroxide favors charring to a greater degree than ATH (8).

The main disadvantage is the high loading required; for example about 60% $Mg(OH)_2$ is needed to reach V-0 in polypropylene. Some synergists have been found to lower this level somewhat (10). The stiffening effect is less detrimental in softer polymers such as polyolefin or ethylene vinyl acetate cable jacket or TPO roofing membranes.

Antimony Oxides. Antimony oxide is available both as the commodity antimony trioxide (Sb_2O_3) [1309-64-4], and various specialty products such as colloidal antimony pentoxide (Sb_2O_5) [1314-60-9] or sodium antimonate [15432-85-6]. There are also various proprietary combinations such as zinc/antimony oxide. Antimony oxides are not primary flame retardants but are important synergists for the halogen flame-retardant additives and halogen-containing plastics. Antimony trioxide is sold by Albemarle, Great Lakes Chemical, Anzon, Atofina, Campine, Harcros, Laurel, PQ, and others, and is largely supplied from China.

Antimony trioxide is a white powder, dusty unless oil-treated or pelletized. It remains solid at all polymer-processing temperatures. The synergism with halogen results from thermal formation of $SbCl_3$ or $SbBr_3$, which inhibit flame by scavenging hydrogen atoms and other radicals.

In contrast to antimony trioxide, which acts as a white pigment, the particle size of antimony pentoxide (colloidal), available as powders, dispersions, or polymer concentrates from Nyacol Nano Technologies, is small enough to cause minimal light scattering and thus able to produce translucent or transparent polymer formulations. It is more costly than antimony trioxide but this may be partially offset by lower loadings.

In acid-sensitive thermoplastic polyesters such as PET, PBT, or PC, sodium antimonate is advantageous since it avoids some undesired catalytic action of the oxide itself.

Borates.

Boric Acid [10043-35-3]. This powdered solid, sold by U.S. Borax and others, serves to prevent smoldering combustion of cotton batting (11), and is used in mattresses and furniture, where it is mixed in mechanically, its binding to the fibers aided by oil. Boric acid probably works by melting and coating the cellulose, although some vapor action is also likely.

Sodium Borates (11). These water-soluble salts, made by U.S. Borax and others, have been known since the eighteenth century as nondurable flame retardants for cotton, rope, canvas, and paper. The hydrated salts can act as endothermic heat sinks and moreover the salt fuses to a nonflammable glassy barrier layer. Sodium borates, in particular borax (sodium tetraborate decahydrate [1303-96-4]), are used in disposable paper and nonwoven cellulosic products, and as wood flame retardants where their water solubility can be tolerated. The borate salts are effective on flaming combustion but allow severe afterglow; they are best used in formulations with afterglow preventatives, and often used with boric acid.

Zinc Borates. These are usually used as hydrates, one of the most common being U.S. Borax's FIREBRAKE ZB, which is $2ZnO \cdot 3B_2O_3 \cdot 3.5H_2O$ [138265-88-0]. These hydrated salts have an endothermic action and also, at the elevated temperature of burning, they can flux with or sinter with other minerals such as alumina to form nonflammable barriers. For plastics processed at higher temperature, a lower hydrate FIREBRAKE 415, $4ZnO \cdot B_2O_3 \cdot H_2O$ [149749-62-2 or 1332-07-6] is used. A main use of zinc borates is as smoke suppressants and flame-retardant synergists in PVC or in other polymers with halogen additives. They can replace all or part of the usual antimony oxide synergist, often with the result that the smoke evolution during burning is lowered (12). The endothermic loss of water from these hydrates is a substantial part of their mode of action; in the case of PVC, they also induce dehydrochlorination at fire exposure temperatures.

Zinc borates, including the very thermally stable anhydrous $2ZnO \cdot 3B_2O_3$ [12767-90-7 or 1332-07-6], FIREBRAKE 500, have been found to act as synergists with magnesium hydroxide or aluminum trihydroxide in polyolefin and other thermoplastic formulations, by promoting char/ceramic barrier formation (13–15). Several other zinc borates are available from R. J. Marshall Co., Barium metaborate (Chapman Chemical's FLAMEBLOC 550), calcium borates, and magnesium borates are also used as flame retardants and smoke suppressants. These borates can serve also as anticorrosives and preservatives, especially in coatings.

Other Inorganics.

Molybdates. Calcium molybdates and zinc molybdates and various modifications thereof (15) are commercially available from Sherwin Williams as KEMGARDS, and are principally used in PVC as smoke suppressants (15).

Ammonium octamolybdate (AOM), $(NH_4)_4Mo_8O_{26}$ [12411-64-2], a slightly water-soluble crystalline salt, is a smoke suppressant for PVC (15). It is used in wire and cable, mass transit vehicle interiors, and carpet backing. It is believed to work by forming a barrier and by modifying the decomposition of the PVC.

Stannates. Zinc stannate [12036-37-2], Alcan's FLAMTARD S, and zinc hydroxystannate [12027-96-2], FLAMTARD HS, are both white water-insoluble powders useful as smoke suppressants in PVC. They can partly replace antimony oxide as flame-retardant synergists in halogen-containing flame-retardant formulations, with reduced smoke (16,17).

Zinc Sulfide [1314-98-3]. This stable white pigment shows synergistic flame-retardant action in PVC and can be partially substituted for antimony oxide. It can enhance other flame retardants in nylons and nylon blends (18).

Potassium Hexafluorozirconate [16923-95-8]. This water-soluble compound is a flame retardant for wool by the "Zirpro" process. Applied in combination with formic acid and citric acid, the fluorozirconate exhausts onto wool and after mild heating, provides a fairly wash-durable flame-retardant finish. Wool upholstery for aircraft makes use of this treatment (19).

Layered Clays ("Nanoclays") and Other Finely Divided Inorganic Additives. Layered clays such as montmorillonite or hectorite, when treated with substances which can penetrate between the layers, such as quaternary ammonium compounds, can be made to separate (exfoliate) into individual layers with nanometer thicknesses. At loadings of only a few percent in many polymers, physical properties such as modulus and heat deflection temperature may be improved. Moreover, the rate of heat release during burning as measured by cone calorimetry can be greatly reduced (20,21). Generally, this effect is not enough to pass typical flame retardancy requirements except in combination with some other flame retardant, and frequently faster ignition is an undesirable side-effect. However, commercially useful flame retardancy improvements with nanoclays in combination with, for example, alumina trihydrate, can be achieved in polyolefin cable (22). Synthetic platy silicates can be used in place of the montmorillonite (23). Besides the layered clays, some other finely divided minerals such as attapulgite, kaolinite, talc, or silica can have this beneficial effect, which may be related to heat-transfer- or mass-transfer-barrier formation or barrier strengthening in cooperation with char formation. In polycarbonates or polycarbonate blends, nanodimensioned titania or boehmite can be used in conjunction with other flame retardants (24).

At higher loadings, as are often used in elastomer formulations, nonlayered clays such as kaolin clays and attapulgite serve to impart flame retardance by dilution of the combustible material, and heat sink action enhanced by water loss if the clays are not calcined.

Expandable Graphite Flake. This product, which has long been known, is made by treating graphite flake with nitric and sulfuric acid, which intercalate between the graphite layers. It is available commercially from Graftech and Nyacol in the United States and from Asian manufacturers. When heated by fire exposure to above about 160°C, gases generated by the action of the oxidizing acids on the graphite cause the flakes to swell up greatly to form elongated twisted "wormlike" fibrils. This expanded material is an excellent heat insulator. Elastomeric polymers, such as flexible foams and coatings, putties, and firestop products can be flame retarded with expandable graphite, used by itself or compounded with other flame retardants.

Halogenated Flame Retardants

The products containing both halogen and phosphorus are discussed under Phosphorus. Brominated products have their own section because they are the largest category of flame retardants.

The mode of action of halogenated flame retardants is often described as proceeding with the production of hydrogen halide (or, in the presence of antimony oxide, antimony trihalide), which enters the flame zone and serves as a flame inhibitor. Part of this flame inhibition is generally believed to result from the scavenging of free hydrogen atoms, which are responsible for the rate-controlling chain branching steps in flame chemistry; however another part of the mode of action appears to be physical dilution, heat capacity, and endothermicity (25,26).

Chlorine-Containing Flame Retardants.

Chloroparaffins. These range from pourable liquids to waxes to rather high melting solids, depending on the chain length of the paraffin and the level of chlorination. The liquid lower chlorinated ones are mainly of interest in metal cutting formulations. Some highly chlorinated liquid chloroparaffins are used in PVC and elastomers to function as secondary plasticizers and as flame retardants. A wide range of chloroparaffins is available from Dover Chemical Co.

At or above 70% chlorine content, the materials are solids with softening temperatures from 103 to 160°C. These are useful as flame-retardant additives particularly for polyolefins, rubber, paints and adhesives. A typical formula for meeting UL 94 V-0 with polyethylene uses 20–24% chloroparaffin and 8–10% antimony oxide (27). Above the 13-carbon chain length, the toxicological characteristics of the long-chain chloroparaffins [63449-39-8] is very favorable.

Polycyclic Chlorohydrocarbon (DECHLORANE PLUS) [13560-89-9]. There is only one commercial additive flame retardant in this group, Oxychem's DECHLORANE PLUS, which is a polycyclic chlorohydrocarbon of the structure

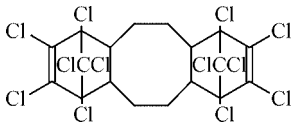

in which all of the chlorine atoms are so positioned that dehydrochlorination cannot readily occur. Thus, the molecule is thermally very stable.

It was originally developed for polyethylene and other polyolefins, and is still used to some extent in those applications, but its use in polyamide 6,6 has become more important.

DECHLORANE PLUS can be synergized by antimony oxide, but better results including lower smoke levels are achieved by use of some iron oxide as synergist or as cosynergist with antimony oxide (28).

Chlorendic Anhydride (HET Anhydride) [115-27-5]. This compound is the Diels–Alder adduct of hexachlorocyclopentadiene and maleic anhydride, having the following structure:

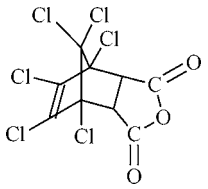

It has been used since the 1960s as a component of unsaturated polyester resins, where it imparts, besides flame retardancy, an enhanced degree of corrosion resistance (solvent resistance) and thus resins made from it are useful for industrial vessels and ducts.

Brominated Flame Retardants

This is the largest flame retardant category, in terms of economic value. At present, the leading US sources are Great Lakes Chemical Co. and Albemarle, both of whom have access to the warm bromine-rich brine found in Arkansas, and an Israeli producer, Dead Sea Bromine Group (DSBG), using the bromine-rich Dead Sea brine. Recently, these American producers have also begun to use bromine from the Dead Sea. Overviews of the usage of brominated flame retardants and the environmental aspects are available (29,30).

Additive Brominated Flame Retardants.

Hexabromocyclododecane [25637-99-4]. This product is a solid mixture (31,32) of stereoisomers, mp about 175–195°C. It is available from Great Lakes, Albemarle, and DSBG. The main application is in expanded polystyrene foam. It is generally used without antimony oxide, and allows for the melt-flow mode of extinguishment in addition to quenching the flame by evolved hydrogen bromide. It may be synergized with a small amount of a peroxide or other free-radical generator which probably work by degrading the polymer under fire-exposure conditions, thus aiding extinguishment by dripping. A heat-stabilized grade (32) can also be used in polypropylene to reach UL 94 V-2 ratings such as for building/construction applications in pipe, lamp sockets, and stadium seats. Hexabromocyclododecane is also useful in textile flame-retardant backcoating, in combination with antimony oxide and a binder. A recent review for the CPSC by a toxicology panel gave a favorable report to this use (33).

Pentabromodiphenyl Ether [32534-81-9]. This is a very viscous liquid or low melting solid, mp <30°C. It is made as Great Lakes Chemical's DE-71 by direct catalyzed bromination of diphenyl ether. It has been used in admixture with a triaryl phosphate as a flame retardant for flexible polyurethane slab-stock foam, the major advantage in that application being its stability and freedom from causing "scorch" (discoloration and deterioration of the foam at the peak temperature of water-initiated blowing). In this kind of mixture, it has been marketed as Akzo Nobel's FYROL PBR and Great Lakes Chemicals's DE-60(F) or DE-61.

In recent years, pentabromodiphenyl ether has been detected widely in the environment such as in marine animals and the milk of nursing mothers. In view of concern regarding possible chronic toxicity (34), it has been largely discontinued and the only US producer is halting production in 2004.

Octabromodiphenyl Ether[32536-52-0]. This is a solid melting in the range 70–150°C, comprising a mixture of several isomers of octa- with lower and higher brominated diphenyl ethers. It has been a preferred flame-retardant additive for ABS, polyamides, or PBT because it does not reduce the impact strength as badly as less soluble additives.

Recently (in 2003), the EU required that the use of this product be discontinued because of toxicological concerns. In 2003, it was banned in California (effective as of 2007) but its use has already declined.

Decabromodiphenyl Ether[1163-19-5]. This is the second largest brominated flame retardant, and is used in HIPS, textile backcoating, and in polyolefins, generally together with antimony oxide. It is made, as are the other members of this series, by bromination of diphenyl ether and is commercially available by Albemarle as SAYTEX 102, Great Lakes Chemical as DE-83, and Dead Sea Bromine (DSBG) as FR-1210. In view of the large volume and multiple producers, it is priced favorably. The structure is as follows:

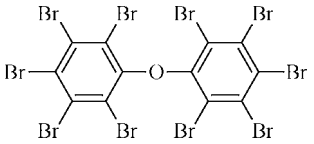

Decabromodiphenyl ether is a solid, melting at about 304–309°C, substantially insoluble in water, and with negligible vapor pressure. In contrast to the lower brominated diphenyl ethers, it has only rarely been found as an environmental pollutant and is low in toxicity. Risk studies conducted in the United States and the European Union (33,35) indicate a low degree of risk in the use of this flame retardant. It is the major flame retardant used in high impact polystyrene (HIPS) with antimony oxide, and has substantial use in polyolefin wire and cable as well as electrical parts made of other plastics such as polyamides and thermoplastic polyesters.

Tetradecabromodiphenoxybenzene [58965-66-5]. This product has an advantage for use in polyamide 6,6 because it has less tendency to "bloom" (to come to the surface) than decabromodiphenyl ether. It is available from Albemarle as SAYTEX 120.

1,2-Bis(2,4,6-tribromophenoxy)ethane [37853-59-1]. This product, mp 223–225°C, containing 70% Br, sold by Great Lakes as FIREMASTER 680, is used mainly in ABS where it appears compatible and has only a moderate tendency to bloom.

Decabromodiphenylethane (1,2-Bis[pentabromophenyl]ethane) [84852-53-9]. This solid additive, Albemarle SAYTEX 8010, is an alternative to the polybromodiphenyl ethers. It has 80% Br, a very high melting point (above 350°C), excellent thermal stability (good recyclability), fair UV stability, and gives performance similar to decabromodiphenyl ether in polyolefins and styrenics. An important use is in HIPS for TV and other electrical or electronic enclosures.

Octabromo-1-phenyl-1,3,3-trimethylindane [155613-93-7]. This is a solid 73% bromine additive, mp 240–255°C, produced by DSBG as FR-1808, which can also be substituted for decabromodiphenyl ether. The structure is as follows:

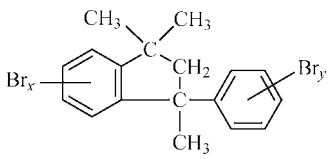

In styrenics, polyamide 6,6, and engineering thermoplastics, it is effective with antimony oxide and has good flow and impact properties even in filled formulations (36).

Ethylenebis(tetrabromophthalimide) [32588-76-4]. This is a high melting crystalline compound, mp 450–455°C, made from tetrabromophthalic anhydride and ethylenediamine. It is available from Albemarle as SAYTEX BT-93.

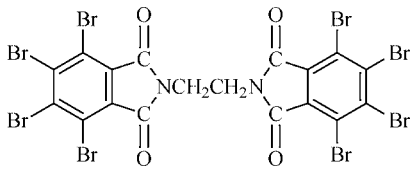

It has better sunlight stability than the polybrominated diphenyl ethers and thus can be used in nonyellowing polyolefins and styrenics. By removal of a small impurity, Albemarle has made available a grade SAYTEX BT-93W with even better color photostability.

Tris(2,4,6-tribromophenoxy)-1,3,5-triazine [25713-60-4]. This is a newer member of the bromine additive family made by DSBG as FR-245 from 2,4,6-tribromophenol and cyanuric chloride. It is a white solid, mp 230°C, containing 67% Br. It can be substituted for decabromodiphenyl ether in styrenics and their alloys, and has melt flow advantages (permitting shorter cycle times and thinner walls) as well as good impact and UV stability (36).

Tetrabromobisphenol A Bis(2,3-dibromopropyl) Ether [21850-44-2]. This is a rather low melting (∼95–111°C) colorless solid containing 68% bromine which is effective as an economical flame retardant in polypropylene, olefin copolymers, and HIPS. It is available from Albemarle as SAYTEX HP-800A, from DSBG as FR-720, and from Tosoh as FLAMECUT 121K. Principal uses are in wire and cable, and in electrical sockets to achieve a UL 94 V-2 rating.

Poly(2,6-dibromophenylene Oxide) [69882-11-7]. This is a light tan melt-processable solid, softening range 210–240°C, containing about 64% Br. It is used in unfilled and reinforced PBT and PET, and polyamides 6 and 66. It allows good chemical resistance and light stability. It is available from Great Lakes Chemical as PO-64P and from Unitex as UNIPLEX FRP-64.

Tetrabromobisphenol A Polycarbonate Oligomer (Tribromophenyl End Capped) [71342-77-3]. This is a thermally stable resinous solid made from tetrabromobisphenol A and phosgene. It is principally used as a flame-retardant additive for PBT, ABS, and polycarbonate for electrical and electronic apparatus housing. It is available from Great Lakes Chemical as BC-58.

Brominated Epoxy Oligomers (BEO) [68928-70-1] as Additives. The reaction of tetrabromobisphenol A with epichlorohydrin can be conducted in a ratio to make either diglycidyl ether or to make oligomers of reduced epoxy functionality, or end capped with tribromophenol to avoid functionality. These oligomers are mainly used as melt-blendable additives useful in many thermoplastics, notably in ABS, HIPS, and polyamides. Processing and UV stability advantages are often superior to those of decabromodiphenyl ether, and a good balance of properties is obtained for use in ABS in business machine applications (37). These

additives are available from DSBG and a similar series from Resolution Performance Products. The lower molecular weight members have enough epoxy functionality for use as reactives in epoxy, phenolic, and unsaturated polyester resins.

Brominated Polystyrenes. There are two main classes of brominated polystyrenes. The older class, suitable for the principal polyamides, is made by brominating a low molecular weight polystyrene, probably with bromine chloride or a mixture of bromine and chlorine. A version with 68% Br and improved thermal stability has been developed by Albemarle as SAYTEX HP-7010, particularly for glass-filled engineering resins (38). The other class of brominated polystyrenes, more thermally stable and preferred for use in higher temperature polyamides, is made from brominated styrene monomers. A further variant is a copolymer of dibromo- and tribromostyrene with some glycidyl methacrylate (Great Lakes FIREMASTER CP-44HF which improves melt flow, compatibility, and mechanical properties in engineering thermoplastics.

Bis(2-ethylhexyl) Tetrabromophthalate [20566-35-2][26040-51-7]. This liquid ester with plasticizing character and containing 45% Br is available from Great Lakes Chemical as DP-45, by Oxychem as PYRONYL 45, and by Unitex as UNIPLEX FRP-45. It is mainly used in PVC wire and cable insulation, coatings, and elastomers.

2-Ethylhexyl Tetrabromobenzoate [183658-27-7]. This liquid ester was recently introduced by Great Lakes Chemical as FIREMASTER BZ-54 mainly for use in combination with a triaryl phosphate as a nonscorching flame retardant for water-blown flexible polyurethane foam slab stock.

Poly(pentabromobenzyl acrylate) [59447-57-3]. This polymeric additive, DSBG's FR-1025, is melt-blendable with polyolefins, and at 8.5% in polypropylene produces a V-2-rated formulation. It is also useful in engineering thermoplastics such as PBT and polyamides.

Disodium Tetrabromophthalate [25357-79-3]. This is a water-soluble salt, available as Great Lakes FR-756, used in nondurable textile flame-retardant finishing.

Reactive Bromine Compounds.

Tetrabromophthalic Anhydride [632-79-1]. This is a reactive aromatic bromine compound, available from Albemarle as SAYTEX RB-49 and from Great Lakes as PHT-4, with several diverse uses in flame retardancy. It can be reacted with diols and, generally, maleic anhydride to make polyesters, which are then diluted with styrene to produce flame-retardant unsaturated polyester resins suitable for panels and bulkheads in buildings and public transport.

Tetrabromophthalic anhydride can be reacted with ethylenediamine to make the bisphthalimide additive discussed above, and also converted to a diol, discussed below.

Hydroxethoxyethyl Hydroxypropyl Tetrabromophthalate [20566-35-2]. This diol, a viscous liquid, is available from Albemarle as SAYTEX RB-79 and from Great Lakes Chemical as PHT4-DIOL. It has the following main component:

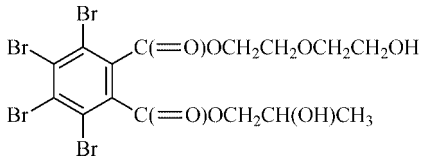

It is useful for the preparation of flame-retardant flexible or rigid polyurethane foams. In the foam applications, where it is often used as a blend with a triaryl phosphate such as in SAYTEX RB 7980 (higher hydroxyl number) or RX 8500 (lower hydroxyl number). Its advantage is that it allows flexible polyurethane foam to reach high temperatures in the water-blown foaming step without "scorch" (thermal damage).

More recently, a more reactive analog was introduced by Great Lakes Chemical as FIREMASTER 520. This probably has a hydroxyethyl group instead of hydroxypropyl.

Dibromoneopentyl Glycol [3296-90-0]. This diol, available from DSBG as FR-522, is made by reaction of pentaerythritol with hydrogen bromide. It is a crystalline compound, mp 109–110°C, and has been used in flame-retardant unsaturated polyester resins and polyurethane foams.

Tribromoneopentyl Alcohol [1522-92-5]. This is also made by DSBG as FR-513 by reaction of pentaerythritol with hydrogen bromide. It is a crystalline compound, mp 62-67°C, with the following structure:

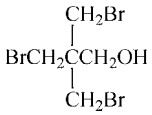

It can be used by itself or more conveniently in a liquid mixture with a triaryl phosphate as a reactive for the preparation of nonscorching flexible polyurethane foams.

Another use for this alcohol is as a precursor of tris(tribromoneopentyl) phosphate, discussed below in the Phosphorus Flame Retardants section.

Tetrabromobisphenol A [79-94-7]. This compound, a solid, mp 179-181°C is the largest of the bromine-containing flame retardants. Tetrabromobisphenol A is available from Albemarle as SAYTEX CP-2000, Dead Sea Bromine as FR-1524, and Great Lakes Chemical as BA-59P.

The largest volume use is in epoxy circuit boards (printed wiring boards) to meet the FR-4 standard in electronic equipment (computers, printers, communication equipment). The usual mode of usage is as a "chain extender," wherein it is reacted with a nonhalogenated epoxy resin.

A related use is to produce the diglycidyl ether of tetrabromobisphenol A, which can be used as such in epoxy thermoset fabrication but is mainly reacted with methacrylic acid to make flame-retardant vinyl ester resins. These are useful for making fiber-reinforced corrosion resistant containers and ducts. The diglycidyl ether can also be chain extended with more tetrabromobisphenol A to make a family of, mainly, additives for thermoplastics.

Another important mode of usage of tetrabromobisphenol A is as an additive in styrenics, particularly in dark-pigmented ABS. It is typically used at 18–22% plus 4–8% antimony oxide. This application is favored by the low cost of tetrabromobisphenol A.

Pentabromobenzyl Acrylate[59447-55-1]. This monomer, available from DSBG as FR-1025M, can be used in reactive extrusion to graft onto polypropylene

and various other thermoplastics. Dyeable flame-retardant polypropylene fibers can be produced. The homopolymer is discussed under Additives.

Vinyl Bromide[593-60-2]. This low boiling monomer (bp 15.8°C) is mainly used for copolymerization with other vinyl monomers to make modacrylic fibers, for inherently flame-retardant textiles. Copolymers with vinyl chloride are also useful in flame-retardant coatings.

Commercial Phosphorus-Based Flame Retardants

Phosphorus compounds comprise, value-wise, the second largest group of flame retardants, and are probably the fastest growing segment as a result of environmental concerns with various bromine–antimony retardants. An earlier review is available (39).

Inorganic Phosphorus Compounds.

Red Phosphorus [7723-14-0]. This polymeric form of phosphorus is relatively nontoxic, not spontaneously flammable, and stable up to ~450°C. In finely divided, coated, and stabilized form it is available from Clariant, Rhodia, Italmatch, and Tosoh. It has been found to be a powerful flame-retardant additive (40) effective at relatively low loadings. In Europe, it is used in molded nylon electrical parts in a coated and stabilized form. Handling hazards and color have deterred usage in the United States. The development of masterbatches by Italmatch overcomes the flammable dust problem, but evolution of trace phosphine from reaction with water is still a concern (41).

Ammonium Phosphates. Monoammonium Phosphate [7722-76-1], $NH_4H_2PO_4$, and diammonium phosphate [7783-28-0], $(NH_4)_2HPO_4$ (or mixtures of the two), have long been used for low cost flame retarding and afterglow prevention of paper, textiles, disposable nonwoven cellulosic fabrics, and wood products (42–44). Ammonium phosphate finishes are resistant to dry-cleaning solvents but not to water.

Formulations of ammonium phosphates and ammonium bromide, sometimes with wetting and softening agents, are sold for use on cellulosic–synthetic fiber blends. A large-volume use in the United States for ammonium phosphate is in forest fire control, usually by aerial application and often combined with ammonium sulfate.

Water-soluble ammonium pyrophosphates and lower molecular weight (water-soluble) ammonium polyphosphates have uses on textile and paper similarly to ammonium phosphates but have less tendency to crystallize and to impair the texture.

Insoluble Ammonium Polyphosphate. When ammonium phosphates are heated in the presence of urea, relatively water-insoluble ammonium polyphosphate [68333-79-9] is produced (45) consisting of long chains of repeating —$OP(O)(ONH_4)$— units.There are several crystal forms (type II is the least-soluble), and the commercial products, available from a number of manufacturers, differ in molecular weight, particle size, solubility, and surface coating (46). These finely divided solids are principal ingredients of intumescent paint and mastics (47). In such formulations, ammonium polyphosphate is considered to function as a catalyst for charring an organic component such as pentaerythritol or an

aminoplast resin (48,49). A blowing agent such as melamine or chlorowax is also present to impart a foamed character to the char, thus forming a fire-resistant insulating barrier. In addition, the intumescent formulations typically contain resinous binders, pigments, ceramic components, and other fillers.

A series of compounded flame retardants, based on finely divided insoluble ammonium polyphosphate together with char-forming nitrogenous resins, has been developed for polyolefins, ethylene–vinyl acetate, and urethane elastomers (50–56). Ammonium polyphosphate is also an efficient flame retardant in rigid polyurethane foam, with minimal adverse effects on other foam properties (57).

Additive Organic Phosphorus Flame Retardants.

Melamine Phosphates and Other Amine Phosphates. Commercial products in this group include melamine orthophosphate [20208-95-1], $C_3H_6N_6 \cdot H_3O_4P$, and melamine pyrophosphate [15541-60-3], $2C_3H_6N_6 \cdot H_4O_7P_2$. The pyrophosphate, available from Cytec, Chemische Fabrik Budenheim, and Broadview Technology, is less water-soluble (0.09 g/100 mL water) and also more thermally stable. These are available as finely divided solids and used principally in flame-retardant coatings (58), although plastic and elastomer applications also show promise (59). A detailed study of the thermal decomposition of the these compounds has been published (60).

A more recent member of this family is melamine polyphosphate (MELAPUR 200, originally from DSM, now from Ciba), which has a thermal stability advantage for use in polyamide 6 and 66 (61) and in combination with char-assisting additives, in polyolefins such as those used for stadium seating.

Ethylenediamine Salt of Phosphoric Acid. This is a finely divided solid, mp 250°C, slightly soluble in water. It was introduced by Albright & Wilson as Amgard EDAP and is now available as Broadview Technology's INTUMAX AC-3, mainly as an additive for polyolefins, EVA, and PVC. Unlike ammonium polyphosphate, it is self-intumescent and does not require a char-forming synergist (62). It is synergized by melamine or melamine pyrophosphate, and is available as a blend with these, respectively from Unitex Corp. and Broadview Corp.

Triethyl Phosphate. Triethyl phosphate [78-40-0], $C_6H_{15}O_4P$, is a colorless liquid boiling at 209–218°C containing 17 wt% phosphorus, made by Eastman from diethyl ether and phosphorus pentoxide (63,64). Triethyl phosphate has been used commercially as an additive for polyester laminates and in cellulosics. In polyester resins, it functions as a viscosity depressant as well as a flame retardant, and permits high loadings of alumina trihydrate (65).

Dimethyl Methylphosphonate (DMMP) [756-79-6]. This is a water-soluble liquid, bp 185°C, with the formula $CH_3P(=O)(OCH_3)_2$, contains 25% phosphorus, which is near the maximum possible for a phosphorus ester, and therefore highly efficient as a flame retardant. It is sold by Akzo Nobel as FYROL DMMP. Applications include use as a viscosity depressant and flame retardant in alumina trihydrate (ATH)-filled polyester resins (66) such as used for bathtubs and shower stalls. Some applications have been found in rigid polyurethane foams and as an intermediate for making other flame retardants. In Europe, DMMP has an "R46" (mutagen) classification, which deters its use.

Diethyl Ethylphosphonate (DEEP) [78-38-6]. This is a liquid compound introduced by Bayer as LEVAGARD VP AC 4048 for applications similar to those

of DMMP. It is less susceptible to undesirable interactions with blowing agents or amine catalysts. It has a less toxic European rating than DMMP.

Dimethyl Propylphosphonate (DMPP) [18755-43-6]. This liquid additive was recently introduced by Bayer as LEVAGARD DMPP, an alternative to the chloroalkyl phosphates for flame-retarding rigid polyurethane foams.

Aluminum Diethylphosphinate. This solid additive, available in combination with a melamine or inorganic synergist as Clariant's EXOLIT OP 1311 and 1312, is a highly effective additive in polyamides, PBT, and epoxy (67–69).

Oligomeric Ethyl Phosphates. An oligomeric ethyl phosphate additive containing 19% phosphorus has been introduced for use in flexible polyurethane foams by Akzo Nobel as FYROL PNX. Because of the high percentage of phosphorus, it is quite efficient and as little as 5 php is effective in passing the California 117 test and MVSS 302 in a 1.5–1.8 lb/cu.ft. foam. For automotive applications, this low-volatility additive has the advantage of not causing windshield fogging. A lower viscosity version is available as FYROL PNX-S.

Halogenated Aliphatic Phosphates and Phosphonates. The principal use of these additives is in polyurethane foams; broader reviews of this important flame retardant application area have been published (70,71).

2-Chloroethanol Phosphate (3:1). Tris(2-chloroethyl) phosphate [115-96-8], $C_6H_{12}Cl_3O_4P$ [2-chloroethanol phosphate (3:1)], is a low viscosity liquid product that has found widespread usage because of low cost, low odor, high percentage of phosphorus, and compatibility with essentially all polymers containing polar groups. Akzo Nobel's FYROL CEF contains 10.8% phosphorus and 36.7% chlorine, and is made from ethylene oxide and phosphorus oxychloride (72). This phosphate is used in rigid polyurethane and polyisocyanurate foams, carpet backing, flame-laminated and rebonded flexible foam, flame-retardant coatings, most classes of thermosets, adhesives, cast acrylic sheet, and wood–resin composites such as particle board. It is used with melamine in flexible urethane foam cushions and institutional mattresses.

1-Chloro-2-Propanol Phosphate (3:1). Tris(1-chloro-2-propyl) phosphate [13674-84-5], $C_9H_{18}Cl_3O_4P$, is a liquid containing 33% chlorine and 9.5% phosphorus. It is produced by reaction of propylene oxide and phosphorus oxychloride. Because of the branchy structure, this phosphate is much lower in reactivity to water and bases than the 2-chloroethyl homologue (73). It is sold as Akzo Nobel's FYROL PCF, Bayer's LEVAGARD PP, or Albright & Wilson's (now Albemarle's) ANTIBLAZE 80 or TMCP and is a preferred additive for rigid urethane foams where good storage stability in the isocyanate or the polyol–catalyst mixture is required. It is used in isocyanurate foam to reduce friability and brittleness, and is also used on a large scale in flexible urethane foams, often with melamine.

1,3-Dichloro-2-Propanol Phosphate (3:1). Tris(1,3-dichloro-2-propyl) phosphate [13674-87-8], $C_9H_{15}Cl_6O_4P$, sold by Akzo Nobel as FYROL FR-2 and by Albright & Wilson (now Albemarle) as ANTIBLAZE 180 or 195, contains 49% chlorine and 7.2% phosphorus. It is made from epichlorohydrin and phosphorus oxychloride . The principal structure has 1,3-dichloro-2-propyl groups with a minor percentage of 2,3-dichloro-1-propyl groups.

Compared to the foregoing chloroalkyl phosphates, this product has a greatly reduced volatility, much lower water solubility, and high stability toward the

amine catalysts used in foam manufacture. It is a long-established and a leading additive for flexible urethane foams (74) and can be added to the isocyanate or the polyol-catalyst mixture. This phosphate shows little tendency to scorch, ie to cause discoloration and degradation, except in some low density water-blown foams. Flexible foam formulations containing this and other haloalkyl phosphates can be further stabilized against scorch by appropriate antioxidants and acid acceptors (75–78). Scorch is believed to be aggravated if the flame retardant can alkylate an aminoaryl group resulting from hydrolysis of isocyanate (79).

Combinations of tris(dichloroisopropyl) phosphate or tris(1-chloro-2-propyl) phosphate with melamine are used in cushioning formulations and are effective for passing antismoldering requirements (80) as well as stringent British furniture standards. Tris(dichloroisopropyl) phosphate is also useful as a flame retardant in styrene–butadiene and acrylic lattices for textile backcoating and binding of nonwovens.

The mode of action of tris(dichloroisopropyl) phosphate in flexible polyurethane foams appears to be both physical and chemical (81).

Oligomeric 2-Chloroethyl 1-Ethylidine Phosphonate. This is made from the reaction of tris(2- chloroethyl) phosphite with acetaldehyde, and has the following structure:

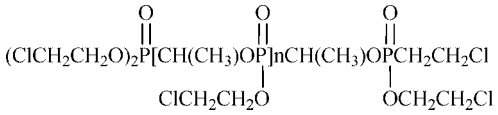

This liquid oligomer, Clariant's EXOLIT 5087, contains 27–28% Cl and 15% P, and is useful as an additive flame retardant for transparent cast polymethyl methacrylate, unsaturated polyester resins, or rigid polyurethane foams. It has good light stability, but is not stable to heat above about 180°C.

Aliphatic Diphosphates. These have low volatility and good to fair thermal stability, and are thus useful in those open-cell (flexible) foams which have requirements for improved resistance to dry and humid aging.

A diphosphate introduced originally as Monsanto's Phosgard 2XC20 [38051-10-4], $C_{13}H_{24}Cl_6O_8P_2$, is now available as Albemarle's) ANTIBLAZE 100 or V6. The compound has the following structure:

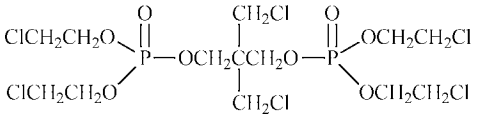

This compound has enhanced hydrolytic stability in addition to low volatility. It is useful in many types of flexible foam, as well as in adhesives and epoxy- or phenolic-based laminates.

Oligomeric 2-Chloroethyl Phosphate. Akzo Nobel's FYROL 99 [109640-81-5] (82,83) is low in volatility and useful in resin-impregnated air filters, in flexible urethane foam, rebonded foam, structural foam and flame-retardant coatings.

Tris(tribromoneopentyl) Phosphate [19186-97-1]. This solid, mp 181°C, compound has stable but highly efficient bromine. It can be used as an additive, with or without an antimony oxide synergist, in a wide range of thermoplastics including polypropylene and HIPS (84). It is particularly advantageous in polypropylene fiber, since it melts at the spinning temperature, does not require high loadings, and can be used without antimony oxide. It has good light stability and favorable toxicology. It is available from DSBG at FR-370 (special carpet fiber grade as FR-372) and from Unitex as BAP-370. It can be synergized to favor the melt-flow mode of extinguishment by small amounts of a hydrocarbon radical generator (Akzo Nobel's PERKADOX 30) (85).

Cycloaliphatic Phosphates and Phosphonates.

Oligomeric Cyclic Phosphonates. AMGARD CU or CT, also Clariant's EXOLIT OP 910, and AMGARD 1045 are mixtures of the diphosphonate and triphosphonate with the following structures ($C_9H_{20}O_6P_2$ [41203-81-0], and $C_{15}H_{31}O_9P_3$ [42595-49-9]).

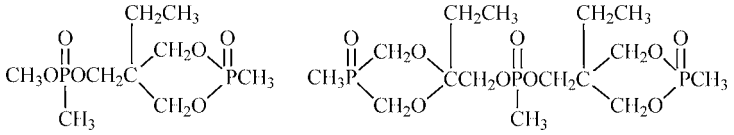

These are made via the bicyclic phosphite from trimethylolpropane subjected to the Arbuzov reaction with dimethyl methylphosphonate (86,87). The bicyclic phosphite intermediate is highly neurotoxic, but, after the ring-opening step, the product is low in toxicity. AMGARD CU (higher viscosity) or CT (lower viscosity) is largely the diphosphonate. AMGARD 1045 (high viscosity) contains a larger amount of the triphosphonate. Both materials are water-soluble, thermally stable low volatility liquids having about 20–21 % phosphorus content and no halogen. AMGARD CU or CT is used as a flame-retardant finish for polyester fabric by the "thermosol" process. After the phosphonate is applied from an aqueous solution, the fabric is heated to swell and soften the fibers, allowing the phosphonate to be absorbed and strongly held after the fabric cools. Many formulated polyester textile finishes are on the market based on this active ingredient.

AMGARD 1045 can advantageously be added to polyethylene terephthalate melt before spinning. These products are also useful flame retardants for other thermoplastics, thermoset polyester resins, polyurethanes, polycarbonates, nylon 6, and textile backcoating.

Pentaerythritol Phosphates. These products take advantage of the excellent char-forming ability of the pentaerythritol structure (88).

A bicyclic pentaerythritol phosphate, Great Lakes CN-1197 or Unitex UNIPLEX FRX 44-33, [5301-78-0], was introduced for use in thermosets, preferably in combination with melamine or ammonium polyphosphate (89). It is a high melting solid with the following structure:

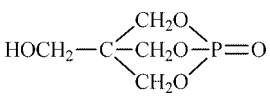

Cyclic Neopentyl Thiophosphoric Anhydride. This solid additive, SANDOFLAM 5060, was commercialized in Europe by Sandoz (sold now by Clariant as EXOLIT 5060) for use in viscose rayon (regenerated cellulose) (90,91). It is sold as an aqueous dispersion or wet filter cake, and has the following structure [4090-50-1]:

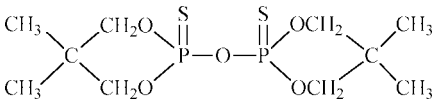

Despite the anhydride structure, it is remarkably stable, surviving addition to the highly alkaline viscose, the acidic coagulating bath, and also resisting multiple laundering of the rayon fabric. Typical levels of addition are 12–22%.

2,2-Bis(chloromethyl)propanediol Bis(cyclic neopentyl phosphate). This solid additive, originally commercialized by Sandoz (90,91), has been sold by Clariant as EXOLIT 5085 (VP). It has the following structure:

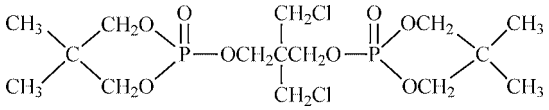

The neopentyl structure increases thermal stability, so that this compound is useful as a flame-retardant additive in extruded polymethyl methacrylate sheet.

Aryl Phosphates. Aryl phosphates were introduced into commercial use early in the twentieth century as plasticizers (qv) for flammable plastics such as cellulose nitrate and later for cellulose acetate and PVC (92). Principal applications are in wire and cable insulation, connectors, automotive interiors, vinyl moisture barriers, plastic greenhouses (Japan), furniture upholstery, conveyer belts (especially in mining), and vinyl foams (93).

In vinyls, the aryl phosphates are frequently used in combinations with phthalate plasticizers. The proportion of the more expensive phosphate is usually chosen so as to permit the product to reliably pass the flammability specifications. In plasticized vinyls used in automotive interiors, these phosphates are used to pass the Federal Motor Vehicle Safety Standard 302.

Triaryl phosphates are also used on a large scale as flame-retardant hydraulic fluids, lubricants, and lubricant additives. Smaller amounts are used as nonflammable dispersing media for peroxide catalysts.

Triaryl phosphates are produced from the corresponding phenols (usually mixtures) by reaction with phosphorus oxychloride, usually in the presence of a catalyst (94,95). Tricresyl phosphate was originally made from petroleum-derived or coal-tar-derived cresylic acids (cresols). Discovery of the neurotoxicity of the ortho-cresyl isomers led manufacturers to select cresols having very little ortho-isomer.

In the 1960–1980 period, the use of more economical synthetic isopropyl- and *t*-butylphenols as alternatives to cresols was developed (96,97). Commercial triaryl phosphates such as FMC's (now Great Lakes') KRONITEX 100 and Akzo Nobel's PHOSFLEX 31P and 41B are based on partially isopropylated or *t*-butylated

phenol. The relative volatilities and oxidative stabilities of these phosphates have been compared; the *t*-butylphenyl phosphates are the most oxidatively stable of the alkylphenyl phosphates (98).

Triphenyl Phosphate [115-86-6]. This is a colorless solid, mp 48–49°C, usually produced in the form of flakes or shipped in heated vessels as a liquid. It is available from Akzo Nobel as PHOSFLEX TPP. An early application was as a flame retardant for cellulose acetate safety film. It is also used in cellulose nitrate, various coatings, triacetate film and sheet, and rigid urethane foam. It has been used as a flame-retardant additive for engineering thermoplastics such as polyphenylene oxide–high impact polystyrene and ABS–polycarbonate blends.

Cresyl Diphenyl Phosphate [26444-49-5]. This is the most efficient plasticizer of the liquid phosphates, but it is relatively volatile. It is used, especially in Europe, in vinyls and in ABS–polycarbonate blends.

Tricresyl Phosphate [1330-78-5] and Trixylyl Phosphate [25155-23-1]. The commercial tricresyl phosphate has been for many years a mainly *m*,*p*-isomer mixture to avoid the neurotoxicity caused by the *o*-cresyl isomer. Typical products of this class are Akzo Nobel's LINDOL [1330-78-5], $C_{21}H_{21}O_4P$, or FMC's (now Great Lakes') KRONITEX TCP [68952-35-2]. These are nearly colorless liquids, bp about 260–275°C at 1.3 kPa (10 mm Hg). Tricresyl phosphate is used as a relatively flame-retardant plasticizer in flexible and semi-rigid PVC, cellulose nitrate, ethylcellulose coatings, and various rubbers. Typical applications are vinyl tarpaulins, mine conveyer belts, air ducts, wire and cable insulation, and vinyl films. Trixylenyl phosphate is a related product of lower volatility and less extractability, having advantages for wire and cable insulation.

Isopropylphenyl Diphenyl Phosphate [28108-99-8], [68937-41-7], [68782-95-6]. The plasticizer efficiency is close to that of tricresyl phosphate. It is made from the product of isopropylation of phenol by propylene. The phosphate is a mixture of mainly *o*- and *p*-isomers and contains a distribution of different levels of alkylation (99–101). It is sold by Akzo Nobel in the PHOSFLEX series and by Great Lakes in the REOFOS series. Main uses are in PVC and as a component of nonscorching or non-windshield-fogging formulations for flexible polyurethane foams (97a). There are also functional fluid applications outside the scope of this article.

tert-Butylphenyl Diphenyl Phosphate [56803-37-3], [68937-40-6]. This is a slightly less efficient plasticizer than the isopropyl homolog although in admixture with dialkyl phthalates the difference can be minimal and it can be used in such formulations as a PVC plasticizer with reduced flammability. It has been used as a flame retardant in engineering thermoplastics (102) and as a fire-retardant hydraulic fluid. The products from different manufacturers (Akzo, Great Lakes) are somewhat different in isomer distribution and alkylation levels.

Alkyl Diphenyl Phosphates. These are products originally developed to provide improved low temperature flexibility, a fault of triaryl phosphate plasticizers in PVC (103). These phosphates generally provide slightly less flame-retardant efficacy but are generally superior to the triaryl phosphates in regard to smoke when the vinyl formulation is burned. Two commercial products of this family are 2-ethylhexyl diphenyl phosphate [1241-94-7], $C_{20}H_{27}O_4P$, Ferro's SANTICIZER 141 or Akzo Nobel's PHOSFLEX 362, and isodecyl diphenyl phosphate [29761-21-5], $C_{22}H_{31}O_4P$, Ferro's SANTICIZER 148 or Akzo Nobel's PHOSFLEX 390. A

newer member of this group was introduced by Monsanto; it is believed to be a slightly higher alkyl chain length and has improved low temperature properties with reduced volatility (104).

Aromatic Diphosphates and Oligomeric Phosphates.

Tetraphenyl Resorcinol Diphosphate [57583-54-7]. This is the main component of an oligomeric phosphate flame retardant, Akzo Nobel's FYROLFLEX RDP or Great Lakes Chemical's REOFOS RDP, designed for use in engineering thermoplastics such as polyphenylene oxide blends (105,106), thermoplastic polyesters, polyamides, polycarbonates, and ABS–polycarbonate blends. A major use was in PPO–HIPS blends and later in ABS–polycarbonate blends (107). It is a colorless to light-yellow liquid, viscosity 400–800 mPa · s at 25°C, and a pour point of −12°C. It is less volatile than the triaryl phosphates and has a higher percentage of phosphorus (11% P) than triphenyl phosphate.

A closely related diphosphate with 2,6-dimethylphenyl groups is available from Daihachi (Japan), and has improved hydrolytic resistance but is higher in price.

Tetraphenyl Bisphenol-A Diphosphate [5945-33-5]. This is the main component of an oligomer, Akzo Nobel's FYROLFLEX BDP, Great Lakes' REOFOS BAPP, or Albemarle's NCendX P30, and is used for the same applications as the RDP discussed above. RDP and BDP are mainly the diphosphates with small amounts of the higher oligomers. Although BDP has a lower percentage of phosphorus (9%) than RDP (11%), it is lower in cost, and has a substantial hydrolytic stability advantage (108), a factor of particular importance for the application in polycarbonate–ABS blends.

Substantial development work has been done on other tetraaryl diphosphates and higher oligomers thereof, such as with aliphatic linking groups (109).

Reactive Organic Phosphorus Compounds.

Organophosphorus Monomers. Many vinyl monomers containing phosphorus have been described in the literature (110,111), but few have gone beyond the laboratory. Methacryloxyethyl acid phosphates are commercially available but appear to be used in coatings as adhesion improvers, not as flame retardants. Bis(2-chloroethyl) vinylphosphonate [115-98-0] and the corresponding acid are available from Rhodia but do not seem to have commercial use as flame retardants probably due to cost. These and related monomers have been reviewed and their copolymerization behavior has been studied (110,111).

Phosphorus-Containing Diols and Polyols. The commercial development of several phosphorus-containing diols occurred in response to the need to flame retard rigid urethane foam insulation used in transportation and construction. There are a large number of references to phosphorus polyols (112) but only a few of these have been used commercially.

Albright & Wilson's (now Albemarle's) VIRCOL 82 is a mixed diol mixture containing bis(hydroxypropyl) dibutyl propanediol diphosphates (113). The neutral liquid has an OH number of 205 mg KOH/g and contains 11.3% phosphorus. It is used in rigid foam.

Diethyl N,N-bis(2-hydroxyethyl)aminomethylphosphonate [2781-11-5]. Over several decades, commercial usage (limited by cost) has been made of this phosphonate diol (Akzo Nobel's FYROL 6, Bayer's LEVAGARD 4090N) (114), $(HOCH_2CH_2)_2NCH_2P(O)(OC_2H_5)_2$.

The product contains 12.6% phosphorus and has an OH number in the 450 mg KOH/g range. FYROL 6 is used to impart a permanent Class II E-84 flame-spread rating to rigid foam for insulating walls and roofs. Particular advantages are low viscosity, stability in polyol-catalyst mixtures, and outstanding humid aging resistance. FYROL 6 is used in spray foam, froth, pour-in-place, and slab stock. Its mode of action is believed to be increased char formation (115).

Oligomeric Ethyl Ethylene Phosphate Diol. This halogen-free phosphorus-containing diol was developed by Hoechst for rigid or flexible foams and is now marketed as EXOLIT 550 by Clariant (116). The product is a hydroxyethyl-terminated ethyl ethyleneglycol phosphate oligomer with about 17% phosphorus content and is said to be useful for rigid and flexible foams, especially molded or high density slabstock.

Oligomeric Phosphate—Phosphonate. A commercially used reactive oligomeric alcohol, Akzo Nobel's FYROL 51 [70715-06-9], is a mixture of methylphosphonate units and methyl phosphate units with mainly hydroxy end groups. A typical component has the structure as follows (110):

$$HOCH_2CH_2O[P(O)(CH_3)OCH_2CH_2O]_x[P(O)(OCH_3)OCH_2CH_2O]_yH$$

FYROL 51 is a water-soluble liquid containing about 21% phosphorus. The end groups are principally primary hydroxyl and the compound can thus be incorporated chemically into aminoplasts, phenolic resins, and polyurethanes. FYROL 51, or 58 (diluted) is used with amino resins to produce a flame-retardant resin finish on paper used for automotive air filters, or for backcoating of upholstery fabric to pass the British or California flammability standards. Under the trade name FYROLTEX HP (Akzo Nobel), it has been in development for cotton textile finishing, in combination with an amino resin (117).

Combinations with FYROL 6 permit the OH number to be adjusted to typical values used in flexible foam, urethane coating, or reaction injection molding (RIM) applications (118,119).

Reactive Organophosphorus Compounds in Textile Finishing. The flame retarding of cotton requires the application of a textile finish. Markets for finishes have been in military goods, industrial protective clothing, curtains, hospital goods, and children's sleepwear. An extensive review is available (120).

Tetrakis(hydroxymethyl)phosphonium Salts. The reaction of formaldehyde and phosphine in aqueous hydrochloric or sulfuric acid yields tetrakis-(hydroxymethyl)phosphonium chloride [124-62-1 or the sulfate [55566-30-8]. These are made by Rhodia, Cytex, and Chinese producers. The salts have the general structure $(HOCH_2)_4P^+X^-$. They are water-soluble crystalline compounds sold as concentrated aqueous solutions. The methylol groups are highly reactive (121–125) and capable of being cured on the fabric by reaction with ammonia or amino compounds and post-oxidized to form durable cross-linked phosphine oxide structures.

Finishes based on these reagents are durable to numerous launderings. This finish is primarily used on work clothing. This finishing process, developed by Albright & Wilson (now marketed by Rhodia), is known as the PROBAN process, which employs a precondensate of the phosphonium compound with urea (125, 126).

Dimethyl N-Methylolphosphonopropionamide or 3-([Hydroxymethyl]-Amino)-3-oxopropyl)Phosphonic Acid, Dimethyl Ester. This cotton finish, Ciba's PYROVATEX CP, was introduced by Geigy (later Ciba) in the 1970s especially for children's sleepwear and upholstery. It has the structure $(CH_3O)_2P(O)CH_2CH_2C(O)NHCH_2OH$ with some related compounds (127). The methylol group is the reactive part of the molecule. PYROVATEX CP coreacts on cellulose with an amino resin such as a methylolmelamine in the presence of a phosphoric acid catalyst or latent acid catalyst, to produce finishes durable to as many as 50 washes (128,129). A higher assay version, PYROVATEX CP New, has been introduced. An apparently similar product, PEKOFLAM DPN, is available from Clariant. This finish is practiced in Europe and the Far East but very little in North America. Recent efforts have been made to lower the formaldehyde emissions from this system (130).

Phosphorus-Containing Polymers as Textile Fibers. A large number of addition and condensation polymers having phosphorus built in have been described, but few have been commercialized (131). No general statement seems warranted regarding the efficacy of built-in vs additive phosphorus (132). However, in textile fibers, there is greater assurance of permanency.

Polyester Fibers Containing Phosphorus. Numerous patents describe poly(ethylene terephthalate) (PET) flame retarded with phosphorus-containing difunctional reactants. At least two of these appear to be commercial (see POLYESTERS, FIBERS).

Hoechst-Celanese's TREVIRA 271 (now practiced by KoSa) appears to be based on a cyclic phosphinic carboxylic anhydride [15171-48-9] which is reacted with glycol and then introduced into the PET backbone to produce a flame-retardant polyester [82690-14-0], having phosphinate units of the structure $-OP(O)(CH_3)CH_2CH_2COO-$ (133,134). FR TREVIRA 271 is used for children's sleepwear, work clothing, and home furnishings. A phosphorus content as low as 0.6% is reported to be sufficient to pass drapery and upholstery tests.

Toyobo's HEIM II (former GH) is apparently based on the following chemistry via a phosphinate intermediate dihydrooxaphosphaphenanthrene oxide (DOPO) [63562-31-2] produced from *o*-phenylphenol and phosphorus trichloride (135):

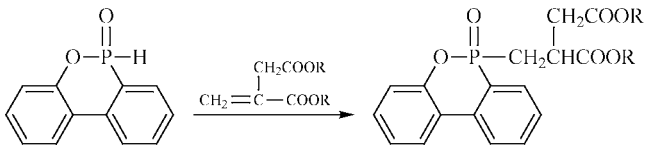

This dicarboxylic ester is then copolycondensed with the other reactants in PET manufacture to produce a flame-retardant polyester [63745-01-7]. The advantage of this rather unusual phosphinate structure is its high thermal and hydrolytic stability. The fabric is probably used mainly for furnishings in public buildings in Japan.

Phosphorus-Containing Printed Wiring Boards. This same phosphinate intermediate, dihydrooxaphosphaphenanthrene oxide (DOPO), is also the subject of substantial efforts in the Far East and Europe to react it into epoxy printed wiring boards and encapsulated electronic circuit elements as a

hypothetically "green" alternative to the established use of tetrabromobisphenol A (136). A number of other approaches to use of reacted-in phosphorus structures have been proposed and are in field trials at present (136).

Sulfur-Containing Flame Retardants

Ammonium Sulfate [7723-20-2]. This is a very inexpensive water-soluble salt used as a paper or wood flame retardant. In combination with ammonium phosphates, it is used in fighting forest fires from the air. In cellulosics, its acidity can cause discoloration and strength loss, so it is usually used in disposable items such as temporary decorations.

Ammonium Sulfamate [7773-06-0]. This salt is similar to ammonium sulfate but somewhat less acidic and corrosive. It is applied as an aqueous solution to paper or cellulosic fabric to obtain a flame retardant finish nondurable to washing. It has fairly good afterglow retardation.

Potassium Perfluorobutylsulfonate [29420-49-3] (3M's FR-2025), Potassium Diphenylsulfonesulfonate [63336-43-8] (Sloss Industries and Seal Sands, Ltd.), and Sodium Trichlorophenylsulfonate [53423-65-7] (Sloss Industries). These substantially neutral salts are used at levels below 1% as flame retardants in polycarbonate, often in combination with other retardants. These sulfonates permit clear formulations. At levels as low as 0.2%, the sulfonates accelerate carbon dioxide evolution and the breakdown of the polymer to phenolic fragments, thence to char (137).

Nitrogen-Based Flame Retardants

Melamine [108-78-1]. This inexpensive solid melts with vaporization at about 350°C and, if evaporation is constrained, decomposition also occurs to ammonia and nonvolatile condensation products—melam, melem, and eventually melone. It is occasionally used by itself as a flame retardant but more often used as a blowing agent and flame-retardant adjuvant in intumescent coatings, elastomers, and plastic formulations (138) as well as in flexible polyurethane foams (139,140).

Melamine Cyanurate [37640-57-6]. This 1:1 adduct (salt) of melamine and cyanuric acid, decomposition temperature ~413°C, is a leading flame retardant for unfilled polyamide 6, where it is typically used at 5–10% by weight, but it does not work very well in most glass-filled polyamide 6. It is also less efficient in polyamide 6,6. It is available from Ciba and several other producers. The mode of action has been studied (141–143).

Hindered Amine Ethers. This unusual new family of flame retardants (or synergists) was discovered by Ciba, which had been exploring the light stabilizer family of 2,2,6,6-tetramethylpiperidine derivatives (see UV STABILIZERS). The *N*-alkoxy or cycloalkoxy derivatives appear to have flame-retardant action particularly in polyolefins. One member of this group, where the *N*-cyclohexyloxy-2,2,6,6-tetramethylpiperidinyl group is attached to an oligomeric polymer chain, has been in market development as Ciba's NOR 116 (144).

Health, Safety and Environmental Aspects

Several factors should be considered: the toxicity of the compounds themselves, the effect of the flame retardants on combustion product toxicity and visible smoke, and environmental effects.

Broad Studies of Flame Retardants. Several broad studies of health, safety, and environmental factors of flame retardants have been published by public agencies. A critical review by a US government–appointed toxicology panel was conducted to facilitate CPSC regulations on flammability of furniture upholstery (145). The panel found ammonium polyphosphate, alumina trihydrate, zinc borate, hexabromocyclododecane, decabromodiphenyl ether (oxide), PYROVATEX CP, and THPC to be usable with minimum risk on residential furniture even with worst-case assumptions. Antimony trioxide, several organophosphates, chlorinated paraffins, and molybdate salts were said to need more exposure studies.

A study at the University of Surrey sponsored by the UK Department of Trade and Industry weighed health risks (toxicity and exposure) of a wide range of flame retardants *vs* their benefits (146). This study encompassed alumina trihydrate, antimony trioxide, decabromodiphenyl ether, tetrabromobisphenol A, and tris(chloroisopropyl) phosphate, and in general found that the benefits outweighed the risks.

An overview of the health, exposure, and environmental aspects of flame retardants was issued in 1997 by the International Programme on Chemical Safety of the World Health Organization, International Labor Organization, and UN Environment Programme (147).

Toxicity, exposure, and environmental data on many of the commercial flame retardants can be found conveniently in an Australian database (148), which is supplemented as new products are imported. Ongoing assessments of flame retardants in use, particularly the brominated ones, and possible alternatives are published by the Danish Environmental Department (149).

Comparative fire tests with a variety of flame-retarded items such as might be found in a typical room *vs* the same set of items without flame retardants have been run under the auspices of the National Institute of Standards and Technology. These tests showed that the room with the flame-retardant objects afforded 15-fold better escape time, lower material consumption, less heat, and less carbon monoxide (150).

A number of risk assessments are being done on flame retardants under EU auspices, and reasonably current status reports are available (151,152). Prioritization factors for the assessments, including tonnage, recognized aquatic hazards, bioamplification and persistence have been summarized as of 2004 (153).

Broad studies of the emissions of brominated and phosphorus flame retardants from consumer products and building materials show, as expected, that the more volatile ones such as tris(1-chloro-2-propyl) phosphate, triphenyl phosphate, and the brominated additives up to 6 bromine atoms are detectible in indoor air (154,155).

Organohalogens. Much attention has been directed to organohalogen products, in view of the legacy of environmental concern over such materials as DDT insecticide, PCB transformer fluid, and PBB (a flame retardant which in one incident contaminated cattle feed).

Some halogenated flame retardants, such as the polychlorinated polycyclic hydrocarbon DECHLORANE PLUS, have escaped adverse reports. Chloroparaffins have been found to be of toxicological concern at the low molecular weight end of the series (IARC 2B rating: possible carcinogen) but above C13, the chloroparaffins are rated as noncarcinogenic (156,157). Likewise, the aquatic toxicity favors the long-chain chloroparaffins.

Many workshops and conferences on the bromine compounds have been held under auspices of government/nongovernmental organizations and industry (examples: References 158–160). Concern has lately focused on the lower brominated diphenyl ethers (such as penta-) which are detected widely in the environment. In a review, Dutch researchers conclude that the toxicity mechanism of polybrominated diphenyl ethers is the same as that of the dioxins, and, although the present concentrations are not a large risk, these ethers are accumulative. Decabromodiphenyl oxide is less toxic than the less-brominated congeners, and its absorption from the gastrointestinal tract is low.

At the present time, pentabromodiphenyl ether and octabromodiphenyl ether have been judged by authorities in California and the European Union to have enough environmental presence and health risk to require a ban (161). Decabromodiphenyl ether, which is of large commercial importance as a flame retardant, seems much less of an environmental contamination problem, and its toxicology per se elicits less concern. However, its photolytic and biological debromination to lower brominated diphenyl ethers (162,163) is a factor which is being weighed by the EU and California authorities. A final decision as to its regulatory status is not available at the time of writing.

Risk analyses are underway (2004) in the European Union on hexabromocyclododecane.

Militating against a ban to include all of the polybrominated additives is the evidence that the high thermal and hydrolytic stability of decabromodiphenyl ether and related polyhalogenated flame retardants makes it feasible to recycle the flame-retarded plastics, which is more difficult with the halogen-free flame retardants (164). An overview, from an industry standpoint, of the effects of regulations on the bromine-containing flame retardants is available as of early 2004 (165). Recyclability of these plastics appears to provide an advantage.

Antimony Oxide. Antimony oxide is used very often as a synergist with halogenated flame retardants. There are some toxicological concerns about antimony oxide because of some equivocal carcinogenicity data, but, on balance, the risk is deemed acceptable (particularly since it is extremely water-insoluble and poorly bioavailable). It is still used in large amounts (166,167). A World Health Organization toxicology critique and drinking water guideline is available (2003) as a draft (168).

Phosphorus Flame Retardants. The original version of tricresyl phosphate was found in the 1930–1940 period to cause paralysis on ingestion as a food or liquor adulterant. However, as a result of basic studies, it was shown that the neurotoxicity characteristic was related to the *o*-cresyl isomer and the manufacturers thereafter have avoided using *o*-cresol to make triaryl phosphates (169). The newer isopropylphenyl and *t*-butylphenyl phosphates have little or no neurotoxicity (170).

The structure–toxicity relationships of organophosphorus compounds have been extensively researched and are relatively well understood (169–174).

A critical review of the toxicity of the haloalkyl phosphates and the potential metabolic products is available (175). The flame retardant "tris" (tris-2,3-dibromopropyl) phosphate was found to be mutagenic in laboratory tests; its production and use were discontinued in the 1970s. Tris(2-chloroethyl) phosphate and tris(dichloroisopropyl) phosphate have voluntary "R40" labels (limited evidence of carcinogenicity in animal tests). Tris(chloroisopropyl) phosphate does not require special classification. The chloroalkyl phosphates are undergoing (as of 2004) an EU risk assessment. They have been detected at various locales in municipal waste water (176), indoor dust, or indoor air (177,178).

Analytical data indicates the emission of trace vapors of triphenyl phosphate, which is controversially claimed to have some allergenic properties, from warm HIPS TV cabinetry (179). However, this emission results in air concentrations far below those which might be considered hazardous (180). The higher molecular weight diphosphates and oligomers appear to avoid toxicological problems (181).

Effect of Flame Retardants on Combustion Products. There appears to be no documented case of any type of fire retardant contributing to human fire casualties. There is ample evidence that carbon monoxide is the main acute toxicant in flames, although oxygen depletion and other toxic gases may contribute. This topic has been studied intensively (182–185).

It appears that in a large fire (which cause most of the casualties), the carbon monoxide yield and the overall smoke toxicity are almost independent of the material burning; this belief has had a dampening effect on combustion toxicology studies (186–188).

Although hydrogen halides (from halogen-containing plastics) are toxic, it is difficult to find cases of fire deaths attributable to them. Using quantitative assessment methods for the fire gases, the Federal Aviation Authority (189,190) model does not ascribe a heavy contribution by HCl and HBr compared to CO and HCN.

The concern about halogens in combustion often focuses on the formation, environmental contamination, and chronic (not acute) toxicity of halogenated dibenzodioxin ("dioxin") or halogenated dibenzofurans, particularly during disposal of halogen-containing plastics by incineration. Much study has been done on the dioxins by analytical chemists, toxicologists, and epidemiologists, a copious literature including books has been produced (191,192), and major international conferences are held annually (159) (A thorough overview of the chemistry, biochemistry, toxicology, environmental occurrence, and risk aspects can be found in Reference 193.). Some but not all authorities consider the dioxins to be carcinogenic; they may be cocarcinogens. The linkage of human health problems to incineration products is tenuous and the link to dioxins even more so. It has been shown that dioxins are produced by all chlorine- or bromine-containing fuels, and predate the era of plastics. EPA data shows that present-day government-approved incinerator–scrubber installations (waste-to-energy facilities) have reduced dioxin emissions to very low levels (194,195). Certain metal smelters such as Boliden in Sweden have also been found to handle halogen-containing waste with acceptably minimal dioxin emissions (165).

A survey of data from small-scale combustion or pyrolysis experiments revealed no consistent pattern of decrease or increase in the yields of toxic gases (CO, HCN) when phosphorus flame retardants were present (196). Experimental conditions (such as burning temperature) seem to dominate over the composition of the material being burned (197).

Effects on Visible Smoke. Smoke is a main impediment to egress from a burning building. In general, the halogen–antimony systems tend to increase the smoke yield relative to the mass burned, but when successful as retardants, they may reduce the total smoke by lessening the mass burned (198,199).

A comparative study of fire performance of halogenated and nonhalogenated cables discusses the smoke performance (200).

Chlorine–antimony systems or chlorine–bromine–antimony systems usually tend to be less smoky than bromine–antimony (201), and it is also possible to lower smoke in some plastics by use of further additives such as zinc borate, molybdates, or iron oxides. In general, the use of ATH or $Mg(OH)_2$ as part of the flame-retardant system results in lower smoke with most polymers (202,203).

Although some examples are known where specific phosphorus flame retardants increased visible smoke in small-scale tests, other instances are reported where the presence of the retardant reduced smoke. The effect appears to be a complex function of burning conditions and of other ingredients in the formulation (204,205). In one careful study, ammonium phosphate was found to raise or lower visible smoke from wood depending on the pyrolysis temperature (206). Where the phosphorus flame retardant functions by char enhancement, lower smoke levels are likely to be observed.

Environmental Considerations. The halogenated flame retardants differ greatly in environmental contamination. As mentioned already, pentabromodiphenyl ether has become widely dispersed, but decabromodiphenyl ether much less so due to its negligible solubility and vapor pressure. Antimony trioxide also is nonmigratory because of its very low solubility and negligible vapor pressure but nonetheless is under close scrutiny from the regulatory authorities (166,207).

The newer families of polymeric or oligomeric or reacted-in bromine, as well as very high molecular weight chlorine- or bromine-containing flame retardants are well designed to avoid migration and to be innocuous environmentally, since they have essentially no water solubility or vapor pressure.

The phosphate flame retardants have come under close environmental scrutiny. Results published to date on acute toxicity to aquatic algae, invertebrates, and fish indicate substantial differences between the various aryl phosphates (208–212). It has been found that the higher molecular weight phosphorus compounds are much better in terms of toxicity to aquatic organisms (213,214).

Tests in pure water, river water, and activated sludge showed that commercial triaryl phosphates and alkyl diphenyl phosphates undergo reasonably facile degradation by hydrolysis and biodegradation (215,216), the chloroalkyl phosphates less so.

Several risk–benefit analyses have favored the use of the flame retardants, since fire and smoke cause severe environmental injury besides the direct losses of life and property. For example, the polycyclic aromatic hydrocarbons which occur in copious amounts in soot have been indicated to be orders of magnitude more

serious than the dioxins, as was revealed in life-cycle assessments of TV sets (217) and furniture (218) with and without flame retardants. The fact that fire is, itself, a severe environmental pollutant, in the absence of a flame retardant, is reemphasized (219).

Nevertheless, environmental pressures continue to impact the flame retardant field, in some cases reinforced by "green" marketing strategies, "eco labels" and misleading generalizations about entire families of chemicals. These pressures have stimulated serious effort, some already successful, to find flame retardants less subject to criticism. Current research and development efforts are in the direction of halogen-free phosphorus compounds, inorganics, high molecular weight halogen compounds, polymeric additives, reactives, flame-retardant polymer modifications and blends.

BIBLIOGRAPHY

"Fire Retardancy" in *EPST* 1st ed., Vol. 7, pp. 1–64, by Raymond B. Hindersinn and George Wagner; Suppl. Vol. 2, pp. 270–339, by Raymond Hindersinn, Hooker Research Corp.; "Flammability" in *EPSE* 2nd ed., Vol. 7, pp. 154–210, by Richard G. Gann and Richard A. Dipert, U.S. National Bureau of Standards, and Michael J. Drews, Clemson University.

1. A. H. Tullo, *Chem. Eng. News* **43** (Nov. 7, 2003).
2. F. Gastrock (of BRG Townsend), personal communication, Feb. 2004.
3. W. E. Horn Jr., in A. F. Grand and C. A. Wilkie, eds., *Fire Retardancy of Polymeric Materials*, Marcel Dekker, Inc., New York, 2000, pp. 285–352.
4. T. J. Lynch, T. Chen, and D. Riley, *Reinf. Plast*. 44–46 (Sept. 2003).
5. T. Chen, in *52nd International Wire and Cable Symposium/Focus*, Nov. 16–20, 2003.
6. R. Sauerwein, in *Flame Retardants '04*, Conference Proceedings, Jan. 2004, Interscience Communications, London, 2004.
7. R. Rothon and B. Ritchie, *Flame Retardants 2000, Proceedings of the 9th Conference*, Interscience Communications, London, 2000, pp. 113–120.
8. J. Innes, A. W. Cox, and M. W. Walter, *Proc. Intl. Conf. Fire Sci.* **25**, 303–314.
9. H. C. Ashton, T. Chen, and T. J. Lynch, in *Polyolefins 2003*, SPE, Houston, 2003, pp. 395–406.
10. E. D. Weil, M. Lewin, and H.-S. Lin, *J. Fire Sci.* **16**, 383–404 (1998).
11. L. T. Arthur and K. Quill, in Plastics & Rubber Institute, eds., *Flame Retardants '92*, Elsevier Science, London, 1992, pp. 223–237.
12. K. Shen, in *Recent Adv. Flame Retard. Polym. Mater.* **11**, 213–221 (2000).
13. K. Shen and R. M. Leeuwendahl, in *14th Annual BCC Conference on Flame Retardancy*, Stamford, Conn., June 2–4, 2003.
14. S. Bourbigot, R. Leeuwendal, K. Shen, and D. Schubert, *Polym. Degrad. Stabil.* **64**, 419–425 (1999).
15. L. L. Musselman, F. W. Moore, and W. J. Kennelly, "Flame-Retarding and Smoke-Suppressing Molybdates and Borates," in J. Edenbaum, ed., *Plastics Additives and Modifiers Handbook*, Kluwer Academic Publishers, Dordrecht, the Netherlands, 1992.
16. D. Chaplin and S. C. Brown, *Flame Retardants '90*, British Plastics Federation, Elsevier Applied Science, London, 1990, pp. 114–125.
17. P. Cusack, *Flame Retardants '90*, British Plastics Federation, Elsevier Applied Science, London, 1990, pp. 176–190.
18. E. D. Weil, M. Lewin, and V. Barinov, in *13th Annual BCC Conference on Flame Retardancy*, Stamford, Conn., June 3–5, 2002.

19. S. A. Hasselbrack, in *Improved Fire- and Smoke-Resistant Materials for Commercial Aircraft Interiors*, National Materials Advisory Board, National Academies Press, Washington, 1995, pp. 165–174.
20. J. Markarian, *Plast. Add. Compdg*. Nov.–Dec. 2003, 32–36.
21. T. Kashiwagi, J. R. Shields, R. H. Harris Jr., and W. H. Awad, in *14th Annual BCC Conference on Recent Advances in Flame Retardancy of Polymeric Materials*, Stamford, Conn., June 2–4, 2003.
22. G. Beyer, *Plast. Add. Compdg.* **4**(10), 22–28 (2002).
23. J. M. Cogen, T. S. Lin, A. B. Morgan, and J. M. Garcés, in *Proceedings of the 52nd International Wire and Cable Symposium*, Nov. 17–20, 2003.
24. U.S. Pat. 5,849,827 (1998), M. Bödiger, T. Eckel, D. Wittmann, and H. Alberts (to Bayer).
25. E. Larsen, in *Kirk–Othmer Encyclopedia of Chemical Technology*, 2nd ed., Vol. 10, John Wiley & Sons, Inc., New York, pp. 373–379.
26. E. D. Weil and M. Lewin, in A. R. Horrocks and D. Price, eds., *Fire Retardant Materials*, Woodhead Publishing Ltd., Cambridge, U.K., 2001, pp. 31–68.
27. D. Stein and D. Stevenson, in *Polyolefins 2003, SPE International Conference on Polyolefins*, Houston, Tex., Feb. 23–26, 2003, pp. 601–624.
28. R. Markezich, in *Proceedings of 51st International Wire and Cable Symposium 2000*, pp. 413–417.
29. "Brominated Flame Retardants, Substance Flow Analysis and Assessment of Alternatives," Danish Environmental Protection Agency, June 1999. http://www.mst.dk/19908pubs/87-7909-416-3/default.htm.
30. *2nd International Workshop on Brominated Flame Retardants*, May 14–18, 2001, sponsored by Swedish Ministry of the Environment, Swedish Academy of Science, and World Health Organization.
31. E. R. Larsen and E. L. Ecker, *J. Fire Sci.* **4**, 261–276 (1986); *J. Fire Sci.* **6**(2), 139–159 (1988).
32. B. M. Valange, S. E. Calewarts, G. A. Bonner, F. A. Pettigrew, and R. A. Schliefstein, in *Flame Retardants '90 [Proc.]*, Elsevier, London, 1990, pp. 67–77.
33. National Academy of Science, *Toxicological Risks of Selected Flame Retardant Chemicals*, National Academy Press, Washington, D.C., 2000.
34. P. O. Darnerud, *Environ. Int.* **29**, 841–853 (2003).
35. "Bis(pentabromophenyl) Ether," European Union Risk Assessment Report, EUR 20402, First Priority List, Vol. 17, 2002.
36. P. Georlette, *Plast. Add. Compdg.* **3**(4), 28–33 (2001).
37. F. Heine, R. Braibant, A. Fonze, B. Plaitin, and J. Rivière, in *World Compounding Congress 2000*, Dec. 5–7, 2000, Neuss/Düsseldorf, Germany.
38. D. De Schryver, S. D. Landry, and J. S. Reed, *Polym. Degrad. Stabil.* **64**, 471–477 (1999).
39. E. D. Weil, in *Kirk-Othmer Encyclopedia of Chemical Technology*, John Wiley & Sons, Inc., New York, 2001. (online)
40. E. N. Peters, *J. Appl. Polym. Sci.* **24**, 1457–1464 (1979).
41. E. Weil, in *11th Annual BCC Conference on Recent Advances in Flame Retardancy of Polymeric Materials*, Stamford, Conn., May 22–24, 2000.
42. M. Lewin, in M. Lewin and S. Sello, eds., *Handbook of Fiber Science and Technology: Chemical Processing of Fibers and Fabrics*, Vol. 2, Marcel Dekker, Inc., New York, 1984, Part B, pp. 1–141.
43. R. H. Barker and J. E. Hendrix, in W. C. Kuryla and A. J. Papa, eds., *Flame Retardancy of Polymeric Materials*, Vol. 5, Marcel Dekker, Inc., New York, 1979, pp. 1–65.
44. S. LeVan, in R. Rowell, ed., *The Chemistry of Solid Wood*, American Chemical Society, Adv. Chem. Ser. 207, Washington, D.C., 1984, pp. 531–574.

45. C. Y. Shen, N. E. Stahlheber, and D. R. Dyroff, *J. Am. Chem. Soc.* **91**, 62–67 (1969).
46. O. Schacker, *Plast. Add. Compdg.* **4**(4), 28–30, 32–33 (2002).
47. H. J. Vandersall, *J. Fire Flamm.* **2**, 97–140 (1971).
48. G. Camino and L. Costa, *Rev. Inorg. Chem.* **8**(1–2), 69–100 (1986).
49. D. Scharf, in *Fire Retardant Engineering Polymers & Alloys*, Fire Retardant Chemicals Association, Lancaster, Pa., 1989, pp. 183–202.
50. R. Mount, in *International Conference on Fire Safety*, Fire Retardant Chemicals Association, New Orleans, Mar. 25–28, 1990, pp. 253–267.
51. Ger. Pat. Appl. 3,720,094 (Mar. 3, 1988), H. Staendeke and D. Scharf (to Hoechst Celanese).
52. U.S. Pat. 4,579,894 (Apr. 1, 1986), G. Bertelli and R. Locatelli (to Montedison SpA).
53. U.S. Pat. 4,336,182 (June 22, 1982), G. Landoni, S. Fontani, and O. Cicchetti (to Montedison SpA).
54. G. Montaudo, E. Scamporrino, and D. Vitalini, *J. Polym. Sci.* **21**, 3321–3331, 3361–3371 (1983).
55. U.S. Pat. 4,504,610 (Mar. 12, 1985), R. Fontanelli, G. Landoni, and G. Legnani (to Montedison SpA).
56. M. Le Bras, G. Camino, S. Bourbigot, and R. Delobel, eds., *Fire Retardancy of Polymers: The Use of Intumescence*, Royal Society of Chemistry Special Publication 224, Springer Verlag, Berlin, 1998.
57. R. Walz, C. Schuetz, and M. Sicken, *Kunststoffe Plast. Europe* **86**(2), pp. 34–36 (1996).
58. E. D. Weil and B. McSwigan, *J. Coat. Technol.* **66**(839), 75–82 (1994).
59. E. Weil and B. McSwigan, *Plast. Compdg*. 31–39, May–June 1994.
60. L. Costa, G. Camino, and M. P. Luda di Cortemiglia, in G. Nelson, ed., *Fire & Polymers*, American Chemical Society Symposium Series, No. 425, Washington, D.C., 1990, pp. 211–238.
61. R. Grabner, in *Addcon World 99* (5th), Prague, Czech Republic, Oct. 27–28, 1999, RAPRA Conference Proceedings 1999.
62. C. L. Goin and M. T. Huggard, in M. Lewin and G. S. Kirshenbaum, eds., *Recent Advances in Flame Retardancy of Polymeric Materials*, Vol. II, Business Communication Co., Inc., Norwalk, Conn., 1992, pp. 94–101.
63. U.S. Pat. 2,430,569 (Nov. 11, 1947) D. C. Hull and A. H. Agett (to Eastman Kodak Co.).
64. U.S. Pat. 2,407,279 (Sept. 10, 1946), D. C. Hull and J. R. Snodgrass (to Eastman Kodak Co.).
65. U.S. Pat. 3,909,484 (Sept. 30, 1975), A. N. Beavon (to Universal-Rundle Corp.).
66. P. V. Bonsignore and J. H. Manhart, *Proc. 29th Annu. Conf. Reinf. Plast. Compos. Inst. SPE* **23C**, 1–8 (1974).
67. U.S. Pat. 6,255,371 (2001), E. Schlosser, B. Nass, and W. Wanzke (to Clariant GmbH).
68. U.S. Pat. 6,547,992 (2003), E. Schlosser, B. Nass, and W. Wanzke (to Clariant GmbH).
69. O. Schacker, W. Wanzke, and D. Scharf, in *New Century of FR Compounding*, Fire Retardant Chemicals Association Fall Conference, Cleveland, Ohio, Oct. 20–22, 2002, pp. 101–111.
70. E. D. Weil and S. Levchik, *J. Fire Sci.* **22**, 183–209 (2004).
71. E. D. Weil and S. Levchik, *Polym. Int*. (in press).
72. U.S. Pat. 3,100,220 (Aug. 6, 1963), A. L. Smith (to Celanese Corp.).
73. J. W. Crook and G. A. Haggis, *J. Cell. Plast*. 119–122, Mar./Apr. 1969.
74. U.S. Pat. 3,041,293 (June 26, 1962), R. Polacek (to Celanese Corp.).
75. U.S. Pat. 4,477,600 (Oct. 16, 1984), G. Fesman (to Stauffer Chemical Co.).
76. U.S. Pat. 4,794,126 (Dec. 27, 1988), G. Fesman, B. Jacobs, and B. Williams (to Akzo America Inc.).
77. S. Andrews, in J. Kresta, ed., *60 Years of Polyurethanes*, Technomics Publishing Co., Lancaster, Pa., 1998.

78. R. L. Gray and R. L. Lee, in G. Pritchard, ed., *Plastics Additives*, Chapman Hall, London, pp. 567–575.
79. M. L. Luda, P. Bracco, L. Costa, and S. V. Levchik, *Polym. Degrad. Stabil.* **82**, 215–220 (2004).
80. O. M. Grace and co-workers, in *Proceedings of the Polyurethanes World Congress*, Sept. 29–Oct. 2, 1987, Aachen, Germany.
81. M. Ravey, I. Keidar, E. D. Weil, and E. M. Pearce, *J. Appl. Polym. Sci.* **68**, 217–228, 231–254 (1998).
82. U.S. Pat. 3,896,187 (July 22, 1975), E. D. Weil (to Stauffer Chemical Co.).
83. U.S. Pats. 4,382,042 (May 3, 1983) and 4,458,035 (July 3, 1984), T. A. Hardy and F. Jaffe (both to Stauffer Chemical Co.).
84. U.S. Pat. 6,150,442 (Nov. 21, 2001), D. Chundusry and R. Sanford (to Ferro Corp.).
85. Eur. Pat. Appl. 1,239,005 (Nov. 9, 2002), Y. Bar Yakov and S. Hini (to Bromine Compounds, Ltd.).
86. U.S. Pat. 3,789,091 (Jan. 29, 1974), J. J. Anderson, J. G. Camacho, and R. E. Kinney (to Mobil Oil Corp.).
87. U.S. Pat. 3,849,368 (Nov. 19, 1974), J. J. Anderson, J. G. Camacho, and R. E. Kinney (to Mobil Oil Corp.).
88. Y. Halpern, M. Mott, and R. H. Niswander, *Ind. Eng. Chem. Prod. Res. Dev.* **23**, 233–238 (1984).
89. E. Termine and K. G. Taylor, in *Additive Approaches to Polymer Modification*, SPE RETEC Conference Papers, Toronto, Ontario, Canada, Sept. 1989.
90. U.S. Pat. 4,220,472 (Sept. 2, 1980), C. Mauric and R. Wolf (to Sandoz Ltd.).
91. R. Wolf, *Ind. Eng. Chem., Prod. Res. Dev.* **20**, 413–420 (1981).
92. D. L. Buszard, *Chem. Ind. (London)* **16**, 610–615 (1978).
93. L. G. Krauskopf, in L. I. Nass and C. A. Heiberger, eds., *Encyclopedia of PVC*, 2nd ed., Vol. 2, Marcel Dekker, Inc., New York, 1988, pp. 143–261.
94. T. W. Lapp, Report NTIS PB-251678, Midwest Research Institute, Feb. 1976.
95. F. A. Lowenheim and M. K. Moran, *Faith, Keyes and Clark's Industrial Chemicals*, 4th ed., John Wiley & Sons, Inc., New York, 1975, pp. 849–853.
96. J. M. Heaps, *Plastics (London)* **33**, 410–413 (1969).
97. U.S. Pat. 3,919,158 (Nov. 11, 1975), D. R. Randell and W. Pickles (to CIBA-GEIGY AG).
98. S. G. Shankwalkar and D. G. Placek, *Ind. Eng. Chem. Res.* **31**, 1810–1813 (1992).
99. A. J. Duke, *Chimia* **32**, 457–463 (1978).
100. E. R. Nobile, S. W. Page, and P. Lombardo, *Bull. Environ. Contam. Toxicol.* **25**, 755–761 (1980).
101. J. Andrews, A. Noonan, L. Timberlake, and R. Rose, in *11th International Flame Retardancy Conference*, London, Jan. 27–28, 2004.
102. U.S. Pat. 6,140,399 (2000), S. Munro (to Great Lakes Chemical).
103. J. R. Darby and J. K. Sears, in N. M. Bikales, ed., *Encyclopedia of Polymer Science and Technology*, Wiley-Interscience, New York, 1975, pp. 229–306.
104. D. H. Paul, in *Fire Retardant Chemicals Association*, Coronado, Calif., Oct. 20–23, 1991, pp. 79–108.
105. Eur. Pat. Appl. 356,633 (Mar. 7, 1990), C. A. A. Claesen and J. H. G. Lohmeijer (to General Electric Co.).
106. D. Bright, S. Dashevsky, P. Moy, and K.-M. Tu, *Annu. Tech. Conf. Soc. Plast. Eng.* **56**, 2875–2879 (1998).
107. E. A. Murashko, G. F. Levchik, S. V. Levchik, D. A. Bright, and S. Dashevsky, *J. Fire Sci.* **16**, 233–249, 278–296 (1998).
108. S. V. Levchik, D. A. Bright, G. Alessio, and S. Dashevsky, *J. Vinyl Add. Technol.* **7**(2), 98–103 (2001).

109. PCT Intl. Appl. WO 03 55,940 (July 10, 2003), B. A. Williams, D. A. Bright, and E. Pinzoni (to Akzo Nobel NV).
110. E. D. Weil, R. B. Fearing, and F. Jaffe, *J. Fire Retard. Chem.* **9**(1), 39–49 (1982).
111. R. Gallagher and J. C. H. Hwa, *J. Polym. Sci., Polym. Symp.* **64**, 329–337 (1978).
112. A. J. Papa, *Ind. Eng. Chem. Prod. Res. Dev.* **9**, 478–496 (1970).
113. Br. Pat. 954,792 (Apr. 8, 1964) (to Virginia-Carolina Chem. Co.).
114. U.S. Pat. 3,235,517 (Feb. 16, 1966), T. M. Beck and E. N. Walsh (to Stauffer Chemical Co.).
115. X. L. Wang, K. K. Yang, and Y. Z. Wang, *J. Appl. Polym. Sci.* **82**, 276–282 (2001).
116. M. Sicken, C. Schutz, and S. Jung, in *Polyurethanes Expo '96*, Las Vegas, Nev., Oct. 20–23, 1996, pp. 460–466.
117. C. Q. Yang, W. Wu, and J. Stowell, in *14th Annual BCC Conference on Recent Advances in Flame Retardancy of Polymeric Materials*, Stamford, Conn., June 2–4, 2003.
118. Eur. Pat. Publ. 138,204 (Apr. 24, 1985), G. Fesman, R. Y. Lin, and R. A. Raeder (to Stauffer Chemical Co.).
119. Eur. Pat. Appl. 255,381 (Feb. 3, 1988), D. M. Konkus and P. Kraft (to Stauffer Chemical Co.).
120. A. R. Horrocks, *Rev. Prog. Coloration* **16**, 62–101 (1986).
121. S. L. Vail, D. J. Daigle, and A. W. Frank, *Text. Res. J.* **52**, 678–692 (1982).
122. A. W. Frank, D. J. Daigle, and S. L. Vail, *Text. Res. J.* **52**, 738–750 (1982).
123. D. J. Daigle and A. W. Frank, *Text. Res. J.* **52**, 751–755 (1982).
124. W. A. Reeves, G. Drake, J. Beninate, and R. Perkins, *Text. Chem. Color.* **2**, 283–285 (1969).
125. Br. Pat. 1,439,607 (1976), R. Cole and J. Stephenson (to Albright and Wilson Ltd.).
126. U.S. Pat. 4,311, 855 (1976), R. Cole and J. Stephenson (to Albright and Wilson Ltd.).
127. A. Kapura, *J. Fire Sci.* **12**(1), 3–13 (1994); *J. Fire Sci.* **14**(3), 169–185 (1996).
128. R. Aenishanslin and co-workers, *Text. Res. J.* **39**, 375–381 (1969).
129. R. Aenishanslin and N. Bigler, *Textilveredlung* **3**, 467–474 (1968).
130. R. Horrocks and D. Roberts, *Exotextile '98: Sustainable Development*, Bolton, U.K., Apr. 7–8, 1998, Woodhead Publ. Ltd., Cambridge, U.K., 1999.
131. E. D. Weil, in J. I. Kroschwitz, ed., *Encyclopedia of Polymer Science and Engineering*, Vol. 11, John Wiley & Sons, Inc., New York, 1988, pp. 96–126.
132. R. Stackman, in C. H. Carraher and M. Tsuda, eds., *Modification of Polymers*, American Chemical Society Symposium Series, No. 121, Washington, D.C., 1980, pp. 425–434.
133. U.S. Pat. 3,941,752 (Mar. 2, 1976), H. J. Kleiner, M. Finke, U. Bollert, and W. Herwig (to Hoechst AG).
134. U.S. Pat. 4,033,936 (July 5, 1977), U. Bollert, E. Lohmar, and A. Ohorodnik (to Hoechst AG).
135. U.S. Pat. 4,127,590 (Nov. 28, 1978), S. Endo, T. Kashihara, A. Osako, T. Shizuki, and T. Ikegami (to Toyo Boseki KK).
136. E. D. Weil and S. Levchik, *J. Fire Sci.* **22**, 25–39 (2004).
137. A. Ballistreri, G. Montaudo, E. Scamporrino, C. Puglisi, and D. Vitalini, *J. Polym. Sci., Part A.: Polym. Chem* **26**, 2113–2127 (1988).
138. E. D. Weil and V. Choudhary, *J. Fire Sci.* **13**, 104–126 (1995).
139. O. M. Grace, R. E. Mericle, and J. D. Taylor, *J. Cell. Plast.* **21**, 311–317 (1985).
140. B. Bastin, R. Paleja, and J. Lefebvre, in *Polyurethanes Expo 2002 Proceedings*, Boston, Oct. 13–16, 2002, API, pp. 244–254.
141. J. Kersjes and C. Furst, in *Interflam '99, Proceedings of the 8th International Conference*, Vol. 2 Interscience Communications Ltd., London, 1999, pp. 1211–1216.
142. A. Casu, G. Camino, M. De Giorgi, D. Flath, V. Morone, and R. Zenoni, *Polym. Degrad. Stabil.* **58**, 297–302 (1997).

143. G. Stern and H. Horacek, *Int. J. Polym. Mater.* **25**, 255–268 (1994).
144. R. Srinivasan and B. Rotzinger, in *Polyolefins 2000, International Conference on Polyolefins*, Houston, Tex., Feb. 27-Mar. 1, 2000, SPE, pp. 571–581.
145. "Toxicological Risks of Selected Flame Retardant Chemicals," Subcommittee on Flame Retardant Chemicals, Committee on Toxicology, Board on Environmental Studies and Toxicology, National Research Council, 2000, National Academy Press, Washington, D.C., 2000. Full text at http://books.nap.edu/catalog/9841.html?onpi.newsdoc042700.
146. G. C. Stevens and A. H. Mann, "Risks and Benefits in the Use of Flame Retardants in Consumer Products: A Report for the Department of Trade and Industry," Polymer Research Centre, School of Physical Sciences and School of Biological Sciences, University of Surrey, Guildford, Surrey GU2 5XH, U.K., Jan. 1999.
147. "Flame Retardants: A General Introduction," Environmental Health Criteria 192, International Programme on Chemical Safety, World Health Organization, International Labor Organization and UN Environment Programme, 1992. Full text at http://www.inchem.org/documents/ehc/ehc/ehc192.htm.
148. Public Chemical Assessment Reports, National Industrial Chemical Notification and Assessment Scheme (NICNAS), Australian Department of Environment and Heritage. Index at http://www.nicnas.gov.au/publications/car/pec/pecindex.htm.
149. "Brominated Flame Retardants in Widespread Use," Danish Environment Agency, 2002; http://www.mst.dk/project/NyViden/2000/05130000.htm for more recent update.
150. V. Babrauskas, R. H. Harris Jr., R. G. Gann, B. C. Levin, B. T. Lee, R. D. Peacock, M. Paabo, W. Twilley, M. F. Yoklavich, and H. M. Clark, "Fire Hazard Comparison of Fire-Retarded and Non-Fire-Retarded Products," NBS Special Publication, No. 749, U.S. Dept. of Commerce, Washington, July 1988. Available on the Internet at http://fire.nist.gov/bfrlpubs/fire88/art003.html.
151. "Summaries of EU Risk Assessments Carried Out for Flame Retardants, and Status of EU Risk Assessments Underway," http://www.cefic-efra.org/pdf/1202/EFRA˙sum˙Risk˙2002.pdf.
152. V. Steukers and S. Kroon, in *Flame Retardants, '04*, Conference Proceedings, Jan. 2004, Interscience Communications, London, 2004.
153. S. Dungey, in *Flame Retardants, '04*, Conference Proceedings, Jan. 2004, Interscience Communications, London, 2004.
154. O. Hahn, S. Kemmlein, O. Jann, S. Kalus, and D. Stolle, in *Flame Retardants, '04*, Conference Proceedings, Jan. 2004, Interscience Communications, London, 2004.
155. G. C. Stevens, R. Ghanem, J. L. Thomas, A. R. Horrocks, and B. Kandola, in *Flame Retardants. '04*, Conference Proceedings, Jan. 2004, Interscience Communications, London, 2004.
156. "Long Chain Chlorinated Paraffin," U.K. Environment Agency Risk Assessment, 2001 (draft).
157. "Updated Risk Assessment of Alkanes, C10–C13 Chloro-," U.K. Environment Agency, 2003 (draft).
158. Brominated Flame Retardants and Foam Furniture Conference and Roundtable, Apr. 29–30, 2003, Environmental Finance Center, EPA Region 9, San Francisco, CA. Text of most papers at http://www.greenstart.org/efc9/2003˙Conf.htm.
159. *Dioxin 2003, 23rd International Symposium on Halogenated Organic and Persistent Organic Pollutants*, Boston, Mass., Aug. 24–29. Proceedings are reported in *Organohalogen Compd.* 61–65 (2003). Papers specifically dealing with the brominated flame retardants are reported in http://www.dioxin2003.org/BFR%20Highlights.pdf.
160. K. Moss, "Toxicology of Flame Retardants," lecture at Workshop on Toxic Use Reduction at Toxic Use Reduction Institute, Amherst, Mass., Dec. 12, 2002.

161. C. Hogue, *Chem. Eng. News* **81**(46), 49–51 (2003).
162. G. Soderstrom, U. Sellstrom, C. A. de Wit, and M. Tysklind, *Environ. Sci. Technol.* **38**(1), 127–132 (2004).
163. H. M. Stapleton, M. Alaee, R. J. Letcher, and J. E. Baker, *Environ. Sci. Technol.* **38**(1), 112–119 (2004).
164. T. Imai, S. Hamm, and K. Rothenbacher, *Environ. Sci. Technol.* **37**, 652–656 (2003).
165. D. Drohmann and L. Tange, in *Flame Retardants. '04*, Conference Proceedings, Jan. 2004, Interscience Communication, London, 2004.
166. K. Van de Velde, in *E & E Conference*, Brussels, Belgium, Mar. 5–6, 2003. Updates available at IAOIA, contact Karine.vandevelde@campine.be.
167. T. Long, in *Flame Retardants in Our New World, Papers Presented at Fire Retardant Chemicals Association [Spring Conference]*, San Antonio, Tex., Mar. 10–13, 2002, pp. 57–58.
168. Revised Document for WHO Drinking Water Guidelines, 3rd ed. Draft available as: http://www.who.int/docstore/water˙sanitation˙health/GDWQ/draftchemicals/antimony2003.pdf.
169. D. C. G. Muir, in O. Hutzinger, ed., *Anthropogenic Compounds, Handbook of Environmental Chemistry*, Vol. 3, Springer-Verlag, Berlin, 1984, Part C, pp. 41–66.
170. Environmental Protection Agency, *Fed. Regist.* **57**, 2138–2159 (1992).
171. M. B. Abou-Donia, in K. Blum and L. Manzo, eds., *Neurotoxicology*, Marcel Dekker, Inc., New York, 1985, pp. 423–444.
172. M. B. Abou-Donia and D. M. Lapadula, *Annu. Rev. Pharmacol. Toxicol.* **30**, 405–440 (1990).
173. M. K. Johnson, *Toxicol. Appl. Pharmacol.* **102**, 385–399 (1990).
174. M. L. Weiner and B. S. Jortner, *Neurotoxicology* **20**, 653–674 (1999).
175. J. W. Holleman, *Health Effects of Haloalkyl Phosphate Flame Retardants and Potential Metabolic Products*, Oak Ridge National Laboratory, Tenn., 1984, DOE/NBM-4006848 (DE84 006848),
176. J. Prosch, W. Puchert, and M. Gluschke, *Vom Wasser* **95**, 87–95 (2000); *Chem. Abstr.* **137**: 388853s (2002).
177. G. Ingerowski, A. Friedle, and J. Thumella, *Indoor Air* **11**(3), 145–149 (2001).
178. T. Salthammer, F. Fuhrmann, and E. Uhde, *Indoor Air* **13**(1), 49–52 (2003).
179. H. Carlsson, U. Nilsson, and C. Ostman, *Environ. Sci. Technol.* **34**, 3885–3889 (2000).
180. European Flame Retardant Association, "Position Paper Triphenyl Phosphate," 2001. Available at http://www.cefic-efra.org/pdf/DOC-01-00%20Revised.pdf.
181. R. Henrich, R. I. Freudenthal, B. M. Ryan, R. L. Sherwood, and co-workers, *Intl. J. Toxicol.* **19**, 223–276 (2000).
182. M. M. Hirschler, S. M. Debanne, J. B. Larsen, and G. L. Nelson, eds., *Carbon Monoxide and Human Lethality: Fire and Non-Fire Studies*, Elsevier Science Publishers, Ltd., London, 1993.
183. B. C. Levin, *Toxicology* **115**, 89–106 (1996).
184. D. Purser, in A. F. Grand and C. A. Wilkie, eds., *Fire Retardancy of Polymeric Materials*, Marcel Dekker, New York, 2000, pp. 450–499.
185. R. G. Gann and co-workers, International Study of the Sublethal Effects of Fire Smoke on Survivability and Health (SEFS): Phase I Final Report, NIST Technical Note 1439, National Institute of Standards and Technology, U.S. Dept. of Commerce, Gaithersburg, Md., Aug. 2001.
186. M. M. Hirschler, in *BCC Flame Retardancy Conference*, Stamford, Con., May 23–25, 1995.
187. J. R. Hall Jr., *Fire Technology* **32**, 351–371 (1996).
188. G. Hartzell, *Toxicology* **115**, 7–23 (1996).

189. L. C. Speitel, Final Report, July 1995, DOT/FAA/AR-95/5, Office of Aviation Research, Washington, D.C.
190. L. C. Speitel, *Toxicology* **115**, 167–177 (1996).
191. W. B. Crummett, *Decades of Dioxin*, Xlibris Corp., Princeton, N.J., 2002.
192. "Dioxins and Dioxin-Like Compounds in the Food Supply: Strategies to Decrease Exposure," Committee on the Implications of Dioxin in the Food Supply, National Research Council, National Academies Press, 2003. Full text on line at http://www.nap.edu/catalog/10763.html.
193. A. Schechter, ed., *Dioxins and Health*, Plenum Press, New York, 1994, pp. 625.
194. N. J. Themelis, *Waste Management World*, 2003–2004 Review Issue, July–Aug. 2003, pp. 40–47. Full text at http://www.seas.columbia.edu/earth/papers/global_waste_to_energy.html.
195. P. Deriziotis and N. J. Themelis, in *North American Waste-to-Energy Conference*, ASME Intl., Tampa, Fla., Apr. 2003.
196. E. D. Weil and A. M. Aaronson, in *Proceedings of the 1st European Conference on Flammability and Fire Retardants, Brussels, BE, July 1977*, Technomic Publishing Co., Westport, Conn., 1978.
197. C. Herpol, *Fire Mater.* **1**(1), 29–35 (1976).
198. F. B. Clarke, *Fire Mater.* **23**(3), 109–116 (1999).
199. A. Heijboer, L. Utevskii, I. B. Yaakov, I. Finberg, and P. Georlette, in *Advances in Plastics Technology APT '97*, International Conference, Katowice, Poland, Dec. 9–11, 1997, pp. 7/1–7/16.
200. M. A. Barnes, P. J. Briggs, M. M. Hirschler, A. F. Matheson, and T. J. O'Neill, *Fire Mater.* **20**(1), 1–37 (1996).
201. R. L. Markezich, R. F. Mundhenke, and D. G. Aschbacher, in *Flame Retardants '94 [Proc. Conf.], 6th*, Interscience Communications, London, 1994, pp. 203–211.
202. M. Rai and S. Brown, in *Flame Retardants '98 [Proc. Conf.], 8th*, Interscience Communications, London, 1998, pp. 83–91.
203. D. H. Park, M. J. Ahn, S. C. Kim, and G. J. Lee, in *Proceedings of International Wire & Cable Symposium, 50th*, 2001, pp. 409–414.
204. T. C. Mathis and J. D. Hinchen, in *31st Annual Technical Conference of SPE, Technical Papers*, Vol. 19, 1973, pp. 343–348.
205. U.S. Pat. 3,869,420 (1975), T. C. Mathis and J. D. Hinchen (to Monsanto Co.)
206. Y. Uehara and Y. Ogawa, in V. M. Bhatnagar, ed., *Advances in Fire Retardant Textiles*, Prog. Fire Ret. Series, Vol. 5, Technomic Publishing Co., Westport, Conn., 1975, pp. 507–599.
207. T. L. Long, in *Papers Presented at Fire Retardant Chemicals Association [Spring Conference]*, San Antonio, Tex, Mar. 10–13, 2002, Fire Retardant Chemicals Association, Lancaster, Pa., 2002, pp. 57–58.
208. L. Cleveland, F. L. Mayer, D. R. Buckler, and D. U. Pulaski, *Environ. Toxicol. Chem.* **5**, 273–282 (1986).
209. D. C. G. Muir, in O. Hutzinger, ed., *Handbook of Environmental Chemistry*, Vol. 3, Springer, Berlin, 1984, Issue Part C, pp. 41–66.
210. J. E. Chambers and P. E. Levi, eds., *Organophosphates, Chemistry, Fate and Effects*, Academic Press, New York, 1992.
211. B.-E. Bengtsson and co-workers, *Environ. Toxicol. Chem.* **5**, 853–861 (1986).
212. R. S. Boethling and J. C. Cooper, *Residue Rev.* **94**, 49–99 (1985).
213. R. T. Henrigh, R. L. Freudenthal and co-workers, *Int. J. Toxicol.* **19**, 223–275 (2000).
214. Akzo Nobel Functional Chemicals LLC, Material Safety Data Sheet on FYROLFLEX BDP.
215. Y. Kawagoshi, S. Nakamura, and I. Fukunaga, *Chemosphere* **48**, 219–225 (2002).
216. W. Mabey and T. Mill, *J. Phys. Chem. Ref. Data* **7**, 383–415 (1978).

217. M. Simonson, C. Tullin, and H. Stripple, *Chemosphere* **46**, 737–744 (2002).
218. P. Andersson, M. Simonson, and H. Stripple, SP Report 2003:22, Swedish National Testing and Research Institute and IVL Swedish Environmental Research Institute, 2003.
219. J. Troitzsch, *Polym. Degrad. Stabil.* **64**, 557–560 (1999).

EDWARD D. WEIL
Polymer Research Institute, Polytechnic University

FORENSIC ANALYSIS

Introduction

Sir Arthur Conan Doyle is believed by many to have first popularized the application of forensic analysis through his newspaper serials originally published in 1887 featuring the fictional character Sherlock Holmes. This work is thought to have inspired many of the early forensic scientists. One of these was Frenchman Edmond Locard, who proposed that when two objects come into contact with one another, a cross-transfer of evidence occurs (1,2). This is the basis of Locard's Exchange Principle and is the foundation of how we can often use physical evidence to link or at least associate a suspect to a crime scene or a victim. Depending on the nature of the evidence, a wide range of analytical methods are used in forensic casework.

A broad definition of the term *forensic*, according to *Webster's New World Dictionary*, is "suitable for a law court or public debate." With the application of forensic science, one must demonstrate in court that the evidence analyzed has relevance to the case in question. The significance of evidence related to a case is often determined by whether the physical evidence has individual or class characteristic properties. Individual characteristics are properties of evidence that can be attributed to a common source with an extremely high degree of certainty. Class characteristics are properties of evidence that can only be associated with a group and never with a single source. (3)

Fingerprint and DNA evidence are accepted as having individual characteristics. Fibers or copy toners, however, are identified by their class characteristics, and because of the large production of these materials, they cannot be

Encyclopedia of Polymer Science and Technology. Copyright John Wiley & Sons, Inc. All rights reserved.

individualized. The strength of fiber evidence depends on the likelihood of those type fibers being randomly found on the suspect. Common fibers such as blue or white cotton from jeans or shirts, respectively, have little evidential value. But, blue Nylon 6,6 fibers with an unusual cross section would have more significant value because there are fewer in existence. Forensic scientists have thoroughly developed statistical values for DNA and fingerprint data to demonstrate individual characteristics. Statistics are more difficult to apply to class evidence, but approaches to apply them are being investigated. The information obtained during polymer analysis is usually characteristic of classes of materials, but in some instances the identification of specific components and physical properties demonstrates an uncommon characteristic. If a contaminant found on an evidential material is identified as a rare substance specific to the crime scene, the evidence would demonstrate a high likelihood of originating from the crime scene. Therefore, forensic polymer analysis is used to identify chemical and physical properties that contribute in varying degrees to the evidential value in criminal forensic analysis.

Forensic science is a hybrid, applied science encompassing any of the natural, engineering, or medical sciences that may be used in analysis for the administration of criminal or civil justice. Criminalistics is a branch of forensic science. Although variously defined, it is generally thought of as utilizing the physical sciences, especially chemistry, physics, and biology to characterize, identify, compare, and individualize items of physical evidence. The forensic scientist may be a full-time employee of a municipal, state, federal, or private laboratory, or a specialist from an academic or industrial laboratory, who is called upon to conduct forensic examinations and provide expert testimony in courts of law.

A forensic scientist must not only possess expertise in an area of specialization, but must also be able to communicate with clarity, because of the importance of conveying accurate scientific results and their interpretation to the court. The forensic scientist, whose qualifications have been accepted by the court, is given the status of expert. This status allows the scientist/witness to offer opinions on the basis of reasonable scientific certainty—an option not allowed by lay witnesses. Because a person's property, reputation, and, very often, life may be at stake in a trial, a special burden of responsibility is placed on the scientist who testifies as an expert.

Polymers as Evidence

This article is concerned principally with the utilization of polymers as items of trace evidence. The small size of samples usually available makes their examination nonroutine. Methods such as tensile testing, fractography, and burning are rarely conducted on a microscale in forensic investigations. A significant part of the forensic examination of polymeric substances is concerned with factors other than those derived from the polymer itself. Criminalistics is distinguished from the other sciences by its unique attempt to individualize as opposed to most natural sciences, where the emphasis is on generalization and the establishment of laws that can be universally applied.

It has only recently become possible to identify microscopic polymer samples by spectroscopic and other instrumental methods. Even with this advantage, and

in spite of the many possible modifications in polymer composition, it is the trace components that serve to individualize these substances and distinguish them from their close relatives. The identification of low concentration additives makes polymer materials more specific, and therefore more evidentially important. However, when trace elements, resulting as random constituents of polymer starting materials and fillers, are identified and quantified, they can render the sample as unique. When crime scene material in question and a known material in the possession of a suspect are analytically identical to these random trace elements, a strong link is realized. This is an area that has not been significantly explored and is open to extensive research.

It is not only important to analyze the composition of a polymer, but to look for and identify subtle post-manufacturing changes that may have occurred. Changes resulting from mechanical or environmental effects can make a sample uniquely identifiable to its source.

Polymers are of interest to the forensic scientist for one or the following reasons:

Trace Evidence. Polymers may be crushed to powder, melted, left behind or carried away, burned, or broken. Particles—usually microscopic—of fibers, paint chips or smears, and rubber or plastic particles may be transferred to the clothing or environment of a suspect or victim. Evidence may also be in the form of soluble or dispersable polymers, such as gums, resins, adhesives, asphalts, etc.

Failures. Polymeric materials, like others, fail. Such failures are often studied as a result of civil liability litigation; however, they occasionally bear importance in criminal cases. Examples include the failure of a suture in an operation, peeling paint from a bridge or building, or failure of plastic parts in a prosthetic implant.

Burned Polymers. Most cases of this type are civil, but on occasion may arise in a criminal investigation. Examples include the flammability of various fabrics or plastics and their suitability for a particular use, determination of the quantity and identity of toxic gases that may have been given off by polymer products in a fire, and the determination of the fiber composition of a fabric after a fire.

Evidence Collection

Successful forensic trace evidence analysis is characterized by the ability to locate, collect, manipulate, identify, and compare microscopic particles. However, sample poverty is common in legal investigations. The sample size is frequently limited, and oftentimes only a portion of the sample can be used, pending the need for additional analysis. This places a further burden on the analyst, techniques, or instruments used. Accordingly, microscopy is the first choice for most forensic examinations.

Once particles of interest are located, they must be isolated for further study and analysis. This may be accomplished by handpicking with fine, pointed forceps

or sharpened tungsten needles while observing through a stereomicroscope. In some cases, the evidence may be collected with sticky, transparent tape. This collection method is not recommended for paint or lacquer particles because of the inevitable mixing of the polymeric evidence and adhesive. In other cases, vacuuming, washing, or scraping with a spatula are useful techniques. Criteria for choosing the proper collection method are given in the literature (4–6).

It is rare that an item of trace evidence can be completely examined *in situ*. Since the original location of the specimen is changed and at least a portion of the specimen is frequently altered in testing, photography at each step of the examination is recommended, and often required, particularly in civil cases. Equipment should be available for ordinary studio photography, macrophotography, and photomicrography. The recent widespread use of digital cameras has made recording images almost routine. These permanent records not only serve to document the course of the investigation, but also help to explain the examination to a jury in the courtroom or to enhance written reports. The value of such exhibits to help the court understand the process cannot be overemphasized. For example, a comparison color photomicrograph of polished cross sections of known and questioned multiple layered paint flakes from a hit-and-run accident offers the jury a visual presentation that is easier to understand than a statement that the paint chips have the same layer structure. Photographs showing the colors of the coat layers, especially a repainted vehicle, can show a vivid match of two compared paints.

Alphabetical/numerical designations are used to label evidence exhibits of known and suspect samples for comparison. In the example cited above, the questioned paint chips recovered from the victims clothing could be labeled "Q-1," and the street where the accident took place labeled "Q-2." Paint samples from the suspect vehicle would have a known origin and be designated with K-numbers, eg, K-1 "Paint from damage to the driver's side fender." This provided systematic references that are easily understood.

Analysis

In most cases, the analytical methods of the forensic chemist are different from those of the usual analytical, quality control, or materials chemists. The most important tests are usually those that lead to identification of the substances under examination. Tests, such as those found in compilations of standard methods of analysis, are rarely of use in the criminalistics laboratory, because they generally require more sample than is available and are usually intended to measure some quantitative aspect of a material. For forensic purposes, initially, a qualitative identification is more important than a quantitative determination. Before the analyst can compare or attempt to individualize a trace sample, it is essential that it be identified. Comparisons performed on traces that have not been accurately identified represent a *fault in principle* and may come back to haunt the scientist during cross-examination.

Microscopical methods are most commonly employed, because they allow the examination of minute specimens and are usually nondestructive. Table 1 describes many of the microscopes and instruments useful for the examination of polymer microtraces. Other equipment less frequently used, because larger

Table 1. Methods for Examining Minute Specimens

Methods	Uses	Refs.
Microscopical		
Stereo binocular		
May be equipped for reflected and transmitted light; a boom stand is a useful accessory for studying bulk objects, clothing, etc	Upright image and long-working distance are excellent for particle manipulation and preliminary examination	7
Comparison		
Two microscopes joined by an optical bridge so that images from both microscopes can be seen on either side of a fine dividing line in the same field of view	Comparison of hairs and fibers, paint chips, layer structure; physical matches	8,9
Polarizing (PLM)		
Standard petrographic microscope; the addition of tilting compensators and a hot stage are useful for the study of synthetic fibers	Essential for the identification of vegetable and synthetic fibers	10–12
Phase contrast and interference contrast	Qualitative systems allow image enhancement; qualitative interference systems permit the most accurate measurement of refractive indexes of synthetic fibers for patent work	12,13
Fluorescence	Autofluorescence can distinguish certain plastics and various layers of white house paints; optical brighteners can be detected on single fibers; fluorochromes can be used to detect substance such as polymer coatings on fibers	14
Scanning electron microscope (SEM)		
Useful alone but enhanced by energy dispersive X-ray analyzer (EDS) system	Of exceptional use in the study of fractures and failure of fibers; the elemental-analysis capability assists in identifying polymers containing characteristic elements, egg, silicone (Si), and neoprene (Cl)	15
Analytical electron microscopy (AEM)		
Transmission (TEM) and scanning transmission electron microscopy (STEM) coupled with elemental analysis and electron diffraction	Identification of phases in polymers, location of copolymers in blends, and identification of inorganic pigments and fillers	16

Table 1. (Continued)

Methods	Uses	Refs.
Micro-Fourier transform infrared spectroscopy (FT-IR)		
The addition of a microscope to an FT-IR, especially when coupled to a mecury cadmium telluried (MCT) detector, allows the collection of ir spectra on particles down to ~10 μm in size	The single most useful instrument for identifying microtraces of polymers of all types	17–20
Micro-Raman spectroscopy	Identification of polymers and pigments	21–23
Ultraviolet, visible, and fluorescence microspectrophotometry (MSP)	Comparison of questioned and known materials, especially fibers and paints, by their spectral characteristics	24
Electron microprobe analyzer		
A more dedicated elemental analyzer than the SEM, although the distinction between electron microprobes and SEM has lessened with time	Quantitative analysis of element in small particles; detects elements of low atomic number	25
Surface analytical		
Secondary ion mass spectrometry (SIMS)	Provides elemental and chemical analysis of surfaces; can reveal thin layers of corrosion of deposition	26
Auger spectroscopy		
Electron spectroscopy for chemical analysis (ESCA)		
Separation		
Pyrolysis gas chromatography (Py-GC)	Sensitive separation of components of polymer mixtures and blends; identification by mass spectra	27–29
Pyrolysis gas chromatography/mass spectrometry (Py-GC/MS)		
Thin-layer chromatography		
High performance liquid chromatography (HPLC)		

samples are required, include those used to perform other tests such as Instron testers, thermal analysis instruments (differential thermal analysis, differential scanning calorimetry, thermogravimetric analysis) and apparatiuses for determining molecular weights, such as size exclusion chromatography. Micromodifications of some of these instruments and techniques have been described and may have occasional significance in forensic investigations (30,31).

Separation methods such as thin layer chromatography (TLC) and pyrolysis-gas chromatography (Py-GC) are useful for comparison of questioned and known specimens when there is sufficient material and the destruction of the specimens is not an issue. In order to identify polymers and certain additives, numerous trace evidence examiners have established libraries of known Py-GC. Commercial

libraries of Py-GC chromatograms have not successfully been established, because analysts have difficulty on agreeing to standard GC conditions. Pyrolysis-gas chromatography/mass spectrometry (Py-GC/MS) can be used successfully to identify materials with commercial mass spectrometry libraries.

The nature of the specimen and the question that has been raised about it determine the course of action and the avenue of the analysis. After consideration of all known facts, and after nondestructive observations are completed, a particular test is selected in an attempt to answer a specific question. The results of this test determine the next step chosen. Some of the methods that may be employed for specific groups of polymers are discussed in the following sections. Microscopic and spectroscopic methods yield a great amount of information in the least amount of time, and, subsequently, are most frequently used by forensic trace examiners. Therefore, microscopy and spectroscopy are discussed in the greatest depth.

Microscopy. Visual light microscopes come in several optical configurations that are used for specific purposes. Low magnification *stereomicroscopes* (SMs) are of particular value in searching large areas for items of question and then separating them as potential evidence. The areas could include portions of garments to scan for foreign debris. Pill boxes of garment scrapings are scanned with SMs to seek potential fibers for comparisons. In addition, they are used for manipulation of the items that have been isolated to preparae toward more detailed microscopical or instrumental analysis. SMs are required in virtually any laboratory that examines micro-traces regardless of what other microscopes or instruments are employed.

The most useful microscope in the hands of a trained microscopist is the *polarizing light microscope* (PLM). Although considerable training and experience are necessary to fully utilize the capabilities of this microscope, a relatively short period of training can give a chemist the necessary skills to use the microscope to identify both natural and synthetic fibers. With minimal training, one can utilize morphological and optical properties to compare polymers regardless of their form or composition when received as items of trace evidence.

Additional microscopes include the *comparison microscope* that permits the microscopist to look at two specimens side by side. This is a useful early step in the comparison of two fibers or paint chips believed to have originated from the same source. The items can be observed and photographed side by side, permitting detailed scrutiny by both the forensic scientist and the court. Other light microscopes such as *fluorescence*, *hot stage*, *phase contrast*, and *interference* instruments may be of value in certain investigations, as shown in Table 1.

The scanning electron microscope (SEM) has some value to the forensic study of polymers, but it is principally the elemental information provided by an energy dispersive X-ray spectrometer (EDS) attached to most SEMs that usually gives the most information in forensic analyses. Using an EDS, the elemental composition of an isolated paint smear or fiber dye may be determined on even the smallest samples. The SEM provides high magnification images of the surfaces of materials. It is less useful for the examination of the interior of a particle of evidence. In this case, microtomed cross sections and freeze fractures can be used to look at interiors. A fairly recent and valuable application of the imaging capability of the SEM in the study of polymers is the examination of the ends of fibers to determine the cause of failure. Cutting with various instruments, crushing, breaking, etc, can

all be studied with the SEM and conclusions can be drawn by careful analysis of the images. Care must be taken, however, since all of the fibers in a multistrand cord or rope may not show the same characteristics as the fibers that initially failed. For example, some of the strands may have been cut with a knife under tension and the rest of the fibers (once there were too few to support the load) may have failed under tension. Other scanning microscopes, such as atomic force microscope (AFM), and instruments have yet to find significant forensic applications (see ATOMIC FORCE MICROSCOPY).

Spectroscopy. The ability to obtain spectroscopic information from microscopic samples has considerably increased the value of spectroscopy in the forensic study of microtraces. Vibrational Spectroscopy (qv) is applicable to a wide range of physical evidence. Polymeric materials, such as fibers, paints, and adhesive tapes, are frequently analyzed to identify characteristic information regarding the composition. Modern infrared and Raman spectrometers with microscopes attached are capable of obtaining chemical information from even the smallest samples. With the development of Fourier transform infrared (FT-IR) spectroscopy, the application of infrared to forensic analysis became more prevalent because of the increased speed and sensitivity of FT-IR. The development of diffuse reflection (DR) accessories provides ease of sample introduction for several forensic applications. Samples with matte-finished surfaces can be directly analyzed with no sample preparation, thus avoiding difficult pellet preparation by grinding the sample and subsequent mixing in potassium bromide. Internal reflectance spectroscopy (IRS), commonly referred to as attenuated total reflectance (ATR), has become widely used with a variety of recently developed accessories. Sample areas of less than one millimeter in diameter can be analyzed using single-reflection bench compartment accessories and diameters on the order of 10 μm can be analyzed with microscope attachments. Raman spectroscopy requires even less sample preparation than FT-IR, and artist's pigments are being identified today by their Raman spectra obtained directly from a painting without removal of sample material (32).

Applications, General Polymers

Because polymers are so common and vary so widely in composition, they are frequently found at crime scenes and subsequently play an evidentiary role in criminal cases. Polymeric materials, such as fibers, paints, and adhesive tapes, are frequently analyzed to identify characteristic information regarding their composition. Physical and chemical information on these materials is increasingly being stored in computer databases to help determine the manufacturer or supplier, or simply to discriminate between many similar samples of material. Some of the available databases will be described as a part of the analyses mentioned in the following pages. Other general polymeric materials found as evidence do not fall into a particular category and must be studied on a case-by-case basis without the aid of comparison to similar material in a database.

The following is a case example where a polymeric material became important evidence. Early one morning on a luxury cruise ship off the coast of California, a man reported to the captain that his wife had been blown overboard. Considering

the minimal wind conditions, the captain became suspicious and alerted the law enforcement authorities. Several hours after the overboard report, the woman's body was recovered by the U.S. Coast Guard. The clothing that both the man and woman were wearing at the time of the incident was forwarded to the FBI Laboratory. The woman's running pants appeared soiled with an orange substance on both legs. Careful examination of her pants with a stereomicroscope revealed orange colored, rubbery particles. Examination of the man's running pants also revealed rubbery particles that appeared identical. On the ship's deck, at the location of the overboard incident, there was an orange colored, rubberized running track. A portion of the track material was removed from the ship and forwarded to the laboratory for analysis. The particles were removed from both pairs of running pants and flattened in a compression cell to make them sufficiently thin to perform transmission analysis using an FT-IR microscope system. Particles from the track material were prepared in the same way and the spectra of all three samples were compared as shown in Figure 1.

The three spectra of the rubberized material compared closely. The material was heavily filled with calcite (hexagonal $CaCO_3$), identified by the intense, broad C—O asymmetric stretch near 1450 cm^{-1}, and narrow out-of-plane and in-plane bends near 880 and 710 cm^{-1}, respectively. To determine the force required to embed the particles in the pants, a fabric similar to that of the pants was rubbed across the removed track piece at different degrees of pressure. The investigators found that it was necessary to rub the fabric with significant pressure, such as in the case of dragging a person, to cause the transfer and embed the material in the fabric. They determined that the transfer of particles suggested an altercation

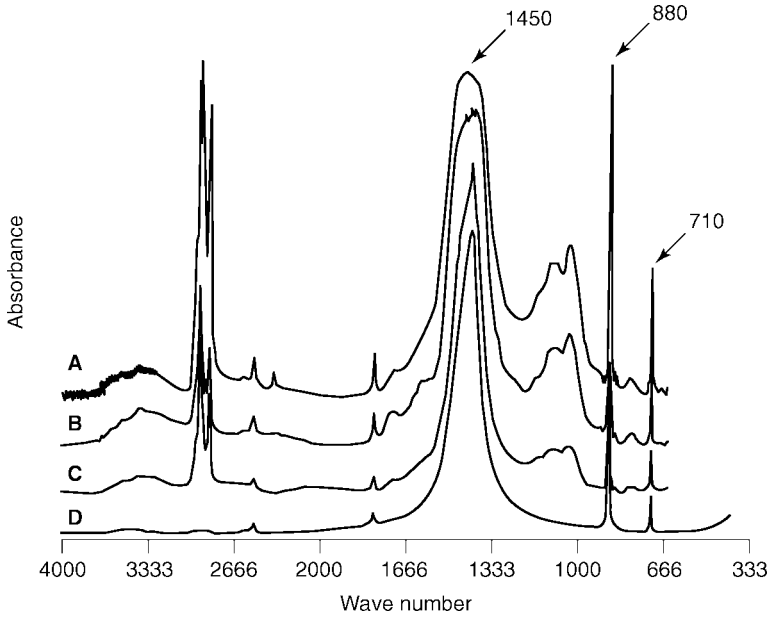

Fig. 1. Cruise ship homicide case. Spectra of rubber particle evidence from, sweat pants from both (**A**) victim and (**B**) the suspect, (**C**) running track and (**D**) calcite reference.

between the individuals, and, therefore, this evidence was heavily weighed and resulted in a homicide conviction. The combined comparison of evidential materials by microscopical examination, infrared analysis, and physical testing played a significant role in this case without witnesses.

Particles of plastic or rubber are often recovered from crime scenes or from victim's and suspect's clothing. Occasionally, these have forensic significance and must be identified and compared as described above. Rubber particles mounted on a microscope slide are recognizable because they can be compressed when pressure is applied to the coverslip with a needle, and recover fully when the pressure is released. Plastics are more easily recognized by an experienced eye by ruling out other types of particles. Particles of plastic are readily identified today by FT-IR analysis.

Plastics may provide evidence in determining passenger location with vehicles in serious accidents when questions arise as to who was driving when the accident occurred. This question is often answered by examination of hairs embedded in the dashboard, sun visor, etc. It has been shown that many thermoplastics can melt and transfer to clothing in the high energy environment that momentarily exists during a high impact collision. Molten plastic from clothing (eg, nylon jackets, cotton polyester shirts) can be collected from dashboards, airbags, and window pillars and identified. Colored polymers may sometimes be compared by light microscopy alone, but any comparison of unknown polymers should always be confirmed by FT-IR spectroscopy.

Fiber Applications

In cases of sexual assault and homicide, the transfer of single fibers often have important forensic significance. The case that most significantly impacted the realization of the importance of fiber evidence was the Atlanta murders that occurred between 1979 and 1981 (33,34). The bodies of 28 boys and young men were found under similar conditions. Although many of the bodies contained fiber and hair evidence that compared closely, Wayne Williams was prosecuted and convicted for only two of the homicides. The conviction was based solely on multiple transferred hairs and fibers with an emphasis on uncommon carpet fiber found in the bedroom of Williams's home.

In the forensic study of fibers, five questions are commonly asked:

(1) What is the polymeric composition of the fiber?
(2) Could the questioned fiber have the same source as the known?
(3) How was the fiber broken?
(4) Who manufactured the fiber or fabric?
(5) What is the commonality of the fiber?

The first question can almost always be answered by PLM, and often more specifically by FT-IR microspectroscopy, regardless of how little fiber is available. The other four may often be more difficult.

In fiber examinations, the analyst receives evidence fibers from a known source and fibers from a suspect source that must be compared to decide whether or not the questioned and known fibers could have a common origin. As part of this comparison, the fibers must be classified according to their generic type. The foremost method of analysis for this type of evidence is light microscopy; however, IR is often valuable to further specify fiber type. Fibers from the clothing of the victim and suspect are screened microscopically for similarity by closely comparing physical and optical properties of the fibers. Laboratories that collect fibrous evidence on clear tape now have the option of using fiber finders that automatically search for target fibers, which saves considerable time in complex cases involving many exhibits. The useful properties may vary significantly because of the color, shape, texture, and chemistry of the fibers. Polarized light microscopy is used to determine the generic classification (eg, nylon, polyester, acrylic) and FT-IR microspectroscopy plays an important role in identifying subclasses of synthetic and regenerated fibers. A spectral library of 83 polymeric fiber types, obtained by transmission spectroscopy on flattened single fibers, was developed to aid forensic examiners in the identification of fiber composition (35–37). IR spectroscopy is particularly useful for subclassifying acrylic fibers that are seen frequently as a wool alternative in sweaters. These fibers are readily transferred between individuals during contact. According to U.S. Federal Trade Commission rules, acrylic fibers must contain at least 85% polyacrylonitrile (38). The other 15% may be copolymers and ionic end groups that enhance the dying properties of the otherwise undyeable fibers. Figure 2 shows spectra of the three most common acrylic

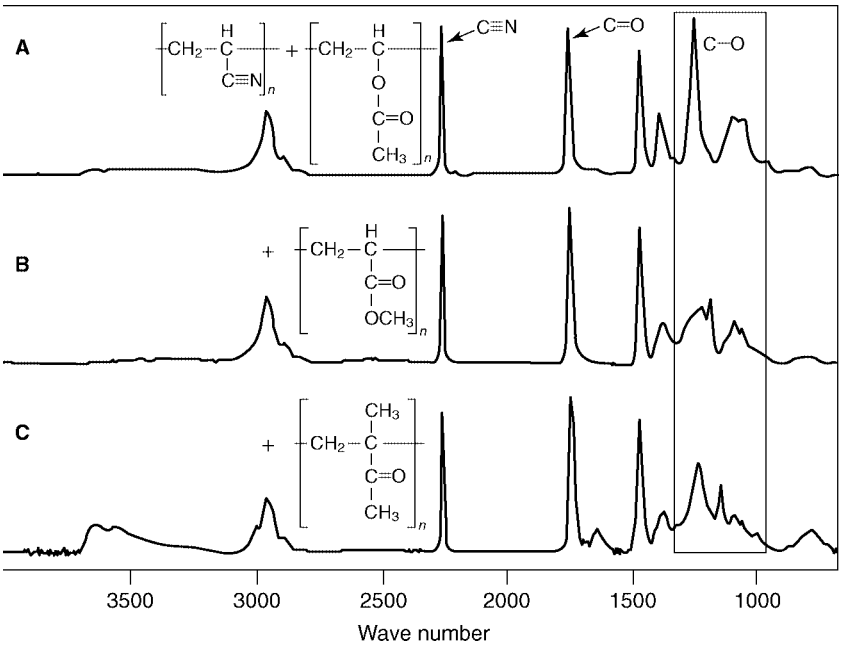

Fig. 2. IR spectra of acrylic copolymer fibers: (**A**) poly(acrylonitrile:vinyl acetate); (**B**) poly(acrylonitrile:methyl acrylate); and (**C**) poly(acrylonitrile:methyl methacrylate).

copolymers. The band shape of the C—O stretch, as shown in the region between 1300 and 1000 cm^{-1}, varies as a result of its position or environment within the different comonomer structures. Over 20 variations of acrylics can be identified by IR (39). Thus, IR is a very useful tool in providing information that further discriminates fiber types in order to enhance the evidential value of a sample.

Tests designed to distinguish the fibers from each other are used to complete a comparison. If the fibers cannot be distinguished at the conclusion of the tests, they are reported as nondistinguishable and it can be said that they may have a common origin. However, at best, fibers provide class-type evidence; they are not as individual as fingerprints or body fluids. It is not the number of tests that are performed, but the discriminating power of each test selected, as well as the independence of each test performed from the others, that determines the completeness of the examination and thus the strength of the conclusions that can be drawn. Table 2 lists various measurements and tests that can be performed on synthetic fibers. Most of the methods shown in Table 2 are applicable to regenerated fibers as well as synthetics. For identification of vegetable fibers (natural cellulose polymer), one must rely almost entirely on a detailed study of morphology for identification. Identification to the genus level of the plant from which the fibers originate is usually as far as a comparison can be taken. For example, having identified both known and questioned fibers as ramie (*Boehmeria nivea*), other tests of comparison are not possible (other than dyed or oiled cordage or rope), since the fibers consist of almost pure cellulose.

The optical and morphological properties of fibers are useful in comparisons when trying to determine possible end use and in manufacturer of the fiber. The optical properties of fibers include color (as well as pleochroism and fluorescence), refractive indices (parallel and perpendicular to the length of the fiber), birefringence (the numerical difference between the two refractive indices), and sign of elongation. The latter is determined by convention. A fiber is said to have a positive sign of elongation if the higher refractive index is parallel to the length of the fiber. The possibility of determining the manufacturer of a single fiber is nearly impossible in most cases. However, in some cases, where the fiber possessed a very characteristic property and manufacturers have given assistance, it has been done. In the Atlanta murder case the manufacturer of the carpet fibers from Williams's home was determined from the unique cross-sectional shape.

The solution of a child murder in Alaska was brought to a successful conclusion by a forensic examination of particles of polymeric trace evidence recovered from her body, which was found lying in a secluded area, not far from her home. These included short ($\sim$1 mm long), brittle red and blue polypropylene fibers and single layered particles of paint in a wide variety of colors. Iron spheres and fragments were also found on the victim's clothing. The girl was freshly dressed when she went off to meet her friend after school. There was no source of particles such as these in her normal environment. A suspect developed in the case had a workshop surrounded by nonfunctioning automobiles and trucks, and he often did repairs on children's bicycles.

It was possible to trace the manufacturer of the fibers by an examination of their cross sections, which were made with difficulty, because of their brittle nature. Infrared microspectroscopy revealed that the fibers were photo-oxidized on the basis of a significant carbonyl absorption band of $\sim$1730 cm^{-1}. The fibers were

Table 2. Fiber Comparison Techniques for Single Fibers and Fiber Fragments

Method	Measurement	Information
Comparison microscope	Side-by side viewing	Diameter, color, pigment, and/or delustrant density and distribution
Polarized light microscopy	Crystallographic properties: refractive indexes[a]	Fiber-identity differences in draw ratio, heat setting
	Sign of elongation	Distinguishes fibers with high bond polarization perpendicular to fiber axis, eg, acrylics
	Birefringence	Fiber identity (qualitative), draw ratio, and end use (quantitative)
Cross section	May be deduced to some extent by logitudinal view; most information is obtained from cut sections	Determination of fineness (tex or denier), modification ratio: can aid in manufacturer identification
Fluorescence microscopy	Autofluorescence	Blues and blue-whites indicate optical brighteners: other colors due to dyes
Microspectrophotometry	Visible spectrophotometry on a microscale	Dye comparison of dye components from known and questioned fibers
Thin-layer chromatography	Separation of dyes	Comparison of dye components from known and questioned fibers
Electron microprobe	Elemental composition	Identity of catalyst residue and elemental tags for comparison and manufacturing origin
Micro FT-IR and Raman	Polymer comparison	Recognition of coploymers in acrylics and modification to polyesters, etc
Thermal microscopy	Melting range	Distinguishes nylon; crystallinity differences

[a]The refractive indexes measured perpendicular ($\eta_{\text{perpendicular}}$) and parallel ($\eta_{\text{parallel}}$) to the length of the fiber. The isotropic refractive index (η_{iso}) is the refractive index the fiber would exhibit in the absence of orientation.

made by Phillip's Fibers and consultation with experts at the company suggested that, most likely, they originated from a "fake" oriental rug that had been left out-of-doors. This carpet, if it ever existed, was never found, but the fibers from the suspect's environment made their way onto the body of the victim.

Fibers identical in all respects to those found on the victim's body were discovered in the truck and workshop of the suspect. Single-layered paint chips in a wide variety of colors and metal particles and spheres were also found in the suspect's workshop. The finding of particles identical to those from the suspect's environment on the victim was a practical example of Locard's Exchange Principle. Since the girl did not have these particles on her clothing when she left the

house with fresh clothing and she did not move after she was murdered, the particles must have been associated with the environment of the murderer. The jury convicted the suspect of the child's murder.

Raman spectrometry promises to complement IR analysis of textile fibers because of the ease of sampling and the additional information it can provide. Light microscopy analysis requires fiber samples to be mounted in a liquid medium, under coverslips, on a glass slide. Because glass absorbs strongly in the IR, the fibers must be removed and cleaned prior to IR analysis. Raman analysis, on the other hand, has been successfully performed on single fibers while mounted on glass microscope slides (21), thus omitting the need to remove the fibers from the slide mount. The additional sample preparation time is not required and, once mounted, the chance of fiber loss is minimal. Figure 3 illustrates the process of obtaining a Nylon 6 fiber spectrum using microscopical Raman analysis. Figure 3**A** includes spectral contributions from the fiber, Permount mounting medium, and glass from the coverslip. Figure 3**B** shows the result of Permount subtracted from the original spectrum. The Nylon 6 spectrum that remains after the glass contributions are subtracted is shown in Figure 3**C**. The baseline is flattened for the final spectrum in Figure 3**D**. The signal-to-noise ratio is less than obtaining a spectrum without being mounted under a coverslip, but it is sufficient to identify the fiber by the prominent characteristic bands as labeled. The band assignments of the major peaks are labeled in accordance with Hendra and coworkers (40). Raman spectra differ from IR spectra, because the selection rules

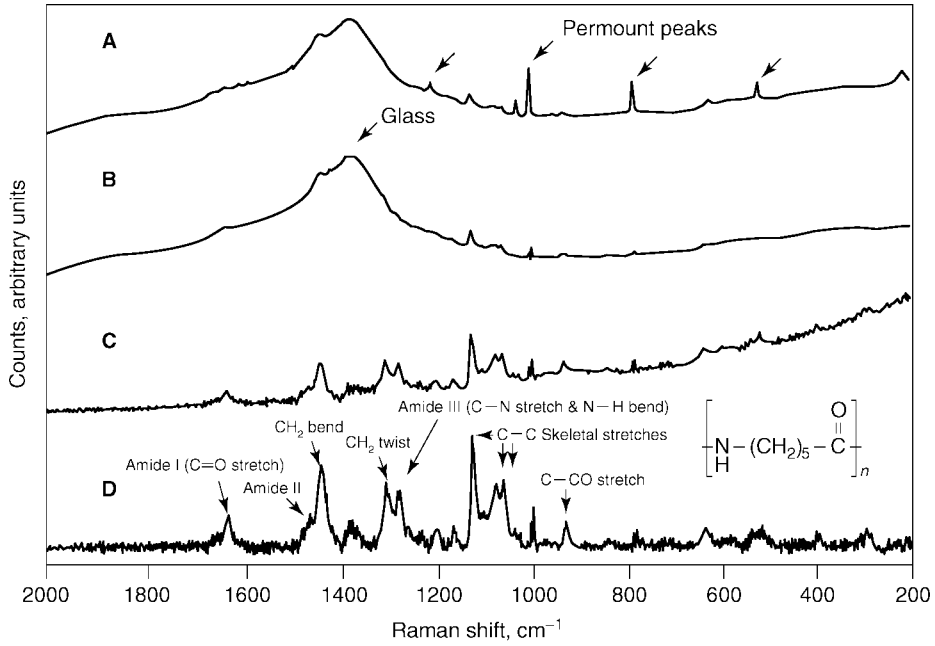

Fig. 3. Raman spectra of a nylon-6 fiber mounted under a coverslip on a glass microscope slide: (**A**) original spectrum; (**B**) Permount mounting medium subtracted; and (**C**) baseline flattened with the major characteristic bands labeled.

for Raman vary from that of IR, thereby producing complementary information. The information obtained by Raman is at times more definitive in determining the polymeric structure. Since Raman spectroscopy demonstrates spectral response from dyes, the dye information can be useful. However, the dye spectral features can interfere with identification of the polymeric composition of fibers. To further characterize the fibers, dye spectral features could provide information regarding the dye type. Studies have been conducted using surface enhanced Raman spectroscopy (SERS) to study dye composition using silver colloid substrates (41,42). While the spectral features are significantly enhanced by SERS, this method requires that the fibers are removed from the glass slides, resulting in an additional step and chance of fiber loss. Raman analysis has demonstrated certain advantages over IR, but the strengths and limitations of both are still under study to determine where each of the methods can be used to obtain the greatest information with the most convenient analysis procedure.

Paint

Paint evidence is usually submitted to the forensic scientist for comparison with paint from a known source. Automotive, architectural, art, marine, aircraft, tool, and other types of paints may become evidence in a variety of crime scenarios (43). Within the United States, most of these examinations involve automotive finishes as related to automotive accidents and hit-and-run cases. The question frequently posed is, what kind of vehicle could have contributed the paint flakes recovered from the scene of a hit-and-run homicide case? Additionally, house paints may be examined in connection with burglaries, and paint from tools in cases involving industrial sabotage. Rarely is it necessary to determine the manufacturer of a particular paint.

The examination proceeds differently, depending on whether the questioned evidence is in the form of flakes or a smear. Individual spray-paint spheres are occasionally encountered and treated in the same manner as individual particles from a smear. Table 3 summarizes the comparison methods employed.

After light microscopy, IR analysis offers the most information in forensic paint examinations. The organic binders are frequently identified by IR, and both organic and inorganic pigments can often be identified. Since the 1970s, scientists from the Royal Canadian Mounted Police (RCMP) have been classifying automotive paints on the basis of chemical composition (50–52). The original analysis was performed with the use of high pressure diamond anvil cells in beam condensers on dispersive IR spectrometers. Since then, the RCMP and other analysts have changed to using the less cumbersome, low pressure, compression diamond cells with beam condensers in FT-IR systems. Inorganic pigment components in paints have revealing spectral features at the lower wave numbers. Beam condensers are used rather than FT-IR microscopes to overcome the limited frequency range of liquid nitrogen cooled mercury cadmium telluride (MCT) detectors used in IR microscopes. For paint analysis, the extended range to near 200 cm^{-1} is obtained with CsI optics and a standard deuterated triglycine sulfate (DTGS) detector in the spectrometer bench.

Table 3. Comparative Methods for Paint Traces

Methods	Measurement	Information	Refs.
Color comparison	Chips laid side by side under a stereo microscope	Visual matching, adhering debris, possible to automotive-paint reference collection	
Spectrophotometry	Visible spectrum	Nonsubjective comparison of color and aid in identifying some pigments	24,44
Cross section	Layer structure	Proof of similarity or dissimilarity for multilayered flakes; even white house paints can be studied by staining with rhodamine and observing with a fluorescence microscope	45
Physical match	Observation of fit between two chips of paint	Only positive form of paint identification; a physical match is regarded as the equivalent of a fingerprint	
Polarized light microscopy	Magnification, optical properties	Observation of properties; identification of a filler	
Microchemical tests	Identification of chemical and physical properties		
	Solvent tests (emperical or select)	Behavior to selected solvents	
	Microchemical reaction	Identification of inorganic fillers and crystalline organic pigments	43,46,47
X-ray diffraction	Identifies crystalline phases	Identification of inorganic fillers and crystalline organic pigments	48
Electron microprobe	Elemental analysis	Identification of inorganic pigments and fillers	
Micro FT-IR	IR spectrum	Identification of polymers and copolymer comprising vehicle; limited identification of pigment	19,43,49
Pyrolysis gas chromatography	Separation of pyrolysis product	"Fingerprint" for comparison; some limited chemical information on chemical type	28

Databases are maintained to search for unknown automotive paints from hit-and-run cases. The FBI Laboratory in Quantico, Va, maintains the National Automotive Paint File, which is the largest automotive paint collection in the United States. The largest forensic collection in the world, with over 50,000 samples, is maintained at the Bundeskriminalamt Research Laboratory in Wiesbaden,

Germany. Scientists at the RCMP have developed a software package called PDQ, ie, Paint Data Query (53). This database uses microscopic and IR spectroscopic analysis results to search for automotive information leading to the identity of make, model, and year of vehicles in question, typically from hit-and-run cases. Through the FBI-sponsored Scientific Working Group for Materials Examination (SWGMAT), this database has expanded to include entries from North American, European, Japanese, and Australian Collections. The international cooperation of forensic scientists has served to assist in casework involving paint evidence from international automobiles that have a global market. This worldwide effort helps everyone that applies the PDQ database for searching an unknown automobile paint found on a hit-and-run victim.

When two paint samples are compared, and comparison results are analytically the same, the analyst may report that the two are similar in all respects and that they may, therefore, have originated from the same source. Comparisons of two paint specimens are made on the layer structure, elemental composition, polymer identity, fillers, and pigments. The analyst must take great care to point out that in the case of an automotive finish, this does not mean that the paint necessarily came from a particular car. From the scientifically determined facts, it could have originated from any of hundreds, or perhaps thousands, of vehicles painted with the same topcoat. However, significance would be attached to the fact that the suspect car was registered and driven in the state where the accident occurred; that this particular car sustained damage to the front end, for example, and that evidence stuck to the bumper was in the form of fiber fragments identical to the fibers from the victim's trousers. If a fragment of paint from the victim's clothing or the accident scene can be found and fits like a jigsaw puzzle in the damaged areas of the suspect car, the association is unequivocal.

Most paints do not usually display as much diversity in chemistry, color, and layer structure as do automotive ones. Therefore, a wider variety of analytical instruments are often used to characterize them. Along with microscopy and IR spectroscopy, other methods frequently used are pyrolysis GC/MS and inorganic elemental analysis by X-ray spectroscopy in the SEM. X-ray diffraction is also of use in the identification of crystalline pigments and fillers.

The study of coatings is also important in litigation concerning peeling paint. The examination in these cases focuses on the two surfaces that were once in contact with each other. Light and scanning electron microscopy of the surfaces are often able to pinpoint the cause, usually improper or inadequate surface preparation. In a very few cases, the surfaces appear to be perfectly clean and yet will still not adhere to each other. Surface analysis techniques such as electron spectroscopy for chemical analysis and Auger spectroscopy can reveal thin layers of otherwise invisible coatings on the surface of the substrate. The chemical composition of these thin coatings can be determined with these techniques, which in turn can help assess the cause of nonadhesion. FT-IR microspectroscopy was used to identify crystals that were implicated in a peeling paint problem. The IR spectra identified the crystals as a fungicide which had exsolved from the paint and recrystallized on the undersurface, pushing the film away from the wood substrate.

Paint comparisons are most often conducted in conjunction with criminal proceedings, but civil cases often arise. In one civil case, the owners of a high rise

office building suspected that their building, especially the windows, was being coated by paint from a bridge a half-mile away that was being spray-painted. Microscopical examination of the glass windows revealed the presence of tiny green spherical particles that were compared visually and by visible microspectrophotometry. The elemental composition was determined using energy-dispersive X-ray spectroscopy and the polymer was identified by FT-IR. These tests could all be conducted on a single sphere and compared with spheres that had formed and fallen around the bridge. The paints from both sources were identical in all respects and the painting contractors were held liable for the damage to the high rise.

A criminalist in California was assigned to rework a murder investigation originally tried in the early 1960s in 1987 after the U.S. Supreme Court overturned

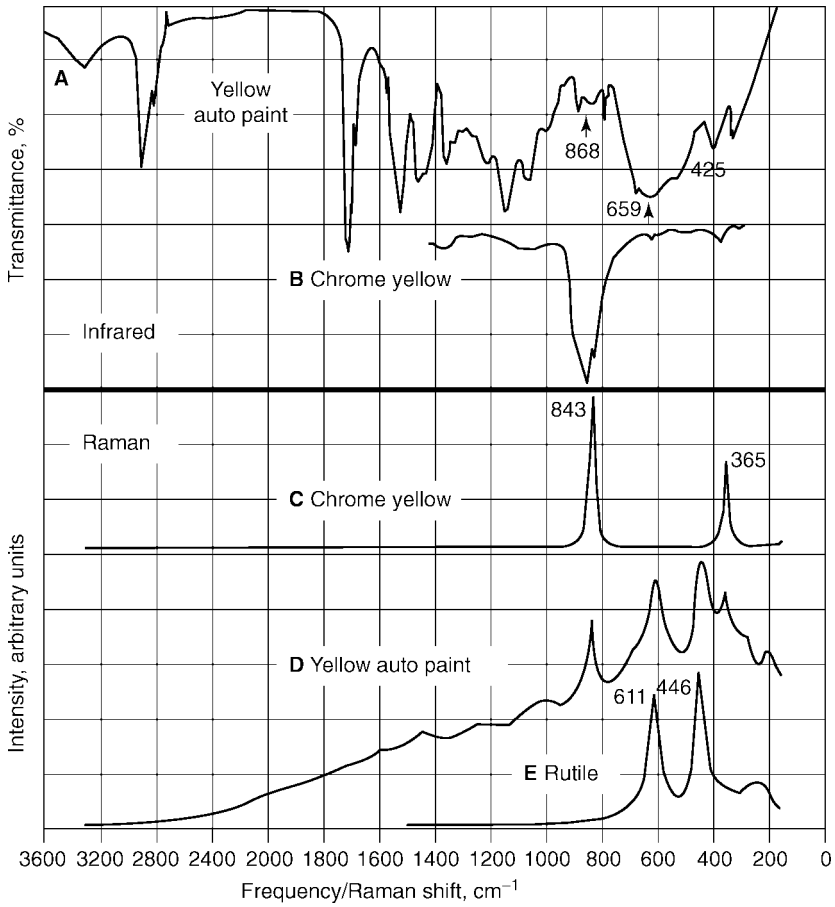

Fig. 4. IR and Raman spectra of yellow acrylic melamine enamel auto paint with pigments: (**A**) IR spectrum of the auto paint; (**B**) IR spectrum of chrome yellow pigment; (**C**) Raman spectrum of chrome yellow pigment; (**D**) Raman spectrum of the yellow auto paint; (**E**) Raman spectrum of rutile. Spectra provided by E. Suzuki, Washington State Patrol, Forensic Laboratory, Seattle, Wash.

the conviction of the defendant on a technical issue. The murdered 16-year-old girl was found in a dry drainage canal near the California desert, some distance from her home. The original suspect in the case was placed at the crime scene on the basis of a partial footprint and tire track in the soil outside the victim's home. During the reinvestigation, the criminalist was surprised to find small, pale green football-shaped particles among the items of evidence associated with the victim and the suspect. Consulting a forensic microscopist, he was informed that they were originally wet spheres of spray paint that had deformed by capillary action because they had a fiber running through them. These particles, whatever their origin, were significant because they were associated with both the suspect and the victim. They had been observed during the original investigation 25 years earlier, but the analysts involved did not feel that they could be analyzed by the techniques available at the time. The forensic microscopist took over the investigation of the particles when the criminalist discovered their source. The headliner of the suspect's vehicle, which was still in custody, had been spray-painted green. The headliner was cotton at that time and many of the droplets dried around the fibers. When the cotton became brittle, the particles broke away and dusted the car with these green football shaped particles. Microanalysis of the particles was conducted for the purpose of comparing the particles from the victim (shoelace, dust from her house, etc) and the suspect (his clothing, dust from his hotel room, etc) to the paint particles from the vehicle headliner. The analysis was exhaustive and it was possible to say that the paint from all three sources was identical in elemental composition, polymer composition, color, fluorescence, and microscopical examination of the fillers and pigments in terms of size and quantity. In addition, the particles were all spray paint, and all of the particles had been sprayed over cotton fibers. These fibers also had the same properties among the three sources. The jury convicted the defendant for the murder a second time.

Researchers are beginning to demonstrate the usefulness of Raman analysis for organic and inorganic pigment identification in paint (22,23). Figure 4 compares IR and Raman paint spectra of a yellow acrylic melamine enamel automotive paint. The IR spectrum in Figure 4**A** clearly shows the resin binder features. The N—H stretch near 3350 cm^{-1}, the C—H stretching near 3000 cm^{-1}, the C═O stretch near 1730 cm^{-1}, the C—N stretch near 1540 cm^{-1}, and the typical C—O envelope from 1300 to 1000 cm^{-1} are observed in the IR. Of particular interest in paint analysis are any contributions by pigments. The weak, broad band at 868 cm^{-1} appears to be contributed by chrome yellow, as shown in the Figure 4**B** reference spectrum. However, because of the band's comparatively low intensity and lack of detail in the paint spectrum, it would be difficult to positively identify chrome yellow by this method alone. The peaks labeled at 659, 425, and 357 cm^{-1} are rutile, a polymorph of titanium dioxide. Figure 4**D** is the Raman spectrum of the yellow auto paint. The major peaks at 843 and 365 cm^{-1} match up with the Raman spectrum of chrome yellow shown in Figure 4**C**. Peaks at 611 and 446 cm^{-1} are contributed by rutile, as shown in Figure 4**E**. With Raman spectroscopy, the high scattering efficiency of some of the pigments, relative to those of the binders, helps to easily determine the pigment components, as interfering binder peaks are not a problem.

BIBLIOGRAPHY

"Forensic Aspects" in *EPSE* 2nd ed., Vol. 7, pp. 279–289, by Skip Palenik, Walter C. McCrone Associates, Inc.

1. E. Locard, *Police J.* **1**, 177 (1928).
2. E. Locard, *Am. J. Police Sci.* **1**, 276 (1930).
3. R. Saferstein, *Criminalistics, An Introduction to Forensic Science*, 7th ed., Prentice-Hall, Upper Saddle River, N.J., 2001, p. 64.
4. S. J. Palenik, in R. Saferstein, ed., *Forensic Science Handbook*, Vol. II, Prentice-Hall, Inc., Englewood Cliffs, N.J., 1988, p. 161.
5. M. Frei-Sulzer, *Kriminalistik* **19**, 190 (1951).
6. P. L. Kirk, *Crime Investigation*, Interscience Publishers, Inc., New York, 1953, p. 83.
7. A. Teetsov, in W. C. McCrone and J. G. Delly, eds., *The Particle Atlas*, Ann Arbor Science Publishers, Ann Arbor, Mich., 1973, p. 204.
8. Ref. 6, p. 69.
9. P. R. Deforest, in R. Saferstein, ed., *Forensic Science Handbook*, 2nd ed., Vol. I, Prentice-Hall, Inc., Upper Saddle River, N.J., 2002, p. 215.
10. W. C. McCrone, L. B. McCrone, and J. G. Delly, *Applied Polarized Light Microscopy*, Ann Arbor Science Publishers, Ann Arbor, Mich., 1978.
11. N. H. Hartshorne and A. Stuart, *Crystals and the Polarizing Light Microscope*, Edward Arnold, Ltd., London, 1970.
12. D. A. Hemsley, *The Light Microscopy of Synthetic Polymers*, Oxford University Press and the Royal Microscopical Society, London, 1984.
13. O. Heuse and F. P. Adolf, *J. Forensic Sci.* **22**(2), 103 (1982).
14. F. R. Rothery and M. A. White, *J. Soc. Dyers Colour* **98**, 11 (1983).
15. L. Engel, H. Klingele, and G. W. Ehrenstein, *An Atlas of Polymer Damage*, Prentice-Hall, Inc., Englewood Cliffs, N.J., 1981.
16. L. C. Sawyer, *Polymer Microscopy*, 2nd ed., Chapman and Hall, Ltd., New York, 1995.
17. H. J. Humecki and R. Z. Muggli, in K. F. J. Heinrich, ed., *Microbeam Analysis*, San Francisco Press, Inc., San Francisco, Calif, 1982, p. 243.
18. H. J. Humecki, *Solid State Technol.* **28**(4), 309 (1985).
19. E. M. Suzuki, in R. Saferstein, ed., *Forensic Science Handbook*, Vol. III, Prentice-Hall, Inc., Englewood Cliffs., N.J., 1993, p. 71.
20. E. G. Bartick and M. W. Tungol, in R. Saferstein, ed., *Forensic Science Handbook*, Vol. III, Prentice-Hall, Inc., Englewood Cliffs., N.J., 1993, p. 196.
21. J. V. Miller and E. G. Bartick, *Appl. Spectrosc.* **55**, 1729 (2001).
22. G. Massonnet and W. Stoecklein, *Sci. Just.* **39**, 181 (1999).
23. E. M. Suzuki and M. Carrabba, *J. Forensic Sci.* **46**(5), 1053 (2001).
24. M. E. Eyring, in R. Saferstein ed., *Forensic Science Handbook*, Vol. I, 2nd ed., Prentice-Hall, Inc., Upper Saddle River, N.J., 2002, p. 321.
25. V. D. Scott and G. Love, *Quantitative Electron-Probe Microanalysis*, John Wiley & Sons, Inc., New York, 1983.
26. P. Echlin, ed., *Analysis of Organic and Biological Surfaces*, John Wiley & Sons, Inc., New York, 1984.
27. M. Blazso, *J. Anal. Appl. Pyrolysis* **39**, 1 (1997).
28. T. Wampler, *J. Chromatogr. A* **842**, 207 (1999).
29. D. Northrop, in R. Saferstein, ed., *Forensic Science Handbook*, Vol. I, 2nd ed., Prentice-Hall, Inc., Upper Saddle River, N.J., 2002, p. 41.
30. T. G. Rochow, *Microscope* **31**(1), 75 (1983).

31. R. Breese and N. J. Street, *Forensic Sci. Int.* **17**, 167 (1981).
32. R. J. H. Clark, in J. M. Chalmers and P. R. Griffiths, eds., *Handbook of Vibrational Spectroscopy*, Vol. IV, John Wiley & Sons, Inc., New York, 2002, p. 2977.
33. H. A. Deadman, *FBI Law Enforcement Bull.* **53**(3), 12 (1984).
34. H. A. Deadman, *FBI Law Enforcement Bull.* **53**(5), 10 (1984).
35. M. W. Tungol, E. G. Bartick, and A. Montaser, *Appl. Spectrosc.* **44**, 543–549 (1990).
36. M. W. Tungol, E. G. Bartick, and A. Montaser, *Spectrochemica Acta Electronica* **46B**, 1535E–1544E (1991).
37. M. W. Tungol, E. G. Bartick, and A. Montaser, in H. Humecki, ed., *Practical Guide to Infrared Microspectroscopy*, Marcel Decker, Inc., New York, 1995, p. 245.
38. Federal Trade Commission Rules and Regulations under the Textile Products Identification Act, *U.S. Code*, Section 70, Title 15, *et seq.* 16 C.F.R. 303.7.
39. M. C. Grieve, *Sci. Just.* **35**, 179 (1995).
40. P. J. Hendra, W. F. Maddams, I. A. M. Royaud, H. A. Willis, and V. Zichy, *Spectrachim. Acta* **46A**, 747 (1990).
41. P. C. White, C. H. Munro, and W. E. Smith, *Analyst* **121**, 835 (1996).
42. P. C. White, C. Rodger, V. Rutherford, Y. Finnon, W. E. Smith, and M. Fitzgerald, *SPIE* **3576**, 77 (1999).
43. S. G. Ryland, in H. Humecki ed., *Practical Guide to Infrared Microspectroscopy*, Marcel Decker, Inc., New York, 1995, p. 163.
44. D. R. Cousins, C. R. Platoni, and L. W. Russell, *Forensic Sci. Int.* **24**(3), 183 (1984).
45. B. Beattle, R. J. Dudley, and K. W. Smalldon, HOCRE Report No. 259, Home Office Central Research Establishment, Aldermaston, U.K., Jan. 1978.
46. J. Thornton, in R. Saferstein, ed., *Forensic Science Handbook*, Vol. I, 2nd ed., Prentice-Hall, Inc., Upper Saddle River, N.J., 2002, p. 429.
47. F. Feigle, *Spot Tests in Organic Analysis*, Elsevier, Amsterdam, 1966.
48. C. J. Curry, D. F. Rendle, and A. Rogers, *J. Forensic Sci. Soc.* **22**, 173 (1982).
49. H. K. Raaschau Nielsen, *J. Coatings Technol.* **56**, 173 (1984).
50. P. G. Rogers, R. Cameron, N. S. Cartwright, W. H. Clark, J. S. Deak, and E. W. W. Norman, *Can. Soc. Forensic Sci. J.* **9**, 1 (1976).
51. P. G. Rogers, R. Cameron, N. S. Cartwright, W. H. Clark, J. S. Deak, and E. W. W. Norman, *Can. Soc. Forensic Sci. J.* **9**, 49 (1976).
52. P. G. Rogers, R. Cameron, N. S. Cartwright, W. H. Clark, J. S. Deak, and E. W. W. Norman, *Can. Soc. Forensic Sci. J.* **9**, 103 (1976).
53. J. L. Buckle, D. A. MacDougall, and R. R. Grant, *Can. Soc. Forens. Sci. J.* **30**, 9 (1997).

EDWARD G. BARTICK
Counterterrrorism and Forensic Science Research Unit,
FBI Academy
SKIP PALENIK
Microtrace

FRACTIONATION

Introduction

Synthetic polymers are heterogeneous materials. Measuring this heterogeneity is the key to understand structure-property relationships, polymerization mechanisms and kinetics, and polymer reaction engineering. Polymer fractionation techniques attempt to fractionate polymers according to specific characteristics of their microstructures as defined by their distributions of molecular weight, chemical composition, comonomer sequence length, tacticity, and long-chain branching.

All synthetic and some natural polymers have a distribution of molecular weights caused by the statistical nature of the polymerization mechanism. Polymers produced via living polymerization have the narrowest molecular weight distributions, while long-chain branched polymers or polymers made with multiple-site catalysts such as heterogeneous Ziegler–Natta catalysts have the broadest molecular weight distributions. Nonetheless, regardless of the polymerization mechanism involved in their production, all polymers have a molecular weight distribution that must be quantified to unequivocally define their microstructures and their physical properties. This explains why the vast majority of polymer fractionation techniques were developed to fractionate polymers according to molecular weight.

For instance, the instantaneous chain-length distribution of many polymers is given by Flory–Schultz's most probable distribution (1),

$$f_n = \frac{1}{N_\mathrm{n}} \exp\left(-\frac{n}{N_\mathrm{n}}\right) \tag{1}$$

where f_n is the number distribution of chains of length n, and N_n is the number-average chain-length. The molecular weight distribution can be obtained from the chain-length distribution by multiplying the latter by the molecular weight of the repeating unit.

The equivalent weight chain-length distribution, w_n, is given by

$$w_n = \frac{n}{N_\mathrm{n}^2} \exp\left(-\frac{n}{N_\mathrm{n}}\right) \tag{2}$$

Polymers whose chain-length distributions follow equation 1 have a polydispersity index $N_\mathrm{w}/N_\mathrm{n}$ of 2, where N_w is the weight-average chain length of the polymer. Figure 1 shows the number and weight chain-length distributions of a polymer with $N_\mathrm{n} = 1000$. Notice that, even for the relatively narrow polydispersity of 2, a significant range of chain lengths is encompassed by the distribution.

Nowadays the most common technique for determining the molecular weight distribution of polymers is size-exclusion chromatography (SEC), also known as gel-permeation chromatography (GPC). Other methods for measuring molecular weight distributions exist, but the ease of use and universality of SEC makes it the technique of choice for this type of fractionation.

Copolymerization adds another level of complexity to polymer microstructure. Superimposed on the molecular weight distribution, we now have to

Encyclopedia of Polymer Science and Technology. Copyright John Wiley & Sons, Inc. All rights reserved.

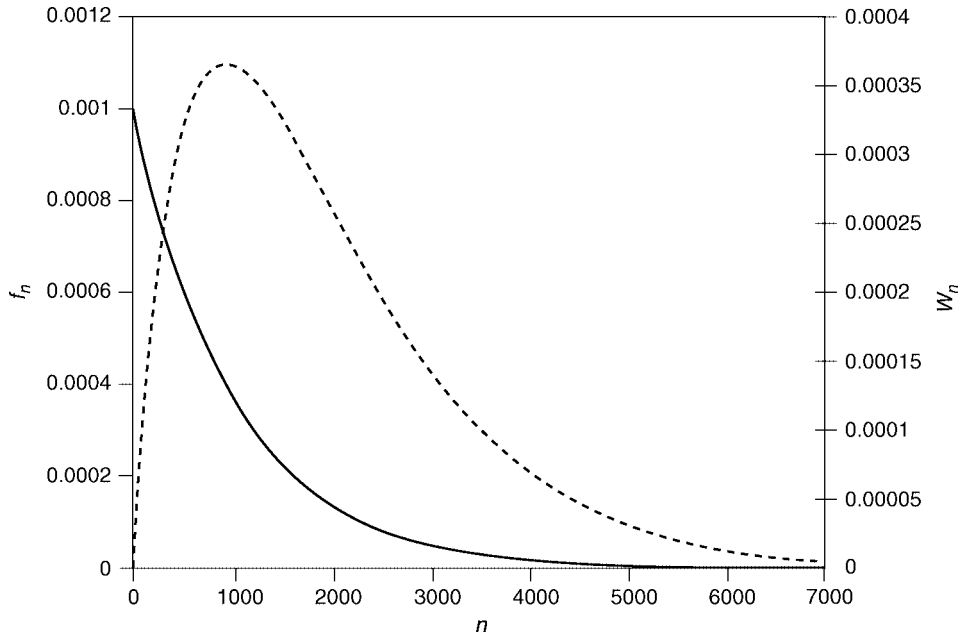

Fig. 1. Flory–Schultz's most probable chain length distributions for $N_n = 1000$. f_n (——) Number distribution; w_n (– – –) weight distribution.

account for the distributions of chemical composition and comonomer sequence length. The instantaneous bivariate weight distribution of chain length and chemical composition, $w_{n,y}$, of many linear binary copolymers was derived by Stockmayer (2):

$$w_{n,y} = \frac{n}{N_n^2} \exp\left(-\frac{n}{N_n}\right)\sqrt{\frac{n}{2\pi F_1(1-F_1)\kappa}} \exp\left(-\frac{ny^2}{2F_1(1-F_1)\kappa}\right) \tag{3}$$

where y is the deviation from the average fraction of monomer 1 in the copolymer F_1. The parameter κ is defined as a function of F_1 and the reactivity ratios r_1 and r_2:

$$\kappa = \sqrt{1 - 4F_1(1-F_1)(1-r_1r_2)} \tag{4}$$

The average fraction of comonomer in the copolymer can be estimated as usual using the Mayo–Lewis equation:

$$F_1 = \frac{(r_1-1)f_1^{\,2} + f_1}{(r_1+r_2-2)f_1^{\,2} + 2(1-r_2)f_1 + r_2} \tag{5}$$

where f_1 is the molar fraction of monomer 1 in the reactor.

Notice that equation 3 reduces to Flory–Schultz's most probable distribution upon integration over all copolymer compositions, ie integrating y from $-\infty$ to

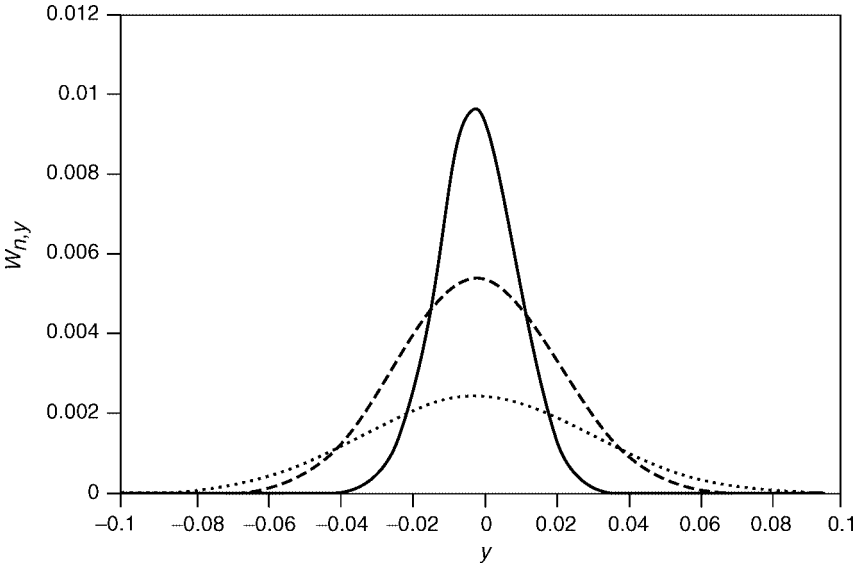

Fig. 2. Stockmayer's distribution for chains of different length of a model random copolymer ($r_1r_2 = 1.0$) with $F_1 = 0.5$ and $N_n = 1000$. - - - $n = 250$; ▬ ▬ $n = 500$; ——— $n = 2000$.

$+\infty$. Consequently, linear binary copolymers described by Stockmayer's bivariate distribution also obey Flory–Schultz's distribution for chain length.

Figure 2 compares the chemical composition distribution of polymers of different chain lengths for a random binary copolymer ($r_1r_2 = 1.0$). Notice how the distribution gets broader with decreasing chain-lengths. It is easy to understand this behaviour considering that, as chain length tends to infinity, the composition of all copolymer chains should be the same for a given probability of polymerization of monomer 1 and monomer 2. On the other hand, chains with short lengths are more likely to deviate from the average copolymer composition on purely statistical grounds, in the same way as it is more likely to get three consecutive heads by tossing a coin three times than it is to get one hundred consecutive heads by tossing a coin one hundred times.

Figure 3 shows how the chemical composition distribution of copolymer chains of the same length varies when the comonomer incorporation varies from alternating ($r_1r_2 \to 0$) to random ($r_1r_2 = 1$) to block ($r_1r_2 \to \infty$). As expected, the distribution gets broader with increasing tendency to form comonomer blocks: all chains of a perfectly alternating binary copolymer have the same composition (ie $F_1 = F_2 = 0.5$) but the tendency to form long comonomer sequences or blocks ($r_1r_2 \to \infty$) may broaden the distribution considerably.

There are no general analytical solutions to describe the chemical composition distribution of ternary or higher copolymers, although an analytical solution for the particular case of random multicomponent copolymers has been derived (3). For nonrandom polymerizations, the chemical composition distribution of multicomponent copolymers can be calculated using techniques such as Monte Carlo simulation or population balances (4).

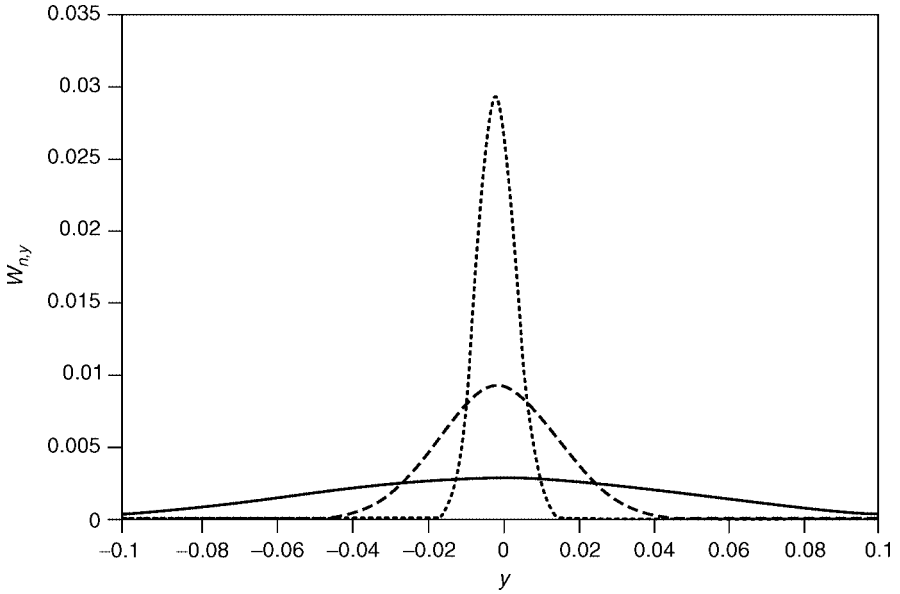

Fig. 3. Stockmayer's distribution for chains with $F_1 = 0.5$ and $N_n = 1000$ as a function of reactivity ratio product. Alternating: $r_1r_2 = 0.01$; random: $r_1r_2 = 1$; and block: $r_1r_2 = 10$. - - - $r_1r_2 = 0.01$; —— —— $r_1r_2 = 1.0$; ———— $r_1r_2 = 10$.

Asymmetrical monomers such as propylene and styrene form polymers with different tacticity. Isotactic and syndiotactic chains have regular molecular structures and are generally semicrystalline, while atactic polymers are amorphous because of the random placement of the monomer units in the chain. The tacticity distribution may be modeled as a comonomer distribution, where the different monomer orientations during chain insertion (meso or racemic) are treated as pseudo-comonomer types. Therefore, at least in principle, Stockmayer's distribution can be used to approximate the tacticity distribution of homopolymers.

The most common techniques to measure the chemical composition distribution of semicrystalline copolymers are temperature rising elution fractionation (TREF) and crystallization analysis fractionation (Crystaf). These two techniques are based on the differences among the crystallizabilities of copolymer chains with distinct comonomer contents. Because variations in tacticity affects polymer crystallinity, Crystaf and TREF have also been used to measure the tacticity distribution of polymers. No direct methods are available for measuring the complete chemical composition distribution of amorphous copolymers, although some field flow fractionation, ultracentrifugation, and chromatography methods are sensitive to differences in comonomer content. The use of matrix-assisted laser desorption ionization time-of-flight (MALDI-TOF) mass spectrometry as a detector for SEC has also been proposed to determine the bivariate distribution of molecular weight and chemical composition of some copolymers, either semicrystalline or amorphous.

The last and most complex polymer microstructural distribution is the one for long-chain branching. Long-chain branches can be formed according to very

different mechanisms, and analytical solutions for long-chain branch distributions are only known for a few particular cases. For the case of terminal branching with coordination catalysts, the instantaneous joint distribution of chain-length, chemical composition, and long-chain branching, $w_{i,n,y}$, is given by the equation (5,6)

$$w_{i,n,y} = \frac{1}{(2i+1)!}\frac{n^{2i+1}}{N_n^{2i+2}}\exp\left(-\frac{n}{N_n}\right)\sqrt{\frac{n}{2\pi F_1(1-F_1)\kappa}}\exp\left(-\frac{ny^2}{2F_1(1-F_1)\kappa}\right) \quad (6)$$

where i is the number of long-chain branches per chain. Notice that Stockmayer's distribution, equation 3, is a particular solution of equation 6 for linear chains, ie for $i = 0$.

Figure 4 and Figure 5 illustrate how the distributions of chain length and chemical composition vary as a function of the number of long-chain branches per chain for a model copolymer. Notice how chains with more long-chain branches are longer and have narrower distributions of chain length and chemical composition. The increase in average chain length with increasing branching is self-explanatory; the narrowing of the distributions is caused by the averaging effect of randomly combining chains of different lengths and compositions via long-chain branch-formation reactions.

Unfortunately, there are no techniques that can be used to fractionate polymers exclusively according to long-chain branching. A measure of average long-chain branching as a function of molecular weight can be obtained when SEC is combined with a viscometer or a light-scattering detector, but the results are

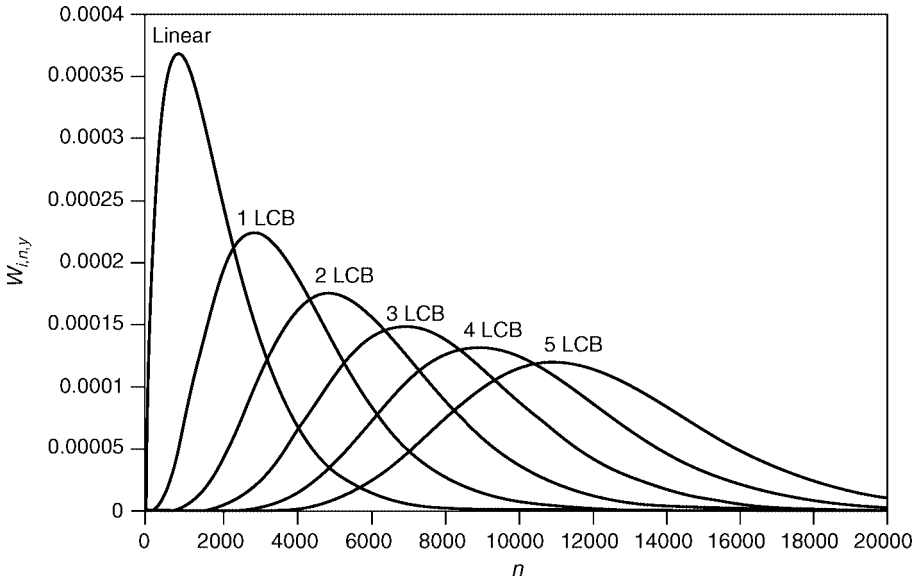

Fig. 4. Chain-length distribution as a function of long-chain branching frequency for a model polymer with $N_n = 1000$, $F_1 = 0.5$, and $r_1 r_2 = 1.0$. The curves are obtained by integrating equation 6 over the entire composition range, $-\infty < y < +\infty$. For details see Ref. 6.

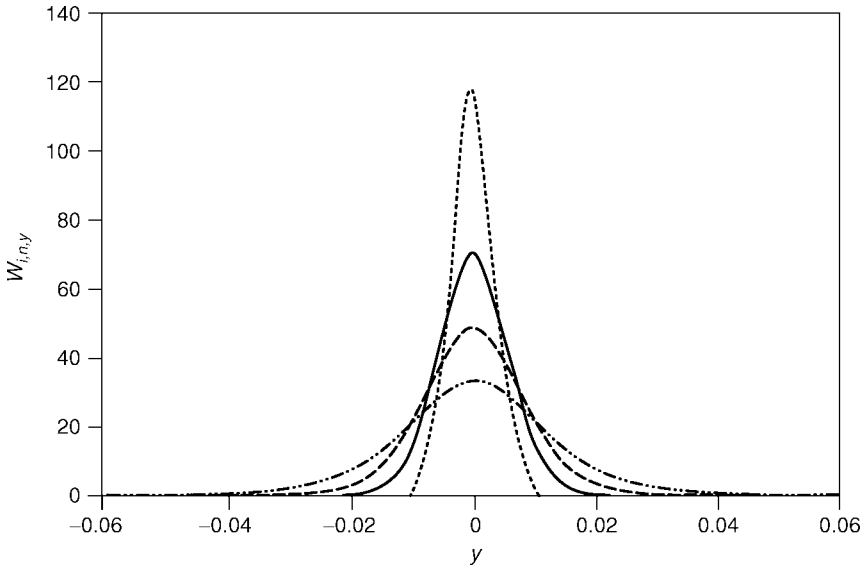

Fig. 5. Chemical composition distribution as a function of long-chain branching frequency for a model polymer with $N_n = 1000$, $F_1 = 0.5$, and $r_1 r_2 = 1.0$.— - -—Linear;▬ ▬ 1 LCB;▬▬ 3 LCB;_ _ _ 10 LCB. The curves are obtained by integrating equation 6 over the entire chain-length range, $0 < n < \infty$. For details see Ref. 6.

semiquantitative at the best for most polymers because of the complex fractionation process that takes place in nonuniformly branched polymers. Considering the importance that long-chain branching has on altering rheological and mechanical properties of polymers, this poses a significant limitation on the understanding of a very important class of polymers.

These three theoretical distributions describe only a very small portion of the diversity of polymer microstructures that are produced every day in academia and industry. Even for the polymerization systems they describe, they are only strictly valid as instantaneous distributions. If conditions in the polymerization reactor fluctuate as a function of time or spatial location, the distributions for the polymer product may be considerably more complex. In this case, it is very difficult to find a mathematical model precise enough to describe the complete polymer microstructure, and we must rely solely on experimental fractionation for its determination. In fact, the comparison of experimentally-measured microstructural distributions with the ones predicted by theory is a powerful tool to investigate polymerization mechanisms and understand polymer reactor nonidealities. Nonetheless, these distributions are essential to realize the complexity of polymer microstructure and the interdependency of the distributions of molecular weight, chemical composition (or tacticity), and long-chain branching. This interdependency should always be kept in mind when interpreting the fractionation data from any experimental technique.

In this article we will review some relevant fractionation techniques that can be used to elucidate the main aspects of the polymer microstructures delineated above.

Batch Fractionation

It has been claimed that polymer batch fractionation is almost as old as polymer science itself (7). Batch fractionation relies on the separation of polymer chains, initially present in a dilute solution, in two phases (liquid–liquid or liquid–solid). Fractionation occurs by altering the goodness of the solvent, either by changing the ratio of solvent to nonsolvent or by varying the temperature of the polymer solution. The nonsolvent, most often, must be miscible with the solvent, but should not be able to dissolve the polymer.

Batch fractionation was developed to determine the molecular weight distribution of polymers. Even though molecular weight fractionations nowadays are more efficiently achieved with chromatographic techniques such as size-exclusion fractionation, batch fractionation is still important when the objective is to obtain large fractions of polymers with narrow molecular weight distributions that may be required, for instance, to establish structure-property relationships or to elucidate polymerization mechanisms. In this way, batch fractionation is still relevant today, albeit to serve a different purpose from which it was originally developed.

Semicrystalline polymers can be fractionated according to their molecular weights by the solvent/nonsolvent approach at temperatures above their melting point, or by crystallizability by the temperature variation approach. Amorphous polymers are fractionated only according to their molecular weights. We will describe the fractionation of amorphous polymers first, followed by a discussion on the fractionation of semicrystalline polymers later.

A comprehensive compendium of laboratory procedures for batch fractionation of polymers was written by Francuskiewicz (8). The readers are directed to this reference for more specific details on the several experimental techniques described below.

Fractionation of Amorphous and Semicrystalline Polymers by Molecular Weight. Flory–Huggin's theory for dilute polymer solutions is still convenient to describe the liquid–liquid batch fractionation of amorphous polymers between a polymer-rich phase and a polymer-lean phase. Even though Flory–Huggin's theory for dilute solution is based on several simplifying assumptions, it correctly describes the trends during the batch fractionation of polymers and provides a useful theoretical framework to rationalize its qualitative features. The discussion in this section will follow closely the elegant development adopted by Flory in his remarkable book on polymer chemistry (9).

Semicrystalline polymers can be fractionated by either molecular weight or crystallizability. All the considerations that will be made in this section for the fractionation of amorphous polymers by chain length are equally valid for semicrystalline polymers, provided that the polymer is kept above its melting point throughout the fractionation to eliminate chain crystallization effects.

For a liquid–liquid system, the volume fractions of polymer of chain length n in the polymer-rich phase, $\upsilon_n{}^*$, and in the polymer-lean phase, υ_n, are conveniently described by the simple exponential equation:

$$\frac{\upsilon_n^*}{\upsilon_n} = e^{\sigma n} \tag{7}$$

The parameter σ can be estimated with the expression

$$\sigma = \upsilon_S\left(1-\frac{1}{N_n}\right) - \upsilon_S^*\left(1-\frac{1}{N_n^*}\right) + \chi\left[(1-\upsilon_S)^2 - \left(1-\upsilon_S^*\right)^2\right] \tag{8}$$

where N_n is the number average chain length, χ is the Flory–Huggin's interaction parameter between polymer and solvent, and $\upsilon_S{}^*$ and υ_S are the volume fractions of solvent in the polymer-rich and polymer-lean phases, respectively. In the following discussion, the exact value of the parameter σ is immaterial; it suffices to know that σ depends on the properties of the polymer and solvent(s) used in the fractionation.

Calling V and V^* the volume fractions of the polymer-lean and polymer-rich phases, respectively, and defining $R = \frac{V^*}{V}$, the fraction of polymer chains with chain length n in the polymer-lean phase, f_n, is given by

$$f_n = \frac{V\upsilon_n}{V\upsilon_n + V^*\upsilon_n^*} = \frac{1}{1+R\frac{\upsilon_n^*}{\upsilon_n}} = \frac{1}{1+Re^{\sigma n}} \tag{9}$$

Similarly, the fraction of polymer with chain length n in the polymer-rich phase, $f_n{}^*$, is given by the expression

$$f_n^* = 1 - f_n = \frac{Re^{\sigma n}}{1+Re^{\sigma n}} \tag{10}$$

Equation 7 shows that, for positive values of σ, the *partition ratio* $\frac{\upsilon_n^*}{\upsilon_n}$ is always greater than 1. Therefore, the polymer chains, independently of their chain lengths, will always have a higher volume fraction in the polymer-rich phase. Since the partition ratio increases exponentially with chain length, longer chains will be more selective towards the polymer-rich phase than shorter chains. This simply reflects the fact that shorter chains have fewer units to interact with the poor solvent in the polymer-lean phase, and therefore are less discriminating than the longer chains. Batch fractionation of amorphous polymers relies solely on this small selectivity difference among chains of different lengths.

Precipitation Fractionation. In this method, fractions of decreasing molecular weights are obtained in each successive fractionation step. Because of the decreasing molecular weight of the fractions, this technique is also called *downward* precipitation fractionation, to distinguish it from another variant named *upward* precipitation fractionation that will be described later in this section. In either case, it is instructive to notice that precipitation fractionation is a misnomer, since the polymer does not in fact precipitate, but rather forms a separate polymer-rich liquid phase.

The precipitation fractionation method starts with a dilute polymer solution. Liquid–liquid separation, with the formation of a polymer-rich and a polymer-lean phase, is induced by either decreasing the temperature or by adding a specified amount of a nonsolvent. A third, less common technique, involves the evaporation of solvent from a solvent/nonsolvent mixture. All these procedures increase the value of χ, until it eventually exceeds its critical value, thus leading to phase separation.

The Flory–Huggin's interaction parameter, χ, is defined by the equation

$$\chi = \frac{V_S}{RT}(\delta_S - \delta_P)^2 \tag{11}$$

where V_S is the molar volume of the solvent, T is the temperature, R is the gas constant, and δ_S and δ_P are the solubility parameters for the solvent and polymer, respectively. Therefore, a decrease in temperature will increase the value of χ, and consequently the value of σ as well (cf eq. 8). An exception to this rule may happen for systems that have a lower critical solution temperature (LCST). In the latter case, an increase in temperature will instead increase the value of χ.

Similarly, if the solubility parameter for the solvent/nonsolvent mixture is calculated by the simple additive rule

$$\delta_S = \upsilon_{\text{solvent}}\delta_{\text{solvent}} + \upsilon_{\text{nonsolvent}}\delta_{\text{nonsolvent}} \tag{12}$$

then adding a nonsolvent to the solution will increase the term $(\delta_S - \delta_P)^2$ in equation 11 and accordingly increase the value of χ, leading to the formation of the polymer-rich phase.

If the initial polymer solution is very dilute, the volume of the polymer-rich phase, V^*, will be much smaller than the volume of the polymer-lean phase, V; ie $R \ll 1$. Since the partition ratio for longer chains is higher than for shorter chains, the concentration of longer chains will be higher than the concentration of the shorter chains in the polymer-rich phase. Because of this selective partition, it is advantageous to assure that the volume of the polymer-lean phase is much larger than the volume of the polymer-rich phase. In this case, the majority of the less selective shorter chains will stay in the polymer-lean phase, simply because its volume is much larger than the volume of the polymer-rich phase. This effect is illustrated, in a rather exaggerated manner, in Figure 6, where a plot of f_n versus n for several R values is shown when the value of the parameter σ was selected (arbitrarily) so that $f_{2000} = \frac{1}{2}$. Notice how the separation efficiency gets increasingly better as R tends to zero. In this theoretical limit, an almost perfect partition between the phases would be possible, but evidently this operation condition cannot be reached experimentally.

The polymer-rich phase is then separated from the polymer-lean phase, and a new fraction of lower molecular weight can be collected by either further lowering the temperature or by adding more nonsolvent. The polymer-rich phase is once more separated from the polymer-lean phase, and the process is repeated as many times as required.

Since chains of all molecular weights will be partitioned between the two phases, precipitation fractionation is not capable, even at very high dilutions, to obtain polymer fractions of very sharp chain-length distributions. This effect is illustrated in Figure 7 for a model polymer that follows the most probable chain-length distribution given by equation 2. Notice that even at high dilutions (small R), there is significant overlapping of the distributions of each of the fractions.

This interesting phenomenon is further illustrated in Figure 8 for the simulated fractionation of a model polymer into five fractions. The dotted lines indicate the chain-length distributions of the polymer in the polymer-lean phase,

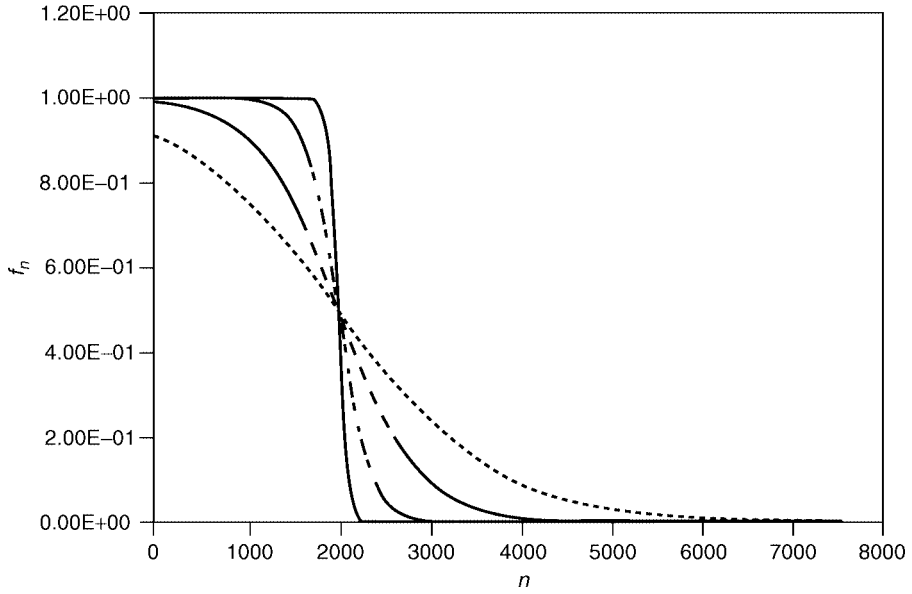

Fig. 6. Molar fraction of polymer in the polymer-lean phase (f_n) as a function of chain length (n) and the ratio of the volume of polymer-rich to polymer-lean phases (R). R = 1.0 E-1; R = 1.0 E-2; R = 1.0 E-5; R = 1.0 E-20. The value of the parameter σ was selected so that $f_{2000} = \frac{1}{2}$.

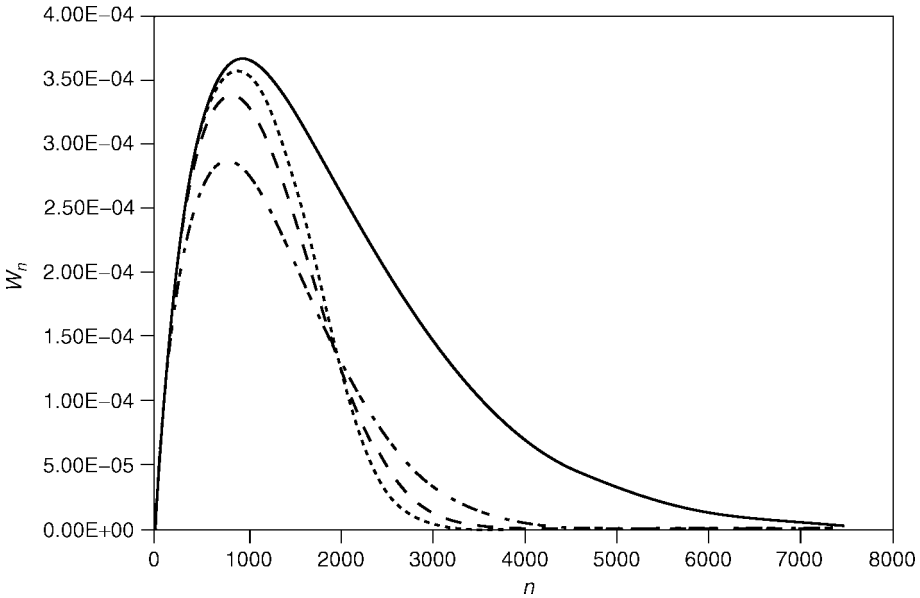

Fig. 7. Chain-length distributions in the polymer-lean fraction as a function of the ratio of volumes of polymer-rich to polymer-lean phases (R). Parent distribution; R = 1.0 E-1; R = 1.0 E-2; R = 1.0 E-3.

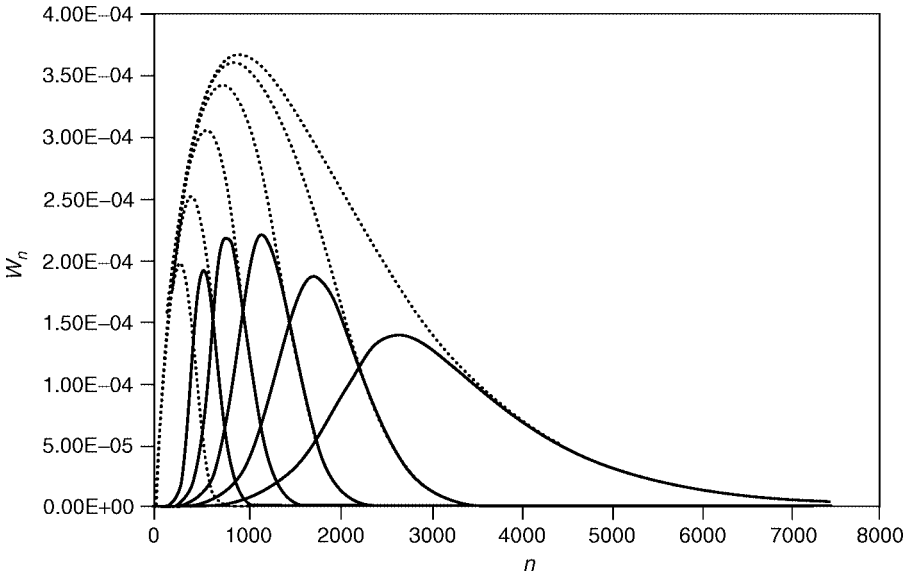

Fig. 8. Simulated chain-length distributions for precipitation fractionation of a model polymer sample that follows Flory–Schultz's distribution with $N_n = 1000$. The following parameters were used to simulate the fractionation: $R = 1 \times 10^{-3}$ and $\sigma = 3 \times 10^{-3}$, 4.5×10^{-3}, 6.75×10^{-3}, 1.01×10^{-2}, and 1.52×10^{-2}.

and the solid lines the chain-length distributions in the polymer-rich phase. The chain-length distribution of the original model polymer follows the most probable distribution with $N_n = 1000$. The parameter σ is arbitrarily increased from fractions 1 to 5 to simulate either a decrease in temperature or the addition of a nonsolvent. The distribution of the first polymer-rich solution is given by $w_n[1 - f_n^{(1)}]$, where w_n is the most probable chain-length distribution of the parent resin. Similarly, the distribution of the first polymer-lean phase is simply $w_n f_n^{(1)}$. After separation of the polymer-rich phase, the second fraction is obtained by decreasing the temperature of (or adding nonsolvent to) the polymer-lean phase. The distribution of the second polymer-rich phase is $w_n f_n^{(1)}[1 - f_n^{(2)}]$, and that of the polymer-lean phase is $w_n f_n^{(1)} f_n^{(2)}$. It is easy to see that this process can be repeated for k fractions, leading to the following equations for the chain-length distributions of polymer in the two phases:

$$w_n^{(k)} = w_n \prod_{i=1}^{k} f_n^{(i)}, \text{ polymer-lean phase} \tag{13}$$

$$w_n^{*(k)} = w_n \left[\prod_{i=1}^{k-1} f_n^{(i)} \right] \left(1 - f_n^{(k)}\right) = w_n^{(k-1)} \left(1 - f_n^{(k)}\right), \text{ polymer-rich phase} \tag{14}$$

where $w_n^{(k)}$ is the chain-length distribution of the kth fraction and the asterisk superscript indicates the polymer-rich phase. Notice that even though the chain-length distributions of the fractions is narrower than that of the parent sample,

significant overlapping takes place in all fractions because of the lower values of the partition ratios for the shorter chains. The reader is directed to the review by Kamide (7) for extensive and more rigorous simulations of batch fractionations of polymer solutions.

Rigorously speaking, for the case of solvent/nonsolvent precipitation fractionation the general mathematical treatment described above must be modified to treat the ternary solvent/nonsolvent/polymer system, but the trends are the same. It has been proposed that solvent/nonsolvent fractionation can be more effective for chain-length fractionation than temperature reduction, and in fact solvent/nonsolvent fractionation is generally a more commonly used technique to fractionate polymer chains according to molecular weight.

Upward Precipitation Fractionation. In this method, fractions of increasing molecular weights are obtained in each successive fractionation step. A large amount of nonsolvent is added to the original polymer solution, driving most of the polymer to the polymer-rich phase. Contrarily to the downward precipitation fractionation discussed above, in this method most of the polymer will be concentrated in the polymer-rich phase. The polymer-lean phase is recovered as the first fraction with the lowest average molecular weight. The remaining polymer-rich phase is completely redissolved and more nonsolvent is added, preferentially driving the high molecular weight chains into the polymer-rich phase. The polymer-lean phase is recovered as the second fraction with higher molecular weight and the cycle of redissolutions and solvent/nonsolvent additions is repeated. A similar result can be obtained by altering the temperature of the solution. The mathematical description adopted above for the downward precipitation fractionation method is also adequate for the upward precipitation fractionation method.

Notice that the high molecular weight fractions are only obtained after several fractions of lower molecular weights have been recovered. Considering the lower phase selectivity of the low molecular weight chains, the upward precipitation fractionation method can remove most of the shorter chains before isolating the high molecular weight fractions. As a consequence, the high molecular weight fractions isolated with the upward precipitation fractionation method will have narrower molecular weight distributions than the ones obtained with the downward precipitation fractionation technique.

It should be clear that both upward and downward precipitation fractionations require the use of very large amounts of solvent to ensure the low polymer concentration necessary for efficient fractionation. To minimize this inconvenience, several refractionation mechanisms have been suggested. The refractionation schemes involve the fractionation of polymer-rich solutions into two fractions that must subsequently be refractionated several times until the required degree of separation is achieved (10).

An informative summary of the several steps required to fractionate polymers by precipitation fractionation is given in Figure 9.

Extraction or Solution Fractionation. In extraction fractionation, polymer chains of increasing molecular weights are extracted from the polymer-rich phase by gradually increasing the goodness of the solvent, either by increasing the temperature or the ratio of solvent to nonsolvent. Many of the considerations made above for the precipitation fractionation methods are also valid for the extraction fractionation techniques.

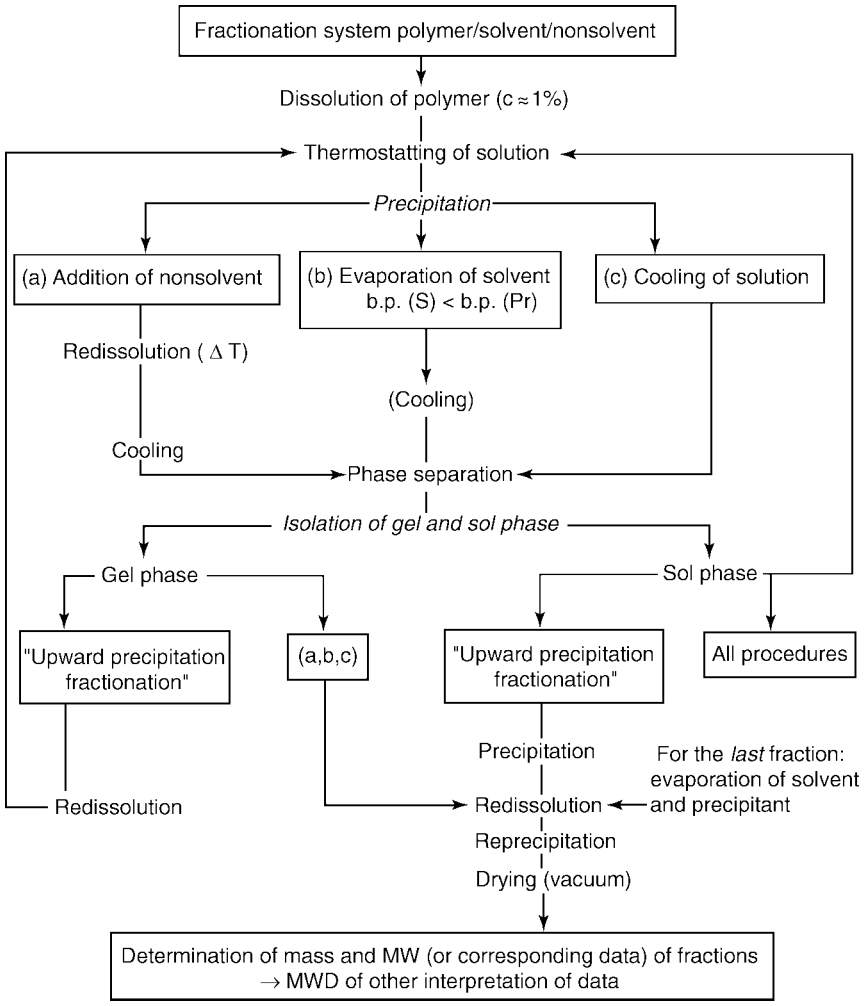

Fig. 9. Steps required for precipitation fractionation. From Table 5.2 in Ref. 8. Copyright (1994) Springer-Verlag.

A large contact area between the polymer-rich and polymer-lean phases is a very important requirement in extraction fractionation to reduce mass-transfer limitations between the phases during extraction. In the simplest extraction technique, *direct extraction*, this is achieved by using finely divided polymer particles or powder. Direct extraction is commonly performed in Sohxlet extractors. Diffusion limitations, polymer swelling, and equipment plugging make direct extraction a technique of limited use.

The contact area between the phases can be enlarged in *film extraction* and *column extraction*. The discussion of column extraction techniques will be postponed to the section on TREF. In film extraction, a thin polymer film is deposited onto a support material with a large surface area. This technique can also be performed inside Sohxlet extractors, but it is also prone to several experimental difficulties (11).

In *coacervate extraction* the polymer is initially present as a dilute solution. A large amount of nonsolvent is added, causing most of the polymer to separate into the polymer-rich phase. The polymer-lean phase, containing the low molecular weight chains, is recovered as the first fraction. Then more solvent is added to the polymer-rich phase. The liquid–liquid mixture is vigorously stirred to ensure good contact between the phases. Upon equilibration, the newly formed lean phase is recovered as the second fraction and the process is repeated as many times as required. A similar fractionation can be obtained by increasing the temperature of the solution.

As apparent from the last paragraph, coacervate extraction is similar to upward precipitation fractionation. However, differently from the last technique, the polymer-rich phase is not redissolved during coacervate extraction. As a consequence, smaller volumes of solvent and nonsolvent are required, but care must be taken to avoid occlusion of chains in the polymer-rich phase and mass-transfer limitations during fractionation. Similarly to upward precipitation fractionation, coacervate extraction is more adequate to isolate high molecular weight fractions with narrower molecular weight distributions.

Fractionation Equipment. Until recently, no fully automated instrument existed to perform batch fractionation of polymers. Most of the older experimental apparatuses consisted of simple glassware equipment that required considerable operator time and the manipulation of sizeable amounts of solvent. Some of these experimental fractionation systems have been thoroughly described by Francuskiewicz (8).

A fully automated batch fractionation instrument called mc2-PREP is now available. Figure 10 shows a schematic of mc2-PREP. The two stirred fractionation vessels placed inside a temperature-programmable oven can fractionate polymers into eight fractions by either solvent/nonsolvent or temperature variation techniques. Operator intervention is only required to precipitate and filter the polymer fractions after they are isolated from the parent polymer solution.

The coacervate extraction method is recommended in the molecular weight fractionation mode of mc2-PREP (the "m" in mc2-PREP), although the precipitation method (both upward and downward) is also possible in principle. As usual, the initial polymer solution is precipitated by the addition of a large amount of nonsolvent or reducing the temperature. The polymer-lean phase is transferred from the fractionation vessel to a fraction collection vial between each solvent/nonsolvent injection or temperature-increase steps through the transfer line located inside the fractionation vessel. The two fractionation vessels can be operated in parallel, with either the same or different samples. At the end of the fractionation, the fractions collected in the fraction collection vials are precipitated and filtered. mc2-PREP can also be used to fractionate polymers according to crystallizability, as described in the next section.

Fractionation of Semicrystalline Polymers by Crystallizability. The temperature variation method is the most common approach to fractionate semicrystalline polymer chains according to crystallizability. In this case, since chain crystallization is the main fractionation mechanism, the temperature should be lowered below the melting point of the polymer in solution during the fractionation.

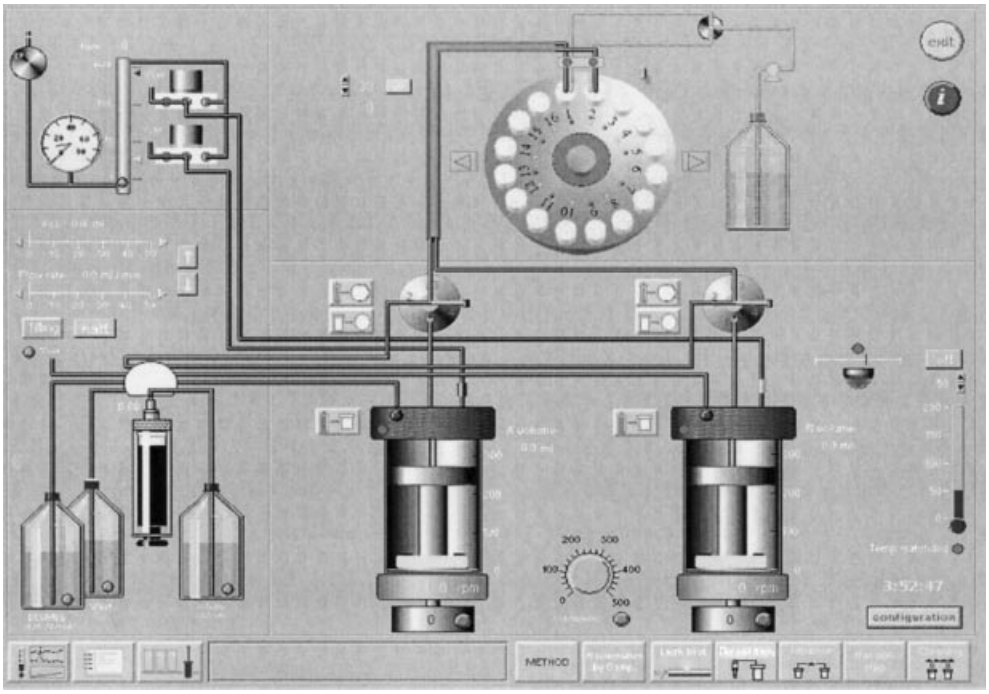

Fig. 10. Diagram of mc2-PREP. Courtesy of Polymer C*h*ar.

Chain crystallizability is strongly influenced by the degree of regularity of the chains. In the case of binary copolymers, generally the comonomer present in the smallest fraction does not crystallize and acts as a chain defect. The melting temperature, therefore, decreases with increasing amounts of this comonomer. Typical examples are copolymers of ethylene and α-olefins, where the α-olefin molecules are generally too large to be included in the crystalline lattice and lead to the formation of smaller polymer crystallites with lower melting temperatures. For the case when the two comonomers crystallize, such as for ethylene/propylene copolymers, the comonomer present in less amount acts as a defect and the melting temperature passes through a minimum located between the melting points of the two semicrystalline homopolymers. A similar phenomenon takes place with stereoregular homopolymers such as isotactic polypropylene. In this case, propylene molecules inserted in a racemic configuration will decrease the melting temperature of the isotactic polymer. Similarly, regioirregular insertions will also decrease the melting point of the polymer (12).

The melting point depression of a random binary AB copolymer, where the comonomer B does not crystallize, is described by the equation 15

$$\frac{1}{T_m} - \frac{1}{T_m^0} = -\frac{R}{\Delta H_u} \ln x_A \tag{15}$$

where $T_m{}^0$ is the melting point of an infinitely long-chain of homopolymer A, T_m is the melting temperature of the random copolymer AB, ΔH_u is enthalpy of melting

of the repeating unit A, and x_A is the molar fraction of the crystallizable unit A. In principle, this equation can also be used to describe the melting point depression of stereoregular homopolymers due to stereoirregular insertions. For instance, in the case of isotactic polypropylene, x_A could represent the molar fraction of meso insertions and $(1 - x_A)$ would then represent the molar fraction of racemic insertions.

Fractionation by crystallizability takes place by either decreasing or increasing the temperature, similarly to what is done in the methods of fractional precipitation or coacervate extraction for molecular weight fractionation. However, differently from those, solid–liquid phase separation occurs during fractionation by crystallizability. We will call *Crystaf-mode* the fractionation that takes place upon cooling the polymer solution, and *TREF-mode* the fractionation that takes place by dissolving previously precipitated polymer crystallites. This nomenclature is consistent with the continuous analysis techniques of Crystaf and TREF, which will be described later in this article, and is more adequate for fractionation by crystallizability.

Irrespective of the fractionation mode, one starts with a dilute polymer solution at high temperature. In Crystaf-mode, fractions of decreasing crystallinity (increasing noncrystallizable comonomer content) are obtained as the temperature is reduced. The more crystalline chains are precipitated at higher temperatures and separated from the remaining solution before the temperature is lowered to obtain the next polymer fraction. In TREF-mode, all or most of the polymer is precipitated by reducing the temperature to its lowest value at the beginning of the fractionation. The first fraction is collected at the lowest fractionation temperature and it is, therefore, the one that has the highest fraction of the non-crystallizable comonomer. Fractions with increasing crystallizabilities and lower comonomer contents are collected by increasing the temperature at predetermined intervals. A slow cooling rate is a requirement for good fractionation even in the TREF-mode, since it permits the growth of well-formed crystals and enhances the resolution of the fractionation.

Fractionation Equipment. Similar to molecular weight fractionation, most of the conventional equipment for crystallization fraction is rather simple and requires significant operator time. Fully automated crystallization fractionations are possible using mc2-PREP, in both Crystaf-mode and TREF-mode (the "c2" in mc2-PREP stands for these two fractionation modes).

In TREF-mode the polymer solution is initially placed inside a crystallization vessel at high temperature. The temperature is then slowly reduced, precipitating most of the polymer. The polymer that remains in solution is transferred via the in-line filter to a fraction collection vial as the first, least crystalline fraction. More solvent is transferred to the fractionation vessel and the temperature is increased by a predetermined amount, dissolving the next, more crystalline fraction. The process is then repeated with the recovery of polymer solutions at increasing dissolution temperatures. Two polymer samples can be fractionated simultaneously in the TREF-mode, one in each fractionation vessel.

The two fractionation vessels are required to fractionate one sample in Crystaf-mode. The polymer solution is initially placed in one of the fractionation vessels at high temperature (vessel 1). The temperature is then decreased, causing part of the polymer to crystallize out of solution. The polymer solution

is transferred from vessel 1 to vessel 2 via an in-line filter to avoid sampling the polymer crystallites that constitute the first, high crystallinity fraction. The crystallized polymer remaining in vessel 1 is then redissolved and the resulting solution is transferred to a fraction collection vial. The fractionation process is then repeated by decreasing the temperature in vessel 2, transferring the remaining solution to vessel 1, and recovering the polymer precipitated in vessel 2 as the second fraction. These steps can be repeated several times to obtain the number of polymer fractions of decreasing crystallinity required by the fractionation.

Several of the issues related to the fractionation efficiency of these two techniques have been investigated with their continuous counterparts, Crystaf and TREF, and will be discussed in the next section.

Crystallization Analysis Fractionation

Crystallization analysis fractionation (Crystaf) fractionates polymer chains according to differences in crystallizability. Crystaf can be used to fractionate polymers due to differences in chemical composition, comonomer sequence length, and tacticity. It may also respond to long-chain branching, provided that the polymer is branched enough to affect its crystallinity. The fractionation principle operative in Crystaf was discussed in the section on batch fractionation for the case of slowly cooling (or warming) solutions of semicrystalline polymers.

In Crystaf, a dilute solution of a semicrystalline polymer is slowly cooled from a high temperature to room or subambient temperatures, while the polymer concentration is monitored as a function of crystallization temperature by an on-line mass detector to obtain its *cumulative distribution*. The *differential distribution* is calculated by taking the first derivative of the cumulative distribution with respect to the crystallization temperature. Both cumulative and differential Crystaf curves for a bimodal blend of two ethylene/α-olefin copolymers are shown in Figure 11. A calibration curve must be used to translate the crystallization temperature distribution into a polymer microstructural distribution, as will be explained later in this section.

The Crystaf apparatus shown in Figure 12 has five crystallization vessels that can be operated in parallel. Sample injection, dissolution, analysis, and disposal are completely automated. Small aliquots of the solution are taken through an in-line filter to avoid sampling polymer crystals with the polymer solution and sent to the on-line mass detector. The mass detector is commonly an infrared cell that is less sensitive to temperature fluctuations of the polymer solution. Additional detectors can also be installed on the sampling line to measure complementary properties, such as viscosity and copolymer composition.

Usually, Crystaf is operated at a cooling rate of 0.1°C/min. It will be shown later that cooling rates can significantly influence the results of Crystaf analysis. The concentration of the polymer solution is not considered to affect the fractionation results, provided it is kept in the range of 0.2–1.0 mg/mL (14). The type of solvent only affects the crystallization temperature: polymers crystallize at lower temperatures in the presence of better solvents, but the effect on fractionation efficiency is negligible (15).

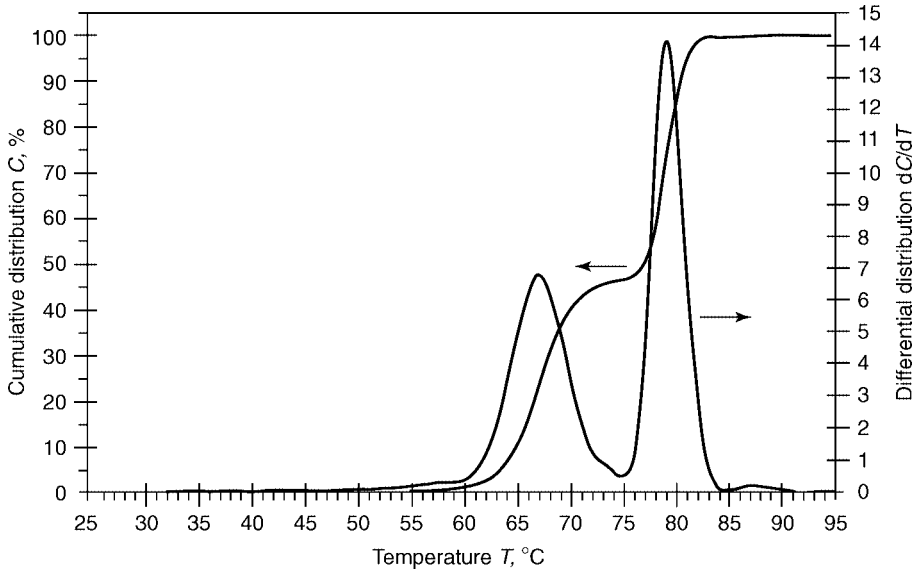

Fig. 11. Cumulative and differential Crystaf curves of a blend of polyolefins.

The raw Crystaf profile provides information about the distribution of crystallizabilities of the polymer sample that can be correlated to molecular structure with the use of a proper calibration curve. Contrary to SEC, there is no universal calibration curve for Crystaf: for quantitative analysis, calibration curves should be prepared with narrow standards that have microstructures as similar as possible to the sample being analyzed.

Calibration standards for Crystaf are not commercially available and have to be prepared by either preparative fractionation of a broad sample with similar characteristics (generally obtained by using the batch fractionation techniques described previously) or by synthesis of samples with narrow distributions. Figure 13 shows the Crystaf profiles of a set of calibration standards for ethylene/1-hexene random copolymers, and Figure 14 is the resulting calibration curve (16). The calibration curves for Crystaf for random (or near random) copolymers are generally linear, in good agreement with the prediction of equation 15 for copolymers with small amounts of comonomer. In this case, the following approximations apply:

$$\frac{1}{T_{\mathrm{m}}} - \frac{1}{T_{\mathrm{m}}^0} = \frac{T_{\mathrm{m}}^0 - T_{\mathrm{m}}}{T_{\mathrm{m}} T_{\mathrm{m}}^0} \cong \frac{T_{\mathrm{m}}^0 - T_{\mathrm{m}}}{\left(T_{\mathrm{m}}^0\right)^2} \tag{16}$$

$$\ln x_A = -(1 - x_A) = -x_B \tag{17}$$

Substituting these expressions in equation 15,

$$T_{\mathrm{m}} \cong T_{\mathrm{m}}^0 - \frac{R\left(T_{\mathrm{m}}^0\right)^2}{\Delta H_{\mathrm{u}}} x_B \tag{18}$$

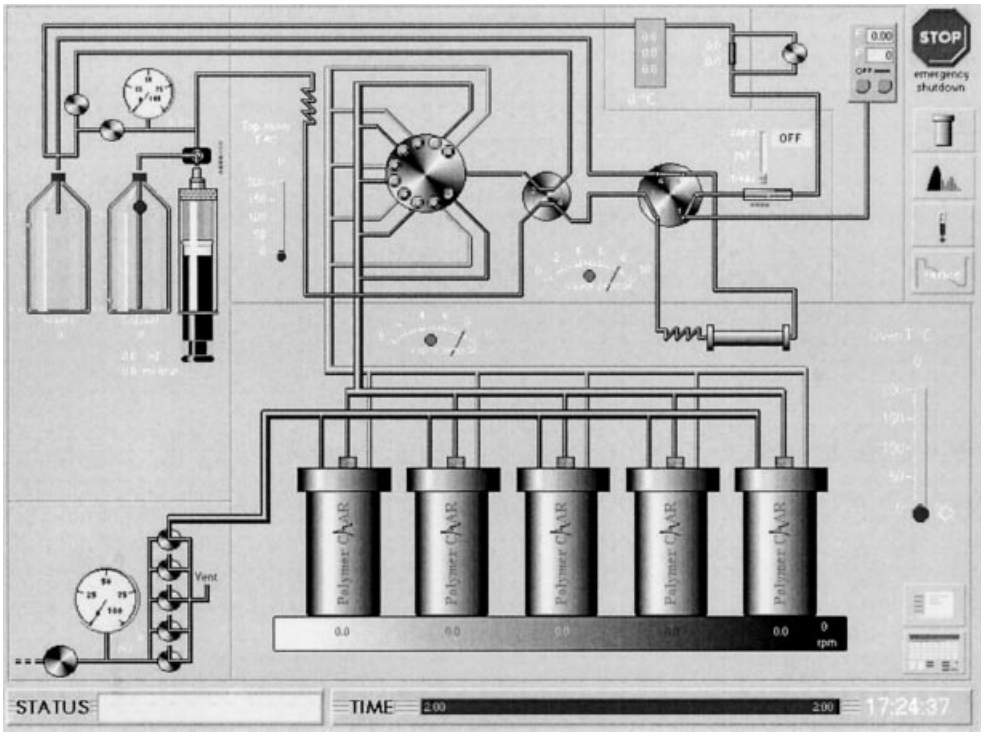

Fig. 12. Schematic of Crystaf. Courtesy of Polymer C*h*ar.

which shows that the melting temperature depression is a linear function of the fraction of non-crystallizable comonomer in the copolymer.

One of the main difficulties for the quantification of Crystaf is the nonuniversality of its calibration curves. Even for a series of ethylene/α-olefin copolymers, the calibration curves will vary as a function of comonomer type, as illustrated in Figure 15. The general rule of thumb for these copolymers (from propene to 1-octene) is, the longer the α-olefin, the lower the crystallization temperature for a given α-olefin molar fraction. This has been explained by several authors on the basis of the difference in the degree of inclusion of the α-olefin in the crystalline lattice: shorter α-olefins are more likely to cocrystallize with ethylene and therefore depress the crystallization temperature to a lesser extent.

Sequence length distribution is another factor that may affect calibration curves in Crystaf. This is easy to visualize if we compare the extreme cases of block and random ethylene/α-olefin copolymers with the same α-olefin content. We start by assuming that the α-olefin units cannot crystallize and the crystallization temperature is a function only of the average length of the ethylene sequences in the chain. Since the average sequence of crystallizable ethylene units is much longer in block copolymers than in random copolymers with the same comonomer content, block copolymers will have much higher crystallization temperatures than random copolymers. This limitation is easily overcome by using calibration standards with microstructure similar to the polymers being analyzed.

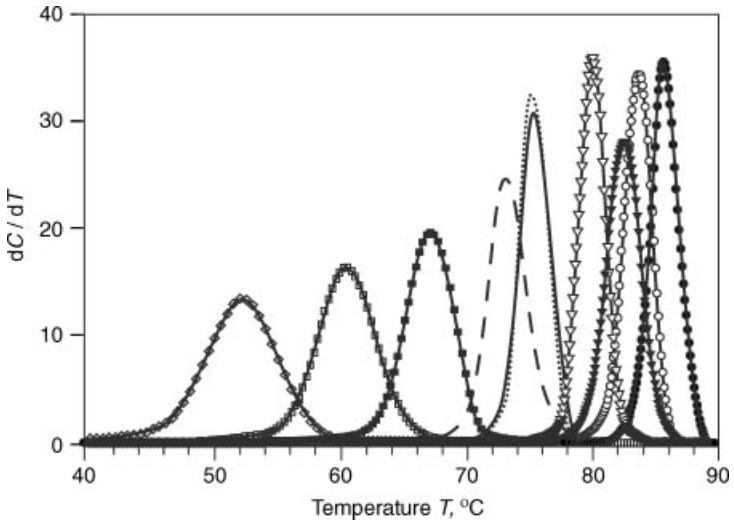

Fig. 13. Crystaf profiles for a set of random ethylene/1-hexene copolymer calibration standards. —●— 0r (0 mL); —○— 5d (0.5 mL); —▼— 10e (1.0 mL); —▽— 23b (2.3 mL); _____ 41a (4.1 mL); . . . 41e (4.1 mL); — —65b (6.5 mL); —■— 100f (10.0 mL); —□— 150a (15.0 mL); —◇— 200a (20.0 mL). From Ref. 16.

Molecular weight effects are practically negligible in determining the Crystaf peak temperatures for polyethylene chains with molecular weights higher than 5000, and even these effects can be corrected by taking into account the terminal methyl groups of the chains. Likewise, small amounts of long-chain branching (in the range of 1 to 4 LCB per 1000 C atoms) do not influence Crystaf profiles appreciably. On the other hand, the shape of Crystaf profiles is affected by molecular

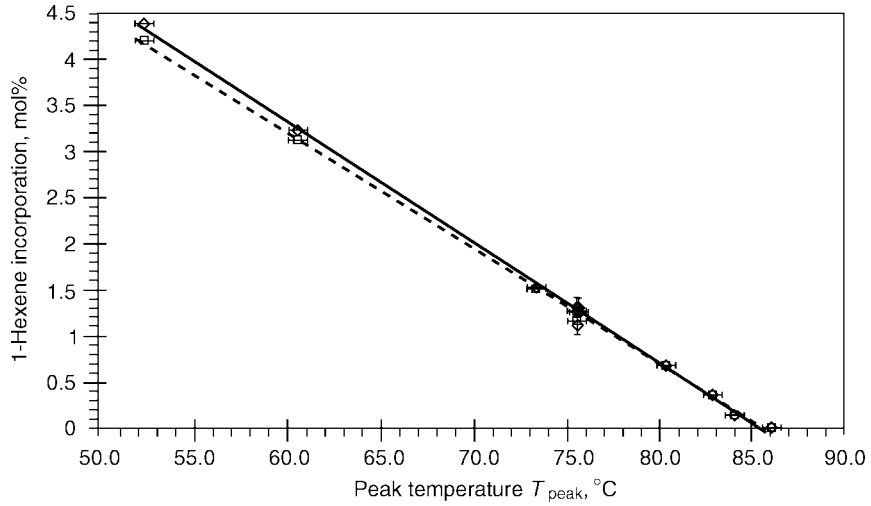

Fig. 14. Crystaf calibration curve for random ethylene/1-hexene copolymers. □ ASTM; – – – % incorporation = $-0.1263 \cdot \text{Tpeak} + 10.8065$; ◇ dePooter; _____ % incorporation = $-0.1317 \cdot \text{Tpeak} + 11.2467$. From Ref. 16.

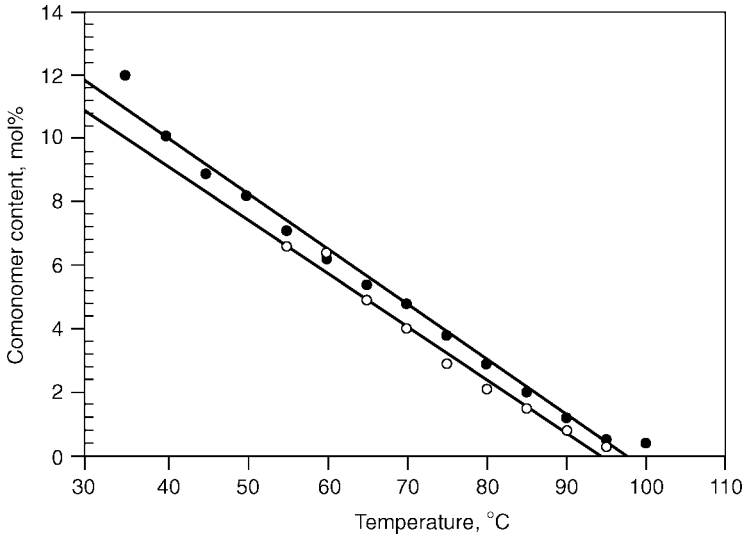

Fig. 15. Crystaf calibration curves for ethylene/1-butene (EB-01) and ethylene/1-octene (EO-01) copolymers. ● EB-01; ○ EO-01. From Ref. 17. Copyright (2000) Wiley-VCH.

weight: distributions with a low molecular weight tail are characterized by a low crystallinity tail in Crystaf, perhaps because the low molecular weight chains crystallize at lower temperatures (18,19).

Cooling rate is the most important operating variable in Crystaf. It significantly affects Crystaf peak temperatures (Fig. 16) and the cocrystallization of

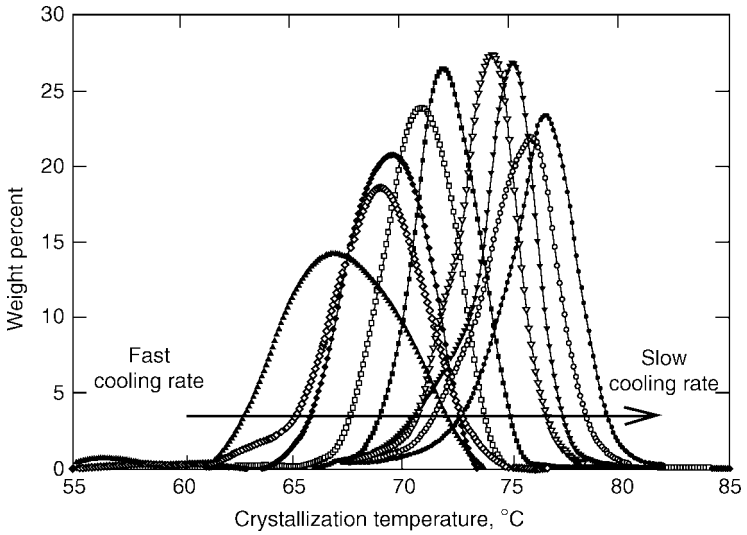

Fig. 16. Crystaf peak temperatures as a function of cooling rate for an ethylene/1-hexene copolymer sample. —●— 0.0033 CPM; —○— 0.01 CPM; —▼— 0.02 CPM; —▽— 0.05 CPM; —■— 0.1 CPM; —□— 0.2 CPM; —◆— 0.5 CPM; —◇— 1 CPM; —▲— 2 CPM. CPM = °C per minute. From Ref. 14.

chains with different average comonomer contents. This is particularly important to keep in mind when analyzing polymers made with multiple-site catalysts, such as heterogeneous Ziegler–Natta systems, where chain populations with different comonomer contents are present (17). Good resolution among these populations can only be achieved under very slow cooling rates, often slower than the standard Crystaf rates of 0.1°C/min. Figure 17 illustrates this situation for ternary blends of ethylene/1-hexene copolymers made with a metallocene catalyst. The dotted lines represent the Crystaf profile estimated for the blend if no cocrystallization takes place. Cocrystallization becomes more significant with increasing cooling rate and proximity of the crystallization peaks of the different polymer populations. Interestingly, the type of α-olefin does not seem to play a role in the cocrystallization phenomena (20).

Temperature Rising Elution Fractionation

Temperature rising elution fractionation (TREF) is based on the same principles of Crystaf, but involves two consecutive steps: precipitation (or crystallization) and elution. In the precipitation step, polymer is crystallized from a dilute solution by slowly decreasing the temperature inside a column packed with an inert support. Alternatively, the precipitation step can be done in a stirred vessel in the presence of the support and the polymer-coated support is subsequently transferred to the TREF column for the elution step. In the elution step, the polymer deposited onto the support is eluted from the column with a continuous flow of solvent at increasing temperatures. An on-line detector measures the concentration of the polymer solution exiting the column as a function of elution temperature. Figure 18 shows a schematic of a TREF apparatus and a typical TREF curve for linear low density polyethylene.

Polymer fractionation takes place during the precipitation step according to crystallizability. The precipitation step in TREF is essentially analogous to the crystallization that takes place in Crystaf. As for Crystaf, a slow cooling rate is the most important requirement to minimize cocrystallization of polymer populations with different crystallizabilities and enhance peak resolution. Since there is no monitoring of the polymer solution concentration during the precipitation step, the elution step is required to measure the concentration of polymer recovered as a function of elution temperature.

Given that the fractionation mechanism in Crystaf and TREF are very similar, they both provide analogous information about polymer microstructure, with the TREF profiles shifted to higher temperatures due to the supercooling effect in Crystaf, as exemplified in Figure 19. Crystaf analysis times tend to be shorter because of the extra time required by the additional elution step in TREF.

Table 1 compares the analysis times for Crystaf and TREF at different cooling and heating rates (14). Similar to Crystaf, TREF calibration curves are not universal and depend on the microstructure of the polymer being analyzed (21).

It has long been considered that the elution step in TREF was mainly required to recover and monitor the concentration of the polymer already fractionated during the precipitation step. However, recent studies with ethylene/α-olefin copolymer blends indicate that for the same cooling rate, TREF can better resolve

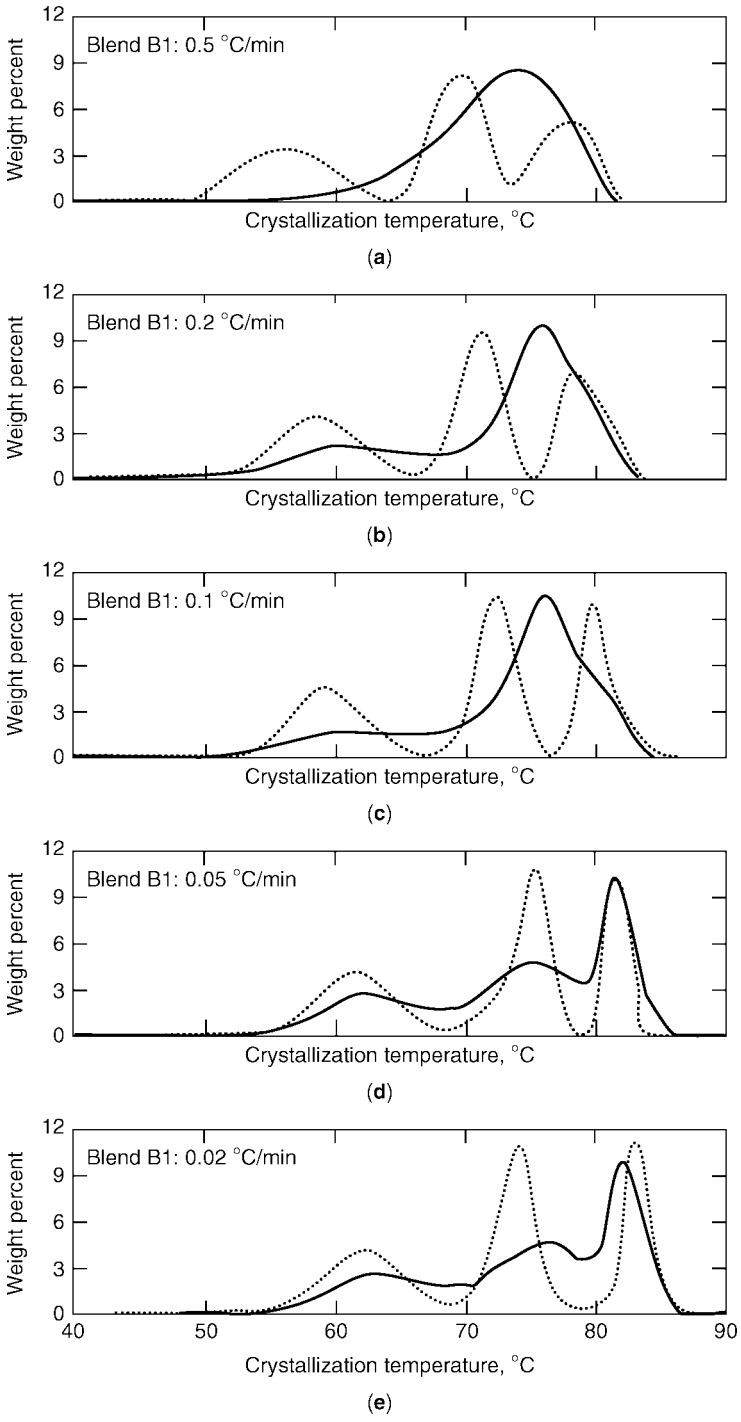

Fig. 17. Cocrystallization of ethylene/1-hexene copolymers in Crystaf as a function of cooling rate. Dotted lines are the profiles calculated from the Crystaf analyses of the individual components in the blend. . . . Calculation; ——— experiment. From Ref. 14.

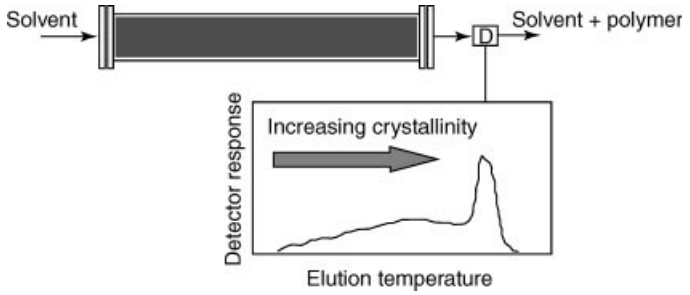

Fig. 18. TREF schematic and typical TREF profiles of a Ziegler–Natta linear low density polyethylene.

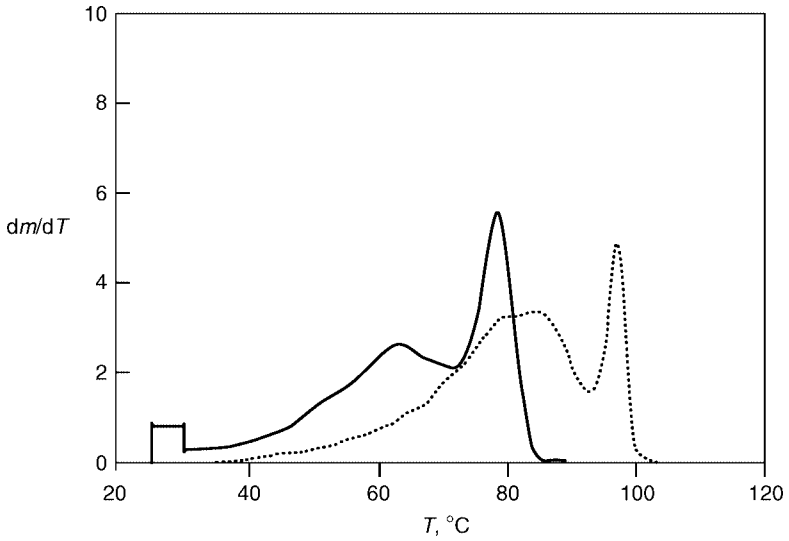

Fig. 19. Comparison of Crystaf and TREF profiles for an ethylene/1-butene Ziegler–Natta copolymer. ——— EB-01 Crystaf; - - - - - EB-01 TREF. From Ref. 17. Copyright (2000) Wiley-VCH.

Table 1. Comparison of Crystaf and TREF Analysis Times[a]

Cooling rate, °C/min	Crystaf analysis time, min	Tref analysis time for several heating rates		
		0.5°C/min	0.2°C/min	0.1°C/min
0.5	235	425	620	945
0.2	430	620	815	1140
0.1	755	945	1140	1465
0.05	1405	1595	1790	2115
0.02	3355	3545	3740	4065
0.01	6605	6795	6990	7315

[a]From Ref. 14.

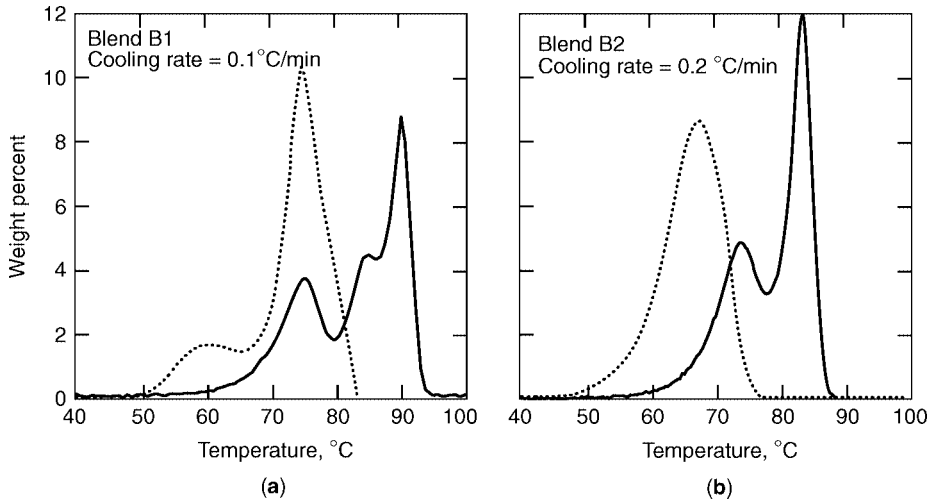

Fig. 20. Comparison of TREF and Crystaf blend peak resolution for ethylene/1-hexene copolymers as a function of cooling rate. ——— Tref; . . . Crystaf. From Ref. 14.

the peaks of the individual populations, as indicated in Figure 20. The slow heating during the elution step may lead to recrystallization of the crystals formed during the precipitation step, enhancing the peak resolution of TREF as compared to Crystaf. This is an attractive TREF feature when analyzing complex blends or polymers made with multiple-site catalysts (14).

The performance of TREF is relatively insensitive to polymer concentration in the range of 1–4 mg/mL. When compared to Crystaf, TREF peak positions are less dependent on the cooling rate, maybe because of recrystallization during the elution step. Solvent flow rate and heating rate can also affect peak position and breadth, but it has been demonstrated that these variations can be eliminated by operating TREF at constant ratio of heating rate to solvent flow rate, as illustrated in Figure 21. These conditions ensure that each volume element exiting the column contains polymer chains that were eluted during the same time/temperature interval (14).

Solvent and support type have only a minor effect on TREF fractionation. Better solvents lead to lower elution temperatures. The effect of different support types has not been systematically investigated, although some authors claim that it may lead to peak broadening in TREF (15,21).

TREF can also be operated in preparative mode. In this case, a larger column is used and samples are collected at predetermined time intervals for posterior analysis by other techniques. The efficiency of TREF preparative fractionation is essentially the same as for batch fractionation by temperature.

An interesting variation of TREF uses supercritical fluids as solvents and columns containing a high surface stainless steel mesh packing. The main advantage of supercritical TREF (CITREF: critical, isobaric TREF) over conventional TREF is that supercritical solvents such as propane can be easily separated from the polymer by pressure reduction after the column, recompressed, and recycled back to the column in a closed loop. Because of this, CITREF can be used as a

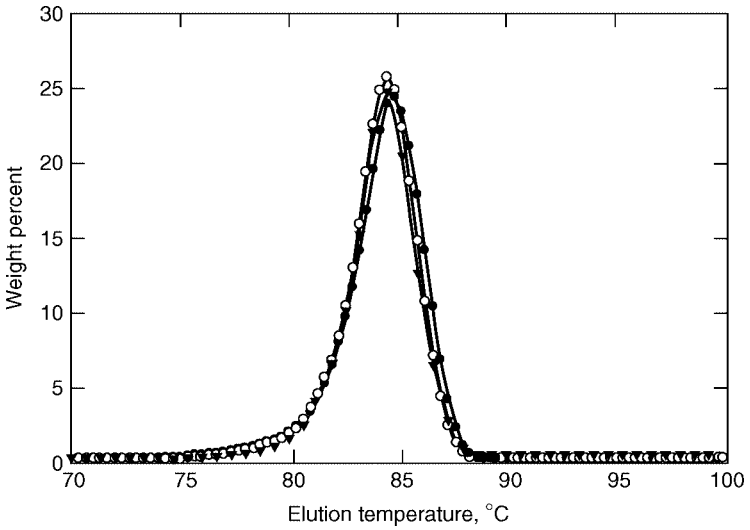

Fig. 21. Comparison of the TREF profiles for an ethylene/1-hexene sample measured at a ratio of 1:1:1 for cooling rate: heating rate: solvent flow rate. —●— Rate = 0.1°C/min; —○— rate = 0.2°C/min; —▼— rate = 0.5°C/min. From Ref. 14.

preparative method to fractionate much larger polymer samples than can be practically accomplished with conventional TREF using organic chlorinated solvents (22–24). Interestingly, because the density of supercritical fluids can be changed over a wide range of values by varying the pressure, CITREF can also be operated at constant temperature and varying pressure to fractionate polymers according to their molecular weights (25), provided they are kept above their melting points for the case of semicrystalline polymers. In this way, the term $(\delta_S - \delta_P)^2$ in equation 11 can be regulated by varying the pressure of the supercritical fluid without the addition of a nonsolvent.

Mathematical Models for Crystaf and TREF. Existing mathematical models for Crystaf and TREF suffer from several limitations because of the complex nature of the fractionation process that takes place in these techniques. For binary linear copolymers made with single site catalysts, Stockmayer's distribution (eq. 3) can be used to model the chemical composition distribution, but its translation into actual Crystaf and TREF curves is a much harder task.

A very simple model relating Crystaf or TREF curves to Stockmayer's distribution has been proposed (26), but this approach was later found to be unsatisfactory to describe quantitatively the chemical composition distribution of polyolefins made with single site catalysts, as illustrated in Figure 22 (27). Notice, however, that even though the Crystaf profiles and Stockmayer's distribution do not agree quantitatively, Stockmayer's distribution predicts the correct trends, particularly the broadening of the chemical composition distribution with decreasing molecular weight of the samples. A new model was proposed on the basis of the crystallization of the longest crystallizable monomer sequence per chain (28). In this approach, the longest ethylene sequence per chain, and not the overall comonomer distribution, determines the temperature at which the chain crystallizes in Crystaf or

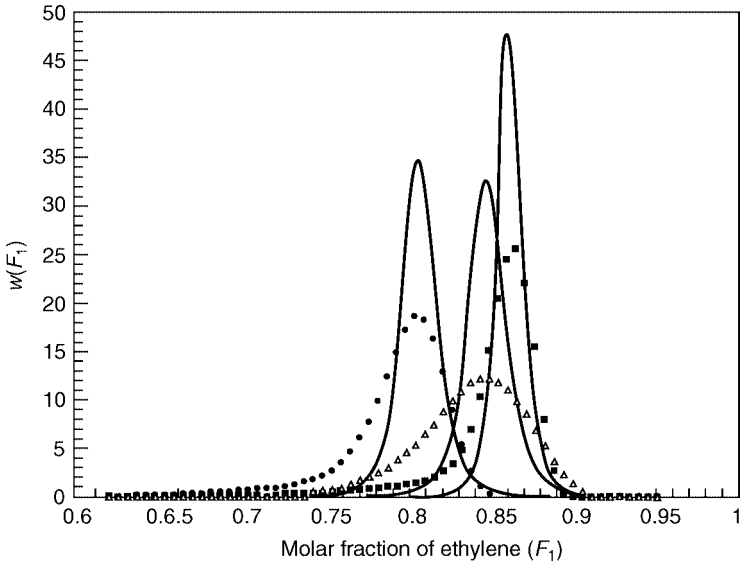

Fig. 22. Comparison of Crystaf profiles and Stockmayer's distributions for a series of ethylene/1-octene copolymers. Experimental Crystaf curves are indicated with symbols and the solid curves are the respective Stockmayer's distributions. ● Sample A; ◆ sample D; △ sample H. Molecular weights of samples A: $M_n = 29\,600$; D: $M_n = 38\,000$; H: $M_n = 19\,800$. From Ref. 27. Copyright (1998) Wiley-VCH.

elutes in TREF. Therefore, the distribution of the longest ethylene sequences, and not the chemical composition distribution, is used to model the fractionation with Crystaf and TREF. This approach led to modest success for some ethylene/1-octene copolymers, but was later found not to be generally applicable to a broader range of polymer samples. It is certain that crystallization kinetics play a very important role in both Crystaf and TREF fractionations and that models that rely simply on thermodynamic equilibrium assumptions are not capable of describing these techniques quantitatively (18). Much more research is still required to obtain reliable phenomenological models for these two fractionation techniques.

Size-Exclusion Chromatography

Size-exclusion chromatography (SEC), also known as gel-permeation chromatography (GPC), is currently the standard technique to fractionate polymers according to molecular weight due to its short analysis time and good reproducibility (see CHROMATOGRAPHY, SIZE EXCLUSION). There exist many excellent reviews and book chapters covering different aspects of SEC fractionation (29–35). SEC is a standard liquid chromatographic technique and, as such, involves the transport of a polymer sample dissolved in a mobile phase through a packed column. Even though SEC can be run in preparative mode using large columns to fractionate sizeable polymer samples, it is much more commonly operated in analytical mode with small columns and only a few milligrams of polymer.

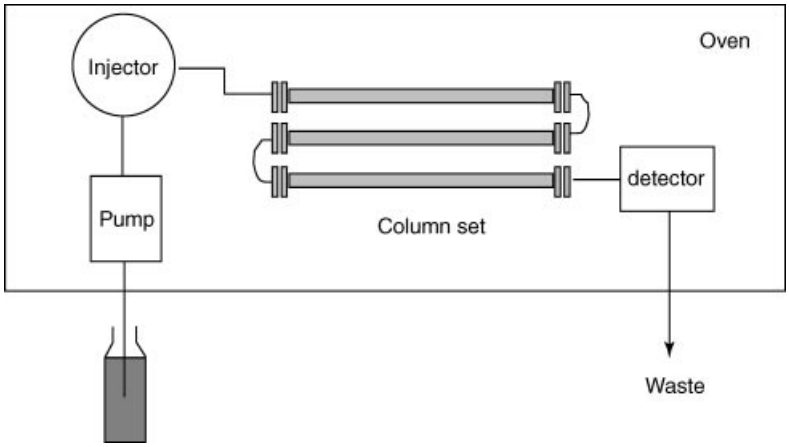

Fig. 23. SEC schematic.

SEC is commonly referred as *room-temperature SEC* or high temperature SEC, but the separation mechanism for both techniques is the same. As the name indicates, room-temperature SEC is used for polymers that are soluble at room temperature in the mobile phase; tetrahydrofuran is a commonly used solvent in this case, but many other solvents are equally adequate. High temperature SEC is mostly used for polyolefins and their copolymers since they are only soluble at temperatures from 120 to 150°C in solvents such as trichlorobenzene. In general, solvent type does not play a very important role in SEC, provided that it does not interfere with the column pore structure (when cross-linked polymer beads are used) and with the on-line detectors at the exit of the columns. However, care must be taken to avoid non size-exclusion effects, particularly for room-temperature SEC.

Figure 23 shows a schematic of SEC. The principle of SEC operation can be succinctly described as follows: the polymer sample, present as a dilute solution in a vial, is injected into the mobile phase as a narrow pulse and continuously flows through a series of columns containing packing with variable pore sizes. The elution time of the polymer chains depends on their size in solution or hydrodynamic radius: chains with higher volumes penetrate into fewer pores and elute first, while chains with smaller volumes penetrate into more pores (or penetrate deeper into the pores) and elute later. An on-line detector at the exit of the columns, most commonly a refractive index detector, is used to monitor the concentration of polymer chains eluting from the last column in the series, and a calibration curve is applied to relate elution volumes to molecular weights. *Retention time* is the time taken by a polymer fraction to elute from the columns. Likewise, *elution volume* is the volume of mobile phase required to elute a given polymer fraction from the columns.

In reality, even if all the pores were of the same diameter, fractionation by size would still take place since, because of solute-to-wall exclusion effects inside the pores, the available pore volume is higher for smaller chains than for larger ones, as illustrated in Figure 24. In practice, columns with a range of pore sizes are always used.

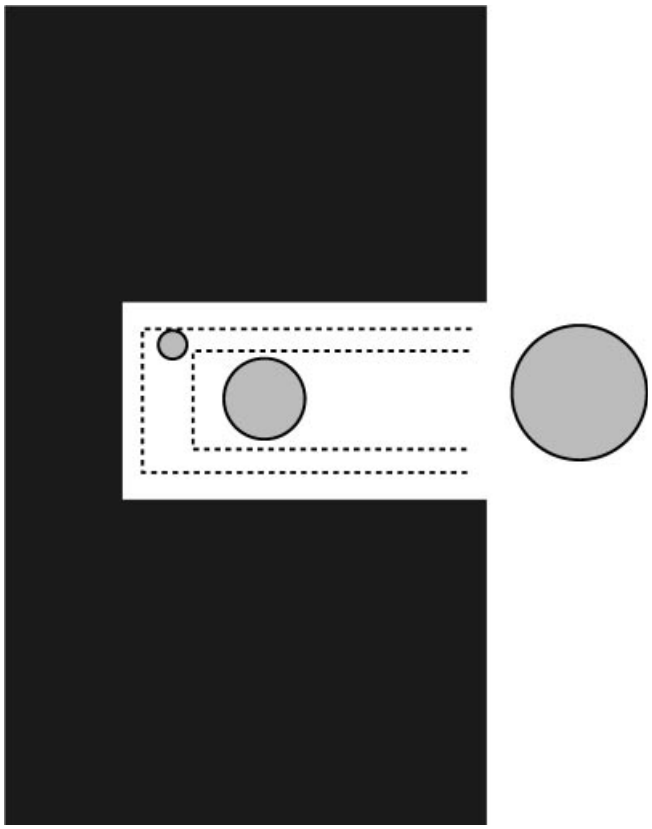

Fig. 24. Mechanism of SEC separation. Dotted lines indicate solution-to-wall exclusion volumes.

The relation between elution volume in the column and chain size in solution can be described with the simple equation:

$$V_R = V_i + KV_p \tag{19}$$

where V_R is the total elution volume, V_i is the interstitial volume between the packing particles, V_p is the pore volume of the packing particles, and K is a partition coefficient for the polymer chains between the stationary and the mobile phases. The partition coefficient K depends on the sizes of pores and polymer chains. It is equal to zero ($K = 0$) for chains that are too large to penetrate into any of the pores (*total exclusion limit*), and equal to one ($K = 1$) for chains that are small enough to diffuse into all pores (*total permeation* or *penetration limit*). These two limits, indicated in Figure 25, set the boundaries for polymer size resolution in SEC. Chains whose sizes are below the total permeation limit or above the total exclusion limit cannot be fractionated by SEC. Some mathematical models have been proposed to relate the value of K to pore sizes and radius of gyration of the polymer chains (32,36).

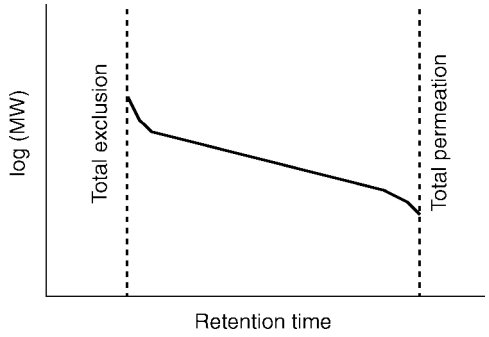

Fig. 25. An SEC calibration curve, showing the total permeation and total exclusion limits.

The partition coefficient can also be understood from a thermodynamic point of view with equation (37):

$$K = \exp\left(-\frac{\Delta G}{RT}\right) = \exp\left(\frac{\Delta S}{R} - \frac{\Delta H}{RT}\right) \tag{20}$$

Ideally, enthalpic effects are completely absent and SEC fractionation takes place on a size-exclusion basis only, ie

$$K \cong \exp\left(\frac{\Delta S}{R}\right) \tag{21}$$

Therefore, the value of K is proportional to the decrease in entropy experienced as the polymer chains diffuse into the pores of the packing and $0 \leq K \leq 1$.

The size of polymer chains in solution is a function of their chain length and topology, as well as solvent type and temperature. For linear chains, the size in solution is directly proportional to chain length, but for chains containing long-chain branches this relation depends on the type, number, and topology of the branches, making the quantification of SEC results significantly more complex (33).

In principle, SEC can be calibrated with standards of narrow molecular weight distribution of the polymer that one wishes to analyze. In this way, a calibration curve relating molecular weight to elution volume is obtained, in a fashion similar to what is done for the calibration of TREF or crystallization analysis fractionation. This approach, however, suffers from the limitation that the calibration curve is only applicable to one specific polymer. Additionally, narrow standards are not available for many different types of polymers. In principle, the batch fractionation techniques discussed above could be used to obtain such narrow standards, but these processes are time-consuming and, as explained, do not permit the isolation of samples with very narrow molecular weight distributions.

One of the great advantages of SEC is that it can be calibrated using a *universal calibration curve* that is independent of polymer type, provided that the chains behave like random coils in solution. This remarkably elegant solution to a rather complex problem is often taken for granted, but it is perhaps the most important reason why SEC is so widely applicable to different polymer types. The

universal calibration curve relies on the principle that polymer chains with the same volume in solution will elute at the same time from an SEC column. In other words, chains with the same hydrodynamic volume have the same retention time and elution volume.

The product of the molecular weight M and the intrinsic viscosity $[\eta]$ is called the *hydrodynamic volume* and is proportional to the size of polymer chains in solution:

$$[\eta]M = \Phi\left(\bar{r_0^2}\right)^{3/2}\alpha^3 \tag{22}$$

In equation 22, $\bar{r_0^2}$is the root-mean-square end-to-end distance of the polymer chain, and α and Φ are constants that depend on the type of solvent and polymer (30). When the logarithm of the hydrodynamic volume is plotted as a function of elution volume, an elegant relationship arises that is independent of polymer type, as illustrated in Figure 26 (31).

According to equation 22, polymers with the same root-mean-square end-to-end distances have the same hydrodynamic volume. Polystyrene standards spanning a wide range of molecular weight averages with very narrow molecular weight distributions (with polydispersity indices typically below 1.1) can be produced via living anionic polymerization and are, therefore, ideal calibration standards for SEC. The hydrodynamic volume of an unknown polymer, x, can be compared to that of a polystyrene standard, ps, with the equation:

$$M_{\mathrm{ps}}[\eta]_{\mathrm{ps}} = M_x[\eta]_x \tag{23}$$

The choice of a polystyrene standard is one of mere convenience; in principle, any other polymer standard with narrow molecular weight distribution could be used to generate the universal calibration curve. Equation 23 can be made more useful by substituting the Mark–Houwink relationship,

$$[\eta] = KM^a \tag{24}$$

and solving for M_x to obtain

$$\log M_x = \left(\frac{1}{1+a_x}\right)\log\frac{K_{\mathrm{ps}}}{K_x} + \frac{1+a_{\mathrm{ps}}}{1+a_x}\log M_{\mathrm{ps}} \tag{25}$$

Calibration curves for polystyrene narrow standards are very often linear functions in the general form,

$$V_{\mathrm{R}} = a - b\log M_{\mathrm{ps}} \tag{26}$$

where a and b are positive constants determined empirically. Higher degree polynomials are used when a simple linear regression is not adequate. The experimentally-measured SEC elution profile for polymer x is converted into the molecular weight distribution as follows: for each retention volume V_{R}, the

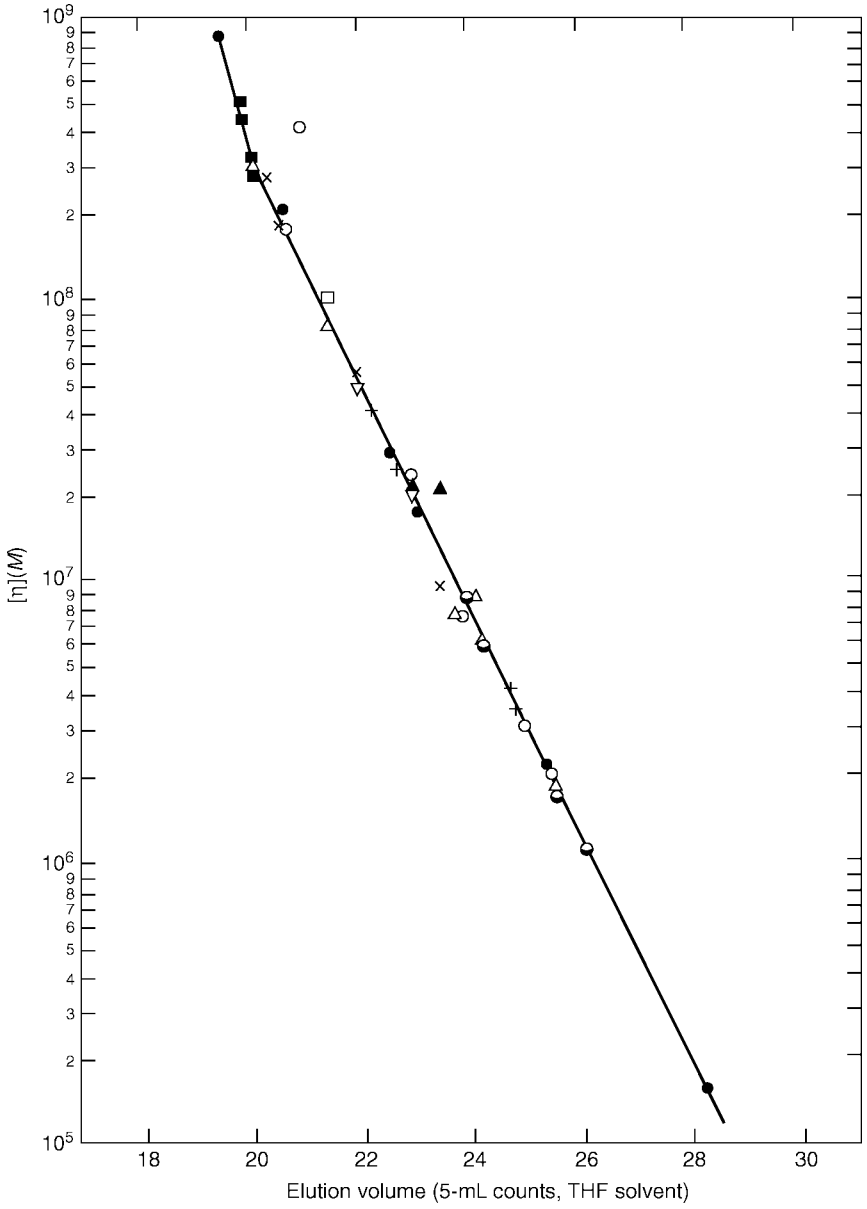

Fig. 26. Universal calibration curve for SEC. ● Polystyrene (linear); ○ polystyrene ("comb"); + polystyrene ("star"); △ polystyrene–poly(methylmethacrylate) copolymer (heterograft); × poly(methylmethacrylate) (linear); ◒ poly(vinylchloride); ▽ polystyrene–poly(methylmethacrylate) copolymer (graft-comb); ■ poly(phenyl siloxane); ▲ polystyrene–poly(methylmethacrylate) copolymer (statistical-linear); □ polybutadiene. From Ref. 31.

polystyrene-equivalent molecular weight, M_{ps}, is calculated using the universal calibration curve (eq. 26). This value is then substituted into equation 25 and the molecular weight of the sample, M_x, is calculated provided that the Mark–Houwink constants are known for polystyrene and the polymer sample at the

required analysis temperature and solvent. Calibration curves using broad standards may also be used, but are less common than the ones that use narrow standards (30).

Once the molecular weight distribution is established, molecular weight averages are calculated according to the following expressions:

$$M_n = \frac{1}{\int \frac{w(M)}{M}\,\mathrm{d}M} \tag{27}$$

$$M_w = \int M w(M)\,\mathrm{d}M \tag{28}$$

$$M_z = \frac{\int M^2 w(M)\,\mathrm{d}M}{\int w(M)\,\mathrm{d}M} \tag{29}$$

$$M_v = \left[\int M^\alpha w(M)\,\mathrm{d}M\right]^{1/2} \tag{30}$$

where $w(M)$ is the differential molar mass distribution measured by the mass on-line detector:

$$w(M) = \frac{\mathrm{d}W_V}{\mathrm{d}M} = \frac{\mathrm{d}W_V}{\mathrm{d}V}\frac{\mathrm{d}V}{\mathrm{d}(\log M)}\frac{\mathrm{d}(\log M)}{\mathrm{d}M} = \frac{\mathrm{d}W_V}{\mathrm{d}V}\frac{\mathrm{d}V}{\mathrm{d}(\log M)}\frac{1}{M} \tag{31}$$

The term $\frac{\mathrm{d}W_V}{\mathrm{d}V}$ is the height of the chromatogram and $\frac{\mathrm{d}V}{\mathrm{d}(\log M)}$ is the slope of the calibration curve, both measured at the elution volume V.

Many modern SEC instruments are provided with on-line viscometers to measure the intrinsic viscosity of the polymer sample during the analysis. In this case, the Mark–Houwink constants are estimated during the SEC analysis and do not need to be known *a priori*.

Many round-robins have been performed to test the intra- and inter-laboratory reproducibility of SEC. D'Agnillo and co-workers (38) reviewed the previous literature in the area and provided the most recent round-robin for high temperature SEC.

Fractionation Equipment. The main requirements for a commercial SEC unit are as follows: (*1*) reliable solvent pumps to keep a constant flow of mobile phase; (*2*) fractionation columns in the right range of porosity to fractionate a wide range of molecular weights; (*3*) an injection system capable of injecting the polymer sample without significantly disturbing the flow of the mobile phase; (*4*) an efficient mass detector and, optionally, chain-length or composition-sensitive detectors; and (*5*) an automated data acquisition system. All of the commercially available SEC units have incorporated these required features.

A reliable high pressure liquid pumping system (generally reciprocating-dual piston design to avoid pressure fluctuations) is one of the most important parts of SEC. Since SEC calibration is based on the retention time in the columns and the logarithm of the molecular weight varies very often as a linear function

of the elution volume or retention time, any fluctuation in flow rate will lead to significantly inaccurate molecular weight distributions. Pump pressures generally vary from 1000 to 4000 psi. These high pressures are required to overcome the pressure loss in the columns due to the small particle sizes of the packing. The flow rate of the mobile phase is kept in the range of 1–3 mL/min.

The injection system should be able to inject a small sample aliquot with precision, with injection volumes usually varying from 10 to 200 μL. The polymer sample solutions are commonly prepared with concentrations varying from 0.05 to 0.1% wt/vol. For high temperature SEC, polymer solutions are generally prepared directly in the injection compartment under spinning and filtering, if required. Off-line sample preparation setups are also available. The sample injection systems are provided with a sample carousel to permit the sequential injection of several samples.

SEC columns are commonly packed with microporous glass beads or cross-linked styrene–divinylbenzene gels, the latter being more common especially for applications involving chains soluble in organic solvents. Several other, less commonly used packings, are also available (33,39). The column packing can have pores of constant size or a distribution of pore sizes; the latter are called linear columns since they generally lead to a linear calibration curve. For polystyrene–divinylbenzene columns, the pore sizes depend on the degree of cross-linking since they are formed by swelling the packing with solvent. Pore sizes in the range of 50 to 10^7 Å correspond to the effective size range of most polymer molecules in solution. The size of the particles in the packing is also important: gel particle sizes in the range of 5–10 μm allow good packing and minimum channeling; 3-μm particles with increased pore volume packing, providing enhanced resolution at low molecular weights, are also available. SEC columns are generally 300–600-mm long and 7.5 mm in diameter, but shorter mini-bore columns 250-mm long and 4.6 mm in diameter can also be used to decrease solvent usage. Generally two or three columns are used in series, preceded by a shorter guard column to filter polymer gels and other impurities that may plug or damage the columns. All columns will degrade with usage, particularly polystyrene/divinylbenzene columns used at high temperatures. Column degradation alters their porosity and, consequently, polymer retention time. Because of this, SEC columns must be recalibrated at regular intervals to ensure that the results are reliable. It is common practice to monitor the state of the columns by injecting broad and narrow standards during the analysis of other unknown samples. Eventually, column degradation will lead to peak broadening and loss of resolution.

Differential refractive index detectors are the standard SEC mass detectors. They have the advantage of being able to respond to all polymer types, provided that the choice of solvent is adequate. To maximize detector response, the refractive indices of the polymer and solvent should differ significantly. Infrared and ultraviolet detectors have also been used successfully as mass detectors. Viscometers can be added to allow the calculation of the intrinsic viscosity of unknown polymer samples. They are also essential for the analysis of polymers with long-chain branches. Light-scattering detectors permit the direct measurement of the weight-average molecular weight of the polymer fraction present in the detector cell and can, therefore, be used to determine molecular weight distributions as an absolute technique dispensing the use of calibration curves. The combination of

SEC with refractive index, viscosity, and light-scattering detectors is referred to as *triple detector system*. This powerful configuration has found many applications in industry and academia, but it is also more complex to operate than single-detector SEC systems.

As any other liquid chromatographic technique, SEC analysis can be influenced by peak broadening due to axial dispersion and flow irregularities. A description of this phenomenon is beyond the scope of this article. For more information, see the brief summary presented by Styring and Hamielec and the related references cited by these authors (33).

SEC of Complex Polymers. For the case of linear homopolymers and linear and chemically homogeneous copolymers, there exists a direct relationship between the size of the polymer chains in solution and molecular weight. In this case, the separation mechanism operative in SEC will lead to fractionation by molecular weight only. On the other hand, complex polymers may have long-chain branches and, in the case of copolymers, are heterogeneous in chemical composition. Since the radius of gyration (or size in solution) is affected by both long-chain branching and chemical composition, chains with different molecular weights may have the same retention volume, and consequently the species present in the detector cell may have a distribution of molecular weights. In this case, other microstructural factors besides molecular weight affect SEC fractionation. Interaction chromatography (IC) is sometimes used to resolve these polymers. IC makes use of the enthalpic term of equation 20 to achieve the fractionation. Since the enthalpic term is influenced by the chemical nature of the polymer, chains with distinct chemical compositions can be fractionated. Chang recently published a comprehensive review on this subject (37).

Field Flow Fractionation

The power of field flow fractionation (FFF) lies in the simplicity of the design of its main component, the FFF separation channel. In FFF, a pulse of a polymer solution is injected into a carrier liquid and flows through a rectangular thin channel. An external physical field is applied perpendicularly to the axial flow, acting as a driving force for the fractionation of the polymer molecules according to molecular weight and/or other microstructural properties. Figure 27 shows a schematic of a FFF channel. Contrarily to chromatographic techniques such as SEC, the FFF channels contain no packing and can, therefore, be used to analyze polymer chains with a broader range of hydrodynamic radii from 1 nm to 100 μm. Several books and reviews have been recently published on this topic (40–45). The reader is referred to the review by Cölfen and Antonietti (43) for a comprehensive and up-to-date overview of principles, techniques, and applications of several FFF methods.

The nature of the external field determines the type of fractionation achieved in FFF. Even though many different types of fields have been examined, the most common are thermal, flow, and gravitational/centrifugal. Figure 28 summarizes some types of FFF methods with their respective dates of invention.

The fractionation mechanism in FFF is as simple as it is elegant (Fig. 29). Since the axial flow is laminar, a parabolic velocity profile is established in the rectangular channel. Consider first the case of flow-FFF (*Fl*-FFF) of a linear

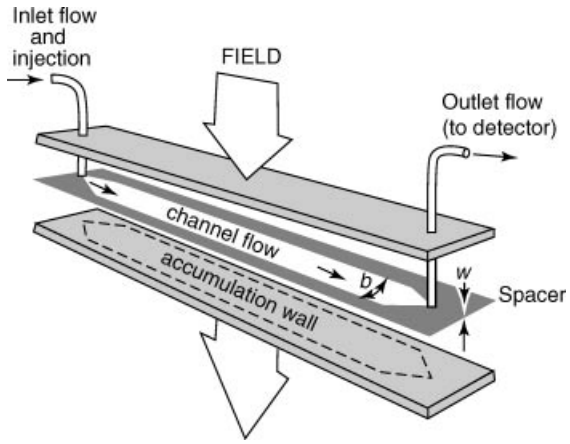

Fig. 27. Schematic of a FFF channel. From Ref. 40.

homopolymer: the carrier liquid flows perpendicularly through the porous walls of the channel, establishing an external flow field that is normal to the axial flow (*cross flow*). A narrow pulse of polymer solution is injected at one end of the column and the axial flow is stopped for a short period of time. The cross flow forces the polymer molecules to accumulate near the opposite wall (*accumulation wall*), generating a transversal polymer concentration gradient. According to Fick's law, this concentration gradient will act as the driving force for molecular diffusion in the opposite direction of the external field. After a short time, a

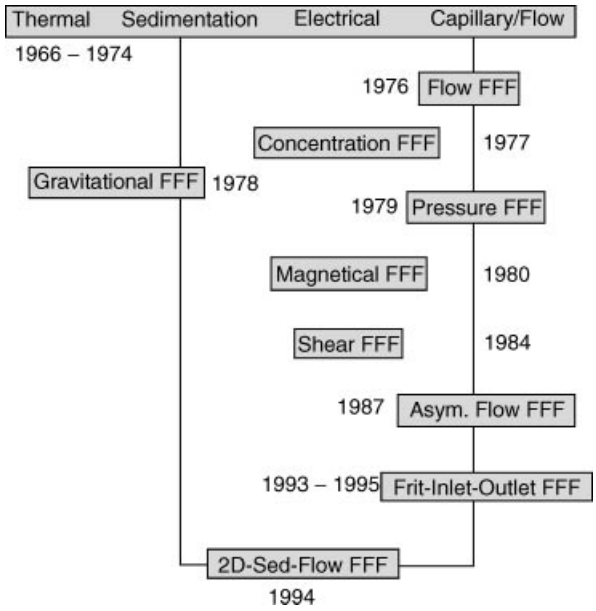

Fig. 28. Some types of FFF with their times of invention. From Ref. 43. Copyright (2000) Springer-Verlag.

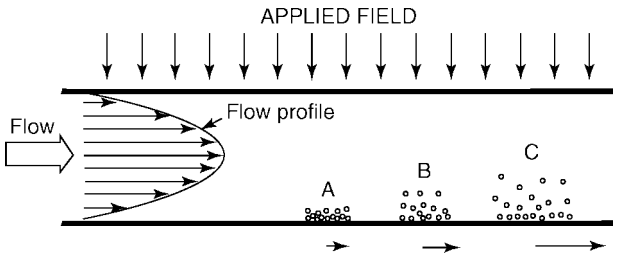

Fig. 29. FFF flow profiles and mechanism of fractionation. The molecular weight of the particles increases in the order A > B > C. From Ref. 40.

steady state is reached in a process called *relaxation* with the establishment of a polymer layer of a given thickness near the accumulation wall. Chains with smaller hydrodynamic radii (smaller molecular weights) have higher diffusion coefficients and will move farther away from the accumulation wall than chains with higher hydrodynamic radii. When the axial flow is restarted, generating a parabolic velocity profile inside the channel, smaller chains will, on average, be transported with higher axial velocities than larger chains and will consequently elute from the channel at shorter residence times (or shorter elution volumes). This mode of operation, where the intensity of the driving force is constant throughout the channel, is called the *classic* or *normal* model of operation. The intensity of the driving forces can be varied as a function of analysis time to permit the fractionation of polymers with broad molecular weight distributions. This mode of operation is called *field intensity programming*. Some other FFF modes of operation include steric-FFF (46), hyperlayer-FFF (47), and focusing-FFF (48). Hydrodynamic chromatography can also be seen as a special case of FFF where the external driving forces are absent (43). More details about these modes of operation can be found in the cited references.

Among all FFF techniques, *Fl*-FFF is the most universal, since the separation relies only on the difference between the diffusion coefficients of the solute species. It can be applied to fractionate polymers (down to molecular weights of 10^3 g/mol), colloids, and particles with hydrodynamic radii from 1 nm to 50 μm in either water or organic solvents, although it has been used much more frequently for water-soluble polymers. The transversal flow driving force has the same effect on molecules of all chain lengths, and thus forces them towards the accumulation wall regardless of their sizes. However, since Fick's diffusivity is inversely proportional to molecular weight, the shorter chains will diffuse away from the accumulation wall faster than the longer ones. As a consequence, in *Fl*-FFF the fractionation mechanism is regulated mainly by molecular weight. In symmetric *Fl*-FFF, the two walls are permeable to the transversal flow, while in asymmetric *Fl*-FFF only one of the walls is permeable. Figure 30 shows an example of *Fl*-FFF used in the fractionation of proteins.

In thermal-FFF (*Th*-FFF), a temperature gradient is imposed on the FFF channel (generally 10–100 K), causing the chains to diffuse towards the cold wall by a mechanism called thermal diffusion (Soret effect). *Th*-FFF is commonly used to fractionate synthetic polymers soluble in organic solvents with molecular weights from 10^4 to 10^7 g/mol. In principle, it can also be used to fractionate

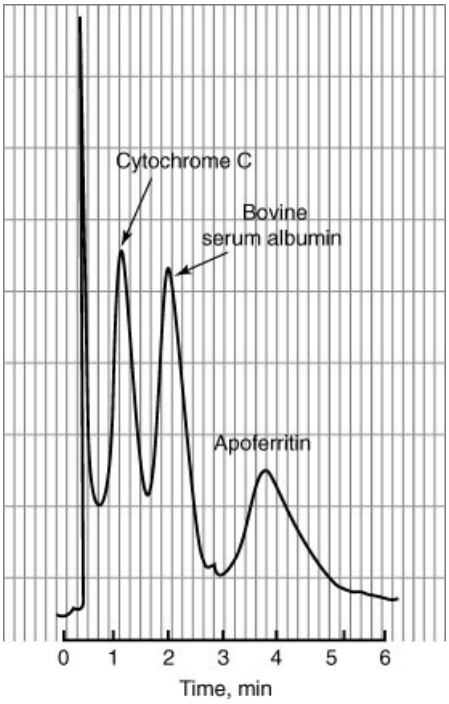

Fig. 30. *Fl*-FFF fractionation of three proteins. From Ref. 40.

hydrophilic polymers, but in practice *Fl*-FFF is the predominant technique for these polymers. *Th*-FFF is very useful for shear-sensitive chains with very high molecular weights or macromolecular aggregates. Unfortunately, the fractionation of shorter polymer chains requires the use of very high temperature gradients that may cause several operational problems.

The ratio of the thermal diffusivity D_T, to the molecular diffusivity D is the main fractionation parameter in *Th*-FFF. D_T depends on polymer and solvent composition, but it is virtually independent of chain length and long-chain branching. For random copolymers, D_T varies linearly with monomer composition, but more complex behavior is observed for block copolymers. In principle, this dependency on chemical composition can be used to fractionate copolymers according to their composition, as is beautifully illustrated in Figure 31 (49).

Gravitational or centrifugal forces are used to promote fractionation in sedimentation FFF (*S*-FFF). *S*-FFF is applicable for polymers with molecular weights higher than 10^6 g/mol and colloids or particles with diameters larger than 30 nm, both in water and organic solvents. The fractionation is regulated basically by the differences in density and the intensity of the centrifugal forces. It is mostly used to fractionate large biopolymers, polymer latexes, inorganic particles, emulsions, biological cells, etc. Figure 32 shows the schematic of an *S*-FFF channel coiled around a centrifugal rotor. An example of fractionation of polystyrene latex beads by *S*-FFF is illustrated in Figure 33.

Theoretical Considerations. The laminar flow patterns inside the FFF channel are well understood from basic fluid dynamic models and permit a very

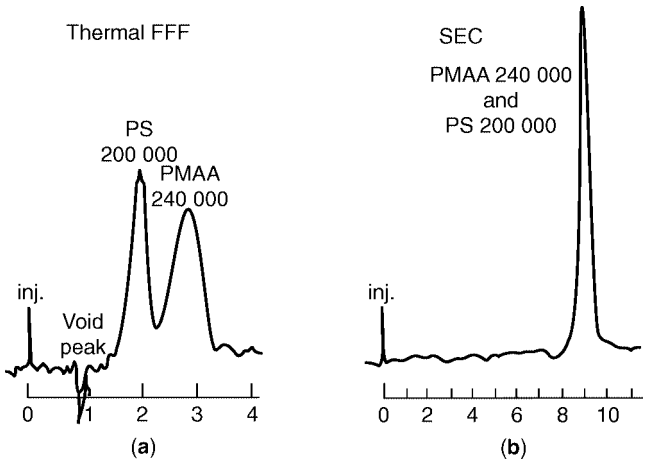

Fig. 31. *Th*-FFF according to chemical composition. From Ref. 49. Copyright (1989) Springer-Verlag.

elegant theoretical treatment for different FFF modes of operation, as opposed to chromatographic techniques where the internal packing generates flow patterns that are difficult to describe rigorously with simple mathematical models. Because of this precise mathematical treatment, FFF can be used not only as a fractionation technique, but also to determine fundamental physicochemical properties of the sample under analysis. This also allows a new concept for a universal

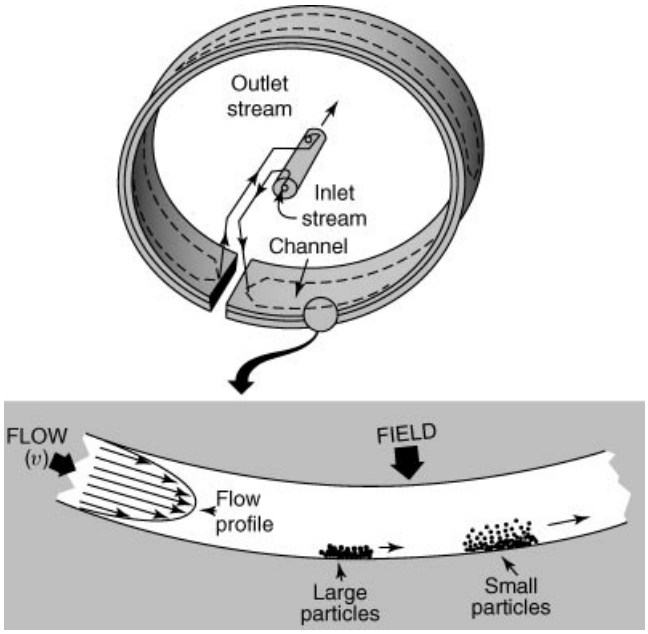

Fig. 32. *S*-FFF channel. From Ref. 40.

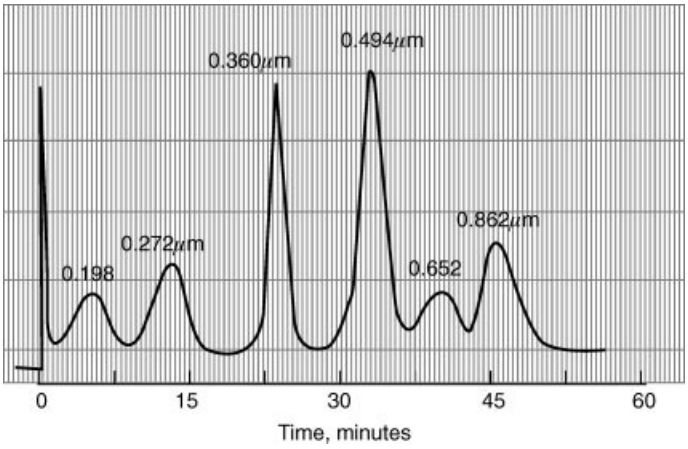

Fig. 33. *S*-FFF of polystyrene beads of different diameters. From Ref. 40.

calibration curve for fractionation by molecular weight. Basic mathematical relationships for *Th*-FFF, *Fl*-FFF, and *S*-FFF will be developed in this section, but the readers should be aware that significant deviations from this ideal behavior may occur during actual fractionation experiments. For a more elaborate mathematical treatment of these techniques, the reader is referred to the review by Cölfen and Antonietti (43).

Very concise expressions can be developed for FFF if the following assumptions are made: (*1*) the FFF channel can be modeled as the space between two parallel infinite plates, (*2*) the flow profile is parabolic, (*3*) a steady state concentration profile is established in the channel, and (*4*) the external field is uniform. With these assumptions, a simple mass balance across the cross section of the channel leads to the expression for the transversal flux J_x,

$$J_x = u_x c(x) - D\frac{\mathrm{d}c(x)}{\mathrm{d}x} \tag{32}$$

where u_x is the drift velocity of the chains toward the accumulation wall caused by the external field, $c(x)$ is the concentration profile of solute molecules as a function of the distance x from the accumulation wall, and D is their diffusion coefficient. The diffusion coefficient of polymers is a function of their molecular weight and other microstructural characteristics.

Solving this equation at the steady state, ie $J_x = 0$, leads to an exponential solution for $c(x)$,

$$c(x) = c_0 \exp\left(-\frac{x|u_x|}{D}\right) \tag{33}$$

where c_0 is the polymer concentration at the accumulation wall. Therefore, the normal mode of operation generates an exponential concentration profile with thickness inversely proportional to the molecular weight of the polymer solute. (In the case of focusing FFF, the external forces are varied in such a way as to balance

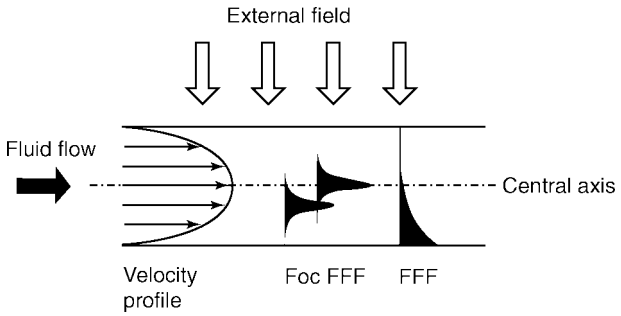

Fig. 34. Concentration gradients in classical and focused FFF. Reprinted from Ref. 45 by courtesy of Marcel Dekker, Inc.

the opposing diffusional forces, creating a focused band at a defined position above the accumulation wall where the external force is exactly counterbalanced, as illustrated in Figure 34.)

The two most important parameters in FFF are the dimensionless retention parameter λ and the ratio of the retention time of an unretained solution to the retention time of a retained solution, $R = \frac{t_0}{t_r}$. An unretained solution is one whose retention time is not affected by the external field (the carrier liquid, for instance). The retention parameter is defined by the equation

$$\lambda = \frac{l}{w} = \frac{kT}{Fw} \tag{34}$$

where l is the thickness of the solute separation layer, w is the width of the FFF channel, k is Boltzmann's constant, T is the temperature, and F is the transversal force that acts on the solute molecules. The parameter λ is, therefore, the fraction of the channel width occupied by the solute molecules.

The parameter λ cannot be measured directly, but must be related to R via the equation

$$R = \frac{t_0}{t_r} = \frac{V_0}{V_r} = 6\lambda\left[\coth\left(\frac{1}{2\lambda}\right) - 2\lambda\right] \tag{35}$$

where V_0 is the volume of the separation channel and V_r is the retention volume for the retained solution.

Since $\lambda \ll 1$ for most cases, the following approximation applies:

$$R \cong 6(\lambda - 2\lambda^2) \cong 6\lambda \tag{36}$$

Once λ is estimated from an experimentally-measured value of R, it can be used to calculate the values of several physicochemical parameters for the polymer chains. For *Fl*-FFF, the following expression holds:

$$\lambda = \frac{Dw}{\dot{V}_c} \tag{37}$$

where $\dot{V}_c$ is the transversal flow rate. The equivalent expressions for *Th*-FFF and *S*-FFF are as follows:

$$\lambda = \frac{D}{D_T(\mathrm{d}T/\mathrm{d}x)w} \tag{38}$$

$$\lambda = \frac{RT}{\varpi^2 rM\left(1 - \frac{\rho}{\rho_s}\right)w} \tag{39}$$

where D_T is the thermal diffusion coefficient, $\mathrm{d}T/\mathrm{d}x$ is the temperature gradient across the channel, $\varpi^2 r$ is the centrifugal acceleration, M is the molecular mass of the solute, R is the gas constant, and ρ and ρ_s are the solvent and solute densities, respectively. Equations 37 to 39 are very helpful to understand the basic physical parameters that affect separation inside FFF channels. Notice that the layer thickness, as estimated by the parameter λ, is always inversely proportional to the field strength, ie, $\dot{V}_c$, $\mathrm{d}T/\mathrm{d}x$, or $\varpi^2 r$. This permits the fractionation of a very broad range of molecular sizes by simply decreasing the intensity of the external field, as done in the mode of operation called *field intensity programming*. For instance, the analysis of a sample with broad molecular weight distribution can be started at high field intensity. If this intensity was kept throughout the fractionation, very large elution times would be required to elute the highest molecular weight species. Decreasing the field intensity in a programmed way leads to a reduction of the retention time of larger chains, thus shortening the analysis time. This procedure, however, increases the complexity of the analytical procedure and may also lead to undesirable secondary relaxation phenomena: solute–solute and solute-accumulation wall interactions at high field strengths.

Use of *Fl*-FFF and *Th*-FFF for Molecular Weight Fractionation. *Th*-FFF and SEC have been often compared since both techniques are generally used to obtain the molecular weight distribution of synthetic polymers in organic solvents. Nonetheless, SEC is much more widely used than FFF, despite the fact that these techniques can be seen as complementary. One of the advantages of SEC is the existence of a universal calibration curve applicable to all polymer types. Even though universal calibration curves can also be obtained for FFF, their concept is radically different from that of the universal calibration curve for SEC. For SEC, the universal calibration curve can be used for all polymers in the same SEC instrument and column set, but will differ from instrument to instrument. Even in the same instrument, the calibration curves will "drift" as the columns age and change their pore structure, particularly for high temperature SEC. Contrarily, the universal calibration curve for FFF is applicable, in principle, to a given polymer–solvent combination in all FFF setups, but will be different for each polymer–solvent system. Another practical advantage of SEC that may explain its predominance over FFF is a more straightforward mode of operation. Many of the operation modes of FFF, while very efficient, require considerably more expertise from the analyst.

In general, SEC is capable of analyzing lower molecular weight chains (using packing with small pore radii) but has limitations for very high molecular weight chains that can suffer chain scission because of the high shear stresses inside the

SEC columns and/or generate very high viscosities and pressure drops. On the other hand, *Th*-FFF is not very effective for fractionating low molecular weight chains because a very high temperature gradient is required (D is large for small chains, cf eq. 38), but becomes more attractive for higher molecular weight chains. Additionally, a series of SEC columns can be used to fractionate samples with very broad molecular weight distributions (up to five decades or more) since the elution volume in SEC is a linear (or quasi-linear) function of the logarithm of the molecular weight. Calibration curves for FFF, however, show a now-linear relation between elution volume and the logarithm of the molecular weight, as indicated in equation 40 below. This implies that in the normal mode of operation, FFF fractionation is limited to samples with narrow molecular weight distributions. As we have seen, this limitation can be reduced by operating FFF in the field programming mode, but at the price of a more elaborate analysis procedure (43).

FFF molecular weight calibration curves can be represented by the relation

$$\log V_r = a + S_m \log M \tag{40}$$

where V_r is the retention volume, M is the molar mass of the polymer, and a and S_m are constants for a given polymer–solvent system. The power of this approach is that the calibration constants can be related to the characteristics of the FFF equipment used to obtain the calibration curve and then extended to any other FFF setup. In other words, after equation 40 is determined for a given polymer-solution system in one FFF setup, in principle it can be used in any other FFF setup, even if some of the operation conditions and channel dimensions are different. This procedure will be outlined in the next paragraphs.

The following expressions apply for linear or uniformly branched polymers:

$$\frac{D}{D_T} = \varphi_0 M^{-n} \tag{41}$$

$$D = AM^{-b} \tag{42}$$

where the parameters φ_0, n, A, and b are universal constants for a given polymer–solvent system. Substituting equation 42 in equation 41, the following expression results:

$$\frac{AM^{-b}}{D_T} = \varphi_0 M^{-n} \tag{43}$$

Since it is know that D_T is nearly independent of molecular weight, then $b \approx n$ provided that the measurements are made at the same temperature.

Equations 41 and 42 can be substituted into their respective definitions of λ, equations 38 and 37, to obtain

$$\lambda = \frac{\varphi_0 M^{-n}}{(dT/dx)w} = \frac{\varphi_0 M^{-n}}{(\Delta T/w)w} = \frac{\varphi_0}{\Delta T} M^{-n} \tag{44}$$

$$\lambda = \frac{wA}{\dot{V}_c} M^{-b} \tag{45}$$

The parameter λ can be calculated from the experimentally-measured value of R using equation 35. Using the approximation $R = 6\lambda$ (accurate within 2% when $R < 0.06$), it is possible to obtain closed-form expressions for the dependency of the retention volume on molecular weight:

$$V_r = \frac{V_0 \Delta T}{6\varphi_0} M^n \text{ for } Th\text{-FFF} \tag{46}$$

$$V_r = \frac{V_0 \dot{V}_c}{6Aw} M^b \text{ for } Fl\text{-FFF} \tag{47}$$

Comparing equations 46 and 47 with the universal calibration curve, equation 40, the following expressions for the calibration constants are obtained:

$$a = \log \frac{V_0 \Delta T}{6\varphi_0} \text{ and } S_m = n \text{ for } Th\text{-FFF} \tag{48}$$

$$a = \log \frac{V_0 \dot{V}_c}{6Aw} \text{ and } S_m = b \text{ for } Fl\text{-FFF} \tag{49}$$

The beauty of these equations is that they are related only to the dimensions of the FFF channel, w and V_0; the strength of the external fields, ΔT or $\dot{V}_c$; and the polymer–solvent specific constants, φ_0, A, n and b. (For more rigorous calibrations, some corrections of these equations may be required.) They can, therefore, be applied to analyze a known polymer–solvent system in different FFF instruments under a wide range of experimental conditions (50).

Fractionation Equipment. The basic setup of FFF is essentially the same required for chromatographic techniques, with the chromatographic columns replaced by the FFF channel. The same requirements for precise sample injection, stable flow of the carrier liquid, and adequate sample detection described for SEC also apply to FFF.

FFF channels are usually 50- to 500-μm thick, 10- to 100-cm long, and have an aspect ratio of 20 to 200 (width/thickness). Particular details such as materials of construction, geometry of the channels, and specific arrangements of flow inlets and outlets can vary among different setups and operation modes. Details for several equipment configurations can be found in the references cited in this section.

Differential refractive index detectors are the most common choice for FFF mass detectors. As also the case for SEC, the use of multiple detectors is becoming increasingly important with FFF. Low angle laser light scattering (LALLS) and multiangle laser light scattering (MALLS) detectors are used for absolute determination of molecular weights. Many other detectors (UV, ICP-MS, differential viscometer, IR, electrospray mass spectroscopy) have also been used with FFF.

FFF is manly an analytical technique, but some effort has be made to run it in preparative or at least micro-preparative mode. The use of modified continuous FFF techniques or SPLITT channels (where the incoming polydisperse sample is split into two outlet flows with narrower distributions) is briefly described by Cölfen and Antonietti (43).

Continuous Polymer Fractionation

Continuous polymer fractionation (CPF) is a liquid–liquid extraction technique developed to fractionate large amounts of polymer (51). It was originally developed to fractionate homopolymers by molecular weight and has been applied for polyvinyl chloride (52), polyisobutylene (53,54), polyethylene (55), and polycarbonate (56). Recently, attempts to extend CPF to copolymers have been made (57) and it was shown that, under certain operational conditions, fractionation by chemical composition could also be achieved (58).

Being continuous, the advantage of CPF over the other techniques previously discussed lies in the fact that larger polymer samples can be fractionated in relatively shorter times. This is particularly important if large fractions with narrow MWD or CCD are required for the establishment of structure-property relationships or to remove, on a technical scale, chain populations that are undesirable for a given application of specialty polymers.

In a CPF liquid–liquid extraction column, the feed stream containing the polymer solution (polymer rich phase) flows countercurrently to the eluent stream containing the extracting agent. Chains with low molecular weight present in the polymer-rich phase (gel phase) are extracted by the eluent stream (sol phase), and the two phases exit from the bottom and top of the column because of their density differences. Mixed (solvent/nonsolvent) or single solvents can be used with CPF, but mixed solvents provide more flexible operational conditions. The same principles discussed before for batch fractionation can be extended to CPF. Weinmann and co-workers provide detailed theoretical treatment of CPF (56). Naturally, a single pass through a CPF column only permits the fractionation into two low–high molecular weight fractions. If more fractions are required, it is necessary to use columns in series, in which case successive extractions of the low molecular weight components can be achieved by changing the solvent/nonsolvent ratio or column temperature in the series.

A recent article describes two configurations for CPF columns (57): both were glass columns with high diameter ratios of 2.4 m/3.5 cm and 1.9 m/1.5 cm. The larger column was filled with glass beads of 8- and 10-mm diameter in a 1:1 ratio, while the smaller one with glass beads of 6 and 8 mm in a 3:1 ratio. The feed inlet was positioned at 3/4 of the total column high, since theoretical and experimental results indicate that this placement increases the separation efficiency (56). In this case, the temperature of the upper $\frac{1}{4}$ of the column can be decreased, creating a reflux effect that is beneficial to the fractionation. Two to three theoretical plates per meter and a fractionation capacity of 10–100 kg of polymer per hour and square meter of cross section have been reported for these columns (51).

A related technique for the fractionation of large amounts of polymer, continuous spin fractionation (CSF), has also been recently disclosed (59).

Mass Spectrometry

Traditional mass spectrometry techniques involving the study of ions in the gas phase are not adequate for the analysis of polymers because of their very low vapor pressures and their tendency to suffer chain scission during ionization. On the

other hand, recent developments on soft ionization techniques such as electrospray ionization (ESI) and matrix-assisted laser desorption ionization (MALDI) mass spectrometry have found many applications in the polymer field (60–63). Since ESI is more commonly used with biopolymers (63) and most common applications of mass spectrometry (qv) for synthetic polymers use MALDI, we will restrict our discussion in this section to the later technique.

Mass spectrometry experiments consist of two equally important steps: ionization/vaporization and detection. Although traditional techniques such as electron impact ionization are too harsh and lead to the fragmentation of polymer molecules, the softer ionization technique of MALDI can be successfully used to fractionate polymers of narrow molecular weight distribution. The ionized analyte is accelerated through a magnetic field with voltage V, acquiring a velocity that is proportional to its mass-to-charge ratio (m/z). Time-of-flight (TOF) analyzers have been found to be the most adequate for polymer analysis. In the TOF spectrometer, the ions are separated according to their velocities and their m/z is evaluated on the basis of the time it takes for the ionized molecules to travel a flight path of length L to the detector (64):

$$t = \left(\frac{m}{2zeV}\right)^{1/2} L \tag{50}$$

Commercial MALDI-TOF instruments in the range up to 10,000 g/mol can have a resolution of up to 4 g/mol, which permits a remarkable resolution of molecular weight distributions (65). This impressive resolution is illustrated in Figure 35 for the molecular weight distribution of a polymethylmethacrylate sample (66).

The original promise of obtaining the complete molecular weight distribution of polymers with MALDI-TOF did not hold true except for polymers with very narrow distributions (polydispersity indices less than 1.2), in which case the analysis can be very accurate and reproducible (67). The reasons for this are complex and mainly caused by the fact that both the ionization process and the detector are mass-sensitive and discriminate towards the shorter chains in the population. The detector effect can be easily understood from inspection of Figure 1, where the number and weight chain length distributions of a polymer that follows Flory–Schultz's most probable distribution are compared. It is clear that the number of shorter chains greatly exceeds the number of longer chains, but the longer chains account for a much higher mass fraction of the sample. The signal of refractive index detectors, commonly used with SEC and FFF, is proportional to the mass of the polymer in the detection cell and is therefore very sensitive to the high molecular weight end of the distribution. On the other hand, the TOF detector is sensitive to the number, not the weight, of chains, and therefore the signal for the longer chains is quickly lost in the background noise. This is elegantly illustrated in Figure 36, where the molecular weight distributions of three polydimethylsiloxane samples measured by MALDI-TOF are much narrower and shifted to the low molecular weight end of the distribution than the ones measured by SEC.

In order to circumvent this limitation but still preserve the detailed molecular weight information generated by this powerful detection technique, MALDI-TOF has been used as an absolute detector, both on-line and off-line, for

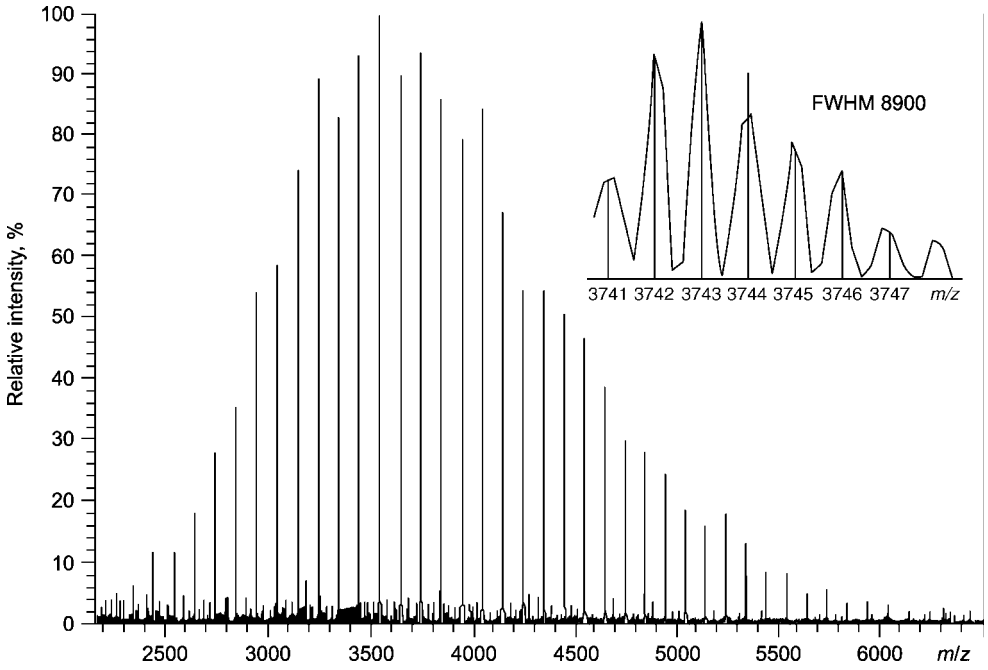

Fig. 35. MALDI analysis of a polymethylmethacrylate resin. _____ Raw data; ..... Theoretical isotope distribution. From Ref. 66.

narrow molecular weight fractions obtained by SEC (65,69,70). When applied to molecular weight measurements of homopolymers alone, MALDI-TOF brings little advantages to the already sophisticated SEC triple detector systems discussed above. However, when applied to copolymers, this approach permits the simultaneous estimation of the bivariate distribution of molecular weight and chemical composition, as explained by Suddaby and co-workers (65) and illustrated in Figure 37. In brief, this methodology consists in matching the molecular weights of the MALDI peaks for each SEC fraction to combinations of the molar masses of the comonomers using a polymerization kinetics model. Therefore, SEC/MALDI-TOF may have the potential to surpass any other known technique for the elucidation of the microstructure of synthetic copolymers.

Moreover, even though the complete molecular weight distribution for broad polymers may not be accurately recovered by MALDI-TOF alone, the very detailed molecular weight information provided for the lower molecular weight species is ideally suitable for the study of polymerization reaction mechanisms, chain end types, dendrimer analyses, and polymer identification (60–63,68).

Mass spectrometry experiments in general, and MALDI-TOF in particular, require the sample to be in the gas phase and ionized. Ionization is commonly achieved by the complexation of a cation with the polymer molecule. Polymers containing heteroatoms such as polyethers, polyamides, polyesters, polymethylmetacrylates, polysiloxanes, and polycarbonates are reasonably simple to be cationized by the addition of sodium or potassium salts. Apolar polymers containing double bonds such as polystyrene, polybutadiene, and polyisoprene can also

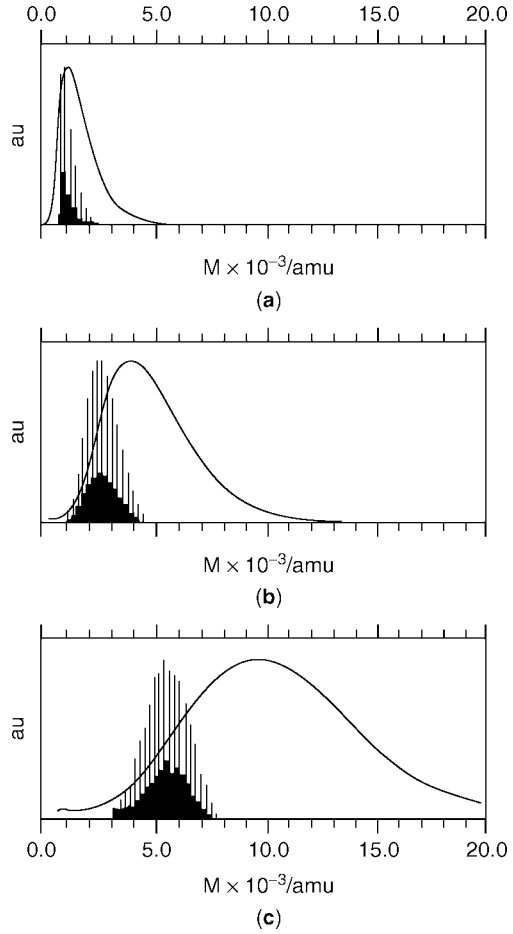

Fig. 36. Overlay of SEC and MALDI-TOF profiles for three poly(dimethylsiloxane) samples. From Ref. 67. Copyright (2000) Wiley-VCH.

be cationized with silver or copper salts. Until recently, apolar polymers with no functional groups, such as polyethylene and polypropylene, could not be analyzed by MALDI [with the exception of low molecular weight waxes and long alkanes (67)], but some alternative routes involving the functionalization of their terminal double bonds have been developed and seem to lead to sound analytical results (71–74). This is particularly attractive for the analysis of polyethylene made with metallocene catalysts that generally contains a large fraction of vinyl-terminated chains. Unfortunately, polymer–cation interactions are still the subject of much debate, even for polymer containing heteroatoms. For instance, varying the cation type in the analysis of polymethylmethacrylate samples can cause changes of 20–35% in their estimated molecular weight distributions (60).

The selection of the matrix for MALDI analysis is also far from trivial. In his comprehensive review, Nielen listed a table with more than 200 polymer/matrix/solvents entries for MALDI-TOF analysis. Homogeneous

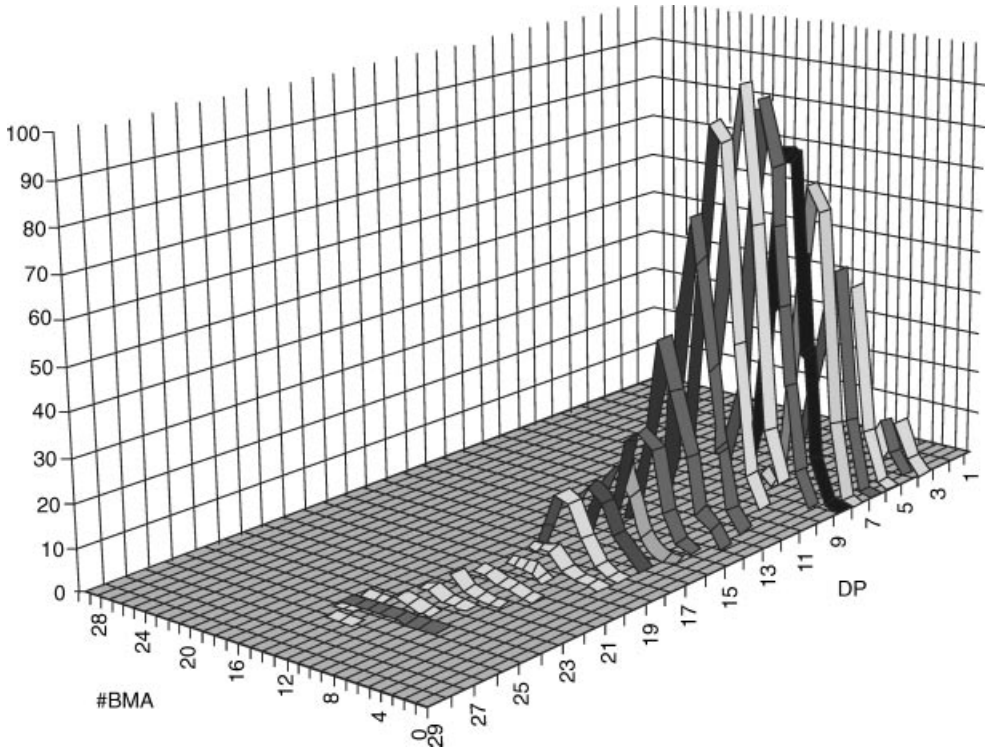

Fig. 37. Bivariate distribution of degree of polymerization (DP) and chemical composition for a copolymer of methylmethacrylate and *n*-butylmethacrylate determined by SEC–MALDI. Reprinted with permission from Ref. 65. Copyright (1996) American Chemical Society.

cocrystallization of matrix and polymer sample is essential for accurate analysis with MALDI. Generally, it is recommended that the polarities of matrix and polymer be close, but often a trial-and-error process is required. Several methods also exist for transferring the mixture of matrix, salt, and sample solutions onto the MALDI target, with electrospray deposition being considered the best approach (60).

Interaction Chromatography and Other Polymer Fractionation Techniques

The fractionation techniques described above are the ones that have proved to be applicable to the widest class of synthetic polymers over the last decades. Evidently, many more fractionation techniques have been used with many polymer types. Some of these methods will be described very briefly in the next paragraphs.

Ultracentrifugation has been used mainly for the characterization of biopolymers and gels in aqueous solutions. Some recent equipment developments have

stirred renewed interest in this fractionation method (75,76). Ultracentrifugation can be used in three main modes of operations: sedimentation velocity, equilibrium, and density gradient. In the *sedimentation-velocity* method, the centrifuge is operated at high rotational speed (above 40,000 rpm), generating a concentration profile in the fractionation cell that can be correlated to the molecular weight distribution of the polymer. In the *equilibrium* method, the centrifuge is operated at lower rotational speeds and long analysis times are required to establish the equilibrium between sedimentation and diffusion. The *density-gradient* method is mainly used to estimate the chemical composition or tacticity distributions of polymers and involves the use of two solvents of different densities. More details on centrifugation methods, including the description of new equipment apparatuses can be found in Borchard and co-workers (75).

Turbidimetric methods have also found some applications for the detection of polymer fractionation. In this case, polymer precipitation is promoted via the addition of a nonsolvent or temperature variation, according to the methods described for batch fractionation, and the turbidity created by the precipitation of the polymer chains is measured with a photometer. Both molecular weight and chemical composition fractionations can be achieved, based on the precipitation method utilized. However, only qualitative information about the distributions of molecular weight or chemical composition of the samples can be achieved by this method, because it is very difficult to relate the detector response to the actual microstructural distributions. Since this method of detection does not require the recovery of the individual polymer fractions, it may be very attractive for samples that form very viscous solutions, such as high molecular weight polymers, or samples containing inorganic fillers that would otherwise clog continuous fractionation equipment such as TREF, Crystaf, or SEC. *Cloud-point titration* is a variation of this method, used for the detection of incipient turbidity in a polymer solution. It is especially useful for the determination of the theta composition of polymer solutions. The principles of turbidimetric methods have been reviewed by Elias (77).

Many variations of interaction or adsorption chromatography have also been used to fractionate polymers. Although powerful, they are very often polymer-specific and beyond the scope of the present review. The reader is referred to the chapter of fractionation of polymers in the *Polymer Handbook* for an overview of some of these techniques (78) and to the review by Chang (37) for more details.

The power of interaction chromatography techniques will be briefly illustrated with a well-designed example for the fractionation by molecular weight of the six polystyrene samples shown in Figure 38 (79). The samples were analyzed in a high performance liquid chromatography (HPLC) system equipped with C18 bonded silica columns with various pores sizes using a solvent mixture containing a good solvent, CH_2Cl_2, and a poor solvent, CH_3CN, for polystyrene. At the highest concentration of the good solvent (65% CH_2Cl_2 by volume) the entropic effects dominate (recall eq. 20) and size exclusion is the main mechanism of separation. Thus, the chains with higher molecular weight have lower retention times. As the fraction of the good solvent CH_2Cl_2 decreases to 57%, the fractionation resolution is totally lost and all samples elute at the same retention time. At this operation condition, called the *chromatographic critical point* or the *adsorption-size exclusion transition point*, enthalpic and entropic effects cancel each other and

no separation takes place. For higher concentrations of nonsolvent, solute-support interaction effects start to dominate, increasing the enthalpic term in equation 20. At these conditions, longer chains having more repeating units interact strongly with the support and are retained longer in the columns, reversing the sequence of retention times observed during the size-exclusion mode of fractionation. A similar behavior is observed when the solvent mixture composition remains the same (CH_2Cl_2/CH_3CN: 57/43, the chromatographic critical point at 30.5°C) and the temperature is allowed to vary. According to equation 20, it is expected that the enthalpic effects will decrease as the temperature increases, and therefore fractionation by size exclusion will predominate at higher fractionation temperatures. This is indeed observed in the series of fractionations varying from 20 to 50°C, as indicated in Figure 38.

Interaction chromatography can also be used to fractionate model polymers according to long-chain branching. An application for star-shaped polystyrenes was presented by Chang and co-workers (79).

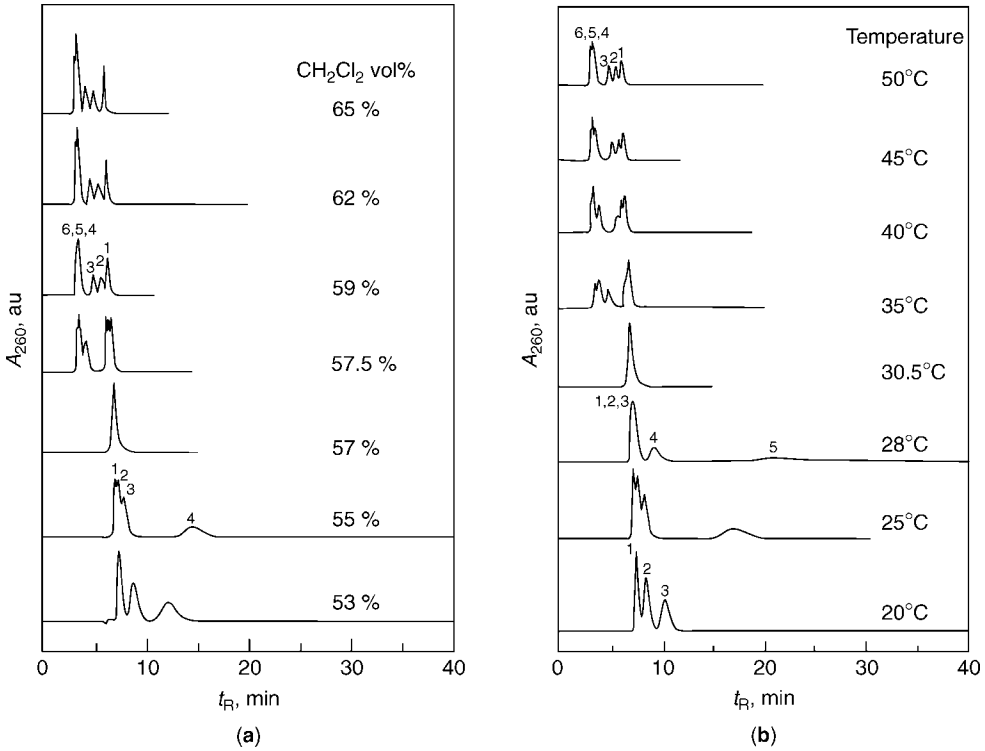

Fig. 38. Solvent composition and temperature effects for the fractionation of six polystyrene samples of different molecular weights M_w: (*1*) 2.5×10^3, (*2*) 12×10^3, (*3*) 29×10^3, (*4*) 165×10^3, (*5*) 502×10^3, and (*6*) 1800×10^3. The solvent mixture is CH_2Cl_2/CH_3CN. CH_2Cl_2 is a good solvent and CH_3CN is a poor solvent for polystyrene. The chromatograms on the left were measured at a constant temperature of 30.5°C and the ones on the right were measured at a constant ratio CH_2Cl_2/CH_3CN of 57/43 (vol/vol). From Ref. 79. Copyright (1996) Wiley-VCH.

Cross-Fractionation Chromatography and Related Techniques

Cross fractionation, also called *orthogonal fractionation*, is a term that can be applied to any technique that permits the fractionation of polymers according to two or more microstructural characteristics. For instance, polymer chains can be first separated into several fractions with narrow chemical composition distributions by TREF and each fraction can then be analyzed by SEC to recover their molecular weight distributions. When done off-line, these TREF–SEC fractionations are very time-consuming but can generate a wealth of information on polymer microstructure (80,81).

The term *cross-fractionation chromatography* (CFC) has been lately applied to a more specific method that combines TREF and SEC fractionation in an automated cross-fractionation instrument. The TREF fractions are collected in stepwise mode at predetermined temperature intervals and directly injected into the SEC columns (82). This system is very attractive because it permits the direct estimation of the bivariate distribution of molecular weight and chemical composition distribution of semicrystalline polymers. Evidently, all the considerations made above for the fractionation of complex polymers with TREF and SEC must be kept in mind when interpreting the results of these fractionations, since the separation mechanisms are not truly based on molecular weight and chemical composition but rather on hydrodynamic volume and crystallizability. CFC has been used in a large number of investigations, especially to study the polymerization mechanism of ethylene, propylene, and higher α-olefins with single- and multiple-site catalysts (83–89). Figure 39 shows the bivariate distribution of an ethylene/propylene copolymer measured by CFC and illustrates well the potential of this technique.

Interaction chromatographic separation methods that are sensitive to chemical composition have also been coupled with SEC to achieve similar cross-fractionation results for other polymer types (90–94), and fully automated instruments have been developed for HPLC–SEC orthogonal fractionations (95). It is generally preferred that the samples be first fractionated according to chemical composition by HPLC and then separated according to molecular weight by SEC.

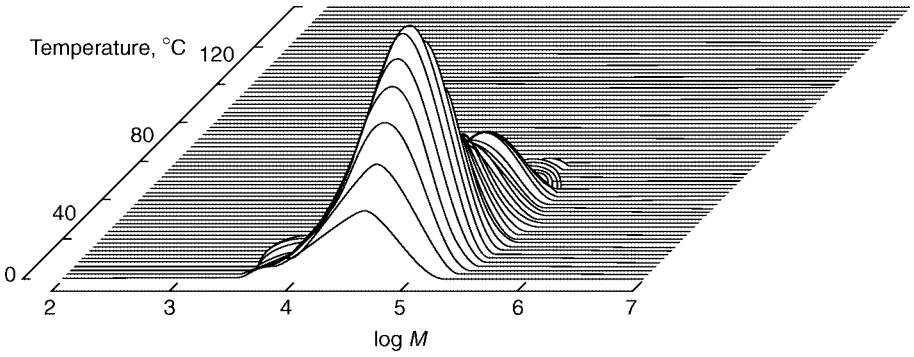

Fig. 39. Cross-fractionation chromatograph of an ethylene–propylene sample. Reprinted From Ref. 86. Copyright (2001), with permission from Elsevier.

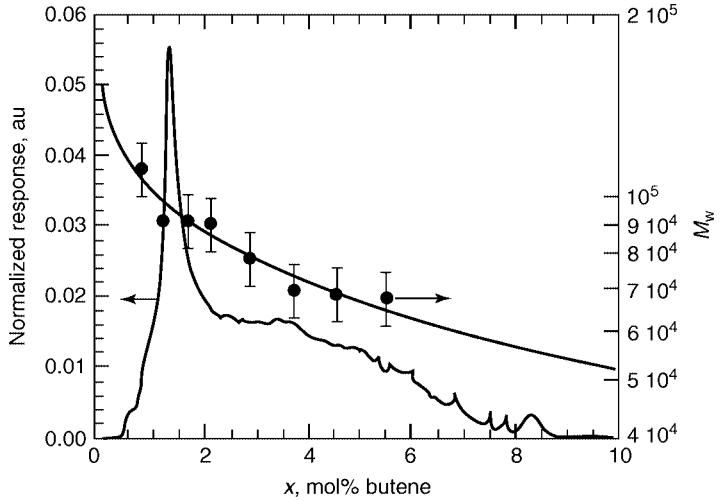

Fig. 40. Molecular weight distribution and average comonomer content for an ethylene/1-butene sample made with a Ziegler–Natta catalyst. Reprinted from Ref. 99. Copyright (2001), with permission from Elsevier.

The advantage of this sequence lies in the fact that SEC of complex copolymers responds to both molecular weight and chemical composition, while the influence of molecular weight on HPLC fractionation can be minimized by the selection of adequate analysis conditions. The importance of polymer cross-fractionation techniques is increasing because of the rapidly growing use of polymers with complex microstructures and would require a separate chapter for complete discussion. The interested reader is referred to the article by Pasch for a review on recent advances in the field of cross fractionation of polymers (96).

A simpler approach to CFC consists in measuring the average chemical composition of polymer eluting from SEC columns using an on-line Fourier transform infrared (FTIR) detector. Even though liquid flow cells can be used, signal-to-noise ratio problems may arise because of the low concentration of polymer species in the detector cell. Alternatively, the SEC effluent can be sent to a solvent evaporative interface where the polymer is deposited as a thin layer onto the surface of a germanium disk. After SEC fractionation, the disk is attached to an infrared spectrometer and the polymer microstructure is analyzed as a function of elution time (97,98). Unfortunately, this technique is not free of experimental difficulties either because it is very often difficult to obtain a uniform film deposited onto the disk. The type of information that can be obtained with SEC–FTIR is illustrated in Figure 40 for an ethylene/1-butene copolymer made with a heterogeneous Ziegler–Natta catalyst.

The SEC–FTIR combination, although attractive due to its simplicity, is not able to recover the bivariate distribution of molecular weight and chemical composition, but can only measure average composition as a function of molecular weight. Consequently, it is not a true cross-fractionation technique. A method to recover the chemical composition component of the distribution was proposed for the case of polyolefins made with single and multiple-site catalysts using a

polymerization kinetics model and molecular weight distribution deconvolution techniques (99,100).

BIBLIOGRAPHY

"Fractionation" in *EPST* 1st ed., Vol. 7, pp. 231–260, by Julien S. Johnson and Manfred J. R. Cantow, Chevron Research Co., and Roger S. Porter, University of Massachusetts; in *EPSE* 2nd ed., Vol. 7, pp. 298–327, by L. H. Tung, The Dow Chemical Co.

1. P. J. Flory, *Principles of Polymer Chemistry*, Cornell University Press, Ithaca, 1953, p. 321.
2. W. H. Stockmayer, *J. Chem. Phys.* **13**, 199 (1945).
3. S. Anantawaraskul, J. B. P. Soares, and P. Wood-Adams, *Macromol. Theory Simul.* **12**, 229 (2003).
4. J. B. P. Soares, *Chem. Eng. Sci.* **56**, 4131 (2001).
5. J. B. P. Soares and A. E. Hamielec, *Macromol. Theory Simul.* **5**, 547 (1996).
6. J. B. P. Soares and A. E. Hamielec, *Macromol. Theory Simul.* **6**, 591 (1997).
7. K. Kamide, in L. H. Tung, ed., *Fractionation of Synthetic Polymers* Marcel Dekker, Inc., New York, 1977, p. 103.
8. F. Francuskiewicz, *Polymer Fractionation*, Springer-Verlag, Berlin, 1994.
9. Ref. 1, pp. 559–563.
10. H. F. Mark, ed., *Encyclopedia of Polymer Science and Engineering*, 2nd ed., Vol. 7, John Wiley & Sons, Inc., New York, 1985, p. 298.
11. Ref. 8, pp. 66–67.
12. L. Mandelkern, *Crystallization of Polymers*, Cambridge University Press, Cambridge, 2002.
13. Ref. 1, p. 569.
14. S. Anatawaraskul, J. B. P. Soares, and P. M. Wood Adams, *J. Polym. Sci., Part B: Polym. Phys.* **41**, 1762 (2003).
15. L. Wild, *Adv. Polym. Sci.* **98**, 1 (1990).
16. D. M. Sarzotti, J. B. P. Soares, and A. Penlidis, *J. Polym. Sci., Part B: Polym. Phys.* **40**, 2595 (2002).
17. A. A. da Silva Filho, J. B. P. Soares, and G. B. de Galland, *Macromol. Chem. Phys.* **201**, 1226 (2000).
18. S. Anantawaraskul, J. B. P. Soares, P. M. Wood-Adams, and B. Monrabal, *Polymer* **44**, 2393 (2003).
19. J. Nieto, T. Oswald, F. Blanco, J. B. P. Soares, and B. Monrabal, *J. Polym. Sci., Part B: Polym. Phys.* **39**, 1616 (2001).
20. S. Anantawaraskul, J. B. P. Soares, and P. M. Wood-Adams, *Macromol. Chem. Phys*. (in press).
21. J. B. P. Soares and A. E. Hamielec, in R. A. Pethrick and J. V. Dawkins, eds., *Modern Techniques for Polymer Characterisation*, John Wiley & Sons, Inc., Chichester, U.K., 1999, p. 15.
22. M. McHugh and V. Krukonis, *Supercritical Fluid Extraction—Principles and Practice*, 2nd ed., Butterworth-Heinemann, Boston, 1994.
23. B. Folie, M. Keltchtermanns, J. R. Schutt, H. Schonemann, and V. Krukonis, *J. Appl. Polym. Sci.* **64**, 2015 (1997).
24. J. J. Watkins, V. J. Krukonis, P. D. Condo, D. Pradham, and P. Ehrlich, *J. Supercrit. Fluids* **4**, 24 (1991).
25. L. J. D. Britto, J. B. P. Soares, A. Penlidis, and V. Krukonis, *J. Polym. Sci., Part B: Polym. Phys.* **37**, 553 (1999).

26. J. B. P. Soares and A. E. Hamielec, *Macromol. Theory Simul.* **4**, 305 (1995).
27. J. B. P. Soares, B. Monrabal, J. Nieto, and J. Blanco, *Macromol. Chem. Phys.* **199**, 1917 (1998).
28. D. Beigzadeh, J. B. P. Soares, and T. A. Duever, *J. Appl. Polym. Sci.* **80**, 2200 (2001).
29. D. Campbell, R. A. Pethrick, and J. R. White, *Polymer Characterization*, 2nd ed., Stanley Thornes Publishers Ltd., Cheltenham, U.K., 2000, pp. 38–49.
30. G. Glöckner, *J. Chromatogr. Libr.* **34**, 116–137 (1987).
31. Z. Grubisic, P. Rempp, and H. Benoit, *Polym. Lett.* **5**, 753 (1967).
32. L. H. Tung and J. C. Moore, in L. H. Tung, ed., *Fractionation of Synthetic Polymers*, Marcel Dekker, Inc., New York, 1977, p. 545.
33. M. G. Styring and A. E. Hamielec, in A. R. Cooper, ed., *Determination of Molecular Weight*, John Wiley & Sons, Inc., New York, 1989, p. 263.
34. G. L. Hagnauer, *Anal. Chem.* **54**, 265R (1982).
35. W. W. Yau, J. J. Kirkland, and D. D. Bly, *Modern Size-Exclusion Liquid Chromatography: Practice of Gel Permeation and Gel Filtration Chromatography*, John Wiley & Sons, Inc., New York, 1979.
36. E. F. Cassassa, *Macromolecules* **9**, 182 (1976).
37. T. Chang, *Adv. Polym. Sci.* **163**, 1 (2003).
38. L. D'Agnillo, J. B. P. Soares, and A. Penlidis, *J. Polym. Sci., Part B: Polym. Chem.* **40**, 905 (2002).
39. H. G. Barth, B. E. Boyles, and C. Jackson, *Anal. Chem.* **70**, 251R (1998).
40. J. C. Giddins, *Unified Separation Science*, John Wiley & Sons, Inc., New York, 1991, pp. 200–215.
41. J. C. Giddings, *Unified Separation Science*, John Wiley & Sons, Inc., New York, 1991.
42. M. E. Schimpf, *Trends Polym. Sci.* **4**, 114 (1996).
43. H. Cölfen, and M. Antonietti, *Adv. Polym. Sci.* **150**, 67 (2000).
44. J. Janca, in R. A. Pethrick and J. V. Dawkins, eds., *Modern Techniques for Polymer Characterization* John Wiley & Sons, Inc., Chichester, U.K., 1999, p. 57.
45. J. Janca, *Field-Flow Fractionation: Analysis of Macromolecules and Particles*, Marcel Dekker, Inc., New York, 1988.
46. J. C. Giddins, *Sep. Sci. Technol.* **13**, 241 (1978).
47. J. C. Giddins, *Sep. Sci. Technol.* **18**, 765 (1983).
48. J. Janca, *Makromol. Chem., Rapid Commun.* **3**, 887 (1982).
49. J. J. Gunderson and J. C. Giddings, in C. Booth and C. Price, eds., *Polymer Characterization* Pergamon Press, Oxford, 1989, p. 279.
50. J. C. Giddins, *Anal. Chem.* **66**, 2783 (1994).
51. B. A. Wolf, in D. Bloor, M. C. Flemings, R. J. Brooks, and S. Mahajan, eds, *The Encyclopedia of Advanced Materials*, Pergamon Press, Oxford, 1994, p. 881.
52. H. Geerissen, J. Roos, and B. A. Wolf, *Makromol. Chem.* **186**, 735 (1985).
53. H. Geerissen, J. Roos, P. Schützeichel, and B. A. Wolf, *J. Appl. Polym. Chem.* **34**, 271 (1987).
54. H. Geerissen, P. Schützeichel, and B. A. Wolf, *J. Appl. Polyn. Sci.* **34**, 287 (1987).
55. H. Geerissen, P. Schützeichel, and B. A. Wolf, *Makromol. Chem.* **191**, 659 (1990).
56. K. Weinmann, B. A. Wolf, M. T. Rätzsch, and L. Tschersich, *J. Appl. Polym. Sci.* **45**, 1265 (1992).
57. A. C. Hagenaars, Ch. Bailly, A. Schneider, and B. A. Wolf, *Polymer* **43**, 2663 (2002).
58. S. Loske, A. Schneider, and B. A. Wolf, *Macromolecules* **36**, 5008 (2003).
59. WO Pat. Appl. PCT/EP03/00755, J. Eckelt, T. Haase, S. Loske, and B. A. Wolf.
60. M. W. F. Nielen, *Mass Spectrom. Rev.* **18**, 309 (1999).
61. G. Montaudo, *Trends Polym. Sci.* **4**, 81 (1996).
62. D. M. Haddleton, in A. J. Ryan, ed., *Emerging Themes in Polymer Science* The Royal Society of Chemistry, Cambridge, 2001, p. 61.

63. E. Scamporrino and D. Vitalini, in R. A. Pethrick and J. V. Dawkins, eds., *Modern Techniques for Polymer Characterization* John Wiley & Sons, Inc., Chichester, U.K., 1999, p. 233.
64. J. R. Chapman, *Practical Organic Mass Spectrometry: A Guide for Chemical and Biochemical Analysis*, 2nd ed., John Wiley & Sons, Inc., Chichester, U.K., 1983, p. 11.
65. K. G. Suddaby, K. H. Hunt, and D. M. Haddleton, *Macromolecules* **29**, 8642 (1996).
66. A. T. Jackson, H. T. Yates, C. I. Lindsay, Y. Didier, J. A. Segal, J. H. Scrivens, G. Critchley, and J. Brown, *Rapid Commun. Mass Spectrom.* **11**, 520 (1997).
67. C. M. Guttman, S. J. Wetzel, W. E. Wallace, W. R. Blair, R. M. Goldschmidt, D. L. Vanderhart, and B. M. Fanconi, *Polym. Prepr.* **41**, 678 (2000).
68. D. M. Haddleton, S. A. F. Bon, K. L. Robinson, N. J. Emery, and I. Moss, *Macromol. Chem. Phys.* **201**, 694 (2000).
69. M. S. Montaudo, C. Puglisi, F. Samperi, and G. Montaudo, *Polym. Prepr.* **41**, 686 (2000).
70. M. S. Montaudo, *Polymer* **43**, 1587 (2002).
71. R. Chen, T. Yalcin, W. E. Wallace, C. M. Guttman, and L. Li, *J. Am. Soc. Mass Spectrom.* **12**, 1186 (2001).
72. B. J. Bauer, W. E. Wallace, B. M. Fanconi, and C. M. Guttman, *Polymer* **42**, 9949 (2001).
73. S. Lin-Gibson, L. Brunner, D. L. Vanderhart, B. J. Bauer, B. M. Fanconi, C. M. Guttman, and W. E. Wallace, *Macromolecules* **35**, 7149 (2002).
74. H. Ji, N. Sato, Y. Nakamura, Y. Wan, A. Howell, Q. A. Thomas, R. F. Storey, W. K. Nonidez, and J. W. Mays, *Macromolecules* **35**, 1196 (2002).
75. W. Borchard and E. Selic, in R. A. Pethrick and J. V. Dawkins, eds., *Modern Techniques for Polymer Characterization* John Wiley & Sons, Inc., Chichester, U.K., 1999, p. 317.
76. H. Cölfen, *Polym. News* **23**, 152 (1998).
77. H. G. Elias, in L. H. Tung, ed., *Fractionation of Synthetic Polymers* Marcel Dekker, Inc., New York, 1977, p. 345.
78. J. M. Barrales-Rienda, A. Bello, P. Bello, and G. M. Guzmán, in J. Brandup, E. H. Immergut, and E. A. Grulke, eds., *Polymer Handbook* 4th ed., John Wiley & Sons, Inc., New York, 1999, Chapt. VII, p. 327.
79. T. Chang, H. C. Lee, W. Lee, S. Park, and C. Ko, *Macromol. Chem. Phys.* **200**, 2188 (1999).
80. J. B. P. Soares and A. E. Hamielec, *Polymer* **37**, 4606 (1996).
81. M. Zhang, D. T. Lynch, and S. E. Wanke, *J. Appl. Polym. Sci.* **75**, 960 (2000).
82. S. Nakamo and Y. Goto, *J. Appl. Polym. Sci.* **26**, 4217 (1981).
83. N. Aust, I. Beytollahi-Amtmann, and K. Lederer, *Int. J. Polym. Anal. Charact.* **1**, 245 (1995).
84. M. Yamahiro, H. Mori, K. Nitta, and M. Terano, *Polymer* **40**, 5265 (1999).
85. K. Nomura, K. Oya, and Y. Imanishi, *Polymer* **41**, 2755 (2000).
86. M. C. Haag, C. Krug, J. Dupont, G. B. de Galland, J. H. Z. dos Santos, T. Uozumi, T. Sano, and K. Soga, *J. Mol. Catal. A: Chem.* **169**, 275 (2001).
87. F. Shimizu, J. T. M. Pater, and G. Weickert, *J. Appl. Polym. Sci.* **81**, 1035 (2001).
88. K. Nomura, H. Okumura, T. Komatsu, and N. Naga, *Macromolecules* **35** (2002).
89. N. Naga and Y. Imanishi *J. Polym. Sci., Part A: Polym. Chem.* **41**, 441 (2003).
90. G. Glöckner, M. Strickler, and W. Wunderlich, *J. Appl. Polym. Sci.* **37**, 3147 (1989).
91. M. Augenstein and M. Stickler, *Makromol. Chem.* **191**, 415 (1990).
92. S. Mori, *J. Chromatogr.* **503**, 411 (1990).
93. S. Mori, *Anal. Chem.* **60**, 1125 (1988).
94. S. Mori, *Anal. Chem.* **53**, 1813 (1981).
95. P. Kilz, R. P. Krüger, H. Much, and G. Schulz, *ACS Adv. Chem.* **247**, 223 (1995).
96. H. Pasch, *Adv. Polym. Sci.* **150**, 1 (2000).
97. L. M. Wheeler and J. N. Willis, *Appl. Spectrosc.* **47**, 1128 (1993).

98. T. Provder, M. Whited, D. Huddleston, and C. Y. Kuo, *Prog. Org. Coat.* **32**, 155 (1997).
99. A. Faldi and J. B. P. Soares, *Polymer* **42**, 3057 (2001).
100. J. B. P. Soares, R. F. Abbott, J. N. Willis, and X. Liu, *Macromol. Chem. Phys.* **197**, 3383 (1996).

JOAO B. P. SOARES
University of Waterloo

FRACTOGRAPHY. See Volume 2.

FRACTURE. See Volume 2.

FREE RADICAL POLYMERIZATION. See RADICAL POLYMERIZATION.

FRP. See RADICAL POLYMERIZATION.

GEL POINT

Introduction

The gel point (GP) marks the transition of a material from liquid to solid. The transition is caused by the growth of structure in the material, a structure that correlates molecular or supramolecular motion over large distances. At GP, the correlation length diverges to infinite size. This appearance of long-range connectivity is most easily seen in a rheological experiment (1).

The growth of connected structure is called *gelation* and its opposite, the decay of connectivity, is called *reverse gelation*. Depending on connectivity mechanism, the wide variety of gels can be grouped into two classes (2,3), the three-dimensionally connected networks and all the others for which the connectivity mechanism is less clearly defined. This second group of gels goes under many different names such as "jamming," "soft glass," "colloidal glass," "self-assembly," "granular gel" to mention a few. For lack of a specific term, here we call this second group the *glassy gels* since they often involve nonequilibrium states. As a common property of both classes of gels, the material structure immobilizes as it assumes a state of minimal internal energy that would get disturbed by flow. GP is marked by the divergence of regions of immobile structure to infinite size. Below GP connectivity, the material is able to flow and to relax while, beyond the gel point, a yield stress needs to be overcome before flow may happen.

Since a polymer at its gel point is in a critical state (4–9), it commonly is called a *critical gel* (10) to distinguish it from the various materials that are commonly called gel. It is interesting to explore the properties of the critical gel and use these as reference for describing the properties in the vicinity of the gel point. The critical gel affords universal rheological properties that are intermediate between liquid and solid, including the temperature shift factors that are also in between (11). It combines extreme ductility and fragility when subjected to large strain. Its

Encyclopedia of Polymer Science and Technology. Copyright John Wiley & Sons, Inc. All rights reserved.

high adhesion strength (tackiness) is also an expression of the intermediate state; the critical gel still maintains the wetting properties of the liquid (low molecular weight polymer) while starting to gain the cohesive strength of the solid. The adhesion behavior must be accounted for when designing experiments with gels. It also suggests future applications of gels as adhesives.

The information most needed can be summed up in the following questions:

(1) When does GP occur?
(2) How soft or stiff is the material at GP?
(3) How fast does the material pass through GP?

These questions can be answered with the knowledge of the properties at GP. The simplicity and universality of the GP behavior, as shown below, suggests the use of the critical gel as reference state for developing soft materials.

Rheological Properties of the Critical Gel

The evolution of equilibrium mechanical properties during gelation is schematically shown in Figure 1 (using the example of chemical gelation). The steady shear viscosity of the liquid state grows as the connectivity increases. In the approach to GP, the steady shear viscosity diverges (ie, an infinite time would be necessary for the flow to reach steady state). Beyond GP, the equilibrium modulus starts to grow. At GP, the viscosity is infinite while the equilibrium modulus is still zero

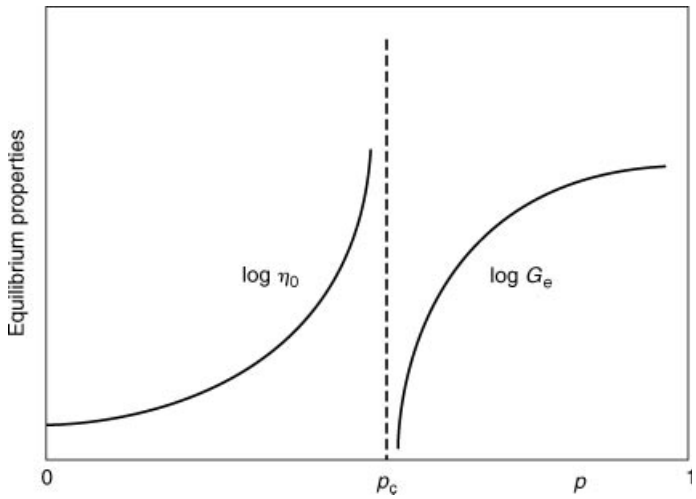

Fig. 1. Evolution of mechanical properties of a cross-linking polymer as a function of extent of cross-linking p (schematic). Representative properties are the steady shear viscosity for the liquid state (sol) and the equilibrium modulus for the solid state (gel). All viscoelastic liquid states are in between the Newtonian liquid ($p = 0$) and the critical gel ($p = p_c$). Equivalently, all viscoelastic solids are in between the critical gel and the Hookean solid ($p = 1$).

because the stress in a deformed critical gel can still relax completely. This shows that the conventional equations for a liquid (characterized by a steady shear viscosity) or for a solid (characterized by an equilibrium modulus) do not apply at GP. The critical gel has its own rheological behavior (1). The critical gel

a. requires infinite time to relax and
b. relaxes in a broad distribution of shorter modes which are self-similar.

This expresses itself in slow power law dynamics for both the linear relaxation modulus $G(t)$ and the relaxation time spectrum $H(\lambda)$ (12–14)

$$G(t) = St^{-n_c}; \qquad H(\lambda) = \frac{S\lambda^{-n_c}}{\Gamma(n_c)} \quad \text{for} \quad \lambda_0 < t < \infty \tag{1}$$

This rheological pattern seems to be a universal rheological property, since it occurs with both network gels and glassy gels at GP. Experiments with a large variety of chemically or physically gelling materials show this self-similar behavior without exception. The gamma function $\Gamma(n_c)$, arises naturally in the conversion of $G(t)$ into $H(\lambda)$. The two material parameters are the stiffnes S and the relaxation exponent n_c. Subscript c is used here to identify the critical state at the gel point. λ_0 is a crossover time to small-scale dynamics of the building blocks of the critical gel.

In comparison, a power law behavior has been predicted for molecules of self-similar (fractal) structure (15,16), suggesting that the critical gel is self-similar over a wide range of length scales (10,17). It also has been shown, without use of an analogy, that the onset of rigidity in a randomly cross-linked system is a continuous phase transition (18); at the transition, the correlation length diverges and the system is necessarily self-similar. The scaling behavior is then an automatic consequence of statistical thermodynamics (qv). Several theories have been proposed for the critical gel behavior (19–22).

The relaxation exponent n_c may assume values in the range $0 < n_c < 1$ (21). Its value cannot be predicted since a systematic study of the effect of molecular architecture on the value of the relaxation exponent is still missing. Typical experimental values are as follows:

$n_c \cong 0.5$ for end-linking networks with balanced stoichiometry (12,14,23)
$n_c \cong 0.5$–0.7 for end-linking networks with imbalanced stoichiometry (12,13,24)
$n_c \cong 0.7$ for epoxies (25)
$n_c \cong 0.8$ for PVC plastisol (26)
$n_c \cong 0.3$ for radiation cross-linked polyethylene (27)
$n_c \cong 0.5$ for micellar block polyelectrolytes (28)

The gel strength S depends on the value of n_c. A large value of S is always associated with a small value of n_c. Very little information is available about n_c of glassy gels.

The dynamic modulus of the critical gel, as described by equation 1, is also a power law:

$$G^*(\omega, p_c) = \Gamma(1 - n_c)\, S(i\omega)n_c \tag{2}$$

The real (the storage modulus G') and imaginary (loss modulus G'') parts are related as

$$G'(\omega, p_c) = \frac{G''(\omega,p_c)}{\tan(\frac{n_c\pi}{2})} = \Gamma(1 - n_c)S\omega^n \cos\left(\frac{n_c\pi}{2}\right) \tag{3}$$

The phase shift δ as defined by the loss tangent $\tan\,\delta = G''/G'$, is proportional to the slope of the dynamic modulus at GP (13):

$$\delta_c = \frac{n_c\pi}{2} \tag{4}$$

Introduced into a general constitutive equation for linear Viscoelasticity (qv) (29,30), the above relaxation modulus results in the constitutive equation for critical gels, the Winter–Chambon gel equation: (12,13)

$$\tau(t) = S\int_{-\infty}^{t} \mathrm{d}t'(t - t')^{-n_c}\dot{\gamma}(t') \tag{5}$$

The gel equation predicts all known rheological properties of critical gels, such as infinite viscosity and zero equilibrium modulus, as long as the applied strain is small. For large strains, a suitable strain measure must be introduced (12). Large strain behavior and breaking of the structure (reverse gelation by mechanical field) is not included in this equation. The breaking of critical gels (31) is a topic which needs to be investigated more closely in the future.

Chemical Gel Point

Chemically cross-linking polymers belong to the group of network gels. Molecules cross-link into large clusters through covalent bonds. The independent variable of the cross-linking process is the extent of reaction, p, which can be understood as bond probability. The polymer reaches the GP at a critical extent of the cross-linking reaction, $p \rightarrow p_c$. At GP, the second moment of the cluster size distribution diverges (7) and the molecular weight distribution is infinitely broad ($M_w/M_n \rightarrow \infty$) as molecules range from the smallest unreacted oligomer to the infinite cluster. The molecular motions are correlated over large distances but the critical gel has no intrinsic size scale. The liquid polymer before the GP, $p < p_c$, is called a *sol* because it is soluble in good solvents. The solid polymer beyond the GP, $p_c < p$, called a *gel* is not soluble any more, even in a good solvent. However, unattached molecules (sol fraction) are still extractable from the gel.

Prediction of the Chemical Gel Point. The classical mean field theories (32–34) are able to predict the critical conversion p_c quite accurately (35,36). The

predictions are mainly based on the assumptions that all functional groups of the same type are equally reactive, all groups react independently of one another, and no intramolecular reactions occur in finite species. The threshold p_c depends on the geometry of the network-forming species. Special cases follow.

Case 1. Homopolymerization of similar f-functional molecules:

$$p_c = \frac{1}{f-1} \tag{6}$$

The same relation is found for the end-linking of molecules of low functionality ($f = 3$ or 4) and for the vulcanization of long molecular chains. The average number of cross-linking sites along the chain is defined as

$$f = \frac{\sum_i f_i^2 n_f}{\sum_i f_i n_f} \tag{7}$$

with n_f being the number of molecules of functionality f_i.

Case 2. Cross-linking of f-functional molecules A_f with g-functional molecules B_g, which are mixed at a molar ratio

$$r = \frac{f(A_f)}{g(B_g)}$$

reaches the gel point at a conversion

$$p_{A,c} = [r(f-1)(g-1)]^{-1/2} \tag{8}$$

with $p_B = r p_A$. For the formation of a gel, the stoichiometric ratio must be chosen between a lower and upper critical value:

$$r_l = [(f-1)(g-1)]^{-1} \quad \text{and} \quad r_u = 1/r_l \tag{9}$$

Otherwise the reaction stops before reaching the gel point. The relations in equation 9 follow from equation 8 when considering species A_f or species B_g fully reacted, respectively.

Instead of the extent of reaction, the *stoichiometric ratio* is often chosen as independent variable of a chemical gelation experiment. Consider a system that consists of cross-linker A (average functionality $f = 3$ or $f = 4$, etc) and chain extender B (functionality $g = 2$). Assuming that the reaction is always brought to completion, the degree of cross-linking would depend on the stoichiometric ratio r (ratio of cross-linker sites to chain extender sites). The stoichiometry dependence of equilibrium mechanical properties is sketched in Figure 2. The cross-link density is a maximum for balanced stoichiometry. The viscosity diverges at a lower and an upper critical ratio r_l and r_u of equation 9. Solid behavior is found everywhere at intermediate stoichiometry $r_l < r < r_u$. Critical gels are formed at $r = r_l$ and $r = r_u$.

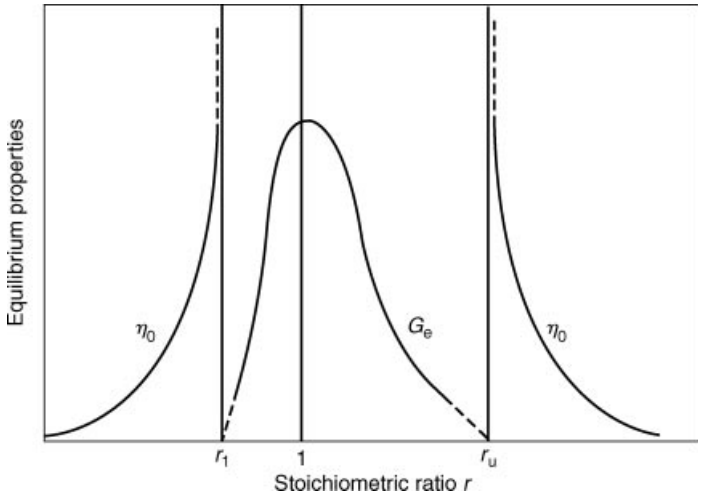

Fig. 2. Steady-state mechanical properties (schematic) of cross-linking polymers with different stoichiometric ratios r, defined as ratio of cross-linking sites of two reacting polymers. The reaction is presumably brought to completion. Steady critical gel behavior is found at the lower and the upper critical values, r_l and r_u.

Physical Gel Point

Physical gels are able to form sample-spanning, supermolecular structures. Connectivity has been found with a wide range of mechanisms which have been reviewed extensively by te Nijenhuis (37), Larson (38), and Nishinari (39). Physical gels come as both network materials (associative networks) and glassy gels. Such glassy gels can energetically associate into a sample-spanning structure, by repulsion as well as by attraction, leading to nonequilibrum states (soft glasses) (3,28). In analogy to chemical gelation, the physical gelation is defined by the growth of physically connected aggregates and the physical gel point is reached when the correlation length of molecular (or supramolecular) motion diverges to infinity. For temperature-dependent connectivity these materials are called *thermoreversible* (40); however, other variables might determine the connectivity such as pH value, concentration of connecting component, charge density, or stress level.

The principal differences between chemical and physical gels lie in the lifetime and the functionality of the junctions. Chemical bonds are considered to be permanent while the physical junctions have finite lifetimes. Physical junctions are constantly created and destroyed, however, at very low rates so that the network appears to be permanently connected if the time of observation is shorter than the lifetime of the physical network. For longer times of loading, the material flows and is characterized as a liquid even beyond its gel point. The analogy between chemical and physical gelation applies very well to systems with long-living bonds. It becomes less defined when renewal of physical bonds occurs on the time scale of observation and the system behaves as a liquid. In this case, a characteristic renewal time, λ_{pg}, of the physical bonds determines long-time ordering processes and rheology of a physical gel.

The analogy between physical and chemical gelation applies only to time scales shorter than the characteristic renewal time. Equation 1 changes into

$$G(t) = S_c t^{-n_c} \quad \text{for} \quad \lambda_0 < t < \lambda_{pg} \tag{10}$$

Physical gels typically have a yield stress beyond which the structure gets broken and liquid behavior sets in. Below the yield stress, the physical gel is a solid at experimental times shorter than the renewal time and it is a liquid at experimental times longer than the renewal time.

Range of the Power Law

The power law of the critical gel of a cross-linking polydimethylsiloxane (PDMS) was found for G' and G'' to extend over a frequency range of more than five decades (13,14), the entire experimental range. A lower frequency limit is given by the correlation length, which is the linear size of a typical cluster of the self-similar structure. This correlation length diverges at GP and the lower frequency limit of the power law could theoretically be extended to zero. However, a practical lower frequency limit is given by the finite sample size, ie, at a scale of observation that exceeds the size of the sample in the rheometer. The upper frequency limit of the power law behavior very much depends on the small scale structure of the critical gel.

For chemical gelation, the upper frequency limit (and the corresponding lower time limit, λ_0, of eqs. 1 and 10) typically depends on the following two molecular sizes:

(1) *Size of the chains between cross-links*: The randomly coiled chains exhibit self-similar behavior and the transition from the self-similar critical gel to the self-similar chain (between network junctions) is difficult to detect experimentally.
(2) *Glass length*: At very high frequency, the scale of observation decreases below the lower scaling length of the polymer called the *glass length*. The *glass length* is given by the size of the network element that determines the transition to glassy behavior at low temperature. This smallest network element depends on the specific molecular structure. It could be the distance between cross-links or the length of a chain unit. At this small-length scale, vitrification becomes important and deviation from equilibrium self-similar behavior is expected. In this description of chemical gelation, it is tacitly assumed that the scale of observation is sufficiently larger than the glass length. The details of the molecular structure are neglected by neglecting the high frequency transition to the glass behavior of the chemical networks.

Physical critical gels typically have a very limited power law region. The slow dynamics is governed by the transition to flow behavior as an expression of the finite lifetime of the physical junctions. The faster dynamics undergoes transition to the dynamics of the structural building blocks. These building blocks

are typically quite large in physical gels so that their dynamics can be seen at already low frequency. Between these two phenomena, little may remain of the self-similar dynamics of the critical gel. General relations are difficult to find because of the large variety of connectivity mechanisms, especially is glassy gels. Nonequilibrium states make the power law parameters path-dependent, ie they depend on the history of the glassy gel formation.

Vicinity of the Gel Point

The power law region seems to stretch out and then contract again, having its widest range at GP. The slope gradually decreases during gelation. This phenomenon is visible on cross-linking of PDMS (13,14), and it is very pronounced for radiation cross-linking of polyethylene (27). It is found in physical gels (26,28,41–44) as well as in chemical gels.

The longest relaxation time λ_{max} first grows to infinity and then decays again. In the vicinity of GP, this may be expressed in power laws (45):

$$\lambda_{max} \sim \begin{cases} (p-p_c)^{-s/(1-n_c)} & \text{for} \quad p<p_c \\ (p_c-p)^{-z/n_c} & \text{for} \quad p_c<p \end{cases} \tag{11}$$

These equations hold for small introduce absolute value signs $|p - p_c|$, ie, in the vicinity of GP. Materials near GP are often called *nearly critical gels*. The exponents depend not only on the dynamic critical exponent (relaxation exponent n_c) but also on the dynamic exponents s and z for the viscosity $\eta \sim (p_c - p)^{-s}$ and the equilibrium modulus $G_e \sim (p - p_c)^z$. If one, in addition, assumes symmetry of the diverging λ_{max} near the gel point

$$\frac{s}{1-n_c} = \frac{z}{n_c} \tag{12}$$

then the critical exponents are related as (45,46)

$$n_c = \frac{s}{s+z} \tag{13}$$

Into these relations one may introduce specific values (s, z) from percolation theory or from branching theory and determine the corresponding values for n_c. The wide range of values for the relaxation exponent $0 < n_c < 1$ lets us expect that the dynamic exponents s and z are nonuniversal. Since s and z can be predicted from theory (47), n_c values can be calculated from equation 13. This result, however, relies on the symmetry hypothesis, which does not seem to be generally valid, at least not for highly entangled polybutadienes (48).

The slow dynamics of a system, for which the relaxation time goes through a singularity, can be described with a discrete relaxation time spectrum with a

longest relaxation time $\lambda_{max}(p)$ that diverges at GP:

$$G(t,p) = G_e + \frac{S}{n\ \Gamma(n)\lambda_{max}^n} \sum_{i=1}^{\infty} \exp\left(- \frac{ti^{1/n}}{\lambda_{max}} \right) \tag{14}$$

Its four parameters G_e, S, λ_{max}, and n all depend on the bond probability p. In the liquid below GP and at GP, the equilibrium modulus is equal to zero, $G_e = 0$. For $n = 0.5$ and $G_e = 0$, this spectrum reduces to the well-known Rouse spectrum. It is remarkable that depending on the value of λ_{max}, the Rouse spectrum describes a viscoelastic liquid that includes the Newtonian liquid ($\lambda_{max} \to 0$) and the critical gel ($\lambda_{max} \to \infty$) as limiting cases.

Alternatively to equation 14, a cutoff function $F(t, \lambda_{max})$ may be applied to the equation of the critical gel, equation 1:

$$G(t,p) = G_e + St^{-n}F(t, \lambda_{max}) \tag{15}$$

The model reduces to the power law at the gel point $F(t, \lambda_{max}) \to 1$ for $\lambda_{max} \to \infty$. The stretched exponential cutoff function (49)

$$F(t, \lambda_{max}) = e^{-(t/\lambda_{max})^{\beta}} \quad \text{with} \quad 0 < \beta < 1 \tag{16}$$

was found to give good results with a curing epoxy (50).

Measurements of Instant of Gelation

Equilibrium Rheological Measurements. The appearance of an equilibrium modulus or the divergence of the steady shear viscosity might be used to estimate the position of the gel point by extrapolation. Extrapolation is necessary because these measurements fail in the close vicinity of GP. Measurement of the equilibrium modulus (51,52) is extremely difficult because its value remains below the detection limit for a considerable time and it, theoretically, requires an infinite time to perform the measurement. The diverging steady shear viscosity (53–55) indicates the location of GP. The simplicity of this experiment may lead to neglect of the severe shortcomings that can be summed up as follows:

(1) GP is found by extrapolation of an experiment which never can reach steady state since the longest relaxation time diverges at GP.
(2) The network structure near GP is very fragile and most probably gets broken during the viscosity measurement, causing an apparent delay in gelation or may induce reverse gelation.

For these reasons, steady-state measurements give only an apparent gel point. The real and the apparent gel point might be close together, but additional experiments will be needed for confirming such an assumption.

Transient Rheological Measurement. The nature of the critical gel suggests transient measurements, which are possible even if the longest relaxation

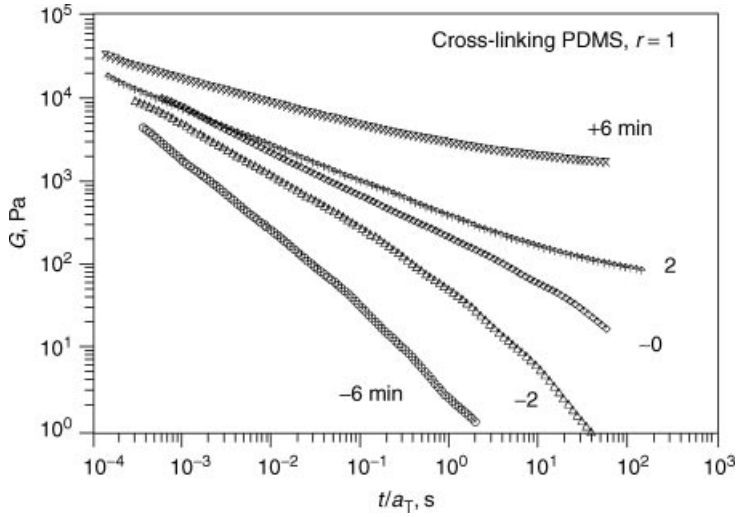

Fig. 3. Evolution of relaxation modulus of a cross-linking polymer as shown with five samples of increased cross-link density. Parameter is the reaction time distance from the gel point ($t - t_c$). The values are calculated from dynamic mechanical data (13). The power law relaxation is limiting behavior for the liquid and the solid. One of the samples is very close to the critical gel. However, at very long times it deviates from the power law behavior. It is still a fluid.

time diverges. A typical evolution of the relaxation modulus is shown in Figure 3. The power law is distinguished from the other states by being a straight line. It shows that the entire relaxation time spectrum is affected by the gel transition. It is surprising to find that intermediate relaxation modes, which are accessible to experiment, are affected by the diverging longest relaxation time in a way that makes it possible to distinguish between a sol and a gel (1,13,14). It is not necessary to measure the diverging longest relaxation time; measurement of intermediate relaxation modes suffice for detecting the gel point in many different ways. Three examples are as follows:

(1) the loss tangent $\tan \delta = G''/G'$ of the critical gel is independent of the frequency of the dynamic experiment. GP is detected by the intersect of $\tan \delta$ curves (see Fig. 4). A multifrequency experiment has been designed for detecting the GP based on this approach (56).

(2) For start-up of shear flow at constant rate, the transient viscosity grows in a power law with time. This might be utilized for detecting GP. The total strain must be kept small because, near GP, stress relaxation is infinitely slow and shear modification cannot be avoided even at extremely low rates of deformation.

(3) It is especially simple to detect the instant of gelation of a material whose critical relaxation exponent n_c is known. For any frequency (within the power law region) and any temperature, in a small amplitude oscillatory shear experiment at constant ω_0, GP is reached at the instant at which functions $G'(\omega_0, t)/\cos(n_c\pi/2)$ and $G''(\omega_0, t)/\sin(n_c\pi/2)$ intersect (see eq. 3).

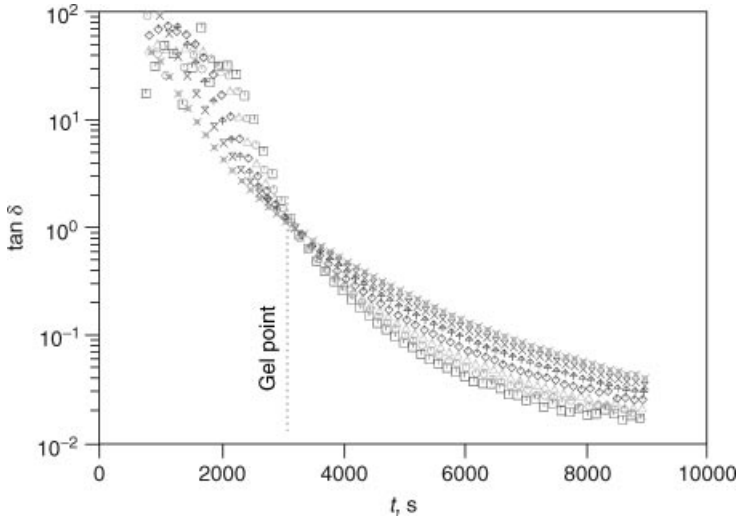

Fig. 4. Loss tangent of a chemically cross-linking polybutadiene as function of reaction time (48). Data were taken at several frequencies. The GP is marked by the instant at which the loss tangent is independent of frequency. All data are taken at low frequencies where the self-similar behavior prevails.

In the special case of $n_c = 0.5$, this relation simplifies even further. It should be noted that an intersect of G' and G'' is not necessarily indicating a gel point in spite of many published claims to the contrary.

With dynamic mechanical experiments, the instant of gelation can be measured as precisely as the accuracy of the rheometer permits, a significant advantage over extrapolation methods. An additional advantage is that the strain is kept small and shear modification of the molecular structure is avoided. The main limitation is the experimental time that tends to get long as low probing frequency is chosen. Rapidly gelling materials do not give sufficient time to the experimentalist to perform mechanical spectroscopy near the gel point.

Nonrheological Methods. Dynamic light scattering has been developed as nondestructive and real-time determination of GP for both chemical and physical systems (57–59). Time-resolved dynamic light scattering not only allows one to determine the gelation threshold but also to investigate critical dynamics near the gelation threshold. At GP, a power law appears in the intensity–time correlation function. Specific features originate from some unique aspects of gels: nonergodicity, frozen inhomogeneities, in addition to the divergence of the connectivity correlation.

Specific Methods for Chemical Gelation. The predictability of the threshold p_c suggests that GP can be found by monitoring the degree of cross-linking until it has reached the theoretical p_c value. However, the degree of cross-linking is difficult to measure accurately. Side reactions that parallel the cross-linking reaction (60,61) might interfere with the measurement. For practical purposes, these difficulties are avoided by saying that the polymer is before the gel point (sol state) if it can be completely dissolved in a good solvent and beyond the gel

point (gel state) if it cannot be dissolved completely. Numerous solution swelling experiments have confirmed that the rheologically observed GP coincides with the transition from a completely soluble state to an insoluble state (13,14,23).

Applications

For many applications in polymer processing, it is sufficient to know when the liquid–solid transition occurs for the purpose of avoiding it. For example, shaping must occur before the gel point while the polymer is still able to flow and the stress can relax to zero. Polymers around the gel point are used in a broad spectrum of applications such as gel processing, reactive processing (gel as intermediate state), and the development of new polymeric materials (adhesives, absorbents, porous catalysts, vibration dampers, membranes, colloidal glasses). They are also important outside the polymer field, for example, in food technology or in blood clotting.

BIBLIOGRAPHY

"Gel Point" in *EPSE* 2nd ed., Suppl. Vol., pp. 343–352, by H. H. Winter, University of Massachusetts, Amherst, Mass.

1. H. H. Winter and M. Mours, *Adv. Polym. Sci.* **134**, 165–234 (1997).
2. P. S. Russo, *Reversible Polymer Gels and Related Systems* (ACS Symposium Series No. 350), American Chemical Society, Washington, D.C., 1987.
3. D. Bonn, H. Kellay, H. Tanaka, G. Wegdam, and J. Meunier, *Langmuir* **15**, 7534–7536 (1999).
4. A. Coniglio and H. E. Stanley, *Phys. Rev. Lett.* **42**, 518 (1979).
5. A. Coniglio, H. E. Stanley, and W. Klein, *Phys. Rev. B* **25**, 6805 (1982).
6. P. G. de Gennes, *Scaling Concepts in Polymer Physics*, Cornell University Press, Ithaca, 1979.
7. D. Staufer, A. Coniglio, and M. Adam, *Adv. Polym. Sci.* **44**, 103 (1982).
8. D. Stauffer, *Introduction to Percolation Theory*, Taylor & Francis, Philadelphia, 1985.
9. H. E. Stanley, *Introduction to Phase Transitions and Critical Phenomena*, Oxford Press, New York, 1985.
10. T. Vilgis and H. H. Winter, *Progr. Colloid Polym. Sci.* **26**, 494–500 (1988).
11. A. Izuka, H. H. Winter, and T. Hashimoto, *Macromolecules* **27**, 6883–6888 (1994).
12. H. H. Winter and F. Chambon, *J. Rheol.* **30**, 367–382 (1986).
13. F. Chambon and H. H. Winter, *J. Rheol.* **31**, 683–697 (1987).
14. F. Chambon and H. H. Winter, *Polym. Bull.* **13**, 499–503 (1985).
15. M. Muthukumar, *J. Chem. Phys.* **83**, 3161 (1985).
16. M. E. Cates, *J. Phys.* **46**, 1059 (1985).
17. M. Muthukumar and H. H. Winter, *Macromolecules* **19**, 1284–1285 (1986).
18. P. Goldbart and N. Goldenfeld, *Phys. Rev. Lett.* **58**, 2676 (1987).
19. W. Hess, T. Vilgis, and H. H. Winter, *Macromolecules* **21**, 2536–2542 (1988).
20. J. E. Martin, D. Adolf, and J. P. Wilcoxon, *Phys. Rev. Lett.* **61**, 2620–2623 (1988).
21. M. Muthukumar, *Macromolecules* **22**, 4656 (1989).
22. R. H. Colby, M. Rubinstein, J. R. Gillmor, and T. H. Mourey, *Macromolecules* **25**, 7180 (1992).
23. F. Chambon, Z. S. Petrovic, W. J. MacKnight, and H. H. Winter, *Macromolecules* **19**, 2146 (1986).

24. D. Durand, M. Delsanti, M. Adam, and J. M. Luck, *Europhys. Lett.* **3**, 297 (1987).
25. D. Adolf, J. E. Martin, J. P. Wilcoxon, *Macromolecules* **23**, 527–531 (1990).
26. K. te Nijenhuis and H. H. Winter, *Macromolecules* **22**, 411 (1989).
27. E. M. Valles, J. M. Carella, H. H. Winter, and M. Baumgärtel, *Rheol Acta* **29**, 535–542 (1990).
28. S. R. Bhatia and A. Mourchid, *Langmuir* **18**, 6469–6472 (2002).
29. J. D. Ferry, *Viscoelastic Properties of Polymers*, 3rd ed., John Wiley & Sons, Inc., New York, 1980.
30. R. B. Bird, R. Armstrong, and O. Hassager, *Dynamics of Polymeric Liquids*, Vol. **1**, John Wiley & Sons, New York, 1987.
31. S. K. Venkataraman and H. H. Winter, *Rheol. Acta* **29**, 423–432 (1990).
32. P. J. Flory, *J. Am. Chem. Soc.* **63**, 3083 (1941); *J. Phys. Chem.* **46**, 132 (1942).
33. W. H. Stockmayer, *J. Chem. Phys.* **11**, 45–55 (1943).
34. W. H. Stockmayer, *J. Chem. Phys.* **11**, 45 (1944).
35. C. W. Macosko and D. R. Miller *Macromolecules* **9**, 199 (1976).
36. K. Dusek and D. Patterson, *J. Polym Sci A* **26**, 1209 (1986).
37. K. te Nijenhuis, *Adv. Polym. Sci.* **130**, 1–252 (1997).
38. R. Larson, *The Structure and Rheology of Complex Fluids*, Oxford University Press, Oxford, 1999.
39. K. Nishinari, *Rep. Progr. Polym. Phys.* **43** (special issue), 163–192 (2000).
40. J. M. Guenet, *Thermoreversible Gelation of Polymers and Biopolymers*, Academic Press, New York, 1992.
41. L. Li and Y. Aoki, *Macromolecules* **30**, 7835–7841 (1997).
42. H. Soenen, H. Berghmans, H. H. Winter, and N. Overbergh, *Polymer* **38**, 5653–5660 (1997).
43. B. D. Chin and H. H. Winter, *Rheol. Acta* **41**, 265 (2002).
44. R. H. Horst and H. H. Winter, *Macromolecules* **33**, 7538–7543 (2000).
45. H. H. Winter, *Progr. Colloid Polym. Sci.* **75**, 104–110 (1987).
46. Martin and co-workers, 1989.
47. C. P. Lusignan, T. H. Mourey, J. C. Wilson, and R. H. Colby, *Phys. Rev. E* **60**, 5657 (1999).
48. M. Mours and H. H. Winter, *Macromolecules* **29**, 7221–7229 (1996).
49. C. Friedrich and L. Heymann, *J. Rheol.* **32**, 235 (1988).
50. D. Adolf and J. E. Martin, *Macromolecules* **23**, 3700 (1990).
51. R. J. Farris and C. Lee, *Polym. Eng. Sci.* **23**, 586 (1983).
52. M. Adam, M. Delsanti, and D. Durand, *Macromolecules* **18**, 2285 (1985).
53. S. Lipshitz and C. W. Macosko, *Polym. Eng. Sci.* **16**, 803 (1976).
54. J. M. Castro, C. W. Macosko, and S. J. Perry, *Polym. Commun.* **25** (1984).
55. S. A. Bidstrup, Ph.D. dissertation, University of Minnesota, 1986.
56. E. E. Holly, S. K. Venkataraman, F. Chambon, and H. H. Winter, *J. Non-Newtonion Fluid Mech.* **27**, 17–26. (1988).
57. P. Lang and W. Burchard, *Macromolecules* **24**, 814–815 (1991).
58. M. Shibayama and T. Norisuye, *Bull. Chem. Soc. Jpn.* **75**(4), 641–659 (2002).
59. J. E. Martin, *Phys. Rev. A* **36**, 3415 (1987); J. E. Martin and K. D. Keefer, *Phys. Rev. A* **34**, 4988–4992 (1987).
60. C. W. Macosko and J. C. Saam, *ACS Polym. Prepr.* **26**, 48 (1985).
61. A. Fisher and M. Gottlieb, In *Proc. of Networks 86*, Elsinor, Denmark, Aug. 1986.
62. J. E. Martin, J. P. Wilcoxon, and D. Adolf, *Phys. Rev. A* **36**, 1803 (1987).

H. HENNING WINTER
University of Massachusetts

GELATIN. See Volume 6.

GELS. See HYDROGELS.

GENE-DELIVERY POLYMERS. See Volume 6.

GENETIC METHODS OF POLYMER SYNTHESIS

Introduction

Polymers have found enormous technological significance in a variety of areas including plastics, resins, fibers, and biomaterials. Both the chemical nature of the polymer and its structure are critical in determining its properties; the importance of polymer structure in dictating function has, for many decades, fueled the development of synthetic strategies for creating well-defined macromolecules. During the past 15 years, the application of biosynthetic strategies has gained increasing prominence as a polymer synthetic method, owing to the fact that the biosynthesis of macromolecules offers precise control of monomer sequence and macromolecular structure. This control is the source of the information storage, hierarchical assembly, mechanical strength, and enzymatic properties of natural macromolecules such as nucleic acids and proteins, which serve as an inspiration to the polymer chemist. Genetic methods of polymer synthesis have therefore been used to create protein-based polymeric materials inspired by natural molecules such as collagen, silk, and elastin, as well as materials comprising amino acid sequences with no natural counterpart. The macromolecules produced by these strategies exhibit novel and well-controlled properties, and genetically directed synthetic methods promise the contribution of additional advanced materials in the future.

Properties of Synthetic Polymers

Synthetic polymers, used here to describe polymers produced by chemical (ie, nonbiological) methods, have enjoyed great technological success since the beginning of their development in the early 20th century. A nearly limitless set of monomers can be polymerized by a vast variety of chemical transformations, which has contributed to the successful application of polymers in disparate applications, such as textiles, high temperature materials, and biomaterials. The properties of polymers are controlled by their chemical composition and by structural parameters such as polymer chain length, stereochemistry, monomer sequence, and topology. Because chemical polymerizations are statistical processes, synthetic polymers exist as a population of different molecules of varying structure, rather than as a collection of identical molecules. The properties of a synthetic polymer can therefore only be characterized with respect to the average properties of the chain

Encyclopedia of Polymer Science and Technology. Copyright John Wiley & Sons, Inc. All rights reserved.

population and the distribution around this average. Such heterogeneity has not adversely affected the use of these macromolecules in bulk application, but does have profound consequences when attempting to engineer polymer properties on the nanometer length scale. In this regime, important parameters such as functional group placement and macromolecular assembly are directly affected by variations in molecular weight, sequence, stereochemistry, and topology.

There have been many advances in synthetic polymer chemistry that have increased the control of polymer structure. These advances began most notably in the 1950s with the implementation of Ziegler–Natta polymerizations (1,2) and living polymerizations (3–5), which permitted, for the first time, control over architectural parameters such as stereochemistry and molecular weight, respectively. The development of these methods was critical to developing an understanding of structure–property relationships in polymeric materials and for the production of useful plastics, fibers, and elastomers. Since that time, a variety of novel chemical strategies for controlling polymerizations have continued to evolve, including the use of organometallic catalysts to control stereochemistry in olefinic polymers; atom-transfer radical polymerizations that permit living free-radical polymerization; living *N*-carboxyanhydride polymerizations; and living ruthenium-catalyzed ring opening metathesis polymerizations (2,6–15). These methods have been extremely important for producing stereoregular materials, synthetic macromolecules with unusual self-assembly properties and phase separation behavior, polymers with triggered and controlled response, and functionalized polymers with controlled molecular weight. Despite these advances, precise control of functional group placement remains elusive in polymers produced by chemical methods, which can limit their utility in applications where precise molecular recognition, catalysis, and assembly is desired. Because genetically directed methods of polymer synthesis offer precise control over molecular weight, stereochemistry, and sequence, they have been increasingly applied over the last 15 years toward the synthesis of exactly defined protein based materials that have potential uses in materials, biomedical, and nanotechnology applications.

Biosynthesis of Proteins

The control over protein synthesis in living organisms is derived from the templated nature of the genetically directed polymerization (Fig. 1). A DNA message encoding an amino acid sequence—naturally derived or artificial—is transcribed (converted) to a messenger RNA (mRNA) sequence. This sequence is translated (decoded) by transfer RNA (tRNA) molecules, which deliver amino acids to the ribosome. At the ribosome, the corresponding amino acid sequence is linked together enzymatically to form the protein. The tRNA molecules carry the appropriate amino acid to its exactly specified location along the protein chain via codon–anticodon pairing, and are charged with the appropriate amino acid by a highly selective class of enzymes, the aminoacyl tRNA synthetases. These enzymes exhibit an extremely small error frequency in amino acid incorporation—fewer than one in 10,000 errors (16)—so the amino acid sequence is preserved with great fidelity during protein biosynthesis; this permits the exact control of the placement of over 20 different amino acids along the protein backbone. This primary sequence

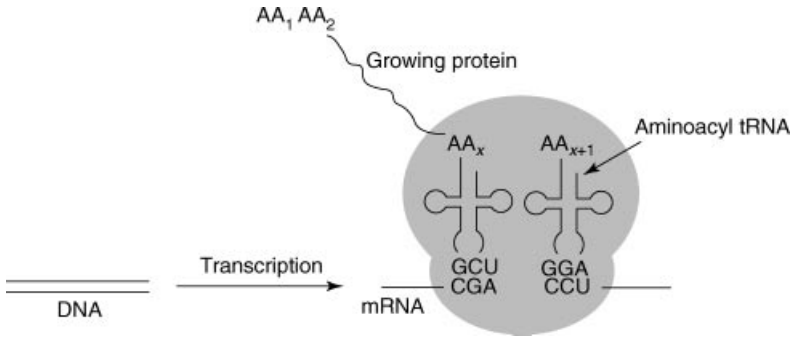

Fig. 1. Schematic of protein biosynthesis.

directs the formation of regular secondary structure (helical, coil, or sheet) and mediates the 3-D structure, assembly, and molecular recognition that are the hallmark of biological materials and the source of their remarkable properties. The strict sequence control, then, allows the synthesis of a remarkably diverse set of materials from a single set of building blocks. For example, the range of properties of Silk (qv), Collagen (qv), and elastin, which are each synthesized from the same set of 20 natural amino acids, arises from differences in their primary sequences and consequently different conformations and assembly.

The mechanical properties of these natural proteins, which can be comparable to and sometimes exceed those of high performance synthetic materials (Table 1), coupled with their potential biological activity, have been a motivation for the synthesis of polymers via genetic methods. Capturing these properties in genetically engineered artificial protein polymers offers the possibility of biologically derived performance materials and other protein materials that can be engineered with properties not currently found in the natural protein repertoire (eg, novel folding motifs and assemblies). Furthermore, the exact molecular weight control and precise specification of amino acid position of genetically directed methods provides materials that carry sufficient information to exactly control their folding and assembly. Because proteins assume thermodynamically stable structures in solution, the 3-D placement of functional groups on the atomic

Table 1. Representative Properties of Several Natural Proteins and Synthetic Fibers[a]

Material	UTS, MPa	Modulus, GPa	% Strain at break
B. mori silk	740	10	20
N. clavipes silk	875–972	11–13	17–18
Collagen (mammalian tendon)	120	1.2	13
Elastin (bovine ligament)[b]	2	0.0011	150
Polylactic acid, 50,000–300,000 MW	28–50	1.2–3.0	2–6
Bone	160	20	3
Kevlar (49 fiber)	3600	130	2.7
Synthetic rubber	50	0.001	850

[a]Adapted from Ref. 17, with permission from Elsevier.
[b]From Ref. 18.

length scale, with assembly controlling placement on longer length scales, is possible; the advantages of this assembly include the purposeful control of the mechanical, chemical, and biological properties of the artificial protein polymer chain. The variety of amino acid sequences that can be constructed and produced in cellular hosts via protein engineering methods provides access to a wide variety of protein polymers with diverse properties. Additionally, the incorporation of non-natural amino acids in these polymers has also significantly broadened the versatility of *in vivo* protein synthesis as a route to producing polymeric materials.

Genetically Directed Synthetic Strategies

Recombinant DNA methods have been traditionally used in site-directed mutagenesis studies designed to probe protein folding or enzymatic activity. The ease with which genetic sequences can be constructed has, however, led to the increased use of these methods for the synthesis of proteins with repetitive sequences. Naturally occurring materials with desired properties can be produced in organisms such as bacteria and yeast, simply by transferring the DNA encoding the natural protein into the appropriate expression host. Alternatively, short, repetitive amino acid sequences that are found in naturally occurring proteins can be linked together to form an artificial protein (one that does not exist in nature). Finally, since the folding of certain amino acid motifs is understood, amino acid sequences not found in nature can be designed from scratch (*de novo* design) to produce artificial proteins with desired chemical, biological, and/or physical behavior.

The production of naturally occurring proteins, such as silk, collagen, or elastin, is motivated by their excellent mechanical properties. In one approach for producing these proteins, the cDNA encoding the natural protein is isolated from an organism that produces the protein of interest and is cloned into an expression plasmid that carries the necessary genetic information to direct the expression host to produce both RNA and protein. While this approach guarantees that the polymer sequence will match that of the natural protein, difficulties with gene stability and protein synthesis can be encountered when the genes are extremely long and repetitive and when the coding preferences of the organism from which the DNA is isolated are different than those of the expression host. In many cases, it is not possible or necessary to construct a single amino acid sequence that encodes the full-length protein, and so shortened DNA sequences from the natural protein can be used.

Since many natural structural proteins comprise highly repetitive amino acid sequences, strategies to produce artificial repetitive proteins with properties analogous to those of the natural proteins have also been developed. The artificial repetitive proteins are either based on naturally occurring amino acid sequences or on sequences identified via *de novo* design. The overall strategy for gene design and expression is summarized in Figure 2. Synthetic genes encoding the artificial proteins are produced via standard molecular biological protocols; the genes for short amino acid sequences (30–40 amino acids, 90–120 base pairs) are first produced by solid-phase chemical synthesis and are then ligated into circular plasmid DNA, which serves as a source of the DNA "monomer" for future experiments. The initial solid-phase synthesis of the short genes permits use of DNA sequences

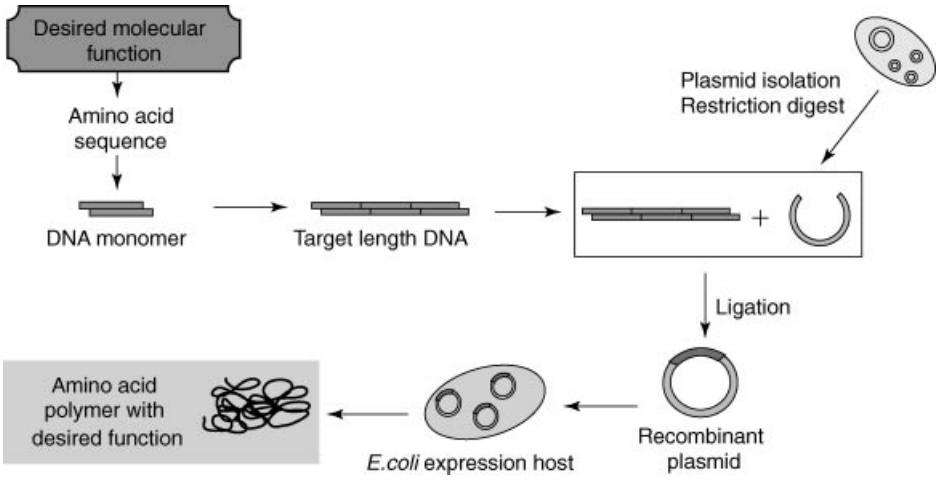

Fig. 2. Protein engineering strategy for the genetically directed synthesis of protein polymers.

that reflect the natural coding preferences of the organism in which the protein will be expressed and allows reduction of repetition in codon usage. It also permits the inclusion of amino acids with desired chemical functionality, or the insertion of biologically active sequences, to capture a variety of desired materials properties in the resulting protein. After the sequence of the gene in the plasmid in confirmed, the monomer is isolated from the plasmid and multimerized enzymatically. The multimerization proceeds in a head-to-tail orientation to form genes that can have lengths of up to 5000 base pairs (approximately 1675 amino acids); these genes are ultimately ligated into an expression plasmid (*vide infra*).

There are several different strategies (random, iterative, and recursive) that have emerged for the construction of multimers, as outlined in Figure 3, although the use of one strategy is not exclusive of another; ie, a combination of these approaches can be used in the construction of a single artificial gene (19). In random approaches, as the general one described above, DNA monomers are oligomerized in a single step, creating a population of oligomers of different lengths. In iterative approaches, a DNA segment is oligomerized in a series of uniform steps, each step adding one DNA segment to the growing oligomer. In recursive approaches, the DNA monomers are joined sequentially, with the length of the ligated segments doubling at each step. Random approaches offer the advantage of rapid creation of a library of repetitive genes of different lengths in a single step. Although this method does not guarantee the synthesis of a specific gene of desired length, it has been the most widely adopted of the multimerization strategies, owing to its simplicity and the fact that ligation conditions can be controlled to increase the probability of obtaining multimers of a given molecular weight range. Iterative and recursive approaches offer the advantage of production of genes with a specific and predetermined molecular weight, which is desirable if the effects of sequential changes in molecular weight or the impact of a precise and alternating block copolymer architecture are of interest. These methods requires repetitive cloning steps, the exact number depending on the desired

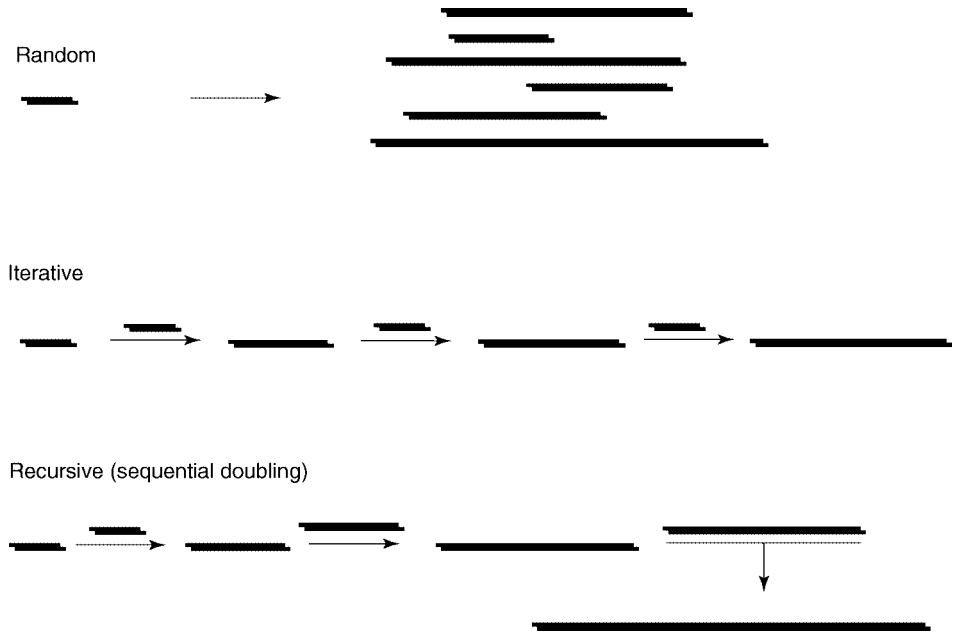

Fig. 3. Multimerization strategies employed for the construction of artificial genes. Adapted from Ref. 19, with permission from Elsevier.

length of the gene. The different approaches are used depending on the requirements of a specific macromolecular design, and demonstrate the flexibility of genetic methods of polymer synthesis for the production of varied types of polymer architectures.

Once the appropriate gene library is constructed, individual genes are incorporated into an expression plasmid, which is then incorporated into an expression host, most commonly *E. coli*. Because only one type of plasmid is maintained per cell, the plasmid DNA of individual bacterial colonies can be screened to identify and isolate a specific synthetic gene of desired length. The chosen synthetic gene is expressed from an expression plasmid (Fig. 2), which directs the synthesis of mRNA and protein in the cell. The expression plasmid also contains a promoter that regulates protein production and that can be controlled by inexpensive external means (eg, addition of chemicals, change in temperature). During protein expression, host cells are grown to a desired density, and then protein synthesis is initiated by simple addition of chemicals or change in temperature. Protein polymers can be produced at high levels in host cells; protein generally accumulates intracellularly (although it can also be transported out of the cell) and is then isolated from the cellular proteins via cell lysis, washing, precipitation, and chromatographic methods. The proteins are analyzed via amino acid analysis, chromatographic methods, mass spectrometry, NMR, and immunochemical analysis to confirm their identity; the pure product is absolutely homogeneous in both molecular weight and sequence. A variety of protein polymers based on silk, collagen, elastin, mussel adhesive proteins, and viral spike proteins have been produced by these methods, and there are also reports of the production of

hybrid polymeric materials comprising synthetic polymers coupled to genetically engineered motifs. There are limited reports of the synthesis of the mussel adhesive and viral spike protein polymers (20,21) and the hybrid polymers (22–24). The vast majority of materials have been produced from silk, collagen, elastin, and artificial amino acid sequences (Table 2); research in the design, synthesis, and characterization of these materials will therefore by presented below.

Silk-Like Protein Polymers

Naturally occurring silk (qv) is produced by a variety of organisms such as the silkworm (eg, *Bombyx mori*), spider (eg, *Nephila clavipes*), and scorpion, and the toughness and mechanical properties of the silk fiber has interested materials scientists for its use as a lightweight, high performance fiber, and in composite applications. Of all the silks, those from *B. mori* and from the dragline of *N. clavipes* have been the most extensively studied. The silk from the silkworm *B. mori* has been cultivated for centuries and used as a textile fiber. Spider silks, in contrast, are a family of proteins, in which there are multiple types of silk; for example, *N. clavipes* has seven different types of silk, each of which is tailored for a specific function. All silks have a highly repetitive amino acid sequence, which is characteristic of the fibrous proteins (eg, silk, collagen, and elastin) that serve a mechanical or structural function; globular proteins that serve catalytic or molecular recognition functions do not contain such repetitive sequences. The exact nature of the repetitive amino acid sequence depends on the type of silk, but includes alanine- and glycine-rich regions that have a high propensity for β-sheet formation via intrachain hydrogen bonding, interrupted by less crystalline or amorphous domains. The crystalline region from *B. mori* fibroin, for example, has the sequence [GAGAGSGAAG(SGAGAG)$_8$Y], and it is estimated to occur approximately 70 times within the protein (101). The repeated motifs from spider silk are less conserved, but a 13 amino acid repeat, (YGGLGSQGAGRGG), based on cDNA sequences, has been identified (102); this consensus region is generally followed by a short polyalanine sequence. The novel mechanical properties of silks are believed to arise from the folding of the protein into small β-sheet crystallites that are dispersed in a noncrystalline matrix (103); shear forces during fiber spinning permit processing and alignment of the crystallites to produce excellent fiber properties. The dragline of *N. clavipes*, for example, dissipates energy over a large surface area and balances stiffness (modulus of 10–50 GPa), strength (tensile strength of near 1.0 GPa), and extensibility (elongation to break of 10–30%) (104) (Table 1). These mechanical properties compare will to those of synthetic high performance materials, with a high tensile strength that approaches that of Kevlar, a toughness 3 times that of aramid fibers, and a strength 5 times that of steel by weight.

Protein engineering strategies have been widely employed for the production of silk-like proteins, both in research investigations aimed at understanding the molecular basis for the excellent mechanical properties of silk, as well as in commercial applications that employ protein engineering methods as a source of specialty materials (or potentially materials for bulk fiber applications). Protein engineering of silk is motivated in large part by the difficulty of isolating

Table 2. Representative Consensus Sequences Used for Genetically Synthesized Protein Polymers[a]

Protein	Natural protein model	Expression host	Ref.
Silk-like proteins			
$(GAGAGS)_x$	*B. mori* silk	*E. coli*	26
$[(GAGAGS)_9GAAGY)_x$	*B. mori* silk	*E. coli*	26,61
$[(GAGAGS)_n$-(GAAVTG-RGDSPASAAGY$)_m]_x$	*B. mori* silk/fibronectin	*E. coli*	27,61
$[(GAGAGS)_n$-(GAAPGAS-IKVAVSAGPSAGY$)]_x$	*B. mori* silk/laminin	*E. coli*	61
[GGAGSGYGGGYGHGYGSDGG-$(GAGAGS)_3]_{2,4,6}$	*S. c. ricini*/*B. mori* silks	*E. coli*	28
$[(GXG)_n$-$(A)_m]_x$	*N. clavipes* dragline silk	*E. coli*, *B. subtilis*, *P. pastoris*	29–33
$[(GPGGYGPGQQ)_n$-$(A)_m]_x$	*N. clavipes* dragline silk	*E. coli*, *B. subtilis*, *P. pastoris*	29–33
$[GLGGQGGGAGQGGYG]_x$	*N. clavipes* dragline silk	*E. coli*	35
$[SGRGGLGGQGAGA_{10}$-GGAGQGGYGGLGSQGT$]_x$	*N. clavipes* dragline silk	*E. coli*	34
$[SGRGGLGGQGAGA_5$-GGAGQYGGLGSQG$]_x$	*N. clavipes* dragline silk	*E. coli*	41–43
$[SGRGGLGGQGAGMA_5$M-GGAGQYGGLGSQG$]_x$	*N. clavipes* dragline silk	*E. coli*	41–43
$[SGRGYSLGGQGAGA_5$-GGAGQYGGLGSQG$]_x$	*N. clavipes* dragline silk	*E. coli*	41,44
$[SGPGGYGPGQQT]_x$	*N. clavipes* dragline silk	*E. coli*	34
$[(GPGGSGPGGY)_2$-GPGGK$]_{11}$	*N. clavipes* flagelliform silk	*E. coli*	46
$[\{(AEAEAKAK)_2$ AG$(GPGQQ)_6GS\}_9$-$(AEAEAKAK)_2$AG(GPGQQ)]	*N. clavipes* flagelliform silk	*E. coli*	47
$[A_{18}$TS(GVGAGYGAGAGYGV-GAGYGAGVGYGAGAGY)TS$]_4$	*S. cynthia ricini*/*B. mori* silk	*E. coli*	45
Partial cDNA construct	*N. clavipes* dragline silk	*E. coli*, mammalian, transgenic plants	25,38,40 36,37
Partial cDNA construct	A. diadematus silk	Mammalian, transgenic animals	38,39
Collagen, cDNA constructs			
proα1	Human type I, III collagen	*P. pastoris*, *S. frugiperda*	50 48,55
proα1 and proα2	Human type I collagen	*P. pastoris*	49

Table 2. (Continued)

Protein	Natural protein model	Expression host	Ref.
proα1	Human type I collagen	H. *polymorpha*	54
proα2	Human type I collagen	Transgenic mouse	51
proα1	Human type I collagen	Transgenic mouse	52
Collagen-like proteins			
(GESGREGAPGAEGSP-GRDGSPGAKGDRGET)$_6$	Human type I collagen	*B. brevis*	57
(GAPGAPGAPGPVGPA-GKSGDRGETGPAGPP)$_{8,10}$	Human type I collagen	*B. brevis*	57
Partial cDNA	Mouse type I, rat type III collagens	*P. pastoris*	53
GPE[{(GPQ)(GPE)$_4$}$_2$]$_x$	Bovine collagen	*S. cerevisiae*	56
GXP-GXQ-rich random polymers	Collagen-like	*P. pastoris*	58
(GPP)$_{32}$	Collagen-like	*E. coli*	59,60
[GAP(GPP)$_4$]$_x$	Collagen-like	*E. coli*	61
[(GAP(GPP)$_4$)$_2$GLPGPKGDRGD-AGPKGADGSPGPAGPA-GPVGSP]$_n$	Collagen-like, Cell binding	*E. coli*	61
(GAPGAPGSQGAPGLQ)$_{52}$	Collagen-like	*E. coli*	61–63
Elastin-like proteins			
(VPGXG)$_x$	Mammalian elastin	*E. coli*, yeast, transgenic plants	61,64–74
[(VPGVG)$_n$(VPGXG)$_m$]$_x$	Mammalian elastin	*E. coli*	67,73,80,81
[(VPGVG)$_n$(VPGAG)$_m$(VPGGG)$_p$]$_x$[b]	Mammalian elastin	*E. coli*	19,68,76
[GVGVP GVG(F/V)P GXG(F/V)P-(GVGVP)$_3$]$_n$	Mammalian elastin	*E. coli*	75
[GVGVP GVG(F/V)P GXG(F/V)P-GVGVP GVGFP G(V/F)GFP]$_n$	Mammalian elastin	*E. coli*	75
[GVGVP GVG(F/K)P GEGFP-GVGVP GVG(F/V)P G(F/K)GVP]$_n$	Mammalian elastin	*E. coli*	75
[GVGIP GFGEP GEGFP GVGVP-GFGFP GFGIP]$_n$	Mammalian elastin	*E. coli*	75
(GVGIP)$_x$, (AVGVP)$_x$	Mammalian elastin	*E. coli*	75
AB[c]	Mammalian elastin	*E. coli*	77–79
BAB[c]	Mammalian elastin	*E. coli*	77–79

Table 2. (Continued)

Protein	Natural protein model	Expression host	Ref.
$(GVG(V/I)P)_{10}GVGVPGRGDSP-(GVG(V/I)P)_{10}$	Elastin/cell-binding domain	*E. coli*	75
$[LD\text{-}CS5^{d}\text{-}(GVPGI)_x]_y$	Fibronectin/elastin	*E. coli*	66
$[LD\text{-}CS5\text{-}G(VPGIG)_{20}VP]_5$	Fibronectin/elastin	*E. coli*	88
$RKTMG[LD\text{-}CS5\text{-}G(VPGIG)_{20,25}VP]_{5,3,1}\text{-}LEKAAKLE$	Fibronectin/elastin	*E. coli*	88
$[LD\text{-}CS5\text{-}G((VPGIG)_2VPGKG(VPGIG)_2)_4\text{-}VP]_3$	Fibronectin/elastin	*E. coli*	89
Silk-elastin-like proteins			
$[(GVGVP)_n(GAGAGS)_m]_x$	Elastin/*B. mori* silk	*E. coli*	61,82,87
$[(GVGVP)_n(GAGAGS)_m\text{-}(GAAVTGRGDSPASAAGY)\text{-}(GAGAGS)_p]_x$	Elastin/*B. mori* silk/fibronectin	*E. coli*	61,82
$[(GVGVP)_n(GEGVP)\text{-}(GVGVP)_m(GAGAGS)_p]_x$	Elastin/*B. mori* silk	*E. coli*	83,84
$[(GAGAGS)_n(GVGVP)_m\text{-}(GKGVP)(GVGVP)_p]_x$	*B. mori* silk/elastin	*E. coli*	82,85–87
Artificial proteins			
$[(AG)_nPEG]_x$	Random coil	*E. coli*	100
$[(AG)_nEG]_x$	Silk mimetic sequence	*E. coli*	90
$[(GA)_3GX]_x$	Silk mimetic sequence	*E. coli*	91,98,99
$ED(E_{17}D)_xEE$, benzylated	Helical	*E. coli*	92–94
$Helix\text{-}[(AG)_3PEG]_{10}\text{-}Helix^{e}$	Leucine zipper	*E. coli*	95
$Helix\text{-}[(AG)_3PEG]_{10}$	Leucine zipper	*E. coli*	95
Helix	Leucine zipper	*E. coli*	95
$[(AAAQ)_x(AAAE)(AAAQ)_x]_y$	Helical	*E. coli*	96
$[GKGSAQA]_x$	Random coil	*E. coli*	97
$[AKPSYPPTYK]_x$	Mussel adhesive mimetic	*E. coli*	20
$[LSVQTSAPLTVSDGK]_{16}$	Viral spike protein	*E. coli*	21
$[SGLDFDNNALRIKLG]_{26}$	Viral spike protein	*E. coli*	21
$[QLSLRVSEPLDTSHGV]_{64}$	Viral spike protein	*E. coli*	21

[a] One-letter abbreviations of the amino acids are employed except as noted in the table. The letter X indicates positions in which several different amino acids have been encoded. Only general consensus repeats are given; minor linker regions, fusion tags, random sequences of amino acids, and minor substitutions in isolated repeats are deleted for simplification.

[b] The A and G residues are dispersed randomly throughout the sequence to reduce gene repetition.

[c] A blocks: $[VPGEG(IPGAG)_4]_{14}$, $[(APGGVPGGAPGG)_2]_x$, $[VPGVG(IPGVGVPGVG)_2]_{19}$, $[VPGEG(VPGVG)_4]_{30}$, $[VPGEG(VPGVG)_4]_{48}$, $[(VPGMG)_5]_x$; B blocks: $[VPAVG(IPAVG)_4]_{16}$, $[VPGFG(IPGVG)_4]_{14}$.

[d] CS5 = GEEIQIGHIPREDVDYHLYP; CS5 is a cell-binding domain from fibronectin.

[e] Helix = SGDLENEVAQLEREVRSLEDEAAELEQKVSRLKNEIEDLKAE.

these proteins in large quantities from the predatory spider, which cannot be cultivated like the silkworm. Despite advances in recombinant DNA methods, no complete cDNA or genomic DNA sequence of a natural silk protein has been successfully utilized for protein expression. The difficulties arise primarily because of the extreme length and repetitiveness of these genes, and also potentially because of the poor codon correspondence between the animal and the expression host, which places an unbalanced demand on aminoacyl-tRNA pools during bacterial protein expression. As a result of these difficulties, genetic deletions and/or premature termination during protein synthesis are often observed. However, the relatively simple, repetitive amino acid sequences that comprise silk proteins can be easily used to construct artificial silk-like proteins, and this approach has addressed the instability and poor production of protein from the expression plasmids prepared from the natural cDNA. Indeed, these approaches have been used to produce silk-like protein polymers containing nearly 1000 amino acids from bacterial expression systems, and somewhat longer polymers in yeast, indicating the flexibility of the method. Limitations in predicting protein polymer structure and function from the properties of the repetitive amino acid sequences can occur, but have not caused serious problems in the design of silk-like artificial proteins; the repetition of consensus sequences of natural silks provides protein-based polymers in which the conformational properties of the original protein are well preserved.

The instability of long cDNA sequences has limited their lengths to less than 2.5 kb. Recently, a 1.5-kb partial cDNA fragment of *N. clavipes* dragline silk has been cloned and the 43-kDa protein has been expressed from *E. coli* (25). However, most work has focused on the bacterial expression of silk-like proteins from synthetic genes, as mentioned above. Earliest reports of this approach date back to the work of Cappello and co-workers in 1990 (26). In these initial studies, a variety of different silk-like protein sequences with the repetitive sequence $(GAGAGS)_n$ were constructed, (where G is glycine, A is alanine, and S is serine) on the basis of the *B. mori* silk fibroin. The 108-bp monomer, flanked by Ban I restriction sites which permit only head-to-tail ligation of monomers, was multimerized enzymatically, and the multimers were fractionated and ligated into an expression system controlled by a strong, temperature-sensitive promoter that permits induction of protein expression by simply raising temperature to above 40°C. The $(GAGAGS)_n$ sequence proved intractable because of the formation of very stable and insoluble β-sheet structures, and so more complex sequences with improved solubility have been produced via introduction of noncrystalline regions dispersed between the β-sheet crystalline regions. For example, artificial proteins designed to contain both the crystalline segments of silk fibroin and the cell adhesion domain of fibronectin have also been synthesized by Cappello and co-workers, and have been shown via wide-angle X-ray scattering and molecular simulations to crystallize according to the models for Silk I (27). More recently, a sequence that alternates the $(GAGAGS)_4$ repeat from *B. mori* with a $(VPGVG)_8$ repeat from elastin has been produced, and the protein maintains excellent materials properties based on the combination of crystallinity and elasticity imparted by the two repetitive domains of the 832-amino acid artificial protein (105). Copolymers of the crystalline region of *B. mori* silk fibroins with the unordered glycine-rich region of *Samia*

cynthia ricini have also been produced to improve the tractability of the *B. mori* crystalline domain (28).

Similar success has been observed for the expression of repetitive artificial proteins based on spider silk amino acid sequences. Genes for partial amino acid sequences from *N. clavipes* have been generated, and repetitive genes of these sequences have been produced via recursive multimerization strategies. Proteins comprising 8 or 16 repeats of a poly(alanine) β-sheet hard segment with either interspersed (GXG) variants or (GPGGY) and (GPGQQ) alternating pentamers as the soft segment have been expressed in both *E. coli* and *Bacillus subtilis* by Fahnestock and co-workers (29–31). When expressed in *E. coli* under control of the strong promoter of the bacteriophage T7, approximately 10–30% of the soluble cell protein is the expression target sequence, although some truncated products are formed in these expression systems. The proteins are easily purified via chromatographic methods or via solubility differences between the artificial repetitive protein and other cellular proteins (31,32). When expressed in the yeast *Pichia pastoris*, from genes employing the codon preferences for *Pichia* (33), truncated products are eliminated and protein yields are increased, with silk-like proteins comprising 10% of the total protein (yields of 1 g/L). A chromosomal integration strategy is used to establish the genes in *Pichia* by homologous recombination, and expression is controlled by the strong promoter AOX1, which is induced by addition of small amounts of methanol. Fusing the target protein to secretion signals and prosequences of *Saccharomyces cerevisiae* permits efficient secretion of the target protein from the cell and into the extracellular medium, although at much lower yields. The advantages of this system include the fact that *P. pastoris* is a useful host for large-scale fermentation, and that extracellular localization of an expression protein target has many potential advantages for low cost production (simpler recovery, purification, and the potential for expression from immobilized cells). Circular dichroism (CD) characterization of these proteins in dilute aqueous solution indicates that the protein polymer adopts a random coil conformation, with increasing β-sheet content upon drying, consistent with the reported behavior of natural silk proteins upon spinning into fibers.

The production of other synthetic genes based on the amino acid sequences of dragline silk from *N. clavipes* has also been achieved by Kaplan and co-workers. From the partial cDNA sequences of this silk, two consensus repeats (NCMAG1 and NCMAG2, abbreviated for *N. clavipes* major ampullate gland) have been identified: (GGAGQGGYGGLGSQGAGRGGLGGQGAG), followed by a polyalanine region, and (GPGGYGPGQQGPGGYAPGQQPSGPGS), also followed by a polyalanine region. Repetitive proteins with sequences based on NCMAG1 and NCMAG2 have been produced from *E. coli* via expression of artificial repetitive genes from a pQE9 expression vector under control of a bacteriophage T5 promoter (34); these proteins contain a hexahistidine fusion to facilitate purification via metal chelate affinity chromatography. Yields of approximately 15 mg/L have been observed, although the yield of the silk-like repetitive proteins decreases with increasing length. Characterization via CD confirms the expected presence of β-sheet structure in these proteins. Additional silk-like proteins, also modeled after the dragline silk of *N. clavipes*, have been produced in *E. coli* by other research groups (35,106); in general, these proteins have molecular weights ranging

from 10 to 160 kDa (molecular weights of natural spider silk proteins can reach 740 kDa), with yields of purified protein ranging from 2 to 20 mg/L.

In addition to expression from bacterial and yeast expression hosts, silk proteins have also been expressed from transgenic hosts, motivated in part by the low expression yields obtained in microorganisms. Tobacco and potato plants have been successfully utilized as transgenic hosts for producing silk-like proteins based on dragline silk (36,37). In these investigations, at least 2% of the total soluble protein in the endoplasmic reticulum of the tobacco and potato leaves and potato tubers is reported to be silk. In addition, partial cDNA clones of the silk protein from *Araneus diadematus* and from *N. clavipes* have been expressed in mammalian cells [baby hamster kidney (BHK) cells] to yield several grams of protein that is recovered in soluble form by ammonium sulfate precipitation. The 25–50-mg/L yields provide an ultimate yield of more than 12 g of material purified from conditioned culture media (38). For production of larger amounts of these recombinant silk-like proteins, expression from goat milk may prove a viable alternative, and is currently under development; transgenic goats that express silk proteins in their milk have been produced by Nexia Biotechnologies, Inc., and methods to purify these proteins have been developed (39,107–109).

Additional areas of active research have been to mimic the fiber spinning conditions of the spider and to control β-sheet assembly in order to produce artificial silk protein materials that have mechanical properties similar to those of the natural silk protein fibers. In general, the spinning of recombinant, silk-like artificial proteins requires dissolution in harsh solvents such as hexafluoroisopropanol, formic acid, or 9 *M* lithium bromide. For example, fibers have been spun from solutions of these proteins in hexafluoroisopropanol with quenching in methanol and wet drawing. Such fibers exhibit the properties [tenacities of 2 g/denier (gpd) and 8–10% elongation] of traditional textile fibers, but do not match the properties of natural dragline silk (110). Silk proteins produced from bacterial sources have also been spun into fibers from more benign aqueous processing conditions that better mimic those of the spider. In 2002, Arcidiacono and co-workers reported the aqueous solution spinning of silk sequences derived from *N. clavipes* dragline silk and expressed from *E. coli* (40). The proteins are produced via expression of the C-terminal cDNA of *N. clavipes* dragline (42.9 kDa), or via expression of the consensus sequences NCMAG1 and NCMAG2 of *N. clavipes* (55 kDa). The key to the successful spinning of these proteins from aqueous solution has been to eliminate the drying of the protein at any stage of purification and processing, by increasing protein concentration via removal of water during purification, with processing in dilute denaturing buffer (160 m*M*–1 *M* urea). The content of β-sheet structure in the fibers increases with time, as expected, and fiber diameters range from 10 to 60 μm in diameter, depending on the weight percentage of the spin dope and the identity of the protein. Fibers are insoluble in water and birefringent, indicating the formation of oriented fibers, although no mechanical property measurements have been reported. The *A. diadematus*-derived protein produced in mammalian cells (38) has also been processed in a similar manner—first concentrated into an aqueous spin dope exceeding 23% (w/v) protein, coagulated in methanol/water, and exposed to wet draw conditions. The fibers isolated via these methods exhibit a tenacity of 2.26 gpd and 55–130% extensibility, which yield a toughness equivalent to that of silk, although the properties do not exactly mimic

natural silk fibers, which have a tenacity of 7–11 gpd and an extensibility of 30% (*vide supra*).

The difficulties in processing silk proteins is largely a result of the spontaneous assembly into β sheets of the poly(alanine) sequences of dragline silk, especially under conditions of shear. In an effort to understand the architectural variables that will permit purposeful control of β-sheet formation and hierarchical assembly during processing, protein engineering methods have been employed toward the design and synthesis of silk protein sequences in which amino acids and amino acid sequences are included for control of β-sheet formation. Incorporating sequences that can trigger β-sheet assembly, for example, as demonstrated by Kaplan and co-workers, has been one approach to control protein properties. In one design, methionine residues have been included to flank the (AAAAA) units of the NCMAG1-based repetitive proteins (41–43). Under reducing conditions, these polymers readily form β-sheet structures as assessed by CD and Fourier transform infrared (FTIR) spectroscopies; β-sheet assembly is disrupted upon oxidation of methionine to the larger and more hydrophilic sulfoxide. These researchers have also introduced sites of enzymatic phosphorylation that flank the alanine-rich sequences, in order to alter the size and charge of serine residues and control β-sheet formation (41,44). When the serine hydroxyl group in the sequence RGYSLG is phosphorylated by cAMP protein kinase, β-sheet formation is prevented; upon dephosphorylation by alkaline phosphatase, the ability to form β sheets is recovered. In other investigations aimed at controlling solubility and processability of silk-like proteins, Asakura and co-workers (45) have designed a chimeric sequence that combines the crystalline polyalanine sequence $(Ala)_{18}$ of *Samia cynthia ricini* silk with a noncrystalline (GX)-rich sequence (GVGAGYGAGAGYGVGAGYGAGVGYGAGAGY) found in the silk fibroin of *B. mori*. The introduction of the glycine-rich noncrystalline sequence in the protein results in improved solubility of this silk-like protein and prevents β-sheet formation in the polyalanine region of the protein, as assessed via solid-state ^{13}C CP/MAS NMR studies.

The materials properties of other members of the spider silk family are also becoming of increasing research interest. Sequences based on the flagelliform silk protein, which produces the unique elastomeric properties of the capture spiral of spider webs, have been recently studied by Conticello and co-workers (46). A protein containing 11 repeats of the flagelliform-derived amino acid sequence $\{(GPGGSGPGGY)_2GPGGK\}$ can be expressed in *E. coli*, and has been characterized by a combination of techniques including CD, FTIR, and NMR, which indicate that these molecules adopt a β-turn conformation. These results suggest that the elastomeric properties of the flagelliform sequence may have similar origins as those found in other β-turn-forming proteins such as elastin. The mechanical properties of protein polymers that contain flagelliform-like amino acid sequences can also be controlled by the inclusion of peptide motifs that are known to form β-sheet crystallites but that are not naturally found in silk proteins.

Conticello and co-workers (47) have also produced alternating block copolymers containing a flagelliform-like sequence $(GPGQQ)_6$, which is derived from the *A. diadematus* dragline silk fibroin, and the amphiphilic sequence $(AEAEAKAK)_2$. Although the (AEAEAKAK) sequence is not a silk-derived sequence, it has been shown to form very stable β-sheet structures in aqueous solution (111). Proteins

containing these sequences assemble into β-sheet linked membranes from concentrated aqueous solution, and membrane formation is responsive to conditions that alter the conformation of the (AEAEAKAK) units in the polymer (47).

The application of silk-like protein polymers in many disparate applications such as textiles, medical applications, and cosmetics will be possible, given their demonstrated synthesis and favorable properties. One difficulty to be overcome in the synthesis of artificial silk-like proteins from bacterial hosts is the generally low expression yields, which can be as low as 1–10 mg/L. Yeast systems offer advantages in this regard, with potential yields of 300–1000 mg/L possible, although difficulties in purifying the protein from these expression hosts have been encountered. While the mechanical properties of spider silk are a desirable goal, it has remained difficult to reproduce the properties in the laboratory environment, although continued progress is being made in this direction, owing to increased understanding of the processing of these proteins and the ability to control the solubility of the proteins via protein engineering strategies. Improved understanding of the impact of synthesis and processing on the resulting mechanical properties of silk-like materials will increase the number of applications in which these polymers will find use. Coupled with the fact that silk-like proteins can also be useful in supporting cell growth and tissue function, the proteins will find use in both materials science and medical applications, such as in fibers, threads, membranes, and scaffolds. The genetic tailoring of their sequence and the ability to include repeats of other structural proteins such as collagen or elastin (*vide infra*) has also resulted in a variety of silk-based proteins that can be useful in varied materials applications, including fiber reinforcement, controlled release, and scaffolds for tissue engineering, and will continue to expand the number of uses in which these polymers will find application.

Collagen-Like Protein Polymers

Collagen (qv) is another important fibrous structural protein that has been produced by protein engineering methods for applications in materials science and biology. The collagens comprise a highly abundant family of extracellular matrix proteins that are found in all connective tissues. They represent 30% of the total body proteins in mammals and are found in tendons, ligaments, cartilage, bone, and skin. Although there are at least 20 genetically distinct types of collagen (the most abundant in mammals being types I–III), all are composed of three helical chains that have the general amino acid sequence Gly-X-Y, in which X is primarily proline, and Y is primarily hydroxyproline. The monomeric helical sequence first assembles into a triple helix with dimensions of 300 nm in length and 1.5 nm in diameter, which then forms larger-scale hierarchical structures that ultimately assemble into high strength elastic fibers that form connective tissue (112). In addition to its structural role, collagen is also involved in a variety of important biological events such as early development, cell attachment and proliferation, wound healing, and tissue remodeling. This combination of mechanical strength, higher order assembly, and biological activity of collagen has made it a broadly used protein-based biomaterial. Collagen I, in particular, is the most abundant structural protein in animals, and has been

widely exploited for medical use, cosmetics, therapeutics, and also as its denatured form (gelatin) in food and photographic emulsions. Although collagen is available in large quantities from mammalian sources, extraction from animal tissues poses the risk of contamination by viral or infectious agents, which has become of increasing concern in recent years. Owing to this potential risk, the simplicity of the repetitive sequence, the wide biological and materials uses of collagen, and the ability to tailor collagen amino acid sequences, protein engineering strategies have become more prevalent for the production of recombinant collagen.

In contrast to the production of silk-like proteins, recombinant production of collagen-like proteins has focused primarily on the production of cDNA sequences isolated from natural sources. Fibrillar collagens have been produced in mammalian cells (113,114), insect cells (48,49), yeast (51,115–118), and transgenic animals (51,52,118) and plants (119,120). Yields generally range from 15 to 500 mg/L, although a triple-helical, 160-kDa human type I collagen has been produced in mouse milk at 1–8-mg/mL yields (52), and a 21-kDa fragment of mouse collagen I (from cDNA fragments) can be produced from *P. pastoris* at yields of 14.8 g/L of clarified broth (53).

To obtain correctly assembled collagen fibrils, most organisms employ extensive post-translational modification of procollagens, and the enzymes that mediate these modifications have been incorporated into expression systems for collagen production. One of the most important considerations is the hydroxylation of proline residues to 4-hydroxylproline via the action of the tetrameric (α_2 β_2) enzyme prolyl 4-hydroxylase. In almost all collagens (with the exception of some marine invertebrate collagens), hydroxylation of the proline is required for correct fibril formation and to maintain the melting temperature of the collagen at physiologically relevant levels (approximately 40°C). A lack of hydroxylation reduces (and can, under physiological conditions, eliminate) the propagation of banded fibril formation, lowers the melting transition temperature, and can render the collagen useless for biological applications (120). Most bacterial and yeast expression hosts do not contain the genes for prolyl 4-hydroxylase, and some insect and mammalian expression hosts do not generate sufficient amounts of this enzyme. Coexpression of collagen with the subunits of prolyl 4-hydroxylase has therefore been used to permit recombinant production of functional collagen. Another consideration in collagen expression is that the protein is generally expressed as procollagen, which contains N- and C-terminal peptides to impart solubility. The genes for the proteolytic enzymes N-proteinase and C-proteinase are also often included in expression hosts to allow processing of the procollagen, via removal of the N- and C-terminal peptides, into the assembling collagen form. It has been recently reported, however, that human type I collagen proteins lacking the propeptides can be produced from *S. cerevisiae* expression hosts that lack the genes for the prolyl 4-hydroxylase (117) and can still correctly fold. Generally, in expression systems in which the proteinases are not included, procollagen can be cleaved with pepsin post-translationally to liberate the N- and C-terminal propeptides and permit fibrillar assembly of collagen.

Vuorela and co-workers (50) have demonstrated that coexpression of subunits of human prolyl 4-hydroxylase with the proα1 (III) chains of human type III procollagen in *P. pastoris* yeast expression systems permits production of

approximately 15 mg/L of properly folded homotrimeric type III procollagen that is resistant to pepsin digestion. The yeast expression hosts also demonstrate an expected increased level of prolyl 4-hydroxylase activity, and can be used in the large-scale production of different types of recombinant collagen. Similar strategies have also been employed for the production of high levels of human type I collagen in *P. pastoris* (121). In these investigations, the genes for the proα1 and proα_2 chains of type I procollagen are expressed, along with the genes for both the α and β subunits of prolyl 4-hydroxylase. The correct assembly of proα1 and proα_2 chains is observed (2:1 ratio), and high expression yields of 500 mg/L are obtained. In contrast to these other yeast systems, properly hydroxylated, 28-kDa mouse α1 (I) collagen fragments can be expressed from the yeast *Hansenula polymorpha* without coexpression of prolyl 4-hydroxylase (54). Successful expression of the procollagen chains from insect cells has also been observed. Proα1 chains of human type III collagen have been expressed from baculovirus vectors in *S. frugiperda* Sf9 or High Five cells (48), as have wild-type and modified proα chains of human type I collagen (55). With coexpression of human prolyl 4-hydroxylase, correctly assembling procollagen molecules can be produced at yields of 10–20 mg/L.

Mammary gland expression has also been explored as a route to produce procollagens, although this has been more limited in scope and use to date. The general method involves the expression of genomic or cDNA transgene sequences in conjunction with mammary-gland–specific promoters, which drives the expression of the proteins in milk. It has been achieved for procollagen via two different approaches. In one strategy, the cDNA encoding a shortened version of recombinant pro α_2 procollagen chains has been integrated into the mouse genome, and the procollagen has been coexpressed with the α and β subunits of prolyl 4-hydroxylase. The expression of a thermally stable triple helical artificial α_2(I) homotrimer at 50–200 mg/L is possible in this system (51). In another instance, transgenic mice were generated that contained the αS1-casein mammary-gland–specific promoter linked to a 37-kb segment of the human α1(I) procollagen structural gene. Very high levels of triple helical procollagen are produced via this system (8 mg/mL) (52). An advantage for transgenic expression of protein polymers in milk is that the expression levels of proteins can be increased via the use of a species with a higher volume production of milk (eg, mouse to rabbit to pig or goat).

Although recombinant natural collagen sequences have been of significant academic and commercial interest (115,122,123), the production of collagen-based proteins with additional functions has also been explored. For example, in an effort to design advanced biomaterials, Fertala and co-workers (124) have identified specific regions in collagen that are responsible for particular biological activity. These researchers have developed a cDNA cassette expression system (125) that allows systematic removal of specific amino acid sequences in collagen II. By removal of certain D blocks in collagen II, followed by expression of the modified protein in mammalian cells (HT-1080 cells), purification, and assessment of human chondrocyte (cartilage cell) spreading and migration, the amino acid region 704-938 has been identified as critical for the spreading of chondrocytes (124). The studies demonstrate that collagen (II) domains differ in their ability to support attachment and migration of chondrocytes, and suggest that advanced collagen-based materials could be designed to present multiple copies of the critical domains, permitting support of a greater number of cells and potential improvements in

tissue regeneration. In other efforts to produce collagen-based materials with improved biological activity, Hayashi and co-workers have produced a collagen III epidermal growth factor (EGF) chimeric protein from Sf9 insect cells (126). The proteins maintain the fibril-forming properties of the collagen domain, and films of the protein also improve cell growth via the action of the EGF; the chimeric protein may therefore be useful for cell culturing, wound healing, and tissue engineering applications. Together, these studies point to the utility of protein engineering strategies to identify and to produce materials containing multifunctional domains that impart desired biological and materials properties.

In addition to protein engineering investigations that have been based on natural collagen sequences, there is also significant interest in creating artificial collagen-like sequences with novel chemical and physical properties. Accordingly, genetically directed methods have been employed to produce artificial protein polymers containing the collagen-based GXY repeat, with substitutions in the X and Y positions to impart desired chemical functionality. The proteins have been expressed in yeast and bacterial systems. For expression from yeast (*Saccharomyces cerevisiae*) and certain bacteria (*Bacillus brevis*), fusion of the α-mating factor secretion signal permits secretion of the collagen-like proteins (CLPs) into the medium (53,56,57), which simplifies purification and points to the feasibility of commercial scale production of the proteins. Kajino and co-workers (57) have designed DNA sequences encoding human α1 collagen repeats $(GESGREGAPGAEGSPGRDGSPGAKGDRGET)_6$ and $(GAPGAPGAPGPVGPAGKSGDRGETGPAGPP)_{8,10}$ according to the codon usage of *B. brevis*. The proteins are expressed in *B. brevis* at estimated yields of 500 mg/L, and they exhibit reversible sol-gel behavior similar to that of native gelatin. Nonhydroxylated gelatins, with sequences based on partial cDNA sequences from mouse type I and rat type III collagen, have been produced in higher yields of 14.8 g/L from *P. pastoris*, using the *S. cerevisiae* α-mating factor (53). Completely synthetic, 36.8-kDa collagen sequences that are rich in GXP and GXQ sequences can also be produced, without degradation, in *P. pastoris* at high yields of approximately 3–6 g/L (58).

Expression from *E. coli* has not been as successful as the yeast and *B. brevis* expression systems. In early attempts to express CLPs from bacterial expression systems (59,60), a 22-kDa CLP with the sequence $(Gly\text{-}Pro\text{-}Pro)_{32}$ was produced in *E. coli* under control of a thermally inducible promoter. The resulting protein degraded in this cellular host, although use of an appropriate mutant host minimized this problem. Reducing the proline content of the collagen-like proteins appears to minimize stability problems, as less proline-rich proteins with sequences such as $\{GAP(GPP)_4\}_x$ and $\{\{GAP(GPP)_4\}_2GPAGPVGSP\}_x$ have been successfully produced from *E. coli* by Ferrari and Cappello (61). Recently, the sequence $(GAPGAPGSQGAPGLQ)_{52}$, which has an even lower proline content than previously produced CLPs, has been expressed in *E. coli*; the protein can be expressed in soluble form, at 100–200-mg/L yields, in low cell density, small-scale experiments (62,63).

The tensile strengths and availability of type I collagen render it the most widely used natural polymer in the medical field, with uses in tissue engineering, delivery systems, and cosmetic surgery; the denatured form of collagen (gelatin) finds widespread use as a food additive and photographic emulsion. In addition to

minimizing risks associated with isolation of collagen from animal sources, genetically directed strategies for the production of recombinant collagen-like protein polymers are also appealing as a result of the potential for CLPs in the above applications. The progress toward expression of collagen-like proteins from bacterial and other expression systems may permit the rational design of artificial CLPs with specialized materials uses; for example, understanding the individual roles of collagen domains in eliciting biological responses may result in the design of CLP-based scaffolds for directed interactions with cells. The ability to produce designer collagen and gelatin polymers via genetically directed methods may therefore drive the growth of these strategies as a large-scale source of recombinant human collagens and artificial collagen-like polymers for a variety of additional applications in nanotechnology, materials science, and medicine.

Elastin-Like Protein Polymers

Elastin is another protein found in connective tissues, and provides strength, flexibility, and elasticity to organs and tissue. When expressed in tissue, elastin is produced as the 750–800 amino acid protein tropoelastin, which then assembles into microfibrils, is modified via hydroxylation of proline, and is cross-linked via lysyl oxidase oxidation of lysine-rich domains (127). This assembly and insolubilization of tropoelastin results in the mature elastin network, which confers elastic and biological functionality to tissue. Elastin is composed of large, mobile, highly hydrated hydrophobic domains and smaller alanine-rich regions. The hydrophobic domains of elastin contain proline, alanine, valine, leucine, isoleucine, and glycine, with valine and glycine being most abundant. The sequence of the hydrophobic domain is highly repetitive, containing repeats of the general sequences GX, PX, GGX, or PGX (X = G, A, V, L, or I); the common repeat in mammalian elastin is VPGVG, with up to 11 consecutive pentapeptide repeats (127,128). In contrast to silk and collagen, elastin, even at high molecular weights, is soluble in aqueous solution, which, along with the highly repetitive nature of the hydrophobic regions of this functional protein, has fueled an enormous amount of interest in the use of elastin-based repeats in genetically engineered protein polymers. Whereas protein engineering has been employed in the production of tropoelastins for studies of biological activity, essentially all materials investigations have focused on the biosynthesis of elastin-like proteins (ELPs) comprising repetitions of the VP(LCST)GVG motif.

One unique feature of the VPGVG sequence is that, although it is generally soluble, it exhibits a lower critical solution temperature (LCST), which causes aqueous solutions of the protein to separate into solvent-rich and polymer-rich phases upon heating. This transition is analogous to that of the well-known poly(*N*-isopropylacrylamide) polymers, in which an entropy-driven dehydration of the polymer chain results in phase separation above a critical temperature. The ability of elastin-like polymers to undergo an LCST transition is conserved as long as the glycine and valine residues are present. The LCST transition is observed even with substitution, in the repeat sequence VPGXG, of any amino acid X (except proline); indeed, choice of the amino acid residue X can be used to control the LCST of the protein. This unique behavior of elastin confers mechanical properties

that make it a versatile platform for the engineering of protein-based materials for a variety of applications such as biomaterials, drug delivery, responsive silica membranes, and tissue engineering.

Because of this versatility, both chemical and protein engineering methods have been used widely for the synthesis of elastin-based protein materials based on the VPGXG sequence. A single repeat of the VPGVG unit is sufficient to observe the random coil to β-turn transition (129), which has made chemical strategies accessible for the synthesis of elastin-based peptide materials. However, limitations of solid-phase peptide synthesis plague these materials at higher molecular weights, since the presence of hard-to-purify deletion products significantly alters the properties of the materials (64). Protein engineering methods have therefore been used widely for synthesis, with relatively high yields (generally 50–100 mg/L, and up to 800 mg/L) facilitating the characterization and use of these materials for commercial applications. Elastin-like proteins have been produced in *E. coli* (64–68), fungi (69), chloroplasts (70), and plants (71), although most materials investigations with elastin-like proteins utilize bacterial expression.

The broad range of interest in elastin-like protein polymers has fueled the development of new genetic strategies for the assembly of the genes encoding the elastin repeats (70,74). Seamless cloning methods (72) permit the assembly of high molecular weight genes, in a controlled head-to-tail fashion, directly into the expression vector. Clones of up to 5000 bp (200 kDa) have been prepared via these strategies, with yields commonly on the order of 200–800 mg/L. Since the multimerization is random in nature, seamless cloning results in the formation of a library of genes of different lengths, although the exact length of the genes cannot be controlled purposefully. Recursive strategies have therefore also been applied for the synthesis of repetitive artificial proteins with specific and predetermined chain lengths (68) to enable control of elastin-like protein transition temperature via purposeful control of ELP molecular weight and block architecture. By sequential cloning steps, gene products carrying a specified number of repeats can be produced. A variety of $(VPGXG)_n$ ELPs have been produced via these strategies, with molecular weights up to 130 kDa (330 pentapeptide repeats).

The elastin-like proteins produced by genetic methods have proven useful for a number of applications in biotechnology, materials science, and medicine. In early demonstrations by Urry and co-workers (64), ELPs with the general sequence G–$(VPGVG)_{19}$–VPGV have been expressed from *E. coli*, are easily purified from cellular proteins, and exhibit a sharp LCST at approximately 48°C, as expected for a VPGVG sequence of this molecular weight. By appropriate design of the elastin-like polymer, thermal, chemical, and electrochemical stimuli can all be used to alter and control the LCST of ELPs (64). Urry and coworkers have demonstrated, for example, that substitution of any of the natural amino acids in the fourth position of the VPGVG pentapeptide provides a range of LCST transitions. Attachment of redox-active cofactors such as FAD/$FADH_2$ (flavin adenine dinucleotide) or NAD/NADH (nicotinamide adenine dinucleotide) to glutamic acids in a VPGEG repeat permits electrochemical control over the hydrophobic collapse of the protein (73). Upon reduction of FAD to $FADH_2$ or of NAD to NADH, the increased hydrophobicity of the pentapeptide results in the hydrophobic collapse of the elastin-like polymer at substantially lower temperatures (73). If the two different states of the ELP (oxidized and reduced) have LCSTs

above and below room temperature, the electrochemical transition can stimulate an observable transition under ambient conditions.

Following up on the extensive body of work by Urry (74,75,130), others have also taken advantage of the control of LCST possible for these elastin-like polymers in the design of ELPs for drug delivery applications. In one example, Chilkoti and co-workers (19,68,76) have produced a family of polymers of the general sequence VPGXG in *E. coli*, where X = V, A, and/or G. The ratios of V:A:G are varied in order to tune the LCST, with one library containing no A or G, and two others containing the residues in ratios of 5:2:3 and 1:8:7. The A and G substitutions in the fourth position of the pentamer are dispersed throughout the sequence to reduce the repetition within the gene. These polymers have 120 to 330 pentapeptide repeats and molecular weights of 50 kDa to 130 kDa, and the LCST of the polymers is dependent on both the molecular weight and the guest residue sequence. Transition temperatures that vary smoothly between approximately 28°C and 78°C are obtained, demonstrating the potential for genetically designing an ELP with a desired transition temperature for drug delivery applications. In addition, ELPs designed to exhibit an LCST at 35°C (131) exhibit complex shear moduli similar to those observed for collagen and hyaluronan at physiological temperature, and are able to support cartilaginous cell growth. The combination of these results suggests that these materials may also be useful as injectable scaffolds for cartilaginous tissue repair (131), although chemical crosslinking would likely be required to impart sufficient mechanical integrity upon gel formation. These investigators have also designed block copolymers based on the VPGXG sequences, with one block comprising 64 repeats of the V:A:G composition 1:8:7 (LCST > 90°) and the other comprising 60 repeats of VPGVG (LCST = 35°C). Upon heating, these block copolymers form 40–100-nm size nanoparticles, owing to the hydrophobic collapse and aggregation of the VPGVG block. The mechanical, chemical, and/or biological properties can be tuned to enable self-assembly with incremental changes in temperature, pH, and ionic strength, making these block copolymers attractive candidates for controlled delivery, tissue engineering applications, and stimuli responsive surfaces and membranes (132,133).

Genetically directed synthetic strategies also permit the preparation of other complex block copolymers with tunable properties. Conticello and co-workers (77,78) have designed and synthesized a series of elastin-mimetic diblock (AB) and triblock (BAB) copolymers for assembly on the mesoscopic scale, and have expressed these polymers in *E. coli*. The B blocks consist primarily of the hydrophobic elastin repeats $\{VPAVG(IPAVG)_4\}_{16}$, and the A blocks comprise more hydrophilic repeats such as $\{VPGEG(IPGAG)_4\}_{14}$, $\{VPGEG(VPGVG)_4\}_{30}$, and $\{VPGEG(VPGVG)_4\}_{48}$ (see Table 2). The hydrophobic B blocks exhibit an LCST below 37°C, which is desired so that collapse of the hydrophobic block occurs under physiologically relevant conditions. The substitution of alanine (A) in place of glycine (G) in position three of the pentamer results in a change of mechanical properties of the material from elastomeric to plastic, which permits control of the mechanical properties of the block. The hydrophilic blocks are chosen because of their high LCST values, so that phase separation of the two blocks occurs at physiological conditions to form ordered polymeric structures. Indeed, BAB block copolymers with an A block comprising $\{VPGEG(VPGVG)_4\}_{30}$ undergo a reversible sol–gel transition at 23°C. The same group has demonstrated

that diblock copolymers of the general sequence $\{VPGEG(IPGAG)_4\}_{14}VPGEG–\{VPGFG(IPGVG)_4\}_{16}VPGFG$ assemble into spherical particles and beaded filaments in water at 25°C (79).

There are also significant opportunities for controlling the mechanical properties of ELP materials via covalent cross-linking strategies. Several different strategies have been employed to cross-link soluble elastin molecules into a cross-linked, elastomeric network. Early work by Urry employed γ irradiation for cross-linking, which yields elastomeric networks with an elastic modulus very similar to native elastin. Although this method does not require a specific amino acid for cross-linking, it affords little control over the position of cross-linking and can also result in chain scission. Therefore, in addition to γ irradiation (134), other radical-based cross-linking methods employing dicumyl peroxide have been developed, as well as chemical cross-linking strategies such as carbodiimide coupling (80) and chemical reactions with electrophilic reagents. Chemical cross-linking approaches, explored by several groups, offer the advantage of control of the positions of the chemically reactive cross-linking sites, which can in turn control cross-linking density, molecular weight between cross-links, and resultant mechanical properties. Elastin-like proteins with the repetitive sequences $\{(VPGVG)_4VPGKG\}_{39}$ have been produced by the Conticello group; the lysines are reacted with the electrophilic *N*-hydroxysuccinimide esters of bifunctional carboxylic acids, bis(sulfosuccinimidyl)suberate (in phosphate buffer), or disuccinimidylsuberate (in DMSO) to produce cross-linked gels (67). The elastin-mimetic hydrogels exhibit expected elastomeric behavior, with a reversible contraction (62.4%) and expansion upon cycling between 10 and 45°C. Trifunctional tris-succinimidyl aminotriacetate has also been used by other groups to cross-link elastin-like polymers $\{VPGKG(VPGVG)_6\}_n$ (with $n = 56$, 112, and 224) and $\{VPGKG(VPGVG)_{16}\}_n$ (with $n = 51$, 102, and 204) (81). The mechanical properties of the cross-linked hydrogels are dependent on molecular weight, the density of lysine residues, and temperature, and range from 0.24 to 15 KPa. Cross-linked elastin-like polymer hydrogels exhibit an LCST, although one that is gradual, as compared to the abrupt LCST transition observed for soluble elastin-like polymers. In additional studies by Urry and co-workers (80), polymers with the general sequence $\{(GVGVP)_2(GXGVP)(GVGVP)_2\}_n$, with X = lysine or glutamic acid, have been mixed and cross-linked via carbodiimide-mediated coupling. The swelling of the cross-linked materials varies as a function of the cross-linking reaction temperature, and filamentous structures are formed in elastin-like polymers cross-linked above their LCST.

Methods to produce elastomeric fibers from ELPs have also been investigated. Uncross-linked polymers can be spun into fibrous mats via electrospinning protocols (135), with long uniform fibers resulting from spinning solutions greater than 10 wt% in polymer; tensile strengths of 35 MPa and a material modulus of 1.8 GPa are possible via these strategies. Acrylate groups have been incorporated via reaction with the lysine (K) amines to permit production of cross-linked elastin-mimetic fibers (136), which exhibit increased tensile strengths and moduli that are similar to those reported for native elastin.

Alternate strategies to control the mechanical properties of elastin-like proteins, via combination with amino acid sequences from different fibrous proteins, have also been explored. Combining the temperature-responsiveness

of elastin-based repeats with the excellent mechanical properties of silk-like proteins (*vide supra*) yields protein polymers that have properties similar to those observed in segmented polyurethanes, with the advantage of controlled sensitivity to stimuli (pH and temperature). Cappello and co-workers have combined the (GVGVP) repeat from mammalian elastin with the (GAGAGS) sequence from *B. mori* silk to create copolymers of over 10 different compositions (82). The relative lengths of the silk-like and elastin-like blocks are varied, and the ionic sensitivity of the polymers is controlled via the selection of amino acids in the elastin-like block. Representative copolymer compositions include the sequences $\{(GVGVP)_4(GEGVP)(GVGVP)_3(GAGAGS)\}_{16}$ and $\{(GVGVP)_4(GXGVP)(GVGVP)_4(GAGAGS)\}_{11}$, where X is either glutamic acid or valine (83,84); these silk-elastin-like polymers (SELPs) are easily expressed from *E. coli* hosts. Characterization of the physical behavior of these proteins via turbidity measurements indicates that the transition temperature (LCST) of the polymers containing glutamic acid is sensitive to pH, and that the LCST of both the glutamic acid- and valine-containing polymers can be modulated with changes in ionic strength, temperature, polymer concentration, and polymer length (83,84). The simultaneous control over amino acid sequence and molecular weight afforded by genetically directed methods of polymer synthesis therefore provides opportunities for fine-tuning the stimuli-responsive behavior of these polymers. The materials have potential applications as injectible urethral bulking agents for treating incontinence, cell culture coatings, drug delivery systems, or soft-tissue augmentation or bone repair.

Cappello and co-workers have also investigated polymers in which the number of silk-like domains in the polymer is increased to produce polymers that spontaneously form hydrogels in aqueous solution. For example, the sequence $\{(GVGVP)_4(GKGVP)(GVGVP)_3(GAGAGS)_4\}_{12}$ undergoes an irreversible sol-gel transition in aqueous solution of physiological pH and ionic strength, mediated by hydrogen-bond controlled crystallization of the silk-like domains (85), unlike the polymers above, which contain fewer silk-like repeats and do not form hydrogels. The hydrogels (12 wt%) exhibit mechanical and swelling properties that do not change as a function of temperature, as the presence of the silk domains eliminates their temperature sensitivity (86). X-ray diffraction patterns of SELP polymers are very similar to those of simple silk-like polymers (SLPs), confirming the presence of similar crystalline arrangements of silk-like blocks in both SELPs and SLPs. Crystalline silk-fibroin domains are also observed, via NMR, in the solid state of other SELPs (137). Proteins and DNA can be delivered from the hydrogels without loss of activity (85,87,138,139); bioactive DNA can be released from the gels for up to 28 days, with the rate of release for 2.6–11-kb plasmids being dependent on the size of the plasmid DNA (87,139). DNA released from these gels can also be delivered in the active form in a mouse breast cancer model (139). These results suggest the potential use of these polymers as *in situ* gel-forming implants for protein and gene delivery applications (140,141).

Protein engineering strategies have also allowed the incorporation of biological function into elastin-like protein polymers and SELPs. The incorporation of cell-binding amino acid sequences, such as RGD (82,142) and REDV (from the CS5 domain of fibronectin) (66) (Table 2), permits endothelial cell adhesion to

these materials for their application in tissue engineering. Tirrell and co-workers have also incorporated cross-linking domains into biologically active elastin-like polymers (Table 2) to permit the production of biologically active, cross-linked materials with mechanical properties similar to those of native elastin. The incorporation of lysine residues at the termini or in the VPGXG repeat of elastin-CS5 copolymers permits cross-linking via gluteraldehyde or *N*-hydroxysuccinimide activated suberic acids (88,89). Molecules of the general sequence RKTMG{LD-CS5-G$(VPGIG)_{20}VP\}_x$LEKAAKLE, with $x = 1$, 3, and 5, have been cross-linked via reaction with gluteraldehyde. The observed molecular weight between cross-links (M_c) and mechanical properties of the cross-linked polymers approximate those of elastin (0.3–0.6 MPa), with elongation-to-break values of 100–220% (88). A broader range of mechanical properties can be obtained from elastin-based proteins in which lysine residues are incorporated in the VPGXG repeats. Proteins of the general sequence $\{LD\text{-}CS5\text{-}G((VPGIG)_2(VPGKG)(VPGIG)_2)_4VP\}_3$, when cross-linked via reaction with NHS-activated suberic acids, yield cross-linked materials with Young's moduli ranging from 0.07–0.97 MPa, with M_c values of 3,000–38,000 (89). These values span the range of mechanical properties of natural elastins and vary as expected with measured extents of cross-linking. Films prepared from these proteins have also been shown to support endothelial cell adhesion under shear stresses that mimic those in blood vessels (143). The polymers are therefore being considered for applications in engineered artificial grafts for the surgical reconstruction of small- and medium-diameter blood vessels.

Overall, the applications for elastin-based protein polymers are numerous, given their useful elastomeric properties, biological behavior, and low immunogenicity. The versatility of these systems includes the ability to engineer the LCST behavior of $(VPGXG)_n$ polymers via choice of the X residue, to produce cross-linked elastomeric gels, and to synthesize elastin-like block copolymers that assemble into nanoparticles. The amino acid sequence of these polymers can also be engineered to allow the incorporation of biologically active domains. Their possible applications as drug and gene delivery vehicles, membranes, elastomeric fibers, and vascular grafts have continued to motivate interest in their scientific and technological potential, and a variety of academic and industrial research groups continue to investigate these polymers.

Artificial Proteins Designed *de Novo*

In addition to the design of protein polymers based on repetitive amino acid sequences found in naturally occurring proteins, *de novo* design has also been applied to the production of artificial proteins with desired conformational properties. Knowledge of the secondary structure preferences (ie, α-helix, β-sheet, coiled-coil, reverse turn, etc) of amino acids and amino acid sequences has permitted the design of completely artificial proteins with prescribed structures, chemical reactivity, and assembly. These short amino acid sequences are encoded into genes and multimerized into target polymer lengths via the genetic strategies previously described. Proteins are expressed from *E. coli*, purified by appropriate protocols, and their structure and assembly is characterized. A variety of novel protein materials, such as crystalline lamellar solids, smectic-like liquid crystals, and reversible

hydrogels have been produced via these methods, and showcase the control over macromolecular structure and function that can be achieved by genetically directed polymer synthesis.

The earliest example of this approach involved the design and synthesis of crystalline lamellar solids by Tirrell and co-workers. Although the folded chain lamellar crystal is a well-known motif in polymer science, this architecture is formed in synthetic polymers for largely kinetic reasons. The trapping of the polymer chain into a folded conformation upon cooling makes it essentially impossible to precisely control the thickness and surface chemistry of such chain-folded lamellar structures. The genetic engineering approach, however, has afforded such folded structures in which both variables can be controlled, simply by controlling the sequence of amino acids in a protein polymer. Polymers with the general sequence $\{(AG)_xEG\}_y$(with x ranging from 3 to 6, and y ranging from 5 to 54) have been designed on the basis of the knowledge that alanyl–glycyl dyads form thermodynamically stable β-sheets in natural silk proteins. When precipitated from formic acid, this family of proteins forms crystalline solids with primarily β-sheet structure, as ascertained from infrared and Raman spectroscopic analysis, cross polarization/magic angle spinning NMR, and wide-angle X-ray diffraction (WAXD) (90,144). X-ray diffraction investigations indicate that the lamellar thickness is always shorter than the chain length of the polymers, as expected for the chain-folded architecture, and consistent with this observation, X-ray structure refinement identifies an antiparallel β-sheet arrangement of the chains as the best fit to experimental X-ray data. The glutamic acid residues of this sequence would be expected to lie at the lamellar surface, and indeed, deprotonation of the carboxylic acid groups does not cause any change in the chain conformation or intersheet packing distance as observed via vibrational spectroscopy and WAXD, respectively (145). Consistent with these results, X-ray diffraction characterization of crystalline lamellar solids of $\{(AG)_3XG\}$ sequences (with X = Asn, Phe, Ser, Val, or Tyr) demonstrates that the interlamellar spacing increases linearly with the increasing volume of the amino acid side chain in position X (91), but that neither the turn length nor the intrasheet packing distance is altered. These results suggest that crystal surface functionality can be designed via the choice of the amino acid in position X of the $\{(AG)_3XG\}_y$ sequences.

The self-assembling properties of certain β-sheet-forming peptides have also been captured in protein polymers. Sequences of alternating polar and nonpolar residues comprise a prevalent sequence motif in the antiparallel β-sheet regions of natural proteins, and accordingly, the peptide $(AEAEAKAK)_2$ has been demonstrated by Zhang and co-workers to self-assemble into an organized supramolecular structure (111). Protein polymers of the sequence $(AEAEAKAKAEAEAKAK)_9$ have been produced by Goeden-Wood and co-workers in an effort to capture the self-assembling characteristics of the peptides while improving the mechanical properties of the supramolecular gels (146,147). The proteins (which contain a decahistidine fusion sequence) can be expressed from *E. coli* and purified via metal-chelate affinity chromatography with yields of approximately 5 mg/L. The protein is shown, via CD and FTIR investigations, to adopt a stable β-sheet structure, and is suggested to form β-sheet fibrils via Congo Red dye binding assays and characterization by scanning electron microscopy (SEM). Under physiological conditions, the protein forms hydrogels with a storage modulus of approximately

100 Pa, suggesting the potential application of these polymers in soft tissue engineering or drug delivery applications.

In addition to the *de novo* design of β-sheet forming protein polymers in which self-assembly is controlled by monomer sequence, the design of helical proteins in which assembly is controlled by molecular weight has also been demonstrated. Helical rods form well-defined self-assembled structures; one particularly well-studied example is poly(γ-benzyl-α,L-glutamate) (PBLG), which forms oriented films and liquid crystalline solutions. The large dipole moment along the helical axis permits orientation of these rod-like polymers via the use of an electric field to yield materials with interesting piezoelectric and nonlinear optical properties. Since the conventional approach for making these molecules utilizes the ring-opening polymerization of *N*-carboxy-α-amino acid anhydrides, molecules made by this method have broad molecular weight distributions, and therefore form cholesteric liquid crystalline phases in which there is orientational order but no longitudinal registry of individual chains. Smectic liquid crystalline phases, in which there is both orientational order and longitudinal registry, are not observed for PBLG synthesized by the chemical methods. In contrast, genetically directed synthetic strategies permit the synthesis of monodisperse poly(α,L-glutamic acid) (PLGA), which can be chemically benzylated to form biosynthetically derived PBLGs capable of forming smectic-like liquid crystalline phases in solution (92,93). Monodisperse polypeptides with the sequence $ED(E_{17}D)_xEE$ (referred to as PBLG-*x* after benzylation), where $x = 3$–6, have been produced in *E. coli* (93,94). Aspartic acid (D) is included periodically to provide recognition sites for the enzyme *BbsI* and to preserve the genetic stability of the repetitive glutamic acid sequence. The biosynthetically produced PLGAs are benzylated by alkylation of the PLGA with phenyldiazomethane, and analysis by NMR indicates 94–98% benzylation. Small-angle X-ray diffraction patterns of films dried from solutions of PBLG-4 and PBLG-5 (in a 97/3 mixture of chloroform and trifluoroacetic acid) show well-defined spacings of 114.5 and 140 Å, respectively. These values almost exactly match the expected lengths of the monodisperse PBLG helices (114.5 and 141 Å) (92,93), suggesting alignment of the helical molecules in a smectic-like liquid crystalline phase. The films are thought to specifically orient in a twisted grain boundary (TGB)-like phase, owing to the superposition of a smectic-A layering (from the monodisperse PBLG) and the chirality of the helical rod (148).

Additional helical polymers in which assembly is controlled by monomer sequence have also been designed by Tirrell and co-workers and by Kaplan and McGrath, and have proven fruitful for assembly of protein-based materials. Helical coiled-coil motifs (comprising leucine zipper peptides) are found in transcription factors and play an important role in controlling protein dimerization and DNA binding; related helical motifs are also found in structural proteins such as keratin (the main structural protein in hair and nails). The primary structural feature of the leucine zipper peptides is the heptad repeat sequence *abcdefg*, in which hydrophobic amino acids occupy positions *a* and *d* (*d* is primarily leucine), while charged residues generally occupy positions *e* and *g*. Under appropriate pH and temperatures, these amino acid sequences adopt helical conformations that array the hydrophobic residues *a* and *d* along a single face of the helix. Assembly of these helices, most often in the form of dimeric coiled-coils, is controlled by aggregation of the hydrophobic face, with the stability of specific associations

modulated by the charged residues *e* and *g*. The coiled-coil stability, aggregation number, and aggregate specificity can be manipulated though control of the heptad amino acid sequence and the chain length. Thus, these helical motifs serve as versatile structures for the assembly of novel protein-based materials.

Earliest work in this area by Kaplan and McGrath focused on the synthesis of a variety of isolated leucine zipper peptides with controlled assembly properties (149,150). Expanding the approach, Tirrell and co-workers have designed hydrogel-forming, triblock copolymers carrying short leucine zipper end blocks flanking a water-soluble polyelectrolyte domain (95). In this triblock copolymer, there are three main considerations in the design of the protein sequence: (*1*) the hydrophobic face of the leucine zipper block is modeled after the a/d residue pattern of the *Jun* oncogene product; (*2*) the *b*, *c*, and f positions are chosen on the basis of the residues that most commonly reside in those positions in naturally occurring coiled-coil proteins; and (*3*) nine of the 12 *e* and *g* positions in the sequence are occupied by Glu residues in order to facilitate pH control of gelation and viscoelastic behavior. The triblock protein polymer comprises two leucine zipper end blocks of six heptad repeats, with a central polyelectrolyte block of the sequence $\{(AG)_3PEG\}_{10}$. It has been expressed in *E. coli*, and CD characterization of the purified protein confirms the presence of both helical and random coil structures. At low pH and ambient temperature, these materials form elastic gels; increases in pH or temperature produce a viscous solution of nonassociated protein (95). Solid-state NMR investigations of the protein hydrogel show that the central polyelectrolyte domain is isotropically mobile on the microsecond time scale, while the leucine zipper domains are rigid, which is consistent with the association of the leucine zippers as the basis for hydrogel formation (151). On the millisecond time scale, the leucine zipper domains exhibit rigid body motion, which supports the hypothesis that the domains act as continuously exchanging physical cross-links.

Alteration of the composition of these proteins via genetic methods may prove to be a successful strategy for modulating the physical behavior of protein-based hydrogels. For example, alteration of the acid/base balance in the helical domains (positions *e* and *g*) can alter the stability of the coiled-coil association, which will in turn control the stability of the hydrogel network and alter the pH and temperature at which these macromolecular structures assemble into hydrogels. Inclusion of cross-linking or lysis domains and/or cellular or molecular recognition sequences will permit the design of hydrogels with predetermined physical and biological properties and may expand their uses as reagents for encapsulation and controlled delivery.

Genetically directed synthetic methods are also being exploited for the structure-based design of protein polymers that display desired functional groups. Kiick and co-workers have designed a series of functionalized, alanine-rich helical proteins with the general sequence $\{(AAAQ)_x(AAAE)(AAAQ)_x\}_h$, in which the position and number of the glutamic acid residues (E) can be varied systematically. Members of this family of proteins can be produced in *E. coli* and are easily purified via metal chelate affinity chromatography at yields of 10–20 mg/L. The proteins are shown, via CD spectroscopy, to be highly helical under ambient conditions (96), and, along with related random coil sequences, have intended applications for purposeful display of biologically active groups and/or organic moieties.

In all of the cases described above, genetically directed methods have been used to produce protein polymers with predesigned secondary structures that control the folding, assembly, and/or the mechanical and biological properties of the resulting polymer. However, genetically directed methods of polymer synthesis have also been applied to the production of protein polymers in which a lack of regular secondary structure is desired. Recursive multimerization strategies have been used by Won and Barron (97) to produce genes that encode random coil protein polymers of the general sequence $(GKGSAQA)_x$, with molecular weights up to 46.25 kDa. Protein polymers of this repetitive, nonnatural sequence have been produced in *E. coli* at yields of approximately 15 mg/L, and CD studies confirm the random coil nature of the protein. The ultimate goal of this line of investigation is the creation of long, repetitive water-soluble proteins for diverse biomaterials and tissue engineering applications. Inclusion of the lysine residues (K) at regular intervals in this random-coil, water-soluble protein is intended for the attachment of bioactive factors or for cross-linking.

Multisite Incorporation of Nonnatural Amino Acids

A very important recent development in these synthetic methods is the expansion of their chemical versatility via the incorporation of nonnatural amino acids. Standard methods of *in vivo* protein synthesis employ the 20 naturally occurring amino acids normally encoded by the mRNA templates. This repertoire of amino acids includes carboxylic acids, amines, and thiols as the primary chemically reactive sites, which limits the chemical versatility of protein polymers. Accordingly, there has been a great deal of interest in incorporating functional groups such as alkenes, alkynes, halogens, or azides into proteins. Such incorporation would permit chemical modification of protein polymers via reactions that are orthogonal to those of the natural amino acids and would also afford opportunities to alter surface properties, impart photosensitivity, and control association of protein polymers. However, investigations of this kind have been challenging owing to the strict controls over the fidelity of protein biosynthesis exerted by the aminoacyl-tRNA synthetases (aaRS), the class of enzymes that controls the incorporation of amino acids into proteins *in vivo*.

There are several strategies for incorporating nonnatural amino acids into proteins that circumvent the discriminatory power of the aaRS; for example, nonnatural amino acids can be incorporated directly into polypeptides via chemical synthesis strategies. Whereas the number of nonnatural amino acids that can be incorporated in this fashion is essentially limitless, there are several disadvantages. In solution-based *N*-carboxyanhydride polymerizations (13), sequence control is lost, while in solid-phase peptide synthetic methods (152), the less than perfect efficiency of the amino acid coupling step limits peptide length to approximately 50–75 amino acids, which is generally insufficient for materials applications.

A second strategy that avoids the synthetases combines both chemical and biological synthesis. Chemical aminoacylation methods were introduced by Hecht and co-workers in the late 1970s (153) and have since been exploited by a variety of other investigators (154–157). In these strategies, the nonnatural amino acid is

chemically attached to a suppressor tRNA, which decodes a single stop codon that is engineered into the mRNA sequence of a target protein. The nonnatural amino acid is then incorporated into the protein by suppression (decoding) of the stop codon by the suppressor rRNA during *in vitro* translation. This method permits the site-specific incorporation of nonnatural amino acids into proteins, and the chemical aminoacylation step permits the incorporation of essentially any nonnatural amino acid. The *in vitro* translation protocols, however, yield only microgram quantities of protein. To address these low protein yields, *in vivo* strategies employing heterologous synthetases have been developed for the site-specific incorporation of nonnatural amino acids into proteins produced from *E. coli* and from yeast (158–163); these methods have proven a versatile strategy for the site-specific incorporation of electrophilic, acetylenic, azido-functionalized, and redox-active amino acids into proteins (164–166). Such strategies require the inclusion, in the expression host, of both a suppressor tRNA that decodes the stop codon during protein synthesis (and is not recognized by any of the *E. coli* aaRS) and a synthetase that will aminoacylate only the suppressor tRNA (and none of the endogenous *E. coli* tRNAs) with only the nonnatural amino acid. A recent advance in this line of investigation is the generation of a bacterial expression host that carries the heterologous synthetases necessary for site-specific, *in vivo* incorporation of a nonnatural amino acid and that can also synthesize the nonnatural amino acid from basic carbon sources (167).

Although suppression-based methods permit the incorporation of a variety of nonnatural amino acids, modest suppression efficiencies limit the incorporation of the nonnatural amino acid to a single site in the protein. Whereas in many instances it may be desirable to limit incorporation to a single site (eg, studies of protein folding or enzymatic activity), multisite incorporation has many distinct advantages in the synthesis of protein polymer materials, in which alteration of bulk material properties is desirable. In multisite incorporation strategies, nonnatural amino acids are incorporated into protein polymers at some or all of the positions normally occupied by the natural amino acid, generally via the utilization of the nonnatural amino acid by the protein biosynthetic apparatus of the expression host. These strategies therefore also afford the opportunity to control the placement of the nonnatural amino acids in the protein polymer, which offers additional advantages in macromolecular synthesis.

Perhaps surprisingly, given the extremely high fidelity of amino acid incorporation during protein biosynthesis, it has been known for decades that a number of nonnatural amino acids are able to replace natural amino acids in bacterial proteins. For example, selenomethionine is incorporated in place of methionine in *E. coli*, can be used in all steps of protein biosynthesis, and supports cell growth (168–170). Amino acids that differ in structure and functionality from the natural amino acids, such as *p*-fluorophenylalanine, norleucine, and trifluoroleucine, have also been known for decades to replace the natural amino acids in bacterially synthesized proteins (170–172). Over the past several years, a variety of additional nonnatural amino acids bearing novel chemical functionality have also been incorporated into protein polymers *in vivo* (Fig. 4). Unsaturated, azido-functionalized, and ketone-decorated analogues have been incorporated and subsequently modified via chemical strategies that are orthogonal to the chemistries of natural amino acid side chains (173–175). Fluorinated amino acids offer opportunities for

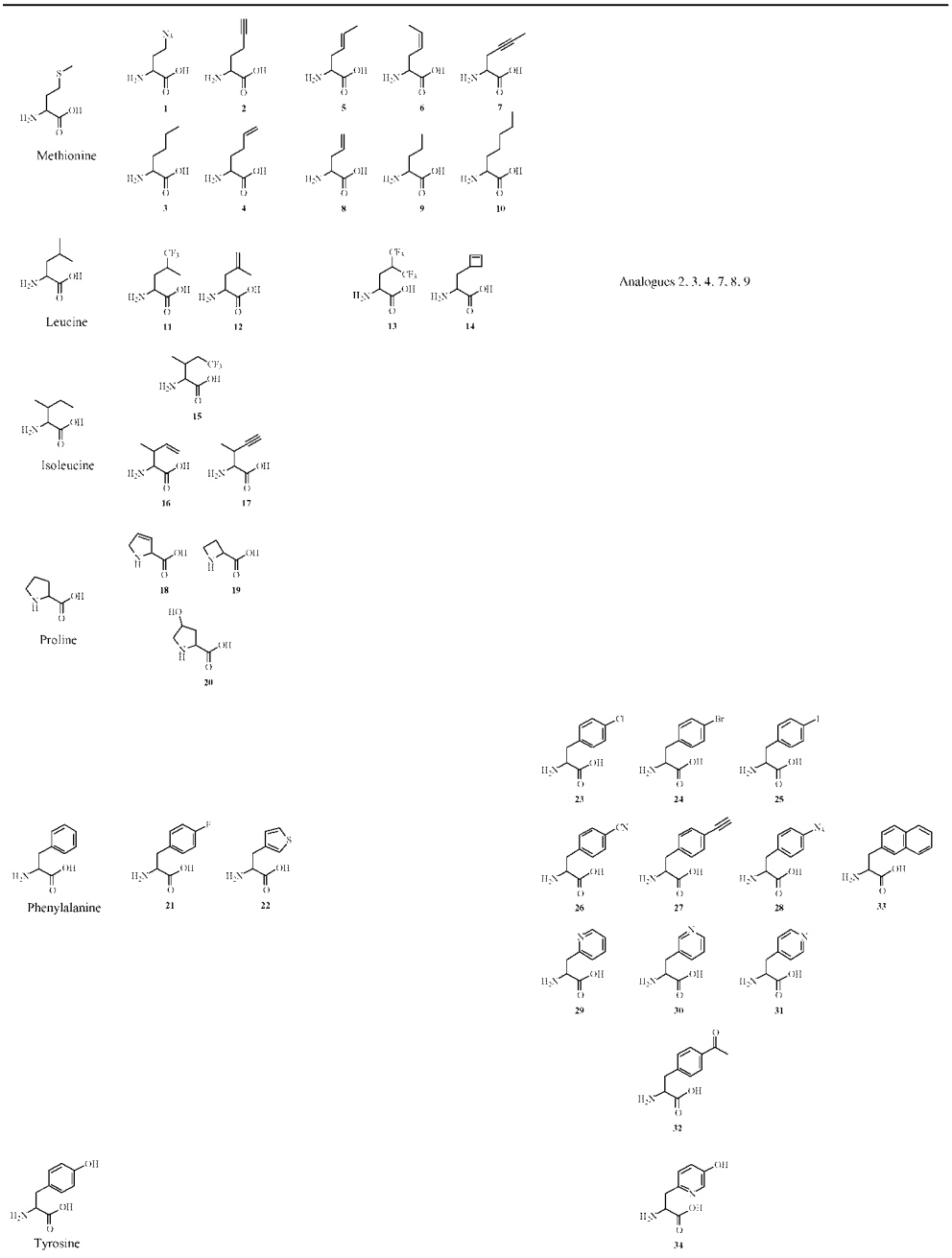

Fig. 4. Nonnatural amino acids and the strategies used for their multisite incorporation into proteins.

controlling the surface properties of protein films (98), and also afford strategies for increasing the thermodynamic stability of protein assemblies (176). Incorporation of aryl halide function permits chemical modification of proteins via palladium-catalyzed reactions, and also offers new opportunities for protein structure determination (177,178).

The incorporation of nonnatural amino acids into proteins *in vivo* requires that the nonnatural amino acid meet several criteria. First the analogue must be transported across the cell membrane into the cell, either by amino acid specific or general transport mechanisms, and it must not be degraded once inside the cell. Second, the nonnatural amino acid must be recognized by the aaRS during translation, and must also be able to form a stable aminoacyl-tRNA that is not subject to the aaRS editing mechanisms that normally prevent misacylation of tRNA. Finally, the nonnatural amino acid must be an efficient substrate for the elongation factor Tu (EF-Tu) and must be accepted at the ribosomal A site. Transport into the cell does not appear to be limiting, based on the number of nonnatural amino acids that have been demonstrated to replace natural amino acids in biosynthetically derived proteins. Recognition of the misacylated-tRNA by EF-Tu and acceptance at the ribosomal A site are also not suggested to be limiting factors, based on the enormous number of nonnatural amino acids that can be incorporated into proteins by *in vitro* translation protocols. Many different investigations have indicated that the key determinant to the success of the *in vivo* approach, therefore, is the ability of the nonnatural amino acid to be charged to a tRNA by an aminoacyl-tRNA synthetase.

The high specificity and efficiency that the aaRS exhibit for the natural amino acids requires that the concentration of natural amino acid in the culture medium during protein expression must be strictly limited relative to the concentration of the nonnatural amino acid, so that incorporation of the nonnatural amino acid will be favored. This requires that the natural amino acid that will be replaced must be chosen prior to protein expression, and the appropriate bacterial auxotroph (a strain that is unable to synthesize the chosen natural amino acid) must be obtained/produced. The general experimental procedure for nonnatural amino acid incorporation involves several steps. The auxotroph is grown first in medium that contains the natural amino acid (to maximize the number of protein-producing cells), and then at a desired cell density the cells are centrifuged and washed quickly in order to remove the natural amino acid, and are then resuspended in a medium that contains the nonnatural amino acid but not the natural amino acid. Protein expression is then induced, and in cases where the nonnatural amino acid supports protein biosynthesis, the protein is isolated and purified. The extent of amino acid replacement (ie, nonnatural amino acid incorporation) can be determined via amino acid analysis, Edman degradation analysis, mass spectrometry, tryptic digest/mass spectrometry, and/or NMR, depending on the identity of the nonnatural amino acid.

One of the more recent developments in the *in vivo* incorporation of nonnatural amino acids has been the correlation of the activation of a nonnatural amino acid by an aaRS with the ability of the nonnatural amino acid to support protein biosynthesis (ie, to be incorporated into proteins *in vivo*). The covalent attachment of an amino acid to its cognate tRNA proceeds in two steps, activation and

aminoacylation:

$$\text{aaRS} + \text{aa} + \text{ATP} \rightleftharpoons [\text{aaRS} : \text{aa}{\sim}\text{AMP}] + \text{PP}_i$$
$$[\text{aaRS} : \text{aa}{\sim}\text{AMP}] + \text{tRNA}^{\text{aa}} \rightleftharpoons \text{aaRS} + \text{AMP} + \text{aa}{\sim}\text{tRNA}^{\text{aa}}$$

where aaRS is the aminoacyl-tRNA synthetase, aa is the amino acid, ATP is adenosine triphosphate, AMP is adenosine monophosphate, PP_i is pyrophosphate, aaRS:aa∼AMP is the aminoacyladenylate complexed with the enzyme, and aa∼$tRNA^{aa}$ is the aminoacyl-tRNA. The rate of activation of the amino acid by the enzyme can be measured in assays that monitor the rate at which radiolabeled pyrophosphate is incorporated into ATP (the reverse of the top reaction). The rate of ATP–PP_i exchange is measured as a function of analogue concentration, and the data are fit to a standard Michaelis–Menten model to determine $k_{\text{cat}}/K_{\text{m}}$, which can be used to compare the relative rates of activation of different amino acids by a given aaRS. The measured rates of activation of a variety of nonnatural amino acids by the appropriate aaRS have been shown by Tirrell and co-workers to correlate well with the ability of the bacterial host to utilize the amino acids during protein biosynthesis.

The quantitative establishment of the direct role of the aaRS in the multisite incorporation of nonnatural amino acids has resulted in the development of several strategic approaches that can be taken to control incorporation. The first relies on the ability of the wild-type biosynthetic apparatus to utilize nonnatural amino acids, and uses a standard auxotrophic expression host for protein synthesis. The second approach relies on increasing the level of activity of the wild-type aaRS in the bacterial host by engineering the host to produce extra copies of the desired enzyme. In the third approach, the aaRS is also engineered; the active site can be altered to permit activation of a broader set of nonnatural amino acids, and/or the editing activity of the aaRS can be abolished so that misacylated tRNAs are no longer destroyed by the editing pathway of the enzyme. The mutant aaRS is then overexpressed in the bacterial host. An additional strategy, which permits simultaneous incorporation of both a nonnatural amino acid and its natural counterpart in specified positions, expands the genetic code by the expression of a heterologous aaRS/tRNA pair. The aaRS with desired new activities can be identified via evolutionary-based mutagenesis strategies and/or by rational computational approaches. The application of these methods, as described in more detail below, has resulted in a large set of nonnatural amino acids that can be incorporated into proteins *in vivo* (Fig. 4).

Strategies for Nonnatural Amino Acid Incorporation that Employ the Wild-Type Biosynthetic Apparatus

Methionine. Of the investigations on the incorporation of nonnatural amino acids into proteins, the incorporation of methionine analogues is among the earliest studied. Methionine has been an interesting target for replacement by nonnatural amino acids, as the promiscuity of the biosynthetic apparatus toward methionine has been known for decades, and a variety of methionine analogues

are able to replace methionine during protein biosynthesis. There are no editing mechanisms for hydrolysis of misacylated $tRNA^{Met}$, which suggests that methionine analogues of varying side-chain structures and chemical function may be readily incorporated into proteins. In addition, methionine-rich interfaces are known to mediate a variety of protein–protein assembly processes, and the replacement of methionine may therefore provide opportunities for purposeful manipulation of protein–protein interactions.

The first report of multisite inclusion of nonnatural amino acids into genetically engineered protein polymers was reported by Tirrell and co-workers in the early 1990s, with the inclusion of selenomethionine (in place of methionine) into the repetitive β-sheet-forming polypeptide $\{(GA)_3GM\}_9$ (99). A methionine auxotroph was transformed with an expression plasmid that contained the DNA sequence encoding the polypeptide. The ratio of selenomethionine to methionine in the product protein, as determined via radiolabelling assays, correlated linearly with the ratio in the growth medium, indicating that selenomethionine is capable of essentially perfect replacement of methionine. Standard auxotrophic expression hosts were used to produce the selenomethionine-containing proteins, with the wild-type protein biosynthetic machinery accepting selenomethionine in place of methionine in every stage of protein biosynthesis.

In addition to the selenomethionine example above, telluromethionine, norleucine, trifluoromethionine, and ethionine have all demonstrated translational activity in wild-type bacterial hosts as well (179–181). The translational activity (ie, ability to support protein biosynthesis) of several additional chemically novel methionine analogues (**1-10**) has therefore been investigated (Figure 4). In all of these studies, the incorporation of methionine analogues into the target protein murine dihydrofolate reductase (mDHFR) has been determined; mDHFR carries methionine in 8 positions, and therefore serves as a reasonably stringent test of incorporation of methionine analogues. The mDHFR is encoded in a commercially available pQE15 expression plasmid, which is transformed into an *E. coli* methionine auxotroph.

Methionine analogues **1**, **2**, **3**, and **4** have been shown to replace methionine *in vivo* in these conventional bacterial expression hosts (174,182,183); the remaining methionine analogues, **5-10**, do not support protein biosynthesis under similar assay conditions. Analogues **1** (azidohomoalanine, Aha) and **2** (homopropargylglycine, Hpg) replace methionine quantitatively, as assessed via amino acid analysis, Edman degradation, and mass spectrometry. Furthermore, cultures supplemented with these analogues support the production of mDHFR in the same yields as cultures supplemented with methionine (approximately 40 mg/L) (174,183). Analogue **4** (homoallylglycine, Hag) replaces methionine at levels of approximately 92%, although yields of mDHFR from cultures supplemented with Hag are approximately 28% of those from cultures supplemented with methionine. Further assessment of the activation of the methionine analogues by MetRS has also been conducted and has suggested additional strategies for the incorporation of analogues **5–10** (*vide infra*).

These results suggest that the replacement of methionine by chemically reactive analogues can be used in the synthesis of chemically and physically novel protein polymers. Indeed, mDHFR decorated with the azido-functionalized Aha

(**1**) can be selectively modified by Staudinger-type reactions with triarylphosphine reagents (174), in both its purified form as well as in whole cell lysates. Cell-surface proteins equipped with Aha can also be efficiently modified with alkyne-functionalized biotinylating reagents via copper(I)-catalyzed triazole formation (184). Upon incubation with an avidin-functionalized fluorescent agent after biotinylation, cells decorated with Aha can be differentiated from cells decorated with methionine via flow cytometry methods (184). These results suggest opportunities for chemical modification of protein polymers and for labeling of proteins *in vivo*.

Fluorinated Amino Acids. Synthetic fluoropolymers exhibit many useful surface properties, such as low surface energy, low friction coefficient, excellent solvent resistance and hydrolytic stability, and chemical and biological inertness, and this has enabled these polymers to find use in many disparate applications, such as Teflon-coated pans, self-lubricating parts, pipe liners, membranes, and vascular grafts. The possibility of imparting similar properties to well-defined protein architectures has been of long-term research interest. Fluorinated leucine analogues have been of particular focus owing to leucine's abundance in natural proteins, and substitution by leucine analogues may provide a general strategy for controlling protein folding and function. Furthermore, 5,5,5-Trifluoroleucine (Tfl, **11**) has been known for over 30 years to support bacterial cell growth and to be incorporated into proteins in the absence of leucine. Tfl has been incorporated into β-sheet forming polypeptides with the general sequence $\{(GA)_3GL\}_{12}$, via protein expression in a standard leucine auxotroph, in an attempt to produce protein materials with similar surface characteristics as fluoropolymers. The incorporation of Tfl significantly lowers the surface energy of resulting protein films; contact angles of hexadecane on fluorinated protein films (70°) are much higher than those on the unfluorinated, leucine-containing protein (17°) (98). The fluorinated analogue *p*-fluorophenylalanine (Pff, **21**) can also be incorporated into the similar sequences $\{(GA)_3GF\}_{13}$ (98). FTIR and WAXD studies of protein solids containing Tfl or Pff confirm the antiparallel β-sheet architecture, suggesting that the fluorinated surface may be formed by presentation of the fluorinated amino acids in the fold regions of the β-sheet proteins.

The incorporation of fluorinated amino acids into proteins also confers other potential materials property advantages. Since many organofluorine compounds exhibit lower solubility in water than their hydrocarbon equivalents, fluorinated amino acids may act as hyper-hydrophobic analogues of the hydrophobic amino acids, which may impart increased stability to assembled protein structures stabilized by hydrophobic interactions. The fact that the fluorinated amino acids are nearly isosteric to their natural counterparts also suggests that fluorinated amino acids could be incorporated into proteins without disrupting protein structure. These factors have motivated the investigation of the effect of fluorinated analogues of leucine on the assembly and stability of coiled-coil proteins produced *in vivo*. In experiments to test Tfl incorporation, the pQE9-derived expression plasmid encoding the leucine zipper protein (*vide supra*) is transformed into a leucine auxotroph, and the cells are grown on cultures supplemented with Tfl (**11**). As might be expected on the basis of many previous reports of the translational activity of Tfl, the analogue supports the synthesis of the leucine zipper protein (176), with a maximum level of incorporation of 92%, as indicated by

amino acid analysis and MALDI-MS. Varying the ratio of leucine to Tfl in the culture medium permits various amounts of each amino acid to be incorporated into the protein, although the yields of protein decrease steadily to 20 mg/L (from 40 mg/L) as the percentage of Tfl in the culture medium is increased to 100%. Analysis of the purified proteins via CD indicates that the protein outfitted with Tfl exhibits essentially identical secondary structures as the leucine-containing protein, with greater than 90% helicity. Additionally, the proteins show increasing stability to thermal and chemical denaturation with increasing degrees of fluorination, with "melting" temperatures increased to a maximum of 67°C as compared to 54°C for the leucine-containing protein (176). The increased stability of these assembled structures with respect to thermal and chemical denaturation may have important consequences on controlling the stability and stimuli-responsiveness of not only leucine zipper based, but other types of protein-based materials as well.

Similar strategies have also been employed to incorporate trifluoroisoleucine (Tfi, **15**) into proteins *in vivo* (185). The analogue Tfi was used to supplement cultures of an *E. coli* isoleucine auxotroph equipped with a pQE-15-derived expression plasmid encoding mDHFR (which contains 14 Ile residues). In this bacterial expression host, Tfi was shown to support protein synthesis, with levels of replacement of 93% (185). In an effort to deduce the impact of the incorporation of fluorinated amino acids on protein function, Tfi was also incorporated into murine interleukin-2 (mIL-2), which contains five isoleucine residues in the helical core of the protein. Fluorinated mIL-2 elicits an equivalent maximal proliferative response as the wild-type mIL-2, which indicates that the fluorinated protein still folds into an active, native structure. The combination of the results for the isoleucine and leucine analogues suggests that at least some protein domains will tolerate side-chain fluorination without loss of function. They also indicate the potential for maintaining desired secondary structures and biological activity in repetitive artificial proteins equipped with nonnatural amino acids.

Unsaturated and Structural Amino Acids. The earliest investigations of the incorporation of unsaturated analogues into genetically engineered proteins were conducted in the 1990s. Unsaturated proline analogues were of initial interest for their potential ability to modify protein folding behavior and present reactive chemical functionality at fold surfaces; the potential for substitution of proline had been indicated by earlier studies indicating incorporation of proline analogues into cellular proteins (186). Polymers of the repeating unit $\{(AG)_3PEG\}_x$ had been successfully produced in *E. coli* hosts (100) but were difficult to crystallize, presumably because the conformationally restricted proline residue prevents alignment and hydrogen bonding of the alanylglycyl diads in the repetitive polymer. The incorporation of the analogues dehydroproline (Dhp, **18**) and azetidine-2-carboxylic acid (Aze, **19**) has therefore been assessed via expression of $\{(AG)_3PEG\}_{16}$ in cultures of a proline auxotroph grown on media supplemented with Dhp or Aze (173,187). The Dhp is most readily incorporated (nearly 100%), while the Aze is incorporated at levels of approximately 40%, as determined by ^{1}H NMR spectroscopy and amino acid analysis.

The physical properties of the Dhp variant are qualitatively very similar to those of the proline-containing variant; both form optically clear, amorphous

solids and are water-soluble, indicating a lack of crystallization. The chemical properties of the Dhp variant, however, are strikingly different, as reaction of the protein with H_2O_2 or Br_2 produces hydroxylated and brominated forms of Dhp in quantitative reactions, as determined by the loss of the alkene resonance in the NMR spectrum of the modified protein (173). Whereas the Aze variant is not chemically reactive, the physical structure of this protein is very different than the proline-containing protein, with FTIR spectroscopy indicating β-sheet structure (187). The smaller size of the Aze appears to increase the chain flexibility sufficiently to permit folding; the fact that the addition of only 4 to 6 Aze residues out of 148 amino acids can cause such a pronounced change in physical properties may also have important consequences for purposeful control of polymer physical and chemical behavior. Incorporation of the unsaturated leucine analogue **12** and isoleucine analogues **16** and **17** into the test protein mDHFR has also been reported and may have similar potential for modification of protein folding and reactivity (188,189). The isoleucine analogues can support protein synthesis at levels of approximately 50% of that observed in cultures supplemented with isoleucine, and can replace isoleucine with extents of replacement of 80% (**16**) and 70% (**17**).

The modification of protein structural properties via incorporation of nonnatural amino acids has also recently been realized for human type I collagen expressed in *E. coli*. Proline residues in collagen are hydroxylated to permit folding and to improve the stability of the collagen triple helix (*vide supra*). In mammalian systems, this enzymatic post-translational modification permits the accumulation of correctly folded protein. In prokaryotic systems, however, these enzymes are not present, and thus the modification of the proline has been accomplished via the introduction of the enzyme prolyl 4-hydroxylase in the expression host. The direct incorporation of trans-4-hydroxyproline (Hyp, **20**) in place of proline would obviate the need for the introduction of such additional enzymatic pathways. Buechter and co-workers have demonstrated the feasibility of this approach by the expression, in *E. coli*, of a protein with a sequence derived from the α_1 fragment of human type I collagen; the protein contains 64 Gly-X-Y repeating units and 52 proline residues in both positions X and Y (190). The protein has been expressed in an *E. coli* proline auxotroph, under conditions in which the auxotroph is grown in proline-depleted cultures that contain hydroxyproline and hyperosmotic concentrations of sodium chloride (500 m*M*). Mass spectrometry and amino acid analysis of the protein indicate quantitative replacement of Pro by Hyp in proteins isolated from these cultures. Hyp is activated 5 orders of magnitude less efficiently than Pro by ProRS *in vitro* (190), and therefore does not support protein biosynthesis under normal culture conditions. However, subjecting *E. coli* to hyperosmotic conditions increases the intracellular Hyp concentration sufficiently to recover its ability to support protein biosynthesis; it may be accumulated via mechanisms similar to those that cause active accumulation of Pro under hyperosmotic conditions (191). The Hyp-containing collagen fragments fold into the correct triple-helical structure, as assessed via CD spectroscopy (190), indicating that the global substitution of Hyp for Pro does not appear to destabilize the triple helix, even though Hyp is normally only found in the Y position of Gly-X-Y repeats in vertebrate collagens. Full-length fragments of α_1(I) chain, with

338 G-X-Y repeats and 255 proline residues, have also been expressed in proline-depleted cultures supplemented with Hyp under hyperosmotic conditions, and although the extent of Hyp substitution has not been quantitatively determined, these results suggest that Hyp can replace Pro in even very large numbers of Propositions.

Electroactive Amino Acids. Conducting polymers have been actively investigated for decades because of their potential applications in lightweight batteries, electrodes, nanowires, and nerve regeneration. The production of conducting polymers, however, is often plagued by the insolubility of the highly conjugated, rigid polymer. The incorporation of electroactive amino acids into genetically engineered protein polymers has been explored as a strategy for circumventing these solubility issues, as well as for generating biomedically relevant materials with combined biological and electrical function useful for nerve regeneration. Early investigations explored the incorporation of 3-thienylalanine (3TA, **22**) into the repetitive sequence $\{(GA)_3GF\}_{13}$; protein polymers were expressed from a pET-derived plasmid in a phenylalanine auxotroph grown on media supplemented with 3TA. The 3TA replaces Phe at levels of approximately 85%, as determined by ^{1}H NMR spectroscopy, amino acid analysis, and UV spectroscopy (192). The 3TA analogue alone can be oxidatively polymerized to produce conjugated systems (193), which could be used for the formation of electroactive films or the direct electropolymerization and attachment of biologically active motifs to electrode surfaces.

Nonnatural Amino Acid Incorporation via Overexpression of Wild-Type Aminoacyl-tRNA Synthetases

The examples above demonstrate the flexibility of the wild-type translational apparatus for the incorporation of nonnatural amino acids. Nevertheless, the range of chemical functionality available via utilization of a wild-type bacterial host is substantially more limited than that available via chemical polymerization methods, which has prompted further investigation of the promiscuity of the aaRS in the incorporation of nonnatural amino acids. Such investigations have relied on developing an understanding of the relationship between the rates of activation of a nonnatural amino acid by its cognate aaRS and the ability of the nonnatural amino acid to be incorporated into proteins *in vivo*.

Studies by Kiick and Tirrell have demonstrated the correlation between the kinetics of MetRS-catalyzed analogue activation *in vitro* and methionine analogue incorporation into proteins *in vivo*. The results of ATP-PP_i activation assays indicate that the translationally active analogues **1**, **2**, **3**, and **4** are activated by *E. coli* MetRS, although they are 390-, 500-, 1050- and 1850-fold poorer substrates for the enzyme than methionine, respectively (174,194). In the case of analogues **1** and **2**, the lower rates of activation do not impede the rate of protein synthesis or the extent of incorporation of the analogue (*vide supra*). At the sufficiently lower rates of activation of analogues **3** and **4**, however, the yield of protein recovered from cultures supplemented with the analogue correlates with the rate of activation of

the analogue (57% and 28% yields, respectively). Analogues **5-10** are increasingly poor substrates for the MetRS, consistent with their lack of translational activity in a conventional bacterial host (195).

Overexpression of MetRS in a bacterial expression host has been successfully employed as a strategy for incorporation of methionine analogues **5-10**. In this approach, the *E. coli metG* gene and its promoter are ligated into the expression plasmid pQE-15; bacterial hosts equipped with this plasmid (pQE15-MRS) exhibit approximately 50-fold increased rates of methionine activation. When this modified bacterial expression host is grown in cultures supplemented with analogue **5**, the rate of activation of analogue **5** is increased sufficiently to permit its incorporation into proteins at levels of replacement of approximately 92% (with protein yields of approximately 12 mg/L) (196). The analogues **6-10**, which are activated up to 340,000 more slowly than methionine, can also be incorporated into proteins via similar strategies (195), although the engineered expression host must be grown in medium supplemented with large amounts of the analogue (500 mg/L). In protein produced under these conditions, the level of methionine replacement by analogues **6-10** is 60–98%. Overexpression of the MetRS has also been shown to increase protein yields from cultures supplemented with poor substrates of MetRS.

Overexpression of wild-type aaRS has also been used to expand the number of fluorinated amino acid analogues that can be incorporated into proteins (197). The successful modification of protein properties via incorporation of Tfl, **11**, suggests fluorination as a strategy for modifying surface properties and assembly, and substitution by Hfl, **13**, which carries six fluorine atoms, may have a correspondingly greater impact on protein stabilization. ATP-PP_i exchange assays indicate that Tfl is only 240-fold poorer a substrate for LeuRS relative to Leu, consistent with its ability to replace Leu in proteins produced by a conventional bacterial host. These assays, however, show that Hfl is approximately a 4000-fold poorer substrate for LeuRS versus leucine. Overexpression of the wild-type LeuRS in an engineered expression host has therefore been employed as a strategy to permit incorporation of Hfl (197). The *E. coli leuS* gene and its promoter were ligated into the expression vector pQEA1 (which encodes the leucine zipper motif), to yield plasmid pA1EL. Bacterial hosts equipped with the pA1EL plasmid exhibit LeuRS activity that is elevated approximately 8 times that of unmodified bacterial hosts. Leucine zipper proteins produced from Hfl-supplemented cultures of this bacterial host show a maximum level of Hfl incorporation of 74%, as assessed via amino acid analysis and MALDI-MS. CD measurements confirm that the Hfl-containing protein is >90% helical, and that the melting transition temperature for this fluorinated protein is elevated to 76°C [which is 22°C greater than that of the leucine-containing protein and 9°C greater than that of the Tfl containing protein (*vide supra*)]. The Hfl-containing protein remains 100% folded in urea concentrations up to 4 *M* (197). Overexpression of the LeuRS has also permitted the incorporation of cyclobutenylglycine, **14**, into leucine zipper proteins (198); the side-chain functionality of this analogue may have uses for chemical modification or graft polymerization via ring-opening metathesis polymerization methods. Combined, these results suggest that overexpression of a wild-type aaRS is a general strategy for expanding the set of nonnatural amino acid analogues that can be incorporated into proteins *in vivo*.

Nonnatural Amino Acid Incorporation via Overexpression of Mutant Aminoacyl-tRNA Synthetases

Active Site Mutations. Alteration of the amino acid specificity of the aminoacyl-tRNA synthetases offers another strategy for incorporating into proteins nonnatural amino acids that are not utilized by the wild-type translational apparatus. Such alteration was initially demonstrated in investigations focused primarily on altering the specificity of an aaRS for different natural amino acids (199,200). More recently, investigations by Tirrell and co-workers have expanded the number of nonnatural amino acids that can be incorporated into proteins via mutagenesis of the active site of PheRS (175,177,178). Wild-type PheRS is active toward phenylalanine and *p*-fluorophenylalanine (Pff, **21**), but not toward *p*-chlorophenylalanine (Pcf, **23**), presumably because the additional steric bulk of the chlorine substituent precludes acceptance of Pcf at the active site of PheRS. In 1991, an engineered mutant form of this enzyme that charges $tRNA^{Phe}$ with Pcf was reported (201); the enzyme carries the mutation A294G, in which the alanine residue at position 294 has been mutated to glycine. This mutation effectively enlarges the active site and permits the activation of phenylalanine analogues that carry larger substituents in the *para* position; indeed, investigations indicated that the mutant PheRS permitted incorporation of Pcf into proteins *in vivo* (202). Overexpression of this mutant PheRS in *E. coli* has also permitted the multisite incorporation of a larger set of chemically diverse phenylalanine analogues into target proteins; analogues incorporated include *p*-bromo (**24**) (177), *p*-iodo (**25**), p-cyano (**26**), *p*-ethynyl- (**27**), and *p*-azido-phenylalanine (**28**), and 2-, 3-, and 4-pyridylalanine (**29-31**) (178).

To achieve these results, the mutant α subunit of PheRS is encoded on an expression plasmid that also encodes the target protein mDHFR (which contains nine Phe residues). The resulting plasmid is transformed into an *E. coli* phenylalanine auxotroph (177), and the auxotroph is grown in media depleted of Phe and supplemented with one of the phenylalanine analogues (250–500 mg/L). Target protein isolated from these cultures is then characterized to determine the level of analogue incorporation. The analogue *p*-Br-Phe, **24**, is incorporated into mDHFR at levels of replacement of 88% (as determined via amino acid analysis), with protein yields of 20–25 mg/L (approximately 70% of the expression levels of cultures supplemented with Phe) (177). The other phenylalanine analogues, **25-31**, can be incorporated into mDHFR with levels of replacement ranging from 45 to 90%, with protein yields of 6–18 mg/L (178). The UV spectra of proteins outfitted with analogues **27**, **28**, **29**, **30**, or **31** show peaks whose positions and intensities are consistent with those of the free amino acid analogues, indicating that the functional groups are not modified by the bacterial host during protein biosynthesis or modified by photodegradation.

The introduction of these functional groups provides numerous opportunities to engineer protein polymer properties. Introduction of aryl halide functionality into engineered proteins, for example, opens possibilities for a variety of controlled chemical modifications of proteins via chemistries that are orthogonal to existing methods of protein modification, such as transition metal-catalyzed coupling, amidation, and cyanation. The aryl azide side chain provides the capacity for intramolecular photoactivated cross-linking via the liberation of an amine group

upon exposure to UV light. The use of such modification strategies would allow new approaches to side-chain modification, immobilization on surfaces, cross-linking, and synthesis of graft copolymers. Several of the phenylalanine analogues also show distinct photophysical behavior in the X-ray, UV, and IR regions that may facilitate crystal structure determination via X-ray diffraction and biophysical studies of protein folding and assembly. Bromination, for example, has been explored as a new tool for use in X-ray diffraction studies of protein structure via multiwavelength anomalous diffraction methods.

The potential for incorporating additional Phe analogues via further mutagenesis of the PheRS has also been investigated by the Tirrell group. The crystal structure of the *Thermus thermophilus* wild-type PheRS complexed with Phe (203) has served as a starting point for the design for additional mutant *E. coli* PheRS. Computational approaches have been used to identify important cavity-forming mutations in the *T. thermophilus* enzyme (175), and show that mutation of Ala314 (Ala294 in *E. coli*) to Gly, and Val261 (Thr251 in *E. coli*) to Gly, enlarges the active site. Overexpression of the double mutant PheRS (A294G and T251G) in a bacterial expression host (via similar strategies as those above) permits incorporation of *p*-acetophenylalanine (Paf, **32**) into mDHFR, at levels of replacement of approximately 80% and yields of 20 mg/L (60% of those obtained from cultures supplemented with Phe) (175). The Paf-containing mDHFR has been shown to be active toward hydrazide reagents, without chain cleavage. These studies demonstrate the power of computational approaches for the design of aaRS that permit incorporation of new nonnatural amino acids. They also demonstrate the versatility of the biosynthetic apparatus for production of proteins containing chemically novel nonnatural amino acids.

In addition to these investigations of PheRS, other investigations have suggested the potential for altering the amino acid specificity of TyrRS (199,204) to permit incorporation of tyrosine analogues. An active site mutant of TyrRS, F130S, shows an increased specificity for azatyrosine, **34**, via *in vitro* assays of aminoacylation. The mutant TyrRS is overexpressed in *E. coli* expression hosts, and when cultures of the host are grown on media supplemented with radiolabelled ^{3}H-azatyrosine, azatyrosine is incorporated into *E. coli* cellular proteins, as assessed via SDS-PAGE with detection via film exposure (204). The results for cellular protein uptake are likely to be generally applicable to the incorporation of similar analogues into artificial repetitive protein polymers.

Editing Site Mutations. Mutations of aaRS editing sites have also been a target for increasing the number of nonnatural amino acids that can be incorporated into proteins. IleRS, LeuRS, and ValRS all exhibit an editing mechanism in which a separate editing domain of the aaRS controls hydrolysis of noncognate aminoacyladenylates and misaminoacylated tRNAs on the basis of the size and hydrophilicity of the noncognate amino acid side chain. LeuRS, in particular, employs this editing mechanism to prevent the incorporation of methionine and isoleucine in place of leucine during protein biosynthesis. Tang and Tirrell have reported the generation of a T252Y editing site mutant of *E. coli* LeuRS with impaired editing activity, as assessed via *in vitro* aminoacylation assays (205). A leucine zipper target protein (*vide supra*) has been produced in cultures of a leucine auxotroph that overexpresses the mutant LeuRS; the cultures are supplemented with various nonnatural amino acids but are depleted of leucine,

methionine, isoleucine, and valine. Analysis of the target protein via amino acid analysis and tryptic digest mass spectrometry indicates that the methionine analogues norleucine (**3**) and norvaline (**9**) are incorporated at the leucine sites in the leucine zipper protein at levels of 91 and 79%, respectively (205), consistent with the attenuation of the editing activity of LeuRS against methionine. The analogues also replace methionine at levels of 92 and 68%, respectively (205), as is expected on the basis of the reported ability of these analogues to replace methionine *in vivo* (*vide supra*). Overexpression of the mutant LeuRS also permits the incorporation of the unsaturated methionine analogues homopropargylglycine (**2**), homoallylglycine (**4**), 2-butynylglycine (**7**), and allylglycine (**8**), at levels of 74, 37, 37, and 76%, respectively, as assessed via mass spectrometric analysis. In other investigations, mutations at the editing site of valyl-tRNA synthetase have also been demonstrated to permit the incorporation of aminobutyrate in place of valine in cellular proteins produced by *E. coli* (206). Modulation of the editing activities of select aaRS therefore provides an additional strategy for incorporation of novel amino acids into proteins *in vivo*.

Nonnatural Amino Acid Incorporation via Introduction of Heterologous aaRS/tRNA Pairs

The multisite incorporation of nonnatural amino acids in protein polymers has relied on the replacement of a given natural amino acid by a desired nonnatural amino acid. Protein polymers that contain both a natural amino acid and its analogue can be produced via methods in which the ratio of the amino acids in the culture medium is controlled (*vide supra*). These strategies, however, do not permit precise control of the placement of the natural and nonnatural amino acids in the protein chain, since the nonnatural amino acid must "share" codons with the natural amino acid it replaces. The degeneracy of the genetic code, which arises from the use by the protein biosynthetic apparatus of 61 mRNA sense codons to direct the templated polymerization of 20 amino acid monomers, can be used to overcome this limitation. The ability to reassign degenerate triplet codons to nonnatural amino acids offers possibilities for expanding the combinations of building blocks (natural and nonnatural) that can be used to construct artificial proteins. Tirrell and co-workers have recently demonstrated the feasibility of this strategy for the simultaneous incorporation of phenylalanine and its analogue 3-(2-naphthyl)alanine (Nal, **33**) at specified positions in a target protein (207).

Phenylalanine is encoded by two codons, UUC and UUU, and both codons are read by a single $tRNA^{Phe}$, which carries the anticodon GAA. Introduction of a $tRNA^{Phe}$ with an AAA anticodon, therefore, offers a strategy to incorporate nonnatural amino acids only at phenylalanine positions encoded by UUU, while maintaining the incorporation of Phe at positions encoded by UUC. To achieve this experimentally, Kwon and co-workers have introduced a heterologous PheRS and its cognate $tRNA^{Phe}$ into an *E. coli* expression host (207). Specifically, the investigations have employed a yeast $tRNA^{Phe}$ (with an AAA anticodon, $ytRNA^{Phe}_{AAA}$), which is not charged by *E. coli* PheRS, and a mutant yeast PheRS (T415G) that charges only the yeast $tRNA^{Phe}$ and preferentially activates Nal over Phe (Fig. 5).

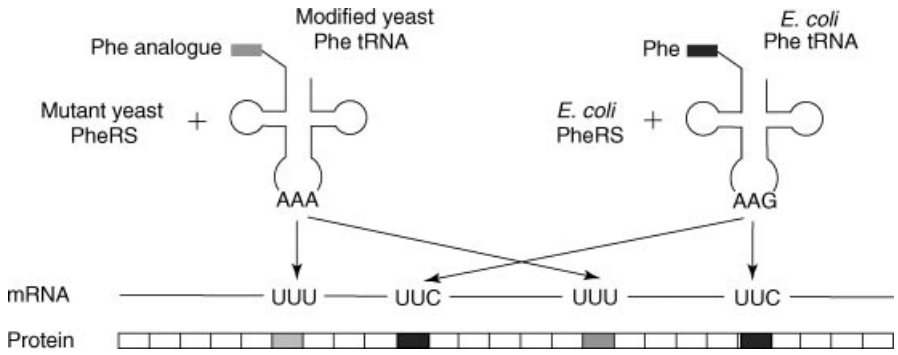

Fig. 5. Strategy for specific multisite incorporation of both natural and non-natural amino acids. Adapted, with permission, from Ref. 208.

The mutant yeast PheRS gene is encoded on an expression plasmid that also encodes the target protein mDHFR, which contains four Phe residues encoded by UUC and five by UUU; the yeast $tRNA^{Phe}_{AAA}$ is encoded on the repressor plasmid pREP4. Protein expression is induced in cultures of a Phe auxotroph that is equipped with these plasmids; the culture medium is supplemented with Nal and depleted of Phe. Amino acid analysis of the isolated target protein indicates that 4.4 of the 9 Phe residues are replaced by Nal, and mass spectral analysis shows replacement of 5 phenylalanine residues by Nal, which corresponds exactly with the number of UUU codons present in the mDHFR gene. Analysis, via MALDI-MS, of tryptic digest fragments of mDHFR indicates that Nal is indeed incorporated at positions encoded by UUU, while Phe is incorporated at positions encoded by UUC (207). This approach will have important consequences for the engineering of protein polymers, particularly upon the identification of additional heterologous aaRS that can charge specific tRNAs with desired nonnatural amino acids.

The versatility of nonnatural amino acid incorporation afforded by overexpression of mutagenized aaRS suggests the potential of evolutionary-based and rational strategies for the design of aaRS with engineered activity toward specific nonnatural analogues. Directed evolution strategies developed by Arnold (209) can be applied to the random mutagenesis of aaRS, followed by appropriate screening to identify aaRS that can charge its tRNA with a desired nonnatural amino acid. Such evolutionary strategies have been applied by Schultz and co-workers to the production of heterologous aaRS that can aminoacylate suppressor tRNAs with nonnatural amino acids *in vivo* (158,162–167); similar strategies should be applicable to the design of aaRS/tRNA pairs for multisite incorporation as well. Rational methods are also potentially powerful approaches to aaRS design. Goddard and co-workers have recently applied computational methods for the determination of Phe analogue/PheRS binding energies, and have demonstrated the correlation between computationally determined binding energies and the incorporation of the Phe analogues into proteins *in vivo* (210). Given the expanding kinetic data now available for a variety of nonnatural amino acid/aaRS pairs, these computational methods can be further developed to allow the rational design of new sets of amino acid/aaRS pairs that will find application in protein polymer engineering. The prospects are therefore promising for utilizing both evolutionary and rational

approaches to engineer the biosynthetic apparatus for the purposeful production of chemically and physically novel protein polymers.

Prospects and Commercial Viability

The expansion in the design and synthesis of *de novo* designed protein polymers over the last decade has had important consequences in polymer science. The genetically directed synthesis of protein polymers has allowed elucidation of structure-function relationships in protein polymers and has experienced enormous growth as an approach to the design of new polymeric materials, with both interesting academic and commercial applications. Protein polymers modeled after natural fibrous proteins have shown novel mechanical, assembly, and biological properties. Artificial protein polymers that exhibit controlled chain folded architectures, liquid crystalline phases, and self-assembled hydrogels on the basis of sequence and molecular weight control have been produced. The development of additional artificial protein polymers will offer continued opportunities for the production of novel materials that display functional groups in a manner that controls materials assembly, mediates interactions with biological targets, and yields polymers with interesting mechanical, biological, and/or surface properties. The expansion of the synthetic methods to include the incorporation of a wide array of nonnatural amino acids also suggests a variety of new strategies for macromolecular synthesis.

In addition to the functional advantages offered by protein-based polymers, continued interest in exploring their commercial use is motivated by the fact that the polymers are produced from renewable resources and are environmentally friendly materials from production through disposal. Practically, the relative cost and amount of time required to design and synthesize a protein polymer with desired physical and chemical characteristics can be much higher than the costs of designing and producing a chemically derived polymer. However, once the protein is designed and methods for its reliable production are defined, the costs of producing the protein polymer via fermentation is generally independent of the complexity of the polymer produced, and can therefore be much lower than the costs of chemical synthesis of complex macromolecules, since chemical synthesis costs increase quickly with increasing polymer complexity and control of monomer sequence. The costs associated with the biosynthesis of protein-based polymers depend on the costs of the materials used in synthesis and the scale of the synthesis; the raw materials are often as simple as glucose or methanol, ammonia, and salts. Larger-scale synthesis is achieved via the use of high cell density fermentation procedures, in which oxygen, glucose, and pH levels are controlled to allow high cell density growth in large quantities of culture medium; in the laboratory, multigram quantities ($>$25 g) of protein can be produced from *E. coli* via such strategies, and yields as high as 15g/L are possible from yeast. Given that commercial fermentations can be scaled to thousands of liters of culture, yields of proteins suitable for technological and market applications are possible. Hundreds of tons of protein per year can be produced via technologies currently in place for the production of amino acids, antibiotics, and protein therapeutics.

The costs of purification of protein polymers can be high if purification requires multiple chromatographic separations; however, most repetitive protein polymers have physicochemical properties very different from cellular proteins, and can be separated from these proteins by selective precipitation methods involving changes in temperature and pH. Similarly, protein polymers whose sequences alone may not permit such simple purification strategies can be expressed with fusion tags that facilitate purification. Secretion into the culture medium can also simplify purification and provide opportunities for less complicated large-scale syntheses, as expression hosts could be immobilized on a solid support, and protein removed in a continuous fashion without the requirement to turn over the culture entirely.

Recombinant enzymes have been produced and purified via these methods at market costs as low as $23/lb (110); these costs are likely acceptable for protein polymers with a primary commercial use as a high value biomedical material. For large commercial materials applications, however, lower cost production and purification will be required. Additional advances in fermentation, such as the use of secretion, may help drive costs down, although currently the yields of protein obtained by protein secretion systems have generally tended to be much lower than those of the standard intracellular accumulation systems.

Nevertheless, production of protein-based materials continues to progress in the areas of biomedically related polymers and fibers, and both prokaryotic and eukaryotic expression systems are used commercially. Since 1988, Protein Polymer Technologies, Inc (PPTI) has been a pioneer in protein polymer design and synthesis, and has extensive patent literature in the area of silk-based and elastin-based polymeric materials. The high molecular weight, genetically engineered biomaterials are processed into products with properties tailored to specific clinical needs; over 50 protein polymer sequences have been designed by PPTI for commercial application, and some can be produced in kilogram quantities. Targeted products include urethral bulking agents for the treatment of stress urinary incontinence, dermal augmentation products for cosmetic and reconstructive surgery, tissue adhesives and sealants, scaffolds for wound healing and tissue engineering, and depots for local drug delivery. The first commercial product of PPTI combined the *B. mori* silk motif with a cell adhesion sequence of fibronectin to yield protein polymers that form autoclavable, stable coatings on plastic and glass via adsorption of the β-sheet blocks of the polymer; these polymers are now sold as cell-culture products by Sanyo Chemical Industries. Silk-elastin-like proteins are used for injectable hydrogels; after injection, stable, water-insoluble hydrogels are formed via β-sheet hydrogen bonding and can be used for both surgical and drug delivery applications. In addition to medical applications, industrial applications are also of interest for the protein polymers, and Genencor International, Inc has obtained a worldwide exclusive license to develop PPTI's protein polymers in both industrial and personal care applications. Nexia Biotechnologies Inc manufactures complex recombinant proteins with industrial and medical applications; its lead product, BioSteel, is based on recombinant spider-silk proteins, and production of these proteins from transgenic goats is under continued development. Targeted applications for these materials include medical sutures, surgical meshes, and artificial ligaments, as well as materials applications such as technical sporting gear (eg, biodegradable fishing lines), soft body armor, and composites.

The challenges facing commercial implementation of protein polymers has not quenched motivation for research and technological progress in this area. In fact, many important contributions have been published first as patent applications because of their potential commercial significance. Numerous patents have been awarded, with topics focused on natural protein sequences, construction and expression of artificial genes/proteins, specific application needs addressed by the unique properties of protein materials, and the incorporation of nonnatural amino acids.

BIBLIOGRAPHY

1. G. Moretti and P. Pino, *Polymer* **28**, 683–692 (1987).
2. P. Corradini, *Macromol. Symp.* **89**, 1–11 (1995).
3. M. Szwarc, *Nature* **178**, 1168–1169 (1956).
4. R. Waack, A. Rembaum, J. D. Coombes, and M. Szwarc, *J. Am. Chem. Soc.* **79**, 2026–2027 (1957).
5. M. Szwarc and M. VanBeylen, *Ionic Polymerization and Living Polymers*, Chapman and Hall, New York, 1993.
6. R. Faust and J. P. Kennedy, *Polym. Bull.* **15**, 317–323 (1986).
7. R. R. Schrock, *Acc. Chem. Res.* **23**, 158–165 (1990).
8. H. H. Brintzinger, D. Fischer, R. Mulhaupt, B. Rieger, and R. M. Waymouth, *Angew. Chem., Int. Ed. Engl.* **34**, 1143–1170 (1995).
9. K. Matyjaszewski, K. Davis, T. E. Patten, and M. Wei, *Tetrahedron* **53**, 15321–15329 (1997).
10. E. L. Dias, T. N. SonBinh, and R. H. Grubbs, *J. Am. Chem. Soc.* **119**, 3887–3897 (1997).
11. J. Chiefari, Y. K. Chong, F. Ercole, J. Krstina, J. Jeffery, T. P. T. Le, R. T. A. Mayadunne, G. F. Meijs, C. L. Moad, G. Moad, E. Rizzardo, and S. H. Thang, *Macromolecules* **31**, 5559–5562 (1998).
12. D. M. Lynn, S. Kanaoka, and R. H. Grubbs, *J. Am. Chem. Soc.* **118**, 784–790 (1998).
13. T. J. Deming, *Nature* **390**, 386–389 (1997).
14. M. Cheng, A. B. Attygalle, E. B. Lobkovsky, and G. W. Coates, *J. Am. Chem. Soc.* **121**, 11583–11584 (1999).
15. J. Louie, C. W. Bielawski, and R. H. Grubbs, *J. Am. Chem. Soc.* **123**, 11312–11313 (2001).
16. J. Parker, *Microbiol. Rev.* **53**, 273–298 (1989).
17. G. H. Altman, F. Diaz, C. Jakuba, T. Calabro, R. L. Horan, J. Chen, H. Lu, J. Richmond, and D. L. Kaplan, *Biomaterials* **24**, 401–416 (2003).
18. J. Gosline, M. Lillie, E. Carrington, P. Guerette, C. Ortlepp, and K. Savage, *Philos. Trans. R. Soc. London, B* **357**, 121–132 (2002).
19. A. Chilkoti, M. R. Dreher, and D. E. Meyer, *Adv. Drug Deliv. Rev.* **54**, 1093–1111 (2002).
20. U.S. Pat. 5,149,657 (Sept. 22, 1992), K. J. Maugh and D. M. Anderson (to Enzon Labs, Inc.).
21. J. P. O'Brien, R. H. Hoess, K. H. Gardner, R. L. Lock, Z. R. Wasserman, P. C. Wever, and F. R. Salemme, in D. Kaplan, W. W. Adams, B. Farmer, and C. Viney, eds., *Silk Polymers*, American Chemical Society, Washington, D.C., 1994.
22. C. Wang, R. J. Stewart, and J. Kopecek, *Nature* **397**, 417–420 (1999).
23. L. Chen, J. Kopecek, and R. J. Stewart, *Bioconjugate Chem.* **11**, 734–740 (2000).

24. S. Halstenberg, A. Panitch, S. Rizzi, H. Hall, and J. A. Hubbell, *Biomacromolecules* **3**, 710–723 (2002).
25. S. Arcidiacono, C. Mello, D. L. Kaplan, S. Cheley, and H. Bayley, *Appl. Microbiol. Biotechnol.* **49**, 31–38 (1998).
26. J. Cappello, J. Crissman, M. Dorman, M. Mikolajczak, G. Textor, M. Marquet, and F. Ferrari, *Biotechnol. Prog.* **6**, 198–202 (1990).
27. J. P. Anderson, J. Cappello, and D. C. Martin, *Biopolymers* **34**, 1049–1058 (1994).
28. T. Asakura, H. Kato, J. Yao, R. Kishore, and M. Shirai, *Polymer J.* **34**, 936–943 (2002).
29. World Patent 9429450 (Dec. 22, 1994), S. R. Fahnestock, (to E.I. du Pont de Nemours & Co.).
30. S. R. Fahnestock and S. L. Irwin, *Appl. Microbiol. Biotechnol.* **47**, 23–32 (1997).
31. U.S. Pat. 6,268,169 (July 31, 2001), S. R. Fahnestock (to E. I. du Pont de Nemours & Co.).
32. S. R. Fahnestock, Z. Yao, and L. A. Bedzyk, *Rev. Mol. Biotechnol.* **74**, 105–119 (2000).
33. S. R. Fahnestock, and L. A. Bedzyk, *Appl. Microbiol. Biotechnol.* **47**, 33–39 (1997).
34. J. T. Prince, K. P. McGrath, C. M. DiGirolamo, and D. L. Kaplan, *Biochemistry* **34**, 10879–10884 (1995).
35. Y. Fukushima, *Biopolymers* **45**, 269–279 (1998).
36. E. E. Hood and J. M. Jilka, *Curr. Opin. Biotechnol.* **10**, 382–386 (2000).
37. J. Scheller, K.-H. Guhrs, F. Grosse, and U. Conrad, *Nature Biotechnol.* **19**, 573–577 (2001).
38. A. Lazaris, S. Arcidiacono, Y. Huang, J.-F. Zhou F. Duguay, N. Chretien, E. A. Welsh, J. W. Soares, and C. N. Karatzas, *Science* **295**, 472–476 (2002).
39. U.S. Pat. 2001042255 (Nov. 15, 2001), A. L. Karatzas, C. N. Karatzas, and J. D. Turner (to Nexia Biotechnologies, Inc.).
40. S. Arcidiacono, C. M. Mello, M. Butler, E. Welsh, J. W. Soares, A. Allen, D. Ziegler, T. Laue, and S. Chase, *Macromolecules* **35**, 1262–1266 (2002).
41. S. Winkler, S. Szela, P. Avtges, R. Valluzzi, D. A. Kirschner, and D. Kaplan, *Int. J. Biol. Macromol.* **24**, 265–270 (1999).
42. R. Valluzzi, S. Szela, P. Avtges, D. Kirschner, and D. Kaplan, *J. Phys. Chem. B.* **103**, 11382–11392 (1999).
43. S. Szela, P. Avtges, R. Valluzzi, S. Winkler, D. Wilson, D. Kirschner, and D. L. Kaplan, *Biomacromolecules* **1**, 534–542 (2000).
44. S. Winkler, D. Wilson, and D. L. Kaplan, *Biochemistry* **39**, 12739–12746 (2000).
45. T. Asakura, K. Nitta, M. Yang, J. Yao, Y. Nakazawa, and D. L. Kaplan, *Biomacromolecules* **4**, 815–820 (2003).
46. Y. T. Zhou, S. X. Wu, and V. P. Conticello, *Biomacromolecules* **2**, 111–125 (2001).
47. Y. Qu, S. C. Payne, R. P. Apkarian, and V. P. Conticello, *J. Am. Chem. Soc.* **122**, 5014–5015 (2000).
48. A. Lamberg, T. Helaakoski, J. Myllyharju, S. Peltonen, H. Notbohm, T. Pihlajaniemi, and K. I. Kivirikko, *J. Biol. Chem.* **271**, 11988–11995 (1996).
49. M. Nokelainen, T. Helaakoski, J. Myllyharju, H. Notbohm, T. Pihlajaniemi, P. P. Fietzek, and K. I. Kivirikko, *Matrix Biol.* **16**, 329–338 (1998).
50. A. Vuorela, J. Myllyharju, R. Nissi, T. Pihlajaniemi, and K. I. Kivirikko, *EMBO J.* **16**, 6702–6712 (1997).
51. D. C. A. John, R. Watson, A. J. Kind, A. R. Scott, K. E. Kadler, and N. J. Bulleid, *Nature Biotechnol.* **17**, 385–389 (1999).
52. P. D. Toman, F. Pieper, N. Sakai, C. Karatzas, E. Platenburg, I. de Wit, C. Samuel, A. Dekker, G. A. Daniels, R. A. Berg, and G. J. Platenburg, *Transgenic Res.* **8**, 415–427 (1999).
53. M. W. T. Werten, T. J. van den Bosch, R. D. Wind, H. Mooibroek, and F. A. de Wolf, *Yeast* **15**, 1087–1096 (1999).

54. E. C. de Bruin, M. W. T. Werten, C. Laane, and F. A. de Wolf, *FEMS Yeast Res.* **1**, 291–298 (2002).
55. J. Myllyharju, A. Lamberg, H. Notbohm, P. P. Fietzek, T. Pihlajaniemi, and K. I. Kivirikko, *J. Biol. Chem.* **272**, 21824–21830 (1997).
56. U.S. Pat. 5,670,616 (Sept. 23, 1997), S. C. Weber and J. A. McElver (to Eastman Kodak Co.).
57. T. Kajino, H. Takahashi, M. Hirai, and Y. Yamada, *Appl. Environ. Microbiol.* **66**, 304–309 (2000).
58. M. W. T. Werten, W. H. Wisselink, T. J. Jansen-van den Bosch, E. C. de Bruin, and F. A. de Wolf, *Protein Eng.* **14**, 447–454 (2001).
59. I. Goldberg, A. J. Salerno, T. Patterson, and J. I. Williams, *Gene* **80**, 305–314 (1989).
60. I. Goldberg and A. J. Salerno, in P. C. Rieke, P. D. Calvert, and M. Alper, eds., *Materials Synthesis Utilizing Biological Processes*, Materials Research Society, Pittsburgh, Pa., 1990, pp. 229–236.
61. F. A. Ferrari and J. Cappello, in K. McGrath and D. Kaplan, eds., *Protein Based Materials*, Birkhauser, Boston, 1997, pp. 37–60.
62. U.S. Pat. 5,773,249 (June 30, 1998), J. Cappello and F. A. Ferrari (to Protein Polymer Technologies, Inc.).
63. J. Yin, J. Lin, W. Li, and D. I. C. Wang, *J. Biotechnol.* **100**, 181–191 (2003).
64. D. T. McPherson, C. Morrow, D. S. Minehan, J. Wu, E. Hunter, and D. W. Urry, *Biotechnol. Prog.* **8**, 347–352 (1992).
65. C. Guda, X. Shang, D. T. McPherson, J. H. Cherry, D. W. Urry, and H. Daniell, *Biotechnol. Lett.* **17**, 745–750 (1995).
66. A. Panitch, T. Yamaoka, M. J. Fournier, T. L. Mason, and D. A. Tirrell, *Macromolecules* **32**, 1701–1703 (1999).
67. R. A. McMillan and V. P. Conticello, *Macromolecules* **33**, 4809–4821 (2000).
68. D. E. Meyer and A. Chilkoti, *Biomacromolecules* **3**, 357–367 (2002).
69. R. W. Herzog, N. K. Singh, D. W. Urry, and H. Daniell, *Appl. Microbiol. Biotechnol.* **47**, 368–372 (1997).
70. C. Guda, S. B. Lee, and H. Daniell, *Plant Cell Rep.* **19**, 257–262 (2000).
71. X. Zhang, D. W. Urry, and H. Daniell, *Plant Cell Rep.* **16**, 174–179 (1996).
72. R. A. McMillan, T. A. T. Lee, and V. P. Conticello, *Macromolecules* **32**, 3643–3648 (1999).
73. D. W. Urry, A. Q. Peng, L. C. Hayes, D. McPherson, J. Xu, T. C. Woods, D. C. Gowda, and A. Pattanaik, *Biotech. Bioeng.* **58**, 175–190 (1998).
74. D. W. Urry, *Prog. Biophys. Mol. Biol.* **57**, 23–57 (1992).
75. D. W. Urry, A. Pattanaik, M. A. Accavitti, C.-X. Luan, D. T. McPherson, J. Xu, D. C. Gowda, T. M. Parker, C. M. Harris, and J. Naijie, in A. J. Domb, J. Kost, and D. M. Wiseman, eds., *Drug Targeting and Delivery, Handbook of Biodegradable Polymers*, Vol. 7, Harwood Academic Publishers, Amsterdam, 1997, pp. 367–386.
76. D. E. Meyer, B. C. Shin, G. A. Kong, M. W. Dewhirst, and A. Chilkoti, *J. Controlled Release* **74**, 213–224 (2001).
77. E. R. Wright and V. P. Conticello, *Adv. Drug Delivery Rev.* **54**, 1057–1073 (2002).
78. E. R. Wright, R. A. McMillan, A. Cooper, R. P. Apkarian, and V. P. Conticello, *Adv. Funct. Mater.* **12**, 149–154 (2002).
79. T. A. T. Lee, A. Cooper, R. P. Apkarian, and V. P. Conticello, *Adv. Mater.* **12**, 1105–1110 (2000).
80. J. Lee, C. W. Macosko, and D. W. Urry, *Biomacromolecules* **2**, 170–179 (2001).
81. K. Trabbic-Carlson, L. A. Setton, and A. Chilkoti, *Biomacromolecules* **4**, 572–580 (2003).
82. Z. Megeed, J. Cappello, and H. Ghandehari, *Adv. Drug Delivery Rev.* **54**, 1075–1091 (2002).

83. A. Nagarsekar, J. Crissman, M. Crissman, F. Ferrari, J. Cappello, and H. Ghandehari, *J. Biomed. Mater. Res.* **62**, 195–203 (2002).
84. A. Nagarsekar, J. Crissman, M. Crissman, F. Ferrari, J. Cappello, and H. Ghandehari, *Biomacromolecules* **4**, 602–607 (2003).
85. J. Cappello, J. W. Crissman, M. Crissman, F. A. Ferrari, G. Textor, O. Wallis, J. R. Whitledge, X. Zhou, D. Burman, L. Aukerman, and E. R. Stedronsky, *J. Controlled Release* **53**, 105–117 (1998).
86. A. A. Dinerman, J. Cappello, H. Ghandehari, and S. W. Hoag, *Biomaterials* **23**, 4203–4210 (2002).
87. Z. Megeed, J. Cappello, and H. Ghandehari, *Pharm. Res.* **19**, 954–959 (2002).
88. E. R. Welsh and D. A. Tirrell, *Biomacromolecules* **1**, 23–30 (2000).
89. K. Di Zio and D. A. Tirrell, *Macromolecules* **36**, 1553–1558 (2003).
90. M. T. Krejchi, E. D. T. Atkins, A. J. Waddon, M. J. Fournier, T. L. Mason, and D. A. Tirrell, *Science* **265**, 1427–1432 (1994).
91. E. J. Cantor, E. D. Atkins, S. J. Cooper, M. J. Fournier, T. L. Mason, and D. A. Tirrell, *J. Biochem.* **122**, 217–225 (1997).
92. S. M. Yu, V. Conticello, G. Zhang, C. Kayser, M. J. Fournier, T. L. Mason, and D. A. Tirrell, *Nature* **389**, 187–190 (1997).
93. S. M. Yu, C. M. Soto, and D. A. Tirrell, *J. Am. Chem. Soc.* **122**, 6552–6559 (2000).
94. G. Zhang, M. J. Fournier, T. L. Mason, and D. A. Tirrell, *Macromolecules* **25**, 3601–3603 (1992).
95. W. A. Petka, J. L. Hardin, K. P. McGrath, D. Wirtz, and D. A. Tirrell, *Science* **281**, 389–392 (1998).
96. R. S. Farmer and K. L. Kiick, manuscript in preparation.
97. J.-I. Won and A. E. Barron, *Macromolecules* **35**, 8281–8287 (2002).
98. E. Yoshikawa, M. J. Fournier, T. L. Mason, and D. A. Tirrell, *Macromolecules* **27**, 5471–5475 (1994).
99. M. J. Dougherty, S. Kothakota, T. L. Mason, D. A. Tirrell, and M. J. Fournier, *Macromolecules* **26**, 1779–1781 (1993).
100. K. P. McGrath, M. J. Fournier, T. L. Mason, and D. A. Tirrell, *J. Am. Chem. Soc.* **114**, 727–733 (1992).
101. Y. Tsujimoto and Y. Suzuki, *Cell* **18**, 591–600 (1979).
102. M. Xu and R. V. Lewis, *Proc. Natl. Acad. Sci. USA* **87**, 7120–7124 (1990).
103. J. D. van Beek, S. Hess, F. Vollrath, and B. H. Meier, *Proc. Natl. Acad. Sci. U.S.A.* **99**, 10266–10271 (2002).
104. F. Vollrath and D. P. Knight, *Nature* **410**, 541–548 (2001).
105. U.S. Pat. 6,380,154 (Apr. 30, 2002), J. Cappello and E. R. Stedronsky (to Protein Polymer Technologies, Inc.).
106. R. V. Lewis, M. Hinman, S. Kothakota, and M. J. Fournier, *Protein Expr. Purif.* **7**, 400–406 (1996).
107. World Pat. 03057720 (July 17, 2003), C. N. Karatzas, Y. Huang, and C. Turcotte (to Nexia Biotechnologies, Inc.).
108. World Pat. 03057727 (July 17, 2003), C. N. Karatzas and C. Turcotte (to Nexia Biotechnologies, Inc.).
109. World Pat. 03060099 (July 24, 2003), C. N. Karatzas, A. Rodenheiser, A. Alwattari, and S. Islam (to Nexia Biotechnologies, Inc.).
110. S. Fahnestock, in S. Fahnestock and A. Steinbuchel, eds., *Biopolymers, Vol. 8: Polyamides and Complex Proteinaceous Materials II*, Wiley-VCH, Weinheim, 2003, pp. 47–79.
111. S. Zhang, T. Holmes, C. Lockshin, and A. Rich, *Proc. Natl. Acad. Sci. U.S.A.* **90**, 3334–3338 (1993).

112. K. E. Kadler, D. F. Holmes, J. A. Trotter, and J. A. Chapman, *Biochem. J.* **316**, 1–11 (1996).
113. World Pat. 9307889 (Apr. 29, 1993), D. J. Prockop, L. Ala-Kokko, A. Fertala, A. Sieron, K. I. Kivirikko, and A. Geddis (to Thomas Jefferson University).
114. A. Fichard, E. Tillet, F. Delacoux, R. Garrone, and F. Ruggiero, *J. Biol. Chem.* **272**, 30083–30087 (1997).
115. World Pat. 9818918 (May 7, 1998), P. R. Vaughan, M. Galanis, J. A. M. Ramshaw, and J. A. Werkmeister (to Commonwealth Scientific and Industrial Research Organisation).
116. P. D. Toman, G. Chisholm, H. McMullin, L. M. Giere, D. R. Olsen, R. J. Kovach, S. D. Leigh, B. E. Fong, R. Chang, G. A. Daniels, R. A. Berg, and R. A. Hitzemann, *J. Biol. Chem.* **275**, 23303–23309 (2000).
117. D. Olsen, S. D. Leigh, R. Chang, H. McMullin, W. Ong, E. Tai, G. Chisholm, D. E. Birk, R. A. Berg, R. A. Hitzeman, and P. D. Toman, *J. Biol. Chem.* **276**, 24038–24043 (2001).
118. U.S. Pat. 5,895,833 (Apr. 20, 1999), R. A. Berg (to Cohesion Technologies, Inc.).
119. F. Ruggiero, J.-Y. Exposito, P. Bournat, V. Gruber, S. Perret, J. Comte, B. Olagnier, R. Garrone, and M. Theisen, *FEBS Lett.* **469**, 132–136 (2000).
120. S. Perret, C. Merle, S. Bernocco, P. Berland, R. Garrone, D. J. S. Hulmes, M. Theisen, and F. Ruggiero, *J. Biol. Chem.* **276**, 43693–43698 (2001).
121. M. Nokelainen, H. Tu, A. Vuorela, H. Notbohm, K. I. Kivirikko, and J. Myllyharju, *Yeast* **18**, 797–806 (2001).
122. World Pat. 9714431 (Apr. 24, 1997), P. D. Toman, R. A. Berg, G. A. Daniels, R. A. Hitzeman, and G. E. Chisholm (to Collagen Corporation and Genotypes, Inc.).
123. World Pat. 9738710 (Oct. 23, 1997), K. I. Kivirikko and T. Pihlajaniemi (to Fibrogen, Inc.; Academy of Finland).
124. A. Fertala, W. B. Han, and F. K. Ko, *J. Biomed. Mater. Res.* **57**, 48–58 (2001).
125. W. V. Arnold, A. L. Sieron, A. Fertala, H. P. Gachinger, D. Mechling, and D. J. Prockop, *Matrix Biol.* **16**, 105–116 (1997).
126. M. Hayashi, M. Tomita, and K. Yoshizato, *Biochim. Biophys. Acta* **1528**, 187–195 (2001).
127. L. Debelle and A. M. Tamburro, *Int. J. Biochem. Cell. Biol.* **31**, 261–272 (1999).
128. D. W. Urry, T. M. Parker, M. C. Reid, and D. C. Gowda, *J. Bioact. Compat. Polym.* **6**, 263–282 (1991).
129. H. Reiersen, A. R. Clarke, and A. R. Rees, *J. Mol. Biol.* **283**, 255–264 (1998).
130. D. W. Urry, *J. Phys. Chem. B.* **101**, 11007–11028 (1997).
131. H. Betre, L. A. Setton, D. E. Meyer, and A. Chilkoti, *Biomacromolecules* **3**, 910–916 (2002).
132. G. V. R. Rao, S. Balamurugan, D. E. Meyer, A. Chilkoti, and G. P. Lopez, *Langmuir* **18**, 1819–1824 (2002).
133. N. Nath and A. Chilkoti, *Anal. Chem.* **75**, 709–715 (2003).
134. J. Lee, C. W. Macosko, and D. W. Urry, *Macromolecules* **34**, 5968–5974 (2001).
135. L. Huang, R. A. McMillan, R. P. Apkarian, B. Pourdeyhimi, V. P. Conticello, and E. L. Chaikof, *Macromolecules* **33**, 2989–2997 (2000).
136. K. Nagapudi, W. T. Brinkman, J. E. Leisen, L. Huang, R. A. McMillan, R. P. Apkarian, V. P. Conticello, and E. L. Chaikof, *Macromolecules* **35**, 1730–1737 (2002).
137. J. M. Yao and T. Asakura, *J. Biochem.* **133**, 147–154 (2003).
138. A. Dinerman, J. Cappello, H. Ghandehari, and S. Hoag, *J. Controlled Release* **82**, 277–287 (2002).
139. A. Megeed, M. Haider, D. Li, J. B. W. O'Malley, J. Cappello, and H. Ghandehari, *J. Controlled Release* **94**, 433–445 (2004).
140. M. Haider, Z. Megeed, and H. Ghandehari, *J. Controlled Release* **95**, 1–26 (2004).
141. Z. Megeed, H. Ghandehari, in M. Amiji, ed., *Polymeric Gene Delivery: Principles and Applications*, CRC Press, Boca Raton, Fla., in press.

142. A. Nicol, D. C. Gowda, T. M. Parker, and D. W. Urry, in C. Gebelein and C. Carraher, eds., *Biotechnology and Bioactive Polymers*, Plenum, New York, 1994, p. 95.
143. S. C. Heilshorn, K. A. DiZio, E. R. Welsh, and D. A. Tirrell, *Biomaterials* **24**, 4245–4252 (2003).
144. M. T. Krejchi, S. J. Cooper, Y. Deguchi, E. D. T. Atkins, M. J. Fournier, T. L. Mason, and D. A. Tirrell, *Macromolecules* **30**, 5012–5024 (1997).
145. C. C. Chen, M. T. Krejchi, D. A. Tirrell, and S. L. Hsu, *Macromolecules* **28**, 1464–1469 (1995).
146. N. L. Goeden-Wood, V. P. Conticello, S. L. Muller, and J. D. Keasling, *Biomacromolecules* **3**, 874–879 (2002).
147. N. L. Goeden-Wood, J. D. Keasling, and S. J. Muller, *Macromolecules* **36**, 2932–2938 (2003).
148. S.-J. He, C. Lee, S. P. Gido, S. M. Yu, and D. A. Tirrell, *Macromolecules* **31**, 9387–9389 (1998).
149. K. P. McGrath and D. L. Kaplan, *Macromol. Symp.* **77**, 183–189 (1994).
150. K. P. McGrath, M. M. Butler, C. M. DiGirolamo, D. L. Kaplan, W. A. Petka, and T. M. Laue, *J. Bioact. Compat. Polym.* **15**, 334–356 (2000).
151. S. B. Kennedy, E. R. deAzevedo, W. A. Pekta, T. P. Russell, D. A. Tirrell, and M. Hong, *Macromolecules* **34**, 8675–8685 (2001).
152. R. B. Merrifield, *Pure Appl. Chem.* **50**, 643–653 (1978).
153. S. M. Hecht, B. L. Alford, Y. Kuroda, and S. Kitano, *J. Biol. Chem.* **253**, 4517–4520 (1978).
154. C. J. Noren, S. J. Anthony-Cahill, M. C. Griffith, and P. G. Schultz, *Science* **244**, 182–188 (1989).
155. J. D. Bain, C. G. Glabe, T. A. Dix, and A. R. Chamberlin, *J. Am. Chem. Soc.* **111**, 8013–8014 (1989).
156. V. W. Cornish, D. Mendel, and P. Schultz, *Angew. Chem., Int. Ed. Engl.* **34**, 621–633 (1995).
157. T. Hohsaka, Y. Ashizuka, H. Sasaki, H. Murakami, and M. Sisido, *J. Am. Chem. Soc.* **121**, 12194–12195 (1999).
158. D. R. Liu, T. J. Magliery, M. Pastrnak, and P. G. Schultz, *Proc. Natl. Acad. Sci. U.S.A.* **94**, 10092–10097 (1997).
159. S. Ohno, T. Yokogawa, I. Fujii, H. Asahara, H. Inokuchi, and K. Nishikawa, *J. Biochem.* **124**, 1065–1068 (1998).
160. R. Furter, *Protein Sci.* **7**, 419–426 (1998).
161. A. K. Kowal, C. Kohrer, and U. L. RajBhandary, *Proc. Natl. Acad. Sci. U.S.A.* **98**, 2268–2273 (2001).
162. A. Zhang, L. Wang, A. Brock, and P. G. Schultz, *Angew. Chem., Int. Ed. Engl.* **41**, 2840–2842 (2002).
163. J. W. Chin, T. A. Cropp, J. C. Anderson, M. Mukherji, Z. Zhang, and P. G. Schultz, *Science* **301**, 964–967 (2003).
164. L. Wang, Z. Zhang, A. Brock, and P. G. Schultz, *Proc. Natl. Acad. Sci. U.S.A.* **100**, 56–61 (2003).
165. A. Dieters, T. A. Cropp, M. Mukherji, J. W. Chin, J. C. Anderson, and P. G. Schultz, *J. Am. Chem. Soc.* **125**, 11782–11783 (2003).
166. L. Alfonta, Z. Zhang, S. Uryu, J. A. Loo, and P. G. Schultz, *J. Am. Chem. Soc.* **125**, 14662–14663 (2003).
167. R. A. Mehl, J. C. Anderson, S. W. Santoro, L. Wang, A. B. Martin, D. S. King, D. M. Horn, and P. G. Schultz, *J. Am. Chem. Soc.* **125**, 935–939 (2003).
168. T. Tuve and H. Williams, *J. Am. Chem. Soc.* **79**, 5830–5831 (1957).
169. D. B. Cowie and G. N. Cohen, *Biochim. Biophys. Acta* **26**, 252–261 (1957).

170. D. B. Cowie, G. N. Cohen, E. T. Bolton, and H. D. Robichon-Szulmajster, *Biochim. Biophys. Acta* **34**, 39–46 (1959).
171. E. D. Fenster and H. S. Anker, *Biochemistry* **8**, 269–274 (1969).
172. M. H. Richmond, *J. Mol. Biol.* **6**, 284–294 (1963).
173. T. J. Deming, M. J. Fournier, T. L. Mason, and D. A. Tirrell, *J. Macromol. Sci., Pure Appl. Chem.* **A34**, 2143–2150 (1997).
174. K. L. Kiick, E. Saxon, D. A. Tirrell, and C. R. Bertozzi, *Proc. Natl. Acad. Sci. U.S.A.* **99**, 19–24 (2002).
175. D. Datta, P. Wang, I. S. Carrico, S. L. Mayo, and D. A. Tirrell, *J. Am. Chem. Soc.* **124**, 5652–5653 (2002).
176. Y. Tang, G. Ghirlanda, W. A. Petka, T. Nakajima, W. F. DeGrado, and D. A. Tirrell, *Angew. Chem., Int. Ed. Engl.* **40**, 1494–1496 (2001).
177. N. Sharma, R. Furter, P. Kast, and D. A. Tirrell, *FEBS Lett.* **467**, 37–40 (2000).
178. K. Kirshenbaum, I. S. Carrico, and D. A. Tirrell, *Chem. BioChem.* **2–3**, 235–237 (2002).
179. W. A. Hendrickson, J. R. Horton, and D. M. LeMaster, *EMBO J.* **9**, 1665–1672 (1990).
180. N. Budisa, B. Steipe, P. Demange, C. Eckerskorn, J. Kellermann, and R. Huber, *Eur. J. Biochem.* **230**, 788–796 (1995).
181. H. Duewel, E. Daub, V. Robinson, and J. F. Honek, *Biochemistry* **36**, 3404–3416 (1997).
182. J. C. M. van Hest and D. A. Tirrell, *FEBS Lett.* **428**, 68–70 (1998).
183. J. C. M. van Hest, K. L. Kiick, and D. A. Tirrell, *J. Am. Chem. Soc.* **122**, 1282–1288 (2000).
184. A. J. Link and D. A. Tirrell, *J. Am. Chem. Soc.* **125**, 11164–11165 (2003).
185. P. Wang, Y. Tang, and D. A. Tirrell, *J. Am. Chem. Soc.* **125**, 6900–6906 (2003).
186. A. B. Mauger and B. Witkop, *Chem. Rev.* **66**, 47–86 (1966).
187. T. J. Deming, M. J. Fournier, T. L. Mason, and D. A. Tirrell, *Macromolecules* **29**, 1442–1444 (1996).
188. T. Michon, F. Barbot, and D. Tirrell, *Royal Soc. Chem.* **276**, 63–72 (2002).
189. M. Mock, T. Michon, and D. A. Tirrell, *Polym. Prep.* **44**, 1065–1066 (2003).
190. D. D. Buechter, D. N. Paolella, G. S. Leslie, M. S. Brown, K. A. Mehos, and E. A. Gruskin, *J. Biol. Chem.* **278**, 645–650 (2003).
191. J. L. Milner, S. Grothe, and J. M. Wood, *J. Biol. Chem.* **263**, 14900–14905 (1988).
192. S. Kothakota, T. L. Mason, D. A. Tirrell, and M. J. Fournier, *J. Am. Chem. Soc.* **117**, 536–537 (1995).
193. D. W. Flanagan and D. A. Tirrell, *Polym. Prep.* **44**, 892–893 (2003).
194. K. L. Kiick and D. A. Tirrell, *Tetrahedron* **56**, 9487–9493 (2000).
195. K. L. Kiick, R. Weberskirch, and D. A. Tirrell, *FEBS Lett.* **502**, 25–30 (2001).
196. K. L. Kiick, J. C. M. van Hest, and D. A. Tirrell, *Angew. Chem., Int. Ed. Engl.* **39**, 2148–2152 (2000).
197. Y. Tang and D. A. Tirrell, *J. Am. Chem. Soc.* **123**, 11089–11090 (2001).
198. D. A. Tirrell, Y. Tang, and I. S. Carrico, *Abstr. Pap. Am. Chem. Soc.* **222**, U45–U45 (2001).
199. G. D. Gay, H. W. Duckworth, and A. R. Fersht, *FEBS Lett.* **318**, 167–171 (1993).
200. F. Agou, S. Quevillon, P. Kerjan, and M. Mirande, *Biochemistry* **37**, 11309–11314 (1998).
201. P. Kast and H. Hennecke, *J. Mol. Biol.* **222**, 99–124 (1991).
202. M. Ibba and H. Hennecke, *FEBS Lett.* **364**, 273–275 (1995).
203. L. Reshetnikova, N. Moor, O. Lavrik, and D. G. Vassylyev, *J. Mol. Biol.* **287**, 555–568 (1999).
204. F. Hamano-Takaku, T. Iwama, S. Saito-Yano, K. Takaku, Y. Monden, M. Kitabatake, D. Soll, and S. N., *J. Biol. Chem.* **275**, 40324–40328 (2000).
205. Y. Tang and D. A. Tirrell, *Biochemistry* **41**, 10635–10645 (2002).

206. V. Doring, H. D. Mootz, L. A. Nangle, T. L. Hendrickson, V. de Crecy-Lagard, P. Schimmel, and P. Marliere, *Science* **292**, 501–504 (2001).
207. I. Kwon, K. Kirshenbaum, and D. A. Tirrell, *J. Am. Chem. Soc.* **125**, 7512–7513 (2003).
208. *Chem. Eng. News* 40–43 (June 23, 2003).
209. F. H. Arnold, *Chem. Eng. Sci.* **51**, 5091–5102 (1996).
210. P. Wang, N. Vaidehi, D. A. Tirrell, and W. A. I. Goddard, *J. Am. Chem. Soc.* **124**, 14442–14449 (2002).

READING LIST

L. Debelle and A. M. Tamburro, *Int. J. Biochem. Cell Biol.* **31**, 261–272 (1999).
S. Fahnestock, in S. Fahnestock and A. Steinbüchel, eds., *Biopolymers, Vol. 8: Polyamides and Complex Proteinaceous Materials II*, Wiley-VCH, Weinheim, 2003, pp. 47–79.
C. W. P. Foo and D. L. Kaplan, *Adv. Drug Delivery Rev.* **54**, 1131–1143 (2002).
R. W. Old and S. B. Primrose, *Principles of Gene Manipulation*, 5th ed., Blackwell Science, Cambridge, Mass., 1994.
K. McGrath and D. Kaplan, eds., *Protein Based Materials*, Birkhauser, Boston, 1997.
J. Sambrook and D. W. Russell, *Molecular Cloning: A Laboratory Manual*, 3rd ed., Cold Spring Harbor Press, Cold Spring Harbor, N.Y., 2001.
R. K. Scopes, *Protein Purification: Principles and Practice*, 3rd ed., Springer, New York, 1994.
J. C. M. van Hest and D. A. Tirrell, *Chem. Commum*. 1897–1904 (2001).

KRISTI L. KIICK
University of Delaware

List of Abbreviations and Symbols

Natural amino acids, three-letter and one-letter abbreviations

Ala, A	alanine
Arg, R	arginine
Asn, N	asparagine
Asp, D	aspartic acid
Cys, C	cysteine
Gln, Q	glutamine
Glu, E	glutamic acid
Gly, G	glycine
His, H	histidine
Ile, I	isoleucine
Leu, L	leucine
Lys, K	lysine
Met, M	methionine
Phe, F	phenylalanine
Pro, P	proline
Ser, S	serine
Thr, T	threonine
Trp, W	tryptophan

Tyr, Y	tyrosine
Val, V	valine
	Other abbreviations and symbols
AAA	adenine adenine adenine
CCU	cytosine cytosine uracil
cDNA	complementary deoxyribonucleic acid
CGA	cytosine guanine adenine
DNA	deoxyribonucleic acid
GAA	guanine adenine adenine
GCU	guanine cytosine uracil
GGA	guanine guanine adenine
k_{cat}	turnover number
K_m	Michaelis constant
mRNA	messenger ribonucleic acid
RNA	ribonucleic acid
SDS–PAGE	sodium dodecyl sulfate–polyacrylamide gel electrophoresis
tRNA	transfer ribonucleic acid
UUC	uracil uracil cytosine
UUU	uracil uracil uracil

GLASS TRANSITION. See Volume 2.

GRAFT COPOLYMERS. See Volume 6.

GREEN PLASTICS. See ENVIRONMENTALLY DEGRADABLE POLYMER.

HIGH PERFORMANCE FIBERS

Introduction

High performance fibers are generally characterized by remarkably high unit tensile strength and modulus as well as resistance to heat, flame, and chemical agents that normally degrade conventional fibers. Applications include uses in the aerospace, biomedical, civil engineering, construction, protective apparel, geotextiles, and electronic areas.

For many years, plastics reinforced with polymer fibers have been utilized in the manufacture of boats and sports cars. More recently, ultrahigh strength, high modulus fibers have been invented and combined into composites whose strength and stiffness on a specific basis are unmatched by conventional construction materials. Composites are now replacing metals in such crucial applications as aircraft and the space shuttle. The polymeric composites contain carbon or aramid fibers several times stiffer, weight for weight, than steel. In composite materials, the fibers support the load which is distributed by the plastic which also prevents fatigue and failure (1–4) (see COMPOSITE MATERIALS).

In addition to their role in composites, high performance fibers are also found in coated and laminated textile products, three-dimensional fabric structures, multifunctional property improvement, and intelligent or self-adaptive materials.

Encyclopedia of Polymer Science and Technology. Copyright John Wiley & Sons, Inc. All rights reserved.

In this article, the preparation and properties of typical high performance fibers are discussed, then their applications are classified and detailed. The principal classes of high performance fibers are derived from rigid-rod polymers (qv), gel-spun fibers, modified carbon fibers (qv), carbon–nanotube composite fibers, ceramic fibers, and synthetic vitreous fibers.

Rigid-Rod Polymers

Rigid-rod polymers are often liquid crystalline polymers classified as lyotropic, such as the aramid Kevlar (DuPont), or thermotropic liquid crystalline polymers, such as Vectran (Celanese) (see POLYAMIDES, AROMATIC; LIQUID CRYSTALLINE POLYMERS, MAIN-CHAIN; LIQUID CRYSTALLINE THERMOSETS).

Liquid Crystallinity. The liquid-crystalline state is characterized by orientationally ordered molecules. The molecules are characteristically rod- or lathe-shaped and can exist in three principal structural arrangements: nematic, cholesteric, smectic, and discotic (5,6).

In the nematic phase, within volume elements of the macroscopic sample, the axes of the molecules are oriented on average in a specific direction in various domains. The centers of gravity of the molecules are arranged in a random fashion, and consequently no positional long-range order exists. The molecules are arranged in essentially parallel arrays. Without the presence of an orienting magnetic or physical force, the molecules exist in random parallel arrays. When an orienting force is applied, these domains orient easily. The nematic phase is amenable to translational mobility of constituent molecules.

The cholesteric phase may be considered a modification of the nematic phase since its molecular structure is similar. The cholesteric phase is characterized by a continuous change in the direction of the long axes of the molecules in adjacent layers within the sample. This leads to a twist about an axis perpendicular to the long axes of the molecules. If the pitch of the helical structure is the same as a wavelength of visible light, selective reflection of monochromatic light can be observed in the form of iridescent colors.

In the smectic phase, the centers of gravity of the rod-like molecules are arranged in equidistant planes, ie, the ends of the molecules are correlated. The planes may move perpendicular to the layer normal, and within layers different arrangements of the molecules are possible. The long axes of the molecules may be parallel to the layer normal or tilted with respect to it. A two-dimensional short- or long-range order may exist within the smectic layers. The smectic modifications are labeled according to the arrangement of the molecules within the layers using the symbols A–K.

In the smectic A phase, the director is perpendicular to the planes, while in the smectic C phase, the director is tilted at an angle less than 90° to the planes. In the smectic A and C phases, the molecules diffuse randomly and as a result, no positional order exists within the planes (positional order exists only in one dimension). However, other smectic liquid crystal phases exist in which the molcules have some degree of order within each plane that results in three-dimensional positional order (or quasi-three-dimensional order). In this case, molecules diffusing through the plane spend more time at certain locations than at other locations.

The smectic B phase is a more ordered analog of the smectic A phase in which the molecules adopt hexagonal order over distances of ca 150–600 Å (6). The hexagonal S_B phase has two tilted analogs called the smectic I and smectic F phases, in which the hexagonal lattices tilt toward the apex and the side, respectively. In the crystal B phase, the molecules adopt hexagonal order similar to that of the smectic B phase; however, the hexagonal lattices show long-range (three-dimensional) positional order. Crystal J and G phases represent hexagonal lattices with long-range positional order which are analogs of S_I and S_F, respectively. The crystal E phase results from contraction of a hexagonal lattice which leads to a herringbone-like structure with restricted rotation. Crystal K and H phases are the respective tilted analogs of the crystal E phase.

In the discotic phase, disclike molecules form liquid crystal phases in which the axis perpendicular to the planes of the molecules, orients along a specific direction. The nematic discotic phase has orientational order but no positional order. In the columnar discotic phase, the disclike molecules form columns and therefore exhibit orientational and positional order. In a chiral discotic liquid crystal, the director rotates in a helical path throughout the system.

Poly(1,4-benzamide) (PBA) (7) was the first nonpeptide synthetic polymer reported to form a liquid crystalline solution. In order to obtain liquid-crystalline solutions of poly(1,4-benzamide), it was first necessary to prepare the polymer in the proper solvent. Preparation of the polymer in *N,N*-dialkylamide solvents at low temperatures from *p*-aminobenzoyl chloride hydrochloride produces tractable PBA polymers with inherent viscosities of as much as 5 dL/g. In solvents such as *N,N*-dimethylacetamide [127-19-5] and *N,N,N′,N′*-tetramethylurea [632-22-4] a coupled polymerization–spinning process in liquid-crystalline solution has been developed. If polymerization is initiated at temperatures greater than 25°C, lower molecular weight polymer is formed. Above 25°C, chain termination by reaction of acid chloride chain ends with *N,N*-dialkylamide is significant. To obtain high molecular weights, a lithium base such as lithium hydride, lithium carbonate, or lithium hydroxide is added to the polymerization solution after the first 1–2 h of reaction time to neutralize the hydrogen chloride generated. As the reaction proceeds, the polymerization rate decreases because the increasing amounts of hydrogen chloride consequently produce fewer free-terminal amine groups.

When pure needle-like crystals of *p*-aminobenzoyl chloride are polymerized in a high temperature, nonsolvent process, or a low temperature, slurry process, polymer is obtained which maintains the needle-like appearance of monomer. PBA of inherent viscosity, 4.1 dL/g, has been obtained in a hexane slurry with pyridine as the acid acceptor. Therefore, PBA of fiber-forming molecular weight can be prepared in the solid state.

In 1975, the synthesis of the first main-chain thermotropic polymers, three polyesters of 4,4′-dihydroxy-α, α'-dimethylbenzalazine with 6, 8, and 10 methylene groups in the aliphatic chain, was reported (8). Shortly thereafter, at the Tennessee Eastman Co. thermotropic polyesters were synthesized by the acidolysis of poly(ethylene terephthalate) by *p*-acetoxybenzoic acid (9). Copolymer compositions that contained 40–70 mol% of the oxybenzoyl unit formed anisotropic, turbid melts which were easily oriented.

Polyesters such as poly(*p*-phenylene terephthalate), which would be expected to form liquid crystalline phases, decompose at temperatures below the melting point. Three principal methods have been used for lowering the melting

temperatures of thermotropic copolyesters: (*1*) the use of flexible groups as spacers to decouple the mesogenic units and reduce the axial ratio; (*2*) the use of unsymmetrical groups on mesogenic units; and (*3*) the copolymerization of rigid units with nonlinear, bent units which add a "kink" to the rod-like system.

According to patents obtained by Carborundum (10–12), Celanese (13), DuPont (14–17), and Eastman (9,18) most industrial main-chain thermotropics are prepared by condensation polymerization involving transesterification. Hydroxy-substituted monomers are acetylated before polymerization by acetic anhydride in the presence of a suitable catalyst. The transesterification reactions involve acetylated diol, or monosubstituted hydroxybenzoic or hydroxynaphthoic acids, and diacids. The polymerizations are carried out in an inert atmosphere to prevent oxidation. A stainless steel stirrer is utilized to improve mixing and to accelerate the release of the reaction by-products. The polymerizations are carried out at 50–80°C above the melting point of the highest melting monomer. After a low melt viscosity prepolymer is obtained, a vacuum is applied to remove the additional acetic acid and increase the molecular weight of the polymer. Finally, solid-state polymerization under reduced pressure or in nitrogen at a temperature of 10–30°C below the melting point may be utilized to increase the molecular weight. The heat treatment of spun fibers under these conditions leads to spectacular increases in tensile strength and modulus.

Researchers at DuPont used hydroquinone asymmetrically substituted with chloro, methyl, or phenyl substituents and swivel or nonlinear bent substituted phenyl molecules such as 3,4- or 4,4′-disubstituted diphenyl ether, sulfide, or ketone monomers. For example, poly(chloro-1,4-phenylene-*trans*-hexahydroterephthalate) and related copolymers were prepared in a melt-polymerization process involving the reaction of molar equivalents of the diacetoxy derivatives of diphenols and hexahydroterephthalic acid (19). During polymerization, a phase transition from isotropic to anisotropic occurred soon after the rapid melting of the intermediates to form a clear, colorless liquid.

Also in 1972 (20), Carborundum researchers described a family of aromatic copolyesters that were recognized later to form liquid-crystalline melts. The polymers are based on a bisphenol monomer. In 1976, in a patent assigned to Carborundum, a hydroxybenzoic acid–terephthalic acid–bisphenol system, modified and softened with isophthalic acid, was reported to be melt spinnable to produce fiber (21).

Industrial Lyotropic Liquid-Crystalline Polymers (Aramid Fibers). The first polyaramid fiber (MPD-1) was based on poly(*m*-phenylene isophthalamide) [24938-60-1]. The fiber was not liquid crystalline but was the first aramid fiber to be commercialized by DuPont under the trade name Nomex nylon in 1963 and changed to Nomex aramid in 1972 (22). The principal market niche for Nomex (DuPont) was as a heat-resistant material. Teijin also introduced a fiber (trademark Conex) based on MPD-1 in the early 1970s. Fenilon, also based on MPD-1, was produced in the former USSR for civilian, military, and space exploration applications. In 1970, DuPont introduced an aramid fiber, Fiber B, for use in tires, which was probably based on polybenzamide PBA spun from an organic solvent. Fiber B had high strength and exceptionally high modulus. Another version of Fiber B, based on poly(*p*-phenylene terephthalamide) [24938-64-5] (PPT) was introduced in the 1970s. This version of Fiber B was spun from sulfuric acid and had a tensile strength approximately twice that of the Fiber B based on MPD-1.

An even higher modulus fiber based on PPT, in which the modulus was increased by the drawing of the as-spun fiber, was introduced under the name PRD-49 for use in rigid composites. The undrawn and drawn fibers were later announced as Kevlar-29 and Kevlar-49, respectively. In 1975, Akzo of the Netherlands reported the commercialization of an aramid fiber, Twaron (Akzo), based on PPT.

Nomex. This fiber was commercialized for applications requiring unusually high thermal and flame resistance. Nomex (DuPont) fiber retains useful properties at temperatures as high as 370°C. Nomex has low flammability and has been found to be self-extinguishing when removed from the flame. On exposure to a flame, a Nomex fabric hardens, starts to melt, discolors, and chars thereby forming a protective coating (23). Therefore an outstanding characteristic is low smoke generation on burning. The limiting oxygen index (LOI) value (top down) for Nomex fabrics is 26.0 (24). Nomex has a tga weight loss of 10% at 450°C and a use temperature of 370°C. Nomex has good to excellent strength, a tenacity of 0.42–0.51N/tex (4.8–5.8 gf/den) (25), good extendability, and a modulus greater than that of nylon-6,6. The density is 1.38 g/cm^3 (26). Nomex is more difficult to dye than nylon, but the use of dye carriers allows dyeing to proceed at high temperatures with temperature-resistant basic dyes (27). The structure of Nomex may be represented as follows:

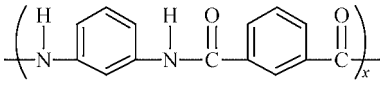

Nomex

MPD-1 fibers may be obtained by the polymerization of isophthaloyl chloride [99-63-8] and *m*-phenylenediamine [108-45-2] in dimethylacetamide with 5% lithium chloride (26). The reactants must be very carefully dried since the presence of water would upset the stoichiometry and lead to low molecular weight products. Temperatures in the range of 0 to −40°C are desirable to avoid such side reactions as transamidation by the amide solvent and acylation of *m*-phenylenediamine by the amide solvent. Both reactions would lead to an imbalance in the stoichiometry and result in forming low molecular weight polymer. Fibers may be either dry spun or wet spun directly from solution.

Kevlar. In the 1970s, researchers at DuPont reported that the processing of extended chain all para-aromatic polyamides from liquid crystalline solutions produced ultrahigh strength, ultrahigh modulus fibers. The greatly increased order and the long relaxation times in the liquid crystalline state compared to conventional systems led to fibers with highly oriented domains of polymer molecules. The most common lyotropic aramid fiber is poly(*p*-phenyleneterephthalamide) (PPT) which is marketed as Kevlar by DuPont. Aramid fiber is available from Akzo under the trade name Twaron. These fibers are used in body armor, cables, and composites for sports and space applications. Kevlar has the following structure:

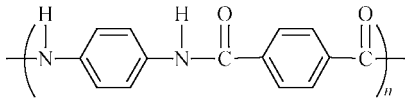

Kevlar

PPT of high molecular weight (inherent viscosity of 22 dL/g, corresponding to a molecular weight of 123,000) can be prepared by low temperature polymerization in various solvents (28). PPT is less soluble in amide solvents than PBA and the most successful polymerization solvents are a mixture of hexamethylphosphoramide [680-31-9] (HMPA) and *N*-methylpyrrolidinone [872-50-4] (NMP) or NMP-containing calcium chloride (29,30). These solvent systems yield fiber-forming polymer. As the molecular weight increases rapidly during the first few seconds of the polymerization, the critical concentration is exceeded and the solution develops the opalescence characteristic of the liquid-crystalline state. The critical factors influencing the molecular weight include stoichiometry, solvent composition, temperature, and solids concentration (31). At low monomer concentrations, side reactions can occur between the acid chloride chain ends and the amide solvents. At higher solids concentrations, gelation acts to limit the development of high molecular weights. It is of critical importance to keep the initial temperature low in order to prevent the reaction of the amide solvents with the acid chloride groups.

The preparation of high molecular weight PPT in HMPA/NMP shows a strong dependence of inherent viscosity on reactant concentrations. In 2:1 (by volume) HMPA/NMP, the highest inherent viscosity polymer is obtained when each reactant is present in concentrations of ca 0.25 *M* (32,33); higher and lower concentrations result in the formation of polymer of lower inherent viscosities. A typical procedure (31) is as follows: 1,4-phenylenediamine [106-50-3], HMPA, and NMP are added to an oven-dried resin kettle equipped with a stirrer and stirred for ca 15 min with cooling to −15°C, followed by the addition of powdered terephthaloyl chloride [100-20-9] to the rapidly stirred solution. The reaction mixture changes to a thick, opalescent, paste-like gel in ca 5 min.

The manufacturing process utilized (34,35) is continuous polymerization in order to minimize cost. A continuous stream of *p*-phenylenediamine solution is added to a continuous stream of molten terephthaloyl chloride. Volumetric control is easily achieved because both reactants are in the liquid state. Residence time in the mixing apparatus is on the order of 1 s. Next, the reactants enter a high shear, continuous screw mixer, in which the inherent viscosity of the polymer increases to 4–4.5 dL/g. The minimum inherent viscosity required for fiber spinning in sulfuric acid is 4 dL/g. The residence time is less than 15 s so the polymer solution which enters the third stage is still a fluid. The third stage is a high shear, twin-screw mixer with blades positioned for a number of recycle zones within the mixer, thereby achieving lower temperatures, higher residence times, and higher molecular weights.

An alternative polymerization process utilizes a slurry of calcium chloride in NMP as the polymerization medium (30). The solubility of calcium chloride is only 6% at 20°C; however, the salt continues to dissolve as conversion of monomers to polymer proceeds and calcium chloride/polyamide complexes are formed. Polymer molecular weight is further increased by the addition of *N,N*-dimethylaniline [121-69-7] as an acid acceptor. This solvent system produces fiber-forming polymer of molecular weights comparable to that formed in HMPA/NMP.

Since PPT melts with decomposition at ca 560°C (36), melt spinning cannot be employed. Thus, solution spinning techniques (31) must be used to prepare fibers. Although dry, wet, and dry jet-wet spinning methods have all been used to

prepare fibers, ordinarily PPT is spun from nematic sulfuric acid solutions using the dry jet-wet spinning process with cold water as the coagulant. In the dry spinning process, a polymer solution is passed through a spinnerette followed by flash evaporation of the solvent in a heated chamber and subsequent winding of the fiber produced on a bobbin. In the wet spinning process, the polymer solution is passed through a spinnerette located in a coagulation bath. The fiber formed is then drawn to increase molecular orientation, tenacity, and modulus. In dry jet-wet spinning, the polymer solution is allowed to flow through a spinnerette into a separated coagulation bath. Therefore, the temperatures of the spinnerette and coagulation baths may be independently controlled. The liquid crystalline nature of the PPT dopes and the dry jet-wet spinning technology are principally responsible for the development of commercial high performance Kevlar fibers.

Drawdown of the coagulated fiber is an essential element in high performance fiber technology (31). Under shear, the unoriented domains become oriented in the direction of stretch. In the fiber manufacturing process, the unoriented liquid-crystalline domains are oriented in the spinnerette, followed by retention and perfection of the highly ordered nematic phase by the elongational forces in the air gap and further drawdown in the coagulation medium (37). Coagulation sets the high degree of orientational order achieved by stretching. Tenacity increases with increasing drawdown and inherent viscosity as well as decreasing air gap (between the spinnerette and coagulation bath). Modulus increases with increasing drawdown and total spinning strain.

Because of their rigid-chain structure, PPT and related *p*-aramids exhibit liquid-crystalline behavior in solution. The rod-like molecules aggregate in nematic, ordered domains. When solutions of these materials are exposed to shear, these ordered domains tend to orient in the direction of flow. On passing through a spinnerette, liquid-crystalline solutions retain the high degree of orientation acquired in the spinning process, leading to as-spun fibers with extraordinary degrees of crystallinity and orientation. As-spun fibers of PPT, obtained by spinning a 20% solution of PPT in 100% sulfuric acid, have a crystalline orientation angle of ca 12° (determined from wide-angle X-ray diffraction) and a modulus of ca 72 GPa (38). Heat treatment increases the degree of crystalline alignment. Correspondingly, heat-treated fibers have an orientation of ca 9° and a modulus of ca 120 GPa.

In a typical commercial dry jet-wet spinning process, PPT polymer of inherent viscosity 6.0 dL/g is added to 99.7% sulfuric acid in a water-jacketed commercial mixer in a ratio of 46 g of polymer to 100 mL of acid (39). The mixture is sealed in a vacuum of 68.5–76 mL of mercury. Mixing takes place for 2 h at temperatures of 77–85°C. The dope is then transferred to a glass-lined, water-jacketed kettle at 90°C. Any air or bubbles caused by the transfer are removed under vacuum for about 30 min. The dope is then pumped through a heated (90°C) transfer line to an electrically heated spinning block with an associated gear pump. The gear pump then meters the dope through a heated (80°C) 1.25-cm diameter spinnerette containing 100 holes of 51 μm diameter. The dope is extruded from the spinnerette at a velocity of ca 63 m/min vertically through a 0.5-cm layer of air (air gap) into water at a temperature of 1°C. The yarn is wound on a bobbin under a 50°C water spray. The bobbin is then submerged in 0.1 *N* $NaHCO_3$ solution and then further extracted with water at 70°C.

Dramatic increases in the mechanical properties of aramid fibers are observed on heat treatment under tension. Tenacity and modulus increase exponentially with increasing temperature (and draw ratios) of wet spun fibers at temperatures of ca 360°C (the glass-transition temperature, T_g) to 550°C (the melting temperature). Dry jet-wet spun yarns heat treated under tension show substantial increases in modulus at temperatures greater than 200°C; the already high values of tenacity remain essentially unchanged. An intermediate modulus, high tenacity dry jet-wet spun yarn is thus converted into high modulus, high strength fiber.

Because the inherent viscosities of the heated yarns remain constant, it is postulated that the changes are physical. Yarns with as-spun moduli of 8.8–88 N/tex (100–1000 gf/den) may be obtained directly by dry jet-wet spinning. Yarns with as-spun tenacities of greater than 1.8 N/tex (20 gf/den) are obtained by dry jet-wet spinning. Kevlar-29 has a tenacity of ca 2.5 N/tex (28 gf/den) and a specific modulus of ca 41 N/tex (464 gf/den) (40). Kevlar-49 has a tenacity of ca 2.5 N/tex (28 gf/den) and a specific modulus of ca 86 N/tex (980 gf/den). A relatively new fiber, Kevlar-149, is the highest tensile modulus aramid fiber currently available. Its specific modulus is ca 126 N/tex (1430 gf/den) and tenacity ca 2.3 N/tex (26 gf/den).

The crystal structure of PPT is pseudo-orthorhombic (essentially monoclinic) with $a = 0.785$ nm; $b = 0.515$ nm; c (fiber axis) $= 1.28$ nm and $\gamma = 90°$ (41). The molecules are arranged in parallel hydrogen-bonded sheets. There are two chains in a unit cell and the theoretical crystal density is 1.48 g/cm^3. The observed fiber density is 1.45 g/cm^3. Based on electron microscopy studies of peeled sections of Kevlar-49, the supramolecular structure consists of radially oriented crystallites. The fiber contains a pleated structure along the fiber axis, with a periodicity of 500–600 nm.

Technora. In 1985, Teijin Ltd. introduced Technora fiber, previously known as HM-50, into the high performance fiber market. Technora is based on the 1:1 copolyterephthalamide of 3,4′-diaminodiphenyl ether and *p*-phenylenediamine (42). Technora is a wholly aromatic copolyamide of PPT, modified with a crankshaft-shaped comonomer, which results in the formation of isotropic solutions that then become anisotropic during the shear alignment during spinning. The polymer is synthesized by the low temperature polymerization of *p*-phenylenediamine, 3,4′-diaminophenyl ether, and terephthaloyl chloride in an amide solvent containing a small amount of an alkali salt. Calcium chloride or lithium chloride is used as the alkali salt. The solvents used are hexamethylphosphormide (HMPA), *N*-methyl-2-pyrrolidinine (NMP), and dimethylacetamide (DMAc). The structure of Technora is as follows:

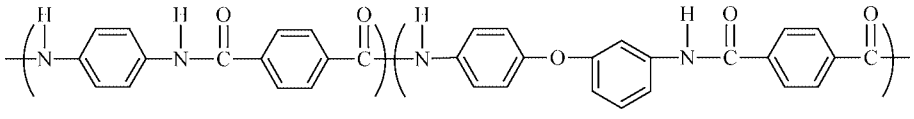

Technora

The polymerization is carried out at temperatures of 0–80°C in 1–5 h at a solids concentration of 6–12%. The polymerization is terminated by neutralizing

agents such as calcium hydroxide, calcium oxide, calcium carbonate, or lithium hydroxide. Inherent viscosities of 2–4 dL/g are obtained at 3,4′-diaminodiphenyl ether contents of 35–50 mol%. Because of the introduction of nonlinearity into the PPT chain by the inclusion of 3,4′-diaminodiphenyl ether kinks, the copolymer shows improved tractability and may be wet or dry jet-wet spun from the polymerization solvent. The fibers are best coagulated in an aqueous equilibrium bath containing less than 50 vol% of polymerization solvent and from 35 to 50% of calcium chloride or magnesium chloride.

The copolymer fiber shows a high degree of drawability. The spun fibers of the copolymer were highly drawn over a wide range of conditions to produce fibers with tensile properties comparable to PPT fibers spun from liquid-crystalline dopes. There is a strong correlation between draw ratio and tenacity. Typical tenacity and tensile modulus values of 2.2 N/tex (25 gf/den) and 50 N/tex (570 gf/den), respectively, have been reported for Technora fiber (42).

Heterocyclic Rigid-Rod Polymers.

PBO, PBZ, and PIPD. PBZ, a family of *p*-phenylene-heterocyclic rigid-rod and extended chain polymers includes poly(*p*-phenylene-2,6-benzobisthiazole) [69794-31-6] (*trans*-PBZT), poly(*p*-phenylene-2,6-benzobisoxazole) [60871-72-9] (*cis*-PBO), and poly[2,6-diimadazo[4,5-b:4′,5′-e]pyridinylene-1,4(2,5-dihydroxy)phenylene (PIPD). PBZT and PBO were initially prepared at the Air Force Materials Laboratory at Wright–Patterson Air Force Base, Dayton, Ohio (43). PBZT was prepared by the reaction of 2,5-diamino-1,4-benzenedithiol dihydrochloride with terephthalic acid [100-21-0] in polyphosphoric acid (PPA) and PBO by the reaction of 4,6-diamino-1,3-benzenediol dihydrochloride with terephthalic acid in PPA. The PIPD was prepared by the reaction of 2,3,5,6-tetraaminopyridine with 2,5-dihydroxyterephthalic acid. PIPD was initially prepared at Akzo Nobel Central Research (44).

Although the crystal structures of the 2,6-diphenyl- *cis*- and *trans*-benzobisoxazole compounds have colinear exocyclic bonds with the coplanar condensed rings (45), and the phenyl rings coplanar with the heterocycles (46), the central ring of the 2,6-diphenyl-*cis*-benzobisthiazole system is bent (47). The exocyclic bonds of the 2,6-diphenyl-*cis*-benzobisthiazole system are bent out of linearity. The central, condensed ring system of 2,6-diphenyl-*trans*-benzobisthiazole is planar with the exocyclic bonds showing a deviation of only 0.06 nm from colinearity. The phenyl rings of 2,6-diphenyl-*trans*-benzobisthiazole deviate from planarity with a dihedral angle of ca 23°. The phenylene rings in the *trans*-PBZT polymers are coplanar with the central condensed heterocyclic ring system. Wide-angle X-ray diffraction studies of PIPD revealed a hydrogen bonding scheme consisting of intramolecular O–H–N hydrogen bonds and intermolecular N—H—O hydrogen bonds. The crystal structure of heat-treated PIPD fiber (M5 fiber) showed monoclinic symmetry (48). Crystal structure analysis showed that the neighboring chains are shifted along the *c*-axis (chain axis) relative to one another by 2.0 Å units. Each polymer chain is linked by bidirectional intermolecular hydrogen bonds to its four axially shifted neighbors. The presence of bidirectional intermolecular hydrogen bonding in PIPD is considered to be the basis for the exceptionally good compressive properties of PIPD. The relatively high compressive strength of PPT as compared to PBO and PBZT (4) is attributed to interchain hydrogen bonding. The additional bidirectional hydrogen bonding in

PIPD compared to PPT would explain the exceptionally high level of compressive strength for PIPD. Sikkema and co-workers (49) reported that while other polymers have compressive strengths between 0.2 and 0.6 GPa, M5 fiber spun from PIPD has a compressive strength of 1.7 GPa. The structures of PBO, PBZT, and PIPD are as follows:

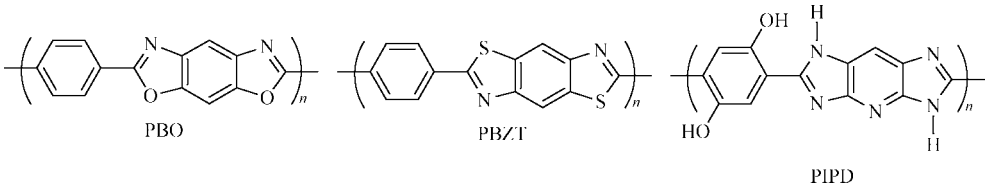

The early syntheses of *cis*-PBO and *trans*-PBZT were conducted at polymer concentrations of 3 wt% or less. Since these isotropic solutions had high bulk viscosities, polymerizations had to be carried out at low solids concentrations to maintain tractability. When the concentration of *trans*-PBZT was raised to 5–10 wt%, nematic solutions were formed and polymers with intrinsic viscosities as high as 31 dL/g were obtained. Initially, the formation of *trans*-PBZT solutions of concentrations greater than 10% caused foaming problems during the polymerization and low molecular weights. The discovery of the P_2O_5 adjustment method was the breakthrough that resulted in the production of nematic spinnable dopes.

The P_2O_5 adjustment method involves adding P_2O_5 to the PPA polymerization solvent to maintain an effective PPA composition as the PPA acts as solvent, catalyst, and dehydrating agent. PPA acts as the solvent for monomer, oligomers, and polymer. PPA also activates the functional groups for polymerization and removes the water of condensation. Also, P_2O_5 is added at the end of the polymerization to achieve the viscosity necessary for spinning. At the end of the polymerization process, the P_2O_5 content must be greater than 82% to keep all the components in solution and less than 84% to give a solution of the proper viscosity for spinning. The temperatures of the PBO and PBZT polymerizations are raised in steps from 100 to 200°C to avoid decomposition of monomers. The temperature of the PIPD polymerization was raised stepwise from 100 to 180°C.

These rigid-rod polymers are spun using the dry jet-wet spinning technique also used for the spinning of aramid dopes. The solution is extruded under heat and pressure through a single or multihole spinnerette and an air gap into a coagulation bath, followed by washing, drying, and heat setting. PBO and PBZT have been spun in PPA and methanesulfonic acid. Water, dilute phosphoric acid, methanol, and ammonia have been used as coagulants. Heat treatment involves temperatures of 500–700°C with residence times on the order of a few seconds to several minutes. The nematic PPA solution formed in the polymerization may be used as the spinning dope. The typical molecular weight range used to spin fibers is 50,000–100,000 daltons. PIPD as-polymerized solutions of M_w 60,000–150,000 were air-gap wet spun at 180°C into a water or dilute phosphoric acid bath, followed by washing to a low phosphorus content and drawing at a temperature above 400°C to produce the final high modulus M5 fiber.

In thermogravimetric analyses (50) of the ordered polymers, the extrapolated onset of degradation of PBO and PBZT is reported to be 620°C in air. The

extrapolated onset of degradation of PBO in helium is over 700°C. In isothermal aging studies in air at 343°C, PBO and PBZT retain ca 90% of the weight after 200 h. At 371°C in air, PBO and PBZT retain ca 78 and 71% of the original weight, respectively. PBZ polymers degrade without the observation of crystalline melting points or glass-transition temperatures. The onset of thermal decomposition in air for PIPD was reported to be 530°C.

Toyobo (Zylon) has marketed the PBO fiber and Magellan Systems International has brought M5 fiber to the marketplace. PBO fibers have the highest reported tensile modulus of any known polymeric fiber, 280–360 GPa (41–52 $\times$ 10^6 psi). PBO and PBZT are among the most radiation-resistant polymers. Although the compressive strengths of PBO and PBZT are approximately an order of magnitude less than the tensile strengths, alloys of these fibers with high compressive strength fibers can be produced. The polymers are now being evaluated for other applications such as nonlinear optics. Possible PBO applications include reinforcing fibers in composites, multilayer circuit boards, athletic equipment, marine applications, woven fabrics, and fire-resistant fibers (1). Magellan Systems International reports a tenacity of 5.3 GPa, a modulus of 350 GPa, and a compressive strength of 1.6 GPa for M5 fiber (51). Possible M5 applications include advanced lightweight composites, hard and soft ballistic armour, high strength cables, advanced fabrics and textiles, and high performance fire retardant materials.

Polybenzimidazole (PBI) Fibers. Poly[(2,2′-*m*-phenylene)-5,5′-bisbenzimidazole] [25734-65-0] is a textile fiber originally marketed by the Celanese Corp. (52) which does not form liquid-crystalline solutions due to its bent meta backbone monomeric component. PBI (Celanese) has an excellent resistance to high temperature and chemicals.

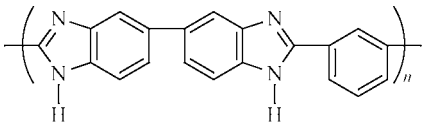

PBI

PBI is being marketed as a replacement for asbestos and as a high temperature filtration fabric with excellent textile apparel properties. The synthesis of wholly aromatic polybenzimidazoles with improved thermal stabilities was reported in 1961 (53). The Non-Metallic Materials and Manufacturing Technology Division of the U.S. Air Force Materials Laboratory, Wright–Patterson Air Force Base, awarded a contract to the Narmco Research and Development Division of the Whittaker Corp. for development of these materials into high temperature adhesives and laminates.

Poly[2,2′-(*m*-phenylene)-5,5′-bisbenzimidazole] was chosen as the most promising candidate for further development as a fibrous material. Under the terms of an Air Force contract, DuPont was able to spin fibers from both dimethylsulfoxide and dimethylacetamide solutions to form relatively strong, thermally stable fibers. In 1963, an Air Force contract was awarded to Celanese Research Co. for the development of a manufacturing process for the scale-up of PBI production. PBI fiber of tenacities 0.31–0.44 N/tex (3.5–5.0 gf/den) were produced in sufficient quantity for large-scale evaluation. The fiber was discovered to have

a soft hand in addition to possessing a high degree of nonflammability. In the limited oxygen index (LOI) test, the concentration of oxygen required for sustained, steady-state burning was 41%. A new development program was started at Celanese with funding from NASA and the Air Force to develop a flight suit material, fabrics for fatigues worn in space capsules, and utility equipment such as ropes and bungee cords.

Further field tests demonstrated that in spite of the excellent thermal and fire resistance, shrinking of the fabrics occurred above the glass-transition temperature which might expose the wearer to flames. Based on the results obtained in an Air Force contract at Dynatech Co., the Celanese Research Co. developed a two-stage process that reduced the shrinkage from 50 to 6%. The process was also amenable to on-line processing. The sulfonated derivative is the fiber which was marketed by the Celanese Corp. Some end uses include replacement of asbestos, thermal and chemical safety apparel, and stack gas filter bags, airline seat covers, firemen turn coats, and race car driver suits.

Development efforts at Celanese Research Co. established solid-state polymerization as the most practical process for engineering scale-up. Homogeneous solution polymerization of PBI in polyphosphoric acid was eliminated because of the need to work with low solid compositions (in the range of 3–5%) during the precipitation, neutralization, and washing steps required for isolation of the product.

In the first stage of the engineering scale-up process (54), a 189 L oil-jacketed, stainless steel reactor is charged with diphenyl isophthalate [744-45-6] (DPIP) and 3,3′,4,4′-tetraaminobiphenyl (TAB). The reactor is deoxygenated by alternative application of vacuum and filling with nitrogen three times, followed by agitation and heating to 250°C under a stream of nitrogen, followed by heating at 290°C for 1.5–3.0 h in the absence of agitation before cooling. In the second stage of the process, the polymer obtained in three to four runs is ground to 0.84 mm (20 mesh) and charged into a 38 L oil-heated stainless steel reactor for a final heating step with agitation at 370–390°C for 3–4 h. Initially, large amounts of foam were produced in the first stage of the process. Foam reduction involves the addition of 10–20% by weight of an organic additive such as diphenyl ether. At the lower temperature of the first stage, the additive acts to prevent foaming and the additive is then removed at the higher temperatures involved in the second stage. Although the foam volume is significantly reduced, the additive residues are removed only with considerable difficulty.

The spinning process used to produce PBI fibers is dry spinning (55). The preferred solvent for dry spinning of PBI is dimethylacetamide (DMAc). The powdered polymer is dissolved in DMAc at high temperatures (ca 250°C) to form ca 23% wt/wt concentration spinning dopes. The spinning dope is fed by a metering pump through a spinnerette (following filtering) into a countercurrent of hot nitrogen gas in the spinning column. Nitrogen gas is used to prevent oxidation of the oxidatively sensitive filaments formed as the hot gas evaporates the DMAc. The filaments pass to a godet roll and then onto a winder. Washing of the fiber takes place on perforated bobbins to remove lithium chloride stabilizer and residual solvent. The fiber is drawn to achieve improved mechanical properties by passing it from feed rolls to draw rolls through an oven set at temperatures greater than 400°C while under a positive nitrogen pressure. Acid treatment to minimize

shrinkage involves the use of aqueous sulfuric acid to produce an acid salt followed by heat treatment to form sulfonic acid groups. If all the imidazole rings were substituted, the final stabilized product would contain 8% sulfur; however, the level of sulfur ordinarily obtained (ca 6%) is sufficient for the required improvement in dimensional stability.

Typical properties of stabilized PBI (56) are a tenacity of 0.27 N/tex (3.1 gf/den), a fiber breaking elongation of 30%, an initial modulus of 3.9 N/tex (45 gf/den), a density of 1.43 gf/cm^3, and a moisture regain of 15% (at 21°C and 65% relative humidity).

Solution dyeing of PBI is necessary (57) because the glass-transition temperature (T_g) of PBI is greater than 400°C, and as a result dye molecules only slowly diffuse into the PBI fiber structure. Since the pigments are added to the spinning dope, the pigments must be capable of withstanding the high temperatures used in the various fiber-forming processes.

Industrial Thermotropic LCPs. Vectran (Celanese), poly(6-hydroxy-2-naphthoic acid-*co*-4-hydroxybenzoic acid) [81843-52-9], was the first thermotropic fiber to become commercially available (58). Vectran is synthesized by the melt acidolysis of *p*-acetoxybenzoic acid and 6-acetoxy-2-naphthoic acid.

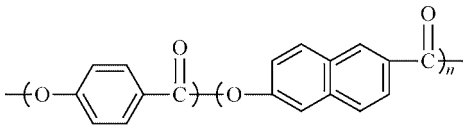

Vectran

First, *p*-hydroxybenzoic acid (HBA) [99-96-7] and 6-hydroxy-2-naphthoic acid (HNA) [16712-64-4] are acetylated to produce the low melting acetate esters which are molten at 200°C. In an inert gas, the two monomers are melted together at 200°C. The temperature is raised to 250–280°C and acetic acid is collected for 0.5–3 h. The temperature is raised to 280–340°C and additional acetic acid is removed in vacuum for a period of 10–60 min. The opalescent polymer melt produced is extruded through a spinning jet, followed by melt drawdown. The use of the parallel offset monomer, acetylated HNA, results in the formation of a series of random copolyesters of different compositions, many of which fall within the commercially acceptable melting range of 250–310°C. Characteristically, these nematic melts show the persistence of orientational order under the influence of elongational flow fields which results in low melt viscosities under typical fiber formation conditions even at high molecular weights.

Axial orientation develops quickly during melt drawdown with a concomitant increase in fiber modulus. At a drawdown ratio of ca 10, the fiber achieves a maximum modulus in the range of 44.1–61.7 N/tex (500–700 gf/den). Neither cold drawing nor annealing led to additional increases in modulus. The high level of mechanical properties is the result of the comparative ease of axial orientation of the nematic phase leading to a highly oriented rod-like fiber structure. This is borne out by X-ray fiber analysis which shows well-defined meridonal maxima characteristic of highly oriented parallel arrays of polymer chains with poor lateral spacing.

Heat treatment of the as-spun fibers results in an increase in tenacity but no attendant increase in modulus. Typically, the as-spun fibers are heat treated in an inert environment at temperatures 10–20°C below the melting point for from 10 min to several hours. There is a corresponding increase in chemical resistance and melting temperatures, presumably due to increases in molecular weight rather than improvements in structural perfection. This is in agreement with X-ray fiber diagram results which show no increase in orientation of mesophases during the heat-treatment process. Vectran HS fibers are reported to have typical tensile strength and modulus values of 2 N/tex (23 gf/den) and 46 N/tex (550 gf/den) (59), respectively. The melting point and density are reported to be 330°C and 1.4 g/cm^3. The fibers have an excellent chemical resistance except for their resistance to alkali.

Gel-Spun Fibers

In the mid-1970s, it was discovered at the Dutch States Mines Co. (DSM) that through an ingenious new method of gel spinning ultrahigh molecular weight polyethylene it was possible to produce fibers having twice the tenacity of Kevlar, which was then considered to be the strongest known fiber (60). The discovery was important not only because of the exciting 3.8 N/tex (44 gf/den) strengths these new fibers displayed, but also because it clearly demonstrated that factors other than monomer polarity were critical in controlling fiber performance characteristics. These high performance polyethylene fibers (HPPE) produced by the DSM subsidiary company Stamicarbon were called Dyneema and those produced by the Allied Signal Corp. in the United States are sold under the trade name of Spectra 1000. The commercial products have somewhat lower strengths than the laboratory fibers but still are in the high 2.6 N/tex (30 gf/den) range (61).

Process. In the gel spinning process, 1–8% solutions of polyethylene are prepared by dissolving polymer of molecular weights of 1–4 million in hot hydrocarbon liquids such as decalin, melted waxes, or mineral oils at ca 150°C. These hot solutions are then screw extruded through spinnerettes having holes of 0.5–2.0 mm diameter and an L/D ratio of 25 to control the viscoelastic flow properties of the fluid. The fibers are spun into a cooling bath which yield disoriented highly crystalline gel fibers of sufficient stability to be wound onto a first godet at several meter per minute. These gel fibers are then processed in solvents at about 50°C to remove the hydrocarbons. The solvent-free gels are then stretched in progressively hotter zones at temperatures from 120 to 160°C with an overall final windup/extrusion speed of about 1000/1 or whatever is required to give the final desired strengths of 1.7–3.5 N/tex (20–40 gf/den) (62).

The patent literature indicates that the AlliedSignal process uses lower boiling solvents such as chlorofluorocarbons as the cooling/extraction baths (63), whereas the processes of Stamicarbon indicate the use of decalin solvent followed by cooling and slow removal of the decalin in successively hotter chambers while stretching (64).

Properties. Fiber property comparisons for the different products are given in Table 1.

Table 1. Properties of Commercial HPPE Fibers[a]

Fiber	Tenacity, N/tex	Initial modulus, N/tex	Elongation at break, %
Dyneema	1.01–3.57	57–128	3–7
Spectra 1000	3.4–3.57	162–171	3–7

[a] Refs. 63 and 64.

The attributes of HPPE fibers include high strength; high abrasion resistance; high UV stability as compared to other synthetics; high resistance to acids, alkali, organic chemicals, and solvents; and low density. Disadvantages are a low melting point of about 150°C (1), which means performance is limited to no more than 120°C; difficult processing; and poor surface adhesion properties.

It is difficult to process HPPE staple fibers mechanically because of so-called married fibers which are bundles of 4–6 fibers that firmly adhere to each other and resist separation by conventional processing. Although HPPE fibers like to adhere to each other, they exhibit poor adhesion to other materials.

It is possible to modify HPPE to overcome the poor adhesion of the fiber surfaces by using corona discharge in an oxygen atmosphere previously developed for polyolefin films or by the addition of fillers to the polymer solution prior to spinning. The melting point of HPPE fibers embedded in polymer matrices is increased by about 8°C (65,66). Temperature performance can also be enhanced by wrapping the HPPE fibers with other fire-resistant or fire-retardant fibers (67,68). Other ultrahigh molecular weight polymers have also been spun via the gel spinning process. These include polypropylene, polyacrylonitrile, poly(vinyl alcohol), and nylon-6. However, the property improvements in these cases evidently have not warranted commercialization.

Modified Carbon Fibers (Elongatable Carbonaceous Fiber)

Carbon Fibers (qv) are made by the nonoxidative high temperature pyrolysis of fibers originally spun from either rayon, polyacrylonitrile (PAN) [25014-41-9] or mesomorphic hydrocarbon tar (MT or pitch) materials. Of these three staring materials the most work has been done with rayon because the carbon fibers produced from rayon have the best overall physical and performance characteristics (69).

For example, rayon-based carbon fibers have the lowest density followed by those from PAN, with those from the tar base having the highest density. A similar trend is found in physical strength test results. Of paramount importance for space vehicle use, the carbon fibers from rayon exhibit the best ablative performance with the least loss of weight during re-entry into earth's atmosphere. The carbon fibers used in space projects require a special classified type of rayon and special carbonizing conditions to reach peak performance. During the early 1990s such rayon was in short supply due to the closing of the main producer having effluent pollution problems. However, a second new supply was developed with no delay to the space program. Due to their low elongation and resulting high brittleness, essentially all rayon-based carbon fibers are used as reinforcement fibers for laminate structures with polyphenolic and other resins. Carbon fiber

cloth can only be woven on special types of textile looms. Acrylonitrile copolymers and terpolymers can be used to make carbon type fibers with higher elongations that are much more applicable for textile operations.

Liquid-crystalline mesophase pitch is employed for high modulus carbon fiber production by stress graphitization. Carbon fibers prepared from this process were commercialized in the early 1980s (1). Petroleum, coal tar, and poly(vinyl chloride) are common sources of the pitch used in the preparation of carbon fibers.

It is difficult to weave or knit regular carbon fiber. For any fiber to be considered as a satisfactory textile fiber it should have an elongation of at least 3% and preferably more in the range of 5–8%. The extreme brittleness, high modulus, and low elongation of standard carbon fibers restrict them to be woven only on a special type of rigid rapier loom. To overcome these drawbacks, an exciting new modification of carbon fiber technology was developed; by using less stringent carbonizing conditions and only partially carbonizing the precursor fibers, improved textile fiber properties have been achieved (70).

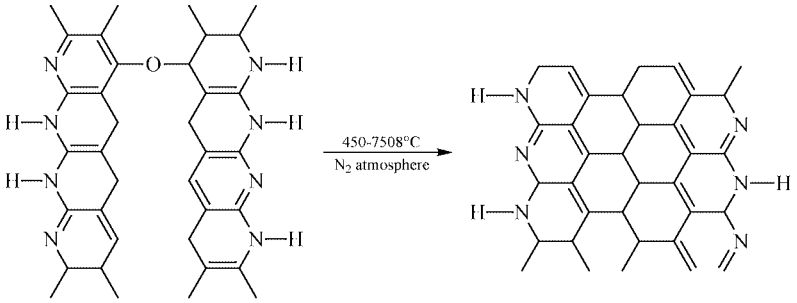

OPF EDF

Process. Any standard precursor material can be used, such as oxidized polyacrylonitrile (PAN) fiber (OPF). This OPF (Dow) is treated in a nitrogen atmosphere at 450–750°C, preferably 525–595°C, to give fibers having between 69 and 70% C, 19% N; density less than 2.5 g/mL; and a specific resistivity under $10^{10}\ \Omega \cdot$cm. If crimp is desired, the fibers are first knit into a sock before heat treating and then de-knit. Controlled carbonization of precursor filaments results in a linear Dow fiber (LDF), whereas controlled carbonization of knit precursor fibers results in a curly carbonaceous fiber (EDF) (Dow). At higher carbonizing temperatures of 1000–1400°C the fibers become electrically conductive (71).

Properties. Unlike regular carbon fibers, these new products do not conduct electricity, but do exhibit good textile processing properties and possess exceptional ignition-resistant, flame-retardant, and even fire-blocking properties. The limiting oxygen index (LOI) defines the percentage of oxygen necessary in an oxygen/nitrogen mixture before a material supports combustion. Typical LOI values for various fibers are given in Table 2.

Previous results with ignition-resistant (IR) blends, where such fibers as aramids or PBI (Celanese) are used as the high LOI fibers, show that they need at least 65% and typically 85% fiber content to pass the vertical burn test for lightweight nonwoven batting. In contrast only 7–20% of either the Dow EDF or LDF mixed with flammable natural and synthetic fibers allow the blends to

Table 2. Limiting Oxygen Values of Fibers[a]

Fiber	LOI, %
Polyethylene	17
Polystyrene	19
Cotton	20
Nylon	20
Polycarbonate	22
DuPont Nomex	26
PPO	26
Polysulfone	30
Polyimide	37
Rigid PVC	40–44
Oxidized PAN	>40
Hoechst–Celanese PBI	41
Dow EDF	45–55
Phillips PPS	44
Graphite	55
PTFE	95

[a] Refs. 70 and 71.

pass such tests while still retaining most of the base natural or synthetic fiber properties. Blends of 50/50 EDF/polyester also passed the stringent FAA airlines ignition resistance tests with zero flame length and no after-burn, whereas other blends of 65% LOI fiber/40% synthetic blends gave burn lengths of 20 cm and 15 s after-burn, clearly demonstrating the superiority of the lower level carbonaceous fiber as a flame blocker (71,72). Such nonwoven batting has exceptional thermal and sound insulation properties and has been successfully tested by the U.S. Navy for pilot's arctic wear.

Carbon–Nanotube Fibers

In 2000, Poulin and co-workers reported a carbon–nanotube spinning method (73) in which surfactant-dispersed single-walled nanotubes were injected at a rate of 10–100 ml/h into a cylindrical container holding a 5% poly(vinyl alcohol) (PVA) aqueous solution. The cylinder was rotated at speeds of 30–150 rpm. By pumping out the PVA solution, meter-long ribbons were obtained. After the ribbons were washed and rinsed with pure water to remove PVA and surfactant and drying, fibers several tens of centimeters long were made by slowly pulling the ribbons out of water. Young's moduli of the fibers varied between 9 and 15 GPa.

In 2003, Baughman and co-workers reported that by modifying the Poulin process (74), they were able to spin 100-m lengths of nanotube composite fiber in a continuous process at a rate of more than 70 cm/min. In their process, the spinning gel was injected into a cylindrical pipe in which a a PVA coagulation solution was allowed to flow, resulting in collapse of the spinning solution into nanotube fiber subsequently wound on a mandrel. The second stage of the process

involved unwinding the fibers on a series of godets that transport them through an acetone wash-bath, followed by drying and wrapping on a mandrel.

Baughman reported that these composite fibers were tougher than any natural or synthetic fibers described to date. The composite fibers were approximately 50 μm in diameter and contained ca 60% single-wall nanotubes by weight. They reported a tensile strength of 1.8 GPa (which is comparable to that of spider silk) and an energy-to-break of 570 J/g that is higher than that of spider dragline silk (165 J/g), Kevlar fibers (33 J/g), and graphite fiber (12 J/g). Baughman and co-workers have used the nanotube composite fibers to make nanotube supercapacitors which were woven into textiles. Suggested potential applications for the carbon–nanotube fibers include distributed sensors, electronic interconnects, electromagnetic shields, and attennas and batteries.

Silicon Carbide Ceramic Fibers

The commercially produced continuous and multifilament Nicalon (Hercules) fiber is produced from polydimethylsilane; however other organosilicon polymers have been used for the production of silicon carbide fiber. Polydimethylsilane is first distilled to remove the low molecular weight components, and polymer of average molecular weight 1500 is melt spun at 280°C and cured in air at 200°C. The fiber is then heat treated between 800 and 1500°C in nitrogen or vacuum. Optimum mechanical properties are achieved at ca 1250°C. Listed properties of the Nicalon fiber are modulus: 200 GPa; and tensile strength: 2.8 GPa (1).

Continuous SiC fibers can also be prepared by using chemical vapor deposition (CVD). For this process, tungsten or a carbon substrate fiber and vapors of CH_3SiHCl_2, $C_2H_5SiCl_3$, or CH_3SiCl_3 have been used. A SiC fiber with a reported modulus of 400 GPa and tensile strength of 3.45 GPa (1) is produced in a tubular glass reactor by a CVD process on a carbon monofilament substrate melt-spun from coal tar pitch. The process is carried out in two steps : (*1*) approximately 1 μm thick pyrolytic graphite is deposited to render the substrate fiber smooth and enhance its electrical conductivity, and (*2*) the coated substrate fiber is exposed to the silane vapors. Decomposition at the surface occurs at temperatures of ca 1300°C to form β-SiC continuously on the substrate.

Silicon carbide has high thermooxidative stability and good thermal and electrical insulation properties. In composite applications, this fiber can be used to reinforce polymer, metal, and ceramic matrices.

Vitreous Fibers

Man-made vitreous fibers (MMVF) comprise a number of glass and specialty glass fibers and also refractory ceramic fibers. The vitreous state in glass is somewhat analogous to the amorphous state in polymers. However, unlike organic polymers, it is not desirable to achieve the crystalline state in glass. Glasses are produced from glass-forming compounds such as SiO_2, P_2O_5, etc, which are mixed with other intermediate oxides such as Al_2O_3, TiO_2, or ZnO, and modifiers or fluxes like MgO, Li_2O, BaO, CaO, Na_2O, and K_2O (1).

The purpose of the fluxes is to break down the SiO_2 network so that the molten glass has the proper viscosity characteristics to allow it to cool to the desired vitreous state. Glasses with large fractions of noncross-linking monovalent alkaline fluxes allow the melts to form at lower temperatures but correspondingly have lower chemical resistance. For example, sodium silicate glasses with larger amounts of Na_2O are sold as water solutions (water glass).

A wide range of glass compositions is available to suit many textile fiber needs; the three most common glass compositions are referred to as E, S, and AR glasses. AR glass is a special glass with higher contents of Zr_2O designed to resist the calcium hydroxide in the cementitious products where it is used. S glass is a magnesium–aluminum–silicate cross-linked glass used where high mechanical strength or higher application temperatures are desired. E glass is a member of the calcium–aluminum–silicate family containing less than 2% alkali (see composition in ASTM specification D578-89a) and is the predominant glass used to make textile and continuous filament fibers.

Glass fibers $<3\ \mu$m are to be avoided because these are classified as respirable fibers which can enter and damage lung passages. Most glass fiber products have sufficient fiber lengths to prevent lung entry even if their diameters are $<3\ \mu$m.

Manufacture. Vitreous fibers are produced by several processes (75).

Continuous Drawing Process. Textile glass filaments are made by a process different from that used for making discontinuous fibers, but literally parallel to a standard organic polymer melt spinning operation that does not employ a screw extruder. Premelted glass or glass marbles are fed into an electrically-heated furnace called a bushing which contains platinum nozzles. The exiting glass filaments are drawn down into the desired diameters, water sprayed, coated with a sizing, and the multiple filaments are collected as bundles of strands which are then wound onto a suitable cone.

Rotary Process. This process is much like the making of cotton candy except that molten glass is used in place of molten sugar. The melted glass is dropped into a rotating spinner with sidewall perforations and the exiting glass filaments are drawn to a fine diameter by the centrifugal force. These fibers are collected and coated with a protective spray containing either lubricants, binders, or antistatic and wetting agents. Other versions of the rotary process are (*1*) the wheel centrifugal process where molten glass is cascaded over spinning wheels and the formed fibers are stretched and broken by variations in the wheel speeds prior to being collected, and (*2*) the Downey process where molten glass is dropped onto a centrifuge wheel and then exits into a stream of high velocity air much like the melt blown process for making textile nonwovens.

Flame Attenuation. This process closely resembles the continuous drawing process except that the melted strand is not wound onto a cone. Rather, the exiting strand is blown at right angles with a high velocity gas burner so as to remelt and reform the glass as small fibers, which are collected as a mat onto a moving belt. A modification of this process simply uses the high velocity flame at right angles to a dropping melted stream of glass to fibrillate the mass into minute fibers.

Properties. Glass fibers made from various compositions have softening points in the range 650–970°C. Fiber length and diameter distributions are significant factors in determining thermal and acoustical insulation properties. Slag wool and rock wool fibers are prepared from the slag from pig iron blast furnaces.

They contain significant amounts of iron oxides and have a glass-transition temperature of 760–870°C. Slag and rock wool fibers are used to prevent fires from spreading. At temperatures above 850°C, these fibers partially devitrify and form polycrystalline material that melts at 1225–1360°C, which is high enough to contain the fires for several hours. Seventy percent of the slag wool in the United States is used for ceiling tiles.

Refractory Ceramic Fibers (RCF). These MMVF materials constitute only about 1% of the vitreous fiber market but have exceptional high temperature performance characteristics. They are produced by using high percentages of Al_2O_3 about 50/50 with SiO_2 as is or modified with other oxides like ZrO_2 or by using Kaolin clay which has similar high amounts of Al_2O_3. Different compositions result in modifying end use temperatures from about 1050°C or higher for the kaolin-based products to 1425°C and above for the zirconium-containing materials. At temperatures above 1000°C these ceramic fibers tend to devitrify and partially crystallize. Specially prepared ceramic fibers are used to protect space vehicles on re-entry and can withstand temperatures above 1250°C.

Structure/Property Classification

Commercial high performance fibers and high technology textile products have become an increasingly important segment of fiber and textile consumption worldwide. Although breakdown of the numerous applications by weight and/or economic value is impractical, one review indicated that high technology textile uses would account for 50% of all worldwide fiber consumption by the year 2000 compared to 10–15% in 1990 (76). In some instances various technologies and concepts are combined or refined to produce a textile product for the desired application(s). Thus, sophistication and enhancement of properties may be introduced at the fiber, yarn, and/or fabric levels.

The relationship between structure and properties of textile or fibrous substrates and their applications is one method of classifying nontraditional or high technology textiles. At the fiber level, the distinguishing high performance characteristics are high tenacity/strength fibers, hollow fibers, very fine or microtex (microdenier) fibers (hollow or nonhollow), fibers with unique porosities, bicomponent and biconstituent fibers, and fibers with superior resistance to extreme heat, flame, and/or chemical agents (Table 3). At the fabric or product level, the classes may be described as coated and laminated fabrics, composites and fiber-reinforced materials, three-dimensional fabric structures, and fabrics containing polymers or structural features that impart multifunctional properties or allow the fibrous substrate to act as an intelligent material. Although some of these fiber and fabric characteristics also apply to conventional textile uses and products, many of these concepts have evolved from the production and use of high performance fibers and products.

Fiber Properties.

High Strength Fibers. Super fibers or fibers with very high tenacities and Young's moduli have been defined as those with a tenacity of at least 2.5 GPa (255 kgf/mm^2) and a modulus of at least 55 GPa (5600 kgf/mm^2) (77). Fibers meeting these criteria are glass fibers, aramids such as Kevlar and Twaron, gel spun

Table 3. Classification of High Performance Fibers and High Technology Fibers by Properties[a]

Property	Fiber types	Applications
High tenacity and modulus	Aramids, gel spun polyethylene, PBO, PIPD, polyarylate	Tires, antiballistics, ropes, optical cables
Resistant to heat and flame	Aramids, PEEK (Victrex), PBI, polyimides, EDF	Protective clothing for various applications
Resistance to chemical agents	Fluorocarbons, polyolefins	Filters, geotextiles, marine applications
Microtex and hollow fibers	Most synthetics and regenerated fibers	Filtration, leisure, insulation, biomedical fashion, fragrances
Intricate shapes and porosities	Most synthetics and regenerated fibers	Antimicrobial, fiber optics, specialty wipes

[a]Ref. 3.

polyethylene such as Dyneema and Spectra, and various carbon fibers and aromatic liquid-crystalline polyesters such as Vectran. Representative applications are for antiballistic clothing, building materials, aerospace, and as reinforcing material in composites for various applications.

Heat-Resistant Fibers. Inherently flame- and heat-resistant fibers have other criteria for performance in addition to high tenacity and modulus. These fibers must be suitable for protective clothing or for use as a material in a particular application such as firefighters' uniforms, race car drivers apparel for protection from hot metals and gas explosions, and as components in commercial and military aircraft. Dimensional stability and strength retention on exposure to intense heat sources as well as a limiting oxygen index (LOI) above 30 are essential for most of these applications. Fiber types and blends meeting these criteria are various aramids such as Nomex and Kevlar, polybenzimidazole (PBI), poly(phenylene sulfide) (PPS) such as Ryton (Phillips Petroleum), Dow's EDF, and wool blends with these various inherently flame-resistant fibers.

Chemically-Resistant Fibers. Fibers with excellent chemical resistance to corrosive and/or chemical warfare agents or extreme pH conditions (eg, very acidic or very alkaline) were initially used for protective clothing. However, applications for filtration of gases and liquids in numerous industrial facilities are now more important. For example, PPS is suitable for use in filter fabrics for coal-fired boilers because of its outstanding chemical and heat resistance to acidic flue gases and its excellent durability under these end use conditions. Many high tenacity fibers are also chemically inert or relatively unaffected under a variety of conditions. Aramids, gel spun polyethylene, polypropylene, fluorocarbon, and carbon fibers meet these criteria and have been used or are being considered for applications where chemical resistance is important.

Fine and Hollow Fibers. Controlling and designing the geometry, fineness or denier, and porosities of fibers (and occasionally of yarns) have led to novel and high technology textile products for diverse applications. Hollow fibers derived from regenerated cellulose or from synthetic fibers have been used in the development of artificial body organs such as the kidney, pancreas, and lung. Hollow fibers

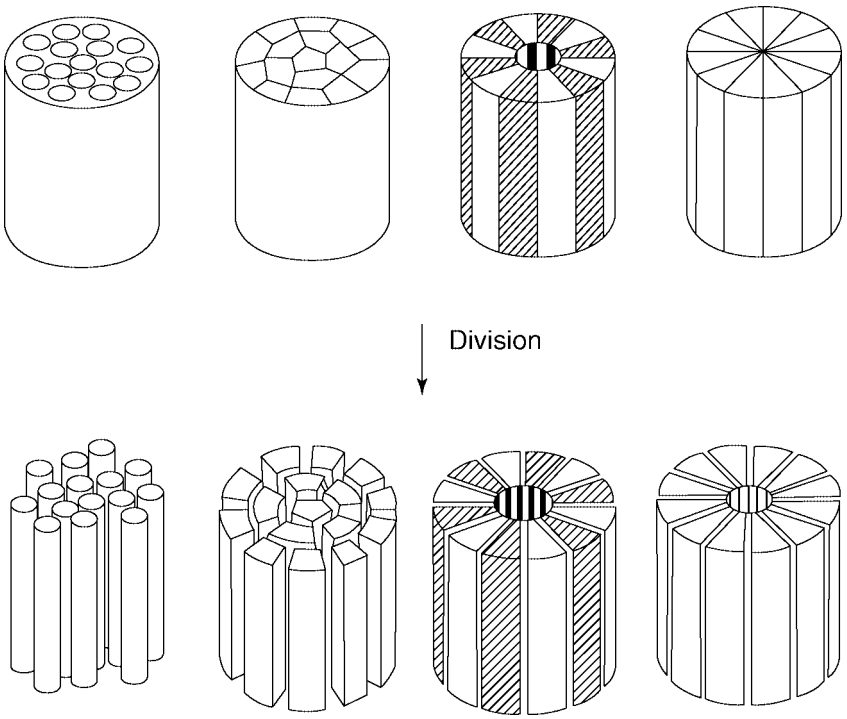

Fig. 1. Ultrafine fibers are produced by spinning bicomponent or biconstituent polymer mixtures, highly stretching such products to ultrafine deniers, and extracting or otherwise removing the undesired matrix carrier to release the desired ultrafine fibers (78). For example, spinning polyester islands in a matrix of polystyrene and then, after stretching, dissolving the polystyrene to leave the polyester fibers; cospinning polyester with polyamides, then stretching, removing the polyester by caustic treatment, leaving 100% nylon ultrafine fibers.

have also frequently been employed to increase the insulation value of garments due to the benefits of the air trapped inside the fiber cavity. A variety of ultrafine fibers, ranging in tex (denier) from as little as 0.0011 (0.01) up to 0.011 (0.1) have been commercialized (primarily in Japan) to impart various surface characteristics that change fabric hand and appearance. Because spinning ultrafine fibers directly is technically difficult, such fibers may be produced by spinning bicomponent or biconstituent polymer mixtures, highly stretching them to form ultrafine deniers, and extracting or otherwise removing the undesired matrix carrier material to release the desired ultrafine fibers (Fig. 1) (78). Another technique used to prepare ultrafine (nanofibers) fibers is electrospinning (79). Controlling the porosity of fibers has been advantageously used to release antimicrobial agents at different rates for specific applications. Novel core/sheath yarns that control selective distribution of both components are being evaluated for numerous applications.

Product Types.

Composites. Various composite materials have evolved over the years as a significant class of high performance textile products. The prototype composite is carbon fiber with an epoxy resin matrix for structural aircraft components

and other aerospace and military applications. Carbon fiber composites are also used in various leisure and sporting items such as golf clubs, tennis rackets, and lightweight bicycle frames. However, other types of applications and composites are also entering the marketplace. For example, short cellulose fiber/rubber composites are used for hoses, belting, and pneumatic tire components.

3D Structures. Three-dimensional textile structures have been developed primarily for architectural, civil engineering, and aerospace applications. Such structures fall into four different categories: nonwoven orthogonals (straight, continuous fibers arranged in three directions with no interlacing); multilayer woven (multiple layers interlaced at selected points); multilayer knitted or stitched (multiple layers of yarns stitched in diverse or desired directions); and three-dimensional braids (intertwining of multiple yarns so that a particular yarn follows a path taking it completely across the structure several times) (80).

Multifunctional Materials. Multifunctional property improvement by binding of specific polymers to fibers and fibrous products has been extensively investigated and reviewed (81). With poly(ethylene glycol) as the bound polymer, functional and aesthetic property improvements include thermal comfort, liquid absorbency/repellancy, increased wear life, soil release, resistance to static charge, antimicrobial activity, and resiliency. Numerous applications such as sportswear/ski wear, protective clothing for health care workers, durable and nondurable hygienic items, work uniforms, and space suits are being commercialized and evaluated.

Smart Materials. The field of intelligent or self-adaptive materials is in its infancy, particularly with regard to textile products. Conceptually, any material that is responsive to one or more external stimuli (heat, force, light, moisture, electrical current) and that responds to such exposure by changing shape or related characteristics is classified as an intelligent material. Synthetic gels that act like artificial muscle and fabrics that self-repair to avoid tensile and other forms of mechanical failure are examples of ongoing research and uses (82).

Classification by Types of Application

Another way to classify high performance fibers and high technology textile materials or products is by types of applications. A scheme of 10 main categories has been adopted (Table 4) and is similar to several classification schemes previously reported (76).

Transportation. High performance fibers and high technology textile products have many applications in the transportation area. Composites are increasingly used as structural materials in aircraft components such as horizontal stabilizers, fins, landing gear doors, fan blades, and nose spin cones. In addition to carbon and glass fibers in composites, aramid and polyimide fibers are also used in conjunction with epoxy resins. Safety requirements by the U.S. Federal Aeronautics Administration (FAA) have led to the development of flame- and heat-resistant seals and structural components in civilian aircraft cabins. Wool blend fabrics containing aramids, poly(phenylene sulfide), EDF (Dow), and other inherently flame-resistant fibers and fabrics containing only these highly heat- and flame-resistant fibers are the types most frequently used in these applications.

Table 4. Classification of High Performance and High Technology Textiles by Types of Applications[a]

Application class	Subcategories	Examples of specific products
Transportation	Civilian and military aircraft, traffic	Components of aircraft, air bags, seats in planes and cars
Manufacturing	Electronics, information, and communication	Optical fibers for telecommunications and computers, printed circuit boards, industrial filters and belts
Agriculture and forestry	Horticulture, erosion control, barriers	Greenhouse covers, control of drainage, land nets cultivation of plants
Civil engineering and construction	Geotextiles and geomembranes architectural	Road reinforcement, pond liners, and dams, fabric roofs, soil stabilization
Fishery and marine	Pollution containment, aquatic life, industrial and leisure marine equipment and vehicles	Breeding of corrosion resistant composites, conveyers floating backwaters, screens for fish breeding, speedboat components
Protective clothing	Chemical/environmental/biological security, heat and flame	Firefighters' uniforms, bulletproof vests, protection from toxins and diseases
Sports and leisure	Sporting goods and vehicles, spas and pools	Golf clubs, tennis rackets, snowmobiles, bicycle frames, spa and pool parts, ski wear and sportswear, luxury apparel
Biomedical and health care	Devices, artificial organs, sutures, wound care, prostheses	Kidneys and artificial limbs, bioimplants, dressings for wounds, hydrogel composites
Defense and aerospace	Chemical/biological protection, camouflage, components for weapons	Chemical/biological warfare protection composites for armour and other weapons, space suits and materials for space travel
Energy use and conversion	insulation, containment of hazardous waste, shields from high energy sources	All types of insulation, waste containers, electromagnetic shielding

[a]Ref. 76.

The introduction of air bags into automobiles represented a new and enormous market for high performance textiles. Polyamide-coated fabrics are primarily used because of the high strength of the polyamide, but there have been marketing and technical studies that indicate the feasibility of using high tenacity polyester as the base fabric. Performance requirements for air bags include tear; tensile, seam, and bursting strength; dimensional stability;

resistance to puncture, abrasion, and buckling; flame resistance; and resistance to delamination (83). It has been estimated that by the end of the century more than 41×10^6 m^2 of coated fabrics would be used in the United States alone to make automobile air bags (84).

Manufacturing. The use of advanced textile materials in manufacturing is a diverse and expanding market. Optical fibers are being increasingly used in telecommunications, computers, cable television, and to facilitate process control in the nuclear, petrochemical and chemical, and food industries. Although most optical fibers are glass or of related inorganic composition, there are optical fibers for special applications comprised of poly(methyl methacrylate), polystyrene, and polycarbonate that are coextruded with fluorinated acrylate polymers. Polyacetal, ie, poly(oxymethylene) fiber has also been used as a reinforcing material for optical fibers. Basic fiber properties required for an optical fiber are (*1*) a structure with a high refractive index core and a low refractive index cladding (sheath bonded to core under high temperature and pressure); (*2*) fiber with a low attenuation or low power loss of light over distance; and (*3*) fiber with low dispersion or pulse broadening as light travels down the fiber (85).

Electronics and electrical insulation are other manufacturing areas in which advanced fibers are extensively used. Manufacturing of computer components such as printed circuit boards and printed wiring boards require use of reinforced fibers that have good dielectric properties, thermal and dimensional stability, chemical resistance, and low moisture regain. For electrical insulation applications, fiber requirements are high dielectric strength, low power loss, and good thermal and chemical resistance. Although inorganic fibers are extensively used for both electronic and electrical applications, aramid fibers are also now used for both types of applications. A variety of natural and synthetic fibers are also used for various electrical applications (86).

A third area that has rapidly expanded in the manufacturing sector is the demand for clean room working garments. The primary electronics and computer industries have the most stringent requirements for cleanliness in their manufacturing environments; clean room garments are also used by personnel in the pharmaceutical, food, precision engineering, and biotechnology/biomedical industries. Requirements for clean room garments and the increasingly stringent standards for both particle size and number of acceptable particles have been critically reviewed and discussed (87). Required properties for garments in clean rooms include fabrics or materials that are dustproof, antistatic, durable to laundering and sterilization procedures, and that are comfortable. Garments have been designed with ability to filter air by mechanical or electrostatic concepts and collect fine particles. Microtex polyester fibers are most frequently used to make these clean room garments. Diameters of particles to be removed have progressed from about 1 μm in the early 1970s to only 0.1 μm in the 1990s. Industry standards for the corresponding degree of cleanliness (particles/m^3) have decreased from 35,000 to 35 (10,000 to 1 per ft^3). Thermal comfort of many of the garments is unacceptable due to their low moisture content, but some efforts are being made to develop microporous coatings to provide both comfort and function required for this application.

The fourth area of manufacturing for advanced fibrous materials is that of filtration of liquids and gases. Filters have diverse requirements for different

industries and environments to which they are exposed. The use of cellulose acetate and aramid hollow fibers to desalinate water by a reverse osmosis process is an example of one of the earlier applications for filtration. Important fiber properties for such filtration are hydrolytic, oxidative, and biological stability over wide pH ranges. Separation of gases by ultrafiltration for a variety of industries is another example of the importance of advanced fibrous substrates. Because of the diversity of exposure to extreme temperature changes and corrosive chemical agents, many of the high temperature, high tenacity, and inert fibers are replacing more conventional types of fibers for such filtration. Poly(phenylene sulfide), polysulfone, aramids, polyimide, PEEK (Victrex), fluorocarbon, and related fibers are examples of high performance fibers effective for gas and liquid filtration under extreme and rapidly changing environmental conditions.

Agriculture and Forestry. Agricultural and silvicultural applications for high performance textile materials range from geotextile and geomembrane materials to horticultural uses to facilitate the growth, yield, and production of edible and ornamental plants. Geotextile structures, either permanent or biodegradable, are inexpensive alternatives to more expensive, conventional concrete or other materials for prevention and control of gully formation. Also, drainage and soil erosion control on farm acreage have been facilitated by geotextiles. Wind fences and other geotextile barriers have also been advantageously used.

If the geotextile is above ground, it should be stable to sunlight, air pollution, rot, and mildew-producing fungi besides having mechanical integrity and dimensional stability. If the textile is below ground, it should be dimensionally stable and inert to most chemical agents and have good long-term permeability so that it does not become easily clogged with soil particles.

Other examples of agricultural applications are flexible and lightweight silos constructed from geotextiles that hold grain, manure, or any other agricultural commodity of interest. Polypropylene fiber is used primarily in most geotextile (agricultural, civil engineering, and other applications) structures because of its excellent inertness to chemical and biological agents and its dimensional stability over long periods of use. Polyester and glass fibers are also used to some extent in geotextiles.

Horticultural applications include use of greenhouse thermal screens, rowcrop and turf covers, conveyer belts to process agricultural products, and other similar items. High performance fibers are not normally used in these applications, but high strength fibers are preferable for conveyer belts. Environmentally inert low cost fibers such as polypropylene are used for many of the outdoor horticultural applications.

Civil Engineering and Construction. These textile applications can be classified as civil engineering applications (also commonly referred to as geotextiles) and architectural applications. High performance fibers are not currently used to any great extent in these applications due to their high unit cost. However, mechanical and environmental requirements for such applications demand that even conventional fibers withstand challenging structural demands and sustained long-term performance outdoors. Polypropylene fibers have captured a sizable portion of the geotextile market because of their excellent dimensional stability and chemical inertness. Polyester and glass fibers are two other types of fibers used in geotextile applications. Reinforcement of highways and roadbeds is by far the

principal use of geotextiles. Their primary function is to serve as a soil stabilizer by spreading the impact load of vehicles over a larger area thus prolonging the useful life of roadways. As in agricultural applications, geotextiles are also used to prevent or minimize soil erosion and facilitate drainage. These materials have been utilized in important projects such as reinforcement of dikes in Holland and to construct dams in the United States. Mechanisms for geotextile failure have been critically evaluated and discussed (88). The types of failure must be evaluated relative to the function of the geotextile. Failure modes include piping of soils through or clogging of the geotextile, reduced tensile resisting force, deformation of the fabric, reduced resistance to puncture, and reduced in-plane flow of liquids.

Most architectural fabrics are usually flexible composites comprised of glass fibers coated with fluorocarbons to resist wind, mechanical forces, and outdoor environmental degradation. The airport terminal in Saudi Arabia, and the roofs for the Hubert Humphrey Dome in Minneapolis and the Tokyo Dome Stadium are a few examples of the successful use of architectural fabrics.

Fishery and Marine. Marine applications for textiles include (*1*) those concerned with fishing and fishing industries, (*2*) leisure items and components, and (*3*) industrial, including control of various types of environmental pollution and influences (89,90). The earliest use of textiles in fishery and marine applications were for high strength nets, lines, and ropes. Conventional natural and synthetic fibers are being replaced by high performance fibers such as aramids, gel spun polyethylene, and polyacetal. However, cost is still a factor because the latter fibers are still much more expensive than the conventional fibers. More advanced applications for fishing and marine industries include the construction of artificial seaweed beds comprised of synthetic fiber membranes that facilitate fish breeding.

Advanced composites and fiber-reinforced materials are used in sailcloth, speedboat, and other types of boat components, and leisure and commercial fishing gear. Aramid and polyethylene fibers are currently used in conveyer belts to collect valuable offshore minerals such as cobalt, uranium, and manganese. Construction of oil-adsorbing fences made of high performance fabrics is being evaluated in Japan as well as the construction of other pollution control textile materials for maritime use. For most marine uses, the textile materials must be resistant to biodeterioration and to a variety of aqueous pollutants and environmental conditions.

Protective Clothing. Protection against adverse chemical and biological environments, from heat and/or flame, and antiballistic protection are the principal applications of protective clothing. Several high performance fibers are finding increasing use in many protective clothing applications due to their high strength, resistance to cutting and firearms, and their ability to withstand temperature extremes and corrosive chemical agents. Aramids such as Kevlar and polyethylene fibers such as Spectra are used in many bulletproof vests and other types of security garments. PBI is used in firemen turn coats and race car driver suits.

Aramids are also used in firefighters' uniforms for their excellent flame resistance. The new Dow Curlon EDF fibers have exceptional flame resistance both by themselves and in combination with other flammable fibers. At only 20% by weight, Curlon has been shown to totally prevent the flaming of polyester and other similar flammable materials. This property along with Curlon's good textile processibility will undoubtedly lead to many new applications in the protective

garment area (70–72). Garments derived from blends of polybenzimidazole (PBI) and aramid fibers have excellent chemical resistance and a low propensity to severe burns as shown by tests in a gas pit where temperatures could rise as high as 1100°C (91).

There are distinct performance differences for garments that are resistant to flame alone compared to those that are resistant to both heat buildup and flammability. Appropriate tests have been devised that measure the thermal protective performance of fabrics when exposed to a radiant heat source. Sophisticated constructions against biohazards need further development to produce materials that are both thermally comfortable and impermeable to blood-borne pathogens and other deleterious microorganisms. The most promising approaches are materials that are laminated or coated fabrics that are permeable to vapor but impermeable to liquids. Statistics included in recent OSHA standards for protection against blood-borne pathogens (eg, hepatitis and AIDS viruses) estimate that currently close to six million persons in the United States (health care workers and many other occupations) require protective clothing and other types of safeguards against these biohazards (92).

Sports and Leisure. The application of high technology fiber properties and complex structures for sports and leisure are identifiable in three areas: components for sporting goods, boats, and other rigid structures; high technology sportswear and ski wear; and luxury apparel. Although most components for sporting goods (such as tennis rackets, golf clubs, lightweight bicycle frames, spa components, speedboat components) are usually carbon–fiber reinforced composites, the high performance aramids and polyethylene are now being used to manufacture items such as bicycle helmets and other sports items. For these end uses, impact and overall tensile strength, dimensional stability, and resistance to specific environmental agents are required. High technology sportswear and ski wear evolved with the advent of Gore Tex.

Gore-Tex. Gore-Tex (WL Gore) was the first fabric comprised of a microporous polytetrafluoroethylene film laminated to a polyamide fabric. The microporosity of the film allowed the garment to be breathable or allow passage of water vapor yet be waterproof or resistant to liquid penetration. Since that time, a variety of microporous materials or related structures have been developed in the United States and Japan. Another example for high technology sportswear is the latent heat and high water absorbency of a cross-linked poly(ethylene glycol) coating on fabrics that makes it possible for the garment to be thermally adaptable in hot and cold environments (81). Also, microencapsulation of zirconium carbide into polyamide or polyester fibers produces a ski wear garment (called Solar-α) that absorbs sunlight and converts it into heat.

Numerous high touch fibers have been produced and commercialized (primarily in Japan) for luxury apparel. Conceptually, the geometry and fineness of the fibers are carefully modified and controlled to produce fabrics with desirable sensual responses of touch, sight, sound, comfort, and even odor (78,93). There are several techniques for producing ultrafine fibers and this has led to the production and commercialization of materials such as Ultrasuede, artificial leather and silk, fabrics with a peach-fuzz sensation, perfumed hosiery, fabrics that change color due to microencapsulation of cholesteric liquid crystals, and numerous other luxury and novelty textile products.

Biomedical and Health Care. This area is an extremely diverse and expanding market for high performance fiber concepts and their reduction to the desired end use performance. Although the complexity of the human body and its physiological functions are difficult to mimic with artificial materials, significant progress has been made in the introduction of biomaterials and related health care products. The numerous uses of fibers in medicine have been critically and concisely reviewed, including nonimplantable items (such as surgical dressings, gowns, drapes, pressure bandages), extra corporeal devices (components of dialyzers and oxygenators, catheters) and implants (sutures, vascular grafts, artificial organs, fibers and fabrics for surgical reinforcement, optical fibers for medical procedures, and orthopedic devices) (94). In addition to having the desired mechanical and functional integrity for the particular biomedical application, the fibrous product must be nonallergenic, usually nonthrombogenic, noncarcinogenic, sterilizable, and biocompatible. Nonimplant items are usually derived from conventional fibers and fabrics, except for clean room garments. Examples of extra corporeal devices or components are regenerated hollow cellulose fibers for the artificial kidneys or dialyzers and hollow fibers or flatsheet fibrous membranes derived from polypropylene, polytetrafluoroethylene, and various coated fabrics in blood oxygenation devices.

Implants generally can be classified as those that are designed to be bioabsorbable (eg, sutures) and those that are designed for more permanent function (nonabsorbable sutures, vascular grafts, and artificial organs). Bioabsorbable materials have been critically reviewed with emphasis on sutures and related fibrous products (95). Bioabsorbable sutures were originally derived from catgut or collagen, but now a variety of poly(glycolic acid) homo- and copolymers as well as poly(dioxanones) are used. Hydrogel fibrous composites have become important as wound dressings and as implants. Many of these hydrogel composites are poly(ethylene oxide) homopolymers and/or copolymers of poly(acrylic acid), polyacrylamide, or other related structures (96). Nonabsorbable sutures and reinforced structures for vascular grafts and artificial organs are derived from high tenacity polyamide, polypropylene, polyester, polytetrafluoroethylene, and various coated fibers and fabrics. Optical fibers for endoscopy and angioplasty procedures are usually composed of glass or poly(methyl methacrylate). In addition to these classifications, the production of biomimetic fibers, ie, fibrous materials that are specifically designed to mimic physiological and other anatomical functions of living organisms, has been described (97). Applications include artificial cells, nerves and muscles, biosensors, and artificial bones and teeth.

Defense and Aerospace. Military applications for high performance fibers and high technology textiles generally parallel those discussed earlier for civilian aircraft and protective clothing. Protective clothing is usually designed to be impermeable to chemical and biological warfare agents such as nerve and mustard gas. Design of protective clothing for these purposes is usually classified information, but it is reasonable to assume that the clothing assembly consists of microporous membranes and elaborate filtration devices. Another military application is the design of combat uniforms that are dyed in such a manner that they provide effective camouflage and are not detectable by night surveillance devices. Not surprisingly such materials have been adapted to civilian use by hunters to give better camouflage against deer and turkeys, which see UV reflections. Printing of aramid fabrics for this purpose has been described (98).

Requirements for space suits are more complex and frequently involve garments that can circulate water and/or air through the fibrous assembly. Laminated and/or coated garments with specific requirements to pressure, radiation, temperature, and humidity are more structurally complex as a textile product relative to the types of fibers used in this aerospace fabrication.

Fiber composites and three-dimensional textile structures are frequently used in advanced military weapons and aircraft such as extended use armor tracks, materials for engine parts (nose spin cones and fan blades), and primary and secondary structural components of aircraft (main wings, horizontal tail and stabilizer, speed brakes, high performance gaskets, fins, and ailerons). Although many of these materials are carbon fiber–epoxy resin composites or glass fiber–epoxy resin composites, there is an increase in the use of aramid, polyimide, and polytheretherketone (PEEK) fibers because of their excellent strength and thermal/oxidative and chemical stabilities.

Energy Use and Conservation. A variety of materials are needed for high performance thermal insulation, particularly as components of nuclear reactors. Replacements for asbestos fibers are needed for components such as reactor core flooring, plumbing, and packaging. The fibers must be very resistant to high temperatures with outstanding dimensional stability and resistance to compression.

Filters for nuclear fuel reprocessing and replacement of fibrous composites to reduce or prevent radiation leaks are two other areas of application. Advanced fiber composites, aramids, and high tenacity polyethylene for specific applications are types of high performance fibers and structures being considered (3). Metal-coated fibers and fabrics have been effective in electromagnetic shielding applications. High performance fabrics have also been used for containment of hazardous waste in addition to being used for conservation of energy and improving the safety of nuclear power plants (99). The same considerations that apply to geotextiles for other applications also apply to geotextiles used for waste containment. However, there are additional performance requirements such as excellent resistance to municipal waste leachate. Thus, polypropylene and to a lesser extent polyethylene fibers are used in the construction of geotextiles for this type of application.

BIBLIOGRAPHY

1. S. Kumar, *Indian J. Fibre Textile Res.* **16**, 52 (1991).
2. L. L. Chapoy, *Recent Advances in Liquid Crystal Polymers*, Elsevier Applied Science Publishers, Ltd., New York, 1985.
3. T. Hongu and G. O. Phillips, *New Fibers*, 2nd ed., Woodhead Pub. Ltd., Cambridge, England, 1997.
4. X.-D. Hu, S. E. Jenkins, B. G. Min, M. B. Polk, and S. Kumar, *Macromol. Mater. Eng.* **288**, 823 (2003).
5. P. J. Collings and M. Hird, *Introduction to Liquid Crystals: Chemistry and Physics*, Taylor & Francis, London, 1997.
6. P. J. Collings, *Liquid Crystals*, 2nd ed., Princeton University Press, Princeton, N.J, 2002.
7. S. L. Kwolek and P. W. Movgan, *Macromolecules* **10**, 1390 (1977).
8. A. Roviello and A. Sirigu, *J. Polym. Sci. Polym. Lett. Ed*. **13**, 455 (1975).
9. W. J. Jackson and H. F. Kuhfuss, *J. Polym. Sci. Polym. Chem. Ed*. **14**, 2043 (1976).

10. Ger. Pat. 2,052,971 (1970) (to Carborundum).
11. U.S. Pat. 3,829,406 (1971) (to Carborundum).
12. Ger. Pat. 2,507,066 (1976) (to Carborundum).
13. U.S. Pat. 4,161,470 (1980) (to Celanese).
14. U.S. Pat. 3,991,013 (1976) (to DuPont).
15. U.S. Pat. 3,991,014 (1976) (to DuPont).
16. U.S. Pat. 4,066,620 (1978) (to DuPont).
17. U.S. Pat. 4,118,372 (1978) (to DuPont).
18. W. J. Jackson and H. F. Kuhfuss, *J. Polym. Sci. Polym. Chem.* **14**, 2043 (1976).
19. S. L. Kwolek and R. R. Luise, *Macromolecules* **19**, 1789 (1986).
20. U.S. Pat. 3,637,595 (1972) (to Carborundum).
21. U.S. Pat. 3,975,487 (1976) (to Carborundum).
22. H. H. Yang, in M. Lewin and J. Preston, eds., *Handbook of Fiber Science and Technology*, Vol. **3**, Part C, Marcel Dekker, New York, 1983, p. 105.
23. H. H. Yang, in M. Lewin and J. Preston, eds., *Handbook of Fiber Science and Technology*, Vol. **3**, Part C, Marcel Dekker, New York, 1983, Ref. 22, p. 130.
24. Properties of Nomex High Temperature Resistant Nylon Fiber, NP-33, Bulletin, E. I. DuPont de Nemours & Co., Wilmington, Del., Oct. 1969.
25. U.S. Pat. 3,049,518 (1962) (to DuPont).
26. U.S. Pat. 3,287,324 (1966) (to DuPont).
27. Dyeing and Finishing Nomex Type 450 Aramid Bulletin, NX-1, E. I. DuPont de Nemours & Co., Inc., Wilmington, Del., May 1976.
28. J. R. Schaefgen, V. S. Fold, F. M. Logullo, V. H. Good, L. W. Gulrich, and F. L. Killian, *Polym. Prepr.* **17**, 69 (1976).
29. U.S. Pat. 4,172,938 (1979) (to Teijin).
30. Brit. Pat. 1,547,802 (1979) (to AKZO).
31. M. Jaffee and R. S. Jones, in M. Lewin and J. Preston, eds., *Handbook of Fiber Science and Technology*, Vol. **3**, Part A, Marcel Dekker, New York, 1983, Chapt. 9.
32. T. I. Bair, P. W. Morgan, and F. L. Killian, *Macromolecules* **10**, 1396 (1977).
33. J. Preston, *Polym. Eng. Sci.* **15**, 199 (1975).
34. U.S. Pat. 3,850,888 (1974) (to DuPont).
35. U.S. Pat. 3,884,881 (1975) (to DuPont).
36. M. Jaffe, in E. Turi, ed., *Thermal Characterization of Polymeric Fibers*, Academic Press, New York, Chapt. 7, 1981.
37. E. T. Samulski, M. M. Denn, D. B. Du Pre, N. D. Field, A. C. Griffin, M. Jaffe, S. L. Kwolek, M. B. Polk, D. C. Prevorsek, M. T. Shaw, U. Sutev, and D. J. Williams, *Liquid Crystalline Polymers: Report of the Committee on Liquid Crystalline Polymers*, National Materials Advisory Board, NMAB-453, National Academy Press, Washington, D.C., 1990, p. 28.
38. E. E. Magat, *Philos. Trans. R. Soc. London, Ser. A* **294**, 463 (1980).
39. U.S. Pat. 3,767,756 (1973) (to DuPont).
40. H. H. Yang, *Kevlar Aramid Fiber*, John Wiley & Sons, Inc., New York, 1993.
41. M. G. Northholt, *Eur. Polym. J.* **10**, 799 (1974).
42. S. Ozawa and K. Matsuda, in M. Lewin and J. Preston, eds., *Handbook of Fiber Science and Technology*, Vol. **3**, Part B, Marcel Dekker, New York, 1983, p. 1.
43. J. F. Wolfe, in H. F. Mark, N. M. Bikales, C. G. Overberger, and J. I. Kroschwitz, eds., *Encyclopedia of Polymer Science and Engineering*, 2nd ed., Vol. **11**, 1988, p. 601.
44. D. J. Sikkema, *Polymer* **39**, 5981 (1998).
45. D. Bhaumilk, W. J. Welsh, and J. E. Mark, *Macromolecules* **14**, 947 (1981).
46. M. W. Wellman, W. W. Adams, D. R. Wiff, and A. V. Fratini, Part 1, AFML-TR-79-4184 U. S. Air Force Materials Laboratory, Wright–Patterson Air Force Base, Dayton, OH, Feb. 1980.

47. M. W. Wellman, W. W. Adams, R. A. Wolfe, D. S. Dudis, D. R. Wiff, and A. V. Fratini, *Macromolecules* **14**, 935 (1981).
48. E. A. Klop and M. Lammers, *Polymer* **39**, 5987 (1998).
49. M. Lammers, E. A. Klop, M. G. Northolt, and D. J. Sikkema, *Polymer* **39**, 5999 (1998).
50. L. R. Denny, I. J. Goldfarb, and E. J. Soloski, *Mater. Res. Soc. Symp. Proc.* **134**, 395 (1989).
51. http://www.m5fiber.com/fiber.htm.
52. A. B. Conciatori, A. Buckley, and D. E. Stuetz, in M. Lewin and J. Preston, eds., *Handbook of Fiber Science and Technology*, Vol. **3**, Part A, Marcel Dekker, New York, 1983, p. 221.
53. H. Vogel and C. S. Marvel, *J. Polym. Sci.* **50**, 511 (1961).
54. A. B. Conciatori, A. Buckley, and D. E. Stuetz, in Ref. 52, p. 230.
55. A. B. Conciatori, A. Buckley, and D. E. Stuetz, in Ref. 52, p. 240.
56. A. Buckley, D. E. Stuetz, and G. A. Serad, in I. Kroschwitz, ed., *High Performance Polymers and Composites*, John Wiley & Sons, Inc., New York, 1991, p. 589.
57. A. B. Conciatori, A. Buckley, and D. E. Stuetz, in Ref. 52, p. 251.
58. M. Jaffe, G. W. Calundann, and H.-N. Yoon, in Ref. 42, p. 83.
59. Nippon Chemtec Consulting, Inc., Report V-8-113-1; V-8-134-2.
60. U.S. Pat. 4,137,394 (1976) (to Stamicarbon, B.V.).
61. U.S. Pat. 4,536,536 (1985) (to Allied corp.).
62. *Textiltechnik* (**4**), 175 (1985).
63. U.S. Pat. 4,403,012 (1983) (to Allied Corp.).
64. Eur. Pat. 77,590 (1983) (to Stamicarbon, B.V.); Ger. Pat. 3,023,726 (1981) (to Stamicarbon, B.V.).
65. Eur. Pat. 144,997 (1985) (to Stamicarbon, B.V.).
66. Eur. Pat. 55,001 (1992) (to Stamicarbon, B.V.).
67. A. P. S. Sawhney, K. Q. Robert, G. F. Ruppenicker, and L. B. Kimmel, *Text. Res. J.* **62**(1), 21 (1992).
68. U.S. Pat. 4,976,096 (1990) (to U.S.A.).
69. P. Ehrburger and J.-B. Donnet, in Ref. 52, p. 169.
70. U.S. Pat. 4,837,076 (1989) (to Dow).
71. F. P. McCullough and B. C. Goswami, Novel fibers and their ignition behavior in *Hi-Tech Conference*, Clemson University, S.C., July 21, 1993.
72. U.S. Pats. 4,879,168; 4,943,478; 4,950,533; 4,950,540; 4,980,233; 4,997,716; 4,999,236; 5,024,877 (to Dow).
73. B. Vigolo, A. Penicaud, C. Coulon, C. Sauder, R. Pailler, C. Journet, P. Bernier, and P. Poulin, *Science* **290**, 1331 (2000).
74. A. B. Dalton, S. Collins, E. Munoz, J. M. Razal, V. H. Ebron, J. P. Ferraris, J. N. Ferraris, J. N. Coleman, B. G. Kim, and R. Baughman, *Nature* **423**, 703 (2003).
75. W. Eastes, ed., *Man-Made Vitreous Fibers*, TIMA Inc., Mar. 1993.
76. K. Matsumoto, *Jpn. Textile News* **456**, 59 (Nov., 1992).
77. Ref. 3, Chapt. 2.
78. M. Takahashi, in L. Rebenfeld, ed., *Science and Technology of Fibers and Related Materials*, Wiley-Interscience, New York, 1991, p. 38.
79. H. Fong and D. H. Reneker, in D. R. Salem, ed., *Structure Formation in Polymeric Fibers*, Hanser, Munich, 2000, Chapt. 6.
80. P. S. Tung and S. Jayaraman, in T. L. Vigo and A. F. Turbak, eds., *High-Tech Fibrous Materials*, American Chemical Society, Washington, D.C., 1991, Chapt. 4.
81. T. L. Vigo and J. S. Bruno, *Proc. NASA Tech. Conf. 2002* **2**, 307 (1993).
82. K. Kajiwara and S. B. Ross-Murphy, *Nature* **355**, 208 (Jan. 16, 1992).
83. *Chem. / Textil-Industrie* **39**(5), T146/E68 (May, 1989).
84. *High Performance Textiles* 12 (Jan., 1991).

85. E. L. Barish and B. Tariyal, in M. Lewin and J. Preston, eds., *High Technology Fibers, Part C*, Marcel Dekker, Inc., New York, 1993, Chapt. 1.
86. A. K. Dinghra and H. G. Lauterbach, in J. Kroschwitz, ed., *Encyclopedia of Polymer Science and Engineering*, Vol. **6**, John Wiley & Sons, Inc., New York, 1986, p. 756.
87. Ref. 3, Chapt. 6.
88. C. J. Sprague and G. W. Davis, in Ref. 80, Chapt. 20.
89. *Jpn. Textile News* **391**, 48 (June, 1987).
90. M. Issi, *Jpn. Textile News* **456**, 63 (Nov., 1992).
91. N. Fahl and M. Faile, in Ref. 80, Chapt. 14.
92. T. L. Vigo, in M. Raheel, ed., *Protective Clothing*, Marcel Dekker, Inc., New York, 1996, Chapt. 9.
93. Ref. 3, Chapt. 3.
94. D. Lyman, in Ref. 80, Chapt. 8.
95. Y. Ikada, in Ref. 42, Part B, Chapt. 8.
96. P. H. Corkhill, C. J. Hamilton, and B. J. Tighe, *Biomaterials* **10**(1), 3 (1989).
97. Ref. 3, Chapt. 4.
98. J. D. Hodge and E. A. Dodgson, in Ref. 83, Chapt. 17.
99. S. D. Menhoff, J. W. Stenborg, and M. J. Rodgers, in Ref. 83, Chapt. 23.

GENERAL REFERENCES

References 80 and 91.
M. Lewin and J. Preston, eds., *High Technology Fibers, Part A*, Marcel Dekker, Inc., New York, 1985, p. 397.
M. Lewin and J. Preston, eds., *High Technology Fibers, Part B*, Marcel Dekker, Inc., New York, 1989, p. 332.
M. Lewin and J. Preston, eds., *High Technology Fibers, Part C*, Marcel Dekker, Inc., New York, 1993, p. 376.
T. L. Vigo and B. J. Kinzig, eds., *Composite Applications: The Role of Matrix, Fiber, and Interface*, VCH Publishers, New York, 1992, p. 407.
T. L. Vigo and A. F. Turbak, eds., *High-Tech Fibrous Materials: Composites, Biomedical Materials, Protective Clothing, and Geotextiles*, American Chemical Society, Washington, D.C., 1991, p. 398.

MALCOLM POLK
Georgia Institute of Technology
TYRONE L. VIGO (DECEASED)
U.S. Department of Agriculture
ALBIN F. TURBAK
Falcon Consultants, Inc.,
University of Georgia

HYDROGELS. See Volume 2.

β-HYDROXYALKANOATES. See POLY3-(HYDROXYALKANOATES).

HYPERBRANCHED POLYMERS. See Volume 2.

INTELLIGENT POLYMER SYSTEMS

Introduction

Intelligent polymer systems possess the ability to sense, process information, and actuate responses. Energy is usually required to implement these functions and so energy conversion/storage capabilities are desirable if the system is to be truly autonomous. Ideally, these functions would be integrated at the molecular level.

It has been clearly demonstrated over the past 20 years that inherently conducting polymers (ICPs) are capable of providing all of the above functions and as such they have a critical role to play in the development of intelligent polymer systems (see ELECTRICALLY ACTIVE POLYMERS).

This article briefly reviews the properties of ICPs and their ability to function as sensors, processors, actuators, and energy conversion/storage systems.

To illustrate the ability of ICPs to provide the range of functions required for intelligent polymer systems, we will draw on examples that utilize polypyrroles (**1**) or polythiophenes (**2**).

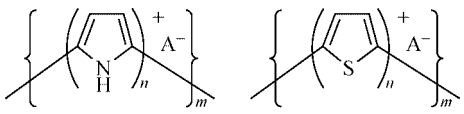

1 **2**

Encyclopedia of Polymer Science and Technology. Copyright John Wiley & Sons, Inc. All rights reserved.

For polypyrroles and polythiophenes, n is usually ~3–4 for optimal conductivity; ie, there is a positive charge on every third or fourth pyrrole or thiophene along the polymer chain, near which the dopant anion A^- is electrostatically attached.

Polyanilines are also of interest but they are less amenable to use in a wide range of environments because of the need to retain protonation to ensure conductivity. Consequently, most of the examples here will focus on polypyrrole and polythiophene.

Each of these materials may be produced via either chemical or electrochemical oxidation of the appropriate monomer (1). For polypyrrole the electrodeposition process is described simplistically in equation 1.

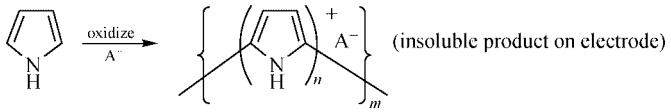

(1)

A dopant counterion (A^-) is incorporated during electrosynthesis to balance the charge on the polymer backbone. A wide range of dopants can be incorporated using this approach. Common chemical oxidants such as $FeCl_3$ and $(NH_4)_2S_2O_8$ may also be used and these provide the anion from the oxidant, as the dopant anion A^-. In general, chemical oxidation provides ICPs as powders, while electrochemical synthesis leads to films.

An important feature of ICPs is that they are amenable to oxidation/reduction processes that can be initiated at moderate potentials. For polypyrroles and polythiophenes, two oxidation states can be reversibly switched, as shown in equation 2 (Z = NH or S). The oxidized forms exhibit good electrical conductivity (σ = 1–100 $S \cdot cm^{-1}$), while the reduced forms have very low conductivity ($\sigma \sim 10^{-8}$ $S \cdot cm^{-1}$).

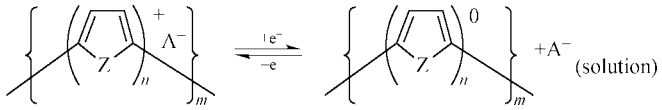

(2)

If the dopant anion A^- is small and mobile (eg, Cl^-) and the polymer has a high surface-area-to-volume ratio, then upon reduction the anion will be efficiently ejected from the polymer. However, if the dopant is large and immobile (eg, if A^- is a polyelectrolyte such as polystyrene sulfonate) then an electrically induced cation-exchange process occurs, according to equation 3:

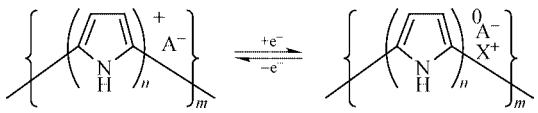

(3)

where the cation (X^+) is incorporated from the supporting electrolyte solution (2). The exact nature of the reduction process has a dramatic effect on the physical and

chemical properties of the polymer. These changes are important in determining the sensing, information processing, and actuation capabilities of the systems as discussed below.

Sensing

Nature has developed recognition systems that are able to discriminate on the basis of highly specific molecule–molecule interactions generating a unique signal. Alternatively, nature utilizes arrays of less specific sensors to collect information that is deciphered using pattern recognition processes carried out in the brain. Both approaches have also been pursued using ICPs in the development of synthetic sensors, as both chemical and physical sensors.

As chemical sensors, specificity can be induced by using molecular recognition components from nature. For example, the ICP may be used as an immobilization platform for enzymes (3–5), antibodies (6–10), oligonucelotides (11–13), or even whole living cells (14,15). The bioactive component may be incorporated during the polymerization process and the ICP provides signal transduction and transmission capabilities (Figure 1**a**). The majority of enzyme-containing ICP sensors generate a signal because of the enzymatic generation of an electroactive product (eg, H_2O_2) or the consumption of an electroactive product (eg, O_2). Alternatively, the bioevent may trigger a change in pH of the analyte solution that alters the resistance of the polymer (16). The mechanism of signal generation with antibody-containing conducting polymer sensors appears to be associated

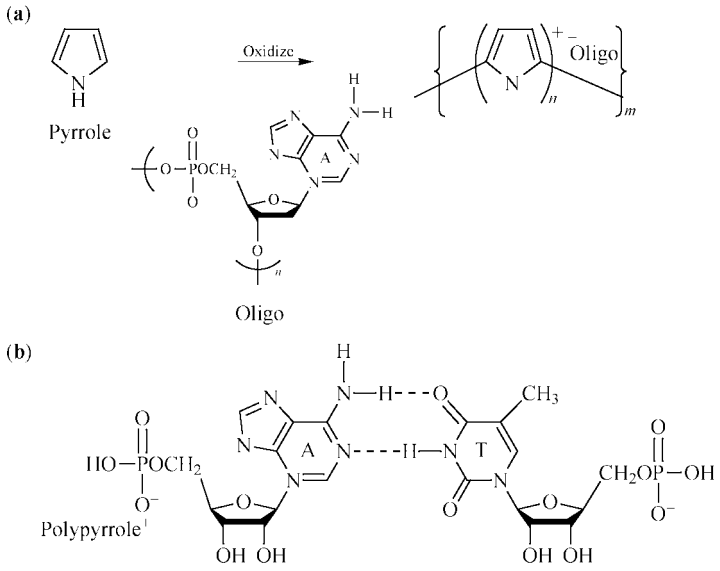

Fig. 1. (**a**) Polymeriztaion of polypyrrole onto an electrode using an oligonucleotide (A) as the dopant. The oligonucleotide is physically entrapped within the polymer during synthesis. (**b**) As a target oligonucleotide (T) passes across the surface of the oligonucleotide (A) doped polypyrrole electrode, a hybridization reaction occurs (indicated by the dashed lines). This results in a change in the current/potential response observed at the electrode.

with the modification of cation movement into and out of the polymer upon oxidation/reduction in the presence of the antigen (17,18). In the case of complementary oligonucleotide binding, only limited examples use direct electrochemical signal transduction (19,20), and here the mechanism of signal generation is not clear (Figure 1**b**).

The selective detection of metal ions has also been achieved by the covalent attachment of molecular recognition moieties to the ICP backbone. The usual approach has been to synthesize a monomer or dimer containing the appropriate recognition group and this is subsequently polymerized (21). Swager (22) have prepared polythiophenes containing crown ethers and calixarenes covalently bound to the bithiophene repeat units, which exhibit controllable selectivity toward Li^+, Na^+, and K^+ ions.

An alternative route to appropriately functionalized ICPs is the use of sulfonated species containing the desired molecular recognition/receptor site as the dopant anion for the conducting polymer chains. For example, calixarene-containing polypyrroles (23) and polyanilines (24) have recently been prepared via the use of sulfonated calixarenes as dopant anions. Similarly, the incorporation of metal complexing agents such as sulfonated 8-hydroxyquinoline as dopants in polypyrroles provides a simple route to metal ion-selective ICPs (25).

ICPs have also been assembled as microsensing arrays with a view to collecting less specific data subsequently deciphered using pattern recognition software. The so-called electronic noses are based on this principle (26–30). A range of conducting polymers with differing molecular selectivity respond (by changes in electronic resistance of the polymer) to a complex mixture to produce a unique pattern of responses. This approach has been used to differentiate beers (26), to detect microorganisms (28,29), for wastewater management (31,32), and for wine characterization (33). Stuetz and co-workers (31) demonstrated the ability of a nonspecific sensor array (consisting of 12 conducting polymers) to detect changes in the organic content of a wastewater sample. These researchers were able to draw a comparison between the odor profiles of sewage liquids and corresponding BOD, GOD, and TOC measurements using this sensor array. Using a nonspecific conducting polymer sensor array, Bourgeois and co-workers (32) developed an on-line continuous measurement system that monitored changes in water and wastewater quality. By analyzing the headspace gas from sparged samples, which flowed over the sensor array, they were able to successfully monitor samples both in a laboratory and in field setting. Guadarrama and co-workers (33) used the response of a conducting polymer sensor array to characterize varieties of Spanish wine. Using static and dynamic headspace sampling combined with statistical analysis utilizing pattern recognition techniques, they were able to characterize these wines by considering the sensitivity of the polymer films to moisture and ethanol content.

The array approach has also been developed for amperometric sensing when used in solution. Change in amperometric responses in the presence of different ions is used as the signal transduction method. This has been used by us to discriminate between simple ions (34,35) and even proteins (36). The approach used is similar to the “electronic nose” in that none of the sensing elements is specific; however, each polymer has a different selectivity series, giving rise to a unique pattern of responses for any given protein.

Actuating

ICPs are capable of undergoing transformations at the molecular level through to the macro-molecular level. The former can be used to build responsive molecule release systems, while the latter forms the basis of artificial muscles. A change in oxidation state of the polymer (see equations 2 and 3) is accompanied by dramatic changes in chemical and physical properties. Chemical changes have been studied at the molecular level using a technique known as *inverse chromatography* both in solution (37,38) and in gas phase (39,40). These studies revealed that, at least when the dopant A^- is small and mobile, reduction decreases the anion-exchange capacity of the polymer and increases the hydrophobicity of the polymer backbone. The dopants can be chosen so that the release process has the desired effect on the chemical composition of the immediate environment. For example, Miller described the triggered release of glutamate (41) and salicylate (42) among other compounds.

The movement of ions has also been tracked using electrochemical quartz crystal microbalance techniques (43–45). As ions move in and out of the polymer matrix, upon oxidation and reduction, a resonant frequency shift is observed for the polymer coated quartz crystal. The magnitude of the frequency shift is indicative of the amount of ions moving either in or out of the polymer. The direction of ion flow has been shown to be dependent upon the nature of the dopant bound within the polymer. Small spherical-like anions are known to move easily in and out of the polymer matrix. When the polymer is oxidized the backbone becomes cationic (p-type) and anions move into the polymer, effectively doping the polymer. Upon reduction of the polymer backbone, the cationic characteristics of the polymer are lost and the anions are expelled under the negative electric field of the reduction potential. Ion flux can be reversed by the incorporation of large anion species into the polymer during the growth phase, such as dodecylbenzene sulfonate (46,47) or polyelectrolytes such as polystyrene sulfonate (48). Upon reduction of the polymer the bulky anion cannot be expelled while the polymer backbone looses its net cationic charge, resulting in the bulk material having an anionic character. The result of this process is that cation species are incorporated into the polymer to achieve electrostatic balance.

The incorporation of either anions or cations during redox cycling results in polymer swelling. This principle has been exploited in applications such as polymer actuators. These incorporation/exclusion events at the molecular level also result in changes in the overall volume (dimensions) of the polymer (49). It was these volume changes that led Baughman and colleagues to the concept of electromechanical actuators (artificial muscles) based on conducting polymers.

Massoumi and Entezami (50,51) utilized conducting polymer bilayers to demonstrate that active cations and electrolyte cations (ie, sulfosalicylic acid and 2-ethylhexyl phosphate) can be transported in to and out (controlled release) of the bilayer outer film.

Pyo and Reynolds (52,53) reported the selective releasing of ions, such as adenosine 5′-triphosphate and heparin respectively, from conducting polymer bilayer structures. Piro and co-workers (54) successfully incorporated oligonucleotides into conducting polymer films using a two-step polymerization process. The release of these trapped oligonucleotides was also investigated, where the

release exhibited a three-step profile: a "burst" period during the first 5 min, followed by an intermediate and a very slow release stage lasting up to several days. The uptake and release of dopamine were investigated with a quinone-containing conducting polymer film (55). This study found that dopamine, once incorporated into the polymer, could be released by applying an oxidative potential. Pernaut and Reynolds (56) studied the controlled release of a polypyyrole membrane "loaded" up with adenosine triphosphate (ATP). Electrochemical triggering allowed ATP to be delivered with a variety of release profiles and adjustable rates.

Controlled-release devices that utilize the unique properties of conducting polymer membranes can also be configured. It has been shown that the transport properties of ICPs are dependent on the oxidation state of the membrane. This has been demonstrated both in solution (57) and for transport of volatiles (58). Extraordinary selectivity factors have been reported for the separation of some volatiles; for example, selectivity factors of 3590 for H_2/N_2, 30 for O_2/N_2, and 336 for CO_2/CH_4 were reported (59). With membranes operational in solution, the controlled transport of simple ions (60), metal ions (61,62), small organic molecules (63), and even proteins (64,65) has been demonstrated.

The transitions that occur within the conducting polymers also result in dramatic changes in physical properties. For example, upon reduction the materials become more transparent (66), making them useful in electrochromic devices (67,68).

By producing simple laminated membrane structures (Figure 2) containing the ICP, force generation occurs upon oxidation/reduction of the active polymers, and movement follows. A number of detailed studies on the effect of polymer composition, supporting electrolyte and rate of stimulation on the forces generated, have been carried out (69–72).

In recent studies it has been shown that the electrolyte used for ICP-based devices including artificial muscles is critical (73). Subsequent to this, it was discovered that a new class of electrolytes, ionic liquids, have characteristics that are particularly useful for ICPs (74,75).

Ionic liquids (ILs) have received a great deal of attention in recent years (see Ionic Liquids, Polymerization in). ILs have unique solvent properties and low volatility that provide advantages over conventional electrolyte systems with a wide range of application in green chemistry. Attention has been mainly directed toward modifying ILs to manipulate the solvent and electrical properties. Properties that are unique to ionic liquids include tunable hydrophobicity (76) and

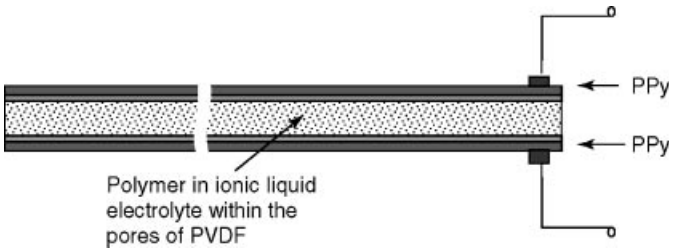

Fig. 2. Cross section of a polypyrrole double-sided PVDF [poly(vinylidene fluoride)] electromechanical actuator, with the pores of PVDF filled with electrolyte.

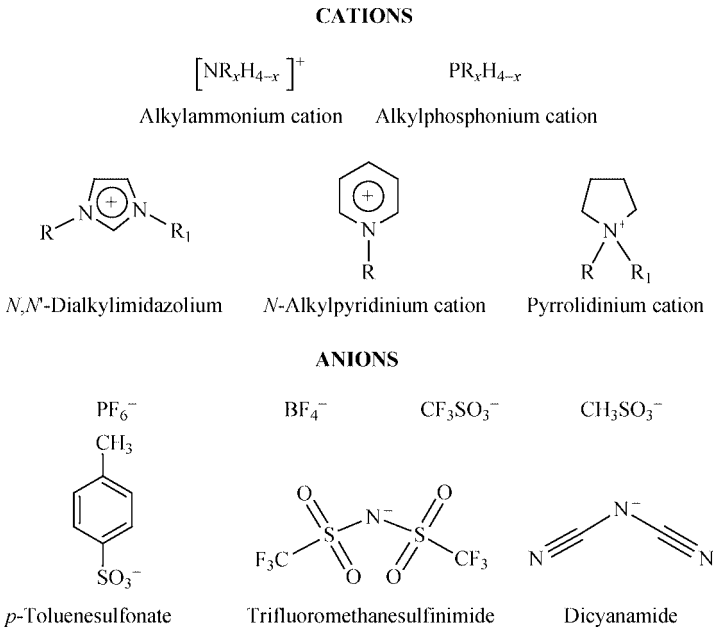

Fig. 3. Typical ionic liquid ions.

choice of anion (77). ILs generally have excellent thermal stability (78) and low volatility (79) and, in some instances, offer unique solubility properties as a result of following different dissolution rules with respect to common organic solvents (80). The minimal vapor pressure they exhibit also leads to good environmentally stability. ILs also offer wide electrochemical potential windows, which can be manipulated by choice of the anion and cation system (81,82). There are potentially thousands of IL systems yet to be discovered based on the combination of organic cation structures with the myriad of anions that are potentially available. Figure 3 shows a number of cation systems that have been reported with anions such as PF_6^-, BF_4^-, NO_3^-, Cl^-, $CF_3SO_3^-$, and trifluoromethanesulfonimide, to list but a few.

Given the intimate interaction of ICPs with the electrolyte, especially during oxidation/reduction of the polymer the chemical nature of the ionic liquid is also important. The versatility of ionic liquids in this regard has proven extremely useful. For example, the use of imidazolium cations during oxidation/reduction of PPy PF_6 used as electromechanical actuators has been shown to not only give markedly improved stability (increasing cycles length from hundreds to hundreds of thousands of cycles) but also increased performance. The latter feature arises from the inclusion of the imidazolium cation during reduction, a process that apparently preserves the inherent modulus of the materials (83).

Another interesting form of these electrolytes involves their use as solid electrolytes. By performing polymerization in the ionic liquid a solid can be produced (84). A highly stable, easily handled actuator can be constructed using this electrolyte.

All of the above responses (actuators) are initiated by creating an appropriate electrical potential that causes the polymer to change form. This is usually achieved by imposition of a potential from an external source.

Electrochromic Devices

Electrochromic devices (ECDs) have been extensively researched as potential large area electrochromic windows. The technology is in direct competition with liquid crystal display devices. ECDs have a distinct advantage over the LCD in that the device color remains even after the driving potential has been removed (68) (see Electrochromic Polymers). The use of ICPs in electrochromic devices has been discussed and reviewed in a number of recent articles (85–88). The observed color changes of these devices are ideally reversible and can undergo thousands of cycles without degradation. Device scale-up is strongly dependent upon the electrochemical behavior of the polymer in the electrolyte, which has a strong influence upon the redox reversibility of the polymer. Solvent-based electrolytes, although shown to be effective in the laboratory, suffer from component evaporation, often leading to device failure. Sealing the unit to prevent solvent leakage has also proven to be a challenge. This issue has been addressed by the adoption of solid polymer electrolyte systems. More recently, the application of nonvolatile ionic liquids (74–91) to electrochromic devices has produced devices capable of millions of cycles, with little loss of performance over the device lifetime (92).

Electrochromic effects in conducting polymers are achieved by varying the band gap (HOMO − LUMO) of the π–π^* transition and is associated with π-bond conjugation. Band gap, and therefore color, is influenced by the type of monomer repeat unit, the polymer conjugation length, and, ultimately, the level of polymer oxidation. Copolymerization of different monomers has also been used as a method of modifying these band gaps. Polypyrroles have a color shift from blue-violet (670 nm) to yellow-green (420 nm) when oxidized and reduced respectively. Polyanilines have three redox states that are yellow when fully reduced to the leucoemeraldine state (300–400 nm), green in the mid-oxidation emeraldine salt state (400 and $>$750 nm), and blue when fully oxidized as the pernigraniline salt (600 nm). Polythiophene is blue when oxidized (730 nm) and red when reduced (470 nm) (93).

The challenge that remains for conducting polymer electrochromic applications is clearly in the domain of device scale-up. The application of these materials to large area devices, such as windows, requires uniform real-time switching of the polymer oxidation state to access different color regions. Although this has been demonstrated for small-scale devices, it is difficult at larger scales.

Information Processing

The use of inorganic, silicon-based materials in the development of complex circuitry that is capable of processing vast amounts of information is a well-developed

industrial technology. The concept of plastic electronics has only attracted considerable interest in recent years.

Polymers are increasingly being utilized as new materials for electronics and optics. Necessary elements for this imperative are of course the functional properties but with the added advantage of polymer processability and flexibility in structural design (94). In fact, replacement of traditional inorganic semiconductors by organic molecules, polymeric or even biological materials have recently been termed as *molecular electronics* (ME) (95). Rambidi (96) identified one of the main directions in the development of devices for molecular information processing to be based on the concept of distributed molecular (chemical) information processing media. It has been proposed that the electrical conduction in ICPs occurs via nonlinear (or topographic) defects (solitons/polarons) generated either during synthesis or as a result of doping. Solitons and polarons have recently been shown to have implications in the technical development of molecular electronic devices (97).

To realize molecular electronics, one of the key issues is how to fabricate the ordered structures in a planned manner since various properties of organic molecules are of anisotropic nature, and consequently the functions of molecular assemblies depend strongly on the way molecules are arranged in them (97). Much research has been done on the molecular engineering of these assembly processes, namely Langmuir–Blodgett film (98,99) and self-assembly techniques (100,101). Pal and co-workers (102) used the Langmuir–Blodgett technique to develop polymeric light-emitting diodes (LEDs) (see LANGMUIR-BLODGETT FILMS). Both dc and ac LEDs were fabricated with a precise thickness ranging from a few molecular layers to tens of layers. In dc LEDs, they showed that as few as three layers of active polymer can yield the same luminance as the thicker ones. Zhang and co-workers (103) fabricated binary DNA/surfactant-modified arrays on a heterogeneous patterned surface through a controlled condensation and dewetting process using the SAM (self-assembled monolayers) technique. Studies on the formation of DNA SAMs at surfaces were driven by an inherent interest in understanding different aspects of this molecule and its importance in biomimetic materials science and molecular electronics.

ICPs have been studied for their application to such molecular electronic devices as diodes (104,105), field effect transistors (FETs) (106,107), and light emitting diodes (LEDs) (108,109) (Figure 4). Rectifying junctions are the basic element of many electronic components. Since their discovery, ICP rectifying junctions such as p–n junction and Schottky junction have been studied (97). Chen and Fang (111) found that the acid doping of free-standing polyaniline film can cause a higher rectifying behavior and photovoltaic conversion. It has been shown that increased diode performance is observed when the device is fabricated from regioregular polymers having a short alkyl substituent and/or by the presence of electron-withdrawing groups (97).

The performance of ICP-based FETs are quite encouraging and recent use of these devices in logic circuits or active matrix emissive displays has geared up the research in this direction immensely (112,113). In conventional semiconductor devices, "field effect" has been used to improve performance (114). Control of current passing through a "gate electrode" using the field-effect phenomenon opens the possibility of a transistor action without requiring the existence of p–n junctions,

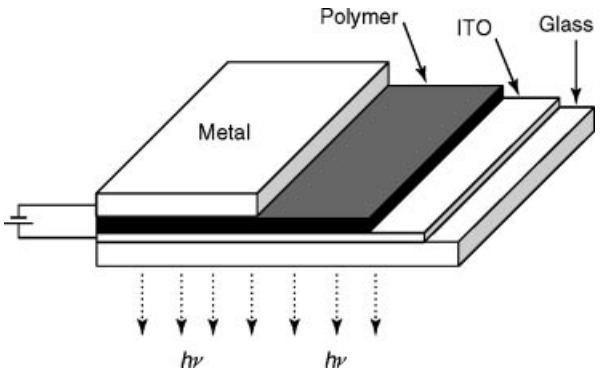

Fig. 4. Schematic of a polymer LED device configuration (110).

which in turn improves the device characteristics (97). Koezuka and co-workers (106) were the first to use this phenomenon to fabricate ICP-based FETs.

ICPs have been demonstrated to exhibit light emission in the entire visible spectrum, quantum efficiency over 4%, fast response time, brightness of 10^6 cd $\cdot$ m^{-2}, and device lifetime more than 2 months (97). Heeger (115) reported that the operating life of polymer LEDs, with an initial brightness of 400–500 cd $\cdot$ m^{-2} at room temperature, approached several thousand hours. This equates to operating lifetimes in excess of 10^4 h at display brightness. The current interest in exploring the luminescent properties of ICPs is for flat-panel displays used in information processing devices, such as laptop computers, cellular telephones, small handheld devices, large panel displays, and notebook computers (97). The main advantages of these ICP materials over conventional luminescent materials are the tuning of wavelength emitted by chemical modification, low operating voltages, flexibility, easy processing, low cost, possibility of making large area device, and output color in whole visible spectrum (97).

Energy Conversion/Storage

The intelligent polymer system must also be capable of converting energy from a natural source, such as sunlight, and storing it until required. ICPs that are capable of carrying out these functions have potential as a replacement for Si photovoltaic cell technology as well as energy storage in rechargeable battery systems.

Polymer Photovoltaics. The potential of making lightweight, low cost, and flexible solar cells has driven growing interest in device development. It has been demonstrated that ICPs are capable of functioning as the active layer in photovoltaic devices (116–120). Upon irradiation of the ICP electron–hole pairs (excitons) are generated. If these excitons are transported to an interface where they can be split before recombination occurs, then electrical energy is generated. Both Schottky devices (121) and photoelectrochemical cell (122–124) configurations have been used. Photovoltaic responses were obtained early on from a variety of ICPs in single-polymer Schottky devices with quantum efficiencies up to

Table 1. Summary of Photovoltaic Performance of Some Conducting Polymers

Polymer system	Device	Voc,[a] V	Isc,[b] mA/cm^2	FF,[c]	Y,[d] %
Polyacetylene (PA)	n-Si/p-PA	0.53	18.18	0.32	4.3
Polymethylthiophene	Al/PMT/Au	0.23	0.16 (x10^{-3})	0.30	—
Polypyrrole (PP)	PP/n-Si	0.29	9.0	0.46	1.2
Polyaniline (PAn)	Al/PAn/ITO	0.43	—	0.70	0.8[e]
Polythiophene	Photoelectrochemical cell	0.41	0.35 ($\times 10^{-3}$)	—	0.6[f]

[a]Voc: open circuit voltage.
[b]Isc: short circuit current.
[c]FF: fill factor.
[d]Y: engineering conversion efficiency.
[e]Power conversion efficiency.
[f]Monochromatic photon to current efficiency.

1% (125–127); the best results have been obtained using interpenetrating blends of functionalized polyphenylenevinylenes (128,129) and/or polythiophenes (130) with quantum efficiencies up to 29% and energy conversion efficiencies up to 2%. The addition of dyes (131–133) and electron acceptors (134–136) to such devices has also increased the overall power conversion efficiency to around 3%. Performance parameters for some typical conducting polymers are listed in Table 1. Although the performance of these materials is significantly low than what has been achieved for traditional silicon-based technologies, the production of these devices are still highly attractive as device manufacture can be undertaken without the need for a clean room, the relatively low cost with respect to silicon, technology, and the potential for large-scale flexible cells.

Energy Storage. A number of strategies have been adopted for the utilization of conducting polymers as rechargeable battery devices. Many studies have looked at the potential of replacing either the anode or cathode electrode with a conducting polymer, more typically the cathode, as tradition metal anodes have significantly higher energy densities, gravimetrically, than do polymers (137). A more interesting possibility is the development of all polymer batteries where an electroactive polymer comprises both the ahde and cathode supported on inert conducting supports such as graphite and platinum. Killian and co-workers were the first group to report the assembly of an all-polymer battery structure (138) utilizing both p- and n-dopable polypyrrole with a specific charge capacity of 22 mAh $\cdot$ g^{-1} at a cell potential of 0.4 V. The cells showed no loss in capacity when cycled 100 times. The observed cell potential was clearly limited by the n-doping ability of the cathode.

More recently, an all-polymer battery based on derivatized polythiophenes supported on graphite-coated supports was described (139). In this instance, polythiophene functioned more effectively in the n-doping region and provided an improved cell discharge voltage of 2.4 V and capacities of 9.5–1.5 mAh $\cdot$ g^{-1}. A recent approach is the development of a polymer/polymer battery based on polyaniline anode and poly-1-naphthol cathode (140). This device has been reported with an impressive cell voltage of 1.4 V, a specific capacity of 150 Ah g^{-1}, and a loss of 15% of cell capacity after 100 cycles. Other attempts at fabricating battery systems have been made (141) with polyacetylene, polypyrrole, and polyaniline (142),

where the batteries were shown to compare favorably on a gravimetric basis. On a volumetric basis, more traditional inorganic insertion compound electrodes were found to outperform these systems. The application of conducting polymers as either a cathode or anode combined with more traditional inorganic or metallic electrodes has been extensively reviewed by others (137,139).

Polymer Processing

All of the foregoing applications of ICPs have significant commercial potential. However, in most cases, exploitation has been limited because of the lack of convenient polymer processing and device fabrication protocols. For example, polypyrroles exhibit the desirable properties mentioned above; however, polymerization usually results in the formation of an insoluble, infusible material not amenable to subsequent fabrication. Conducting polythiophene salts are similarly intractable. Several approaches have recently been employed to overcome this problem of intractability.

Solubility has been induced for polypyrroles by attaching alkyl (143,144) or alkyl sulfonate (145,146) groups to produce 3-substituted pyrrole monomer prior to polymerization. This results in markedly enhanced solubility in organic or aqueous medias respectively. Polythiophenes can also be rendered either organic-solvent-soluble (147) or water-soluble (148) using these derivitization approaches. These improvements in solubility achieved above via ring substitution generally result in significant loss in electrical conductivity of the final polymer. Consequently, formation of colloidal dispersions is an attractive alternative route to solution processing in water, as this allows for post-synthesis handling while retaining reasonable conductivity.

Conducting polymer colloids can be produced by chemical (149) or electrochemical (150,151) oxidation of monomer in the presence of a steric stabilizer. Colloids produced electrochemically are formed by intercepting the polymer deposition on the electrode surface utilizing hydrodynamic control. This is facilitated by the presence of a steric stabilizer in solution. The electrochemical approach is advantageous in that the polymer properties can be altered by accurate control of the oxidation potential during polymerization. This technique also allows a wide range of dopants to be incorporated into the polymer to give different properties. For example, proteins can be incorporated into conducting polymers while retaining their biological integrity (151).

Emulsion polymerization is the most appropriate method for producing submicrometer (nano) particles owing to its versatility and relative simplicity. Formation of ICP nanodispersions consisting of highly conducting nanoparticles dispersed in either organic or aqueous solution has been achieved using polyaniline (152), polypyrrole (153), and regioregular polythiophene (154). Jang and Oh (155) used thermodynamically stable microemulsion micelles as nanoreactors to synthesize, at low temperatures, polypyrrole nanoparticles with dimensions of several nanometers. Deng and co-workers (156), using a core–shell approach, synthesized magnetic and conducting Fe_3O_4–polypyrrole nanoparticles (30–40 nm in diameter) in the presence of Fe_3O_4 magnetic fluid (core material) in aqueous solution containing sodium dodecylbenzenesulfonate as a surfactant and dopant.

The successful polymerization of polythiophene nanoparticles has been plagued by the insolubility of most thiophene monomers, and their subsequent polymer. Although advances have been made in solubilizing the monomer, in particular the utilization of surfactants, polymerization normally results in either precipitated powders or deposition of solid films. In recent times the substituted thiophene, poly(3,4-ethylenedioxythiophene) (PEDOT) has received much attention owing to its excellent environment stability. Baytron (PEDOT/PSS), a polythiophene dispersion commercially available from Bayer Corp., is widely used in electrochromic and antistatic device fabrication (157). Advances in substituted thiophene monomer synthesis are now providing a means of polymerizing polythiophenes that are stable as nanoparticle solutions. Edder and Frechet (158) recently synthesized a series of bridged oligothiophenes where their novel molecular architecture is expected to improve their utility as electroactive surfactants for semiconducting nanoparticles or organic electronics.

Device Fabrication

For the final device, the functional properties of ICPs must be integrated within a host structure that provides the mechanical/physical properties required.

ICPs have been assembled inside a number of host polymers including polyacrylonitrile, polyvinyl alcohol, and others (159). A number of attempts have been made to form composites with improved processability and mechanical properties while maintaining the inherent properties of the conducting polymer (160). Conducting polyaniline blends and composites are prepared mostly via the chemical oxidation route, although electrochemical synthesis is also employed in some cases (161,162). Using the chemical approach *in situ* polymerization of monomer in the presence of a host polymeric matrix has been reported (163–165). Polyaniline–poly(ethylene terephthalate) (163) and polyaniline–polystyrene (164) composites have been prepared using this approach.

Emulsion polymerization in heterogeneous systems (166) has been used to prepare processable conductive composites of polyaniline–poly(alkyl methacrylate). Polyaniline composites have also been prepared via dispersion polymerization (167–169). In such studies colloidal dispersions of electrically conductive polyaniline particles have been prepared using vinyl methyl ether (168) or methyl cellulose (170) stabilizers.

ICPs have also been assembled inside hydrogels, retaining both the electronic properties of ICPs and the water adsorption properties of gels (171,172).

Conducting polymers have also been prepared as coatings on both natural and synthetic fibers and fabrics. For example, silk and wool (173,174) or nylon (175) have been coated. Electrospinning (176,177) is another method for the production of ICP composite fibers and nanofibers. This simple approach is based on the electrostatic fiber spinning of composite fibers of polyaniline with polyethylene oxide, polystyrene, and polyacrylonitrile. These fibers are formed when a high electric field (5–14 kV) is placed between the tip of a metallic anodic spinning needle loaded with the dissolved polymer solution (0.5–4 wt% PAn and 2–4 wt% host polymer) and an opposing cathode plate separated by 20 cm. The presence of the high electric field results in the surface tension of the polymer-loaded solution

at the needle tip to be exceeded, expelling a polymer fiber from the surface toward the opposing cathodic plate. The transit time from anode tip to the cathode plate is accompanied by a desolvation and drying process in part assisted by the electrostatic charges placed upon the solvent molecules which undergo electrostatic repulsion processes. The resulting nanofiber composite is reported to have lengths in the meter range collected as an interwoven mesh with large surface to volume ratios ($\sim 10^3$ $m^2 \cdot g^{-1}$). Fiber dimensions of less than 100 nm have been routinely produced by this technique. More recently (176) fibers of PAn have been directly spun from a 20 wt% solution of polyaniline (Versicon, JGB Enterprises, Inc., Liverpool, NY) in 98% sulfuric acid at 5 kV.

The ability to provide more processable ICPs, as described above, enables new approaches to device fabrication, including ink-jet printing (178) and screen printing (179). Photolithography has also been used to produce ICP patterns (180–182), while spin coating has been used to produce thin, even films (183).

Screen printing is a simple and environmentally friendly way to produce electronic circuitry and make interconnections (184). Bao and Lovinger (185) used screen printing to develop organic transistors with high field-effect mobilities (approx 0.015–0.045 $cm^2 \cdot V^{-1} \cdot s^{-1}$) using regioregular poly(3-hexylthiophene). Garnier and co-workers (186) have demonstrated the usefulness of printing in organic FET fabrication, while Gustafsson (187) showed it was possible to print polyaniline to form the gate electrode. While screen printing is a highly efficient and relatively simple way to fabricate intricate electronics and circuits, this technique suffers from low resolution; in most instances, screen printing is used to pattern the parts of the circuits that do not demand high resolution (188).

Because of the ability to print, typically at higher resolution, ink-jet printing has emerged as an attractive patterning technique for conjugated polymers in areas such as LEDs (189). Patterning of organic molecules by ink-jet printing can be achieved either by printing a solution of the molecule (in organic solvent) or by printing dispersions of the molecule in water or organic solvents. Magdassi and Ben Moshe (190) have demonstrated the concept of direct patterning of water-insoluble organic molecules in the form of nanoparticles contained in a microemulsion droplet, which are converted into organic nanoparticles upon impact with the substrate surface due to evaporation of the volatile solvent. Rogers and co-workers used microcontact printing techniques to fabricate various electronic components, such as transistors (191) and logic gates (192) from conducting polymer dispersions and conducting polymer composites. While these printing techniques mentioned above offer higher resolution than conventional screen printing techniques, these still suffer from resolution limitations for some circuit designs. Sirringhaus and co-workers (193) developed a method to print high-resolution all-polymer transistor circuits utilizing hydrophobic surface patterning which confines the spreading of water-based conducting polymer ink droplets upon ink-jet printing.

BIBLIOGRAPHY

1. G. G. Wallace, G. M. Spinks, L. A. P. Kane-Maguire, and P. R. Teasdale, *Conductive Electroactive Polymers: Intelligent Material Systems*, 2nd ed., CRC Press, Boca Raton, Fla, 2003.

2. X. Ren and P. G. Pickup, *J. Phys. Chem.* **97**, 5356 (1993).
3. M. Umana and J. Waller, *Anal. Chem.* **58**, 2979 (1986).
4. N. C. Foulds and C. R. Lave, *Anal. Chem.* **60**, 2473 (1988).
5. S. B. Adeloju, J. N. Barisci, and G. G. Wallace, *Anal. Chim. Acta.* **332**, 145 (1996).
6. O. A. Sadik and G. G. Wallace, *Anal. Chim. Acta.* **279**, 200 (1993).
7. D. Barnett, O. A. Sadik, M. J. John, and G. G. Wallace, *Analyst* **119**, 1997 (1994).
8. S. Bender and O. A. Sadik, *Environ. Sci. Technol.* **32**, 788 (1998).
9. A. Sargent and O. A. Sadik, *Anal. Chim. Acta.* **376**, 125 (1998).
10. A. Sargent and O. A. Sadik, *Electrochim. Acta.* **44**, 4667 (1999).
11. G. Bidan, M. Billan, K. Galasso, T. Livache, G. Mathis, A. Reget, L. M. Torres-Rodriguez, and E. Vieil, *Appl. Biochem.*, in press.
12. F. Garnier, H. K. Karri-Youssoufi, P. Srivastava, B. Mandrand, and T. Delair, *Synth. Met.* **100**, 89 (1999).
13. J. Wang, M. Jiang, and A.-N. Kawde, *Electroanal.* **13**, 537 (2001).
14. T. E. Campbell, A. J. Hodgson, and G. G. Wallace, *Electroanalysis*, in press.
15. M. V. Deshpande and E. A. H. Hall, *Biosens. Bioelectron.* **5**, 431 (1990).
16. M. Nishizawa, T. Matsue, and J. Uchida, *Anal. Chem.* **64**, 2642 (1992).
17. J. N. Barisci, D. Hughes, A. I. Minett, and G. G. Wallace, *Anal. Chim. Acta.* **371**, 39 (1998).
18. J. J. Gooding, C. Wasiowych, D. Barnett, B. Hibbert, J. N. Barisci, and G. G. Wallace, *Biosens. Bioelectron*, in press.
19. J. Wang, M. Jiang, A. Fortes, and B. Mukherjee, *Anal. Chim. Acta* **402**, 7 (1999).
20. M. Jiang and J. Wang, *J. Electroanal. Chem.* **500**, 584 (2001).
21. S. Higgins, *J. Chem. Soc. Rev.* **26**, 247 (1997).
22. T. M. Swager, *Acc. Chem. Res.* **31**, 201 (1998). and references cited therein.
23. G. Bidan and M.-A. Niel, *Synth. Met.* **84**, 255 (1997).
24. M. Davey, S. Ralph and G. G. Wallace, *Unpublished results*.
25. V. Misoska, *Chemistry Honors Thesis*, University of Wollongong, 1998.
26. H. V. Shurmer, P. Corcoran, and J. W. Gardner, *Sens. Actuators, B* **4**, 29 (1991).
27. J. W. Gardner, T. C. Pearce, and S. Friel, *Sens. Actuators, B* **240**, 118–119 (1994).
28. T. D. Gibson, O. Prouser, J. N. Halbert, R. W. Marshall, P. Corcoran, P. Lowery, E. A. Ruck-kerene, and S. Heron, *Sens. Actuators, B* **44**, 413 (1997).
29. P. K. Namdev, Y. Alroy, and V. Singh, *Biotechnol. Prog.* **14**, 75 (1998).
30. M. C. Lonergan, E. J. Severin, B. J. Doleman, S. A. Beaber, R. H. Grubbs, and N. S. Lewis, *Chem. Mater.* **8**, 2298 (1996).
31. R. M. Stuetz, R. A. Fenner, S. T. Hall, I. Stratful, and D. Loke, *Water Sci. Technol.* **41**, 41–47 (2000).
32. W. Bourgeois, P. Hogben, A. Pike, and R. M. Stuetz, *Sens. Actuators, B* **88**, 312–319 (2003).
33. A. Guadarrama, J. A. Fernandez, M. Iniguez, J. Souto, and J. A. de Saja, *Anal. Chim. Acta* **411**, 193–200 (2000).
34. R. John, D. Ongarato, and G. G. Wallace, *Electroanalysis* **8**, 623 (1996).
35. T. A. Nguyen, J. N. Barisci, A. Partridge, and G. G. Wallace, *Synth. Met.* **137**, 1445–1446 (2003).
36. W. Lu, T. Nguyen, and G. G. Wallace, *Electroanalysis* **10**, 1101 (1998).
37. P. R. Teasdale and G. G. Wallace, *Polym. Int.* **35**, 197 (1994).
38. H. Chriswanto and G. G. Wallace, *Chromatographia* **42**, 191 (1996).
39. M. M. Chehimi in N. P. Cheremisinoff and P. N. Cheremisinoff, eds., *Handbook of Advanced Materials Testing*, Marcel Dekker, New York, 1995.
40. M. M. Chehimi, M. L. Abel, and Z. Sahraoui, *J. Adhesion. Sci. Technol.* **10**, 287 (1996).
41. B. Zinger and L. L. Miller, *J. Am. Chem. Soc.* **196**, 6861 (1987).
42. Q. X. Zhou, L. L. Miller, and J. R. Valentine, *J. Electroanal. Chem.* **261**, 147 (1989).

43. A. Khalkhali, W. E. Price, and G. G. Wallace, *React. Funct. Polym.* **56**, 141 (2003).
44. A. Mirmohseni, W. E. Price, and G. G. Wallace, *Synth. Met.* **84**, 823 (1997).
45. R. Bilger and J. Heinze, *Synth. Met.* **43**, 2893 (1991).
46. M-A. De Paoli, R. C. D. Peres, S. Panero, and B. Scrosati, *Electrochim. Acta* **37**, 1173 (1992).
47. R. C. D. Peres, M. A. De Paoli, and R. M. Torresi, *Synth. Met.* **48**, 259 (1992).
48. K. Naoi, M. Lien, and W. H. Smyrl, *J. Electrochem. Soc.* **138**, 440 (1991).
49. R. H. Baughman, L. W. Shacklette, R. L. Elsenbaumer, E. Plichta, and C. Becht, *Conjugated Polymeric Materials: Opportunities in Electronics, Optoelectronics and Molecular Electronics*, Kluwer Academic, the Netherlands, 1990, pp. 599–682.
50. B. Massoumi and A. Entezami, *Eur. Polym. J.* **37**, 1015–1020 (2001).
51. B. Massoumi and A. Entezami, *Polym. Int.* **51**, 55–560 (2000).
52. M. Pyo and J. R. Reynolds, *Synth. Met.* **71**, 2233 (1995).
53. M. Pyo and J. R. Reynolds, *Am. Chem. Soc. Polym. Mater. Sci. Eng. Proc.* **71**, 715 (1994).
54. B. Piro, M. C. Phma, and T. Ledoan, *J. Biomed. Mater. Res.* **46**, 566–572 (1999).
55. B. Piro, T. A. Nguyen, J. Tannguy, and M. C. Pham, *J. Electroanal. Chem.* **499**, 103–111 (2001).
56. J. M. Pernaut and J. R. Reynolds, *J. Phys. Chem. B.* **104**, 4080–4090 (2000).
57. H. Zhao, W. E. Price, C. O. Too, G. G. Wallace, and D. J. Zhou, *Memb. Sci.* **119**, 199–212 (1996), and references cited threin.
58. M. R. Anderson, B. R. Mattes, H. Reiss, and R. B. Kaner, *Science* **252**, 1412 (1991).
59. R. Parhasarathy, V. P. Menon, and C. R. Martin, *Chem. Mater.* **9**, 560 (1997).
60. W. E. Price, G. G. Wallace, and H. J. Zhao, *Electroanal. Chem.* **334**, 111 (1992).
61. M. J. Davey, S. F. Ralph, C. O. Too, A. C. Partridge, and G. G. Wallace, *React. Funct. Polym.* **49**, 87 (2001).
62. V. Misoska, J. Ding, J. M. Davey, W. E. Price, S. F. Ralph, and G. G. Wallace, *Polymer* **42**, 8571 (2001).
63. H. Zhao, W. E. Price, and G. G. Wallace, *J. Memb. Sci.* **100**, 239 (1995).
64. H. Zhao, C. O. Too, and G. G. Wallace, *J. Int. Mat. Syst. Struct.* **8**, 1052 (1997).
65. D. Zhou, C. O. Too, A. M. Hodges, A. W. H. Mau, and G. G. Wallace, *React. Funct. Polym.* **45**, 217 (2000).
66. K. Hyodo, *Electrochim. Acta* **39**, 265 (1994).
67. R. J. Mortimer, *Chem. Soc. Rev.* **26**, 147 (1997).
68. K. Gurunathan, A. V. Murugan, R. Marimuthu, U. P. Mulik, and D. P. Amalnerkar, *Mater. Chem. Phys.* **61**, 173 (1999).
69. M. Ghandi, P. Murray, G. M. Spinks, and G. G. Wallace, *Synth. Met.* **73**, 247 (1995).
70. T. W. Lewis, S. E. Moulton, G. M. Spinks, and G. G. Wallace, *Synth. Met.* **85**, 1419, (1997); T. W. Lewis, G. M. Spinks, G. G. Wallace, D. De Rossi, and M. Pachetti, *Polym. Prepr. (Am. Chem. Soc., Div. Polym. Chem.)* **38**, 520 (1997).
71. S. Shakuda, S. Morita, T. Kawai, and K. Yoshiro, *Jpn. J. Appl. Phys.* **32**, 5143 (1993).
72. T. F. Otero and J. M. Samsinena, *Bioelectrochem. Bioenerg.* **42**, 117 (1997).
73. J. Ding, L. Lu, G. M. Spinks, D. Zhou, S. Forsyth, M. Forsyth, D. MacFarlane, and G. G. Wallace, *Proc. SPIE Smart Struct. Mater.* **4695**, 8 (2002).
74. W. Lu, A. G. Fadeev, B. Qi, E. Smela, B. R. Mattes, J. Ding, G. M. Spinks, J. Mazurkiewicz, D. Zhou, D. R. MacFarlane, S. A. Forsyth, M. Forsyth, and G. G. Wallace, *Science* **297**, 983–987 (2002).
75. J. Ding, D. Zhou, G. Spinks, S. Forsyth, M. Forsyth, D. MacFarlane, and G. Wallace, *Chemi. Mater.* **15**, 2392–2398 (2003).
76. K. R. Seddon, A. Stark, and M. J. Torres, *Pure Appl. Chem.* **72**, 2275 (2000).
77. S. A. Forsyth, D. R. MacFarlane, R. J. Thomson, and M. von Itzstein, *Chem. Commun.* **7**, 714 (2002).

78. D. R. MacFarlane, J. Sun, J. Golding, P. Meakin, and M. Forsyth, *Electrochim. Acta* **45**, 1271 (2000).
79. J. Sun, M. Forsyth, and D. R. MacFarlane, *J. Phys. Chem. B.* **102**, 8858 (1998).
80. A. E. Visser, R. P. Swatloski, W. M. Reichert, R. Mayton, S. Sheff, A. Wierzbicki, J. H. Davis, and R. D. Rogers, *Chem. Commun.* **135**, (2001).
81. V. R. Koch, L. A. Dominey, C. Nanjundiah, and M. J. Ondrechen, *J. Electrochem. Soc.* **143**, 798 (1996).
82. J. Fuller, R. T. Carlin, and R. A. Osteryoung, *J. Electrochem. Soc.* **144**, 3881 (1997).
83. J. Ding, D. Zhou, G. Spinks, S. Forsyth, M. Forsyth, D. MacFarlane, and G. Wallace, *Chem. Mater.* **15**, 2392 (2003).
84. D. Zhou, G. M. Spinks, C. Tiyapiboonchaiya, D. R. MacFarlane, M. Forsyth, J. Sun, and G. G. Wallace, *Electrochim. Acta* **48**, 2355 (2003).
85. B. C. Thompson, P. Schottland, K. Zong, and J. R. Reynolds, *Chem. Mater.* **12**, 1563–1571 (2000).
86. D. R. Rosseinsky and R. Mortimer, *J. Adv. Mater.* **13**, 783–793 (2001).
87. P. R. Somani and S. Radhakrishnan, *Mater. Chem. Phys.* **77**, 117–133 (2002).
88. P. Chandrasekhar, B. J. Zay, G. C. Birur, S. Rawal, E. A. Pierson, L. Kauder, and T. Swanson, *Adv. Funct. Mater.* **12**, 95–103 (2002).
89. J. D. Holbrey and K. R. Seddon, *Clean Prod. Processes* **1**, 223 (1999).
90. M. J. Earle and K. R. Seddon, *Pure Appl. Chem.* **72**, 1391 (2000).
91. D. Fitzmaurice, *Phys World* **15**, 25, (2002).
92. PCT Int. Appl. Pat. WO 2002053808, W. Lu, B. R. Mattes, A. G. Fadeev, and B. Qi
93. P. R. Somani and S. Radhakrishnan, *Mater. Chem. Phys.* **77**, 117 (2002).
94. S. Tripathy, D. Y. Kim, L. Li, and J. Kumar, *Pure Appl. Chem.* **70**, 1267–1270 (1998).
95. K. Curunathan, A. Vadivel Murugan, R. Marimuthu, U. P. Mulik, and D. P. Amalnerkar, *Mater. Chem. Phys.* **61**, 173–191 (1999).
96. N. G. Rambidi, *Microelectron. Eng.* **69**, 485–500 (2003).
97. V. Saxena and B. D. Malhotra, *Curr. Appl. Phys.* **3**, 293–305 (2003).
98. M. K. Ram, E. Maccioni, and C. Nicolini, *Thin Solid Films* **303**, 27 (1997).
99. A. Marletta, D. Goncalves, O. N. Oliveira Jr, R. M. Faria, and F. E. G. Guimaraes, *Synth. Met.* **119**, 207 (2001).
100. J. J. Apperloo, P. R. L. Malenfant, J. M. J. Frechet, and R. A. J. Janssen, *Synth. Met.* **121**, 1259 (2001).
101. L. Peters, Sano, J. J. Morrison, N. Feeder, A. B. Holmes, and A. Kraft, *Synth. Met.* **119**, 175 (2001).
102. A. J. Pal, T. P. Ostergard, R. M. Osterbacka, J. Paloheimo, and H. Stubb, *IEEE J. Selected Top. Quantum Electron.* **4**(1), 137–143 (1998).
103. G. Zhang, X. Yan, X. L. Hou, G. Lu, B. Yang, L. X. Wu, and J. C. Shen, *Langmuir* **19**, 9850–9854 (2003).
104. J. Lei, W. Liang, C. S. Brumlik, and C. R. Martin, *Synth. Met.* **47**, 351 (1992).
105. M. Narashimhan, M. Hagler, V. Commarata, and M. Thakur, *Appl. Phys. Lett.* **72**, 1063 (1998).
106. A. Tsumura, M. Koezuka, and T. Ando, *Appl. Phys. Lett.* **49**, 1210 (1986).
107. A. Tsumura, H. Fuchigami, and H. Koezuka, *Synth. Met.* **1181**, 41–43 (1991).
108. M. Koehler and I. A. Hummelgen, *J. Appl. Phys.* **87**, 3074 (2000).
109. G. G. Malliaries and J. C. Scott, *J. Appl. Phys.* **85**, 7426 (1999).
110. W. H. Kim, A. J. Makinen, N. Nikolov, R. Shashidhar, H. Kim, and Z. H. Kafafib, *Appl. Phys. Lett.* **80**, 3844–3846 (2002).
111. S. Chen and Y. Fang, *Synth. Met.* **60**, 215–222 (1993).
112. C. J. Dury, C. M. J. Mutsaers, C. M. Hrat, M. Matters, and D. M. de Leeuw, *Appl. Phys. Lett.* **73**, 108 (1999).

113. Y. Y. Lin, A. Dodabalapur, R. Sarpeshkar, Z. Bao, W. Li, K. Baldwin, V. R. Raju, and H. E. Katz, *Appl. Phys. Lett.* **74**, 2714 (1999).
114. S. M. Sze, *Physics of Semiconductor Devices*, 2nd ed., John Wiley & Sons, Inc., New York, 1981.
115. A. J. Heeger, *Solid State Commun.* **107**, 673–679 (1998).
116. P. Dastoor, D. L. Officer, C. O. Too, and G. G. Wallace, *Chem. Innovation*, 15–22 (2000).
117. N. S. Saricifci and A. J. Heeger, *Int. J. Mod. Phys. B* **8**, 237 (1994).
118. N. S. Sariciftci, L. Smilowitz, and A. J. Heeger, *F. Wudl, Science* **258**, 1474 (1992).
119. J. J. M. Halls, K. Pichler, R. H. Friend, S. C. Moratti, and A. B. Holmes, *Appl. Phys. Lett.* **68**, 3120 (1996).
120. J. Chen, C. O. Too, A. K. Burrell, G. E. Collis, D. L. Officer, and G. G. Wallace, *Synth. Met.* **137**, 1373 (2003).
121. C. J. Brabec, N. Sacrifici, and J. C. Hummelen, *Adv. Funct. Mat.* **11**, 15 (2001).
122. W. A. Gazotti, A. F. Nogueira, E. M. Grotto, M. C. Gallazi, and M. A. De Paoli, *Synth. Met.* **108**, 151–157 (2000).
123. T. Yohannes, T. Solomon, and O. Inganas, *Synth. Met.* **82**, 215 (1996).
124. C. A. Cutler, A. K. Burrell, G. E. Collis, D. L. Officer, C. O. Too, and G. G. Wallace, *Synth. Met.* **123**, 225–237 (2001).
125. Y. Kunugi, Y. Harima, and K. Yamashita, *J. Chem. Soc., Chem. Commun.* **787**, (1995).
126. H. Shirakawa and S. Ikeda, *Kobunshi Ronbunshu* **28**, 369 (1979).
127. T. Yohannes, T. Solomon, and O. Inganaes, *Synth. Met.* **82**, 215 (1996).
128. J. J. M. Halls, C. A. Walsh, N. C. Greenham, E. A. Marseglia, R. H. Friend, S. C. Moratti, and A. B. Holmes, *Nature* **376**, 498 (1995).
129. G. Yu and A. J. Heeger, *J. Appl. Phys.* **78**, 4510 (1995).
130. M. Granstrom, K. Petritsch, A. C. Arias, A. Lux, M. R. Andersson, and R. H. Friend, *Nature* **395**, 257 (1998).
131. N. R. Armstrong and J. Porphyrins, *Phthalocyanines* **4**, 414 (2000).
132. K. Yoshino, K. Tada, A. Fujii, E. M. Conwell, and A. A. Zakhidov, *IEEE Trans. Electron Devices* **44**, 1315 (1997).
133. T. Yamaue, T. Kawai, M. Onoda, and K. Yoshino, *J. Appl. Phys.* **85**, 1626 (1999).
134. J. J. M. Halls and R. H. Friend, *Synth. Met.* **85**, 1307 (1997).
135. G. Yu, J. Gao, J. C. Hummelen, F. Wudl, and A. J. Heeger, *Science* **270**, 1789 (1995).
136. C. J. Brabec, N. S. Sariciftci and J. C. Hummelen, *Adv. Funct. Mater.* **11**, 15 (2001).
137. P. Novak, K. Muller, K. S. V. Santhanam, and O. Hass, *Chem. Rev.* **97**, 207 (1997).
138. J. G. Killian, B. M. Coffey, F. Gao, T. O. Poehler, and P. C. Searson, *J. Electrochem. Soc.* **143**, 936 (1996).
139. Y. Gofer, H. Sarker, J. G. Killian, J. Giaccai, T. O. Poehler, and P. C. Searson, *Biomed. Inst. Tech.* **32**, 33 (1998).
140. H. H. Rehan, *J. Power Sources* **113**, 57 (2003).
141. M. D. Levi, Y. Gofer, and D. Aurbach, *Polym. Adv. Tech.* **13**, 697 (2002).
142. L. W. Shaklette, M. Maxfield, S. Gould, J. F. Wolfg, T. R. Jow, and R. H. Baughman, *Synth. Met.* **18**, 611 (1987).
143. H. Masuda and K. Kaeriyama, *J. Mat. Sci.* **26**, 5637 (1991).
144. S. A. Ashraf, F. Chen, C. O. Too, and G. G. Wallace, *Polymer* **37**, 2811 (1996).
145. A. O. Patil, Y. Ikenoue, F. Wudl, and A. J. Heeger, *J. Am. Chem. Soc.* **109**, 1858 (1987).
146. E. E. Havinga, W. ten Hoeve, E. W. Meijer, and H. Wynberg, *Chem. Mater.* **1**, 650 (1989).
147. M. R. Bryce, A. Chissel, P. Kathirgamanathan, D. Parker, and R. M. Smith, *J. Chem. Soc., Chem. Comm.* 466 (1987).
148. J. N. Barisci, J. Mansouri, G. M. Spinks, G. G. Wallace, C. Y. Kim, D. Y. Kim, and J. Y. Kim, *Colloids Surf.* **126**, 129 (1997).
149. M. Aldissi and S. P. Armes, *Progr. Org. Coat.* **19**, 21 (1991).

150. H. Eisazadeh, G. Spinks, and G. G. Wallace, *Polymer* **35**, 3801 (1994).
151. J. N. Barisci, A. J. Hodgson, L. Liu, G. G. Wallace, and G. Harper, *React. Polym.* **39**, 269 (1999).
152. P. Ghosh, S. K. Siddhanta, S. R. Haque, and A. Chakrabarti, *Synth. Met.* **123**, 83–89 (2001).
153. M. Omastova, M. Trchova, J. Kovarova, and J. Stejskal, *Synth. Met.* **138**, 447–455 (2003).
154. F. Brustolin, F. Goldoni, E. W. Meijer, and N. A. J. M. Sommerdijk, *Macromolecules* **35**, 1054–1059 (2002).
155. J. Jang and J. H. Oh, *Chem. Commun.* **19**, 2200–2201 (2002).
156. J. G. Deng, Y. X. Peng, C. L. He, X. P. Long, P. Li, and A. S. C. Chan, *Polym. Int.* **52**, 1182–1187 (2003).
157. H. W. Heuer, R. Wehrmann, and S. Kirchmeyer, *Adv. Funct. Mater.* **12**, 89–94 (2002).
158. C. Edder and J. M. Frechet, *J. Org. Lett.* **5**, 1879–1882 (2003).
159. J. Jagur-Grodzinski, *Polym. Adv. Tech.* **13**, 615, (2002), and references cited therein.
160. A. Mirmohseni and G. G. Wallace, *Polymers* **44**, 3523 (2003).
161. M. Karakisla, M. Sacak, and U. Akbulut, *J. Appl. Polym. Sci.* **59**, 1347 (1996).
162. D. A. W. Soares and A. A. A. de Queiroz, *Macromol. Sym.* **170**, 221 (2001).
163. A. A. Pud, S. P. Rogalsky, G. S. Shapoval, and A. A. Korzhenko, *Synth. Met.* **99**, 175 (1999).
164. S. Y. Oh, H. C. Koh, J. W. Choi, H. W. Rhee, and H. S. Kim, *Polym. J.* **29**, 404 (1997).
165. Q. Xiang and H. Q. Xie, *European Polym. J.* **32**, 865 (1996).
166. S. Y. Yang and E. Ruckenstein, *Synth. Met.* **59**, 1 (1993).
167. B. Vincent and J. Waterson, *J. Chem. Soc.* 683, (1990).
168. P. Banerjee, M. L. Digar, S. N. Bhattacharyya, and B. M. Mandal, *Eur. Polymer. J.* **30**(4), 499, (1994).
169. P. Armes and M. Aldissi, *J. Chem. Soc.* **88** (1989).
170. D. Chattopadhyay and B. M. Mandal, *Langmuir* **12**, 1585 (1996).
171. K. Gilmore, A. J. Hodgson, B. Luan, C. J. Small, and G. G. Wallace, *Polym. Gels Networks* **2**, 135 (1994).
172. C. J. Small, C. O. Too, and G. G. Wallace, *Polym. Gels Networks* **5**, 251 (1997).
173. S. N. Bhadani, S. K. Sen Gupta, G. C. Sahu, and M. Kumari, *J. Appl. Polym. Sci.* **61**, 207 (1996).
174. S. W. Tan and H. Ge, *Polymer* **37**, 965 (1996).
175. D. Abraham and A. Bharati, Subramanyam, *Polymer* **23**, 5295 (1996).
176. A. G. MacDiarmid, W. E. Jones, I. D. Norris, J. Gao, A. T. Johnson, N. J. Pinto, J. Hone, B. Han, F. K. Ko, H. Okuzaki, and M. Llaguno, *Synth. Met.* **119**, 27 (2001).
177. I. D. Norris, M. M. Shaker, F. K. Ko, and A. G. MacDiarmid, *Synth. Met.* **114**, 109 (2000).
178. D. Pede, G. Serra, and D. De Rossi, *Mat. Sci. Eng.* **C5**, 89, (1998).
179. J. P. Hart and S. A. Wring, *TrAc.* **16**, 89 (1997).
180. A. Nannini and G. Serra, *J. Mol. Electron.* **6**, 81 (1990).
181. M. S. A. Abdou, G. A. Diaz-Guijada, M. I. Arroyo, and S. Holdcraft, *Chem. Mater.* **3**, 1003 (1991).
182. D. G. Li dzey, M. A. Pate, M. S. Weaver, T. A. Fisher, and D. D. C. Bradley, *Synth. Met.* **82**, 141 (1996).
183. D. Chinn and J. Janata, *Thin. Solid. Films* **252**, 145 (1994).
184. K. Gilleo, *Polymer Thick Films*, Van Nostrand Reinhold, New York, 1996.
185. Z. Bao and A. J. Lovinger, *Chem. Mater.* **11**, 2607–2612 (1999).
186. F. Garnier, R. Hajlaoui, A. Yassar, and P. Srivastava, *Science* **265**, 1684 (1994).
187. G. Gustafsson, Y. Cao, G. M. Treacy, F. Klavetter, N. Colaneri, and A. J. Heeger, *Nature* **357**, 477–479 (1992).

188. J. A. Rogers and Z. Bao, *J. Polym. Sci., Part A: Polym. Chem.* **40**, 3327–3334 (2002).
189. T. R. Hebner, C. C. Wu, D. Marcy, M. H. Lu, and J. C. Sturm, *Appl. Phys. Lett.* **72**, 519 (1998).
190. S. Magdassi and M. Ben Moshe, *Langmuir* **19**, 939–942 (2003).
191. G. B. Blanchet, Y. L. Loo, J. A. Rogers, F. Gao, and C. R. Fincher, *Appl. Phys. Lett.* **82**, 463–465 (2003).
192. M. Lefenfeld, G. Blanchet, and J. A. Rogers, *Adv. Mater.* **15**, 1188–1194 (2003).
193. H. Sirringhaus, T. Kawase, R. H. Friend, T. Shimoda, M. Inbasekaran, W. Wu, and E. P. Woo, *Science* **290**, 2123–2126 (2000).

G. G. WALLACE
P. C. INNIS
S. E. MOULTON
University of Wollongong

INTERCALATION POLYMERIZATION

Introduction

The term *intercalation* is used by chemists to describe the insertion of mobile guest species (atoms, molecules, or ions) into a crystalline host lattice containing an interconnected system of empty lattice sites (□) of appropriate size, according to the general equation (see Reference 1)

$$x\,\text{Guest} + \square_x\,[\text{Host}] \longleftrightarrow (\text{Guest})_x[\text{Host}]$$

Usually reversible and occurring near room temperature, intercalation reactions are considered as topochemical processes, since the structural integrity of the host lattice is formally conserved. A wide range of inorganic host lattices have been found to undergo these intercalation reactions including (2) (Fig. 1) (*1*) framework lattices made of interconnected or parallel isolated channels and (*2*) layered lattices and chain-type structures made of inorganic slabs or chains, respectively. The framework lattices (zeolite-type structures, tungsten bronzes, etc) are characterized by rigid vacant channels with constant pore volume. Therefore, the uptake of guest species is limited by the minimal channel cross section which results in guest shape selective intercalation behavior ("molecular sieve" phenomenon). On the other hand, the structures resulting from the weak association of slabs or chains provide flexible "pores," since the dimensions of the interslab or interchain spaces can adapt to the dimensions of the guest species. In practice, the chain structures, such as $(NbSe_3)_8$, $(Mo_3Se_3)_8$, and $(RuBr_3)_8$, have low structural stability and therefore relatively few studies have been carried out on their intercalation chemistry (1).

Thus, the present review is mainly devoted to the synthetic aspects of the intercalation of organic monomers in layered inorganic lattices and their *in situ*

Encyclopedia of Polymer Science and Technology. Copyright John Wiley & Sons, Inc. All rights reserved.

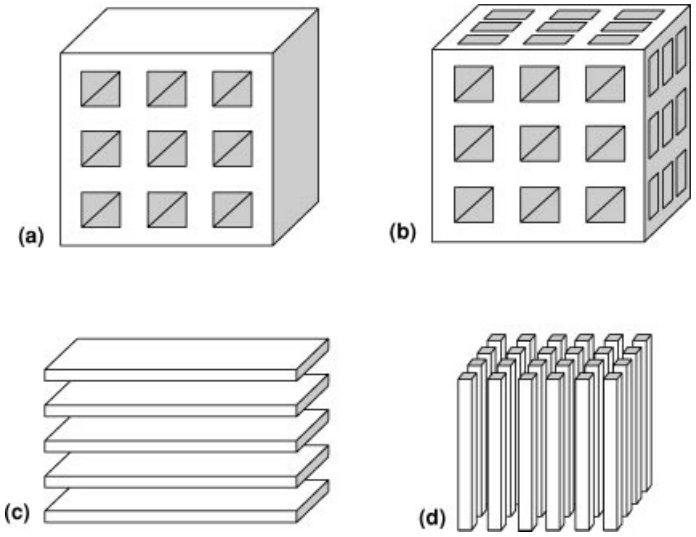

Fig. 1. Schematic representation of inorganic host lattices: framework lattices made of parallel isolated channels (**a**) or interconnected channels (**b**), layered lattices (**c**), and chain-like structures (**d**).

polymerization leading to hybrid monophasic compounds, also called layered nanocomposites, made of the alternation of inorganic and polymer layers. Nevertheless, it may be noticed that these topochemical reactions are not the only routes to obtain such layered nanocomposites (Fig. 2): the synthesis of the mineral slabs from soluble precursors in a macromolecular solution (3,4) or the mineral slab exfoliation and their subsequent restacking after adsorption of macromolecules (encapsulative precipitation) (5,6) are other already investigated routes, which will not be reported in this article.

Under specific experimental conditions, such materials may be obtained as delaminated (or exfoliated) nanocomposites, which may be described as single inorganic slabs uniformly and randomly dispersed within a polymer matrix. Readers interested by the synthesis and the properties of these delaminated nanocomposites, especially in the field of clays, should see Nanocomposites, Polymer–Clay and other recent reviews (7–9). These materials have unusual and versatile properties, such as barrier materials and reinforced materials, (see BARRIER POLYMERS; REINFORCEMENT).

Nevertheless, considerable interest has also focused in recent years upon the synthesis of layered nanocomposites. Polymer-layered nanocomposites have advantages over their small-molecule analogues in compositional stability and mechanical strength, which make them more suitable for applications. On the other hand, it is expected that the thermal or oxidative stability of the polymer could be enhanced through encapsulation. The constrained environment is also expected to lead to a higher degree of polymer ordering, which would enhance their properties by orders of magnitude (ie, electronic conductivity or nonlinear optical susceptibility for conjugated polymers). A more potentially rewarding benefit arises, however, when the two lattices have ionic and/or electronically conductive

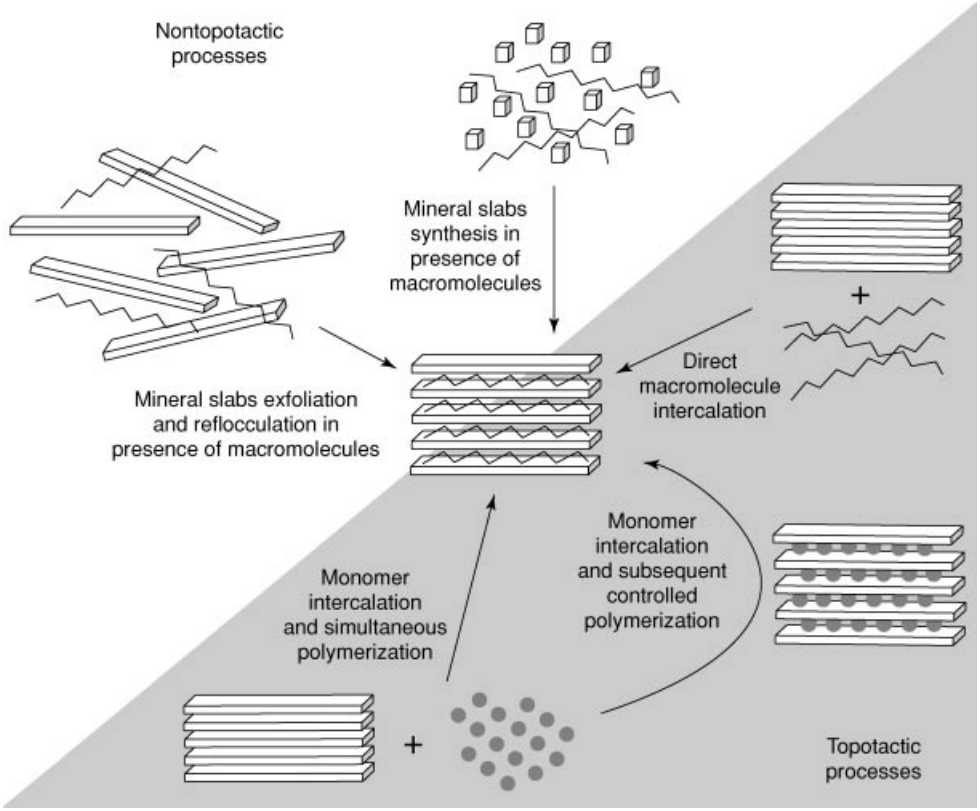

Fig. 2. Schematic representation of the synthetic routes leading to polymer-layered nanocomposites (where ○ and □ symbolize organic monomer and inorganic slab precursor, respectively).

properties. The goal is to design systems such that two lattices interact in such a way so as to enhance the properties of both.

The advantages of the polymer-layered nanocomposites are not only connected to the properties of the materials themselves. The presence of intercalated macromolecules may provide also a unique interslab environment for photofunctional molecules or probes. The photoluminescent behavior of tris(2,2′, -bipyridine)ruthenium(II) is gratefully enhanced in the interslab space of fluorotetrasilicic mica by the presence of poly(vinylpyrrolidinone)(PVP) (10). Moreover, layered nanocomposites may also be the precursors of inorganic ceramics (β-sialon, SiC, AlN, $Al_4Si_2C_5$, etc) through carbothermal reduction, because inorganic slabs and organic substances can contact at a molecular level and therefore prevent phase separation phenomena and the crystallization of parasitic phases (11). Lastly, from the viewpoint of the polymer chemist, polymerization reactions carried out in the confined 2-D space between inorganic slabs may further the synthesis of (*1*) macromolecules with stereospecific sequences, if the arrangement of intercalated monomers may be controlled through their interactions with the inorganic slabs and/or with cointercalated species, and (*2*) planar macromolecules

by using the interslab space as a polymerization nanoreactor where the polymer growth is prevented in the third direction by the slab presence.

Inorganic Layered Hosts and Intercalation Driving Forces

The majority of layered phases are characterized by strong intralayer covalent bonding and weak interlayer interactions. The slabs may be electrically neutral or may possess an overall charge which may be either positive or negative (Table 1). In molecular layered compounds, the slabs are electrically neutral and stacked on each other by Van der Waals forces or hydrogen bonds and the interslab space is a connected network of empty lattice sites. In the charged layered systems, the slabs are held together by weak electrostatic forces and the interslab spaces are partially or completely filled by ions or by a combination of ions and solvent molecules. The interslab distance, corresponding to the first line at lower 2θ values on x-ray diffraction (XRD) patterns, is directly affected by the presence, the concentration, and the conformation of any guest intercalated species. It should be noticed that this interslab distance corresponds to the basal spacing which is indeed the sum of the thickness of the interslab space and the thickness of the slab itself (Fig. 3). It is generally the first recorded parameter for checking the intercalation success and determining the guest arrangement.

Intercalation Through Electron Transfer. The direct intercalation of electrically neutral molecules in layered neutral crystals is only possible if these guest molecules are Lewis bases (organic amines, phosphines, thiols, etc) or strong electron donors (alkali metals) and if the host lattice is reducible. Indeed, the electron transfer mechanism from the intercalated guest to the host lattice is governed

Table 1. Examples of Some Layered Host Structures That Exhibit Intercalation Reactions[a]

Lattice Type	Illustrative examples[b]	Slab charge
Metal chalcogenides	$\mathbf{MX_2}$ where M = Ti, Ta, Mo, etc; X = S, Se	Neutral
	$\mathbf{MPX_3}$ where M = Mn, Cd, etc; X = S, Se	Neutral
Metal oxides	$\mathbf{MoO_3}$	Neutral
	$\mathbf{V_2O_5}$ or $\mathbf{V_2O_5} \cdot n\mathrm{H_2O}$ (xerogel)	Neutral
Metal oxy-halides	**MOX** where M = Fe, Ti, V, etc; X = Cl, Br	Neutral
Metal halides	α-$\mathbf{RuCl_3}$	Neutral
Hydrous metal oxides	$[\mathbf{M^{II}_{1-x}M'^{III}_x(OH)_2}]^{x+}[A^{n-}_{x/n}]^{x-} \cdot n\mathrm{H_2O}$ where M = Mg, Ni, etc; M′ = Al, Co, Fe, etc; A = Cl, NO_3, CO_3, etc	Positive
Metal hydrogen phosphates	$\mathbf{M(HOPO_3)_2} \cdot \mathrm{H_2O}$ where M = Ti, Zr, Hf, Ce, Sn	Neutral
Hydrogen uranyl phosphate	$\mathrm{H}\mathbf{UO_2PO_4} \cdot 4\mathrm{H_2O}$	Negative
Metal phosphates	$\mathbf{MOPO_4}$ where M = Ti, V, etc	Neutral
Smectite clays and silicates	Kaolinite $\mathbf{Al_4Si_4O_{10}(OH)_8}$	Neutral
	(Fluoro)Hectorite $\mathrm{Na_{0.6}}\mathbf{(Li_{0.6}Mg_{5.4})Si_8O_{20}(OH,F)_4}$	Negative
	Montmorillonite $\mathrm{Ca_{0.35}}\mathbf{(Mg_{0.7}Al_{3.3})Si_8O_{20}(OH)_4}$	Negative

[a] For their crystalline structure and intercalation chemistry, see for instance Ref. 1.
[b] The chemical component in bold type constitutes the slab (the other ones are in the interslab space).

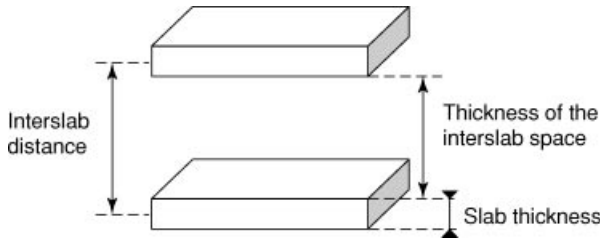

Fig. 3. Schematic representation of the characteristic distances describing the interslab space: the interslab distance is directly derived from XRD patterns (distance corresponding to the first line at lower 2θ values); the thickness of the interslab space is derived from the latter after deduction of the slab thickness.

by the oxidizing power of the metal within the slabs: the layered structure is generally preserved if the guest molecules are just on the reducing side of the host. Intercalation reactions are performed under anhydrous conditions at temperatures up to 200°C with neat reactants, if the potential guests are liquid or low melting solids. Solid guests are dissolved in polar organic solvents (toluene, acetonitrile, dimethoxyethane, dimethylformamide, etc) which often accelerate the intercalation process, but may also cointercalate with the guest molecules. On intercalation, the electric band structures of the layered crystals are changed greatly: some layered semiconductors are changed into metallic compounds and even changed into superconductors (12).

Intercalation Through Ion Exchange. Such mechanisms are observed in layered lattices made of negative or positive slabs, where the net charge is balanced in the interslab space by the presence of cations or anions, respectively. These ions can often be replaced by immersing the material in a concentrated solution of other ions of the same charge. These exchange reactions are driven by the great excess of the replacement ion. Intercalation reactions involving clay hosts all generally proceed by cation-exchange processes, with various kinds of inorganic as well as organic cations, such as voluminous quarternary alkyl ammonium ions.

Intercalation Through Dipole–Ion Interactions. Neutral polar molecules can also directly intercalate into the interslab spaces of ion-exchangeable layered crystals. The driving force for the intercalation is mainly due to dipole–cation interactions similar to the interactions involved in the solvation of cations in an electrolyte solution. The intercalation occurs only if such interactions are strong enough to compensate the energy necessary for the guest molecules to spread the slabs.

Surfactant-Mediated Intercalation. In general, nonpolar molecules are not able to intercalate between the slabs of pristine inorganic layered materials. The preintercalation of ionic surfactants by ion-exchange reactions is the only route allowing to make the interslab space sufficiently open and organophilic for accommodating non polar guest molecules. This route is especially used in the field of clays with commercial organically modified clay precursors, called organoclays.

Intercalation Through Acid–Base Interactions. Such mechanisms are observed in layered host lattices (metal phosphates; layered perovskites $HCa_2Nb_3O_{10}$, $HCa_2Nb_2MO_9$ with M = Al, Fe, $HMM' O_6 \cdot H_2O$ with M = Nb,

Ta and M′ = W, Mo), where acidic protons, present within or between the slabs, may be neutralized by guest Brønsted bases.

Intercalation Through Guest Displacement. Kaolinite is atypical among silicates, because neither cations nor anions are present in the interslab space and the inherent hydrogen bondings between the slabs limit the intercalation chemistry. Today, the most effective technique for kaolinite is a guest displacement reaction, in which preintercalated organic species (DMSO, NMF, methanol, etc) can be displaced with various types of organic molecules. Multistep displacement is also possible by using these compounds as second intermediates (11).

Direct Intercalation of Preformed Macromolecules

In addition to the rapidly expanding field of exfoliated clay–polymer nanocomposites (see NANOCOMPOSITES, POLYMER-CLAY), direct intercalation of macromolecules into inorganic layered materials with retention of the layered nature is also an excellent way of constructing nanocomposites with original properties. The synthetic pathways have to overcome large entropic barriers.

One of the first successful attempts for intercalating preformed macromolecules was reported in the field of clays (13). Poly(ethylene oxide)(PEO) macromolecules ($M_w = 6 \times 10^2 - 6 \times 10^5$ g/mol) were intercalated from acetonitrile solutions into montmorillonite or hectorite where interslab cations were Li^+, Na^+, K^+, Ba^{2+}, etc. The resulting compounds exhibit good chemical and thermal stability, preserving their ion-exchange properties. The corresponding increase in the interslab distance (between 0.6 and 0.8 nm according to the cation nature) does not depend on the PEO molar mass and is consistent with a single-layer intercalated polymer adopting a helical conformation in the interslab space (Fig. 4). Such an arrangement, checked by IR, ^{13}C, and ^{23}Na NMR spectroscopies, indicates that interslab cations remain associated with the PEO oxygen atoms and this allows one to infer that the intercalation driving force is the well-known PEO affinity for cationic species (dipole–cation interaction) (14,15). PEO–clay nanocomposites show higher ionic conductivities than the parent silicate (up to $10^{-5} - 10^{-4}$ S/cm in the direction parallel to the layer plane) and their potential use as polymer electrolyte in solid-state lithium batteries as a substitute for conventional PEO–salt complexes is argued by the fact that in these nanocomposite systems the typical problem of ion pair formation is avoided, because only the cations are able to move (16). Similar routes, based on the PEO affinity for cations, were also successfully investigated with MPS_3 (with M = Mn, Cd) (17,18) or MoO_3 (19) materials preintercalated with alkali cations. In transition-metal phosphorous trisulfides, the concept was extended to poly(ethylene imine) (20) and PVP (21).

Cation exchange reactions, as intercalation driving force, were investigated with ionomer macromolecules such as poly(*p*-xylylene-α-dimethylsulfonium chloride) ($M_w = 10^5$ g/mol) in MoO_3 after the preintercalation of hydrated alkali cations and partial swelling in water (22). The ionomer was *in situ* converted to poly(*p*-phenylenevinylene) (PPV) by heating up to 250°C for eliminating HCl and $S(CH_3)_2$ (eq. 1). The interslab distance is in good agreement with an orientation of the aromatic ring planes perpendicularly to the oxide slabs. The increase of electronic

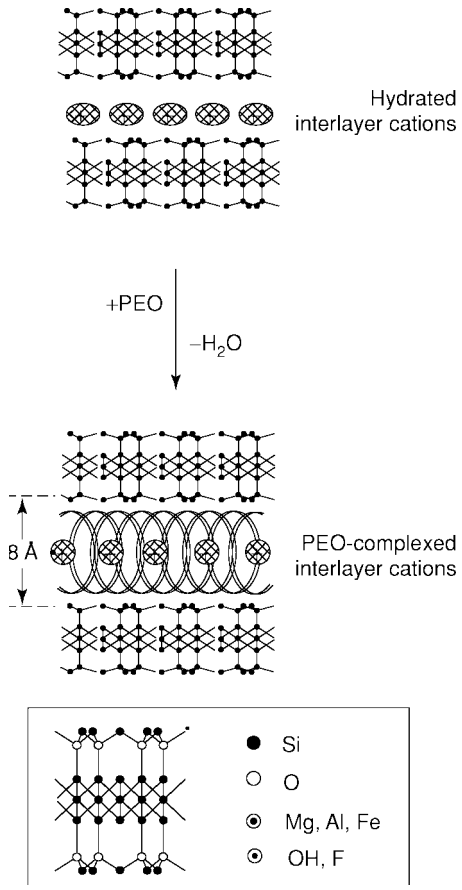

Fig. 4. Schematic representation of the helical arrangement of PEO macromolecules into smectite clays. From Ref. 14, with permission.

conductivity, together with x-ray photoelectron spectroscopy (XPS) data, is consistent with the formation of p-doped PPV in the oxide lattice.

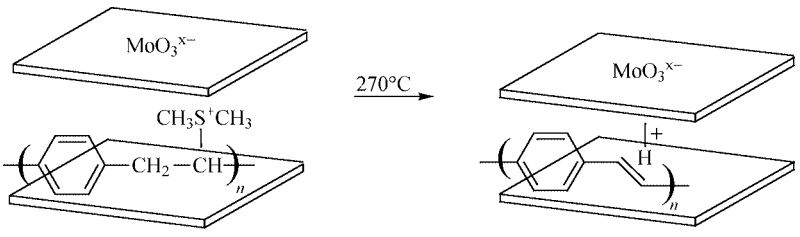

(Reprinted with permission from Ref. 22. Copyright (1192) American Chemical Society.)

(1)

Another example of direct macromolecule intercalation is the insertion of hydrophilic chains, such as PEO, PVP, poly(propylene glycol) (PPG), and

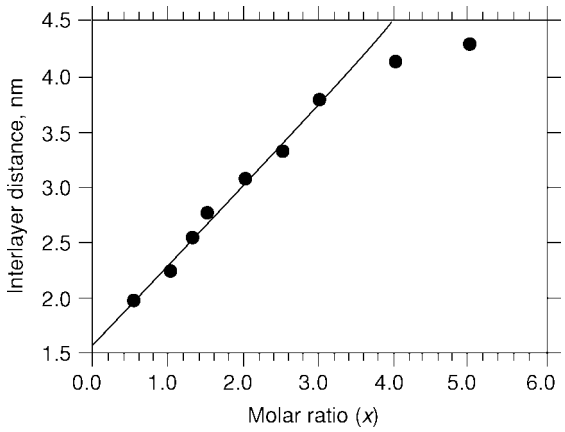

Fig. 5. Variation of the interslab distance as a function of x in $(PVP)_xV_2O_5 \cdot nH_2O$ nanocomposite. From Ref. 24, with permission.

methylcellulose, between the slabs of vanadium oxide xerogel, which is infinitely swellable in water (23–25). In practice, the nanocomposites were carried out by mixing aqueous solutions of macromolecules with a $V_2O_5 \cdot nH_2O$ solution in various stoichiometries and obtained as red self-supporting films. It may be noticed that, in the case of $(PVP)_xV_2O_5 \cdot nH_2O$ materials, single phases are obtained when $1 \leq x \leq 5$. Interestingly, as x increases, the interslab distance increases continuously and linearly up to $x = 3$ with the increment being 0.7 nm per mole of PVP (Fig. 5). At $x > 3$, significant deviations from the linear relationship begin to appear, showing that the interslab space become saturated and that any additional polymer deposits outside the host. Moreover, the nanocomposite films are flexible with methylcellulose, but brittle with PPG and PVP.

Last typical examples, which may be taken in the literature, are surfactant-mediated intercalation with the incorporation of poly(*p*-phenylene) into MoO_3 (26) (Fig. 6) or poly(ethylene glycol)–kaolinite (27) and PVP–kaolinite (28) by refined guest displacement methods.

The main disadvantage of the route based on the direct intercalation of preformed macromolecules is the slow kinetics for the transport of macromolecules in the interslab spaces. In practice, the intercalation experiments require several days to complete at room temperature and their duration is inversely proportional

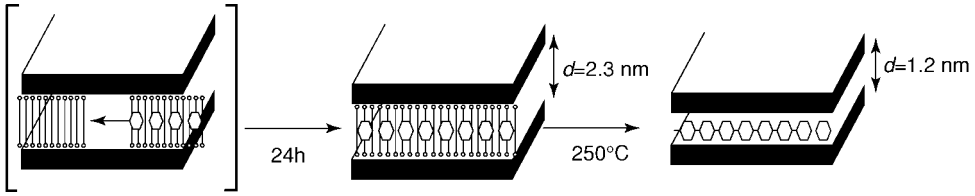

Fig. 6. Schematic representation of the surfactant-mediated intercalation of poly(*p*-phenylene) into MoO_3. Reprinted with permission from Ref. 26. Copyright (1998) American Chemical Society.

to the molar mass of macromolecules. Another limit is the inability of this method for accommodating nonlinear and insoluble macromolecules, such as the majority of conducting organic polymers. That is why parallel efforts have been focused on two-step routes, such as monomer intercalation and *in situ* polymerization. Further advantage of such synthetic routes based on polymerization in constrained environment is that, in theory, they offer the possibility for designing: (*1*) macromolecules with stereospecific sequences, if the arrangement of intercalated monomers may be controlled through their interactions with the inorganic slabs and/or with cointercalated species and (*2*) two dimensional macromolecules by using the interslab space as a polymerization nanoreactor where the polymer growth is prevented in the third direction by the slab presence.

Monomer Intercalation and Simultaneous Polymerization

In a significant number of cases, the contact between organic monomers and inorganic layered materials leads to the spontaneous polymerization of the monomers between the slabs. Even if all the mechanisms involved are not completely elucidated, it is possible to distinguish several scenarios.

Spontaneous Polymerization in Layered Aluminosilicates. Layered aluminosilicates are known not only to intercalate organic species but also to trigger spontaneous polymerization of some organic monomers. Brønsted acidity and/or transition-metal cations populating the surface of the slabs have been reported to be responsible for initiating the polymerization.

Forty years ago, it was shown that bringing into contact Na-montmorillonite and 4-vinylpyridine at ambient temperature leads to the formation of an intercalated monolayer of poly(4-vinylpyridine) whose aromatic rings are oriented perpendicularly to the slabs (29). Melted acrylamide was also successfully intercalated and polymerized, but the attempted intercalation/polymerization of styrene was less conclusive. At the time, the assumption of an ionic polymerization mechanism initiated by chemisorbed hydronium or hydroxyl ions derived from water was made.

In the case of transition-metal-exchanged smectite clays such as montmorillonite or hectorite, the interaction of the organic monomer with the transition-metal ions is followed by a relatively slow electron transfer reaction which produces reactive organic free radicals (30). These radicals then serve to initiate polymerization of guest monomers, such as benzene, aniline, pyrrole, and thiophene on hectorite films. According to the nature of the monomer and therefore to the strength of its interaction with the transition cation, the polymerization occurs on the film surface and/or in the interslab spaces, as checked by scanning force microscopy (SFM) and x-ray diffraction (XRD). For example, aniline vapor readily polymerizes in both sites of Cu^{2+}-exchanged hectorite (31). On the basis of the results of electron spin resonance (ESR) experiments, a plausible polymerization mechanism was proposed, where the first step is the oxidation of one aniline molecule by Cu^{2+}, leading to an aniline radical-cation able to initiate the polymerization. Atmospheric O_2 is also involved in the propagation step, with the subsequent formation of polyaniline in the leucoemeraldine form. Other easily oxidized monomers, such as pyrrole and thiophene, react in a similar way. On

the other hand, with benzene, the extent of polymerization is much lower, with macromolecules essentially located between the slabs (30).

The intercalative polymerization of aniline may also be carried out using a Cu^{2+}-exchanged synthetic hectorite (fluorohectorite) (32). The electronic absorption spectrum of the resulting nanocomposites showed the characteristic insulating poly(aniline) form (ie the emeraldine base). To obtain conducting materials it is necessary to dope the nanocomposite by exposure to HCl vapors. As a consequence of this treatment, the emeraldine salt is formed within the interslab space and a significant increase in the electrical conductivity is observed, which reaches high in-plane d.c. conductivity values (0.05 S/cm) with an anisotropic ratio $\sigma_{\parallel}/\sigma_{\perp}$ close to 10^5. Similar experiments are also successful with pyrrole, leading to polymerized nanocomposites where the variation in the basal spacing is consistent with heterocyclic rings oriented parallel to the silicate slabs (33). A broad infrared band extending from about 1800 cm^{-1} into the near-infrared region is indicative of the presence of polarons/bipolarons in conducting polypyrrole. Doping of polypyrrole–fluorohectorite nanocomposites with iodine vapors produces a strong increase in the d.c. conductivity from 2×10^{-5} to 0.12 S/cm. The electrical conductivity increases with temperature in the 100–400 K range, but above 400 K the observed dramatic decrease is interpreted as strong oxidation of polypyrrole (16).

Methyl methacrylate (MMA) and styrene, adsorbed on transition-metal-exchanged hectorite, may undergo polymerization by mechanisms that do not involve electron transfer and the reduction of the metal cation in the interslab spaces. This type of polymerization occurs relatively slowly (3 days to a week) compared with the redox reactions previously described and the resulting polymer seems, in most cases, to be primarily located on the surface of the clay film or in defects in this film (34). The ESR technique showed no evidence for the formation of organic free radicals during the polymerization. A possible cationic mechanism would rely on the enhanced Brønsted acidity of the intercalated transition metals, due to the high degree of dissociation of the water molecules associated to these metals, and the potential for the stabilization of cationic species by the negatively charged silicate slabs. While cationic polymerization of MMA may be unusual, this species could act as a Lewis acid, and in the presence of small amounts of water as a Brønsted acid (30).

A last example concerns the spontaneous polymerization of 2-ethynylpyridine within the interslab spaces of montmorillonite with different exchangeable cations (35,36). When the colorless acetylenic monomer is added into the aluminosilicate suspension in benzene, the color of the mixture readily turns reddish brown and darkens gradually. The macromolecules may be liberated through dissolution of the clay with hydrofluoric acid and on their infrared spectrum a strong band at 1630 cm^{-1}, due to —C=C— stretching, is observed, indicating the formation of a polymer with extensive conjugation. Additional evidence for polymerization is provided by the large bathochromic shift in the UV–vis absorption spectrum of the polymer, with an absorption peak at 470 nm, while poly(2-ethynylpyridine) from thermal polymerization in bulk absorbs at 370 nm, indicating a more extensively conjugated structure of the former. Thermogravimetric experiments show that the macromolecules confined to the interslab spaces have a higher thermal stability than the liberated polymer. The

polymerization rate of 2-ethynylpyridine increases with acidity of the montmorillonites, consistently with a spontaneous mechanism wherein the acetylenic triple bond would be activated via quaternization of the pyridine nitrogen. These sources of protons could be polarized water molecules on the surface of aluminosilicates, particularly water molecules associated with compensating cations.

Redox Intercalative Polymerization in Highly Oxidizing Hosts. The *in situ* redox intercalative polymerization (RIP) reaction is a direct and topotactic intercalation method (37). This type of reaction requires a strongly oxidizing host to provide the driving force to pull the monomers into the interslab spaces and oxidize them into polymers. In addition, the host should be able to distribute efficiently those electrons throughout the structure. These hosts are essentially FeOCl, V_2O_5, $VOPO_4$, and α-$RuCl_3$. The monomers may be polymerized through an oxidative mechanism, and therefore they mainly derive from aniline, pyrrole, thiophene, or furan structures, leading to conductive macromolecules. Generally prepared through chemical or electrochemical routes, the electronically conductive polymers are obtained as amorphous and insoluble powders, whose microstructure morphology characteristics (overall chain conformation and packing, degree of cross-linking, etc) are largely uncontrollable. Therefore, the charge transport mechanisms remain poorly understood and the following examples result from synthesis efforts for designing well-defined 2-D architectures isolated from each other through the use of the interslab spaces as nanoscale templates. Moreover, it has been clearly shown according to spectroscopic data that the role of the oxidizing transition-metal ions (such as Fe^{III} in FeOCl or V^{IV} in $VOPO_4$) determines the conducting form of the polymer and, therefore, the electrical behavior of the resulting nanocomposite (38,39).

The transition-metal oxyhalide FeOCl was the first investigated host (38). In a typical synthesis, a mixture of FeOCl and monomer (neat or in acetonitrile solution) is stirred at ~40–50°C for several days. The violet solid turns brown-black gradually with a shiny metallic luster and, few days later, it is recovered by filtration, washed, and dried. The success of the redox intercalative polymerization is strongly dependent on the first anodic potential (E_{pa}) of the heterocyclic monomers with respect toward the reduction potential of the inorganic phase. Although the precise redox potential of FeOCl under the reaction conditions is not known, it may be inferred from RIP experiments with different monomers that this value is comprised between 1.32 and 1.86 V versus SCE (40). These lower and upper bounds indeed correspond to the E_{pa} of the most oxidizible monomers which are readily polymerized within the slabs of FeOCl (2,2′-bithiophene) and the E_{pa} of the less oxidizible monomers which cannot be polymerized in similar conditions, respectively (Fig. 7). The fact that pyrrole and 2,2′-bithiophene may be spontaneously intercalated and polymerized, contrarily to thiophene (structurally very close to pyrrole), suggest that thermodynamic rather than kinetic factors are important in these intercalative polymerization reactions. It should be also pointed out that for RIP to occur in a five-membered ring heterocycle, the 2 and 5 positions must not be blocked by substituents. For example, use of 2,5-dimethylpyrrole, which has a less positive E_{pa} than pyrrole itself, does not form a conductive polymer nor an intercalation compound. This of course derives from the fact that polymerization proceeds through coupling at the 2 and 5 positions. Elemental analyses were consistent with the stoichiometries $(C_4H_3N)_{0.34}FeOCl$ and $(C_4H_2S)_{0.28}FeOCl$ and

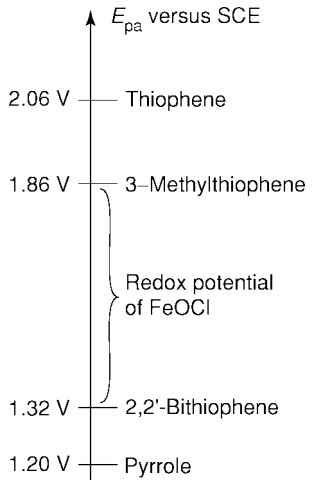

Fig. 7. Thermodynamic factors explaining why the redox intercalative polymerization in FeOCl is possible for pyrrole and 2,2′-bithiophene and not for 3-methylthiophene and thiophene.

XRD patterns with heterocyclic rings oriented perpendicular to FeOCl slabs. If the intercalation reaction is carried out at higher temperatures (>80°C) and for longer times (>2 weeks), the scanning electron microscopy (SEM) photographs show what appears to be amorphous polymeric film covering the crystal surfaces. XRD patterns of these overreacted samples show broad diffraction peaks, suggesting considerable decrease in the crystallite size and/or severe disorder resulting from the disruption of the FeOCl lattice. The ^{57}Fe Mössbauer spectroscopy allowed to check the partial reduction of FeOCl. Consistently with the RIP mechanism, electrons are transferred to the host slabs and are delocalized over all Fe sites, thus yielding an average formal oxidation state of Fe less than +3. Four-probe electrical conductivity data (in the range 4–300 K) measured on compressed pellets of the pyrrole or 2,2′-bithiophene based nanocomposites show a decrease in conductivity with falling temperature, with room temperature, conductivity of about 1 S/cm.

FeOCl host was also investigated for the redox intercalative polymerization of aniline (41). The success of this reaction strongly depends on the experimental conditions of the reaction: the most defined nanocomposites are obtained with acetonitrile as solvent and with a mole ratio of aniline to FeOCl > 8 in order to drive the reaction to completion. The reaction is accelerated by raising the temperature and/or performing it under air, indicating that oxygen is involved in the RIP mechanism. When large single crystals of FeOCl (as long as 0.5 mm) are used, the reaction rate is much slower, but the resulting products contain amounts of poly(aniline) similar to the microcrystalline samples. Elemental analyses show stoichiometry $(C_6H_4NH)_{0.3}FeOCl$ which corresponds to the maximum value calculated on the basis of the molecular sizes of FeOCl and poly(aniline). The macromolecules may be extracted from the nanocomposite by dissolution of the mineral slabs in HCl. Molecular weight studies via size exclusion chromatography (SEC) analysis suggest $M_w \sim 6100$ and $M_n \sim 3500$ versus $M_w \sim 69000$ and $M_n \sim 7700$ observed for polyaniline obtained independently in bulk. So, chain

lengths obtained in the interslab spaces are shorter than those obtained in bulk conditions, but show narrower length distribution. Infrared spectra of the intercalated macromolecules show the characteristic fingerprint of the emeraldine positive form, whose counter anions are the reduced FeOCl slabs.

Vanadium pentoxide is one of the most extensively studied inorganic layered host in the field of conductive polymers (35). The inorganic starting matrix could be either crystalline V_2O_5 or the quasi-amorphous $V_2O_5 \cdot nH_2O$ xerogel materials obtained by drying the gel resulting from the acidic hydrolysis of vanadate. Nevertheless, V_2O_5 gels can form highly oriented films that yield characteristic powder XRD patterns with enhanced 00l peaks. The strongly oxidizing character of the oxide induces the redox polymerization of the organic monomer. It is worth remarking that while the intercalated polymer is effectively p-doped (partially oxidized) during this process, the V_2O_5 suffers itself a partial reduction that renders it an n-doped (partially reduced) electrically conductive mixed-valence (V^{IV}/V^{V}) oxide. Such redox intercalation reactions alter the band structure of vanadium oxide forming bronze-like electrically conductive materials with mixed electronic charge-transport properties. So, these nanocomposites could be characterized as conductive polymer bronzes by analogy to alkali metal or molecular bronzes (42). First attempts of RIP experiments in V_2O_5 were performed with pyrrole and *N*-methylpyrrole (43), 2,2′-bithiophene (44), 2,5-dimercapto-1,3,4-thiadiazole (45), 3,4-ethylene dioxythiophene (46), and aniline (42,47,48). In this last case, the redox intercalation reaction and the subsequent spontaneous polymerization were studied in detail. In practice, it occurs instantly upon contact of the xerogel with aniline and is associated with an immediate and dramatic color change to dark blue. Despite this, the reaction takes several hours to go to completion because of the diminishing diffusion of the growing guest species into the interslab spaces. As neat aniline is not able to swell the xerogel and as other solvents such as DMSO or DMF are too readily cointercalated, water seems to be the most suitable solvent because a lot of it is expelled from the slightly hydrophobic interslab space, allowing more polymer to be inserted. When a wet xerogel (preswollen by water) of V_2O_5 is used, the reaction is complete within minutes but the final product is nearly amorphous, and sometimes the V_2O_5 framework is severely disrupted as checked by the dramatic changes on the V—O stretching region of the infrared spectrum. Experiments carried under air show that in such conditions the reaction completion times are shorter and the products tend to possess better lamellar order. The reaction steps of aniline and V_2O_5 in air are very complicated and could be summarized by the following overall equation:

$$x\ C_6H_5NH_2 + V_2O_5 \cdot nH_2O + (2x - 3y)/2\ O_2 \rightarrow$$
$$[(C_6H_4NH)_{x-y}(C_6H_5NH_3)_y]V_2O_5 \cdot mH_2O + (2x - 3y)/2\ H_2O_2 + (n - m)H_2O$$

Aging the samples in the presence of O_2 causes simultaneously the partial reoxidation of the reduced V_2O_5 framework and the oxidative coupling of polyaniline oligomers and anilinium ions inside the interslab spaces to form longer chains. So, oxygen acts as an electron acceptor during the *in situ* reaction and long after intercalation is complete. Further experiments carried out with 4-anilinoaniline or 4-anilinoanilinium iodide as monomers in $V_2O_5 \cdot nH_2O$ xerogel leads to the

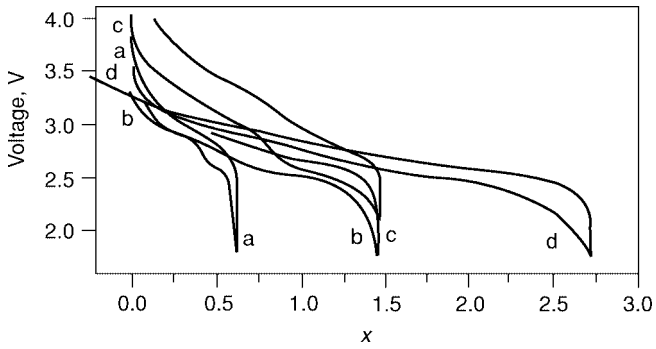

Fig. 8. First discharge curves of (a) V_2O_5 xerogel dried at 100°C, (b) poly(aniline)–V_2O_5 nanocomposite as prepared, without treatment, (c) V_2O_5 xerogel dried at 250°C, and (d) poly(aniline)–V_2O_5 nanocomposite treated at 80°C for 5 h, as a cathode material by coupling with a lithium metal anode using 1 *M* $LiClO_4$ in a 1:1 mixture of ethylene carbonate/dimethoxyethane as electrolyte (note: x is the ratio intercalated Li^+/V_2O_5). From Ref. 51, with permission.

intercalation of 4-anilinoanilinium cation moieties, followed by their polymerization (49). The oligomers obtained through this route exhibit a relatively low molecular weight dispersion, which cannot be obtained by the oligomerization reactions of 4-anilinoaniline in liquid phase. Electrochemical Li insertion into these polyaniline/V_2O_5 nanocomposites is enhanced because the intercalated conductive macromolecules facilitate Li diffusion kinetics and increase the capacity (50). The electrochemical performance indeed is very sensitive to the nature of the conductive polymer, the synthesis conditions, and subsequent treatments. For example, O_2 treatment, which has an important effect on the final molecular weight of the macromolecules and on the oxidation state of the oxide, is of great help in controlling the specific capacity of these nanocomposite cathodes, which can reach values as high as 300 A · h/g (measured at a low discharge rate) (51) (Fig. 8). So, there are features like this increased capacity or the improved diffusion of lithium [Li^+ diffusion coefficients were found to be one order of magnitude higher in the nanocomposites than in pristine V_2O_5 (50)] that make the performance of the nanocomposite materials superior to the sum of its components (52). Unfortunately, owing to the possible presence of benzidine moieties in the polyaniline backbone, the application of such nanocomposites is limited since they might yield toxic (carcinogenic) products upon degradation. So, the intercalation of the more "environment-friendly" poly(3,4-ethylene dioxythiophene) (PEDOT) in vanadium pentoxide was investigated (46). These experiments were performed with crystalline V_2O_5 and 3,4-ethylene dioxythiophene in water refluxing for 12 h. Interestingly, as a function of the EDOT amount, the interslab spacing of V_2O_5 expands in two stages, consistently with the intercalation of a first monolayer of PEDOT for low monomer concentration and the intercalation of a second monolayer for higher concentrations. The application potential of these nanocomposites as cathode materials in rechargeable lithium batteries was demonstrated by the electrochemical insertion of lithium, showing a discharge capacity superior to 300 mA · h/g (compared to 140 mA · h/g for pristine V_2O_5) with a better

reversibility, presumably because of the structural stabilization of the crystalline oxide as the consequence of the polymer presence between its slabs (53).

Oxovanadium phosphates, $VOPO_4$ and more expanded α-$VOPO_4 \cdot 2H_2O$, are layered compounds obtained by refluxing V_2O_5 in phosphoric acid and also known for accommodating organic and organometallic compounds between their slabs through redox reactions. Methyl-substituted pyrrole derivatives (3-methylpyrrole and 3,4-dimethylpyrrole) can be oxidatively polymerized in the $VOPO_4$ interslab space, whereas pyrrole is polymerized only on the grain surface without intercalation (54). The oligomerization indeed would occur at the interface of the $VOPO_4$ lattice and the intercalation of these oligomers would indeed depend on the regularity of their chain structure: poly(3-methylpyrrole) and poly(3,4-dimethylpyrrole) form a straight-chain structure which would be suitable for intercalation, whereas partially branched chains of polypyrrole could not be inserted (Fig. 9). Indeed, further experiments showed that intercalated polypyrrole can be obtained more readily in cast films by contact with pyrrole vapors (39). In the case of aniline (but also of 4-anilinoaniline and 4-anilinoanilinium iodide), its intercalation as anilinium cation was shown, but it does not polymerize spontaneously in the interslab space (49) or it gives short oligomers unable to enhance the electrical conductivity of the nanocomposite (55). So, the reactivity of $VOPO_4$ would be likely different from that of V_2O_5 xerogel and it was suggested that a possible reason could be the longer distance between intercalated monomer and the nearest-neighboring vanadium

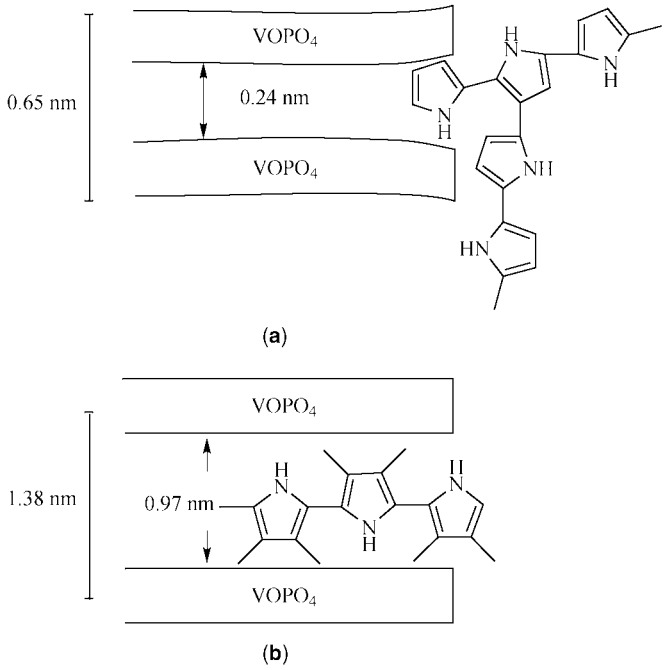

Fig. 9. Schematic representation of the intercalation of (**a**) polypyrrole and (**b**) poly(3,4-dimethylpyrrole) moieties into the $VOPO_4$ interslab space. Reproduced from Ref. 54, with permission of The Royal Society of Chemistry.

atoms in the case of the phosphate (49). Nevertheless, the *in situ* polymerization of aniline may be achieved by treatment with Cu^{2+} ions ($CuCl_2$) (56).

In contrast to layered metal chalcogenides, oxides, and thiophosphates, layered transition-metal halides have not received much attention in the study of intercalation, because most of them are not very stable, even under mild conditions in which they are generally hydrolyzed, solubilized, or decomposed. α-$RuCl_3$ is a notable exception and is very stable under these conditions. Cations can be intercalated reductively or through ion exchange, while neutral polar molecules can be incorporated through solvent exchange. It was recently demonstrated that it is also a suitable host for macromolecules (encapsulative precipitation) (57) and in particular for polyaniline through a RIP process (37). The reaction is carried out from a solution of aniline in acetonitrile in open air at ambient temperature for 1 week. XRD and infrared spectroscopy data are consistent with the formation of the conductive polymer (emeraldine salt form) in the interslab space. Similar to the intercalative polymerization of aniline into FeOCl and V_2O_5, the presence of oxygen is key to a successful outcome of the reaction. So, heating the product at 120°C in air for 5 days allows to complete the polymerization. On the other hand, a control experiment in the absence of air or oxygen showed that no intercalation reaction occurred after 23 days. The electrical conductivity of the nanocomposite at room temperature is ~2 S/cm, three orders of magnitude higher than that of α-$RuCl_3$. Moreover, in contrast to pristine α-$RuCl_3$, which shows antiferromagnetic ordering below 15.6 K, the nanocomposite does not exhibit this transition, because of the presence of diamagnetic Ru^{2+} centers (due to the partial reduction of Ru^{3+} through the RIP process) and the increased separation of the $RuCl_3$ slabs. The potential applications of such polyaniline/α-$RuCl_3$ nanocomposites will probably be derived from the combination of the high conductivity of polyaniline and the wide-ranging catalytic properties of $RuCl_3$, providing new materials with valuable electrocatalytic properties.

Monomer Intercalation and Subsequent Controlled *In Situ* Polymerization

The observation of the spontaneous polymerization of intercalated monomers is essentially limited to the cases of very oxidizing hosts accommodating monomers able to oxidatively polymerize (leading to electroactive polymers) or to very acidic and/or transition-metal-exchanged aluminosilicates. In all other cases, the polymerization is generally not spontaneous and it has to be initiated or catalyzed in a second step through the use of an external compound.

Oxidative polymerization. In Na-exchanged or Cs-exchanged montmorillonites, anilinium chloride may be readily intercalated by ion-exchange reaction at ambient temperature in a few hours. The oxidative polymerization may be performed by electropolymerization (58): the anilinium/montmorillonite nanocomposite is used as electrode and electrolyzed galvanostatically at 20 $\mu A/cm^2$ in 2 *M* HCl up to 20 mC/cm^2. The clay-modified electrode changes its color from white to blue and this blue color cannot be removed (even by washing with organic solvents) suggesting that the intercalated aniline is polymerized during the electrolysis. Another polymerization route consists in using an external oxidant

such as ammonium peroxodisulfate at 0°C for 1 day in water, where the nanocomposite is dispersed (59). Peroxodisulfate may also be used for oxidizing aniline in other layered hosts, whose intrinsic redox potential is not sufficient: MoO_3 (60) or layered Brønsted acids, such as $HCa_2Nb_3O_{10}$, $HCa_2Nb_2MO_9$ (M = Al, Fe) (61), and $AlH_2P_3O_{10} \cdot 2H_2O$ (62), where aniline is previously intercalated through acid–base interaction. In other examples, the aniline intercalated in MoO3 is oxidized by iron(III) chloride (63), aqueous H_2O_2, or iodine vapor (64). These oxidants are generally used in the proportion of 2 equiv per equivalent of aniline. Sometimes, atmospheric oxygen through a thermal treatment at 130°C in air is efficient enough, for instance when aniline is intercalated in layered metal phosphate $HUO_2PO_4 \cdot 4H_2O$ (65,66) or α-$M(HOPO_3)_2 \cdot H_2O$ (M = Zr, Ti) (66) and in trirutile-like layered oxides $HMWO_6 \cdot nH_2O$ (67) or $HMMoO_6 \cdot H_2O$ (68) (M = Nb, Ta).

Free-Radical Polymerization. The earliest works in these layered nanocomposites are also more complete from the point of view of the polymer chemistry (69). These studies concerned the adsorption of MMA monolayers (through dipole–ion interactions) between the slabs of Na-exchanged montmorillonite and the free-radical polymerization MMA initiated by thermolysis of cointercalated benzoyl peroxide or azobisisobutyronitrile or with γ-ray initiation. It was shown that γ-ray doses or initiator concentrations necessary to induce the polymerization are higher than those allowing comparable bulk polymerizations. The polymerized nanocomposites appeared to resist thermal degradation under conditions at which complete degradation of free polymer was found (70). This effect would be due to steric factors hindering the thermal motion of the macromolecule segments sandwiched between the slabs of montmorillonite. Moreover, it would appear that the macromolecules liberated by dissolution of the mineral by HF have a greater thermal stability than macromolecules made in a conventional free-radical technique. An NMR spectroscopy study of the liberated macromolecules showed a pronounced isotactic component which is weak in the reference PMMA (71). Isotacticity increases as the monomer intercalation yield decreases and it reaches a plateau for yields corresponding to a monolayer arrangement between the slabs, indicating that the mechanism which leads to stereospecificity is confined to the interslab space. A model was proposed where the exchangeable cations (such as sodium), which randomly populate the interslab space, interact through dipole–ion interactions with the carbonyl group of two monomers (Fig. 10). Thus coordinated, both

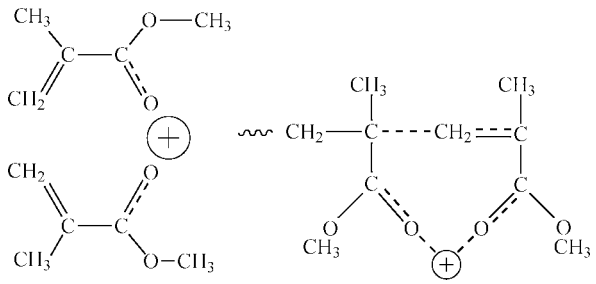

Fig. 10. Schematic representation showing how in the interslab space the dipole–ion interactions between two MMA monomers and one exchangeable cation would lead to the formation of an isotactic diad. From Ref. 71, with permission.

monomers would lead to the formation of an isotactic diad, increasing therefore the stereoregularity of the macromolecules. By varying the nature of the exchangeable cations, it was observed that the percentage of isotactic triads increases with increasing strength of the dipole–ion interactions (72). At least, the polymerization conversion yield depends strongly on the nature of the exchangeable cations: $Na^+ < K^+ < Cs^+$ and $Mg^{2+} < Ca^{2+} < Sr^{2+} < Ba^{2+}$, ie, with increasing interaction energy (73). The polymerization rate does not depend significantly on monomer surface concentration up to a critical value below which the rate drops dramatically. The overall energy of activation was found to be similar to the value for bulk polymerization and it was suggested that steric effects, reducing the mobility of monomer molecules within the interslab space, are responsible for the decrease in polymerization rates. A further example of γ-ray-initiated polymerization was reported with vinyl acetate intercalated in Na-exchanged montmorillonite (74).

Propargylamine and aminoacetonitrile may be readily intercalated through acid–base interaction within the interslab spaces of α-$M(HOPO_3)_2 \cdot H_2O$ (M = Zr, Sn) (75). Their subsequent thermal treatment (150–180°C for 24 h in air) or UV irradiation (550 W medium pressure Hg lamp for 11 days) results in polymerization of the guest molecules. However, if the photochemical reaction does not reduce the crystallinity of the initial materials, its extent is more limited, as observed by ^{13}C CP-MAS NMR spectroscopy. In all cases, these polymerized nanocomposites are insulators as pressed powder pellets ($\sigma < 10^{-8}$ S/cm). Heating these compounds to 300°C in argon turns them black and at temperature over 750°C the graphitization reaction leads to conductivities up to 1 S/cm.

Last examples are taken in the fields of layered double hydroxides (LDH) whose general formula is $[M^{II}_{1-x}M'^{III}_x(OH)_2]^{x+}_{\text{slab}}\,[A^{n-}_{x/n} \cdot mH_2O]^{x-}_{\text{interslab space}}$ and the structure derives from the natural hydrotalcite (M = Mg; M′ = Al, $A^{n-} = CO_3^{2-}$ and $0.22 < x < 0.33$). Partial M^{II} to M^{III} substitution induces a positive charge for the layers, balanced with the presence of exchangeable anions A^{n-} between the slabs. So, acrylate anions were intercalated through anion exchange and subsequently polymerized by thermal treatment at 80°C in the presence of potassium peroxodisulfate (76). The interslab distance was found to slightly decrease from 1.38 to 1.34 nm. Infrared data confirmed the disappearance of the C=C vibration band. Acrylate anions are also readily intercalated in nickel-based LDH, leading to $[Ni_{0.7}M'_{0.3}(OH)_2]^{0.3+}[(\text{acrylate})^-_{0.3} \cdot \frac{1}{2}H_2O]^-$ where M′ = Fe or Co, through the reduction of the corresponding layered γ-oxyhydroxide in dispersion in an aqueous solution of acrylate (77,78). The nature of the substituting cation in the slabs appears to strongly influence the polymerization mechanism. When M′ = Fe, the LDH containing monomer anions may be isolated and then interslab free-radical polymerization of acrylate anions was successfully initiated by potassium peroxodisulfate. On the contrary, a one-step process occurs if M′ = Co, leading straight to LDH containing polyacrylate anions. The true role of the substituting cation M′ is not yet well understood, nevertheless it would seem that in this last case, a free-radical polymerization mechanism could also be suggested, but involving a redox initiation step where a few acrylate anions would be oxidized during the intercalation reaction and would lead to the formation of radical carbonium ions. The *in situ* polymerized macromolecules were extracted from interslab spaces by anionic exchange, derivatized into poly(methyl acrylate),

and analyzed by SEC. Only oligomers were detected with weight-average molar masses ranging from 300 to 2900 g/mol vs. polystyrene standards (79).

Miscellaneous Polymerization. Pioneering works demonstrated the feasibility of the intercalation of 6-aminocaproic acid between the slabs of various Na^+-, Ca^{2+}-, Mg^{2+}-, Co^{2+}-, and Cu^{2+}-exchanged montmorillonites, where it arranges as a monolayer or a bilayer as a function of the intercalated amount (80). It was found from infrared data that Cu in Cu^{2+}-exchanged nanocomposites was strongly bonded to the amino acid. In a second step, 6-aminocaproic acid was *in situ* polymerized by thermal treatment at 250°C for 1 h in nitrogen flow. A step polymerization mechanism was suggested with the condensation of protonated $-NH_3^+$ groups with —COOH ones. Thermogravimetric results showed that the thermal stability of the polymerized nanocomposites is lower in Cu^{2+}-exchanged montmorillonite than in the other materials, probably because of a lesser degree of polymerization partially inhibited by the strong bonding between cations and monomers. Similar results were observed in α-$Zr(HOPO_3)_2 \cdot H_2O$, where the head-by-tail arrangement of the 6-aminocaproic acid monomers organized by the host matrix is conducive to polyamide formation (81). Evidence for *in situ* polymerization came again from thermogravimetric analysis, infrared spectroscopy, and ^{13}CCP-MAS NMR spectroscopy data. From differential thermal analysis results, it was found that, in contrast to the bulk polymer, which shows a melting transition at 229°C, the polyamide-based nanocomposite shows no thermal events over the range 80–320°C. This difference in behavior between bulk and confined macromolecules is attributed to inhibited formation of polymer crystallites within a spatially restricted environment of a layered matrix. More recently, negatively charged aspartic acid was intercalated within the interslab space of LDH based on magnesium and aluminum through a coprecipitation technique involving simultaneous formation of the inorganic slabs and intercalation of the anionic species (encapsulative precipitation) (82). *In situ* thermal polycondensation of aspartate monomer was performed at 220°C in air for 24 h leading to a poly(α,β-aspartate) based nanocomposite. The observed decrease in basal spacing and structural order was attributed at once to the polycondensation reaction and to the loss of intercalated water molecules. A last example concerns the intercalation of β-alanine into kaolinite by the guest displacement method using ammonium acetate based kaolinite as the intermediate (83). Zwitterionic β-alanine was ordered in a monolayer arrangement between the layers. Although the intercalated monomer was mostly polymerized by thermal treatment at 250°C for 10 h under nitrogen atmosphere, a part of the guest species was decomposed to acrylic acid and NH_3 gas.

The *in situ* thermal polymerization of ε-caprolactone in Cr^{3+}-exchanged fluorohectorite was also reported (84). The basal spacing observed prior to polymerization was found to be consistent with the orientation of the ε-caprolactone ring perpendicular to the silicate layers (Fig. 11). After polymerization, the decrease in the basal spacing is consistent with the dimensional change accompanying the ring-opening polymerization. The polymerization reaction appears to proceed through cleavage of the acyl-oxygen bond catalyzed by the interslab Cr^{3+} ions. It may be noticed that, in that example, between the monomer intercalation step at room temperature and the polymerization step at 100°C, the excess monomer was not removed. Therefore, the final material may be described as poly(ε-caprolactone) intercalated silicate particles embedded in the same polymer matrix. In similar

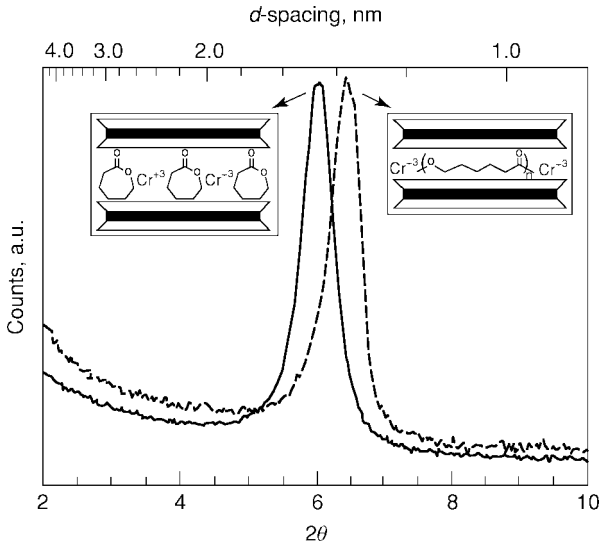

Fig. 11. Powder XRD patterns of ε-caprolactone–fluorohectorite nanocomposite before (solid line) and after (dashed line) polymerization. Insets are schematic illustrations (not drawn to scale) corresponding to the intercalated monomer (left) and intercalated macromolecule (right). Reprinted with permission from Ref. 84. Copyright (1993) American Chemical Society.

cases, the delamination is often observed leading to delaminated (or exfoliated) nanocomposites, especially in the field of aluminosilicates (see NANOCOMPOSITES, POLYMER-CLAY).

In this article, a great number of synthetic pathways leading to polymer-layered nanocomposites have been reported. The structure and the original properties of these new materials were greatly investigated, in particular from the viewpoint of their ionic or electron conductivity and their thermal stability. Nevertheless, only a small part of these works were focused on the study of the polymerization mechanisms at work and/or on the thorough analysis of the stereoregularity and the skeletal structure of intercalated macromolecules. So, a lot of research remains to be carried out in order to fully understand these factors and to prove that such routes are of industrial interest for the synthesis of well-defined polymers.

BIBLIOGRAPHY

1. D. O'Hare, in D. W. Bruce and D. O'Hare, eds., *Inorganic Materials*, John Wiley & Sons, Inc., New York, 1992, pp. 166, 235.
2. R. Schöllhorn, *Chem. Mater.* **8**, 1747 (1996).
3. P. B. Messersmith and S. I. Stupp, *J. Mater. Res.* **7**, 2599 (1992).
4. C. O. Oriakhi, I. V. Farr, and M. M. Lerner, *J. Mater. Chem.* **6**(1), 103 (1996).
5. E. Ruiz-Hitzky, R. Jimenez, B. Casal, V. Manriquez, A. Santa Ana, and G. Gonzalez, *Adv. Mater.* **5**, 738 (1993).

6. M. G. Kanatzidis, R. Bissessur, D. C. DeGroot, J. L. Schindler, and C. R. Kannewurf, *Chem. Mater.* **5**, 595 (1993).
7. M. Alexandre and P. Dubois, *Mater. Sci. Eng.* **28**, 1 (2000).
8. T. J. Pinnavaia and G. W. Beall, eds., *Polymer-Clay Nanocomposites*, John Wiley & Sons, Ltd., New York, 2001.
9. R. A. Vaia and E. P. Giannelis,*MRS Bull.*, 394 (2001).
10. M. Ogawa, M. Inagaki, N. Kodama, K. Kuroda, and C. Kato, *J. Phys. Chem.* **97**, 3819 (1993).
11. Y. Komori and K. Kuroda, in Ref. 8, pp. 4, 18.
12. S. Yamanaka, *Ceram. Bull.* **70**, 1056 (1991).
13. E. Ruiz-Hitzky and P. Aranda, *Adv. Mater.* **2**, 545 (1990).
14. P. Aranda and E. Ruiz-Hitzky, *Acta Polym.* **45**, 59 (1994).
15. P. Aranda and E. Ruiz-Hitzky, *Chem. Mater.* **4**, 1395 (1992).
16. E. Ruiz-Hitzky and P. Aranda, in Ref. 8, pp. 19, 46.
17. I. Lagadic, A. Léaustic, and C. Clément, *J. Chem. Soc., Chem. Commun.*, 1396 (1992).
18. P. Jeevanandam and S. Vasudevan, *Chem. Mater.* **10**, 1276 (1998).
19. L. F. Nazar, H. Wu, and W. P. Power, *J. Mater. Chem.* **5**, 1985 (1995).
20. C. O. Oriakhi, R. L. Nafshun, and M. M. Lerner, *Mater. Res. Bull.* **31**, 1513 (1996).
21. D. Yang and R. F. Frindt, *J. Mater. Res.* **15**, 2408 (2000).
22. L. F. Nazar, Z. Zhang, and D. Zinkweg, *J. Am. Chem. Soc.* **114**, 6239 (1992).
23. Y. J. Liu, D. C. DeGroot, J. L. Schindler, C. R. Kannewurf, and M. G. Kanatzidis, *Chem. Mater.* **3**, 992 (1991).
24. Y. J. Liu, D. C. DeGroot, J. L. Schindler, C. R. Kannewurf, and M. G. Kanatzidis, *Adv. Mater.* **5**, 369 (1993).
25. E. Ruiz-Hitzky, P. Aranda, and B. Casal, *J. Mater. Chem.* **2**, 581 (1992).
26. T. A. Kerr, F. Leroux, and L. F. Nazar, *Chem. Mater.* **10**, 2588 (1998).
27. J. J. Tunney and C. Detellier, *Chem. Mater.* **8**, 927 (1996).
28. Y. Komori, Y. Sugahara, and K. Kuroda, *Chem. Mater.* **11**, 3 (1999).
29. H. Z. Friedlander and C. R. Frink, *J. Polym. Sci., Polym. Lett.* **2**, 475 (1964).
30. M. P. Eastman and T. L. Porter, in Ref. 8, pp. 65, 93.
31. T. L. Porter, M. P. Eastman, D. Y. Zhang, and M. E. Hagerman, *J. Phys. Chem., B* **101**, 11106 (1997).
32. V. Mehrotra and E. P. Giannelis, *Solid State Commun.* **77**, 155 (1991).
33. V. Mehrotra and E. P. Giannelis, *Solid State Ionics* **51**, 115 (1992).
34. M. P. Eastman, E. Bain, T. L. Porter, K. Manygoats, R. Whitehorse, R. A. Parnell, and M. E. Hagerman, *Appl. Clay Sci.* **15**, 173 (1999).
35. H. B. Liu, D. W. Kim, A. Blumstein, J. Kumar, and S. K. Tripathy, *Chem. Mater.* **13**, 2756 (2001).
36. D. W. Kim, A. Blumstein, H. Liu, M. J. Downey, J. Kumar, and S. K. Tripathy, *J. Macromol. Sci.: Pure Appl. Chem., A* **38**, 1405 (2001).
37. L. Wang, P. Brazis, M. Rocci, C. R. Kannewurf, and M. G. Kanatzidis, *Chem. Mater.* **10**, 3298 (1998).
38. M. G. Kanatzidis, L. M. Tonge, and T. J. Marks, *J. Am. Chem. Soc.* **109**, 3797 (1987).
39. A. De Stefanis, S. Foglia, and A. A. G. Tomlinson, *J. Mater. Chem.* **5**, 475 (1995).
40. M. G. Kanatzidis, H. O. Marcy, W. J. McCarthy, C. R. Kannewurf, and T. J. Marks, *Solid State Ionics*, **32/33**, 594 (1989).
41. C. G. Wu, D. C. DeGroot, H. O. Marcy, J. L. Schindler, C. R. Kannewurf, T. Bakas, V. Papaefthymiou, W. Hirpo, J. P. Yesinowski, Y. J. Liu, and M. G. Kanatzidis, *J. Am. Chem. Soc.* **117**, 9229 (1995).
42. M. G. Kanatzidis and C. G. Wu, *J. Am. Chem. Soc.* **111**, 4139 (1989).
43. C. G. Wu, M. G. Kanatzidis, H. O. Marcy, D. C. DeGroot, and C. R. Kannewurf, *Polym. Mater. Sci. Eng.* **61**, 969 (1989).

44. M. G. Kanatzidis, C. G. Wu, H. O. Marcy, D. C. DeGroot, and C. R. Kannewurf, *Chem. Mater.* **2**, 222 (1990).
45. E. Shouji and D. A. Buttry, *Langmuir* **15**, 669 (1999).
46. A. V. Murugan, B. B. Kale, C. W. Kwon, G. Campet, and K. Vijayamohanan, *J. Mater. Chem.* **11**, 2470 (2001).
47. Y. J. Liu, D. C. DeGroot, J. L. Schindler, C. R. Kannewurf, and M. G. Kanatzidis, *J. Chem. Soc., Chem. Commun.* **1993**, 593 (1993).
48. C. G. Wu, D. C. DeGroot, H. O. Marcy, J. L. Schindler, C. R. Kannewurf, Y. J. Liu, W. Hirpo, and M. G. Kanatzidis, *Chem. Mater.* **8**, 1992 (1996).
49. H. Nakajima and G. Matsubayashi, *J. Mater. Chem.* **5**, 105 (1995).
50. F. Leroux, G. Goward, W. P. Power, and L. F. Nazar, *J. Electrochem. Soc.* **144**, 3886 (1997).
51. M. Lira-Cantu and P. Gomez-Romero, *J. Electrochem. Soc.* **146**, 2029 (1999).
52. P. Gomez-Romero, *Adv. Mater.* **13**, 163 (2001).
53. A. V. Murugan, C. W. Kwon, G. Campet, B. B. Kale, T. Maddanimath, and K. Vijayamohanan, *J. Power Sources* **105**, 1 (2002).
54. H. Nakajima and G. Matsubayashi, *J. Mater. Chem.* **4**, 1325 (1994).
55. N. Kinomura, T. Toyama, and N. Kumada, *Solid State Ionics* **78**, 281 (1995).
56. H. Nakajima and G. Matsubayashi, *Chem. Lett.*, 423 (1993).
57. L. Wang, M. Rocci-Lane, P. Brazis, C. R. Kannewurf, Y. I. Kim, W. Lee, J. H. Choy, and M. G. Kanatzidis, *J. Am. Chem. Soc.* **122**, 6629 (2000).
58. H. Inoue and H. Yoneyama, *J. Electroanal. Chem.* **233**, 291 (1987).
59. T. C. Chang, S. Y. Ho, and K. J. Chao, *J. Chin. Chem. Soc.* **39**, 209 (1992).
60. R. Bissessur, D. C. DeGroot, J. L. Schindler, C. R. Kannewurf, and M. G. Kanatzidis, *J. Chem. Soc., Chem. Commun.* **1993**, 687 (1993).
61. S. Uma and J. Gopalakrishnan, *Mater. Sci. Eng., B* **34**, 175 (1995).
62. H. Tagaya, S. Shigemitsu, N. Kuramoto, J. I. Kadokawa, M. Karasu, and K. Chiba, *J. Incl. Phenom. Mol. Recognit. Chem.* **18**, 193 (1994).
63. T. A. Kerr, H. Wu, and L. F. Nazar, *Chem. Mater.* **8**, 2005 (1996).
64. P. G. Hill, P. J. S. Foot, and R. Davis, *Mater. Sci. Forum* **191**, 43 (1995).
65. Y. J. Liu and M. G. Kanatzidis, *Inorg. Chem.* **32**, 2989 (1993).
66. Y. J. Liu and M. G. Kanatzidis, *Chem. Mater.* **7**, 1525 (1995).
67. B. E. Koene and L. F. Nazar, *Solid State Ionics* **89**, 147 (1996).
68. N. S. P. Bhuvanesh and J. Gopalakrishnan, *Mater. Sci. Eng., B* **53**, 267 (1998).
69. A. Blumstein, *J. Polym. Sci.* **3**, 2653 (1965).
70. A. Blumstein, *J. Polym. Sci.* **3**, 2665 (1965).
71. A. Blumstein, S. L. Malhotra, and A. C. Watterson, *J. Polym. Sci.: Part A-2* **8**, 1599 (1970).
72. A. Blumstein, K. K. Parikh, L. Shadi, and R. Blumstein, *J. Polym. Sci.* **9**, 1681 (1971).
73. S. L. Malhotra, K. K. Parikh, and A. Blumstein, *J. Colloid. Inter. Sci.* **41**, 318 (1972).
74. N. Sonobe, T. Kyotani, and A. Tomita, *Carbon* **28**, 483 (1990).
75. J. E. Pillion and M. E. Thompson, *Chem. Mater.* **3**, 777 (1991).
76. M. Tanaka, I. Y. Park, K. Kuroda, and C. Kato, *Bull. Chem. Soc. Jpn.* **62**, 3442 (1989).
77. S. Rey, J. Mérida-Robles, K. S. Han, L. Guerlou-Demourgues, C. Delmas, and E. Duguet, *Polym. Int.* **48**, 277 (1999).
78. C. Vaysse, L. Guerlou-Demourgues, E. Duguet, and C. Delmas, *Inorg. Chem.* **42**, 4559 (2003).
79. C. Vaysse, L. Guerlou-Demourgues, C. Delmas, and E. Duguet, *Macromolecules* **37**, 45 (2004).
80. C. Kato, K. Kuroda, and M. Misawa, *Clays Clay Miner.* **27**, 129 (1979).
81. Y. Ding, D. J. Jones, P. Maireles Torres, and J. Rozière, *Chem. Mater.* **7**, 562 (1995).

82. N. T. Whilton, P. J. Vickers, and S. Mann, *J. Mater. Chem.* **7**, 1623 (1997).
83. T. Itagaki, Y. Komori, Y. Sugahara, and K. Kuroda, *J. Mater. Chem.* **11**, 3291 (2001).
84. P. B. Messersmith and E. P. Giannelis, *Chem. Mater.* **5**, 1064 (1993).

ETIENNE DUGUET
STÉPHANIE REY
JOSEPHA MARIA MERIDA ROBLES
Institut de Chimie de la Matière Condensée de Bordeaux, CNRS &
Université des Sciences et Technologies de Bordeaux

INTERFACIAL PROPERTIES.

See SURFACE PROPERTIES.

INTERPENETRATING POLYMER NETWORKS

Introduction

An *interpenetrating polymer network*, IPN, is defined as a combination of two polymers in network form, at least one of which is synthesized and/or cross-linked in the immediate presence of the other (1). An IPN is distinguished from other multipolymer combinations such as Polymer Blends (qv), blocks, and grafts in two ways: (*1*) An IPN swells, but does not dissolve in solvents; and (*2*) creep and flow are suppressed (see BLOCK COPOLYMERS; GRAFT COPOLYMERS).

The above represents the classical definition of an IPN. The term *interpenetrating polymer network* was coined before the extent or consequences of phase separation were fully realized. This article covers sequential and simultaneous types of IPNs made in bulk and also includes such materials as IPNs based on latexes and suspension-sized particles; thermoplastic IPNs, which contain physical cross-links in one or both polymers, and hence may be (partly) soluble; and a number of other closely related materials.

Some applications of IPNs of note include sound and vibration damping, biomedical applications, natural products and renewable resources, tough and impact-resistant materials, etc. IPN review articles include those by Sperling and Hu (2), Lipatov (3), and Athawale and co-workers (4). There are also papers of note by Srivastava and co-workers (5), and edited books by Klempner and co-workers (6), and Kim and Sperling (7). Two older books review early references, and develop the concepts of IPNs (1,8).

Nomenclature. The IPNs have a well-developed nomenclature (9), as do most multicomponent polymeric materials (10). Thus, a cross-linked polymer network is indicated by the prefix *net-*, and an IPN is indicated by the connective *-ipn-*. Thus, an IPN of polybutadiene and polystyrene is written as

Encyclopedia of Polymer Science and Technology. Copyright John Wiley & Sons, Inc. All rights reserved.

(*net*-polybutadiene)-*ipn*-(*net*-polystyrene)

and if copolymers and/or two-worded mer structures are needed, brackets are employed:

{*net*-poly(styrene-*stat*-butadiene)}-*ipn*-{*net*-poly(ethyl acrylate)}

Synthesis and Structure of IPN and SIN Materials

Figure 1 models the structure of interpenetrating polymer networks and related materials. Solid and dotted lines indicate polymer 1 and polymer 2, respectively. The dots indicate cross-links. Structure a indicates a polymer blend, where the two polymers are mixed, but not bonded together anywhere. Structure b indicates a graft copolymer (qv), where polymer 2 is bonded along the side of polymer 1. Structure c indicates a block copolymer (qv), where polymers 1 and 2 are bonded end-on-end. These three structures are all thermoplastic, in that, not being cross-linked, they flow if heated above their glass transition and/or melting temperatures.

Structure d illustrates an AB–cross-linked copolymer. In this case, polymers 1 and 2 are bonded to each other. Structure e indicates an IPN, sometimes called a

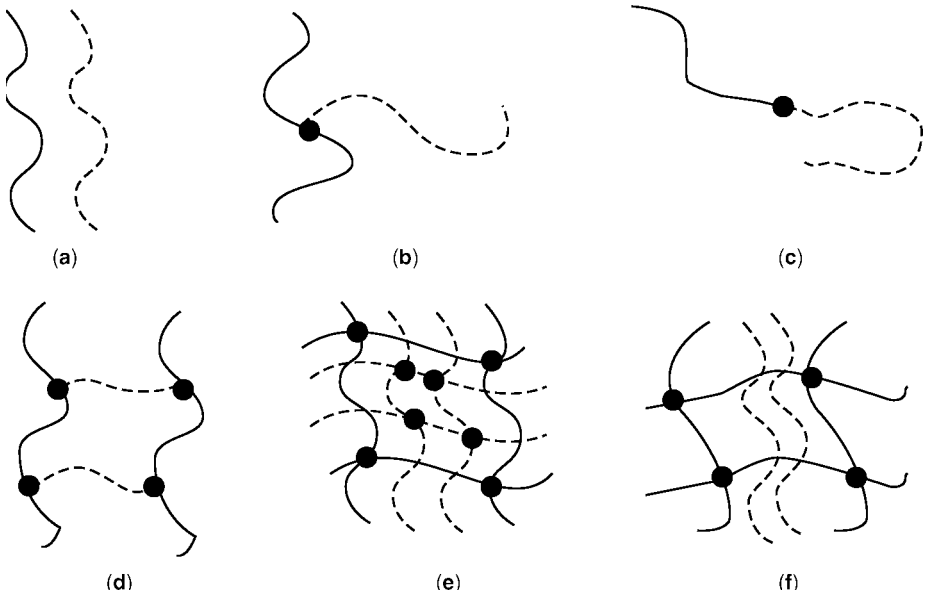

Fig. 1. Six basic combinations of two polymers, represented by solid and dashed lines, respectively, and the dots representing covalent bonds. (**a**) A polymer blend, with no bonding between the chains; (**b**) a graft copolymer, with the dashed polymer bonded to the side of the solid line polymer; (**c**) a block copolymer, where the chains are bonded end-on-end; (**d**) an AB-cross-linked copolymer, where one polymer is bonded to the other, but not to itself; (**e**) an interpenetrating polymer network of two cross-linked polymers; (**f**) a semi-interpenetrating polymer network, where only one of the polymers is cross-linked.

full IPN, where both polymers are cross-linked. Structure f illustrates a semi-IPN, where one polymer, but not both, are cross-linked. These last three structures are all thermoset, because at least one polymer network pervades the entire material. Thus, they will not flow on heating.

Of course, one may imagine many related structures and/or more complex topologies. By simple analogy, three or more polymers may coexist in any one of the topologies of Figure 1. Some quite different materials include the polyrotaxanes, where rings encircle a polymer chain (11); catenanes (12), where a series of rings form a chain (13); and dendrimers. These latter are hyperbranched, fractal-like structures emanating from a central core and containing a large number of terminal groups (14) (see DENDRONIZED POLYMERS). Noting that the polyrotaxanes, catenanes, and dendrimers are usually one-phase polymers, their behavior is quite different from that of any of the structures shown in Figure 1.

Figure 2 (15) outlines the two basic methods of IPN synthesis. In Figure 2, the boxes indicate monomers, the X's indicate cross-links, and the subscripts indicate whether it goes to make up polymer 1 or polymer 2. As in Figure 1, the lines indicate the polymers and the dots indicate cross-links. The P_1 and P_2 above the arrows indicate polymerization of polymer 1 and polymer 2, respectively.

The general procedure to synthesize a sequential IPN calls for mixing monomer 1 and cross-linker 1 and polymerizing to form network 1. Then, monomer 2 and cross-linker 2 are swollen in, and polymerized *in situ*.

A simultaneous interpenetrating network, SIN, as the name suggests, starts with a mix of both monomers and both polymers. These are polymerized simultaneously, but by different routes, such as chain and step polymerization. Thus, while reacting, the two polymers do not interfere with each other, but merely dilute

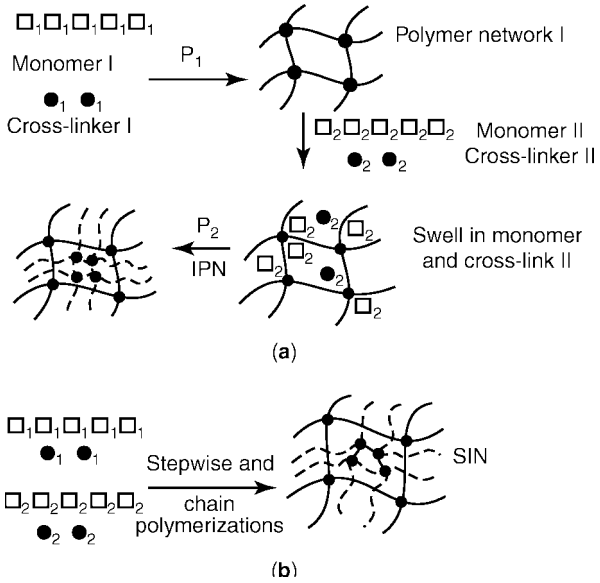

Fig. 2. Two basic synthetic methods of preparing IPNs, sequentially and simultaneously. (**a**) Sequential IPNs; (**b**) simultaneous interpenetrating network (SIN).

each other. Of course, the rates of the two reactions need not be equal. As explored below, if one polymer or the other reacts faster, different morphologies may result, with concomitant different physical and mechanical behavior patterns.

Besides sequential and simultaneous IPN synthetic methods, there are several other methods of preparation:

Latex IPNs. The polymers are made via emulsion polymerization, each particle constituting a micro-IPN. Frequently, one monomer and cross-linker are polymerized, followed by addition of a second monomer and cross-linker, which is also polymerized. Depending on the rates of monomer addition relative to the rates of polymerization, various degrees of interpenetrating and/or core-shell morphologies may result.

Gradient IPNs. The overall composition and/or cross-link density of the material varies from location to location on the macroscopic scale. One way of preparing these materials involves partial swelling of the first polymer network by the second monomer mix, followed by rapid polymerization before diffusional equilibrium takes place.

Thermoplastic IPNs. These materials utilize physical cross-links rather than chemical cross-links. Thus, the materials may be made to flow at elevated temperatures. As such, they are hybrids between polymer blends and IPNs. Such cross-links may involve block copolymers, ionomers, and/or semicrystallinity.

Semi-IPN. As illustrated in Figure 1**f**, a semi-IPN is composed of a cross-linked polymer and a linear polymer. If one is making a sequential synthesis, the terminology semi-I and semi-II IPNs refers to having the first or second polymer cross-linked, respectively.

Homo-IPNs. These materials consist of two networks prepared from substantially the same cross-linked polymer.

Special Considerations in IPN and SIN Synthesis. Most of the IPNs and SINs made to date rely on chain and/or step polymerization, although other methods, such as anionic polymerization, have been occasionally employed. Of course, appropriate cross-linkers, initiators, and so forth must be added.

For very many IPN and SIN syntheses, except for phase separation aspects, the interaction between the two materials during polymerization has often been ignored. However, to greater or lesser extents in real systems, of course, there is some interaction. A few examples are helpful:

(1) In sequential IPNs, if polymer I is based on a diene, and monomer II (such as styrene) is polymerized *via* free-radical polymerization, some grafting will occur. Of course, this grafting is important for interfacial bonding in such related materials as high impact polystyrene (HIPS) and acrylonitrile–butadiene–styrene (ABS) materials.

(2) If polymer I is an acrylic, the labile hydrogen may be abstracted, providing another type of grafting site.

(3) In a SIN polymerization, the high viscosity of one of the polymers, or its lack of high viscosity as a slow-polymerizing component, may alter the phase morphology or other features.

(4) Vitrification of one of the polymers may slow or stop the polymerization of the other component.

Some specific investigations of the chemical interactions include the following:

Tabka and Widmaier (16,17) undertook the study of the interactions of azo-bis(isobutyronitrile) (AIBN), free-radical initiators with stannous and stannic organotin polyurethane catalysts. These workers found a synergistic effect of stannous octoate on the AIBN on the radical polymerization (qv) of methyl methacrylate, increasing the reaction rate and shortening the gelation time. While there was a severe deactivation of the tin(II) atom by the AIBN, there was no measurable effect using organotin(IV) stannic catalysts.

Michal'chuk and co-workers (18) investigated the changes in mobility during formation on the basis of epoxy and allylic oligomers. Using pulse NMR spectroscopy, these workers concluded that SIN formation results in mutual hindrances to the full conversion of the reactive groups, and a concomitant increase in the number of defects in the IPNs. This results in greater molecular mobility in the final materials than might otherwise be expected.

Polymer Blend and IPN Classification Scheme. Of course, all of the various compositions of matter composed of two polymers are related to each other. Figure 3 (19) illustrates how the major kinds of polymeric materials based on two kinds of mers are related to each other. The IPNs are shown here under the *occasional grafts* heading, because many of the preparations have a few grafts between the two polymers as a consequence of free-radical chemistry, etc. Since one network of these materials is always polymerized in the presence of the other

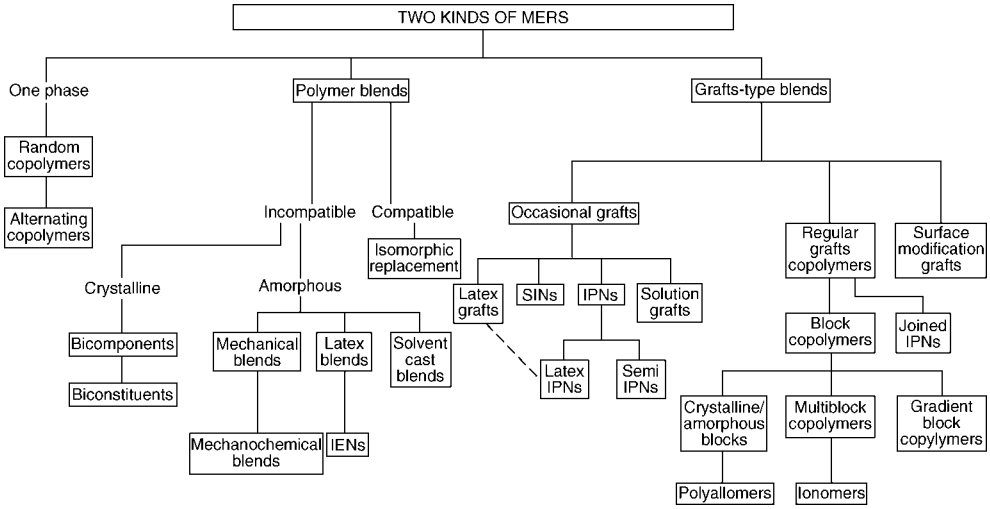

Fig. 3. A polymer blend classification scheme.

network, some grafting is hard to avoid, and in many cases is desired. However, an IPN (or SIN) can be distinguished from a graft copolymer (qv) because the morphology (qv) and mechanical behavior are primarily controlled by the cross-links rather than the grafts.

IPN Morphology and Physical Behavior

Most compositions of matter made up of two polymers (see Fig. 1) exhibit some degree of phase separation. This is caused by the very small entropy of mixing two high molecular weight materials, and the very frequent positive heat of mixing of two different chemical structures. In simple polymer blends (qv), the mixing tends to be relatively coarse, although many routes to complex and relatively finely divided morphologies have been developed. Block copolymers (qv) domain sizes are largely controlled by the molecular weight of the individual blocks, and the domain shape by the relative proportions of the two blocks (20,21).

Electron Microscopy Studies. In sequential IPNs and semi-IPNs, the size and shape of the polymer II domains are controlled by the cross-link density of polymer I and the relative proportions of the two polymers. Figure 4 illustrates

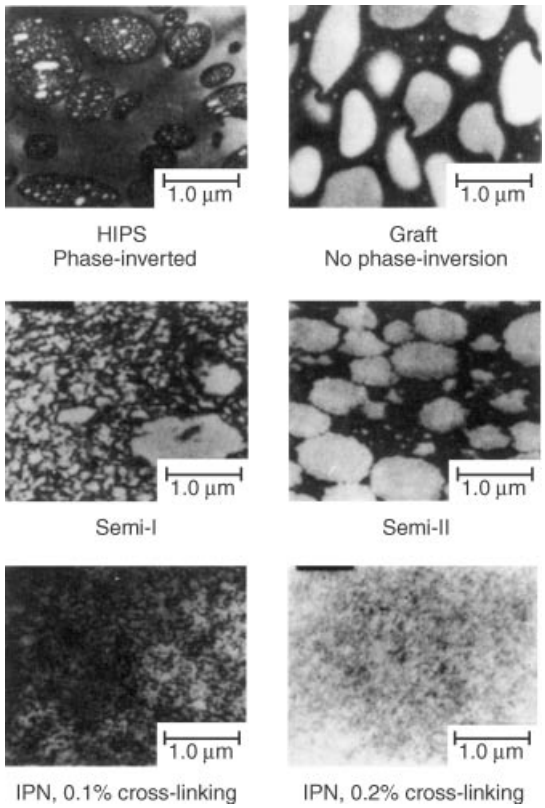

Fig. 4. Transmission electron microscopy of OsO_4-stained polybutadiene and polystyrene (white) combinations.

the two-phased morphology of IPNs, semi-IPNs, and polymer blends prepared from styrene-butadiene copolymers (qv) (SBR) and polystyrene (22) (see STYRENE POLYMERS). The double bonds in the butadiene polymers (qv) are stained dark with osmium tetroxide. In this series of transmission electron micrographs, the samples are sliced to about 60 nm thickness, sometimes called *salami slices*.

The upper left photo in Figure 4 is of HIPS, a material known for its toughness (23). This material is a type of polymer blend made by dissolving polybutadiene or SBR in styrene monomer, and polymerizing *with stirring*. The SBR is first soluble in the styrene monomer, but phase separates after a few percent conversion. Part of HIPS toughness comes from having grafts between the polybutadiene and the polystyrene, and part of the toughness comes from a phase-within-a-phase-within-a-phase morphology (24). Shortly after polymerization is initiated, the growing quantity of polystyrene makes the SBR insoluble in the mix. At first, the SBR phase is the continuous phase. On continued polymerization, the growing volume and increasing viscosity of the polystyrene-rich phase causes a phase inversion, helped by the stirring.

Of course, the styrene within the polybutadiene droplets is also polymerizing, but cannot get out. It forms a very fine structure, also visible in the upper left photo of Figure 4.

HIPS gets its toughness in part from this fine structure, and in part from the grafting that takes place between the SBR and the polystyrene, increasing the interfacial bond strength. (Commercially, block copolymers of polybutadiene and polystyrene are often added to further increase the interfacial bond strength.)

The upper right photo has substantially the same composition as that in the upper left, but was made without stirring. This material was first made in 1927 (25). It did not undergo phase inversion, and hence the SBR remains the continuous phase. This material is adhesive in nature, but not commercial.

The corresponding sequential IPN morphology of the same overall composition is shown in the lower left photo. In this case, a sheet of SBR was cross-linked, followed by swelling in styrene plus divinyl benzene and polymerizing *in situ*. The phase domains are of the order of 100 nm, with both phases exhibiting co-continuity. An increased cross-link level for the SBR results in a finer phase domain structure, as shown in the lower right of Figure 4.

The two semi-IPNs are shown in the middle left and right photos of Figure 4. The semi-I IPN resembles the full IPN, but the morphology is coarser. The semi-II IPN resembles the upper right morphology. Of significant interest here was that the HIPS exhibited a toughness value of about 80 J/m (1.5 ft·lb/in.) of notch, while the middle left had about 160 J/m (3.0 ft·lb/in.), and the lower left had about 267 J/m (5.0 ft·lb/in.) of notch.

The development of the morphology in both the HIPS-type material and the IPNs requires several steps (see Fig. 5) (26). The original polymer I swollen with monomer II solution first has one phase. After a few percent of polymerization, it phase separates via nucleation and growth kinetics. This tends to produce spheroidal-shaped particles, the white material in Figure 5**a**. (Super-saturated salt solutions often follow nucleation and growth phase separation kinetics.) On further polymerization, the phase separation kinetics follows spinodal decomposition, leading to interconnected cylinders (Fig. 5**b**) (27–29). Close examination of both the HIPS and IPN morphologies strongly suggests that spinodal

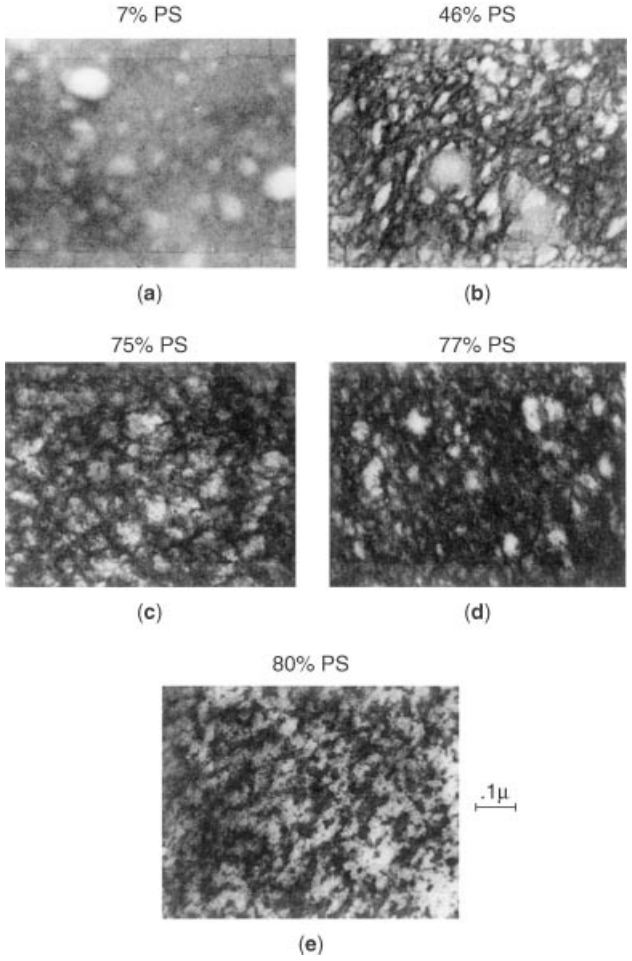

Fig. 5. Transmission electron microscopy of the polymerization of substantially the same composition as shown in the lower left portion of Figure 4.

decomposition plays a strong role in the final morphology of these materials. (Note that a thin section of a cylinder cut at an angle looks like an ellipsoid.) Figures 5**c**, 5**d**, and 5**e** have something of an appearance of a snowstorm, because the continued cross-linking limits phase separation.

Thus, as illustrated in Figure 6, the initial mix first has one phase, then undergoes a region of nucleation and growth. Then, the composition enters the spinodal decomposition region, arriving at the final morphology. Note that if phase separation is more or less complete, the final composition will be a mix of nearly pure polymer I and polymer II, with the final composition being an average.

Phase diagrams of IPNs have also been researched. Sophia and co-workers (30) found that the phase diagram of a semi-IPN indicates a lower critical solution temperature for these materials (Fig. 7), similar to that of polymer blends. Seemingly strange, these materials are more mutually soluble at lower temperatures than at higher temperatures, a consequence of their low entropy of mixing.

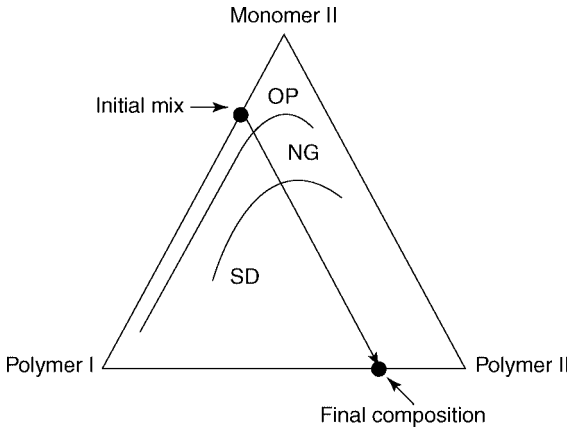

Fig. 6. A generalized phase diagram for the polymerization shown in Figure 5. OP = One phase, NG = nucleation and growth, and SD = spinodal decomposition.

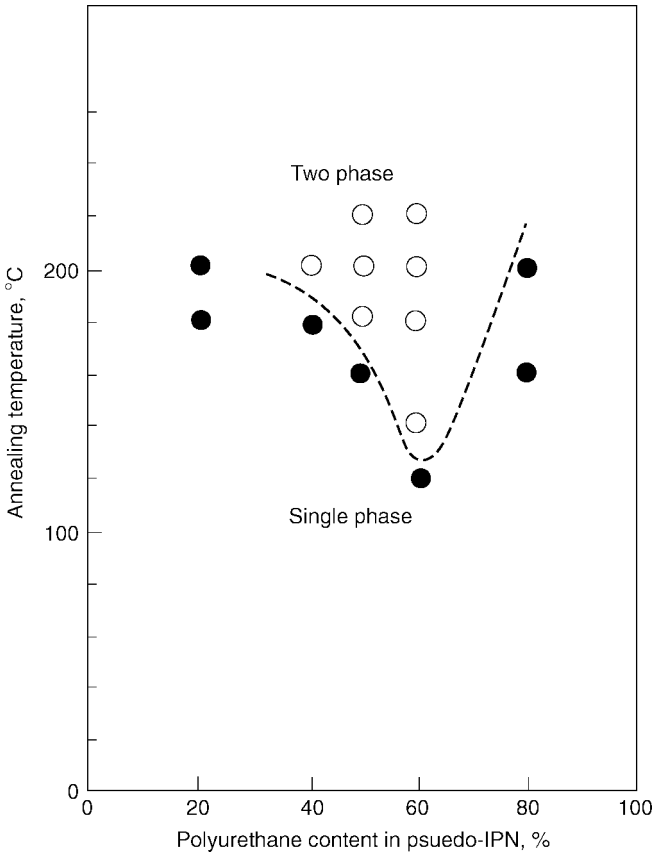

Fig. 7. A phase diagram of a polyurethane–poly(vinyl chloride) semi-IPN, showing a lower critical solution temperature.

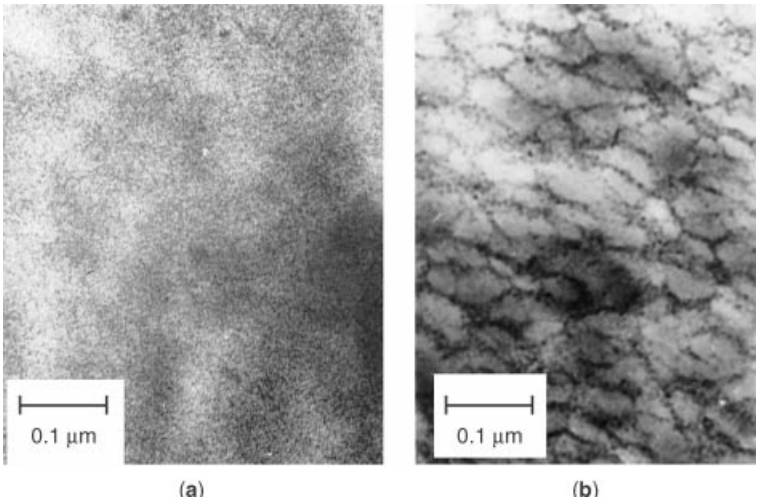

Fig. 8. A comparison of two possible morphologies of IPNs, based on (**a**) {poly(ethyl acrylate)}-*ipn*-{poly(methyl methacrylate)} and (**b**) {poly(ethyl acrylate)}-*ipn*-polystyrene.

The relative miscibility (qv) of the two polymers in IPNs is controlled not only by the thermodynamics of mixing, but to some extend also by the cross-link density and exact method of preparation. Huelck and co-workers (31) learned that while IPNs of poly(ethyl acrylate) and polystyrene exhibited two distinct glass transitions (qv) and two observable phases via transmission electron microscopy, the corresponding {*net*-poly(ethyl acrylate)}-*ipn*-{*net*-poly(methyl methacrylate)} compositions, being isomeric, had a microheterogeneous morphology (see Fig. 8).

Ma and Tang (32) showed that increasing cross-link density of SINs of poly(*n*-butyl acrylate) and epoxy 10:90 compositions tends to increase molecular interpenetration, and thus entanglement between the two networks.

Glass-Transition Behavior. Sánchez and co-workers (33) studied the system {*net*-poly(methyl acrylate)}-*ipn*-{*net*-poly(methyl methacrylate)}, which is not chemically isomeric, but close to being so. They varied the cross-linking level of both polymers of these sequential IPNs. When the poly(methyl acrylate) was cross-linked with 10% of ethylene glycol dimethacrylate (EGDMA), dynamic mechanical studies on midrange compositions showed that the system had a single glass transition, showing it to be substantially miscible (see Fig. 9) (33). The poly(methyl acrylate) network was polymerized first with 0.1% (open circles), 0.5% (squares), and 10% (triangles). In each case, the PMMA network contained 10% EGDMA.

It must be noted that this apparent miscibility is only mechanical in nature, a product of the high cross-link level of a sequential IPN. Sánchez and co-workers (33) note that the key factor controlling the apparent miscibility in sequential IPNs is the cross-linking density of the network polymerized first.

In related work, Dueñas and co-workers (34) found a similar effect with the system poly(butyl acrylate) and poly(butyl methacrylate). At 10% cross-linking level, the forced miscibility was sufficient to allow the glass transitions of the IPNs to follow the Fox equation (35).

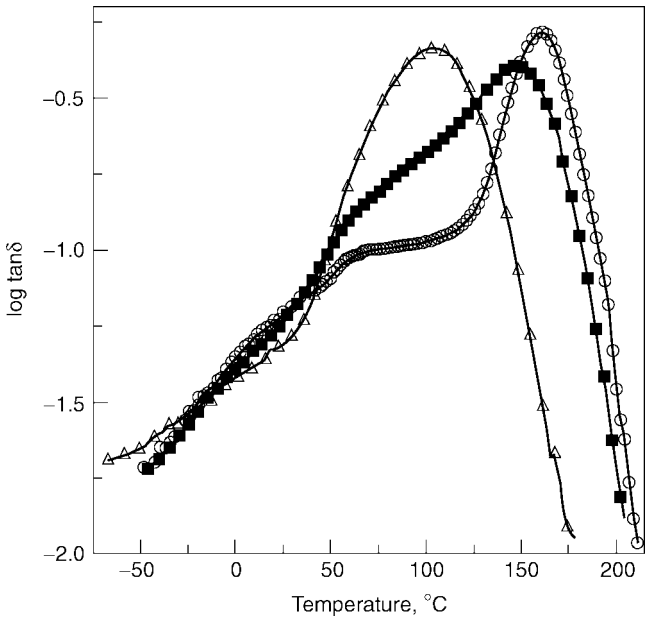

Fig. 9. Sequential IPNs of poly(methyl acrylate) and poly(methyl methacrylate) as a function of cross-linking level with EGDMA.

In block copolymers composed of random-coiled polymers, the molecular weight of the blocks and their relative proportions controls the domain size and shape (36,37). A somewhat similar relationship exists in IPN.

Domain Size Theory. Assuming spherical domains, Yeo and co-workers (38) derived equations for the domain size in sequential IPNs. The domain diameter of polymer II, D_{II}, was related to the interfacial tension γ, the absolute temperature T times the gas constant R, and the concentration of effective network chains, c_I and c_{II}, occupying volume fractions v_I and v_{II}, respectively:

$$D_{II} = \frac{4\gamma}{RT(Ac_I + Bc_{II})} \tag{1}$$

where

$$A = \frac{1}{2v_{II}}\left(3v_I^{1/3} - 3v_I^{4/3} - v_I \ln v_I\right) \tag{1a}$$

and

$$B = \frac{1}{2}\left(\ln v_{II} - 3v_{II}^{2/3} + 3\right) \tag{1b}$$

The quantity γ is experimentally determined from the work to create a unit interface. For many polymer/polymer interfaces, the value is in the range of 20–60 J/μm^2 (39). Although equation 1 was derived for spheres, it yields a reasonable estimation of the cylindrical diameter of spinodally phase-separated IPNs.

Phase Continuity in Sequential IPNs. The question has been repeatedly raised: Do IPN morphologies really exhibit dual phase continuity? Evidence for dual phase continuity in sequential IPNs was examined by Widmaier and Sperling (40,41). A series of sequential IPNs were prepared from poly(*n*-butyl acrylate) and polystyrene. Two cross-linkers were used, divinyl benzene (DVB), which forms ordinary covalent cross-links, and acrylic anhydride (AA), which forms labile cross-links. The AA cross-links were cut by soaking the samples in a 10% aqueous ammonium hydroxide solution for about 12 hours.

Some of the samples had the AA cross-links in the acrylic component and some of them had it in the styrenic component. After de–cross-linking one component or the other, the materials were subjected to a Soxhlet extractor. The remaining materials were examined by scanning electron microscopy. The density of the remaining material was also determined.

For both types, nearly the whole amount of de–cross-linked polymer could be extraced, indicating a low level of chemical grafting between the two polymers, and/or little entrapped material. When polymer II (polystyrene) was de–cross-linked and extracted, one still recovered polymer I (the acrylic) without substantial damage as shown by its density, equilibrium swelling degree, and scanning electron micrographs.

When polymer network I was de–cross-linked and extracted, the remaining network II presented a porous structure as indicated by reduced density and scanning electron microscopy. The void regions, corresponding to the location of the poly(*n*-butyl acrylate) before extraction, appeared interconnected. However, the extent of continuity of polymer II depended on its concentration. For midrange compositions, there was good evidence for dual phase continuity. However, when the amount of polymer II was decreased below 30%, the sample crumbled by itself, indicating a macroscopically discontinuous second phase. At a microscopic level, though, some degree of connectivity could still be detected. In summary, greater than 20–30% of polymer network II, its phase domain structure was continuous. Throughout the composition range studied, polymer network I was continuous.

The foregoing finding was important especially in the light of transmission electron micrograph studies, resulting in thin salami slices of osmium tetroxide stained samples. The observation of polymer network II could be interpreted as spherical domains in many such cases, but suggestive of ellipsoidal structures in others. The above discussion leads to the conclusion that the spherical and/or ellipsoidal structures, being two-dimensional, are better interpreted as interconnecting structures containing spheroidal and other morphologies (26,42). The modulus evidence for dual phase continuity will be presented below.

Modulus vs Composition. The modulus of IPNs as a function of composition yields information about their relative phase continuity. The first such study on polyacrylate/polyurethane latex interpenetrating elastomeric networks (IENs) was carried out by Matsuo and co-workers (Fig. 7) (43). Note that in the midrange of composition, the modulus begins to follow the parallel Takayanagi model (44). This suggests that the stiffer acrylic phase is becoming a continuous phase, as predicted from percolation models of three-dimensional mosaics of compressed spheroidal structures.

Yeo and co-workers (Fig. 10) (45) compared several models of phase continuity with the behavior of {*net*-poly(butyl acrylate)}-*ipn*-(*net*-polystyrene). The

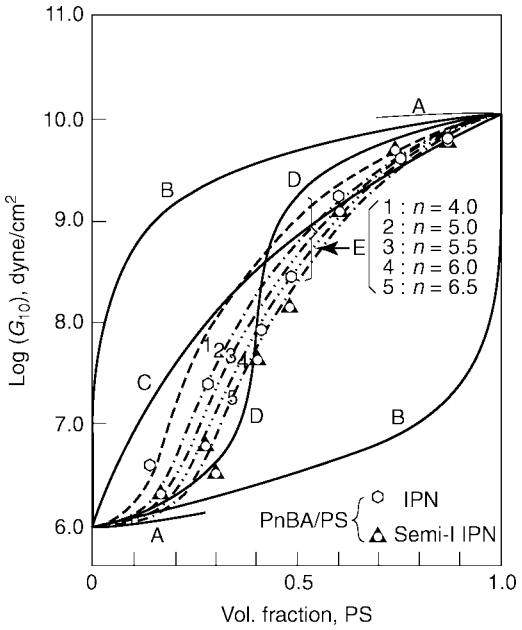

Fig. 10. Sequential IPNs of poly(butyl acrylate) and polystyrene as a function of composition. **A**: Upper–Lower Bound Model; **B**: Hashin–Shtrikman Model; **C**: Davies Model; **D**: Budiansky Model; and **E**: Coran–Patel Model. dyne/cm^2 = 0.1 Pa.

S-shaped curve has the greatest slope near the 50/50 composition. The Budiansky model (46,47) was the only model to follow the S-shaped curve.

Ramis and co-workers (48) made a similar study of SINs prepared from unsaturated polyester–styrene mixes with MDI-poly(propylene glycol). When the storage modulus, E', was plotted through a range of compositions, the Budiansky equation (47) was again found to fit better than several other relationships.

Phase Separation and Gelation Studies. A phase diagram of linear poly(ethylene oxide) (LPEO) and divinyl benzene (DVB) cross-linked poly(methyl methacrylate) as a function of polymerization of the latter was also researched by duPrez and co-workers (49) (Fig. 11). The temperature of measurement was also a variable, but the curve separating the one-phased system from the two-phased system did not change much in the narrow temperature range covered.

A time–temperature-transformation (TTT) diagram (50,51) study on a poly(ether sulfone)-*ipn-net*-epoxy semi-II IPN was carried out by Kim and coworkers (Fig. 12) (52). Note the several regions delineated by the progressive polymerization and cross-linking of the epoxy. Several steps in the transformation during polymerization were identified:

(1) Onset of phase separation
(2) Gelation of the epoxy
(3) Fixation of the phase-separated morphology
(4) End of phase separation
(5) Vitrification (glass forming) of the epoxy phase.

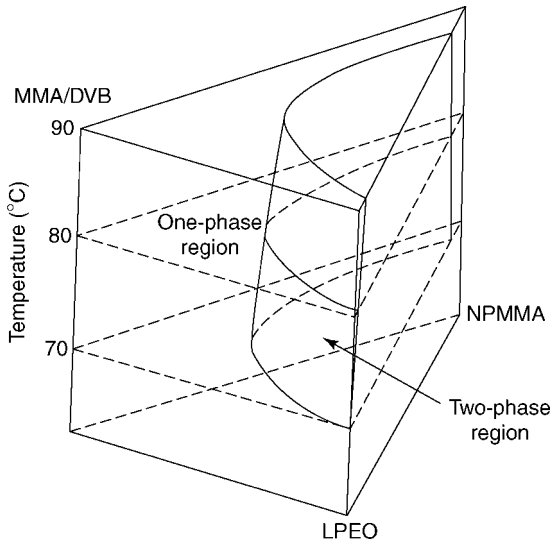

Fig. 11. A ternary phase diagram of the semi-IPN based on methyl methacrylate, poly(methyl methacrylate), and linear poly(ethylene oxide).

These workers also found that the lower critical solution temperature for the material was at 265°C.

The development of SINs requires three steps: gelation of polymer I, gelation of polymer 2, and phase separation of 1 from 2. Since these three events may occur

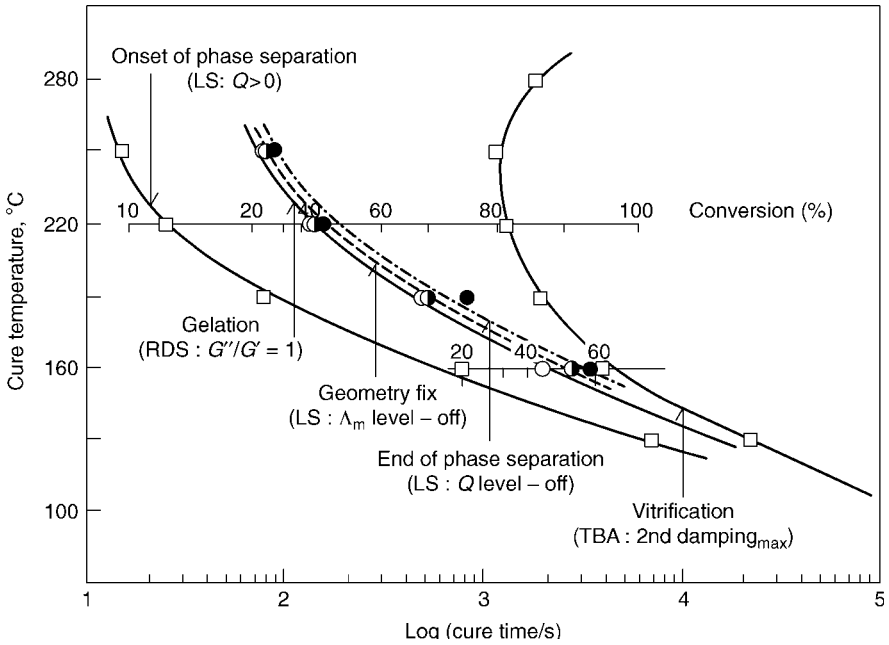

Fig. 12. A time–temperature-transformation (TTT) cure diagram for the system poly(ether sulfone)-*ipn*-epoxy.

in any order depending on concentration, cross-linker level, initiator, temperature, etc, there are 3! = 6 different morphologies and physical behavior patterns that may be observed.

This led to the development of a series of metastable phase diagrams for (*net*-polyurethane)-*ipn*-{poly(methyl methacrylate)} SINs (see Figs. 13 and 14) (53). The term *metastable* derived from the realization that none of the IPNs or SINs are truly at thermodynamic equilibrium relative to phase separation. Two figures were utilized to illustrate the phenomena more clearly. Since both monomers and both polymers needed to be represented, a tetrahedron structure was utilized, where the four pure components occupy the four vertices. The four triangular faces of both figures represent the ternary systems delineated by the compositions indicated in the vertices. Since the methyl methacrylate mix contained 0.5% tetraethylene glycol dimethacrylate as a cross-linker, it gelled after about 8% conversion, indicated by the G_1-U-PU plane in Figure 13. The phase separation curve for the ternary system MMA-PMMA-"U" on polymerization of only the methyl methacrylate is indicated by the points C-D-A-E. In a similar fashion, the phase separation curve for the MMA-PMMA-PU system, rear triangle in Figure 13, is shown by the points J-B-K-L. The entire tetrahedron volume is divided into two regions: one phase-separated and the other single-phased, separated by C-D-A-E-L-K-B-J. Tracing the sail-like characteristics of this surface aids in following the separation of the two regions of space. The curvilinear line A-B indicates the intersection of the PMMA gelation plane with that of the phase

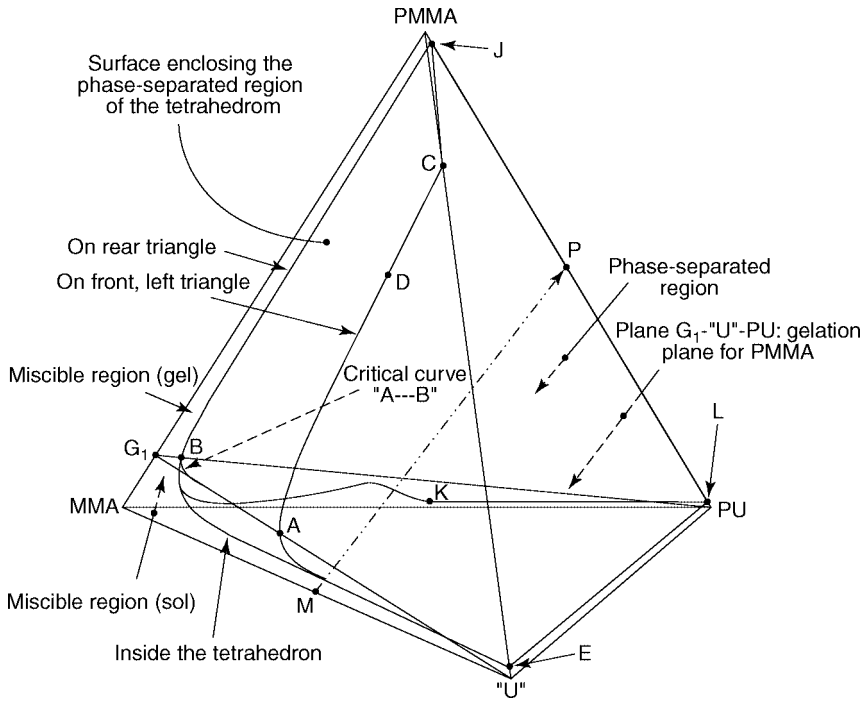

Fig. 13. A tetrahedron metastable phase diagram for the SIN polymerization of poly(methyl methacrylate) and polyurethane.

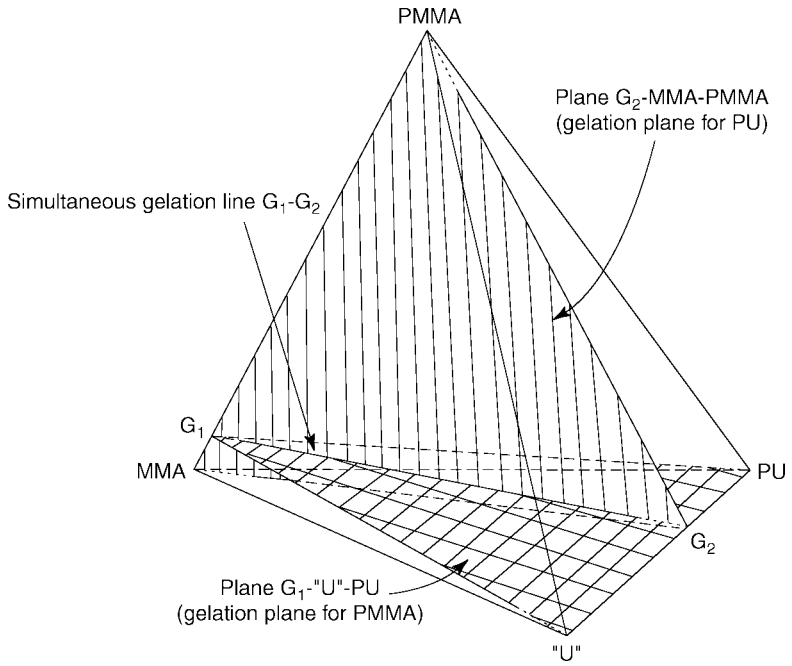

Fig. 14. Continuation of Figure 13, illustrating the gelation planes of both the poly(methyl methacrylate), G_1 and polyurethane, G_2.

separation sail-like surface. It represents the critical line along which there is simultaneous gelation of the PMMA and phase separation of the PU from that of the PMMA. Thus, reactions moving to the left of this curve will have the PMMA gel before phase separation, while reactions to the right of A-B phase separation before gelation.

Figure 14 illustrates the gelation plane of the polyurethane, G_2-MMA-PMMA, as well as the G_1 gelation plane of the PMMA (also shown in Figure 13). The intersection of the two planes, G_1-G_2, indicates the line of simultaneous gelation of both polymers. The line G_1-G_2 also intersects the line A-B of Figure 13, not shown. This intersection represent a triple critical point. Here, both polymers simultaneously gel and phase-separate. This defines an ideal SIN synthesis.

All SIN and IPN polymerizations must begin somewhere along the edge of the line MMA-"U", and end along the edge line PMMA-PU. However, the lines need not be straight or even single lines. When phase separation ensues, the line divides into two portions, ending at points J and L of Figure 13.

Since the polymerization rates can be controlled, and in general will not be equal, and the cross-linker levels independently control the gelation planes, all six possibilities of SIN morphologies can be envisioned. Also, as an extreme, a sequential IPN synthesis can also be traced on these figures. The semi-IPNs will clearly lack one of the gelation planes. A polymer blend polymerization will have only the phase separation curvilinear plane, without either gelation plane. Thus, Figures 13 and 14 provide a kind of map to determine how and why different morphologies and concomitant physical and mechanical behavior patterns emerge.

Of course, these maps serve as a guide to bring about specific morphologies and concomitant behavior profiles of the IPNs.

Following the work of Mishra and co-workers (53), Dean and co-workers (54,55) investigated the SIN syntheses of dimethacrylate- and epoxy-based materials by near-infrared and other methods. The rates and order of the polymerizations were systematically altered. The final conversion of the dimethacrylate was limited by the vitrification or topological restraint of the SIN. Whether one or two glass transitions are observed depends on the relative rates and order of the polymerizations.

Of course, the relative reaction rates of the two polymers in SINs may be controlled by the quantity of cross-linker, temperature, initiator level, concentration of the two monomers, level of light intensity, time and completeness of phase separation, etc. The above assumes that there is no interference between the two reactions, except for the mutual dilution effect.

Thermoplastic IPNs

Thermoplastic IPNs are hybrids between the polymer blends and the IPNs. Often, physical cross-links are used to bond the chains in one or both polymers. In other cases, one of the phases actually has chemical cross-links, but it constitutes a discontinuous phase so as to allow flow. In this latter case, the discontinuous case is often cylindrical in shape, highly elongated.

The most important commercial thermoplastic elastomers are based on polypropylene (PP) and ethylene–propylene–diene monomer (EPDM) elastomer (see ETHYLENE-PROPYLENE ELASTOMERS). The diene portion of the elastomer is cross-linked, frequently by dynamic vulcanization, ie, chemical cross-linking during melt shearing.

The PP/EPDM thermoplastic elastomer was modeled by Kresge (56) to show the morphology of the material after crystallization (see Fig. 15). To allow for extraction of the elastomer, he used EPM, lacking in chemical cross-linking. The PP clearly exhibits phase continuity, resembling an open-celled sponge with micron-sized porosity. Careful examination of the micrograph indicated that the voids were also continuous. (Otherwise, the EPM could not have been extracted.) Therefore, the material formed an interpenetrating two-phased structure. However, it is probable that the increase in viscosity of the EPDM phase, brought about by cross-linking, would reduce the continuity of the elastomer phase.

Coran and Patel (57) point out several examples of the improvements achieved:

(1) Reduced permanent set
(2) Greater ultimate mechanical strength
(3) Greater fatigue resistance
(4) Improved fluid resistance to hot oils
(5) Greater high-temperature stability
(6) Greater stability of the phase morphology in the melt; the phase domain size does not increase.

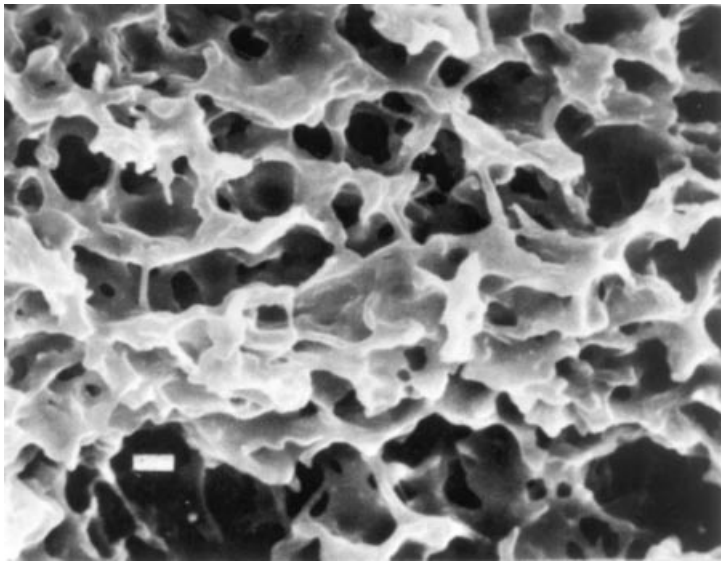

Fig. 15. A scanning electron micrograph of a model thermoplastic IPN based on a binary (70/30) blend of EPM and polypropylene. The EPM phase was removed, then the sample fractured under liquid nitrogen to illustrate the dual phase continuity of the material.

(7) Greater green strength, ie, greater melt strength
(8) More reliable fabricability

The PP/EPDM materials are most famous for being tough, energy-absorbing materials, which led them to be used as the plastic component of automotive bumpers.

Davison and Gergen prepared thermoplastic IPNs based on block copolymers and semicrystalline polymers (see Table 1) (58). Here, a hydrogenated version of the styrene–butadiene–styrene triblock copolymer was utilized, ie, SEBS, where the EB stands for ethylene-butylene (saturated 1,2-polymerized butadiene mers).

Table 1. Composition of Co-Continuous Interlocking Network Phases

	Composition by parts	
Component	A	B
25,000-100,000-25,000 SEBS	100	100
Poly(butylene terephthalate)	100	70
Shellflex 790 extending oil	100	–
Tuffto 6050 oil	–	50
Polypropylene	10	10
Irganox 1010 antioxidant	0.2	0.2
Dilaurothiodipropionate antioxidant	0.5	0.5
TiO_2	5	5

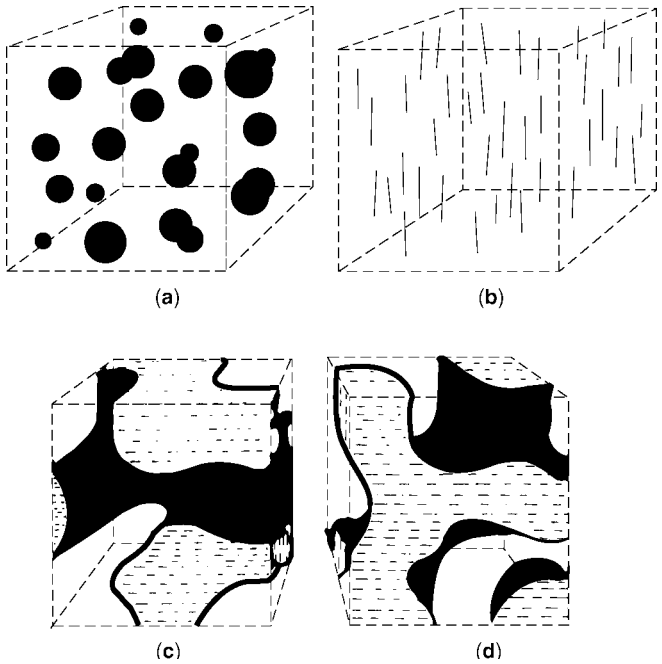

Fig. 16. Various morphologies illustrating the development of dual-phase continuity. (**a**) Dispersed sphere, clearly discontinuous in space; (**b**) dispersed fibers or cylinders. Figures (**c**) and (**d**) together illustrate dual-phase continuity, where both phases are interlocked in a kind of three-dimensional puzzle.

By blending these polymers, taking care to match melt viscosities and volume fractions (see eq. 2 below), dual-phase continuity can be achieved (see Fig. 16) (59). In Figure 16**a**, droplets of material are dispersed in a continuous matrix, a morphology observed in rubber-toughened plastics. Figure 16**b** illustrates dispersed fibers, observed in liquid crystal polymers and some thermoplastic elastomers. If the fibers or cylinders are infinitely long, they exhibit one-dimensional phase continuity.

Figures 16**c** and 16**d** constitute the important figures that model the materials in Table 1. These two figures together depict a co-continuous morphology, where the two phases are interlocked or interpenetrating. Note that three polymers are presented in Table 1. The major components are the SEBS and the poly(butylene terephthalate). The third polymer is the polypropylene, used as a compatibilizer. It appears at the interfaces between Figures 16**c** and 16**d**. Thus, *three* co-continuous phases are formed in this material! These materials are useful as under-the-hood electrical insulators because they have substantially constant modulus between the glass transition of the EB center block and the melting temperature of the poly(butylene terephthalate).

The requirements for both dual phase continuity and phase inversion for polymer blends and thermoplastic IPNs alike require the specification of the melt viscosity and the volume fraction of each component. Some melt shearing is assumed. These concepts were formulated quantitatively by Paul and Barlow (60)

and Jordhamo and co-workers (61):

$$\frac{V_1}{V_2} \times \frac{\eta_2}{\eta_1} = X \tag{2}$$

where if

$X > 1$, phase 1 is continuous
$X \approx 1$, dual phase continuity or phase inversion
$X < 1$, phase 2 is continuous

In equation 2, V represents the volume fraction and η represents the melt viscosity of phase 1 or 2, as per subscript. Equation 2 is true in the limiting case for zero shear. Utracki (62) proposed somewhat more complex relationships for finite shear rates.

However, in many experimental and industrial situations, equation 2 provides a reasonable approximation, as reviewed by Jordhamo and co-workers (see Fig. 17) (61). Note especially the dual phase continuity region in Figure 17. If the shearing action is stopped while the composition is within this region, it may remain dual phase continuous. Here, the phase continuity of a number of materials was examined and plotted. It must be noted that dual-phase continuity and/or phase inversion took place over about a factor of 4 in the data. Thus, some aspect of dual phase continuity exists via equation 2 as X varies from about 0.5 to about 2.

Thermoplastic IPN technology was also explored by Han and co-workers (63). In this case, thermoplastic IPNs based on polypropylene (PP) and EPDM were prepared using supercritical solution technology. Propane was used as the supercritical fluid. The synthesis steps were as follows:

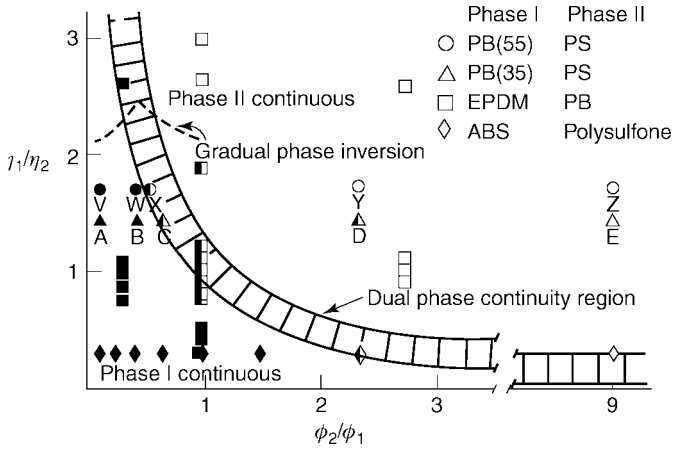

Fig. 17. Phase continuity and inversion diagram for polymer blends and IPNs during polymerization and under shear.

(1) PP and EPDM were dissolved in propane; a homogeneous solution was formed.
(2) *t*-Butyl peroxide was injected.
(3) EPDM was cross-linked for one hour at 175°C and 65 MPa.
(4) The polymers could be precipitated by two independent methods:
    a. Reducing the pressure below the cloud point, followed by lowering the temperature; or
    b. Isobaric cooling to ambient temperature, then reducing the pressure.
(5) Residual solvent was vented.
(6) Dried thermoplastic IPN was recovered.

The morphologies using the 4a route were fibrous in nature (64); those utilizing route 4b resulted in a porous spheroidal structure for the PP phase (65). In all cases, the morphology was significantly finer than that available with the then commercial routes of preparing PP/EPDM thermoplastic IPNs.

Siegfried and co-workers (66,67) investigated thermoplastic IPNs based on SEBS triblock copolymers with a polystyrene ionomer. Two subclasses of thermoplastic IPNs were identified: those prepared by a sequential polymerization method, and those prepared by mechanically blending separately synthesized polymers. In each case, a polystyrene acid sulfate was neutralized dynamically in the melt with a concentrated solution of sodium hydroxide. The water steamed off rapidly under the reaction conditions. The first subclass resulted in lower melt viscosities, but more nearly equal dual-phase continuity was achieved with the second subclass. The subject of thermoplastic IPNs was recently reviewed by Sperling (68).

Latex IPNs

Latex IPNs, by definition, have their origin in emulsion polymerization. Several types of latex IPNs exist. If one blends two kinds of latex particles, followed by film formation and cross-linking of both polymers, the material is called an *interpenetrating elastomeric network*, IEN. Usually, IENs form a three-dimensional mosaic structure (69,70).

Latex IPNs are often made by sequential polymerization of two (or more) cross-linked polymers utilizing emulsion polymerization (71). For core-shell latex IPN synthesis, first a cross-linked seed latex of polymer 1 is synthesized (2). Then, a second monomer and cross-linker are added to the system, usually with no added surfactant. Often, a starved polymerization route is employed, ie, the rate of polymerization equals or exceeds the rate of monomer addition. This reduces the swelling of the seed latex by the monomer 2 mix, producing a two-layer latex having a spherical core, and an overlaying shell. Obviously, multiple shells can be added for different purposes.

Some possible morphologies of latex IPNs having three polymers are illustrated in Figure 18 (72). Note that in Figure 18**a**, the monomer B mix first dissolves

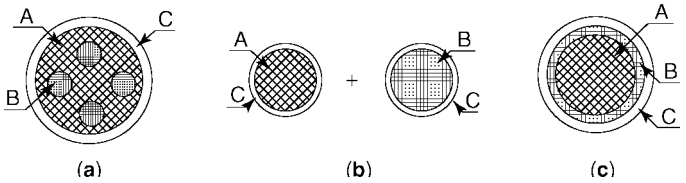

Fig. 18. Some possible latex IPN particle morphologies. (**a**) IPN core/shell particles; (**b**) separated core/shell particles; and (**c**) multilayered particles.

in polymer A, then polymerizes and phase separates to form internal domains. Then, polymer network C forms a shell around the A-B core.

If the glass transitions of the three polymers are sufficiently different, and the three polymers are phase-separated, then one obtains three glass transitions, as illustrated in Figure 19 (73). In this case, the three polymers were obtained by blending two latexes having different cores but the same shell, as in Figure 18**b**. G' and G'' represent the dynamic shear modulus. Both latexes have a core of poly(butadiene-*stat*-styrene), with some of the latexes having a SAN shell and some having a shell of poly(ethylhexyl methacrylate-*stat*-styrene). In both cases, the polymerizations were carried out under starved conditions.

Silverstein and co-workers (74), Silverstein and Narkis (75), and Nemirovski and Narkis (76) studied the morphology and rheological behavior of latex IPNs and related materials (see Fig. 20) (75). After water evaporation, some degree of phase continuity of individual phase domains is achieved in this case. All of these compositions were based on polyacrylates and polystyrene. After polymerizing and drying, the latex particles do not interdiffuse to form a monolithic solid because of the cross-links in each latex particle. However, being moderately soft, they flow together as modeled in Figure 20 (75). The solid black spheres represent polystyrene domains, and the cross-hatched material represents an acrylic

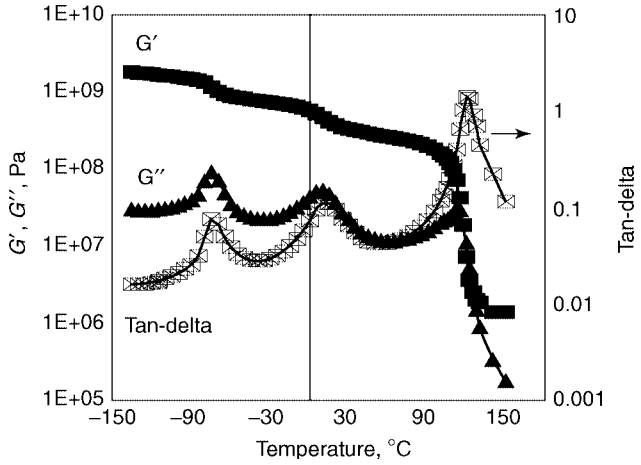

Fig. 19. The dynamic mechanical behavior of a mix of two latexes or the morphologies represented by Figure 18**b**.

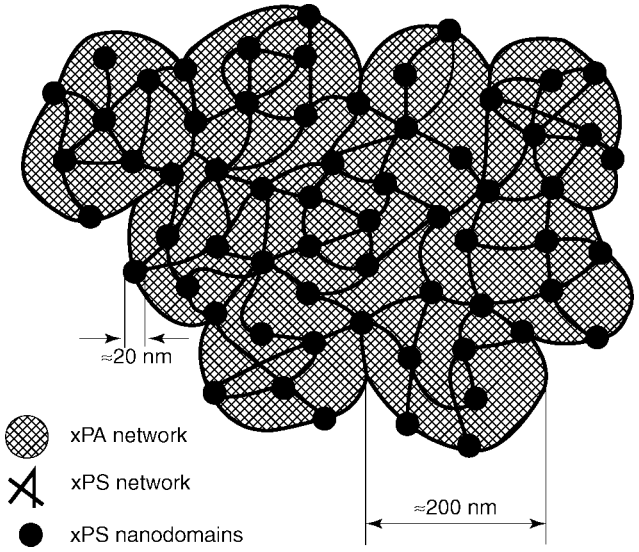

Fig. 20. Model of a latex IPN.

network. The rheological behavior of these materials resembles the flow behavior that might be expected for a room full of underinflated beach balls.

Sound and Vibration Damping Behavior

Sound and vibration damping are important throughout the world today for the automotive industry, appliances, aircraft, tall buildings, submarine technology, etc. However, the frequencies of the sound or vibration differ greatly, from a fraction of a Hertz for tall buildings to 10^3–10^4 Hz for cars and appliances. This is important, because the WLF equation shows that the glass transition increases some 6–7°C with each decade of frequency increase (77). One of the most important methods of damping involves polymeric materials in or near their glass transitions temperatures where the loss tangent tan δ and/or the loss modulus E″ are high.

Many IPNs exhibit a microheterogeneous morphology. When the domains are of the order of 10–20 nm, the whole system becomes substantially all interphase material, ie, it is extensively but incompletely mixed, with different microregions having different compositions (see Fig. 8) (31). In the transmission electron micrograph of Figure 8**a**, the microheterogeneous morphology is made from the isomeric pair, poly(ethyl acrylate) and poly(methyl methacrylate). When polystyrene is used as the second polymer, the cellular structure in Figure 8**b** emerges.

Whereas an immiscible IPN pair will have two distinct glass transitions, the microheterogeneous morphology often results in one broad glass transition, covering the temperature range between both homopolymer glass transitions. Thus, more or less constant E″ or tan δ can be obtained.

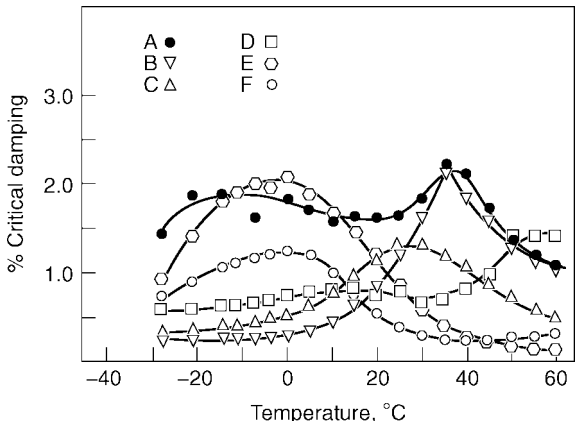

Fig. 21. Damping effectiveness as a function of temperature for several commercial materials compared to an IPN, composition A.

There are two basic engineering mechanisms for the use of damping polymers:

(1) Extensional damping, where a polymer is placed as a free layer on the resonating vibrating system; and
(2) Constrained layer damping, where a stiff material is placed on the top of the damping polymer to increase the shearing action. Sometimes a simple sandwich arrangement is used, where two thin layers of sheet metal (the bread) have a thin layer of polymer between them (the jelly).

The damping of an IPN constrained layer system based on an acrylic/methacrylic IPN and an epoxy constraining layer is compared with several other commercial homopolymers and statistical copolymers in Figure 21 (78). Hitachi Chemical has a high temperature sound and vibration damping material based on vinyl–phenolic compositions (79).

Natural Products/Renewable Resource-Based IPNs

Of increasing importance in modern society are polymeric materials that either originate from plants or animals, are naturally degradable, or both. One of the major approaches utilizes triglyceride oils with functionality other than double bonds. For example, most of the edible oils such as corn oil are triglycerides containing one or more double bonds in the side chains. Usually, the double bonds are structurally *cis*. An exception is tallow, which is a saturated oil.

Castor Oil-Based IPNs. Those triglyceride oils with functionality other than double bonds such as hydroxyl or carbonyl groups are generally considered inedible, although they are sometimes used for medicinal purposes. Prime among

these materials is castor oil, containing one hydroxyl group per side chain (see eq. 3):

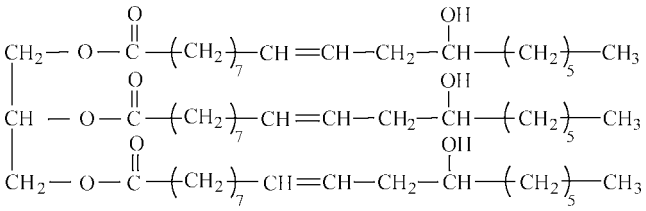

(3)

In medicinal applications, the hydroxyl group irritates the stomach lining. Chemically, the hydroxyl group can react to form urethanes or esters, and hence form a polymer network. Polyurethane foam rubber frequently contains large amounts of reacted castor oil, for example. The glass transition of castor oil polyesters are of the order of −50°C (80).

If styrene (or other vinyl monomer) plus cross-linker is swollen in and polymerized, an IPN is formed. The products tend to be tough, leathery materials. Research on castor oil-based IPNs began in 1974 as a cooperative research program between the Universidad Industrial de Santander, Bucaramanga, Colombia, and Lehigh University in the United States (81,82).

Castor oil hydroxyl groups can be easily reacted with either isocyanate groups to form polyurethanes, or with carboxyl groups to form polyesters. The synthesis scheme for forming polyester-based SINs from castor oil is illustrated in Figure 22 (80). Here, sebacic acid (itself a derivative of castor oil) is reacted with

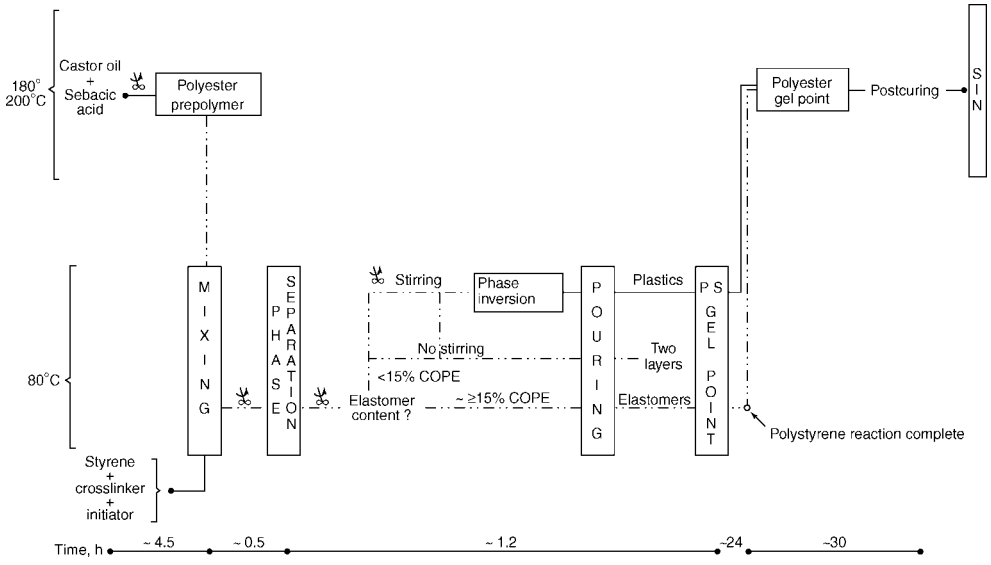

Fig. 22. A synthesis scheme for castor oil-polyester based SINs with polystyrene being the second component. ▬ ▪ ▬ ▪ ▬ = polyester is the continuous phase; ▬▬ = polystyrene is the continuous phase; and ⁂ = Stirring.

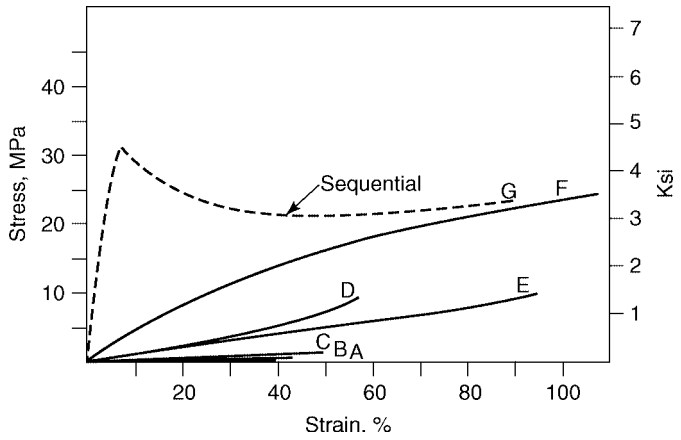

Fig. 23. Stress–strain curves for several castor oil (CO), polyester (PE), polyurethane (PU), and polystyrene network (PSN) materials. A: COPEN; B: COPEUN; C: COPUN; D: 40/60 COPEN/PSN; E: 40/60 COPEUN/PSN; F: 40/60 COPUN/PSN; and G: 40/60 COPUN/PSN.

castor oil. Note that stirring is required after phase separation to obtain phase inversion.

A number of polyester, polyurethane, and mixed structures were made into IPN. Stress–strain curves on these compositions are illustrated in Figure 23 (83). In some cases, the castor oil was first reacted with a diacid, then finished with an isocyanate to form a urethane. Here, COPEN stands for castor oil polyester network, U stands for urethane, and EU stands for the mixed ester–urethane derivative. PSN stands for polystyrene network. Compositions 1, 2, and 3 are relatively soft and weak. Compositions 4 and 5 are somewhat higher modulus, more energy-absorbing materials. Composition 6 is much tougher. The sequential IPN, composition 7, is identical to composition 6, except that the sequential mode of IPN formation replaced the SIN mode. The yield point in the stress–strain curve of composition 7 suggests greater phase separation with the polystyrene being a more continuous phase. It must be pointed out that composition 6 is tough enough to make long-lasting shoe heels.

Castor oil has also been made into semi-IPNs with poly(ethylene terephthalate) (PET). Typical time–temperature reaction conditions are shown in Figure 24 (84). Since the castor oil is an ester as well as the PET, significant bond interchange takes place at elevated temperatures, as indicated. If the material is heated too long, a statistical copolymer will result. Under the given reaction conditions, the mix goes from a two-phase mix to a one-phase mix. On cooling, it phase separates again.

Tan (85) investigated SIN compositions based on castor oil polyurethanes and styrene–acrylic mixes. Under these conditions, there is considerable grafting. Abrasion resistance to jetting sand was very high, leading to a coating application of the Ge Zhou Ba hydroelectric power station dam in the desert region of western China (86).

Other triglyceride oils that are being investigated as IPN monomers include vernonia oil and lesquerella oil. Vernonia oil, a naturally epoxidized oil,

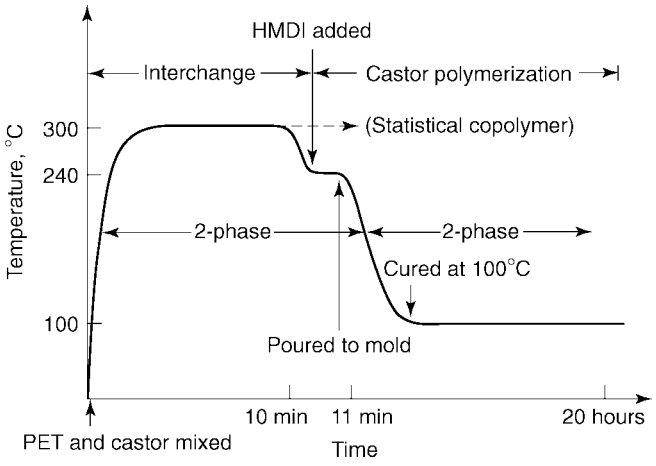

Fig. 24. A typical time–temperature cure cycle illustrating bond interchange and phase behavior of castor oil/urethanes and poly(ethylene terephthalate) semi-IPNs. Axes not drawn to scale.

was combined with poly(ethylene terephthalate) to make semi-IPNs (87). Lesquerella oil comes from a wild flower growing in the desert of southwest United States and Mexico. It, too, makes tough IPNs (88). It is thought that lesquerella could be grown where no crop exists today. Other functionalized oils of interest include crambe, epoxidized linseed oil, and epoxidized soybean oil (89).

Natural Rubber Latex-Based IPNs. Another kind of natural product IPN is based on natural rubber latexes. After processing, this rubber is in wide use today for truck and aircraft tires (see RUBBER, NATURAL). While still in the latex form, these latexes can be treated just like their synthetic counterparts and used as the core material for IPN production. An interesting material, prepared by polymerizing methyl methacrylate in the rubber latex, is called Hevea Plus MG (90–92). This makes an impact-resistant composition somewhat resembling ABS. Polystyrene as well as PMMA was used variously as the second polymer. Notched Izod impact strengths were increased over those of the pure plastics by a range of 10–15, reaching over 30 kJ/m^2.

Polysaccharide-Based IPNs. Cellulose (qv) and cellulose derivatives have been the largest tonnage single polymer sold in the world since the beginning of civilization until the present. Kamath and co-workers (93) prepared IPNs and related AB–cross-linked copolymers using compositions such as allyl cellulose cinnamonate and cross-linked acrylics, polystyrenes, or vinyl acetates. An improved thermal stability was noted. Hydrogel materials prepared from cellulose esters and polyacrylamide have also been investigated (94) (see HYDROGELS).

Combinations of both polysaccharides and castor-oil–based polyurethanes have also been investigated. Semi-IPNs of castor-oil–based polyurethanes and nitrokonjac glucomannan (NKGM) were investigated by Gao and Zhang (95). The konjac glucomannan is a natural polysaccharide, and was nitrated for these studies. Possible substitution of the semi-IPN for some petrochemical products was mentioned, along with biodegradability. Films made from the semi-IPN were found to be highly transparent, with a breaking strength of some 30 MPa.

Table 2. History of IPNs and Related Materials

Event	Investigators	Year	Ref.
Vulcanization of rubber	Goodyear	1844	96
First IPN	Aylsworth	1914	97
Macromolecular Hypothesis	Staudinger	1920	98
Graft Copolymers	Ostromislensky	1927	25
Homo-IPNs	Staudinger and Hutchinson	1951	99
Block copolymers	Dunn and Melville	1952	100
HIPS and ABS	Amos, McCurdy, and McIntire	1954	23
Block copolymer surfactants	Lunsted	1954	101
Interpenetrating polymer network term used	Millar	1960	102
Thermoplastic elastomers	Holden and Milkovich	1966	103
AB–Cross-linked copolymers	Bamford, Dyson, and Eastmond	1967	104
Interphase characteristics of IPNs	Lipatov and Sergeeva	1967	105
Sequential IPNs	Sperling and Friedman	1969	106
Latex IENs	Frisch, Klempner, and Frisch	1969	107
SINs	Sperling and Arnts	1971	108
Thermoplastic IPNs	Davison and Gergen	1977	109
Modern IPN nomenclature	Kahovec and co-workers	1997	9

History of Interpenetrating Polymer Networks and Related Materials

The patent literature shows that IPNs were invented over and over again, beginning in 1914 (see Table 2). Each time, the idea was lost and reinvented.

Aylsworth (97) was the first person known to invent an IPN. In 1914 he combined the then new phenol–formaldehyde compositions with natural rubber and sulfur. Of some historical interest is that Jonas Aylsworth was Thomas Edison's chief chemist (110). Edison had just switched from the cylinder-type record to the platter, using the new phenol–formaldehyde materials. However, these phenol–formaldehyde materials were brittle, and the first phonograph records had to be made very thick to prevent breakage.

In effect, by adding natural rubber and sulfur, Aylsworth made not only the first IPN, but also the world's first rubber-toughened plastic. This was decades before rubber-toughened styrenics were commercial. The West Orange, NJ, Edison Museum has evidence that Aylsworth's composition was used for toughening phonograph records from 1914 to 1929, stopping only when Edison left the phonograph record business. Then, the idea was apparently lost.

Aylsworth's patent (97), however, does not mention IPNs and polymer networks, or even use the term polymer. Note that that date was six years prior to H. Staudinger's enunciation of the macromolecular hypothesis, which was, of course, the first statement that certain colloids had the structure of long chains.

Several other independent discoveries of IPNs followed. J. J. Staudinger (son of H. Staudinger) and Hutchinson have a 1951 patent (with a 1941 application date!) to smooth the surfaces of transparent plastic sheeting for esthetic purposes (99). These men took sheets of cross-linked polystyrene or PMMA and swelled the

sheets with the same monomer mix as the first network. This stretched the sheets, and after polymerization of the second monomer mix the waviness or surface imperfections of the original material were reduced. These were the first homo-IPNs.

The next independent invention of IPNs was by Solt in 1955 (111). Solt invented anionic–cationic ion exchange resins with the idea of having both charges on the *same* suspension-sized particle. The idea was that the exchange efficiency would be improved if both charges were in juxtaposition, but still separated in space. Indeed, the charges must be separated, even by a fraction of a nanometer, to prevent coacervation.

The term *interpenetrating polymer network* was first coined by Millar in 1960 (102). These were polystyrene–polystyrene homo-IPN suspension-sized particles. The idea was that some particles, the *fines*, were too small. On adding more monomer and cross-linker, larger and more satisfactory particles could be made. Early works by Shibayama and Suzuki (112), Lipatov and Sergeeva (105), Frisch and co-workers (107), and Sperling and Friedman (106) set the pace for the modern development, founding the field of IPNs (1).

In Table 2, there is an apparent gap of two decades (1977–1997) between thermoplastic IPNs and the modern IPN nomenclature; in fact many people were busy characterizing a number of new materials and developing their applications, as described above. Application-oriented papers and patents are delineated below.

Actual or Proposed IPN Applications

A number of commercial IPN materials and their applications are summarized in Table 3. The value of IPNs to society, of course, lies in their usefulness. IPNs can and are being made into rubber-toughened plastics and a special value seems to lie in their capability of forming tough but flexible materials. IPNs often have another unusual property: that of forming co-continuous, very finely divided phases. These tough but flexible materials have suggested biomedical applications.

Biomedical Applications. Dillon (114) synthesized IPN membranes from polytetrafluoroethylene (PTFE) and poly(dimethyl siloxane) (PDMS) (see PERFLUORINATED POLYMERS, POLYTETRAFLUOROETHYLENE; SILICONES). These flexible membranes are used for a variety of medical purposes, especially second-degree burn care. These materials are commercially available under the trade name Silon. The PDMS component rapidly transports body fluids away from the burn site, while the PTFE provides mechanical strength. The PTFE is also waterproof, so that when the wound area is washed, water beads up on the film. An additional valuable feature is that the films are highly transparent, so that the doctor can observe the wound area easily, making early treatment of any infection or other problem possible.

Salmerón Sánchez and co-workers (115) prepared sequential IPNs based on {*net*-poly(ethyl acrylate)-*ipn*-{*net*-poly(hydroxyethyl acrylate)}. These two polymers differ primarily in the presence or absence of a hydroxyl group. Investigation via differential scanning calorimetry indicated three qualitatively different kinds of thermograms depending on the initial quantity of water present. The water present is primarily associated with the poly(hydroxyethyl acrylate), but the

Table 3. Selected Commercial IPN Materials[a]

Manufacturer	Trade Name	Composition	Application
Shell Chemical Co.	Kraton IPN	SEBS–polyester	Automotive parts
LNP Plastics	Rimplast	Silicone rubber–nylon or PU	Gears or medical
DSM N.V.	Kelburon	PP–EP or rubber–PE	Automotive parts
Uniroyal (Reichhold Chemical Co.)	TPR	EPDM–PP	Auto bumper parts
Rohm & Haas	–	Anionic–cationic	Ion-exchange resins
Monsanto	Santoprene	EPDM–PP	Tires, hoses, belts, and gaskets
BF Goodrich	Telcar	EPDM–PP or PE	Tubing, liners, and wire and cable insulation
Exxon	Vistalon	EPDM–PP	Paintable automotive parts
Cook Composites	Acpol	Acrylic–urethane–polystyrene	Sheet molding compounds
Dentsply International	Trubyte, Bioform	Acrylic–based	Artificial teeth
Hitachi Chemical	–	Vinyl-phenolics	Damping compounds
Bio Med Sciences	Silon	PDMS–PTFE	Burn dressing, scar abatement

[a]Updated from Table 10.5 in Ref. 113.

poly(ethyl acrylate) component clearly interferes with water transport and freezing. Whereas this was a basic study of hydrogel behavior, other systems examined below have several potential applications, particularly to the biomedical field (see HYDROGELS).

Polymer gels based on poly(*N*-isopropylacrylamide) [P(N-iPAAm)] in aqueous media undergo a temperature-induced collapse of the chains from a perturbed random coil to a globular structure known as a *coil-to-globular transition*. This is macroscopically observable as a sudden decrease of the degree of swelling at a sharp first-order phase transition known as a *lower critical solution temperature* (LCST) at 32°C. The P(N-iPAAm) gels exhibit the sharpest transition of the class of thermosensitive alkylacrylamide polymers examined (116) (see ACRYLAMIDE POLYMERS).

Since this LCST occurs between room temperature and body temperature, there has been great interest in this and related materials from a biomedical point of view. In order to adjust the LCST to meet various proposed objectives, a number of copolymers and IPNs of P(N-iPAAm) and have been prepared.

Zhang and Peppas (117) examined sequential IPNs of poly(methacrylic acid) (PMAA) and P(N-iPAAm) hydrogels as a function of pH and temperature. pH is critically important to studies involving PMAA, since the carboxyl group is ionized at higher pH but in the acid form below about 5.5. The IPNs had a swelling/deswelling transition in a range that included that of pure P(N-iPAAm), 32°C, but was broader.

An important possible use of such IPNs involves drug delivery. A number of model drugs was examined by Zhang and Peppas (117). As expected, higher

permeability was observed for the smaller model drug compounds (see CONTROLLED RELEASE TECHNOLOGY).

At low water contents, the LCST depends on the water concentration for P(N-iPAAm) (118), being constant for high swelling ratios (as most often needed), but shifting to higher temperatures when the initial water concentration is below 50%. Hydrophilic poly(acrylic acid) (PAA), when added in IPN form, tends to increase the LCST. In the case of P(N-iPAAm) and PAA sequential IPNs, the association between the complementary binding sites produces complexes that decrease the ability of the hydrogel to swell in water. For the various copolymers and IPNs, a major effect was the broadening of the transition.

The first-order LCST of P(N-iPAAm) leads to many possible applications in the biomedical field. Wu and Jiang patented an IPN hydrogel based on {*net*-poly(*N*-isopropylacrylamide)}-*ipn*-{*net*-gelatin} (119). These materials also swell greatly at room temperature, but can be made to undergo a rapid reduction in volume at blood temperature, 37°C. When formed into a tube, these hydrogels can be placed over the cut ends of a blood vessel. The material shrinks rapidly as the material increases in temperature from room temperature to body temperature, grasping both ends of the blood vessel and allowing blood to be temporarily transported in a normal manner.

There are two ways of bending light. The most common is to present the light with a material surface at an angle to the direction of the light's travel. However, light waves can also be *bent* by changing the refractive index internally in the material. This latter fact has been used to prepare gradient IPN compositions in soft contact lenses. By using computer-controlled laser polymerization of polymer II in gradient IPNs (polymers of two different refractive indices), it is possible to have improved astigmatism control (120,121).

Another class of IPNs are the homo-IPNs, made of two more or less identical polymers. An example are the homo-IPNs prepared from cross-linked poly(methyl methacrylate) (PMMA) (122,123). In this case, densely cross-linked material of suspension-sized PMMA particles are prepared. These are mixed with a very similar monomer mix, and polymerized. Some, but not all, of the second monomer mix swells into the suspension particles.

Homo-IPNs of PMMA are used commercially for artificial teeth, the kind that come out at night (122,123). One trade name is Bioform IPN (Table 3). In one example, suspension-sized particles of cross-linked PMMA were mixed with linear PMMA, MMA monomer, cross-linker, and initiator. After polymerization, the teeth have two superior properties. First, because a suspension polymerization route is used, the dentist can grind the teeth to a fine powder. This is important when fitting the new teeth to the opposing set of teeth. They can be ground better because the interface between the suspension-sized particles and the surrounding phase is slightly weaker than the bulk material. A single network of a similar composition may char under the dentist's drill.

Second, a densely cross-linked polymer is required. Salad oil, butter, and similar materials are excellent plasticizers (qv) for linear PMMA, which cause the teeth to swell.

Smart Materials. Eck and co-workers (124) developed a smart material for solar energy management. It seems that the use of solar energy to heat water in some tropical areas results in water that is *too hot*. Usually, the water pipes to

be heated are in a panel covered by glass, and exposed to the sun. The material of Eck and co-workers makes use of a lower critical solution temperature (see Fig. 7 for example) with an IPN based on {*net*-poly(propylene oxide)}-*ipn*-{*net*-poly(styrene-*stat*-2-hydroxymethyl acrylate)}. A film of this material is placed on the underside of the glass. At low temperatures, the film is clear, transmitting the light. When the temperature exceeds a certain value, the film clouds up, increasing reflection back into the atmosphere.

A polymer blend of the same or similar composition cannot be used because the phase domains that will form will become large enough to take many hours to diffuse back to a single phase. The IPN forms domains of only some tens of nanometers, allowing diffusion back and forth between one phase and two phases in minutes. Interestingly, this appears to be the only application suggested for the LCST of polymer blends or IPNs.

Pervaporation Membranes. Pervaporation membranes for separation of ethanol and water and other types of solutions are being investigated by Kim and his students (125,126). Some of these membranes are anionic/cationic IPNs. Starting with a 10% ethanol feed, after three stages the retentate is 94% ethanol. Water vapor passes through the membrane as the pervaporate.

Other Applications. Another new material, developed by Lipatov and Karbanova (127) and Bukhbinder and Kosjakov (128) flies under the designation gradans. Cylindrical glass or polymer fibers are widely used to transmit light or other electromagnetic energy for communication purposes, optoelectronics, integrated optics, and medical engineering. A major problem is that the electromagnetic energy tends to leak out of the surface of the fiber, shortening the useful path. If the fiber is made so that its refractive index has an increasing gradient from the center to the surface, the energy will be bent back towards the center as it moves through the fiber. One way to accomplish this is through making a gradient IPN, with the second monomer making a polymer of higher refractive index than the first.

Some of the materials mentioned in Table 3 have already been discussed. The reader will recognize the Silon and Bioform materials described above. Kraton IPN is also discussed above (see Figs. 16**c** and 16**d** and Table 1). Several of the materials manufactured are based on EPDM–PP thermoplastic IPNs.

Current Literature Suggestions and Applications. In 2004, the production of IPN-based papers is averaging about 100 papers a year. This contrasts to the fact that up to 1979, there was a *total* of about 125 scientific papers and about 75 patents issued on the subject. The number of IPN-related patents has also increased accordingly.

Many of the most recent papers mention possible applications (see Table 4). Again, possible medical applications stand out the most.

Kim and Kim describe a most interesting material in Reference 134 of Table 4. The need for synthetic blood vessel sections is great. A blood vessel must be both flexible and strong. However, a major problem with materials has been that the inner surface may abrade red blood cells and cause adsorption of materials such as the fibrinogens and platelets, important in coagulating blood. (The lifetime of red blood cells passing various surfaces is inversely related to the modulus of the material of contact.) Fibrinogen is one of the most important globular proteins circulating in the blood, playing a central role in the regulation of hemostasis

Table 4. Actual and Proposed IPN Applications from Select Recent Literature

Composition	Application	Ref.
Biomedical/Pharmaceutical		
Poly(ε-caprolactone) semi-homo-IPNs	Bone implant composites with hydroxyapatite	129
Poly(*N*-isopropylacrylamide-*stat*-acrylic acid) + grafted polyacrylamide copolymers	Engineered cartilage, polymer scaffolds	130
Acrylic resin IPNs	Acrylic false teeth	131
Poly(acrylic acid) + cross-linked gelatin	Hydrogel drug release systems.	132
Segmented polyurethane + poly(2-methacryloyloxyethyl phosphoryl chloride)	Blood compatibility, no platelet adhesion	133
Polyurethane + polystyrene with pendant poly(ethylene oxide) chains	Blood compatibility; adsorption of fibrinogens and platelets suppressed.	134
Chitosan + poly(ethylene oxide) semi-IPN	Drug release	135
Sodium alginate + cross-linked gelatin or egg albumin	Controlled release of medication	136
Poly(vinyl alcohol) + poly(dimethyl siloxane) hydrogels	Drug release	137
Chondroitin + poly(acrylic acid) semi-II IPN	Controlled drug release	138
Polyurethane + polystyrene IPNs	Adhesion of endothelial cells	139
Poly(hydroxyethyl methacrylate) + poly(ethylene glycol) semi-IPN	Antithrombogenic material	140
Polypropylene + polyacrylamide mix	Controlled release of drugs	141
Poly(vinyl alcohol) + poly(2-hydroxyethyl methacrylate)	Prosthetic disc nucleus	142
Poly(2-hydroxyethyl methacrylate) + chitosan	Lysozyme adsorption	143
Polysiloxane + poly(vinyl alcohol) with ferromagnetic derivate	Immobilize antigens	144
Electrical		
Polystyrene or poly(methyl methacrylate) + modified epoxy	Underfill adhesive for electronic applications	145
Castor oil-based polyurethane + poly(methyl methacrylate) + polyaniline	Electrical conducting properties	146
Polyaniline + poly(vinyl alcohol) semi-IPN	Electrical conducting materials	147
Poly(vinyl alcohol) + chitosan hydrogel	Bends in electric field; smart material	148
Polyaniline + poly(vinyl acetate) semi-II IPN	Electrical conductivity	149
Polyaniline + melamine-urea	Electrical conductivity	150
Poly[methoxyoligo(oxyethylene) methacrylate] + poly(methyl methacrylate)	Electrochemical conductivity	151
Poly(sodium acrylate) + poly(*N*-isopropyl acrylamide) semi-II IPN	Intelligent hydrogels, thermovolume sensitive, heavy metal ion recovery	152

Table 4. (Continued)

Composition	Application	Ref.
Poly(vinyl alcohol) + poly(diallyl dimethyl ammonium chloride)	Samples bend in electric field	153
Damping		
Vegetable oils	Damping materials	154
Polyester + epoxy with carbon black	Heat-resistant damping	155
Poly(dimethyl siloxane) + polyacrylates + polymethacrylates	High temperature damping	156
Polysiloxanes + poly(methyl methacrylate)	Sound and vibration damping	157
Ion exchange		
Sulfonated polystyrene + poly(vinyl chloride) semi-I IPNs	Cation exchange membranes	158
Poly(hydroxyethyl methacrylate) + chitosan	Removal of heavy metal ions from aquatic systems	159
Poly(vinyl chloride) + polystyrene with cation exchange groups	Cation exchange membrane	160
General		
Polyimides + alkoxysilane dye	Second-order nonlinear optics	161
Epoxy + unsaturated polyester	Rubber-toughened plastics	162
Poly(vinyl alcohol) grafted with acrylamide + sodium alginate	Pesticide release	163
Poly(acrylic acid) + poly(butyl methacrylate-*stat*-methyl methacrylate)	Pervaporation membrane	164
Natural rubber + polystyrene	High transport membranes	165
Carboxymethyl cellulose + poly(ethylene glycol) + cross-linked polyacrylamide	Controlled release of KNO_3 agricultural fertilizer	166
Unsaturated polyester + poly(2-hydroxyethyl methacrylate)	Improved flame resistance	167

and thrombosis. It participates in blood coagulation and facilitates adhesion and aggregation of platelets. The result might be thrombosis in the patient.

Mother Nature makes the inner lining of blood vessels very soft, so that the probability of coagulation is far reduced. The hydrophilic pendant poly(ethylene oxide) (PEO) chains, described in Reference 134, stick out from the inner side of the blood vessel, creating a soft gel environment. The presence of the pendant PEO chains significantly suppresses the adhesion of fibrinogens and platelets on the surface of the polymeric blood vessel by steric repulsion. In these IPNs, the blood compatibility increases with both the length of the pendent chains and the density of grafting.

Thus, the polyurethane and polystyrene, main components of the IPN, provide both the strength and the flexibility, and the grafted PEO provides a soft, gelatinous inner surface, mimicking Mother Nature. Besides possible use as artificial blood vessels, there is a wide range of blood-handling equipment now in use for surgery, etc, as possible applications.

A similar effect arises in the materials described in Reference 133 of Table 4. Segmented polyurethanes, of course, are a type of block copolymer. These

materials are very strong elastomers, which are in wide use as the elastic fiber in undergarments, bathing suits, etc. The poly(2-methacryloyloxyethyl phosphoryl chloride) forms a highly swollen, soft gel partly exposed on the IPN blood vessel surface.

However, there are possible applications to optoelectronics, agriculture, and other topics as well. References 148, 152, and 153 in Table 4 mention smart materials, particularly those that bend in an electric field. These are widely being investigated as sensors of various kinds.

Concluding Comments

In a certain sense, the term *interpenetrating polymer networks* is a misnomer, since most of these materials phase separate, rather than being mutually soluble on the molecular level. One could argue that the phases interpenetrate, and/or that true molecular interpenetration takes place at the interphase. However, the term describes the general synthesis and structure of the materials.

The field of interpenetrating polymer networks now takes its place parallel to the fields of polymer blends, grafts, and blocks. Indeed, most of these materials are useful because they undergo some kind of phase separation. Many IPNs seem to work best when the degree of phase separation is only partial or the size of the domains is in the tens of nanometer range. Those IPNs composed of an elastomer and a plastic to make flexible materials seem to be the most unique among these materials.

BIBLIOGRAPHY

"Interpenetrating Polymer Networks" in *EPST* 1st ed., Suppl. Vol. 1, pp. 288–306, by L. H. Sperling, Lehigh University; "Interpenetrating Polymer Networks" in *EPSE* 2nd ed., Vol. 8, pp. 279–341, by D. Klempner, University of Detroit, and L. Berkowski, BASF Corp.

1. L. H. Sperling, *Interpenetrating Polymer Networks and Related Materials*, Plenum Press, New York, 1981.
2. L. H. Sperling and R. Hu, in L. A. Utracki, ed., *Polymer Blends Handbook*, Kluwer Academic Publishers, The Netherlands, 2004.
3. Y. S. Lipatov, *Prog. Polym. Sci.* **27**, 1721 (2002).
4. V. D. Athawale, S. L. Kolekar, and S. S. Raut, *J. Macromol. Sci., Polym. Revs.* **C43**(1), 1 (2003).
5. M. Kamel and A. K. Srivastava, *Polym. Int.* **52**, 692 (2003).
6. D. Klempner, L. H. Sperling, and L. A. Utracki, eds., *Interpenetrating Polymer Networks*, American Chemical Society, Washington, D.C., 1994.
7. S. C. Kim and L. H. Sperling, eds., *IPNs Around the World: Science and Engineering*, John Wiley & Sons, Inc., Chichester, England, 1997.
8. Y. S. Lipatov and L. M. Sergeeva, *Interpenetrating Polymeric Networks*, Naukova Dumka, Kiev, 1979.
9. J. Kahovec, P. Kratochvil, A. D. Jenkins, I. Mitra, I. M. Papisov, L. H. Sperling, and R. F. T. Stepto, *Pure Appl. Chem.* **69**, 2511 (1997).
10. W. Ring, I. Mita, A. D. Jenkins, and N. M. Bikales, *Pure and Appl. Chem.* **57**, 1427 (1985).

11. P. E. Mason, W. S. Bryant, and H. W. Gibson, *Macromolecules* **32**, 1559 (1999).
12. J. P. Sauvage, *Science* **291**, 2105 (2001).
13. S. Menzer, A. J. P. White, D. J. Williams, M. Belohradsky, C. Hamers, F. M. Raymo, A. N. Shipway, and J. F. Stoddart, *Macromolecules* **31**, 295 (1998).
14. C. L. Jackson, H. D. Chanzy, F. P. Booy, B. J. Drake, D. A. Tomalia, B. J. Bauer, and E. J. Amis, *Macromolecules* **31**, 6259 (1998).
15. R. E. Touhsaent, D. A. Thomas, and L. H. Sperling, *J. Polym. Sci.* **46**, 175 (1974).
16. M. T. Tabka and J. M. Widmaier, *Macromolecules* **32**, 2520 (1999).
17. T. M. Tabka and J. M. Widmaier, *J. Appl. Polym. Sci.* **85**, 1929 (2002).
18. V. M. Michal'chuk, A. N. Nikolaevskii, L. I. Maklakov, and Y. S. Lipatov, *Polymer* **42**, 1691 (2001).
19. L. H. Sperling, ed., *Recent Advances in Polymer Blends, Grafts, and Blocks*, Plenum, New York, 1974.
20. A. K. Khandpur, S. Forster, F. S. Bates, I. W. Hamley, A. J. Ryan, W. Bras, K. Almdal, and K. Mortensem, *Macromolecules* **28**, 8796 (1995).
21. D. A. Hajduk, H. Takenouchi, M. A. Hillmyer, F. S. Bates, M. E. Vigild, and K. Almdal, *Macromolecules* **30**, 3788 (1997).
22. A. A. Donatelli, L. H. Sperling, and D. A. Thomas, *Macromolecules* **9**, 671, 676 (1976).
23. U.S. Pat. 2,694,692 (1954), J. L. Amos, J. L. McCurdy, and O. R. McIntire.
24. M. E. Soderquist and R. P. Dion, in J. I. Kroschwitz, ed., Encyclopedia of Polymer Science and Engineering, John Wiley & Sons, Inc., New York, 1989.
25. U.S. Pat. 1,613,673 (1927), I. Ostromislensky.
26. L. H. Sperling, in D. Klempner, L. H. Sperling, and L. A. Utracki, eds., *Interpenetrating Polymer Networks*, American Chemical Society, Washington, D.C., 1994.
27. J. W. Cahn, *J. Chem. Phys.* **42**, 93 (1965).
28. J. W. Cahn and J. E. Hilliard, *Chem. Phys.* **28**, 258 (1958).
29. J. W. Cahn and J. E. Hilliard, *Chem. Phys.* **31**, 688 (1959).
30. D. Sophia, D. Klempner, V. Sendijarevic, B. Suthar, and K. C. Frisch, in D. Klempner, L. H. Sperling, and L. A. Utracki, eds., *Interpenetrating Polymer Networks*, ACS Symposium Series 239, ACS Books, Washington, D.C., 1994.
31. V. Huelck, D. A. Thomas, and L. H. Sperling, *Macromolecules* **5**, 340, 348 (1972).
32. S. Ma and X. Tang, in D. Klempner, L. H. Sperling, and L. A. Utracki, eds., *Interpenetrating Polymer Networks*, American Chemical Society, Washington, D.C., 1994.
33. M. S. Sánchez, G. G. Ferrir, C. T. Cabanilles, J. M. Dueñas, M. M. Pradas and J. L. G. Ribelles, *Polymer* **42**, 10071 (2001).
34. J. M. M. Dueñas, D. T. Escuriola, G. G. Ferrer, M. M. Pradas, J. L. G. Ribelles, P. Pissis, and A. Kyritsis, *Macromolecules* **34**, 5525 (2001).
35. T. G. Fox, *Bull. Am. Phys. Soc.* **1**, 123 (1956).
36. D. J. Meier, *Polym. Prepr.* **11**, 400 (1970).
37. D. J. Meier, *J. Polym. Sci.* **26C**, 81 (1969).
38. J. K. Yeo, L. H. Sperling, and D. A. Thomas, *Polymer* **24**, 307 (1983).
39. S. Wu, *Polymer Interface and Adhesion*, Marcel Dekker, New York, 1982.
40. J. M. Widmaier and L. H. Sperling, *Macromolecules* **15**, 625 (1982).
41. L. H. Sperling, *Polym. Eng. Sci.* **23**, 693 (1983).
42. A. M. Fernandez, Ph.D. Thesis, Lehigh University, 1984.
43. M. Matsuo, T. K. Kwei, D. Klempner, and H. L. Frisch, *Polym. Eng. Sci.* **10**, 327 (1970).
44. M. Takayanagi, *Mem. Fac. Eng. Kyushu Univ.* **23**, 11 (1963).
45. J. K. Yeo, L. H. Sperling, and D. A. Thomas, *Polym. Eng. Sci.* **21**, 696 (1981).
46. B. Budiansky, *J. Compos. Mater.* **4**, 286 (1971).
47. B. Budiansky, *J. Mech. Phys. Solids* **13**, 223 (1965).
48. X. Ramis, A. Cadenato, J. M. Morancho, and J. M. Salla, *Polymer* **42**, 9469 (2001).
49. F. E. duPrez, P. Tan, and E. J. Goethals, *Polym. Adv. Technol.* **7**, 257 (1996).

50. J. K. Gillham, *Polym. Eng. Sci.* **19**, 676 (1979).
51. M. T. DeMuse, J. K. Gillham, and F. Parodi, *J. Appl. Polym. Sci.* **64**, 15 (1997).
52. B. S. Kim, T. Chiba, and T. Inoue, *Polymer* **34**, 2809 (1993).
53. V. Mishra, F. E. DuPrez, E. Gosen, E. J. Goethals, and L. H. Sperling, *J. Appl. Polym. Sci.* **58**, 331 (1995).
54. K. Dean, W. D. Cook, W. D. Ray, J. Galy, and H. Sautereau, *Macromolecules* **34**, 6623 (2001).
55. K. Dean and W. D. Cook, *Macromolecules* **35**, 7942 (2002).
56. E. N. Kresge, in D. R. Paul, and S. Newman, eds., *Polymer Blends*, Academic Press, New York, 1978.
57. A. Y. Coran and R. P. Patel, in G. Holden, N. R. Legge, R. Quirk, and H. E. Schroeder eds., *Thermoplastic Elastomers*, Hanser, Munich, 1996.
58. U.S. Pat. 4,101,605 (1978), W. P. Gergen and S. Davison.
59. W. P. Gergen, *Kautsch. Gummi, Kunstst.* **37**, 284 (1984).
60. D. R. Paul and J. W. Barlow, *J. Macromol. Sci. Rev. Macromol. Chem.* **C18**, 109 (1980).
61. G. M. Jordhamo, J. A. Manson, and L. H. Sperling, *Polym. Eng. Sci.* **26**, 518 (1986).
62. L. A. Utracki, *Polymer Alloys and Blends: Thermodynamics and Rheology*, Hanser, Munich, 1990.
63. S. J. Han, Ph.D. Dissertation, Lehigh University, Bethlehem, Pa, 1998.
64. S. J. Han, D. J. Lohse, M. Radosz, and L. H. Sperling, *J. Appl. Polym. Sci.* **77**, 1478 (2000).
65. S. J. Han, D. J. Lohse, M. Radosz, and L. H. Sperling, *Macromolecules* **31**, 5407 (1998).
66. D. L. Siegfried, D. A. Thomas, and L. H. Sperling, *J. Appl. Polym. Sci.* **26**, 177 (1981).
67. D. L. Siegfried, D. A. Thomas, and L. H. Sperling, *Polym. Eng. Sci.* **21**, 39 (1981).
68. L. H. Sperling, in G. Holden, H. R. Kricheldorf, J. E. McGrath, and R. Quirk, eds., *Thermoplastic Elastomers*, 3rd ed., Hanser, Munich, 2004.
69. H. L. Frisch and D. Klempner, *Adv. Macromolec. Chem.* **2**, 149 (1970).
70. Ger. Pat. 2,153,987 (1972), K. C. Frisch, H. L. Frisch, and D. Klempner.
71. P. A. Lovell and M. S. El-Aasser, eds., *Emulsion Polymerization, and Emulsion Polymers*, John Wiley & Sons, Inc., Chichester, England, 1997.
72. R. Hu, V. L. Dimonie, M. S. El-Aasser, R. A. Pearson, A. Hiltner, S. G. Mylonakis, and L. H. Sperling, *J. Polym. Sci. B: Polym. Phys.* **35**, 1501 (1997).
73. R. Hu, V. L. Dimonie, M. S. El-Aasser, R. A. Pearson, A. Hiltner, S. G. Mylonakis, and L. H. Sperling, *J. Polym. Sci. A: Polymer. Chem.* **35**, 2193 (1997).
74. M. S. Silverstein, Y. Talmon, and M. Narkis, *Polymer* **30**, 416 (1989).
75. M. S. Silverstein and M. Narkis, *J. Appl. Polym. Sci.* **33**, 2529 (1987).
76. N. Nemirovski and M. Narkis, in D. Klempner, L. H. Sperling, and L. A. Utracki, eds., *Interpenetrating Polymer Networks*, American Chemical Society, Washington, D.C., 1994.
77. J. D. Ferry, *Viscoelastic Properties of Polymers*, 3rd ed., John Wiley & Sons, Inc., New York, 1980.
78. L. H. Sperling, T. W. Chiu, R. G. Gramlich, and D. A. Thomas, *J. Paint Technol.* **46**, 4 (1974).
79. K. Yamamoto and A. Takahashi, in R. D. Corsaro, and L. H. Sperling, eds., *Sound and Vibration Damping with Polymers*, American Chemical Society, Washington, D.C., 1990.
80. N. Devia, J. A. Manson, L. H. Sperling, and A. Conde, *Macromolecules* **12**, 360 (1979).
81. L. W. Barrett, L. H. Sperling, and C. J. Murphy, *JAOCS* **70**, 523 (1993).
82. L. W. Barrett, L. H. Sperling, E. Gilmer, and S. G. Mylonakis, *J. Appl. Polym. Sci.* **48**, 1035 (1993).
83. N. Devia, J. A. Manson, L. H. Sperling, and A. Conde, *Polym. Eng. Sci.* **19**, 878 (1979).

84. L. W. Barrett, L. H. Sperling, J. W. Gilmer, and S. G. Mylonakis, in D. Klempner, L. H. Sperling, and L. A. Utracki, eds., *Interpenetrating Polymer Networks*, ACS Books, Washington, D.C., 1994.
85. P. Tan, in D. Klempner, L. H. Sperling, and L. A. Utracki, *Interpenetrating Polymer Networks*, American Chemical Society, Washington, D.C., 1994.
86. *The Report of the Application Result of IPN Materials*, Institute of Science Research of the Engineering Bureau of Ge Zhou Ba, China, 1987.
87. L. W. Barrett, O. L. Shaffer, and L. H. Sperling, *J. Appl. Polym. Sci.* **48**, 953 (1993).
88. L. H. Sperling, J. A. Manson, and M. A. Linne, *J. Polym. Mater.* **1**, 54 (1984).
89. I. Frischinger and S. Dirlikov, in D. Klempner, L. H. Sperling, and L. A. Utracki, eds., *Interpenetrating Polymer Networks*, American Chemical Society, Washington, D.C., 1994.
90. Technical Information Sheet No. 9, Rev., Natural Rubber Producers Research Association, Kuala Lumpur, Malaysia, 1977.
91. D. J. Hourston and J. Romaine, *J. Appl. Polym. Sci.* **39**, 1587 (1990).
92. M. Schneider, T. Pith, and M. Lambla, *Polym. Adv. Technol.* **6**, 326 (1995).
93. M. Kamath, J. Kincaid, and B. Mandal, *J. Appl. Polym. Sci.* **59**, 45 (1996).
94. P. H. Corkhill, J. H. Fitton, and B. J. Tighe, *J. Biomater. Sci. Polym. Edn.* **4**, 615 (1993).
95. S. Gao and L. Zhang, *Macromolecules* **34**, 2202 (2001).
96. U.S. Pat. 3,633 (1844), C. Goodyear.
97. U.S. Pat. 1,111,284 (1914), J. W. Aylsworth.
98. H. Staudinger, *Ber. Dtsch. Chem. Ges.* **53**, 1073 (1920).
99. U.S. Pat. 2,539,377 (1951), J. J. P. Staudinger and H. M. Hutchinson.
100. A. S. Dunn and H. W. Melville, *Nature* **169**, 699 (1952).
101. U.S. Pat. 2,674,619 (1954), L. G. Lunsted.
102. J. R. Millar, *J. Chem. Soc.* 1311 (1960).
103. U.S. Pat. 3,265,765 (1966), G. Holden and R. Milkovich.
104. C. H. Bamford, R. W. Dyson, and G. C. Eastmond, *J. Polym. Sci.* **16C**, 2425 (1967).
105. Y. S. Lipatov and L. M. Sergeeva, *Russ. Chem. Rev.* **45**(1), 63 (1967).
106. L. H. Sperling and D. W. Friedman, *J. Polym. Sci. A-2* **7**, 425 (1969).
107. H. L. Frisch, D. Klempner, and K. C. Frisch, *Polym. Lett.* **7**, 775 (1969).
108. L. H. Sperling and R. R. Arnts, *J. Appl. Polym. Sci.* **15**, 2317 (1971).
109. U.S. Pat. 4,041,103 (1977), S. Davison and W. P. Gergen.
110. L. H. Sperling, *Polymer News* **132**, 332 (1987).
111. U.K. Pat. 728,508 (1955), G. S. Solt.
112. K. Shibayama and Y. Suzuki, *Rubber Chem. Technol.* **40**, 476 (1967).
113. L. H. Sperling, *Polymeric Multicomponent Materials: An Introduction*, Wiley-Interscience, New York, 1997.
114. M. E. Dillon, in D. Klempner, L. H. Sperling, and L. A. Utracki, eds., *Interpenetrating Polymer Networks*, American Chemical Society, Washington, D.C., 1994.
115. M. S. Sánchez, G. G. Ferrer, M. M. Pradas, and J. L. G. Ribelles, *Macromolecules* **36**, 860 (2003).
116. Y. H. Bae, T. Okano, and S. W. Kim, *J. Polym. Sci., Part B: Polym. Phys.* **28**, 923 (1990).
117. J. Zhang and N. A. Peppas, *Macromolecules* **33**, 102 (2000).
118. E. Diez-Peña, I. Quijada-Garrído, P. Futos, and J. M. Barreles-Rienda, *Macromolecules* **35**, 2667 (2002).
119. U.S. Pat. 6,030,634 (2000), C. Wu and S. Jiang.
120. I. Calderara, D. Baude, D. Joyeux, and D. J. Lougnot, *Polym. Mat. Sci. Eng. (Prepr.)* **75**, 244 (1996).
121. Eur. Pat. 486638B1 (1995), D. Lougnot and D. Baude.
122. U.S. Pat. 4,396,377 (1983), F. D. Roemer and L. H. Tateosian.
123. U.S. Pat. 4,396,476 (1983), F. D. Roemer and L. H. Tateosian.

124. W. Eck, H. R. Wilson, and H. J. Cantow, *Adv. Mater.* **7**, 800 (1995).
125. Y. K. Lee, T. M. Tak, D. S. Lee, and S. C. Kim, *Polym. J.* **23**, 429 (1991).
126. Y. K. Lee, T. M. Tak, D. S. Lee, and S. C. Kim, *J. Membrane Sci.* **52**, 157 (1990).
127. Y. S. Lipatov and L. V. Karbanova, *J. Mater. Sci.* **30**, 2475 (1995).
128. T. L. Bukhbinder and V. I. Kosjakov, *Vysokomolekuljarny Soedineniya, Ser. B* **28**, 625 (1996).
129. J. Y. Hao, Y. Liu, S. B. Zhou, Z. Li, and X. M. Deng, *Biomaterials* **24**, 153 (2003).
130. R. A. Stile, K. R. Shull, and K. E. Healy, *Langmuir* **19**, 1853 (2003).
131. R. L. Schneider, E. R. Curtis, and J. M. S. Clancy, *J. Prosthetic Dentistry* **88**, 145 (2002).
132. M. Changez, K. Burugapalli, V. Koul, and V. Choudhary, *Biomaterials* **24**, 527 (2003).
133. N. Morimoto, Y. Iwasaki, N. Nakabayashi, and K. Ishihara, *Biomaterials* **23**, 4881 (2002).
134. J. H. Kim and S. C. Kim, *Biomaterials* **23**, 2015 (2002).
135. M. N. Khalid, F. Agnely, N. Yagoubi, J. J. Grossiord, and G. Couarraze, *Eur. J. Pharm. Sci.* **15**, 425 (2002).
136. A. R. Kulkarni, K. S. Soppimath, T. M. Aminabhavi, and A. M. Dave, *J. Appl. Polym. Sci.* **85**, 911 (2002).
137. M. S. Shin, S. J. Kim, I. Y. Kim, N. G. Kim, C. G. Song, and S. I. Kim, *J. Appl. Polym. Sci.* **85**, 957 (2002).
138. L. F. Wang, J. M. Wang, and Y. L. Chiang, *J. Appl. Polym. Sci.* **85**, 114 (2002).
139. J. H. Kim, S. H. Kim, H. K. Kim, T. Akaike, and S. C. Kim, *J. Biomed. Mater. Res.* **62**, 613 (2002).
140. A. K. Baipai and M. Shrivastava, *J. Macromol. Sci., Pure Appl. Chem.* **39**, 667 (2002).
141. M. H. Wu, J. Chen, Q. Qian, and B. R. Bao, *J. Radioanal. Nucl. Chem.* **252**, 531 (2002).
142. D. Darwis, P. Stasica, M. T. Razzak, and J. M. Rosiak, *Radiat. Phys. Chem.* **63**, 539 (2002).
143. G. Bayramoglu and M. Y. Arica, *Colloid Surf. A. Physicochem. Eng. Asp.* **202**, 41 (2002).
144. R. A. L. Coelho, G. A. Jaques, A. D. Barbosa, G. Veldzquez, S. M. L. Montenegro, W. M. Azevedo, and L. B. Carvalho, *Biotech. Lett.* **24**, 1705 (2002).
145. L. Fan and C. P. Wong, *IEEE Trans. Comp. Packag. Technol.* **25**, 148 (2002).
146. T. Jeevananda and Siddaramaiah, *Eur. Polym. J.* **39**, 569 (2003).
147. R. Gangopadhyay and A. De, *Synth. Met.* **132**, 21 (2002).
148. S. J. Kim, S. J. Park, I. Y. Kim, M. S. Shin, and S. I. Kim, *J. Appl. Polym. Sci.* **86**, 2285 (2002).
149. J. Q. Ma, H. H. Song, H. L. Frisch, S. Maaref, and S. S. Sun, *J. Appl. Polym. Sci.* **85**, 2287 (2002).
150. Y. J. Wang, X. H. Wang, X. J. Zhao, J. Li, Z. S. Mo, T. B. Jing, and F. S. Wang, *Macromol. Rapid Commun.* **23**, 118 (2002).
151. X. P. Hou and K. S. Siow, *Solid State Ionics* **147**, 291 (2002).
152. K. Yamashita, T. Nishimura, and M. Nango, *Polym. Adv. Technol.* **14**, 189 (2003).
153. S. J. Kim, S. G. Yoon, Y. M. Lee, and S. I. Kim, *Sens. Actuators, B-Chem.* **88**, 286 (2003).
154. Y. P. Yin, S. R. Yao, and X. Y. Zhou, *J. App. Polym. Sci.* **88**, 1840 (2003).
155. Y. F. Shih and R. J. Jeng, *J. Appl. Polym. Sci.* **86**, 1904 (2002).
156. G. S. Huang, Z. Li, and L. X. Jiang, *J. Appl. Polym. Sci.* **85**, 545 (2002).
157. S. Z. Wu, S. L. Yao, Z. Z. Huang, H. Y. Xi, and J. R. Shen, *Macromol. Mater. Eng.* **287**, 231 (2002).
158. Y. J. Choi, M. S. Kang, and S. H. Moon, *J. Appl. Polym. Sci.* **88**, 1488 (2003).
159. O. Genc, C. Arpa, G. Bayramoglu, M. Y. Arica, and S. Bektas, *Hydrometallurgy* **67**, 53 (2002).
160. Y. J. Choi, M. S. Kang, and S. H. Moon, *Desalination* **146**, 287 (2002).
161. R. J. Jeng, W. Y. Hung, C. P. Chen, and G. H. Hsiue, *Polym. Adv. Technol.* **14**, 66 (2003).

162. Z. G. Shaker, R. M. Browne, H. A. Stretz, P. E. Cassidy, and M. T. Blanda, *J. Appl. Polym. Sci.* **84**, 2283 (2002).
163. S. G. Kumbar and T. M. Aminabhavi, *J. Appl. Polym. Sci.* **84**, 552 (2002).
164. B. Y. Lim and S. C. Kim, *J. Membr. Sci.* **209**, 293 (2002).
165. A. P. Mathew, S. Packivisamy, R. Stephen, and S. Thomas, *J. Membr. Sci.* **201**, 213 (2002).
166. A. K. Baipai and A. Giri, *J. Macromol. Sci., Pure Appl. Chem.* **39**, 667 (2002).
167. Y. F. Shih, R. J. Jeng, *Polym. Degrad. Stab.* **77**, 67 (2002).

L. H. SPERLING
Lehigh University

IONOMERS. See Volume 6.

ISOBUTYLENE POLYMERS. See BUTYL RUBBER.

ISOCYANATE-DERIVED POLYMERS. See Volume 6.

LATEX TECHNOLOGY

Introduction

Latex technology encompasses colloidal and polymer chemistry in the preparation, processing, and conversion of natural and synthetic latices into useful products.

Latex technology vernacular is not always consistent. By definition a *latex* is a colloidal suspension of polymer particles stabilized by dispersing agents in an aqueous medium. The dispersing agents are conventional ionic or nonionic surfactants or polymeric surfactants made from block or graft copolymers derived from monomers with different hydrophobicities. An *emulsion* (1) is a dispersion of two or more (2) immiscible liquid phases (one being water) stabilized by amphiphilic materials. A latex is a specific type of emulsion; one where the organic phase is a polymer particle. The terms latex and emulsion are often used interchangably partly because emulsion polymerization is the principal synthetic route to latices. Emulsion polymerization is one type of heterophase polymerization involving organic and aqueous phases. Others include suspension, dispersion, and precipitation polymerization which generate water-borne particles different from latices. Heterophase Polymerization (qv) can also involve two immiscible organic phases as in nonaqueous polymer dispersions and polymer microgels. Finally, polymers prepared via homogeneous polymerization, whether in solution or neat, can be inverted into a polymer dispersion in water using surfactants. Similar to latices, these materials can have very different molecular weight and functional group distributions and thus form a separate class of materials.

Latices have been in use for a very long time and the history of latices and polymer development are closely linked. The Mayas (3), around 1600 BC, used the sap of trees like the sparse *Hevea brasiliensis* of South America (4) to make rubber products and waterproof clothing. The Mayas called the sap "caa o-chu," literally translated as "weeping tree." *Caoutchouc* is now the French word for rubber. The

Encyclopedia of Polymer Science and Technology. Copyright John Wiley & Sons, Inc. All rights reserved.

natural rubber derived from this sap was shown to be 93–95% *cis*-1-4-isoprene by Faraday (5) in the early 19th century. Goodyear's invention of vulcanization, and later the automobile, increased natural rubber demand through the beginning of the 20th century (6). Large rubber plantations in Malaya, Ceylon, Indonesia, and Indochina increased the world's natural rubber production to 200,000 t by 1920. Enhanced supply led to rapid growth of natural rubber products and improvements in latex processing. The Allied blockade of Germany during World War I led to the first process for making synthetic latex (7). Gottlob (8) and others were early developers of emulsion polymerization (at first using methods to duplicate how natural rubber is produced in nature). Soon thereafter, U.S. companies began producing commercial synthetic latices: Buna S (butadiene–styrene copolymer), also known as Government Rubber–Styrene or GR–S rubber; Neoprene (polychloroprene) (9); and Thiokol (polysulfides) (see STYRENE-BUTADIENE COPOLYMERS). Japan's seizure of the Southeast Asia rubber plantations during World War II led to intensive research in synthetic rubber production (10). Today synthetic latex production accounts for 60% of the 18×10^6-t total rubber market (11,12) which has been growing at 2–5% over the last decade. Synthetic latices account for ca 2.5% of the world polymer market (13,14). Allergic reactions to proteins in natural latex and other natural latex market drivers have recently created more opportunities for synthetic latices (15). Over 70% of the natural latex market is converted to solid polymer for use in tires.

Many synthetic latices exist (16–18). They contain butadiene and styrene copolymers (elastomeric), styrene–butadiene copolymers (resinous), butadiene and acrylonitrile copolymers, butadiene with styrene and acrylonitrile, chloroprene copolymers, methacrylate and acrylate ester copolymers, vinyl acetate copolymers, vinyl and vinylidene chloride copolymers, ethylene copolymers, fluorinated copolymers, acrylamide copolymers, styrene–acrolein copolymers, and pyrrole and pyrrole copolymers. Many of these latices also have carboxylated versions.

Traditional applications for latices are adhesives, binders for fibers and particulate matter, protective and decorative coatings (qv), dipped goods (especially without allergens), foam, paper coatings including water-proofing paper (19), backings for carpet and upholstery, modifiers for bitumens and concrete, and thread and textile modifiers to improve feel or properties such as flame retardence. More recently latices have found use in biomedical applications as protein immobilizers; as visual detectors in immunoassays, as release agents in drug delivery (20), wound treatment, and synthetic blood (21), in electronic applications as photoresists for circuit boards; in batteries, conductive paint, copy machines; as key components in molecular electronic devices; in specialty coatings for seeds (22), in artificial turf plastics; and as an important component of oil recovery techniques (23). The application of even more specialized latices can be surprisingly complex (24).

Latex Properties

The observable properties of a latex, ie, stability, rheology, film properties, interfacial reactivity, and substrate adhesion, are determined by the colloidal and polymeric properties of the latex particles. Important colloidal properties include ionic charge, stability, particle size and morphology distribution, viscosity, solids,

and pH. Important polymer properties include molecular weight distribution, monomer sequence distribution, glass-transition temperature, crystallinity, degree of cross-linking, and free monomer. Methods for analyzing each of these properties exist, depending on the end use of the product. Overviews of the various polymer colloid characterization methods are available (25–27) (see also COATINGS).

Stability. For a latex to be a useful product, control of polymer isolation is crucial. The individual polymer particles must be stable enough to avoid coagulation resulting from perturbances like high temperature, freeze–thaw cycles, high shear in handling, electrolyte addition, and organic solvent addition during processing, but not so stabilized that polymer isolation is impossible. Stability is related to the surface properties of the latex particles, and these are usually determined during latex manufacture (28). Visual detection of coagulation is easy; more sophisticated optical techniques are possible (29). The types of initiator, emulsifier, and monomers used are the key determinants.

Electrostatic Stabilization. The electrical charges on the surface of a latex particle are balanced by an electrical double layer of oppositely and then similarly charged counterions. The outer layer is known as the diffuse electrical double layer, and its potential controls the colloidal stability of the latex particles (30). The diffuse electrical double-layer potential is closely related to the zeta potential. Electrophoresis measurements at various pH and ionic strengths are a means of calculating the zeta potential (31,32). As two particles approach, their individual diffuse double layers begin to overlap and the particles repulse one another. As the particles get even closer, attractive forces build and the particles coagulate. The energy required to overcome the repulsive forces depends on the ionic strength of the bulk phase, the temperature, and the nature of the ions balancing the latex particle charge. Latex particles coagulate at zeta potentials close to zero and are very stable at zeta potentials above 50 mV. One way to coagulate particles is to reduce the energy barrier between particles by adding electrolyte. The Derjaguin–Landau–Verwey–Overbeek (DLVO) theory (33) is a method for predicting the amount of electrolyte needed to coagulate a latex by first predicting the critical coagulation concentration. DLVO theory does not account for the chemical nature of the electrolyte nor the interaction of the ions with water. Additional mechanisms must often be added to the extended DLVO theory to model more complicated systems (34). Aluminum compounds, such as aluminum alginate, coagulate latices with varying effectiveness depending on the pH of the latex system (35). Protein behavior (36) and even nonaqueous stabilization can be modeled in a similar fashion (37).

Steric Stabilization. Nonionic surfactants, usually containing ethylene oxide units, are able to stabilize particles by adsorbing their hydrocarbon chain ends on the hydrophobic polymer zones of the surface of the latex particle. The ethylene oxide groups extend into the water phase. These compounds suffer from temperature and dilution sensitivity. A–B block copolymers where A is compatible with the latex polymer and B with the dispersion medium offer a more robust method of steric stabilization. Triblock and star block methacrylate copolymers can also act as surfactants providing steric stabilization (38). Reactive macromonomers with affinity toward the dispersion medium copolymerized with hydrophobic monomer offer a chemical way of grafting the stabilizer to the surface of the latex particle (39). Organic solvent addition is used to coagulate sterically stabilized latices (40).

Addition of soluble homopolymer can lead to reversible and irreversible flocculation by depletion and bridging flocculations (41).

In general, electrostatic stabilization leads to smaller and more uniform particle size when compared with syntheses involving similar amounts of steric stabilizers. An advantage of non-ionic surfactants over electrostatic stabilization is improved humidity resistance (42). A given class of stabilizer can provide both electrostatic and steric stabilization depending on the length of the steric moieties in the surfactant molecule (43).

Other Stabilizers. In addition to anionic, cationic, and nonionic surfactants used in manufacture of the latex, other specialized surfactants can be added or compounded to the latex after manufacture to increase the stability of the latex. For example, amphoteric surfactants such as *c*-cetyl betaine are used to improve the mechanical stability of low pH anionic compounds. Quaternary ammonium salts are used to improve the mechanical stability of cationic latices and their compounds. They are used either alone or in combination with a nonionic surfactant. Sequestrants (44) such as sodium silicate, sodium polyphosphate, and the sodium salt of ethylene diamine tetraacetic acid are added to anionic latices to retard the destabilizing action of cations that get leached slowly from compounding ingredients containing multivalent ions. The addition of these ingredients is also beneficial if the use of hard water is unavoidable in making and using the anionic latex compound. Care must be taken to avoid shocking the latex during compounding with these additional surfactants.

Rheology. Flow properties of latices are important during processing and in many latex applications such as dipped goods, paint, and fabric coatings. Rheology is used to characterize the stability of latices (45). For dilute, nonionic latices, the relative latex viscosity is a power–law expansion of the particle volume fraction. The terms in the expansion account for flow around the particles and particle–particle interactions. For ionic latices, electrostatic contributions to the flow around the diffuse double layer and enhanced particle–particle interactions must be considered (46). A relative viscosity relationship for concentrated latices was first presented in 1972 (47). A review of empirical relative viscosity models is available (46). In practice, latex viscosity measurements are carried out with rotational viscometers (see RHEOLOGICAL MEASUREMENTS).

It is possible to increase the viscosity of a latex after manufacture using thickeners. Thickening occurs through increases in medium viscosity or polymer particle aggregation. If considerable aggregation occurs without a corresponding increase in medium viscosity, undesirable separation or creaming occurs. Methylcellulose, caseinates, and polyacrylate salts are typical thickeners. Ease of adding the thickener, ability to maintain viscosity, and undesirable side effects must be considered when selecting a thickener. Some thickeners slowly hydrolyze in the latex and lose their effectiveness over time. The full range of the effects of adding thickener develops over time; some of them are much faster than others. To avoid exceeding the desired viscosity, it is advisable to add thickener in small increments, waiting after each for the viscosity to reach equilibrium before adding the next one.

The viscosity of the latex can also be dependent on pH. In the case of some latices, lowering the pH with a weak acid such as glycine is an effective method for raising the viscosity without destabilizing the system. Latices made with

poly(vinyl alcohol) as the primary emulsifier can be thickened by increasing the pH with a strong alkali.

Particle size influences the viscosity of a latex, and the industrial demand for high solids latices has led to bimodal and multimodal particle-size distributions (48). Solids levels approaching 70 wt% are possible. The smaller the particle size, the higher the viscosity.

Particle Size. The particle-size distribution of a latex is a determinant of its performance in application. Particles are almost always spherical, although nonspherical particles are possible (49,50). Particle-size distributions are now routinely measured using scattering methods, light scattering being the most common and most effective on particles >300 nm. Small-angle neutron scattering (SANS) is useful for concentrated latices and smaller (< ca 300 nm) particle sizes (51). Microscopic techniques are also a reliable method. Two of the newer techniques are sedimentation field-flow fractionation (52) and capillary hydrodynamic fractionation (53). The particle-size distribution has an impact on stability, rheology, morphology, and film-forming properties. Stability is predicted for larger particles, with broadly distributed particle sizes showing a greater tendency to coagulate owing to interactions between the smaller particles (54). Viscosity effects are weighted to the larger particles. Morphology is affected by particle size, as in the case where the particle size of the polystyrene latex used to seed polystyrene core–poly(ethyl methacrylate) shell particles determined the morphology of the final latex. When the seed was less than 200 nm in diameter, the final particles were prolate spheroids of near-hemispherical polystyrene and poly(ethyl acrylate) domains. When the seed was 300 nm in diameter, spherical polystyrene particles embedded with circular patches of poly(ethyl methacrylate) were the result (55). A review of the fundamental aspects of morpology control has been written by Sundberg and Durant (56).

Film Properties. Dehydration (57) at temperatures above the polymer glass-transition temperature is the principal means for forming film from latex. Interdiffusion of the polymer chains between particles is thought to be the limiting step in film formation (58). The final properties of the film depend on the polymer in the latex particles. Significant differences can exist between films made from solution polymer and latex polymer, respectively, because of the colloidal debris remaining on the latex polymer (59). Important film properties include hardness, flexibility, clarity, conductance, impact strength, and toughness. Core–shell particles have seen extensive use as rubber-toughening agents.

Improving Properties Through Compounding. The potential value of most polymers can be realized only after proper compounding. Materials used to enhance polymer properties or reduce polymer cost include antioxidants (qv), cross-linking agents, accelerators, fillers (qv), plasticizers (qv), adhesion promoters, pigments, etc. Antioxidants are essential to retard degradation in unsaturated polymers. Cross-linking agents are used to build modulus, resistance to permanent deformation, and greater solvent resistance in many types of polymers. Accelerators are frequently used to reduce the time and temperature required to affect the cross-linking. Fillers, such as carbon black (qv) and clays, do not reinforce latex polymers as they do their dry polymer counterparts. Rather, they are used in most latex applications to adjust processing rheology and to lower raw material costs of the product, or to impart specific effects, eg, aluminum trihydrate to increase resistance to flame degradation, or carbon black to increase resistance

to UV degradation. Plasticizers and oils are used to soften and increase flexibility at lower temperatures, improve resistance to crystallization, or depress the brittle point of the product. Hydrocarbon process oils, glycols, vegetable oils, ester plasticizers, and low melting point resins are some of the common materials used. Many types of resins are added to enhance the tackiness of polymers. Generally, within a class of tackifying resins, the lower the melting point, the greater the tack developed in the compounded polymer. The optimum amount of any resin for maximum tack depends on the type of polymer to which it is added. Resins added as solvent-cut emulsions rather than as solventless emulsion or dispersions develop more tack in the polymer, because the residual solvent in the polymer contributes to the tack of the polymer resin blend. Pigments and dyes are used to impart color. Some pigments with some polymers also impart other effects such as improved water resistance or reduced flammability.

Latex Applications

Adhesives. Latices are used as additives (qv) in the construction market, in tires and belt fabrication, in furniture manufacture, in packaging, and in tapes, labels, envelopes, and bookbinding. The adhesives are used in wet or dry laminations. In wet lamination, the adhesive is not dried before assembly; hence at least one of the substrates must be porous to allow for the water to evaporate. Wet lamination has the advantage that the surfaces to be adhered can be repositioned during assembly, provided the solids content remains below the level at which the adhesive begins to form a film. The disadvantage of wet lamination is the slower development of cohesive strength in the adhesive film and the need for closer control of timing when the two substrates are to be brought together; if this occurs too soon, the adhesive film is too weak to hold the assembly together, and if it occurs too late, the adhesive is too dry to effect a satisfactory bond.

Binders. Latices are used as fiber binders in the paper and textile industries. The two principal methods of application are (*1*) wet-end addition, wherein the ionic latex is added to a fiber slurry and then coagulated in the slurry prior to sheet formation; and (*2*) saturation of the latex into a formed fiber web, wherein the latex is coagulated by dehydration. Latices are also used as binders for particulate matter such as rubber scrap.

Coatings. Latices are used in residential and industrial paints, coated paper and paperboard, seeds (60), fabric coatings, backing for carpet, upholstery, and drapery; as basecoats for wallpaper and flooring; and in insulation coatings (see COATINGS). Application methods include brushing, squeegee, spraying, dipping, and frothing (see COATING METHODS, SURVEY).

Dipped Goods. Latices are used in various dipping processes to produce balloons, bladders, gloves, extruded thread, and tubing. Manufacturing techniques include multiple dip and dry, and coagulant dipping employing a colloidal destabilizer (61,62).

Foam Products. Latices are made into foams for use in cushioning applications. The latices are frothed with air and then chemically coagulated for thick applications, or heated to induce coagulation for thinner applications. The latter method allows for infinite pot life during production (see CELLULAR MATERIALS).

Modifiers. Latices are added to bitumens, mortars, and concrete to improve impact resistance and reduce stress cracking. Key to the use of latices in these technologies is compatibility between the latex and the construction materials.

Synthetic Latex Manufacture

The history of emulsion polymerization has been well documented (63). Early efforts to produce synthetic rubber coupled bulk polymerization with subsequent emulsification (64). The first attempts at emulsion polymerization arose from problems controlling the heat generated during bulk polymerization. In emulsion polymerization, hydrophobic monomers are added to water, emulsified by a surfactant into small particles, and polymerized using a water-soluble initiator. The result is a colloidal suspension of fine particles, 50–1000 nm in diameter, usually comprising 30–50 wt% of the latex product. By 1935 emulsion polymerization became the method of choice in making synthetic rubber because of its many advantages (65): (*1*) the reaction mass viscosity remains low throughout the polymerization, providing for improved heat transfer, agitation, and product handling; (*2*) the sensible heat of the water in the emulsion balances the heat of reaction generated by free-radical polymerization; and (*3*) the rate of reaction is rapid, while producing very high molecular weight.

Kinetics and Mechanisms. Early researchers misunderstood the fast reaction rates and high molecular weights of emulsion polymerization (66). In 1945 the first recognized qualitative theory of emulsion polymerization was presented (67). This mechanism for classic emulsion preparation was quantified (68) and the polymerization separated into three stages: nucleation, particle growth while monomer droplets exist, and particle growth once monomer droplets have disappeared.

Stage I: Particle Nucleation. During stage 1 of a typical emulsion polymerization, the reaction mass consists of an aqueous phase containing small amounts of soluble monomer, small spherical micelles, and much larger monomer droplets. The micelles are typically 5–30 nm in diameter and are saturated with monomer emulsified by the surfactant. The monomer droplets are larger, 1000–10,000 nm in diameter, and are also stabilized by the surfactant.

Water-soluble initiator is added to the reaction mass to generate radicals which can enter the very small diameter micelles. Polymerization starts in the mcielle, converting it into a growing polymer particle. As monomer within the particle converts to polymer, it is replenished by diffusion from the monomer droplets. The concentration of monomer in the particle remains high (5–7 M), as long as monomer droplets exist. The growing polymer particles require more surfactant to remain stable, supplied from the uninitiated micelles. Stage I is complete once the micelles have disappeared, usually at or before 10% monomer conversion. Typically, 1 in 100 micelles are converted into latex particles, the others sacrificing their surfactant to the larger latex particles.

Primary radicals generated from water-soluble initiator rarely enter a micelle (69) because of differences in surface-charge density. The radicals formed from decomposition of water-soluble initiator are ionic in nature and very soluble

in the aqueous phase. The ionic radical water solubility is reduced by polymerization with monomer dissolved in the aqueous phase, a key first step, and the growing ionic oligomer chains become less soluble in the aqueous phase and readily enter the micelles. Radical entry is a thermodynamic balance based on solubility (70). Other theories exist to explain how water-soluble radicals enter micelles (71). The micelles are presumed to be the principal locus of particle nucleation (72) because of the large surface area of micelles relative to the monomer droplets.

However, in the case of miniemulsion, processing methods reduce the size of the monomer droplets closer to the size of the micelle, leading to significant particle nucleation in the monomer droplets (73) and therefore lack of dependence on monomer tranpsort across the aqueous phase. Intense agitation, cosurfactant, and dilution are used to reduce monomer droplet size. Additives such as cetyl alcohol are used to retard the diffusion of monomer from the droplets to the micelles, in order to further promote monomer droplet nucleation (74). The benefits of miniemulsions include inclusion of hydrophobic moieties in latex particles (75), faster reaction rates (76), improved shear stability, and the control of particle-size distributions to produce high solids latices (77). Microemulsion Polymerization (qv) (78) employs very high surfactant levels to make very small latex particles.

An expression for the number of particles formed during stage I was developed, assuming micellar entry as the formation mechanism (68), where k is a constant varying from 0.37 to 0.53 depending on the relative rates of radical adsorption in micelles and polymer particles, r_i is the rate of radical generation, m is the rate of particle growth, a_s is the surface area covered by one surfactant molecule, and S is the total concentration of soap molecules.

$$N_\mathrm{p} = k(r_i/m)^{0.4}(a_\mathrm{s}S)^{0.6} \tag{1}$$

During stage I, the number of polymer particles range from 10^{13} to 10^{15} per mL. As the particles grow they adsorb more emulsifier and eventually reduce the soap concentration below its critical micelle concentration (CMC). Once below the CMC, the micelles disappear and emulsifier is distributed between the growing polymer particles, monomer droplets, and aqueous phase.

The Smith–Ewart expression (eq. 1) accurately predicts the particle number for hydrophobic monomers such as styrene and butadiene (79), but fails to predict the particle number (80) for more hydrophilic monomers such as methyl methacrylate and vinyl acetate. A new theory based on homogeneous particle nucleation, called the HUFT theory after Hansen, Ugelstad, Fitch, and Tsai, was developed (81) to explain the hydrophilic monomer data yielding more accurate particle number predictions. The HUFT theory has been extended to include precursor and mature latex particle formation (82,83). In homogeneous coagulation theory (82), very small diameter precursors, containing only small amounts of monomer, transform into mature particles through coagulation. Mature particles form only near the end of the nucleation stage and positively skewed particle-size distributions are the result (83).

The debate as to which mechanism, controls particle nucleation continues. There is strong evidence that the HUFT and coagulation theories hold true for the more water-soluble monomers. What remains at issue are the relative rates of

micellar entry, homogeneous particle nucleation, and coagulative nucleation when surfactant is present at concentrations above its CMC. It is reasonable to assume that each mechanism plays a role, depending on the nature and conditions of the polymerization (84).

Whatever the nucleation mechanism, the final particle size of the latex is determined during stage I, provided no additional particle nucleation or coalesence occurs in the later stages. Monomer added during stages II and III only serves to increase the size of the existing particles.

Stage II: Growth in Polymer Particles Saturated with Monomer. Stage II begins once most of the micelles have been converted into polymer particles. At constant particle number the rate of polymerization, R_p, as given by Smith–Ewart kinetics is as follows: (85)

$$R_p = \frac{10^3 N k_p [M] \bar{n}}{N_A} \tag{2}$$

where k_p is the propagation rate constant, $[M]$ is the concentration of monomer in the particle, N is the concentration of growing polymer particles, $\bar{n}$ is the average number of radicals per particle, and N_A is Avogadro's number.

During stage II the growing particles maintain a nearly constant monomer concentration. The concentration of monomer is particle-size dependent, with smaller particles having lower concentrations (86).

During stages II and III the average concentration of radicals within the particle determines the rate of polymerization. To solve for $\bar{n}$ the fate of a given radical was balanced across the possible adsorption, desorption, and termination events. Initially, a solution was provided for three physically limiting cases. Subsequently, n was solved for explicitly without limitation using a generating function to solve the Smith–Ewart recursion formula (87). This analysis for the case of very slow rates of radical desorption was improved on (88), and later radical readsorption was accounted for and the Smith–Ewart recursion formula solved via the method of continuous fractions (89). More recently, an algebraic solution (90) to the Smith–Ewart recursion formula was put forth that greatly simplifies the calculation.

The nature of the radical within the latex particle determines its fate; ie, its propensity to desorp, propagate, chain transfer, or terminate. It seems reasonable that an ionic radical will not penetrate deeply into a latex particle but rather anchor its ionic head on the surface or palisade of the latex particle, much the way a surfactant molecule does. Once anchored, the nonpolar tail containing the radical will penetrate into the particle, and reactively diffuse throughout the polymer and monomer solution until either the ionic radical desorbs back into the aqueous phase, the ionic radical terminates with another radical within the particle, or the ionic radical undergoes a chain transfer event with either the monomer, polymer, or a chain-transfer agent within the latex particle. Once a chain transfer event occurs, the new radical becomes nonionic and has a markedly different solublity in the particle and aqueous phases. As the nonionic radical grows in chain length within the particle, it becomes even less soluble in the aqueous phase and becomes less likely to desorb. Such a qualitative description of radical fate was quantified

(91) and used to properly calculate the rate of polymerization in a macromonomer-mediated emulsion polymerization of methyl methacrylate.

As the particles grow, they require more soap to remain stable. If soap is not available the particles can destabilize, causing product and process problems.

Stage III: Growth in Polymer Particles with a Decreasing Monomer Concentration. Stage III begins once the monomer droplets disappear. The rate of polymerization decreases with reduced particle monomer concentration. At high monomer conversion, diffusion control of termination can cause an apparent increase in the rate of polymerization (92). Still further conversion can lead to diffusion control of propagation and a marked reduction in rate of polymerization (93). High free monomer in the final latex can result (94–96) causing product odor and handling problems.

The Smith–Ewart kinetics described assume homogeneous conditions within the particle. An alternative view, where monomer polymerizes only on the surface of the particle, has been put forth (97) and supported (98). The nature of the intraparticle reaction environment remains an important question.

Basic Components. The principal components in emulsion polymerization are deionized water, monomer, initiator, emulsifier, buffer, and chain-transfer agent. A typical formula consists of 20–60% monomer, 2–10-wt% emulsifier on monomer, 0.1–1.0-wt% initiator on monomer, 0.1–1.0-wt% chain-transfer agent on monomer, various small amounts of buffers and bacteria control agents, and the balance deionized water.

Water. Latices should be made with deionized water or condensate water. The resistivity of the water should be at least $10^5\Omega$. Long-term storage of water should be avoided to prevent bacteria growth. If the ionic nature of the water is poor, problems of poor latex stability and failed redox systems can occur. Antifreeze additives are added to the water when polymerization below 0°C is required (99). Low temperature polymerization is used to limit polymer branching, thereby increasing crystallinity.

Monomers. A wide variety of monomers can be used, and they are chosen on the basis of cost and ability to impart specific properties to the final product. Water solubilities of industrially important monomers are shown in Table 1 (100). The solubility of the monomer in water affects the physical chemistry of the polymerization. Functional monomers such as methacrylic and acrylic acid, infinitely soluble in water, are also used. These monomers impart long-term shelf stability to latices by acting as emulsifiers. The polymerization behavior of some monomers, such as methacrylic acid, as well as the final latex properties are influenced by pH. For optimum results with these acids, polymerization is best performed at a pH of ca 2. After polymerization, the latex is neutralized to give adequate shelf stability at tractable viscosities.

When monomers of drastically different solubility (101) or hydrophobicity are used or when staged polymerizations (102,103) are carried out, core–shell morphologies are possible. A wide variety of core–shell latices have found application in paints and impact modifiers, and as carriers for biomolecules. In staged polymerizations, spherical core–shell particles are made when polymer made from the first monomer is more hydrophobic than polymer made from the second monomer (104). When the first polymer made is less hydrophobic than the second, complex

Table 1. Water Solubilities of Monomers Common to Latex Production

Monomer	CAS Registry Number	Solubility in water at 25°C, mM
n-Octyl acrylate	[2499-59-4]	0.34
Dimethylstyrene		0.45
Vinyltoluene	[25012-15-4]	1.0
n-Hexyl acrylate	[2499-95-8]	1.2
Styrene	[100-42-5]	3.5
n-Butyl acrylate	[141-32-2]	11
Chloroprene	[126-99-8]	13
Butadiene	[106-99-0]	15
Vinylidene chloride	[75-35-4]	66
Ethyl acrylate	[140-88-5]	150
Methyl methacrylate	[80-62-6]	150
Vinyl chloride	[75-01-4]	170
Vinyl acetate	[108-05-4]	290
Methyl acrylate	[96-33-3]	650
Acrylonitrile	[107-13-1]	1600
Acrolein	[107-02-8]	3100

morphologies are possible including voids and half-moons (105), although spherical particles still occur (106).

Surfactants. Surfactants perform many functions in emulsion polymerization, including solubilizing hydrophobic monomers, determining the number and size of the latex particles formed, providing latex stability as particles grow, and providing latex stability during post-polymerization processing.

Emulsification is the process by which a hydrophobic monomer, such as styrene, is dispersed into micelles and monomer droplets. A measure of a surfactant's ability to solubilize a monomer is its CMC. Below the CMC the surfactant is dissolved in the aqueous phase and does not serve to solubilize monomer. At and above the CMC the surfactant forms spherical micelles, usually 50–200 soap molecules per micelle. Many properties, such as electrical conductivity, interfacial tension, surface tension, refractive index, and viscosity, show a sudden decrease at the CMC (107). The CMC is temperature- and chain-length-dependent for a given class of surfactants (108). The CMCs of nonionic surfactants are higher than those of ionic surfactants (109).

Surfactants also stabilize the growing polymer particles by overcoming the attractive forces between particles. Anionic and cationic surfactants use electrostatic repulsion forces to negate the attraction. Nonionic surfactants use steric forces to repel the attraction. Figure 1 compares the two stabilizing mechanisms. The ability of a given surfactant to stabilize latex particles is dependent on many factors (110), including surfactant type and concentration, aqueous solubility of the monomer and polymer, agitation and shear rate, temperature, surface tension, ionic strength, and concentration of the monomer and polymer (111).

An a priori method for choosing a surfactant was attempted by several researchers (112) using the hydrophile–lipophile balance or HLB system (113). In the HLB system a surfactant soluble in oil has a value of 1 and a surfactant soluble in water has a value of 20. Optimum HLB values have been reported

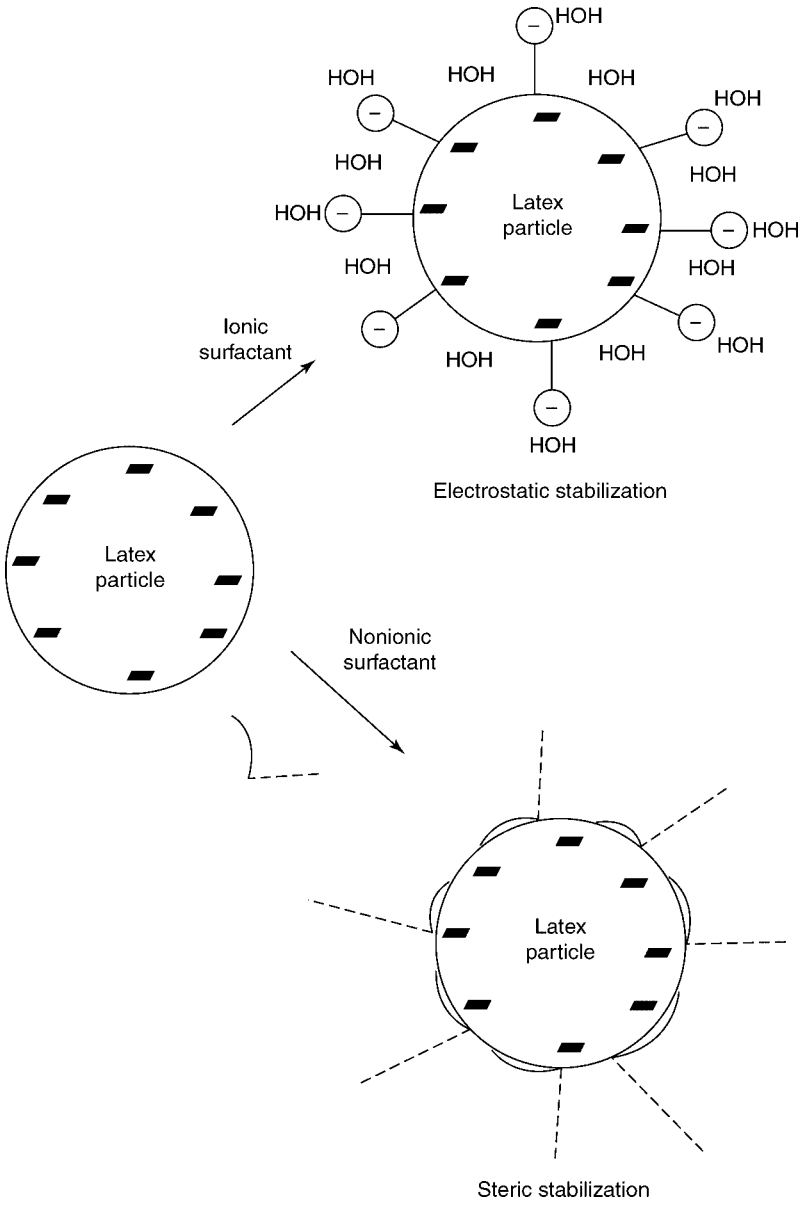

Fig. 1. Surfactant stabilization mechanisms.

for latices made from styrene, vinyl acetate, methyl methacrylate, ethyl acrylate, acrylonitrile, and their copolymers and range from 11 to 18. The HLB system has been criticized as being imprecise (114).

Three generations of latices as characterized by the type of surfactant used in manufacture have been defined (115). The first generation includes latices made with conventional (*1*) anionic surfactants such as fatty acid soaps, alkyl carboxylates, alkyl sulfates, and alkyl sulfonates (116); (*2*) nonionic surfactants such as

poly(ethylene oxide) or poly(vinyl alcohol) used to improve freeze–thaw and shear stability; and (*3*) cationic surfactants such as amines, nitriles, and other nitrogen bases, rarely used because of incompatibility problems. Portland cement latex modifiers are one example where cationic surfactants are used. Anionic surfactants yield smaller particles than nonionic surfactants (117). Often a combination of anionic surfactants or anionic and nonionic surfactants is used to provide improved stability. The stabilizing ability of anionic fatty acid soaps diminishes at lower pH as the soaps revert to their acids. First-generation latices also suffer from the presence of soap on the polymer particles at the end of the polymerization. Steam and vacuum stripping methods are often used to remove the soap and unreacted monomer from the final product (118,119).

The second generation includes latices made with functional monomers such as methacrylic acid, 2-hydroxyethyl acrylate [818-61-1], acrylamide [79-06-1], 2-dimethylaminoethylmethacrylate [2867-47-2], and sodium *p*-vinylbenzenesulfonate [98-70-4] that create *in situ* polymeric emulsifier. The initiator decomposition products, such as the sulfate groups arising from persulfate decomposition, can also act as chemically bound surfactants. These surfactants are difficult to remove from the latex particle.

The third generation are latices made with independently prepared surfactant to mimic the *in situ* prepared functional monomer surfactant. These emulsifiers are often A–B block polymers where A is compatible with the polymer and B with the aqueous phase. In this way, surface adsorption of the surfactant is more likely.

Any of these surfactant classes can involve surfactants that react onto the latex particle. These surfactants are known as *surfmers*. If the surfactant also acts as a chain-transfer agent, it is dubbed a *transurf*. Reversible addition fragmentation agents can act as transurfs (120).

Initiators. The initiators most commonly used in emulsion polymerization are water-soluble although partially soluble and oil-soluble initiators have also been used (121). Normally only one initiator type is used for a given polymerization. In some cases a finishing initiator is used (122). At high conversion the concentration of monomer in the aqueous phase is very low, leading to much radical–radical termination. An oil-soluble initiator makes its way more readily into the polymer particles, promoting conversion of monomer to polymer more effectively.

The most common water-soluble initiators are ammonium persulfate, potassium persulfate, and hydrogen peroxide. These can be made to decompose by high temperature or through redox reactions. The latter method offers versatility in choosing the temperature of polymerization with −50 to 70°C possible. A typical redox system combines a persulfate with ferrous ion:

$$S_2O_8^{2-} + Fe^{2+} \rightarrow Fe^{3+} + SO_4^{2-} + SO_4^{-} \quad (3)$$

Reducing agents are employed to return the Fe^{3+} to Fe^{2+}. By starting at a lower temperature, the heat of reaction can be balanced by the sensible heat of the water in the emulsion. Temperature profiles from 20 to 70°C are typical for such systems. Care must be taken when working with redox systems to eliminate oxygen from the reactor before beginning the polymerization. The effectiveness of

the redox system can be pH-dependent, with the optimum pH range depending on the type of the redox system (123). For higher temperature polymerizations, eg, above 70°C, thermal decomposition of the initiator is used.

A third source of initiator for emulsion polymerization is hydroxyl radicals created by γ-radiation of water. A review of radiation-induced emulsion polymerization detailed efforts to use γ-radiation to produce styrene, acrylonitrile, methyl methacrylate, and other similar polymers (124). The economics of γ-radiation processes are claimed to compare favorably with conventional techniques although worldwide industrial application of γ-radiation processes has yet to occur. Use of γ-radiation has been made for laboratory study because radical generation can be turned on and off quickly and at various rates (125).

The ionic nature of the radicals generated, by whatever technique, can contribute to the stabilization of latex particles. Soapless emulsion polymerizations can be carried out using potassium persulfate as initiator (126). It is often important to control pH with buffers during soapless emulsion polymerization.

Chain-Transfer Agents. The most commonly employed chain-transfer agents in emulsion polymerization are mercaptans, disulfides, carbon tetrabromide, and carbon tetrachloride. They are added to control the molecular weight of a polymer, P_n, by transferring a propagating radical to the chain-transfer agent AX (127):

$$P_n^{\bullet} + \mathrm{AX} \rightarrow P_n\mathrm{X} + \mathrm{A}^{\bullet} \tag{4}$$

The newly formed short-chain radical $\mathrm{A}^{\bullet}$ then quickly reacts with a monomer molecule to create a primary radical. If subsequent initiation is not fast, AX is considered an inhibitor. Many have studied the influence of chain-transfer reactions on emulsion polymerization because of the interesting complexities arising from enhanced radical desorption rates from the growing polymer particles (128,129). Chain transfer reactions are not limited to chain transfer agents. Chain transfer to monomer is in many cases the main chain termination event in emulsion polymerization. Chain transfer to polymer leads to branching which can greatly impact final product properties (130).

Other Ingredients. During polymerization and post-processing, the pH of the emulsion is important. Increasing the pH to improve latex stability is achieved usually by adding sodium hydroxide, potassium hydroxide, or ammonia. To avoid causing any localized flocculation because of a rapid increase in electrolyte in a confined area, these ingredients must be added as dilute solutions of around 3% with mild agitation. In some cases, some surfactant may be required to be added along with the dilute alkali. Antimicrobial agents are added for protection against bacteria attack.

Process. Commercial processes (131) manufacturing latex can be divided into batch, semibatch, and continuous methods. A schematic of typical equipment is shown in Figure 2. The reactor is usually glass-lined, including agitator and thermowell. The remaining tanks are constructed of stainless steel. The reactor is jacketed to allow for heating and cooling between 0 and 100°C. Reactor agitation is chosen to provide adequate mixing while avoiding shear-induced coagulation. The reactor is equipped with a small condenser; reflux is to be avoided to prevent coagulum from forming. A monomer–soap solution is emulsified by a centrifugal pump

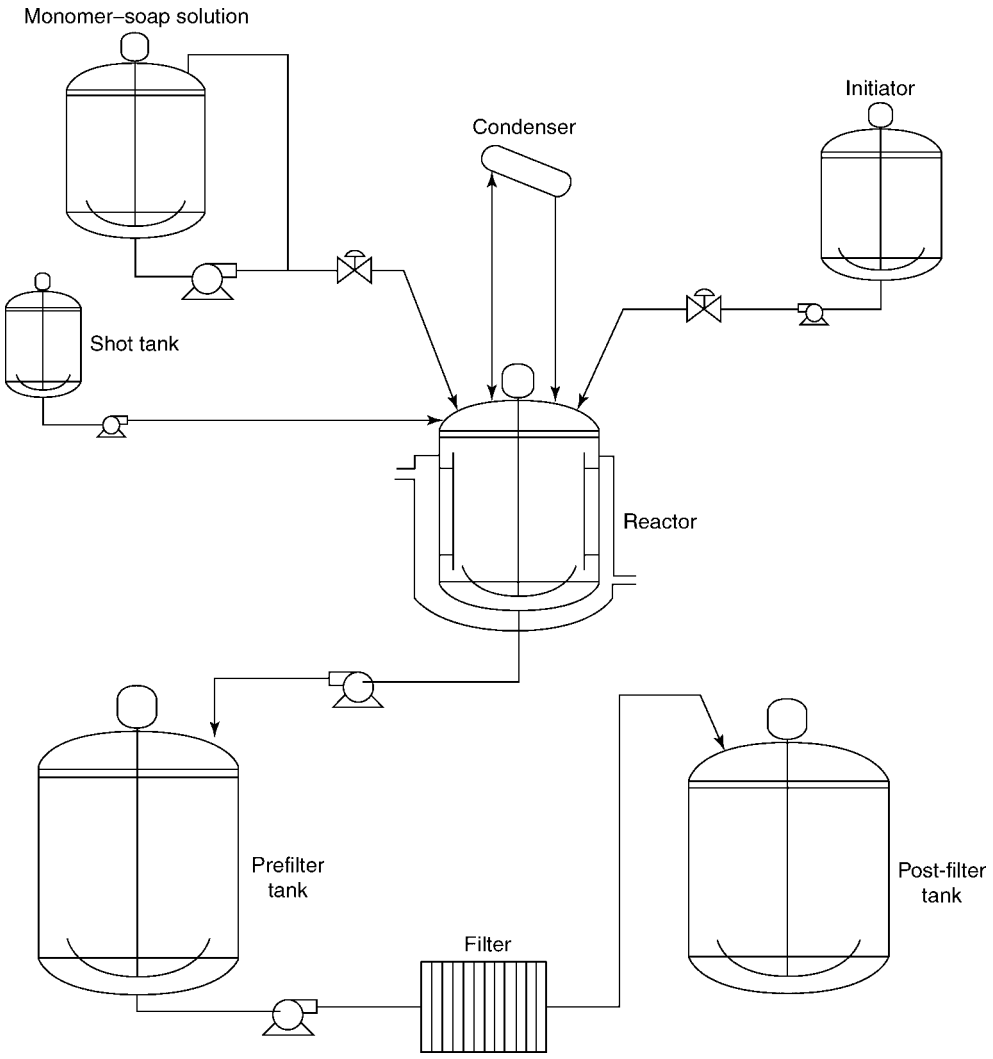

Fig. 2. Typical latex manufacturing equipment.

and fed to the reactor along with initiator, using suitable flow control. Premixing monomer and initiator is to be avoided to prevent premature polymerization in the feed tank. A shot tank is usually required to allow for addition of ingredients in minor amounts.

In the most common production method, the semibatch process, about 10% of the preemulsified monomer is added to the deionized water in the reactor. A shot of initiator is added to the reactor to create the seed. Some manufacturers use master batches of seed to avoid variation in this step. Having set the number of particles in the pot, the remaining monomer and, in some cases, additional initiator are added over time. Typical feed times are 1–4 h. Lengthening the feeds tempers heat generation and provides for uniform comonomer sequence distributions (132). Sometimes skewed monomer feeds are used to offset differences in monomer

reactivity ratios. In some cases a second monomer charge is made to produce core–shell latices. In-line instruments can help determine monomer consumption rates and are becoming more frequently employed, especially in the development of new materials (133). At the end of the process, pH adjustments are often made. The product is then pumped to a prefilter tank, filtered, and pumped to a post-filter tank where additional processing can occur. When the feed rate of monomer during semibatch production is very low, the reactor is said to be monomer-starved. Under these conditions, monomer droplets are not present, and intraparticle polymerization takes place under high polymer–low monomer concentrations. These conditions can lead to branched polymer with bi- and trimodal molecular weight distributions (134).

The batch process is similar to the semibatch process, except that most or all of the ingredients are added at the beginning of the reaction. Heat generation during a pure batch process makes reactor temperature control difficult, especially for high solids latices. Seed, usually at 5–10% solids, is routinely made via a batch process to produce a uniform particle-size distribution. Most kinetic studies and models are based on batch processes (135).

Continuous processes have been developed for many of the larger volume synthetic latices (136–140). Most of these processes involve the use of several continuously stirred tank reactors (CSTR) in series. The exponential residence time distribution of a CSTR is broad relative to a batch reactor, leading to broad particle-size distributions. By placing many CSTRs in series, the effective residence time and corresponding particle-size distributions are narrowed. CSTR processes can also suffer from sustained oscillations and multiple steady states, leading to poor reactor and product performance (141). The cause of the oscillations is related to new particle formation. To avoid such oscillations, many processes use a seed latex in the feed stream (142). If premanufacture of seed is not desirable, a tubular reactor can be used to produce seed of uniform particle size (143). Tubular reactors have also been used as loop reactors, where feeds enter and leave a tubular loop in which the circulating flow is much greater than the throughput (144). Cooling water is sprayed directly on the tube to control the reaction temperature. Recently, coagulum has been successfully controlled during tubular production of a latex using pulsatile flow (145).

Foaming represents a persistent problem in the processing and handling of latices. The most effective way to eliminate the presence of foam is to simply avoid its generation. Ways to reduce foam include eliminating the free fall of latex by using dip-pipes, not stirring air into the latex by not agitating with exposed impellers, and not adding dry ingredients laden with adsorbed air directly to the latex. There are many proprietary additives for minimizing generation of foam (antifoaming agents) or eliminating foam (defoaming agents), but there is no one type that works for all latices (see ANTIFOAMING AGENTS). Only by trial and error can the most effective agent be found for a given compound or process. With any of them, the minimum amount required should be used since their addition tends to cause localized flocculation, poor wetting, lower water resistance, and "fisheyes" in films. Many antifoam agents get absorbed into the polymer or other ingredients in the compound and thus lose their effectiveness over time, particularly if the compound is being recirculated during processing. These conditions necessitate augmentation with additional amounts of antifoaming agent to counter these effects.

Process Modeling. The complexity of emulsion polymerization makes reliable computer models valuable. Many attempts have been made to simulate the emulsion polymerization process for different monomer systems (146–148).

Other Routes.

High Solids Emulsions. Latices are made at the highest possible solids content consistent with acceptable viscosity. Latices solids can be increased by centrifuging, creaming, electrodecantation, or evaporation. The latter two techniques, however, are not of commercial importance. Natural rubber latex, 25–40-wt% solids to start, is concentrated to about 60-wt% solids by centrifuging with milk/cream separator equipment. Creaming is commonly used with synthetic polymer latices. Creaming is accelerated by adding solutions such as ammonium alginate and surfactant to the latex. Depending on the initial solids content and type of latex, solids contents of 58–65 wt% are possible.

Soap-starved recipes have been developed that yield 60-wt% solids low viscosity polymer emulsions without concentrating. It is possible to make latices for application as membranes and similar products via emulsion polymerization at even higher solids (149). Solids levels of 70–80 wt% are possible. The paste-like material is made in batch reactors and extruded as product.

Inversion of Nonacqueous Polymers. Many polymers such as polyurethanes, polyesters, polypropylene, epoxy resins, and silicones that cannot be made via emulsion polymerization are converted into latices. Such polymers are dissolved in solvent and inverted via emulsification, followed by solvent stripping (150). Solid polymers are milled with long-chain fatty acids and diluted in weak alkali solutions until dispersion occurs (151). Such latices usually have lower polymer concentrations after the solvent has been removed. For commercial uses the latex solids are increased by techniques such as creaming.

BIBLIOGRAPHY

"Latexes" in *EPST* 1st ed., Vol. 8, pp. 164–195, by Richard Stagg, Marbon Chemical Division, Borg Warner Corp., in *EPSE* 2nd ed., Vol. 8, pp. 647–677, by D. C. Blackley, London School of Polymer Technology.

1. H. Warson, *Applications of Synthetic Resin Latices*, Vol. 1, John Wiley & Sons, Inc., Chichester, U.K., 2001, pp. 49–89.
2. V. R. Sinner and A. Kumar, *Indian J. Pharmaceutical Sci.* **64**(3), 191–199 (2002).
3. M. Antonietti and K. Tauer, *Macromol. Chem. Phys.* **204**, 207–219 (2003).
4. M. Morton, *Introduction to Rubber Technology*, Reinhold Publishing Corp., New York, 1959.
5. M. Faraday, *Q. J. Sci. Lit. Art* **21**, 19 (1826).
6. P. G. Cook, *Latex—Natural and Synthetic*, Reinhold Publishing Corp., New York, 1956.
7. U.S. Pat. 1,864,078 (1932), C. Hueck (to I.G. Farbenindustrie AG).
8. Ger. Pat. 150,690 (1909); Ger. Pat. 558,890 (1927); Ger. DRP 568,907 (1930).
9. W. H. Carothers, G. J. Berechet, and A. M. Collins, *J. Am. Chem. Soc.* **54**, 4066 (1932); W. H. Carothers, I. Williams, and J. E. Kirby, *J. Am. Chem. Soc.* **53**, 4203 (1931).
10. G. G. Winspear, ed., *The Vanderbilt Latex Handbook*, R. T. Vanderbilt Co., New York, 1954.
11. Rubber Statistical Bulletin, International Rubber Study Group, London, 2003.
12. J. W. Vanderhoff, *Chem. Eng. Sci.* **48**, 203–217 (1993).

13. H. Mooibroek and K. Cornish, *Appl. Micrbiol. Biotechnol.* **53**, 355 (2000).
14. D. Urban and K. Takamura, eds., *Polymer Dispersions and Their Industrial Applications*, Wiley-VCH, New York, 2002.
15. R. H. D. Beswick, *Latex 2002 International Conference on Latex and Latex Based Products*, Rapra Technology Ltd., Shrewsbury, U.K., Dec. 2002, pp. 45–59.
16. E. Daniels, E. D. Sudol, and M. S. El-Aasser, eds., *Polymer Latexes: Preparation, Characterization and Applications*, ACS Symposium Series, Vol. 492, American Chemical Society, Washington, D.C., 1992.
17. J. C. Carl, *Neoprene Latex*, E. I. du Pont de Nemours & Co., Inc., Wilmington, Del., 1962.
18. H.-G. Vogt, H.-J. Erb, and S. Butz, *Latex 2001 International Liquid Elastomers Conference*, Rapra Technology Ltd., Shrewsbury, U.K., Dec. 2001, pp. 51–60.
19. K. Arai, *Kami Parupu Gijutsu Taimusu* **43**(7), 23–30, (2000).
20. K. M. Scholsky and R. M. Fitch, *J. Controlled Release* **3**, 87–108 (1986).
21. P. E. Keipert, *Blood Substitutes* **2**, 127–156 (1998).
22. J. K. Bernard and co-workers, *J. Dairy Sci.,* **86**, 3661–3666 (2003).
23. G. W. Sams and M. Zaouk, *Energy Fuels* **14**, 31–37 (2000).
24. S. Muroi, *Colloids Surf. A: Physiochem. Eng. Aspects* **153**, 3–10 (1999).
25. M. S. El-Aasser and co-workers, in M. S. El-Aasser and J. W. Vanderhoff, eds., *Emulsion Polymerization of Vinyl Acetate*, Applied Science Publishers, London, 1981, p. 215.
26. P. A. Lovell, *Royal Soc. Chem.* **263**, 74–86, (2001). Special publication.
27. A. Guyot , T. McKenna and M. Schneider, *Microspheres, Microcapsules and Liposomes*, 2002, pp. 39–76.
28. U.-R. Cho, *Eylasutoma,* **37**(1), 31–38 (2002).
29. R. H. Ottewill, *J. Polym. Sci., Polym. Lett.* **111**, 131 (1973).
30. R. L. Rowell, *J. Polym. Sci., Polym. Lett.* **111**, 201–204 (1973).
31. E. J. W. Verwey and J. Th. G. Overbeek, *Theory of the Stability of Lyophobic Colloids*, Elsevier, Amsterdam, the Netherlands, 1948.
32. B. V. Derjaguin and L. Landau, *Acta Physiochim. URSS* **14**, 633 (1941); S. Croll, *Prog. Org. Coat.* **44**(2), 131–146 (2002).
33. C. G. Force and E. Matijevic, *Kolloid. Z. Z. Polym.* **224**, 51 (1968).
34. M. S. Romero-Cano and co-workers, *Langmuir* **17**, 3505–3511 (2001).
35. D. H. Napper, *Polymeric Stabilization of Colloidal Dispersions*, Academic Press, London, 1983.
36. F. B. Sheinerman and co-workers, *Curr. Opin. Struct. Biol.* **10**(2), 153–159 (2000).
37. R. M. Raj and R. W. Cannon, *Surf. Sci. Ser.* **104**, 27–61 (2002).
38. S. Pascual, P. Narrainen and D. M. Haddleton, *ACS*, 221st Poly 007 (2001).
39. D. H. Napper, *J. Colloid Interface Sci.* **58**, 390 (1977); X. E. E. Reynhout and co-workers, *J. Polym. Sci., Part A: Polym. Chem.* **41**, 2985–2995 (2003).
40. A. P. Gast, C. K. Hall, and W. B. Russell, *Faraday Discuss. Chem. Soc.* **76**, 189 (1983).
41. Ref. 99, p. 406.
42. Y. Tang, F. Zhong, G. Liu, and Y. Sun, *Huaxue Wuli Xuebao* **16**, 321–325 (2003).
43. A.-M. Sung and I. Piirma, *Langmuir* **10**, 1393–1398 (1994).
44. J. W. Goodwin, *J. Polym. Sci., Polym. Lett.* **111**, 212–215 (1973).
45. M. Shaffer and H. Bui, *25th Proceedings of the International Waterborne, High-Solids and Powder Coatings Symposium*, 1998, pp. 93–104.
46. I. M. Krieger, *Adv. Colloid Interface Sci.* **3**, 111 (1972).
47. J. W. Vanderhoff, H. R. Sheu, and M. S. El-Aasser, *J. Polym. Sci., Polym. Lett.* **111**, 529–565 (1973); B. S. Casey, *Mater. Forum* **16**, 117–122 (1992).
48. I. T. Kim and P. Luckman, *Powder Technol.* **77**, 21 (1993).
49. R. H. Ottewill, in Ref. 25, pp. 253–276.

50. M. F. Mills and co-workers, *Macromolecules* **26**, 3553–3562 (1993); R. H. Ottewill, *Pure Appl. Chem.* **64**, 1697–1702 (1992).
51. S. Lee, M. N. Meyers, R. Beckett, and J. C. Gidding, *Anal. Chem.* **60**, 1129 (1988).
52. J. G. DosRamos and C. A. Silebi, *J. Colloid Interface Sci.* **135**, 165 (1990).
53. J. N. Shaw and R. H. Ottewill, *Discuss. Faraday Soc.* **42**, 154 (1966); A. Kithara and H. Ushiyama, *J. Colloid Soc.* **43**, 73 (1972); B. A. Mathews and C. T. Rhoades, *J. Colloid Soc.* **32**, 332 (1970).
54. J. W. Vanderhoff, in Ref. 25, pp. 43–44.
55. G. L. Brown, *J. Polym. Sci.* **22**, 423 (1956); D. P. Sheetz, *J. Appl. Polym. Sci.* **9**, 3759 (1965); J. W. Vanderhoff, E. B. Bradford, and W. K. Carrington, *J. Polym. Sci., Part C* **41**, 155 (1973).
56. D. C. Sundberg and Y. G. Durant, *Polym. React. Eng.* **11**, 379–432 (2003).
57. K. Hahn, G. Ley, and R. Oberthur, *J. Polym. Sci., Polym. Lett.* **111**, 463–479 (1973).
58. C. H. Gelbert and H. E. Berkheimer, Paper C in Educational Symposium No. 18 on Latex Technology, Rubber Division of the American Chemical Society, Montreal, Canada, 1987.
59. L. A. Cannon and R. A. Pethrick, *Polymer* **43**, 6429–6438 (2002).
60. R. M. Herbert, *Pesticide Formulations and Application Systems*, ASTM Special Technical Publication, (STP 1449) Vol. 23, 2003, pp. 55–67.
61. R. E. Partch and co-workers, in Ref. 17, pp. 368–386.
62. P. Espiard and co-workers, in Ref. 17, pp. 387–404.
63. R. M. Fitch, *Polym. React. Eng.* **11**, 911–953, (2003); J.-C. Daniel, *Surf. Sci. Ser.* **115**, 1–22, (2003); R. G. Gilbert, *Chinese J. Poly. Sci.* **18**(3), 189–193 (2000); K. Tauer, *Surf. Sci. Ser.* **100**, 429–453 (2001); P. Flesher, *J. Soc. Leather Technologists Chemists* **78**(3), 71–84 (1994).
64. G. Odian, *Principles of Polymerization*, 2nd ed., John Wiley & Sons, Inc., New York, 1981, p. 319.
65. H. Fikentscher, *Angew. Chem.* **51**, 433 (1938); J. H. Baxendale and co-workers, *J. Polym. Sci.* **1**, 466 (1946); W. P. Hohenstein and H. Mark, *J. Polym. Sci.* **1**, 549 (1946).
66. W. D. Harkins, *J. Chem. Phys.* **13**, 381 (1945); *J. Amer. Chem. Soc.* **69**, 1428 (1947).
67. W. V. Smith and R. H. Ewart, *J. Chem. Phys.* **16**, 592 (1948).
68. R. G. Gilbert and G. T. Russell, Course Notes from a Short Course on Emulsion Polymers at Sydney University, Sydney, Australia, 1992, p. 18.
69. F. K. Hansen, *Chem. Eng. Sci.* **48**, 437–444, (Jan. 1993).
70. M. C. Grady, Sc. D. dissertation ETH 11945, Zürich, 1996.
71. M. S. El-Aasser, in F. Candau and R. H. Ottewill, eds., *Scientific Methods for the Study of Polymer Colloids and Their Applications*, Kluwer Academic Publishers, Dordrecht, the Netherlands, 1990, pp. 12–15.
72. J. Ugelstad and co-workers, *J. Polym. Sci., Polym. Lett.* **111**, 503 (1973).
73. P. L. Tang and co-workers, in Ref. 17, pp. 72–98.
74. K. Fontenot and F. J. Schork, *J. Appl. Polym. Sci.* **49**, 663–655 (1993); D. T. Barnett and F. J. Schort, *Chem. Eng. Commun.* **80**, 113–125 (1989); E. Elbing and co-workers, *Aust. J. Chem.* **42**, 2085–2094 (1989).
75. K. Landfester and co-workers, *Macromol. Chem. Phys.* **201**, 81, (2000).
76. M. S. El-Aasser, in F. Candau and R. H. Ottewill, eds., *An Introduction to Polymer Colloids*, Kluwer Academic Publishers, Dordrecht, the Netherlands, 1990, p. 15.
77. H. Gerrens, *Fortschr. Hochpolym. Forsch.* **1**, 234–238.
78. M. Antonietti and co-workers, *Macromolecules* **24**, 6636, (1991).
79. V. I. Yeliseyeva, in I. Piirma, ed., *Emulsion Polymerization*, Academic Press, New York, 1982, p. 248.
80. R. M. Fitch and C. H. Tsai, *Polym. Lett.* **8**, 703 (1970).

81. D. H. Napper and R. G. Gilbert, *Makromol. Chem., Macromol. Symp.* **10/11**, 503 (1987).
82. D. H. Nappera and R. G. Gilbert, in Ref. 72, p. 167.
83. A. S. Dunn, in Ref. 17, pp. 45–54.
84. W. V. Smith, *J. Am. Chem. Soc.* **70**, 3695 (1948).
85. M. Morton, S. Kaizerman, and M. W. Altier, *J. Colloid Sci.* **9**, 300 (1954).
86. W. H. Stockmayer, *J. Polym. Sci.* **24**, 314 (1957).
87. J. T. O'Toole, *J. Appl. Polym. Sci.* **9**, 1291 (1965); *J. Polym. Sci., Part C* **27**, 171 (1969).
88. J. Ugelstad, P. C. Mork, and J. O. Aasen, *J. Polym. Sci., Part A-1* **5**, 2281 (1967).
89. G. T. Russell and co-workers, *Macromolecules* **21**, 2133 (1988).
90. B.-G. Li and B. W. Brooks, *J. Polym. Sci.: Part A: Polym. Chem.* **31**, 2397–2402 (1993).
91. M. C. Grady, Presentation at the *North American Research Conference Series Science and Technology of Emulsion Polymers/Polymer Colloids*, Nov. 1999.
92. M. J. Ballard and co-workers, *Macromolecules* **19**, 1303 (1986).
93. I. A. Maxwell, E. M. F. J. Verdurmen, and A. L. German, *Makromol. Chem.* **193**, 2677–2695 (1992).
94. S. S. Medvedev, *Proc. Int. Symp. Makromol. Chem. Prague 1957*, Pergamon Press, New York, 1958, p. 174.
95. S. S. Medvedev, Kinet. Mech. Polyreactions, IUPAC Int. Symp. Makromol. Chem., Plenary Main Lect. 1969, p. 39.
96. S. S. Medvedev and co-workers, *J. Macromol. Sci. Chem. A* **7**, 715 (1973).
97. M. R. Grancio and D. J. Williams, *J. Polym. Sci., Part A-1* **8**, 2617 (1971).
98. D. C. Blackley, *Emulsion Polymerization*, Applied Science Publishers Ltd., London, 1975.
99. E. R. Blout and co-workers, *Monomers*, Interscience Publishers, New York, 1949.
100. Y. C. Chen, V. Dimonie, and M. S. El-Aasser, *Pure Appl. Chem.* **64**, 1691–1696 (1992); Y. C. Chen, V. L. Dimonie, O. L. Shaffer, and M. S. El-Aasser, *Polym. Int.* **30**, 185–194 (1993).
101. S. Lee and A. Rudin, in Ref. 17, pp. 234–254.
102. S. Laferty and I. Piirma, in Ref. 17, pp. 255–271.
103. M. Okubo, A. Yamada, and T. Matsumoto, *J. Polym. Sci., Polym. Chem. Ed.* **16**, 3219 (1980).
104. T. J. Min, A. Klein, M. S. El-Aasser, and J. W. Vanderhoff, *J. Polym. Sci,. Polym. Lett. Ed.* **21**, 2845 (1981).
105. Y. C. Chen, V. L. Dimonie, O. L. Shaffer, and M. S. El-Aasser, *Polym. Int.* **30**, 185–194 (1993).
106. H. Gerrens and G. Hirsch, in J. Brandrup and E. H. Immergut, eds., *Polymer Handbook*, 2nd ed., John Wiley & Sons, Inc., New York, 1975, pp. II–483.
107. B. D. Flockhart, *J. Colloid. Sci.* **16**, 484–492 (1961); J. K. Weil and co-workers, *J. Am. Oil Chem. Soc.* **40**, 538–540 (1963).
108. K. Shinoda, T. Nakagawa, B. I. Tamamushi, and T. Isemura, *Colloidal Surfactants*, Academic Press, Inc., New York, 1963.
109. R. H. Ottewill, in Ref. 80, pp. 1–6.
110. K. Fontenot and F. J. Schork, *Ind. Eng. Chem. Res.* **32**, 374 (1993).
111. M. P. Merkel, M. S. dissertation, Lehigh University, Bethlehem, Pa., 1982.
112. W. C. Griffin, *Off. Dig. Fed. Paint Varnish Prod*. Clubs 28 (June 1956).
113. M. S. El-Aasser, in Ref. 72, p. 17.
114. J. W. Vanderhoff, *Chem. Eng. Sci.* **48**, 212 (1993).
115. Ref. 65, p. 333.
116. A. S. Dunn, in Ref. 17, p. 51.
117. Rus. Pat. 4-239506 (1992), S. Takao, H. Nakano, and H. Kobayashi.
118. M. Nomura and K. Fujita, *Makromol. Chem., Rapid Commun.* **10**, 581–587 (1989).
119. M. Nomura, J. Ikoma, and K. Fujita, in Ref. 17, pp. 55–71.

120. A. Guyot, *Macromol. Symp.* **179**, 105–132 (2001); O. Soula and co-workers, *J. Poly. Sci., Part A: Polym., Chem.* **37**, 4205–4217 (1999).
121. A. E. Hamielec and J. F. MacGregor, in Ref. 80, p. 330.
122. H. Warson, in I. Piirma and J. L. Gardon, eds., *Emulsion Polymerization*, ACS Symposium Series, Vol. 24, American Chemical Society, Washington, D.C., 1976, p. 228.
123. V. T. Stannett, in Ref. 80, pp. 415–450.
124. Ref. 69, p. 59.
125. A. R. Goodall, J. Hearn, and M. C. Wilkinson, *Brit. Polym. J.* **10**, 141 (1978); *J. Polym. Sci., Polym. Chem. Ed.* **17**, 1019 (1979).
126. Ref. 65, pp. 226–242.
127. H. Lee and G. W. Pohlein, *Polym. Process. Eng.* **5**(1), 37–74 (1987).
128. B. C. Wang and co-workers, *J. Polym. Sci., Polym. Lett. Ed.* **18**, 711 (1980).
129. P. A. Lovell, T. H. Shah, and F. Heatley, in Ref. 17, pp. 188.
130. K. Chujo and co-workers, *J. Polym. Sci., Part C* **27**, 321 (1969).
131. E. Saravanakumar, *Paintindia* **52**(10), 41–52 (2002).
132. J. Guillot, A. Guyot, and C. Pichot, in Ref. 72 , p. 103.
133. J. R. Leiza and J. M. Asua, in J. M. Asua ed., *Polymeric Dispersions: Principles and Applications*, Kluwer Academic Publishers, London, 1997, p. 363.
134. W. H. Ray, *ACM Symposium Series* 226, 1983.
135. G. W. Pohlein, in Ref. 80, pp. 357–382.
136. G. Ley and H. Gerrens, *Chem. Ing. Tech.* **43**, 693 (1971).
137. A. W. DeGraff, Ph.D. dissertation, Lehigh University, Bethlehem, Pa., 1970.
138. F. J. Schork, Ph.D. dissertation, University of Wisconsin-Madison, 1981.
139. R. K. Greene, R. A. Gonzales, and G. W. Pohlein, in Ref. 59, pp. 367–378.
140. C. Kiparissides, Ph.D. dissertation, McMaster University, Hamilton, Ontario, Canada, 1978.
141. H. C. Lee and G. W. Pohlein, *Chem. Eng. Sci.* **41**, 1023–1030 (1986).
142. R. A. Gonzalez, M.S. dissertation, Lehigh University, Bethlehem, Pa., 1974.
143. U.S. Pat. 3,551,996, R. Lanthier (to Gulf Oil Canada, Ltd.).
144. D. A. Paquet, Ph.D. dissertation, University of Wisconsin-Madison, 1993.
145. K. W. Min and W. H. Ray, *J. Appl. Polym. Sci.* **22**, 89 (1978); J. B. Rawlings and W. H. Ray, *Polym. Eng. Sci.* **28**, 237 (1988).
146. M. Morbidelli, G. Storti, and S. Carra, *J. Appl. Polym. Sci.* **28**, 961 (1983).
147. J. R. Richards, J. P. Congalidis, and R. G. Gilbert, *J. Appl. Polym. Sci.* **37**, 2727–2756 (1989).
148. E. Ruckenstein and F. Sun, *J. Appl. Polym. Sci.* **46**, 1271–1277 (1992).
149. Ref. 123; J. Ugelstad and co-workers, in Ref. 80, pp. 383–413.
150. S. P. Suskind, *J. Appl. Polym. Sci.* **9**, 2451 (1965).
151. R. H. Ottewill and co-workers, in M. S. El-Aasser and R. M. Fitch, eds., *Future Directions in Polymer Colloids*, Martinus Nijhoff Publishers, Dordrecht, Germany, 1987, pp. 243–251.
152. P. J. Tarcha and co-workers, in Ref. 17, pp. 347–367.

MICHAEL C. GRADY
DuPont Company

LDPE. See ETHYLENE POLYMERS, LDPE.

LIGHT-EMITTING DIODES. See Volume 3.

LIGNIN. See Volume 3.

LINEAR LOW DENSITY POLYETHYLENE.
See ETHYLENE POLYMERS, LLDPE.

LIQUID CRYSTALLINE POLYMERS, MAIN-CHAIN.
See Volume 3.

LIQUID CRYSTALLINE THERMOSETS. See Volume 3.

LITERATURE OF POLYMERS. See INFORMATION RETRIEVAL.

LITHOGRAPHIC RESISTS. See Volume 6.

LIVING POLYMERIZATION, ANIONIC.
See ANIONIC POLYMERIZATION.

LIVING POLYMERIZATION, CATIONIC.
See CARBOCATIONIC POLYMERIZATION.

LIVING RADICAL POLYMERIZATION. See Volume 6.

LLDPE. See ETHYLENE POLYMERS, LLDPE.

LOW DENSITY POLYETHYLENE. See ETHYLENE POLYMERS, LDPE.

MECHANICAL PERFORMANCE OF PLASTICS

Introduction and Scope

Since 1950 or so revolutionary developments have taken place in synthesis, characterization, structure–property relations, performance, and applications of synthetic polymers. Applications of these materials have permeated all aspects of our daily life, including health, medicine, clothing, transportation, housing, defence, energy, electronics and photonics, information technology, employment, and trade (1). This has been possible because of unique attributes of polymer-based materials including low density, high specific strength and modulus, high corrosion resistance, full ranges (from very low to very high) of electrical and thermal conductivities, easy and low energy processing into intricate shapes by fast processing techniques (such as injection molding or extrusion), moth and fungus resistance, controlled biodegradability, low permeability of water vapors and other gases, and great aesthetic appeal. One property alone, namely low densities, causes gradual conversion in automotive, aviation, aerospace, and other industries from metal parts to polymer-based parts.

On top of the above attributes, polymer materials are generally less expensive than most alternative materials. Mechanical properties are most important in the design and selection of engineering plastics because all applications require necessarily a certain degree of mechanical loading.

Consider now polymer-based materials from the point of view of a materials user. A user can be an industrialist who buys truckloads of polymer-based components for his plant, a housewife, a little girl playing with a plastic doll—in fact anybody. The user typically has no interest (and little knowledge) of chemical synthesis of polymers, thermodynamics, polymer processing—in fact of any

Encyclopedia of Polymer Science and Technology. Copyright John Wiley & Sons, Inc. All rights reserved.

of the areas of polymer science and engineering. There is only one aspect of interest common to scientists, engineers, and laymen alike—and that is the *performance*. Since performance involves mechanical properties, there will be necessarily certain overlaps with other articles of this *Encyclopedia* which in various ways deal with these properties, eg, Elasticity, Rubber-like (qv), Viscoelasticity (qv), Fracture (qv), Fatigue (qv), Impact Resistance (qv), Dynamic Mechanical Analysis (qv), Micromechanical Properties (qv), and Yield and Crazing (qv). The present article focuses on performance and its constituent *reliability*.

Problems in polymer science and engineering can be solved on the basis of information acquired in experiments, by developing models and theories, and also by performing computer simulations. All these three kinds of approaches are useful when dealing with performance and reliability.

Relaxational and Destructive Processes: Chain Relaxation Capability

The Importance of Reliability. The reliability of a material or component—not necessarily polymeric—constitutes its most important characteristics. The two questions concerning polymer-based materials that are being asked the most often are

(1) Will a material or component serve as much time as I need it, or will it fail prematurely?
(2) Is there a material or component with better properties?

Although both questions are often asked simultaneously, the second question deals with development of new materials and will be considered in other articles. The first question shows that failure is related to prediction of service performance under given service conditions.

Chain Relaxation Capability. What is the key factor of deciding whether a material will serve—rather than deform and fracture into pieces? To answer this, we need to remember that polymer-based materials are viscoelastic. The "face" each polymer shows to the observer—elastic, viscous flow, or a combination of both—depends on the rate and duration of force application as well as on the nature of the material and external conditions including the temperature. Later there will be a more detailed discussion of the nature of viscoelasticity. At this point let us stress that properties of viscoelastic materials vary with time—while for elastic materials time plays no role at all.

A component in service is "attacked" from the outside, perhaps by an impact (in impact testing we are actually hitting the specimen with a hammer) or else by slow extension (as in tensile testing). In general, forces with various duration, direction(s), and application rate

$$U = U_0 - U_b - U_r \tag{1}$$

Here U is the energy provided from the outside which at a given time has not yet been spent one way or the other; U_b ("b" for bond breaking) at the same time

has been spent on destructive processes (such as crack formation or propagation); U_r at the given time has been dissipated, in other words spent on nondestructive processes. Dissipation in a viscoelastic material is largely related to relaxational processes; the subscript "r" stands for relaxation. The quantities in equation 1 may refer to the material as a whole, but it is usually more convenient to take them as pertaining each to a unit weight of polymer such as 1 g.

The question whether the component will survive in fact hinges on U_r. The energy U_r is related to the chain relaxation capability (CRC) which has been defined (2–4) as the amount of external energy dissipated by relaxation in a unit of time per unit weight of polymer.

We shall use the abbreviation CRC for the concept and the symbol U_{CRC} for the respective amount of energy. Thus, at a given time t

$$U_r = \int_0^t U_{CRC}\, dt \tag{2}$$

It takes approximately 1000 times more external energy to break a primary chemical bond (such as a carbon–carbon bond in a carbonic chain, what corresponds to U_b and to crack propagation) than to execute a conformational rearrangement. This is the basis of the following key statement (2–4): Relaxational processes have priority in the utilization of external energy. The excess energy, which cannot be dissipated by such processes, goes into *destructive* processes.

In other words, the viscoelastic material will try to relax rather than fracture—as long as it can go on relaxing. Unless there is a high concentration of external energy at a particular location, so that a number of primary chemical bonds will break starting a crack, that energy will be dissipated. In contrast to metals and other nonchain materials, when we pull at a polymeric chain, we gradually engage all segments of it; this by itself lowers the probability of local concentration of the external energy and thus the probability of destruction.

We can distinguish at least four constituents of CRC (2–4):

(1) Transmission of energy across the chain, producing intensified vibrations of the segments;
(2) Transmission—mainly by entanglements but also by segment motions—of energy from the chain to its neighbors;
(3) Conformational rearrangements (such as cis into trans) executed by the chains;
(4) Elastic energy storage resulting from bond stretching and angle changes. This last factor is often excluded from considerations even though for a number of processes, it might be quite important.

Chain relaxation capability depends strongly on free volume, that is the amount of space in which polymer chain segments can move around and relax. This connection will be explored and used to advantage later on in this article.

The concepts defined above will serve to evaluate reliability of polymer-based materials, but first methods of experimental determination of mechanical properties and also the responses of materials to deformation should be reviewed (5).

Quasi-Static Mechanical Testing

Types of Applied Stress. Mechanical behavior of polymer-based materials depends on composition, structures, and interactions at molecular and supermolecular levels (5–7). The structures are much dependent on primary chemical (mostly covalent) bonding inside the chains and secondary bonding (dispersion: van der Waals, induction, electrostatic, and hydrogen bonding, the last being the strongest in this category) forces in between chains (8). The composition often includes additives aimed at an improvement of a particular property.

When a body is subjected to an applied force F, the resultant stress σ induces a finite deformation or strain ε within the body. The deformation can be recoverable (elastic) irrecoverable (plastic), gradually partly recoverable (viscoelastic) and can lead to fracture of the body, depending on amplitude of load, rate of deformation, and temperature. The recoverable deformation may be instantaneous, small (energetic elastic in nature due to the bending and stretching of the interatomic bonds of plastic materials), or large (rubbery or entropic, also elastic in nature due to coiling and uncoiling of polymer chains). The irrecoverable or plastic deformation may lead to permanent deformation or may be recoverable after heating the polymeric material above its glass-transition temperature T_g. The viscoelastic deformation is generally a function of temperature T since it depends on free volume v^f (much more of which is discussed later).

Simple *fracture* is the separation of the body into two or more parts in response to an imposed stress that can be acting slowly (for instance the gravitational field of the earth), rapidly (impact), or anything in between.

The applied stress may be tensile, compressive, shear, hydrostatic, or torsional (see Fig. 1). Two fracture models are possible, *ductile* and *brittle*. In ductile materials fracture is preceded by substantial plastic deformation with high energy absorption. By contrast, there is normally little or no plastic deformation and low energy absorption accompanying a brittle fracture. The ductility is a function of temperature of the material, the strain rate, and the stress state. Depending on these factors, a material considered ductile material may actually fail in a brittle manner.

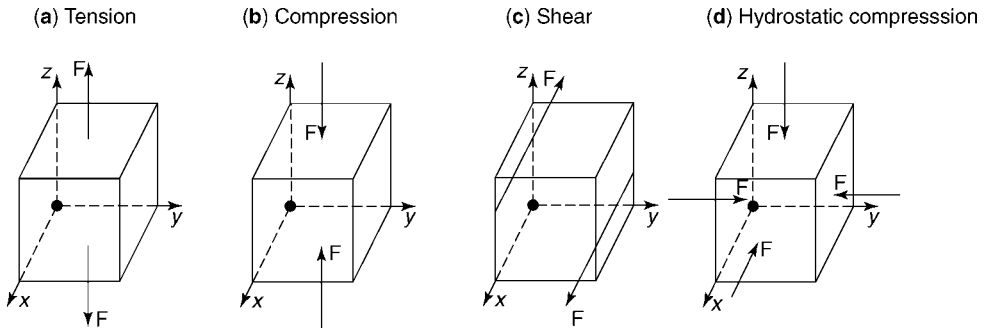

Fig. 1. Typical modes of stress application to polymeric materials: (**a**) Tension, (**b**) Compression, (**c**) Shear, (**d**) Hydrostatic pressure.

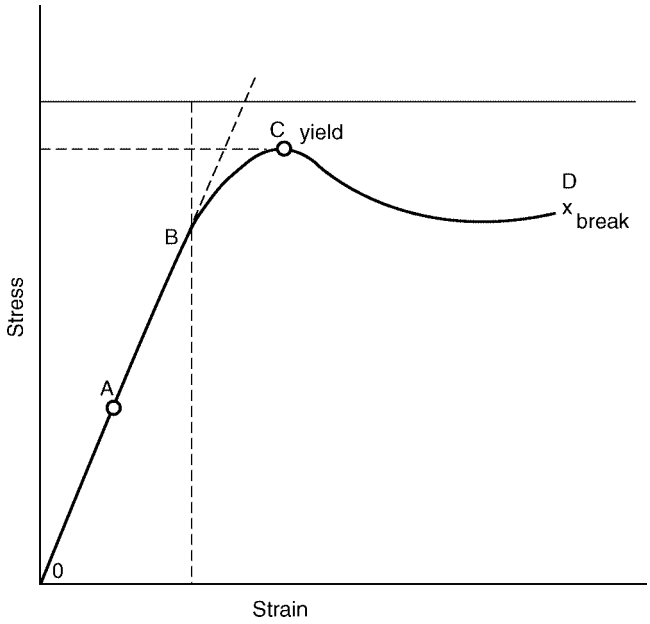

Fig. 2. A stress–strain curve in tension typical for engineering plastics.

Stress–Strain Behavior. The determination of stress–strain behavior in tension is one of the most important test methods for mechanical properties of engineering plastics and is of high importance to the design engineer (see ENGINEERING THERMOPLASTICS, OVERVIEW). The tensile test is usually performed by monitoring the force that develops as the sample is elongated at a constant rate of extension. An often encountered stress–strain curve of a plastics material at equilibrium with any environment can be represented as depicted in Figure 2.

The behavior seen in Figure 2, typical as it is, is by no means the only one. A hard and brittle material such as a phenolic resins (qv) is characterized by a high modulus of elasticity, no well-defined yield point, and low strain at break (Fig. 3**a**). It may not yield before break. A hard and strong material is characterized by a high modulus, high yield stress, and high strength with low strain at break, such as a polyoxymethylene (Fig. 3**b**). A hard and tough material such as polycarbonate (qv) is characterized by high modulus, high yield stress, and high elongation at break (Fig. 3**c**). A soft but tough material such as polyethylene (PE) exhibits low modulus and low yield stress with very high elongation at break (Fig. 3**d**) (see ETHYLENE POLYMERS, HDPE; ETHYLENE POLYMERS, LDPE; ETHYLENE POLYMERS, LLDPE). A soft and weak material, such as polytetrafluoroethelene (PTFE, Teflon) is characterized by low modulus and low yield stress with moderate elongation at break (see PERFLUORINATED POLYMERS, POLYTETRAFLUOROETHYLENE).

The area under stress–strain curve is proportional to the energy required to break and is a measure of the *toughness* of the material. Typical engineering plastics exhibit curves characteristic of hard and strong or hard and tough materials.

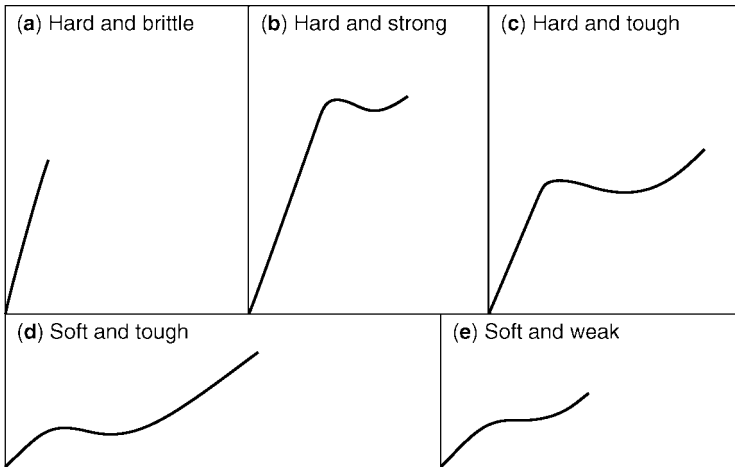

Fig. 3. Tensile stress–strain curves for several categories of plastics.

Elastic Modulae. The mechanical behavior is in general terms concerned with the deformation that occurs under loading. Generalized equations that relate stress to strain are called *constitutive relations*. The simplest form of such a relation is Hooke's Law which relates the stress s to the strain e for uniaxial deformation of the ideal elastic isotropic solid:

$$\sigma = E\,\varepsilon \tag{3}$$

E is the Young's modulus and is clearly a measure of resistance of the material to deformation; the reciprocal of the modulus $D = 1/E$ is called *compliance*.

In reality, the mechanical behavior of polymeric solids deviates from equation 3. The following factors are at play:

(1) Only at very small deformations the stress is exactly proportional to the strain and Hooke's Law is obeyed. In general, the constitutive equations are *nonlinear*. Unlike metals, polymers can recover from strains beyond the proportional limit without any permanent deviations.

(2) The loading rate and time affect the deformations in polymeric solids. As already pointed out, viscoelastic materials show simultaneously the "face" of an elastic solid and that of a flowing viscous liquid. This implies that the simplest constitutive relation for a polymeric solid should, in general, contain *time* and *frequency* as variables in addition to stress and strain.

(3) There is incomplete and time-dependent recovery when loads are removed.

(4) Polymer-based materials are often anisotropic—as in cases of films and synthetic fibers.

(5) Temperature and other environmental factors affect the mechanical behavior. Thus, polymers can show all features of a glassy brittle solid, an elastic rubber, or a viscous liquid depending on the temperature and time scale of measurements. At low temperatures or high frequencies, a polymeric

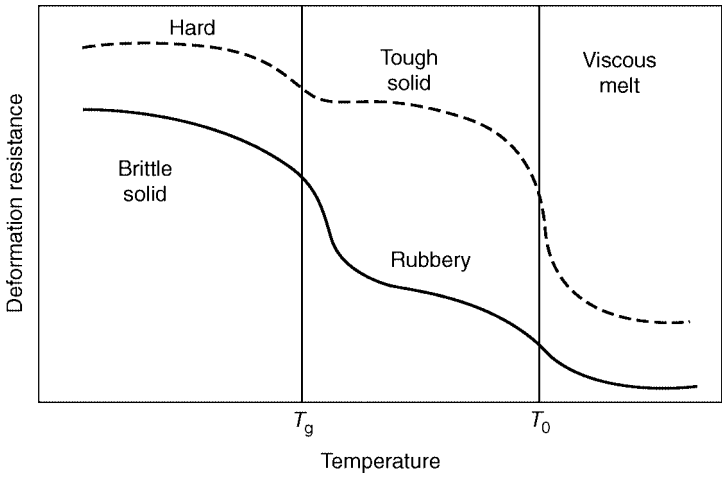

Fig. 4. Variation of Young's modulus with temperature for amorphous (solid line) and semicrystalline (broken line) polymers.

material may be glass-like with the Young's modulus of 10^9–10^{10} N/m^2 and will break or flow at strains greater than 5%. At high temperatures or low frequencies, the same polymeric material may be rubber-like with a modulus of 10^6–10^7 N/m^2 withstanding large extensions (≈100%) without permanent deformation. At still higher temperatures, permanent deformation occurs under load and the material behaves like a highly viscous liquid. In an intermediate temperature or frequency range (glass-transition range), the material is not glassy or rubber-like. Here it shows an intermediate modulus (viscoelastic modulus) and may dissipate a considerable amount of energy on being strained. Figure 4 shows the variation of Young's modulus with temperature. Note that the diagram pertains to uncross-linked elastomers (=rubbers) since in the cross-linked ones the plateau in the middle part remains also at high temperatures; see next section for more on elastomers. The glass-transition temperature is also highly influential in semicrystalline plastics where a brittle-tough transition in the solid state can be observed in response to an applied stress. Young's modulus decreases drastically on traversing the melting temperature T_m as melt is formed. The extent of crystallization determines the rate of change of the modulus—providing temperature characteristics both across and within the primary thermal transition.

(6) The whole range of the behaviors shown in Figure 5 can be displayed by a single polymer, depending on the temperature and strain rate. The figure displays the load extension behavior of a single polymer at various temperatures. At the lowest temperature we observe low extensibility followed by brittle behavior (Fig. 5**a**). Figure 5**b** shows a distinct yield point (maximum load) with subsequent failure by neck instability. Necking and cold drawing is seen in Figure 5**c** with orientational hardening and eventual failure in the highly oriented neck at high strain levels exceeding often 300%. Behaviors

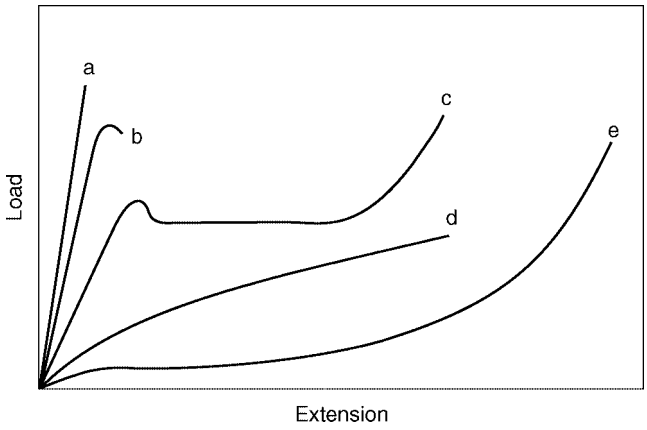

Fig. 5. Stress–strain curves at various temperatures (increasing from a to e): (**a**) low extensibility followed by brittle fracture at the lowest temperature; (**b**) localized yielding followed by fracture; (**c**) necking and cold drawing; (**d**) homogeneous deformation with indistinct yield; (**e**) rubber-like behavior.

seen in Figures 5**d** and 5**e** are characteristics of rubber elastic response, which is typical for amorphous and low crystalline materials at temperatures just above the glass-transition temperature T_g. These deformations are mainly elastic—characterized by low stress and high extensibility—unless there is significant stress-induced crystallization during drawing process.

(7) Similar curves can be obtained by changing the strain rate rather than temperature (see Fig. 6).

The elastic modulus E is only one of four elastic constants or modulae (8). Another one is the Poisson ratio ν defined as

$$\nu = -\varepsilon_r/\varepsilon \tag{4}$$

where ε_r is the linear strain in the direction perpendicular to the tensile stress σ producing the strain ε along the direction of the force application. ε_r has the opposite sign to that of ε, and hence the minus sign is incorporated in the definition to make ν positive for most materials. On application of a tensile stress on one pair of perpendicular faces of unit cube (Fig. 7**a**), the cube transforms to the shape seen in Figure 7**b**.

The bulk modulus k_b is defined by

$$k_b = -V\,dP/dV = -dP/(dV/V) \tag{5}$$

Here V is the volume of material and dP is the hydrostatic pressure applied from all sides. The negative sign has again been introduced to render the modulus positive.

The shear modulus G, the last of the four modulae, is defined in terms of the shear strain θ divided by the shear stress σ. Assuming θ to be very small

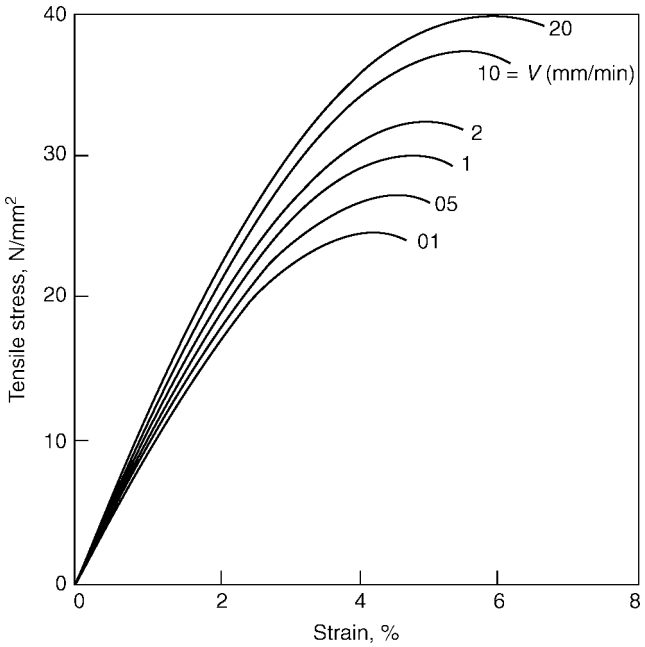

Fig. 6. Tensile stress–strain curves up to the yield point at various strain rates.

(see Fig. 7**c**), we have

$$G = \sigma/\theta \tag{6}$$

The linear theory of elasticity provides relationships between the modulae:

$$E = 2G(1+\nu) = 3\,k_b(1-2\nu) \tag{7}$$

The forces involved in the elasticity of amorphous polymers (qv) are not only of the van der Waals (dispersive) type but involve a high proportion of bonded interactions between atoms. The conformations of the polymer chain are "frozen in" so that the forces required in order to stretch bonds, change bond angles, and rotate segments of polymer chain around bonds are very important in determining the elastic properties. These forces are stronger than van der Waals forces and cause higher modulus.

Calculation of the modulae of semicrystalline polymers (qv) is fairly tedious and involves several operations: (*1*) calculation of modulae of amorphous polymers; (*2*) calculation of the elastic constants of anisotropic crystalline polymers; (*3*) averaging of elastic constants of the crystalline materials to provide an effective isotropic modulus; (*4*) the averaging of the isotropic amorphous and crystalline modulae to obtain the overall modulus. Only the second of these steps is accurate, the other are approximate.

In a semicrystalline material the chains are constrained because of the crystallization process. The constraints give the material different properties from those of a purely amorphous rubbery polymer. The states of stress and strain

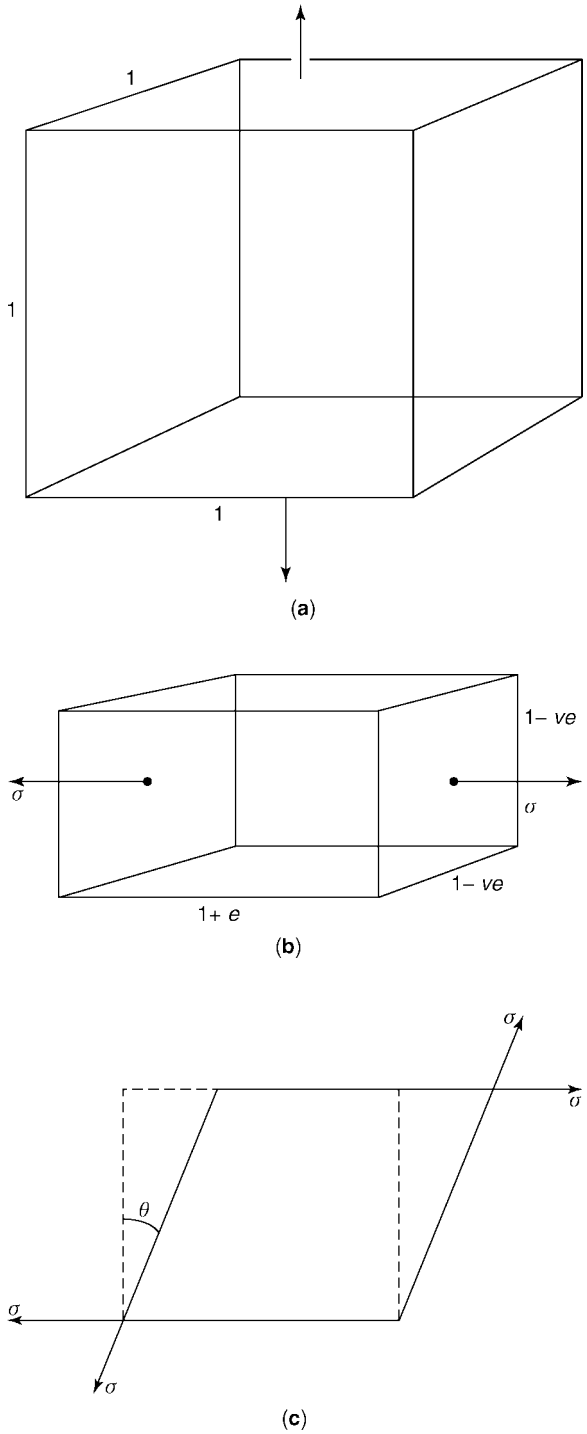

Fig. 7. The effect of application of tensile stress σ on a unit cube before (**a**) and after (**b**); (**c**) the application of shear stress τ to the unit cube.

are not homogeneous in a material comprising components with different elastic properties. In the operations just described, the assumption of uniform stress gives results closer to the experiment than does the assumption of uniform strain.

Rubber Elasticity

Unlike ordinary plastics, elastomers (also called rubbers) are capable of undergoing very large recoverable deformations under the influence of very small loads. A typical rubber may be stretched up to 10 times of its original length with essentially no visual or nonrecoverable strain. The rubber-like materials consist of relatively long polymeric chains that have a high degree of flexibility and mobility and are joined into a network structure. That structure leads to solid-like features where chains are prevented from flowing relative to each other under external stresses. The phenomenon is known as *rubber elasticity*. It is entropy-driven and is endowed with a thermoelastic effect. Rubber elasticity has been discussed by Gedde (9) and in much detail by Mark and his colleagues (10–12) (see ELASTICITY, RUBBER-LIKE). Important facts include

(1) A stretched rubber sample subjected to uniaxial load contracts reversibly on heating.
(2) The rubber sample gives out heat reversibly when stretched.
(3) The elastic forces are due to changes in conformational entropy. The long-chain molecules are stretched out to statistically less favorable states. The instantaneous deformation occurring in rubbers is due to high segmental mobility and thus results in rapid changes in chain conformation of the molecules. The energy barriers between different conformational states must be therefore small compared to the thermal energy.

The above features of rubbery materials have long been known. The quantitative measurements of mechanical and thermodynamic properties of natural and other elastomers go back to 1805 and some of the studies were conducted by luminaries like Joule and Maxwell. The first molecular theory in polymer science dealt with the rubber elasticity (9–12).

The first rubbery material discovered was natural rubber obtained from latex of the tree called *Hevea brasiliensis*. At this writing we have quite a variety of synthetic rubber or synthetic elastomers. The double bonds in natural rubber are all in cis configuration; a change in molecular conformation corresponding to a rotation around any of three single bonds per repeat unit requires very little energy. There are many single bonds in the backbone and there are no stiffening groups such as ring structures and bulky side chains. Another important feature is that the glass-transition temperatures T_g for all these materials are low and below the room temperature; hence they are in the rubbery state at ambient temperatures. Elastomers typically have low melting temperatures but some of them do undergo crystallization upon sufficiently large deformations.

Examples of typical elastomers include natural rubber, butyl rubber, poly(dimethyl siloxane), polyethyl acrylate, styrene–butadiene copolymer, and ethylene–propylene copolymer. Some polymers are not elastomers under normal

conditions but can be made so by raising the temperature or adding plasticizers (qv).

Quantitative statistical theories of rubber elasticity are based on the premise that contributions to the elasticity from to changes in the internal energy on stretching are negligible compared with the contributions due to changes in entropy (9–12). (see STATISTICAL THERMODYNAMICS). Essentially, the aim of the statistical theory is the calculation of the change in entropy when a rubber is deformed. By relating the change of entropy to the work done, strain energy function can be derived for isothermal stretching. Currently, one typically assumes that the network consists of phantom Gaussian chains, that all network changes are entropic, that the volume remains constant, and that one needs to take into account interchain interactions. In the phantom network theory, the positions of junctions are allowed to fluctuate about the mean positions prescribed by the affine deformation ratio. One finds that the modulus is proportional to the absolute temperature and also increases with increasing cross-link density.

The network theory gives a good representation of the experimental results only for moderate strains ($\varepsilon < 1.5$). For larger extensions, the theory overpredicts the stress because the conformational states are no longer adequately represented by the Gaussian distribution. At still higher extensions ($\varepsilon > 6$), the observed stress rapidly rises because of development of strain-induced crystallization [see Fig. 8 (here λ = strain ε)].

The values of Young's modulus for isotropic glassy and semicrystalline polymers are typically two orders of magnitude lower than those of metals. These materials can be either brittle with fracture at strains of a few percent or ductile leading to large but nonrecoverable deformation. Young's modulae for elastomers are typically four orders of magnitude smaller than, say, steel—which is how recoverable extensions up to ≈1000% are possible.

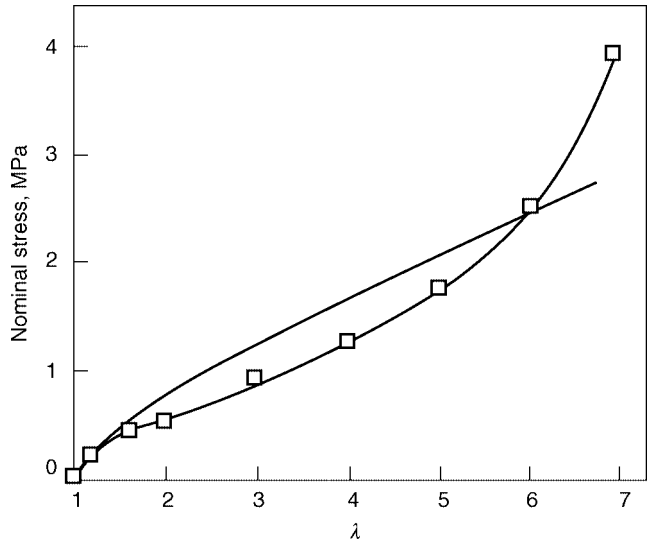

Fig. 8. Variation of nominal stress with extension ratio in a cross-linked rubber. —□— Experimental; ———Theoretical.

Creep, Stress Relaxation, and Dynamic Mechanical Behavior

Viscoelasticity. As already noted, the time-dependent properties of polymer-based materials are due to the phenomenon of viscoelasticity (qv), a combination of solid-like elastic behavior with liquid-like flow behavior. During deformation, equations 3 and 6 above applied to an isotropic, perfectly elastic solid. The work done on such a solid is stored as the energy of deformation; that energy is released completely when the stresses are removed and the original shape is restored. A metal spring approximates this behavior.

In contrast, a viscous liquid has no definite shape and flows irreversibly under the action of external forces; the work done by shearing stress is dissipated as heat. The so-called perfect liquid obeys the law of Newton:

$$\sigma = \eta \, \mathrm{d}\gamma/\mathrm{d}t \tag{8}$$

where $\mathrm{d}\gamma/\mathrm{d}t$ is the rate of change of shear strain with time t; the proportionality factor η is the shear viscosity. A dashpot is quite often used to represent the ideal viscous flow behavior according to equation 8. A dashpot is full of a purely viscous liquid; the plunger moves through the liquid at a rate proportional to the stress.

Since by definition the viscoelastic material in shear exhibits both the behavior governed by equation 6 and than represented by equation 8, the constitutive relation for the linear viscoelastic solid can be written as

$$\sigma = G\gamma + \eta \, \mathrm{d}\gamma/\mathrm{d}t \tag{9}$$

We have to remember that equation 9 applies only at small strains.

The linear viscoelastic materials obey the so-called Boltzmann Superposition Principle. As noted by Tschoegl (13), this was the only foray of the Viennese statistical physicist Ludwig Boltzmann into mechanics. The principle states that in linear viscoelasticity effects are simply additive; it matters at which instant an effect is created and it is assumed that each increment of stress makes an independent contribution.

Two manifestations of linear viscoelasticity are *creep* and *stress relaxation*; the respective two testing methods are known as *transient tests*. One can also apply sinusoidal load, an increasingly more used method of study of viscoelasticity by dynamic mechanical analysis (qv) (DMA). We shall now briefly discuss each of these three approaches.

Creep. Creep is a time-dependent strain increase under a constant stress. As already mentioned, the constant stress can be quite simply provided by a gravitational field of the earth. The creep behavior is most often analyzed in terms of the Kelvin–Voigt model in which a spring and a dashpot are parallel. The model is characterized by a constant representing the elastic (modulus) and viscous flow (viscosity) deformations. From the geometry of model, individual strain in each element is equal to total strain and applied stress is supported jointly by the spring and dashpot.

In nature viscoelasticity rarely follows the Kelvin–Voigt model. A way out is to make a combination of springs and dashpots so as to describe the observed behavior. Such combined models are convenient for calculations. Needless to say,

they do *not* explain anything. The explanation has to be found in the morphology of the phases present and still deeper at the level of chemical structures and interactions between chain segments.

Stress Relaxation. The phenomenon of stress relaxation is the time-dependent stress decay under a constant strain condition. There exists a simple Maxwell model of the process, which consists of a spring and dashpot in series. If a fixed strain is applied, the spring is immediately extended and a stress is produced in it. The dashpot begins to be displaced. The strain and stress in the spring thus decay to zero as dashpot is displaced at decreasing rate until the displacement becomes equal to the original strain of the spring. Thus the stress relaxes to zero according to the model.

In reality, the stress decays to a constant value called the *residual stress* (14–16). Moreover, Kubat has discovered a curious phenomenon (14,15): the stress σ vs time t curves for stress relaxation of metals and polymers look practically the same. This in spite of claims by some hardened metallurgists that plastics should not be even called materials and in spite of behavior of some polymer scientists who simply ignore metals and alloys. Kubat has shown that even the slope of the large central descending part is virtually independent of the kind of material.

Trying to expain this curious phenomenon, Kubat has assumed that the relaxation occurs in *clusters*. That is, neither individual atoms in metals nor the polymer segments relax individually, but both kinds of units relax collectively. On the basis of this assumption, Kubat succeeded in developing a general theory of stress relaxation that provides predictions agreeing precisely with experiments (16).

Every theory makes certain assumptions. Computer simulations of polymers provide us with information inaccessible experimentally (17); the section Fracture Mechanics and Crack Propagation deals more on this subject. The simulations also make possible testing theoretical models. If there is a disagreement between the behavior of a computer-generated material and the prediction, one cannot blame it on errors of the experiment.

Molecular dynamics computer simulations have been used to test the basic assumptions of the Kubat theory (18,19). At first, the right shape of the stress vs time curve was seen, but the residual stress was seen after 1.5 decades of time; in reality for both metals and polymers it takes 4.3 or so decades of time. The computer-generated materials had no defects; to make the materials more realistic, some 2 or 3 vol% of defects were introduced. Then the stress relaxation curves took more than 4 decades of time—in agreement with the experiment (see Fig. 9).

More importantly, the molecular dynamics simulations show that the metal atoms and polymer chain segments rarely relax individually. They relax in clusters—just as Kubat has assumed. This is why it does not matter whether the material is a metal or a polymer. Kubat has also derived an equation for the distribution of cluster sizes (16). Simulations show that his size distribution equation is close to the behavior of computer-simulated materials (20). This is a beautiful example where experiments, theory, and computer simulations all coincide.

Dynamic Mechanical Analysis (DMA). Dynamic mechanical analysis (DMA) consists in imposition of a sinusoidal stress at a specified angular frequency ω and temperature T. In elastic materials strains are in the same phase

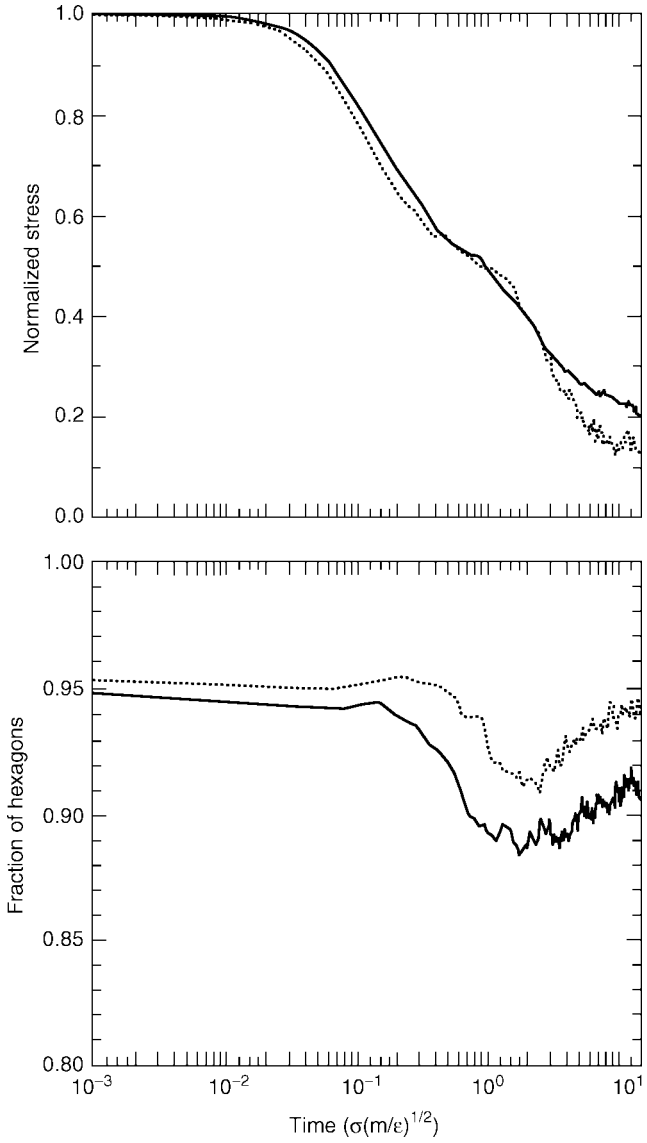

Fig. 9. Computer simulation of stress relaxation; after. ——— Polymer; . . . . . Metal (15).

as stresses and are related by a unique modulus value. By contrast, in viscoelastic materials there is a strain lag. The more liquid-like the material is, the larger the lag; the more solid-like it is, the smaller the lag. This is why DMA is a technique *par excellence* to characterize viscoelasticity of polymer-based materials. The experiment can be represented by

$$\varepsilon = \varepsilon_0 \exp(i\omega t) \tag{10a}$$

$$\sigma = \sigma_0 \exp\{i(\omega t + \partial)\} \tag{10b}$$

where ∂ represents the lag. The complex modulus is defined by

$$G^* = \sigma/\varepsilon = (\sigma_0/\varepsilon_0)\exp(i\partial) = (\sigma_0/\varepsilon_0)(\cos\theta + i\sin\theta) = G' + iG'' \tag{11}$$

Convenient parameters to work with are G' and G''. The former is called the *storage modulus* and represents the elastic solid-like contribution to the viscoelastic response of the material. The latter is called the *loss modulus* and represents the liquid-like response.

Some researchers like to work with just one parameter to characterize viscoelastic behavior, either G^* defined above or the so-called *loss factor*

$$G''/G' = \tan\partial \tag{12}$$

We find it more convenient to deal with G' and G'' separately. However, when one deals simultaneously with many polymer-based materials then one diagram per material might be sufficient. An example of behavior of a polymer is shown in Figure 10 as a function of the logarithmic angular frquency. Here G' is called G_1, G'' is called G_2, and tan ∂ is also displayed.

It can be shown that the energy ΔU dissipated per cycle per unit volume of the material is given by

$$\Delta U = \Pi G'' \varepsilon_0^2 \tag{13}$$

As more and more polymer-based materials are in use, their viscoelastic characteristics become more and more important. Some industry practitioners are apprehensive of imaginary and complex quantities such as those that appear in equations 10a, 10b and 11. Fortunately, a unique book on DMA (21) is aimed

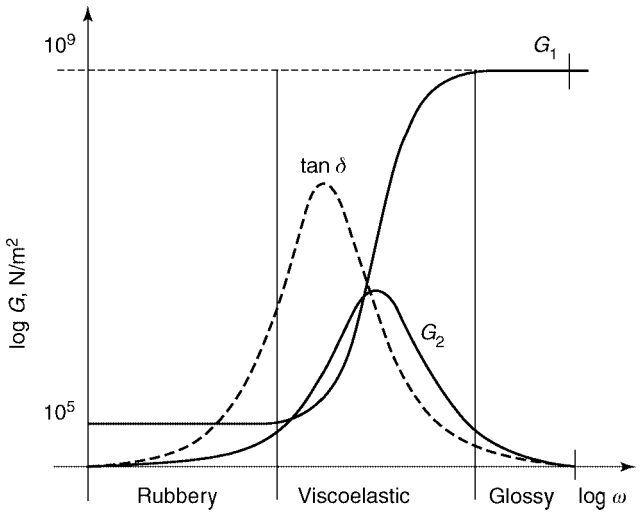

Fig. 10. DMA characteristics of a polymer. The variations of G', G'', and tan ∂ with the logarithmic frequency ω. Explanations in text.

precisely at the apprehensive practitioners—although it provides a wealth of information for the initiated as well. A much shorter story on the subject also by Menard can be found as a chapter in a collective book (22).

Yield Behavior

Yield Stress. For ideal linear viscoelastic material, if the load is removed at any time, the material recovers fully. These conditions are approximately satisfied at low stresses for several polymers. The elastic strains occur because of increase in the intermolecular distances, the bond angles, or a small shifting (without destruction) of the fluctuation network linkage points. At a certain stress level called the *yield stress*, the strain increases without a further increase in the stress. If the material has been strained beyond the yield stress, a nonrecoverable strain remains. Thus the yield point of a material is the highest stress that it can endure without manifesting a permanent strain upon unloading (see YIELD AND CRAZING).

The phenomenon of yielding occurs in all materials, including semicrystalline and glassy polymers. Yielding is associated with stress levels necessary to produce the initial permanent strain called the *plastic strain*. However, as so much in mechanics, also this definition has been first devised for metals. For polymers it is not unique because under some conditions polymers will manifest a strain after unloading which may persist only for a certain period of time. Thus the definition of what is the permanent strain in polymer-based materials from a practical point of view is arbitrary. For those materials whose stress–strain curves are monotonic, the 0.2% offset method is often used to determine yield stress. A line is constructed parallel to the elastic portion of the stress–strain curve at the offset strain such as 0.002. The stress corresponding to the intersection of this line with the stress–strain curve as it bends over into the plastic region is then defined as the yield strength σ_y. When the material exhibits a maximum in the stress–strain curve just beyond the elastic region, in this case the maximum stress is recognized as the yield stress.

Most of polymers except for the glass-transition region exhibit a maximum in the stress vs strain curve and it is this maximum stress that is usually referred as the yield point in what follows. At the yield point, molecular chain segments are able to slip past each other and the deformation process occurring either in crystalline or amorphous phase is entirely irreversible and is exemplified by a sharp drop in the stress–strain curve. The lateral sample dimensions are immediately narrowed; this observation has become known as *necking* and is most often seen in semicrystalline polymers above T_g. True stress (load/actual area of cross section at the particular load) rises in vicinity of the necked region, so that further deformation may occur preferentially in the elements of materials close to this point. However, the molecules become highly aligned in the direction of applied stress. Local stiffness increases as a result and a point is reached where the enhanced resistance to deformation in the plastically deformed anisotropic region compensates the simultaneous increase in true stress. The post-yield necking process becomes stable in this way; further deformation results in neck propagation along the waist of the material. This process is called *cold drawing*; it occurs at a drawing stress often independent of strain level. At the point where the relatively

compliant and isotropic material has all been highly strained because of formation of chain-extended crystalline morphology during cold drawing, the load rises since the applied deformation is resisted by the uniaxially oriented microstructure of high stiffness. The strength and stiffness properties have been enhanced parallel to the draw direction. The adjacent segments of the parallel chains are generally held only by secondary bond forces giving rise to fibrillization as precursor to eventual fracture when the material in the remaining cross section is unable to support to applied load.

The shapes of stress–strain curves for various temperatures are shown in Figure 11. The yield stress decreases with increasing temperature. The segments shift in the process of cold drawing of flow of a glassy polymer under the effect of stress—not because of thermal motion, but because the latter is almost absent in the glassy state. However, there is definite storage of thermal energy in the polymer even when $T < T_g$. With the elevation of temperature in the region below T_g, the storage of energy in the segments grows and a smaller and smaller external mechanical energy is needed to shift the segments and to develop cold

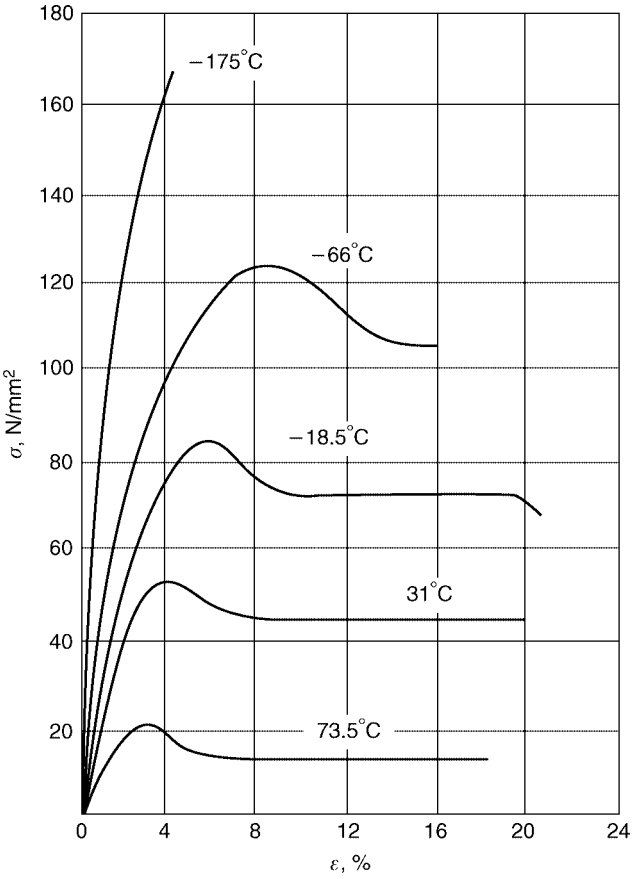

Fig. 11. The tensile stress–strain curves for poly(vinyl chloride) (PVC) at several temperatures.

flow. Lowering of temperature causes not only an increase in yield stress but also straightening of curve and diminution of yielding. The specimen may fail even before the yield stress is reached. The failure occurs at very low strain such as fraction of 1%. This means that the polymer at low temperatures behave like a brittle one that is not capable of not only highly elastic strains but also of cold flow.

After withdrawal of high stresses below T_g, the large strains do not disappear. However, if the polymer is then heated above T_g, the specimen recovers its original size completely. Thus the deformation of glassy polymers is recoverable.

Shear Yielding. In consideration of yielding of polymer-based materials, a major distinction must be made between two different microstructural phenomena, *shear yielding* and *craze yielding*. Shear yielding basically involves the shear flow with little or no change in density up to the yield point. Craze yielding or dilatational yielding is highly localized in the form of thin crazes which consist of a very porous fibrillar region.

The yielding of solids under multiaxial stresses gives rise to question about the yield criteria. One of the simplest yield criteria was proposed by Tresca already in 1864. It states that yielding occurs when the maximum shear stress exceeds a critical value. In terms of principal stresses we have (23):

$$(\sigma_1 - \sigma_3)/2 > \sigma_y \tag{14}$$

Here $\sigma_1 > \sigma_2 > \sigma_3$ so that σ_1 is the largest principal stress. A negative stress is always smaller than a positive one and σ_y is the shear yield point. Since the criterion holds for all possible values of the principal stresses, it also holds for the uniaxial stress field. In this case the criterion reduces to

$$(\sigma_1 - \sigma_3) > \sigma_y \tag{15}$$

The Tresca criterion works well for polycrystalline materials. It has been observed that the following criterion proposed by van Mises is somewhat better (23):

$$(\sigma_1 - \sigma_3)^2 + (\sigma_2 - \sigma_3)^2 + (\sigma_3 - \sigma_1)^2 = 2\sigma_y \tag{16}$$

The differences between the two criteria is usually ≈15%. The Tresca criterion is often used because its form is simpler and because for engineering applications it gives a more conservative prediction for shear failure.

Both Tresca and van Mises criteria are not affected by the addition of hydrostatic pressure because that pressure simply adds a constant to each of the principal stresses and the two criteria depend only on the differences between the principal stresses. However, many experiments with multiaxial stresses show that the yield criteria for polymers have to include the hydrostatic component of the stress tensor $\boldsymbol{P}$, where

$$\boldsymbol{P} = (\sigma_1 + \sigma_2 + \sigma_3)/3 \tag{17}$$

$\boldsymbol{P}$ affects the yield stress as well as the shape of the stress–strain curve. This is reflected by the difference between uniaxial tension and compression stress–strain curves; a pure shear curve lies between them.

Given limited applicability of earlier equations, Brown and co-workers (23,24) have developed the following equation for uniaxially oriented polymers:

$$B_9(\sigma_2-\sigma_3)^2+B_{10}(\sigma_2-\sigma_1+\sigma_i)^2+B_{11}(\sigma_1-\sigma_i+\sigma_2)^2 + 2\mathrm{L}\tau_{23}^2+2M\tau_{32}^2+2N\tau_{12}^2=(1-\boldsymbol{QP})^2 \quad (18)$$

Here σ_i is the difference between the yield point in tension and in compression in the direction of orientation. Thus, according to equation 18, eight parameters are required to describe completely the yield stress of a uniaxially oriented polymer.

The crystalline regions become more prominent at low temperature relative to amorphous regions and they may permit easy slip at low temperatures probably via a dislocation mechanism. However, there is no evidence of dislocations in semicrystalline polymers. In PTFE the increase in yield point with decreasing crystallinity may be due to grain size effect. As the crystallinity is reduced, the lamella size also decreases. It is most likely that the direction of easy slip is parallel to the chain direction. Since the chains are parallel to the thin dimension of the crystal, it is likely that the lamella thickness should directly affect the yield point at low temperatures—as was observed experimentally (25).

Molecular Theories of Yielding. Several models of yielding of amorphous polymers are based on continuum mechanics invoking the concepts of free volume, springs and dashpots, and viscosity. Some of the theories take molecular point of view. Robertson (26,27) assumed chain bending as the fundamental mechanism for yielding. He postulated that the yield point corresponds to the state where the amount of bends produced by the stress were equivalent to the number of bends that occur at T_g.

In another molecular approach Argon (28) has proposed a theory of yielding for glassy polymers based on the concept that deformation at molecular level consists in the formation of a pair of molecular kinks. The resistance to double kink formation is considered to arise from the elastic interactions between chain molecule and its neighbors, ie, from intermolecular forces. This is in contrast to the Robertson theory, where intramolecular forces are of primary consideration. We need to recall that the intramolecular forces are by several orders of magnitude stronger than the intermolecular ones—except for entanglements which operate as if they were primary chemical bonds.

Brown (24,29) proposed a model of homogeneous yielding based on the Mie (Lennard–Jones) interaction potential. According to Brown, there are three types of molecular motions in an amorphous polymer up to shear yield strain:

(1) shearons which consist of the motion of molecular segments whose covalent bonds lie in the plane of shear;
(2) rotons which are like shearons except that covalent bonds make an angle with the plane of shear; and
(3) tubons which require a force parallel to the covalent bond that allows the molecular segments to move along the shear plane.

The macroscopic yield point is calculated in the Brown model on the basis of cooperative and nearly homogeneous motion of all molecular segments. The value of the yield point is calculated from the friction and shear resistance of each type of molecular motion produced by shearons, rotons, and tubons.

Crazing. As noted in the beginning of the Shear Yielding section, shear yielding is different from craze yielding. We need also to note that crazes constitute one source of cracks. Crazes are observed in glassy polymers except thermosets. Originally, it was thought that crazes are just tiny cracks, but this turned out not to be true. We now recognize three kinds of these structures: surface crazes, internal crazes, and crazes at the crack tip. All three kinds consist of elongated voids and fibrils. The fibrils are composed of highly oriented chains and each fibril is oriented approximately at 90° to the craze axis. The fibrils span the craze top to bottom, resulting in an internal sponge-like structure (see Yield and Crazing).

Extensive studies of crazes and their behavior under loads have been conducted by Kramer and co-workers (30–40). We know from this work that there are two unique regions within the craze: (*1*) the craze/bulk interface, a thin (10–25 nm) strain-softened polymer layer in which the fibrillation (and thus craze widening) takes place and (*2*) the craze midrib, a somewhat thicker (50–100 nm wide) layer in the craze center, which forms immediately behind the advancing craze. The relative position of the midrib does not change as the craze widens. By contrast, as the phase boundaries advance, continuously new locally strain-softened regions are generated, while strain-hardened craze fibrils are left behind.

In general, externally provided energy in excess of CRC may be absorbed by crazing, shear yielding, or cracking. Therefore, we need to compare crazing to shear yielding. In the latter, oriented regions are formed at 45° angles to the stress. The shear bands are birefringent; in contrast to crazes, no void space is produced.

Of course, cracks are the "really dangerous" ones. We talk more about cracks as such in the following section. The crazes are capable of bearing significant loads thanks to the fibrils. Therefore, the question arises, under what conditions can crazes transform into cracks? The fibril breakdown must precede crack nucleation. Kramer and his colleagues have established that an important variable governing craze fibril stability is the average number of effectively entangled strands n_e that survive the formation of fibril surfaces. Equations for calculating the original number of strands n_0 as well as the number n_e have been provided by Kramer and Berger (36). It turns out that polymers with $n_e > 11.0 \times 10^{25}$ strands/m^3 and concomitantly a short entanglement length I_e are ductile and deform by shear yielding. Such materials exhibit strains up to $\varepsilon = 0.25$ or even more prior to macroscopic fracture. Polymers with $n_e < 4 \times 10^{25}$ strands/m^3 and thus with large I_e are brittle and deform exclusively by crazing. For polymers with intermediate values of n_e (and I_e), competition between shear deformation and crazing is observed.

The presence of liquids or vapors in the environment of a polymeric component affects the response to external mechanical forces (24,41). Thus, for instance polyarylate under uniaxial extension exhibits exclusively shear yielding without crazing. However, exposure to organic vapor (methyl ethyl ketone) results in crystallization, embrittlement, and conversion of the response to deformation from shear yielding to crazing (41).

Fracture Mechanics and Crack Propagation

Stress Concentrators and Stress Concentration Factor. Just as all materials, polymer-based materials exhibit structure imperfections of various kinds. They appear already in processing, during handling in transport, as well as in service. Because of the presence of crazes, scratches, cracks, and other imperfections, mechanical properties of real polymeric materials are not as good as they theoretically could be. In this section we deal particularly with stress concentrators such as *cracks* (which appear although we did not want them) and *notches* (which are made on purpose to have well-defined cracks).

As said, imperfections appear already in processing. We have *knit lines*: areas in injection-molded parts made of thermoplastics in which, during manufacturing, separate polymer melt flows arise, meet, and melt more or less into one another. Consequences of the presence of knit lines on mechanical properties are discussed by Criens and Moslé (42). They also discuss methods of mitigating effects of knit lines on performance. The simplest such method, namely raising the processing temperature, is also a costly one.

The deteriorating effects of cracks and notches on material properties are represented by the *stress concentration factor*

$$K_t = 1 + 2(h/r)^{1/2} \tag{19}$$

Here h is the depth (length) of the crack or notch, or one-half of the length of the major axis in an elliptical hole; and r is the radius of curvature at the bottom (tip) of the notch, or at each end of the major axis of an elliptical crack. The name stress concentration factor is very appropriate. Tensile tests were discussed under Quasi-Static Mechanical Testing. Consider again a tensile test with the stress σ applied to the ends of the specimen. The lines of force applied to these ends cannot go through the air; they must go through the material—and therefore around the crack. As a consequence, when the lines meet (or separate, depending on the direction) at the crack tip, that tip is subjected not to the nominal stress σ but to the stress which is K_t time larger. Equation 19 is also applicable in everyday life, not only in an industrial plant or a testing laboratory. When one wants to cut a plastic sheet into halves, a small incision in one side of the sheet helps. Such an incision is in fact a notch, and creates the stress concentration defined by equation 19.

Stress Intensity Factor. In some applications, a somewhat different measure of the "evil" produced by a crack or notch called the stress intensity factor is in use:

$$K_I = \alpha^* \Pi^{1/2} \sigma h^{1/2} \tag{20}$$

K_I characterizes the stress distribution field near the crack tip. The Roman one, I, refers to the opening or tensile mode of crack extension; α^* is a geometric factor appropriate to a particular crack and component shape; the remaining symbols are the same as in equation 19. It is unfortunate that K_t and K_I have similar symbols, similar names, and are expressed in terms of the same quantities—but we do not propose to fight the existing habits in this article. For an infinite plate in

plane stress, the geometric factor $\alpha^* = 1$. *Plane stress* means that the stress along the z-axis perpendicular to the plate surface is almost—although not exactly—equal to zero. For other geometries there exist tabulations of α^* values (43).

Griffith's Theory of Fracture. Fracture (qv) of polymers and polymer-based composites is of course a subject on which entire books have been written. General fracture mechanics has been presented fairly succinctly by Pascoe (44). Here we shall quote the most important results.

Already in 1921 Griffith (45,46) considered for elastic bodies the question: when will a crack propagate? Starting with basic thermodynamics, he replied: this will happen if the crack growth will lower the overall energy. He considered three contributions to the energy:

(1) the potential energy of the external forces which are doing work on the body deforming it;
(2) the stored elastic strain energy; and
(3) the work done against the cohesive forces as the new crack surfaces are formed.

On this basis Griffith derived an equation which in modern notation can be written as

$$\sigma_{cr} = (2\Gamma E/\Pi h)^{1/2} \tag{21}$$

σ_{cr} is the stress level at and above which the crack will propagate; Γ is the surface energy per unit area (corresponds to the last of the three factors just named); E is the elastic modulus; and h is the same as in equations 19 and 20.

Thus, if the actual stress imposed $\sigma < \sigma_{cr}$, the material will sustain that stress without the crack growing. The equation is identical for both constant load and constant displacement conditions, and hence it should work also for any intermediate conditions. Equation 21 has been the inspiration for much further work. Pascoe (44) provides a fairly detailed discussion of the Griffith theory.

Crack Propagation and Its Prevention. To begin with, there is a need to distinguish rapid crack propagation (RCP) and slow crack propagation (SCP). RCP is a dangerous process; velocities of 100–400 m/s (that is 300–1400 ft/s) have been observed in PE pipes. Since such pipes are being used for distribution of fuel gas within localities, RCP might be accompanied by an explosion of the gas pressurized inside. However, a criterion was developed which allows prediction of whether RCP will occur (47); the criterion is also discussed in Reference 4. Briefly, from the determination of impact strength of the material, that is, the energy absorbed by the material when fracturing under impact, one can predict whether RCP will or will not occur. The criterion is based on CRC concepts; the impact strength is used here as the appropriate measure of the CRC for rapid crack propagation.

Slow crack propagation is not limited to fuel plastic pipes, not at all spectacular, and "quiet" and insidious. The crack propagation rate dh/dt might be only, say, 1 mm per month; an observation for, say, 2 weeks after installing a polymeric component in service might not show anything.

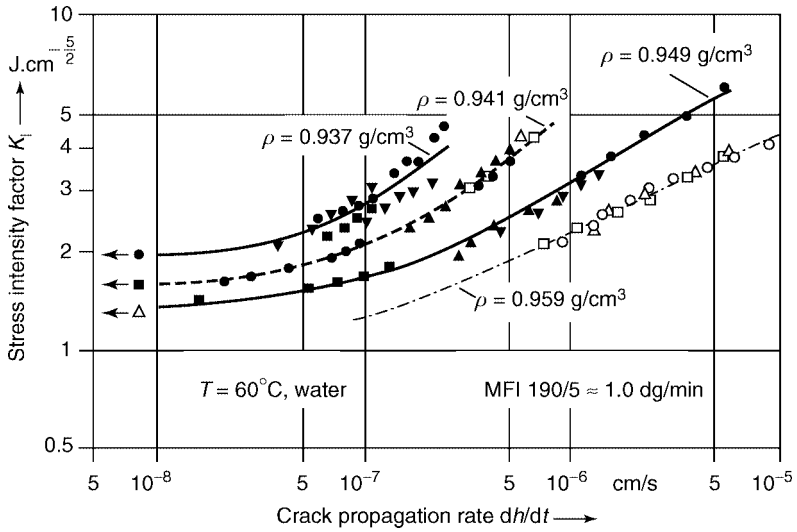

Fig. 12. Crack propagation rate vs the stress intensity factor for Hoechst polyethylenes (48).

Experimentalists customarily present the dh/dt rates as a function of the logarithmic stress intensity factor log K_{I} as defined by equation 20. The problem of relating dh/dt to K_{I} was solved by using the CRC approach (48) in conjunction with the Griffith fracture mechanics including our equation 21. The result is

$$\log K_{\mathrm{I}} = \frac{1}{2}\log\left(\alpha^{*2} 2\Gamma E\right) + \frac{1}{2}\log[1 + (1/\beta h_{\mathrm{cr}})\mathrm{d}h/\mathrm{d}t] \tag{22}$$

Here β is a time-independent factor characteristic for a material. In the derivation of the last equation, both the stress level σ and the initial crack length h_0 were used (48). However, these quantities canceled out—with the unexpected result that the crack propagation rate is independent of both.

The experimental results support equation 22—as shown for instance in Figure 12 for Hoechst PEs studied under tension in water medium at 60°C. Each kind of symbol pertains to a different stress level and a different original notch length. We have called SCP "insidious." The lowest crack propagation rate shown in the figure is $\mathrm{d}h/\mathrm{d}t = 10^{-8}$ cm/s; this is only 0.315 cm per year, but the crack does grow. This fact gives us an idea of the usefulness of equation 22.

As mentioned, equation 22 was derived on the basis of the CRC concept. The larger is the CRC, the better the material defends itself against external forces. We can write a series of approximate proportionalities (4):

$$\mathrm{CRC} \sim v^{\mathrm{f}} \sim T \sim \omega^{-1} \sim \rho^{-1} \tag{23}$$

where ρ is the mass density and ω is the frequency used in the Dynamic Mechanical Analysis Section. The expression (23) will be discussed more in a later section. Now we see that Figure 12 provides a direct proof of validity of the CRC approach

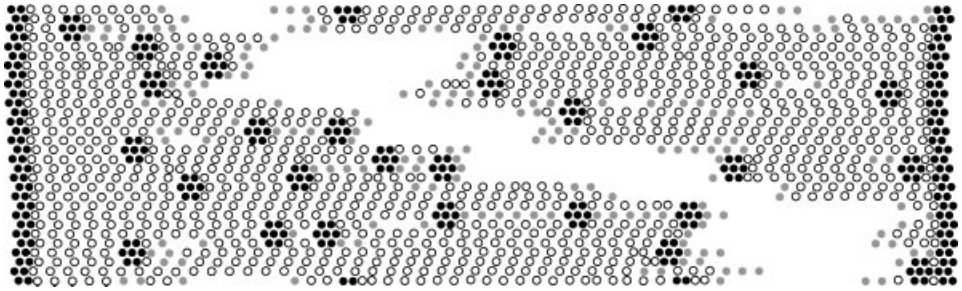

Fig. 13. Tensile deformation leading to crack propagation in a two-phase (PLC islands + flexible matrix) polymer (51).

and of the expression 23. The material with the lowest density has necessarily the highest free volume v^f and, therefore, the lowest crack propagation rate dh/dt.

Computer Simulation of Crack Propagation. A typical experimental procedure for investigating fracture consists in looking at the fracture surface with a scanning electron microscope (SEM) or a transmission electron microscope (TEM) (49,50). This provides us with the morphology at the time of fracture, which is useful information. However, the microscopic techniques do not tell us where and how the crack(s) which eventually led to fracture had started.

The whole story from the crack initiation to fracture can be seen in molecular dynamics (MD) computer simulations (51–53). We have already talked about MD simulations of stress relaxation in a previous section. The question to be answered by MD was: where in two-phase materials formed by polymer liquid crystals (PLCs) the cracks start? They could start in the flexible polymer matrix because it is relatively weak, or inside the LC-rich *islands* which are more brittle, or at the interface from the matrix side, or else at the interface from the island side.

An example of the answer is shown in Figure 13 (51). A large crack which is going to cause fracture is formed at the interfaces on the matrix side. The beauty of computer simulations is that we can watch the cracks form and propagate until fracture. Animations of this process are made for added perspicuity.

Ductile–Brittle Transition. As seen in expression 23, CRC is also proportional to the temperature T. At low temperatures polymer-based materials are brittle and more prone to crack propagation. There exists the *ductile–brittle impact transition temperature* below which the material is brittle and above which ductile. A successful method of prediction of that temperature as a function of the stress concentration factor (eq. 19) is described in Reference 3.

Crack Healing. Finally, let us mention that *crack healing* takes place. Experiments of this kind have been conducted by Wool and his collaborators and described in detail (54,55). As Wool says, when two similar pieces of a bulk polymer are brought into contact at a temperature above the glass transition, the interface gradually disappears and mechanical strength develops as the crack—or weld—heals. This takes place in both cracks and welds in spite of the differences between them. Healing is mainly due to the diffusion of chains across the interface. This fact is the origin of a method of crack healing with *molecular nails*—also discussed by Wool (54,55).

Healing manifests itself not only in mechanics but also in tribology; see Section on Tribology.

Long-Term Service Prediction

Free Volume as the Prediction Tool. For obvious reasons, prediction of long-term performance from short-term tests is needed. Such prediction methods exist and are in fact quite powerful. Unfortunately, numerous papers and reports are still based on a false assumption that *nothing can be predicted and therefore everything has to be measured*. Much information can be obtained from a limited amount of experimental data—and also from computer simulations discussed at various locations in this article.

To be able to make long-term predictions, some definitions are needed. We have already noted that the more the free volume v^f, the larger is the maneuvering ability of the chains, and the higher CRC. Using specific quantities (typically per 1 g), we write

$$v = v^* + v^f \tag{24}$$

where v is the total specific volume and v^* is the characteristic (incompressible or hard-core) volume. The last two names are based on the qualitative picture of applying an infinitely high pressure so that all free volume is "squeezed out" and only v^* remains. Some people like to work instead with the reduced volume defined as

$$\tilde{v} = v/v^* = 1 + v^f/v^* \tag{25}$$

Equation 24 or 25 is usable only in conjunction with a specific equation of state of the general form $P = P(v, T)$. We also need two more reduced parameters defined in an analogous way as in equation 25:

$$\tilde{P} = P/P^* \quad \tilde{T} = T/T^* \tag{26}$$

P denotes pressure and T (thermodynamic) temperature; P^* and T^* are, like v^*, characteristic (hard-core) parameters for a given material. T^* constitutes a measure of the strength of interactions in the material. It has been found repeatedly that good results are obtained when using the Hartmann equation of state (56–58):

$$\tilde{P}\tilde{v}^5 = \tilde{T}^{3/2} - \ln \tilde{v} \tag{27a}$$

At the atmospheric pressure the term containing $\tilde{P}$ becomes negligible, and we have simply

$$\tilde{v} = \exp(\tilde{T}^{3/2}) \tag{27b}$$

Evaluation of the necessary characteristic parameters in equation 27a proceeds as follows. One can use the thermomechanical analysis (TMA) in the expansion mode and determine at the atmospheric pressure, the dependence of specific volume v on temperature T. By fitting the experimental results to equation 27b one obtains the characteristic parameters v^* and T^*. If one performs full P–V–T determination [this can be done with the so-called Gnomix apparatus (59) used also by us to advantage (60)], then one represents experimental results by equation 27a and finds by a least-squares procedure the parameters P^*, v^*, and T^*.

Time–Temperature Correspondence. The next step consists in using the so-called correspondence principles. The most often used is the principle of time–temperature correspondence advocated and used extensively by Ferry (61). To formulate the correspondence (also called equivalence) principle, consider a conformation rearrangement in the chain so fast that we cannot record it at the room (laboratory) temperature. What we can do is to lower the temperature. At a temperature low enough, the process will be slowed down to the extent that we shall be able to "catch" it. This approach works in the opposite direction as well. Instead of conducting experiments for 100 years at the ambient temperature, we can go to a higher temperature, thus produce higher free volume v^f in the material, and "catch" within, say, 10 h the same series of events. This is the basis for the time–temperature correspondence.

As discussed earlier, we can perform DMA by applying an oscillating force to a polymer-based material. If the frequency ω of the oscillations is low, the chains will be able within one half-cycle to adjust better to the externally imposed field, just as they do at higher temperatures. The inverse is true also: high frequencies will provide very little opportunity for such rearrangements, just as if the free volume was low and the temperature low also. We infer that high frequencies cause similar effects as low temperatures and also vice versa. This is the reason for the series of proportionalities (eq. 23) provided above and also for the time–frequency correspondence principle.

To see how one makes long-term predictions, consider for instance dependence of tan ∂ for high density polyethylene (HDPE) as a function of the logarithmic reciprocal frequency log ω^{-1} (62). One can make a series of isothermal measurements of this quantity. Then, taking advantage of the time–frequency correspondence, one can shift the isothermal curves—except for one—so that they would form a single curve. This is shown (62) in Figure 14. The diagram is called the *master curve* and pertains to the reference temperature T_0 for which the curve was *not* moved.

We see in the axis explanation for Figure 14 the *shift factor* a_T. It tells us how much a given isothermal curve needs to be shifted; thus, a_T is the key to the long-term prediction. One of us has derived a general equation for a_T (2,3):

$$\ln a_T = A_T + B/(\bar{v} - 1) \tag{28}$$

where A_T and B are material constants; B is called the Doolittle constant since it comes from the Doolittle equation connecting viscosity and free volume (see also Reference 62 for the cases involving predrawing). Since the reduced volume as defined in equation 25 appears in equation 28, we also need an equation of state such as the Hartmann equation (eq. 27a).

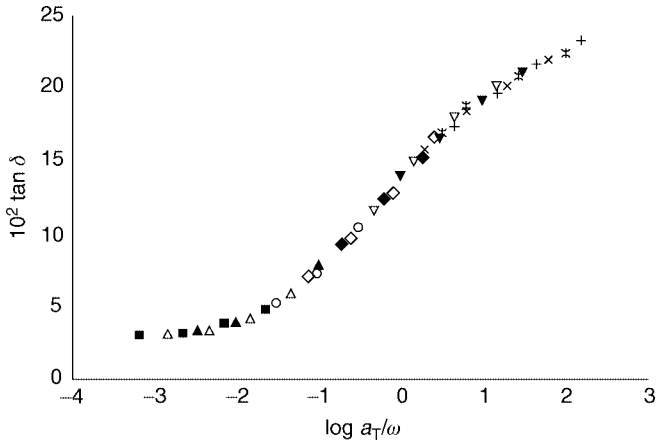

Fig. 14. The master curve of tan ∂ vs log ω^{-1} for HDPE at 40°C (62). Each kind of symbols pertains to a different isotherm.

The master curve for HDPE shown in Figure 14 was obtained using equation 28 in conjunction with equation 27a. In Figure 15 we see the results of the calculation presented as a continuous curve. The experimental points have been obtained by shifting the curves until the best visual fit. Clearly the equation works.

The correspondence principles accomplish an important goal: prediction of long-term behavior from short-term tests. However, some polymer scientists and engineers do not believe that the prediction methods work apparently, because they think that the time–temperature equivalence is the same thing as the so-called WLF equation of 1955 (63) for the shift factor a_T. Ferry who co-created WLF warned (61) that the use of that equation is limited to a temperature range

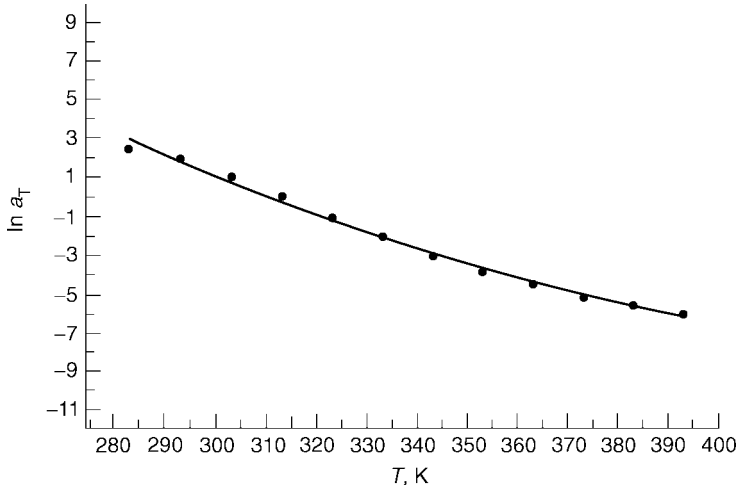

Fig. 15. The temperature shift factor a_T as a function of the temperature T for the master curve shown in Figure 14; filled circles are the experimental points from creep, the continuous line calculated from equation 28 together with equation 27a (62).

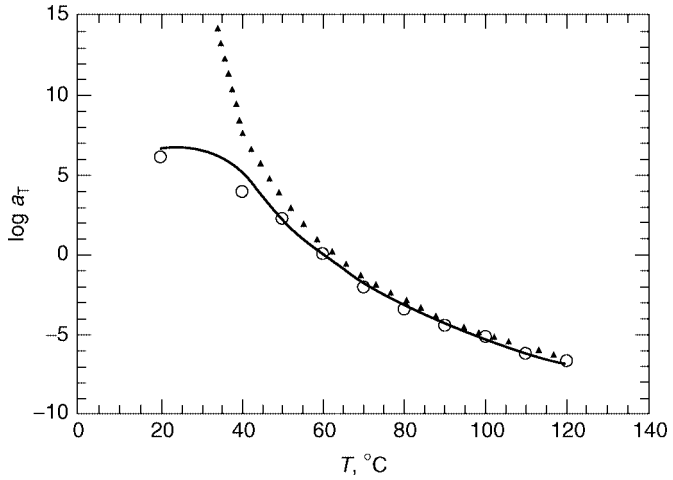

Fig. 16. The temperature shift factor a_T (T) for PET/0.6PHB polymer liquid crystal (PET = poly(ethylene terephthalate, PHB = *p*-hydroxybenzoic acid, 0.6 = mole fraction of PHB in the PLC copolymer). Explanations in text (64).

from the glass temperature T_g to $\approx (T_g + 50)$ K. When the WLF equation is used outside of its applicability range, bad results are likely.

The prediction methods are applicable not only to one-phase polymer-based materials, but also to multiphase systems. A polymer liquid crystal which forms *four phases* in its service temperature range has been studied and predictions accomplished over 16 decades of time. Each experiment was made over 4 decades only (64) and the same equations 27a and 28 were used. Let us look at the diagram of the logarithmic temperature shift factor log a_T as a function of the temperature T for that PLC in Figure 16. The circles are the experimental values corresponding to shifting resulting in a 16 decade master curve. The continuous line was calculated from equations 27a and 28. We include also as triangles values of a_T calculated from the WLF equation. We see that at higher temperatures the WLF results agree well with the experiment—the reason why that equation is still in use. We also see that at low temperatures the WLF equation leads to disastrous results.

There is also the issue whether the temperature shift factor a_T depends on the technique used or is it a property of the material independent of the kind of experiments performed. In derivation of equation 28 it was assumed that a_T is a material property (2,3). This is confirmed by experiments. The continuous line seen in Figure 16 agrees with the experimental shift factors obtained from creep (shown as circles) equally well as with a_T values obtained from stress relaxation results (64).

Time–Stress Correspondence. In 1948 O'Shaughnessy demonstrated experimentally the existence of a different equivalence principle, namely between time and stress (65). Several compliance D values for rayon at different stress levels were shifted forming what we now call a master curve. Some work on this basis was performed at the Latvian Institute of Polymer Mechanics in Riga and is described by Goldman (5). However, generally the O'Shaughnessy principle attracted much less attention than the time–temperature–frequency correspondence. The

reason was that there was no equation which would enable calculations based on this principle—not even a bad one.

In 2000 (66) an equation was derived for the stress shift factor:

$$\ln a_\sigma = A_\sigma + \ln v(\sigma)/V_{\text{ref}} + B/(\bar{v}-1) + C(\sigma - \sigma_{\text{ref}}) \tag{29}$$

where the index "ref" pertains to the reference state for which no shifting occurs. The parameter A_σ is analogous to A_T in equation 28; B is the same Doolittle constant; and C is another material parameter.

Actually in Reference 66 a more general shift factor equation was derived which deals with changes of both the temperature T and stress σ:

$$\ln a_{T,\alpha} = A_{T,\sigma} + \ln T_{\text{ref}}/T + \ln v/v_{\text{ref}} + B(\bar{v}-1) + C(\sigma - \sigma_{\text{ref}}) \tag{30}$$

When we assume a constant stress $\sigma = \sigma_{\text{ref}}$ then equation 30 reduced to equation 28 as it should. When we need a shift factor dependent on the stress level σ only for $T = T_{\text{ref}} =$ constant then equation 30 reduced to equation 29 as it also should.

Equation 29 was tested experimentally with good results (67,68). However, we defer showing an example of its application to the following section.

Long-Term Predictions from a Minimum of Data. One problem with the use of the correspondence principles to make long-term prediction seemed unresolved: the amount of data needed. Thus, in Reference 64 experimental creep and stress relaxation results for the PET/0.6PHB PLC were obtained at 10 temperatures. Similarly, in Reference 67 creep compliance was determined at 9 stress levels. Can we get away with doing experiments at two or three temperatures—or at two or three stress levels—and get valid predictions? The answer is yes, and procedures for that purpose have been developed. When one works with the time–stress correspondence, then the minimum data procedure (68) is naturally based on equation 29. Similarly, when we use the time–temperature correspondence, the minimum data procedure (69) is based on equation 28.

Here is an example of the minimum data procedure for the application of the time–stress correspondence. In Figure 17 we show creep compliance of the same PET/0.6PHB PLC as a function of logarithmic time. This is a master curve—and only two sets of experimental data (for two stress levels) have been used to create it.

As a proof of the validity of the prediction, in Figure 18 we show the stress shift factor a_σ as a function of the stress level σ. The continuous curve with asterisks has been calculated using all experimental results available, that is 9 sets for 9 stress levels. The broken line with open circles is based on two extreme sets of results only, for 10 J/cm^3 and 50 J/cm^3, the same as seen as points in Figure 17. Both curves have been obtained from experimental data via equation 29. We see that the differences are small. The values calculated from two stress levels deviate from those based on the full set on the average by $\pm 0.73\%$ (68). Thus, not only prediction of reliability and long-term behavior from short-term tests seems possible for many polymer-based materials. The amount of experimental data needed for the prediction is lower than widely believed.

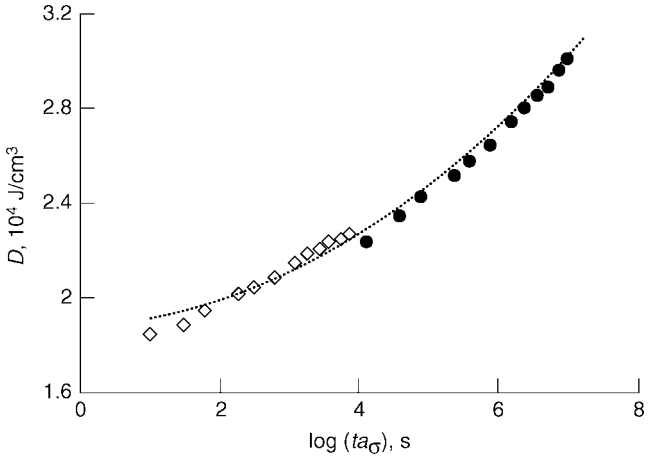

Fig. 17. Master curve of creep compliance of PET/0.6PHB for $\sigma_{ref} = 10$ J/cm^3 (= 10 MPa = 10 MN/m^2). Open circles are experimental points for 10 J/cm^3, filled circles for 50 J/cm^3 (68).

Tribology: Scratch and Wear Resistance

In the section under Fracture Mechanics and Crack Propagation, cracks and notches were discussed as stress concentrators. Scratches are also stress concentrators which affect the reliability. Therefore, we now need to move from the mechanics of polymer-based materials to their tribology. Tribology deals with friction, wear, scratch resistance, and design of interactive surfaces in relative motion (70). It is an underappreciated science. Rabinowicz (71) says the following about the so-called Jost report on tribology prepared for the British Government:

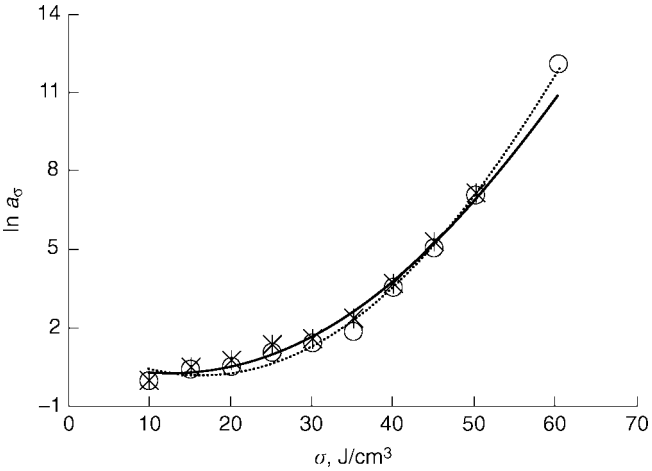

Fig. 18. Logarithmic stress shift factor a_σ as a function of stress level σ for the master curve shown in Figure 17. The continuous line is based on experimental results for nine stress levels; the discontinuous one on two levels only, 10 J/cm^3 and 50 J/cm^3. -✳- Experimental; -⊖- Calculated (10–50) (68).

"At the time the Jost Report appeared it was widely felt that the Report greatly exaggerated the savings that might result from improved tribological expertise. It has now become clear that, on the contrary, the Jost Report greatly underestimates the financial importance of tribology. The Report paid little attention to wear, which happens to be (from the economical point of view) the most significant tribological phenomenon" (see SCRATCH BEHAVIOR OF POLYMERS).

Scratch testing involves the determination of the instantaneous depth (penetration depth R_p) caused by an indentor and also of the final (*after healing*) residual depth R_h. Healing is a consequence of viscoelasticity. It is clear that in terms of reliability, R_h (rather than R_p) is important; the shallower the residual depth, the higher the scratch resistance.

Can we improve the scratch resistance of polymer-based materials? Fortunately, the answer is yes. One way is to apply a low concentration additive to a given polymer-based material. This is much easier said than done—but possible (72,73). In Figure 19 we see the residual depth R_h in a commercial epoxy as a function of concentration of an added fluoropolymer for various forces applied by

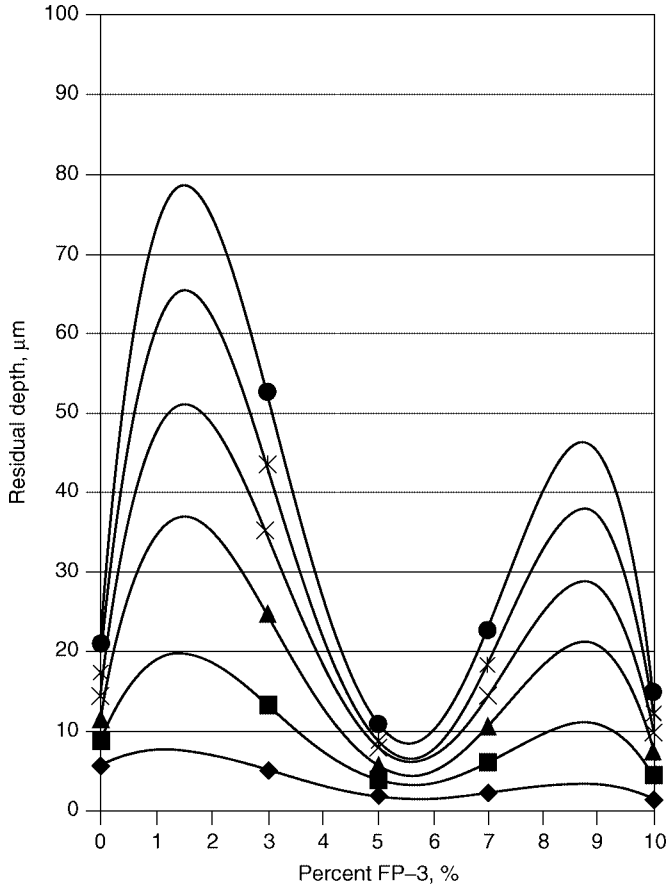

Fig. 19. The residual depth R_h of a commercial epoxy as a function of weight % concentration of a fluoropolymer additive; after (73). ◆ 2N, ■ 4N, ▲ 6N, × 8N, ⁎10N, ● 12N.

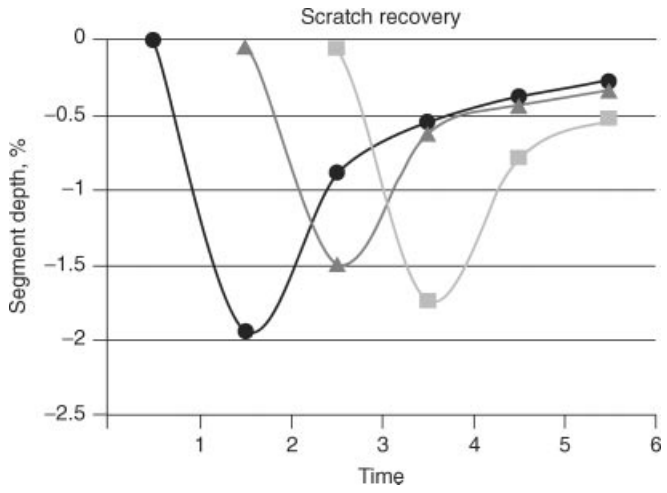

Fig. 20. Changes with time of vertical locations of surface segments in scratch testing simulation. —●— Segment 1, —▲— Segment 2, —■— Segment 3 (76).

a diamond indentor. We see that first the curves go through maxima. That is, if somebody would stop experiments at 3 wt% of the additive, one would conclude that the additive lowers the scratch resistance instead of enhancing it.

Wear can be defined as the unwanted loss of material from solid surfaces owing to mechanical interaction (71). When dealing with metal surfaces, one often uses external lubricants. For polymers and polymer-based materials this is not advisable. The polymer might absorb the lubricant and swell; the results would be worse than without the lubricant.

One option of lowering wear which is widely used is lowering the friction. *Friction* can be defined as the tangential force of resistance to a relative motion of two contacting surfaces (71). One distinguishes *static friction* which appears when starting relative motion and *dynamic friction* which manifests itself when sustaining the motion. Again, an appropriate additive might lower the friction. This has been done also for a commercial epoxy with a fluoropolymer additive (74).

Another option of lowering wear has been discovered recently. It turns out that multiple scratching might result after 15 times or so in *polymer hardening* so that consecutive scratch runs do not make the groove any deeper (75). This has been found for instance for polypropylene and also for TFPE (Teflon). This in spite of the fact that Teflon is a material with notoriously low scratch resistance—as known to anybody who has ever used frying pans.

As in other topics discussed above, molecular dynamics computer simulations also here elucidate the phenomena that take place. In Figure 20 we show the first ever computer simulation of scratch testing (76).

BIBLIOGRAPHY

"Mechanical Properties" in *EPST* 1st ed., Vol. 8, pp. 445–516, by V. A. Kargin and G. L. Slonimsky, Akademii Nauk SSSR; "Mechanical Properties" in *EPSE* 2nd ed., Vol. 9, pp. 379–466, by D. W. Hadley, University of Reading, and I. M. Ward, University of Leeds.

1. *Polymer Science and Engineering: The Shifting Research Frontiers*, National Academy Press, Washington, D.C., 1994.
2. W. Brostow, *Mater. Chem. Phys.* **13**, 47 (1985).
3. W. Brostow, in Ref. 6, Chapt. 10.
4. W. Brostow, in Ref. 7, Chapt. 5.
5. A. Y. Goldman, *Prediction of the Deformation Properties of Polymeric and Composite Materials*, American Chemical Society, Washington, D.C., 1994.
6. W. Brostow and R. D. Corneliussen, eds., *Failure of Plastics*, Hanser, Munich, 1986.
7. W. Brostow, ed., *Performance of Plastics*, Hanser, Munich, 2000.
8. W. Brostow, *Science of Materials*, R. E. Krieger, Malabar, FL, 1985; W. Brostow, *Introducción a la ciencia de los materiales*, Editorial Limusa, Mexico, D.F., 1981; W. Brostow, *Einstieg in die moderne Werkstoffwissenschaft*, Hanser, München, 1985; W. Brostow, *Materialoznavstvo*, Lvivska Politechnika, Lviv, 2004.
9. U. W. Gedde, *Polymer Physics*, Chapman and Hall, London, 1996.
10. B. Erman and J. E. Mark, *Structures and Properties of Rubberlike Networks*, Oxford University Press, 1997.
11. J. E. Mark and B. Erman, *Rubberlike Elasticity—A Molecular Primer*, John Wiley & Sons, Inc., New York, 1998.
12. J. E. Mark and B. Erman, in Ref. 7, Chapt. 17.
13. N. W. Tschoegl, *The Phenomenological Theory of Linear Viscoelastic Behaviour—An Introduction*, Springer, Berlin, 1989.
14. J. Kubat, *Nature* **204**, 378 (1965).
15. J. Kubat and L. A. Nilson, *Mater. Sci. Eng.* **24**, 223 (1976).
16. J. Kubat and M. Rigdahl, in Ref. 6, Chapt. 4.
17. S. A. Fossey, in Ref. 7, Chapt. 4.
18. W. Brostow and J. Kubat, *Phys. Rev. B* **47**, 7659 (1993).
19. S. Blonski, W. Brostow, and J. Kubat, *Phys. Rev. B* **49**, 6494 (1994).
20. W. Brostow, J. Kubat, and M. J. Kubat, *Mater. Res. Soc. Symp. Proc.* **321**, 99 (1994).
21. K. P. Menard, *Dynamic Mechanical Analysis—A Practical Introduction*, CRC Press, Boca Raton, Fla., 1999.
22. K. P. Menard, in Ref. 7, Chapt. 8.
23. N. Brown, R. A. Duckett, and I. M. Ward, *Philos. Mag.* **18**, 483 (1973).
24. N. Brown, in Ref. 6, Chapt. 6.
25. S. Fischer and N. Brown, *J. Appl. Phys.* **44**, 4322 (1973).
26. R. E. Robertson, *J. Chem. Phys.* **44**, 3950 (1966).
27. R. E. Robertson and J.-H. Kim, in Ref. 7, Chapt. 14.
28. A. S. Argon, *Philos Mag.* **28**, 830 (1973).
29. N. Brown, *J. Mater. Sci.* **18**, 2241 (1983).
30. A. M. Donald and E. J. Kramer, *J. Mater. Sci.* **17**, 1871 (1982).
31. E. J. Kramer, *Adv. Polym. Sci.* **52/53**, 1 (1983).
32. E. J. Kramer, *Polym. Eng. Sci.* **24**, 761 (1984).
33. C. S. Henkee and E. J. Kramer, *J. Mater. Sci.* **21**, 1398 (1986).
34. L. L. Berger and E. J. Kramer, *J. Mater. Sci.* **22**, 2739 (1987).
35. L. L. Berger and E. J. Kramer, *J. Mater. Sci.* **23**, 3536 (1988).
36. E. J. Kramer and L. L. Berger, *Adv. Polym. Sci.* **91/92**, 1 (1990).
37. L. L. Berger, *Macromolecules* **22**, 3162 (1989).
38. L. L. Berger, *Macromolecules* **23**, 2926 (1990).
39. C. J. G. Plummer and A. M. Donald, *Polymer* **32**, 409 (1991).
40. A. M. Donald, in Ref. 7, Chapt. 13.
41. L. L. Berger, *J. Polym. Sci. Phys.* **27**, 1629 (1989).
42. R. M. Criens and H.-G. Moslé, in Ref. 6, Chapt. 21.

43. J. E. Shigley and C. R. Mischke, *Mechanical Engineering Design*, McGraw-Hill, New York, 1989.
44. K. J. Pascoe, in Ref. 6, Chapt. 7.
45. A. A. Griffith, *Philos. Trans. R. Soc. A* **211**, 163 (1921).
46. A. A. Griffith, In *Proc. 1st Int. Congress Appl. Mech.*, Delft, 1924 p. 55.
47. W. Brostow and W. F. Müller, *Polymer* **27**, 76 (1986).
48. W. Brostow, M. Fleissner, and W. F. Müller, *Polymer* **32**, 419 (1991).
49. A. Lustiger, in Ref. 6, Chapt. 16.
50. G. H. Michler, *Kunststoff-Mikromechanik*, Hanser, München, 1992.
51. W. Brostow, M. Donahue III, C. E. Karashin, and R. Simoes, *Mater. Res. Innovat.* **4**, 75 (2001).
52. W. Brostow, A. M. Cunha, J. Quintanilla, and R. Simoes, *Macromol. Theory Simul.* **11**, 308 (2002).
53. W. Brostow, A. M. Cunha, and R. Simoes, *Mater. Res. Innovat.* **7**, 19 (2003).
54. R. P. Wool, *Polymer Interfaces*, Hanser, Munich, 1995.
55. R. P. Wool, in Ref. 7, Chapt. 15.
56. B. Hartmann, *Proc. Can. High Polym. Forum* **22**, 20 (1983).
57. B. Hartmann and M. A. Haque, *J. Appl. Phys.* **58**, 2831 (1985).
58. B. Hartmann and M. A. Haque, *J. Appl. Polym. Sci.* **30**, 1553 (1985).
59. P. Zoller, P. Bolli, V. Pahud, and H. Ackermann, *Rev. Sci. Instrum.* **47**, 948 (1976).
60. J. M. Berry, W. Brostow, M. Hess, and E. G. Jacobs, *Polymer* **39**, 4081 (1998).
61. J. D. Ferry, *Viscoelastic Properties of Polymers*, 3rd ed., John Wiley & Sons, Inc., New York, 1980.
62. Yu. M. Boyko, W. Brostow, A. Y. Goldman, and A. C. Ramamurthy, *Polymer* **36**, 1383 (1995).
63. M. L. Williams, R. F. Landel, and J. D. Ferry, *J. Am. Chem. Soc.* **77**, 3701 (1955).
64. W. Brostow, N. A. D'Souza, J. Kubat, and R. Maksimov, *J. Chem. Phys.* **110**, 9706 (1999).
65. M. T. O'Shaughnessy, *Textile Res. J.* **18**, 263 (1948).
66. W. Brostow, *Mater. Res. Innovat.* **3**, 347 (2000).
67. A. E. Akinay, W. Brostow, and R. Maksimov, *Polym. Eng. Sci.* **41**, 977 (2001).
68. A. E. Akinay and W. Brostow, *Polymer* **42**, 4527 (2001).
69. A. E. Akinay, W. Brostow, V. M. Castaño, R. Maksimov, and P. Olszynski, *Polymer* **43**, 3593 (2002).
70. W. Brostow, J.-L. Deborde, M. Jaklewicz, and P. Olszynski, *J. Mater. Ed.* (in press).
71. E. Rabinowicz, *Friction and Wear of Materials*, 2nd ed., John Wiley & Sons. Inc., New York, 1995.
72. W. Brostow, B. Bujard, P. E. Cassidy, H. E. Hagg, and P. E. Montemartini, *Mater. Res. Innovat.* **6**, 7 (2002).
73. W. Brostow, B. Bujard, P. E. Cassidy, and S. Venumbaka, *Int. J. Polym. Mater.* (in press).
74. W. Brostow, P. E. Cassidy, H. E. Hagg, M. Jaklewicz, and P. E. Montemartini, *Polymer* **42**, 7971 (2001).
75. W. Brostow, G. Damarla, J. Howe, and D. Pietkiewicz, *Mater. Res. Innovat* (to be published).
76. W. Brostow, J. A. Hinze, and R. Simoes, in preparation.

WITOLD BROSTOW
Department of Materials Science and Engineering,
University of North Texas
RAM PRAKASH SINGH
Materials Science Centre,
Indian Institute of Technology—Kharagpur

MECHANICAL TESTING. See MECHANICAL PERFORMANCE.

MELAMINE–FORMALDEHYDE RESINS

Introduction

Melamine-based resins represent an important class of aminoplastic resins (1–6) and are made by the reaction of formaldehyde with mainly melamine, using urea, phenol, or other components as comonomers. The raw material and the basic chemistry of melamine–formaldehyde (MF) resins, their history, their basic industrial manufacturing procedures, as well as their use as laminating resins, molding compounds, coatings, textile finishes, and other applications have been described earlier (7,8) (see AMINO RESINS). This article concentrates on melamine-based resins used as wood adhesives, which is by far the biggest area of application, as well as on various special chemical aspects such as cocondensation and analysis (see also WOOD COMPOSITES). SciFinder (1960–2003) comprises approximately 2500 citations for MF resins (all types), implying the still high significance of research in this area.

For most applications as wood adhesives, the melamine resins are in liquid form; for special applications powdered (spray dried) types are used. The resins consist of linear or branched oligomeric and polymeric molecules in an aqueous solution, and sometimes partly as a dispersion of molecules in an aqueous phase. The resins show duroplastic hardening behavior, leading to three-dimensional cross-linking and hence to insoluble and nonmeltable networks. The resins, however, always contain some residual monomers, especially free formaldehyde, even in the hardened state.

Even with only the three monomers melamine, formaldehyde, and urea, a variety of different types of resins exists which can fulfill nearly all requirements given in the wood-based panels industry. This field of application involves the production of wood-based panels like particleboards, medium density fiberboard (MDF), oriented strand board (OSB), plywood, blockboards, and others. In rare cases the resins and panels are also used in the furniture industry. According to the raw materials used, various types of melamine resins are possible:

MF	melamine–formaldehyde resin
MUF	melamine–urea–formaldehyde cocondensation resin
mUF	melamine-fortified UF resins
MF + UF	mixture of a MF and an UF resin
PMF	phenol–melamine–formaldehyde cocondensation resin
MUPF, PMUF	melamine–urea–phenol–formaldehyde cocondensation resin

Composition of the Resins and Basic Reactions

The generation of melamine–formaldehyde resins usually follows a two-step mechanism (Fig. 1). The first step (methylolation step) leads to the formation of

Encyclopedia of Polymer Science and Technology. Copyright John Wiley & Sons, Inc. All rights reserved.

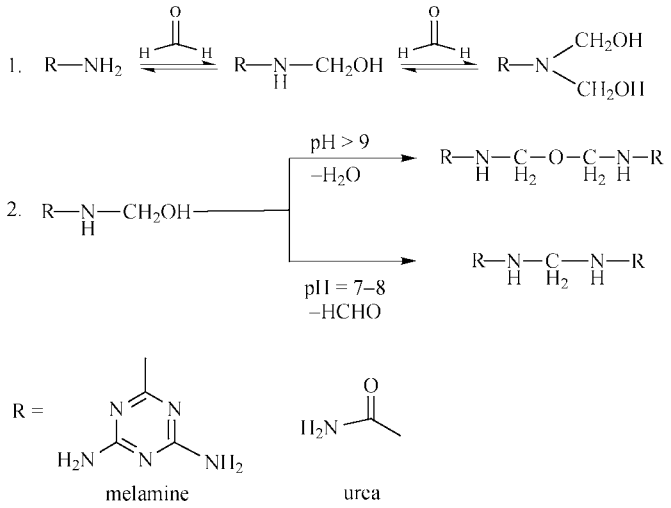

Fig. 1. Reaction mechanism for the formation of formaldehyde-based amino resins. 1, methylolation; 2, condensation.

methylolated melamine species by reaction with formaldehyde. The second step (bridging) forms ether or methylene bridges by condensation, either water or free formaldehyde is generated depending on pH. Both steps can be either base- or acid-catalyzed and are equilibrium reactions.

The most important parameters for the melamine–formaldehyde resins are

(1) the type of the monomers (melamine, urea, phenol)

(2) the molar ratio or mass ratio of the various monomers in the resin:

F/M	Molar ratio of formaldehyde to melamine
$F/(NH_2)_2$	Molar ratio of formaldehyde to amide groups, whereby urea counts for two NH_2 groups, and melamine for three NH_2 groups
M/U	Molar ratio of melamine to urea
F/U/M	Triple molar ratio
% melamine	Mass portion of melamine in the resin: (a) based on the liquid resin, (b) based on the resin solids content, or (c) based on the sum of urea and melamine in the resin

(3) the purity of the different raw materials, eg residual methanol or formic acid in formaldehyde or ammeline/ammelide in melamine (9,10), with ammeline–melamine–formaldehyde resins described in the literature (11,12)

(4) the "cooking" procedure, which usually is a multi step procedure with both alkaline and acidic steps:

a. pH-program

b. temperature program

c. types and amounts of alkaline and acidic catalysts

d. sequence of addition of the different raw materials

e. duration of the different steps of the cooking procedure

The melamine molecule contains three primary amine groups, each of which has the potential of reacting with two moles of formaldehyde forming up to a hexa-substituted product if the molar ratio F/M is high enough. Because of the significant higher reactivity of these melamine amine groups towards substitution with formaldehyde than urea, the melamine resins show the ability to form polymer structures with a much higher cross-link density compared to UF resins.

The production of pure MF resins is usually performed by the reaction of melamine with formaldehyde in an aqueous solution yielding a precondensate mixture of different monomeric as well as short linear and branched oligomeric melamine–formaldehyde compounds; all these reactions are determined mainly by temperature, length of condensation, pH of condensation, as well as the order and time course of heating and reagent addition (13). Usually all types of methylolated melamine species together with oligomeric parts (usually more than six melamine residues are linked from the beginning of the reaction) are present in the reaction mixture (see Fig. 2). Kinetic investigations (14–17) indicate the following order of reactivity towards methylolation of functional groups : (a) the rate of the methylolation decreases with increasing number of methylol groups/melamine; (b) the methylolation of secondary nitrogens is favored over tertiary nitrogens; and (c) secondary nitrogens (ie, already methylolated $-NH_2$ moieties) deactivate the methylolation of neighbored nitrogen atoms. Further important parameters

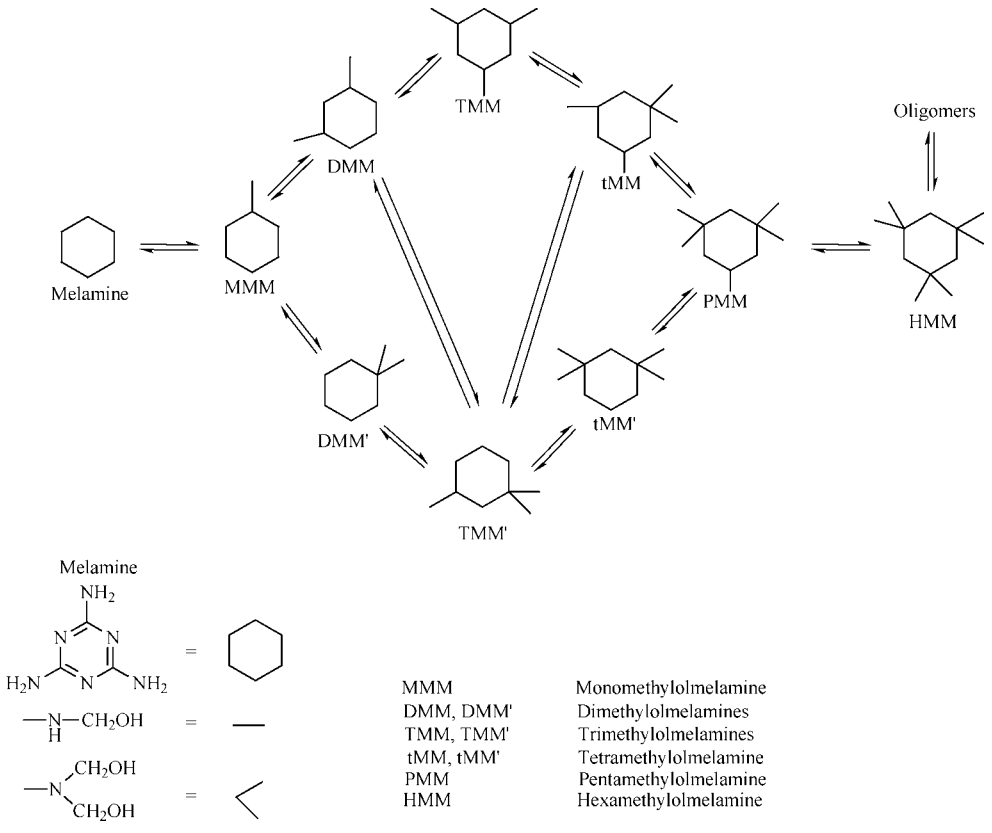

Fig. 2. Formation pathways of methylolated melamines.

are changes in the pH due to parallel running Canizarro reactions and the grain size of the melamine used (18,19).

The obtained liquid resins are colorless and normally of low viscosity. Such MF solutions are cured in a second stage by the application of heat, pressure, or an acid catalyst to give an insoluble, highly cross-linked resin. The long-term storage stability of the resins mainly requires stable rheological properties. Possible thixotropic behavior during storage at room temperature and chemical cross-linking or alterations due to further condensation are the drawbacks (20,21).

The molar mass distributions of melamine-based condensation and cocondensation resins are much broader than for other synthetic polymers. The low molar mass monomers comprise free formaldehyde (M = 30 g/mol) as well as residual and nonreacted post-added urea (M = 60g/mol). Monomeric methylols are generated, eg, in the case of MUF resins, by the reaction of this post-added urea with the free formaldehyde. The oligomeric compounds with two to five molecules of melamine are linked by methylene or methylene ether bridges. Free formaldehyde in the resin has positive and negative effects: on the one hand it induces the hardening reaction by reaction with the aminoplastic hardener and functions as an additional cross-linker; on the other hand it causes formaldehyde emission during the press cycle. Addditionally the residual formaldehyde leads to the displeasing subsequent formaldehyde emission from the pressed boards. Because of the stringent formaldehyde emission regulations worldwide, especially Germany/Austria and Japan ["E1"; "E Zero"; "Super E Zero"/"Four star" (22)] and hence the necessity to limit the subsequent formaldehyde emission, the molar ratio $F/(NH_2)_2$ has been decreased drastically within the last two decades.

The molar ratio of formaldehyde/reactive amino groups [$F/(NH_2)_2$] distinctly determines reactivity, the possible degree of cross-linking, and hence the bonding strength. If the molar ratio is decreased in order to lower the formaldehyde emission, the reactivity as well as the degree of hardening (degree of cross-linking) decreases (see Table 1).

An increase in the M/U molar ratio at a fixed F/(M + U) molar ratio enhances the bond performance. MUF resins with high melamine content have a more highly branched cross-linked structure and free melamine compared to

Table 1. $F/(NH_2)_2$ Molar Ratio of Melamine-Based Resins[a]

1.20 to 1.35	Resins for water-resistant plywood; addition of a formaldehyde catcher is necessary
0.98 to 1.15	E1-particleboard- and E1-MDF-resin for water-resistant boards (PB: EN 312-5 and 312-7; MDF: EN 622-5). Especially for MDF production, formaldehyde catchers are added.
Distinctly below 1.00	Special resins for boards with a very low subsequent formaldehyde emission

[a] (mUF, MUF, MUPF, and others) currently in use in the wood-based panels industry.

resins with low melamine content even if there is no significant difference in the linkage structure (23).

Influence of the Degree of Condensation. The higher the degree of condensation (higher molar masses), the higher is the viscosity at the same solid content. Besides a reduced water dilutibility of the resin, the flowing ability and the penetration into the wood surface are diminished. Additional effects are a decreased wetting behavior of a wood surface and a reduced distribution of the resin on the wood surface (particles, fibers). For mixtures MF + UF the degrees of condensation of the two components determine the viscosity of the mix according to the composition.

Correlations between the molar mass distribution (degree of condensation) and mechanical and hygroscopic properties of the produced boards are rather uncertain. The influence of the degree of condensation shows itself during the application and the hardening reaction (wetting behavior, penetration into the wood surface in dependence of the degree of condensation, drying out behavior after the application of the resin onto the surface).

Hydrolysis Resistance. The deterioration of a bond line, and hence its durability under the conditions of weathering, is determined essentially by

(1) failure of the resin (low hydrolysis resistance, degradation of the hardened resin causing loss of bonding strength);
(2) failure of the interface between the resin and wood surface due to the replacement of physical bonds between resin and reactive wood surface sites by water or other nonresin chemicals; and
(3) breaking of bonds due to mechanical forces and stresses: the influence of water causes swelling, and therefore movement of the structural components of the wood-based panels (cyclic stresses due to swelling and shrinking, including stress rupture).

The different behavior and resistance against hydrolysis depends on the type of the formaldehyde based resin and is determined at the molecular level. The aminomethylene links in urea–formaldehyde resins (UF) are susceptible to hydrolysis and therefore not stable at higher relative humidity or increased moisture contents, especially at elevated temperatures (24,25). A higher hydrolysis resistance can be achieved by incorporating melamine into the resin (melamine fortified UF resins, MUF, PMF, MUPF, PMUF), whereby the bonding between the nitrogen of the melamine and the carbon of the methylol group shows an increased stability against hydrolysis. The stabilization of the C—N bond arises from the conjugated double bonds of the aromatic ring structure of the melamine. An additional stabilization effect is exerted by the slower decrease of the pH in the bond line due to the buffering capacity of melamine (26).

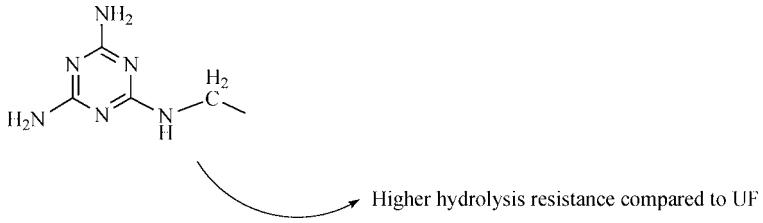

Because of the high costs of melamine as raw material, the costs for melamine-based resins are, however, much higher than for UF resins. Therefore the content of melamine in these resins is always as high as necessary but as low as possible. Pure melamine–formaldehyde resins are found mainly in mixtures with UF resins. The possible higher hydrolysis resistance as the most important advantage of these pure MF resins is counteracted by their low storage stability in liquid form and their exceedingly high price. The melamine content in the resins can vary between a few percent in melamine-fortified UF glue resins and more than 30%. Additionally, the mode of incorporation of the melamine can be very different. This knowledge is usually proprietary, and therefore description in the literature is rare (27,28). The higher the content of melamine, the higher is the stability (hydrolysis resistance) of the hardened resin against the influence of humidity and water (2, 29, 30). The stability of a resin against hydrolysis can be evaluated by monitoring the formaldehyde emanation during hydrolysis caused by boiling water or the influence of diluted acids at higher temperatures (31).

The reaction progress and end point can be monitored *in situ* under actual reaction conditions using FTIR spectroscopy for functional groups in real time, whereby the concentration of key reaction species can be followed directly using their isolated IR bands (32).

Melamine-fortified resins with a melamine content of up to approximately 10% based on liquid resin are used for various applications where straight UF resins cannot provide the desired combination of processing tolerance, formaldehyde emission, and specific board properties such as a low thickness swelling. MUF resins with higher content of melamine (up to 30% based on liquid resin) find applications in enhanced performance grade boards for use in humid conditions (moisture-resistant application).

Cocondensation Resins. Cocondensation of MF resins with urea, phenols, and other components is possible in many ways. One of the most interesting tasks is to clarify whether there is a real cocondensation within these resins or rather whether two independent, interpenetrating networks are formed (see INTERPENETRATING POLYMER NETWORKS). Cocondensation between urea and melamine via methylene bridges and methylene ether bridges has been strongly suggested or proven (33), but precise analysis cannot always be attained (34).

The production of MUF resins of various content of melamine can follow various paths:

(1) Direct cocondensation of melamine, urea, and formaldehyde in a multistep reaction with varying sequences of addition of the components (35–41), in particular of melamine and urea (27). Subsequent partial etherification leads to improved storage stability of the MUF resins with a low content of formaldehyde (42) and an improved reactivity (43).

(2) Direct mixing of an MF resin with a UF resin (28,44–46).

(3) Addition of melamine in various forms (pure melamine, MF/MUF-powder resin) to a UF resin during the application of the resin. In the case of the addition of pure melamine, the UF resin must have a rather high molar ratio of at least F/U = 1.5 approximately. Otherwise there is not enough formaldehyde available to react with the melamine in order to incorporate it into the resin.

(4) Melamine can also be added in the form of melamine salts, such as acetates, formiates, or oxalates (47–53), which decompose in the aqueous resin mix at higher temperatures. The melamine is then incorporated into the UF resin, forming an MUF resin and generating acids as latent hardeners. Furthermore it has been reported that using this procedure with melamine salts, the amount of melamine needed is much lower than in other MUF resins (47–52). MUF resins can also contain various other compounds that can react with formaldehyde such as urea derivatives, guanamines, or amides (54,55).

MUPF resins (PMUF resins) are mainly used for the production of particleboards according to DIN 68763 and EN 312 (quality P5 and P7, option 2 "V100"), as well as of OSB (quality type OSB3 and OSB4 according to EN 300). They usually contain small amounts of a phenol component. Production procedures are described in patents and in the literature (56–66). Newly developed MUPF resins enable a distinct reduction of the necessary resin consumption in the OSB face layers (67,68).

PMF/PMUF resins usually contain little or no urea. The analysis of the molecular structure of these resins has shown that there is no cocondensation between the phenol and the melamine, but that there exist two separate networks (69–72). This can be explained on the basis of a different reactivity of the phenol methylols and the melamine methylols, depending on the existing pH.

Under acidic conditions there are two steps in the hardening of a PMF resin (73): in the first, quick step, the condensation of the melamine dominates; in the second, rather slow step, the phenol is incorporated into the network. Under alkaline conditions a cocondensation between phenol and melamine could be detected (74,75). A PMUF resin with a distinctly higher portion of phenol and also a high content of melamine can be produced by starting with a PF condensation, followed by addition of melamine and further formaldehyde; urea is then added at the end of the procedure to decrease the molar content of free formaldehyde (76).

There are interesting niche markets for resins with very low content of formaldehyde and hence boards with extremely low subsequent formaldehyde emission. Since pure UF resins are too weak to be used for this purpose (low mechanical strength, high thickness swelling), melamine-fortified resins or MUF resins are used. The necessary content of melamine in these resins can vary distinctly and depends on the level of subsequent formaldehyde emission, on the board type as well as on other board requirements; eg, a certain thickness swelling (77–80).

Melamine-based resins with extreme low molar ratios [$F/(NH_2)_2 < 0.5$] can be used as so-called formaldehyde scavenger resins (81). They are mixed mainly with UF resins during the application for the production of wood-based panels with low subsequent formaldehyde emission.

MUF honeymoon adhesive systems for bonding of timber of high moisture content (wet gluing) to produce laminated wood (glulam) and finger-jointing are composed of two components: (*1*) a MUF resin at a pH of approximately 10 with no fillers added, and (*2*) a low pH aqueous solution of carboxymethylcellulose and formic acid lacking resorcinol in the system (82–85).

Correlations Between the Composition of Melamine Resins and Properties of Hardened Glue Lines and Wood-Based Panels

Only a few investigations have been done concerning the prediction of adhesive bond strengths and other properties based on the composition of the resin. Equations for evaluating a possible correlation between the chemical structures in various MUF resins with different molar ratios $[F/(NH_2)_2]$ and different types of preparation and the achievable internal bond together with the subsequent formaldehyde emission have been investigated. For this purpose, various structural components have been determined by means of NMR, and several ratios of the amounts of the various structural components have been calculated, eg,

(1) for MF resins (86):
   a. unreacted melamine to monosubstituted melamine
   b. unreacted melamine to total melamine
   c. methylene bridges related to methylol groups
   d. degree of branching: number of branching sites at methylene bridges related to total number of bondings at methylene bridges

(2) for MUF-resins (87,88) typical ratios determined are
   a. sum of unreacted melamine and urea to the sum of substituted melamine and urea
   b. methylene bridges related to methylols or to the sum of methylene bridges and methylols.

Applications

Depending on the various requirements different resin types are selected for use. Boards with low requirements (interior use) are usually UF-bonded. The incorporation of melamine (MUF, MF + UF), and sometimes phenol (MUPF), improves the low resistance of UF bonds to the influence of humidity, water, and weather. Fields of application for the various melamine-based wood adhesives resins are boards with reduced thickness swelling; eg, as laminate flooring cores and boards for use in humid conditions [according to EN 312 for particleboard, EN 300 for OSB, EN 622-5 for MDF, EN 314 for plywood and prEN 12775, prEN 13353, prEN 13017, and prEN 13354 for blockboard (solid wood panels)].

Impregnation of wood with MF impregnating resins has shown considerable potential to improve various wood properties such as surface hardness and weathering resistance. Using UV micro spectroscopy, it has been shown that water-soluble MF resins diffused well into the secondary cell wall and the middle lamella of wood (89–92).

Laminate floorings require a very low long-term (24 h) thickness swelling of the MDF/HDF- or particleboard cores. Requirements usually are less than 8% or 10%, respectively, sometimes less than 6% or even lower. Such a low thickness swelling usually cannot be obtained with UF resins; the incorporation of melamine is a suitable way to achieve the desired results. The necessary melamine content

Table 2. MUF–Glue Resin Mixes for Particleboard, MDF, and Plywood

Components/resin mixes	A[a]	B[b]	C[c]	D[d]
MUF resin[e]	100	100	—	—
MUF resin[f]	—	—	100	—
MUF resin[g]	—	—	—	100
Extender[h]	—	—	—	10
Water	—	10–20	20–50	up to 10
Urea solution[i]	up to 5	up to 5	up to 10	—
Hardener solution[j]	15	6	up to 4	—
Powder hardener[k]	—	—	—	3

[a]Glue mix A: particleboard for use in humid conditions (core layer).
[b]Glue mix B: particleboard for use in humid conditions (face layer).
[c]Glue mix C: MDF board for use in humid conditions.
[d]Glue mix D: plywood, class 2 or class 3 (EN 314).
[e]MUF resin with $F/(NH_2)_2 \approx 1.03–1.08$.
[f]MUF resin with $F/(NH_2)_2 \approx 0.95–1.03$.
[g]MUF plywood resin with $F/(NH_2)_2 \approx 1.2–1.4$.
[h]Extender: rye or wheat flour, containing in case some inorganic fraction.
[i]Urea solution (40%).
[j]eg, Ammonium sulfate solution (20%).
[k]eg, Ammonium sulfate in powder form.

in the resin depends on various parameters; eg, the type of wood furnish, the pressing parameters (pressure profile, density profile), and the resin consumption. Another important parameter is the cooking procedure of the resin, which considerably influences the thickness swelling of the boards even at the same gluing factor and the same content of melamine. It is especially important to use the formaldehyde present in the system as efficiently as possible by maximizing the content of methylene bridges compared to methylene ether bridges.

Combination of Melamine Resins with Other Adhesives. PMDI can be used as an accelerator and as a special cross-linker for MUF resins, with additions of approximately 1–2% based on dry particles (46,93–95).

For the purpose of special effects, combinations of adhesives or glue resins might be used; eg, the combination of adhesives in the particleboard or OSB production with PMDI in the core layer and a MU(P)F resin in the face layer.

Glue Resin Mixes for the Application of Melamine Resins. Table 2 summarizes some glue resin mixes for different applications in the production of particleboard, MDF, and plywood.

Hardening of Melamine Resins

During the curing process of a thermosetting adhesive resin, a three-dimensional network is built up. This yields an insoluble resin which is no longer thermoformable. The acid hardening conditions can be adjusted (*1*) by the addition of a so-called latent hardener (eg, ammonium sulfate or ammonium nitrate), or (*2*) by the direct addition of acids (maleic acid anhydride, formic acid, phosphoric acid and others) or of acidic substances, which dissociate in water (eg aluminium

sulfate). Ammonium sulfate reacts with the free formaldehyde in the resin to generate sulfuric acid, which decreases the pH. These acidic conditions hence enable the condensation reaction to restart, and finally the gelling and hardening of the resin. The rate of decrease of the pH during the hardening process depends upon the amount of available free formaldehyde and on the amount of hardener. An acceleration of the hardening process is achieved by heat (26,96), whereas the addition of melamine to a UF resin slows down the pH drop after the addition of the hardener (26) and thus yields an increase in the gel time.

The mechanism of the hardening reaction of MUPF/PMUF resins is not entirely clear. Such resins harden under similar acid conditions as MUF resins, whereas phenolic resins have a minimum of reactivity under these conditions; hence the phenolic portion of the resin might not really be incorporated into the aminoplastic portion of the resin during hardening (66).

During the hardening of PMF resins, no cocondensation reaction occurs. Therefore in the hardened state, two independent interpenetrating networks exist (69–72,97). Indications for a cocondensation via methylene bridges between the phenolic nucleus and the amido group of the melamine have been found by ^{1}H NMR only in model reactions between methylolated phenols and melamine (97).

The hardening of MUF resins can be enhanced by the addition of formaldehyde-based accelerator mixtures and monitored via rheology, gel time measurements, as well as the so-called ABES tests (98,99). Analyses indicate that cured MUF resins are mainly composed of separate MF and UF networks. Thus particleboards glued with an MUF/accelerator mixture exhibit improved mechanical properties compared to boards produced with commercially used MUF adhesives. The swelling properties of particleboards glued with an MUF/accelerator mixture are comparable to boards made from a commercial MUF resin (100).

Imino-amino methylene base intermediates obtained by the decomposition of hexamethylenetetramine (hexamine) stabilized by the presence of strong anions (hexamine sulfate) have been shown to markedly improve the water and weather resistance of hardened MUF resins used as wood adhesives (101–105). Even with only small additions between 1% and 5% the use of MUF resins of much lower melamine content with constant performance of the boards is possible.

Analytical Chemistry of MF Resins

The analytical chemistry of MF resins requires modern and sophisticated analytical methods because of the chemical complexity of the resin mixture. Several tens of components, ranging from defined low molecular component to oligomeric and polymeric components, can be identified within the resin mixture. Usually analytical methods are performed to achieve information on the following points : (*1*) the detailed composition (structure and amount) of low molecular components, (*2*) the estimation of the amount of characteristic functional moieties, and (*3*) the structure of the hardened thermoplastic networks. A complete overview of analytical methods concerning MF resins can be found in the literature (1).

Nuclear Magnetic Resonance (qv) (86,106) in the liquid state has proven one of the most efficient and valuable tools for analyzing the composition of MF and related resin materials. Besides ^{1}H NMR (16,107) spectroscopy, whose

Table 3. ^{13}C Chemical Shifts for Selected Functional Groups in MF Resins

Assignment	^{13}C Chemical shift (ppm)[a]
—NH$\underline{C}$H$_2$NH—	47
=N$\underline{C}$H$_2$NH—	52
=NCH$_2$O$\underline{C}$H$_3$/—N(CH$_2$O$\underline{C}$H$_3$)$_2$	58
=N$\underline{C}$H$_2$N=	64
=NH$\underline{C}$H$_2$OH	68–69
—N($\underline{C}$H$_2$OH)$_2$	68–69
—NH$\underline{C}$H$_2$OCH$_2$NH—	73
=N$\underline{C}$H$_2$OCH$_2$NH—	73
—NH$\underline{C}$H$_2$OCH$_3$	77.3
—N($\underline{C}$H$_2$OCH$_3$)$_2$	77
HO$\underline{C}$H$_2$OH	82
($\underline{C}$H$_2$O)$_n$ oligomers	85.2

[a] Chemical shift in ppm relative to TMS in DMSO.

resolution is limited by the small spectral range (~15 ppm), ^{13}C NMR spectroscopy (15,108,109) (spectral range ~200 ppm) is very effective for the analysis of hydrated or lyophilized samples in dimethyl sulfoxide (DMSO) or aqueous solution. Table 3 and Table 4 show the relevant resonances together with the assignment to the corresponding structural units (17,110). Values are shown for methylolated as well as methoxylated MF resins. Additional information on MUF (87) and M(U)PF resins (69–71,111) is reported in the literature. Degrees of branching as well as distinct molecular species can be identified with this method. The molecular mobility of resins components can be analyzed by gel-phase NMR spectroscopy on native MF resins (13). The changes of the concentration of various structural elements during the condensation of an MF resin can be followed by ^{13}C NMR (112).

Table 4. ^{13}C Chemical Shifts of the Triazine Region

		^{13}C Chemical shift (ppm)[a]	
Assignment		R = H	R = CH$_3$
	Melamine	167,4	167,4
	MMM	167,2	overlapped
	N,*N*′-DMM	167,0	overlapped
	MMM	166,3	166,7
	N,*N*′DMM	166,0	166,7
	N,*N*′,*N*″-TMM	165,8	166,7
	N,*N*,*N*′,*N*′-TMM	165,2	167,4
	PMM	165,2	167,4
	HMM	165,2	167,4

[a] ^{13}C Chemical shift in 40% DMSO/60% H$_2$O.

The lower the pH during the condensation, the higher is the portion of methylene bridges compared to ether linkages.

Hardened MF resins can be analyzed by solid-state NMR spectroscopy (113,114) detecting ^{13}C NMR and ^{15}N nuclei (requiring ^{15}N-enriched material). The chemical shift values from Table 3 and Table 4 are valid because of the equivalence between chemical shifts in solution and solid-state NMR spectra. The usual limited resolution of these spectra, however, limits the detailed analysis possible by liquid NMR spectroscopy. An analysis of molecular mobility within the hardened networks can be achieved by ^{13}C solid-state NMR spectroscopy.

IR spectroscopy is used frequently for the analysis of MF-type resin materials. Despite its broad use and availability, the information is quite limited for the analysis of distinct chemical species because of broad bands and overlap with water signals (see VIBRATIONAL SPECTROSCOPY). Information on cocondensation between phenolic resins and melamine (72,115), the structural analysis of hydroxymethylated melamines (116,117), as well as the chemistry of hardening (118) can be followed.

The analysis of MF resins as well as alkoxylated MF resins by chromatographic methods has been described vastly in the literature (119,120) and allows the separation and identification of oligomeric methylolated melamines by conventional UV- or refractive index based detection. The most direct method for the determination of methylolated melamines within a MF resin is the coupling between HPLC methods and Mass Spectrometry (qv), enabling the direct structural analysis by HPLC-MS methods on methoxylated (121–124) and butoxylated MF resins (see CHROMATOGRAPHY, HPLC) (125). Favored ionization methods use ESI-MS ionization methods to achieve an efficient ionization process. The detection of up to pentameric melamine units can be achieved by this method.

High pressure DSC coupled with both HPLC and GPC can characterize the polymerization or cure of MF resins (126). DSC was used to calculate the kinetics of the reaction resin during curing, and GPC monitored the change in molar masses.

The effects of cure temperature and amount of catalyst on the rheokinetical behavior of an MF resin can be followed using dynamical mechanical techniques (127), and time–temperature–transformation (TTT) cure diagrams can be constructed using the results of these methods (127–129) (see DYNAMIC MECHANICAL ANALYSIS).

Other, more historic methods for analyzing the chemical composition of MF resins rely on size-exclusion chromatography (SEC) (130,131) and thin-layer chromatography (132) (see CHROMATOGRAPHY, SIZE EXCLUSION).

Economic Aspects

Out of the approximately 6.5 million ton of formaldehyde-based resins (in dry form) used as adhesives in the wood-based panels industry, more than 900,000 ton are based on melamine (133). The resins are produced mainly by the chemical industry itself, as well as partly by the wood-based panels industry on its so-called megasites. In 1999 approximately 28%, or 196,000 ton, of the melamine that was produced worldwide was converted into wood adhesives (133).

BIBLIOGRAPHY

1. M. Dunky and P. Niemz, *Wood Based Panels and Glue Resins: Technology and Influence Parameters*, Springer, Heidelberg, 2002, p. 978.
2. A. Pizzi, *Advanced Wood Adhesives Technology*, Marcel Dekker, Inc., New York, 1994, pp. 67–88.
3. M. Dunky and A. Pizzi, in D. A. Dillard and A. V. Pocius, eds., *Adhesion Science and Engineering, Vol. 2: Issue Surfaces, Chemistry and Applications*, Elsevier Science B.V., Amsterdam, 2003, pp. 1039–1103.
4. M. Dunky, in A. Pizzi and K. L. Mittal, eds., *Handbook of Adhesive Technology*, 2nd ed., Marcel Dekker, Inc., New York, 2003, pp. 887–956.
5. A. Pizzi, in A. Pizzi and K. L. Mittal, eds., *Handbook of Adhesive Technology*, 2nd ed., Marcel Dekker, Inc., New York, 2003, pp. 653–680.
6. B. Broline, in *Proceedings of Wood Adhesives 2000*, Lake Tahoe, Nev., June 22–23, 2000, pp. 469–473.
7. L. L. Williams, in A. Seidel, ed., *Encyclopedia of Chemical Technology*, 5th ed., Wiley-Interscience, New York, 2004, pp. 618–652.
8. H. Diem and G. Matthias, *Ullmann's Encyclopedia of Industrial Chemistry*, 6th ed., Electronic Release, Wiley-VCH, Weinheim, 1998.
9. J. Shen and G. M. Crews, *Polym. Prepr.* **74**, 238–239 (1996).
10. S. Ono, T. Funato, Y. Inoue, T. Munechika, T. Yoshimura, H. Morita, S.-I. Rengakuji, and C. Shimasaki, *J. Chromatogr.* **A 815**, 197–204 (1998).
11. J. Shen, G.-M. Crews, C. U. Pittman Jr., Y. Wang, and R. Ran, *J. Polym. Sci: Part A: Polym. Chem.* **34**, 2543–2561 (1996).
12. C. U. Pittman Jr., M. G. Kim, D. D. Nicholas, L. Wang, F. R. A. Kabir, T. P. Schultz, and L. L. Ingram Jr., *J. Wood Chem. Technol.* **14**, 577–603 (1994).
13. J. Mijatovic, W. H. Binder, F. Kubel, and W. Kantner, *Macromol. Symp.* **181**, 373–382 (2002).
14. B. Tomita, *J. Appl. Polym. Sci., Polym. Chem. Ed.* **15**, 2347–2365 (1977).
15. B. Tomita and H. Ono, *J. Appl. Polym. Sci., Polym. Chem. Ed.* **17**, 3205–3215 (1979).
16. J. R. Ebdon, J. E. B. Hunt, and W. T. S. O'Rourke, *Br. Polym. J.* **19**, 197–203 (1987).
17. J. R. Ebdon, J. E. B. Hunt, W. T. S. O'Rourke, and J. Parkin, *Br. Polym. J.* **20**, 327–334 (1988).
18. D. Braun and V. Legradic, *Angew. Makromol. Chem.* **25**, 193–196 (1972).
19. D. Braun and V. Legradic, *Angew. Makromol. Chem.* **34**, 35–53 (1973).
20. T. Gebregiorgis and M. Gordo, *J. Chem. Soc. Faraday Trans.* **180**, 359–382 (1984).
21. S. Jahromi, *Macromol. Chem. Phys.* **200**, 2230–2239 (1999).
22. JIS A 5905 (May 2003), *Fiberboards*; JIS A 5908 (2003), *Particleboards*.
23. S. Tohmura, A. Inoue, and S. H. Sahari, *J. Wood Sci.* **47**, 451–457 (2001).
24. H. Yamaguchi, M. Higuchi, and I. Sakata, *Mokuzai Gakkaishi* **26**, 199–204 (1980).
25. H. Yamaguchi, M. Higuchi, and I. Sakata, *Mokuzai Gakkaishi* **35**, 801–806 (1989).
26. M. Higuchi, H. Shimokawa, and I. Sakata, *Mokuzai Gakkaishi* **25**, 630–635 (1979).
27. T. A. Mercer and A. Pizzi, *Holzforsch. Holzverwert.* **46**, 51–54 (1994).
28. R. Maylor, in *Proceedings of Wood Adhesives 1995*, Portland, Oreg., June 29–30, 1995, pp. 115–121.
29. S. Chow and K. J. Pickles, *Wood Sci.* **9**, 80–83 (1976).
30. H. Neusser and W. Schall, *Holzforsch. Holzverwert.* **24**, 108–116 (1972).
31. H. G. Freeman and R. E. Kreibich, *For. Prod. J.* **18**(7), 39–43 (1968).
32. M. Pavlovsky, R. Ferwerda, M. Scheepers, and J. J. Nusselder, in *TAPPI Plastics Laminates Symposium*, Atlanta, Ga., Aug. 21–23, 2000, pp. 43–45.
33. B. Tomita and C.-Y. Hse, *Mokuzai Gakkaishi* **41**, 349–354 (1995).

34. B. Tomita and C.-Y. Hse, *Mokuzai Gakkaishi* **41**, 490–497 (1995).
35. Ger. Pat. DE 2,455,420 (Nov. 22, 1974), H. Czepel (to Lentia GmbH.).
36. Eur. Pat. EP 62,389 (Apr. 7, 1982), J. J. Hoetjer (to Methanol Chemie Nederland V.o.F.).
37. U.S. Pat. 4,123,579 (Mar. 30, 1977), H. O. McCaskey Jr. (to Westinghouse Electric Corp.).
38. U.S. Pat. 5,681,917 (Mar. 26, 1996), R. A. Breyer, S. G. Hollis, and J. J. Jural (to Georgia-Pacific Resins, Inc.).
39. Eur. Pat. EP 185,205 (Nov. 16, 1985), H. Etling, H. Diem, W. Eisele, and M. Siegler (to BASF AG).
40. Eur. Pat. EP 913,411 (Oct. 28, 1998), J. Lalo and R. Garrigue (to Elf Atochem S.A.).
41. Eur. Pat EP 1,088,838 (Sept. 29, 2000), J. Lalo (to Atofina).
42. Eur. Pat. EP 864,603 (Feb. 17, 1998) O. Wittmann, M. Kummer, and H. Schatz (to BASF AG).
43. Ger. Pat. DE 4,011,159 (Apr. 6, 1990), G. Matthias, E. Weber, and H. Diem (to BASF AG).
44. Ger. Pat. DE 3,116,547 (Apr. 25, 1981), F. Kaesbauer and W. Bolz (to BASF AG).
45. Eur. Pat. EP 52,212 (Oct. 3, 1981), H. Etling, C. Dudeck, H. Diem, and M. Siegler (to BASF AG).
46. Eur. Pat. EP 107,260 (Oct. 25, 1983), A. Tinkelenburg, H. W. L. M. Vaessen, and J. G. J. Dirix (to Methanol Chemie Nederland V.o.F.).
47. C. Cremonini and A. Pizzi, *Holzforsch. Holzverwert.* **49**, 11–15 (1997).
48. C. Cremonini and A. Pizzi, *Holz Roh. Werkst.* **57**, 318 (1999).
49. C. Kamoun and A. Pizzi, *Holz Roh. Werkst.* **56**, 86 (1998).
50. M. Prestifilippo, A. Pizzi, H. Norback, and P. Lavisci, *Holz Roh. Werkst.* **54**, 393–398 (1996).
51. M. Zanetti and A. Pizzi, *J. Appl. Polym. Sci.* **88**, 287–292 (2003).
52. A. Pizzi, in *Proceedings of Wood Adhesives 2000*, Lake Tahoe, Nev., June 22–23, 2000, pp. 219–239.
53. A. Weinstabl, W. H. Binder, H. Gruber, and W. Kantner, *J. Appl. Polym. Sci.* **81**, 1654–1661 (2001).
54. Ger. Pat. DE 19,532,719 (Sept. 5, 1995), A. Meier, C. Hittinger, H. Schatz, G. Lehmann, T. Reiner, and M. Niessner (to BASF AG).
55. U.S. Pat. 6,566,459 (Apr. 29, 2002), P. G. Dopico, S. L. Wertz, J. C. Phillips, and G. E. Mirous (to Georgia-Pacific Resins, Inc.).
56. Ger. Pat. DE 2,020,481 (Apr. 27, 1970), J. Mayer and C. Schmidt-Hellerau (to BASF AG).
57. Eur. Pat. EP 69,267 (June 19, 1982), H. Diem, R. Fritsch, H. Lehnert, G. Matthias, H. Schatz, and O. Wittmann (to BASF AG).
58. Ger. Pat. DE 3,145,328 (Nov. 14, 1981), H. Diem, R. Fritsch, H. Lehnert, G. Matthias, H. Schatz, and O. Wittmann (to BASF AG).
59. U.S. Pat. 4,285,848 (July 31, 1978), C. H. Hickson (to Borden, Inc.).
60. Ger. Pat. DE 3,807,403 (Mar. 7, 1988), C. Schmidt-Hellerau, E. Weber, and G. Matthias (to BASF AG).
61. Eur. Pat. EP 31,533 (Dec. 13, 1980), H. Schatz, C. Dudeck, H. Diem, J. Mayer, and C. Schmidt-Hellerau (to BASF AG).
62. Eur. Pat. EP 337,093 (Feb. 28, 1989), C. Schmidt-Hellerau, E. Weber, and G. Matthias (to BASF AG).
63. U.S. Pat. 4,285,848 (Aug. 25, 1981), C. H. Hickson (to Borden, Inc.).
64. Ger. Pat. DE 3,027,203 (July 18, 1980), H. Schittek (to Deutsche Texaco AG).
65. M. Prestifilippo and A. Pizzi, *Holz Roh. Werkst.* **54**, 272 (1996).
66. C. Cremonini, A. Pizzi, and P. Tekely, *Holz Roh. Werkst.* **54**, 85–88 (1996).

67. J. Gomez-Bueso, J. Mattheij, L. Evers, W. Kantner, and M. Dunky, in *Proceedings of the Seventh European Panel Products Symposium*, Llandudno, North Wales, U.K., 2003, pp. 75–81.
68. J. Gomez-Bueso, J. Mattheij, L. Evers, W. Kantner, and M. Dunky, *Holz Zentr. Bl.* **129**, 1226 (2003).
69. D. Braun and W. Krausse, *Angew. Makromol. Chem.* **108**, 141–159 (1982).
70. D. Braun and W. Krausse, *Angew. Makromol. Chem.* **118**, 165–182 (1983).
71. D. Braun and H.-J. Ritzert, *Angew. Makromol. Chem.* **125**, 9–26 (1984).
72. D. Braun and H.-J. Ritzert, *Angew. Makromol. Chem.* **125**, 27–36 (1984).
73. J.-K. Roh, M. Higuchi, and I. Sakata, *Mokuzai Gakkaishi* **35**, 320–327 (1989).
74. J.-K. Roh, M. Higuchi, and I. Sakata, *Mokuzai Gakkaishi* **36**, 36–41 (1990).
75. J.-K. Roh, M. Higuchi, and I. Sakata, *Mokuzai Gakkaishi* **36**, 42–48 (1990).
76. Eur. Pat. EP 915,141 (Oct. 21, 1998), M. Paventi (to Arc Resin Corp.)
77. M. Dunky, unpublished results, 2001.
78. F. Wolf, in *Proceedings of the First European Panel Products Symposium*, Llandudno, North Wales, U.K. 1997, pp. 243–249.
79. G. Lehmann, in *Proceedings of Adhesives for Wood Based Panels and Fiber Form Parts (Klebstoffe für Holzwerkstoffe und Faserformteile)*, Braunschweig, Germany, 1997.
80. R. M. Rammon, in *Proceedings of the 31st Washington State University International Particleboard / Composite Materials Symposium*, Pullmann, Wash. 1997, pp. 177–181.
81. U.S. Pat. 5,684,118 (Mar. 26, 1996), R. A. Breyer, B. R. Arndell, and S. Stompel (to Georgia-Pacific Resins, Inc.).
82. M. Properzi, A. Pizzi, and L. Uzielli, *Holz Roh. Werkst.* **61**, 77–78 (2003).
83. M. Properzi, A. Pizzi, and L. Uzielli, *Holzforschung Holzverwert.* **53**, 73–77 (2001).
84. M. Properzi, A. Pizzi, and L. Uzielli, *Holz Roh. Werkst.* **59**, 413–421 (2001).
85. M. Properzi, C. Simon, A. Pizzi, B. George, L. Uzielli, and G. Elbez, *Holzforschung Holzverwert.* **54**, 18–20 (2002).
86. T. A. Mercer and A. Pizzi, *J. Appl. Polym. Sci.* **61**, 1697–1702 (1996).
87. T. A. Mercer and A. Pizzi, *J. Appl. Polym. Sci.* **61**, 1687–1695 (1996).
88. L. A. Panangama and A. Pizzi, *J. Appl. Polym. Sci.* **59**, 2055–2068 (1996).
89. W. Gindl, F. Zargar-Yaghubi, and R. Wimmer, *Bioresour. Technol.* **87**, 325–330 (2003).
90. W. Gindl, E. Dessipri, and R. Wimmer, *Holzforschung* **56**, 103–107 (2002).
91. D. Lukowsky, *Holz Roh. Werkst.* **60**, 349–355 (2002).
92. W. Gindl, H. S. Gupta, *Compos. Part A: Appl. Sci. Manufact.* **33**, 1141–1145 (2002).
93. A. Tinkelenberg, H. W. L. M. Vassen, K. W. Suen, and P. G. J. Leusink, *J. Adhesi.* **14**, 219–231 (1982).
94. Eur. Pat. EP 25,245 (Aug. 28, 1980), A. Tinkelenberg, H. W. L. M. Vassen, and K. W. Suen (to Methanol Chemie Nederland V.o.F.)
95. H.-J. Deppe, *Holz Zentr. Bl.* **111**, 1433–1435 (1985).
96. M. Higuchi and I. Sakata, *Mokuzai Gakkaishi* **25**, 496–502 (1979).
97. M. Higuchi, S. Tohmura, and I. Sakata, *Mokuzai Gakkaishi* **40**, 604–611 (1994).
98. P. E. Humphrey, in *Proceedings of the Third Pacific Rim Bio-Based Composites Symposium*, Kyoto, Japan, 1996, pp. 366–373.
99. U.S. Pat. 5,176,028 (Oct. 1, 1990), P. E. Humphrey (to The State of Oregon, Oregon State University).
100. J. Mijatovic, M. Dunky, and W. Kantner, in *Proceedings of the Seventh European Panel Products Symposium*, Poster Session, Llandudno, North Wales, U.K., 2003, pp. T15–T19.
101. M. Zanetti, A. Pizzi, and C. Kamoun, *Holz Roh. Werkst.* **61**, 55–65 (2003).
102. A. Pizzi, P. Tekely, and L. A. Panamgama, *Holzforschung* **50**, 481–485 (1996).
103. M. Zanetti and A. Pizzi, in *Proceedings of the Sixth European Panel Products Symposium*, Llandudno, North Wales, U.K., 2002, pp. 231–248.

104. M. Zanetti and A. Pizzi, *J. Appl. Polym. Sci.* **90**, 215–226 (2003).
105. C. Kamoun, A. Pizzi, and M. Zanetti, *J. Appl. Polym. Sci.* **90**, 203–214 (2003).
106. R. P. Subrayan and F. N. Jones, *J. Appl. Polym. Sci.* **62**, 1237–1251 (1996).
107. H. Schindlbauer and J. Anderer, *Fresenius Z. Anal. Chem.* **301**, 210–214 (1980).
108. B. Tomita, *J. Polym. Sci.* **15**, 2347–2365 (1977).
109. A. J. J. de Breet, W. Dankelman, W. G. B. Huysmans, and J. de Wit, *Angew. Makromol. Chem.* **62**, 7–31 (1977).
110. M. Dawbarn, J. R. Ebdon, S. J. Hewitt, J. E. B. Hunt, I. E. Williams, and A. R. Westwood, *Polymer* **19**, 1309–1312 (1978).
111. D. Braun and R. Unvericht, *Angew. Markomol. Chem.* **226**, 183–195 (1995).
112. V. M. L. J. Aarts, M. L. Scheepers, and P. M. Brandts, in *Proceedings of the European Plastic Laminates Forum*, Heidelberg, Germany, 1995, pp. 17–25.
113. M. Andreis, J. L. Koenig, M. Gupta, and S. Ramesh, *J. Polym. Sci. Part B: Polym. Physics* **33**, 1449–1460 (1995).
114. J. R. Ebdon, P. E. Heaton, T. N. Huckerby, W. T. S. O'Rourke, and J. Parkin, *Polymer* **25**, 821–825 (1984).
115. D. Braun and V. Vargha, *Angew. Markomol. Chem.* **163**, 169–193 (1988).
116. D. Braun and V. Legradic, *Angew. Markomol. Chem.* **36**, 41–55 (1974).
117. D. Braun and V. Legradic, *Angew. Makromol. Chem.* **34**, 35–53 (1973).
118. K. Umemura, S. Kawai, H. Sasaki, R. Hamada, and Y. Mizuno, *J. Adhes.* **59**, 87–100 (1996).
119. S. Kawai, H. Nagano, and T. Maji, *J. Chromatogr.* **477**, 467–470 (1989).
120. T. T. Chang, *Progr. Org. Coat.* **29**, 45–53 (1996).
121. A. Marcelli, D. Favretto, and P. Traldi, *Rapid. Commun. Mass. Spectram* **11**, 1321–1328 (1997).
122. T. T. Chang, *Anal. Chem.* **66**, 3267–3273 (1994).
123. T. T. Chang, *Polym. Prepr.* **37**(1), 292–293 (1996).
124. E. Longordo, L. A. Papazian, T. L. Chang, *J. Liq. Chromatogr.* **14**(11), 2043–2063 (1991).
125. D. Favretto, P. Traldi, and A. Marcelli, *Eur. Mass Spectrom.* **4**, 371–378 (1998).
126. E. W. Kendall, L. D. Benton, and B. R. Trethewey Jr., *Proc. TAPPI Plast. Laminates Symp.* 117–132, (2000).
127. P.-O. Hagstrand, C. Klason, L. Svensson, and S. Lundmark, in *Proceedings of the XIIIth International Congress on Rheology*, Cambridge, U.K., 2000, Vol. 1, pp. 157–159.
128. P.-O. Hagstrand and C. Klason, *Polym. Eng. Sci.* **39**, 2019–2029 (1999).
129. M. Properzi, A. Pizzi, and L. Uzielli, *J. Appl. Polym. Sci.* **81**, 2821–2825 (2001).
130. D. Braun and W. Pandjojo, *Angew. Makromol. Chem.* **80**, 195–205 (1979).
131. K. Dietrich, J. Moskalenko, K. Wiener, and W. Teige, *Acta Polym.* **37**(4), 252–253 (1986).
132. D. Braun and W. Pandjojo, *Fresenius Z. Anal. Chem.* **294**, 375–378 (1979).
133. A. C. L. M. van der Waals, J. J. H. Nusselder, and T. Bacon, in *Proceedings of Wood Adhesives 2000*, Portland, Oreg., 2000, pp. 193–195.

WOLFGANG H. BINDER
Institute of Applied Synthetic Chemistry, Technical University of Vienna
MANFRED DUNKY
Dynea Austria GmbH

MEMBRANE TECHNOLOGY. See Volume 3.

METAL-CONTAINING POLYMERS. See Volume 7.

METALLOCENE CATALYSTS. See SINGLE-SITE CATALYSTS.

METALLOCENES. See Volume 7.

METHACRYLIC ESTER POLYMERS. See Volume 3.

MICROCELLULAR PLASTICS. See Volume 7.

MICROEMULSION POLYMERIZATION. See Volume 7.

MICROGELS. See SMART MATERIALS, MICROGELS.

MICROMECHANICAL PROPERTIES. See Volume 3.

MISCIBILITY. See Volume 7.

MODELING OF POLYMER PROCESSING AND PROPERTIES. See Volume 3.

MOLECULAR MODELING. See Volume 7.

MOLECULAR RECOGNITION IN DENDRIMERS

Introduction

Dendrimers are highly branched polymers that can be obtained with a very high degree of control (1–10). The degree of control that is obtainable in dendrimers is often touted as being matched by those only seen with biopolymers. Ever since the first report of dendrimer synthesis (11), a number of possible applications for these molecules were envisioned (7,12). Several of those imaginative ideas are being brought to practice with these new macromolecular architectures. The seminal work of Newkome and Tomalia also has to be credited for bringing this area of research to the forefront (13,14). A particular theme that has emerged out of these new molecules is to use these scaffolds for molecular recognition (15). Structurally, dendrimers have three different locations of interest: a core, highly branched interior building blocks, and functionalities in the periphery. The features that render these macromolecules as ideal candidates for molecular recognition are that (*1*) dendrimers can be obtained in a highly monodisperse form, ie, with a high degree of control over molecular weight; (*2*) They adapt a globular conformation at higher generations, thereby generating space in its interior for binding guest molecules; (*3*) The core of the dendrimer is often well-encapsulated from the solvent environment; (*4*) The ability to functionalize the periphery of the dendrimers allows for a high density presentation of functionalities.

Encyclopedia of Polymer Science and Technology. Copyright John Wiley & Sons, Inc. All rights reserved.

Binding events between two molecules (a host and a guest) occur due to certain attractive forces. These could be dispersion forces such as π-stacking, metal–ligand interactions, hydrogen bonding, hydrophobic interaction, ionic interaction, or other electrostatic attractions. In this article, we will focus mainly on hydrogen-bonding-based recognition and hydrophobic forces. We will make occasional reference to ionic interactions and π-stacking within the two topics above. Dendrimers based on metal–ligand interactions are not included in this review and interested readers are referred to other recent review articles on this topic (6,16,17) (see also DENDRONIZED POLYMERS).

Synthesis of Dendrimers

Syntheses of dendrimers can be achieved mainly through two complementary methods: (*1*) a divergent approach and (*2*) a convergent approach (18). Both approaches use AB_n monomer units and utilize protection–deprotection (or masking–unmasking methodologies) to grow the dendrimer. The divergent synthesis starts from the core and the periphery grows as more synthetic iterations are performed on the same molecule (Fig. 1). Therefore, the reactive functionalities are always in the periphery of the dendrimer. In the convergent synthesis, the dendritic growth occurs at the focal point of the dendron or dendrimer, since the growth takes place from the periphery to the core (Fig. 2). The divergent approach and the convergent approach are shown schematically in Figures 1 and 2, respectively.

There are advantages and disadvantages to both of these approaches. Since the reactive functionalities are in the periphery of the growing dendrimer in the divergent approach, the reactivity of these groups is retained even at high generations. However, in the convergent synthesis, since the reactive functional group is at the focal point of the dendrimer, this functionality tends to get encapsulated at higher generations. Therefore, it becomes less reactive and it is difficult to

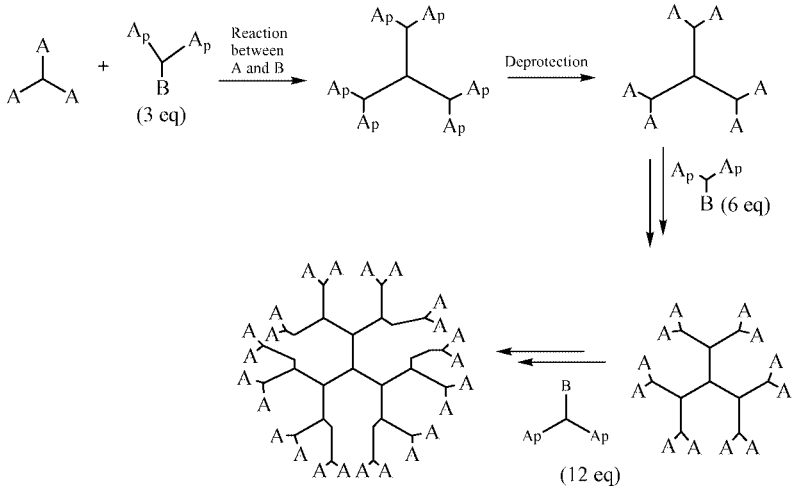

Fig. 1. Schematic representation of the divergent approach.

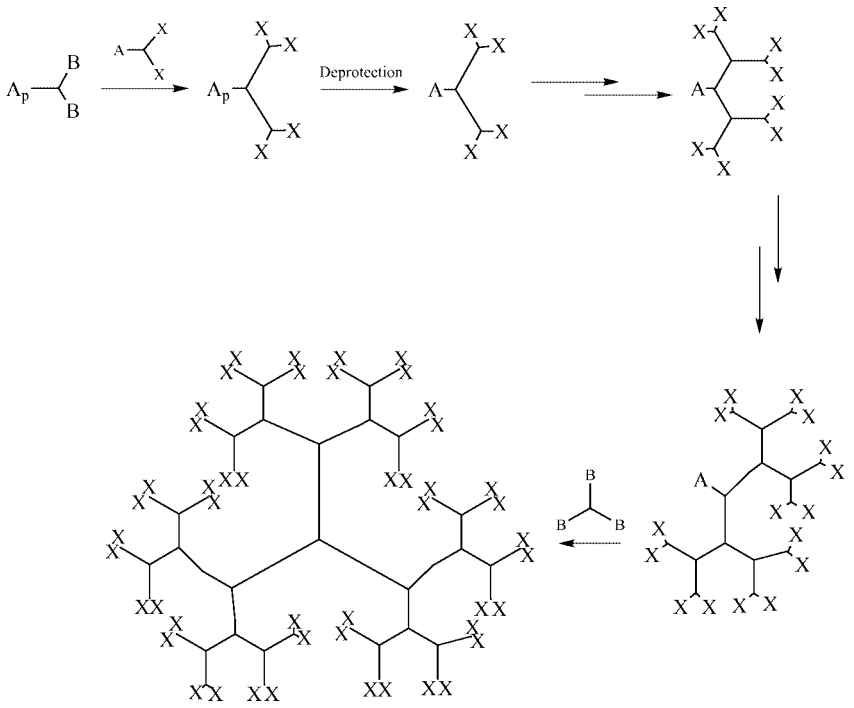

Fig. 2. Schematic representation of the convergent approach.

produce very high generations using the convergent approach. Also, note that the number of reactions that needs to be done on a single dendrimer molecule doubles with each generation in the divergent synthesis (Fig. 1). This results in defects in the dendrimer structures at higher generations. In the convergent synthesis, the number of reactions to be performed in a particular molecule always remains the same, independent of the generation. Therefore, achieving a pure, monodisperse dendrimer is more likely. Dendritic systems such as the commercially available polyamidoamine (PAMAM) and poly(propylene)imine (PPI) dendrimers are synthesized through a divergent approach. Dendrimers such as the Newkome dendrimer, silane-based dendrimers, and the phosphorus based dendrimers are also made using a divergent approach (13,19,20). Benzyl ether and phenylacetylene dendrimers are the two main classes of dendrimers that have been synthesized using a convergent approach (4,5).

Since dendrimers are often pursued as globular protein mimics, it is useful to be able to vary each monomer unit from the other, ie introduce sequences within dendrimers. For achieving such a possibility, the convergent approach is an ideal synthetic protocol. The Thayumanavan group has developed two synthetic protocols in which the peripheral functionalities of the dendrimers are all different from each other (21,22). In the first approach, we used an AB_2 monomer unit in which one of the B units is protected. This approach was demonstrated by the monoprotection of one of the phenolic groups of 3,5-dihydroxybenzyl alcohol with an allyl moiety. The resultant monomer was treated with one alkylating agent to

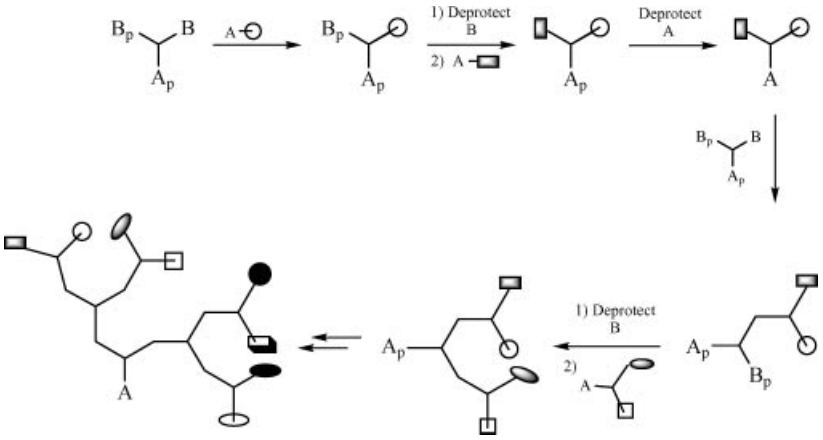

Fig. 3. Schematic representation of ABB_p sequencing methodology.

cleanly afford the monosubstituted compound. The allyl group was deprotected and the resultant phenol was then treated with a second electrophile to afford the differentially substituted G1 dendron. Conversion of the hydroxymethyl moiety to bromomethyl group and iterations of the above-mentioned steps resulted in higher generation dendrons, as schematically shown in Figure 3.

In an alternate approach, an ABB′ monomer was used as the building block unit. In this monomer, under a certain condition the functionality B reacts with A selectively, while A can react with B′ under a different set of conditions. The repeat unit used for this purpose was ethyl 3-hydroxy-5-hydroxymethylbenzoate. Here B is the phenol, B′ is the primary alcohol, and the masked form of A is the ester group. This approach is schematically shown in Figure 4. Another facile route that is capable of introducing sequences within dendrimers was developed by Simanek, where three different functionalities can be reacted one at a time with a traizine core (23).

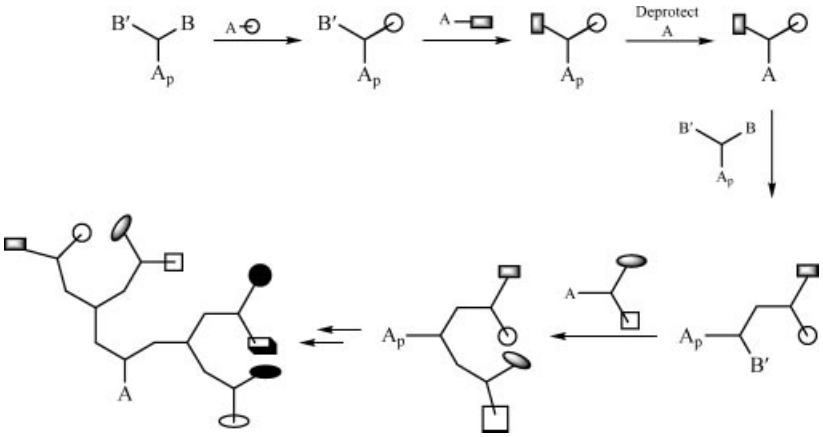

Fig. 4. Schematic representation of ABB′ sequencing methodology.

Hydrogen Bonding

Hydrogen bonding has been a fascinating tool for molecular recognition for chemists, since it is ubiquitous in nature's recognition processes and is highly directional. The directional nature of hydrogen bonds allows control over the relative orientation of the host–guest molecular framework. Hydrogen-bonding-based interactions are often weak in the presence of polar and/or protic solvents or in the presence of other competitive guest molecules. This feature has led to the design of the reversible incorporation of guest molecules that could find use in applications such as catalysis, separations, and controlled drug release.

Hydrogen Bonding within Dendritic Interiors. Newkome and co-workers incorporated 2,6-diaminopyridine units as the host recognition functionalities within dendrimers (24). The dendrimer host containing the donor–acceptor–donor (DAD) hydrogen-bonding receptor was able to bind glutarimide containing the complementary acceptor–donor–acceptor (ADA) units with 1:1 functional stoichiometry (Fig. 5). The apparent association constant was found to be about 62–70 M^{-1}. Newkome also noted that the analysis was complicated by additional complexation sites within the dendrimer backbone, as they weakly compete for the guest molecule. Similarly, Santo and Fox have also studied the hydrogen-bonding interaction between dendrimers and several heterocyclic guest molecules (25). These authors noticed that the binding efficiency depends on the nature of the peripheral functionalities of PAMAM dendrimers. It is also interesting to note that PAMAM dendrimers have been shown to be capable of accommodating guest molecules such as 2-naphthol in their interior, which can then be released upon a pH change (26). These interactions are presumed to be due to hydrogen bonding.

Specific binding between a dendrimer host and a complementary guest molecule was also achieved by Zimmerman and co-workers, where they used benzyl ether or phenyleneethynylene dendrimer backbone (27). In this work, naphthyridine units were incorporated into the focal point of dendrimers, and complementary benzamidinium-based molecules were used as guests (Fig. 6). The authors found the association constant (K_a) of this host–guest interaction to be independent of the dendrimer generation and is dependent only on the nature of the solvent in which it is measured. These results were taken to suggest

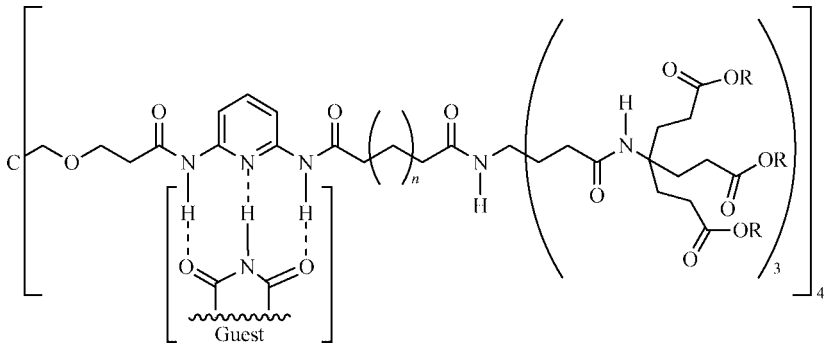

Fig. 5. Structure of the Newkome dendrimer that binds glutarimide.

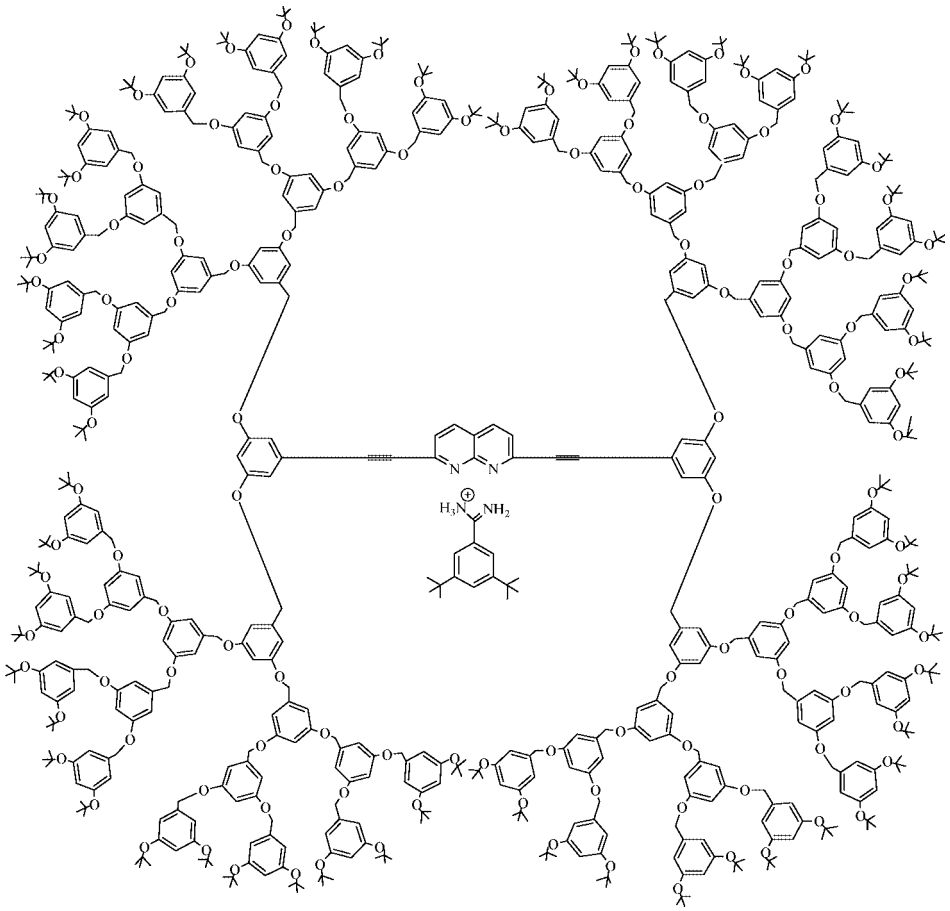

Fig. 6. Structure of the dendrimer with a naphthyridine core.

that dendrimers are highly porous in nature and that the dendritic interiors are solvent-filled. This is an interesting result, considering the report by Fréchet, where the solvatochromic shifts of a chromophore incorporated in the core suggests that the polarity of the dendritic interior is dictated by the dendrimer backbone and not the bulk solvent (28).

Diederich and co-workers incorporated optically active binaphthol at the core of benzyl ether dendrimers (29). The diol moiety in the core was converted to the corresponding phosphates, which were used for carbohydrate recognition (30). Although, they observed a 1:1 association with glycosidic guest molecules, the binding selectivity was observed to be weak. Also, the association strength did not change significantly with dendrimer generation. This observation is consistent with Zimmerman's results mentioned above. Fluorescence-based enantioselective recognition of amino alcohols was also attempted with BINOL-cored dendrimers (31). The proof-of-principle for such a possibility is reported, although the enantiodiscrimination using these dendrimers is moderate. The fact that the fluorescence quenching is not dependent on amino alcohol concentration leads to the

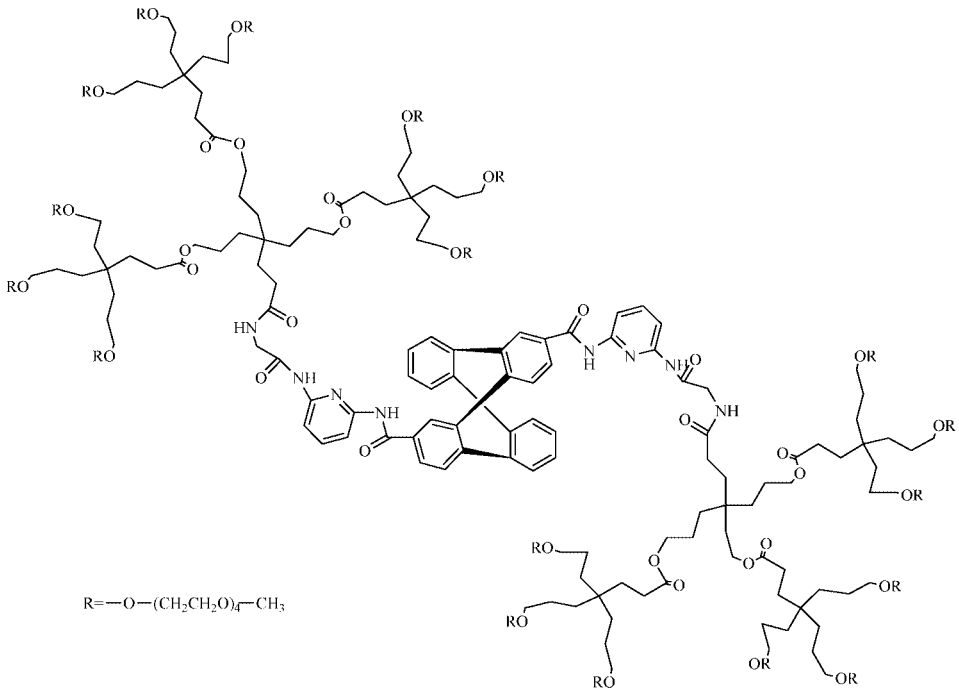

Fig. 7. Structure of a dendrocleft.

conclusion that the quenching occurs because of the hydrogen bonding between the core of the dendrimer and the amino alcohols.

Carbohydrate recognition has also been achieved with dendrimers by Smith and Diederich (32). These so-called dendroclefts are made up of a 9,9′-spirobi[9*H*-fluorene] initiator core containing 2,6-di(carboxamido)pyridine moieties (Fig. 7). Upon increasing the dendrimer generation, it was noted that the discrimination of enantiomeric guest molecules became poorer, whereas discrimination between diastereomeric guest molecules became better. This was attributed to the difference in steric demands of the dendritic shell or to the possible participation of the peripheral functionalities in the host–guest hydrogen-bonding network.

Molecularly imprinted polymers have been approached as a possible mode of performing host–guest chemistry in recent years (33). However, the limitations of these methods include incomplete template removal, broad guest affinities, and slow mass transfer. The molecular homogeneity, monodispersity, and large solubility of dendrimers make them good choice for the molecular imprinting process. Recently, Zimmerman and co-workers used their cored-dendrimer concept (34) to template porphyrins with benzyl ether dendrimer (35). The hollow core of the dendrimer contained eight carboxyl groups inside the dendritic core, capable of hydrogen bonding with complementary guest molecules. They showed that different porphyrin-based guest molecules can bind reversibly to the host structure (Fig. 8) (36).

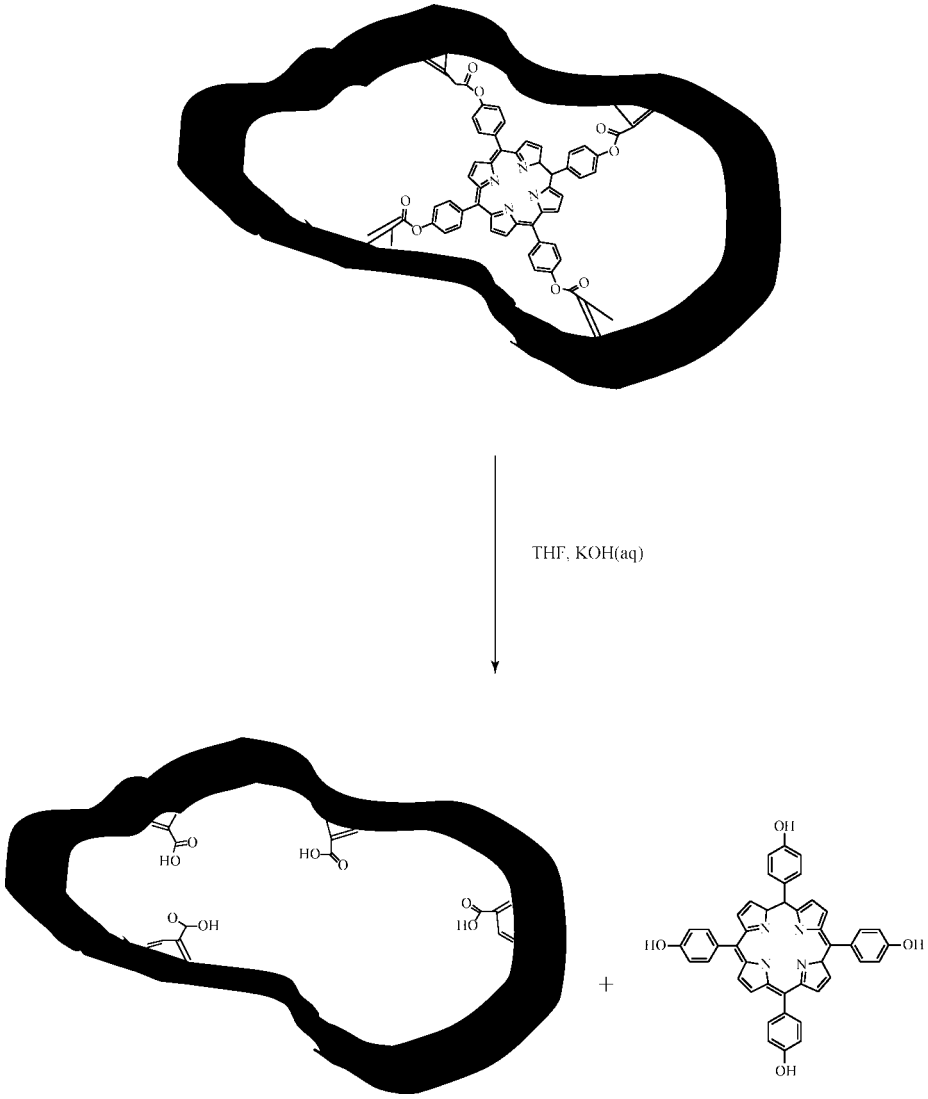

Fig. 8. Molecularly imprinted dendrimers.

Hydrogen Bonding in the Dendritic Periphery. While host–guest interaction in the dendritic interior is interesting because of the unique environment that dendrimers often provide in their interiors, reversible modification of dendritic periphery is also interesting. Meijer and co-workers showed that PPI dendrimers with modified urea functionalities can be utilized to bind guest molecules that are also urea-based (37). It was also shown later that a thiourea-based host functionality is better than urea itself for the urea-based guests (Fig. 9) (38). The observation was confirmed by isothermal calorimetry studies. Since both host and guest molecules are based on urea functionalities and since the periphery of the dendrimers contains a high density of the urea functionalities, there is

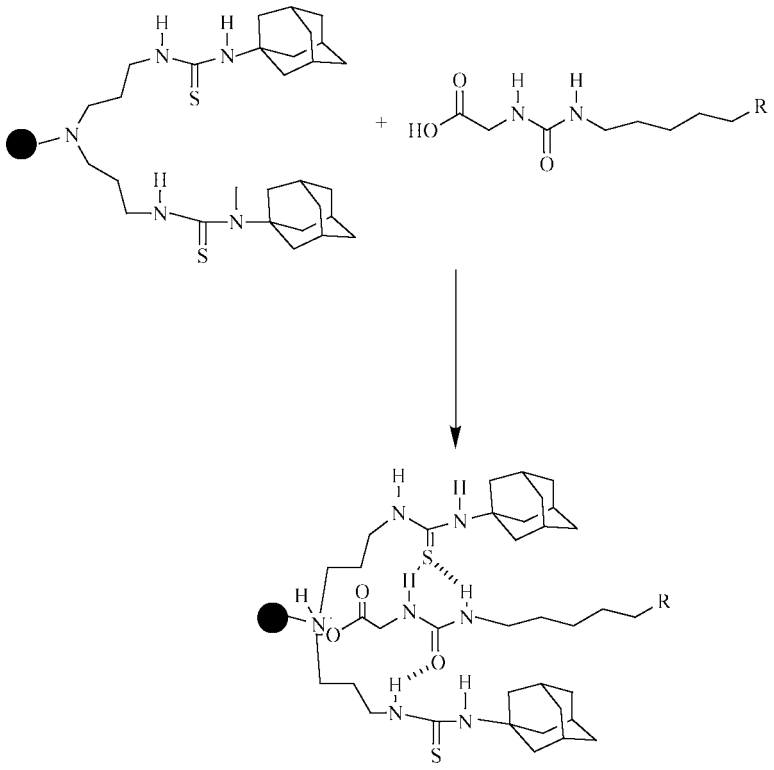

Fig. 9. Binding of urea guest molecules with thiourea functionalities in the dendritic periphery.

an obvious opportunity for intramolecular hydrogen bonding in these dendrimers. When there is an increased intramolecular hydrogen-bonding interaction, it was observed that the host–guest interaction is weaker. The authors attributed this observation as the probable reason for thiourea being a better host. They suggest that the soft interaction between the molecules owing to the presence of sulfur compared to oxygen provides a less dense structure, which is more accessible to guest molecules.

An elegant application of this method was shown by Reek and Meijer, where this type of dendrimer was used as catalytic support for palladium-catalyzed allylic amination reactions (39). The periphery of the dendrimer contains many adamantyl-functionalized urea groups (Fig. 10), and the catalyst was designed to have complementary hydrogen-bonding elements along with a triphenyl phosphine moiety, a ubiquitous ligand in organometallic catalysis. The presence of multiple catalytic sites in a single dendrimeric support did not hamper the reaction rate, showing that the phosphine ligands were independent of each other. It was also easy to recover the ligand from the support, which could then be reused.

An interesting work by Kim showed that the periphery of the dendrimers can be reversibly manipulated through noncovalent interactions (40). They used Cucurbituril as the molecular bead that encapsulates the amino butane peripheral units (Fig. 11). The pseudorotaxane-terminated dendrimers not only gave a

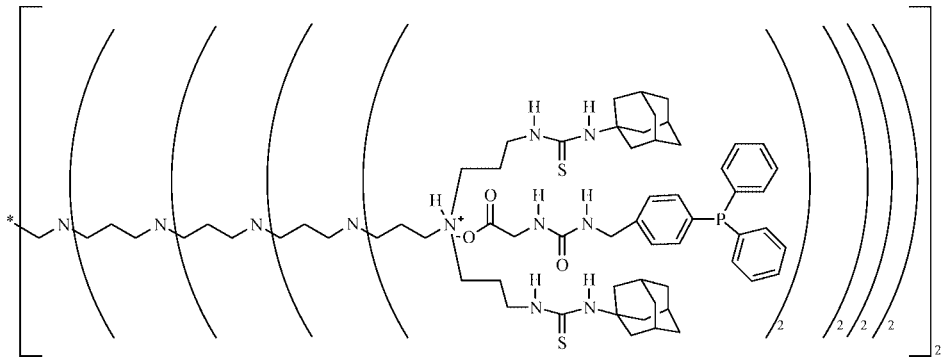

Fig. 10. A recoverable catalyst using hydrogen-bonded host–guest dendrimer.

topologically novel dendritic structure but also suggested that these structures can be useful for applications such as drug delivery upon appropriate redesign.

Intramolecular hydrogen bonding among the periphery units in dendrimers has been effectively used for binding guest molecules. Meijer's group has shown that the intramolecular hydrogen bonding among the peripheral units can be used to construct a so-called dendritic box. Intramolecular hydrogen bonding is

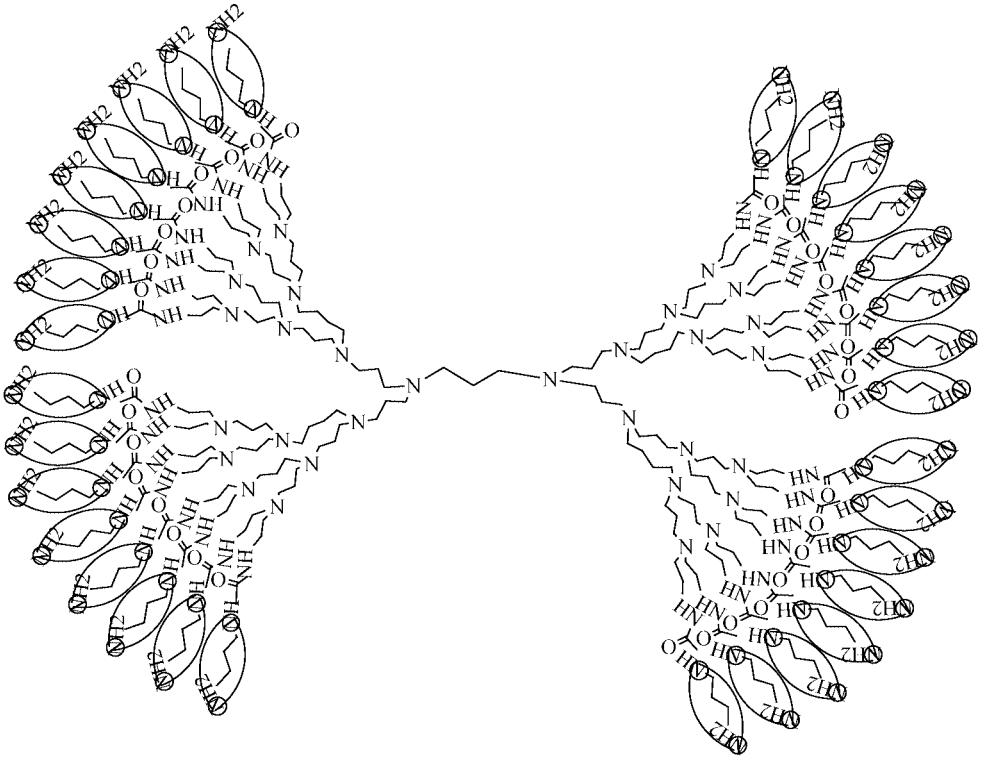

Fig. 11. Dendrimers with noncovalently bound cucurbiturils (the cylindrical objects denote cucurbiturils).

shown to result in dendrimers with a solid-shell structure and a flexible core (41,42). The hydrogen bonding units were generated from the derivatization of the primary amino groups in PPI dendrimers with Boc-protected amino acids. Guests were incorporated inside the dendrimers while functionalizing the peripheral amino groups. Typical guest molecules used include 3-carboxy-PROXYL radical, erichrome black, and rose bengal. All these guest molecules contain carboxylic or sulfonic acid functionalities, which bind to the dendritic interior containing tertiary amines presumably through acid–base interactions. Note that the role of hydrogen-bonding periphery in these dendrimers is not to provide specific interactions with the guest molecules, but rather to provide a solid shell to trap the guest molecules. Meijer noted that size-selective release of the trapped guest molecules is possible by first deprotecting the Boc groups and then by hydrolyzing the amino acids from the dendrimer under rather harsh conditions (Fig. 12) (43,44).

Biomimetic Materials. The large structure of dendrimers and their globular shape has attracted significant attention because of its potential application as biomimetics, especially as enzyme mimics. The work by Aida and co-workers showed the function of dendrimers as a hemoglobin mimic (45). Aryl ether dendrimers were used to encapsulate iron(II)–porphyrin 1-methylimidazole complex (Fig. 13). The oxygen-binding ability of the complex increased with the dendrimer generation where the dioxygen molecule binds to the complex, instead of the μ-oxo-dimer formation observed for lower generations of the dendrimers. Another important result from this study was that the oxygenated complex was very stable toward carbon monoxide, which holds exciting possibilities in itself. However, in this work, the use of 1-methylimidazole apparently complicated the study of oxygen affinity measurements.

Interestingly, Collman and co-workers used 1,2-dimethylimidazole (dimim) which formed 1:1 high spin iron(II) adduct (Fig. 14) (46). It was found that the ratio of the two binding constants K_{CO}/K_{O2} of this complex was very low, as compared to T-state hemoglobin and the picket fence Fe(II)–dimim complex. The probable reason is that the bound dioxygen molecule formed hydrogen bonding with the amide NH-groups of the dendritic backbone used. The destabilization of the CO ligand was thought to be an unfavorable steric interaction between the CO and the dendritic branch. These results were further supported in a later publication, where the O_2 binding studies were performed (47). It was noted that the complexation of first and second generation of the amide-based dendrimers show efficient O_2 binding, whereas the control molecule without the amide bonds showed reduced stability for the dioxygen complex. Also for the first and second generation of the amide-based dendrimer, it was seen that in the presence of solvents like water, the oxygen affinity of these compounds decreased, clearly showing the effect of competing hydrogen bonding between water and the dendritic branches.

The emission properties of tryptophan (Trp) have been widely used in biophysical studies of proteins. Recently, Smith and Müller used Trp to probe the dendritic microenvironment by attaching the amino acid to polyether dendrimers and studying their fluorescence spectra (Fig. 15) (48). It was observed that in the presence of non-hydrogen-bonding solvents, the dendritic effect (shift of λ_{max}) was profound. The argument was that in presence of non-hydrogen bonding solvents, there was effective hydrogen-bonding interaction between the amide H-atom of

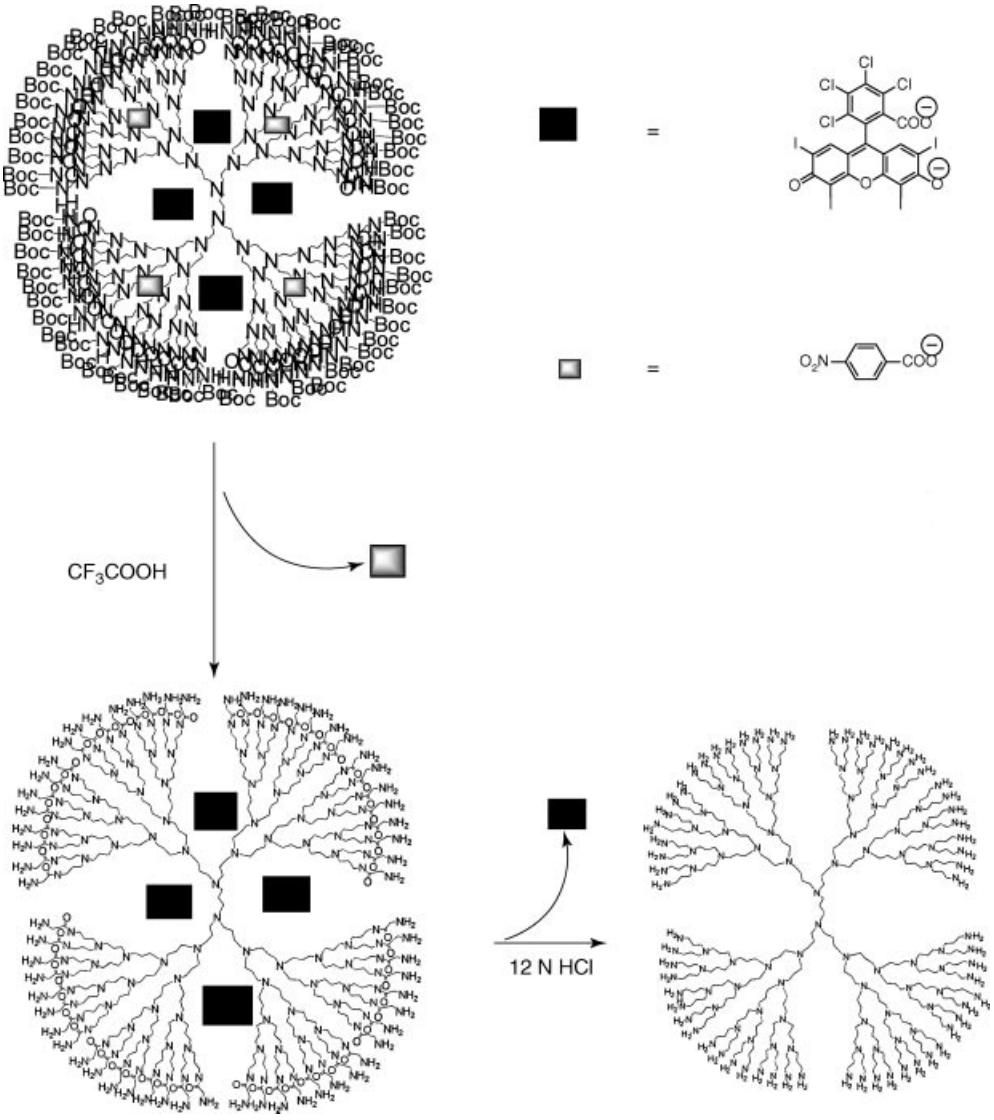

Fig. 12. Dendritic box and selective guest release.

Trp and the carbonyl groups of the dendrimer, which leads to the shift in the emission spectra. It was seen that the hydrogen bond acceptor solvents do not change the character of the spectra much, which is understandable. Also, the hydrogen bond donor–acceptor solvents showed negative dendritic effect owing to the competition faced by the Trp, from the solvents. It was proposed that strong hydrogen bonding between the Trp and dendritic branch resulted in a change of the polarity of Trp's microenvironment, resulting in an emission shift. This proposal was further supported in a later publication where they took Trp along with another compound where the —NH group of the indole ring has been changed to N—Me (49). No dendritic effect was observed in this case.

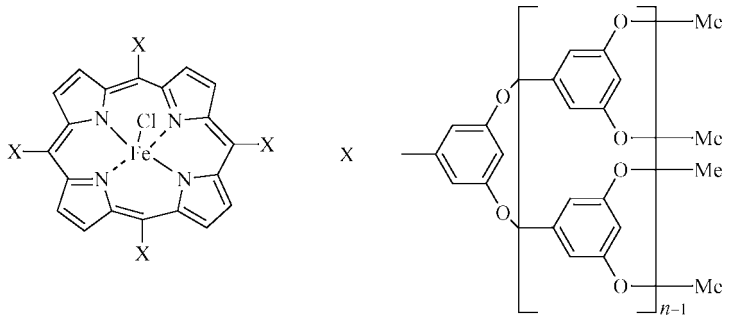

Fig. 13. Porphyrin dendrimer with oxygen-binding ability.

Parquette and Huang showed that the hydrogen-bonding effects within the dendritic interior could result in a particular helical bias in a dendrimer, and that the chirality can be transferred from the core to the periphery. Working with pyridine-2,6-dicarboxamide, they first showed the synthesis and characterization of dendrimers whose conformations at different levels are somewhat restricted because of intramolecular hydrogen bonding (Fig. 16) (50). The stability of helical secondary structure in these dendrimers is dramatically enhanced by linking each generational shell through an anthranilamide turn unit (51). Circular dichroism studies on these intramolecularly hydrogen-bonded dendrimers revealed that the interconversion between the two diastereomeric helical conformations (M and P helices) relating a pair of anthranilamide termini depends on solvent, temperature, and dendrimer generation (52). More recently, they have shown that the compaction levels of these dendrimers can be modified by varying the linkers in the central core of the dendrimer (53).

Sensors. An obvious application of molecular recognition is in the area of sensory materials. Several aspects described above can be exploited to generate sensors. There have been a particular interest in anion sensing with dendritic structures. Significant contributions in this field have been made independently by Astruc and Kaifer. Astruc and co-workers studied the binding effect of several anions, including HSO_4^-, $H_2PO_4^-$, and Cl^-, on different dendrimer generations (54). The dendritic effect was most pronounced with $H_2PO_4^-$ anions. Using polyamido ferrocene dendrimers, they showed that with increase in generations, the $E_{1/2}$ value for ferrocene wave increased with the addition of the $H_2PO_4^-$ anions (Fig. 17). It was proposed that the $H_2PO_4^-$ anion interacts with the dendrimers via a synergy between electrostatic and hydrogen-bonding interactions. The fact that more $H_2PO_4^-$ anions are needed for higher generations of dendrimer was taken to suggest that the $H_2PO_4^-$ units are interacting with the amide moieties present in the dendritic backbone. The sensory effect was maximum for the dendrimer with 18 ferrocene units, indicating that the steric factors become important in larger generations. This work was extended further by attaching AB3 phenol units *p*-OH—$C_6H_4C(CH_2CH{=}CH_2)_3$ and *p*-OH—$C_6H_4C[(CH_2)_3SiMe_2{-}CH_2NHCOFc]_3$, with different generations of polypropyleneimine dendrimers (55). The molecules here were assembled by hydrogen bonding. The characterization by cyclic voltammetry (CV) and NMR methods proved that the

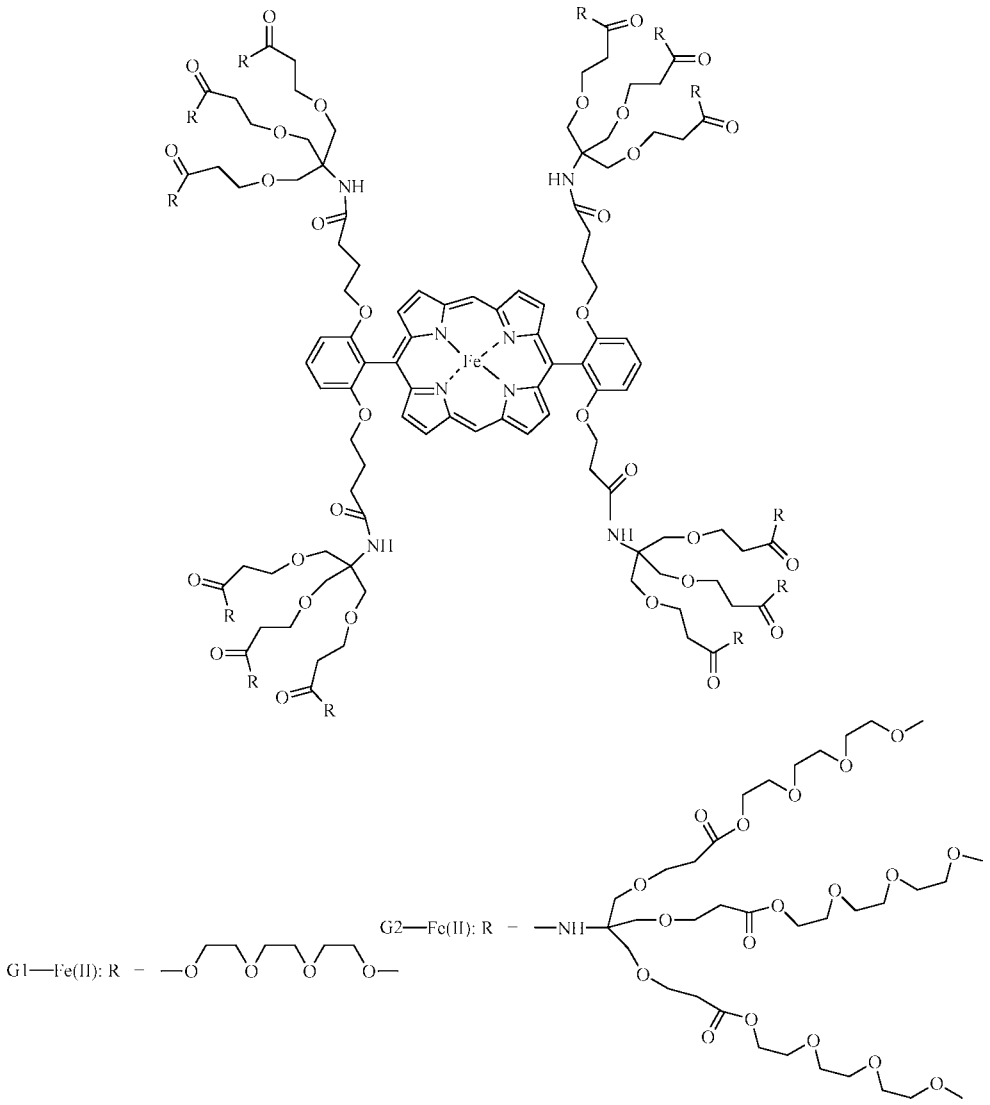

Fig. 14. Iron–porphyrin dendrimer by Collman and Diederich.

sudden wave changes, alterations of half stoichiometry, and decrease of peak intensity in CV are all affected by dendrimer generations. On a similar note, Kaifer and co-workers showed that similar hydrogen-bonding-mediated anion sensing can be performed via ferrocenyl urea dendrimers (56). The results here are significant since all the studies were done in DMSO, where the competing solvent effects would seem to make the anion sensing less feasible.

Dendrimer Assemblies. Supramolecular assembly is not a new area of research and chemists have been involved in this field for a long time. However, controlled assembly of well-defined macromolecules is often seen only in nature. Dendrimers are ideal scaffolds as artificial proteins and enzyme mimics, since

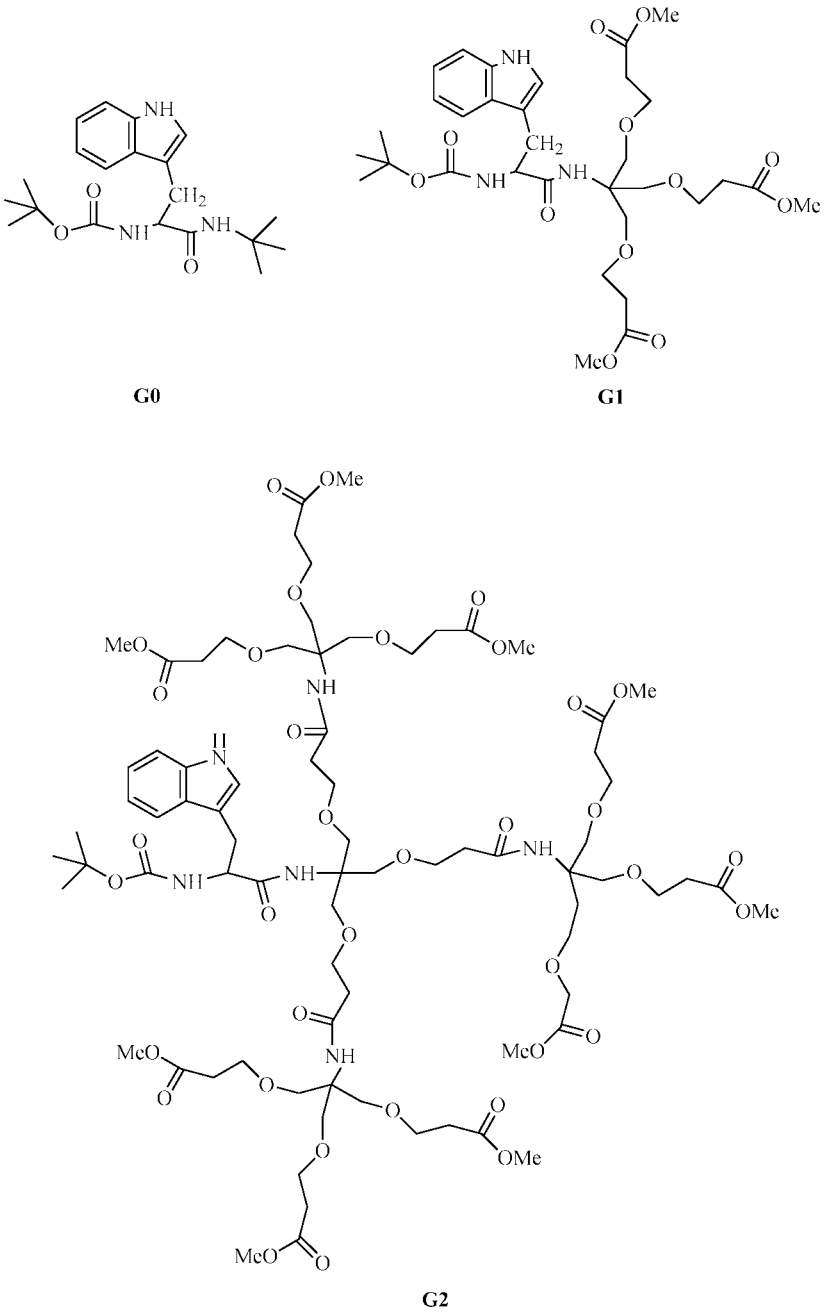

Fig. 15. Tryptophan dendrimers.

they have large molecular weights, are monodisperse, and are easy to functionally manipulate. Zimmerman showed that hydrogen-bonding-mediated assembly of didendrons can be achieved by complexing monodendrons with a 1,9,10-anthyridine core and ditopic complementary guest molecule (Fig. 18). A 2:1 complex was

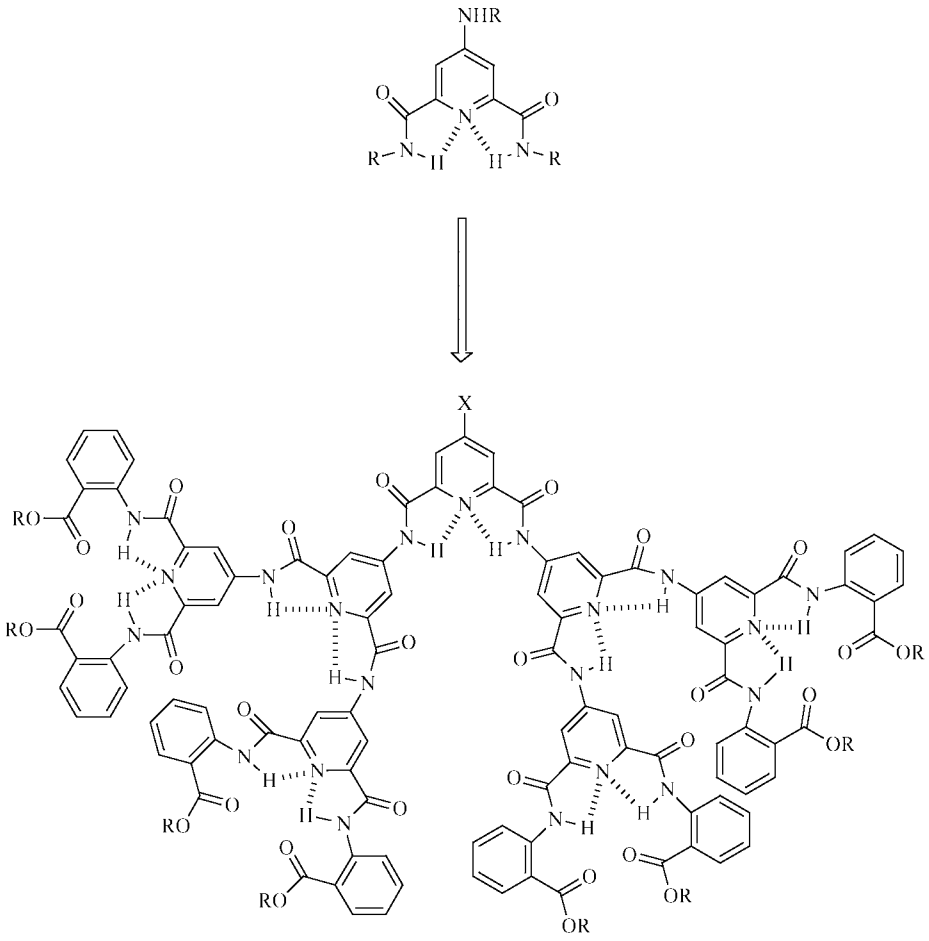

Fig. 16. Dendrimers with helical bias due to intramolecular hydrogen bonding.

observed between the anthyridine core with three hydrogen bond acceptor functionalities (AAA) and guest molecules containing benzamidine groups with two hydrogen bond donor abilities (DD). High association constants were observed between these complementary hydrogen-bonding motifs. A small molecule containing two benzamidine group was used to assemble two dendrons containing the naphthyridine core (57).

Similarly, Smith and co-workers showed the scope of dendritic assembly through the interaction between a crown-ether core and divalent ammonium ions (58). Lysine-based dendrons were built with crown ethers at the focal point. These dendrons assembled into didendrons upon a 2:1 binding with a guest molecule containing two ammonium moieties. This supramolecular assembly of dendrons was easily dislodged using K^+ ions, as the latter competes for the crown ether (Fig. 19). In a later publication, the same group reported the supramolecular assembly of the similar dendrimers based on aliphatic diamines (59). The two-component gel-phase materials reported here are attributed to the length

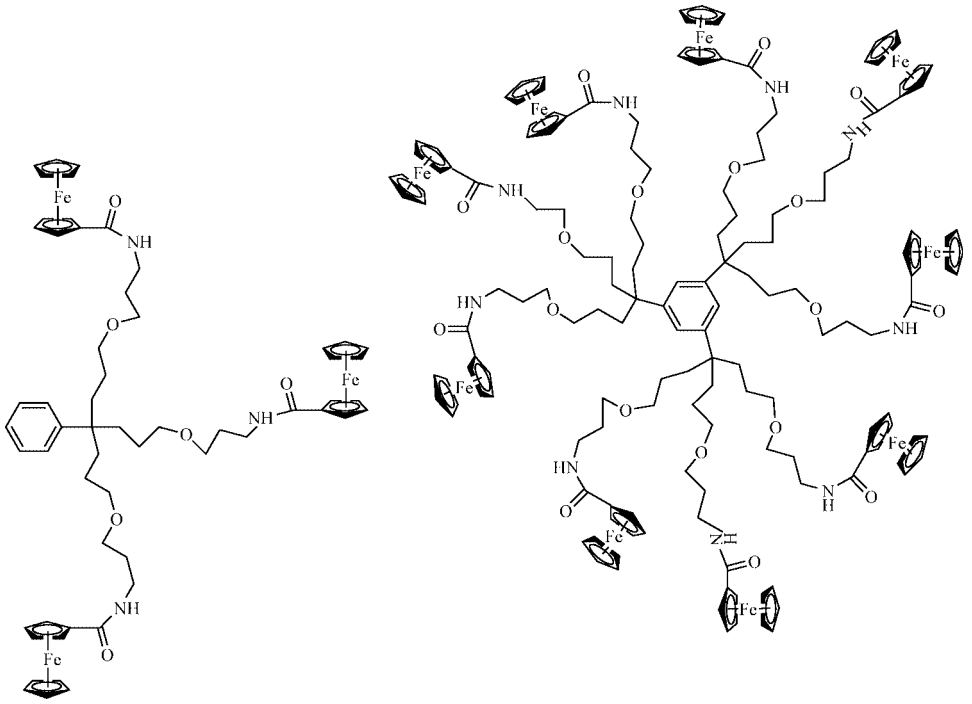

Fig. 17. Anion sensing ferrocene dendrimers.

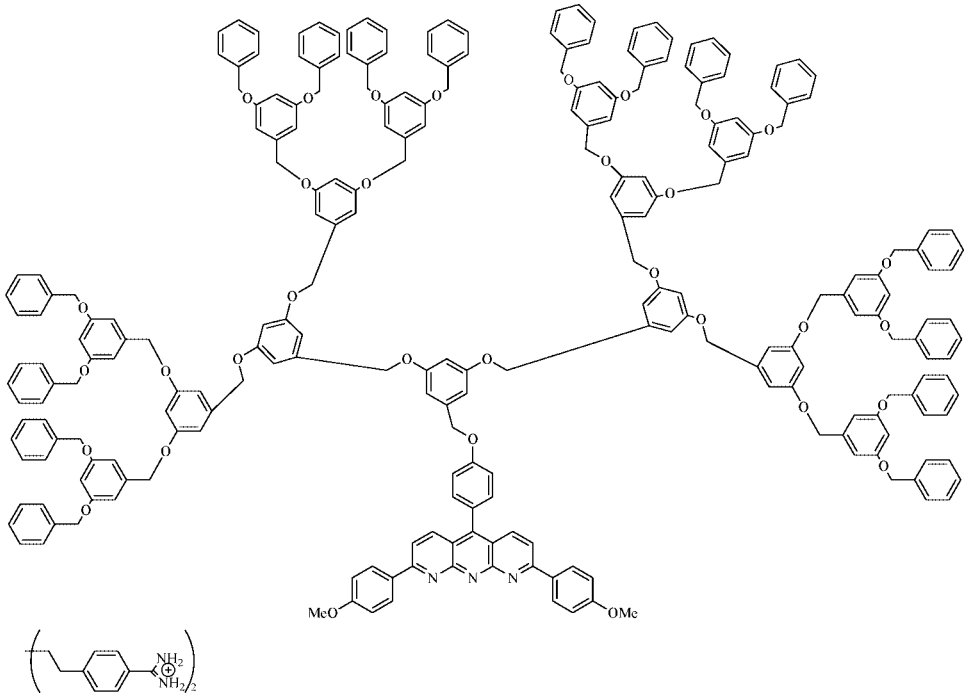

Fig. 18. Dendron with the DDD motif and the complementary guest.

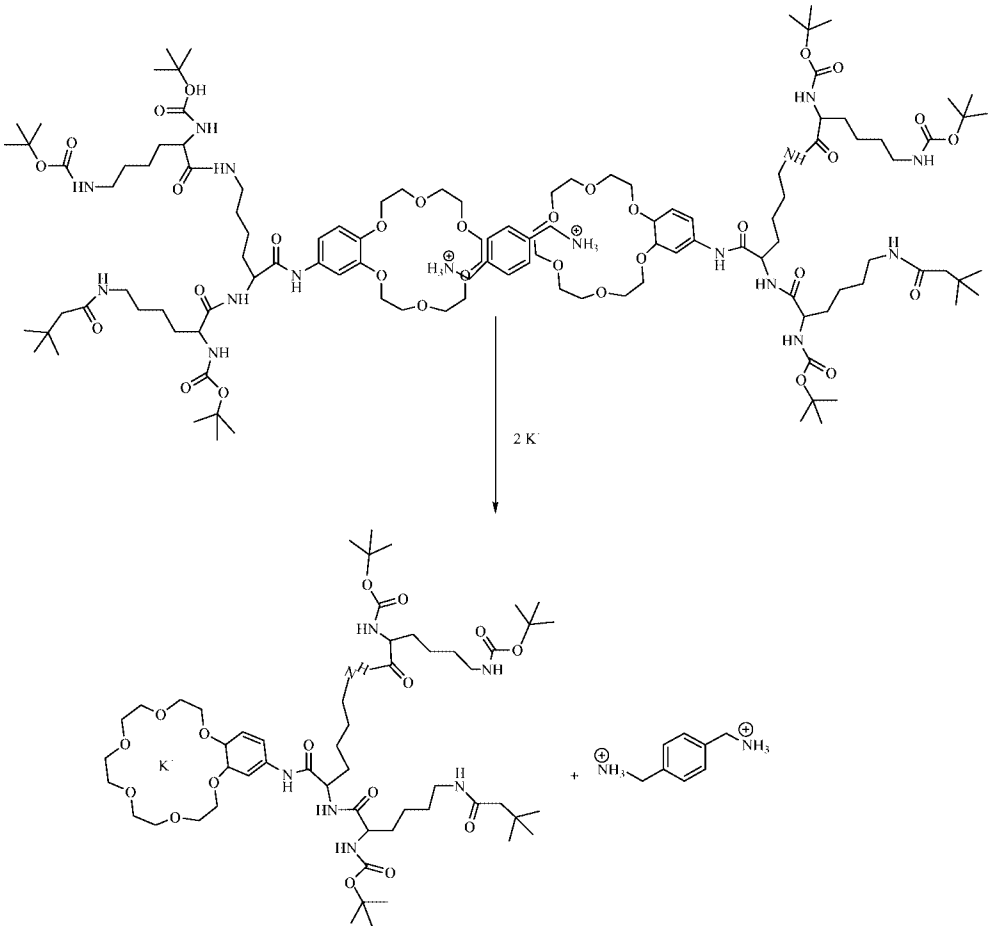

Fig. 19. Deaggregation of crown-cored dendrons.

of the hydrophobic spacer and the potential hydrogen-bonding units within the amino acid branches. Similarly, Gibson reported a tritopic $R_2NH_2^+$ moiety, which exhibited the ability to assemble dendrons cooperatively (60,61).

Another interesting dendrimeric assembly strategy was shown by Stoddart and co-workers, where they introduced the concept of mechanically interlocked branching units in the dendrimer (62,63). Here the dendrons are attached to particular components, which are involved in mechanical bonding with catenanes or rotaxanes. A bis-dibenzo[24]crown-8 core was attached to $R_2NH_2^+$ type compound, where R is a benzylic group. The association constant for those assemblies was found to be quite high. After association, benzyl ether dendrimers were attached while maintaining the association in good yield (Fig. 20). Stoddart also reported a similar assembly of dendrimers by a slippage methodology (64).

Assemblies higher than dimeric and trimeric ones have also been reported with dendrimers. Zimmerman attached benzyl ether dendrimers to a core containing two-isophthalic acid units (65). The self-complementary nature of carboxylic acids is expected to provide either a polymeric or a hexameric aggregate

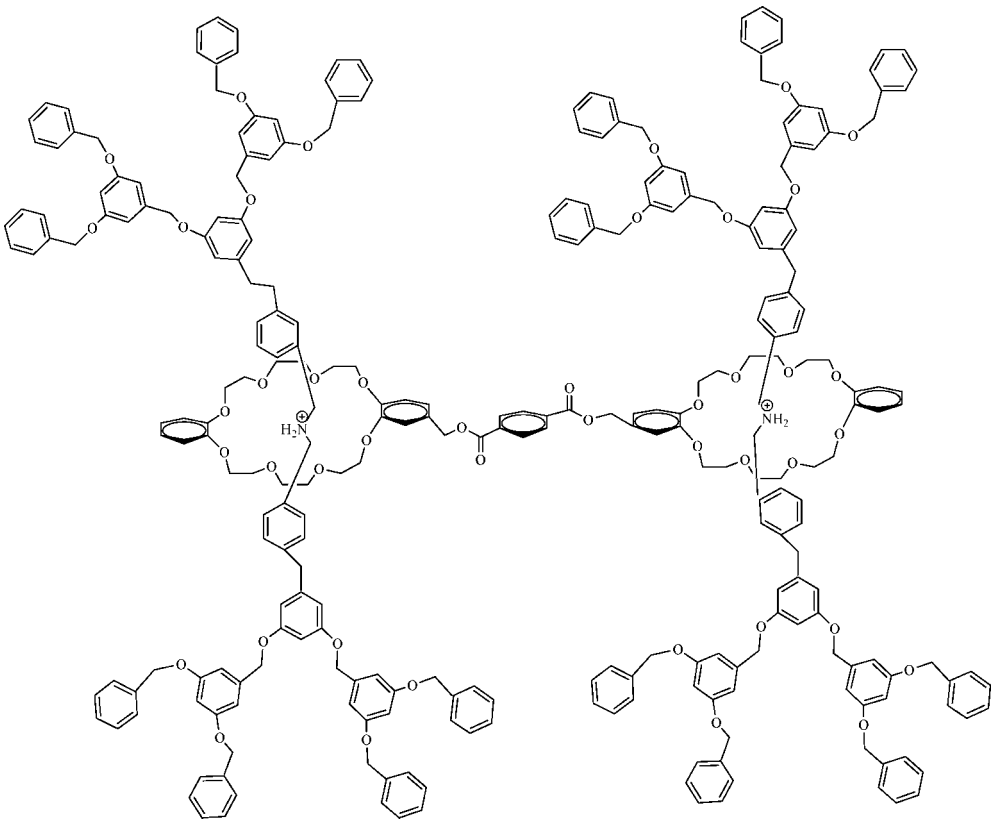

Fig. 20. Dendrimers with mechanical branching.

via hydrogen bonding (Fig. 21). The SEC and NMR data showed the hexameric structure to be predominant. An advantage for the hexamer aggregation was the subtle interplay between favorable hydrogen bonding and van der Waal's interaction, and the unfavorable steric interactions between the adjacent dendrimers in competing aggregates. The hexameric aggregate structure was further supported by SANS (small-angle neutron scattering) studies (66).

The hexameric assembly based on carboxylic acid moieties mentioned above exhibited low stability in moderately competitive solvents like THF. Also, only certain generations of dendrimers (G2 and G3) formed hexameric aggregates, while G1 did not form any stable hexameric assembly. Keeping this in mind and also the fact that nature has chosen heterocycles to form hydrogen bonds in nucleic acids, Zimmerman and Kolotuchin synthesized and characterized a new molecule capable of forming hexameric assemblies (Fig. 22) (67). This compound formed hexameric aggregates and were stable in dilute THF solutions. Encouraged by this result, they attached different generation dendrons to this species and characterized the assemblies (68). From NMR titration data, it was shown that the stability of the hexameric assemblies was (A)6-G1 > (A)6-G2 > (A)6-G3. Also when (A)6-G1 and (A)6-G3 were mixed together, they formed one structure out of about 13 possible structures. This indicated that the discrete aggregates were

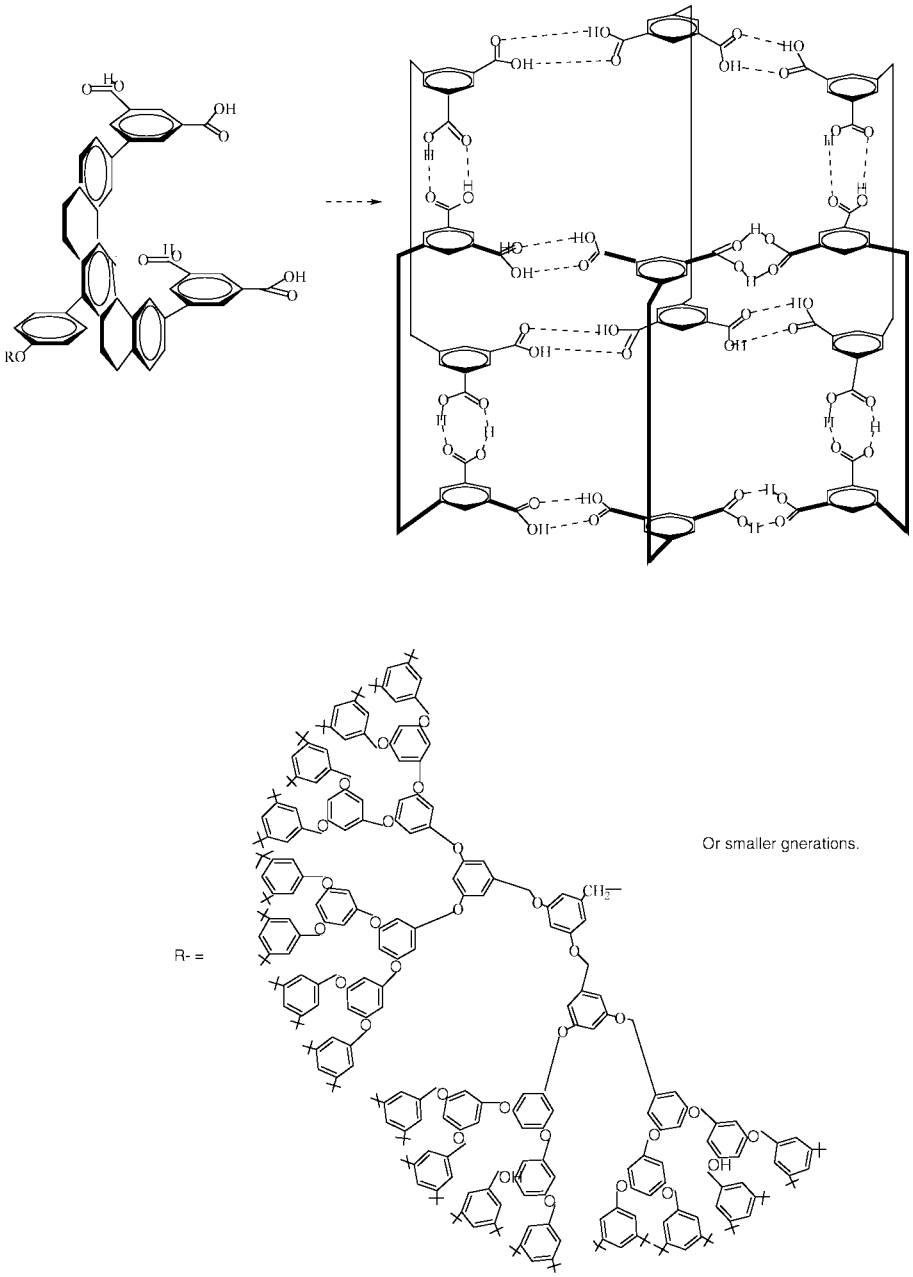

Fig. 21. Carboxylic acid based hexameric dendrimer assembly.

self-selected, and one can play with the supramolecular structures by making subtle variations in different parameters like temperature, solvent, and steric effects (69). Even higher order assemblies using liquid crystalline dendrimers have been achieved by the elegant work of Percec and co-workers (70,71). Discussion of those structures is beyond the scope of this review. Similarly, dendrimers also have been

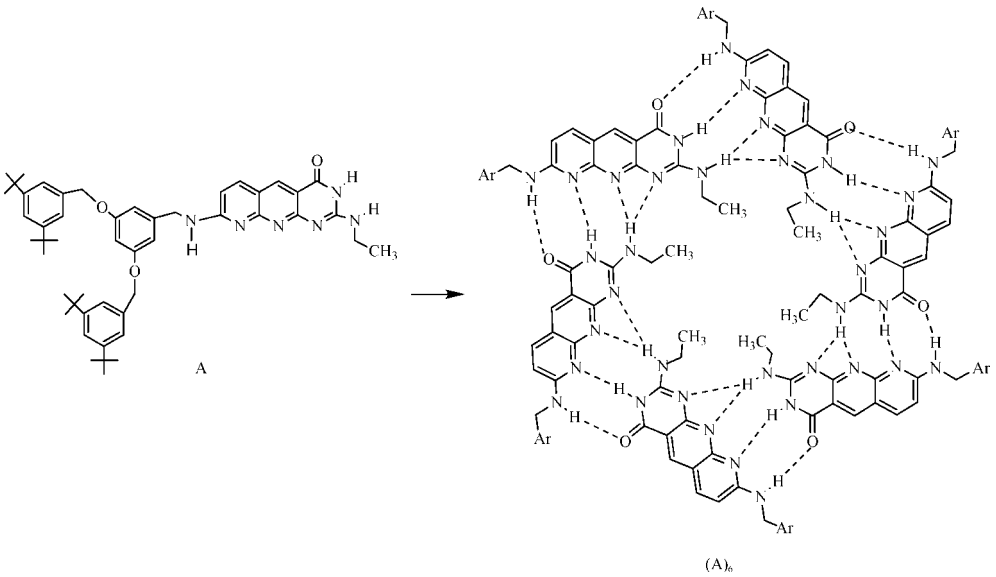

Fig. 22. Stable hexameric assemblies designed by Zimmerman.

shown to form hydrogen-bonding-based network assemblies with themselves or with other polymers, the discussion of which is not included in this article (72–77).

Host–Guest Interaction Based on Amphiphilicity

The globular nature of dendrimers at high generations provides significant opportunities for dendrimers to be used as hosts in a variety of ways. One of the most prominent interactions involves the formation of dendrimers with micellar or inverse-micellar characteristics. In this section, we will discuss host–guest interactions based on hydrophobic or solvophobic pressure. We will also discuss binding based on ionic attractions including acid–base interactions within this section, since these have been used along with amphiphilicity to enhance binding in several cases.

Dendrimers as Micelles. In their seminal work, Newkome and coworkers designed and synthesized a dendrimer called micellanoic acid with an all-hydrocarbon interior and carboxylic acid periphery (Fig. 23) (78). They showed that these dendrimers are water-soluble and are capable of sequestering hydrophobic substituents in their interior. The guest molecules include spectral probes such as phenol blue, naphthalene, pinacyanol chloride, and diphenylhexatriene. By comparison with classical amphiphiles such as SDS, it was shown that the critical micelle concentration (cmc) of these dendrimers is very low. Therefore, they called these dendrimers as unimolecular micelles (79). Binding abilities of some of these amphiphilic dendrimers have also been investigated using electrokinetic chromatography and electrochemistry (80–83).

Similarly, amphiphilic dendrimers with carboxylic acid peripheral groups and benzyl ether interior were synthesized by Fréchet and co-workers (Fig. 24)

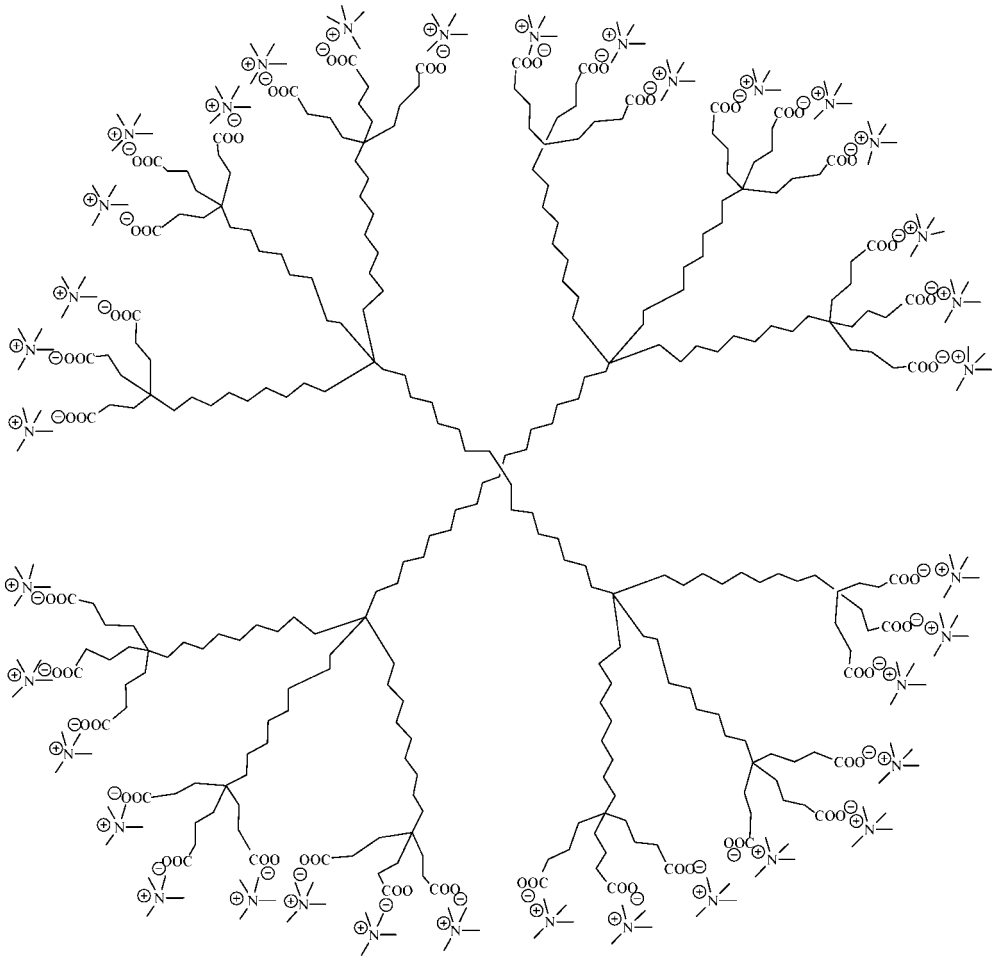

Fig. 23. Structure of micellanoic acid.

(84). The carboxylate salts of these dendrimers are water-soluble and are capable of sequestering apolar guest molecules, such as pyrene. Spectral analysis indicated that about 0.45 molecules of pyrene was found per dendrimer. Fréchet also demonstrated that this could be increased to 0.7 molecule of pyrene per dendrimer by increasing the ionic strength of the solvent. This is a significant number and is comparable to classical micelles based on small molecule amphiphiles. The cmc values for these dendrimers seem to be nonexistent or below the detectable limits, reiterating the ability of dendrimers to function as unimolecular micelles. These dendrimers also demonstrated the ability to act as recyclable solubilizing agents.

Kraska and Seyferth synthesized water-soluble carbosilane dendrimers based on simple hydrosilation and alkylation reactions (19). The sulfonate-terminated and tetralkylammonium-terminated amphiphilic dendrimers have been shown to act as micelles. These dendrimers are capable of sequestering alkyl benzenes (toluene, ethyl benzene, or propyl benzene). It was estimated that a

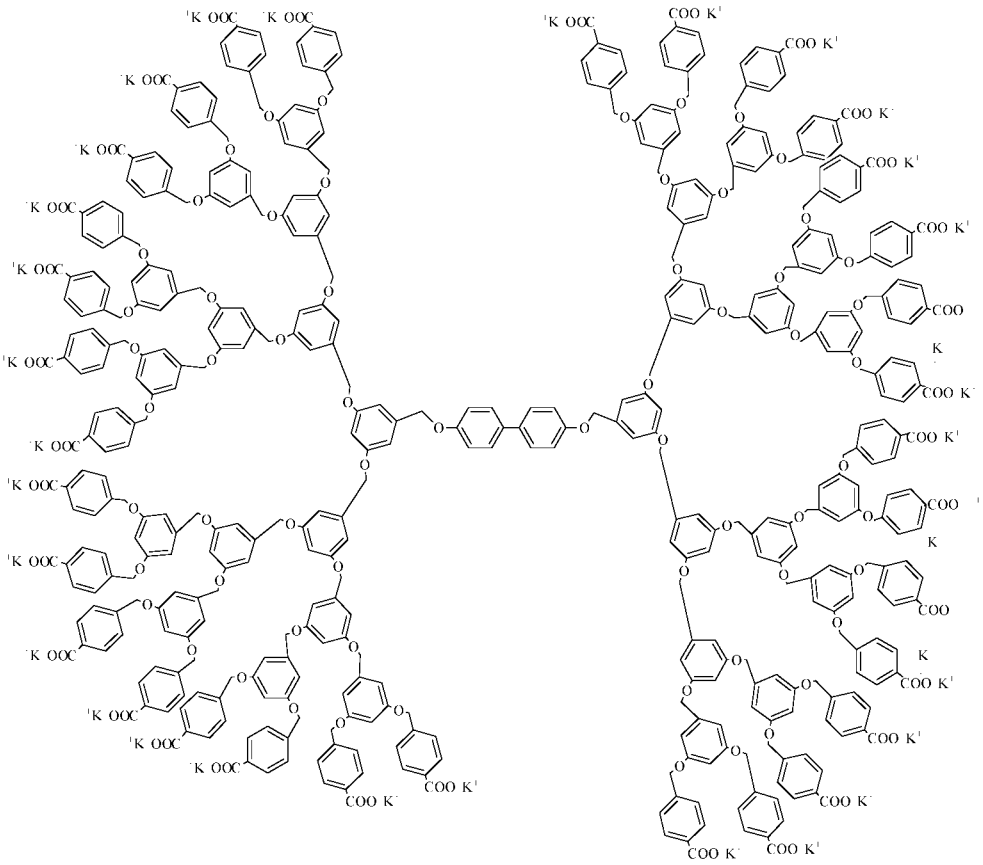

Fig. 24. Structure of micellar benzyl ether dendrimer.

second-generation dendrimer with 16 sulfonate groups in the periphery was able to sequester about two to three alkyl benzene molecules in its interior.

Turro and co-workers studied amphiphilic PAMAM dendrimers with different alkyl chain lengths at their core (85). Specifically, diamino derivatives of ethane, butane, octane, and dodecane were studied. The amino groups were placed at the terminal carbons of these *n*-alkanes. The ability of these dendrimers to sequester hydrophobic derivatives was studied by using Nile red as the guest molecule. They observed that the sequestering ability depends both on the dendrimer generation and the length of the alkyl chain in the core. They were able to demonstrate that the dye molecule is bound closer to the alkyl chain at the core, in case of long alkyl chains. It was also shown that the ability of the dendrimers to sequester apolar guest molecules is enhanced by adding a surfactant to the aqueous solution of the dendrimer. The location of the dye molecule in this case also depends on the length of the alkyl chain at the core, as shown in Figure 25. Note that the ability to generate both amine-terminated and carboxylic-terminated PAMAM dendrimers render them capable of sequestering guest molecules based on ionic interactions. This capability has been exploited by the research groups of Turro and Tomalia (86,87).

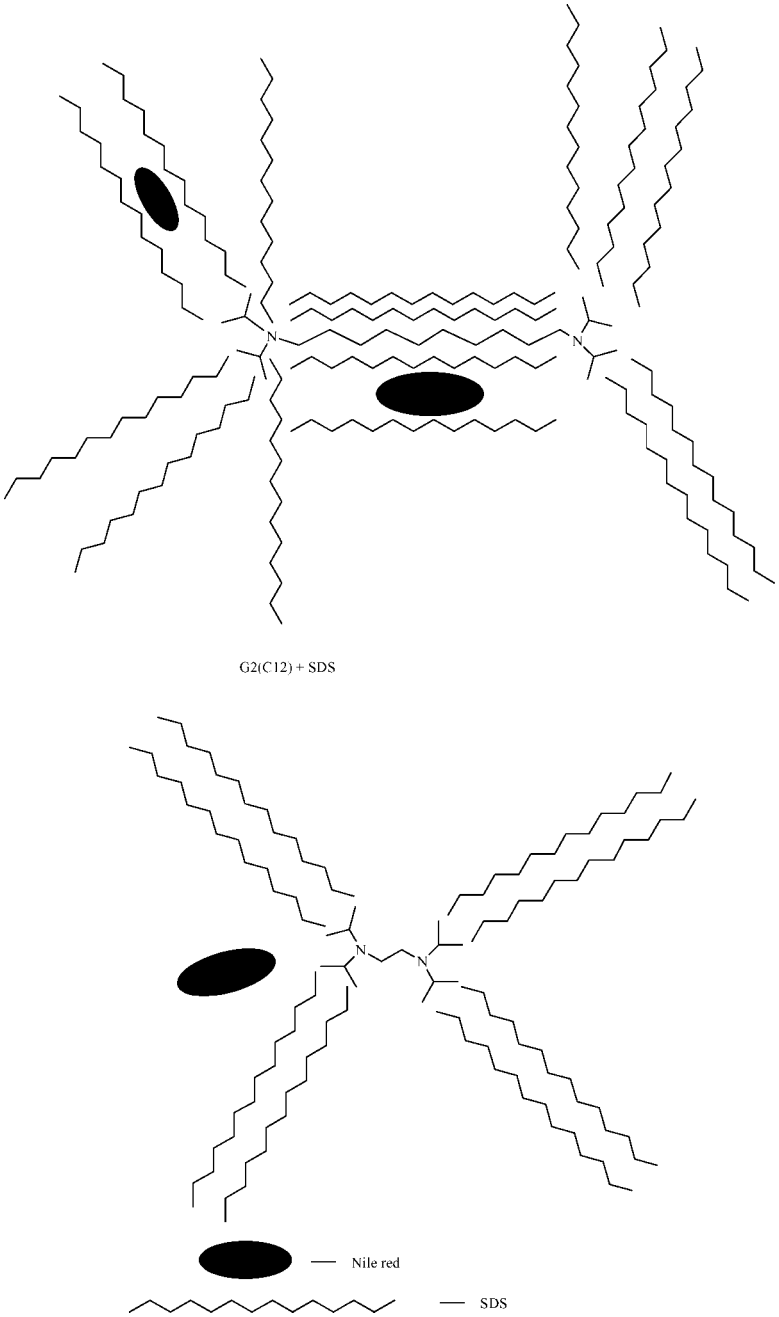

Fig. 25. Location of the dye in amphiphilic PAMAM dendrimers and surfactant mixture.

An interesting variation to the amphiphilic dendrimers shown above was synthesized by Pan and Ford (88,89). PPI dendrimers were derivatized at their periphery with both alkyl chains and triethyleneglycol monomethyl ether (TEG) moieties (Fig. 26). They observed that these dendrimers are not soluble in water,

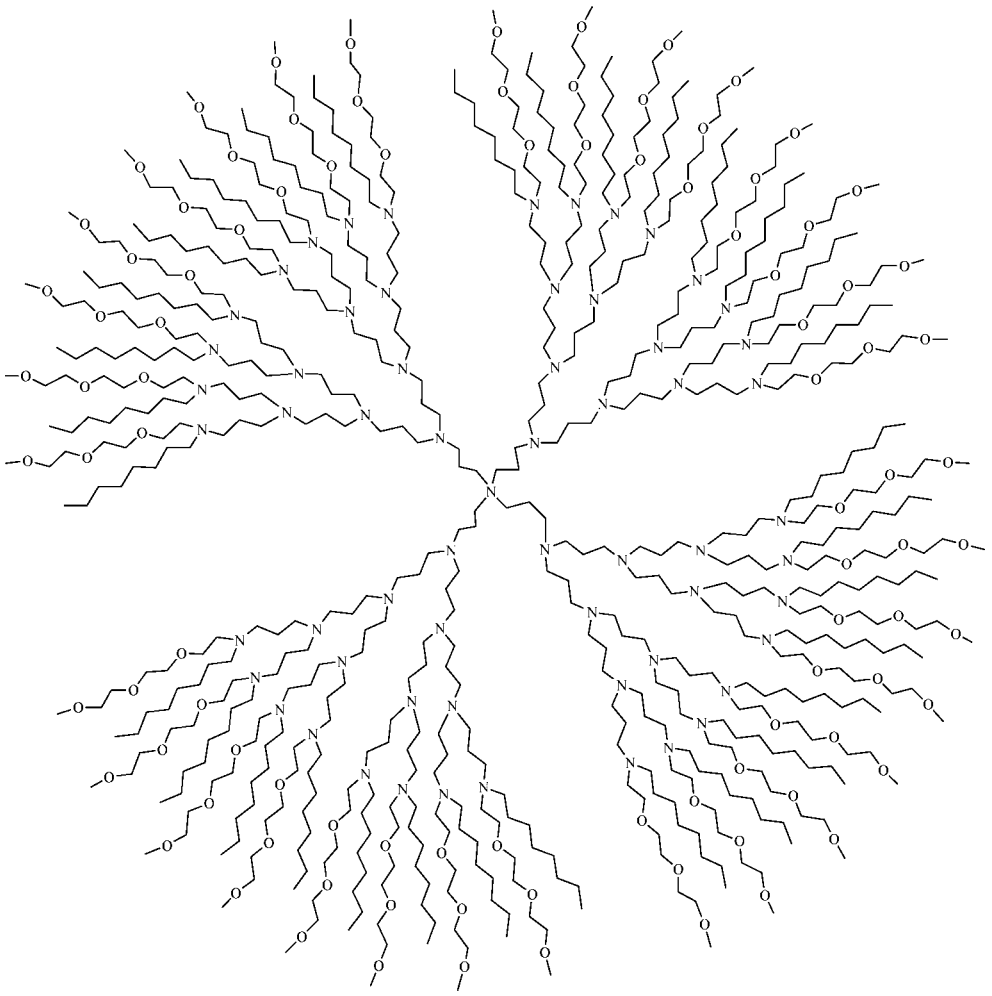

Fig. 26. Structure of amphiphilically modified peripheries designed by Ford.

surprisingly even at low pH. However, they were able to render these dendrimers soluble in water by further derivatizing these dendrimers into quaternary ammonium salts. Aqueous solutions of these dendrimers were able to accommodate apolar guests such as pyrene or Reichardt's dye. Furthermore, these dendrimers also exhibited the ability to catalyze the decarboxylation reaction of 6-nitrobenzoisoxazole-3-carboxylate ion. A rate increase of 200–500 times was observed in the presence of the dendrimer, compared to the rate of the reaction in pure water.

In proteins, almost all the side chains of hydrophobic amino acids are directed toward the interiors in globular proteins. Similarly, the hydrophilic amino acid side chains are directed toward the exterior of these proteins with significant consistency. These biomacromolecules can therefore be also considered as unimolecular micelles as well. Noting this structural theme in proteins, it is clear that an important structural requirement that will further enhance dendrimers' repertoire

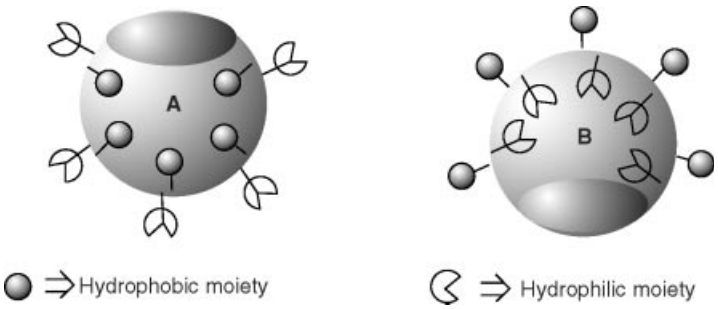

Fig. 27. The possible conformations (**A** and **B**) of the amphiphilic dendrimer in polar and apolar solvents respectively.

in this arena involves the ability to selectively functionalize the concave interiors of these macromolecules, ie, selectively direct functional groups toward the interior of the globular dendrimer. A flexible backbone is a prerequisite to obtain globular shape at high generations. Attaining conformational control over the orientation of the functional groups is nontrivial, when the molecules are built with flexible linkers. Thayumanavan and co-workers proposed an approach to achieve control over functional group orientation by rendering the macromolecules facially amphiphilic (90). In this design, the dendrimers are uniformly amphiphilic over the entire globular surface; that is, when the convex face of the dendrimer is hydrophilic, the concave face will be hydrophobic and vice versa. The nature of the functional groups directed toward the concave interior of the dendrimer will be driven by solvophobic interactions. In this design, the inherent flexibility of the dendritic backbone can be expected to yield the different solvent-dependent conformations 27**A** and 27**B**, as shown in Figure 27.

The monomer design involves a unit that has the AB_2 functional groups for the dendrimer growth and the amphiphilic functional groups in orthogonal planes (Fig. 28). The amphiphilic substituents are placed on opposite sides of the plane containing the AB_2 moieties. Such relative placement of the functional groups dictates that the amphiphilic moieties are in a plane perpendicular to that of the macromolecular backbone upon assembly of the dendrimer. The geometric arrangement of the dendrimer also dictates that the hydrophobic and the hydrophilic functionalities are in opposite faces of the globular dendrimer, and thus the structures 27**A** and 27**B** should result (Figs. 27 and 28). A monomer unit that satisfies these structural requirements is represented by the biphenyl molecule shown in Figure 28, in which the hydrophilic unit is a TEG moiety and the hydrophobic unit is an *n*-butyl group. Synthesis of dendrons up to the fourth generation has been reported. However, solubility problems hampered the studies that would support the structural hypothesis proposed. Experiments are under way to modify the functional groups and render the dendrimers soluble in both polar and apolar solvents.

In addition to utilizing dendrimers themselves as micelles, there have been several reports on utilizing block-*co*-polymers containing a hydrophilic linear polymer and a hydrophobic dendrimer. These studies are not included in this review. We recommend some key references in this area for an interested reader (91–104).

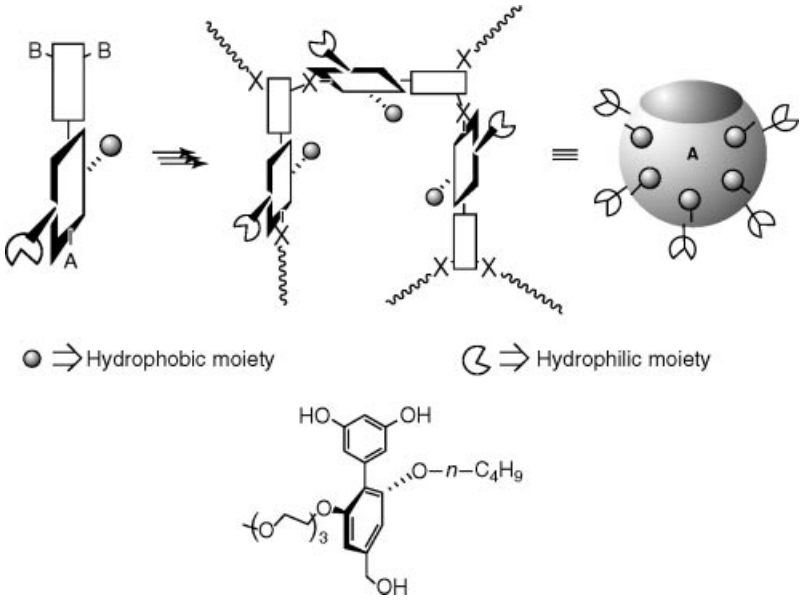

Fig. 28. Cartoon of the AB_2 monomer with the amphiphilic groups on the orthogonal plane, the dendrimer growth, and its conformation in a hydrophilic solvent is represented.

Biomimetic Dendritic Amphiphiles. The active sites of globular proteins are often buried in their hydrophobic binding pockets. Inspired by globular proteins, Diederich has developed a class of dendrimers called dendrophanes (105). These are dendrimers that contain a hydrophobic cyclophane cavity and polar peripheral functionalities. Diederich showed that the size of the guest molecules that could be accommodated in these hydrophobic cavities depend on the size of the cyclophane core. Two different cyclophanes were reported; one that is capable of binding benzene and naphthalene guests and a larger one that is capable of binding large steroidal substrates (106,107). Guest molecules were shown to be bound specifically at the cyclophane core and the nonspecific binding, if any, is negligible. The binding constants were found to be independent of the dendrimer generation. The micropolarity of the cyclophane core is significantly reduced and is comparable to ethanol. The exchange kinetics of the host–guest binding events were found to be fast. The combination of these properties led to the idea of developing these molecules into possible artificial globular enzymes. In order to mimic the enzyme pyruvate oxidase, Diederich and co-workers incorporated thiazolium ions into the cyclophanes and studied the catalytic ability of these compounds in the oxidation of naphthalene-2-carboxyaldehyde to naphthalene-2-carboxylate (Fig. 29) (108). The observed acceleration of the reaction was attributed to both the reduced polarity in the dendritic interior and fast exchange rates.

More recently, Hecht and Fréchet have synthesized an amphiphilic dendrimer that is capable of acting as a photoreactor to catalyze a cycloaddition reaction between cyclopentadiene and singlet oxygen (109). In this case, an apolar functionality capable of sensitizing singlet oxygen (benzophenone) was attached to dendrons containing hydrophilic peripheral groups. The cyclopentadiene

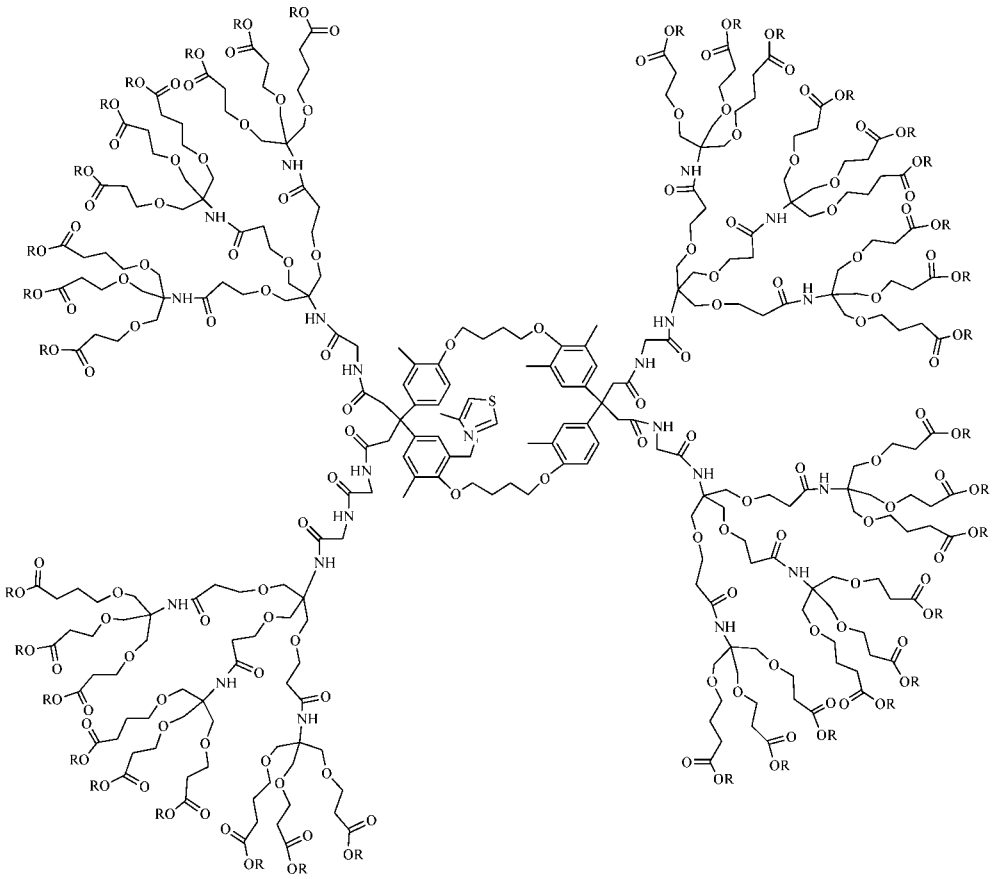

Fig. 29. Structure of the dendritic enzyme.

substrate was concentrated closer to the benzophenone core owing to the relatively apolar nature of the core. Since the singlet oxygen is also generated near the benzophenone core, the dendrimer was able to serve as a nanoreactor for this reaction (Fig. 30).

Dendrimers as Inverted Micelles. The inherently polar building blocks of PAMAM and poly(propylene imine) dendrimers make these molecules attractive candidates for the creation of unimolecular inverted micelles. Meijer modified the PPI dendrimers with apolar end groups such as the palmitoyl chains and studied the inverted micellar character of these dendrimers (Fig. 31) (110,111). These dendrimers are capable of sequestering anionic guest molecules from aqueous solutions. The binding process is attributed to the combination of hydrophobic effect, hydrogen bonding, and ionic interactions. It was also noted that the efficiency of binding is dependent on pH and were better at lower pH. It is also interesting to note that these dendrimers exhibited significant selectivity in the sequestration of guest molecules from the aqueous solution. For example, a fifth-generation dendrimer was able to extract only 1 or 2 molecules of fluorescein, whereas the same host was able to extract about 50 molecules of rose bengal. This selectivity is

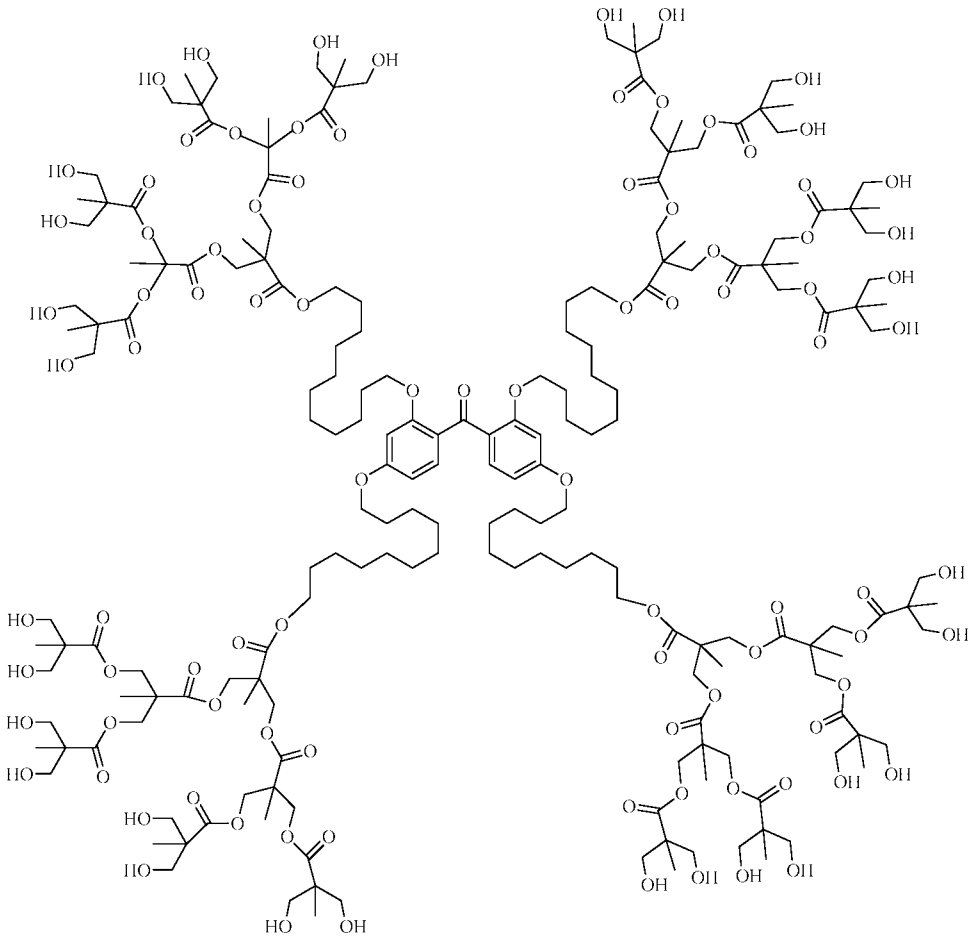

Fig. 30. Structure of the dendrimer with a singlet oxygen sensitizing core.

magnified in an experiment where it was demonstrated that even at pH 10, the dendrimer was able to selectively extract rose bengal out of a mixture containing a 10,000:1 ratio of fluorescein to rose bengal. Meijer also utilized PPI dendrimers that are modified with oligo(*p*-phenylenevinylenes) as the peripheral apolar functionality to study energy transfer in supramolecular assemblies containing the dendrimer host and an anionic dye molecule as the guest (112). Similarly, Balzani and Vögtle have shown that PPI dendrimers functionalized with dansyl groups in their periphery can extract eosin red from aqueous solutions into the organic layer (113,114). When dendrimers are functionalized with fluorocarbon chains at their periphery, these macromolecules were soluble in supercritical carbon dioxide and fluorocarbon solvents and were capable of solubilizing polar substrates in these solvents (115,116). This is of considerable significance, since this process could have implications in environmentally benign catalytic processes.

Tomalia and co-workers reported the hydrophobic modification of PAMAM dendrimers by treating the terminal primary amines with various epoxyalkanes (117). Similar to the PPI dendrimers reported above, these dendrimers also

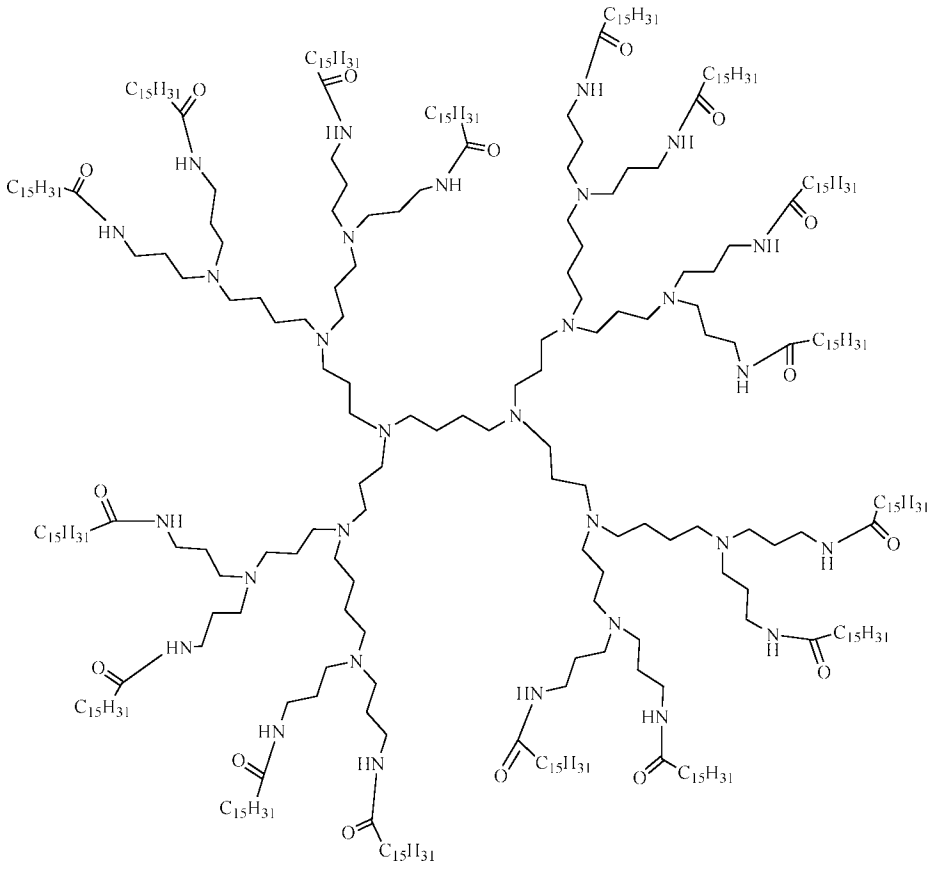

Fig. 31. Inverted micelles based on poly(propylene imine) dendrimer.

exhibited the inverted micelle properties that are capable of sequestering polar guest molecules. More specifically, Tomalia showed that these dendrimers are capable of transporting copper(II) ions from an aqueous solution into an organic phase.

An elegant experiment by Crooks showed that the hydrophobic modification of PAMAM dendrimers by noncovalent interactions could also result in macromolecules that behave like inverted micelles (118). The spontaneous assembly between the fatty acids and amino periphery of the PAMAM dendrimer was driven by ionic interactions (Fig. 32). These dendrimers were shown to be capable of extracting hydrophilic dyes such as methyl orange from water into toluene. Similarly, these dendrimers were also shown to be excellent molecular containers for catalytically active metal nanoparticles. The inverted micellar nature of various dendrimers have been used by Crooks and others for the preparation of a variety of nanoparticles (119–122). A related macromolecule, but an architecture with less of a control, is a hyperbranched polymer. Hydrophobically modified hyperbranched polymers have also been shown to be capable of acting as inverted micelles (123,124).

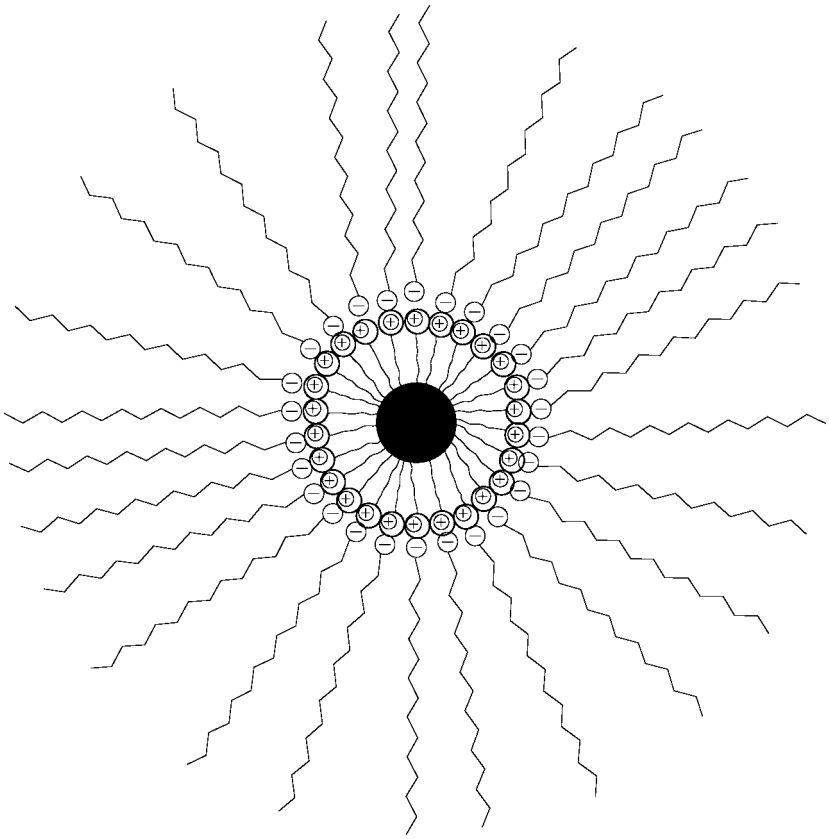

Fig. 32. Supramolecular assembly of inverted micelles by Crooks.

Binding at the Dendritic Periphery. Dendrimers with ferrocene substitutions at their periphery have been synthesized to achieve new electrochemical sensors for anions such as $H_2PO_4^-$ (54–56,125). These ferrocene dendrimers are often insoluble in aqueous media. However, if the peripheral ferrocenes are efficiently complexed with cyclodextrins, the resultant complex can be rendered water-soluble (Fig. 33). Kaifer and co-workers were able to demonstrate that such complexes are indeed more soluble (126). They also noted that the solubility depends on the efficiency of complexation, which decreased with increasing generation possibly because of steric crowding. Since the binding of ferrocene with cyclodextrin is based on the hydrophobic effect, there is a significant difference in binding between ferrocene and ferrocenium ions. The weaker binding of ferrocenium ions provides the opportunity to release these complexes with electrochemical control. Similarly, the difference in association constants between cobaltocenium ion and cabaltocene provides a system in which the binding increases upon an electrochemical trigger (127).

Similar to ferrocene, admantane is also considered an excellent guest moiety for β-cyclodextrin. Reinhoudt showed that adamantyl-terminated PPI dendrimers can bind to several β-cyclodextrin molecules (128–130). The complex was most

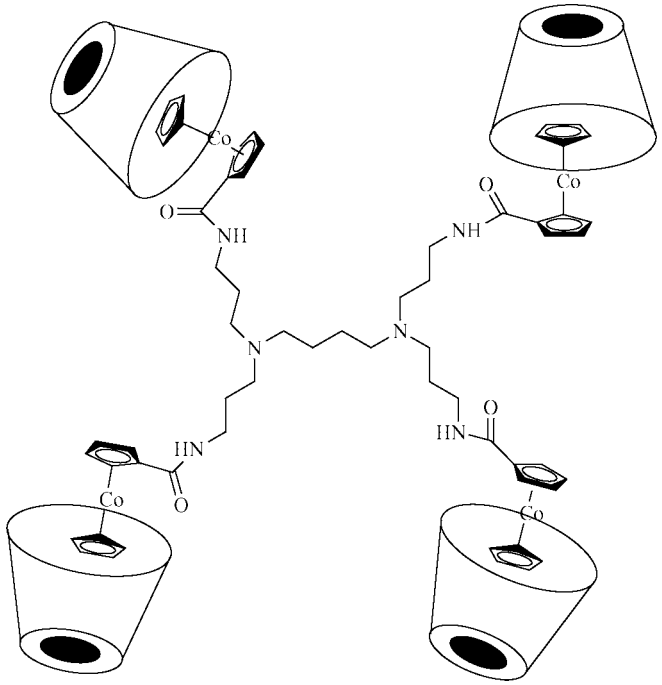

Fig. 33. Dendrimer with cyclodextrin caps.

stable at pH 2, at which point the internal tertiary amines are all protonated. The possible extended conformation of the protonated dendrimer is suggested to be responsible for the complete complexation of cyclodextrins with dendrimers up to the fourth generation. Reinhoudt was able to show that the stoichiometry of binding up to fourth-generation dendrimer between the cyclodextrin and adamantyl groups was 1:1. This ratio decreased in the fifth generation and is attributed to the possible steric crowding.

Small surfactant molecules also have been used as guest molecules to bind to the surface of the dendrimers, often through the combination of hydrophobic effect and ionic interactions (131–136). Ottaviani and co-workers studied the characteristics of the PAMAM dendrimers using noncovalently incorporated nitroxide radical based surfactant (131). The dendrimers were terminated with carboxylate moieties, while the nitroxide radical was functionalized with a quaternary ammonium functionality. They noted that the nitroxide surfactants were able to act as micellar hosts for low generation dendrimers. However, for higher generation dendrimers (>3.5), the dendrimer was able to act as a host for the nitroxide surfactant molecule. The binding was proposed to be due to ionic and hydrophobic interactions. Using EPR (electron paramagnetic resonance) studies, they were also able to show that the nitroxide radical probes are trapped in a restricted space in proximity to the dendrimer surface. On the basis of this observation, a mode of binding was proposed as seen in Figure 34 (132). Similarly, Majoral has utilized this strategy to functionalize the periphery of phosphorus-based dendrimers noncovalently with carbohydrates (136).

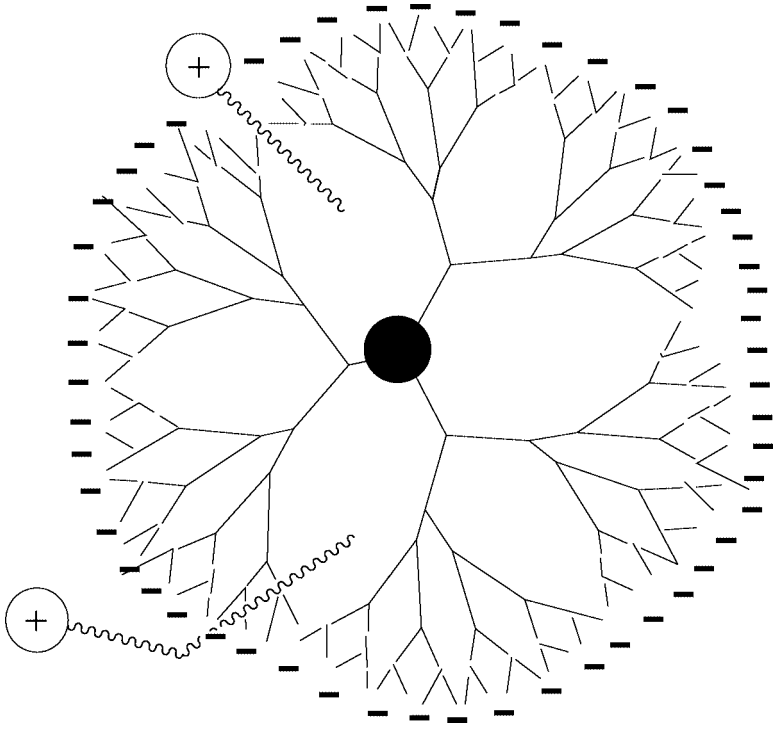

Fig. 34. Binding small molecule surfactants in dendrimers with hydrophobic chains buried inside.

Catalysis with Amphiphilic Dendrimers. An example of biomimetic catalysis with amphiphilic dendrimers has already been mentioned above (108). Similarly other micellar dendrimers have been used to catalyze reactions either within the hydrophobic interior or at the interface. An interesting example was provided by the research group of Rico-Lattes, in which PAMAM dendrimers were functionalized using D-gluconolactone (137–139). The resultant chiral dendrimers were tested for their capabilities in the asymmetric reduction of prochiral ketones using sodium borohydride as the reagent. While these dendrimers provide moderate or poor asymmetric induction in a homogeneous phase (water), the chiral induction was very high in THF. The selectivity is attributed to the supramolecular ordering of the prochiral ketone at the chiral solvating interface. The third-generation dendrimer was found to be a particularly suitable vehicle for this chiral induction. Similarly, binding based on hydrophobic interaction is also attributed to the catalysis of aminolysis reactions of *p*-nitrophenyl esters using amine-terminated PAMAM dendrimers (140,141).

Hawker and co-workers reported the synthesis of unimolecular inverse micelles based on benzyl ether dendrimers with hydroxyl groups in its interior (142). They showed that this dendrimer was able to catalyze the E1 elimination reaction of 2-iodo-2-methylheptane. The tridendron of G4 seems to be particularly effective in catalyzing this reaction. The conversions to products were found to be greater than 90%. The regioselectivity of the elimination was moderate. Turnover

numbers as high as 17,400 were observed with these dendrimers. The catalysis of the dendrimer was attributed to the ability of the internal hydroxy groups to stabilize the cationic transition state of the elimination reaction.

Dendrimer Assembly Based on Hydrophobic Interactions. Noncovalent assembly of dendrimers using hydrogen-bonding interactions was discussed earlier in this article. Noncovalent assembly of dendrimers based on hydrophobic interactions is also very attractive, since these assemblies can be achieved in aqueous solutions or other polar solvents. The strong association between adamantyl groups and β-cyclodextrin is a well-known phenomenon. Newkome and co-workers used this interaction in an attempt to assemble dendrimers (83). They synthesized a bis-ester of admantane carboxylic acid with tetraethyleneglycol and attempted to complex this bis(adamantane ester) to a β-cyclodextrin derivatized with amide dendrons (Fig. 35). On the basis of a dye-displacement assay, the efficiency of the dendrimer assembly was found to be not very high. They attributed this to the possible steric encumbrance of the bis(admantane ester) owing to the chain compaction by the sodium ions present in solution.

Diederich has used the previously described association between steroids and cyclophanes to noncovalently assemble dendrimers (143). A bis(testosterone) derivative that contains a rigid phenylacetylene-based linker is used as the ditopic ligand (Fig. 36). The linker contains positively charged amino groups, which are useful both to solubilize these compounds in aqueous solutions and to have ionic interactions with the negatively charged periphery of the dendrons. Using ^{1}H NMR, it was ascertained that the steroid, not the phenylacetylene linker, is bound to the cyclophane. The association constants for a 1:1 complex were high in all cases. However, the association for a 2:1 complex was dependent on the length of the bis(steroid) linker. It was observed that for higher generation dendrimers, the possible repulsion between the negative charges of the dendrons inhibits the

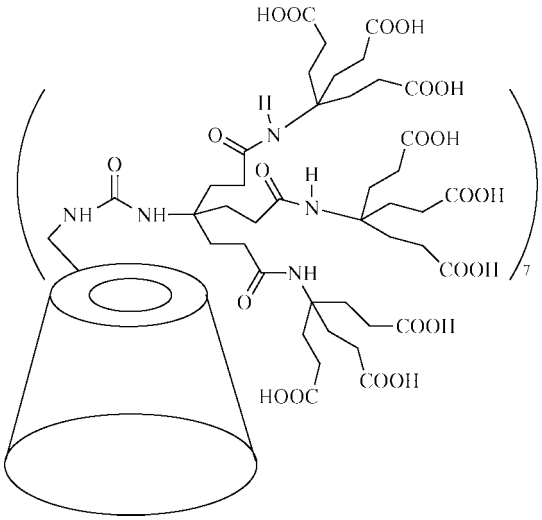

Fig. 35. Cyclodextrin cored dendrimer synthesized by newkome.

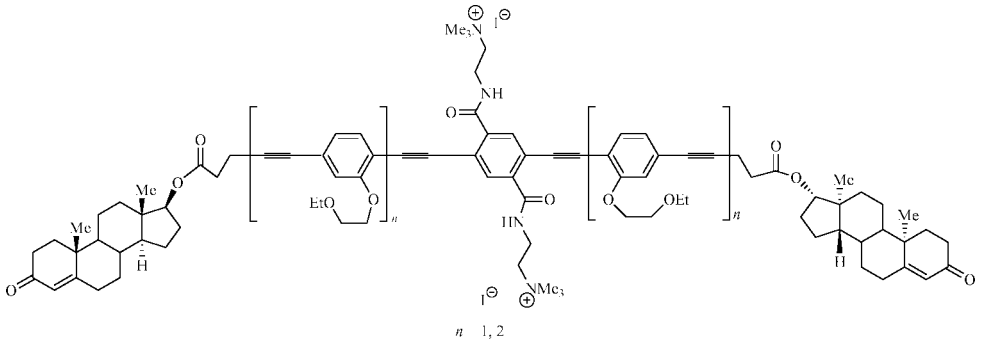

Fig. 36. Structure of the ditopic steroidal guest molecule (structure of the dendrimer is similar to the one shown in Fig. 29, but with a larger cyclophane core).

formation of a 2:1 complex. This repulsive interaction is reduced for dimerizing the dendrons by using a longer phenylacetylene linker.

Summary

Ever since the first reports on the synthesis of dendrimers, these macromolecules have attracted the attention of researchers from biology to engineering. The compactness of the three-dimensional architecture, the opportunity to present a high density of functional groups in the periphery, the opportunity to encapsulate functionalities in the core, and the globular structure of these molecules make them extremely versatile. Each of these features makes these molecules attractive for different applications in a variety of areas. Some of these features make them ideal architectures for binding guest molecules in its interior, periphery, or the interface. In this article, we have mainly discussed hydrogen bonding and amphiphilic interactions with frequent inference to ionic interactions. Molecular recognition using dendritic scaffolds will have lasting implications in nanotechnology and biology (144–154).

BIBLIOGRAPHY

1. A. W. Bosman, H. M. Janssen, and E. W. Meijer, *Chem. Rev.* **99**, 1665–1688 (1999).
2. M. Fischer and F. Vögtle, *Angew. Chem., Int. Ed. Engl.* **38**, 884–905 (1999).
3. J. M. J. Fréchet, *Science* **263**, 1710–1715 (1994).
4. S. M. Grayson and J. M. Fréchet, *J. Chem. Rev.* **101**, 3819–3868 (2001).
5. J. S. Moore, *Acc. Chem. Res.* **30**, 402–413 (1997).
6. G. R. Newkome, E. He, and C. N. Moorefield, *Chem. Rev.* **99**, 1689–1746 (1999).
7. D. A. Tomalia, A. M. Naylor, and W. A. Goddard III, *Angew. Chem., Int. Ed. Engl.* **29**, 138–175 (1990).
8. D. A. Tomalia, *Adv. Mater.* **6**, 529–539 (1994).
9. S. C. Zimmerman and L. Lawless, *J. Top. Curr. Chem.* **217**, 95–120 (2001).
10. F. Zeng and S. C. Zimmerman, *Chem. Rev.* **97**, 1681–1712 (1997).
11. E. Buhleier, W. Wehner, and F. Vögtle, *Synthesis* 155–1158 (1978).

12. M. Maciejewski, **A17**, 689–703 (1982).
13. G. R. Newkome, Z. Q. Yao, G. R. Baker, and V. K. Gupta, *J. Org. Chem.* **50**, 2003–2004 (1985).
14. D. A. Tomalia, H. Baker, J. Dewald, M. Hall, G. Kallos, S. Martin, J. Roeck, J. Ryder, and P. Smith, *Polym. J.* **17**, 117–132 (1985).
15. F. Vögtle, ed., *Dendrimers II: Architecturre, Nanostructure and Supramolecular Chemistry*, Vol. 210, Springer, Berlin, 2000.
16. V. Balzani, A. Juris, M. Pink, M. Venturi, S. Campagna, and S. Serroni, in J. L. Brédas, ed., *Conjugated Oligomers, Polymers, and Dendrimers: From Polyacetylene to DNA*, 1999, p. 291.
17. K. Onitsuka and S. Takahashi, *Top. Curr. Chem.* **228**, 39–63 (2003).
18. G. R. Newkome, C. N. Moorefield, and F. Vögtle, *Dendrimers and Dendrons: Concepts, Syntheses, Applications*, 2nd ed., Wiley-VCH, Weinheim, Germany, 2001.
19. S. W. Kraska and D. Seyferth, *J. Am. Chem. Soc.* **120**, 3604–3612 (1998).
20. M. Slany, M. Bardají, M. J. Cassnove, A. M. Caminade, J. P. Majoral, and B. Chaudret, *J. Am. Chem. Soc.* **117**, 9764–9765 (1995).
21. K. Sivanandan, D. Vutukuri, and S. Thayumanavan, *Org. Lett.* **4**, 3751–3753 (2002).
22. D. Vutukuri, K. Sivanandan, and S. Thayumanavan, *Chem. Commun*. 796–797. (2003).
23. W. Zeng, D. T. Nowlan III, L. M. Thomson, W. M. Lackowski, and E. E. Simanek, *J. Am. Chem. Soc.* **123**, 8914–8922 (2001).
24. G. R. Newkome, B. D. Woosley, E. He, C. N. Moorefield, R. Güther, G. R. Baker, G. H. Escamilla, and H. Luftmann, *Chem. Commun*. 2737–2738 (1996).
25. M. Santo and M. A. Fox, *J. Phys. Org. Chem.* **12**, 293–307 (1999).
26. M. H. Kleinman, J. H. Flory, D. A. Tomalia, and N. J. Turro, *J. Phys. Chem. B* **104**, 11472–11479 (2000).
27. S. C. Zimmerman, Y. Wang, P. Bharathi, and J. S. Moore, *J. Am. Chem. Soc.* **120**, 2172–2173 (1998).
28. C. J. Hawker, K. L. Wooley, J. M. J. Fréchet, *J. Am. Chem. Soc.* **115**, 4375–4376 (1993).
29. A. Bähr, B. Felber, K. Schneider, and F. Diederich, *Helv. Chim. Acta* **83**, 1346–1376 (2000).
30. T. D. James, H. Shinmori, M. Takeuchi, and S. Shinkai, *Chem. Commun*. 705–706 (1996).
31. V. J. Pugh, Q.-S. Hu, X. Zuo, F. D. Lewis, and L. Pu, *J. Org. Chem.* **66**, 6136–6140 (2001).
32. D. K. Smith and F. Diederich, *Chem. Commun*. 2501–2502 (1998).
33. G. Wulff, *Angew. Chem., Int. Ed. Engl.* **34**, 1812–1832 (1995).
34. M. S. Wendland and S. C. Zimmerman, *J. Am. Chem. Soc.* **121**, 1389–1390 (1999).
35. S. C. Zimmerman, M. S. Wendland, N. A. Rakow, I. Zharov, and K. S. Suslick, *Nature* **418**, 399–403 (2002).
36. S. C. Zimmerman, I. Zharov, M. S. Wendland, N. A. Rakow, and K. S. Suslick, *J. Am. Chem. Soc.* **125**, 13504–13518 (2003).
37. M. W. P. L. Baars, A. J. Karlsson, V. de Sorokin, B. F. W. Waal, and E. W. Meijer, *Angew. Chem., Int. Ed.* **39**, 4262–4265 (2000).
38. U. Boas, A. J. Karlsson, B. F. M. de Waal, and E. W. Meijer, *J. Org. Chem.* **66**, 2136–2145 (2001).
39. D. de Groot, B. F. M. de Waal, J. N. H. Reek, A. P. H. J. Schenning, P. C. J. Kamer, E. W. Meijer, and P. W. N. M. van Leeuwen, *J. Am. Chem. Soc.* **123**, 8453–8458 (2001).
40. J. W. Lee, Y. H. Ko, S.-H. Park, K. Yamaguchi, and K. Kim, *Angew. Chem., Int. Ed.* **40**, 746–749 (2001).
41. J. F. G. A. Jansen, E. M. M. d. B. van den Berg, E. W. Meijer, *Science* **266**, 1226–1229 (1994).

42. F. G. A. J. Jansen, H. W. I. Peerings, E. M. M. d. B. van den Berg, and E. W. Meijer, *Angew. Chem., Int. Ed. Engl.* **34**, 1206–1209 (1995).
43. J. F. G. A. Jansen, E. W. Meijer, and E. M. M. d. B. van den Berg, *J. Am. Chem. Soc.* **117**, 4417–4418 (1995).
44. M. W. P. L. Baars, R. Kleppinger, M. H. J. Koch, S.-L. Yeu, and E. W. Meijer, *Angew. Chem., Int. Ed. Engl.* **39**, 1285–1288 (2000).
45. D. L. Jiang and T. Aida, *Chem. Commun*. 1523–1524 (1996).
46. J. P. Collman, L. Fu, A. Zingg, and F. Diederich, *Chem. Commun*. 193–194 (1997).
47. A. Zingg, B. Felber, V. Gramlich, L. Fu, J. P. Collman, and F. Diederich, *Helv. Chim. Acta* **85**, 333–351 (2002).
48. D. K. Smith and L. Müller, *Chem. Commun*. 1915–1916 (1999).
49. S. Koenig, L. Müller, and D. K. Smith, *Chem. Eur. J.* **7**, 979–986 (2001).
50. B. Huang and J. R. Parquette, *Org. Lett.* **2**, 239–242 (2000).
51. B. Huang and J. R. Parquette, *J. Am. Chem. Soc.* **123**, 2689–2690 (2001).
52. J. Recker, D. J. Tomcik, and J. R. Parquette, *J. Am. Chem. Soc.* **122**, 10298–10307 (2000).
53. B. Huang, M. A. Prantil, T. L. Gustafson, and J. R. Parquette, *J. Am. Chem. Soc.* **125**, 14518–14530 (2003).
54. C. Valério, J. L. Fillaut, J. Ruiz, J. Guittard, J. C. Blais, and D. Astruc, *J. Am. Chem. Soc.* **119**, 2588–2589 (1997).
55. M. C. Daniel, J. Ruiz, and D. Astruc, *J. Am. Chem. Soc.* **125**, 1150–1151 (2003).
56. B. Alonso, C. M. Casado, I. Cuadrado, M. Morán, and A. E. Kaifer, *Chem. Commun*. 1778–1779 (2002).
57. Y. Wang, F. Zeng, and S. C. Zimmerman, *Tetrahedron Lett.* **38**, 5459–5462 (1997).
58. G. M. Dykes, D. K. Smith, and G. Seeley, *J. Angew. Chem., Int. Ed.* **41**, 3254–3257 (2002).
59. G. M. Dykes and D. K. Smith, *Tetrahedron* **59**, 3999–4009 (2003).
60. H. W. Gibson, N. Yamaguchi, L. Hamilton, and J. W. Jones, *J. Am. Chem. Soc.* **124**, 4653–4665 (2002).
61. T. Nagasaki, O. Kimura, M. Ukon, S. Arimori, I. Hamachi, and S. Shinkai, *J. Chem. Soc., Perkin Trans.* **1**, 75–81 (1994).
62. A. M. Elizarov, S.-H. Chiu, P. T. Glink, and J. F. Stoddart, *Org. Lett.* **5**, 679–682 (2002).
63. F. Zeng, S. C. Zimmerman, S. V. Kolotuchin, D. E. C. Reichert, and Y. Ma, *Tetrahedron* **58**, 825–843 (2002).
64. A. M. Elizarov, T. Chang, S.-H. Chiu, and J. F. Stoddart, *Org. Lett.* **5**, 3565–3568 (2002).
65. S. C. Zimmerman, F. Zeng, D. E. C. Reichert, and S. V. Kolotuchin, *Science* **271**, 1095–1098 (1996).
66. P. Thiyagarajan, F. Zeng, C. Y. Ku, and S. C. Zimmerman, *J. Mater. Chem.* **7**, 1221–1226 (1997).
67. S. V. Kolotuchin and S. C. Zimmerman, *J. Am. Chem. Soc.* **120**, 9092–9093 (1998).
68. Y. Ma, S. V. Kolotuchin, and S. C. Zimmerman, *J. Am. Chem. Soc.* **124**, 13757–13769 (2002).
69. P. S. Corbin, L. J. Lawless, Z. Li, Y. Ma, M. J. Witmer, and S. C. Zimmerman, *Proc. Natl. Acad. Sci.* **99**, 5099–5104 (2002).
70. V. Percec, C.-H. Ahn, T. K. Bera, G. Ungar, and D. J. P. Yeardley, *Chem. Eur. J.* **5**, 1070–1083 (1999).
71. V. Percec, T. K. Bera, M. Glodde, Q. Fu, V. S. K. Balagurusamy, and P. A. Heiney, *Chem. Eur. J.* **9**, 921–935 (2003).
72. W.-D. Jang, E.-L. Jiang, and T. Aida, *J. Am. Chem. Soc.* **122**, 3232–3233 (2000).
73. W. Zhang, S. O. Gonzalez, and E. E. Simanek, *Macromolecules* **35**, 9015–9021 (2002).
74. H. R. Strapert, N. Nishiyama, and D.-L. Jiang, T. Aida, and K. Kataoka, *Langmuir* **16**, 8182–8188 (2000).

75. T. Imae, T. Hirota, K. Funayama, K. Aoi, and M. Okada, *J. Colloid Interface Sci.* **263**, 306–311 (2003).
76. H. Zhang, Y. Fu, D. Wang, L. Wang, Z. Wang, and X. Zhang, *Langmuir* **19**, 8497–8502 (2003).
77. F. Huo, H. Xu, L. Zhang, Y. Fu, Z. Wang, and X. Zhang, *Chem. Commun*. 874–875 (2003).
78. G. R. Newkome, C. N. Moorefield, G. R. Baker, M. J. Saunders, and S. H. Grossman, *Angew. Chem., Int. Ed. Engl.* **30**, 1178–1180 (1991).
79. Y. H. Kim and O. W. Webster, *J. Am. Chem. Soc.* **112**, 4592–4593 (1990).
80. S. A. Kuzdzal, C. A. Monnig, G. R. Newkome, and C. N. Moorefield, *J. Am. Chem. Soc.* **119**, 2255–2261 (1997).
81. S. A. Kuzdzal, C. A. Monnig, G. R. Newkome, and C. N. Moorefield, *J. Chem. Soc., Chem. Commun*. 2139–2140 (1994).
82. C. M. Cardona, T. D. McCarley, and A. E. Kaifer, *J. Org. Chem.* **65**, 1857–1864 (2000).
83. G. R. Newkome, L. A. Godínez, and C. N. Moorefield, *Chem. Commun*. 1821 (1998).
84. C. J. Hawker, K. L. Wooley, and J. M. J. Fréchet, *J. Chem. Soc., Perkin Trans.* **1**, 1287–1297 (1993).
85. D. M. Watkins, Y. Sayed–Sweet, J. W. Klimash, N. J. Turro, and D. A. Tomalia, *Langmuir* **13**, 3136–3141 (1997).
86. K. R. Gopidas, A. R. Leheny, G. Caminati, N. J. Turro, and D. A. Tomalia, *J. Am. Chem. Soc.* **113**, 7335–7342 (1991).
87. N. J. Turro, J. K. Barton, and D. A. Tomalia, *Acc. Chem. Res.* **24**, 332–340 (1991).
88. Y. Pan and W. T. Ford, *Macromolecules* **32**, 5468–5470 (1999).
89. Y. Pan and W. T. Ford, *Macromolecules* **33**, 3731–3738 (2000).
90. P. Bharathi, H. Zhao, and S. Thayumanavan, *Org. Lett.* **3**, 1961–1964 (2001).
91. T. M. Chapman, G. L. Hillyer, E. J. Mahan, and K. A. Shaffer, *J. Am. Chem. Soc.* **116**, 11195–11196 (1994).
92. J. M. J. Fréchet, I. Gitsov, T. Monteil, S. Rochat, J.-F. Sassi, C. Vergelati, and D. Yu, *Chem. Mater.* **11**, 1267–1274 (1999).
93. I. Gitsov, K. L. Wooley, and J. M. Fréchet, *J. Angew. Chem., Int. Ed. Engl.* **31**, 1200–1202 (1992).
94. I. Gitsov and J. M. Fréchet, *J. Macromolecules* **26**, 6536–6546 (1993).
95. I. Gitsov, K. L. Wooley, C. J. Hawker, P. T. Ivanova, and J. M. Fréchet, *J. Macromolecules* **26**, 5621–5627 (1993).
96. I. Gitsov and J. M. J. Fréchet, *J. Am. Chem. Soc.* **118**, 3785–3786 (1996).
97. Y. Chang, Y. C. Kwon, S. C. Lee, and C. Kim, *Macromolecules* **33**, 4496–4500 (2000).
98. Y. Chang, C. Kim, *J. Polym. Sci., Part A: Polym. Chem.* **39**, 918–926 (2001).
99. I. Gitsov, K. R. Lambrych, V. A. Remnant, and R. Pracitto, *J. Polym. Sci., Part A: Polym. Chem.* **38**, 2711–2727 (2000).
100. J. Iyer, K. Fleming, and P. T. Hammond, *Macromolecules* **31**, 8757–8765 (1998).
101. Z. Bo, J. P. Rabe, and A. D. Schlüter, *Angew. Chem., Int. Ed. Engl.* **38**, 2370–2372 (1999).
102. J. C. M. v. Hest, D. A. P. Delnoye, M. W. P. L. Baars, M. H. P. v. Genderen, and E. W. Meijer, *Science* **268**, 1592–1595 (1995).
103. J. C. M. v. Hest, M. W. P. L. Baars, C. Elissen–Román, M. H. P. v. Genderen, and E. W. Meijer, *Macromolecules* **28**, 6689–6691 (1995).
104. J. C. M. v. Hest, D. A. P. Delnoye, M. W. P. L. Baars, C. Elissen–Román, M. H. P. v. Genderen, and E. W. Meijer, *Chem. Eur. J.* **2**, 1616–1626 (1996).
105. F. Diederich and B. Felber, *Proc. Natl. Acad. Sci.* **59**, 4778–4781 (2002).
106. P. Wallimann, S. Mattei, P. Seiler, and F. Diederich, *Helv. Chim. Acta* **80**, 2369–2390 (1997).

107. S. Mattei, P. Wallimann, B. Kenda, W. Amrein, and F. Diederich, *Helv. Chim. Acta.* **80**, 2391–2417 (1997).
108. T. Habicher, F. Diederich, and V. Gramlich, *Helv. Chim. Acta.* **82**, 1066–1095 (1999).
109. S. Hecht and J. M. J. Fréchet, *J. Am. Chem. Soc.* **123**, 6959–6960 (2001).
110. S. Stevelmans, J. C. M. v. Hest, J. F. G. A. Jansen, D. A. F. J. v. Boxtel, E. M. M. d. B. van den Berg, and E. W. Meijer, *J. Am. Chem. Soc.* **118**, 7398–7399 (1996).
111. M. W. P. L. Baars, P. E. Froehling, and E. W. Meijer, *Chem. Commun*. 1959–1960 (1997).
112. A. P. H. J. Schenning, E. Peeters, and E. W. Meijer, *J. Am. Chem. Soc.* **122**, 4489–4495 (2000).
113. V. Balzani, P. Ceroni, S. Gestermann, M. Gorka, C. Kauffmann, and F. Vögtle, *Tetrahedron* **58**, 629–637 (2002).
114. F. Vögtle, S. Gestermann, C. Kauffmann, P. Ceroni, V. Vicinelli, and V. Balzani, *J. Am. Chem. Soc.* **122**, 10398–10404 (2000).
115. A. I. Cooper, J. D. Londono, G. Wignall, J. B. McClain, E. T. Samulski, J. S. Lin, A. Dobrynin, M. Rubinstein, A. L. C. Burke, and J. M. J. Fréchet, J. M. DeSimone, *Nature* **389**, 368–371 (1997).
116. B. A. Omotova and J. M. Shreeve, *Macromolecules* **36**, 8336–8345 (2003).
117. Y. Sayed–Sweet, D. M. Hedstrand, R. Spinder, and D. A. Tomalia, *J. Mater. Chem.* **7**, 1199–1205 (1997).
118. V. Chechik, M. Zhao, and R. M. Crooks, *J. Am. Chem. Soc.* **121**, 4910–4911 (1999).
119. Y. Niu and R. M. Crooks, *Chem. Mater.* **15**, 3463–3467 (2003).
120. F. Gröhn, B. J. Bauer, and E. Amis, *J. Macromolecules* **34**, 6701–6707 (2001).
121. C. Zhang, S. O'Brien, and L. Balogh, *J. Phys. Chem. B* **106**, 10316–10321 (2002).
122. F. Gröhn, X. Gu, H. Grüll, J. C. Meredith, G. Nisato, B. J. Bauer, A. Karim, and E. J. Amis, *Macromolecules* **35**, 4852–4854 (2002).
123. S.-E. Stiriba, H. Kautz, and H. Frey, *J. Am. Chem. Soc.* **124**, 9698–9699 (2002).
124. A. Sunder, M. Krämer, R. Hanselmann, R. Mülhaupt, and H. Frey, *Angew. Chem., Int. Ed.* **38**, 3552–3555 (1999).
125. M.-C. Daniel, J. Ruiz, S. Nlate, J.-C. Blais, and D. Astruc, *J. Am. Chem. Soc.* **125**, 2617–2628 (2003).
126. R. Castro, I. Caudrado, B. Alonso, C. M. Casado, M. Morán, and A. E. Kaifer, *J. Am. Chem. Soc.* **119**, 5760–5761 (1997).
127. B. González, C. M. Casado, B. Alonso, I. Caudrado, M. Morán, Y. Wang, and A. E. Kaifer, *Chem. Commun*. 2569–2570 (1998).
128. J. J. Michels, M. W. P. L. Baars, E. W. Meijer, J. Huskens, and D. N. Reinhoudt, *J. Chem. Soc., Perkin Trans.* **2**, 1914–1918 (2000).
129. J. Huskens, M. A. Deij, and D. N. Reinhoudt, *Angew. Chem., Int. Ed.* **41**, 4467–4471 (2002).
130. K. J. C. van Bommel, G. A. Metselaar, W. Verboom, and D. N. Reinhoudt, *J. Org. Chem.* **66**, 5405–5412 (2001).
131. M. F. Ottaviani, N. J. Turro, S. Jokusch, and D. A. Tomalia, *J. Phys. Chem.* **100**, 13675–13686 (1996).
132. M. F. Ottaviani, E. Cossu, N. J. Turro, and D. A. Tomalia, *J. Am. Chem. Soc.* **117**, 4387–4398 (1995).
133. Y. C. Li, C. A. McMilan, D. M. Bloor, J. Penfold, J. Warr, J. F. Holzwarth, E. Wyn-Jones, *Langmuir* **16**, 7999–8004 (2000).
134. S. M. Ghoreishi, Y. Li, J. F. Holzwarth, E. Khosdel, J. Warr, D. M. Bloor, and E. Wyn-Jones, *Langmuir* **15**, 1938–1944 (1999).
135. X. Li, A. C. H. Ng, C. Wu, and D. K. P. Ng, *Macromolecules* **33**, 2119–2123 (2000).
136. M. Blanzat, C.-O. Turrin, E. Perez, I. Rico-Lattes, A.-M. Caminade, and J.-P. Majoral, *Chem. Commun*. 1864–1865 (2002).

137. A. Schmitzer, S. Franceschi, E. Perez, I. Rico–Lattes, A. Lattes, L. Thion, M. Erard, and C. Vidal, *J. Am. Chem. Soc.* **123**, 5956–5961 (2001).
138. A. Schmitzer, E. Perez, I. Rico–Lattes, and A. Lattes, *Tetrahedron Lett.* **40**, 2947–2950 (1999).
139. A. Schmitzer, E. Perez, I. Rico–Lattes, A. Lattes, and S. Rosca, *Langmuir* **15**, 4397–4403 (1999).
140. I. K. Martin and L. Twyman, *J. Tetrahedron Lett.* **42**, 1123–1126 (2001).
141. J. L. Burnett, A. S. H. King, I. K. Martin, and L. Twyman, *J. Tetrahedron Lett.* **43**, 2431–2433 (2002).
142. M. E. Piotti, F. Rivera Jr., R. Bond, C. J. Hawker, and J. M. J. Fréchet, *J. Am. Chem. Soc.* **121**, 9471–9472 (1999).
143. B. Kenda and F. Diederich, *Angew. Chem., Int. Ed.* **37**, 3154–3158 (1998).
144. R. G. Ispasoiu, L. Balogh, O. P. Varnavski, D. A. Tomalia, and T. Goodson III, *J. Am. Chem. Soc.* **122**, 11005–11006 (2000).
145. H. Stephan, H. Spies, B. Johannsen, C. Kauffmann, and F. Vögtle, *Org. Lett.* **2**, 2343–2346 (2000).
146. M. Zhao, L. Sun, and R. M. Crooks, *J. Am. Chem. Soc.* **120**, 4877–4878 (1998).
147. G. Pistolis, A. Malliaris, D. Tsiourvas, and C. M. Paleos, *Chem. Eur. J.* **5**, 1440–1444 (1999).
148. J. D. Reuter, A. Myc, M. M. Hayes, Z. Gan, R. Roy, D. Qin, R. Yin, L. T. Piehler, R. Esfand, D. A. Tomalia, and J. R. Baker, *Bioconjugate Chem.* **10**, 271–278 (1999).
149. S. Andre, P. J. C. Ortega, M. A. Perez, R. Roy, and H. J. Gabius, *Glycobiology* **9**, 1253–1261 (1999).
150. D. Page, D. Zanini, and R. Roy, *Biorg. Med. Chem.* **4**, 1949–1961 (1996).
151. R. Roy, *Curr. Opin. Struct. Biol.* **6**, 692–702 (1996).
152. R. Roy, *Top. Curr. Chem.* **187**, 241–274 (1997).
153. R. Roy, M. G. Baek, and K. Rittenhouse-Olson, *J. Am. Chem. Soc.* **123**, 1809–1816 (2001).
154. C. Z. Chen, and S. L. Cooper, *Adv. Mater.* **12**, 843–846 (2000).

SUBHADEEP BASU
BRITTO S. SANDANARAJ
S. THAYUMANAVAN
University of Massachusetts

MOLECULAR SELF-ASSEMBLY

Introduction

Molecular self-assembly is an extremely versatile tool for the thermodynamically controlled generation of higher order constructs (1). Nature uses self-assembly extensively in biological systems with "lock and key" specificity to give the diverse range of highly ordered systems observed in living organisms. Applying the self-assembly strategy to the reversible synthesis and controlled aggregation of

Encyclopedia of Polymer Science and Technology. Copyright John Wiley & Sons, Inc. All rights reserved.

macromolecules has garnered considerable interest in recent years. The utility of directional and highly specific noncovalent interactions has been demonstrated to be a particularly attractive method of controlling polymer aggregation, using the abundance of recognition elements developed by supramolecular chemists (1). The high degree of modularity makes this approach extremely versatile in that the assembling units can be precisely tuned with directed synthesis to customize the selectivity, directionality, and association strength of the noncovalent interaction. Also, the strength of the noncovalent interactions that embody molecular self-assembly is thermally dependent, allowing for reversible control over the assembly process which contributes to the design of unique material properties with defect correction and self-healing capabilities.

Recently, a number of contributions have been published that detail a growing field of synthetic polymer chemistry: supramolecular polymers/polymerization (2,3). Supramolecular polymers are macromolecules containing monomers held together by noncovalent interactions. As listed in Table 1, these interactions can be divided into six commonly used categories which include hydrogen bonding (4) (often multiple hydrogen bonds acting in tandem), π stacking of aromatic systems (5), metal–ligand interactions (6), London dispersion forces (7), electrostatics, and hydrophobics. As formed, these novel supramolecular polymers should exhibit similar material properties to their covalently bound counterparts with the added functionality of reversible binding. In addition to the supramolecular polymerization of main chain polymers, it is also conceivable to modify covalently bound linear polymers with pendant sidechains capable of noncovalent binding. In theory, this combination provides the most advantageous properties from both components: intrinsic materials properties dictated by the choice of polymer backbone with the reversible lock and key nature of supramolecular interactions.

Main-Chain Versus Side-Chain Supramolecular Polymers

The present concept of supramolecular polymers containing multiple hydrogen bonding units was first introduced over a decade ago by Jean-Marie Lehn (8). Three-point hydrogen bonds between bisfunctional diaminopyridine and thymine derivatives form supramolecular polymer chains exhibiting liquid crystalinity (Fig. 1**a**). Lehn and co-workers expanded the scope of this methodology to include bisfunctional molecules joined by chiral tartaric acid spacers (9) and rigid anthracene-based linkers (10). The utility of this approach has been demonstrated many times over in the years since, as can be ascertained by numerous contributions from many researchers (11,12).

Building upon Lehn's three-point hydrogen bound supramolecular polymers is the work done by E. W. Meijer using self-complementary ureidopyrimidinones, recognition elements capable of quadruple hydrogen bonding (Fig 1**b**). The quadruple hydrogen bonding system has two major differences with complementary three-point hydrogen bonding between thymine and diamidopyridines: an extremely high degree of association ($K_{\mathrm{dim}} > 10^6\ \mathrm{M}^{-1}$) and self-complementarity that eliminates stoichiometric concerns. The high dimerization constant of ureidopyrimidinone makes this an excellent system for supramolecular polymerizations, as the resulting polymers will possess a high degree of polymerization in

Table 1. Six Categories of Noncovalent Intermolecular Interactions[a]

Interaction	Description and bond strengths	Selected example
(London) Dispersion forces	> 4 kJ/mol. Temporarily induced dipole–dipole interactions	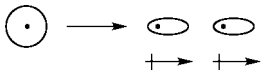
π–π stacking	8–12 kJ/mol (face–face), 12–21 kJ/mol (edge–face). Attractive forces between electron-rich interior with electron-poor exterior	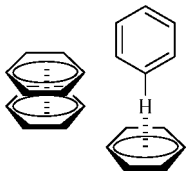
Hydrophobic	4–42 kJ/mol. Association of nonpolar complements in aqueous or polar media	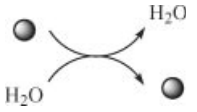
Hydrogen bonding	> 4kJ/mol (weak), 4–17 kJ/mol (moderate), 21–42 kJ/mol (strong). Donor–acceptor interaction involving hydrogen atom as proton donor and base (electron pair) as proton acceptor	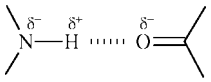
Electrostatic	4–42 kJ/mol (dipole–dipole), 42–125 kJ/mol (ion–dipole), >188 kJ/mol (ion–ion). Coulombic attraction between opposite charges	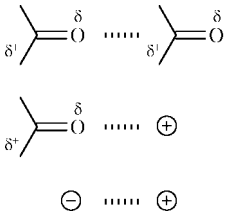
Dative bonding	21–377 kJ/mol. Metal–ligand coordination. Ligand donates electron pair(s) to center	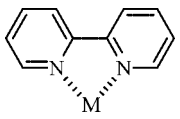

[a]Association strengths are for systems in chloroform.

solution. The resulting macromolecules generate excellent materials that have many advantages, such as strongly temperature-dependent viscoelastic properties. However, substantially more energy is required to induce complete dissociation to overcome the high degree of association.

In contrast to the above supramolecular polymers, recognition groups covalently attached as pendant polymer side chains (13) have been investigated for their potential elastomeric properties, first by Stadler and co-workers (14) in 1986 to increase miscibility between incompatible polybutadiene and polyisoprene blends by employing the relatively weak dimerization of urazole moieties ($K_{\mathrm{dim}} < 10^2\ \mathrm{M}^{-1}$), and later in 2001 where G. W. Coates and co-workers

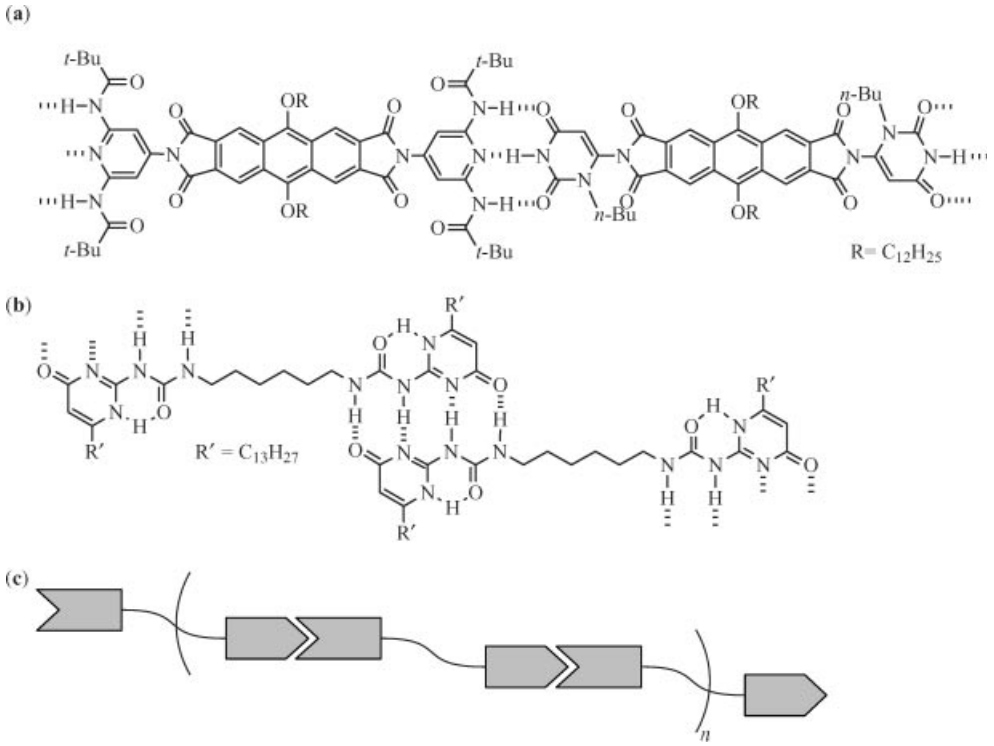

Fig. 1. Supramolecular polymers developed by (**a**) Lehn employing three-point hydrogen bonds between diamidopyridine and thymine residues and (**b**) Meijer employing self-complementary, quadruple hydrogen bonds. (**c**) A simplified schematic depicting the extended chain of repeating bisfunctional monomers fashioning the backbone of a supramolecular polymer.

(15) demonstrated the synthesis of elastomeric polyolefins equipped with thermoreversible cross-links between ureidopyrimidinone pendant groups. Kato and co-workers (16,17) have made large contributions to this field by exploring side-chain polymers as liquid crystalline materials. Furthermore, these motifs have been investigated by M. Weck and co-workers (18) for their dual functionality in catalysis and self-assembly, as well as by Sleiman and co-workers for their "DNA-mimetic" supramolecular aggregation properties yielding potentially functional morphologies (19).

As will be detailed in the following section, polymer assemblies can be formed very efficiently with moderate strength association constants $\sim$500–600 M^{-1} ($\sim$14.6 kJ/mol = 3.5 kcal/mol), especially when many of these interactions are working cooperatively. These moderate strength interactions contribute to overall constructs that are quite dynamic and require minimal amounts of energy for disassembly. These characteristics provide an elegant and potent means for controlling solution-state polymer structure, and applications are envisioned ranging in diversity including, but not limited to transport, encapsulation, delivery systems, sensors, devices, and other environmentally responsive materials.

"Plug and Play" Polymers

As mentioned earlier, the recognition elements inducing main-chain supramolecular polymerizations appear in many varieties. Analogously, these assembling units can also be effectively utilized as assembling units on polymer side chains. There exist two methods of generating pendant side chains containing supramolecular elements: (*1*) polymerizing or copolymerizing the monomer with a presynthesized recognition moiety, and (*2*) polymerizing a monomer with an active site that does not participate in the polymerization but is capable of post-polymerization modification. The latter scenario will be discussed throughout the rest of this article, as it avoids issues of blockiness (nonrandom blocks of functionality due to cooperativity during polymerization) and solubility associated with aggregation during copolymerization processes.

Supramolecular assembly is dynamic by nature. Further enhancing this characteristic is the modular nature of noncovalent interactions that permit a divergent approach to polymer structure, allowing multiple systems to be assembled using a single polymer backbone (Fig. 2). These polymers provide flexible backbones, are synthesized readily using free-radical–initiated polymerizations

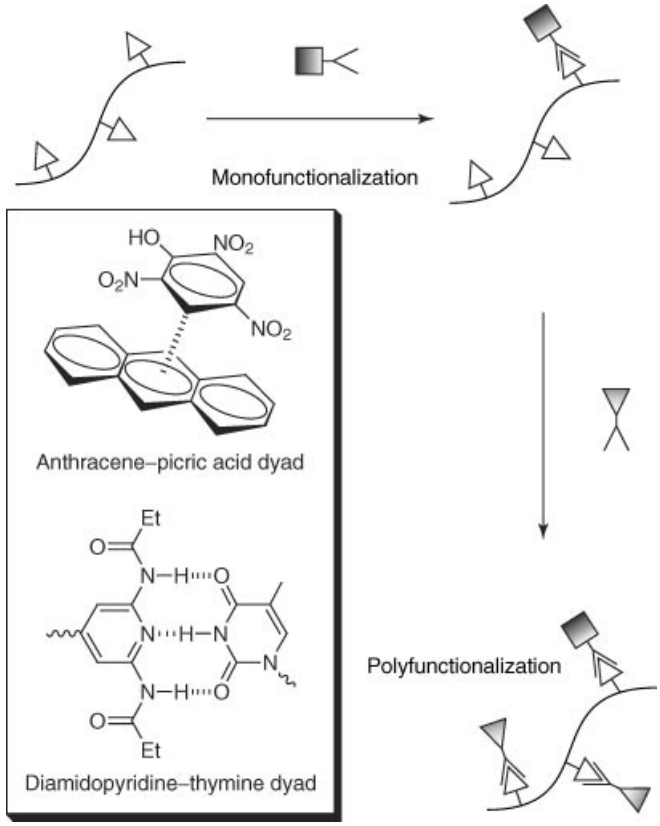

Fig. 2. Schematic representation of versatility of reversible, supramolecular side-chain modification, and selected examples of interactions that can be employed (inset).

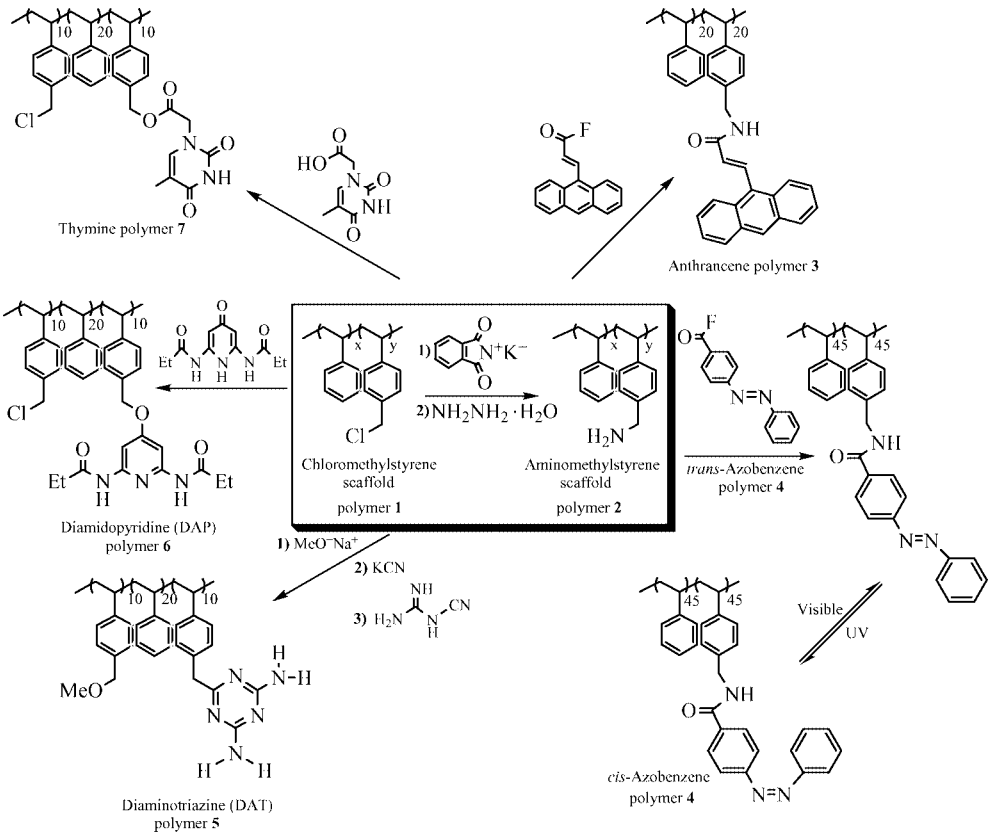

Fig. 3. Schematic illustration of versatile polymer scaffolds providing a divergent approach to polymer structure.

in multigram scales, and contain numerous monomers with sites for facile substitution. [Styrene and *p*-(chloromethyl)styrene polymerize with similar reactivity rates; therefore the desired 1:1 monomer ratio was achieved by initiating the polymerization in the presence of a 1:1 molar ratio of monomers]. The versatility of this polymer is demonstrated in Figure 3. For example, the chloromethyl sites can be directly functionalized via nucleophilic substitution, or easily converted to amines which react quantitatively with active esters, acid halides, or other electrophiles.

Our first investigations into polymer structural control were achieved utilizing aromatic stacking interactions. Employing polymers **3** and **4**, obtained from amine-functionalized polymer **2**, anthracene and azobenzene moieties were introduced quantitatively onto the styrene backbone. Anthracene polymer **3** adopts a highly folded, compact globular structure in solution because of numerous favorable anthracene–anthracene and anthracene–benzene interactions. (20) Capitalizing on the electron-rich nature of the pendant anthracene side chains, electron-deficient picric acid (Fig. 4**a**) was introduced into the system to induce a swelling of the polymer structure. The increased electrostatic interaction between the electron-rich anthracenes and electron-poor picric acid causes picric acid to

intercalate between anthracenes, affecting a swelling of the polymer globule. The hydrodynamic radius of the polymeric globule is dependent upon the concentration of picric acid, allowing for facile control over polymer size. Also, addition of picric acid causes this system to exhibit an increased thermal stability due to increased electrostatic interactions between anthracene–picric acid over anthracene–anthracene (Fig. 4).

Later, it was also demonstrated that pendant azobenzene units provide for photochemical control over polymer structure (21). Azobenzene is an extremely versatile photochrome; its structure can be controlled by the absorption of light,

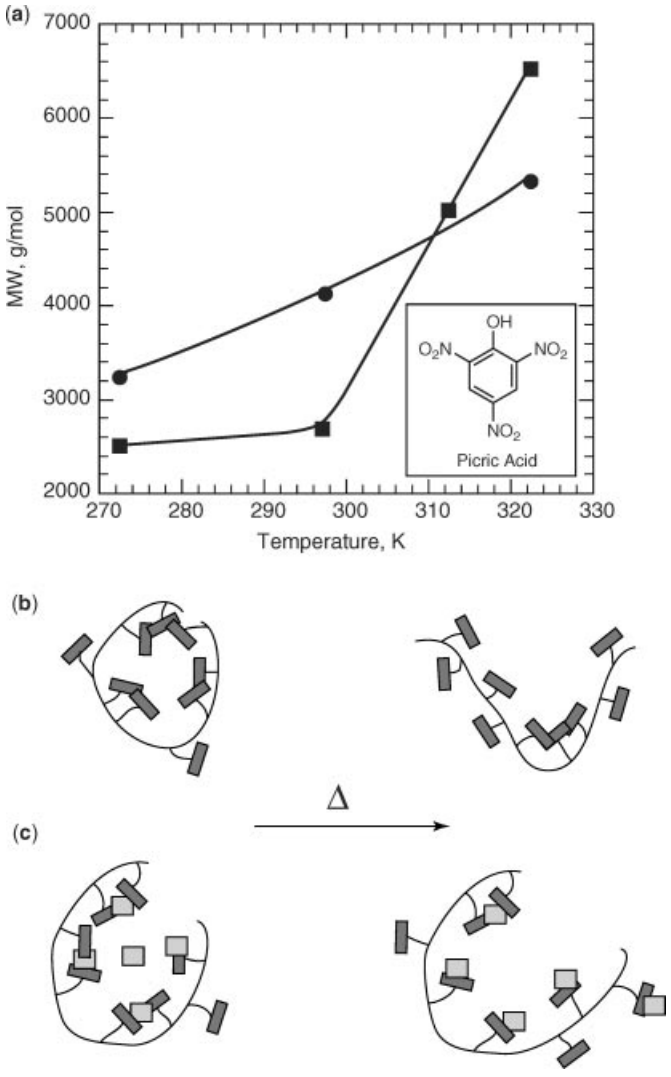

Fig. 4. Graphical and schematic illustrations of thermal unfolding process. (**a**) Variations in relative sizes of polymer **3** with and without picric acid. Apparent molecular weight obtained relative to polystyrene standards, (**b**) polymer **3**, and (**c**) polymer **3** with picric acid. Picric acid was introduced as component of elution solvent, 1.0×10^{-4}M.

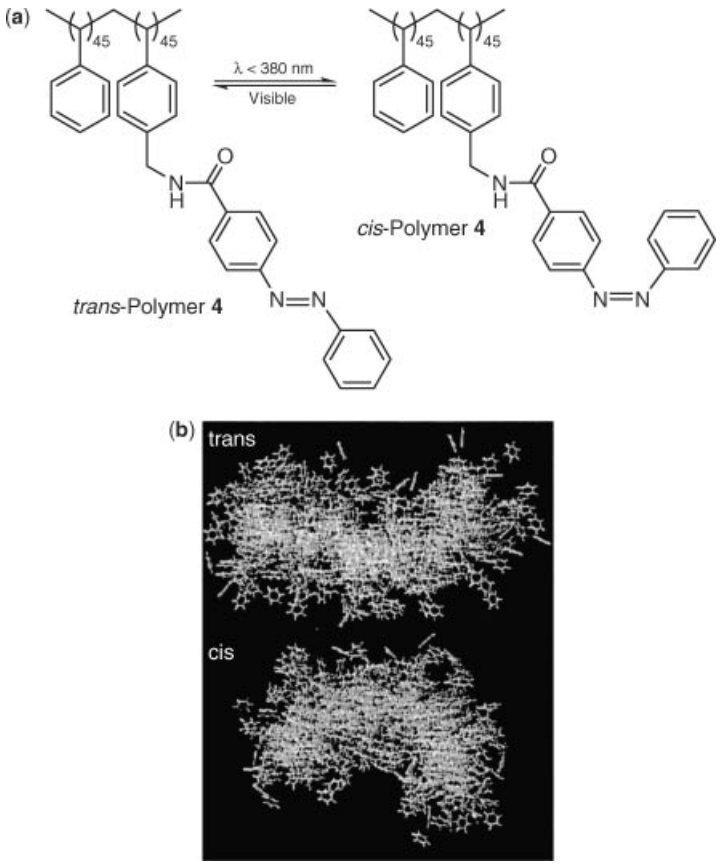

Fig. 5. (**a**) Azobenzene polymer **4** and reversible photochemical behavior. (**b**) Molecular dynamics simulation (300 K, $CHCl_3$) of trans and cis forms of polymer **4**.

often used for the creation of light-driven devices. (22) Photochemical isomerization of the azobenzene chromophore (UV irradiation induces trans to cis isomerization) causes the hydrodynamic radius to decrease as a result of the more compact cis isomer allowing for a greater degree of side-chain–side-chain aromatic stacking (Figs. 5 and 6). This isomerization process is reversible and directly linked to the UV–vis behavior of azobenzene.

To extend the methodology and demonstrate the modularity of reversible side-chain modification using specific noncovalent interactions, recognition elements capable of three-point hydrogen bonding were attached to the polymer scaffold. Diaminotriazine is a suitable recognition element for noncovalent side-chain modification through its donor–acceptor–donor hydrogen bonding units. However, attachment of triazine to the chloromethylstyrene scaffold (polymer **1**), fashioning polymer **5**, generates a polymer with a highly folded, micelle-like structure in noncompetitive solvents such as $CHCl_3$ as a result of the multiple modes of intrapolymeric hydrogen bonding between diaminotriazine moieties (23). This compact macromolecular conformation creates a system that inefficiently

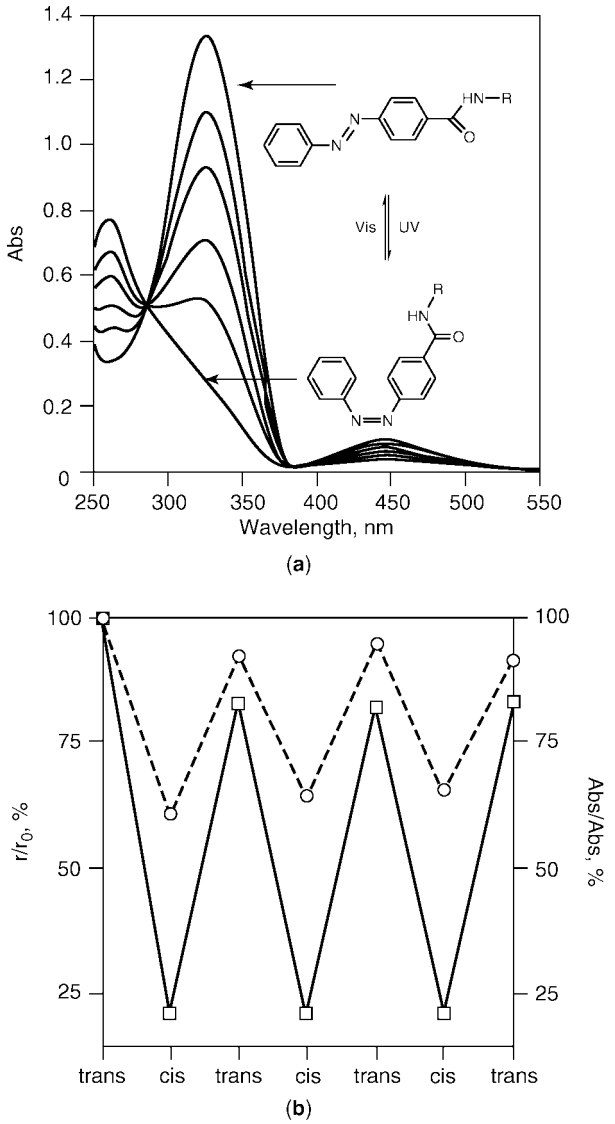

Fig. 6. (**a**) Absorption spectra variations of polymer **4** upon irradiation with UV and visible lights, and (**b**) variations in the relative radius of gyration (solid line) and absorption (dashed line) of **4** during irradiation.

complexes external guests because of competition between polymer–polymer and polymer–guest interactions. However, this conformation is very attractive for encapsulation since site isolation is a major advantage in catalysis and data storage. Specifically, ferroceneuracil **8** is able to penetrate the highly compact structure of **5** and bind multiple triazine units in the polar core (24). This guest is equipped with an additional hydrogen bond donor, N—H(1) in Figure 7, not in a linear array with the three-point DAD motif, creating a "wraparound" effect that maximizes favorable contacts between host and guest.

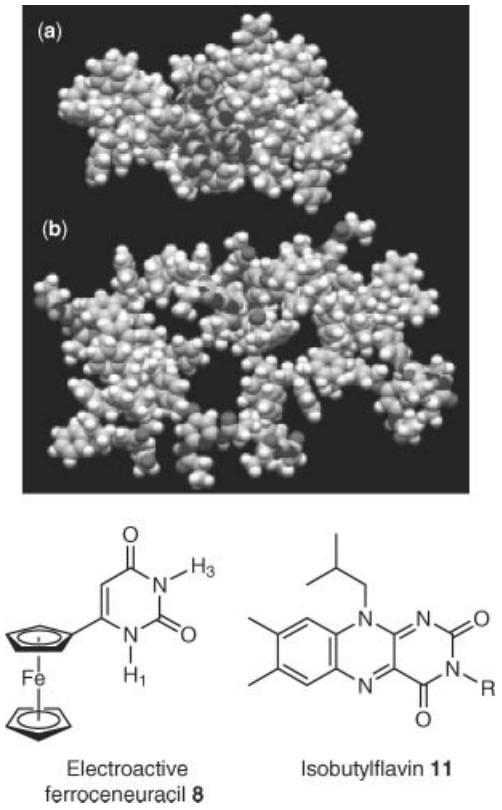

Fig. 7. Molecular dynamics runs (300 K, $CHCl_3$) of polymers (**a**) **5** and (**b**) **6** (40 repeat units each, schematically represented in Figure 3). Electroactive guest **8** and fluorescent guest **11** employed to probe binding efficiencies of **5** and **6**.

Efforts to provide more efficiency in guest complexation resulted in the replacement of diaminotriazine with diacyldiamidopyridine. Diacyldiamidopyridine is a highly analogous molecule containing the very same donor–acceptor–donor motif as diaminotriazine; however, diacyldiamidopyridine self-associates to a lesser extent resulting in a less-folded polymer capable of more efficient guest complexation.

To probe the binding efficiencies with the polymers above, a guest, isobutylflavin **11**, was employed. Isobutylflavin **11** contains the complementary acceptor–donor–acceptor recognition moiety required for specific complexation. Figure 8**a** shows that there is a significant reduction in binding efficiency of the triazine derivative compared to the diamidopyridine derivative. As previously mentioned, implicit in the bimolecular recognition of intrapolymerically associated triazine polymers is a decrease in the efficiency of interpolymeric binding. This inefficiency is explained by the requirement for polymer **5** to first uncoil prior to the recognition event (Fig. 8**b**).

The previous paragraphs have outlined a few methodologies by which we have demonstrated control over solution-state polymer structure by reversibly

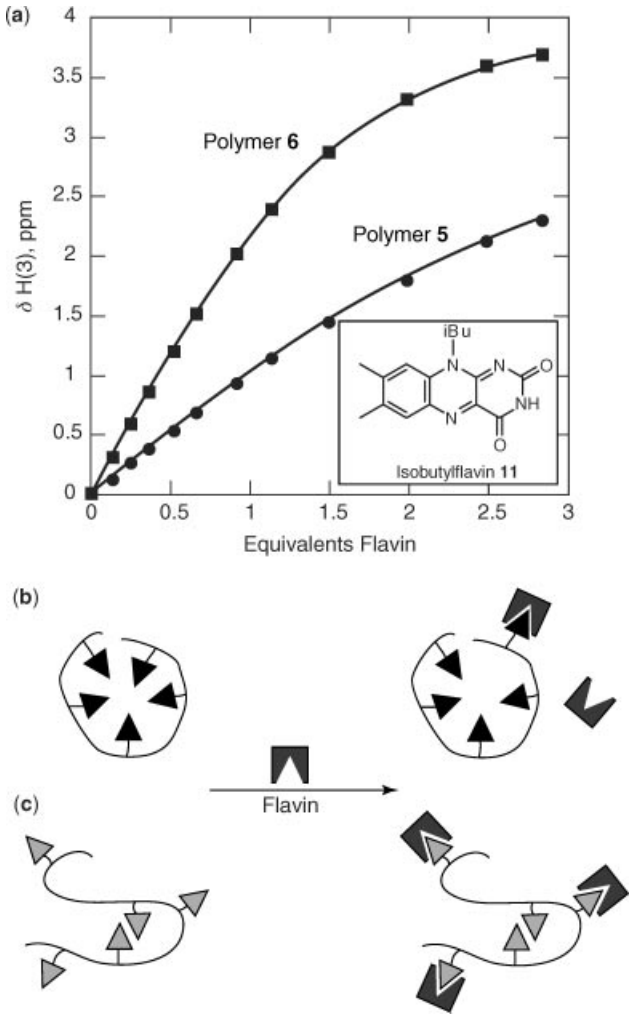

Fig. 8. (**a**) Graphical representation of the downfield shift of the imide proton of polymer **11** upon introduction to polymers **5** and **6**. Schematic representations of the recognition behavior of (**b**) polymers **5** and (**c**) **6** with **11**.

binding small guests to the pendant side chains of a flexible polymer scaffold or through reversible interactions of the pendant side chains with themselves. As such, this "plug and play" methodology has proven to be a very versatile approach to supramolecular polymer engineering.

Formation of Highly Structured, Functional Microscale Systems

Reversible side-chain modification has been demonstrated to be quite useful and very versatile at controlling the structure of single polymer strands in solution. This approach can also be very effectively used for solution-state assembly of

many polymer strands into higher order structures such as vesicles (25), micelles (26), and gels (27). As specific molecular recognition processes provide a tool for obtaining molecular-level control over higher order assembly processes (28), so too will integration of the "lock and key" selectivity with the phase-separated, three-dimensional nature of vesicular and micellar templates present a new opportunity for the creation of systems featuring novel structural and dynamic properties.

Combination of complementary diacyldiamidopyridine- and thymine-functionalized polymers **6** and **7**, respectively, in nonpolar media results spontaneously in the formation of giant vesicular aggregates, or recognition-induced polymersomes (RIPs). (Fig. 9) (29). In contrast to reports of di-block copolymer-based polymersomes that rely upon solvophobicity and phase

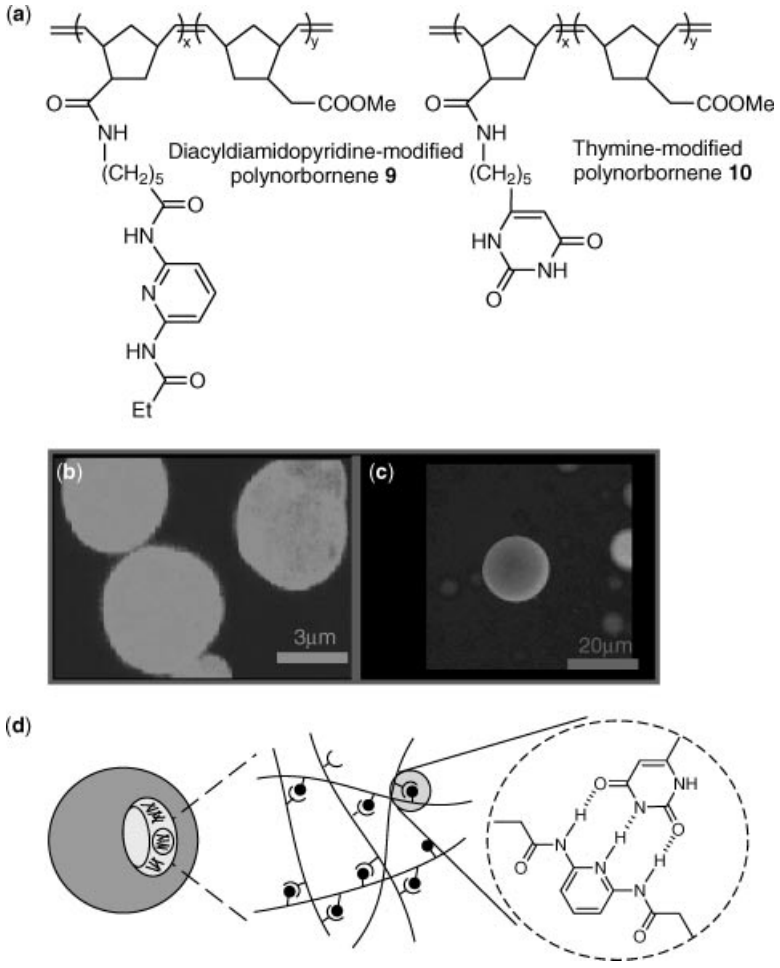

Fig. 9. (**a**) Random polynorbornene-based copolymers **9** and **10** that assemble into RIPs analogous to copolymers **6** and **7**. Laser confocal scanning micrographs of polymersomes formed through combination of complementary polymers (**b**) **6** and **7**, and (**c**) **9** and **10**. (**d**) Schematic illustration of specific interstrand hydrogen bonding driving polymersome formation.

segregation for self-assembly (18), these RIPs are formed through highly specific interactions between the complementary pendant side chains (Fig. 9**d**) as the polymers do not aggregate unless functionalized post-polymerization with recognition elements. Interestingly, these highly unusual, ordered microstructures from disordered, random copolymers are not unique to flexible polystyrene backbones; the more rigid polynorbornene scaffold, when derivatized with diacyldiamidopyridine (polymer **9**) and thymine (polymer **10**), also self-assembles in nonpolar media into RIPs (30) (Fig. 9**b**).

The formation of vesicular architectures from random copolymers lacking well-defined headgroups was unprecedented, proving a new method for the creation of supramolecular assemblies. This mode of assembly provides a new tool for the control of vesicle structure; complementary monovalent and multivalent guests would be expected to distort or disrupt vesicle structure through competitive binding to the polymer recognition sites (31). (see POLYMER VESICLES).

Initially, flavin was introduced into a solution of preformed RIPs to specifically and reversibly incorporate a fluorescent tag into the vesicular structure as an extension of our plug and play approach to polymer side-chain modification. As expected, the monodentate flavin caused a disruption in RIP structure appearing as an immediate swelling upon contact (Fig. 10**b**). However, this result was briefly lived as RIP diameter slowly returned to that of original, preformed RIPs (Fig. 11).

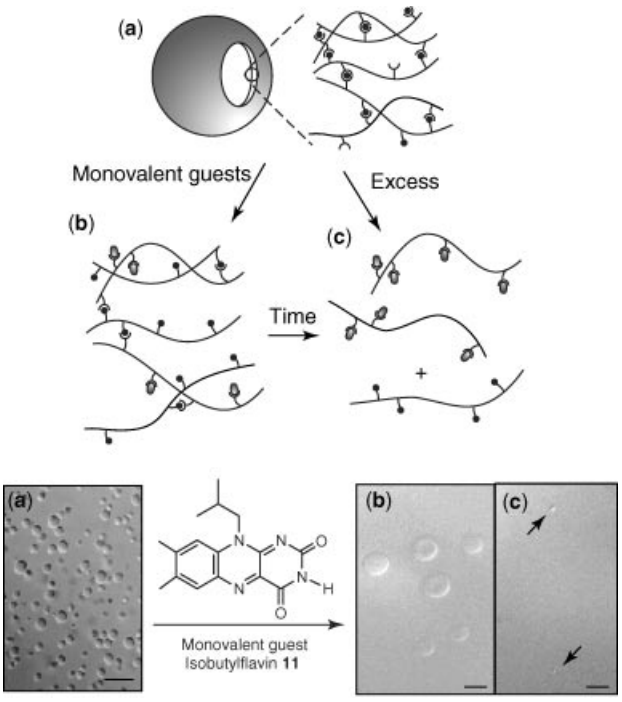

Fig. 10. Differential interference contrast micrographs of RIP–guest interactions with corresponding schematics: (**a**) native, undoped RIPs; (**b**) swollen RIPs 30 s after monovalent guest **11** addition; and (**c**) equilibrated RIPs 50 min after addition of 11. Scale bars represent 10 μm.

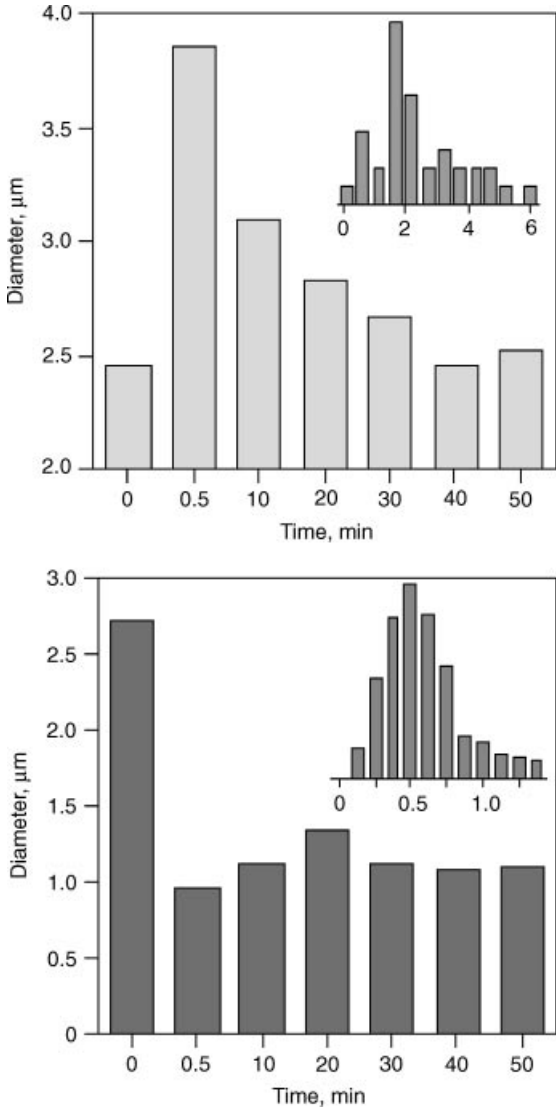

Fig. 11. Graphical representations of size changes occurring upon introduction of mono- and multivalent guests. Flavin (top) affects an immediate but temporary RIP swelling. Thy–Au (bottom) constricts polymer strands within RIPs resulting in submicrometer constructs. The insets on each graph are histograms of the equilibrated system 50 min after guest addition.

Presumably, this is due to the dynamic nature of these specific recognition processes. Flavin competitively binds with the DAP moiety of polymer **6**; over time, strands of polymer **6** become saturated with **11**, causing these polymers to leave the aggregate, in turn resulting in a return to original RIP size. Since RIP size distribution (Fig. 11**a**) and average diameter return to that of original, undoped RIPs firmly suggest that flavin is not incorporated into the final, equilibrated RIP system.

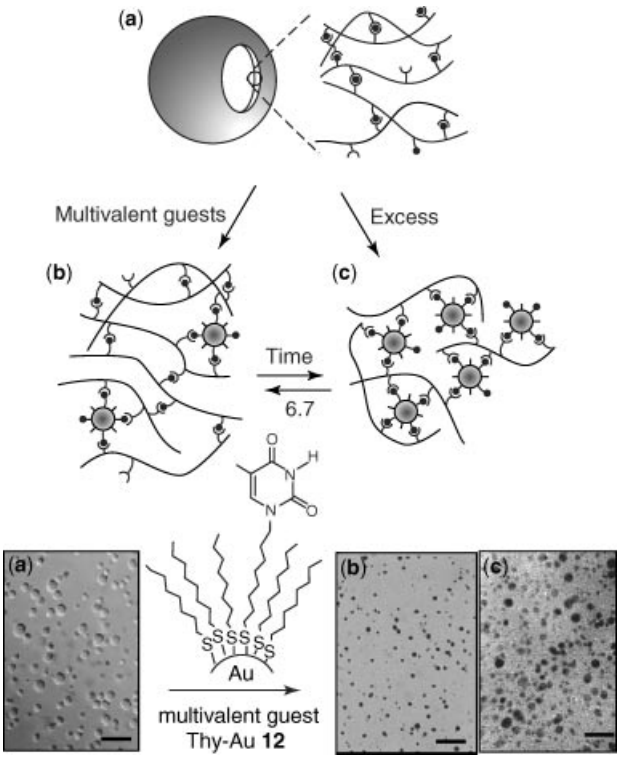

Fig. 12. Differential interference contrast micrographs of RIP–guest interactions with corresponding schematics: (**a**) native, undoped RIPs; (**b**) smaller RIPs 30 s after multivalent guest **12** addition (scale bars represent 10 μm); (**c**) submicrometer polymer–nanoparticle assemblies 50 min after Thy–Au addition. Scale bar represents 1 μm.

As already mentioned, multivalent guests were expected to act very differently with RIPs because of the greater number of contacts that, potentially, can be formed between the multifunctional Thy–Au and RIP (Fig. 12). In previous studies, we have demonstrated that analogous polymers interact specifically with Thy–Au to form solid spherical assemblies (32). The gold nanoparticles are excellent guests for these investigations because of their discrete structure, solubility in nonaqueous media, facile place exchange of ligands, and desired multifunctionality. From this, we predicted and confirmed that Thy–Au specifically embeds within the RIP and then causes a major reorganization of the component polymers. This process can followed qualitatively by phase contrast microscopy as RIPs are initially observed to be translucent in solution. The solution darkened upon addition of an aliquot of Thy–Au, but the solution cleared very rapidly ($\sim$30 s), indicating Thy–Au is rapidly incorporated into the RIP wall. However, this rapid incorporation was followed by an overall decrease in average diameter (Fig. 12**b**). Addition of Thy–Au constricts the component polymers, resulting in an immediate decrease in RIP diameter. However, the structures do not equilibrate back to original size, as seen in the flavin system, but rather new self-assembled spheres on the submicrometer scale forms.

To demonstrate the specific nature of these observed effects, highly analogous *N*-methylated versions of guests were synthesized and employed in the same capacity. The methyl groups cause only minimal changes in guest structure; however, these groups drastically change guest activity in solution as the methyl group effectively disrupts three-point hydrogen bonding, making these excellent molecules for control experiments. In both cases, no size changes or morphological effects were observed, clearly indicating the specific nature of these interactions.

Extension of this self-assembly approach to supramolecular engineering has led to an alternate motif for noncovalent cross-linking, a series of bisthymines that are complementary to the diamidopyridine side chains of polymer **6** (33). Upon combination in non-polar media thermally reversible, micrometer scale spherical aggregates were formed (Figs. 13**b** and 13**c**).

From the LCSM micrographs in Figure 13, the solid fluorescence profile of these spherical assemblies is indicative of a filled sphere rather than the vesicular morphology. Moreover, it is apparent that the fluorescence emission tapers off with microsphere radius; fluorescence is more intense in the microsphere center

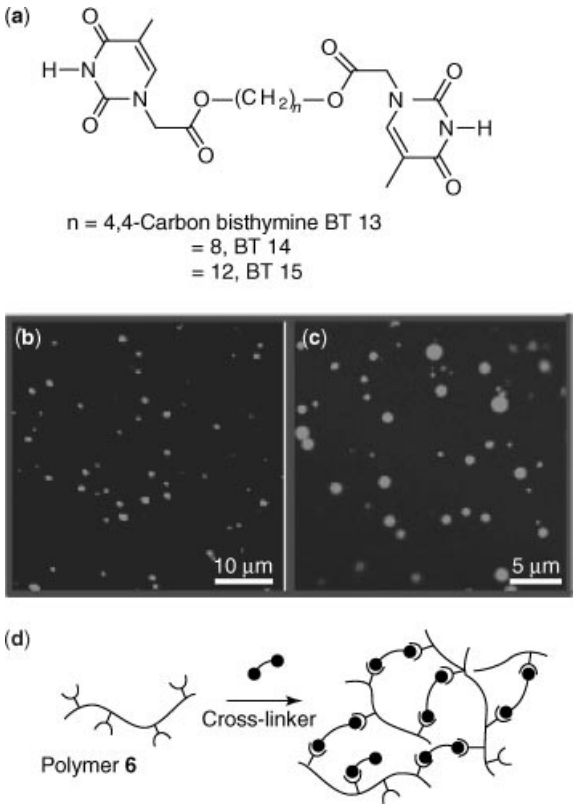

Fig. 13. (**a**) Bisthymine cross-linkers 13–15. (**b**,**c**) LCSM micrographs of microspheres generated from combination of polymer **6** and bisthymine (BT) **16**. (**d**) Schematic depiction of noncovalent polymer cross-linking.

indicating the presence of a microgel morphology. Also, the highly localized fluorescence observed in the micrographs indicates that very little flavin-tagged polymer exists free in solution, demonstrating the effectiveness of the cross-linking process.

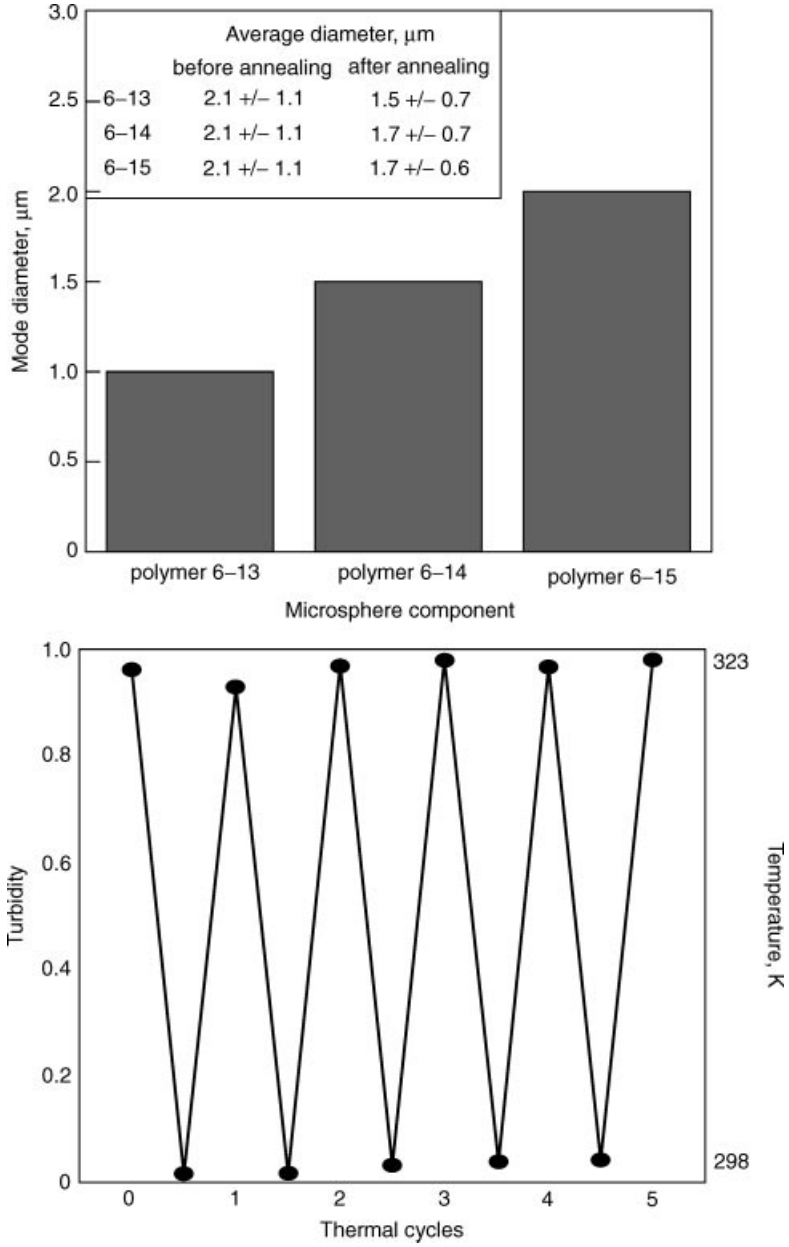

Fig. 14. Graphical representations of increasing microsphere diameter with increasing cross-linker length and average diameters (top) before and after thermal annealing cycles (inset), and solution turbidity during annealing cycles (bottom).

Interestingly, the overall size distribution of the resulting microspheres was found to be dependent on cross-linker preorganization; varying the alkyl spacer between thymines on the cross-linker translates into a stepwise growth in overall diameter on the microscale (Fig. 14). In accord with self-assembled systems, these microspheres could be thermally cycled, with complete disassociation of system components at elevated temperatures. Although small variations in turbidity are detected, microspheres after thermal annealing appear to retain less polydisperse, smaller overall diameters. Presumably, this change in distribution is the result of thermal cycling of the initial kinetic structures to thermodynamically more stable aggregates.

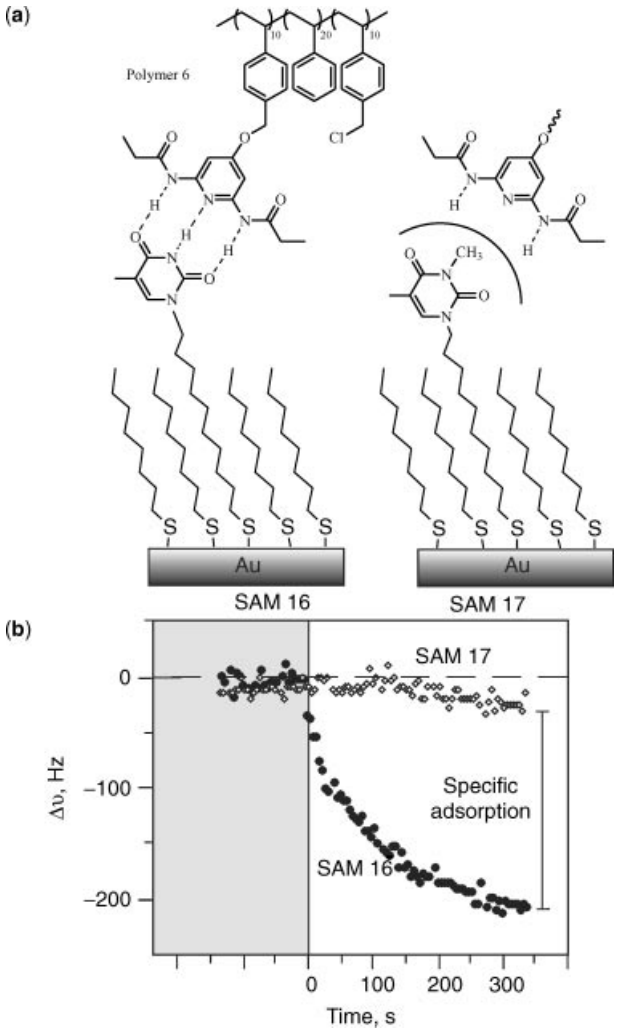

Fig. 15. (**a**) Self-assembled monolayers (SAMs) featuring imide functionality **16** and *N*-methylated control **17**. (**b**) Graphical representation clearly illustrating the essential role specific hydrogen bonding plays in polymer deposition.

Surface Modification

The concepts of supramolecular chemistry are also well suited to interactions at the solid–liquid interface. This provides an effective and efficient means of reversibly controlling the physical and chemical properties of a surface. There currently exist many well-established techniques for surface modification, such as electrostatics, ionic coordination, chemisorption, and Langmuir–Blodgett deposition; however, introducing specific hydrogen bonding interactions allows one to enhance the interfacial specificity between the surface and adsorbate while maintaining surface-charge neutrality, a prerequisite when designing materials with biocompatibility. To this end, self-assembled monolayers (SAMs) allow the incorporation of specific amounts of diverse functionality to investigate polymer deposition using noncovalent interactions (Fig. 15) (34).

Quartz crystal microbalance (QCM) is a well-established technique for monitoring surface deposition as the natural frequency of quartz decreases when mass is deposited onto the chip. This frequency change can be directly related to film formation and can be monitored in real time. The QCM experiment in Figure 15**b** depicts this phenomenon and indicates that polymer is rapidly adsorbed onto SAMs with the selectively expected from the DAP–Thy recognition dyad. These data also provide a method for determining the varying contributions of adsorption from nonspecific or specific interactions. Any frequency change in the case of *N*-methylated SAM **17** is due to nonspecific adsorption and can be subtracted from the response observed with SAM **16** to isolate the contribution of specific adsorption processes.

BIBLIOGRAPHY

1. L. J. Prins, D. N. Reinhoudt, and P. Timmerman, *Angew. Chem., Int. Ed.* **40**, 2383–2426 (2001).
2. J. M. Lehn, *Supramolecular Chemistry–Concepts and Perspectives*, VCH, Weinheim, 1995.
3. R. P. Sijbesma, F. H. Beijer, L. Brunsveld, B. J. B. Folmer, Jhkk Hirschberg, R. F. M. Lange, J. K. L. Lowe, and E. W. Meijer, *Science* **278**, 1601–1604 (1997); L. Brunsveld, B. J. B. Folmer, E. W. Meijer, and R. P. Sijbesma, *Chem. Rev.* **101**, 4071–4097 (2001); A. Ciferri, *Macromol. Rapid Commun.* **23**, 511–529 (2002); J. S. Moore, *Curr. Opin. Colloid Interface Sci.* **4**, 108–116 (1999); J. Huff, J. A. Preece, and J. F. Stoddart, *Macromol. Symp.* **102**, 1–8 (1996); V. Percec, J. Heck, G. Johansson, D. Tomazos, M. Kawasumi, and G. Ungar, *J. Macromol. Sci., Pure Appl. Chem.* **A31**, 1031–1070 (1994); H. A. Klok, J. J. Hwang, J. D. Hartgerink, and S. I. Stupp, *Macromolecules* **35**, 6101–6111 (2002); R. K. Castellano, D. M. Rudkevich, and J. Rebek Jr., *Proc. Natl. Acad. Sci. U.S.A.* **94**, 7132–7137 (1997); R. K. Castellano, K. Clark, S. L. Craig, C. Nuckolls, and J. Rebek Jr., *Proc. Natl. Acad. Sci. U.S.A.* **97**, 12418–12421 (2000).
4. R. P. Sijbesma and E. W. Meijer, *Chem Commun*. 5–16 (2003); D. C. Sherrington and K. A. Taskinen, *Chem. Soc. Rev.* **30**, 83–93 (2001).
5. D. H. Zhao and J. S. Moore, *Macromolecules* **36**, 2712–2720 (2003); S. Tsuzuki, K. Honda, and R. Azumi, *J. Am. Chem. Soc.* **124**, 12200–12209 (2002); D. J. Hill and J. S. Moore, *Proc. Natl. Acad. Sci. U.S.A.* **99**, 5053–5057 (2002); J. D. Hartgerink,

E. R. Zubarev, and S. I. Stupp, *Curr. Opin., Solid State Mater. Sci.* **5**, 355–361 (2001); V. Berl, I. Huc, R. G. Khoury, M. J. Krische, and J. M. Lehn, *Nature* **407**, 720–723 (2000).

6. B. G. G. Lohmeijer and U. S. Schubert, *J. Polym. Sci., Part A: Polym. Chem.* **41**, 1413–1427 (2003); K. J. Calzia and G. N. Tew, *Macromolecules* **35**, 6090–6093 (2002); Y. Chujo, K. Sada, and T. Saegusa, *Macromolecules* **26**, 6320–6323 (1993); Y. Chujo, K. Sada, and T. Saegusa, *Macromolecules* **26**, 6315–6319 (1993).
7. A. D. Stroock, R. S. Kane, M. Weck, S. J. Metallo, and G. M. Whitesides, *Langmuir* **19**, 2466–2472 (2003); J. Slager and A. J. Domb, *Adv. Drug Deliv. Rev.* **55**, 549–583 (2003); A. A. Louis, *Philos. Trans. R. Soc. London, Ser. A* **359**, 939–960 (2001); E. Pefferkorn, *J. Coll. Interface Sci.* **216**, 197–220 (1999); J. Li, L. Wang, Y. H. Ying, and Y. Yang, *J. Acta Chim. Sin.* **60**, 1700–1706 (2002).
8. J. M. Lehn, *Science* **260**, 1762–1763 (1993); J. M. Lehn, *Makromol. Chem. Macromol. Symp.* **69**, 1–17 (1993); J. M. Lehn, *Polym. Int.* **51**, 825–839 (2002); V. Berl, M. Schmutz, M. J. Krische, R. G. Khoury, and J. M. Lehn, *Chem. Eur. J.* **8**, 1227–1244 (2002).
9. T. Gulikkrzywicki, C. Fouquey, and J. M. Lehn, *Proc. Natl. Acad. Sci. U.S.A.* **90**, 163–167 (1993).
10. M. Kotera, J. M. Lehn, and J. P. Vigneron, *Tetrahedron* **51**, 1953–1972 (1995); M. Kotera, J. M. Lehn, and J. P. Vigneron, *J. Chem. Soc. Chem. Commun.* **2**, 197–199 (1994).
11. H. W. Gibson, L. Hamilton, and N. Yamaguchi, *Polym. Adv. Technol.* **11**, 791–797 (2000); K. Yamauchi, J. R. Lizotte, D. M. Hercules, M. J. Vergne, and T. E. Long, *J. Am. Chem. Soc.* **124**, 8599–8604 (2002); K. Yamauchi, J. R. Lizotte, and T. E. Long, *Macromolecules* **35**, 8745–8750 (2002); E. A. Archer, N. T. Goldberg, V. Lynch, and M. J. Krische, *J. Am. Chem. Soc.* **122**, 5006–5007 (2000); K. M. Chen, X. P. Jiang, L. C. Kimerling, and P. T. Hammond, *Langmuir* **16**, 7825–7834 (2000); T. H. Galow, A. K. Boal, and V. M. Rotello, *Adv. Mater.* **12**, 576–579 (2000).
12. S. C. Zimmerman and L. J. Lawless, *Supramolecular Chemistry of Dendrimers*, Vol. 217, Springer-Verlag, Berlin, 2001, pp. 95–120.
13. R. F. M. Lange and E. W. Meijer, *Macromolecules* **28**, 782–783 (1995); M. Born and H. Ritter, *Makromol. Chem. Rapid Commun.* **12**, 471–476 (1991); H. Ritter, *Macromol. Symp.* **77**, 73–38 (1994); C. B. St. Pourcain and A. C. Griffin, *Macromolecules* **28**, 4116–4121 (1995).
14. R. Stadler and J. Burgert, *Makromol. Chem. Macromol. Chem. Phys.* **187**, 1681–1690 (1986); C. Hilger and R. Stadler, *Polymer* **32**, 3244–3249 (1991); C. Hilger, M. Drager, and R. Stadler, *Macromolecules* **25**, 2498–2501 (1992); C. Hilger and R. Stadler, *Macromolecules* **25**, 6670–6680 (1992).
15. L. R. Rieth, R. F. Eaton, and G. W. Coates, *Angew. Chem., Int. Ed. Engl.* **40**, 2153–2156 (2001).
16. T. Kato, *Molecular Self-Assembly*, Vol. 96, Springer-Verlag, Berlin, 2000, pp. 95–146.
17. T. Kato and J. M. J. Frechet, *J. Am. Chem. Soc.* **111**, 8533–8534 (1989); T. Kato, H. Kihara, U. Kumar, T. Uryu, and J. M. J. Frechet, *Angew. Chem., Int. Ed. Engl.* **33**, 1644–1645 (1994); T. Kato, H. Kihara, T. Uryu, A. Fujishima, and J. M. J. Frechet, *Macromolecules* **25**, 6836–6841 (1992); T. Kato, *Kobunshi Ronbunshu* **54**, 855–862 (1997).
18. J. M. Pollino and M. Weck, *Synthesis (Stuttgart)* 1277–1285 (2002); J. M. Pollino and M. Weck, *Org. Lett.* **4**, 753–756 (2002).
19. H. S. Bazzi and H. F. Sleiman, *Macromolecules* **35**, 9617–9620 (2002); J. Dalphond, H. S. Bazzi, K. Kahrim, and H. F. Sleiman, *Macromol. Chem. Phys.* **203**, 1988–1994 (2002).

20. F. Ilhan, M. Gray, K. Blanchette, and V. M. Rotello, *Macromolecules* **32**, 6159–6162 (1999).
21. G. Clavier, F. Ilhan, and V. M. Rotello, *Macromolecules* **33**, 9173–9175 (2000).
22. M. S. Vollmer, T. D. Clark, C. Steinem, and M. R. Ghadiri, *Angew. Chem., Int. Ed. Engl.* **38**, 1598–1601 (1999); I. Willner, D. Rubin, R. Shatzmiller, and T. Zor, *J. Am. Chem. Soc.* **115**, 8690–8694 (1993); M. Ueda, N. Fukushima, K. Kudo, and K. Ichimura, *J. Mater. Chem.* **7**, 641–645 (1997).
23. F. Ilhan, M. Gray, and V. M. Rotello, *Macromolecules* **34**, 2597–2601 (2001).
24. T. H. Galow, F. Ilhan, G. Cooke, and V. M. Rotello, *J. Am. Chem. Soc.* **122**, 3595–3598 (2000).
25. B. M. Discher, Y. Y. Won, D. S. Ege, J. C. M. Lee, F. S. Bates, D. E. Discher, and D. A. Hammer, *Science* **284**, 1143–1146 (1999); B. M. Discher, D. A. Hammer, F. S. Bates, and D. E. Discher, *Curr. Opin. Coll. Interface Sci.* **5**, 125–131 (2000); F. Checot, S. Lecommandoux, H. A. Klok, and Y. Gnanou, *Eur. Phys. J.* **10**, 25–35 (2003); H. Kukula, H. Schlaad, M. Antonietti, and S. Forster, *J. Am. Chem. Soc.* **124**, 1658–1663 (2002); F. H. Meng, C. Hiemstra, G. H. M. Engbers, and J. Feijen, *Macromolecules* **36**, 3004–3006 (2003).
26. S. E. Webber, *J. Phys. Chem. B* **102**, 2618–2626 (1998); K. L. Wooley, *J. Poly. Sci., Part A: Polym. Chem.* **38**, 1397–1407 (2000); K. B. Thurmond, H. Y. Huang, C. G. Clark, T. Kowalewski, and K. L. Wooley, *Coll. Surf. B: Biointerfaces* **16**, 45–54 (1999); H. Y. Huang, E. E. Remsen, and K. L. Wooley, *Chem. Commun*. 1415–1416 (1998); Y. Zheng, Y. Y. Won, F. S. Bates, H. T. Davis, L. E. Scriven, and Y. Talmon, *J. Phys. Chem. B* **103**, 10331–10334 (1999).
27. M. Annaka and T. Tanaka, *Nature* **355**, 430–432 (1992); A. P. Nowak, V. Breedveld, L. Pakstis, B. Ozbas, D. J. Pine, D. Pochan, and T. J. Deming, *Nature* **417**, 424–428 (2002); Y. Osada and J. P. Gong, *Adv. Mater.* **10**, 827–837 (1998); S. Varghese, A. K. Lele, D. Srinivas, M. Sastry, and R. A. Mashelkar, *Adv. Mater.* **13**, 1544–1548 (2001).
28. T. A. Taton, C. A. Mirkin, and R. L. Letsinger, *Science* **289**, 1757–1760 (2000); T. H. Galow, A. K. Boal, and V. M. Rotello, *Adv. Mater.* **12**, 576–579 (2000).
29. F. Ilhan, T. H. Galow, M. Gray, G. Clavier, and V. M. Rotello, *J. Am. Chem. Soc.* **122**, 5895–5896 (2000).
30. U. Drechsler, R. J. Thibault, and V. M. Rotello, *Macromolecules* **35**, 9621–9623 (2002).
31. R. J. Thibault, T. H. Galow, E. T. Turnberg, M. Gray, P. H. Hotchkiss, and V. M. Rotello, *J. Am. Chem. Soc.* **124**, 15249–15254 (2002).
32. A. K. Boal, F. Ilhan, J. E. DeRouchey, T. Thurn-Albrecht, T. P. Russell, and V. M. Rotello, *Nature* **404**, 746–748 (2000).
33. R. J. Thibault, P. Hotchkiss, M. Gray, and V. M. Rotello, *J. Am. Chem. Soc.* **125**, 11249–11252 (2003).
34. T. Norsten, E. Jeoung, R. J. Thibault, and V. M. Rotello, *Langmuir* **19**, 7089–7093 (2003).

RAYMOND J. THIBAULT
VINCENT M. ROTELLO
Department of Chemistry, University of Massachusetts

MOLECULARLY IMPRINTED POLYMERS.

See Volume 7.

MORPHOLOGY.

See Volume 7.

MOLECULAR WEIGHT DETERMINATION

Introduction

This article discusses the theory and methods for the determination of molecular weight averages and molecular weight distributions of oligomeric and polymeric materials. The more important methods are described in greater detail in separate articles (see CHROMATOGRAPHY, SIZE EXCLUSION; FRACTIONATION; CHARACTERIZATION OF POLYMERS).

Molecular Weight Averages and Distributions

Most polymeric materials are comprised of mixtures of molecules of various sizes. This distribution of molecular weights is a result of the statistical nature of the polymerization proces (1). A complete description of the molecular weight distribution of a homopolymer is necessary to understand its physical, rheological, and mechanical properties. Structural variations, such as chain branching, and copolymer or higher mer polymers with various degrees of structural randomness further complicate a complete description of the molecular ensemble. Copolymers and higher mer polymers also need to be characterized for molecular composition as a function of molecular weight. Block copolymers and polymer mixtures also offer significant challenges to evaluate their molecular weight distribution. Failure mechanisms and practical lifetimes of polymeric materials may also be established through molecular weight measurements.

Most classical techniques for molecular weight determination are only capable of yielding one of the molecular weight averages of the distribution. These traditional methods are used nowadays only on a limited basis, and only a limited number of commercial instrumentation is available.

These averages are defined in terms of the molecular weight M_i and the number of moles n_i or the weight w_i of the component molecules. The molecular weight averages are defined by equations 1-4.

Number-average molecular weight:

$$\bar{M}_{\mathrm{n}} = \frac{\sum n_i M_i}{\sum n_i} = \frac{\sum w_i}{\sum w_i / M_i} \tag{1}$$

Weight-average molecular weight:

$$\bar{M}_{\mathrm{w}} = \frac{\sum n_i M_i^{\,2}}{\sum n_i M_i} = \frac{\sum w_i M_i}{\sum w_i} \tag{2}$$

z-Average molecular weight:

$$\bar{M}_z = \frac{\sum n_i M_i^{\,3}}{\sum n_i M_i^{\,2}} = \frac{\sum w_i M_i^{\,2}}{\sum w_i M_i} \tag{3}$$

Encyclopedia of Polymer Science and Technology. Copyright John Wiley & Sons, Inc. All rights reserved.

$(z + 1)$-*Average molecular weight*:

$$\bar{M}_{z+1} = \frac{\sum n_i M_i^4}{\sum n_i M_i^3} = \frac{\sum w_i M_i^3}{\sum w_i M_i^2} \tag{4}$$

Viscosity-average molecular weight:

$$\bar{M}_{\mathrm{v}} = \left[\frac{\sum n_i M_i^{1+a}}{\sum n_i M_i} \right]^{1/a} = \left[\frac{\sum w_i M_i^a}{\sum w_i} \right]^{1/a} \tag{5}$$

Equation 5 is an important practical molecular weight average derived from viscometry. To calculate this average, the exponent a and the constant K of the Mark–Houwink relationship relating intrinsic viscosity $[\eta]$ to molecular weight must be known.

$$[\eta] = KM^a \tag{6}$$

The value of a lies between 0.5 and 1.0 for random coils, depending on the solvent employed to determine the relationship of the intrinsic viscosity to molecular weight. For rigid rod molecules, the value of a is expected to be ~1.8. With these limits for a, it may be seen that $\bar{M}_{\mathrm{v}}$ is always larger than $\bar{M}_{\mathrm{n}}$ but can equal $\bar{M}_{\mathrm{w}}$ when the upper limit of a is reached for random coils.

If molecular weight is considered a continuous variable, the molecular weight distribution may be described by a set of moments μ_r given by the integrals

$$\mu_r = \int_0^x M^r f(M)\, \mathrm{d}M$$

where r = 0, 1, 2, 3, etc; $f(M)$ is the number-density distribution; and $f(M)dM$ is the number of moles of molecules with molecular weight between M and $(M + dM)$.

The average molecular weights are defined as

$$\bar{M}_{\mathrm{n}} = \frac{\mu_1}{\mu_0}$$
$$\bar{M}_{\mathrm{w}} = \frac{\mu_2}{\mu_1}$$
$$\bar{M}_z = \frac{\mu_3}{\mu_2}$$
$$\bar{M}_{z+1} = \frac{\mu_4}{\mu_3}$$

Molecular weight averages can be determined from these moments (2).

Molecular Weight Distribution Functions

Various mathematical functions have been employed to describe the distribution of molecular weights. Some of the more common functions are shown in Table 1 in terms of the mole fraction X. Further details are available (3).

Width of Molecular Weight Distributions. The width of the Gaussian distribution function may be expressed in terms of the standard deviation of the mole fraction MWD function σ_n or the mass fraction MWD function σ_w:

$$\sigma_n = (\bar{M}_w \bar{M}_n - \bar{M}_n)^{0.5}$$
$$\sigma_w = (\bar{M}_z \bar{M}_w - \bar{M}_w)^{0.5}$$

The standard deviation is an absolute measure of the width for the Gaussian function only. Widths of molecular weight distribution for other functions have to be calculated for each case from the distribution function itself.

The relationships between molecular weight averages and parameters in the molecular weight distribution functions are as follows:
which leads to

$$\exp(\sigma_w)^2 = \frac{\bar{M}_w}{\bar{M}_n} = \frac{\bar{M}_z}{\bar{M}_w}$$

Thus the ratios of two adjacent averages are constant.

Poisson distribution function.

The ratio of the weight-average to number average molecular weight is given by

$$\frac{\bar{M}_w}{\bar{M}_n} = 1 + \left(\frac{1}{\bar{M}_n}\right) - \left(\frac{1}{\bar{M}_n}\right)^2$$

Table 1. Molecular Weight Distribution Functions

Name	Function	Comments
Gaussian	$X(M) = \frac{1}{\sigma_n (2\pi)^{1/2}} \exp\left[\frac{(M - M_m)^2}{2\sigma_n^2}\right]$	M_m = median value equal to $\bar{M}_n$
Log-normal	$X(M) = \frac{1}{\sigma_n (2\pi)^{1/2}} \exp\left[\frac{(\ln M - \ln M_m)^2}{2\sigma_n^2}\right]$	M_m = geometric mean
Poisson[a]	$X(M) = \frac{\nu^{M-1}}{\Gamma(M)} \exp(-\nu)$	$\nu = \bar{M}_n - 1$
Flory–Schulz[b]	$X(M) = \frac{\beta^{k+1} M^{k-1} \bar{M}_n}{\Gamma(k+1)} \exp(-\beta M)$	k = degree of coupling $\beta = \frac{k}{\bar{M}_n}$

[a] $\Gamma(M) = \gamma$-function.
[b] $\Gamma(k+1) = \gamma$-function.

Gaussian distribution function
mole-fraction distribution function median value $= \bar{M}_n$
mass-fraction distribution function median value $= \bar{M}_w$

Log-normal distribution function
mass-fraction distribution function median value $= M_m$

$$\bar{M}_n = M_m \exp[(\sigma_w)^2/2]$$

$$\bar{M}_w = M_m \exp[3(\sigma_w)^2/2]$$

$$\bar{M}_z = M_m \exp[5(\sigma_w)^2/2]$$

and therefore depends only on $\bar{M}_n$.

Flory–Schulz distribution function
The molecular weight averages this function are related by

$$\frac{\bar{M}_n}{k} = \frac{\bar{M}_w}{k+1} = \frac{\bar{M}_z}{k+2}$$

where k is the coupling constant, defined as the number of independently growing chains required to form one dead chain.

Polydispersity
Traditionally, polydispersity Q has been defined as

$$Q = \bar{M}_w/\bar{M}_n = U + 1$$

where U, the molecular inhomogeneity, has a numerical value of one less than Q. The width of molecular weight distributions increases with increasing Q and U. Except for the Gaussian distribution function, the standard deviation is only a relative measure of distribution width (4,5).

Determination of Molecular Weight

Several books have been published since this article was last written (6–9).

Number-Average Molecular Weight.

End-Group Analysis. In end-group analysis the concentration of an end group is measured by a suitable technique, and then, from the known structure of the polymer, the value for $\bar{M}_n$ may be calculated (10–15). In condensation polymers one end of the polymer should have a specific group that can be titrated by appropriate means. Polyesters (13), polyamides (13), and polyurethanes (16) have been subjected to this analysis. Polyethers have been analyzed by hydroxyl-group titrations similar to those used for polyesters or by reaction with excess phenyl isocyanate followed by reaction with excess di-*n*-butylamine; the latter was back-titrated with perchloric acid (17). Nonaqueous titrations (18) have been used to

characterize polysulfones with $\bar{M}_n$ values of up to 25,000. Potentiometric titration in aqueous and nonaqueous media have been used to determine molecular weights of acrylamide and acrylonitrile polymers (19). Spectrophotometric analyses have also been widely utilized (14), notably uv–visible, infrared techniques, and NMR (20). Examples include the determination of phenolic end groups in polymers by uv spectroscopy (21) and potentiometric titration (18). Infrared spectroscopy has been used (22) to estimate carboxyl groups in the presence of carbonyl groups by reaction of the former with SF_4; the resulting thionyl halides were quantitatively measured. NMR spectroscopy (^1H) has been used to characterize $\bar{M}_n$ of hydroxyl end-capped polystyrenes (A. D. Edwards and M. J. R. Loadman, Malaysian Rubber Producers Research Association, unpublished data, 1976). Reaction of the single proton on the hydroxyl group yields a trimethylsilyl group containing nine protons. The enhanced sensitivity allows determination of $\bar{M}_n$ values of up to 80,000. A similar method has been reported for hydroxy-terminated polybutadienes (23), polyester polyurethanes (24), epoxides (25), and other polymers (26–28). Acid end groups in polyethylene terephthalate have been characterized (29) by reaction with hexafluoroisopropanol and ^{19}F NMR.

In certain cases extremely high sensitivity may be attained with radioactive labeling (30). Using radiolabeled (^{35}S) bisulfite initiator, the number-average molecular weight of Teflon samples was determined in the range of 389,000–8,900,000 (31). This is a particularly useful technique for insoluble polymers.

Measurement of Colligative Properties. Colligative properties are those that depend on the number of species present rather than on their kind (32,33). From thermodynamic arguments it may be shown that for very dilute ideal solutions

$$\ln a_1 = -X_2$$

where a_1 is the activity of the solvent and X_2 is the mole fraction of solute. From this relationship the solute molecular weight may be calculated if the weight fraction w_2 is known.

$$x_2 = \frac{n_2}{n_1} = \frac{w_2 M_1}{M_2 w_1}$$

This equation demonstrates that the activity, measurable by several methods, is proportional to the number of solute molecules. Thus in the case of polydisperse solutes, the number-average molecular weight is the average determined. At higher concentrations and molecular weights, the solutions become nonideal, and higher powers of the solute concentration are introduced into the equations. Measurements of several solute concentrations are required, and appropriate extrapolation techniques must be used.

Lowering of Vapor Pressure. The partial vapor pressure p_1 of solvent 1 over a solution is lower than the vapor pressure over the pure solvent $p_1{}^0$. This is expressed by Raoult's law:

$$P_1 = X_1 p_1{}^0$$

where X_1 is the mole fraction of the solvent.

For a binary solution containing a mole fraction X_2 of solute then,

$$X_2 = \frac{p_1^0 - p_1}{p_1^0} = \frac{\Delta p_1}{p_1^0} \tag{7}$$

For a dilute solution,

$$X_2 = \frac{n_2}{n_1} = \frac{w_2 M_1}{M_2 w_1} \tag{8}$$

Combining equations 7 and 8 yields

$$M_2 = w_2 \frac{M_1}{w_1} \frac{p_1^0}{\Delta p_1}$$

The unknown molecular weight of solute M_2 may be calculated from the lowering of the vapor pressure caused by the addition of w_2 grams of solute to form a binary solution; $\bar{M}_n$ values of up to 1000 may be determined (34–37).

A variation of this technique, the isopiestic method (38–40), was devised to avoid the difficulty of accurately determining the small difference in vapor pressure caused by the addition of solute. In this method (41) two limbs of a container joined by a common vapor space are filled, one with a reference solution of known weight concentration w_s and molecular weight M_s and the other with the unknown solution of known weight concentration w_2 and unknown molar concentration. The apparatus is immersed in a constant-temperature bath controlled to $\pm 0.001^\circ$C; the absolute temperature is not important. Distillation of the solvent continues until the vapor pressures above the solutions in each limb are equal, and thus the solutions contain equal mole fractions of solute. At equilibrium, which may require several weeks, the final volumes V_s, and V_2 of the known and unknown solutions are read from the calibrations on each limb.

$$\bar{M}_n = \frac{w_2 M_s V_s}{V_2 w_s}$$

$\bar{M}_n$values of up to 20,000 have been determined by this method.

Ebulliometry. Ebulliometry (34,42–47) is another technique for determining the depression of the solvent activity by the solute. In this case the elevation of the boiling point is determined. The boiling-point elevation ΔT_b is measured with sensitive thermocouples or matched thermistors in a Wheatstone bridge. The molecular weight $\bar{M}_n$ is calculated from

$$\bar{M}_n = \frac{K_b c}{\Delta T_b}$$

where c is the concentration of solute in g/1000 g of solvent and

$$K_b = \frac{R T_b^2 M}{1000\ \Delta H_v} \tag{9}$$

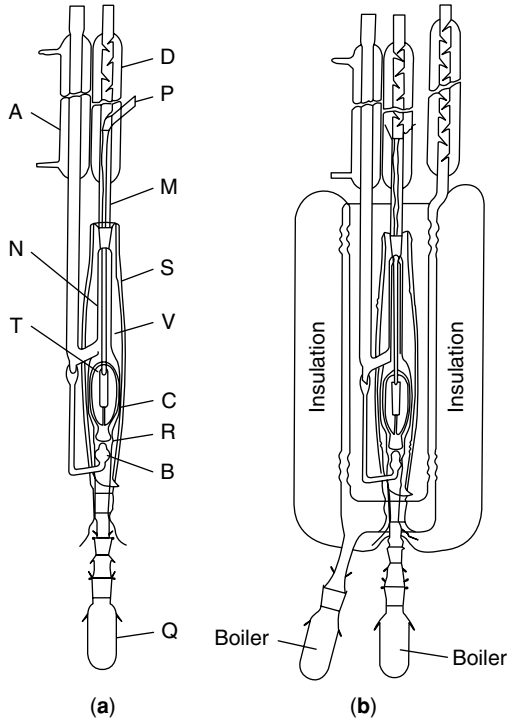

Fig. 1. (**a**) Ebulliometer design for molecular weight determination of up to $\bar{M}_n = 100{,}000$. A denotes ebulliometer cooler; B, boiler; C, Cottrell pump; D, adiabatic jacket cooler; M, thermopile; N, upper thermopile weldings; P, thermopile terminals connected with detector; Q, adiabatic jacket boiler; R, platinum resistance; T, lower thermopile weldings; and V, vacuum jacket circulated by solvent vapor. (**b**) Complete ebulliometer with adiabatic jackets and insulating apparatus (50). Courtesy of Huethig and Wepf Verlag.

is the molal ebullioscopic constant. M is the molecular weight of the solvent and T_b its boiling point; ΔH_v is the molar latent heat of vaporization of the solvent.

The ebullioscopic constant may be evaluated directly from equation 9 and thus provides an absolute method. However, the value for K_b is often determined by using a high purity solute of known molecular weight.

Currently, a sensitivity of 1×10^{-5}°C or 2.4×10^{-6}°C is attainable using a 160-junction thermocouple (48) or thermistors (49), respectively. The upper limit of molecular weight, which may be determined by this method, also depends on the solvent and solution nonideality. With careful measurements and good ebulliometer design, $\bar{M}_n$ values of up to 100,000 may be determined on isotactic polypropylene (50). The apparatus employed is shown in Figure 1. This technique has been applied to aqueous solutions (51). An ebulliometer of simple design having a temperature sensitivity of 50×10^{-6}°C has recently been reported (52). A rotating ebulliometer attempts to overcome the superheating problem (53). Errors in the methods for treating ebullioscopic data to obtain molecular weight have been discussed (54).

Cryoscopy. The freezing point of a solution is depressed below that of the pure solvent by an amount proportional to the mole fraction of solute. The value

for $\bar{M}_n$ is obtained from

$$\bar{M}_n = \frac{K_f c}{\Delta T_b}$$

where c is the concentration of solute in g/1000 g of solvent and

$$K_f = \frac{RT_m^2 M}{1000\ \Delta H_{fus}}$$

is the molal cryoscopic constant; M is the molecular weight of the solvent and T_m its melting point; ΔH_{fus} is the molar latent heat of fusion of the solvent.

Some materials, such as camphor, have very large cryoscopic constants and may be used to increase the sensitivity of the method. The method is used to determine $\bar{M}_n$ of polymers (55–59), such as polyesters (60) and ethylene-vinyl acetate copolymers (61).

A novel variation of this technique (62) involves depression of the first-order, nematic–isotropic melting transition of *N*-(*p*-ethoxybenzylidene)-*p*-*n*-butylaniline. Polystyrene and poly(ethylene oxide) are soluble in both phases, and $\bar{M}_n$ values of up to 10^6 have been studied.

Vapor-Pressure Osmometry. When a drop of solution is exposed to pure solvent vapor, the solvent vapor condenses onto the droplet, because the solute lowers the vapor pressure of the drop (63–68). The heat of condensation causes the temperature of the drop to rise, until theoretically the solution vapor pressure is increased to equal that of the solvent. In practice this does not occur, but a state of equilibrium is reached, where the heat losses from the droplet are matched by the heat of condensation (GB/T 6579-86). The temperature increase is proportional to the number of moles of solute present. A standardized method is available (H. Knauer, Berlin, unpublished data).

The design of a commercial instrument is given in Figure 2 (H. Knauer, Berlin, unpublished data). The temperature stability needed is 0.001°C. In another design, by Wescan Instruments, Inc., small platinum mesh screens ensure that a constant amount of solvent or solution is present on the thermistor. The resistance value ΔR, which is proportional to the temperature difference, is measured with a bridge circuit in all instruments. A calibration curve of ΔR vs molality m is determined by employing a solute of known molecular weight. After several minutes ΔR reaches a constant value; the calibration curve is often highly linear, but may not go through the zero point (66).

$$\Delta R = a + bm$$

The number-average molecular weight of the unknown sample may then be calculated from equation 10:

$$\bar{M}_n = \frac{bc}{\Delta R - a} \tag{10}$$

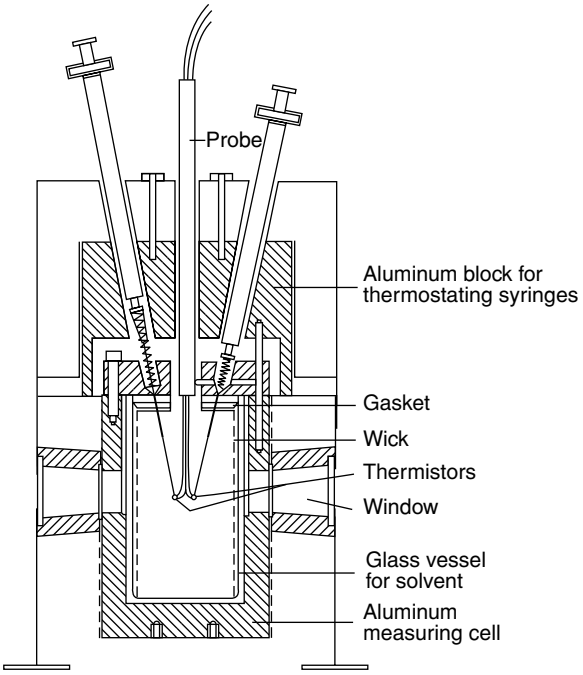

Fig. 2. Vapor-pressure osmometer apparatus (H. Knauer, Berlin, unpublished data, 1987). Courtesy of Dr. -Ing. Herbert Knauer GmbH.

where c is the concentration of solute in g/1000 g of solvent. In older osmometers the calibration curve depended on the material used to perform the calibration. For the Wescan instrument and another research vapor-pressure osmometer (69), both based on the same design (70), the calibration constant was independent of the material. These instruments have determined polystyrene $\bar{M}_n$ values of 400,000 (71), 100,000 (72), and 100,000 (69); polyolefins have been characterized at 140°C (73) and styrene/methylmethacrylate copolymers (32). For higher molecular weight solutes, the virial coefficients become important. In this case $\Delta R/c$ must be plotted against c in order to extrapolate the $\Delta R/c$ value to infinite dilution. When the plot is not linear, it is necessary to plot $(\Delta R/c)^{1/2}$ vs c to obtain a linear extrapolation to infinite dilution.

Membrane Osmometry. Membrane osmometry is a well-established technique (68,74–81). Commercial instrumentation is available (Gonotec GmbH, Knauer). A standardized method is available (GB/T 6596-86). The main problem is membrane permeation by lower molecular weight species (82). Improvements in membranes with well-defined, low molecular weight cutoffs can be expected as a consequence of the renewed interest in membrane-separation techniques (83,84) (see MEMBRANE TECHNOLOGY). Membrane osmometry has been applied to a wide variety of polymers, including operation at high temperatures for polymers difficult to dissolve. Comb-like polymers have been characterized and the results compared with those from gel permeation chromatography (GPC) (85). Preliminary results of an online osmometer for GPC detection have been described (86,87). The upper limit for molecular weight determination is ca 1×10^6. The lower limit

depends on the molecular weight distribution, ie, the details of the composition of the low molecular weight tail. In most cases the concentration dependence of osmotic pressure Π must be determined and Π/c extrapolated to zero concentration by plotting Π/c vs c, or $(\Pi/c)^{1/2}$ vs c.

Viscosity-Average Molecular Weight. The viscosity of dilute polymer solutions may be related to the molecular weight of the polymer by the appropriate calibration (see Viscometry). The polymer is usually separated into narrow molecular weight distribution fractions, which are characterized by absolute molecular weight methods. The molecular weight is related to the intrinsic viscosity $[\eta]$ by the Mark–Houwink relationship (eq. 6).

The intrinsic viscosity is obtained using viscometer types of viscometer tubes and plotting the reduced or inherent viscosity of a series of polymer solutions with various concentrations against the solution concentration. Extrapolation to zero concentration yields the intrinsic viscosity. The technique has found widespread application (88–92), and compilations of Mark–Houwink constants are available (93). A novel method to determine intrinsic viscosity using a flow piezoelectric quartz crystal has been developed (94). Static and continuous measurements of intrinsic viscosity using a differential viscometer (Viscotek) have been reviewed (95). If the Mark–Houwink constants are determined using narrow molecular weight distribution materials, the average molecular weight obtained from equation 6 is the viscosity-average molecular weight $\bar{M}_v$. The range of molecular weights that may be characterized is very large. Special precautions are required for extremely high molecular weight samples to avoid degradation during the solution process or the measurement (96). Dilute solution viscometry for measurement of molecular weight, branching, and other physical parameters have been reviewed (97). A method to calculate the viscosity average molecular weight from GPC for a polymer with unknown Mark–Houwink constants has been reported (98).

Weight-Average Molecular Weight.

Light Scattering. Laser Light Scattering (qv) is a technique (99–106) widely used to characterize polymeric materials. Standardized methods are available (ASTD D4001 and GB/T 6598-86). Commercial instrumentation is available to measure the light-scattering properties of polymer solutions and the refractive index increment (107). Older instrumentation includes the Brice Phoenix Photometer, the Sofica Light Scattering Photometer, as well as the Chromatix product. Wyatt Technology and Malvern Instruments currently produce instruments. Lasers are used as light sources to measure scattering at small angles to the beam. This is important since the data obtained must be extrapolated to zero concentration and zero scattering angle using Zimm plots (108). The weight-average molecular weight is determined by this technique, and the molecular weights accessible range from a few hundred to several million. The solutions employed must be free of dust and are usually subjected to filtration or centrifugation. Solutions of high molecular weight degradable polymers are the most difficult to clarify. The solvent is selected to give a reasonable difference in refractive index with the solute. The technique has been applied to determine the molecular weight of difficultly soluble polymers such as polyethylene (109,110) and of polytetrafluoroethylene and its copolymers with ethylene (111–113). Copolymers with homogeneous distribution of monomer units in the polymer chain may be analyzed by the same methods as homopolymers. If the composition varies as a function of molecular weight, the analysis is more complicated (114). Terpolymers have also been considered (115).

True molecular weights and heterogeneity of styrene-butyl acrylate copolymers have been determined using static low angle laser light scattering (LALLS) and GPC/LALLS (116) and styrene–polydimethylsiloxane block copolymers (117) using GPC/LALLS. Multi-angle laser light scattering (MALLS) has been used as a GPC detector to characterize molecular weight, molecular size, and branching of organic and water soluble polymers (118).

Dynamic light scattering (119) has been used to determine the number average molecular weight (120) and molecular weight distribution of polymers in solution (121–123). There are several mathematical approaches to determine the molecular weight distribution from PCS data. Comparisons with GPC and numerical simulation have been made (124). The resolution of bimodal distributions has been demonstrated (125).

Pulse-induced critical scattering (126,127), although not utilized as a method for molecular weight characterization, may be a sensitive procedure for detecting small differences in molecular weight distribution.

X-ray (128) and neutron scattering (qv) (129,130) may also be used to determine weight-average molecular weights. The main drawback is the greater expense and the lack of suitable facilities.

Ultracentrifuge. The ultracentrifuge is used to determine molecular weights (131–133). Sedimentation velocity employs a sufficiently high centrifugal field so that the sedimentation rate may be measured. The sedimentation coefficient S is empirically corrected for concentration and pressure effects to give S_0, the sedimentation coefficient at zero concentration. The method also requires the measurement of the diffusion coefficient at infinite dilution D_0. The molecular weight is calculated from the Svedberg equation

$$\frac{S_0}{D_0} = \frac{M(1 - \nu\rho)}{RT}$$

where ν is the partial specific volume of the solute and ρ the density of the solution. For a polydisperse solute the correct averages for S and D are combined in the Svedberg equation to yield a well-defined average molecular weight. If D is obtained from intensity-fluctuation spectroscopy (134) and combined with the weight average S value, the weight-average molecular weight is obtained. The application of the sedimentation velocity method to calculate molecular weight distribution is extremely complex, but has been successful in special studies (135).

In the sedimentation equilibrium method, a lower centrifugal field is maintained for a period of time in such a way that sedimentation is balanced by diffusion and an equilibrium distribution of polymer is established in the cell. Although $\bar{M}_w$ and $\bar{M}_z$ are easily determined, the length of time of the experiment is a disadvantage. In contrast to light scattering, this method is not affected by dust particles, and no calibration is needed. The molecular weight distribution may be obtained from the sedimentation velocity data, but not without mathematical difficulties (136) or requiring additional data at other rotor speeds (137,138). An improved detection system for the analytical ultracentrifuge has been reported (139,140). A new 8-cell rotor that allows increased throughput of samples has been described (141).

Improved data analysis has led to the simultaneous determination of the sedimentation coefficient and diffusion coefficient, and a calculation of the molecular weight from the Svedberg equation (142). The Svedberg method is capable of determining molecular weights of up to 40×10^6 (96) on an absolute basis. Sedimentation equilibrium in a density gradient has been used to determine the compositional analysis of copolymers, eg, butadiene-styrene (143).

Munk (144) has recently reviewed the use of sedimentation velocity and sedimentation equilibrium to characterize molecular weight. A new absolute method for the determination of molecular weight distribution based on band sedimentation and LALLS has been applied to water-soluble polymers (145).

Higher Molecular Weight Averages. Classical techniques often cannot be used for higher molecular weight averages ($\bar{M}_z$, $\bar{M}_{z+1}$, etc). These are usually measured by determining the molecular weight distribution by fractionation (qv) or affinity chromatography (qv) and back-calculating the averages from the distribution.

Determination of Molecular Weight Distribution

Fractionation. Polymers may be separated on the basis of molecular weight by precipitation or phase-separation techniques (146–149). The polymer that is originally in solution separates on the basis of molecular weight when the thermodynamic quality of the solvents is changed, ie, by changing the solvent composition or temperature. The principal techniques are *fractional precipitation* and *coacervate extraction*, both solution-based (Fig. 3). The former is based on the removal of material from the polymer-rich precipitated phase and the latter on the removal of fractions from the polymer-lean solution phase. Computer simulations and experimental results have shown the coacervate extraction technique (150) to yield narrower molecular weight distribution fractions than the fractional precipitation method (151–153).

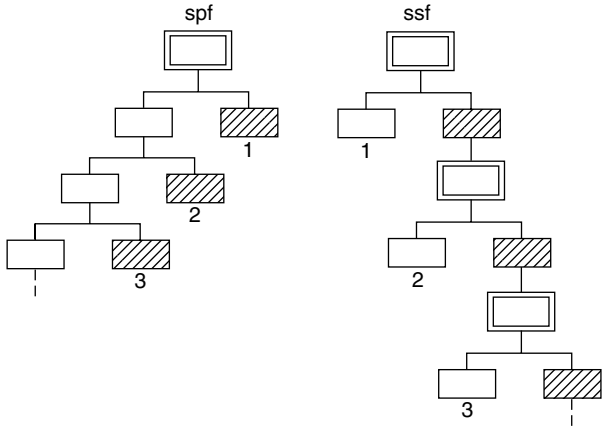

Fig. 3. Successive precipitation (SPF) and solution fractionation (SSF) (coacervate extraction): ▭, mother solution; ▭, polymer rich phase; and ▨, polymer-lean phase. Numbers denote fraction numbers (148). Courtesy of Society of Chemical Industry.

To obtain the molecular weight distribution, the fractions of known mass must be characterized by a molecular weight technique. The integral and differential molecular weight distribution may be evaluated using a method (154) that assumes no particular molecular weight distribution function for the fraction or treatments that assume a particular model for the molecular weight distribution of the fractions (155). Fractionation may also be achieved by crystallization from dilute solution (156).

In column fractionation (157,158) the polymer is precipitated onto an inert support, which is placed at the top of a packed column (159). A solvent mixture of increasing solvent power is pumped through the column; a temperature gradient is often maintained. This is known as *Baker–Williams fractionation* (160). This technique is applicable to all amorphous homopolymers and crystalline homopolymers above the melting point. For copolymers and more complex compositions, the same technique may be employed, but the analysis is considerably more difficult.

Temperature rising elution fractionation (TREF) (161,162) is a useful fractionation technique which gives information on the compositional distribution.

Chromatography. The determination of molecular weight distribution and chemical composition by chromatographic techniques has been discussed (163).

Gel Permeation (Size-Exclusion) Chromatography. GPC has been in use since the 1960s and has been a most important development in molecular weight determination (164–169). For this technique the polymer must be soluble, and calibration with suitable standards is required. The method is extremely efficient; it requires 0.5–2 h per sample and only a few milligrams of material. Standardized methods are available (GB/T 6599-86, ASTM D5296-97, and A83 ASTM D6747-99). Commercial instrumentation capable of operating up to 150°C is available from Waters and Polymer Laboratories. Detection is normally accomplished by differential refractometry, although uv and ir (170) absorption spectrometry have also been employed. The chromatographic columns are packed with spherical- or irregular-shaped porous beads. The packing may be a crosslinked polymer, a porous glass, or a silica material. The pore size distribution determines the separation range of the columns. Calibration is normally performed using well-characterized narrow MWD standards. Calibration can be performed using broad MWD materials (171). Typical calibration curves (172) are shown in Figure 4. By combining columns in series, a separation range may be achieved covering the molecular weight distribution of the sample. Mathematical treatments of the chromatogram and calibration curve to calculate the molecular weight distribution are given (173). Broadening by the chromatographic process must be calibrated for and corrections applied to produce true molecular weight distributions. *Chemimetrics* has been applied to GPC calibration equations (174) and helped to establish the best equations. Data reduction in GPC (175) has been described. A new solvent system which allows polyesters and polyamides to be characterized by GPC at room temperature has been developed (176). High speed GPC of low molecular weight polymers has been described (177).

The design and use of a continuous, viscometric detector (178,179) has further advanced the application of the GPC technique, and a commercial viscometric detector is on the market from Viscotek Corp (180,181).

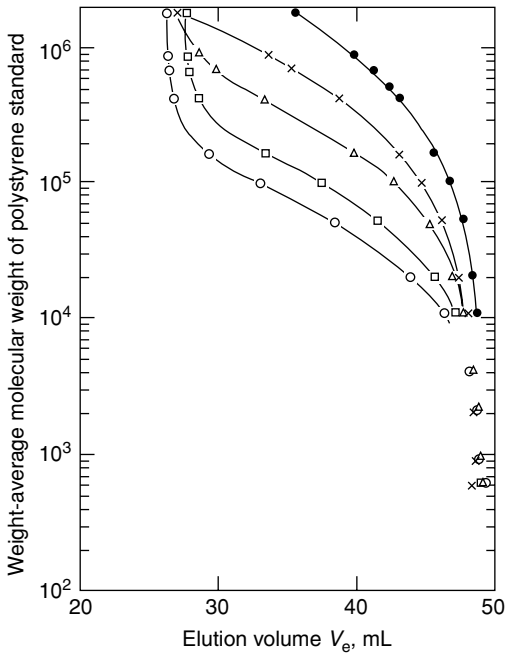

Fig. 4. GPC calibration curve for Corning porous glasses with various pore sizes: ○, CPG 10–240; □, CPG 10–370; ×, CPG 10–1250; and ●, CPG 10–2000 (172). Courtesy of John Wiley & Sons, Inc.

Direct determination of the polymer molecular weight in the detector cell after separation by GPC is possible by LALLS. The technique (182–184) is applicable to the dilute polymer solutions emerging from the chromatographic column; commercial equipment is available, older models (Chromatix KMX6 and LSD100 from LDC/Milton Roy) and newer instruments (Wyatt and Polymer Labs). A review of prior development and a description of a methodology for correcting for dispersion in the concentration detector and the light scattering detector has been published (185). A review of GPC and the application of molecular weight detectors and related separation techniques has been published (186). The characterization of complex polymers by GPC and high performance liquid chromatography (HPLC) has been discussed (187). Quantitative high temperature GPC of polyolefins using refractive index and differential viscometer detection (188) and differential viscometer and light scattering detectors (189) has been reported. This method has been used for on-line molecular weight measurement and branching characterization of water-soluble polymers (185,190). Shear degradation during the chromatographic process may be a problem (191), but can be detected by viscometry and LALLS. A triple detector employing a concentration detector, a viscometer, and a light scattering detector is available (Viscotek). Three detectors, an evaporative light scattering detector to measure concentration, a refractometer, and LALLS, have been used to determine MWD of copolymers (EPM and EPDM) (192). LALLS has proven useful in detecting and eliminating aggregates in dilute polymer solutions which would affect the GPC results (193). Nuclear magnetic resonance,

NMR, has been employed as an on-line detector for GPC (194). Goldwasser (195) developed an analysis which allows the calculation of absolute values for $\bar{M}_n$ from the combined results from GPC and differential viscometry. Mass spectrometry has been coupled with GPC to characterize a variety of polymers (196–198). A comparison of the most probably peak value of polymer distributions has been evaluated between MALDI MS and GPC (199).

Analyses by GPC of block and statistical copolymers (200,201) and copolymers (202) and polymer mixtures (203) have been reported. Full copolymer characterization by combining GPC-NMR with GPC-MALDI has been demonstrated (204).

Other detectors that are capable of determining the polymer concentration in the effluent are based on dielectric constant (205) and density (206–213). Mass can be determined directly with a piezoelectric quartz sensor having a sensitivity of 10^{-10} g (214). A universal mass detector, evaporative light scattering Detector (ELSD) based on the formation of droplets in a nebulizer gas and detection by light scattering using a laser, has been developed and applied to GPC (215). Commercial ELSD units are available from Alltech, Varex Corp., and Polymer Laboratories.

A direct molecular weight method (216) employs the LALLS detector, but uses sedimentation velocity instead of GPC to separate the polymers.

Round robin tests for reproducibility of GPC results have been reported (217). Twenty-four laboratories used calibration standards from two different sources and three test polymers. The results for the three samples varied from 3 to 14% depending on which calibration was used. Similar results for number-average molecular weights have been documented (218). Round robin characterization of polyethylene by high temperature GPC in 15 laboratories has been documented (219).

High Performance Liquid Chromatography and Supercritical Fluid Chromatography. For lower molecular weights, HPLC and supercritical fluid chromatography (SFC) (220) offer higher resolution than GPC. Higher molecular weights may produce multiple peaks from monodisperse standards (221). The oligomers are resolved into individual peaks, and molecular weight averages are calculated (222). HPLC is more common and has been applied to phenol-formaldehyde resins (223), polyurethanes (224), polyesters (225), and polycarbonates (226). Since solvent gradients are often used in HPLC the refractometer detector cannot be used, and ultraviolet/visible spectrometers and/or ELSDs must be used. The ELSD may also be used in SFC. SFC can resolve higher oligomers than HPLC. Polystyrene oligomers of up to $n = 50$ may be resolved by SFC; the process requires 18 h (227). Several commercial SFC units are available and their availability should rapidly increase the application of this technique to characterize oligomeric species. A review of supercritical fractionation of polymers and copolymers has been published (228). Mass spectrometry has been used in conjunction with SFC and capillary GPC to characterize polypropylene glycol (229).

Liquid adsorption chromatography (LAV) and GPC have been used to determine chemical composition distribution (CCD) and MWD of styrene–methyacrylate copolymers (230).

Thin-Layer Chromatography. Thin-layer chromatography (TLC) is widely applicable to polymer characterization and has been used to characterize

molecular weight distribution and compositional distribution (231–233). Cellulose nitrate has been fractionated by this method on the basis of molecular weight or nitrogen content (234).

Mass Spectrometry. Advances in soft ionization techniques and developments in high resolution mass spectrometers has led to the possibility of determining intact molecular ions up to 1×10^6 Da and the measurement of the entire MWD (235,236). The application of mass spectrometry techniques to characterize polymer molecular weight distribution has evaluated (237–243). The MWD of polystyrene SRM 1487 and a narrow MND polymethylmethacrylate (MW 6300) determined by MALDI TOF mass spectrometry have been compared with results from the ultracentrifuge and GPC (244).

Phase-Distribution Chromatography. A chromatographic fractionation is achieved in this method (245,246), by partitioning a solute between a solvent flowing through a column, packed with a support coated with a thin layer of high molecular weight, non-cross-linked polymer. The temperature of operation is below the Θ-temperature of the solute, and separation efficiency increases sharply with decreasing temperature. A fully automated chromatograph has been designed (247), and applications have been reported (248–250).

Field–Flow Fractionation. Field-flow fractionation (FFF) employs a one-phase chromatographic system (251,252). Commercial instrumentation is available from Postnova Analytics and Tecan. Separation occurs in a thin channel containing a single moving fluid. The field applied across the channel may be selected on the basis of the solute. Possible fields include sedimentation, cross-flow, concentration, dielectric, thermal, and magnetic. A book (253) and a review (254) of this technique and its comparison with GPC for the characterization of polymer molecular weights have been published.

Thermal fields have been used for the separation of polymers in organic solvents (255). Methods for calculation of MWD from thermal FFF have been published (256). For aqueous systems a cross-flow of solvent has been used to separate polyelectrolytes (257) and high molecular weight polyacrylamides (258). Water-soluble polymers have also been characterized by this technique (259,260), in conjunction with LALLS detector (261) and MALLS (262). Extremely high molecular weights of up to 10^{12} can be determined (263); because no abrupt changes occur in the forces imposed on the polymer molecules, no degradation takes place. Sedimentation fields were investigated (264), and small samples were quickly fractionated. Compositional heterogeneity has been determined by sequential GPC and FFF (265).

Electrophoresis. Electrophoresis is widely practiced on biopolymers (266–268) for the determination of molecular weights of proteins and their subunits. Typically, a polyacrylamide bed is used to separate or characterize these solutes under the influence of an electric field, on the basis of charge and molecular size. The proteins are frequently denatured with sodium dodecyl sulfonate (SDS), and these subunit-SDS complexes are separated on the basis of molecular size. A densitometer employing a soft laser scanning device is commercially available to automate the data-reduction process (269).

Rheological Measurements. Some polymers are difficult to dissolve. Mechanical spectroscopy or rheological measurements (qv) offer a way to determine the molecular weight distribution of these materials. Mechanical spectroscopy has

been applied to characterize the MWD of polyolefins (270) Rheological data has been used to determine the MWD of polybutadiene and polypropylene (271). Measurements of ethylene–tetrafluorethylene copolymers using dynamic mechanical analysis of the melts showed broader distributions than those determined by high temperature laser light scattering (272).

Other Techniques. Atomization of polymer solutions to form single molecules deposited in a solvent-free state on a surface has been demonstrated for a wide variety of polymers (273). The electron microscope is used at 20,000–30,000 × after platinum shadowing to determine size and size distribution (274). The scanning transmission electron microscope is employed for biological macromolecules (275). For extremely high molecular weight polymers hydrodynamic chromatography (HDC) may be a viable technique. Columns are packed with solid spheres and the diameter determines the separation range. Solid particles between 5 and 300 nm may be separated. Columns are available from Polymer Laboratories, and using a high temperature infrared detector cell the composition of polyolefin copolymers can be characterized. A mathematical model for HDC and GPC for porous column packings has been published (276). Methods to characterize insoluble polymers have been discussed (277,278).

BIBLIOGRAPHY

"Molecular Weight Determination" in *EPST* 1st ed., Vol. 9, pp. 182–193, by Manfred J. R. Cantow, Airco Central Research Laboratories, and Julian F. Johnson, Chevron Research Co; in *EPST* 2nd ed., Vol. 10, pp. 1–19, by Anthony R. Cooper, Lockheed Missiles and Space Co.

1. L. H. Peebles, *Molecular Weight Distributions in Polymers*, Wiley-Interscience, New York, 1971.
2. K. W. Min, *J. Appl. Polym. Sci.* **22**, 589 (1978).
3. G. C. Berry, in M. B. Bever, ed., *Encyclopedia of Materials Science and Engineering*, Pergamon Press, Oxford, 1986, pp. 3759–3768.
4. C. W. Pyun, *J. Polym. Sci., Polym. Phys. Ed.* **17**, 2111 (1979).
5. C. W. Pyun, *J. Polym. Sci., Polym. Phys. Ed.* **24**, 229 (1986).
6. A. R. Cooper and J. D. Winefordner, ed., Determination of Molecular Weight, Vol. 103 in Chemical Analysis, A Series of Monographs on Analytical Chemistry and Its Applications, John Wiley & Sons, Inc., New York, 1989.
7. R. A. Pethrick and J. V. Dawkins, eds., *Modern Techniques for Polymer Characterisation*, John Wiley & Sons, Inc., New York, 1999.
8. D. Campbell, R. A. Pethrick, and J. R. White, *Polymer Characterisation—Physical Techniques*, 2nd ed., Stanley Thornes, Cheltenham, U.K., 2000.
9. R. A. Pethrick and R. S. Stein, eds., *Experimental Methods for Polymer Characterization*, John Wiley & Sons, Inc., Sussex, U.K., 1999.
10. N. C. Billingham, *Molar Mass Measurements in Polymer Science*, Halsted Press, a division of John Wiley & Sons, Inc., New York, 1977, Chapt. 9, p. 234.
11. G. F. Price, in P. W. Allen, ed., *Techniques of Polymer Characterization*, Butterworth & Co. (Publishers) Ltd., London, 1959, Chapt. VII.
12. S. R. Rafikov, S. A. Pavlova, and I. I. Tverdokhlebora, *Determination of Molecular Weights and Polydispersity of High Polymers*, Israel Programme for Scientific Translation, Jerusalem, Israel, 1964, Chapt. 8.

13. R. G. Garmon, in P. E. Slade, Jr., ed., *Polymer Molecular Weights*, Marcel Dekker, Inc., New York, 1975, Chapt. 3.
14. J. Urbanski, N. Czerwinski, K. Janicka, F. Majewska, and H. Zowall, *Handbook of Analysis of Synthetic Polymers and Plastics*, Wiley-Interscience, New York, 1977.
15. A. R. Cooper, in Ref. 6, Chapt. 2.
16. D. J. David and H. B. Staley, *Analytical Chemistry of Polyurethanes*, Wiley-Interscience, New York, 1959.
17. D. H. Reed, F. E. Critchfield, and D. K. Elder, *Anal. Chem.* **35**, 571 (1963).
18. A. J. Wnuk, T. F. Davidson, and J. E. McGrath, *J. Appl. Polym. Sci., Appl. Polym. Symp.* **34**, 89 (1978).
19. A. S. Sarac, B. Ustamehmetoglu, and C. Erbil, *Polym. Bull.* **32**(1), 91–95 (1994).
20. J. R. Ebdon, in L. S. Bark and N. S. Allen, eds., *Analysis of Polymer Systems*, Applied Science Publishers, London, 1982, p. 21.
21. E. Shchori and J. E. McGrath, *J. Appl. Polym. Sci., Appl. Polym. Symp.* **34**, 103 (1978).
22. J. F. Heacock, *J. Appl. Polym. Sci.* **7**, 2319 (1963).
23. G. Fages and Q. T. Pham, *Makromol. Chem.* **180**, 2435 (1979).
24. F. W. Yeager and J. W. Becker, *Anal. Chem.* **49**, 722 (1977).
25. W. B. Moniz and C. F. Poranski, Jr., in R. S. Bauer, ed., *Epoxy Resin Chemistry*, ACS Symposium Series 114, American Chemical Society, Washington, D. C., 1979.
26. S. Amiya, K. Mathumura, and T. Taniguchi, *Anal. Sci.* **7**, 1649 (1991).
27. A. M. Kenwright, S. K. Pierce, R. W. Richards, A. Bunn, and W. A. MacDonald, *Polymer* **40**, 2035–2040 (1999).
28. T. Amari, K. Nishimura, K. Minio, A. Kawabata, and Y. Ozika, *J. Polym. Sci., Polym. Chem.* **39**, 665 (2001).
29. Y. Ma, U. S. Agarwal, J. A. J. M. Vekemans, and D. J. Sikkema, *Polymer* **44**, 4429–4434 (2003).
30. K. L. Berry and J. H. Peterson, *J. Am. Chem. Soc.* **73**, 5195 (1951).
31. R. C. Dobau, A. C. Knight, J. H. Peterson, and C. A. Sperati, *130th Meeting of the American Chemical Society*, Atlantic City, N. J., Sept. 1956.
32. H. Suzuki and K. Kamide, in Ref. 7, pp. 375–387.
33. A. R. Cooper, in Ref. 6, Chapt. 2.
34. D. F. Rushman, in Ref. 11, p. 113.
35. I. M. Kolthoff and P. J. Elving, eds., *Treatise on Analytical Chemistry, Theory and Practice*, Vol. 7, Part 1, Wiley-Interscience, New York, 1978, p. 4446.
36. G. Radakoff, *Z. Chem.* **1**, 135 (1961).
37. R. U. Bonnar, M. Dimbat, and F. H. Stross, *Number Average Molecular Weights*, Wiley-Interscience, New York, 1958, p. 275.
38. Ref. 35, p. 114.
39. Ref. 36, p. 4448.
40. Ref. 38, p. 268.
41. R. L. Parette, *J. Polym. Sci.* **15**, 450 (1955).
42. Ref. 38, p. 113.
43. Ref. 36, p. 4450.
44. M. Ezrin, in M. McIntyre, ed., *Characterization of Macromolecular Structure, Publication 1573*, National Academy of Science, Washington, D. C., 1968, p. 3.
45. C. A. Glover, in Ref. 13, Part I, p. 105.
46. C. A. Glover, in M. Ezrin, ed., *Polymer Molecular Weight Methods, Advances in Chemistry Series 125*, American Chemical Society, Washington, D. C., p. 1.
47. G. Davison, in Ref. 20, p. 209.
48. C. A. Glover, C. N. Reilly, and F. W. McLafferty, eds., *Advances in Analytical Chemistry and Instrumentation*, Vol. 5 Wiley-Interscience, New York, 1966, p. 1.
49. E. Zichy, *SCI Monogr* **17**, 122 (1963).

50. P. Parrini and M. S. Vacanti, *Die Makromol. Chem.* **175**, 935 (1974).
51. W. De Oliveira, *Differential Ebulliometry*, Ph. D. thesis, Clarkson College of Technology, Potsdam, N. Y., 1975.
52. W. De Oliveira and G. Francisco, *Chem. Biomed. Environ. Instrum.* **10**, 189 (1980).
53. J.-T. Chen, H. Sotobayashi, and F. Asmussen, *Colloid Polym. Sci.* **259**, 1202 (1981).
54. J. Melsheimer and H. Sotobayashi, *Die Makromol. Chem.* **179**, 2913 (1978).
55. Ref. 46, p. 124.
56. E. J. Newitt and V. Kokle, *J. Polym. Sci., Part A-2* **4**, 705 (1966).
57. Ref. 35, p. 125.
58. Ref. 38, p. 17.
59. Ref. 12, p. 255.
60. L. Carbonnel, R. Guieu, C. Ponge, and J. C. Rosso, *J. Chim. Phys. Physicochim. Biol.* **70**, 1400 (1973).
61. A. Ya Ryasnyanskaya, S. L. Lyubimova, V. V. Kalashnikov, R. A. Terteryan, V. N. Mosastyrskii, and B. V. Gryaznov, *Neftepererab. Neftekhim. Moscow* 69 (1973).
62. B. Kronberg and D. Patterson, *Macromolecules* **12**, 916 (1979).
63. A. V. Hill, *Proc. R. Soc. London, Ser. A* **127**, 9 (1930).
64. C. A. Glover, in Ref. 13, p. 142.
65. Ref. 10, p. 81.
66. M. J. R. Cantow, R. S. Porter, and J. F. Johnson, *J. Polym. Sci., Part A* **2**, 2547 (1964).
67. C. E. M. Morris, in Ref. 6, Chapt. 3.
68. B. Hunt, in Ref. 7, Chapt. 9.
69. K. Kamide, T. Terakuwa, and H. Uchiki, *Makromol. Chem.* **177**, 1447 (1976).
70. R. E. Dohner, A. H. Wachter, and W. Simon, *Helv. Chim. Acta* **50**, 2193 (1967).
71. A. H. Wachter and W. Simon, *Anal. Chem.* **41**, 90 (1969).
72. D. E. Burge, *J. Appl. Polym. Sci.* **24**, 293 (1979).
73. F. M. Mirabella, *J. Appl. Poly. Sci.* **25**, 1775 (1980).
74. Ref. 38, p. 191.
75. Ref. 10, p. 44.
76. Ref. 11, p. 68.
77. H. Coll and F. H. Stross, in Ref. 47, p. 10.
78. R. D. Ulrich, in Ref. 46, p. 9.
79. W. R. Krigbaum and R.-J. Roe, in Ref. 36, p. 4461.
80. D. E. Burge, *Am. Lab.* 41 (June 1977).
81. H. Coll, in Ref. 6, Chapt. 4.
82. H. Coll, *J. Polym. Sci., Makromol. Rev.* **5**, 541 (1971).
83. A. R. Cooper, ed., in *Polymer Science and Technology*, Vol. 16, Plenum Press, New York, 1982.
84. A. R. Cooper, ed., *in Polymer Science and Technology*, Vol. 13, Plenum Press, New York (1981).
85. K. Yokota, T. Hirabayashi, and Y. Inai, *Polym. J. (Japan)* **26**(4), 105–108 (1994).
86. W. W. Yau, *J. Appl. Polym. Sci., Appl. Polym. Symp.* **48**, 85–94 (1991).
87. U. Lehman, W. Kohler, and W. Albrecht, *Macromolecules* **29**, 3212–3215 (1996).
88. K. Kamide and M. Saito, in Ref. 6, Chapt. 8.
89. P. F. Onyon, in Ref. 11, Chapt. VI.
90. D. K. Carpenter and L. Westerman, in Ref. 13, Part II, p. 441.
91. M. Van Oene, in Ref. 47, p. 353.
92. Ref. 10, p. 172.
93. M. Kurata and Y. Tsunashima, in J. Brandrup and E. H. Immergut, eds., *Polymer Handbook*, 3rd ed., Wiley-Interscience, New York, 1989, Chapt. VII.
94. Y. Mao, W. Wei, J. Zhang, and Y. Li, *J. Appl. Polym. Sci., A* **12**, 82, 63 (2001).

95. J. W. Mays and N. Hadgjichristidis, in H. G. Barth and J. W. Mays, eds., *Modern Methods of Polymer Characterization*, John Wiley & Sons, Inc., New York, Chapt. 7, 1997.
96. B. Appelt and G. Meyerhoff, *Macromolecules* **13**, 657 (1980).
97. J. W. Mays and N. Hadjichristidis, in Ref. 7, pp. 227–269.
98. H. Kh. Mahabadi, *J. Polym. Sci., Polym. Phys.* **22**, 449–457 (1984).
99. M. B. Huglin, ed., *Light Scattering from Polymer Solutions*, Academic Press, Inc., Orlando, Fla., 1972.
100. M. Kerker, *The Scattering of Light*, Academic Press, Inc., Orlando, Fla., 1969.
101. H. Yamakawa, *Modern Theory of Polymer Solutions*, Harper & Row (Publishers), Inc., New York, 1971.
102. G. C. Berry, in R. A. Meyers, ed., *Encyclopedia of Analytical Chemistry*, John Wiley & Sons, Inc., Sussex, U.K., 2000.
103. G. C. Berry and P. M. Coutts, in Ref. 9, p. 721.
104. G. C. Berry, in H. F. Mark, N. M. Bikales, C. G. Ovèrberger, G. Menges, and J. I. Kroshwitz, eds., Encyclopedia of Polymer Science and Engineering, Vol. 8, John Wiley & Sons, Inc., New York, 1987, pp. 721–794.
105. B. Chu, in Ref. 6, Chapt. 5, pp. 53–86.
106. G. Berry and P. M. Cotts, in Ref. 7, Chapt. 4.
107. H. Utiyama, in Ref. 99, Chapt. 3.
108. B. H. Zimm, *J. Chem. Phys.* **16**, 1093 (1948).
109. B. Chu, M. Onclin, and J. R. Ford, *J. Phys. Chem.* **88**, 6566 (1984).
110. J. W. Pope and B. Chu, *Macromolecules* **17**, 2633 (1984).
111. B. Chu and C. Wu, *Macromolecules* **19**, 1285 (1986).
112. B. Chu and C. Wu, *Macromolecules* **20**, 93 (1987).
113. C. Wu, W. Buck, and B. Chu, *Macromolecules* **20**, 98 (1987).
114. E. F. Cassassa and G. C. Berry, in Ref. 8, Part I, p. 161.
115. H. Kambe, Y. Kambe, and C. Honda, *Polymer* **14**, 460 (1973).
116. F. B. Mahili, C. Y. Kuo, and T. Provder, *J. Appl. Polym. Sci.* **29**, 925–931 (1984).
117. T. Dumelow, S. R. Holding, L. J. Maisey, and J. V. Dawkins, *Polymer* **27**, 1170–1176 (1986).
118. S. Podzimek, *J. Appl. Polym. Sci.* **54**(1), 91–103 (1994).
119. B. Chu, *Laser Light Scattering*, 2nd ed., Academic Press, Inc., Boston, 1991.
120. J. C. Selser, *Macromolecules* **12**, 909 (1979).
121. Q. Ying, B. Chu, R. Qian, J. Bao, J. Zhang, and C. Xu, *Polymer* **26**, 1401 (1985).
122. B. Chu, Q. Ying, C. Wu, J. R. Ford, and M. S. Dhadal, *Polymer* **26**, 1408 (1985).
123. D. Caroline, in J. V. Dawkins, ed., *Developments in Characterization*, Vol. 5, Elsevier Applied Science, London, 1986.
124. I. Tomka and G. Vancso in J. Mitchell, Jr., ed., *Applied Polymer Analysis and Characterization*, Hanser, Munich, 1987, p. 237.
125. G. Vansco, I. Tomka, and K. Vansco-Polacsek, *Macromolecules* **21**, 415 (1988).
126. M. Gordon, J. Goldsbrough, B. W. Ready, and K. W. Derham, in J. H. S. Green and R. Dietz, eds., *Industrial Polymers: Characterization by Molecular Weight*, Transcripta Books, London, 1973, p. 45.
127. H. Galina, M. Gordon, P. Irvine, and L. A. Kleintjens, *Pure Appl. Chem.* **54**, 365 (1982).
128. D. Glotter and O. Kratky, *Small Angle X-Ray Scattering*, Academic Press, Ltd., London, 1982.
129. R. W. Richards, in J. V. Dawkins, ed., *Developments in Polymer Characterization*, Vol. 5, Elsevier Applied Science Publishers, Ltd., Barking, U.K., 1986.
130. R. W. Richards, in Ref. 6, Chapt. 6, pp. 87–116.
131. H. Fujita, *Mathematical Theory of Sedimentation Analysis*, Academic Press, Inc., Orlando, Fla., 1962.

132. A. R. Cooper, in Ref. 6, Chapt. 7, pp. 117–144.
133. H. Borchard and E. Selic, in Ref. 7, Chapt. 11.
134. D. N. Pussey, in Ref. 126, p. 26.
135. R. Dietz, in Ref. 126, p. 19.
136. D. A. Lee, *J. Polym. Sci., Part A-2* **8**, 1039 (1970).
137. T. G. Scholte, *J. Polym. Sci., Part A-2* **6**, 11 (1968).
138. T. G. Scholte, *Eur. Polym. J.* **6**, 51 (1970).
139. J. Flossdorf, H. Schillig, and K. P. Schindler, *Makromol. Chem.* **179**, 1617 (1978).
140. J. Flossdorf, *Makromol. Chem.* **181**, 715 (1980).
141. N. Machtle and U. Klodwig, *Makromol. Chem.* **180**, 2507 (1979).
142. R. Wohlschiess, K. F. Elgert, and H.-J. Cantow, *Angew. Makromol. Chem.* **74**, 323 (1978).
143. C. J. Stacy, *J. Appl. Polym. Sci.* **21**, 2231 (1977).
144. P. Munk, *Modern Methods of Polymer Characterization*, John Wiley & Sons, Inc., New York, 1991, 271–312.
145. G. Holzwarth, L. Soni, and D. N. Schulz, *Macromolecules* **19**, 422–426 (1986).
146. M. J. R. Cantow, ed., *Polymer Fractionation*, Marcel Dekker, Inc., New York, 1967.
147. L. H. Tung, ed., *Fractionation of Synthetic Polymers*, Marcel Dekker, Inc., New York, 1977.
148. K. Kamide, Y. Miyazaki, and T. Abe, *Br. Polym. J.* **13**, 168 (1981).
149. K. Kamide and S. Matsuda, in Ref. 6, Chapt. 9.
150. K. Kamide and Y. Miyazaki, *Polym. J.* **12**, 153 (1980).
151. K. Kamide, in Ref. 146, p. 103.
152. K. Kamide, Y. Miyazaki, and T. Abe, *Makromol. Chem.* **117**, 485 (1976).
153. K. Kamide, Y. Miyazaki, and T. Abe, *Polym. J.* **9**, 395 (1977).
154. G. V. Schulz, *Z. Phys. Chem. Abt. B* **46**, 137 (1940).
155. K. Kamide, T. Ogawa, M. Sanada, and M. Matsumoto, *Kobunshi Kagaku* **25**, 440 (1968).
156. R. Koningsveld and A. J. Pennings, *Recl. Trav. Chim. Pays-Bas Belg.* **83**, 552 (1964).
157. J. H. Elliot, in Ref. 146, p. 67.
158. E. M. Barrall, II, J. F. Johnson, and A. R. Cooper, in Ref. 147, p. 267.
159. V. Desreux and M. C. Spiegels, *Bull. Soc. Chim. Belg.* **59**, 476 (1950).
160. C. A. Baker and R. J. P. Williams, *J. Chem. Soc.* 2352 (1956).
161. C. Fonseca and I. Harrison, in Ref. 7, Chapt. 1.
162. J. Soares and A. Hamielec, in Ref. 7, Chapt. 2.
163. B. Trathnigg, *Prog. Polym. Sci.* **20**, 615–650 (1995).
164. K. H. Altgelt and L. Segal, eds., *Gel Permeation Chromatography*, Marcel Dekker, Inc., New York, 1971.
165. W. W. Yau, J. J. Kirkland, and D. D. Bly, eds., *Modern Size Exclusion Chromatography*, Wiley Interscience, New York, 1979.
166. J. Janca, ed., *Steric Exclusion Liquid Chromatography of Polymers*, Marcel Dekker, Inc., New York, 1984.
167. A. R. Cooper, in Ref. 129, p. 131.
168. A. R. Cooper, in Ref. 20, p. 243.
169. M. G. Styring and A. E. Hamielec, in Ref. 6, Chapt. 10, pp. 263–300.
170. L. M. Wheeler and J. N. Willis, *Appl. Spectrosc.* **47**, 1128–1130 (1993).
171. S. Mori, *Anal. Chem.* **53**, 1813–1818 (1981).
172. A. R. Cooper, A. R. Bruzzone, J. H. Cain, and E. M. Barrall, II, *J. Appl. Polym. Sci.* **15**, 571 (1971).
173. J. Janca, in J. C. Giddings, E. Grushka, J. Cazes, and P. R. Brown, eds., *Advances in Chromatography*, Vol. 19, Marcel Dekker, Inc., New York, 1981, p. 37.

174. S. T. Balke, *Applied Polymer Symposia*, Vol. 43, John Wiley & Sons, Inc., New York, 1989, pp. 5–38.
175. G. R. Miera, *Modern Methods of Polymer Characterization*, John Wiley & Sons, Inc., New York, 1991, pp. 67–101.
176. T. H. Mourey, T. G. Bryan, and J. Greener, *J. Chromatogr. A, No* **2**, 377–385 (1993).
177. L. Mrkvickova, J. Liq, *Chromatogr. Rel. Technol.* **20**, 403–411 (1997).
178. A. C. Ouano, *J. Polym. Sci., Part A-1* **10**, 2169 (1972).
179. A. C. Ouano, D. L. Horne, and A. R. Gregges, *J. Polym. Sci. Polym. Phys. Ed.* **12**, 307 (1974).
180. M. A. Haney, *J. Appl. Polym. Sci.* **30**, 3023 (1985).
181. M. A. Haney, *J. Appl. Polym. Sci.* **30**, 3037 (1985).
182. W. Kaye, *Anal. Chem.* **45**, 221 (1973).
183. A. C. Ouano and W. Kaye, *J. Polym. Sci.* **12**, 1151 (1974).
184. A. C. Ouano, *J. Chromatogr.* **118**, 303 (1976).
185. A. E. Hamielec and H. Meyer, in Ref. 129, pp. 95–130.
186. H. G. Barth, B. E. Boyes, and C. Jackson, *Anal. Chem.* **70**, 251–278 (1998).
187. S. T. Balke, *Modern Methods of Polymer Characterization*, John Wiley & Sons, Inc., New York, 1991, pp. 1–66.
188. R. Lew, D. Suwandra, S. T. Balke, and T. H. Moury, *Applied Polymer Symposium Proceedings*, Vol. 52, John Wiley & Sons, Inc., New York, 1993, pp. 125–144.
189. P. Simon and A. Rudin, *J. Appl. Polm. Sci.* **46**, 763–773 (1992).
190. D. J. Nagy, *J. Polym. Sci., Polym. Lett. Ed.* **24**, 87 (1986).
191. H. G. Barth and F. J. Carlin, Jr., *J. Liq. Chromatogr.* **7**, 1717 (1984).
192. V. Grinspun and A. Rudin, *J. Appl. Polym. Sci.* **32**, 4303–4311 (1986).
193. V. Grinshpun, *Diss. Abs. Int.* **47**(5) (1986).
194. K. Hatada, T. Kityama, and K. Tahiro, *Polymer Yearbook*, Vol. 8, Harwood Academic Publishers, U.K., 1991, pp. 221–232.
195. J. M. Goldwasser, *Chromatography of Polymers*, ACS Symposium Series 521, American Chemical Society, Washington, D.C., pp. 243–251.
196. S. D. Hanton and X. M. Liu, *Anal. Chem.* **72**, 4550–4554 (2000).
197. M. Maeda, Y. Ohzeki, P. O. Danis, K. Waddell, T. Kehoe, and K. Seta, *Chromatography* **20**, 408–409 (1999).
198. C. E. Kassis, J. M. DeSimone, R. W. Linton, E. E. Remsen, G. W. Lange, and R. M. Friedman, *Rapid Commun. Mass. Spectrom* **11**, 1134–1138 (1997).
199. C. Jackson, B. Larsen, and C. McEwen, *Anal. Chem.* **68**, 12303–1308 (1996).
200. J. M. Goldwasser and A. Rudin, *J. Liq. Chromatogr.* **6**, 2433–2464 (1983).
201. V. V. Nesterov, O. I. Kurenbin, V. D. Krasikov, and B. G. Belenkii, *Talanta* **34**(1), 161–165 (1987).
202. K. Q. Wang and H. H. Huang, *J. Liq. Chrom. Rel. Technol.* **23**, 523–529 (2000).
203. J. M. Goldwasser, A. Rudin, and E. L. Elsdon, *J. Liq. Chromatogr.* **5**, 2253–2257 (1982).
204. M. S. Montaudo, *Polymer* **43**, 1587–1597 (2002).
205. R. A. Sanford, R. K. Bade, and E. N. Fuller, *Am. Lab*. 99 (Mar. 1983).
206. J. Francois, M. Jacot, Z. Crubisic-Gallot, and H. Benoit, *J. Appl. Polym. Sci.* **22**, 1159 (1978).
207. D. Sarazin, J. LeMoigne, and J. Francois, *J. Appl. Polym. Sci.* **22**, 1377 (1978).
208. H. Leopold and B. Trathnigg, *Die Angew. Makromol. Chem.* **68**, 185 (1978).
209. B. Trathnigg, *Monatsh. Chem.* **109**, 467 (1978).
210. B. Trathnigg, *Die Angew. Makromol. Chem.* **89**, 65 (1980).
211. B. Trathnigg, *Die Angew. Makromol. Chem.* **89**, 73 (1980).
212. B. Trathnigg, *Makromol. Chem. Rapid Commun.* **1**, 569 (1980).
213. W. L. Elsdon, J. M. Goldwasser, and A. Rudin, *J. Polym. Sci., Polym. Chem.* **20**, 3271–3283 (1982).

214. W. W. Schulz and W. H. King, Jr., *J. Chromatogr. Sci.* **11**, 343 (1973).
215. H. S. Huang and H. G. Barth, in *Antec '85, Conference Proceedings of the SPE 43rd Annual Technology Conference*, Washington, D. C., 1985, p. 277.
216. G. Holzworth, L. Soni, and D. N. Schulz, *Macromolecules* **19**, 422 (1986).
217. S. Mori and co-workers, *Bunseki Kagaku* **46**, 837–844 (1997).
218. S. Hirayanagi, *Bunseki Kagaku* **46**, 795–797 (1998).
219. L. D'Agnillo, J. B. P. Soares, and A. Pendlis, *J. Polym. Sci., Polym. Phys. Ed.* **40**, 905–921 (2002).
220. B. E. Richter, in Ref. 6, Chapt. 13.
221. A. Shalliker, P. E. J. Kavanaugh, and I. Russell, *18th Australian Polymer Symposium*, Bendigo, Australia, Feb. 4–8, 1990, Paper 29.012.
222. S. Mori, *J. Chromatogr.* **156**, 111 (1978).
223. A. Sebenik and S. Lapanje, *J. Chromatogr.* **106**, 454 (1975).
224. P. McFadyen, *J. Chromatogr.* **123**, 468 (1976).
225. L. M. Zaborsky, II, *Anal. Chem.* **49**, 1166 (1977).
226. C. Bailly, D. Daoust, R. Legras, J. P. Mercier, and M. de Valck, *Polymer* **27**, 776 (1986).
227. E. Klesper and W. Hartmann, *J. Polym. Sci., Polym. Lett. Ed.* **15**, 9 (1977).
228. M. A. McHugh, V. J. Krukonis, and J. A. Pratt, *Trends Polym. Sci.* **2**, 301–307 (1994).
229. H. Yun, S. V. Olesik, and E. H. Marti, *J. Microcolumn Sep.* **11**(1), 53–61 (1999).
230. S. Mori, *Anal. Chem.* **60**, 1125–1128 (1988).
231. B. G. Belenkii and E. S. Gankina, *J. Chromatogr. Rev.* **141**(1), 13–90 (1977).
232. H. Inagaki and T. Tanaka, in J. V. Dawkins, ed., *Developments in Polymer Characterization*, Vol. 3, Applied Science Publishers, London, 1982, p. 1.
233. H. Inagaki, in Ref. 147, p. 649.
234. K. Kamide, T. Okada, T. Terakawa, and K. Kaneo, *Polym. J.* **10**, 547 (1978).
235. C. A. Jackson and W. J. Simonsick Jr., *Curr. Opin. Solid State Mater. Sci.* **2**, 661–667 (1977).
236. G. Montaudo, *Trends Polym. Sci.* **4**(3), 81–86 (1996).
237. L. Li, *Am. Chem. Soc., Polym. Prepr. Div. Polym. Chem.* **41**, 627–628 (2000).
238. W. E. Rudzinski and T. M. Abraham, *Polym. News* **25**, 213–214 (2000).
239. J. W. Kwang and R. W. Odom, *Anal. Chem.* **70**, 456A–461A (1998).
240. T. Q. Ngyen, H. H. Kausch, and G. Yu, *Macromol. Symp.* **110**, 97–106 (1996).
241. M. Dey, J. A. Castoro and C. L. Williams, *Anal Chem.* **67**, 1575–1579 (1995).
242. R. P. Lattimer, R. E. Harris and H.-R. Schulten, in Ref. 6, Chapt. 14.
243. E. Scamporrino and D. Vitalini, in Ref. 7, Chapt. 8.
244. C. M. Guttman, W. R. Blair, and P. O. Dennis, *Soc. Plast. Eng., Antec 98* **2**, 2109–2113 (1998).
245. R. H. Casper and G. V. Schulz, *Sep. Sci.* **6**, 321 (1971).
246. G. S. Greschner, in Ref. 6, Chapt. 11.
247. G. S. Greschner, *Makromol. Chem.* **180**, 2551 (1979).
248. G. S. Greschner, *Makromol. Chem.* **181**, 1435 (1980).
249. G. S. Greschner, *Makromol. Chem.* **182**, 2845 (1981).
250. G. S. Greschner, *Advances in Polymer Science*, Vol. 73, Springer-Verlag, Berlin, 1985, p. 1.
251. J. C. Giddings, *Pure Appl. Chem.* **51**, 1459 (1979).
252. G. C. Giddings, K. D. Caldwell and L. F. Kesner, in Ref. 6, Chapt. 12.
253. T. Provder, ed., *Chromatography of Polymers: Characterization by SEC, Size Exclusion Chromatography and FFF Field Flow Fractionation*, American Chemical Society, Washington, D.C., 1993.
254. K. D. Caldwell, *Modern Methods of Polymer Characterization*, John Wiley & Sons, Inc., New York, 1991, pp. 113–150.
255. J. C. Giddings, M. N. Myers, G. C. Lin, and M. Martin, *J. Chromatogr.* **142**, 23 (1977).

256. M. T. Nyugen and R. Beckett, *18th Australian Polymer Symposium*, Bendigo, Australia, Feb. 4–8, 1990, Paper 16.012.
257. J. C. Giddings, G. C. Lin, and M. N. Myers, *J. Liq. Chromatogr.* **1**, 1 (1978).
258. R. Hecker, P. D. Fawell, A. Jefferson, and J. B. Farrow, *J. Chromatogr. A* **837**, 139–151 (1999).
259. J. C. Giddings, M. A. Benincasa, M. K. Liu, and L. Ping, *J. Liq. Chromatogr.* **15**, 1729–1747 (1992).
260. M. A. Benincasa and J. C. Giddings, *Anal. Chem.* **64**, 790–798 (1992).
261. Y. Jiang, M. Miller, P. Li, and M. Hansen, *Polym. Mater. Sci. Eng.* **79**, 57–58 (1998).
262. Y. Jiang, M. E. Miller, P. Li and M. E. Hansen, *Am. Lab*. 98–108 (Feb. 2002).
263. J. C. Giddings, *J. Chromatogr.* **125**, 3 (1976).
264. J. J. Kirkland, W. W. Yau, and W. A. Doerner, *Anal. Chem.* **52**, 1944 (1980).
265. A. C. Van Asten, R. J. Van Dam, W. T. Kok, R. Tijssen, and H. Poppe, *J. Chromatogr. A* **703**(1/2), 245–263 (1995).
266. P. C. Allen, E. A. Hill, and A. M. Stokes, *Plasma Proteins, Analytical and Preparative Techniques*, Blackwell Scientific Publications, Oxford, U.K., 1978, p. 7.
267. T. J. Mantle, *Techniques in Protein and Enzyme Biochemistry*, B105b, 1978, p. 1.
268. C. Viney and L. Gilliland, in Ref. 7, Chapt. 10.
269. J. A. Zeineh, M. M. Zeineh, and R. A. Zeineh, *Am. Lab*. 124 (June 1986).
270. F. Leonardi, A. Allal, and G. Marin, *Rheol. Acta* **37**, 199–213 (1998).
271. D. W. Mead, *J. Rheol.* **38**, 1797–1827 (1994).
272. W. H. Tuminello, W. H. Buck, and D. L. Kerbow, *Macromolecules* **26**, 499–503 (1992).
273. D. V. Quayle, *Br. Polym. J.* **1**, 15 (1969).
274. G. Koszterszitzs and G. V. Schulz, *Makromol. Chem.* **178**, 2437 (1977).
275. R. Freeman and K. R. Leonard, *J. Microsc.* **122**, 275 (1980).
276. G. Stegman, J. C. Kraak, and H. Poppe, *J. Chromatogr.* **550**, 721–739 (1991).
277. J. P. Queslel and J. E. Mark, in Ref. 6, Chapt. 16.
278. A. M. Zaper, J. L. Koenig, in Ref. 6, Chapt. 15.

GENERAL REFERENCES

Refs. 1,11,12,38,45,47,99,100,120,127, and 166 are good general references.
M. J. Forrest, Rapra Review Report, Vol. 12, No. 7, Rapra Technology Ltd., London, 2001, p. 148.
R. A. Pethrick and J. V. Dawkins, eds., *Modern Techniques for Polymer Characterisation*, John Wiley & Sons, Inc., New York, 1999.
T. Provder, ed., *Chromatography of Polymers: Hyphenated and Multidimensional Techniques*, ACS Books, Washington, D.C., 1999.
H. G. Barth and J. W. Mays, eds., *Modern Methods of Polymer Characterization*, John Wiley & Sons, Inc., New York, 1997.
S. Holding, *Polymer Testing 97, Conference Proceedings, Paper 8 9T*, Rapra Technology Ltd., London, 1997.
C. G. Smith, P. B. Smith, A. J. Pasztor, M. L. McKelvy, D. M. Meunier, and S. W. Froelicher, *Anal. Chem.* **67**(12), 97R–126R (1995).
S. R. Holding and E. Meecham, Rapra Review Report, Vol. 7, No. 11, Rapra Technology Ltd., London, 1995, p. 148.
B. J. Hunt and M. I. James, *Polymer Characterization*, Kluwer, London, 1993.
T. R. Crompton, *Practical Polymer Analysis*, Plenum Press, New York, 1993.
J. Springer, M. D. Lechner, H. Dautzenberg, and W. M. Kulicke, *Makrolmol. Chem., Macromol. Symp.* **61**, 1–23 (Aug 1992).
D. Campbell and J. R. White, *Polymer Characterisation—Physical Techniques*, Chapman and Hall, London, 1989.

E. Schroeder, G. Muller, and K.-F. Arndt, *Polymer Characterization (retroactive coverage)*, Carl Hanser Verlag, Munich, Germany, 1989.
A. R. Cooper, *Polym. Eng. Sci.* **29**, 1 (1989).
L. J. V. Dawkins, ed., *Developments in Polymer Characterization*, Vols. 1–5, Elsevier Applied Science Publishers, Ltd., Barking, U.K., 1986.
J. Janca, ed., *Steric Exclusion Liquid Chromatography of Polymers*, Marcel Dekker, Inc., New York, 1984.
S. Bark and N. S. Allen, eds., *Analysis of Polymer Systems*, Applied Science Publishers, London, 1982.
W. W. Yau, J. J. Kirkland, and D. D. Bly, eds., *Modern Size Exclusion Chromatography*, Wiley-Interscience, New York, 1979.
N. C. Billingham, *Molar Mass Measurements in Polymer Science*, Halsted Press, a division of John Wiley & Sons, Inc., New York, 1977.
L. H. Tung, ed. *Fractionation of Synthetic Polymers*, Marcel Dekker, Inc., New York, 1977.
P. E. Slade, Jr., ed., *Polymer Molecular Weights, Parts I and II*, Marcel Dekker, Inc., New York, 1975.

ANTHONY R. COOPER
Lockheed Martin Space Systems

MOLECULAR WEIGHT DISTRIBUTION.

See MOLECULAR WEIGHT DETERMINATION.

MOLECULARLY IMPRINTED POLYMERS.

See Volume 7.

MORPHOLOGY.

See Volume 7.

MOLECULAR WEIGHT DETERMINATION

Introduction

This article discusses the theory and methods for the determination of molecular weight averages and molecular weight distributions of oligomeric and polymeric materials. The more important methods are described in greater detail in separate articles (see CHROMATOGRAPHY, SIZE EXCLUSION; FRACTIONATION; CHARACTERIZATION OF POLYMERS).

Molecular Weight Averages and Distributions

Most polymeric materials are comprised of mixtures of molecules of various sizes. This distribution of molecular weights is a result of the statistical nature of the polymerization proces (1). A complete description of the molecular weight distribution of a homopolymer is necessary to understand its physical, rheological, and mechanical properties. Structural variations, such as chain branching, and copolymer or higher mer polymers with various degrees of structural randomness further complicate a complete description of the molecular ensemble. Copolymers and higher mer polymers also need to be characterized for molecular composition as a function of molecular weight. Block copolymers and polymer mixtures also offer significant challenges to evaluate their molecular weight distribution. Failure mechanisms and practical lifetimes of polymeric materials may also be established through molecular weight measurements.

Most classical techniques for molecular weight determination are only capable of yielding one of the molecular weight averages of the distribution. These traditional methods are used nowadays only on a limited basis, and only a limited number of commercial instrumentation is available.

These averages are defined in terms of the molecular weight M_i and the number of moles n_i or the weight w_i of the component molecules. The molecular weight averages are defined by equations 1-4.

Number-average molecular weight:

$$\bar{M}_{\mathrm{n}} = \frac{\sum n_i M_i}{\sum n_i} = \frac{\sum w_i}{\sum w_i / M_i} \tag{1}$$

Weight-average molecular weight:

$$\bar{M}_{\mathrm{w}} = \frac{\sum n_i M_i^{\,2}}{\sum n_i M_i} = \frac{\sum w_i M_i}{\sum w_i} \tag{2}$$

z-Average molecular weight:

$$\bar{M}_z = \frac{\sum n_i M_i^{\,3}}{\sum n_i M_i^{\,2}} = \frac{\sum w_i M_i^{\,2}}{\sum w_i M_i} \tag{3}$$

Encyclopedia of Polymer Science and Technology. Copyright John Wiley & Sons, Inc. All rights reserved.

$(z + 1)$-*Average molecular weight*:

$$\bar{M}_{z+1} = \frac{\sum n_i M_i^4}{\sum n_i M_i^3} = \frac{\sum w_i M_i^3}{\sum w_i M_i^2} \tag{4}$$

Viscosity-average molecular weight:

$$\bar{M}_{\mathrm{v}} = \left[\frac{\sum n_i M_i^{1+a}}{\sum n_i M_i} \right]^{1/a} = \left[\frac{\sum w_i M_i^a}{\sum w_i} \right]^{1/a} \tag{5}$$

Equation 5 is an important practical molecular weight average derived from viscometry. To calculate this average, the exponent a and the constant K of the Mark–Houwink relationship relating intrinsic viscosity $[\eta]$ to molecular weight must be known.

$$[\eta] = KM^a \tag{6}$$

The value of a lies between 0.5 and 1.0 for random coils, depending on the solvent employed to determine the relationship of the intrinsic viscosity to molecular weight. For rigid rod molecules, the value of a is expected to be ~1.8. With these limits for a, it may be seen that $\bar{M}_{\mathrm{v}}$ is always larger than $\bar{M}_{\mathrm{n}}$ but can equal $\bar{M}_{\mathrm{w}}$ when the upper limit of a is reached for random coils.

If molecular weight is considered a continuous variable, the molecular weight distribution may be described by a set of moments μ_r given by the integrals

$$\mu_r = \int_0^x M^r f(M)\, \mathrm{d}M$$

where r = 0, 1, 2, 3, etc; $f(M)$ is the number-density distribution; and $f(M)dM$ is the number of moles of molecules with molecular weight between M and $(M + dM)$.

The average molecular weights are defined as

$$\bar{M}_{\mathrm{n}} = \frac{\mu_1}{\mu_0}$$
$$\bar{M}_{\mathrm{w}} = \frac{\mu_2}{\mu_1}$$
$$\bar{M}_z = \frac{\mu_3}{\mu_2}$$
$$\bar{M}_{z+1} = \frac{\mu_4}{\mu_3}$$

Molecular weight averages can be determined from these moments (2).

Molecular Weight Distribution Functions

Various mathematical functions have been employed to describe the distribution of molecular weights. Some of the more common functions are shown in Table 1 in terms of the mole fraction X. Further details are available (3).

Width of Molecular Weight Distributions. The width of the Gaussian distribution function may be expressed in terms of the standard deviation of the mole fraction MWD function σ_n or the mass fraction MWD function σ_w:

$$\sigma_n = (\bar{M}_w \bar{M}_n - \bar{M}_n)^{0.5}$$
$$\sigma_w = (\bar{M}_z \bar{M}_w - \bar{M}_w)^{0.5}$$

The standard deviation is an absolute measure of the width for the Gaussian function only. Widths of molecular weight distribution for other functions have to be calculated for each case from the distribution function itself.

The relationships between molecular weight averages and parameters in the molecular weight distribution functions are as follows:
which leads to

$$\exp(\sigma_w)^2 = \frac{\bar{M}_w}{\bar{M}_n} = \frac{\bar{M}_z}{\bar{M}_w}$$

Thus the ratios of two adjacent averages are constant.

Poisson distribution function.

The ratio of the weight-average to number average molecular weight is given by

$$\frac{\bar{M}_w}{\bar{M}_n} = 1 + \left(\frac{1}{\bar{M}_n}\right) - \left(\frac{1}{\bar{M}_n}\right)^2$$

Table 1. Molecular Weight Distribution Functions

Name	Function	Comments
Gaussian	$X(M) = \frac{1}{\sigma_n (2\pi)^{1/2}} \exp\left[\frac{(M - M_m)^2}{2\sigma_n^2}\right]$	M_m = median value equal to $\bar{M}_n$
Log-normal	$X(M) = \frac{1}{\sigma_n (2\pi)^{1/2}} \exp\left[\frac{(\ln M - \ln M_m)^2}{2\sigma_n^2}\right]$	M_m = geometric mean
Poisson[a]	$X(M) = \frac{\nu^{M-1}}{\Gamma(M)} \exp(-\nu)$	$\nu = \bar{M}_n - 1$
Flory–Schulz[b]	$X(M) = \frac{\beta^{k+1} M^{k-1} \bar{M}_n}{\Gamma(k+1)} \exp(-\beta M)$	k = degree of coupling $\beta = \frac{k}{\bar{M}_n}$

[a] $\Gamma(M) = \gamma$-function.
[b] $\Gamma(k+1) = \gamma$-function.

Gaussian distribution function
mole-fraction distribution function median value $= \bar{M}_n$
mass-fraction distribution function median value $= \bar{M}_w$

Log-normal distribution function
mass-fraction distribution function median value $= M_m$

$$\bar{M}_n = M_m \exp[(\sigma_w)^2/2]$$

$$\bar{M}_w = M_m \exp[3(\sigma_w)^2/2]$$

$$\bar{M}_z = M_m \exp[5(\sigma_w)^2/2]$$

and therefore depends only on $\bar{M}_n$.

Flory–Schulz distribution function
The molecular weight averages this function are related by

$$\frac{\bar{M}_n}{k} = \frac{\bar{M}_w}{k+1} = \frac{\bar{M}_z}{k+2}$$

where k is the coupling constant, defined as the number of independently growing chains required to form one dead chain.

Polydispersity
Traditionally, polydispersity Q has been defined as

$$Q = \bar{M}_w/\bar{M}_n = U + 1$$

where U, the molecular inhomogeneity, has a numerical value of one less than Q. The width of molecular weight distributions increases with increasing Q and U. Except for the Gaussian distribution function, the standard deviation is only a relative measure of distribution width (4,5).

Determination of Molecular Weight

Several books have been published since this article was last written (6–9).

Number-Average Molecular Weight.

End-Group Analysis. In end-group analysis the concentration of an end group is measured by a suitable technique, and then, from the known structure of the polymer, the value for $\bar{M}_n$ may be calculated (10–15). In condensation polymers one end of the polymer should have a specific group that can be titrated by appropriate means. Polyesters (13), polyamides (13), and polyurethanes (16) have been subjected to this analysis. Polyethers have been analyzed by hydroxyl-group titrations similar to those used for polyesters or by reaction with excess phenyl isocyanate followed by reaction with excess di-*n*-butylamine; the latter was back-titrated with perchloric acid (17). Nonaqueous titrations (18) have been used to

characterize polysulfones with $\bar{M}_n$ values of up to 25,000. Potentiometric titration in aqueous and nonaqueous media have been used to determine molecular weights of acrylamide and acrylonitrile polymers (19). Spectrophotometric analyses have also been widely utilized (14), notably uv–visible, infrared techniques, and NMR (20). Examples include the determination of phenolic end groups in polymers by uv spectroscopy (21) and potentiometric titration (18). Infrared spectroscopy has been used (22) to estimate carboxyl groups in the presence of carbonyl groups by reaction of the former with SF_4; the resulting thionyl halides were quantitatively measured. NMR spectroscopy (^1H) has been used to characterize $\bar{M}_n$ of hydroxyl end-capped polystyrenes (A. D. Edwards and M. J. R. Loadman, Malaysian Rubber Producers Research Association, unpublished data, 1976). Reaction of the single proton on the hydroxyl group yields a trimethylsilyl group containing nine protons. The enhanced sensitivity allows determination of $\bar{M}_n$ values of up to 80,000. A similar method has been reported for hydroxy-terminated polybutadienes (23), polyester polyurethanes (24), epoxides (25), and other polymers (26–28). Acid end groups in polyethylene terephthalate have been characterized (29) by reaction with hexafluoroisopropanol and ^{19}F NMR.

In certain cases extremely high sensitivity may be attained with radioactive labeling (30). Using radiolabeled (^{35}S) bisulfite initiator, the number-average molecular weight of Teflon samples was determined in the range of 389,000–8,900,000 (31). This is a particularly useful technique for insoluble polymers.

Measurement of Colligative Properties. Colligative properties are those that depend on the number of species present rather than on their kind (32,33). From thermodynamic arguments it may be shown that for very dilute ideal solutions

$$\ln a_1 = -X_2$$

where a_1 is the activity of the solvent and X_2 is the mole fraction of solute. From this relationship the solute molecular weight may be calculated if the weight fraction w_2 is known.

$$x_2 = \frac{n_2}{n_1} = \frac{w_2 M_1}{M_2 w_1}$$

This equation demonstrates that the activity, measurable by several methods, is proportional to the number of solute molecules. Thus in the case of polydisperse solutes, the number-average molecular weight is the average determined. At higher concentrations and molecular weights, the solutions become nonideal, and higher powers of the solute concentration are introduced into the equations. Measurements of several solute concentrations are required, and appropriate extrapolation techniques must be used.

Lowering of Vapor Pressure. The partial vapor pressure p_1 of solvent 1 over a solution is lower than the vapor pressure over the pure solvent $p_1{}^0$. This is expressed by Raoult's law:

$$P_1 = X_1 p_1{}^0$$

where X_1 is the mole fraction of the solvent.

For a binary solution containing a mole fraction X_2 of solute then,

$$X_2 = \frac{p_1^0 - p_1}{p_1^0} = \frac{\Delta p_1}{p_1^0} \tag{7}$$

For a dilute solution,

$$X_2 = \frac{n_2}{n_1} = \frac{w_2 M_1}{M_2 w_1} \tag{8}$$

Combining equations 7 and 8 yields

$$M_2 = w_2 \frac{M_1}{w_1} \frac{p_1^0}{\Delta p_1}$$

The unknown molecular weight of solute M_2 may be calculated from the lowering of the vapor pressure caused by the addition of w_2 grams of solute to form a binary solution; $\bar{M}_n$ values of up to 1000 may be determined (34–37).

A variation of this technique, the isopiestic method (38–40), was devised to avoid the difficulty of accurately determining the small difference in vapor pressure caused by the addition of solute. In this method (41) two limbs of a container joined by a common vapor space are filled, one with a reference solution of known weight concentration w_s and molecular weight M_s and the other with the unknown solution of known weight concentration w_2 and unknown molar concentration. The apparatus is immersed in a constant-temperature bath controlled to $\pm 0.001^\circ$C; the absolute temperature is not important. Distillation of the solvent continues until the vapor pressures above the solutions in each limb are equal, and thus the solutions contain equal mole fractions of solute. At equilibrium, which may require several weeks, the final volumes V_s, and V_2 of the known and unknown solutions are read from the calibrations on each limb.

$$\bar{M}_n = \frac{w_2 M_s V_s}{V_2 w_s}$$

$\bar{M}_n$values of up to 20,000 have been determined by this method.

Ebulliometry. Ebulliometry (34,42–47) is another technique for determining the depression of the solvent activity by the solute. In this case the elevation of the boiling point is determined. The boiling-point elevation ΔT_b is measured with sensitive thermocouples or matched thermistors in a Wheatstone bridge. The molecular weight $\bar{M}_n$ is calculated from

$$\bar{M}_n = \frac{K_b c}{\Delta T_b}$$

where c is the concentration of solute in g/1000 g of solvent and

$$K_b = \frac{R T_b^2 M}{1000\ \Delta H_v} \tag{9}$$

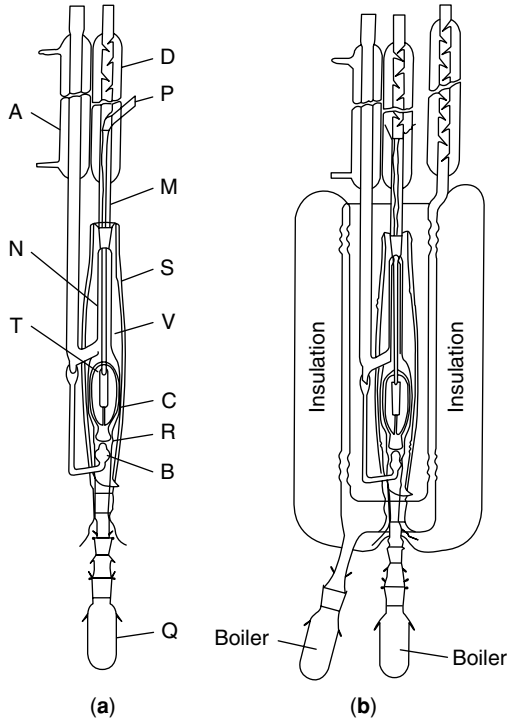

Fig. 1. (**a**) Ebulliometer design for molecular weight determination of up to $\bar{M}_n = 100{,}000$. A denotes ebulliometer cooler; B, boiler; C, Cottrell pump; D, adiabatic jacket cooler; M, thermopile; N, upper thermopile weldings; P, thermopile terminals connected with detector; Q, adiabatic jacket boiler; R, platinum resistance; T, lower thermopile weldings; and V, vacuum jacket circulated by solvent vapor. (**b**) Complete ebulliometer with adiabatic jackets and insulating apparatus (50). Courtesy of Huethig and Wepf Verlag.

is the molal ebullioscopic constant. M is the molecular weight of the solvent and T_b its boiling point; ΔH_v is the molar latent heat of vaporization of the solvent.

The ebullioscopic constant may be evaluated directly from equation 9 and thus provides an absolute method. However, the value for K_b is often determined by using a high purity solute of known molecular weight.

Currently, a sensitivity of 1×10^{-5}°C or 2.4×10^{-6}°C is attainable using a 160-junction thermocouple (48) or thermistors (49), respectively. The upper limit of molecular weight, which may be determined by this method, also depends on the solvent and solution nonideality. With careful measurements and good ebulliometer design, $\bar{M}_n$ values of up to 100,000 may be determined on isotactic polypropylene (50). The apparatus employed is shown in Figure 1. This technique has been applied to aqueous solutions (51). An ebulliometer of simple design having a temperature sensitivity of 50×10^{-6}°C has recently been reported (52). A rotating ebulliometer attempts to overcome the superheating problem (53). Errors in the methods for treating ebullioscopic data to obtain molecular weight have been discussed (54).

Cryoscopy. The freezing point of a solution is depressed below that of the pure solvent by an amount proportional to the mole fraction of solute. The value

for $\bar{M}_n$ is obtained from

$$\bar{M}_n = \frac{K_f c}{\Delta T_b}$$

where c is the concentration of solute in g/1000 g of solvent and

$$K_f = \frac{RT_m^2 M}{1000\ \Delta H_{fus}}$$

is the molal cryoscopic constant; M is the molecular weight of the solvent and T_m its melting point; ΔH_{fus} is the molar latent heat of fusion of the solvent.

Some materials, such as camphor, have very large cryoscopic constants and may be used to increase the sensitivity of the method. The method is used to determine $\bar{M}_n$ of polymers (55–59), such as polyesters (60) and ethylene-vinyl acetate copolymers (61).

A novel variation of this technique (62) involves depression of the first-order, nematic–isotropic melting transition of *N*-(*p*-ethoxybenzylidene)-*p*-*n*-butylaniline. Polystyrene and poly(ethylene oxide) are soluble in both phases, and $\bar{M}_n$ values of up to 10^6 have been studied.

Vapor-Pressure Osmometry. When a drop of solution is exposed to pure solvent vapor, the solvent vapor condenses onto the droplet, because the solute lowers the vapor pressure of the drop (63–68). The heat of condensation causes the temperature of the drop to rise, until theoretically the solution vapor pressure is increased to equal that of the solvent. In practice this does not occur, but a state of equilibrium is reached, where the heat losses from the droplet are matched by the heat of condensation (GB/T 6579-86). The temperature increase is proportional to the number of moles of solute present. A standardized method is available (H. Knauer, Berlin, unpublished data).

The design of a commercial instrument is given in Figure 2 (H. Knauer, Berlin, unpublished data). The temperature stability needed is 0.001°C. In another design, by Wescan Instruments, Inc., small platinum mesh screens ensure that a constant amount of solvent or solution is present on the thermistor. The resistance value ΔR, which is proportional to the temperature difference, is measured with a bridge circuit in all instruments. A calibration curve of ΔR vs molality m is determined by employing a solute of known molecular weight. After several minutes ΔR reaches a constant value; the calibration curve is often highly linear, but may not go through the zero point (66).

$$\Delta R = a + bm$$

The number-average molecular weight of the unknown sample may then be calculated from equation 10:

$$\bar{M}_n = \frac{bc}{\Delta R - a} \tag{10}$$

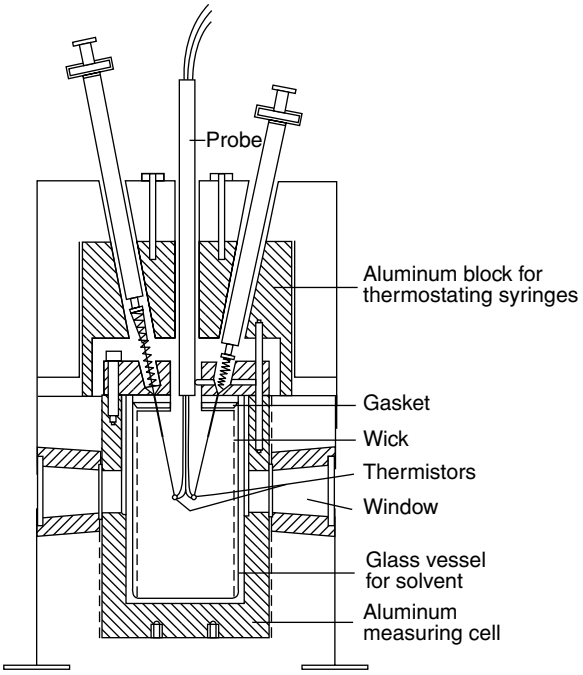

Fig. 2. Vapor-pressure osmometer apparatus (H. Knauer, Berlin, unpublished data, 1987). Courtesy of Dr. -Ing. Herbert Knauer GmbH.

where c is the concentration of solute in g/1000 g of solvent. In older osmometers the calibration curve depended on the material used to perform the calibration. For the Wescan instrument and another research vapor-pressure osmometer (69), both based on the same design (70), the calibration constant was independent of the material. These instruments have determined polystyrene $\bar{M}_n$ values of 400,000 (71), 100,000 (72), and 100,000 (69); polyolefins have been characterized at 140°C (73) and styrene/methylmethacrylate copolymers (32). For higher molecular weight solutes, the virial coefficients become important. In this case $\Delta R/c$ must be plotted against c in order to extrapolate the $\Delta R/c$ value to infinite dilution. When the plot is not linear, it is necessary to plot $(\Delta R/c)^{1/2}$ vs c to obtain a linear extrapolation to infinite dilution.

Membrane Osmometry. Membrane osmometry is a well-established technique (68,74–81). Commercial instrumentation is available (Gonotec GmbH, Knauer). A standardized method is available (GB/T 6596-86). The main problem is membrane permeation by lower molecular weight species (82). Improvements in membranes with well-defined, low molecular weight cutoffs can be expected as a consequence of the renewed interest in membrane-separation techniques (83,84) (see MEMBRANE TECHNOLOGY). Membrane osmometry has been applied to a wide variety of polymers, including operation at high temperatures for polymers difficult to dissolve. Comb-like polymers have been characterized and the results compared with those from gel permeation chromatography (GPC) (85). Preliminary results of an online osmometer for GPC detection have been described (86,87). The upper limit for molecular weight determination is ca 1×10^6. The lower limit

depends on the molecular weight distribution, ie, the details of the composition of the low molecular weight tail. In most cases the concentration dependence of osmotic pressure Π must be determined and Π/c extrapolated to zero concentration by plotting Π/c vs c, or $(\Pi/c)^{1/2}$ vs c.

Viscosity-Average Molecular Weight. The viscosity of dilute polymer solutions may be related to the molecular weight of the polymer by the appropriate calibration (see Viscometry). The polymer is usually separated into narrow molecular weight distribution fractions, which are characterized by absolute molecular weight methods. The molecular weight is related to the intrinsic viscosity $[\eta]$ by the Mark–Houwink relationship (eq. 6).

The intrinsic viscosity is obtained using viscometer types of viscometer tubes and plotting the reduced or inherent viscosity of a series of polymer solutions with various concentrations against the solution concentration. Extrapolation to zero concentration yields the intrinsic viscosity. The technique has found widespread application (88–92), and compilations of Mark–Houwink constants are available (93). A novel method to determine intrinsic viscosity using a flow piezoelectric quartz crystal has been developed (94). Static and continuous measurements of intrinsic viscosity using a differential viscometer (Viscotek) have been reviewed (95). If the Mark–Houwink constants are determined using narrow molecular weight distribution materials, the average molecular weight obtained from equation 6 is the viscosity-average molecular weight $\bar{M}_v$. The range of molecular weights that may be characterized is very large. Special precautions are required for extremely high molecular weight samples to avoid degradation during the solution process or the measurement (96). Dilute solution viscometry for measurement of molecular weight, branching, and other physical parameters have been reviewed (97). A method to calculate the viscosity average molecular weight from GPC for a polymer with unknown Mark–Houwink constants has been reported (98).

Weight-Average Molecular Weight.

Light Scattering. Laser Light Scattering (qv) is a technique (99–106) widely used to characterize polymeric materials. Standardized methods are available (ASTD D4001 and GB/T 6598-86). Commercial instrumentation is available to measure the light-scattering properties of polymer solutions and the refractive index increment (107). Older instrumentation includes the Brice Phoenix Photometer, the Sofica Light Scattering Photometer, as well as the Chromatix product. Wyatt Technology and Malvern Instruments currently produce instruments. Lasers are used as light sources to measure scattering at small angles to the beam. This is important since the data obtained must be extrapolated to zero concentration and zero scattering angle using Zimm plots (108). The weight-average molecular weight is determined by this technique, and the molecular weights accessible range from a few hundred to several million. The solutions employed must be free of dust and are usually subjected to filtration or centrifugation. Solutions of high molecular weight degradable polymers are the most difficult to clarify. The solvent is selected to give a reasonable difference in refractive index with the solute. The technique has been applied to determine the molecular weight of difficultly soluble polymers such as polyethylene (109,110) and of polytetrafluoroethylene and its copolymers with ethylene (111–113). Copolymers with homogeneous distribution of monomer units in the polymer chain may be analyzed by the same methods as homopolymers. If the composition varies as a function of molecular weight, the analysis is more complicated (114). Terpolymers have also been considered (115).

True molecular weights and heterogeneity of styrene-butyl acrylate copolymers have been determined using static low angle laser light scattering (LALLS) and GPC/LALLS (116) and styrene–polydimethylsiloxane block copolymers (117) using GPC/LALLS. Multi-angle laser light scattering (MALLS) has been used as a GPC detector to characterize molecular weight, molecular size, and branching of organic and water soluble polymers (118).

Dynamic light scattering (119) has been used to determine the number average molecular weight (120) and molecular weight distribution of polymers in solution (121–123). There are several mathematical approaches to determine the molecular weight distribution from PCS data. Comparisons with GPC and numerical simulation have been made (124). The resolution of bimodal distributions has been demonstrated (125).

Pulse-induced critical scattering (126,127), although not utilized as a method for molecular weight characterization, may be a sensitive procedure for detecting small differences in molecular weight distribution.

X-ray (128) and neutron scattering (qv) (129,130) may also be used to determine weight-average molecular weights. The main drawback is the greater expense and the lack of suitable facilities.

Ultracentrifuge. The ultracentrifuge is used to determine molecular weights (131–133). Sedimentation velocity employs a sufficiently high centrifugal field so that the sedimentation rate may be measured. The sedimentation coefficient S is empirically corrected for concentration and pressure effects to give S_0, the sedimentation coefficient at zero concentration. The method also requires the measurement of the diffusion coefficient at infinite dilution D_0. The molecular weight is calculated from the Svedberg equation

$$\frac{S_0}{D_0} = \frac{M(1 - \nu\rho)}{RT}$$

where ν is the partial specific volume of the solute and ρ the density of the solution. For a polydisperse solute the correct averages for S and D are combined in the Svedberg equation to yield a well-defined average molecular weight. If D is obtained from intensity-fluctuation spectroscopy (134) and combined with the weight average S value, the weight-average molecular weight is obtained. The application of the sedimentation velocity method to calculate molecular weight distribution is extremely complex, but has been successful in special studies (135).

In the sedimentation equilibrium method, a lower centrifugal field is maintained for a period of time in such a way that sedimentation is balanced by diffusion and an equilibrium distribution of polymer is established in the cell. Although $\bar{M}_w$ and $\bar{M}_z$ are easily determined, the length of time of the experiment is a disadvantage. In contrast to light scattering, this method is not affected by dust particles, and no calibration is needed. The molecular weight distribution may be obtained from the sedimentation velocity data, but not without mathematical difficulties (136) or requiring additional data at other rotor speeds (137,138). An improved detection system for the analytical ultracentrifuge has been reported (139,140). A new 8-cell rotor that allows increased throughput of samples has been described (141).

Improved data analysis has led to the simultaneous determination of the sedimentation coefficient and diffusion coefficient, and a calculation of the molecular weight from the Svedberg equation (142). The Svedberg method is capable of determining molecular weights of up to 40×10^6 (96) on an absolute basis. Sedimentation equilibrium in a density gradient has been used to determine the compositional analysis of copolymers, eg, butadiene-styrene (143).

Munk (144) has recently reviewed the use of sedimentation velocity and sedimentation equilibrium to characterize molecular weight. A new absolute method for the determination of molecular weight distribution based on band sedimentation and LALLS has been applied to water-soluble polymers (145).

Higher Molecular Weight Averages. Classical techniques often cannot be used for higher molecular weight averages ($\bar{M}_z$, $\bar{M}_{z+1}$, etc). These are usually measured by determining the molecular weight distribution by fractionation (qv) or affinity chromatography (qv) and back-calculating the averages from the distribution.

Determination of Molecular Weight Distribution

Fractionation. Polymers may be separated on the basis of molecular weight by precipitation or phase-separation techniques (146–149). The polymer that is originally in solution separates on the basis of molecular weight when the thermodynamic quality of the solvents is changed, ie, by changing the solvent composition or temperature. The principal techniques are *fractional precipitation* and *coacervate extraction*, both solution-based (Fig. 3). The former is based on the removal of material from the polymer-rich precipitated phase and the latter on the removal of fractions from the polymer-lean solution phase. Computer simulations and experimental results have shown the coacervate extraction technique (150) to yield narrower molecular weight distribution fractions than the fractional precipitation method (151–153).

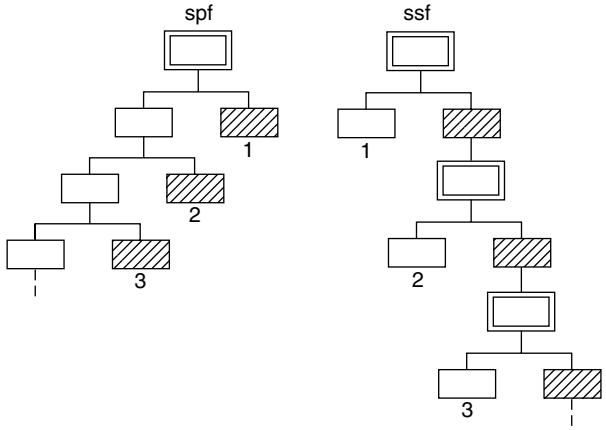

Fig. 3. Successive precipitation (SPF) and solution fractionation (SSF) (coacervate extraction): ▭, mother solution; ▭, polymer rich phase; and ▨, polymer-lean phase. Numbers denote fraction numbers (148). Courtesy of Society of Chemical Industry.

To obtain the molecular weight distribution, the fractions of known mass must be characterized by a molecular weight technique. The integral and differential molecular weight distribution may be evaluated using a method (154) that assumes no particular molecular weight distribution function for the fraction or treatments that assume a particular model for the molecular weight distribution of the fractions (155). Fractionation may also be achieved by crystallization from dilute solution (156).

In column fractionation (157,158) the polymer is precipitated onto an inert support, which is placed at the top of a packed column (159). A solvent mixture of increasing solvent power is pumped through the column; a temperature gradient is often maintained. This is known as *Baker–Williams fractionation* (160). This technique is applicable to all amorphous homopolymers and crystalline homopolymers above the melting point. For copolymers and more complex compositions, the same technique may be employed, but the analysis is considerably more difficult.

Temperature rising elution fractionation (TREF) (161,162) is a useful fractionation technique which gives information on the compositional distribution.

Chromatography. The determination of molecular weight distribution and chemical composition by chromatographic techniques has been discussed (163).

Gel Permeation (Size-Exclusion) Chromatography. GPC has been in use since the 1960s and has been a most important development in molecular weight determination (164–169). For this technique the polymer must be soluble, and calibration with suitable standards is required. The method is extremely efficient; it requires 0.5–2 h per sample and only a few milligrams of material. Standardized methods are available (GB/T 6599-86, ASTM D5296-97, and A83 ASTM D6747-99). Commercial instrumentation capable of operating up to 150°C is available from Waters and Polymer Laboratories. Detection is normally accomplished by differential refractometry, although uv and ir (170) absorption spectrometry have also been employed. The chromatographic columns are packed with spherical- or irregular-shaped porous beads. The packing may be a crosslinked polymer, a porous glass, or a silica material. The pore size distribution determines the separation range of the columns. Calibration is normally performed using well-characterized narrow MWD standards. Calibration can be performed using broad MWD materials (171). Typical calibration curves (172) are shown in Figure 4. By combining columns in series, a separation range may be achieved covering the molecular weight distribution of the sample. Mathematical treatments of the chromatogram and calibration curve to calculate the molecular weight distribution are given (173). Broadening by the chromatographic process must be calibrated for and corrections applied to produce true molecular weight distributions. *Chemimetrics* has been applied to GPC calibration equations (174) and helped to establish the best equations. Data reduction in GPC (175) has been described. A new solvent system which allows polyesters and polyamides to be characterized by GPC at room temperature has been developed (176). High speed GPC of low molecular weight polymers has been described (177).

The design and use of a continuous, viscometric detector (178,179) has further advanced the application of the GPC technique, and a commercial viscometric detector is on the market from Viscotek Corp (180,181).

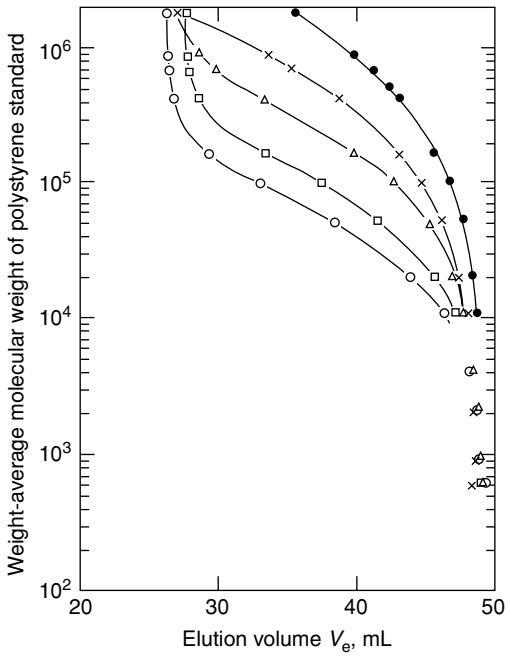

Fig. 4. GPC calibration curve for Corning porous glasses with various pore sizes: ○, CPG 10–240; □, CPG 10–370; ×, CPG 10–1250; and ●, CPG 10–2000 (172). Courtesy of John Wiley & Sons, Inc.

Direct determination of the polymer molecular weight in the detector cell after separation by GPC is possible by LALLS. The technique (182–184) is applicable to the dilute polymer solutions emerging from the chromatographic column; commercial equipment is available, older models (Chromatix KMX6 and LSD100 from LDC/Milton Roy) and newer instruments (Wyatt and Polymer Labs). A review of prior development and a description of a methodology for correcting for dispersion in the concentration detector and the light scattering detector has been published (185). A review of GPC and the application of molecular weight detectors and related separation techniques has been published (186). The characterization of complex polymers by GPC and high performance liquid chromatography (HPLC) has been discussed (187). Quantitative high temperature GPC of polyolefins using refractive index and differential viscometer detection (188) and differential viscometer and light scattering detectors (189) has been reported. This method has been used for on-line molecular weight measurement and branching characterization of water-soluble polymers (185,190). Shear degradation during the chromatographic process may be a problem (191), but can be detected by viscometry and LALLS. A triple detector employing a concentration detector, a viscometer, and a light scattering detector is available (Viscotek). Three detectors, an evaporative light scattering detector to measure concentration, a refractometer, and LALLS, have been used to determine MWD of copolymers (EPM and EPDM) (192). LALLS has proven useful in detecting and eliminating aggregates in dilute polymer solutions which would affect the GPC results (193). Nuclear magnetic resonance,

NMR, has been employed as an on-line detector for GPC (194). Goldwasser (195) developed an analysis which allows the calculation of absolute values for $\bar{M}_n$ from the combined results from GPC and differential viscometry. Mass spectrometry has been coupled with GPC to characterize a variety of polymers (196–198). A comparison of the most probably peak value of polymer distributions has been evaluated between MALDI MS and GPC (199).

Analyses by GPC of block and statistical copolymers (200,201) and copolymers (202) and polymer mixtures (203) have been reported. Full copolymer characterization by combining GPC-NMR with GPC-MALDI has been demonstrated (204).

Other detectors that are capable of determining the polymer concentration in the effluent are based on dielectric constant (205) and density (206–213). Mass can be determined directly with a piezoelectric quartz sensor having a sensitivity of 10^{-10} g (214). A universal mass detector, evaporative light scattering Detector (ELSD) based on the formation of droplets in a nebulizer gas and detection by light scattering using a laser, has been developed and applied to GPC (215). Commercial ELSD units are available from Alltech, Varex Corp., and Polymer Laboratories.

A direct molecular weight method (216) employs the LALLS detector, but uses sedimentation velocity instead of GPC to separate the polymers.

Round robin tests for reproducibility of GPC results have been reported (217). Twenty-four laboratories used calibration standards from two different sources and three test polymers. The results for the three samples varied from 3 to 14% depending on which calibration was used. Similar results for number-average molecular weights have been documented (218). Round robin characterization of polyethylene by high temperature GPC in 15 laboratories has been documented (219).

High Performance Liquid Chromatography and Supercritical Fluid Chromatography. For lower molecular weights, HPLC and supercritical fluid chromatography (SFC) (220) offer higher resolution than GPC. Higher molecular weights may produce multiple peaks from monodisperse standards (221). The oligomers are resolved into individual peaks, and molecular weight averages are calculated (222). HPLC is more common and has been applied to phenol-formaldehyde resins (223), polyurethanes (224), polyesters (225), and polycarbonates (226). Since solvent gradients are often used in HPLC the refractometer detector cannot be used, and ultraviolet/visible spectrometers and/or ELSDs must be used. The ELSD may also be used in SFC. SFC can resolve higher oligomers than HPLC. Polystyrene oligomers of up to $n = 50$ may be resolved by SFC; the process requires 18 h (227). Several commercial SFC units are available and their availability should rapidly increase the application of this technique to characterize oligomeric species. A review of supercritical fractionation of polymers and copolymers has been published (228). Mass spectrometry has been used in conjunction with SFC and capillary GPC to characterize polypropylene glycol (229).

Liquid adsorption chromatography (LAV) and GPC have been used to determine chemical composition distribution (CCD) and MWD of styrene–methyacrylate copolymers (230).

Thin-Layer Chromatography. Thin-layer chromatography (TLC) is widely applicable to polymer characterization and has been used to characterize

molecular weight distribution and compositional distribution (231–233). Cellulose nitrate has been fractionated by this method on the basis of molecular weight or nitrogen content (234).

Mass Spectrometry. Advances in soft ionization techniques and developments in high resolution mass spectrometers has led to the possibility of determining intact molecular ions up to 1×10^6 Da and the measurement of the entire MWD (235,236). The application of mass spectrometry techniques to characterize polymer molecular weight distribution has evaluated (237–243). The MWD of polystyrene SRM 1487 and a narrow MND polymethylmethacrylate (MW 6300) determined by MALDI TOF mass spectrometry have been compared with results from the ultracentrifuge and GPC (244).

Phase-Distribution Chromatography. A chromatographic fractionation is achieved in this method (245,246), by partitioning a solute between a solvent flowing through a column, packed with a support coated with a thin layer of high molecular weight, non-cross-linked polymer. The temperature of operation is below the Θ-temperature of the solute, and separation efficiency increases sharply with decreasing temperature. A fully automated chromatograph has been designed (247), and applications have been reported (248–250).

Field–Flow Fractionation. Field-flow fractionation (FFF) employs a one-phase chromatographic system (251,252). Commercial instrumentation is available from Postnova Analytics and Tecan. Separation occurs in a thin channel containing a single moving fluid. The field applied across the channel may be selected on the basis of the solute. Possible fields include sedimentation, cross-flow, concentration, dielectric, thermal, and magnetic. A book (253) and a review (254) of this technique and its comparison with GPC for the characterization of polymer molecular weights have been published.

Thermal fields have been used for the separation of polymers in organic solvents (255). Methods for calculation of MWD from thermal FFF have been published (256). For aqueous systems a cross-flow of solvent has been used to separate polyelectrolytes (257) and high molecular weight polyacrylamides (258). Water-soluble polymers have also been characterized by this technique (259,260), in conjunction with LALLS detector (261) and MALLS (262). Extremely high molecular weights of up to 10^{12} can be determined (263); because no abrupt changes occur in the forces imposed on the polymer molecules, no degradation takes place. Sedimentation fields were investigated (264), and small samples were quickly fractionated. Compositional heterogeneity has been determined by sequential GPC and FFF (265).

Electrophoresis. Electrophoresis is widely practiced on biopolymers (266–268) for the determination of molecular weights of proteins and their subunits. Typically, a polyacrylamide bed is used to separate or characterize these solutes under the influence of an electric field, on the basis of charge and molecular size. The proteins are frequently denatured with sodium dodecyl sulfonate (SDS), and these subunit-SDS complexes are separated on the basis of molecular size. A densitometer employing a soft laser scanning device is commercially available to automate the data-reduction process (269).

Rheological Measurements. Some polymers are difficult to dissolve. Mechanical spectroscopy or rheological measurements (qv) offer a way to determine the molecular weight distribution of these materials. Mechanical spectroscopy has

been applied to characterize the MWD of polyolefins (270) Rheological data has been used to determine the MWD of polybutadiene and polypropylene (271). Measurements of ethylene–tetrafluorethylene copolymers using dynamic mechanical analysis of the melts showed broader distributions than those determined by high temperature laser light scattering (272).

Other Techniques. Atomization of polymer solutions to form single molecules deposited in a solvent-free state on a surface has been demonstrated for a wide variety of polymers (273). The electron microscope is used at 20,000–30,000 × after platinum shadowing to determine size and size distribution (274). The scanning transmission electron microscope is employed for biological macromolecules (275). For extremely high molecular weight polymers hydrodynamic chromatography (HDC) may be a viable technique. Columns are packed with solid spheres and the diameter determines the separation range. Solid particles between 5 and 300 nm may be separated. Columns are available from Polymer Laboratories, and using a high temperature infrared detector cell the composition of polyolefin copolymers can be characterized. A mathematical model for HDC and GPC for porous column packings has been published (276). Methods to characterize insoluble polymers have been discussed (277,278).

BIBLIOGRAPHY

"Molecular Weight Determination" in *EPST* 1st ed., Vol. 9, pp. 182–193, by Manfred J. R. Cantow, Airco Central Research Laboratories, and Julian F. Johnson, Chevron Research Co; in *EPST* 2nd ed., Vol. 10, pp. 1–19, by Anthony R. Cooper, Lockheed Missiles and Space Co.

1. L. H. Peebles, *Molecular Weight Distributions in Polymers*, Wiley-Interscience, New York, 1971.
2. K. W. Min, *J. Appl. Polym. Sci.* **22**, 589 (1978).
3. G. C. Berry, in M. B. Bever, ed., *Encyclopedia of Materials Science and Engineering*, Pergamon Press, Oxford, 1986, pp. 3759–3768.
4. C. W. Pyun, *J. Polym. Sci., Polym. Phys. Ed.* **17**, 2111 (1979).
5. C. W. Pyun, *J. Polym. Sci., Polym. Phys. Ed.* **24**, 229 (1986).
6. A. R. Cooper and J. D. Winefordner, ed., Determination of Molecular Weight, Vol. 103 in Chemical Analysis, A Series of Monographs on Analytical Chemistry and Its Applications, John Wiley & Sons, Inc., New York, 1989.
7. R. A. Pethrick and J. V. Dawkins, eds., *Modern Techniques for Polymer Characterisation*, John Wiley & Sons, Inc., New York, 1999.
8. D. Campbell, R. A. Pethrick, and J. R. White, *Polymer Characterisation—Physical Techniques*, 2nd ed., Stanley Thornes, Cheltenham, U.K., 2000.
9. R. A. Pethrick and R. S. Stein, eds., *Experimental Methods for Polymer Characterization*, John Wiley & Sons, Inc., Sussex, U.K., 1999.
10. N. C. Billingham, *Molar Mass Measurements in Polymer Science*, Halsted Press, a division of John Wiley & Sons, Inc., New York, 1977, Chapt. 9, p. 234.
11. G. F. Price, in P. W. Allen, ed., *Techniques of Polymer Characterization*, Butterworth & Co. (Publishers) Ltd., London, 1959, Chapt. VII.
12. S. R. Rafikov, S. A. Pavlova, and I. I. Tverdokhlebora, *Determination of Molecular Weights and Polydispersity of High Polymers*, Israel Programme for Scientific Translation, Jerusalem, Israel, 1964, Chapt. 8.

13. R. G. Garmon, in P. E. Slade, Jr., ed., *Polymer Molecular Weights*, Marcel Dekker, Inc., New York, 1975, Chapt. 3.
14. J. Urbanski, N. Czerwinski, K. Janicka, F. Majewska, and H. Zowall, *Handbook of Analysis of Synthetic Polymers and Plastics*, Wiley-Interscience, New York, 1977.
15. A. R. Cooper, in Ref. 6, Chapt. 2.
16. D. J. David and H. B. Staley, *Analytical Chemistry of Polyurethanes*, Wiley-Interscience, New York, 1959.
17. D. H. Reed, F. E. Critchfield, and D. K. Elder, *Anal. Chem.* **35**, 571 (1963).
18. A. J. Wnuk, T. F. Davidson, and J. E. McGrath, *J. Appl. Polym. Sci., Appl. Polym. Symp.* **34**, 89 (1978).
19. A. S. Sarac, B. Ustamehmetoglu, and C. Erbil, *Polym. Bull.* **32**(1), 91–95 (1994).
20. J. R. Ebdon, in L. S. Bark and N. S. Allen, eds., *Analysis of Polymer Systems*, Applied Science Publishers, London, 1982, p. 21.
21. E. Shchori and J. E. McGrath, *J. Appl. Polym. Sci., Appl. Polym. Symp.* **34**, 103 (1978).
22. J. F. Heacock, *J. Appl. Polym. Sci.* **7**, 2319 (1963).
23. G. Fages and Q. T. Pham, *Makromol. Chem.* **180**, 2435 (1979).
24. F. W. Yeager and J. W. Becker, *Anal. Chem.* **49**, 722 (1977).
25. W. B. Moniz and C. F. Poranski, Jr., in R. S. Bauer, ed., *Epoxy Resin Chemistry*, ACS Symposium Series 114, American Chemical Society, Washington, D. C., 1979.
26. S. Amiya, K. Mathumura, and T. Taniguchi, *Anal. Sci.* **7**, 1649 (1991).
27. A. M. Kenwright, S. K. Pierce, R. W. Richards, A. Bunn, and W. A. MacDonald, *Polymer* **40**, 2035–2040 (1999).
28. T. Amari, K. Nishimura, K. Minio, A. Kawabata, and Y. Ozika, *J. Polym. Sci., Polym. Chem.* **39**, 665 (2001).
29. Y. Ma, U. S. Agarwal, J. A. J. M. Vekemans, and D. J. Sikkema, *Polymer* **44**, 4429–4434 (2003).
30. K. L. Berry and J. H. Peterson, *J. Am. Chem. Soc.* **73**, 5195 (1951).
31. R. C. Dobau, A. C. Knight, J. H. Peterson, and C. A. Sperati, *130th Meeting of the American Chemical Society*, Atlantic City, N. J., Sept. 1956.
32. H. Suzuki and K. Kamide, in Ref. 7, pp. 375–387.
33. A. R. Cooper, in Ref. 6, Chapt. 2.
34. D. F. Rushman, in Ref. 11, p. 113.
35. I. M. Kolthoff and P. J. Elving, eds., *Treatise on Analytical Chemistry, Theory and Practice*, Vol. 7, Part 1, Wiley-Interscience, New York, 1978, p. 4446.
36. G. Radakoff, *Z. Chem.* **1**, 135 (1961).
37. R. U. Bonnar, M. Dimbat, and F. H. Stross, *Number Average Molecular Weights*, Wiley-Interscience, New York, 1958, p. 275.
38. Ref. 35, p. 114.
39. Ref. 36, p. 4448.
40. Ref. 38, p. 268.
41. R. L. Parette, *J. Polym. Sci.* **15**, 450 (1955).
42. Ref. 38, p. 113.
43. Ref. 36, p. 4450.
44. M. Ezrin, in M. McIntyre, ed., *Characterization of Macromolecular Structure, Publication 1573*, National Academy of Science, Washington, D. C., 1968, p. 3.
45. C. A. Glover, in Ref. 13, Part I, p. 105.
46. C. A. Glover, in M. Ezrin, ed., *Polymer Molecular Weight Methods, Advances in Chemistry Series 125*, American Chemical Society, Washington, D. C., p. 1.
47. G. Davison, in Ref. 20, p. 209.
48. C. A. Glover, C. N. Reilly, and F. W. McLafferty, eds., *Advances in Analytical Chemistry and Instrumentation*, Vol. 5 Wiley-Interscience, New York, 1966, p. 1.
49. E. Zichy, *SCI Monogr* **17**, 122 (1963).

50. P. Parrini and M. S. Vacanti, *Die Makromol. Chem.* **175**, 935 (1974).
51. W. De Oliveira, *Differential Ebulliometry*, Ph. D. thesis, Clarkson College of Technology, Potsdam, N. Y., 1975.
52. W. De Oliveira and G. Francisco, *Chem. Biomed. Environ. Instrum.* **10**, 189 (1980).
53. J.-T. Chen, H. Sotobayashi, and F. Asmussen, *Colloid Polym. Sci.* **259**, 1202 (1981).
54. J. Melsheimer and H. Sotobayashi, *Die Makromol. Chem.* **179**, 2913 (1978).
55. Ref. 46, p. 124.
56. E. J. Newitt and V. Kokle, *J. Polym. Sci., Part A-2* **4**, 705 (1966).
57. Ref. 35, p. 125.
58. Ref. 38, p. 17.
59. Ref. 12, p. 255.
60. L. Carbonnel, R. Guieu, C. Ponge, and J. C. Rosso, *J. Chim. Phys. Physicochim. Biol.* **70**, 1400 (1973).
61. A. Ya Ryasnyanskaya, S. L. Lyubimova, V. V. Kalashnikov, R. A. Terteryan, V. N. Mosastyrskii, and B. V. Gryaznov, *Neftepererab. Neftekhim. Moscow* 69 (1973).
62. B. Kronberg and D. Patterson, *Macromolecules* **12**, 916 (1979).
63. A. V. Hill, *Proc. R. Soc. London, Ser. A* **127**, 9 (1930).
64. C. A. Glover, in Ref. 13, p. 142.
65. Ref. 10, p. 81.
66. M. J. R. Cantow, R. S. Porter, and J. F. Johnson, *J. Polym. Sci., Part A* **2**, 2547 (1964).
67. C. E. M. Morris, in Ref. 6, Chapt. 3.
68. B. Hunt, in Ref. 7, Chapt. 9.
69. K. Kamide, T. Terakuwa, and H. Uchiki, *Makromol. Chem.* **177**, 1447 (1976).
70. R. E. Dohner, A. H. Wachter, and W. Simon, *Helv. Chim. Acta* **50**, 2193 (1967).
71. A. H. Wachter and W. Simon, *Anal. Chem.* **41**, 90 (1969).
72. D. E. Burge, *J. Appl. Polym. Sci.* **24**, 293 (1979).
73. F. M. Mirabella, *J. Appl. Poly. Sci.* **25**, 1775 (1980).
74. Ref. 38, p. 191.
75. Ref. 10, p. 44.
76. Ref. 11, p. 68.
77. H. Coll and F. H. Stross, in Ref. 47, p. 10.
78. R. D. Ulrich, in Ref. 46, p. 9.
79. W. R. Krigbaum and R.-J. Roe, in Ref. 36, p. 4461.
80. D. E. Burge, *Am. Lab.* 41 (June 1977).
81. H. Coll, in Ref. 6, Chapt. 4.
82. H. Coll, *J. Polym. Sci., Makromol. Rev.* **5**, 541 (1971).
83. A. R. Cooper, ed., in *Polymer Science and Technology*, Vol. 16, Plenum Press, New York, 1982.
84. A. R. Cooper, ed., *in Polymer Science and Technology*, Vol. 13, Plenum Press, New York (1981).
85. K. Yokota, T. Hirabayashi, and Y. Inai, *Polym. J. (Japan)* **26**(4), 105–108 (1994).
86. W. W. Yau, *J. Appl. Polym. Sci., Appl. Polym. Symp.* **48**, 85–94 (1991).
87. U. Lehman, W. Kohler, and W. Albrecht, *Macromolecules* **29**, 3212–3215 (1996).
88. K. Kamide and M. Saito, in Ref. 6, Chapt. 8.
89. P. F. Onyon, in Ref. 11, Chapt. VI.
90. D. K. Carpenter and L. Westerman, in Ref. 13, Part II, p. 441.
91. M. Van Oene, in Ref. 47, p. 353.
92. Ref. 10, p. 172.
93. M. Kurata and Y. Tsunashima, in J. Brandrup and E. H. Immergut, eds., *Polymer Handbook*, 3rd ed., Wiley-Interscience, New York, 1989, Chapt. VII.
94. Y. Mao, W. Wei, J. Zhang, and Y. Li, *J. Appl. Polym. Sci., A* **12**, 82, 63 (2001).

95. J. W. Mays and N. Hadgjichristidis, in H. G. Barth and J. W. Mays, eds., *Modern Methods of Polymer Characterization*, John Wiley & Sons, Inc., New York, Chapt. 7, 1997.
96. B. Appelt and G. Meyerhoff, *Macromolecules* **13**, 657 (1980).
97. J. W. Mays and N. Hadjichristidis, in Ref. 7, pp. 227–269.
98. H. Kh. Mahabadi, *J. Polym. Sci., Polym. Phys.* **22**, 449–457 (1984).
99. M. B. Huglin, ed., *Light Scattering from Polymer Solutions*, Academic Press, Inc., Orlando, Fla., 1972.
100. M. Kerker, *The Scattering of Light*, Academic Press, Inc., Orlando, Fla., 1969.
101. H. Yamakawa, *Modern Theory of Polymer Solutions*, Harper & Row (Publishers), Inc., New York, 1971.
102. G. C. Berry, in R. A. Meyers, ed., *Encyclopedia of Analytical Chemistry*, John Wiley & Sons, Inc., Sussex, U.K., 2000.
103. G. C. Berry and P. M. Coutts, in Ref. 9, p. 721.
104. G. C. Berry, in H. F. Mark, N. M. Bikales, C. G. Ovèrberger, G. Menges, and J. I. Kroshwitz, eds., Encyclopedia of Polymer Science and Engineering, Vol. 8, John Wiley & Sons, Inc., New York, 1987, pp. 721–794.
105. B. Chu, in Ref. 6, Chapt. 5, pp. 53–86.
106. G. Berry and P. M. Cotts, in Ref. 7, Chapt. 4.
107. H. Utiyama, in Ref. 99, Chapt. 3.
108. B. H. Zimm, *J. Chem. Phys.* **16**, 1093 (1948).
109. B. Chu, M. Onclin, and J. R. Ford, *J. Phys. Chem.* **88**, 6566 (1984).
110. J. W. Pope and B. Chu, *Macromolecules* **17**, 2633 (1984).
111. B. Chu and C. Wu, *Macromolecules* **19**, 1285 (1986).
112. B. Chu and C. Wu, *Macromolecules* **20**, 93 (1987).
113. C. Wu, W. Buck, and B. Chu, *Macromolecules* **20**, 98 (1987).
114. E. F. Cassassa and G. C. Berry, in Ref. 8, Part I, p. 161.
115. H. Kambe, Y. Kambe, and C. Honda, *Polymer* **14**, 460 (1973).
116. F. B. Mahili, C. Y. Kuo, and T. Provder, *J. Appl. Polym. Sci.* **29**, 925–931 (1984).
117. T. Dumelow, S. R. Holding, L. J. Maisey, and J. V. Dawkins, *Polymer* **27**, 1170–1176 (1986).
118. S. Podzimek, *J. Appl. Polym. Sci.* **54**(1), 91–103 (1994).
119. B. Chu, *Laser Light Scattering*, 2nd ed., Academic Press, Inc., Boston, 1991.
120. J. C. Selser, *Macromolecules* **12**, 909 (1979).
121. Q. Ying, B. Chu, R. Qian, J. Bao, J. Zhang, and C. Xu, *Polymer* **26**, 1401 (1985).
122. B. Chu, Q. Ying, C. Wu, J. R. Ford, and M. S. Dhadal, *Polymer* **26**, 1408 (1985).
123. D. Caroline, in J. V. Dawkins, ed., *Developments in Characterization*, Vol. 5, Elsevier Applied Science, London, 1986.
124. I. Tomka and G. Vancso in J. Mitchell, Jr., ed., *Applied Polymer Analysis and Characterization*, Hanser, Munich, 1987, p. 237.
125. G. Vansco, I. Tomka, and K. Vansco-Polacsek, *Macromolecules* **21**, 415 (1988).
126. M. Gordon, J. Goldsbrough, B. W. Ready, and K. W. Derham, in J. H. S. Green and R. Dietz, eds., *Industrial Polymers: Characterization by Molecular Weight*, Transcripta Books, London, 1973, p. 45.
127. H. Galina, M. Gordon, P. Irvine, and L. A. Kleintjens, *Pure Appl. Chem.* **54**, 365 (1982).
128. D. Glotter and O. Kratky, *Small Angle X-Ray Scattering*, Academic Press, Ltd., London, 1982.
129. R. W. Richards, in J. V. Dawkins, ed., *Developments in Polymer Characterization*, Vol. 5, Elsevier Applied Science Publishers, Ltd., Barking, U.K., 1986.
130. R. W. Richards, in Ref. 6, Chapt. 6, pp. 87–116.
131. H. Fujita, *Mathematical Theory of Sedimentation Analysis*, Academic Press, Inc., Orlando, Fla., 1962.

132. A. R. Cooper, in Ref. 6, Chapt. 7, pp. 117–144.
133. H. Borchard and E. Selic, in Ref. 7, Chapt. 11.
134. D. N. Pussey, in Ref. 126, p. 26.
135. R. Dietz, in Ref. 126, p. 19.
136. D. A. Lee, *J. Polym. Sci., Part A-2* **8**, 1039 (1970).
137. T. G. Scholte, *J. Polym. Sci., Part A-2* **6**, 11 (1968).
138. T. G. Scholte, *Eur. Polym. J.* **6**, 51 (1970).
139. J. Flossdorf, H. Schillig, and K. P. Schindler, *Makromol. Chem.* **179**, 1617 (1978).
140. J. Flossdorf, *Makromol. Chem.* **181**, 715 (1980).
141. N. Machtle and U. Klodwig, *Makromol. Chem.* **180**, 2507 (1979).
142. R. Wohlschiess, K. F. Elgert, and H.-J. Cantow, *Angew. Makromol. Chem.* **74**, 323 (1978).
143. C. J. Stacy, *J. Appl. Polym. Sci.* **21**, 2231 (1977).
144. P. Munk, *Modern Methods of Polymer Characterization*, John Wiley & Sons, Inc., New York, 1991, 271–312.
145. G. Holzwarth, L. Soni, and D. N. Schulz, *Macromolecules* **19**, 422–426 (1986).
146. M. J. R. Cantow, ed., *Polymer Fractionation*, Marcel Dekker, Inc., New York, 1967.
147. L. H. Tung, ed., *Fractionation of Synthetic Polymers*, Marcel Dekker, Inc., New York, 1977.
148. K. Kamide, Y. Miyazaki, and T. Abe, *Br. Polym. J.* **13**, 168 (1981).
149. K. Kamide and S. Matsuda, in Ref. 6, Chapt. 9.
150. K. Kamide and Y. Miyazaki, *Polym. J.* **12**, 153 (1980).
151. K. Kamide, in Ref. 146, p. 103.
152. K. Kamide, Y. Miyazaki, and T. Abe, *Makromol. Chem.* **117**, 485 (1976).
153. K. Kamide, Y. Miyazaki, and T. Abe, *Polym. J.* **9**, 395 (1977).
154. G. V. Schulz, *Z. Phys. Chem. Abt. B* **46**, 137 (1940).
155. K. Kamide, T. Ogawa, M. Sanada, and M. Matsumoto, *Kobunshi Kagaku* **25**, 440 (1968).
156. R. Koningsveld and A. J. Pennings, *Recl. Trav. Chim. Pays-Bas Belg.* **83**, 552 (1964).
157. J. H. Elliot, in Ref. 146, p. 67.
158. E. M. Barrall, II, J. F. Johnson, and A. R. Cooper, in Ref. 147, p. 267.
159. V. Desreux and M. C. Spiegels, *Bull. Soc. Chim. Belg.* **59**, 476 (1950).
160. C. A. Baker and R. J. P. Williams, *J. Chem. Soc.* 2352 (1956).
161. C. Fonseca and I. Harrison, in Ref. 7, Chapt. 1.
162. J. Soares and A. Hamielec, in Ref. 7, Chapt. 2.
163. B. Trathnigg, *Prog. Polym. Sci.* **20**, 615–650 (1995).
164. K. H. Altgelt and L. Segal, eds., *Gel Permeation Chromatography*, Marcel Dekker, Inc., New York, 1971.
165. W. W. Yau, J. J. Kirkland, and D. D. Bly, eds., *Modern Size Exclusion Chromatography*, Wiley Interscience, New York, 1979.
166. J. Janca, ed., *Steric Exclusion Liquid Chromatography of Polymers*, Marcel Dekker, Inc., New York, 1984.
167. A. R. Cooper, in Ref. 129, p. 131.
168. A. R. Cooper, in Ref. 20, p. 243.
169. M. G. Styring and A. E. Hamielec, in Ref. 6, Chapt. 10, pp. 263–300.
170. L. M. Wheeler and J. N. Willis, *Appl. Spectrosc.* **47**, 1128–1130 (1993).
171. S. Mori, *Anal. Chem.* **53**, 1813–1818 (1981).
172. A. R. Cooper, A. R. Bruzzone, J. H. Cain, and E. M. Barrall, II, *J. Appl. Polym. Sci.* **15**, 571 (1971).
173. J. Janca, in J. C. Giddings, E. Grushka, J. Cazes, and P. R. Brown, eds., *Advances in Chromatography*, Vol. 19, Marcel Dekker, Inc., New York, 1981, p. 37.

174. S. T. Balke, *Applied Polymer Symposia*, Vol. 43, John Wiley & Sons, Inc., New York, 1989, pp. 5–38.
175. G. R. Miera, *Modern Methods of Polymer Characterization*, John Wiley & Sons, Inc., New York, 1991, pp. 67–101.
176. T. H. Mourey, T. G. Bryan, and J. Greener, *J. Chromatogr. A, No* **2**, 377–385 (1993).
177. L. Mrkvickova, J. Liq, *Chromatogr. Rel. Technol.* **20**, 403–411 (1997).
178. A. C. Ouano, *J. Polym. Sci., Part A-1* **10**, 2169 (1972).
179. A. C. Ouano, D. L. Horne, and A. R. Gregges, *J. Polym. Sci. Polym. Phys. Ed.* **12**, 307 (1974).
180. M. A. Haney, *J. Appl. Polym. Sci.* **30**, 3023 (1985).
181. M. A. Haney, *J. Appl. Polym. Sci.* **30**, 3037 (1985).
182. W. Kaye, *Anal. Chem.* **45**, 221 (1973).
183. A. C. Ouano and W. Kaye, *J. Polym. Sci.* **12**, 1151 (1974).
184. A. C. Ouano, *J. Chromatogr.* **118**, 303 (1976).
185. A. E. Hamielec and H. Meyer, in Ref. 129, pp. 95–130.
186. H. G. Barth, B. E. Boyes, and C. Jackson, *Anal. Chem.* **70**, 251–278 (1998).
187. S. T. Balke, *Modern Methods of Polymer Characterization*, John Wiley & Sons, Inc., New York, 1991, pp. 1–66.
188. R. Lew, D. Suwandra, S. T. Balke, and T. H. Moury, *Applied Polymer Symposium Proceedings*, Vol. 52, John Wiley & Sons, Inc., New York, 1993, pp. 125–144.
189. P. Simon and A. Rudin, *J. Appl. Polm. Sci.* **46**, 763–773 (1992).
190. D. J. Nagy, *J. Polym. Sci., Polym. Lett. Ed.* **24**, 87 (1986).
191. H. G. Barth and F. J. Carlin, Jr., *J. Liq. Chromatogr.* **7**, 1717 (1984).
192. V. Grinspun and A. Rudin, *J. Appl. Polym. Sci.* **32**, 4303–4311 (1986).
193. V. Grinshpun, *Diss. Abs. Int.* **47**(5) (1986).
194. K. Hatada, T. Kityama, and K. Tahiro, *Polymer Yearbook*, Vol. 8, Harwood Academic Publishers, U.K., 1991, pp. 221–232.
195. J. M. Goldwasser, *Chromatography of Polymers*, ACS Symposium Series 521, American Chemical Society, Washington, D.C., pp. 243–251.
196. S. D. Hanton and X. M. Liu, *Anal. Chem.* **72**, 4550–4554 (2000).
197. M. Maeda, Y. Ohzeki, P. O. Danis, K. Waddell, T. Kehoe, and K. Seta, *Chromatography* **20**, 408–409 (1999).
198. C. E. Kassis, J. M. DeSimone, R. W. Linton, E. E. Remsen, G. W. Lange, and R. M. Friedman, *Rapid Commun. Mass. Spectrom* **11**, 1134–1138 (1997).
199. C. Jackson, B. Larsen, and C. McEwen, *Anal. Chem.* **68**, 12303–1308 (1996).
200. J. M. Goldwasser and A. Rudin, *J. Liq. Chromatogr.* **6**, 2433–2464 (1983).
201. V. V. Nesterov, O. I. Kurenbin, V. D. Krasikov, and B. G. Belenkii, *Talanta* **34**(1), 161–165 (1987).
202. K. Q. Wang and H. H. Huang, *J. Liq. Chrom. Rel. Technol.* **23**, 523–529 (2000).
203. J. M. Goldwasser, A. Rudin, and E. L. Elsdon, *J. Liq. Chromatogr.* **5**, 2253–2257 (1982).
204. M. S. Montaudo, *Polymer* **43**, 1587–1597 (2002).
205. R. A. Sanford, R. K. Bade, and E. N. Fuller, *Am. Lab*. 99 (Mar. 1983).
206. J. Francois, M. Jacot, Z. Crubisic-Gallot, and H. Benoit, *J. Appl. Polym. Sci.* **22**, 1159 (1978).
207. D. Sarazin, J. LeMoigne, and J. Francois, *J. Appl. Polym. Sci.* **22**, 1377 (1978).
208. H. Leopold and B. Trathnigg, *Die Angew. Makromol. Chem.* **68**, 185 (1978).
209. B. Trathnigg, *Monatsh. Chem.* **109**, 467 (1978).
210. B. Trathnigg, *Die Angew. Makromol. Chem.* **89**, 65 (1980).
211. B. Trathnigg, *Die Angew. Makromol. Chem.* **89**, 73 (1980).
212. B. Trathnigg, *Makromol. Chem. Rapid Commun.* **1**, 569 (1980).
213. W. L. Elsdon, J. M. Goldwasser, and A. Rudin, *J. Polym. Sci., Polym. Chem.* **20**, 3271–3283 (1982).

214. W. W. Schulz and W. H. King, Jr., *J. Chromatogr. Sci.* **11**, 343 (1973).
215. H. S. Huang and H. G. Barth, in *Antec '85, Conference Proceedings of the SPE 43rd Annual Technology Conference*, Washington, D. C., 1985, p. 277.
216. G. Holzworth, L. Soni, and D. N. Schulz, *Macromolecules* **19**, 422 (1986).
217. S. Mori and co-workers, *Bunseki Kagaku* **46**, 837–844 (1997).
218. S. Hirayanagi, *Bunseki Kagaku* **46**, 795–797 (1998).
219. L. D'Agnillo, J. B. P. Soares, and A. Pendlis, *J. Polym. Sci., Polym. Phys. Ed.* **40**, 905–921 (2002).
220. B. E. Richter, in Ref. 6, Chapt. 13.
221. A. Shalliker, P. E. J. Kavanaugh, and I. Russell, *18th Australian Polymer Symposium*, Bendigo, Australia, Feb. 4–8, 1990, Paper 29.012.
222. S. Mori, *J. Chromatogr.* **156**, 111 (1978).
223. A. Sebenik and S. Lapanje, *J. Chromatogr.* **106**, 454 (1975).
224. P. McFadyen, *J. Chromatogr.* **123**, 468 (1976).
225. L. M. Zaborsky, II, *Anal. Chem.* **49**, 1166 (1977).
226. C. Bailly, D. Daoust, R. Legras, J. P. Mercier, and M. de Valck, *Polymer* **27**, 776 (1986).
227. E. Klesper and W. Hartmann, *J. Polym. Sci., Polym. Lett. Ed.* **15**, 9 (1977).
228. M. A. McHugh, V. J. Krukonis, and J. A. Pratt, *Trends Polym. Sci.* **2**, 301–307 (1994).
229. H. Yun, S. V. Olesik, and E. H. Marti, *J. Microcolumn Sep.* **11**(1), 53–61 (1999).
230. S. Mori, *Anal. Chem.* **60**, 1125–1128 (1988).
231. B. G. Belenkii and E. S. Gankina, *J. Chromatogr. Rev.* **141**(1), 13–90 (1977).
232. H. Inagaki and T. Tanaka, in J. V. Dawkins, ed., *Developments in Polymer Characterization*, Vol. 3, Applied Science Publishers, London, 1982, p. 1.
233. H. Inagaki, in Ref. 147, p. 649.
234. K. Kamide, T. Okada, T. Terakawa, and K. Kaneo, *Polym. J.* **10**, 547 (1978).
235. C. A. Jackson and W. J. Simonsick Jr., *Curr. Opin. Solid State Mater. Sci.* **2**, 661–667 (1977).
236. G. Montaudo, *Trends Polym. Sci.* **4**(3), 81–86 (1996).
237. L. Li, *Am. Chem. Soc., Polym. Prepr. Div. Polym. Chem.* **41**, 627–628 (2000).
238. W. E. Rudzinski and T. M. Abraham, *Polym. News* **25**, 213–214 (2000).
239. J. W. Kwang and R. W. Odom, *Anal. Chem.* **70**, 456A–461A (1998).
240. T. Q. Ngyen, H. H. Kausch, and G. Yu, *Macromol. Symp.* **110**, 97–106 (1996).
241. M. Dey, J. A. Castoro and C. L. Williams, *Anal Chem.* **67**, 1575–1579 (1995).
242. R. P. Lattimer, R. E. Harris and H.-R. Schulten, in Ref. 6, Chapt. 14.
243. E. Scamporrino and D. Vitalini, in Ref. 7, Chapt. 8.
244. C. M. Guttman, W. R. Blair, and P. O. Dennis, *Soc. Plast. Eng., Antec 98* **2**, 2109–2113 (1998).
245. R. H. Casper and G. V. Schulz, *Sep. Sci.* **6**, 321 (1971).
246. G. S. Greschner, in Ref. 6, Chapt. 11.
247. G. S. Greschner, *Makromol. Chem.* **180**, 2551 (1979).
248. G. S. Greschner, *Makromol. Chem.* **181**, 1435 (1980).
249. G. S. Greschner, *Makromol. Chem.* **182**, 2845 (1981).
250. G. S. Greschner, *Advances in Polymer Science*, Vol. 73, Springer-Verlag, Berlin, 1985, p. 1.
251. J. C. Giddings, *Pure Appl. Chem.* **51**, 1459 (1979).
252. G. C. Giddings, K. D. Caldwell and L. F. Kesner, in Ref. 6, Chapt. 12.
253. T. Provder, ed., *Chromatography of Polymers: Characterization by SEC, Size Exclusion Chromatography and FFF Field Flow Fractionation*, American Chemical Society, Washington, D.C., 1993.
254. K. D. Caldwell, *Modern Methods of Polymer Characterization*, John Wiley & Sons, Inc., New York, 1991, pp. 113–150.
255. J. C. Giddings, M. N. Myers, G. C. Lin, and M. Martin, *J. Chromatogr.* **142**, 23 (1977).

256. M. T. Nyugen and R. Beckett, *18th Australian Polymer Symposium*, Bendigo, Australia, Feb. 4–8, 1990, Paper 16.012.
257. J. C. Giddings, G. C. Lin, and M. N. Myers, *J. Liq. Chromatogr.* **1**, 1 (1978).
258. R. Hecker, P. D. Fawell, A. Jefferson, and J. B. Farrow, *J. Chromatogr. A* **837**, 139–151 (1999).
259. J. C. Giddings, M. A. Benincasa, M. K. Liu, and L. Ping, *J. Liq. Chromatogr.* **15**, 1729–1747 (1992).
260. M. A. Benincasa and J. C. Giddings, *Anal. Chem.* **64**, 790–798 (1992).
261. Y. Jiang, M. Miller, P. Li, and M. Hansen, *Polym. Mater. Sci. Eng.* **79**, 57–58 (1998).
262. Y. Jiang, M. E. Miller, P. Li and M. E. Hansen, *Am. Lab*. 98–108 (Feb. 2002).
263. J. C. Giddings, *J. Chromatogr.* **125**, 3 (1976).
264. J. J. Kirkland, W. W. Yau, and W. A. Doerner, *Anal. Chem.* **52**, 1944 (1980).
265. A. C. Van Asten, R. J. Van Dam, W. T. Kok, R. Tijssen, and H. Poppe, *J. Chromatogr. A* **703**(1/2), 245–263 (1995).
266. P. C. Allen, E. A. Hill, and A. M. Stokes, *Plasma Proteins, Analytical and Preparative Techniques*, Blackwell Scientific Publications, Oxford, U.K., 1978, p. 7.
267. T. J. Mantle, *Techniques in Protein and Enzyme Biochemistry*, B105b, 1978, p. 1.
268. C. Viney and L. Gilliland, in Ref. 7, Chapt. 10.
269. J. A. Zeineh, M. M. Zeineh, and R. A. Zeineh, *Am. Lab*. 124 (June 1986).
270. F. Leonardi, A. Allal, and G. Marin, *Rheol. Acta* **37**, 199–213 (1998).
271. D. W. Mead, *J. Rheol.* **38**, 1797–1827 (1994).
272. W. H. Tuminello, W. H. Buck, and D. L. Kerbow, *Macromolecules* **26**, 499–503 (1992).
273. D. V. Quayle, *Br. Polym. J.* **1**, 15 (1969).
274. G. Koszterszitzs and G. V. Schulz, *Makromol. Chem.* **178**, 2437 (1977).
275. R. Freeman and K. R. Leonard, *J. Microsc.* **122**, 275 (1980).
276. G. Stegman, J. C. Kraak, and H. Poppe, *J. Chromatogr.* **550**, 721–739 (1991).
277. J. P. Queslel and J. E. Mark, in Ref. 6, Chapt. 16.
278. A. M. Zaper, J. L. Koenig, in Ref. 6, Chapt. 15.

GENERAL REFERENCES

Refs. 1,11,12,38,45,47,99,100,120,127, and 166 are good general references.
M. J. Forrest, Rapra Review Report, Vol. 12, No. 7, Rapra Technology Ltd., London, 2001, p. 148.
R. A. Pethrick and J. V. Dawkins, eds., *Modern Techniques for Polymer Characterisation*, John Wiley & Sons, Inc., New York, 1999.
T. Provder, ed., *Chromatography of Polymers: Hyphenated and Multidimensional Techniques*, ACS Books, Washington, D.C., 1999.
H. G. Barth and J. W. Mays, eds., *Modern Methods of Polymer Characterization*, John Wiley & Sons, Inc., New York, 1997.
S. Holding, *Polymer Testing 97, Conference Proceedings, Paper 8 9T*, Rapra Technology Ltd., London, 1997.
C. G. Smith, P. B. Smith, A. J. Pasztor, M. L. McKelvy, D. M. Meunier, and S. W. Froelicher, *Anal. Chem.* **67**(12), 97R–126R (1995).
S. R. Holding and E. Meecham, Rapra Review Report, Vol. 7, No. 11, Rapra Technology Ltd., London, 1995, p. 148.
B. J. Hunt and M. I. James, *Polymer Characterization*, Kluwer, London, 1993.
T. R. Crompton, *Practical Polymer Analysis*, Plenum Press, New York, 1993.
J. Springer, M. D. Lechner, H. Dautzenberg, and W. M. Kulicke, *Makrolmol. Chem., Macromol. Symp.* **61**, 1–23 (Aug 1992).
D. Campbell and J. R. White, *Polymer Characterisation—Physical Techniques*, Chapman and Hall, London, 1989.

E. Schroeder, G. Muller, and K.-F. Arndt, *Polymer Characterization (retroactive coverage)*, Carl Hanser Verlag, Munich, Germany, 1989.
A. R. Cooper, *Polym. Eng. Sci.* **29**, 1 (1989).
L. J. V. Dawkins, ed., *Developments in Polymer Characterization*, Vols. 1–5, Elsevier Applied Science Publishers, Ltd., Barking, U.K., 1986.
J. Janca, ed., *Steric Exclusion Liquid Chromatography of Polymers*, Marcel Dekker, Inc., New York, 1984.
S. Bark and N. S. Allen, eds., *Analysis of Polymer Systems*, Applied Science Publishers, London, 1982.
W. W. Yau, J. J. Kirkland, and D. D. Bly, eds., *Modern Size Exclusion Chromatography*, Wiley-Interscience, New York, 1979.
N. C. Billingham, *Molar Mass Measurements in Polymer Science*, Halsted Press, a division of John Wiley & Sons, Inc., New York, 1977.
L. H. Tung, ed. *Fractionation of Synthetic Polymers*, Marcel Dekker, Inc., New York, 1977.
P. E. Slade, Jr., ed., *Polymer Molecular Weights, Parts I and II*, Marcel Dekker, Inc., New York, 1975.

ANTHONY R. COOPER
Lockheed Martin Space Systems

MOLECULAR WEIGHT DISTRIBUTION.

See MOLECULAR WEIGHT DETERMINATION.

MOLECULARLY IMPRINTED POLYMERS.

See Volume 7.

MORPHOLOGY.

See Volume 7.

NANOCOMPOSITES, LAYER-BY-LAYER ASSEMBLY

Introduction

Advanced materials from inorganic nanoparticles (NPs) and other nanocolloids such as single wall carbon nanotubes (SWNT) are currently one of the most dynamic areas of today's science. They represent significant fundamental and commercial interest with a wide range of applications including the next generation optics, electronics, and sensors (1–6). Synthetic methods of colloidal chemistry afford manipulation of their size, surface structure, and hence, their properties (7). In optical, electrical, and magnetic devices, nanocolloids will be mostly used as thin films. Currently, such films are typically made by spin coating, spraying, or sometimes by simple painting of nanoparticle–matrix mixtures. The layer-by-layer assembly (LBL) is one of the most promising new methods of thin film deposition, which is often used for oppositely charged polyelectrolytes (PE) (8,9). It has also been successfully applied to thin films of nanocolloids (10–33). One of the major advantages of LBL is simplicity: the process requires neither sophisticated hardware nor high purity of the components. At the same time under optimal conditions, the method produces high quality of coatings with thickness controllable at the nanometer level (26). This deposition technique is also quite universal: for virtually any aqueous dispersion of NPs, one can find a matching polyelectrolyte and deposition conditions yielding a steady film buildup (34). The lateral packing of the NPs and SWNTs in individual adsorption layers can also be controlled by different means producing densely packed coatings (15,27,34). The LBL coatings are also highly homogeneous unlike the composite polymer/NP coatings obtained by other means (35), where phase separation may occur (36). Last but not the least, LBL affords combining NPs with other functional materials often used by

Encyclopedia of Polymer Science and Technology. Copyright John Wiley & Sons, Inc. All rights reserved.

this technique such as dyes, proteins, and DNAs, leading to a palette of multifunctional nanostructured materials (37). In essence, LBL can be a convenient method for processing NPs in thin films, which opens broad perspectives for this technique, both in research and in industry. This article attempts to summarize the current status of understanding of the LBL deposition of NPs, the structure of produced films and the future applications for these materials.

Layer-By-Layer Assembly

Layer-by-layer assembly can be described as the sequential adsorption of positively and negatively charged species, say A and B, by dipping a substrate alternatively into their solutions. Rinsing with water between adsorption steps removes the excess of the previous solution and leaves a thin layer of charged species on the surface, thereby preparing the surface for the next adsorption step. The dynamic development of LBL that has been seen recently was sparked mainly by its great success with assembly of polyelectrolytes (9,30,38–40); However, similar ideas were previously used (41) for the assembly of colloids, for production of semiconductor films (42,43), and for the assembly of NP/PE magnetic films (10). The description of experimental details of the technique can be found in the original publications of the respected authors (see also COLLOIDS; POLYELECTROLYTES; LANGMUIR-BLODGETT FILMS).

From the analysis of the abundant literature on LBL, one can say that A and B are preferentially chosen to be of relatively high molecular weight. The experimental work on polymers with different chain lengths indicates that the increase of the molecular mass of species promotes stable LBL growth (15,44–46), which is related to the diverse nature of intermolecular interactions involved in the process (see SWNT/Polyelectrolyte Composites). Although for relatively low molecular weight species such as multicharged metal ions (47–51) and molecular dyes (52–54), the LBL assembly was also reported, and their tendency to leach out should be accentuated (55). Heavy mass and the multiple points of attachment of A and B render the absorption sufficiently irreversible to allow for the deposition of the next layer. Either A or B is almost always a PE, while the other LBL partner can be a dispersion of NPs, clay sheets, proteins, dyes, vesicles, DNA, viruses or other species. The omnipresence of PEs in LBL assemblies acquired popularity in the 1990s is explained by their ability to cover irregularities owing to the rod-like conformation of the charged macromolecules in aqueous solutions (9,56).

Ultrastrong Materials

The mass–strength ratio of materials is of exceptional importance for many different applications. The critical parts of different vehicles and crafts depend on strength and toughness of the materials they are made of, while strict limitations on the weight of the different components are placed by the modern air and spacecraft technology. SWNT presents significant potential as a basic material for space applications. Exceptional mechanical properties of SWNT (57–62) have prompted

intensive studies of SWNT composites. These qualities can also be used in a variety of other technologies from automotive to military and medical. However, the present composites have shown only a moderate strength enhancement when compared to other hybrid materials (53–65). Although substantial advances have been made (66), mechanical characteristics of SWNT-doped polymers are noticeably below their highly anticipated potential. Pristine SWNTs are well known for poor solubilization, which leads to phase segregation of composites. Severe structural inhomogeneities result in the premature failure of the hybrid SWNT/polymer materials. Connectivity with and uniform distribution within the matrix are essential structural requirements for strong SWNT composites (67–69). A new processing approach based on sequential layering of chemically-modified nanotubes and polyelectrolytes can greatly diminish the phase segregation and render SWNT composites highly homogeneous. Combined with chemical cross-linking, this processing leads to drastically improved mechanical properties. Tensile strength of the composites is several times higher than that of SWNT composites made via mixing; it approaches values seen for hard ceramics. The universality of the layering approach applicable to a wide range of functional materials makes possible successful incorporation of SWNT into a variety of composites imparting to them required mechanical properties.

The thin film membranes that are obtained as a result of the layer-by-layer process can be used as an intermediate or as a component of ultrastrong laminates. At the same time, the prepared membranes can also be utilized in the as-prepared form for space and biomedical technologies because they combine the strength and multiple functionality of the SWNT membranes.

SWNT composites are typically prepared by blending, *in situ* polymerization, and extrusion. After extensive surface modification, such as grafting or polymer wrapping (68–70), the phase segregation from a macromolecular matrix is smaller than for pristine SWNT, but still remains high owing to the high affinity of SWNTs to each other. Vastly different molecular mobilities of both components also contribute to widespread phase separation. Very intense research on appropriate surface modification of SWNT is currently under way in many groups around the world. Nevertheless, most common loadings of nanotubes in the polymer matrix are within the 1–15 wt% range, whereas more than 50% of the SWNT content is needed for materials with special mechanical performance without compromising the homogeneity of the composite at the nanometer level. This high loading of the nanotubes is particularly important when both electrical and mechanical qualities of the nanotubes are going to be utilized.

The phase segregation between dissimilar materials can be circumvented by applying a layer-by-layer assembly (LBL) (71). The immobilization of the macromolecular compounds and strong interdigitation of the nanometer-thick film allows for the close-to-perfect molecular blending of the components (72,73).

SWNT/Polyelectrolyte Composites. The SWNT/polyelectrolyte composites produced in this study were assembled onto a solid support via alternate dipping of a solid substrate (glass slides, Si wafers) into dispersions of SWNT and polyelectrolyte solutions (74–76). The individual assembly steps, ie adsorption of SWNT and polyelectrolyte monolayers, were interlaced by rinsing steps to remove the excess of assembling materials. When the LBL procedure

was complete, the multilayer films were lifted off the substrate to obtain uniform free-standing membranes, which can be handled as regular composites (77). Such films make possible straightforward testing of their mechanical properties.

SWNT were produced by laser ablation and subsequently purified via acid treatment. Single-wall nanotubes were manufactured by laser vaporization of carbon rods doped with Co, Ni and FeS in an atmosphere of $Ar:H_2$. Standard SWNT products made by HiPCO and other methods contain significant amount of sooth, graphite flakes, and remnants of the catalyst, which need to be removed prior to the assembly. The quality of the dispersion directly affects the mechanical performance of the resulting composite.

A suspension of SWNT raw material was refluxed in 65% HNO_3 and subsequently purified by centrifugation. Supplemented by sonication, this treatment results in the partial oxidation of ca 5% of the total number of carbon atoms both in caps and walls of SWNT (78). A similar type of dispersion can also be made following other recipes such as polymer wrapping the nanotubes, and chemical derivatization. Optimization of the aqueous nanotube dispersions should be considered as one of the most critical direction of the optimization of the carbon nanotube composites and speed and quality of their processing in the composites. Dispersions made by other methods are expected to be also applicable for the preparation of LBL films. The strength and other mechanical properties will depend though on energy of attractive interactions between the coating agent and the matrix as well as between SWNT and the coating agent.

In slightly oxidized nanotubes, the presence of carboxylic acid groups affords the preparation of metastable SWNT dispersions after 1 min sonication in deionized water without any additional surfactant. Thus prepared negatively charged SWNT with zetapotential of -0.08 V can be layer-by-layer assembled with positively charged polyelectrolyte, such as branched poly(ethyleneimine), $M_w = 70{,}000$ (PEI) (Fig. 1). Since the overall negative charge of the SWNT used here was fairly small, after every 5th deposition cycle, a layer of SWNT was replaced with a layer of poly(acrylic acid), $M_w = 450{,}000$ (PAA) (Fig. 1). These additional layers improve

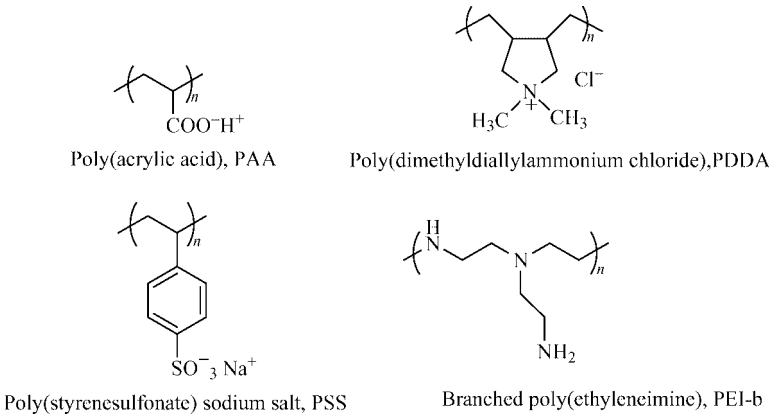

Fig. 1. Common polyelectrolytes, used for LBL process.

the linearity of the deposition process and present a convenient chemical anchor for subsequent chemical modification. For the same reasons, a single PEI/PAA bilayer was deposited on a bare glass or Si substrate prior to the SWNT assembly. The assembly conditions of the entire procedure (pH, ionic strength, concentrations, etc) were optimized so that the dipping cycles can be repeated as many times as needed with linear growth of the multilayers (Fig. 2**a**). This enables the preparation of films with any desirable thickness and architecture tailored to different applications. The ionic conditions of LBL assembly were the following: 1% solution of PEI at pH 8.5; 1% PAA at pH 6 (pH 3 for wafer coating); SWNT at pH 6.8. All solutions were made in 18 MΩ deionized (DI) water without addition of any extra salt or other low molecular weigh electrolyte. DI water was also used for rinsing at pH 8.5 adjusted by NaOH. Wafers/glass slides were cleaned in piranha solution, rinsed with DI water, sonicated for 15 min and again thoroughly rinsed with DI water. After that, they were coated with a precursor layer: PEI (10 min) + PAA (15 min, pH 3), followed by the deposition of $(PEI/SWNT)_5$. The layer sequence of $(PEI/PAA)(PEI/SWNT)_5$ was repeated until the desirable thickness is obtained. Exposure times of 10 and 60 min was used for polylectrolytes and SWNT baths, respectively.

Multilayer stacks with a cumulative structure of $((PEI/PAA)(PEI/SWNT)_5)_6$ and $((PEI/PAA)(PEI/SWNT)_5)_8$ containing 30 and 40 (PEI/SWNT) bilayers, respectively, were typically used in this study.

Currently, other methods are being investigated for dispersing SWNT in water to avoid excessive damage to the SWNT wall such as wrapping of the nanotubes with copolymers, which can equally well work on the SWNT and multiwall carbon nanotubes (MWNT). For some applications, MWNTs can be a preferred materials due to lower cost.

Similarly to other polyelectrolyte LBL systems (71), a submonolayer of SWNT is deposited in each deposition cycle. The final morphology of the multilayers can be described as a mixture of individual carbon nanotubes and their 4–9 nm bundles intricately interwoven together in a fine fabric (Fig. 2**c**) (74,75). Two important structural characteristics should be pointed out. SWNT uniformly cover the entire surface of the substrate without any evidence of phase separation. Also, the presence of oxidized flat graphite sheets and other forms of carbon colloids in the experiments was very small. Both these factors contributed to the mechanical properties of the composites. The quality of the nanotube material was also assessed by Raman spectroscopy. (Raman measurements were performed in a backscattering configuration with a 50 mW of 514.5 nm laser light was incident on the samples.) The characteristic Raman peaks for SWNTs, eg the radial breathing mode at $\sim$182 cm^{-1} and the tangential C–C stretching modes located at $\sim$1560 cm^{-1} (G1 mode) and $\sim$1583 cm^{-1} (G2 mode), were very sharp and narrow indicating the high uniformity of the SWNT and low level of impurities present in the films. A barely visible peak at $\sim$1340 cm^{-1} (D mode) revealed the presence of residual amounts of disordered carbon structures. Using the correlation between the frequency of the radial breathing mode, ν, and the SWNT diameter, d, expressed as $d = 223.75/\nu$ (79), a value of $d = 1.2$ nm is obtained, which is in a good agreement with the SWNT diameters obtained from AFM images of many individual nanotubes. From these images, the length of the nanotubes was estimated to be 2–7 μm.

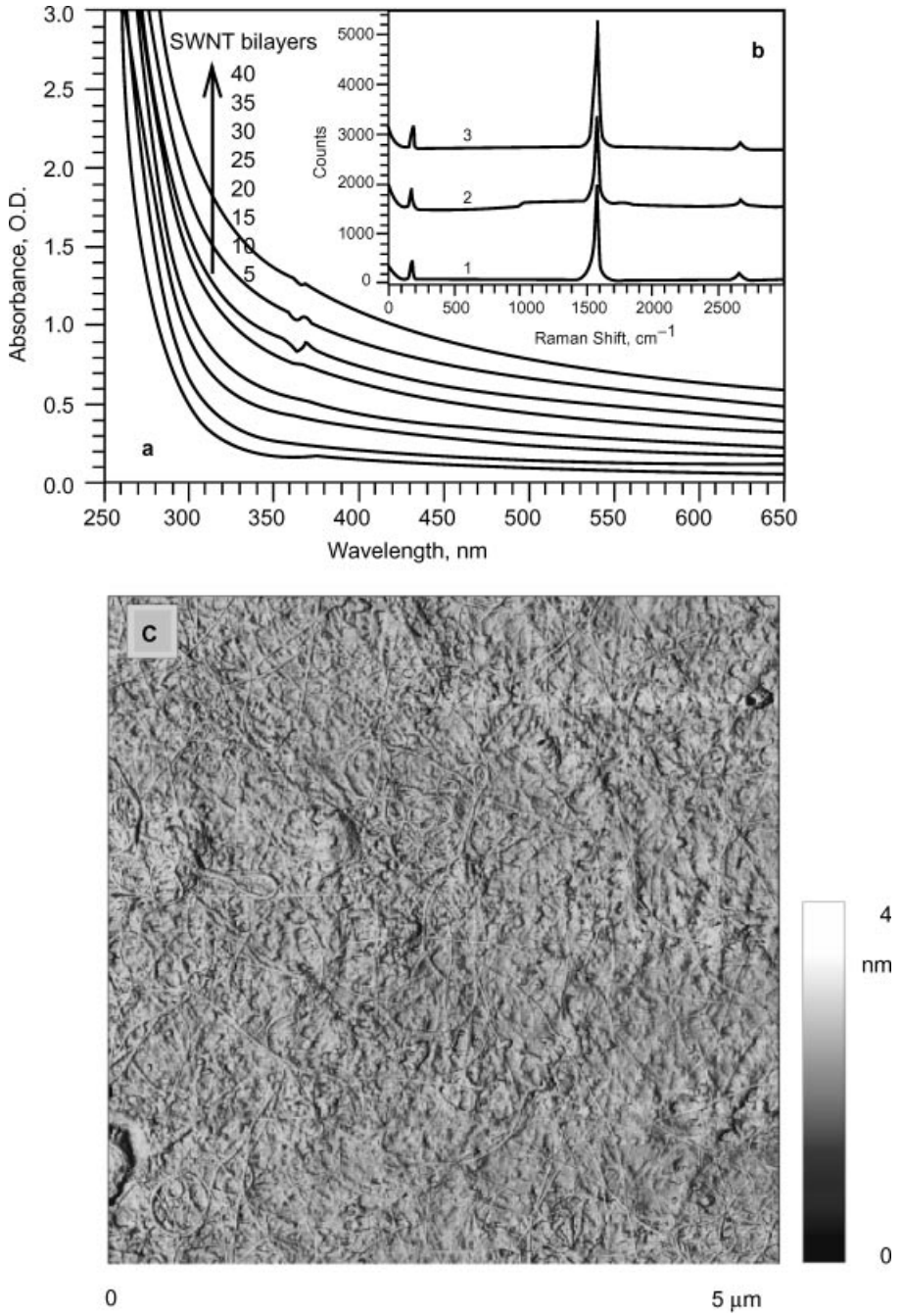

Fig. 2. Structural characterization of SWNT multilayers. (**a**) Sequential UV–vis spectra of a glass substrate in the course of the LBL deposition of SWNT. The spectra were taken for a total number of (PEI/SWNT) bilayers indicated in the graph. (**b**) Raman scattering spectra of SWNT dispersion (*1*), LBL film on a glass substrate (*2*) and free-standing film (*3*). (**c**) Tapping mode AFM image (DI, multimode IIIA) of a Si wafer bearing (PEI/PAA)(PEI/SWNT)$_5$. See Refs. 74,75.

PEI was utilized as the LBL partner of SWNT because of terminal $-NH_2$ and backbone —NH— groups in the main chain and branches suitable for the subsequent chemical modification of the composite (80). The PEI chains can be cross-linked (*1*) with each other and (*2*) with carboxyl groups on SWNT and PAA. Chemical stitching increases the connectivity of the polyelectrolyte matrix with SWNT, and therefore, load transfer in the composite (80). The combination of both modification pathways was used. SWNT/PEI/PAA composite was heated to 130°C after the deposition of each layer. According to the study by Sullivan and co-workers (81), this treatment should result in amide bonds between a variety of protonated and nonprotonated functional groups of PEI, PAA, and SWNT complementing the intrinsic ionic cross-linking of the LBL films (81). Subsequently, the film was exposed to glutaraldehyde at room temperature. This treatment is well known to produce covalent bonds with primary amine groups present in the polyelectrolyte. Samples were cross-linked in 0.5% glutardialdehyde solution in phosphonate buffer (0.054 *M* Na_2HPO_4, 0.013 *M* NaH_2PO_4, pH 7.4) for 1 h at room temperature. To remove unreacted glutaraldidehyde, the film was rinsed with tap water for 3 × 10 min and then with DI water the same number of times. This reaction produces a tight network of polymeric chains and nanotubes connected by dialdehyde linkages. It was found that if only 1% of all carbon atoms of SWNT are chemically bonded to the polymer matrix, such as cross-linking drastically increases the shear between them by an order of magnitude (80). Therefore, a 5% density of —COOH groups on the SWNT surface cited above should be sufficient to obtain good connectivity with the polyelectrolyte matrix. Note these groups are not completely utilized at the moment, because of the relatively low temperature of amide bond cross-linking step.

Mechanical Properties and Testing

The mechanical properties of the LBL-assembled SWNT thin films were studied in their free-standing form prepared by the chemical delamination from the substrate (77). SWNT multilayers were separated from the silicon wafers by immersion into 0.5% aqueous HF for 3 min. The Raman scattering spectrum of the separated film is almost identical to that of the supported film and original nanotubes (Fig. 2**b**), demonstrating that the structure of SWNT remains mostly unaltered during the cross-linking and delamination. The breathing mode frequency shifts from 185 cm^{-1} in the assembled film to 182 cm^{-1} in the cross-linked self-standing films indicating a small expansion of the tube diameters.

The delaminated thin films (Fig. 3**a**), can be easily handled in a variety of ways. They can be made of any desirable size or shape determined only by the dimensions of the substrate. The films that we routinely prepare in this study were ca 1 × 3 cm. Assemblies with a structure of $((PEI/PAA)(PEI/SWNT)_5)_6$ and $((PEI/PAA)(PEI/SWNT)_5)_8$ displayed an SWNT content of 50 ± 5 wt% as calculated from carbon and nitrogen EDAX peak integrals. Previously reported composites made with modified SWNT revealed strong inhomogeneities even at SWNT loadings as low as 6–8% (64,65). The cross-sectional image of the free-standing film (Figs. 4**a** and 4**b**) clearly demonstrates the absence of micrometer-scale inhomogeneities although the occasional inclusion of a round 30–60 nm particles can be

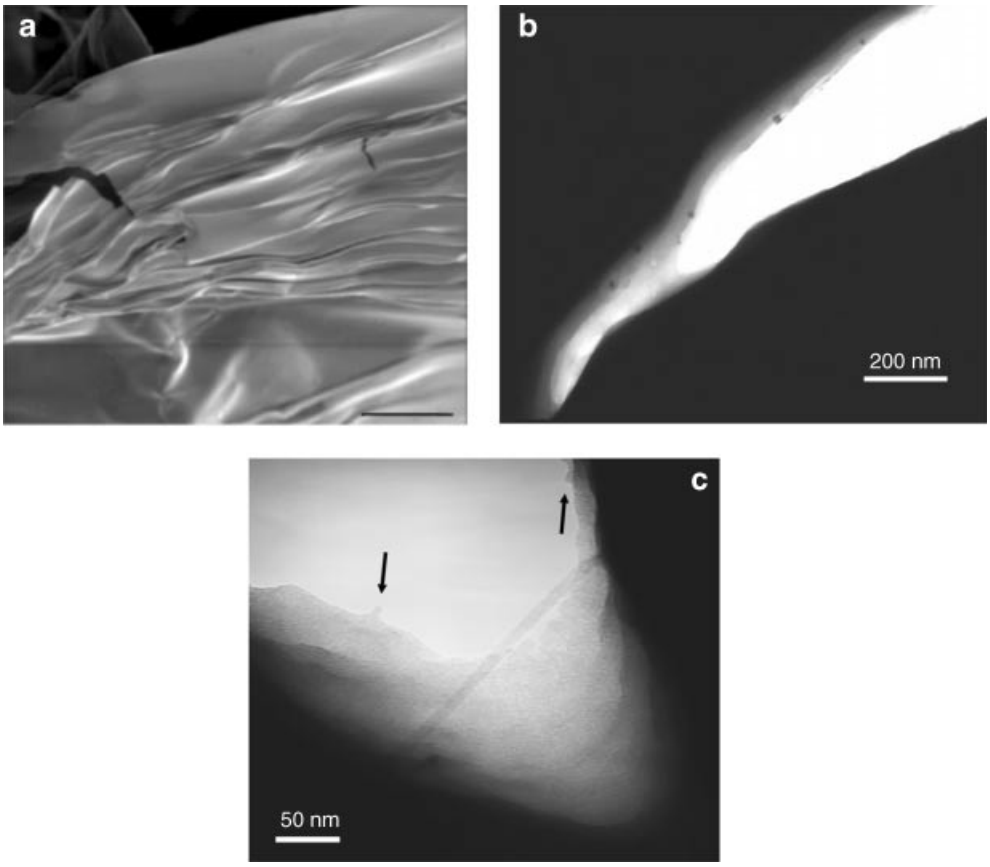

Fig. 3. Electron microscopy of the rupture region in SWNT multilayers. (**a**) SEM image of the surface and broken edges of $((PEI/PAA)(PEI/SWNT)_5)_8$. (**b**) and (**c**) TEM images of ruptured areas of the freestanding films. The arrows indicate the likely stubs of the broken nanotubes bundles. They were identified as such because (*1*) the diameter of both of them is equal to theat of the actual SWNT bundle bridging the gap and (*2*) their mutual positioning presents a virtually perfect match with the expected location of the ends of a bundle broken during gap opening.

seen (possibly dust). The slight variations in the gray scale contrast between different strata show the actual variations in SWNT distribution within the sample. They originate from small deviations in SWNT adsorption conditions, such as dispersion concentration and pH, during the buildup procedure. In SEM microscopy (Fig. 3**a**), the surface of the sample also appears smooth and continuous. Typically, the separation of single/multiwall carbon nanotubes and their bundles in mixed polymer composites can be observed as whiskers clearly visible in TEM and SEM images (60,82). The TEM examination of the initial stages of rupturing showed that virtually no fiber pullout occurs in the LBL multilayers (Fig. 3**b**). This can be contrasted by extensive nanotube pullout reported before by several groups (60,82). For many TEM images obtained in different areas of the self-standing films, we were able to observe only one SWNT bundle bridging the break region

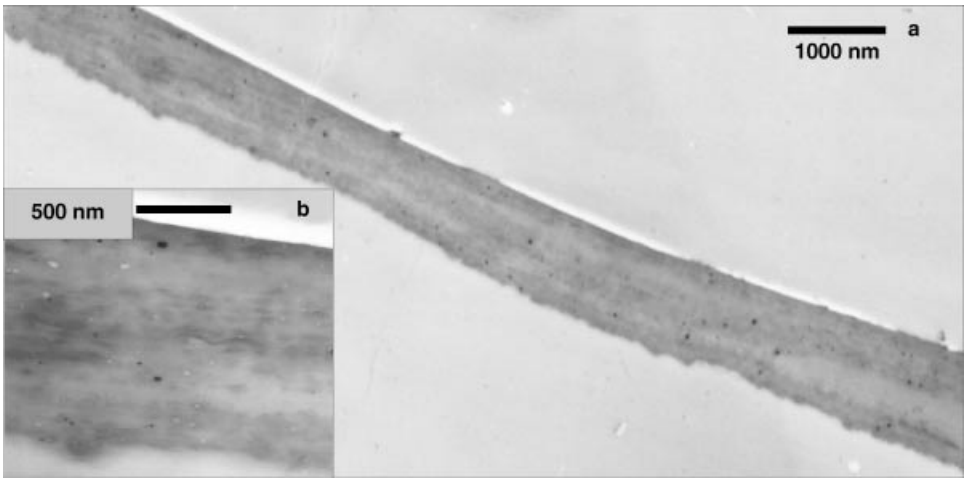

Fig. 4. TEM examination of the homogeneity of the SWNT LBL film. Survey (**a**) and closeup (**b**) TEM images of SWNT film cross sections. The top and botom sides of the film are slightly different in roughness: the one that was adjacent to the flat substrate is smoother than the "growth" surface of the film. See Refs. 74,75.

(Fig. 3**c**). The same image also shows two broken carbon fiber stubs imbedded in the walls of the crack (marked by arrows in Fig. 3**c**). In total, the microscopy results indicate efficient load transfer in the LBL composite. Currently, similar films are prepared from multiwall carbon nanotubes utilizing polymer wrapping (Fig. 5).

The mechanical properties of the layered composites were tested on a custom-made thin film tensile strength tester (McAllister Inc.) recording the displacement and applied force by using pieces cut from $((PEI/PAA)(PEI/SWNT)_5)_6$ and $((PEI/PAA)(PEI/SWNT)_5)_8$ free-standing films. The tester was calibrated on similar pieces made from cellulose acetate membranes and Nylon threads. $((PEI/PAA)(PEI/SWNT)_5)_6$ and $((PEI/PAA)(PEI/SWNT)_5)_8$ samples had an average TEM thickness of 0.75 and 1.0 μm, respectively. Their typical stress (σ) vs strain (ε) curves differed quite markedly from stretching curves seen previously

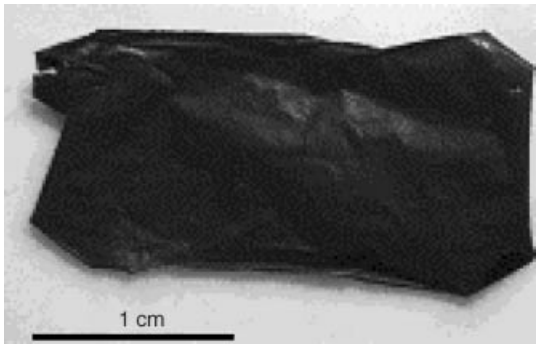

Fig. 5. Optical photograph of the freestanding LBL films made from multiwall carbon nanotubes.

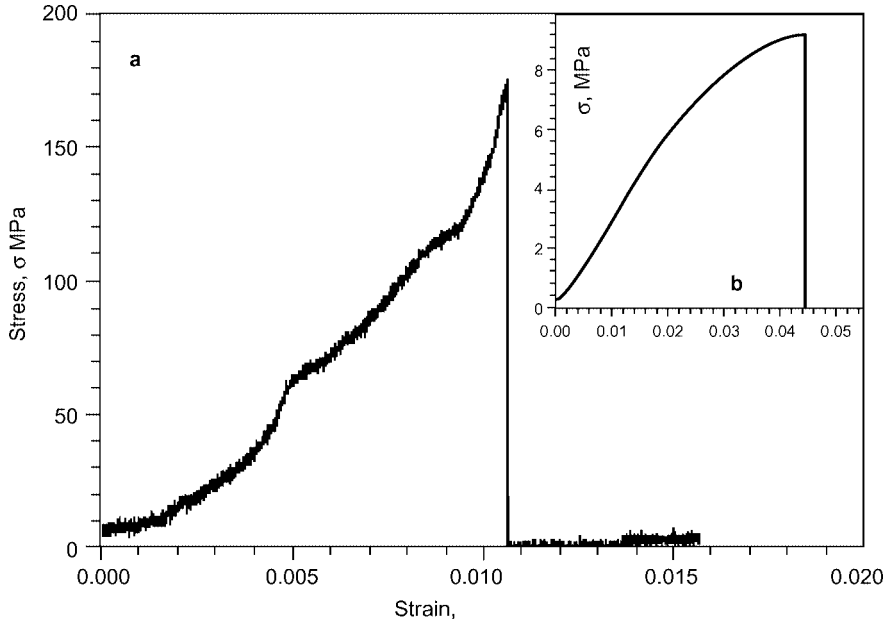

Fig. 6. Typical tensile strength curves of the SWNT LBL films. Stress–strain dependence for (**a**) $((PEI/PAA)(PEI/SWNT)_5)_8$ and (**b**) a similar free-standing multilayer film made solely from polyelectrolytes. The dependence of the mechanical properties of the cross-linked LBL composites on humidity was tested in the range of relative humidity of 30–100%, $T = 298^{\circ}C$, and was found to be negligible See Refs. 74,75.

for SWNT composites (66) and for LBL films made solely from polyelectrolytes, $(PEI/PAA)_{40}$, obtained by the same assembly procedure (Fig. 6**b**). They displayed a characteristic wave-like pattern, gradual increase of $d\sigma/d\varepsilon$ derivative, and the complete absence of the plateau region for high strains corresponding to plastic deformations (Fig. 6**a**). The latter correlates well with the enhanced connectivity of SWNT with the polymer matrix (Fig. 3). Other mentioned stretching features indicate the reorganization of the layered composite under stress. A process similar to the sequential breakage of cross-linked parts of coiled molecules (see AFM image in Figure 2) observed in natural nanocomposites, such as seashells and bones (83,84), is likely to be responsible for the wave-like pattern and the increase of the stretching curve slope.

Considering the complexity of the deformation process, the assessment of elastic and inelastic behavior in each part of the curve will be done upon detailed microscopy investigation. Meanwhile, the values of $d\sigma/d\varepsilon$ exceeding 50 GPa should be noted.

The comparison with stretching curves for polyelectrolytes (Fig. 6**b**) shows that the incorporation of nanotubes in the LBL structure resulted in the transfer of the SWNT strength to the entire assembly. The stretching curves of the SWNT multilayers display a clear break point. The ultimate tensile strength, T, was found to be 220 ± 40 MPa with some readings being as high as 325 MPa. This is several times to an order of magnitude greater than the tensile strength of

strong industrial plastics with $T = 20$–66 MPa (85). It is also substantially higher than the tensile strength of carbon fiber composites made by mixing: polypropylene filled with 50 vol% Carbon Fibers (qv) has $T = 53$ MPa (86). A recent study on SWNT/poly(vinyl alcohol) ribbons with axially aligned nanotubes reported a tensile strength of 150 MPa (66). The T values obtained for SWNT LBL films are, in fact, close to those of ultrahard ceramics and cermets such as tungsten monocarbide, $T = 340$ MPa, silicon monocarbide, $T = 300$ MPa, and tantalum monocarbide, $T = 290$ MPa (85). Such strength and failure strain greater than in cermets (ca >1% in SWNT LBL vs. 0.2–0.6% in carbides) displayed by an organic composite is quite remarkable.

The tensile strength of single carbon nanotubes was experimentally determined to be between 13 and 50 GPa (82,87). The lower values obtained for the SWNT multilayers should be mainly attributed to the contribution of polyelectrolytes and some uncertainty in the actual cross-sectional area at the break point and a degree of cross-linking. The mixing law predicts that a polyelectrolyte matrix with $T = 9$ MPa makes a negligible contribution to the strength of the composite while taking about 50% of its volume fraction (SWNT is $d = 1.14$ g/cm^3). Since the density of the polyelectrolytes used for the preparation of the multilaters, ie PDDA $d = 1.04$ g/cm^3, PAA $d = 1.14$ g/cm^3 is almost the same, the volume fraction of SWNT in the composite can be considered to be equal to the mass fraction). Additionally, the decrease of the mechanical strength of the nanotubes in the process of ionic functionalization (estimate 15%) (88) should also be considered as a factor affecting the strength of these composites. These issues are pointed out as means of further optimization of the multilayers. Tuning of their molecular structure and composition should lead to vast improvement of their mechanical properties that could possibly approach those of pristine carbon nanotubes.

It is also interesting to compare the T values for SWNT composite films to those obtained for other LBL films made with other inorganic components such as montmorillonite platelets, M, and nanoparticles, NP, for instance 8–10 nm magnetite nanoparticles. The free-standing films $(PDDA/NP)_{40}$ and $(PDDA/NP/PDDA/M)_{40}$ made according to Reference (77) revealed T equal to 40 and 72 MPa, respectively. In conjunction with the tensile strength data (see above), it can be concluded that inorganic or SWNT components act as a molecular armor in the layered composites significantly reinforcing them. The molecular organization of the material made possible the transfer of a part of their strength to the entire assembly.

The high structural homogeneity and interconnectivity of the structural components of the LBL films combined with high SWNT loading leads to significant increase of the strength of SWNT composites, being somewhat weaker than some other organic and carbon fiber materials but at the same time being far beyond their potential as ultrastrong composites. The described technique minimizes the structural defects originating from phase segregation and opens a possibility for the molecular design of layered hybrid structural materials from different polymers and other nanoscale building blocks. The prepared free-standing membranes can serve as a unique component for a variety of technologies. One of the great advantages of it in respect to other technologies is the ability to prepare ultrathin, ultrastrong membranes with minimal heterogeneity.

BIBLIOGRAPHY

1. A. P. Alivisatos, *J. Phys. Chem.* **100**, 13226–13239 (1996).
2. D. L. Klein, R. Roth, A. K. L. Lim, A. P. Alivisatos, and P. L. Mceuen, *Nature* **389**, 699–701 (1997).
3. M. Bruchez Jr., M. Moronne, P. Gin, S. Weiss, and A. P. Alivisatos, *Science* **281**, 2013–2016 (1998).
4. M. G. Bawendi, *Abstr. Pap. Am. Chem. Soc.* **212**, 149-Inor (1996).
5. H. Weller, *Curr. Opin. Colloid Interface S.* **3**, 194–199 (1998).
6. W. C. W. Chan and S. Nie, *Science* **281**, 2016–2018 (1998).
7. A. P. Alivisatos, *Science* **271**, 933–937 (1996).
8. G. Decher and J. D. Hong, *Ber. Bunsen-Ges. Phys. Chem. Chem.* **95**, 1430 (1991).
9. G. Decher, *Science* **277**, 1232–1237 (1997).
10. C. A. Bruce, A. M. Homola, and M. R. Lorentz, *Preparation of Thin, Aligned Magnetic Coatings*, IBM Corporation. PCT 259,270[4,333,961], Issue Date: June 8, 1982, Filing date Apr. 30, 1981.
11. F. Aliev, M. Correa-Duarte, A. Mamedov, J. W. Ostrander, M. Giersig, L. Liz-Marzan, and N. Kotov, *Adv. Mater.* **11**, 1006–1010 (1999).
12. K. Ariga, Y. Lvov, I. Ichinose, and T. Kunitake, *Appl. Clay Sci.* **15**, 137–152 (1999).
13. F. Caruso, H. Lichtenfeld, M. Giersig, and H. Möhwald, *J. Am. Chem. Soc.* **120**, 8523–8524 (1998).
14. F. Caruso, R. A. Caruso, and H. Möhwald, *Science (Washington, D.C.)* **282**, 1111–1114 (1998).
15. M. A. Correa-Duarte, M. Giersig, N. A. Kotov, and L. M. Liz-Marzan, *Langmuir* **14**, 6430–6435 (1998).
16. M. A. Correa-Duarte, M. Giersig, N. A. Kotov, and L. M. Liz-Marzan, *Langmuir* **14**, 6430–6435 (1998).
17. D. L. Feldheim, K. C. Grabar, M. J. Natan, and T. E. Mallouk, *J. Am. Chem. Soc.* **118**, 7640–7641 (1996).
18. M. Y. Gao, B. Richter, S. Kirstein, and H. Möhwald, *J. Phys. Chem. B* **102**, 4096–4103 (1998).
19. M. Gao, S. Kirstein, A. L. Rogach, H. Weller, and H. Möhwald, *Adv. Sci. Technol. (Faenza, Italy)* **27**, 347–358 (1999).
20. N. A. Kotov, I. Dekany, and J. H. Fendler, *J. Phys. Chem.* **99**, 13065–13069 (1995).
21. Y. Liu, Y. Wang, and R. O. Claus, *Chem. Phys. Lett.* **298**, 315–319 (1998).
22. Y. Liu, W. Zhao, Y. X. Wang, and R. O. Claus, *Proc. Spie-Int. Soc. Opt. Eng.* **3324**, 45–48 (1998).
23. Y. Lvov, K. Ariga, M. Onda, I. Ichinose, and T. Kunitake, *Langmuir* **13**, 6195–6203 (1997).
24. Y. M. Lvov, J. F. Rusling, D. L. Thomsen, F. Papadimitrakopoulos, T. Kawakami, and T. Kunitake, *Chem. Commun*. 1229–1230 (1998).
25. Y. Lvov, K. Ariga, M. Onda, I. Ichinose, and T. Kunitake, *Langmuir* **13**, 6195–6203 (1997).
26. A. Mamedov, J. Ostrander, F. Aliev, and N. A. Kotov, *Langmuir* **16**, 3941–3949 (2000).
27. I. Pastoriza-Santos, D. S. Koktysh, A. A. Mamedov, M. Giersig, N. A. Kotov, and L. M. Liz-Marzan, *Langmuir* **16**, 2731–2735 (2000).
28. G. S. Ferguson and E. R. Kleinfeld, *Adv. Mater.* **7**, 414–416 (1995).
29. E. R. Kleinfeld and G. S. Ferguson, *Science* **265**, 370–373 (1994).
30. C. M. Bell, M. F. Arendt, L. Gomez, R. H. Schmehl, and T. E. Mallouk, *J. Am. Chem. Soc.* **116**, 8374–8375 (1994).
31. T. Cassagneau, T. E. Mallouk, and J. H. Fendler, *J. Am. Chem. Soc.* **120**, 7848–7859 (1998).

32. S. W. Keller, H. N. Kim, and T. E. Mallouk, *J. Am. Chem. Soc.* **116**, 8817–8818 (1994).
33. N. I. Kovtyukhova, P. J. Ollivier, B. R. Martin, T. E. Mallouk, S. A. Chizhik, E. V. Buzaneva, and A. D. Gorchinskiy, *Chem. Mater.* **11**, 771–778 (1999).
34. J. W. Ostrander, A. A. Mamedov, and N. A. Kotov, *J. Am. Chem. Soc.* **123**, 1101–1110 (2001).
35. A. L. Rogach, D. S. Koktysh, M. Harrison, and N. A. Kotov, *Chem. Mater.* **12**, 1526–1528 (2000).
36. H. Mattoussi, L. H. Radzilowski, B. O. Dabbousi, D. E. Fogg, R. R. Schrock, E. L. Thomas, M. F. Rubner, and M. G. Bawendi, *J. Appl. Phys.* **86**, 4390–4399 (1999).
37. A. A. Mamedov and N. A. Kotov, *Langmuir* **16**, 5530–5533 (2000).
38. G. Decher and J. D. Hong, *Macromol. Chem., Macromol. Symp.* **46**, 321 (1991).
39. M. Ferreira, J. H. Cheung, and M. F. Rubner, *Thin Solid Films* **244**, 806–809 (1994).
40. Y. Lvov, G. Decher, and H. Möhwald, *Langmuir* **9**, 481–486 (1993).
41. I. J. Iler, *J. Colloid Interface Sci.* **21**, 569 (1966).
42. Y. F. Nicolau, *Appl. Surf. Sci.* **22–23**, 1061–1074 (1985).
43. Y. F. Nicolau and J. C. Menard, *J. Cryst. Growth* **92**, 128–142 (1988).
44. Y. Shimazaki, R. Nakamura, S. Ito, and M. Yamamoto, *Langmuir* **17**, 953–956 (2001).
45. N. A. Kotov, S. Magonov, and E. Tropsha, *Chem. Mater.* **10**, 886–895 (1998).
46. W. B. Stockton and M. F. Rubner, *Macromolecules* **30**, 2717–2725 (1997).
47. S. H. Lee, J. Kumar, and S. K. Tripathy, *Langmuir* **16**, 10482–10489 (2000).
48. B. A. Snopok, Y. G. Goltsov, E. V. Kostyukevich, L. Matkovskaya, I. A. Koshets, E. V. Rengevich, P. E. Strizhak, Y. M. Shirshov, and E. F. Venger, in *Book of Abstracts, 219th ACS National Meeting*, San Francisco, CA, March 26–30, 2000.
49. H. Hong, I. Benjamin, S. Kirstein, Y. Avny, R. Neumann, and D. Davidov, *Synth. Met.* **102**, 1215–1216 (1999).
50. J. Kim, S. K. Tripathy, J. Kumar, and K. G. Chittibabu, *Mater. Sci. Eng. C* **C7**, 11–18 (1999).
51. J. Kim, H. C. Wang, J. Kumar, S. K. Tripathy, K. G. Chittibabu, M. J. Cazeca, and W. Kim, *Chem. Mater.* **11**, 2250–2256 (1999).
52. K. Ariga, Y. Lvov, and T. Kunitake, *J. Am. Chem. Soc.* **119**, 2224–2231 (1997).
53. C. Tedeschi, H. Möhwald, and S. Kirstein, *J. Am. Chem. Soc.* **123**, 954–960 (2001).
54. C. Tedeschi, F. Caruso, H. Möhwald, and S. Kirstein, *J. Am. Chem. Soc.* **122**, 5841–5848 (2000).
55. D. S. Koktysh and N. A. Kotov, *Rhodamine 6G in PAA/PDDA Films*, unpublished results, 2001.
56. N. A. Kotov, T. Haraszti, L. Turi, G. Zavala, R. E. Geer, I. Dekany, and J. H. Fendler, *J. Am. Chem. Soc.* **119**, 6821–6832 (1997).
57. E. W. Wong, P. E. Sheehan, and C. M. Lieber, *Science (Washington, D.C.)* **277**, 1971–1975 (1997).
58. V. N. Popov, V. E. Van Doren, and M. Balkanski, *Phys. Rev. B* **61**, 3078–3084 (2000).
59. R. H. Baughman and co-workers, *Science (Washington, D.C.)* **284**, 1340–1344 (1999).
60. D. Qian, E. C. Dickey, R. Andrews, and T. Rantell, *Appl. Phys. Lett.* **76**, 2868–2870 (2000).
61. M. F. Yu and co-workers, *Science (Washington, D.C.)* **287**, 637–640 (2000).
62. J. P. Salvetat and co-workers, *Adv. Mater. (Weinheim, Ger.)* **11**, 161–165 (1999).
63. M. S. P. Shaffer and A. H. Windle, *Adv. Mater. (Weinheim, Ger.)* **11**, 937–941 (1999).
64. R. Haggenmueller, H. H. Gommans, A. G. Rinzler, J. E. Fischer, and K. I. Winey, *Chem. Phys. Lett.* **330**, 219–225 (2000).
65. P. C. P. Watts and co-workers, *J. Mater Chem.* **11**, 2482–2488 (2001).
66. B. Vigolo and co-workers, *Science* **290**, 1331–1334.
67. J. P. Salvetat and co-workers, *Phys. Rev. Lett.* **82**, 944–947 (1999).
68. J. Chen and co-workers, *J. Phys. Chem. B* **105**, 2525–2528 (2001).

69. S. J. V. Frankland, A. Caglar, D. W. Brenner, and M. Griebel, *J. Phys. Chem. B* **106**, 3046–3048 (2002).
70. A. Star and co-workers, *Angew. Chem., Int. Ed.* **40**, 1721–1725 (2001).
71. G. Decher, *Science* **277**, 1232–1237 (1997).
72. A. Wu, D. Yoo, J. K. Lee, and M. F. Rubner, *J. Am. Chem. Soc.* **121**, 4883–4891 (1999).
73. A. A. Mamedov, A. Belov, M. Giersig, N. N. Mamedova, and N. A. Kotov, *J. Am. Chem. Soc.* **123**, 7738–7739 (2001).
74. A. A. Mamedov, N. A. Kotov, M. Prato, D. Guldi, J. P. Wicksted, A. Hirsch, *Nat. Mater.* **1**, 190–194 (2002).
75. A. A. Mamedov, D. M. Guldi, M. Prato, and N. A. Kotov, in *Abstracts of Papers, 223rd ACS National Meeting*, Orlando, FL, United States, Apr. 7–11, 2002.
76. J. H. Rouse, Z. Ounaies, P. T. Lellehei, and E. J. Siochi, *Abstracts of Papers, 223rd ACS National Meeting*, Orlando, FL, United States, April 7–11, 2002.
77. A. A. Mamedov and N. A. Kotov, *Langmuir* **16**, 5530–5533 (2000).
78. D. B. Mawhinney and co-workers, *Chem. Phys. Lett.* **324**, 213–216 (2000).
79. S. Rols and co-workers, *Eur. Phys. J. B* **18**, 201–205 (2000).
80. S. Westenhoff and N. A. Kotov, *J. Am. Chem. Soc.* **124**, 2448–2449 (2002).
81. D. M. Sullivan and M. L. Bruening, *J. Am. Chem. Soc.* **123**, 11805–11806 (2001).
82. F. Li, H. M. Cheng, S. Bai, G. Su, and M. S. Dresselhaus, *Appl. Phys. Lett.* **77**, 3161–3163 (2000).
83. J. B. Thompson and co-workers, *Nature (London)* **414**, 773–776 (2001).
84. B. L. Smith and co-workers, *Nature (London)* **399**, 761–763 (1999).
85. *CRC Materials Science and Engineering Handbook*, CRC, Boca Raton, FL, 1992.
86. S. Y. Fu and co-workers, *J. Mater. Sci.* **36**, 1243–1251 (2001).
87. M. F. Yu, B. S. Files, S. Arepalli, and R. S. Ruoff, *Phys. Rev. Lett.* **84**, 5552–5555 (2000).
88. A. Garg and S. B. Sinnott, *Chem. Phys. Lett.* **295**, 273–278 (1998).
89. Z. Tang, N. A. Kotov, S. Magonov, and B. Ozturtk, *Nat. Mater.* **2**, 413–418 (2003).

NICHOLAS A. KOTOV
ARIF A. MAMEDOV
University of Michigan
DIRK M. GULDI
University of Notre Dame
MAURIZIO PRATO
Università di Trieste
JAMES WICKSTED
Oklahoma State University
ANDREAS HIRSCH
Universität Erlangen-Nürnberg

NANOCOMPOSITES, METAL-FILLED

Introduction

Atomic clusters of transition metals embedded into polymeric matrices represent a very attractive class of materials which combine properties belonging to the nanometer-sized metal phase (such as certain magnetic, electronic, optical, or catalytic properties) and the polymer phase (such as processability and film-forming properties) (1). By the careful selection and combination of both components, tailor-made functional materials exhibiting unique characteristics (2) can be obtained, with the advantage of using the well-established, low cost technologies available for polymer processing, such as printing, spraying, or spin-coating.

Polymeric dispersions of nanometer-sized metal particles offer the possibility of functionalizing the polymer by properties coming from the large number of surface atoms (3) and the quantum-size effects (4). Nanometric metals show properties that differ significantly from that of bulk metals, which makes these nanocomposite systems intriguing for scientific study and potentially useful for a number of technological applications (5–12). The control of nanoparticle morphology becomes a very important aspect, since morphology profoundly influences the material performance. As a long-term goal the ability to control and vary particle size, distributions, shapes, and composition independently from one another is very desierable, in order to allow the tuning of nanocomposite properties. A broad area of nanoparticle features, ranging from nanosized single crystals to somewhat larger (in the range of about 100–200 nm) yet well-stabilized nonagglomerates, gain significant technological importance.

Polymer-embedded nanostructures are potentially useful for a number of technological applications, especially as advanced functional materials (eg, high energy radiation shielding materials, microwave absorbers, optical limiters, polarizers, sensors, hydrogen storage systems) (5–12). In addition to the intrinsic nanoscopic material properties, the presence of a very large interface area in these polymer-based nanocomposites can affect significantly polymer characteristics (eg, glass-transition temperature, crystallinity, free volume content, ignition temperature), allowing the appearance of further technologically exploitable mechanical and physical properties (eg, fire-resistance, low gas diffusivity).

Historical Background

The fundamental knowledge on the preparation and nature of metal/polymer nanocomposites looks back at a long history which is connected to the names of many illustrious scientists (2).

The oldest technique for the preparation of metal/polymer nanocomposites that can be found in the literature was described in detail in an abstract in 1835 (13). The original article appeared in 1833 (*J. Erdmann, p. 22*). In an aqueous solution, a gold salt was reduced in the presence of gum-arabic, and subsequently a nanocomposite material was obtained in the form of a purple solid simply by coprecipitation with ethanol.

Encyclopedia of Polymer Science and Technology. Copyright John Wiley & Sons, Inc. All rights reserved.

Around 1900, widely forgotten reports indicated the preparation of polymer nanocomposites with uniaxially oriented inorganic particles, and their remarkable optical properties (14,15). Dichroic plants and animal fibrils (eg, linen, cotton, spruce, or chitin, amongst others) were prepared by impregnation with solutions of silver nitrate, silver acetate, or gold chloride, followed by reduction of the corresponding metal ions under the action of light (16).

Dichroic films were also obtained using gold chloride treated gelatin which was subsequently drawn, dried, and finally exposed to light (17). Similar results were obtained when gelatin was mixed with colloidal gold before drying and drawing (18). The gold or silver content in such systems amounted typically to ca 1% by weight (19).

In 1904, Kirchner and Zsigmondy (Nobel Laureate in Chemistry, 1925) reported that nanocomposites of colloidal gold and gelatin reversibly changed color from blue to red upon swelling with water (20). In order to explain the mechanism of nanocomposite color change, they suggested that the material absorption must also be influenced by the distance between the embedded particles. In addition, around the same time, the color of gold particles embedded in dielectric matrices was subject of detailed theoretical analyses by Maxwell Garnett who explained the color shifts upon variation of particle size and volume fraction in a medium (21,22).

During the following three decades, dichroic fibers were prepared with many different elements (ie, Os, Rh, Pd, Pt, Cu, Ag, Au, Hg, P, As, Sb, Bi, S, Se, Te, Br, I) (23–27). The dichroism was found to depend strongly on the employed element, and optical spectra of dichroic nanocomposites, made of stretched poly(vinyl alcohol) films containing gold, silver, or mercury, were presented in 1946 (however, the preparative scheme used is not really clear) (28). It was assumed already in the early reports that dichroism was originated by the linear arrangement of small particles (29) or by polycrystalline rod-like particles (30) located in the uniaxially oriented spaces present in the fibers. An electron micrograph depicted in 1951 showed that tellurium needles with typical dimensions of ca 5×50 nm were present inside a dichroic film made of stretched poly(vinyl alcohol), however also in this case, just a limited number of details were given about the technique used for sample preparation (31).

In 1910, Kolbe was the first to prove that dichroic nanocomposite samples based on gold contained the metal indeed in its zero-valence state. Such affirmation was confirmed a few years later by X-ray scattering. In particular, it was shown that zero-valence silver and gold were present in the respective nanocomposites made with oriented ramie fibers, and the ring-like interference patterns of the metal crystallites showed that the individual primary crystallites were not oriented (32). Based on Scherrer's equation, which was developed just in this period, the average particle diameter of silver and gold crystallites was determined in fibers of ramie, hemp, bamboo, silk, wool, viscose, and cellulose acetate to be between 5 and 14 nm (33).

Basic Concepts

A nanocomposite is a material made of two or more phases one of which has at least one dimension in a nanometric size range. Metal/polymer nanocomposites

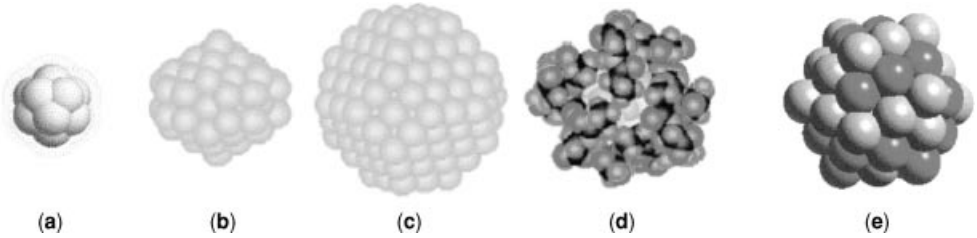

Fig. 1. Structure of atomic clusters of metals: (**a**) elemental cluster, (**b**) small cluster, (**c**) large cluster, (**d**) thiol-derivatized cluster, and (**e**) alloyed cluster.

are made of a continuous polymeric matrix embedding nanosized metal domains. Thermoplastic polymers, elastomers, and thermosetting resins can be potentially used as matrix, but amorphous linear polymers, like optical plastics (eg, polystyrene, poly(methyl methacrylate)) and conductive polymers are the most frequently used. About the metallic filler, very small clusters and nanoparticles with a pseudospherical shape are frequently employed (see Fig. 1). The use of nanorods and nanowires has also been described (2).

In these materials, the polymer has the function of protecting the nanostructures and allowing their manipulation, whereas the nanosized filler provides the polymeric matrix with unique properties coming from "small-size" effects (ie, *mesoscopic properties*). To allow the appearance of mesoscopic properties, the nanoparticle size is required to be very small; usually a dimension less than 30 nm is necessary for most metallic materials. In particular, the metal domain size, where electrons move, needs to be comparable to the critical lengths of physical phenomena (eg, wavelength of the electrons at the Fermi edge, mean free paths of electrons or phonons, coherency length, screening length). Such phenomenon is named *electron confinement* (4). In addition, on this size scale, also phenomena related to the high percentage of surface atoms appear in the material (3).

Different topologies can result in the preparation of polymer-embedded metal clusters. To prepare materials characterized by the properties of surface atoms or with characteristics coming from the confinement effect, a contact-free dispersion of clusters must result in the polymer matrix, since only in this case the large amount of surface atoms present allows the surface properties of matter to prevail on that of bulk. Both regular (eg, uniaxially oriented pearl-necklace type of arrays of nanoparticles) and irregular metal cluster distributions are used in technological applications.

The properties of nanometric particles strictly depend on their microscopical structure (ie, chemical composition, shape, size, percentage of defects, microstrain concentration, etc). For example, the characteristic surface plasmon absorption of a system of metal nanoparticles dispersed into a dielectric matrix is related to the particle shape and size (34). To prepare a color filter, identical particles should be used, otherwise the material will appear black. The presence of a single type of microscopic structure allows each particle to provide the same contribution to the composite properties. From a theoretical point of view, an ideal nanostructured composite should be made of identical metal domains uniformly dispersed into the polymeric matrix. However, since it is very difficult to prepare a sample of

identical metal grains, the only practically possible situation is a system of single crystals with a narrow size distribution.

Because of the high surface chemical reactivity, metal clusters can be easily oxidized or contaminated by nucleophilic molecules. The surface reactivity of small clusters is so high that even noble metals (eg, Pt, Pd, Ag) can be oxidized by air. Since small molecules present in the air (eg, oxygen, water, sulfur dioxide) are dissolved in polymers and can diffuse through it, the polymeric matrix cannot prevent metal from surface reactions. Finally, the polymer matrix has only the function to freeze particles, avoiding their diffusion and aggregation by sintering. For such a reason the nanoparticles need to be passivated before their embedding in polymers. The surface treatment (eg, thiol-derivatization, see Fig. 1d) prevents particle aggregation by short-range steric repulsion and stabilizes the metal core principally by electronic effects. Surface passivation offers also the possibility to disperse filler into most of liquid monomers and organic solvents where polymers are soluble.

Classification

Nanocomposites are biphasic materials that can be classified on the basis of their microstructure by the self-connectivity concept, that is the number of space directions (X, Y, Z) in which each phase inside the composite physically contacts itself. Composite classification based on self-connectivity has been proposed for the first time by Newnham in 1978 (35). Because of the discontinuous nature of most nanocomposite materials, the self-connectivity concept needs to be applied to a limited but representative composite portion (ie, a local self-connectivity definition should be used). In particular, like in macro- and microcomposite systems, each phase in a nano-composite material can be locally self-connected in zero, one, two, or three dimensions. It is natural to confine the attention to three perpendicular axes since all property tensors are generally referred to such a system. In general, for a n-phase system the number of possible self-connectivity patterns is given by $(n + 3)!/3!n!$. Therefore, inside a biphasic system ($n = 2$) there are 10 different self-connectivity patterns: $(0–0)^*$, $(1–0)^*$, $(2–0)^*$, $(3–0)^*$, $(1–1)^*$, $(2–1)^*$, $(3–1)^*$, $(2–2)^*$, $(3–2)^*$, and $(3–3)^*$. The first number in the notation represents the physical connectivity of one of the two phases and the second number refers to connectivity of the other one. A schematic representation of these 10 types of self-connectivities is given in Figure 2, using a cube as the basic building block. Arrows are used in Figure 2 to indicate the connected directions, and an asterisk has been introduced in the symbol to indicate the local connectivity.

Properties of Nanosized Metals

Nanosized metals are characterized by novel thermodynamic, chemical, catalytic, optical, magnetic, and transport properties which are much different from those of corresponding massive metals. For this reason a 3-D periodic table of elements has been frequently proposed by chemists working in this material science field (36).

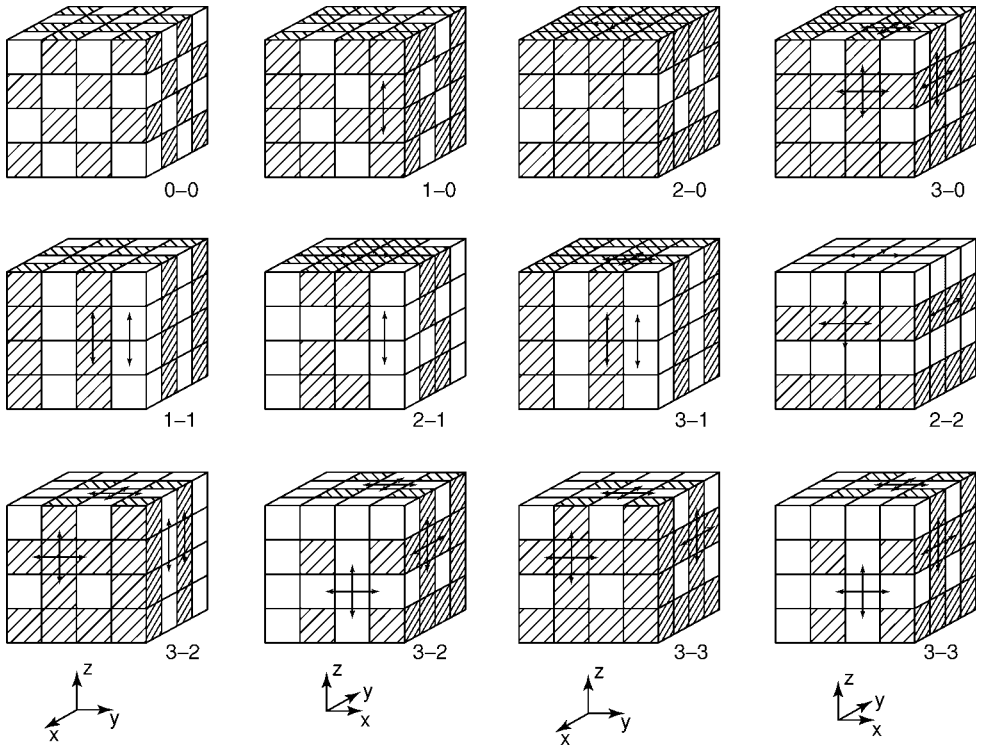

Fig. 2. The connectivity patterns of a biphasic solid (35).

The thermodynamic properties of matter are classically described as natural constants; however, they change significantly when the dimension approaches a few nanometers (37). The first small-size effect which has been observed for metals is the change in the melting point (38–43). When a solid is heated, it melts, and the melting temperature is normally considered one of the most important characteristics of a material. Nanometer-size crystals melt at much lower temperatures than extended ones. This can be understood in two ways. First, the cohesive energy of a crystal arises by the sum of all pairwise interactions between the atoms. In a very small crystal the number of surface atoms is large, and therefore the cohesive energy per atom has not yet converged on the bulk value. A second picture is more thermodynamic: as a solid is heated, melting takes place at the temperature where the chemical potentials of solid and liquid are equal. In addition to the usual term in the chemical potential, a very small crystal also has a term in it for the surface energy. In general, the surface energy of liquids is less than that of solids, because a liquid can readily assume the lowest surface area shape, a sphere. As a consequence, the smaller the crystal the lower is the melting temperature, and the reduction in the melting temperature is proportional to the surface to volume ratio, or inversely proportional to the nanocrystal radius. This scaling law for melting temperature reduction has been verified in many metals (37).

Several interesting chemical properties arise as the grain size of a metal is decreased to a nanometer-size range (eg, enhanced reactivity, stoichiometric behavior of heterogeneous reactions, new reaction routes). Theoretical computations

(37) showed that the fraction of metal atoms residing on the surface of a 100-nm grain increases from 1–2% up to 85–95% for grain sizes in the range of 1–2 nm. The importance of this observation is that the chemistry of such surfaces is much different from that of the same atoms contained within larger grains. If the size of a cubic crystal is decreased from 100 nm down to the 3–5 nm range, the fraction of atoms contained in edge sites as compared to those contained in basal planes increases to 70%. The consequence of this observation is that as the crystal size decreases, the fraction of atoms located in low coordination sites increases sharply, which inherently imparts a higher chemical reactivity to such materials (activated metals). High surface areas and intrinsically high surface reactivities of hyperfine reactants allow surface reactions to approach stoichiometric conversion. With the development of hyperfine powders, the heterogeneous phase reaction can be carried out much faster and at lower temperatures (44,45). Finally, gas–solid reactions and liquid–solid reactions take on a new dimension, and hyperfine solids enter now in the chemist's arsenal as novel chemical reagents.

The properties of nanosized metals in heterogeneous catalysis are well established, since heterogeneous catalysts represent one of the pioneering fields of nanotechnology (3). The increasing portion of surface atoms with decreasing particle size, compared with bulk metals, makes small metal particles as highly reactive catalysts, since surface atoms are the active centers for catalytic elementary processes. Among the surface atoms, those sitting on the crystal edges and corners (see Fig. 3) are more reactive than those on basal planes. The percentage of edge

Fig. 3. SEM micrograph of 3-D self-organized poly(methyl methacrylate) particles. If beads are considered as atoms, the picture can be used to visualize the different catalytic sites on the surface of a metal crystal.

and corner atoms also increases with decreasing size and this is the reason for the enhanced catalytic activity (ie, supercatalytic effect) and different selectivity of very small metal catalysts.

If metal particles become very small, reaching the nanometer-size scale, a color may occur. This is a typical phenomenon of nanometric metals. Actually, optical absorption may result in the ultraviolet or visible part of the spectrum, and this arises from a surface plasmon resonance. This is due to a collective electron plasma oscillation (plasmon) that is coupled to an external transverse electromagnetic field through the particle surface. It is possible to quantitatively relate the absorption coefficient to the wavelength of the exciting radiation by the Mie theory for spherical inclusions in a dielectric matrix (34). Far-IR luminescence is another optical phenomenon frequently observed with nanosized metals (46).

New magnetic properties appear in metals when the size approaches the nanometric regime (47). The so-called odd–even effect is a phenomenon observed when diamagnetic metals are reduced to a nanometric-size regime. In particular, diamagnetic materials have only spin-paired electrons. However, in practice it cannot be assumed that a macroscopic piece of a diamagnetic metal does not have one or more unpaired electrons. This cannot be measured because of the effectively infinite number of atoms and electrons. However, if the particle size is small enough to make one unpaired electron measurable, the odd–even effect should become visible. Among small diamagnetic metal particles there should be an equal percentage of odd and even numbers of electrons.

For magnetic materials such as Fe, Co, and Ni, the magnetic properties are size-dependent (47). In particular, the coercivity force H_c needed to reverse an internal magnetic field within the particle changes with particle size and it is maximum for single-domain particles. Further, the strength of the internal magnetic field of a single particle can be size-dependent.

Giant magnetostriction, magnetoresistivity, and magnetocaloric effects represent further examples of new properties arising from the small size of magnetic domains (48).

Also transport properties, which are strictly related to the electronic structure of a metal particle, critically depend on size (37). For small particles, the electronic states are not continuous, but discrete, because of the confinement of electron wave function. Consequently, also properties like electrical and thermal conductivity may exhibit quantum-size effects.

Most of these unique chemical and physical characteristics of nanosized metals can be used for the functionalization of plastic materials.

Preparation Methods

A limited number of methods have been developed for the preparation of metal/polymer nanocomposites. Usually, such techniques consist of highly specific approaches, which can be classified as *in situ* and *ex situ* methods. In the *in situ* methods two steps are needed: firstly, the monomer is polymerized in solution, with metal ions introduced before or after polymerization. Secondly, metal ions in the polymer matrix are reduced chemically, thermally, or by UV/γ- irradiation. In the *ex situ* processes, the metal nanoparticles are chemically synthesized,

and their surface is organically passivated. The derivatized nanoparticles are dispersed into a liquid monomer which is then polymerized.

***In situ* Methods.** A simple, direct, and versatile *in situ* method was proposed by Watkins and McCarthy (49). In this method, an organometallic precursor is dissolved in supercritical fluid (SCF) carbon dioxide and infused into a solid polymer as SCF solution. Chemical or thermal reduction of the precursor to the zero-valence metal either in presence of SCF or subsequent to its removal produces metal domains within the solid polymer matrix. Such technique has been used in the synthesis of nanoscale platinum clusters embedded into poly(4-methyl-1-pentene) and poly(tetrafluoroethylene), using dimethyl(cyclooctadiene)Pt(II) as metal precursor. There are multiple advantages associated with this approach: first, the high permeation of CO_2 in virtually all polymers and the wide range of organic and organometallic reagents which are soluble in CO_2 render this technique a generally useful scheme for the synthesis of polymer composites. Neither the polymer substrate nor the reaction product needs to be soluble in CO_2. Second, the sorption of CO_2 is a very fast process which significantly enhances the kinetics of the penetrant absorption. The degree of polymer swelling, diffusion rates within the substrate, and the partitioning of penetrates between the SCF and the swollen polymer can be controlled by density mediated adjustments of solvent strength via changes in temperature and pressure. Coupled with manipulation of reaction rates, SCFs offer unprecedented control over composite composition and morphology. In addition, SCFs such as CO_2 are gases at ambient conditions and the solvent dissipates rapidly upon the release of pressure. In the case of metalation using dimethyl(cyclooctadiene)Pt(II), the process effluent consists of CO_2 and light hydrocarbons (methane and cyclooctane) derived from the precursor ligands.

Bronstein and co-workers (50) reported an *in situ* method for the preparation of polymer-cobalt nanocomposites by mixing $CO_2(CO)_8$ with a polyacrylonitrile copolymer or an aromatic polyamide in dimethylformamide (DMF). The cobalt carbonyl interacts with DMF giving the complex $[Co(DMF)_6]^{2+}[Co(CO)_4]^{2-}$, which is then converted to nanodispersed Co particles by thermolysis.

Analogously, silver/polyimide nanocomposites have been prepared by Fragalà and co-workers (51) by thermolysis of a mixture of a metallorganic silver complex and polyamidic acid (PPA). The PAA precursor transforms in polyimide (PI) at a curing temperature compatible with the metallorganic precursor reduction temperature, so that at the same time the precursor decomposes, giving metallic silver particles, and the PAA transforms itself in PI, allowing the silver particles to remain trapped in the polymeric cage.

Copper/polymer nanocomposites have been prepared in the solid state by Lyons and co-workers (52). A soluble precursor was synthesized by complexing poly(2-vinylpyridine) with copper formate (ie, $Cu(HCO_2)_2$) in methanol. The thermal decomposition of the complex results in a redox reaction whereby Cu(II) is reduced to copper metal and the formate anion is oxidized to CO_2 and H_2. By incorporating a reducing agent into the complex, the thermal decomposition reaction is not diffusion-limited, and nanocrystalline copper particles can be prepared in the solid state.

Chen and co-workers (53) describe the synthesis of iron nanoparticles dispersed in poly(4-vinylpyridine) homopolymer and vinylstyrene-4-vinylpyridine copolymers by chemical reduction of thin films of iron chloride/polymer

nanocomposite precursors swollen by DMF. Idrazine was used as reducing agent. Such approach can be used because the metal ions have a high tendency to form ionic clusters in a polymeric matrix. The produced microscopic phases, which are separated by the hydrophobic portions of the polymer, have a diameter ranging from 2 to 10 nm. The chemical reduction of the dispersed ionic metal domains produces ultrafine metal particles.

Huang and co-workers (54) prepared copper/poly(itaconic acid-*co*-acrylic acid) nanocomposites via *in situ* chemical reduction of the Cu^{2+}–polymer complex by hydrazine hydrate aqueous solution.

Metal/polymer nanocomposites were prepared by Chen and co-workers (55) using dispersion of metal chlorides in polyurethane. Both polyurethane and metal salts were dissolved in *N*,*N*′-dimethylacetamide, followed by film casting and reduction of the metal salts by sodium borohydrate. The metal particle size depended on the type of metal salt used and on its concentration.

Zhu and co-workers (56) developed a method for the preparation of metal/polymer nanocomposites based on γ-irradiation. In this method, the metal salt was dissolved in the organic monomer, and the formation of nanocrystalline metal particles and monomer polymerization was obtained simultaneously in solution by irradiation with a ^{60}Co γ-ray source, leading to a homogeneous dispersion of nanocrystalline metal particles in the polymer matrix. Also UV-irradiation has been used for the reduction of metal ions dispersed in polymer matrices (57).

Wizel and co-workers (58) have described the use of ultrasounds in the *in situ* synthesis of composite materials made of polystyrene and iron. The propagation of ultrasound waves through a fluid causes the formation of cavitation bubbles. The collapse of these bubbles, described as an implosion in the hot-spot theory, is the origin of extreme local conditions: high temperatures (5000–25,000 K) and high pressures (1000 atm). The cooling rates obtained during the bubble collapse are greater than $10^7\ K \cdot s^{-1}$. These high cooling rates have been utilized in the sonication of $Fe(CO)_5$ as a neat liquid or in solution, to produce amorphous iron nanoparticles. In addition, ultrasound radiation has been widely used for the preparation of polymers without the use of initiators (59). These two chemical processes have been combined for the fabrication of metal/polymer nanocomposites by sonication of styrene solution of iron carbonyl.

***Ex Situ* Methods.** Because of the high optical purity that can be achieved in the final product, the *ex situ* synthesis of metal/polymer nanocomposites is a very attractive technique, especially in the preparation of materials for optical applications. The particulate material of the required size, as obtained by a solution chemistry route, is stabilized by legand chemisorption (eg, thiols) in order to reduce their surface reactivity and tendency to agglomeration, and then it is incorporated into a castable polymeric matrix. Usually, the passivated nanoparticles are dispersed into a liquid monomer–initiator mixture (eg, styrene or methyl methacrylate activated by benzoyl peroxide), which is then thermally polymerized. Because a little amount of filler is required, the polymerization behavior of the monomer is not significantly influenced by the presence of passivated nanoparticles (the reaction rate is only slightly decreased (60)). Gonsalves and co-workers (60,61) have prepared surface-derivatized gold particles by phase-transfer reaction of gold ions with dodecanthiol and used these particles for the synthesis of poly(methyl methacrylate) based nanocomposites. Carotenuto (62) has developed

a new technique for the preparation of bulk quantities of atomic clusters of gold, derivatized by thiols by a modification of the well-known *Polyol Process* technique (63). The *ex situ* approach has been used also in the synthesis of silver/polyethylene nanocomposites (64,65). A variety of high nuclearity metal cluster compounds which can be used for the polymeric nanocomposite preparation have been recently synthesized and studied (66–76).

Clusters of noble and easily reducible metals (eg, Ag, Au, Pd) can be obtained by alcoholic reduction of metal ions in presence of polymeric stabilizers. Poly(vinylpyrrolidinone), poly(vinyl alcohol), poly(methylvinyl ether), etc are usually utilized. High quality polymer-protected metal clusters can be obtained at the end of reaction simply by addition of a nonsolvent liquid which causes the nanocomposite separation from the reactive mixture (coprecipitation) (77–79). However, the use of such nanocomposites is limited because of their excessive moisture sensitivity.

Characterization Techniques

For the comprehension of mechanisms involved in the appearance of novel properties in polymer-embedded metal nanostructures, their characterization represents the fundamental starting point. The microstructural characterization of nanofillers and nanocomposite materials is performed mainly by transmission electron microscopy (TEM), large-angle X-ray diffraction (XRD), and optical spectroscopy (UV–vis). These three techniques are very effective to determine particle morphology, crystal structure, composition, and grain size (48).

Of the many techniques which have been used to study the structure of metal/polymer nanocomposites, TEM has undoubtedly been the most useful. This technique is currently used to probe the internal morphology of nanocomposites. As visible in Figure 4, high quality images can be obtained because of the presence, in the sample, of regions that do not allow the high voltage electron beam passage (ie, the metallic domains) and region perfectly transparent to the electron beam (ie, the polymeric matrix). High resolution TEM (HRTEM) allows morphological investigations with a resolution of 0.1nm, and thus this technique makes possible to accurately image nanoparticle sizes, shapes, and in some cases even inner atoms (80) (see Fig. 5).

Large-angle X-ray powder diffraction (XRD) has been one of the most versatile techniques utilized for the structural characterization of nanocrystalline metal powders. The modern improvements in electronics, computers, and X-ray sources have allowed it to become an indispensable tool for identifying nanocrystalline phases as well as crystal size and crystal strain (see Fig. 6). The comparison of the crystallite size obtained by the XRD diffractogram using the Scherrer formula with the grain size obtained from the TEM image allows to establish if the nanoparticles have a mono- or polycrystalline nature (11).

Metal clusters are characterized by the surface plasmon resonance, which is an oscillation of the surface plasma electrons induced by the electromagnetic field, and consequently their microstructure can be indirectly investigated by optical spectroscopy (UV–vis spectroscopy). The characteristics of this absorption (shape, intensity, position, etc) are strictly related to the nature, structure, topology, etc

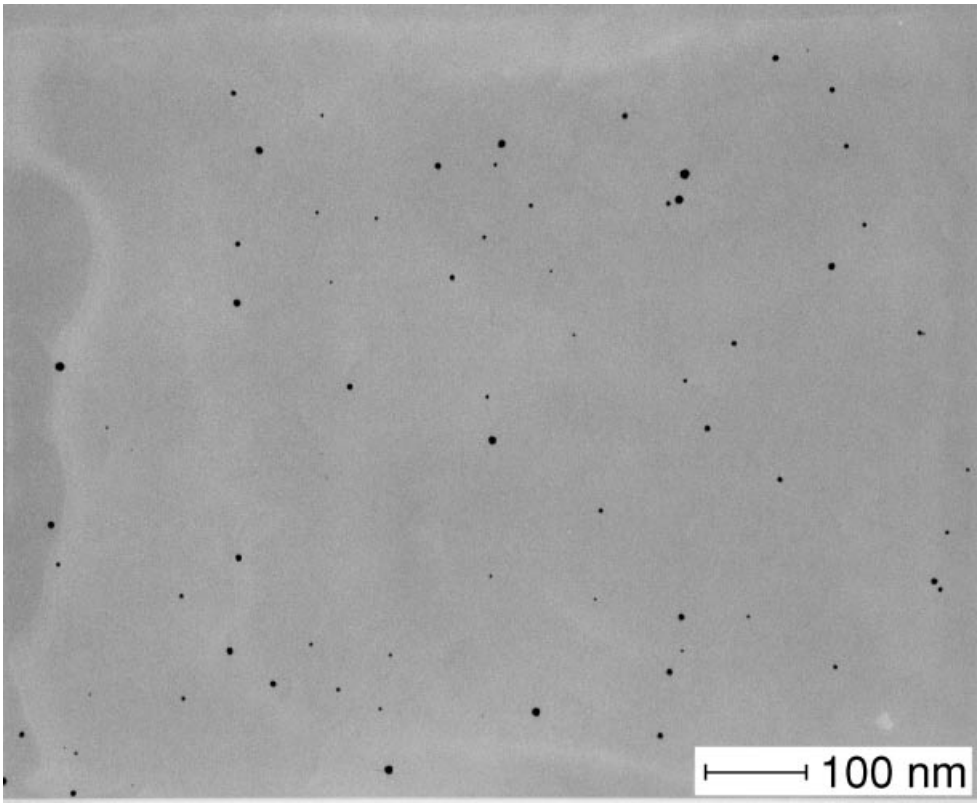

Fig. 4. TEM micrograph of metal gold clusters embedded in poly(vinylpyrrolidinone).

of the cluster system. In fact, the absorption frequency is a fingerprint of the particular metal, the eventual peak splitting reflects aggregation phenomena, the intensity of the peak is related to the particle size, the absorption wavelength is related to the particle shape, the shift of the absorption with increasing of temperature is indicative of a cluster melting, and so on. For bimetallic particles information about inner structure (intermetallic or core/shell) and composition can be obtained from the maximum absorption frequency (81). Differently from *out-line* techniques (eg, TEM, XRD) this method allows *on-line* and *in situ* cluster sizing and monitoring of morphological evolution of the system (see Fig. 7). This method has been used also in the study of cluster nucleation and growth mechanisms (82,83). In addition to multielectron transition (ie, plasmon absorption) also single-electron transition (interband transition) can be detected and studied by optical spectroscopy in order to obtain important microstructural information.

This outline of the principal characterization techniques for nanocomposite materials and nanosized metal fillers is far from being complete. Advances in Raman spectroscopy, energy dispersive spectroscopy, infrared spectroscopy, and many other techniques are of considerable importance as well. In fact, the success that nanostructured materials are having in the last few years is strictly related to the advanced characterization techniques which are available today.

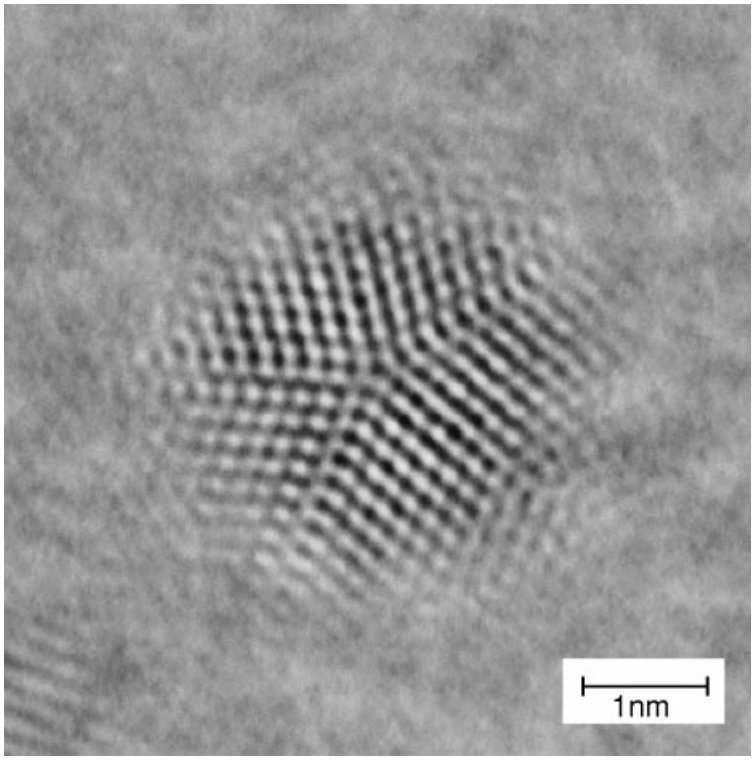

Fig. 5. HRTEM image of a very small metal cluster.

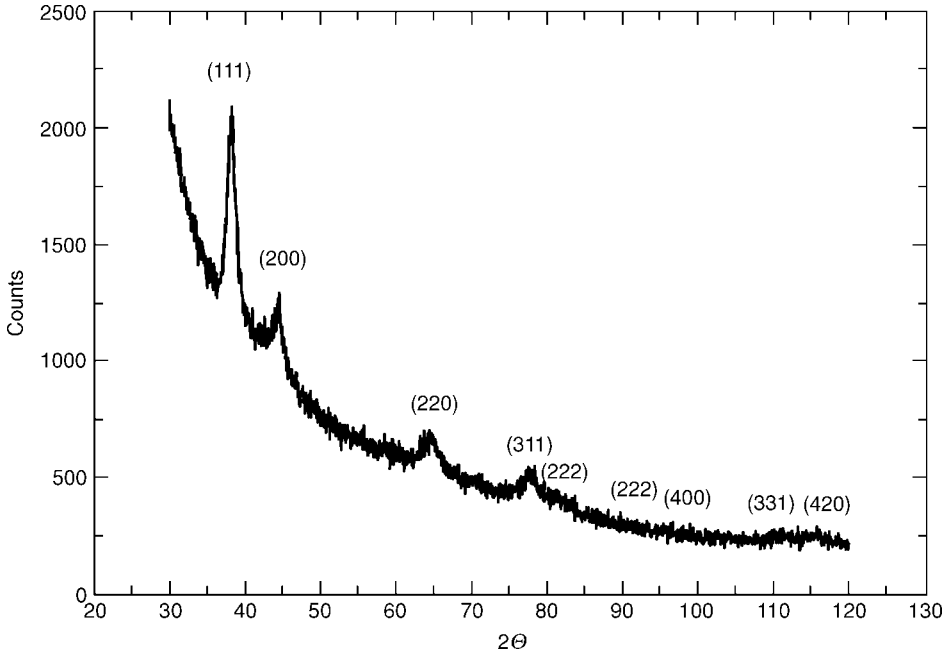

Fig. 6. XRD pattern of nanosized gold clusters.

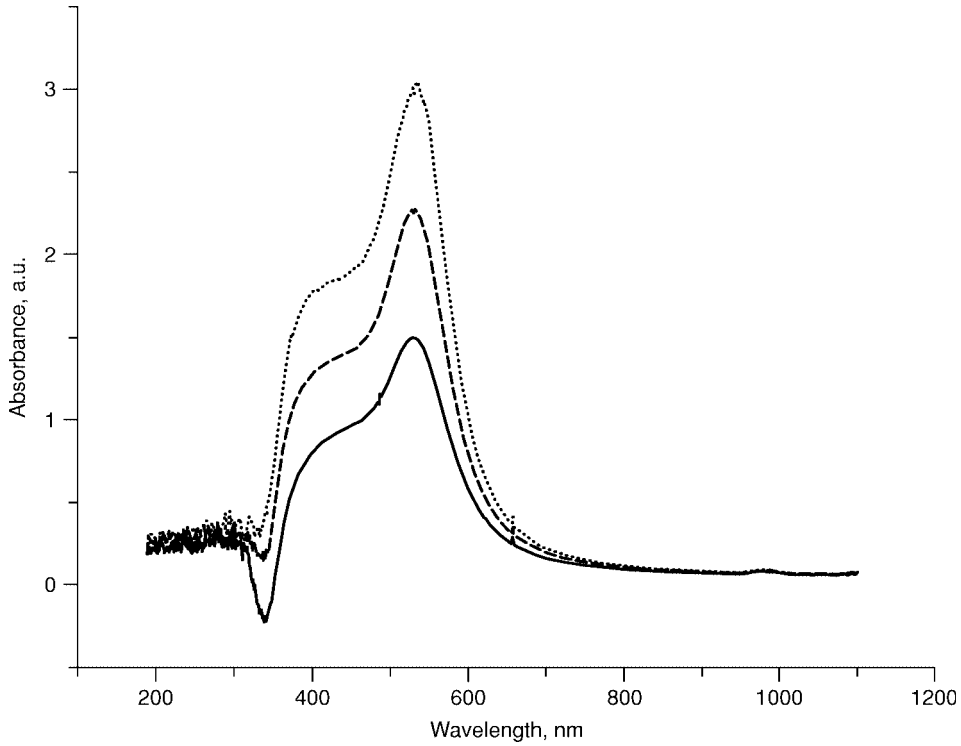

Fig. 7. UV–vis spectra of a colloidal gold suspension during the cluster growth. Temperature = 60°C; —— 5 min, – – – – 10 min, - - - - 15 min.

Applications

Applications of metal/polymer nanocomposites have already been made in different technological fields. However the use of a much larger number of devices based on these materials is predicted for the near future.

Because of the plasmon surface absorption band, atomic clusters of metals can be used as pigments for optical plastics. The color of the resulting nanocomposites is light-fast and intensive, and these materials are perfectly transparent, since the cluster size is much lower than light wavelength. Gold, silver, and copper can be used for color filter application. Also UV absorbers can be made for example by using Pd clusters. The plasmon surface absorption frequency is modulated by making intermetallic particles (eg, Pd/Ag, Au/Ag) of adequate composition.

As shown in Figure 8, polymeric films containing uniaxially oriented pearl-necklace type of arrays of nanoparticles exhibit a polarization-dependent and tunable color (64,65,84–86). The color of these systems is very bright and can change strongly, modifying the light polarization direction. These materials are obtained by dispersing metal nanoparticles in polymeric thin films and subsequently reorganizing the dispersed phase into pearl-necklace arrays by solid-state drawing at temperature below the polymer melting point. The formation of these arrays in the films is the cause of a strong polarization-direction-dependent color which can

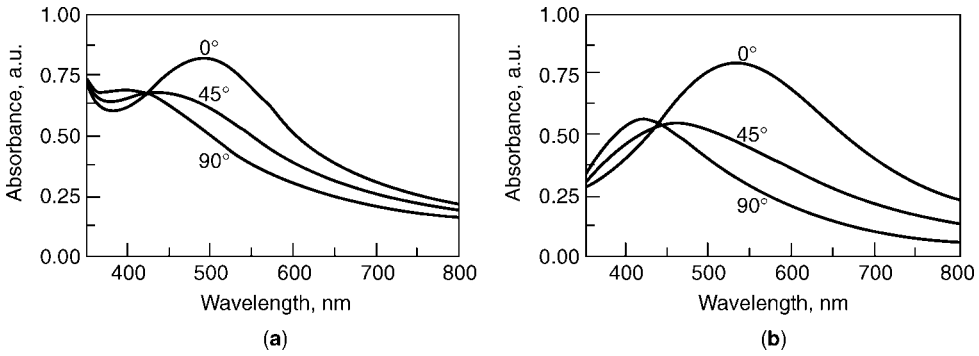

Fig. 8. (**a**) UV–vis spectra of drawn polyethylene/silver nanocomposites containing 4 wt% dodecanethiol coated silver nanoparticles in linearly polarized light. (**b**) Absorption spectra of drawn polyethylene/silver nanocomposite film annealed for 15 h at 180°C. The angle between the polarization direction of the light and the drawing direction of the film is given (64).

be used in the fabrication of liquid-crystal color display (see Fig. 9) and special electrooptical devices (see Fig. 10).

Surface plasmon resonance has been used to produce a wide variety of optical sensors, eg, systems which are able to change their color in presence of specific analytes. These devices can be used as sensors for immunoassay, gas, and liquid (see Fig. 11) (48).

Metals are characterized by ultrahigh/low refractive indices and therefore they can be used to modify the refractive index of optical plastics (87–89). Ultrahigh/low refractive index optical plastics can be used in the waveguide technology (eg, planar waveguides and optical fibers).

Plastics doped by atomic clusters of ferromagnetic metals show magnetooptical properties (ie, when subject to a strong magnetic field, they can rotate the vibration plane of a plane-polarized light) and therefore they can be used

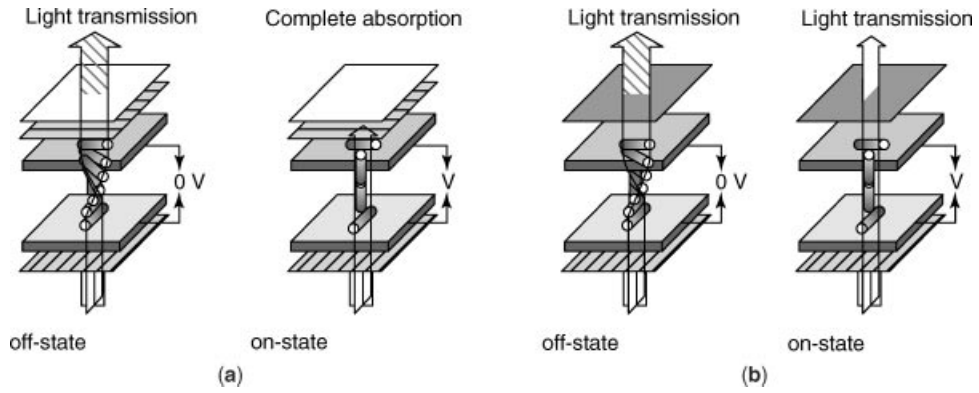

Fig. 9. Schematic representation of (**a**) a conventional color twisted nematic liquid-crystal display; and (**b**) display set-up containing a color polarizing filter (64).

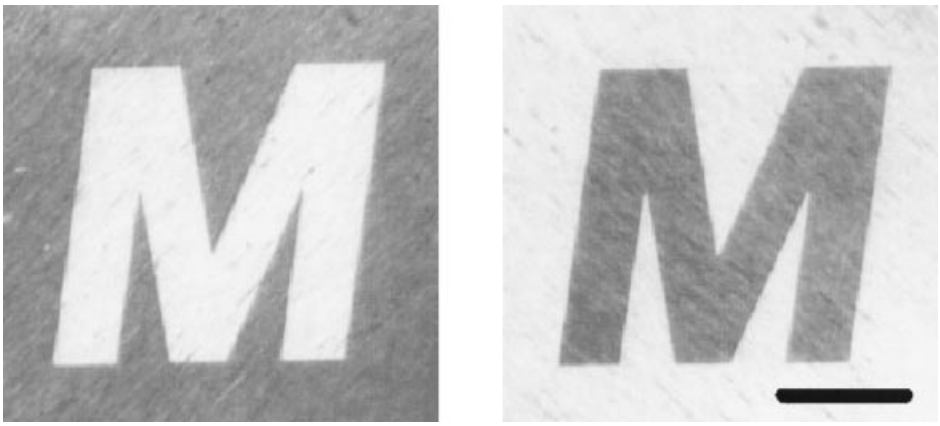

Fig. 10. Twisted nematic liquid-crystal cell equipped with a polyethylene/silver nanocomposite filter (65).

as Faraday rotators (90,91). These devices have a number of important optical applications (eg, magneto-optic modulators, optical isolators, optical shutters).

Nanosized metals (eg, gold, silver) have attracted much interest because of the nonlinear optical polarizability, which is caused by the quantum confinement of the metal's electron cloud (92) (see NONLINEAR OPTICAL PROPERTIES). When irradiated with light above a certain threshold power, the optical polarizability deviates from the usual linear dependence on that power. By incorporating these particles into a clear polymeric matrix, nonlinear optical devices can be made in a readily processable form (61). These materials are used to prepare a number of devices for photonics and electrooptics (see ELECTROOPTICAL APPLICATIONS).

Contact-free dispersion of noble metal clusters in polymer can be also used as nonporous catalytic membranes (93–95). Traditionally, nonporous catalytic separation layers are composed of palladium or palladium alloy foils. Reduction in

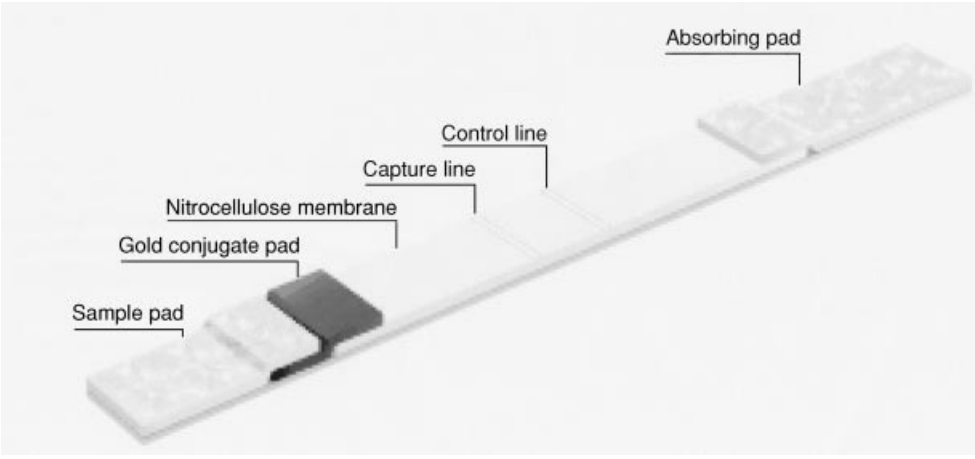

Fig. 11. Nanosized gold-based optical sensor for biological assay.

thickness by metal film deposition on special supports increases the hydrogen permeability and reduces the costs for the precious metal. Polymeric matrix filled by a catalytic nanosized metal offers in addition to the above advantages, the possibility of using the catalytic properties of nanoscale metal catalysts.

One of the most important characteristics of polymers filled by metal microclusters is their ability to absorb microwave radiation, producing heat (96). These plastic materials can be processed by using new technologies based on the microwave heating and can be used for food packaging, microwave shielding, RADAR camouflage, plastic welding by microwaves, etc.

Metal/polymer nanocomposites can have many other important applications. For example, nanoparticles embedded into poly(vinylpyrrolidinone) can be used for the electroless plating of polymeric, ceramic, and semiconductor substrates (93–98). These materials have also been used for the preparation of "smart" systems that experience a reversible alteration of their properties upon exposure to light. They are used as infrared barriers against exposures to intense solar light or fires (99).

Summary

Metal cluster–polymer systems are receiving increased attention because of the interesting properties and large potentialities for technological applications. In particular, these nanocomposite systems can provide simple, low cost options for obtaining tailored materials with high promise for various catalytic, optical, magnetic, and electronic applications. Usually, the control of the nanoparticle morphology, ie, particle size, size distribution, shape, and composition, is of main interest. Nanoparticle features can be varied by selection of preparation method and variation of experimental conditions. In addition to the versatility of the nanoparticle features and the polymer morphologies, options can be provided to tailor the topology of the metal–polymer systems. This includes for example the uniaxially oriented pearl-necklace type distribution of metal nanoparticles within the polymer matrix. For a variety of applications special topologies are important and determining factors for tuning the composite material performance.

In conclusion, further research activity in this field is extremely important for the development of advanced devices for functional applications based on these materials.

BIBLIOGRAPHY

1. A. B. R. Mayer, *Mater. Sci. Eng., C* **6**, 155 (1998).
2. W. Caseri, *Macromol. Rapid Commun.* **21**, 705 (2000).
3. W. R. Moser, *Advanced Catalysts and Nanostructured Materials: Modern Synthetic Methods*, Chapman & Hall, New York, 1996.
4. R. C. Ashoori, *Nature* **379**, 413 (1996).
5. G. Carotenuto, *Polym. News* **25**, 191 (2000).
6. G. Carotenuto, *Polym. News* **25**, 260 (2000).
7. G. Carotenuto, *Polym. News* **25**, 365 (2000).

8. G. Carotenuto, *Polym. News* **26**, 48 (2001).
9. G. Carotenuto, *Polym. News* **26**, 119 (2001).
10. G. Carotenuto, *Polym. News* **26**, 234 (2001).
11. G. Carotenuto, *Polym. News* **26**, 278 (2001).
12. G. Carotenuto, *Polym. News* **26**, 342 (2001).
13. C. U. Shepard, *Sill. J. (Am. J. Sci. Arts)* **28**(1), 145 (1835).
14. H. Ambronn, *Kgl. Sächs. Ges. Wiss.* **8**, 613 (1896).
15. H. Ambronn and R. Zsigmondy, *Ber. Sächs. Ges. Wiss.* **51**, 13 (1899).
16. H. Ambronn, *Kgl. Sächs. Ges. Wiss.* **8**, 613 (1896).
17. H. Ambronn, *Kgl. Sächs. Ges. Wiss.* **8**, 613 (1896).
18. H. Ambronn and R. Zsigmondy, *Ber. Sächs. Ges. Wiss.* **51**, 13 (1899).
19. E. Kolbe, Ph.D. dissertation, Jena, Germany, 1913 (cited by A. Frey-Wyssling, *Protoplasma* **27**, 372 (1937)).
20. F. Kirchner and R. Zsigmondy, *Ann. Phys., vierte Folge (Drude's Ann.)* **15**, 573 (1904).
21. J. C. Maxwell *Garnett, Philos. Trans. R. Soc. London, A* **203**, 385 (1904).
22. J. C. Maxwell *Garnett, Philos. Trans. R. Soc. London, A* **205**, 237 (1906).
23. F. Braun, *Ann. Phys., vierte Folge (Drude's Ann.)* **16**, 238 (1905).
24. A. Frey, *Jahrbuch Wiss. Bot.* **67**, 597 (1927).
25. A. Frey, *Z. Wiss. Mikrosk* **42**, 421 (1925).
26. A. Frey, *Naturwiss* **13**, 403 (1925).
27. F. Bion, *Helv. Phys. Acta* **1**, 165 (1928).
28. E. H. Land and C. D. West, in J. Alexander, ed., *Colloid Chemistry*, Reinhold, New York, 1946, p. 160.
29. H. Ambronn, *Z. Wiss. Mikrosk.* **22**, 349 (1906).
30. A. Frey-Wyssling, *Protoplasma* **27**, 563 (1937).
31. E. H. Land, *J. Opt. Soc. Am.* **41**, 957 (1952).
32. S. Berkman, J. Bohm, and H. Zocher, *Z. Phys. Chem.* **124**, 83 (1926).
33. A. Frey-Wyssling, *Protoplasma* **27**, 372 (1937).
34. U. Kreibig and M. Vollmer, in J. P. Toennies, ed., *Optical Properties of Metal Cluster*, Springer-Verlag, Berlin, 1993.
35. R. E. Newnham, D. P. Skinner, and L. E. Cross, *Mater. Res. Bull.* **13**, 525 (1978).
36. A. Rosén, *Adv. Quantum Chem.* **30**, 235 (1998).
37. K. J. Klabunde, ed., *Nanoscale Materials in Chemistry*, Wiley-Interscience, New York, 2001.
38. M. Wautelet, *Solid State Commun.* **74**, 1237 (1990).
39. Ph. Buffat and J. P. Borel, *Phys. Rev. A* **13**, 2287 (1997).
40. Q. Jiang, Z. Zhang, D. T. Hsu, H. Y. Tong, and M. Iskandar, *J. Mater. Sci.* **34**, 5919 (1999).
41. G. L. Allen, R. A. Bayles, W. W. Gile, and W. A. Jesser, *Thin Solid Films* **144**, 297 (1986).
42. C. R. M. Wronski, *Br. J. Appl. Phys.* **18**, 1731 (1967).
43. Z. L. Wang, J. M. Petroski, T. C. Green, and M. A. El-Sayed, *J. Phys. Chem. B* **102**, 6145 (1998).
44. Y. Zhang, S. Liao, Y. Fan, J. Xu, and F. Wang, *J. Nanoparticle Res.* **3**, 23 (2001).
45. R. D. Rieke and S. E. Bales, *J. Am. Chem. Soc.* **96**, 1775 (1974).
46. J. Zhang, Z. Wang, J. Liu, S. Chen, and G. Liu, *Self-Assembled Nanostructures*, Kluwer Academic, New York, 2003.
47. J. S. Miller and M. Drillon, eds., *Magnetism: Molecules to Materials III, Nanosized Magnetic Materials*, Wiley-VCH, Weinheim, Germany, 2002.
48. H. S. Nalwa, ed., *Nanostructured Materials and Nanotechnology*, Academic Press, San Diego, Calif., 2001.
49. J. J. Watkins and T. J. McCarthy, *Chem. Mater.* **7**, 1991 (1995).

50. M. Bronstein, E. Sh. Mirzoeva, M. V. Seregina, P. M. Valetsky, S. P. Solodovnikov and R. A. Register, *ACS Symp. Ser.* **622**, 102 (1996).
51. M. E. Fragalà, G. Compagnini, G. Malandrino, C. Spinella, and O. Puglisi, *Eur. Phys. J. D* **9**, 631 (1999).
52. A. M. Lyons, S. Nakahara, M. A. Marcus, E. M. Pearce, and J. V. Waszczak, *J. Phys. Chem.* **95**, 1098 (1991).
53. L. Chen, W. J. Yang, and C. Z. Yang, *J. Mater. Sci.* **32**, 3571 (1997).
54. C. Huang and C. Z. Yang, *Appl. Phys. Lett.* **74**, 1692 (1999).
55. G. M. Nasr and M. M. Badawy, *Polym. Int.* **38**, 249 (1995).
56. Y. Zhu, Y. Qian, X. Li and M. Zhang, *Chem. Commun.* 1081 (1997).
57. M. Zheng, M. Gu, Y. Jin and G. Jin, *Mater. Res. Bull.* **36**, 853 (2001).
58. S. Wizel, S. Margel and A. Gedanken, *Polym. Int.* **49**, 445 (2000).
59. P. Kruus, M. O'Neill and D. Robertson, *Ultrasonics* **28**, 304 (1990).
60. K. E. Gonsalves, G. Carlson, X. Chen, S. K. Gayen, R. Perez and M. Jose-Yacaman, *Nanostruct. Mater.* **7**, 293 (1996).
61. K. E. Gonsalves, G. Carlson, X. Chen, J. Kumar, F. Aranda, R. Perez and M. Jose-Yacaman, *J. Mater. Sci. Lett.* **15**, 948 (1996).
62. G. Carotenuto and L. Nicolais, *J. Mater. Chem.* **13**, 1038 (2003).
63. T. Sugimoto, ed., *Fine Particles Synthesis, Characterization, and Mechanism of Growth*, Marcel Dekker, Inc., New York, 2000, p. 460–496.
64. Y. Dirix, C. Bastiaansen, W. Caseri and P. Smith, *J. Mater. Sci.* **34**, 3859 (1999).
65. Y. Dirix, C. Bastiaansen, W. Caseri and P. Smith, *Adv. Mater.* **11**, 223 (1999).
66. R. L. Whetten, J. T. Khoury, M. M. Alvarez, S. Murty, I. Vezmar, Z. L. Wang, P. W. Stephens, C. L. Cleveland, W. D. Luedtke and U. Landman, *Adv. Mater.* **8**, 428 (1996).
67. R. L. Whetten, M. N. Shafigullin, J. T. Koury, T. G. Scaaff, I. Vezmar, M. M. Alvarez and A. Wilkinson, *Acc. Chem. Res.* **32**, 397 (1999).
68. W. D. Luedtke and U. Landman, *J. Phys. Chem.* **100**, 13324 (1996).
69. P. C. Ohara, D. V. Leff, J. R. Heath and W. M. Gelbart, *Phys. Rev. Lett.* **75**, 3466 (1995).
70. R. L. Whetten, M. N. Shafigullin, J. T. Khoury, T. G. Schaaff, I. Vezmar, M. M. Alvarez and A. Wilkinson, *Acc. Chem. Res.* **32**, 397 (1999).
71. Z. L. Wang, S. A. Harfenist, R. L. Whetten, J. Bentley and N. D. Evans, *J. Phys. Chem. B* **102**, 3068 (1998).
72. M. M. Alvarez, J. T. Khoury, T. G. Scheeff, M. Shafigullin, I. Vezmar and R. L. Whetten, *Chem. Phys. Lett.* **266**, 91 (1997).
73. A. Badia, W. Gao, S. Singh, L. Demers, L. Cuccia and L. Reven, *Langmuir* **12**, 1262 (1996).
74. C. B. Murray, S. Sun, W. Gaschler, H. Doyle, T. A. Betley and C. R. Kagan, *IBM J. Res. Dev.* **45**, 47 (2001).
75. G. Katabi, Y. Koltypin, X. Cao and A. Gedanken, *J. Cryst. Growth* **166**, 760 (1996).
76. Z. L. Wang, S. A. Harfenist, I. Vezmar, R. L. Whetten, J. Bentley, N. D. Evans and K. B. Alexander, *Adv. Mater.* **10**, 808 (1998).
77. G. Carotenuto, G. P. Pepe, and L. Nicolais, *Eur. Phys. J. B* **16**, 11 (2000).
78. G. Carotenuto, G. P. Pepe, L. Parlato, and L. Nicolais, *Mater. Eng.* **11**, 261 (2000).
79. G. Carotenuto, *Appl. Organomet. Chem.* **15**, 1 (2001).
80. M. J. Y. Yacaman, R. Perez, P. Santiago, M. Banaissa, K. Gonsalves, and G. Carlson, *Appl. Phys. Lett.* **69**, 913 (1996).
81. H. Remita, J. Khatouri, M. Treguer, J. Amblard, and J. Belloni, *Z. Phys. D* **40**, 127 (1997).
82. G. Carotenuto, S. DeNicola, G. P. Pepe, and L. Nicolais, *Eur. Phys. J. B* **24**, 437 (2001).
83. G. Carotenuto, S. DeNicola, and L. Nicolais, *J. of Nanoparticle Res.* **3**, 469 (2001).
84. N. A. F. Al-Rawashdeh, M. L. Sanfrock, C. J. Seugling, and C. A. Foss, *J. Phys. Chem.* **102**, 361 (1998).

85. J. C. Wittmann and P. Smith, *Nature* **352**, 414 (1991).
86. A. H. Lu, G. H. Lu, A. M. Kessinger, and C. A. Foss, *J. Phys. Chem. B* **101**, 9139 (1997).
87. L. Zimmerman, M. Weibel, W. Caseri, and U. W. Suter, *J. Mater. Res.* **8**, 1742 (1993).
88. M. Weibel, W. Caseri, U. W. Suter, H. Kiess, and E. Wehrli, *Polym. Adv. Technol.* **2**, 75 (1991).
89. L. Zimmerman, M. Weibel, W. Caseri, U. W. Suter, and P. Walther, *Polym. Adv. Technol.* **4**, 1 (1992).
90. A. H. Lu, G. H. Lu, A. M. Kessinger, and C. A. Foss, *J. Phys. Chem. B* **101**, 9139 (1997).
91. K. Baba, F. Takase, and M. Miyagi, *Opt. Commun.* **139**, 35 (1997).
92. K. Puech and W. J. Blau, *J. Nanoparticle Res.* **3**, 13 (2001).
93. L. Troger, H. Hunnefeld, S. Nunes, M. Oehring, and D. Fritsch, *Z. Phys. D* **40**, 81 (1997).
94. D. Fritsch and K. V. Peinemann, *Catal. Today* **25**, 277 (1995).
95. M. Ohtaki, M. Komiyama, H. Hirai and N. Toshima, *Macromolecules* **24**, 5567 (1991).
96. D. Acierno, C. Leonelli, G. C. Pellacani, eds., *Application of the Microwave Technology*, Mucchi Editore, Modena, Italy, 2000.
97. E. P. Boonekamp, J. J. Kelly, and L. G. J. Fokkink, *Langmuir* **10**, 4089 (1994).
98. A. M. T. Van der Putten, J. W. G. De Bakker, and L. G. J. Fokkink, *J. Electrochem. Soc.* **139**, 3475 (1992).
99. G. A. Gaddy, J. Mclain, S.-W. Huang, B. L. Slaten, and G. Mills, in *Proceedings 67th Annual Meeting of the APS Southeastern Section*, Mississippi State, 2000.

G. CAROTENUTO
L. NICOLAIS
Institute for the Composite Material Technology,
National Research Council

NANOCOMPOSITES, POLYMER–CLAY. See Volume 3.

NEUTRON SCATTERING

Introduction

"Scattering" to most polymer scientists means light scattering, and the extent of their experience with the experiment is often the description in a course of how light scattering can be used to determine the molecular weight and radius of gyration of a polymer in solution, as well as the second virial coefficient of the solution, by measuring the scattered light intensity from a series of dilute solutions for multiple angles. (1–4) This data is then plotted as a Zimm plot to obtain the desired characteristics of the polymer chain and solution. Or maybe the polymer scientist is interested in the crystal structure of a commercial polymer and uses X-ray diffraction to provide details of the local ordering of the pertinent long-chain molecule. (5–7) The X-ray scatterer may not see the correlation between the diffraction peaks and the information in the Zimm plot, but there is one. The

Encyclopedia of Polymer Science and Technology. Copyright John Wiley & Sons, Inc. All rights reserved.

angular dependence of scattered radiation provides direct information on the spatial distribution and microscopic structure of the scattering particles, whether in light scattering, X-ray diffraction, or neutron scattering experiments. For X-ray diffraction this information is on the order of angstroms and provides the arrangement of atoms on an ordered lattice, while (small-angle) light scattering provides data on the average size of a complete polymer chain on a length scale of a few to tens of nanometers.

In fact, scattering is a powerful analytical method that can be utilized to determine the structure and dynamics of a range of "soft" materials (colloids, polymers, proteins, etc) using X-rays, light, and neutrons. Moreover, the fundamental physics of the correlation between the angular dependence of the scattered intensity to the microscopic structure of the scattering particle is identical for all types of radiation; it is only the manner in which the data is treated and analyzed to provide information on the structure that makes them appear different. A given analysis can be used with any type of radiation; the same analyses that are used in X-ray diffraction are used in neutron diffraction, and can be used in light-diffraction experiments, if it will provide important data on the ordering of the particles that are diffracting (scattering) the incoming radiation. Small-angle X-ray, neutron, and light-scattering experiments are commonly reported in journals, with similar analyses and types of results. The primary difference is the type of radiation that shines on the sample and its interaction with the scattering particle.

The Scattering Experiment

Differences among radiation types can best be explained through a discussion of the scattering experiment itself. A scattering experiment can be depicted as in Figure 1, where the radiation shines on the sample, interacts with the sample, and is scattered in all directions. The intensity of the scattered radiation (I) is then measured at a detector for multiple angles (θ) and can be plotted as shown in the I vs θ plot in Figure 1. For most geometries and samples, the scattering intensity is a maximum at zero angle and drops with increasing angle. In this diagram the wavelength of the incident radiation (λ_i) and the wavelength of the scattered radiation (λ_s) are equal, and thus this is an elastic scattering event. The angular dependence of the scattering intensity can then be analyzed to provide information on the size, shape, and orientation of the scattering particle in the sample. This type of experiment is often termed a *static* scattering experiment as the information garnered is related to the static structure of the scattering particle, not its dynamics.

However, in order to obtain a useful I vs θ curve, a number of specific criteria must be met. Two of the most important criteria are that the measurement be taken in the correct angular range and that there be sufficient contrast in the sample for scattering to occur.

The correct angular range and sufficient contrast in the sample depends intimately on the type of radiation that is used in the scattering experiment, and a more detailed discussion of the scattering process is necessary to clarify this point.

Consider two vials, one that contains pure solvent and another that contains a solution with particles that may scatter light. Figure 2 shows a beam of light

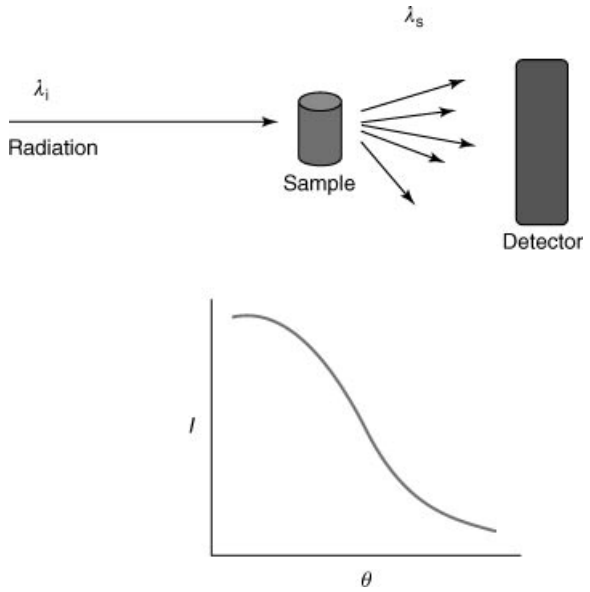

Fig. 1. (**a**) Schematic of an experiment to determine the angular dependence of the scattering of an incident radiation by a sample; (**b**) Typical intensity of scattered radiation vs scattering angle plot.

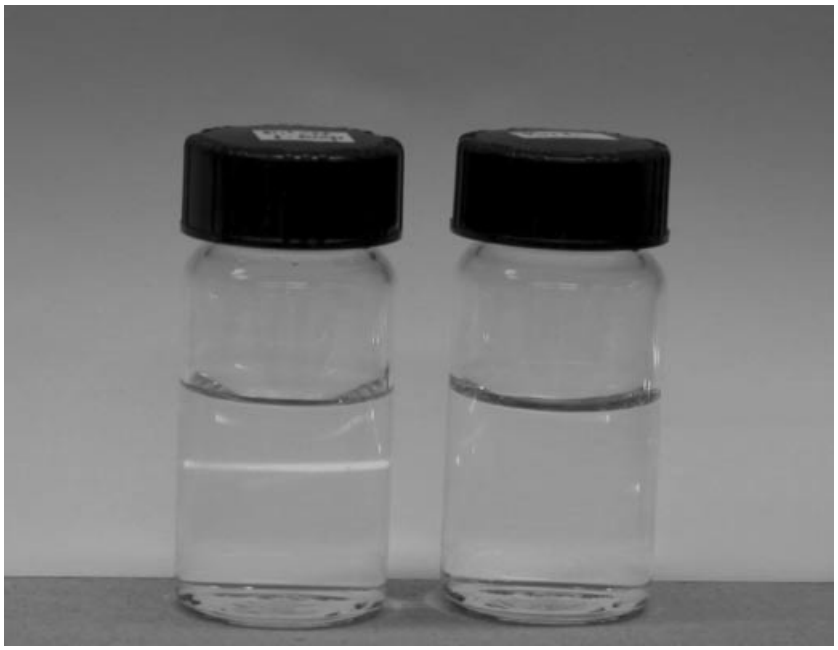

Fig. 2. Illustration of scattering power. The left vial contains polystyrene spheres that have a different refractive index than water, which provides contrast that results in scattering of the laser that is observable by the human eye.

from a laser pointer shining through two vials, where the right-hand one is pure water and the left is a 0.0002% solution of polystyrene (PS) microspheres (0.4 μm) in water. Notice how the laser light is strongly scattered by the solution, but not the pure solvent. That is because the solution contains PS particles that have a different refractive index than the water solvent that it is immersed in. This difference in the refractive index of the solute (PS, $n = 1.59$) and the solvent (water, $n = 1.33$) provides the contrast that is needed to observe scattering. Notice that in the pure water, there is no portion of the sample that has a different refractive index than the rest of the sample, and thus there is no observable scattering because there is no contrast. It is important to emphasize that it is possible to have a solution, but still not have sufficient contrast between the solvent and solute to observe scattering. For instance, if you have a solution where the solute and solvent have refractive indices that are identical, there will be no portion of the sample that has a different refractive index than the rest of the sample, and therefore there is no significant scattering. This phenomenon is termed *contrast matching* and is utilized in some scattering experiments to extract the scattering from a single component in a multicomponent sample.

This concept of "contrast" also holds true for the scattering of X-rays and neutrons by a polymer solution. However, when X-rays are being scattered by a particle, the X-rays interact with electrons of an atom and thus the intensity of scattering from a given atom depends on the electron density of that atom, not the refractive index. The electron density increases with atomic number on the periodic chart. Thus, for a polymer solution to strongly scatter X-rays, the electron density of the polymer and solvent must be significantly different. Finally, when neutrons are scattered, the neutrons interact with the nucleus of the atom and thus the intensity of the scattered radiation depends on the structure of the nucleus. This scattering power is quantified by the scattering length density b of a given atom and can vary by isotope. Therefore, to observe significant scattering from a polymer in solution, the scattering length density of the polymer must differ from that of the solvent. This has dramatic consequences for studying polymers and other soft matter by neutron scattering, as the scattering length densities of hydrogen and deuterium are significantly different. Thus, by changing the level of deuteration of a polymer (or solvent), the contrast (and thus amount of scattering) of a polymer in solution can be tuned without dramatically altering the thermodynamics of the mixture. (8–10)

This control of contrast in polymer mixtures by selective deuteration results is a unique and powerful aspect of neutron scattering in studying polymer systems; by the dispersion of a deuterated polymer chain in a matrix of identical hydrogenated chains, neutron scattering can be used to examine the structure and dynamics of a polymer in the melt or concentrated solution. This ability to "highlight" a single molecule in a matrix of identical polymer chains is illustrated in Figure 3. In Figure 3**a**, groups of polymer chains are shown, all drawn the same color. Because there is no contrast between the various chains, it is difficult to pick out one single chain. In Figure 3**b**, the color of one of the chains has been changed slightly, modeling the system where the scattering length density of one chain is slightly different than that of the matrix. Although this chain may now be observable, it is still difficult to examine. Finally in Figure 3**c**, a single chain is much darker than the remainder and is easy to pick out from the matrix and examine

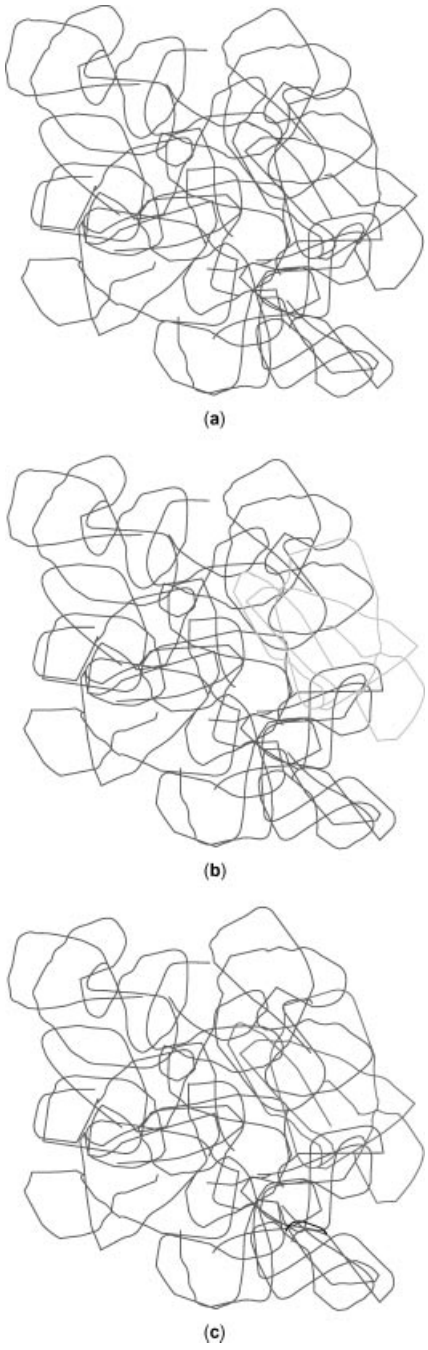

Fig. 3. Illustration of contrast. Figure **a** contains 10 polymer chains, where each chain is the same color, and thus there is no contrast between chains and it is difficult to differentiate one chain from the rest. Figure **b** contains the same 10 chains, but one has a slightly different color than the remaining chains, and thus this chain may be examined with difficulty. Figure **c** contains the same 10 chains, where one is now much darker than the remaining chains, providing a mechanism to clearly study this chain.

precisely. This picture illustrates the system where that chain is deuterated while the matrix of chains remains protonated with respect to neutron scattering. This one chains stands out as different from the matrix and can be selectively studied by neutron scattering.

The other criterion that is required to successfully utilize scattering to study polymer systems involves completing a scattering experiment in the correct angular range to extract useful information concerning the structure of the scattering particle from the angular dependence of the scattering intensity. This can best be exemplified in Figure 4, which shows the resultant I vs θ plots for scattering experiments that are completed in the wrong angular range. The I vs θ plot shown in Figure 4**a** shows a quick drop in intensity at low angle and very little scattering at higher angles. This type of curve is the result of measuring over too wide of an angular range so that the important information in the small-angle region is not resolved. Alternatively, Figure 4**b** shows a modest drop in intensity with angle, but no significant change in scattering intensity over the angular range of the scattering. In this case, the angular range is too small and there is insufficient data to quantify the drop in intensity with angle that can provide information on the structure and size of the scattering particle.

The quantification of this "correct" angular range requirement provides a correlation of the length scales that can be studied by radiation of a given wavelength. At small angles, the length scale that is measured, d, is approximately λ/θ, where λ is the wavelength of the radiation and θ is the scattering angle. This approximation demonstrates that neutrons are indeed ideal to examine the structure of proteins and polymers; for cold neutrons, $\lambda = 0.5 - 1.5$ nm, and small-angle scattering instruments provide a range of θ that allows the observation of the structure of soft matter over length scales ranging from 1 to 100 nm, perfect to determine the structure of a macromolecule from the local to global length scales.

Scattering with Neutrons. Thus, observing the scattering of neutrons by a polymeric system is a very powerful tool to determine the structure and dynamics of polymers over the correct length scales, primarily because of the ability to tune the contrast between components by selectively deuterating the particles (or portions of particles) that are of interest. Additionally, neutrons offer further benefits, including their ability to penetrate matter. Because the neutrons interact with the nucleus of an atom, a large portion of the neutrons that impact a sample will be transmitted through it without absorption or scattering. One useful result of this is that the sample holder can be quite large and complex as the neutrons are then able to penetrate a large sample holder and scatter from the sample. Thus, it is possible to complete neutron-scattering experiments from a broad range of sample environments including *in situ* steady shear (11–13), high pressure (14,15), oscillatory shear (16), and even when the sample is an aerosol (17,18).

However, there are some drawbacks to using neutron scattering. Most notably, the production of neutrons is a very costly process, as the neutrons are most often produced for scattering experiments by nuclear fission in a nuclear reactor or by spallation. *Spallation* is the process where energetic subatomic particles, such as protons, strike a target and eject particles, including many neutrons from the nuclei of the atoms in the target. These neutrons then serve as the source of the radiation for the neutron-scattering experiments. In either case, the cost of a

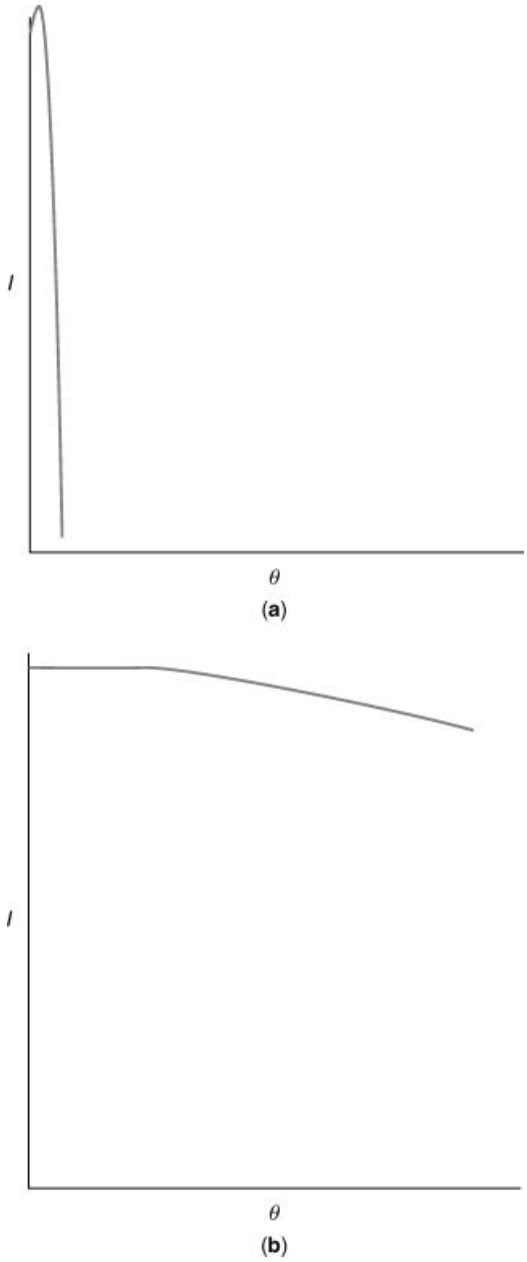

Fig. 4. Examples of the measured angular dependence of the scattering intensity for poorly designed experiments. The angular range in (**a**) is too broad, while the experiment shown in (**b**) is the result of an experiment where the angular range is too narrow.

nuclear reactor or spallation source is beyond most companies or laboratories and thus is in the domain of government agencies. Thus, there exist a handful of facilities in the United States, with more spread out around the world, where a polymer scientist can complete neutron-scattering experiments, and their completion

requires the time and expense of travel. Additionally, the current flux of neutrons requires significant sample size (usually, ~0.1–1.0 g), with larger sizes needed for exotic sample environments, such as a shear cell. This may be a particular problem for biological and exotic samples, where it is difficult to create more than a few milligrams of a given material. However, the Spallation Neutron source that is currently being built in Oak Ridge, Tennessee, will provide much greater intensity of neutrons on the sample, and thus allow faster measurements on smaller samples.

Even given these limitations, neutron scattering is a unique and very powerful technique that can provide information on the microscopic structure and dynamics of a polymeric material that is not obtainable by any other method. For instance, no other method provides a direct measure of the size of a polymer chain in the melt that is available by measuring the scattered intensity of neutrons from a blend of deuterated and protonated versions of the same polymer. Similarly, the shape and thermodynamic interactions of polymers in concentrated mixtures are most effectively monitored by carefully designed neutron-scattering experiments, some of which will be described in detail later in the article.

Structure from the Scattering Curve

There are a number of excellent reviews that detail the relationship between the angular dependence of the scattering intensity to the density distribution of the scattering system, and that will not be duplicated here (19,20). Rather, the methods to extract the structural information of the scattering system from the scattering pattern will be emphasized.

Classical scattering theory shows that the coherent scattering from a one-component system is proportional to the Fourier transform of the density correlation function, $C(\mathbf{r})$, of the particles in the system (19,21,22):

$$\left(\frac{\partial\sigma}{\partial\Omega}\right) \propto \int_V \exp(-i\mathbf{q}\cdot\mathbf{r})\, C(\mathbf{r})\mathrm{d}\mathbf{r} \tag{1}$$

where $(\frac{\partial\sigma}{\partial\Omega})$ is the number of scattered neutrons per second per solid angle $\partial\Omega$ in the neutron-scattering experiment. For simplicity, this quantity will be replaced by $I(q)$ in the remainder of this article. In equation 1, $\mathbf{q}$ is the scattering or momentum transfer vector, and has a magnitude $|\mathbf{q}| = q = 4\pi/\lambda \sin(\theta/2)$, where λ is the wavelength of the scattered radiation and θ is the scattering angle.

In a multicomponent system, such as a mixture of two constituents (component 1 and component 2), the scattering intensity now has contributions from correlations among particles of type 1, correlations among particles of type 2, and correlations between type 1 and type 2 particles, resulting in a scattering intensity $I(q)$ that can be described as

$$I(q) = b_1^2 S_{11}(q) + b_2^2 S_{22}(q) + 2b_1 b_2\, S_{12}(q) \tag{2}$$

Where b_i is the scattering length of component i and S_{ij} is the partial structure factor that describes the contribution to the scattering of the correlations between components i and j and is

$$S_{ij} = \int_{V,} \int_{V'} \langle n_i(\mathbf{r}) n_j(\mathbf{r}') \rangle \exp[-i\mathbf{q} \cdot (\mathbf{r}' - \mathbf{r})] d\mathbf{r}\ d\mathbf{r}' \tag{3}$$

where n_i ($\mathbf{r}$) is the local density of component i at point $\mathbf{r}$ and $\langle \ldots \rangle$ denotes an average over the scattering volume. Note that comparing equation 1 and equation 3, the density distribution function of the scattering particles $C(\mathbf{r}'') = \langle n_i(\mathbf{r}) n_j(\mathbf{r}') \rangle$ where $\mathbf{r}'' = \mathbf{r} - \mathbf{r}'$. Thus, the partial structure factor is the Fourier transform of the density distribution of the scattering particles, and if it can be extracted from the measured scattering intensity, it will provide information on the structure of the scattering particles; ie, $S_{11}(q)$ will provide information on the spatial distribution of the particles of type 1.

At first glance, the sum of three partial structure factors appears to add significant complexity to analyzing the $I(q)$ to determine the correlation between measured scattering patterns and structure of the scattering sample. However, it is relatively straightforward to show that, for two scattering particles of equal volumes, $S_{11}(q) = S_{22}(q) = -\frac{1}{2} S_{12}(q)$, which simplifies equation 2 to (23,24)

$$I(q) = (b_1 - b_2)^2 S_{11}(q) = (b_1 - b_2)^2 S_{22}(q) = -(b_1 - b_2)^2 S_{12}(q) \tag{4}$$

Thus, the angular dependence of the scattering intensity of a binary mixture can be analyzed as the Fourier transform of the density correlation function of any of the scattering particles scaled by the square of the difference in scattering lengths of the two components.

Let us assume that component 1 is a polymer and component 2 is a solvent. The requirement that the scattering particles (1 and 2) have equal volume for equation 4 to be valid requires that "particle 1" be equivalent to a section of the polymer chain that is the same volume as the solvent. Approximating this as a monomer segment of the polymer chain leads to an interesting result. Equation 4 tells us that $I(q) = (b_1 – b_2)^2 S_{11}(q)$; therefore the scattering pattern from a polymer/solvent mixture will provide a direct measure of the spatial distribution of the monomers (as they have been defined as the scattering particles of type 1). Moreover, if the polymer molecules are sufficiently dilute to be independent of each other, the q dependence of the scattering pattern is the Fourier transform of the spatial distribution of the monomers in a single-particle chain. This quantity is known as the *Particle Form Factor* of the polymer chain, $P(q)$, and Debye has shown that the Fourier transform of a Gaussian segment distribution, known as the *Debye Function*, is (25)

$$P(q) = 2\frac{[\upsilon^2 - 1 + \exp(-\upsilon)^2]}{\upsilon^4} \tag{5}$$

where $\upsilon = qR_g$, and R_g is the radius of gyration of the polymer molecule. Thus, by fitting the experimentally determined scattering pattern to equation 5, the radius of gyration and random coil nature of the polymer chain can be determined.

If the polymer molecules are not dilute, then a term for the *intermolecular* correlation between monomer segments [$Q(q)$] also contributes to the scattering pattern and must be accounted for in any subsequent data analysis. Fortuitously, when analyzing the scattering pattern of a mixture of two identical polymers, where one is deuterated and the other is not, $Q(q)$ can be related to the single particle form factor $P(q)$, and thus the scattering intensity pattern, $I(q)$, from this type of mixture can be directly correlated to the single-particle form factor, $P(q)$. Therefore the scattering from a mixture of deuterated and protonated identical polymers *at any concentration* can be readily analyzed to provide information on the structure of a polymer chain in the melt (23,24)

$$I(q) = (b_d - b_h)^2 x(1-x) N z^2 P(q) \tag{6}$$

where b_d is the scattering length of the deuterated polymer, b_h is the scattering length of the protonated polymer, x is the volume fraction of deuterated polymer, N is the total number of polymer molecules, and z is the number of monomer segments in the polymers.

Thus, from a practical standpoint, the scattering intensity of neutrons from a polymeric system as a function of angle can be measured. This scattering pattern is the Fourier transform of the density distribution of the scattering particles and, therefore, can be analyzed to provide information on the spatial distribution of the scattering particles. More specifically, in dilute mixtures or when a deuterated polymer is dispersed in its protonated counterpart, the size (R_g) and structure (does it obey the Gaussian distribution and is thus a random coil?) of the polymer chain can be readily determined from this scattering intensity pattern. Other single-particle form factors can also be used to model scattering data, such as that for a rigid rod, hollow sphere, or cylinder (26,27), which can provide size and structural information on other objects beyond random coils. For instance, the packing of a thermotropic, semiflexible liquid crystalline polymer has been shown to pack into a cylindrical conformation by fitting the resultant neutron scattering to the single particle form factor of a cylinder, where the radius and length of the cylinder are readily obtained from the fit (28).

Moreover, it is not difficult to design other experiments and apply broader analysis techniques to the measured $I(q)$ to provide information on the structure and thermodynamics of polymeric systems beyond the conformation of a polymer chain in the melt. Rather than describe the exact conditions and analyses for each of these opportunities, the remainder of this article will detail specific examples that describe efforts to examine particular structural aspects of polymeric systems with small-angle neutron scattering.

The Conformation of a Polymer Chain in the Melt

The most well-known examples of neutron-scattering experiments were completed in the early 1970s to unequivocally determine the conformation of a polymer chain

in the melt. Over 20 years earlier, Flory had predicted that a polymer chain that is dispersed in a matrix of identical polymer chains would follow random walk statistics (29) rather than the more obvious self-avoiding walk statistics that polymers are known to adopt in a good solvent. Unfortunately, there were no available techniques at the time to determine the conformational statistics of a single chain in the melt to test this prediction. However, the advent of neutron scattering provided a mechanism to determine the structure of a single polymer chain in the melt by selectively deuterating one molecule, dispersing it in a matrix of nearly identical protonated polymers, and examining it.

The design of these experiments was straightforward; the researchers dispersed protonated poly(methyl methacrylate) in deuterated poly(methyl methacrylate) at a level of a few percent and analyzed the resulting neutron-scattering intensity patterns to determine the radius of gyration of the polymer as well as the second virial coefficient of this solution. These results show that the polymer attains the same radius of gyration as that measured in a theta solvent and that the second virial coefficient of this mixture is zero (30–32). Similar experiments on mixtures of protonated polystyrene and deuterated polystyrene were completed that provided information on the scaling relationship between the radius of gyration and molecular weight for this polymer (33,34). All of these experiments demonstrated that the R_g scales as $M^{0.5}$ in the melt and obeys the Debye function down to a length scale of 1 nm, as would be expected from random walk statistics and was predicted by Flory.

In fact, further experiments over the years have shown that the R_g scales as $M_w^{0.5}$ for a range of polymers in the melt or glassy state with the proportionality constant equal to that which is observed in a theta solvent, verifying that flexible polymer chains in the melt attain a configuration that is accurately modeled as random coil. These results are tabulated in Table 1, where the data are taken from Reference 19 (see also CONFORMATIONS AND CONFIGURATION).

Table 1. Conformation of Polymer Chain in the Melt and in a θ Solvent

		Bulk	In θ solvent
Polymer	State	$R_g{}^a/M_w^{0.5}$,Å/(g/mol)$^{0.5}$	$R_g{}^a/M_w^{0.5}$,Å/(g/mol)$^{0.5}$
Atactic poly(methyl methacrylate)	Glass	0.25–0.27	0.25
Isotactic poly(methyl methacrylate)	Glass	0.30	0.28
Syndiotactic poly(methyl methacrylate)	Glass	0.29	0.24
Polybutadiene	Melt	0.35	0.34–0.42
Atactic polystyrene	Glass	0.265–0.28	0.27–0.28
Atactic polystyrene	Melt	0.275	0.27–0.28
Poly(vinyl chloride)	Glass	0.40	0.37
Polyisobutylene	Melt	0.31	0.30
Poly(ethylene terephthalate)	Glass	0.39	0.42
Polyethylene	Melt	0.45–0.46	0.45

[a] To convert Å to nm, divide by 10.

The Location of End Groups in Dendrimers

Dendrimers are highly branched polymers that can be synthesized by the consecutive addition of multifunctional monomers to a multifunctional core to form a tree-like structure (35,36), where an illustration of a dendrimer formed from trifunctional monomers is presented in Figure 5 (see DENDRONIZED POLYMERS). These macromolecules have recently attracted significant attention as possible sensors, drug carriers, lubricants, and surface-active agents. As the molecule is synthesized and becomes larger, more active sites remain at the outer edge of the molecules with each successive generation. As the number of active growth sites increases with size, the mass of the molecule increases exponentially with the number of generations. Clearly, the packing of each new generation becomes more dense, until the density saturates and the size of the molecule reaches a maximum.

The density profile of these unique structures has been the subject of much investigation. DeGennes first predicted that the dendrimer will have a density minimum at the center of the molecule, increase with radius, and reach a maximum at the outer edge of the spherical molecule (37). This structure provides a cavity in the center of the molecule that would provide an ideal structure for its use as a carrier. However, further theoretical and simulation studies have suggested that the molecule is not hollow, but has a density maximum at the center that decreases with radius (38–40).

Small-angle X-ray scattering and other studies have not clarified the radial structure of these intriguing molecules (41,42); however, a recent study of the radial density profile by small-angle neutron scattering has provided a clearer picture of its structure (43). Lindner and co-workers have used contrast variation small angle neutron scattering to unequivocally show that these molecules have a density maximum at the center, and a density profile that decreases with radius.

The specifics of this set of experiments take advantage of the ability to control the contrast between the dendrimer and the solvent by varying the extent of deuteration of the solvent, which is accomplished by mixing deuterated dimethyl acetamide (DMA-D_9) and protonated dimethyl acetamide (DMA-H_9). These

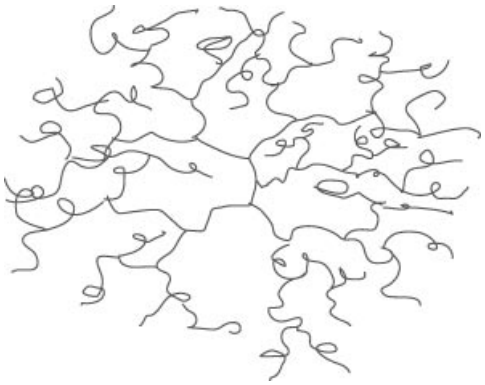

Fig. 5. Illustration of a dendrimer that is formed from trifunctional monomers, grown to the fourth generation.

researchers determined the scattering pattern of a fifth-generation dendrimer dissolved in DMA at various concentrations and varying ratios of DMA-D_9 to DMA-H_9. The authors analyze this data to extract the portion of the scattering that is due solely to the shape of the dendrimer [I_s (q)] from the measured scattering intensity which also contains contributions due to inhomogeneities of the dendritic structure, which may result from imperfections in the structure and the fact that the building blocks of the dendrimer may not all have the same structure (and thus scattering length). This careful analysis provides a measure of the average scattering length density of the dendrimer, which provides an exact measure of the molecular weight of the dendrimer. A comparison of this value to the ideal fifth-generation dendrimer indicates that the structure is not perfect.

Finally, the authors extract the radial density profile of the dendrimer from I_s (q) by its Fourier inversion to show that the density of the dendrimer is a maximum at the center that decreases smoothly to the outer edge. Moreover, the results demonstrate that the dendrimer radius extends to 6 nm and is thus a fluctuating, not a dense, structure. This analysis is further verified by comparing the scattering intensity [I_s (q)] to the Fourier transform of this density distribution and to the Fourier transform of the homogeneous sphere, where this comparison shows a clear coincidence to the experimentally determined density profile and clear deviations from that of the homogeneous sphere.

Thus the ability to systematically vary the contrast between the solute and solvent by mixing deuterated and protonated solvents provides a mechanism to unequivocally extract the scattering from the solute, and thus determine the structure of that solute. These results show that the end groups of this dendrimer are not confined to the outer layer of this centrosymmetric structure, which would result in a core-shell density profile. Rather, the end groups are distributed throughout the volume of the macromolecule. This information will have significant impact on the utilization of these novel macromolecules and their use in the design of molecular scale sensors, drug carriers, and lubricants.

The Radius of Gyration of Polymers in Ultrathin Films

It is well known that confining a polymer molecule to a thin film or near a surface lowers its configurational entropy. This confinement may also alter the configuration of the polymer, which may impact its adhesive and thermal properties, among others. One can easily imagine that a polymer chain that is confined to a thin film that is on the order of (or less than) its radius of gyration may be flattened. Moreover, as devices become smaller, polymers are often utilized in applications where the confinement of the polymer chain is significant. Thus, the alteration of the configuration of a polymer chain by confinement is of importance to their use in micro- and nanoscale devices. It is, therefore, important to understand how confinement alters the size and shape of a polymer chain, with the expectation that this data can provide fundamental information to predict, understand, and control the properties of polymers in these environments.

As polymers in miniature devices are mostly melts, neutron scattering becomes an ideal experimental technique to provide this information. Clearly, by

dispersing a fraction of deuterated polymer in a protonated thin film of the polymer, SANS can be used to determine the radius of gyration of a polymer confined to the film, as a function of film thickness, in a similar way to the bulk measurements in the 1970s that verified the random coil nature of the polymer chain in the melt (30,32,33). However, the relatively low intensity of neutrons that strike the sample in a scattering experiment introduces a complication into this planned experiment. In a scattering experiment, the intensity of scattered radiation is proportional to the amount of sample in the beam. In a bulk SANS experiment, a sample usually contains on the order of 0.1–0.5 g to optimize the signal to noise. However, with a radius of a neutron beam that is on the order of a centimeter, a thin film of polymer that is only as thick as the radius of gyration of a polymer will only provide 0.000785 mg of sample in the beam, clearly an amount that is insufficient to provide adequate signal-to-noise ratio to accurately determine the radius of gyration of a polymer. Researchers who have completed such a study overcame this obstacle by simultaneously scattering from multiple, identical thin films, thus effectively increasing the sample size (44,45).

The authors of this study measured the neutron-scattering intensity of isotopic blends that contain 25 wt% deuterated polystyrene and 75 wt% protonated polystyrene in thin films that vary in thickness (D) from 1 μm down to 10 nm. These thicknesses correspond to $D/R_{g,bulk}$ that range from 50 to 0.5. The samples were annealed at high temperature and quenched to ensure that the samples were at equilibrium. The data were analyzed by accounting for scattering from interfacial roughness in the form of capillary waves and incoherent scattering to extract the scattering due to the dispersion of the deuterated polymers in the protonated matrix $I_s(q)$. This scattering, $I_s(q)$, was then analyzed using the RPA model and the Kratky approach (q^2I vs q^2) to determine the radius of gyration of the deuterated polymers and test the Gaussian nature of the confined chains, respectively. The R_g results are shown in Figure 6, which shows that the size of

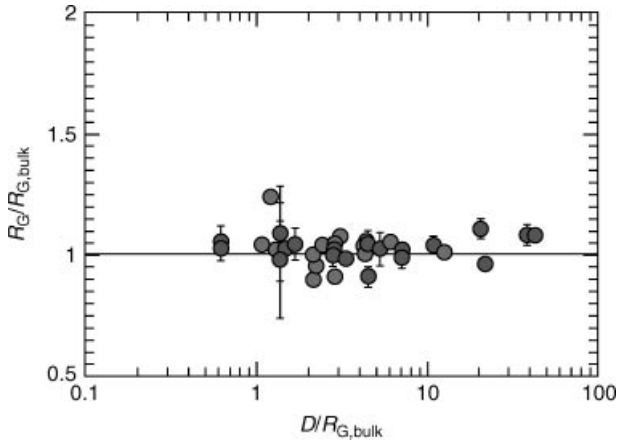

Fig. 6. The radius of gyration of deuterated polystyrene in a thin film normalized to its radius of gyration in the bulk as a function of film thickness that is also normalized to the radius of gyration of the polymer in the bulk. ● $M_w = 270$ K, ● $M_w = 650$ K. Reprinted with permission from Ref. 44. Copyright (2001) American Chemical Society.

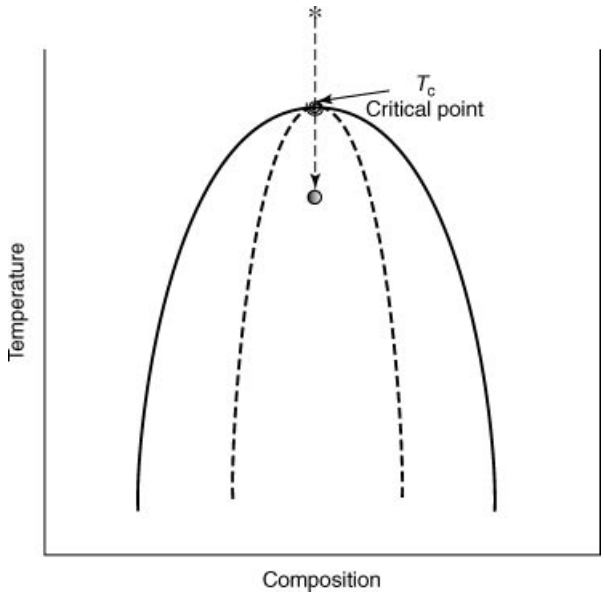

Fig. 7. Representative phase diagram of a binary mixture of two molecules that have similar sizes.

the polymer chain in the plane of the surface does not change from that of the chain in the bulk, even when the thickness of the film is less than the R_g of the bulk chain. The data also verify that the chains do retain their Gaussian character for all film thicknesses studied. This result agrees with recent simulation and theoretical studies and will have implications on the properties and dynamics of a polymer chain in confined geometries.

Polymer Blends

The Spinodal Decomposition Process in Polymer Blends. For many mixtures, there exists a temperature range where the system will remain miscible for all compositions, while a change in temperature will alter the balance of the enthalpy and entropy of mixing to create a thermodynamic state where the most stable system is one where two phases coexist and the mixture, therefore, phase separates. This situation is illustrated in Figure 7, which shows the phase diagram of a regular solution (46). When below the critical temperature, the outer line of this phase diagram denotes the compositions of the two phases that coexist at a given temperature. Therefore, for this system, it is possible to design a temperature program where the system is brought from the one-phase state at high temperature to a phase-separated system at low temperature.

In fact, the kinetics of the process by which the system goes from a homogeneous, one-phase system to the final equilibrium state of two coexisting phases is extremely important to both industrial and academic researchers. From an industrial standpoint, understanding and control of the morphology of the

phase-separated system can provide a mechanism to create new materials with novel properties. From an academic point of view, the self-assembling process of the phase separation and resultant morphologies provide insight into nonequilibrium thermodynamics. Of particular interest, a more complete understanding of the kinetics of spinodal decomposition as a phase separation process has been an area of intense study (47–51).

It is known from thermodynamics that in the region of the phase diagram below the spinodal line (dotted line in Figure 7) that a one-phase system is absolutely unstable and the system will phase separate spontaneously via the spinodal decomposition mechanism (SD). Moreover, the time evolution of the change in concentration is well described in the early stages of SD by the theory first presented by Cahn for small molecules (52,53). This theory predicts that there exists a dominant length scale for the phase separation process that does not change with time in this early stage and that the amplitude of the concentration fluctuations [$\Delta\phi$ (**r**,t)] that occur on this length scale grows exponentially with time. Unfortunately, these predictions were difficult to observe in small molecular mixtures, as the time scale of the early stage is too brief (ie $<$1 s) for experimental measurements. However, because polymers are larger and slower, the time scale over which this early stage lasts is minutes, providing sufficient time to monitor the time dependence of the growth of the concentration fluctuations to test this theory. Moreover, small-angle neutron scattering is an ideal tool to monitor these changes, as the scattering intensity [$I(q)$] of the mixture provides direct information on the distribution of the scattering particles, and thus can be used to observe the variation of the spatial distribution of the concentration fluctuations as a function of time.

Time-resolved small-angle neutron scattering has, thus, been used to determine the coarsening kinetics of spinodal decomposition in polymer blends. Blends systems that have been investigated include mixtures of hydrogenated and deuterated polybutadiene as well as deuterated polystyrene and poly(vinyl methyl ether) (49–51) where the deuteration of one component in the blend provides the necessary contrast to complete the experiments. In these experiments, the researchers create a polymer blend that is initially in the one phase-region (* in Fig. 7). This mixture is then quickly brought to a temperature in the phase-separated regime, below the spinodal decomposition line ($\circ$ in Fig. 7), and subsequently the scattering intensity [$I(q)$] for the system as a function of time is measured. The resultant scattering patterns can then be fit to the Fourier transform of the theoretically predicted concentration fluctuation distribution (47), which provides a direct mechanism to test the theories of the kinetics of spinodal decomposition.

These results confirm that $\Delta\phi$ (**r**,t) grows exponentially with time while the characteristic length scale **r** remains constant in the early stage (54). Further experiments have documented that at later times, in the intermediate stage of SD, the phase-separated morphology coarsens with time, resulting in a nonexponential growth of $\Delta\phi$ (**r**,t) and an increase in **r** with time. At even later times, in the late stage of the SD process, the interface between the separate domains narrows and $\Delta\phi$ (**r**,t) reaches an equilibrium value, which is defined by the specifics of the phase diagram. These domains can coarsen further (though more slowly than earlier stages) and thus, the length scale of the domains, **r**, continues to grow slowly.

Thus, the ability of small-angle neutron scattering to tune the contrast of the phase separating blends combined with its ability to examine the correct length

scales of this phase separation process make SANS an ideal technique to determine the kinetics of the concentration fluctuation growth during spinodal decomposition. Moreover, the results show that the linearized Cahn–Hilliard–Cook theory of SD (52,53,55) accurately describes the early stage of spinodal decomposition, and that the intermediate and late stage kinetics obey universal kinetics.

The Crossover from Mean-Field to Ising Behavior in Critical Polymer Blends. Polymer systems have long been known to follow mean-field behavior at most temperatures, as long-range fluctuations are readily damped because of their slow relaxation processes and intimate mixing of chains (56,57). However, it is expected from critical theory that as a mean field system approaches a critical point, fluctuations will become more prevalent and impact the structure of the system. The increased importance of the fluctuations results in a polymer mixture transitioning to behave as a non-mean-field (Ising) system (58). The point where this transition occurs is known as the *Ginzburg criterion* (59). This transition from mean-field to non-mean-field behavior can be determined by monitoring the temperature dependence of concentration fluctuation size (ξ), where it is expected that $\xi \sim (T - T_c)^{-\nu}$ and $\nu = 0.5$ for a system that obeys mean-field behavior and $\nu = 0.63$ for an Ising type system.

As neutron scattering measures the fluctuation in the scattering length density of a system, it is an ideal tool to monitor the presence and growth of concentration fluctuations in a polymer/polymer mixture. In fact, the inverse of the zero-angle scattering, $I^{-1}(q{=}0)$, is proportional to the second derivative of the free energy of the mixture with respect to the blend concentration, which is the osmotic compressibility of a mixture. Theories of cooperative phenomena show that $I^{-1}(q{=}0) \sim (T - T_c)^{-2\nu}$ (60) and thus the determination of $I^{-1}(q)$ extrapolated to $q{=}0$ for a polymer blend at a series of temperatures near T_c will provide a method to verify the existence of this crossover and its influence on the mixing behavior of two polymers (61,62).

To test this prediction of the crossover from mean-field to Ising-type behavior, very precise small-angle neutron scattering measurements were completed on blends of deuterated polystyrene (d-PS) and poly(vinyl methyl ether) (PVME) at the critical concentration for a series of temperatures as the one-phase mixture approaches the temperature of phase separation (ie, the critical point T_c in Fig. 7) (61). The data were analyzed by fitting the measured $I\ (q)$ to the random phase approximation to estimate $I(q{=}0)$ for each temperature, where the temperature is controlled to ± 0.01 K.

Far away from the critical temperature, Schwahn and co-workers found that the inverse of the scattering intensity at zero angle, $I^{-1}(q{=}0)$, scales with $(T_c - T)$ where T is the temperature at which the scattering is measured, as would be expected from a mean-field system. However, as the temperature approached the critical temperature, $I^{-1}\ (q{=}0)$ diverges from a linear relationship with $(T_c\text{-}T)$ within 3 K of T_c. Moreover, in this narrow region near the critical point, $I^{-1}(0)$ scales as $(T_c\text{-}T)^{1.26}$ as one would expect from a system that obeys Ising-type behavior. This transition is shown in Figure 8, taken from Reference 61.

This result emphasizes that mean-field theory is a very accurate model to describe the behavior of polymer systems for most of the phase diagram, except in a narrow window near the critical temperature and concentration. This implies that concentration fluctuations do not significantly influence the phase behavior

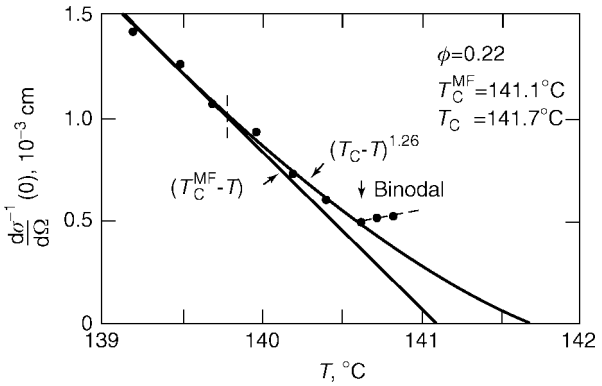

Fig. 8. The inverse of the zero-angle scattering of a polymer blend (d-PS/PVME) as it approaches the phase separation temperature. Note the deviation from mean-field behavior just below 140 °C. Reprinted with permission from Ref. 61. Copyright (1987) by the American Physical Society.

of polymers, whereas for small molecule mixtures, it is known that composition fluctuations can influence the system throughout the phase diagram of the mixture and neutron scattering is an instrumental technique in defining these differences.

Flow-Induced Structure in Polymers

In order to create a useful polymeric product, the material will have to undergo some level of processing where a shear flow is applied to a polymer melt or solution to create the desired shape. However, it is well known that the application of a shear field onto a polymer melt or solution can modify its structure (63). One interesting phenomenon that has been observed is the enhancement of concentration fluctuations by the application of a shear field. In other words, a polymer solution that is miscible at rest appears to phase separate when it is sheared. This phenomenon has been well studied, but is not completely understood (64–67).

As neutron scattering provides information on the spatial distribution of concentration fluctuations by virtue of its ability to provide direct evidence of the spatial distribution of the scattering particles, it is an ideal technique to examine the changes that occur during this phenomenon on length scales ranging from the monomeric level to that of many chains. Moreover, if combined with light scattering, which provides information on larger length scales than that of neutrons, an understanding of the development and deformation of the concentration fluctuations as a function of parameters such as shear rate and temperature over length scales ranging from submolecular to micrometers can be found. There exist a number of articles describing the monitoring of the structures that are induced in polymer blends, phase-separated block copolymer, liquid crystalline polymer solutions and melts, and polymer solutions by an applied shear field; but to exemplify the utility of this technique, the work of Hashimoto and Lindner on the impact of temperature and shear rate on the enhancement and deformation of concentration fluctuations in polystyrene/dioctyl phthalate solutions (PS/DOP) using neutron- and light-scattering experiments will be discussed (68).

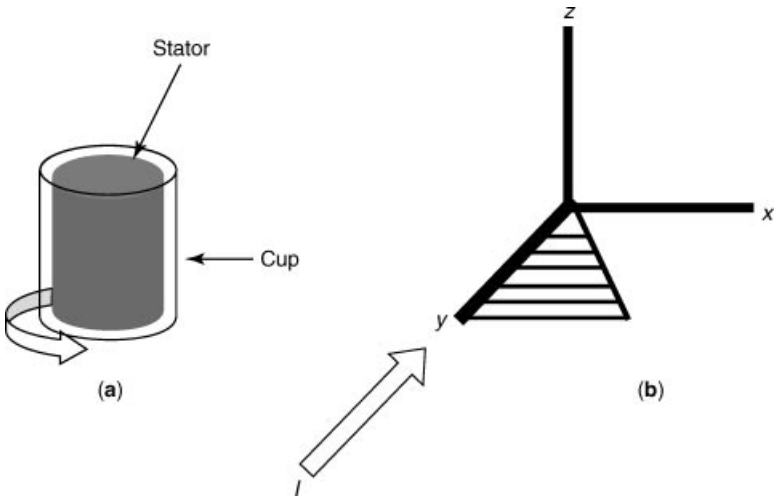

Fig. 9. (**a**) Diagrammatic representation of a couette shear cell. (**b**) The resultant geometry of the shear field, where the x-axis is the flow direction, the y-axis is the shear gradient and the z-axis is the vorticity direction. Note that the incident radiation is also along the y-axis, and the measured scattering intensity is in the flow–vorticity plane.

In this work, the investigators measured the scattering patterns of PS/DOP while they were being sheared. This requires that a sample holder be designed whereby the material can be constantly sheared during the time that the scattering pattern is collected. A geometry that has provided significant success at collecting the scattering of polymer systems *in situ*, during shear flow, is a couette cell as shown in Figure 9. In this cell, an outer cup is made out of a material that is relatively transparent to neutrons, such as quartz. This cup then contains a stator that fits symmetrically into the cup, but leaves a thin annulus between the cup and the stator into which the polymer melt or solution can be filled (11). It is important that the stator also be manufactured from a material that allows large transmission of neutrons. Stators have been successfully made from quartz and oxygen free copper, where the copper provides better heat transport and higher use temperatures, and thus provides the ability to measure shear effects on bulk polymer materials as well as solutions.

The SALS and SANS data were combined to provide information on the structure of the concentration fluctuations on length scales ranging from tens of angstroms to 10 microns. The authors were able to fit the data to model the scattering from the structure of the thermal concentration fluctuations as well as the contributions from the demixed phases. The scattering pattern was, thus, fit to the sum of an Ornstein–Zernike function (to model thermal fluctuations) and a modified squared Lorentzian function (to model the demixed phases). From these fits, the authors were able to provide quantitative information regarding the size and shape of the demixing domains as a function of temperature, shear rate, and polymer molecular weight. Moreover, the results provide a data set that can be used to test current and pioneering theoretical models of this phenomenon and find that earlier theoretical treatments do not agree well with this broad set of results.

The results, however, do appear to agree with more recent theoretical models and thus provide critical insight into the physics of this unique phenomenon.

Thus, the combination of neutron scattering and light scattering is a valuable tool set that allows these researchers to monitor the structures that exist in the phase-separating mixture on a broad range of length scales. It is only with the information of the structure of this polymer solution over these length scales that allows the researchers to critically evaluate theoretical models of shear-induced phase separation in polymer mixtures.

Structure of Proteins by Contrast Variation

The mechanism by which biological enzymes become active, bind with substrates, and affect a catalytic reaction is of broad interest. Specific details on how the enzymes coordinate and interact with regulators are of particular importance in understanding enzymatic activity. For instance, calmodulin is a receptor for calcium that is responsible for binding of Ca^{2+} in calcium-dependent regulation of cellular processes via interactions with enzymes (69). A model system for this regulation of enzymatic activity is the calcium/calmodulin activation of myosin light chain kinase (MLCK) (70,71). MLCK contains a catalytic cleft that is normally inhibited by a regulatory sequence within the MLCK. The binding of the Ca^{2+}/calmodulin (CaM) to the MLCK activates the catalytic cleft, and enables target enzyme recognition and substrate binding. However, the specific structural mechanism by which the CaM complex activates the catalytic cleft was not verified until Trewhella and co-workers utilized small-angle neutron scattering experiments with contrast variation to elucidate the change in structure of the CaM complex and MLCK upon binding that results in the activation of the catalytic cleft. (72,73)

In these experiments (73), the authors determined the scattering patterns for CaM–MLCK (in which the CaM is deuterated) complexes in H_2O/D_2O mixtures that were 0, 20, 75, 82, and 85% D_2O. This range of mixtures provided the needed information to extract the individual shape functions of the MLCK and CaM structures at various stages of the binding process. This is accomplished by analyzing the measured scattering function $I\,(q, \Delta b_c, \Delta b_K)$ with the following equation

$$I\,(q, \Delta b_c, \Delta b_K) = \Delta b_c^2\, I_c\,(q) + \Delta b_c\, \Delta b_K\, I_{CK}\,(q) + \Delta b_K^2\, I_K\,(q) \qquad (7)$$

where subscripts c and K denote deuterated CaM and MLCK, respectively, Δb_i is the contrast between the scattering length density of component i and solvent ($b_i - b_s$) and $I_c\,(q)$, $I_K\,(q)$, and $I_{CK}(q)$ denote the contribution to the total scattering from the structure of the CaM, the structure of the MLCK, and the correlation between the structures of CaM and MLCK, respectively. Note that by completing the experiments for a series of D_2O/H_2O mixtures, a series of equations that fit equation 7 are created, and the scattering from each individual structure [$I_c\,(q)$ and $I_K\,(q)$] can be extracted and analyzed.

The authors do precisely that: they fit the resulting individual form factors to those of two ellipsoids that provide information on the size, shape, and relative

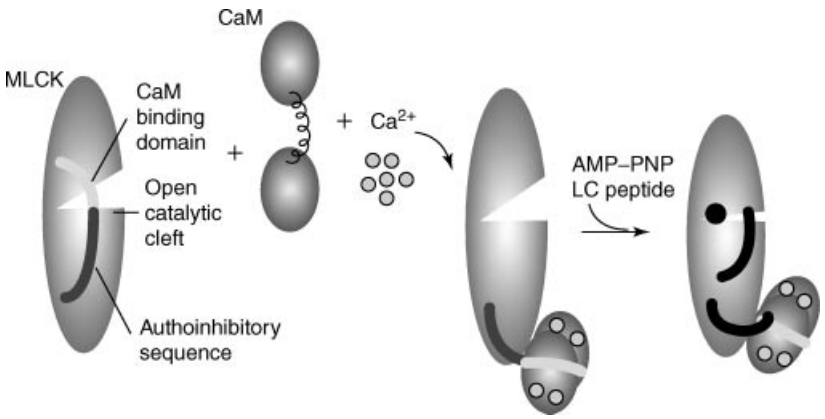

Fig. 10. Diagram that depicts the interaction of CaM to MLCK that results in the activation of the catalytic cleft of MLCK to enzymatic activity. Reprinted with permission from Ref. 73. Copyright (1998) American Chemical Society.

dispositions of the CaM and MLCK. This information provides a very precise picture of how the two molecular components come together, interact, and activate the catalytic cleft of the MLCK, which is illustrated in Figure 10 (from Reference 73). The scattering results indicate that a regulatory sequence within the MLCK keeps its catalytic cleft open. The binding of Ca^{2+} to CaM opens hydrophobic clefts in the CaM. Upon binding of the CaM with MLCK, the hydrophobic clefts on the CaM interact with hydrophobic residues of the MLCK sequence, which induces movement of the MLCK regulatory sequence away from its catalytic cleft, relieving the MLCK auto-inhibition and providing an activated structure that can now bind with substrates and thus enable enzymatic activity.

This example further demonstrates the power of neutron scattering to extract structural information of individual components in a complex system by use of the contrast variation method. Contrast variation provides an additional sample preparation technique that allows the extraction of the scattering of a single component in a multicomponent mixture and broadens the utility of neutron scattering into fields such as the study of biological complexes and the structure of diblock copolymers (74).

BIBLIOGRAPHY

"Neutron Scattering" in *EPSE* 2nd ed., Vol 10, pp. 112–184, by G. D. Wignall, Oak Ridge National Laboratory.

1. P. C. Painter and M. M. Coleman, *Fundamentals of Polymer Science, An Introductory Text*, Technomic Press, Lancaster, Pa., 1997.
2. P. C. Hiemenz, *Polymer Chemistry, The Basic Concepts*, Marcel Dekker, New York, 1984.
3. A. Rudin, *The Elements of Polymer Science*, Academic Press, New York, 1999.
4. L. H. Sperling, *Introduction to Physical Polymer Science*, Wiley-Interscience, New York, 1992.
5. B. D. Cullity, *Elements of X-ray Diffraction*, Addison Wesley, Reading, Mass., 1978.

6. A. Guinier, *X-Ray Diffraction in Crystals, Imperfect Crystals, and Amorphous Bodies*, Freeman, San Francisco, 1963.
7. M. Kakudo and N. Kasai, *X-Ray Diffraction by Polymers*, Elssevier, Amsterdam, 1972.
8. F. S. Bates, G. D. Wignall, and W. C. Koehler, *Phys. Rev. Lett.* **55**, 2425 (1985).
9. F. S. Bates, L. J. Fetters, and G. D. Wignall, *Macromolecules* **21**, 1086 (1988).
10. F. S. Bates, M. Muthukumar, G. D. Wignall, and L. J. Fetters, *J. Chem. Phys.* **89**, 535 (1988).
11. A. I. Nakatani, H. Kim, and C. C. Han, *J. Res. Natl. Inst. Stand. Tech.* **95**, 7 (1990).
12. F. A. Morrison, J. W. Mays, M. Muthukumar, A. I. Nakatani, and C. C. Han, *Macromolecules* **26**, 5271 (1993).
13. M. D. Dadmun and C. C. Han, *Macromolecules* **27**, 7522 (1994).
14. B. Hammouda, N. P. Balsara, and A. A. Lefebvre, *Macromolecules* **30**, 5572 (1997).
15. A. A. Lefebvre, J. H. Lee, N. P. Balsara, and B. Hammouda, *Macromolecules* **33**, 7977 (2000).
16. K. A. Koppi, M. Tirrell, and F. S. Bates, *Phys. Rev. Lett.* **70**, 1449 (1993).
17. B. E. Wyslouzil, J. L. Cheung, G. Wilemski, and R. Strey, *Phys. Rev. Lett.* **79**, 431 (1997).
18. C. H. Heath, K. A. Streletzky, B. E. Wyslouzil, J. Wolk, and R. Strey, *J. Chem. Phys.* **118**, 5465 (2003).
19. J. S. Higgins and H. C. Benoit, *Polymers and Neutron Scattering*, Oxford University Press, Oxford, 1994.
20. R. J. Roe, *Methods of X-ray and Neutron Scattering in Polymer Science*, Oxford University Press, Oxford, 2000.
21. G. E. Bacon, *Neutron Diffraction*, Oxford University Press, Oxford, 1975.
22. G. L. Squires, *Introduction to the Theory of Thermal Neutron Scattering*, Cambridge University Press, Cambridge, (1978).
23. M. Daoud, J. P. Cotton, B. Farnoux, G. Jannink, G. Sarma, and H. Benoit, *Macromolecules* **8**, 804 (1975).
24. A. Akcasu, G. C. Summerfield, S. N. Jahshan, C. C. Han, C. Y. Kim, and H. Yu, *J. Polym. Sci., Polym. Phys.* **18**, 863 (1980).
25. P. J. Debye, *J. Appl. Phys.* **15**, 338 (1944).
26. T. Neugebauer, *Annalen der Physik* **42**, 509 (1943).
27. A. Guinier and G. Fournet, *Small Angle Scattering of X-Rays*, John Wiley and Sons, Inc., New York, 1955.
28. F. Hardouin, G. Sigaud, M. F. Achard, A. Brulet, J. P. Cotton, D. Y. Yoon, V. Percec, and M. Kawasumi, *Macromolecules* **28**, 5427 (1995).
29. P. J. Flory, *J. Chem. Phys.* **17**, 303 (1949).
30. R. G. Kirste, W. A. Kruse, and J. Schelten, *J. Makromol. Chem.* **162**, 299 (1973).
31. R. G. Kirste, W. A. Kruse, and J. Schelten, *Angew. Chem. Int. Ed.* **12**, 431 (1973).
32. J. Schelten, W. A. Kruse, and R. G. Kirste, *Kolloid Z. Z. Polym.* **251**, 919 (1973).
33. D. G. H. Ballard, G. D. Wignall, and J. Schelten, *Eur. Polym. J.* **10**, 861 (1974).
34. J. M. Guenet, C. Picot, and H. Benoit, *Macromolecules* **12**, 86 (1979).
35. D. A. Tomalia, A. Naylor, and W. A. Goddard, *Angew. Chem. Int. Ed.* **29**, 138 (1990).
36. G. R. Newkome, C. N. Moorefield, and F. Vögtle, *Dendritic Molecules*, VCH, Weinheim, Germany, 1996.
37. P. G. DeGennes and H. Hervet, *J. Phys. (Paris)* **44**, L351 (1983).
38. R. L. Lescanec and M. Muthukumar, *Macromolecules* **23**, 2280 (1990).
39. M. Murat and G. S. Grest, *Macromolecules* **29**, 1278 (1996).
40. D. Boris and M. Rubinstein, *Macromolecules* **29**, 7251 (1996).
41. T. J. Prosa, B. J. Bauer, E. J. Amis, D. A. Tomalia, and R. Scherrenburg, *J. Polym. Sci., Part B: Polym. Phys.* **35**, 2913 (1997).
42. R. Scherrenburg, B. Coussens, P. van Vliet, G. Edouard, J. Brackman, E. de Brabander, and K. Mortensen, *Macromolecules* **31**, 456 (1998).

43. D. Pötschke, M. Baullauff, P. Lindner, M. Fischer, and F. Vögtle, *Macromolecules* **32**, 4079 (1999).
44. R. L. Jones, S. K. Kumar, D. L. Ho, R. M. Briber, and T. P. Russell, *Macromolecules* **34**, 559 (2001).
45. R. L. Jones, S. K. Kumar, D. L. Ho, R. M. Briber, and T. P. Russell, *Nature* **400**, 146 (1999).
46. J. Hildebrand, *J. Am. Chem. Soc.* **51**, 66 (1929).
47. T. Hashimoto, *Phase Transitions* **12**, 47 (1988).
48. H. L. Snyder and P. Meakin, *J. Chem. Phys.* **79**, 5588 (1983).
49. T. Hashimoto, M. Itakura, and N. Shimizu, *J. Chem. Phys.* **85**, 6773 (1986).
50. T. Sato and C. C. Han, *J. Chem. Phys.* **88**, 2057 (1988).
51. F. S. Bates and P. Wiltzius, *J. Chem. Phys.* **91**, 3528 (1989).
52. J. W. Cahn, *Acta Metall.* **9**, 795 (1961).
53. J. W. Cahn, *J. Chem. Phys.* **42**, 93 (1965).
54. H. Jinnai, H. Hasegawa, T. Hashimoto, and C. C. Han, *J. Chem. Phys.* **99**, 4845 (1993).
55. H. E. Cook, *Acta Metall.* **18**, 287 (1970).
56. M. Kurata, *Thermodynamics of Polymer Solutions*, MMI Press, New York, 1982.
57. P. G. deGennes, *Scaling Concepts in Polymer Physics*, Cornell University Press, Ithaca, N.Y., 1979.
58. K. Binder, *Phys. Rev. A* **29**, 341 (1984).
59. V. L. Ginzburg, *Sov. Phys. Solid State* **2**, 1824 (1960).
60. H. E. Stanley, *Introduction to Phase Transitions and Critical Phenomena*, Oxford University Press, Oxford, 1971.
61. D. Schwahn, K. Mortensen, and H. Yee-Madeira, *Phys. Rev. Lett.* **58**, 1544 (1987).
62. F. S. Bates, J. H. Rosedale, P. Stepanek, T. P. Lodge, P. Wiltzius, G. H. Fredrickson, and R. P. Hjelm, *Phys. Rev. Lett.* **65**, 1893 (1990).
63. A. I. Nakatani and M. D. Dadmun, eds., *Flow-Induced Structure in Polymers*, ACS Symposium Series 597, American Chemical Society, Washington, D.C. 1995.
64. E. Helfand and G. H. Fredrickson, *Phys. Rev. Lett.* **62**, 2468 (1989).
65. S. T. Milner, *Phys. Rev. E* **48**, 3674 (1993).
66. A. Onuki, *J. Phys.: Condens. Matter.* **9**, 6119 (1997).
67. A. Onuki, R. Yamamoto, and T. Taniguchi, *J. Phys. II* **7**, 295 (1997).
68. S. Saito, T. Hashimoto, I. Morfin, P. Lindner, and F. Boue, *Macromolecules* **35**, 445 (2002).
69. J. T. Stull, in P. Cohen and B. C. Klee, eds., *Molecular Aspects of Cellular Regulation*, Elsevier, Amsterdam, 1988.
70. B. E. Kemp, M. W. Parker, S. H. Hu, T. Tiganis, and C. House, *Trends Biochem. Sci.* **19**, 440 (1994).
71. J. K. Krueer, R. C. Padre, and J. T. Stull, *J. Biol. Chem.* **270**, 16848 (1995).
72. D. B. Heidorn, P. A. Seeger, S. E. Rokop, D. K. Blumenthal, A. R. Means, H. Crespi, and J. Trewhella, *Biochemistry* **28**, 6757 (1989).
73. J. K. Kreuger, G. Zhi, J. T. Stull, and J. Trewhella, *Biochemistry* **37**, 13997 (1998).
74. L. Ionescu, C. Picot, R. Duplessix, M. Duval, H. Benoit, J. P. Lingelser, and Y. Gallot, *J. Polym. Sci.: Polym. Phys. Ed.* **19**, 1033 (1981).

MARK D. DADMUN
University of Tennessee

NOMENCLATURE. See Volume 7.

NONLINEAR OPTICAL PROPERTIES

Introduction

This article introduces the field of nonlinear optics and the electronic nonlinear optical (NLO) response of polymers and polymer composites. Both second- and third-order NLO phenomena are included, with primary emphasis on harmonic generation, the intensity-dependent refractive index, and nonlinear (multiphoton) absorption effects. The beginning sections introduce the phenomena and explain how the order of the nonlinearity can be understood from a series expansion of the polarization in powers of the electric-field. In addition to listing the variety of nonlinear optical phenomena and some applications, some of the advantages of polymeric materials for NLO applications are also surveyed.

Structure-property relationships that are important to the NLO response are explored in later sections. The approach taken in this article is to work backwards from the bulk effects, described first, to their origin at the molecular level. Thus, Section 5 describes the connection between the constituent molecular NLO hyperpolarizabilities and the macroscopic NLO response. Topics include local field effects, orientation of molecules and polymers, methods of incorporating NLO chromophores into polymers, and limitations on the application of simple summative models. Particular molecular properties that determine the microscopic NLO response are discussed and a few distinct models and parameters useful for optimizing second-order and third-order material properties are provided. The emphasis is on understanding the influence of π-electrons and electron delocalization, as well as on the nature and scaling of polymer repeat units for third-order materials. Also briefly reviewed are several categories of polymer structures that have been studied, and their advantages and disadvantages for NLO applications. Finally, major test methods for measuring the NLO properties of materials are surveyed.

The research literature on nonlinear optics and NLO polymers is vast, whereas this article is, of necessity, intended to serve primarily as a starting point for further investigation. Major topics of related NLO research are left to other articles in this Encyclopedia and to the reading list and bibliography. The reading list at the end of this article recommends books, proceedings, and special journal issues devoted to nonlinear optics and the NLO properties of molecular organic materials and polymers. (See, especially, References 1–7). The article is also focused primarily on all-optical nonlinearities. See article ELECTROOPTICAL APPLICATIONS for a discussion of the changes in the optical response of polymers due to an applied AC or DC electric-field from the so-called Pockels or Kerr effects. Nonlinearities arising primarily from vibrational or rotational/orientational motion (8) are not considered here. Also omitted are the unique NLO properties of many specialized classes of polymers, such as liquid crystalline polymers (see LIQUID CRYSTALLINE POLYMERS, MAIN-CHAIN), organometallic polymers (see METAL-CONTAINING POLYMERS), chiral and biological polymers, and magneto-optical polymers. Similarly, promising studies of polymer-based nanoscale structures, the optical properties of conducting polymers (9) and their application to the development of electroluminescent polymers for organic light-emitting diodes (LEDs) and lasers are outside the scope of this article (see LIGHT-EMITTING DIODES).

Encyclopedia of Polymer Science and Technology. Copyright John Wiley & Sons, Inc. All rights reserved.

Overview of Nonlinear Susceptibilities

Linear and Nonlinear Optics Compared. A simple comparison with the characteristics of linear optics illustrates some of the unique phenomena associated with nonlinear optics. Light bends (refracts) at an optical interface between two media because of the change in speed of propagation of light, as described by each media's refractive index. In linear optics, the refractive index n of the material does not change with the intensity of the light at ordinary light levels. (Otherwise one would need different power eyeglasses for low levels of light and for bright sunshine.) Also, the light transmitted by a linear transparent material does not change frequency upon passing through it. An incident red light emerges red. For both linear and nonlinear optics, media are dispersive, so that the index of refraction changes with the frequency of the light, and a medium may absorb visible light at some frequencies, giving the material a distinctive color. If the optical properties are linear, however, both the dispersion and the relative fraction of power absorbed are independent of the intensity of the light.

If the incident light is sufficiently intense, as in a laser, these simple linear relationships are no longer sufficient to describe the optical response of so-called nonlinear media (or any media, for that matter, if the measurement is precise enough or the intensity is high enough and the material is not destroyed in the process). When the optical properties of the material become nonlinear, the refractive index may change with the intensity of the incident light, thereby changing the optical path length and the focusing properties of an optical element made from that material. In addition, the presence of one beam may amplify another or change its polarization when the beams overlap in the medium, as in an optical switch. Also, the material's absorption (the imaginary part of the index of refraction) may vary with incident intensity. For example, in an optical limiter, the material may appear to be transparent to low levels of light, but a sufficiently intense beam will trigger significant absorption. Conversely, the absorption of a so-called saturable absorber decreases as the intensity of the light increases. Finally, the frequency response of the medium may also be altered when nonlinear effects become apparent. For example, an intense infrared laser may produce a significant visible frequency component upon passing through a material, through harmonic generation, or through another frequency conversion process.

Anharmonic Oscillator Model. At the microscopic level, materials respond to light (or more specifically to the oscillations of the electric-field of the light) through the back-and-forth movement of charges. As an example of how the nonlinear displacement of the charge affects the detected response, it is helpful to view the effects of the oscillating optical electric-field on a material using an anharmonic oscillator model (10). Ignoring the vector nature of the field for the present, the force on the electron in an electric-field E is simply $F_e = eE$, where e is the electron charge. For linear media, the restoring force on the electrons in the presence of the optical field is directly proportional to the electron displacement x from equilibrium, just like the restoring force for a simple spring, $F_{\text{restore}} = -kx = -m\omega_0{}^2x$, where k is the spring constant, ω_0 the resonant frequency, and m the mass. The resulting equation of motion for the electron, ignoring damping of the oscillations, is then simply $eE - m\omega_0^2 x = m\frac{d^2x}{dt^2}$. The solution to this equation in

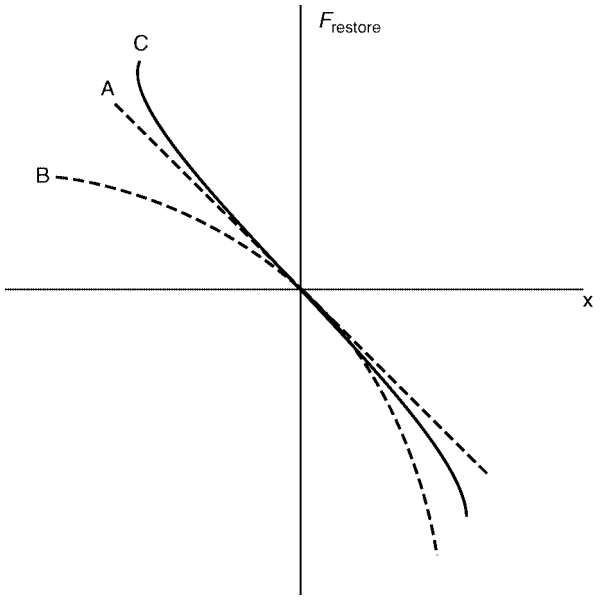

Fig. 1. Examples of restoring forces $F_{restore}$ as functions of x for (A) a linear restoring force, (B) a restoring force with a quadratic nonlinear term, and (C) a restoring force with a cubic nonlinear term.

the case of a monochromatic optical field oscillating at ω ($E = E_0 \cos\omega t$) is

$$x = -\frac{e}{m}\frac{E}{\left(\omega_0^2 - \omega^2\right)} \tag{1}$$

As the pull of the applied field becomes stronger, however, the electron's spring-like response becomes distorted. The restoring force must include additional, nonlinear terms proportional to the square of the displacement for second-order processes ($F_{restore} = -kx - ax^2$) or the cube of the displacement for third-order processes ($F_{restore} = -kx - bx^3$). (Coefficients a and b may be positive or negative. Figure 1 shows examples of quadratic and cubic nonlinear restoring forces for positive coefficients.) The solution to the equation of motion in the case of an anharmonic restoring force is not possible in closed form, but the solution can be expressed as a series expansion, $x = x_1 + x_2 + x_3 + \cdots$, where x_1 is the solution without any anharmonic term in the restoring force (given by equation 1). Given a single monochromatic incident optical field as a driving force for the oscillator, again expressed as $E = E_0 \cos \omega t$, the simplest nonlinear contributions turn out to be proportional to the square $x_2 \sim {E_0}^2 \cos^2\omega t$ and the cube $x_3 \sim {E_0}^3 \cos^3\omega t$ of the incident field (11). Application of simple trigonometric identities to the expressions for x_2 and x_3 reveals typical resulting phenomena. Using the identity $\cos^2 \omega t = \frac{1}{2} + \frac{1}{2} \cos 2\omega t$, the $\cos^2\omega t$ term may be expressed as a combination of a second-harmonic response ($2\omega = \omega + \omega$) and a constant DC field response called optical rectification ($0 = \omega - \omega$). The expansion $\cos^3\omega t = \frac{3}{4} \cos\omega t + \frac{1}{4} \cos 3\omega t$ similarly leads to a third harmonic response ($3\omega = \omega + \omega + \omega$) and a response at the incident

frequency ($\omega = \omega + \omega - \omega$). The latter is responsible for the intensity-dependent refractive index change in the material (12).

Nonlinear Susceptibilities. Nonlinear optical effects are formally understood through the series expansion of the ith component of the polarization (average dipole moment per unit volume) $\boldsymbol{P}$ of a material in powers of the electric-field in the medium $\boldsymbol{E}$ (typically on the order of 10^6 V/m or greater for nonlinear effects to appear), as in (13)

$$P_i^{\omega} = P_i + \varepsilon_0\left[\chi_{ij}^{(1)}(-\omega;\omega)E_j^{\omega} + \chi_{ijk}^{(2)}(-\omega;\omega_1,\omega_2)E_j^{\omega_1}E_k^{\omega_2} + \chi_{ijkl}^{(3)}(-\omega;\omega_1,\omega_2,\omega_3)E_j^{\omega_1}E_k^{\omega_2}E_l^{\omega_3} + \cdots\right] \tag{2}$$

where summation over repeated coordinate indices (i, j, k) is assumed, ε_0 is the permittivity of free space, and the frequency dependence will vary with the NLO process under investigation. [Equation 2 expresses the components of the polarization in the frequency domain, which is the customary approach appropriate for monochromatic or nearly monochromatic fields. In some cases, such as recent research using ultrashort pulses, an analogous and more general time-domain expansion may be preferable (14).] The resultant response frequency ω is a combination (sum and/or difference) of the incident frequencies ω_n. The negative sign is included as a reminder that photon energy (and momentum) is conserved in these parametric processes. Thus, the sum of the frequencies given within each of the parentheses equals zero. The first term on the right, P_i, represents the permanent dipole moment per unit volume in the material. The second term provides the linear contribution to the refractive index (and, if $\chi^{(1)}$ is complex, the absorption coefficient) through the usual second-rank tensor for the linear susceptibility $\chi^{(1)}$. (Recall, in the case of linear homogeneous, isotropic, transparent media, the index of refraction is related to $\chi^{(1)}$ by $n = \sqrt{1+\chi^{(1)}}$.) The remaining terms are responsible for the NLO properties of the material, primarily through the second- and third-order susceptibility tensors, $\chi^{(2)}$ and $\chi^{(3)}$. Although including an arbitrarily large number of terms in the expansion of the polarization in equation 2 is possible, categorizing nonlinear phenomena as either second-order or third-order, using just the terms explicitly shown in equation 2, is practically sufficient. Higher order terms are usually of greatly diminished strength (15).

Centrosymmetric vs Noncentrosymmetric Bulk Media. The distinction between second- and third-order nonlinearities is particularly important for the design of NLO materials for different applications. The terms with even powers in the series expansion of the polarization (eq. 2) are identically zero for centrosymmetric materials. Only noncentrosymmetric materials can exhibit second-order ($\chi^{(2)}$) NLO properties, such as second harmonic generation. [All materials, however, are noncentrosymmetric at their surfaces, and researchers have used surface techniques, such as surface second-harmonic generation, to study centrosymmetric materials (16). For recent reviews, see Reference 17.] The presence of second-order effects depends on the asymmetry both of the individual molecules and on the arrangement of those molecules. The requisite asymmetry is not found naturally in bulk amorphous polymers. The amorphous nature of most polymers requires special preparation to produce the requisite asymmetry, such as

electric-field poling (18), a liquid crystalline phase (19), self-assembly (20), or film formation techniques, as in a Langmuir–Blodgett film (21,22). Most of these techniques are used to align dipolar donor–acceptor groups that are either dissolved in a guest–host system or attached to a polymer to produce macroscopic asymmetry, as discussed in Section 5.4 on incorporating chromophores into polymers. These film preparation techniques and the material properties based on them are beyond the scope of this article, but the references above provide starting points for further investigation (see also LANGMUIR-BLODGETT FILMS; LIQUID CRYSTALLINE POLYMERS, MAIN-CHAIN). Polymer orientation is also discussed at length in the article Electrooptical Applications (qv) because the second-order susceptibility is critical to linear electrooptic devices.

Nonlinear Susceptibility Tensor Elements. In general, the nonlinear susceptibilities, $\chi^{(2)}$ and $\chi^{(3)}$, are complex third- and fourth- rank tensors and, therefore, are comprised of 3^3 and 3^4 different complex numbers, respectively. Fortunately, various symmetries significantly restrict the number of independent tensor elements. Kleinman showed that in certain circumstances, the susceptibility tensor elements are identical for rearrangements of the tensor indices (23). For second-harmonic generation in lossless media, for example, Kleinman's symmetry reduces the number of elements of $\chi^{(2)}$ to 10. In this case, an abbreviated notation has been introduced, $d_{il} = \frac{1}{2}\chi^{(2)}_{ijk,}$, where l represents the six permuted combinations of the jk indices ($l = 1, 2, 3, 4, 5$, and 6, corresponding to the respective index combinations $11, 22, 33, 23 = 32, 13 = 31$, and $12 = 21$), and the ijk indices can be freely permuted (10). Thus, for example, $2d_{13} = \chi^{(2)}_{133} = \chi^{(2)}_{313} = \chi^{(2)}_{331} = 2d_{35}$ and $2d_{33} = \chi^{(2)}_{333}$. For cylindrically symmetric materials (a poled polymer, for example) only two tensor elements are important: the element d_{33}, which describes interactions parallel to the dipolar axis, and the element d_{31}, which describes interactions perpendicular to the dipolar axis (24).

For centrosymmetric materials, such as amorphous polymers, the lowest order nonzero nonlinear susceptibility is $\chi^{(3)}$. For an isotropic polymer, the number of independent $\chi^{(3)}_{ijkl}$ elements is only three, generally, because no direction can be preferred over any other and each direction must appear at least twice (leading to $\chi^{(3)}_{1111} = \chi^{(3)}_{1122} + \chi^{(3)}_{1212} + \chi^{(3)}_{1221}$) [It should be noted that an isotropic solution of chiral molecules will exhibit second-order nonlinearities, but not second-harmonic generation (25)]. For third-harmonic generation, the susceptibility elements simplify to only one ($\chi^{(3)}_{1122} = \chi^{(3)}_{1212} = \chi^{(3)}_{1221}$), and for the nonlinear refractive index, the number of elements needed is only two ($\chi^{(3)}_{1122} = \chi^{(3)}_{1212}$). Furthermore, the nature of the physical mechanism leading to the nonlinear refractive index can sometimes be determined from the ratio of the elements. For example, the relation $\chi^{(3)}_{1122} = \chi^{(3)}_{1221}$ applies if the refractive index change is only due to the nonresonant electronic response of the charges, but $\chi^{(3)}_{1221} = 6\chi^{(3)}_{1122}$ applies if the refractive index change is due to molecular reorientation (26). Fortunately, in many cases it is not necessary to specify individual tensor elements. Unless otherwise stated, the effective nonlinear susceptibility appropriate for the geometry of the material and configuration of the experiment should be assumed.

Problems With Conventions, Reference Standards, and Units. The expression for the relationship between the response and the input fields given by equation 2 is not the only expression commonly used in the literature. Variations

include expanding the polarization in a Taylor series instead of a power series (27), and defining the relationship between the field and the polarization differently (28). Differences between conventions often make it difficult to compare bulk nonlinear susceptibilities and the related molecular susceptibilities (or hyperpolarizabilities) obtained by different experimental methods and by different researchers (29). A more complete theoretical discussion of the problem of comparing conventions as well as the inconsistent use of reference standards for NLO process can be found in Reference 28. For purposes of this article, trends in structure-property relationships will be emphasized, rather than precise values of the NLO coefficients measured. Nonetheless, typical SI values for $\chi^{(2)}$ are $10^{-12} - 10^{-9}$ m/V and for $\chi^{(3)}$ are $10^{-22} - 10^{-18}$ m^2/V^2. Dramatic variations in these values are possible, particularly near a resonance where thermal effects and saturated absorption also contribute to the NLO response. Slower, nonelectronic effects, such as reorientation and electrostriction, also can increase the effective nonlinear susceptibility by orders of magnitude (30). The permittivity factor ε_0 in equation 2 is appropriate for SI units. Most researchers publish results in electrostatic units (esu), however, sometimes without even specifying the fundamental dimensions to which these units refer. Conversion to SI is a straightforward, though not always obvious process. For example, a typical polymer $\chi^{(3)}$ value of 10^{-12} esu $= 10^{-12}$ cm^2/statvolt^2 converts to $4\pi/9 \times 10^{-20}$ m^2/V^2 in SI units, whereas a typical poled polymer $\chi^{(2)}$ value of 10^{-8} esu $= 10^{-8}$ cm/statvolt becomes $4\pi/3$ pm/V in SI. A detailed discussion of the unit conversion process can be found in Reference 31, with the caveat that different conversions are required between SI and esu depending upon the choice of convention for the series expansion of the polarization (28). For example, many authors choose to omit the factor of 4π in the conversion (32).

Nonlinear Phenomena

This section surveys the most widely studied phenomena included among NLO effects that arise due to the electronic contributions to the real and imaginary parts of $\chi^{(2)}$ and $\chi^{(3)}$. This review will be primarily concerned with phenomena related to harmonic generation, the intensity-dependent refractive index, and multiphoton absorption.

Parametric Processes. Parametric processes are those in which photon energy is conserved while the light propagates through the medium. Parametric phenomena of particular interest for devices due to the real part of the nonlinear susceptibility tensors include

(1) second-harmonic generation (SHG) given by

$$P_i^{2\omega} = \frac{1}{2}\varepsilon_0 \chi_{ijk}^{(2)}(-2\omega; \omega, \omega) E_j^{\omega} E_k^{\omega} \tag{3}$$

(2) third-harmonic generation (THG) given by

$$P_i^{3\omega} = \frac{1}{4}\varepsilon_0 \chi_{ijkl}^{(3)}(-3\omega;\, \omega,\, \omega,\, \omega) E_j^{\omega} E_k^{\omega} E_l^{\omega}, \tag{4}$$

(3) degenerate four-wave mixing, (DFWM or the all-optical Kerr effect, OKE) given by

$$P_i^{\omega} = \frac{3}{4}\varepsilon_0 \chi_{ijkl}^{(3)}(-\omega;\, \omega,\, \omega,\, -\omega) E_j^{\omega} E_k^{\omega} E_l^{-\omega} \tag{5}$$

In each case above, the fractional prefactor accounts for the indistinguishability (degeneracy) of the frequencies of the incident fields so that different expressions yield the same susceptibilities in the zero-frequency limit. This convention is common, but not universally adopted (33).

Harmonic Generation. Nonlinear frequency conversion, especially harmonic generation, is important for the development of sources of coherent light at frequencies not otherwise accessible by efficient lasers, in particular the blue, violet, and UV frequencies needed for dense data storage. Harmonic generation is also useful for nonlinear spectroscopic studies, which probe excited states in materials (34).

For harmonic conversion, the conversion efficiency (the ratio of harmonic to fundamental power, η) is largely determined by the size of the effective nonlinearity, the input power P_ω, the interaction length l, and the ability to phase-match the spatial frequencies of the second harmonic and the fundamental light (35). For purposes of illustration, in the limit where only a small fraction of the power is converted and the index of refraction, n_ω, in the material is assumed to be real (lossless) and isotropic, the conversion efficiency can be expressed as (36)

$$\eta = \frac{128\pi^5 \left(\chi_{\text{eff}}^{(2)}\right)^2 l^2 P_\omega}{n_{2\omega} n_\omega^2 \lambda^2 c} \left(\frac{\sin\Delta\varphi/2}{\Delta\varphi/2}\right)^2 \tag{6}$$

Here, $\Delta\varphi = \pi l/\lambda\,(n_{2\omega} - n_\omega)$ is the phase shift between the propagating fundamental and the generated harmonic light, λ is the wavelength in free space, and c is the speed of light. If $\Delta\varphi = 0$, then the factor $(\sin(\Delta\varphi/2)/\Delta\varphi/2)$ in equation 6 takes on its maximum value 1. If the indices of refraction at the second harmonic ($n_{2\omega}$) and the fundamental (n_ω) are not equal, however, the resulting efficiency oscillates with rapidly diminishing peaks as the interaction length increases. The process of minimizing $\Delta\phi$ by making the *effective* refractive indices the same for the fundamental and harmonic light is called *phase-matching*. Techniques for phase-matching are discussed in later in connection with the discussion of using harmonic generation as a technique for characterizing the NLO properties of a polymeric material and for device applications. Poled polymers, have been studied extensively for use in second harmonic generation and other frequency conversion devices.

Degenerate Four-Wave Mixing. DFWM involves input and output light all at the same frequency. When applied to a single input beam, this effect is responsible for applications such as self-focusing and defocusing due to differences

in intensity across the beam profile. When two distinct input beams overlap in a sample, another effect of DFWM may be the transfer of energy between the beams, which is useful for many applications such as single-frequency, all-optical switching (37).

DFWM is best understood in terms of an intensity-dependent refractive index. The two lowest order terms in the refractive index expansion for isotropic media may be written simply as

$$n = n_0 + n_2 I \tag{7}$$

where I is the incident intensity, n_0 is the usual linear index (as seen for lower light levels), and

$$n_2 = \frac{3}{4\varepsilon_0 c n_0^2} \mathrm{Re}\left[\chi^{(3)}\right] \tag{8}$$

The key parameter in optical switching is the intensity-dependent phase-shift (as might appear between the arms of a Mach–Zehnder interferometer (38) or in a directional coupler (39), for example) given by

$$\Delta\varphi(\lambda, L) = \frac{2\pi L n_2 I}{\lambda} \tag{9}$$

where L is the interaction length, and n_2 also depends upon the wavelength λ (40). Phase shifts of π or greater are required for most devices, though some applications require only a shift of $\pi/2$ (41).

Sum and Difference Frequencies; Nondegenerate Four-Wave Mixing. In addition to the phenomena described above, interesting NLO phenomena may also result from a combination of monochromatic fields of different frequencies, as in sum ($\omega = \omega_1 + \omega_2$) and difference ($\omega = \omega_1 - \omega_2$) frequency generation in second-order processes, or nondegenerate four-wave mixing, a third-order process in which the detected frequency may be any combination of the input frequencies (for example, $\omega = 2\omega_1 - \omega_2$ or $\omega = \omega_1 + 2\omega_2$). These phenomena have historically been of less importance for polymer device applications, though commercial applications for optical parametric generation using inorganic crystals, such as β-barium borate are well developed. Finally, third-order, nondegenerate, four-wave mixing may also involve the use of light of one frequency to cause a change in the refractive index of the medium that is experienced by a second beam at a different frequency ($\omega = \omega_1 - \omega_1 + \omega_2$) (42,43).

Resonant Nonlinear Phenomena. The susceptibility tensors $\chi^{(2)}$ and $\chi^{(3)}$ may be complex, indicating the presence of multiphoton resonances and nonlinear absorption effects. The effects of nonlinear absorption are of significant interest in polymer device applications and are typically expressed in a power series in the incident intensity with the transmitted intensity I_1 given by (44)

$$\frac{\mathrm{d}I_1}{\mathrm{d}z} = -\alpha^{(1)} I_1 - \alpha^{(2)} I_1 I_2 - \alpha^{(3)} I_1 I_2 I_3 - \cdots \tag{10}$$

where the light propagates in the z-direction and the different subscripts 1, 2, 3 allow for light of different wavelengths to impact the transmission at wavelength 1. The two-photon absorption coefficient $\alpha^{(2)}$ is related to the imaginary part of the complex third-order susceptibility for an isotropic medium by

$$\alpha^{(2)} = \frac{3\omega}{2\varepsilon_0 c^2 n_0^2} \operatorname{Im}\left[\chi^{(3)}\right] \tag{11}$$

One figure of merit for all-optical switching is the relative two-photon absorption that accompanies an intensity-dependent change in refractive index. The quantity $2\alpha^{(2)}\lambda/n_2$ must be less than unity for switching to be possible (45).

In some resonant phenomena, such as saturated absorption, the use of a power series as shown in equation 10 may be inappropriate because of the contributions from higher order processes. For a dye in a solid polymer matrix, the intensity-dependent absorption coefficient, based on inhomogeneous broadening of the absorption, is often expressed in terms of the saturation intensity I_s at which the population of excited states in the dye from decay processes matches the decay rate from the excited states (46):

$$\alpha(I) = \frac{\alpha^{(1)}}{(I + I_s)^{\frac{1}{2}}} \tag{12}$$

Multiphoton absorption is already widely used for spectroscopic analysis. As discussed later in this article, linear absorption spectra of centrosymmetric molecules only give transitions between states of opposite parity. Two-photon absorption is capable of providing information about transitions between states of the same parity, or so-called two-photon states. In addition, even in noncentrosymmetric materials, two-photon absorption can probe the bulk properties of the medium at frequencies near the linear absorption band where a linear probe may be absorbed at the material surface (44). Two-photon absorption promises to be useful for ultrafast optical limiters, which protect against damage due to high power laser pulses. Polymers containing metal centers or carbon-60 (fullerene) have been especially interesting for this application (47–49). Multiphoton absorption effects are also being investigated currently for their application to laser mode locking, optical pulse shaping, and other beam processing applications (50).

Other Effects.

Combination with Static Fields. A common technique, useful for optoelectronic devices, is to combine a monochromatic optical field with a DC or quasi-static field. This combination can lead to refractive index and absorption changes (linear or quadratic electrooptic effects and electroabsorption), or to electric-field induced second-harmonic generation (EFISH or DC-SHG, $2\omega = \omega + \omega + 0$) in a quasi-third-order process. In EFISH, the DC field orients the molecular dipole moments to enable or enhance the second-harmonic response of the material to the applied laser frequency. The combination of a DC field component with a single optical field is referred to as the linear electrooptic (Pockels) effect ($\omega = \omega + 0$), or the quadratic electrooptic (Kerr) effect ($\omega = \omega + 0 + 0$). These electrooptic effects are discussed extensively in the article Electrooptical Applications (qv). EFISH is

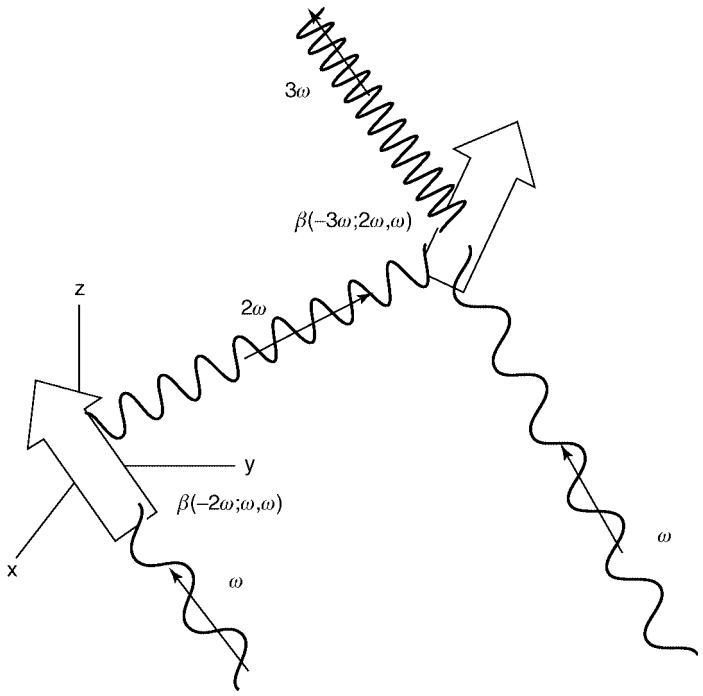

Fig. 2. Schematic showing a cascaded optical nonlinearity in which the second harmonic generated at one molecule combines with the fundamental by sum frequency generation at a nearby molecule to result in a third harmonic generated through a cascade of second-order processes.

discussed in this article, however, for the important role that it has played in the characterization of nonlinear optical materials for other applications.

Cascading. In most cases, the distinction between second- and third-order nonlinearities is evident from the different phenomena each produce. That distinction blurs, however, when one considers the cascading of second-order effects to produce third-order nonlinear phenomena (51). In a cascaded process, the nonlinear optical field generated as a second-order response at one place combines anew with the incident field in a subsequent second-order process. Figure 2 shows a schematic of this effect at the molecular level where second-order effects in noncentrosymmetric molecules combine to yield a third-order response that may be difficult to separate from a pure third-order process. This form of cascading is complicated by the near-field relationships that appear in the interaction between molecules, but analysis of cascaded phenomena is of interest, because it provides a way to explore local fields and the correlations between orientations of dipoles in a centrosymmetric material (52).

Another form of cascading takes advantage of nonlocal, phase-matched cascading of successive $\chi^{(2)}$ processes to produce third-order nonlinear phase shifts (53). These cascading effects have been investigated for their ability to lead to large intensity-dependent refractive indices in poled waveguide materials (54). For example, two successive second-order effects, such as second-harmonic generation, followed by down conversion ($\omega = 2\omega - \omega$), or optical rectification, followed by the

linear electrooptic effect, lead to an intensity-dependent refractive index based on successive $\chi^{(2)}$:$\chi^{(2)}$ interactions (55). The interested reader is referred to the references for a more complete discussion of the enhancements that have been achieved through cascaded nonlinearities.

Nonlinear Light Scattering. Other forms of frequency conversion processes and nonlinear spectral broadening are possible through nonlinear light scattering. When the scattering is due to fluctuations in the molecular susceptibility, the result provides yet another method for investigating NLO properties referred to as hyper-Rayleigh scattering (HRS) (56,57). A brief description of HRS is included later because of its growing use in measuring optical nonlinearities of organic chromophores incorporated into NLO polymers, especially octupolar molecules and conducting solutions, not amenable to investigation through EFISH. Other nonlinear optical scattering processes are generally beyond the scope of this article, but are mentioned here for completeness. Stimulated Raman scattering and coherent anti-Stokes Raman spectroscopy (CARS), for example, involve light scattering from optical phonons and are widely used to convert available laser output frequencies to a variety of infrared, visible or even ultra-violet wavelengths, via so-called Stokes and anti-Stokes shifts (58,59). Stimulated Brillouin scattering involves light scattering from sound waves, a photon/acoustic phonon interaction through electrostriction (60). Rayleigh scattering leads to frequency shifts from inhomogeneities in the material and is called Rayleigh wing-scattering if due to fluctuations in the orientation of anisotropic molecules (61).

Advantages of NLO Polymers

Optical second-harmonic generation (SHG) in an organic material was first reported in 1964 (62). The first measurements of the third-order NLO response of a polymer were performed on polydiacetylene crystalline polymers by Sauteret and co-workers in 1976 (63). Interest in polymeric second-order materials increased dramatically in the early 1980s when Meredith and co-workers performed the first studies on dye-doped glass-forming systems (64) and Singer and co-workers developed the process of electric-field poling to lock in the orientation of the chromophores in a guest–host system (65).

Why Polymers?. Though most current commercial NLO applications use inorganic crystals and semiconductors, polymeric materials have been found to offer many advantages over their inorganic counterparts. These advantages include fast (subpicosecond) response times for nonresonant electronic effects, high optical damage thresholds, large susceptibilities combined with low dielectric constants, ease of processability as thin films or as fibers, ability to be integrated into silicon-based semiconductor structures or onto almost any substrate through spin-coating or other film deposition techniques, and, most importantly, compositional flexibility, which allows their physical and chemical properties to be tailored for specific end use applications through custom-functional design. These advantages, in turn, lead to large figures of merit for device applications. Disadvantages to be overcome, however, include lower thermal stability at high and low temperatures, lower mechanical strength, and, in some cases, higher linear optical absorption and scattering.

Generally, the suitability of a material for device applications requires a balance between optical nonlinearity, thermal and chemical stability, optical losses, and processability. Tradeoffs are to be expected as higher nonlinearities near resonance, for example, lead to increased absorption losses. For third-order materials, the all-optical device applications are especially diverse and promising. These devices include all-optical switches (66), logic gates, optical memories, optical limiters, light modulators, ultrafast shutters, directional couplers (67), nonlinear amplifiers (68), and phase conjugators (69). The application of polymers to waveguide devices is a very important area of applied research, though the details are beyond the scope of this article. Polymer fibers have also been studied for their ability to provide high quality long-length interaction for nonlinear effects with low losses and large bandwidth (70–72). Though no devices have yet been put into mass production (41), the basic figures of merit for switching device applications have been met by several materials and methods, including polydiacetylene waveguides (38) and poly(methyl methacrylate) fibers (73), and through the use of cascaded nonlinearities (74).

Connecting Macroscopic Properties to Microscopic Unit Properties

The foregoing sections described how various NLO phenomena can be understood in terms of the nonlinear susceptibilities. In this section, those susceptibilities are described in terms of the polarizabilities and hyperpolarizabilities, which characterize the separation of charge due to the electric-field at the molecular level. Major factors considered in bridging between the microscopic and the macroscopic properties include (*1*) local field effects, (*2*) orientation effects, (*3*) methods for incorporating NLO chromophores into a polymer to optimize the bulk properties, and (*4*) limits to the optimization of bulk properties through additive effects of the microscopic response.

Relating Macroscopic and Molecular Properties. For many organic/polymeric materials, the bulk polarization is best understood through averaging of the molecular polarizabilities of the weakly-interacting constituent materials. The molecular polarizability is expressed in a series expansion, similar to equation 2 for the polarization, (28)

$$p_I^{\omega} = \mu_I + \alpha_{IJ}(-\omega;\omega)F_J^{\omega} + \beta_{IJK}(-\omega;\omega_1,\omega_2)F_J^{\omega_1}F_K^{\omega_2} + \gamma_{IJKL}(-\omega;\omega_1,\omega_2,\omega_3)F_J^{\omega_1}F_K^{\omega_2}F_L^{\omega_3} + \cdots \tag{13}$$

where $\boldsymbol{F}$ represents the *local* electric-field at the molecule. It is helpful to note the terminology differences between the macroscopic and molecular levels. Upper case subscripts are used to distinguish the molecular coordinate system from the laboratory coordinate system in which the macroscopic properties are measured. μ is the permanent dipole moment of the molecule. α is the linear polarizability tensor (not the absorption coefficient found in equation 10). The $\chi^{(2)}$ and $\chi^{(3)}$ tensors are referred to as *second*- and *third*-order susceptibilities; the corresponding molecular level tensors, β and γ, are called the *first* and *second* hyperpolarizabilities. Values for β and γ are usually given in esu, where a typical chromophore

value for β of 10^{-30} esu $= 10^{-30}$ cm^4/statvolt becomes 4.2×10^{-40} m^4/V in SI units and a value for γ of 10^{-33} esu $= 10^{-33}$ cm^5/statvolt^2 becomes 1.4×10^{-47} m^5/V^2 in SI (28). The reader is warned, however, that different unit conventions, and different conversion factors, are also used (75).

Local Fields. Relating the macroscopic nonlinear susceptibilities to the hyperpolarizabilities requires (*1*) incorporating the effects of the local fields at the molecules, and (*2*) averaging over the arrangement of molecules in the bulk. In general, finding the relationship between the local field in equation 13 and the macroscopic field found in equation 2 is a highly nonlinear and difficult problem (the "local field problem") (49). (Analysis in the case of monomolecular films is simpler because local field corrections are less important and the materials are highly oriented (76)). The local field $\boldsymbol{F}$ acting on the molecule is the vector sum of the applied field and the polarization field. The polarization field is the difference between the field due to nearest neighbor molecules and the collective field of a large number of molecules in a carefully defined volume around the molecule. The local field problem is solved satisfactorily for homogeneous materials by approximating the polarization by the linear term in the series expansion of equation 2 and assuming that the molecule exists in a spherical cavity in a homogenous media (77). This method of analysis, first described by Lorentz, leads to the so-called Lorentz local field factors, $f_\omega = (n_\omega^2 + 2)/3$, where n_ω is the linear index of refraction of the medium at frequency ω. (If static fields are involved, an Onsager local field treatment provides a first approximation to a more detailed treatment. In this case, the relevant local field factor becomes $f_0 = [\varepsilon(n^2 + 3)]/(n^2 + 2\varepsilon)$ where ε represents the relative permittivity (78)). Thus, for homogeneous isotropic media and optical fields only,

$$\chi^{(2)}(-\omega; \omega_1, \omega_2) = N/\varepsilon_0 \times f_\omega f_{\omega_2} f_{\omega_1} \times \langle \beta(-\omega; \omega_1, \omega_2) \rangle \tag{14}$$

$$\chi^{(3)}(-\omega; \omega_1, \omega_2, \omega_3) = N/\varepsilon_0 \times f_\omega f_{\omega_3} f_{\omega_2} f_{\omega_1} \times \langle \gamma(-\omega; \omega_1, \omega_2, \omega_3) \rangle \tag{15}$$

with N being the number density of the molecules and $\langle\ \rangle$ representing orientational averaging, which is discussed in the following section.

The local field effects for *composite* materials require more detailed analysis and can lead to a significant enhancement of the NLO response. For example, a promising method for enhancing the nonlinearity by several orders of magnitude through local field effects is to embed either finely distributed or fractal clusters of metal particles (79) in a polymer matrix.

Orientational Averaging. In general, orientational averaging requires careful consideration of the tensor nature of the hyperpolarizabilities and susceptibilities, and an appropriate choice of distribution functions for the geometries of the molecules involved and their arrangement in the bulk. The orientational averaging of γ (or β) is given formally by the integration of γ (or β), weighted by an appropriate distribution function for the range of orientations, over the appropriate range of angular orientations (79)

$$\langle \gamma \rangle = \frac{\int G(\Omega)\gamma(\Omega)\, \mathrm{d}\Omega}{\int G(\Omega)\, \mathrm{d}\Omega} \tag{16}$$

In the case of an isotropic polymer, the weighting function $G(\Omega)$ is a constant for all orientations. See also Reference 80 for a discussion of theoretical models used to calculate the appropriate order parameters used to perform the orientational averaging for β.

Electric-Field Poling for Second-Order NLO Polymers. As previously discussed, only noncentrosymmetric media have nonzero $\chi^{(2)}$ values. Similarly, the molecular constituents of the media must have nonzero β. Moreover, in amorphous polymers, the bulk is centrosymmetric with $\chi^{(2)} = 0$, even if β is nonzero, due to the random orientation of the molecules. Thus, it is necessary to align the polar constituents in the polymer in order to generate second-harmonic or produce other $\chi^{(2)}$ effects (though second-harmonic generation through hyper-Rayleigh scattering is still possible). Alignment is usually accomplished through electric-field poling, as illustrated in Figure 3. Poling involves heating the polymer, with the NLO chromophore incorporated into it, to a temperature above the temperature at which the polymer becomes rubbery, called the glass-transition temperature, T_g. (See GLASS TRANSITION) At and above T_g, the dipoles can be aligned simply by the

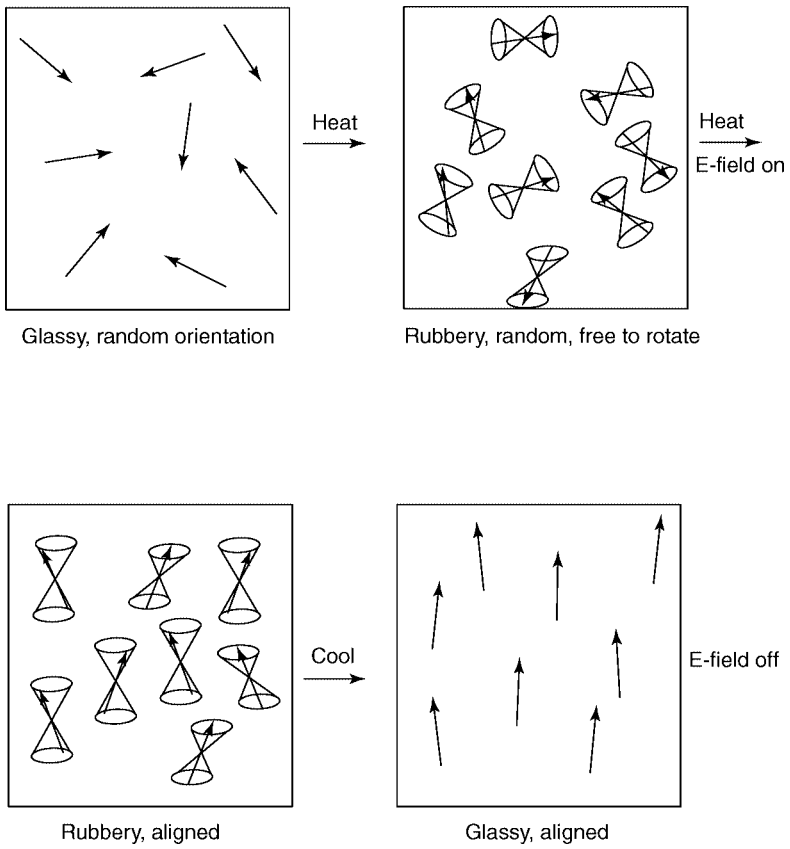

Fig. 3. Illustration of the electric-field poling process where the arrows represent the dipole moment orientation for NLO chromophores dissolved in a polymer matrix. (First appearing in Reference 81. Reprinted with permission.)

application of an external electric (poling) field, typically on the order of 100 MV/m. With the poling field maintained, the polymer is cooled back to room temperature, locking in the polar alignment (at least temporarily). See Reference (78) for a more complete description of the poling process and its implications for orientational averaging and long-term thermal stability. The foregoing section assumes that T_g is lower than the chromophore decomposition temperature. Hybrid pressure poling and all-optical poling methods are also in use. These utilize other optical effects such as photoisomerization to assist the poling process (82).

For an isotropic, poled polymer film of essentially one-dimensional NLO molecules, the orientational average is expressed in terms of the average angle between the ground-state dipole moments of the chromophores and the direction in the film they would be pointing if perfectly aligned (83). For a polymer film in which the nonlinear component or moiety is rotationally symmetric about the film normal (z-axis), the only two nonzero susceptibility components can be determined from the angle (θ) between the film normal and the molecular Z-axis, (84)

$$\chi^{(2)}_{zzz} = N\beta^*_{ZZZ}\langle\cos^3\theta\rangle \qquad \chi^{(2)}_{xxz} = \frac{1}{2}N\beta^*_{XXZ}\langle\cos\theta\,\sin^2\theta\rangle \tag{17}$$

where * indicates that appropriate local field corrections are already incorporated into the hyperpolarizabilities. For poled polymer materials, the orientational averages shown in equation 17 are determined thermodynamically by the coupling between the poling field E_p and the nonzero molecular dipole moment μ. (The ground state dipole moment can be determined from measurements of the permittivity and refractive index as a function of concentration (85)). The only two tensor components of χ^2 can then be expressed simply as

$$\chi^{(2)}_{zzz} = N\beta^*\frac{\mu^* E_p}{5\varepsilon_0 kT} \qquad \chi^{(2)}_{xxz} = N\beta^*\frac{\mu^* E_p}{15\varepsilon_0 kT} \tag{18}$$

where kT is the Boltzman energy. When poling is needed to induce polar order, the molecular figure of merit is the $\mu\beta$ product. Nonresonant values of $\mu\beta$ as great as 10×10^{-45} esu have been reported for 3-phenyl-5-isoxazolone, for example (86). In the absence of dipolar interactions, such as assemblies of octupolar multidimensional molecules, a more complicated analysis is required. In these cases, the desired alignment may be a highly ordered octupolar state without dipolar interactions (87). A later section briefly discusses polymeric materials with multidimensional constituents.

Maintaining polar order in a poled polymer is of great importance for second-order applications (88,89). The dielectric relaxation process leading to decay in the orientation of ordered polymers has been studied extensively and is the subject of another article (see DIELECTRIC RELAXATION). Several models that describe the chromophore reorientation for NLO materials have been proposed, including the Kohlrausch–Williams–Watts (KWW) model (90,91), biexponential and triexponential decay models (92), time-dependent Debye relaxation time models (93), and the Liu–Ramkrishna–Lackritz (LRL) model (94). For further information on

these and other issues relating to dielectric relaxation in poled polymers, see also Reference 95.

One more example of the difficulties that can arise in comparing the hyperpolarizabilities and bulk susceptibilities is seen in the case of EFISH. Although EFISH is a macroscopic third-order process, the microscopic–macroscopic transition for EFISH is expressed as

$$\chi^{(3)}_{ijkl}(-2\omega;\omega,\omega,0) = N[\langle\gamma^{*}_{\mathrm{IJKL}}(-2\omega;\omega,\omega,0)\rangle_{ijkl} + \langle\mu^{*}_{I}(-0;0)\beta^{*}_{JKL}(-2\omega;\omega,\omega)\rangle_{ijkl}] \quad (19)$$

The second term on the right side of equation 19 ultimately determines the usefulness of the molecule when incorporated into a polymer for second-order applications (96). A DC field aligns the dipole moment μ so that the first hyperpolarizability, β, can contribute to the bulk response. A similar expression is applied to poled polymers (24). The assumption that γ is negligible compared to β is usually valid for nonlinear chromophores, but not for extended π-electron donor–acceptor systems because γ increases with conjugation length faster than β (97).

Orientational Effects in Third-Order Polymers. Bulk asymmetry is not required for a third-order NLO response, but orientation of polymer chains remains an important factor even if $\beta = 0$. For one-dimensional, π-electron conjugated polymers, the largest contribution to the NLO response occurs for light polarized parallel to the direction of the conjugated chain. Therefore, alignment of polymer chains, which restricts electron delocalization to one-dimension, enhances the magnitude of the NLO response of the polymer. Polymers with high levels of anisotropy exhibit significantly larger NLO response when the applied electric-field is polarized in a direction parallel to the chain orientation. The NLO response of an unoriented film of linear chain molecules has been shown to be one-fifth the NLO response of oriented film when the electric-field is applied parallel to the molecules (98). The implication is that processing polymers on a microscopic level is one method of enhancing the third order response of the polymer. A common method used to align polymer chains is stretch orientation of thin films (99). See also Reference 79 for an example of the application of the orientational averaging process to third-order materials.

Incorporating Chromophores into Polymers. The dominant approach used to enhance the second-order NLO response of organic materials is to incorporate optimized chromophores into a polymer matrix. The method used for incorporating the chromophore varies. The choice of polymer depends upon linear optical and other properties that make the polymer suitable for devices (81).

Guest–Host Polymers. The simplest, but not optimal, approach to incorporating NLO chromophores into a polymer is to dissolve the dye molecules into the polymer in a guest–host solid solution system (see Fig. 4**a**). (Poly (methyl methacrylate) has been one of the most commonly used polymers for this purpose for its ease of processability.) There are several significant drawbacks, however, to using a guest–host system. (*1*) The amount of dye that can be dissolved is usually very limited. (*2*) The glass transition temperature drops with increased doping due to plasticization. (*3*) The chromophore tends to leave the polymer at elevated temperatures. (*4*) Finally, the alignment of the molecular dipoles is less stable, so that a poled guest–host system is unlikely to retain its orientation for long periods

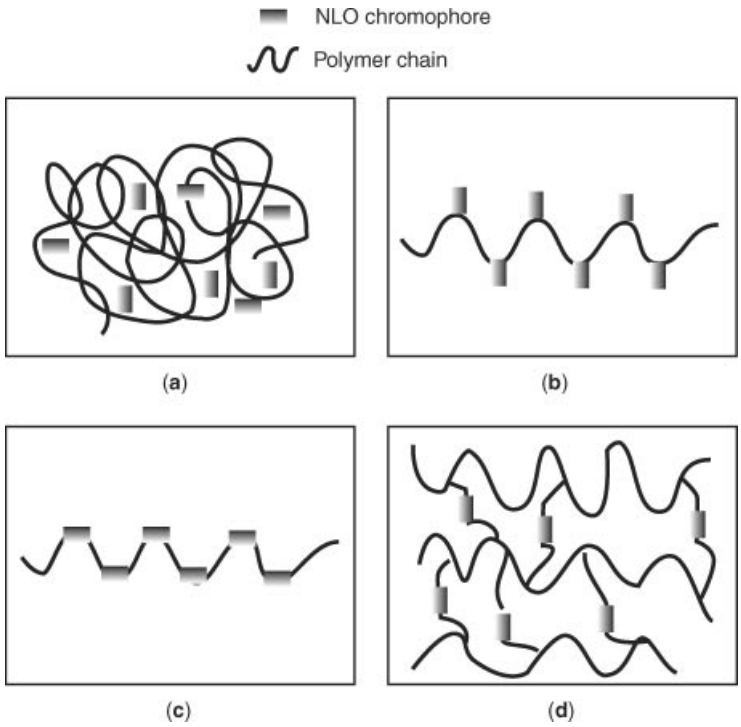

Fig. 4. Schematic of methods for incorporating NLO chromophores into a polymer, including (**a**) guest–host system, (**b**) side-chain functionalized system, (**c**) main-chain functionalized system, and (**d**) cross-linking system.

(24). Methods to overcome these limitations include using high glass-transition temperature polymers, such as polyimides or polyetherketones, doped with relatively miscible chromophores (100,101).

Side-Chain Polymers. Though more challenging to produce than a guest–host system, a side-chain functionalized system in which at least one end of each of the chromophores is attached as a side chain to the polymer backbone, avoids some of the limitations of the guest–host system (see Fig. 4**b**). The resultant polymer retains the nonlinearity of the dopant molecules and permits greater chromophore concentration for a larger NLO response. Still, packing problems may appear if the chromophore concentration becomes too high. Attaching the chromophore as a side chain causes the orientational stability and other thermal properties of the system to depend more on the thermal properties of the polymer. For example, a polyimide with a high T_g is better able to preserve the polar order of the chromophore if the chromophore is incorporated as a side chain, rather than a simple solute (102).

Main-Chain Polymers. Main-chain polymers incorporate the chromophore directly into the chain by linking both ends of the chromophore, in either head-to-tail (isoregic) or head-to-head (syndioregic) configuration or some combination. Though a main chain configuration should add stability, establishing polar order in these polymers is not always obvious. The syndioregic configuration offers the possibility of folding the polymer like an accordion so that the chromophores will align (103) (see Figure 4**c**).

Cross-Linked Polymers. Perhaps the greatest promise for long-term stability in molecular materials comes from cross-linked polymers (see Fig. 4**d**). Cross-linking must be performed during poling, but can be accomplished with guest–host (104), side-chain, or main-chain systems. The cross-linking must be done carefully to avoid the introduction of defects. One promising approach is the use of interpenetrating polymer networks (105).

Limitations to Relating the Polymer Response to Molecular and Oligomeric Properties. In many cases, the NLO response of the polymer can be derived entirely from the response of the molecular NLO chromophore units and their concentration in the polymer as a medium. The assumption that the system is weakly interacting is justified if the nonlinearity is a linear function of molecular concentration (106,107). For large concentrations of molecules in a polymer matrix, the assumption of a weakly interacting system may break down, however, as dimerization or aggregation become important (108).

Oligomers. Similarly, the third-order NLO properties of π-conjugated polymers are often extrapolated from oligomeric structure studies. Effective conjugation length scaling laws and band gap narrowing are examples of properties that have been investigated in terms of the oligomeric unit (109,110). Unfortunately, some aspects of a polymeric system cannot be modeled by smaller molecules, and extending oligomeric structure–property relationships to polymeric materials can be problematic. For instance, saturation effects in electron delocalization become apparent as conjugated chains become very long. Also, it is known that the excited state structure of a polymer may differ from its corresponding oligomer (111), and the effect that substitution may have on a polymer is not reflected by substitution on its related oligomeric or polyeneic structure (112). Many other issues that surround the extension of oligomer structure–property relationships to polymer relationships have been considered and much literature is available on the topic (113). With these caveats in mind, the next section discusses the electronic character of constituent NLO materials for the purpose of understanding the origin of the hyperpolarizabilities.

Structure–Property Relationships: Understanding Constituent NLO Properties

How macroscopic NLO properties of a material are determined from the response of its microscopic constituents was shown in the previous section. The origin of the NLO properties of these constituents is discussed here. A fundamental theoretical problem is to calculate the NLO response directly from the electronic configuration of the molecules. This section explores the molecular parameters that contribute to large hyperpolarizabilities. Particular emphasis is on sum rule calculations and essential states models as guides to obtaining the optimal NLO response.

The discussion necessarily divides into separate consideration of the structure–property relationships for the molecular constituents, which particularly impact the $\chi^{(2)}$ response, and the nature of the supramolecular and polymeric effects, especially relevant to $\chi^{(3)}$ materials. Fundamental factors affecting each are discussed, including symmetry, donor–acceptor groups and

charge transfer, conjugation or π-electron delocalization length, the nature of the π-electron bonding sequence, bond length alternation (or bond order alternation), aromaticity, multidimensionality, and the substitution of alternate atoms into the conjugated structure.

Brief Overview of Quantum Calculations. Most organic and polymeric systems, unlike inorganic systems, owe their nonlinear response to virtual electron excitations occurring in the individual molecular or monomeric units. A complete theoretical understanding of the NLO response requires extensive quantum mechanical calculations, which encompass every structural aspect of the system. These aspects include the positions and electron configuration of each atom, the nature of the bonds between atoms, and the full electronic energy band structure, including all interactions. The linear and nonlinear properties can be deduced from the wavefunction of the system, which is the solution to the Schroedinger equation $H\Psi = E\Psi$, where H is the suitably chosen Hamiltonian operator including interactions among all the charges and E is the energy of the system. The molecular orbital (MO) approach expands the wavefunction in a self-consistent set of basis functions with appropriate configuration interactions (CI), using a linear combination of atomic orbitals (114). The number of CI integrals to be calculated increases as the fourth power or higher of the number of basis functions in the molecule, so that calculations even for small molecules can be time-consuming (115).

At least three different approaches are used to calculate the nonlinear response from quantum chemical considerations (40,116). In so-called "derivative" techniques, the polarizability and hyperpolarizabilities are found by taking derivatives of the dipole moment components with respect to the various electric-field components.

$$\alpha_{ij} = \frac{\partial \mu_i}{\partial E_j}$$
$$\beta_{ijk} = \frac{\partial^2 \mu_i}{\partial E_j \partial E_k} \tag{20}$$
$$\gamma_{ijkl} = \frac{\partial^3 \mu_i}{\partial E_j \partial E_k \partial E}$$

These derivatives are evaluated using so-called coupled Hartree–Fock techniques and either static or oscillating fields (117). A second approach is to model the nonlinear media as a set of coupled anharmonic oscillators, with resonant frequencies corresponding to excited state transition frequencies. The strength of the coupling is a function of the proximity of the external field frequency to the resonant frequency of the oscillator.

A third approach, the one most important for the current discussions, is to treat the electric-field as a source of perturbation of the total molecular energy using real and virtual excited state transitions. This approach uses electronic wave functions either for all of the electrons of the molecule (ab initio calculations) or for only the valence electrons (so-called semiempirical theories). Semiempirical Hamiltonians may ignore electron interactions completely (Huckel theory). They may assume one π-orbital per carbon and assume no overlap between adjacent electron orbitals (Pariser–Parr–Pople or PPP). Or, they may include both the σ and

π electrons and either no overlap (so-called complete neglect of differential overlap or CNDO), or only include overlap between orbitals on the same atom (intermediate neglect of differential overlap or INDO). The goal of each of these techniques is to compute the energy levels, transition moments, and dipole moment differences for essential energy states of a molecule (118). These parameters are used in a sum-over-states perturbation approach to determine the hyperpolarizabilities. See, for example, References (40,119–121). An advantage of the perturbation approach is the explicit appearance of the frequency response and the role that different excited states play in the frequency response.

Sum-Over-Essential States Models for Molecular Materials.

The Two-Level Model for β. For NLO organic chromophores (dyes) used to provide a large second-order nonlinear response, the sum-over-states approach has proven to be a particularly valuable predictor of β and its spectral dispersion. In the sum-over-states approach, hyperpolarizabilities may be calculated in theory by including contributions from virtual and real transitions to and from *all* of the excited states or energy levels of the molecules. In practice, however, only a few states are expected to contribute measurably. The key to using this approach for optimizing β (or γ) is to identify and characterize the contributions of the most important excited states of the molecule in the spectral region of interest. In fact, β is often well understood by truncating the sum to include only the ground state and *one* excited state, a so-called two-level model. The energy difference between these two states is sometimes called the optical gap, and the nature and location of the transition (gap) between the two states is particularly important for its dominant role in the linear absorption spectrum. The two-level model yields a simple formula for β in the case of second-harmonic generation (122):

$$\beta_{\text{two-level}} = \frac{3}{2\hbar^2} \frac{\omega^2 \left|\mu_{01}^2\right| \Delta\mu_{10}}{\left[\omega_{10}^2 - \omega^2\right]\left[\omega_{10}^2 - 4\omega^2\right]} \tag{21}$$

where $\hbar\omega_{10}$ is the energy difference between the ground and excited state, μ_{01} is the transition dipole moment between the two states, "0" (the ground state) and "1" (the excited state), and $\Delta\mu_{10} = \mu_{11} - \mu_{00}$ is the difference between dipole moments of these two states. The transition dipole moment μ_{01} can be determined by numerical integration of the absorption spectra. The ground state dipole moment μ_{00} is determined through concentration-dependent measurements of the relative permittivity and refractive index. The excited state dipole moment μ_{11} is typically found by analysis of spectral shifts in the absorption band due to changes in the local electric-field (electrochromism or solvatochromism) (85).

The two-level model justifies the dominant approach for optimization of the second-order NLO response, which is to couple the largest transition moment with the largest dipole moment difference. This combination of a large transition moment and large dipole moment difference is usually accompanied by a sharp absorption peak. A general rule-of-thumb, which has been adopted by many researchers into second-order molecular materials is summed up by the adage, "Redder is better." In effect, the lower the energy of the dominant absorption peak of the chromophore, the greater is the nonlinear response. (Interestingly, some highly nonlinear organic chromophores such as Foron brilliant blue and squaraine dyes

(123,124) have sharp absorption peaks shifted so far into the visible so as to absorb the red wavelengths, yet transmit higher energy blue wavelengths, prompting the enigmatic description that such chromophores "are so red, they're blue!")

The two-level model has guided researchers in finding optimal chromophores for nonlinear polymers ever since the original work by Oudar and Chemla in the early 1970's (125). More recent theoretical analysis by Kuzyk of sum-rule-restricted off-resonance contributions to the optical nonlinearity shows that a full quantum sum-rule analysis provides a physical limit to the maximum diagonal tensor component, *off resonance*, for *both* β (126), and γ (127). This study indicates that the key to increasing β and γ is to design molecules that have *one* dominant excited state at an energy close to the ground state with as many double (or triple) bonds (delocalized electrons) as possible. Molecules with a single dominant excited state are, therefore, particularly well-suited to a two-level model analysis. Kuzyk has also extended this work to off-diagonal tensor components to show that the maximum off-diagonal components can be no larger than the largest possible diagonal component (128). (The off-diagonal components for a particular molecule, however, may be larger than the available diagonal components for that molecule (25)).

Donor–Acceptor Groups. The difference between the ground state and excited state dipole moments, $\Delta\mu_{01}$, is important in designing optimal second-order NLO chromophores because $\Delta\mu_{01}$ quantifies the ability of the electrons in the molecule to shift preferentially in one direction along the molecule with the application of an oscillating electric-field. To impart such a bias, initial studies used aromatic and long-chain π-electron systems with an electron donating group at one end and an accepting group at the other. A prototypical dye molecule with these features, dimethylaminonitrostilbene (DANS), is shown in Figure 5. Recall that the dipole moment is simply a measure of the separation of a unit charge along the length of the molecule. The effect of substitution of different electron donor and acceptor groups has been the subject of extensive study, and tables of values for different groups can be found in References 129 and 130.

Nature of π-Electron Bonding, Aromaticity, and Bond Length Alternation. A comparison between the ground and excited state structures in Figure 5 introduces another line of inquiry for optimizing β. In the charge-transfer (CT) excited state,

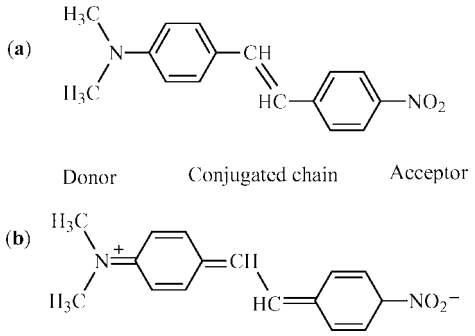

Fig. 5. Typical linear donor–acceptor chromophore (DANS) (**a**) ground state and (**b**) first excited state structures.

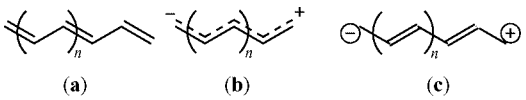

Fig. 6. The nature of π-electron bonding varies between the (**a**) polyene, (**b**) cyanine, and (**c**) zwitterionic limits.

the charge configuration will change from the aromatic structure of Figure 5**a** to the more quinonal (and zwitterionic) structure represented in Figure 5**b**. In this case, the CT state has lost "aromaticity," as can be seen by the loss of conjugation in the rings. Marder and co-workers have studied CT processes and found that a larger effective donor–acceptor strength will often result from a degenerate ground state in which the π-electrons are optimally delocalized along the chain. In this case, the CT state gains aromaticity and the $\Delta\mu_{01}$ factor will be negative, leading to a negative β off-resonance (131).

The relative contributions to the ground-state energy of different electron configurations (as those shown in Figs. 5**a** and 5**b** can be described by the tendency of the ground state to exhibit pronounced bond length alternation (BLA). In general, BLA refers to the difference in the bond lengths between adjacent carbon atoms within the backbone chain of the molecule. (Similarly, bond order alternation refers to the extent of alternating single, double, or triple bonds along the backbone, where single bonds are longest and triple shortest.) The nature of the π-electron bonding can be seen also in Figure 6, which illustrates the difference between polyene, cyanine, and zwitterionic forms for the conjugated chain. The polyene and zwitterionic structures show significant bond length alternation, while the cyanine shows none (131). Tuning between these forms is possible through changing solvent polarity and the strength of the donor and acceptor end groups (118).

Studies by Meyers and co-workers have shown that the NLO response of many strong donor-acceptor molecules suffer from too much bond length alternation (on the order of 0.01 nm), which inhibits charge transfer in the excited state (132). β is zero in the cyanine limit, however, when there is no bond length alternation. Interestingly, β peaks with opposite sign when the BLA is either intermediate between the polyene/cyanine structure or intermediate between a cyanine/zwitterionic structure (BLA $\sim \pm 0.004$ nm) (133). One important result from these studies is that the relative amount of charge separation is a function not only of the end groups involved, but also of the molecular environment due to solvatochromic effects (118). For a more extensive discussion of the balance of factors represented in the two-level model and techniques for optimizing β, see also Reference 134. A discussion of methods for determining the dependence of β on other parameters may also be found in Reference 135.

Conjugation Length. The dominant characteristics for second-order materials are π-electron delocalization and strong acceptor–donor dipolar charge transfer. Thus, the distance and magnitude of the charge transfer of the π-electrons in the excited state determines the magnitude of β. β increases with charge separation (electron delocalization) only if strong coupling through the conjugated bridge unit between the donor and the acceptor ends is preserved. Studies of the conjugation length dependence of β have shown an initial increase as the third

power in that length, at least for the first 12 π-electrons or more (136). However, studies have demonstrated that the donor–acceptor interaction stops increasing after a certain chain length, limiting the electron delocalization, and the result is an observable saturation effect (137,138). Unfortunately, increased conjugation length correlates with increased absorption, leading to reduced linear optical transparency. The significance of conjugation length is also explored further below in connection with third-order materials.

The Two-Level Model for γ and Its Limitations. Generally, essential-states-model calculations have been very successful in explaining and predicting the second-order response of noncentrosymmetric materials, but considerable work remains for understanding third-order materials. As a starting point, consider again the two-level model, which can be expressed for third-harmonic generation as (139)

$$\gamma_{\text{two-level}} = \frac{\mu_{01}^2}{4\hbar^3}\left[\Delta\mu_{10}^2 D_{111} - \mu_{01}^2 D_{11}\right] \tag{22}$$

The dependence on the energy difference between the ground state and excited state and the incident photon energy is given by the denominator "D" factors (omitting resonance damping effects near the excited state transition energies)

$$\begin{aligned} D_{111} = {} & [(\omega_{10} - 3\omega)(\omega_{10} - 2\omega)(\omega_{10} - \omega)]^{-1} + [(\omega_{10} + \omega)(\omega_{10} - 2\omega)(\omega_{10} - \omega)]^{-1} \\ & + [(\omega_{10} + \omega)(\omega_{10} + 2\omega)(\omega_{10} - \omega)]^{-1} + [(\omega_{10} + \omega)(\omega_{10} + 2\omega)(\omega_{10} + 3\omega)]^{-1} \end{aligned}$$

and

$$\begin{aligned} D_{11} = {} & \left[(\omega_{10} - \omega)^2(\omega_{10} - 3\omega)\right]^{-1} + \left[(\omega_{10} + \omega)(\omega_{10} - \omega)^2\right]^{-1} \\ & + \left[(\omega_{10} + \omega)^2(\omega_{10} - \omega)\right]^{-1} + \left[(\omega_{10} + \omega)^2(\omega_{10} + 3\omega)\right]^{-1} \end{aligned} \tag{23}$$

A major difference between $\beta_{\text{two-level}}$ and $\gamma_{\text{two-level}}$ is the presence of two competing terms in equation 22. (Only the second term will contribute, however, with a centrosymmetric material, yielding a negative γ if D_{111} and D_{11} are positive, as they must be below resonance.) Competition between the two terms of the model results for noncentrosymmetric molecules. Fundamental calculations by Kuzyk show that the maximum theoretical result for noncentrosymmetric molecules is positive and four times the value in the centrosymmetric case (127).

Two-Photon Resonant Enhancement. The frequency dependence of the essential states models is also important as indicated by the potential for resonant enhancement in the denominators "D" of the sum-over-states (with appropriate damping effects not indicated in eq. 23). Generally, it is undesirable to operate near a resonance with either the fundamental input frequency ω or the desired harmonic output. When 2ω approaches ω_{10}, however, an important intermediate two-photon resonance is evident from the second D_{111} term. In this case, resonant enhancement appears without undesirable absorption effects. The $(\omega_{10}-2\omega)$ denominator term also appears in expressions for other types of frequency conversion and even the nonlinear refractive index. Intermediate resonant enhancement applies not only to the two-level model. Absorption and/or resonant enhancement

are possible whenever there are real energy levels close to the one, two, or three photon transitions (140).

Bond Length Alternation Revisited. Meyers and co-workers have also theoretically examined simple donor–acceptor polyenes by applying an external, static homogeneous electric-field to tune to different degrees of bond length alternation and mimic the effects of varying solvent polarity. Their studies indicate that for highly bond-length alternated molecules, such as polyenes, the off-resonant γ is positive, but, as the bond alternation is decreased, γ changes sign and peaks negatively in the cyanine limit (133).

Extension to Multilevel Models for Constituent Materials.

Symmetry and Excited States. It should be emphasized that Kuzyk's sum-rule calculations, which highlight the importance of the energy difference between the ground and the first excited states, only provide upper bounds on the values of β and γ. Predicting actual values require more complex relationships. Similarly, the two-level model has been shown to be inadequate even as a starting point for many materials, (139,141) failing to account even for the sign of γ. For example, measurements, as well as full quantum chemical calculations, show that centrosymmetric polyene-like molecular materials show a positive off-resonant nonlinearity. The two-level model predicts only negative γ off-resonance for centrosymmetric systems (142). In contrast, linear cyanines have been modeled theoretically in detail by Pierce, who found that, below resonance, $\gamma < 0$ for all-trans linear centrosymmetric cyanines. His calculations, as well as several experimental studies, however, show that the two-level model is still inadequate for these molecules and higher lying two-photon states must be included (143,144).

To understand the effects of additional states beyond the two-level model in centrosymmetric molecular materials, it is helpful to analyze symmetry conditions that dictate allowable transitions between states. Because the ground state (also called the 1Ag state) is of Ag symmetry, the lowest optically allowed one-photon transition is to the 1Bu state (of opposite symmetry), which is the lowest lying one-photon excited state in the linear absorption spectrum. The 1Bu state is not necessarily the lowest lying excited state, however. One fundamental difference between centrosymmetric polyenes and cyanines is the location of another excited state, the lowest lying two-photon state or 2Ag state. Studies show that the 2Ag state lies energetically below the linear absorption peak (1Bu state) for polyenes, but above the peak for cyanines. Electron correlations that lower the 2Ag state below the 1Bu state create a nonradiative decay pathway for the 1Bu state and can significantly detract from the nonlinear response (145).

Excited-State Enhancements. Several studies also consider further enhancements that may be possible if starting *from* an excited state (146). By optically pumping to increase the population of an excited state, Heflin and co-workers observed a two-order magnitude enhancement (147). The reasons for this increase can be seen again from the terms of the two-level model in equations 21 and 22. By starting from an excited state, one can take advantage of larger optical transition moments μ_{nm}, where n and m are both excited states, and smaller energy differences, $\hbar\omega_{nm}$, between the populated excited state n and the excited state m.

Some Structure–Property Relationships for Third-Order Polymers and Macromolecules. The preferred approach for developing dipolar second-order materials has been to find optimized chromophores and incorporate these

into a polymer with appropriate functionalization. For third-order applications chromophore doping is sometimes used, but is not necessary as the conjugated polymer itself contributes significantly to the NLO response. Third-order materials more often focus on the polymer matrix itself as a system for maximizing extended π-electron conjugation, though researchers have probed third-order phenomena through the use of smaller, simpler monomers and oligomers. Polymers systems are more difficult to probe because of their size and complexity. Optimization parameters include conjugation length (limited by significant saturation effects, and optimizing interaction among the electrons through chain conformation) and the introduction of spacers and donor–acceptor groups, sometimes leading to increased dimensionality of the polymer system.

Conjugation Length and Saturation Effects. The effective conjugation length of a polymer heavily influences the size of the third-order NLO response (148). The free-electron model of Rustagi and Ducuing showed that γ increases exponentially with the number of repeat units in the chain (L) by, $\gamma \sim L^n$, where $n = 5$ for short chains (149). Experimental studies agree (150), in general, with this relationship, though the scaling exponent varies in the range of $n \sim 3$–5.4 (151). The scaling exponent n is dependant upon factors such as the chemical structure of the material and substituent groups. For instance, ($n \sim 2.5$) was reported by Samuel and co-workers for unsubstituted polyacetylene (152), and various substituted polyacetylenes values of n between 2.3 and 4.6 were reported by Neher and co-workers (153). The effect of electron correlations on the scaling has also been investigated, but is beyond the scope of this article. See, for example, Reference 154.

Oligomeric studies have also shown, however, that the NLO response of a conjugated polymer can become quickly saturated as the quantity of repeat units in the chain is increased beyond a certain, critical value. For example, very long chain polyene oligomers showed a saturation of γ at 60 double bonds (155), and poly(triacetylene) oligomers showed saturation of NLO values at 10 repeat units (110). Another study by Yang and co-workers provided evidence that suggested that the exponential scaling factor n in longer conjugated chains actually becomes dependant upon the number of repeat units (L) in the chain (156). This function, $n(L)$, can be used to gain a more detailed understanding of the phenomena that occurs during the transition from a very short chain oligomer to a very long chain oligomer and ultimately a polymer.

Donor–Acceptor Groups, Spacers, and Planar Structure for Third-Order Polymers. A rigid planar structure in a polymeric material increases the third-order nonlinear optical response by maximizing the overlap area of the π-electron orbitals, thereby enhancing electron delocalization (157). Electron donor–acceptor groups are sometimes incorporated in conjugated, third-order polymer systems to enhance electron delocalization. As with second-order NLO chromophores, these "push–pull" groups can be added as end groups, or can be inserted directly into the conjugated backbone structure. A recent study by Gubler and co-workers showed that inserting various spacer groups in the conjugated pathway of a polyene molecule increased γ for the molecule due to increased electron delocalization (158). The relationship between the presence of spacers and the maintenance of a rigid planar structure can be complicated. In the Gubler study, when the polyene to which spacers were added was polymerized, the third-order response of related polymeric materials did not maintain the increased NLO response of the polyenes.

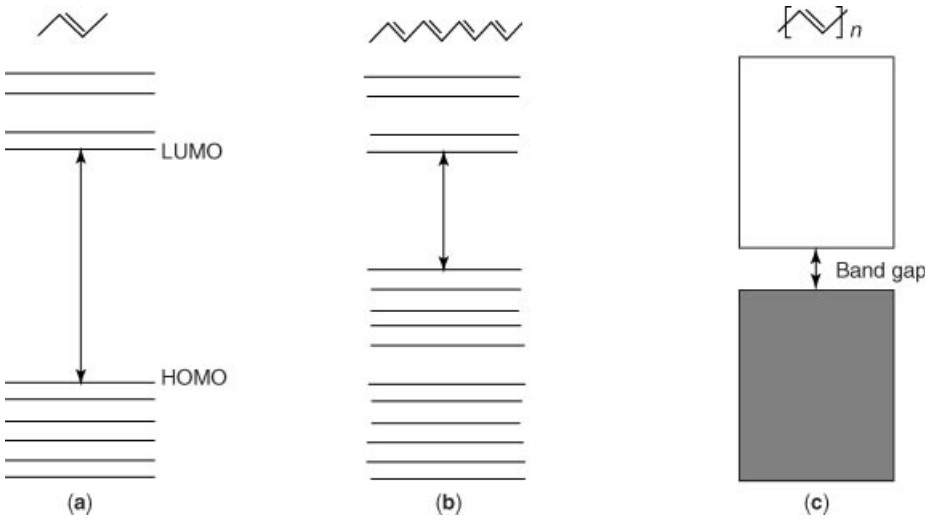

Fig. 7. Electronic effects upon increasing the number of repeat units in a conjugated chain. In a very long chain, discrete energy levels are replaced by valence and conduction bands, and as the conjugation length is increased, the band gap is typically reduced. (**a**) π-conjugated chain with few repeat units, (**b**) π-conjugated chain with increased number of repeat units, and (**c**) π-conjugated polymer chain.

This loss in scaling was attributed to a decrease in electron delocalization due to a loss of planar structure that occurred in the polymer sample as a result of the interchain spacers. Other studies have also indicated that the planarity of the polymer is a dominating factor in deciding the third-order nonlinear response of the polymer (159). Further investigation of the effect of the spacers and the effect of the substitution on third-order materials is needed.

Band Gap. A common model for characterizing the effects of excited states for extended polymer systems is to consider the so-called band gap in the polymer. π-Conjugated polymers are sometimes considered organic semiconductors because the energies of their electrons exist in energy bands rather than discrete energy levels. The transition of the electronic structure (of a growing π-conjugated chain), from energy levels to energy bands, occurs as monomer units are added to a growing chain (see Fig. 7). As units are added, the number of valance and conduction energy bands increases as does the amount of electron delocalization. When the chain is sufficiently long, the energy levels are forced together so closely that energy bands are formed and discrete energy levels no longer exist.

The band gap is considered to be the energy difference that exists between the highest occupied molecular orbital (HOMO) in the ground state and the lowest unoccupied molecular orbital (LUMO) in the excited state. Theoretically, the *band gap* is defined as the amount of energy required for an electron to transition from the ground state to the first dipole-allowed (one-photon) excited state. Experimentally, the band gap of a π-conjugated material is quantified by measuring by the longest wavelength electronic absorption maximum (λ_{max}) (160). In general, reducing the band gap causes an increase in electron delocalization along a conjugated chain and therefore an increase in the third-order NLO response.

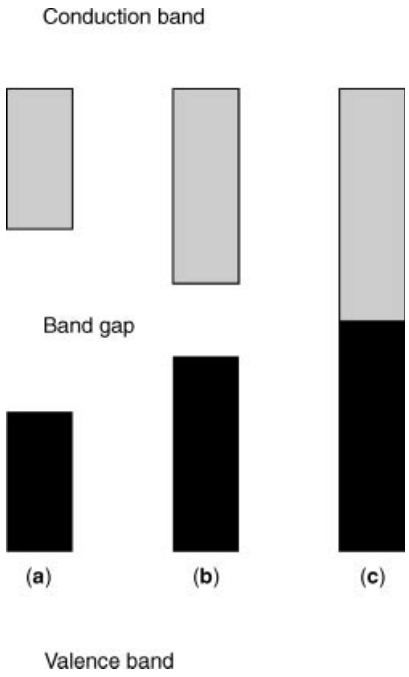

Fig. 8. Band gaps in (**a**) an insulator, where the gap is large and electrons are unable to pass from valence band to conduction band; (**b**) a semiconductor, where electrons with sufficient energy are able to pass from the valence to the conduction band; and (**c**) a conductor, where no band gap exists.

Much research in third-order π-conjugated materials is driven towards reducing the band gap to a semiconductor (161) or even intrinsically conducting status, as illustrated in Figure 8 (162). Two important approaches to minimizing the band gap of π-conjugated materials are minimizing BLA and incorporating donor–acceptor groups (163). Polyacetylene, for instance, would have a zero band gap (and be a intrinsically conducting polymer) if the adjacent carbons atoms along the chain were all equidistant; in other words, if the BLA value were zero. This is not the case, however, due to the alternating single and double bonds along the PA chain. Therefore PA has a finite band gap. Consider a thiophene monomer, which can have either an aromatic or quinoid structure. The structure that is exclusively quinoid has a relatively large band gap because the bonds between the thiophene repeat units are completely double bond in nature. Similarly, the linkages between the aromatic repeat units are fully single bond in character. The ideal strategy in reducing the band gap of a polythiophene is synthesizing a structure in which the quinoid and aromatic structures balance in such a way that the BLA is effectively zero.

The excited states in semiconducting materials can be viewed as containing electrons and "holes" (vacancies left by the absence of an electron), which are formed from the ground state by promoting electrons from filled (valence band) orbitals to the empty (conduction band) orbitals. In the free charge continuum, these electrons and holes are uncorrelated, meaning that the knowledge of the

position of either an electron or a hole does not yield any information about the location of the other. Any state that lies below the band edge of the continuum is known as an excitonic state. In these states, the motion of the electron and hole are correlated, and the combination is referred to as an "exciton." At energies close to a one-photon resonance, double-excited states or "biexcitons" can play a major role in the two-photon absorption spectrum (164).

Multidimensional Molecular Materials. Current trends in the field have shifted away from quasi-one-dimensional or dipolar intermolecular charge transfer materials, and towards inherently two- or three-dimensional and octupolar molecules (165). The hyperpolarizabilities of these molecules do not follow the rules of Kleinman symmetry referred to earlier. The electrons move in at least two dimensions, allowing for polarization-independent applications (25). A main advantage of pushing beyond traditional one-dimensional materials is that alignment of nondipolar materials enables high density packing arrangements not feasible in the presence of dipolar interactions (166). The scope of materials that can be utilized is also much increased. Materials studied include tight-packing donor–acceptor–donor Λ-shaped molecules, stretchable chains to induce axial nonpolar alignment (87), and a variety of chiral shapes, including chiral bulk materials made from achiral molecules arranged in a chiral fashion, such as a threefold propeller-like arrangement (167).

Second-order studies have also begun to focus on large-scale dendritic structures for which large β are seen in HRS measurements without the need for bulk alignment (168,169). Functionalized dendrimers have been also investigated recently for second- and third-order applications. In these large structures, the nonlinear chromophore is placed in the core, along a branch, or at the ends of the dendrimeric structure depending on the application (170). Phthalocyanines and organometallics are interesting second- and third-order nonlinear materials, in part due to their generally high chemical and thermal stability. The π-electron behavior in the molecule is altered by the presence of a metal in the conjugated structure. Ligand-metal bonding leads to transfer of electron density between the metal atom and the ligand systems, causing the electron orbitals of the metal and the ligands to overlap, leading to large hyperpolarizabilities. This class of materials includes polysilanes, metalloporphyrin complexes and metallophthallocyanines (171).

Polymer Structures for NLO Applications. Polymers with π-electron conjugated backbones are favored and widely researched candidates for third-order NLO studies (172–176). The broad categories of π-electron conjugated polymers considered for third-order include linearly conjugated polymers such as polyacetylene (PA), polydiacetylene (PDA), polyazines (PAZ), and linear polyimides (PI); polyheterocyclic polymers such as polypyrrole (Ppy) (177), heterocyclic polyimides, polyquinoline (PQ) (178) polythiophene (PT), polyvinylenes (PV), and polyanilines (PANI) (179); Rigid-Rod Polymers (qv) such as poly(*p*-phenylene benzobisoxazole) (PBZO) and poly(*p*-phenylene benzobisthiazole) (PBZT); and benzimidaxobenzophenanthroline-type (BBB or BBL) ladder polymers. Though localized σ-bonds in carbon chains generally contribute little to the nonlinear response, silicon-based polymers, polysilianes (180), have been studied for their advantages as a third-order material. These polymers are σ-electron conjugated, and therefore maintain the fundamental electron delocalization required for large

Table 1. Representative Nonresonant Enhanced χ^3 Values for Prominent Third-Order π-Conjugated Polymeric Materials

Polymer[a]	Structure	χ^3 (esu) $\times 10^{-12}$	Technique	Wavelength, μm	Reference
PDA	**1** (R′ = R″ = H)	1.4	THG	1.907	181,182
PDA-PTS	[b]	160	THG	2.62	59
PDA-4-BCMU	[c]	49	THG	1.064	183
trans-PA	**2**	1300	THG	1.907	184,185
PAZ	**3**	8	THG	1.5	186,187
PI	**4**	1.2	DFWM	.602	188,189
PQ	**5**	2.2	THG	2.38	190,191
PPV	**6**	7.8	THG	1.85	192,193
PT	**7**	30	DFWM	1.604	194,195
PBZO	**8**	8.1	THG	2.4	196,197
PBZT	**9**	8	DFWM	.602	197,198
BBL	**10**	15	DFWM	1.604	197,199
BBB	**11**	5.5	DFWM	1.604	197,200

[a]PDA: polydiacetylene; BMCU: butoxycarbonylmethylurathane group; PTS: *para*-toluene sulfonate; *trans*-PA: *trans*-polyacetylene; PAZ: polyazine; PI: poyimide; PQ: polyquinoline; PPV:poly(*p*-phenylene vinylene); PT: polythiophene; PBZO: poly(*p*-phenylene benzobisoxazole); PBZT: poly(*p*-phenylene benzobisthiazole); BBL and BBB: benzimidazophenanthroline-type heteroaromatic ladder polymer.
[b]PDA structure (**1**): R′ = R″ = CH_2—O—SO_2—$C_6H_4CH_3$
[c]PDA structure (**1**): R′ = R″ = $(CH_2)_3$—O—CO—NH—CH_2—COO—C_4H_9

third-order NLO response. A short survey of some of the more widely studied of these basic polymeric structures, follows; see also Table 1.

Polydiacetylene—First NLO Polymer Research. Polydiacetylene (**1**) was the first polymer to be investigated for third-order NLO properties. In the late 1970s, Sauteret and co-workers published the first documentation of a large third-order NLO response in a single *p*-toluene sulfate crystal of polydiacetylene (63). The crystal displayed a fast response time (10^{-14} s), a high NLO response (on the order of 10^{-11} esu), and a high laser damage threshold (50 Gw/cm^2 with picosecond response times for a single crystal). Subsequent reports have given third-order susceptibility values ranging over several orders of magnitude (201–203). Influencing factors are chemical structure, resonance enhancement, and measurement techniques.

Polydiacetylenes are linear polymers with highly conjugated π-electron backbones (see DIACETYLENE AND TRIACETYLENE POLYMERS). They can be synthesized via a solid-state polymerization reaction, namely a 1,4-topochemical polymerization of diacetylene monomeric units (204–206). This synthesis mechanism is unique because the polymer product retains the crystalline structure of its monomeric precursors, whereas most polymers have a predominately amorphous structure and limited regions of crystallinity. This type of polymerization has been achieved for polydiacetylene thin films (207,208), Langmuir–Blodgett films (209–211) monolayers (212), single crystals (62), and solutions (213,214). The crystalline structure offers enhanced third-order NLO properties due to high levels of anisotropy (215), but preparation of crystals with high optical quality can be difficult.

One of the most promising of all materials studied for third-order applications is the polydiacetylene, poly(diacetylene *para*-toluene-sulfonate), commonly

referred to as PTS. PTS is thermally stable to ∼180°C, and so less prone to optically induced thermal effects. It can be processed into waveguide structures for device applications and is one of the very few materials that have been shown to meet the standard figures of merit for optical switching devices (38).

Polydiacetylene has been useful in probing third-order phenomena for several reasons. Its centrosymmetric structure excludes second-order NLO effects. Also, polydiacetylenes exhibit chromism in response to such external influences as temperature and solvents (216). Thermochromic and solvatochromic properties have been used to probe third-order effects as a function of conjugation (217). The high degree of structural control that is possible through side-chain substitution allows a wide variety of polydiacetylene polymers to be synthesized (216). It is common to substitute a long alkyl chain as one side group and a carboxylic group as the second. Undergoing this type of substitution allows the polymer to be processed as a Langmuir–Blodgett film. Butoxycarbonylmethylurathane (BCMU)-type polydiacetylenes (**1**) have side groups $R_1 = R_2 =$ $-(CH_2)_3-O-CO-NH-CH_2-COO-C_nH_{2n+1}$ widely studied due to their high solubility in aqueous and nonaqueous solvents, the planar structure, and alternation of color observable with change in conjugation (218–220). Many other polydiactylene-type polymers have been investigated for their third-order NLO properties (181). Future efforts will likely include methodologies such as engineering diacetylene monomers to obtain polymers with enhanced optical properties and processability, and synthesizing a polydiacetylene with a ladder polymer structure (221).

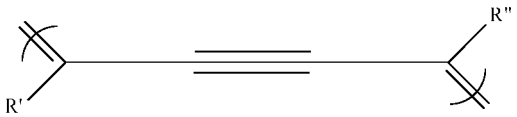

1

Polyacetylenes. Another widely-studied class of linear conjugated polymer are polyacetylenes, (222) which exist in both the trans and cis isomeric states. The trans isomer (**2**) exhibits cubic susceptibility values an order of magnitude greater than the cis isomer, over the entire range of the optical spectrum (223). This phenomenon has been attributed to the twofold degenerate ground state (224). A ground state is degenerate if the single and double bonds along the chain can be interchanged with no change in corresponding conformational energy. Soliton formation is unique to structures that have degenerate ground states (225). Within the class of NLO π-conjugated polymers, soliton formation is common in *trans*-polyacetylene and some forms of polyaniline (the reduced leucoemeraldine-base or LB (226), and the fully oxidized form, polypernigraniline (227)) In a nondegenerate ground state, exchanging of single and double bonds results in a higher and a lower energy configuration (228,229). Solitons form on a chain when the ground state has twofold degeneracy, which means that two energetically equivalent conformations are possible. A region of degeneracy is formed on the same chain and is separated by a transition region (which is the soliton) in which the BLA decreases and ultimately becomes zero at the center. One energy level is formed directly in the center of the band gap. Soliton movement is not analogous to that of polaron

(discussed below under Polyazines) in that a soliton is a topological defect that cannot pass from chain to chain or through another soliton on the same chain.

Polyacetylenes have very good mechanical properties and high electrical conductivity values, as compared to other conducting polymers. (Although electrical conductivity is not directly linked to NLO activity, a polymer with high electrical conductivity and large NLO response could be a promising candidate for device applications.) Polyacetylene is an air-sensitive and insoluble polymer (230). Attempts have been made to alter the polymer to afford increased solubility and environmental stability (222). A graft copolymer of polyacetylene and poly (methyl methacrylate), for example, has displayed enhanced solubility and stability (231). Substituting a phenyl ring onto polyacetylene offers increased stability. This polymer, poly(phenyl acetylene), has a lesser NLO response as compared to polyacetylene. One method used to increase the NLO response of poly(phenyl acetylene) is further substitution on the phenyl ring itself (232) (see ACETYLENIC POLYMERS, SUBSTITUTED).

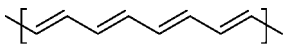

2

Polyazines. Polyazines (**3**) are one-dimensional π-conjugated, arylene-type polymers that are isoelectric to polyacetylene. The differentiating factor is that polyazines have nitrogen atoms substituted into the backbone structure, whereas polyacetylene backbone contains carbon atoms exclusively. Polyazine, like most conjugated polymers, has a nondegenerate ground state, which means that, unlike *trans*-polyacetylene, no solitons will be present in the polymer. It is thought, however, that polyazines contain polaron and bipolaron defects. Polaron-type excitations are common to π-conjugated chains and can be formed by adding an electron (or an electron hole) to a conjugated chain, leading to changes in chain conformation, energy levels, and electron delocalization. (See Reference 233 for a comprehensive discussion of excited states in conjugated polymers.) Incorporating nitrogen increases the environmental stability and optical transparency of polyazine polymers. The chief advantages of polyazines are extreme architectural flexibility, environmental stability, and solubility; and the characteristic disadvantage is the high optical absorption. Compensation for absorption is possible, however, through chemical modification.

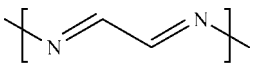

3

Polyimides. Polyimides (**4**) contain carbon–nitrogen double bonds. Linearly conjugated polyimides exist as both thermoplastics and thermosets. High mechanical strength, good insulating properties, processability from a soluble precursor, long-term chemical and orientational stability, and high thermal stability are among the characteristics that make polyimides a useful contender for optical applications (234). Heterocyclic polyimides have also been investigated due to increase in electron delocalization inherent to the ring structure. Polyimides (qv) are

commonly synthesized under severe reaction conditions which limits the ability to chemically modify the polymer (by either NLO chromophore addition or other NLO enhancing substituents) (235).

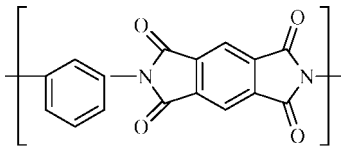

4

Polyquinolines. The high mechanical strength, solubility in organic solvents, ability to be easily processed into thin films with desirable optical properties (such as low optical loss), and thermal stability (at temperatures as high as 600°C) make polyquinolines good candidates for device application studies. Polyquinolines (**5**) are commonly used as the host in guest host polymer systems, and are therefore the subject of much second-order poling research (236). They have also been studied as NLO chromophore functionalized polymers (235). In addition to good end use and processability properties, polyquinolines also have large third-order susceptibilities because of the electron delocalization occurring between carbon–nitrogen double bonds. One recent study reported off-resonant $\chi^{(3)}$ values as large as 1.1×10^{-10} esu for a polyquinoline copolymer with flourene chromophores [the chromophores were incorporated to increase planarity and rigidity of the polymer which enhances the third-order NLO response (237)].

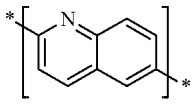

5

Polyvinylenes. Polyvinylenes, particularly poly(*p*-phenylenevinylene) (qv) (238,239), have been studied for their large $\chi^{(3)}$ values on the order of magnitude of 10^{-11}esu (but varying over several orders of magnitude) (240). Polyvinylenes (**6**) can be prepared via a soluble precursor, which is of interest for device applications because the polymer solution can be easily processed and then converted, via thermal polymerization, to its finalized solid-state form (241). Good optical quality thin films have been achieved, which exhibit high mechanical strength, large optical damage thresholds, high electrical conductivity values upon doping, and a high degree of orientational anisotropy (242). For dipolar polymers, a high degree of anisotropy increases the third-order NLO response under conditions where the incident polarization is directed parallel to the polymer backbone (243).

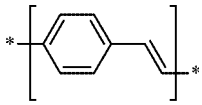

6

Polythiophenes. Polythiophenes (**7**) are polyheterocylic polymers that have a thiophene ring as a repeating backbone unit. Polythiophenes exhibit high electrical conductivity values, yet offer increased environmental stability (244) as compared to polyacetylenes (see ELECTRICALLY ACTIVE POLYMERS). Doping polythiophenes changes their electrical conductivity, but the third-order response of the polymer has been reported to be the same in doped and undoped samples, suggesting that electrical conductivity and NLO response originate from dissimilar origins (245). They are intensely colored materials due to high optical absorptions, and have large resonant third-order responses (246). Polythiophenes are not soluble in organic solvents. Successful efforts to countermand this disadvantage include incorporating methyl methacrylate units in the main chain via copolymerization (247), and substitution of an alkyl chain at the 3-position on the thiophene ring of the polymer (248).

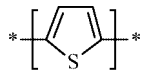

7

Rigid Rod Polymers. One class of rigid polymers that has been commonly studied for its optical, as well as electrical, properties is poly(*p*-phenylenebenzazoles) (PBX). The rigid rod structure of these polymers provides excellent mechanical strength and thermal and thermo-oxidative stability, and they are classed as high performance polymers (249). Two PBX-type polymers that have been of particular interest to NLO applications are poly(*p*-phenylenebenzobisoxazole) (**8**) (PBZO or PBO) and poly(*p*-phenylenebenzobisthiazole) (**9**) (PBZT or PBT) (251). The backbones of these polymers are uniquely conjugated, collinear, and coplanar, which makes intramolecular charge mobility possible, and allows for a large third-order NLO response (see RIGID-ROD POLYMERS).

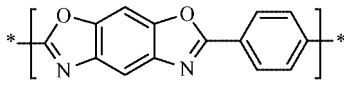

8

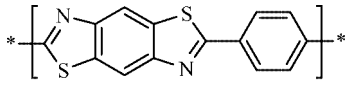

9

Heteroaromatic Ladder Polymers. BBB and BBL are benzimidazophenanthroline ladder polymers which lend themselves to third-order NLOs through their planar conformation, quasi-two-dimensional structure, and to end use applications through their mechanical and thermal stability and electrical properties (252). BBL and BBB are very similar in their repeat unit structure; the manner in which the monomer units are linked together, however, is different. BBL (**10**) has a full-ladder structure, which means that the monomeric units are linked by two covalent bonds, whereas BBB (**11**) has a semi ladder structure because its

monomer units are linked by a single covalent bond. As a result, the $\chi^{(3)}$ of BBL is about three times larger than that of BBB. BBL has a larger NLO response due to the increased planarity of the full-ladder structure of the polymer.

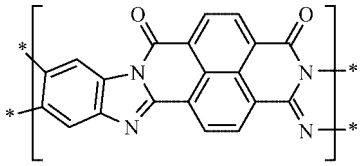

10

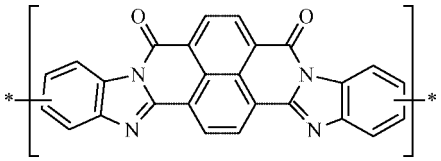

11

Measurement Techniques and Devices

For every nonlinear optical effect, one would expect that there is a measurement technique to characterize it. Not all of NLO effects, however, are subject to measurements that are convenient or informative for comparative purposes or device applications. This section highlights a few of the more common test methods for NLO organic molecules and polymers, and provides references for more detailed explanations of these techniques. Significant omissions here are techniques based on the linear and quadratic electrooptic effect, which are discussed in the article ELECTROOPTICAL APPLICATIONS.

Just as there are two broad categories of nonlinear effects, (*1*) changes in the frequency of the output, and (*2*) changes in the refractive index or absorption, so also there are two types of measurements that are typically performed to quantify these effects. The first type includes measurements based on frequency mixing where the input and detected frequencies differ, as in harmonic generation, nondegenerate four-wave mixing, and hyper-Rayleigh scattering. The second type measures changes in the refractive index through birefringence, diffraction, or other methods, as in the optical Kerr effect and degenerate four-wave mixing. Both types of measurements can be adapted to spectral studies and determination of the real and the imaginary parts of the nonlinear susceptibilities, and, in turn, the related hyperpolarizabilities.

The nonlinear susceptibility can be determined either through absolute or relative methods (253). Absolute measurements are very difficult to implement, however, because they require an accurate determination of the incident and harmonic powers. Even for standard reference materials with relatively large nonlinearities, inconsistent reporting and disagreement over the appropriate values has complicated comparisons (28). Whether the standard values can be agreed upon or

not, determination of the susceptibilities relative to common accepted standards is the favored approach for reporting nonlinearities of new materials.

Frequency Mixing Techniques: Harmonic Generation, Hyper-Rayleigh Scattering, and Nondegenerate Four-Wave Mixing. A major advantage of frequency mixing techniques is their ability to distinguish electronic contributions to the nonlinear susceptibility from contributions due to vibrational, orientational, and thermal effects, and to distinguish resonant and nonresonant electronic motions. The price paid for this advantage is the requirement of very high powered lasers, especially for third harmonic and other third-order effects, and the need for careful filtering and weak-signal detection of non-phase-matched outputs.

Harmonic Generation. In a typical relative measurement involving harmonic generation, the input laser radiation is split into two beams, one incident upon the sample to be measured and the second on a suitable reference standard, such as quartz glass for second-harmonic generation or BK-7 glass for third-harmonic generation, or carbon disulfide for other third-order processes. By simultaneously measuring the harmonic response of both the sample and the reference, the effects of laser fluctuations in power are greatly diminished. After suitable spectral filtering of the output beams to detect only the harmonic (typically using photomultiplier tubes or avalanche photodiodes), the harmonics from the previously characterized reference and the sample are compared.

Simply placing the source and reference in the laser's path is not sufficient, however, to ensure a useful relative measurement. The magnitude of the harmonic response is a function of the path length in the material, and harmonic intensity generated fluctuates through the mismatch in propagation phase between the fundamental and the harmonic wave. The typical sample is not "phase-matched" in that the harmonic and fundamental do not propagate at the same speed through the sample. In second-harmonic generation, the coherence length is the spatial period of the oscillation in the output and, thus, a measure of the effective length in the material for efficiently generating second harmonic. The coherence length of the output in this case is defined as

$$\ell_{\text{coh}} = \frac{\pi}{\Delta k} \qquad \Delta k = \frac{2\omega(n_{2\omega} - n_{\omega})}{c} \tag{24}$$

where n_{ω} is the refractive index at ω. The coherence length for a polymer is typically on the order of 20 μm (254). For samples approaching that thickness or greater, the optical path length through the material must be systematically altered during measurement either by translating a wedge-shaped sample and reference through the beam during measurement, or by rotating the sample and reference each about an axis through and perpendicular to the beam path. The resulting interference patterns (sometimes called Maker fringes (255)) are then analyzed in terms of both their magnitudes and their periodicity to determine the nonlinear susceptibility (256). The second harmonic output, for example, is given

by

$$I_{2\omega} \propto \frac{\left|\chi^{(2)}(-2\omega;\omega,\omega)\right|^2 (I_\omega)^2 L^2}{\lambda_{2\omega}^2 n_\omega^2 n_{2\omega} \varepsilon_0^2} \frac{\sin^2(2\pi L/\ell_{\text{coh}})}{2\pi L/\ell_{\text{coh}}} \tag{25}$$

where I_ω is the incident intensity and L is the interaction length (thickness) in the sample. The accuracy and interpretation of these measurements depends also on careful measurements of the linear optical properties and geometries of the samples and setup, including the effects of multiple reflections at the interfaces (257). Significant birefringence and/or absorption further complicate the analysis, (258) but also provide information about the imaginary parts of the nonlinear susceptibilities.

Phase-Matching. As indicated previously, due to spectral dispersion, $n_{2\omega}$ and n_ω are generally not equal in an isotropic material. In regions of ordinary dispersion, for example, the refractive index at the second harmonic is always greater than the refractive index of the fundamental for two beams of the same polarization propagating in the same direction. Second-order materials are *not* isotropic, however, so that the natural birefringence of these materials (that is, the different refractive indices for different light polarizations) can be used to achieve a reasonable degree of phase matching. The nature of the birefringence of a material depends upon its crystal class. Poled polymers, being cylindrically symmetric about the polar axis, are classed as ∞mm materials because they have a unique axis "3" in the poling direction about which there is an infinite-fold rotation, and an infinity of mirror planes (259,260). In a positive uniaxial crystal, for example, as well as some poled polymers (261), the index of refraction, n_0, for light polarized perpendicular to the plane of incidence and so also perpendicular to poling direction (a so-called ordinary ray) is smaller than that for light having a component parallel to the optic axis or poling direction (an extraordinary ray with index n_e). For a negative uniaxial crystal, the relative values of the extraordinary indices are smaller than the ordinary index.

For poled polymers, if light is polarized along the poling axis, it will couple more strongly to the charge-transfer axis, which should have a larger polarizability and hence larger refractive index. So n_e should be greater than n_0 leading to a positive uniaxial material. For polymers like polyimides, however, it is possible that the index for the polymer dominates, and polyimides molecules tend to lie in the plane of the film. So in general, the birefringence of the polymer would tend to give a larger index in the plane, and the molecule would tend to give a larger index perpendicular to the plane of the film. Depending on the concentrations and polarizabilities, the overall birefringence could have either sign (K. D. Singer, private communication).

Because both the extraordinary ray and the optic axis are in the plane of incidence, the index of refraction seen by the extraordinary ray depends upon the angle of incidence. Thus, a common method for achieving phase-matching, called "Type I" phase-matching as shown in Figure 9, is to find the angle at which the index of refraction of the fundamental extraordinary ray, $n_e(\theta)$, at ω equals that of the harmonic ordinary ray, n_0, at 2ω. Another common method, called "Type II," is for the fundamental to consist of two orthogonal polarizations that average to

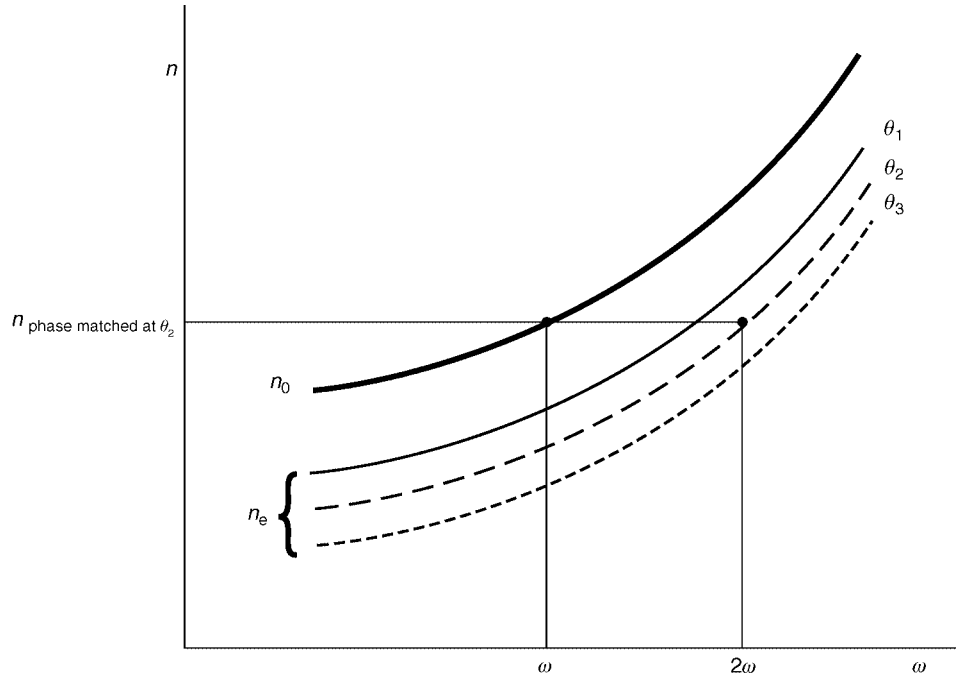

Fig. 9. Sample ordinary and extraordinary dispersion curves in the normal dispersion regime for a negative birefringent material for which the possible extraordinary indices are smaller than the ordinary indices. For the frequencies shown, the phase-matching condition is met for the second harmonic when the light propagates at θ_2 with respect to the optic axis.

the same index of refraction as that experienced by the harmonic. For further details, See Reference 262. A significant drawback of these methods is that the different indices of refraction for the orthogonal polarizations also lead to different angles of refraction for the fundamental and harmonic rays. Thus, the interaction length is further constrained by the walk-off of the rays from one another due to birefringence. If can arrange that the angle for optimal phase-matching is 90° (as might be seen in a single-mode guided wave), then there will be no walk-off.

Another method for phase-matching, which does not require that the rays have different polarization directions and so avoids the problem of walk-off, is to arrange the harmonic conversion frequencies and material properties so that the device operates in a spectral region where there is an absorption peak at frequencies between the fundamental and the harmonic. In this case, a region of anomalous dispersion where the index of refraction is a decreasing function of frequency, accompanies the presence of the intermediate absorption. By carefully combining materials, so that the resulting composite has the same index of refraction at both the fundamental and harmonic, phase-matching results for that pair of frequencies (263) (see Fig. 10).

In integrated optics devices, phase matching must occur in a waveguide structure. The quantized effective indices of refraction vary for different modes of propagation in the waveguide, and the dispersion in the effective mode

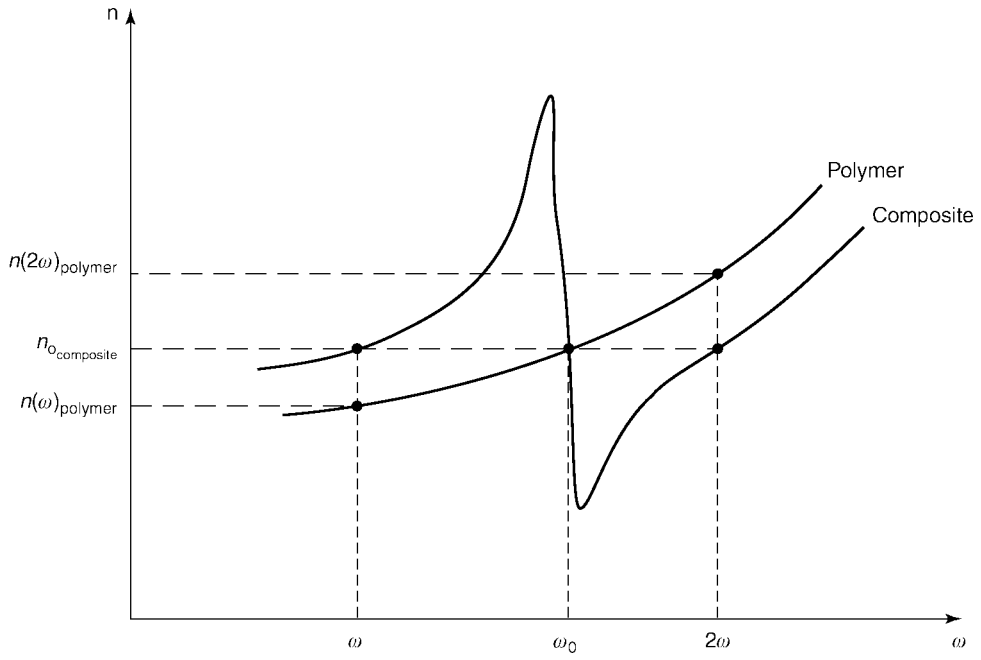

Fig. 10. An example of anomalous dispersion phase-matching in which the dopant molecule exhibits a strong absorption at frequency ω_0 between the fundamental (ω) and harmonic (2ω), leading to a lower index of refraction at the harmonic. The dopant is added to a polymer exhibiting normal dispersion resulting in a composite with equal refractive indices at the fundamental and harmonic, n_0.

index of refraction is generally greater than that of the bulk index of refraction. Phase-matching may be achieved by propagating the fundamental in one mode and polarization and the harmonic in a different mode or different polarization. The details of this procedure can be found in Reference 264. A major drawback of phase-matching in different modes in a waveguide is that light rays propagating in different modes do not necessarily overlap well in the waveguide, limiting their interaction.

Phase-matching in a waveguide is also accomplished by spatial periodic poling (so-called quasi-phase-matching), where the direction of poling is either reversed or polar order is inhibited in the waveguide at regular intervals so that the length of each interaction region is at or shorter than the coherence length (the length over which the phase-mismatch begins to decrease the harmonic output.) Figure 11 illustrates this process by showing the growth in second-harmonic intensity as a function of interaction length. This method has also been applied to cascaded nonlinearities where it induces effective cubic nonlinearities (265).

Electric-Field-Induced Second Harmonic Generation. As previously discussed, in almost all cases the bulk NLO second-order response can be understood through summation over molecular nonlinearities of the constituents. Thus, the key measurements for optimizing polymeric NLO materials are aimed at characterizing their molecular constituents. The wedged cell technique described above has been applied to liquids containing dissolved organic chromophores, through

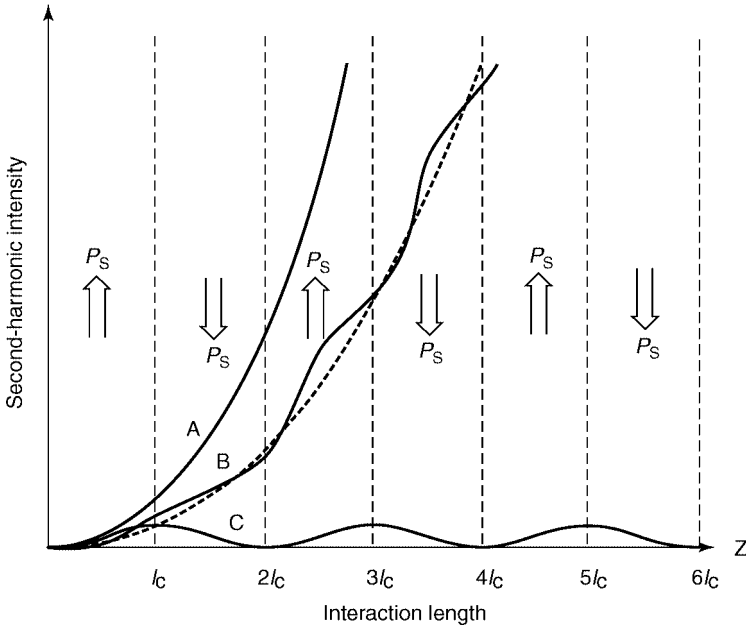

Fig. 11. Variation of second-harmonic intensity as a function of interaction length represented for (A) a phase-matched system, (B) a periodically poled system for which the poling field, and therefore the nonlinearity, changes direction every coherence length, and (C) a non-phase-matched process for which the power flows back from the harmonic completely back to the fundamental during every other coherence length of interaction. (From Reference 6, p. 262. Reprinted with permission.)

electric-field-induced second harmonic generation. The major additional factor in this case is that solutions of polar molecules lack the requisite bulk asymmetry needed for second harmonic generation. To align the dipoles and break the symmetry, a large, but usually very short, DC voltage is applied across the solution just as the beam passes through it (266). (The relationship between the $\chi^{(3)}$ value obtained through this measurement and the molecular properties of the dipoles is given by equation 19).

Hyper-Rayleigh Scattering. EFISH cannot be used, however, on ionic or conductive solutions, due to the need for a large DC field, or on molecules that have no dipole moment, but only have an octupolar moment. Instead, researchers often prefer to use hyper-Rayleigh scattering (HRS) to make measurements, which can be used for all types of molecules, including multidimensional structures, chiral molecules, and stretched polymers (56,267). In the HRS technique, the nonlinear response of the sample is measured from the *scattered* second harmonic, rather than second harmonic transmitted through the sample, again by comparison to a known reference. Careful comparisons between the EFISH and HRS response, including spectral dispersion of each, have shown the consistency of these two methods (268). Ostroverkhova and co-workers have shown that with measurements based on just two different polarizations, the full hyper-Rayleigh scattering tensor can be expressed in terms of its rotationally invariant components for

β, and that figures of merit corresponding to each of the rotationally invariant tensors can be determined (269). The range of information that can be obtained by HRS is expanded by varying the polarization of the detected light, including circular and elliptical polarizations, (270) and by varying the angle at which the scattered light is measured to determine the relative tensor components to the susceptibility. HRS measurements are complicated by the need to account for solvent effects and background fluorescence. The β values obtained are combinations of β-tensor components.

Measuring Nonlinear Refractive Index Changes.

Z-Scan. Z-scan is one of the simpler methods to implement and rapidly measure both the nonlinear refractive index and the nonlinear absorption in a solid, liquid, or solution (271). Many different variations on the basic idea behind z-scan exist and interpretation of the results of a z-scan measurement can be complicated. The most common z-scan technique, illustrated in Figure 12, involves focusing a laser beam on a point in space and translating the sample through the focal point for a distance a few times greater than the diffraction length, $Z_0 = \pi {w_0}^2/\lambda$ (where w_0 is the focal spot half-width at $1/e^2$ of the maximum irradiance and λ is the laser wavelength). The detector is placed behind a fixed aperture on the other side of the sample for measuring the transmitted light in the far-field. As the location of the sample changes, so does the amount of transmission through the aperture according to the placement of the sample in the path, the thickness of the sample and its index of refraction, and, most importantly, the changes in the sample's refractive index with intensity. As the sample approaches the focal point from the far side of the aperture, the light through the aperture is diminished by a self-focusing nonlinearity ($\Delta n > 0$). The sample acts so as to enhance the focusing power of the lens, thus taking the focal point away from the aperture and reducing transmission through the aperture to the detector. As the sample passes through the focal point, the situation is reversed and the same positive Δn in the

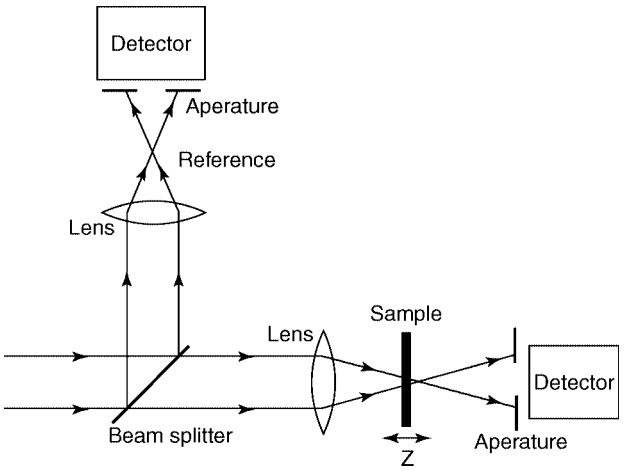

Fig. 12. Schematic for z-scan technique. By varying the placement of the sample along the optic axis, the amount of light being detected through the aperture changes due to the intensity-dependent refractive index of the sample.

sample will tend to reduce the divergence of the light, increasing the transmission through the aperture. For $\Delta n < 0$ and self-defocusing, the result is reversed in that the transmission through the aperture is increased when the sample is on the far side of focal point and decreased on the near side from the aperture (272).

Interpretation of the resulting normalized transmittance can yield both the nonlinear refractive index (based on the change in optical path length) and the nonlinear absorption coefficient (based on the change in absorption by the sample). The results depend upon knowing the laser beams spatial and temporal profile, power content, and stability. One disadvantage of the technique is that it cannot be used to identify the origin of the nonlinearity, as it treats nonlinearities arising from electronic processes the same as orientational and other processes by giving only time-averaged results. Thus, the results must be interpreted based on the theoretical origin of the nonlinearity. Furthermore, the z-scan technique is more difficult to apply with thick samples where the nonlinearity may cause changes in the beam profile through diffraction or self-focusing inside the sample.

Many parameters for and variations on z-scan must be omitted here, but some of the variations include (*1*) open aperture z-scans, (273) where all the transmitted light is collected in order to determine two-photon absorption effects, (*2*) eclipsing z-scan (EZ-scan), (274) which replaces the aperture with a block and collects the light at the outer edges, (*3*) excite-probe and two-color z-scans, (275) which use two collinear beams that differ in either polarization or wavelength and can be time-resolved, and (*4*) non-Gaussian beam or top-hat beam z-scans, (276) which use a beam with a steeper curvature gradient spatial profile to increase the z-scan's sensitivity.

Optical Kerr Effect. Another important method used to characterize polymers is the optical Kerr effect (OKE). The optical Kerr effect differs from the quadratic electrooptic effect in that the birefringence effects are induced solely by an optical field (37). In this measurement, an intense linearly polarized pump pulse induces birefringence in the nonlinear sample through an intensity-dependent refractive index change. The sample is placed between crossed polarizers and a weak, typically tunable, continuous wave (cw) probe laser (usually at a different wavelength and polarized at 45° to the pump pulse) overlaps the pumped region. The increased transmission of the probe beam when the pump pulse arrives is proportional to $(\chi_{\text{eff}}^{(3)})^2$, a combination of elements of the $\chi^{(1)}$ tensor. Many variations on this technique have been used including (*1*) use of a pulsed probe beam to reduce the effects of stray probe light, (277) (*2*) use of a nonlinear mixing crystal, after the analyzer in which a portion of the pump beam is frequency mixed with the probe to enhance the signal to noise ratio by creating an optical gate for the probe coincident with the pump pulse, (278) (*3*) use of an optical heterodyne technique in which a slightly uncrossed analyzer polarization allows for interference between the optical Kerr effect signal and the unaltered probe beam, (279) and (*4*) use of circularly and elliptically polarized pump beams tuned near a Raman active vibration in the sample to determine the Raman spectrum and $\chi_{\text{eff}}^{(3)}$ simultaneously (called the Raman-induced optical Kerr effect) (280). OKE measurements using pulsed probes and time-domain studies are especially helpful for characterizing molecular mechanisms contributing to the effect (281). The optical Kerr effect is especially significant in characterizing polymers for applications such as ultrafast light gates or optical shutters.

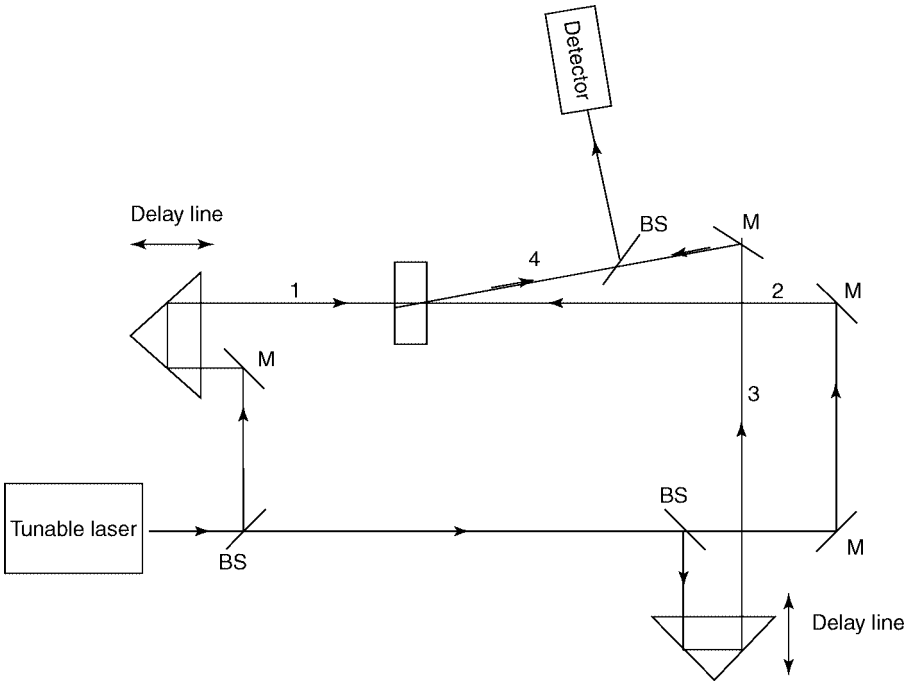

Fig. 13. Schematic for backward scattered (phase conjugate) degenerate four-wave mixing. (BS = beam splitter, M = mirror.) The pump beams (1) and (2) are collinear and counterpropagating. The probe beam (3) when incident on the sample leads to the creation of the phase conjugate beam (4), which is detected and compared to a suitable reference. The delay lines are included so that the timing of pulsed light arriving at the sample via paths (1), (2), and (3) can be varied.

Degenerate Four-Wave Mixing. A slightly more complex configuration for studying real third-order nonlinearities is one in which a single laser beam is split into two or more beams, which are then crossed at the sample, leading to intensity-dependent diffraction. There are two common geometries of this so-called degenerate four-wave mixing (DFWM) (*1*) backward or phase conjugate scattering and (*2*) forward scattering. In the former case, shown in Figure 13, two counter propagating pump beams will be incident on the sample with approximately equal intensities, and a third, probe beam, will cross these at the sample. The result of the nonlinear interaction is a backward scattering of the probe beam. The backward scattered beam is the phase conjugate of the probe and the ratio of the phase conjugate reflectivity to the incident probe intensity yields $\chi^{(3)}_{\text{eff}}$, as a function of the sample length, absorption, and field amplitudes on both sides of the sample (37).

In the forward scattering, or two-wave mixing geometry, two strong pump beams with wave vectors $\boldsymbol{k}_1$ and $\boldsymbol{k}_2$ cross to generate a diffracted beam that conserves momentum with the wave vector direction $2\boldsymbol{k}_1 + \boldsymbol{k}_2$. By varying the delay between the two beams arrival, real-time studies of grating dynamics can be used to distinguish nonresonant electronic nonlinearities. DFWM is a favored technique for studying photorefraction in NLO polymers and other materials.

Nonlinear Absorption. In theory, any of the above measurement techniques could be applied to materials in the presence of nonlinear absorption and interpreted to provide the two-photon absorption coefficient $\alpha^{(2)}$ or the two-photon cross-section $\sigma^{(2)}$. The study of multiphoton absorption is, of course, inherently spectroscopic, probing the multiphoton resonances that impact various nonlinear phenomena. Third-harmonic generation in thin films has been used to characterize the phase of the complex $\chi^{(3)}$ and thus $\alpha^{(2)}$, but the experimental technique requires additional steps and interpretation may be complicated by excited state absorption and three-photon resonances (282). The presence of an imaginary component of $\chi^{(3)}$ significantly complicates DFWM measurements by adding additional phase grating components to the phase conjugate beam, including thermal gratings. Separation of the different contributions to the imaginary part of $\chi^{(3)}$ has been accomplished by time-resolved (283) and picosecond time-scale (284) measurements.

If the primary aim is to characterize the nonlinear absorption, several direct techniques are more easily implemented or interpreted. Conceptually, the simplest technique is to measure the transmitted intensity as a function of the incident intensity on the sample. Separating the linear and nonlinear contributions depends upon the spatial and temporal characteristics of the laser, however, as well as the thickness L and reflectivity R of the sample surfaces. For example, if the laser provides a CW beam of uniform spatial intensity, normally incident on a sample, the transmission T may be expressed as a product $T = T_L T_{NL}$ of the linear transmission $T_L = (1-R^2) \quad e^{-\alpha^{(1)}L}$ and a nonlinear factor $T_{NL} = 1/(1+f)$ where

$$f = \frac{\alpha^{(2)}(1-R)I_1\left(1-e^{-\alpha^{(1)}L}\right)}{\alpha^{(1)}} \tag{26}$$

Of course, the illumination is more commonly of nonuniform spatial and temporal quality, leading to more complicated expressions for T_{NL} (44). Instead, it may be easier to use relative measures of nonlinear absorption by splitting the beam between the sample and a reference, such as ZnSe (285).

Another technique is to use a z-scan setup with an open aperture so that the change in collected light as the sample is translated through the focal point is determined solely by the relative absorption in the sample rather than the focusing or defocusing effects of the sample. This technique includes both two-photon effects and excited-state absorption. Van Stryland and co-workers have shown that the two effects can be separated by comparing the absorption for equal incident energies, but different powers, by adjusting the pulse duration. The two-photon absorption depends upon the intensity, whereas the excited-state absorption depends upon the fluence of the pulse (286).

Many other techniques have been used in addition to those discussed. For example, additional absorption techniques, generally beyond the scope of this article include two-photon luminescence (287), thermal lensing (288), photoacoustic techniques (289), and white-light continuum spectroscopy (290). For further information, the reader is referred particularly to Reference 1.

BIBLIOGRAPHY

1. M. G. Kuzyk and C. W. Dirk, eds. *Characterization Techniques and Tabulations for Organic Nonlinear Optical Materials*, Marcel Dekker, Inc., New York, 1998.
2. H. S. Nalwa, ed., *Handbook of Advanced Electronic and Photonic Materials and Devices, Vol. 9: Nonlinear Optical Materials*, Academic Press, San Diego, Calif., 2001.
3. J. Zyss, ed., *Molecular Nonlinear Optics: Materials, Physics, and Devices*, Academic Press, San Diego, Calif., 1994.
4. H. S. Nalwa, ed., *Handbook of Organic Conductive Molecules and Polymers*, Vol. 4, John Wiley & Sons, Inc., New York, 1997.
5. G. A. Lindsay and K. D. Singer, eds., *Polymers for Second-Order Nonlinear Optics* (ACS Symposium Series 601), American Chemical Society, Washington, D.C., 1995.
6. P. N. Prasad and D. J. Williams, *Introduction to Nonlinear Optical Effects in Molecules and Polymers*, John Wiley & Sons, Inc., New York, 1991.
7. H. S. Nalwa and S. Miyata, eds., *Nonlinear Optics of Organic Molecules and Polymers*, CRC Press, Boca Raton, Fla., 1997.
8. D. M. Bishop, *Rev. Mod. Phys.* **62**, 343–374 (1990).
9. F. Hide, M. A. Diaz-Garcia, B. J. Schwartz, M. R. Andersson, Q. Pei, and A. J. Heeger, *Science.* **273**, 1833 (1996).
10. R. W. Boyd, *Nonlinear Optics*, 2nd ed., Academic Press, Inc., San Diego, Calif., 2002, Chapt. 1.
11. Ref. 6, p. 20.
12. M. Pope and C. E. Swenberg, *Electronic Processes in Organic Crystals and Polymers*, 2nd ed., Oxford University Press, New York, 1999.
13. Y. R. Shen, *The Principles of Nonlinear Optics*, John Wiley & Sons, Inc., New York, 1984.
14. P. N. Butcher and D. Cotter, *The Elements of Nonlinear Optics*, Cambridge University Press, Cambridge, 1990, p. 28.
15. A. A. Said, C. Wamsley, D. J. Hagan, E. W. Van Stryland, B. A. Reinhardt, P. Roderer, and A. G. Dillard, *Chem Phys. Lett.* **228**, 646–650 (1995); K. Yang, J. Kumar, D.-C. Lee, D. J. Sandman, and S. Tripathy, *Opt. Lett.* **25**, 1186–1188 (2000).
16. Y. R. Shen, *Nature* **337**, 519–525 (1989).
17. K. B. Eisenthal, *Chem. Rev.* **96**, 1343–1360 (1996); R. M. Corn and D. A. Higgins, *Chem. Rev.* **94**, 107–126 (1994).
18. K. D. Singer, M. G. Kuzyk, R. B. Comizzoli, H. E. Katz, M. L. Schilling, J. E. Sohn, and S. J. Lalama, *Appl. Phys. Lett.* **53**, 1800–1802 (1988).
19. I. C. Khoo, *Liquid Crystals: Physical Properties and Nonlinear Optical Phenomena*, Wiley-Interscience, New York, 1994.
20. Y. Liu, R. O. Claus, D. Marciu, C. Figura, and J. R. Heflin, in B. Kippelen, H. S. Lackritz, and R. O. Claus, eds., *Organic Nonlinear Optical Materials and Devices*, Materials Research Society, Warrendale, Pa., 1999, pp. 29–32. Symposium Proceedings, Vol. 561.
21. A. Ulman, *An Introduction to Ultrathin Organic Films*, Academic Press, New York, 1991.
22. D. M. Nguyen, T. M. Mayer, S. F. Hubbard, K. D. Singer, J. A. Mann Jr., and J. B. Lando, *Macromolecules* **30**, 6150–6157 (1997).
23. D. A. Kleinman, *Phys. Rev.* **126**, 1977–1979 (1962).
24. G. A. Lindsay, in Ref. 5, pp. 1–19.
25. V. Ostroverkhova, O. Ostroverkhova, R. G. Petschek, K. D. Singer, L. Sukhomlinova, and R. J. Twieg, *IEEE J. Quantum Electron.* **7**, 781–792 (2001).
26. Ref. 10, pp. 193–209.
27. D. M. Bishop, *Rev. Mod. Phys.* **62**, 343–374 (1990).

28. R. F. Shi, and A. F. Garito, in Ref. 1, Chapt. 1, pp. 1–36.
29. D. M. Burland, C. A. Walsh, F. Kajzar, and C. Sentein, *J. Opt. Soc. Am, B* **8**, 2269–2281 (1991).
30. Ref. 10, p. 193.
31. I. M. Skinner and S. J. Garth, *Am. J. Phys.* **58**, 177–181 (1990).
32. Ref. 12, p. 1145.
33. J. R. Heflin, Y. M. Cai, and A. F. Garito, *J. Opt. Soc. Am B* **8**, 2132–2147 (1991).
34. S. Mukamel, *Principles of Nonlinear Optical Spectroscopy*, Oxford University Press, New York, 1995.
35. K. D. Singer, S. F. Hubbard, A. Schober, L. M. Hayden, and K. Johnson, in Ref. 1, pp. 311–514.
36. Ref. 6, p. 89.
37. R. A. Norwood, in Ref. 1, Chapt. 4, pp. 693–765.
38. M. Thakur and D. M. Kroi, *Appl. Phys. Lett.* **56**, 1213–1215 (1990).
39. G. Assanto, G. Stegeman, M. Sheik-Bahae, and E. Van Stryland, *Appl. Phys. Lett.* **62**, 1323–1325 (1993).
40. J. L. Bredas, C. Adant, P. Tackx, and A. Persoons, *Chem. Rev.* **94**, 243–278 (1994).
41. G. I. Stegeman and A. Miller, in J. E. Midwinter, ed., *Photonics in Switching*, Vol. 1, Academic Press, San Diego, Calif., 1993, pp. 81–145.
42. R. Adair, L. L. Chase, and S. Payne, *J. Opt. Soc. Am. B* **4**, 875–881 (1987).
43. M. D. Levenson, *Introduction to Nonlinear Spectroscopy*, Academic Press, New York, 1982.
44. S. Kershaw, in Ref. 1, Chapt. 7, pp. 515–654.
45. V. Mizrahi, K. W. DeLong, G. I. Stegman, M. A. Saifi, and M. J. Andrejco, *Opt. Lett.* **14**, 1140–1142 (1989).
46. K. K. Sharma, K. D. Rao, and G. R. Kumar, *Opt. Quantum Electron* **26**, 1–23 (1994).
47. S. R. Mishra and S. C. Mehnendale, in Ref. 2, Chapt. 8 pp. 347–367.
48. R. Crane, K. Lewis, E. Van Stryland, and M. Khoshnevisan, eds., *Materials for Optical Limiting, Mater. Res. Soc. Proc.*, Vol. 374, 1995.
49. J. Venturini, E. Koudoumas, S. Couris, J. M. Janot, P. Seta, C. Mathis, and S. Leach, *J. Mater. Chem.* **12**, 2071–2076, (2002).
50. J. W. Perry, in Ref. 7, pp. 813–860.
51. G. R. Meredith, *J. Chem. Phys.* **77**, 5863–5873 (1982).
52. J. H. Andrews, K. L. Kowalski, and K. D. Singer, *Phys. Rev. A* **46**, 4172–4184 (1992).
53. G. I. Stegeman, *Quantum Semiclass. Opt.* **9**, 139–153 (1997); G. I. Stegeman, D. J. Hagan, and L. Torner, *Opt. Quantum Electron.* **28**, 1691 (1996).
54. D. Y. Kim, W. E. Torruellas, J. Kang, C. Bosshard, G. I. Stegeman, P. Vidakovic, J. Zyss, W. E. Moerner, R. Twieg, and G. Bjorklund, *Opt. Lett.* **19**, 868–70 (1994); Y. Ueno, G. I. Stegeman, and K. Tajima, *Jpn. J. Appl. Phys., Part 2 Lett.* **36**, 613–615 (1997).
55. J. B. Khurgin, A. Obeidat, S. J. Lee, and Y. J. Ding, *J. Opt. Soc. Am. B* **14**, 1977–1983 (1997).
56. G. J. T. Heeskin, A. G. T. Ruiter, N. F. van Hulst, and B. Bolger, *Phys. Rev. Lett.* **71**, 999–1002 (1995).
57. K. Clays and A. Persoons, in H. S. Nalwa, ed., *Handbook of Advanced Electronic and Photonic Materials and Devices, Vol. 9: Nonlinear Optical Materials*, Academic Press, San Diego, Calif., 2001, pp. 229–265.
58. E. P. C. Lai and H. S. Ghaziaskar, *Appl. Spectrosc.* **48**, 1011–1014 (1994); H. S. Ghaziaskar, W. M. Mullett and E. P. C. Lai, *Vib. Spectrosc.* **5**, 337–344 (1993).
59. S. J. Cyvin, J. E. Rauch, and J. C. Decius, *J. Chem. Phys.* **43**, 4083–4095 (1965).

60. S. Y. Lehman, L. E. Mcneil, and R. J. Albalak, *J. Polym. Sci., Part B: Polym. Phys.* **38**, 2170–2178 (2000); J. K. Kruger, J. Embs, J. Brierley, and R. Jimenez, *J. Phys. D: Appl. Phys.* **31**, 1913–1917 (1998).
61. I. W. Shepherd, *Rep. Prog. Phys.* **38**, 565–620 (1975); R. Y. Chiao, P. L. Kelley, and E. Garmire, *Phys. Rev. Lett.* **17**, 1158–1161 (1966).
62. P. M. Rentzepis and Y. H. Pao, *Appl. Phys. Lett.* **5**, 156–158 (1964).
63. C. Sauteret, J. P. Hermann, R. Frey, F. Rradere, J. Ducing, R. H. Baughman, and R. R. Chance, *Phys. Rev. Lett.* **36**, 956–959 (1976).
64. G. R. Meredith, J. G. VanDusen, and D. J. Williams, *Macromolecules* **15**, 1385–1389 (1982).
65. K. D. Singer, J. E. Sohn, and S. L. Lalama, *Appl. Phys. Lett.* **49**, 248–250 (1986).
66. D. J. Welker and M. G. Kuzyk, *Appl. Phys. Lett.* **69**, 1835–1836 (1996).
67. S. R. Vigil, Z. Zhou, B. K. Canfield, J. Tostenrude, and M. G. Kuzyk, *J. Opt. Soc. Am B* **15**, 895–900 (1998).
68. T. Tagaya, Y. Koike, T. Kinoshita, E. Nihei, T. Yamamoto, and K. Sasaki, *Appl. Phys. Lett.* **63**, 883–884 (1993).
69. H. Watanabe, T. Omatsu, T. Hirose, A. Hasegawa, and M. Tateda, *Opt. Lett.* **24**, 1620–1622 (1999).
70. Y. Ohtsuka, E. Nihei, and Y. Koike, *Appl. Phys. Lett.* **57**, 120–122 (1990).
71. R. F. Shi, C. Koeppen, G. Jiang, J. Wang, and A. F. Garito, *Appl. Phys. Lett.* **71**, 3625–3627 (1997).
72. M. G. Kuzyk, ed., *Proc. SPIE* **3473**, 1–151 (1998). Session 2 papers.
73. M. G. Kuzyk, D. W. Garvey, S. R. Vigil, and D. J. Welker, *Chem. Phys.* **245**, 533–544 (1999).
74. Y. Baek, R. Schiek, G. I. Stegeman, G. Krijnen, I. Baumann, and W. Sohler, *Appl. Phys. Lett.* **68**, 2055–2057 (1996).
75. K. D. Singer, S. F. Hubbard, A. Schober, L. M. Hayden, and K. Johnson, in Ref. 1, pp. 311–514.
76. T. F. Heinz, H. W. K. Tom, and Y. R. Shen, *Phys. Rev. A* **28**, 1883–1885 (1983).
77. J. D. Jackson, *Classical Electrodynamics*, 2nd ed., John Wiley & Sons, Inc., New York, 1975.
78. K. D. Singer and J. H. Andrews, in J. Zyss ed., *Molecular Nonlinear Optics: Materials Physics, and Devices*, Academic Press, San Diego, Calif., 1994, pp. 245–298.
79. M. G. Kuzyk, in Ref. 1, pp. 111–220.
80. K. D. Singer, M. G. Kuzyk, and J. E. Sohn, *J. Opt. Soc. Am B* **4**, 968–976 (1987).
81. R. D. Small, K. D. Singer, J. E. Sohn, M. G. Kuzyk, and S. J. Lalama, *Proc. SPIE* **682**, 160–169 (1986).
82. A.-C. Etile, C. Fiorini, F. Charra, and J.-M. Nunzi, *Phys. Rev. A* **56**, 3888–3896 (1997); J. Si, J. Qiu, and K. Hirao, *J. Appl. Phys.* **90**, 4895–4899 (2001).
83. F. Ghebremichael, M. G. Kuzyk, K. D. Singer, and J. H. Andrews, *J. Opt. Soc. Am B* **15**, 2294–2297 (1998).
84. T. F. Heinz, H. W. K. Tom, and Y. R. Shen, *Phys. Rev. A* **28**, 1883 (1983).
85. F. Wurthner, F. Effenberger, R. Wortmann, and P. Kramer, *Chem. Phys.* **173**, 305–314 (1993).
86. S. R. Marder, L. T. Cheng, B. G. Tiemann, A. C. Friedli, M. Blanchard-Desce, J. W. Perry, and J. Skindhøj, *Science* **263**, 511–514 (1994).
87. V. Ostroverkhov, K. D. Singer, and R. G. Petschek, *J. Opt. Soc. Am. B* **18**, 1858–1865 (2001).
88. C. P. J. M. van der Vorst, and S. J. Picken, *J. Opt. Soc. Am B* **7**, 320–325 (1990).
89. H. S. Lackritz and J. M. Torkelson, in J. Zyss ed., *Molecular Nonlinear Optics: Materials Physics, and Devices*, Academic Press, San Diego, Calif., 1994, Chapt. 8, pp. 339–377.

90. G. Williams and D. C. Watts, *Trans. Faraday. Soc.* **66**, 80 (1970); M. L. Williams, R. F. Landel, and J. P. Ferry, *J. Am. Chem. Soc.* **77**, 3701–3707 (1955).
91. A. Dhinojwala, G. K. Wong, and J. M. Torkleson, *J. Chem. Phys.* **100**, 6046–6054 (1994).
92. H. L. Hampsch, J. Yang, G. K. Wong, and J. M. Torkelson, *Macromol.* **23**, 3640–3647 (1990).
93. T. Goodson and C. H. Wang, *J. Phys. Chem.* **100**, 13920–13926 (1996).
94. L. Liu, D. Ramkrishna, and H. S. Lackritz, *Macromolecules* **27**, 5987–5999 (1994).
95. Y. S. Fu, M. H. Ostrowski, and H. S. Lackritz, in J. P. Runt and J. J. Fitzgerald, eds., *Dielectric Spectroscopy of Polymeric Materials*, Oxford University Press, Oxford, 1997, Chapt. 14.
96. M. Barzoukas, D. Josse, P. Fremaux, J. Zyss, J. F. Nicoud, and J. O. Morely, *J. Opt. Soc. Am B* **4**, 977–986 (1987).
97. D. M. Burland, C. A. Walsh, F. Kajzar, and C. Sentein, *J. Opt. Soc. Am B* **8**, 2269–2281 (1991).
98. M. Sinclair, D. Moses, K. Akagi, and A. J. Heeger, *Phys. Rev. B* **38**, 10724–10733 (1987).
99. C. C. Fay, D. M. Stoakley, and A. K. Clair, *High Performance Polym.* **11**, 145–156 (1999).
100. A. J. Beuhler, D. A. Wargowski, K. D. Singer, and T. Kowalczyk, *IEEE Trans. Comp. Pack. Manuf. Technol. B* **18**, 232 (1995).
101. W. Shi, Y. J. Ding, X. Mu, C. Fang, Q. Pan, and Q. Gu, *J. Opt. Soc. Am. B* **19**, 215–221 (2002).
102. W. Sotoyama, S. Tatsuura, and T. Yoshimura, *Appl. Phys. Lett.* **64**, 2197–2199 (1994).
103. J. D. Stenger-Smith, R. A. Henry, A. P. Chafin, and L. H. Merwin, in Ref. 5, pp. 1–19.
104. T. C. Kowalczyk, T. Z. Kosc, K. D. Singer, A. J. Beuhler, D. A. Wargowski, P. A. Cahill, C. H. Seager, and M. B. Meinhardt, in Ref. 5, pp. 381–400.
105. S. Marturunkakul, J. I. Chen, L. Li, X. L. Jiang, R. J. Jeng, S. K. Sengupta, J. Kumar, and S. K. Tripathy, in Ref. 5, pp. 198–204.
106. R. Tykwinski, U. Gubler, R. Martin, F. Diederich, Ch. Bosshard, and P. Günter, *J. Phys. Chem. B* **102**, 4451–4465 (1998).
107. U. Gubler, *Third Order Nonlinear Optical Effects in Polymers*, Ph. D. dissertation, Swiss Fed. Inst. Tech., Zurich, 2000. Available at http://ecollection.ethbib.ethz.ch/cgi-bin/show.pl?type = diss&nr = 13605 (Accessed September 12, 2003).
108. G. J. Ashwell, P. Leeson, G. S. Bahra, and C. R. Brown, *J. Opt. Soc. Am. B* **15**, 484–488 (1998).
109. Y. Aoki, T. Tada, and Y. Orimoto, *Phys. Rev. B.* **66**, 1931041–1931044 (2002).
110. R. E. Martin, U. Gubler, J. Cornil, M. Balakina, C. Boudon, Ch. Bosshard, J.-P. Gisselbrecht, F. Diederich, P. Günter, M. Gross, and J.-L. Brédas, *Chem.—Eur. J.* **6**, 3622–3635 (2000).
111. J. Seixas de Malo, L. M. Silva, and L. G. Arnaut, *J. Chem. Phys.* **111**, 5427–5433 (1999).
112. Ref. 4, p. 339.
113. E. H. Sargent, M. D'Iorio, J. Zyss, C. Andraud, and P. W. E. Smith, eds., in *J. Opt. A: Pure Appl. Opt.* **4**, 593–671 (2002).
114. M. A. Pasquinelli, *An Effective Particle Approach to the Photophysics of Conjugated Polymers*, Ph.D. dissertation, Carnegie-Mellon University, January, 2002. Available at www.chem.cmu.edu/groups/yaron/pdf/pasquinellithesis.pdf. Accessed September 12, 2003.
115. D. P. Shelton and J. E. Rice, *Chem. Rev.* **94**, 3–30 (1994).
116. J. M. Andre, J. Delhalle, and J. L. Bredas, *Quantum Chemistry Aided Design of Organic Polymers. An Introduction to the Quantum Chemistry of Polymers and Its Applications*, World Scientific, Singapore, 1991.

117. S. P. Karna, G. B. Talapatra, W. M. K. P. Wijekoon, and P. N. Prasad, *Phys. Rev. A* **45**, 2763–2770 (1992).
118. I. D. L. Albert, T. J. Marks, and M. A. Ratner, in Ref. 1, pp. 37–110.
119. B. J. Orr and J. F. Ward, *Mol. Phys.* **20**, 513–526 (1971).
120. W. Liptay, in E. C. Lim, ed., *Excited States*, Academic Press, New York, 1974.
121. B. Champagne and B. Kirtman, in Ref. 2.
122. J. Zyss and J. L. Oudar, *Phys. Rev. A* **26**, 2028–2048 (1982).
123. C. W. Dirk, L. T. Cheng, and M. G. Kuzyk, *Int. J. Quantum Chem.* **43**, 27–36 (1992).
124. H. Ikeda, T. Sakai, and K. Kawasaki, *Chem. Phys. Lett.* **179**, 551–554 (1991).
125. J. L. Oudar and D. S. Chemla, *J. Chem. Phys.* **66**, 2664–2668 (1977).
126. M. G. Kuzyk, *Phys. Rev. Lett.* **85**, 1218–1221 (2000).
127. M. G. Kuzyk, *Opt. Lett.* **25**, 1183–1185 (2000); errata in *Opt. Lett.* **28**, 135 (2003).
128. M. G. Kuzyk, *IEEE J. Quantum Electron.* **7**, 774–780 (2001).
129. K. D. Singer, S. F. Hubbard, A. Schober, L. M. Hayden, and K. Johnson, in Ref. 1, pp. 311–514.
130. H. S. Nalwa, T. Watanabe, and S. Miyata, in Ref. 7, pp. 89–350.
131. S. R. Marder, B. Kippelen, A. K.-Y. Jen, and N. Peyghambarian, *Nature* **388**, 845–851 (1997).
132. S. R. Marder, C. B. Gorman, F. Meyers, J. W. Perry, G. Bourhill, J. L. Bredas, and B. M. Pierce, *Science* **265**, 632–635 (1994).
133. F. Meyers, S. R. Marder, B. M. Pierce, and J. L. Bredas, *J. Am. Chem. Soc.* **116**, 10703–10714 (1994).
134. S. R. Marder, D. N. Beratan, and L. Cheng, *Science* **252**, 103–106 (1991).
135. K. D. Singer, H. E. Katz, J. E. Sohn, C. W. Dirk, L. A. King, and H. M. Gordon, *J. Opt. Soc. Am. B* **6**, 1339–1350 (1989).
136. L. T. Cheng, W. Tam, S. R. Marder, A. E. Stiegman, G. Rikken, and C. W. Spangler, *J. Phys. Chem.* **95**, 10643–10652 (1991).
137. V. Alain, *J. Phys. Chem.* **95**, 10643–10652 (1991).
138. V. Alain, L. Thouin, M. Blanchard-Desce, U. Gubler, C. Bosshard, P. Gunter, J. Muller, A. Fort, and M. Barzoukas, *Adv. Mater.* **11**, 1210–1214 (1999).
139. M. G. Kuzyk and C. W. Dirk, *Phys. Rev. A* **41**, 5098–5109 (1990).
140. Z. G. Soos and D. Mukhopadhyay, *J. Chem. Phys.* **101**, 5155 (1994).
141. J. H. Andrews, J. D. V. Khaydarov, K. D. Singer, D. L. Hull, K. C. Chuang, *J. Opt. Soc. Am. B* **12**, 2360–2371 (1995).
142. S. Mazumdar and F. Guo, *J. Chem. Phys.* **100**, 1665–1672 (1994).
143. B. M. Pierce, *Proc. SPIE.* **1560**, pp. 148–161 (1991).
144. K. S. Mathias, M. G. Kuzyk, C. W. Dirk, A. Tan, S. Martinez, and G. Gampos, *J. Opt. Soc. Am. B* **15** 871–883 (1998).
145. J. W. Wu, J. R. Heflin, R. A. Norwood, K. Y. Wong, O. Zamani-Khamiri, A. F. Garito, P. Kalyanaraman, and J. Sounik, *J. Opt. Soc. Am. B* **6**, 707–720 (1989).
146. J. R. Heflin, D. C. Rodenberger, R. F. Shi, M. Wu, N. Q. Wang, Y. M. Cai, A. F. Garito, *Phys. Rev. A* **45**, 4233–4236 (2002).
147. D. C. Rodenberger, J. R. Heflin, and A. F. Garito, *Nature* **359**, 309–311 (1992).
148. M. T. Zhao, M. Samoc, P. H. Singh, P. N. Prasad, *J. Chem Phys.* **93**, 7916–7920 (1989).
149. Ref. 12, p. 1148.
150. Ref. 6, p. 235.
151. R. R. Tykwinski, U. Gubler, R. E. Martin, F. Diederich, C. Bosshard, and P. Gunter, *J. Phys. Chem. B.* **102**, 4451–4465 (1998).
152. I. D. W. Samuel, I. Ledoux, C. Dhenaut, J. Zyss, H. H. Fox, R. R. Schrock, and J. Sibley, *Science* **256**, 1070–1072 (1994).
153. D. Neher, A. Kaltbeitzel, A. Wolf, C. Bubeck, G. C. Wegner, *J. Phys. D: Appl. Phys.* **24**, 1193–1202 (1991).

154. C. Q. Wu, *Cond. Mat.* **23**, 1–22 (1992). Also available at http://arxiv.org/PS˙cache/cond-mat/pdf/9210/9210022.pdf.
155. I. Ledoux, I. D. W. Samuel, J. Zyss, S. N. Aliraki, F. J. Schattenmann, R. R. Schock, and R. J. Silbey, *Chem. Phys.* **245**, 1–16 (1999).
156. H. Meier, D. Ickenroth, U. Stalmach, K. Koynov, A. Bahtiar, and C. Bubck, *Eur. J. Org. Chem.* **2001**, 4431–4443 (2001).
157. J.-T. Lin, J.-H. Sheu, and S.-L. Lee, *Chem. Phys. Lett.* **345**, 228–234 (2001).
158. U. Gubler, S. Concilio, Ch. Bosshard, I. Biaggio, P. Gunter, R. E. Martin, M. J. Edelmann, J. A. Wytko, and F. Diederich, *Appl. Phys. Lett.* **81**, 2322–2324 (2002).
159. X. Zhan, Y. Liu, D. Zhu, W. Huang, and Q. Gong, *J. Chem. Phys. B* **106**, 1884–1888 (2002).
160. J. Ma, S. Li, and Y. Jiang, *Macromolecules* **35**, 1109–1115 (2002).
161. D.-H. Hwang, J.-H. Chang, H.-K. Shim, and T. Zyung, *Synth. Met.* **119**, 393–394 (2001).
162. M. Jayakannan, P. A. van Hal, and R. Janssen, *J. Poly. Sci. A.* **40**, 251–261 (2002).
163. H. A. M. van Mullekom, J. A. J. M. Vekemans, E. E. Havinga, and E. W. Meijer, *Mater. Sci. Eng: R.-Rep.* **32**, 1–40 (2001).
164. V. A. Shakin and S. Abe, *Phys. Rev. B* **50**, 4306–4315 (1994).
165. J. Zyss and S. Brasselet, *C. R. Acad. Sci.* **4**, 601–608 (2000).
166. D. Beljonne, W. Wenseleers, E. Zojer, Z. Shuai, H. Vogel, S. Pond, J. Perry, S. Marder, and J. Bredas, *Adv. Funct. Mater.* **12**, 631–641 (2002).
167. S. Van Elshocht, T. Verbiest, M. Kauranen, L. Ma, H. Cheng, K. Musick, L. Pu, and A. Persoons, *Chem. Phys. Lett.* **309**, 315–320 (1999).
168. S. Mukamel, *Nature* **388**, 425–427 (1997).
169. M. Kauranen, T. Verbiest, C. Boutton, M. N. Teerenstra, K. Clays, A. J. Schouten, R. J. M. Nolte, and A. Persoons, *Science* **270**, 966–969 (1995).
170. H. Ma and A. K.-Y. Jen, *Jen, Adv. Mater.* **13**, 1201–1205 (2001).
171. K. S. Suslick, N. A. Rakow, M. E. Kosal, and J.-H. Chou, *J. Porphyrins and Phthalocyanines* **4**, 407–413 (2000).
172. W. R. Salaneck, I Lundström, and B. Rånby, eds., *Conjugated Polymers and Related Materials: Interconnection of Chemical and Electronic Structure*, Oxford University Press, Oxford, 1993.
173. G. Zerbi, ed., *Organic Materials for Photonics*, North-Holland, Amsterdam, 1993.
174. J. L. Brédas and R. Sibley, eds., *Conjugated Polymers*, Kluwer, Dordrecht, Netherlands, 1991.
175. J. Messier, F. Kajzar, and P. Prasad, eds., *Organic Molecules for Nonlinear Optics and Photonics*, Vol. 94 of NATO Advanced Study Institute, Series E, Applied Sciences, Kluwer, Dordrecht, the Netherlands, 1991.
176. Ref. 4, p. 309.
177. Y. Matsuzaki, M. Nakano, K. Yamaguchi, K. Tanaka, and T. Yamabe, *Chem. Phys. Lett.* **263**, 119–125 (1996).
178. A. K. Agrawal, S. Jenekhe, H. Vanherzeele, and J. S. Meth, *J. Phys. Chem.* **96**, 2837–2843 (1992).
179. J. A. Osahemi, S. Jenekhe, H. Vanherzeele, S. Meth, Y. Sun, and A. G. MacMiarmid, *J. Phys. Chem.* **96**, 2830–2836 (1992).
180. E. A. Perpète, J.-M. André, and B. Champagne, *J. Chem. Phys.* **109**, 4624–4637 (1998).
181. Ref. 7, pp. 648–649.
182. K. Kubodera and T. Kaino, in T. Kobayashi, ed., *Springer Proceedings in Physics*, Vol. 36, Springer, Berlin, 1989, p. 163.
183. C. Hsu, Y. Kawabe, Z. Ho, N. Ppeyghambarian, J. N. Polky, W. Krug, E. Miao, *J. Appl. Phys. Lett.* **67**, 7199–7203 (1990).
184. F. Kajzar, S. Etemad, G. L. Baker, and J. Messier, *Solid State Commun.* **63**, 1113–1117 (1987).

185. Ref. 7, p. 665.
186. H. S. Nalwa, A. Kakuta, A. Mukoh, *J. Appl. Phys.* **73**, 4743–4745 (1993).
187. Ref. 7, p. 704.
188. Ref. 7, p. 715.
189. R. O. Ebewele, *Polymer Science and Technology*, CRC Press, New York, 2002, p. 442.
190. Ref. 7, p. 700.
191. Ref. 7, p. 702.
192. T. Kaino, K. Kubodera, S. Tomaru, T. Kurihara, S. Saito, T. Tsutsui, S. Tokito, *Electron Lett.* **23**, 1095 (1987).
193. Ref. 6, p. 235.
194. D. D. C. Bradley, Y. Mori, *Jn. J. Appl. Phys.* **28**, 74 (1989).
195. Ref. 7, p. 688.
196. S. A. Jenekhe, J. A. Osaheni, J. S. Meth, and H. Vanherzeele, *Chem. Mater.* **4**, 683–687 (1992).
197. Ref. 7, p. 697.
198. Ref. 7, p. 699.
199. J. R. Lindle, F. J. Bartoli, C. A. Hoffman, O. K. Kim, Y. S. Lee, J. S. Shirk, and Z. H. Kafafi, *Appl. Phys. Lett.* **56**, 712–714 (1990).
200. Ref. 4, p. 336.
201. Ref. 7, pp. 658–660.
202. Ref. 4, p. 322.
203. Ref. 6, p. 232.
204. D. Sandman, I. Kim, J. M. Njus, D. Lee, A. Cholli, and S. Sahoo, *Macromol. Symp.* **192**, 99–113 (2003).
205. G. Wegner, *Naturforsch Z, B* **24**, 824 (1969).
206. M. Schott and G. Wegner, in D. S. Chemla and J. Zyss, eds., *Nonlinear Optical Properties of Organic Molecules and Crystals*, Vol. 2, Academic Press, New York, 1987, pp. 3–46.
207. J. LeMoigne, M. Moroni, H. Coles, A. Thierry, and F. Kajzar, *Mater. Res. Soc. Symp. Proc.* **247**, 65 (1992).
208. T. Kanetake, K. Ishikawa, T. Hasewaga, T. Koda, K. Takeda, M. Hasewaga, K. Kubodera, and H. Kobayaski, *Appl. Phys. Lett.* **54**, 2287–2289 (1989).
209. P. A. Chollet, F. Kajzar, and J. Messier, *Synth. Met.* **18**, 459–464 (1987).
210. F. Kajzar and J. Messier, *Thin Solid Films* **132**, 11–19 (1985).
211. E. Geiger, P. Hug, and A. Keller, *Macromol. Chem. Phys.* **203**, 2422–2431 (2002).
212. M. D. Mowery, M. Cai, H. Menzel, and C. E. Evans, *J. Vac. Sci. Technol., A* **17**, 2136–2141 (1999).
213. M. Chandross, Y. Shimoi, and S. Mazumdar, *Synth. Met.* **85**, 1001–1006 (1997).
214. A. Sarkar, S. Okada, H. Matsuda, and H. Nakanish, *Polym. Bull.* **41**, 425–431 (1998).
215. C. C. Hsu, Y. Kawabe, Z. Z. Ho, N. Peyghambarain, J. M. Polky, W. Krug, and E. Miao, *J. Appl. Phys.* **67**, 7199–7203 (1990).
216. Ref. 7, p. 648.
217. Ref. 6, p. 234.
218. C. C. Hsu, Y. Kawabe, Z. Z. Ho, N. Peyghambarain, J. N. Polky, W. Krug, and E. Miao, *J. Appl. Phys.* **67**, 7199–7203 (1990).
219. S. Okada, T. Doi, A. Mito, K. Hayamizu, A. Ticktin, H. Matsuda, N. Kikuchi, A. Masaki, N. Minami, K. Haas, and H. Nakanishi, *Nonlinear Opt.* **8**, 121 (1994).
220. Ref. 6, p. 235.
221. A. Sarkar, S. Okada, H. Matsuzawa, H. Matsuda, and H. Nakanishi, *J. Mater. Chem.* **10**, 819–828 (2000).
222. A. S. M. Karim, R. Nomura, H. Kajii, R. Hidayat, K. Yoshino, and T. Masuda, *J. Polym. Sci. Part A: Polym. Chem.* **38**, 4717–4723 (2000).

223. Ref. 7, p. 666.
224. Ref. 7, p. 664.
225. M. V. Mostovoy, M. T. Figge, J. Knoester, *Europhys. Lett.* **38**, 687–692 (1997).
226. J. M. Grinder, A. P. Epstein, *Phys. Rev. B* **41**, 10674–10684 (1990).
227. M. C. dos Santos, J. L. Bredas, *Phys. Rev. Lett.* **62**, 2499–2505 (1989).
228. Ref. 4, p. 336.
229. A. J. Heeger, S. Kivelson, J. R. Schrieffer, and W.-P. Su, *Rev. Mod. Phys.* **60**, 781–850 (1988).
230. G. Costa, in G. Allen, ed., *Comprehensive Polymer Science*, Oxford University Press, New York, 1989, Chapt. 9, p. 155.
231. Ref. 6, p. 238.
232. D. Neher, A. Wolf, M. Leclerc, A. Kaltbeizel, C. Bubeck, G. Wegner, *Synth. Met.* **37**, 249–253 (1990).
233. Y. Furukawa, N. S. Sariciftci, eds., in *Primary Photoexcitations in Conjugated Polymers*, World Scientific, Singapore, 1997, Chapt. 17, pp. 511–519. Available at http://www.ipc.uni˙linz.acat/publ/book/Chapter17.pdf. Accessed August 27 2003.
234. K. Y. Kim, S. Jang, F. W. Harris, *Macromoleules.* **34**, 8925–8933 (2001).
235. A. K.-Y. Jen, X. Wu, and H. Ma, *Chem. Mater.* **10**, 471–473 (1998).
236. Y. M. Cal and A. K.-Y. Jen, *Appl. Phys. Lett.* **67**, 299–301 (1995).
237. X. W. Zhan, Y. Q. Liu, D. B. Zhu, G. Xu, X. C. Liu, P. X. Ye, *Appl. Phys. A* **77**, 375–378 (2003).
238. M. Guohong, L. Guo, J. Mi, Y. Lui, Q. Shixiong, J. Liu, G. He, and Y. Li, *Physica B* **305**, 147–154 (2001).
239. D. R. Gagnon, J. D. Capistran, F. E. Karasz, R. W. Lenz, S. Antoun, *Polymer* **28**, 567–573 (1987).
240. Ref. 7, p. 684.
241. A. Samoc, M. Samoc, M. Woodruff, and B. Luther-Davies, in D. L. Wise, D. J. Trantolo, G. E. Wnek, T. M. Cooper, and J. D. Gresser, eds., *Photonic Polymer Systems*, Marcel Dekker, Inc., New York, 1998, pp. 373–436.
242. R. Riehn, A. Charas, J. Morgado, F. Cacialli, *Appl. Phys. Lett.* **82**, 526–528 (2003).
243. McBranch, M. Sinclaire, A. J. Heeger, A. O. Patil, S. Shi, S. Askari, and F. Wudl, *Synth. Met.* **29**, 85–90 (1989).
244. E. Ando, S. Onodera, M. Iino, O. Ito, *Carbon* **39**, 101–108 (2001).
245. T. Kaino, K. Kubodera, T. Kobayashi, S. Kurihara, T. Sato, T. Tsutsui, S. Takito, and H. Murata, *Appl. Phys. Lett.* **53**, 2002–2004 (1988).
246. H. S. Nalwa, *J. Appl. Phys. D.* **23**, 745–747 (1990).
247. H. S. Nalwa, *Thin Solid Films* **225**, 175–181 (1993).
248. Ref. 4, p. 687.
249. Z. Wu, F. Li, L. Huang, Y. Shi, X. Jin, S. Fang, K. Chuang, R. E. Lyon, F. W. Harris, and S. Z. D. Cheng, *J. Therm. Anal. Calorimetry* **59**, 361–373 (2000).
250. S. A. Jenekhe, J. A. Osaheni, J. S. Meth, H. Vanherzeele, *Chem. Mater.* **4**, 683–687 (1992); H. Vanherzeele, J. S. Meth, S. Jenekhe, M. F. Roberts, *J. Opt. Soc. Am. B* **9**, 524–533 (1992).
251. R. J. Gehr, G. L. Fischer, R. W. Boyd, J. E. Sipe, *Phys. Rev. A* **53**, 2792–2798 (1995).
252. J. R. Lindle, F. J. Bartolli, C. A. Hoffman, O.-K. Kim, Y. S. Lee, J. S. Shirk, Z. H. Kafafi, *Appl. Phys. Lett.* **56**, 712–714 (1989).
253. K. D. Singer, S. F. Hubbard, A. Schober, L. M. Hayden, and K. Johnson, in Ref. 1, pp. 311–514.
254. M. G. Kuzyk, R. C. Moore, and L. A. King, *J. Opt. Soc. Am B* **7**, 64–72 (1990).
255. P. D. Maker, R. W. Terhune, M. Nisenhoff, and C. M. Savage, *Phys. Rev. Lett.* **8**, 21–22 (1962).
256. J. Jerphagnon and S. K. Kurtz, *J. Appl. Phys.* **41**, 1667–1681 (1970).

257. D. Neher, A. Wolf, C. Bubek, and G. Wegner, *Chem. Phys. Lett.* **163**, 116 (1989).
258. W. N. Herman and L. M. Hayden, *J. Opt. Soc. Am B* **12**, 416–427 (1995).
259. K. D. Singer, M. G. Kuzyk, and J. E. Sohn, *J. Opt. Soc. Am B* **4**, 968–976 (1987).
260. K. D. Singer and J. H. Andrews, in J. Zyss, ed., *Molecular Nonlinear Optics: Materials Physics, and Devices*, Academic Press, San Diego, Calif., 1994, p. 254.
261. D. Jungbauer, I. Teraoka, D. Y. Yoon, B. Reck, J. D. Swalen, R. Tweig, and C. G. Willson, *J. Appl. Phys.* **69**, 8011–8017 (1991).
262. Ref. 6, Chapt. 5.
263. T. Dai, K. D. Singer, R. J. Twieg, and T. C. Kowalczyk, *J. Opt. Soc. Am. B* **17**, 412–421 (2000).
264. G. I. Stegeman and R. H. Stolen, *J. Opt. Soc. Am B* **6**, 652–662 (1989).
265. C. Balslev Clausen, O. Bang, and Y. S. Kivshar, *Phys. Rev. Lett.* **78**, 4749–4752 (1997).
266. K. D. Singer and A. F. Garito, *J. Chem. Phys.* **75**, 3572 (1981).
267. V. Ostroverkhov, O. Ostroverkhova, R. G. Petschek, K. D. Singer, L. Sukhomlinova, R. J. Twieg, S.-X. Wang, and L. C. Chien, *Chem. Phys.* **257**, 263–274 (2000).
268. S. F. Hubbard, R. G. Petschek, and K. D. Singer, *Opt. Lett.* **21**, 1774–1776 (1996).
269. S. F. Hubbard, R. G. Petschek, K. D. Singer, N. D'Sidocky, C. Hudson, L. C. Chien, C. C. Henderson, and P. A. Cahill, *J. Opt. Soc. Am. B* **15**, 289–301 (1998); V. Ostroverkhov, R. G. Petschek, K. D. Singer, L. Sukhomlinova, R. J. Twieg, S.-X. Wang, and L. C. Chien, *J. Opt. Soc. Am. B* **17**, 1531–1542 (2000).
270. P. Kaatz and D. P. Shelton, *J. Chem. Phys.* **105**, 3918–3929 (1996).
271. M. Sheik-Bahae, A. A. Said, and E. W. Van *Stryland, Opt. Lett.* **14**, 955–957 (1989).
272. E. W. Van Stryland and M. Sheik-Bahae, in Ref. 1. pp. 655–692.
273. M. Sheik-Bahae, A. A. Said, T. H. Wei, D. J. Hagan, and E. W. Van Stryland, *J. Quantum Electron.* **26**, 760–769 (1990).
274. T. Xia, D. J. Hagan, M. Sheik-Bahae, and E. W. Van Stryland, *Opt. Lett.* **19**, 317–319 (1994).
275. M. Sheik-Bahae, J. Wang, J. R. DeSalvo, D. J. Hagan, and E. W. Van Stryland, *Opt. Lett.* **17**, 258–260 (1992).
276. W. Zhao and P. Palffy-Muhoray, *Appl. Phys. Lett.* **65**, 673–675 (1994).
277. L. Yang, R. Dorsinville, P. P. Ho, W. K. Zou, N. L. Yang, and R. R. Alfano, *Appl. Phys. Lett.* **53**, 2009–2010 (1988).
278. M. G. Kuzyk, R. A. Norwood, J. W. Wu, and A. F. Garito, *J. Opt. Soc. Am. B* **6**, 154–164 (1989).
279. B. Blaszczak, *Opt. Commun.* **58**, 439–443 (1986).
280. D. Heiman, R. W. Hellwarth, M. D. Levenson, and G. Martin, *Phys. Rev. Lett.* **36**, 189–192 (1976).
281. M. J. Feldstein, P. Vohringer, and N. F. Scherer, *J. Opt. Soc. Am. B* **12**, 1500 (1995).
282. T. Hasegawa, Y. Iwasa, H. Kishida, T. Koda, Y. Tokura, H. Tachibana, and Y. Kawabata, *Phys. Rev. B* **45**, 6317–6320 (1992).
283. R. L. Sutherland, E. Rea, V. Natarajan, T. Pottenger, and P. A. Fleitz, *J. Chem. Phys.* **98**, 2593–2603 (1993).
284. M. Zhao, Y. Cui, M. Samoc, P. N. Prasad, M. R. Unroe, and B. A. Reinhardt, *J. Chem. Phys.* **95**, 3991–4001 (1991).
285. E. W. Van Stryland, M. A. Woodall, H. Vanherzeele, and M. J. Soileau, *Opt. Lett.* **10**, 490–492 (1985).
286. T. H. Wei, D. J. Hagan, M. J. Spence, E. W. Van Stryland, J. W. Perry, and D. R. Coulter, *Appl. Phys. B. B* **54**, 46–51 (1992).
287. C. H. Chen and M. P. McCann, *Opt. Commun.* **63**, 335–338 (1987).
288. P. Foggi, P. R. Salvi, R. Bini, and E. Castellucci, *J. Mol. Struct.* **175**, 147–152 (1988).

289. R. Philip, P. Sathy, V. P. N. Nampoori, J. Philip, and C. P. G. Vallabhan, *J. Phys. B* **25**, 155–161 (1992).
290. R. A. Negres, J. M. Hales, A. Kobyakov, D. J. Hagan, and E. W. VanStryland, *Opt. Lett.* **27**, 270–272 (2002).

READING LIST

With respect to polymeric and organic molecular materials, there are several monographs and numerous collections of research works to consider. Annual proceedings presenting current research were published through 1997 by the Society of Photo-optical Instrumentation Engineers (SPIE) under the title *Nonlinear Optical Properties of Organic Materials*, Vols. I–X. Since 2001, this series has been superceded by the annual series *Linear and Nonlinear Optics of Organic Materials*, Vols. I–III, currently edited by M. Kuzyk. Additional recent relevant proceedings from SPIE include:

M. G. Kuzyk, *Third Order Nonlinear Optical Materials*, 3473 SPIE, Bellingham, Wash., 1998.

M. Eich, *Organic Nonlinear Optical Materials*, 3796 SPIE, Bellingham, Wash., 1999.

The proceedings of the October 2003 annual meeting, entitled *Organic Materials and Nanotechnology*, CDS 100 SPIE, Bellingham, Wash., 2004, promise to provide an up-to-date account of research in that field.

Noteworthy collections and monographs include:

K.-S. Lee, ed., *Polymers for Photonics Applications, Vol. 1: Advances in Polymer Science*, Vol. 158, Springer, Berlin, 2002.

H. S. Nalwa, ed., *Supramolecular Photosensitive and Electroactive Materials*, Academic Press, San Diego, Calif., 2001.

H. S. Nalwa, ed., *Handbook of Advanced Electronic and Photonic Materials and Devices, Vol. 9: Nonlinear Optical Materials*, Academic Press, San Diego, Calif., 2001.

M. Pope and C. E. Swenberg, *Electronic Processes in Organic Crystals and Polymers*, 2nd ed., Oxford University Press, New York, 1999.

H. S. Nalwa, ed., *Handbook of Organic Conductive Molecules and Polymers*, CRC Press, Inc., Boca Raton, 1997.

M. G. Kuzyk and C. W. Dirk, eds., *Characterization Techniques and Tabulations for Organic Nonlinear Optical Materials*, Marcel Dekker, Inc., New York, 1998.

S. Miyata, and H. Sasabe, eds., *Poled Polymers and Their Applications to SHG and EO Devices*, Gordon and Breach, Queensland, Australia, 1997.

H. S. Nalwa and S. Miyata, eds., *Nonlinear Optics of Organic Molecules and Polymers*, CRC Press, Boca Raton, Fla., 1997.

G. A. Lindsay And K. D. Singer, ed., *Polymers for Second-Order Nonlinear Optics* (ACS Symposium Series No. 601), American Chemical Society, Washington, D.C., 1995.

S. Mukamel, *Principles of Nonlinear Optical Spectroscopy*, Oxford University Press, New York, 1995.

J. Zyss, ed., *Molecular Nonlinear Optics: Materials, Physics, and Devices*, Academic Press, Inc., San Diego, Calif., 1994; and its predecessor volumes D. S. Chemla and J. Zyss, *Nonlinear Optical Properties of Organic Molecules and Crystals*, Vols. 1 and 2, Academic Press, Inc., San Diego, Calif., 1987.

L. A. Hornak, ed., *Polymers for Lightwave and Integrated Optics*, Marcel Dekker, Inc., New York, 1992.

P. N. Prasad and D. J. Williams, *Introduction to Nonlinear Optical Effects in Molecules and Polymers*, John Wiley & Sons, Inc., New York, 1991.

S. Miyata and H. Sasabe, *Light Wave Manipulation using Organic Nonlinear Optical Materials*, Gordon and Breach, Amsterdam, 2000.

Ch. Bosshard, K. Sutter, Ph. Pretre, J. Hullinger, M. Florsheimer, P. Kantz, and P. Gunter, in A. F. Garito and F. Kajzar, eds., *Advances in Nonlinear Optics, Vol. 1: Organic Nonlinear Optical Materials*, Gordon and Breach, Basil, Switzerland, 1995.

Because the field of nonlinear optical properties of polymers is cross-disciplinary among optical sciences, material sciences, polymer chemistry, and other disciplines, important research is published in a wide variety of journals, including those of the Materials Research Society (MRS), the Optical Society of America (OSA), the Institute of Physics (IOP), the American Chemical Society (ACS), the American Physical Society (APS), and the IEEE Lasers and Electro-Optics Society. Particularly noteworthy are the special issues on organic materials for nonlinear optics and photonics, including:

N. Peyghambarian and S. Marder, eds., *IEEE Selected Top. Quantum. Electron.* **7**, 757–863 (2001).

C. Hooker, W. R. Burghardt, and J. M. Torkelson, eds., *Chem. Phys.* **245**, 1–568 (1999).

M. G. Kuzyk, K. D. Singer, and R. J. Twieg, eds, *J. Opt. Soc. Am. B.* **15**(1, 2), 254–488 and 724–932 (1998).

J. Michl, ed., *Chem. Rev.* **94**(1), 1–278 (1994).

Finally, the following texts provide a broad selection of views on the field of nonlinear optics.

R. W. Boyd, *Nonlinear Optics*, 2nd ed., Academic Press, San Diego, Calif., 2002.

G. S. He and S. H. Liu, *Physics of Nonlinear Optics*, World Scientific, Singapore, 1999.

E. G. Sauter, *Nonlinear Optics*, John Wiley & Sons, Inc., New York, 1996.

R. L. Sutherland, *Handbook of Nonlinear Optics*, Marcel Dekker, Inc., New York, 1996.

P. N. Butcher and D. Cotter, *The Elements of Nonlinear Optics*, Cambridge University Press, New York, 1990.

Y. R. Shen, *The Principles of Nonlinear Optics*, John Wiley & Sons, Inc., New York, 1984.

N. Bloembergen, *Nonlinear Optics*, W. A. Benjamin, New York, 1965.

JAMES H. ANDREWS
KIMBERLY A. GUZAN
Youngstown State University

NONWOVEN FABRICS, SPUNBONDED

Introduction

In 2001, the global production of spunbonded fabrics reached a record 1,400,000 t with an annual growth rate of between 6 and 8% (1). There are approximately 260 individual production lines in operation throughout the world. Spunbonded fabrics are distinguished from other nonwoven fabrics in their one-step manufacturing process which provides either a complete chemical-to-fabric or polymer-to-fabric process. Although the use of monomers as part of the in-line process is no longer in commercial use, in either instance the manufacturing process integrates the spinning, laydown, consolidation, and bonding of continuous filaments to form a

Encyclopedia of Polymer Science and Technology. Copyright John Wiley & Sons, Inc. All rights reserved.

fabric. Commercialization of this process dates to the early 1960s in the United States and Western Europe (2,3) and in the early 1970s in Japan (4). Many of the first plants constructed are still in operation attesting to the usefulness of the method. New production plants continue to be built (1,5) to supply the growing demand (Table 1).

The large investment required for a turnkey spunbonded plant ($15–50 million, 2002 U.S. dollars) is offset by their high productivity. Spunbonded production was originally limited to western Europe, the United States, and Japan, but has since spread to virtually all areas of the world. Production lines, mainly nonproprietary, have been installed throughout Asia, South America, and the Middle East, areas and countries that previously did not participate in the technology. Considerable ownership changes occurred in the United States and Europe as the strategies of companies committed to the technology evolved (6).

Early marketing efforts for spunbonded fabrics centered on their substitution for existing (ie, woven) textile fabrics. Generally, success was achieved in areas where only functionality was important. Extremely slow progress has occurred in areas where textile-like aesthetics are required. Only in the area of disposable protective clothing has success been achieved for the garment market. Nevertheless, spunbonded fabrics are recognized as a unique class of materials within the general category of nonwoven fabrics (see NONWOVEN FABRICS, STAPLE FIBERS).

The area of largest growth for spunbonded fabrics continues to be disposable diaper coverstock, that accounts for approximately 70% of the U.S. coverstock market. Forecasts for the future growth of spunbonded fabrics continue to be favorable as consumption in both durable and disposable areas continues to grow. Growth is forecast to generally exceed the growth of all nonwovens, which itself is expected to grow at 3–6% per annum (1,6). In addition to diaper coverstock and hygiene, growth is anticipated in geotextiles, roofing, carpet backing, medical wrap, and durable paper applications such as envelopes (6).

New plant construction will bring increased capacity to levels of regional overcapacity, which will force producers to export large quantities of product to keep supply and demand in balance. Considerable consolidation of ownership has occurred during the last five years and the investment and output for each new line has grown enormously. New production lines can produce up to 1 billion m^2 of coverstock per year more than doubling the annual output of lines built only 5 years ago. Environmental issues have had relatively little effect on either production or products. Consumers prefer the convenience of disposable diapers, and studies have shown that diapers are still a relatively small contributor to landfill space.

Although producers have benefited from the generally stable prices for crude oil, a sudden increase in these prices or decrease in availability of resin feedstocks would adversely impact both profitability and growth. Producers who have not upgraded to newer, faster, and more efficient lines have experienced low or negative profitability. There appear to be no new fiber technologies that would radically change the manner in which spunbonded structures are produced. Any serious challenges to existing markets will likely come from film, airlay, or advances in alternative technologies within a specific market segment.

Table 1. Spunbond Producers by Region

Company	Polymer base[a]	Technology base
North America		
Ahlstrom	PP	Nordson
American Nonwovens	PP	Ason Neumag
Avgol	PP	Reifenhauser
BBA Nonwovens	PET	via DuPont[b]
	PP	via duPont[c]
		Self-developed
		Reifenhauser
Colbond	PET/PA	via Akzo[d]
DuPont	HDPE, PET	Self-developed[e]
First Quality	PP	Reifenhauser
Freudenberg	PET	Self-developed[f]
Johns Manville	PET	via Hoechst[g]
Kimberly-Clark	PP	Self-developed
PGI Nonwovens	PP	Reifenhauser
		STP Impianti
Texbond	PP	STP Impianti
Western Nonwovens	PA	via Monsanto[h]
Europe		
BP	PP	Reifenhauser
BBA Nonwovens	PP	Reifenhauser
		Lurgi
		Self-developed
NWI (Cartiere Mirano)	PP	NWT
Colbond	PET, PET/PA	via Akzo[d]
Don & Low	PP	Reifenhauser
DuPont	HDPE	Self-developed[e]
	PP	Self-developed[c]
Fibertex	PP	Reifenhauser
Freudenberg	PET	Self-developed[f]
Johns Manville	PET	via Hoechst[g]
Pegas	PP	Reifenhauser
Politex-Freudenberg	PET	Self-developed
Polyfelt	PP	Lurgi
Tenotex	PP	Self-developed
Texbond	PP	STP Impianti
		Self-developed
Terram BBA	PP/PE	via ICI
South America		
Bidim BBA	PET	via Rhone Poulenc
Companhia Providencia	PP	Reifenhauser
Kami	PP	Reifenhauser
Fitesa	PP	STP Impianti
PGI	PP	Reifenhauser
Japan		
Asahi	PP, PET, Cupra	Self-developed
Chisso	PP, PP/PE	Reifenhauser
Idemitsu	PP	Reifenhauser

Table 1. (Continued)

Company	Polymer base[a]	Technology base
Futamura	Rayon	Self-developed
Mitsui	PP	Self-developed Reifenhauser
OJI Paper	PP	Reifenhauser
Teijin	PET, PP	Self-developed
Toray	PET	Self-developed
Toyobo	PET	Self-developed
Unitika	PET, PA	Self-developed
Other Areas		
Avgol (Israel)	PP	Reifenhauser
Cheil (S. Korea)	PP	Reifenhauser
Freudenberg (Taiwan)	PET	Self-developed[f]
Hanil (S. Korea)	PP/PET	Kobelco
IndoSyntec (Indonesia)	PET	NWT
Kaymac Industries	PET	via Rhone Poulenc
Kimberly-Clark (Australia)	PP	Self-developed
Kolon (S. Korea)	PP/PET	Self-developed
Nan Ya (Taiwan)	PP	Lurgi & Reifenhauser
PGI (China)	PP	Reifenhauser
SAAF (Saudi Arabia)	PP	Reifenhauser
Spuntec (S. Africa)	PP	Reifenhauser
Thai Tusco (Indonesia)	PP/PET	via Unitika
Yuhan-Kimberly (S. Korea)	PP	Self-developed

[a] PP = polypropene; PET = poly(ethylene terephthalate); PA = ; HD PE = high density polyethylene.
[b] Reemay process.
[c] Typar process.
[d] Split process.
[e] Flashspun Tyvek process (HDPE).
[f] Lutradur process.
[g] Began with RhonePoulenc license.
[h] Cerex process.

General Characteristics

Spunbonded fabrics are filament sheets made through an integrated process of spinning, attenuation, deposition, bonding, and winding into roll goods. The fabrics are made up to 5.2 m wide and usually not $>$ 3.0 m in order to facilitate productivity. Fiber sizes range from 0.1 to 50 dtex although a range of 2–20 dtex is most common. A combination of thickness, fiber fineness (denier), and number of fibers per unit area determines the fabric basis weight which ranges from 8–800 g/m^2; 13–180 g/m^2 is typical. Average basis weights in hygiene have fallen by 20% or more because of improvements in process technology.

Most spunbonded processes yield a sheet having planar–isotropic properties owing to the random laydown of the fibers (Table 2). Unlike woven fabrics, spunbonded sheets are generally nondirectional and can be cut and used without concern for higher stretching in the bias direction or unraveling at the edges.

Table 2. Physical Properties of Spunbonded Products

Product	Basis weight, g/m^2	Thickness, mm	Tensile strength,[a] N[b]	Tear strength,[a] N[b]	Mullen burst, kPa[c]	Bonding method
Accord	69		144 MD 175 XD	36 MD 40 XD	323	Point thermal
Bidim	150		495	280	1545	Needle-punch
Cerex	34	0.14	135 MD 90 XD	40 MD 32 XD	240	Chemically induced area
Colback	100	0.6	300[d]	120		Area thermal (sheath-core)
Corovin	75		130	15		Point thermal
Lutradur	84	0.44	225 MD 297 XD	85 MD 90 XD	598	Copolymer area thermal
Polyfelt	137		585	225	1445	Needle-punch
Reemay	68	0.29	225 MD 180 XD	45 MD 50 XD	330	copolymer area thermal
Terram	137	0.7	850	250	1100	Area thermal (sheath-core)
Trevira	155		630 MD 495 XD	270 MD 248 XD	1512	Needle-punch
Typar	103	0.305	540 MD 495 XD	207 MD 235 XD	825	Undrawn segments Area thermal
Tyvek	54	0.15	4.6[e] MD 5.1[e] XD	4.5 MD 4.5 XD		Area and point thermal

[a]MD = Machine direction; XD = cross-direction.
[b]Unless otherwise noted. To convert N to pound-force, divide by 4.448.
[c]To convert kPa to psi, multiply by 0.145.
[d]300 N/5 cm = 34.5 ppi.
[e]N/mm; to convert N/mm to ppi, divide by 0.175.

It is possible to produce nonisotropic properties by controlling the orientation of the fibers in the web during laydown. Although it is not readily apparent, most sheets are layered or shingled structures with the number of layers increasing with higher basis weights for a given product. Fabric thickness varies from 0.1 to 4.0 mm; the range 0.15–1.5 mm represents the majority of fabrics in demand. The method of bonding greatly affects the thickness of the sheets, as well as other characteristics. Fiber webs bonded by thermal calendering are thinner than the same web that has been needle-punched, because calendering compresses the structure through pressure, whereas needle-punching moves fibers from the x–y plane of the fabric into the z (thickness) direction.

The structure of traditional woven and knit fabrics permits the fibers to readily move within the fabric when in-plane shear forces are applied, resulting in a fabric that readily conforms in three dimensions. Because calender bonding of a spun web causes some of the fibers to fuse together, thus giving the sheet integrity, the structure has a relatively stiff hand or drape compared to traditional textile fabrics. This is a result of the immobilization of fibers in the areas of fiber-to-fiber fusion. The immobilization may be moderated by limiting the bonds to very small areas (points) or by entangling the fibers mechanically or hydraulically. Saturation bonding of spun webs with chemical binders such as acrylic emulsions can bond the structure throughout and result in very stiff sheets. This technique is used to provide thermal and mechanical dimensional stability to certain structures whereby the emulsion binder functions as a nonthermoplastic component within the thermoplastic matrix.

Other approaches include powder bonding, although this method may be more suitable for bonding nonwoven fabrics made from staple fibers (7,8) (see NONWOVEN FABRICS, STAPLE FIBERS).

The method of fabric manufacture dictates many of the characteristics of the sheet, but intrinsic properties are firmly established by the base polymer selected. Properties such as fiber density, temperature resistance, chemical and light stability, ease of coloration, surface energies, and others are a function of the base polymer. Thus, because nylon absorbs more moisture than polypropylene, spunbonded fabrics made from nylon are more water-absorbent than fabrics of polypropylene.

The majority of spunbonded fabrics are based on either isotactic polypropylene or polyester (Table 1). Small quantities are made from nylon-6,6 and an increasing tonnage from (flashspun) high density polyethylene. Table 3 illustrates the basic characteristics of fibers made from different base polymers. Although

Table 3. Fibers for Spunbonded Nonwoven Fabrics

Fiber type	Breaking tenacity, N/tex[a]	Elongation, %	Specific gravity	Moisture regain,[b] %	Approximate melt point, °C
Polyester	0.17–0.84	12–150	1.38	0.4	248–260
Nylon-6,6	0.26–0.88	12–70	1.14	4.0	248–260
Polypropylene	0.22–0.48	20–100	0.91	~0.0	162–171

[a] To convert N/tex to gf/den, multiply by 11.3.
[b] At 21°C and 65% rh.

some interest has been seen in the use of linear low density polyethylene (LLDPE) as a base polymer, largely because of potential increases in the softness of the final fabric (9), economic factors continue to favor polypropylene (see PROPYLENE POLYMERS (PP)). Bicomponent technology will allow polyethylene to be used in a more economical way by directing it only to the surfaces where it brings a useful property.

Isotactic polypropylene is the most widely used polymer in spunbonded production because it is the least expensive fiber-forming polymer that provides the highest yield (fiber per weight) and covering power owing to its low density. Isotactic polypropylene is only ca 70% the density of most types of polyesters, and thus equivalent yields of fiber require a greater weight of more expensive polyester. Large advances have been made in the manufacture of polypropylene resins and additives since the first spunbonded polypropylene fabrics were commercialized in the 1960s. Unstabilized polypropylene fibers are readily degraded by ultraviolet UV light, but dramatic improvements in additives permit years of outdoor exposure to occur before fiber properties are significantly affected. Metallocene polypropylene resins are the latest major resin improvement available for spun bonding.

Polypropylene fibers are neither dyeable by conventional methods nor readily stained because dye receptor sites do not naturally exist along the molecular backbone. However, some spunbonded polypropylene fabrics are colored by the addition of a pigment to the polymer melt, wherein the pigment becomes encased within the fiber interior. Advantages to this method include higher resistance to fading and bleeding and ease of reproducibility of color shades from lot to lot. A key disadvantage is the generation of small to large quantities of off-quality production during the transitions into and out of a particular color, and coloration normally occurs only on low output lines. A delustering pigment, eg TiO_2, is often added to polypropylene as it almost always is with the manufacture of nylon fibers.

Most off-quality or scrap polypropylene fibers may be repelletized and blended in small percentages with virgin polymer to produce first-grade spunbonded fabrics. The economics are of great importance in a process where high yields are required in order to be competitive. Some manufacturing equipment directly recycles edge-trim back into an extruder, where it is blended back into the polymer melt (see OLEFIN FIBERS).

Polyester fiber has several performance advantages versus polypropylene, although it is less economical. Polyester can produce higher tensile strength and modulus fabrics that are dimensionally stable at higher temperatures than polypropylene. This is of importance in selected applications such as roofing, automotive carpet backing, and dryer sheets. Polyester fabrics are easily dyed and printed with conventional equipment which is of extreme importance in apparel and face fabrics, although of lesser importance in most spunbonded applications (see POLYESTERS, FIBERS).

Spunbonded fabrics have been made from both nylon-6 and nylon-6,6 polymers. Because nylon is more costly and highly energy-intensive, it is less economical than either polyethylene or polypropylene. Although a considerable body of knowledge exists in the preparation of nylon polymers, such as end group control, it has been of little advantage in spunbonded fabric production. Historically, nylon-6,6 spunbonded fabrics have been commercially produced at weights as low

as 10 g/m^2 with excellent cover and strength, but recently this has been achieved with polypropylene as well. Unlike the olefins and polyesters, fabrics made from nylon absorb water quite readily through hydrogen bonding between the amide group and water molecules (see POLYAMIDES, FIBERS).

Traditional melt spun methods have not utilized polyethylene as the base polymer because the resin is more expensive and the physical properties obtained have been lower compared to those obtained with polypropylene. Advances in polyethylene technology have resulted in the commercialization of new spunbonded structures having characteristics, such as softness, not attainable with polypropylene. Although fiber-grade polyethylene resin was announced in late 1986, it has seen limited acceptance because of higher costs and continuing improvements in polypropylene resin technology (see ETHYLENE POLYMERS).

Flashspun high density polyethylene fabrics have been commercial since the early 1960s; however, this is a proprietary and radically different process of manufacturing a spunbonded fabric, more technically challenging to produce, and highly capital-intensive. Today, there is only one manufacturer of flashspun fabrics, although they are produced in both Europe and the United States.

Some fabrics are composed of combinations of polymers where a lower melting polymer functions as the binder element. The binder element may be a separate fiber interspersed with higher melting fibers (10), or the two polymers may be combined in one fiber type (11). In the latter case, the so-called bicomponent fiber may have the lower melting portion as a sheath covering a core of the higher melting polymer (Fig. 1). Bicomponent fibers can also be spun, whereby the two polymers are extruded side by side. The polymer composition of the binder element in such structures may be either polyethylene, nylon-6, and polyester copolymers typically modified by lowering the terephthalic acid content by substitution with isophthalic acid. Great advances have been made in bicomponent spinning and a large variety of intrafiber structures can be easily produced from turnkey spinbeams (Fig. 2) (12). Bicomponent webs can be subjected to mechanical stresses such as water jet impact which causes the individual filament to fracture into its components yielding a new number of filaments equal to the number of components or segments created in the filament during spinning. Thus, a single filament containing 16 pie segments will fracture into 16 smaller wedge-shaped filaments.

Spunbonded fabrics with elastomeric properties are now commercial. One type of structure has been commercialized in Japan on the basis of thermoplastic polyurethanes, but the process is more similar to melt blowing than spun bonding (13). This represented the first commercial production of such fabrics, although spunbonded urethane fabrics have been previously discussed (14). A more economical approach using polypropylene has recently become commercial and is used in medical and hygienic applications (15). High costs and inferior performance versus woven fabrics continue to exclude these fabrics from the huge apparel markets. Elastomeric fabrics may also be created using the meltblown process for specialty applications.

There is an almost unlimited number of ways to characterize spunbonded fabrics. Many tests in use were originally developed for the characterization of textiles and paper products. When taken together, properties such as tensile, tear, and burst strength; toughness; elongation to break; basis weight; thickness; air porosity; dimensional stability; and resistance to heat and chemicals are often

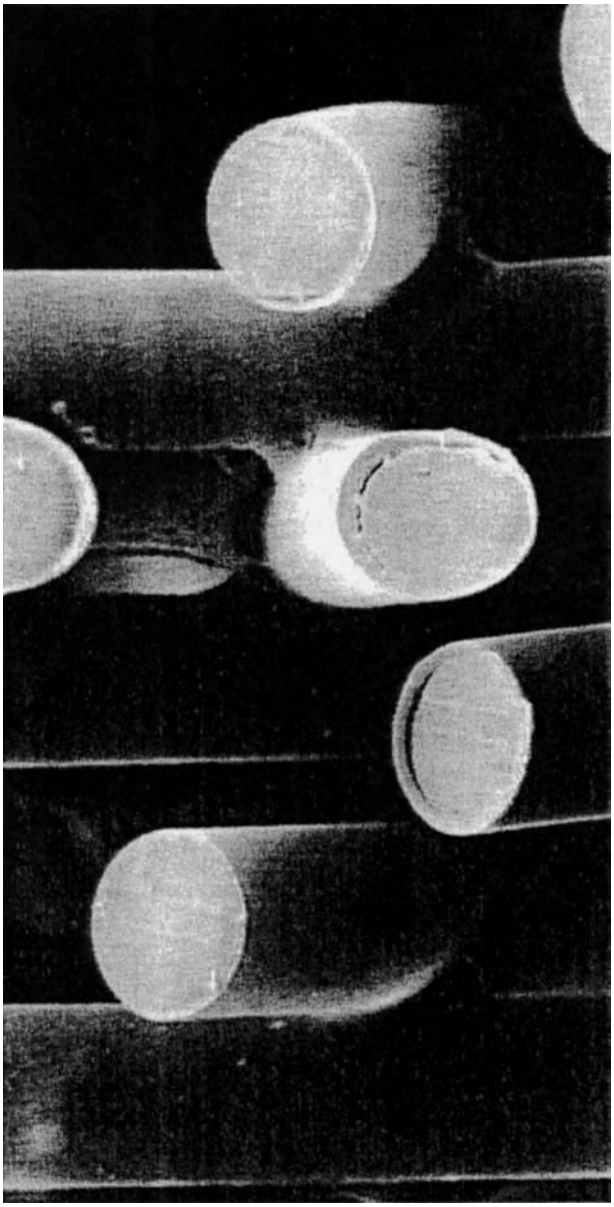

Fig. 1. Microstereo view of the cross-section of skin core filaments.

sufficient to uniquely describe one product. The reason is that these properties reflect both the fabric composition and its structure, the latter being defined by a manufacturing process unique to that fabric. Compare, eg, the differing shapes of the generic stress–strain curves of thermally bonded and needle-punch bonded fabrics (Fig. 3). The shape of each curve is largely a function of the freedom of the filaments to move when the fabric is placed under stress, and is thus a function of fabric structure.

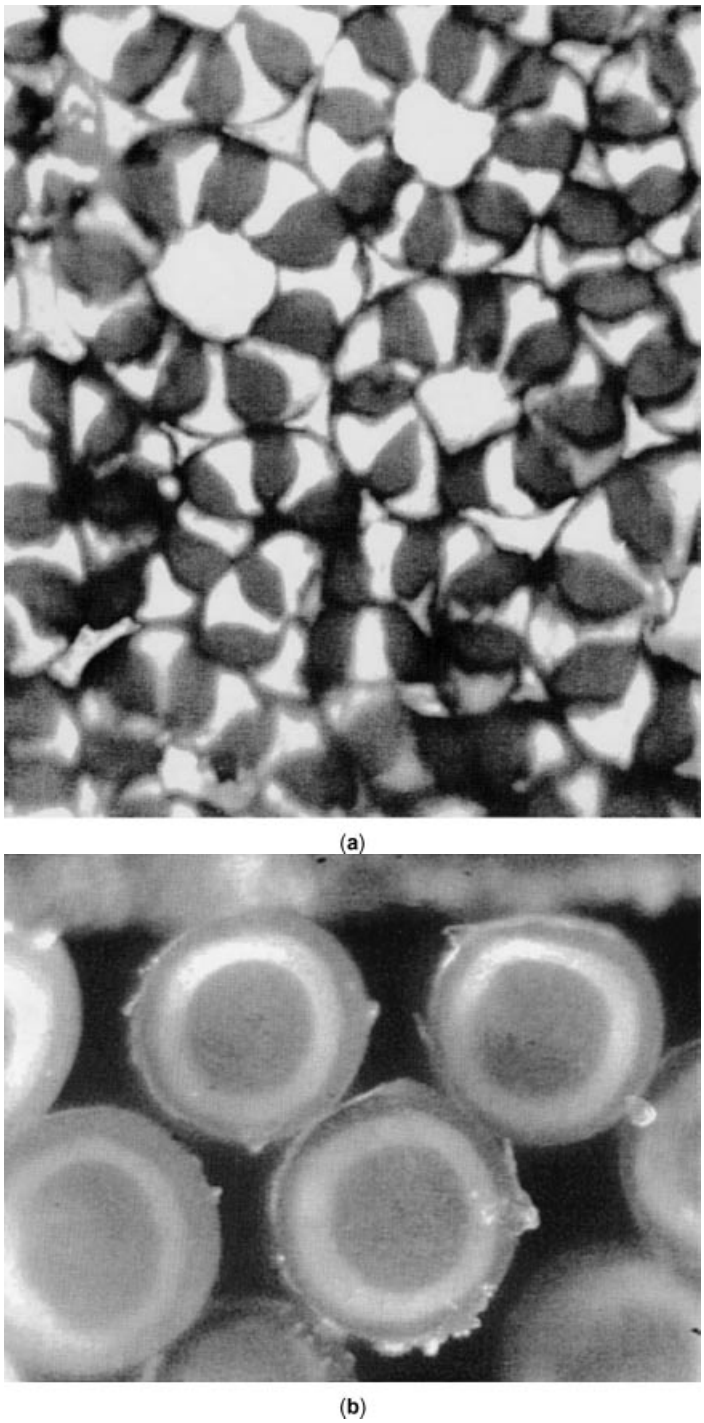

Fig. 2. Bicomponent filament structures. (**a**) Hollowpie; (**b**) sheathcore—large. Courtesy Hills Inc..

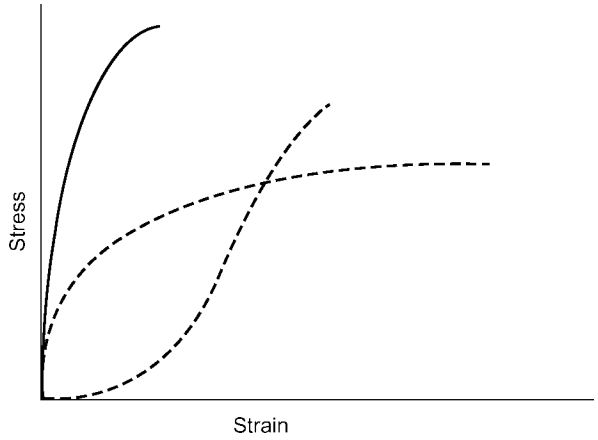

Fig. 3. Typical stress–strain curves of nonwoven fabrics, where (——) is woven; (– – –), thermally bonded nonwoven; and (- - -), needle-punched nonwoven.

Diverse applications for the fabric sometimes demand specialized tests, such as for moisture vapor, liquid transport barrier to fluids, coefficient of friction, seam strength, resistance to sunlight, oxidation and burning, and/or comparative aesthetic properties. Most properties can be determined using standardized test procedures that have been published as nonwoven standards. Test methods adopted in the USA are published by INDA, while those adopted in Europe are published by EDANA. A comparison of typical physical properties for selected spunbonded products is shown in Table (2).

Spinning and Web Formation

Spunbonded fabric production couples the fiber spinning operation with the formation and consolidation of the web in order to maximize productivity. It is the coupling of these processes that distinguishes the spunbonded process from traditional methods of fabric formation where fiber is first spun and collected, then formed into a fabric by a separate process such as weaving or carded into a web. If the bonding device is placed in line with spinning and web formation, the web is converted into bonded fabric in one step (Fig. 4). In some arrangements, the web is bonded off-line in a separate step which appears at first to be less efficient; however, this offers the advantage of being more flexible if more than one type of bonding is to be performed on the web being produced. Some specialty processes also separate the spinning and the laydown steps which adds cost but provides high control on the fiber properties and ensures few breaks in laydown.

The basic spinning process is similar to the production of continuous filament yarns and utilizes similar extruder conditions for a given polymer (16). Fibers are formed as the molten polymer exits the 500 or more tiny holes (ca 0.2 mm) of each spinnerette, where it is immediately quenched by chilled air. Since a key objective of the process is to produce a relatively wide (eg, 3–4 m) web, individual spinnerettes are placed side by side in order that sufficient fibers be generated

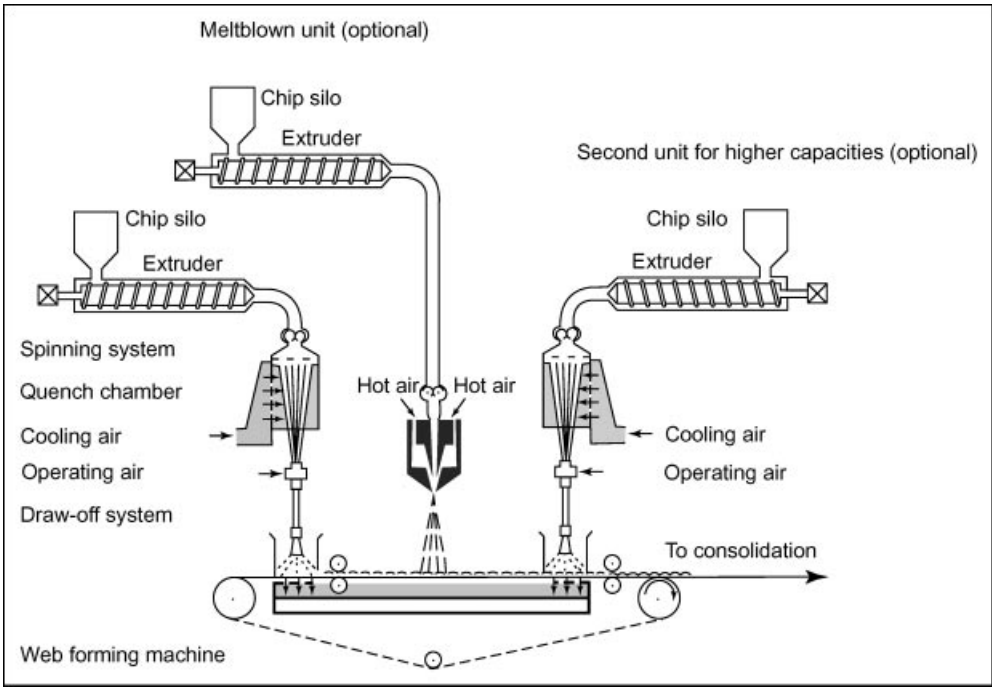

Fig. 4. Typical multibeam spunbonded process (3).

across the width. This entire grouping of spinnerettes is often called a block or bank, and in commercial production it is common for between two and four blocks, but as many as eight, to be used in tandem in order to increase the coverage and uniformity of laydown of the fibers in the web.

Most spunbond machinery producers now utilize large rectilinear spinplates in lieu of multiple small individual spinnerettes. In effect, the spinning plate is slightly wider than the desired web, and a continuous curtain of filaments is formed providing uniformity from point to point relative to multiple side by-side-spinnerettes in a block. Each spinbeam can contain up to 30,000 holes and it is common for multiple spinbeams to be used in tandem to further improve uniformity and increase throughput.

Prior to deposition on a moving belt or screen, the molten polymer threads from a spinnerette must be attenuated to orient the molecular chains of the fibers in order to increase fiber strength and decrease extendibility. This is accomplished by hauling the plastic fibers off immediately after they have exited the spinnerette. In practice, this is done by accelerating the fibers either mechanically (17) or pneumatically (17–19). In older processes, the fibers are pneumatically accelerated in multiple filament bundles; however, most new installations accelerate an entire beam or curtain of filaments (20–22).

In traditional textile spinning, some orientation of fibers is achieved by winding up the filaments at a rate of 3000–5000 m/min to produce the so-called partially oriented yarns (POYs) (23). The POYs can then be mechanically drawn in a separate step to achieve maximum strength. In spunbonded production, filament

bundles are partially oriented by being pneumatically accelerated at speeds of 6000 m/min or greater (19,24). Accelerating the filaments at such great speeds not only achieves a partial orientation but results in extremely high rates for web formation, particularly for lightweight structures (eg, 15 g/m^2). The formation of wide webs at high speeds results in a high efficiency of manufacture. Newer processes have been commercialized, that can accelerate filaments at speeds up to 8000 m/min and simultaneously create very small fiber deniers with high throughput (25).

For many applications this partial degree of orientation imparts a sufficient increase in strength and decrease in extendibility to make the final bonded fabric perfectly functional; eg, diaper coverstock. However, some applications, such as geotextiles and primary carpet backing, demand that the filaments achieve a very high tensile strength and low degree of extension. This requires subsequent additional attenuation, such as the mechanical drawing of filaments, a process usually accomplished over heated rolls with a typical draw ratio of ca 3.5:1 (17). After drawing, the filaments are pneumatically deposited onto a moving belt or screen. Because drawing rolls cannot normally dispatch filaments as fast as pneumatic jets, the web-forming process is usually less rapid, although the resulting web has greater physical strength.

The pneumatic deposition of the filament bundles onto the moving belt results in formation of the web. A pneumatic gun uses high pressure air to move the filaments through a constricted area of lower pressure but higher velocity, as in a venturi tube. Pneumatic jets used in spunbonded production have been described (17,24). Unfortunately, the excellent filament uniformity coming out of the spinnerette is lost when the filaments are consolidated going through a gun.

In order for the web to achieve maximum uniformity and cover, it is imperative that the individual filaments be separate from each other prior to reaching the belt. Failure to sufficiently separate individual filaments results in the appearance of "ropes" in the web. One method used to effect this state of separation is to induce an electrostatic charge onto the bundle while still under tension and prior to pneumatic deposition. The charge may be induced either triboelectrically or more typically by applying a high voltage charge to the filaments (26). The level of electrostatic charge on the filaments must be at least 30,000 esu/m^2 of filament surface area (16) to be effective. After deposition onto the moving belt, it is necessary to discharge the filaments; this is usually accomplished by bringing the filaments in contact with a conductive grounded surface. In some cases, the deposition belt is made of conductive wire and connected to ground. The electrostatic repulsion method has the advantage of being relatively simple and reliable. Producing webs by spinning rectilinearly arranged filaments through a so-called slot jet reduces or eliminates the need for such bundle-separating devices (20,21), because the filament bundles are not collapsed en route to the belt as they are in a pneumatic gun.

Other routes to reachieving filament separation have been described and rely on mechanical or aerodynamic forces to affect separation. Figure 5 illustrates one method that utilizes a rotating deflector plane to force the filaments apart while depositing the opened filaments in overlapping loops (27). After the splayed filaments fall to the deposition surface or forming screen, a suction from below the disposition surface holds the fiber mass in place.

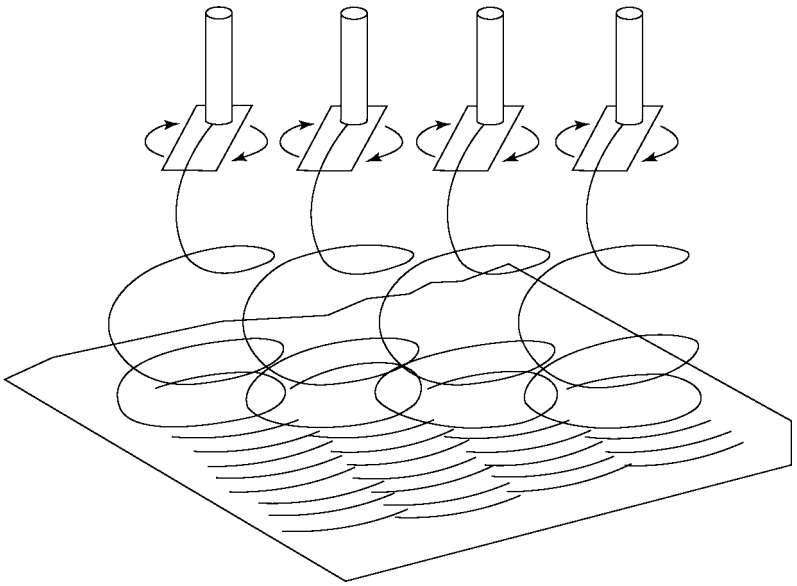

Fig. 5. Deflector plane for separation of filaments.

For many applications, it is acceptable or desirable to lay down the filaments in a random fashion without orienting the filament bundles with respect to the direction of the laydown belt (24). However, it is sometimes desirable to control the directionality of the splayed filaments on the laydown belt in order to achieve a particular characteristic in the final fabric. Directionality can be controlled by traversing the filament bundles either mechanically (19,27) or aerodynamically (17,28) as they travel downward toward the collecting belt. The aerodynamic method consists of supplying alternating pulses of air on either side of the filaments as they emerge from the pneumatic jet. By properly arranging the spinnerette blocks and the directing jets, laydown can be achieved predominately in the desired direction. Figure 6 illustrates the production of a web with predominately machine and cross-machine direction filament laydown (17). It is possible to generate highly ordered laydown patterns by oscillating filament bundles between closely spaced plates to achieve a high degree of parallelism.

If the laydown belt is moving and filaments are rapidly traversed across this direction of motion, the filaments are deposited in a zigzag or sine wave pattern on the surface of the moving belt. The effect of the traverse motion on the coverage and uniformity of the web have been described mathematically (29). The relationships between the collecting belt speed, period of traverse, and the width of filament curtain being traversed determine the appearance of the formed web upon the laydown belt. Figure 7 illustrates the laydown for a process where the collecting belt travels a distance equal to the width of the filament curtain, x, during one complete period of traverse across a belt width y. If the belt speed is v_b and the traverse speed is v_t, the number of layers deposited, z, is calculated by the formula, $z = (x \cdot v_t)(y \cdot v_b)$. It can be seen that if the traverse speed is twice the belt speed and if x and y are equal, then a double coverage will occur over all areas of the belt.

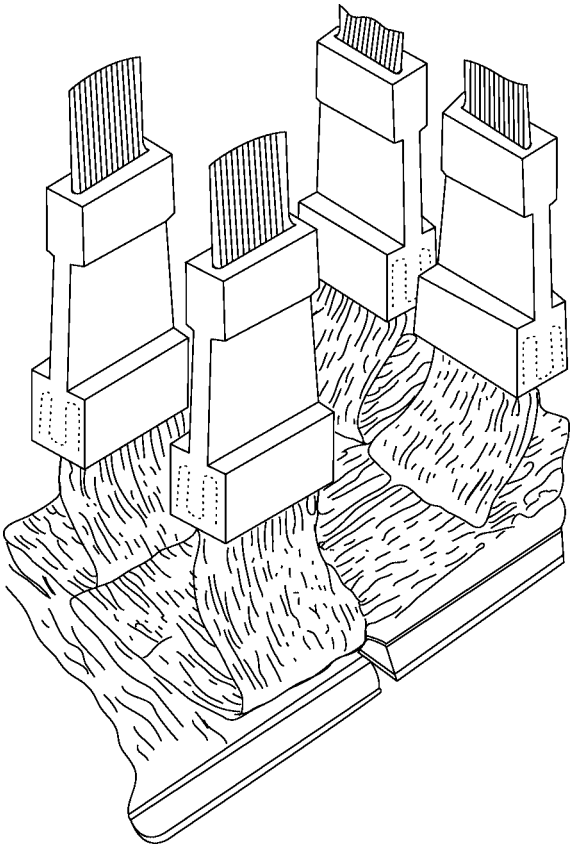

Fig. 6. Web production with predominantly machine and cross-machine direction.

The alternative to the use of multiple spinnerettes per bank, and now the most widely utilized process, is the so-called curtain spin process, which utilizes a single plate of the width of the desired web which has been drilled with holes for fiber formation. The advantage to this approach is that it results in a uniform distribution of filaments within the curtain of continuous fibers produced from the

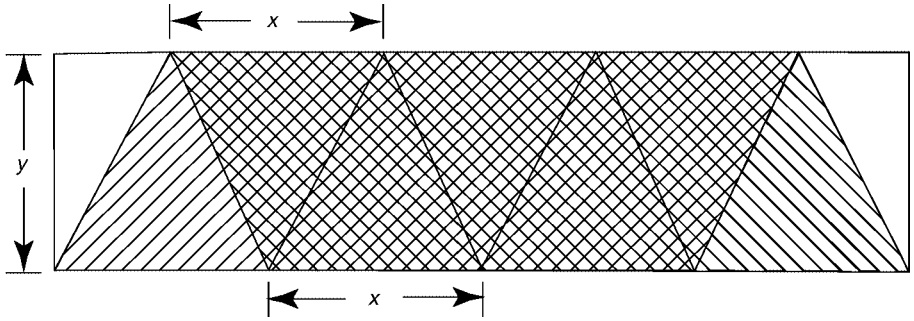

Fig. 7. Laydown pattern diagram.

spinning plate. The use of the single uniform distribution of filaments within the curtain of continuous fibers is produced from the spinning plate. The use of the single spinning plate automatically places the fibers in a uniformly distributed array and thereby presents a curtain of high uniformity filaments to the fiber attenuation mechanism. Care must be taken to keep individual filaments from sticking while they are still plastic, which is normally in the quench or cooling area between the spin plate and the laydown jet.

By comparison, the multiple spinnerette per bank process requires additional effort prior to laydown in order to compensate for the gaps between the individual spinnerettes. Failure to present a uniformly distributed filament array to the laydown screen will result in spot-to-spot variations in fiber density and a web that has the appearance of blotch.

In general, once the curtain of filaments has been produced, it is necessary to attenuate the filaments in order to provide strength and resistance to deformation. The most commonly practiced approach is to utilize a single slot, which is at least the width of the curtain, at a point below the spinning plate and above the laydown screen. There are three practical approaches taken. The first utilizes the injection of low pressure air at a point above the slot so that the fibers attain sufficient acceleration in the slot to provide adequate draw (21) (Fig. 8). The second utilizes a low pressure vacuum below a venturi to provide the pressure differential required for sufficient acceleration and resulting attenuation (30). The third utilizes an acceleration slot immediately below the spin plate with little or no quench or cooling of the filaments (25).

One of the limitations of the curtain–slot draw process has been that the amount of fiber attenuation is constrained because of the short distance generally allowed between the spinnerette and the venturi slot, and the use of relatively low pressure air for drawing so as not to induce high turbulence in the area of the laydown. In order to adapt this concept for the production of polyester fabrics that inherently require much higher fiber acceleration to attain the desired polyester fiber properties, a new process has been commercialized (25).

Bonding

Many methods can be used to bind the fibers in the spun web. Although most procedures were originally developed for use with nonwoven staple fibers, three were adapted for use with continuous filaments: mechanical needling, thermal, and chemical/binder. Thermal and chemical–binder methods may bond the web by fusion or adhesion of fibers using either large or small regions, generally referred to as area bonding and point bonding, respectively. Point bonding results in the fusion of fibers at discrete points with fibers remaining relatively free in between the point bonds. Other methods that are used with staple fiber webs, but which are not routinely used with continuous filament webs, are stitchbonding (29,31), ultrasonic fusing (8,32), and hydraulic entanglement (33). Hydraulic entanglement is currently being developed as a high speed bonding process for spunlaid webs as a way to achieve superior softness. It has the potential to produce the most radically different continuous filament structures; however, it has the disadvantage of being a more costly and complex bonding process.

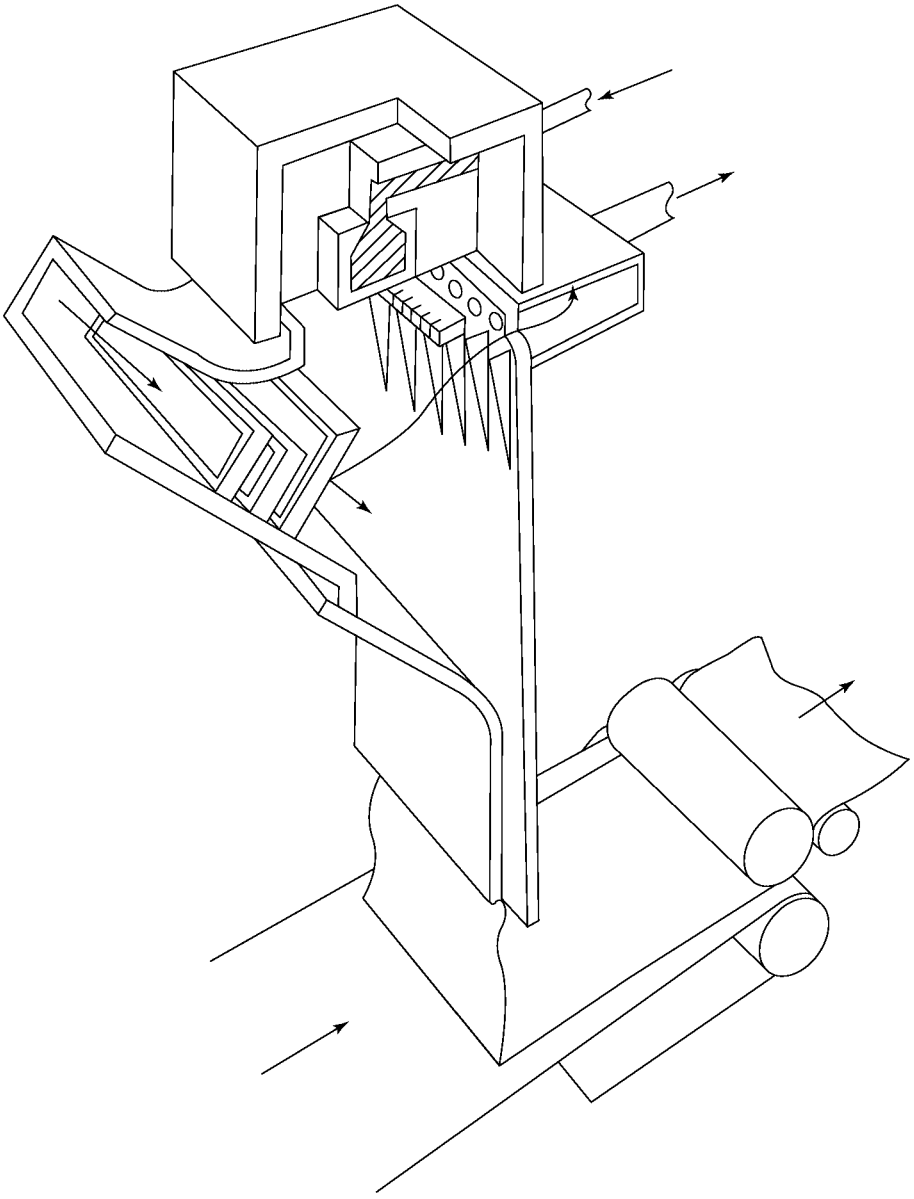

Fig. 8. Curtain spinning process (22).

Of the three standard bonding methods used in spunbonded manufacturing, mechanical needling, also called needle punching or needle bonding, is the simplest and least expensive. Although it is the oldest process, it continues to be widely used. Significant improvements in throughput and flexibility have resulted in the sales growth of needle-bonded fabrics, particularly for geotextiles (qv) and roofing. An excellent review of mechanical needling technology has been published (29).

In the needle-punching process, a continuous filament web is subjected to barbed needles which are rapidly passed through the plane of the moving spun web (see NONWOVEN FABRICS, STAPLE FIBERS). The needles pass in and out of the web at frequencies exceeding 3,000 strokes/min that can result in as many as 500 penetrations/cm^2 depending on the needle density and the line speed, which can be as high as 150 m/min (34). The effect of this operation is to interlace the fibers and thus bond the structure together, relying only on the mechanical entanglement and fiber-to-fiber friction. The fabric produced tends to be more conformable and bulky than fabrics bonded by thermal or chemical/binder methods. Because the fibers have freedom to move over each other, the fabric is easily deformed and exhibits a low initial modulus (Fig. 2).

The principal variables in needle-punching are the needle design, punch density, and depth of punch. Considerable research has been conducted on the shape and design of the needles and how this affects the interlacing of the fibers (29). Needling produces a fabric that is 100% fiber with no points or areas of fusion or melting, thus it is easily adapted to most fiber webs and requires less precise control than thermal bonding. In addition it is the only bonding method suitable for the production of spunbonded fabrics of very high basis weights, eg, 800 g/m^2. It is, however, only suitable for the production of uniform fabrics greater than ca 80 g/m^2 because needling tends to concentrate fibers in areas resulting in loss of visual uniformity at lower weights.

Unlike mechanical needling, both thermal and chemical/binder bonding depend on fiber-to-fiber attachment as the means of establishing fabric integrity. It is the degree and extent of attachment that determines many of the fabric qualities, most notably the hand or softness. Because point bonding can be accomplished using as little as 10% bonding area, (ie, 90% unbonded area), such fabrics are considerably softer than area-bonded structures. Fiber mobility is retained, in part or in total, outside the areas of the point bonds. Thermal bonding is far more common than chemical–binder bonding and is generally more economical because the latter method adds the cost of resin and still requires a thermal curing treatment as the final step. Both area and point thermal bonding are rapid processes having line speeds in excess of 300 m/min and up to 800 m/min during production of lightweight fabrics.

Area thermal bonding can be accomplished by passing the spun web through a source of heat, usually steam or hot air. Prior to entering the bonding area, the spun web may be consolidated by passing it under compressional restraint through a heated prebonding area which adds integrity to the web (10). While in the bonder, the consolidated web is exposed to hot air or pressurized steam that causes fusion to occur between some, but not all, of the fiber crossover points. Complete fusion leads to a paper-like structure with low resistance to tearing. The spun web may contain small percentages, typically 5–30%, of a lower melting fiber (10), or the filaments may contain undrawn segments that are lower melting than the drawn or matrix segment (28). Heterofilament structures utilize a lower melting covering (sheath) on the outside of the filaments to effect fusion. Both polyethylene and nylon-6 have been used as the lower melting sheath in commercial spunbonded products.

The use of steam is generally limited to polypropylene and polyethylene fusion because impractical pressures are required to reach the temperature levels

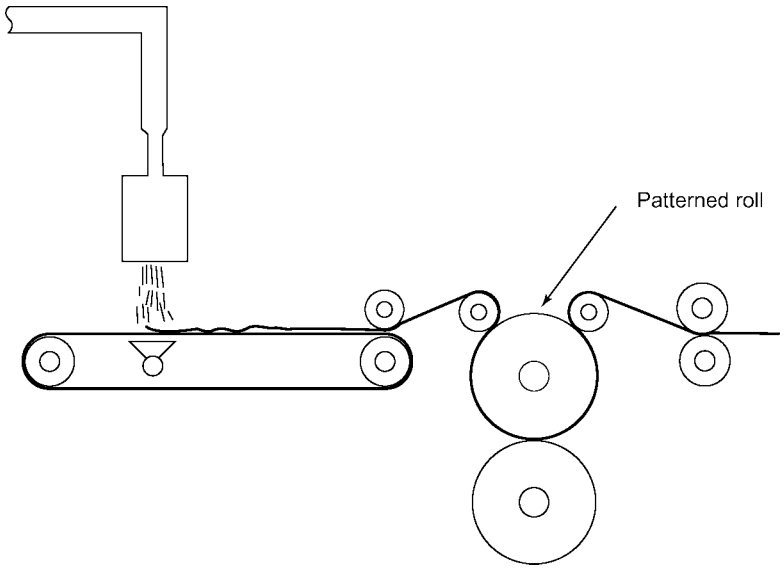

Fig. 9. Pattern bonding roll at the end of a spun bonding line.

(eg, >200°C) required for bonding polyesters. In general, greater temperature control is required for area bonding polypropylene than for other polymers because the temperature difference between the matrix and binder fibers can be only 3°C (28).

Whereas thermal area bonding uses temperature as the variable to a great degree and relies on sophisticated web structures containing binder fibers, thermal point bonding utilizes both temperature and pressure to affect fiber-to-fiber fusion. Thus it is a simpler approach to bonding because it does not require the web to contain lower melting fibers or segments and is less demanding of the technology required to produce the web. Point bonding is usually accomplished by passing a web, previously consolidated or compacted with either heated or unheated press rolls, through heated nip rolls, one of which contains a raised pattern on its surface (Fig. 9). When bonding, polypropylene roll temperatures generally do not exceed 170°C; however, pressures on the raised points are quite high, preferably 138–310 MPa (20,000–45,000 psi) (35). The degree of bonding between the points can be controlled by varying the ratio of heights of the raised points to the depth of the web (36). Typically only 10–25% of the surface available for bonding is converted to fused, compacted areas of bonding.

Optimum conditions of pressure and temperature are dependent on many variables including, but not limited to, the nature of the web, line speed, and engraved pattern. Optimized conditions are best obtained through detailed investigations and much experience. Even subtle changes in any of these variables can result in significant changes in the properties of the finished fabric (7,8). New designs for bonding calenders continue to refine the process (37).

Because engraved point bonding rolls can be as wide as 5 m, the problem of maintaining uniform pressure across the width must be addressed. Small differences in pressure across the width can produce an unacceptably variable product.

Hydraulic pressure is applied at the ends to the roll causing a slight deflection that results in less pressure being applied in the center compared to the ends. A number of solutions to this problem have been devised (37), including cambering wherein the roll diameter decreases slightly from the center to the ends and mechanical means such as pressurizing the external shell of one of the two nip rollers.

Chemical–binder bonding is used less frequently than thermal bonding in the production of spunbonded fabrics, and in a shift over the past decade the same is also true for staple fiber nonwovens. Resin binders are occasionally used with spunbonded webs to achieve special characteristics that are unattainable thermally (38). In a typical case, acrylic resin(s) are applied to saturate the web, excess resin is removed by nip rolls, and the wet web is passed through a drying oven to remove excess water and cure the resin which tends to concentrate at fiber–fiber junctions. By curing the resin, a thermoset binder conveys high thermal dimensional stability to the web for applications such as roofing.

Resin binders may alternatively be applied in discreet points in a pattern so as to immobilize fewer fibers and produce a softer fabric; however, it is difficult to accurately control the diffusion of the resin, and the drying step requirements make it less attractive than thermal bonding.

Chemical bonding with hydrogen chloride gas has been used with spun webs of nylon-6,6 to commercially produce spunbonded nylon fabrics (39). In this bonding process, the activating hydrogen chloride gas is passed over web fibers held in close contact by tension. The hydrogen chloride disrupts hydrogen bonds between the polymer chains and forms a complex with the amide group. When the gas is desorbed the process reverses, this time with new hydrogen bonds formed between polymer chains in different fibers. This basic method has been further refined to permit only the formation of pattern bonds, whereby fiber mobility is retained between the bonded areas yielding a softer hand to the bonded fabric (40).

Bonding a web by any means allows for certain generalizations. If the web is highly bonded, most of the fibers are bonded to another fiber. The resulting structure is relatively stiff, paper-like, and has higher tensile and modulus but lower resistance to tear propagation. On the other hand, if the web is only slightly bonded fewer fiber-to-fiber bonds are present and the structure is more conformable with lower tensile and modulus but higher resistance to tear propagation due to bunching of filaments. Additionally, webs that are only slightly bonded exhibit low surface abrasion resistance. In comparing area to point bonding, greater varieties of structures are achievable through point bonding because of the various bonding roll patterns available. The expense associated with the manufacture of the pattern roll generally dictates the careful selection of the pattern, however.

Meltblown Fabrics

Meltblown fabrics differ from the traditional spunbonded fabrics by having lower fiber denier (fineness) and by usually being composed of discontinuous filaments. Although meltblown fabrics are not generally referred to as spunbonded, the integration of spinning, attenuation (although slight), laydown, and bonding during the production of meltblown webs describes a process traditionally defined as spun

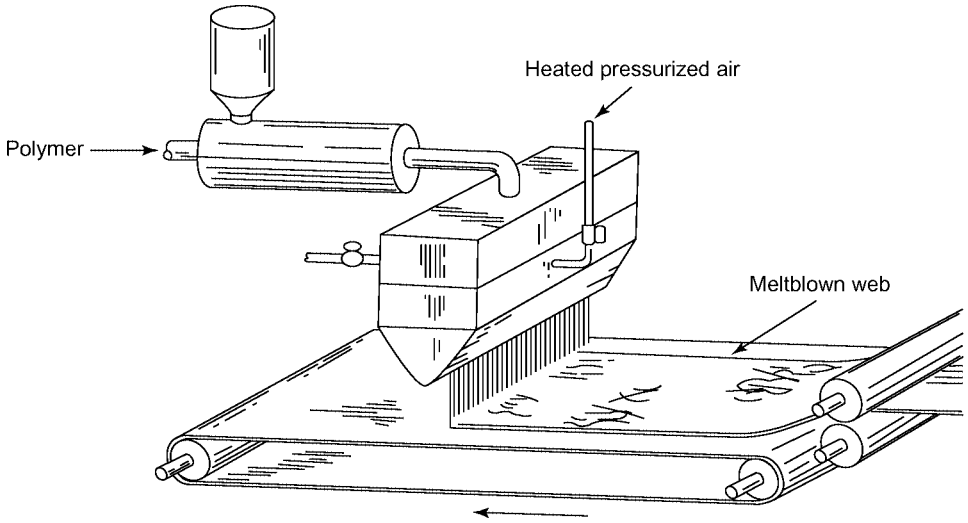

Fig. 10. Schematic of the meltdown process.

bonding. The inherent fiber entanglement often makes additional bonding unnecessary, however. Fibers produced by melt blowing are very fine, having typical diameters of 3 μm (41,42), smaller by nearly an order of magnitude than traditional spunbonded fibers. The fibers are extremely fine and largely unoriented, causing the webs to be quite weak and easily distorted. Most thermoplastic polymers have been meltblown, but the majority of commercial products are produced from high melt flow grade polypropylene.

In the manufacture of meltblown fabrics, a special die is used in which heated, pressurized air attenuates the molten polymer filament as it exits the orifice of the dye or nozzle (Fig. 10). Air temperatures range from 260 to 480°C with sonic velocity flow rates (43).

The rapidly moving hot air greatly attenuates the fibers as they exit from the orifices to create their small diameters. The fibers are relatively weak and deposited on the forming screen as a random entangled web that may be thermally point bonded to improve strength and appearance. The web may also be deposited onto a conventional spun web, then thermally bonded. Sandwich structures, called SMS, are routinely created with the meltblown web in the middle between two conventional spunbonded webs (44). Other materials, eg, cellulosics, have been blended into the meltblown filament stream to yield a meltblown structure with a unique combination of properties (45). Mixtures of meltblown and crimped bulking fibers have been sold as thin thermal insulation for use in outdoor clothing and gear (46). Meltblown technology has also been adapted to produce nontraditional spunbonded fabrics, such as elastomeric webs (47).

The great quantity of very fine fibers in a meltblown web creates several unique properties such as large surface areas and small (<1 μm) pore sizes. These have been used in creating new structures for hospital gowns, sterile wrap, incontinence devices, oil spill absorbers, battery separators, and special requirement filters. During the last decade, meltblown technology has experienced large growth mainly in the form of SMS or SMMS sandwich structures in hygiene (6).

Flashspun Fabrics

The process of producing spunbonded webs by flash spinning is a radical departure from the conventional melt spinning approach. In melt spinning, a molten polymer is typically extruded through a spin plate containing ~20,000 tiny holes. This produces a fiber curtain containing ~20,000 fibers, each typically 15–50 μm in diameter. The fibers are kept separate from each other until the bonding operation connects some or all of them.

By contrast, flash spinning begins with a 10–15% polymer solution prepared by dissolving a solid polymer, such as high density polyethylene, with a suitable solvent, such as pentane, trichlorofluoromethane, or methylene chloride (48). The solution is heated to approximately 200°C, pressurized to ~4.5 MPa (653 psi), and the pressurized vessel is connected to a spinnerette containing a single hole. When the pressurized solution is permitted to expand rapidly through the hole, the low boiling solvent is instantaneously flashed off leaving behind a three-dimensional film–fibril network referred to as a plexifilament. The three-dimensionality results from the cross-linking interconnection of the fine fibers which produces a film thickness of 4 μm or less (48). Thus many individual but interconnected fibers are created from a single-hole spinnerette.

It is believed that bubbles form rapidly as the pressurized solution undergoes depressurization during spinning and the bubbles may grow and rupture, thus forming the plexifilamental network (48). Gases that are effectively insoluble in the solvent may be added to the pressurized solution in order to facilitate high rates of bubble nucleation.

When a multiplicity of single-hole spinnerettes are assembled across a width, the plexifilaments produced can form a wide web that can be thermally bonded to produce a flat sheet structure (49). The web-forming procedure is ameliorated by use of a baffle that deflects the stream of plexifilaments after exiting the spinnerette.

Unlike fine fibers prepared by melt blowing, the plexifilaments from flash spinning are substantially oriented and possess relatively high tenacities [0.08 N/tex ($>$1g $\cdot$ f/den)]. The plexifilaments scatter light effectively as a result of high surface areas (ca 2 m^2/g) and thus form opaque webs. In addition, the fineness of the plexifilament fibrils also results in a web structure of exceptional softness. Webs are either area or point bonded to yield paper- or cloth-like aesthetics, respectively. The paper-like sheets are used as durable papers and may be printed using conventional inks (qv) and printing equipment, whereas the point-bonded structures are very soft and find use in disposable protective clothing.

Flash spinning is the most complex and sophisticated method for manufacturing spunbonded fabrics. A single production line can require an investment of nearly $200 million, and serious safety issues must be addressed in the plant's design and operation. Although the process has been in use since 1962, the need to spin heated and pressurized solutions under precise conditions has resulted in only one company (DuPont) practicing the technology as a route to these unique spunbonded products. A second producer (Asahi) stopped producing in Japan some years ago after forming a marketing joint venture with Du Pont. Hydrocarbon solvents are now being used for the process since chlorofluorocarbons, the traditional solvents, are restricted because of environmental regulations (50).

The physical properties of flashspun fabrics are unique and not attainable via the melt-spun spunbond process. Even bicomponent melt spinning cannot produce similar structures. As a result the profitability of a flashspun operation is very high when the capacity of a line is fully utilized.

Test Methods

Spunbonded fabrics are characterized by standardized test procedures originally developed for textile fabrics and paper products. The Association of the Nonwoven Fabrics Industry (INDA) has published a list of test procedures (Table 4) (51) which are routinely used in determining specific physical characteristics of spunbonded and other nonwoven fabrics. Analogous test methods are published in Europe by EDANA, the European Association of Nonwoven Fabrics. INDA and EDANA are working together to develop and publish harmonized international test procedures. Many tests are established for the evaluation of nonstrength-related properties such as washability, stiffness, and softness. Great strides have been made in the test methodology used to evaluate the hand of materials for textile applications such as clothing. A methodology and equipment, permitting quantitative evaluation of fabric hand, have been developed (52).

As applications are developed, the need for new end use specific test methods grows. Geotextile uses are a good example of how a large new application requires the design of new test methods (54). In addition to break, stretch, tear, and burst resistances described in Table 4, geotextile fabrics are tested for puncture, maximum opening size, permittivity, and asphalt retention, according to IST 180.1–9. The puncture test notes the resistance to being punctured by a probe with either a flat or spherical tip. Maximum opening measures the largest size glass beads that can pass through a fabric, thereby reflecting the size of soil particles that can be stopped by a geotextile. Permittivity is how fast water, at a given pressure, passes through a geotextile. Asphalt retention is judged by how much asphalt cement is left in a geotextile after it is dipped in the cement and allowed to drain, and what change in area the geotextile undergoes.

Long-term applications also demand test methodology on the aging characteristics of spunbonded fabrics. Roofing applications, for example, require that the saturated fabrics retain their strength for many years despite a hostile environment. By heating the fabric at several different temperatures higher than the expected nominal conditions, and measuring the time it takes to observe a significant property change, for instance loss of 50% tensile strength, effects can be plotted to permit some extrapolation back to expected nominal conditions (55). The importance of aging tests will increase as more long-term applications are developed for synthetic fabrics. The Swedish Building Institute has developed heat aging tests and standards for films and fabrics used in building construction. Canada has established a number of longevity and performance test procedures for construction fabrics, such as housewrap.

In medical applications, many test procedures have been developed for screening the efficiency of fabrics to block the passage of viruses, blood-borne pathogens, etc. Spunbonded SMS sandwich fabrics are widely used as protective

Table 4. INDA Test Methods[a]

Property	Description	IST number
Absorbency	Amtount of liquid absorbed and speed of absorption	10.1–3
Abrasion	Resistance of nonwovens to being worn away	20.1–5
Bursting strength	Force to rupture nonwoven under water pressure	30.1
Electrostatic properties	Amt of charge that can build up on a sample	40.1–2
Optical properties	Opacity: resistance to light being passed brightness: whiteness	60.1–2
Permeability	Ease of air or water vapor passage under pressure	70.1–2
Repellency	Resistance of nonwovens to wetting and penetration after exposure to water, salt solutions, alcohol, and hydrocarbon solvents and oils	80.1–9
Bacterial	Resistance of a nonwoven to penetratration by bacteria in a salt solution under water pressure	
Stiffness		
Cantilever	Tendency for a nonlimp nonwoven to droop as it is pushed over the edge of a surface	90.1
Curly	Ability of a heavy, stiff nonwoven to push a pendulum aside as it is moved past it	90.2
Handle-O-Meter	ability of a soft, lightweight nonwoven to flex and not drag as it is pushed through an opening	90.3
Tear	Resistance of a nonwoven to continue to tear after being cut and pulled from both sides	100.1–3
Breaking load and elongation	Force to break a nonwoven when it is pulled from both ends; extent of stretching before breaking	110.1–4
Seam breaking	Force needed to break a seam holding two pieces of nonwoven together when the sample is pulled from both ends	
Bond strength of laminates	Force to separate a nonwoven from another material after they have been laminated together	
Internal bond strength	Force to pull a nonwoven fabric into two plies	
Thickness	How thick a nonwoven is when it is held between a weight and a surface	120.1–2
Coefficient of friction	Drag when a nonwoven is slid over itself or over a polished surface	140.1
Dry cleaning and laundering	Shrinkage, loss of strength, ability to be peeled apart experienced by a single fabric or laminate	150.1
Linting	Extent of particles loosened from nonwoven as it is bent and flexed in air stream	160.1
Extraction	Amt of material leached out of nonwoven after exposure to hot solvents	190.1

[a] Ref. 53.

gowns in hospital operating rooms because of their combination of barrier and comfort.

Overall, the test methods published by INDA (Table (4)) continue to be the general tests used to characterize fabrics; however, specific market applications often generate special test procedures to fulfill unique needs.

Applications for Spunbonded Fabrics

Uses for spunbonded fabrics have traditionally been segmented into durable and disposable categories. In the early 1970s, consumption of spunbondeds was predominately for durable uses such as carpet backing, furniture, bedding, and geotextiles. By 1980, however, disposable applications accounted for an increasingly large percentage because of the acceptance of lightweight (eg, 17 g/m^2) spunbonded polypropylene fabrics as a coverstock for diapers and incontinence devices (6). In the 1990s, the use of new diaper and training pants designs have increased the demand for lightweight fabrics far beyond earlier predictions.

Both the durable and disposable markets for spunbondeds have experienced dramatic growth (~6% per year). Disposable applications utilize the vast majority of the yardage produced although only ~50% on a tonnage basis (56). Significant areas of durable growth have been in the building and construction industries where spunbondeds are used in geotextiles, roofing membranes, and Housewrap. Growth has also been achieved in primary carpet backing in automotive carpets and carpet tiles, where moldability and high dimensional stability, respectively, were achieved through the use of polyester spunbonds.

With the possible exception of Housewrap, however, there have been virtually no new markets established as a result of the special characteristics of spunbonded fabrics. Growth has come about in an evolutionary fashion where spunbonded fabrics were substituted for woven fabrics, other nonwoven fabrics (including knits), paper or film in previously existing applications, or where the cost–property relationship has permitted an extension of an existing application, such as the redesign of diapers. The principal contributions that spunbondeds have made in these markets generally have been attractive economics, or improved processibility and performance in the final product. This combination has greatly accelerated the use of the products within an application and consequently contributed to the growth of specific markets. General market opportunities for nonwovens have been reviewed (6,7,56).

Of the four basic polymer types available in spunbonded form (ie, polypropylene, polyethylene, polyester, and nylon), both polyester and nylon are more costly polymer forms than either of the olefins. It is possible for this cost advantage to be offset by other factors, such as production of the fabric in lighter unit weight, but in general olefin-based products have an economic advantage for an equivalent weight fabric. In addition, the lower density of olefinic polymers provides a greater "yield" of more fibers per unit area, which provides better cover and performance. In some applications, however, this advantage is moot if the olefin-based product cannot perform properly. An example of this is in roofing membranes where a key requirement is dimensional stability to hot bitumen at temperatures approaching 200°C, which is above the melting point of both polypropylene and polyethylene

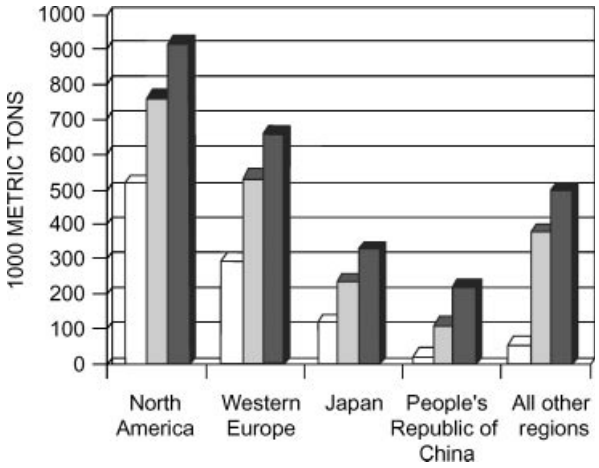

Fig. 11. Global demand forcost for nonwoven fabrics. □ 1988; ■ 1996; ■ 2001 (57).

but well within the performance limits of polyester. To a great extent this one property, ie, higher temperature resistance, largely differentiates the opportunities for polyester spunbondeds versus olefinic counterparts. Although polyester fibers exhibit higher modulus and more flexible dyeing, these properties seem to be of little advantage in the markets for spunbonded fabrics.

Spunbonded Markets: Durable Applications. A summary of late 1990s markets for nonwoven fabrics in the United States and western Europe is shown in Figures 11, 12, and 13. Approximately 37% of total global nonwoven production for 2001 was estimated as being spunbonded (1). In North America this represents 550,000 t of spunbonded production with volume growth of 8.5% per year for the period 1996–2001 (1). The principal durable applications center around construction and automotive applications although there are other smaller areas.

One of the first durable applications was the use of spunbonded polypropylene in primary carpet backing. First introduced in the mid-1960s as a replacement for woven jute, it is still used in specialty carpets and holds a unique position in applications that require isotropic planar properties for dimensional stability such as printed or patterned carpets. The finer fiber versus woven ribbons or jute also allows tufting needles to penetrate with little deflection where fine-gauge tufting is desired. Finally, because the spunbonded backing is bonded at many fiber junctions, it offers the advantage of maintaining clean edges after cutting or trimming, making it attractive for use in small rugs where the unraveling feature of woven ribbon backings can be a concern. Although the first spunbonded primary carpet backing was made from polypropylene, other spunbonded products based on polyester and polyester–nylon were later commercialized as tuftable carpet backing products, mainly for automotive uses.

An extremely successful application for spunbonded fabrics is in the area of furniture, bedding, and home furnishings. In furniture construction the use of lower cost spunbonded fabrics has become routine, whereas in the 1970s woven sheeting dominated the market. Spunbondeds are used in hidden areas requiring

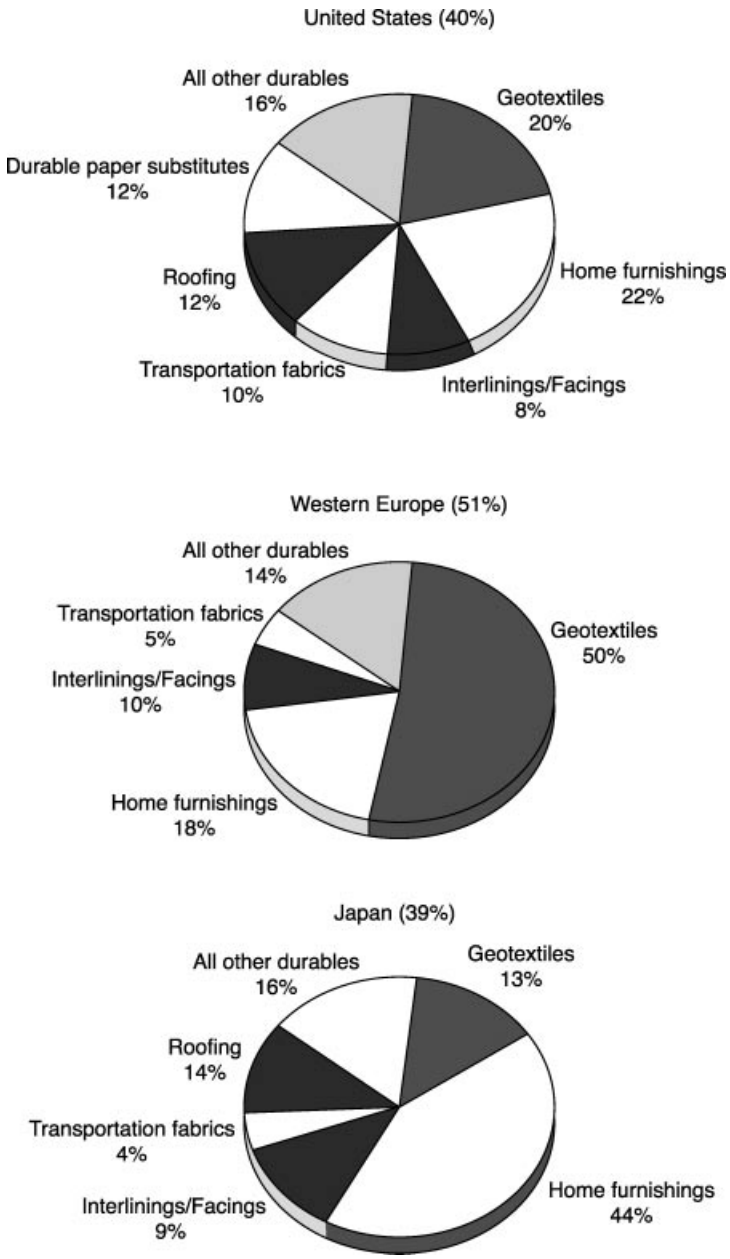

Fig. 12. Durable nonwovens market demand by applications and region (58).

high strength and support in chairs, sofas, and other seating. The bottoms of chairs are often covered with dust covers made of spunbonded fabrics because of the nonfraying characteristics, high porosity, excellent cover, and low cost. An inherent resistance to rot and mildew versus natural fabrics also adds to the popularity of spunbonded fabrics in home uses.

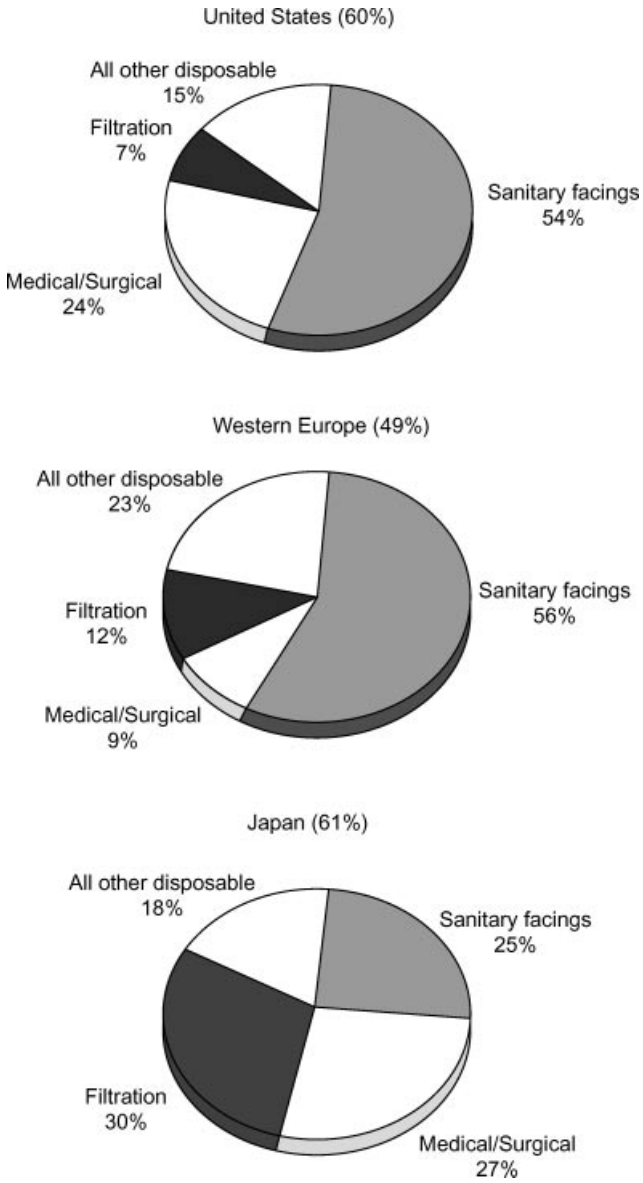

Fig. 13. Disposable nonwovens market demand by applications and region (59).

In bedding, spunbondeds are used as spring insulators, spring wrapping in mattress construction, dust covers under box springs, and facing cloth for quilting. Home furnishing uses include mattress pad covers where the spunbonded fabric serves as the top and bottom of a sandwich structure with a middle layer of fiberfill and fastened by ultrasonic quilting. Draperies also have used spunbonded fabrics wherein the lightweight fabric serves as a stitching medium for use with stitch-bonding equipment. Spunbonded fabrics are also used in blinds, both vertical and

horizontal, wherein the fabric, which must be extremely uniform, may be saturated with colored resins to form opaque and optionally pleatable blinds.

A high growth application for spunbonded fabrics is the air infiltration barrier whereby the penultimate vertical surfaces of old or newly constructed houses are covered with a layer of spunbonded fabric followed by the application of the ultimate external sheathing such as siding or masonry. The objective is to construct a barrier to the infiltration of air into the wall cavity and to the insides of homes, thus lowering the cost of heating and cooling. Tests conducted by the National Bureau of Standards and the National Association of Homebuilders confirmed the effectiveness of the air infiltration barrier concept as a means of lowering the cost of heating a home (60). Certain spunbonded fabrics are well suited for this application because they possess a unique combination of properties required for functionality. These include resistance to the penetration of liquid water and low porosity to air currents, but with a simultaneously high transport of moisture vapor. In a winter climate, warm moist air from inside the house can penetrate through the wall cavity and to the outside. If the air barrier material is not sufficiently permeable to moisture vapor, condensation can occur inside the wall cavity where damage from moisture can occur. In addition, the effective R-value of the insulation (eg, fiber glass) inside the wall cavity is diminished by the presence of liquid and solid water. Trapped moisture in wall cavities provides an opportunity for the growth of molds, a growing concern in warm moist climates. The combination of water and air current resistance combined with breathability to moisture vapor and high tensile and tear strength is a difficult combination of properties to assemble. Spunbonded technology can provide these characteristics in economical form.

Uses for nonwovens in automobiles have grown from a rather modest beginning in the 1970s to a position of significance (58). Although needle-punched nonwoven fabrics have been used in large-area applications, such as backing for vinyl seats and landau tops, spunbonded fabrics have, historically, been utilized in lower volume applications such as labels for seat belts, spring insulators, listings in seats, and as coated fabrics for ducting. Spunbonded polyester has become accepted as a tuftable backing in molded carpets where the use of spunbonded backing allows for greater molding precision, improved dimensional stability, and resistance to puncture. Newer applications include headliners, which are often complex composites that can be molded into sophisticated shapes. Lightweight spunbonds are used as sound insulators in between dashboard components, and as the base fabric in interior door panels and sun visors.

Material acceptance in roofing applications has changed significantly since the mid-1970s, particularly for spunbonded fabrics. The market opportunity is extremely large and is thought to exceed 1.86×10^8 m^2 for commercial buildings (flat roofing) in the United States alone. Much of the development for roofing applications was done in Europe and slowly became accepted in the United States. Although fiber glass fabrics have been the largest volume nonwoven consumed in roofing, spunbonded polyester and polypropylene have made considerable penetration (61). A significant difference between glass and polyester is the ability of polyester to flex and stretch without damage to the filaments. Because rooftops are known to expand and contract with seasonal changes, fabrics of polyester are less susceptible to damage from sudden temperature fluctuations which induce rapid dimensional changes.

Spunbonded polyester is basically a carrier for bituminous waterproofing membrane. Here spunbonded fabric is saturated with bitumen and serves to provide integrity and dimensional stability to the bitumen. As bitumen coatings modified with elastomeric polymers, such as atatic polypropylene (APP) or sequenced butadiene–styrene (SBS), became accepted as improvements over unmodified bitumen, changes occurred in the installation and manufacture of membranes. Historically, built-up roofs were made *in situ* by mopping hot bitumen into organic felts that had been placed on the roof decking. In the 1990s, the roof membrane was manufactured under tightly controlled conditions in a factory distant from the site of application. The spunbonded fabric is typically saturated with modified bitumen by dipping into tanks of hot bitumen which are heated up to 200°C. Excess bitumen is metered off and the cooled surfaces are coated with a release material such as talc to prevent blocking together on the roll. The composite is packaged into rolls approximately 1 m wide and 50 m long. The rolls are then shipped to the job site and applied to the flat roof surface by slowly unrolling while heating the underside to tackiness with a propane torch to enable it to adhere to the roof deck. Adjacent rolls are lap seamed to provide for watertightness across the roll width of the roof. Spunbonded polyester is also used in the so-called cold roof method, typically used for roof maintenance. In this method, a cold mastic is applied over a fiber glass base sheet, followed by more mastic, another layer of polyester, more mastic, and a final topcoat.

In Europe, particularly France and Germany, bitumen-coated spunbonded polypropylene fabrics are widely accepted as rooflinings under concrete, clay, or ceramic tiles for pitched-roof construction. In this use, the spunbonded fabric is a critical element of the membrane because the rooflining is draped between roof rafters and depends on the strength of the spunbonded for self-support during the life of the roof. The bitumen coating renders the spunbonded waterproof and allows it to shed any water that might leak between the tiles during snow and rainstorms. Spunbonded fabrics coated with nonbituminous materials such as acrylics have also been used in Europe. Rooflinings represent a considerable opportunity for spunbonded fabrics in Europe and in the sunbelt areas of the United States.

Nonwoven fabrics have played an important part in the development of geotextile applications. Needle-punch fabrics manufactured from either staple fibers or spunbonded continuous filaments have found worldwide acceptance on the basis of field performance. In 2000, it is estimated that North America consumed approximately 300 million m^2 of geotextiles (62).

Many fabric manufacturers have dedicated considerable effort to the marketing of their products in order to participate in this growth area. Geotextile fabrics function by being porous to water but not to the fines of the soil, thereby permitting them to effectively separate or partition soil fines from other elements. The net effect is keeping the soil from eroding or moving position. For example, in the construction of a new road the geotextile can separate the subsoil from the gravel or aggregate. By maintaining this separation, the aggregate is not driven into the subsoil base by the weight of vehicles nor are soil fines pumped up into the aggregate since the geotextile filters out their passage. However, water is freely transported through the fabric, enabling proper drainage without buildup of hydrostatic pressures. Thus the road resists rutting and sustains the weight of traffic more effectively while permitting proper drainage of water through the fabric. In

drainage ditches, perforated drainage pipes are often wrapped with a geotextile prior to installation to prevent them from becoming clogged.

Spunbonded fabrics are effective filters in that they are layered structures of relatively fine fibers, the three-dimensional structure of which creates a torturous path. Even relatively thin spunbonded fabrics (eg, 0.2–0.25 mm) present a significant challenge to the passage of soil fines and are suitable for use in some filtration applications. The porosity of geotextile fabrics is classified by means of several procedures such as flux (volume flow/area per time) and equivalent opening size (EOS), which is a measure of the apparent pore size of the openings in the fabric. The flux measures the porosity to liquid water, and the EOS measures the porosity to solid particles of a known diameter. Literature is available on limitations of particular styles of fabrics within an application.

Growing university research ensures that users and specifiers will continue to become more sophisticated in their methodology and more demanding of manufacturers. Excellent textbooks are available for both students and practicing engineers (53,63).

A growing use for spunbond fabrics is in landscaping where lightweight (eg, 70–100 gsm) fabrics are sold as landscape fabrics for weed control. Typically these fabrics are placed in landscape beds over the soil and covered with stones or mulch where they resist the emergence of weeds from the soil while allowing water to drain through into the soil. They will not, however, prevent seed germination in the mulch, and they should be viewed as only a partial solution for weed control.

Other durable applications such as interlinings and coating/laminating substrates do not appear to offer much near-term opportunity for growth for spunbonded fabrics. In interlinings, however, spunlaced nonwovens have received wider acceptance because of the outstanding drape and softness, previously unavailable from any other fabric.

Spunbonded fabrics have a relatively small percentage of the coated fabric market which is dominated by other nonwovens. Needle-punched nonwovens offer more of the bulk and resiliency required for functionality in automotive and furniture seating.

Many filtration requirements are fulfilled by spunbonded structures, and a growing but technically complex market has developed since the 1970s (64). Applications include pool and spa, air particulate, coolant, milk, and sediment for household water.

A recent development is the automatic shaping of heavyweight spunbonded and needlepunched fabrics into three-dimensional honeycomb-shaped structures that allows, for the first time, the use of spunbonded fabrics as a three-dimensional solid object (65). This platform process opens up vast new applications previously unreachable by the two dimensional nature of these fabrics. Spunbond fabrics can be automatically converted into products as diverse as matresses, sandwich panels, air-flow straighteners, sand walls for temporary dikes, and drainage containment blocks. There is high interest in third world areas for the very inexpensive mattresses that can be produced from spunbond lines already in place in these areas. This process holds promise to open up large new markets for existing spunbonded fabrics.

Spunbonded Markets: Disposable Applications. The outlook for spunbonded disposable applications indicates a 5–7% compounded annual growth

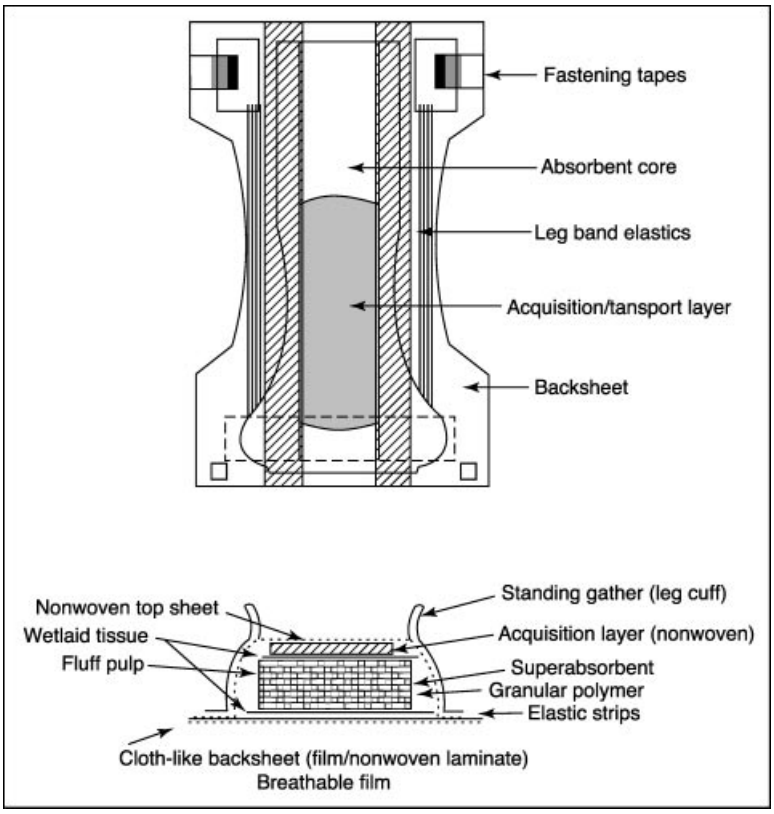

Fig. 14. Components of a modern disposable diaper (56).

forecast (1,6). Spunbonded plant capacity installed or announced since the 1980s has been aimed at satisfying increased demand largely for disposable applications. Key markets are components for baby diapers, training pants, incontinence devices, surgical gowns and drapes, medical sterilization wrap, protective clothing, and envelopes (see Fig 13, Ref. 69).

The use of spunbonded fabrics as coverstock for diapers and incontinence devices has grown dramatically since 1980, and by 1995 consumption exceeded 2 billion m^2 in the United States and is forecast to reach 3.5 billion within five years (67). A coverstock functions as a one-way medium through which urine is transported into the absorbent core. The laminar structural feature of the coverstock helps keep the skin of the user dry and comfortable. Figure 14 shows the uses of nonwovens in a premium price diaper (68). Although 17 g/m^2 spunbonded polyester was originally used in diaper coverstock, it has been supplanted entirely by 15–17 gsm weight spunbonded polypropylene.

Changes in diaper design have made disposable diapers among the most highly engineered disposable products in the world, and involve not only coverstock but the nature of the absorbent layer and design of the diaper itself. The use of form-fitting legs with leg cuffs for leak protection, as well as refastenable closures, has accelerated the acceptance of disposable diapers for both infants and

adults. Spunbonded fabrics are used in several major components of the diaper, including coverstock, leg cuffs, and backsheet (68). Spunbonded coverstock is also widely used in feminine napkins and, to a limited extent, in tampons. The conversion of eastern European countries to market economies has created increasing demand for disposable diapers and consequently spunbonded polypropylene coverstock. Other areas of the world showing higher penetration of disposable diapers are South America and China.

The uses of spunbonded fabrics as fabrics in diapers and other personal absorbent devices will most likely remain unchallenged for the near term. Virtually any other nonwoven production method appears to be at a cost disadvantage opposite spunbonded polypropylene. Perforated films lack tactile feel and are largely limited to use in femine napkins. There have been composite products developed from meltblown and spunbonded combinations, generally where improved hydrophobicity is desired. These products can be produced on-line at relatively low additional cost and offer high value to diaper manufacturers.

In medical applications, great progress has been made in the substitution of traditional reuseable woven materials with higher performing spunbondeds (69). Historically, flashspunbonded polyethylene was the first 100% spunbonded to find limited acceptance in medical uses such as disposable operating room gowns, shoe covers, and sterilizable packaging. Other spunbonded fabrics of polypropylene or nylon found some acceptance as cellulosic composites with the lightweight spunbonded serving to add physical strength to the composite. Over the last decade, composite structures of spunbond-meltblown-spunbond polypropylene (SMS) have gained wide acceptance in operating room gowns and sterilizable (CSR) wrap. Structures made of spunlaced polyester–cellulose are also widely used but have lost market share to SMS because of the higher barrier of SMS.

Operating room gowns worn by members of the surgical team place very high demands on fabric properties. Key requirements include breathability for comfort, low noise, absolute barrier to fluid penetration, low particle generation (linting), sterilizability, and impermeability to bacteria and viral particles. Woven cotton fabric gowns were worn for many years but had to be reused because of high cost. This required the added expense of laundering the garments and the need to decide when each garment was no longer suitable for use in the operating room. Several studies comparing disposable and reusable fabrics have been conducted in an attempt to correlate the effect of fabric linting with post-operative infections. Although no correlation has yet been established, some studies have demonstrated that single-use fabrics generate significantly fewer particles than cotton fabrics (70). Other studies have indicated that the rate of postoperative wound infection is reduced with the use of high barrier spunbonded olefin gowns and drapes. Concern for viral transmission (eg, AIDS) has increased the demand for disposable, higher barrier fabrics without loss of comfort.

Medical devices or trays of devices are often sterilized after the nonsterile device is sealed in a package. A part of this package, such as the lid, is made from flashspun or spunbonded/meltblown fabric because it possesses the unique property of permitting the sterilizing gas of ethylene oxide to pass through while remaining impenetrable to bacteria. These fabrics are manufactured to tightly controlled standards to ensure the highest resistance to bacterial/viral

penetration. The superiority of a spunbonded fabric to the alternative coated papers has been reviewed (71).

Spunbonded fabrics have been utilized as shoe covers in the operating room. The covers are usually sewn with an elastic band at the top to allow them to be held snugly in place. The fabric requirements are toughness, some porosity for comfort, nonlinting, resistance to slippage, and a nonstatic characteristic. In order to achieve the last property, the fabric is usually treated with an antistatic coating. Failure to use a nonstatic fabric may cause sparks to be generated in the operating room environment, which could damage sensitive electronic devices or lead to fire. Other medical applications for spunbonded fabrics include head covers, face masks, drapes, and other uses requiring breathable/barrier properties.

A large-volume area for spunbonded fabrics is the disposable protective clothing market (72). To a great extent the demand for high performance disposable protective clothing has tracked high technology manufacturing, environmental demands, and more recently the concern from biological or chemical terrorism. The manufacture of particulate sensitive electronic components, such as silicon chip integrated circuits, resulted in the construction of clean rooms where the generation of any particulate was in part controlled through the use of nonlinting yet comfortable clothing made from spunbonded fabrics. Because the spunbonded fabrics are made of continuous filaments, practically no linting results. At the same time the structure allows the passage of moisture and air, thus helping the wearer to remain comfortable. The spunbonded garment is worn over other clothing; therefore the maximum pore size must be sufficiently small to prevent the passage of lint and other particles through the garment and into the clean room.

The 1980s saw the beginning of the removal of large quantities of asbestos (qv) from schools and buildings, creating the need for clothing which could not be penetrated by small asbestos fibrils, yet inexpensive enough to permit daily disposal. Certain spunbonded and spunbond/meltblown laminate fabrics demonstrate excellent resistance to asbestos penetration from particles as small as 0.5 μm.

Similarly the handling of hazardous materials has prompted the need for affordable, disposable protective clothing. Once exposed to toxic waste, pesticides, or radioactive materials, the clothing itself is transformed into a hazardous material and must be disposed of to prevent spreading of contamination. Garments that demand the utmost in protection at the lowest price are often made by extrusion coating, laminating spunbonded fabrics with polyethylene, or laminating the fabric to poly(vinylidene chloride) film.

Packaging applications for spunbonded fabrics are for the most part a specialty area in which paper products or plastic films do not adequately perform. One of the largest packaging applications for spunbonded fabric is high performance envelopes. Although lightweight tear- and puncture-resistant envelopes are not in demand by individual consumers, both large and small businesses have found spunbonded envelopes to outperform those made from conventional paper products. The lighter weight of the spunbonded envelope allows for postal savings, and some corporations specializing in overnight delivery have successfully used spunbonded envelopes with excellent results. Coated spunbonded fabrics are used as the outerwrap of coils of steel and aluminum where they outperform alternative materials such as films and papers.

A significant percentage of U.S. synthetic staple fiber production is packaged in bales of extrusion coated spunbonded fabrics, so treated to render the fabric impervious. Synthetic fibers have been shipped worldwide in this manner with great success.

Although other nonwoven processes such as spunlacing have experienced large growth in disposable wipes, spunbonded fabrics have not participated in this segment generally because some cellulosic fibers are required in the wipe and spun bonding cannot readily utilize such fibers.

A reverse-wipe application is seen in the clothes dryer fabric softener sheet wherein the spunbonded fabric is coated with a complex combination of wax, surfactants, and perfumes which are released into the environment of a hot clothes dryer to soften and perfume the clothes, as well as provide an antistatic quality. The spunbonded sheet, which must be made of polyester or nylon for temperature resistance, provides a simple and cost-effective medium to store the chemical compounds prior to release in the dryer.

There are many other smaller specialty disposable applications for spunbonded fabrics which vary widely from country to country. These applications include candy wrapping, agricultural coverings, wall covering, and packaging.

BIBLIOGRAPHY

"Nonwoven Fabrics, Spunbonded" in *EPSE* 2nd ed., Vol. 10, pp. 227–253, by Ronald L. Smorada, Reemay, Inc.

1. T. Wirtz, in *12th Annual TANDEC Conference*, Nov. 19–21, 2002, Knoxville, Tenn.
2. R. L. Smorada, *INDA J. Nonwovens Res.* **3**(4) (Fall 1991).
3. D. T. Ward, *ITB Nonwovens Ind. Text.* 27–33 (Feb. 1998).
4. K. Ohmura, *Nonwovens Ind.* **36** (Nov. 1999).
5. K. Ohmura, *Nonwovens Ind.* **26** (July 2002).
6. J. R. Starr, *Nonwovens World* 68–73 (Feb.–Mar. 1999).
7. *Nonwovens World* **5**(1), 16 (Jan. 1990).
8. *Nonwovens Ind.* **24**(10), 54–63 (Oct. 1993).
9. *Guide to Nonwoven Fabrics*, INDA, Cary, N.C., p. 24.
10. U.S. Pat. 3,989,788 (Nov. 2, 1976), L. L. Estes, A. F. Fridrichsen, and V. S. Koshkin (to Du Pont).
11. Brit. Pat. 1,157,437 (July 9, 1969), B. L. Davies (to ICI Ltd.).
12. J. Hagwood, in *12th Annual TANDEC Conference*, Nov. 19–21, 2002, Knoxville, Tenn.
13. Y. Ogawa, *Spunbonded Technology Today 2*, Miller-Freeman, San Francisco, 1992, p. 123.
14. U.S. Pat. 3,439,085 (Apr. 15, 1969), L. Hartmann (to C. Freudenberg).
15. U.S. Pat. 6,225,243 (May 1, 2001), J. Austin (to BBA Nonwovens).
16. U.S. Pat. 3,338,992 (Aug. 29, 1967), G. A. Kinney (to E. I. du Pont de Nemours & Co., Inc.).
17. U.S. Pat. 3,991,244 (Nov. 9, 1976), S. C. Debbas (to E. I. du Pont de Nemours & Co., Inc.).
18. Brit. Pat. 1,436,545 (May 19, 1976), J. Brock (to ICI Ltd.).
19. U.S. Pat. 4,017,580 (Apr. 12, 1977), J. Barbey (to Rhône-Poulenc).
20. U.S. Pat. 3,502,763 (Mar. 24, 1970), L. Hartmann (to C. Freudenberg).
21. U.S. Pat. 4,405,297 (Sept. 20, 1983), D. W. Appel and M. T. Morman (to Kimberly-Clark Corp.).

22. U.S. Pat. 5,545,371 (Aug. 13, 1996), F. Lu (to Ason Engineering Inc.).
23. U.S. Pat. 3,771,307 (Nov. 13, 1973), D. G. Petrille (to E. I. du Pont de Nemours & Co., Inc.).
24. U.S. Pat. 3,692,618 (Sept. 19, 1972), O. Dorschner, F. Carduck, and C. Storkebaum (to Metallgesellschaft AG).
25. U.S. Pat. 6,183,684 (Feb. 6, 2001), F. Lu (to Ason Engineering Inc.).
26. U.S. Pat. 5,225,018 (July 6, 1993), L. M. Zeldin, R. E. Lamkin, and J. E. Werner (to Fiberweb North America).
27. U.S. Pat. 4,163,305 (Aug. 7, 1979), V. Semjonow and J. Foedrowitz (to Hoechst AG).
28. U.S. Pat. 3,322,607 (May 30, 1967), S. L. Jung (to E. I. du Pont de Nemours & Co., Inc.).
29. H. Külter, in J. Lunenschloss and W. Albrecht, eds., *Non-Woven Bonded Fabrics*, Ellis Horwood Ltd., Chichester, U.K., 1985, p. 178.
30. U.S. Pat. 4,813,864 (Mar. 21, 1989). H. Balk (to Reifenhauser GmbH).
31. R. G. Mansfield, *Textile World* (June 2002).
32. J. Neuwirth, *Nonwovens World* 136–139, April–May 2002.
33. K. Völker, *Nonwovens World* 97–103, Apr.–May 2002.
34. K. Bitz, *Nonwovens Ind.* 45–50 (Feb. 2002).
35. U.S. Pat. 3,855,046 (Dec. 17, 1974), P. B. Hansen and L. B. Pennings (to Kimberly-Clark Corp.).
36. U.S. Pat. 3,855,045 (Dec. 17, 1974), R. J. Brock (to Kimberly-Clark Corp.).
37. I. H. Doring, *Ind. Text.* 51–52 (Dec. 2000).
38. U.S. Pat. 4,125,663 (Nov. 14, 1978), P. Eckhart (to Hoechst AG).
39. U.S. Pat. 3,542,615 (Nov. 24, 1970), E. J. Dobo, D. W. Kim, and W. C. Mallonee (to Monsanto Corp.).
40. U.S. Pat. 3,322,607 (May 30, 1967), S. L. Jung (to E. I. du Pont de Nemours & Co., Inc.).
41. J. R. Collier and co-workers, in *12th Annual International TANDEC Conference*, Nov. 19–21, Knoxville, Tenn.
42. E. Schwartz, in *32nd Clemson Nonwovens Fabrics Forum*, June 25–28, 2001, Clemson Univ., Clemson, S.C.
43. U.S. Pat. 3,972,759 (Aug. 3, 1976), R. R. Buntin (to Exxon).
44. U.S. Pat. 4,374,888 (Feb. 22, 1983), S. R. Bornslaeger (to Kimberly-Clark Corp.).
45. U.S. Pat. 4,100,324 (July 11, 1978), R. A. Anderson, R. C. Sokolowski, and K. W. Ostermeier (to Kimberly-Clark Corp.).
46. U.S. Pat. 4,118,531 (Oct. 3, 1978), E. R. Hauser (to 3M Co.).
47. Y. Ogawa, *Nonwovens World* 79–81 (May–June 1986).
48. U.S. Pat. 3,081,519 (Mar. 19, 1963), H. Blades and J. R. White (to E. I. du Pont de Nemours & Co., Inc.).
49. U.S. Pat. 3,442,740 (May 6, 1969), J. C. David (to E. I. du Pont de Nemours & Co., Inc.).
50. U.S. Pat. 5,081,177 (Jan. 14, 1992), H. Shin (to E. I. du Pont de Nemours & Co., Inc.).
51. *Nonwoven Fabrics Handbook*, INDA, Cary, N.C., pp. 77–79.
52. S. Kawabata, *The Standardization and Analysis of Hand Evaluation*, 2nd ed., Textile Machinery Society of Japan, Osaka, Japan, 1980.
53. *Standard Test Methods Manual*, INDA, Cary, N.C., pp. 168–177.
54. R. M. Koerner, *Designing with Geosynthetics*, 4th ed., Prentice-Hall, Englewood Cliffs, N.J., 1999, pp. 93–146.
55. Ref. 54, p. 137.
56. K. Shariq, *Nonwovens World* 90–96 (Winter 1998).
57. Ref. 56, p. 90.
58. Ref. 56, p. 94.
59. Ref. 56, p. 93.
60. *Du Pont Tyvek Literature*, Bulletin E-60658.
61. C. E. Frei, *Nonwovens Ind.* 56–60 (Oct. 1999).

62. C. E. Pelc, *Nonwovens Ind.* p. 42 (Oct. 2000).
63. A. A. Balkema, in R. Veldhuijzen Van Zanten, ed., *Geotextiles and Geomembranes in Civil Engineering*, Rotterdam/Boston, Mass., 1986.
64. C. E. Pelc, *Nonwovens Ind.* pp. 30–36 (Nov. 2000).
65. R. L. Smorada, *Nonwovens World* pp. 49–52 (Feb.–Mar. 2002).
66. D. K. Smith, *Nonwovens World* pp. 64–70 (Winter 1998).
67. P. Hannah, *Nonwovens World* pp. 79–86 (Winter 1998).
68. C. White, *Nonwovens Ind.* pp. 26–39 (Jan. 1999).
69. D. K. Lickfield, *Technical Text. Technol.* pp. 18–20 (Mar. 2003).
70. S. P. Scheinberg, J. H. O'Toole, and S. K. Rudys, *Partic. Microbiol. Cont.* (July/Aug. 1983).
71. Th. Mengen and A. Jordy, in *8th Symposium of the Austrian Society for Hygiene, Microbiology and Preventative Medicine*, Vienna, Austria, 1984.
72. A. Teng, *Nonwovens Ind.* pp. 38–44 (Mar. 2003).
73. Arthur D. Little Report C87352 (May 1982).

RONALD S. SMORADA
Versacore Industrial Corporation

NONWOVEN FABRICS, STAPLE FIBERS

Introduction

A nonwoven fabric is a textile structure made from fibers, without a yarn being first made; knitted and woven fabrics, require yarns. A nonwoven fabric normally comprises a network of fibers or continuous filament yarns strengthened by mechanical, chemical, or thermally interlocking processes. Examples are bonding with binders such as latex polymers, needling, hydroentanglement, and stitchbonding.

History. Johnson and Johnson became involved in nonwovens in the 1930s (1). After 10 years of experimentation its nonwovens department became part of Chicopee Manufacturing Corp. Viscose rayon was used to make a wide range of products including bedpads, surgical towels, disposable diapers, sanitary napkins, and wiping cloths. In the 1970s water jets were being used to bond fibers together to make surgical gauze.

Other companies with an early involvement in developing nonwovens to replace textiles include Avondale Mills, Kimberly-Clark, The Kendall Co., and the West Point Manufacturing Co. Freudenberg started trying to make a leather substitute in the 1930s (2).

The spunbond process transforms polymer directly to fabric by extruding filaments, orienting them as bundles or groupings, layering them on a conveying screen, and interlocking them by thermal fusion, mechanical entanglement, chemical binders, or combinations of these. The technology was developed by Freudenberg and DuPont in the 1950s (see NONWOVEN FABRICS, SPUNBONDED).

Encyclopedia of Polymer Science and Technology. Copyright John Wiley & Sons, Inc. All rights reserved.

Meltblown fabrics are also made directly from thermoplastic resins. Polymer granules are melted and extruded. As soon as the melt passes through the extrusion orifice, it is blown with air at high temperature. The airstreams attenuate the molten polymer and solidify it into a random array of very fine fibers. The fibers are then separated from the air stream as a randomly entangled web and compressed between heated rolls. The combination of fine-diameter fibers, random entanglement, and close packing results in a fabric structure with a large surface area and many small pores.

After the development of spunbonded and meltblown processes, combined systems such as SMS (spunbonded/meltblown/spunbonded) were developed to combine the benefits of each fabric type. In the late 1990s bicomponent spunbonded technology was introduced.

Definitions. The Textile Institute defines nonwovens as "textile structures made directly from fibre rather than yarn. These fabrics are normally made from continuous filaments or from fibre webs or batts strengthened by bonding using various techniques: these include adhesive bonding, mechanical interlocking by needling or fluid jet entanglement, thermal bonding and stitch bonding."

The ISO 9092 definition is as follows: "A manufactured sheet, web or batt of directionally or randomly orientated fibres, bonded by friction, and/or cohesion and/or adhesion, excluding paper and products which are woven, knitted, tufted, stitch-bonded incorporating binding yarns or filaments, or felted by wet-milling, whether or not additionally needled. The fibres may be of natural or manufactured origin. They may be staple or continuous filaments or be formed in situ." Various notes are included in this definition including clarification on the difference between a wet-laid nonwoven and a wet-laid paper—in essence, the difference depends on the presence of a substantial proportion of fibers.

Nonwoven structures need not be considered as substitutes for knitted or woven fabrics—they are a class in their own, enabling a unique range of engineered properties and aesthetics to be achieved.

Nonwoven Processes

The basic concept employed in making a nonwoven fabric is to transform fiber-based materials into two-dimensional sheet structures with fabric-like properties. These are flexibility, porosity, and mechanical integrity. Their manufacturing processes can be split into four groups: dry-laid webs, extrusion-formed webs, wet-laid webs, and web-bonding.

Dry-Laid Processes. These include mechanical, eg carded, and aerodynamic, eg air-laid routes. Dry-laid nonwovens are made with staple fiber processing machinery such as cards and garnetts, which are designed to manipulate staple fibers in the dry state. Also included in this category are nonwovens made from filaments in the form of tow, and fabrics composed of staple fibers and stitching filaments or yarns, ie, stitchbonded nonwovens.

Extrusion-Formed Webs. Examples include spunbonded and meltblown. Extrusion technology is used to produce spunbond, meltblown and porous-film nonwovens. These fabrics are made with machinery associated with polymer

extrusion methods such as melt-spinning, film casting and extrusion coating (see EXTRUSION).

Wet-Laid Processes. Papermaking technology is used to process wood pulp fibers, synthetic fibers longer than wood pulp, and other fibers that differ in other ways from pulps. Included in this category are methods for producing dry-laid pulp and wet-laid nonwovens. These fabrics are made with machinery associated with pulp fiberizing, such as hammer mills, and paperforming, ie slurry pumping onto continuous screens which are designed to manipulate short fibers in a fluid.

Web-Bonding Processes. These can be split into chemical and physical. Chemical bonding refers to the use of water-based and solvent-based polymers to bind together the fibrous webs. These binders can be applied by saturation (impregnation), spraying, printing, or application as a foam. Physical bonding processes include thermal processes such as calendering and hot air bonding, and mechanical processes such as needling and hydroentangling.

The various nonwoven processes and the fabrics made from each have a number of common characteristics. In general, textile technology-based processes provide maximum product versatility, because most textile fibers and bonding systems can be utilized and conventional textile web processing equipment can be readily adapted at minimal cost. Extrusion technology-based processes provide somewhat less versatility in product properties, but yield fabric structures with exceptional strength-to-weight ratios, as is the case with spunbonds; high surface area-to-weight characteristics, a benefit of using meltblown technology; or high property uniformity per unit weight, as is the case with textured films, at modest cost.

Paper technology-based nonwoven processes provide the least product versatility and require a high investment at the outset, but yield outstandingly uniform products at exceptional speeds. Hybrid processes provide combined technological advantages for specific applications.

Fibers for Nonwovens

Nonwoven fabrics made directly from polymers are discussed elsewhere. The properties of nonwoven fabrics are highly influenced by the properties of their constituent fibers.

Technically, a fiber is a material characterized by fineness, flexibility, and by having a high ratio of length to thickness. Textile fibers also exhibit sufficient strength and extensibility, elasticity, flexibility, and temperature stability to endure the environments in which they are to be used. They can be divided into continuous filaments or staple forms. Staple fibers range in length from about 2 to 20 mm. Fibers with thicknesses greater than about 100 μm are generally considered coarse bristles; fibers with lengths less than a centimeter are generally not processed on textile-based processing machinery.

Typical textile fibers used, for example, in a needle-punched filter fabric, are a blend of 3.3 and 6.6 dtex polyester staple fibers. These are about 5 cm long, have diameters ranging from 18 to 25 μm, linear density of 350–650 mg per 1000 m and length-to-width ratios in the order of 1000 to 1.

Table 1. Properties of Some Commercially Available Textile Fibers

Fiber	Density, g/mL	Modulus, N/tex[a]	Tenacity, N/tex[a]	Elongation, %	Regain, %	T_m, °C
Cotton	1.52	4.85	0.26–0.44	7	7	
Jute	1.52	17.2	044–052	2	12	
Wool	1.31	2.38	0.08–0.17	40	13	
Rayon	1.54	4.85–7.5	0.8–0.44	8–20	11	177
Acetate	1.32	3.53	0.11	25–45	6.5	260
Nylon	1.14	2.65	0.44–0.79	15–50	3–5	260
Polyester	1.38	4.41–8.38	0.35–0.71	15–50	0.4	254
Acrylic	1.16	6.44	0.17–0.26	20–30	1–1.5	
Polypropylene	0.91	7.76	0.26–2.64	20	0.01–0.1	177
Nomex[b]	1.38	8.83	0.35–0.44	20–30	4	371
Kevlar[b]	1.44	42.34	0.79–1.14	1.5–4	5	482
Sulfur	1.37	2.65–3.53	0.26–0.35	25–35	0.6	285
Glass	2.56	30.89	0.79–1.76	2–5	0	1482

[a] To covert N/tex to g/den, multiply by 11.33.
[b] Polyamides.

Virtually all fibers (an important exception is glass fibers) are composed of long-chain molecules or polymers arranged along the fiber axis. Essential requirements for fiber formation include long-chain molecules with no bulky side groups, strong main-chain bonding, parallel arrangement of polymer chains, and chain-to-chain attraction or bonding. Basic phases in the fiber formation process are obtaining a suitable polymeric material, converting the material to liquid form, solidifying the material into fiber dimensions, and treating the fiber to bring about desired properties. These four phases are present in the formation of natural as well as manufactured synthetic fibers, the principal differences being the amount of time and energy required.

A selection of fiber properties is given in Table 1. In general, fiber diameters range from 5 to over 40 μm for natural fibers, and from less than 10 μm (microfibers) upwards for manufactured fibers.

Almost all the fibers used in nonwovens are synthetic. The split is approximately as follows: Polypropylene 63%; polyester 23%; viscose rayon 7%; acrylic 2%; polyamide 2%; other 3%; (see PROPYLENE POLYMERS (PP); OLEFIN FIBERS; POLYESTERS, FIBERS; CELLULOSE FIBERS, REGENERATED; ACRYLIC FIBERS; POLYAMIDES, FIBERS).

With the increasing need to reduce cost and achieve sustainability, there has been a growth in interest in using recycled fibers, eg, from polyester bottles.

Web Formation

Web formation, the second phase in manufacturing nonwoven fabrics, transforms fibers or filaments from linear elements into planar arrays in the form of preferentially arranged layers of lofty and loosely held fiber networks termed webs, batts, or sheets. Mechanical and fluid means are used to achieve the fiber arrangement. Basic fabric parameters established at web formation, in addition to fiber orientation, are the unfinished product weight per unit area and the manufactured

width. In all nonwoven manufacturing systems, the fiber material is deposited or laid on a forming or conveying surface. The physical environment at this phase is dry when textile technology is used, wet when papermaking technology is used, and molten when extrusion technology is used.

Webs are prepared by opening, blending, and carding.

Opening and Blending. A bale of fibers needs to be broken apart and the closely packed fibers in the tufts need separating before further processing can be carried out. This is an important first stage to forming a web—once the web has been formed it cannot be made more even by further processing, and any irregularities will adversely affect product performance. So it is important to open the fiber tufts, remove any contamination, and even out bale-to-bale variation before further processing.

Textile Carding. Carding is the process of disentangling, cleaning, and intermixing fibers to make a web for further processing into a nonwoven. The aim is to take a mass of fiber tufts and produce a uniform, clean web. The process predominantly aligns the fibers which are held together as a web by slight mechanical entanglement and fiber–fiber friction. The main type of card is a roller card. The carding action is the combing or working of fibers between the points of saw-tooth wire clothing on a series of interworking card rollers. Short fibers and foreign bodies are removed, the fiber tufts are opened, and the fibers are arranged more or less parallel. The carding or parallelization of fibers occurs when one of the surfaces moves at a speed greater than the other. Fibers are removed, or "stripped," when the points are arranged in the same direction and the more quickly moving surface removes or transfers the fibers from the more slowly moving surface.

Woollen cards, for example, were designed to process a rather wide range of fiber lengths ($<$1–20 cm) and diameters ($<$20–50 μm) with additional objectives of removing contaminants, mixing fibers, preserving fiber length, extracting as few fibers as possible, and delivering as many as 100 slivers. Conventional woollen cards, consequently, consist of a series of relatively wide and large cylinders to achieve productivity and accommodate fiber length requirements; multiple rolls to work and mix fibers on the large cylinders; and smaller cylinders and rolls to take fibers to and transfer them from each working area.

Cotton cards, on the other hand, were designed to process shorter fibers (15–30 mm) and a more narrow range of fiber diameters (15–30 μms). Additional requirements include eliminating very short fiber segments and extracting nonfibrous material such as seed coat particles and leaf fragments. A traditional cotton card consists of a roll-to-plate mat feeding assembly, a fiber-from-mat separating roll (lickerin), one large cylinder and several curvilinear surfaces (revolving flats) between which the carding action takes place, a smaller cylinder which removes fibers (doffs) from the carding cylinder, and a web-condensing and sliver-coiling assembly.

When short (35–50 mm) synthetic fibers are processed on cotton cards, the flats are often replaced with stationary granular surfaces in order to minimize the fiber extraction and damage. Fibers up to 150 mm in length are processed on cotton cards with workers and strippers (Fig. 1).

Garnetts were designed to thoroughly disentangle textile fibers which were reclaimed from various fiber or textile manufacturing operations or regenerated from threads and rags. Garnetts are compact, versatile, and highly productive. Most have a feeding section, a gentle opening section, a working section consisting

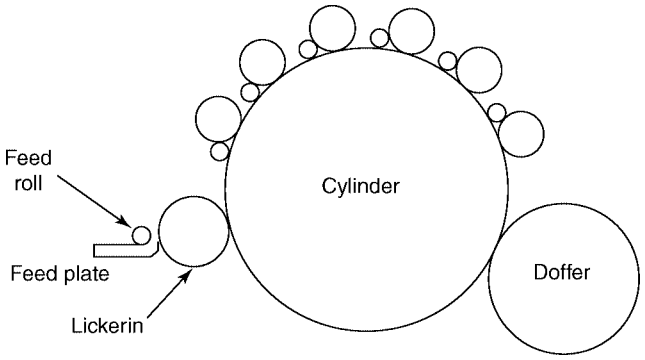

Fig. 1. Cotton card with workers and strippers (doffers).

of one to four cylinders with or without a worker and stripper rolls, and one to four doffers.

The choice between using a cotton card, a woollen card, or a garnett depended on fiber dimensions. Woollen cards were used for long, coarse fibers, cotton cards for finer, shorter fibers, and garnetts for fibers having a wide range of dimensions.

Nonwoven Cards. Modern, high speed cards designed to produce nonwoven webs show evidence of either a cotton or wool fiber-processing heritage and have processing rate capabilities comparable to those of garnetts. Contemporary nonwoven cards are available up to 5 m and are configured with one or more main cylinders, roller or stationary tops, one or two doffers, or various combinations of these principal components.

Single-cylinder cards are usually used for products requiring machine-direction or parallel-fiber orientation. Double-cylinder cards, frequently called tandem cards, are basically two single-cylinder cards linked together by a section of stripper and feed rolls to transport and feed the web from the first working area to the second. The coupling of two carding units in tandem distributes the working area and permits greater fiber throughput at web quality levels comparable to slower single-cylinder machines.

Roller-top cards have five to seven sets of workers and strippers to mix and card the fibers carried on the cylinder. The multiple transferring action and reintroduction of new groupings of fibers to the carding zones provides a doubling effect which enhances web uniformity. Stationary-top cards have strips of metallic clothing mounted on plates positioned concavely around the upper periphery of the cylinder. The additional carding surfaces thus established provide expanded fiber alignment with minimum fiber extraction.

Double-doffer cards are generally used to conserve manufacturing space or optimize throughput while maintaining web quality. The double-doffer configuration splits the web, which essentially doubles the output of lightweight structures or yields an additional doubling action for heavier ones (Fig. 2).

Web Layering

Forming fibers into a web on a carding or garnetting machine takes place at the doffer. The web forms as the doffer strips and accumulates fibers from the cylinder. The number of fibers accumulated and the mass of each fiber determine the weight

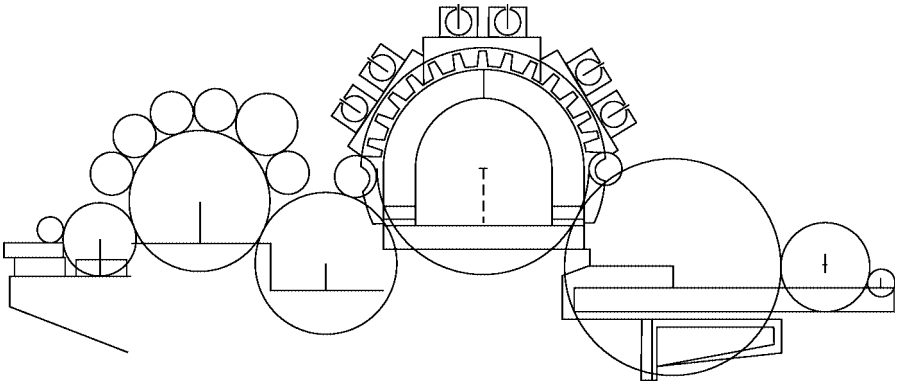

Fig. 2. Contemporary nonwoven card configuration.

of the web. For a given fiber orientation, web weight per unit area is limited by the ratio of the surface speed of the cylinder to the surface speed of the doffer. This is typically 10–15. The result is that cotton cards give up to 10 g/m^2 per doffer, woollen cards up to 25 g/m^2, and garnetts up to 50 g/m^2.

Nonwoven fabrics are made in weights ranging from less than 10 to several hundred grams per square meter, and fiber orientations ranging from parallel to random. Webs can be built up or layered to achieve the desired weight. This can be done by folding from one machine, collection from multiple forming machines, or cross-lapping.

Web folders or straight plaiters are used with cotton cards to produce surgical waddings, and with woollen cards and garnetts to produce padding and cushion filler. The resulting batt is limited in width to the width of the forming machine. Delivery is in the form of individual stacks of parallel fiber layers. Layering of webs from two or more cards or garnetts arranged in tandem onto a conveying apron or screen provides continuous delivery. Tandemly arranged, roller-top cotton carding lines are used to form webs for diaper and feminine pad facings, interlinings, and wipes. In this instance, web weight is controlled by the number of cards included and finite adjustment of cylinder or doffer speed ratios. Density gradient and multifiber laminate webs can be formed by processing fibers of different sizes and chemical types on individual cards in the line. Web characteristics include a high degree of fiber parallelization and increased uniformity due to the doubling effect of layering.

Parallel laid webs can only be the width of the card web and they remain anisotropic; cross-laid webs can be wider and more uniform.

Cross-lapping is essentially the plaiting or folding of a fiber web onto a conveying device placed at an angle of 90° to the forming unit. Delivery is continuous and fiber orientation is biaxial. In addition to being a means of determining a range of product weights, cross-lapping is also a means of determining a range of product widths. Additives, such as binder and particulate matter, can also be deposited onto individual web layers at the lapping stage.

Cross-lapping can be achieved by doffing webs onto reciprocating floor aprons, inclined aprons (camel back) reciprocating onto stationary floor aprons or conveyors, or runout (horizontal) apron folders reciprocating onto stationary floor

aprons or conveyors. Cross-lapped web widths may range from several centimeters to several meters. Cross-lapped webs are used in the production of highloft and needled structures.

Web Spreading and Web Drafting. Spreading layers of parallel fiber webs is a means of simultaneously increasing web width, decreasing web weight, and altering fiber orientation. Controlled stretching or drafting web layers is a means of simultaneously increasing web throughput, decreasing web weight, and altering fiber orientation.

Spreading devices typically consist of modules of bowed rolls of increasingly wider widths operating at speeds slightly greater than the conveying speed of the input web. Fibers move longitudinally but mostly horizontally past one another, resulting in a lateral stretching or drafting of the web and overall repositioning of individual fibers. Width increases of 50–250% are common. Web-drafting devices consist of a series of top-and-bottom roll sets of the same width operating at successively increasing speeds. When heavy cross-lapped layers are drafted, a more isotropic arrangement of fibers is achieved. Draft ratios of six and higher are practiced in some nonwoven operations. Web drafters are also used as a means for in-line weight control.

Random Cards. Fiber orientation ratios as low as 3:1 can be achieved on cards by expanding the condensing action at doffing through the addition of scrambling or randomizing rolls operating at successively slower surface speeds. Proper selection of clothing wire and speed ratios can yield webs with increased *z*-direction fiber orientation, resulting in increased thickness and loft; throughput speed, however, is decreased. Cards specifically designed to produce random webs at contemporary throughputs are configured with several small cylinders that hurl the fibers onto adjacent doffers or cylinders, which in turn transfer the fibers centrifugally onto subsequent cylinders. Figure 3**a** shows the roll arrangement for lightweight nonwovens and Figure 3**b** for heavier weight nonwovens.

Aerodynamic Web Formation. Heavy webs, especially of coarse fibers, cannot easily be made on a mechanical system such as carding. Air-laying is the preferred manufacturing route. By this means it is possible to make a heavy fabric as a single layer, unlike carding or folding for which the layers can split. The principle is that the fibers are well-opened before being directed by air currents onto a collector which can be a flat conveyor or a drum. In principle a better balance of properties in the CD and MD directions should be possible, with a significant proportion of fiber elements in the thickness direction.

Air-laid nonwovens can be grouped into two categories: those formed from natural or synthetic textile fibers and those formed from natural or synthetic pulps. The basic elements are a preformed feed mat, a feeding arrangement, a fiber separation device, an air-generating means, an air-regulation means, and a fiber collection or condensing means.

As fibers in the feed mat pass between the feed roll and feed plate, they are separated by metallic wire teeth on the lickerin roll and carried to an air venturi where they are stripped and tumbled until they strike a moving, perforated collection surface (Fig. 4). At the collection surface, the airborne fibers follow paths of least resistance and accumulate in a self-levelling manner while the air passes through perforations. Fiber orientation in the web is isotropic in layers corresponding to the number of fibers transferred from the wire teeth to

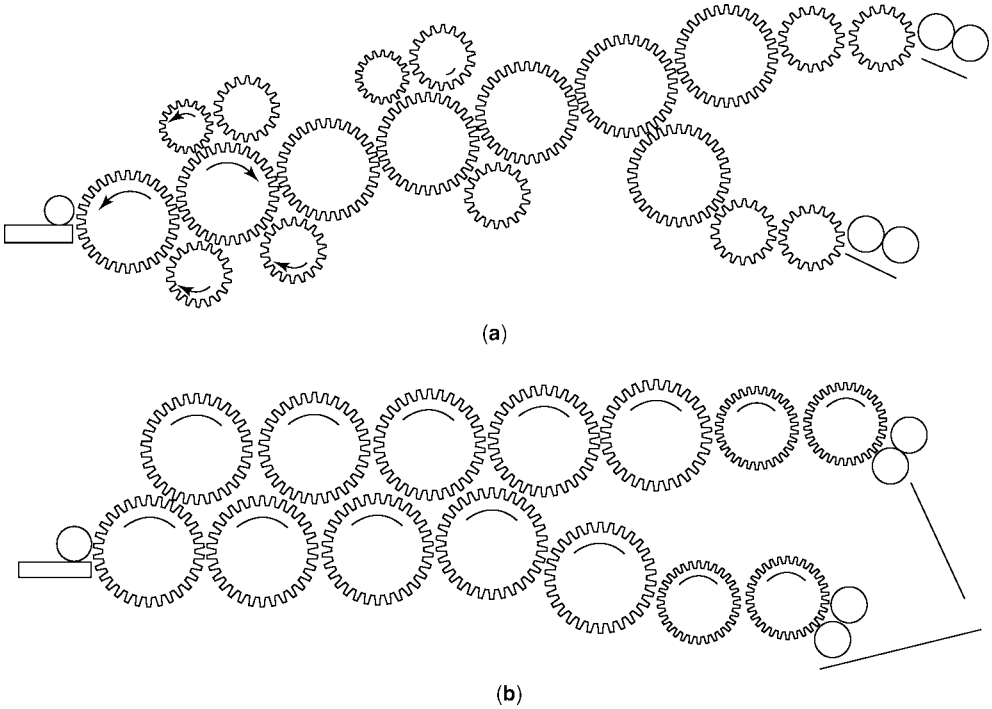

Fig. 3. Random card roll arrangements designed for (a) lightweight nonwovens and (b) highloft nonwovens.

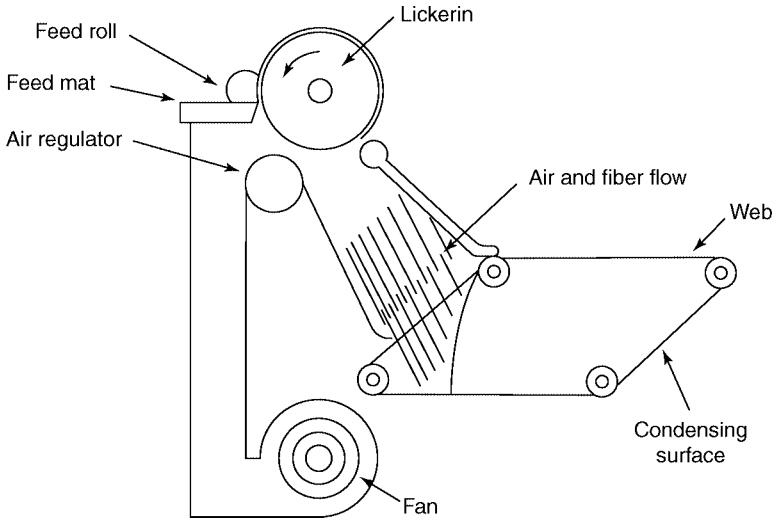

Fig. 4. Aerodynamic web formation.

the air-transportation zone, the intensity of the air, and the speed of the collection surface.

Other configurations include a standard roller card with a series of workers and clearers to open the fiber, with various arrangements of air distribution, eg overpressure or under pressure to direct the fibers and lay them on the perforated collector.

Three-dimensional webs can be made on air-forming machines, provided the fibers used are relatively short and stiff and the webs made are of relatively low density. Air-forming machines allow for production of web thicknesses up to several centimeters, and weights ranging from 30 to 3000 g/m^2 at widths from one to several meters.

Textile fibers can be air-formed directly into end-use configuration by including a shaped condensing surface or, as in the production of pillows, an air-permeable screen drum or belt. Aerodynamic web formation is a suitable means of processing brittle fibers such as glass and ceramics.

Fibers of different diameters, lengths, shapes, and densities break up when processed together in air streams. This fractionation results in the formation of webs with different top and bottom surface characteristics, as well as varying density and porosity gradients. Such structures have been used in filtration.

Short Fiber Systems. The web formation phase of the papermaking process occurs between the headbox and the forming wire. In this area, the fibers, suspended in a dilute water slurry, are deposited on a moving screen which permits the water to pass and the fibers to collect. Traditional papers use a variety of wood pulps or other short cellulosic fibers which pack together to form relatively dense, nonporous, self-adhered sheets. The use of textile fibers, instead of cellulose-based materials, with papermaking machinery distinguishes wet-laid nonwoven manufacturing from traditional paper manufacturing. Both manufacturing methods, however, transport the fibers in a water slurry. The use of papermaking fibers on air-laid nonwoven machinery bridges a gap between textile and paper systems. In both technologies, the transport medium is a fluid: water in wet-laid nonwovens and air in dry-laid pulps.

Dry-Laid Pulp. A principal objective of using air to form webs from natural and synthetic fiber pulps is to produce relatively lofty, porous structures from short fibers, without using water. Air or dry-laid pulp machinery can be imagined as a series of forming-unit modules. Each module consists of two to four perforated drums through which airborne fibers are circulated and further agitated by mechanical beaters placed in close proximity to the inner drum surfaces. As the fibers circulate and separate by the force of the air and the sweeping action of the beaters, they are pulled through the drum perforations by a vacuum onto a condensing conveyor.

Air-laid pulp-forming lines generally consist of three or more forming heads in tandem. Web weights range 70–2000 g/m^2 at throughputs of about 1000 kg/h.

Wet-Laid Web Formation. In the wet-lay or wet-forming process, fibers are suspended in water, brought to a forming unit where the water is drained off through a forming screen, and the fibers are deposited on the screen wire. A principal objective of wet-laid nonwoven manufacture is to produce structures with textile characteristics, primarily flexibility and strength, at papermaking speeds. This can be done by incorporating textile fibers at web formation.

In general, however, it is difficult to incorporate textile fibers because they do not readily wet out, are difficult to disperse, and tend to tangle with one another. Consequently, large amounts of water are needed to keep the fibers in suspension. Also, if the slurry is not handled properly, the fibers tangle and cause poor sheet formation. This can be overcome by increasing the slurry dilution and controlling fiber orientation.

Forming machine designs that have been commercially successful include the inclined-wire fourdrinier and the cylinder former. Inclining the forming wire and suction boxes on a fourdrinier machine to an angle of 5°–30° expands the forming area, which in turn decreases the flow requirements for web formation, increases drainage, and aligns fibers along the machine direction. The cylinder former configuration also provides an expanded forming area. Another benefit of this design is that higher vacuum pressures can be used, which results in the ability to produce both heavy and dense as well as light and relatively impermeable structures.

Web Consolidation

Nonwoven bonding processes interlock webs or layers of fibers, filaments, or yarns by mechanical, chemical, or thermal means. The extent of bonding is a significant factor in determining fabric strength, flexibility, porosity, density, loft, and thickness. Bonding is normally a sequential operation performed in tandem with web formation but it is also carried out as a separate and distinct operation.

In some fabric constructions, more than one bonding process is used, for example, sometimes a needled fabric is thermally bonded and then chemically bonded with the aim of achieving high stiffness.

Needle-Punching. In this method, fiber webs are mechanically interlocked by physically moving some of the fibers or elements of the length of some fibers from a near-horizontal to a near-vertical position. This is achieved by intermittently passing an array of barbed needles into the web to move groups of fibers, and then withdrawing the needles without significantly disturbing the newly-positioned fibers. The degree of interlocking depends on the extent to which the needles penetrate the web (depth of penetration), the needling density (penetrations per unit area of fabric), and the number of groups of fibers or fiber elements which are repositioned per penetration. The latter depends on the design of the needles used.

The basic parts of a needleloom are the web-feeding mechanism, the needle beam which comprises a needleboard which holds the needles, a stripper plate, a bed plate, and a fabric take-up mechanism. (Fig. 5).

The fiber web, sometimes carried or reinforced by a scrim or other fabric, is guided between bed and stripper plates, which have openings corresponding to the arrangement of needles in the needle board. During the downstroke of the needle beam, each barb carries groups of fibers, corresponding in number to the number of needles and number of barbs per needle, into subsequent web layers to a distance corresponding to the penetration depth. During the upstroke of the needle beam, the fibers are released from the barbs, and interlocking is accomplished. At the end of the upstroke, the fabric is advanced by the take-up, and the cycle is repeated.

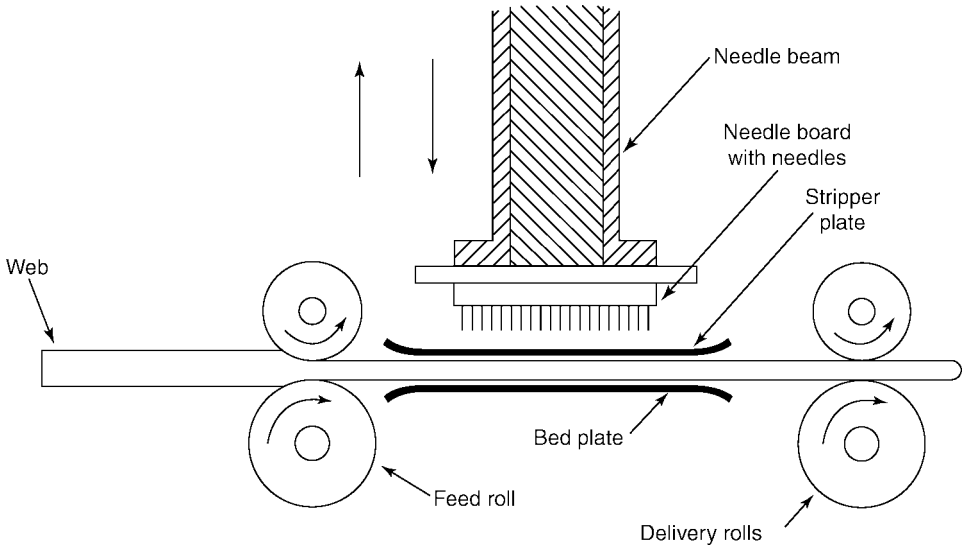

Fig. 5. Basic elements of a needle-punch machine.

Needling density is determined by both the distance advanced and the number of penetrations per stroke.

The development of a mechanical process for producing felt is dated to 1820 and has been attributed to J.R. Williams (3). The transition from interlocking fibers by working the scales on adjacent fiber surfaces against one another to working the fibers by a scaled external member in the form of a barbed penetrating device took place during the last quarter of the nineteenth century. This transition was made possible by the development of the mechanisms and machinery to produce needled nonwovens in a factory environment.

Needle looms are produced in widths ranging from several centimeters to several meters. Virtually all needle looms employ reciprocating motion to provide the penetration action. The most common needle loom configuration is the single upper-board, downstroke arrangement. Other arrangements include double upper-board, single upper- and lower-board, and double upper- and lower-board. To achieve high penetration densities on both sides of a fabric, needle looms of differing configurations are often placed in tandem.

Needle looms with low density boards are used to lightly consolidate webs and are termed pre-needlers or tackers. Machines with multiple or high density needle capabilities are referred to as consolidation or finishing needle looms. Machines designed to produce patterned or raised surfaces are termed structuring looms and are used as a mechanical finishing process.

Fabric weights range from 50 to 5000 g/m^2, and needling densities range from fewer than a hundred to several thousand penetrations per square centimeter.

Most needled fabric is made in flat form; however, tubular fabric, ranging in diameter from a few millimeters to papermakers' felt dimensions, can be made on some machines.

Needled nonwovens are sometimes mistaken for fabrics which have been felted or fabrics made directly from fibers which have been interlocked by a

combination of mechanical work, chemical action, moisture, and heat. Fabrics which have been felted are generally composed of yarns spun from wool fibers and have undergone a controlled shrinkage by subjection to the fulling process, a mechanical beating in the presence of lubricating agents. Fabrics made directly from fibers which have been interlocked by a combination of mechanical work, chemical action, moisture, and heat are felts. Felts are generally composed of wool or fur fibers and are physically held together by the interlocking of scales on individual fibers. Fiber interlocking in a felt is achieved by a process called *hardening*, which consists of passing fiber webs between oscillating and vibrating plates in the presence of steam. Following hardening, the felt is subjected to a fulling process. Felt density, stiffness, and tenacity are dependent on web weight and extent of hardening and fulling.

On the other hand, a needled felt is a fabric composed of natural, synthetic, or a combination of natural and synthetic fibers physically interlocked by the action of a needle loom with or without combination of other textile fabrics and with or without suitable combination of mechanical work, chemical action, moisture, and heat, but without weaving, knitting, stitching, thermal bonding, or adhesives (4).

Early needle-punched nonwovens were made from coarse animal hair and vegetable fibers and were used as carpet underlays and padding for mattresses and furniture. By the late 1950s needled synthetic products were being introduced for home furnishings and apparel. Several attempts were made to make synthetic leather in the 1960s, with the needled fabric as a substrate.

The main applications of needle-punched fabrics are automotive, geotextiles, footwear components, insulation, and roofing substrates.

Stitchbonding. This is a mechanical bonding method that uses knitting elements, with or without yarn, to interlock fiber webs. Sometimes called stitchthrough or web knitting, this technology was developed in eastern Europe in the late 1940s. Maliwatt and Arachne machines use yarn; Malivlies and Arabeva machines use modified knitting needles to interlock the fibers. Both families of machines operate essentially on the same principle, but differ in the positioning of the knitting elements, direction of web passage, and type of needles used.

The sequence of operations for a web-consolidation cycle on an Arachne machine is as follows. The web is guided upward and positioned between the web-holder table and knock-over table and penetrated by the needle. After passing through the web, the hook of the needle is provided with a yarn properly placed by the closing motion of the yarn guide. When the needle reaches the end of the upward stroke, the yarn is pulled through the previously formed loop, the loop is cast off, the fabric is advanced, and the cycle is repeated. Similar functions are served by the Arachne web-holder table and the needle loom bed plate, the Arachne knock-over table and the needle loom stripper plate, and the Arachne knitting needle and the needle loom needle. Thus, when yarn is eliminated, stitchbonding and needle-felting methods interlock fibers similarly.

Stitchbonded fabrics are used in home furnishings, footwear, filtration, and coating.

Hydroentanglement. This is a generic term for a nonwoven process that can be used for web consolidation, fabric surface-texturing purposes, or both. The mechanism is one of fiber rearrangement within a preformed web by means of fluid forces. When used for bonding, hydroentanglement repositions individual fibers

into configurations that result in frictional interlocking. When used as a surface-texturing means, hydroentanglement repositions fibers into open-patterned arrangements.

Also termed spunlaced or jet-laced nonwovens, fabrics of this type have been sold commercially since the early 1970s and have been successfully used in applications such as interlinings, wipes, wound dressings, and surgical gowns. The earliest hydroentangled fabrics were lightweight but now weights of up to 400 g/m^2 are possible.

The hydroentanglement process, as illustrated by DuPont patent drawings (5), involves subjecting the web and its conveying device to increasingly higher pressure jets of water. When the water jet strikes the web, it moves individual fibers away from the high points of the conveying means and is deflected by the conveying surface. As a result, voids are created in the web, and fibers intermingle. Whether the fabric surface is visibly smooth or openly patterned depends on the wire design or surface geometry. When highly interlocked, mechanically bonded (spunlace) structures are desired, high water pressure and plain mesh wire are used. The resulting fabric surface is comparatively smooth and the overall structure is relatively strong because of a large amount of individual fiber entanglement. When open-surface (apertured) structures are desired, lower water pressure and conveying wire combinations or surfaces with preferred patterning configurations and depths are used, and a fabric surface with an overall aperture geometry reflective of wire or surface contour is established. A wide variety of aperture shapes and lines are possible. Individual aperture shape or hole clarity is a function of fiber dimensions, jetting pressure, and wire interlacing or embossment shape and height.

Chemical Bonding. Sometimes called resin bonding, chemical bonding is a general term describing the technologies employed to interlock fibers by the application and curing of a chemical binder. The chemical binder most frequently used to bond nonwovens is waterborne latex. Most latex binders are made from vinyl polymers, such as vinyl acetate, vinyl chloride, styrene, butadiene, acrylic, or combinations thereof. The monomer is polymerized in water, and the polymeric material takes the form of suspended (emulsified) particles. Thus the emulsion polymerization of vinyl acetate yields a vinyl acetate polymer binder and the copolymerization of styrene and butadiene yields styrene–butadiene copolymer (qv) or styrene-butadiene rubber (SBR) binder.

Latexes (or latices) are widely used as nonwoven binders because they are versatile, can be easily applied, and are effective adhesives. The chemical composition of the monomer determines stiffness and softness properties, strength, water affinity, elasticity, and durability. The type and nature of functional side groups determine solvent resistance, adhesive characteristics, and cross-linking nature. The type and quantity of surfactant used influence the polymerization process and application method. The ability to incorporate additives such as colorants, water repellents, bacteriastats, flame retardants, wetting agents, and lubricants expands this versatility even further (see LATEX TECHNOLOGY).

Chemical binders are applied to webs in amounts ranging from about 5 to 60 wt%. In some instances when clays or other weight additives are included, add-on levels can approach or even exceed the weight of the web. Waterborne binders are applied by spray, saturation, print, and foam methods. A general objective of

each method is to apply the binder material in a manner sufficient to interlock the fibers and provide chemical and mechanical properties sufficient for the intended use of the fabric.

Spray bonding is used for fabric applications which require the maintenance of high loft or bulk, such as fiberfill. The binder is atomized by air pressure, hydraulic pressure, or centrifugal force, and is applied to the upper surfaces of the web in droplet form using a system of nozzles. To apply binder to the lower surface, the web direction is reversed on a second conveyor and the web passes under a second spray station. After each spraying, the web is passed through a heating zone to remove water. The binder is cured, or cross-linked, upon passage through a third heating zone. Drying and curing is frequently done in a three-pass oven. Binder addition levels commonly range from 30 to 60% of the fiber weight.

Saturation bonding (sometimes simply called "impregnation") is used in conjunction with processes that require rapid binder addition, such as card-bond systems, and for fabric applications that require strength and maximum fiber encapsulation, such as carrier fabrics or some shoe stiffeners. Fiber encapsulation is achieved by totally immersing the web in a binder bath or by flooding the web as it enters the nip point of a set of pressure rolls. Excess binder is removed by vacuum or roll pressure. There are three variations of saturation bonding: screen, dip-squeeze, and size-press. Screen saturation is used for medium weight nonwovens, such as interlinings. Dip-squeeze saturation is used for web structures with sufficient strength to withstand immersion without support. Size-press saturation is used in high speed processes, such as wet-laid nonwovens. Through-air ovens or perforated drum dryers are used to remove water and cure the resin. Binder addition levels range from 20 to 60% of fiber weight.

In print bonding, binder is applied in predetermined areas or patterns. This method is used for fabric applications that require some areas of the fabric to be binder-free, such as wipes and coverstocks. Many lightweight nonwovens are print-bonded. Printing patterns are designed to enhance strength, fluid transport, softness, hand, and drape. Print bonding is most often carried out with gravure rolls arranged as shown in Figure 6**a**. Binder addition levels are dependent on both engraved area and depth, and the binder-solids level. Increased pattern versatility can be achieved by using rotary-screen rolls arranged as shown in Figure 6**b**. Drying and curing are carried out on heated drums or steam-heated cans.

Foam bonding is used when low water and high binder-solids concentration levels are desired. The basic concept involves using air as well as water as the binder carrier medium. Foam-bonded nonwovens generally require less drying and curing energy because less water is used. The foam is generated by concurrently aerating and mechanically agitating the binder compound. Air/binder dilutions (blow ratios) range from 5 to 25. The addition of a stabilizing agent to the binder solution causes the foam to resist collapse during application and curing, and yields a fabric with enhanced loft, hand, and resilience.

Nonstabilized foams are referred to as froths; froth-bonded fabrics are similar in properties to some saturation-bonded nonwovens. Typical foams used as nonwoven binder solutions have a consistency similar to shaving cream. Application methods include knife-edge layering onto a horizontal web surface followed by vacuum penetration, and saturation and penetration of a vertical web surface

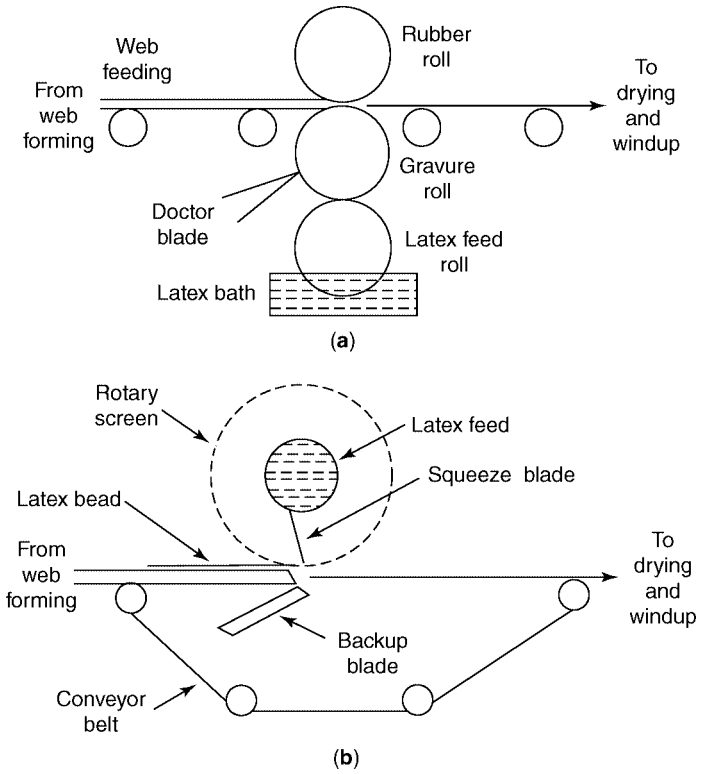

Fig. 6. Print bonding methods where (a) is gravure and (b) is rotary-screen printing.

using a horizontal-nip pad. Drying and curing are carried out in ovens, drum dryers, or steam cans.

Thermal Bonding. In thermal bonding, heat energy is used to activate an adhesive, which in turn flows to fiber intersections and interlocks the fibers upon cooling. The adhesive may be individual fibers, portions of individual fibers, or powders. Advantages of thermal bonding include low cost and the wide availability of binder materials and machines. The use of thermal bonding is increasing and replacing chemical bonding in medium weight nonwovens.

Thermal bonding is achieved as the result of a sequence of three events: heating, flowing, and cooling. The adhesive component, distributed in a nonwoven web in the form of a unicomponent fiber, bicomponent fiber, or powder particle, is subjected to heat. For binder fibers and powders, initial heat softens the binder surface and expands its contact area with other fibers; additional heat induces binder flow, resulting in molten binder–fiber wetting and broader binder-to-fiber contact. As the adhesive approaches its melting point, its surface softens, and contact areas with more stable fibers expand further to form potential bonding sites. Upon melting, the adhesive, now in liquid form, becomes attached to a network fiber. It then flows along the network fiber into a crossing of two or more fibers, or forms an adhesive bead. Upon cooling, the adhesive solidifies and forms a bond at each fiber contact.

In addition to the melt-flow properties of the adhesive, bond strength is a function of the percentage of fiber surface area joined or shared at fiber intersections, the heating and cooling times, and bonding temperature. Bond effectiveness is also dependent on binder distribution and binder concentration. Fabric strength, resilience, softness, and drape are affected by bond strength, bond position, and total bonded area. A properly produced thermal-bonded nonwoven can approach the idealized nonwoven structure, namely, one in which individual fibers are connected at crossings with each other.

Three basic methods of heating are used for thermal bonding: conduction, radiation, and convection. Conduction technologies include fixed contact with a heated surface and ultrasonic welding. Direct contact heating is done with heated calender rolls. For area or surface glazing, smooth rolls are used. For point bonding, patterned or embossed rolls are used. Thermal calendering is most efficient in terms of heat loss, but heavy roll pressures tend to destroy fabric loft.

For fabrics containing a significant proportion of thermoplastic material which is usually thermoplastic fibers but could be powder, bonding, including in patterns, can be done ultrasonically. An illustration of the basic elements of an ultrasonic bonding unit is given in Figure 7. In this bonding method, a web is placed between a high frequency oscillator or horn, and a patterned roll. As the waves pass through the web and are concentrated on the raised points of the patterned roll, sound energy heats the fibers. If they are thermoplastic, they will soften and start to melt, bonding the fabric together in patterns corresponding to those on the surface of the roll.

Radiation heating concentrates fiber bonding on the surface. For lofty or thick structures, this effect yields a bond intensity gradient throughout the fabric thickness. Radiant heating systems are used mostly for applications which require

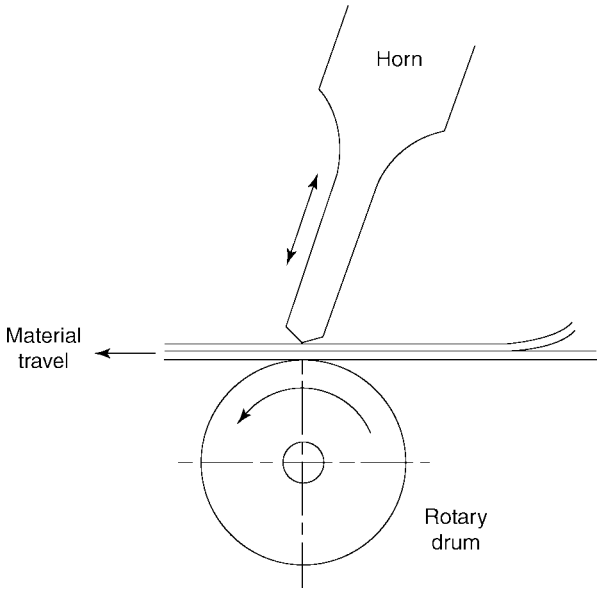

Fig. 7. Basic elements of ultrasonic bonding.

instant heating and concentrated heating zones. Convection heating methods pass heated air through the nonwoven web and are used to bond many medium and heavy weight nonwovens. Two common commercial configurations are multizone through-air ovens and compact through-air ovens. Multizone ovens transport the nonwoven web through heating and cooling zones on a flat conveyor, with production speed and dwell time requirements being accommodated by increasing oven length. Compact through-air ovens use felt or perforated belts to guide the webs around perforated drums. In these systems, hot air is recirculated through the fabric, drum, and heat exchanger by low speed radial fans. The belt guide conveyor serves to stabilize the nonwoven batt during heating, and also controls fabric loft and shrinkage.

From an energy standpoint, modern thermal bonding, ie web consolidation with no heat requirement for water removal, is very efficient. Manufacturing lines for thermal-bonded nonwovens also require less floor space and operate at higher production rates. Thermal-bonded nonwovens are generally softer and drier, have greater strength per unit weight, and are absorbent and porous because of smaller bonding points.

Thermal bonding also provides the opportunity to design fabrics which are more easily recyclable than chemically bonded fabrics.

Finishing

Commercial nonwoven fabrics are transported from the manufacturing plant to the customer in the form of rolls of varying dimensions to accommodate the fabric end-use application or subsequent conversion processes. Slitting and winding are finishing processes common to all nonwoven manufacturing methods. Roll width is determined at the slitting operation, and roll length is determined at the winding operation.

The fabric may also be given one or more of a number of other finishing treatments, either in tandem with web formation and bonding or off-line as a separate operation, as a means of enhancing fabric performance or aesthetic properties. Performance properties include functional characteristics such as moisture transport, absorbency, or repellency, flame retardancy, electrical conductivity, abrasion resistance, and frictional behavior. Aesthetic properties include appearance, surface texture, and smell.

Generally, nonwoven finishing processes can be categorized as either chemical, mechanical, or thermomechanical. Chemical finishing involves the application of chemical coatings to fabric surfaces or the impregnation of fabrics with chemical additives or fillers. Mechanical finishing involves altering the texture of fabric surfaces by physically reorienting or shaping fibers on or near the fabric surface. Thermomechanical finishing involves altering fabric dimensions or physical properties through the use of heat and pressure.

Finishing may also be viewed as another means for providing nonwovens with additional application-dependent chemical and/or physical properties. Finishing processes bring about value-added fabrics with technically sophisticated properties for specific end-use applications.

Chemical Finishing. For many nonwovens, chemical finishing is an extension of the binder application process through the use of technology associated with fabric coating. In most instances, the coating process is applied to enhance the properties of the nonwoven; however, in some applications, the nonwoven is used as a carrier to transmit the properties of the coating material. The coating may be applied as a continuous covering or as a pattern; it is most frequently applied in aqueous solution form. With many nonwoven substrates, special care must be taken because of the delicate nature of the structure itself or the arrangement of fibers on or near the fabric surface.

A number of different methods are used to coat nonwovens depending on the viscosity requirements of the coating material and the amount and location of coating desired. Knife-over-roll (blade coating), reverse-roll, air-knife, wire-wound rod, transfer-roll, rotary screen, and slot-die methods are used to apply continuous coatings to single surfaces. Double-surface coating of relatively nonporous nonwovens with high viscosity materials can be achieved by using dip saturators or size presses with gapped or low pressure squeeze rolls. Impregnation of substantially porous nonwovens can be achieved by using the same equipment at higher roll pressures. Patterned coatings or decorative printing can be achieved with the use of gravure rolls or rotary screens. Likewise, fabrics can be impregnated with different impregnants either side, using rotary screens followed by a pair of nip rolls.

Transfer roll, rotary screen, saturation, size press, and gravure apparatus are similar to those used for resin bonding. Reverse-roll coaters are similar in configuration to gravure print-bonding apparatus, but differ in the surface patterning and direction of rotation of the applicator roll. The amount of material applied when using this method is controlled by adjusting the relative speeds of the applicator roll and the rate of fabric passage through the coating system.

In knife-over-roll or blade coating, the coating material is placed on the fabric surface behind a knife, or doctor blade, and metered according to the gap set between the blade and the fabric surface. This method is used to apply thick coatings of highly viscous materials such as pastes, plastisols, or foams.

Air-knife coating is a high speed process used to apply continuous coatings of relatively low viscosity materials onto nonwovens with irregular surfaces. The principal components of this system are illustrated in Figure 8. Following an initial application, the coating material is metered by air impingement.

Wire-bar (Mayer) coating is used to uniformly coat lightweight material applications. As in air-knife coating, the material is applied initially at a first station, but in this system, the coating material is metered and levelled by a wire-wound rod. Coating weight and uniformity are controlled by changing wire thickness and pitch on the metering rod.

Transfer-roll or flexographic coating is used to apply continuous coatings of low or medium viscosity materials at high speeds. This system is particularly suitable for coating stiff or irregularly surfaced nonwovens and for applying abrasives. With high viscosity materials and appropriately designed gravure rolls, flexographic coaters can be used as pattern applicators for decorative prints.

Rotary-screen coating is also used to apply either continuous or discontinuous coatings to nonwovens. The screen is a sleeve, perforated according to a mesh size which corresponds to the size and number of hole per unit area of surface. A

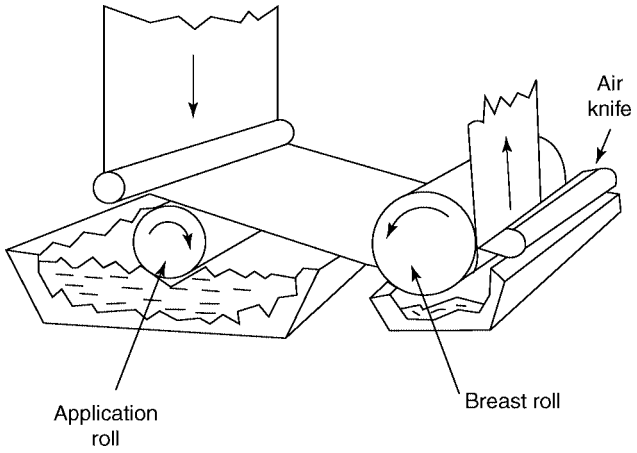

Fig. 8. Components of an air-knife coating apparatus.

material supply tube and squeegee blade are fitted inside the screen. The coating material, in the form of a paste or foam, is forced by the blade through the perforations of the rotating screen onto the nonwoven. For a given coating material, coating weight and penetration are controlled by varying mesh size and squeegee pressure. Patterned coatings or printed designs can be achieved by blocking out selected perforations.

Slot-die or extrusion coating involves the application of molten polymer resin through a slot die directly onto the surface of a nonwoven. Upon extrusion, the resin is smoothed and quenched by a cooling roll. Coating weight is controlled by slot size and extrusion rate. In a variant of this method, nonwoven fabrics are combined with an extruded film just after the die and before the roll-stack. The fabrics can be subsequently chemically bonded to give a sandwich structure. Such products are used as waterproof insales in shoes.

Various chemical finishes can be applied by impregnation, spraying, etc. These include softeners, flame retardants, and antistatic, antisoil, water-repellent, and antibacteria finishes.

Finally dyeing and printing can be included as examples of chemical finishing of nonwovens.

Mechanical and Thermomechanical Methods. These methods provide nonwovens with patterned surface structures, enhance the surface texture of nonwovens, or both. Patterned surfaces may be established by embossing, by compressive shrinkage, and for needle-felted nonwovens, by creating loops or pile. Surface textures, ranging from flat and smooth to raised and levelled, may be created or altered by calendering, sueding, napping, polishing, brushing, or shearing. In general, mechanical finishing processes operate at speeds slower than web-consolidation processes and, consequently, are carried out off-line or as a separate batch process.

Smooth surfaces are normally established by calendering, a process which subjects the fabric at the nip point(s) of two or more rolls to the influence of controlled time, temperature and pressure. When calendering is used as a

thermal-bonding process, the rolls are of the same dimension and composition and are independently driven. However, when calendering is used as a fabric finishing operation, the rolls are frequently of different dimensions and composition and are not always independently driven.

Specific terms have been designated according to the function and composition of various rolls. Steel rolls that impose pressure, transmit heat, and emboss a pattern onto the fabric are known as pattern rolls. Flexible surface rolls that transport the fabric and permit pressure transmission to the fabric are termed bowl rolls or bowls. Bowl rolls are usually larger in diameter than pattern rolls. The material used to make these types of rolls is chosen according to the depth of surface smoothness to be placed on the fabric being calendered, and must be compatible with the pattern roll.

Calender designations include embossing calenders, friction calenders, and compaction calenders. Most embossing calenders are fitted with a main pattern roll and either one or two bowl rolls which are positively driven by the pattern roll through interconnecting gearing. In friction calendering, the rubbing action is accomplished by operating the pattern rolls at higher rates than their bowl counterparts. Compaction calendering establishes desired fabric thicknesses or calliper through adjustable gapping or roll spacing.

Sueding is a mechanical finishing process in which fibers on the surface of a fabric are cut by the abrasive action of a sanding roll operating at relatively high speed. The cut fibers are oriented in the direction of the sand roll rotation and protrude about a millimeter from the surface. The primary components of a sueding machine are the guiding system, sanding roll, support roll, and roll spacing structure and control. Sueding is sometimes used to reduce the gauge and raise the surface of synthetic leather materials.

The napping process mechanically raises fibers to the surface of a lubricated fabric by withdrawing the fibers from the interior of the fabric. A planetary napping machine configuration is shown in Figure 9; basic components include a series of working rolls wound with hooked wire and a fabric guiding system. The working rolls are operated in a direction opposite the fabric and at surface speeds greater than the fabric passage speed. The napping action takes place as

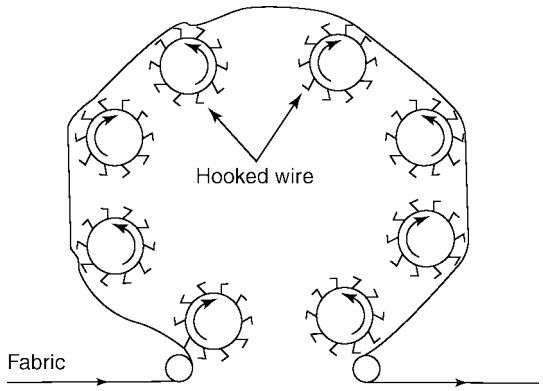

Fig. 9. Planetary napping machine configuration.

the wires of the working rolls penetrate the fabric, withdraw fibers, and form a nap of raised fibers on the surface of the fabric. Depending on wire design, wire wrapping pattern, roll arrangement, number of rolls, and relative roll rotation and direction, nappers can be used to produce a wide range of either loop or velour surface effects.

Polishing is a thermomechanical process that aligns the pile of a raised fabric surface. Polishing machine components include a guiding system consisting of a tension blanket and a spirally grooved heated cylinder. The mechanical action of the rotating edge of the roll groove against the tensioned fabric surface results in a static charging of the pile fibers, which in turn aligns the fibers in a parallel orientation. Rotation of the spiral roll in the direction that momentarily entraps fibers in the grooves results in a raised, parallel pile surface. Rotation of the spiral roll in the opposite direction results in a flat, parallel pile surface.

Brushing is a mechanical finishing process that lifts fibers to the fabric surface and aligns the raised fibers along the machine direction of the fabric. Brushing machinery is similar in configuration to both sueding and napping machinery, but the composition of the working roll is different. Straight-wire clothing is used in brushing machine rolls. As the working roll rotates against the fabric surface, the straight wire withdraws and orients the fibers along the direction of fabric passage through the machine. The length of fiber withdrawn is determined by the gap adjustment between the working and support rolls.

Shearing cuts raised fibers to uniform heights. Fabric shearing generally follows a brushing operation and consists of subjecting the fabric surface to a series of spirally wound shearing blades rotating over a stationary ledger blade. The working elements of a shearing machine are similar in configuration to a reel-type lawn mower. In operation, the fabric is guided under the shear blades while the pile is held in a raised position by vacuum. As the fabric passes a shearing point, the raised fibers strike the ledger blade and are cut by the rotating shear blades. Cut pile height is controlled by adjustment of the distance between the fabric guide and the rotating blades.

Tumbling can be used to soften chemically bonded fabrics—this technology was developed for leather and involves breaking of internal bonds in the structure to provide increased softness and suppleness.

The addition of some shrinkage fibers enables the fabric to be shrunk by heating to an appropriate temperature. This technique is often used to increase the density of a needled fabric and is employed in the manufacture of synthetic leather—after needling, the fabric is shrunk and then chemically bonded.

Another process commonly used in synthetic leather manufacture is splitting. A thick and dense, chemically bonded needlefelt is split up to six times to provide material for shoe-linings, handbags, etc.

Production

Total consumption of nonwovens in 2001 was around 3 million tons and was thought to be growing to about 4 million tons by 2005. Ninetynine percent of all nonwovens are made from synthetic fibers. Polypropylene predominates (63%), with polyester being second (23%) and viscose rayon third (7%).

The United States continues to be the major nonwoven producer (37%), then Western Europe (29%), followed by Japan (8%) and China (6%). Production in China is growing quickly—especially in spunbonded and spunlace fabrics.

Production according to manufacturing technology is approximately as follows: highloft 26%, spunbonded 17%, needlepunched 10%, bonded pulp 8%, thermal-bonded carded webs 7%, hybrids 7%, resin-bonded carded webs 6%, spunlace 5%, wet-laid 5%, meltblown 4%, and the rest 5%.

The majority of card-resin-bonded and card-thermal-bonded fabrics are used as coverstock; interlinings, wipes, and carrier sheets account for most of the remainder. More than half the highloft volume is used in furniture and sleeping applications; filtration, apparel, insulation, healthcare, with geotextiles accounting for most of the remainder. Stitchbonded fabrics are used in bedding, shoe linings, and a variety of coated products. Needlepunch fabrics are used in automotive, geotextiles, filtration, bedding, and home furnishing applications.

The major use for spunlace fabrics is in medical products; other applications include wipes, industrial apparel, interlinings, absorbent components, filtration, and coating. Medical applications account for about a third of all wet-laid nonwovens. Most bonded pulp fabrics are used as wipes or as absorbent components.

Spunbondeds are commonly used for coverstock, geotextiles, roofing substrates, carpet-backing, medical products, filtration, furniture, and packaging. Meltblown fabrics, because of their relatively fine fiber structure, is commonly used in filtration, sorbents, wipes, and sanitary products.

Applications

Nonwoven goods applications split into disposables and durables, with disposables being the major share.

Coverstock is the nonwoven fabric placed on the user's side of sanitary absorbent products such as baby diapers, nappy liners, adult diapers, incontinence products, and feminine hygiene products. Medical and surgical products include protective wrap for hospital items which are distributed through the central supply room; surgical drapes, packs, and gowns; other protective products such as face masks, caps, aprons, bibs, and shoe covers; absorbent products such as surgical dressings and sponges; and other hospital products such as isolation gowns, examination gowns, sheets, shrouds, underpads, and bedding.

Nonwoven wipes includes products for babies and adults, the food service and electronics industries, medical and clean room applications, dusters, shoe cleaning cloths and hand towels. Nonwoven fabrics are used to filter air, water, petroleum, food, and beverages. Nonwovens loaded with abrasives, cleansers, or finishes are used in a wide range of products for cleaning and scouring. Also, many protective garments are made from nonwoven fabrics.

Durable products include geotextiles, for example, to stabilize earth works, roads, landscaping, etc. In agriculture, nonwovens are used as protective or capillary mats, shading, and windbreaks.

In aircraft, nonwovens are used as reinforcement media in composites and lightweight insulation. In electronic components, nonwovens are used as battery separators, and in cable insulation—nonwovens of superabsorbent fiber have been

used as cablewrap to protect the core from the ingress of water. Vehicle applications include moldable carpet backings, headlinings, and interior trim. In building construction, nonwovens are used for roofing, insulation, and water-impermeable wrappings. In furniture and bedding, nonwovens are used as decking and ticking, quilt backings, carpet backings, underlays, wallcoverings, and padding. In shoes, chemically bonded nonwovens are used as shoe stiffeners and insoles. Uppers and linings are made from synthetic leather which comprises chemically bonded nonwovens made from microfibers.

BIBLIOGRAPHY

"Nonwoven Fabrics, Survey" in *EPSE* 2nd ed., Vol. 10, pp. 204–227, by A. Drelich, Chicopee.
1. R. Johnson, *Robert Johnson Talks It Over*, Johnson & Johnson, New Brunswick, N.J., 1949.
2. J. N. Balboni, in *INDA-TEC'93*, INDA, Cary, N.C., 1993.
3. E. A. Vaughn, *J. Nonwovens Res.* **4**, 1 (1992).
4. ASTM Designation D2475-77, American Society for Testing and Materials, Philadelphia, Pa.
5. U.S. Pat. 3,485,706 (Dec. 23, 1969), F. J. Evans (to E. I. du Pont de Nemours & Co., Inc.).

ROGER CHAPMAN
Texon UK Limited

NOVOLAKS. See PHENOLIC RESINS.

NUCLEAR MAGNETIC RESONANCE

Introduction

An important objective in materials science is the establishment of relationships between the microscopic structure or molecular dynamics and the resulting macroscopic properties. Once established, this knowledge then allows the design of improved materials. Thus, the availability of powerful analytical tools such as NMR spectroscopy (1–13) is one of the key issues in polymer science. Its unique chemical selectivity and high flexibility allows one to study structure, chain conformation and molecular dynamics in much detail and depth. NMR in its different variants provides information from the molecular to the macroscopic length scale and on molecular motions from 1 to 10^{10} Hz. It can be applied to crystalline as well as to amorphous samples which is of particular importance for the study of polymers.

Encyclopedia of Polymer Science and Technology. Copyright John Wiley & Sons, Inc. All rights reserved.

Moreover, NMR can be conveniently applied to polymers since they contain predominantly nuclei that are NMR sensitive such as ^{1}H and ^{13}C.

Although well established for liquid-like samples such as macromolecules in solutions (14,15), the applications of NMR to solid or solid-like polymers is more demanding because of the presence of anisotropic interactions that complicate the analysis of the results. Several techniques for the removal of these interactions have thus been developed and are nowadays in a state where they could be routinely applied. Nonaveraged anisotropic interactions on the other hand provide valuable information that is lost in the solution state. Thus, while it is often necessary to remove the anisotropic interactions, in many cases one would simultaneously like to preserve them in order to exploit their information content.

This is where two-dimensional (2D) spectroscopy comes into play (1), for instance, by correlating one-dimension where the anisotropic interactions are preserved with a (high resolution) dimension where they are removed. Multidimensional NMR spectroscopy proves to be a powerful method to reveal structural and dynamical information at the molecular level in elastomers (16). Residual dipolar couplings can be measured site-selectively and correlated with the cross-link density and mechanical stress. The local segmental order and information on local molecular motions can also be obtained with newly developed 2D NMR methods (16). The information at the molecular level can be correlated with macroscopic properties of elastomers and provides the basis for a better design of material properties for specific applications.

From the viewpoint of NMR, elastomers, and other viscoelastic polymers above their glass-transition temperature exhibit both, solid-like and liquid-like features (12). Whereas the segmental motions give rise to the liquid-like behavior, the presence of permanent or nonpermanent cross-links leads to residual dipolar couplings, that is responsible for the solid-like properties. This promises that both properties can be exploited, but the application of 2D techniques to viscoelastic materials has to deal with the difficulties related to both, rigid and mobile samples (16). Compared with the wealth of applications in solution and in the solid state, NMR has not been widely applied to viscoelastic polymers, although it can provide information on such important areas as the chain dynamics in elastomers, the local structure, residual couplings (induced by chemical cross-links and topological constraints), dynamic order parameters, internuclear distances, intermolecular interactions (which are important for instance for the miscibility), the effects of fillers on molecular motions, and segmental orientation under mechanical stress and others.

NMR imaging finds most of its applications in medical diagnostics of humans and pathology studies of animal models (17–22). The success of the method is based on noninvasiveness of the nuclear magnetic resonance and the unsurpassed soft-matter contrast, which is hard to achieve with competitive methods like X-ray or computer tomography. The same advantages can be exploited in imaging studies related to materials science (19,22). Here, an important class of soft-matter materials is given by synthetic polymers above the glass transition temperature. Apart from Semicrystalline Polymers (qv) like polyethylene, polypropylene, some polyamides, and polymer melts, elastomers constitute the most striking class of synthetic soft matter with a modulus similar to many biological tissues. Applications of imaging for which nondestructiveness or contrast are essential, are

competitive with other imaging techniques in the information gained and the cost of the experiment. Such applications to elastomers concern distributions in temperature, stress, cross-link density, modulus, and the dynamics of fluid absorption and swelling.

The nucleus imaged most often is the proton. The reason is not only sensitivity but also the weak dipolar couplings between protons in a chemical group and between different chemical groups which dominate the signal decay by relaxation. These dipolar couplings are motionally averaged by the often fast but nearly always anisotropic motion of intercross-link chains. This motion and consequently the value of the residual dipolar couplings are affected by chain stiffness, cross-link density, chain orientation, temperature, and additives, etc. Given that the residual dipolar interactions are too strong to obtain chemical-shift resolution without sample spinning or multipulse techniques, relaxation techniques that probe different time regimes of molecular motion provide the primary access to contrast in imaging of elastomers.

After a brief introduction of the basic principles of NMR, the one-dimensional (1D) and two-dimensional (2D) methods that have been applied to viscoelastic materials will be reviewed. NMR imaging which can be considered as a special form of multidimensional NMR will be introduced by discussing principles and image contrast. Illustrative examples of NMR imaging to elastomer materials are given.

Basic Principles of NMR

Magnetic Resonance Phenomenon. Magnetic resonance is a branch of spectroscopy that detects the quantum-mechanical transitions induced by electromagnetic radiation in a system of discrete energy levels of electron or nuclei placed in a static magnetic field. Nuclear magnetic resonance (NMR) employs electromagnetic waves in the radio-frequency range between 900 MHz and 2 kHz.

Nuclear magnetic resonance is one of the most powerful method for structural and dynamics investigation on matter in different states of aggregation. This is due to the following features: (*1*) The interaction of nuclear magnetic moments are very weak compared with the thermal energy, therefore, we deal with nuclear paramagnetism. Moreover, the energy delivered by the radio-frequency generator are much larger compared with the strength of these internuclear couplings. That leads to the possibility to manipulate these interactions in a specific way and to simplify the spectral response. (*2*) The radio-frequency photons have much lower energy compared with the energy of chemical bonds. Therefore, the interaction of electromagnetic radiation with the matter, especially, biomolecules is nonionising. (*3*) The number of radio-frequency photons with a specific frequency is very large. Hence, the phase of the associated electromagnetic wave is very well defined. The high degree of coherence of radio-frequency radiation is essential for implementation of NMR experiments including magnetic resonance imaging (MRI).

The appearance of NMR spectra, and consequently the molecular structure they are able to provide, arises from the discrete nature of the energy levels pertaining to a nuclear spin system. The energy levels are mainly a result of the

Zeeman interaction $-\vec{\mu}\cdot\vec{B}_0$ between the static magnetic field of induction $\vec{B}_0$ and nuclear magnetic moment $\vec{\mu}$. The quantum-mechanical quantity called spin momentum $\vec{I}$ is related to magnetic moment by $\vec{\mu}=\gamma\hbar\vec{I}$, where γ is the magnetogyric ratio and $\hbar$ is the Planck constant divided by 2π.

In the absence of the magnetic field the nuclear spin states are degenerated (see Fig. 1**a**). The application of a static magnetic field $\vec{B}_0$ induces a magnetic interaction described by the Zeeman Hamiltonian $H=-\vec{\mu}\cdot\vec{B}_0$. Taking the magnetic field orientation to be along the z-direction we get

$$H=-\gamma\hbar B_0 I_z \tag{1}$$

The eigenvalues E_m of this Hamiltonian can be evaluated from the Schrödinger equation

$$H|m\rangle=-\gamma\hbar B_0 m|m\rangle \tag{2}$$

where $|m\rangle$ is the eigenstate corresponding to the eigenvalue $E_m=-\gamma\hbar B_0 m$. The magnetic quantum number is m where $m=I, I-1,\ldots, -I$. Therefore, the equidistant energy differences are for the single-quantum transitions $\Delta m=\pm 1$ given by

$$\Delta E=\hbar\omega_0 \tag{3}$$

where the Larmor frequency is $\nu_0=\nu_{\mathrm{L}}=\omega_0/2\pi$. Energy level diagrams of a spin $I=1/2$ and $I=1$ are shown in Figure 1.

Another important ingredient for a magnetic resonance experiment is represented by the presence of the radio-frequency (rf) field. Only the magnetic component of the electromagnetic field, ie, $\vec{B}_1(t)=\vec{B}_{10}\cos(2\pi\nu t)$ interacts with the magnetic moment of the nuclei. The amplitude of the rf field is $\vec{B}_{10}$ and ν is the carrier frequency. This field is produced by a rf coil and leads to a perturbation Hamiltonian

$$H_{\mathrm{p}}=-\gamma\hbar\vec{B}_{10}\cdot\vec{I}\cos(2\pi\nu t) \tag{4}$$

From time-dependent perturbation theory of quantum-mechanics, it can be stated that a transition between two states $|\psi\rangle$ and $|\phi\rangle$ is allowed provided that $\langle\psi|H_{\mathrm{p}}|\phi\rangle\neq 0$. This takes place if $\nu\approx\nu_0$ (ie, the resonance condition) and the alternative magnetic field $\vec{B}_1(t)$ is polarized perpendicularly to the static magnetic field $\vec{B}_0$. Concerning a spin $I=1$ (Fig. 1**b**), similar calculations show that only the single-quantum transitions $|0\rangle\rightarrow|1\rangle$ and $|-1\rangle\rightarrow|0\rangle$ (and those in the opposite directions) are allowed in the first approximation and occur at the same frequency, given by equation 3.

Quantitative spin system evolution in the presence of the interspin couplings has to be described in the language of quantum-mechanics. This is a reflection of the quantum-mechanical nature of the spins and the fact that the spin couplings via propagator operators encode NMR observables. Nevertheless, the description of nuclear magnetization relaxation processes is done by a semiclassical approach

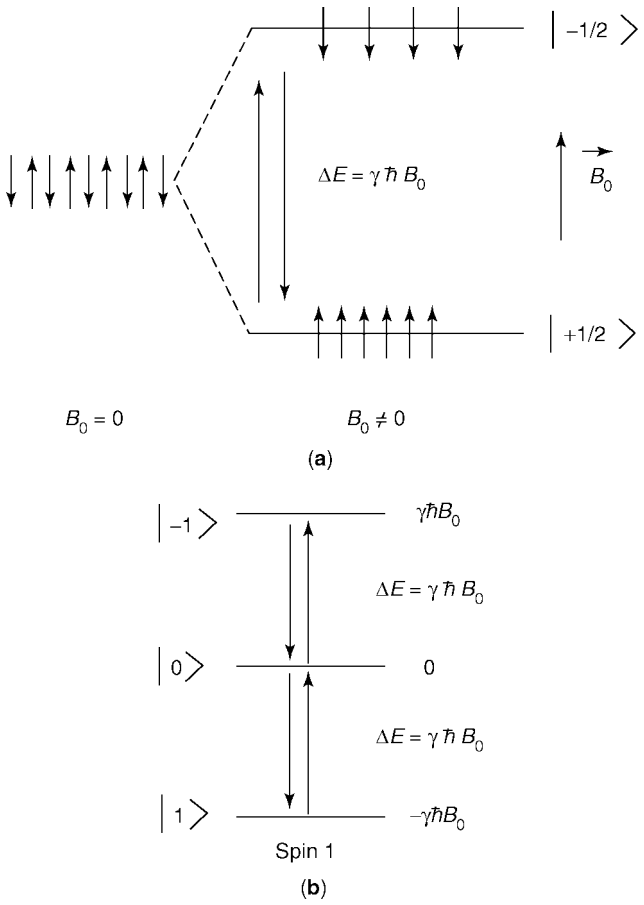

Fig. 1. (**a**) Energy levels diagram and allowed transitions of an ensemble of spins with $I = 1/2$ in the absence and the presence of $\vec{B}_0$. The small arrows indicate the orientation of nuclear spins relative to $\vec{B}_0$. (**b**) Energy diagram and allowed single-quantum transitions for spins with $I = 1$.

where the thermal bath is described classically and the spin system by a quantum-mechanical formalism.

In general, the NMR experiments are performed at high temperatures employing a large number of spins. These features lead to the possibility to treat classically some aspects of the experiments. The excess of spins oriented along the static magnetic field $\vec{B}_0$ with respect of those oriented in the opposite direction (cf Fig. 1**a**) results in a macroscopic nuclear magnetization $\vec{M}$ aligned along the static magnetic field, which is called equilibrium magnetization (cf Fig. 2**a**). It can be displaced from this equilibrium by an appropriate perturbation, for instance, by a rf excitation. It is then subject to a precessional motion around $\vec{B}_0$ with the Larmor frequency ν_L (Fig. 2**b**). The electromagnetic perturbation which brings $\vec{M}$ into a plane perpendicular to $\vec{B}_0$ allows the observation of the Larmor precession through an electromotive force which occurs in a coil whose axis is

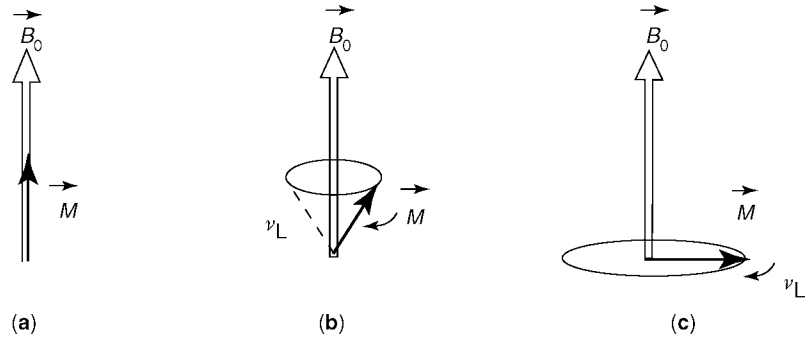

Fig. 2. (**a**) At thermal equilibrium, the nuclear magnetization $\vec{M}$ is collinear with $\vec{B}_0$. (**b**) Under the action of an electromagnetic perturbation $\vec{M}$ is displaced from equilibrium position. It starts undergoes precessional motion around $\vec{B}_0$ at the Larmor frequency $\nu_L = \nu_0$. (**c**) After the action of a 90° rf pulse the magnetization $\vec{M}$ is brought in a transverse plane to $\vec{B}_0$.

contained in that plane (Fig. 2**c**). This can be done by rotation of the nuclear magnetization using a resonant 90° rf pulse. The nuclear magnetization M can be oriented antiparallel to $\vec{B}_0$ by the action of 180° pulse. The majority of NMR experiments used pulse sequences composed of 90° and 180° rf pulses.

Magnetic and Electric Spin Interactions. The nuclear spins can experience various external and internal interactions. These interactions can have magnetic or electric origin. The external interactions are, in general, represented by the Zeeman interactions with static and rf magnetic fields and the gradients of these fields.

The chemical shielding, dipole–dipole, spin–spin indirect coupling or J-coupling, spin-rotation, and hyperfine couplings represent the major internal magnetic interactions. The quadrupolar interaction has an electrostatic character. All these interactions have a tensorial character, ie, are function on the orientation of the principal axes of the tensor relative to the direction of $\vec{B}_0$. They are relevant for solid polymers below and around the glass transition temperatures. For polymer in solution or for soft polymers fast molecular motions average these anisotropic interactions to isotropic or residual values which can be zero. Detailed description of the properties of these spin interactions can be found in References 1–9.

In the studies of elastomers by NMR experiments dipolar and quadrupolar interactions have been mainly used. The presence of the high magnetic field already imposes a manipulation of the spin system which separates certain parts of the spin interaction Hamiltonian. This process is called truncation and the secular dipolar Hamiltonian of two spins I and S has the general form

$$H_{\mathrm{d}}^{(0)} = -\left(\frac{\mu_0}{4\pi}\right)\frac{\gamma_I\gamma_S}{r^3}\frac{1}{2}(3\cos^2\theta_{IS} - 1)(3I_zS_z - \vec{I}\cdot\vec{S}) \qquad (5)$$

The factor $\mu_0/4\pi$, where μ_0 is the magnetic susceptibility of vacuum has been introduced in conformity with MKSA units. The magnetogyric ratios are γ_I and

γ_S. The spin operators are denoted by $\vec{I}$ and $\vec{S}$. The space encoded part of the dipolar Hamiltonian depends on the distance r of spins I and S and the angle θ_{IS} between $\vec{r}$ and $\vec{B}_0$. The anisotropic segmental motions average the space part of $H_{\mathrm{d}}^{(0)}$ to a residual value.

Finally, the truncated form of the axially symmetric quadrupolar Hamiltonian for nuclei with spin I larger than 1/2 can be expressed as

$$H_{\mathrm{Q}}^{(0)} = C_{\mathrm{Q}}\left[3I_z^2 - \vec{I}^{\,2}\right] \tag{6}$$

The quadrupolar coupling C_{Q} is defined by

$$C_Q = \frac{eQV_{\mathrm{ZZ}}}{4hI\,(2I-1)} \tag{7}$$

where eQ is the quadrupolar moment of a specific isotope and V_{ZZ} is the Z component of the electric field tensor at the position of the nucleus. In the presence of anisotropic molecular motions, the electric field gradient tensor is averaged to a residual value.

The spin interactions can be classified as inhomogeneous and homogeneous (4). The NMR spectrum generated by the inhomogeneous spin interaction which is linear in the spin operator I_z, is a sum of independent individual lines. A selective rf irradiation can saturate only a group of spins producing a hole in the spectrum. For homogeneous lines the NMR spectrum is a sum of individual lines with no shift with respect to each other. The spin interactions bilinear in the spin operators generate these spectra. The excitation of the spectrum with a selective pulse will affect all the spectral frequencies.

Magnetization Relaxation. One of the important sources of information about molecular motions is related to the relaxation of the longitudinal (M_z) and transverse (M_x and M_y) components of the macroscopic nuclear magnetization. The molecular motions modulate the spin interactions that lead to the exchange of energy between the nuclear energy levels and the lattice or thermal bath represented by the molecular degree of freedom. This process is described by a time constant T_1 the so-called longitudinal relaxation time. The dephasing of the transverse magnetization components M_x and M_y, which is related to the increase of the entropy of the spin system is described by the transverse relaxation time T_2.

The molecular motions responsible for the relaxation include: (*1*) overall translational or rotational motions, (*2*) local motions such as internal rotations around C—C bonds or molecular axis of symmetry or segmental motions of polymer chains, and (*3*) exchange between two different distinct chemical sites within the same molecule or different molecules.

In the simplest assumption, the time evolution of the nuclear magnetization under relaxation processes can be described by the Bloch equations (see (19), and

references therein)

$$\frac{dM_{x,y}(t)}{dt} = \frac{M_{x,y}(t)}{T_2}$$
$$\frac{dM_z(t)}{dt} = -\frac{M_z(t) - M_0}{T_1} \tag{8}$$

where M_0 is the magnetization of the spin system in the thermodynamic equilibrium. The time evolution of $\vec{M}(t)$ vector under relaxation processes described by equation 8 is given by exponential functions. This approximation is not valid in many cases for polymer or other macromolecular systems where complex relaxation mechanisms are present (23,24). In such cases, a complete treatment requires additional relaxation parameters such as cross-relaxation or cross-correlation rates (1,23–25). Such a situation occurs whenever two spins A and X interact by a random fluctuating spin interactions. For this cross-relaxation process A spins magnetizations induces a modification of X magnetization which add up to the specific evolution of X magnetization. More formally, this coupling can be expressed via the Solomon equations (see for instance, Reference 25) which contain besides the longitudinal relaxation rates of spins A and X also cross-relaxation rate which reflects the coupling between the A and X spin magnetizations. Several two-dimensional NMR experiments (see below) can measure cross-relaxation rates that enhance our knowledge about molecular motions in complex systems (1,25).

The longitudinal magnetization relaxation can be measured using different methods (5,18,19,25) based on the scheme:

$$\text{Initial perturbation} - \text{Evolution}\ (\tau) - \text{Detection}$$

The initial perturbation brings the spin system in a state on nonequilibrium and can be represented by an inversion pulse of 180° (ie, $M_z(0) \rightarrow -M_0$) or a saturation train of 90° pulses (ie, $M_z(0) = 0$). The detection is performed by a standard 90° pulse under low or high resolution conditions.

The transverse relaxation measurements are performed using a Hahn echo (see below) or Carr–Purcell–Meiboom–Gill (CPMG) pulse sequences (18,19). The first method uses the pulse scheme: $90^\circ_x - \tau - 180^\circ_{x,y} - \tau -$ Hahn echo and measure the time evolution of the amplitude of the Hahn echo as a function of echo time 2τ. CPMG scheme, $90^\circ_x - [\tau - 180^\circ_y - \tau -$ Hahn echo$]_N$ allows measuring the transverse magnetization decay in a single scan using a train of N Hahn echoes.

The mechanisms of relaxation are produced by local magnetic fields originating from randomly fluctuating spin interactions like homonuclear or heteronuclear dipolar, quadrupolar or chemical shielding interactions. They would induce quantum-mechanical transitions in the Zeeman energy levels manifold whose effect would be to take the nuclear magnetization back to the equilibrium configuration. When performing a spectra decomposition of these fluctuating local fields $\vec{h}(t)$ (which are in general, tensorial quantities), we can find a nonzero component frequencies equal to those of the various transitions which can exist within the Zeeman energy level diagram. Efficiency of the local magnetic fields to induce

transitions can be appreciated by the quantities named spectral densities of the form

$$J_i(\omega) = \int_0^\infty \overline{h_i(t)h_i(0)}\, \exp(-i\omega t)\, dt \tag{9}$$

where $h_i(t)$ is the random fluctuating i component of local fields. The bar denotes an average over the ensemble of spin systems. On the other hand, a quantum-mechanical transition can be induced by a fluctuating local field at the condition that a certain degree of coherence is present. The autocorrelation function $C(t) = \overline{h_i(t)h_i(0)}$ is indicative of this coherence that essentially persists for a time equal with the correlation time τ_c. A more general correlation function is represented by space–time autocorrelation function $C(\vec{x}, t)$, where $\vec{x}$ is a general spatial coordinate meant to represent translational or rotational coordinates. These correlation functions will turn out to be necessary in the context of characterization of two-dimensional (2D) exchange spectra (2). Moreover, a three-dimensional (3D) spectrum, being a three-time distribution, contains information that cannot be directly retrieved from the 2D spectrum. The detailed information on the nature of the nonexponential loss of correlation in polymers obtained from reduced four-dimensional (4D) exchange spectrum is also not accessible in the corresponding one-dimensional relaxation measurements and the 2D exchange spectrum (2).

Molecular processes with a single correlation time are rarely found in partially or strongly disordered solids like semicrystalline or amorphous polymers. A distribution of the correlation times $g(\tau)$ has to be introduced in order to evaluate the correlation function (2), ie,

$$C(t) = \int_0^\infty \exp\left\{-\frac{t}{\tau}\right\} g(\tau)\, d\tau \tag{10}$$

Such distribution has been shown to span several orders of magnitude for instance in the case of local motions in the glassy state. Instead of the distribution function, other fitting functions for correlation function $C(t)$ are considered. One of these functions is the stretched exponential Kohlraush–Williams–Watts function $\exp\{-(t/\tau_{\mathrm{kww}})^\beta\}$ that has been found to fit the data quite universally (2).

Spin Coherences. In all NMR experiments the spin system evolves under internal and external spin interactions. For isolated spins, the spin dynamics can be described in terms of the motion of classical magnetization vectors. Many structural and molecular dynamics problems in NMR involve couples spins. In this case, it is necessary to recourse to a quantum—mechanical formalism where a density operator describes the state of the system (1).

The density operator $\rho(t)$ is a generalized wave function which describes a so-called mixed state. This state corresponds to a statistical ensemble of quantum-mechanical objects, which in our case is a collection of nuclei with magnetic moments. Therefore, the statistics specific of these objects and the statistics of an ensemble are simultaneously present.

The equation of motion for the density operator is given by Liouville–von-Neumann equation

$$i\frac{\partial\rho(t)}{\partial t} = [H(t), \rho(t)] \tag{11}$$

where $H(t)$ is the Hamiltonian or total energy operator of the system expressed in angular frequency units, which may itself be time dependent. In general, equation 11 does not have an exact solution. Several mathematical methods have been applied to obtain an approximate solution for $\rho(t)$ one of the most efficient and accurate being the Floquet technique (1). The dynamics of the spin system detected via an observable $\langle O(t)\rangle$ described by a quantum-mechanical operator O can be evaluated by

$$\langle O(t)\rangle = \mathrm{Tr}\{O\rho(t)\} \tag{12}$$

Thus, the expectation value is found by evaluating the trace of the product of the observable operator and the density operator.

A particularly simple interpretation of the density matrix is possible in the eigenbase of the Hamiltonian H. The diagonal element ρ_{rr} is equal to the probability that the spin system is found in the eingenstate $|r\rangle$. The population of state $|r\rangle$ is P_r and therefore, $\rho_{rr} = P_r$. The off-diagonal element is defined by

$$\rho_{rs} = \langle r|\rho(t)|s\rangle = \overline{c_r(t)c_s^*(t)} \tag{13}$$

where the bar indicates an ensemble average. These elements describe a "coherent superposition" of eigenstates $c_r(t)|r\rangle + c_s(t)|s\rangle$ in the sense that the time dependence and the phase of the various members of the ensemble are correlated with respect to $|r\rangle$ and $|s\rangle$. Such a coherent superposition is simply called "coherences". A spin coherence can be associated with a transition between two eigenvalues specified by the eigenstates $|r\rangle$ and $|s\rangle$. If the two states span an allowed transitions with a difference in magnetic quantum numbers $\Delta M_{rs} = M_r - M_s = \pm 1$, the coherences ρ_{rs} is related to the NMR observables represented by the transverse magnetization components $M_x^{(rs)} \pm iM_y^{(rs)}$. In general, a matrix element of the density operator ρ_{rs} represents p-quantum coherence for which $p = M_r - M_s$, which, for $p \neq \pm 1$, does not lead to observable magnetization and can only be detected indirectly by two-dimensional spectroscopy (1,26).

The density operator $\rho(t)$ has been formulated for the entire quantum-mechanical system. For magnetic resonance applications, it is usually sufficient to calculate expectation values of a restricted set of operators which act exclusively on nuclear variables. The remaining degrees of freedom are referred to as "lattice". The reduced spin density operator is defined by $\sigma(t) = \mathrm{Tr}_1\{\rho(t)\}$, where Tr_1 denotes a partial trace over the lattice variables. The reduced density operator can be represented as a vector in a Liouville space of dimension

n^2, ie,

$$\sigma(t) = \sum_{r}^{1,n^2} b_r(t) B_r \tag{14}$$

where n is the dimension of the Hilbert space of all admissible state functions and $\{B_r\}$ is a complete set of orthogonal base operators. A proper selection of this base is often essential to ease the solution of a particular spin dynamics problem. For instance, for systems with spins $I_k = 1/2$ the product of the Cartesian spin operators is a convenient base operators (1,27). As an example, the complete set of product operators $\{B_r\}$ for two J or dipolar coupled nuclei with spin $I = 1/2$ consists of $2^{2\times 2} = 16$ operators, ie,

$$\frac{1}{2}E \text{ (E is the unity operator)}, I_{ix}, I_{iy}, I_{iz}$$

$$2I_{ix}I_{jx}, 2I_{iy}I_{jy}, 2I_{iz}I_{jz}, 2I_{ix}I_{jy}, 2I_{ix}I_{jz}, \text{ for } i,j = 1,2 \tag{15}$$

The spin modes described by the product operators of equation 15 are the matrix elements of the density operator

$$\rho = \begin{pmatrix} P_1 & \text{SQ} & \text{SQ} & \text{DQ} \\ \text{SQ} & P_2 & \text{ZQ} & \text{SQ} \\ \text{SQ} & \text{ZQ} & P_3 & \text{SQ} \\ \text{DQ} & \text{SQ} & \text{SQ} & P_4 \end{pmatrix} \tag{16}$$

The above product operators can be detected by a proper design NMR experiment (1,26) and reflect different features of the spin systems related to the structure, spin interaction topology, and molecular dynamics. The most popular spin modes are represented by single-quantum coherences (SQ) of spin i, I_{ix} and I_{iy} that are related to x- and y-magnetizations, respectively. Two-spin coherences of spin i and j consist of superposition of $p = 0$ (zero-quantum (ZQ)) and $p = \pm 2$ (double-quantum (DQ)) quantum coherences. The former is insensitive to the inhomogeneity of the magnetic field and the latter is reflecting the existence of spin couplings. Not only the existence of J- or dipolar couplings can be detected by editing DQ coherences but also the strength of these couplings can be measured including internuclear distances and dihedral angles (27–29).

Spin-Echoes. The evolution of spin coherences under nonfluctuating spin interactions is a reversible process. The strength and sign of the spin Hamiltonians can be manipulated by rf pulses and/or sample rotation such that the evolution of the spin system during a period of time is refocused during the spin system evolution at a latter time.

The spin interactions described by inhomogeneous or homogeneous spin Hamiltonians lead to inhomogeneous and homogeneous spin-echoes. If a linear superposition of both types of spin Hamiltonians is present, a mixed spin-echo can be generated. The most common used inhomogeneous echoes are: Hahn (30),

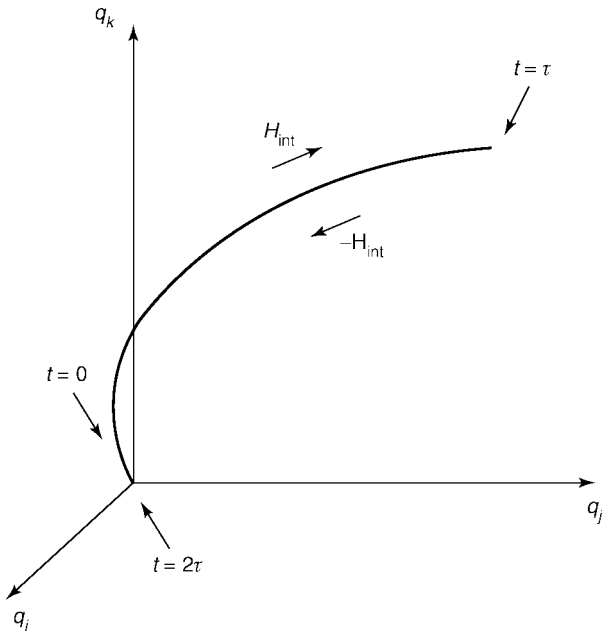

Fig. 3. Evolution of the quantum-mechanical state of a spin system in a Liouville space. The evolution from the initial time $t = 0$ to an intermediate time $t = \tau$ takes place under a Hamiltonian H_{int} which describes internal and external spin interactions. At this time, a pulse sequence change the sign of the spin Hamiltonian. The spin system evolves on the same generalized trajectory and after total evolution time $t = 2\tau$ the initial state is refocused under a spin echo.

stimulated (30), and gradient echoes (5,18). Solid (31) and magic (32–34) echoes are the most familiar types of homogeneous echoes.

In order to understand how a spin echo can be produced, we shall consider a spin system composed of N nuclei, which interact, or not between themselves. The quantum-mechanical state of such a system can be described by a linear superposition of spin coherences represented by a vector evolving in a Liouville space of dimension 2^{2N} (cf Fig. 3). In this abstract space, the state of the spin system at time $t = 0$ is represented by a configurational point. This state corresponds in many cases to the single-quantum coherences excited after a 90° rf pulse. The spin system evolves in laboratory or rotating reference frames for a time τ, evolution described by the propagator operator $E_{\text{evolution}} = \exp\{-\text{i}H_{\text{int}}\tau\}$, where H_{int} is the spin-interaction Hamiltonian. At the end of this evolution period, a pulse or a complex pulse sequence is applied which change the sign of the Hamiltonian H_{int}. During the refocusing period of duration τ the evolution operator is now $E_{\text{refocusing}} = \exp\{-\text{i}(-H_{\text{int}})\tau\}$. This is formally equivalent with a time reversal, ie, $\tau \rightarrow -\tau$. For the full evolution period 2τ, the propagator is $E_{\text{evolution}}\, E_{\text{refocusing}} = E$, where E is the unity operator and the spin system is reaching the initial state. Hence, a spin echo was generated with an amplitude identical with the free induction decay as long as the magnetization relaxation processes are neglected.

The pulse sequence used for generation of inhomogeneous spin-echo of the Hahn type is shown in Fig. 4**a**. The spin systems for which this echo can be

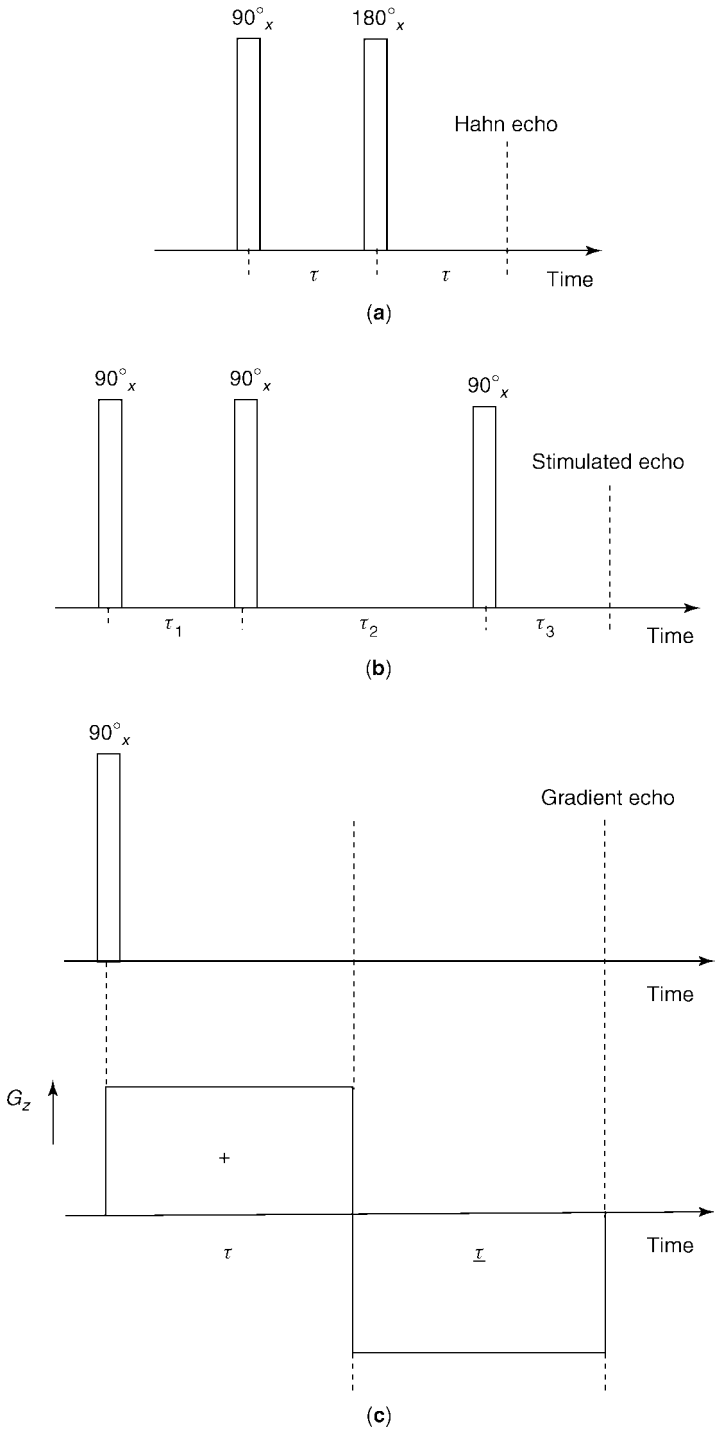

Fig. 4. Pulse sequences used for Hahn echo (**a**), stimulated echo (**b**), and gradient echo (**c**) are shown.

produced are characterized by the Hamiltonian $H_{\text{int}} = -\delta I_z$, where δ describes the inhomogeneity of the magnetic fields or chemical shift distributions. By the action of refocusing 180°_y pulses, the spin operator I_z becomes $-I_z$ and the spin Hamiltonian changes the sign, ie, $H_{\text{int}} = -H_{\text{int}}$. If the transverse magnetization relaxation is neglected, the amplitude of the Hahn echo is equal with the amplitude of the free induction decay generated after 90°_x preparation pulse (cf Fig. 4**a**). The relaxation encoding is given by the factor $\exp\{-2\tau/T_2\}$, where T_2 is the transverse relaxation time. The Hahn echo represents an important tool for measuring residual dipolar couplings, correlation function of molecular motions, and encoding of spatial information and mass transport. If the 180°_x pulse is split in two 90°_x pulses separated by a time τ_2 (cf Fig. 4**b**), a stimulated echo is produced at time τ_1 after the action of the last pulse. This spin-echo has under ideal conditions the amplitude half of the amplitude of FID and the lifetime is much longer compared with that of the Hahn echo. Therefore, it is an ideal instrument for measuring self-diffusion coefficients.

The scheme used for gradient echo is presented in Figure 4**c**. The evolution of the single-quantum excited by a preparation 90°_x pulse under a field gradient G_z is refocused by the filed gradient with the opposite direction $-G_z$. The amplitude of the echo is affected by the presence of the magnetic field gradients inside the sample. This effect is exploited for enhancement of the contrast in MRI.

In many rigid or soft polymers, the protons are dipolar coupled in a complex network. The dipolar Hamiltonian is bilinear in spin operators representing a homogenous interaction. Pulse sequences can be designed that change the sign of the dipolar Hamiltonian H_{d}, ie, $H_{\text{d}} \rightarrow -kH_{\text{d}}$, where k is a scaling factor. An example of such a homogeneous spin-echo is given by magic echo for which $k = 1/2$ (cf Fig. 5**b**). The most simple homogeneous spin echo is represented by solid echo

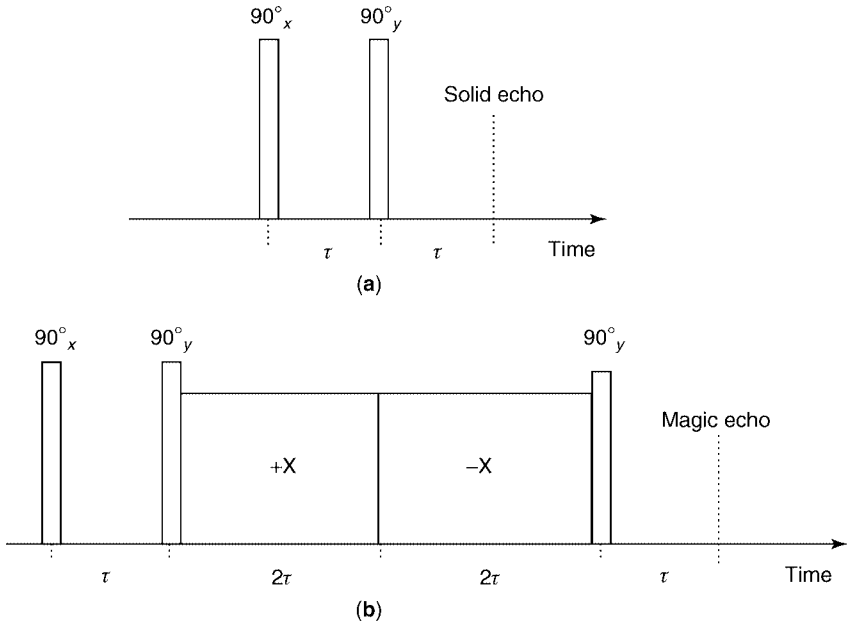

Fig. 5. Pulse sequences used for solid echo (**a**) and magic echo (**b**) are shown.

(Fig. 5**a**). For a spin system composed of spin-1/2 pairs the spin evolution is fully refocused by the solid echo. This is not the case for a multispin dipolar network. These echoes can be used for high resolution NMR spectroscopy of solids, measurement of residual spin interactions, and NMR imaging of rigid polymers.

Two-dimensional Fourier Spectroscopy. Two-dimensional (2D) spectroscopy is a general concept that can be applied to different brunches of spectroscopy which make it possible to acquire more detailed information about the molecular system under investigation. Since the first proposal in the 1971 (35) and the first experimental realization in the 1974 (36–38) a large number of 2D NMR methods have been invented and applied (1) to solve structural and dynamical problems in physics, chemistry, biology, and medicine.

Several strategies can be employed for obtaining a 2D spectrum, which is a signal function $S(\omega_1, \omega_2)$ of two independent frequency variables (ω_1, ω_2) (1). The most popular one is based on the 2D time-domain experiments. In this approach, a time-domain signal $s(t_1, t_2)$ is obtained by incrementing the time interval t_1 parametrically from experiment to experiment, and recording the free induction signal as a function of t_2. In a general case, for a 2D experiment, we distinguish four intervals:

$$[\text{Preparation } (t_p)]-[\text{Evolution } (t_1)]-[\text{Mixing } (t_m)]-[\text{Detection } (t_2)]$$

The four basic intervals have the following qualitative features: (*1*) *Preparation period*: In the course of this period of fixed length the spin system is prepared in a coherent nonequilibrium state. In the simplest experiments, the preparation periods consists of a single rf pulse. However, this period can involve more sophisticated procedures like cross-polarization (39,40) and excitation of multiple-quantum coherences (1,41). (*2*) *Evolution period*: During this period, in general, the spin system evolves under a spin Hamiltonian, which may be modified by heteronuclear decoupling (42), sample spinning (43,44), or homonuclear decoupling pulse sequences (45,46). The evolution during this indirect dimension of the 2D experiment determines the frequencies in the ω_1-domain. (*3*) *Mixing period*: This period may consists of one or more rf pulses, separated by intervals with fixed or variable durations. During the mixing period, transfer of coherences or polarization can take place. For instance, mixing process transforms single (SQ)-, multiple (MQ)- or zero-quantum (ZQ) coherences into observable transverse magnetization. In many cases, the 2D spectrum may be regarded as a visual representation of the pathways of the mixing process. (*4*) *Detection period*: In the course of the detection period, the SQ coherences evolution is measured as a function of time-domain variable t_2. The spin system can be manipulated by the action of coherent averaging pulse sequences and/or sample spinning, or by polarization transfer to nuclei with higher sensitivity. Finally, a complex 2D spectrum is obtain for the time-domain data by a complex 2D Fourier transformation defined by

$$S(\omega_1, \omega_2) = \int_{-\infty}^{\infty} \mathrm{d}t_1 \exp\{-\mathrm{i}\omega_1 t_1\} \int_{-\infty}^{\infty} \mathrm{d}t_2 \exp\{-\mathrm{i}\omega_2 t_2\} s(t_1, t_2) \tag{17}$$

The major advantages of 2D NMR spectroscopy are related to the assignment of complex spectra, of revealing the correlated transitions to establish J- or dipolar

coupling topologies or for studying complex dynamic processes. These features lead to a classification of 2D spectroscopic experiments in three groups (1).

The interpretation of NMR spectra is often impeded by the complexity of overlapping resonances. When the interactions responsible for the multiplet structure are different such as chemical shielding, dipolar, or scalar couplings, it is often possible to render spectra more intelligible by *separating* various interactions in orthogonal frequency domains. In the course of *2D separation* experiments the number of peaks is conserved.

The second group of 2D experiments is represented by *2D correlation* methods based on coherence transfer. These experiments allow interpretation of NMR spectra of networks of coupled spins by establishing the connectivities of nuclear spins coupled by J or dipolar interactions. The appearance of cross-peaks in 2D correlation spectra constitutes a proof of the existence of resolved scalar or dipolar couplings, and allows one to correlate the chemical shifts of coupled partners. These experiments are designed to correlate transitions of coupled spins by transferring magnetization of MQ coherences from one transition to another in the course of a suitable designed mixing process.

A third class of 2D time-domain experiments is concerned with studying *dynamic processes* such as cross-relaxation, nuclear Overhauser effects, chemical exchange, and magnetization exchange including spin diffusion (1,2). These methods have a number of advantages particularly when the system comprises an extended network of exchange processes that occur simultaneously. Moreover, the 2D methods are most useful for studying slow dynamic processes with rates that are two low to affect the lineshapes. The basic idea of 2D exchange spectroscopy is the "frequency labeling" of the longitudinal magnetization of various chemical sites before chemical or magnetization exchange takes place, such that after exchange the pathways of the magnetization can be traced back to their origins.

The magnetic resonance imaging (MRI) techniques used most frequently for applications to soft polymers are directly related to the multidimensional Fourier transform (5,18,19,47). Just like in 2D spectroscopy, the phase of the signal acquired during the detection period (time domain t_2) is modulated by the coherence phases present in the evolution period (t_1). The idea is that the accumulated signal phase is primarily a result of the applied gradient which induces a position encoding. A 2D Fourier transformation then produces a 2D image of the object.

One-Dimensional NMR Studies of Molecular Motions and Dynamic Order

NMR methods can probe molecular dynamics in polymers on various time scales from relatively fast segmental motions (with correlation times of the order of 10^{-10} s) down to slow motions in the 10^{-3} s range or even slower (2–6,48). Dynamics in the range of around 10^{-10} s can be investigated by T_1 measurements that are sensitive to motions around the Larmor frequency. Particularly useful for such investigations is the field cycling technique, where the magnetic field and thus also the Larmor frequency ω can be varied over several orders of magnitudes

down to the 10 kHz regime. By acquiring $T_1(\omega)$, molecular dynamics can be probed over the corresponding range ((5), and references therein).

Slow motions can be studied using so-called longitudinal relaxation in the rotating frame ($T_{1\rho}$) (5). In these experiments, a radio-frequency field ("spin-lock pulse") with field strength of around 10–100 kHz plays the same role as the main magnetic field does for T_1. For instance, the changes in the phase structure under mechanical deformation of thermoplastic elastomers have been investigated by $T_{1\rho}$ measurements of ^{13}C nuclei under MAS (49).

Transverse relaxation (T_2) and lineshape analysis has also been the topic of many studies of molecular dynamics in viscoelastic media ((12,13,50,51), and references therein). It was found to be indicative of heterogeneities of molecular motions (12,13). Transverse relaxation curves therefore often turn out to be composed of a superposition of multiexponential and the Gaussian decays. Measurement of residual dipolar couplings, molecular motions, and other parameters have been performed by this relaxation technique on different nuclei like ^{1}H, ^{13}C, ^{15}N, ^{31}P, and ^{29}Si and could be related to material properties such as the cross-link density (12,13). In order to separate the liquid-like and solid-like contributions of the T_2 decay, a linear combination of Hahn echoes and solid echoes have been used (52,53). While Hahn spin-echo amplitudes are encoded by irreversible dephasing due to molecular motions and by reversible residual dipolar couplings, only the first effect encodes the amplitudes of solid echo (actually mixed echo) to first approximation. The appropriate combination of these spin-echoes thus gives access to residual dipolar couplings and the fluctuation rate (52,53). The method was applied to measure the degree of segmental order induced in natural rubber upon stretching (53).

A powerful technique for the study of orientation and dynamics in viscoelastic media is lineshape analysis in deuteron NMR spectroscopy (2,50,51,53). Recent reviews on this topic were published (50,51). For instance, the average orientation of chain segments in elastomer networks upon macroscopic strain can be determined by this technique (54–60). For a nondeformed rubber, a single resonance line in the deuterium NMR spectrum is observed (57) while the spectrum splits into a well-defined doublet structure under uniaxial deformation. It was shown that the usual network constraint on the end-to-end vector determines the deuterium lineshape under deformation, while the interchain (excluded volume) interactions lead to splitting (57–60). Deuterium NMR is thus able to monitor the average segmental orientation due to the cross-links and mean field separately (60).

The network structure of unfilled and filled elastomers was probed by the analysis of the quadrupolar splitting in ^{2}H solid echo spectra of uniaxially strained samples (55) (see Fig. 6). The local chain order at a given elongation is larger by a factor of 1.5–2 in the filled system. A decrease of local chain mobility in the absorption layer is observed under stress. The same method was applied to investigate molecular dynamic in thermoplastic elastomer based on hydrogen bonding complexes (61,62).

The 1D NMR techniques described above already allow a detailed investigation of polymer dynamics but they are mostly not selective in the sense that they do not provide information on the averaging of particular couplings. For the interpretation of some of the above results therefore a representative spin pair

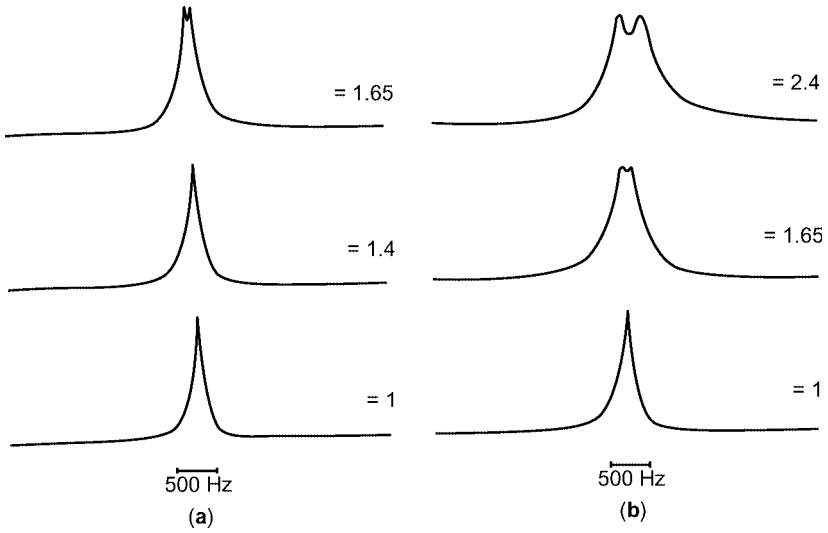

Fig. 6. Deuterium solid echo spectra of unfilled (**a**) and filled (**b**) poly[dimethylsiloxane] networks at 305 K with and without mechanical stress as given by the parameter λ. Reproduced from Ref. 55, with permission from Wiley-VCH.

along the chain was assumed, thus neglecting local site-specific motions as well as the geometry of the bonds. This is where multidimensional NMR techniques come into play.

Residual van Vleck Moments. The difficulties related to these measurements are due to the small values of the residual spin couplings compared to those of other spin interactions, the many-body character of the dipolar couplings and the presence of molecular motions which produce a supplementary encoding of the spin system response.

One-dimensional (1D) NMR methods based on the dipolar correlation effect in combination with the Hahn and solid echoes (52,63), the stimulated echo (5), the magic echo (64), magnetization-exchange (65), and cross-relaxation dynamics (66) provide access only to the second van Vleck moment via a model which takes into account the solid-like and liquid-like contributions to the spin system response (67). Model free access is given by the analysis of multiple-quantum builtup (68) and decay (69) curves recorded in the initial regime of the excitation/reconversion periods.

In the following, we discuss a method to measure model free the residual dipolar van Vleck moments without contributions from inhomogeneous spin interactions originating from static magnetic field inhomogeneities, local susceptibility effects, and heteronuclear dipolar interactions (70). Moreover, in the first approximation this method is insensitive to the transverse relaxation produced by the fluctuating dipolar interactions.

Principles of the Method. The method is based on the mixed echo composed of the Hahn and the magic echo (33,71,72). The Hahn echo explores the magic echo shape generated by an accordion magic sandwich (cf Fig. 7).

One possibility to have the amplitude of the Hahn echo encoded by the homonuclear dipolar interactions is to employ a mismatched magic sandwich

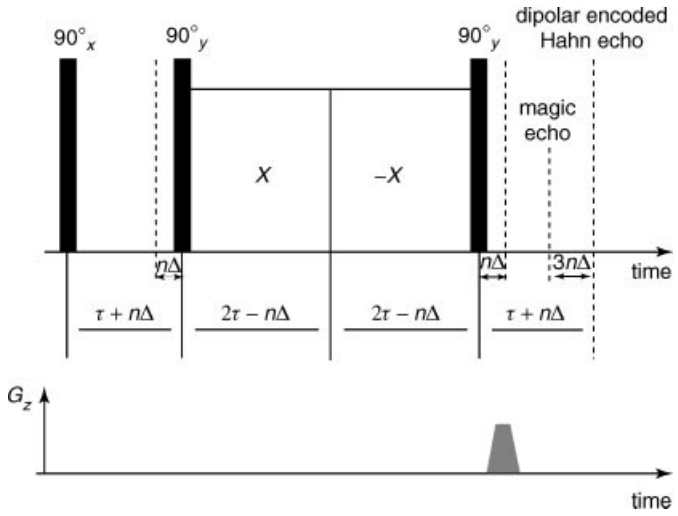

Fig. 7. AIMS pulse sequence used for generation of a mixed echo composed of a magic and a Hahn echo. A dephasing gradient pulse is applied at the end of the sequence. Reproduced from Ref. 70, with permission from Elsevier.

(MS), ie, $90^{\circ}_{x} - (\tau + n\Delta) - 90^{\circ}_{y}$ – Burst Pulse$_{x}$ $(2\tau - n\Delta)$ – Burst Pulse$_{\overline{x}}$ $(2\tau - n\Delta)$ – $90^{\circ}_{y} - (\tau + n\Delta)$ – Mixed Echo (see Fig. 7), where n is a positive and negative integer number and Δ is the time decrement and increment, respectively. We call this mismatched MS composite pulse with variable n the *accordion magic sandwich* (hereafter the method will be called AIMS).

The spin system response to the AIMS sequence was evaluated in Reference 70 for a multispin dipolar network characteristic to elastomers and other soft polymers. It was shown that the normalized amplitude of the Hahn echo measured at time $t = 6\ \tau$ is encoded only by the homonuclear dipolar couplings and relaxation, ie,

$$\frac{S(3n\Delta)}{S(0)} = \frac{\mathrm{Tr}\left\{I_y \exp\left\{-\mathrm{i}\hat{\bar{H}}_d^{(0)}(3|n|\Delta)\right\}I_y\right\}}{\mathrm{Tr}\{I_y^2\}} \exp\left\{-2n\Delta\left(\frac{1}{T_2^*} - \frac{1}{T_{2\rho}^*}\right)\right\} \tag{18}$$

where T_2^* and $T_{2\rho}^*$ are the effective transverse relaxation times in the laboratory and rotating frames, respectively. It is easy to see from the above equation that a combination of signals taken with $+|n|$ and $-|n|$ is given by

$$\frac{S(3|n|\Delta)S(-3|n|\Delta)}{S(0)^2} = G(3|n|\Delta)^2 \tag{19}$$

This composite NMR signal is not encoded by the transverse relaxation. The function $G(t)$ describes the magic echo shape and is given by (4)

$$G(t) = \frac{\mathrm{Tr}\left\{I_y \exp\left\{-\mathrm{i}\hat{\bar{H}}_d^{(0)} t\right\}I_y\right\}}{\mathrm{Tr}\{I_y^2\}} \tag{20}$$

In the short-time limit, ie, for $3|n|\Delta\omega_d \ll 1$, we obtain from the above equations,

$$\frac{S(3|n|\Delta)S(-3|n|\Delta)}{S(0)^2} \cong 1 - \bar{M}_2(3|n|\Delta)^2 + \frac{1}{12}\bar{M}_4(3|n|\Delta)^4 - \cdots \quad (21)$$

where $\bar{M}_2$ and $\bar{M}_4$ are the residual second and forth van Vleck moments, respectively (4).

In conclusion, the AIMS pulse sequence produces a disentanglement of the magic and Hahn echoes in time. The dipolar encoding of the signal occurs because the Hahn echo samples the magic echo shape.

^1H Residual van Vleck Second Moments of Cross-Linked Series of Natural Rubber. Proton residual second and fourth van Vleck moments were measured by AIMS for the samples of cross-linked series of natural rubber (NR). The residual van Vleck moments $\bar{M}_2$ and $\bar{M}_4$ can be evaluated by the best fits of the composite signals with equation 21 and these results are shown in Figures 8**a** and 8**b**, respectively, for the whole NR series.

The measured values of $\bar{M}_2$ are in good agreement with the values measured on the same series using the model dependent dipolar correlation function (64). The best fit of the dependence of $\bar{M}_2$ and $\bar{M}_4$ on shear modulus G is given by continuous lines in figures 9**a** and 9**b**. These are described, in general, by a polynomial $\sum_1^m (-1)^p a_p G^p$ up to the powers four and eight in G, respectively. This polynomial dependence can be justified by considering high order corrections to a Gaussian distribution of the end-to-end vectors (68). The classical Gaussian distribution will lead only to dependences of powers two and four in G which are shown by the dashed lines in these figures. Nevertheless, in the case of samples with low values of the cross-link density the Gaussian approximation is able to describe the experimental data sufficiently well (see the insets of figures 8**a** and 8**b**). These results also show that high order van Vleck moments are more sensitive to cross-link density compared to the second van Vleck moment which is usually used.

The value of the ratio $\bar{M}_4/\bar{M}_2{}^2$ on shear modulus is shown in figure 8**c**. The ^{1}H NMR absorption lineshape is quasi-Lorentzian for all samples but starts to deviate towards a Gaussian lineshape for higher values of the cross-link density.

Residual Dipolar Couplings by ^{1}H Multiple-Quantum NMR. The measurements of residual dipolar couplings in elastomer system is desirable, because they reflect the hindrance to molecular motions by the cross-linking, topological constraints, and the external factors like mechanical stress. Dipolar-encoded longitudinal magnetization (DELM) NMR decay curves, double-quantum (DQ) and triple-quantum (TQ) NMR buildup intensities for measuring the residual dipolar couplings and the associated dynamic order parameters were discussed in Reference 68. These methods allow measuring residual dipolar couplings model free and in the limit of short excitation time regime the effective dipolar network is simplified.

Principles of the Method. One of the important features of the MQ spectroscopy is the possibility to edit the strongest dipolar couplings. This feature is based on the fact that the efficiency of MQ pumping is a nonlinear function of the dipolar coupling strength. For instance, the pumping efficiencies of DQ and TQ coherences in the initial excitation time regime are proportional to $(D^{ij})^2$

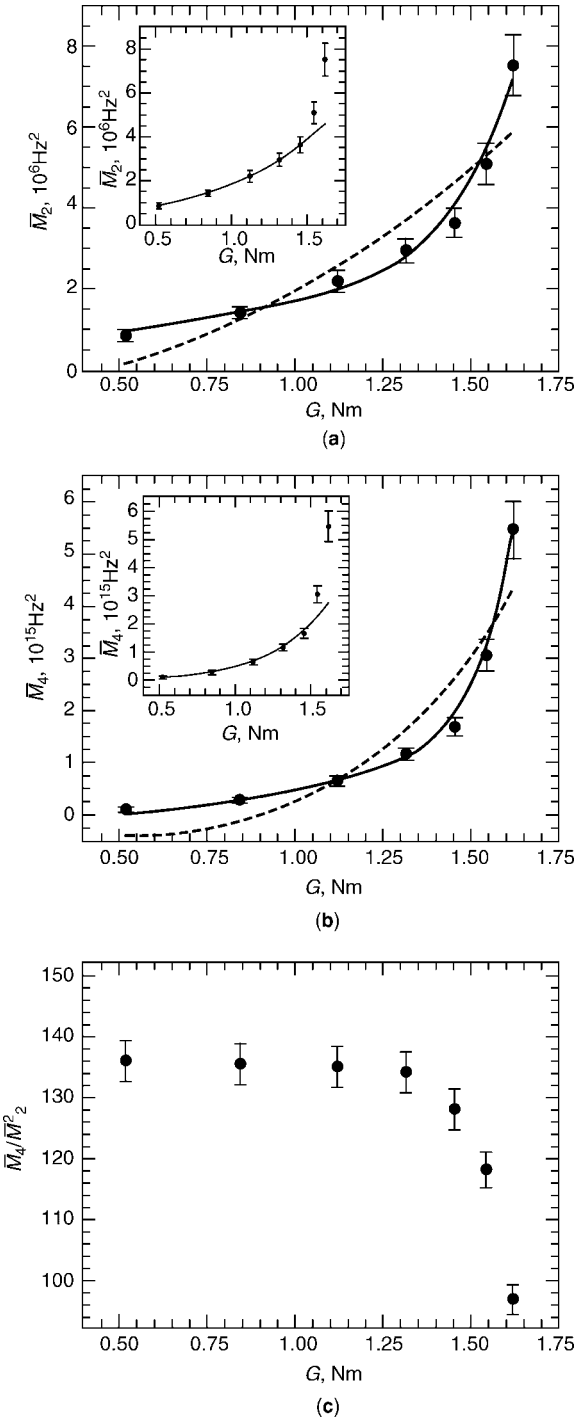

Fig. 8. Proton residual van Vleck moments $\bar{M}_2$ (**a**), $\bar{M}_4$ (**b**), and the ratio $\bar{M}_4/\bar{M}_2{}^2$ (**c**) measured by AIMS for the samples of a series of cross-linked natural rubber versus the shear modulus G. Reproduced from Ref. 70, with permission from Elsevier.

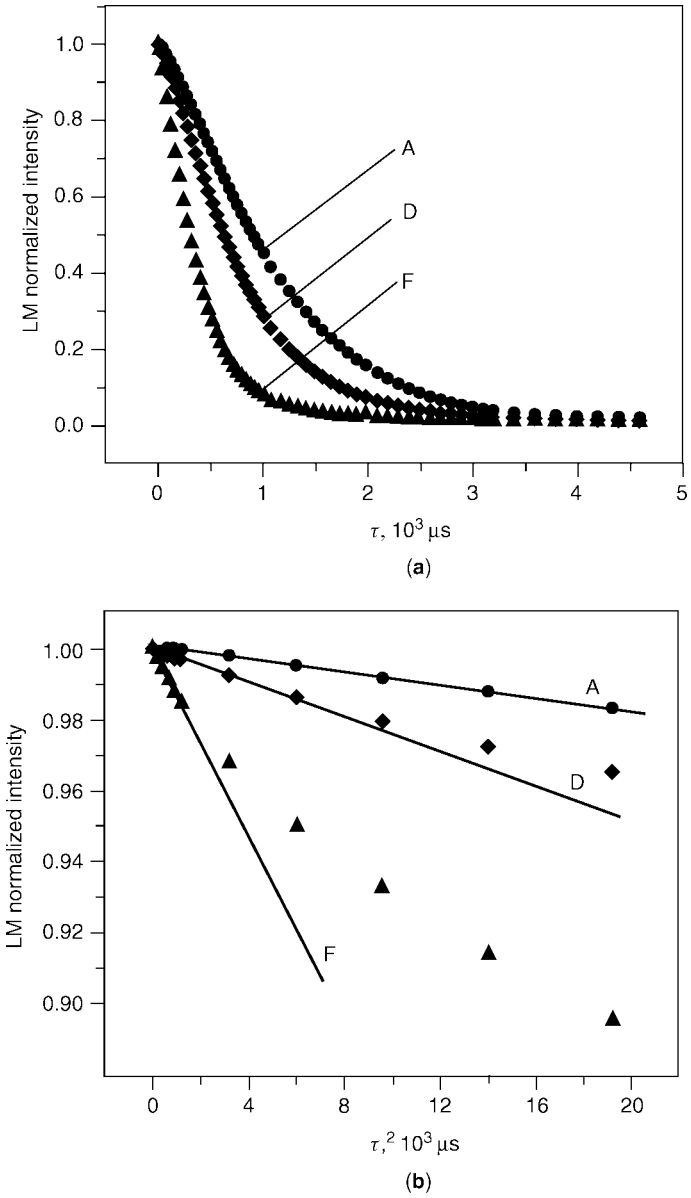

Fig. 9. (**a**) Proton dipolar-encoded longitudinal magnetization decay curves for a series of synthetic polyisoprene samples with different cross-link densities. (**b**) The initial time behavior of DELM decays exhibits a linear dependence in τ^2 (solid lines). Reproduced from Ref. 68, with permission from American Institute of Physics.

and $(D^{ij})^4$, respectively, where D^{ij} is the dipolar strength between protons i and j (73–75). Therefore, we can estimate that the pumping efficiency of DQ coherences for methylene protons is about six times higher compared to that of methyl protons. The editing capabilities are expected to be even better for the intergroup

dipolar interactions. In the case of TQ coherences, the maximum pumping efficiency is expected for the methyl group.

The possibility to implement a MQ dipolar filter has already been demonstrated. For instance, by use of a ^{13}C–^{13}C DQ dipolar filter working in the initial excitation time regime the signal of the crystalline domains in polyethylene could be enhanced (74). The possibility of functional group editing by MQ NMR methods is also supported by DQ experiments performed on static and rotating elastomers. The 2D ^{1}H DQ MAS spectrum of polyisoprene (68) shows that for short excitation times the response of the methylene protons can be approximated well by an isolated spin pair. Moreover, the experiment shows that the DQ coherences at which methyl protons participate are mainly originating from the CH_3 group. This also leads to the conclusion that TQ coherences excited in the initial time regime can be attributed mainly to the methyl groups. Weak dipolar coupling of CH_2 and CH_3 protons with CH protons is demonstrated (68). But, the contribution of the methine protons to the overall NMR signal is only about 12% so that these couplings are negligible in a good approximation.

The spin system response to the pulse sequence used for excitation of different multipolar spin states can be evaluated in the limit of short dipolar encoding time. For DELM, it is possible to write (68)

$$\begin{aligned} S_{\mathrm{DELM}}(\tau) \approx 1 - \left\{ l_2 \left[D^{(2)} S_s^{(2)} \right]^2 + l_3 \left[D^{(3)} S_s^{(3)} \right]^2 + \text{intergroup} \right\} \tau^2 - \cdots \\ \equiv 1 - [D_{\mathrm{eff}}]^2 \tau^2 - \cdots \end{aligned} \tag{22}$$

where the numerical coefficients are $l_2 = 21/80$, and $l_3 = 63/190$ and correspond to the CH_2 and CH_3 groups. D_{eff} is the effective residual dipolar coupling describing contributions from both CH_2 and CH_3 groups as well as intergroup residual dipolar couplings. Nevertheless, the residual dipolar couplings of methylene and methyl protons dominate the intergroup couplings and the slope of the LM decay curve versus the square of the excitation time τ is given by a weighted sum of the squares of dynamic order parameters of CH_2 and CH_3 groups.

The DQ signal can be evaluated in a similar manner, and finally one can write

$$\begin{aligned} S_{\mathrm{DQ}}(\tau) \approx \left(d_2 \left[D^{(2)} S_s^{(2)} \right]^2 + d_3 \left[D^{(3)} S_s^{(3)} \right]^2 + \text{intergroup} \right) \tau^2 + \cdots \\ \equiv [D'_{\mathrm{eff}}]^2 \tau^2 + \cdots \end{aligned} \tag{23}$$

where the numerical coefficients are $d_2 = 21/40$ and $d_3 = 9/200$. An effective residual dipolar coupling D'_{eff} similar (but not identical) to D_{eff} for dipolar encoded longitudinal magnetization can be introduced describing DQ-edited residual dipolar couplings.

In the regime of short excitation times the TQ coherences are derived mainly from the methyl protons. The spin system response to the pulse sequence (68) for a proton triad rotating rapidly around the C_3 axis in a static sample can be evaluated similar to the procedure used for DQ coherences. In the limit of short excitation

times, the normalized TQ-filtered signal is given by

$$S_{TQ}(\tau) \approx \left(r_3\left[D^{(3)}S_s^{(3)}\right]^4 + \text{intergroup}\right)\tau^4 + \cdots \equiv [D''_{\text{eff}}]^4\tau^4 + \cdots \quad (24)$$

where $r_3 = 39/4$. Again as above, an effective residual dipolar coupling D''_{eff} can be introduced for the full dipolar network. These effective residual dipolar couplings, introduced by the above equations, depend on the dipolar network edited by the experiments and it is therefore not easy to express them in terms of site-specific dynamic order parameters. Nevertheless, D''_{eff} is expected to be dominated by the methyl protons.

Dynamic Order Parameters. Dipolar-encoded longitudinal magnetization decay curves were measured for ^{1}H in a series of cross-linked synthetic polyisoprene samples (68). The decays for three samples (A, D, and F with the cross-link density of 0.75, 5.0, and 15.0, respectively) are shown in Figure 9.

The decay curves show a dependence on the cross-link density. In the short-time regime, the dipolar-encoded LM decays display a linear dependence in τ^2, in accordance with equation 22, (cf Fig. 9**b**). DQ buildup curves for the same samples are shown in figure 10 for the full range of excitation time τ. Systematic dependence of the DQ-filtered signal intensity on the cross-link density is evidenced in Figure 10**a**. Based on equation 23, an initial dependence of the signal amplitude on τ^2 will be shown by the DQ signals with a slope related to the scaled dynamic order parameters of methylene and methyl protons (cf Fig. 10**b**). TQ buildup curves for protons in polyisoprene also show a clear dependence on the cross-link density similar to the case of the DQ buildup curves.

Within the limit of experimental errors scaled dynamic order parameters measured from the MQ experiments show a linear dependence on cross-link density (cf Fig. 11).

This is expected because the dynamic order parameters $S_s^{(2)}$ and $S_s^{(3)}$ are inversely proportional to the number N of statistical segments. The same dependence on N is expected for cross-link density as measured in parts per hundred of rubber (phr) of cross-linking agent. For the whole series, the dynamic order parameters of methyl protons are slightly larger than those of the methylene protons. This reflects the hindrance imposed to the motion of methyl groups attributed to backbone chain by the short-range interactions between segments belonging to different chains in comparison with the case of the methylene proton located along the polymer chain.

The values of the effective ^{1}H residual dipolar couplings $D_{\text{eff}}/2\pi$ measured from the initial decays of the LM are shown as a function of cross-link density in Figure 11**b**. In the good approximation, the dipolar couplings are linearly proportional to cross-link density. These quantities can also be evaluated from equations 23 and 24 by using the dynamic-order parameters measured site-selectively from DQ and TQ buildup curves. These $D_{\text{eff}}/2\pi$ are plotted versus cross-linked density in Figure 11**b**, again showing a linear dependence on cross-linked density. They are systematically lower than the values measured from the LM

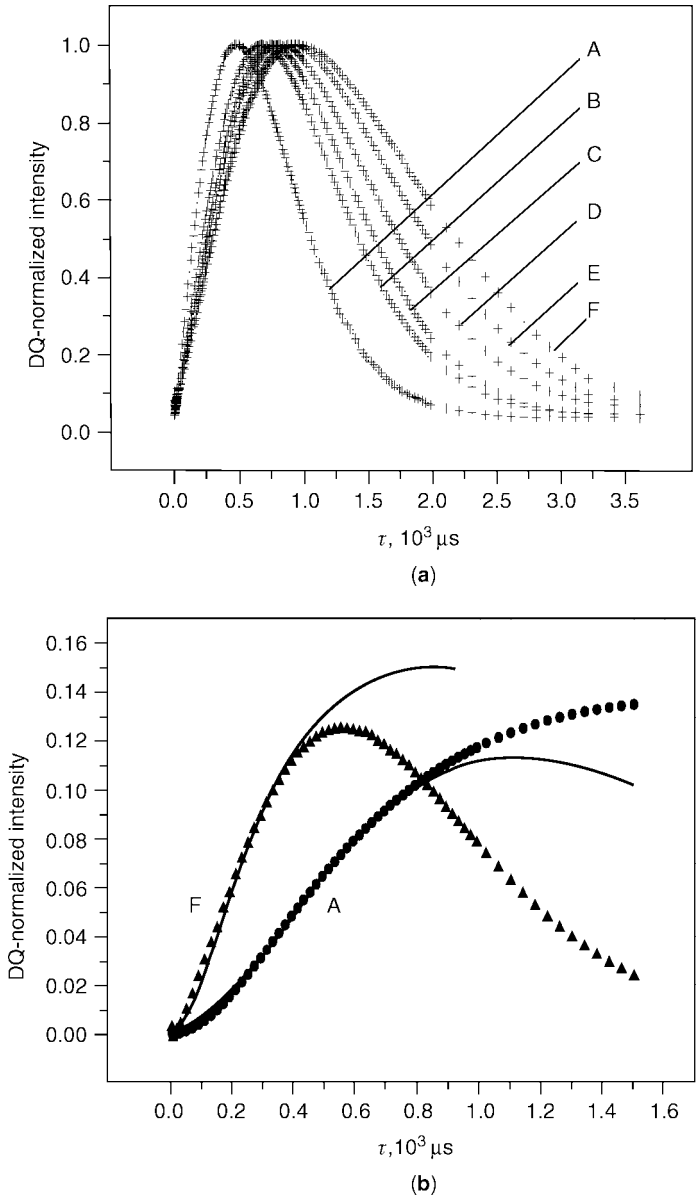

Fig. 10. Proton DQ buildup curves for a series of synthetic polyisoprene samples with different cross-link densities increasing from samples A to F. (**a**) The signal dependence on excitation and reconversion times τ for the full time domain. (**b**) The initial time regime of the DQ buildup curves for samples A and F together with the simulated curves including transverse relaxation (continuous lines). Reproduced from Ref. 68, with permission from American Institute of Physics.

decays. This fact can be due to the shorter time scale used for extraction of $D_{\text{eff}}/2\pi$ from LM decays compared to that used in DQ and TQ buildup curves.

The dynamic order parameters determined by the above methods can be compared to those measured by other NMR techniques if the specific dynamic

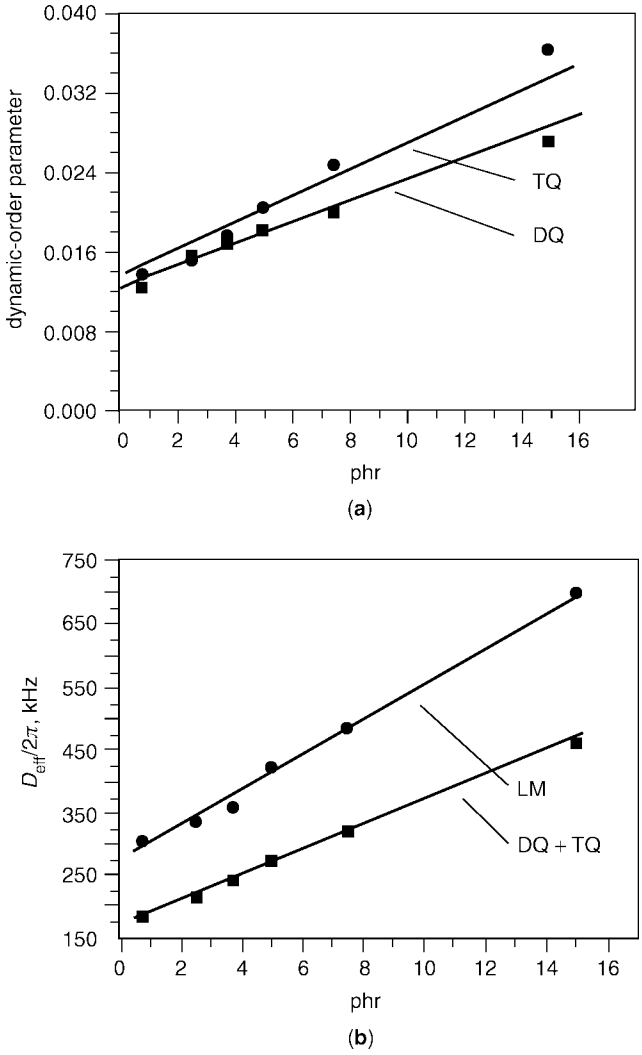

Fig. 11. (**a**) The dependence of dynamic-order parameters measured from DQ (squares) and TQ (circles) buildup curves on the cross-link density for synthetic polyisoprene. (**b**) The effective residual dipolar coupling D_{eff} (circles) measured from dipolar encoded longitudinal magnetization decays together with the D_{eff} values (squares) computed from dynamic-order parameters. A linear dependence on the cross-link density is evidenced in all cases (solid lines). Reproduced from Ref. 68, with permission from American Institute of Physics.

time scale is considered. It was shown that residual dipolar couplings measured in the initial time regime of the LM decays, DQ, and TQ buildup curves are more sensitive to cross-link density as compared to, for instance, transverse relaxation rates (68).

The proposed methods are generally applicable to partially averaged proton dipolar interactions and can be applied for studying segmental order and its associated dynamics in a variety of polymer networks or entangled melts and solutions

(transient networks) without the need for isotopic labeling, sample rotation, or the use of cross-polarization.

Heterogeneity in Segmental Chain Order of Grafted Polymers. Proton multiple-quantum NMR was also used for investigation of heterogeneity in segmental chain order of grafted polymers. The measurements were performed on a series of samples of poly(dimethylsiloxane) (PDMS) layers chemically attached to the surface of hydrophilic silica (76). These grafted PDMS layers consists of partially immobilized chain segments at the PDMS–silica interface and mobile chain portions outside the interface which is probed by measurements of homonuclear double- and triple-quantum buildup curves. These curves reveal a bimodal distribution of the residual dipolar couplings along the PDMS chain (see Fig. 12).

The segmental orientation detected in the interface and mobile regions are related to the average chain length and reflects the competing effects of the surface-induced orientation and chain conformations.

The ^{1}H DQ (and TQ) buildup curves were measured at two temperatures $T = 298$ K and $T = 227$ K for the three grafted PDMS samples with different chain lengths (N_t) and the results are shown in Figure 12. The buildup curves display two maxima. The first maximum shows a relatively sharply defined value of the excitation and reconversion time τ. The second maximum at longer τ values are more difficult to identify in sample PDMS3 ($N_t = 4.5$) and less pronounced in sample PDMS2 ($N_t = 6.2$) due to the small amount of the mobile fraction and the broadness of the signal. Nevertheless, the second maximum is enhanced at lower temperature (cf Fig. 12**b**) due to reduced mobility and therefore increasing residual dipolar coupling. The maximum at short τ values are due to the segments at the interface, and those present at longer τ correspond to the mobile fractions of the grafted PDMS chains. The first maximum occurs at the same τ value for the three samples indicating the same chain immobilization in the interface of all three samples. The immobilizations are caused by a loss of conformation entropy due to chain anchoring to the silica surface and by excluded volume effects from the silica surface and neighboring chains. Thus, the averaged residual dipolar couplings of the interface have the same values independent of N_t. These results are both reflected in the ^{1}H DQ as well as in the ^{1}H TQ buildup curves (76).

The positions of the second maximum of the three samples are also indicative of the anisotropy of chain motions outside the interface. Assuming the same thickness of the interface in all three samples, we deduce that the fraction of the mobile chain fragments decreases from sample PDMS1 ($N_t = 7.7$) to PDMS3 ($N_t = 4.5$). This results in a shorter τ value for the position of the second maximum for sample PDMS3 versus samples PDMS2 and PDMS1 that can be detected in the DQ as well as the TQ buildup curves (76).

A bimodal distribution of the segmental-chain orientation corresponding to the interface and the mobile regions of PDMS chains grafted onto silica was detected by ^{1}H multiple-quantum NMR spectroscopy. The size of the interface is found to be independent of the total length of the PDMS chains. A broad distribution of segmental orientation prevails in the mobile region, and the segmental mobility is proportional to its fraction and therefore to the chain length. At lower temperatures, the mobility decreases until at $T = 198$ K the whole chain appears to be immobile at the time scale of the NMR experiment of about 10^{-5} s.

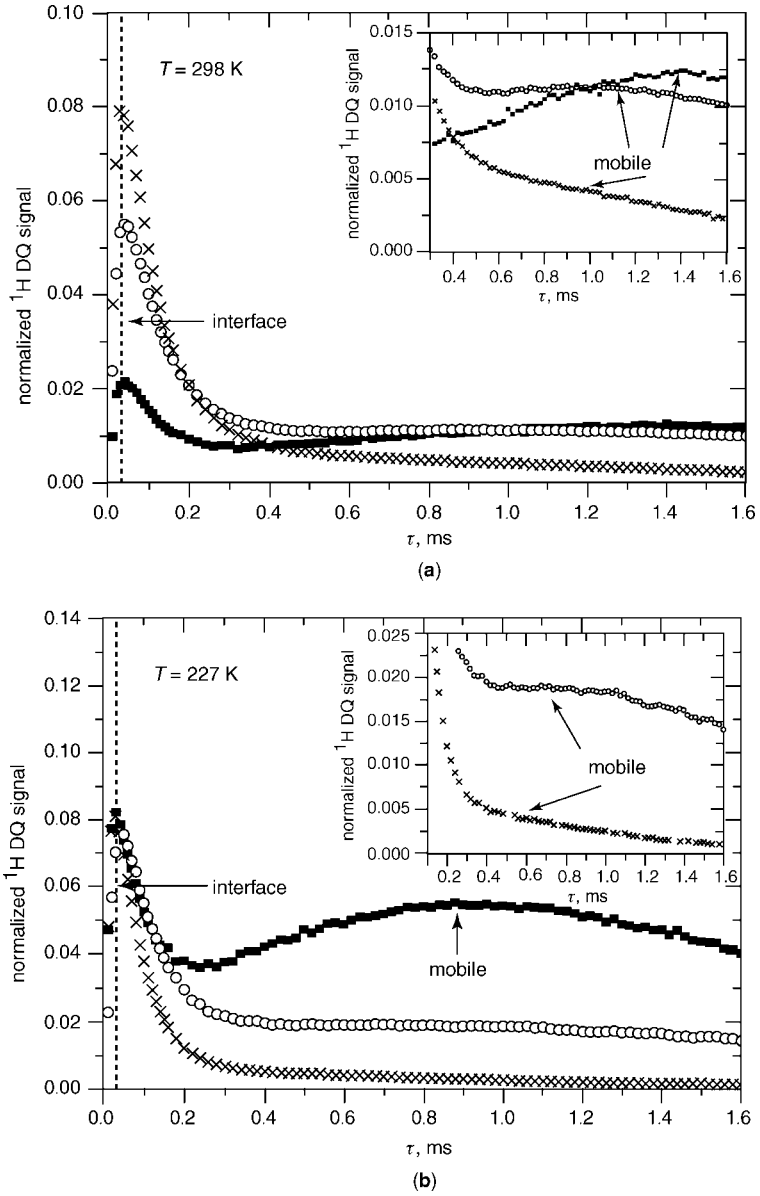

Fig. 12. Proton DQ buildup curves of grafted PDMS samples recorded at $T = 298$ K (**a**) and $T = 227$ K (**b**). (■) PDMS1, (○) PDMS2, and (×) PDMS3. The region of the DQ buildup curves after the first maximum is enlarged in the insets. Reproduced from Ref. 76, with permission from American Chemical Society.

The measurements using transverse ^{1}H relaxation shown that this quantity is also highly sensitive to the heterogeneous mobility of PDMS chains grafted onto a silica surface (77). This method allowed the distinction between a dense brush-like structure of the grafted layer containing chains of a fairly uniform

length and a layer containing a significant fraction of long-chain loops outside the grafted layer. The mobility of the chain outside the interface was found to increase with increasing average length of the grafted chains in agreement with the measurements performed by MQ NMR (76).

Local Segmental Anisotropy Induced by Mechanical Deformation. A well-known consequence of the theory of rubber elasticity is bond orientation (78,79). Deformation of an elastomer induces anisotropy of the backbone bonds of the polymer coil. In recent NMR studies of rubber elasticity, the mechanism of deformation and the orientation of network chains have received increasing attention (50,51). The local segmental anisotropy induced by a uniaxial applied force in elastomers was also investigated by NMR in terms of ^{1}H dipolar encoded longitudinal magnetization decays and double-quantum coherences buildup curves (80). These multipolar nuclear spin states were measured as a function of the angle θ between the static magnetic field and the direction of the applied force. The experimentally determined angular dependence of the effective residual dipolar couplings shows a minimum around the magic angle. These NMR methods offer the possibility to investigate in great detail the mechanisms responsible for the induced local anisotropy in strained polymer networks without contributions from the dipolar correlation effect (*vide infra*) and without need for chain deuteration.

Network Properties by Transverse Magnetization Relaxation. The transverse relaxation reflects mainly the loss of quantum phase coherence of spins. The axial symmetry induced by the presence of static magnetic field is of particular interest for observing the broad spectrum of relaxation rates related to the hierarchy of fluctuations, which affect any polymer chain in a melt or network (from about 10^9 s^{-1} down to less than 1 s^{-1}). For protons attached to polymer chains, the irreversible dynamics of the longitudinal magnetization is sensitive to properties generated by the local viscosity, which governs the random rotations of monomeric units. With regard to the transverse magnetization, the relaxation process cannot by analyzed without considering the time interval allotted for the full random rotations of chemical units that is close to the time interval (about 1 s or more) required for the full renewal of the chain configurations. However, this is to long a process for inducing any magnetic relaxation mechanism; consequently, the transverse magnetization is sensitive to a part of the hierarchy of chain fluctuations, only. In other words, random motions of units are detected as nonisotropic rotations generated by the topological constraints and the irreversible dynamics of the transverse magnetization is thus governed by the nonzero average of the dipolar interactions. A solid-like behavior of the transverse relaxation is expected to be associated with the property of elasticity, provided the time scale of the renewal of configurations is longer than the NMR scale of observation. This effect is considerably enhanced when permanent networks are observed.

Models for Transverse Relaxation. The simplest model to describe chain statistics from the NMR point of view is a chain of freely jointed segments of fixed length (12). Such a chain may be rescaled in several hierarchical steps according to the time scale of the motions which takes place at different space scales, compared to the time scale defined by the NMR spin interactions. All intrachain motions are assumed to be fast enough to average elementary interactions, whereas junction average positions are static.

Let us consider a linear chain of N statistical segments, fixed at its extremities. An average orientation is induced along the chain by these constrains. To estimate the effect of this average orientation on NMR parameters, the simplest picture is to consider that each segment carries an isolated pairs of spins, usually protons (two-spin approximation). Within this framework, the time evolution of the transverse magnetization $M_{\vec{R}}(t)$ for a spin pair attached to a chain may be written in the very simple form

$$M_{\vec{R}}(t) = \mathrm{Re}\left[M_0 \exp\left\{-\frac{t}{T_2}\right\} \exp\{\mathrm{i}\omega_{\vec{R}}\,\mathrm{t}\}\right] \tag{25}$$

where $M_{\vec{R}}(t)$ is the initial polarization, T_2 is the transverse relaxation time related to the fluctuating part of the dipolar Hamiltonian, and $\omega_{\vec{R}}$ is the residual dipolar interaction in angular frequency units. Other theories of transverse relaxation ((13), and references therein) are more complex that this simple approach. A polymer network is considerably disordered. To model this disorder, the end-to-end vector components $\vec{R}(x, y, z)$ may be supposed to obey ideal, the Gaussian statistics, ie,

$$P(\vec{R}) = \left(\frac{3}{2\pi N a^2}\right)^{3/2} \exp\left\{-\frac{3}{2}\frac{\vec{R}^2}{Na^2}\right\} \tag{26}$$

where a is the length of the statistical segment. The overall evolution of the complex transverse magnetization is then obtained by averaging equation 25 over end-to-end vector distribution. This yields (67)

$$M(t) = \mathrm{Re}\left[M_0\left(1 - \frac{2}{3}\mathrm{i}D_{ij}N_{\mathrm{e}}^{-1}t\right)^{-1/2}\left(1 + \frac{1}{3}\mathrm{i}D_{ij}N_e^{-1}t\right)^{-1}\exp\left\{-\frac{t}{T_2}\right\}\right] \tag{27}$$

where D_{ij} is the dipolar coupling constant for a spin pair and N_{e} is the effective number of statistical segments. At short times, ie, for $\Delta^2 N_{\mathrm{e}}{}^{-1}t^2 \ll 1$ the transverse relaxation decay has a Gaussian behavior corresponding to the presence of the residual dipolar couplings.

Experimental transverse relaxation decays cannot be usually described from exponential time functions but integral treatments of these curves yield standard parameters equivalent to relaxation rates (81). Without entering into too many details, it may be worth noting that the integral treatment amount to calculating several moments of the function $P(\vec{R})$. The first and the third moments of the distribution function are obtained from the two following integral treatments of the experimental relaxation curves

$$A_1 = \int_0^\infty \frac{M(t)}{\sqrt{t}}\,\mathrm{d}t, \text{ and } A_3 = \int_0^\infty \frac{\mathrm{d}M(t)/\mathrm{d}t}{\sqrt{t}}\,\mathrm{d}t \tag{28}$$

A NMR structural parameter χ_{c} was introduced which is defined as $\chi_{\mathrm{c}} = A_3/A_1$. The quantity $1/\chi_{\mathrm{c}}$ is proportional to the correlation length of segments between two consecutive nodes. Thermal behavior, swelling effects,

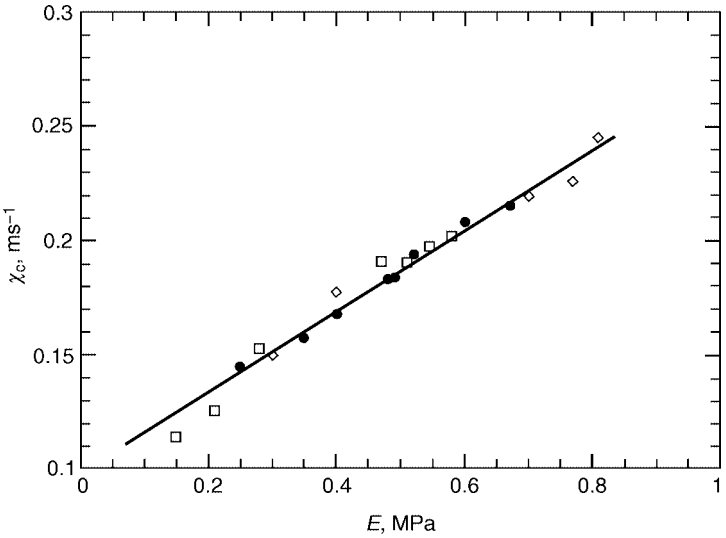

Fig. 13. Relaxation rate parameter χ_c as a function of the Young modulus E for randomly cross-link PDMS chains. NMR measurements were performed without any sample deformation. Reproduced from Ref. 82, with permission from American Chemical Society.

NMR-vulcanization, and NMR-elasticity relationships can be derived using the χ_c parameter ((81), and references therein). For instance, linear dependence of the NMR relaxation rate χ_c on the modulus of elasticity E measured on randomly PDMS chains (82) are shown in Figure 13.

Segmental fluctuations involved in the linear mechanical response to a small strain are directly observed from the transverse magnetization relaxation, in the absence of any strain.

Characterization of Polymer Networks by Transverse Relaxation. The NMR transverse magnetisation relaxation experiments were extensively used for quantitative analysis of the density of chemical cross-links, temporary and trapped chain entanglements and physical network junctions which are formed in filled rubbers, semicrystalline and ionic containing elastomers, and for determination of the molecular-scale heterogeneity of polymer networks ((83), and reference therein).

Several types of heterogeneity may occur in rubbery materials: (*1*) molecular-scale heterogeneity, which is caused by the chemical heterogeneity of uncured elastomers, network defects, and heterogeneous distribution of network junctions on a molecular level; (*2*) morphological heterogeneity of rubbery compounds due to a spatially heterogeneous distribution of components and filler in the compound; (*3*) spatial heterogeneity due to a difference in curing conditions such as temperature and concentration of vulcanisation agents throughout the sample volume.

A significant difference between the large spatial-scale mobility of network chains and that of network defects allows us to determine the degree of network heterogeneity. The most reliable data are obtained for swollen samples, because an increasing solvent content results in the disentanglement of network defects from network chains (84–86). The molecular mobility of network chains is consequently

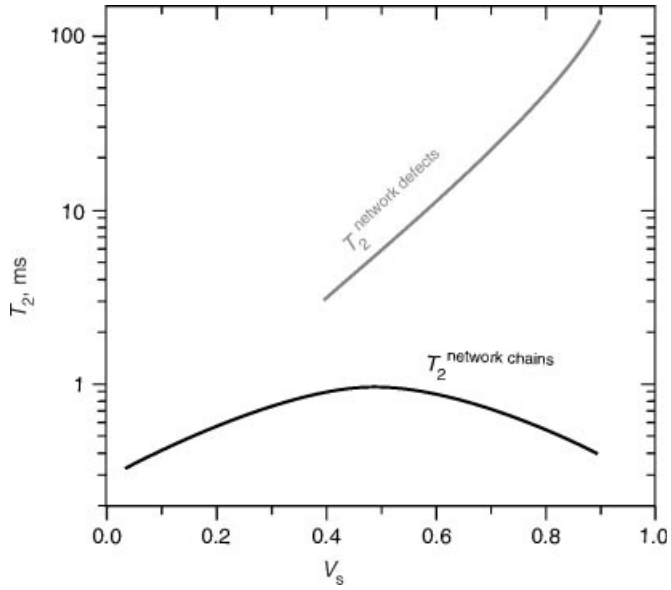

Fig. 14. The transverse relaxation time for a polymer network with defects against the volume fraction of a good solvent. Reproduced from Ref. 84, with permission from American Chemical Society.

decoupled from that of network defects, resulting in a major distinction in the relaxation behavior.

One example is given by the monoexponential T_2 decay of a cured acrylate that is splitted into two components upon swelling. This behavior is most clearly observable at high solvent concentrations (84,85). One component has short decay time (T_2^s), which is comparable with that of the original sample. This component apparently derives from network chains. Starting at a low volume solvent content (see Fig. 14), V_s, T_2^s shows an increase, which may be attributable to the following phenomena: (*1*) the disentanglement of network chains, (*2*) an increase in the frequency of the large spatial-scale chain motion, and (*3*) a slight decrease in the strength of the interchain proton dipole–dipole interactions. At $V_s \approx 40$–50 vol%, T_2^s reaches a maximum value. A value of T_2^s at the maximum, $(T_2^s)^{max}$, is related to the molecular mass of the network chains between chemical cross-links and trapped chain entanglements. At higher values of V_s, T_2^s decreases until the state of equilibrium swelling is reached. This decrease in T_2^s is thought to reflect the increase in the interchain proton dipole–dipole interactions as a result of the network chain elongation following a progressive increase in the solvent fraction in a swollen gel (12).

The long decay time (T_2^l) of the other component is typical of semidiluted polymer solutions. A T_2^l value continuously increases with an increasing solvent content. This component is apparently originated from the relaxation of network defects which are disentangled from network chains in a swollen state. At the equilibrium swelling degree, the relative fraction of the T_2^l relaxation component could be used as a measure of the fraction of highly mobile network defects. The

described behavior of T_2 relaxation decay following a progressive increase in the solvent fraction is typical of networks containing a significant fraction of network defects.

Distinct T_2 relaxation components with widely differing mean decay times suggest molecular or macroscopic heterogeneity of the material. In such cases, the submolecules concept can be used to describe the relaxation behavior (12). In a simplified interpretation, the overall T_2 relaxation decay of a heterogeneous elastomer is the weighted sum of the decays originating from the submolecules, which are defined as the network chains that are formed by the chemical and physical junctions, and network defects, ie, chains that are not attached to the network, chain loops and dangling chain ends. The large spatial-scale mobility of these submolecules differs substantially, and so does their relaxation behavior. The relative contribution of the submolecules to the overall decay is proportional to the number of protons attached to these chain fragments.

A quantitative analysis of the shape of the decay curve is not always straightforward due to the complex origin of the relaxation function itself (12,81,87–89) and the structural heterogeneity of the long-chain molecules. Nevertheless, several examples of the detection of structural heterogeneity by T_2 experiments have been published, for example the analysis of the gel/sol content in cured (90,91) and filled elastomers (85,86), the estimation of the fraction of chain-end blocks in linear and network elastomers (91,92), and the determination of a distribution function for the molecular mass of network chains in cross-linked elastomers (93,94).

Chain Orientation and Slow Dynamics by Dipolar Correlation Effect. An important 1D NMR method used for investigating anisotropy of chain dynamics and segmental order in polymer networks is given by the decay of the solid echo (12,63), a combination of Hahn and solid echoes (52), and a normalized stimulated echo (95–97). For all these cases, the echo amplitude decays can be described by a residual dipolar or quadrupolar correlation function (DCF) (for an introduction, see Reference 5). This function describes the autocorrelation of dipolar or quadrupolar randomly fluctuating interactions around the residual nuclear spin interactions that have been preaveraged by the fast dynamics of the chains and functional groups. Measurement of the DCF together with a corresponding theoretical model reveals important information about local segmental order and slow-chain dynamics under various experimental conditions. The possibility to measure the DCF using a combination of a solid echo, a Hahn echo and the free induction decay of protons, and deuterons has been discussed in Reference 63. An improved method was introduced later by Callaghan and Samulski (52) which exploits the fact that Hahn echo refocuses chemical shielding interactions and magnetic field inhomogeneities. Moreover, the Hahn echo amplitude is encoded by the molecular motions and residual dipolar couplings. The fluctuation of the dipolar interactions encodes the amplitude of the solid echo (actually a mixed echo) to a first approximation. The appropriate combination of these echoes, thus, gives access to residual dipolar couplings and the fluctuation rates. From the viewpoint of the spin system response, the solid echo completely refocuses the evolution of coherences of quadrupolar nuclei of spin $I = 1$ like ^{2}H and of a pair of 1/2 spins other than the ^{1}H multispin dipolar interactions. Therefore, the solid echo is strongly affected by the residual multispin interaction which makes the measurements of

DCF inaccurate. Moreover, the time scale of the dipolar or quadrupolar interaction fluctuations is limited to the time of the solid echo decay which is shorter than the transverse magnetization relaxation time. A considerably longer NMR time-window is offered by the DCF recorded with a stimulated echo (95–97). However, the amplitude of the stimulated echo is smaller than that of the solid echo and is affected by the multispin residual dipolar couplings as well as by the fluctuating dipolar fields. Furthermore, the evolution of the chemical shift Hamiltonian before storage of the z-magnetization encodes the stimulated echo evolution. Moreover, magnetization exchange competes with the dipolar correlation effect.

In all the cases discussed above, only the response of the spin system composed of dipolar coupled spin-1/2 pairs was considered. Proton DQ-NMR spectroscopy on elastomers—static and spinning at the magic angle—proved that the consideration of isolated spin-1/2 pairs is a crude approximation (68). The dipolar couplings between the protons belonging to various functional groups are shown to be active in two-dimensional DQ-MAS spectra for high excitation/reconversion times (68,73).

Dipolar correlation function can be measured for a multispin dipolar coupled network, for example, for the protons in functional groups attached to polymer chains in elastomers by a mixed echo given by the combination of the magic and the Hahn echo. The magic echo refocuses the residual multispin dipolar Hamiltonian with high efficiency (71–73,98). In a good approximation, the amplitude of the mixed echo is independent of residual (quasistatic) multispin couplings and inhomogeneous spin interactions including chemical shielding interaction. The following gives an evaluation of the dipolar correlation function describing slow chain motions within the limits of an exponential correlation function and a distribution of correlation times.

Mixed Echo Decay. The mixed echo amplitude decay can be expressed in terms of the autocorrelation function of the dipolar Hamiltonian (64). Transverse relaxation processes described by a single correlation time are rarely found in amorphous polymers including elastomers. If a normalized distribution of correlation times $g(\tau_c)$ is introduced, than the mixed echo decay is given by (64)

$$S_{ME}(6\tau) \cong 1 - \bar{M}_2 \int_0^\infty {\tau_c}^2 \left\{ e^{-\frac{6\tau}{\tau_c}} - 3\, e^{-\frac{5\tau}{\tau_c}} + \frac{9}{4}\, e^{-\frac{4\tau}{\tau_c}} + 3\, e^{-\frac{\tau}{\tau_c}} + \frac{3\tau}{\tau_c} - \frac{13}{4} \right\} g(\tau_c)\, d\tau_c \tag{29}$$

where τ_c is the correlation time. It is obvious form equation 29 that the measurement of DCF leads to a mixture of contributions from residual van Vlevk second moment and the distribution function of correlation times that is model dependent.

A particularly simple form for the function $g(\tau_c)$ is related to the log-Gaussian distribution (see for instance Reference 2), ie,

$$g(\tau_c) \equiv \frac{1}{\tau_c} F_G(\ln \tau_c) \tag{30}$$

where

$$F_{\mathrm{G}}(\ln\tau_c) \equiv \frac{1}{\sigma_{\ln}\sqrt{2\pi}} \exp\left\{ - \frac{[\ln(\tau_{\mathrm{c}}/\tau_{\mathrm{c0}})]}{2\sigma_{\ln}^2} \right\} \tag{31}$$

The center of gravity of the correlation time distribution is given by $\ln(\tau_{\mathrm{c0}})$ and the width of the distribution is $\Delta_{1/2} = 1.02\,\sigma_{\ln}$.

Parameters of the Dipolar Correlation Function for a Cross-Linked Elastomer Series. The mixed echo decays were measured for a series of cross-linked natural rubber (64). The model involving the distribution of correlation times (see eq. 29) was used to fit the mixed echo decay. The residual second van Vleck moments obtained from fits as a function of shear modulus G.

For ideal polymer coils, the most significant and distinctive property is the Gaussian distribution of the end-to-end distances. By considering the different segments of the freely jointed chain which are statistically independent and can be represented by a Markov chain, one can derive the correction to the Gaussian distribution of the end-to end distances (see Reference 99).

Using the corrected Gaussian distribution function one than gets (64)

$$\langle M_2 \rangle \propto \frac{5}{3}\frac{1}{N^2} - \frac{2}{3}\frac{1}{N^3} \tag{32}$$

Within the limit of the approximation used, it is concluded that the residual second van Vleck moment scales with $1/N^2$ for high numbers of statistical segments, ie, for $N \gg 1$, which means for low cross-link densities. However, this regime is invalid for the series of cross-linked natural rubber investigated using DCF (64). The effective number of statistical segments N is defined by the number of segments $N^{(0)}$ between physical cross-links or topological constraints and the number $N^{(\mathrm{C})}$ of segments between chemical cross-links. If we assume that the contributions to the residual dipolar coupling are additive and topological constraints are independent of the degree of chemical cross-linking, we can write $(N)^{-1} \approx (N^{(0)})^{-1} + (N^{(\mathrm{C})})^{-1}$. In this case, one expects (cf equation 32) that $\langle M_2 \rangle$ has a polynomial dependence on cross-link density or shear modulus.

Based on the dependence of the residual second moment on $1/N$ given by equation 32, the measured $\langle M_2 \rangle$ values can be fitted by a polynomial up to the forth power in the shear modulus G, ie,

$$\langle M_2 \rangle = a_0 - a_1 G + a_2 G^2 - a_3 G^3 + a_4 G^4 \tag{33}$$

This dependence is similar with that shown in Figure 8**a** measured using AIMS method (70). If only the first four values of $\langle M_2 \rangle$ corresponding to an intermediate regime of cross-linking are considered, the G^2 term dominates the dependence as it is expected from a Gaussian distribution of end-to-end vectors. The DCF measurements also reveal that the centre of gravity, as well as the logarithmic width of the distribution function of correlation time—which describes the slow motion of the network chains—scale with the cross-link density in a complex manner (64).

The development of NMR methods that allow accurate measurements of residual second van Vleck moments and the distribution of correlation times yields new tools to test polymer network theories that are more sophisticated than the theory of the freely jointed chain corresponding to a Markov chain.

Viscoelastic Polymers by Two-Dimensional NMR Spectroscopy

The investigation of molecular dynamics and local segmental orientation by two-dimensional (2D) NMR spectroscopy has a number of advantages (1,2) particularly when dealing with complicated spin systems such as viscoelastic polymers. Below, we will discuss examples of such investigations, concentrating on techniques that are particularly sensitive to the viscoelastic regime that is, NMR techniques for measuring residual dipolar couplings and dynamic order parameters. Readers interested in a more general overview of multidimensional NMR of polymers are referred to references (2,3,6).

Chain Orientation from 2D ^{1}H Magnetization Exchange Spectroscopy. Two-dimensional ^{1}H magnetization-exchange spectroscopy and its reduced one-dimensional (1D) variant have been used to probe residual dipole–dipole couplings between different functional groups of a SBR sample, namely between the CH and CH_2 groups of the butadiene units (65,100). The intergroup residual dipolar couplings can then be correlated with the shear modulus that is an independent measure of the cross-link density (65). Hence, the dynamic local-order parameter associated with the partially averaged dipolar coupling can be evaluated taking the average over the relevant dynamic processes.

Principle of the Method. Following the general scheme of 2D NMR spectroscopy, an evolution period of duration t_1 follows the excitation pulse. This interval ends with a flip-back pulse and the system is allowed to exchange during the mixing period t_m. After a third pulse the remaining signal is acquired during the detection interval t_2 (1). The intensity of the cross-peaks in the resulting 2D spectra then reflects the degree of exchange between the corresponding groups. Since full 2D NMR spectroscopy is time-consuming, for quantitative evaluations also a reduced 1D form has been used. In this case, the time t_1 is fixed and adjusted such that it acts as a chemical-shift filter (2) for one of the two butadiene lines in the static SBR spectrum. The reappearance of the filtered line with increasing mixing time is then a measure of the magnetization exchange between the protons of the CH and CH_2 groups. Note, that unlike the 500 MHz spectrum the styrene line and the CH line could not be distinguished in these experiments so that only the CH and CH_2 lines of the butadiene units are resolved. They are separated by about 3.35 ppm, corresponding to 1 kHz at the Larmor frequency of 300 MHz.

The theory needed for the evaluation of the exchange process was also developed (65,100). The model of the spin system used is depicted in Figure 15.

For short mixing times, the measurable exchange of ^{1}H longitudinal magnetization is predominantly determined by the protons belonging to nearest-neighbor CH and CH_2 groups. At longer mixing times on the other hand, a much larger spin system along the polymer chain must be considered, in principle. In Reference 100, however, it was shown that even in this case the intergroup residual dipolar

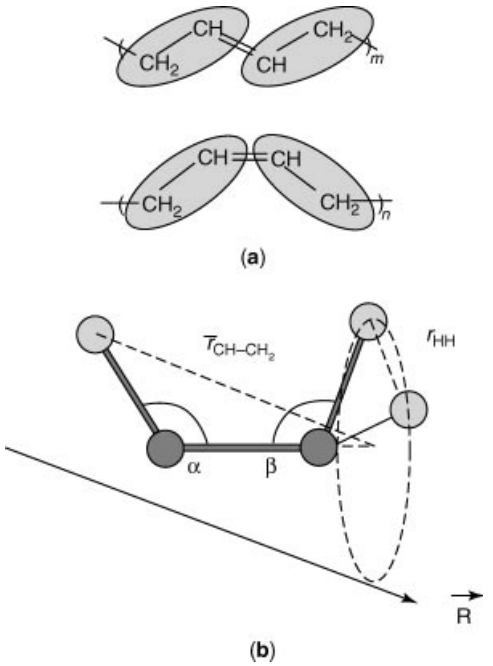

Fig. 15. (**a**) The monomer unit of *trans*- and *cis*-1,4-butadiene. The alternating sequence of CH—CH_2 groups, for which the magnetization-exchange process is treated. (**b**) The geometry of the CH—CH_2 spin system. The shaded circles represent protons and the black circles carbon atoms. The conformational jumps of the methylene protons lead to an average CH—CH_2 proton distance $\bar{r}_{CH—CH_2}$. Reproduced from Ref. 65, with permission from American Institute of Physics.

coupling can be measured from the initial-time regime of the magnetization-exchange decay curve.

In the limit of short mixing times t_m, the initial decay rates for the CH line were found (65,100) to depend only on the intergroup residual dipolar coupling $\bar{D}^{CH—CH_2}$ according to

$$\langle\langle I_z(t_m)\rangle\rangle = 1 - \frac{1}{2}\langle(\bar{D}^{CH—CH_2})^2\rangle t_m^2 \tag{34}$$

where $\langle\langle I_2(t_m)\rangle\rangle$ is the observable for the CH protons (for the CH_2 protons the factor 1/2 must be substituted by 1/4 in equation 34). The symbol $\langle\ \rangle$ represents the statistical ensemble average of the space part of the dipolar coupling in a disordered elastomer. Note, that from such measurements, the intergroup dipolar coupling $\bar{D}^{CH—CH_2}$ can be determined which is largely parallel to the segment axis. That is, it is much more informative with respect to the detection of chain order and chain motion than intragroup couplings would be.

Two-Dimensional ^1H Magnetization-Exchange Processes in Cross-Linked SBR. From the point of view of molecular motion, cross-linked elastomers are highly heterogeneous systems and a solid-like behavior is present together with slow and fast motions of both chains segments and functional

groups. Hence, the magnetization-exchange process is expected to be also heterogeneous, that is, driven by different mechanisms.

In order to investigate this heterogeneity, a series of static 2D NMR experiments was performed on SBR for increasing mixing time (100). As already discussed above, the aromatic and the olefinic protons are not resolved under the applied experimental conditions as can be seen in the 2D spectra shown in Figure 16.

A remarkable feature of the diagonal 2D spectrum for short mixing times is that the width of the diagonal peaks perpendicular to the (ω_1, ω_2) diagonal is much smaller than the widths along the diagonal. This indicates that the ^{1}H NMR spectrum is heterogeneously broadened (65). The width of each line along the diagonal reflects both the solid- and the liquid-like contributions, whereas the width perpendicular to the diagonal reflects selectively the liquid-like line width only. This feature is very pronounced for the CH diagonal peak and less for the CH_2 diagonal peak because of the strong proton–proton coupling within the methylene group. A similar result was already found in a ^{13}C magnetization-exchange experiment on natural rubber aimed to detect chain diffusion (101). While no chain diffusion was detected, the lines were also found to be spread out along the diagonal.

In the ^{1}H magnetization-exchange experiment on SBR not much cross-peak signal is found for mixing times shorter than 2.5 ms (see Fig. 16**a**). This indicates that within this time scale the CH and CH_2 functional groups can be considered in reasonable approximation to be isolated. The intergroup residual dipolar coupling leads to magnetization exchange for longer mixing times. Intense positive cross-peaks are thus present for $t_m = 30$ ms (see Figs. 16**d** and 16**e**). Such positive cross-peaks can arise for two reasons: from the exchange process mediated by residual dipolar couplings and from cross-relaxation induced by segmental motions with correlation times τ_c longer than ${\omega_0}^{-1}$ (1).

Proton Intergroup Residual Dipolar Couplings. The residual dipolar couplings between the protons of the CH and the CH_2 groups were determined from the t_m dependence of the peak intensities. The decay of the longitudinal magnetization $M(t_m)$ of the diagonal signals (normalized to the value M_0 that corresponds to zero mixing time) is recorded for short mixing times for the CH group. According to equation 34, the magnetization-exchange dynamics should show an initial quadratic dependence on t_m. This dependence is indeed found in the experiments and is shown in Figure 17**a** for SBR as an example.

From the slope of the initial magnetization decay, the values of the effective residual dipolar couplings $D_{\mathrm{eff}}^{\mathrm{CH{-}CH_2}} \equiv \langle (\bar{D}_{\mathrm{eff}}^{\mathrm{CH{-}CH_2}})^2 \rangle^{1/2}$ could be evaluated and it could be shown that these couplings scale with the cross-link density (65,100). The correlation of the coupling constant $D_{\mathrm{eff}}^{\mathrm{CH{-}CH_2}}$ with the shear modulus G as an independent measure of the cross-link density demonstrates this behavior (Fig. 17**b**). Note, however, that the line in Figure 17**b** does not cross the origin but provides a significant value for $D_{\mathrm{eff}}^{\mathrm{CH{-}CH_2}}$ at G = 0. This is not in contradiction with the applied model, but reflects the influence of local chain order (physical cross-links). From extrapolating to $G = 0$ in Figure 17**b**, the intergroup residual coupling of an uncross-linked SBR melt was determined to be $\bar{D}_{\mathrm{eff}}^{\mathrm{CH{-}CH_2}} \approx 533$ Hz. Using average internuclear distances and bond angles for SBR, one can extract the value for the dynamic-order parameter $S_{\mathrm{H{-}H_2}}$ of the CH—CH_2 intergroup linkage

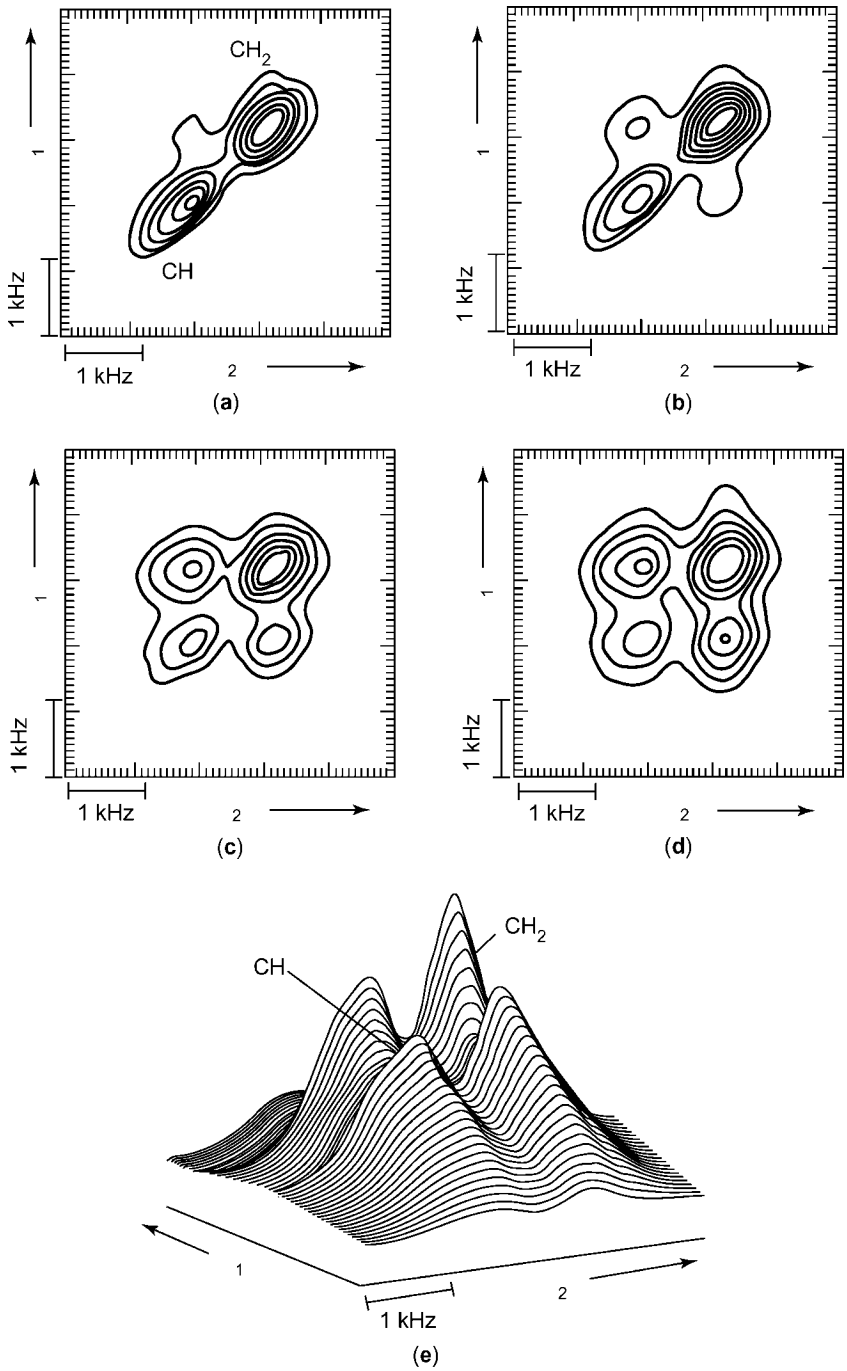

Fig. 16. Two-dimensional ^{1}H magnetization-exchange spectra of a SBR recorded with different mixing times have been used: $t_m = 2.5$ ms (**a**), 5 ms (**b**), 15 ms (**c**), and 30 ms (**d**). The 2D surface representation for $t_m = 30$ ms in (**e**) shows that all cross-peaks are positive. Reproduced from Ref. 65, with permission from American Institute of Physics.

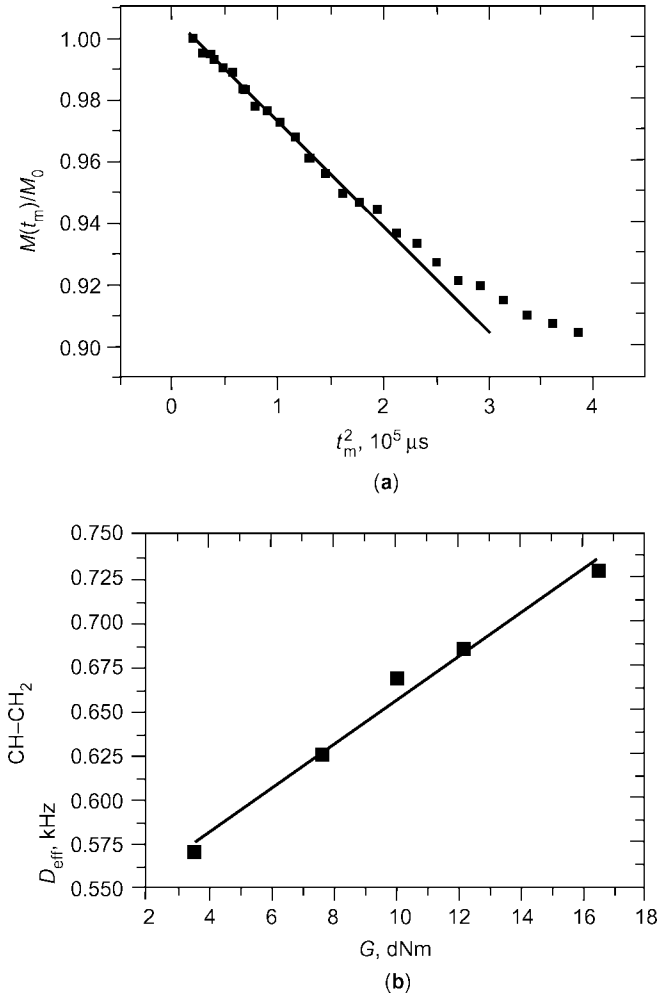

Fig. 17. (**a**) The initial decays of the proton magnetization for the exchange process CH → CH_2. The initial part of the magnetization-exchange data (starting with $t_m = 100\ \mu s$) shows the predicted dependence in t_m^2. The effective CH—CH_2 intergroup dipolar coupling constant $D_{eff}^{CH—CH_2}$ can be evaluated by fitting the theoretical curve. (**b**) $D_{eff}^{CH—CH_2}$ as a function of the shear modulus G for a series of differently cross-linked SBR samples. Reproduced from Ref. 65, with permission from American Institute of Physics.

$\vec{r}_{CH—CH_2}$ according to $\bar{D}_{eff}^{CH—CH_2} = D_{rigid}^{CH—CH_2} S_{H—H_2}$. This yields $S_{H—H_2} \approx 0.1$ and suggests an even higher value for the dynamic-order parameter for the corresponding carbon–carbon bond $S_{C—C} \approx 0.13$, since $\vec{r}_{CH—CH_2}$ and $\vec{r}_{C—C}$ forms an angle of 24°. Thus, even in polymer melts the chain motion can be largely anisotropic, as shown previously for poly(methacrylates) (102).

Magnetization-exchange NMR spectroscopy offers a convenient means for measuring the residual dipolar couplings between functional groups along the polymer chains. The intergroup dipolar coupling is remarkably high even in uncross-linked melts representing relatively high local segmental order. In

cross-linked samples, it scales with the cross-link density as predicted by the scale-invariant model of residual dipolar couplings (12), emphasing its relation to viscoelastic properties of the elastomers.

Segmental Motions by 2D NOESY-MAS Spectroscopy. In the previous paragraph, we have discussed the coherent magnetization-exchange process by ^{1}H non vanishing average dipolar couplings. Under fast MAS conditions, however, the residual couplings responsible for the exchange are largely refocused for full rotor periods and cross-relaxation by the fluctuating part of the dipolar interaction predominates. This so-called nuclear Overhauser effect (NOE) (103) takes place if the spins system is not in internal equilibrium. It corresponds to relaxation between dipolar-coupled nuclei such as ^{13}C and ^{1}H or between different nonequivalent magnetically sites of the same type of nucleus. NOE spectroscopy (NOESY) is well known in liquid-state NMR where it is one of the standard 2D techniques to elucidate and assign structures of macromolecules in solution (1).

Following the success of the technique in solution state, NOESY has been also applied to polymers or viscoelastic materials (104–110). As in solution experiments, one takes advantage of the fluctuating part of the dipolar coupling to extract useful structural and dynamical information. Using this method, nuclear Overhauser enhancement factors have been measured in polyisoprene over a range of temperatures with static ^{13}C NOE spectroscopy (104). A molecular-weight independent change of regime was observed at around 60°C for the backbone motion reflecting a loss of motional cooperativity with increasing temperature. Also the temperature-independent correlation time of the internal rotation of the methyl group could be inferred.

The polymer miscibility in polymer blends (PS/PVME) was probed by ^{13}C NOE spectroscopy under MAS (105). This study takes advantage of the fact that cross-peaks appear only between spins that are neighbors of each other, thus establishing NOE as a probe for the degree of mixture on the molecular level. Additional information on the molecular structure of the blend could be obtained from the NOE growth rates. The results suggest that there exists a specific interaction between the phenyl ring of the PS and the PVME methyl group. In Reference 106 the same technique was applied for investigating methyl groups as a source of cross-relaxation in solid polymers such as polycarbonate or polystyrene.

Static ^{1}H 2D NOE spectroscopy was applied in a first experiment showing that the technique can be used to measure interchain interactions (107). This work was then continued by applying the technique under MAS to investigate the intermolecular interactions responsible for the miscibility in polybutadiene/polyisoprene blends above the glass-transition temperature (108). It could be shown that intermolecular association can be probed by this technique and the results reveal the existence of weak intermolecular interactions between the polyisoprene methyl group and the vinyl side chain of the polybutadiene.

Segmental Motions of Elastomers. NOESY experiment under MAS on protons was used to study molecular motions in technical relevant materials such as rubbers (109,110). For the evaluation of these parameters, it is necessary to understand the cross-relaxation process in the presence of anisotropic motions and under sample spinning. Such a treatment is provided in Reference 110 and the cross-relaxation rates were found to weakly depend on fast motions in the Larmor frequency range and strongly on slow motions of the order of the spinning

frequency ν_R. Explicit expressions for the ν_R dependent cross-relaxation rates were derived for different motional models. Examples explicitly discussed were based on a heterogeneous distribution of correlation times (2,12,111) or on a multistep process in the most simple case assuming a bimodal distribution of correlation times (112–114).

The derived relationships were tested experimentally on a cross-linking series of styrene–butadiene rubbers and the cross-relaxation was studied as a function of the rotor frequency ν_R. As an illustration of such measurements, Figure 18**a** shows a surface representation of the gradient-selected 2D NOESY spectrum of a SBR sample acquired with a mixing time of 2.7 ms at a rotor frequency of 8 kHz. The lines corresponding to the aliphatic, the olefinic, and the aromatic protons are well resolved and can be assigned as indicated. Already at short mixing times pronounced cross-peaks are visible, in particular between the olefinic CH and the CH_2 group.

Figure 18**b** shows the decay curve of the diagonal peaks for mixing times up to 3 ms. Unlike in the magnetization-exchange case (65), the decay is found to be approximately linear in t_m in the short mixing time regime and exponential or biexponential for long times (110). A similar curve can be plotted for the increase of the cross-peaks. In order to investigate the effect of the sample spinning on the cross-relaxation rates, series of 2D NOESY-MAS spectra were acquired as a function of the rotor frequency. The rates evaluated from these series were found to decrease linearly with rotor frequency that is an indication that cross-relaxation in elastomers is dominated by slow motions in the 10 kHz regime rather than by motions in the Larmor frequency range as in case of liquids. The cross-relaxation rates at room temperature were found to depend moderately only on the cross-link density that is another indication that cross-relaxation is dominated by the α process.

The experimental rates were analyzed in terms of the explicit expressions derived by the theoretical treatment (110). As expected for a statistical copolymer, segmental motions in the SBR samples cannot be described by a single correlation time (2). From T_1 data that were also measured the correlation time should be in the range of 10^{-8} s while the rotor frequency ν_R dependence of the cross-relaxation rates requires a correlation time of 10^{-5} s. So it is clear that at least two different correlation times are necessary to account for the experimental findings. The relaxation dispersion data T_1 (ω) (ω being the Larmor frequency) (96), however, show no discontinuity that would indicate the presence of two distinct motional processes. Thus, the data were analyzed in terms of a broad distribution of correlation times for almost isotropic segmental motions (α relaxation). With a simple log-Gaussian distribution function of reasonable parameters (110) it was found that one could account for both the T_1 values and the ν_R-dependent cross-relaxation rates. From the center of gravity of the distribution, the glass-transition temperature could be estimated as $T_g = 230$ K using the well-known Williams–Landel–Ferry (WLF) equation (2). This value compares favorably with the known value of $T_g = 220$ K for uncross-linked SBR-1500.

Selective Residual Dipolar Couplings by ^{1}H Multiple-Quantum NMR Spectroscopy. Multiple-quantum MQ NMR spectroscopy is well established for structural studies of liquids and highly mobile solutes in liquid crystals (1,26).

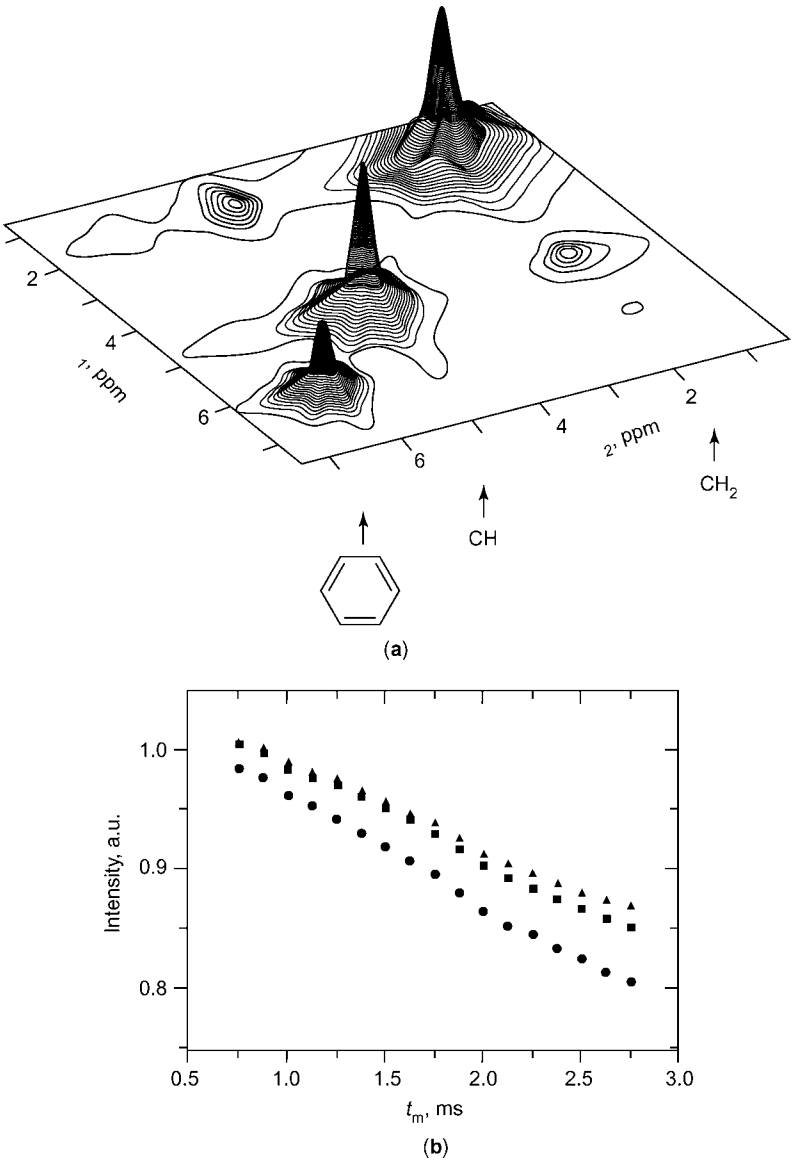

Fig. 18. (**a**) 2D ^{1}H-NOESY surface spectrum of SBR acquired for a mixing time of 2.7 ms and under 8 kHz MAS. Already at this short mixing time pronounced cross-peaks are visible. (**b**) Short-time decay of the cross-peak intensity evaluated from a series of 2D spectra. Such curves can be analyzed providing information on internuclear distances and segmental dynamics (■) aromatic CH, (●) olefinic CH, (▲) CH. Reproduced from Ref. 110, with permission from Taylor & Francis Ltd.

In recent years, there has been a sustained effort to obtain homonuclear (73,115–119) and heteronuclear (120–122) high resolution MQ NMR spectra also for organic solids using fast MAS to increase resolution and sensitivity. Such MQ spectra proved to be valuable tools for determining dipolar connectivities between

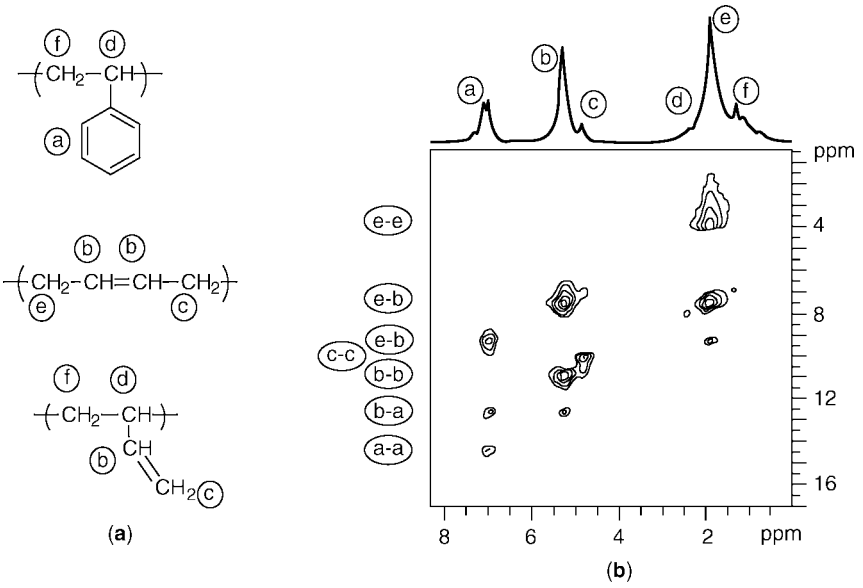

Fig. 19. Proton DQ MAS spectrum of a SBR sample with a low value of cross-link density (0.8–0.8 phr sulfur accelerator). The rotor frequency was 10 kHz and the t_1 increment was 15 μs. The diagonal peaks and the cross-peaks of the functional groups are assigned as indicated (compare (**a**) and (**b**)). Reproduced from Ref. 73, with permission Elsevier.

spin-1/2 nuclei (74,75,116). More quantitatively, dipolar couplings, internuclear distances, and molecular torsion angles can be measured by these techniques (74). For viscoelastic materials, it was recently shown that ^{1}H high resolution MQ NMR spectroscopy offers the possibility to measure site-selective residual dipolar couplings between all resolved protons (73,119). The MQ technique thus is an attractive tool for studying structure and dynamics in polymer melts (119) and elastomers (68,73).

Dipolar Connectivities from the High Resolution ^{1}H DQ MAS Spectroscopy. Figure 19 shows the ^{1}H DQ spectrum of a cross-linked SBR sample that has been acquired at a spinning frequency of 10 kHz (73).

The peaks in the 2D DQ spectrum correspond to double-quantum coherences between two spins which must be relatively close neighbors in space in order to contribute significantly to the peak intensity as follows from the strong distance sensitivity of the dipolar coupling. From the existence of the corresponding peaks therefore through space dipolar connectivities can be easily established.

The assignment of the peaks is shown along the ω_1 dimension by pairs of letters a–f (see Fig. 19**a**) which indicates the functional groups that are involved in the generation of the corresponding DQ peaks. From a simple qualitative inspection of the DQ spectrum, it can be seen that there are dipolar connectivities between practically all functional groups. The strongest DQ signals are found between protons of the polybutadiene groups, but also DQ peaks of considerable intensity are visible between the polybutadiene protons and the aromatic protons of the styrene units. This indicates a good mixture of the different functional

groups on the nanometer length scale as is found for instance in the case of a statistical copolymer.

Another recent example of the use of ^{1}H DQ MAS NMR spectroscopy is given by the study of molecular scale miscibility of poly(butylenes terephtalate)-*block*-poly(tetramethylene oxide) multiblock (PBT-*block*-PTMO) copolymers (123) by looking for correlation peaks between signals from the hard and soft blocks.

Previous ^{13}C NMR MAS relaxation experiments revealed a large, bimodal-like heterogeneity of the PTMO chain mobility, which were explained by microphase separation of the amorphous phase into a highly mobile PTMO-rich phase and a less mobile PBT/PTMO mixed phase (PBT/PTMO interface) (124). However, the motional heterogeneity of the PTMO blocks can also originate from a dynamical interface due to anchoring of PTMO blocks to rigid PBT domains, which can cause apparent "two-phase" behavior. 2D NMR experiments can provide direct information on the molecular scale miscibility in polymeric materials. ^{1}H DQ correlation spectroscopy under fast MAS using the back-to-back (BABA) sequence is used in the present study to determine the proximity of the PBT and PTMO chain units in the block copolymers.

The ^{1}H MAS NMR spectrum of PBT-*block*-PTMO consists of resonances at 8.0, 4.4, 3.4, and 1.6 ppm that originate from the aromatic protons of PBT, OCH_2 protons of PBT, OCH_2 protons of PTMO, and the $(CH_2)_2$ protons of PBT and PTMO, respectively. It is noted that the OCH_2 protons of PBT and PTMO at the transition from PBT to PTMO blocks along the chain have slightly different chemical shifts, as measured by ^{1}H solution NMR spectra, ie, 4.35 and 3.45 ppm for PBT and PTMO, respectively. However, these resonances are not resolved in the solid state NMR spectra. Figure 20 shows the phase-sensitive 2D spectrum of sample A1000/35 measured using the BABA sequence (123). The single-quantum (SQ) and double-quantum (DQ) dimensions are shown on the horizontal and vertical axes, respectively. The signals in the DQ dimension are situated at the sum of the frequencies of the two-coupled protons. Therefore, a DQ signal between two protons with identical chemical shifts will be on the diagonal, and signals between two protons with different chemical shifts will be off-diagonal giving rise to two signals equally spaced from the diagonal. One should note the different positions of off-diagonal signals are compared to COSY/NOESY spectra.

As expected, all resonances of PBT and PTMO blocks are present in the 2D spectrum, ie, all diagonal peaks and off-diagonal correlation peaks between the aromatic and the OCH_2 protons of PBT as well as a correlation peak between the CH_2 and OCH_2 peaks of PTMO. Additionally, there is a correlation peak between the aromatic protons from PBT and the OCH_2 groups from PTMO, suggesting a close proximity of these two chain fragments. The signal is in fact much more intense than one would expect (*1*) from a small fraction (only 14%) of PTMO chain units that are located at the transition from PBT to PTMO blocks in a single chain and (*2*) from the rather long intrachain distance between aromatic PBT and the OCH_2 protons of PTMO at the transition from the hard to the soft blocks along the chain. The correlation peak cannot be explained by spin diffusion during the 1ms *z*-magnetization delay after the reconversion period. Therefore, the DQ BABA MAS experiment is not affected essentially by the spin diffusion process and gives information about the molecular scale mixing. This correlation peak has to come primarily from intermolecular couplings between the PBT and PTMO protons

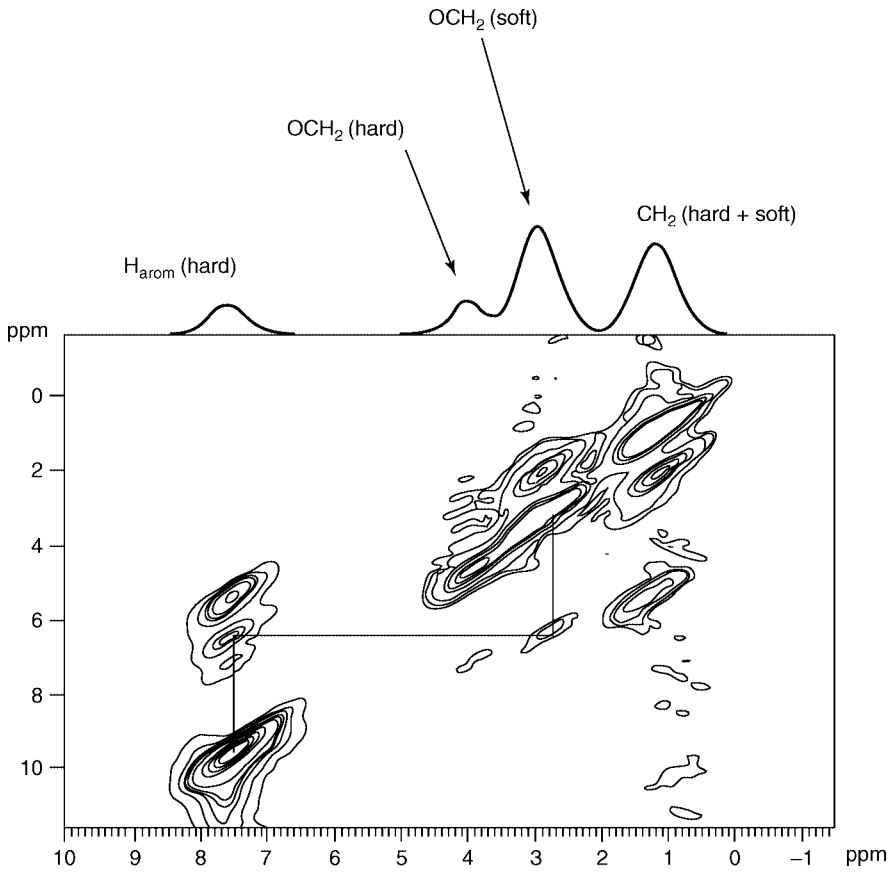

Fig. 20. Two-dimensional ^{1}H DQ MAS spectrum for thermoplastic elastomers PBT-*block*-PTMO with a length of PTMO block of 1000 g/mol and amount of PTMO block of 35% in weight (sample A1000/35) showing the dipolar correlation between the resonances of PBT and PTMO chain units, as indicated by the lines connecting the peak positions. Reproduced from Ref. 123, with permission from American Chemical Society.

of adjacent chains. In fact, it was shown that a DQ correlation signal arises at short recoupling times, which in our case, marks an interproton distance below 0.5 nm. Therefore, this correlation peak can be unambiguously attributed to PBT and PTMO units in a mixed PBT/PTMO phase.

Site-Selective Double-Quantum Buildup Curves and Correlation with Cross-Link Density. A more quantitative evaluation of the DQ peak intensities is possible by acquiring the experimental DQ buildup curves for each of the peaks performing a series of DQ experiments with increasing excitation time. As an example, the buildup curves for the three main contributions are shown in Figure 21 for two SBR samples with different cross-link densities (73).

A fit of the experimental DQ builtup curves using a relationship derived in the spin-pair approximation allows the ratio of the corresponding residual dipolar couplings to be determined, ie, $(\bar{D}^{CH_2} S_s^{CH_2}) : (\bar{D}^{CH_2-CH} S_s^{CH_2-CH}) : (\bar{D}^{CH-CH} S_s^{CH-CH})$, where $\bar{D}^{ij}$ represents a preaveraged dipolar coupling constant and S_s^{ij} the

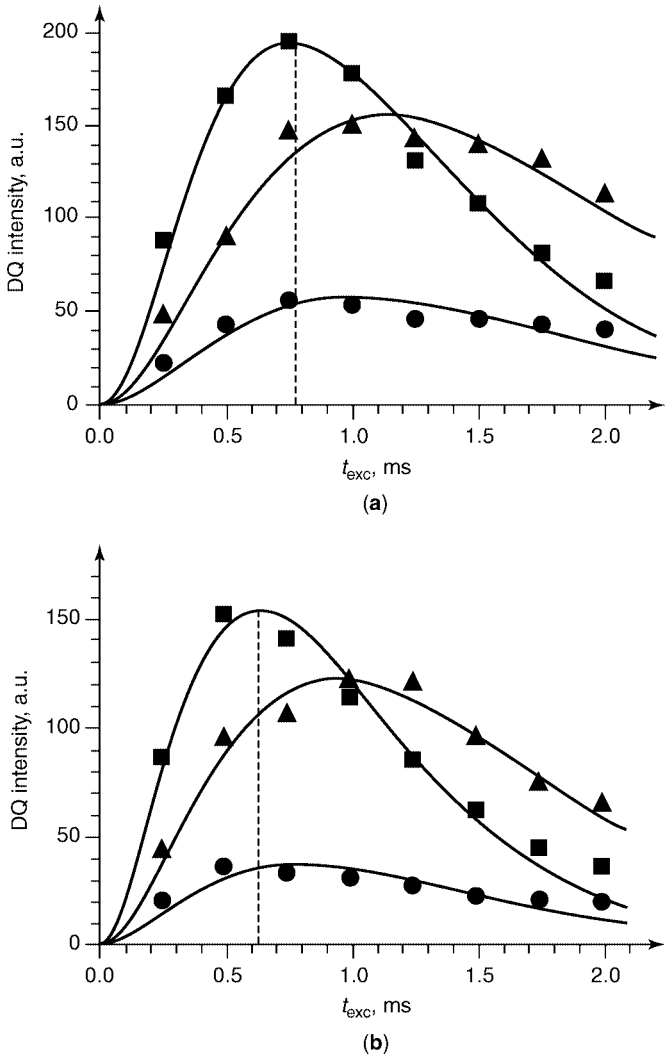

Fig. 21. Site-selective ^{1}H DQ buildup curves for low (**a**) and high (**b**) cross-linked SBR samples. The DQ signals correspond to the —CH_2— (■), CH_2—CH— (▲) and CH═CH coherences (●). The vertical dashed lines mark the excitation times for the maximum signal for the methylene protons, which differs for the two cases. Reproduced from Ref. 123, with permission from Elsevier.

corresponding scaled dynamic-order parameter (73,119). The order parameter $S_s^{CH_2—CH}$ (calibrated using a 1D MAS sideband pattern) is found to be close to the value $S_s^{CH_2—CH} = 0.1$ that has been estimated for SBR samples by the magnetization-exchange experiments described above (65). The order parameter corresponding to the CH—CH coupling is even higher (73). This coupling provides the best measure for the chain dynamics since it is predominantly aligned along the segmental axis.

For investigating a series of samples with different cross-link densities, however, the procedure described above is very time-consuming. In this case, a somewhat less detailed 1D measurement of the integral DQ-filtered signal can be used to establish the relationship between the total DQ intensity and the cross-link density. The square root of the DQ intensity is found to be an approximately linear function of the cross-link density but, more important, the topological constraints that are already present in the melt are found to dominate the residual couplings (see also Reference 119). Hence, the technique is not so much a sensitive measure of the cross-link density but is a rather sensitive and selective probe for local dynamic chain order.

The strongest residual dipolar couplings were also edited in a nonrotating cross-linked polyisoprene series by exciting double- and triple-quantum coherences in the short time regime (68). From this, the dynamic order parameters of the methylene and methyl groups were estimated and correlated with the cross-link density. Essentially, the same behavior was found as for SBR.

Residual Local Dipolar Fields by Heteronuclear Correlation Experiments. The NMR spectrum of rare spins (e.g. ^{13}C) contains extremely useful information because of the usually high chemical-shift dispersion and the possibility to easily eliminate undesired spin interactions. It would thus be advantageous to combine this high resolution dimension with ^{1}H spectroscopy in form of a heteronuclear correlation experiment (1). In the following, we will concentrate on the so-called wide-line separation (WISE) experiment (2,125–128), in which ^{1}H broadline information is correlated with the ^{13}C spectroscopic information. There are however also other possibilities for including heteronuclear information in a 2D experiment, for instance, 2D heteronuclear *J*-resolved spectroscopy which was applied for the investigation of filled natural rubber in Reference 101. It was concluded that there must be a high degree of motion in order to allow the scalar ^{13}C—^{1}H couplings to be revealed by magic-angle spinning alone. The ^{13}C line width was found to be determined by susceptibility effects due to the presence of the filler.

While the (heteronuclear and homonuclear) residual dipolar couplings have to be eliminated in such *J*-resolved experiments, they are the main source of information in the WISE experiment described below. For the investigation of viscoelastic materials the experiment thus must be performed under static conditions or under slow magic-angle spinning. The method is discussed in the previous section.

^{13}C–^{1}H Local Residual Dipolar Couplings by WISE-MAS Experiments. For elastomers and rubbery-like materials well above the glass-transition temperature T_g, the high molecular mobility reduces the dipolar couplings dramatically. The WISE experiment allows one to investigate site-selectively residual dipolar interactions and thus molecular dynamics by editing the corresponding proton slices of the 2D data set.

In References 129 and 130 ^{13}C-edited ^{1}H transverse relaxation was investigated in a nonrotating SBR cross-linking series. A short contact time was used to avoid ^{1}H spin diffusion. As a consequence of this, only ^{1}H atoms directly bonded to ^{13}C atoms are observed and the ^{1}H transverse relaxation is thus found to be mainly governed by ^{1}H—^{13}C heteronuclear couplings which makes analysis simple. The ^{13}C-edited ^{1}H transverse relaxation could be fitted with only one adjustable

parameter, the effective number of statistical segments (129). This was invoked as a justification for the heterogeneous model used to describe transverse relaxation. Moreover, the effect of cross-linking could be investigated and it was shown that it affects the dynamics of all functional groups to the same extend (125).

A similar experiment has been performed in (125) but under MAS conditions. For a series of cross-linked natural rubber samples (A-F1), ^{13}C-edited ^{1}H spinning sidebands have been extracted from the 2D spectrum. These sideband patterns are encoded by the residual dipolar couplings of the corresponding functional groups and are presented in Figure 22.

For the experimental conditions given, the spectra are found to be dominated by heteronuclear dipolar interactions which leads to relatively narrow, well-separated dipolar spinning sidebands. The heteronuclear dipolar couplings could be evaluated by simulating the spectra on this basis (see right column in Figure 22). They where found to be between 0.9 and 1.5 kHz for the samples of the series (the intercross-link masses M_c were between 6700 and 11,000 g/mol). A practically identical envelope of the spinning-sidebands intensities in the indirect dimension is found for all functional groups. This indicates that the effective ^{1}H—^{13}C vectors of different segments are affected in approximately the same way by internal motions.

Spin diffusion as an alternative explanation of this effect could be excluded by a similar experiment with additional ^{13}C decoupling during the evolution period t_1 which eliminates the encoding by the heteronuclear dipolar couplings (125). Distinct features are then visible for the spinning sideband patterns of the CH_3, CH_2 and CH groups (see Reference 125) proving that different functional groups are relatively isolated from each other on the time scale of the experiment as a consequence of the reduction of homonuclear dipolar interactions by high segmental mobility and magic-angle sample spinning. Therefore, the indirect detection of the spinning sideband patterns via cross-polarization ^{13}C spectroscopy allows for selective measurements of residual dipolar interactions on different functional groups (125).

Deuterium NMR Studies on Thermoplastic Elastomers. For the investigation of the molecular dynamics in polymers, deuteron solid-state nuclear magnetic resonance (^{2}D-NMR) spectroscopy has been shown to be a powerful method (2). In the field of viscoelastic polymers, segmental dynamics of poly(urethanes) has been studied intensively by ^{2}D-NMR (131,132). In addition to 1D NMR Spectoscopy, 2D NMR exchange spectroscopy was used to extend the time scale of molecular dynamics up to the order of milliseconds or even seconds. In combination with line-shape simulation, this technique allows one to obtain correlation times and correlation-time distributions of the molecular mobility as well as detailed information about the geometry of the motional process (2).

Principles of the Method. The scheme typically used for such 2D-exchange NMR experiments corresponds to that given in References 1 and 2, however, in case of deuterons often a solid echo sequence is used for detection instead of the last pulse. During the mixing time t_m of the experiment, molecular reorientations are allowed to take place. If the molecular orientation of a C—^{2}H bond has changed due to slow molecular motions, the signal continues to evolve with a new frequency. For reorientation about a well-defined angle θ, the 2D exchange spectrum exhibits

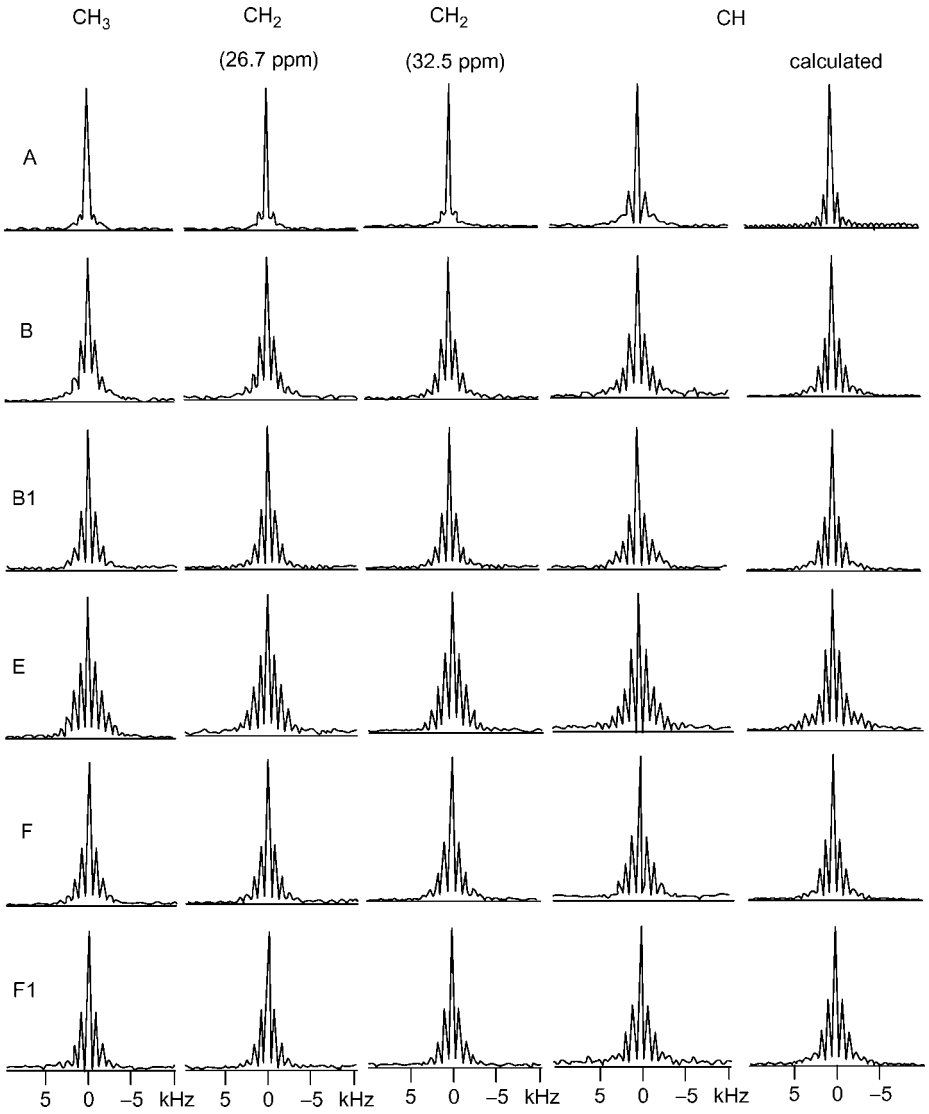

Fig. 22. Slices from a 2D experiment corresponding to $^{13}C—^{1}H$ WISE experiment performed on a series of cross-linked natural rubber samples A—F1 under magic-angle spinning. The slices reflecting proton sideband pattern for the different functional groups that are encoded by the ^{1}H residual dipolar couplings. The distinct features of dipolar slices prove that the different functional groups may be considered as relatively isolated groups of spins on the time scale of the evolution and cross-polarization. Reproduced from Ref. 125, with permission from Rapra Technology.

characteristic ridges in the form of ellipses that can be analyzed with respect to motions (for details about the analysis we refer to literature (2)).

Local Motions and Segmental Orientation in Supramolecular Hydrogen Bond Assemblies. In the field of viscoelastic materials, the technique has been mainly applied to thermoplastic elastomers. One interesting elastomer belonging

to this class consists of polybutadiene chains functionalised by 4-(3,5-dioxo-1,2,4-triazolidin-4-yl) benzoic acid (U4A) units which act as effective junctions zones. The molecular dynamics of the phenyl rings of the U4A units has been probed by 1D and 2D ^{2}H-NMR (see Reference 133, and references therein). In this system, there are three spatially separated environments that are reflected in the mobility of the polar units. Phenyl rings which are incorporated in the structure are either rigid or undergo 180° phenyl flips. The small fraction of free functional groups move isotropically and their mobility is coupled to the dynamics of the polymer matrix. The 1D ^{2}H-NMR spectra can be described quantitatively assuming a distribution of correlation times over 2–3 decades and the geometry of the motional processes is defined by the environment in the clusters up to the order–disorder transition temperature. 2D spectra of the model compounds show an elliptical exchange patterns, indicating well-defined slow 180° phenyl flips on a time scale of 100 ms up to 3 s.

Principles of NMR Imaging Methods

In polymers, the spatial distribution of the nuclei and the spin interactions as well as motions can be probed by NMR at different length scales using different strategies. The NMR techniques suitable for investigation of spatial structures are identified in Figure 23 together with the appropriate spatial resolution scale. In the nanoscale range, spectroscopic methods based on manipulation of spin interactions can measure internuclear distances and bond angles ((27), and references therein).

The field gradients are used for selection of the coherence pathways and encoding of molecular diffusion but many methods perform without the demand for field gradients. In the mesoscopic range, spin diffusion ((2), and references therein) can be used for measuring domain sizes and morphology. The domain of NMR imaging of polymers (134–138), which uses space encoding by field gradients can probe today only the macroscopically distributed heterogeneities, ie, in the order of 10–100 μm.

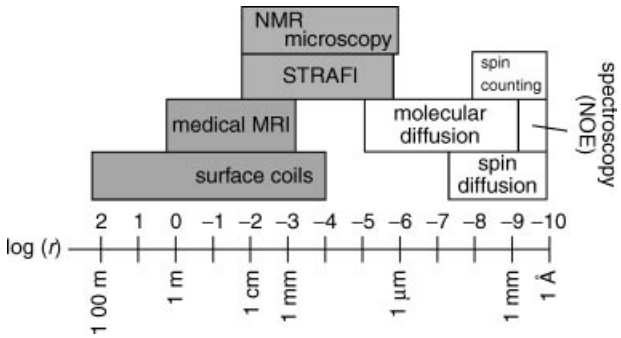

Fig. 23. Range of spatial resolution available from different NMR experiments that covers over teen orders of magnitude. The methods using direct space encoding by gradient are shaded, but all other spatial information can be included for creation of image contrast. Reproduced from Ref. 136, with permission from Wiley.

In recent years, the field of spatially resolved magnetic resonance which includes imaging, microscopy, and volume localized spectroscopy of materials (5,18) has been advanced by the introduction of several new techniques and improvement of the existing ones designed to overcome, mainly, the dipolar interactions of abundant proton spins in rigid polymers that contribute to broadening of the NMR resonance lines. The well-known condition $\Delta x = 2\pi\,\Delta\nu_{1/2}/(\gamma G_x)$ (see for instance, Reference 47) for the spatial resolution Δx^{-1} by frequency encoding, where γ is the magnetogiric ratio, $\Delta\nu_{1/2}$ is the full width at half height of NMR spectrum and G_x is the field gradient strength in the x-direction, can define the strategies for improving the quality of NMR images. There are, in principle, two possibilities: either the gradient strength can be increased or the line width be reduced (47,139–141). This can be achieved by manipulation of the spin or the space part of the interaction Hamiltonian or both, or by dilution manipulations (4). Increasing the gradient, strength might seem the simpler approach. However, the difficulty of using a large gradient is that the receiver bandwidth must be increased to accommodate the spread in resonance frequencies and therefore more noise is introduced into the resultant image. The noise content is proportional to the square root of the receiver bandwidth, and hence the time to acquire a given quality image, in both resolution and sensitivity, depends on the line width.

Many solid-state imaging techniques use spin coherences refocused by *echoes* for different purposes: (*1*) To record very short free induction decays present, in general, for solids and/or in the presence of strong field gradients. (*2*) For space encoding during the echo time. (*3*) For line narrowing by homonuclear or heteronuclear dipolar decoupling. (*4*) Reconversion of multiple-quantum (MQ) coherences into detectable single-quantum coherences. The properties of the spin echoes that refocus inhomogeneous and homogeneopus spin interactions have been discussed in the previous section. Also mixed echoes can be produced which eliminate all internal and external spin interactions. In the maximum of a mixed echo, each individual spin is fully isolated in the rotating reference frame in the absence of relaxation processes; a "time-suspension" process is taking place.

Methods of liquid-state imaging which can be applied, for instance, for analysis of elastomers or polymer swelling have been reviewed on several occasions (see for instance, References 19,47,135, and 139–141). Many of the methods used to record NMR images of solids can be combined with spectroscopic information. This unique feature and the richness in parameter contrast compensate for the relatively modest spatial resolution in many applications. If the spatial information is phase encoded, ie, indirectly detected, then the spectroscopic dimension is scanned directly, in many cases, by means of spin-echoes and in the absence of gradients. This approach is referred to as spectral frequency encoding. On the other hand, the spectroscopic information can be phase encoded or detected indirectly in the same way as in conventional two-dimensional spectroscopy. This approach is referred to as spectral phase encoding.

Spin System Response for a Heterogeneous Sample. In the following, a heterogeneous sample having magnetically equivalent nuclei with magnetogiric ratio γ and the local spin density $\rho(\vec{r})$ is considered. The space localized thermodynamic equilibrium magnetization corresponding to a voxel with coordinates (x, y, z) of the position vector $\vec{r}$ is given by $m_0\,(x, y, z) = C\rho(x, y, z)$, where C is the Curie constant. In the rotating reference frame at the resonance frequency,

the single-pulse NMR spin system response $s(\vec{r},t)$ can be expressed by the local free induction decay (FID) $f(\vec{r}, t)$,

$$s(\vec{r},t) = C\rho(\vec{r})f(\vec{r},t) \tag{35}$$

Spatially resolved NMR is concerned with unraveling the spatial distribution of $\rho(x, y, z)$ and measuring associated NMR parameters at individual "volume cells", or voxels at space point specified by the vector $\vec{r}$. If many contiguous voxels are investigated on a plane, or if a projection is investigated, one refers to NMR *imaging*, if individual voxels are investigated one refers to volume-selective NMR.

The spin density distribution can be resolved by different techniques. The standard approach exploits the possibility of introducing space dependence to the resonance frequency ω in each voxel by superposing a magnetic field gradient to a homogeneous magnetic field $\vec{B}_0(0,0,B_0)$ by the use of additional coils. In general, the field gradient is a Cartesian tensor with nine components related by the Maxwell equations. In the limit of large static magnetic field and small gradient, the gradient tensor can be reduced to a gradient vector $\vec{G}$ for an approximate description of the imaging experiments with good accuracy. Then the resonance frequency becomes dependent on the space vector $\vec{r}$, ie, $\omega(\vec{r}) = \gamma(B_0 + \vec{G}\cdot\vec{r}) = \omega_0 + \gamma\vec{G}\cdot\vec{r}$, where the field gradient vector collects the derivatives of the magnetic field in the z-direction with respect to the space coordinates defined by the component of the field gradient: $\vec{G}(\partial B_0/\partial x, \partial B_0/\partial y, \partial B_0/\partial z)$.

The total time-dependent signal of an inhomogeneous object of volume V measured in a magnetic field gradient and in rotating frame at the angular frequency ω_0 is given by

$$S(t) \propto C\iiint_V \rho(x,y,z)f(x,y,z,t)\exp\{\mathrm{i}\gamma\vec{G}\cdot\vec{r}t\}\,\mathrm{d}x\,\mathrm{d}y\,\mathrm{d}z \tag{36}$$

In high magnetic field the spatial dependence of the Curie constant can be neglected in a good approximation.

In order to illustrate the basic concepts of space encoding time-dependent gradients $\vec{G}(t)$ shall be admitted. The wave vector $\vec{k}$ can be introduced which is the Fourier conjugate to the space variable $\vec{r}$,

$$\vec{k}(t) = \gamma\int_0^t \vec{G}(t')\,\mathrm{d}t'. \tag{37}$$

In this notation, the single-pulse response signal in time-dependent main field gradients becomes

$$S(t) \propto C\iiint_V \rho(x,y,z)f(x,y,z,t)\exp\{\mathrm{i}\vec{k}(t)\cdot\vec{r}\}\,\mathrm{d}x\,\mathrm{d}y\,\mathrm{d}z. \tag{38}$$

This equation is the starting point for the discussion of spatial resolved NMR basic procedures.

Spatial Resolution by Frequency Encoding. The principle of the spatial resolution of NMR imaging by frequency encoding is discussed in the following in the presence of a pulsed uniform gradient, say $G_x = \partial B_0/\partial x$. After the radio-frequency excitation pulse the quantity $k_x(t)$ grows linearly with time according to equation 37, ie, $k_x(t) = \gamma G_x t$. Thus, $\vec{k}$ space is sampled in the direction of k_x, and time t and k_x are equivalent variables. If t is replaced by $k_x/(\gamma G_x)$ the spin system response given by equation 38 becomes

$$S(k_x/(\gamma G_x)) \propto C \iiint_V \rho(x, y, z) f(x, y, z, k_x/(\gamma G_x)) \exp\{i\gamma k_x \cdot x\} \, dx \, dy \, dz \tag{39}$$

The complex FID signal acquired in this way is composed of contributions evolving according to the local offset resonance frequency $\gamma G_x x$ labeling the nuclei responsible for this local transverse magnetization, hence, the term frequency encoding. Note that this is the conventional way of encoding in the Fourier transform spectroscopy. However, in context with NMR imaging, signals are processed in terms of the wave numbers k_x rather than of offset frequencies. The Fourier transform over k_x produces the convolution of the Fourier transform of the functions $\rho(x, y, z)$ and $f(x, y, z, k_x/(\gamma G_x))$. If $f(x, y, z, k_x/(\gamma G_x)) \approx f(k_x/(\gamma G_x))$, the Fourier transform of the FID is the space-dependent spectral response $F(x)$ and the Fourier transform of the triple integral is a projection $P(x) = \int\int \rho(x, y, z) \, dy \, dz$ of the spin density on the x-axis. Then, the Fourier transform of equation 39, can be written as

$$S(x) \propto C \int_{x_{\text{sample}}} F(x - x') P(x') \, dx' \tag{40}$$

where x_{sample} represents the sample size in the x-direction. A faithful representation of the spin-density projection $P(x)$ would be obtained by this method of frequency encoding only if the spectrum $F(x - x')$ is a Dirac function $\delta(x - x')$, or a narrow NMR absorption line like for liquid samples.

The above discussion is illustrated in Figure 24. If the samples are liquid, a narrow NMR absorption line is observed for both samples in a homogeneous magnetic field and a projection of the object along the x-axis is measured in the presence of the field gradient G_x. The signal amplitude at each resonance frequency or space coordinate is determined by the number of spins that experience the same magnetic field strength. If the spectrum in a homogeneous field is broad like in the solid samples (bottom traces) then the convolution (cf eq. 40) of the projection of the spin density by the line shape becomes noticeable, and the spatial features are smeared out. Thus, the minimum distance Δx which can be resolved is defined by the ratio of the full width at half spectral intensity $\Delta\omega_{1/2}$ of spectral features to the spread of the resonances introduced by the field gradient, ie,

$$\Delta x = \frac{\Delta\omega_{1/2}}{\gamma G_x} \tag{41}$$

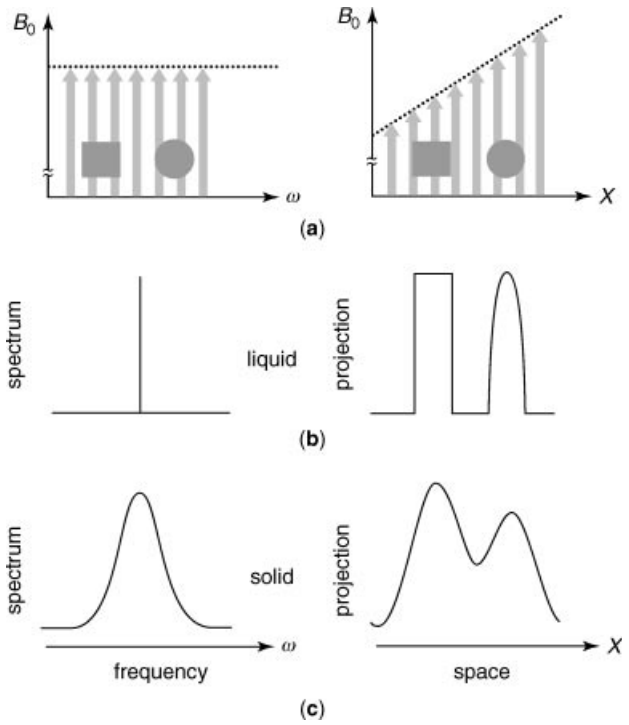

Fig. 24. Effect of field gradient on the NMR signal. The samples consists of a rectangular and a circular object. (**a**) Homogeneous magnetic field (left) and magnetic field with a linear space dependence (right). (**b**) Spectroscopic response for a liquid sample with a single, narrow line in the NMR spectrum. (**c**) Spectroscopic response for a solid sample with a single, broad line in the NMR spectrum. Reproduced from Ref. 136, with permission from Wiley.

Clearly, equation 41 indicates that when the line width increases, the gradient strength G_x also has to be increased, at least when the resolution Δx is to be kept constant.

Spatial Resolution by Phase Encoding. Broadening of the projection by the NMR spectrum (cf eq. 40 can be avoided if the spatial information is detected indirectly in the fashion of the multidimensional Fourier NMR spectroscopy (1). For instance, a magnetic-field gradient G_y is switched on for an evolution time t_1 following a radio-frequency excitation pulse, and the signal is acquired in a detection time t_2 after the gradient has been switched off. For this 2D scheme, the NMR signal can be written as

$$S(t_1, t_2) \propto Cf(t_1) f(t_2) \int_{y_{\text{sample}}} P(y) \exp\{i\gamma k_y y\} \, dy \tag{42}$$

where k_y- $\gamma G_y t_1$ and $P(y) = \int\int \rho(x, y, z) \, dx \, dz$. It becomes clear that there are two ways to perform the experiment: either t_1 is varied in the custom of 2D NMR spectroscopy, or t_1 is kept constant and G_y is stepped in increments ΔG_y. The first

case bears no advantage compared to direct frequency encoding discussed above. As time t_1 proceeds, not only does k_y increase, but also the free induction decay $f(t_1)$ evolve and deteriorate the signal intensity and finally the spatial resolution. But, if t_1 is kept constant $f(t_1)$ has a fixed value, and the phase change of the signal in the evolution period depends only on the wave vector k_y. Thus, the spatial resolution achievable for phase encoding depends on the maximum gradient strength available and on the signal-to-noise ratio, because the signal strength decreases with increasing $\vec{k}$.

The digital resolution or the pixel resolution of an NMR image can be much higher than the actual space resolution. The digital resolution $1/\Delta y$ of the NMR imaging in y-direction is determined by the maximum value of k_y or equivalently by the number n_y of complex signal values and the $\vec{k}$ space sampling intervals Δk_y, ie, $1/\Delta y = n_y\ \Delta k_y/(2\pi)$. To avoid signal aliasing, k_y has to be stepped in small enough intervals so that the signal-phase increment $y_{\max}\ \Delta k_y$ for the maximum object coordinate $y_{\max}$ never exceeds 2π.

Sampling $\vec{k}$ Space. Different imaging schemes are often discriminated against the way $\vec{k}$ space is sampled (for more details see Reference 19).

Two elementary 2D NMR imaging methods are illustrated in Figure 25: 2D Fourier imaging (2DFI, Fig. 25**a**) and back-projection imaging (BPI, Fig. 25**b**). Orthogonal gradients are switched subsequently in 2DFI and simultaneously in BPI. As a consequence, $\vec{k}$ space is sampled in orthogonal coordinates for 2DFI.

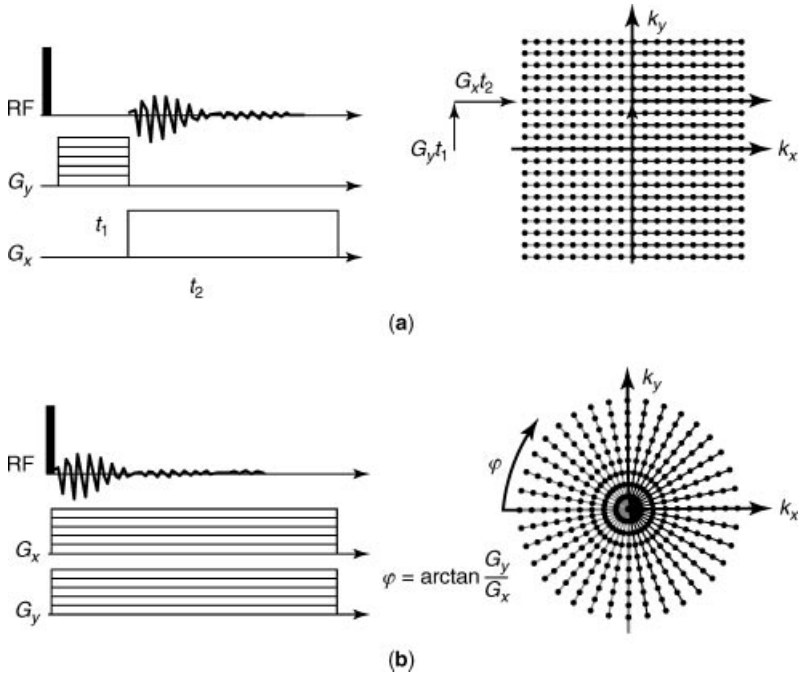

Fig. 25. Schemes for acquisition of 2D NMR images. Excitation and detection schemes (left) and maps in $\vec{k}$ space, where NMR signals is acquired (right). Reproduced from Ref. 136, with permission from Wiley.

When applied simultaneously, the direction of the resulting gradient changes depending on the relative strengths of G_x and G_y gradients. In this way, $\vec{k}$ space can be sampled in cylindrical coordinates in BPI. In either case, the image is obtained by the Fourier transformation of the $\vec{k}$-space data.

Often phase and frequency encoding are combined for acquisition of two-dimensional (2D) images (cf Fig. 25**a**, left). Then the gradient G_y is called the phase encoding gradient, and G_x is the frequency encoding gradient. This is one of the most used methods for recording images in elastomers materials that are soft solids with NMR line widths $\Delta\nu_{1/2} \approx 100$ Hz/1 kHz.

Contrast in NMR Imaging. Compared with other image-forming methods, the NMR imaging is characterized by the abundance of parameters that can be exploited for producing contrast (142,143). Many features invisible to other image-forming techniques can thus be visualized with NMR. To exploit the diversity of contrast features, it is useful to optimize the imaging experiment for generation of maximum contrast. The local contrast C is defined as the relative difference in image intensities M of neighboring structures i and j (17)

$$C = \frac{|M(\vec{r}_i) - M(\vec{r}_j)|}{|M_{\max}|} \tag{43}$$

where $|M_{\max}|$ is the absolute maximum of $M(\vec{r}_i)$ and $M(\vec{r}_j)$, where $\vec{r}_i$ and $\vec{r}_j$ are the space coordinates of voxels i and j under consideration.

Contrast Parameters and Material Properties. The contrast parameters relevant for polymer characterization by NMR imaging are directly related to the spin density, static and fluctuating nuclear spin interactions, and to the mass transport parameters. Even if the above quantities can change on molecular or mesoscopic scale only the variation of them on the space domains larger than the resolution of image can be detected in NMR imaging. The residual dipolar and quadrupolar interactions are related to the NMR parameters like van Vleck moments (4) and relaxation times (144). The fluctuating part of spin interactions leads to a variety of contrast parameters of magnetization relaxation type like spin-lattice relaxation in the laboratory reference frame (T_1), rotating frame (T_{1r}), transverse relaxation (T_2), solid echo or coherent averaging pulse sequences decay time (T_{2e}) (4), and dipolar correlation decays (5). The relaxation NMR parameters are also related to the manipulation of sample by contrast agents like paramagnetic relaxation agents, ferromagnetic particles (17), and hyperpolarized xenon (145,146).

The chemical shielding interaction leads to chemical contrast parameters related to the chemical composition as well as molecular orientation. Differences in magnetic susceptibility and the distribution of magnetic fields produced by electrical currents can be also detected via chemical shift (19).

The NMR quantities defining the contrast of NMR images depend on various macroscopic and microscopic physical and chemical parameters of the investigated samples that affect the nuclear spin interactions or molecular transport parameters. They can be classified as internal and external. Moreover, they can be state parameters that are stationary quantities like stress, strain, moduli of shear and compression, cross-link density, distribution and agglomeration of filler particles, molecular orientation, fibril orientation and domain size distribution,

distribution of voids, and the temperature distribution. Transition parameters or kinetic parameters characterize the time evolution of the polymer system. They are determined in *in situ* NMR experiments or in stop-and-go experiments. Examples are characteristic times of chemical and physical aging (147,148) of vulcanization (149) and curing (150) processes of heat dissipation and fluid permeation (151,152).

Transition parameters can be determined directly from the analysis of the time evolution of changes in NMR images, but state parameters must be related to NMR parameters either by theory or calibration. Theories have been published that relate the cross-link density of unfilled and filled elastomers to the parameters of transverse relaxation parameters (153) and others relating dynamic storage modulus of polymers to the cross-polarization rate (154).

A simpler approach is based on empirical correlations between NMR parameters and sample properties, which often can be established by calibration of an NMR parameter against a material parameter (155,156). An example of stress–strain calibration is given in Figure 26 by calibration of T_2 of filled poly(dimethyl siloxane) rubber against strain (153), (cf Fig. 26**a**). By use of the stress–strain curve (Fig. 26**b**) from mechanical measurements, T_2 can be calibrated against stress (see Fig. 26**c**).

The procedure can be used to translate the spatially resolved NMR parameters T_2 into values related to the strength of local stress.

Another possibility is given by the observation of the quadrupole splitting in deuteron NMR (155,157). For small strain, the splitting Δ_Q is linearly proportional to $\Lambda^2 - \Lambda^{-1}$ where $\Lambda = \frac{L}{L_0}$ is the elongation ratio, L and L_0 are the length of polymer band after stretching and in the relaxed state, respectively (see Fig. 27).

The rubber samples are prepared by swelling in a solution of deuterated spy molecules, these molecules follow the polymer network alignment under strain and the residual quadrupolar coupling that results from their anisotropic motion is observed either by spectroscopic imaging or by double-quantum imaging (158,159). The above deuteration procedure leads to the modification of the network and to potential modulation of the NMR signal encoding by the self-diffusion of the incorporated oligomers.

The above adverse effects can be avoided if ^{1}H residual dipolar couplings of elastomer chains (68) were used to generate contrast in NMR imaging of stretched samples. Dipolar contrast filters can be implemented based on dipolar encoded longitudinal magnetization as well as double- and triple-quantum coherences (160,161). The associated contrast filter parameters were investigated by measurements of the line width in ^{1}H multiple-quantum filtered spectra, the dipolar encoded longitudinal magnetization decay curves, and the double- and triple-quantum buildup curves as a function of the extension ratio for a natural rubber band. Together with stress–strain measurements, these results allow for correlation of ^{1}H residual dipolar couplings with stress values in stretched natural rubber.

Magnetization Filters. The contrast generation in NMR imaging is directly related to the concept of magnetization or coherences filters. Various molecular (internal) or external parameter weights are introduced by the use of magnetization or coherences filters (Fig. 28), which block part of the incoming signal originating from the thermodynamic equilibrium magnetization.

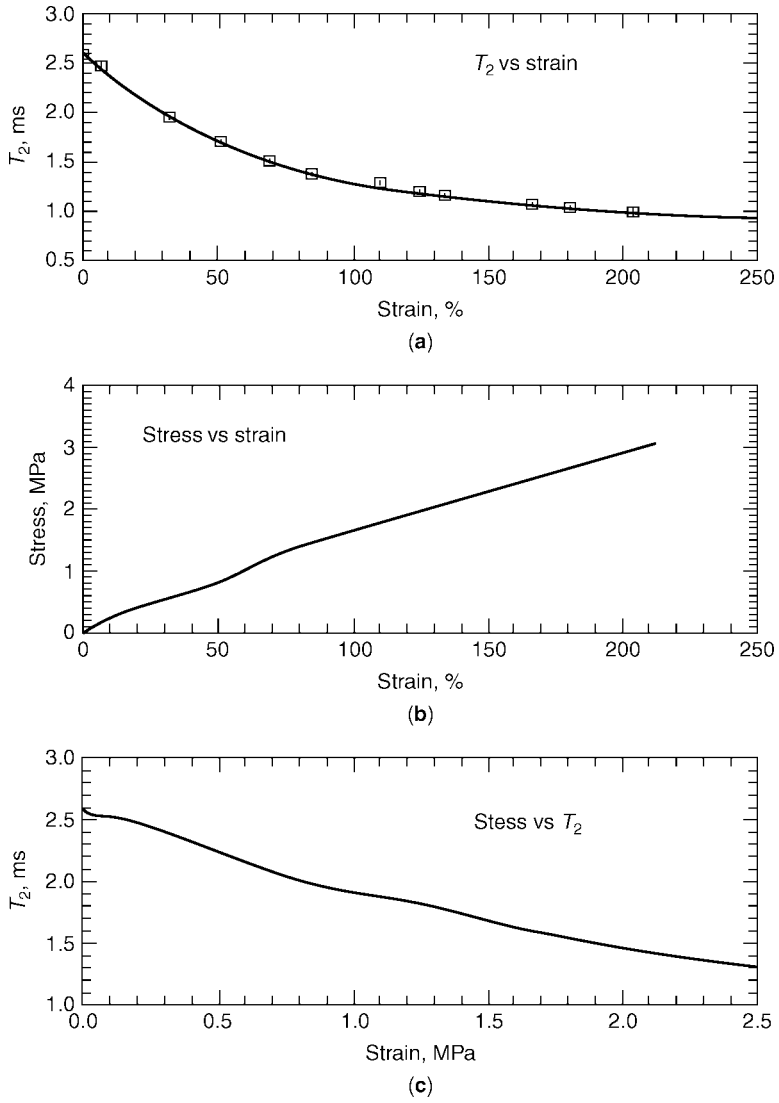

Fig. 26. Calibration of T_2 values measured for different strain (**a**) of filled poly(dimethyl siloxane) against stress (**c**) by use of the mechanical stress–strain curve (**b**). Reproduced from Ref. 142, with permission from Wiley.

As a result, there is a gain in selectivity of the output signal at the expense of a deterioration of signal-to-noise ratio.

A generic scheme for contrast optimisation in the Fourier NMR imaging is illustrated in Figure 28**b**, (142). In general, three periods are distinguished: a filter period, a space-encoding period, and a spectroscopy period. For image contrast other than the often-uninformative spin density, the space-encoding period must be combined either with a magnetization filter or with spectroscopic data acquisition or both. The signal detected after the action of the general pulse sequence

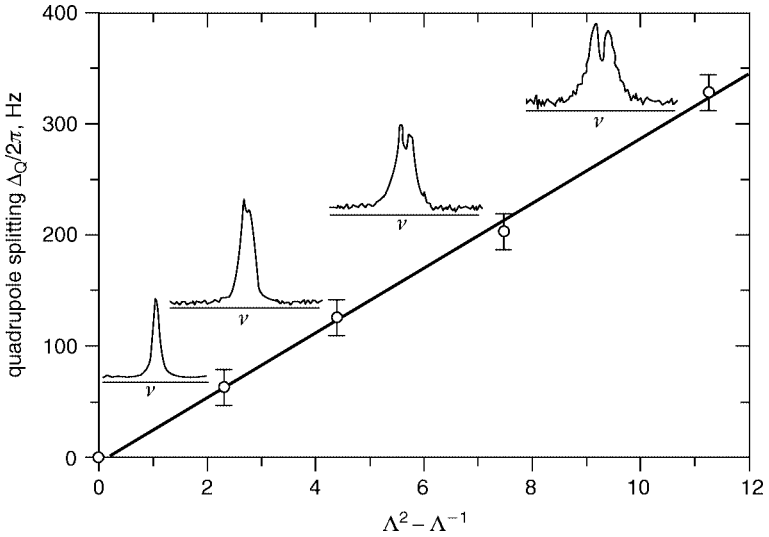

Fig. 27. Deuteron quadrupolar splitting of 1,4-tetra-deuterated butadiene oligomers from natural rubber bands for different strains. Reproduced from Ref. 142, with permission from Wiley.

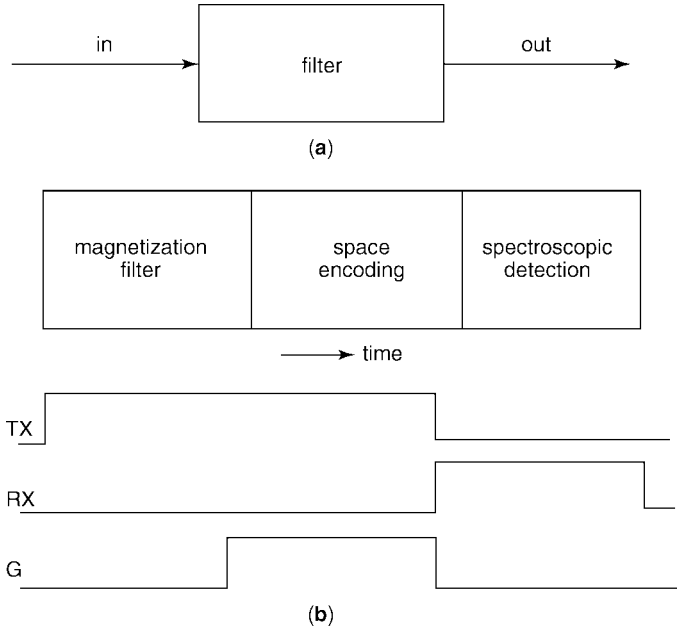

Fig. 28. (**a**) A magnetization filter blocks part of the incoming magnetization or spin coherences. (**b**) General scheme for generation of NMR image contrast. Initial nuclear magnetization is filtered by the radio-frequency irradiation of resonant nuclei (TX) before or also during space encoding period by magnetic-field gradients ($\vec{G}$). In the absence of gradients, the NMR signal is detected (RX) for the extraction of spectroscopic information. Reproduced from Ref. 143, with permission from Wiley.

designed to introduce image contrast can be written as (162)

$$S(\vec{k}) = \int \rho(\vec{r}) F_c(\{p\}, \vec{r}) \exp[-i\,2\pi \vec{k} \cdot \vec{r}]\, d\vec{r} \tag{44}$$

where the contrast parameter manifold is denoted by $\{p\}$ and $F_c(\{p\}, \vec{r})$ is the combined local contrast function. This function could be a product of several parameter contrast functions, such as

$$F_c(\{p\}, \vec{r}) \equiv F_c(T_1, \vec{r}) F_c(T_{1\rho}, \vec{r}) F_c(T_2, \vec{r}) F_c(\delta_i, \vec{r}) F_c(\vec{q}, \vec{r}) \cdots \tag{45}$$

where for instance, the contrast factors in the right-hand side of equation 45 representing the effects of longitudinal (T_1 and $T_{1\rho}$) and transverse (T_2) relaxation times, chemical shift (δ), and the effect of coherent and incoherent molecular translation motions described in the $\vec{q}$ space (18).

There are two basic approaches by which the image contrast can be studied. The first makes the pulse sequence sensitive to a particular contrast parameter p so that the image intensity bears or is weighted by the influence of that contrast. This approach offers the advantage of time efficiency but is only qualitative. The quantitative information can be obtained by the second approach that include inter alia two-image scheme (162). This method requires two imaging experiments under two contrast conditions. The final parameter map is computed from the two images, voxel by voxel, by means of some mathematical calculation, such as division.

The first approach is illustrated in Figure 29 for the simple case of spin-lock-filtered projections of a composite piece of rubber cut from the tread of a car tire. Such a filter imposes a $T_{1\rho}$ weight on the spin density (cf Fig. 29**a**). From the space distributed magnetization decays, the parameter map of $T_{1\rho}$ can be obtained (cf Fig. 29**b**) independent of spin densities.

An important class of magnetization filters are mobility filters which select magnetization based on the time scale of segmental motions ((19), and references therein). The parameters for discrimination are the amplitude and characteristic frequency or the correlation time τ_c of molecular motions. The effect a filter exerts on a NMR signal can be represented by the filter transfer function. Examples are given in Figure 30 (163,164) with transfer function for filters, which select magnetization based on the time scale of molecular motion.

Depending on the time scale, different pulse sequences can be used. In the fast motion regime, T_1 filters are applicable. Both saturation recovery and the stimulated echo can be used for this, but the transfer function of both filters is complementary. The spin-echo or Hahn echo filter has a transfer function similar to that of the saturation recovery filter, but because T_2 processes are efficient at slower molecular motions, the filter cut off is shifted to longer correlation times. The dipolar filter exploits the strength of the dipolar couplings averaged by the molecular motions. The residual dipolar filters can use ^{1}H double- and triple-quantum coherences (160,161) as well as ^{1}H–^{1}H magnetization exchange (165). Dipolar correlation effect detected via stimulated echo can be used for a mixed residual dipolar coupling/slow motion filter (166). Resolved splitting of the residual quadrupolar coupling of ^{2}H of spy molecules has been used as quadrupolar

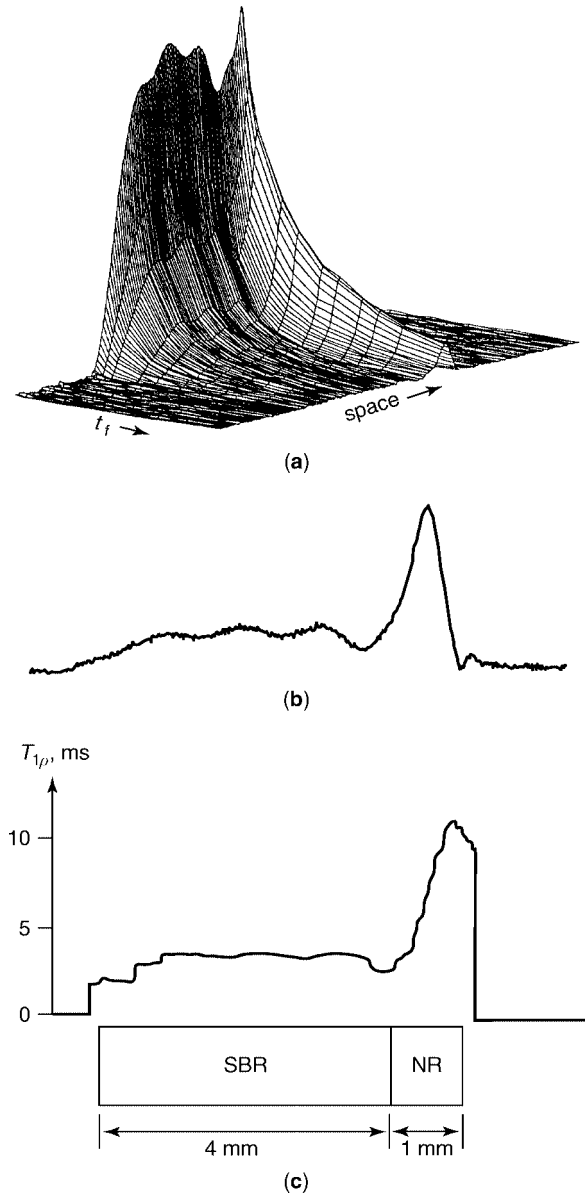

Fig. 29. Filter-weighted and spin-lattice relaxation in the rotating frame $T_{1\rho}$ of an elastomer composite of SBR and natural rubber cut from the tread of a car tire. (**a**) A stack of one-dimensional ^{1}H images with variable duration t_f of the spin-lock radio-frequency magnetic field. (**b**) A $T_{1\rho}$ parameter map obtained from the decay shown in (**a**). Reproduced from Ref. 143, with permission from Wiley.

coupling filter (158,159). The spin-lattice relaxation in the rotating frame or $T_{1\rho}$ filter is efficient at slow motions with correlation times of the order of the inverse of the angular frequency of the spin-look radio-frequency pulse. The transverse magnetization decay for a train of solid echoes or magic echoes is characterized

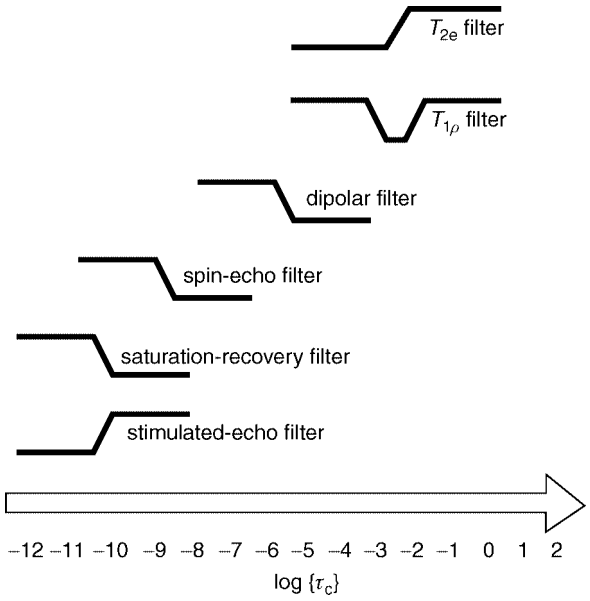

Fig. 30. Time scale of molecular motion and filter transfer functions of pulse sequences, which can be used for selecting magnetization according to the time scale of the molecular motion. Reproduced from Ref. 143, with permission from Wiley.

by the effective transverse relaxation time T_{2e} (68) a parameter sensitive to the slow segmental motion like $T_{1\rho}$.

The identification of material heterogeneities based on differences in molecular motion is an important feature of NMR imaging. The importance of slow molecular motion for image contrast is demonstrated in Figure 31 with relaxation time parameter images through a partially aged sheet of carbon-black-filled styrene-*co*-butadiene rubber (SBR) (147).

The one-dimensional space scale starts at the unaged center of the rubber sheet at $\Delta r = 0$ and ends at the aged surface at $\Delta r = 700$ μm. Two curves are shown for each relaxation parameters as a function of space. The top curve is for unaged material and it varies little with space. The bottom curve is for the aged material. Both curves overlap in the center of the sheet and split toward the surface. The splitting is a direct measure of image contrast. The contrast is largest for those relaxation times that are sensitive to slow molecular motions. the contrast is largest for T_{2e} and $T_{1\rho}$ images and almost zero for T_1.

NMR Imaging of Elastomers

Potentially rather useful applications of NMR imaging are in elastomer industry. This section features some selected examples that illustrate the type of information obtained by imaging of elastomers. Such applications to elastomers concern distribution in temperature stress, cross-link density, modulus, and the dynamics of fluid absorption and swelling.

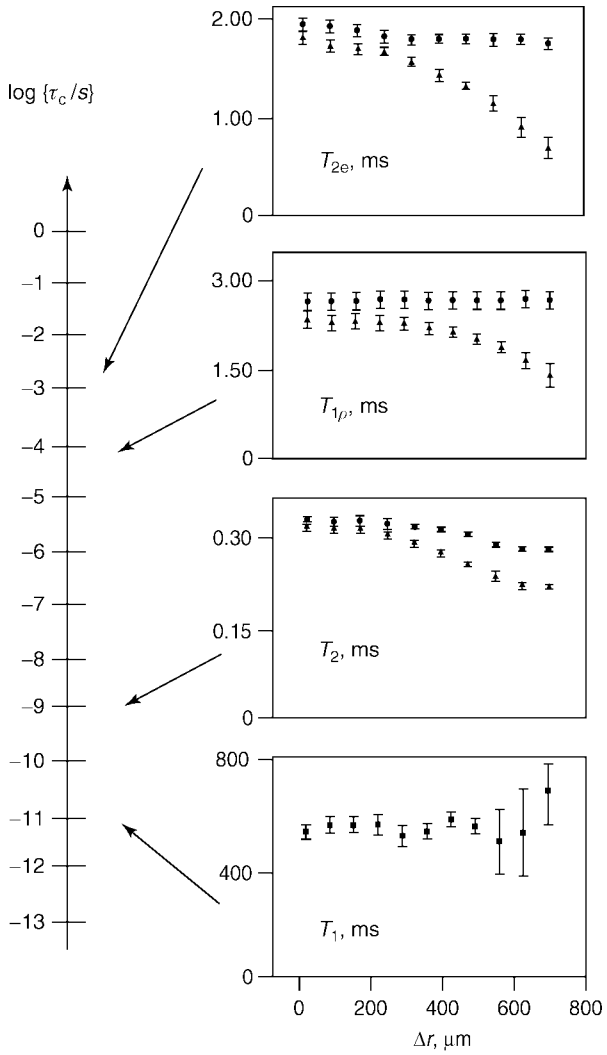

Fig. 31. Relaxation parameters T_1, T_2, $T_{1\rho}$, and T_{2e} for contrast in thermal oxidative aging of SBR. The insets depict the space distribution of relaxation times for a partially aged (lower curve) and an unaged (upper curve) rubber sheet. Reproduced from Ref. 147, with permission from Wiley.

Heterogeneities in Elastomers. Heterogeneities in elastomers materials are related to the defects induced in the process of preparation. The processes that lead to the defects are as follows.

Mixing Processes. Technical elastomers are blends of up to about 30 different compounds like natural rubber, styrene–butadiene rubber, silicate and carbon-black fillers, and mobile components like oils and waxes. Improper mixing leads to inhomogeneities with corresponding variation in mechanical and thermal properties. An important source of heterogeneities of this type is represented by filler

clusters. Even the variance of the distribution statistics of active filler may lead to heterogeneities detected as an average over a volume cell or voxel with the spatial resolution of NMR imaging.

Vulcanization. Heterogeneous structures arise from effects of thermal conductivity, which lead to space-dependent temperature profile during the vulcanization process depending on the position of the heat source and on heat dissipation. As a result, inhomogeneous cross-link densities may be established (167). If the process of cross-linking is incomplete the defects represents by the free chains are also presents. The changes in segmental mobility from progress of the vulcanization reaction and from the associated sample temperature distribution can be monitored directly by the NMR imaging *in situ* (149). In the covulcanization of blends and sheets from different formulations, inhomogeneities in cross-link density max arise from differences in solubility and diffusion of curatives (168).

Aging. Aging processes are often induced by ultraviolet (UV) irradiation or other ionization radiations (169), exposure to heat and oxygen, and by biological mechanisms. Depending on the load applied, different aging processes are observed (170). The action of electromagnetic radiation with high energy of the associated photons as well as nuclear irradiation will produce chain scission with decrease in the cross-link density and associated increase in chain mobility. Thermal oxidative aging usually leads to the formation of hardened surface layers in natural rubber (NR) as well as synthetic rubber (styrene-*co*-butadiene rubber (SBR) (147,148,171–174). Typically, these layers approach a thickness of 200–300 μm and inhibit progress of the aging process further into the bulk of thin sample. The material hardening is explained by an increase in cross-link density. In the absence of oxygen, chain scission may dominate at elevated temperatures with an associated increase in the segmental mobility. Other types of aging involve aggressive fluids and gases. In this context, a sample of degraded rubber hose gas been investigated (175), but also the degradation of polyethylene pipes and the enzymatic degradation of biologically synthesized polymers (176) have been studied through NMR imaging. Related investigations have been carried out on asphalts (177). Aging associated with swelling of the rubber particles has been observed in crumb-rubber modified asphalts (178).

Mechanical Load. Static mechanical load by strain leads to stretching of random-coil polymer chains in the direction of sample elongation and chain compression in the orthogonal directions. The value of the residual dipolar and quadrupolar couplings is increased by the mechanical load, and moreover, the distribution of the correlation times is also modified. Therefore, many NMR parameters sensitive to the residual dipolar couplings and slow motions can be used for characterization of the local strain–stress effects in heterogeneous elastomers (158,160,161,179). Dynamics mechanical load leads to sample heating where the temperature distribution in dynamic equilibrium is determined by the temperature-dependent loss-modulus and the thermal conductivity of the sample. Because transverse relaxation rate (approximated by the T_2 relaxation) scales with the temperature for carbon filled SBR, a T_2 map provides a temperature map of the sample. Such temperature maps have been measured for carbon-black filled SBR cylinders for different filler contents and mechanical load (180).

NMR Images and Parameter Maps in Elastomers. NMR of elastomers including NMR imaging appears to address one of the industrially most relevant applications of NMR. Applications of the one- (1D) and two-dimensional (2D) NMR images and parameter maps for characterization of elastomer materials with heterogeneous mesoscopic and macroscopic structure will be reviewed in the following.

Vulcanization and Covulcanization. The main effect taking place during the vulcanization process is the space distribution in the cross-link density. One source of this variation is the spatial distribution of the rubber formulation, although short-scale variations are often smoothed by component diffusion during the vulcanization process. Differences on the millimeter scale can lead to interfacial structures.

Another source of variations in cross-link density on the millimeter scale is the curing process in combination with the sample geometry. Heat is supplied to the sample for a certain time and after vulcanization is removed from the sample in certain time. Near the heat source the cross-linking process induced by vulcanization is set in first and near the heat sink is sets in last. Depending on the time dependence of the heat from the source and sink, surface and the thermal properties of the sample, complicated time-dependent temperature profiles are established in the sample.

The vulcanization process has been followed across a thick disk from unfilled SBR by NMR imaging of the effective transverse signal decay (149). The measurements were carried out in a magnetic field slightly inhomogeneous from the construction of a special vulcanization probe and the effective transverse relaxation time T_2^* was measured (see Fig 32). Despite accelerated signal decay from the field inhomogeneities, T_2^* still turned out to be sensitive to chain mobility because of a sufficiently strong contribution from T_2.

A nonlinear relationship between the effective transverse relaxation rate $1/T_2^*$ and the reduced shear modulus was found. Nevertheless, the relationship that low modulus corresponds to high T_2^* and high modulus to low T_2^* can be used to interpret the imaging data across the SBR sheet measured during the vulcanization process (see Fig. 32). Immediately after sample heating, chain mobility is high and so is T_2^*. With the formation of the cross-links chain mobility decreases and so does T_2^*. The vulcanization front is defined by the center of change in T_2^*. It can be seen to migrate through the thin sample on a time scale of about half an hour with the temperature in the range between 140 and 170°C across the sample. With increasing time the slope of the T_2^* curve flattens indicating a broadening of the reactive vulcanization zone.

Another example of spatial determination of the local cross-link density in inhomogeneous vulcanized elastomers by means of the spatially dependent T_2^* decay times was discussed on poly(isobutylene-*p*-methylstyrene-*p*-bromon-ethylstryrene) (PIB-PMS/BrPMS) (181). It was shown that by swelling the elastomers in the aprotic solvent CCl_4, the proton signal in the magnetic resonance images originates almost exclusively from the rubber methyl protons (182). This makes it possible to acquire selective images of the rubbery phase, which were demonstrated to be superior toward the visualization of the network homogeneity. Moreover, swelling of these elastomers in an appropriate solvent enhances the molecular chain mobility and reduces the

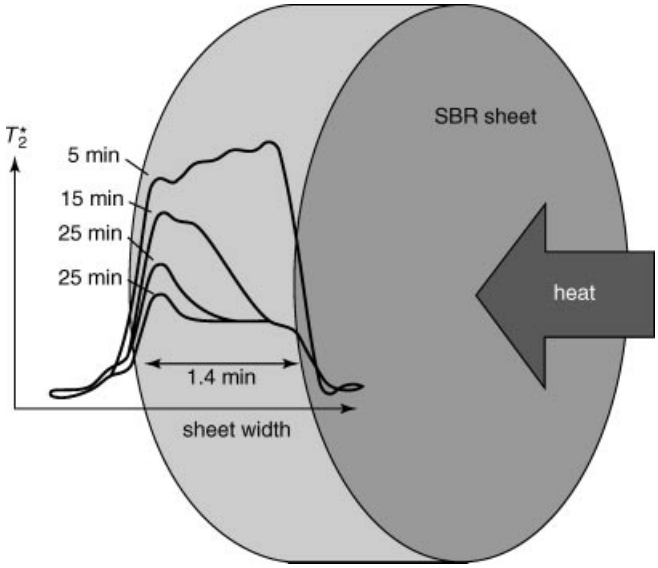

Fig. 32. Time-resolved T_2^* parameter one-dimensional images across a 1.4 mm thick sheet of SBR following the vulcanisation process. Reproduced from Ref. 149, with permission from Rapra Technology.

proton line width to an extent acceptable for recording magnetic resonance images.

The gravimetric Flory–Rehner (183) experiments are combined with NMR imaging to study spatially dependent degree of cross-linking, in unfilled, 1,6-hexamethylenediamine-cured PIB-PMS/BrPMS therpolymers (181). Localized relaxometry reveals two proton T_2^* relaxation decay times in CCl_4 swollen specimens: a fast decaying component reflecting the constrained chain segments near the cross-links and topological constraints (T_{2s}^*) and a slow decaying component originating from less constrained, remote chains (T_{2l}^*). On the basis of a linear relation between the bulk number-average molecular weight between effective cross-link ($M_{n,\mathrm{eff}}^{\mathrm{bulk}}$) and the volume average T_2^*, magnetic resonance images allow the determination of the local cross-link density in inhomogeneous cross-link PIB terpolymer samples by means of the spatially-dependent effective transverse relaxation. The measurements of the localized T_{2s}^*, and T_{2l}^* allow to deduce the localized molecular weight between the effective cross-links $M_{n,\mathrm{eff}}(\vec{r})$ for each region of interest labeled 1–10 in Fig. 33. This method reveals that the sample 1 exposes a very heterogeneous network structure as is illustrated by a large variation in the localized $M_{n,\mathrm{eff}}(\vec{r})$. This indicates an unfavourable mixing. This in strong contrast to specimen 2, having a rather homogeneous network structure as is demonstrated by the small variation in $M_{\mathrm{n,eff}}(\vec{r})$ as a result of a uniform curing. The homogeneity of mixing and curing of the specimens 3 and 4 (cf Fig. 33) is somewhere in between. These results clearly demonstrate that NMR image is a useful technique to investigate the homogeneity of mixing and curing of elastomers.

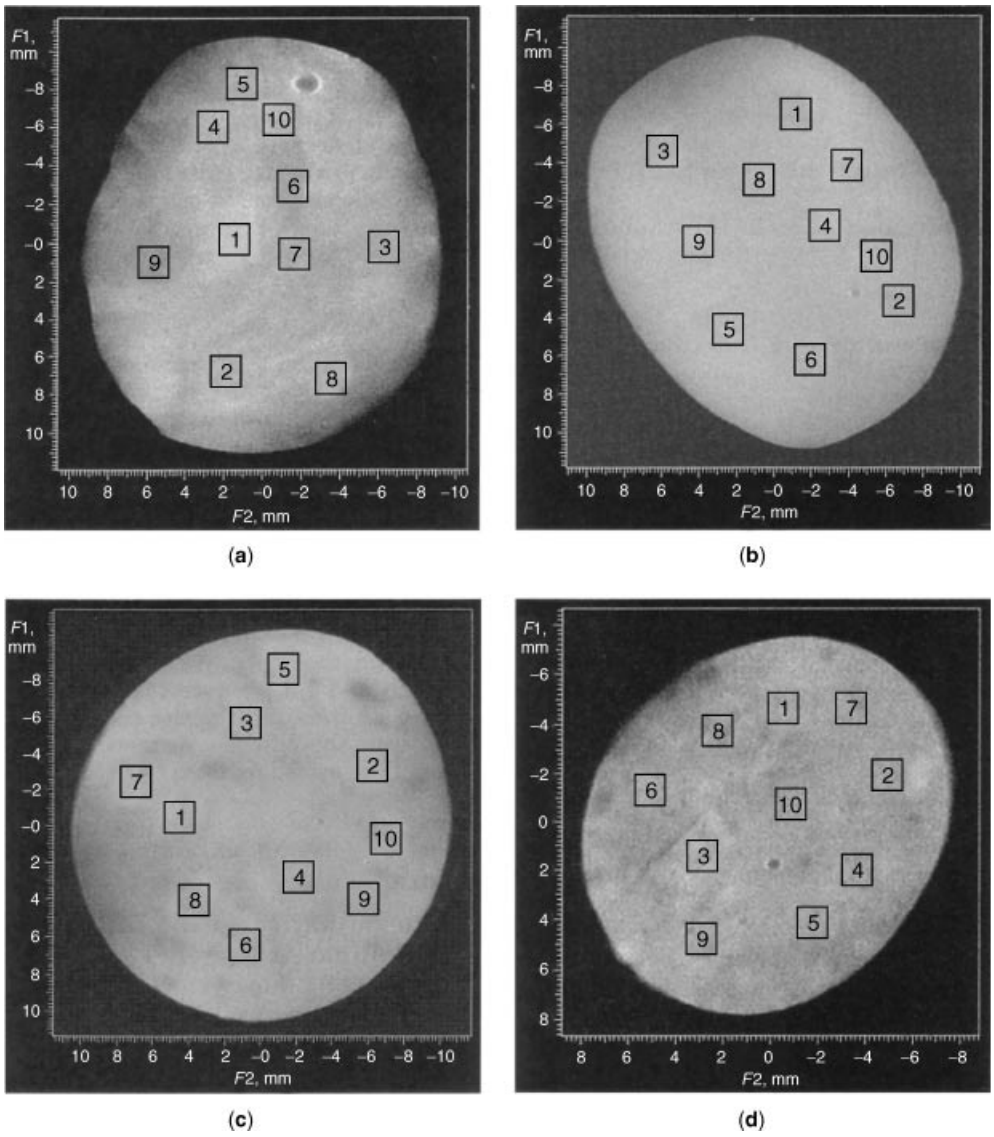

Fig. 33. Proton NMR images of unfilled polyisobutilene-based elastomers, cured with 1,6-hexamethylenediamine, after equilibrium swelling in CCl_4. The degree of cross-linking increases from samples 1 to 4. The regions of interest indicate the locations used to determine the local relaxation decay times. Reproduced from Ref. 181, with permission from American Chemical Society.

During fabrication of elastomer products like car tires different elastomer formulations often need to be covulcanizes. At the interface between an SBR and an NR layer, an interfacial layer with a modulus higher than either SBR and NR had been detected (145,171). In images detected using Hahn-echo method

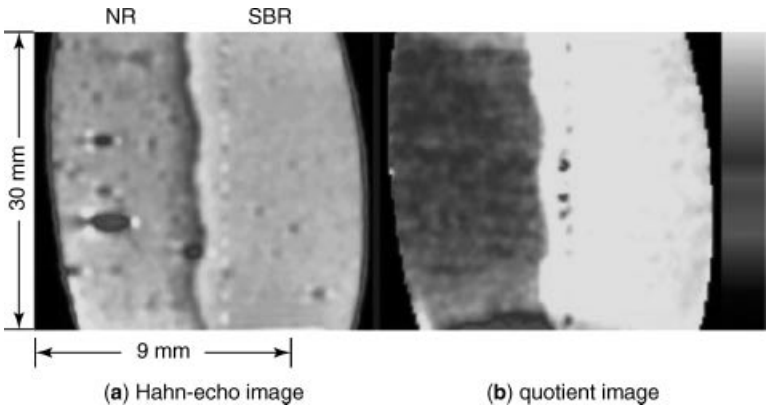

Fig. 34. Proton T_2^*-weighted Hahn-echo image (**a**) of an unfilled SBR/NR covulcanisate with dimensions 9 mm × 30 mm. The image has been acquired with an echo time of $t_E = 3.3$ ms. A quotient image (**b**) computed as the quotient of two Hahn-echo images acquired with different echo times of 4.2 and 3.4 ms. Reproduced from Ref. 145, with permission from Rapra Technology.

the interface is identified by a dark line paralleled to a slightly brighter line (see Fig. 34).

A mixture of spin density and relaxation forms contrast in the Hahn-echo image. Contrast in the quotient image is determined only by transverse relaxation. In this image, the interface appears abrupt and well defined. The image of the interface shows a transition from the hard SBR component to the soft NR component with a width of the order of 0–5 mm (184,185). This is the space scale on which the modulus changes. The shape and dimension of the interface are defined by the concentration differences in the vulcanizing agents, which diffuse at elevated temperatures across the interface until their diffusion is hampered by their role in the vulcanization reaction. Thus, the interface arises from a delicate balance between diffusion, reaction, heat supply, and removal.

Blending. Interfaces similar to those encountered during covulcanization may arise in blends with incomplete mixing. In unvulcanized samples, heterogeneities from blending can be deduced by gradient echo imaging, where the contrast is enhanced by differences in magnetic susceptibility of the components (186). However, fine structures are usually homogenized during the vulcanization process. Larger structures survive, in particular, when one component had already been vulcanized.

An example of such a case is illustrated in Figure 35 by two orthogonal slices through a block of a vulcanised blend from a soft (bright) and a previously vulcanised hard (dark) component (141). In slice (a), the structures invoked by mixing of components appear course but random, but slice (b) reveals stream lines of material flow in the rolling mill.

The presence of carbon-black filler usually does not affect the NMR data in contrast to functionalized silicate filler. This is attributed to rapid transverse relaxation of network chain segments near carbon-black filler particles caused by paramagnetic centers in the filler. Thus, for the technologically important

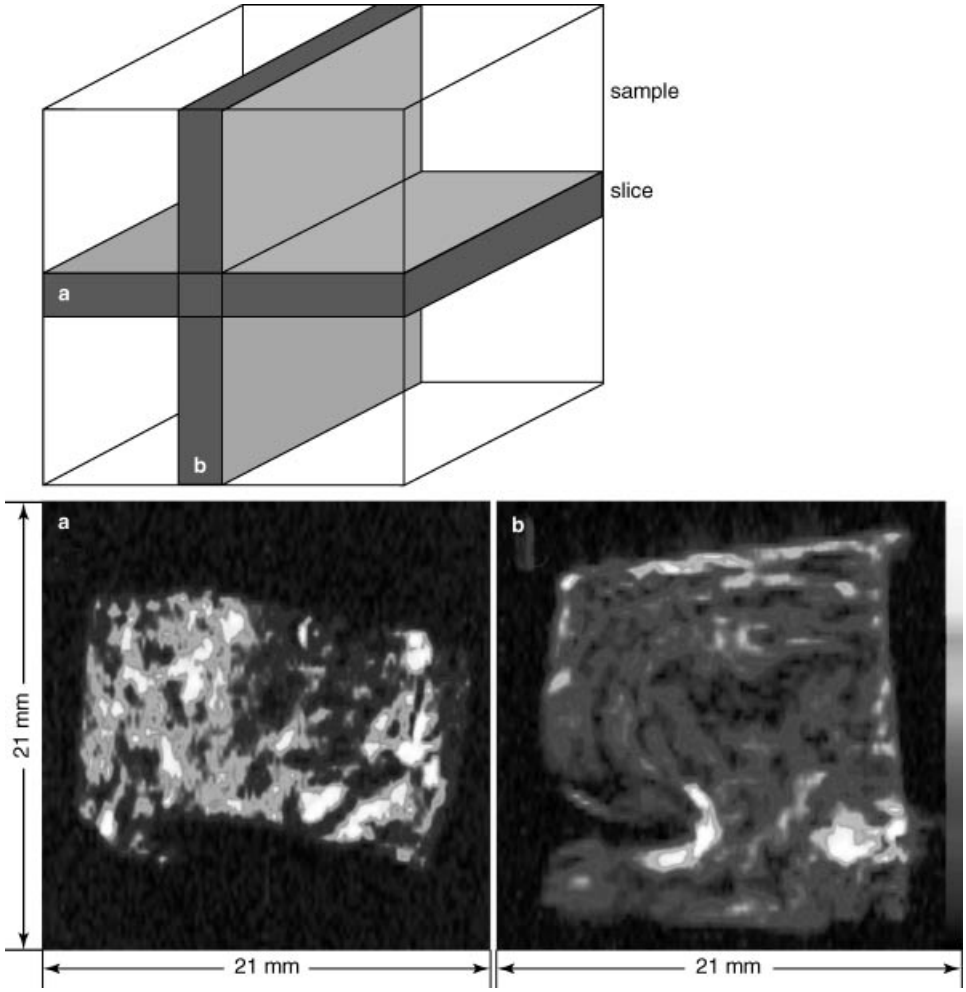

Fig. 35. (**a**) Proton T_2^*-weighted orthogonal slices of a carbon-black filled blend with a soft (bright) and a hard (dark) component. Insufficient blending in a rolling mill is visualized by the stream lines in slice (**b**). Reproduced from Ref. 145, with permission from Rapra Technology.

class of carbon-filled elastomers, NMR can provide the chemical cross-link density.

Aging. Aging of elastomers is a process that affects the mobility of intercross-link chains by packing, chain scission, and formation of new cross-links. Thermooxidative aging of many elastomers including SBR and NR leads to the formation of a brittle surface layer with reduced mobility that appears dark in ^{1}H Hahn-echo images. Often this region is followed by a zone of brighter image intensity, which can be attributed to chain scission or the accumulation of low molecular-weight additives (148).

The time evolution of the thermooxidative aging in SBR has been studied by NMR imaging (see Ref. 145). In order to detect the aged surface layer with reduced

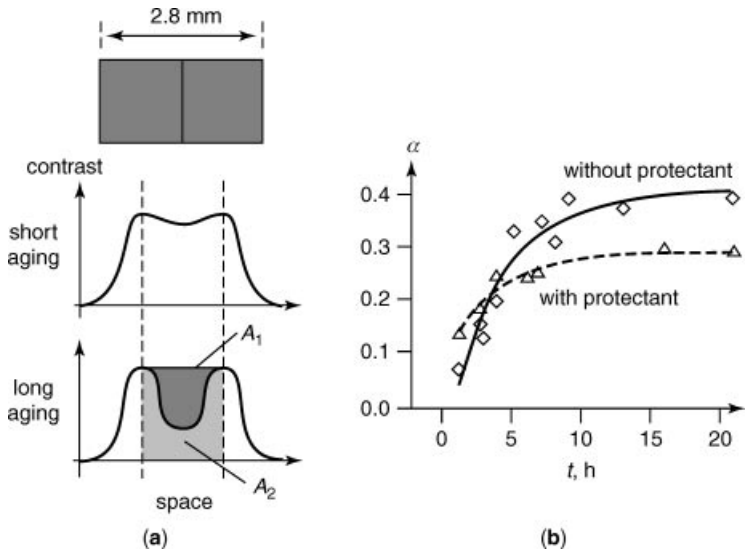

Fig. 36. Analysis of thermal oxidative aging by T_2^*-weighted Hahn-echo imaging. (**a**) Two SBR layers stacked after aging. The aged layer suffers a signal loss marked by the area A_1. The relative signal decrease defines the aging parameter α. (**b**) The progress in aging can be followed by evaluating the aging parameter α as a function of aging time t. Reproduced from Ref. 145, with permission from Rapra Technology.

signal intensity in Hahn-echo images, two aged sheets were stacked and the stack was imaged along its axis. In this way, the signal from the soft core delineated the hardened surface layers (cf Fig. 36).

Sample Deformation. Sample deformations modify the number of accessible conformations of intercross-link chains, so that they can be detected by analysis of relaxation and residual dipolar and quadrupolar couplings. For instance, dynamic mechanical load on elastomers is often exerted at small deformations and low deformation rates but over extended time periods. Then part of the mechanical energy is dissipated into heat depending on the value of the loss modulus. As a consequence, a temperature profile is established within the sample. Then the modulus varies across the sample depending on the temperature profile and properties determined for thick samples under dynamic load are average quantities.

The temperature profile associated with sample heating during weak dynamic shear deformation of carbon-black filled SBR cylinders of 10 mm diameter and 10 mm in height has been imaged by NMR by use of a specially designed probe (180).

The transverse relaxation time strongly depends on temperature (cf Fig. 37**a**), so that the temperature can be mapped by parameter imaging of T_2. Axial parameter projections have been acquired in dynamic equilibrium at a shear rate of 10 Hz and for carbon-black contents ranging from 10 to 70 phr. One-dimensional cross sections through those projections are depicted in Figure 37**b**. An increase of the temperature in the center of the sample is observed with increasing carbon-black contents which scales with the increasing loss modulus of

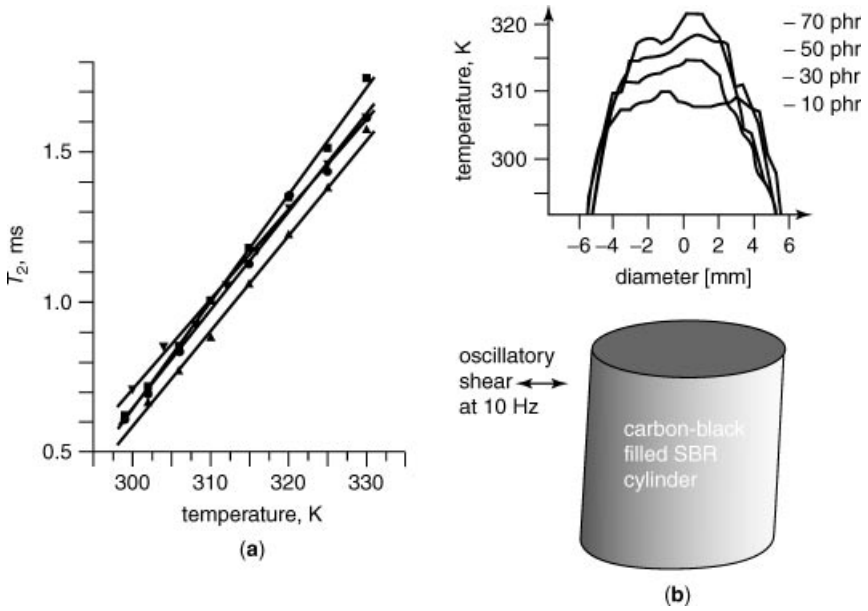

Fig. 37. Temperature profiles from T_2 parameter images of SBR cylinders with different carbon-black filler contents undergoing oscillatory shear deformations. (**a**) Temperature calibration curves and (**b**) temperature profiles across the cylinders. (■) 10 phr (●) 30 phr, (▲) 50 phr, and (▼) 70 phr. The pixel resolution was 0.4 × 0.4 mm^2. Reproduced from Ref. 180, with permission from Rapra Technology.

the sample. The 70 phr sample is warmer by over 10°C in the center of the sample than the 10 phr sample.

NMR Mobile Sensor for Quality Control of Elastomers. Over the last few years, a mobile NMR surface scanner called NMR-MOUSE has been developed for the nondestructive investigation of arbitrarily large objects (187,188). The NMR-MOUSE is a palm-size NMR device which is built up from two permanent magnets. The magnets are mounted on an iron yoke with antiparallel polarization to form the classical horseshoe geometry. The main direction of the polarization magnetic field $\boldsymbol{B}_0$ is across the gap and the field strength decreases rapidly with increasing distance from the surface. The radio-frequency (rf) field $\boldsymbol{B}_1$ is generated by a surface coil which is mounted in the gap. The NMR-MOUSE is characterized by strong inhomogeneities in the static and radio-frequency magnetic fields. Due to these fields inhomogeneities, NMR spectroscopy of the chemical shift is not possible, but magnetization relaxation times and parameters of translational motion can be measured by echo techniques (189–192). Moreover, the orientation dependence of NMR parameters can be easily investigated with the mobile NMR sensor for large samples on stretching devices (191).

Some selected applications of the NMR-MOUSE to elastomers are summarized in Figure 38 (193). In Figure 38**a**, transverse relaxation times have been measured for a series of carbon-filled NR samples with different curing times. Normalized values measured at high and homogeneous magnetic field (7 T, DMX 300) are compared to those measured with the NMR-MOUSE (0.5 T). Although

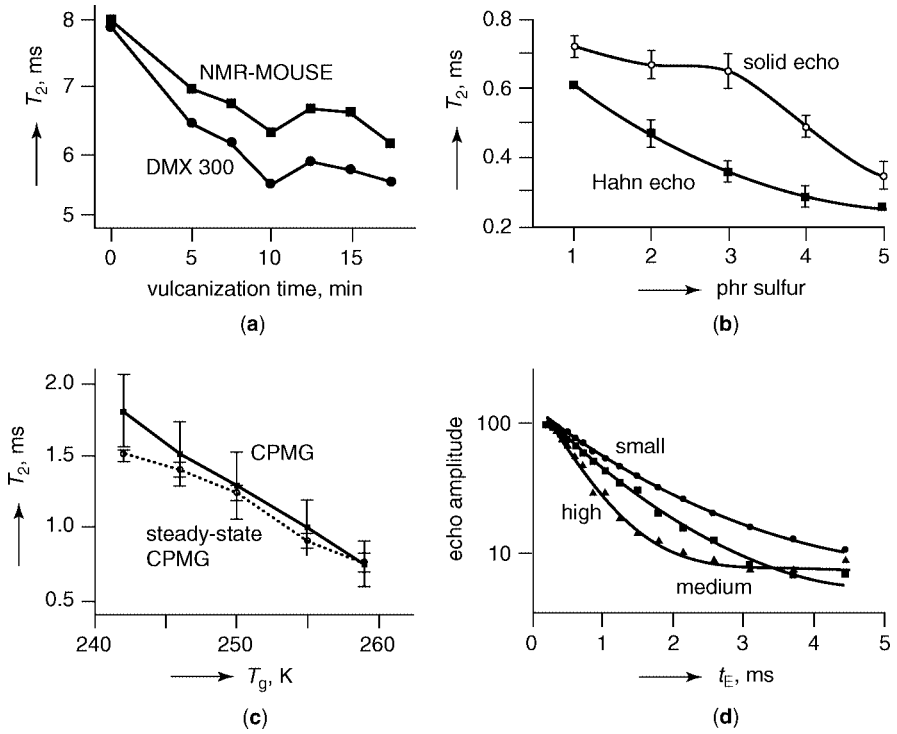

Fig. 38. Applications of the NMR-MOUSE to elastomer materials. (**a**) Values of ^{1}H T_2 for a curing series of carbon-black filled NR. The measurements made with NMR-MOUSE are compared with the values obtained at 300 MHz in high homogeneous field. (**b**) T_2 of a cross-link series of unfilled SBR with different sulfur contents. (**c**) T_2 versus glass-transition temperature T_g of unfilled SBR by the CPMG and steady-state CPMG methods. (**d**) Normalized Hahn-echo decays for polybutadiene latex samples for small, medium, and large cross-link densities. Reproduced from Refs. 189 and 190, with permission from Rapra Technology.

the values differ because of different $\boldsymbol{B}_0$ field strengths, they closely follow the same trend. This confirms that relaxation measurements by the NMR-MOUSE are a valid alternative to relaxation measurements at homogeneous magnetic fields.

In Figure 38**b**, relaxation times are shown for a series unfilled SBR samples with variations in sulfur content. With increasing sulfur content the chemical cross-link density increases. Relaxation times are given for measurements with Hahn echoes and with solid echoes. The change in relaxation times and thus the sensitivity of the method is larger for the Hahn-echo measurements at small cross-link density and for the solid echo measurements at high cross-link density. Solid echoes reduce the signal attenuation from the dipole–dipole interaction between two spins in addition to producing a Hahn echo. At high cross-link density multi-center dipolar couplings become effective and the solid echo becomes less effective in reducing signal attenuation from dipolar interactions. The Hahn echo does not

affect the dipole–dipole interaction at all. This explains the difference in contrast obtained with both methods.

A reduction in measurement time is gained when the measurements are performed in dynamic equilibrium between radio-frequency excitation and longitudinal relaxation (1). NMR methods which operate in this regime are referred to as steady-state methods. They deliver equivalent information compared to methods which demand complete relaxation to thermodynamic equilibrium between scans. T_2 measurements performed with the CPMG and the steady-state CPMG method are depicted in Figure 38**c** and correlated with the glass-transition temperature T_g of unfilled SBR laboratory samples of different cross-link densities. The NMR measurements were done at room temperature, whereas T_g had been determined by temperature-dependent measurements of the dynamic-mechanical loss modulus (189,190). The correlation between both measurements is not surprizing, because both probe the network dynamics. These data demonstrate that in certain cases T_g can be determined locally and nondestructively on large samples at room temperature by the NMR-MOUSE.

The large magnetic-field gradients give rise to rapid signal loss from molecules with translational motion, so that signal from low molecular-weight fluids is suppressed at echo times t_E of the order of 1 ms and more. The signal detected at larger echo times is from larger molecules or particles. This effect of solvent suppression is exploited in the characterization of cross-link density in polybutadiene latex samples (see Fig. 38**d**). The signal decay for weak cross-link density is slow compared to that for large cross-link density. In summary, Figure 38 demonstrates that the NMR-MOUSE is a suitable device for determination of relative cross-link density in a number of different soft materials.

The possibility to excite and detect proton NMR double-quantum coherences in inhomogeneous static and radio-frequency magnetic fields was also investigated (194,195). For this purpose, specialized pulse sequences which partially refocus the strongly inhomogeneous evolution of the spin system and generate double-quantum buildup and decay curves were implemented on the NMR-MOUSE. It was shown that DQ decay curves have a better signal-to-noise ratio in the initial time regime compared to DQ buildup curves. The double-quantum buildup and decay curves were recorded for a series of cross-linked natural rubber samples. These curves give access to quantitative values of the ratio of proton total residual dipolar couplings that are in good agreement with those measured in homogeneous fields. A linear dependence of these ratios on the sulfur-accelerator content was reported.

The self-diffusion coefficient (D) of swollen liquids in elastomers can be measured using NMR-MOUSE with a bar magnet (192). The method was shown to be particularly useful for measuring D of small penetrant molecules in elastomers without the need for measurements of the transverse relaxation rates. The self-diffusion coefficient of toluene in a series of cross-linked natural rubber samples was measured and correlated with the cross-link density.

The NMR-MOUSE is simple mobile NMR sensor suitable for operation in an industrial environment. Its use for quality control is demonstrated in Figure 39 by the T_2 statistics measured at both sides of a conveyor belt with steel cords (193). The magnetic field $\boldsymbol{B}_0$ distortions from the steel cords were minimized by suitable orientation of the NMR-MOUSE with respect to the direction of the cords.

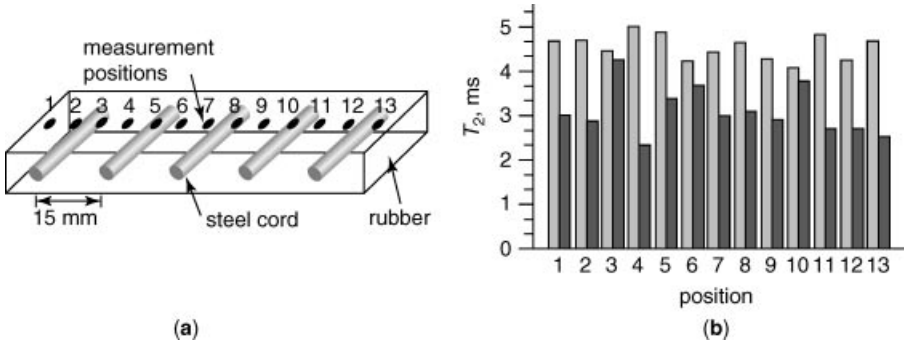

Fig. 39. Quality control of a conveyor-belt section with steel cords. (**a**) Position of measurement points. (**b**) T_2 values for upper and lower sides determined with the CPMG pulse sequence (▒) upper side and (■) lower side. Reproduced from Ref. 193, with permission from Rapra Technology.

The upper side of the belt exhibits a higher average T_2 value than the lower side, which indicates lower cross-link density. In addition to that the variance of the measured values is larger for the lower side indicating a better quality material on the upper side.

Images can be obtained with the NMR-MOUSE by measuring voxels individually by lateral displacement of the device or a change of excitation frequency to shift the sensitive volume in depth (193). On the other hand, also pulsed magnetic field gradients can be employed for phase encoding of the space information. Frequency encoding is hampered by the nonlinear magnetic field profile together with the inaccessibility of the FID.

In direction parallel to the magnetic gap, the magnetic field gradient is weakest, and a sensitive volume of a centimeter and more in width can be excited by a short rf pulse. Solenoidal gradient coils can readily be incorporated into the gap and pulsed to produce antiparallel magnetic fields (196,197). Then a gradient field is established along the gap and spatial resolution can be introduced into the measurement by phase-encoding techniques similar to single-point imaging. The effects of the background field inhomogeneity $B_z - B_0$ and of chemical shift on the magnetization phase are balanced in the peak of the Hahn echo and the only phase evolution from the pulsed field gradient remains. By applying gradient pulses with different amplitudes, $\boldsymbol{k}$ space can be scanned in the direction along the gap, so that the Fourier transformation of the acquired signal produces a one-dimensional image (196). This measurement protocol has been applied in a study of a rubber sheet with parallel textile fibers. The fibers do not contribute to the detected signal, so that their positions can be located by the dips in the 1D profile.

Clearly, the basic imaging scheme can be extended to include relaxation-time contrast for discrimination of variations in cross-link density and strain, and the 1D MRI-MOUSE (magnetic resonance imaging MOUSE) can be extended with further gradient coils to permit imaging in three dimensions. Recently, a two-dimensional imaging with a single-sided NMR probe was reported (197). Numerous applications of the MRI-MOUSE can be envisioned in soft-matter analysis, in

particular in those areas, where imaging with conventional equipment has proven to be successful and where smaller, less expensive, and mobile devices are in need.

BIBLIOGRAPHY

"Nuclear Magnetic Resonance" in *EPST* 1st ed., Vol. 9, pp. 356–396, by F. A. Bovey, Bell Telephone Laboratories; in *EPSE* 2nd ed., Vol. 104, pp. 254–327, by F. A. Bovey and L. W. Jelinski, AT&T Bell Laboratories.

1. R. R. Ernst, G. Bodenhausen, and A. Wokaun, *Principles of Nuclear Magnetic Resonance in One and Two Dimensions*, Clarendon Press, Oxford, 1987.
2. K. Schmidt-Rohr and H. W. Spiess, *Multidimensional Solid State NMR and Polymers*, Academic Press, New York, 1994.
3. V. J. McBrierty and K. J. Parker, *Nuclear Magnetic Resonance in Solid Polymers*, Cambridge University Press, Cambridge, 1993.
4. M. Mehring, *Principles of High Resolution NMR Spectroscopy in Solids*, 2nd ed., Springer, Berlin, 1983.
5. R. Kimmich, *NMR: Tomography, Diffusiometry, Relaxometry*, Springer, Berlin, 1997.
6. F. A. Bovey and P. A. Mireau, *NMR of Polymers*, Academic Press, San Diego, 1996.
7. F. Horii, in I. Ando and T. Asakura, eds., *Solid State NMR in Polymers*, Elsevier, Amsterdam, 1998.
8. H. W. Beckham and H. W. Spiess, *NMR Basic Princ. Prog.* **32**, 163 (1994).
9. H. W. Spiess, *Annu. Rep. NMR Spectrosc.* **34**, 1 (1997).
10. P. A. Mirau, S. A. Heffner, G. Koegler, and F. Bovey, *Polym. Int.* **26**, 29 (1991).
11. B. F. Chmelka, K. Schmidt-Rohr, and H. W. Spiess, in R. Tycko, ed., *Nuclear Magnetic Resonance Probes of Molecular Dynamics*, Kluwer Academic Publishes, the Netherlands, 1994, p. 113.
12. J.-P. Cohen Addad, *Prog. NMR Spectros.* **25**, 1 (1994).
13. V. D. Fedotov and H. Schneider, Structure and dynamics of bulk polymers by NMR method, *NMR, Basic Principles and Progress* Vol. 21, Springer, Berlin, 1989.
14. F. A. Bovey, *High Resolution NMR of Macromolecules*, Academic Press, New York, 1972.
15. J. N. S. Evans, *Biomolecular NMR Spectroscopy*, Oxford University Press, New York, 1995.
16. D. E. Demco, S. Hafner, and H. W. Spiess, Multidimensional NMR techniques for characterization of viscoelastic materials, in V. M. Litvinov and P. P. De, eds., *Handbook of Spectroscopy of Rubbery Materials*, Rapra Technology Ltd., Shawbury, 2002.
17. P. Mansfield and P. G. Morris, NMR imaging in biomedicine, *Advanced Magnetic Resonance*, Suppl. 2, Academic Press, New York, 1982.
18. P. T. Callaghan, *Principles of Nuclear Magnetic Resonance Microscopy*, Clarendon Press, Oxford, 1991.
19. B. Blümich, *NMR Imaging of Materials*, Clarendon Press, Oxford, 2000.
20. E. M. Haacke, R. W. Brown, M. R. Thompson, and R. Venkatesan, *Magnetic Resonance Imaging, Physical Principles and Sequence Design*, Wiley-Liss, New York, 1999.
21. M. T. Vlaardingerbroek and J. A. den Boer, *Magnetic Resonance Imaging*, 2nd ed., Springer, Berlin, 1999.
22. B. Blümich and D. E. Demco, NMR Imaging of Elastomers, in V. M. Litvinov, and P. P. De, eds., *Handbook of Spectroscopy of Rubbery Materials*, Rapra Technology Ltd., Shawbury, 2002.

23. J.-J. Delpuech, ed., *Dynamics of Solutions and Fluid Mixtures by NMR*, John Wiley & Sons, Ltd., Chichester, 1995.
24. R. Tycko, ed., *Nuclear Magnetic Resonance of Molecular Dynamics*, Kluwer Academic Publishers, Dordrecht, 1994.
25. D. Canet, *Nuclear Magnetic Resonance. Concepts and Methods*, John Wiley & Sons, Ltd., Chichester, 1996.
26. M. Munowitz and A. Pines, *Adv. Chem. Phys.* **66**, 1 (1987).
27. M. H. Levitt, *Spin Dynamics*, John Wiley & Sons, Ltd., Chichester, 2001, and references therein.
28. I. Schnell and H. W. Spiess, *J. Magn. Reson. Adv. Magn. Reson.* **151**, 153 (2001).
29. S. B. Brown and H. W. Spiess, *Chem. Rev.* **101**, 4125 (2001).
30. E. Hahn, *Phys. Rev.* **80**, 580 (1950).
31. J. G. Powles and P. Mansfield, *Phys. Lett.* **2**, 58 (1962).
32. H. Schneider and H. Schmiedel, *Phys. Lett.* **30A**, 298 (1969).
33. W.-K. Rhim, A. Pines, and J. S. Waugh, *Phys. Rev. B* **3**, 684 (1971).
34. D. E. Demco, *Phys. Lett.* **45A**, 113 (1973).
35. J. Jeener, Ampere International Summer School, Basko Polje, Yugoslavia, 1971
36. R. R. Ernst, *Chemia* **29**, 179 (1975).
37. L. Müller, A. Kumar, and R. R. Ernst, *J. Chem. Phys.* **63**, 5490 (1975).
38. W. P. Aue, E. Bertholdi, and R. R. Ernst, *J. Chem. Phys.* **64**, 2229 (1976).
39. S. R. Hartmann and E. L. Hahn, *Phys. Rev.* **128**, 2042 (1962).
40. A. Pines, M. G. Gibby, and J. S. Waugh, *J. Chem. Phys.* **59**, 569 (1973).
41. M. Munowitz and A. Pines, *Adv. Chem. Phys.* **66**, 1 (1987).
42. R. Freeman, *Spin Choreography. Basic Steps in High Resolution NMR*, Spektrum, Oxford, 1997, and references therein.
43. E. R. Andrew, A. Bradbury, and R. G. Eades, *Nature* **182**, 1659 (1958).
44. I. J. Lowe, *Phys. Rev. Lett.* **2**, 285 (1959).
45. J. S. Waugh, L. M. Huber, and U. Haeberlen, *Phys. Rev. Lett.* **20**, 180 (1968).
46. P. Mansfield, M. J. Orchard, D. C. Stalker, and K. H. B. Richards, *Phys. Rev. B* **7**, 90 (1973).
47. P. Mansfield and P. G. Morris, NMR imaging in biomedicine, *Advanced Magnetic Resonance*, Suppl. 2, Academic Press, New York, 1982.
48. A. K. Whittaker, *Annu. Rep. NMR Spectrosc* **34**, 106 (1997).
49. A. Schmidt, W. S. Veeman, V. M. Litvinov, and W. Gabrielse, *Macromolecules* **31**, 1652 (1998).
50. B. Deloche and P. Sotta, in V. M. Litvinov and P. P. De, eds., *Handbook of Spectroscopy of Rubbery Materials*, Rapra Technology Ltd., Shawbury, 2002.
51. P. G. Klein and M. E. Ries, *Prog. NMR Spectrosc.* **42**, 31 (2003).
52. P. T. Callaghan and E. T. Samulski, *Macromolecules* **30**, 113 (1997).
53. R. Ball, P. T. Callaghan, and E. T. Samulski, *J. Chem. Phys.* **106**, 7352 (1997).
54. B. Deloch, A. Dubault, and D. Durand, *J. Polym. Sci., Part B: Polym. Phys.* **30**, 1419 (1992).
55. V. M. Litvinov and H. W. Spiess, *Makromol. Chem.* **193**, 1181 (1992).
56. P. Sotta and B. Deloch, *J. Chem. Phys.* **100**, 4591 (1994).
57. P. Sotta, *Macromolecules* **31**, 3872 (1998).
58. M. G. Brereton and E. R. Ries, *Macromolecules* **29**, 2644 (1996).
59. M. G. Brereton, *Macromolecules* **24**, 6160 (1991).
60. M. E. Ries, M. G. Brereton, P. K. Klein, I. M. Ward, P. Ekanayake, H. Menge, and H. Schneider, *Macromolecules* **32**, 4961 (1999).
61. A. Dardin, R. R. Stadler, C. Boeffel, and H. W. Spiess, *Makromol. Chem.* **194**, 3467 (1993).

62. A. Dardin, H. W. Spiess, R. R. Stadler, and E. T. Samulski, *Polym. Gel Networks* **5**, 37 (1997).
63. J. Collignon, H. Sillescu, and H. W. Spiess, *Colloid Polym. Sci.* **259**, 220 (1981).
64. R. Fechete, D. E. Demco, and B. Blümich, *J. Chem. Phys.* **118**, 2411 (2003).
65. D. E. Demco, S. Hafner, C. Fülber, R. Graf, and H. W. Spiess, *J. Chem. Phys.* **105**, 11285 (1996).
66. C. Fülber, D. E. Demco, O. Weintraub, and B. Blümich, *Macromol. Chem. Phys.* **197**, 581 (1996).
67. P. Sotta, C. Fülber, D. E. Demco, B. Blümich, and H. W. Spiess, *Macromolecules* **29**, 6222 (1996).
68. M. Schneider, L. Gasper, D. E. Demco, and B. Blümich, *J. Chem. Phys.* **111**, 402 (1999).
69. A. Wiesmath, C. Filip, D. E. Demco, and B. Blümich, *J. Magn. Reson.* **149**, 258 (2001).
70. D. E. Demco, R. Fechete, and B. Blümich, *Chem. Phys. Lett.* **375**, 406 (2003).
71. A. Pines, W.-K. Rhim, and J. S. Waugh, *J. Magn. Reson.* **6**, 457 (1972).
72. S. Matsui, *Chem. Phys. Lett.* **179**, 187 (1991).
73. R. Graf, D. E. Demco, S. Hafner, and H. W. Spiess, *Solid State Nucl. Magn. Reson.* **12**, 139 (1998).
74. R. Graf, D. E. Demco, S. Hafner, and H. W. Spiess, *J. Chem. Phys.* **106**, 885 (1997).
75. J. Gottwald, D. E. Demco, R. Graf, and H. W. Spiess, *Chem. Phys. Lett.* **243**, 314 (1995).
76. M. Wang, M. Bertmer, D. E. Demco, B. Blümich, V. M. Litvinov, and H. Barthel, *Macromolecules* **36**, 4411 (2003).
77. V. M. Litvinov, H. Barthel, and J. Weis, *Macromolecules* **35**, 4356 (2002).
78. L. R. G. Treloar, *The Physics of Rubber Elasticity*, Clarendon Press, Oxford, 1975.
79. B. Erman and J. Mark, *Structures and Properties of Rubberlike Networks*, Oxford University Press, Oxford, 1997.
80. R. Fechete, D. E. Demco, and B. Blümich, *Macromolecules* **35**, 6083 (2003).
81. J.-P. Cohen Addad, in V. M. Litvinov and P. P. De, eds., *Handbook of Spectroscopy of Rubbery Materials*, Rapra Technology Ltd., Shawbury, 2002, p. 291.
82. J.-P. Cohen Addad, B. Phan Thanh, and H. Montes, *Macromolecules* **30**, 4374 (1997).
83. V. M. Litvinov, in V. M. Litvinov and P. P. De, eds., *Handbook of Spectroscopy of Rubbery Materials*, Rapra Technology Ltd., Shawbury, 2002, p. 353.
84. V. M. Litvinov and A. A. Dias, *Macromolecules* **34**, 4051 (2001).
85. V. M. Litvinov and P. A. M. Steeman, *Macromolecules* **32**, 8476 (1999).
86. V. M. Litvinov, *Int. Polym. Sci. Technol.* **15**, T/28 (1988).
87. M. G. Brereton, *Macromolecules* **23**, 1119 (1990).
88. M. G. Brereton, *Macromolecules* **24**, 2068 (1991).
89. J. P. Cohen-Addad and O. Girard, *Macromolecules* **25**, 593 (1992).
90. T. P. Kulagina, V. M. Litvinov, and K. T. Summanen, *J. Polym. Sci., Part B: Polym. Phys.* **31**, 241 (1993).
91. H. W. Weber and R. Kimmich, *Macromolecules* **26**, 2597 (1993).
92. R. Kimmich, M. Köpf, and P. T. Callaghan, *J. Polym. Sci., Part B: Polym. Phys.* **29**, 1025 (1991).
93. G. I. Sandakov, V. P. Tarasov, N. N. Volkova, Y. A. Ol'khov, L. P. Smirnov, L. N. Erofeev, and A. K. Khitrin, *Vysokomol. Soedin., Ser. B* **31**, 821 (1989).
94. N. N. Volkova, G. I. Sandakov, A. I. Sosikov, Y. A. Ol'khov, L. P. Smirnov, and K. T. Summanen, *Polym. Sci. U.S.S.R.* **34**, 127 (1992).
95. R. Kimmich, E. Fischer, P. Callaghan, and N. Fatkullin, *J. Magn. Reson. A* **117**, 53 (1995).
96. E. Fischer, F. Grinberg, R. Kimmich, and S. Hafner, *J. Chem. Phys.* **109**, 846 (1998).
97. F. Grinberg, M. Garbarczyk, and W. Kuhn, *J. Chem. Phys.* **111**, 11222 (1999).

98. D. E. Demco, S. Hafner, and R. Kimmich, *J. Magn. Reson.* **96**, 307 (1992).
99. A. Y. Grosberg and A. R. Khokhov, *Statistical Physics of Macromolecules*, American Institute of Physics, Woodbury, NY, 1994.
100. L. Gasper, D. E. Demco, and B. Blümich, *Solid State Nucl. Magn. Reson.* **14**, 105 (1999).
101. A. P. M. Kentgens, W. S. Veeman, and J. van Bree, *Macromolecules* **20**, 1234 (1987).
102. A. S. Kulik, D. Radloff, and H. W. Spiess, *Macromolecules* **27**, 433 (1994).
103. A. W. Overhauser, *Phys. Rev.* **92**, 411 (1953).
104. J. Denault and J. Prud'homme, *Macromolecules* **22**, 1307 (1989).
105. J. L. White and P. Mirau, *Macromolecules* **26**, 3049 (1993).
106. J. L. White, *Solid State NMR* **10**, 79 (1997).
107. P. Mirau, P. H. Tanaka, and F. Bovey, *Macromolecules* **21**, 2929 (1988).
108. S. A. Heffner and P. Mirau, *Macromolecules* **27**, 7283 (1994).
109. T. Fritzhanns, S. Hafner, D. E. Demco, H. W. Spiess, and F. H. Laukien, *J. Magn. Reson.* **134**, 355 (1998).
110. T. Fritzhanns, D. E. Demco, S. Hafner, and H. W. Spiess, *Mol. Phys.* **97**, 931 (1999).
111. E. Fischer, R. Kimmich, U. Beginn, M. Möller, and N. Fatkulin, *Phys. Rev. E* **59**, 4079 (1999).
112. G. Lipardi and A. Szabo, *J. Am. Chem. Soc.* **104**, 4546 (1982).
113. G. Lipardi and A. Szabo, *J. Am. Chem. Soc.* **104**, 4559 (1982).
114. G. Simon, K. Baumann, and W. Gronski, *Macromolecules* **25**, 3624 (1992).
115. H. Geen, J. J. Titman, J. Gottwald, and H. W. Spiess, *Chem. Phys. Lett.* **227**, 79 (1994).
116. M. Feike, D. E. Demco, R. Graf, J. Gottwald, S. Hafner, and H. W. Spiess, *J. Magn. Reson.* **122**, 241 (1996).
117. C. Filip, X. Filip, M. Bertmer, D. E. Demco, and B. Blümich, *J. Magn. Reson.* **150**, 184 (2001).
118. X. Feng, P. J. E. Verdegem, Y. K. Lee, D. Sandström, M. Edén, P. Bovee-Geurts, W. J. de Grip, J. Lugtenburg, H. J. M. de Grott, and M. H. Levitt, *J. Am. Chem. Soc.* **119**, 6853 (1997).
119. R. Graf, A. Heuer, and H. W. Spiess, *Phys. Rev. Lett.* **80**, 5738 (1998).
120. W. Sommer, J. Gottwald, D. E. Demco, and H. W. Spiess, *J. Magn. Reson. A* **112**, 131 (1995).
121. M. Hong, J. D. Gross, and R. G. Griffin, *J. Phys. Chem. B* **101**, 5869 (1997).
122. K. Saalwächter, R. Graf, D. E. Demco, and H. W. Spiess, *J. Magn. Reson.* **139**, 287 (1999).
123. V. M. Litvinov, M. Bertmer, L. Gasper, D. E. Demco, and B. Blümich, *Macromolecules* **36**, 7598 (2003).
124. W. Gabrielse, M. Suliman, and K. Dijkstra, *Macromolecules* **34**, 1685 (2001).
125. C. Malveau, P. Tekely, and D. Canet, *Solid State NMR* **7**, 271 (1997).
126. P. Tekely, D. Nicole, J. Brondeau, and J. J. Delpuech, *J. Phys. Chem.* **90**, 5608 (1986).
127. N. Zumbulyadis, *Phys. Rev. B* **33**, 6495 (1986).
128. K. Schmidt-Rohr, J. Clauss, and H. W. Spiess, *Macromolecules* **25**, 3273 (1992).
129. P. Sotta, C. Fülber, D. E. Demco, B. Blümich, and H. W. Spiess, *Macromolecules* **29**, 6222 (1996).
130. C. Fülber, D. E. Demco, O. Weintraub, and B. Blümich, *Macromol. Chem. Phys.* **197**, 581 (1996).
131. A. D. Meltzer, H. W. Spiess, C. D. Eisenbach, and H. Hayen, *Makromol. Chem. Rapid Commun.* **12**, 261 (1991).
132. J. A. Kornfield, H. W. Spiess, H. Nefzger, H. Hayen, and C. D. Eisenbach, *Macromolecules* **24**, 4787 (1991).

133. A. Dardin, C. Boeffel, H. W. Spiess, R. Stadler, and E. T. Samulski, *Acta Polym.* **46**, 291 (1995).
134. P. Blümler and B. Blümich, *Rubber Chem. Technol.* **70**, 469 (1997).
135. B. Blümich and D. E. Demco, in V. M. Litvinov and P. P. De, eds., *Spectroscopy of Rubbery Materials*, Rapra Technology Ltd., Shrewsbury, 2001.
136. D. E. Demco and B. Blümich, *Conc. Magn. Reson.* **10**, 19 (1997).
137. D. E. Demco and B. Blümich, *Conc. Magn. Reson.* **10**, 269 (1997).
138. D. G. Cory, *Annu. Rep. NMR Spectrosc.* **24**, 88 (1992).
139. P. Blümler and B. Blümich, *NMR Basic Princ. Prog.* **30**, 211 (1994).
140. J. H. Strange, *Phil. Trans. Soc. Lond. A* **333**, 427 (1990).
141. P. J. McDonald, *Prog. NMR Spectrosc.* **30**, 69 (1997).
142. B. Blümich, *Conc. Magn. Reson.* **10**, 19 (1998).
143. B. Blümich, *Conc. Magn. Reson.* **11**, 71 (1998).
144. A. Abragam, *Principles of Nuclear Magnetism*, Oxford Academic Press, London, 1961.
145. D. Raftery and B. F. Chmelka, *NMR Basis Princ. Prog.* **30**, 111 (1994).
146. D. E. Demco and B. Blümich, *Curr. Opp. Solid State Mater. Sci.* **5**, 195 (2001), and references therein.
147. C. Fülber, B. Blümich, K. Unseld, and V. Herrmann, *Kautsch. Gummi Kunstst.* **48**, 254 (1995).
148. P. Blümler and B. Blümich, *Macromolecules* **24**, 2183 (1991).
149. C. Fülber, K. Unseld, V. Herrmann, K. H. Jakob, and B. Blümich, *Colloid Polym. Sci.* **274**, 191 (1996).
150. R. L. Armstrong, A. Tzalmona, M. Menzinger, A. Cross, and C. Lemaire, in B. Blümich and W. Kuhn, eds., *Magnetic Resonance Microscopy*, VCH, Weinheim, 1992, p. 309.
151. P. Mansfield, R. Bowtell, and S. Blackband, *J. Magn. Reson.* **99**, 507 (1992).
152. M. A. Rana and J. L. Koenig, *Macromolecules* **27**, 3727 (1994).
153. G. Simon and H. Schneider, *Macromol. Chem. Macromol. Symp.* **52**, 233 (1991).
154. A. A. Parker, J. J. Marcinko, P. Rinaldi, D. P. Hendrick, and W. Ritchey, *J. Appl. Polym.* **48**, 667 (1993).
155. P. Blümler and B. Blümich, *Acta Polym.* **24**, 2183 (1991).
156. C. Schwarzbauer, J. Zange, H. Adolf, R. Deichnmann, U. Nöth, and A. Haase, *J. Magn. Reson. B* **100**, 178 (1995).
157. P. Sotta, B. Deloche, J. Herz, A. Lapp, D. Durand, and J.-C. Rabadeux, *Macromolecules* **20**, 2769 (1987).
158. M. Klinkenberg, P. Blümler, and B. Blümich, *Macromolecules* **30**, 1038 (1997).
159. M. Klinkenberg, P. Blümler, and B. Blümich, *J. Magn. Reson. A* **119**, 197 (1996).
160. M. Schneider, D. E. Demco, and B. Blümich, *Macromolecules* **34**, 4019 (2001).
161. M. Schneider, D. E. Demco, and B. Blümich, *J. Magn. Reson.* **140**, 432 (1999).
162. Y. Xia, *Conc. Magn. Reson.* **8**, 205 (1996).
163. P. Blümler and B. Blümich, *Magn. Reson. Imag.* **10**, 779 (1992).
164. B. Blümich and P. Blümler, *Makroml. Chem.* **194**, 2133 (1993).
165. L. Gasper, D. E. Demco, and B. Blümich, *Solid State Nucl. Magn. Reson.* **14**, 105 (1999).
166. F. Grindberg, M. Heidenreich, and W. Kuhn, *J. Magn. Reson.* **159**, 87 (2002).
167. S. R. Smith and J. L. Koening, *Macromolecules* **24**, 3498 (1991).
168. B. Klei and J. L. Koenig, *Acta Polym.* **48**, 199 (1997).
169. P. Palmas, R. Colsenet, L. Lemaire, and M. Sebbare, *Polymer* **44**, 4889 (2003).
170. P. Denner, B. Walker, and T. Willing, *Macromol. Symp.* **119**, 339 (1997).
171. P. Blümler, B. Blümich, and H. Dumler, *Kautsch. Gummi. Kunstst.* **45**, 699 (1992).
172. M. Knörgen, U. Heuert, H. Schneider, P. Barth, and W. Kuhn, *Polym. Bull.* **38**, 101 (1997).

173. M. Knörgen, U. Heuert, H. Menge, and H. Schneider, *Angew. Makromol. Chem.* **261/262**, 123 (1998).
174. J. A. Chudek and G. Hunter, *J. Mater. Sci. Lett.* **11**, 222 (1992).
175. M. Sardashti, B. A. Baldwin, and D. J. O'Donnell, *J. Polym. Sci., B: Polym. Phys.* **33**, 571 (1995).
176. A. Spyros, R. Kimmich, B. H. Briese, and D. Jenddrossek, *Macromolecules* **30**, 8218 (1997).
177. F. P. Miknis, A. T. Pauli, L. C. Michon, and D. A. Netzel, *Fuel* **77**, 399 (1998).
178. F. P. Miknis and L. C. Michon, *Fuel* **77**, 393 (1998).
179. P. Blümler and B. Blümich, *Acta Polym.* **44**, 125 (1993).
180. D. Hauck, P. Blümlr, and B. Blümich, *Macromol. Chem. Phys.* **198**, 2729 (1997).
181. P. Adriaensens, A. Pollaris, M. Kelchtermans, and J. Gelan, *Macromolecules* **36**, 706 (2003).
182. P. Adriaensens, A. Pollaris, D. Vanderzande, J. Gelan, J. L. White, A. J. Dias, and M. Kelchtermans, *Macromolecules* **32**, 4692 (1999).
183. P. J. Flory, *J. Chem. Phys.* **18**, 108 (1950).
184. P. Prado, L. Gasper, G. Fink, B. Blümich, V. Herrmann, K. Unseld, H-B. Fuchs, H. Möhler, and M. Rühl, *Macromol. Mater. Eng.* **274**, 13 (2000).
185. P. Prado, L. Gasper, G. Fink, and B. Blümich, *Appl. Magn. Reson.* **18**, 1 (2000).
186. P. Blümler, V. Litvinov, H. G. Dikland, and M. van Duin, *Kautsch. Gummi. Kundstst.* **51**, 865 (1998).
187. G. Eidmann, R. Salvesberg, P. Blümler, and B. Blümich, *J. Magn. Reson. A* **122**, 104 (1992).
188. F. Balibanu, K. Hailu, R. Eymael, D. E. Demco, and B. Blümich, *J. Magn. Reson.* **145**, 246 (2000).
189. G Zimmer, A. Guthausen, and B. Blümich, *Solid State Nucl. Magn. Reson.* **12**, 183 (1998).
190. A. Guthausen, G. Zimmer, P. Blümler, and B. Blümich, *J. Magn. Reson.* **130**, 1 (1998).
191. K. Hailu, R. Fechete, D. E. Demco, and B. Blümich, *Solid State Nucl. Magn. Reson.* **22**, 327 (2002).
192. M. Klein, R. Fechete, D. E. Demco, and B. Blümich, *J. Magn. Reson.* **164**, 310 (2003).
193. B. Blümich and D. E. Demco, in V. M. Litvinov and P. P. De, eds., *Spectroscopy of Rubbery Materials*, Rapra Technology Ltd., Shrewsbury, 2001.
194. A. Wiesmath, C. Filip, D. E. Demco, and B. Blümich, *J. Magn. Reson.* **149**, 258 (2001).
195. A. Wiesmath, C. Filip, D. E. Demco, and B. Blümich, *J. Magn. Reson.* **154**, 60 (2002).
196. I. P. Prado and B. Blümich, *J. Magn. Reson.* **144**, 200 (2000).
197. F. Casanova and B. Blümich, *J. Magn. Reson.* **163**, 38 (2003).

D. E. DEMCO
B. BLÜMICH
Institut für Technische Chemie und Makromolekulare Chemie,
Rheinisch-Westfälische Technische Hochschule

NUCLEIC ACIDS. See POLYNUCLEOTIDES.

NYLON. See POLYAMIDES.

OLEFIN FIBERS

Introduction

Olefin fibers, also called polyolefin fibers, are defined as manufactured fibers in which the fiber-forming substance is a synthetic polymer of at least 85 wt% ethylene, propylene, or other olefin units (1). Several olefin polymers are capable of forming fibers, but only polypropylene [9003-07-0] (PP) and, to a much lesser extent, polyethylene [9002-88-4] (PE) are of practical importance. Olefin polymers are hydrophobic and resistant to most solvents. These properties impart resistance to staining but cause the polymers to be essentially undyeable in an unmodified form.

The first commercial application of olefin fibers was for automobile seat covers in the late 1940s. These fibers, made from low density polyethylene (LDPE) by melt extrusion, were not very successful. They lacked dimensional stability, abrasion resistance, resilience, and light stability. The success of olefin fibers began when high density polyethylene (HDPE) was introduced in the late 1950s (see ETHYLENE POLYMERS, HDPE). Yarns made from this highly crystalline, linear polyethylene have higher tenacity than yarns made from the less crystalline, branched form (LDPE) (see ETHYLENE POLYMERS, LDPE). Markets were developed for HDPE fiber in marine rope where water resistance and buoyancy are important. However, the fibers also possess a low melting point, lack resilience, and have poor light stability. These traits caused the polyethylene fibers to have limited applications.

Isotactic polypropylene, based on the stereospecific polymerization catalysts discovered by Ziegler and Natta, was introduced commercially in the United States in 1957. Commercial polypropylene fibers followed in 1961. The first market of significance, contract carpet, was based on a three-ply, crimper-textured yarn. It competed favorably against wool and rayon–wool blends because of its lighter

Encyclopedia of Polymer Science and Technology. Copyright John Wiley & Sons, Inc. All rights reserved.

weight, longer wear, and lower cost. In the mid-1960s, the discovery of improved light stabilizers led to the development of outdoor carpeting based on polypropylene. In 1967, woven carpet backing based on a film warp and fine-filament fill was produced. In the early 1970s, a bulked-continuous-filament (BCF) yarn was introduced for woven, texturized upholstery. In the mid-1970s, further improvement in light stabilization of polypropylene led to a staple product for automotive interiors and nonwoven velours for floor and wall carpet tiles. In the early 1980s, polypropylene was introduced as a fine-filament staple for thermal bonded nonwovens.

The growth of polyolefin fibers continues. Advances in olefin polymerization provide a wide range of polymer properties to the fiber producer. Inroads into new markets are being made through improvements in stabilization, and new and improved methods of extrusion and production, including multicomponent extrusion and spunbonded and meltblown nonwovens.

Properties

Physical Properties. Table 1 (2) shows that olefin fibers differ from other synthetic fibers in two important respects: (*1*) olefin fibers have very low moisture absorption and thus excellent stain resistance and almost equal wet and dry properties, and (*2*) the low density of olefin fibers allows a much lighter weight product at a specified size or coverage. Thus 1 kg of polypropylene fiber can produce a fabric, carpet, etc, with much more fiber per unit area than a kilogram of most other fibers.

Tensile Strength. Tensile properties of all polymers are a function of molecular weight, morphology, and testing conditions. The effect of temperature on the tensile properties of a typical polypropylene fiber is shown in Figure 1 (3). Tensile properties are also affected by strain rate, as shown in Figure 2 (3).

Table 1. Physical Properties of Commercial Fibers[a]

Polymer	Standard tenacity, GPa[b]	Breaking elongation, %	Modulus, GPa[b]	Density, kg/m^3	Moisture regain[c]
Olefin	0.16–0.44	20–200	0.24–3.22	910	0.01
Polyester	0.37–0.73	13–40	2.1–3.7	1380	0.4
Carbon	3.1	1	227	1730	
Nylon	0.23–0.60	25–65	0.5–2.4	1130	4–5
Rayon	0.25–0.42	8–30	0.8–5.3	1500	11–13
Acetate	0.14–0.16	25–45	0.41–0.64	1320	6
Acrylic	0.22–0.27	35–55	0.51–1.02	1160	1.5
Glass	4.6	5.3–5.7	89	2490	
Aramid	2.8	2.5–4.0	113	1440	4.5–7
Fluorocarbon	0.18–0.74	5–140	0.18–1.48	2100	
Polybenzimidazole	0.33–0.38	25–30	1.14–1.52	1430	15

[a] Ref. 2.
[b] To convert GPa to psi, multiply by 145,000.
[c] At 21°C and 65% rh.

Lower temperature and higher strain rate result in higher breaking stresses at lower elongations, consistent with the general viscoelastic behavior of polymeric materials. Similar effects are observed on other fiber tensile properties, such as tenacity or stress at break, energy to rupture, and extension at break (4). Under the same spinning, processing, and testing conditions, higher molecular weight results in higher tensile strength. The effect of molecular weight distribution on tensile properties is complex because of the interaction with spinning conditions (4,5). In general, narrower molecular weight distributions result in higher breaking tenacity and lower elongation (4,6). The variation of tenacity and elongation with draw ratio for a given spun yarn correlates well with amorphous orientation (7,8). However, when different spun yarns are compared, neither average nor amorphous orientation completely explains these variations (9–11). Theory suggests that the number of tie molecules, both from molecules traversing the interlamellar region and especially those resulting from entanglements in the interlamellar region, defines the range of tensile properties achievable using draw-induced orientation (12,13). Increased entanglements (more ties) result in higher tenacity and lower elongation.

Creep, Stress Relaxation, and Elastic Recovery. Olefin fibers exhibit creep, or time-dependent deformation under load, and undergo stress relaxation, or the spontaneous relief of internal stress. Because of the variety of molecular sizes and morphological states present in semicrystalline polymers, the creep and stress relaxation properties for materials such as polypropylene cannot be represented in one curve by using time–temperature superposition principles (14). However, given a spun yarn and thus a given structural state, curves for creep fracture (time to break under variable load) can be developed for different draw ratios, as shown in Figure 3 (15), indicating the importance of spun-yarn structure in a crystallizable polyolefin fiber. The same superposition can be carried out up to 110°C, where substantial reordering of polymer crystalline structure occurs (16).

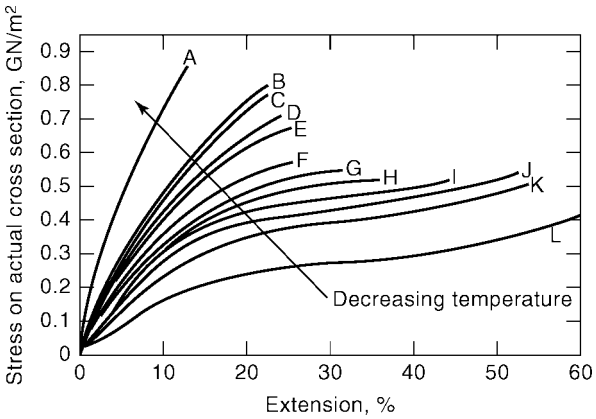

Fig. 1. Effect of temperature on tensile properties of polypropylene (3); strain rate = 6.47×10^{-4} s^{-1}. In degrees Kelvin: A, 90; B, 200; C, 213; D, 227; E, 243; F, 257; G, 266; H, 273; I, 278; J, 283; K, 293; and L, 308 (broken at 74.8% extension, 4.84×10^8 N/m^2). To convert GN/m^2 to dyne/cm^2, multiply by 10^{10}.

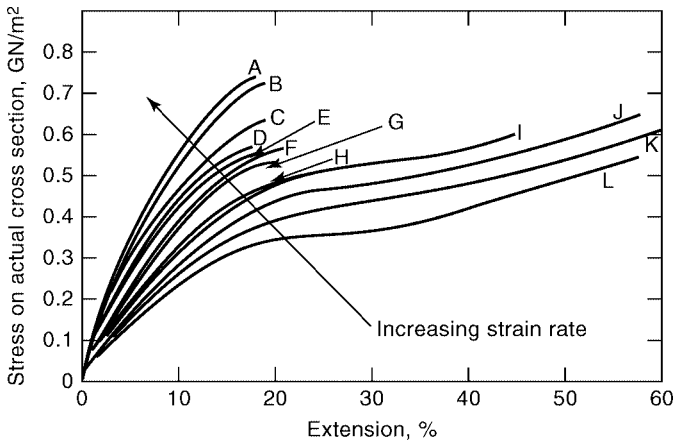

Fig. 2. Effect of strain rate on tensile properties of polypropylene at 20°C (3). In s^{-1}: A, 4.9×10^2; B, 2.48×10^2; C, 1.26×10^2; D, 6.3×10^1; E, 3.2×10^1; F, 2.87×10^1; G, 2.3×10^{-1}; H, 3.3×10^{-2}; I, 1.33×10^{-2}; J, 4.17×10^{-3}; K, 1.67×10^{-3}; and L, 3.3×10^{-4}. To convert GN/m^2 to $dyne/cm^2$, multiply by 10^{10}.

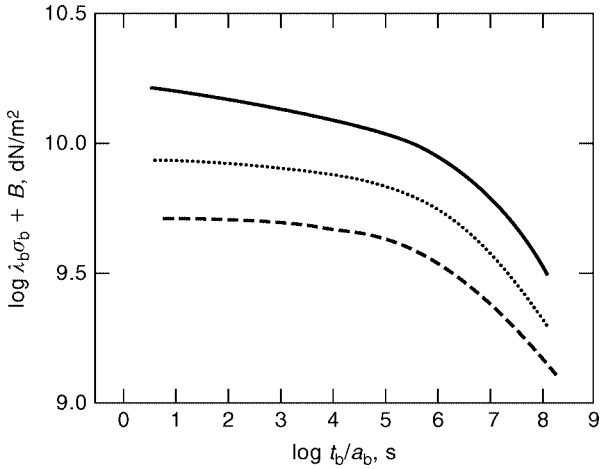

Fig. 3. Composite curve of true stress at break $\lambda_b\sigma_b$ at 40°C vs reduced time to break t_b/a_b for polypropylene fibers of three draw ratios (15): (———), 2.7 × draw, **B** = 0; (·····), 3.5 × draw, $B = 0.2$ (– – –), 4.5 × draw, $B = 0.4$. Values of B are arbitrary.

High molecular weight and high orientation reduce creep. At a fixed molecular weight, the stress-relaxation modulus is higher for a highly crystalline sample prepared by slow cooling than for a smectic sample prepared by rapid quench (14). Annealing the smectic sample raises the relaxation modulus slightly, but not to the degree present in the fiber prepared by slow cooling.

Elastic recovery or resilience is the recovery of length upon release of stress after extension or compression. A fiber, fabric, or carpet must possess this property in order to spring back to its original shape after being crushed or wrinkled. Polyolefin fibers have poorer resilience than nylon; this is thought to be partially

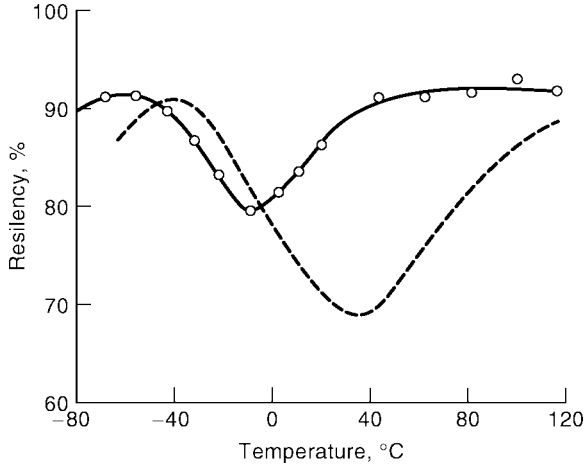

Fig. 4. Resiliency of polypropylene (—○—) and polyethylene (– – –), multifilament yarns as a function of temperature (17).

related to the creep properties of the polyolefins. Recovery from small strain cyclic loading is a function of temperature, as shown in Figure 4, and found to be a minimum for polypropylene at 10°C, near the glass-transition temperature T_g (17). The minimum for polyethylene is at 30°C, higher than the amorphous T_g. This minimum is thought to be associated with motions in the crystalline phase of the highly oriented crystalline structure (17).

Chemical Properties. The hydrocarbon nature of olefin fibers, lacking any polarity, imparts high hydrophobicity and, consequently, resistance to soiling or staining by polar materials, a property important in carpet and upholstery applications. Unlike the condensation polymer fibers, such as polyester and nylon, olefin fibers are resistant to acids and bases. At room temperature, polyolefins are resistant to most organic solvents, except for some swelling in chlorinated hydrocarbon solvents. At higher temperatures, polyolefins dissolve in aromatic or chlorinated aromatic solvents, and show some solubility in high boiling hydrocarbon solvents. At high temperatures, polyolefins are degraded by strong oxidizing acids.

Thermal and Oxidative Stability. The thermal transitions of several polyolefins are compared to other polymers in Table 2. In general, polyolefins undergo thermal transitions at much lower temperatures than condensation polymers, and thus the thermal and oxidative stability of polyolefin fibers are comparatively poor (18). They are highly sensitive to oxygen, which must be carefully controlled in all processing. The tertiary hydrogen in polypropylene imparts sensitivity to oxidative degradation by chain scission resulting in molecular weight degradation. Polyolefins are stabilized by hindered phenols or phosphites. Hindered phenol stabilizers provide moderate melt stability and good long-term heat aging, but undergo gas yellowing, which is a chemical reaction of phenolic compounds and nitrous oxide gases producing yellow-colored compounds. Typical sources of nitrous oxides are gas-fired heaters, dryers, and tenters, and propane-fueled lift trucks used in warehouses. Phosphites are good melt stabilizers and do not gas

Table 2. Thermal Properties of Olefins and Other Fiber-Forming Polymers

Polymer[a]	T_g, °C	T_m, °C	Softening temperature, °C	Thermal degradation temperature, °C
High density polyethylene (HDPE)	−120	130	125	
i-Polypropylene (PP)	−20	165	160	290
i-Poly(1-butene)	−25	128		
i-Poly(3-methyl-1-butene)		315		
i-Poly(4-methyl-1-pentene)	18	250	244	
Poly(ethylene terephthalate) (PET)	70	265	235	400
Nylon-6,6	50	264	248	360

[a] i = isotactic.

yellow, but have poor long-term heat aging. Preferred stabilizers are highly substituted phenols such as Cyanox 1790 and Irganox 1010, or phosphites such as Ultranox 626 and Irgafos 168 (see ANTIOXIDANTS; HEAT STABILIZERS).

Ultraviolet Degradation. Polyolefins are subject to light-induced degradation (19); polyethylene is more resistant than polypropylene. Although the mechanism of UV degradation is different from thermal degradation, the resulting chain scission and molecular weight degradation is similar. In fiber applications, stabilization against light is necessary to prevent loss of properties. The stabilizer must be compatible, have low volatility, be resistant to light and thermal degradation itself, and must last over the lifetime of the fiber. Chemical and physical interactions with other additives must be avoided. Minimal odor and toxicity, colorlessness, resistance to gas yellowing, and low cost are additional requirements (see UV STABILIZERS).

Stabilizers that act as UV screens or energy quenchers are usually ineffective by themselves. Because polyolefins readily form hydroperoxides, the more effective light stabilizers are radical scavengers. Hindered amine light stabilizers (HALS) are favored, especially high molecular weight and polymeric amines that have lower mobility and less tendency to migrate to the surface of the fiber (20,21). This migration is commonly called *bloom*. Test results for some typical stabilizers are given in Table 3 (22).

Table 3. Stabilization of Polypropylene Fiber by Polymeric HALS[a]

HALS	Manufacturer	Carbon arc T50, h[b]	Florida T50, kJ/m^2[c,d]
None		70	<105
Chimassorb 944	CIBA-GEIGY Corp.	300	293–418
Cyasorb 3346	American Cyanamid Co.	320	418
Spinuvex A-36	Montedison Corp.	370–400	293

[a] Test specimens were 0.5 tex (4.5 den) filaments containing 0.25% specified HALS (22).
[b] Hours to 50% retention of initial tensile strength under carbon arc exposure.
[c] kJ/m^2 to 50% retention of tensile strength; Florida under glass exposure.
[d] To convert kJ/m^2 to Langley, multiply by 239.

Flammability. Flammability of polymeric materials is measured by many methods, most commonly by the limiting-oxygen-index test (ASTM D2863), which defines the minimum oxygen concentration necessary to support combustion, or the UL 94 vertical-burn test, which measures the burn length of a fabric. Most polyolefins can be made fire retardant using a stabilizer, usually a bromine-containing organic compound, and a synergist such as antimony oxide (23). However, the required loadings are usually too high for fibers to be spun. Fire-retardant polypropylene fibers exhibit reduced light and thermal resistance. Commercial fire-retardant polyolefin fibers have just recently been introduced, but as expected the fibers have limited light stability and poor luster. Where applications require fire retardancy, it is usually conferred by fabric finishes or incorporation of fire retardants in a latex, such as in latex-bonded nonwovens and latex-coated wovens.

Dyeing Properties. Because of their nonionic chemical nature, olefin fibers are difficult to dye. Oil-soluble dispersed dyes diffuse into polypropylene but readily bloom and rub off. In the first commercial dyeing of olefin fibers, nickel dyes such as UV-1084, also a light stabilizer, were used. The dyed fibers were colorfast but dull and hazy. A broad variety of polymeric dye-sites have been blended with polypropylene; nitrogen-containing copolymers are the most favored (24–26). A commercial acid-dyeable polypropylene fiber is prepared by blending the polypropylene with a basic amino-polyamide terpolymer (27). In apparel applications where dyeing is important, dyeable blends are expensive and create problems in spinning fine denier fibers. Hence, olefin fibers are usually colored by pigment blending during manufacture, called *solution dyeing* in the trade.

Manufacture and Processing

Olefin fibers are manufactured commercially by melt spinning, similar to the methods employed for polyester and polyamide fibers (see POLYESTERS, FIBERS; POLYAMIDES, FIBERS). The basic process of melt spinning is illustrated in Figure 5. The polymer resin and ingredients, primarily stabilizers, pigments, and rheological modifiers, are fed into a screw extruder, melted, and extruded through fine diameter holes. The plate containing the holes is commonly called a *spinnerette*. A metering pump and a mixing device are usually installed in front of the spinneret to ensure uniform delivery and mixing to facilitate uniform drawdown at high speeds. In the traditional or long spinning process, the fiber is pulled through a long cooling stack-type quench chamber by a take-up device at speeds in the range of 50–2000 m/min and discontinuously routed to downstream finishing operations. In the short spinning process, filaments are cooled within a few centimeters of the spinneret at speeds of 50–150 m/min. Because of the lower speeds, fiber can be continuously routed to downstream finishing operations in a one-step process (28). Finishing operations include drawing the fiber to as much as six times its original length, heat treatment to relieve internal stresses, and texturizing processes, which are combinations of deformational and heat treatments. These treatments were developed to impart specific characteristics to the olefin fiber dependent on its end use. Commercial olefin fibers are produced in a broad range of linear densities, from 0.1 to 12 tex (1.1–110 den), to fit a variety of applications, as shown in Figure 6 (29).

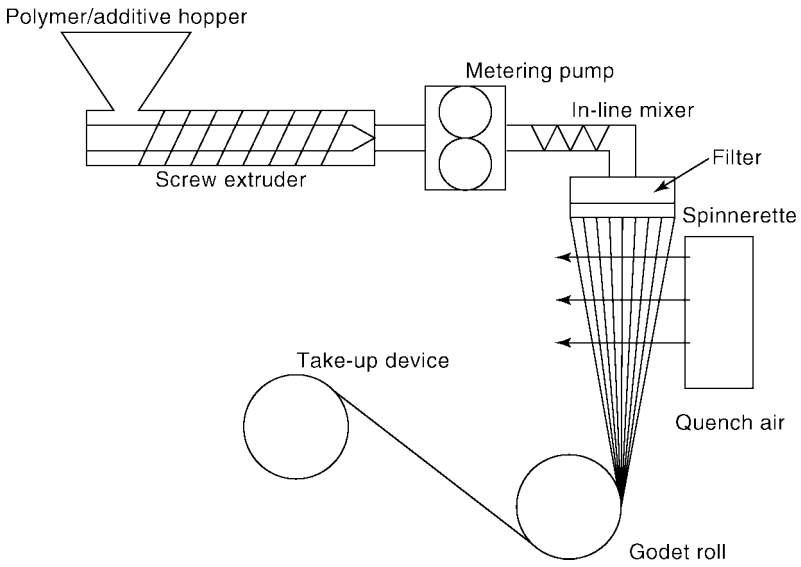

Fig. 5. Melt spinning process.

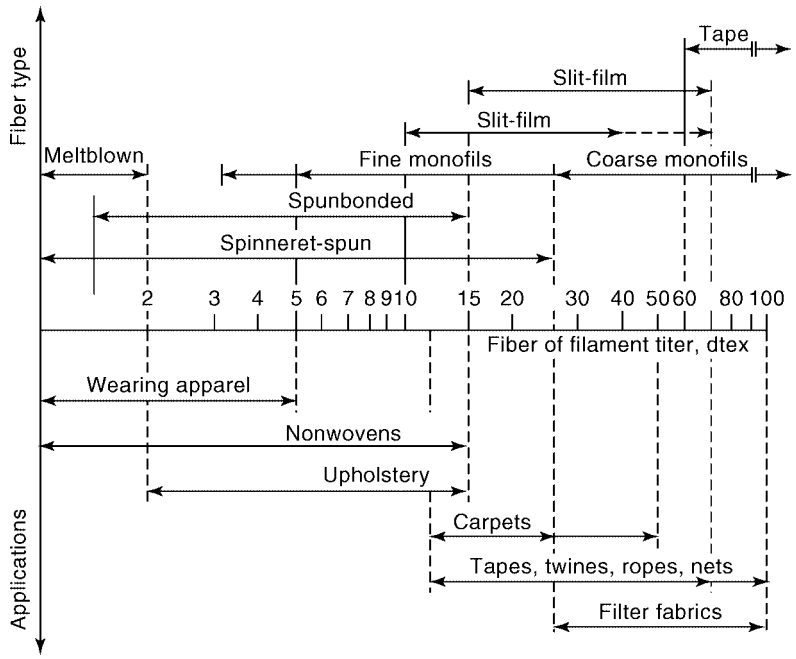

Fig. 6. Linear density of olefin fibers in various applications (29); dtex = 1.1 den.

Extrusion. Polymer resin and additives are melted and pumped through an extruder into a spinning pump. The pump meters the molten polymer through a filter system which removes particles from the molten polymer stream that might clog the capillaries of the spinneret or cause discontinuities in fine diameter fiber. These filters are typically either sand packs or metal screens. The polymer continues to a spinneret, where it is extruded through holes under pressure. These holes or capillaries define the size and shape of the extruded fiber. A spinneret may contain up to several thousand capillaries, typically 0.3–0.5 mm in diameter. The length of the capillary is sized to the melt viscosity of the polymer. Typical length-to-diameter ratios of spinneret capillaries are 2:1 to 8:1. The spinneret holes can be arranged in a variety of hole spacings and patterns, including rectangular, round, and annular. Considerations include throughput rate, heat transfer required to quench the fiber, and fiber diameter.

The extrusion of olefin fibers is largely controlled by the polymer. Polyolefin melts are strongly viscoelastic, and melt extrusion of polyolefin fibers differs from that of polyesters and polyamides. Polyolefins are manufactured in a broad range of molecular weights and ratios of weight-average to number-average molecular weight (M_w/M_n). Unlike the condensation polymers, which typically have molecular weights of 10,000–15,000 and M_w/M_n of approximately 2, polyolefins have weight-average molecular weights ranging from 50,000 to 1,000,000 and, as polymerized, M_w/M_n ranges from 4 to 15. Further control of molecular weight and distribution is obtained by chemical or thermal degradation. The full range of molecular weights used in olefin fiber manufacture is above 20,000, and M_w/M_n varies from 2 to 15. As molecular weight increases and molecular weight distribution broadens, the polymer melt becomes more pseudoplastic as indicated in Table 4 and shown in Figure 7 (30). In the sizing of extrusion equipment for olefin fiber production, the wide range of shear viscosities and thinning effects must be considered because these affect both power requirements and mixing efficiencies.

Table 4. Molecular Weight Characterization Data for Polypropylene Samples[a,b]

Code[c]	Melt flow rate[d]	$M_w \times 10^{-5}$	M_w/M_n	M_z/M_w	$M_v \times 10^{-5}$
High molecular weight polypropylene					
○ Narrow	4.2	2.84	6.4	2.59	2.40
△ Regular-broad	5.0	3.03	9.0	3.57	2.42
□ Broad-regular	3.7	3.39	7.7	3.54	2.71
Middle molecular weight polypropylene					
◍ Narrow	11.6	2.32	4.7	2.81	1.92
▲ Regular	12.4	2.79	7.8	4.82	2.13
▥ Broad	11.0	2.68	9.0	4.46	2.07
Low molecular weight polypropylene					
⊕ Narrow	25.0	1.79	4.6	2.47	1.52
◑ Regular-narrow	23.0	2.02	6.7	3.18	1.66

[a] Ref. 30.
[b] Figs. 7-9.
[c] Narrow, regular, and broad refer to molecular weight distribution.
[d] ASTM D1238 (Condition L; 230/2.16).

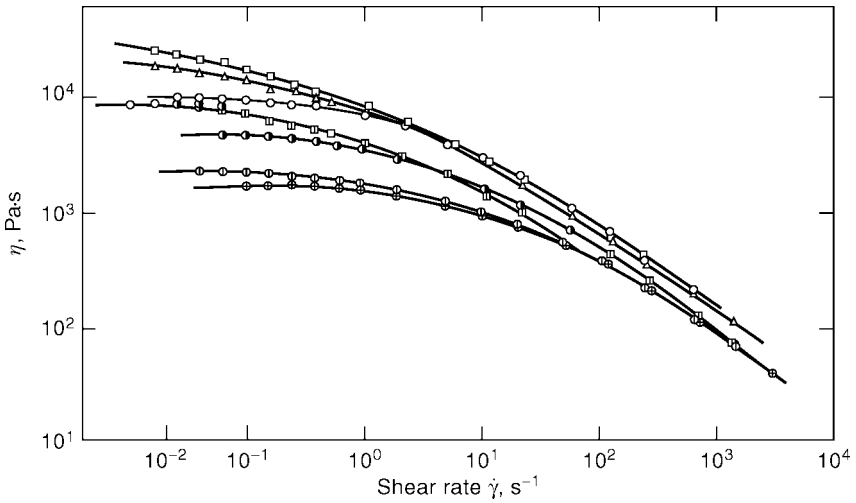

Fig. 7. Shear viscosity at 180°C of polypropylene of different molecular weight and distribution vs shear rate (30); see Table 4 for key. $Pa \cdot s = 0.1$ P.

Fiber spinning is a uniaxial extension process, and the elongational viscosity behavior, which is the stress–strain relationship in uniaxial extension, is more important than the shear viscosity behavior. The narrower molecular weight distributions tend to be less thinning, and as shown in Figure 8 (30), elongational viscosity increases at higher extension rates. This leads to higher melt orientation, which in turn is reflected in higher spun fiber orientation, higher tenacity, and lower extensibility. In contrast, the broad molecular weight distributions tend to be more thinning and hence more prone to necking and fracture at high spinning speeds (30,31), but yield a less oriented, higher elongation spun fiber. The

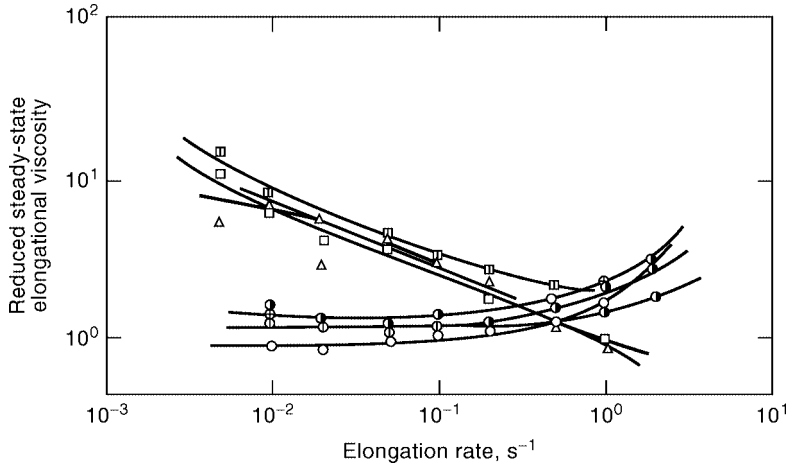

Fig. 8. Elongational viscosity at 180°C of polypropylene of different molecular weight and distribution (30); see Table 4 for key.

choice of an optimum molecular weight and molecular weight distribution is determined by the desired properties of the fiber and the process continuity on available equipment.

Because of the high melt viscosity of polyolefins, normal spinning melt temperatures are 240–310°C, which is 80–150°C above the crystalline melting point. Because of the high melt temperatures used for polyolefin fiber spinning, thermal stabilizers such as substituted hindered phenols are added. In the presence of pigments, the melt temperature must be carefully controlled to prevent color degradation and to obtain uniform color dispersion.

Polyolefin melts have a high degree of viscoelastic memory or elasticity. First normal stress differences of polyolefins, a rheological measure of melt elasticity, are shown in Figure 9 (30). At a fixed molecular weight and shear rate, the first normal stress difference increases as M_w/M_n increases. The high shear rate obtained in fine capillaries, typically on the order of 10^3–10^4 s^{-1}, coupled with the viscoelastic memory, causes the filament to swell (die swell or extrudate swell) upon leaving the capillary. On a molecular scale, the residence time in the region of die swell is sufficient to allow relaxation of any shear-induced orientation. However, high die swell significantly affects the drawdown or extension rate, leading to threadline breaks. Die swell can be reduced by lower molecular weight, narrower molecular weight distribution, or higher melt temperature.

Quench. Attempts have been made to model this nonisothermal process (32–35), but the complexity of the actual system makes quench design an art.

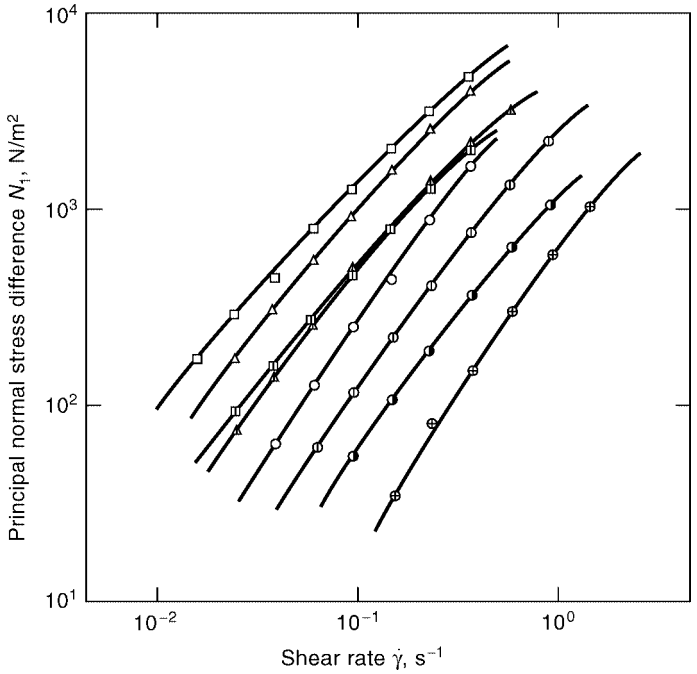

Fig. 9. First normal stress differences of polypropylene of different molecular weight and distribution (30); see Table 4 for key. To convert N/m^2 to dyne/cm^2, multiply by 10.

Arrangements include straight-through, and outside-in and inside-out radial patterns (36). The optimum configuration depends on spinneret size, hole pattern, filament size, quench-chamber dimensions, take-up rate, and desired physical properties. Process continuity and final fiber properties are governed by the temperature profile and extension rate.

Polypropylene and other linear polyolefins crystallize more rapidly than most other crystallizable polymers. Unlike polyester, which is normally amorphous as spun, the fiber morphology of polyolefins is fixed in the spinning process; this limits the range of properties in subsequent drawing and annealing operations. In a low crystallinity state, sometimes called the paracrystalline or smectic form, a large degree of local order still exists. It can be reached by extruding low molecular weight polyolefins, processing at low draw ratio, or by a rapid quench such as by using a cold water bath (37).

Quench is more commonly practiced commercially by a controlled air quench in which the rate of cooling is controlled by the velocity and temperature of the air. During normal cooling, crystallization occurs in the threadline. In-line X-ray scattering studies demonstrate that crystallization is extremely rapid; the full crystalline structure is almost completely developed in fractions of a second (38). Fiber spinning is an extensional process during which significant molecular orientation occurs. Under rapid crystallization, this orientation is fixed during the spinning process. Small-angle neutron-scattering studies of quiescent polypropylene crystallization show that the chain dimensions in both melt and crystallized forms are comparable (39). Although there may be significant relaxation of the amorphous region after spinning, the primary structure of the fiber is fixed during spinning and controls subsequent drawing and texturizing of the fiber. For fixed extrusion and take-up rates, a more rapid quench reduces the average melt-deformation temperature, increases relaxation times, and gives a more entangled melt when crystallization begins. The rapidly quenched fiber usually gives lower elongation and higher tenacity during subsequent draw (40). Using a very rapid quench, the melt may not be able to relax fast enough to sustain drawdown, resulting in melt fracture. Under conditions of a slow quench, the melt may totally relax, leading to ductile failure of the threadline.

A common measurement useful in predicting threadline behavior is fiber tension, frequently misnamed spinline stress. It is normally measured after the crystallization point in the threadline when the steady state is reached and the threadline is no longer deformed. Fiber tension increases as take-up velocity increases (38) and molecular weight increases. Tension decreases as temperature increases (41). Crystallinity increases slightly as fiber tension is increased (38). At low tension, the birefringence increases as tension is increased, leveling off at a spinline tension of 10 MPa (1450 psi) (38).

Take-Up. Take-up devices attenuate the spinline to the desired linear density and collect the spun yarn in a form suitable for further processing. A godet wheel is typically used to control the take-up velocity which varies from 1–2 m/s for heavy monofilaments to 10–33 m/s for fine yarns. The yarn can be stacked in cans, taken up on bobbins, or directly transferred to drawing and texturizing equipment.

In the spunbond process (Fig. 10), an aspiratory is used to draw the fibers in spinning and directly deposit them as a web of continuous, randomly oriented

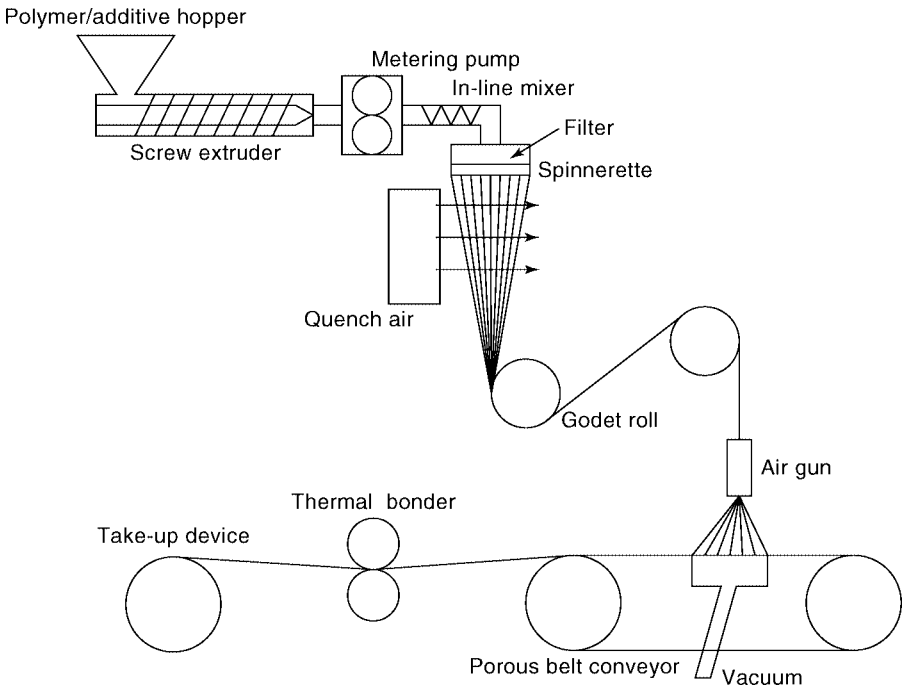

Fig. 10. Flow sheet for typical spunbond fabric manufacture.

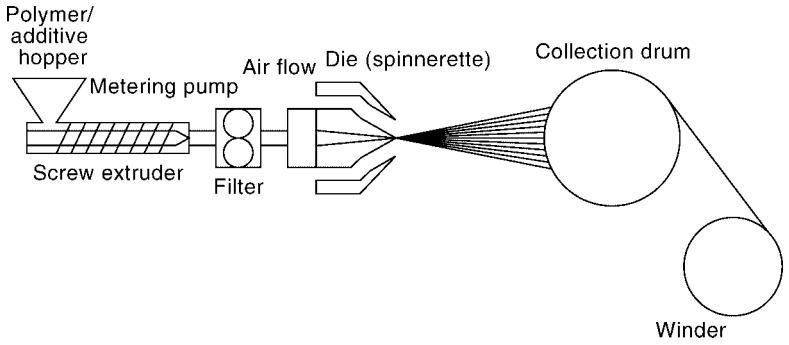

Fig. 11. Flow sheet for typical meltblown fabric manufacture.

filaments onto a moving conveyor belt. In the meltblown process (Fig. 11), high velocity air is used to draw the extruded melt into fine-denier fibers that are laid down in a continuous web on a collector drum.

Draw. Polyolefin fibers are usually drawn to increase orientation and further modify the physical properties of the fiber. Linear density, necessary to control the textile properties, is more easily reduced during drawing than in spinning. The draw step can be accomplished in-line with spinning in a continuous spin–draw–texturing process (36,42) or in a second processing step. This second processing step allows simultaneous mixing of colors in a multi-ply continuous

filament yarn for textiles. For staple fiber production, large bundles or tows consisting of up to a million or more filaments are stretched, texturized (crimped), and cut.

In secondary drawing operations, the aging properties of the spun yarn must be considered. Because polypropylene fibers have a low T_g, the spun yarn is restructured between spinning and drawing; this is more important as the smectic content is increased (43). The aging process depends on whether the yarn is stored on bobbins under tension or coiled in cans with no tension on the fiber. The aging of quick-quenched (smectic) polypropylene films has been studied (43). Stored at room temperature, the increase in yield stress is 5% in 24 hours. Similar data on polypropylene spun fibers have not been published, but aging effects are similar. Drawn fiber properties, such as density, stress relaxation modulus, and heat of fusion, age because of collapse of excess free volume in the noncrystalline fraction (44).

The crystalline structure of the spun yarn affects the draw process. Monoclinic yarns tend to exhibit higher tenacity and lower elongation at low draw ratios than smectic yarns (6). They exhibit lower maximum draw ratios, undergo brittle fracture, and form microvoids (45) at significantly lower draw temperatures, which creates a chalky appearance. Studies of the effect of spun-yarn structure on drawing behavior show that the as-spun orientation and morphology determine fiber properties at a given draw ratio, as shown in Figure 12 (9,45,46). However, final fiber properties can be correlated with birefringence, a measure of the average orientation, as shown in Figure 13 (9,45). Fiber properties and amorphous orientation show good correlation in some studies (Fig. 14) (7,8), but in most studies the range of spun-yarn properties is limited. Such studies suggest that the deformation during draw primarily affects the interlamellar amorphous region

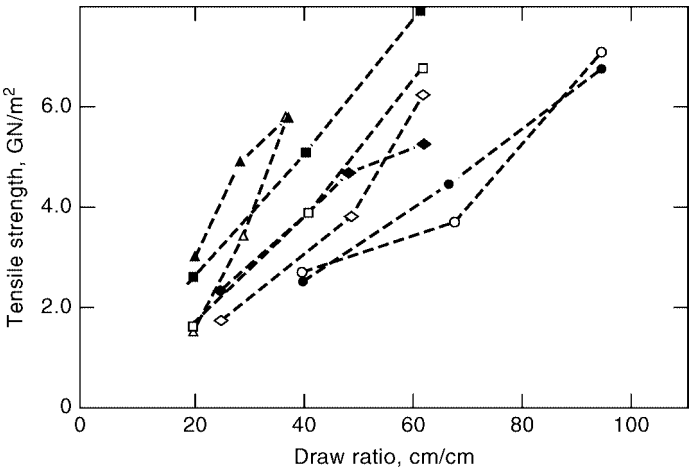

Fig. 12. Tensile strength vs draw ratio (6): 0.42 melt index spun at 50 m/min, ■, □; and 500 m/min, ▲, △; 12.0 melt index spun at 100 m/min, ●, ○; and 500 m/min, ♦ ◇. Open symbols = cold drawn and annealed at 140°C; filled symbols = drawn at 140°C. To convert GN/m^2 to $dyne/cm^2$, multiply by 10^{10}.

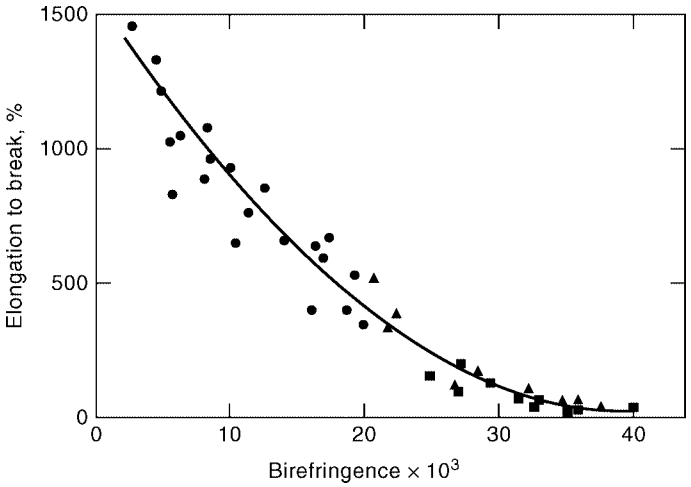

Fig. 13. Elongation to break as a function of birefringence for undrawn, hot-drawn, and cold-drawn annealed fibers (6): ●, undrawn; ▲, cold-drawn, annealed at 140°C; ■, hot-drawn at 140°C.

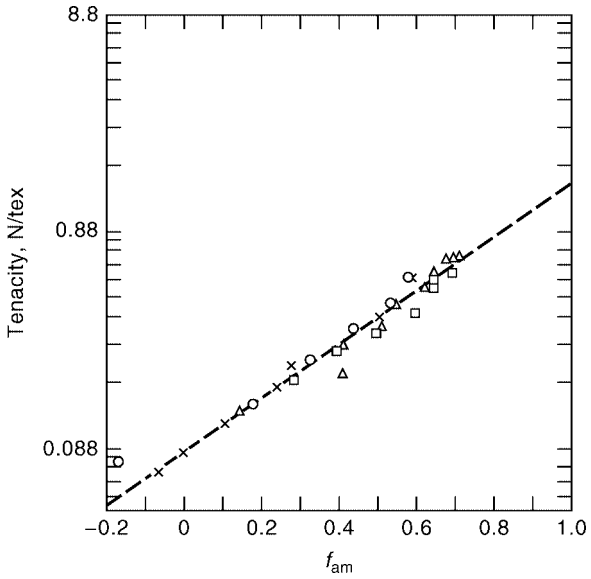

Fig. 14. Tenacity as a function of amorphous orientation (f_{am}) for polypropylene fibers and films (7). Film drawn at 135°C (○), 110°C (×), and 90°C (□). △, Heat-set fiber. To convert N/tex to gf/den, multiply by 11.3. $\text{Tenacity}_{max} = 1.3$ N/tex (15 gf/den).

at low draw ratio. At higher draw ratio, the crystalline structure is substantially disrupted.

Texturing. The final step in olefin fiber production is texturing; the method depends primarily on the application. For carpet and upholstery, the fiber is usually bulked, a procedure in which fiber is deformed by hot air or steam jet turbulence in a nozzle and deposited on a moving screen to cool. The fiber takes

on a three-dimensional crimp that aids in developing bulk and coverage in the final fabric. Stuffer box crimping, a process in which heated tow is overfed into a restricted outlet box, imparts a two-dimensional sawtooth crimp commonly found in olefin staple used in carded nonwovens and upholstery yarns.

Slit-Film Fiber. A substantial volume of olefin fiber is produced by slit-film or film-to-fiber technology (29). For producing filaments with high linear density, above 0.7 tex (6.6 den), the production economics are more favorable than monofilament spinning (29). The fibers are used primarily for carpet backing and rope or cordage applications. The processes used to make slit-film fibers are versatile and economical.

The equipment for the slit-film fiber process is shown in Figure 15 (29). An olefin film is cast, and, as in melt spinning, the morphology and composition of the film determine the processing characteristics. Fibers may be produced by cutting or slitting the film, or by chemomechanical fibrillation. The film is fibrillated mechanically by rubbing or brushing. Immiscible polymers, such as polyethylene or polystyrene (PS), may be added to polypropylene to promote fibrillation. Many common fiber-texturing techniques such as stuffer-box, false-twist, or knife-edge treatments improve the textile characteristics of slit-film fibers.

Several more recent variations of the film-to-fiber approach result in direct conversion of film to fabric. The film may be embossed in a controlled pattern and subsequently drawn uniaxially or biaxially to produce a variety of nonwoven products (47). Addition of chemical blowing agents to the film causes fibrillation upon extrusion. Nonwovens can be formed directly from blown film using a unique radial die and control of the biaxial draw ratio (48) (see NONWOVEN FABRICS, STAPLE FIBERS).

Bicomponent Fibers. Polypropylene fibers have made substantial inroads into nonwoven markets because they are easily thermal bonded. Further enhancement in thermal bonding is obtained using bicomponent fibers (49). In

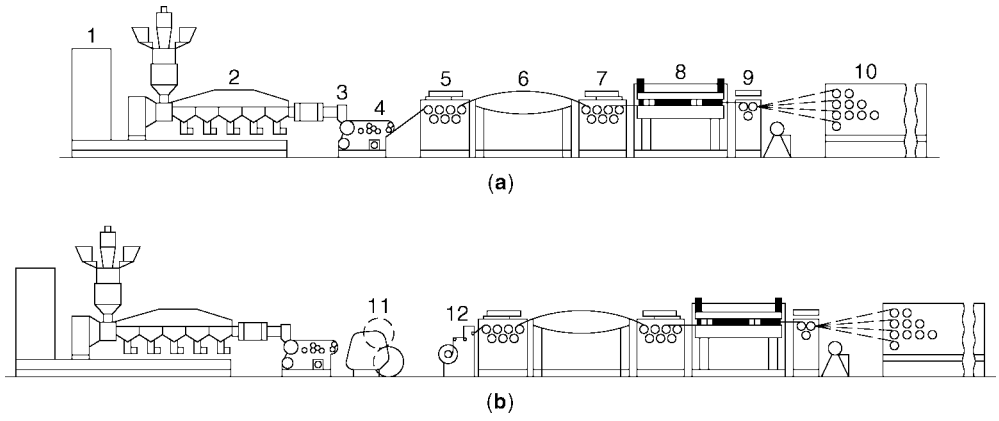

Fig. 15. Production lines for stretched film tape (29): (**a**) continuous production line for film tape; (**b**) discontinuous production lines for film and film tape. 1, Control cabinet; 2, extruder; 3, flat die; 4, chill roll; 5, septet (seven rolls); 6, hot plate; 7, septet (seven rolls); 8, heat-setting oven; 9, trio (three rolls); 10, bobbin winder; 11, film winder; and 12, film-unrolling stand.

these fibers, two incompatible polymers, such as polypropylene and polyethylene, polyester and polyethylene, or polyester and polypropylene, are spun together to give a fiber with a side-by-side or core–sheath arrangement of the two materials. The lower melting polymer can melt and form adhesive bonds to other fibers; the higher melting component causes the fiber to retain some of its textile characteristics.

Bicomponent fibers have also provided a route to self-texturing (self-crimping) fibers. The crimp results from the length differential developed during processing caused by differential shrinkage in the two polymers in side-by-side or eccentric core–sheath configurations (50).

Conventional spinning technology is limited in the production of very fine denier filaments because of spinning and mass uniformity problems as the melt drawdown is increased. Ultrafine filaments (microfibers) can be produced through bicomponent technology by extruding two or more components together as a single fiber and later separating the components through chemical or mechanical processes. Fibers of 0.1–0.001 tex (~1–0.01 den) per filament can be produced (50,51).

Meltblown, Spunbond, and Spurted Fibers. A variety of directly formed nonwovens exhibiting excellent filtration characteristics are made by meltblown processes (52), producing very fine, submicrometer filaments. A simple schematic of the die is shown in Figure 11. A stream of high velocity hot air is directed on the molten polymer filaments as they are extruded from a spinneret. This air attenuates, entangles, and transports the fiber to a collection device. Because the fiber cannot be separated and wound for subsequent processing, a nonwoven web is directly formed. Mechanical integrity of the web is usually obtained by thermal bonding or needling, although other methods, such as latex bonding, can be used. Meltblown fabrics are made commercially from polypropylene and polyethylene. The webs are soft, breathable, and drapable (53–55).

In the spunbond process, the fiber is spun similarly to conventional melt spinning, but the fibers are attenuated by air drag applied at a distance from the spinneret (see NONWOVEN FABRICS). This allows a reasonably high level of filament orientation to be developed. The fibers are directly deposited onto a moving conveyor belt as a web of continuous randomly oriented filaments. As with meltblown webs, the fibers are usually thermal bonded or needled (53).

Pulp-like olefin fibers are produced by a high pressure spurting process developed by Hercules, Inc. and Solvay, Inc. Polypropylene or polyethylene is dissolved in volatile solvents at high temperature and pressure. After the solution is released, the solvent is volatilized, and the polymer expands into a highly fluffed, pulp-like product. Additives are included to modify the surface characteristics of the pulp. Uses include felted fabrics, substitution in whole or in part for wood pulp in papermaking, and replacement of asbestos in reinforcing applications (56).

High Strength Fibers. The properties of commercial olefin fibers are far inferior to those theoretically attainable. Theoretical and actual strengths of common commercial fibers are listed in Table 5 (57). A number of methods, including superdrawing (58), high pressure extrusion (59), spinning of liquid crystalline polymers or solutions (60), gel spinning (61–65), and hot drawing

Table 5. Theoretical and Actual Strengths of Commercial Fibers[a]

Polymer	Density, kg/m^3	Molecular area, nm^2	Theoretical strength, GPa[b]	Strength of commercial fiber, GPa[b]
Polyethylene	960	0.193	31.6	0.76
Polypropylene	910	0.348	17.6	0.72
Nylon-6	1140	0.192	31.9	0.96
Polyoxymethylene	1410	0.185	32.9	
Poly(vinyl alcohol)	1280	0.228	26.7	1.08
Poly(*p*-benzamide)	1430	0.205	29.7	3.16
Poly(ethylene terephthalate)	1370	0.217	28.1	1.15
Poly(vinyl chloride)	1390	0.294	20.8	0.49
Rayon	1500	0.346	17.7	0.69
Poly(methyl methacrylate)	1190	0.667	9.2	

[a]Ref. 56.
[b]To convert GPa to psi, multiply by 145,000.

Table 6. Properties of Commercial High Strength Fibers[a]

Fiber	Density, kg/m^3	Strength, GPa[b]	Modulus, GPa[b]	Elongation to break, %	Filament diameter, mm
Polyethylene	970	2.6	117	3.5	0.038
Aramid	1440	2.8	113	2.8	0.012
S-glass	2490	4.6	89	5.4	0.009
Graphite	1730	3.1	227	1.2	0.006
Steel whiskers	7860	2.3	207	1.3	0.250

[a]Ref. 66.
[b]To convert GPa to psi, multiply by 145,000.

(66) produce higher strengths than those given in Table 5 for commercial fibers, but these methods are tedious and uneconomical for olefin fibers. A high modulus commercial polyethylene fiber with properties approaching those of aramid and graphite fibers (Table 6) (67) is prepared by gel spinning (68) (see CARBON FIBERS; POLYAMIDES, AROMATIC). Although most of these techniques produce substantial increases in modulus, higher tensile strengths are currently available only from gel spinning or dilute fibrillar crystal growth. Even using these techniques, the maximum strengths observed to date are only a fraction of the theoretical strengths.

Hard-Elastic Fibers. Hard-elastic fibers are prepared by annealing a moderately oriented spun yarn at high temperature under tension. They are prepared from a variety of olefin polymers, acetal copolymers, and polypivalolactone (69,70). Whereas the strengths observed are comparable to those of highly drawn commercial fiber, in the range 0.52–0.61 N/tex (6–7 gf/den), the recovery from elongation is substantially better. Hard-elastic fibers typically exhibit 90% recovery from 50% elongation, whereas highly drawn, high tenacity commercial fibers exhibit only 50–75% recovery from 5% elongation. The mechanism of elastic recovery

differs from the entropic models normally used to explain plastic properties. The hard elastic fibers are thought to deform through opening of the lamellae stacked structure, resulting in void formations; recovery is controlled by energy considerations. Although there are potential uses in applications involving substantial deformation, products such as stretch fabrics and hard-elastic fibers are not yet used commercially.

Economic Aspects

Polyolefin fiber (from polypropylene or ethylene polymers) has continued to be one of the fastest growing segments of the synthetic fiber industry. Worldwide production has been increasing at an annul rate of 6% since 1996 and reached 5.5 million ton in 1999. Polyolefin fibers account for 18% of the worldwide synthetic fibers market. Polypropylene fibers predominate and account for 89–95% of the polyolefin production in Western Europe and the United State. The remainder is manufactured from polyethylene. Polypropylene fibers account for 80% usage in Japan (71).

The principal use for polyolefin fibers is in consumer products. The primary use is the production of carpets and rugs, and includes backings. Polyolefins in the form of nonwoven fabrics is the second largest use.

Nonwoven fabrics continue to be the largest growing segment in the textile industry. In 2001, worldwide consumption was 3.5 billion ton valued at over $14 billion. Between 1997 and 2001, world consumption grew at a rate of 11.2%/year. For much of the past decade, solid growth has occurred in industrialized nations. Double-digit growth is now seen in developing nations (primarily Aisa). In 2001, developing countries consumed 39% of all nonwovens produced. Consumption is up from 11% in 1988. Use should continue to grow at the rate of 10–12% through 2006 (72).

Demand for nonwoven roll goods currently exceeds local capacity by 50%. Growth, particularly in China, has seen expansion of local manufacturing capabilities. In North America, Western Europe, and Japan, damand for nonwovens is expected to increase at 3–5%/year through 2006.

Industrial applications of polyolefin fibers include woven and nonwoven geotextiles, agriculatural fabrics, construction sheeting, automobile fabrics, filtration media, rope/twine, woven bags, narrow-woven web and tapes, tents, and tarpaulins. Geosynthetic fabrics will continue to be a growing market for polypropylene nonwovens.

Applications

Olefin fibers are used for a variety of purposes from home furnishings to industrial applications. These include carpets, upholstery, drapery, rope, geotextiles, and both disposable and nondisposable nonwovens. Fiber mechanical properties, relative chemical inertness, low moisture absorption, and low density contribute to desirable product properties. Olefin fiber use in apparel has been restricted by low melting temperatures, which make machine drying and ironing of polyethylene

and polypropylene fabrics difficult or impossible. However, this market is increasing as manufacturers take advantage of the wicking properties (moisture transport) as in lightweight sportswear (73).

Polypropylene fibers are used in every aspect of carpet construction from face fiber to primary and secondary backings. Polypropylene's advantages over jute as carpet backing are dimensional stability and minimal moisture absorption. Drawbacks include difficulty in dyeing and higher cost. Bulked-continuous-filament (BCF) carpet yarns provide face fiber with improved crimp and elasticity. BCF carpet yarns are especially important in contract carpets, characterized by low dense loops, where easy cleaning is an advantage.

Olefin fiber is an important material for nonwovens (74). The geotextile market is still small, despite expectations that polypropylene is to be the principal fiber in such applications. Disposable nonwoven applications include hygienic coverstock, sanitary wipes, and medical roll goods. The two competing processes for the coverstock market are thermal-bonded carded staple and spunbond, both of which have displaced latex-bonded polyester because of improved strength, softness, and inertness.

A special use for meltblown olefin fiber is in filtration media such as surgical masks and industrial filters (75). The high surface area of these ultrafine filament fibers permits preparation of nonwoven filters with effective pore sizes as small as 0.5 μm.

Other applications, including rope, cordage, outdoor furniture webbing, bags, and synthetic turf, make up the remaining segments of the olefin fiber market. Spunbond polyethylene is used in packaging applications requiring high strength and low weight. Specialty olefin fibers are employed in asphalt and concrete reinforcement (76–79). Hollow fibers have been tested in several filtration applications (80,81). Ultrafine fibers are used in synthetic leather, silk-like fabrics, and special filters (50,51). These fibers are also used in sports outerwear, where the tight weaves produce fabrics that are windproof and waterproof, but are able to pass vapors from perspiration and thus keep the wearer cool and dry (51). If the economics of the high modulus olefin fibers becomes more favorable, substantial markets could be developed in reinforced composites such as boat hulls (67).

BIBLIOGRAPHY

"Olefin Fibers" in *EPST* 1st ed., Vol. 9, pp. 403–440, by Victor L. Erlich, Reeves Brothers, Inc.; in *EPSE* 2nd ed., Vol. 10, pp. 373–395, by L. M. Landoll, Hercules, Inc.

1. The Textile Fiber Products Identification Act, Public Law 85–897, Washington, D.C. (Sept. 1958).
2. *Text. World* **134**, 49 (Nov. 1984).
3. I. M. Hall, *J. Polym. Sci.* **54**, 505 (1961).
4. F. Lu and J. E. Spruiell, *J. Appl. Polym. Sci.* **34**, 1521 (1987).
5. J. E. Flood and S. A. Nulf, *Polym. Eng. Sci.* **30**, 1504 (1990).
6. H. S. Brown, T. L. Nemzek, and C. W. Schroeder, paper presented at *The 1983 Fiber Producer Conference*, Greenville, S.C., Apr. 13, 1983, sponsored by Fiber World, Brilliam Publishing Co., Atlanta, Ga.

7. R. J. Samuels, *Structural Polymer Properties*, Wiley-Interscience, New York, 1974.
8. F. Geleji and co-workers, *J. Polym. Sci. Polym. Symp.* **58**, 253 (1977).
9. H. P. Nadella, J. E. Spruiell, and J. L. White, *J. Appl. Polym. Sci.* **22**, 3121 (1978).
10. A. J. de Vries, *Pure Appl. Chem.* **53**, 1011 (1981).
11. A. J. de Vries, *Pure Appl. Chem.* **54**, 647 (1982).
12. D. T. Grubb, *J. Polym. Sci., Polym. Phys. Ed.* **21**, 165 (1983).
13. D. Thirion and J. F. Tassin, *J. Polym. Sci., Polym. Phys. Ed.* **21**, 2097 (1983).
14. G. Attalla, I. B. Guanella, and R. E. Cohen, *Polym. Eng. Sci.* **23**, 883 (1983).
15. A. Takaku, *J. Appl. Polym. Sci.* **26**, 3565 (1981).
16. A. Takaku, *J. Appl. Polym. Sci.* **25**, 1861 (1980).
17. G. M. Bryant, *Text. Res. J.* **37**, 552 (1967).
18. L. Reich and S. S. Stivala, *Rev. Macromol. Chem.* **1**, 249 (1966).
19. D. J. Carlsson and D. M. Wiles, *J. Macromol. Sci. Rev., Macromol. Chem.* **14**, 65 (1976).
20. D. J. Carlsson, A. Garton, and D. M. Wiles, in G. Scott, ed., *Developments in Polymer Stabilisation*, Applied Science Publishers, London, 1979, p. 219.
21. F. Gugumaus, in Ref. 20, p. 261.
22. L. M. Landoll and A. C. Schmalz, private communication, Hercules Inc., Oxford, Ga., 1986.
23. J. Green, in M. Lewin, S. M. Atlas, and E. M. Pierce, eds., *Flame-Retardant Polymeric Materials*, Vol. 3, Plenum Press, New York, 1982, Chapt. 1.
24. U.S. Pat. 3,873,646 (Mar. 25, 1975), H. D. Irwin (to Lubrizol Corp.).
25. U.S. Pat. 3,653,803 (Apr. 4, 1972), H. C. Frederick (to E. I. du Pont de Nemours & Co., Inc.).
26. U.S. Pat. 3,639,513 (Feb. 1, 1972), K. Sadakata, Mitaka-shi, M. Sasaki, H. Masahiro, Yamaguchi-ken, Y. Nakamura, Y. Mikida, K. Ito, and K. Kimura (to Mitsubishi Rayon Co., Ltd.).
27. U.S. Pat. 3,433,853 (Mar. 18, 1969), R. H. Earle, A. C. Schmalz, and C. A. Soucek (to Hercules Inc.).
28. K. Hawn and R. Meriggi, *Nonwovens World* 44 (Sept. 1987).
29. H. Krassig, *J. Polym. Sci., Macromol. Rev.* **12**, 321 (1977).
30. W. Minoshima, J. L. White, and J. E. Spruiell, *Polym. Eng. Sci.* **20**, 1166 (1980).
31. O. Ishizuka and co-workers, *Sen-i Gakkaishi* **31**, T372 (1975).
32. S. Kase and T. Matsuo, *J. Polym. Sci., Part A* **3**, 2541 (1965).
33. S. Kase and T. Matsuo, *J. Appl. Polym. Sci.* **11**, 251 (1967).
34. C. D. Han and R. R. Lamonte, *Trans. Soc. Rheol.* **16**, 447 (1972).
35. R. R. Lamonte and C. D. Han, *J. Appl. Polym. Sci.* **16**, 3285 (1972).
36. F. Fourne, *IFJ* **3**, 30 (Aug., 1988).
37. C. Prost and co-workers, *Makromol. Chem., Macromol. Symp.* **23**, 173 (1989).
38. H. P. Nadella, H. M. Henson, J. E. Spruiell, and J. L. White, *J. Appl. Polym. Sci.* **21**, 3003 (1977).
39. D. G. H Ballard and co-workers, *Polymer* **20**, 399 (1979); **23**, 1875 (1982).
40. W. C. Sheehan and T. B. Cole, *J. Appl. Polym. Sci.* **8**, 2359 (1964).
41. Ref. 20, p. 1541.
42. R. Wiedermann, *Chemiefasern Textilind.* **28/80**, 888 (1978).
43. D. M. Gezovich and P. H. Geil, *Polym. Eng. Sci.* **8**, 210 (1968).
44. C. P. Buckley and M. Habibullah, *J. Appl. Polym. Sci.* **26**, 2613 (1981).
45. H. Bodaghi, J. E. Spruiell, and J. L. White, *Intern. Polym. Processing* **III**, 100 (1988).
46. A. Garten and co-workers, *J. Polym. Sci., Polym. Phys. Ed.* **15**, 2013 (1977).
47. U.S. Pat. 3,137,746 (June 16, 1964), D. E. Seymour and D. J. Ketteridge (to Smith and Nephew, Ltd.).
48. U.S. Pat. 4,085,175 (Apr. 18, 1978), H. W. Keuchel (to PNC Corp.).

49. *Text. Month* 10 (Aug. 1983).
50. D. O. Taurat, *IFJ* **3**, 24 (May 1988).
51. W. R. Baker, *IFJ* **7**, 7 (Apr. 1992).
52. R. R. Buntin and D. T. Lohkamp, *TAPPI* **56**, 74 (1973).
53. J. Zhou and J. E. Spruiell, *Nonwovens—An Advanced Tutorial*, TAPPI Press, Atlanta, Ga., 1989.
54. L. C. Wadsworth and A. M. Jones, Paper presented at *INDA/TEC, The International Nonwovens Technological Conference*, Philadelphia, Pa., June 2–6, 1986.
55. A. M. Jones and L. C. Wadsworth, Paper presented at *TAPPI 1986 Nonwovens Conference*, Atlanta, Ga., Apr. 21–24, 1986.
56. T. W. Rave, *Chemtech* **15**, 54 (Jan. 1985).
57. T. Ohta, *Polym. Eng. Sci.* **23**, 697 (1983).
58. M. Kamezawa, K. Yamada, and M. Takayanagi, *J. Appl. Polym. Sci.* **24**, 1227 (1979).
59. H. H. Chuah and R. S. Porter, *J. Polym. Sci., Polym. Phys. Ed.* **22**, 1353 (1984).
60. J. L. White and J. F. Fellers, *J. Appl. Polym. Sci., Appl. Polym. Symp.* **33**, 137 (1978).
61. P. Smith and P. J. Lemstra, *Makromol. Chem.* **180**, 2983 (1979).
62. P. Smith and P. J. Lemstra, *J. Mater. Sci.* **15**, 505 (1980).
63. P. Smith and P. J. Lemstra, *Polymer* **21**, 1341 (1980).
64. B. Kalb and A. J. Pennings, *Polymer* **21**, 3 (1980).
65. B. Kalb and A. J. Pennings, *J. Mater. Sci.* **15**, 2584 (1980).
66. A. F. Wills, G. Capaccio, and I. M. Ward, *J. Polym. Sci., Polym. Phys. Ed.* **18**, 493 (1980).
67. R. C. Wincklhofer, Paper presented at *TAPPI 1985 Nonwovens Symposium*, Myrtle Beach, S.C., Apr. 21–25, 1985.
68. U.S. Pat. 4,413,110 (Nov. 1, 1983), S. Kavesh and D. C. Prevorsek (to Allied-Signal Inc.).
69. R. J. Samuels, *J. Polym. Sci., Polym. Phys. Ed.* **17**, 535 (1979).
70. S. L. Cannon, G. B. McKenna, and W. O. Statton, *J. Polym. Sci., Macromol. Rev.* **11**, 209 (1976).
71. B. Davenport, W. Cox, F. Dubois, and M. Yoneyama, *Chemical Economics Handbook*, SRI International, Menlo Park, Calif., Nov. 2000.
72. B. F. Hadjuk, T. Sasano, and S. Schlag, *Chemical Economics Handbook*, SRI International, Menlo Park, Calif., Jan. 2003.
73. *Am. Tex.* **13**, 44 (Dec. 1984).
74. R. G. Mansfield, *Nonwovens Ind.* **16**, 26 (Feb. 1985).
75. W. Shoemaker, *Nonwovens Ind.* **15**, 52 (Oct. 1984).
76. D. J. Hannant, *Fiber Cements and Fiber Concretes*, John Wiley & Sons, Inc., New York, 1978.
77. *Nonwovens Rept.* **87**, 1 (July 1978).
78. U.S. Pat. 4,492,781 (Jan. 8, 1985), F. J. Duszak, J. P. Modrak, and D. Deaver (to Hercules Inc.).
79. J. P. Modrak, Paper presented at *19th Paving Conference and Symposium*, Albuquerque, N. Mex., Jan. 12, 1982.
80. A. G. Bondarenko and co-workers, *Fibre Chem.* **14**, 246 (May–June 1982).
81. *Daily News Record* **11**, 12 (May 4, 1981).

CARL J. WUST
FiberVisions
ERIK GRANN GAMMELGAARD
FiberVisions

OLEFIN-SULFUR DIOXIDE POLYMERS. See POLYSULFONES.

OPTICAL PROPERTIES. See Volume 7.

ORGANOMETALLIC POLYMERS. See METAL CONTAINING POLYMERS.

ORIENTED FILMS. See FILMS, ORIENTATION.

OXIDATIVE POLYMERIZATION

Introduction

Oxidative polymerization is, formally, abstraction of two hydrogen atoms from a monomer to give a polymer, and thus may be classified as polycondensation. The applicable monomers are mainly aromatic compounds. Electrical and chemical oxidation methods are often used, in which catalysis with dioxygen or hydrogen peroxide is the most favorable; the reaction temperature is moderate and the by-product is water only. Oxidative polymerization is one of the cleanest and lowest loading methods in polycondensation. However, the reaction mechanism is unclear in many cases and the coupling selectivity is not generally easy to control.

This article deals with oxidative polymerization of phenols, anilines, thiophenol derivatives, aromatic hydrocarbons, heterocyclic aromatics, and other monomers. The reaction mechanism, the coupling selectivity, and the characteristics of the resulting polymers are discussed.

2,6-Disubstituted Phenols

Until the 1950s, oxidation of 2,6-dimethylphenol (2,6-Me_2P) by an oxidant like benzoyl peroxide (1) or alkaline ferricyanide (2) mainly gave 3,3′,5,5′-tetramethyldiphenoquinone (DPQ) (Fig. 1). In 1959, oxidative polymerization of 2,6-Me_2P catalyzed by CuCl/pyridine (Py) under dioxygen leading to poly(2,6-dimethyl-1,4-phenylene oxide) (Poly-2,6-Me_2P) was discovered (3). Various catalysts such as copper/substituted-ethylenediamine complexes were developed and Poly-2,6-Me_2P was found completely miscible with polystyrene (4) (see POLYETHERS, AROMATIC).

Oxidative Coupling Mechanism. Poly-2,6-Me_2P is a C—O coupling product and DPQ is a product via C—C coupling. Control of the C—O coupling is a most important question (5). Three possible reaction mechanisms for the C—O coupling

Encyclopedia of Polymer Science and Technology. Copyright John Wiley & Sons, Inc. All rights reserved.

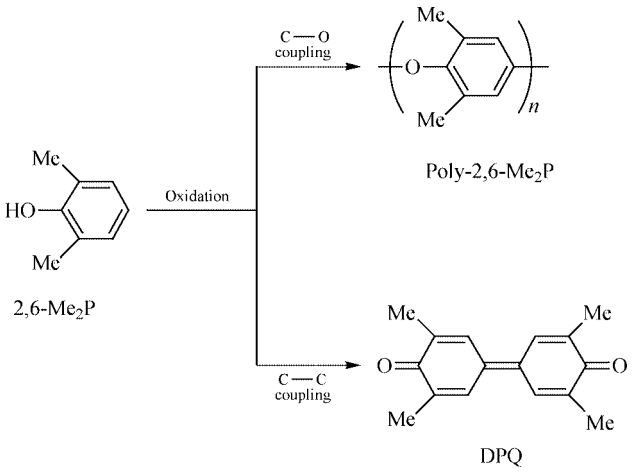

Fig. 1. Oxidation of 2,6-dimethylphenol.

selectivity have been proposed as follows: (*1*) coupling of free phenoxy radicals resulting from one-electron-oxidation of 2,6-Me_2P, (*2*) coupling of phenoxy radicals coordinated to a catalyst complex, and (*3*) coupling through phenoxonium cation formed by two-electron-oxidation of 2,6-Me_2P (Fig. 2).

Coupling of Phenoxy Radicals Coordinated to Catalyst Complex. Because the oxidative coupling of 2,6-Me_2P with benzoyl peroxide or alkaline ferricyanide affords DPQ as the main product (1,2), it seems that the free phenoxy radical leads to C—C coupling. C—O coupling results from the phenoxy radical

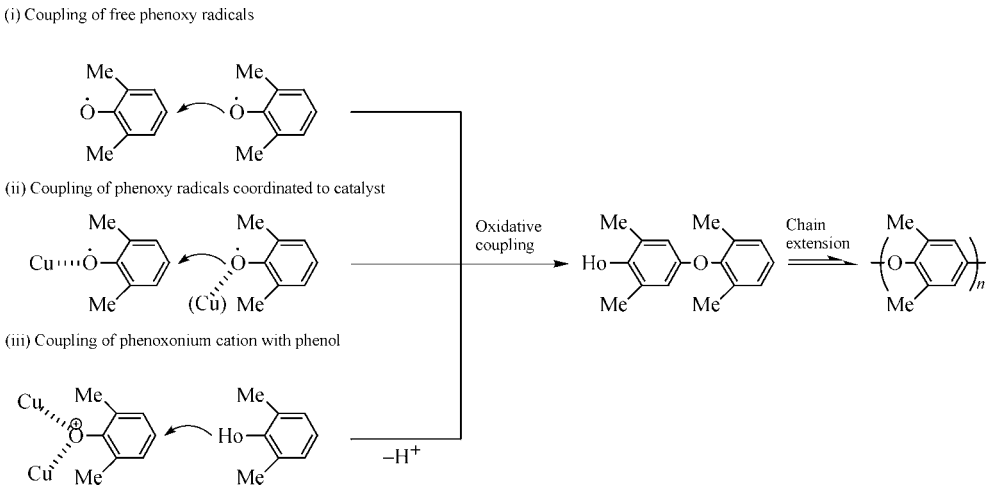

Fig. 2. Three possible mechanisms for C—O coupling in the oxidative polymerization of 2,6-dimethylphenol.

coordinated to the copper complex [(ii) in Fig. 2]. In CuCl/Py catalysis, increasing the amount of Py to copper (6,7) favors the C—O coupling. Substituents at the 2,6-positions of Py (6) or high reaction temperature (8) makes the C—C coupling favorable.

The kinetic study of Cu/Py catalysis showed that the oxidative polymerization proceeded by a Michaelis–Menten-type reaction mechanism and the C—O coupling is preferred when at least one of the radicals is coordinated to copper (9). ESR measurements using a copper(II) acetate/Py complex (10), where Py/Cu = 20, showed two phenoxo-copper(II) complexes, and the oxidative polymerization gave mainly Poly-2,6-Me_2P. For Py/Cu = 2, none of phenoxo-copper(II) complexes was detected and the major product was DPQ. Thus, these data suggest that coupling via the coordinated phenoxy radicals mainly leads to the C—O coupling.

Coupling of Phenoxonium Cation with 2,6-Dimethylphenol. No ESR signals of free phenoxy radicals in the oxidation of 2,6-Me_2P with a [CuCl(OCH_3)Py] complex were detected (11). It was assumed that the phenoxy radical was oxidized by the Cu(II) complex (totally two-electron-oxidation from the phenol) to give the phenoxonium cation, which can couple with the phenol leading to C—O coupling [(iii) in Fig. 2]. For a Cu/*N*-methylimidazole (NMI) catalyst, the reaction order in copper changed from 1.22 at NMI/Cu=10 to 1.70 at NMI/Cu=75, and the selectivity for the C—O coupling reached a maximum at the NMI/Cu ratio of at least 30 (12). From the data, the key intermediate may be a μ-phenoxo dicopper(II) complex, in which two-electron-transfer from phenoxo moiety to two copper atoms can give a phenoxonium cation.

By ab initio calculation, the atomic charges for the phenol, phenolate anion, phenoxy radical, phenoxonium cations of 2,6-Me_2P were determined (13). Since the oxygen atoms in all the species were negative, it was considered that the species susceptible to the C—O coupling has positive charge on the *para*-carbon, and therefore, it should be the phenoxonium cation. The coupling of the phenoxy radicals was excluded, because the treatment of 2,6-Me_2P with benzoyl peroxide yielded DPQ (1). The reaction between the phenoxy radical and phenol was ruled out, because 2,6-dimethylanisole did not react in the oxidative polymerization of 2,6-Me_2P (14).

If the oxidative coupling of 2,6-Me_2P proceeds via the phenoxonium cation, in the presence of a nucleophilic reagent in excess to the phenol, the phenoxo cation should react with the nucleophile, and hence, Poly-2,6-Me_2P cannot be obtained. In fact, it was found that the oxidative polymerization of 2,6-Me_2P catalyzed by a Cu(tmed) (tmed: *N,N,N′,N′*-tetramethylethylenediamine) complex with an excess amount of *n*-pentylamine produced Poly-2,6-Me_2P in 75% yields (5). The nucleophilicity of *n*-pentylamine toward benzyl chloride was confirmed to be much greater than that of 2,6-Me_2P. These facts strongly indicate that such electrophilic intermediates as a phenoxonium cation are not involved in the oxidative polymerization.

Coupling of Free Phenoxy Radicals. The above two mechanisms [(ii) and (iii) in Fig. 2] are based on the assumption that the coupling via free phenoxy radicals of 2,6-Me_2P leads to the C—C coupling mainly. With alkaline ferricyanide (2), DPQ was produced in 45–50% but the other half of the oxidized material was a yellow nonketonic polymer, probably Poly-2,6-Me_2P. On the other hand, the oxidation with benzoyl peroxide afforded the C—C coupling products in total 60% yield (1).

However, detailed analysis for this oxidation reaction showed that the reaction mechanism did not involve radical intermediates but rather a benzoyl perester intermediate (15). It was reported that the thermal decomposition of benzoyl 2,6-dimethylphenyl carbonate, which should generate the phenoxy radical, produced Poly-2,6-Me_2P and DPQ in 35–38% and 10% yield, respectively (16). From these studies, it seems that some complicated experimental results and different understandings were involved in the above assumption of the C—C coupling selectivity in the free-radical coupling, which was pointed out before (17).

In addition, many studies on the oxidative coupling of 2,6-Me_2P with inorganic oxidants were performed, and in some cases the free radical was observed. The oxidation with MnO_2, PbO_2, and Ag_2O produced Poly-2,6-Me_2P in 60–95% yields. For MnO_2 (18) and Ag_2O (19), the free radicals of 2,6-Me_2P and Poly-2,6-Me_2P were detected by ESR measurements. By the addition of increasing amount of triethylamine in oxidative polymerization with PbO_2, the formation of DPQ was suppressed and the yield of Poly-2,6-Me_2P was increased (20). On the other hand, the oxidation by hexachloroiridate(IV) anion in an acidic aqueous solution afforded DPQ in 55–65% (21).

It was considered from the above studies (20,21) that the selectivity for the C—O or C—C coupling of 2,6-Me_2P was much affected by a coexisting base or acid. Recently, oxidative coupling of 2,6-Me_2P with Ag_2CO_3 was examined in the presence of excess *n*-pentylamine (nPA) or acetic acid (AcOH) (5). The ratio of the products Poly-2,6-Me_2P and DPQ was 50/50 without these additives, >99/∼0 with nPA, and 0/100 with AcOH. These data indicate that generally in the oxidative coupling of 2,6-Me_2P the addition of a base would lead to the C—O coupling and that of an acid to the C—C coupling.

The above observations may be explained by the following proposal (22): in basic reaction media, a free phenoxy radical is formed leading to C—O coupling [(i) in Fig. 2], and in acidic reaction media, a phenoxonium cation could be generated to give the C—C coupling. In the electrochemical oxidation of 2,6-Me_2P, the oxidation above pH 5.2 takes place via two monoelectronic steps, the first of which forms the free phenoxy radical; the oxidation below pH 5.2 undergoes one dielectronic step, which might generate the phenoxonium cation (23). It is still unclear whether or not the phenoxonium cation is really involved as the intermediate in the oxidative coupling; however, at least the phenoxonium cation should be easier to form under acidic conditions than under basic conditions.

To summarize on the above observations about the reaction mechanisms, the C—O/C—C coupling selectivity in the oxidative polymerization of 2,6-Me_2P appears to be as follows (5).

(1) The coupling via coordinated phenoxy radicals and the coupling of free phenoxy radicals under basic conditions would mainly lead to the C—O coupling.
(2) The coupling of free phenoxy radicals under acidic conditions or the coupling of phenoxonium cations from the two electron oxidation with phenol would favor the C—C coupling.

Chain Extension Mechanism. The chain extension mechanism in the oxidative polymerization of 2,6-Me_2P has been almost established (Fig. 3). It has

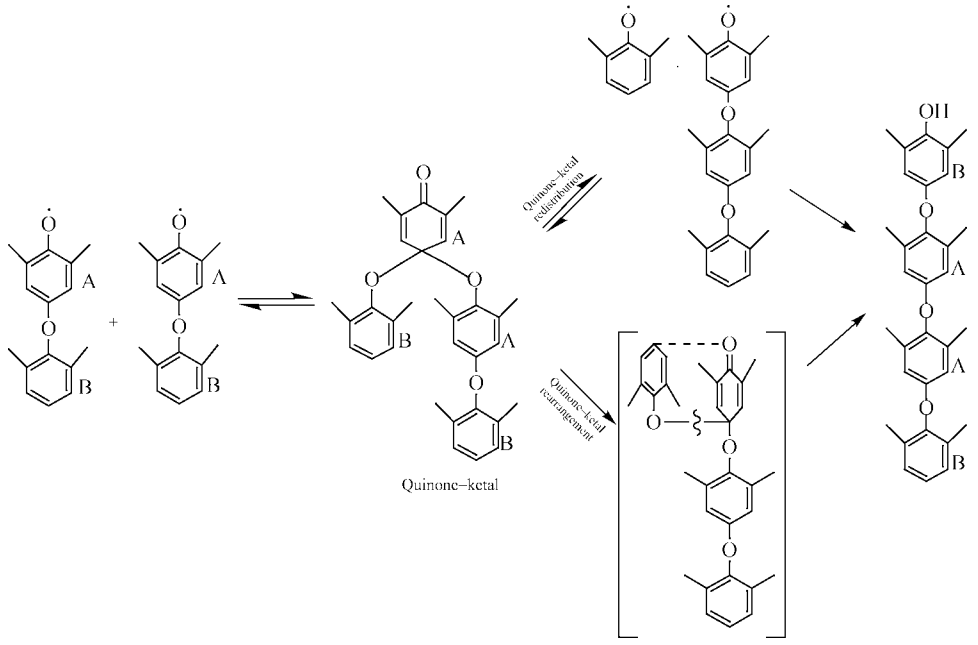

Fig. 3. Chain extension in the oxidative polymerization of 2,6-dimethylphenol.

been widely accepted that two dimeric phenoxy radicals couple with each other to give a quinone-ketal intermediate, which has not been detected. No reactivity of the tail phenoxy group (marked B in Fig. 3) was observed, because the π-conjugation is cut off by the ether bond (25); ie, the head-tail coupling mechanism, in which the oxygen atom of head phenol unit couples at the *para*-carbon atom of tail phenoxy group (24), is excluded. The oxidation of a 4-phenoxyphenol marked with methyl group (let it be A-B as two distinguishable aromatic rings) yielded none of the dimer through a head-tail coupling (A-B-A-B) but the dimer through a quinone-ketal intermediate (B-A-A-B) (26).

Two reaction routes from a quinone-ketal intermediate to a tetramer were proposed; one is a quinone-ketal redistribution to give a monomer radical and a trimer radical (27), and the other is a quinone-ketal intramolecular rearrangement (28). The oxidative polymerization from 2,6-Me_2P dimer produced the oligomers of even numbers such as 2,6-Me_2P itself and the trimer (27,29). From these data, the extension mechanism for the oxidative polymerization of 2,6-Me_2P definitely involves quinone-ketal redistribution and it is unclear whether or not quinone-ketal rearrangement actually occurs. For 2-methyl substituted and 2,6-unsubstituted 4-phenoxyphenols, only quinone-ketal rearrangement took place at a low temperature; however, at higher reaction temperatures, quinone-ketal redistribution also occurred (26). Application of the redistribution mechanism resulted in the modification (30–32) and depolymerization (33) of Poly-2,6-Me_2P.

In general, the oxidative polymerization of phenols undergoes a stepwise growth mechanism, although the electrochemical oxidative polymerization has been suggested to be a chain reaction mechanism (34). However, phenolic dimers

and higher oligomers have electron-donating phenoxy groups at *p*-positions and become easier to oxidize (more reactive) than phenolic monomers. Therefore, until the monomer is almost consumed, the reaction mixture consists mainly of the monomer and polymer, and so it often seems to proceed formally via chain reaction mechanism, but it is actually reactive intermediate polycondensation (35).

Other 2,6-Disubstituted Monomers. Various poly(2,6-substituted-1,4-phenylene oxide)s possessing alkyl, aryl, alkoxyl, and halogen groups have been produced (see POLYETHERS, AROMATIC). Recently, some functional polymers (36–39) were synthesized, one of which was converted to a heterocyclic ladder polymer (39). Poly(2,6-difluoro-1,4-phenylene oxide)s with crystallinity (40) and no crystallinity (41) were synthesized. By enzyme catalysis, oxidative polymerization of 3,5-disubstituted-4-hydroxybenzoic acids, with liberation of carbon dioxide, produced poly(2,6-disubstituted-1,4-phenylene oxide)s (42,43).

2- and/or 6-Unsubstituted Phenols

A phenoxy radical intermediate has four reactive positions: the oxygen and *para*-carbon as well as two *ortho*-carbons. Therefore, for *o*-unsubstituted phenols, it is difficult to regulate the coupling selectivity. Enzyme catalysts and enzyme model catalysts have been studied for the control of the polymerization of 2- and/or 6-unsubstituted phenols.

Enzyme Catalyst. Oxidative coupling of phenols is involved in some biological reactions; for example, formation of lignin (qv) or melanin is catalyzed by oxidoreductase enzymes such as peroxidase, oxidase, or oxygenase (44,45). In 1983, horse radish peroxidase (HRP) catalyst was used to remove phenols from waste water, affording water-insoluble low molecular weight phenolic polymers (46). Since HRP was employed as the polymerization catalyst (47–49), the polymerization of various phenols by using HRP with hydrogen peroxide or laccase (an oxidase) with dioxygen has been extensively investigated (50,51). These enzymes show high catalytic activity for generating free radicals from phenols, but are unable to control the coupling selectivity (52).

In oxidative polymerization of phenol by HRP catalyst (53,54), soluble polyphenol was obtained for the first time by controlling the polymer structure and molecular weight (55). Regio-controlled poly(hydroxyphenylene) was synthesized by using poly(ethylene glycol) (PEG) as template (eq. 1) (56). The enzyme-catalyzed oxidative polymerizations of alkylphenols (57–61), biphenols (62–64), and various functional phenols (65–70) were also performed. For glucose-β-D-hydroquinone, only C—C coupling at *o*-positions was claimed (eq. 2) (65). Chemoselective polymerization of a phenolic monomer having a methacryloyl group (eq. 3) (71) and an ethynyl group (72) was achieved and gave the corresponding polyphenol. "Artificial urushi" was prepared by laccase-catalyzed cross-linking reactions of urushiol analogues (73,74). (see ENZYMATIC POLYMERIZATION).

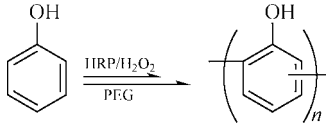

(1)

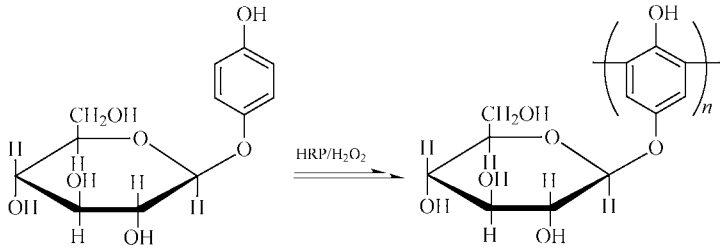

(2)

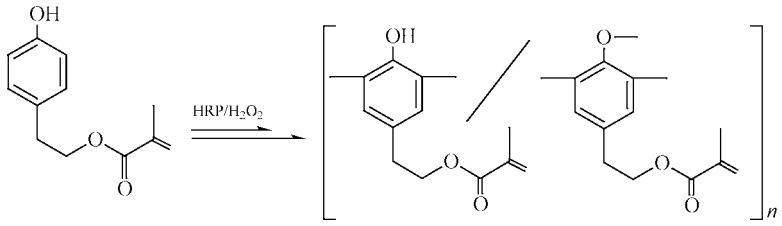

(3)

Peroxidase Model Catalyst. An *N,N′*-bis(salicylidene)ethylenediamino iron [Fe(salen)] complex was found to be a cheap peroxidase model catalyst for oxidative polymerization of phenols with hydrogen peroxide (75–79). Hematin also polymerized ethylphenol in a reaction mechanism similar to that for HRP (80).

Tyrosinase Model Catalyst ("Radical-Controlled" Oxidative Polymerization Catalyst). Conventional copper catalysts were not able to give useful polymers from phenols having at least one *o*-position unsubstituted (26,81,82). Peroxidase (HRP), oxidase (laccase), and peroxidase-model [Fe(salen)] catalysts also showed a limited ability for controlling the coupling selectivity of such phenols (5,53). New copper catalysts were then studied. Copper(I)/diamine complexes, typical conventional catalysts, reacted with dioxygen to give bis(μ-oxo) dicopper(III) complexes (83). In the reaction of HRP with hydrogen peroxide, Fe(IV)=O intermediates were formed (84). These active oxygen complexes were subjected to the reaction with phenols to afford "free" phenoxy radical species (83,85). These data suggest that the regioselective coupling cannot be achieved by the catalysts generating "electrophilic" or "radical" active oxygen species.

Then, a working hypothesis was made (Fig. 4) (86,87): if a catalyst generates only a "nucleophilic," strictly speaking "basic," μ-η^2:η^2-peroxo dicopper(II)complex **1** (88,89), it will abstract a proton (not a hydrogen atom) from phenol to give phenoxo–copper(II) complex **2**, equivalent to phenoxy radical–copper(I) complex **3**. Intermediate species **2** and/or **3** are not "free" radicals but "controlled" radicals, and therefore regioselectivity of the subsequent coupling will be entirely regulated. The difficulty for conventional catalysts to control the regioselectivity (90,91) is probably due to generation of free radicals. This new concept is characterized by the exclusive formation of controlled phenoxy radicals, and hence the new concept was termed a "radical-controlled" oxidative polymerization (87).

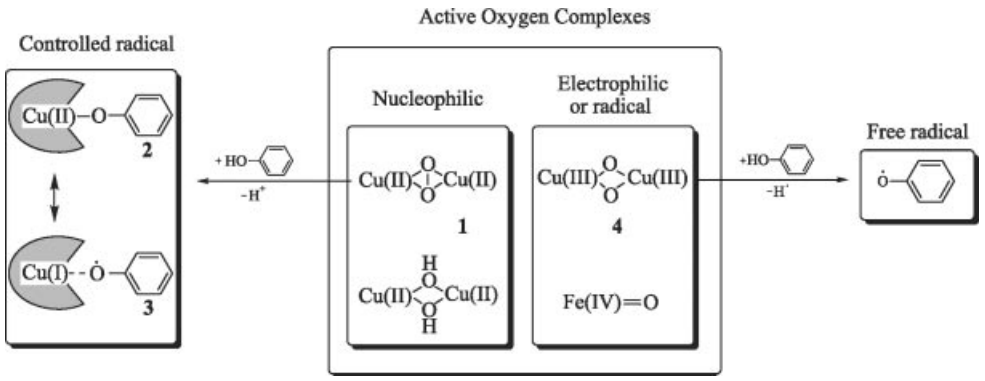

Fig. 4. Nucleophilic vs electrophilic active oxygen complexes.

Oxidative Polymerization of 4-Phenoxyphenol by Tyrosinase Model Catalyst. "Radical-controlled" oxidative polymerization of 4-phenoxyphenol (PPL) catalyzed by tyrosinase model complexes has been developed (eq. 4)(86,87,92,93).

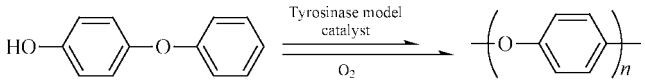

PPL PPO (4)

This was the first simple synthesis of crystalline poly(1,4-phenylene oxide) (PPO) having a melting point by the catalytic oxidative polymerization method, although other time-consuming synthesis procedures have been reported (94–96). As the tyrosinase model, (hydrotris(3,5-diphenyl-1-pyrazolyl)borate) copper [Cu(Tpzb)] complex (**5**) and (1,4,7-R_3-1,4,7-triazacyclononane) copper [$Cu(L^R)$: R = isopropyl (iPr), cyclohexyl (cHex), and *n*-butyl (nBu)] complexes (**6**) were employed.

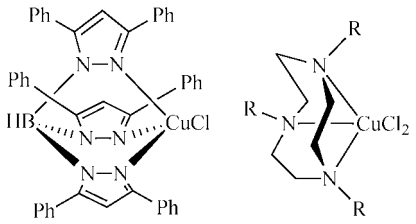

5 **6**

To examine the coupling selectivity, the ratio of oxidative coupling dimers formed at the initial stage of polymerization of PPL was investigated (Table 1) (86,87). CuCl/*N*,*N*,*N*′,*N*′-tetraethylethylenediamine (teed), which was the sole catalyst reported for oxidative coupling of PPL (26), was also employed (entry 7). As a model system of free phenoxy radical coupling, an equimolar amount of 2,2′-azobisisobutyronitrile (AIBN) was used for the oxidation of PPL (entry 8). In the

Table 1. Dimer Ratio at Initial Stage of Oxidative Polymerization of 4-Phenoxyphenol

				Initial dimer ratio, %			
Entry	Catalyst	Oxidant	Solvent	**7**	**8**	**9**	**10**
1	Cu(Tpzb)Cl[a]	O_2	Toluene	91	9	0	0
2	Cu(Tpzb)Cl[a]	O_2	THF	91	9	0	0
3	$Cu(L^{iPr})Cl_2$[a]	O_2	Toluene	93	7	0	0
4	$Cu(L^{iPr})Cl_2$[a]	O_2	THF	89	7	1	3
5	$Cu(L^{cHex})Cl_2$[a]	O_2	Toluene	95	5	0	0
6	$Cu(L^{nBu})Cl_2$[a]	O_2	Toluene	90	9	0	1
7	CuCl/teed[a]	O_2	Toluene	79	6	2	13
8	[b]	AIBN	Toluene	82	4	2	12

[a] Polymerization of PPL (0.60 mmol) with Cu complex (0.030 mmol) and 2,6-diphenylpyridine (0.30 mmol) in solvent (1.2 g) under dioxygen (101.3 kPa) at 40°C. CuCl (0.030 mmol) and teed (0.015 mmol) was used as the Cu complex in entry 7.
[b] Oxidized by AIBN (0.60 mmol) under nitrogen at 40°C.

case of CuCl/teed, four dimers were detected and the structures of the dimers were identified as **7**, **8**, **9**, and **10**. Products **7** and **8** are formed by C—O coupling, and formation of **9** and **10** is based on C—C coupling.

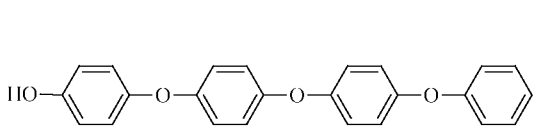

7

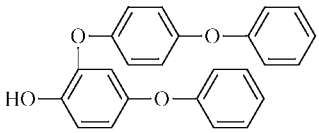

8

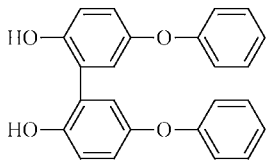

9

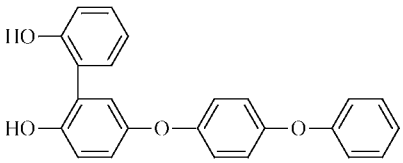

10

For the CuCl/teed catalyst, considerable amounts of the two C—C coupling dimers of **9** and **10** were detected and **7** selectivity was low (79%). The dimer ratio was very similar to that via free-radical coupling by AIBN oxidation, in which considerable amounts of the C—C coupling dimers were observed. However, for Cu(Tpzb) (**5**) in toluene and in THF, and for the $Cu(L^{iPr})$, $Cu(L^{cHex})$, and $Cu(L^{nBu})$ (**6**) in toluene, none or very little of the C—C coupling dimers were detected, showing high regioselectivity of **7**. The order of **7** selectivity was $Cu(L^{nBu})$ (90%) < $Cu(L^{iPr})$ (93%) < $Cu(L^{cHex})$ (95%), in good agreement with that of steric hindrance of the substituents (87). These data show that the regioselectivity of phenoxy radical coupling can be controlled by these catalysts. The dimerization catalyzed by the $Cu(L^{iPr})$ in THF gave C—C coupling dimers to some extent.

The resulting polymer was isolated as a methanol-insoluble part. In the cases with little or no C—C dimer formation (entries 1–3,5,6), white powdery polymers

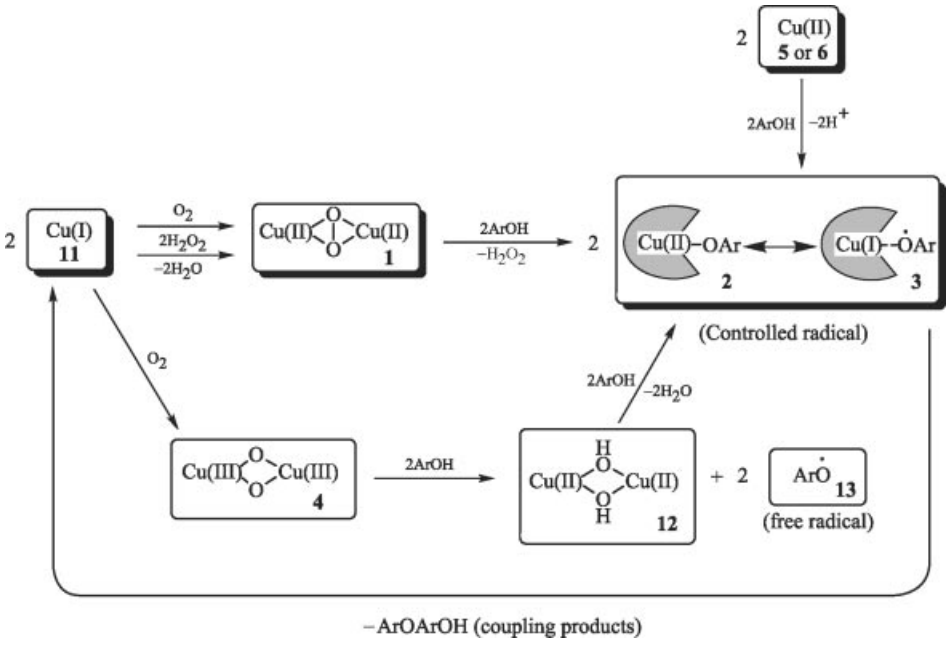

Fig. 5. Reaction mechanism for copper complex catalysis of oxidative polymerization.

with M_w of 700–4700 were obtained. The IR spectrum patterns of the polymers were very similar to that of PPO synthesized by Ullmann condensation (95). From the DSC analysis, the polymers showed melting points (T_m) at 171–194°C. In polymerizations giving considerable amounts of the C—C dimers (entries 4,7,8), the brownish polymers showed no clear melting points in the DSC traces.

Reaction Mechanism of Catalytic Cycle. On the basis of the above data, the reaction mechanism for the copper complex catalysis is postulated as follows (Fig. 5). First, the starting copper(II) chloride complex Cu(Tpzb)Cl (**5**) or $Cu(L^R)Cl_2$ (**6**) reacts with PPL or oligomers of PPL to give phenoxo-copper(II) complex (**2**), equivalent to phenoxy radical-copper(I) complex (**3**). Regioselective coupling takes place between two molecules of **2** and/or 3 to produce copper(I) complexes (**11**) as well as the phenylene oxide products having *p*-linkage selectively, because the steric hindrance of the catalysts blocks the coupling at *o*-positions.

In case of the Cu(Tpzb) complex (**5**), formation of μ-η^2:η^2-peroxo dicopper(II) complex (**1**) from **11** was confirmed under dioxygen (89) in both toluene and THF. For the $Cu(L^{iPr})$ complex as well as the $Cu(L^{cHex})$ and $Cu(L^{nBu})$ complexes (**6**), it was reported that **11** afforded complex **1** in nonpolar solvents such as toluene (97). **1** reacts with phenols to regenerate **2** (98) and hydrogen peroxide (99). Hence, this catalytic system would allow only the regioselective coupling process from **2** and/or **3** and completely exclude free-radical coupling reactions; the present reaction is thus recognized as "radical-controlled" oxidative polymerization.

For the $Cu(L^{iPr})$ complex under dioxygen in THF, **11** gave bis(μ-oxo) dicopper(III) complex (**4**) (97). **4** abstracts hydrogen atoms from phenols to give bis(μ-hydroxo) dicopper(II) complex (**12**) and free phenoxy radical (**13**). Therefore,

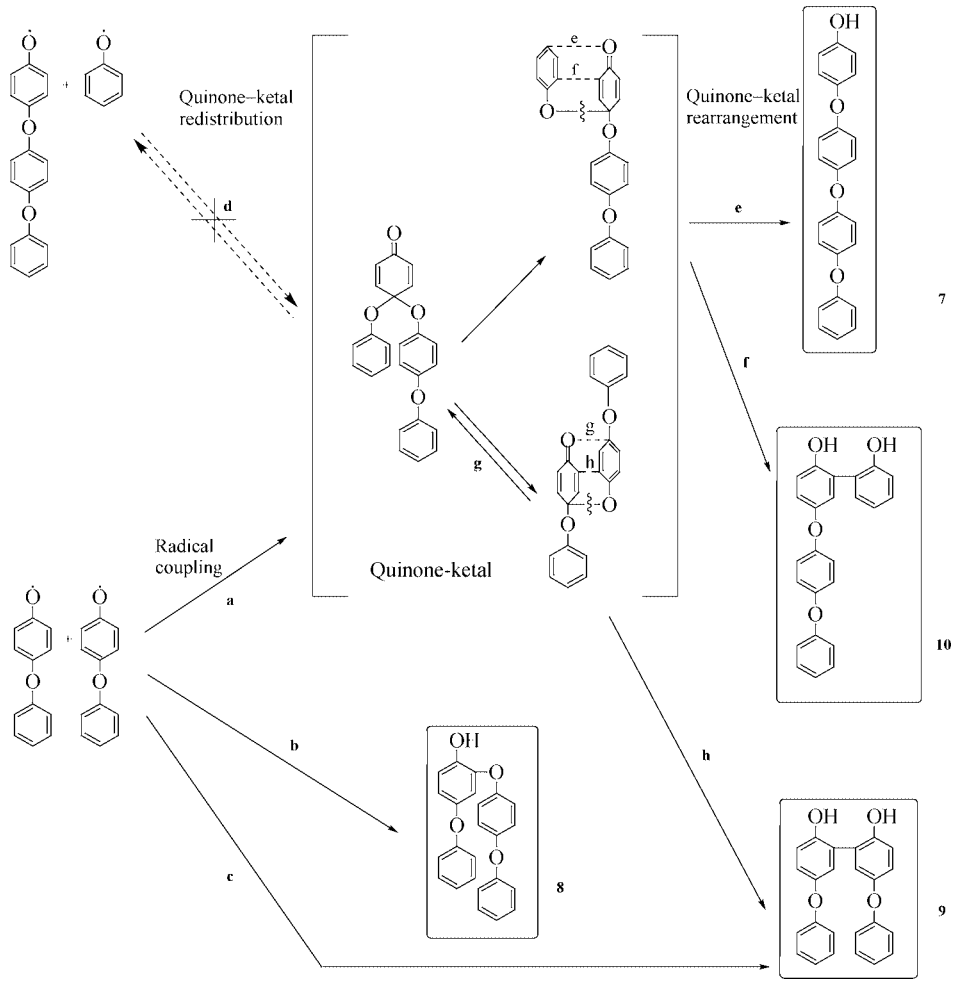

Fig. 6. Reaction mechanism for oxidative coupling and chain extension of 4-phenoxyphenol.

this catalytic cycle involves the free-radical coupling with the formation of C—C linkages, although production of **2** from complex **12** also takes place (100). The CuCl/teed complex also reacts with dioxygen to give **4** (83).

Two computational studies have been performed; one disagreed with the above reaction mechanism (101), but the other was in good agreement (102).

Reaction Mechanism of Oxidative Coupling and Chain Extension. Figure 6 shows a specrulative reaction mechanism for oxidative coupling of PPL to produce dimers (87,92). For simplicity, the mechanism is argued here by expressing intermediate structures in the form of free radical rather than controlled radicals. First, two phenoxy radicals are generated from PPL and couple to each other (radical coupling); then only three reaction routes (**a**, **b**, and **c**) can take place, giving rise to a quinone-ketal intermediate, **8** and **9**, respectively. From the quinone-ketal, the redistribution path (quinone-ketal redistribution, **d**) was

ruled out, and therefore the rearrangement path (quinone-ketal rearrangement) is proposed in the oxidative coupling of PPL. On cleavage of the ketal C—O bond, synchronous bond formation of route **e** to **7**, that of **f** to **10**, and that of **h** to **9** can occur, but that of **g** regenerates the quinone-ketal.

In the "radical-controlled" oxidative coupling of PPL, the radical coupling takes place from controlled phenoxy radical–copper(I) intermediate. Therefore, the steric effect of the catalyst would suppress **8** formation (route **b**) and inhibit **9** formation (route **c**), mainly giving quinone-ketal intermediate (route **a**). Moreover, almost no detection of **10** as well as **9** shows that the catalyst must be kept interacting with the quinone-ketal intermediate during the rearrangement. Probably, the carbonyl group of the quinone-ketal coordinates to the copper(I) atom of the catalyst. Thereby, bond formation at the *o*-position to **10** and **9** via routes **f** and **h**, respectively, would be protected and give **7** predominantly via route **e**. Further chain extension follows in a similar way to that of dimerization.

Oxidative Polymerization of Other Phenols by Tyrosinase Model Catalyst. The substituent effect of phenol monomers on the reaction rates has been investigated (103). For the Cu(tmed) catalyst, the reaction rates were governed by the O—H homolytic bond dissociation energies of the monomers, which are closely related to the electronic effect of substituents. On the other hand, for the Cu(L^{iPr}) catalyst, the steric effect of substituents at the *o*-positions depressed the reaction rates.

In the oxidative polymerization of phenol, the Cu(L^{iPr}) catalyst showed high selectivity for C—O coupling; however, it did not exclude the formation of C—C coupling (104). The resulting polymer consisted mainly of a 1,4-phenylene oxide unit but contained a considerable amount of C—C coupling structures, showing no crystallinity. The oxidative polymerization of 2- and 3-methylphenol regioselectively produced soluble poly(phenylene oxide)s, showing good thermal stability (105,106).

The polymers obtained from 2,5-dialkylphenols [2,5-R_2P: R = methyl (Me), ethyl (Et), *n*-propyl (nPr)] are noteworthy (107) (eq. 5). The oxidative polymerization of 2,5-Me_2P catalyzed by Cu(L^{iPr})Cl_2 in toluene under dioxygen produced a white polymer. The M_w was 19,300 and the structure was composed exclusively of a 2,5-dimethyl-1,4-phenylene oxide unit. The melting temperatures in the first and second scan (T_{m1} and T_{m2}) were detected at 308 and 303°C, respectively. Poly-2,5-Me_2P (eq. 5) showing heat-reversible crystallinity was synthesized for the first time. The isomeric polymer Poly-2,6-Me_2P (Fig. 1) showed a melting point at 237°C (T_{m1}), but once the crystaline part had been totally melted, recrystallization never occurred (T_{m2} not detected) by slow cooling or after annealing (108). Since thermoplastic polymers are mainly used as melt-moldings, Poly-2,6-Me_2P is generally accepted as an amorphous polymer; however, Poly-2,5-Me_2P is considered as a crystalline one.

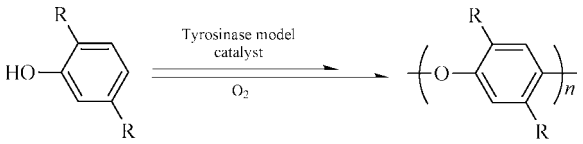

2,5-R_2P P-2,5-R_2P (5)

In the oxidative polymerization of 2,5-Et_2P and 2,5-n-Pr_2P (107), white polymers with M_w of 23,100 and 32,200, respectively, possessed only the 1,4-phenylene oxide units. The latter showed heat-reversible crystallinity with T_{m2} at 276°C, however, the former did not show a detectable T_{m2}. The recrystallization for poly(alkylated phenylene oxide)s after melting seems to be governed by both the position and nature of alkyl substituents.

Oxidative Polymerization of Naphthol Derivatives. Oxidative polymerization of 2-naphtol (109) and 1,5-dihydroxynaphthalene (110) has been done using enzyme catalysts. Solid-state polycondensation of 2,6-dihydroxynaphthalene with $FeCl_3$ catalyst (111) has been accomplished. Asymmetric oxidative coupling polymerization of 2,3-dihydroxynaphthalenes and their derivatives was achieved by chiral copper catalysts (112–115).

Oxidative Polymerization of Anilines

Oxidative polymerization of aniline produces polyaniline (PAN) (eq. 6). This polymer was obtained as aniline black about a century ago (116,117) and has been revived as an electrically conducting polymer (see ELECTRICALLY ACTIVE POLYMERS).

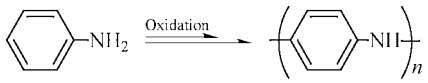

(6)

Polyaniline has been synthesized electrochemically (118,119) and with chemical oxidizing agents (120–123); a typical oxidizing agent is ammonium persulfate (120,121). Catalytic oxidative polymerization of aniline using iron salt catalyst (124) or HRP enzyme catalyst (125–129) with hydrogen peroxide, iron salt catalyst with ozone (130), and copper salt catalyst with dioxygen (131) has been done. A photo-induced catalytic system (132,133) and a gas-phase plasma method (134) have also been reported. Strongly acidic reaction conditions in the polymerization are normally selected, because polymer structure and electrical conductivity of PAN depend on the pH of the polymerization reaction (135,136).

The reaction mechanism of oxidative polymerization of aniline has been a big controversy (Fig. 7). The dimerization step is generally proposed as (i), in which aniline is one-electron-oxidized to a cation radical, followed by coupling of two molecules of the cation radical to a dimer. The subsequent steps of chain extension are under discussion; routes involving coupling of cation radicals such as (ii)–(iv) (137–140) and routes via electrophilic attack of a two-electron-oxidized quinodal diiminium ion (v) or nitrenium ion (vi) (141,142) have been proposed. The addition of electron-rich arenes does not inhibit the polymerization, and therefore the route through the nitrenium ion (vi) seems to be rejected (137).

Protonic doping is necessary to convert PAN from an insulator to a conductor (136), and so various dopants such as acid-substituted polymers (143–146) and chiral sulfonic acids (147–149) have been employed. Emulsion polymerization of aniline-afforded PAN particles (150–156) and PAN–silica particles (157,158). Polyaniline nanofibers have been synthesized by template-guided polymerization

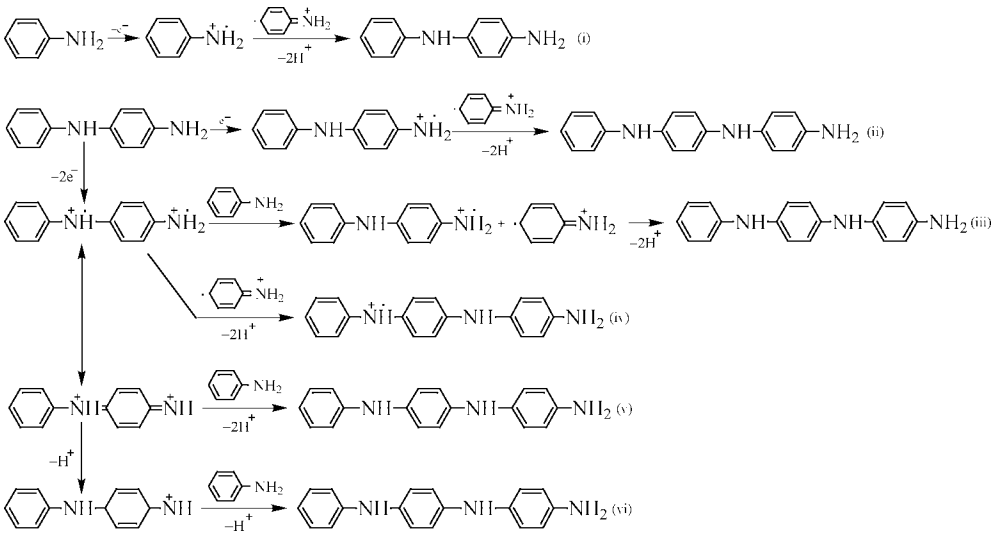

Fig. 7. Reaction mechanism for oxidative polymerization of aniline.

(159,160) and aqueous/organic interfacial polymerization (161–163). Intercalated PANs in V_2O_5 (164), $VOPO_4$ (165), MoO_3 (166), and FeOCl (167) have been obtained, and included PANs in zeolite molecular sieves (168) and mesoporous channel hosts (169).

Many substituted polyanilines were also synthesized (170). Typical examples are self-doping polymers, such as sulfonic acid ring-substituted PANs (171–177), mercaptopropanesulfonic acid substituted PANs (178), *N*-alkylsulfonic acid substituted PANs (179–181), and *N*-phenylsulfonic acid substituted PANs (182,183). Polyanilines having boronic acid for detecting sugar and dopamine (184,185) and for controlling self-doped states (186) have been produced. Long-chain-substituted anilines were polymerized at an air–water interface by the Langmuir–Blodgett technique (138,187,188). (see LANGMUIR-BLODGETT FILMS). Polyanilines with liquid crystalline substituents (189,190) and redox-active disulfide unit (191) were synthesized. Oxidative polymerization of 1-aminonaphthlenes gave PAN-like polymers (192,193).

Oxidative Polymerization of Thiophenols and Their Derivatives

Thiophenol is oxidatively coupled to give diphenyldisulfide (eq. 7), because formation of an S—S bond, resulting from the coupling of thiophenoxyl radicals, happens more readily than formation of a C—S bond (194). Oxidative polymerization of 1,3-dimercaptobenzene afforded poly(1,3-phenylenedisulfide) (195–197).

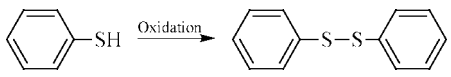

(7)

Poly(phenylene sulfide) (PPS) has been synthesized by oxidative polymerization of diphenyl disulfide, which was obtained via oxidation of thiophenol (eq. 8) (198–208). PPS is an engineering plastic with a high melting point, which is manufactured by condensation polymerization eliminating a salt.

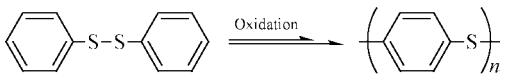

(8)

The oxidative polymerization of diphenyl disulfide was carried out in the presence of a strong acid by electrolysis (198) and by reaction with Lewis acids such as $SbCl_5$ (199–201) or quinones such as 2,3-dichloro-5,6-dicyano-1,4-benzoquinone (202–205). VO catalysts such as vanadyl acetylacetonate with O_2 have also been used for the oxidative polymerization (206–208), and the catalytic reaction mechanism involving four-electron reduction of O_2 has been discussed (209–215).

The chain extension mechanism is shown in Figure 8 (201). Diphenyl disulfide is oxidized to a cation radical, which reacts with diphenyl disulfide to give phenylbis(phenylthio)sulfonium cation, followed by electophilic attack of diphenyl sulfide on the cation.

The use of various diaryl disulfides as the monomer produced PPSs substituted with methyl groups at the 2- or 3-, 2,3-, 2,5-, or 2,6-positions, methoxy at the 2-position, etc. (204,207). Reactive functionalized oligomers (216) and block polymers containing alkylene and perfluoroalkylene groups (217,218) have been obtained. Cyclic hexakis(1,4-phenylene sulfide) was synthesized (219), and ring-opening polymerization of such cyclic oligomers was also found (220).

The synthesis of PPS via poly(sulfonium cation) as a soluble precursor (221) was developed through oxidative polymerization of methyl 4-(phenylthio)phenyl sulfide (222), followed by dealkylation (eq. 9) (223–225).

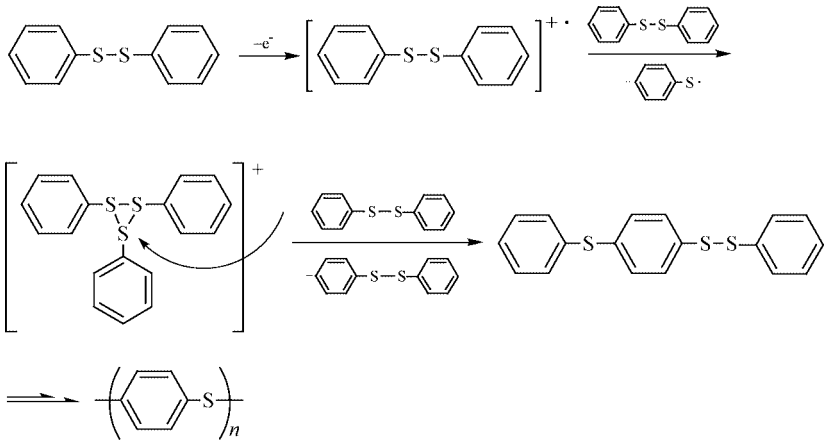

Fig. 8. Reaction mechanism for oxidative polymerization of diphenyl disulfide.

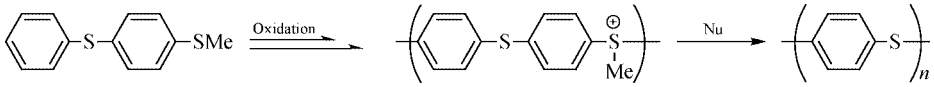

(9)

Oxidative Polymerization of Aromatic Hydrocarbons

In the 1960s, oxidative polymerization of benzene by $CuCl_2$-$AlCl_3$ was discovered (eq. 10) (226). Other oxidants such as $AlCl_3$-MnO_2, $FeCl_3$, and $MoCl_5$ were employed. These systems allowed the polymerization of various monomers such as toluene, chlorobenzene, diphenyl, naphthalene, and phenanthrene (227).

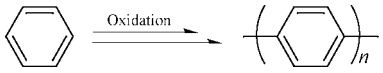

(10)

Oxidative polymerization of bis(1-naphthoxy) monomers is known as the Sholl Reaction (eq. 11) (228). 1,4-Dialkoxybenzenes have been polymerized using $FeCl_3$ (229,230) and oxovanadium catalyst with dioxygen (231) to give poly(2,5-dialkoxy-1,4-phenylene)s (eq. 12). Poly(4,6-di-*n*-butyl-1,3-phenylene) was also obtained (232).

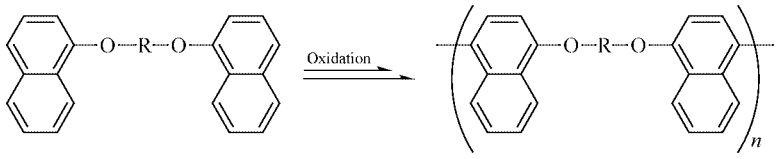

(11)

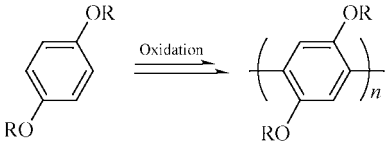

(12)

Three reaction mechanisms of C—C coupling in oxidative polymerization of benzenes have been reported (Fig. 9). The first step of each mechanism is one electron oxidation of a monomer to give a cation radical. The next step may be (i) coupling of two cation radicals (233,234), (ii) coupling of one cation radical with one neutral molecule (226,228), or (iii) coupling of one cation radical with many neutral molecules (stair-step mechanism) (235).

Oxidative Polymerization of Heterocyclic Aromatics

Oxidative polymerization of pyrrole (236), thiophene (237), furan (238), and selenophene (239) was performed with electrical methods around two decades ago

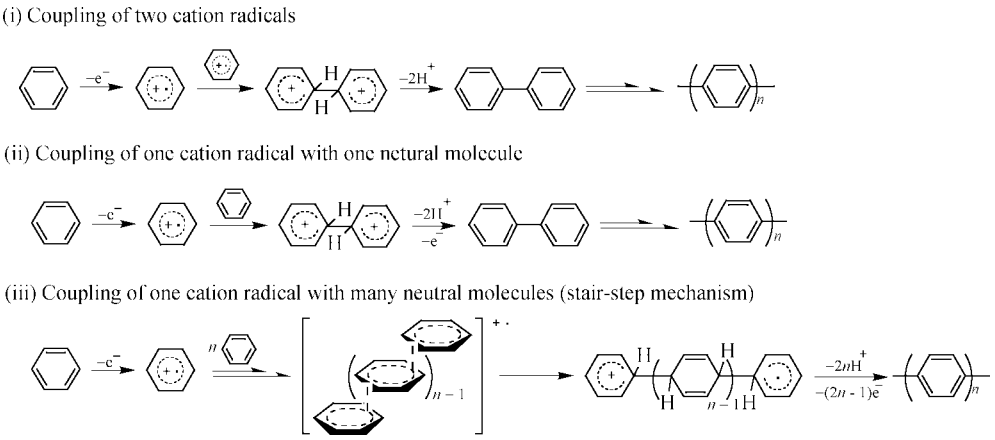

Fig. 9. Reaction mechanism for oxidative polymerization of benzene.

(eq. 13). More recently, numerous studies on the resulting polymers, particularly polypyrroles and polythiophenes, have been performed in terms of electrical conductivity (see ELECTRICALLY ACTIVE POLYMERS).

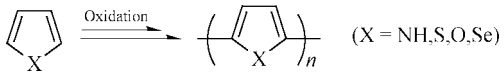

(13)

For the oxidative polymerization of heterocyclic aromatics, two reaction mechanisms, similar to that of benzenes, have been proposed (Fig. 10). One is coupling of two cation radicals [(i) in Fig. 10] (240,241), and the other is coupling of one cation radical with one neutral molecule [(ii) in Fig. 10] (242,243).

Oxidative Polymerization of Pyrroles. The synthesis of pyrrole blacks was performed by chemical oxidative polymerization with a variety of oxidizing agents such as hydrogen peroxide, lead dioxide, quinines, ferric chloride, and persulfates (244) before the electrical method was employed (236). The catalytic oxidative polymerization under dioxygen to give polypyrrole (PPY) has also been developed (245–247).

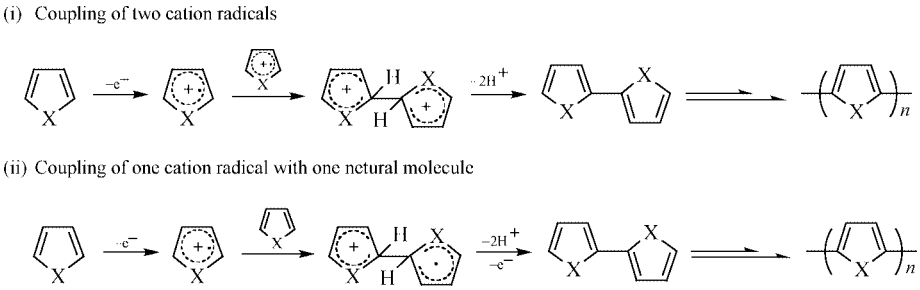

Fig. 10. Reaction mechanism for oxidative polymerization of heterocyclic aromatics.

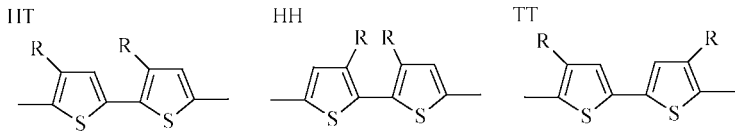

Fig. 11. Regioisomers of 3-substituted polythiophenes.

Various PPYs having 1-substituted (248), 3-substituted (249,250), and 3,4-disubstituted (251–253) groups, and transition metal complex moieties (254–256) have been obtained.

PPY particles were produced by colloidal dispersion method (257–259). Monolayer and multilayer PPYs were obtained by thiol–Au interaction (260,261), by deposition on $YBa_2Cu_3O_{7-\delta}$ (262,263), by intercalation in FeOCl (264), and by monomer amphiphilicity (265). PPY wires (266–268), PPY tubes (269–271), and PPY microcontainers (272,273) have also been synthesized.

Oxidative Polymerization of Thiophenes. Thiophene is oxidatively polymerized to give polythiophene (PTH) by electrochemical oxidation (237); by chemical oxidation with AsF_5 (274), NO salts (275), and $FeCl_3$ (276); and by catalytic oxidation with dioxygen (277).

PTH can be substituted at the 3- and/or 4-positions (278). 3-Substituted PTHs have regioisomers (Fig. 11), and the regioregularity greatly affects conjugation length and electronic properties. For poly(3-alkylthiophene)s, high regioselectivity of 91–98% HT has been obtained by organometalic reaction (279,280); however, a maximum 89% HT (Fig. 11) has been obtained by oxidative polymerization (281,282). In oxidative polymerization of 3-arylthiophenes (283–285) and 3-alkoxy-4-methylthiophenes (286), 94–96% HT contents were achieved. This regioselectivity has been discussed as arising from the spin density of the radical cations (287,288).

Poly(3,4-ethylenedioxythiophene) was developed around 1990, and its combination with poly(styrene sulfonic acid) became practical because of its high film-formability, conductivity, transparency, and stability (289). Many functional PTHs were prepared possessing crown ether (290,291), tetrathiafluvalene-like structures (292,293), C_{60}-attachment (294,295), probes for affinity chromism (296–298), and various metal complexes (299–306).

PTH film obtained by electrochemical deposition was stronger than aluminum film (307). PTH fibers were produced by using capillary flow cell (308) and with electrically independent connections (309). PTHs were included in zeolite (310,311) and such PTH wires (312) were obtained. PTH catenanes and rotaxanes have also been synthesized (313,314).

Oxidative Polymerization of Other Monomers

Treatment of *m*-diethynylbenzene with a copper catalyst and dioxygen gave a poly(phenylene butadiynylene) (315). Use of Cu-incorporated mesoporous materials as the oxidative polymerization catalyst for 1,4-diethynylbenzene produced highly conjugated poly(1,4-phenylene-1,4-butadiynylene) (316).

Bifunctional *p*-tolylcyanoacetic esters (317) and monofunctional phenylcyanoacetic esters (318) were oxidatively polymerized using a copper catalyst with dioxygen.

BIBLIOGRAPHY

"Oxidative Polymerization" in *EPSE* 2nd ed., Vol. 10, pp. 670–683, by Martin B. Jones, University of North Dekota, and Peter Kovacic, University of Wisconsin-Milwaukee.

1. S. L. Cosgrove and W. A. Waters, *J. Chem. Soc*. 388 (1951).
2. C. G. Haynes and co-workers, *J. Chem. Soc*. 2823 (1956).
3. A. S. Hay and co-workers, *J. Am. Chem. Soc.* **81**, 6335 (1959).
4. A. S. Hay, *J. Polym. Sci., Part A: Polym. Chem.* **36**, 505 (1998).
5. S. Kobayashi and H. Higashimura, *Prog. Polym. Sci.* **28**, 1015 (2003).
6. G. F. Endres and co-workers, *J. Org. Chem.* **28**, 1300 (1963).
7. H. Finkbeiner and co-workers, *J. Org. Chem.* **31**, 549 (1966).
8. E. Tsuchida and co-workers, *Makromol. Chem.* **176**, 1349 (1975).
9. E. Tsuchida and co-workers, *Makromol. Chem.* **151**, 221 (1972).
10. E. P. Talsi and co-workers, *J. Mol. Catal.* **57**, 325 (1990).
11. J. Kresta and co-workers, *Makromol. Chem.* **176**, 157 (1975).
12. P. J. Baesjou and co-workers, *J. Mol. Catal., A: Chem.* **110**, 195 (1996).
13. P. J. Baesjou and co-workers, *J. Am. Chem. Soc.* **119**, 12590 (1997).
14. A. S. Hay, *Adv. Polym. Sci.* **4**, 496 (1967).
15. C. Walling and R. B. Hodgdon Jr., *J. Am. Chem. Soc.* **80**, 228 (1958).
16. V. A. Dodonov and W. A. Waters, *J. Chem. Soc*. 2459 (1965).
17. C. C. Price and K. Nakaoka, *Macromolecules* **4**, 363 (1971).
18. E. McNelis, *J. Org. Chem.* **31**, 1255 (1966).
19. W. G. B. Huysmans and W. A. Waters, *J. Chem. Soc. B* 1163 (1967).
20. H. M. van Dort and co-workers, *J. Polym. Sci., Part C* **22**, 431 (1968).
21. R. Cecil and J. S. Littler, *J. Chem. Soc. B* 1420 (1968).
22. W. A. Waters, *J. Chem. Soc. B* 2026 (1971).
23. J.-L. Roubaty and co-workers, *Makromol. Chem.* **179**, 1151 (1978).
24. W. A. Butte Jr. and C. C. Price, *J. Am. Chem. Soc.* **84**, 3567 (1962).
25. D. A. Bolon, *J. Am. Chem. Soc.* **88**, 3148 (1966).
26. W. J. Mijs and co-workers, *Tetrahedron* **23**, 2253 (1967).
27. G. D. Cooper and co-workers, *J. Am. Chem. Soc.* **87**, 3996 (1965).
28. B. Miller, *J. Am. Chem. Soc.* **86**, 1127 (1964).
29. P. J. Baesjou and co-workers, *Macromolecules* **32**, 270 (1999).
30. D. M. White, *J. Org. Chem.* **34**, 297 (1969).
31. H. A. M. van Aert and co-workers, *Macromolecules* **28**, 7967 (1995).
32. H. A. M. van Aert and co-workers, *Macromolecules* **30**, 6056 (1997).
33. K. Saito and co-workers, *Chem.—Eur. J.* **9**, 4240 (2003).
34. E. Tsuchida and co-workers, *Reactive Oligomers*, American Chemical Society, Washington, D.C., 1985, p. 175.
35. W. Koch and co-workers, *Makromol. Chem., Suppl.* **12**, 105 (1985).
36. S.-H. Hyun and co-workers, *Bull. Chem. Soc. Jpn.* **61**, 1319 (1988).
37. E. Tsuchida and co-workers, *Macromolecules* **28**, 7917 (1995).
38. K. Takeshi and coworkers, *Chem. Lett.* **28**, 393 (1999).
39. K. Oyaizu and co-workers, *Macromolecules* **35**, 67 (2002).
40. R. Ikeda and co-workers, *Macromolecules* **33**, 6648 (2000).
41. K. Oyaizu and co-workers, *Macromolecules* **33**, 5766 (2000).

42. R. Ikeda and co-workers, *Macromolecules* **29**, 3053 (1996).
43. R. Ikeda and co-workers, *Polym. Int.* **47**, 295 (1998).
44. K. Sarkanen, *Lignins*, Wiley-Interscience, New York, 1971.
45. H. S. Mason, *J. Biol. Chem.* **172**, 83 (1948).
46. A. M. Klibanov and co-workers, *Science* **221**, 259 (1983).
47. M. Schnitzer and co-workers, *Soil Biol. Biochem.* **16**, 371 (1984).
48. J. S. Dordick and co-workers, *Biotech. Bioeng.* **30**, 31 (1987).
49. J. A. Akkara and co-workers, *J. Polym. Sci., Part A: Polym. Chem.* **23**, **29**, 1561 (1991).
50. S. Kobayashi, *J. Polym. Sci.: Part A: Polym. Chem.* **24**, **37**, 3041 (1999).
51. S. Kobayashi and co-workers, *Chem. Rev.* **101**, 3793 (2001).
52. L. B. Davin and co-workers, *Science* **275**, 362 (1997).
53. H. Uyama and co-workers, *Chem. Lett*. 423 (1994).
54. H. Uyama and co-workers, *Chem. Lett*. 795 (1995).
55. T. Oguchi and co-workers, *Macromol. Rapid Commun.* **20**, 401 (1999).
56. Y.-J. Kim and co-workers, *Macromolecules* **36**, 5058 (2003).
57. H. Uyama and co-workers, *J. Polym. Sci., Part A: Polym. Chem.* **35**, 1453 (1997).
58. F. F. Bruno and co-workers, *Langmuir* **11**, 889 (1995).
59. N. Mita and co-workers, *Chem. Lett.* **31**, 402 (2002).
60. H. Tonami and co-workers, *Macromol. Chem. Phys.* **200**, 2365 (1999).
61. T. Fukoka and co-workers, *Macromolecules* **36**, 8213 (2003).
62. S. Kobayashi and co-workers, *Macromol. Rapid Commun.* **17**, 503 (1996).
63. S. Kobayashi and co-workers, *Macromol. Chem. Phys.* **199**, 777 (1998).
64. T. Fukuoka and co-workers, *Macromolecules* **33**, 9152 (2000).
65. P. Wang and co-workers, *J. Am. Chem. Soc.* **117**, 12885 (1995).
66. H. Tonami and co-workers, *Macromol. Chem. Phys.* **200**, 1998 (1999).
67. P. Wang and J. S. Dordick, *Macromolecules* **31**, 941 (1998).
68. T. Fukuoka and co-workers, *Biomacromolecules* **3**, 768 (2002).
69. W. Liu and co-workers, *Chem. Mater.* **12**, 1577 (2000).
70. W. Liu and co-workers, *Macromolecules* **34**, 3522 (2001).
71. H. Uyama and co-workers, *Macromolecules* **31**, 554 (1998).
72. H. Tonami and co-workers, *Biomacromolecules* **1**, 149 (2000).
73. S. Kobayashi and co-workers, *Chem. Lett.* **29**, 1214 (2000).
74. S. Kobayashi and co-workers, *Chem.—Eur. J.* **7**, 4755 (2001).
75. Jpn. Kokai Tokkyo Koho, JP 08053545 (1996), A. Terahara and H. Higashimura (to Sumitomo-Chemical Co.) (in English); *Chem. Abstr.* **125**, 11750 (1996).
76. H. Tonami and co-workers, *Polym. Bull.* **42**, 125 (1999).
77. T. Tsujimoto and co-workers, *Chem. Lett.* **29**, 1122 (2000).
78. R. Ikeda and co-workers, *Macromol. Rapid Commun.* **21**, 496 (2000).
79. T. Fukuoka and co-workers, *Macromol. Rapid Commun.* **23**, 698 (2002).
80. J. A. Akkara and co-workers, *Macromolecules* **33**, 2377 (2000).
81. A. S. Hay, *J. Polym. Sci.* **58**, 581 (1962).
82. E. Tsuchida and co-workers, *Makromol. Chem.* **164**, 203 (1973).
83. V. Mahadevan and co-workers, *J. Am. Chem. Soc.* **119**, 11996 (1997).
84. J. E. Penner-Hahn and co-workers, *J. Am. Chem. Soc.* **108**, 7819 (1986).
85. M. Valoti and co-workers, *Arch. Biochem. Biophys.* **269**, 423 (1989).
86. H. Higashimura and co-workers, *J. Am. Chem. Soc.* **120**, 8529 (1998).
87. H. Higashimura and co-workers, *Macromolecules* **33**, 1986 (2000).
88. N. Kitajima and co-workers, *J. Am. Chem. Soc.* **111**, 8975 (1989).
89. N. Kitajima and co-workers, *J. Am. Chem. Soc.* **114**, 1277 (1992).
90. A. S. Hay and G. F. Endres, *Polym. Lett.* **3**, 887 (1965).
91. A. S. Hay, *Polym. Eng. Sci.* **16**, 1 (1976).
92. H. Higashimura and co-workers, *J. Polym. Sci., Part A: Polym. Chem.* **38**, 4792 (2000).

93. H. Higashimura and co-workers, *J. Mol. Catal., A, Chem.* **161**, 233 (2000).
94. E. Tsuchida and co-workers, *J. Macromol. Sci., Chem. A* **21**, 1081 (1984).
95. H. M. van Dort and co-workers, *Eur. Polym. J.* **4**, 275 (1968).
96. M. Kubo and co-workers, *Macromolecules* **31**, 3469 (1998).
97. J. A. Halfen and co-workers, *Science* **271**, 1397 (1996).
98. N. Kitajima and Y. Moro-oka, *Chem. Rev.* **94**, 737 (1994).
99. S. Mahapatra and co-workers, *J. Am. Chem. Soc.* **116**, 9785 (1994).
100. K. Fujisawa and co-workers, *Chem. Lett.* **28**, 739 (1999).
101. E. Tkatchouk and co-workers, *Macromolecules* **36**, 5607 (2003).
102. M. Kubota and co-workers, *Bull. Chem. Soc. Jpn.* **77**, 813 (2004).
103. H. Higashimura and co-workers, *Polym. Adv. Tech.* **11**, 733 (2000).
104. H. Higashimura and co-workers, *Polym. Prepr. Jpn.* **48**, 706 (1999).
105. H. Higashimura and co-workers, *Appl. Catal., A: Gen.* **194–195**, 427 (2000).
106. H. Higashimura and co-workers, *J. Mol. Catal., A: Chem.* **155**, 201 (2000).
107. H. Higashimura and co-workers, *Macromol. Rapid Commun.* **21**, 1121 (2000).
108. S. Z. D. Cheng and B. Wunderlich, *Macromolecules* **20**, 1630 (1987).
109. R. S. Premachandran and co-workers, *Macromolecules* **29**, 6452 (1996).
110. L. Wang and co-workers, *J. Polym. Sci., Part A: Polym. Chem.* **31**, 2855 (1993).
111. M. Suzuki and Y. Yatsugi, *Chem. Commun*. 162 (2002).
112. S. Habaue and co-workers, *Macromolecules* **36**, 2604 (2003).
113. S. Habaue and co-workers, *Macromolecules* **35**, 2437 (2002).
114. S. Habaue and co-workers, *Polym. J.* **35**, 592 (2003).
115. X. Xie and co-workers, *Angew. Chem. Int. Ed.* **42**, 2168 (2003).
116. R. Willstätter and S. Dorogi, *Chem. Ber.* **42**, 4118 (1909).
117. A. G. Green and A. E. Woodhead, *J. Chem. Soc*. 2388 (1910).
118. D. M. Mohilner and co-workers, *J. Am. Chem. Soc.* **84**, 3618 (1962).
119. E. M. Geniés and co-workers, *Synth. Met.* **36**, 139 (1990).
120. W.-S. Huang and co-workers, *J. Chem. Soc., Faraday Trans. 1* **82**, 2385 (1986).
121. A. Pron and co-workers, *Synth. Met.* **24**, 193 (1988).
122. M. Inoue and co-workers, *Synth. Met.* **30**, 199 (1989).
123. N. Toshima and H. Yan, *Bull. Chem. Soc. Jpn.* **68**, 1056 (1995).
124. D. K. Moon and co-workers, *Makromol. Chem.* **193**, 1723 (1992).
125. J. A. Akkara and co-workers, *Indian J. Chem.* **31B**, 855 (1992).
126. L. A. Samuelson and co-workers, *Macromolecules* **31**, 4376 (1998).
127. W. Liu and co-workers, *J. Am. Chem. Soc.* **121**, 71 (1999).
128. W. Liu and co-workers, *J. Am. Chem. Soc.* **121**, 11345 (1999).
129. R. Nagarajan and co-workers, *Macromolecules* **33**, 9542 (2000).
130. N. Toshima and co-workers, *Chem. Lett.* **29**, 1428 (2000).
131. N. Toshima and co-workers, *Bull. Chem. Soc. Jpn.* **67**, 1947 (1994).
132. K. Teshima and co-workers, *Chem. Commun*. 829 (1996).
133. K. Teshima and co-workers, *Macromolecules* **31**, 6783 (1998).
134. R. Hernandez and co-workers, *J. Phys. Chem.* **88**, 3333 (1984).
135. F. Lux, *Polymer* **35**, 2915 (1994).
136. A. G. Macdiarmid and co-workers, *Mol. Cryst. Liq. Cryst.* **121**, 173 (1985).
137. Y. Ding and co-workers, *J. Polym. Sci., Part A: Polym. Chem.* **37**, 2569 (1999).
138. R. R. Bodalia and R. S. Duran, *J. Am. Chem. Soc.* **115**, 11467 (1993).
139. K. Tzou and R. V. Gregory, *Synth. Met.* **47**, 267 (1992).
140. E. M. Genies and C. Tsintavis, *J. Electroanal. Chem.* **195**, 109 (1985).
141. Y. Wei and co-workers, *J. Phys. Chem.* **94**, 7716 (1990).
142. E. M. Genies and M. Lapkowski, *J. Electroanal. Chem.* **236**, 189 (1987).
143. N. Kuramoto and co-workers, *J. Chem. Soc., Chem. Commun*. 1478 (1990).
144. K. Shannon and J. E. Fernandez, *J. Chem. Soc., Chem. Commun*. 643 (1994).

145. I. Kulszewicz-Bajer and co-workers, *J. Chem. Soc., Chem. Commun*. 641 (1994).
146. S.-A. Chen and H.-T. Lee, *Macromolecules* **28**, 2858 (1995).
147. P. C. Innis and co-workers, *Macromolecules* **31**, 6521 (1998).
148. W. Li and co-workers, *Macromolecules* **35**, 9975 (2002).
149. G.-L. Yuan and N. Kuramoto, *Macromolecules* **36**, 7939 (2003).
150. S. P. Armes and M. Aldissi, *J. Chem. Soc., Chem. Commun*. 88 (1989).
151. B. Vincent and J. Waterson, *J. Chem. Soc., Chem. Commun*. 683 (1990).
152. N. Gospodinova and co-workers, *J. Chem. Soc., Chem. Commun*. 923 (1992).
153. P. J. Kinlen and co-workers, *Macromolecules* **31**, 1735 (1998).
154. D. Kim and co-workers, *Macromolecules* **35**, 5314 (2002).
155. P. S. Rao and co-workers, *Macromolecules* **35**, 4988 (2002).
156. E. Marie and co-workers, *Macromolecules* **36**, 3967 (2003).
157. M. Gill and co-workers, *J. Chem. Soc., Chem. Commun*. 108 (1992).
158. J. Stejskal and co-workers, *Macromolecules* **29**, 6814 (1996).
159. J.-M. Liu and S. C. Yang, *J. Chem. Soc., Chem. Commun*. 1529 (1991).
160. L. Yu and co-workers, *J. Appl. Polym. Sci.* **88**, 1550 (2003).
161. J. C. Michaelson and A. J. McEvoy, *J. Chem. Soc., Chem. Commun*. 79 (1994).
162. J. Huang and co-workers, *J. Am. Chem. Soc.* **125**, 314 (2003).
163. J. Huang and R. B. Kaner, *J. Am. Chem. Soc.* **126**, 851 (2004).
164. M. G. Kanatzidis and C.-G. Wu, *J. Am. Chem. Soc.* **111**, 4139 (1989).
165. H. Nakajima and G. Matsubayashi, *Chem. Lett.* **22**, 423 (1993).
166. R. Bissessur and co-workers, *J. Chem. Soc., Chem. Commun*. 687 (1993).
167. C.-G. Wu and co-workers, *J. Am. Chem. Soc.* **117**, 9229 (1995).
168. P. Enzel and T. Bein, *J. Phys. Chem.* **93**, 6270 (1989).
169. C.-G. Wu and T. Bein, *Science* **264**, 1757 (1994).
170. M. Leclerc and co-workers, *Macromolecules* **22**, 649 (1989).
171. J. Yue and A. J. Epstein, *J. Am. Chem. Soc.* **112**, 2800 (1990).
172. J. Yue and co-workers, *J. Am. Chem. Soc.* **113**, 2665 (1991).
173. J. Yue and A. J. Epstein, *Macromolecules* **24**, 4441 (1991).
174. X.-L. Wei and co-workers, *J. Am. Chem. Soc.* **118**, 2545 (1996).
175. H. S. O. Chan and co-workers, *Chem. Commun*. 1327 (1998).
176. K. Krishnamoorthy and co-workers, *Chem. Commun*. 240 (2002).
177. T. Yamamoto and co-workers, *Macromolecules* **36**, 7075 (2003).
178. C.-C. Han and co-workers, *Macromolecules* **36**, 7908 (2003).
179. P. Hany and co-workers, *Synth. Met.* **31**, 369 (1989).
180. J.-Y. Bergeron and co-workers, *J. Chem. Soc., Chem. Commun*. 180 (1990).
181. S.-A. Chen and G.-W. Hwang, *J. Am. Chem. Soc.* **116**, 7939 (1994).
182. C. DeArmitt and co-workers, *Polymer* **34**, 158 (1993).
183. M. T. Nguyen and co-workers, *Macromolecules* **27**, 3625 (1994).
184. E. Shoji and M. S. Freund, *J. Am. Chem. Soc.* **124**, 12486 (2002).
185. B. Fabre and L. Taillebois, *Chem. Commun*. 2982 (2003).
186. B. A. Deore and co-workers, *J. Am. Chem. Soc.* **126**, 52 (2004).
187. L. J. Kloeppner and R. S. Duran, *Langmuir* **14**, 6734 (1998).
188. L. J. Kloeppner and co-workers, *Macromolecules* **33**, 8006 (2000).
189. L. I. Gabaston and co-workers, *Chem. Commun*. 429 (1996).
190. H. Goto and K. Akagi, *Macromolecules* **35**, 2545 (2002).
191. J.-S. Cho and co-workers, *Macromolecules* **34**, 2751 (2001).
192. D.-K. Moon and co-workers, *Macromolecules* **26**, 6992 (1993).
193. E. P. Cintra and co-workers, *Macromolecules* **36**, 2079 (2003).
194. F. Magno and co-workers, *J. Electroanal. Chem.* **30**, 375 (1971).
195. U.S. Pat. 3,294,760 (1966), A. S. Hay (to General Electric Co.).
196. C. Della and co-workers, *J. Polym. Sci., Polym. Lett. Ed.* **23**, 323 (1985).

197. E. Shouji and D. A. Buttry, *J. Phys. Chem. B* **102**, 1444 (1998).
198. E. Tsuchida and co-workers, *Macromolecules* **20**, 2315 (1987).
199. E. Tsuchida and co-workers, *Macromolecules* **20**, 2030 (1987).
200. K. Yamamoto and co-workers, *Bull. Chem. Soc. Jpn.* **62**, 3655 (1989).
201. E. Tsuchida and co-workers, *Macromolecules* **23**, 2101 (1990).
202. E. Tsuchida and co-workers, *Macromolecules* **23**, 930 (1990).
203. K. Yamamoto and co-workers, *J. Polym. Sci., Part A: Polym. Chem.* **29**, 1359 (1991).
204. K. Yamamoto and co-workers, *Macromolecules* **25**, 2698 (1992).
205. K. Oyaizu and co-workers, *Bull. Chem. Soc. Jpn.* **67**, 1456 (1994).
206. E. Tsuchida and co-workers, *Macromolecules* **22**, 4138 (1989).
207. K. Yamamoto and co-workers, *Macromolecules* **26**, 3432 (1993).
208. K. Yamamoto and co-workers, *Bull. Chem. Soc. Jpn.* **67**, 251 (1994).
209. E. Tsuchida and co-workers, *Inorg. Chem.* **33**, 1056 (1994).
210. K. Yamamoto and co-workers, *J. Am. Chem. Soc.* **118**, 12665 (1996).
211. K. Oyaizu and co-workers, *Inorg. Chem.* **35**, 6634 (1996).
212. E. Tsuchida and co-workers, *Inorg. Chem.* **38**, 3704 (1999).
213. Z. Liu and F. C. Anson, *Inorg. Chem.* **39**, 274 (2000).
214. Z. Liu and F. C. Anson, *Inorg. Chem.* **40**, 1329 (2001).
215. K. Oyaizu and co-workers, *Inorg. Chem.* **42**, 1070 (2003).
216. E. Tsuchida and co-workers, *Macromolecules* **28**, 409 (1995).
217. K. Yamamoto and co-workers, *Macromolecules* **27**, 4312 (1994).
218. E. Tsuchida and co-workers, *Macromolecules* **27**, 7504 (1994).
219. K. Miyatake and co-workers, *Macromolecules* **30**, 4502 (1997).
220. E. Tsuchida and co-workers, *Macromolecules* **31**, 6469 (1998).
221. K. Yamamoto and co-workers, *J. Am. Chem. Soc.* **115**, 5819 (1993).
222. K. Yamamoto and co-workers, *J. Org. Chem.* **61**, 1912 (1996).
223. E. Tsuchida and co-workers, *Macromolecules* **26**, 7144 (1993).
224. E. Tsuchida and co-workers, *Macromolecules* **27**, 1057 (1994).
225. K. Yamamoto and co-workers, *J. Org. Chem.* **60**, 452 (1995).
226. P. Kovacic and A. Kyriakis, *J. Am. Chem. Soc.* **85**, 454 (1963).
227. P. Kovacic and M. B. Jones, *Chem. Rev.* **87**, 357 (1987).
228. V. Percec and H. Nava, *J. Polym. Sci., Part A: Polym. Chem.* **26**, 783 (1988).
229. K. Mukai and co-workers, *J. Polym. Sci., Polym. Chem. Ed.* **23**, 1259 (1985).
230. M. Ueda and co-workers, *Macromolecules* **25**, 5125 (1992).
231. T. Okada and co-workers, *Macromolecules* **29**, 7645 (1996).
232. T. Okada and co-workers, *J. Polym. Sci., Part A: Polym. Chem.* **35**, 2259 (1997).
233. L. M. Goldenberg and P. C. Lacaze, *Synth. Met.* **58**, 271 (1993).
234. K. Yamamoto and co-workers, *Bull. Chem. Soc. Jpn.* **61**, 1731 (1988).
235. S. A. Milosevich and co-workers, *J. Am. Chem. Soc.* **105**, 1088 (1983).
236. A. F. Diaz and co-workers, *J. Chem. Soc., Chem. Commun*. 635 (1979).
237. A. F. Diaz and co-workers, *J. Electroanal. Chem.* **121**, 355 (1981).
238. G. Tourillon and F. Garnier, *J. Electroanal. Chem.* **135**, 173 (1982).
239. K. Yoshino and co-workers, *Jpn. J. Appl. Phys. Part 2* **22**, L701 (1983).
240. E. M. Genies and co-workers, *J. Electroanal. Chem.* **149**, 101 (1983).
241. Y. Wei and co-workers, *Chem. Mater.* **3**, 888 (1991).
242. T. Inoue and T. Yamase, *Bull. Chem. Soc. Jpn.* **56**, 985 (1983).
243. G. Koßmehl, *Makromol. Chem. Macromol. Symp.* **4**, 45 (1986).
244. G. P. Gardini, *Adv. Heterocycl. Chem.* **15**, 67 (1973).
245. N. Toshima and J. Tayanagi, *Chem. Lett.* **19**, 1369 (1990).
246. S. Izumi and N. Toshima, *Bull. Chem. Soc. Jpn.* **67**, 539 (1994).
247. E. Tsuchida and co-workers, *J. Electroanal. Chem.* **438**, 167 (1997).
248. J. R. Reynolds and co-workers, *Macromolecules* **20**, 958 (1987).

249. J. Rühe and co-workers, *Synth. Met.* **28**, C177 (1989).
250. D.-K. Moon and co-workers, *Macromolecules* **28**, 6205 (1995).
251. A. Nazzal and G. B. Street, *J. Chem. Soc., Chem. Commun*. 83 (1984).
252. V. Enkelmann and co-workers, *Synth. Met.* **37**, 79 (1990).
253. P. Schottland and co-workers, *Macromolecules* **33**, 7051 (2000).
254. A. Deronzier and J.-C. Moutet, *Acc. Chem. Res.* **22**, 249 (1989).
255. C. J. Pickett and co-workers, *J. Chem. Soc., Chem. Commun*. 694 (1992).
256. G. Bidan and co-workers, *J. Am. Chem. Soc.* **114**, 5986 (1992).
257. S. P. Armes and B. Vincent, *J. Chem. Soc., Chem. Commun*. 288 (1987).
258. N. Cawdery and co-workers, *J. Chem. Soc., Chem. Commun*. 1189 (1988).
259. M. L. Digar and co-workers, *J. Chem. Soc., Chem. Commun*. 18 (1992).
260. R. J. Willicut and R. L. McCarley, *J. Am. Chem. Soc.* **116**, 10823 (1994).
261. R. L. McCarley and R. J. Willicut, *J. Am. Chem. Soc.* **120**, 9296 (1998).
262. S. G. Haupt and co-workers, *J. Am. Chem. Soc.* **116**, 9979 (1994).
263. R.-K. Lo and co-workers, *J. Am. Chem. Soc.* **118**, 11295 (1996).
264. M. G. Kanatzidis and co-workers, *J. Am. Chem. Soc.* **109**, 3797 (1987).
265. D. M. Collard and M. A. Fox, *J. Am. Chem. Soc.* **113**, 9414 (1991).
266. C. Jérôme and R. Jérôme, *Angew. Chem. Int. Ed.* **37**, 2488 (1998).
267. T. Bein and P. Enzel, *Angew. Chem. Int. Ed.* **28**, 1692 (1989).
268. M. Ikegami and co-workers, *Angew. Chem. Int. Ed.* **42**, 2154 (2003).
269. C. R. Martin and co-workers, *J. Am. Chem. Soc.* **112**, 8976 (1990).
270. C. R. Martin, *Science* **266**, 1961 (1994).
271. M. R. Ghadiri and co-workers, *Nature* **369**, 301 (1994).
272. L. Qu and G. Shi, *Chem. Commun*. 206 (2003).
273. L. Qu and co-workers, *Macromolecules* **36**, 1063 (2003).
274. G. Koßmehl and G. Chatzitheodorou, *Makromol. Rapid Commun.* **2**, 551 (1981).
275. G. Koßmehl and G. Chatzitheodorou, *Makromol. Rapid Commun.* **4**, 639 (1983).
276. K. Yoshino and co-workers, *Jpn. J. Appl. Phys.* **23**, L899 (1984).
277. S. Yu and co-workers, *Chem. Lett.* **28**, 559 (1999).
278. J. Roncali, *Chem. Rev.* **92**, 711 (1992).
279. T.-A. Chen and R. D. Rieke, *J. Am. Chem. Soc.* **114**, 10087 (1992).
280. R. D. McCullough and R. D. Lowe, *J. Chem. Soc., Chem. Commun*. 70 (1992).
281. M. Leclerc and co-workers, *Makromol. Chem.* **190**, 3105 (1989).
282. S. Amou and co-workers, *J. Polym. Sci., Part A: Polym. Chem.* **37**, 1943 (1999).
283. M. R. Andersson and co-workers, *Macromolecules* **27**, 6503 (1994).
284. T. Hayakawa and co-workers, *J. Polym. Sci: Part A: Polym. Chem.* **39**, 2287 (2001).
285. M. Miyasaka and co-workers, *Macromolecules* **33**, 8211 (2000).
286. G. Daoust and M. Leclerc, *Macromolecules* **24**, 455 (1991).
287. M. Fréchette and co-workers, *Synth. Met.* **84**, 223 (1997).
288. S. Ando and M. Ueda, *Synth. Met.* **129**, 207 (2002).
289. L. B. Groenendaal and co-workers, *Adv. Mater.* **12**, 481 (2000).
290. M. J. Marsella and T. M. Swager, *J. Am. Chem. Soc.* **115**, 12214 (1993).
291. S. Scheib and P. Bäuerle, *J. Mater. Chem.* **9**, 2139 (1999).
292. P. J. Skabara and co-workers, *Chem. Commun*. 1005 (2000).
293. P. J. Skabara and co-workers, *Macromolecules* **34**, 2232 (2001).
294. T. Benincori and co-workers, *Angew. Chem. Int. Ed.* **35**, 648 (1996).
295. B. Jousselme and co-workers, *Macromolecules* **36**, 3020 (2003).
296. S. Bernier and co-workers, *J. Am. Chem. Soc.* **124**, 12463 (2002).
297. H. A. Ho and co-workers, *Angew. Chem. Int. Ed.* **41**, 1548 (2002).
298. H. A. Ho and M. Leclerc, *J. Am. Chem. Soc.* **125**, 4412 (2003).
299. R. P. Kingsborough and T. M. Swager, *J. Am. Chem. Soc.* **121**, 8825 (1999).
300. R. P. Kingsborough and T. M. Swager, *Angew. Chem. Int. Ed.* **39**, 2897 (2000).

301. C. L. Kean and P. G. Pickup, *Chem. Commun*. 815 (2001).
302. O. Clot and co-workers, *J. Am. Chem. Soc.* **122**, 10456 (2000).
303. O. Clot and co-workers, *J. Am. Chem. Soc.* **123**, 9963 (2001).
304. D. A. Weinberger and co-workers, *J. Am. Chem. Soc.* **123**, 2503 (2001).
305. D. H. Kim and co-workers, *J. Org. Chem.* **608**, 133 (2000).
306. A. Vigalok and co-workers, *J. Am. Chem. Soc.* **123**, 7917 (2001).
307. G. Shi and co-workers, *Science* **267**, 994 (1995).
308. S. Li and co-workers, *Science* **259**, 957 (1993).
309. C. L. Curtis and co-workers, *Science* **262**, 2014 (1993).
310. P. Enzel and T. Bein, *J. Chem. Soc., Chem. Commun*. 1326 (1989).
311. J. V. Caspar and co-workers, *J. Am. Chem. Soc.* **113**, 600 (1991).
312. G. Li and co-workers, *Angew. Chem. Int. Ed.* **42**, 3818 (2003).
313. D. L. Simone and T. M. Swager, *J. Am. Chem. Soc.* **122**, 9300 (2000).
314. J. Buey and T. M. Swager, *Angew. Chem. Int. Ed.* **39**, 608 (2000).
315. A. S. Hay, *J. Org. Chem.* **25**, 1275 (1960).
316. V. S.-Y. Lin and co-workers, *J. Am. Chem. Soc.* **124**, 9040 (2002).
317. H. A. P. de Jongh and co-workers, *J. Polym. Sci., Polym. Chem. Ed.* **11**, 345 (1973).
318. H. A. P. de Jongh and co-workers, *J. Org. Chem.* **36**, 3160 (1971).

HIDEYUKI HIGASHIMURA
Sumitomo Chemical Company Ltd.
SHIRO KOBAYASHI
Kyoto University

PHASE TRANSFORMATION

Introduction

Phase transformations of polymeric materials, such as unmixing of a polymer solution or polymer blend, or the crystallization of a polymer melt or its glass transition into an amorphous structure, are very common phenomena and have important applications. This article briefly summarizes some key theoretical concepts about these phenomena, discusses the extent to which they differ from related phenomena in other materials (1) and mentions a few typical experiments to introduce the main techniques used to study such phase transitions.

Some transitions that are only known for macromolecules, however, will not be mentioned at all since they are covered elsewhere in this Encyclopedia (see, eg. GEL POINT). Also we shall not be concerned here with the transformations from the molten state to the solid state of polymeric materials, since this is the subject of separate treatments (see CRYSTALLIZATION KINETICS; GLASS TRANSITION; VISCOELASTICITY). Unlike other materials, polymers in the solid state rarely reach full thermal equilibrium. Of course, all amorphous materials can be considered as frozen fluids (see GLASS TRANSITION) Rather perfect crystals exist for metals, oxides, semiconductors etc, whereas polymers typically are semicrystalline, where amorphous regions alternate with crystalline lamellae, and the detailed structure and properties are history-dependent (see SEMICRYSTALLINE POLYMERS). Such out-of-equilibrium aspects are out of the scope of the present article, which rather emphasizes general facts of the statistical thermodynamics (qv) of phase transitions and their applications to polymers in fluid phases.

Thermodynamics

According to the Gibbs phase rule, a system containing z "components," ie, chemically different constituents, and r phases, has $f = z + 2 - r$ degrees of freedom (such as temperature T, pressure p, or relative concentration c_i of the ith component (2)). When one applies this formula to systems containing polymers, one usually treats one chemical type of polymer as one component, even if it is polydisperse. Strictly speaking, each fraction with a specific molecular weight needs to be treated as a distinct component (see THERMODYNAMIC PROPERTIES OF POLYMERS). For many practical purposes this complication can be neglected. Special effects on phase transitions (3) due to polydispersity will be mentioned when appropriate.

"Phases" in thermodynamic systems are then macroscopic homogeneous parts with distinct physical properties. For example, densities of "extensive thermodynamical variables," such as particle number N_i of the ith species, enthalpy U, volume V, entropy S, and possible order parameters, such as the nematic order parameter for a liquid crystalline polymer etc, differ in such coexisting phases. In equilibrium, "intensive thermodynamic variables," namely T, p, and the chemical potentials μ_i have to be the same in all phases. Coexisting phases are separated by well-defined interfaces (the width and internal structure of such interfaces play an important role in the kinetics of the phase transformation (1) and in other

Encyclopedia of Polymer Science and Technology. Copyright John Wiley & Sons, Inc. All rights reserved.

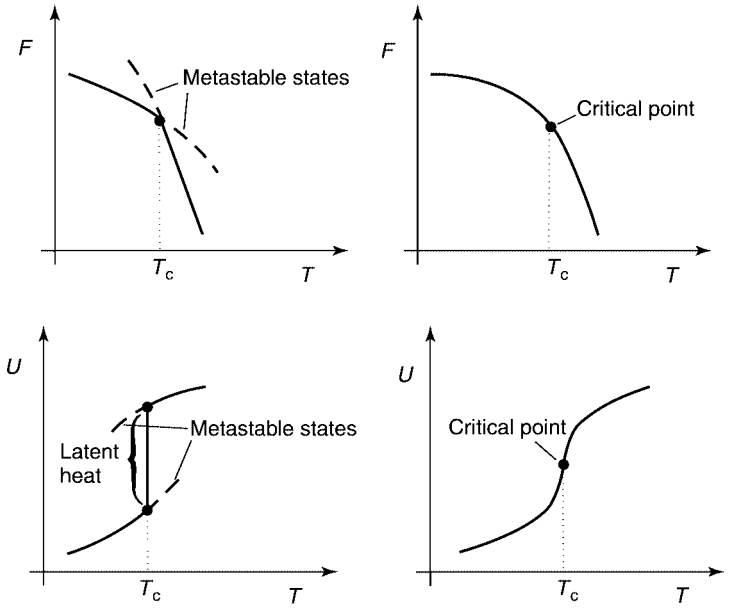

Fig. 1. Schematic variation of the Gibbs free energy F of a single-component system with temperature at constant pressure for a first-order transition (upper part left) and a second-order transition (upper part right). Lower part shows the corresponding behavior of the internal energy U.

material properties, see eg (4,5)). Phase transformations can be brought about eg by varying parameters such as temperature (Fig. 1) or pressure. In magnetic systems and superconductors also the magnetic field H is a suitable control parameter, in dielectric materials the electric field E. These variables will be ignored here throughout, although the switching of block copolymer mesophase structures by electric fields in thin films is of interest (6).

Figure 1 shows that one must distinguish first-order phase transitions [where first derivatives of the appropriate thermodynamic potential F, such as the enthalpy $U = [\partial(\beta F)/\partial\beta]_p$, where $\beta = 1/k_B T$, k_B being Boltzmann's constant, or volume $V \equiv (\partial F/\partial p)_T$ exhibit a jump] and second-order transitions, where U,V are continuous, but second derivatives are singular (1,2,7). The classical example for the latter case is the gas–liquid critical point, where the specific heat $C_p = (\partial U/\partial T)_p$ or the isothermal compressibility $\kappa_T = -(1/V)(\partial V/\partial p)_T$ diverge,

$$\kappa_T = \hat{\kappa}_T (T/T_c - 1)^{-\gamma}, \qquad p = p_c, \qquad T \to T_c^+ \tag{1}$$

where p_c is the critical pressure, T_c the critical temperature, $\hat{\kappa}_T$ is called a "critical amplitude" and γ a "critical exponent," which has the value $\gamma_{MF} = 1$ according to van der Waals theory and related mean-field theories (7,8), while $\gamma_I \approx 1.24$ according to the Ising model "universality class" (7–10). Here we have already invoked the notion that the critical exponents that describe the asymptotic singular behavior as a critical point is approached do not depend upon which specific material is

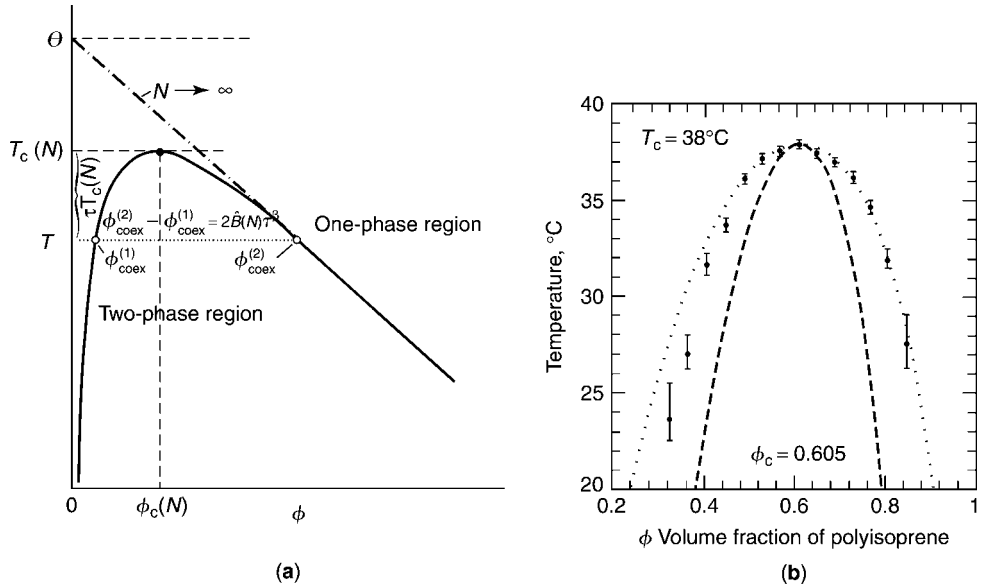

Fig. 2. (**a**) Schematic phase diagram of a polymer solution, at constant pressure, using temperature T and volume fraction ϕ of the polymer as variables. Phase separation into a dilute or semidilute solution (with volume fraction $\phi_{coex}^{(1)}$) and a more concentrated solution (with volume fraction $\phi_{coex}^{(2)})_{occurs}$ for states (T, ϕ) that fall in the two-phase region underneath the coexistence curve (binodal). The binodal ends in the critical point $\phi_c(N)$, $T_c(N)$, where N is the degree of polymerization of the polymer. For $N \to \infty$ the critical point merges with the theta point of the dilute solution, ie, $T = \Theta$, $\phi_c(N \to \infty) = 0$. For further explanations cf text. (**b**) Phase diagram of the partially miscible polymer blend poly(isoprene)–poly(ethylene) with molecular weights of 2000 and 5000, respectively. From Ref. 12. Broken curve inside of the coexistence curve (dotted) is the spinodal as estimated from a Flory–Huggins fit.

investigated, but are the same for all systems belonging to the same class. There are only a few classes, eg all systems in $d = 3$ space dimensions, exhibiting for $T < T_c$ a scalar "order parameter" belong to this same class. Of course, the gas–liquid transition is of little relevance for polymers simply because for high molecular weights T_c is too high, so that the polymer would chemically degrade already at much lower temperatures. Only for short alkanes gas–liquid critical phenomena can be studied (eg $T_c = 723$ K for $C_{16}H_{34}$ (11) while for $C_{24}H_{50}$ T_c is no longer available). However, it turns out that the phase diagram of a polymer in a solvent of variable quality (assuming that the quality is controlled by temperature) is isomorphic to the gas–liquid phase diagram of the polymer, see Figure 2**a**. Also phase diagrams of partially miscible polymer blends (qv) (see also MISCIBILITY) belong to the Ising class. Figure 2**b** presents an experimental example (12).

In Figure 2**a**, it was assumed that the pure solvent critical point is much higher than the Θ temperature of the solution, so the latter can be approximated as incompressible for simplicity. Then the role of the pressure for the gas–liquid transition is now played by the osmotic pressure of the polymer in solution, and the volume fraction ϕ rather than the density is used to distinguish the phases. In terms of $t \equiv 1 - T/T_c(N)$ we can introduce another power law for the "order

parameter" of the transition ψ,

$$\psi = \left(\phi_{\text{coex}}^{(2)} - \phi_{\text{coex}}^{(1)}\right)/2 = \hat{B}(N)t^{\beta} \tag{2}$$

where $\hat{B}(N)$ is another critical amplitude, and the exponent β takes the values $\beta_{\text{MF}} = 1/2$ in the mean-field theories and $\beta_{\text{I}} \approx 0.325$ in the Ising class. Here N denotes the degree of polymerization or "chain length" of the flexible linear polymer, respectively.

In Figure 1 we have already emphasized that at a first-order transition one typically finds metastable states. In principle, statistical thermodynamics describes systems in thermal equilibrium only, ie, only those branches of F that are the lower solid ones in the upper part of Figure 1 (left part) can be described, and nothing is said about the dashed continuations describing the metastable states. However, mean-field theories (such as the van der Waals equation of a fluid, or Flory–Huggins theory (13–15) for a polymer mixture) readily yield approximate descriptions of metastable states up to a "limit of metastability" or "spinodal." Such a "spinodal curve" delineating this boundary between metastable and unstable regions in the (T, ϕ) plane of a binary polymer mixture has been drawn in Figure 2**b**. It is important to realize, however, that such spinodals are mean-field concepts. They are meaningful objects in statistical thermodynamics in very special limiting cases only. One such limit is realized for polymer blends when the chain lengths $N_{\text{A}}, N_{\text{B}}$ of the two flexible linear polymers constituting the mixture both tend to infinity (15–17). Then the mean-field spinodal line adopts a well-defined meaning as a sharp dividing line between two distinct kinetic mechanisms of phase separation: Metastable states in between binodal and spinodal (Fig. 2**b**) decay via nucleation and growth, while "unstable states" underneath the spinodal curve of the binary mixture decay by the spontaneous growth of "concentration waves" with wavelengths exceeding a characteristic critical wavelength λ_{c}, which diverges at the spinodal curve (Fig. 3). This mechanism of phase separation is called "spinodal decomposition" (15–20). Theory predicts (15–17) that in the limit $N_{\text{A}} \to \infty$, $N_{\text{B}} \to \infty$ the lifetime of metastable states becomes infinite right up to the spinodal curve, since homogenous nucleation is suppressed. Although there is ample experimental evidence for the occurrence of (nonlinear) spinodal decomposition as a mechanism of phase separation in polymer blends (19), experimental evidence for the specific singularities associated with spinodal lines in the phase diagrams of mixtures is still lacking. Thus, although spinodal curves are often drawn in phase diagrams of real materials, such as in Figure 2**b**, we caution the reader that these curves are either the result of a mean-field fit or of some extrapolation procedure, and hence of limited validity.

Phase Diagrams

When one approaches the critical point in the phase diagram (Figs. 2 and 3), the distinction between the two coexisting phases and also the difference $\phi_{\text{coex}}^{(2)} - \phi_{\text{coex}}^{(1)}$ (cf eq. 2) vanish. Also the two branches of the spinodal curve meet in the critical point of the phase diagram. In Figures 2 and 3, we have assumed that the phase

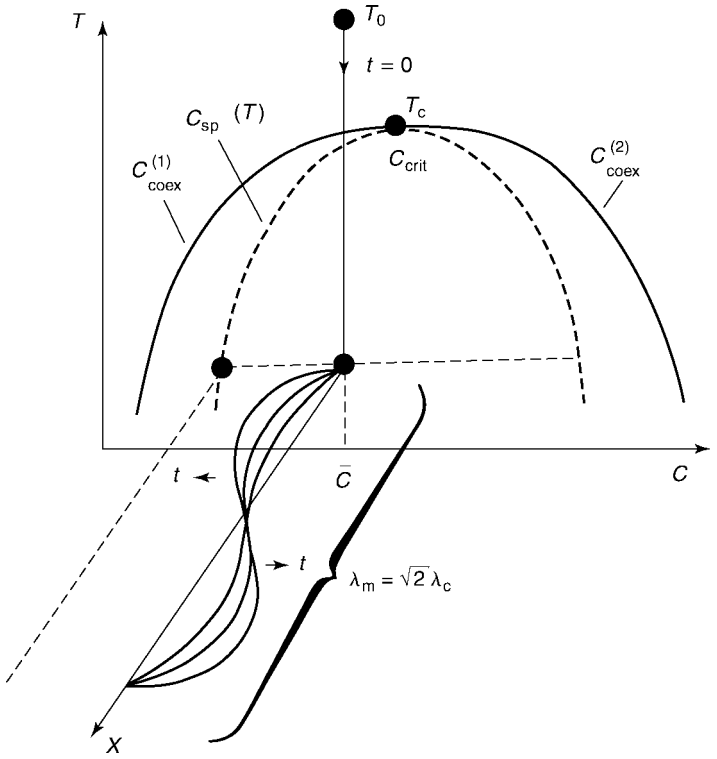

Fig. 3. Schematic illustration of a "quenching experiment" of a binary mixture, where phase separation via "spinodal decomposition" is initiated by a sudden reduction of temperature T from an initial temperature T_0 in the one-phase region to a temperature T in the two-phase region in the temperature concentration (c) plane underneath the spinodal (shown as broken curve) at time $t = 0$. While the average concentration $\bar{c}$ stays constant, of course, in the course of time concentration inhomogeneities spontaneously develop with wavelengths $\lambda_c < \lambda < \infty$. Maximum growth occurs at a wavelength $\lambda_m = \sqrt{2\lambda_c}$, according to the linearized theory of spinodal decomposition (18). This is symbolically indicated by showing growing waves assuming one spatial coordinate x only. In practice there is a band of growing wavelengths, and the phases of the waves and the orientations of the wave vectors are randomly distributed, and hence in real space the concentration pattern is not periodic.

diagram contains a miscibility gap at low temperatures, ie, an "upper critical solution temperature" (UCST) where T_c, ϕ_c is a maximum of both the coexistence curve and the spinodal. In fact, many polymer solutions and polymer blends show the opposite behavior, ie, the phases separate when the temperature is raised, starting at a "lower critical solution temperature" (LCST) (21) and there also are examples of systems that exhibit both LCST and UCST behavior, eg poly(isobutylene) dissolved in benzene (22).

At this point, we mention one important caveat: The assertion that the critical point is at a maximum or minimum of the coexistence curve in the (T, ϕ)-plane is only true if the polymer is strictly monodisperse. One of the characteristic effects of polydispersity is that the critical point no longer coincides with the extremum of the coexistence curve (although it still is an extremum of the spinodal)

(23). An example for this behavior is the LCST mixture of poly(styrene) (PS) and poly(vinylmethylether) (PVME). For example, for molecular weights $\bar{M}_w = 62700$ and $\bar{M}_w = 60000$, obtained from light scattering, one finds the minimum of the binodal at about $\phi_{min} \approx 0.38$ PS while $\phi_c \approx 0.48$ PS (24).

Of course, the concepts of a "limit of metastability" for metastable states at first-order transitions, and the distinction between two mechanisms of phase separation (nucleation and growth of a new phase vs long wavelength instabilities (25,26)) is not only used for solutions or mixtures, but for first-order transitions (Fig. 1) in general. For example, for metallic alloys undergoing order–disorder transitions to ordered superstructures, which in typical cases (such as the Au–Cu system (1)) are of first-order, the concept of "spinodal ordering" was coined (27), and similar phenomena where an order parameter grows spontaneously out of a disordered phase are expected to occur for the order–disorder transition of block copolymers, for instance. As is well known (15,28–36), diblock copolymer melts display an order–disorder transition (ODT; also referred to as "microphase separation transition") from a disordered melt to mesophases with various types of long-ranged order (Fig. 4) when the product of chain length N and Flory–Huggins parameter χ [that characterizes the degree of incompatibility between the partners A and B of the block copolymer, $N = N_A + N_B$, $f = N_A/(N_A + N_B)$] is large enough. Actually, the phase diagrams of Figure 4 are grossly simplified as they assume perfect symmetry between A and B (same size and shape of the monomers, same chain stiffness, etc), and therefore the phase diagrams are perfectly symmetric around $f = 1/2$, which experimentally is known not to be the case (37). Additional phases occur in narrow regions of the phase diagram (such as the gyroid and close-packed spherical phases (33)) which are not displayed in Figure 4. At this point we also mentioned that ordered phases were also observed (37), such as the double diamond and perforated lamellar structure, which are—at least in the idealized mean-field limit—only metastable rather than truly stable phases (33).

While in the mean-field limit the self-assembly of block copolymers into ordered mesophases is only controlled by two parameters, χN and f, this is no longer true when one goes beyond mean-field theory by including the effect of statistical fluctuations (30). Then the chain length N enters as a separate parameter, and the topology of the phase diagram changes (Fig. 4**b**). Only in the limit $N \to \infty$ mean-field theory is recovered, but this limit is hard to achieve since even for an effective chain length $\bar{N} = 10^4 (\bar{N} = [(\sqrt{6}R_g)^3 \rho_c]^2)$, ρ_c being the chain density and R_g the gyration radius) there are appreciable differences between the actual phase diagram (Fig. 4**b**) and the corresponding mean-field limit (Fig. 4**a**). While in the mean-field limit for $f = 1/2$ the ODT is a second-order transition, it is actually weakly of first order. Therefore close to the transition point the ordered phase forms from the disordered one also by nucleation and growth (31). Defining as an order parameter the amplitude A of a concentration wave

$$\phi(\vec{r}) = 2A \cos(q^* \vec{n} \cdot \vec{r} + \varphi), \qquad q^* \approx 1.945/R_g \tag{3}$$

where $\vec{n}$ is a unit vector perpendicular to the lamellas and φ characterizes the phase of the concentration wave, one can derive an effective free-energy functional $f_H(A)$ as shown in Figure 5 (31). When $\chi > \chi_0$, only the disordered phase is stable

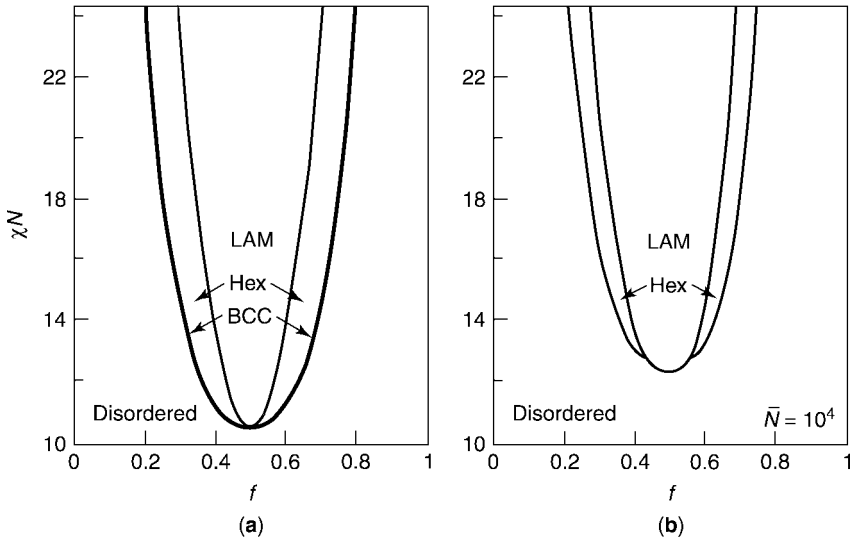

Fig. 4. Theoretically predicted phase diagrams of diblock copolymer $A_f\,B_{1-f}$ melts in the plane of parameters χN (χ = Flory–Huggins parameter, N = chain length) and composition f[where $f = N_A/(N_A + N_B)$], according to the Leibler (29) random phase approximation (**a**) and the Fredrickson-Helfand (30) Hartree approximation (**b**). Mesophases considered are the lamellar (LAM) phase, the hexagonal (HEX) phase where cylinders rich in the minority component are arranged periodically, a cross section perpendicular through the cylinders yielding a triangular lattice, and the body-centered cubic (BCC) lattice of spherical micelles. From Ref. 32.

(single minimum of $f_H(A)$ at $A = 0$, Fig. 5**a**), while at $\chi = \chi_0$ metastable minima with nonzero A appear, which become degenerate in depth with $f_H(A = 0)$ at the transition point, $\chi = \chi_t$, (see Fig. 5**c**). Even for $\chi > \chi_t$ the disordered phase ($A = 0$) is still metastable, since the minimum at $A = 0$ still persists and is separated by barriers from the stable minima. Note that the point $\chi = \chi_0$ is a spinodal point of the ordered phase within the region of the phase diagram where the disordered phase is the stable one. Finally, we recall from equation 3 that the characteristic wavelength $\lambda^* = 2\pi/q^*$ of the ordering is of the same order as the gyration radius of the chains, and hence of a "mesoscopic" scale rather than an atomistic scale. This justifies the name "mesophase" for the ordered structures in Figure 4.

Similar considerations as outlined here for diblock copolymers can be made for other types of orderings (liquid crystals (38,39)) or density functional theory of crystallization (melting transitions (40)). However, we shall not dwell on these topics (rather see LIQUID CRYSTALLINE POLYMERS and CRYSTALLIZATION KINETICS).

Surfaces

The concept of phase transitions can be carried over from bulk systems also to their surfaces (41–47). To be specific, let us consider a binary polymer blend (A,B) in a thin-film geometry (46,47). We suppose the film has a uniform thickness $\mathcal{D}$

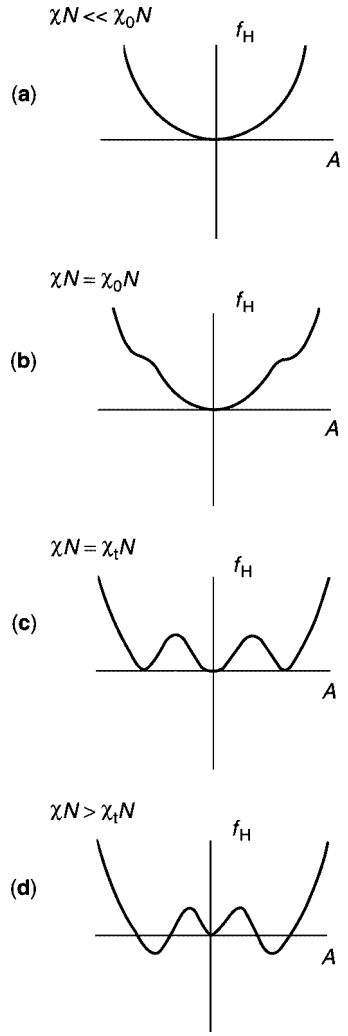

Fig. 5. Schematic free-energy functional $f_H(A)$ of a symmetrical diblock copolymer ($f = 1/2$) plotted vs the amplitude A of the concentration wave characterizing the lamellar ordering in the weak segregation limit. Cases (**a**–**d**) show $f_H(A)$ for regions above (**a**) and at (**b**) the spinodal χ_0 of the ordered phase, at the order–disorder transition (**c**) and below it (**d**). From Ref. 31.

and is bounded by a substrate on its lower surface and by some other material (or gas or vacuum, respectively) on its upper surface, as is the common situation in the application of thin polymer films (4,5). Then the thermodynamic potential F needs to be decomposed into bulk and surface terms (41–47)

$$F = F_{\text{bulk}} + \frac{1}{\mathcal{D}} F_s^{(l)} + \frac{1}{\mathcal{D}} F_s^{(u)}, \qquad \mathcal{D} \to \infty \tag{4}$$

where $F_s^{(l,u)}$ are the surface excess free energies due to the lower (upper) boundary of the thin film. Just as the bulk free energy F may exhibit singularities (Fig. 1) as a function of external control parameters due to phase transitions, also surface excess free energies F_s may exhibit singularities due to surface phase transitions. For example, in a binary polymer blend one expects that one species (eg, B) is preferred by a surface, and hence there is an enrichment layer of B at this surface. A surface phase transition (of first order) then physically corresponds to a jump in thickness of this enrichment layer, caused eg by variation of temperature (if the thickness of the layer jumps from a finite value to infinity, this is called a "wetting transition," while it is called "prewetting transition" if the jump occurs from a smaller to a larger value (48–50). Similar surface-induced ordering can also be considered for block copolymers (46,47,51,52). There is also great interest (both from theory (47,53) and from experiment (54) on surface effects on the kinetics of phase transformations in polymer blends ("surface-directed spinodal decomposition" (55,56). Finally, we mention that related concepts also apply to phase transformations of thin homopolymer films on substrates: If the film is metastable, the dewetting of the substrate starts by the nucleation and growth of holes in the film (57), while for unstable films "spinodal dewetting" (58,59) is predicted. A particular active field is also the study of phase transformations in thin block copolymer films (36,47,60,61).

Critical Phenomena in Polymer Solutions and Blends

In this section we elaborate further on the phenomena that occur in the vicinity of the critical points (cf phase diagrams Figs. 2**a** and 2**b**), since these phenomena were extensively studied in the last decade and a rather definite knowledge about them has been gained.

Of course, a useful starting point of the discussion still is the Flory–Huggins mean-field theory (13–16), where the excess free-energy density of mixing is written as

$$\frac{1}{a^3}\frac{\Delta F_{\mathrm{mix}}}{k_{\mathrm{B}}T} = \frac{\phi_{\mathrm{A}} \ln \phi_{\mathrm{A}}}{N_{\mathrm{A}}} + \frac{\phi_{\mathrm{B}} \ln \phi_{\mathrm{B}}}{N_{\mathrm{B}}} + \chi \phi_{\mathrm{A}} \phi_{\mathrm{B}} \tag{5}$$

where a is the lattice spacing of the underlying lattice model; ϕ_{A}, and $\phi_{\mathrm{B}} = 1 - \phi_{\mathrm{A}}$ are the volume fractions of the two types of (effective) monomers; N_{A}, N_{B} are the chain lengths of the two polymers (formally a polymer solution is obtained putting $N_{\mathrm{A}} = N$, $N_{\mathrm{B}} = 1$); and the Flory–Huggins parameter χ is related to pairwise interaction energies $\varepsilon_{\mathrm{AA}}$, $\varepsilon_{\mathrm{AB}}$, $\varepsilon_{\mathrm{BB}}$ via $\chi = z\,[\varepsilon_{\mathrm{AB}} - (\varepsilon_{\mathrm{AA}} + \varepsilon_{\mathrm{BB}})/2]/k_{\mathrm{B}}T = z(\Delta\varepsilon)/k_{\mathrm{B}}T$, z being the coordination number of the lattice.

Neglecting any possible dependence of χ on ϕ $(= \phi_{\mathrm{A}})$, the condition of the spinodal χ_{s} becomes

$$\left.\frac{\partial^2(\Delta F_{\mathrm{mix}}/k_{\mathrm{B}}T)}{\partial \phi^2}\right|_{\phi=\phi_{\mathrm{s}}(\chi)} = 0 \Rightarrow 2\chi_{\mathrm{s}}(\phi) = \frac{1}{\phi N_{\mathrm{A}}} + \frac{1}{(1-\phi)N_{\mathrm{B}}} \tag{6}$$

For monodisperse polymers, the maximum of the spinodal $\phi_s(\phi)$ yields the critical point

$$\phi_c^{FH} = (\sqrt{N_A/N_B} + 1)^{-1}, \qquad 1/\chi_c^{FH} = 2\left(N_A^{-1/2} + N_B^{-1/2}\right)^{-2} \tag{7}$$

For the special case of a symmetric mixture ($N_A = N_B = N$), we have $\phi_c = 1/2$ and $\chi_c = 2/N$, ie, the critical temperature $k_B T_c = z(\Delta\varepsilon)/\chi_c = z(\Delta\varepsilon)N/2$ scales linearly with N. For the other special case of a polymer solution, $\phi_c \propto 1/\sqrt{N}$ for $N \to \infty$, and $1/\chi_c \to 2$, ie, the theta temperature (Fig. 2**a**) is $\Theta = 2z\,(\Delta\varepsilon)/k_B$. The two branches of the coexistence curve are obtained as

$$\phi_{coex}^{(1,2)} - \phi_c = \pm\hat{B}(\chi/\chi_c - 1)^{1/2} \tag{8}$$

where $\hat{B} = \sqrt{3}/2$ for a symmetric mixture, while $\hat{B} \propto N^{-1/4}$ for a solution. In the latter case equation 8 holds only for $x = \frac{1}{2}\sqrt{N}(\chi/\chi_c - 1) \ll 1$ (62). In the opposite limit $x \gg 1$, one rather finds (62)

$$\phi_{coex}^{(1)} \approx \frac{3}{2}(1 - T/T_c)\exp\left[-\frac{3}{8}(1 - T/T_c)^2 N\right], \qquad \phi_{coex}^{(2)} \approx \frac{3}{2}(1 - T/\Theta) \tag{9}$$

For $N \to \infty$ (keeping $1 - T/\Theta$ fixed) one hence finds $\phi_{coex}^{(2)} - \phi_{coex}^{(2)} \propto (1 - T/\Theta)$, ie, the exponent of the order parameter now is $\beta^t{}_{MF} = 1$, as expected for a tricritical point (62).

Of course, it is of interest to study how the critical properties of a polymer solution scale with $N \to \infty$ (62–68). A standard assumption invokes power laws (66)

$$\hat{B}(N) \propto N^{-x_1}, \qquad \phi_c(N) \propto N^{-x_2}, \qquad \Theta - T_c\ (N) \propto N^{-x_3} \tag{10}$$

which have the mean field values ${x_1}^{MF} = 1/4, {x_2}^{MF} = 1/2, {x_3}^{MF} = 1/2$. Assuming that the mean-field–type scaling behavior $\phi_{coex}^{(2)} - \phi_{coex}^{(1)} \propto N^{-1/2}\tilde{\phi}[N^{1/2}(1 - T/T_c)]$ holds generally but in the vicinity of T_c one must recover equation 2 with the correct Ising universality class exponent $\beta \approx 0.325$ yields instead $x_1 = (1-\beta)/2 \approx 0.34$ (14,62), while the exponents x_1, x_3 would keep their mean-field values. However, the results of many experiments (64,65) and simulations (66,67) agree only with $x_3 = 1/2$ but suggest instead $x_2 \approx 0.38$, if one insists on the simple power laws (eq. 10). The idea involved to explain $x_2 \approx 0.38$, namely that the chains at the critical point are already partially collapsed and no longer ideal Gaussian coils (as they should be at the theta point (14)), is also clearly refuted by the simulations. There are several possibilities to explain the problems with equation 10. For example, one expects logarithmic corrections to the simple power laws near a tricritical point (63)

$$\phi_c(N) \propto (\ln N)^{1/2}/N^{1/2}, \qquad \Theta - T_c(N) \propto N^{-1/2}(\ln N)^{-3/11}, \qquad N \to \infty \tag{11}$$

It is rather likely, however, that neither experiments nor simulations have reached the regime of sufficiently large N yet where equation 11 is observed.

Another possibility is that the crossover between mean field and Ising critical behavior, which is spread out over many decades in $1 - T/T_c$ (68,69), also causes the exponents x_1, x_2, x_3 in equation 10 to be "effective exponents," which show a significant variation when one studies $\hat{B}(N),\phi_c(N)$, etc. over many decades in N. Usually experiments and simulations have only 1 to 2 decades in N at their disposal, and therefore all conclusions on the validity of equations 10 and 11 are still preliminary. However, experiments do allow a study of enough decades in $|1 - T/T_c|$ to confirm the theoretical expectation that the critical exponents β,γ, etc. take the values of the Ising universality class.

While the Flory–Huggins mean-field theory is not a good approximation for the description of critical phenomena in polymer solutions, it works much better for (approximately symmetric) polymer blends. To understand this fact, it is useful to consider the scattering from concentration fluctuation within the framework of the "random phase approximation (RPA)" (14). It is based on the assumption that the chain configurations in the blend are unperturbed Gaussian coils, and it reduces the collective scattering function $S_{coll}(\vec{q})$, q being the scattering wavevector, to the single-chain factors $S_A(\vec{q}),S_B(\vec{q})$ as follows,

$$S_{coll}^{-1}(\vec{q}) = [\phi S_A(\vec{q})]^{-1} + [(1-\phi)S_B(\vec{q})]^{-1} - 2\chi_{eff} \tag{12}$$

where $S_A(q) = Nf_D(R^2_{g,A}q^2)$, $f_D(x)$ being the Debye function $f_D(x) = (2/x^2)[\exp(-x) - 1 + x]$,$R_{g,A} = \sigma_A\sqrt{N_A/6}$ being the gyration radius of the A chains, and σ_A their segment sizes. A similar notation holds for the B component. $\chi_{eff} = \chi$ if χ is strictly independent of χ, otherwise (15,16) $\chi_{eff} = -(1/2)\,\partial^2/\partial\phi^2[\phi(1-\phi)\chi(\phi)]$. The RPA expression is routinely used to extract the Flory–Huggins parameter from small-angle neutron scattering experiments. Unfortunately, the value depends slightly on the system (eg, there are differences between homopolymer blends and block copolymer systems (70)) and on the method (eg, scattering, composition of the coexisting phases and surface enrichment (71)). Expanding equation 12 for small q yields

$$S_{coll}(q) = S_{coll}(0)/(1 + q^2\xi^2) \tag{13}$$

with $S_{coll}^{-1}(0) = (\phi N_A)^{-1} + [(1-\phi)N_B]^{-1} - 2\chi_{eff}$. $1/S_{coll}$ vanishes at the spinodal curves (cf eq. 6, and ξ is the correlation length of the concentration fluctuations. Defining the effective lattice parameter a of the Flory–Huggins lattice by $a^2 = \sigma^2_A(1-\phi) + \sigma^2_B\,\phi$, one finds for $\phi = \phi_c$, $\chi < \chi_c$ that

$$S_{coll}(0) = (2\chi_c)^{-1}(1 - \chi/\chi_c)^{-1}, \qquad \xi = \frac{a}{6}(4N_AN_B)^{1/4}(1 - \chi/\chi_c)^{-1/2} \tag{14}$$

which are special cases of the relations $S_{coll}(0) = \hat{S}(T/T_c - 1)^{-\gamma}$,$\xi = \hat{\xi}(T/T_c - 1)^{-\nu}$ describing the critical singularities of the critical scattering intensity and correlation length, respectively, with $\gamma_{MF} = 1$, $\nu_{MF} = 1/2$, the corresponding mean-field exponents. Equation 14 shows that the critical amplitude $\hat{\xi}$ for a symmetrical polymer mixture is of the same order as the gyration radius R_g (while for a

polymer solution it is much smaller, $\hat{\xi} \propto \sqrt{aR_g}$). This large value of $\hat{\xi}$ is critical for the validity of mean-field theory for $N \to \infty$, as the Ginzburg criterion (72,73) shows. According to this criterion mean-field theory is valid when the fluctuation of the order parameter in a correlation volume is much less than the mean square order parameter itself. This yields (in d dimensions)

$$\hat{S}\hat{\xi}^{-d}/\hat{B}^2 \ll |1 - T/T_c|^{(2-d)/2} \qquad \text{or} \qquad \text{Gi} \ll |1 - T/T_c| \tag{15}$$

where the "Ginzburg number" Gi is proportional to $(\hat{S}\hat{\xi}^{-d}/\hat{B}^2)^{2/(4-d)}$. For a symmetric polymer mixture, $\hat{B}$ is of order unity, while $\hat{S} \propto N$, $\hat{\xi} \propto N^{1/2}$, and hence $\text{Gi} \propto \text{N}^{(2-\text{d})/(4-\text{d})}$ ($= 1/N$ in $d = 3$). Thus for large enough N mean-field theory becomes valid for polymer mixtures in $d = 3$ (but not in $d = 2$, ie, for polymer blends in thin film geometry Gi is of order unity). For polymer solutions, where $\hat{B} \propto N^{-1/4}$, $\hat{S}$ of order unity, $\hat{\xi} \propto N^{1/4}$, one rather finds $\text{Gi} \propto N^{-1/2}$ in $d = 3$. Since equation 8 is only supposed to hold if $\sqrt{N}(1-T/T_c) \ll 1$ but equation 15 requires that $|1 - T/T_c| \gg 1/\sqrt{N}$, we see that Flory–Huggins theory must fail in the critical region of a phase-separating polymer solution, and this is confirmed by experiment (65,69).

For polymer blends in $d = 3$ it then turns out that a crossover scaling description applies (74–76), $t = |1 - T/T_c|$,

$$\phi^{(2)}_{\text{coex}} - \phi^{(1)}_{\text{coex}} \propto \text{t}^{1/2}\tilde{B}(t/\text{Gi}), \qquad S_{\text{coll}}(0) \propto Nt^{-1}\tilde{S}(t/\text{Gi}) \tag{16}$$

where the scaling functions for small values of their arguments behave as $\tilde{B}(x) \propto x^{\beta - 1/2}$,$\tilde{S}(x) \propto x^{1-\gamma}$, to reproduce the critical behavior of the Ising universality class. There exists an analytic approximation (74) for $\tilde{\xi}(x)$ that provides a very good fit to the experimental data (76). However, while the above prediction $\text{Gi} \propto 1/N$ is confirmed by simulations of an idealized lattice model (75) it is not compatible with the experimental data for polymer blends (76,77). This discrepancy is attributed to the compressibility of the blend (which is completely neglected in eqs. 5, 12 and 13, which gives rise to an anomalous pressure dependence of the Ginzburg number (77).

At this point, it is appropriate to critically reexamine to what extent the Flory–Huggins description (Eqs. 5–7) is valid as a phenomenological model. One important qualitative effect that is neglected completely is the "correlation hole effect" (14): For an effective monomer of a chain it is more likely to have other monomers in the neighborhood that belong to the same chain rather than to other chains. Of course, only interchain interactions and no intrachain interaction contribute to macroscopic phase separation, and hence the "effective coordination number" z that enters the Flory–Huggins parameter χ gets reduced. It turns out (78) that this leads to $1/\sqrt{N}$ corrections in $d = 3$, $z = z_\infty + \text{const}/\sqrt{N}$, and similarly $\chi_c = \chi_\infty + \text{const}/\sqrt{N}$, $\phi_c = \phi_c^{\text{FH}} + \text{const}/\sqrt{N}$, etc. In $d = 2$, however, this effect is far more drastic, since the chains can interpenetrate only rather little, and hence $z \propto 1/\sqrt{N} \to 0$ as $\to N \to \infty$, and therefore also (79) $\chi_c \propto 1/\sqrt{N}$ rather than $\chi_c \propto 1/N$ as in the case of $d = 3$. The linear scaling of the critical temperature T_c with N in $d = 3$ has been experimentally verified (80) while no systematic

studies of phase separation of polymer blends in ultrathin films so far have been possible.

Of course, polymer blends are fluids, and a more realistic description of the packing of neighboring atomic groups is needed than can be achieved by Flory–Huggins theory (and its extensions that account for compressibility (81). An approach that attempts to generalize theories of fluid structure and thermodynamics to polymer mixtures is the polymer reference interaction site model (PRISM) (82,83). While this approach is not useful for the critical properties, it clearly is a powerful description of the general interplay between structure and thermodynamics in polymer blends. It shares a disadvantage with the Monte Carlo computer simulation approach (75,78,84,85), namely that extensive numerical computations are mandatory. A complementary approach is the lattice cluster theory of Freed and co-workers (86), which takes better account of asymmetry in size and shape of monomers by using a lattice model with "monomers" occupying several lattice sites. The monomer shape might impart an entropic contribution (87,88) or a composition dependence (88) onto the Flory–Huggins parameter that might result in a significant modification of the phase behavior as a function of temperature and composition. However, there is neither a fully satisfactory approach that could predict the Flory–Huggins parameter (if one uses eq. 5 as an effective description) from atomistic input, nor can one describe the complete phase diagrams of binary and ternary blends and the structure of the coils under the various thermodynamic conditions accurately. Note that the RPA (eq. 12) also is a rough approximation only. In reality, the polymer coils do respond to the conditions of the thermodynamic state in which the system is in; eg, in a polymer blend typically chains of the minority component contract (89,90), while in block copolymer melts pretransitional chain stretching occurs (91,92)—and also is seen in the experiment (93)—because the center of mass of the A block gets separated from that of the B block, so that the polymer coil adopts a dumbbell-like shape. Because of all these limitations, the understanding of more complex phase-separation phenomena—where eg, microphase separation of block copolymers competes with macroscopic phase separation—are much less well understood, and will not be treated here. Such phenomena occur in blends of block copolymers (94) or blends of homopolymers with block copolymers (95).

We only mention, that for homopolymer–block copolymer mixtures RPA predicts that the wavelength λ^* of lamellar ordering may diverge at particular points in the phase diagram, so-called Lifshitz points (96); however, isotropic Lifshitz points are destabilized by statistical fluctuations and hence exist only in the mean field limit, while in reality one expects there a kind of "microemulsion" in the phase diagram. Such microemulsion phases also occur presumably in random copolymer melts (97), interpenetrating polymer networks (98), etc.

Returning now to the phase diagram of polymer solutions, we emphasize also that much more complicated phenomena than envisaged in Figure 2**a** can occur. For example, considering the solution of short alkane chains (eg hexadecane) in carbondioxide, one encounters a competition between gas–liquid transitions of both polymer (C_{16} H_{34}) and solvent (CO_2) and liquid–liquid phase separation (99,100). Thus the phase diagram not only contains (in the space of three variables p,T, and ϕ) various lines of critical points, but special points such as critical end points, triple points, and tricritical points may also occur. Each system then

requires a separate detailed discussion on an atomistic level to understand all the possible phase changes that it can undergo. In this article, we hence have not emphasized these rather specific aspects, but the general feature of the critical-point phenomena involved.

Interfaces between Coexisting Phases

There are two methods to extend equation 5 to the inhomogeneous situation where a domain of the phase rich in polymer coexists with solvent or a domain rich in polymer A coexists with another domain rich in polymer B. The simplest approach (15,16,99,101) amends equation 5 with a $(\nabla\phi)^2$ term; this is appropriate in the "weak segregation limit." In the opposite case ("strong segregation limit") one goes from pure A to pure B in a blend and the method of choice is the self-consistent field theory (102–106), which also is a powerful method for the study of the block copolymer phase diagrams in this strong segregation limit (32–36). These theories predict the "interfacial tension" f_{int} (= excess free energy due to the interface per unit area) and the "intrinsic width" w_0 of the interface. For a polymer solution in the critical region near $T_c(N)$, the mean field theory yields (107)

$$f_{\text{int}} \propto N^{-1/4}[1 - T/T_c(N)]^{3/2}, \qquad w_0 = 2\xi \propto N^{1/4}[1 - T/T_c(N)]^{-1/2} \tag{17}$$

while actually the behavior compatible with Ising universality class is (107), with $\nu \approx 0.63$,

$$f_{\text{int}} \propto \xi^{-2} = N^{\nu-1}[1 - T/T_c(N)]^{2\nu}, \qquad w_0 \propto N^{(1-\nu)/2}[1 - T/T_c(N)]^{-\nu} \tag{18}$$

Conversely, for the symmetrical polymer blend in the mean field critical regime the corresponding results are (15,16)

$$f_{\text{int}} \propto N^{-1/2}(1 - \chi_c/\chi)^{3/2}, \qquad w_0 = 2\xi \propto N^{1/2}(1 - \chi_c/\chi)^{-1/2} \tag{19}$$

while in the Ising critical regime one has

$$f_{\text{int}} \propto \xi^{-2} = N^{2(\nu-1)}(1 - \chi_c/\chi)^{2\nu}, \qquad w_0 = 2\xi \propto N^{1-\nu}(1 - \chi_c/\chi)^{-\nu} \tag{20}$$

Finally, we note the behavior in the strong segregation limit (102), ρ being the monomer density and a the statistical segment length, and a factor $(k_B T)^{-1}$ is absorbed in f_{int}

$$f_{\text{int}} = \rho a \sqrt{\chi/6}, \qquad w_0 = a/\sqrt{6\chi} \tag{21}$$

Equation 20 also holds for a strongly segregated polymer solution (but then χ is of order unity).

Now interfacial widths can be measured by depth-profiling techniques which eg use a nuclear reaction analysis to obtain the concentration profile through a thin polymer film (108,109) or by total reflection of neutrons (110) or X-rays. However, it should be noted that neither in an experiment nor in a simulation can one ever observe the "intrinsic width" of an interface, which is an absolutely hypothetical object (106,111). Rather the observed width always results from a convolution of the intrinsic profile with the capillary wave broadening (106,111,112). On a lateral length scale L, one obtains for the actual mean square width

$$w^2 = w_0^2 + \frac{1}{4f_{\text{int}}}(\ln \mathrm{L} - \ln\lambda_0) \tag{22}$$

where λ_0 is the short wavelength cutoff of the capillary wave spectrum, and it was assumed that the thickness $\mathcal{D}$ of the film is large enough such that the finite size effect due to $\mathcal{D}$ is still negligible. In many circumstances this is not the case (109), and then a much stronger size effect $w^2 \propto (\text{const}\ \mathcal{D})$ may result (113). Now the appropriate choice of λ_0 is still questionable (104–106,114), and while f_{int} can be extracted if one observes the predicted linear variation between w^2 and L, obviously there is no unique separation between $w^2{}_0$ and $\ln \lambda_0/(4 f_{\text{int}})$. In practice, observations of equation 22 are rare, and f_{int} is estimated experimentally by other methods (eg the "capillary rise" method or the "sessile drop" method, see eg Ref. 115).

Since many application properties of amorphous solid polymer blends (which often are phase-separated on a mesoscopic scale) are controlled by the interfaces they contain, a good understanding of the structure and properties of interfaces is very important. Simulations (116) have shown that free volume and chain ends get enriched at the interfaces, and homopolymers become oriented parallel to the interface at strong segregation, while adsorbed block copolymers tend to orient perpendicularly (117). The compatibilizing effect of block copolymers adsorbed to interfaces in unmixed blends is well known.

Once more, we emphasize that our treatment has simplified the topic enormously, and only the most salient features were mentioned. Complications due to the pressure dependence in blends and due to the gas–liquid transitions in polymer solvent-systems may lead to new effects. For example, for the interfaces between gaseous CO_2 bubbles in a $C_{16}H_{34}$ matrix one obtains interfacial wetting of fluid CO_2, which reduces the interfacial tension drastically and hence facilitates nucleation (118). In fact, an understanding of nucleation in polymer blends (119) and solutions (118) is just emerging.

BIBLIOGRAPHY

"Phase Transformations" in *EPSE* 2nd ed., Vol. 11, pp. 30–45, by L. Leibler, Université Pierre et Marie Curie.

1. G. Kostorz, ed., *Phase Transformations in Materials*, Wiley-VCH, Weinheim, 2001.

2. L. D. Landau and E. M. Lifshitz, *Statistical Physics*, Pergamon Press, Oxford, 1958.
3. P. Sollich, *J. Phys.: Condens. Matter* **14**, R79 (2002).
4. I. C. Sanchez, ed., *Physics of Polymer Surfaces and Interfaces*, Butterworth-Heinemann, Boston, 1992.
5. S. Granick, ed., *Polymers in Confined Environments* (Advances in Polymer Science, Vol. 138) Springer, Berlin, 1999.
6. T. Thurn-Albrecht, J. De Rouchy, T. P. Russell, and H. M. Jaeger, *Macromolecules* **33**, 3250 (2000).
7. D. Chowdhury and D. Stauffer, *Principles of Equilibrium Statistical Mechanics*, Wiley-VCH, Weinheim, 2000.
8. M. A. Anisimov and J. V. Sengers, in J. S. V. Sengers, R. F. Kayser, C. J. Peters, and H. J. White, eds., *Equations of State for Fluids and Fluid Mixtures*, Elsevier, Amsterdam, 2000, pp. 381–434.
9. M. E. Fisher, *Rev. Mod. Phys.* **46**, 587 (1974).
10. K. Binder and E. Luijten, *Phys. Rep.* **344**, 179 (2001).
11. M. J. Anselme, A. Gude, and A. S. Teja, *Fluid Phase Equilibria* **57**, 317 (1990).
12. A. Cumming, P. Wiltzius, and F. S. Bates, *Phys. Rev. Lett.* **65**, 863 (1990).
13. P. J. Flory, *Principles of Polymer Chemistry*, Cornell University Press, Ithaca, 1953.
14. P. D. de Gennes, *Scaling Concepts in Polymer Physics*, Cornell University Press, Ithaca, 1979.
15. K. Binder, *Adv. Polym. Sci* **112**, 181 (1994).
16. K. Binder, *J. Chem. Phys.* **79**, 6387 (1983).
17. K. Binder, *Phys. Rev. A: At., Mol., Opt. Phys.* **29**, 341 (1984).
18. J. W. Cahn, *Acta Metall.* **9**, 795 (1961).
19. T. Hashimoto, in E. J. Kramer, ed., *Materials Science and Technology, Vol. 12: Structure and Properties of Polymers*, VCH, Weinheim, 1992.
20. K. Binder and P. Fratzl, in Ref. 1, pp. 409–480.
21. N. P. Balsara, in J. E. Mark, ed., *Physical Properties of Polymers Handbook*, AIP, Woodbury, New York, 1996.
22. J. M. Bardin and D. Patterson, *Polymer* **10**, 247 (1969).
23. R. Koningsveld and L. A. Kleintjens, *Macromolecular Chemistry*, Vol. **1**, Butterworth, London, 1973, p. 97.
24. H. L. Snyder, P. Meakin, and S. Reich, *Macromolecules* **16**, 757 (1983).
25. K. Binder and D. Stauffer, *Adv. Phys.* **25**, 343 (1976).
26. J. D. Gunton, M. San Miguel, and P. S. Sahni, in C. Domb, and J. L. Lebowitz, eds., *Phase Transitions and Critical Phenomena*, Vol. **8**, Academic Press, London, 1983, p. 267.
27. D. De Fontaine and H. E. Cook, in R. E. Miller, E. Ascher and I. Jaffee, eds., *Critical Phenomena in Alloys, Magnets and Superconductors*, McGraw Hill, New York, 1971, p. 257.
28. E. Helfand and Z. R. Wasserman, *Macromolecules* **9**, 879 (1976).
29. L. Leibler, *Macromolecules* **13**, 1602 (1980).
30. G. H. Fredrickson and E. Helfand, *J. Chem. Phys.* **87**, 697 (1987).
31. G. H. Fredrickson and K. Binder, *J. Chem. Phys.* **91**, 7265 (1989).
32. F. S. Bates and G. H. Fredrickson, *Annu. Rev. Phys. Chem.* **41**, 525 (1990).
33. M. W. Matsen and M. Schick, *Curr. Opin. Colloid Interface Sci.* **1**, 329 (1996).
34. I. W. Hamley, *The Physics of Block Copolymers*, Oxford University Press, Oxford, 1998.
35. J. Noolandi and A.-C. Shi, *Curr. Opin. Colliod Interface Sci.* **3**, 436 (1998).
36. M. J. Fasolka and A. M. Mayes, *Annu. Rev. Mater. Sci.* **31**, 323 (2001).

37. F. S. Bates, M. F. Schulz, A. K. Khandpur, S. Förster, and J. H. Rosedale, *Faraday Discuss.* **98**, 7 (1994).
38. P. G. de Gennes, *The Physics of Liquid Crystals*, Clarendon Press, Oxford, 1974.
39. S. Chandrasekhar, *Liquid Crystals*, Cambridge University Press, Cambridge, 1992.
40. M. Baus, *J. Stat. Phys.* **48**, 1129 (1987).
41. K. Binder, in C. Domb and J. L. Lebowitz, eds., *Phase Transitions and Critical Phenomena*, Vol. **8**, Academic Press, London, 1983, p. 1.
42. P. G. de Gennes, *Rev. Mod. Phys.* **57**, 827 (1985).
43. D. E. Sullivan and M. M. Telo da Gama, in C. A. Croxton, ed., *Fluid Interfacial Phenomena*, John Wiley & Sons, Inc., New York, 1986, p. 45.
44. S. Dietrich, in C. Domb and J. L. Lebowitz, eds., *Phase Transitions and Critical Phenomena*, Vol. **12**, Academic Press, London, 1988, p. 1.
45. M. Schick, in J. Charvolin, J. F. Joanny, and J. Zinn-Justin, eds., *Liquids at Interfaces*, North-Holland, Amsterdam, 1990.
46. K. Binder, *Acta Polym.* **46**, 204 (1994).
47. K. Binder, in Ref. 4, pp. 1–89.
48. J. W. Cahn, *J. Chem. Phys.* **66**, 3667 (1977).
49. I. Schmidt and K. Binder, *J. Phys. (France)* **46**, 1631 (1985).
50. M. Müller, K. Binder, and E. V. Albano, *Int. J. Mod. Phys. B* **15**, 1867 (2001).
51. G. H. Fredrickson, *Marcomolecules* **20**, 2535 (1987).
52. K. Binder, H. L. Frisch, and S. Stepanow, *J. Phys. II (Paris)* **7**, 1353 (1997).
53. K. Binder, *J. Nonequil. Thermodyn.* **23**, 114 (1998).
54. G. Krausch, *Mater. Sci. Eng. Rep. R* **14**, 1 (1995).
55. R. A. L. Jones, L. H. Norton, E. J. Kramer, F. S. Bates, and P. Wiltzius, *Phys. Rev. Lett.* **66**, 1326 (1991).
56. S. Puri and K. Binder, *Phys. Rev. A* **46**, R4487 (1992).
57. G. Reiter, *Phys. Rev. Lett.* **68**, 75 (1992).
58. F. Brochard and J. Daillant, *Can. J. Phys.* **68**, 1084 (1990).
59. R. Xie, A. Karim, J. F. Douglas, C. C. Han, and R. A. Weiss, *Phys. Rev. Lett.* **81**, 1251 (1998).
60. T. P. Russell, *Curr. Opin. in Colloid Interface Sci.* **1**, 107 (1996).
61. K. Binder and M. Müller, *Curr. Opin. Colloid Interface Sci.* **5**, 315 (2000).
62. B. Widom, *Physica A* **194**, 532 (1993).
63. B. Duplantier, *J. Phys. (France)* **43**, 991 (1982).
64. I. C. Sanchez, *J. Appl. Phys.* **58**, 2871 (1985).
65. R. Perzynski, A. Delsanti, and M. Adam, *J. Phys. (France)* **48**, 155 (1987).
66. N. B. Wilding, M. Müller, and K. Binder, *J. Chem. Phys.* **105**, 802 (1996).
67. H. Frauenkron and R. Grassberger, *J. Chem. Phys.* **107**, 9599 (1997).
68. A. A. Povodyrev, M. A. Anisimov, and J. V. Sengers, *Physica A* **264**, 345 (1999).
69. Y. B. Melnichenko, M. A. Anisimov, A. A. Povodyrev, G. D. Wignall, J. A. Sengers, and W. A. Van Hook, *Phys. Rev. Lett.* **79**, 5266 (1997).
70. W. W. Maurer, F. S. Bates, T. P. Lodge, K. Almdal, K. Mortensen, and G. H. Fredrickson, *J. Chem. Phys.* **108**, 2989 (1998).
71. J. Klein, T. Kerle, F. Zink, and E. Eiser, *Macromolecules* **33**, 1298 (2000).
72. V. L. Ginzburg, *Sov. Phys. Solid State* **2**, 1824 (1960).
73. P. G. de Gennes, *J. Phys. Lett. (Paris)* **38**, L34 (1997).
74. M. Y. Belyakov and S. B. Kiselev, *Physica A* **190**, 75 (1992).
75. H.-P. Deutsch and K. Binder, *J. Phys. II (France)* **3**, 1049 (1993).
76. D. Schwahn, G. Meier, K. Mortensen, and S. Janssen, *J. Phys. II (France)* **4**, 837 (1994).
77. D. Schwahn, *Macromol. Symp.* **149**, 43 (2000).

78. M. Müller, and K. Binder, *Macromolecules* **28**, 1825 (1995).
79. A. Cavallo, M. Müller, and K. Binder, *Europhys. Lett.* **61**, 214 (2003).
80. M. D. Gehlsen, J. H. Rosedale, F. S. Bates, G. D. Wignall, and K. Almdal, *Phys. Rev. Lett.* **68**, 2452 (1992).
81. I. C. Sanchez and R. H. Lacombe, *Macromolecules* **11**, 1145 (1978).
82. K. S. Schweizer and J. G. Curro, *Adv. Chem. Phys.* **98**, 1 (1997).
83. K. S. Schweizer and A. Yethiraj, *J. Chem. Phys.* **98**, 9053 (1993).
84. K. Binder, in K. Binder, ed., *Monte Carlo and Molecular Dynamics Simulations in Polymer Science*, Oxford University Press, New York, 1995, pp. 356–432.
85. S. K. Kumar, *Macromolecules* **30**, 5085 (1997).
86. K. W. Foreman and K. F. Freed, *Adv. Chem. Phys.* **103**, 335 (1998).
87. J. Dudowicz, K. F. Freed, and J. F. Douglas, *J. Chem. Phys.* **116**, 9983 (2002).
88. M. Müller, *Macromolecules* **28**, 6556 (1995).
89. A. Sariban and K. Binder, *Macromol. Chem.* **189**, 2357 (1988).
90. M. Müller, *Macromolecules* **31**, 9044 (1998).
91. H. Fried and K. Binder, *Europhys. Lett.* **16**, 237 (1991).
92. K. Binder and H. Fried, *Macromolecules* **26**, 6878 (1993).
93. K. Almdal, J. H. Rosedale, F. S. Bates, G. D. Wignall, and G. H. Fredrickson, *Phys. Rev. Lett.* **65**, 1112 (1990).
94. H. Frielinghaus, N. Hermsdorf, K. Almdal, K. Mortensen, L. Messe, L. Corvazier, J. P. A. Fairclough, A. J. Ryan, P. D. Olmsted, and I. W. Hamley, *Europhys. Lett.* **53**, 680 (2001).
95. D. Schwahn, K. Mortensen, H. Frielinghaus, K. Almdal, and L. Kielhorn, *J. Chem. Phys.* **112**, 5454 (2000).
96. D. Broseta and G. H. Fredrickson, *J. Chem. Phys.* **93**, 2927 (1990).
97. J. Houdayer and M. Müller, *Europhys. Lett.* **58**, 660 (2002).
98. S. Stepanow, A. V. Dobrynin, T. A. Vilgis, and K. Binder, *J. Phys. I (Paris)* **6**, 837 (1996).
99. L. G. MacDowell, P. Virnau, M. Müller, and K. Binder, *J. Chem. Phys.* **117**, 6380 (2002).
100. P. Virnau, M. Müller, L. G. MacDowell, and K. Binder, *Comput. Phys. Commun.* **147**, 378 (2002).
101. J. F. Joanny and L. Leibler, *J. Phys. (France)* **39**, 951 (1978).
102. E. Helfand and Y. Tagami, *J. Chem. Phys.* **56**, 3592 (1971).
103. D. Broseta, G. H. Fredrickson, E. Helfand, and L. Leibler, *Macromolecules* **23**, 132 (1990).
104. A. N. Semenov, *Macromolecules* **26**, 6617 (1993).
105. A. N. Semenov, *Macromolecules* **27**, 2732 (1994).
106. A. Werner, F. Schmid, M. Müller, and K. Binder, *Phys. Rev. E* **59**, 728 (1999).
107. B. Widom, *Stat. Phys.* **52**, 1343 (1988).
108. A. Budkowski, *Adv. Polym. Sci.* **142**, 1 (1999).
109. T. Kerle, J. Klein, and K. Binder, *Euro. Phys. J. B* **7**, 401 (1999).
110. M. Stamm and D. W. Schubert, *Annu. Rev. Mater. Sci.* **25**, 325 (1996).
111. K. Binder and M. Müller, *Int. J. Mod. Phys. C* **11**, 1093 (2000).
112. D. Jasnov, *Rep. Prog. Phys.* **47**, 1059 (1984).
113. A. Werner, F. Schmid, M. Müller, and K. Binder, *J. Chem. Phys.* **107**, 8175 (1997).
114. A. Milchev and K. Binder, *Europhys. Lett.* **59**, 8 (2002).
115. K.-Q. Xia, C. Franck, and B. Widom, *J. Chem. Phys.* **97**, 1446 (1992).
116. M. Müller, K. Binder, and W. Oed, *J. Chem. Soc., Faraday Trans.* **91**, 2396 (1995).
117. A. Werner, F. Schmid, K. Binder, and M. Müller, *Macromolecules* **29**, 8241 (1996).

118. M. Müller, L. G. MacDowell, P. Virnau, and K. Binder, *J. Chem. Phys.* **117**, 5480 (2002).
119. S. M. Wood and Z. G. Wang, *J. Chem. Phys.* **116**, 2289 (2002).

KURT BINDER
MARCUS MÜLLER
Institut für Physik, Johannes Gutenberg Universität

PHENOLIC RESINS. See Volume 7.

PHOSGENE. See Volume 3.

PHOSPHORUS-CONTAINING POLYMERS AND OLIGOMERS. See Volume 3.

PHOTOPOLYMERIZATION, CATIONIC

Introduction

Light-induced polymerization reactions, commonly known as *photopolymerizations*, are generally chain reactions in which the propagating active centers (free radicals or cations) are produced by a photochemical event. These reactions may be initiated using ultraviolet or visible light, and offer many advantages when compared to the more common thermal polymerizations in which heat is used to produce active centers. For example, photopolymerization uniquely offers spatial control (since the light may be directed to locations of interest in the system) and temporal control (since the light is readily modulated on and off) of the initiation reaction, and the rate of production of active centers is often independent of temperature. In addition, since active centers can be produced rapidly and efficiently using photochemical processes, photocuring offers high production rates, and is highly energy efficient compared to thermal polymerizations in which the entire system must be raised to elevated temperatures. A major application of photopolymerization that exploits these advantages is films and coatings that exhibit high cure rates without the use of volatile solvents, thereby minimizing emissions of organic compounds.

The vast majority of photopolymerizations used in industry are free-radical polymerizations, which have been studied extensively (for reviews, see references 1–5 as well as Photopolymerization, Free Radical (qv)). By far the most widely used classes of monomers for UV-initiated free-radical photopolymerizations are multifunctional acrylates and methacrylates. Several investigations have demonstrated that free-radical polymerizations of these monomers exhibit unusual kinetic behavior, including immediate onset of autoacceleration, the formation of heterogeneous polymers (2,6–11), and the attainment of a maximum conversion

Encyclopedia of Polymer Science and Technology. Copyright John Wiley & Sons, Inc. All rights reserved.

significantly less than unity (2,12–15). These monomers polymerize very rapidly, and are easily modified on the ester group, allowing materials with a variety of properties to be obtained (2); and a wide range of acrylates and methacrylates are commercially available. However, free-radical photopolymerizations have a number of problems and drawbacks that have lead scientists to examine other photopolymerization systems. For example, many acrylates are relatively volatile (methacrylates are generally less volatile than acrylates), and have an unpleasant odor. Moreover, there has been a growing concern over potential health hazards associated with the acrylates (3,4,16). Finally, the free-radical photopolymerizations are inhibited by oxygen and must be carried out under an inert atmosphere such as nitrogen or under a protective film or mold to achieve the highest reaction rates and the optimal properties of the film or coating.

UV-initiated cationic photopolymerizations exhibit several advantages when compared with the free-radical photopolymerization discussed above. First of all the cationic photopolymerizations are not inhibited by oxygen. This feature provides a significant practical advantage for industrial processes since it is not necessary to blanket the system with nitrogen to achieve rapid cure rates. Secondly, in contrast to the free-radical photopolymerizations which experience a rapid decrease in polymerization rate when the light source is removed (due to radical–radical termination reactions), the cationic polymerizations proceed long after the irradiation has ceased, consuming nearly all of the monomer. Finally, cationic photopolymerization is a very versatile technique and may be used to polymerize important classes of monomers, including epoxides and vinyl ethers. Although these classes of monomers cannot cure by free-radical photopolymerizations, they exhibit many desirable properties, including low volatility, good rheological properties, and low toxicity (3). Furthermore, the cured polymer films associated with these monomers exhibit excellent clarity, adhesion, abrasion resistance, and chemical resistance. In addition, the cationic ring-opening polymerizations of epoxides exhibit less shrinkage, as low as 1–2% (17), than do polymerizations of unsaturated monomers such as acrylates and methacrylates, which is typically 5–20%. However, the presence of water vapor may impede the cationic curing, notably if thin films are cured at a low light intensity.

The reaction kinetics are an important aspect of any photopolymerization system under consideration for an application. For some applications, such as coatings on optical fibers, photopolymerization is perhaps the only way in which cure can be achieved fast enough to meet the requirements of the system. The reaction kinetics fundamentally follow from the mechanism by which the reaction takes place, and chain photopolymerization processes generally begin with an initiation step in which active centers are produced photochemically; proceed by the propagation step in which the active center reacts successively with a number of monomer molecules to link them covalently into a polymer chain; and may end in a termination step in which the active centers are consumed by a chemical reaction. Photopolymerization is distinguished by the fact that it is the absorption of a photon (by a specially designed photoinitiator molecule) that results in the production of active centers. Therefore, it is important to understand the photochemical processes by which the active centers are generated. The fundamental nature of the propagation and termination steps is the same for photo- and thermal polymerizations.

This article provides an overview of the important features of the kinetics of cationic photopolymerization, and a valuable resource for any scientist or engineer who is considering these reactions for a study or an application. The article begins with a description of the photoinitiation step, including the compounds and mechanisms by which cationic active centers are produced by a unimolecular process (typically a photo-induced fragmentation of the initiator), or a bimolecular process (typically an energy or electron-transfer process between a photosensitizer and the initiator). Commonly used photoinitiators and photosensitizers have been described and compared. The photoinitiation step is especially important because it is the step that distinguishes these reactions from their thermally initiated counterparts. Next, a description of traditional cationically polymerizable monomers as well as recently developed, highly reactive monomers is provided. Representative kinetic rate expressions have been presented to illustrate the link between the reaction mechanism and a quantitative description of the polymerization rate, and to illustrate the important variables that affect the rate.

Photoinitiation

Despite the advantages of UV-initiated cationic photopolymerizations discussed above, this technique has received considerably less attention than the analogous free-radical reactions, and most of the studies in the literature have focused on the photoinitiation step. This fact may be attributed to the lack of suitable UV-sensitive cationic photoinitiators until recent years. In fact, applicable photoinitiators for cationic polymerizations were not developed until the late 1970s, several decades after free-radical photoinitiators had been reported. Until then, photoinitiators developed were specific to particular reaction systems. For example, Asai and co-workers (18–23) investigated the use of numerous metal salts such as sodium chloroaurate, silver salts in aromatic solvents, copper perchlorate, vanadium tetrachloride and titanium tetrachloride, as photoinitiators for cationic polymerization of *N*-vinylcarbazole. Photopolymerizations of isobutylene in the presence of Lewis acids such as vanadium chloride, titanium chloride, and tin chloride have been reported (24) via a radical–cation mechanism. A variety of monoepoxides were polymerized using manganese decacarbonyl (25) and methylcyclopentadienyl manganese tricarbonyl (26). Other examples include photocatalyzed polymerization of epichlorohydrin using bis(cyclopentadienyl) iron complex (27), and polymerization of 2-chloroethyl vinyl ether photosensitized by bis(cyclopentadienyl) titanium chloride (28).

The first more generally applicable cationic photoinitiators that achieved some success were diazonium salts of complex metal halide anions (29–35). These diazonium salts were mainly used for the cationic ring-opening photopolymerization of epoxides. Upon photolysis, these salts produce an aryl halide, molecular nitrogen, and a strong Lewis acid capable of initiating cationic polymerization, as illustrated in Figure 1. The efficiency of the diazonium salt depends on the structure of the phenyl ring, which also affects the spectral sensitivity of the molecule, and the nature of the anion moiety (17,34,36,37).

The use of these diazonium salts, however, was limited because of their poor thermal stability requiring the photoinitiators to be added just before the

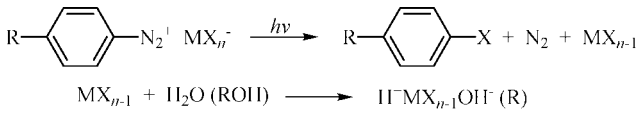

Fig. 1. Reaction mechanism for the photolysis of a diazonium photoinitiator. Here, R denotes substituents on the phenyl ring and MX_n^- represents a metal halide.

irradiation, and the release of nitrogen gas as a by-product which caused bubbles and pinholes in the coatings, for which they were mainly used, rendering practical constraint on the film thickness to be less than 15 μm (38). Some attempts have been made to stabilize these salts by adding additives such as nitriles (39), amides (40), sulfoxides (41), and poly(vinyl pyrrolidone) (42); however, these approaches achieved limited success and were not widely adopted.

Iodonium and Sulfonium Photoinitiators. A breakthrough in the development of cationic photoinitiators occurred in the late 1970s with the development of the first iodonium salt photoinitiators. These initiators, which were developed independently at the General Electric (43) and 3M (44), avoided the shortcomings of the diazonium photoinitiators. Unlike previous initiators, these salts are remarkably stable in the absence of light, are thermally stable at room temperature, and do not degrade in the presence of moisture. Shortly after the iodonium photoinitiators were introduced, Crivello and Lam (45) reported the development of the triarylsulfonium salts as a second class of highly efficient cationic photoinitiators that offered many of the same advantages. Representative molecular structures of the diaryliodonium salts and triarylsulfonium salts are shown as structures **1** and **2** respectively. R denotes substituents selected to enhance solubility in organic monomers and to alter the absorbance characteristics of the photoinitiator, and MX_n^- represents a metal halide.

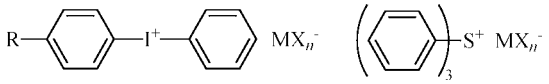

1 **2**

The mechanism by which these compounds produce active centers for polymerization is described in detail below; however, at this point it should be noted that in their latent state, the compounds possess a cationic center (situated on the iodine or sulfur atoms), and possess a large anionic counterion. The aromatic rings can generally be functionalized (typically in the ortho and para positions) to enhance solubility in the organic monomers and to alter the absorbance characteristics of the photoinitiator. A number of excellent reviews are available which provide an account of the development of these initiators as well as a comprehensive list of compounds that have been synthesized (36,46,47).

The cation and the anion in the iodonium and sulfonium salts each play an important role in the performance of the photoinitiator. The cation is the light-absorbing component, and adding substituents to the aromatic rings can alter the UV absorption characteristics (for a review of this topic see Ref. 36,47, and 48). Generally, an unsubstituted iodonium salt will exhibit an absorbance maximum in the deep UV region of the spectrum at around 220 nm, and this absorbance maximum can be redshifted to around 270 nm by the addition of substituents such

as ether groups, or additional aromatic rings. Sulfonium salts generally exhibit their absorbance maximum at longer wavelengths than do the iodonium salts, and may exhibit notable absorbance peaks between 300 and 320 nm. The structure of the cation also controls the quantum yield (number of molecules of active centers produced per photon absorbed) and the thermal stability of the photoinitiator (46). The iodonium salt exhibits high quantum yield (between 0.7 and 0.9) and these yields are generally higher than those for the sulfonium salts. In summary, the cation of the photoinitiator plays the determining role in the production of active centers, including the wavelengths of light for which the compound will be active, the efficiency with which the light will be used to create active centers, and, as described in more detail below, the ability of the salt to be photosensitized. The cation has very little effect on any of the processes (such as propagation) that occur after the active centers are produced and, as described below, it is the anion that plays a defining role in the rate of the propagation reaction.

Before the active center is produced, the anion serves as the counterion for the iodonium or sulfonium cation, and plays a relatively unimportant role at this stage since it has little effect on the absorbance characteristics of the salt. After the active center is produced, however, the anion serves as the counterion for the propagating active center, and at this stage plays a critical role in the rate of the propagation reaction and, therefore, ultimately in the performance of the initiator. For the propagation reaction to progress at a high rate the propagating active center must have access to monomer with which it may react; therefore it is important that the active center is not encumbered with a closely associated counterion. This can be achieved if the counterion is large and the negative charge is dispersed over a large volume. This consideration has led to the use of a variety of nonnucleophilic anions such as BF_4^-, PF_6^-, AsF_6^-, SbF_6^-, $FeCl_4^-$, and $SbCl_6^-$. A nucleophilic anion such as Cl^- quickly quenches any cationic species generated during the photolysis by forming a closely associated ion pair, which prevents propagation. Based upon the above consideration, the rate of the propagation reaction is directly controlled by the counterion, and for the four most commonly used counterions, polymerization rate follows the order: $BF_4^- < PF_6^- < AsF_4^- < SbF_6^-$ (36). Although the use of arsenic and antimony leds to the strongest superacids and the highest polymerization rates, they are toxic heavy metals, and may present problems associated with recycling when used on a large scale. For this reason, Castellanos and co-workers (49) reported a new anion, tetrakis pentafluorophenyl borate, which is as effective as SbF_6^-, but does not contain a heavy metal.

The mechanism by which onium photoinitiators produce active centers is very complex and the details are still under investigation by a number of researchers (47,50–56). The generally accepted photoinitiation reaction mechanism for iodonium salts is shown in Figure 2. Upon absorption of a photon the iodonium salt is promoted to an electronic excited state (denoted by an asterisk in the figure),

$$Ar_2I^+MX_n^- \xrightarrow{h\nu} (Ar_2I^+ MX_n^-)^* \longrightarrow ArI^+\cdot + Ar\cdot + MX_n^-$$

$$ArI^+\cdot + R{-}H \longrightarrow ArI^+H + R\cdot$$

$$ArI^+H + Mx_n^- \longrightarrow ArI + H^+MX_n^-$$

Fig. 2. Reaction mechanism for the photolysis of an iodonium photoinitiator. Here, Ar represents aryl group.

and then undergoes an irreversible photofragmentation in which a carbon–iodine bond is cleaved to produce an aryliodonium radical–cation and an aryl radical. It is unclear that precisely which excited state is involved in the fragmentation reaction, as some investigators (47) have concluded that it is a singlet state, while others (52,53) have concluded that it is a triplet state. In any case, it is generally accepted that the result of the fragmentation reaction is the formation of an iodine radical–cation [this has been observed by transient absorption experiments and is highly reactive with a lifetime of approximately 6 μs (36)]. This highly reactive radical–cation will abstract a hydrogen atom from any convenient source, which can be the monomer, water, alcohol, or other impurities; rate constants for this reaction have been measured to be of the order of $10^6\ M^{-1} \cdot s^{-1}$ (36). This hydrogen abstraction step yields an aryl iodine cation and a neutral organic radical, which can initiate radical polymerizations. The aryl iodine cation will quickly expel a proton to form a neutral aryl iodine molecule and a superacid formed by the proton and the counterion. This superacid initiates the cationic polymerization by addition to the monomer. The mechanism for a sulfonium salt photoinitiator is similar with the cleavage of a carbon–sulfur bond under irradiation.

Other Onium Salts and Organometallic Photoinitiators. The success of the iodonium and sulfonium salts as photoinitiators has led to the investigation of a number of analogous onium salts based on the halides and the Group VIA atoms; however, these alternative initiators have not been widely used for various reasons. For example, chloronium and bromonium salts were prepared (57,58) and they were also found to function as cationic photoinitiators, but these salts are difficult to prepare and they have low thermal stability. Similarly, triarylselenonium salts have also been investigated and found to function as cationic initiators (59); however their preparation has been found to be expensive (60). Other onium salts such as phosphonium and arsonium salts, developed by Abu-Abdoun and co-workers for the photopolymerization of *p*-methylstyrene and styrene, have also been reported (61–63) as successful cationic photoinitiators. Photopolymerization of carbazolyloxiranes with sulfonium and tropylium salts has been reported (64). Dialkylphenacyl sulfonium photoinitiator (65–67) has been reported with excellent solubility in both polar and nonpolar monomers. Pyridinium and isoquinolinium salts have also been reported and they were found useful for polymerizing both the epoxide and vinyl ether monomers (68).

Organometallic compounds which can act as highly efficient photoinitiators for epoxide monomers have been described in the literature (25–27,69–71). The most commonly used organometallic compounds are the photoinitiators based on iron arene complex developed by the investigators at the Ciba-Geigy Corp. (37,69–71). These salts are generally prepared from ferrocene, as reviewed by Lohse and Zweifel (37). The molecular structure of a typical iron–arene complex is shown as (**3**).

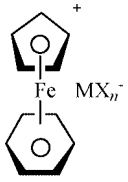

3

Upon irradiation with an appropriate light source, the iron–arene complex looses the uncharged tridentate arene ligand and the positive charge moves to iron, which in association with the anion acts as a Lewis acid capable of polymerization (37). One drawback of these photoinitiators is that they are known to polymerize only the ring-opening monomers and may not be suitable for monomers with unsaturated bonds such as vinyl ethers (46).

Bimolecular Photoinitiation and Photosensitization. As mentioned above, the iodonium and sulfonium photoinitiators generally absorb light in the wavelength range of 200–300 nm. The effective initiating wavelength may be expanded by the use of photosensitizers or co-initiators, which shift the effective spectral window to well above 300 nm (into the near-UV and visible regions of the spectrum). The near-UV region of the spectrum is particularly convenient for initiating polymerizations because most monomers and resins absorb negligibly at these wavelengths, yet industrial medium and high pressure mercury lamps exhibit strong emission bands in this region. In addition, use of a large fraction of the available light contributes to an overall more efficient photolysis of the initiator and, as a consequence, acceleration in the polymerization rate. A variety of compounds can be used as photosensitizers, including heterocyclic and fused-ring aromatic hydrocarbons, organic dyes, and aromatic ketones.

In general, photosensitization results from a direct interaction between an excited photosensitizer molecule (the first excited singlet state or the lowest energy triplet state that takes place due to the absorption of photon by these molecules) and the initiator. This interaction can be either an energy transfer or an electron transfer process. In the energy transfer mechanism the excited-state photosensitizer interacts with a ground-state initiator molecule to form an exciplex. In the exciplex, the excited-state energy is transferred to the initiator by vibrational relaxation that fragments the initiator to create active centers. According to this mechanism, the photosensitizer functions essentially as a catalyst and is regenerated in its ground state. For this energy transfer to be thermodynamically feasible, the excited-state energy of the photosensitizer must be greater than that of the initiator (47), a condition which is rarely met for onium salt photoinitiators.

A second possible mechanism for photosensitization involves electron transfer from the excited state of the photosensitizer to the initiator within the exciplex (47,54,72,73). Figure 3 (73) shows the important photochemical and electron transfer steps in the reaction between anthracene (the photosensitizer) and an iodonium salt. As shown in the figure, when an anthracene molecule is exposed to light it absorbs photons and goes into the first excited singlet state. From this excited state a fraction of anthracene molecules undergoes intersystem crossing to go to the lowest triplet state, where they form an excited-state complex with the initiator molecules. There has been some ambiguity as to whether the exciplex is formed in the triplet state of the sensitizer or the singlet state. Recently, on the basis of a series of fluorescence and phosphorescence lifetime studies, combined with the photochemical rate calculations and triplet state quencher studies, Nelson and co-workers (73) reported that electron transfer occurs predominantly from the triplet excited state of anthracene to the initiator. In this exciplex anthracene may undergo electron transfer to the initiator, forming a radical cation which is capable of initiating cationic polymerization.

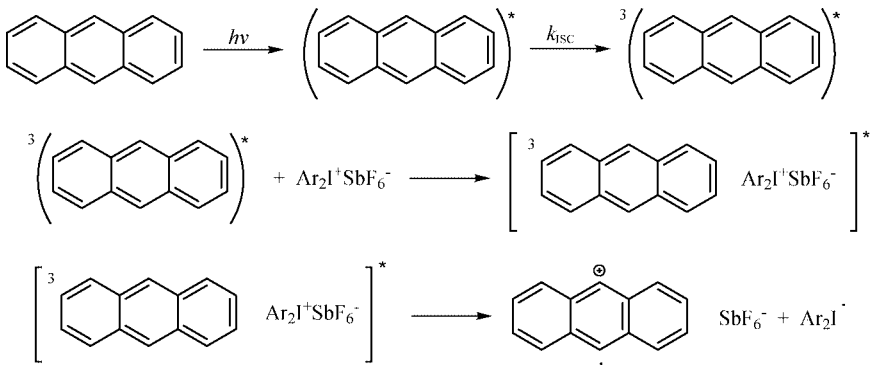

Fig. 3. Photosensitization mechanism based on electron transfer from triplet-state anthracene to the iodonium initiator (see reference 73).

For the electron transfer mechanism, the thermodynamic feasibility is governed by the excited-state energy of the photosensitizer (the state that participates in the electron transfer step), the oxidation potential of the excited-state photosensitizer, and the reduction potential of the initiator. It has generally been accepted that the photosensitization of diaryliodonium initiators most often proceeds by the electron transfer mechanism and a number of researchers have studied these reactions (38,47,54,74–77). Moorjani and co-workers (78) showed that the reaction system viscosity has an important effect on the overall rate of the photosensitization of diaryliodonium salts. As the reaction proceeds and the viscosity of the mixture increases because of polymerization, the rate of photosensitization will decrease substantially. It is therefore expected that the rate of initiation will become extremely low after a certain degree of polymerization, and that any further reaction will be almost exclusively from the propagation of existing active centers. This applies especially to the monomers that form glassy polymers. A number of references are available reporting the use of a variety of sensitizers with iodonium photoinitiators (68,79–85).

Three-Component Photoinitiator Systems. Three-component initiator systems are flexible and versatile photoinitiators that were initially developed for free-radical photopolymerizations, but may, with careful selection of the components, be used for cationic photopolymerizations. These systems generally contain a light absorbing component (often called a dye), an electron donor (typically an amine), and a third component, which is typically an iodonium salt. These initiator systems offer a number of advantages that have been demonstrated in free-radical photopolymerizations, and are also relevant for cationic photopolymerizations. For example, a wide variety of dyes may be used with the same electron donor and iodonium salt, thereby providing tremendous flexibility in selection of the initiating wavelength and therefore the light source. Indeed, effective visible-light-sensitive systems may allow use of very inexpensive light sources such as halogen and tungsten incandescent lamps. In addition, three-component systems have consistently been found to be faster, more efficient, and more sensitive than other photoinitiator systems. A variety of mechanistic investigations of free-radical three-component initiators have been reported, and the results are

generally applicable to the cationic systems as well. For a review of the literature on free radicals literature including a comprehensive list of dyes and electron donors that have been used, as well as a discussion of the mechanisms by which these reaction may proceed, see Reference 86.

Care must be taken to properly design a three-component initiator system for cationic photopolymerizations. Specifically, most of the amine electron donors that are used in free-radical initiator systems are not applicable for cationic polymerizations because they are highly nucleophilic and will terminate the cationic active center. In addition, the iodonium salt must have a nonnucleophilic anion (note that for free-radical initiation, a chloride counterion is commonly used, but is clearly inappropriate for cationic polymerizations). Fewer guidelines have been provided for selection of dyes to initiate cationic photopolymerizations. Bi and Neckers (87) demonstrated cationic photopolymerizations of epoxides initiated using a three-component initiator system containing a variety of xanthene dyes, amines with low basicity, and iodonium salts with a nonnucleophilic anion. Using this system, the polymerization was initiated by a tungsten lamp equipped with filters that eliminated light below 520 nm (where the iodonium salt does not directly absorb light). The authors further reported that presence of all the three components is required for photopolymerization above this wavelength. The authors attributed the reaction to a mechanism with three primary steps: absorption of light by the dye; production of radicals by reaction of the photoexcited dye with the amine; and production of initiating carbocations by oxidation of the radicals by the iodonium salt.

Detailed guidelines for the design of three-component initiator systems for cationic photopolymerizations were provided by Oxman and co-workers (88–91). These investigators studied a variety of electron donors, including a series of amines with systematically varying basicity (characterized by the pK_b), and varying oxidation potential (characterized by the oxidation potential relative to a saturated calomel electrode). They found that to achieve appreciable conversion of epoxide monomer the electron donor should have an oxidation potential less than 1.34 V (to achieve desired photo-induced electron transfer between the electron donor and the onium salt to produce both the cations and the radicals) and a pK_b value greater than 8 (so that the basicity of the reaction system is low enough for the Lewis acid to proceed with the cationic polymerization without getting completely consumed). These authors used the blue-light absorbing dye camphorquinone in their studies. In addition, since these photoinitiator systems produce both radicals and cations, Oxman and co-workers demonstrated their utility for controlled sequential free-radical/cationic photopolymerization of hybrid systems consisting of methacrylates and epoxides.

Monomers for Cationic Photopolymerization

A variety of classes of monomers undergo cationic chain polymerization, including epoxides, vinyl ethers, propenyl ethers, siloxanes, oxetanes, cyclic acetals and formals, cyclic sulfides, lactones, and lactams. Any monomer that undergoes cationic polymerization is a candidate for cationic photopolymerization, and a suitable monomer may be selected based upon the specific requirements of the application.

Note that these cationically polymerizable monomers include both unsaturated monomers that undergo a chain polymerization through the carbon–carbon double bond, and cyclic ethers that undergo ring-opening polymerizations. An unsaturated monomer is capable of cationic polymerization only if a carbon atom that participates in the double bond also has an electron-releasing substituent such as an alkoxy, phenyl, vinyl, or 1,1-dialkyl group (92). Presence of any of these substituents produces an electron-rich double bond susceptible to electrophilic attack by the propagating cation. Cyclic ethers undergo cationic polymerization because of the presence of the accessible ether electron lone pairs, which are also susceptible to electrophilic attack by the propagating cation, as described in more detail below.

Cationic Ring-Opening Photopolymerization. A number of cyclic monomers can be polymerized by the ring-opening process, including ethers (oxiranes, oxetanes, etc), acetals, amides (lactams), esters (lactones), siloxanes, and sulfides (92). Thermodynamically, ring-opening polymerization of cyclic ethers is favored for all except the six-membered ring (the Gibbs free energy is positive for opening a six-membered ring), and the three- and four-membered rings (oxiranes and oxetanes, respectively) exhibit the most strain and therefore the most rapid polymerizations. Copolymerization of oxirane and oxetane has also been studied (93,94) and presence of oxetane has been reported to increase the overall polymerization rate. Figure 4 shows representative molecular structures of some prominent classes of monomers which undergo ring-opening polymerization. By far the most widely used and thoroughly studied monomers are the oxiranes or epoxides and therefore these monomers provide the basis for most of our discussion. Historically, the epoxide monomers were developed for condensation polymerization with other nucleophilic species such as amines and anhydrides, but they were found to be suitable for cationic ring-opening polymerization as well.

The generally accepted propagation mechanism for cationic ring-opening polymerization for ethylene oxide is shown in Figure 5. According to this mechanism, the proton of the superacid (produced from the initiation step as explained in

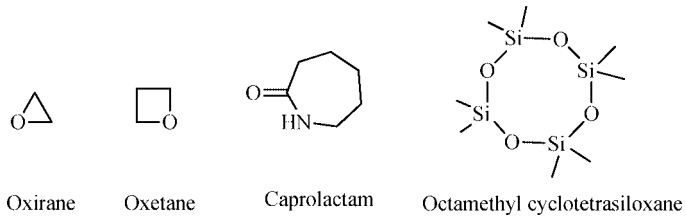

Fig. 4. Molecular structures of representative monomers which undergo cationic ring-opening polymerization.

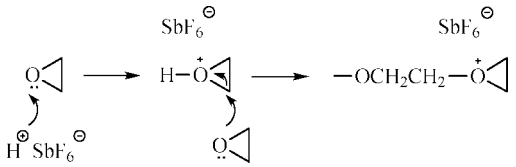

Fig. 5. Propagation step for cationic polymerization of an ethylene oxide monomer.

an earlier section) undergoes an electrophilic addition to the oxygen atom present in the epoxide ring, resulting in the formation of an oxonium ion, which is the propagating species. The α-carbon of the oxonium ion is electron deficient because of its proximity to the positively charged oxygen, and is therefore subject to nucleophilic attack by a monomer unit. This nucleophilic attack opens the epoxide ring (by breaking the carbon–oxygen bond) and produces a new oxonium ion, thereby propagating the active center to the new monomer unit. This process is repeated a number of times to make a polymer chain, and the polymer chain length is determined by the number of propagation steps that occur before the active center undergoes chain transfer or termination. The kinetics of the propagation reaction and the reaction parameters affecting it are examined in more detail in the next section.

Commercial epoxide monomers can be generally categorized into two classes: glycidyl ether resins and cycloaliphatic epoxides. An industry standard cycloaliphatic epoxide is 3,4-epoxycyclohexylmethyl-3,4-epoxycyclohexane carboxylate (**4**).

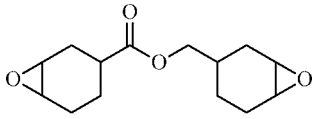

4

The structure of an epoxide plays an important role in the polymerization reactivity, as characterized in a number of papers including References 95 and 96. In general, cycloaliphatic epoxides exhibit shorter cure times than do the glycidyl ether resins because of the enhanced epoxy ring strain, which promotes the ring opening of the oxonium ion during the propagation step (17). In addition, viscosity of the cycloaliphatic epoxides is generally lower than that of the glycidyl ethers and hence they may be used as reactive diluents with the latter.

Cationic Photopolymerization of Unsaturated Monomers. Prominent classes of cationically polymerizable unsaturated monomers include vinyl ethers (**5**), propenyl ethers (**6**), and *N*-vinylcarbazole (**7**).

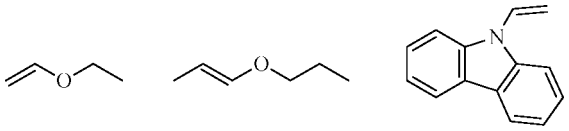

5 **6** **7**

Although a number of unsaturated monomers theoretically may undergo cationic photopolymerizations, there have been few studies of these photopolymerization systems reported in the literature. In the last decade some systematic studies of the cationic photopolymerization of vinyl ethers have been reported; therefore these systems are the focus of our discussion. Vinyl ether and propenyl ether monomers are among the most reactive monomers (which polymerize by a cationic mechanism) and they exhibit low vapor pressure, low toxicity, and relatively low viscosity. Hence, these monomers may be used as reactive diluents to enhance the effective cure rates of epoxide photopolymerizations.

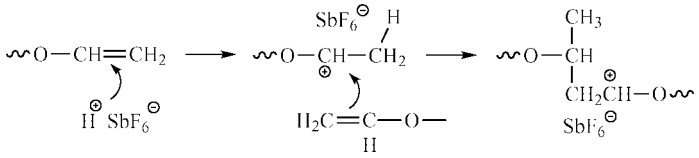

Fig. 6. Propagation step for cationic polymerization of a vinyl ether monomer.

The propagation mechanism for cationic polymerization of a vinyl ether monomer is shown in Figure 6. According to this mechanism, proton of the superacid (produced from the initiation step as explained in an earlier section) breaks the carbon–carbon double bond by attaching itself to one carbon atom, making the other carbon atom electron deficient. This carbocation is subjected to a nucleophilic attack by another monomer molecule which results in the formation of a carbon–carbon bond and transfer of the positive charge to the other carbon atom. This process is repeated a number of times to produce the polymer chain (again, the polymer chain length is determined by the number of propagation steps that occur before the active center undergoes chain transfer or termination).

Development of New Monomers. In the past decade, several new cationically polymerizable monomers exhibiting enhanced reaction rates and desirable film properties have been reported, most notably by Crivello and collaborators. These monomers may not be commercially available; however, a synthetic scheme for preparation of such monomers is usually provided. A detailed account of the utility of each monomer is beyond the scope of this article; however, a list of references that may be useful to the interested reader is provided here. Examples of novel cationically polymerizable monomers include epoxide monomers based on benzyl, allyl, propargyl acetal, and propargyl ether groups (97); epoxide monomers based on α-terpineol (98); difunctional epoxide monomers (99); epoxide monomers based on bisvinyl ethers or propenyl ethers (16,100); monomers based on 1-butenyl ethers (101,102) or 1-butenyl glycidyl ether (103); 1-propenyl ethers (104–107) or 1-propenyl glycidyl ethers (108); aromatic monomers bearing two, three, four, and six cationically polymerizable vinyl, isopropenyl, or propenyl functional groups (109); novel silicon-containing epoxy resins (110–113), oxetanes (114), and 1-propenyl ethers (115,116); novel cycloaliphatic epoxide monomers (117); multifunctional monomers bearing a combination of either epoxy, vinyl ether, cycloaliphatic epoxy, or 1-propenyl ether groups (118,119); ketene acetals (120); epoxy norbornane monomers (121,122); mono-, bi-, and trifunctional oxetanes (123); alkoxy allene monomers (124); monomers based on nopol (125); and dicyclopentadiene (126,127); monomers bearing two, four, and six aryl 2-propenyl groups prepared by isomerization of corresponding allyl groups (128); monomers based on isopropylphenoxy groups (129,130); carbazolyl containing epoxy monomers (131); and novel cycloaliphatic epoxide monomers bearing benzyl ether groups (132). Finally, it should be noted that a wide variety of cationically polymerizable epoxide monomers have been prepared from inexpensive and biorenewable sources such as linseed oil and soybean oil (133–135). In addition, epoxidized soybean oil has also been studied as a reactive diluent with other monomers and the polymerization rate of the reaction system has been characterized (135–137).

Kinetics of Cationic Photopolymerization

Cationic polymerizations, like other chain polymerizations, begin with the initiation step (which results in the production of active centers); then proceed by the propagation step in which the active center reacts successively with a number of monomer molecules to link them covalently into a polymer chain; and finally may end in a termination step in which the active centers are consumed by a chemical reaction. The photoinitiation step, as described in detail in the preceding section, is the only step that is dependent on light. Once the active centers are produced the propagation and termination steps generally proceed by the normal cationic polymerization processes and are subject to the usual reaction variables and kinetic considerations, although the typical counterions for cationic photopolymerization may be different than those used in thermal cationic polymerizations. This may be important since the counterions generally have a marked effect on both the propagation and termination reactions. Finally, in the presence of a Lewis base such as water or alcohols, a growing cationic polymer chain may undergo a chain transfer reaction, which results in the termination of one growing chain and the generation of a proton capable of initiating a new chain. This reaction can have a significant effect on the structure of the polymer, especially in crosslinked systems. In thin coatings exposed to humid air, polymerization may even be suppressed.

The polymer chain length (the number of repeat units per chain, or degree of polymerization) is determined by the number of propagation steps that occur before the active center undergoes chain transfer or termination. In contrast, the kinetic chain length corresponds to the total number of propagation steps that occur during the lifetime of the active center, and therefore corresponds to the number of propagation steps that occur before termination. If no chain transfer occurs the polymer chain length is equal to the kinetic chain length, however, trace amounts of nucleophiles such as water or alcohol are typically present and active center chain transfer is common in cationic polymerization. For this reason the degree of polymerization in cationic photopolymerization is typically significantly lower than the kinetic chain length.

The kinetics of cationic polymerizations are considerably more complex than those of the free-radical polymerizations, and kinetic data is difficult to interpret because of several reasons (92,138–140). For example, in cationic polymerizations the identity and proximity of the counterion has a marked effect on the reactivity of the active center. An active center that is encumbered by a closely associated counterion has a dramatically lower reactivity (typically an order of magnitude lower) than an active center that is separated from the counterion. As described in the section on photoinitiation, this consideration has lead to the development of large, nonnucleophilic counterions; however the reactivity of a cationic active center still depends on the proximity of the counterion. Therefore, at any given time, a variety of propagating species may exist, ranging from ion pairs to separated ions. For this reason, an effective propagation rate constant which includes contributions from all propagating species is usually adopted, as described below. Secondly, unlike free-radical polymerizations, the steady-state approximation for active center concentration is not valid since the cationic active centers are not reactive toward one another, and the rate of active center

generation through initiation is typically much higher than the rate of consumption of active centers through termination. Therefore, the active center concentration generally increases continuously until the photoinitiator is completely consumed, and must be either measured experimentally (which is extremely difficult) or calculated using unsteady-state species balances. Photosensitized polymerizations are further complicated by the fact that the rate of generation of active centers depends upon the system viscosity (which changes appreciably during the course of the reaction). With these general considerations in mind, in this section we provide an overview of the propagation and termination reactions in cationic photopolymerization, focusing on the aspects that will be of greatest value to scientists and engineers considering these systems for studies or applications.

***In Situ* Characterization of the Rate of Cationic Photopolymerization.** Before an examination of the propagation and termination reactions individually, a brief overview of the methods that have been used to obtain profiles of the polymerization rate as a function of time is provided. The photopolymerization rate can be monitored by any technique that measures a physical quantity which changes as the reaction progresses. In theory, a wide variety of analytical techniques could be used for this purpose (139–148), and new methods are continuously being developed (149). The commonly used methods for obtaining complete polymerization rate profiles are differential scanning calorimetry, fluorescence spectroscopy, and vibrational spectroscopies such as Raman and infrared.

Differential scanning calorimeter (DSC) has, perhaps, become the most widely used instrument for studying the kinetics of polymerization reactions (139,141,142). In this calorimetric technique, the reaction rate is monitored by measuring the heat released during the exothermic polymerization. For homopolymerizations, the rate at which heat is released is directly proportional to the polymerization rate, and conversion profiles can be obtained by integrating the reaction rate profiles. The DSC response time is relatively slow (of the order of 2–3 s); therefore this technique cannot be used for rapid photopolymerization systems. Real-time infrared (RTIR) spectroscopy was developed by Decker and Moussa in the early 1990s (143) to investigate the polymerization of acrylates. This technique has also been used to investigate the polymerization of epoxides (144) by simultaneously monitoring the monomer consumption and the polymer formation by using two IR detectors at the wavelengths of 790 and 1100 cm^{-1}, respectively. Infrared spectroscopy (both FTIR and RTIR) has sufficient time resolution to monitor rapid polymerizations. For example, FTIR instruments generally allow spectra to be collected every 40 or 50 ms. Raman spectroscopy has also been used for *in situ* monitoring of photopolymerizations of vinyl ether, acrylates, etc. Raman spectroscopy involves the inelastic scattering of photons rather than their direct absorption or emission by a material; therefore the intrinsic time scale of this method is extremely fast (of the order of femtoseconds). The practical time resolution is determined by the signal intensity, and generally several usable spectra can be acquired in a second (140,145). Fluorescence spectroscopy has been used for real-time monitoring of polymerizations and generally the monitoring schemes are based upon fluorescence probes which exhibit enhanced fluorescence intensity with change in variables such as system viscosity with the progress of polymerization due to decreased nonradiative energy transfer (72,146–148).

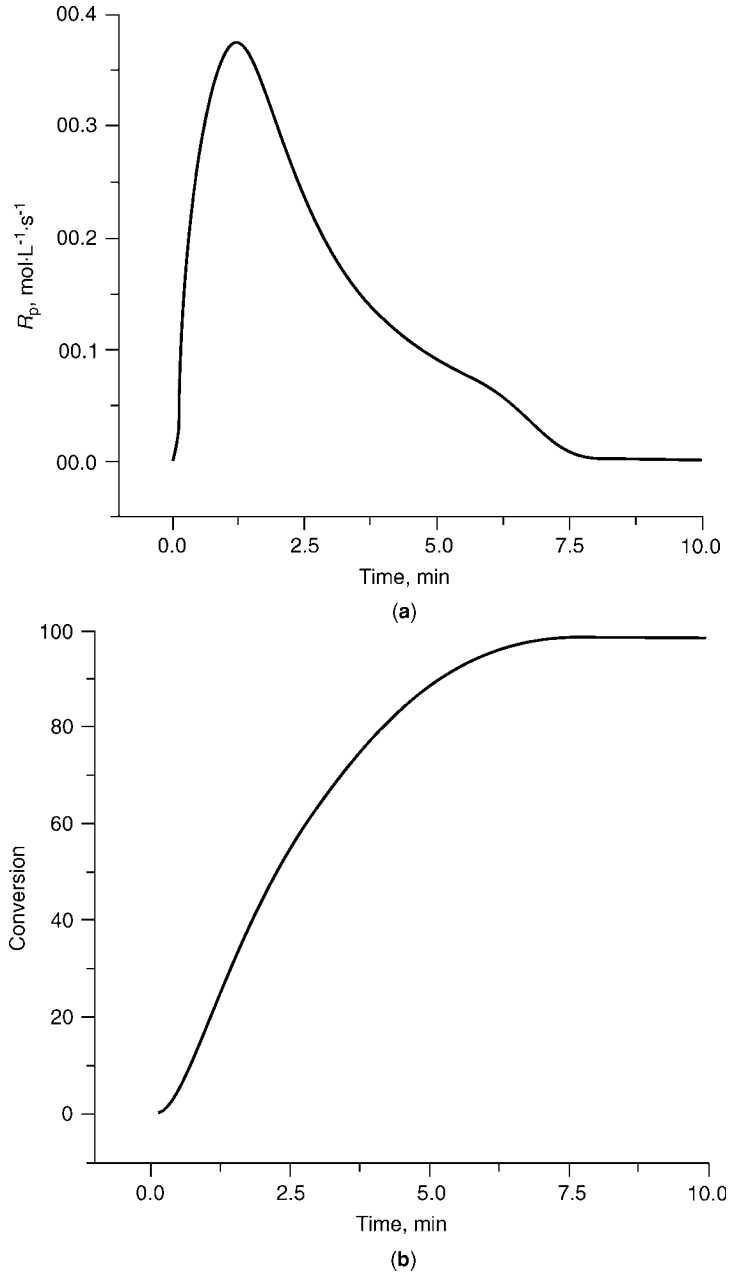

Fig. 7. Polymerization rate and percentage conversion vs time profiles for photopolymerization of phenyl glycidyl ether initiated using 8.86 mM of iodonium tetrakis pentafluorophenyl borate salt at 50°C and light intensity of 25 mW·cm^{-2} (see reference 150).

Figure 7 (150) contains profiles of the polymerization rate and conversion as function of time for cationic photopolymerization of an epoxide monomer obtained using a photo-DSC. As shown in the figure, the reaction rate profile has a general shape that is characteristic of cationic photopolymerizations. Immediately

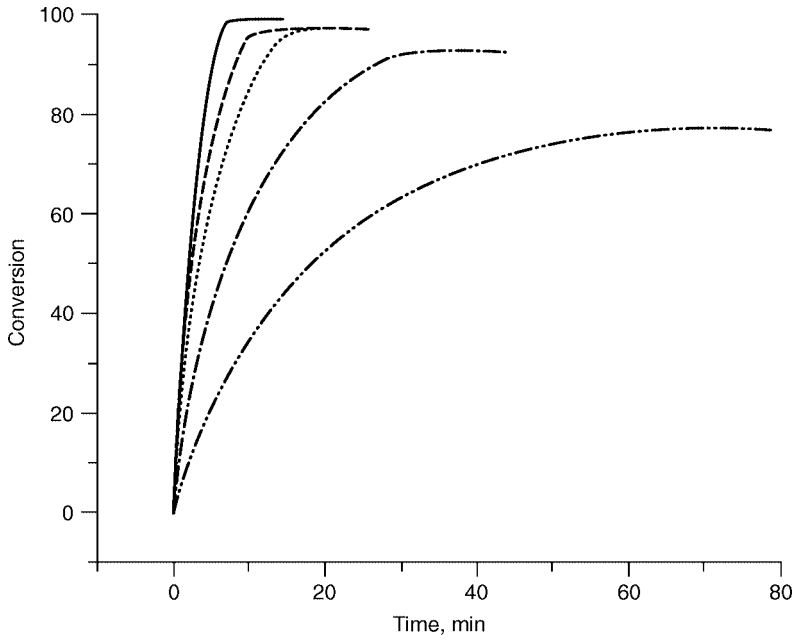

Fig. 8. Profiles of percentage conversion vs time for various illumination times for photopolymerizations of phenyl glycidyl ether initiated using 8.86 m*M* of iodonium tetrakis pentafluorophenyl borate salt at 50°C and light intensity of 25 mW·cm^{-2} (see reference 150). ——; Full illumination; – – 90-s illumination; - - - 60-s illumination; – - – 30-s illumination; – - - – 15-s illumination.

upon illumination, cationic active centers are produced and they react with the surrounding monomer molecules to form a growing polymer chain. The reaction rate increases monotonically because of the increase in the concentration of active centers, reaches a peak, and then decreases, primarily because of the decrease in the concentration of monomer. Typically, as the conversion reaches a high value, the polymerization rate will slow because of diffusional limitations and may ultimately stop at a limiting conversion below 100% if the system turns glassy and vitrification occurs.

One important characteristic of cationic photopolymerization is that the reaction continues for a long time even after the light has been shuttered off. This is strikingly different from free-radical photopolymerization where the reaction stops in a very short time in dark. Figure 8 (150) shows the reaction rate as a function of time for photopolymerization of an epoxide monomer for various illumination times. The figure contains profiles of the conversion as a function of time for five identical reaction systems illuminated for different periods of time ranging from 15 s to the duration of the experiment (full illumination) and it shows that the polymerization reaction proceeds long after the illumination has ceased, often consuming all of the monomer. For example, the sample that was illuminated for only 15 s continues to react for more than an hour in the dark.

Rate Constants for Propagation and Termination. For cationic chain polymerizations, the rate of polymerization is generally accepted to be proportional

to the product of the monomer concentration and the active center concentration, with the proportionality constant being the effective propagation rate constant k_p, as shown in equation 1:

$$R_p = k_p[M][M^+] \quad (1)$$

The propagation rate constant k_p includes contributions from a variety of propagating species ranging from ion pairs to separated ions. The value of k_p depends, of course, on the monomer being polymerized (the previous section contained a description of attempts to create new, highly reactive monomers), and for a given monomer the value of k_p also depends upon the temperature, the photoinitiator anion, and the proximity of the counterion to the active center, as described below. The propagation rate constants for vinyl ether and epoxide monomers have been studied extensively using techniques such as differential scanning calorimetry and Raman spectroscopy (139,140,150,151).

An interesting hypothesis that has been reported in the literature (139,140) is that the value of k_p can change appreciably during the course of the reaction because of a change in the proximity of the counterion and the active center. According to this hypothesis, k_p initially increases sharply, then levels off at a plateau value, and finally as the limiting conversion is reached the value of k_p decreases. At the beginning of the polymerization reaction, it is hypothesized that the active center and the counterion are relatively close to one another since the viscosity is relatively low, and the diffusional mobility of the counterion allows it to move with the cation. As the polymerization progresses there is an increase in the system viscosity, which reduces diffusional mobility of all the species present in the reaction system. The active center retains considerable mobility through propagation since the cation effectively moves through the reaction mixture by reacting with the monomer units (which is termed *reaction diffusion*). The counterion, however, experiences a decrease in mobility as the system viscosity increases, since it has to physically diffuse through the reaction mixture. During this process, the counterion and the active center separate, and since the separated ions are much more reactive than the ion pairs, it leads to a large increase in the value of k_p. Finally, the value of k_p decreases because of the trapping of the active centers. Therefore, a limiting conversion at which the reaction ceases is observed despite the presence of active centers and unreacted monomer.

The rate of termination and, consequently, the active center lifetime for the cationic and radical polymerizations are notably different. Free radicals, which are highly reactive toward one another, have very high termination rate constants (of the order of 10^5 $L \cdot mol^{-1} \cdot s^{-1}$) and have correspondingly short active centers lifetimes (typically less than a second). In contrast, for cationic polymerizations the rate of consumption of active centers is very slow, and generally takes place by some type of nucleophilic attack on the propagating cation. The precise nature of this chemical termination may be system specific, and is generally not well understood. In some cases, termination may occur by combination of the propagating active center with the anion. For example an active center may combine with the metal halide ion such as PF_6^- (the photoinitiator anion), abstract a fluorine atom, and expel a proton, thus regenerating a Lewis acid. Although it has been relatively unstudied, the average cationic active center lifetime has been found to be of the order of tens of minutes (139,140,150).

In addition to this termination by a chemical reaction, the active center may stop propagating owing to trapping. In this case, although the active centers are still present (they have not terminated per se), they are no longer propagating because the surrounding monomer molecules have polymerized and the active centers are unable to access the unreacted monomer. If the "termination" reaction is studied by investigating the reduction of the polymerization rate in the dark, then trapping cannot be distinguished from chemical termination. The termination/trapping of the active centers is commonly modeled as first order, which results in the following equation:

$$\frac{d[M^+]}{dt} = -k_{t/t}[M^+] \tag{2}$$

Here, $[M^+]$ corresponds to the concentration of propagating (untrapped) active centers, while $k_{t/t}$ represents the first-order kinetic rate constant for termination/trapping of active centers.

Effect of Light Intensity. The rate of a cationic photopolymerization depends upon the incident light intensity (radiant flux or photon flux) since an increasing light intensity increases the rate of production of active centers. The rate constants for propagation and termination are independent of light intensity. Therefore, in equation 1, the effect of light intensity is contained within the active center concentration $[M^+]$. The relationship between the light intensity and the active center concentration can be captured within a rate constant for absorbance, k_{abs}, defined as the product of the incident photon flux and the photoinitiator absorption cross section summed over all incident wavelengths (150). The concentration of cationic active centers produced by the photolysis of a photoinitiator (unimolecular initiation) is given by equation 3:

$$[M^+] = \phi I_0(1 - e^{-k_{abs}t}) \tag{3}$$

Here, ϕ is the quantum yield of the photoinitiator cleavage (the number of active centers formed per photon absorbed), and I_0 is the photoinitiator concentration at time $t = 0$. This equation illustrates that the active center concentration is not at steady state, but rather grows with time until the photoinitiator is consumed. Note that this equation accounts only for production of active centers by photolysis. To completely describe the active center concentration, equations 2 and 3 should be combined to account for both the production and the consumption of active centers. It is important to note that while the incident light intensity does affect the rate of polymerization, it generally has no impact on the final limiting conversion (if the temperature is held constant).

Effect of Temperature and Photoinitiator Anion. The polymerization temperature has a significant effect on both the rate of polymerization and the final limiting conversion. For example, Figure 9 contains a series of plots of reaction rate as a function of time for photopolymerization of an epoxide monomer. This figure illustrates that as the temperature is increased, the peak reaction rate increases and the reaction time decreases. The increase in reaction rate with increasing temperature ultimately arises from the effect of temperature on the propagation rate constant (which increases with increasing temperature as described by the Arrhenius equation for the rate constants). The rate of photoinitiation is

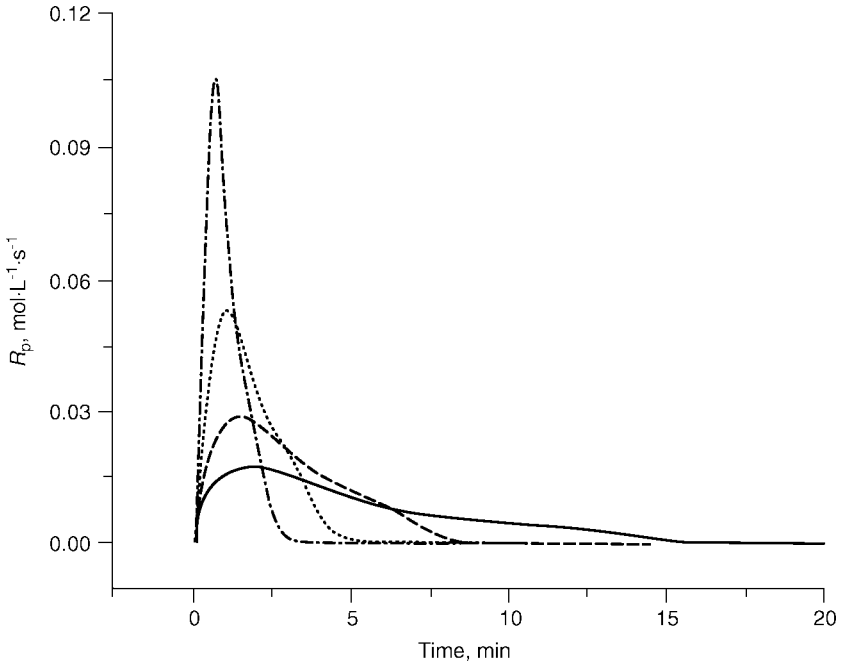

Fig. 9. Effect of temperature on the reaction rate as a function of time for photopolymerizations of phenyl glycidyl ether initiated using 8.86 m*M* of iodonium tetrakis pentafluorophenyl borate salt at light intensity of 25 mW·cm^{-2}. ——— 40°C; - - - - 40°C; ····· 60°C; -·-·- 70°C.

generally independent of temperature (for unimolecular photoinitiation the activation energy is zero since the initiating energy comes from light rather than heat). In addition, as the temperature is increased the final limiting conversion invariably increases because of enhanced mobility of the active centers and diminishing effect of vitrification. The effect of temperature on the propagation and termination rate constants for cationic photopolymerizations of a few vinyl ether and epoxide monomers have been reported (140,150). For example, propagation and termination rate constants for photopolymerization of an epoxide monomer are shown in Table 1 (150).

Table 1. Effect of the Temperature and the Photoinitiator Counterion on the Termination and Propagation Rate Constants[a]

	Iodonium tetrakis pentafluorophenyl borate salt		Iodonium hexafluoroantimonate salt	
Temperature, °C	k_t, s^{-1}	k_p, L·mol^{-1}·s^{-1}	k_t, s^{-1}	k_p, L·mol^{-1}·s^{-1}
50	4.5×10^{-4}	0.6	6.8×10^{-4}	0.4
60	5.5×10^{-4}	1.4	11.3×10^{-4}	0.8

[a] For photopolymerizations of phenyl glycidyl ether monomer at 50°C and 25 mW·cm^{-2} light intensity and at 8.86 m*M* concentration of photoinitiators (see reference 150).

The data in Table 1 also illustrate the effect of the size of the counterion on the values of the propagation and termination rate constant (150,151). This table illustrates that the tetrakis pentafluorophenyl borate anion, which is 14 times more voluminous than the hexafluoroantimonate anion, results in a higher propagation rate constant and lower termination rate constant for the photopolymerization. These are the expected trends since the larger counterion will result in a more weakly associated ion pair.

BIBLIOGRAPHY

"Photopolymerization and Photocross-linking" in *EPST* 1st ed., Vol. 10, pp. 145–156, by G. Oster, Mount Sinai School of Medicine; "Photopolymerization" in *EPSE* 2nd ed., Vol. 11, pp. 186–212, by S. P. Pappas, North Dakota State University.

1. A. Reiser, *Photoreactive Polymers*, John Wiley & Sons, Inc., New York, 1989.
2. J. G. Kloosterboer, *Adv. Polym. Sci.* **84**, 1 (1988).
3. C. G. Roffey, *Photopolymerization of Surface Coatings*, John Wiley & Sons, Inc., New York, 1981.
4. S. P. Pappas, *UV Curing, Science and Technology*, Vol. 2, Technology Marketing Corp., Norwalk, Conn., 1985.
5. M. Kaur and A. K. Srivastava, *J. Macromol. Sci. C: Polym. Rev.* **42**, 481 (2002).
6. H. M. J. Boots, J. G. Kloosterboer, G. M. M. Van de Hei, and R. B. Pandey, *Br. Polym. J.* **17**, 219 (1985).
7. H. Galina, B. N. Kolarz, P. P. Wieczorek, and M. Wojczynska, *Br. Polym. J.* **17**, 215 (1985).
8. W. Funke, *Br. Polym. J.* **21**, 107 (1989).
9. J. Bastide and L. Leibler, *Macromolecules* **21**, 2647 (1988).
10. A. Matsumoto, H. Matsuo, H. Ando, and M. Oiwa, *Eur. Polym. J.* **25**, 237 (1989).
11. J. Baselga, M. A. Llorente, I. Hernandez-Fuentes, and I. F. Pierola, *Eur. Polym. J.* **25**, 471 (1989).
12. D. T. Turner, Z. U. Haque, S. Kalachandra, and T. W. Wilson, *Polym. Mater. Sci. Eng.* **56**, 769 (1987).
13. G. P. Simon, P. E. M. Allen, D. J. Bennett, D. R. G. Williams, and E. H. Williams, *Macromolecules* **22**, 3555 (1989).
14. J. G. Kloosterboer, G. F. C. M. Lijten, and C. P. G. Zegers, *Polym. Mater. Sci. Eng.* **60**, 122 (1989).
15. P. E. M. Allen, D. J. Bennett, S. Hagias, A. M. Hounslow, G. S. Ross, G. P. Simon, D. R. G. Williams, and E. H. Williams, *Eur. Polym. J.* **25**, 785 (1989).
16. S. C. Lapin, in C. E. Hoyle and J. F. Kinstle, eds., ACS Symposium Series, Vol. 417, American Chemical Society, Washington, D.C., 1990, p. 363.
17. J. V. Crivello and K. Dietliker, in G. Bradley, ed., *Photoinitiators for Free Radical Cationic & Anionic Photopolymerisation Volume III*, SITA Technology Ltd., London, 1998, p. 355.
18. M. Asai, K. Kameoka, Y. Takeda, and S. Tazuke, *J. Polym. Sci., Polym. Lett. Ed.* **9**, 247 (1971).
19. M. Asai, S. Tazuke, and S. Okamura, *J. Polym. Sci., Polym. Chem. Ed.* **12**(1), 45 (1974).
20. M. Asai and S. Tazuke, *Macromolecules* **6**, 818 (1973).
21. M. Asai, Y. Takeda, S. Tazuke, and S. Okamura, *Polym. J. (Tokyo)* **7**(3), 359 (1975).
22. Y. Takeda, M. Asai, and S. Tazuke, *Polym. J. (Tokyo)* **7**(3), 366 (1975).
23. M. Asai, H. Matsui, and S. Tazuke, *Bull. Chem. Soc. Jpn.* **47**(4), 864 (1974).
24. M. Marek, L. Toamn, and J. Pilar, *J. Polym. Sci., Polym. Chem. Ed.* **13**(7), 1565 (1975).

25. W. Strohmeier, and P. Hartman, *Z. Naturforsch.* **20b**, 513 (1965).
26. W. S. Anderson, *J. Appl. Polym. Sci.* **15**, 2063 (1971).
27. K. Kaeriyama, *J. Polym. Sci., Polym. Chem. Ed.* **14**, 1547 (1976).
28. K. Kaeriyama, and Y. Shimura, *J. Polym. Sci., Polym. Chem. Ed.* **10**, 2833 (1972).
29. U.S. Pat. 3,708,296 (Jan. 2, 1973), S. I. Schlesinger (to American Can Co.).
30. U.S. Pat. 3,205,157 (1965), J. J. Licari and P. C. Crepeau (to North American Aviation, Inc.).
31. U.S. Pat. 3,829,369 (Aug. 13, 1974), J. H. Feinberg (to American Can Co.).
32. G.B. Pat. 1,404,242 (1975), J. H. Feinberg (to American Can Co.).
33. U.S. Pat. 3,960,684 (1976), J. H. Feinberg (to American Can Co.).
34. S. I. Schlesinger, *Polym. Eng. Sci.* **14**, 513 (1974).
35. M. P. Dreyfuss, J. C. Westfahl, and P. Dreyfuss, *Macromolecules* **1**, 437 (1968).
36. J. P. Fouassier, *Photoinitiation, Photopolymerization, and Photocuring: Fundamentals and Applications*, Hanser/Gardner Publication, Inc., Cincinnati, 1995.
37. F. Lohse and H. Zweifel, *Adv. Polym. Sci.* **78**, 62 (1986).
38. S. P. Pappas, *Prog. Org. Coat.* **13**, 35 (1985).
39. U.S. Pat. 3,721,616 (1974), W. R. Watt (to American Can Co.).
40. U.S. Pat. 3,721,617 (1973), W. R. Watt (to American Can Co.).
41. U.S. Pat. 3,711,391 (1973), J. H. Feinberg (to American Can Co.).
42. U.S. Pat. 3,816,281 (June 11, 1974), J. H. Feinberg (to American Can Co.).
43. J. V. Crivello and J. H. W. Lam, *Macromolecules* **10**(6), 1307 (1977).
44. U.S. Pat. 4,394,403 (July 19, 1983), G. H. Smith (to Minnesota Mining and Manufacturing Co.).
45. J. V. Crivello and J. H. W. Lam, *J. Polym. Sci., Polym. Chem. Ed.* **17**, 977 (1979).
46. J. V. Crivello, *J. Polym. Sci., Part A: Polym. Chem.* **37**, 4241 (1999).
47. J. V. Crivello, *Adv. Polym. Sci.* **62**, 1 (1984).
48. J. V. Crivello, *Dev. Polym. Photochem.* **2**, 1 (1981).
49. F. Castellanos, J. P. Fouassier, C. Priou, and J. Cavezzan, *J. Appl. Polym. Sci.* **60**, 705 (1996).
50. R. S. Davidson and J. W. Goodin, *Eur. Polym. J.* **18**, 589 (1982).
51. J. P. Fouassier, D. Burr, and J. V. Crivello, *J. Macromol. Sci., A: Pure Appl. Chem.* **31**, 677 (1994).
52. R. J. Devoe, M. R. V. Sahyun, N. Serpone, and D. K. Sharma, *Can. J. Chem.* **65**, 2342 (1987).
53. J. L. Dektar and N. P. Hacker, *J. Org. Chem.* **53**, 1835 (1988).
54. J. L. Dektar and N. P. Hacker, *J. Org. Chem.* **55**, 639 (1990).
55. J. L. Dektar and N. P. Hacker, *J. Org. Chem.* **56**, 1838 (1991).
56. V. Jancovicova, V. Brezova, M. Ciganek, and Z. Cibulkova, *J. Photochem. Photobiol., A* **136**, 195 (2000).
57. J. V. Crivello and J. H. W. Lam, *J. Polym. Sci., Polym. Lett. Ed.* **16**, 563 (1978).
58. G. A. Olah, T. Sakakibara, and G. Asensio, *J. Org. Chem.* **43**, 463 (1978).
59. J. V. Crivello and J. H. W. Lam, *J. Polym. Sci., Polym. Chem. Ed.* **17**, 1047 (1979).
60. J. V. Crivello and J. H. W. Lam, *J. Org. Chem.* **43**, 3055 (1978).
61. I. I. Abu-Abdoun and A. Ali, *Macromol. Rep., A* **30**, 327 (1993).
62. D. C. Neckers and I. Abu-Abdoun, *Macromolecules* **17**, 2468 (1984).
63. I. I. Abu-Abdoun and A. Ali, *Eur. Polym. J.* **29**, 1439 (1993).
64. J. V. Gražulevičius, R. Kavaliūnas, R. Lazauskaite, V. M. Getautis, and M. Daškevičienė, *J. Photochem. Photobiol., A:* **110**, 85 (1997).
65. J. V. Crivello and S. Kong, *Macromolecules* **33**, 825 (2000).
66. J. V. Crivello and S. Kong, *Macromolecules* **33**, 833 (2000).
67. J. V. Crivello, *Des. Monomers Polym.* **5**, 141 (2002).
68. W. Schnabel, *Makromol. Rapid Commun.* **21**, 628 (2000).

69. Eur. Pat. 094915 (1984), K. Meier, N. Buehler, H. Zweifel, G. Berner, and F. Lohse (to Ciba-Geigy A.-G.).
70. Eur. Pat. 126712 (1984), K. Meier, G. Eugster, F. Schwarzenback, and H. Zweifel (to Ciba-Geigy A.-G.).
71. K. Meier and H. Zweifel, *J. Imaging Sci.* **30**, 174 (1986).
72. E. W. Nelson, T. P. Carter, and A. B. Scranton, *Macromolecules* **27**, 1013 (1994).
73. E. W. Nelson, T. P. Carter, and A. B. Scranton, *J. Polym. Sci., Part A: Polym. Chem.* **33**, 247 (1995).
74. G. Manivannan and J. P. Fouassier, *J. Polym. Sci., Part A: Polym. Chem.* **29**, 1113 (1991).
75. S. P. Pappas, B. C. Pappas, L. R. Gatechair, and W. Schnabel, *J. Polym. Sci., Polym. Chem. Ed.* **22**, 69 (1984).
76. J. P. Fouassier, D. Burr, and J. V. Crivello, *J. Photochem. Photobiol., A:* **49**, 317 (1989).
77. R. J. Devoe, M. R. V. Sahyun, and E. Schmidt, *J. Imaging Sci.* **33**, 39 (1989).
78. S. Moorjani, B. Rangarajan, and A. B. Scranton, in A. B. Scranton, C. N. Bowman, and R. W. Peiffer, eds., *ACS Symposium Series*, Vol. 673, American Chemical Society, Washington, D. C., 1997, p. 95.
79. Y. Toba, *J. Polym. Sci., Part A: Polym. Chem.* **38**, 982 (2000).
80. J. V. Crivello and M. Sangermano, *J. Polym. Sci., Part A: Polym. Chem.* **39**, 343 (2001).
81. J. V. Crivello and F. Jiang, *Chem. Mater.* **14**, 4858 (2002).
82. Y. Toba, Y. Usui, M. Alam, and O. Ito, *Macromolecules* **31**, 6022 (1998).
83. Y. Toba, M. Saito, and Y. Usui, *Macromolecules* **32**, 3209 (1999).
84. J. L. Jacobs, E. W. Nelson, and A. B. Scranton, *Polym. Mater. Sci. Eng.* **70**, 74 (1993).
85. H. J. Timpe, H. Rautschek, and C. Mueller, *J. Photographic Sci.* **39**, 19 (1991).
86. K. S. Padon and A. B. Scranton, *Recent Res. Dev. Polym. Sci.* **3**, 369 (1999).
87. Y. Bi and D. C. Neckers, *Macromolecules* **27**, 3683 (1994).
88. U.S. Pat. 5,998,495 (Dec. 7, 1999), J. D. Oxman and D. W. Jacobs (to 3M Innovative Properties Co.).
89. U.S. Pat. 6,025,406 (Feb. 15, 2000), J. D. Oxman and D. W. Jacobs (to 3M Innovative Properties Co.).
90. U.S. Pat. 6,187,836 (Feb. 13, 2001), J. D. Oxman, M. C. Trom and D. W. Jacobs (to 3M Innovative Properties Co.).
91. J. D. Oxman, D. W. Jacobs, and M. C. Trom, *Polym. Mater. Sci. Eng.* **88**, 239 (2003).
92. G. Odian, *Principles of Photopolymerization*, John Wiley & Sons, Inc., New York, 1991.
93. H. Sasaki, J. M. Rudzinski, and T. Kakuchi, *J. Polym. Sci., Part A: Polym. Chem.* **33**, 1807 (1995).
94. H. Sasaki, in K. D. Belfield and J. V. Crivello, eds., *ACS Symposium Series*, Vol. 847, American Chemical Society, Washington, D.C., 2003, p. 296.
95. J. V. Crivello and V. Linzer, *Polimery (Warsaw)* **43**, 661 (1998).
96. B. L. Podlogar and D. J. Raber, *J. Org. Chem.* **54**, 5032 (1989).
97. J. V. Crivello and R. A. Ortiz, *J. Polym. Sci., Part A: Polym. Chem.* **39**, 2385 (2001).
98. J. V. Crivello and S. Liu, *Chem. Mater.* **10**, 3724 (1998).
99. J. V. Crivello and A. M. Carter, *J. Polym. Sci., Part A: Polym. Chem.* **31**, 2663 (1993).
100. J. V. Crivello and D. A. Conlon, *J. Polym. Sci., Polym. Chem. Ed.* **21**, 1785 (1983).
101. J. V. Crivello and B. Yang, *J. Polym. Sci., Part A: Polym. Chem.* **33**, 1381 (1995).
102. S. Kaur, J. V. Crivello, and N. Pascuzzi, *J. Polym. Sci., Part A: Polym. Chem.* **37**, 199 (1999).
103. J. V. Crivello and S. S. Liu, *J. Polym. Sci., Part A: Polym. Chem.* **36**, 1179 (1998).
104. J. V. Crivello, K. D. Jo, W. G. Kim, and S. Bratslavsky, in M. K. Mishra, ed., *Macromolecular Engineering: Recent Advances*, Plenum Press, New York, 1995, pp. 85–99. *Proceedings of the International Conference on Advanced Polymers via Macromolecular Engineering*.

105. J. V. Crivello and G. Löhden *J. Polym. Sci., Part A: Polym. Chem.* **34**, 2051 (1996).
106. J. V. Crivello and W. G. Kim, *J. Macromol. Sci., A: Pure Appl. Chem.* **31**, 1105 (1994).
107. J. V. Crivello and S. A. Bratslavsky, *J. Macromol. Sci., A: Pure Appl. Chem.* **31**, 1927 (1994).
108. J. V. Crivello and W. G. Kim, *J. Polym. Sci., Part A: Polym. Chem.* **32**, 1639 (1994).
109. J. V. Crivello, A. Carter, A. Ramdas, and D. H. Suh, *J. Macromol. Sci., A: Pure Appl. Chem.* **31**, 1807 (1994).
110. J. V. Crivello and J. L. Lee, in Ref. 16, p. 398.
111. J. V. Crivello and J. L. Lee, *J. Polym. Sci., Part A: Polym. Chem.* **28**, 479 (1990).
112. R. P. Eckberg and K. D. Riding, in Ref. 16, p. 382.
113. J. V. Crivello, D. Bi, and M. Fan, *J. Macromol. Sci., A: Pure Appl. Chem.* **31**, 1001 (1994).
114. J. V. Crivello and H. Sasaki, *J. Macromol. Sci., A: Pure Appl. Chem.* **30**, 173 (1993).
115. J. V. Crivello, B. Yang, and W. Kim, *J. Polym. Sci., Part A: Polym. Chem.* **33**, 2415 (1995).
116. J. V. Crivello and G. Löhden, *Macromolecules* **28**, 8057 (1995).
117. J. V. Crivello and U. Varlemann, *J. Polym. Sci., Part A: Polym. Chem.* **33**, 2463 (1995).
118. M. Sangermano, G. Malucelli, R. Bongiovanni, A. Priola, U. Annby, and N. Rehnberg, *Polym. Int.* **50**, 998 (2001).
119. S. K. Rajaraman, W. A. Mowers, and J. V. Crivello, *Macromolecules* **32**, 36 (1999).
120. J. V. Crivello, Y. L. Lai, and R. Malik, *J. Polym. Sci., Part A: Polym. Chem.* **34**, 3103 (1996).
121. J. V. Crivello and R. Narayan, *Macromolecules* **29**, 433 (1996).
122. J. V. Crivello and R. Narayan, *Macromolecules* **29**, 439 (1996).
123. O. Nuyken and M. Ruile, *NATO Sci. Ser., Ser. E* **359**, 117 (1999).
124. J. V. Crivello, T. Yoo, and J. A. Dougherty, *J. Polym. Sci., Part A: Polym. Chem.* **33**, 2493 (1995).
125. J. V. Crivello and S. S. Liu, *J. Polym. Sci., Part A: Polym. Chem.* **37**, 1199 (1999).
126. J. V. Crivello and S. Song, *Chem. Mater.* **12**, 3674 (2000).
127. J. V. Crivello and S. Song, *J. Polym. Sci., Part A: Polym. Chem.* **37**, 3427 (1999).
128. J. V. Crivello and D. H. Suh, *J. Polym. Sci., Part A: Polym. Chem.* **31**, 1847 (1993).
129. J. V. Crivello and Y. L. Lai, *J. Polym. Sci., Part A: Polym. Chem.* **33**, 653 (1995).
130. J. V. Crivello and A. Ramdas, *J. Macromol. Sci., A: Pure Appl. Chem.* **29**, 753 (1992).
131. J. V. Gražlevičius, R. Kavaliūas, R. Lazauskaitė, V. M. Getautis, M. Daškevičienė, *Chemija* **1**, 89 (1997).
132. J. V. Crivello and R. A. Ortiz, *J. Polym. Sci., Part A: Polym. Chem.* **39**, 3578 (2001).
133. C. Venturello and R. D'Aloisio, *J. Org. Chem.* **53**, 1553 (1988).
134. J. V. Crivello and R. Narayan, *Chem. Mater.* **4**, 692 (1992).
135. J. Chen, M. D. Soucek, W. J. Simonsick, and R. W. Celikay, *Polymer* **43**, 5379 (2002).
136. C. Decker, T. N. T. Viet, and H. P. Thi, *Polym. Int.* **50**, 986 (2001).
137. A. M. Mathur, V. Narayanan, and A. B. Scranton, in *RadTech '98 North Am. UV/EB Conf. Proc. 1998*, 1998, p. 486.
138. J. P. Kennedy and E. Marechal, *Carbocationic Polymerization*, John Wiley & Sons, Inc., New York, 1982.
139. E. W. Nelson, J. L. Jacobs, A. B. Scranton, K. S. Anseth, and C. N. Bowman, *Polymer* **36**, 4651 (1995).
140. E. W. Nelson, and A. B. Scranton, *J. Polym. Sci., Part A: Polym. Chem.* **34**, 403 (1996).
141. J. M. Barton, *Adv. Polym. Sci.* **72**, 111 (1985).
142. H. Ito, N. Kidokoro, and H. Ishikawa, *J. Photopolym. Sci. Technol.* **5**, 235 (1992).
143. C. Decker and K. Moussa, *J. Coat. Technol.* **62**, 55 (1990).
144. C. Decker and K. Moussa, *J. Polym. Sci., Part A: Polym. Chem.* **28**, 3429 (1990).
145. E. W. Nelson and A. B. Scranton, *J. Raman Spectrosc.* **27**, 137 (1996).

146. J. C. Song and C. S. Sung, *Polym. Prepr. (Am. Chem. Soc., Div. Polym. Chem.)* **32**, 362 (1991).
147. B. Strehmel, J. H. Malpert, A. M. Sarker, and D. C. Neckers, *Macromolecules* **32**, 7476 (1999).
148. B. Strehmel, V. Strehmel, and M. Younes, *J. Polym. Sci., Part A: Polym. Chem.* **37**, 1367 (1999).
149. B. Falk, S. M. Vallinas, and J. V. Crivello, *J. Polym. Sci., Part A: Polym. Chem.* **41**, 579, 2003.
150. V. Sipani and A. B. Scranton, *J. Polym. Sci., Part A: Polym. Chem.* **41**, 2064 (2003).
151. V. Sipani and A. B. Scranton, *J. Photochem. Photobiol., A* **159**, 189 (2003).

VISHAL SIPANI
ALEC B. SCRANTON
University of Iowa

PHOTOPOLYMERIZATION, FREE RADICAL

Introduction

Photopolymerizations, which use light energy (photons) to initiate chain reactions to form polymer materials, are the basis for a growing, billion-dollar industry (1,2). Applications in which photopolymerization is used include films and coatings, inks, adhesives, fiber optics, and dentistry (2–5). Each of these industries has benefited from the high productivity and lower costs afforded by photopolymerization systems.

Photopolymerization has many advantages over thermal and redox polymerizations in which the reaction system is heated to produce active centers. The solvent-free systems used in photopolymerizations eliminate emissions of volatile organic compounds and reduce material costs. Spatial and temporal control of the polymerization is achieved through control of the initiating light. Photopolymerizations also use less energy to effect cure than do thermal means. They produce a more rapid through-cure so that more films and coatings can be processed in less time. Furthermore, photocuring systems are more compact than thermal curing systems and operate at room temperatures. All these characteristics of photopolymerizations translate into lower production costs for industry.

Photopolymerization systems, like thermally initiated systems, contain initiator, monomer, and other additives that impart desired properties (color, strength, flexibility, etc) (6). The reaction is initiated by active centers that are produced when light is absorbed by the photoinitiator. One important class of active centers includes free-radical species, which possess an unpaired electron (5,7). The highly reactive free-radical active centers attack carbon–carbon double bonds in unsaturated monomers to form polymer chains. Although the kinetic treatment of photopolymer systems is similar to that in thermal systems, significant differences arise in the description of the initiation step, which in turn affect the

Encyclopedia of Polymer Science and Technology. Copyright John Wiley & Sons, Inc. All rights reserved.

description of the rate of polymerization. An overview of the components, kinetics, and applications of these free-radical photopolymerization systems is given in this article. More detailed information may be obtained in the references cited.

Photoinitiators

In order to produce free radicals that initiate polymerization, photoinitiators absorb light of a certain frequency. Upon absorption, the photoinitiator molecule is promoted from the ground electronic state to either a singlet or triplet excited electronic state. This excited molecule then undergoes either cleavage or reaction with another molecule to produce initiating free radicals. Numerous photoinitiators have been developed to meet the needs of a variety of photopolymerization systems, as described in a number of recent papers and reviews (3–6,8–12).

In selecting an appropriate photoinitiator system, several key criteria must be fulfilled. First, the absorption spectrum of the initiator must overlap with the emission spectrum of the light source, be it polychromatic (eg, arc lamp) or monochromatic (eg, laser). Good engineering of the system involves optimizing the light absorption of the initiator and, in many cases, minimizing emission lines that do not coincide with the initiator absorption spectrum (ie, are wasted through absorption by other system components). By matching the absorption of the photoinitiator to the light source output, the initiation efficiency can also be optimized. However, the overlap between the initiator and light source must preferably not coincide with the absorption peaks of other components in the photopolymerization system (monomer, pigments, additives, etc.). In systems where there is overlap, such as highly pigmented systems, higher light intensities and photoinitiator concentrations are often used (13). Figure 1 demonstrates a good match of a photoinitiator with a light source and monomer in that there is a clear optical window for the photoinitiator to absorb light in the 300–400-nm region without competition from the monomer.

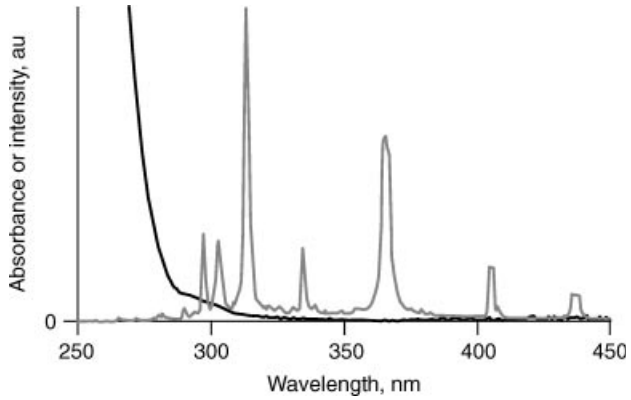

Fig. 1. UV–visible absorption spectra of dimethoxyphenylacetophenone (DMPA) (photoinitiator) and 2-hydroxyethyl methacrylate (HEMA) (monomer) in dichloromethane overlaid with the spectral output of a 200-W Hg(Xe) lamp. ——— DMPA; ——— HEMA; and ——— Hg(Xe) Lamp.

Many free radical photoinitiators are based on the benzoyl chromophore (highlighted in eqs. 1 and 2), which produces free radicals when irradiated with light of the appropriate wavelength. Judicious choice of substituents (R groups) and their placement can alter the absorption spectrum, so that more freedom is available in the choice of lamp (and initiating wavelength) and system components. Secondly, the impact of residual photoinitiator and its photoproducts upon the final products must be considered. This becomes most important in thick films and coatings that must be of a certain color. If the photoinitiator fragments absorb at the same wavelength as the photoinitiator, then light cannot penetrate to the bottom of a thick sample, and full conversion of the monomer will not be attained. Also, some photoinitiator fragments, such as aromatic amines, will "yellow" initially colorless and white coatings and films, especially after long exposure times to sunlight or fluorescent lights (13).

Unimolecular Photoinitiators. Photoinitiators termed unimolecular are so designated because the initiation system involves only one molecular species interacting with the light and producing free-radical active centers. One type includes photoinitiators that form radicals via the cleavage of the initiator molecule. This cleavage may take place at the α or β position with respect to the carbonyl group. Upon illumination, the photoinitiator molecule is excited and undergoes cleavage. In α-cleavage or Norrish Type I, the bond adjacent to the carbonyl is broken to produce two free radicals. Equation 1 demonstrates the α-cleavage of a representative benzyl ketal photoinitiator dimethoxyphenylacetophenone (the dashed box highlights the benzoyl chromophore).

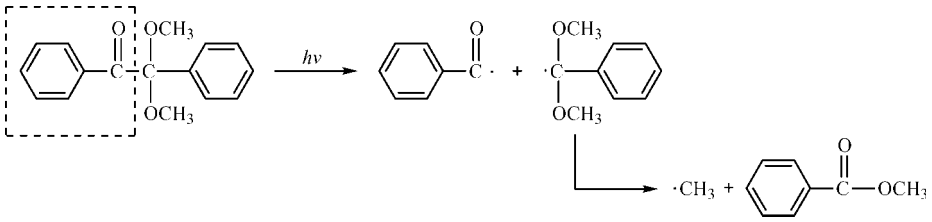

(1)

In this case, the benzoyl radical and a methyl radical produced through the fragmentation of α,α-dimethoxy benzyl radical both initiate polymerization. Other families include benzoin ethers, acetophenone derivatives, amino ketones, and phosphine oxide derivatives (**1–4**) (3,11).

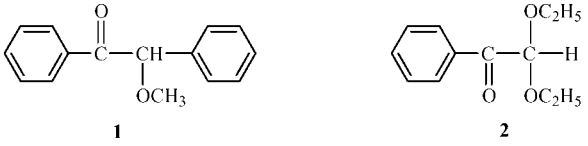

1

2

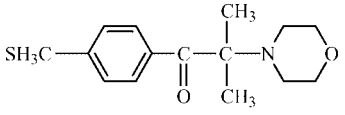

3

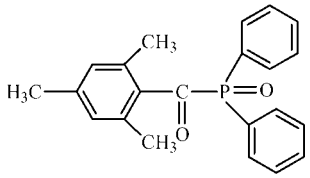

4

β-Cleavage occurs predominately in α-halogenoacetophenones; however, it is also seen in photoinitiators with a C—S or C—O bond adjacent to the benzoyl chromophore, such as β-ketosulfoxides (3,11). Equation 2 demonstrates this cleavage mechanism for the photoinitiator 2,2,2-trichloro-4′-*tert*-butylacetophenone (the dashed box highlights the benzoyl chromophore).

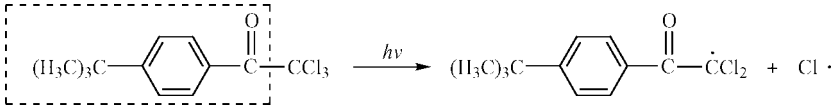

(2)

A second type of unimolecular photoinitiators, also called Norrish Type II, includes those that form biradicals through intramolecular hydrogen abstraction. This occurs in ketones with a γ-hydrogen and is shown in equation 3 for intramoleculer H-abstraction of the photoinitiator 1-phenyl-butan-1-one (14). The resulting ketyl radical participates in termination, while the other radical grows the polymer chain.

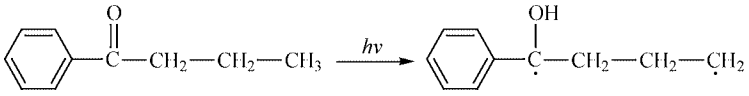

(3)

Bimolecular Photoinitiator Systems. Bimolecular photoinitiators are so-called because two molecular species are needed to form the propagating radical: a photoinitiator that absorbs the light and a co-initiator that serves as a hydrogen or electron donor. Photoinitiator families include benzophenone derivatives, thioxanthones, camphorquinones, benzyls, and ketocoumarins (**5–9**) (3).

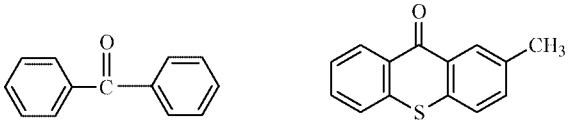

5

6

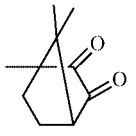

7

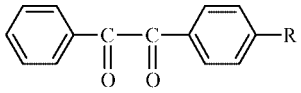

8

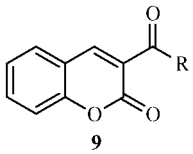

9

The abstraction of a hydrogen molecule from the co-initiator or the transfer of an electron between the two initiating molecules takes place once the photoinitiator is in the excited state. In both cases, free radicals result, one or more of which may actually begin the photopolymerization. Initiation by hydrogen transfer is common in diaryl ketones. The co-initiator is usually an ether or an alcohol with an abstractable α-hydrogen, such as 2-propanol. Equation 4 demonstrates the H-abstraction reaction between the photoinitiator benzophenone and the hydrogen donor tetrahydrofuran. In this case, the ether radical initiates polymerization, and the ketyl radical only participates in termination.

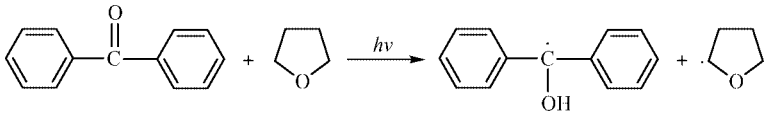

(4)

In photoinitiation by electron transfer, the photoinitiator, after absorption of the initiating light, forms an excited-state complex (exciplex or charge-transfer complex) with the co-initiator, typically an amine. Electron transfer from the amine to the photoinitiator occurs in this exciplex, immediately followed by proton transfer of an α-hydrogen from the amine to the photoinitiator. This results in two radicals: an amine radical that will initiate polymerization and a ketyl-type radical that will most likely terminate by coupling with another free radical species. Figure 2 demonstrates this type of photoinitiation process between benzophenone and an amine co-initiator (3,15).

Bimolecular photoinitiator systems utilize longer wavelengths (thereby requiring less energy) than the unimolecular systems, which are typically constrained to use in the ultraviolet (UV) because of the absorption characteristics of the benzoyl chromophore. However, the production of active centers in bimolecular photoinitiator systems decreases in vitrifying systems (ie, systems in the later stages of conversion where the reaction temperature is less than the glass transition temperature) because diffusion of the initiator and co-initiator molecules

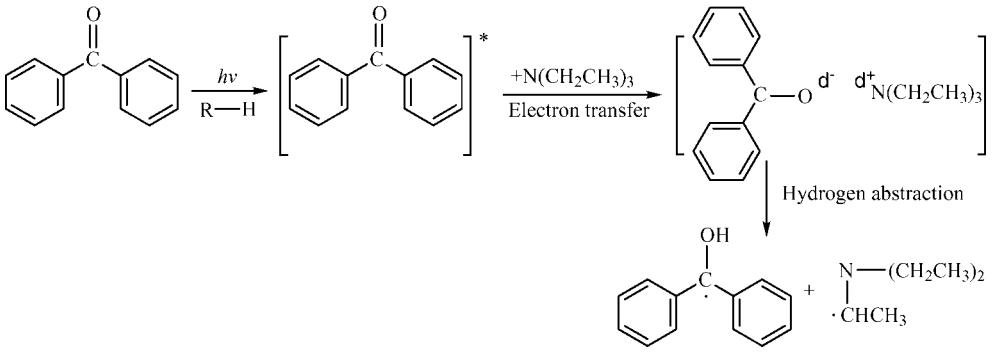

Fig. 2. Electron-transfer reaction with subsequent proton-transfer reaction between the photoinitiator benzophenone and the co-initiator triethylamine.

is strongly suppressed. During this stage in the polymerization, formation of the polymer chains occurs through reactive diffusion.

Photosensitizers. In the bimolecular initiation reactions described above, the co-initiator will not absorb light to initiate polymerization. In contrast, photosensitizers are able to absorb light and are used to enhance the photopolymerization (ie, the photoinitiator is normally able to function without the photosensitizer) (3,4,16). A visible light photosensitizer may be chosen when ultraviolet light is undesirable, such as when working with biological systems or white pigmented systems. If pigments or monomers absorb in the same region as the photoinitiator, a photosensitizer may be used to extend the optical window of the system. A photosensitizer may also be used to improve initiation efficiency by absorbing photons from the light source that the photoinitiator cannot absorb or may do so with a low efficiency.

Two mechanisms have been identified to describe the interaction between photosensitizers and photoinitiators: *energy transfer* and *electron transfer*. In the energy transfer process, the photosensitizer absorbs the light and transfers that energy to the photoinitiator which will then go through either a unimolecular or bimolecular scheme to produce initiating free radicals.

$$PS \xrightarrow{h\nu} PS^*$$

$$PS^* + I \xrightarrow{\text{energy transfer}} PS + I^*$$

$$I^* \longrightarrow R_1^{\cdot} + R_2^{\cdot}$$

In this case, the photosensitizer is not consumed by the reaction and reverts back to its ground state upon transferring its excitation energy to the photoinitiator. For example, the photoinitiator 2-methyl-1-[4-(methylthio)-phenyl]-2-morpholinopropane-1-one (TPMK) absorbs light in the 275–325-nm region, wherear the photosensitizer 3-ethylacetate-2′-methylthioxanthone (ETX) exhibits an absorption peak between 380–420 nm (3). Thus, ETX absorbs light in the visible region of the spectrum and transfers that energy to TPMK, which then undergoes α-cleavage to form the free-radical active centers. In order for this process to occur, the triplet excited electronic state of the photosensitizer must be higher than that of the photoinitiator. Because these states are difficult to match, the energy transfer mechanism is not extensively used.

In the electron transfer mechanism, which is more common, the photosensitizer becomes excited upon illumination and forms an excimer with the photoinitiator. Electron transfer from the photoinitiator to the photosensitizer then occurs, with a subsequent proton transfer. This results in the formation of two radicals. The photosensitizer radical is capable of initiating polymerization, while the photoinitiator radical may not unless it undergoes further reaction (3,13,17). Figure 3 demonstrates this for a representative α-amino ketone photoinitiator and a thioxanthone being used as a photosensitizer.

Specialty Photoinitiators. Photoinitiator systems continue to be developed to meet the needs of industrial applications. Driving forces include increasing reaction speed with higher quantum yields and higher active center reactivities, improving shelf life with greater solubility and stability in the formulations, and

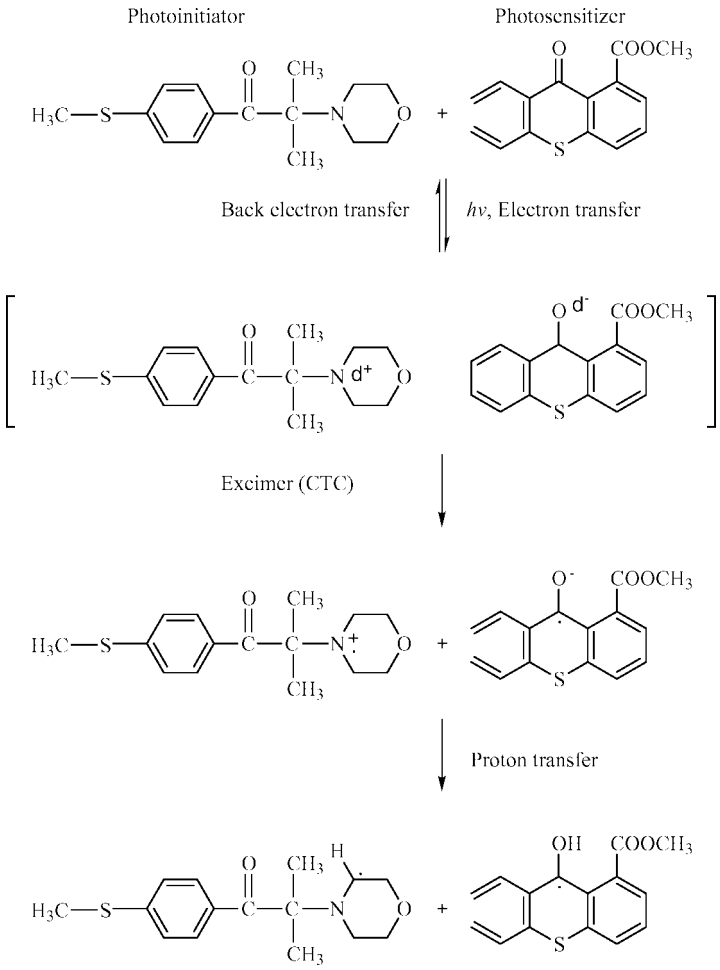

Fig. 3. Electron transfer reaction between the photoinitiator 2-methyl-1-[4-(methylthio)-phenyl]-2-morpholinopropane-1-one and the photosensitizer 9-oxo-9*H*-thioxanthene-1-carboxylic acid methyl ester.

optimizing the absorption spectrum to meet the requirements of the light source and application. Minimizing toxicity of the initiators and yellowing due to photoproducts and sunlight exposure also is important for many applications.

Visible Light Photoinitiators. Visible light photoinitiators are desirable for many applications. Visible light is safer than UV light in that it does not cause cell damage in biological systems. Many common, inexpensive light sources, such as halogen or fluorescent lamps, have strong lines in the visible, which could be used for efficient and cost-effective photoinitiation. In addition, visible lasers are used in photoimaging applications, such as lithography and holography (5). Visible light photoinitiators can also enhance polymerization in systems with pigments, fillers, and UV absorbers (18).

Visible light photoinitiators based on metal salts and complexes have been explored (3,10,12). Some systems generate ionic active centers unless

combined with another molecule (such as a dye or halogenated compound) that will react to produce the initiating free radical. Titanocene complexes, an example of which is bis(η^5-2,4-cyclopentadien-1-yl)-bis-[2,6-difluoro-3-(1*H*-pyrrol-1-yl)phenyl]titanium (**10**), are metal-based photoinitiators that undergo cleavage upon illumination in the 400–550-nm region, with the aryl radical initiating polymerization (12).

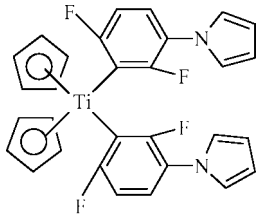

10

Dyes comprise a large fraction of visible light photoinitiators because their excited electronic states are more easily attained. Co-initiators, such as tertiary amines, iodonium salts, triazines, or hexaarylbisimidazoles, are required since dye photochemistry entails either a photoreduction or photo-oxidation mechanism. Numerous dye families are available for selection of an appropriate visible initiation wavelength; an example of a thiazine dye (with an absorption peak around 675 nm) is methylene blue (**11**).

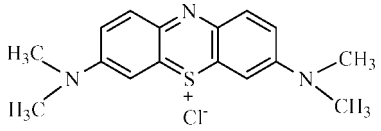

11

Other examples include acridine dyes (with absorption peaks around 475 nm), xanthene dyes (~500–550 nm), fluorone dyes (~450–550 nm), coumarin dyes (~350–450 nm), cyanine dyes (~400–750 nm), and carbazole dyes (~400 nm) (12,19–21). The oxidation or reduction of the dye is dependent on the co-initiator; for example, methylene blue can be photoreduced by accepting an electron from an amine (22) or photo-oxidized by transferring an electron to benzyltrimethylstannane (12). Either mechanism will result in the formation of a free-radical active center capable of initiating a growing polymer chain. For a more detailed discussion of the mechanisms, see Reference 12.

Three-component visible light photoinitiator systems exhibit faster polymerization rates than those seen in the dye-electron donor systems mentioned above. The third component is usually a sulfonium or iodonium salt (an example is diphenyliodonium chloride) (**12**), but may also be a bromocompound, ferrocenium salt, or thiol derivative (3,12,21–24).

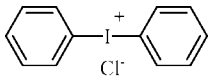

12

The incorporation of the third component has been shown to provide pathways to scavenge oxygen molecules that inhibit free-radical polymerization, to regenerate the dye photoinitiator, and to produce a free-radical active center in place of a terminating dye radical (3,12,13,21). In addition, the wide selection of dyes available for use in three-component systems allows more flexibility in initiating wavelength selection, and the photopolymerization of thick parts is possible if a photobleaching dye is chosen (21).

Water-Soluble Photoinitiators. Water-soluble photoinitiators are needed for systems such as printing inks and emulsion processes, where the reaction system is an aqueous solution rather than simply a monomer. Since free radical photoinitiators are based on the aromatic benzoyl chromophore, the molecules are generally nonpolar and therefore incompatible with water. Research has focused on developing photoinitiators with hydrophilic substituents that increase water solubility (3,25). Both unimolecular and bimolecular systems have been successfully demonstrated. An example of a unimolecular photoinitiator is sodium 4-benzoylbenzenemethane sulfonate (**13**).

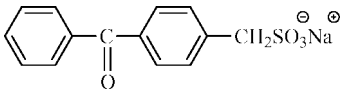

13

Photobleaching Initiators. Photobleaching initiator systems are designed such that the absorption of the photoinitiator byproducts is lower than that of the photoinitiator (13,26). Thus, as the active centers are formed, more light may pass through the system. This is crucial in thick films, where light penetration to the bottom of the sample is hindered by the absorption characteristics of the upper layers. Insufficient light penetration will result in low conversions at the bottom, wrinkling of the surface, and decreased production speeds. Photobleaching is also necessary for colorless or white films and coatings to prevent yellowing. Acylphosphine oxides and bisacylphosphine oxides (**14**), which undergo α-cleavage, are examples of photobleaching initiators widely used today. These photoinitiators absorb well into the visible spectrum; however, once cleavage occurs, the absorption peaks in the visible spectral region disappear.

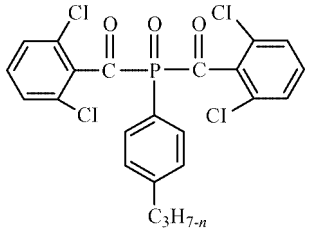

14

Polymerizable and Polymeric Photoinitiators. Growing interest in polymerizable and polymeric photoinitiators is seen in several industries. An example is poly(4,4-dimethyl-1-penten-one) (**15**).

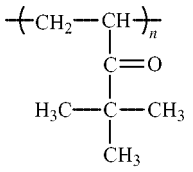

15

In the food-packaging industry, species that migrate from a film or coating may contaminate foods. In the film and coating industries, migrating species may cause yellowing at film surfaces. Thus, tethering or incorporating the photoinitiator on the main polymer chain is an effective means of reducing migration by photoproducts and unreacted photoinitiator (27). These types of photoinitiators exhibit other practical benefits, such as improved compatibility with monomers, longer shelf life, increased reactivity, and reduced volatile emissions (28,29). Polymeric photoinitiators have been synthesized by grafting the initiator molecule onto the backbone of the polymer chain (3,27,30). They have also been created by terminating polymer chains with the initiator molecules (3,27,29,31,32). Polymeric photoinitiators may become entangled within the polymer product or attached to the main polymer chain or network, depending on whether the active center cleaves from or is part of the polymeric photoinitiator chain (27). Polymerizable photoinitiators may be formed by attaching the photoinitiator on a polymeric or oligomeric chain that has one or more functional groups that can enter into the polymerization as well (3). Thus, the photoinitiators become copolymerized with the main polymer chain or network.

In some cases, a monomer may function as a photoinitiator and become incorporated into a copolymer chain. This has been shown for styrene and other conjugated monomers when exposed to deep-UV light; however, the initiation efficiency in these systems is substantially less than when a photoinitiator is present (p. 223 of Ref. 33, and Ref. 34). A better polymerizable initiator scheme is illustrated by the acceptor-donor chemistry of maleimide-donor systems (35–37). Maleimide acts as both photoinitiator and comonomer in the presence of hydrogen donors such as vinyl ethers or vinyl esters (38,39); an example of this copolymerization is shown in equation 5. It shows the molecular structure of the acceptor *tert*-butylmaleimide (left), the donor 4-hydroxy-butyl vinyl ether (right), and their corresponding copolymer repeat unit.

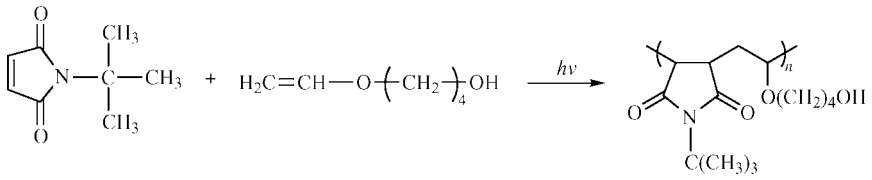

(5)

In these systems, illumination with a subsequent hydrogen abstraction or electron/proton transfer process results in the production of two radicals, both of

which may start a propagating chain by adding either monomer (35–37):

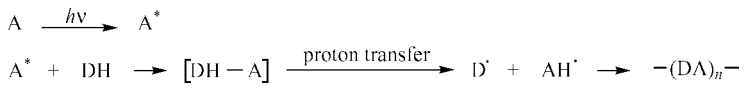

These systems have the added advantage of being photobleaching, as well as less inhibited by oxygen.

Monomers

Unsaturated monomers, which contain a carbon–carbon double bond (C=C), are used extensively in free radical photopolymerizations. The free-radical active center reacts with the monomer by opening the C=C bond and adding the molecule to the growing polymer chain. Most unsaturated monomers are able to undergo radical polymerization (qv) because free-radical species are neutral and do not require electron-donating or electron-withdrawing substituents to delocalize the charge on the propagating center, as is the case with ionic polymerizations. Commercial consideration in formulation development is therefore given to the final properties of the polymer system, as well as the reactivity of the monomer.

(Meth)acrylate Systems. Acrylate and methacrlate monomers are by far most widely used in free-radical photopolymerization processes. The generalized structure of these monomers and their corresponding polymer is shown in Figure 4.

These monomers have very high reaction rates, with acrylates having an even faster reaction rate than their methacrylate counterparts (4). This makes them especially amenable for high speed processing needed in the films and coatings industry. (Meth)acrylate systems are also easily tailored using the ester linkage to obtain the desired chemical, mechanical, and optical properties for a variety of applications (see ACRYLIC ESTER POLYMERS; METHACRYLIC ESTER POLYMERS). Monoacrylates, which have only one C=C group, are generally used as reactive diluents with multiacrylates, which have two or more C=C groups per molecule (Fig. 5). Multiacrylates increase the mechanical strength and solvent resistance of the ultimate polymer by forming cross-linked networks rather than linear polymer chains, whereas monoacrylates reduce the viscosity of the prepolymer mixture for ease of processing (4,6).

One of the drawbacks of acrylate and methacrylate systems is their relatively large polymerization shrinkage. Shrinkage is caused by the formation of covalent

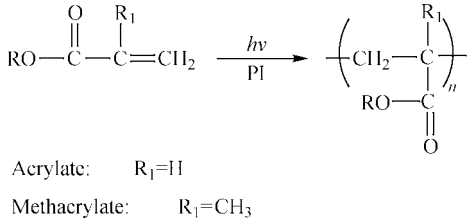

Fig. 4. Molecular structure of a generalized acrylate monomer and its corresponding polymer repeat unit.

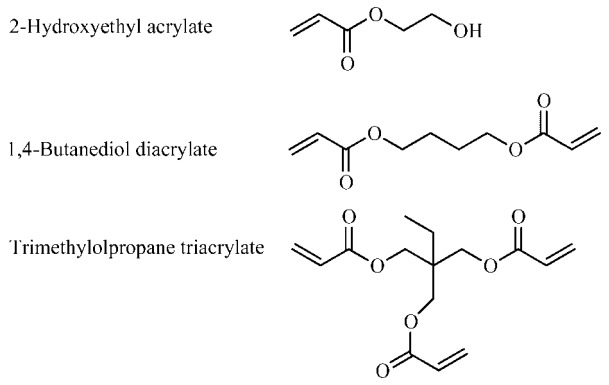

Fig. 5. Molecular structures of monomers with a varying number of acrylate reactive groups: a monoacrylate (top), diacrylate (middle), and triacrylate (bottom).

bonds between monomer molecules. When a covalent bond is formed between two monomer molecules, the distance between them is approximately half as much as that between two molecules experiencing van der Waal's forces in solution. In addition, because the number of conformations that a polymer chain can achieve is less than that for the individual monomer molecules, monomer conversion results in a negative entropy of polymerization and less free volume. Thus, volume shrinkage of 5–25% is observed in these systems (4,40–42). This shrinkage causes stresses in the polymer parts, which can affect their ultimate performance, especially in applications such as stereolithography, dentistry, and coatings. One way to overcome this disadvantage is to develop oligomeric acrylates. These oligomers contain 1 to 12 repeat units formed through step-growth polymerization; the ends are then capped with two or more (meth)acrylate functional groups. Commercially available oligomeric families are shown in Figure 6.

In addition to reducing shrinkage, oliogomeric acrylates offer improved properties of wear resistance and chemical and moisture resistance. They also enable the use of these functional groups in rapid processing applications, which would not be possible using the slower step-growth polymerization mechanism. Because of their size, these oligomers must be combined with other monomers to reduce the resin viscosity. Examples of coating formulations incorporating multiacrylates and oligomeric acrylates are shown in Table 1.

Unsaturated Polyester Systems. Coatings in the furniture industry rely heavily upon resin formulations containing unsaturated polyesters, styrene, and photoinitiator (3,4,13,43,44). The unsaturated polyesters are synthesized using step-growth polymerization (see POLYESTERS, UNSATURATED). Upon illumination, the carbon–carbon double bond in the unsaturated polyester and styrene copolymerize to form a cross-linked network (eq. 6). Equation 6 shows a generalized reaction scheme for an unsaturated polyester system.

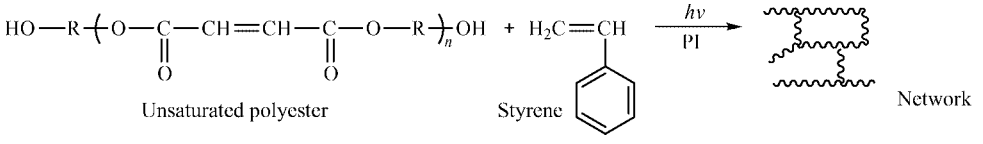

(6)

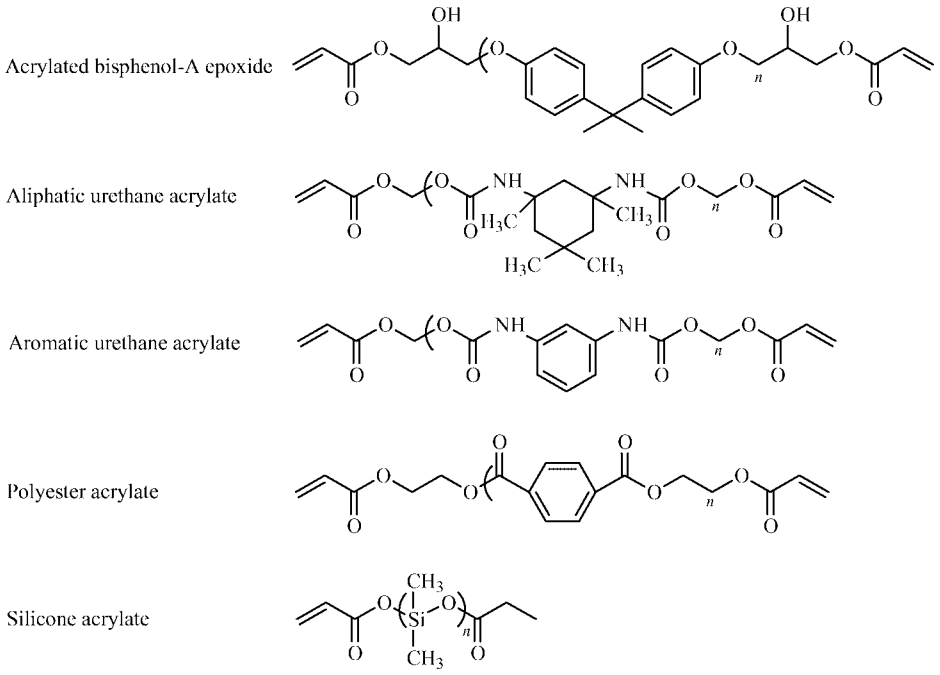

Fig. 6. Molecular structure of some generic acrylated oligomers.

Although these systems polymerize much slower than the acrylate systems, they are low cost and can still polymerize at ambient temperatures.

Thiol–Ene Systems. Systems that combine thiols [such as a trithiol (**16**)] with ene comonomers, such as allyl ethers [like trimethylol propane diallyl ether (**17**)] or acrylates, were first considered in the 1970s; however, because of their unpleasant odor, thiols were abandoned, and acrylates became the monomer of choice for industrial implementation.

Table 1. Sample (Meth)acrylate Formulations

Basic coating	Wood-flooring topcoat	Adhesive resin for dentistry	Resin composite for dentistry
Acrylated epoxy oligomer, 45%	Urethane acrylate, 60%	Dimethacrylated epoxide, 60–70%	Silica filler, 77–87%
Triacrylate, 20%	Diacrylated polyether, 24%	Monomethacrylate, 30–40%	Dimethacrylated epoxide, 5–9%
Diacrylate, 20%	Polyester tetraacrylate, 10%	Camphorquinone, <1%	Dimethacrylated polyether, 5–9%
Amine, 10%	Amine, 10%	Amine, <1%	Camphorquinone, <1%
Benzophenone, 5%	α-Hydroxyketone, 5%		Amine, <1%

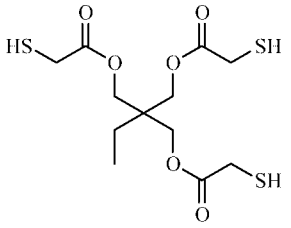

16

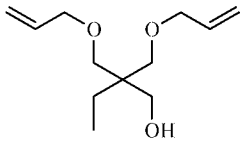

17

Several factors have led to renewed interest in thiol systems. First, the systems require little or no photoinitiator in order to polymerize (45,46). This reduces the cost of formulations (since the photoinitiator is generally the most expensive component), as well as decreases toxicity and purity concerns. In addition, photoinitiator fragments do not interfere with the physical properties of the polymers, such as color and strength. The thiol functions as photoinitiator by producing a thiyl and a hydrogen radical pair through a sulfur–hydrogen bond cleavage when exposed to light (47,48):

$$RSH \xrightarrow{h\nu} RS^{\cdot} + H^{\cdot}$$

Thiol systems are also less sensitive to inhibition by oxygen, a major disadvantage of free-radical polymerizations. The inactive peroxy radical formed through interaction of oxygen and a growing chain end can undergo chain transfer to the thiol to regenerate the active thiyl radical. However, this still results in the incorporation of oxygen into the polymer, which will affect its performance properties. Because most of the double-bond conversion occurs in the liquid state, these systems undergo less volume shrinkage and establish an infinite network (gel point) later in the reaction so that higher conversions, even in systems with multiple functional groups on each monomer, may be reached (49). This is a result of extensive chain transfer during the free-radical chain polymerization, which leads to the formation of very short chains. Long polymer chains and networks are formed through a step-growth mechanism (46–48,50).

Other Monomer Systems. The above sections are by no means an exhaustive list of monomers that are used in free radical photopolymerizations. Diallyldiglycolcarbonate (**18**) has been used for many years in optical components such as lenses (51). Acrylamide (**19**) is used in stereolithography and to prepare holographic materials (52–54). *N*-vinylpyrrolidinone (**20**) is copolymerized with acrylates and methacrylates for cosmetic and biomedical applications (55). Norbornene (**21**) is copolymerized with thiols for optical fiber coatings (56). Liquid crystal polymers (**22**) based on acrylates and thiol–enes are being developed to produce mirror coatings, polarizing films, and liquid crystal displays (57,58).

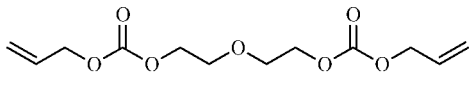

18

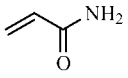

19

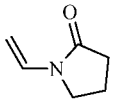

20

21

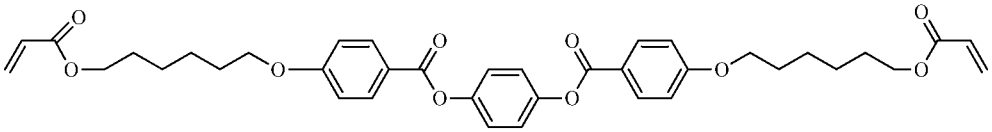

22

Kinetics

The description of free-radical chain polymerization kinetics must take into account four basic steps: *initiation*, which creates free-radical active centers; *propagation*, which grows the polymer chains; *termination*, which destroys the active centers and ends chain growth; and *chain transfer*, which ends a growing chain and begins another. These classical steps also describe thermal polymerizations; however, different descriptions are required for thermal- and photoinitiation.

Initiation. In both thermal- and photopolymerizations, the rate of initiation depends on two processes: the *dissociation* of the initiator and the *initiation* of the propagating chain. The decomposition rate (k_d) of thermal initiators strongly depends on temperature, with the half-life of many thermal initiators at the reaction temperature on the order of minutes or hours. In contrast, for photopolymerizations, the rate at which photons are absorbed at a specific wavelength will determine the decomposition rate of photoinitiators. This process is not temperature-dependent. Thus, in the classic initiation mechanism, the interaction between light of a specific wavelength and a photoinitiator molecule is considered. For a unimolecular photoinitiator, this reaction step can be written as follows:

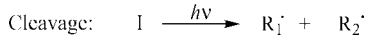

Either one or both of the radicals may then initiate polymerization. Biacetyl is an example of a photoinitiator that generates two identical free-radical groups (eq. 7) (59).

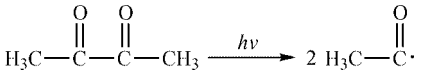

(7)

Benzoin methyl ether is an example of a photoinitiator that generates two dissimilar free radicals, each with a different initiation efficiency (ie, benzoyl radical is more likely to start a propagating chain than the ether radical) (eq. 8) (60).

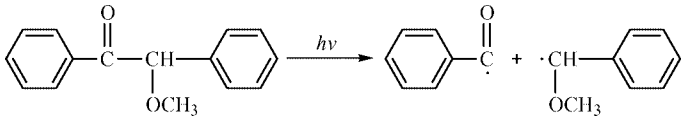

(8)

A similar mechanism may be developed for radical production by electron transfer or hydrogen abstraction:

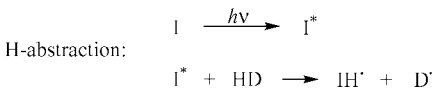

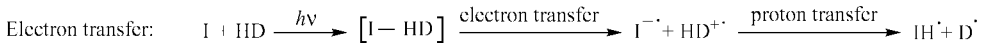

Generally, the donor radical (such as an amine or alcohol) is the initiating species. The reactive radical species ($R^{\bullet}$) then goes on to attack a nearby monomer molecule, thereby starting a propagating chain ($R{-}M^{\bullet}$):

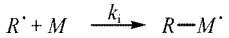

where k_i is the initiation rate constant, usually expressed in L/mol·s. Taking into account these two reactions (production of the free-radical active centers and initiation of the propagating chain), the rate of photoinitiation (R_i), which describes the change in propagating center concentration with respect to time, may be expressed as (33)

$$R_i = \frac{d[R{-}M^{\bullet}]}{dt} = 2f\varphi I_a$$

Here, I_a is the amount of photons absorbed by the photoinitiator molecules expressed in mol photon/L·s or Einstein/L·s; f is the photoinitiator efficiency calculated by determining the moles of propagating chains ($R{-}M^{\bullet}$) started per mole of free-radical active centers ($R^{\bullet}$) generated; and φ is the photoinitiator quantum yield which relates the moles of active center pairs ($R^{\bullet}$) produced per moles photons absorbed (φ is defined such that it is ≤ 1). The integer 2 is included in the expression when both radical species initiate polymerization. If only one of the radical species is active, it is omitted.

Beer's Law, which relates the absorption of light to the concentration of the absorbing species, is used to define I_a for a specified wavelength of light. It is

derived from the partial differential equation used to describe the change in amount of photons as the light passes through an absorbing medium of thickness b:

$$\frac{dI}{db} = -kI \tag{9}$$

where I is the amount of photons in mol photon/(L·s) and k is the absorption coefficient (cm^{-1}), which can also be expressed in terms of the absorbing species concentration and its molar absorptivity as shown below. A bulk-averaged I_a may be obtained by integrating equation 9 over the sample depth:

$$I_a = I_0 - I_t = I_0(1 - e^{-2.3\varepsilon b[I]}) \tag{10}$$

where I_0 is the amount of photons incident upon the sample [mol photon/(L·s)]; I_t is the amount of photons transmitted through the sample [mol photon/(L·s)]; ε is the molar absorptivity of the photoinitiator [L/(mol·cm)]; b is the thickness of reaction system (cm); and [I] is the photoinitiator concentration (mol/L). If the quantity εb[I] is small (<0.01), then equation 10 may be approximated by the first term of its Taylor series expansion (61):

$$I_a = 2.3 I_0 \varepsilon b[I] \tag{11}$$

In systems where the quantity εb[I] is not small, typically in thick systems, equation 10 must be used such that R_i increases proportionally with I_0, but not with [I]. Thus, simply increasing [I] does not result in a homogeneous reaction rate: the upper layers will absorb the largest fraction of the incident light, limiting initiation near the bottom of the system. Therefore, in these systems, conversion at the bottom of the sample is generally much less than at the top unless the initiator concentration and initiating wavelength have been properly chosen.

Several groups have developed models to describe photoinitiation and photopolymerization in thick films or films with high optical densities (62–66). The latest models (62,63) take into account variations in the initiator concentration by solving partial differential equations that describe [I], I_a, and photolysis product concentration as a function of depth and time. If the molar absorptivity, photoinitiator quantum yield, and diffusion properties are known for an initiator system, then these equations can be solved to describe the light intensity gradient in a thick sample and to determine the effects of the initiator absorption characteristics on the efficiency of active center generation for different wavelengths of initiating light.

Propagation. Since chain polymerization kinetics are usually followed for free radically photoinitiated polymerizations, the propagation mechanism involves the addition of monomer to the growing polymer chain:

$$R - M_n^{\cdot} + M \xrightarrow{k_p} R - M_{n+1}^{\cdot} \tag{12}$$

The rate of polymerization (R_p) obtained from this mechanism is as follows:

$$R_p = \frac{d[M]}{dt} = k_p[M][R - M_n^{\bullet}] \tag{13}$$

where k_p is the propagation rate constant [L/(mol·s)] and is generally assumed independent of chain length n. [M] is the reactive group concentration (mol/L), which is equal to the monomer concentration if only one reactive group is present on the monomer molecule.

Termination. Termination of the free-radical active centers may occur either by combination or by disproportionation. In termination by combination, two propagating chains unite to form one long polymer molecule:

$$M_n^{\bullet} + M_m^{\bullet} \xrightarrow{k_{tc}} P_{n+m} \tag{14}$$

In termination by disproportionation, one propagating chain abstracts a hydrogen atom from a neighboring propagating chain, resulting in two polymer molecules, one of them having a terminal double bond:

$$M_n^{\bullet} + M_m^{\bullet} \xrightarrow{k_{td}} P_n + P_m \tag{15}$$

When developing a rate expression for termination, the rate constants for these mechanisms are often lumped in a single termination rate constant, k_t [L/(mol·s)]. The rate of termination, which is generally assumed independent of chain length n, equals the rate of destruction of the propagating active centers ($M^{\bullet}$):

$$R_t = \frac{-d[M_n^{\bullet}]}{dt} = 2k_t[M_n^{\bullet}]^2 \tag{16}$$

Rate of Polymerization. The concentration of growing chains ($R{-}M_n^{\bullet}$) is difficult to measure experimentally; thus, for simplicity, it is often assumed that the change in the concentration of propagating chains over time is very small in comparison to the change in the monomer concentration. According to this pseudo–steady-state assumption, ($d[M_n^{\bullet}]/dt$) is approximated as zero, and the rate of initiation is then equal to the rate of termination. When this is invoked, the rate of polymerization may be written as:

$$R_p = k_p[M]\sqrt{\frac{f\varphi I_a}{k_t}} \tag{17}$$

Similarly, the kinetic chain length (ν), which describes the average number of monomer molecules (or reactive groups for multifunctional monomers) that are consumed per initiating radical, can be calculated as follows:

$$\nu = \frac{R_p}{R_i} \approx \frac{R_p}{R_t} = \frac{k_p[M]}{2\sqrt{k_t f \varphi I_a}} \tag{18}$$

The actual chain length will be shorter if chain transfer reactions occur.

Autoacceleration, where the rate of polymerization increases with conversion in isothermal conditions, is observed in both thermal- and photoinitiated free-radical polymerizations because the termination mechanisms are the same for both. As the chains grow longer, it becomes more difficult for the active centers to diffuse and undergo bimolecular termination; thus, termination frequency decreases and active centers at the chain ends can become trapped. In cases where termination is controlled by diffusion, the pseudo–steady-state assumption is no longer valid and chain length dependent termination (CLDT) may occur (67). As is discussed for chain cross-linking photopolymerizations below, more complicated kinetic treatments must then be considered, including unsteady-state kinetics.

Inhibition. One of the major disadvantages of free-radical photopolymerization is its susceptibility to oxygen inhibition. This is especially troublesome in thin-film and coating applications where oxygen diffusion plays a significant role in increasing cure times and results in incomplete conversion on the surface. When oxygen, which is essentially a biradical in its electronic ground state, reacts with a free-radical active center, it forms a peroxy radical, which is much less reactive (Refs. 3,4, and p. 264 of Ref. 33):

$$\mathrm{M}_\mathrm{n}^\bullet + \mathrm{O}_2 \rightarrow \mathrm{M}_n\text{—O—O}^\bullet$$

$$\mathrm{M}_\mathrm{n}\text{—O—O}^\bullet + \mathrm{M} \rightarrow \text{No reaction}$$

Thus, oxygen effectively acts as a chain terminator and reduces the rate of polymerization until the oxygen in the system has been consumed.

The cost of preventing or minimizing oxygen inhibition is high. In industry, an inert gas such as nitrogen or carbon dioxide may be used to blanket the system. Waxes or shielding films may also be used to prevent oxygen from entering the system. Other methods involve adding oxygen scavengers, dye sensitizers, or antioxidants to capture oxygen and prevent it from reacting with the propagating chains. High photoinitiator concentrations or increased light intensity may also be used to produce a larger number of active centers in order to consume the oxygen in the system faster. However, very close to the surface, it is difficult to consume the oxygen faster than it diffuses into the sample, which can result in tackiness (or incomplete cure) in the surface layers.

Techniques for Measuring Rates and Reactive Intermediates. Kinetic parameters for photopolymerizations may be measured using many different methods or combinations of methods (9,68). Photodifferential scanning calorimetry (PDSC) is a standard technique for obtaining the rate of polymerization (R_p) and conversion (69–73). The conversion of monomer C=C bonds to polymer C—C bonds is an exothermic reaction. The heat flow from the sample (ΔH in W/g) is directly proportional to R_p:

$$R_\mathrm{p} = \frac{\rho \Delta H}{\Delta H_\mathrm{p}}$$

where ρ is the density of the monomer (g/L) and ΔH_p is the heat of polymerization for the reactive group of the monomer (J/mol). The conversion of the sample is

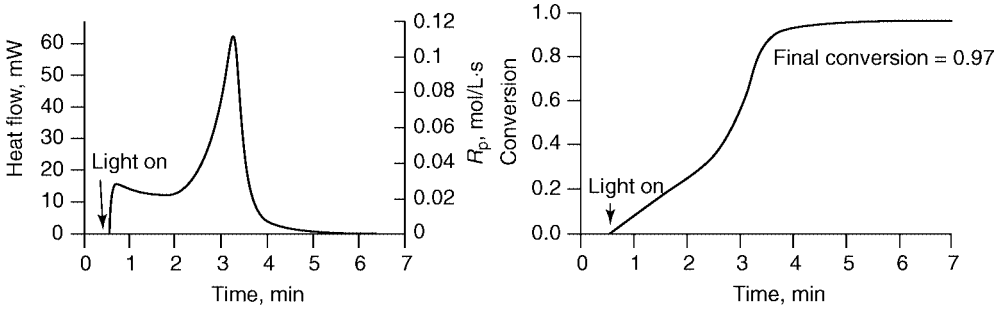

Fig. 7. Photodifferential scanning calorimetry profiles for photopolymerization of 2-hydroxyethyl methacrylate initiated with 2 mmolal dimethoxyphenylacetophenone at 50°C and light intensity of 60 mW/cm^2 with nitrogen purge: polymerization rate (left) and degree of conversion (right).

calculated by integrating the area under the R_p versus time curve, as shown in Figure 7.

Conversion and R_p data may also be obtained using spectroscopic techniques such as Raman spectroscopy (73–75) and infrared spectroscopy (15,50,73,75–77). Here, peaks in these spectra correlate to functional groups within a molecule. As the monomer is converted to polymer, the peaks associated with the C=C bonds decrease. The conversion in the system may be calculated by ratioing this peak height or area at any point in time to the initial peak height or area, as shown in Figure 8:

$$Conversion = 1 - \frac{[M]}{[M]} = 1 - \frac{P_{rxn}(t)/P_{ref}(t)}{P_{rxn}(0)/P_{ref}(0)}$$

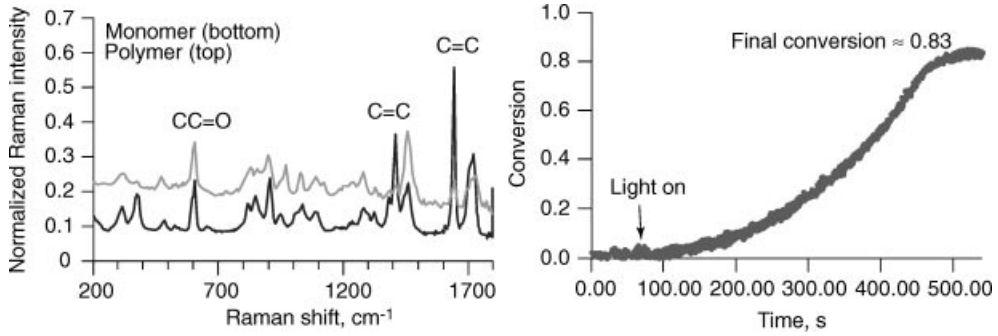

Fig. 8. Raman spectra for photopolymerization of 2-hydroxyethyl methacrylate initiated with 2 mmolal dimethoxyphenylacetophenone at 50°C and light intensity of 75 mW/cm^2: Raman spectra of the monomer and its polymer (left) and degree of monomer conversion based on monitoring the C=C bond depletion at 1640 cm^{-1} (in this system, the internal reference band at 605 cm^{-1} is constant throughout the reaction and cancels out in the conversion ratio) (right).

where P_{rxn} is the peak height or area associated with the reactive functionality and P_{ref} is the peak height or area associated with an internal reference. R_p is then calculated by differentiating the conversion curve over time.

Fluorescence spectroscopy has been used to measure conversion by adding fluorescent molecules to the system that are sensitive to physical parameters (such as polarity or viscosity) that can be correlated to conversion (78–80). Both fluorescence (23) and absorption (35) spectroscopy have been used to follow changes in the photoinitiator spectrum as it absorbs light and produces free radicals. More complicated techniques are used to observe the free-radical active centers generated during polymerization. Since the lifetime of a free-radical active center is very short (typically 10^{-1}–10 s) (p. 274 of Ref. 33), sensitive techniques are needed to determine the structure and concentration of initiating or propagating free radicals. These include the addition of trapping agents that ensnare the free radicals through radical combination or hydrogen abstraction, as well as electron spin resonance (ESR) spectroscopy that allows differentiation of radical species, environment, and concentration during reaction (71,81). Other specialized methods include laser flash photolysis (82–84) and photo-chemically induced dynamic nuclear polarization (photo-CIDNP), which provide information on excited state lifetimes and free-radical intermediates (17,84).

Complex Photopolymerization Systems. Kinetic modeling of free-radical photopolymerizations becomes more complicated as comonomers are added to the reaction system and as different polymerization methods are used to tailor the polymer properties. Although free-radical reaction mechanisms still hold true, rates of propagation and termination must be reconsidered to account for variables such as differences in double bond reactivities, reaction diffusion, and chain transfer.

Chain Cross-Linking Photopolymerizations. In many applications, polymer networks rather than linear chains are desired. The conversion of double bonds in cross-linked systems is often lower because a fraction of the functional groups becomes trapped in areas inaccessible to the active centers. However, polymer networks show improved strength and chemical resistance because degradation of the polymer requires breaking multiple bonds. In order to achieve these types of structures, multifunctional monomers are needed to connect polymer chains together. The monomer itself may then have more than one functional group, as shown in the example (70). Dipentaerythritol pentaacrylate (**23**), a cross-linking monomer, has five reactive sites and is used in protective coating formulations.

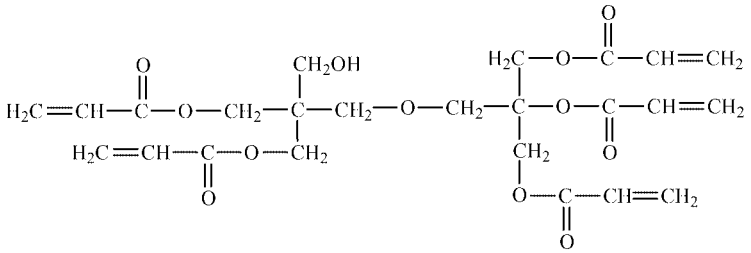

23

Other systems incorporate a monomer with one functional group, which forms the polymer chains, and another monomer with multiple functional groups, which contributes to the chains as well as forming bridges (cross-links) between the chains. For example, 2-hydroxyethyl methacrylate (**24**) and bisphenol A glycidyl methacrylate (**25**) are used in adhesive resins for dental composites:

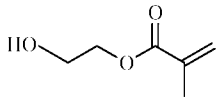

24

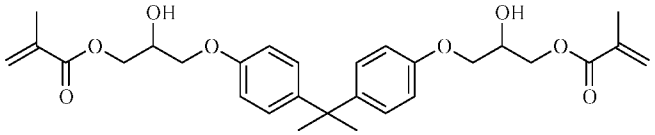

25

Cross-linked systems may also be developed in stages. These monomers have one reactive group that undergoes free-radical polymerization and a second reactive group that undergoes cross-linking by another mechanism, such as cationic photopolymerization. One example is the hybrid monomer (3,4-epoxycyclohexyl) methyl methacrylate (**26**) where the acrylate moiety forms the polymer chains first using free-radical photopolymerization and the epoxy moiety forms the cross-links second using cationic photopolymerization (85):

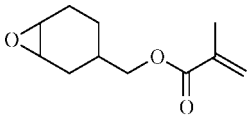

26

The properties of these cross-linked photopolymers are strongly influenced by the cross-link density (ie, the length of the polymer chain between cross-links and the length of the cross-linking molecule itself) (p. 521 of Ref. 33). As the cross-link density increases, hardness and solvent resistance increases, while flexibility decreases (43). The cross-link density can be adjusted by the choice and concentration of the monomers. If different reactive groups are present, then the reactivity ratios of the monomers will determine the rate at which one monomer will react with itself versus the other monomer(s). This will dictate how often a monomer capable of forming a cross-link is added to the main chain. However, in most commercial formulations, mono- and multifunctional monomers with the same type of reactive group (eg, acrylates) are mixed to obtain desired performance properties. Thus, the concentration and number of reactive groups for each monomer will determine the cross-link density.

Kinetic modeling of cross-linked systems is significantly more difficult than for linear systems. Termination mechanisms are more complex because active center trapping (first order or unimolecular termination) and effects of reaction–diffusion must be considered (69,86). Monomers with multiple reactive groups used in highly cross-linking systems may exhibit increased rate of consumption for the pendant reactive groups after the molecule has been included in the polymer chain, resulting in the formation of microgel regions. These structural inhomogeneities are manifested by densely cross-linked regions within a looser polymer

network. Other differences include delayed volume shrinkage with respect to reaction rate (leading to excess free volume) and immediate autoacceleration in the polymerization rate (leading to an increase in radical concentration). Modeling efforts have focused on simulating termination in these systems through incorporating chain-length–dependent termination (67,75,87), combining unimolecular and bimolecular termination equations (69), and considering the impact of diffusion-controlled behavior on the rate constants (72,88,89).

"Living" Free-Radical Photopolymerizations. The ability to control polymer architecture, molecular weight, polydispersity, and end groups enables the development of polymers with improved and specified properties. Living polymerizations, in which propagating chains do not undergo termination or chain transfer reactions and continue to grow until the monomer supply is exhausted, is one way to gain such control (90). Living polymerizations have been successful in systems with ionic active centers; however, bimolecular termination reactions make this difficult to achieve in free-radical polymerizations. Processes such as atom transfer radical polymerization (ATRP) are used in free-radical thermal polymerizations to produce living polymers (91–93) (see LIVING RADICAL POLYMERIZATION). Light-initiated free-radical living polymerizations can be accomplished using iniferters (94). An iniferter participates in the polymerization by serving as an initiator, chain transfer agent, and chain terminator. Photoiniferters generally contain a carbon–sulfur linkage, which cleaves upon illumination to produce a carbon radical and a sulfur radical. Dibenzyl trithiocarbonate (**27**) is an example of such an iniferter (93):

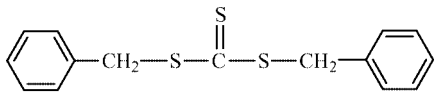

27

The carbon radical ($A^{\bullet}$) is more reactive and serves as the initiation radical, while the sulfur radical ($B^{\bullet}$) is less reactive and serves only as the termination radical (95):

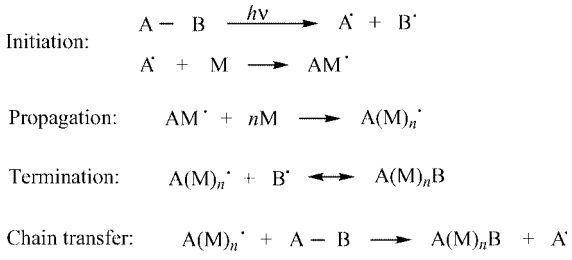

Since termination and chain transfer are still present in iniferter-assisted photopolymerizations, these systems are sometimes described as controlled, rather than living, free-radical polymerizations. Regardless, this approach enables control of bulk free-radical photopolymerizations that is not otherwise

obtainable. Examples of applications include surface modification of substrates (91), three-dimensional nanoscopic patterns (96), and block copolymers (93,97).

Photopolymerization in Microemulsion Systems. Free-radical photopolymerization in microemulsion systems can be used to form stable microlatexes with controlled molecular weight and polydispersity. Microemulsions are two-phase systems, usually consisting of monomer droplets in an aqueous solvent (termed *oil-in-water*) (98,99). Acrylates, methacrylates, and styrenes are typical monomers for microemulsion photopolymerizations. Surfactant molecules are used to stabilize the monomer droplets in solution and to prevent their coalescence. In microemulsions, co-surfactants such as alcohols are often needed to reduce the surface tension of the monomer droplets. This enables further curvature, producing droplets with diameters on the order of 10–50 nm (100). Because of their small size, they do not scatter visible light as do macroemulsions, which are opaque since they contain droplets on the order of 100–1000 nm (101). Thus, microemulsion systems are transparent and allow light to penetrate throughout the system to initiate polymerization within the droplets. Traditional photoinitiators such as benzophenone (102) may be used to generate the free-radical active centers, as well as photoinitiators developed to function as surfactants (103). The kinetics of microemulsion photopolymerizations deviate from the classical bulk kinetics discussed above. Although kinetic expressions for macroemulsions have been developed, a general understanding of microemulsions has not been attained. The surfactant concentration plays an important role in determining the rate of polymerization, along with the light intensity and monomer and photoinitiator concentrations. Termination reactions are suppressed because of the low radical concentration in the droplets and because of diffusional limitations within the droplets, resulting in higher molecular weight polymers (104,105).

Hybrid Photopolymerizations. Hybrid resin systems consist of monomers possessing two different functional groups—one that photopolymerizes by a free-radical active center (such as an acrylate) and the other by a cationic active center (such as an epoxide) (85,106–109). The two functional groups may be combined in one formulation either as separate monomers or as one monomer with both functionalities. If the functional groups are on different molecules, entangled chains or interpenetrating networks will be produced; cross-linked structures will result if the functional groups are on the same molecule because the polymer chains can be connected via either reactive bond.

The systems are designed in order to improve the reaction rate of the mixture and the physical properties of the photopolymer. The flexibility of the two photoinitiation schemes in one system allows for numerous possibilities in achieving greater control of viscosity, conversion, shrinkage, adhesion, and ultimate strength. The kinetics of hybrid photopolymerization systems are more difficult because two reactive systems (free-radical and cationic) must be resolved from one another. Cationic photopolymerization kinetics are more difficult to analyze than free-radical kinetics because the pseudo–steady-state assumption is often not valid for the cationic active center concentration, and the nature and concentration of the cationic active centers is difficult to determine (p. 376 of Ref. 33, see also Photopolymerization, Cationic).

Applications

Free-radical photopolymerizations have been traditionally applied to thin films and coatings where the light penetration is less of an issue (εb[I] is more likely to be small), high production speeds can be achieved, and formulations free from volatile emissions are desirable. In this way, the disadvantages of free-radical photopolymerization, such as poor conversion in thick or strongly absorbing systems, in the presence of oxygen, and in vitrifying systems at ambient temperatures, may be minimized. Despite these limitations, applications of free-radical photopolymerization are far-reaching and encompass the automotive, electronic, medical, optical, graphic arts, flooring, and furniture industries, to name a few. Photopolymerizations continue to expand into previously uncontemplated areas such as topcoats for automobiles, thick parts and composite structures, and biomedical implants as more industries begin to appreciate the advantages these light-induced reactions have over traditional, thermal polymerization methods (1,2,110,111).

Films, Coatings, and Adhesives. Photopolymers may be used as coatings (qv) for a wide range of substrates, including wood, glass, paper, metals, and plastics (2–4,44,110,112–115). These coatings serve to protect surfaces from scratches and chemical exposure, to provide decoration and color, and to allow modification of surface properties. At present, most coatings are applied as a liquid monomer formulation and then photopolymerized; however, photocurable powder coatings are being developed and are expected to have a huge impact in metal-, paper-, and wood-coating applications (2,4). Free radically photopolymerized adhesives provide bonding between laminates, such as glass panes or plastic films. Pressure-sensitive adhesives and release coatings are used to make tapes, labels, and stickers (116,117). Photocurable inks are used on packaging materials and magazines, and photocurable varnishes provide glossy coatings for graphic media.

Optics and Photoimaging. Advanced applications of free-radical photopolymerizations include development of optical devices (118–120). The rapid reaction rates afforded by free-radical photopolymerizations have been able to incorporate liquid crystal order in polymers used for displays, waveguides, and holographic gratings (121,122). Films and coatings for optical components, optical fibers, and eyeglasses also benefit from the flexibility and transparency of these photopolymer materials. In the optical fiber industry alone, several photopolymer coatings are used (123–126). A soft, rubbery primary coating is applied to glass fibers as a cushion against stresses and as a barrier against moisture. A hard secondary coating is applied over the primary coating to prevent damage to the fiber during use. Photoimaging techniques are based on the advantage of spatial control over photoinitiation. This has led to tremendous growth in holographic and lithographic applications and even to rapid prototyping of three-dimensional parts through stereolithography (3,127,128). Patterns for gratings, printed circuit boards, and integrated circuits may be created in photoimageable or photoresist materials using photomasks or computer-controlled lasers (129,130). Microlithography can also be used to develop photopolymer membranes on microfluidic chips to perform chemical separations (131,132).

Biomaterials. In recent years, photopolymerizations have become more prominent in biological applications because these systems can provide superior

products with rapid reaction rates at room temperature. Photopolymerizations for biological applications are more challenging because of the numerous considerations with regard to safety and health. For example, resin formulations and final products must have zero toxicity when introducing these systems into a biological system. Since the migration of small molecules may cause health problems, high conversions of monomer and low concentrations of residual photoinitiator are desirable. When photopolymerizations are conducted *in vivo*, the formulations must be polymerizable by visible light (to prevent cellular damage), and the reactions must not be hampered by atmospheric oxygen or high water concentrations. If the polymers are designed to biodegrade, then the degradation products themselves must not cause health complications (see BIODEGRADABLE POLYMERS, MEDICAL APPLICATIONS). In addition, polymers that will be used *in vivo* must be biocompatible, as well as sterilizable (133). Scaffolding for bone and tissue engineering (qv), bioadhesives for wound closure, and microchips for biochemical analysis are examples of biomaterials produced using free-radical photopolymerizations (134,139).

Hydrogels. Free-radical photopolymerization can be used to produce cross-linked hydrophilic polymer networks that have numerous applications as biomaterials. These hydrogels (qv) are insoluable, but can swell with water to produce soft polymers that have mechanical integrity. Biomedical applications of hydrogels include delivery systems for drugs, enzymes and proteins (140–143); wound dressings (133); and biosensors for detection of glucose and other bioproducts (144). Soft contact lenses are optically transparent hydrogels produced by photopolymerization of mono- and dimethacrylates in a mold (145,146).

Dental Composites. Photopolymers are quickly replacing traditional amalgams for the repair of tooth caries and defects (147) (see DENTAL APPLICATIONS). The photopolymers may be matched to the color of the tooth, and treatment does not require the cutting away of natural tooth structures for bonding. A resin adhesive, which contains a mono-(meth)acrylate as a reactive diluent and a multi-(meth)acrylate as a cross-linker, is applied to the prepped tooth to provide a bond between the tooth and filling. The resin composite, which contains multi-(meth)acrylates for cross-linking and silica fillers to reduce shrinkage stresses, is photopolymerized in incremental layers upon the adhesive base to form the tooth filling. Both the adhesive and composite resins use a visible light free-radical photoinitiator system (camphorquinone with an amine co-initiator) with a blue light source (139,148). Photopolymerization of each layer takes place in less than one minute.

BIBLIOGRAPHY

"Photopolymerization and Photocross-linking" in *EPST* 1st ed., Vol. 10, pp. 145–156, by G. Oster, Mount Sinai School of Medicine; "Photopolymerization" in *EPSE* 2nd ed., Vol. 11, pp. 186–212, by S. P. Pappas, North Dakota State University.

1. A. B. Scranton, *RadTech Rep.* **13**(6), 36 (1999).
2. K. Lawson, *RadTech Rep.* **13**(6), 32 (1999).
3. J. P. Fouassier, *Photoinitiation, Photopolymerization, and Photocuring: Fundamentals and Applications*, Hanser Publishers, New York, 1995.
4. J. V. Koleske, *Radiation Curing of Coatings*, ASTM International, West Conshohocken, Pa., 2002.

5. C. Decker, *Macromol. Rapid Commun.* **23**, 1067 (2002).
6. C. G. Roffey, *Photopolymerization of Surface Coatings*, John Wiley & Sons, Inc., New York, 1982.
7. M. Kaur and A. K. Srivastava, *J. Macromol. Sci., Polym. Rev. C* **42**, 481 (2002).
8. N. S. Allen, *J. Photochem. Photobiol. A* **100**, 101 (1996).
9. H. J. Hageman, *Prog. Org. Coat.* **13**, 123 (1985).
10. B. M. Monroe and G. C. Weed, *Chem. Rev.* **93**, 435 (1993).
11. H. F. Gruber, *Prog. Polym. Sci.* **17**, 953 (1992).
12. J. Jakubiak and J. F. Rabek, *Polimery* **44**, 447 (1999).
13. K. Dietliker, in J. P. Fouassier and J. F. Rabek, eds., *Radiation Curing in Polymer Science and Technology, Vol. II: Photoinitiating Systems*, Elsevier Applied Science, New York, 1993.
14. M. Hamity and J. C. Scaiano, *J. Photochem.* **4**, 229 (1975).
15. J. Segurola, N. Allen, M. Edge, A. Parrondo, and I. Roberts, *J. Photochem. Photobiol. A* **122**, 115 (1999).
16. J. P. Fouassier, D. Ruhlmann, B. Graff, and F. Wieder, *Prog. Org. Coat.* **25**, 169 (1995).
17. G. Rist, A. Borer, K. Dietliker, V. Desobry, J. P. Fouassier, and D. Ruhlmann, *Macromolecules* **25**, 4182 (1992).
18. T. L. Marino, D. Martin, and D. C. Neckers, *Adhes. Age* **38**, 22 (1995).
19. M. Bendyk, B. Jedrzejewska, J. Paczkowski, and L. Linden, *Polimery* **47**, 654 (2002).
20. K. Kawamura, Y. Aotani, and H. Tomioka, *J. Phys. Chem. B* **107**, 4579 (2003).
21. K. S. Padon and A. B. Scranton, *Recent Res. Dev. Polym. Sci.* **3**, 369 (1999).
22. K. S. Padon and A. B. Scranton, *J. Polym. Sci., Part A: Polym. Chem.* **38**, 2057 (2000).
23. K. S. Padon and A. B. Scranton, *J. Polym. Sci., Part A: Polym. Chem.* **39**, 715 (2001).
24. C. Grotzinger, D. Burget, P. Jacques, and J. P. Fouassier, *Polymer* **44**, 3671 (2003).
25. R. S. Davidson, *J. Photochem. Photobiol., A* **73**, 81 (1993).
26. A. B. Scranton, G. A. Miller, L. Gou, and M. El-Maazawi, in *RadTech 2002 Conference Proceedings*, Indianapolic, IN, Apr. 2002, p. 130.
27. C. Carlini and L. Angiolini, *Adv. Polym. Sci.* **123**, 127 (1995).
28. T. Corrales, F. Catalina, C. Peinado, and N. S. Allen, *J. Photochem. Photobiol., A* **159**, 103 (2003).
29. N. Kizilcan and A. Akar, *J. Appl. Polym. Sci.* **85**, 500 (2002).
30. A. M. Sarker, K. Sawabe, B. Strehmel, Y. Kaneko, and D. C. Neckers, *Macromolecules* **32**, 5203 (1999).
31. R. Francis and A. Ajayaghosh, *Macromolecules* **33**, 4699 (2000).
32. N. Kizilcan, *J. Appl. Polym. Sci.* **72**, 927 (1999).
33. G. Odian, *Principles of Polymerization*, 3rd ed., John Wiley & Sons, Inc., New York, 1991.
34. H. S. Taylor and A. A. Vernon, *J. Am. Chem. Soc.* **53**, 2527 (1931).
35. C. W. Miller, E. S. Jönsson, C. E. Hoyle, K. Viswanathan, and E. J. Valente, *J. Phys. Chem. B* **105**, 2707 (2001).
36. S. Jönsson, K. Viswanathan, C. E. Hoyle, S. C. Clark, C. Miller, F. Morel, and C. Decker, *Nucl. Instrum. Methods Phys. Res., Sect. B* **151**, 268 (1999).
37. S. Jönsson, P. E. Sundell, M. Shimose, S. Clark, C. Miller, F. Morel, C. Decker, and C. E. Hoyle, *Nucl. Instrum. Methods Phys. Res., Sect. B* **131**, 276 (1997).
38. C. Decker, F. Morel, S. Jönsson, S. Clark, and C. Hoyle, *Macromol. Chem. Phys.* **200**, 1005 (1999).
39. P. Kohli, A. B. Scranton, and G. J. Blanchard, *Macromolecules* **31**, 5681 (1998).
40. M. P. Patel, M. Braden, and K. W. M. Davy, *Biomaterials* **8**, 53 (1987).
41. J. Stansbury, and J. Ge, *RadTech Rep.* **17**(3), 56 (2003).
42. W. D. Cook, D. R. Derrick, and M. J. Tyas, *Biomaterials* **6**, 362 (1985).
43. C. Decker, *Prog. Polym. Sci.* **21**, 593 (1996).

44. U.S. Pat. 4,999,216 (Aug. 21, 1989), J. Gaske, J. J. Krajewski, and G. K. Noren (to Desoto, Inc.).
45. N. B. Cramer, J. P. Scott, and C. N. Bowman, *Macromolecules* **35**, 5361 (2002).
46. N. B. Cramer, T. Davies, A. K. O'Brien, and C. N. Bowman, *Macromolecules* **36**, 4631 (2003).
47. N. B. Cramer and C. N. Bowman, *J. Polym. Sci., Part A: Polym. Chem.* **39**, 3311 (2001).
48. L. Lecamp, F. Houllier, B. Youssef, and C. Bunel, *Polymer* **42**, 2727 (2001).
49. L. V. Natarajan, C. K. Shepherd, D. M. Brandelik, R. L. Sutherland, S. Chandra, V. P. Tondiglia, D. Tomlin, and T. J. Bunning, *Chem. Mater.* **15**, 2477 (2003).
50. B. Chiou and S. A. Khan, *Macromolecules* **30**, 7322 (1997).
51. I. R. Bellobono and M. Zeni, *Makromol. Chem., Rapid Commun.* **7**, 733 (1986).
52. L. Villegas, M. V. Encinas, A. M. Rufs, C. Bueno, S. Bertolotti, and C. M. Previtali, *J. Polym. Sci., Part A: Polym. Chem.* **39**, 4074 (2001).
53. C. García, A. Fimia, and I. Pascual, *Appl. Phys. B: Lasers Opt.* **72**, 311 (2001).
54. H. Yao, M. Huang, Z. Chen, L. Hou, and F. Gan, *Mater. Lett.* **56**, 3 (2002).
55. L. A. White, C. E. Hoyle, S. Jonsson, and L. J. Mathias, *J. Polym. Sci., Part A: Polym. Chem.* **40**, 694 (2002).
56. U.S. Pat. 5,459,175 (Oct. 17, 1995), J. G. Woods, M. A. Rakas, A. F. Jacobine, L. M. Alberino, P. L. Kropp, D. M. Sutkaitis, D. M. Glaser, and S. T. Nakos (to Loctite Corp.).
57. J. Lub, D. J. Broer, and P. van de Witte, *Prog. Org. Coat.* **45**, 211, 2002.
58. D. J. Broer, J. A. M. M. van Haaren, P. van de Witte, and C. Bastiaansen, *Macromol. Symp.* **154**, 1 (2000).
59. J. Jakubiak and J. F. Rabek, *Polimery* **45**, 485 (2000).
60. H. J. Hageman, F. P. B. van der Maeden, and P. C. G. M. Janssen, *Makromol. Chem.* **180**, 2531 (1979).
61. J. D. Ingle Jr., and S. R. Crouch, *Spectrochemical Analysis*, Prentice Hall, New Jersey 1988, pp. 21.
62. G. A. Miller, L. Gou, V. Narayanan, and A. B. Scranton, *J. Poly. Sci., Part A: Polym. Chem.* **40**, 793 (2002).
63. G. Terrones and A. J. Pearlstein, *Macromolecules* **34**, 8894 (2001).
64. M. D. Goodner and C. N. Bowman, *Chem. Eng. Sci.* **57**, 887 (2002).
65. E. A. Lissi and A. Zanocco, *J. Polym. Sci., Part A: Polym. Chem.* **21**, 2197 (1983).
66. A. R. Shultz and M. G. Joshi, *J. Polym. Sci., Part B: Polym. Phys.* **22**, 1753 (1984).
67. K. A. Berchtold, B. Hacioğlu, L. Lovell, J. Nie, and C. N. Bowman, *Macromolecules* **34**, 5103 (2001).
68. J. F. Rabek, in J. P. Fouassier and J. F. Rabek, eds., *Radiation Curing in Polymer Science and Technology, Vol. I: Photoinitiating Systems*, Elsevier Applied Science, New York, 1993.
69. E. Andrzejewska, M. B. Bogacki, and M. Andrzejewski, *Macromol. Theory Simul.* **10**, 842 (2001).
70. I. V. Khudyakow, J. C. Legg, M. B. Purvis, and B. J. Overton, *Ind. Eng. Chem. Res.* **38**, 3353 (1999).
71. Q. Yu, S. Nauman, J. P. Santerre, and S. Zhu, *J. Appl. Polym. Sci.* **82**, 1107 (2001).
72. L. Lecamp, B. Youssef, C. Bunel, and P. Lebaudy, *Nucl. Instrum. Methods Phys. Res., Sect. B* **151**, 285 (1999).
73. M. Jöhnck, L. Müller, A. Neyer, and J. W. Hofstraat, *Polymer* **40**, 3631 (1999).
74. G. Mailhot and M. Bolte, *J. Photochem. Photobiol. A* **56**, 387 (1991).
75. B. Hacioğlu, K. A. Berchtold, L. G. Lovell, J. Nie, and C. N. Bowman, *Biomaterials* **23**, 4057 (2002).
76. L. Cokbaglan, N. Arsu, Y. Yagci, S. Jockusch, and N. J. Turro, *Macromolecules* **36**, 2649 (2003).

77. C. Decker, F. Masson, and R. Schwalm, *Macromol. Mater. Eng.* **288**, 17 (2003).
78. S. M. Keeny III, J. M. Antonucci, F. W. Wang, and J. A. Tesk, in S. W. Shalaby, Y. Ikada, R. Langer, and J. Williams, eds., *Polymers of Biological and Biomedical Significance*, American Chemical Society, Washington, D. C., 1994.
79. W. F. Jager, A. A. Volkers, and D. C. Neckers, *Macromolecules* **28**, 8153 (1995).
80. J. Paczkowski and D. C. Neckers, *Macromolecules* **25**, 548 (1992).
81. M. V. Encinas, A. M. Rufs, E. Norambuena, and C. Giannotti, *J. Polym. Sci., Part A: Polym. Chem.* **35**, 3095 (1997).
82. A. Wrzyszczyński, P. Filipiak, G. L. Hug, B. Marciniak, and J. Paczkowski, *Macromolecules* **33**, 1577 (2000).
83. M. V. Encinas, A. M. Rufs, S. Bertolotti, C. M. Previtali, *Macromolecules* **34**, 2845 (2001).
84. H. Dreeskamp and W. U. Palm, in J. P. Fouassier and J. F. Rabek, eds., *Lasers in Polymer Science and Technology: Applications*, Vol. II, CRC Press, Inc., Fla., 1990.
85. U.S. Pat. 6,187,836 (Feb. 13, 2001), J. D. Oxman, M. C. Matthew, and D. W. Jacobs (to 3M Innovative Properties Co.).
86. J. Jakubiak and J. F. Rabek, *Polimery* **46**, 10 (2001).
87. J. S. Young and C. N. Bowman, *Macromolecules* **32**, 6073 (1999).
88. D. L. Kurdikar and N. A. Peppas, *Macromolecules* **27**, 4084 (1994).
89. T. M. Lovestead, A. K. O'Brien, and C. N. Bowman, *J. Photochem. Photobiol., A* **159**, 135 (2003).
90. C. J. Hawker, *Acc. Chem. Res.* **30**, 373 (1997).
91. B. de Boer, H. K. Simon, M. P. L. Werts, E. W. van der Vegte, and G. Hadziioannou, *Macromolecules* **33**, 349 (2000).
92. R. Krishnan and K. S. V. Srinivasan, *Macromolecules* **36**, 1769 (2003).
93. Y. You, C. Hong, R. Bai, C. Pan, and J. Wang, *Macromol. Chem. Phys.* **203**, 477 (2002).
94. J. H. Ward, A. Shahar, and N. A. Peppas, *Polymer* **43**, 1745 (2002).
95. T. Otsu, *J. of Polym. Sci., Part A: Polym. Chem.* **38**, 2121 (2000).
96. T. A. von Werne, D. S. Germack, E. C. Hagberg, V. V. Sheares, C. J. Hawker, and K. R. Carter, *J. Am. Chem. Soc.* **125**, 3831 (2003).
97. A. Ajayaghosh and R. Francis, *J. Am. Chem. Soc.* **121**, 6599 (1999).
98. G. David, F. Özer, B. C. Simionescu, H. Zareie, and E. Pişkin, *Eur. Polym. J.* **38**, 73 (2002).
99. P. Kuo, N. J. Turro, C. Tseng, M. S. El-Aasser, and J. W. Vanderhoff, *Macromolecules* **20**, 1216 (1987).
100. I. Capek, *Eur. Polym. J.* **36**, 255 (2000).
101. N. K. Pokhriyal, P. G. Sanghvi, D. O. Shah, and S. Devi, *Langmuir* **16**, 5864 (2000).
102. I. Capek, *Polym. J.* **28**, 400 (1996).
103. L. Wang, X. Liu, and Y. Li, *Macromolecules* **31**, 3446 (1998).
104. I. Capek and J. P. Fouassier, *Eur. Polym. J.* **33**, 173 (1997).
105. C. L. Lester, C. D. Colson, and C. A. Guymon, *Macromolecules* **34**, 4430 (2001).
106. A. Stohr and P. Strohriegl, *Macromol. Chem. Phys.* **199**, 751 (1998).
107. R. Vabrik, I. Czajlik, G. Túry, I. Rusznák, A. Ille, and A. VíG, *J. Appl. Polym. Sci.* **68**, 111 (1998).
108. C. Decker, T. Nguyen Thi Viet, D. Decker, and E. Weber-Koehl, *Polymer* **42**, 5531 (2001).
109. S. Peeters, in J. P. Fouassier and J. F. Rabek, eds., *Radiation Curing in Polymer Science and Technology, Vol. III: Photoinitiating Systems*, Elsevier Applied Science, New York, 1993.
110. C. Bradford, *RadTech Rep.* **13**(6), 19 (1999).

111. D. Harbourne, *RadTech Rep.* **13**(6), 16 (1999).
112. U.S. Pat. 5,888,649 (Aug. 15, 1997), B. S. Curatolo and T. J. Fox (to Avery Dennison Corp.).
113. U.S. Pat. 2002/0143078 A1 (Apr. 3, 2001), M. Awokola, C. Flosbach, H. Loeffler, and V. Paschmann (to E. I. du Pont de Nemours & Co.).
114. U.S. Pat. 2002/0164434 A1 (Sep. 13, 1999), M. Tarvin and M. A. Rau.
115. R. J. Modjewski, *RadTech Rep.* **13**(3), 45 (1999).
116. T. Ozawa, S. Ishiwata, and Y. Kano, *Furukawa Rev.* **20**, 83 (2001).
117. J.-M. Frances, S. Kerr III, and O. Pinto, *Radiat. Curing* **45**(1), 30 (2002).
118. P. Cheben, *Appl. Phys. Lett.* **78**, 1490 (2001).
119. A. Pu and D. Psaltis, *Appl. Opt.* **35**, 2389 (1996).
120. M. L. Schilling, V. L. Colvin, L. Dhar, A. L. Harris, F. C. Schilling, H. E. Katz, T. Wysocki, A. Hale, L. L. Blyler, and C. Boyd, *Chem. Mater.* **11**, 247 (1999).
121. K. Saravanamuttu, X. M. Du, S. I. Najafi, and M. P. Andrews, *Can. J. Chem.* **76**, 1717 (1998).
122. R. Bachelot, C. Ecoffet, D. Deloeil, P. Royer, and D. Lougnot, *Appl. Opt.* **40**, 5860 (2001).
123. J. Zhang, G. Windall, and I. W. Boyd, *Appl. Surface Sci.* **186**, 568 (2002).
124. U.S. Pat. 5,985,952 (Mar. 23, 1998), A. C. Levy (to Alvin C. Levy & Associates, Inc. and Master Adhesives, Inc.).
125. U.S. Pat. 20030100627 A1 (Oct. 9, 2001), T. E. Bishop, P. E. Snowwhite, T. Norlin, J. J. Schouten, J. Southwell, and A. Toussaint (to Pillsbury Winthrop, LLP).
126. U.S. Pat. 6,326,416 (Dec. 30, 1999), C. Chien, E. J. Fewkes, G. F. Jacobs, K. R. Jones, E. H. Urruti, and M. J. Winningham (to Corning, Inc.).
127. U.S. Pat. 5,972,563 (Jul. 28, 1997), B. Steinmann and A. Schulthess (to Ciba Specialty Chemicals Corp.).
128. U.S. Pat. 6,207,347 (Apr. 29, 1999), D. L. Lundy and N. J. Negandhi (to Nichigo-Morton Co. Ltd.).
129. J. Sturge, V. Walworth, and A. Shepp, eds., *Imaging Processes and Materials, Neblette's*, 8th ed., Van Nostrand Reinhold, New York, 1989.
130. U.S. Pat. 5,952,154 (May 29, 1998), R. Barr, D. Lundy, and S. Wheeler (to Morton International, Inc.).
131. C. Yu, M. Xu, F. Svec, and J. M. J. Fréchet, *J. Polym. Sci., Part A: Polym. Chem.* **40**, 755 (2002).
132. C. Yu, F. Svec, and J. M. J. Fréchet, *Electrophoresis* **21**, 120 (2000).
133. J. M. Rosiak and F. Yoshii, *Nucl. Instrum. Methods Phys. Res., Sect. B* **151**, 56 (1999).
134. D. L. Elbert and J. A. Hubbell, *Biomacromolecules* **2**, 430 (2001).
135. A. K. Burkoth and K. S. Anseth, *Biomaterials* **21**, 2395 (2000).
136. J. Elisseeff, W. McIntosh, K. Anseth, S. Riley, P. Ragan, and R. Langer, *J. Biomed. Mater. Res.* **51**, 164 (2000).
137. R. S. Benson, *Nucl. Instrum. Methods Phys. Res., Sect. B* **191**, 752 (2002).
138. M. N. Cooke, J. P. Fisher, D. Dean, C. Rimnac, and A. G. Mikos, *J. Biomed. Mater. Res. Part B: Appl. Biomater.* **64B**, 65 (2002).
139. J. A. Burdick, A. J. Peterson, and K. S. Anseth, *Biomaterials* **22**, 1779 (2001).
140. D. N. Robinson and N. A. Peppas, *Macromolecules* **35**, 3668 (2002).
141. N. P. Desai, A. Sojomihardjo, Z. Yao, N. Ron, and P. Soon-Shiong, *J. Microencapsul.* **17**, 677 (2000).
142. M. Kurisawa, Y. Matsuo, and M. Yui, *Macromol. Chem. Phys.* **199**, 705 (1998).
143. P. Ulanski, I. Janik, S. Kadlubowski, M. Kozicki, P. Kujawa, M. Pietrzak, P. Stasica, and J. M. Rosiak, *Polym. Adv. Technol.* **13**, 951 (2002).
144. K. Sirkar and M. V. Pishko, *Anal. Chem.* **70**, 2888 (1998).

145. EP Pat. 0447169 (Sep. 18, 1991), V. Mcbrierty, J. Magan, and W. Blau (to Bausch & Lomb (US)).
146. U.S. Pat. 6,031,059 (Feb. 29 2000), D. G. Vanderlaan, F. Molock, and G. Fruzzetti (to Johnson & Johnson Vision Products, Inc.).
147. L. G. Lovell, H. Lu, J. E. Elliott, J. W. Stansbury, and C. N. Bowman, *Dent. Mater.* **17**, 504 (2001).
148. J. Nie, L. Å. Lindén, J. F. Rabek, J. P. Fouassier, F. Morlet-Savary, F. Scigalski, A. Wrzyszczynski, and E. Andrzejewska, *Acta Polym.* **49**, 145 (1998).

YING CAI
JULIE L. P. JESSOP
University of Iowa

PHOTORESISTS. See LITHOGRAPHC RESISTS.

PIEZOELECTRIC POLYMERS. See Volume 3.

PLASTICIZERS. See Volume 3.

PLASTICS PROCESSING

Introduction

Plastics are classified as thermoplastic or thermosetting resins, depending on the effect of heat. Thermoplastic resins, when heated during processing, soften and flow as viscous liquids; when cooled, they solidify. The heating/cooling cycle can be repeated many times with little loss in properties. Thermosetting resins liquefy when heated and solidify with continued heating; the polymer undergoes permanent cross-linking and retains its shape during subsequent cooling/heating cycles (see THERMOSETS). Thus, a thermoset cannot be reheated and molded again. However, thermoplastics can be melt-reprocessed, and hence readily recycled (see RECYCLING, PLASTICS).

Thermoplastic Resins. Almost 85% of the resins produced are thermoplastics (1,2). Although a number of chemically different types of thermoplastics are available in the market, they can be divided into two broad classes: amorphous and crystalline. Amorphous thermoplastics shown in Table 1 (3) are characterized by their glass-transition temperature T_g a temperature above which the modulus decreases rapidly and the polymer exhibits liquid-like properties; amorphous thermoplastics are normally processed at temperatures well above their T_g (see AMORPHOUS POLYMERS). Semicrystalline resins shown in Table 2 (3) can have different degrees of crystallinity ranging from 50 to 95%; they are normally processed above the melting point T_m of the crystalline phase (see SEMICRYSTALLINE POLYMERS). Upon cooling, crystallization must occur quickly, ie, in a few seconds. Addition of nucleating agents increases the crystallization rate (see CRYSTALLIZATION KINETICS). Additional crystallization often takes place after cooling and during the first few hours following melt processing.

Over 70% of the total volume of thermoplastics is accounted for by the commodity resins: polyethylene, polypropylene, polystyrene, and poly(vinyl

Encyclopedia of Polymer Science and Technology. Copyright John Wiley & Sons, Inc. All rights reserved.

Table 1. Glass-Transition Temperature of Amorphous Thermoplastics[a]

Polymer	T_g, °C
Polyamideimide (PAI)	295
Polyethersulfone (PES)	230
Polyarylsulfone (PAS)	220
Polyethermide (PEI)	218
Polyarylate (PAR)	198
Polysulfone (PSU)	190
Polyamide, amorphous (PA)	155
Polycarbonate (PC)	145
Styrene–maleic anhydride (SMA)	122
Chlorinated PVC (CPVC)	107
Poly(methyl methacrylate) (PMMA)	105
Styrene–acrylonitrile (SAN)	104
Polystyrene (PS)	100
Acrylonitrile–butadiene–styrene (ABS)	100
Poly(ethylene terephthalate) (PET)	67
Poly(vinyl chloride) (PVC)	65

[a] Ref. 3.

chloride) (PVC) (1) (see ETHYLENE POLYMERS, HDPE; ETHYLENE POLYMERS, LDPE; ETHYLENE POLYMERS, LLDPE; PROPYLENE POLYMERS (PP); STYRENE POLYMERS; VINYL CHLORIDE POLYMERS). They are made in a variety of grades and because of their low cost are the first choice for a variety of applications. Next in performance and in cost are acrylics, cellulosics, and acrylonitrile–butadiene–styrene (ABS)

Table 2. Melting Temperature of Semicrystalline Thermoplastics[a]

Polymer	T_m, °C
Polyetherketone (PEK)	365
Polyetheretherketone (PEEK)	334
Polytetrafluoroethylene (PTFE)	327
Poly(phenylene sulfide) (PPS)	285
Liquid crystal polymer (LCP)	280
Nylon-6,6[b]	265
Poly(ethylene terephthalate) (PET)	260
Nylon-6[b]	220
Nylon-6,12[b]	212
Nylon-11[b]	185
Nylon-12[b]	178
Acetal resin[c]	175
Polypropylene (PP)	170
High density polyethylene (HDPE)	135
Low density polyethylene (LDPE)	112

[a] Ref. 3.
[b] Nylons are polyamides (qv).
[c] Acetal resin in polyoxymethylene (POM).

terpolymers (see ACRYLIC ESTER POLYMERS; ACRYLONITRILE AND ACRYLONITRILE POLYMERS; CELLULOSE ESTERS, INORGANIC). Engineering thermoplastics (qv) such as acetal resins, polyamides (qv), polycarbonates (qv), thermoplastic polyesters (qv), and poly(phenylene sulfide), and advanced materials such as liquid crystal polymers, polysulfones (qv), and polyetheretherketones are used in high performance applications; they are processed at higher temperatures than their commodity counterparts.

With few exceptions, thermoplastics are marketed in the form of pellets. They are shipped in containers of various sizes, from 25-kg bags to railroad hopper cars. Resins are conveyed to silos for storage and from there to the processing equipment. Colored resins are available, but frequently it is more convenient and economical to buy uncolored resins and blend them with color concentrates. Using concentrates avoids handling dusty pigments and ensures uniform color distribution.

The packaging requirements for shipping and storage of thermoplastic resins depend on the moisture that can be absorbed by the resin and its effect when the material is heated to processing temperatures. Excess moisture may result in undesirable degradation during melt processing and inferior properties. Condensation polymers such as nylons and polyesters need to be specially predried to very low moisture levels (4,5), ie, less than 0.2% for nylon-6,6 and as low as 0.005% for poly(ethylene terephthalate) (PET), which hydrolyzes faster.

Thermoplastic Processing. A variety of processing equipment and shaping methods are available to fabricate the desired thermoplastic product (6–10). Extrusion (qv) is the most popular. Approximately 50% of all commodity thermoplastics are used in extrusion process equipment to produce profiles, pipe and tubing, film, sheet, wire, and cable (1). Injection molding (qv) follows as a preferred processing method, accounting for about 15% of all commodity thermoplastics. Other common methods include blow molding (qv), rotational molding (qv), thermoforming (qv), calendering, and, to some extent, compression molding. Details on the amounts of resins converted annually in the United States in terms of processes and products can be found in the following year's January issue of *Modern Plastics*. Computer-aided design software for molds and extruder screws is commercially available. These programs assist in the selection and fabrication of processing equipment, thereby saving research and development time. Modeling and simulation of polymer processing is described in specialized textbooks (11–17).

The range of processes that may be used for fabricating a plastics product is determined by the scale of production, the cost of the machine and the mold, and the capabilities and limitations of the individual processes. For example, complex and precise shapes can be achieved by injection molding, hollow objects via blow molding and rotational molding, and continuous lengths by extrusion.

Thermoplastics processing operations produce emissions into the air, wastewater, and solid waste resulting from both polymers and additives. Most important are volatile organic compounds emitted from heated cylinders and molds. The identification of such volatiles and the development of analytical techniques for measuring their concentration in the workplace are of paramount importance to establish or revise threshold limit values that would minimize exposure to hazardous chemical substances. Environmental issues in polymer processing are reviewed in References 18 and 19.

Extrusion

Extrusion is defined as continuously forcing a molten material through a shaping device. Because the viscosity of most plastic melts is high, extrusion requires the development of pressure in order to force the melt through a die. Manufacturers of plastic resins generally incorporate stabilizers and modifiers and sell the product in the form of cylindrical, spherical, or cubic pellets of about 2–3 mm in diameter. The end-product manufacturers remelt these pellets and extrude specific profiles, such as film, sheet, tubing, wire coating, or as a molten tube of resin (parison) for blow molding or into molds, as in injection molding.

To provide a homogeneous product, incorporation of any additives, such as antioxidants (qv), colorants (qv), and fillers (qv), requires mixing them into the plastic when it is in a molten state. This is done primarily in an extruder. The extruder, as shown in Figure 1, accepts dry solid feed (F, E, J) and melts the plastic by a combination of heat transfer through the barrel (B, C) and dissipation of work energy from the extruder drive motor (I). In the act of melting, and in subsequent sections along the barrel, the required amount of mixing is usually achieved. Venting may also be accomplished to remove undesirable volatile components, usually under vacuum through an additional deep-channel section and side vent port. The final portion of the extruder (L) is used to develop the pressure [$\leq$50 MPa (7500 psi)] for pumping the homogenized melt through a filtering screen (optional) and then through a shaping die attached to the end of the extruder.

Extruders are defined by their screw diameter and length, with the length expressed in terms of the length-to-diameter ratio (L/D). Single-screw extruders

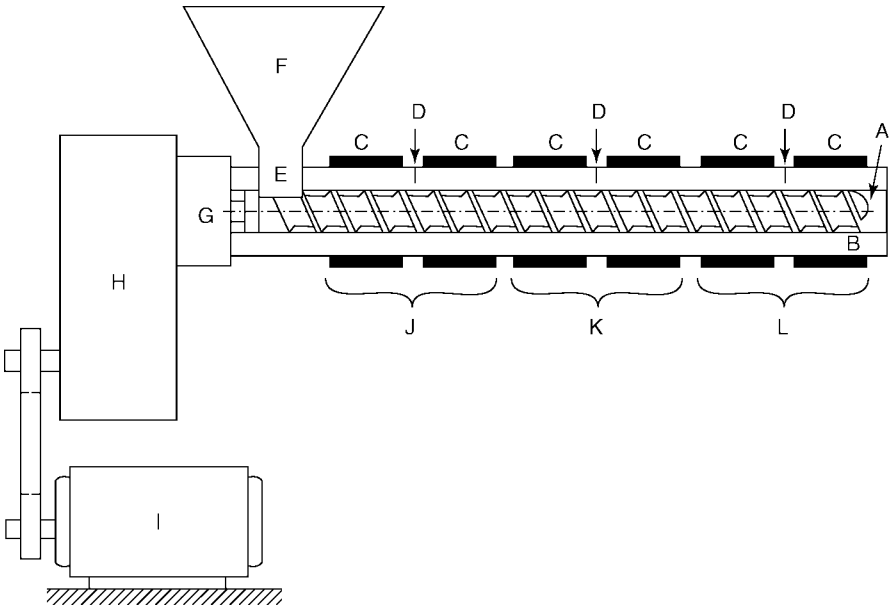

Fig. 1. Parts of an extruder: A, screw; B, barrel; C, heater; D, thermocouple; E, feed throat; F, hopper; G, thrust bearing; H, gear reducer; I, motor; J, deep-channel feed section; K, tapered channel transition section; and L, shallow channel metering section (20).

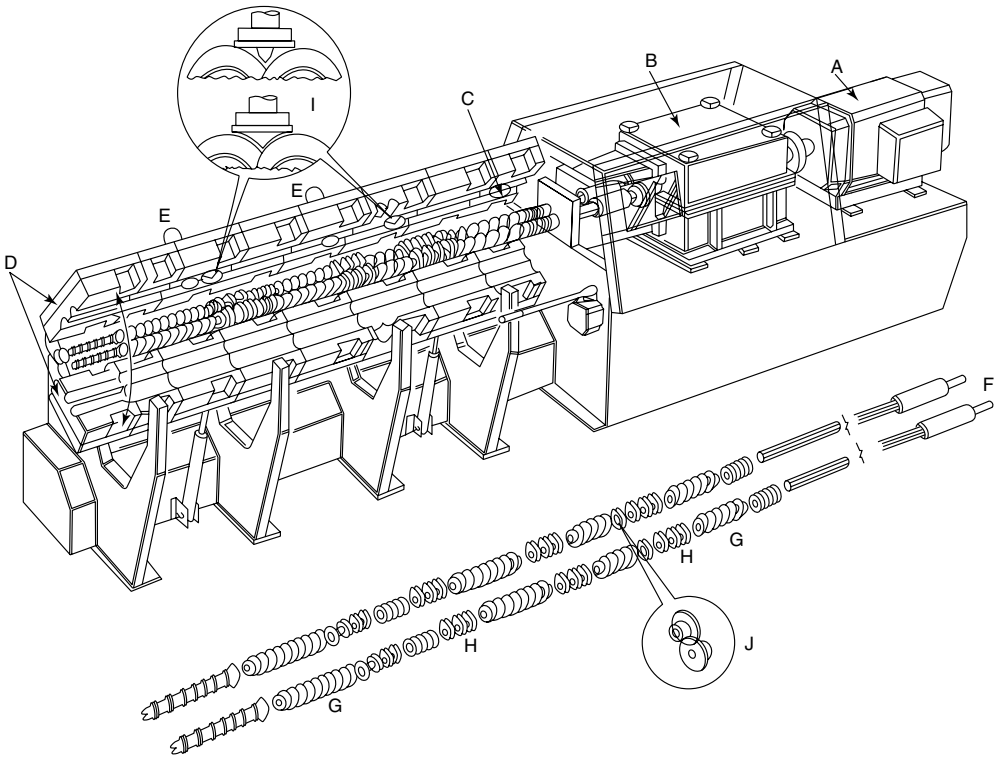

Fig. 2. Intermeshing corotating twin-screw extruder: A, motor; B, gear box; C, feed port; D, clam shell barrel; E, vent port; F, screw shafts; G, conveying screws; H, kneading paddles; I, barrel valve; and J, blister rings. Courtesy of APV Chemical Machinery Inc.

range from small laboratory size (6 mm diameter) to large commercial units (450 mm diameter) capable of processing up to 20 t/h. Melt-fed extruders run at a L/D of about 8; solids-fed extruders run at a L/D of about 20–40 depending on whether intermediate venting is provided.

Varieties of twin-screw extruders are also utilized, particularly when the ingredient mixing requirements are difficult to fulfill or require multiple staging, as in reactive extrusion. Twin-screw extruders are classified as being tangential or intermeshing, and the latter as being counter- or corotating. These extruders are generally supplied with slip-on conveying and kneading screw elements and segmented barrels. These elements, shown in Figure 2, give the processor improved mixing and pumping versatility. Single-screw extruders are usually flood-fed, with the feed rate determined by screw speed. Twin-screw extruders are generally starve-fed. Starve feeding permits greater flexibility in operation as screw speed now becomes a process control variable, independent of feed rate.

Reactive extrusion is the term used to describe the use of an extruder as a continuous reactor for polymerization or polymer modification by chemical reaction (21,22). Extruders are uniquely suitable for carrying out such reactions because of their ability to pump and mix highly viscous materials. Extruders readily permit multiple process steps in a single machine, including melting, metering, mixing, reacting, side-stream addition, and venting.

Recent developments in extrusion equipment include the increased use of microprocessor control systems and a variety of on-line monitoring systems for product quality assurance.

Mechanism of Extruder Operation. An extruder employs drag flow to perform a conveying action that depends on the relative motion between the screw and the barrel. With higher friction on the barrel than on the screw, the solids are conveyed almost as solid plug in the deep-feed channel section. As the channel depth becomes shallower, the compressive action causes more frictional heat, which, combined with the conduction supplied by the barrel heaters, causes the plastic to melt. The molten plastic then enters a constant shallow depth section of the screw called the metering section, where the pumping pressure necessary for extrusion through the final shaping die is developed.

The drag flow or volumetric conveying capability Q_d for the plastic melt is dependent only on screw speed N and the geometry A of the screw:

$$Q_d = AN$$

The drag flow is most easily visualized by unwrapping the screw and dragging a flattened barrel surface diagonally across the channel (Fig. 3).

At the discharge end of the metering section, enough pressure must be generated to overcome the resistance of the transfer piping and the shaping die. This same pressure in effect also causes the plastic melt to want to flow back down the channel and possibly also over the flight tips. This pressure flow Q_p, is dependent on the screw geometry B, pressure driving force ΔP, filled length of the screw L, and melt viscosity μ:

$$Q_p = B\Delta P/\mu L$$

The pressure flow is independent of screw speed, except as the latter affects the viscosity of the melt.

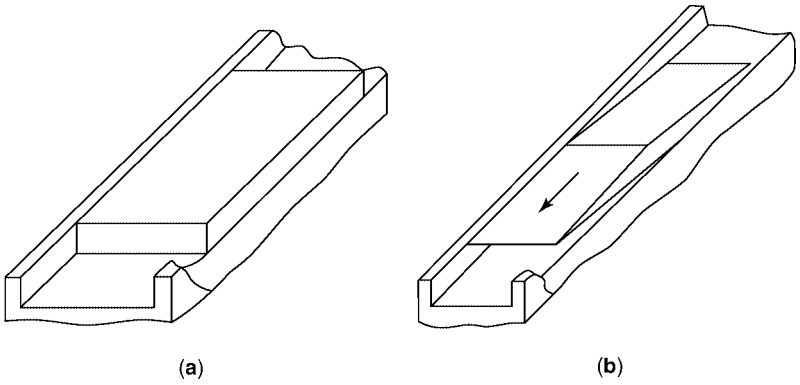

Fig. 3. (**a**) Channel with block of molten plastic; (**b**) channel with moved block of molten plastic; arrow indicates direction of material movement (20).

The net flow Q of an extruder is simply the difference between drag and pressure flows:

$$Q = Q_d - Q_p$$

The pressure and drag flow equations for twin-screw extruders are similar to those expressed above for single-screw extruders but with different geometric constants. The amount being forwarded per revolution (Q_d/N) for fully intermeshing co-rotating twin-screw extruders is one half of the process volume contained in one turn of the screw:

$$Q_d/N = 1.54hDz$$

Where h is the channel depth, D is the screw diameter, and z is the lead length of the screw (23).

Mixing in Extruders. In addition to the conveying and melting steps, extruders perform the vital task of homogenization of additives such as Fillers (qv), stabilizers, and pigments into the base resin (24,25). Incorporation of powdered filters is best accomplished by downstream addition into the barrel after the polymer resin is fully melted. Otherwise, the forces that are generated during melting can cause severe abrasive wear of screws and barrels, and frequently can lead to difficult-to-disperse agglomerates formed by compaction.

If the cross-channel mixing provided by the drag and pressure flows in single-screw extruders is insufficient, various mixing enhancers are available. These generally ensure dispersion by forced passage over a higher shear-restricting slot or an improved distribution by multiple reorientations of flow and sequences of extensional flow.

Mixing in twin-screw extruders benefits from the additional interaction of the two screws with each other as well as with the barrel. Various arrays of kneading paddles are generally used in the most common type, namely the co-rotating, intermeshing, twin-screw extruder. The kneading paddles improve mixing by causing extensive melt reorientation, backmixing, and elongational flow patterns (26).

Further information on extruder operation and plastic processing is available (17,20,27–36). Technology updates and equipment options for specific processing steps are provided annually in publications such as the *Plastics Compounding Redbook* and in *Modern Plastics Encyclopedia*.

Pipe and Tubing. A typical die for extruding tubular products is shown in Figure 4. It is an in-line design, ie, the center of the extruded pipe is concentric with the extruder barrel. The extrudate is formed into a tube by the male and female die parts. The male die part is supported in the center by a spider mandrel. Melt flows around legs of the mandrel and meets on the downstream side. The position of the female die part can be adjusted with bolts; adjustment is required to obtain a tube with a uniform wall thickness.

A vacuum calibrator usually is used for controlled cooling of the tube, as shown in Figure 5. It is a long, closed tank that contains cooling water and uses a vacuum to maintain a constant tube diameter and thickness.

The molten tube enters the tank through a series of cooling rings, and atmospheric pressure inside the tube forces the melt against the rings. The rings

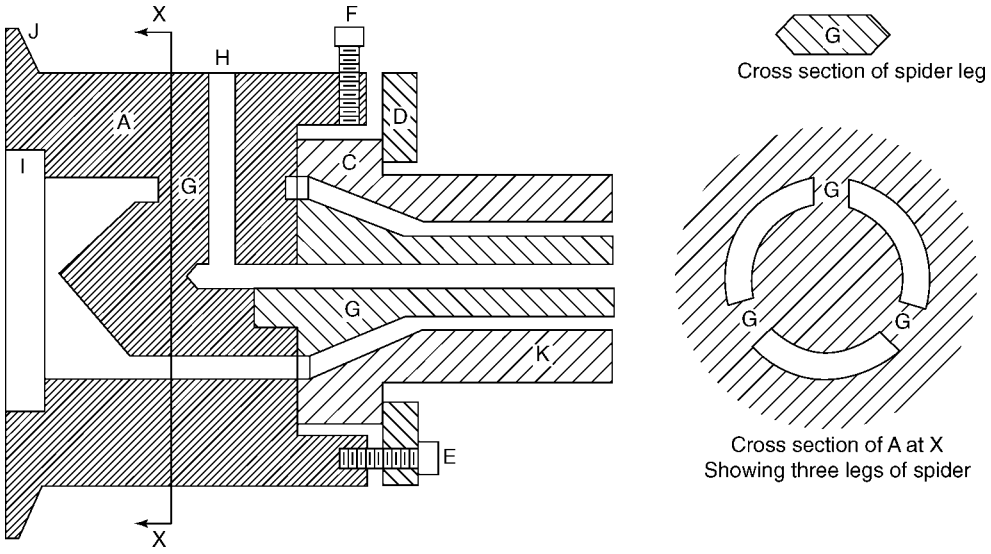

Fig. 4. Pipe or tubing die for in-line extrusion: A, die body; B, mandrel, pin, and male die part; C, die, die bushing, and female part; D, die-retaining ring; E, die-retaining bolt; F, die-centered bolt; G, spider leg; H, air hole; I, seat for breaker plate; J, ring for attachment to extruder; and K, die land (20).

control the expansion of the tube and establish its outside diameters. Water cools the tube and adds strength to it, allowing it to withstand expansion forces. The tube exits the tank through a rubber gasket. A variable-speed takeoff controls the rate at which the tube is pulled through the tank.

Tubing extrusion usually involves drawdown of the resin from the die, ie, the diameter and wall thickness of the tubing are less than that of the die opening. The amount of drawdown is expressed as the ratio of the cross-sectional area of the die opening to the cross-sectional area of the tube wall. Drawdowns in tubing

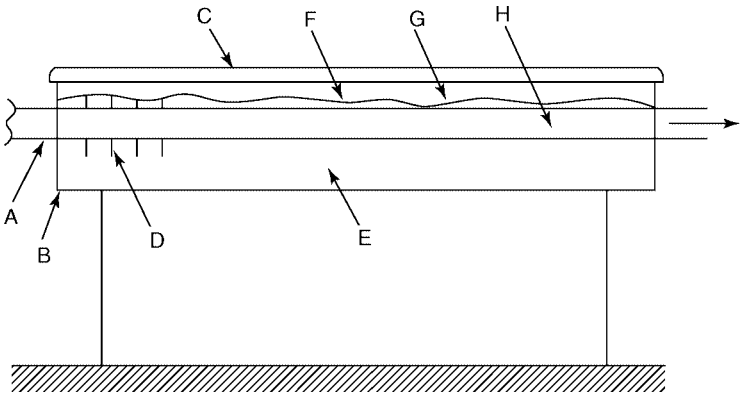

Fig. 5. Vacuum calibrator for pipe and tubing extrusion: A, molten tube from die; B, tank; C, hinged cover with gasket; D, sizing rings; E, circulated and temperature-controlled water; F, water level; G, vacuum; and H, inside of pipe open to atmospheric pressure (20).

extrusion usually range from 2:1 to 8:1. Drawdown in pipe extrusion is often less than 1.1:1. Pipe and tubing may be cut in straight lengths or may be coiled, depending on use and stiffness, eg, polyethylene pipe usually is cut to length, whereas laboratory tubing is coiled. ABS and PVC pipe are made in straight lengths, and soda straws are cut in short lengths.

Pipe extrusion is commonly used in the manufacture of thick-walled products. Die openings are large and resistance to flow is small. Cooling of the pipe is slow because plastics are poor conductors of heat. Long quench tanks and good circulation of cooling water are needed. Low melt temperatures relative to melting or softening points characterize pipe extrusion. Large die openings permit the use of viscous, high molecular weight resins, which yield tougher products.

Profile Extrusion. This method is similar to pipe and tubing extrusion, except that special profile dies are used to produce a variety of asymmetrical products. Typical products include housing siding, window sash molding, decorative trim, plastic lumber, gaskets, and channels. Dies for profile extrusion are designed to allow for shape changes that occur during quenching. Usually, a water trough is used for cooling, but air or cooled metal surfaces are also used. Profile extrusion typically relies on amorphous thermoplastics, such as PVC, ABS, polystyrene, thermoplastic elastomers, etc. The rapid shrinkage accompanying crystallization can result in severe distortion of the profile.

Foam Extrusion. Foamed thermoplastics provide excellent insulating properties because of their very low thermal conductivity, good shape retention, and good resistance to moisture pickup. As such, cylindrical shapes are extruded for pipe insulation, and sheets for building panel insulation. Chemical blowing agents are usually solid powders that can be incorporated into molten plastics without reacting to release their by-product gases until subsequently heated to a higher temperature. Physical blowing agents are dissolved and held in solution by the pressure developed in the extruder (37). As the molten thermoplastic exits the extruder die, the pressure release causes instantaneous foaming. The chlorinated fluorocarbons formerly used as blowing agents have been replaced with more environmentally friendly substitutes, such as hydrochlorofluro carbons (HCFCs) or low molecular weight hydrocarbons such as butane or isopentane. For some thermoplastics, carbon dioxide, nitrogen, or argon can be used (38,39). Critical to the success of most foaming extrusion operations is cooling of the melt just prior to entry to the die. Cooling is most effectively accomplished with a tandem arrangement of two extruders, as shown in Figure 6, wherein the first extruder ensures complete dissolution of the blowing agent, and the second extruder is operated at slow speed for optimum cooling. Additional information on extrusion of foams is contained in References 28,37, and 40 (see CELLULAR MATERIALS).

Film Forming Processes

Blown Film. The blown film process (Fig. 7) uses a tubular die from which the extrudate expands in diameter while traveling upward to a film tower. The top of the tower has a collapsing frame followed by guide and pull rolls to transport the collapsed film to subsequent slitting and windup rolls. The tubular bubble from the die is inflated to the desired diameter by air passing through the center of the

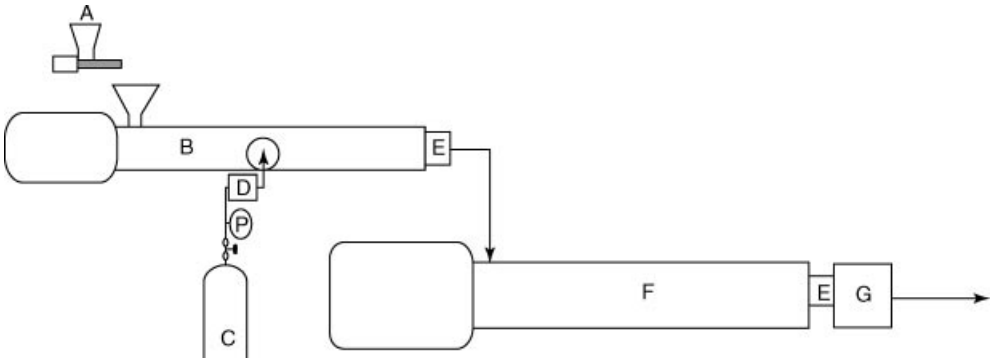

Fig. 6. Foam extrusion line: A, resin feed; B, extruder for melting and gas incorporation; C, gas supply; D, gas metering and compression; E, optical windows; F, cooling extruder; and G, die. P represents a pressure gauge. Courtesy of Polymer Processing Institute.

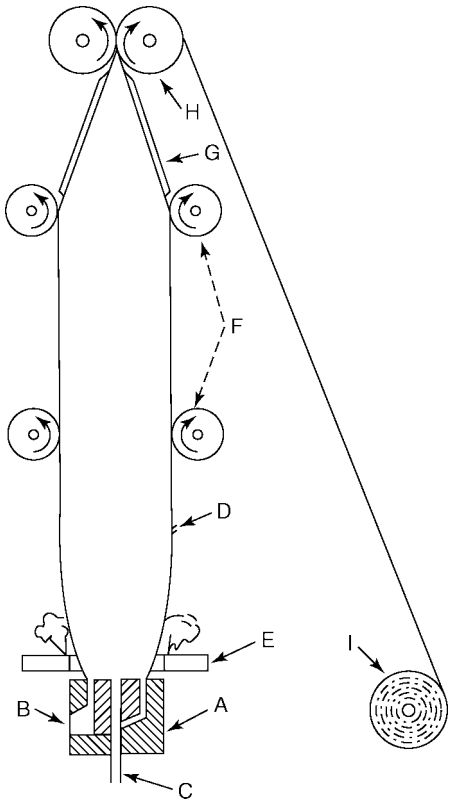

Fig. 7. Extrusion of blown film: A, blown-film die; B, die inlet; C, air hole and valve; D, plastic tube (bubble); E, air ring for cooling; F, guide rolls; G, collapsing frame; H, pull rolls; and I, windup roll (20).

die. Although primary cooling to solidify the melt is supplied by an external air ring, chilled air may also be used internally. Polyethylene is the primary plastic used in most films, especially for packaging and trash bags. Coaxial dies can be used for manufacture of coextruded multilayer films.

The tube is characterized by its blow-up ratio, ie, a larger diameter than the die opening, which is expressed as the ratio of bubble diameter to the die diameter. Typical blow-up ratios range from 2:1 to 4:1. The final film thickness is much thinner than the die gap. Die gaps are slits of ca 0.65 mm. Typical film thicknesses are 0.007–0.125 mm. The process requires a high melt viscosity resin so that the melt can be pulled from the die in an upward direction. Since only air is used for cooling, removal of heat tends to be slow and rate-limiting. Chilled air can also be used internally to improve the efficiency of the air cooling process. The film may be treated for subsequent printing, and it can be slit into various widths and wound onto separate cores.

Cast Film. The cast film process provides a film with gloss and sparkle and can be used with various resins. Figure 8 is an illustration of the essential features of the extrusion equipment. The die opening is a long straight slit with an adjustable gap ca 0.4 mm wide. The die is positioned carefully with respect to the casting roll. The casting or chill roll is highly polished and plated and imparts a smooth and virtually flawless surface to the film. The roll is cooled by rapid circulation of water. Temperature control is critical. A die somewhat longer than the width of the film is needed, because the molten web becomes narrow as it is drawn from the die; this is called neck-in. Edges of the film thicken and are mechanically removed before the film is wound on a roll. The edge trim can be reprocessed.

One of the requirements of this process is that the melt maintain good contact with the chill roll, ie, air must not pass between the film and the roll. Otherwise, air insulates the plastic and causes it to cool at a rate different from the rest of the plastic and this spoils the appearance of an otherwise satisfactory product. The melt should not emit volatiles, which condense on the chill roll, reduce heat

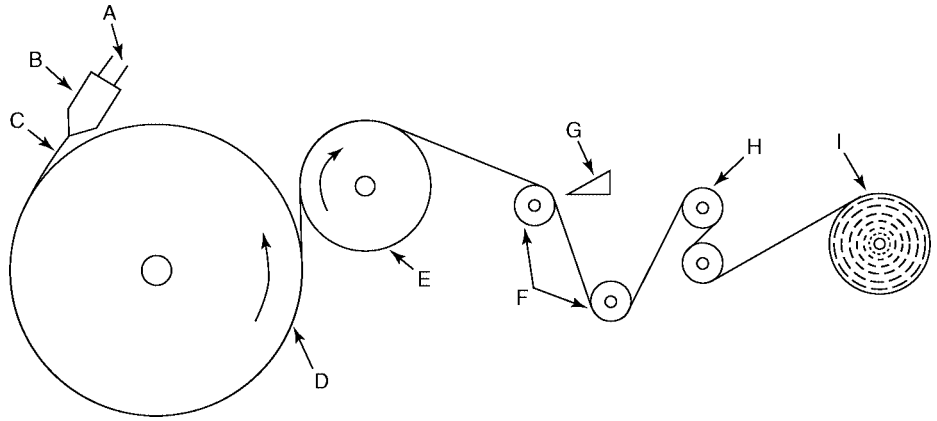

Fig. 8. Extrusion of roll-cast film: A, die inlet; B, cast-film die; C, air gap with molten web; D, casting roll; E, stripping roll; F, idler roll; G, edge-trim slitter; H, pull rolls; and I, windup roll (20).

transfer, and mar the film's appearance. The cast film process allows the use of a higher melt temperature than is characteristic of the blown film process. The higher temperature imparts better optical properties.

Film stretching is a process to impart biaxial orientation in the film by stretching it in two directions simultaneously, the transverse and machine directions, respectively. The process is carried out in a device that grips the edges of the film and extends them to larger widths as the film moves from the inlet to the exit roller. The objective is to increase the modulus and strength of the film uniformly along the entire film plane. Polypropylene and PET have been used successfully in this process (41).

Sheet. The process used to make an extruded plastic sheet is illustrated in Figure 9. Sheeting thicknesses are 0.25–5 mm and widths are as great as 3 m. Heavier gauge sheets are usually cut to a specified length and are stacked. Cooling is controlled by a three-roll stack. The rolls are 25–50 cm in diameter, highly polished, and chrome-plated. They are cored for cooling with circulating water, and the temperature of each roll is controlled by a circulator and temperature control unit. Often the rolls are operated at high temperature to maximize the gloss of the sheeting surface.

A web of molten plastic is pulled from the die into the nip between the top and middle rolls. At the nip, there is a very small rolling bank of melt. Pressure between the rolls is adjusted to produce sheet of the proper thickness and surface appearance. The necessary amount of pressure depends on the viscosity. For a given width, thickness depends on the balance between extruder output rate and the takeoff rate of the pull rolls. A change in either the extruder screw speed or the pull-roll speed affects thickness. A constant thickness across the sheet requires a constant thickness of melt from the die. The die is equipped with bolts for adjusting the die-gap opening and with an adjustable choker bar or dam located inside the die a few centimeters behind the die opening. The choker bar restricts flow in the center of the die, helping to maintain a uniform flow rate across the entire die width.

Drawdown from the die to nip is typically ca 10%. Sheet extrusion requires that the resin be of high melt viscosity to prevent excessive sag of the melt between

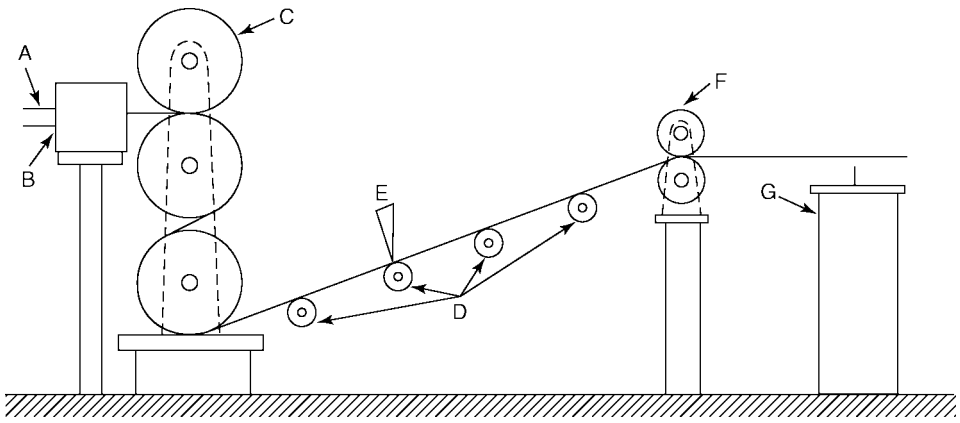

Fig. 9. Sheet extrusion: A, die inlet; B, die; C, three-roll finisher; D, support rollers; E, edge-trim cutter; F, pull rolls; and G, saw or shear (20).

the die and the nip. The melt should reach the nip before touching any other part of the middle roll to prevent uncontrolled cooling of the resin. The appearance of the lower surface of the sheet is determined by the middle roll, ie, its polish, surface temperature, and freedom from condensed materials. The upper surface is cooled by air and has a more glossy appearance. Neither the top roll nor the bottom roll greatly affects the appearance of the top surface of the sheet. Edges of the sheet are trimmed.

Multilayer structures can be formed by simultaneous coextrusion of different layers through a feed block die. The individual layers can be selected for their specific attributes, such as strength, barrier properties, etc, or for incorporation of recycled material. When the basic layers are incompatible, tie layers can also be included to form a cohesive composite structure.

There usually is no need for a high melt temperature to obtain flow through a sheeting die, because die openings are large. Cooling of the sheet is slow because sheeting is thick. Most sheeting is used for thermoforming.

Extrusion Coating. A coating of an appropriate thermoplastic, such as polyethylene, may be applied to a substrate of paper, thin cardboard, or foil to provide a surface property which enables heat sealing or better barrier performance (see BARRIER POLYMERS). Figure 10 is a sketch of the extrusion-coating process. A molten web of resin is extruded downward, and the web and substrate make contact at the nip between a pressure roll and a chill roll. Typical coating thicknesses are 0.005–0.25 mm; the die opening is ca 0.5 mm. The melt web is narrower than the die, which is characteristic of a neck-in, and the edge tends to bead or thicken. Coated substrate is trimmed to the desired width. The highly polished and water-cooled chill roll determines the nature of the surface and removes the heat from the resin. The pressure roll pushes the substrate and the molten resin against the chill roll. Pressure and high melt temperatures are needed for adhesion of resin and substrate.

In contrast to most extrusion processes, extrusion coating involves a hot melt, ca 340°C. The thin web cools rapidly between the die and nip even at high linear rates. Both mechanical and chemical bonding to substrates are involved. Mechanical locking of resin around fibers contributes to the resin's adhesion to paper. Some oxidation of the melt takes place in the air gap, thereby providing

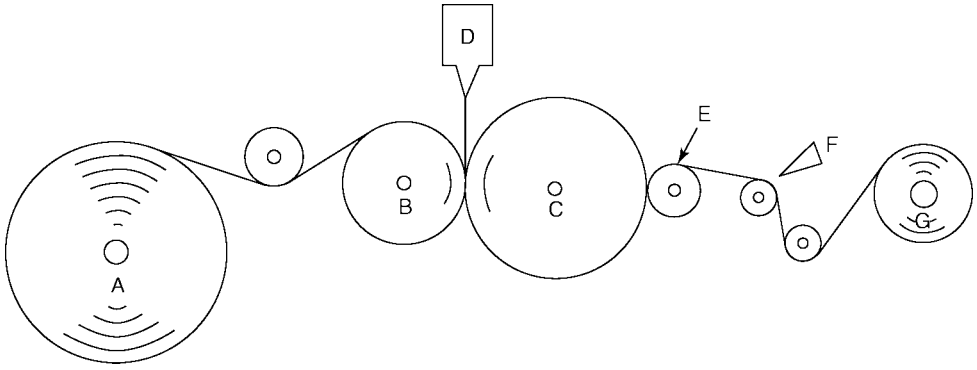

Fig. 10. Extrusion coating: A, unwinding of substrate; B, pressure roll; C, chill roll; D, die; E, stripper roll; F, edge trimmer; and G, windup of coated substrate (20).

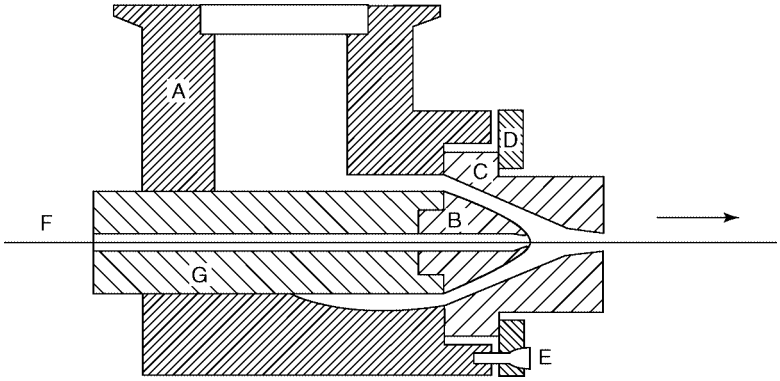

Fig. 11. Wire-coating pressure die: A, die body, crosshead; B, guider tip; C, die; D, die-retaining ring; E, die-retaining bolt; F, wire; and G, core tube (20).

sites for chemical bonding to aluminum foil. Excessive oxidation causes poor heat-sealing characteristics.

Wire and Cable Coating. Protective and insulating coatings can be applied continuously to wire as it is drawn through a cross-head die, as shown in Figure 11. A typical wire coating line consists of a wire payoff, wire preheater, extruder, die, cooling trough, capstan, and wire takeup (Fig. 12).

The melt flows from the extruder into the die where it flows around the bend and around the core tube. On the far side of the core tube, it forms a weld. Melt sticks to and is pulled by the moving wire. Details of the sizes and shapes of the die parts in contact with the melt are important in obtaining a smooth coating at high rates. The die exit usually is the same diameter as that of the coated wire and there is little drawdown. Die openings are small and pressures inside the die are high at ca 35 MPa (5000 psi). Wire take-up systems operate as high as 2000 m/min.

Injection Molding

In injection molding a molten thermoplastic is injected under high pressure into a steel mold. After the plastic solidifies, the mold is opened and a part in the shape

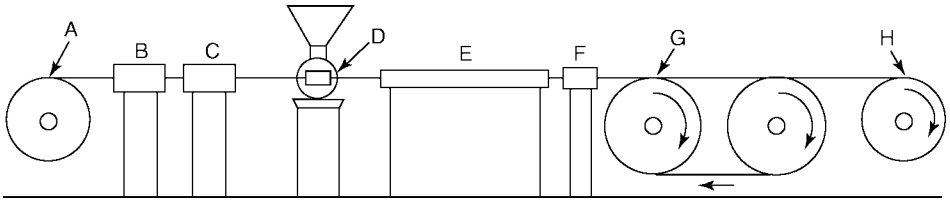

Fig. 12. Wire-coating line: A, unwinding of wire (payoff); B, straightener; C, preheater; D, extruder; E, water trough; F, tester; G, capstan (puller); and H, windup of coated wire (20).

of the mold cavity is removed. General descriptions of the process and related equipment are given in References 2 and 42–45.

Equipment. The machine consists of an injection unit and a clamp unit. The injection unit is usually a reciprocating single-screw extruder that melts the plastic and injects it into the mold or tool. The clamp unit opens, closes, and holds the mold closed against the pressure of injection. The size of an injection molding machine is described by the capacity of its clamping unit, ranging from 50 to 1000 tons. A machine with a given clamp unit can be supplied with a variety of injection units. Injection unit capacity is described by the shot size, which is the maximum volume of melt that can be injected in a single cycle. Shot size is determined by the diameter of the screw and the distance over which it is designed to reciprocate. Shot size is usually expressed as weight or as volume.

An injection molding machine is operated by hydraulic power and equipped with an electric motor and hydraulic pump. The maximum hydraulic oil pressure is ca 14 MPa (2000 psi). A hydraulic cylinder opens and closes the mold and holds the mold closed during injection; another cylinder forces the screw forward, thereby injecting the melt into the mold. A separate hydraulic motor turns the screw to plasticate, homogenize, and pressurize the melt. Control of these movements is a combined function of the hydraulic and electrical systems.

In the injection molding machine shown in Figure 13, the clamp unit is on the left and the injection unit on the right. A mold is shown in position between the platens of the clamp unit with one half of the mold fastened to the fixed platen and the other to the movable platen. When the mold is opened, the movable platen moves away from the fixed platen and the molded part can be removed. After part ejection, the mold is closed in preparation for the next injection cycle. In contrast to extrusion, the screw in the injection unit rotates only during part of molding cycle. When the screw turns, it pumps melt forward. The rearward movement of the screw is controlled by the placement of a limit switch, which stops the hydraulic motor. The maximum length of reciprocation is approximately three screw diameters. The shot size is directly proportional to the amount of screw

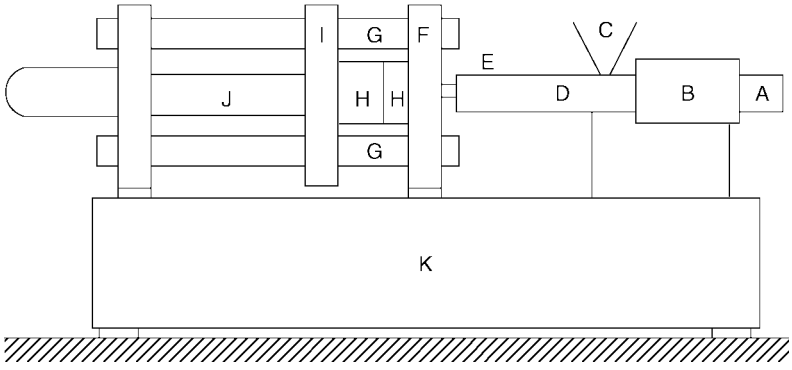

Fig. 13. Injection molding machine: A, hydraulic motor for turning the screw; B, hydraulic cylinder and piston allowing the screw to reciprocate about three diameters; C, hopper; D, injection cylinder (a single-screw extruder); E, nozzle; F, fixed platen; G, tie rods; H, mold; I, movable platen; J, hydraulic cylinder and piston used to move the movable platen and supply the force needed to keep the mold closed; and K, machine base.

reciprocation. The front of the screw is usually equipped with a check valve. While the screw rotates, the melt can move freely forward through the valve. However, the valve closes to prevent any reverse flow. The position of the screw is adjusted in such a way that there is always some melt in front of the screw when the mold is full. This pad or cushion of melt transfers pressure from the screw to the plastic in the mold. After initial filling, some additional melt flows into the mold; this is called packing. The cross section of the hydraulic cylinder, which pushes the screw, is approximately 10 times the cross section of the melt in front of the screw. Thus, 14 MPa (2000 psi) oil pressure corresponds to ca 140 MPa (20,000 psi) melt pressure.

Molding Cycle. The molding cycle begins when the empty mold is closed and full clamp force develops. The screw is then pushed forward in order to inject melt into the mold. The screw holds melt under pressure in the mold for a certain time, often called the injection time, until the gate freezes. When the injection is finished (46,47), the pressure holding the screw forward is reduced to a minimum, the screw starts to rotate, and a mold-closed timer is activated. Before the time expires and the mold opens, the screw stops turning and the next shot is ready for injection. The speed of screw rotation is chosen in such a way that the screw rotation time is less than the mold-closed time. The mold remains open only long enough for the part(s) to be ejected. The length of the molding cycle depends on cooling the part sufficiently so that it may be removed from the mold without distortion. Mold cooling systems are used for cycle reduction. The length of the cycle may also be determined by the appearance of the part; a hotter mold usually imparts a more attractive finish than a cooler mold. Cycle time and quality of moldings are optimized through microprocessor-based controllers that receive inputs from temperature, pressure, and ram position sensors.

Molds and Mold Design. The molds are custom-machined from steel. Cavities must be polished to a very high gloss, since the plastic reproduces the surface in every detail. The cavities are hardened and frequently chrome-plated. Details on mold design are given in References 48–50. A typical shot from a mold, shown in Figure 14, consists of a sprue, runners (43), gates, and two parts. Gate

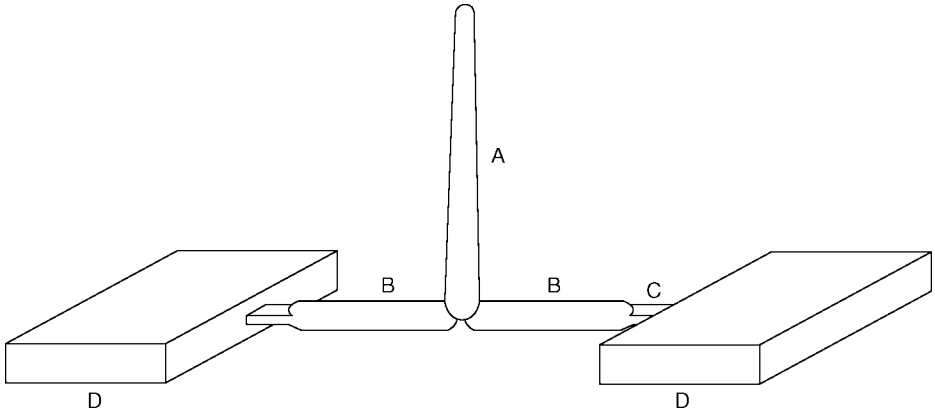

Fig. 14. A full shot: A, sprue; B, runner; C, gate; and D, part.

design is influenced by part geometry, resin type, and processing conditions. Sprue and runners channel the melt into the cavities. After ejection they are separated from the parts, ground, and fed back into the injection unit for reprocessing. Modern mold design tends to reduce or eliminate sprue and runner scrap through a variety of techniques such as hot runners, insulated runners, or by designs that place the nozzle directly against the mold cavity (45,51).

When the mold is opened, the part should be easily removable. Cavities are made with a slight taper to reduce frictional drag of the part on the mold. The half of the mold attached to the movable platen is equipped with ejector pins, which push the part out of the cavity while the mold is being opened. When the mold is closed, the pins are flush with the cavity surface. Release agents or lubricants facilitate ejection and shorten the molding cycle. Some complex parts require that the mold open in several directions in addition to the direction of the platen movement. For a threaded part, eg, a bottle cap, part of the mold must be rotated to remove the article from the mold.

Mold designs must take into account that cooled moldings are always smaller than the cavity, owing to shrinkage. Amorphous plastics shrink less than crystalline plastics (52). In practice, mold shrinkage is expressed as linear shrinkage, rather than volumetric shrinkage. Parts are measured the day after molding and are compared with the size of the mold at room temperature. In actual molding, pressure is maintained to continue packing during cooling to minimize voids and excessive sink marks.

Developments. A variety of process modifications aimed at improving surface finish or weld line integrity, process efficiency, and product costs have been described. They include gas-assisted injection molding developed for the production of hollow plastic parts with separate internal channels, microcellular foam molding that uses supercritical fluids to create microscopic cells throughout the polymer, coinjection, fusible core, multiple live feed, push–pull injection molding, and increasing use of robotic automation for enhanced productivity and part quality (53,57). An important development includes computer-aided design methods, wherein a proposed mold design is simulated by a variety of software packages and the melt flow through it is analyzed (58).

Structural Foam Molding. Structural foam is a modified injection molding process for large articles having a cellular core and an integral solid skin with an overall 20–50% reduction in density, compared to their solid counterparts (40,59,60). It is most frequently used with polyethylene, high impact polystyrene, polypropylene, and several engineering resins. Some modifications to the resin, machine, and mold are required, and a blowing agent must be added to the resin. A chemical blowing agent, which releases gas when heated, is commonly used. The choice of blowing agents depends on the processing temperature required. The most common blowing agent is azodicarbonamide (1,1′-azobisformamide) used at 200–260°C. Upon decomposition, it releases nitrogen, carbon monoxide, and carbon dioxide (qv). Approximately 0.5 wt% of a blowing agent is normally added to the resin pellet as a surface coating or as a pelletized concentrate. Instead of a chemical blowing agent, nitrogen may be mixed with the melt while it is under pressure in an extruder and the mixture maintained under pressure until it is injected into the mold.

The injection molding machine must be equipped with a shutoff nozzle that maintains the melt under pressure while the mold is opened. The screw is retracted only part of the way needed for a full shot, and a short shot is injected into the mold. Without a blowing agent, only a section of a part, ie, a short shot, would be made; the empty space allows the blowing agent to expand the melt, forming the foam structure. Structural foam molding is limited to parts with wall thicknesses of at least 6 mm; below that thickness, reduction in part weight is usually insignificant. Parts, typically, have a dense skin and a foamed interior with various pore sizes. Compared to injection-molded surfaces, the surfaces of structural foam moldings are poor, and are characterized by a rough, swirly finish. Maximum pressure in the mold during foaming is much lower than in injection molding; also, no packing pressure needs to be maintained since the gas keeps the melt front moving. Surface appearance is improved by special techniques.

Because of low injection pressure, some cost savings are possible in mold and press construction. Molding cycles are somewhat longer than for injection molding. The part must be cooled in the mold long enough to be able to resist swelling from internal gas pressure. In structural foam parts there is almost a total absence of sink marks, even in the case of unequal section thickness. Structural foam has replaced wood, concrete, solid plastics, and metals in a variety of applications.

Blow Molding

Blow Molding (qv) is the most common process for making hollow thermoplastic components (61–63). In extrusion blow molding a molten tube of resin called a parison is extruded from a die into an open mold (Fig. 15**a**). In Figure 15**b** the mold is closed around the parison, and the bottom of the parison is pinched together by the mold. Air under pressure is fed through the die into the parison, which expands to fill the mold. The part is cooled as it is held under internal air pressure. Figure 15**c** shows the open mold with the part falling free.

As the parison is extruded, the melt is free to swell and sag. The process requires a viscous resin with consistent swell and sag melt properties. For a large

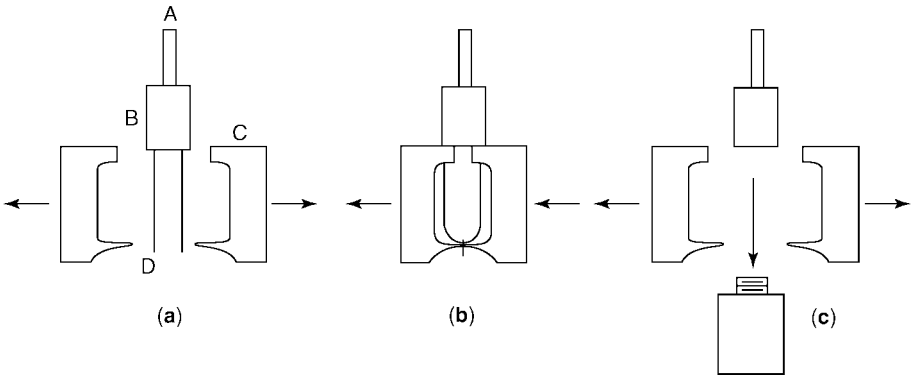

Fig. 15. Three stages of blow molding (**a–c**): A, air line; B, die; C, mold; and D, parison (see text).

container the machine is usually equipped with a cylinder and a piston called an accumulator. The accumulator is filled with melt from the extruder and emptied at a much faster rate to form a large parison; this minimizes the sag of the molten tube.

With a simple parison, the large-diameter sections of the bottle have a thin wall and the small-diameter sections have a thick wall. Certain modifications of the die can control the thickness of the parison wall along its length, which results in a bottle with improved wall thickness distribution and better strength. High density polyethylene (HDPE) is the most common blow-molding resin used to produce containers ranging in size from 30 cm^3 to 200 L.

In injection blow molding, a parison is injection-molded onto a core pin; the parison is then rapidly transferred via the core pin to a blow mold, where it is blown by air into an article. This process is applied to small and intricate bottles.

Soft-drink bottles made from PET are usually made by stretch-blow molding in a two-step process. First, a test-tube-shaped preform is molded, which is then reheated to just above its glass-transition temperature, stretched, and blown. Stretching the PET produces biaxial orientation, which improves transparency, strength, and toughness of the bottle. A one-step process is used for many custom containers that are injection stretch-blow molded.

Development/trends in blow molding focus on the optimization of the viscoelastic properties and improvement in thermal stability of polymers other than HDPE to develop new extrusion/injection blow molding grades; fabrication of small containers by multilayer blow molding for improved barrier properties to water, oxygen, or hydrocarbons; prediction through software packages of wall thickness for parisons and final parts to minimize materials usage.

Other Molding Methods

Rotational Molding. Hollow articles and large, complex shapes are made by rotational molding (qv), usually from polyethylene powder of relatively low viscosity (64–66). The resin is in the form of a fine powder. A measured quantity is placed inside an aluminum mold and the mold is heated in an oven and rotated at low speed. The resin sinters and fuses, coating the inside of the mold. The mold is then cooled by water spray and the part solidifies, duplicating the inside of the mold.

A rotomolding machine has three long arms extending from a central driving mechanism; each arm rotates several molds in two planes. The arms are moved from one process station to the next, ie, from unloading and loading to heating and cooling. Tooling costs are low. The molds are usually made of cast aluminum, but sheet metal is also used. The melt is forced without pressure against the mold surface during heating or cooling, resulting in uniform wall thickness, zero orientation, and high physical properties. Cycle times are long because of the heating and cooling required; they depend on wall thickness and can be as high as 15 min for a 4-mm wall thickness. Common rotomolded products include large tanks and boxes, drums, furniture, and toys. PVC plastisol, a mixture of fine PVC particles and a plasticizer, may also be processed by rotomolding. Plastisols

are liquid at room temperature and are converted to soft solids when heated to ca 180°C. Playballs and toys are made from plastisols.

Among recent trends and developments in rotomolding are the use of microprocessors and temperature sensors for quality assurance, the refinement of methods to produce multiwalled solid or foamed structures all coupled with the continuing availability of new resin grades with suitable viscosities and high thermooxidative stability over the prolonged periods of time in the oven.

Expandable Polystyrene Molding. Molding expandable polystyrene gives foamed products such as insulation board shapes for packaging and disposable food and cup containers. Such processes are also called bead or steam molding (67,68). Expandable polystyrene moldings are manufactured from polystyrene beads 0.25–1.5 mm in diameter containing a blowing agent, such as pentane. These beads, when exposed to heat, expand from 2 to 50 times their original size. The beads are preexpanded by heating with steam or hot air to about the density of the final molded part. After preexpansion, they are stored from 3 to 12 h to let the air diffuse into the cells of the foam. Shaping of the beads is done in special presses and molds, into which the preexpanded beads are transferred by air-conveying systems. Steam causes further expansion and forces the surface fused particles to conform to the shape of the mold. In the manufacture of insulation boards, blocks are molded into cavities up to $5.5 \times 1.2 \times 0.65$ m by injecting steam. After storage and conditioning, the blocks are cut into sheets. Expandable bead molding has been extended to other thermoplastics such as polypropylene.

Thermoforming

Thermoforming (qv) is a process for converting a preform, usually an extruded plastic sheet, into an article such as a thin-wall container or a tray for packaging meat (69–72). Under vacuum the process is called vacuum forming. The sheet is clamped in a frame and exposed to radiant heaters. The sheet softens to a formable condition, is moved over a mold, and sucked against the mold by vacuum. Excess plastic is trimmed and recycled. Timers control the length of the heating and cooling periods, which depend on composition and sheet thickness. Frequently, the process is improved by using mechanical aids (plug-assisted, air-cushioned plug-assisted, drape-assisted). The molds are made of wood, aluminum, steel, or epoxy (73). In some plants the vacuum forming line is run in-line with the sheeting extruder.

Amorphous resins such as styrenics, acrylics, PVC, and some crystalline resins such as polyolefins, PP, and PET are used for thermoforming. Foamed polystyrene sheet is also thermoformed. The polymers must be of fairly high molecular weight because the heated sheet must be form-stable. The significant property is melt elasticity. Sheets of these resins soften but do not sag when heated. Sagging causes thinning; a sagged sheet may have more surface area than the mold, resulting in folds and areas of uneven thickness. Thermoforming is employed for small items such as cups, plates, trays, and larger, deep-drawn moldings such as boats, bath tubs, and freezer liners. Skin packaging, which employs a flexible plastic skin drawn tightly over an article on a card backing, is made by thermoforming.

The process also is used for blister packaging. Thermoforming can be continuous by using rolls of sheet or batch by using precut shapes.

Thermoforming is competing with injection blow molding and rotomolding to prepare hollow parts by refining the twin sheet process by simultaneous or sequential forming of both halves and then compressing at the periphery to effect closure. The growth of thermoforming is also related to the development of software for wall thickness prediction.

Calendering

Calendering is a process uniquely applied to rubbery polymers, mainly semirigid and flexible PVC, for making sheeting of uniform thickness from 0.75–0.05 mm after stretching (74–77). A calender has four heavy, large steel rolls, which are usually assembled in an inverted "L" configuration as shown in Figure 16. This design is preferred for thick sheeting because it gives a long dwell for full heating. The forces generated between the rolls are considerable and sufficient to bend the rolls, resulting in uneven sheet thickness. A common method of compensating for roll bending is by grinding an opposite contour on the roll. A two-roll mill, a Banbury mixer, or an extruder melts the resin, which is subsequently transferred to the calender. Sheet can be made 2.5 m wide and production rates can be as high as 100 m/min. Calendering is often followed by printing, laminating, and embossing. PVC calenders are run at temperatures approaching 200°C to produce highly oriented sheets for items such as shower curtains, rainwear, luggage, and wall paneling.

Casting

Casting refers to the formation of an object in a batch process by pouring a fluid monomer–polymer solution into a mold where it solidifies or by continuously

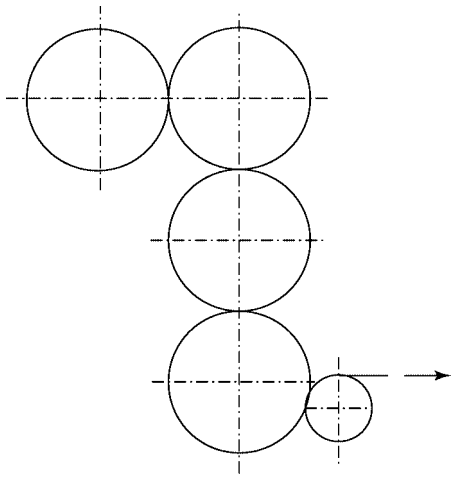

Fig. 16. A four-roll, inverted "L" calender.

pouring the liquid onto a moving belt. The casting process is most frequently used with acrylics. Since the 1950s, cast acrylic sheeting has been made by polymerization of methyl methacrylate in a cell assembled from two glass plates and a flexible gasket. Heating for a few hours until polymerization is complete gives sheets with excellent optical properties. Acrylic sheeting is also made by continuous casting, ie, a monomer–polymer–catalyst mixture is fed onto a stainless steel belt, on which the polymerization is completed. These products are used for glazing and thermoforming. Nylon-6 products with higher molecular weight and crystallinity than extruded or molded resins are also produced by casting in the mold by a process known as *in situ* anionic polymerization.

Thermosetting Resins Processing

Common thermosetting resins are unsaturated polyesters, phenolic resins (qv), amino resins (qv), polyurethanes (qv), epoxy resins (qv), and silicones (qv) (see POLYESTERS, UNSATURATED; URETHANE COATINGS). Less common thermosets (qv) employed in specialized applications are bismaleimides, polyimides (qv), and furan resins. Thermosetting resins are usually low viscosity liquids or low molecular weight solids that are formulated with suitable additives known as cross-linking agents to induce curing; curing involves permanent chemical changes resulting in infusible, insoluble products with excellent thermal and dimensional stability. Thermosetting resins are commonly used in combination with fillers or fibrous reinforcements; as a result, processing methods are often quite different from those employed for thermoplastics (78–80).

Compression, Injection, and Transfer Molding. Compression molding is the oldest process of the plastics industry. General information on the process, which is also applicable to a certain extent to thermoplastics, is found in References 81–85. It is still common, although many thermosetting materials are also injection-molded (86–88). The equipment consists of a vertical hydraulic press with platens for mold attachment. The mold comprises a matched pair of male and female dies. Mold cavities are hardened and highly polished, similar to those of an injection mold. A measured quantity of thermosetting resin compound in granular, sheet, or other form is placed in the hot mold. The mold is closed and the liquified resin through pressure fills the cavity. Continued heating cures the resin within a few minutes, and the part is removed from the mold. Compression molding is commonly employed for phenol–formaldehyde, urea–formaldehyde, melamine–formaldehyde, and polyester molding compounds. To shorten the total cycle, some of these compounds are partially polymerized or preformed into various shapes that are preheated to intermediate temperature before being inserted into the mold. Laminates made of reinforcement layers impregnated with partially polymerized resins are also prepared by compression molding.

Sheet molding compound (SMC) is used in the manufacture of large reinforced compression moldings, which are employed extensively in automotive panels. SMC is prepared as a sandwich, rolled between two polyethylene films; it contains polyester resin, filler (usually calcium carbonate), and 20–30 wt% chopped glass fibers. Other components such as peroxides for cross-linking, thermoplastic additives for shrinkage control, and alkaline-earth oxides and hydroxides to assist maturation are present in smaller amounts. Maturation involves a thickening

chemical reaction that produces within a few days after compounding a tack-free sheet with desirable flow characteristics during molding. The required amount of sheet is then cut to size for placement on the bottom of two matched mold halves to cover at least 70% of the mold area. It is molded at pressures up to 15 MPa (2100 psi) and temperatures in the range 140–180°C. Cure cycles depend on part size and complexity, pressure and heat applied, and formulation characteristics. Cure cycles of 60 s are common. The properties of cured SMC depend on the amount, length, and orientation of the glass fibers.

Bulk molding compound (BMC) is similar to SMC in formulation, but contains shorter glass fibers and higher filler levels (89). The premixed material has the consistency of dough and is supplied in bulk form or as a cylindrical extrudate. BMC is molded by conventional compression or transfer molding; it is also molded in reciprocating screw injection presses equipped with a piston stuffer attached to the barrel to force-feed the material into the screw flights. Other injection-moldable thermoset formulations in granular form (phenolics, amino, epoxy, and diallyl phthalate compounds) are fed through standard gravity hoppers. In thermoset injection molding, screws with low compression ratios are used to convey the material through a short barrel heated typically up to 120°C and decrease its viscosity; this is followed by injection into a hotter mold (typically up to 220°C) where chemical cross-linking takes place. Total cycles may range from 10 to 120 s, depending on part thickness and formulation characteristics.

Transfer molding is a combination of compression molding and injection molding. A measured charge is heated in a reservoir, from which it is injected or transferred through runners to the mold cavity. Forcing the polymer through the entry gate results in a rise in temperature that may promote flow but also accelerates curing. The molten polymer is held at temperature while the cross-linking reaction proceeds to completion.

Open-Mold Processing. Common open-mold processes are hand or mechanized methods such as lay-up and spray-up, that use a single cavity mold and produce one finished surface (90). These techniques are used to produce fiber-reinforced structures containing the reinforcement in the form of cloth, chopped strands, mat, continuous roving, woven roving, etc. Thermosetting resins of choice are liquid unsaturated polyester or epoxy resins. In lay-up, catalyzed resin is used to impregnate the reinforcement that is preplaced on the mold. A spray-up system consists of a resin spray gun, a fiber chopper, and a pumping system; the catalyst is combined with the resin just before deposition with the fibers onto the mold surface. Open-mold processes use little or no pressure during the curing cycle. Cross-linking usually takes place at room or slightly elevated temperature through a proper combination of curing agents. A variety of products such as boat hulls, automotive components, tanks, etc are made by open-mold processing (91). Types of emissions and U.S. environmental regulations for thermoset components and cure reaction by-products are included in Reference 19.

In another open-mold process, filament winding, continuous fibers such as glass, carbon, or aramid are wound on a mandrel surface in a precise geometric pattern (92). Fibers are usually preimpregnated with a low viscosity resin containing a suitable cross-linking agent for room or higher temperature curing. Most common resins are polyesters and epoxies. A tubular component with the fibers in angle-ply arrangement results after curing and the mandrel is withdrawn. The

process, originally developed as a rapid method to manufacture pipes and cylindrical vessels, has expanded to allow more complicated geometries. Products include, among others, helicopter rotor blades, external fuel tanks, pressure bottles, and pipes.

Pultrusion. In pultrusion, reinforcing fibers in a combination of styles are wetted by a resin containing a high temperature cross-linking agent and then pulled through a forming system that positions the fibers into the desired packed structural arrangement; the material then moves through a heated die where curing takes place (93). The process can in principle produce continuous profiles of any length; rods, bars, and other more complex profiles such as I-beams and channels are mostly made from continuous glass fibers and polyester or epoxy resins (94). Glass content can be very high (50–70%) at production rates of about 1.5 m/min (91–93). An analogous method has been used to produce continuous composite lengths by impregnation of fiber bundles with molten thermoplastics which can be chopped to long fiber pellets that are used in injection molding (95).

Reaction Injection Molding. Reaction injection molding (RIM) is used for the production of solid or partially foamed polyurethane moldings by rapid injection of metered streams of polyol and isocyanate into a mold. RIM has been developed around polyurethane and polyurea chemistry; other chemical systems of lesser commercial significance can be processed by RIM (96,97). Articles are produced on a cycle of 3 min or less. The two liquid streams are mixed by impingement before entering the mold. The mold is filled at 0.35–0.70 MPa (50–100 psi), which is a very low pressure compared to that used in standard injection molding. Equipment, and in particular mixing head design, is critical. The cost of the mold and press are less for RIM than for conventional injection molding and the process is particularly suited to the production of large parts.

A wide range of formulations can be used in the RIM process. A typical polyol stream contains 75–80 wt% polyether polyol, 17–20 wt% 1,4-butane-diol, 2–6 wt% blowing agent, and amine and metal catalysts. The most commonly used isocyanates are proprietary products made from 4,4′-methylenedi(phenyl isocyanate). Processing conditions and physical properties depend on the formulation. Often, parts are removed from the mold before curing is complete; then, additional curing is required at elevated temperatures in an oven. Glass fibers and other fillers added for reinforcement and to control shrinkage are dispersed into the polyol component. Another approach is to place continuous fiber mats directly in the mold cavity and inject a low viscosity, reactive mixture through the mat (structural RIM) (98).

Resin Transfer Molding. In resin transfer molding (RTM) a piston-type positive displacement pump injects a premixed resin–catalyst stream into a closed mold thoroughly impregnating a preplaced reinforcement pack. Glass, graphite, or aramid fibers in the form of continuous strand mat, woven rovings, and their combinations are typical reinforcements (99). RTM differs from structural RIM in that it uses slower reacting formulations and injects under lower pressures components that are premixed or homogenized by passing through static mixers. Molds are made of lower cost materials and cycles are longer (10–60 min). RTM machines have been adapted for a variety of resins including polyesters, epoxies, polyurethanes, and isocyanurates (100,101).

Polyurethane Foam Processing.

Flexible Foam. These polyurethane products have varying densities and a relatively low degree of cross-linking (102). They are made from trifunctional polyols (mol wt 3000) and TDI, a mixture of 2,4- and 2,6-toluene diisocyanates, in the presence of tin and amine catalysts, surfactants as foam stabilizers, water, and blowing agents. Physical blowing agents are Freons; CO_2, the reaction product of water and isocyanate, is a chemical blowing agent. Flexible foams are resilient open-cell structures with densities varying from 25 to 650 kg/m^3, depending on the choice of the raw materials. Most flexible foams are produced in the form of a slab or bun in a continuous process in widths up to 2.4 m and thicknesses up to 1.2 m. A liquid foamable mixture is pumped onto a conveyor, which moves through a tunnel where reaction and foaming occur (103). Similar mixtures can be placed in a mold and allowed to foam. This process is used in the manufacture of automobile seats (see Foamed Plastics).

Rigid Foam. These are closed-cell foams with excellent thermal insulation characteristics (104). Most rigid foams are made from a high functionality polyol with ca 500 mol wt and poly(methylene)–poly(phenyl isocyanate), yielding a mixture with a high functionality of 2.7; hence, the foams have a higher degree of cross-linking than the flexible foams. The formulations include blowing agents, catalysts, and foam stabilizers. Rigid foams can be made as continuous slabs that are cut into panels. Other production methods include coating suitable substrates to produce laminated products used for architectural insulation; spraying, as for insulation during construction; and pouring or pumping the foamable mixture into place, as in the manufacture of refrigerators.

BIBLIOGRAPHY

"Plastics Processing" in *EPSE* 2nd ed., Vol. 11, pp. 262–285, by P. N. Richardson, E. I. du Pont de Nemours & Co., Inc.

1. *Mod. Plast.* **71**(1), 73 (1994).
2. N. G. McCrum, C. P. Buckley, and C. B. Bucknall, *Principles of Polymer Engineering*, Oxford University Press, New York, 1997, pp. 1–11.
3. P. G. Kelleher, *Adv. Polym. Technol.* **10**, 219 (1990).
4. P. G. Galanty and G. A. Bujtas, *Modern Plastics Encyclopedia '92*, Vol. 68, No. 11, McGraw-Hill Book Co., Inc., New York, 1991, p. 23.
5. P. J. Rigby, *Modern Plastics Encyclopedia '92*, Vol. 68, No. 11, McGraw-Hill Book Co., Inc., New York, 1991, p. 45.
6. J. F. Chabot Jr., *The Development of Plastics Processing Machinery and Methods*, Society of Plastics Engineers, Brookfield, Conn., 1992.
7. R. C. Progelhof and J. L. Throne, *Polymer Engineering Principles: Properties, Processes and Tests for Design,* Hanser Publishers, Munich, 1993, Chapt. 5.
8. D. H. Morton-Jones, *Polymer Processing*, Chapman and Hall,, New York, 1989.
9. E. A. Grulke, *Polymer Process Engineering*, PTR Prentice-Hall, Englewood Cliffs, N.J., 1994, Chapt. 10.
10. J.-M. Charrier, *Polymeric Materials and Processing: Plastics, Elastomers and Composites*, Hanser Publishers, New York, 1991, Chapt. 5.
11. J. F. Aggasant, P. Avenas, J. Sergent, and P. Carreau, eds., *Polymer Processing: Principles and Modeling*, Hanser Publishers, Munich, 1991.

12. A. I. Isayev, ed., *Modeling of Polymer Processing*, Hanser Publishers, Munich, 1992.
13. N. S. Rao, *Computer Aided Design of Plasticating Screws*, Hanser Publishers, Munich, 1986.
14. K. T. O'Brien, *Computer Modeling for Extrusion and Other Continuous Polymer Processes*, Hanser Publishers, Munich, 1992.
15. C. L. Tucker, *Fundamentals of Computer Modeling for Polymer Processing*, Hanser Publishers, Munich, 1989.
16. J. L. White and H. Potente, eds., *Screw Extrusion: Science and Technology*, Carl Hanser Verlag, Munich, 2003.
17. Society of Plastics Engineers, *The SPE Guide on Extrusion Technology and Troubleshooting*, Brookfield, Conn., 2001.
18. S. H. Patel and M. Xanthos, *Adv. Polym. Technol.* **20**, 222–241 (2001).
19. Radian Corp., *Plastics Processing—Technology and Health Effects*, Noyes Data Corp., Park Ridge, N.J., 1986.
20. P. N. Richardson, *Introduction to Extrusion*, Society of Plastics Engineers, Inc., Brookfield Center, Conn., 1974.
21. M. Xanthos, ed., *Reactive Extrusion: Principles and Practice*, Hanser Publishers, Munich, 1992.
22. W. Baker, C. Scott, and G.-H Hu, eds., *Reactive Polymer Blending*, Carl Hanser Verlag, Munich, 2001.
23. D. B. Todd, *J. Reinforced Plast. and Compos.* **17**, 1607 (1998).
24. D. B. Todd, ed., *Plastics Compounding*, Carl Hanser Verlag, Munich, 2001.
25. J. L. White, A. Koran, and A. Moet, eds., *Polymer Mixing Technology and Engineering*, Carl Hanser Verlag, Munich, 2001.
26. D. B. Todd, *Int. Polym. Proc.* **6**, 143 (1991).
27. E. C. Bernhardt, ed., *Processing of Thermoplastic Materials*, Reinhold Publishing Corp., New York, 1959.
28. Z. Tadmor and C. G. Gogos, *Principles of Polymer Processing*, John Wiley & Sons, Inc., New York, 1979.
29. J. R. Pearson, *Mechanics of Polymer Processing*, Elsevier Science Publishing Co., New York, 1985.
30. Ref. 8, pp. 74–125.
31. C. Rauwendaal, *Polymer Extrusion*, Hanser Publishers, Munich, 1990.
32. J. L. White, *Twin Screw Extrusion: Technology and Principles*, Hanser Publishers, Munich, 1991.
33. M. L. Berins, ed., *Plastics Engineering Handbook of the Society of Plastics Industry*, 5th ed., Van Nostrand Reinhold Co., Inc., New York, 1991, Chapt. 4.
34. W. Michaeli, *Extrusion Dies for Plastics and Rubbers*, Hanser Publishers, Munich, 1992.
35. D. G. Baird and D. I. Collias, *Polymer Processing: Principles and Design*, Wiley Interscience, New York, 1998.
36. C. I. Chung, *Extrusion of Polymers: Theory and Practice*, Carl Hanser Verlag, Munich, 2000.
37. S. T. Lee, ed., *Foam Extrusion: Principles and Practice*, Technomic Publishing Co., Lancaster, Pa., 2000.
38. C. Jacob and S. K. Dey, In *Proceedings of the 52nd SPE Annual Technical Conference*, Vol. 40, Society of Plastics Engineers, Inc., Brookfield Center, Conn., 1994, p. 1964.
39. M. Xanthos, S. K. Dey, Q. Zhang, and J. Quintans, *J. Cel. Plast.* **36**, 102 (2000).
40. D. Klemper and K. C. Frisch, eds., *Handbook of Polymeric Foams and Foam Technology*, Hanser Publishers, Munich, 1992.
41. Ref. 35, p. 265.
42. I. I. Rubin, *Injection Molding—Theory and Practice*, John Wiley & Sons, Inc., New York, 1972.

43. T. Whelan and J. Goff, *Injection Molding of Thermoplastics*, Vols. 1 and 2, Society of Plastics Engineers, Brookfield Center, Conn., 1990.
44. L. Weir, *Introduction to Injection Molding*, Society of Plastics Engineers, Brookfield Center, Conn., 1975.
45. Ref. 8, pp. 146–175.
46. H. W. Cox, C. C. Mentzer, and R. C. Custer, *Polym. Eng. Sci.* **24**, 501 (1984).
47. H. Bangert, *Kunststoffe* **75**, 325 (1985).
48. G. Menges and P. Mohren, *How to Make Injection Molds*, Hanser Publishers, Munich, 1993.
49. K. Stoeckhert, *Mold-Making Handbook*, Hanser Publishers, Munich, 1983.
50. J. H. Dubois and W. Pribble, *Plastics Mold Engineering Handbook*, 4th ed. Van Nostrand Reinhold, Co., Inc., New York, 1987.
51. Mold-Masters Ltd., in Ref. 4, p. 278.
52. R. M. Ogorkiewicz, ed., *Thermoplastics: Effects of Processing*, CRC, Cleveland, Ohio, 1969, p. 118.
53. J. Theberge, *Plast. Eng.* **47**(2), 27 (1991).
54. J. Theberge, in S. H. Munson-McGee, ed., *Opportunities for Innovation: Polymer Composites*, NIST GCR 90-577-1, National Institute of Standards and Technology, Gaithersburg, Md., 1990, pp. 35–44.
55. J. S. Lee, S. Cha, and F. Lai, *Plast. Eng.* **57**(12), 42 (2001).
56. D. Pierick and K. Jacobsen, *Plast. Eng.* **57**(5), 46 (2001).
57. D. C. Preusse, *Plast. Eng.* **58**(5), 18 (2002).
58. L. T. Manzione, ed., *Applications of Computer Aided Engineering in Injection Molding*, Hanser Publishers, Munich, 1987.
59. S. Semerdjiev, *Introduction to Structural Foam*, Society of Plastics Engineers, Brookfield Center, Conn., 1982.
60. E. Hunerberg, *Modern Plastics Encyclopedia '92*, Vol. 68, No. 11, McGraw-Hill Book Co., Inc., New York, 1991, p. 264.
61. Ref. 2, pp. 349–350.
62. D. Rosato and D. Rosato, eds., *Blow Molding Handbook*, Hanser Publishers, Munich, 1989.
63. Ref. 8, pp. 126–137; Ref. 4, pp. 222–227.
64. Ref. 8, pp. 237–241.
65. R. L. Fair, *Modern Plastics Encyclopedia '92*, Vol. 68, No. 11, McGraw-Hill Book Co., Inc., New York, 1991, p. 293.
66. Ref. 33, Chapt. 14.
67. Ref. 33, pp. 593–598.
68. J. M. Joyce, *Modern Plastics Encyclopedia '92*, Vol. 68, No. 11, McGraw-Hill Book Co., Inc., New York, 1991, p. 256.
69. Ref. 2, pp. 346–349.
70. J. L. Throne, *Thermoforming*, Hanser Publishers, Munich, 1987.
71. Ref. 8, pp. 138–145.
72. R. Whiteside, *Modern Plastics Encyclopedia '92*, Vol. 68, No. 11, McGraw-Hill Book Co., Inc., New York, 1991, p. 294.
73. G. R. Garrison, *Modern Plastics Encyclopedia '92*, Vol. 68, No. 11, McGraw-Hill Book Co., Inc., New York, 1991, p. 298.
74. Ref. 8, pp. 186–190.
75. Ref. 33, Chapt. 15.
76. A. Ray and A. V. Shenoy, *J. Appl. Polym. Sci.* **30**, 1 (1985).
77. J. F. Agassant and M. Espy, *Polym., Eng. Sci.* **25**(2), 118 (1985).
78. R. E. Wright, *Molded Thermosets*, Hanser Publishers, Munich, 1992.
79. P. Mallick and S. Newman, *Composites Materials Technology: Processes and Properties*, Hanser Publishers, Munich, 1991.

80. Ref. 2, pp. 350–351.
81. R. G. Whitesides and J. C. O'Brien, *Modern Plastics Encyclopedia '92*, Vol. 68, No. 11, McGraw-Hill Book Co., Inc., New York, 1991, p. 234.
82. Ref. 2, pp. 350–351.
83. G. N. Hartt and J. F. Wilk Jr., in S. H. Munson-McGee, ed., *Opportunities for Innovation: Polymer Composites*, NIST GCR 90-577-1, National Institute of Standards and Technology, Gaithersburg, Md., 1990, pp. 23–34.
84. Ref. 8, pp. 176–184.
85. Ref. 33. Chapt. 9.
86. Ref. 2, pp. 343–344.
87. P. L. Leopold, *Modern Plastics Encyclopedia '92*, Vol. 68, No. 11, McGraw-Hill Book Co., Inc., New York, 1991, p. 272.
88. Ref. 33, Chapt. 8.
89. L. N. Nunnery, *Modern Plastics Encyclopedia '92*, Vol. 68, No. 11, McGraw-Hill Book Co., Inc., New York, 1991, p. 200.
90. L. C. McManus, *Modern Plastics Encyclopedia '92*, Vol. 68, No. 11, McGraw-Hill Book Co., Inc., New York, 1991, p. 286.
91. E. M. Zion, in Ref. 83, pp. 1–22.
92. R. R. Roser, *Modern Plastics Encyclopedia '92*, Vol. 68, No. 11, McGraw-Hill Book Co., Inc., New York, 1991, p. 284.
93. J. Martin, *Modern Plastics Encyclopedia '92*, Vol. 68, No. 11, McGraw-Hill Book Co., Inc., New York, 1991, p. 288.
94. J. E. Sumerak, in Ref. 83, pp. 45–48.
95. P. J. Bates and X. P. Zou, *Int. Polym. Process.* **17**, 376 (2002).
96. J. R. Riley, *Modern Plastics Encyclopedia '92*, Vol. 68, No. 11, McGraw-Hill Book Co., Inc., New York, 1991, p. 281.
97. C. W. Macosko, *RIM, Fundamentals of Reaction Injection Molding*, Hanser, New York, 1989.
98. C. D. Shirrel, in Ref. 83, pp. 59–86.
99. K. A. Jacobs, *Modern Plastics Encyclopedia '92*, Vol. 68, No. 11, McGraw-Hill Book Co., Inc., New York, 1991, p. 290.
100. C. F. Johnson, in Ref. 83, pp. 87–110.
101. G. N. Hartt, J. K. Brew, in Ref. 83, pp. 111–120.
102. R. McBrayer, *Modern Plastics Encyclopedia '92*, Vol. 68, No. 11, McGraw-Hill Book Co., Inc., New York, 1991, p. 260.
103. G. Oertel, ed., *Polyurethane Handbook*, Hanser Publishers, New York, 1993.
104. Ref. 33, Chapt. 19.

M. XANTHOS
D. B. TODD
Polymer Processing Institute

PMMA. See METHACRYLIC ESTER POLYMERS.

POLYACETAL. See ACETAL RESINS.

POLYACRYLAMIDE. See ACRYLAMIDE POLYMERS.

POLYACRYLATES. See ACRYLIC ESTER POLYMERS.

POLYACRYLONITRILE. See ACRYLONITRILE POLYMERS.

POLYAMIDES, AROMATIC. See Volume 3.

POLYAMIDES, FIBERS. See Volume 3.

POLYAMIDES, PLASTICS. See Volume 3.

POLYANHYDRIDES. See Volume 7.

POLYARYLATES. See Volume 7.

POLY(ACRYLIC ACID). See ACRYLIC (AND METHACRYLIC) ACID POLYME.

POLYBENZIMIDAZOLE POLYMERS (PBI). See RIGID ROD POLYMERS.

POLYBENZOTHIAZOLES (PBT). See RIGID ROD POLYMERS.

POLYBENZOXAZOLES (PBO). See RIGID ROD POLYMERS.

POLYBUTADIENE. See BUTADIENE POLYMERS.

POLYBUTENES. See BUTENE POLYMERS.

POLYCARBONATES. See Volume 7.

POLYCARBOSILANES. See Volume 7.

POLYCHLOROPRENE. See CHLOROPRENE POLYMERS.

POLYCYANOACRYLATES. See Volume 3.

POLY(CYCLOHEXYLENE TEREPHTHALATE). See CYCLOHEXANEDIMETHANOL POLYESTERS.

POLYDIACETYLENE. See DIACETYLENE AND TRIACETYLENE POLYME.

POLYELECTROLYTES. See Volume 7.

POLY(ETHYLENE NAPHTHALATE) (PEN)

Introduction

Poly(ethylene naphthalate) (PEN) is a thermoplastic polyester consisting of ethylene naphthalate repeat units:

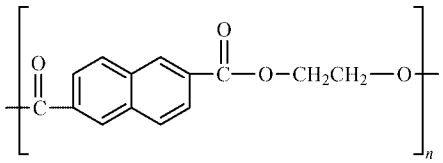

PEN is the polycondensation product of either dimethyl-2,6-naphthalenedicarboxylate (2,6-NDC) or naphthalate dicarboxylic acid (2,6-NDA) with ethylene glycol. To date 2,6-NDC is the preferred feedstock in view of the fact that it can be produced more economically in high purity form relative to purified 2,6-NDA.

Other naphthalate-based polyesters include the butanediol-based analogue, poly(butylene naphthalate) (PBN), as well as copolymers and blends of PET [poly(ethylene terephthalate)] with PEN.

Naphthalate polyesters exhibit physical and mechanical properties generally superior to their terephthalate analogues made from terephthalic acid (TA) or dimethyl terephthalate (DMT), such as PET or poly(butylene terephthalate) (PBT). PEN polymerization was first reported by ICI in 1948 (1). Its superior thermal, mechanical, and physical properties were recognized early on. However, in the 40 years that followed, PEN did not find significant commercialization or application development, due primarily to the lack of commerical availablity of the key monomer, 2,6-NDC. Although studies on PEN film and fiber production and applications were begun by Teijin in the 1960s, it was not until the 1970s that 2,6-NDC became available in sufficient quantities for the first PEN films and fibers to be produced on a semitechnical scale. High value speciality videotapes were found to benefit from the use of PEN film in Japan during the 1980s. In the early 1990s Amoco Chemical Co. announced their plan to invest in a world-scale facility for production of 2,6-NDC in Decatur, Illinois. As a result of the promise of larger scale and more economic raw material supply, plus greater interest from the end market, PEN films were launched commercially in the early 1990s. Since then, the start-up of commercial production at Amoco's (now BP) 30,000 tons/year 2,6-NDC facility has significantly aided the economics of PEN production. This has driven increasing use of PEN in a wide range of applications including films, fibers, and rigid packaging.

An approximate percent breakdown of PEN usage worldwide per end-use segment for the year 2002 is provided in Table 1.

At this time, commercial producers of PEN homopolymer and/or copolymer resins are Teijin Ltd. (Japan), M&G (USA), 3M (USA), KoSa (Europe), Toyobo (Japan), Kolon (Korea), MCC (Japan), Kimex (Mexico), and Shinkong (Taiwan).

Encyclopedia of Polymer Science and Technology. Copyright John Wiley & Sons, Inc. All rights reserved.

Table 1. Major PEN Market Segments and Approximate Percent Breakdown by End-Use Segment[a]

End Use	Approximate consumption, %	Examples
Film	70	Imaging, recording tape, displays, memory storage, insulators, capacitors
Rigid plastic packaging	15	Beer returnable/refillable bottles, pharmaceutical and cosmetic bottles
Fiber	15	Tirecord, hose reinforcement, sailcloth

[a]Data from BP Amoco Chemical Co.

Polymer Properties

Naphthalate polyesters, such as PEN and PBN, derive their performance improvement from the double ring structure of the naphthalene group. Incorporation of this double ring structure in the polymer chain increases thermal, chemical, mechanical, and barrier performance versus polymers based on single aromatic rings. Table 2 illustrates the wide variety of property improvements exhibited by PEN versus PET.

Partial substitution of terephthalate-based polymers with the naphthalate group, in a copolymer or blend form, can provide enhanced properties that are

Table 2. Comparative Properties of PEN vs PET[a]

Property	PEN value	PET value
T_g, °C	122	80
Shrinkage, %		
Dry at 150°C	0.6	1.3
Wet at 100°c	1	5
Mechanical continuous use temperature, °C	160	105
UV absorbance at 360 nm, %	17	1
Radiation resistance, MGy[b]	11	2
Tenacity retention, 45 min. at 150°C, %	99	45
Young's modulus, MPa[c]	5200	3900
Tensile strength, MPa[c]	60	45
Oligomer extraction, mg/m^2	0.8	20
Hydrolysis resistance, h	200	50
Permeability, $\frac{n\ \text{mol}\cdot m}{m^2\cdot s\cdot \text{GPa}}$[d]		
CO_2	12	61
O_2	3	12
Water vapor transmission, $\frac{n\ \text{mol}\cdot m}{m^2\cdot s}$[e]	0.129	0.452

[a]*Source*: Teijin Ltd., Japan.
[b]To convert MGy to Mrad, multiply by 100.
[c]Convert MPa to Psi multiply by 145.
[d]To convert $\frac{n\ \text{mol}\cdot m}{m^2\cdot s\cdot \text{GPa}}$ to $\frac{\text{cm}^3\cdot \text{mm}}{m^2\cdot \text{day}\cdot \text{atm}}$, multiply by 0.2.
[e]To convert $\frac{n\ \text{mol}\cdot m}{m^2\cdot s}$ to $\frac{g\cdot \text{mm}}{m^2\cdot \text{day}}$, multiply by 1.55.

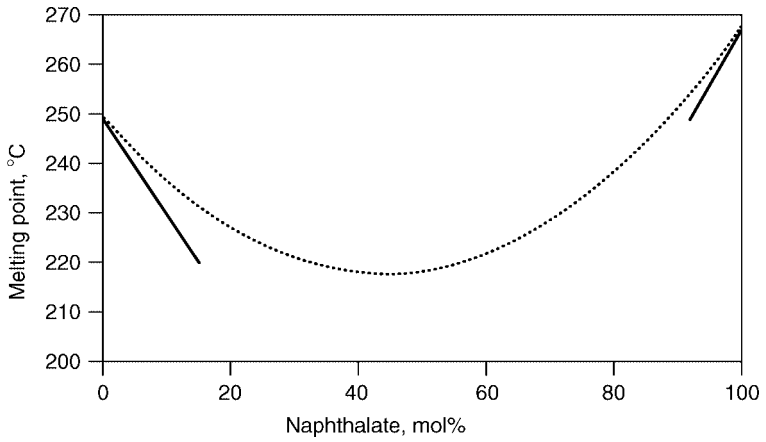

Fig. 1. Melting point of PET/PEN copolymers and blends. ——— Copolymer, - - - - Blend. Data from BP Amoco Chemcial Co.

typically intermediate between the respective homopolymers. A description of key thermal, physical, and mechanical properties is provided below.

Thermal Properties of Naphthalate-Containing Polyesters. Naphthalate homopolymers melt at higher temperatures vs terephthalate homopolymers. Table 3 compares the T_m of PEN and PBN vs PET and PBT respectively.

In random copolymers, where both TA and NDC are present, the melting point decreases as NDC partially substitutes TA (eg, starting from PET) or when TA partially substitutes NDC (eg, starting from PEN). This melting point depression effect is caused by a disruption in the regular crystalline pattern by the minor component (Fig. 1).

Figure 1 shows that the melting point of a PEN copolymer modified with 8 mol% DMT (PENT-8) equals the melting point of a PET homopolymer. Use of the lower melting PENT-8 copolymer in preparing PET/PEN blends is preferred over use of a PEN homopolymer. Not only are lower melt temperatures required in the blending process, which reduces the risk of PET degradation, but there is a better viscosity match between the naphthalate and terephthalate polymers which improves mixing and miscibility.

Within the range of approximately 10–90 mol% NDC, PET/PEN random copolymers (PETN) remain essentially amorphous. On the other hand, PET/PEN blends are capable of crystallizing and exhibiting a melting point at any *T*/*N* ratio, which depends not only on this ratio but also on the degree of randomness or

Table 3. Melting Point of Polyester Homopolymers[a]

Homopolymer	T_m, °C
PET	250
PEN	268
PBT	223
PBN	242

[a] Data from BP Amoco Chemical Co.

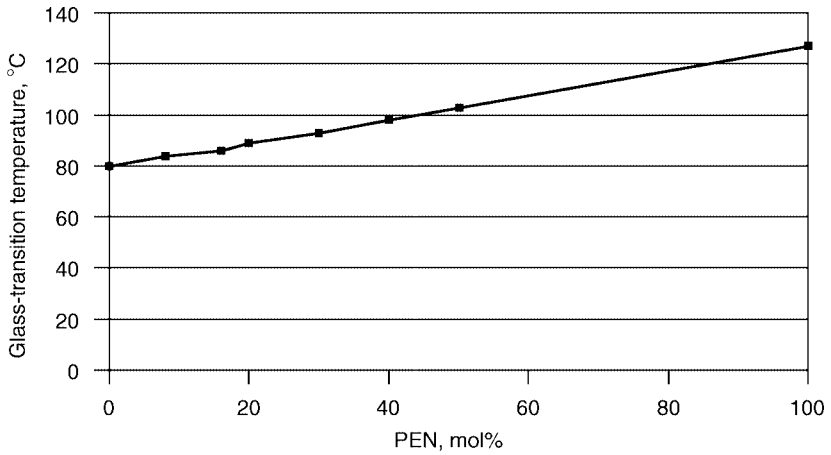

Fig. 2. Glass transition of PET/PEN copolymers and blends. Data from BP Amoco Chemical Co.

transesterification present. The dotted line in Figure 1 provides a cursory representation of this behavior.

Naphthalate homopolymers have a glass-transition temperature significantly higher than the corresponding terephthalate homopolymers (Table 4).

Unlike T_m, the behavior of T_g vs NDC content is linear and follows the mixing rule (Fig. 2).

This linear relationship offers many opportunities for enhancing the thermal resistance of PET by simply blending-in varying amounts of naphthalate. Practical applications include hot-filled, pasteurized, or washable containers, and outdoor glazing.

An increase in T_g also affords improved long-term aging behavior or reduced embrittlement of amorphous parts. It enables a reduction in cycle time during injection molding (eg, of bottle preforms), since the parts can be released hotter. A 20% faster cycle time has been achieved in the case of PEN preforms vs PET. Finally, the higher T_g of PEN contributes greatly to the reduction of thermal shrinkage, which is of value in tire cord and other industrial fiber applications as well as films (see Table 8).

Crystallization. As in the case of PET, PEN can be quenched to amorphous glass. Its amorphous density, 1.325 g/cm^3 [BP Amoco Chemical Co.], is slightly less than that of PET (1.333) (2). Crystallization from the glass or from the melt at low temperatures (<200°C) leads to a triclinic crystal form labeled α (3), whose unit

Table 4. T_g of Polyester Homopolymers[a]

Homopolymer	T_g, °C
PET	80
PEN	125
PBT	46
PBN	82

[a] Data from BP Amoco Chemical Co.

Table 5. PET and PEN Unit Cell Parameters

	PET[a]	α -PEN[b]	β-PEN[c]
Form	Triclinic	Triclinic	Triclinic
a, Å	4.56	6.51	13.14
b, Å	5.94	5.75	9.0.4
c, Å	10.75	13.2	12.19
α, (°)	98.5	81.2	129.31
β, (°)	118	144	88.62
γ, (°)	112	100	90.77
Volume, Å^3	219.2	285.8	1120
Z (rpt units per cell)	1	1	4
Calculated density at 23°C, g/cm^3	1.455	1.407	1.436

[a]Ref. 5.
[b]Ref. 4.
[c]Ref. 3.

cell was determined by Mencik (4). Crystallization from the melt at temperatures above 200°C leads to a more dense crystalline form labeled β (3).

PEN crystallizes in the same crystal pattern as PET, ie, triclinic space group $P\bar{I}$. The unit cell parameters are compared in Table 5.

Gas Permeability. The oxygen, carbon dioxide, and water vapor permeability of polyesters depend not only on composition but also on degree of crystallinity, orientation, and temperature. Regardless of the variable, PEN always exhibits significantly reduced gas permeability relative to PET. Some examples are illustrated in Table 6.

Table 6. Gas Permeability

	PET	PEN	Units and conditions
CO_2 transmission, amorphous sheet	69[a]	15[a]	cc-mil/100 in.^{2}·day·atm @ 23°C and 0% RH
CO_2 transmission, 4 × 4 oriented film (Ref. 8)	31[a]	6.0[a]	cc-mil/100 in.^{2}·day·atm @ 30°C and 0% RH
O_2 transmission, amorphous[b]	10.9[a]	4.4[a]	cc-mil/100 in.^{2}·day·atm @ 23°C and 68% RH
O_2 transmission, oriented film (Ref. 6)	6.1[a]	1.6[a]	cc-mil/100 in^2·day·atm @ 30°C and 68% RH
Water vapor transmission, amorphous	4.31[c]	2.12[c]	g-mil/100 in^2·day·atm @ 38°C and 90% RH
Water vapor transmission, 4 × 4 oriented film (Ref. 6)	1.85[c]	0.52[c]	g-mil/100 in.^{2}·day·atm @ 38°C and 90% RH
Water vapor transmission, commercial biaxially oriented film[d]	0.38[e]	0.09[e]	g·mm/m2·day·atm @ 38°C and 90% RH

[a]For the value with units $\frac{n\ \text{mol}\cdot m}{m^2\cdot s\cdot \text{GPa}}$, multiply by 2.
[b]Data from BP Amoco Chemical Co.
[c]For the value with units $\frac{n\ \text{mol}\cdot m}{m^2\cdot s}$, multiply by 0.253.
[d]*Source*: DuPont Teijin Films (Melinex PET and Kaladex PEN respectively).
[e]For the value with units $\frac{n\ \text{mol}\cdot m}{m^2\cdot s}$, multiply by 0.645.

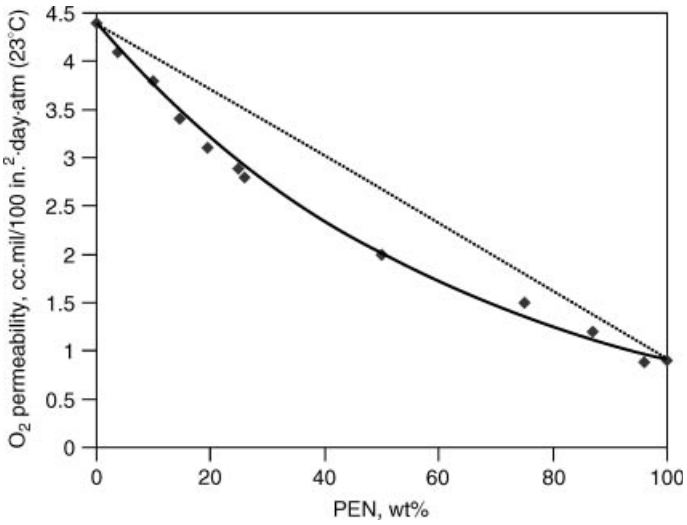

Fig. 3. Oxygen permeability of 4 × 4 biaxially oriented films from PET/PEN blends and copolymers (7). For O_2 permeability values with the units $\frac{n\ \mathrm{mol}\cdot m}{m^2\cdot s\cdot \mathrm{GPa}}$, multiply by 2.

The permeability of PET/PEN copolymers and blends is as good or even lower than that predicted by a linear fit between that of PET homopolymer and PEN homopolymer. For example better-than-linear behavior was reported in the case of O_2 permeability through 4 × 4 biaxially stretched films (Fig. 3).

Chemical Resistance. PEN offers significant improvement in chemical, oxidative, and hydrolytic stability vs PET. This has led to increased use of PEN in demanding engineering resin, fiber, film, and plastics applications and in returnable/refillable, pharmaceutical, and chemical packaging (Table 7).

UV Absorption Characteristics. Naphthalate-containing polyesters demonstrate a dramatically improved barrier to UV radiation. They also exhibit a greater retention of mechanical strength under external exposure or weathering conditions. This behavior is due to the fused aromatic structure of the naphthalate ring of NDC, which absorbs UV light at wavelengths as high as 370 nm. The benzene ring structure of DMT or TA is essentially transparent at wavelengths above 310 nm. This UV absorption behavior is also exhibited in the corresponding polymers (Figs. 4 and 5).

The combination of even very low levels of PEN with PET (by copolymerization or blending) can be a very effective UV barrier. This effectiveness, in the form of transmission versus wavelength through constant thickness (0.33 mm) is illustrated in Figure 6.

Light transmittance T is defined as $T = I/I_0$, where I_0 and I are intensities of incident and transmitted light respectively. The effect of PEN incorporation on light transmission properties at a given wavelength follows the Beer–Lambert Law, $A = \varepsilon CD$, where $A = -\log T$ ("absorbance"), C is PEN concentration, D is light path length, and ε is the naphthalate extinction coefficient at the given wavelength.

Table 7. Comparison of PET and PEN Chemical Resistance[a]

	% Retention of elongation at break	
Chemical Agent	PET	PEN
1% hydrochloric acid		
2 weeks	72	85
5 weeks	74	106
10% hydrochloric acid		
2 weeks	4	69
5 weeks	0	60
1% sodium hydroxide		
2 weeks	76	97
10 weeks	97	126
10% sodium hydroxide		
1 week	0	70
2 weeks	0	50
Ammonia gas		
2 weeks	15	93
10 weeks	0	96
Thermal aging		
2 weeks at 180°C, 0% RH	0	80
2 weeks at 130°C, 100% RH	20	50

[a]From Ref. 8.

Mechanical Properties. Naphthalate presence improves mechanical properties such as modulus and tensile strengths. Like PET, PEN can be oriented uniaxially (fiber) or biaxially (film and bottle) and heat-treated in a variety of ways. Consequently, mechanical properties vary over a wide range depending upon the exact fabrication parameters used. Furthermore, in films, mechanical properties may differ between the machine (MD) and transverse (TD) directions; balanced films have very similar properties between the MD and the TD, whereas in

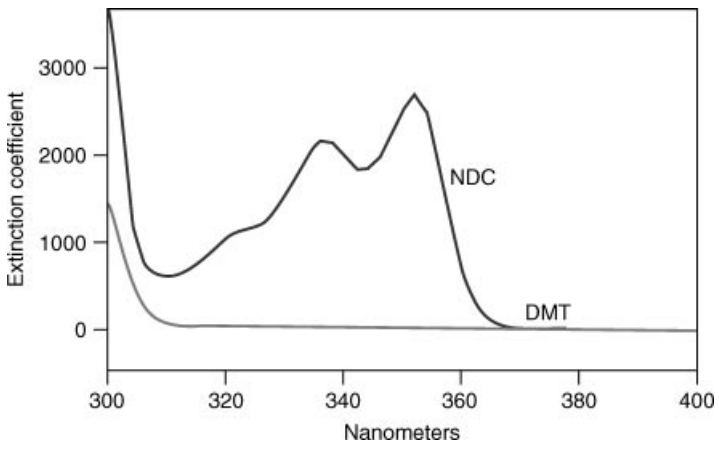

Fig. 4. UV absorption spectrum of NDC vs DMT. Data from BP Amoco Chemical Co.

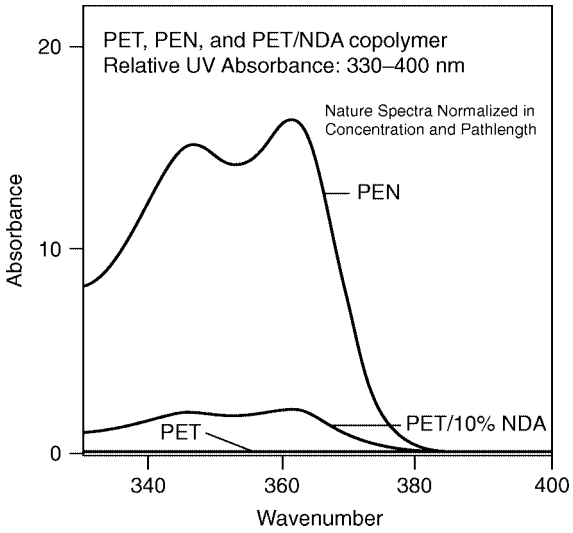

Fig. 5. UV absorption of PEN and PET. Data from BP Amoco Chemical Co.

tensilized films, the properties in MD and TD differ substantially. In general however, PEN bottle sidewalls, fibers, and films are capable of attaining tensile or flex modulus 1.5–3 times higher versus PET. Correspondingly, the elongation at break of PEN is generally lower versus PET.

Table 8 compares mechanical properties of PEN vs PET in typical films and high strength fibers.

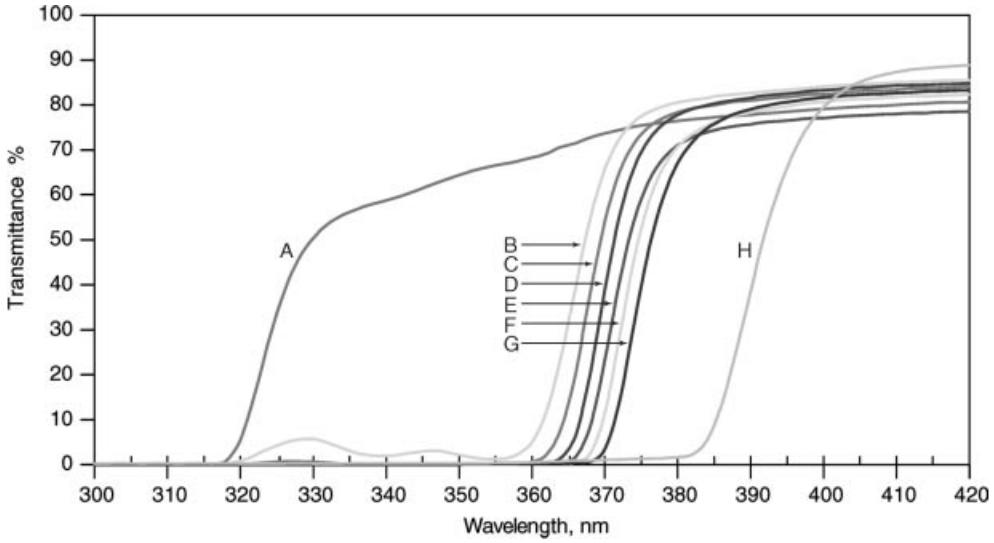

Fig. 6. Light transmission through 0.33 mm for PET, PEN, and PEN/PET combinations. A PET, B 0.3% PEN, C 0.6% PEN, D 1.3% PEN, E 2.5% PEN, F 3.1% PEN G 6.2% PEN, H PEN. Data from BP amoco Chemical Co.

Table 8. Mechanical Properties of PEN and PET Films[a] and Fibers[b]

	PEN	PET
50-μm films		
Young's modulus, Mpa[c]		
MD	5000	3800
TD	5350	4200
Tensile Strength, Mpa[c]		
MD	265	190
TD	150	110
Stress at 5% elongation, MPa[c]		
MD	80	140
TD	70	100
Elongation at break, %		
MD	80	140
TD	70	100
Thermal shrinkage at 150°C, %		
MD	0.6	1.3
TD	0.4	1.3
High strength industrial fibers		
Tenacity, N/tex[d]	0.9	0.8
Modulus, N/tex[d]	32	9.9
Elongation at break, %	8	14
Boiling water shrinkage, %	1	5
Dry heat shrinkage at 177°C, %	4	8

[a] Taken from 1995 DuPont Films PEN Film Brochure.
[b] Refs. 9–11.
[c] To convert MPa to psi, multiply by 145.
[d] To convert N/tex to g/den multiply by 11.33.

PEN Polymerization

Melt-Phase Polymerization. Commercially PEN is produced from 2,6-NDC (abbreviated to "NDC" in the rest of this article) in a process analogous to producing PET from DMT. The reactivity of NDC in a PEN polymerization process is similar to that of DMT in a PET polymerization process and similar catalyst and conditions can be used. Because of this, PEN preparation can be typically accomplished in existing DMT-based polymerization facilities with only minor modification. This modification is generally limited to the NDC feed system and changes required to handle the physical property differences of NDC vs DMT and of PEN vs PET.

Comparative physical properties of DMT and NDC are summarized in Table 9.

The primary differences between PEN and PET polymers from a preparation point of view are the glass-transition temperature and the melt viscosity.

The melt rheology of PEN resin is significantly higher than that of PET even at lower inherent viscosities (IVs) and/or higher temperatures. The rheology of PEN at an IV typically produced in a melt-phase polymerization (0.49–0.53) was

Table 9. Properties of NDC and DMT[a]

	NDC	DMT
Molecular weight	244.26	194.19
Melting point, °C	190	140
Specific gravity	1.35	1.28

[a]Data from BP Amoco Chemical Co.

Table 10. Solubility of NDC in Diols Used in Polyester Polymerization[a]

Ethylene glycol at:	Solubility in g/100 g diol
135°C	1.0
160°C	9.1
167°C	23.1
170°C	31.1
178°C	79.9

[a]Data from PB Amoco Chemical Co.

measured at 295°C and compared to typical PET melt-phase resin. As Figure 7 indicates both PEN IVs had higher viscosities than that of PET.

PEN and copolyesters are readily prepared from NDC and ethylene glycol using either batch or continuous polymerization (12). Solubility data for NDC in ethylene glycol is summarized in Table 10. An example of a typical continuous polymerization process is shown in Figure 8.

NDC, ethylene glycol, and a suitable catalyst are metered into the first of a series of ester-exchange reactors. Normally, several ester exchange reactors provide

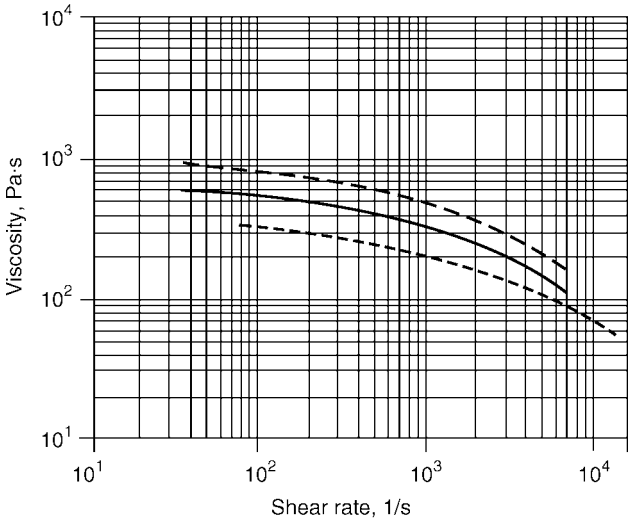

Fig. 7. Viscosity vs shear rate for PEN and PET at 295°C. ——PEN IV = 0.53, — — — PEN IV = 0.49, ▬ ▬ ▬ ▬ PET IV = 0.64. To convert Pa·s to poise, multiply by 10.

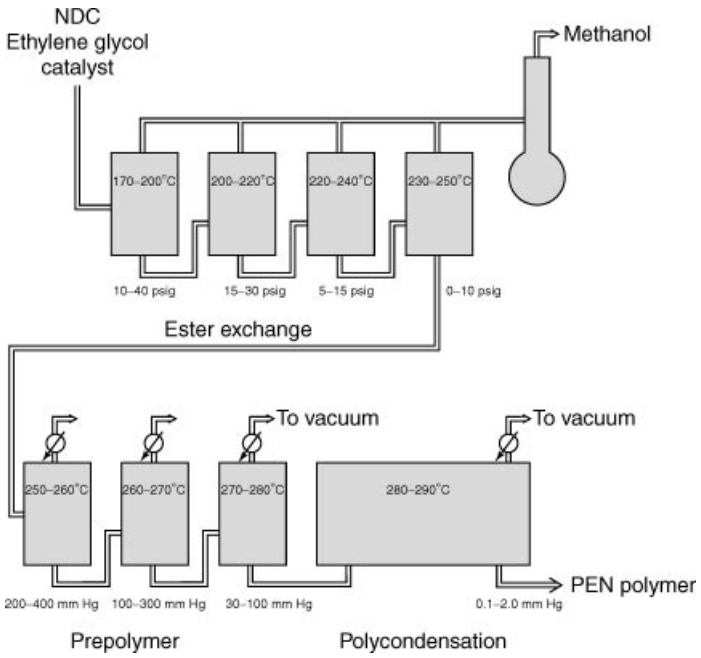

Fig. 8. Continuous PEN polymerization.

control of the temperature profile and conversion to 2-hydroxyethyl terminated oligomers, while the by-product methanol is removed and recovered. Glycol-to-ester feed mole ratios typically range from 1.5 to 3.0, while reactor temperatures range from 170°C in the initial reactor to 250°C in the final reactor. The initial reactor pressure can range from 10 to 40 psig, dropping to 0–10 psig in the final reactor.

The ester-exchange reaction product, a mixture of oligomers, is subsequently metered into the first of a series of prepolymer reactors. Generally, several agitated reactors are used. Operating in a temperature range of 250–280°C, excess ethylene glycol is removed and the resulting prepolymer is metered into a final reactor to complete the polymerization. According to this process, PEN polymer is produced having an IV of 0.4–0.6 dL/g. Examples of suitable final polymerization reactors include the horizontal types supplied by Zimmer AG (Germany) and Hitachi (Japan).

Catalysts, such as manganese, zinc, calcium, cobalt, and titanium, have been widely used as effective ester-exchange catalysts. Polycondensation catalysts, such as antimony, are commonly employed. Phosphorus compounds can be added to increase the thermal stability of the finished resin.

Crystallization/Solid-State Polymerization. As in the case of PET, production of PEN polymer for container or packaging applications will typically include crystallization/solid-state polymerization step. Because PEN has a higher melt viscosity and gas barrier, the volatile byproducts of a solid stating process, such as water, ethylene glycol, or acetaldehyde, are more easily trapped inside the amorphous pellet. This may result in a tendency of the pellets to undergo sudden expansion during crystallization or solid stating.

Several procedures have been described for crystallizing/solid stating PEN. These procedures include adding a devolatilization step (13), or conducting the crystallization under elevated pressure (14) or in the presence of a liquid (15). Because of its higher T_g vs PET, the optimum crystallization temperature range for PEN (180–220 °C) is higher than that of PET (150–190°C). Similarly, because of its higher T_m, the typical SSP temperature of PEN (240–260°C) is higher than that of PET (210–240°C). On the other hand, PEN copolymers with 8–10 mol% TA, which match the PET melting point, should be solid-stated at the same temperature conditions as PET. A typical solid-stated PEN resin has an IV in the range 0.55–0.70 dL/g.

Fiber Applications

The principal applications of PEN and PEN/PET blends and copolymers are as films (see POLYESTER FILMS).

PEN multifilament fibers are commercially available from several polyester fiber producers. These include Teijin in Japan, Honeywell (formally AlliedSignal) in the United States and Europe, Kosa in Europe, and Hyosung in Korea. PEN fibers are produced in a melt spinning/post-drawing process similar to that used in PET fiber manufacture. All production to date is in the form of continuous multifilament yarn, although staple and monofilament fabrication have also been reported.

PEN-based fibers extend the performance of polyesters. PEN fibers have excellent heat resistance, modulus, and dimensional stability relative to PET and demonstrate better retention of mechanical properties in a hot/wet environment and offer improved chemical resistance versus PET fibers (see POLYESTERS, FIBERS). With naphthalate modification, polyester fibers can meet the application requirements, which are currently served by other high performance industrial fibers such as rayon, nylon-6,6, aramids, poly(phenylene sulfide) (PPS), and even steel.

The primary commercial application of PEN fiber today is in rubber reinforcement. Fibers with high molecular weight, crystallinity, and high molecular orientation are required. To produce high orientation PEN fibers requires optimization of both resin design and spinning technology. Typically, high IV (>0.9) solid-stated PEN resin is used. High IV PEN resin is available from suppliers such as M&G and Teijin. In addition to rubber reinforcement (for tires, belts, and hoses) applications for PEN fibers include ropes and cordage, and sailcloth.

Tire Reinforcement. PEN's superior thermal and mechanical properties make it a natural candidate for the reinforcement of radial passenger and light truck tire carcasses. These superior properties are summarized in Table 11.

PEN yarn has higher tenacity and improved modulus vs PET, nylon, and rayon. Its thermal properties, eg, dry heat shrinkage, are also superior. This lower thermal shrinkage is a significant benefit in tire cord manufacture because of the heat-setting treatment and preshrinkage relaxation required to convert yarn to twisted cord. Compared to PET, the lower thermal shrinkage of PEN enables less preshrinkage treatment, which results in a final cord that has improved tenacity and modulus.

Table 11. Physical Properties of High Strength Industrial Yarns Used in Reinforcement

	PEN	PET[a]	Nylon[b]	Rayon[c]	Aramid[d]
Density	1.36	1.39	1.14	1.52	1.44
Tenacity, N/tex	0.9[f]	0.8	0.8	0.44	2
Tensile modulus, N/tex[e]	32[g]	9.7	4.4	11	49
Tensile elongation, %	8[h]	14	15	12	4
Boiling water shrinkage,%	1[g]	5	8	Decomposes	<0.1
Dry heat shrinkage (1 min at 177°C)	4[g]	8	10	6	<0.1

[a] Ref. 11.
[b] Ref. 16.
[c] Ref. 17.
[d] Ref. 18
[e] To convert N/tex to g/den, multiply by 11.33.
[f] Refs. 9 and 10.
[g] Ref. 9.
[h] Ref. 10.

There are multiple opportunities for PEN fiber use in tire construction. Figure 9 is a typical tire construction schematic, showing the three different tire cord textile layers, carcass, belt reinforcement, and cap ply, where PEN fiber can be used.

Cap Ply Reinforcement with PEN. The cap ply is wound over the shoulders or the entire body of the belt to provide a compressive force, which resists the centrifugal forces created in the belt at high rpm. Nylon-6,6 has been typically used for cap ply applications because of its high retractive force at elevated temperatures. PEN cord has been demonstrated to offer similar properties to nylon at 177°C and is an excellent replacement material. Honeywell (formally AlliedSignal) has commercialized high tenacity/high modulus PEN fiber under the trade name PENTEX. In January 1999, Italian tire company Pirelli launched a new

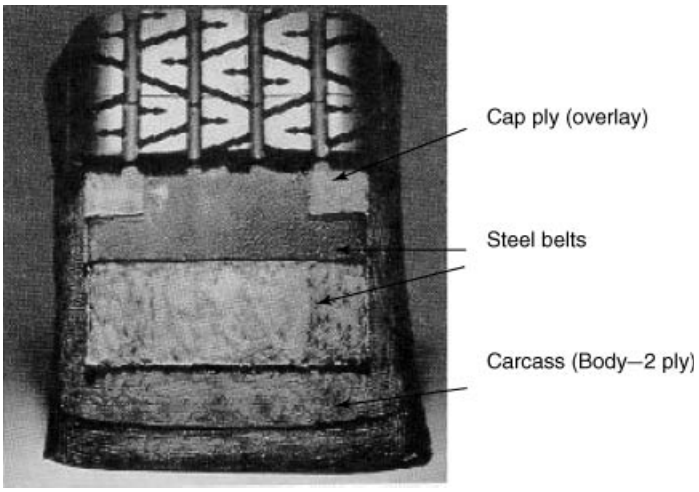

Fig. 9. Radial tire anatomy (19).

tire reinforced with caps made from PENTEX (20). Pirelli uses tire cord made from PENTEX in its Dragon EVO Corsa line of radial motorcycle tires. PEN's significantly higher modulus vs nylon or rayon, 22, 4.4, and 11 N/tex (250, 50, and 125 g/den) respectively, gives it the dimensional stability required for these high performance uses.

Bridgestone, the largest tire company in Japan, is also using PEN cord in nylon cap replacement applications in its Regno GR7000 tire (21). In addition to the dimensional stability improvements, the rigidity that PEN brings to the tire prevents noise generated at the road surface from being transmitted to inside the car. Tests show that these PEN-containing tires reduce road noise by as much as 30%, making the tires ideally suited for high end luxury cars, such as the Lexus.

Carcass Reinforcement. There are several fibers currently used in carcass reinforcement. High modulus/low shrinkage PET is typically used in most radial passenger tires and offers a good mix of properties. Nylon is used extensively in bias ply tires where strength is paramount; this has more value in developing countries with poorly maintained roads and in off-the-road equipment tires. In most of the developed world nylon carcass tires are not longer preferred in passenger cars because of the problem of flat-spotting associated with nylon's high moisture regain. Rayon is the reinforcement cord of choice in Europe for high performance tires, due to its ability to maintain mechanical properties at high temperature.

The performance properties of PEN present opportunities for rayon replacement in carcass construction (22). The use of PEN cord in these applications is currently being evaluated in both Asia and Europe. PEN has a demonstrated acceptable flexural fatigue equivalent to PET and rayon. It has equivalent toughness to rayon, which is important for sidewall impact resistance and curb scuffing resistance. PEN's superior mechanical properties also afford opportunities to use less fiber in carcass construction, enabling production of lighter weight, more fuel-efficient tires.

Steel Belt Replacement with PEN. In radial tires, the carcass provides reinforcement along the radial direction. To provide reinforcement in the rolling direction, belts are necessary. Steel is the traditional material of choice but there has been a drive to replace it with lighter weight synthetic cords. Aramids offer a synthetic alternative but their cost has been prohibitive except for high performance racing tires and luxury cars. PEN has good fatigue at low twist and superior compressive modulus to aramid. This translates into a significant reduction in tire weight and improvement in fuel usage. In addition, use of a polyester fiber-like PEN offers greater opportunity to recycle used tires.

Belts and Hoses. As automotive design trends toward higher engine operating temperatures, the requirements for under the hood reinforcement fibers have changed. Today, fibers not only require good mechanical and thermal properties, but also improved chemical/hydrolytic resistance in a hot-wet environment. PEN fiber meets these more demanding requirements. Performance advantages of PEN include the following:

(1) cost (half compared to aramid)
(2) very low tension decay

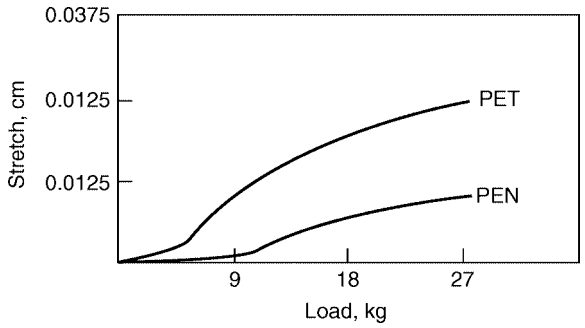

Fig. 10. Stretch at equivalent load of PEN yarn compared to standard polyester (23).

(3) high modulus (two times of PET)
(4) low shrinkage after cure
(5) high adhesion and adhesion retention
(6) improved fatigue resistance

Several types of PEN- or PBN-reinforced belts and hoses, ranging from transmission belts to oil brake hoses, have been produced. Additional applications include timing belts, conveyer belts, high pressure hydraulic, steam, fuel, and coolant hoses, as well as polychain belt cord.

Ropes and Cordage. PEN's high strength, hydrolytic stability, and resistance to UV light degradation create numerous opportunities for its use in rope and cordage applications. The combination of strength and low stretch make PEN cordage the material of choice for rescue rope applications (Fig. 10). For example, Sterling Rope utilized Honeywell's high tenacity PEN yarn, Pentex, in their high performance rescue rope products (24). The dimensional stability of the PEN rescue rope, with less than 1% stretch per 300-lb load, ensures steady support for rescue operations.

Sailcloth. PEN filament yarn has found applications in high performance sailcloth construction. Challenge Sailcloth Inc. has introduced its SuperModulus sailcloth made from Honeywell's high tenacity PEN fiber, Pentex (23). The improved UV resistance of Pentex fibers more than doubles the shelf life of sails in the Caribbean, Mediterranean, and other high UV areas. The low stretch characteristics of PEN also provide a significant advantage in performance and enables production of a much lighter weight sail.

Rigid Packaging Applications

The use of naphthalate-modified polyester resins in packaging applications offers improvement in gas barrier, UV barrier, thermal, and mechanical properties versus PET alone. Naphthalate resins suitable for packaging applications are commercially available in either homopolymer (PEN), PET/PEN copolymers (PETN-x), or PET/PEN blends.

Naphthalate-containing polyester resins at all compositions, from 0 to 100%, are fully regulated for use in food contact applications. Naphthalate polymers are

Table 12. Naphthalate Resin Benefits in Rigid Packaging Applications

Application	Naphthalate Benefit	Typical resin type
Returnable/refillable (Beer, mineral water, water fountain jugs, juice milk)	Improved thermal resistance (washing) Improved chemical resistance (washing) Reduced flavor carryover Reduced adsorption Improve gas barrier (CO_2 loss and O_2 ingress) Increased UV barrier	PEN, copolymers, blends
Beer—one way	Pasteurization capability Increased UV barrier	Copolymers
Small-size carbonated soft drinks (<0.5 L)	Improved barrier against CO_2 loss Increased UV barrier	Copolymers, blends
Hot-fill applications (Foods, sport drinks, fruit juice)	Improved thermal resistance Improved barrier Increased UV barrier	PEN, copolymers, blends
Sterilizable applications (baby bottle)	Improved thermal resistance	PEN, high PEN copolymers
Retort applications (baby food)	Improved thermal resistance	PEN, high PEN copolymers
Pharmaceutical/cosmetic	Improved barrier Improved chemical resistance UV barrier	PEN, copolymers, blends
Industrial and speciality	Improved barrier Improved chemical resistance	PEN, copolymers, blends

permitted for use with all food types and under all conditions of use as defined by the FDA. These include packaging for foods that undergo high temperature sterilization in the container, to frozen foods reheated in the container.

A summary of naphthalate rigid packaging commercial and potential applications is provided in Table 12. Applications of naphthalate-modified polyesters can be segmented by resin type and naphthalate content. This includes PEN homopolymer, medium level PET/PEN blends and PETN-x, or low naphthalate level copolymers. The use of a particular resin type is often dictated by optimization of cost versus the thermal and barrier requirements of the application. Figure 11 summarizes current uses and potential opportunities for naphthalate polyester resins in rigid packaging.

Rigid Packaging Applications for PEN Homopolymer and High PEN Copolymers. PEN homopolymers and high level PEN copolymers are best suited to rigid packaging application requiring the maximum in organoleptics, temperature, and gas barrier improvement. Specific published examples, including market trials and commercial launches, are listed below.

Returnable/Refillable Beer Bottle. In August 1999, Carlsberg A/S launched PEN returnable/refillable bottles for their Carlsberg Lager and Tuborg Green Label brands sold in Denmark (20,25). Danish law requires that all carbonated bottles filled in Denmark are returnable and refillable. Although for one-way

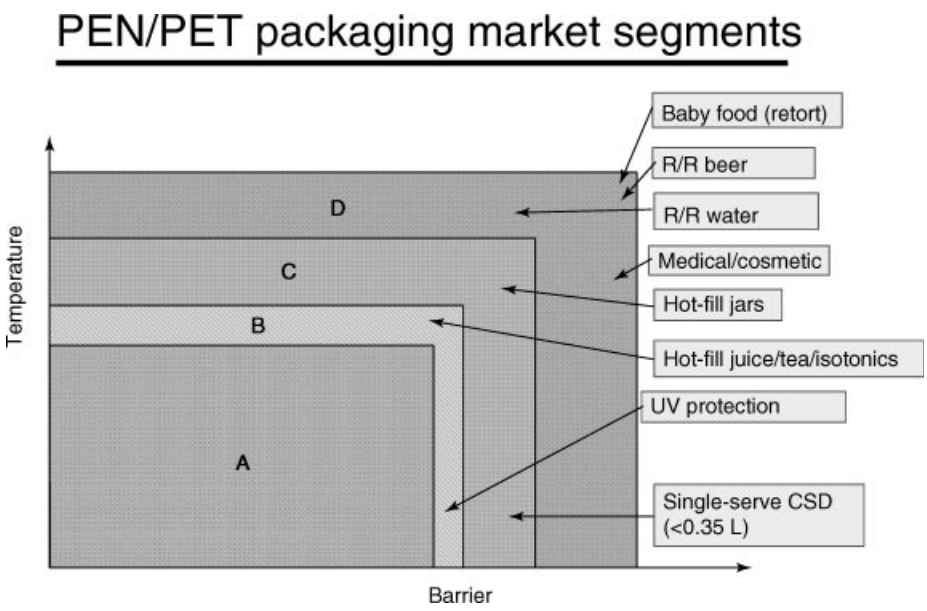

Fig. 11. Opportunities for PEN homopolymers, copolymers, and blends in rigid packaging. A PET, B Low PEN copolymer, C PEN blends, D PEN.

beer coated plastic bottles multilayer PET solutions are available, PEN is the only plastic material that combined the necessary barrier, pasteurization capability and the ability to withstand repeated washings at temperatures used to sterilize glass bottles—up to 85°C. The PEN bottles keep carbon dioxide in and oxygen out, enabling a shelf life of greater than 4 months. The ability to reuse the bottle, an 80% reduction in weight versus glass, makes the PEN return refill package the preferred environmental and total system cost solution. PEN returnable/refillable beer bottles were also launched in Norway and in Brazil (24,25).

PEN Returnable/Refillable Water Bottle. The washing temperature used in returnable/refillable water bottles (up to 90°C in caustic solutions) is higher than the washing temperatures typically used for returnable/refillable carbonated soft drink (CSD) bottles (45–60°C). This is dictated by higher requirements for removal of trace foreign contaminants that might contribute to bad taste. In addition, antiscalping and carbonation retention performance are equally critical. In view of all these factors, PEN, with its high T_g (125°C vs 80°C for PET), high carbonation retention (four times relative to PET) and excellent anti-sorption/desorption characteristics have been an ideal material for packaging returnable/refillable water. In Uruguay, a PEN returnable/refillable bottle was introduced for mineralized water sold under the Bonaqua brand by MONRESA (Montevideos Refrescos, SA), a bottler of The Coca-Cola Co. (26). With PEN bottles, carbonation retention was demonstrated to be four times greater than with PET bottles. The returnable/refillable PEN bottles easily withstand washing with a 2% sodium hydroxide solution at 90°C. No stress cracking and less than 1% dimensional change was shown after 100 washing and refilling cycles.

PEN Cosmetic Bottle. Replacing glass with clear plastic in small bottle applications, like ampules for cosmetics or medicines, requires a polymer that has acceptable resistance against heat distortion, environmental stress cracking, vapor barrier, and creep *in the amorphous state*. This is because the injection blow process used to fabricate clear small containers typically affords an amorphous or low crystalline bottle. PEN homopolymer with its high T_g (125°C) and low gas permeability and chemical resistance is ideal for these applications. One commercial example is a skin care product from Japan's leading mail-order cosmetics company, FANCL (20). Substitution from glass to plastic in this case was driven by two factors: waste disposal in incinerators (glass does not burn) and reduction in total packaging size and cost. With the PEN bottle, FANCL reduced the amount of required protective packing, decreased the size of the box, and substantially reduced the total costs of packaging.

PEN for Medical Applications. Another application for PEN is medical packages, where material selection is driven by chemical resistance, safety, and strength. One example is a package from Abbott Laboratories (24), used for the drug Sevoflurane, a volatile anesthetic used in hospital operating rooms. PEN was chosen to replace glass because of its chemical resistance, low extractables, and strength. The container needs to be able to contain pressure buildup if the contents increase in temperature.

PENT-8 Reusable Baby Milk Bottle. Although polycarbonate (PC) has traditionally been the preferred alternative to glass in reusable baby milk bottles, health concerns with PC usage have been raised in some countries about possible presence of residual bisphenol A. The use of a high PEN-containing copolymer, PENT-8, has been demonstrated to provide a bisphenol A free substitute for PC. In Korea, Kolon has found that PENT-8 has adequate T_g (123°C) to withstand required sterilization in boiling water (20). At the same time, the lower melting point of PENT-8 (250°C) relative to PEN (268°C) makes it processable at PET melt conditions.

PEN School Lunch Tableware. Another example where PEN replaced PC owing to concerns about bisphenol A was in tableware for school cafeterias in Japan (24). The producer, Sanshin, selected PEN homopolymer for its ability to withstand multiple washings and its antiscalping properties.

PEN Bottle Fabrication by Injection Stretch Blow Molding. PEN is semicrystalline polyester-like conventional PET, and those familiar with and skilled in the fabrication of conventional PET should be able to produce good quality bottles from PEN. However, there are some differences between PEN and PET that must be considered when fabricating PEN. The most important of these are the higher glass-transition temperature and melting point of PEN (Tables 2 and 3).

Because of its higher melting point, PEN must be injection-molded at higher temperatures than PET, and because of the higher glass-transition temperature, PEN preforms must be preheated to higher temperature when stretch blow molded.

With respect to preform design, optimization of bottle properties will result from using a slightly higher stretch ratio for PEN than for conventional PET. This is illustrated in Figure 12, which shows stretch ratios of PET and PEN of various IVs. The data were obtained by free blow experiments that were conducted at the

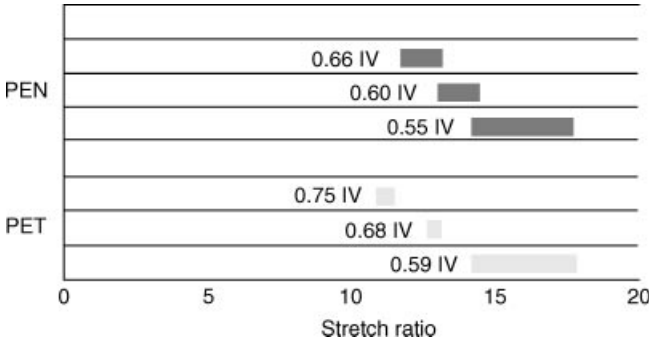

Fig. 12. Stretch ratios of PET and PEN.

optimum stretch temperature range for each resin, which was 105–110°C in the case of PET and 165–170°C in the case of PEN.

The results show that stretch ratio decreases with increasing IV for both PET and PEN but that for a given IV, the stretch ratio of PEN is greater than that of PET. This means that for typical commercial PEN with an IV of about 0.65, one would want to design the preform tooling with a slightly higher stretch ratio than used for typical 0.80 IV commercial PET.

Resin Drying. Like conventional PET, PEN is sensitive to hydrolysis and must be dried prior to melt processing. Recommended drying conditions for PEN are shown in Table 13.

The recommendations are based on a polyester pellet size of 40–50 pellets/g and may need to be adjusted if the pellets are smaller (shorter time) or larger (longer time). The polyester should be dried to a moisture level of 50 ppm or less prior to melt fabrication. Drying temperature greater than 175°C (350°F) should be avoided to prevent discoloration of the polyester.

Preform Injection Molding. PEN homopolymer must be molded at significantly higher temperatures than PET to accommodate the higher melting point and melt viscosity of PEN. In general, for a given injection molding machine, the initial temperature settings should be about 20°C higher for PEN than those typically used for PET. From that starting point, conditions can be adjusted to provide optimum quality preforms. Representative processing conditions for PET and PEN are shown in Table 14 and Figure 13. The data are intended to provide a relative comparison of molding conditions; optimum conditions will depend on the specific resin and injection molding machine used.

Bottle Stretch Blowing. The key difference in stretch blow molding of PEN vs PET is related to the higher glass-transition temperature of PEN. Since the

Table 13. PEN Drying Conditions

Temperature	Drying time, h
150°C (300°F)	6.0
162°C (325°F)	5.0
175°C (350°F)	4.0

Table 14. Indicative Processing Conditions for Making One-Way Amber Beer Bottle Preforms from PEN in Comparison to PET[a]

	PEN	PET
Temp. settings, °C		
Feed zone	291	271
Zone 2	290	270
Zone 3	290	270
Zone 4	290	275
Nozzle	295	275
Back pressure, bar	50	35
Screw speed, m/min	10.0	10.0
Cooling time, s	18.0	18.0
Total cycle time, s	48.8	50.1
Shot size, g	36.9	36.9
Hot runner, °C		
Body	300	275
Tip	305	280

[a]Bottle type: 500 mL, 37 gram weight, long neck with crown finish; preform areal strain: 16.5 for PEN, 13 for PET (see Fig. 13). Amber Colorant: Colormatrix #89-767-1 Tr Amber.

glass-transition temperature of PEN is approximately 40°C higher than that of standard PET, the PEN preforms must be heated approximately 40°C higher than PET preforms prior to stretch blow molding. This can be accomplished by increasing the infrared lamp power settings. If not enough power is available at a given line speed, the next step is to reduce line speed in order to increase residence time in the infrared oven. Since the preform reheat temperature is significantly above the water boiling temperature, it is recommended that amber-colored preforms are kept dry or dried prior to stretch blowing, since the amber colorant particles might nucleate boiling of moisture present, resulting in blistering. A representative set of stretch blow molding conditions (used in blowing the preforms shown in Fig. 13, made according to Table 14) is shown in Table 15. The resulting bottle is shown in Figure 14.

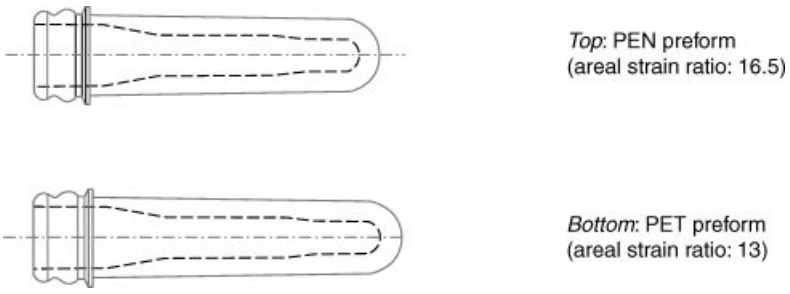

Fig. 13. Difference in preform design for making the same bottle from PEN vs PET (as per Table 14).

Table 15. Representative PEN Stretch Blow Molding Conditions vs PET

	PEN	PET
Speed, bph	500[a]	800
Mold temp., °C	4	4
Mold base temp.	4	4
Overall Oven Power, %	80	60
Oven lamp settings		
Zone 6	50	70
Zone 5	0	70
Zone 4	65	0
Zone 3	30	60
Zone 2	50	32.5
Zone 1	72.5	85
Preform temp., °C	141	99

[a]Slowed down vs. PET to provide additional residence time in the oven for heating up preform to the required temperature (141°C).

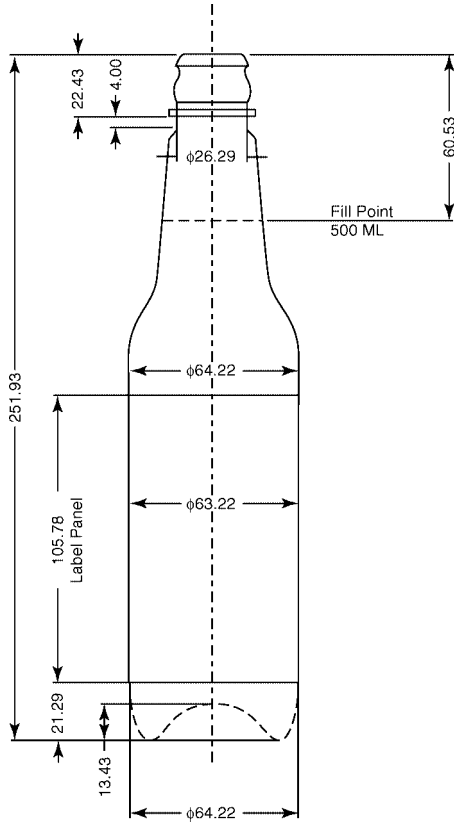

Fig. 14. Schematic of bottle referred to in Table 15

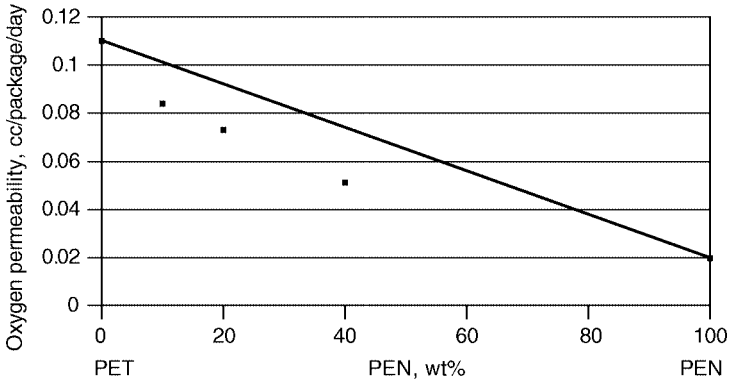

Fig. 15. Oxygen permeation of 0.35-L jars from PET/PEN blends (31).

Rigid Packaging Applications for PET/PEN Blends. Physical blends of PET with PEN are best suited for rigid packaging applications when performance requirements demand a naphthalate content in a range of 15–90%. Random copolymers within this range lack the ability to develop the strain–induced crystallization needed in most bottle applications. Although PET/PEN blends are initially immiscible, melt-blending PET and PEN under conditions where a limited amount of transesterification takes place enhances miscibility, which results in a single T_g and clear blend. The processing window required to produce an acceptable degree of transesterification is wide enough to produce blends that are clear but still capable of developing strain-induced crystallinity. Several studies have been published describing the necessary blending residence time and temperature conditions (27–29). Aoki has reported barrier properties of containers prepared from blends of PET with PEN (30). The data show that the barrier performance observed for 10, 20, and 40 wt% blends exceed that predicted by extrapolation of simple mixtures (Fig. 15), in agreement with the data shown earlier on films (Fig. 3).

Small Hot-Fillable Wide Mouth Jars. PEN/PET blends have been successfully used in wide mouth, nonheat set hot-fill container applications. Aoki and Guelph Food Technology Center established that the hot-fill performance for wide mouth containers made from PET/PEN blends matched closely the glass-transition temperature of the material (31). As shown in Figure 16, containers from each material were tested under a special protocol for hot-filling performance. The jars were filled at various temperatures. The maximum temperature tried at which a jar gave satisfactory performance is marked as "pass" and the next higher temperature tried is marked as "fail." As seen in all cases the material's T_g lies between the "pass" and "fail" temperature.

The biggest benefit of this performance attribute is in the case of small wide-mouth containers, where development of crystallinity during stretching is minimal and application of heat-setting is not practical. A commercial example was a PET/PEN blend container with 40 wt% PEN introduced under the Aran brand in Scotland (32). The size of the container, made on a one-step Aoki machine, was 28 g and the filling was done at 85°C.

CSD Bottles from PET/PEN Blends. As the container size decreases the need for gas barrier (carbonation retention in the case of CSD) increases. This

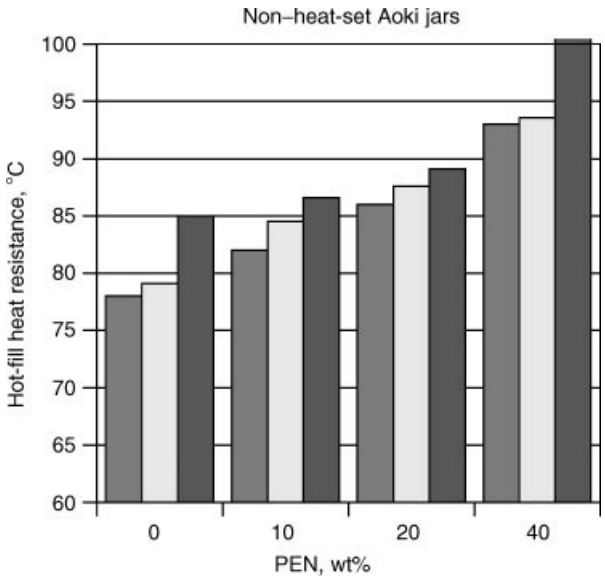

Fig. 16. Hot-fill performance of amorphous jars made from PET/PEN blends. □ Pass ◻ T_g, ■ Fail.

is a direct effect of the increase in specific area or area per unit volume. In general, when considering normal transportation logistics and desired shelf life, the practical CSD bottle size limit attainable with PET is 500 mL. At the same time, market research has shown that smaller single-serve sizes (eg, 350 mL) are desirable in many regions worldwide. The Coca-Cola Co. had demonstrated, through an extended test market introduction in Australia, that a PET/PEN blend is suitable for fabricating a 350-mL bottle that meets the shelf life requirements for Coca-Cola and Diet Coke carbonated beverages (32).

Packaging Applications Using Low PEN Level PET/PEN Copolymers. PETN-x low level copolymers, where $x \leq 1\%$ to typically 10% are used in rigid packaging applications where increased UV barrier resistance or small improvements in thermal performance versus PET are required.

Naphthalate UV Property Benefits in Packaging Applications. As discussed in the Performance Property section, NDC incorporation—even at a low level—into polyesters affords substantial UV-absorber absorption in the 310–370 nm wavelength range. The ability of NDC to function as a UV radiation blocker can be used to protect container contents from the harmful effects of UV light in applications ranging from dairy products to fruit juices and pharmaceuticals. A fundamental advantage offered by NDC-based UV barrier protection in polyester containers is its stability to migration. Unlike many standard UV stabilizers that can leach or migrate out of the polymer matrix, NDC is reacted directly into the polyester backbone and cannot migrate.

Studies completed on model color-sensitive beverages further illustrate the effectiveness of low level naphthalate modification in protecting against UV radiation exposure (33). The model beverage consisted of 20 ppm Yellow #5, 1000 ppm citric acid, 200 ppm sodium benzoate, and 100 ppb iron. This model

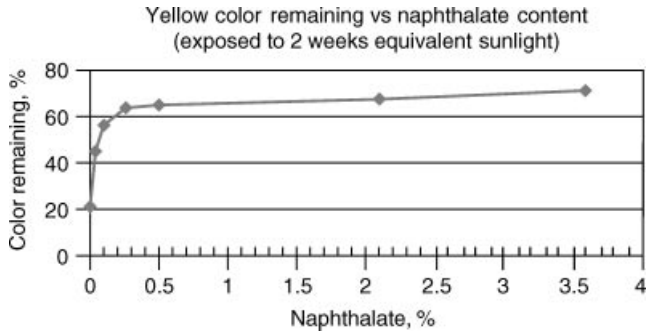

Fig. 17. Color retention of a model beverage in PET and PETN bottles (33).

solution is extremely sensitive to yellow color bleaching upon UV exposure. As Figure 17 illustrates, after accelerated testing in a Xenon weatherometer (corresponding to 2 weeks of equivalent sunlight), substantial protection against color loss occurred even at very low levels of naphthalate content in the PET package. This plot indicates that an NDC level as low as 0.25 mol% should be sufficient for many UV barrier applications.

The same study demonstrated the UV protective capability of PETN copolymers on the color stability of a commercial juice drink containing artificial colorant Blue No. 1. As shown in Figure 18, PET modified with 0.25 mol% NDC offers substantial protection against a dramatic loss in color occurring after only 5 h of sunlight exposure when unmodified PET is used instead.

Low level NDC modification of PET has been used in Japan for Listerine Cool Mint mouthwash, a product of Warner-Lambert Japan. The PETN copolymer in these 80-mL to 700-mL bottles is used to extend shelf life by protection from UV exposure, as well as to prevent absorption of the active ingredients of the mouthwash into the bottle (30). Another commercial packaging application, relying on the UV barrier property of naphthalates, was Fujiya's Lemon Squash (34), packaged in a 1.5-L PETN copolymer bottle. A small amount of naphthalate was incorporated into the PET resin to protect the drink's natural fruit juices and added Vitamin C.

PETN Copolymer Hot-Fill Applications. PETN copolymers at naphthalate modification levels up to 10 mol% are capable of developing strain-induced crystallinity. These copolymers have been used in several bottle geometries and offer both improved thermal resistance and UV barrier versus PET. These advantages derive in part from the increase in T_g (as shown in Fig. 1), and partly from optimizing the bottle stretch blow process and preform design. For example, bottles from PETN that were subjected to a one-stage heat-setting treatment (hot mold) without neck crystallization have been capable of hot-fill temperatures up to 93–95°C. Table 16 shows an example of a hot-fill test comparing a PETN-10 and a PET 500-mL tea-drink bottle.

This increased temperature stability has stimulated several commercial PETN commercial introductions. Examples are illustrated below.

Hero Group, U.K.-based Carters Packaging, had produced a one-way and multitrip container for hot-fill applications (30). Produced on a Sidel standard heat-set, one-wheel blow-molding machine, the package could be hot-filled to 95°C

Table 16. Hot-Water Hot-Fill Test[a,b]

Volume change at:	PET	PETN-10
85°C	−1.0%	−0.2%
90°C	−2.5%	−0.4%
93°C	−2.0%	−0.4%

[a]Data from BP Amoco Chemical Co.
[b]One-step heat-set 500 mL tea-drink bottles, amorphous neck.

after standard aging practices, without having to crystallize the neck to prevent deformation. The one-trip container had a weight of 59 g and a 28-mm neck, while the returnable and rewashable bottle had a weight of 76 g and a 43-mm neck finish. The latter could be washed at 75°C with a 2% caustic solution. For comparison, heat-set PET allows only a washing temperature as high as 59°C.

Säntis Kunstoffe, a Swiss bottle producer, had introduced a 0.5-L PETN-8 container. This bottle contained "Sports + Fit" athletic beverage, which comes in Orange or Citrus Flavor (23). The bottle, which was made on a MAG machine, weighed 40 g and had a filling temperature of 85°C. A similar bottle has been used in Switzerland by the canner Bischofszell AG for its 100% orange juice brand "Sunqueen." which is distributed by the Swiss Migros supermarket chain.

Log Plastics Products Co. of Israel had developed a 1.0-L bottle from PETN copolymer for hot-fill applications (28). The bottle was produced on an Aoki one-step machine. It was used by Gan Schmuel Foods Ltd. for its 100% juices.

Water bottler Powwow has introduced in Europe 5-gallon returnable/refillable containers from PETN copolymers, for use in drinking water fountains, an application typically served by PC (35). Unlike PC containers, which are made by extrusion blow molding, the PETN 5-gallon containers are fabricated by one-step injection/stretch blow molding. Incorporation of PEN repeat units enhances the container's thermal stability against washing with hot caustic solutions, for increased number of trips.

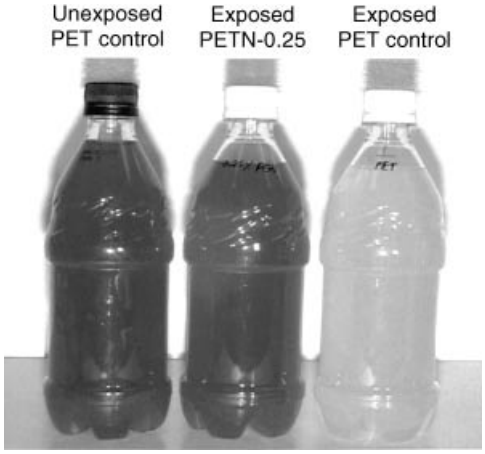

Fig. 18. Blue-colored fruit drink exposed to sunlight for 5 h (33).

BIBLIOGRAPHY

1. BP604,073 (1948), J. G. Cook and co-workers (to ICI).
2. E. Fischer and S. Fakirov, *J. Mater. Sci.* **11**, 104 (1976).
3. J. Liu, J. Myers, P. H. Geil, J. C. Kim, and M. Cakmak, in *ANTEC'97*, Technical Papers Volume XLIII, Society of Plastics Engineers, 1997, p. 740.
4. Z. Mencik, *Chem. Prim.* **17**(2), 78 (1978).
5. C. Bunn and W. Daubney, *Proc. R. Soc.* **226**, 531 (1954).
6. *Research Disclosures* 28,340 (1987).
7. D. C. Hoffman and J. K. Caldwell, in *Specialty Polyesters'95*, pp. 223–242
8. I. Ouchi, H. Aoki, S. Shimotsuma, T. Asai, and H. Hosoi, in *Proc. 17th Japan Congr. Materials Res.*, 1974, p. 217
9. GB Pat. 1,445,464 (1973) (to Teijin).
10. World Pat. WO 93/14252 (1993) (to AlliedSignal)
11. Allied Technical Bulletin P-1, 1300–192.
12. Research Disclosure 29,487 (1988).
13. U.S. Pat. 4,963,644 (Oct. 16, 1990) (to The Goodyear Tire & Rubber Co.).
14. U.S. Pat. 5,750,644 (Dec. 5, 1998) (to Shell Oil Co.).
15. U.S. Pat. 5,744,578 (Apr. 28, 1998) (to Shell Oil Co.).
16. DuPont Technical Bulletin X-272, Type 717.
17. Avtex Fibers Inc. Brochure, Type 120 Yarn.
18. DuPont Technical Bulletin X-272, Kevlar 29, Type 964.
19. F. Fourné, *Synthetic Fibers*, Carl Hansern Verlag, Munich, Germany, 1999, p. 588.
20. BP Amoco "Elements" Naphthalate News Update, Feb. 2000.
21. BP "Elements" Naphthalate News Update, Summer 2001.
22. J.-F. Fritsch (Honeywell Performance Fibers), Technical and Cost Optimization of Textile Constructions for Advanced Reinforcement of Passenger and Van Tires, in *IRC 2000 Rubber Conference*, Helsinki, Finland, June 13, 2000.
23. Amoco NDC "Elements" News Update, Spring 1997.
24. BP "Elements" Naphthalate News Update, Winter 2002.
25. Mod. Plast. 51 (Sept. 2002).
26. Amoco NDC "Elements" News Update, Spring 1995.
27. M. E. Stewart, A. J. Cox, and D. M. Naylor, *Polymer*, **34**, 4060 (1994).
28. Continuing Development of Process Technology for PET/PEN Blend Preforms, by Laura Martin, Husky Injection Molding Systems. Presented at *Bev-Pak America '95*.
29. Further Blow Molding Developments of PET/PEN Blends Bottles, by Luc Desoutter, Group Sidel. Presented at *Bev-Pak America'95*.
30. Fabrication of Naphthalate-Containing Wide Mouth Jars, by I. Nakajima, Aoki. Presented at *Bev-Pak America '95*.
31. A Food Processor's Perspective on Performance Opportunities for Heat Resistant Plastic Packaging, by Nina Goodrich, Ian Britt, and Marvin Tung, Guelph Food Technology Centre. Presented at *1995 Institute of Packaging Professionals* (IDPP).
32. Shell Chemicals Bulletin SC:2306–98, 1998.
33. Barnaby Wallace, End-User Executive Perspective—PET @ Coca-Cola, in *PET Strategies 2001 Conference Proceedings*, Atlanta, Ga.
34. Amoco NDC "Elements" News Update, Autumn 1994.
35. BP "Elements" Naphthalate News Update, Fall 2002.

S. L. SAKELLARIDES
BP Amoco Chemical Company

POLY(ETHYLENE-NORBORNENE). See ETHYLENE-NORBORNENE COPOLYMERS.

POLY(3-HYDROXYALKANOATES). See Volume 3.

POLYIMIDES. See Volume 7.

POLYISOBUTYLENE. See BUTYL RUBBER.

POLYKETONES. See Volume 3.

POLYMER BLENDS. See ARTICLE ONLINE.

POLYESTER FILMS

Introduction

Biaxially drawn polyester film based on poly(ethylene terephthalate) (PET); **1** ($T_m = 255°C$; $T_g = 78°C$) was developed by ICI (1) in Europe and DuPont (2) in the United States in the 19850s with DuPont introducing the first commercial film line in the late 1950s. There was a slow increase in the number of film manufacturers through the 1960s and 1970s, and production increased in the 1980s and 1990s, but in the late 1990s onwards was a major consolidation in the industry with DuPont buying the ICI Films Business and then forming a joint venture with Teijin, Toray acquiring Rhone Poulenc and Chiel, and joint venturing with Saehan, and Mitsubishi acquiring Hoechst. Global capacity of PET film in 2002 was 1,550,000 ton. There are now over 50 producers of PET film worldwide, many in the rapidly expanding Chinese market. DuPont Teijin Films and Toray Saehan Inc. are the largest, with declared capacities of about 290,000 and 280,000 ton respectively. Mitsubishi and SKC form the "second tier" with approximately half the capacity of the top two. The next is Kolon (Korea) with about half the capacity of Mitsubishi and SKC.

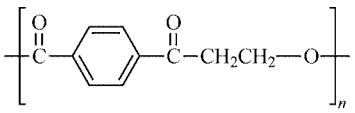

1

The first patent covering poly(ethylene naphthalate) (PEN); **2** ($I_m = 263°C$; $T_g = 120°C$) was filed in 1948 by Cook and co-workers (3) not long after the discovery of PET. However, it was not until the 1970s that the dimethyl ester of 2,6-naphthalene dicarboxylate (2,6-NDC) became available in sufficient quantities for the first PEN films to be produced on a semitechnical scale. Several manufacturers explored this area, with the first PEN film being produced in the early 1970s. However, the raw material continued to be very scarce and costly, and the resulting small scale of film production led to an extremely expensive product compared with PET. This proved to be uneconomic for most applications and there was consequently little commercialization of PEN film until high value speciality videotapes were found to benefit from the use of PEN film in Japan during the 1980s. As a result of the promise of larger scale and more economic raw material supply, plus greater interest from the end market, PEN films were launched commercially in the early 1990s. Since then investment in a world-scale 2,6-NDC production facility by Amoco Chemical Co. (now BP) has significantly aided the economics of PEN film production (see POLY(ETHYLENE NAPHTHALATE) (PEN)). Sales of PEN film are currently of the order of several thousand tonnes and DuPont Teijin Films is the leading producer with its Teonex brand range of films.

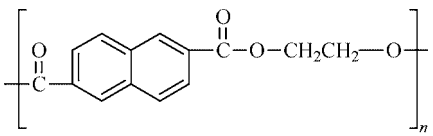

2

Encyclopedia of Polymer Science and Technology. Copyright John Wiley & Sons, Inc. All rights reserved.

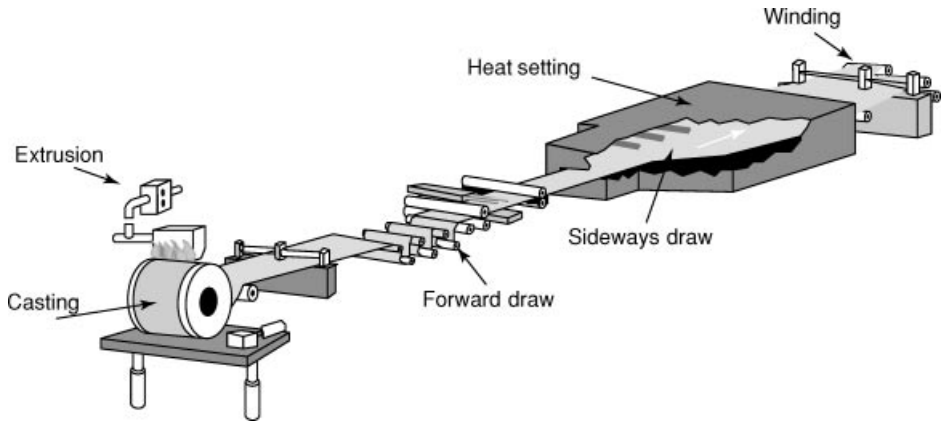

Fig. 1. A Typical film manufacturing process.

The Film Process

Biaxially oriented PET and PEN films are exclusively produced by a stenter process where commonly the amorphous cast film is drawn in the machine direction (MD) by passing it over heated rollers and then fed into a stenter frame to achieve a draw in the transverse direction (TD) (see FILMS, MANUFACTURE; FILMS, ORIENTATION). A schematic of the process is shown in Figure 1.

Normally the sequence of steps is as described above (MD–TD), but the process can be reversed (TD–MD) (4–6); and even a simultaneous stenter process (7) whereby the clips are not interconnected and stretching can therefore be carried out by accelerating the clips in the MD within the diverging TD draw section, has been commercialized. Using this basic process film with thicknesses from 0.6 to 350 μm can be prepared.

The conversion of polymer into film falls into four basic stages:

(1) Polymer preparation and Handling
(2) Extrusion and casting
(3) Drawing and heat setting
(4) Slitting, Winding, and Recovery

The film process and in particular the morphology developed during processing has been described in more detail elsewhere (8,9).

Polymer Preparation and Handling. Polymer can be extruder-fed to the drawing process or it can be directly fed from a continuous polymerizer (CP), but in both cases the virgin polymer tends to be of a number-average molecular weight of about 20,000 although higher and lower molecular weights are filmed. With the extruder-fed film lines the polymer handling involves blending and drying. This is a consequence of the film process never being 100% material efficient and virgin polymer is therefore blended with polymer reclaimed from the film process. Drying is essential in closed (single-screw) extrusion systems as the polyesters are susceptible to hydrolysis, resulting in a reduction in molecular weight, but less commonly, processes have evolved based on vented (twin-screw) extruders where

moisture is removed just after melting. In the drying stage, polymer is crystallized first to avoid the chip sintering during drying and then dried for several hours at 160–180°C to reduce the moisture level to 10–30 ppm. Close-coupled CP film lines do not have this stage and melt is pumped directly through filtration to the die.

Extrusion and Casting. The blended and dried polymer is next melt-extruded through a slot die. There is usually melt filtration before the die to remove degraded polymer, gels, catalyst residues, and pipe deposits. The extrusion system is typically designed to deliver stable output up to about 2.6 ton/h over a wide range of operating conditions and throughputs. Exceptionally, higher outputs are possible, up to about 3.5 ton/h on thick film lines, using complex tandem or parallel extrusion systems (10). More recently twin-screw extruders have been introduced on some film lines to widen the operating window and to provide capital-efficient high throughputs. These are able to cope with a wider range of molecular weights, improve the mixing, and have the advantage of extruding at lower melt temperatures. Other combinations such as tandem single screws with melt pumps are also used to give a stable output. Parallel extrusion systems are also commonly used for high output but these present the problem of ensuring homogeneous melt stream blending. Whichever extrusion system is employed, its purpose is to transport a consistent flow of polymer melt to the flat film die of a stenter process.

The die which can be center- or end-fed converts the melt from a circular cross section to a uniformly thick melt curtain of the required width. The thickness of the film is continuously measured across the web after the stenter process, giving a thickness or gauge profile. This profile data is used to make fine adjustments to flow profile at the die either through thermoviscous heating or by actuation of mechanical bolts (which physically modulate the die gap profile to achieve uniform film thickness profile). Combinations of thermoviscous and mechanical modulation are also employed in some cases.

The purpose of the casting is to produce a continuous uniformly thick film of noncrystalline polymer with no surface blemishes and this is achieved by drawing down the melt curtain onto a casting drum. The polymer melt from the extrusion system will normally be between 280 and 310°C so as to minimize crystallization, which would increase film haze and brittleness and possibly cause a film breakage later in the filming process (9). To ensure this the molten film is cooled as quickly as possible below its glass-transition temperature by cooling the casting drum using recirculated water which passes through a heat exchanger to control its temperature between typically 10 and 15°C. Thin film can be satisfactorily cooled using a single drum, normally of size 600–900 mm in diameter, but for thicker films where the insulating properties of the film prevent cooling through to the air (nondrum) contacting side of the melt, a second drum is used to provide additional cooling.

As the casting drum rotates, air is drawn into the gap between the film of melt and the drum, affecting the contact of the two surfaces and the effectiveness of the cooling. This is avoided by electrostatically charging the film surface by using a pinning wire or blade electrode stretched across the drum just below the die face (11–13). This creates an electrostatic field around the wire or blade which induces a charge on the melt curtain surface. Since the drum is earthed the charge forces the melt curtain onto its surface.

The surface of the casting drum must be of a very high standard so as to avoid imprinting any patterning or "graininess" onto the cast film. The surface must also be hard in order to avoid damage and be resistant to corrosion so that no pitting occurs. Therefore a drum that is hard chrome plated and highly polished is usually favored. During operation the casting drum must be free of vibration and rotate smoothly so as to minimize any source of variation in thickness in the MD of the film.

Drawing and Heat Setting. The cast film initially passes through a preheat zone, where the temperature of the cast film is raised by passage over a series of heated contact rolls until a point, usually about 15°C above its glass transition, T_g, where the material can be readily stretched.

The forward draw stage physically stretches the heated polyester film between two nip roll systems with a surface speed differential and is designed to improve its tensile properties in the MD. Stretch ratios of around 3.5:1 are employed, and the stresses in the structure caused by this step align the molecular chain segments in the direction of the stress and thereby raise its tensile modulus and strength by a factor of about 3.

In the second stage of the stenter oven, the edges of the film web are clipped and led along diverging rails that cause the material to be stretched at temperatures above 100°C (135°C for PEN), for the second occasion, by a factor of between 3 and 4. The object of this step, the sideways draw, is to develop the properties of the film in the TD via orientation at the molecular level, to a point where they balance or approximately balance those measured in the MD (9). The process tends to align molecular chain segments not already aligned in the MD and to realign some MD-oriented crystallites toward the TD. The film at this stage is anisotropic.

The final stage in the stenter oven is designed to develop a crystalline morphology in the film which retains the improved mechanical properties from the drawing stages and which is more stable over time and at elevated temperature.

The heat set or crystallization stage of the process comprises three or more regions of the stenter oven, each with independent temperature control and the capability to adjust the lateral dimension of the web. Thus film can be treated to a range of thermal and strain programs to optimize its final properties. Temperatures of the film can exceed 230°C and although residence time may be only a few seconds this is sufficient for density changes equivalent to a rise of 30–40% in crystallinity to occur. On the same timescale, the noncrystalline regions of the film can exhibit significant molecular relaxation.

Unless all physical anisotropy can be removed from the noncrystalline fraction of biaxial PET film, the product will undergo residual shrinkage at elevated temperature. By managing both the film temperature and a relaxation of strain, achieved by a small convergence of the stenter rails (known as toe-in) during the heat set stage, it is possible to achieve considerable control of this film property (9).

Slitting, Winding, and Recovery. The film in and close to the clips is very thick and cannot be wound into film. This is slit off as the film exits the stenter and reclaimed for reprocessing into film. It is combined with scrap film and is either cut up into flake and compacted into particulate form or is reextruded and formed into pellets. This reclaimed polymer either is fed back in with the virgin polymer at the start of the film process or is fed into the CP process.

The edge trimmed film is then wound up. Rolls of film can be produced either on the stenter, or alternatively they can be slit down off line to the width and lengths required.

Surface and Bulk Properties Control

Film Properties. The film process described produces rolls of PET and PEN films that have the properties required for a standard PET or PEN film, ie high mechanical strength, good flexibility, excellent visual properties, flat and dimensionally stable, and available in a range of thicknesses. The difference in chemical structures of PET and PEN is shown by **1** and **2**. The substitution of the phenyl ring of PET by the naphthalene double ring of PEN has very little effect on the melting point (T_m), which increases by only a few degree Celsius. However, there is a significant effect on the glass-transition temperature (T_g), which increases from 78°C for PET to 120°C for PEN. The result of this is that although the good thermal properties of PET and PEN films enable them to retain physical, chemical, and electrical properties over a wide temperature range, PEN has significantly improved thermal resistance relative to PET. This is particularly noticeable with regard to PEN's higher continuous use temperature (14) Table 1.

The typical properties listed in Tables 1–5 are from DuPont Teijin Films Teonex PEN film datasheet and are for illustrative purposes only and are not intended to be used as design data.

Table 1. Thermal Properties of PET and PEN

Sample thickness, μm	Teonex® PEN film Q51-25 μm		PET film standard Grad-25 μm		Test method
Melting point, °C	269	—	258	—	DSC
Glass-transition temperature, °C	121	—	78	—	
Shrinkage (150°C, 30 min), %					
MD	0.4	—	1.5	—	JIS C-2318 (modified to TDF)
TD	0.0	—	0.2	—	
Shrinkage (200°C, 10 min), %					
MD	2.0	—	4.0	—	Ditto
TD	1.0	—	1.5	—	
Coefficient of thermal expansion (10^{-6}/RH%), –					
MD	13	—	15	—	TDF method
Coefficient of hydrolic expansion (10^{-6}/RH%), –					
MD	11	—	11	—	Ditto
Continuous use temperature, °C					
Mechanical	160 (≥25)	—	105 (all)	—	UL 746B
Electrical	180 (≥25)	—	105 (all)	—	

Table 2. Mechanical Properties of PET and PEN

Property	Typical values	Test method
Tensile strength (MD) at 25°C, MPa[a]	200	ASTM D882-80
Tensile modulus (MD) at 25°C, MPa[a]	3,900	ASTM D882-80
Elongation (MD) at 25°C, %	130	ASTM D882-80
Stress to produce 5% elongation (MD) at 25°C, MPa[a]	105	ASTM D882-80
Density at 25°C, g/cm^3	1,395	ASTM D1505-66
Folding endurance 1 kg loading, 25°C, cycles	100,000	ASTM D2176-63
Tear strength, N/mm		
Initial (Graves) 25°C	294	ASTM D1004-66
Propagating (Elmendorf) 25°C	7.4	ASTM D1922-67
Coefficient of friction (kinetic) at 25°C	0.33	ASTM D1003-61
Refractive index (AB 8E at 25°C), ND25	1.64	ASTM D-542-50
Coefficient of hygroscopic expansion, Mm/mm (%RH)	1.0×10^{-5}	

[a]To convert MPa to psi, multiply by 145.

Table 3. Barrier Properties of PET and PEN

Sample thickness, μm	Teonex® PEN film Q51-25 μm		PET film standard Grad-25 μm		Test method
Water vapor permeability, g/(m^2 · 24 hr)	6.7	—	21.3	—	JIS-Z0208
Gas permeability CO_2, cm^3/(m^2 · 24 h · atm)	97	—	328	—	ASTM D1434-82
Gas permeability O_2, cm^3/(m^2 · 24 h · atm)	21	—	55	—	
Breakdown voltage, KV/mm	300		280		JIS C-2318

Table 4. Electrical Properties of PET and PEN

Sample thickness, μm	Teonex® PEN film Q51-25 μm	PET film standard Grad-25 μm	Test method
Permittivity (25° C)			
60 Hz	3.0	3.2	JIS C-2318
1 kHz	2.9	3.1	
1 GHz	2.9	3.0	
Dissipation factor (25° C)			
60 Hz	0.003	0.002	JIS C-2318
1 kHz	0.005	0.006	
1 GHz	0.005	0.008	
Surface resistivity (25°C), 10^{17} Ω	2	6	JIS C-2151
Volume resistivity (25° C), 10^{17} Ω · cm	10	7	JIS C-2318
UV light permeability at 360 nm, %	0	82	TDF method

Table 5. PET and PEN Films—Comparative Information[a]

	Amorphous		Crystalline			
Properties	PES	PC	PEN	PET	OPP	PPS
T_g, °C	223	150	121	78	−10	90
T_m, °C			263	255	170	285
Young's modulus, GPa[b]	2.2	1.7	6.1	5.3	2.4	6.72
Tensile strength, MPa[c]	83	60	275	225	250	225

[a]Data in this table are gleaned from different datasheets on different thickness films. Data are for comparison between the films only and the numbers should not be taken as absolute.
[b]To convert GPa to psi, multiply by 145,000
[c]To convert MPa to psi, multiply by 145.

PET and PEN retain their physical properties, including tensile strength, Young's modulus, and tear strength over a wide temperature range (−70 to 150°C) (14) (Table 2). PEN is generally a stiffer film than PET for a given thickness. This has been exploited in the development of the advanced photo system for consumer imaging where it has been possible to downgauge the film, resulting in a smaller, thinner reel of photographic film.

The chemical properties of PET and PEN films include excellent resistance to most chemicals. They retain 100% of tensile strength and modulus after 31 days at 23°C in glacial acetic acid, 10% hydrochloric acid, 10% nitric acid, 30% sulfuric acid, 2% sodium hydroxide, 2% ammonium hydroxide, benzyl alcohol, dioxane(1,4), ethyl acetate, ethyl alcohol, methyl ethyl ketone, toluene, trichloroethylene, tetrahydrofuran, cyclohexane, sulfurhexafluoride, 28% hydrogen peroxide, dimethyl formamide, tricresyl phosphate, and 0.25% detergent. PET film is dissolved by hexafluoro-2-propanol, *m*-cresol, *o*-chlorophenol and is attacked by 35% nitric acid, 10% ammonium hydroxide, and *n*-propylamine (14). PET and PEN films also have very low moisture permeability and overall resistance to staining by various chemicals and food products. PEN film has superior barrier properties relative to PET film (Table 3), and the gas and vapor barrier properties can be significantly improved by coating with a barrier coating such as poly(vinylidene chloride) or by vacuum metallization (15) (see BARRIER POLYMERS).

PET and PEN films have excellent electrical insulating properties as shown in Table 4 (14).

Because of their excellent thermal, insulating, and moisture-resistant properties, they are used in a wide variety of electrical applications, with PEN being the preferred candidate in applications that require higher temperatures and good hydrolysis resistance.

However, for many of the specialty applications that PET and PEN films are used in, further modification of either the surface or bulk properties are required as illustrated below.

Coating. PET and PEN are fairly inert polymers and for many applications the surface of the film is altered by coating or adhesive lamination to other materials, eg film for packaging will be lacquered to accept inks or adhesives, or, for photographic applications, primed to accept photosensitive overcoats. Coatings are also applied to achieve other surface effects, such as antistatic, barrier (water, oxygen, carbon dioxide, flavor), release, and frictional characteristics (8,9).

These coatings are usually acrylic-, vinyl-, polyester-, or polyurethane-based, and PET and PEN films are commonly coated either "in-line" or "off-line". "In-line" coating usually involves aqueous-based materials, and is carried out between the forward draw and before entering the stenter, while "off-line" coating involves unwinding and priming the surface of preformed film reels with aqueous- or solvent-based coatings. In both cases, the coating may be applied to one or both sides, and some products have different coatings applied to either sides of the film. Coatings are mostly applied by offset gravure or by direct gravure coating.

Coextrusion. Coextrusion (qv) is used to produce a film with two or more different polymer layers, so that one or both surfaces of the film have different properties to the "core" polymer. In addition, coextrusion allows manufacture of products with layers thinner than can be made and handled as individual layers. Coextrusion provides a means of flexibly configuring a wide range of film laminate structures which cost-effectively meet product requirements.

The basic coextrusion process consists of the generation of two or more melt streams and their confluence while in the melt phase. The number of separate extrusion systems is determined by the number of polymer types. This is typically 2, but occasionally 3 and exceptionally up to 10. Each polymer type to be incorporated in the structure is separately melted, pressurized, and (optionally) filtered in parallel extrusion systems before flowing into the coextrusion hardware. The optimum method of bringing the separate melts together depends primarily on their respective flow behaviors. The melt layers must remain distinct but well bonded in the process from the point(s) of confluence through to solidification. There are basically two hardware configurations in use for common polymers: the multi-manifold die and the injector block. Combinations of the two are also possible for complex structures (8,9).

Fillers. Fillers (qv) are added to PET for two main reasons: either to modify surface properties, or to modify bulk properties. Particulate fillers such as clays and silica, typically a few micrometers in diameter, are added to create surface roughness during the film drawing process. A primary function of the surface roughness is to reduce the blocking or sticking propensity of the otherwise very smooth film surfaces during winding and reel formation. The roughness also enhances dynamic handling behaviour particularly for high speed transport and winding of thin films through subsequent conversion processes. Surface optical properties can also be regulated via filler-induced surface roughness, for example, to control gloss or eliminate Newton's ring fringes between adjacent film layers (9).

Although mechanical properties such as softness, stiffness, and toughness can be addressed, it is most common for optical properties to be modified via particles. Opacity and whiteness are generated by two discrete mechanisms. Simple pigmentation (light scattering from the particle–polymer interface) can be achieved using similar titanium dioxide technology to that employed in the fibers and coatings industries. It is, however, more common for the anatase crystal form to be employed since this is a less abrasive pigment than the more strongly scattering rutile. The second mechanism involves using the additive to generate microvoiding during the film draw. The additive can be inorganic, for example barium sulfate or calcium carbonate, or polymeric, for example, polypropylene. In this mechanism the opacity is derived from scattering between the polymer and the

void. The use of microvoiding confers the potential advantage of a softer film of reduced density.

Shrinkage. Standard PET and PEN films from the stenter process will shrink between 1 and 3% at temperatures above the T_g. For the high level of accuracy required by some electrical applications shrinkages of below 0.1–0.2% are required. In order to meet this the film is unwound and passed through a carefully temperature-controlled oven, with almost no tension in the film. The amount of residual shrinkage in the film after this process is typically less than 0.1% in the MD and the TD for temperatures up to 150°C for PET and 200°C for PEN.

General Comments on Comparison with Other Films. It is not possible in this article to give a detailed comparison of polyester films compared to other films as each class of film has different strengths and weaknesses and serve different markets. Both PET and PEN films are biaxially oriented crystalline films; this imparts unique properties and differentiates them from amorphous films such as polycarbonate (PC) and polyethersulfone (PES) films. As a generalization PET and PEN films are stiffer films compared to amorphous films (Table 5); they have very good solvent resistance and low moisture absorption, but PES film in particular is a higher T_g and higher temperature performance film and PC film has superior clarity. Compared to crystalline films such as oriented polypropylene (OPP), PET and PEN films are higher temperature performance films. Polyphenylene sulfide (PPS) film is a high performance biaxially oriented crystalline film and has a similar continuous use temperature, but a lower T_g compared to PEN film. PEN has better dimensional stability but PPS offers superior flame retardancy and chemical resistance.

The particular strength of polyester films, however, is the wide range of film effects that can be achieved with fillers, coatings, coextrusion, etc, as outlined in the previous sections—this versatility is unique in the films market.

Application. Typical application areas that exploit the properties of polyester film are illustrated in Table 6. It can be seen that usually a combination of properties are required and these are achieved by a combination of base film properties, fillers, coatings, and coextrusion technologies.

Future Trends

The unique blend of properties of PET and PEN films makes them extremely versatile products and the growth in the films market is predicted to be above 5% per annum. However this masks that some areas such as packaging, industrial, and electrical applications are growing at a greater rate whereas the growth in the more traditional markets such as magnetic media or graphic arts materials is more modest. Advances are continually being made in uprating the film process, but in addition new applications for PET and PEN are continually being developed. The trend will be increasingly toward differentiation through the application of new process technologies and advances in the control of the process coupled with the combinations of base polymer, filler, coating, and coextrusion technologies.

Table 6. Examples of Typical Film Applications and the Key Properties Required

Application	Film properties required
Packaging	Seal (peelable through to permanent) Wide heat seal range Barrier (oxygen and aroma) White, clear Surface roughness Pretreats to allow metal, ink, sealant adhesion Stiffness 12–30 μm
Labels	Clear, white, matte, black Durability Adhesion with inks Silicone adhesion 23–175 μm
Imaging • Montage • Microfilm • Digital technology media • APS (PEN)	High opacity, white through to high clarity, flatness, Antistat Dimensional stability Adhesion with inks 50–175 μm Stiffness
Casting and release	Wider range of surface textures from high gloss to very matte Release coats 12–50 μm
Capacitors	Thin film Low shrinkage Electrical–thermomechanical properties 0.9–23 μm
Electronics • Flexible printed circuits, flat flexible cable • Membrane touch switch • Loudspeakers • RFID tags • Automotive wiring (PEN)	Brilliant clarity-white film Electrical properties Low shrinkage Durability Adhesion with inks 12–175 μm High temperature performance Hydrolysis resistance
Coil coating/fiber-reinforced plastics	Heat bondable UV stable 12–125 μm
Electrical insulation • Motors • Cable	High dielectric strength Thermal endurance at elevated temperatures Dimensional stability Durability Chemical resistance 12–350 μm
Magnetic media • Floppy disks	Tensilized film Surface quality

Table 6. (continued)

Application	Film properties required
• Video	Dimensional stability
• High density storage (PEN)	Sublayer for magnetic coating
	Stiffness
Medical test strip	Dimensionally stable
	High stiffness
	Inert and plasticizer free
	Adhesion with ink
	Hydrophilic surface
	Clear (matte or glossy), white (high opacity or translucent)
Electronic displays (PEN)	High temperature stability
	Dimensional stability
	Clarity
	Surface quality
Cards	Durability
	Adhesion with inks
	Heat bondable
	Temperature resistance
	100–350 μm

BIBLIOGRAPHY

1. Br. Pat. 609,797 (1948), J. C. Swallow and D. K. Baird (to ICI).
2. U.S. Pat. 2,823,421 (1958), A. C. Scarlett (to E. I. du Pont de Nemours & Co., Inc.).
3. Br. Pat. 604,073 (1948), J. G. Cook, H. P. W. Huggill, and A. R. Lowe (to ICI).
4. U.S. Pat. 3,256,379 (1966), C. J. Heffelfinger (to E. I. du Pont de Nemours & Co., Inc.).
5. Fr. Pat. 2,529,506A1 (1984), M. Jacquier and J. Barbey (to Rhone Poulenc).
6. Eur Pat. 0,0971,08A1 (1983), M. Jacquier (to Rhone Poulenc).
7. Eur Pat. 008,693 (1979), M. Motegi, I. Kimata, and S. Fujita (to Toray).
8. H. F. Mark, ed., Encyclopedia of Polymer Science and Engineering, 2nd ed., Vol. 12, John Wiley & Sons, Inc., New York, p. 193, and references contained therein.
9. W. A. MacDonald and D. H. Mackerron, in D. W. Brookes and G. A. Giles, eds., *PET Packaging Technology*, Sheffield Academic Press, 2002, pp. 116–157, and references contained therein.
10. F. Hensen and H. Bongaerts, *Plastverarbeiter* **30**, 618, (1979)
11. U.S. Pat. RE 26,951 (1970), A. Vaccaro (to Celanese).
12. U.S. Pat. 3,223,757 (1965), J. Owens and W. Vieth (to E. I. du Pont de Nemours & Co., Inc.).
13. U.S. Pat. 4,309,368 (1982), D. Groves (to ICI).
14. Melinex® PET Film data sheet, DuPont Teijin Films, Luxembourg (http://www.dupontteijinfilms.com).
15. Teonex® PEN Film datasheet, DuPont Teijin Films, Luxembourg (http://www.dupontteijinfilms.com).

W. A. MacDonald
DuPont Teijin Films UK Limited

POLYESTERS, FIBERS. See Volume 3.

POLYESTERS, THERMOPLASTIC. See Volume 7.

POLYESTERS, UNSATURATED

Introduction

Low molecular weight polyesters derived from unsaturated dibasic acids (or anhydrides) dissolved in unsaturated vinyl monomers comprise a versatile family of thermosetting materials known generally as *unsaturated polyester resins*. Prototype resins produced in the early 1940s were used in conjunction with glass fiber reinforcements to produce the first composite plastics. The high strength and radiotransparency of this material expanded its role in radome covers employed in large quantities toward the end of World War II.

Markets for the resins have expanded rapidly; the dominant applications are still in conjunction with glass-fiber reinforcement to form laminar composites known generically as *fiber-glass-reinforced plastic* (FRP) in the United States and *glass-fiber-reinforced plastic* (GRP) in Europe and elsewhere. Resins have also evolved for use in casting processes, which usually contain high loadings of fillers or mineral aggregate and are defined as one form of polymer concrete. By 2002, global production of unsaturated polyester resins had exceeded 1,900,000 t, with the United States being the largest market, at over 780,000 t.

Raw Materials

The properties of polymers formed by the step-growth esterification (1) of glycols and dibasic acids can be manipulated widely by the choice of coreactant raw materials (Table 1) (2). The reactivity fundamental to the majority of commercial resins is derived from maleic anhydride [108-31-6] (MAN) as the unsaturated component in the polymer, and styrene as the coreactant monomer. Propylene glycol [57-55-6] (PG) is the principal glycol used in most compositions, and *ortho*-phthalic anhydride (PA) is the principal dibasic acid incorporated to moderate the reactivity and performance of the final resins.

Isophthalic (*m*-phthalic) acid [121-91-5] (IPA) is selected to enhance thermal endurance as well as to produce stronger, more resilient cross-linked plastics that demonstrate improved resistance to chemical attack. Terephthalic (p-phthalic) acid [100-21-0] (TA) provides similar properties as isophthalic acid; it is also used in corrosion resinstance and a wide variety of other applications.

Other glycols can be used to impart selective properties to these simple compositions. Ethylene glycol [107-21-1] (EG) is used to a limited degree to reduce cost, whereas diethylene glycol [111-46-6] (DEG) produces a more flexible polymer that can resist cracking when impacted. Neopentyl glycol [126-30-7] (NPG) is used in most commercial products to improve uv and water resistance. Alkoxylated derivatives of bisphenol A (BPA) not only impart a high degree of resistance

Encyclopedia of Polymer Science and Technology. Copyright John Wiley & Sons, Inc. All rights reserved.

Table 1. Ingredients of Polyester Resin Formulations in Descending Order of Commercial Significance

Glycol	Dibasic acid or anhydride	Unsaturated acid or anhydride	Unsaturated monomer
Propylene glycol	Phthalic anhydride	Maleic anhydride	Styrene
Diethylene glycol	Dicyclopentadiene–maleic anhydride[a]	Fumaric acid	Vinyltoluene
Ethylene glycol		Methacrylic acid	Methyl methacrylate
Neopentyl glycol	Isophthalic acid	Acrylic acid	Diallyl phthalate
Dipropylene glycol	Adipic acid	Itaconic acid	α-Methylstyrene
Dibromoneopentyl glycol	Chlorendic anhydride[b]		Triallyl cyanurate
Bisphenol A diglycidyl ether	Tetrabromophthalic anhydride		divinylbenzene
Bisphenol A dipropoxy ether	Tetrahydrophthalic anhydride		
Tetrabromobisphenol diethoxy ether	Terephthalic acid		
Propylene oxide	Tetrachlorophthalic anhydride		
1,4-Butanediol			

[a] Acid addition product, formed *in situ*.
[b] 1,4,5,6,7,7-Hexachlorobicyclo(2,2,1)-5-heptene-2,3-dicarboxylic anhydride [115-27-5].

to strong acidic and alkaline environments, but also provide resistance to deformation and creep at elevated temperatures.

Long-chain aliphatic acids such as adipic acid [124-04-9] are generally used to improve flexibility and enhance impact properties, demonstrating subtle improvements over resins modified with the ether glycols (diethylene glycol) and polyether glycols (polypropylene glycol).

Novel polyester compositions have also been derived from dicyclopentadiene [77-73-6] (DCPD), which can enter into two distinct reactions with maleic anhydride to modify properties for lower cost. These compositions have effectively displaced *o*-phthalic resins in marine and bathtub laminating applications.

Recycled poly(ethylene terephthalate) (PET), which offers excellent properties at potentially lower cost, is finding wider use as a raw material component and meeting increasing demands for environmentally compatible resins (see POLYESTERS, THERMOPLASTIC; RECYCLING, PLASTICS).

Other minor raw materials are used for specific needs. Fumaric acid [110-17-8], the geometric isomer of maleic acid, is selected to maximize thermal or corrosion performance and is the sole acid esterified with bisphenol A diol derivatives to obtain optimum polymer performance. Cycloaliphatics such as hydrogenated bisphenol A (HBPA) and cyclohexanedimethanol (CHDM) are used in selective formulations for electrical applications. Tetrahydrophthalic anhydride [85-43-8] (THPA) can be used to improve resilience and impart useful air-drying properties to polyester resins intended for coating or lining applications.

Halogenated intermediates, dibromoneopentyl glycol [3296-90-0] (DBNPG), and alkoxylated derivatives of tetrabromobisphenol A are used extensively in flame-retardant applications. Similar properties can be derived from halogenated

dibasic acids, chlorendic anhydride [115-27-5] (CAN), and tetrabromophthalic anhydride [632-79-1] (TBPA). Processes can be used to produce brominated products by the *in situ* bromination of polymers derived from tetrahydrophthalic anhydride.

Monomers such as methyl methacrylate [80-62-6] are often used in combination with styrene to modify refractive index and improve uv resistance. Vinyltoluene [25013-15-4] and diallyl phthalate [131-17-9] are employed as monomers in selective molding compositions for thermal improvements.

Process Equipment

The polyesterification reaction is normally carried out in stainless steel vessels ranging from 8000–20,000 L, heated and cooled through internal coils (Fig. 1). Blade agitators revolving at 70–200 rpm are effective in stirring the low viscosity mobile reactants, which are maintained under an inert atmosphere of nitrogen or carbon dioxide during the reaction at temperatures up to 240°C.

Weigh tanks or meters measure the liquid glycols into the reactor. Solids are usually added from 25-kg bags or 1000-kg supersacks. Silo and auger are used widely for isophthalic acid, whereas phthalic anhydride [85-44-9] and maleic anhydride are metered in molten form. A packed condenser efficiently separates water from glycol. The glycol is refluxed back into the reactor and the remaining condensate is incinerated on-site using a thermal oxidizer. Once the polymer is formed, it is cooled to below 180°C and drained into a cooled blend tank containing styrene monomer under high agitation.

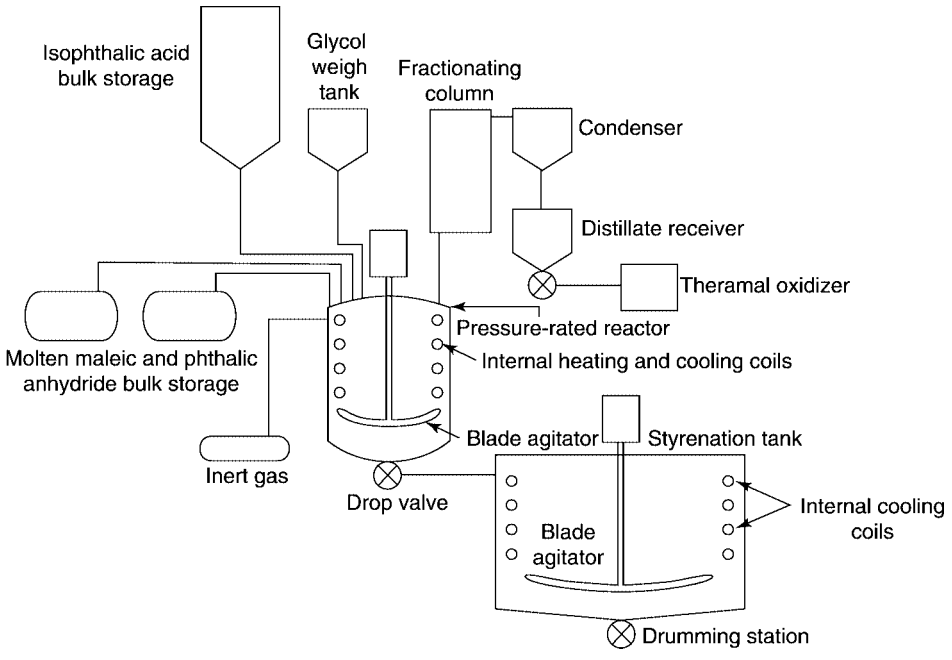

Fig. 1. Reactor system for the manufacture of polyester resins.

Glass-lined reactor systems are used occasionally for halogenated resins to prevent corrosion of the reactor components. Copper and brass fitting should be avoided because of the significant influence on resin cure characteristics.

Polyesterification

The reaction of glycols with dibasic acid anhydrides, such as phthalic and maleic anhydrides, proceeds at above 100°C, ending with the exothermic formation of the acid half-ester produced by the opening of the anhydride ring. The reaction exotherm effectively raises the temperature of the reactants to over 150°C, at which point the half-esters condense into polymers with the evolution of by-product water. As the reaction proceeds, the viscosity of the reactants increases, restricting the release of water, so that the temperatures must be gradually increased to 220°C to maintain a steady evolution of condensate water. Resins normally lose between 8 and 12% of initial charge weight as condensate.

The polyesterification reaction is reversible because it is influenced by the presence of condensate water in equilibrium with the reactants and the polymer. The removal of water in the latter part of the reaction process is essential for the development of optimum molecular weight, on which the ultimate structural performance depends.

The polyesterification reaction is carried out in the presence of an inert gas, such as nitrogen or carbon dioxide, to prevent discoloration. Usually, the sparge rate of the inert gas is increased in the final stages of polyesterification to assist the removal of residual water. Although the removal of water can be facilitated by processing under vacuum, this is rarely used on a commercial scale.

The esterification rate can be accelerated by acid catalysts (3) such as *para*-toluenesulfonic acid and tetrabutyl titanate, but tin salts such as hydrated monobutyl tin oxide are preferred for reasons of product stability during storage. The polyesterification process can be reversed by injecting steam into the reactants; this can be used to control the final molecular weight attained by the polymer. Transesterification during polymer formation also occurs, which leads to changes in the distribution of polymers in the final product. Transesterification is employed on a commercial scale to recycle poly(ethylene terephthalate) waste into useful resins by digesting an equivalent amount of glycol in the presence of catalysts such as tetraisopropyl titanate or zinc acetate. The terephthalate esters subsequently react with maleic anhydride to produce unsaturated terephthalate polymers, which have properties similar to their isophthalic homologues.

The viscosity of the final polymer melt usually limits the progress of molecular weight development, and number-average values (M_n) between 1800 and 2500 are normally observed. Other side reactions also modify molecular weight growth. Side reactions are influenced by the choice of reactants. Ethylene glycol can form cyclic esters with phthalic anhydride; maleic anhydride can produce addition products (4) with lower glycols, forming trifunctional succinate derivatives that lead to high molecular weight branched polymers and the possibility of gelation during esterification. To maintain maximum unsaturation levels during esterification, fumaric acid is often used in place of maleic anhydride. Fumaric acid

is also used widely in formulations involving alkoxylated bisphenol A to obtain optimum thermal and corrosion performance.

Polyesterification involving insoluble reactants such as isophthalic acid is normally carried out in two-stage reactions, in which isophthalic acid reacts first with the glycol to form a clear melt. The balance of the reactants, including maleic anhydride, is then added to complete the polymer, thus avoiding longer cycle times and some discoloration.

Polyester resins can also be rapidly formed by the reaction of propylene oxide (5) with phthalic and maleic anhydride. The reaction is initiated with a small fraction of glycol initiator containing a basic catalyst such as lithium carbonate. Molecular weight development is controlled by the concentration of initiator, and the highly exothermic reaction proceeds without the evolution of any condensate water. Although this technique provides many process benefits, the low extent of maleate isomerization achieved during the rapid formation of the polymer limits the reactivity and ultimate performance of these resins.

Maleic Isomerization. Polyesters are formulated using maleic anhydride (**1**) as the common unsaturated moiety. During the course of the polyesterification reaction at 220°C, the *cis*-maleate ester (**2**) isomerizes to the *trans*-fumarate (**3**). The fundamental reactivity of the final polyester with styrene is directly proportional to the degree of isomerization and the level of fumarate polymers formed during the course of esterification. Maleate polymers in the cis form create strain across the double bond, causing some displacement from a planar configuration; fumarate polymers in the trans configuration are influenced less by steric effects and the double bond can assume a planar configuration conducive to addition copolymerization with styrene. Branched asymmetric reactants such as propylene glycol and bulky aromatic dibasic acids such as isophthalic acid create sufficient steric interference to promote isomerization to the *trans*-fumarate polymers, whereas linear glycols such as ethylene and diethylene glycol and linear dibasic acids such as adipic acid produce resins that have higher levels of the maleate polymer.

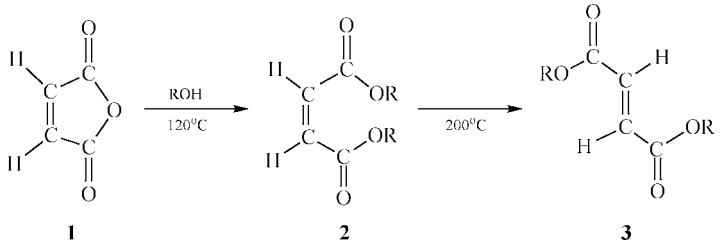

1 **2** **3**

The temperature of esterification has a significant influence on isomerization rate, which does not proceed above 50% at reaction temperatures below 150°C. In resins produced rapidly by using propylene oxide and mixed phthalic and maleic anhydrides at 150°C, the polyester polymers, which can be formed almost exclusively in the maleate conformation, show low cross-linking reaction rates with styrene.

Isomerization is facilitated by esterification at temperatures above 200°C or by using catalysts, such as piperidine and morpholine (6), which are effective

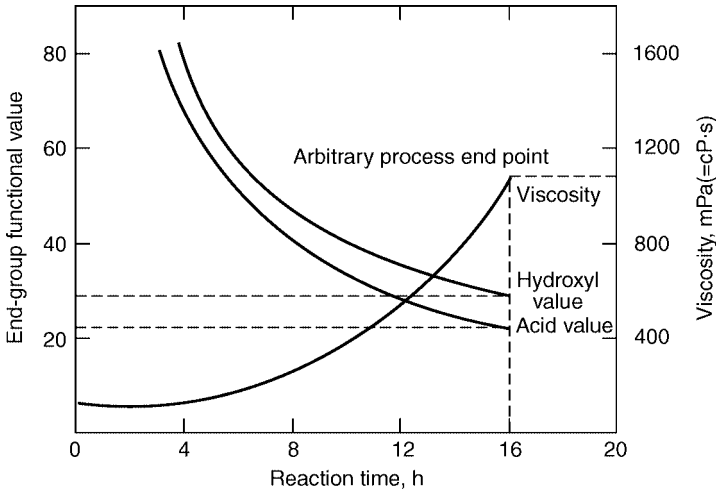

Fig. 2. Functional end groups and solution viscosity during polyester resin manufacture. Acid value is defined as the milligrams of KOH required to neutralize 1 g of polymer; hydroxyl value is defined as the milligrams of acid equivalent required to neutralize 1 g of polymer. Solution viscosities are determined at 60 wt% in styrene.

in raising isomerization of fumarate to 95% completion. Resins made by using fumaric acid are exclusively fumarate polymers, demonstrate higher reactivity rates with styrene, and lead to a complete cross-linking reaction.

End Group Analysis. The reaction of balanced stoichiometric glycol–dibasic acid ingredients theoretically produces polymers with equivalent acid and hydroxyl end groups. Commercial processes, however, normally include an excess of glycol to offset distillation losses. Depending on column efficiency, the polymer can have a higher relative hydroxyl value and a much lower acid value (Fig. 2), and this controls the ultimate molecular size. Most commercial laminating resins have acid values ranging from 25 to 30, whereas higher molecular weight isophthalic resins have values that fall between 10 and 15.

Molecular Weight. Unsaturated polyester resins are relatively low in molecular weight, and are formulated to achieve low working viscosities when dissolved in styrene. The M_n normally falls between 1800 and 2500, although dicyclopentadiene and orthophthalic resins can be useful below this range. The molecular weight follows a Gaussian distribution curve (Fig. 3), the shape of which influences final solution viscosities. In phthalic resins, the presence of a low molecular weight fraction is usually observed, whereas in high maleic resins a high molecular weight shoulder is observed. This indicates significant glycol addition across the double bond to form a trifunctional reactant. Polymers having different chain lengths and compositions exist as a compatible mixture; the ratio of weight-average molecular weight (M_w) and number-average molecular weight (M_n) is defined as the polydispersity D. For o-phthalic and isophthalic resins, D is just over two, but higher molecular weight resins and resins containing high maleic levels are more polydisperse and the distribution curve becomes flatter as the resin viscosity increases.

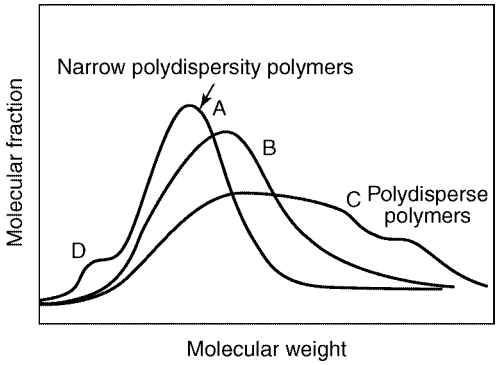

Fig. 3. Molecular weight distribution curves as determined by gel-permeation chromatography. A represents *ortho*-phthalic resins; B, highest molecular weight isophthalic resins; C, high molecular weight polydisperse polymers having high maleic addition reactions; and D, low molecular weight fraction seen in most phthalic resins.

ortho-Phthalic resins consist of chains having an average of 15 ester groups and a narrow distribution curve. The molecular weight development during the manufacturing process is normally followed by using solution viscosity that tends to increase exponentially in the final stages of the reaction. Arbitrary end points are usually established well before this stage to avoid gelation in the reactor (see Fig. 2).

Formulation

***ortho*-Phthalic Resins.** Resins based on *ortho*-phthalic anhydride (Table 2) comprise the largest group of polyester resins and are used in a variety of commercially significant applications, including marine craft, translucent glazing, simulated-marble vanity sets, and buttons. Most laminating and casting processes also rely on both colored and clear gel coats to provide some level of surface protection. The glycol generally controls the required performance; the phthalic–maleic anhydride ratio is adjusted to modify the reactivity according to physical properties required for fabrication needs.

The glycol is charged to the reactor and heated to 50°C under an inert-gas sparge. The lower melting maleic anhydride is metered in, allowing the temperature to rise to 100°C, followed by the phthalic anhydride. A clear solution forms

Table 2. Molar Component Ratio Used in *ortho*-Phthalic Formulations

	Glycol			Acid		
Resin	PG	DEG	NPG	PA	MAN	Styrene monomer
Marine	1.0			0.5	0.5	1.0
Marble	0.8	0.2		0.65	0.35	1.0
Gel-coat	0.5		0.5	0.5	0.5	1.0
Button	0.85	0.15		0.60	0.4	1.0

and the temperature is increased to 120°C to initiate the exothermic reaction between the glycol and anhydride forming the half-ester. The temperature increases rapidly to 150°C as the exotherm heat is released, at which point the half-ester begins to condense into low molecular weight polymers. The increasing viscosity of the melt tends to restrict the release of water vapor, and the reactants can foam into the condenser unless the reaction is controlled through cooling. The temperature is gradually increased to 220°C to maintain a constant removal of the condensate, but falls off as the reaction nears completion, usually in 12 h. Solid phthalic anhydride sublimes out in the latter stages of the reaction, requiring close control of the inert-gas flow and temperature. Some processors have used xylene as an azeotropic solvent to assist water removal while suppressing the sublimation of the phthalic anhydride, but this is not widely applied.

Phthalic resins are usually processed to an acid number of 25–35, yielding a polymer with an average M_n of 1800–2000. The solution viscosity of the polymer is usually followed to ascertain the polymer end point. The resin is cooled to 200°C and hydroquinone stabilizer (150 ppm) is added to prevent premature gelation during the subsequent blending process, with styrene at a maximum temperature of 70°C. The final polymer solution is cooled to 25°C before a final quality check and drumming out for shipment.

Isophthalic Resins. Isophthalic acid (IPA) can be substituted for phthalic anhydride to enhance mechanical and thermal performance and improve resistance to corrosive environments. Significant products include underground gasoline storage tanks and large diameter sewer and water pipe. Although phthalic resins find wide application in ambient fabrication processes, isophthalic resins (Table 3) are more widely used in products employing high temperature forming processes such as pultruded profile and electrical-grade laminate.

Isophthalic resins are manufactured by two-stage processing to facilitate the dissolution of the isophthalic acid. In the first stage, the glycol and isophthalic acid react under pressure at temperatures of 235°C under an inert atmosphere to produce a clear melt. High pressure processing [207 kPa (30 psi)] and, optionally, esterification catalysts such as hydrated monobutyl tin oxide are also widely employed to reduce the cycle times of two-stage processing. Maleic anhydride is added in the second stage and the final resin completed at 220°C to control color and molecular weight development. Isophthalic resins intended for corrosion application are processed to an M_n of 2200–2500; the reaction cycle is about 24 h.

The melting flow of the higher molecular weight isophthalic polymer is much higher than *ortho*-phthalic resins, and blending temperatures in styrene must be increased to avoid freezing the polymer out. Stabilizers such as toluhydroquinone

Table 3. Molar Component Ratio Used in Isophthalic Formulations

	Glycol		Acid		
Resin	PG	DEG	IPA	MAN	Styrene monomer
Tank	1.0		0.5	0.5	1.2
Pipe	0.5	0.5	0.4	0.6	1.2
Pultrusion	0.3	0.7	0.4	0.6	1.0
Electrical	1.0		0.3	0.7	1.0

Table 4. Molar Component Ratio Used in Dicyclopentadiene Formulations

	Glycol					
Resin	PG	EG	DEG	DCPD	MAN	Styrene monomer
Marine		1.0		2.0	2.0	3.0
Molding	1.0			0.5	1.0	1.0
Bathtub			1.0	2.0	2.0	3.0

and benzoquinone are more effective gelation inhibitors for the higher styrene-blending temperatures used for these resins.

Dicyclopentadiene Resins. Dicyclopentadiene (DCPD) can be used as a reactive component in polyester resins in two distinct reactions with maleic anhydride (7). The addition reaction of maleic anhydride in the presence of an equimolar amount of water produces a dicyclopentadiene acid maleate that can condense with ethylene or diethylene glycol to form low molecular weight, highly reactive resins. These resins, introduced commercially in 1980, have largely displaced *ortho*-phthalic resins in marine applications because of beneficial shrinkage properties that reduce surface profile. The inherent low viscosity of these polymers also allows for the use of high levels of fillers, such as alumina trihydrate, to extend the resin-enhancing, flame-retardant properties for application in bathtub products (Table 4).

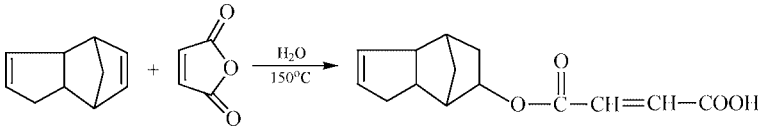

The cleavage of dicyclopentadiene into cyclopentadiene can be accomplished at temperatures above 160°C, producing the heterocyclic Diels–Alder maleic addition product, which opens to the diacid. This product can be esterified with propylene glycol to produce resins that demonstrate enhanced resilience and thermooxidative resistance suitable for molded electrical components.

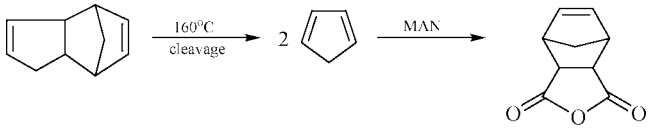

Flame-Retardant Resins. This type of resins are formulated to conform to fire safety specifications developed for construction as well as marine and electrical applications. Resins produced from halogenated intermediates (Table 5) are usually processed at lower temperatures (180°C) to prevent excessive discoloration. Dibromoneopentyl glycol requires glass-lined equipment because of its corrosive nature due to some elimination of bromine during the process at high tempretaures. Tetrabromophthalic anhydride and chlorendic anhydride (8) are formulated with ethylene glycols to maximize flame-retardant properties; reaction

Table 5. Molar Component Ratio Used in Flame-Retardant Formulations

	Glycol		Acid				
Resin	EG	DBNPG	TBPA	PA	CAN	MAN	Styrene monomer
Building	1.0				0.6	0.4	1.5
Glazing		1.0		0.5		0.5	2.0
Marine	1.0		0.15	0.35		0.5	1.0

cycle times are about 12 h. Resins are also produced commercially by the *in situ* bromination of polyester resins derived from tetrahydrophthalic anhydride (9).

Methyl methacrylate (MMA) is often used in combination with styrene to improve light transmission and uv stability in flame-retardant glazing applications. Recently, MMA is used to a limited extent because of new environmental regulations. Phosphate ester (triethyl phosphate) additives are also included to supplement flame-retardant efficiency; benzophenone uv stabilizers are required to prevent yellowing of these uv-sensitive resins.

Bisphenol Resins. Ethoxylated and propoxylated derivatives of bisphenol A form the basis for two distinct resin groups that demonstrate superior thermal and corrosion resistance. The addition product of propylene oxide [75-56-9] and bisphenol A, reacted with fumaric acid and dissolved in styrene monomer, has established commercial significance in applications involving extreme corrosive environments. The resins known generically as bisphenol fumarates (10) have been used since 1955 in the fabrication of tanks and piping used in the chloralkali and pulp and papermaking industries. This resin is unique among polyester compositions in resisting strong alkaline solutions that readily decompose *ortho*-phthalic and isophthalic resins.

Stabilizers. Hydroquinone [123-31-9] (**4**) is widely used in commercial resins to provide stability during the dissolution of the hot polyester resin in styrene during the manufacturing process. Incorporation of oxygen (air) into the styrene containing the resin inhibitor is required to activate them, which is converted to an equilibrium mixture of quinone and the quinhydrone (**5**) (11). At levels of 150 ppm, a shelf life of over 6 months can be expected at ambient temperatures.

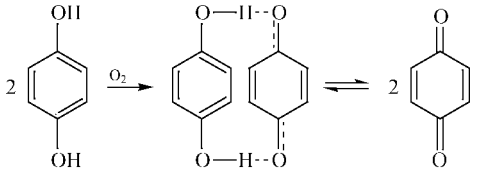

4 **5**

Toluhydroquinone and methyl *tert*-butylhydroquinone provide improved resin color retention; 2,5-di-t-butylhydroquinone also moderates the cure rate of the resin. Quaternary ammonium compounds, such as alkyl trimethylammonium chloride, are effective stabilizers in combination with hydroquinones and also produce beneficial improvements in color when promoted with cobalt octoate. Copper

naphthenate is an active stabilizer at levels of 10 ppm; at higher levels (150 ppm) it influences the reactivity preventing the resin from curing. Tertiary butylcatechol (TBC) is a popular stabilizer used by fabricators to adjust room temperature gelation characteristics.

Cross-Linking Mechanism

The reaction rate of fumarate polyesters with styrene is 20 times that of similar maleate polymers. Commercial phthalic and isophthalic resins usually have fumarate levels in excess of 95% and demonstrate full hardness and property development when catalyzed and cured. The addition polymerization reaction between the fumarate polyester and styrene monomer is initiated by free-radical polymerization. Commercially, benzoyl peroxide (BPO) and methyl ethyl ketone peroxide (MEKP) are the most common initiators used to cross-link unsaturated polyester and styrene. The initiators can be dissociated by heat or redox metal activators into peroxy and hydroperoxy free radicals.

The free radicals initially formed are neutralized by the quinone stabilizers, temporarily delaying the cross-linking reaction between the styrene and the fumarate sites in the polyester. This temporary induction period between catalysis and the change to a semisolid gelatinous mass is referred to as *gelation time* and can be controlled precisely between 1 and 60 min by varying stabilizer and catalyst levels.

As the quinone stabilizer is consumed, the peroxy radicals initiate the addition chain propagation reactions through the formation of styryl radicals. In dilute solutions, the reaction between styrene and fumarate ester follows an alternating sequence. However, in concentrated resin solutions, the alternating addition reaction is impeded at the onset of the physical gel. The liquid resin forms an intractable gel when only 2% of the fumarate unsaturation is cross-linked with styrene. The gel is initiated through small micelles (12) that form the nuclei for the expansion of the cross-linked network. The free styrene monomer is restrained within the gel and further reaction with fumarate groups is determined by the spacial arrangement; the styrene polymerizes in homopolymer blocks as it intercepts fumarate reaction sites. As individual micelles expand and deplete available fumarate sites in the short polymer chains, the remaining styrene forms homopolymer blocks that terminate at the boundaries between overlapping micelles (Fig. 4). Styryl free radicals simultaneously initiate micelle nuclei at points of high fumarate concentration. The micelles continue to expand, interacting with free styrene until the fumarate groups are depleted. The micelles eventually overlap at the boundaries that contain higher levels of terminal styrene homopolymer blocks.

As the micelles expand, the soft gel is transformed into a hard, rubbery transition stage that demonstrates low physical strength before the onset of the exotherm of polymerization. The temperature increases exponentially as the micelle expands. As the temperature subsides, the resulting cross-linked thermoset solid develops superior properties characteristic of the polymer. Generally, optimum strength characteristics are obtained in resins having a styrene/fumarate molar ratio of 2:1. Most resins are formulated with a styrene content consistent

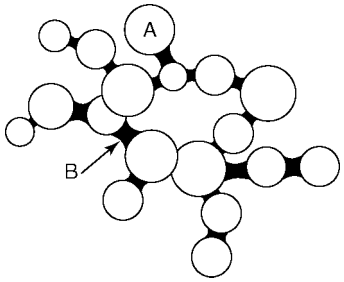

Fig. 4. Micellular gelation mechanism. A shows micelle nuclei, highly cross-linked; B, boundary where micelle growth terminates in styrene block polymers.

with this relationship (Tables 2–5). In resins having equivalent molar ratios of dibasic and unsaturated acid, this equates to resin polymer solutions containing around 40% styrene. However, this imposes some limitation on viscosity and most commercial resins contain between 40 and 45% styrene to achieve lower application viscosities.

In resins having low isomerization levels (80%), the fumarate–styrene reactions run to completion, leaving many unreacted maleate groups within the cross-linked structure. This results in an excess of styrene that inevitably forms larger homopolymer blocks between the intersecting micelles. The performance of such resins is characterized by lower softening temperatures and lower physical properties because of the additional plasticizing effects of the maleate ester group.

The cross-linking reaction mechanism is also influenced by the presence of other monomers. Methyl methacrylate is often used to improve the uv resistance of styrene-based resins. However, the disparate reaction rates of styrene and methacrylate monomer with the fumarate unsaturation not only preclude the use of more than 8% of the methacrylate monomer because of the significant slowing of the cross-linking reaction but also result in undercured products.

Catalyst Selection. The low resin viscosity and ambient temperature cure systems developed from peroxides have facilitated the expansion of polyester resins on a commercial scale, using relatively simple fabrication techniques in open molds at ambient temperatures. The dominant catalyst systems used for ambient fabrication processes are based on metal (redox) promoters used in combination with hydroperoxides and peroxides commonly found in commercial MEKP and related perketones (13). Promoters such as styrene-soluble cobalt octoate undergo controlled reduction–oxidation (redox) reactions with MEKP that generate peroxy free radicals to initiate a controlled cross-linking reaction.

$$\mathrm{ROOH} + \mathrm{Co}^{+2} \rightarrow \mathrm{RO}^{\bullet} + \mathrm{OH}^{-} + \mathrm{Co}^{+3}$$

$$\mathrm{ROOH} + \mathrm{Co}^{+3} \rightarrow \mathrm{ROO}^{\bullet} + \mathrm{Co}^{+2}$$

This catalyst system is temperature-sensitive and does not function effectively at temperatures below 10°C; but at temperatures over 35°C the generation of free radicals can be too prolific, giving rise to incomplete cross-linking

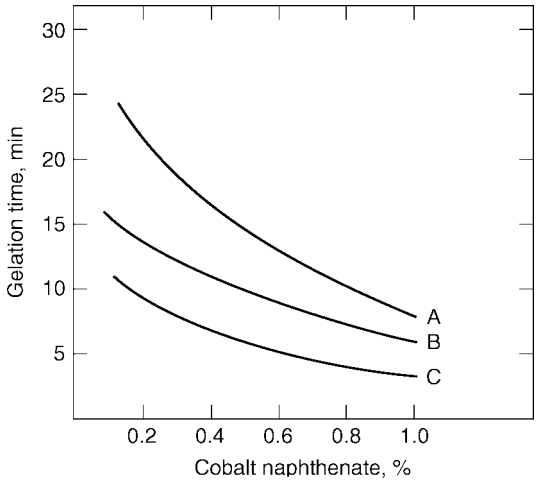

Fig. 5. Influence of catalyst systems on cure rate; gelation time is at 25°C as a function of the initiator concentration. A represents MEKP (1.0%); B, MEKP (1.0%) and dimethylaniline (DMA) (0.05%); and C, MEKP (2.0%).

formation. Redox systems are preferred for fabrication at temperatures ranging from 20 to 30°C (Fig. 5).

Some fabrication processes, such as continuous panel processes, are run at elevated temperatures to improve productivity. Dual-catalyst systems are commonly used to initiate a controlled rapid gel and then a fast cure to complete the cross-linking reaction. Cumene hydroperoxide initiated at 50°C with benzyl trimethylammonium hydroxide and copper naphthenate in combination with *tert*-butyl octoate are preferred for panel products. Other heat-initiated catalysts, such as lauroyl peroxide and *tert*-butyl perbenzoate, are optional systems. For higher temperature molding processes such as pultrusion or matched metal die molding at temperatures of 150°C, dual-catalyst systems are usually employed based on *tert*-butyl perbenzoate and 2,5-dimethyl-2,5-di-2-ethylhexanoylperoxy-hexane (Table 6).

Table 6. Optimal Temperature Range of Conventional Catalyst Systems for Unsaturated Polyesters

Catalyst	CAS registry number	Activator	Processing temperature, °C
Benzoyl peroxide	[94-36-0]	Dimethylaniline	0–25
Methyl ethyl ketone peroxides (MEKP)	[1338-23-4]	Cobalt octoate	20–25
Cumene hydroperoxide	[80-15-9]	Manganese Naphthenate	25–50
Lauroyl peroxide	[105-74-8]	Heat	50–80
tert-Butyl peroctoate	[13467-82-8]	Heat	80-120
Benzoyl peroxide	[94-36-0]	Heat	80–140
2,5-Dimethyl-2,5-di-2-ethyl-hexanoylperoxyhexane	[13052-09-0]	Heat	93–150
tert-Butyl perbenzoate	[614-45-9]	Heat	105–150

The action of redox metal promoters with MEKP appears to be highly specific. Cobalt salts appear to be a unique component of commercial redox systems, although vanadium appears to provide similar activity with MEKP. Cobalt activity can be supplemented by potassium and zinc naphthenates in systems requiring low cured resin color; lithium and lead naphthenates also act in a similar role. Quaternary ammonium salts (14) and tertiary amines accelerate the reaction rate of redox catalyst systems. The tertiary amines form beneficial complexes with the cobalt promoters, facilitating the transition to the lower oxidation state. Copper naphthenate exerts a unique influence over cure rate in redox systems and is widely used to delay cure and reduce exotherm development during the cross-linking reaction.

Another unique redox system used for extending gel times consists of cumene hydroperoxide and manganese naphthenate, which provides consistent gel times of between two and four hours over a temperature range of 25–50°C.

For application temperatures below 10°C or for acceleration of cure rates at room temperature, nonredox systems such as benzoyl peroxide initiated by tertiary amines such as dimethylaniline (DMA) have been applied widely. Even more efficient cures can be achieved using dimethyl-*p*-toluidine (DMPT), whereas moderated cures can be achieved with diethylaniline (DEA).

Tertiary amines are also effective as accelerators in cobalt redox systems to advance the cure rate (Fig. 6). Hardness development measured by Shore D or Barcol D634-1 penetrometer can be used to demonstrate this benefit, which is useful in increasing mold turnover at ambient temperatures.

Cure Exotherm. The cross-linking reaction between the unsaturated polymer and styrene results in a spontaneous change from liquid to a solid state with the onset of the exotherm. The exothermic heat generated is proportional to the fumarate level in the polymer, but increasing styrene levels can enhance

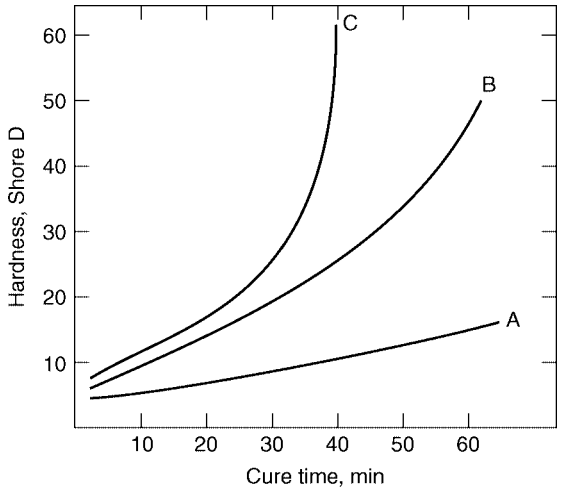

Fig. 6. Influence of catalyst systems on cure rate and effect of dimethylaniline (DMA) on cure rate of cast polymer resin at 25°C. Initiator system contains cobalt naphthenate (0.5%), MEKP (1.0%), and one of the following: A, DMA (0.0%); B, DMA (0.05%); or C, DMA (0.1%).

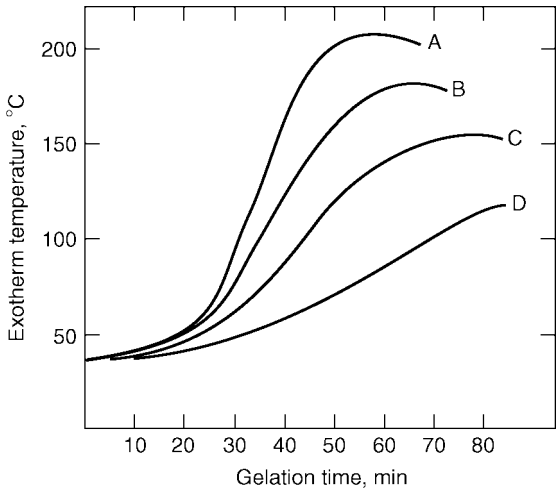

Fig. 7. Influence of copper naphthenate on exotherm temperature. Composition in pph; isophthalic laminating resin is cobalt naphthenate (0.20), dimethylaniline (0.05), and copper naphthenate: A (0.00); B (0.01); C (0.015); or D (0.02).

it further. Although some exotherms can be tolerated in molding processes, these can lead to excessive shrinkage, warpage, and cracking in large moldings or GFR laminations thicker than 9 mm. The cure exotherm can be suppressed in a number of ways to afford a more controllable fabrication system, without adversely affecting the final cure or structural performance.

Copper naphthenate added to the resin at levels between 5 and 20 ppm effectively extends gel and cure characteristics, resulting in a reduction in exothermic heat (Fig. 7). Copper additives are widely used in commercial laminating resins to modify process exothermic effects. α-Methylstyrene [98-83-9] substituted for styrene at levels of 5–8% has also been used effectively in resins cured at above ambient temperatures. The inhibitor 2,5-di-*t*-butylhydroquinone exerts significant exotherm suppression at levels of 200–400 ppm and is useful in high temperature molding processes.

Shrinkage. Polyester resins that undergo cross-linking reactions have as a result a net contraction in volume. Resins dissolved in styrene demonstrate a volumetric shrinkage of 17%. Such high shrinkage can lead to cracking or warping of castings or laminates. Monomers such as vinyltoluene or diallyl phthalate reduce shrinkage; these monomers are often used in high temperature molding compositions to avert warpage or internal voids. With vinyltoluene, volumetric shrinkage during cure is 12.6% and with diallyl phthalate, 11.8%. The effects of shrinkage can also be modified by incorporating soluble poly(vinyl acetate) and related thermoplastic additives into the liquid resins, which phase out during the cross-linking reaction, thus significantly reducing shrinkage. Additional benefits can be obtained by incorporating high filler loadings into resins used in casting or high temperature molding processes.

Air Inhibition. Polyester resins are widely used in open-mold lamination or casting and quite often develop a tacky surface feel after curing. The free-radical polymerization process is sensitive to oxygen, which interferes with the surface

cross-linking mechanism and impedes the cure. Lower molecular weight phthalic resins display a pronounced effect, but higher molecular weight isophthalic resins have less tack. Low molecular weight resins normally produce small fractions of unreactive portions that can migrate to the surface of the resin during the curing process. The lower reactivity of those fractions produce surfaces with high tackiness. Resins based on dicyclopentadiene react with oxygen through an air-drying mechanism and give rise to tack-free surfaces; resins derived from tetrahydrophthalic anhydride have similar air-drying qualities useful for polyester coatings and linings.

Paraffin wax additives are effective in overcoming surface inhibition by forming a monomolecular wax layer at the curing surface. Although effective in excluding oxygen, this waxy layer must be removed for subsequent lamination or bonding processes.

Performance Characteristics. Polyester resins undergo a rapid transformation from a viscous liquid to a solid plastic state that comprises a three-dimensional cross-linked polymer structure. The level of polyester unsaturation determines essential performance characteristics (Table 7), although polymer components can influence subtle features that affect thermal, electrical, and mechanical performance as defined by ASTM procedures.

The cross-linked polymers form a thermoset plastic which cannot be changed or returned to its original condition by heating, as it can with thermoplastics. This thermoset characteristic is beneficial in providing high temperature properties, good solvent and chemical resistance, and high flexural modulus. Cross-linked polyester resins are rigid materials and are highly sensitive to brittle fracture. Reinforcing with glass fiber produces a composite plastic, which has exceptional strength characteristics suitable for replacing conventional fabricating materials such as wood, steel, and concrete. Aggregates and fillers such as ground limestone also improve the strength characteristics of polyester resins and are used widely

Table 7. Standard Test Methods for Polyester Resins and Compounds

Properties	ASTM designation
Specific gravity	D792
Barcol hardness	D2583
Heat Distortion	D648
Flexural strength modulus	D790
Tensile strength modulus, elongation	D638
Tensile impact	D1822
Compressive strength modulus	D695
Izod impact	D256
Shear	D732
Taber abrasion	D1044
Flammability	E84, E162
Dielectric strength	D149
Dissipation factor	D150
Arc resistance	D495
Water absorption	D570
Water vapor transmission	C355
Chemical resistance	C581

in cast objects such as bathroom vanity sets and building components. Polyester resins are used in an unfilled condition in cast objects such as bowling balls and buttons, in thin films for gel coats, and, to a lesser extent, as clear wood coatings.

Mechanical Properties. The performance of various polyester resin compositions can be distinguished by comparing the mechanical properties of thin castings (3 mm) of the neat resin defined in ASTM testing procedures (15). This technique is used widely to characterize subtle changes in flexural, tensile, and compressive properties that are generally overshadowed in highly filled or reinforced laminates.

Resins of higher molecular weight demonstrate higher tensile strength, whereas high fumarate resins have higher flexural modulus. Formulations containing diethylene glycol and adipic acid produce resins that have higher resilience reflected in enhanced tensile and flexural strength but lower flexural modulus. Isophthalic resins provide better mechanical properties than *ortho*-phthalic resins and are consequently preferred in laminate applications requiring higher structural performance. The strength of all polyester resins is enhanced significantly by glass and other fibrous reinforcements. Laminates are usually fabricated from glass fiber mat, having individual fibers 5 cm in length. The structural properties increase in proportion to the glass fiber content, which can be varied from 25 to 40%. Increased reinforcement levels can be achieved by using woven glass roving in alternating plies with chopped strand glass mat. Higher strength can be realized from continuous glass-fiber rovings used in filament-wound structures in the form of pipes or tanks. Helical wind angles are varied to achieve design requirements in hoop or axial directions; a wind angle of 55° can generate twice the strength in the hoop direction. Continuous glass-fiber roving used at reinforcement levels of 65% in pultruded products provides composites that have the highest flexural and tensile properties. Carbon fiber can be useful in developing composites that have higher modulus characteristics, but economics have reduced their wider attractiveness in combinations with polyester resins. Kevlar cloth can be used in combination with unsaturated polyester urethanes to produce light weight, high strength composite plastics for sporting equipment such as kayaks, skis, and bulletproof composites.

Resins filled with ground limestone to levels of 80% by weight are useful in solid-cast products. The fillers reduce sensitivity to brittle fracture and improve modulus, but have little effect on general strength properties (Table 8).

Table 8. Strength Characteristics of Isophthalic Resin and Composite Derivatives

Characteristic	Cast resin	Filled resin	Glass-reinforced laminate	Filament-wound laminate	Pultruded profile
Glass fiber content, %	0	0	30	50	60
Flexural strength, MPa[a]	110	82	193	296	448
Flexural modulus, GPa[b]	3.44	4.68	5.86	13.7	20.6
Tensile strength, MPa[a]	68.9	44.8	110	193	241
Tensile modulus, GPa[b]	3.1	2.6	5.51	12.4	15.1
Tensile elongation, %	2.5	0.5	1.6	1.6	1.5
Compressive strength, MPa[a]	103	110	137	193	200

[a] To convert MPa to psi, multiply by 145.
[b] To convert GPa to psi, multiply by 145,000.

Thermomechanical Properties. The highly cross-linked structure of cured unsaturated polyester resins produces thermoset characteristics in which the resistance to softening and deformation is greatly enhanced at elevated temperatures. The cross-linked network undergoes a structural transition during heating, in which the rigid crystalline state transforms to a softer amorphous condition at the glass-transition temperature T_g, accompanied by a small expansion in volume, thus facilitating some relaxation along the amorphous micellular boundaries and allowing deformation to take place. Aromatic constituents enhance the T_g, as do high fumarate and high styrene levels, whereas aliphatic derivatives (adipic) and reduced fumarate levels lower T_g values. Resins containing high adipic acid levels display rubbery or elastomeric properties at below ambient temperatures. Glass-reinforced products using these resins have exceptional impact properties and demonstrate high tolerance to low temperature cryogenic applications. Deformation at higher temperatures is moderated by fibrous reinforcements. However, as the temperature exceeds the T_g of the cross-linked polymer, laminate properties fall off considerably (Fig. 8).

Although reinforcements can improve the structural behavior of the composite at elevated temperature, the polymer, irrespective of its composition, begins to disassociate chemically in the presence of oxygen. *ortho*-Phthalic resins having the weaker ester bonds depolymerize readily at temperatures over 200°C and form low molecular weight fractions disintegrating the polymer network. Determination of laminate weight loss or flexural property retention indicates that alicyclic diols, including hydrogenated bisphenol A and cyclohexanedimethanol, perform better than lower glycols such as propylene, and neopentyl glycol imparts exceptional thermal stability at temperatures up to 200°C. However, all resins depolymerize spontaneously at around 300°C as the ester groups disassociates from the polymer

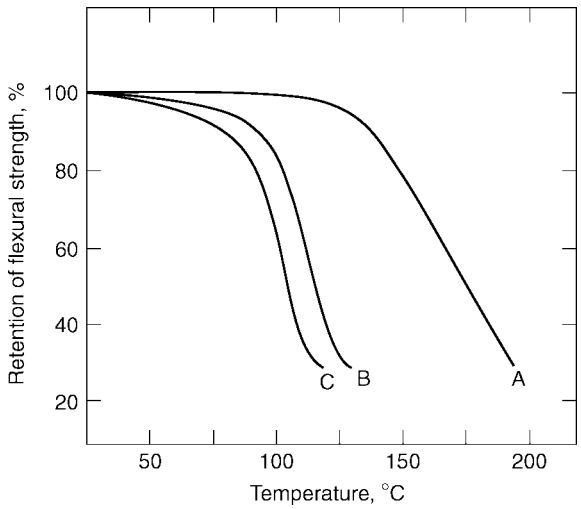

Fig. 8. Flexural properties at elevated temperatures. Laminates constructed from alternating plies of 46.7-g (1.5-az) mat and 746-g/m^2 (24-oz(yd^2) woven roving at a nominal glass content of 45%. A represents bisphenol fumarate (T_g = 130°C); B, isophthalic resin (T_g = 100°C); and C, *ortho*-phthalic resin (T_g = 80°C).

network, producing by-products that include lactones, dimer esters, and glycols. Vinyltoluene provides enhanced thermal performance on account of the increased bond strength resulting from the inductive influence of the methyl group para to the vinyl unsaturation. Oxidative disassociation at elevated temperature can be suppressed with antioxidants, but these eventually interfere with the catalyst's activity, thus reducing cure rate.

Halogenated intermediates based on chlorendic anhydride and alkoxylated brominated bisphenol A are quite stable and are used extensively in flame-retarded high temperature compositions, but brominated alicyclics, such as dibromotetrahydrophthalic resin, are rapidly dehydrohalogenated at lower temperatures.

Cross-linked polyester composites have a relatively low coefficient of thermal conductivity, which can provide beneficial property retention in thick laminates at high temperatures as well as remove the need for secondary insulation. The coefficient of thermal expansion of glass-reinforced composites is similar to aluminum but higher than most common metals.

Dielectric Properties. Polyester resins are nonconductors, have relatively low dipolar characteristics, and provide high dielectric strength and surface resistivity. At high voltage or high current, however, the cross-linked plastics fail due to carbon arcing or tracking caused by the charring of the polymer surface into a conductive carbonaceous residue. Hydrated fillers such as alumina trihydrate (16) suppress surface char formation and are used extensively with glass reinforcement in molding compounds intended for electrical applications. High temperature electrical applications usually specify bisphenol fumarate resins or high molecular weight isophthalic resins having high fumarate reactivity. Dicyclopentadiene resins provide enhanced oxidative resistance, whereas vinyltoluene monomer is used for superior thermal properties. Specialized granulated molding compounds are also formulated by using diallyl phthalate monomers, and are used for injection molding smaller electrical components.

Chemical Properties. The three-dimensional cross-linked network resists penetration and attack by most corrosive chemicals and nonpolar solvents, although weak alkalies and especially polar solvents such as lower ketones, chlorinated aliphatics, and aromatics readily attack *ortho*-phthalic, isophthalic, and dicyclopentadiene resins. Water has wide-ranging effects on different resin compositions as it penetrates into the plastic network. Cross-linking density and the presence of steric constituents local to the ester groups can enhance water resistance. Isophthalic resins have better water absorption characteristics than corresponding *ortho*-phthalic resins. Neopentyl glycol and alkoxylated bisphenol constituents provide maximum performance in aqueous media. Ethylene and diethylene glycols demonstrate high water absorption that leads to the loss of mechanical strength. The presence of glass reinforcements within the cross-linked plastic is also affected by chemical attack. Water absorbed onto surface fibers is carried into the plastic matrix, decoupling the resin–glass fiber interfacial bond in the process. Alkalies compliment this attack on the glass reinforcement and lead to surface blistering and rapid loss of laminate strength. Chemical attack is usually minimized by incorporating surface protection in the form of corrosion-resistant (C glass) surface veils and high surface resin content in laminates intended for chemical service. Reinforced polyester composites or FRPs perform well in

concentrated hydrochloric and phosphoric acids; concentrated sulfuric and nitric acid oxidize and degrade the polymer rapidly. High performance resins based on bisphenol A fumarate and their brominated homologues have featured prominently in FRP piping, tanks, chemical ducting, and scrubbers used to handle corrosive chemicals and emissions in pulp and paper plants, mining and ore classification, and the chloralkali industries. FRP has also emerged as a strategic solution for designing equipment intended for high temperature applications in fossil fuel electric power generating utilities such as chimney stack liners and scrubbers for the control of sulfur dioxide emissions.

Corrosion attack on the polymer is influenced by permeation rate, as well as internal stresses or fatigue, which distorts or fractures the resin glass fiber interface. Localized corrosion failure in large tanks or piping systems can sometimes be explained by stress-induced corrosion failure. FRP composites normally contain air voids that distort into elliptical voids adjacent to the reinforcing fiber. Water and chemicals penetrating these voids set up osmotic cells that plasticize and soften the surrounding polymer, initiating brittle fracture along the fibers and progressively opening up new surface area for corrosion attack in areas under high stress. Nonpolar solvents have little effect on polyester resins and have been used extensively for underground storage of gasoline. However, with the reformulation to unleaded gasoline, the higher aromatic fuels require resins that have higher cross-linking density. This is provided by high fumarate isophthalic or terephthalic derivatives.

Flammability. Polyester resin products ignite and burn by emitting sooty smoke. Flammability can be reduced significantly through halogen-modified components either formulated into the polyester polymer as chlorendic anhydride, tetrabromophthalic anhydride, or dibromoneopentyl glycol, or as part of the monomer system, ie, dibromostyrene. Additives such as phosphate esters are frequently used to enhance flame retardance, whereas antimony trioxide at levels of 5% or less on resin provides optimum retardance in combination with halogenated intermediates. The flame-retardant mechanism depends on the thermal disassociation of the organohalogen component, which, upon exposure to the heat of the flame, releases hydrogen chloride or hydrogen bromide gases that become active as radical transfer agents in suppressing the oxidation–combustion process (17). The activity of the halogen gases is synergized through the formation of antimony oxy halides and trihalides; arsenic and molybdenum salts offer comparable activity. Organophosphorus compounds behave in a supplementary role by forming polyphosphoric acids that induce char at the burning surface. However, phosphates plasticize the polymer and reduce performance at levels exceeding 5%, thus offering marginal benefits. Organoferrous compounds such as ferrocene demonstrate unique synergism with halogenated resins, reducing both flame spread and smoke generation. Also, ferrous oxide (18) is active in chlorendic resins in a similar capacity. The formation of ferric chloride promotes aromatization and enhances char formation and the subsequent reduction of smoke emissions. The exothermic nature of the combustion process can provide sufficient energy for sustained burning, unless halogen modification is used. Nonhalogenated resin systems, based on hydrated fillers such as alumina trihydrate, have emerged. Alumina trihydrate undergoes endothermic disassociation at above 300°C, and can offset the combustion heat and reduce surface temperatures sufficiently to interrupt the high energy oxidation mechanism. Resins incorporating over 40%

by weight of aluminum trihydrate not only qualify for most construction and electrical flammability specifications but also provide significant reduction in smoke emissions. Useful bench-scale tests, such as ASTM E162 and ASTM D2863, have been developed for characterizing flammability and smoke emissions, but the dynamic nature of the combustion process requires large-or full-scale fire testing, such as ASTM E84, to be performed for applications intended for confined areas. Halogenated resins are sensitive to heat and ultraviolet radiation; resins based on tetrabromophthalic anhydride yellow after a few days in direct sunlight. Benzophenone and benzotriazole stabilizers used at levels of 1% are highly effective with chlorendic, dibromoneopentyl, and dibromotetrahydrophthalic derivatives, but resins based on brominated aromatics such as tetrabromophthalic anhydride and tetrabromobisphenol eventually discolor in exterior applications.

Weathering. Polyester resins in the form of laminates, coatings (gel coats), and castings perform well in outdoor exposures; marine craft, tanks, pipes, and architectural facia produced in the 1960s are still in service. Polyesters undergo some change in their surface features in direct sunlight, discoloration or yellowing being most obvious. Dulling and microcrazing occur only in products not appropriately formulated for the exposure. Long-term surface erosion of laminates exposes the glass fibers, which, unless corrected, can lead to rapid loss of structural integrity. Absorption of water influences the interfacial bond between the resin matrix and either the fibrous or aggregate reinforcement, leading to some loss of mechanical properties over 30 years. However, observations indicate that most applications reach this equilibrium after three to five years and do not show much significant change thereafter. Most FRP products are designed with protective and decorative gel coats (19) formulated from neopentyl glycol, which, in combination with some methyl methacrylate monomer and benzophenone uv stabilizers, provides improved weather resistance. Platelet fillers such as talcs and clays, as well as high pigment levels, are incorporated into gel coats to obscure the underlying laminate from the effects of direct sunlight. Surface oxidation and discoloration can also be controlled by using uv-resistant lacquers based on polymethacrylate resins or by cladding with poly(vinyl fluoride) (PVF) or acrylic and poly(ethylene terephthalate) (PET) films.

Application Processes

Open-Mold Process. Polyester resins are fabricated easily in open molds at room temperature. Such processes account for over 80% of production volume, the remaining being fabricated using matched metal dies in high temperature semiautomated processes.

The hand lay-up or spray-up process, used universally for the production of laminar composites incorporating glass-fiber reinforcement, is most efficient for the manufacture of large parts, such as boats, bathtubs, tanks, architectural shapes, and recreational accessories. Resins intended for spray-up processes are usually modified with thixotropic additives, such as fumed silica (1%), to reduce the risk of drainage when applied over large vertical mold surfaces. Molds are also made from FRP for short-run products usually surfaced with a tooling gel coat to provide consistent surface quality and appearance.

Gel coats are pigmented polyester coatings applied to the mold surface and are an integral part of the finished laminate. Gel coats are used widely on hand lay-up and spray-up parts to enhance surface esthetics and coloration, as well as to provide an abrasion-resistant waterproof surface that protects the underlying glass-reinforced structure.

Thermoformed acrylic sheet is displacing gel coats in some bathtub applications; spas have converted almost exclusively to formed acrylic sheet reinforced with glass-reinforced polyester laminations because of higher temperatures and higher structural requirements.

Products of axial symmetry such as pipes and tanks can be produced by filament-winding resin-impregnated glass rovings over a rotating mandrel. This process provides for some versatility in adjusting the winding angle to meet design cost considerations. A winding angle of 55° to the axis produces pipes that have twice the strength in the hoop direction, suitable for conveying high pressure liquids that may be corrosive to metals. Large-diameter piping systems (1–3 m) are also produced by centrifugal casting techniques, by which high levels of silica sand can be used to improve pipe stiffness. FRP pipes have been used extensively as slip linings for deteriorated concrete sewer pipes that avoid costly excavation.

Resins containing fillers and aggregates can be usefully cast into attractive components that simulate marble and granite. Bathroom vanity sets and kitchen countertop components have emerged as a significant commercial outlet for filled resins cast in open molds that often employ gel coats having superior hydrolytic properties to enhance resistance to thermal shock and crazing. Specially formulated isophthalic resins in admixture with sand have been developed for surfacing worn concrete roads and bridges. Polyester resins are also emerging in filled pigmented coatings used as permanent road marking, as some U.S. states displace solvent-based alkyd marking materials. Other products such as buttons and bowling balls are cast from resins containing low filler levels.

Closed-Mold Processes. In an effort to improve the productivity of the hand lay-up process, closed-mold systems containing two mating dies have evolved. In resin-transfer molding (RTM), glass reinforcement is placed in the open mold; once the molds are in place, precatalyzed resin is injected into the cavity under pressure. The process has been further modified to use a vacuum that ensures complete air removal and faster mold filling. The process is adaptable to large components and can be used to encapsulate foam, aluminum, and wood components into the structure. The process is also beneficial in reducing styrene emissions that are regulated under Title III of the U.S. Clean Air Act passed in 1990.

High temperature compression molding has grown rapidly since 1985 as applications for glass-reinforced composites have expanded in the automotive body panel market. Molding compounds incorporating resins, catalysts, fillers, pigments, and glass fiber reinforcements have evolved as bulk molding compounds (BMC) and sheet molding compounds (SMC) to meet requirements in the electrical, business machine, as well as structural automotive markets.

Matched die molding is the most efficient process to produce high volumes of relatively large parts. The mold cycle is under two minutes at 150°C and the process can be incorporated into an automated manufacturing system, reducing labor and scrap while improving quality. Resins have been uniquely formulated to reduce shrinkage and provide composite surfaces that can be primed and coated by using conventional baked enamels. The polyester technology providing these

low profile, low shrink resins is based on the action of thermoplastic additives (20) incorporated into unique polyester resin formulations based on propylene glycol fumarate.

Poly(methyl methacrylate) and poly(vinyl acetate) precipitate from the resin solution as it cures. This mechanism offsets the contraction in volume as the polyester resin cross-links, resulting in a nonshrinking thermoset. Other polymer additives such as poly(butylene adipate) provide similar shrinkage control. The change in volume and compatibility of the polymer produces a whitening of the composite and results in nonuniform coloration in pigmented products. Polystyrene additives used in BMC can be formulated into nonshrinking, pigmentable compounds suitable for colored electrical products and kitchen utensils.

Injection molding of BMC and thick molding compounding (TMC) is expanding to improve the efficiency of the matched die process. TMC is a compound intermediate between BMC and SMC in which the glass-fiber strand integrity is retained in the molded product, thus greatly enhancing strength and impact properties.

High strength composites with linear symmetry can be produced by the pultrusion process (21) using continuous glass-fiber reinforcements in the form of rovings. Special continuous glass mats have also evolved to meet the process requirements of this technology. Glass fiber levels of 65% can be formed into polyester composites that demonstrate exceptional flexural performance characteristics required in such applications as flag poles and automotive springs. The process can also form hollow structures and profiles compatible with extruded aluminum and PVC useful in window and portal construction.

BIBLIOGRAPHY

"Polyesters, Unsaturated" in *EPST* 1st ed., Vol. 11, pp. 129–168, by H. V. Boenig, R&B Plastics, Inc.; in *EPSE* 2nd ed., Vol. 12, pp. 256–290, by Jeffrey Selley, Consultant.

1. W. H. Carothers, *J. Am. Chem. Soc.* **51**, 2548 (1929).
2. H. Boenig, *Unsaturated Polyesters Structures and Properties*, Elsevier Science, Inc., New York, 1964.
3. U.S. Pat. 3,345,339 (Oct. 3, 1967), E. E. Parker and J. G. Baker (to PPG Industries).
4. E. E. Parker, *Ind. Eng. Chem.* **58**, 53 (1966).
5. U.S. Pat. 3,355,434 (Nov. 28, 1967), J. G. Milligan and H. G. Waddill (to Jefferson Chemical Corp.).
6. U.S. Pat. 3,576,909 (Apr. 27, 1971), C. J. Schmidle and A. E. Schmucker (to General Tire and Rubber).
7. D. L. Nelson, *Soc. Plast. Ind. Conf.* **34**, 1G (1979).
8. U.S. Pat. 2,909,501 (Oct. 20, 1959), P. Robitschek and J. L. Olmstead (to Hooker Chemical Corp.).
9. U.S. Pat. 3,536,782 (Oct. 27, 1970), U. Toggwerler and F. Rosselli (to Diamond Shamrock Corp.).
10. U.S. Pat. 2,634,251 (Apr. 7, 1953), P. Kass (to Atlas Powder Co.).
11. C. C. Price and D. H. Read, *J. Polym. Sci.* **1**, 44 (1946).
12. Y.-S. Yang and L. Suspene, *Polym. Eng. Sci. Mater.* **31**(5), 321 (1991).
13. J. Harrison, O. Mageli, and S. Stengel, *Reinforced Plast. Conf.* 15(14) (1960).
14. U.S. Pat. 3,886,113 (May 27, 1975), M. W. Uffner (to Air Products and Chemicals, Inc.).
15. *The American Standards and Testing Methods Manual*, The American Society for Testing and Materials, Philadelphia, Pa., 1992.

16. T. D. Bautista, *Polym. Plast. Technol. Eng.* **18**, 179 (1982).
17. J. E. Selley, *Soc. Plast. Ind. Conf.* **33**, 2E (1978).
18. U.S. Pat. 4,152,368 (May 1, 1979), E. Dorfman, R. R. Hindersinn, and W. T. Schwartz (to Hooker Chemical Corp.).
19. J. H. Davis and S. L. Hillman, *Soc. Plast. Ind. Conf.* **26**, 12C (1971).
20. U.S. Pat. 3,701,748 (Oct. 31, 1972), C. H. Kroekel (to Rohm & Haass Co.).
21. J. E. Sumerak, *Soc. Plast. Ind. Conf.* **40**, 2B (1985).

HILDEBERTO NAVA
Reichhold Chemicals, Inc.

POLYETHERETHERKETONES (PEEK). See ENGINEERING THERMOPLASTICS.

POLYETHERS. See ETHYLENE OXIDE POLYMERS; PROPYLENE OXIDE POLYMERS.

POLYETHERS, AROMATIC

Introduction

Aromatic polyethers are best characterized by their thermal and chemical stabilities and mechanical properties. The aromatic portion of the polyether contributes to the thermal stability and mechanical properties, and the ether functionality facilitates processing but still possesses both oxidative and thermal stability. With these characteristic properties as well as the ability to be processed as molding materials, many of the aromatic polyethers can be classified as engineering thermoplastics (see ENGINEERING THERMOPLASTICS, OVERVIEW).

One class of aromatic polyethers consists of polymers with only aromatic rings and ether linkages in the backbone; poly(phenylene oxide)s are examples and are the principal emphasis of this article. A second type contains a wide variety of other functional groups in the backbone, in addition to the aromatic units and ether linkages. Many of these polymers are covered in other articles, based on the other functionality (see POLYIMIDES; POLYSULFONES).

Poly(phenylene oxide)s, Properties

The poly(phenylene oxide)s are also referred to as polyoxyphenylenes and poly(phenylene ether)s. Variations in the configuration of the ether group, ie, ortho, meta, or para, and in the extent and type of substitution, eg, alkyl, halo, etc, on the aromatic backbone give rise to a large number of possible homo- and copolymers. The polymers with para-oriented ethers have been studied most extensively and several have significant utility. Poly(2,6-dimethyl-1,4-phenylene oxide) [25134-01-4] (DMPPO), prepared by General Electric by the oxidative coupling polymerization of 2,6-dimethylphenol, is marketed as PPO resin. Blends of

Encyclopedia of Polymer Science and Technology. Copyright John Wiley & Sons, Inc. All rights reserved.

DMPPO with polystyrene and additives is marketed under the trade name of Noryl thermoplastic resin. Blends of DMPPO with nylon plus additives are sold as Noryl GTX resin. Other poly(phenylene oxide)s are also of commercial interest. For example, low molecular weight, unsubstituted poly(phenylene oxide)s are of use as heat-transfer fluids and liquid phases for gas chromatography. Poly(2,6-diphenyl-1,4-phenylene oxide) is sold as a gas absorbent and for gas chromatography.

Many newer poly(phenylene oxide)s were reported in the early 1990s. For example, a number of poly(2,6-diphenyl-1,4-phenylene oxide)s were prepared with substituents in the 4-positions of the pendent phenyl groups. Of particular interest is the 4-fluoro substituent, which imparts a lower melting point, enhanced solubility, and a lesser tendency to crystallize than has been found for the parent material (1).

Physical Properties. The glass-transition temperatures and melting points of a variety of poly(1,4-phenylene oxide)s are summarized in Table 1. The very high glass-transition temperatures of DMPPO and poly(2,6-dichloro-1,4-phenylene oxide) relative to their melting points provide polymers with excellent high temperature physical properties. Crystallization of several polymers can be induced with certain liquids, eg, α-pinene, decalin, and toluene for DMPPO, and tetrachloroethane for poly(2,6-diphenyl-1,4-phenylene oxide) (2). Although DMPPO dissolves readily in methylene chloride, a complex of polymer and methylene chloride soon precipitates from the solution (3). Although precipitation of the polymer as the complex can be quantitative, the complex is unstable when separated from the liquid methylene chloride phase and dissociates rapidly to leave the pure polymer. Low molecular weight polymers with very narrow molecular weight distribution ($M_w/M_n = 1.1$) can be prepared by cooling an equilibrating mixture of low molecular weight oligomers in methylene chloride. As the molecular weights of some of the oligomers increase owing to redistribution, these oligomers reach the critical size for complexation and precipitate from solution. The molecular weight at which this occurs is approximately 2000 (4).

Mechanical and electrical properties for DMPPO are given in Table 2.

Chemical Properties. The phenolic end groups in poly(phenylene oxides)s react with oxidizing agents in a variety of ways; the type of product depends in part on other reagents that may be present. Thus, in the presence of other phenols, a catalytic amount of oxidizing agent generates aroxy radicals and the ensuing coredistribution produces low molecular weight products (eq. 1, where $x = 1,2,3,\ldots$) (15). In the absence of the phenol HOAr, and with an equivalent of tetrasubstituted diphenoquinone as an oxidizing agent, biphenyl units are introduced into the polymer at the terminal position and then, through redistribution, internally (16,17) (eq. 2, where $a = 0$, 1, 2, 3, etc). Under acidic conditions with excess oxidizing agent, benzoquinones are generated (eq. 3) (18).

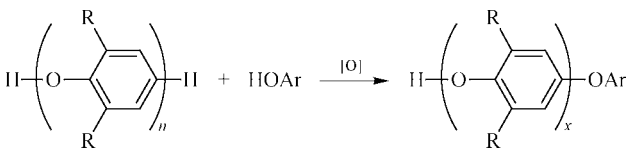

(1)

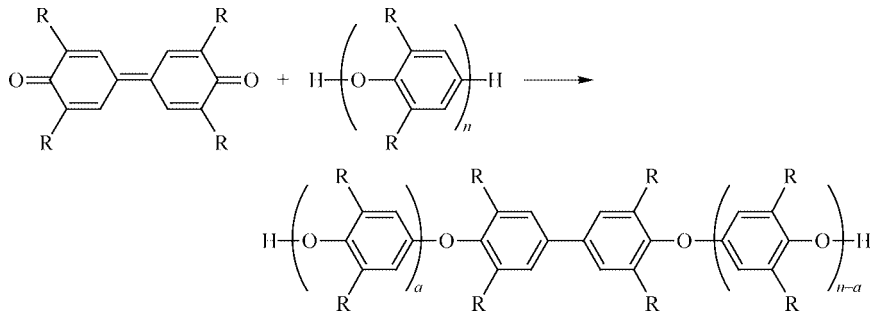

(2)

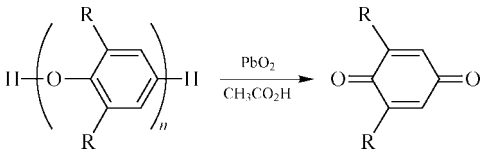

(3)

The preceding reactions do not occur if the terminal hydroxyl group in the polymer is no longer present, eg, if it has been end-capped by acetylation.

Side reactions during polymerization can lead to abnormal end-group formation and branching. For example, when secondary amines are present during a copper-catalyzed polymerization, they are often covalently bound to the methyl group of a head end group (19). With a manganese catalyst system, secondary amines are bound to the polymer analogously if they are present, but if they are absent polymer chains are bound at this site through the oxygen of a head end group to form a benzyl ether linkage. Additional polymerization attaches more units to produce a branched molecule (20), as follows.

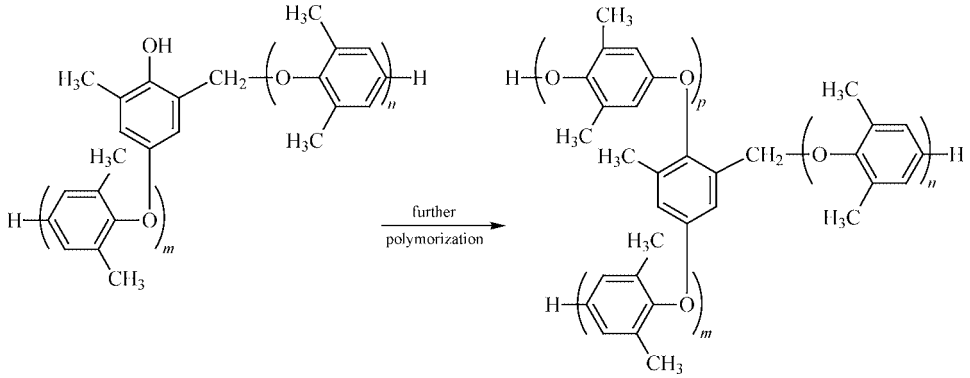

The backbone of poly(phenylene oxide)s is cleaved under certain extreme reaction conditions. Lithium biphenyl reduces DMPPO to low molecular weight products in the dimer and trimer molecular weight range (21) and converts poly(2,6-diphenyl-1,4-phenylene oxide) to 3,5-diphenylphenol in 85% yield (22) (eq. 4).

Table 1. Thermal Properties of Poly(Phenylene Oxides)s 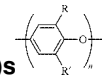

Name	CAS Registry Number	R	R′	T_g, °C	Ref.
Poly(1,4-phenylene oxide)[a]	[25667-40-7]	H	H	82	(5)
Poly(2,6-dimethyl-1,4-phenylene oxide)[b]	[25134-01-4]	CH_3	CH_3	211	(6)
Poly(2-methyl-6-phenyl-1,4-phenylene oxide)	[25805-39-4]	CH_3	C_6H_5	169	(7)
Poly(2-benzyl-6-methyl-1,4-phenylene oxide)	[26545-37-9]	$C_6H_5CH_2$	CH_3	99	(8)
Poly(2-isopropyl-6-methyl-1,4-phenylene oxide)	[31985-12-3]	$(CH_3)_2CH$	CH_3	144	(9)
Poly(2,6-dimethoxy-1,4-phenylene oxide)	[25667-13-4]	CH_3O	CH_3O	167	(10)
Poly(2,6-dichloro-1,4-phenylene oxide)[c]	[26023-26-7]	Cl	Cl	228	(11)
Poly(2,6-diphenyl-1,4-phenylene oxide)[d]	[24938-68-9]	C_6H_5	C_6H_5	230	(12)
Poly(2-*m*-tolyl-6-phenyl-1,4-phenylene oxide)	[79569-12-3]	*m*-Tolyl	C_6H_5	219	(13)
Poly(2-*p*-tolyl-6-phenyl-1,4-phenylene oxide)	[79569-09-8]	*p*-Tolyl	C_6H_5	218	(13)
Poly[2-(4-*t*-butyl)phenyl-6-phenyl-1,4-phenylene oxide]	[79569-10-1]	4-*tert*-Butylphenyl	C_6H_5	240	(13)
Poly(2-naphthyl-6-phenyl-1,4-phenylene oxide)	[79569-11-2]	2-Naphthyl	C_6H_5	234	(13)

[a] Mp = 298°C.
[b] Mp = 268°C.
[c] Mp = 269°C.
[d] Mp = 480°C.

Table 2. Properties of DMPPO[a]

Property	Value
Tensile yield (at 23°C), MPa[b]	80
Tensile modulus, MPa[b]	2,690
Flexural strength, MPa[b]	114
Flexural modulus, MPa[b]	2,590
Izod impact (notched), J/m[c]	64–96
Oxygen index	28–29
Density, g/cm^3	1.06
Dielectric constant (at 60 Hz)	2.54
Dielectric strength (thickness, 3.18 mm), V/mm	20,000

[a]Ref. 14.
[b]To convert MPa to psi, multiply by 145.
[c]To convert J/m to ft · lb/in., divide by 53.38 (ASTM D256).

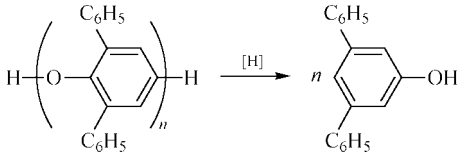

(4)

At temperatures near 370°C, DMPPO undergoes a rearrangement (eq. 5).

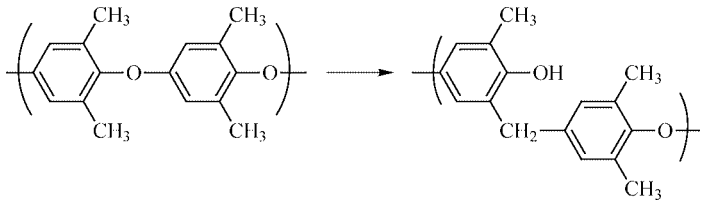

(5)

This appears from model studies to be a radical-chain process (23). Abstraction of a hydrogen from a methyl group, followed by migration of the adjacent phenyl group, generates a phenoxy radical that continues the chain process by abstracting a hydrogen from another methyl group.

Ultraviolet radiation causes cleavage of the aryl ether linkage (24). DMPPO undergoes oxidation when exposed to ultraviolet light and oxygen by direct attack on the aromatic ring to produce a variety of ring-cleaved and quinoidal structures (25–28).

Poly(phenylene oxide)s undergo many substitution reactions (29). A review of substitution reactions as well as degradation reactions. Reactions involving the aromatic rings and the methyl groups of DMPPO include bromination (30), displacement of the resultant bromine with phosphorus or amines (31), lithiation (32), and maleic anhydride grafting (33). Additional reactions at the open 3-position on the ring include nitration, alkylation (34), and amidation with isocyanates (35).

Health and Safety Factors. Animal-feeding studies of DMPPO itself have shown it to be nontoxic on ingestion. The solvents, catalyst, and monomers that are used to prepare the polymers, however, should be handled with caution. For example, for the preparation of DMPPO, the amines used as part of the catalyst are flammable; toxic on ingestion, absorption, and inhalation; and are also severe skin and respiratory irritants. Toluene, a solvent for DMPPO, is not a highly toxic material in inhalation testing; the TLV (77) is set at 375 mg/m^3, and the lowest toxic concentration is reported to be 100–200 ppm (78). Toxicity of 2,6-dimethylphenol is typical of alkylphenols, eg, for mice, the acute dermal toxicity is LD_{50}, 4000 mg/kg, whereas the acute oral toxicity is LD_{50}, 980 mg/kg (79). The Noryl blends of DMPPO and polystyrene have FDA approval for reuse food applications.

Synthesis of Poly(phenylene oxides)

Oxidative Coupling. Many poly(1,4-phenylene oxide)s have been prepared in a one-step polymerization of 2,6-disubstituted phenols by oxidative coupling (36) (see OXIDATIVE POLYMERIZATION). The scope and mechanism of polymerization has been studied in detail by many investigators (37). For the preparation of DMPPO, oxygen is passed through a vigorously stirred solution of 2,6-dimethylphenol and a catalyst at ca 25–50°C. A typical catalyst is composed of a copper halide and one or more aliphatic amines or pyridine. If the catalyst is susceptible to hydrolysis, a desiccant, eg, anhydrous magnesium sulfate, is added to remove the water coproduct. With an amine such as dibutylamine, the drying agent is not required. The polymerization is exothermic and often requires cooling to maintain catalytic activity and attain a high molecular weight product. Catalysts based on manganese and cobalt salts also are effective (38). Noncatalytic oxidizing agents, eg, silver oxide, lead dioxide, and manganese dioxide, when used in excess of the stoichiometric amount, also polymerize many 2,6-disubstituted phenols (39).

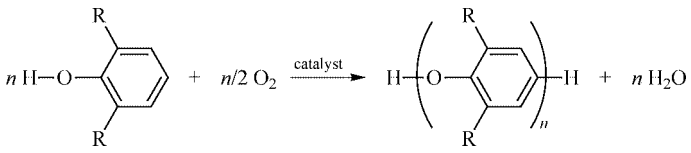

Oxidative coupling polymerizations represent a general reaction for the preparation of high molecular weight linear polymers from many 2,6-di- and 2,3,6-trisubstituted phenols. When the ortho substituents on the phenols are relatively unhindered alkyl or aryl groups, the poly(phenylene oxide) is the chief product (40,41). Bulky ortho substituents, eg, *tert*-butyl, lead to the formation of

the 3,3′,5,5′-tetrasubstituted 4,4′-diphenoquinone (40).

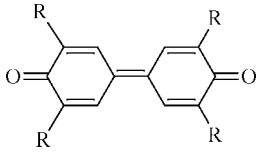

Significant quantities of the diphenoquinone are also produced if the ortho substituents are methoxy groups (40). Phenols with less than two ortho substituents produce branched and colored products from the reactions that occur at the open ortho sites. It is possible to minimize such side reactions in the case of *o*-cresol oxidation by using a bulky ligand on the copper catalyst to block the open ortho position (42).

The selectivity of the oxidation of 2,6-disubstituted phenols depends on the type of oxidizing agent. For example, with a series of cobalt-containing catalysts of the salcomine type, oxidation of 2,6-dimethylphenol produces three products: the poly(phenylene oxide), the diphenoquinone, and 2,6-dimethylbenzoquinone. The product ratio changes with variation in the nature of the ligands (43). The formation of the benzoquinone suggests that ionic processes as well as free-radical reactions take place. Oxidations with reagents that proceed mainly through ionic pathways produce such nonpolymeric products as benzoquinones and cyclohexadienones. Thus, 2,6-dimethylbenzoquinone and its 3-substituted derivatives form when 2,6-dimethylphenol is oxidized with peracids or metal-catalyzed hydrogen peroxide, whereas dimers of 6-hydroxy-2,6-dimethyl-2,4-cyclohexadien-1-one are produced from periodate oxidations (44).

Polymerization Mechanism. The mechanism that accounts for the experimental observations of oxidative coupling of 2,6-disubstituted phenols involves an initial formation of aryloxy radicals from oxidation of the phenol with the oxidized form of the copper–amine complex or other catalytic agent. The aryloxy radicals couple to form cyclohexadienones, which undergo enolization and redistribution steps (36). The initial steps of the polymerization scheme for 2,6-dimethylphenol are as in equation 6.

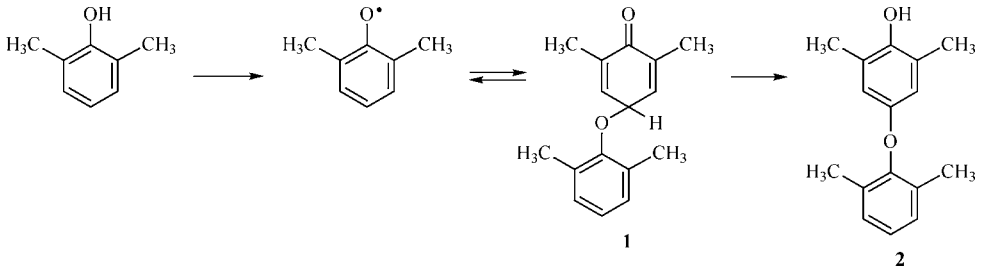

(6)

In equation 6, the dimer (**2**) is formed by enolization of the quinol ether (**1**). Oxidation of the dimer produces the dimer radical, which can couple with other radicals that are present. If it couples with a 2,6-dimethylphenoxy radical

to form a quinol ether, enolization can produce the trimer in a reaction analogous to equation 6. Similarly, oxidation of the trimer followed by coupling with a 2,6-dimethylphenoxy radical and enolization produces tetramer. By this process, each oligomeric product can form the next higher oligomer, and eventually high molecular weights are attained. However, the polymerization does not proceed only by addition of one unit at a time to the growing chain, because coupling also can occur between other combinations of oligomers. Thus, this is a step-growth polymerization rather than a chain-growth polymerization. As an example, dimer radical also can couple with another dimer radical to form a quinone ketal (**3**) (eq. 7) or with a larger oligomeric radical to form an analogous ketal. The reaction proceeds further by dissociation of the ketal to form new oligomeric radicals.

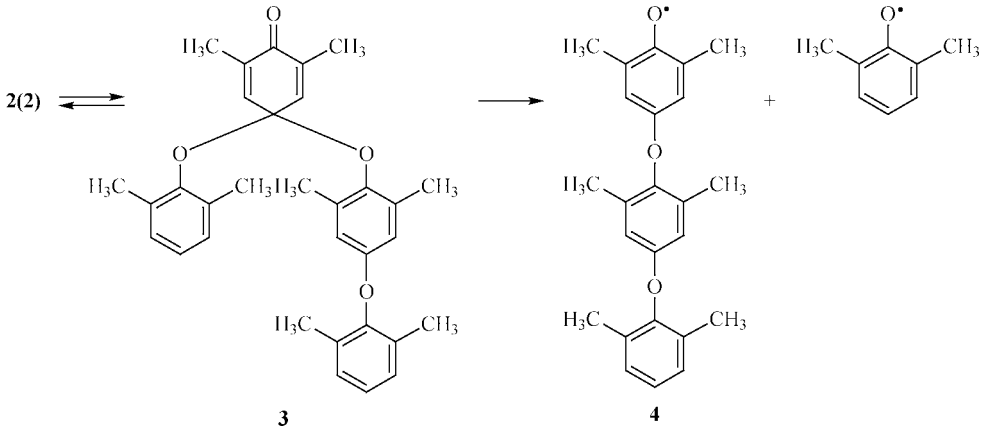

(7)

In equation 7, trimer radical (**4**) is produced when (**3**) dissociates. Whenever (**4**) couples with the other product of equation 7, ie, the 2,6-dimethylphenoxy radical, the tetramer is produced as described. These redistribution reactions of oligomers that proceed by ketal formation and subsequent dissociation ultimately generate terminal quinol ethers which enolize to the more stable terminal phenol (eq. 8).

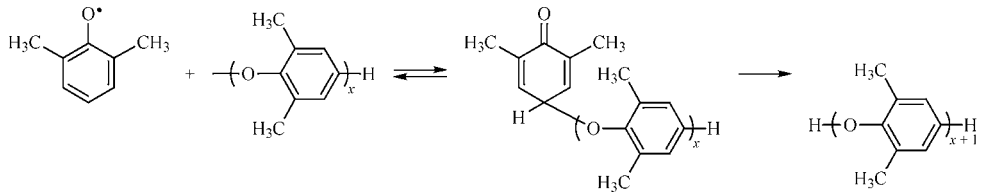

(8)

The enolization aids the attainment of high molecular weights by providing the driving force for the coupling of two oligomeric radicals to form a phenol-terminated oligomer of higher molecular weight, and by generating a phenolic group that can be oxidized to generate a new aryloxy radical which can enter the redistribution–enolization scheme. The overall effect of this combination of

oxidation, radical coupling, dissociation, and enolization is to increase the average molecular weight.

A second process that occurs concurrently with the dissociation–redistribution process is an intermolecular rearrangement by which cyclohexadienone groups move along a polymer chain. The reaction may be represented as two electrocyclic reactions analogous to a double Fries rearrangement. When the cyclohexadienone reaches a terminal position, the intermediate is the same as in equation 8, and enolization converts it to the phenol (eq. 9).

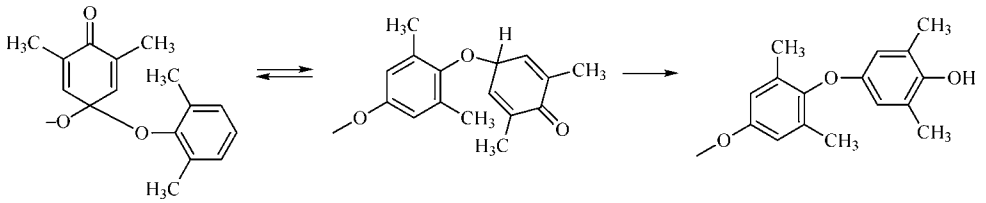

(9)

This process, which predominates at low temperatures, causes migration of internal ketal structures along a chain but does not involve the dissociation to separate aryloxy radicals that occurs during the redistribution process.

Considerable evidence supports these routes and rules out several alternative mechanisms (15,45–51) (see also OXIDATIVE POLYMERIZATION).

2,4,6-Trimethylphenol Polymerization. An unusual aspect of the oxidative coupling of substituted phenols is the formation of DMPPO from 2,4,6-trimethylphenol. Oxidative cleavage of the 4-methyl group produces paraformaldehyde and relatively low molecular weight (M_n = 1000–3000) DMPPO with manganese dioxide (60). DMPPO can also be prepared from 2,4,6-trimethylphenol with oxygen as the oxidizing agent and a catalytic amount of copper halide and an amine (61).

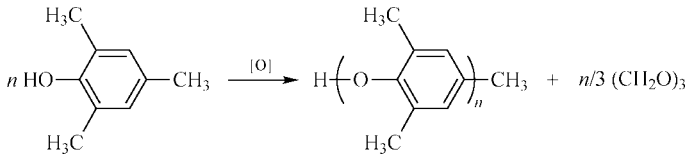

Halogen Displacement. Poly(phenylene oxide)s can also be prepared from 4-halo-2,6-disubstituted phenols by displacement of the halogen to form the ether linkage (52,53). A trace of an oxidizing agent or free radical initiates the displacement reaction. With 4-bromo-2,6-dimethylphenol, the reaction can be represented as in equation 10:

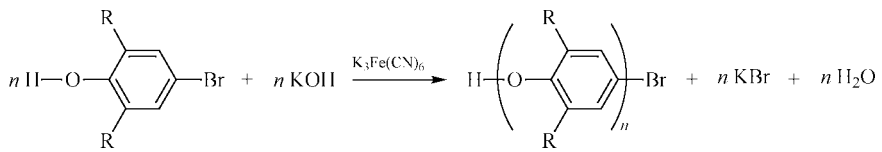

(10)

High molecular weight DMPPO is formed in high yield at room temperature. The reaction is applicable to certain 2,3,5-tri- and 2,3,5,6-tetrasubstituted-4-halophenols. When such compounds have halogens in the 3,4- or 3,4,5-positions only the one in the 4-position is displaced. When a mixture of 3,4-dibromo-2,6-dimethylphenol and 3,4,5-tribromo-2,6-dimethylphenol is polymerized, a random copolymer is formed, where $b = 1$, 2, etc (54,55). The two homopolymers from polymerization of these phenols by themselves are sufficiently insoluble in halogenated and aromatic solvents that they precipitate from the reaction mixture with low molecular weight. The copolymer made from an equimolar mixture of the two monomers is soluble and can be prepared with high molecular weight.

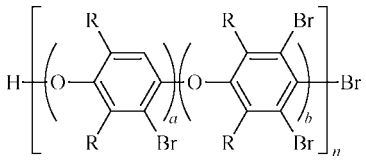

The halogen displacement polymerization proceeds by a combination of the redistribution steps described for oxidative coupling polymerization and a sequence in which a phenoxide ion couples with a phenoxy radical (eq. 11) and then expels a bromide ion. The resultant phenoxy radical can couple with another phenoxide in a manner that is analogous to equation 11 or it can redistribute with other aryloxy radicals in a process analogous to equations 7 and 8.

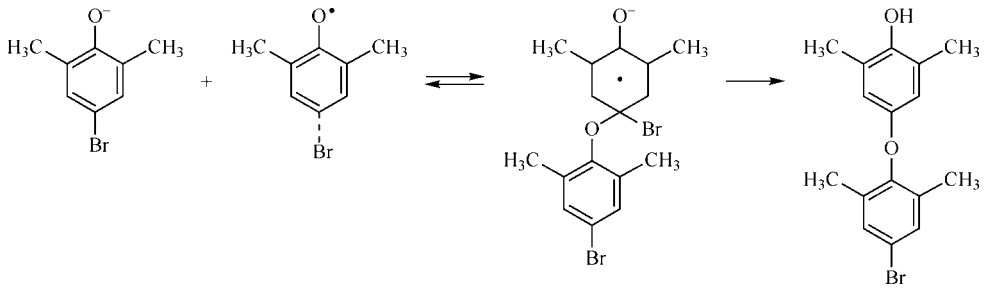

(11)

2,4,6-Trihalophenols can be converted to poly(dihalophenylene oxide)s by a reaction that resembles radical-initiated displacement polymerization. In one procedure, either a copper or silver complex of the phenol is heated to produce a branched product (56). In another procedure, a catalytic quantity of an oxidizing agent and the dry sodium salt in dimethyl sulfoxide produces linear poly(2,6-dichloro-1,4-polyphenylene oxide) (57). The polymer can also be prepared by direct oxidation with a copper–amine catalyst, although branching in the ortho positions

is indicated by chlorine analyses (58).

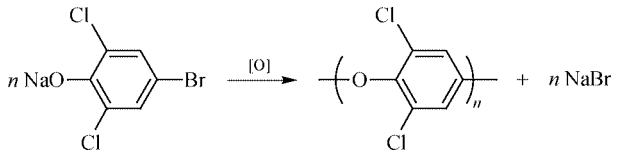

4-Halophenols without 2,6-disubstitution do not polymerize under oxidative displacement conditions. Oxidative side reactions at the ortho position may consume the initiator or interrupt the propagation step of the chain process. To prepare poly(phenylene oxide)s from unsubstituted 4-halophenols, it is necessary to employ the more drastic conditions of the Ullmann ether synthesis. A cuprous chloride–pyridine complex in 1,4-dimethoxybenzene at 200°C converts the sodium salt of 4-bromophenol to poly(phenylene oxide) (1):

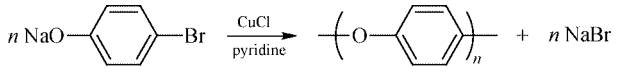

Low molecular weight poly(1,3-phenylene oxide) [25190-64-1] has been prepared from the sodium salt of *m*-chlorophenol with copper as a catalyst (59).

Poly(Phenylene Oxide) Copolymers

Copolymers of poly(phenylene oxide)s can be prepared in several ways. Oxidative coupling of mixtures of phenols, eg, combinations of 2,6-dimethylphenol, and 2-methyl-6-phenylphenol usually provide random copolymers. With a pair of phenols that have different oxidation potentials or that coredistribute at different rates, such as a mixture of 2,6-dimethylphenol and 2,6-diphenylphenol, block copolymers can form (62). Another route is the oxidation of mixed dimers which forms random copolymers (63). Copolymers can also be produced by allowing only some of the rings to undergo reaction in a substitution reaction, eg, bromination of only a fraction of the aromatic rings in DMPPO converts normal units to 3-bromo units (30). Block copolymers have been prepared by condensing the phenolic end groups of DMPPO with other polymers bearing reactive leaving groups on their end groups. For example, block copolymers were formed from aromatic polyesters with α,ω-bis(chloroformyl) end groups by using a phase-transfer catalyst and sodium hydroxide to effect the displacement of the halogen (64). These reactions can be carried out with high yields, thereby enabling the formation of ABA types of block copolymers. In the case of low molecular weight di- or triacyl halides, coupled linear or branched polymers with double or triple the original molecular weight are formed.

Polyether Blends

DMPPO and polystyrene form compatible blends (see POLYMER BLENDS). The two components are miscible in all proportions (65). Reported dynamic–mechanical results that indicate the presence of two phases in some blends apparently are caused by incomplete mixing (66). Transition behavior of thoroughly mixed blends indicates that the polymers are truly compatible on a segmental level (67). Compatibility may be attributed to a π–π interaction between the aromatic rings of the two polymers sufficient to produce a negative heat of mixing. However, the forces are very small, ie, ΔH_{mix} = ca 40 J/mol (9.6 cal/g), and any change in the substitution pattern of either polymer usually makes them incompatible (68). Tensile strength and modulus of blends of DMPPO and crystal polystyrene reach a maximum with a composition containing about 80 wt% DMPPO, but most properties of blends are close to the weighted average for the two polymers (69). Blends with rubber-modified polystyrene, ie, high impact polystyrene (HIPS), also have intermediate property values, but the ductile PPO matrix is toughened more effectively by rubber than is the brittle polystyrene. Therefore, blends of DMPPO with HIPS have much higher impact strength than either material alone (70). This characteristic makes it possible to prepare a family of tough plastics or modified poly(phenylene oxide)s in which some of the high temperature capability of the DMPPO is combined with the easy processibility of polystyrene.

Blends with good mechanical properties can be made from DMPPO and polymers with which DMPPO is incompatible if an appropriate additive, compatibilizing agent, or treatment is used to increase the dispersion of the two phases. Such blends include mixtures of DMPPO with nylon, polycarbonate, polyester, ABS, and poly(phenylene sulfide).

Sulfonation has been used to change some characteristics of blends. Poly(2,6-diphenyl-1,4-phenylene oxide) and polystyrene are immiscible. However, when the polymers were functionalized by sulfonation, even though they remained immiscible when blended, the functionalization increased interfacial interactions and resulted in improved properties (71). In the case of DMPPO and poly(ethyl acrylate), the originally immiscible blends showed increased miscibility with sulfonation (72).

Blends have also been prepared by dissolving DMPPO in a monomer and then polymerizing the monomer. An example is an epoxy–DMPPO blend prepared by curing a solution of DMPPO in Epon 828 at 85°C with an aluminum–tetramethylguanidine catalyst. Some copolymer formation is observed. The solutions can be applied to glass cloth before curing to produce prepregs for composites in applications such as printed circuit boards (73).

Interpenetrating polymer networks (qv) of DMPPO and polymers such as polystyrene, polybutadiene, poly(urethane acrylate), and poly(methyl methacrylate) have been prepared by cross-linking solutions of DMPPO containing bromomethyl groups with ethylenediamine in the presence of the other polymer (74).

Noryl. Noryl engineering thermoplastics are polymer blends formed by melt-blending DMPPO and HIPS or other polymers such as nylon with proprietary stabilizers, flame retardants, impact modifiers, and other additives (75). Because the rubber characteristics that are required for optimum performance in

DMPPO–polystyrene blends are not the same as for polystyrene alone, most of the HIPS that is used in DMPPO blends is designed specifically for this use (76). Noryl is produced as sheet and for vacuum forming, but by far the greatest use is in pellets for injection molding.

Noryl is a rigid dimensionally stable material. Dimensional stability results from a combination of low mold shrinkage, low coefficient of thermal expansion (5.9×10^{-5} per °C), good creep resistance (0.6–0.8% in 300 h at 13.8 MPa (2000 psi)), and the lowest water absorption rate of any of the engineering thermoplastics (0.07% in 24 h at room temperature). Noryl resins are completely stable to hydrolysis. They are not affected by aqueous acids or bases and have good resistance to some organic solvents, but they are attacked by aromatic or chlorinated aliphatic compounds.

Noryl has good impact strength in unfilled grades: Gardner impact strength of 200 to >400 J (150–300 ft·lbf), and notched Izod 0.27–0.53 J/mm (5–10 ft·lb·f/in.) at room temperature and 0.13 J/mm (2.5 ft·lb·f/in.) at 140°C. Other mechanical properties are typical of amorphous engineering thermoplastics: tensile strength 50–70 MPa (8,000–11,000 psi), flexural strength 60–100 MPa (8,000–15,000 psi), and flexural modulus ca 2500 MPa (350,000 psi). Glass- or mineral-filled products have flexural moduli as high as 7600 MPa (1.1×10^6 psi). Dielectric properties are good: dielectric constant is 2.64, dielectric strength is 22 kV/mm at a thickness of 3.18 mm, and it is insensitive to changes in temperature or humidity and to frequencies of 60–10^6 Hz.

DMPPO–polystyrene blends, because of the inherent flame resistance of the DMPPO component (oxygen index ca 29.5), can be made flame retardant without the use of halogenated additives that tend to lower impact strength and melt stability in other polymers. Approximately one-half of total Noryl sales volume is in flame-retarded grades, ie, V0 or V1 in a 1.6-mm section (UL-94).

Properties of DMPPO–polystyrene blends, especially flammability, deflection temperature under load (DTUL) (ASTM D648), and melt viscosity, can be varied over a wide range by changing the ratio of DMPPO to HIPS, the amount and type of additives, and the characteristics of the HIPS. Noryl originally was introduced to fill a price–performance gap between ABS and polycarbonate, but the property range has been extended steadily and 50 standard grades are available with heat-distortion temperatures of 88–150°C; these include products specially designed for foaming, profile extrusion, and electroplating. In addition to the regular grades, approximately equal numbers of special products are available and each is designed primarily for a single application, eg, an easy-flow V0 product for television cabinets, a high heat Noryl for electrical connectors and food packaging for microwave reheating, Noryl GTX blends for automobile parts, etc.

Principal application areas are in water distribution, electrical–electronic applications, business machines, and automobiles. Water distribution applications include pump housings, impellers and filters, shower heads, faucets, valve handles, and other plumbing fixtures. Among the applications in the electrical–electronic areas are cabinets and internal television and radio parts, lighting fixtures, connectors, junction boxes, wiring ducts, cable covers, protective devices, and motor housings. Noryl is used in many small appliances and personal care products, especially those involving exposure to heat and moisture (food processors, hair dryers, steam irons, hot combs, etc) and in console and decorative trim in

dryers, washing machines, and other large appliances. Frames, bases and supports for copiers, display stations, computers, typewriters, printers, and other business machines are commonly made of Noryl. The low temperature impact strength of Noryl and Noryl GTX contribute to its use in a variety of external automotive applications (wheel covers, grilles, fenders, mirror housings steering-column shrouds), instrument panels, electrical connectors, and filler panels.

General Electric is the only U.S. producer of Noryl resin and also has facilities in Japan and Europe. DMPPO is also produced in Japan by Ashahi, Mitsubishi Gas Chemical, and Sumitomo.

Polyethersulfones

The aromatic sulfone polymers are a group of high performance plastics, many of which have relatively closely related structures and similar properties (see POLYSULFONES). Chemically, all are polyethersulfones, ie, they have both aryl ether (ArOAr) and aryl sulfone ($ArSO_2Ar$) linkages in the polymer backbone. The simplest polyethersulfone (**5**) consists of aromatic rings linked alternately by ether and sulfone groups.

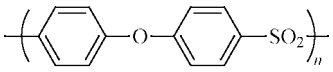

5

Effect of Structure on Properties. The effect of structure on chain flexibility in the series of polymers having the following common structure has been studied by varying the linking group Y (80). The glass-transition temperature changes in a predictable manner with the nature of Y. For example, when Y is a flexible ether, thio, or methylene group, the glass-transition temperature is ca 180°C. Replacement of the hydrogens of the methylene group by alkyl or aryl groups decreases the flexibility and increases the glass-transition temperature; the larger the substituent, the higher the value of T_g. Polar groups, eg, carbonyl and sulfonyl, that are capable of conjugation with the aromatic ring increase the glass-transition temperature, eg, to 245°C for the sulfonyl group, as in (**5**).

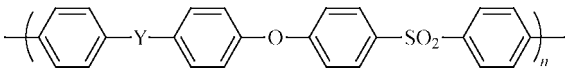

Synthesis. Aromatic polyethersulfones can be prepared by two different routes. In polyetherification, the sulfone group is present in one of the monomers and the ether linkage is formed in the polymerization step. In polysulfonation, the alternative approach is used and the aryl ethers are coupled through a reaction that forms the sulfone linkage. Both processes have been developed commercially. Unlike oxidative coupling polymerization, the mechanisms of both reactions are relatively straightforward, ie, both are polycondensations corresponding to types

of reactions that are well-established in organic chemistry. In general, the two processes are used to produce different types of polymers but some structures, including the basic structure (**5**), are available by either route. Polyetherification and polysulfonation have been reviewed extensively (80–84).

Polyetherification. Aromatic polyethersulfones are formed by reaction of the salts of dihydroxyaromatic compounds with di(haloaryl)sulfones. Reactions of this type, ie, nucleophilic aromatic displacement of halogen in aromatic compounds activated by sulfonyl or other strongly electron-withdrawing groups, are familiar in organic chemistry, but successful application to formation of high molecular weight polymers depends on the accelerating effects of certain dipolar aprotic solvents, which are believed to solvate the cations selectively, thus increasing the reactivity of the phenolate anions. The polar compounds must be stable under the conditions of the reaction and be capable of dissolving both the reactants and the polymer. Dimethyl sulfoxide (DMSO) is commonly employed, and other solvents, eg, tetramethylene sulfone (sulfolane), sometimes are useful when high temperatures are required (80).

The first aromatic sulfone polymer produced commercially was introduced as Bakelite polysulfone but now is sold by Union Carbide under the trade name Udel. It is made by reaction of the disodium salt of bisphenol A (BPA) with 4,4′-dichlorodiphenyl sulfone in a mixed solvent of chlorobenzene and dimethyl sulfoxide (eq. 12).

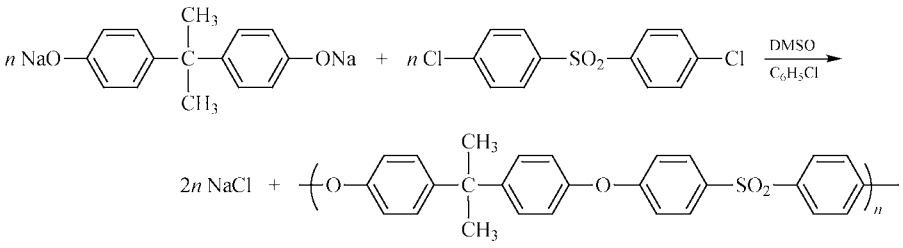

(12)

Polyetherification is similar to a polycondensation process: formation of high molecular weight polymer requires precise adjustment of composition to approximately 1:1 ratio of bisphenol to dihalosulfone. Trace amounts of water greatly reduce the molecular weight attainable owing to side reactions that unbalance the stoichiometry (84). The reactivity of the halosulfone is in the order expected for two-step nucleophilic aromatic displacement reactions: F > Cl > Br. In addition to being the most reactive of the halides, fluorosulfones are the least affected by traces of water. For economic reasons, only the chlorosulfone is used commercially. The reactivity of bisphenols in polyetherification decreases with increasing acidity of the phenol, but aromatic polyethersulfones can be prepared from almost all dihydric phenols under sufficiently vigorous conditions. The hydroxyl group and the active halogen can be combined in the same molecule; for example, (**5**) is produced by the self-condensation of 4-chlorophenyl-4′-hydroxyphenyl sulfone (85). The dichlorosulfone in equation 12 may be replaced by other dihalogen compounds

having strongly electron-withdrawing groups ortho or para to the halogens, such as carbonyl, azo, sulfamido, and nitro groups (86).

5

Copolymers. Copolymers from mixtures of different bisphenols or from mixtures of dichlorosulfone and dichlorobenzophenone have been reported in the patent literature. Bifunctional hydroxyl-terminated polyethersulfone oligomers are prepared readily by the polyetherification reaction simply by providing a suitable excess of the bisphenol. Block copolymers are obtained by reaction of the oligomers with other polymers having end groups capable of reacting with the phenol. Multiblock copolymers of BPA-polysulfone with polysiloxane have been made in this way by reaction with dimethylamino-terminated polydimethylsiloxane; the products are effective impact modifiers for the polyethersulfone (87). Block copolymers with nylon-6 are obtained when chlorine-terminated oligomers, which are prepared by polyetherification with excess dihalosulfone, are used as initiators for polymerization of caprolactam (88).

Polysulfonylation. The polysulfonylation route to aromatic sulfone polymers was developed independently by Minnesota Mining and Manufacturing (3M) and by Imperial Chemical Industries (ICI) at about the same time (89,90). In the polymerization step, sulfone links are formed by reaction of an aromatic sulfonyl chloride with a second aromatic ring. The reaction is similar to the Friedel–Crafts acylation reaction. The key to development of sulfonylation as a polymerization process was the discovery that, unlike the acylation reaction which requires equimolar amounts of aluminum chloride or other strong Lewis acids, sulfonylation can be accomplished with only catalytic amounts of certain halides, eg, $FeCl_3$, $SbCl_5$, and $InCl_3$. The reaction is a typical electrophilic substitution by an arylsulfonium cation (eq. 13).

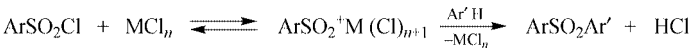

(13)

Reaction of bis(sulfonyl chloride)s with diaryl ether produces polyethersulfones. For example, condensation of diphenyl ether with the disulfonylchloride of diphenyl ether yields polyethersulfone (**5**):

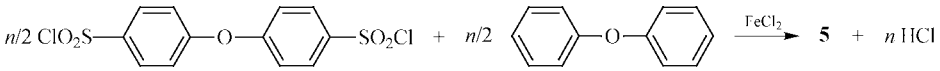

The reaction is carried out either in the melt or in a suitable inert solvent such as acetonitrile; ferric chloride is a preferred catalyst. Successful application of the polysulfonylation reaction to polymer synthesis requires a high degree of para coupling. Chain branching or any substantial degree of ortho coupling without branching results in brittle products. Specificity is improved if the sulfonyl group and the reactive ring are in the same molecule. The process described results in

10–20% of ortho coupling, but self-coupling of the monosulfonyl chloride is without detectable ortho coupling and the product is identical with that obtained by polyetherification. The polysulfonylation reaction is not limited to aryl ethers; it can be applied to most compounds having two or more independent aromatic rings, eg, biphenyl, terphenyl, and naphthalene, but the products are not polyethersulfones unless at least one of the reactants contains the ether linkage. Copolymers of (**5**) in which some of the diphenyl ether units are replaced by other groups are readily available by the sulfonation reaction. Incorporation of rigid biphenyl units by copolymerization of the sulfonyl chlorides of biphenyl and diphenyl ether increases the glass-transition temperature of the polyethersulfones; the Astrel polyethersulfones are of this type (91).

Polyetherketones

The polyetherification route to polyethersulfones can be adapted to the synthesis of polyethers containing strongly electron-withdrawing groups other than sulfone groups. Poly(1,4-oxyphenylenecarbonyl-1,4-phenylene) [27380-27-4] (**6**) is produced by condensation of 4,4′-dihydroxybenzophenone or by the self-condensation of 4-chloro-4′-hydroxybenzophenone. It has a melting point of 367°C and a glass-transition temperature of 154°C (92).

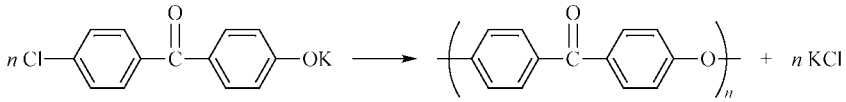

6

A polyetheretherketone (PEEK) (**7**) was introduced by Imperial Chemical Industries on a developmental scale in 1978. It is crystalline with a melting point of 334°C and a glass-transition temperature of ca 145°C (93,94). PEEK can be molded and is used in applications such as liquid chromatography fittings. It is also used for coatings, in electrical insulation for high temperature service, and in composites. Care must be taken on molding composites since the surface of the mold can affect the surface properties of the composite (95,96). Differential scanning calorimetry and microscopic techniques have been used to determine the morphology of molded PEEK graphite composites (97).

Stilan 1000, introduced by RayChem in 1974 and later withdrawn, is a polyetherketone made by a different route:

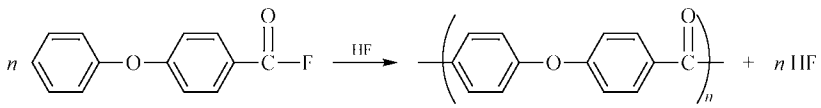

Cyclic aryl ether ketones have been prepared from 1,2-bis(4-fluorobenzoyl)benzene and bisphenols under pseudo high dilution conditions. These materials undergo ring-opening polymerization in the presence of an anionic catalyst (98).

Polyetherimides

A variety of polyetherimides have been described in reviews on polyimides (qv) (99,100). Many more recent materials have additional heterocyclic units such as quinoxaline and benzimidazole units, besides the ether and imide functionalities (101).

An all aromatic polyetherimide is made by DuPont from reaction of pyromellitic dianhydride and 4,4′-oxydianiline and is sold as Kapton. It possesses excellent thermal stability, mechanical characteristics, and electrical properties, as indicated in Table 3. The high heat-deflection temperature of the resin limits its processibility. Kapton is available as general-purpose film and used in applications such as washers and gaskets. Often the resin is not used directly; rather, the more tractable polyamide acid intermediate is applied in solution to a surface and then is thermally imidized as the solvent evaporates.

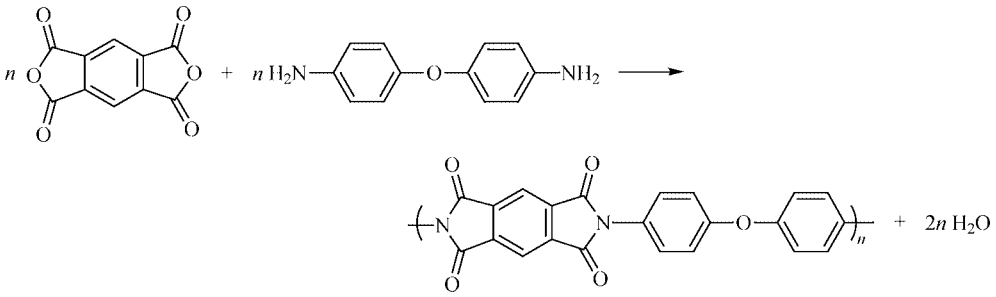

Not all polyetherimides are limited by their tractability, however. Certain aromatic polyetherimides are characterized by a combination of properties that makes them potential engineering thermoplastics (102,103). One of these polymers contains an isopropylidene unit in the backbone to enhance the solubility. It is a molding material introduced by General Electric in 1981 and sold as Ultem resin. Attractive features include high temperature stability, flame resistance without added halogen or phosphorus, high strength, solvent resistance, hydrolytic stability, and injection moldability.

Table 3. Selected Properties of Kapton[a]

Property	Value
CAS Registry Number	[25036-53-7]
Heat deflection temperature, °C	360
Tensile yield (at 23°C), MPa[b]	86
Tensile modulus, MPa[b]	3110
Flexural strength, MPa[b]	131
Flexural modulus, MPa[b]	3110
Oxygen index	36.5
Density, g/cm^3	1.43
Dielectric strength, V/m	58

[a] Ref. 83.
[b] To convert MPa to psi, multiply by 145.

Syntheses. The presence of the ether and imide functionalities provides two general approaches for synthesis. Polyetherimides can be prepared by a nucleophilic displacement polymerization similar to the halide displacement in polysulfone synthesis or by a condensation of dianhydrides and diamines that is similar to normal polyimide synthesis (see POLYIMIDES).

Nitro-Displacement Polymerization. The facile nucleophilic displacement of a nitro group on a phthalimide by an oxyanion has been used to prepare polyetherimides by heating bisphenoxides with bisnitrophthalimides (104). For example with 4,4′-dinitro monomers, a polymer with the Ultem backbone is prepared as follows (105). Because of the high reactivity of the nitro phthalimides, the polymerization can be carried out at temperatures below 75°C. Relative reactivities are nitro compounds over halogens, *N*-aryl imides over *N*-alkyl imides, and 3-substituents over 4-substituents. Solvents are usually dipolar aprotic liquids such as dimethyl sulfoxide, and sometimes an aromatic liquid is used, in addition.

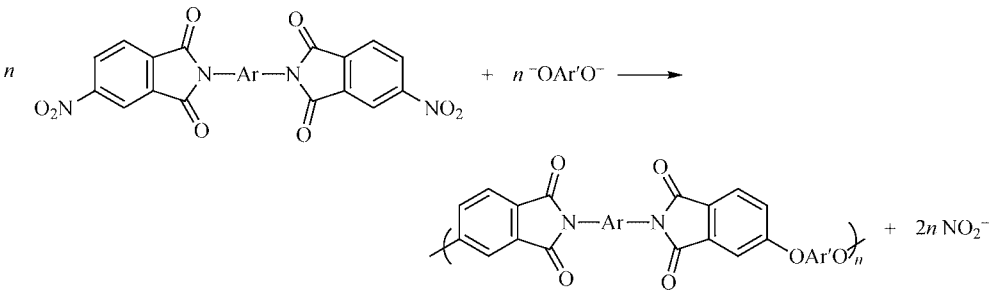

Bisnitrophthalimides can be prepared in high yields and high purity from nitrophthalic anhydrides and diamines under acidic conditions (106).

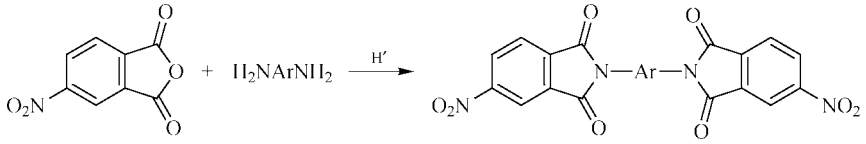

Condensation of Dianhydrides with Diamines. The preparation of polyetherimides by the reaction of a diamine with a dianhydride has advantages over nitro-displacement polymerization: sodium nitrite is not a by-product and thus does not have to be removed from the polymer, and a dipolar aprotic solvent is not required, which makes solvent-free melt polymerization a possibility. Aromatic dianhydride monomers (**8**) can be prepared from *N*-substituted nitrophthalimides by a three-step sequence that utilizes the nitro-displacement reaction in the first step, followed by hydrolysis and then ring closure. For the 4-nitro

compounds, the procedure is as follows.

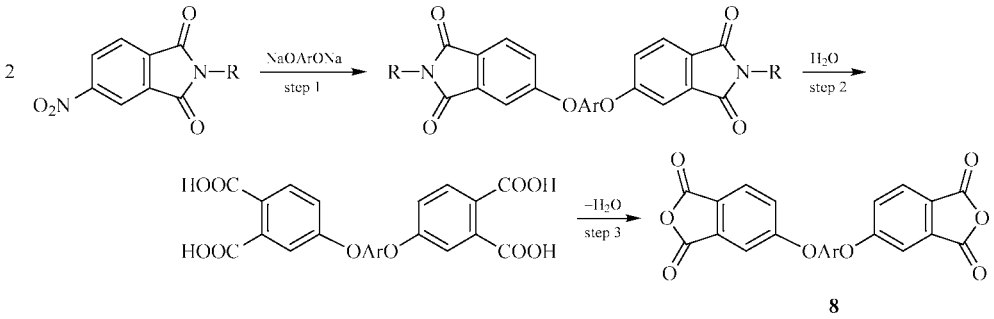

Polymerization of the dianhydride and diamine proceeds through an intermediate poly(amide acid) stage before ring closure converts the adjacent acid and amide groups to the polyetherimide (107). The polymerization can be carried directly to the polyetherimide as a single-step process, or first to an amide–acid-containing prepolymer, which can be isolated, and then to the polyetherimide.

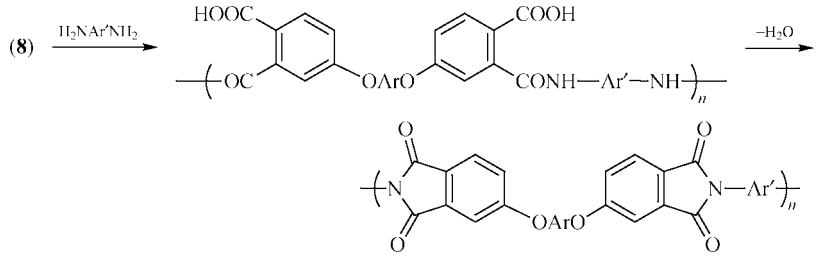

Properties. The mechanical properties and oxygen index of Ultem polyetherimide are listed in Table 4. In flammability testing, the oxygen index of many polyetherimides is high and they are self-extinguishing (V 0), nondripping, and generate little smoke (108). Many polyetherimides with additional chemical functional groups have been reported. Such materials and a variety of polyether-heterocyclics have received only limited commercial attention.

Table 4. Ultem Polyetherimide Properties

Property	Value
Glass-transition temperature, °C	217
Heat-distortion temperature, °C	ca 200
Tensile yield (at 23°C), MPa[a]	103
Tensile modulus, MPa[a]	3000
Flexural strength, MPa[a]	145
Flexural modulus, MPa[a]	3300
Oxygen index	47
Density, g/cm^3	1.28

[a]To convert MPa to psi, multiply by 145.

Ultem polyetherimides have applications in areas where high strength, dimensional stability, creep resistance, and chemical stability at elevated temperatures are important. Uses include electrical connectors, wave guides and printed circuit boards for electronic equipment, food applications (microwaveable containers, utensils, and films), aircraft interior materials, and sterilizable medical equipment.

A large variety of newer poly(ether imide)s has been described. Included among these are perfluorinated polymers (109), poly(ester ether imide)s (110), poly(ether imide)s derived from *N*,*N*′-diamino-1,4,5,8-naphthalenetetracarboxylic bisimide (111), and poly(arylene ether imide ketone)s (112). In addition, many other heterocylic groups have been introduced into polyether systems, eg, poly(pyrazole ether)s (113) and poly(aryl ether phenylquinoxaline)s (114); poly(aryl ether oxazole)s with trifluoromethyl groups (115); and polyethers with other heterolinkages, eg, poly(arylether azine)s (116).

BIBLIOGRAPHY

"Phenols, Oxidative Polymerization" in EPST 1st ed., Vol. 10, pp. 92–111, by A. S. Hay, P. Shenian, A. C. Gowan, P. F. Erhardt, W. R. Haaf, and J. E. Theberge, General Electric Company; "Poly(phenylene ether)" in EPSE 2nd ed., Vol 13, pp. 1–30, by David Aycock, Visaldis Abolins, and Dwain M. White, General Electric Company.

1. H. Yang and A. S. Hay, *J. Polym. Sci. Polym. Chem. Ed.* **31**, 1261, 2015 (1993).
2. W. A. Butte, C. C. Price, and R. E. Hughes, *J. Polym. Sci.* **61**, 528 (1961); S. Horikiri, *J. Polym. Sci., Part A-2* **10**, 1167 (1972); A. R. Schultz and C. R. McCullough, *J. Polym. Sci., Part A-2* **10**, 307 (1972); D. M. Koehen, C. A. Smolders and M. Gordon, *J. Polym. Sci. Polym. Symp.* **61**, 93 (1977); E. Turski and H. Janeczed, *Polymer* **19**, 81 (1978).
3. A. Factor, D. E. Heinsohn, and L. H. Vogt, *Polym. Lett.* **7**, 205 (1969).
4. D. M. White, *Macromolecules* **12**, 1008 (1979).
5. H. M. van Dort and co-workers, *Eur. Polym. J.* **4**, 275 (1968).
6. A. R. Schultz and B. M. Gendron, *J. Appl. Polym. Sci.* **16**, 461 (1972).
7. D. M. White and H. J. Klopfer, *J. Polym. Sci., Part A-1* **10**, 1565 (1972).
8. A. R. Schultz and B. M. Gendron, *J. Polym. Sci. Polym. Symp.* **43**, 89 (1973).
9. *Technical data*, General Electric Co., Selkivk, N.Y., 1976.
10. H. M. van Dort and co-workers, *J. Polym. Sci., Part C* **22**, 431 (1968).
11. G. D. Cooper and A. Katchman, *Addition and Condensation Polymerization Processes, Advances in Chemistry Series No. 91*, American Chemical Society, Washington, D.C., 1969, p. 660.
12. A. S. Hay, *Macromolecules* **2**, 107 (1969).
13. A. S. Hay and R. F. Clark, *Macromolecules* **3**, 533 (1970).
14. *Poly(phenylene oxide)s, Properties Comparison Chart*, General Electric Co., Pittsfield, Mass., 1969.
15. G. D. Cooper, A. R. Gilbert, and H. L. Finkbeiner, *Polym. Prep.* **7**, 166 (1966); D. A. Bolon, *J. Org. Chem.* **32**, 1584 (1967); D. M. White, *J. Org. Chem.* **34**, 297 (1969).
16. D. M. White, *J. Polym. Sci. Polym. Chem. Ed.* **19**, 1008 (1979).
17. U.S. Pat. 4,140,675 (Feb. 20, 1979), D. M. White (to General Electric Co.).
18. H. L. Finkbeiner and A. M. Toothaker, *J. Org. Chem.* **33**, 4347 (1968).
19. D. M. White and S. A. Nye, *Macromolecules* **23**, 1318 (1990).

20. D. M. White and L. A. Socha, *Preprints of the 3rd Pacific Polymer Conference*, Gold Coast, Australia, Dec. 1993.
21. U.S. Pat. 3,442,858 (May 6, 1969), A. S. Hay (to General Electric Co.).
22. P. C. Juliano, J. V. Crivello, and D. E. Floryan, *Polym. Prep.* **15**, 210 (1974).
23. A. Factor, H. Finkbeiner, R. A. Jerussi, and D. M. White, *J. Org. Chem.* **35**, 57 (1970); A. Factor, *J. Polym. Sci., Part A-1* **7**, 363 (1969).
24. H. J. Hageman, W. L. Louwerse, and W. J. Mijs, *Tetrahedron* **26**, 2045 (1970); H. J. Hageman and W. G. B. Huysmans, *Rec. Trav. Chim. Pays-Bas* **91**, 528 (1972).
25. J. E. Pickett, *5th International Conference on Advances in Stabilization and Controlled Degradation of Polymers*, Zurich, Switzerland, 1983.
26. *ACS Symp. Ser.* **280**, 313, 1985.
27. J. Peeling and D. T. Clark, *J. Appl. Polym. Sci.* **26**, 3761 (1981).
28. A. Dilks and D. T. Clark, *J. Polym. Sci. Polym. Chem. Ed.* **19**, 2487 (1981).
29. J. Liska and E. Borsig, *Chem. Listy* **86(12)**, 900 (1992).
30. D. M. White and C. M. Orlando, *Am. Chem. Soc. Symp. Ser.* **6**, 179 (1975).
31. I. Cabasso, J. Jagur-Grodzinski, and D. Vofsi, *J. Polym. Sci., Part A-1* **12**, 1141 (1974).
32. U.S. Pat. 3,378,505 (Apr. 16, 1968), A. S. Hay (to General Electric Co.).
33. J. H. Glans and M. K. Akkapeddi, *Macromolecules* **24**, 384 (1991).
34. A. S. Hay and A. J. Chalk, *Polym. Lett.* **6**, 105 (1668); *J. Polym. Sci., Part A-1* **7**, 691 (1969).
35. S. S. Mahajan, B. D. Sarwade, and P. P. Wadgaonkar, *Polym. Bull.* **20**, 153 (1988).
36. A. S. Hay, H. S. Blanchard, G. F. Endres, and J. W. Eustance, *J. Am. Chem. Soc.* **81**, 6335 (1959).
37. H. L. Finkbeiner, A. S. Hay, and D. M. White, in C. E. Schildknecht and I. S. Skeist, eds., *Polymerization Processes, High Polymers*, Vol. **29**, John Wiley & Sons, Inc., New York, 1977, p. 537.
38. U.S. Pat. 3,965,069 (June 22, 1976), W. K. Olander (to General Electric Co.); U.S. Pat. 3,573,257 (Mar. 30, 1971), S. Nakashio and I. Nakagawa (to Sumitomo Chemical Co.).
39. B. O. Lindgren, *Acta Chem. Scand.* **14**, 1203 (1960); E. J. McNelis, *J. Org. Chem.* **31**, 1255 (1966); M. van Dort, *J. Polym. Sci. Part C* **22**, 431 (1968).
40. A. S. Hay, *J. Polym. Sci.* **58**, 581 (1962).
41. D. M. White and H. J. Klopfer, *J. Polym. Sci Part A-1* **8**, 1427 (1970).
42. A. S. Hay and G. F. Endres, *Polym. Lett.* **3**, 887 (1965).
43. L. H. Vogt, J. G. Wirth, and H. L. Finkbeiner, *J. Org. Chem.* **34**, 273 (1969); D. L. Tomaja, L. H. Vogt, and J. G. Wirth, *J. Org. Chem.* **35**, 2029 (1970).
44. J. D. McClure, *J. Org. Chem.* **28**, 69 (1966); R. G. R. Bacon and A. R. Izzat, *J. Chem. Soc. C* 791 (1963).
45. G. F. Endres and J. Kwiatek, *J. Polym. Sci.* **58**, 593 (1962); G. F. Endres, A. S. Hay, and J. W. Eustance, *J. Org. Chem.* **28**, 1300 (1963).
46. G. D. Cooper, H. S. Blanchard, G. F. Endres, and H. L. Finkbeiner, *J. Am. Chem. Soc.* **87**, 3996 (1965).
47. D. M. White, *Polym. Prep.* **9**(1), 663 (1967).
48. W. J. Mijs, O. E. van Lohuizen, J. Bussink, and L. Volbracht, *Tetrahedron* **23**, 2253 (1967).
49. D. J. Williams and R. Kreilick, *J. Am. Chem. Soc.* **89**, 3408 (1967); *J. Am. Chem. Soc.* **90**, 2775 (1968).
50. H. L. Finkbeiner, G. F. Endres, H. S. Blanchard, and J. W. Eustance, *Polym. Prep.* **2**, 340 (1961).
51. G. D. Cooper and J. G. Bennett, *J. Org. Chem.* **37**, 317 (1972).
52. G. D. Staffin and C. C. Price, *J. Am. Chem. Soc.* **82**, 3632 (1960).
53. U.S. Pat. 3,257,358 (June 21, 1966), G. S. Stamatoff (to E. I. du Pont de Nemours & Co., Inc.).

54. D. M. White, *Polym. Prep.* **15**, 210 (1974).
55. D. M. White and H. J. Klopfer, in E. J. Vandenberg, ed., *Polyethers*, ACS Symposium Series, American Chemical Society, Washington, D.C., 1975, p. 169.
56. H. S. Blanchard, H. L. Finkbeiner, and G. A. Russell, *J. Polym. Sci.* **58**, 469 (1962).
57. U.S. Pat. 3,236,807 (Feb. 22, 1966), G. S. Stamatoff (to E. I. du Pont de Nemours & Co., Inc.).
58. U.S. Pat. 3,431,238 (Mar. 4, 1969), W. Borman (to General Electric Co.).
59. J. H. Beeson and R. E. Pecsar, *Anal. Chem.* **41**, 1678 (1969).
60. E. McNelis, *J. Am. Chem. Soc.* **88**, 1074 (1968).
61. U.S. Pat. 3,749,693 (July 31, 1973), G. D. Cooper (to General Electric Co.).
62. G. D. Cooper, J. G. Bennett Jr., and A. Factor, *Polym. Prep.* **13**, 551 (1972).
63. G. D. Cooper, J. G. Bennett Jr., and A. Factor, Polymerization Kinetics and Technology Advances in Chemistry Series, No. 128, American Chemical Society, Washington, D.C., 1973, p. 230.
64. D. M. White and G. R. Loucks, *Polym. Prep.* **25**(1), 129 (1984).
65. A. R. Schultz and B. M. Beach, *Macromolecules* **7**, 902 (1974).
66. S. Krause, *J. Macromol. Sci. Rev. Macromol. Chem.* **7**, 251 (972).
67. J. Stoelting, F. E. Karasz, and W. J. McKnight, *Polym. Eng. Sci.* **10**(3), 133 (970); A. F. Yee, *Polym. Eng. Sci.* **17**, 213 (1977).
68. W. J. McKnight, F. E. Karasz, and J. R. Fried, *Polymer Blends*, Vol. 1, Academic Press, Inc., New York, 1978, p. 185.
69. L. W. Kleiner, F. E. Karasz, and W. J. McKnight, *Polym. Eng. Sci.* **19**, 519 (1979).
70. U.S. Pat. 3,383,435 (May 14, 1968), E. P. Cizek (to General Electric Co.).
71. D. T. Hseih and D. G. Peiffer, *J. Appl. Polym. Sci.* **44**, 2003 (1992).
72. R. Murali, A. Eisenberg, R. K. Gupta, and F. W. Harris, in D. E. Bergbreiter and C. R. Martin, eds., *Functional Polymers 6th IUCCP Symposium on Functional Polymers*, Plenum Publishing Corp., New York, 1988, p. 37.
73. H. S. Chao and J. M. Whalen, *J. Appl. Polym. Sci.* **49**, 1537 (1993).
74. H. L. Fricsh, D. Klemperner, H. K. Yoon, and K. C. Frisch, *Macromolecules* **13**, 1016 (1980); H. L. Frisch and Y. Hua, *Macromolecules* **22**, 91 (1989); P. C. Mengnjoh and H. L. Frisch, *J. Polym. Sci. Polym. Chem. Ed.* **27**, 3363 (1989); P. C. Mengnjoh and H. L. Frisch, *J. Polym. Sci., Part C, Polym. Lett.* **127**, 285 (1989); S. Singh, H. Ghiradella, and H. L. Frisch, *Macromolecules* **23**, 375 (1990).
75. M. Kramer, *Appl. Polym. Symp.* **15**, 227 (1971).
76. G. D. Cooper, G. F. Lee, A. Katchman, and C. P. Shank, *Mater. Technol*. 12 (1981).
77. J. M. Nielsen, *Solvents and Safety*, General Electric Co., Schenectady, N.Y., 1977, p. 31.
78. *Registry of Toxic Effects of Chemical Substances*, 1979 ed., U.S. Government Printing Office, Washington, D.C., 1980, p. 621.
79. Ref. 78, p. 709.
80. R. N. Johnson, A. G. Farnham, R. A. Clendenning, W. F. Hale, and C. N. Merriam, *J. Polym. Sci., Part A-1* **5**, 2375 (1967).
81. M. E. A. Cudby, R. G. Feasy, B. E. Jennings, M. E. B. Jones, and J. B. Rose, *Polymer* **6**, 589 (1965); M. E. A. Cudby, R. G. Feasy, S. Gaskin, V. Kendall, and J. B. Rose, *Polymer* **9**, 265 (1968).
82. K. J. Ivin and J. B. Rose, in W. M. Pasika, ed., *Advances in Macromolecular Chemistry*, Vol. 1, Academic Press, Inc., New York, 1968, p. 366.
83. V. J. Leslie, G. O. Rudkin Jr., J. B. Rose, and J. Feltzin, *Am. Chem. Soc. Symp. Ser.* **4**, 63 (1974).
84. R. N. Johnson and A. G. Farnham, *J. Polym. Sci., Part A-1* **7**, 2415 (1967).
85. U.S. Pat. 4,105,636 (Aug. 8, 1978), I. C. Taylor (to Imperial Chemical Industries, Ltd.).

86. U.S. Pat. 4,108,837 (Aug. 22, 1978), R. N. Johnson and A. G. Farnham (to Union Carbide Corp.).
87. A. Noshay, M. Matzner, B. P. Barth, and K. W. Watson, *J. Polym. Sci., Part A1* **9**, 3147 (1970).
88. S. E. McGrath, L. M. Robeson, and M. Matzner, in L. M. Sperling, ed., *Recent Advances in Polymer Blends, Grafts and Blocks*, Plenum Press, New York, 1974, p. 195.
89. U.S. Pat. 3,321,449 (May 23, 1967), H. A. Vogel (to Minnesota Mining and Mfg. Co.).
90. Brit. Pat. 1,016,245 (1965), M. E. B. Jones (to Imperial Chemical Industries, Ltd.).
91. T. E. Attwood and co-workers, *Polym. Prep.* **20**(1), 191 (1979).
92. *Plastics for Electronics*, Cordura Publications, Cordura, Calif., 1979.
93. *Plast. World* 11 (May 1980).
94. I. Schmidt and K. J. Binder, *J. Phys. (Paris)* **46**, 1631 (1985).
95. B. R. Prime, *J. Polym. Sci.* **25**, 641, 1986.
96. R. D. McElhaney, D. G. Castner, and B. D. Ratner, in E. Sacher, J. J. Perreaux, and S. P. Kowalczyk, eds., *Metallization of Polymers*, ACS Symp. Series No. 440, American Chemical Society, Washington, D.C., 1990, p. 370.
97. A. Lustiger, F. S. Uralil, and F. M. Newaz, *Polym. Composites* **11**, 65, (1990).
98. K. P. Chan, Y. Wang, and A. S. Hay, *Macromolecules* **28**, 653 (1995).
99. T. Takekoshi, *Advances in Polymer Science*, Vol. 94., Springer-Verlag, Berlin, 1990.
100. C. E. Sroog, *Prog. Polym. Sci.* **16**, 561 (1991).
101. P. M. Hergenrother and S. J. Havens, *Macromolecules* **27**, 4659 (1994).
102. U.S. Pat. 3,838,097 (Sept. 24, 1974), J. G. Wirth and D. R. Heath (to General Electric Co.).
103. U.S. Pat. 3,803,085 (Apr. 9, 1974), T. Takekoshi and J. E. Kochanowski (to General Electric Co.).
104. L. R. Caswell and T. L. Kao, *J. Heterocycl. Chem.* **3**, 333 (1965); F. J. Williams and P. E. Donahue, *J. Org. Chem.* **42**, 3414 (1979).
105. D. M. White and co-workers, *J. Polym. Sci. Polym. Chem. Ed.* **19**, 1635 (1981).
106. T. Takekoshi, J. E. Kochanowski, J. S. Manello, and M. J. Webber, *NASA Contract Report No. CR-145 007*, NASA, Langley, Va., 1976.
107. T. Takekoshi, D. R. Heath, J. E. Kochanowski, J. S. Manello, and M. J. Webber, *Polym. Prep.* **20**(1), 179 (1979).
108. D. E. Floryan and G. L. Nelson, *J. Fire Flammabil.* **11**, 284 (1980).
109. S. Ando, T. Matsuura, and S. Sasaki, *Macromolecules* **25**, 5858 (1992).
110. D. Venkatesan and M. Srinivasan, *J. M. S.—Pure Appl. Chem.* A **30**, 801 (1993).
111. H. Ghassemi and A. S. Hay, *Macromolecules* **27**, 3116 (1994).
112. S. Matsuo and K. Mitsuhashi, *J. Polym. Sci. Polym. Chem. Ed.* **32**, 1969 (1994).
113. J. A. Moore and P. G. Mehta, *Macromolecules* **28**, 444 (1995).
114. J. Hedrick, R. Tweig, T. Matray, and K. Carter, *Macromolecules* **26**, 4833 (1993).
115. G. Maier, R. Hecht, O. Nuyken, K. Borger, and B. Helmreich, *Macromolecules* **26**, 2583 (1993).
116. K. R. Carter and J. L. Hedrick, *Macromolecules* **27**, 3426 (1994).

GARY YEAGER
General Electric Company

POLYETHYLENE. See ETHYLENE POLYMERS.

POLYMER BRUSHES

Introduction

Polymer brushes can be defined as polymer materials prepared and assembled from end-tethered or surface-initiated polymer systems where the average distance between grafting points can be much smaller than the radius of gyration (R_g). This tethering can be of sufficient density such that under equilibrium conditions, these polymer chains stretch along the direction normal to the grafting surface both in the presence or absence of external fields or stimuli (Fig. 1) (1). They can be quite different from that of flexible polymer chains in solutions where the chains are free to adopt a random-walk configuration. In the presence of a good solvent, polymer chains avoid contact with each other in order to maximize polymer–solvent interaction. Also, in the absence of solvent or in melt conditions, polymer chains can stretch away from the interface to avoid overfilling incompressible space (Fig. 2). Moreover, analogous macromolecule systems can be studied and compared to polymer blends (qv), block copolymers (qv), complex polymer architectures, and other functional polymers where confinement in surfaces and interfaces gives unique behavior and properties. In general, the interface to which polymer chains can be tethered may be solid–gas, solid–liquid, liquid–liquid, and liquid–gas. Furthermore, in solid surfaces, polymer chains can be chemically bonded (chemisorption) or may be just physically adsorbed onto the surface (physisorption) of the substrate.

Recently, the investigation of polymer brushes has been focused on the synthesis of new tethered polymer systems primarily through *surface-initiated polymerization* (SIP). Previously, the term polymer brushes has been limited to the investigation of block copolymers (qv) or end-functional linear polymers that have been physically or chemically adsorbed to surfaces, respectively (3,4). Recent synthetic efforts using different polymerization mechanisms have resulted in the discovery of many novel properties of polymer brushes. This has been aided no less than the use of innovative and unique surface-sensitive analysis methods as applied to flat substrates and particles. The study of polymer brushes has benefited from improved dielectric, optical, spectroscopic, and microscopic characterization methods. Understanding the chemistry of these grafting reactions and how

Encyclopedia of Polymer Science and Technology. Copyright John Wiley & Sons, Inc. All rights reserved.

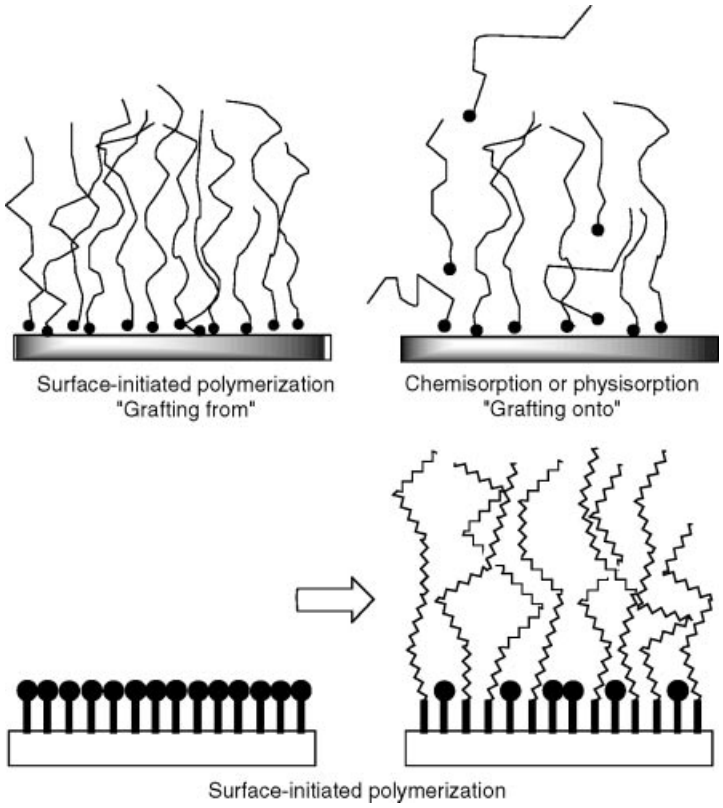

Fig. 1. The polymer brush approach and their classification: grafting to vs grafting from approaches and surface-initiated polymerization (SIP). The influence of grafting density and the enthalphic and entropic factors are clearly present on the "grafting onto" approach. Higher grafting density is expected with the SIP.

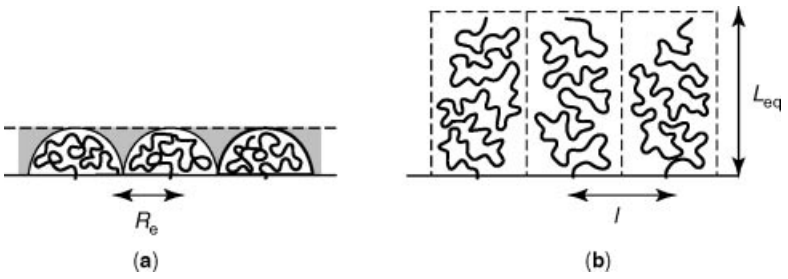

Fig. 2. The two limiting cases of a polymer brush regime, showing (**a**) tethered chains having the critical grafting density $\sigma^* = 1/\pi R_e{}^2$ and (**b**) chains having $\sigma > \sigma^*$ and forming the stretched brush. Other types of brush regime terminologies have been reported in literature. In this case, a characteristic length in the uncompressed brush (**b**) is given by $1 = \sigma^{-1/2}$. From Ref. 2.

changes in monomer type, polymerization conditions, and interfacial properties affect the polymerization kinetics and molecular weight control is essential. It is ideal to have a polymerization technique which affords control over the molecular weight, molecular weight distribution, grafting density, and microstructure of the resulting polymers. In principle, an increase in the molecular weight of polymer chains with monomer conversion and a narrow molecular weight distribution for the grafted chains will give a uniform brush length similar to that observed in living polymerization in solutions. Thus, it is essential to understand the protocols and mechanisms of free-radical, living free radical, anionic, cationic, metathesis polymerizations on surfaces. A number of these polymerization mechanisms have been reviewed in the past by the Tsubokawa and co-workers, including the use of irradiation and plasma ionization techniques to functionalize and polymerize at particle surfaces (5,6). However, of great interest are the recent and current studies on the different polymerization mechanisms on "flat" surfaces and the characterization techniques that can be applied to these systems.

Classification

Grafting onto and Grafting from. The first type of classification that can be used to distinguish polymer brushes is by their source and direction of grafting technique (see GRAFT COPOLYMERS). *Grafting* refers to the tethering or point of anchor for polymer chains. In the case of preformed polymers where an anchoring group was added by design, the polymer is expected to find its way to the surface or interface, where preferential adsorption can take place. This *grafting onto* of preformed functionalized polymers onto the surface could be further divided as a type of *physisorption* or *chemisorption* (another classification). During the grafting procedure, it is expected that the polymer chains will find its way to the surface where enthalpic and entropic considerations will determine the degree of grafting, eg diffusion, steric crowding, solvent quality. On the other hand, in a *grafting from* scheme, the polymer is formed *in situ* from grafting sites (initiators), where the growth of the polymer is limited primarily by reactivity of the active center during propagation, monomer diffusion or availability, and other peculiarities of the interface region, affecting the overall polymerization mechanism. However, to construct a highly dense polymer brush, the *grafting from* technique offers the most promise. This is because the kinetics of adsorption and reactivity is more favorable for smaller molecules, such as the initiator or the monomer (7). Therefore, to achieve a macromolecular design of a dense polymer brush, the SIP technique must be applied.

Physisorption vs Chemisorption. Another important classification involves distinguishing the adsorption process. The *physical adsorption* or *physisorption* of homopolymers or block copolymers have been well reported (4,8). Physical Adsorption (qv) means that noncovalent forces, eg ionic or electrostatic attraction, dipole forces, H-bonding, hydrophobic effect, and van-der Waals forces, are responsible for grafting the polymer to surfaces. A number of macromolecular systems involving the use of linear homopolymers, end-group functional homopolymers, anchor-buoy designated block copolymers, amphiphilic block copolymers, and even star copolymers have been investigated (4). In this case, the polymer is attracted to the surface (both flat or particle) owing to a more

favorable free energy gained by adsorption process (9). However, the problem is that such adsorbed layers are still susceptible to removal, eg by exposure to a thermodynamically good solvent or any subphase conditions that can weaken physical adsorption. Furthermore, it is often difficult to precisely control the physical structure of such adsorbed layers. On the other hand, adhesion between the polymer chains and the substrate may be greatly enhanced if the chains are tethered covalently to organic or inorganic surfaces by *chemical adsorption* or *chemisorption*. This approach involves the reaction of a preformed end-functionalized polymer with appropriate reactive sites on the inorganic surfaces (10). The preformed polymer is synthesized to have a reactive end group that is complementary to another reactive functional group already tethered to a surface (usually by forming self-assembled monolayers or SAM). The polymer end group then finds its way to the surface and a covalent bond is formed between the end-functional polymer and surface-bound complementary functional group. Thus, this method is more thermodynamically favorable than physisorption since the polymer forms a covalent bond anchor, which can only be removed by another chemical reaction. Still, the disadvantage of this method of grafting is that the chains, which are attached at the beginning of the reaction, sterically shields the remaining reactive sites on surfaces (11). Also, not all chemical reactions have the same rates in surfaces as compared to solution and bulk.

Thus, both physisorption and chemisorption have their drawbacks for *grafting onto* surfaces. To this respect, *grafting from* surfaces by SIP has important advantages in terms of polymer brush densities and other physical properties. The rest of this article deals primarily with the subject of polymer brushes prepared by SIP. Other polymer brushes prepared primarily by physisorption or chemisorption is best referred to other review articles and books (12).

Surface-Initiated Polymerization Methods

Polymerization at the interface is governed by thermodynamic and kinetic considerations not necessarily present in bulk or solution. There is a need to understand how these factors affect what is traditionally known about polymerization mechanisms in solution and in bulk. SIP promotes polymerization of monomers directly from initiator sites attached to surfaces, in which case activation of initiator and diffusion of monomers to the reactive sites become primary factors (13). The interface is a highly anisotropic environment where a variety of conditions exists, eg surface energy, polarity, and electrical double layer, not to mention the various geometries, size, shape, and surface properties of the solid-support substrate to which the polymer is bound (14). With the recent popularity of the SIP protocols, unique parameters and conditions toward the various polymerization mechanisms (initiation, propagation, termination, etc) warrant comparison with solution or bulk polymerization methods (15). In terms of chemistries involved at the interface, the homogeneity or heterogeneity of the system and the differences between the bulk phases defines the lifetime of the initiator, the flux of the monomer, and the rate of termination. Because of the high density of grafting sites, it is possible to prepare grafted polymers were the average distance between grafting points is much smaller than R_g. Selective spatial polymer growth is possible by both lithographic and nonlithographic patterning techniques (16). The

behavior of polymer brushes under electric field, temperature gradient, solvent polarity, photochemical effects, and flow gradients can lead to novel types of *field responsive polymers* (17).

Polymer Brushes on Flat Surfaces. By focusing on SIP in flat ideal surfaces, it is possible to take advantage of a wide range of surface-sensitive spectroscopic and microscopic analytical techniques. Flat substrates that have been investigated include glass, quartz, Si wafer, Au-coated glass, and Al-coated glass. There is potential for tailored polymer brush applications via surface modification and patterning (18). Theoretical predictions have been used to calculate molecular weight and polydispersity of polymer brushes grown by SIP on flat surfaces (19). Other theoretical predictions have been made on conformation and dynamic behavior of tethered polymers at flat surfaces (20). For example, it is always interesting to observe theoretical predictions on block copolymer brush behavior with respect to the Flory–Huggins (χ) interaction parameter, Kuhn length, block volume fraction, and substrate surface energies (21).

The number of different polymerization mechanisms reported has increased. Polymer brushes by SIP can be prepared using free-radical (13,22), cationic (23), ring-opening metathesis polymerization (ROMP) (24), atom transfer free-radical polymerization (ATRP) (25), polymerizations using 2,2,6,6-tetramethyl-1-piperidyloxy (TEMPO) (26), and anionic polymerization (27). All these methods are suitable for polymerizing different types of monomers on a variety of flat surfaces, resulting in different polymer growth kinetics and chain densities (Fig. 3). Different polymer brushes by composition (homopolymers, copolymers, mixed polymers) and architecture (block copolymers, hyperbranched, graft, etc) have also been achieved (28). A number of polymers with distinct wetting and polyelectrolyte behavior have been prepared (29).

Since the interface is a highly anisotropic environment, it is typical to use surface-sensitive analytical methods. Innovative use of these analytical tools has allowed elucidation of polymerization mechanisms and physical properties of these tethered polymers *in situ* on flat surfaces. Surface-sensitive spectroscopic and microscopic techniques like atomic force microscopy (AFM), ellipsometry, X-ray reflectometry, etc, have allowed detailed investigations on polymer brush behavior and growth kinetics under glass, melt, or swelling condition. Several articles have focused on reviewing polymer brushes *grafted from* flat surfaces, including SiO_2, Au, and glass (31). It should be emphasized that for each polymerization mechanism, peculiar conditions and parameters have to be optimized for controlled polymer brush growth (length, molecular weight, density, etc). There are parallels or contrasts for the SIP process when applied to flat geometry and particle surfaces.

Polymer Brushes on Particles. SIP from particle surfaces also involves growth of end-tethered polymer brushes under different mechanisms. A variety of initiators, reaction conditions, monomers, and nanoparticles can be employed. Important differences to solution and bulk polymerization can be observed where the nanoparticles with grafted initiators behave as *macroinitiators*. In turn, the development of these materials allow the preparation of thermodynamically and kinetically stable nanocomposites and colloids.

The preparation of polymer brushes grafted on particles and even nanoparticles is by far the more widely studied systems in polymer grafting methods

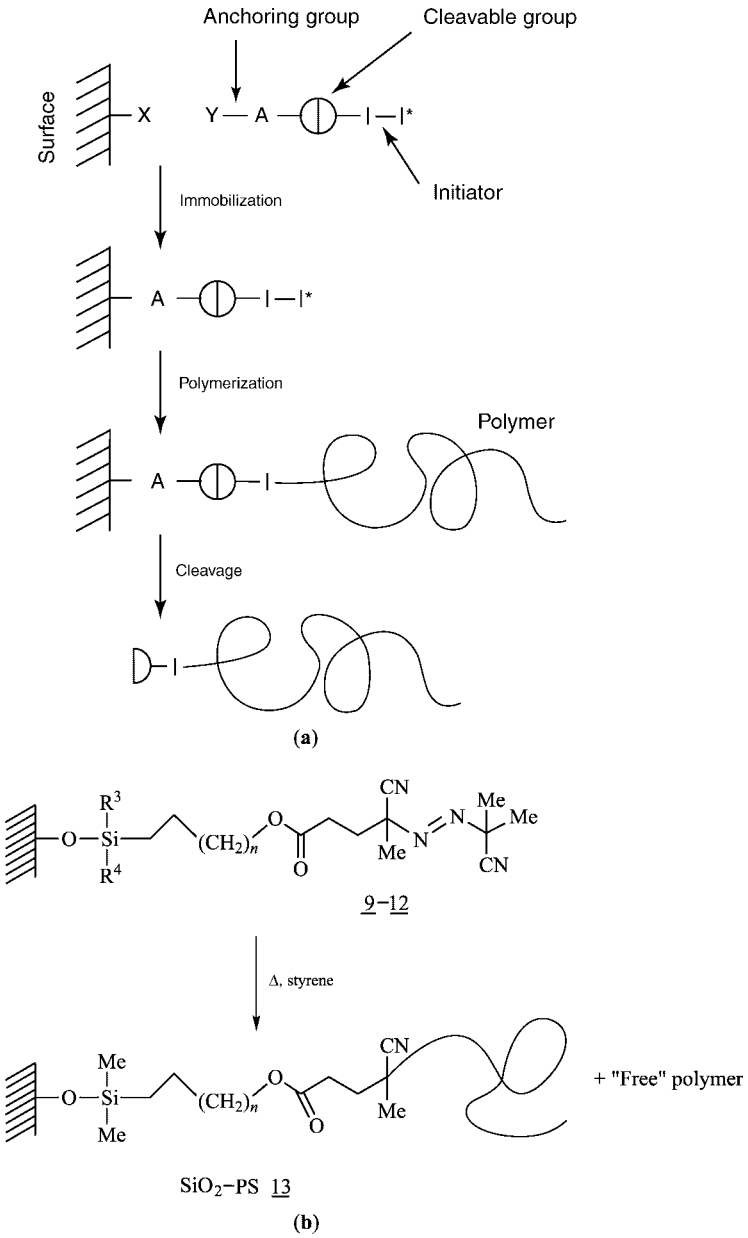

Fig. 3. Protocol for free-radical SIP using AIBN analogue initiators attached to silica nanoparticles. (**a**) general initiator attachment, polymerization, and cleavage scheme; (**b**) AIBN surface initiator. From Ref. 30.

(6). The ease of preparation and analysis of such systems by simple gravimetric methods is one of the most common reasons. Also, particles are readily available and their dispersion properties have been highly studied in industry. In addition, there is great interest in much smaller "nanoparticle" systems as host for the polymerization process (32). The synthesis, characterization, and development of

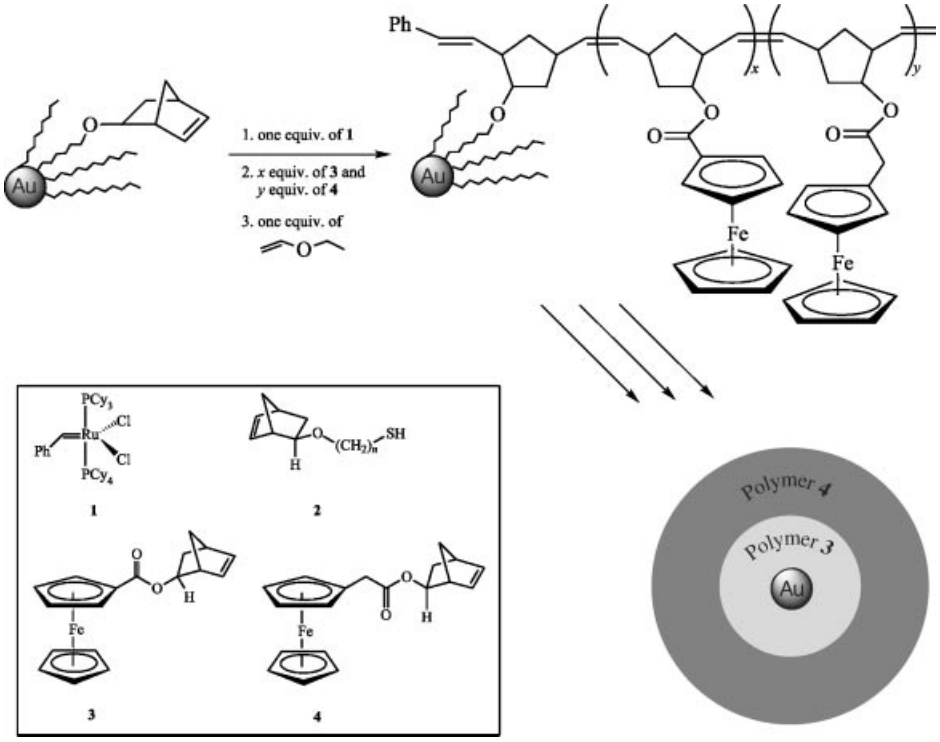

Fig. 4. The protocol for polymer brushes by SIP ring opening metathesis polymerization (ROMP), with initiators attached to Au nanoparticles. From Ref. 39.

new nanoparticle materials have both scientific and technological significance. Primarily through the quantum size effect, a number of these nanoparticle hosts have interesting electrooptical and magnetic properties (33). Different mechanisms are possible on a variety of initiators, reaction conditions, monomers, where a continuum of properties can be possibly observed on going from flat surfaces to high surface-to-volume nanoparticles. A number of polymerization mechanisms for particles have also been reported. This includes free-radical (22), cationic (34), TEMPO (35), anionic (36), ATRP (37), and metathesis (38) (Fig. 4).

Polymerization from particle surfaces is challenging from the perspective of doing surface chemistry with colloids (14). The particle size and geometry vary. Also, the surface energy and solvent polarity changes, which can make a difference in terms of forming stable dispersions in selective solvents at each stage of the polymerization process. There are a number of analytical techniques which have been used to investigate this hybrid systems *in situ*. One of the compelling reasons to do SIP on particles is that it offers the advantage of preparing large quantities of SIP-grown polymers that can be degrafted and extensively analyzed *ex situ*. This is because of the high surface-to-volume ratio afforded by these substrates. However, it is also advantageous to characterize these systems with the polymers still grafted on the particles for the sake of learning more about certain fundamental properties of colloids (14).

Polymerization Mechanisms for Polymer Brushes on Particles

A number of SIP methods on flat surfaces have been the subject of recent reviews (1). More detailed description can be found in this article regarding the various mechanisms used and investigated on flat substrate surfaces. The formation of polymer brushes with various SIP mechanisms on particle systems is the focus of this section. However, as representative polymerization mechanisms, it gives insight into the peculiar aspects for each type of reaction when confined to surfaces.

Surface-Initiated Free-Radical Polymerization. Free-radical SIP of polystyrene from nanoparticle surfaces have been investigated in detail by Ruhe and Prucker (12,32). Using AIBN-type free-radical initiators (qv), they have found that initiation and growth of the polymer at low conversion of a surface-attached initiator are comparable to polymerization in solution. The differences observed were attributed mainly to termination reactions. Another difference between solution polymerization and SIP is that all transfer reactions to either solvent or monomer or transfer agent can lead to termination of growing surface-attached chains via SIP. The consequence is a decrease in the radical efficiency of the initiator in surfaces compared to solution. Similar work on grafting to particles has been reported by Suter and co-workers (40) who tethered azo initiators by ion exchange to mica. A styrene-like initiator has been used to grow polymer brushes from clay surfaces by free-radical SIP (41). Other groups have also reported free radical polymerization (qv) from nanoparticle surfaces (42,43).

Surface-Initiated Atom Transfer Radical Polymerization. Living free radical ATRP show the most promise for polymerization control on surfaces (44,45). It has been shown that typical ATRP conditions proved insufficient for controlled polymerization from flat surfaces (46). The use of a deactivator (Cu(II)) and a "sacrificial" free initiator to the polymerization system afforded molecular weight control. ATRP initiators based on 3-(2-bromopropionyloxy)propyl dimethylethoxysilane have been used to do SIP on surfaces (47). Controlled "living" radical polymerization (qv) was possible through changes in the polymer's grafting density, composition, structure, and molar mass. This was manifested in the linear kinetic plots, linear plots of molecular weight (M_n) versus conversion, increased hydrodynamic diameter with conversion, and narrow molecular weight distributions (M_w/M_n) for the grafted polymer materials. Hybrid nanoparticles possessing well-defined tethered block copolymers are accessible using ATRP (48). Recently, surface-initiated ATRP on silica particles has been demonstrated in aqueous media (49). Other relevant works related to surface-initiated ATRP have been reported (50). Another living free-radical polymerization process called reversible addition-fragmentation chain transfer or RAFT has been applied to surfaces (51). Grafting of polymers to carbon black has been reported using TEMPO (52).

Living Anionic Surface-Initiated Polymerization. Anionic polymerization (qv) is a most versatile method to make well-defined architectures of polymers. It has been employed to grow polymer brushes from various silica gels (53), graphite and carbon black (54), and also flat surfaces (27,55). Results on living anionic polymerization on clay nanoparticles have been reported (56). Special conditions are required since difficulties arise owing to the effects of moisture and other impurities on anionic polymerization. A major limitation of the prior work

by Oosterling and co-workers is that the choice of *tert*-butyllithium (t-C_4H_9Li) as the initiator for styrene polymerization from silica in the presence of toluene is inefficient (54). Yet, despite these difficulties, anionic polymerization remains attractive for the synthesis of complex and well-defined macromolecular architectures (57,58). The Advincula group has recently reported results on living anionic polymerization on clay (59), SiO_2 nanoparticles, and flat surfaces using the initiator precursor 1,1-diphenylethylene (Fig. 5) (27,36,57).

Surface-Initiated Ring-Opening Metathesis Polymerization. Nanoparticles can be coated with alkanethiol-containing and silane-containing initiators for ROMP (39,60). ROMP on surface-functionalized particles makes use of organometallic catalysts to allow metathesis type of polymerization methods. Since this is also a living polymerization process, the advantages of this strategy are numerous, including exceptional control over polymer length and chemical composition as well as particle size, solubility, and shape. Other groups have also reported strategies for ROMP on surfaces (61).

Surface-Initiated Living Cationic Polymerization. Cationic ring-opening surface initiated polymerization reactions can be directed to particle surfaces (34). Using appropriate initiation procedures with 2-oxazoline monomers, a ring-opening cationic polymerization process was observed to proceed in a living manner. Hydroxyundecane-1-thiol-functionalized gold particles were converted to triflate functional groups by exposure to trifluoromethanesulfonic anhydride. Then 2-oxazoline monomer was added and polymerization proceeded under reflux conditions. Termination was done by adding *N*,*N*-di-*n*-octadecylamine. Other groups have reported SIP by living cationic mechanism on a variety of surfaces (62,63).

In summary, different mechanisms are possible and have been successfully demonstrated for grafting polymer brushes. Comparison can be made to their solution or bulk polymerization counterparts. These systems differ in (*1*) rate of polymerization, (*2*) mechanisms and methods of termination, (*3*) consideration of interfacial properties and reaction conditions, and (*4*) methods of analysis and correlation with theoretical trends. Again, different polymerization mechanisms can also be found with polymer brushes on flat surfaces.

Analytical and Characterization Methods

The study of *polymer brushes* has been of great interest not only for their synthesis but also for their unique properties and characterization approaches. The analysis of polymer brushes is a challenge. Because of their reduced dimensionality, assumptions based on analogous solution or bulk systems do not necessarily hold. There is a desire to understand fundamental properties at interfaces and in developing new applications. Since the interface is a highly anisotropic environment, surface energy, polarity, electrical double layer, etc, needs to be taken into account (14). In general, the methods of analysis can be divided into spectroscopic, microscopic, and optical in approach although other classifications can be mentioned. Both *in situ* and *ex situ* methods are possible (see SURFACE ANALYSIS).

Characterization of Polymer Brushes on Flat Substrates. *Ultrathin* organic and polymer films have been the subject of extensive investigations for

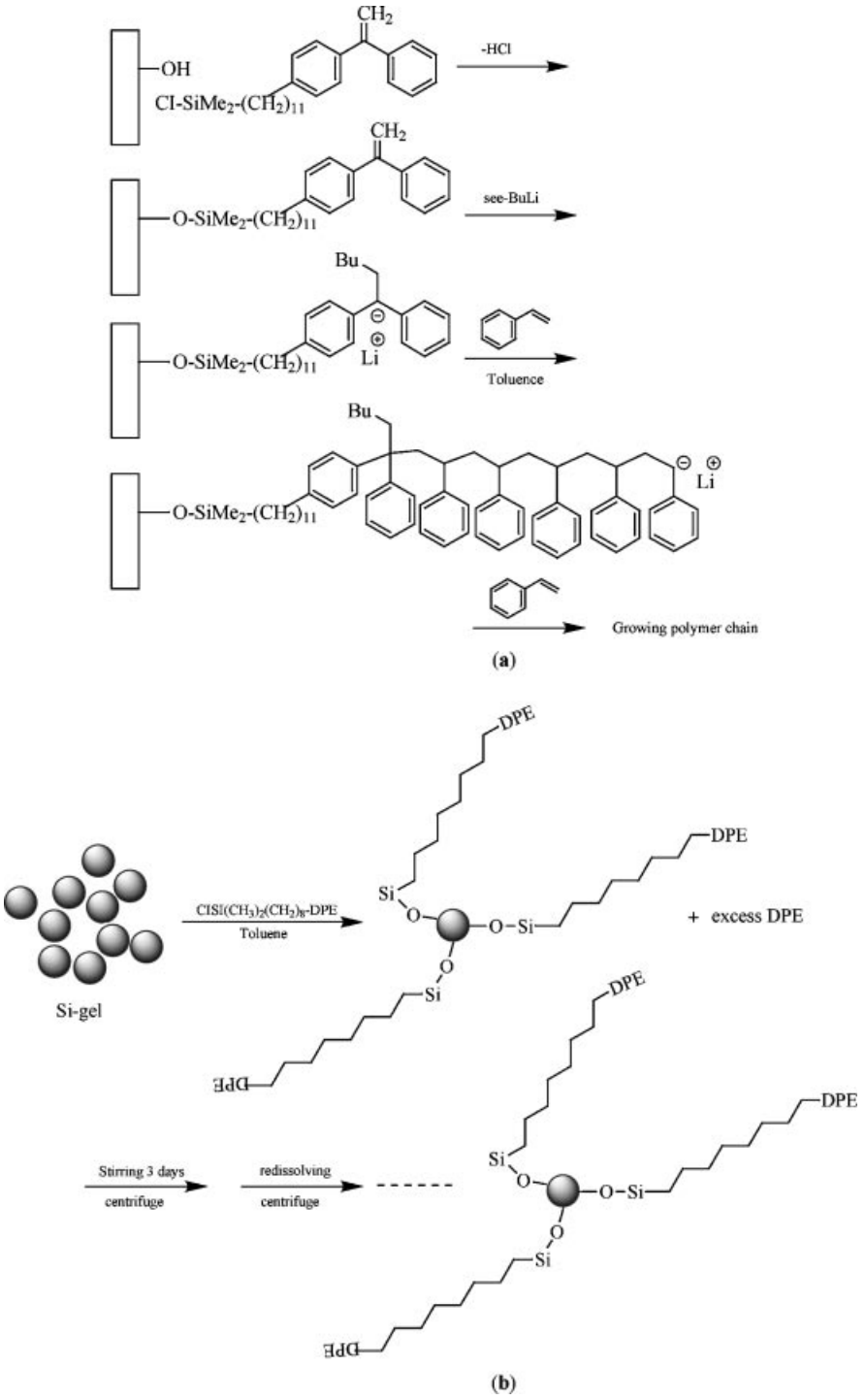

Fig. 5. Protocol for living anionic surface initiated polymerization (LASIP), with initiators attached to silica nanoparticles or clay: (**a**) grafting of initiator and general polymerization scheme; (**b**) nanoparticle grafting procedure. From Ref. 36.

the last few decades (64). They have finite thicknesses of a few to several hundred nanometers, on a variety of solid substrate supported systems. The quasi two-dimensional ordering within layers can be extended into stacked structures perpendicular to the solid substrate. In the investigation of polymer brushes, surface-sensitive spectroscopic and microscopic analytical methods can be applied that have been typically used for investigating other types of organic and polymer ultrathin films which includes spin coating, alternate polyelectrolyte (65), Langmuir–Blodgett technique (66), and self-assembled monolayers (67,68) (see LANGMUIR-BLODGETT FILMS).

Spectroscopic methods such as UV–vis absorbance, fluorescence, and other intensity-sensitive spectroscopic techniques have been used to investigate changes in absorption increase, energy transfer processes, and monitor film growth *in situ* for polymer brushes. The formation of uniform polymer films can also be verified and observed by X-ray reflectivity and other scattering methods (69). Neutron diffraction and reflectometry can be used, relying on deuterated species within layers (70). These techniques are important in probing the mobility of polymer chains, diffusion within layers, and short-range and long-range order parameters that can be correlated with other spectroscopic and microscopic techniques (71).

Techniques for determining the chemical functional group and molecular (elemental) species also include FT-IR and X-ray photoelectron spectroscopy (XPS) (72). XPS in particularly useful for monitoring the presence of different oxidized states of atoms, relative abundance of atomic species, and the presence of the substrate. FT-IR and IR-RAS has been used to monitor specific IR-sensitive functional groups even at monolayer thicknesses (73).

Optical techniques can be used to monitor optical thickness and dielectric constant parameters. This includes ellipsometry, multiple reflection interferometry (74), evanescent wave (75), and surface plasmon resonance spectroscopy techniques (43). Ellipsometry has been used widely and routinely to investigate film thickness of polymer brush films (76). For optical properties of films, it is important that the average film roughness and uniformity is specified. Often, sampling is localized by the "spot" size, such that it is necessary to probe and average different areas of a sample.

Microscopy is very useful especially in monitoring lateral morphologies, layer roughness, domains, or patterns. This includes AFM, scanning electron microscopy (SEM), optical microscopy, and other surface probe microscopy methods (77,78). SEM can be used for relatively thick films combined with microtoming and cryogenic techniques (79). It is very useful for obtaining three-dimensional morphologies and characterization of features of these films. AFM has been used to investigate polymer brushes in a number of ways. This includes (a) general mapping of topology or investigating morphologies (80), (b) identifying features resulting from phase segregations (28), (c) measuring the surface forces involved in different brush geometries (81), (d) estimating the molecular weight of brushes (82), and (e) investigating patterned polymer brushes (Fig. 6) (see ATOMIC FORCE MICROSCOPY).

Other surface-sensitive methods can and have been used

(1) quartz crystal microbalance methods have been used to investigate the deposition process especially *in situ* (84). The value of *in situ*

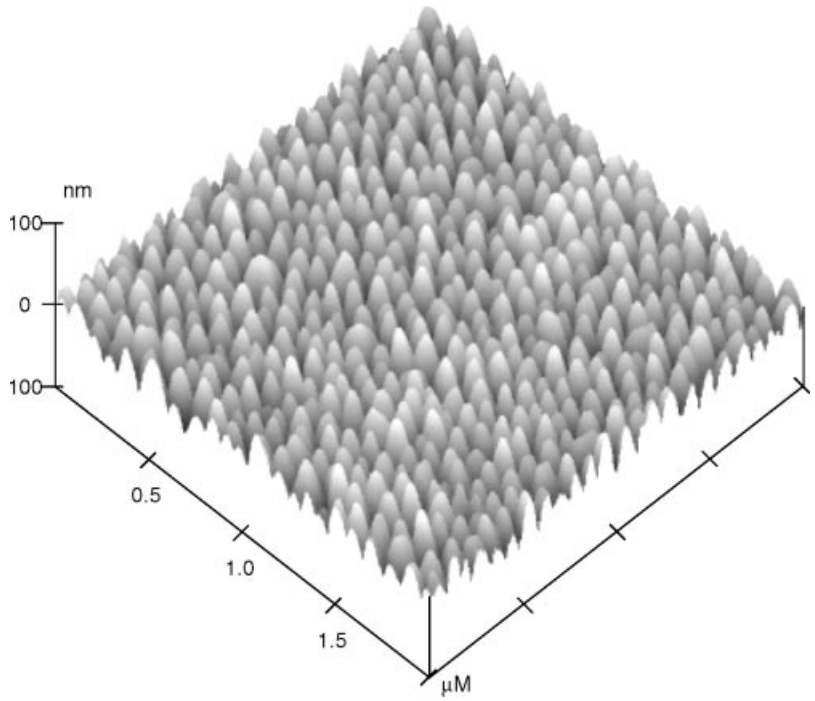

Fig. 6. Formation of a nanopattern from a PS-*b*-PMMA brush with 23-nm PS and 14-nm PMMA as investigated by AFM. From Ref. 83.

monitoring methods is in determining the rate functions of the adsorption process.

(2) Contact angle measurements or surface tensiometry allow determination of surface energy or surface tension on polymer brushes (85). It also gives information on differences in morphology and functional group distribution on surfaces.

(3) Electrochemical methods involve redox behavior of probes or the polymers themselves. It is possible to utilize this technique to investigate permselectivity (86). It can be utilized to probe any redox active species in the polymer films.

(4) Streaming potential measurements with ellipsometry can possibly be applied to polyelectrolyte polymer brushes (87).

(5) A very important technique is the use of a surface force apparatus (SFA) (88). It is capable of measuring the surface forces directly between two molecularly smooth surfaces, eg mica, with a sensitivity of a few millidynes (10 nN) and a distance resolution of about 0.1 nm. These flat smooth surfaces of mica can be covered with polymer brushes to obtain tribological properties between different polymer brush materials. Direct measurement of surface forces is also possible by AFM (89).

Other methods will likely be reported in the future and find unique utility in characterizing and analyzing polymer brushes. It should also be mentioned that

computational and simulation methods are important "tools" for predicting and scaling the observed behavior in polymer brushes and should go hand-in-hand with experimental results (90).

Characterization and Analysis Methods for Polymer Brushes on Particles. There are several important reasons for *in situ* analysis of polymer brushes on particles: (*1*) to monitor grafting of initiator to particle surface, (*2*) to monitor surface functional group conversion, (*3*) to investigate the polymerization mechanism (initiation, propagation, termination), and (*4*) to investigate the properties of a hybrid organic–inorganic particle or nanocomposites. Properties that can be measured include grafting density, polymer shell thickness, swelling and contraction of shell, and polydispersity of polymer brushes. The nature of the particle substrate is important. The analysis of these materials can be further complicated by the fact that different particle and nanoparticle substrates have varying dispersion properties. The particles are governed by size, shape, size distribution, surface charge, hydrophilicity, etc. Each has to be handled properly such that the material is not lost or precipitated with the different polymerization methods.

Direct or *in situ* methods allow monitoring of differences in initiator/monomer composition ratios, time of polymerization, solvent, and temperature conditions. Classical methods for analyzing polymer brush–particle systems include gravimetric (91,92) thermal analysis (93–95) light scattering (96), NMR (97), zeta potential (98,99) and rheology (100). Microscopy methods such as TEM, SEM, and AFM can also be employed, giving direct visualization of core–shell composite architectures (101). An interesting method for investigating polymer–particle dynamics using fluorescence correlation spectroscopy has recently been reported (102). It will be interesting to see in the future how SNOM techniques can be used to probe specific particle–polymer interactions (103). Once polymers have been detached from the substrate, they can be analyzed like any normal polymer product in an *ex situ* manner.

Investigating Polymer Brush Systems on Flat Surface Substrates

Polymer Brush Regimes on Surfaces. In the presence of an interface, the configurational space of polymer chains is limited. The deformation of polymer chains is generally a contribution of both *interaction* and *elastic free energies.* The interplay of these two terms determines the equilibrium thickness and *brush regimes* of tethered polymers. The internal structure and deformation of polymer brushes has also been investigated by numerical and analytical self-consistent field (SCF) calculations, and by computer simulations (104). For example, in densely tethered polymer chains, a strong overlap among the undeformed coils exists at the interface. This increases the polymer-to-polymer contacts and the corresponding interaction energy. The polymer chains are then forced to stretch away along the direction normal to the grafting sites. Stretching lowers the interaction energy per chain, at the price of a high elastic free energy. Thus, different conformational regimes are possible with polymer brushes by the interplay of these two terms. Polymer brushes have equilibrium thicknesses that vary linearly with the degree of polymerization. In contrast, free polymer chains in a theta solvent possess an unperturbed configuration. Research work employing theory, scaling theories, simulation, and surface probe techniques have shown that the

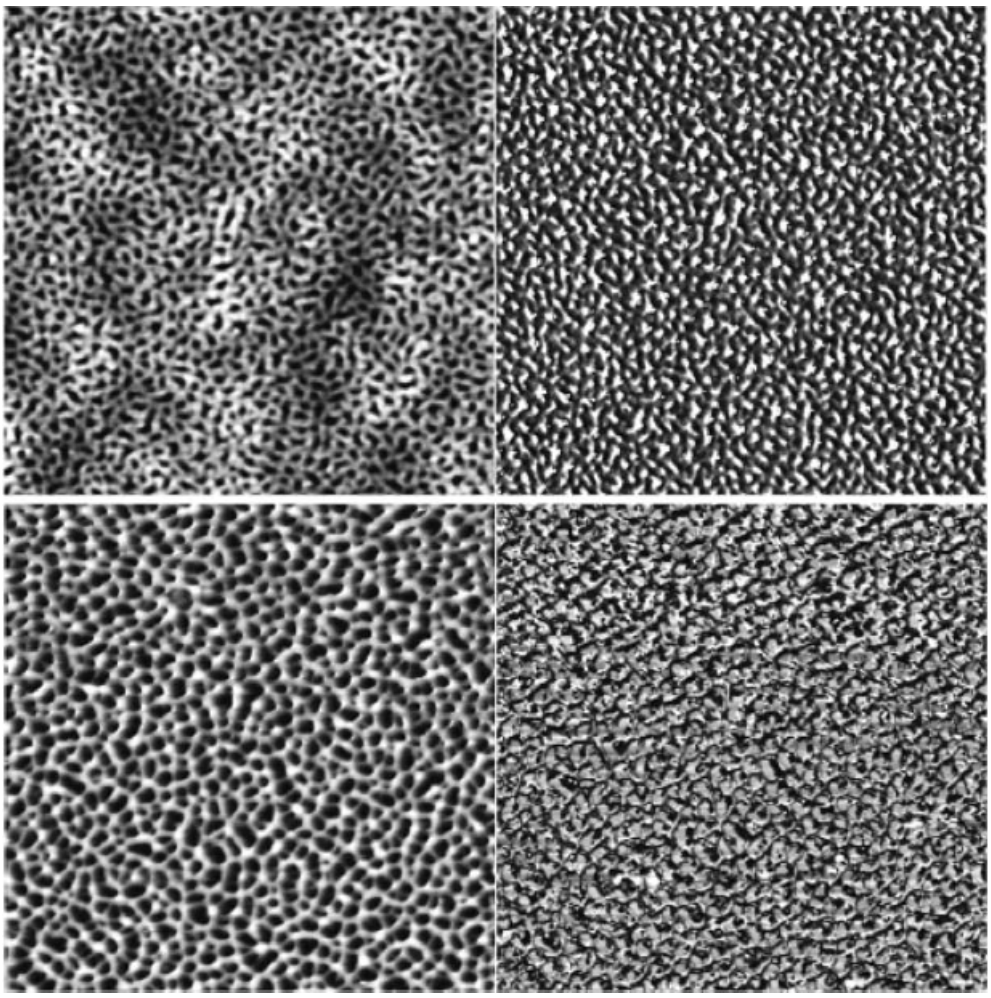

Fig. 7. Investigating phase segregation and formation of patterns in multicomponent polymer brushes as observed by AFM. In this case, glassy and rubbery binary components of grafted polymethacrylate (PMA) and fluorinated polystyrene copolymer (PSF) were sensitively imaged and differentiated between topography (left), phase imaging (right), and glassy (top) and rubbery (bottom) states of the binary brushes. Dimensions at 5×5 μm. From Ref. 107.

different regimes can result from solvent swelling, differences in molecular weight, and differences in grafting density as the tethered polymer chains change their conformation (105). Depending on the equilibrium conditions, densely tethered polymer chains can be deformed and result in a variety of brush regimes which includes "mushroom," "pancakes," "micelle," and "dimples." While such studies have been recently applied to SIP type of polymer brushes, the investigation of brush regimes has long been associated with physisorbed polymers.

Phase Segregation in Multicomponent Polymer Brushes. Phase segregation and ordering in multicomponent polymer brushes have also been extensively studied (Fig. 7) (106,107). In the presence of two tethered immiscible

homopolymers, different ordered phases can be described, similar to lateral microphase separation in bulk (108). The composition varies as a statistical mixture of the two components or as blocks. Theoretical SCF models have been used to examine the equilibrium properties of a binary polymer brush composed of immiscible chains under melt conditions. A number of interesting morphologies and mesophases are possible both by melt and solution conditions (109). By changing the polymer brush architecture, grafting density, chain length, interaction energy between different blocks and interaction energies between blocks and solvents, a variety of novel well-ordered structures have been predicted and observed. Theoretical results indicate that tethered copolymer brushes on a flat substrate are excellent candidates for forming nanopatterned polymer films (110). Recently, this has been a topic of great interest for investigating new morphologies in SIP systems.

Different Stages of the SIP Grafting Technique. SIP on flat substrate surfaces is a step-by-step procedure which begins with the preparation of substrates and ends with characterization of post-polymerized films. Usually the chosen substrate is also dependent on the applicability of various analysis methods. Primarily, the substrate used is determined by the type of SAM technique used to tether initiators on surfaces. In principle, the characterization protocol is typical for investigating SAMs at surfaces but is extended toward macromolecular dimensions once a polymer is attached. The polymerization and post-polymerization characterization is equally important. *However, very few methods are available for in situ characterization during the polymerization itself.* It is difficult to monitor the growth of polymer brushes in real time because the mechanism and kinetics are not necessarily the same as in solution or bulk. The last step, post-polymerization analysis, is a stage where characterization of terminated brushes can be done after several "washing" methods to isolate grafted polymers on surfaces. Any post-polymerization treatments such as cross-linking or functional group conversion of the brush can be examined at this stage. Overall, the step-by-step analysis is useful for characterizing the polymer brush formation and comparing the films "before" and "after" each stage of the grafting or treatment.

Patterning Polymer Brushes. Patterning by both lithographic and nonlithographic technique results in films with features ranging from a few nanometers (nanopatterning) to microns (micropatterning) (111,112). New and simple strategies to fabricate surface-confined patterns with lithographic and nonlithographic methods have been widely reported (113). Nonlithographic methods using microcontact printing (114) and dip-pen nanolithography (DPN) (115) are recently popular. Patterning offers a number of advantages: (*1*) extrinsic, stimuli control of interfacial properties at the micrometer or nanometer scale; (*2*) precisely localized presentation of chemical or topographical features; and (*3*) controlled surface densities, eg required to achieve higher throughput, as in combinatorial methods (116). Various schemes have been reported where microcontact printing and even lithographic methods (18,26) can be used to prepare microscale patterns (Fig. 8). Fabricating nanopatterns by SIP is an interesting goal. One key strategy in the nanopatterning approach is the use of SAM level of initiator self-assembly. In combination with an appropriate nanolithographic technique, such as DPN, interesting future polymeric nanostructures can be prepared.

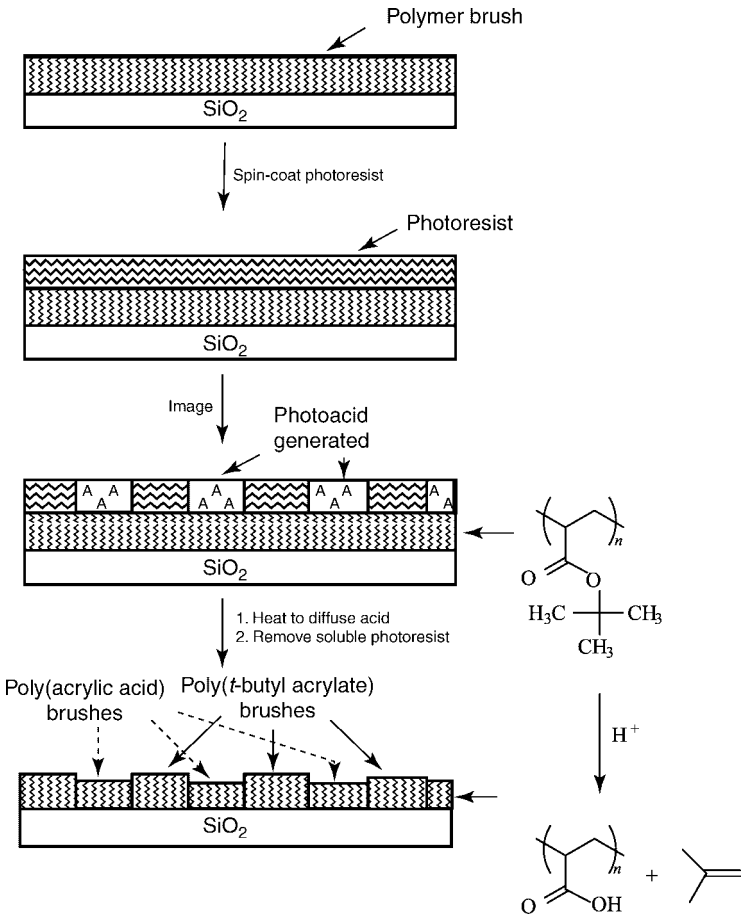

Fig. 8. Scheme for patterning of a polymer brush using a sacrificial photoresist layer and lithographic imaging. From Ref. 18.

Applications

Many applications can be derived from polymer brushes. The most practical use of polymer brushes are modification of surfaces (32), compatible biosurfaces (117), new lubrication materials (118), separations, compatibilizers (119), new adhesives, and polymer composite preparation (120). An interesting application of polymer brushes is in the form of chemical gates (121). Ultrathin and patterned organic films can be prepared which are useful in microelectrics, cell growth control, biomimetic material fabrication, microfluidics, and drug delivery. The versatility of polymer brushes compared to other polymer coating methods is that it allows control of molecular weight, polydispersity, density, composition, block sequencing, and architecture which can be varied for each type of application. Functional polymers observed in solution or in bulk should also have interesting properties when confined to surfaces. This includes liquid crystalline polymers, rigid rods, conjugated polymers, cross-linkable polymers, and polyelectrolytes.

In the area of particles, polymer brushes are of great interest for surface modification and composite material preparation. They have interesting applications in colloidal and interfacial phenomena. In preventing flocculation, the polymer chains, which prefer the solvent to another particle surface, resist overlapping between neighboring particles, resulting in colloidal stabilization. This repulsive force arises from the high osmotic pressure inside these brushes. Strategies have been developed to tailor nanoparticle surfaces by the use of polymer brushes (32). The purpose is to directly tether polymers to nanoparticles, resulting in a *core–shell* type of material architecture. This strategy has lead to the formation of "hairy nanoparticles," which protects the nanoparticle surface and at the same time, increasing the compatibility to polymeric matrices. This is especially important for the preparation of polymer *nanocomposite* materials that can be processed like commercial polymers. A number of inorganic–organic hybrid and nanocomposite materials have been reported (32,118).

BIBLIOGRAPHY

1. B. Zhao and W. J. Brittain, *Progr. Polym. Sci.* **25**, 677 (2000).
2. H. Watanabe, S. M. Kilbry II, and M. Tirrell, *Macromolecules* **33**, 9146 (2000).
3. G. J. Fleer, M. A. Cohen-Stuart, J. M. H. M. Scheutjens, T. Cosgrove, and B. Vincent, *Polymers at Interfaces*, Chapman & Hall, London, 1993.
4. A. Halperin, M. Tirrell, and T. P. Lodge, *Adv. Polym. Sci.* **100**, 31 (1992).
5. N. Tsubokawa, *Prog. Polym. Sci.* **17**, 417 (1992).
6. N. Tsubokawa and A. Kogure, *Polym. J.* **25**, 83 (1993); N. Tsubokawa and A. Kogure, *J. Polym. Sci., Part A: Polym. Chem.* **29**, 697 (1991); N. Tsubokawa and H. Ishida, *Polym. J.* **24**, 809 (1992); N. Tsubokawa, A. Kogure, K. Maruyama, Y. Sone, and M. Shimomura, *Polym. J.* **22**, 827 (1990).
7. F. MacRitchie, *Chemistry of Interfaces*, Academic Press, San Diego, 1990.
8. E. Parsonage, M. Tirrell, H. Watanabe, and R. Nuzzo, *Macromolecules* **24**, 1987 (1987).
9. H. Motschmann, M. Stamm, and C. Toprakcioglu, *Macromolecules* **24**, 3681 (1991).
10. J. Koberstein and C. Laub, *Polym. Prepr.* **40**, 2, 126 (1999); V. Koutsos, E. M. Van der Vegte, and G. Hadziioannou, *Macromolecules* **32**, 1233 (1999); V. Koutsos, E. M. Van der Vegte, G. Hadziioannou, E. Pelletier, and A. Stamouli, *Macromolecules* **30**, 4719 (1997); D. E. Bergbreiter, J. G. Franchina, and K. Kabza, *Macromolecules* **32**, 4993 (1999).
11. A. Balazs and Y. Lyatskaya, *Macromolecules* **31**, 6676 (1998).
12. I. Szleofer and M. A. Carignano, *Adv. Chem. Phys.* **94**, 165 (1996).
13. O. Prucker and J. Ruhe, *Langmuir* **14**, 6893 (1998).
14. A. W. Adamson and A. P. Gast, *Physical Chemistry of Surfaces*, Wiley-VCH, Weinheim, 1997.
15. G. Odian, *Principal of Polymerization*, 3rd ed., Wiley-VCH, Weinheim, 1991.
16. G. Tovar, S. Paul, W. Knoll, O. Prucker, and J. Rühe, *Supramol. Sci.* **2**, 89 (1995).
17. I. M. Khan and J. S. Harrison, *Field Responsive Polymers: Electroresponsive, Photoresponsive, and Responsive Polymers in Chemistry and Biology*, American Chemical Society, Washington, DC, 1999.
18. M. Husemann, M. Morrison, D. Benoit, J. Frommer, M. Mate, W. Hinsberg, J. Hedrick, and C. Hawker, *J. Am. Chem. Soc.* **122**, 1844 (2000).
19. S. T. Milner, T. A. Witten, and M. E. Cates, *Macromolecules* **21**, 2610 (1998); S. Minko, G. Gafijchuk, A. Sidorenko, and S. Voronov, *Macromolecules* **32**, 4525 (1999).

20. S. Alexander, *J. Phys.* **38**, 977 (1977).
21. L. Rockford, S. Mochrie, and T. Russell, *Macromolecules* **34**, 1487 (2001); T. Russell, T. Thurn-Albrecht, M. Tuominen, E. Huang, and C. Hawker, *Macromol. Symp.* **159**, 77 (2000); L. Rockford, Y. Liu, P. Mansky, T. Russell, M. Yoon, and S. Mochrie, *J. Phys. Rev. Lett.* **82**, 2602 (1999); E. B. Zhulina and A. C. Balazs, *Macromolecules* **29**, 6338 (1996).
22. O. Prucker and R. Ruhe, *Macromolecules* **31**, 602 (1998).
23. R. Jordan and A. Ulman, *J. Am. Chem. Soc.* **120**, 243 (1998).
24. M. Weck, J. J. Jackiw, R. R. Rossi, P. S. Weiss, and R. H. Grubbs, *J. Am. Chem. Soc.* **121**, 4088 (1999).
25. M. Ejaz, S. Yamamoto, Y. Tsujii, and T. Fukuda, *Macromolecules* **35**, 1412 (2002); D. M. Jones, A. A. Brown, and W. T. S. Huck, *Langmuir* **18**, 1265 (2002).
26. M. Husseman, E. E. Malmstrom, M. McNamara, M. Mate, D. Mecerreyes, D. Benoit, J. L. Hedrick, P. Mansky, E. Huang, T. P. Russell, and C. J. Hawker, *Macromolecules* **32**, 1424 (1999).
27. R. Advincula, Q. Zhou, M. Park, S. Wang, J. Mays, G. Sakellariou, S. Pispas, and N. Hadjichristidis, *Langmuir* **18**, 8672 (2002); R. Jordan, A. Ulman, J. F. Kang, M. H. Rafailovich, and J. Sokolov, *J. Am. Chem. Soc.* **121**, 1016 (1999); R. P. Quirk, R. T. Mathers, T. Cregger, and M. D. Foster, *Macromolecules* **35**, 9964 (2002).
28. S. G. Boyes, W. J. Brittain, X. Weng, and S. Z. D. Cheng, *Macromolecules* **35**, 4960 (2002).
29. M. Biesalski and J. Ruhe, *Langmuir* **16**, 1943 (2000).
30. J. Ruhe and O. Prucker, *Macromolecules* **31**, 592 (1998).
31. M. Geoghegan, G. Krausch, Y. Tsujii, M. Ejaz, S. Yamamoto, T. Fukuda, K. Shigeto, K. Mibu, and T. Shinjo, *Prog. Polym. Sci.* **28**, 261 (2003).
32. R. Advincula, *J. Dispersion. Sci. Tech.* **24**, 343 (2003).
33. *WTEC Proceedings*, International Technology Institute, Baltimore, Md., 1998, pp. 1–233.
34. R. Jordan, N. West, A. Ulman, Y.-M. Chou, and O. Nuyken, *Macromolecules* **34**, 1606 (2001).
35. S. Yoshikawa, S. Machida, and N. Tsubokawa, *J. Polym. Sci., Polym. Chem.* **36**, 3165 (1998).
36. Q. Zhou, S. Wang, X. Fan, R. Advincula, and J. Mays, *Langmuir* **18**, 3324 (2002).
37. D. M. Jones, A. A. Brown, and W. T. S. Huck, *Langmuir* **18**, 1265 (2002).
38. N. Y. Kim, N. L. Jeon, I. S. Choi, S. Takami, Y. Harada, K. R. Finnie, G. S. Girolami, R. G. Nuzzo, G. M. Whitesides, and P. E. Laibinis, *Macromolecules* **33**, 2793 (2000).
39. K. J. Watson, J. Zhu, S. T. Nguyen, and C. A. Mirkin, *J. Am. Chem. Soc.* **121**, 462 (1999).
40. L. P. Meier, R. A. Shelden, W. R. Caseri, and U. Suter, *Macromolecules* **27**, 1637 (1994).
41. A. Akelah and A. Moet, *J. Mater. Sci.* **31**, 3589 (1996).
42. L. K. Ista, S. Mendez, V. H. Perez-Luna, and G. P. Lopez, *Langmuir* **17**, 2552 (2001); M. J. Percy, C. Barthet, J. C. Lobb, M. A. Khan, S. F. Lascelles, M. Vamvakaki, and S. P. Armes, *Langmuir* **16**, 6913 (2000); R. Schmidit, T. Zhoa, J. B. Green, and D. J. Dyer, *Langmuir* **18**, 1281 (2000); W. Huang, G. Skanth, G. Baker, and M. L. Bruening, *Langmuir* **17**, 1731 (2001).
43. X. Fan, C. Xia, T. Fulghum, M. K. Park, J. Locklin, and R. C. Advincula, *Langmuir* **19**, 916 (2003).
44. J. Pyun and K. Matyjaszewski, *Chem. Mater.* **13**, 3436 (2001).
45. T. von Werne and T. E. Patten, *J. Am. Chem. Soc.* **123**, 7497 (2001).
46. T. von Werne and T. E. Patten, *J. Am. Chem. Soc.* **121**, 7409 (1999).
47. S. C. Farmer and T. E. Patten, *Chem. Mater.* **13**, 3920 (2001).
48. B. Zhao and W. J. Brittain, *Macromolecules* **33**, 8813 (2000).

49. W. Huang, J.-B. Kim, M. L. Bruening, and G. L. Baker, *Macromolecules* **35**, 1175 (2002).
50. B. Filiz Senkal and N. Bicak, *Eur. Polym. J.* **39**, 327 (2003); M. Ejaz, Y. Tsujii, and T. Fukuda, *Polymer* **42**, 6811 (2001); C. R. Vestal and Z. J. Zhang, *J. Am. Chem. Soc.* **124**, 14312 (2002); J. Pyun, K. Matyjaszewski, T. Kowalewski, D. Savin, G. Patterson, G. Kickelbick, and N. Huesing, *J. Am. Chem. Soc.* **123**, 9445 (2001).
51. Y. Tsujii, M. Ejaz, K. Sato, A. Goto, and T. Fukuda, *Macromolecules* **34**, 8872 (2001); M. Baum and W. J. Brittain, *Macromolecules* **35**, 610 (2002).
52. S. Yoshikawa, S. Machida, and N. Tsubokawa, *J. Polym. Sci., Polym. Chem.* **17**, 3165 (1998).
53. M. L. C. M. Oosterling, A. Sein, and A. J. Schouten, *Polymer* **33**, 4394 (1992).
54. N. Tsubokawa, T. Yoshihara, and Y. Sone, *Colloid Polym. Sci.* **269**, 324 (1991).
55. R. Quirk and R. Mathers, *Polym. Bull.* **6**, 471 (2001).
56. Q. Zhou, X. Fan, C. Xia, J. Mays, and R. Advincula, *Chem. Mater.* **13**, 2465 (2001).
57. M. Pitsikalis, S. Pispas, J. Mays, and N. Hadjichristidis, *Adv. Polym Sci.* **135**, 1 (1998).
58. N. Hadjichristidis, H. Iatrou, S. Pispas, and M. Pitsikalis, *J. Polym. Sci., Part A: Polym. Chem.* **38**, 3211 (2000).
59. X. Fan, Q. Zhou, C. Xia, W. Cristofoli, J. Mays, and R. Advincula, *Langmuir* **18**, 4511 (2002).
60. N. Y. Kim, N. L. Jeon, I. S. Choi, S. Takami, Y. Harada, K. R. Finnie, G. S. Girolami, R. G. Nuzzo, G. M. Whitesides, and P. E. Laibinis, *Macromolecules* **33**, 2793 (2000).
61. A. Juang, O. A. Scherman, R. H. Grubbs, and N. S. Lewis, *Langmuir* **17**, 1321 (2001); H. Skaff, M. F. Ilker, E. B. Coughlin, and T. Emrick, *J. Am. Chem. Soc.* **124**, 5729 (2002); M. D. K. Ingall, S. J. Joray, D. J. Duffy, D. P. Long, and P. A. Bianconi, *J. Am. Chem. Soc.* **122**, 7845 (2000).
62. B. Zhao and W. Brittain, *Macromolecules* **33**, 342 (2000).
63. N. Tsubokawa, *Colloids Surf. A* **81**, 195–201 (1993); S. Yoshikawa, T. Iida, and N. Tsubokawa, *Prog. Org. Coatings* **31**, 127–131 (1997); N. Tsubokawa, K. Oyanagi, and S. Yoshikawa, *J. Macromol. Sci. Pure. Appl. Chem.* **37**, 529–548 (2000).
64. C. W. Frank, *Organic Thin Films: Structure and Applications* (ACS Symp. Series 695), American Chemical Society, Washington, DC, 1998.
65. G. Decher and J. D. Hong, *Markomol. Chem., Macromol. Symp.* **46**, 321 (1991).
66. G. Roberts, *Langmuir–Blodgett Films*, Plenum Press, New York, 1990.
67. J. Sagiv, *J. Am. Chem. Soc.* **102**, 92 (1980).
68. A. Ulman, *Organic Thin Films and Surfaces*, Academic Press, San Diego, 1991.
69. R. Mendelsohn, J. W. Brauner, and A. Gericke, *Annu. Rev. Phys. Chem.* **46**, 305 (1995).
70. R. Levy, N. Koneripalli, M. Tirrell, and S. K. Satija, *Macromolecules* **31**, 3731 (1998).
71. E. P. K. Currie, M. Wagemaker, M. A. Cohen Stuart, and A. A van Well, *Phys. B* **283**, 17, 21 (2000).
72. X. Kong, T. Kawai, J. Abe, and T. Iyoda, *Macromolecules* **34**, 1837 (2001).
73. M. Kawaguchi, M. Kawarabayashi, N. Nagata, T. Kato, A. Yoshioka, and A. Takahashi, *Macromolecules* **21**, 1059 (1988).
74. M. R. Munch and A. P. Gast, *Macromolecules* **23**, 2313 (1990).
75. C. Allain, D. Ausserr, and F. Rondelez, *Phys. Rev. Lett.* **49**, 1694 (1981).
76. J. Habicht, M. Schmidt, J. Ruehe, and D. Johannsmann, *Langmuir* **15**, 2460 (1999).
77. S. N. Magonov and M. Whangbo, *Surface Analysis with STM and AFM: Experimental and Theoretical Aspects of Image Analysis*, VCH, New York, 1996.
78. D. W. Bonnell, ed., *Scanning Probe Microscopy and Spectroscopy. Theory, Techniques, and Applications*, 2nd ed., Wiley-VCH, New York, 2001.
79. A. Juang, O. A. Scherman, R. H. Grubbs, and N. S. Lewis, *Langmuir* **17**, 1321 (2001).
80. H. Iwata, I. Hirata, and Y. Ikada, *Langmuir* **13**, 3063 (1997); X. Kong, T. Kawai, J. Abe, and T. Iyoda, *Macromolecules* **34**, 1837 (2001).
81. S. Yamamoto, Y. Tsujii, and T. Fukuda, *Macromolecules* **33**, 5995 (2000).

82. S. Al-Maawali, J. E. Bemis, B. B. Akhremitchev, R. Leecharoen, B. G. Janesko, and G. C. Walker, *J. Phys. Chem. B* **105**, 3965 (2001).
83. B. Zhao, W. J. Brittain, W. Zhou, and S. Z. D. Cheng, *J. Am. Chem. Soc.* **122**(10), 2407 (2000).
84. M. Ivanchenko, H. Kobayashi, E. Kulik, and N. Dobrova, *Anal. Chim. Acta* **314**, 23 (1995); K. A. Marx, *Biomacromolecules* **4**, 1099 (2003).
85. D. Julthongpiput, Y. H. Lin, J. Teng, E. R. Zubarev, and V. V. Tsukruk, *Langmuir* **19**, 7832 (2003).
86. A. Anne and J. Moiroux, *Macromolecules* **32**, 5829 (1999).
87. N. Houbenov, S. Minko, and M. Stamm, *Macromolecules* **36**, 5897 (2003).
88. S. M. Kilbey II, H. Watanabe, and M. Tirrell, *Macromolecules* **34**, 5249 (2001).
89. T. W. Kelley, P. A. Schorr, K. D. Johnson, M. Tirrell, and C. D. Frisbie, *Macromolecules* **31**, 4297 (1998).
90. N. A. Spenley, *Macromolecules* **31**, 4004 (1998); Y. Lyatskaya and A. C. Balazs, *Macromolecules* **30**, 7588 (1997).
91. S. Hayashi, K. Fujiki, and N. Tsubokawa, *React. Funct. Polym.* **46**, 193 (2000).
92. J. I. Amalvy, M. J. Percy, S. P. Armes, and H. Wiese, *Langmuir* **17**, 4770 (2001).
93. M. Z. Rong, Q. L. Ji, M. Q. Zhang, and K. Friedrich, *Eur. Polym. J.* **38**, 1573 (2002).
94. E. Tadd, A. Zeno, M. Zubris, N. Dan, and R. Tannenbaum, *Macromolecules* **36**, 6497 (2003).
95. K.-M. Kim, D.-K. Keum, and Y. Chujo, *Macromolecules* **36**, 867 (2003).
96. W. L. Yu and M. Borkovec, *J. Phys. Chem. B* **106**, 13106 (2002).
97. G. K. Agarwal, J. J. Titman, M. J. Percy, and S. P. Armes, *J. Phys, Chem. B* **107**, 12497 (2003).
98. A. De Sousa Delgado, M. Leonard, and E. Dellacherie, *Langmuir* **17**, 4386 (2001).
99. M. J. Percy, V. Michailidou, S. P. Armes, C. Perruchot, J. F. Watts, and S. J. Greaves, *Langmuir* **19**, 2072 (2003).
100. A. N. Semenov, *Langmuir* **11**, 3560 (1995); U. Raviv, R. Tadmor, and J. Klein, *J. Phys. Chem. B* **105**, 8125 (2001).
101. H. Mori, D. Chan Seng, M. Zhang, and A. H. E. Mueller, *Langmuir* **18**, 3682 (2002); K. Ohno, K. Koh, Y. Tsujii, and T. Fukuda, *Macromolecules* **35**, 8989 (2002).
102. J. J. Zhao, S. C. Bae, F. Xie, and S. Granick, *Macromolecules* **34**, 3123 (2001).
103. R. C. Dunn, *Chem. Rev.* **99**, 2891 (1999).
104. P. G. de Gennes, *Macromolecules* **13**, 1069 (1980); R. Cantor, *Macromolecules* **14**, 1186 (1981); R. R. Netz and M. Schick, *Macromolecules* **31**, 5105 (1998); A. Semenov and S. H. Anastasiadis, *Macromolecules* **33**, 613 (2000).
105. T. Wu, K. Efimenko, P. Vlcek, V. Subr, and J. Genzer, *Macromolecules* **36**, 2448 (2000).
106. I. Luzinov, D. Julthongpiput, and V. V. Tsukruk, *Macromolecules* **33**, 7629 (2000).
107. M. Lemieux, D. Usov, S. Minko, M. Stamm, H. Shulha, and V. V. Tsukruk, *Macromolecules* **36**, 7244 (2003).
108. M. J. Fasolka and A. M. Mayes, *Annu. Rev. Mater. Res.* **31**, 323 (2001).
109. A. Sidorenko, S. Minko, K. Schenk-Meuser, H. Duschner, and M. Stamm, *Langmuir* **15**, 8349 (1999).
110. E. B. Zhulina, C. Singh, and A. C. Balazs, *Macromolecules* **29**, 6338 (1996); E. B. Zhulina and A. C. Balazs, *Macromolecules* **29**, 2667 (1996).
111. C. G. Wilson, in L. F. Thompson, C. G. Willon, and M. J. Bowden, eds., *Introduction to Microlithographay*, 2nd ed., American Chemical Society, Washington, D.C., 1994, p. 139.
112. J. L. Wilbur, A. Kumar, H. Niebuyck, E. Kim, and G. Whitesides, *Nanotechnology* **7**, 452 (1996); S. Clark, M. Montague, and P. Hammond, *Supramol. Sci.* **4**, 141 (1997).
113. Y. Tsujii, M. Ejaz, S. Yamamoto, T. Fukuda, K. Shigeto, K. Mibu, and T. Shinjo, *Polymer* **43**, 3837 (2002).
114. Y. Xia and G. M. Whitesides, *Angew. Chem., Int. Ed. Engl.* **37**, 550 (1998).

115. S. Hong and C. Mirkin, *Science* **288**, 1808 (2000); S. Hong and C. Mirkin, *Science* **286**, 523 (1999).
116. J. C. Meredith, A. P. Smith, A. Karim, and E. J. Amis, *Macromolecules* **33**, 9747 (2000).
117. M. Amiji and K. Park, *J. Biomater. Sci., Polym. Edn.* **4**, 234 (1993).
118. J. F. Joanny, *Langmuir* **8**, 989 (1992).
119. T. Tadros, *The Effect of Polymers on Dispersion Properties*, Academic Press, London, 1982.
120. R. Krishnamoorti and R. Vaia, *Polymer Nanocomposites* (ACS Symposium Series 804), Oxford University Press, North Carolina, 2002.
121. Y. Ito, Y. Ochiai, Y. S. Park, and Y. Imanishi, *J. Am. Chem. Soc.* **119**, 1619 (1997).

RIGOBERTO C. ADVINCULA
University of Houston

POLYMERIC DRUGS. See Volume 7.

POLYMER-SUPPORTED REAGENTS

Introduction

Since the original reports by Merrifield, published some 40 years ago (1), solid supports have been widely used as a synthetic device to avoid expensive and long winded purification processes, principally due to the simplicity of isolating the support and its bound material by direct filtration. There are a number of other advantages when using solid supports; most notably reactions can be driven to completion using high concentrations and mass action of reagents and synthesis can be easily automated (2).

With the introduction of a range of high throughput synthesis methods (3–5), solid supports have become even more indispensable (6), for example, with the use of polymer-supported reagents and catalysts (7), which maintains the target molecules in solution but immobilizes the other component, and renders possible the parallel monitoring of supported reactions but in a solution sense. The most utilized polymer support in solid-phase chemistry is still a copolymer of styrene and divinyl benzene [DVB (2%)], known as a gel-type resin, because of its "gelatinous" and nonmacroporous behavior, originally used by Merrifield for the synthesis of the first tetrapeptide made by solid-phase synthesis (see POLYPEPTIDE SYNTHESIS, SOLID-PHASE METHOD).

Nevertheless, there are some problems correlated with the use of this support, such as its voluminous nature when swollen, its lack of physical stability under harsh handling conditions, and its incompatibility with a number of solvents (8). For this reason, several groups of researchers have investigated a number of alternative solid supports, for solid-phase chemistry, in order to improve resin properties, such as physical robustness, ease of handling, enhancement in loading,

Encyclopedia of Polymer Science and Technology. Copyright John Wiley & Sons, Inc. All rights reserved.

improvement of reaction kinetics, and so forth. This article presents an overview of the materials commonly used in solid-supported chemistry and their evolution.

Styrene–DVB-Based Resins

Polystyrene resins (25–300 μm) are the most commonly used supports in solid-phase chemistry and, in a variety of formats, are extensively used in a wide range of industrial processes (see STYRENE POLYMERS). These basic materials can be easily obtained by radical polymerization of a suspension of an organic phase (the styrene and divinylbenzene monomers in varying proportions) in water, in the presence of a stabilizer (in order to reduce the surface tension of the droplets and to prevent their aggregation) (9). A minimum level (usually at least 0.5%) of DVB is required in order to ensure that the polymer obtained is insoluble in organic solvents. The percentage of DVB (cross-linker), influences the physical and chemical properties of the support. High levels of cross-linking produce more rigid supports; therefore, drastic conditions of reaction such as mechanical stirring and high temperatures are permissible, but on the other hand slower reactions are often observed because of the fact that the reagents cannot easily diffuse within the polymer network (10). On the other hand, low levels of cross-linking produce highly swellable but more fragile beads, which, however, exhibit better reaction kinetics.

In most chemical reactions, the solvent plays a fundamental role and this effect is enhanced in solid-supported chemistry. When in contact with so-called "good" or "poor" solvents, the beads can swell or shrink (this effect depends principally on the level of cross-linking and can be considered akin to the polymer tending to dissolve in the solvent). This phenomenon can increase the ability of reagents to diffuse into the beads, and therefore dramatically influences reaction rates. Reactivity within beads is also highly dependent on resin loading. Loading variations can for example vary, allowing concentrations within beads to range between 50 μM and 0.5 M. As in solution chemistry, such concentration effects can cause huge effects on reaction rates, depending upon the reaction under investigation as a result of electrostatics and/or steric effects of the reagents. To avoid some of these type of issues, spacers are often placed between the polymer and the reactive functionality of the resin (11), but the high concentration of material on a bead is often ignored in solid-phase synthesis.

The reactive functionality (the site of chemistry) on a resin can be added during or after polymerization as shown in Figure 1 (12). Direct functionalization can be performed by including a third monomer into the original monomer mixture, which already bears the desired functional group. Chloromethylstyrene is often used in this regard because it can be easily transformed into a wide range of alternatives (Fig. 2) and is a monomer that incorporates well into styrene/divinyl benzene mixtures (Fig. 1).

Post-functionalization is usually carried out by electrophilic aromatic substitution in the presence of a Lewis acid (27) or by metallation of a brominated resin (Fig. 1) (28).

Good quality polymers are obtained by direct functionalization with the resulting functionality uniformly distributed throughout the bead. However, there are other factors that influence the quality of the polymer. As mentioned by

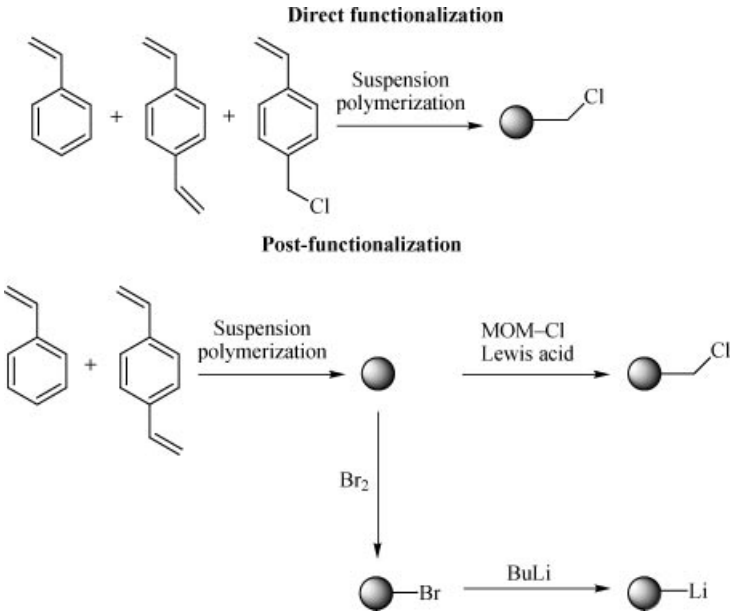

Fig. 1. Functionalization of polystyrene resins.

Czarnik (29), resins from different batches often show different chemical behaviour, as the process of suspension polymerization depends upon many factors such as reactor geometry, agitator design, and agitation rate (30). Uniform, spherical beads are preferred for reproducible chemistry, irregular particles being much more sensitive to mechanical destruction and often falling apart during the reaction. Both 6- and 8-multiparallel polymerization systems have been designed, and these systems show very good reproducibility when used for the synthesis of polymer libraries (Fig. 3) (31), attesting to the parallel advantages of synthesis and maintaining a consistent reaction geometry. A second-generation system allowed 8-multiple polymerizations with the possibility of changing the stirring rate of each reaction vessel.

The level of functional groups or "loading," expressed in mmol/g, can cover a wide range of values (from 0 to virtually 7 mmol/g), but this level varies greatly depending on the application of the support. Generally, the loading and application of polystyrene resins can be grouped as follows:

(1) <0.1 mmol/g, suitable for oligonucleotide synthesis and the synthesis of large peptides/proteins
(2) 0.1–0.7 mmol/g, suitable for supported catalysts (which are added in small amounts)
(3) 0.5–1.5 mmol/g, suitable for solid-phase synthesis (small molecules and peptides) avoiding problems of steric hindrance
(4) >2 mmol/g, preferred for scavenger and reagents based resins, as these types of reagents are added in excess

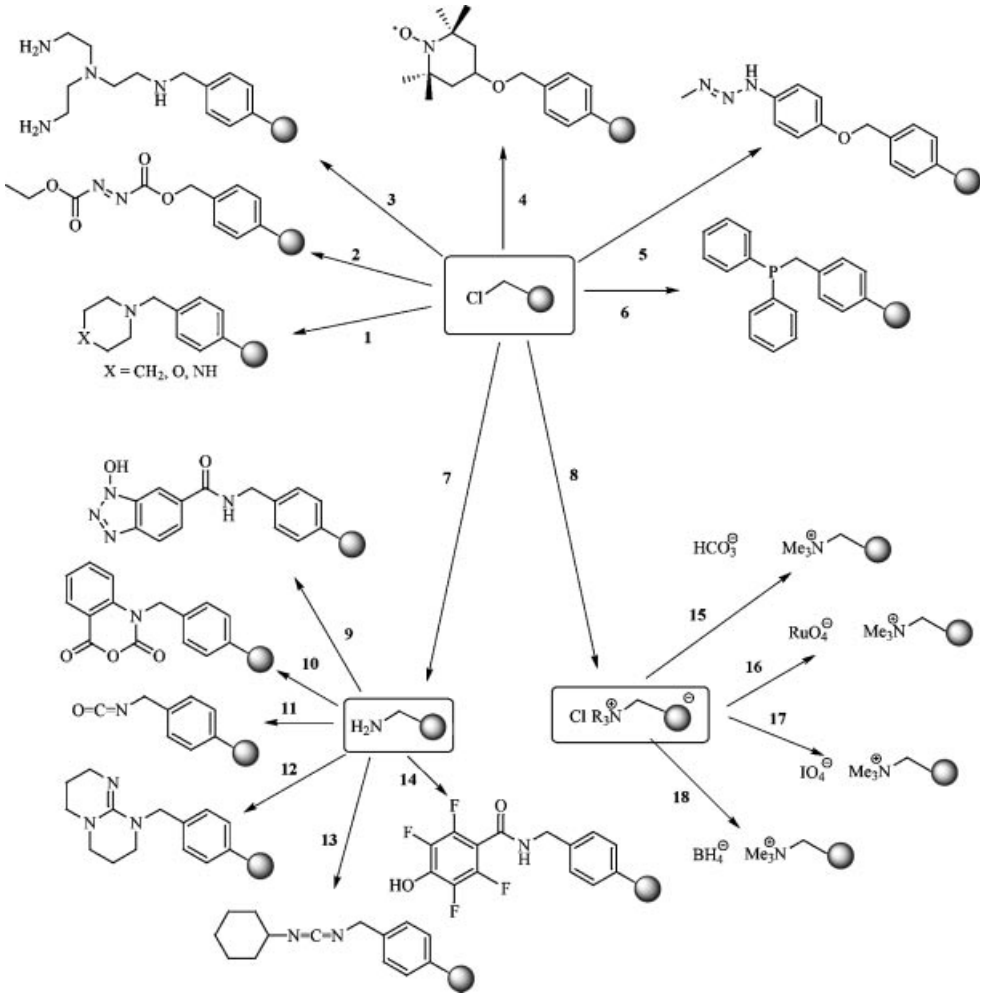

Fig. 2. Preparation of solid-supported reagents and catalysts by derivatization of chloromethyl polystyrene. (**1**: Ref. 13, **2**: Ref. 14, **3**: Ref. 13, **4**: Ref. 15, **5**: Ref. 16, **6**: Ref. 17, **7**: Ref. 18, **8**:NR_3–DMF 110°C, **9**: Ref. 19, **10**: Ref. 20, **11**: Ref. 13, **12**: Ref. 21, **13**: Ref. 22, **14**: Ref. 23, **15**: Ref. 24, **16**: Ref. 25, **17**: Ref. 12, **18**: Ref. 26).

Resin Types

Gel-Type Polystyrenes. Gel-type polystyrenes can be synthesized by radical suspension polymerization of styrene and DVB as reported in 1946 by Hohenstein and Mark (9,32). When suspended in a solvent with good swelling properties, these "white soft beads" assume a gelatinous state; their volume may increase by 6–8 times and they become optically transparent. This process of swelling, as well as the shrinking, occurs from the outside to the inside of the polymer network and the increment of volume is in correlation with its solvation. This plays an important role in chemistry, because it is through such processes that the reactants diffuse into the polymer network where 99% of the functional sites reside (33).

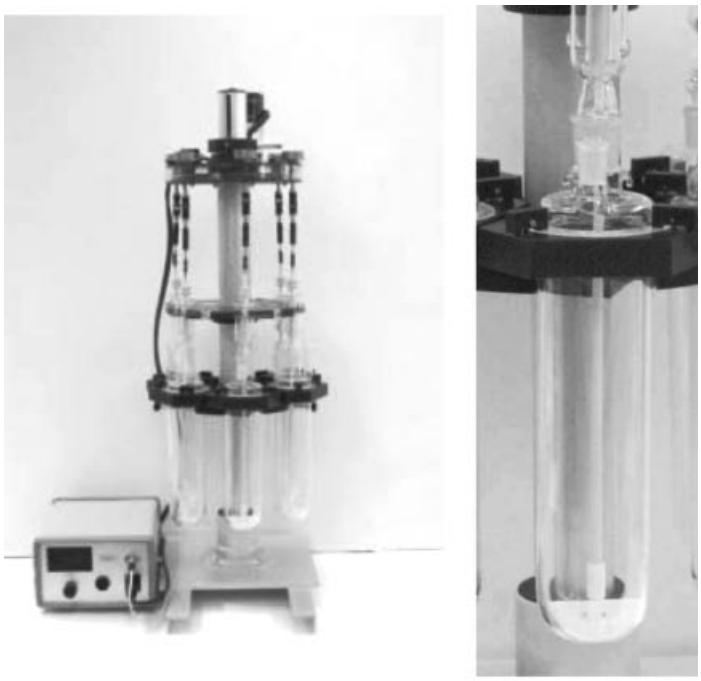

Fig. 3. (**a**) Multiparallel suspension polymerization system; (**b**) close-up of reaction vessel.

As a consequence, the solvent has to be chosen to allow swelling of the resin (34). However, swelling is not the only "solvent dependency", as the type of functionality also affects solvent compatibility. Thus, while Merrifield resins (chloromethyl polystyrene) shrink in highly polar solvents such as water, ion exchange resins show the opposite behavior and do not swell in "good swelling solvents" such as dimethylformamide (DMF). Merrifield observed that the volume of the beads and their behavior with the solvent changed continuously as the supported peptide was grown, attesting to the importance of the resin and the attached molecules, a factor which obviously is influenced by resin loading (35). There are thus a number of other factors which need to be considered when handling and evaluating gel-based supports. If the beads are fully swollen in a "good solvent" and then shrunk rapidly in a bad solvent (eg washing step), "mechanical shock" can take place and the beads may disintegrate, especially with large beads (osmotic shock) (36). To avoid this issue, beads should be washed gradually, starting from a good solvent to a poor solvent, while in the fully swollen state beads should not be agitated with rigid materials, or they may become damaged.

Although a number of issues are correlated with the use of this material, gel-type polystyrene resins are the most used supports in solid-phase chemistry, because of their acceptable loading capacity and relative good kinetics when fully swollen in good solvents.

Macroporous-Type Resins. Macroporous resins were prepared as long ago as 1962 by Millar (37). Macroporous resins have been used for many years

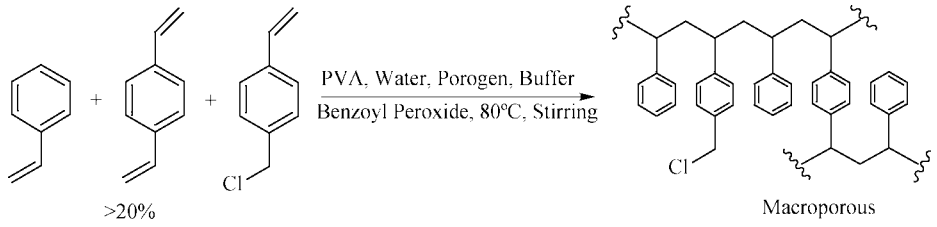

Fig. 4. Synthesis of macroporous polystyrene chloromethyl resin.

as ion-exchange materials, polymeric adsorbents (38), and preparative reverse phases for purification of biomolecules (39), but there are also several examples of this type of support in organic synthesis as carriers for reagents and catalysts (40,41).

Even although the IUPAC definition for macroporous refers to materials that have pores with a diameter greater or equal to 50 nm, the term has been generalized in the resin area to include resins that present a porous structure in the dry state (36).

The formation of the pores occurs when an inert solvent, or porogen, is added to a polymerization mixture containing relatively high levels of cross-linker (Fig. 4). After polymerization, removal of the solvent from the beads leaves intact pores that do not collapse because of the high level of cross-linker used (>20%).

The morphology of the pores (surface area, total pore volume, and average pore diameters) can be adjusted and controlled by an appropriate choice of the type and amount of porogen and the level of cross-linker used (42).

Several porogens (also called diluents) have been used to prepare macroporous resins (43), and they can be divided in three main classes:

(1) Solvating (SOL), such as toluene or dichloroethane (small pore)
(2) Nonsolvating (NONSOL), such as *n*-heptane or alcohols (large pores)
(3) Polymeric (POLY), such as linear polystyrene (very large pores) (44)

Pore formation and their different morphologies have been explained in a recent review (Fig. 5) (36).

When polymerization begins, droplets are formed by the suspension process. The monomer droplets start forming small spherical, so-called microgel, particles.

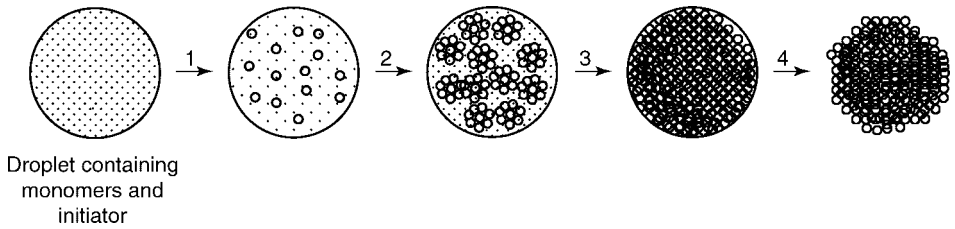

Fig. 5. Pore formation in macroporous resins. (1) Highly solvated swollen microgels, (2) aggregation of swollen microgels, (3) phase separation, (4) solvent removal.

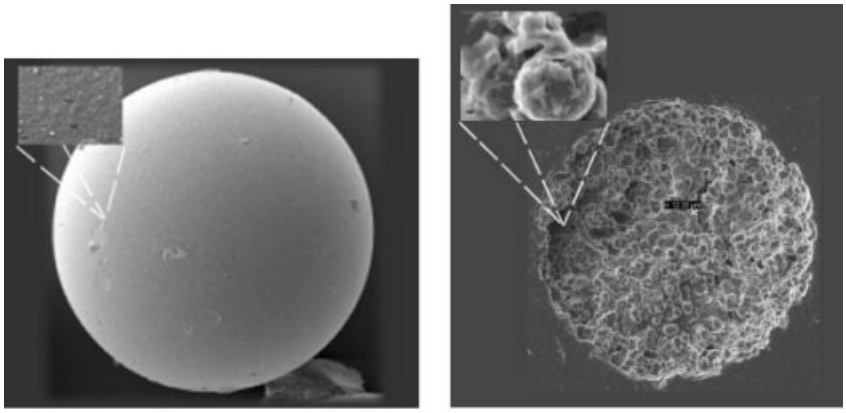

Fig. 6. SEM micrograph of macroporous resins synthesized using (**a**) toluene (solvating) and (**b**) heptane (nonsolvating) porogen.

If these contain a good solvent for the monomers, such as toluene, these particles are fully solvated until there is a high conversion to polymer. Thus, when phase separation takes place (ie, the polymer is no longer soluble in the solvent), the environment within the particle contains only a small amount of unreacted monomer. These particles, therefore, retain their identity and the network of small pores already generated between them is essentially retained. When a nonsolvating porogen, such as heptane, is used, the microgel particles are poorly swollen and phase separation takes place early (low conversion to polymer). In this case the droplet contains a high level of unreacted monomers and these have the effect not only of fusing the microgel particles together, but also of causing significant filling of small pores between the microgel particles. The results of two extreme cases are shown in the Figure 6. Smooth beads polymerized with 200% vol/vol of toluene showed a rough surface only when magnified, whereas beads obtained from heptane (150% vol/vol) gave an irregular morphology.

To improve the benefits of solid-supported reagents and scavengers, macroporous beads need to have a large surface area and large pores. While a high surface area provides more sites for functionalization, large pores provide efficient transport of reagents through the beads. However, as suggested by Sherrington, these two parameters are obviously related (12). If a resin bead has a large surface area and a large number of pores, then each pore is likely to have a small diameter and vice versa. Experimentally, these parameters are measured by nitrogen adsorption/desorption (BET) (45), mercury intrusion porosimetry (46), and electron microscope techniques.

Another consequence of the fixed pores and the rigid structure (high DVB levels) is that macroporous resins have limited swelling. Thus a wide range of solvents commonly used in organic synthesis can be used in solid-phase "macroporous resin assisted chemistry" (even water), without modification of the reaction conditions as required for the use of gel-type resins. Moreover, the rigid structure makes these supports very resistant to mechanical agitation and easy to handle (macroporous resins do not stick like gel type resins).

A comparison between macroporous and 2% gel-based Merrifield resins was performed by Janda (47) who demonstrated the efficiency of washing a dye from pretreated resins was better with a macroporous resin than a gel-type resin. Comparison of a palladium catalyst, for Wacker olefin oxidation, supported on gel-type and macroporous resins gave better results on the macroporous support. Contributions in this area have also been made by Labadie who demonstrated good results using tailored macroporous resins, commonly known as ArgoPore (these resins had surface area, pore volume, and loading well defined for optimal performance in solid-phase chemistry), for example, reactions in water such as the $TiCl_3$-mediated reduction of nitro compounds, periodate-mediated olefin oxidations (48), Suzuki reactions on polymer-supported iodides and bromides (49), and alkylation of supported acids via enolate formation at low temperature (50). Nowadays, it is possible to find a wide range of macroporous polymer-supported reagents and catalysts commercially available. In conclusion, well-designed macroporous resins exhibit better efficiency and kinetics than gel-type resins in highly polar solvents and have become a valid alternative for solid-phase chemistry, without significant swelling and washing issues, although maximum available loadings cannot be as high as the gel-type counterpart (commercially available macroporous resins for solid-phase chemistry have a loading that depends on the manufacturer (ie, Argonaut Technologies: 0.2–1.8 mmol/g; Polymer Labs: 3.0 mmol/g).

Microgel Polystyrenes. Microgels are soluble polymers with a certain degree of cross-linking, but can be precipitated using an appropriate solvent (51). Beads with a diameter of 5–25 μm can be prepared by radical dispersion polymerization in the presence of a surfactant.

It is imperative to use low levels of monomers during preparation to avoid macrogelation due to the aggregation of the microgels to form large-size particles. One of the main characteristics reported for microgels are their ease of handling when solubilized. A consequence of their solubility is that reactions can be easily monitored by classical solution-phase techniques (eg NMR) but that materials can then be readily recovered in a solid-phase manner.

Janda reported a detailed investigation of polymerization parameters such as the type of solvent, percentage of monomer, and level and different type of cross-linker and showed that polymers with good characteristics could be obtained using 5 wt% monomer solution in tetrahydrofuran (THF) (52). Good polymers were achieved using 10% of DVB or 5% of alternative cross-linkers (Fig. 7). Precipitation of the soluble polymers was achieved by addition of cold methanol and filtration through a glass frit.

Becuse of their recent deployment there are only a few examples in literature on the use of this material in solid-phase chemistry. Wulff (53) used microgel

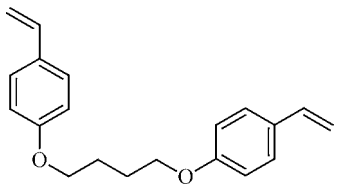

Fig. 7. Cross-linker used in the preparation of microgels.

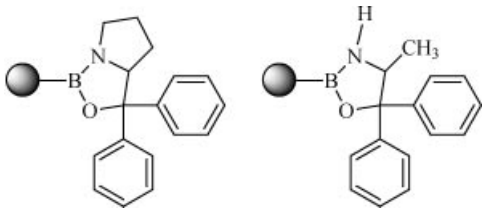

Fig. 8. Microgel-supported oxazaborolidines catalysts.

polymers for the preparation of supported oxazaborolidines as catalysts for asymmetric reduction of ketones (Fig. 8).

This type of catalyst, supported on polystyrene gel type resins, gave results comparable to the homogeneous counterpart. However, because of the poor mechanical properties of the resin under the reaction conditions, a more suitable polymer support was needed. Unfortunately, highly cross-linked resins, with their poor kinetics, decreased the overall selectivity of the catalyst. Although linear polymers were used (54), microgels offered advantages because of their ease of handling. Janda used these supports to perform the solid-phase synthesis of oxazoles (55) and later produced a combinatorial library of phthalimides in good purities and yields using these supports. In addition, microgels were used for the preparation of supported tris(2-aminomethyl)amine and borohydrides to remove isocyanates and to reduce aldehydes respectively.

Polystyrene Nanoparticles. Polymer-based nanoparticles are used in several areas of life science, for example drug delivery (56), and one such polymer matrix commonly used is poly(L-lactic acid) (57). However, nanoparticles with a polystyrene–DVB matrix have been also synthetized (58,59) and used as novel solid supports for organic synthesis (60). The method commonly used to generate these monodisperse particles is Microemulsion Polymerization (qv) (58). However, nanoparticles have also been prepared by precipitation polymerization (61). A microemulsion of styrene and DVB, with an amphiphilic comonomer, in water (three component oil-in-water) (62) allows the preparation of nanobeads with a hard core of polystyrene and the amphiphilic comonomer dispersed on the surface with diameters around 50 and 300 nm that can be precipitated by the addition of methanol. Functionalization of the nanoparticles surface, can be easily achieved using the functionalized amphiphilic comonomer (Fig. 9) (60).

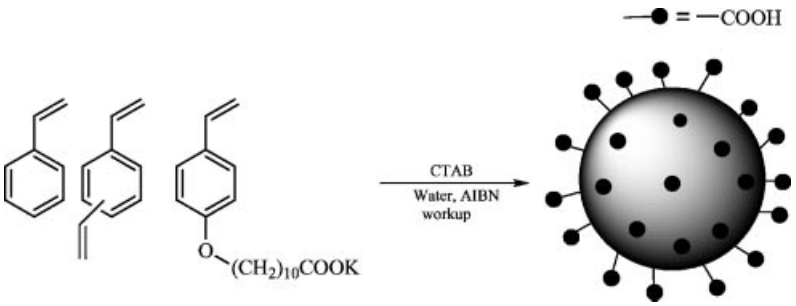

Fig. 9. Synthesis of functionalized polystyrene nanobeads.

These types of beads were used by Cammidge (60) to perform a solid-phase synthesis of porphyrin derivatives following the method described by Leznoff and co-workers (63). Although the final yield of the product was not brilliant (4 and 8% for both the isomers), they were higher than that achieved using "conventional polystyrene resin."

PEG-Grafted Resins

Although gel-type resins are the most widely used supports in solid-phase chemistry, it has been found that such supports are not always the most suitable for peptide synthesis. This is due to two main factors: polystyrene chains are hydrophobic and are not completely compatible with peptides and, furthermore, bulky peptides can adopt unfavorable conformations within the polystyrene cross-linked matrix.

These issues can be avoided by performing the synthesis on linear polymers such as poly(ethylene glycol) (PEG) (64,65), as PEG is soluble in a wide range of organic solvents and, when linked to polypeptides, enhances solubilization. Furthermore, Bayer demonstrated that during coupling reactions, PEG-linked amino acids had the same kinetic properties as amino acid esters (66). However, the main problem in liquid-phase peptide synthesis is the separation of linear PEG from the final polypeptide after cleavage.

Because of its compatibility with peptide chemistry, several authors began to solve the issue of PEG isolation by grafting it onto polystyrene–DVB resin.

As reported by Bayer, polymer grafting by simple reaction with oligomeric PEG and Merrifield resin did not give good results (68), because of the fact that the hydroxylic PEG functionalities could react with two adjacent chloromethyl PS groups, giving an additional degree of cross-linking and reducing the final loading of the resin. However, Barany demonstrated that the grafting of PEG could be achieved by the use of a bifunctional amino-PEG acid (Table 1, entry 2) (69,70). Unfortunately, this support has not found wide use, probably because of its amide linkage.

Bayer described grafting of PEG onto PS resin, by direct anionic polymerization of ethylene oxide onto poly(styryl-methyltetraethylene glycol ether) (68).

The "tentacle polymer" so obtained is commercialized by Rapp Polymere under the name of TentaGel and it is the second most used support for solid-phase organic synthesis after polystyrene resin (Table 1, entry 1) (67). The main characteristic of these resins is their greater swelling in polar solvents such as water, methanol, ethanol, etc, compared to PS resins. As shown in Table 2, entry 2, the swelling of TentaGel is uniform in high to medium polarity solvents. This behavior allows the packing of resins into columns for continuous flow peptide syntheses (68).

Moreover, because of the fact that molecules bound to the highly solvated PEG chains are in a "solution-like" environment and the interactions with the hydrophobic polystyrene backbone are reduced, reaction rates in solid-phase peptide synthesis on TentaGel are greater than on the equivalent Merrifield resins (74,75). Because of the high mobility of PEG chains, gel-phase and MAS NMR result in narrow lines (76). Kinetic comparisons between TentaGel and other supports have been carried out (77,78), and there are several examples of "nonpeptide"

Table 1. PEG Branched Resins

Entry	Resin	Structure	Linkage	Author	References
1	TentaGel	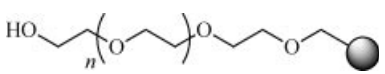	Benzylether[a]	Bayer Rapp	67,68
2	PS–PEG	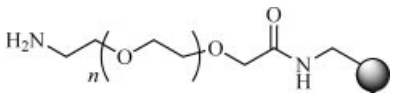	Amide	Barany	69,70
3	ArgoGel	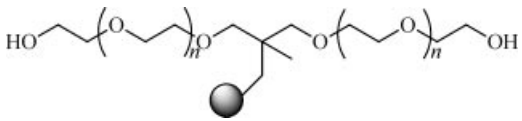	Diol	Gooding	71
4	NovaGel	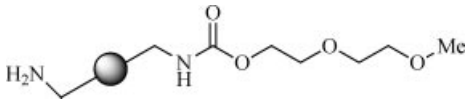	Uretane	Hudson	72
5	PS–MPEG	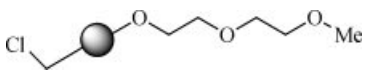	Phenylether	Bradley	73

[a] Original version of TentaGel.

Table 2. Resin Swelling (mL/g of Resin)

Entry	Resin	H_2O	CH_3OH	CH_3CN	DMF	CH_2Cl_2	THF
1	TentaGel[a]	3.6	3.6	4.2	4.7	6.3	5.0
2	PS–PEG[b]	2.8	4.2	3.7	5.1	5.6	3.9
3	ArgoGel[c]	3.9	4.7	—	6.0	7.5	5.8
4	NovaGel[d]	—	4.0	5.0	7.0	10.0	7.5
5	PS–MPEG[e]	2.4	2.8	—	5.8	8.2	8.4
6	Gel-type[f]	—	1.6	3.2	5.6	8.3	8.8

[a] Obtained from Rapp Polymere.
[b] PS–PEG low loading.
[c] Obtained from Argonaut Technologies.
[d] Obtained from Novabiochem.
[e] 7% PEG derivative included.
[f] PS-DVB (1%).

chemistry where the rates are faster on TentaGel than PS resins (ie, Suzuki reactions using supported boronic acids (79), or Sm(II) mediated radical cyclizations (80), or Sharpless asymmetric dihydroxylations) (81). Yan, however, demonstrated that this rule was not always true (82), and found that some reactions, for example terminal modification of aspartic acid or the synthesis of dansyl hydrazones, were faster on PS resins. There are several drawbacks that limit the use of TentaGel resin as a universal support for solid-phase chemistry. The substitutions of TentaGel resins are lower than PS resins although loading can be increased by decreasing the grafting level. However, Lee has demonstrated recently that the swelling of these types of resins depends on the level of grafted PEG (83). When the solvent used was water, there was a direct relationship between PEG level and swelling, but in other solvent systems such as THF or DMF there was a discontinuous trend until the level of PEG was greater than 72% by weight.

A method to increase loading was demonstrated by Bradley by dendrimerization. In this way, TentaGel bead loading was amplified about 10 times (Fig. 10) (84,85).

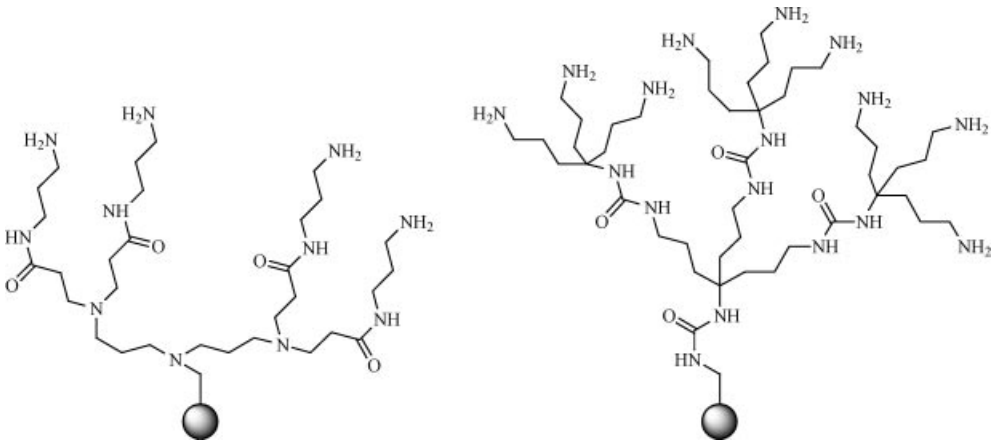

Fig. 10. Dendrimeris for loading improvement.

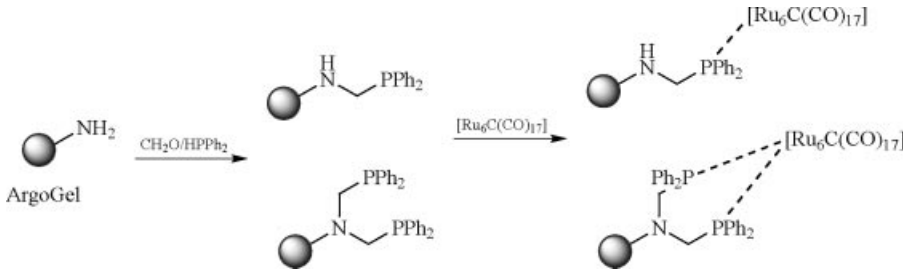

Fig. 11. Preparation of ruthenium-supported catalysts.

There is at least one other main issue that has to be cited. It has been observed that traces of linear PEG are found in final products after cleavage because of the weak benzyl ether bond that links the PEG to the polystyrene backbone.

For this reason, Gooding prepared a PEG-grafted polystyrene resin using a polystyrene diol as a scaffold for the PEG grafting (Table 1, entry 3) (71) [Rapp also used hydroxyethyl PS in the new generation of TentaGel resins (TentaGel S)]. In this way, the chemical stability as well as the loading (0.4–0.5 mmol/g) of such resins was improved. The higher stability of this support was proved by repeated amide cleavages under acidic conditions, where no impurities of linear PEG were found even after long treatments (86). This resin is commercially available from Argonaut Technologies under the name of ArgoGel, and it has been used as a support in the preparation of substituted imidazoles, *N*-alkyl sulfonamides, acylamines, benzofurans, etc (71). De Miguel demonstrated the use of such flexible supports for the immobilization of a highly selective ruthenium cluster catalyst for hydrogenation of olefins and ketones (Fig. 11) (87). Recently, the same group reported the use of such supported catalysts in applications such as gas sensors for H_2S, CO, and SO_2 by color changing of the resin (88).

During his research to improve PEG-grafted resins, Hudson, following the example of Barany, by linking oligomeric PEG chains to aminomethylated resins by a urethane linkage (Table 1, entry 4) (72). These "NovaGel" resins have been commercialized by Novabiochem. The main difference between these supports and the others previously described is that the reactive functionality is still bound to the polystyrene backbone and not to the PEG chains. The effect of the PEG grafting in this case improves swelling as shown in Table 2, entry 4.

However, even if the urethane linkage is more stable than the benzyl ether linkage, leaching of linear PEG can contaminate the final product. Recently, Bradley reported the preparation of novel supports using a principle similar to NovaGel resin, where short PEG chains were linked in the polymer by a phenyl ether and the functionality copolymerized into the beads backbone (Table 1, entry 5). Polystyrene–MPEG nongrafted resins were prepared by adding a new PEG derivative comonomer during polymerization as shown in Table 1, entry 5 (73). Such resins exhibit higher loading capacities (0.63–0.77 mmol/g) compared to PEG-grafted resins and at the same time showed broad solvent compatibility (Table 2, entry 5) and improved resistance to acidic and basic conditions. In addition, during their synthetic evaluations, such supports showed similar, if not better, results compared to grafted polymers without detection of PEG impurities in the final products.

Alternative Cross-Linkers for Polystyrene-Based Resins

To overcome the incompatibility of the hydrophobic polystryrene–DVB matrix with highly polar solvents (aqueous), alternative types of cross-linkers have been utilized over the last few years. Polyethers have been extensively used for this purpose and properties such as swelling and mechanical stability have been improved compared to gel-type resins. The cross-linking agents described herein are (*1*) PEG and (*2*) (poly)tetrahydrofuran based.

Copoly(styrene–PEG). As explained above, PEG grafted onto polystyrene improves its swelling properties in polar solvents (89). One of the major drawbacks of this type of supports is their inherent low loading (0.2–0.6 mmol/g) because a large part of the polymer mass is PEG (∼70%) (48). An alternative to this method is to include PEG in the polymer matrix during polymerization as a cross-linker. Vinyl PEG derivatives have been used to replace DVB as a cross-linker in the synthesis of a polymer matrix (TTEDA–PS: tetraethyleneglycol diacrylate cross-linker–polystyrene) (90). Although this resin showed comparable mechanical properties to gel-type resins, it showed much more effective swelling and solvatation than PS–DVB in polar and nonpolar solvents. The synthesis of an 18-residue peptide on such a chloromethylated resin afforded better yield and purity than PS–DVB. Later bis-styrene–PEG monomers were synthesized, copolymerized with styrene, and used in supporting catalyst in Diels–Alder reactions (91). Oligo(ethylene glycol) styrene derivatives have also been synthesized and copolymerized with styrene by Meldal to prepare polymers used for peptide synthesis (92). Kurth reported an interesting evaluation of the swelling and diffusion properties for these polymers compared to 2% DVB polystyrene (93). In this study several PEG-based cross-linkers, linking two styrene monomers (with different polyether chain lengths, $n = 1, 2, 4, 6$; see Fig. 12), were prepared and used to prepare a library of PEG-based resins using different proportions of PEG cross-linking (2%, 10%, 20%).

As expected, the swelling of these beads in all solvents was much better than their 2% PS–DVB counterpart. At low levels of PEG cross-linking (2%) the swelling was independent of the PEG tether length, but at high levels (20%) better swelling was observed when $n = 6$. In conclusion, the swelling and at the same time the physical stability of the beads were improved. The diffusion of the reagents within these resins was measured by the inclusion of a vinyl dye derivative (dansyl derivative) in the monomer mixture, and the fluorescence quenching of the resulting polymer bound dye was measured by adding triethyloxonium tetrafluoroborate

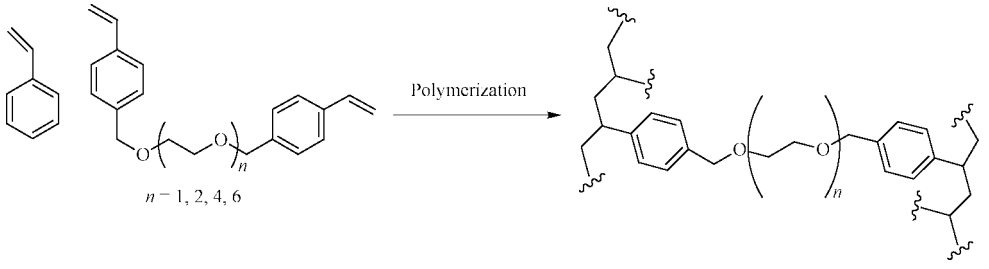

Fig. 12. Synthesis of PEG cross-linked PS resin.

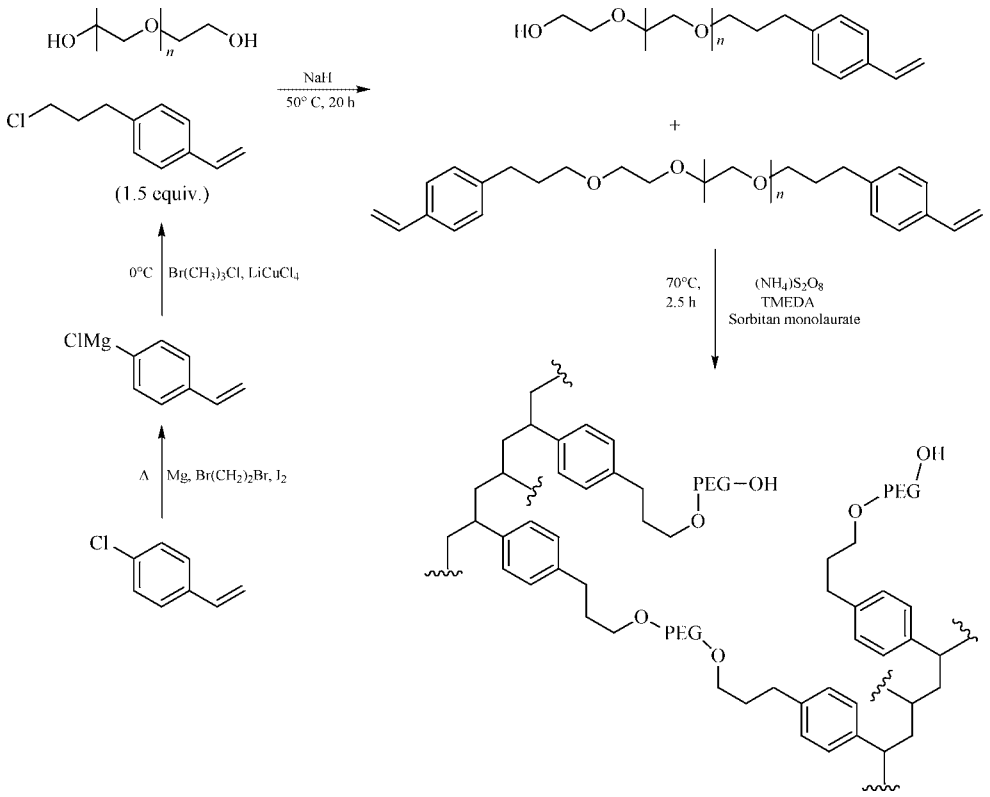

Fig. 13. Synthesis of POEPS-3.

in accordance with the method of Shea (94). These studies showed only a slight difference between conventional PS resins and that modified with PEG cross-linker when the reactions were performed in a good swelling solvent (toluene); however, in poor solvents the PEG-based cross-linked resins showed the best kinetics.

However, one of the drawbacks of using this type of cross-linker is that PEG is connected to the polystyrene backbone by a benzyl ether bond that could be cleaved by the use of Lewis or protic acids. Meldal reported the synthesis and the use of an alternative cross-linker containing a three-carbon spacer between the PEG chain and the polystyrene backbone (85) (Fig. 13).

Properties such as swelling, loading, diffusion, and ability to furnish high quality MAS-NMR have been investigated and compared to commercial counterparts such as TentaGel, ArgoGel, 2% PS-DVB, and macroporous PS (96). The results of this study showed that POEPS-3 was comparable to TentaGel and ArgoPore, in terms of swelling, NMR quality, and diffusion. Moreover, these supports showed better swelling in the range of solvents tested.

Copoly(styrene-butylene glycol). Because of the favorable properties shown by the PEG-based cross-linkers, Janda investigated other types of cross-linkers (97). Because of the tendency of PEG to complex organometallic compounds and its high hydrophilicity, new types of polystyrene resin containing "polytetrahydrofuran"–styrene derivatives as cross-linkers were prepared to allow

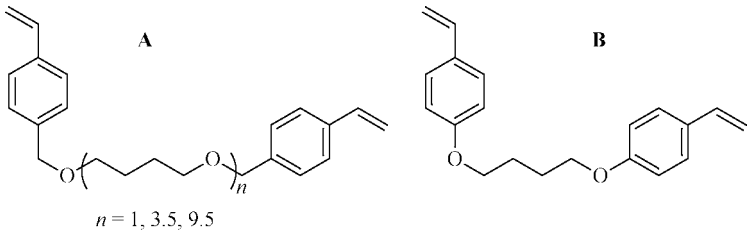

Fig. 14. Cross-linker used in the synthesis of copoly(styrene-tetrahydrofuran) resins.

better solvation of the resin and its functionality that might show reactivity close to homogeneous-phase conditions.

Resins with 1–2% of cross-linker (Fig. 14, **A**) degraded in the presence of strong Lewis acids (TMSOTf) or strong bases (BuLi). However, increasing the cross-linking level (5–10%) gave resins that were unaffected by these conditions. Resins with 1–2% of cross-linker (Fig. 14, **B**) showed good stability under the conditions reported above. The resin synthesized with 2% of cross-linker (Fig. 14, **B**) is commercialized under the name of JandaJel.

The main characteristic of these resins was their incredible swelling in organic solvents, almost doubled compared to conventional gel-type 1% polystyrene resin with 1% DVB (Table 3).

JandaJel was used to prepare a small library of phthalides where the key step of the synthesis was the ortho-lithiation of the supported benzamide (98). The same research group investigated several applications of these resins: Jacobson asymmetric epoxidation with a supported catalyst (99); synthesis of tertiary amines using the REM linker (100); solid-phase synthesis of oligoesters (101); solid-phase peptide synthesis using a routine Boc Protocol (102). Other benefits were reported by Shibasaki during the development of new supported catalysts for Reisser- and Strecker-type reactions (103,104). In a recent publication (105), atom transfer radical polymerization ligands on JandaJel were used to remove a copper catalyst, because of its better solvent compatibility compared to PS–DVB. However, although JandaJel showed less efficiency compared to low molecoular polyethylene capped with appropriate ligands previously developed (106), the reaction times were shorter. In conclusion, JandaJel is more "organic solvent-like" than PS–DVB. However, although its excessive swelling might improve reaction kinetics and yields, it can be a drawback because of the difficulty of handling the support during library synthesis.

Table 3. Swelling Comparison Between Gel-Type and JandaJel Resins[a]

	Volume of swollen resins, mL/g				
Resins (cross-linking)	Dioxane	THF	DMF	Benzene	DCM
Merrifield (1)	6.0	6.4	4.8	6.6	6.0
Merrifield (2)	5.4	5.4	4.2	6.6	5.8
JandaJel (1)	14.8	14.0	10.4	14.6	15.0
JandaJel (2)	7.8	7.4	6.0	8.2	7.4

[a]Ref. 97.

Table 4. Scavenging Efficiencies Using Different Amines

Amine	Solvent	Amount scavenged %
Benzylamine	THF	75
Butylamine	THF	77
Phenylethylamine	DCM	78
Diethylamine	DCM	90
3,5-dimethylamine	THF	48

Alternative Formats for Polystyrene Supports

The synthesis of combinatorial libraries by the split and mix method allows thousands of compounds to be obtained in just a few synthetic steps. In accordance with the original concept, each resin bead bears one single compound, and identification of biologically active compounds can be achieved directly on the beads. The drawback of this process is that the amount of compound that each bead can carry is limited (a few hundreds of picomoles), which is not enough for chemical identifications. To resolve this issue several approaches have been developed. The original method by Bradley was the enhancement of loading by "dendrimerization" (107). Bigger beads can be used, but such supports suffer from poor reaction kinetics and a propensity to disintegrate. Several authors have proposed different formats for solid-supported chemistry for split and mix as well as parallel synthesis applications to improve the issues described above and to improve the ease of handling.

Monoliths and Discs. Fréchet and co-workers introduced the monolith format in the 1990s for applications in chromatography (108) and solid-supported catalysts (109). In 1999, Sherrington described the preparation of polymer discs, cut from monoliths, for synthetic purposes (110). Among the cross-linkers used, PEG_{1000} diacrylates showed better resistance to mechanical stirring and osmotic shock than PS–DVB. After chloromethylations, the discs were coupled with 5-bromosalicylic acid and treated with phenylboronic acid in the presence of $Pd(PPh_3)_4$. Unfortunately, the Suzuki products were not obtained in good yields. In the same year, Fréchet demonstrated the use of their porous-grafted macroporous polystyrene–DVB monolith-disc in so-called "reactive filtration" with good results (111). For the preparation of the monoliths, the monomer mixtures and the porogen were placed into a shrinkable polyethylene tube that acted as a mould inside a glass tube. After polymerization, the glass tube was broken, leaving the monolith tightly trapped in the polyethylene tube which could be cut into 5-mm disc shapes (Fig. 15) (112). The resulting PE-encircled discs showed good mechanical stability and also ease of handling.

To increase the accessibility of the inner reactive groups and also the number of functionalities, the monolith surface was grafted as showed in Figure 16. The chloromethyl polystyrene discs (Fig. 16, **A**) reacted with azobis(4-cyanovaleric acid) (ACVA), a symmetrical azo initiator, to give the polymer-supported acid (Fig. 16, **B** and **C**). The pores were then filled with an appropriate monomer and polymerized to afford the final products (Fig. 16, **D**). The initiator could also react with two chloromethyl groups (Fig. 16, **C**) and this was indeed preferred to obtain

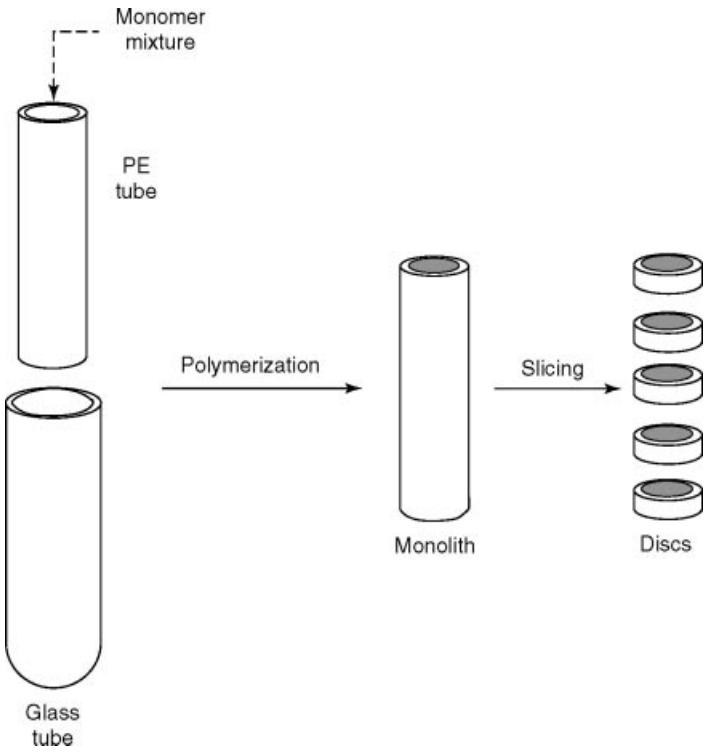

Fig. 15. Preparation of monolithic discs using the method of Fréchet (112).

better grafting as propagation could occur from both the sides of the initiator and, therefore, maximize grafting efficiencies.

Supported disc-reagents were prepared for acylation of several amines in a flow system (113), affording very good conversions into the corresponding amides (114).

The major advantage of this format is that the polymer could be fitted into a cartridge, allowing easy interchangeability during automatic synthesis. Moreover, they could be used to perform synthesis and purification in a flow system (114).

One other application of such monoliths, for the synthesis of a split and mix library, was presented by Janda (115). The preparation of "euclidean-shape" monoliths was performed using a monomer mixture of styrene, chlroromethylstyrene, and 1,4- bis(vinylphenoxy)butane as cross-linker. Dodecanol was used as inert diluent and benzoyl peroxide as initiator.

Films. PS-based films were introduced by Sherrington to be used as an easy device for FTIR *in situ* monitoring (116). Thin films (76mm $\times$ 14mm $\times$ 60–120μm) were obtained by polymerization of monomers in presence of porogen (for macroporous films), and a UV-sensitive initiatior, inserted between two microsocpe slides (Fig. 17). The microscope slides were filled by capillarity, and polymerization initiated by UV irradiation.

Gel-type films were produced using different cross-linkers coupled with styrene and chloromethylstyrene (CMS). The best films were obtained using a

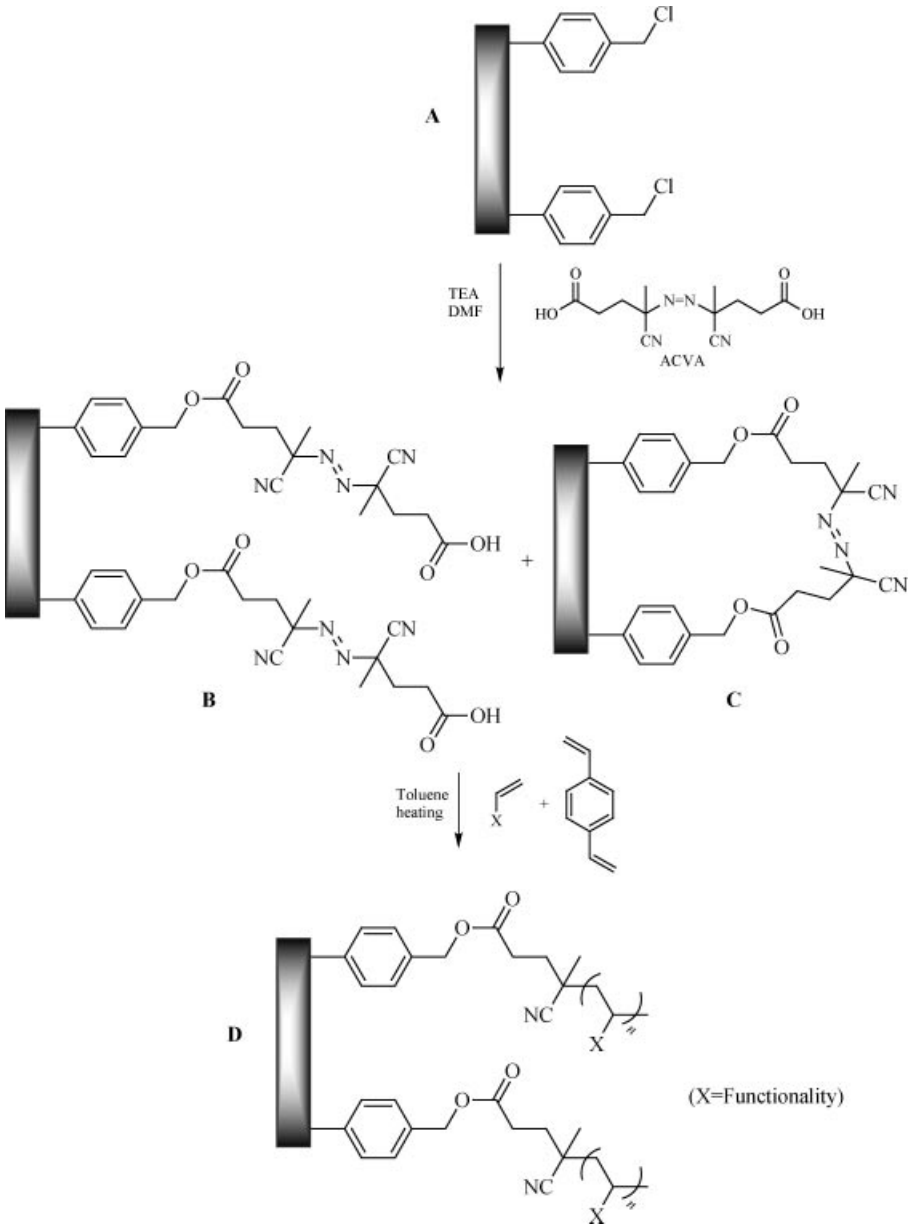

Fig. 16. Grafting of polymer discs.

$PEG_{1000/1500}$-DVB cross-linker, but the PS–DVB films resulting were fragile. The chemistry of these gel-type films was evaluated by nucleophilic displacement of the chlorine with 5-bromosalicylic ester. Macroporous films were also produced using styrene, DVB, and 4-vinylpyridine. Flexible and resistant films were obtained using long-chain alcohols as porogens. To evaluate diffusion through the macroporous films, the pyridine functionality was methylated with methyliodide

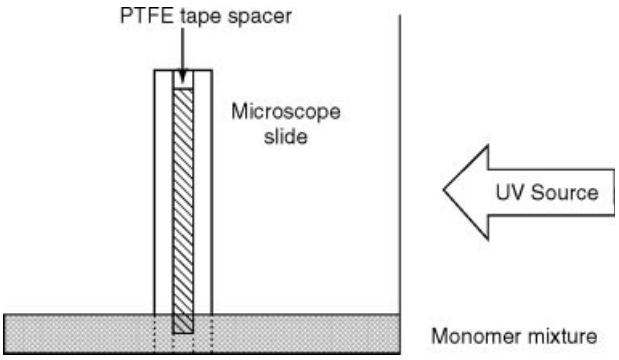

Fig. 17. Preparation of polymeric films (116).

in acetone and the yellow color of the film examined due to the pyridinium iodide charge transfer absorption band. Treatment of the supported pyridinium salt with $KMnO_4$ allowed the film to change color to purple because of the exchange of the iodide with the permanganate. Treating the supported pyridinium salt with $CuSO_4$ caused the film to turn blue because of coordination of the pyridine with Cu(II). The supported-pyridinium salts were also used for the preparation of immobilized rhodium complexes and for mechanistic studies on the carbonylation of olefins by FTIR (117).

Plugs and Tablets. In 2001, Bradley introduced resin plugs as a method to handle polymer supports (118). Plugs were achieved by sintering resin beads with an inert polymer matrix (ultrahigh molecular weight PE). The plugs were obtained in cylindrical forms (9.9-mm length × 7.5-mm diameter) and had loadings between 50 and 150 μmol). Although both PS- and PEG- grafted resins were used for the preparation of the plugs, they are now prepared using StratoSphere resins and commercialized by Polymer Laboratories with the name of StratoSphere Plugs (Fig. 18).

During their evaluations, plugs were used as supports for solid-phase synthesis of small libraries of biaryl compounds, sulfonamides, tertiary amines, ureas, and amides. Although yields and purities were similar to the loose beads counterpart, the reaction times were slightly increased. Because of their mechanical stability and limited swelling, plugs are much easier to handle than the corresponding

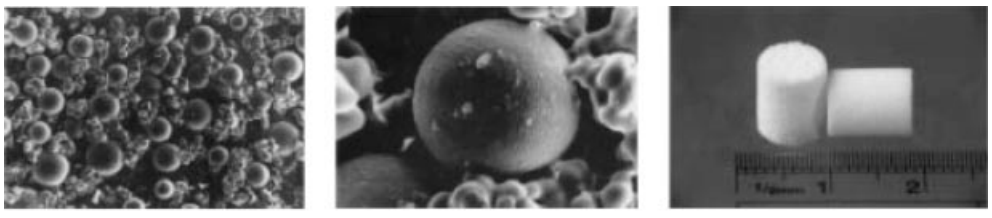

Fig. 18. (**a**) Cross-section of a resin plug (100 × magnification); (**b**) single bead within the matrix of the resin plugs (270 × magnification); (**c**) illustration of the dimension of the resins plugs.

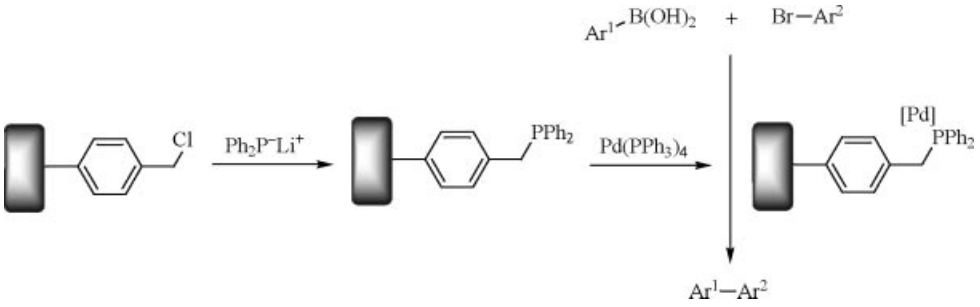

Fig. 19. Preparation and use of palladium plug-supported catalyst.

loose beads. In solution-phase synthesis, plugs have been employed as supports for immobilized palladium catalysts to prepare libraries of biaryl compounds (Fig. 19) with yields comparable to $Pd(PPh_3)_4$ (119).

In conclusion, plug-supported palladium maintained comparable catalytic activities, but were much easier to handle than the homogeneous analogue $Pd(PPh_3)_4$.

An alternative to improve resin handling was introduced by Ruhland, who described the preparation of tablets obtained from the compression of a blend of resin with solid reagents or catalysts (120). The preparation of such tablets involved three steps: swelling of the beads (and the solid reagent or catalyst) in a good solvent; sieving; and compression. The first step was essential for the preparation of mechanically stable tablets. The effect of swelling and drying resulted in agglomerations caused by bead–bead interactions as observed by SEM. Observation of the tablet structure showed that the beads were distorted after compression but not destroyed. The disintegration time of the tablets, measured by gentle shaking, was very solvent-depending and implicated that the swelling of the beads caused disintegration. As a consequence, good solvents such as THF or DCM gave shorter times of disruption (7–16 min) than DMSO or ethanol (>30 min). Functionalized tablets were employed to carry out Mitsunobu reactions and amine acylations, giving results comparable to the corresponding loose resins. During syntheses, tablets were loaded in 48-well plates in only 3 min, whereas the same procedure applied to resin beads took much longer. Moreover, preparation of tablets allowed the protection of sensitive functional groups from moisture or oxygen, and also a drastic reduction in the time of exposure to toxic hazardous and dusty materials in the working environment.

Nonpolystyrene Polymer Matrices

All the polymer supports described so far for solid-phase chemistry have a common factor: the main presence of a polystyrene backbone. Although this polymer matrix has good characteristics, such as chemical and mechanical stability (depending on the type and amount of cross-linker) and favorable loadings in solvent, its compatibility with polar solvents and large biomolecules, such as enzymes and receptors, is quite poor (121). In order to resolve these problems, several authors have replaced hydrophobic polystyrene with a more amphiphilic backbone. In the

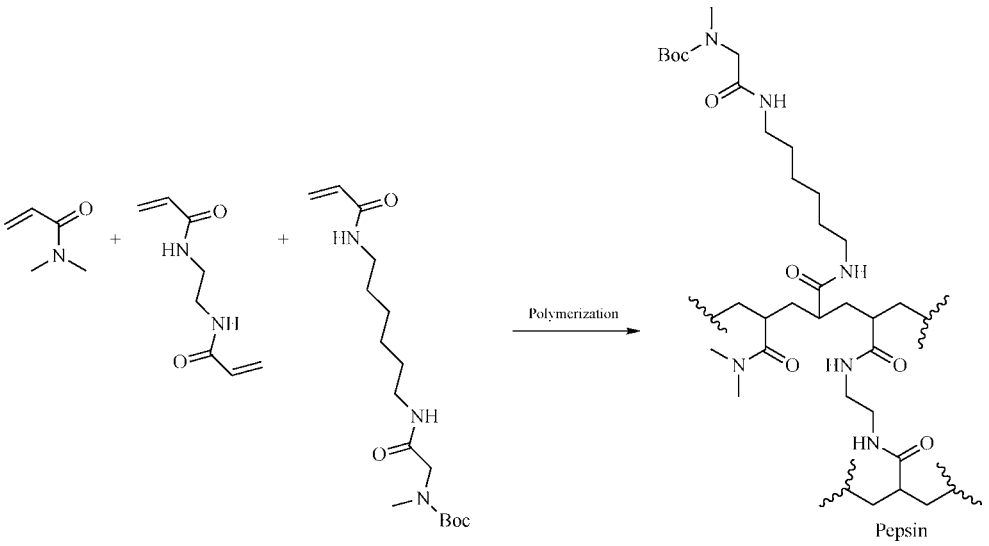

Fig. 20. Preparation of polyamide resins (Pepsin)

early 1970s, Sheppard introduced polyacrylamide supports, prepared by emulsion polymerization (Fig. 20), as an alternative to polystyrene gel-type resin for polypeptide synthesis (122). Such resins showed good swelling in highly polar solvents (see ACRYLAMIDE POLYMERS). Moreover, polypeptides were obtained in higher yields and purities and their syntheses were faster than with traditional polystyrene gel-type resin. These commercialized resins are still in use for large-scale preparation (33).

However, such supports, being very soft and fragile, are difficult to work with (123). Pepsin K was prepared by polymerization of pepsin monomers within rigid macroporous particles to help solve this problem (124).

In the 1990s, Meldal, following the work of Sheppard, developed an improved support which was named PEGA (PEG–polyacrylamide) (125), obtained by inverse suspension polymerization (126) of *N*,*N*-dimethylacrylamide cross-linked with different bis-acrylic-PEG derivatives (Fig. 21, **A**).

Functionalization was introduced by inclusion of acryloyl-PEG-NH_2 monomers (Fig. 21, **C**; loading = 0.08–0.13 mmol/g) or acryloyl-sarcosine

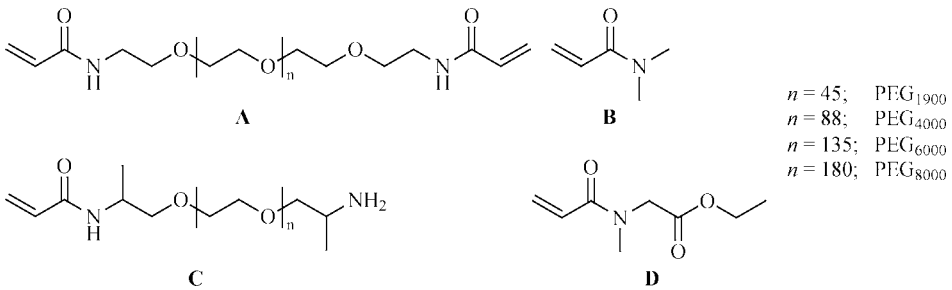

Fig. 21. Monomers used for the preparation of PEGA.

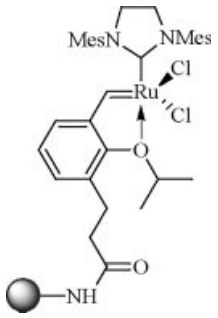

Fig. 22. PEGA supported ruthenium catalyst.

methylester monomer (Fig. 21, **D**; loading = 0.22–1.0 mmol/g) (127). The first version of such resins (PEG_{1900}) allowed the diffusion of biomolecules with a mass of ∼32 kDa into the beads. Although monomer A (Fig. 21), prepared using $PEG_{4000,6000,8000}$, improved the limit (>120 kDa), handling and loadings were poor. Recently, Gardossi observed that the introduction of a positive charge by trialkylammonium species in $PEGA_{1900}$ allowed better swelling than neutral PEGA and consequent inclusion of large proteins (128) although favorable charge–charge interactions are perhaps a more reasonable explanation (but also see Section 3.1). Although the main area of use of PEGA remains for biological based chemistry, because of size accetability (129–131), it has also been used with water-insoluble ruthenium catalysts for metathesis reactions in aqueous and protic solvents (in such conditions the nonsupported catalyst does not work) (Fig. 22) (132).

This catalyst not only showed good activity in metathesis reactions but also did not need to be used in degassed solution, as required by conventional Grubbs catalysts (133). However, the main problem of PEGA is its difficulty of handling: having to be handled in a solvated state as it may disintegrate when dry. A more robust cross-linked ethoxylate acrylate resin (CLEAR) was presented in 1996 by Kempe and Barrany (134). The main component of such supports is a branched PEG-acrylate derivative used in ∼50 mol% (Fig. 23), which gave good swelling in a range of solvents.

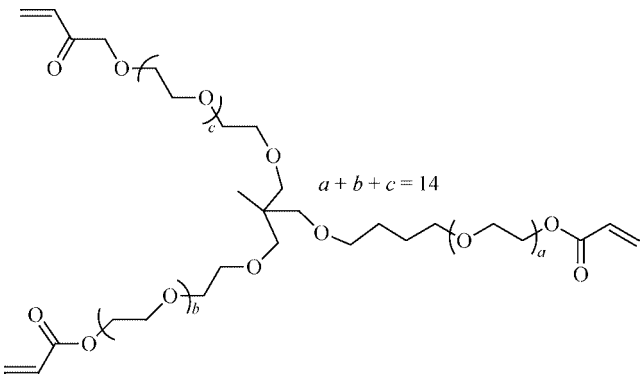

Fig. 23. Trimethylopropane ethoxylate (14/3 EO/OH) triacrylate.

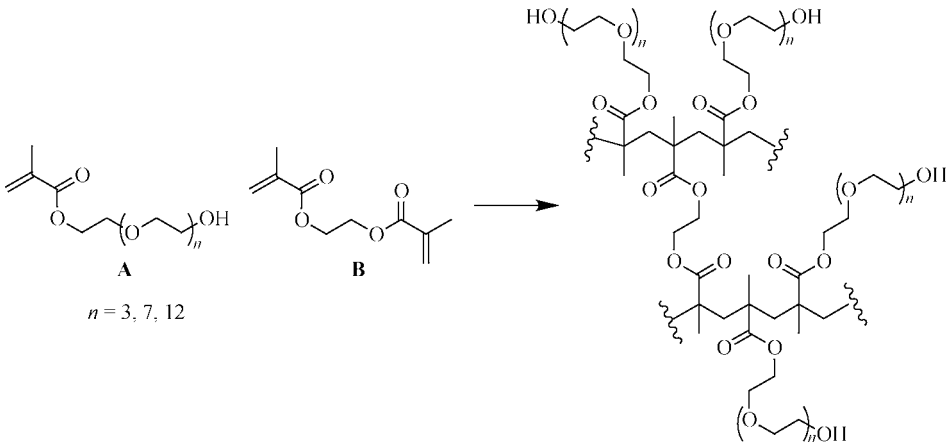

Fig. 24. Preparation of PEG-MA.

Unfortunately, CLEAR is vulnerable to strong bases (such as NaOH or NH_3), although complete polymer dissolution occurs only after long reaction times.

In 2001, Fréchet introduced PEG-MA (PEG methacrylate) (135). The monomers are PEG methacrylate derivatives (Fig. 24, **A**) and ethylene dimethacrylate is used at 2 mol% as a cross-linker (Fig. 24, **B**). Although such monomers are soluble in aqueous media, the preparation of PEG-MA was conducted by a "modified suspension polymerization."

As expected for resins that contained poly(ethylene glycol), PEG-MA was compatible with a broad range of polar and nonpolar solvents. Swelling depended on the chain length of the PEG incorporated in the monomer (Fig. 24, **A**), longer chains giving better swelling. Although loadings calculated were much lower (51–67%) than the ones expected, such values were still much higher than commercial PEG-grafted resins (1.2–1.8 mmol/g). The PEG-MAs were used for the preparation of a small library of hydantoins. The advantages of using PEG clearly reside in the improved property of the tailored polymer matrix. Loading, solvent compatibility (and so, swelling), and mechanical resistance depend on the level of this polymeric monomer. In 2002, Meldal prepared a new class of polymers named SPOCC (superpermeable organic combinatorial chemistry) resins (136). The main characteristic of these polymers was that the backbones and cross-linker both contained PEG. The second generation of such polymers ($SPOCC_{194}$) was prepared by cationic polymerization of the two monomers shown in Figure 25.

Novel SPOCCs exhibit great chemical resistance under various reaction conditions, because there are no benzyl ether, ester, and amide linkages. The use of shorter PEG chains in $SPOCC_{194}$ allowed higher loading compared to the previous generation resins (longer PEG chains), although swelling decreased. Although mainly used in peptide chemistry, SPOCC resins have seen successfully tested in a variety of different organic transformations (136,137). Direct comparison of this support, PS resin, and TentaGel showed comparable if not better kinetics in peptide synthesis.

Cellulose: From Paper to Beads. The first use of cellulose (qv) as a solid support for peptide chemistry can be attributed to Merrifield. Unfortunately, at

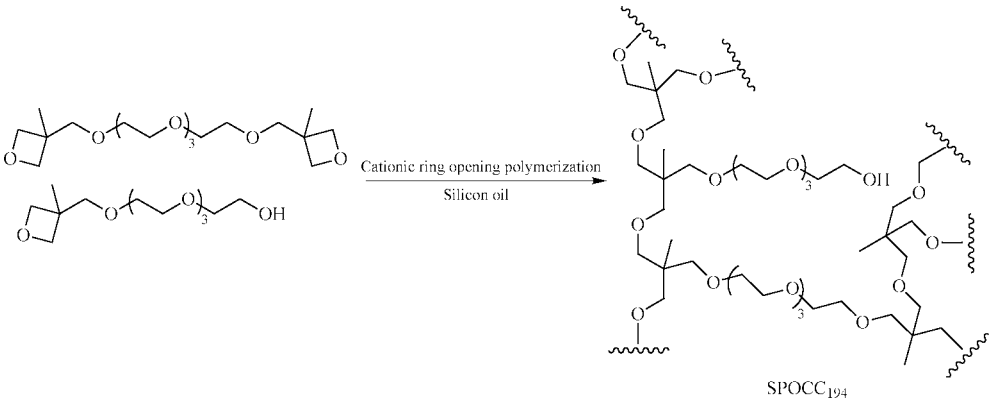

Fig. 25. Preparation of $SPOCC_{194}$.

that time, only a dipeptide was obtained in unsatisfactory yield. Moreover, cellulose was not chemically stable to the conditions used in the synthesis. Merrifield decided to abandon this support and to search for others with better properties (138). Peptides and oligonucleotides have been synthesized on paper and cotton (139,140), and Frank demonstrated, in 1992, the flexibility of cellulose for the preparations of large arrays of peptides on membranes by Spot synthesis (141). At the end of the synthesis, biological assays could be performed directly on each spot on the filter disk, as cellulose is compatible with many binding, enzymatic, and cellular essays (142). However, paper membranes are not suitable for scavenger or supported reagents, because of difficulties in their handling and their limited loading. In 1977, Stamberg found a method to prepare spherical cellulose particles with a certain degree of porosity by heating a viscose suspension (an aqueous solution of sodium cellulose xanthate) in a water-immiscible solvent under stirring (143). Such beads became commercially available under the name of Perloza. Because of the availability of three hydroxyl groups for each glucopyranose monomer, such supports provided very high loadings. Functionalized cellulose beads (0.37–0.65 mmol/g) were used for the synthesis of peptides (5–34 amino acids). The analysis of crude peptides (20 amino acids length) showed better purity when assembled on Perloza than polystyrene (144). The application of cellulose beads in solution-phase chemistry was demonstrated by Chesney and Steel (145). In their procedure, the pendant hydroxyl groups first reacted with allyl bromide; addition of bromine in water was followed by treatment with excess of tris(2-aminoethyl)amine and led to supported branched amino resins (2.2 mmol/g, 4 mmol/g). Such amino resins exhibited good and uniform swelling properties in polar and nonpolar solvents (between 8 and 10 mL/g in all solvents). Moreover, they allowed the synthesis of small libraries of amides and ureas in quite good purities and yields by the scavenging of excess acid chloride and isocyanate derivatives (Fig. 26, **B**). Treatment of Perloza with the enzyme cellulase allowed the complete biodegradation of the beads to glucose that, after treatment with brewers' yeast, led to ethanol, CO_2, and H_2O.

The supported allyl beads were also reactive enough to permit their application as a scavenger of bromine (Fig. 26, **A**) (146). Recently, Perloza aniline

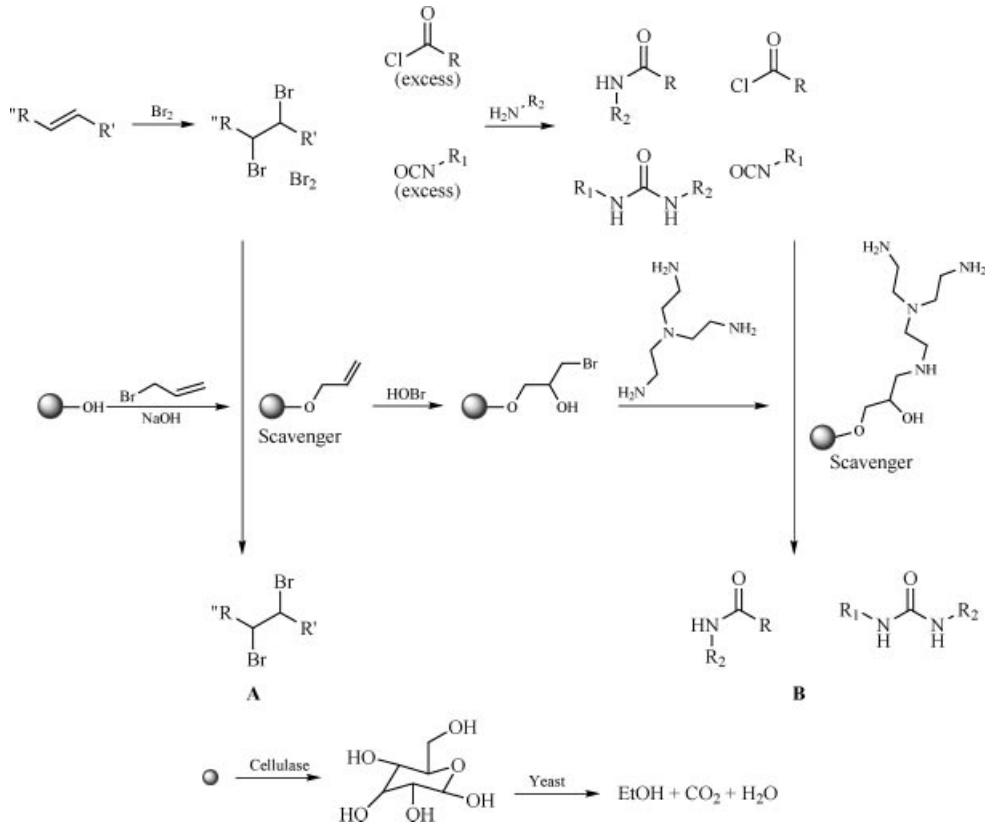

Fig. 26. Scavenger uses of biodegradable cellulose beads.

functionalized beads were used for a synthesis of a library of pyrazoles. Once the reaction conditions were established, the "catch and release" method was adopted and allowed the continuous recycling of the beads without decreasing yields and purities (147).

In conclusion, cellulose beads have interesting properties, such as relatively high loading, cheapness, chemical and mechanical stability, and recycling and easy disposal, factors that could be of use in large-scale industrial processes.

As can be seen, over the years there has been huge development in supports for synthetic applications, with variation of improvement in loading, morphologies, and polymer type.

Gel-type polystyrene resins are still the most widespread supports in solid-phase organic chemistry, exhibiting good characteristics of loading, swelling, and handling. However, they are not universal. Although an ideal support should be inert to reactions conditions, it does not mean that it does not have to interact with the reagents. "Resin beads are like solvents," suggested Czarnic (29), and this concept could be expanded by saying that "different polymer supports are like different solvents." As the choice of a particular solvent can change the course of a reaction, a polymer support has to be considered in the same way. For this reason, research groups continue the early work of Merrifield (139) in order to screen

and synthesize new and enhanced polymer supports for a range of chemical and biological applications.

BIBLIOGRAPHY

"Polymers as Chemical Reagents" in *EPST* 1st ed., Suppl. Vol. 1, pp. 468–492, by A. Patchornik and M. A. Kraus, The Weizman Institute of Science; in *EPSE* 2nd ed., Vol. 12, pp. 618–658, by Philip Hodge, University of Lancaster.

1. R. B. Merrifield, *J. Am. Chem. Soc.* **85**, 2149–2154 (1963).
2. J. A. Porco, T. Deegan, W. Devonport, O. W. Gooding, K. Heisler, J. W. Labadie, B. Newcomb, C. Nguyen, P. van Eikeren, J. Wong, and P. Wright, *Mol. Diversity* **2**, 197–206 (1996).
3. M. Lebl, *J. Comb. Chem.* **1**, 3–24 (1999).
4. J. A. Ellman, *Acc. Chem. Res.* **29**, 132–143 (1996).
5. L. A. Thompson and J. A. Ellman, *Chem. Rev.* **96**, 555–600 (1996).
6. R. C. D. Brown, *J. Chem. Soc., Perkin Trans. 1* **1**, 3293–3320 (1998).
7. S. V. Ley, I. R. Baxendale, R. N. Bream, P. S. Jackson, A. G. Leach, D. A. Longbottom, M. Nesi, J. S. Scott, and R. I. T. S. J. Storer, *J. Chem. Soc., Perkin Trans. 1* 3815–4195 (2000).
8. A. Akelah and D. C. Sherrington, *Chem. Rev.* **81**, 557–587 (1981).
9. W. P. Hohenstein, and H. Mark, *J. Polym. Sci. A* **1**, 127–145 (1946).
10. S. Rana, P. White, and M. Bradley, *J. Comb. Chem.* **3**, 9–15 (2001).
11. F. Guillere, D. Orain, and M. Bradley, *Chem. Rev.* **100**, 2091–2157 (2000).
12. P. Hodge and D. C. Sherrington, eds., *Polymer-Supported Reactions in Organic Synthesis*, John Wiley & Sons, Inc., New York, (1980).
13. R. J. Booth and J. C. Hodges, *J. Am. Chem. Soc.* **119**, 4882 (1997).
14. L. D. Arnold, H. I. Assil, and J. C. Vederas, *J. Am. Chem. Soc.* **111**, 3973–3976 (1989).
15. S. Weik, G. Nicholson, G. Jung, and J. Rademann, *Angew. Chem., Int. Ed.* **40**, 1436–1439 (2000).
16. J. Rademann, J. Smerdka, G. Jung, P., G., and D. Schmid, *Angew. Chem., Int. Ed.* **40**, 381–385 (2001).
17. I. Fenger and C. Le Drian, *Tetrahedron Lett.* **39**, 4287–4290 (1998).
18. M. S. Gibson and R. W. Bradshaw, *Angew. Chem., Int. Ed. Engl.* **7**, 919 (1968).
19. E. P. Iuliana, P. D. Benolt, and A. L. Tartar, *J. Org. Chem.* **62**, 2594–2603 (1997).
20. G. M. Coppola, *Tetrahedron Lett.* **39**, 8233–8236 (1998).
21. K. IIjima, W. Fukuda, and M. Tomoi, *J. Macromol. Sci., Pure Appl. Chem.* **29**, 249–261 (1992).
22. S. Crossigniani, P. D. White, and B. Linclau, *Org. Lett.* **5**, 853–856 (2003).
23. J. M. Salvino, N. V. Kumar, E. Orton, J. Airey, T. Kiesow, K. Crawford, R. Mathew, P. Krolikowski, M. Drew, D. Engers, D. Krolikowski, T. Herpin, M. Gardyan, G. McGeehan, and R. Labaudiniere, *J. Comb. Chem.* **2**, 691–697 (2000).
24. S. R. Stauffer and J. A. Katzenellenbogen, *J. Comb. Chem.* **2**, 318–329 (2000).
25. B. Heinzen and S. V. Ley, *J. Chem. Soc., Perkin Trans. 1* 1907 (1997).
26. H. W. Gibson and J. J. Bailey, *Chem. Commun.* 815 (1977).
27. B. A. Bunin, in E. M. Gordon and J. F. Kerwin eds., *The Combinatorial Index*, Academic Press, San Diego, 1998, pp. 11–15.
28. M. J. Farral and J. M. J. Fréchet, *J. Org. Chem.* **41**, 3877–3882 (1976).
29. A. W. Czarnik, *Biotechnol. Bioeng.* **61**, 77–79 (1998).
30. E. Erbay, T. Bilgic, I. M. Karal, and O. T. Savasci, *Polym. Plast. Technol. Eng.* **31**, 589–605 (1992).

31. S. Alesso, Z. Yu, D. Pears, A. P. Worthington, R. W. A. Luke, and M. Bradley, *J. Comb. Chem.* **3**, 631–633 (2001).
32. R. Arshady, *Colloid. Polym. Sci.* **270**, 717–732 (1992).
33. D. Hudson, *J. Comb. Chem.* **1**, 333–360 (1999).
34. R. Santini and M. C. Griffit, *Tetrahedron Lett.* **39**, 8951–8954 (1998).
35. V. K. Sarin, S. B. H. Kent, and R. B. Merrifield, *J. Am. Chem. Soc.* **102**, 5463–5470 (1980).
36. D. C. Sherrington, *Chem. Commun.* 2275–2286 (1998).
37. J. R. Millar, D. G. Smith, and T. R. E. Kressmann, *J. Chem. Soc.* 304–31 (1965).
38. F. M. B. Couthino, M. A. F. S. Neves, and M. L. Dias, *J. Appl. Polym. Sci.* **65**, 1257–1262 (1997).
39. J. M. J. Fréchet and W. A. Rolls, *J. Chromatogr. A* 97–112 (1990).
40. M. Bernard and W. T. Ford, *J. Org. Chem.* **48**, 326–332 (1983).
41. H. G. Tang and D. C. Sherrington, *J. Mol. Catal.* **94**, 7–17 (1994).
42. K. L. Lewandowski, F. Svec, and J. M. J. Fréchet, *J. App. Polym. Sci.* **67**, 597–607 (1998).
43. O. Okay, *Prog. Polym. Sci.* **25**, 711–719 (2000).
44. I. C. Ponescu and C.-D. Vlad, *Eur. Polym. J.* **33**, 1515–1521 (1997).
45. H. Deleuzel, X. Shultze, and D. C. Sherrington, *Polym. Bull.* **44**, 179–186 (2000).
46. P. A. Webb, C. Orr, *Analytical Methods in Fine Particle Technology, Micrometrics Instrument Corp.*, 1997.
47. M. Hori, J., G. D., P. Wentworth, and K. Janda, *Bioorg. Med. Chem. Lett.* **8**, 2363–2368 (1998).
48. J. W. Labadie, *Curr. Opin. Chem. Biol.* **2**, 346–352 (1998).
49. R. Frenette and R. W. Friesen, *Tetrahedron Lett.* **35**, 9177–9180 (1994).
50. B. J. Backes and J. A. Ellman, *J. Am. Chem. Soc.* **116**, 11171–11172 (1994).
51. W. Funke, O. Okay, and B. Joos-Müller, *Adv. Polym. Sci.* **136**, 139–234 (1998).
52. O. Shinomura, B. Clapham, C. Spanka, S. Mahajan, and K. Janda, *J. Comb. Chem.* **4**, 436–441 (2002).
53. C. Schunicht, A. Biffis, and G. Wulff, *Tetrahedron* **56**, 1693–1699 (2000).
54. G. Giffels, J. Beliezey, M. Felder, and U. Kragl, *Tetrahedron: Asymmetry* **9**, 691–696 (1998).
55. C. Spanka, B. Clapham, and K. Janda, *J. Org. Chem.* **67**, 3045–3050 (2002).
56. B. Jeong, Y. H. Bac, D. S. Lee, and S. W. Kim, *Nature* **388**, 860–862 (1997).
57. A. G. A. Combers, S. Tasker, M. Lindblad, J. Holmgrem, K. Hoste, V. Toncheva, E. Schacht, M. C. Davies, L. Illum, and S. S. Davis, *Biomaterials* **18**, 1153–1161 (1997).
58. M. Pyrasch and B. Tieke, *Colloid Polym. Sci.* **278**, 375–379 (2000).
59. W.-H. Li, K. Li, and H. Stöver, *J. Polym. Sci. A* **37**, 2295–2303 (1999).
60. A. N. Cammidge, S. Downing, and Z. Ngaini, *Tetrahedron Lett.* **44**, 6633–6634 (2003).
61. K. Li and H. Stöver, *J. Polym. Sci. A* **31**, 3257–3263 (1993).
62. M. Dreja, W. Pyckhout-Hintzen, and B. Tieke, *Macromolecules* **31**, 272–280 (1998).
63. C. Leznoff and P. I. Svirskaya, *Angew. Chem., Int. Ed. Engl.* **17**, 947 (1978).
64. E. Bayer and M. Mutter, *Nature* **237**, 512–513 (1972).
65. M. Mutter, H. Hagenmaier, and E. Bayer, *Angew. Chem., Int. Ed. Engl.* **10**, 811–812 (1971).
66. E. Bayer, M. Mutter, R. Uhmann, J. Polster, and H. Mauser, *J. Am. Chem. Soc.* **96**, 7333–7336 (1974).
67. U.S. Pat. 4,908,405 (Mar. 3, 1990), E. Bayer and W. Rapp.
68. E. Bayer, *Angew. Chem., Int. Ed. Engl.* **30**, 113–216 (1991).
69. S. Zalipsky, J. L. Chang, F. Albericio, and G. Barany, *React. Polym.* **22**, 243–258 (1994).
70. S. A. Kates, B. F. McGuinnes, C. Blackburn, G. W. Griffin, N. A. Solé, G. Barany, and F. Albericio *Biopolymers* **47**, 365–380 (1998).

71. O. W. Gooding, S. Baudart, T. L. Deegan, K. Heisler, J. W. Labadie, W. S. Newcomb, J. A. Porco, and P. van Eikeren, *J. Comb. Chem.* **1**, 113–122 (1999).
72. J. H. Adams, R. M. Cook, D. Hudson, V. Jammalamadaka, M. H. Lyttle, and M. F. Songster, *J. Org. Chem.* **63**, 3706–3716 (1998).
73. S. Alesso, Z. Yu, D. Pears, A. P. Worthington, R. W. A. Luke, and M. Bradley, *Tetrahedron* **59**, 7163–7169 (2003).
74. E. Bayer and W. Rapp, in M. E. Harris, ed., *Poly(Ethylene Glycol) Chemistry: Biotechnical and Biomedica Applications*, Plenum Press, New York, 1992, p. 325.
75. S. A. Kates, N. A. Solé, M. Beyermann, G. Barany, and F. Albericio, *Peptide Res.* **9**, 106–113 (1996).
76. E. Bayer, A. Klaus, H. Willisch, W. Rapp, and B. Haemmasi, *Macromolecules* **23**, 1937–1940 (1990).
77. D. P. Walsh, C. Pang, P. B. Parikh, Y.-S. Kim, and Y.-T Chang, *J. Comb. Chem.* **4**, 204–208 (2002).
78. D. Walsh, D. Wu, and Y.-T. Chang, *Curr. Opin. Chem. Biol.* **7**, 353–361 (2003).
79. B. Ruhland, A. Bombrun, and M. A. Gallop, *J. Org. Chem.* **62**, 7820–7826 (1997).
80. X. Du and R. W. Armstrong, *J. Org. Chem.* **62**, 5678–5679 (1997).
81. H. Han and K. Janda, *Angew. Chem., Int. Ed. Engl.* **36**, 1731–1733 (1997).
82. W. Li and B. Yan, *J. Org. Chem.* **63**, 4092–4097 (1998).
83. Y.-S. Lee and B.-D. Park, *React. Fun. Polym.* **44**, 41–46 (2000).
84. V. Swali, N. K. Wells, J. Langley, and M. Bradley, *J. Org. Chem.* **62**, 4902–4903 (1997).
85. S. Lebreton, B. Newcomb, and M. Bradley, *Tetrahedron Lett.* **43**, 2475–2478 (2002).
86. E. Swayze, *Tetrahedron Lett.* **38**, 8465–8468 (1997).
87. C. M. G. Judkins, K. A. Knights, B. F. G. Johnson, Y. R. de Miguel, R. Raja, and J. M. Thomas, *Chem. Commun.* 2624–2625 (2001).
88. C. M. G. Judkins, K. A. Knights, B. F. G. Johnson, and Y. R. de Miguel, *Polyhedron* **22**, 3–7 (2003).
89. Y. Kohno, N. Ogawa, K. B. Chung, and W. Fakuda, *Makromol. Chem.* **193**, 3009–3021 (1992).
90. M. Renil, R. Nagaraj, and V. N. Rajasekharan, *Tetrahedron* **50**, 6681 (1994).
91. K. Kamahori, K. Ito, and S. Itsuno, *J. Org. Chem.* **61**, 8321 (1996).
92. M. Renil and M. Meldal, *Tetrahedron Lett.* **37**, 6185 (1996).
93. M. E. Wilson, K. Paech, W.-J. Zhou, and J. Kurth, *J. Org. Chem.* **63**, 5094–5099 (1998).
94. K. J. Shea, Y. Okahata, and T. K. Dougherty, *Macromolecules* **17**, 296–300 (1984).
95. J. Buchardt and M. Meldal, *Tetrahedron Lett.* **39**, 8695–8698 (1998).
96. M. Grøtli, C. H. Gotfredsen, J. Rademann, J. Buchardt, A. J. Clark, J. Ø. Duus, and M. Meldal, *J. Comb. Chem.* **2**, 108–119 (2000).
97. P. H. Toy and K. Janda, *Tetrahedron Lett.* **40**, 6329–6332 (1999).
98. P. H. Toy, T. S. Reger, P. Garibay, J. C. Garno, J. A. Malikayil, G. Liu, and K. Janda, *J. Comb. Chem.* **3**, 117–124 (2001).
99. T. S. Reger and K. Janda, *J. Am. Chem. Soc.* **122**, 6929–6934 (2000).
100. P. H. Toy, T. S. Reger, and K. Janda, *Org. Lett.* **2**, 2205–2207 (2000).
101. O. Brümmer, B. Clapham, and K. Janda, *Tetrahedron lett.* **42**, 2257–2259 (2001).
102. J. A. Moss, T. J. Dickerson, and K. D. Janda, *Tetrahedron Lett.* **43**, 37–40 (2002).
103. H. Nogami, S. Matsanaga, M. Kanai, and M. Shibasaki, *Tetrahedron Lett.* **42**, 279–283 (2001).
104. M. Takamura, K. Funabashi, M. Kanai, and M. Shibasaki, *J. Am. Chem. Soc.* **123**, 6801–6808 (2001).
105. M. E. Honigfort and W. J. Brittain, *Macromolecules* **36**, 3111–3114 (2003).
106. S. Liou, J. T. Rademarcher, D. Malaba, M. E. Pallack, and W. J. Brittain, *Macromolecules* **33**, 4295–4296 (2000).
107. C. Fromont and M. Bradley, *Chem. Commun.* 283–284 (2000).

108. F. Svec and J. M. J. Fréchet, *J. Anal. Chem.* **64**, 820–822 (1992).
109. F. Svec and J. M. J. Fréchet, *J. Science* **273**, 205–211 (1996).
110. N. Hird, I. Huges, D. Hunter, M. G. J. T. Morrison, D. C. Sherrington, and L. Stevenson, *Tetrahedron* **55**, 9575–9584 (1999).
111. J. A. Tripp, J. A. Stein, F. Svec, and J. M. J. Fréchet, *Org. Lett.* **2**, 195–198 (1999).
112. J. A. Tripp, F. Svec, and J. M. J. Fréchet, *J. Comb. Chem.* **3**, 216–223 (2001).
113. P. Hodge, *Curr. Opin. Chem. Biol.* **7**, 362–373 (2003).
114. J. A. Tripp, F. Svec, and J. M. J. Fréchet, *J. Comb. Chem.* **3**, 604–611 (2001).
115. A. R. Vaino, and K. Janda, *Proc. Natl. Acad. Sci. U.S.A.* **97**, 7692–7696 (2000).
116. P. H. Findlay, S.-M. Leinonen, T., M. G. J., E. E. A. Shepherd, and D. C. Sherrington, *J. Mater. Chem.* **10**, 2031–2034 (2000).
117. BP Chemicals Ltd, Purolite International, Johnson Matthey plc, University of Sheffield, and University of Straclyde, *ACCP News Applied Catalysis and Catalytic Processes*, No. 3, 2000, pp. 6–7.
118. B. Atrash, M. Bradley, R. Kobylecki, D. Cowell, and J. Reader, *Angew. Chem., Int. Ed. Engl.* **40**, 938–941 (2001).
119. B. Atrash and M. Bradley, *Tetrahedron Lett.* **44**, 4779–4782 (2003).
120. T. Ruhland, P. Holm, and K. Andersen, *J. Comb. Chem.* **5**, 842–850 (2003).
121. J. Vagner, G. Barany, K. S. Lam, V. Krchnák, N. F. Sepetov, J. A. Ostrem, P. Strop, and M. Lebl, *Proc. Natl. Acad. Sci. U.S.A.* **93**, 8194–8199 (1996).
122. E. Atherton, D. L. J. Clive, and R. C. Sheppard, *J. Am. Chem. Soc.* **97**, 6584–6585 (1975).
123. E. Atherton, E. Brown, R. C. Sheppard, and A. A. Rosevear, *Chem. Commun.* 1151 (1981).
124. R. Arshady, E. Atherton, D. L. J. Clive, and R. C. Sheppard, *J. Chem. Soc., Perkin Trans. 1* 529–537. (1981).
125. M. Meldal, *Tetrahedron Lett.* **33**, 3077–3080 (1992).
126. R. Arshady, *Colloid. Polym. Sci.* **268**, 948–958 (1990).
127. M. Renil, M. Ferreras, J. M. Delaisse, N. T. Foged, and M. Meldal, *J. Pept. Sci.* **4**, 195–210 (1998).
128. A. Basso, L. De Martin, L. Gardossi, G. Margetts, I. Brazendale, A. Y. Bosma, R. Ulijn, and S. Flitsch, *Chem. Commun.* 1296–1297. (2003).
129. S. Leon, R. Quarrel, and G. Lowe, *Bioorg. Med. Chem. Lett.* **8**, 2997–3002 (1998).
130. H. K. Smith and M. Bradley, *J. Comb. Chem.* **1**, 326–332 (1999).
131. M. Conza and H. Wennemers, *Chem. Commun.* 866–867. (2003).
132. S. J. Connon and S. Blechert, *Bioorg. Med. Chem. Lett.* **12**, 1873–1876 (2002).
133. D. M. Lynn, B. Mohr, L. M. Henling, M. W. Day, and R. H. Grubbs, *J. Am. Chem. Soc.* **122**, 6601 (2000).
134. M. Kempe and G. Barrany, *J. Am. Chem. Soc.* **118**, 7083–7093 (1996).
135. R. Kita, F. Svec, and J. M. J. Fréchet, *J. Comb. Chem.* **3**, 564–571 (2001).
136. J. Rademann, M. Grøtli, M. Meldal, and K. Bock, *J. Am. Chem. Soc.* **121**, 5459–5466 (1999).
137. L. P. Miranda, W. D. Lubell, K. M. Halkes, T. Groth, M. Grøtli, J. Rademann, C. H. Gotfredsen, and M. Meldal, *J. Comb. Chem.* **4**, 523–529 (2002).
138. R. B. Merrifield, in J. I. Seeman, ed., *Profiles, Pathways and Dreams: Autobiographies of Eminents Chemists*, American Chemical Society, Washington, D.C., 1993.
139. R. Frank, W. Heikens, G. Heistberg-Moutsis, and H. Blöcker, *Nucleic Acids Res.* **11**, 4365–4377 (1983).
140. R. Frank and R. Doring, *Tetrahedron* **44**, 6031–6040 (1983).
141. R. Frank, *Tetrahedron* **48**, 9217–9232 (1992).
142. U. Reineke, R. Volkmer-Engert, and J. S. Mergener, *Curr. Opin. Biotechnol.* **12**, 59–64 (2001).

143. U.S. Pat. 4,055,510 (Oct. 25, 1977), J. Peska, J. Stamberg, and Z. Blace. (Ceskoslovenska Akademie Ved).
144. D. R. Englebretsen and D. R. K. Harding, *Int. J. Peptide Protein Res.* **43**, 546–554 (1994).
145. A. Chesney, P. Barnwell, D. F. Stonehouse, and P. G. Steel, *Green Chem.* **2**, 57–62 (2000).
146. A. Chesney, P. G. Steel, and D. F. Stonehouse, *J. Comb. Chem.* **2**, 434–437 (2000).
147. L. De Luca, G. Giacomelli, A. Porcheddu, M. Salaris, and M. Taddei, *J. Comb. Chem.* **5**, 465–471 (2003).

GENERAL REFERENCES

For nice, historical review of solid-supported reagents catalysts, and sorbents, see D. C. Sherrington, *J. Polym. Sci. A* **39**, 2364–2377 (2001), and also D. Hudson, *J. Comb. Chem.* **1**, 336–360 (1999); *J. Comb Chem.* **1**, 403–457 (1999).

MARK BRADLEY
NICOLA GALAFFU
University of Southampton

POLYMETHACRYLATES. See METHACRYLIC ESTER POLYMERS.

POLY(METHACRYLIC ACID). See ACRYLIC (AND METHACRYLIC) ACID POLYMERS.

POLYNUCLEOTIDES. See Volume 3.

POLYOXYMETHYLENE. See ACETAL RESINS.

POLYPEPTIDE SYNTHESIS, SOLID-PHASE METHOD

Introduction

Peptides play key structural and functional roles in biochemistry, pharmacology, and neurobiology, and are important probes for research in enzymology, immunology, and molecular biology. A *peptide* is a chain of 3–50 amino acid building blocks, taken from among the 20 genetically encoded L-residues, or unusual ones. The sequences can be linear, cyclic, or branched. A rapid, efficient, and reliable method for the chemical synthesis of peptides is of utmost importance. Synthesis can confirm structures of naturally occurring substances and make them available in greater quantities for further investigations, can delineate antigenic determinants

Encyclopedia of Polymer Science and Technology. Copyright John Wiley & Sons, Inc. All rights reserved.

to allow preparations of artificial vaccines, and can lead to potent new drugs by judicious chemical substitutions that change functional groups and/or conformations of the parent peptide. These synthetic methods can also be extended to the study of *proteins*, which are defined as polypeptide chains of 50 or more residues.

The last century has witnessed the development of an extraordinary array of techniques for the chemical assembly of amino acids to form peptides. They can be subdivided into solution and solid–phase methods. The former have evolved since the beginning of the twentieth century (1–3); although quite powerful, they also require considerable labor, time, and skill because of the unpredictable solubility characteristics of intermediates and because of the lack of a method for automation. Recognizing the mechanical and physical limitations of the earlier chemical precedents, but retaining their strengths, in 1959 R. B. Merrifield of the Rockefeller University conceived the method of solid–phase peptide synthesis (SPPS). The solid–phase method has since been expanded to include other oligomeric systems, including DNA and polysaccharides, and to include combinatorial libraries. In recognition of the maturation and impact of this body of work, Merrifield was honored with the 1984 Nobel Prize in Chemistry (4). Many comprehensive reviews of SPPS have been written over the years (5–20).

Solid-phase synthesis is based on the covalent attachment (anchoring) of the growing peptide chain to an insoluble polymeric support or resin carrier, so that unreacted soluble reagents can be removed by filtration and washing without loss of the peptide–resin. Subsequently, the insoluble peptide–resin is extended by a series of addition cycles, which are required to proceed with high yields and fidelities. Excess soluble reagents drive the reactions to completion. Because of the speed and simplicity of the repetitive steps, the solid-phase procedure is amenable to automation. After the chain has been established, it is necessary to release (cleave) the crude peptide from the support under conditions that do not affect sensitive residues in the sequence. Purification and characterization follow to ensure and verify that the desired structure has been obtained.

Strategy and Tactics

A general strategy for stepwise solid-phase synthesis of linear polypeptides is shown in Figure 1. An insoluble polymeric support (Resin) is functionalized with a reactive group, typically an aminomethyl moiety. The first amino acid is attached to this functional group through a linker, usually a handle. A handle is defined as a bifunctional spacer that on one end typically contains a carboxyl group for coupling to an aminomethyl group on the polymeric support. The other end attaches to the first amino acid and acts as a permanent protecting group during chain assembly (7). The first amino acid is then attached to the handle by the C^{α}-carboxyl group as either an ester or amide linkage depending on whether the desired peptide will contain a C-terminal acid or amide group, respectively. Each amino acid contains a temporary protecting group (**T**, Fig. 1) on the N^{α}-amino group and a permanent protecting group (**P**, Fig. 1) on a reactive side-chain functional group if necessary. The peptide chain is then elaborated in the C $\rightarrow$ N direction by repeated cycles of deprotection of the temporary N^{α}-protecting group followed by coupling of the next protected amino acid. This deprotection/coupling cycle is repeated until all amino

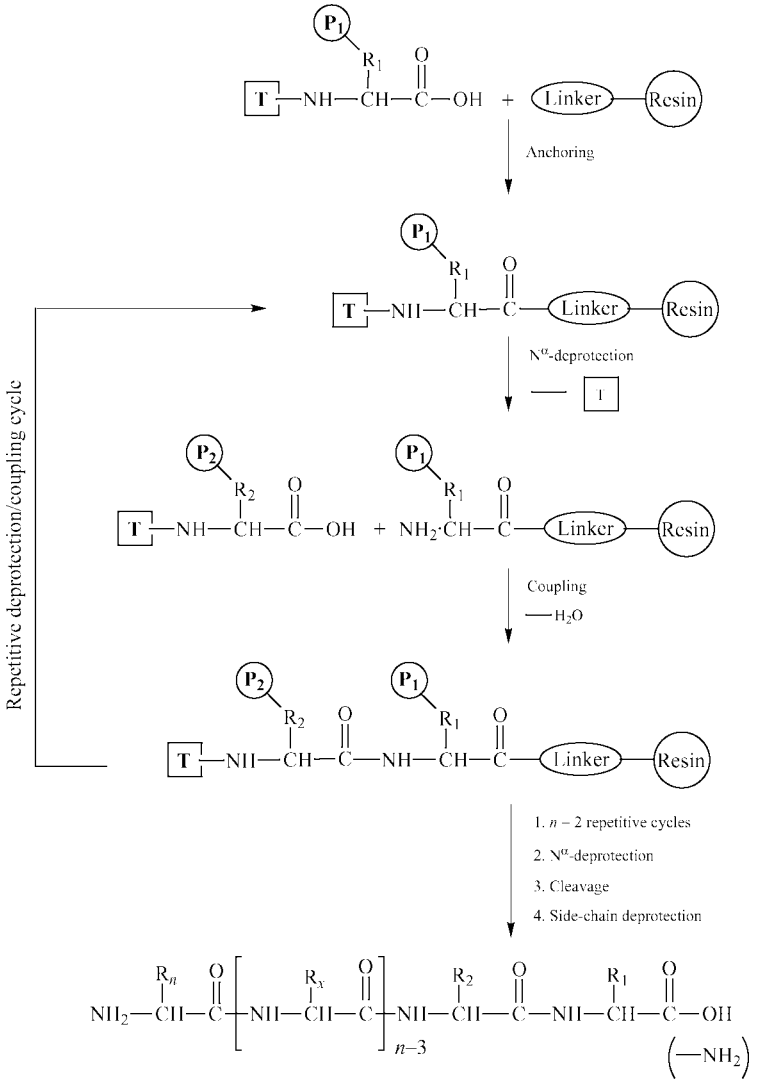

Fig. 1. Generic stepwise solid-phase synthesis of linear polypeptides. **T**, temporary protection; $\mathbf{P}_x$, permanent side-chain protection; $\mathbf{R}_x$, amino acid side chain.

acids of the peptide have been introduced. The peptide is then cleaved from the polymeric support, and the permanent protecting groups are removed; these last two steps are often combined in a single procedure. This strategy with C → N chain assembly offers the advantage that racemization is negligible. Variations on this general scheme exist that allow other C-terminal modifications such as thioesters, esters, or hydrazides to be synthesized. The chain may also be attached to the resin via either a side-chain functional group or the peptide backbone to allow elongation in the N → C direction as well as C → N (bidirectional synthesis) and to allow on-resin cyclization between the termini and/or a side chain for the synthesis

Table 1. Statistics of Chain Assembly in SPPS[a]

Average % yield of repetitive deprotection/coupling cycles	Total number of residues				
	5	10	25	50	100
80.0	32.8	10.7	0.4	0.0	0.0
90.0	59.0	34.9	7.2	0.5	0.0
95.0	77.4	59.9	27.7	7.7	0.6
99.0	95.1	90.4	77.8	60.5	36.6
99.5	97.5	95.1	88.2	77.8	60.6
99.9	99.5	99.0	97.5	95.1	90.5

[a] One can select a sequence length from the column headings and an average percent yield over all deprotection/coupling cycles from the left-most column of numbers. The number at the intersection of the selected column and row represents the theoretical percentage of peptide chains on resin that will contain the correct sequence after linear assembly has been completed. This theoretical percentage yield does not include side reactions and manipulative losses that will result from the cleavage and the purification steps that follow chain assembly in a synthesis.

of lactams, see References 3,5,7,8,10,12, and 16–20 for further information on C-terminal modifications.

Because the growing peptide is not isolated and purified after each repetitive deprotection/coupling cycle (Fig. 1), the fidelity of each step must proceed in near quantitative fashion. Table 1 contains the percent of correct peptide sequence that will be found on the resin at the end of a synthesis as a function of the average percent yield over all deprotection/coupling cycles and as a function of the total number of residues in the sequence. Yields of 95% per cycle, what would be considered fantastic in a solution synthesis, are unacceptably low for even peptides as short as 10 amino acids, as only 59.9% of the correct sequence would be assembled on the resin. Yields must be greater than 99% for each repetitive deprotection/coupling cycle to have any hope of isolating the desired product. The data of Table 1 also show that for sequences of greater than 25 amino acids, increasing the yield of each cycle by a few tenths of a percent makes a substantial difference in the overall yield. Thus, double coupling of each amino acid is routinely done on longer syntheses. Fortunately, the art of peptide synthesis has progressed to the level that yields greater than 99.5% for each repetitive cycle can generally be achieved. The impurities are often deletion peptides that differ from the desired sequence by only one or two amino acids and that may be hard if not impossible to remove during purification. Thus, for longer sequences many peptide chemists routinely include a capping step with acetic anhydride, after double coupling and before deprotection, to terminate the chain before the next cycle is begun. The termination peptides will then differ in length from the desired product by many amino acids and will be easier to remove from the desired product during purification.

In the repetitive deprotection/coupling cycle of Figure 1 are three classes of protecting groups. The first is the temporary N^{α}-protection. The remaining two classes contain permanent groups, the side-chain-protection and the peptide-linker bond, that remain intact during chain assembly. Implicit in this repetitive cycle is that the two permanent classes are stable to the conditions used to remove

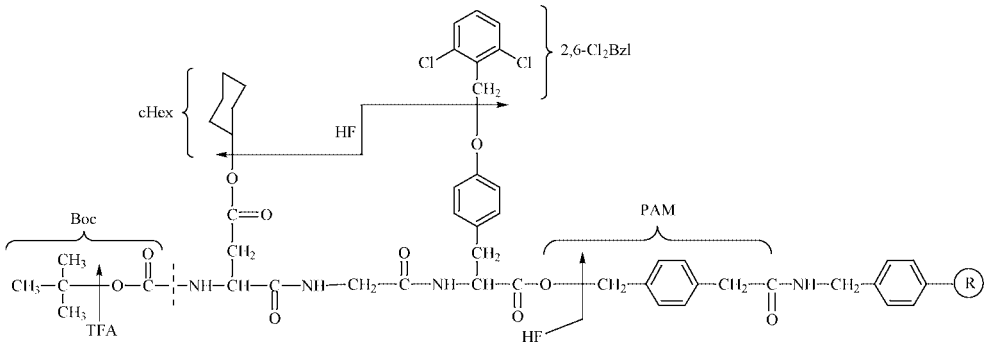

Fig. 2. Commonly used protection scheme based on graduated acidolysis. Temporary N^{α}-amino protection is provided by the *tert*–butyloxycarbonyl (Boc) group, removed at each step by the moderately strong trifluoroacetic acid (TFA). Permanent benyzl- and cyclohexyl-based side-chain–protecting groups and the phenylacetamidomethyl (PAM) ester handle linkage are cleaved simultaneously at the end of the synthesis by HF to yield the free peptide acid.

the temporary N^{α}-protection. If all classes are removed by the same chemical mechanism, for example acidolysis, differential stability between classes can only be achieved by designing protecting groups that are cleaved at different kinetic rates. This often necessitates very harsh conditions for final removal of the two classes of permanent protection. The alternative is to design protecting groups for each class that are cleaved by different or orthogonal mechanisms (7,21). Ideally, a fully orthogonal protection scheme would allow each class of protecting group to be cleaved in any order without removing the other two classes (22). Orthogonal protection schemes allow milder overall conditions, because deprotection strategies are based upon mechanism rather than kinetics.

Many combinations of temporary and permanent protecting groups have been developed over the years. Only two have survived the test of time and are routinely used today. The first is an improved version of the original Merrifield system. This system is a non-orthogonal scheme based on graduated acid lability to differentiate temporary from permanent protecting groups (Fig. 2). The N^{α}-*tert*-butyloxycarbonyl (Boc) group (23–25) is used for temporary protection. The Boc group is stable to alkali and nucleophiles but is rapidly removed by organic and inorganic acids (7). The Boc group is usually removed by trifluoroacetic acid (TFA) (20–50%) in dichloromethane (DCM) or HCl (4N) in dioxane. Permanent side-chain–protecting groups are ether, ester, and urethane derivatives based on benzyl alcohol "fine-tuned" with electron-donating methoxy or methyl groups or electron-withdrawing halogens to achieve the proper level of stability to acid. Alternatively, ether and ester derivatives based on cyclopentyl or cyclohexyl alcohol are sometimes used to mitigate certain side reactions. These permanent side-chain–protecting groups and the peptide-handle linkage are cleaved by the strong Lewis acid anhydrous HF. In neat anhydrous HF, cleaved protecting groups exist as carbocations that may alkylate sensitive side chains of residues such as tryptophan. Thus, acid cleavages are always carried out in the presence of carbocation scavengers such as anisole. Scavengers such as dimethyl sulfide, *p*-cresol,

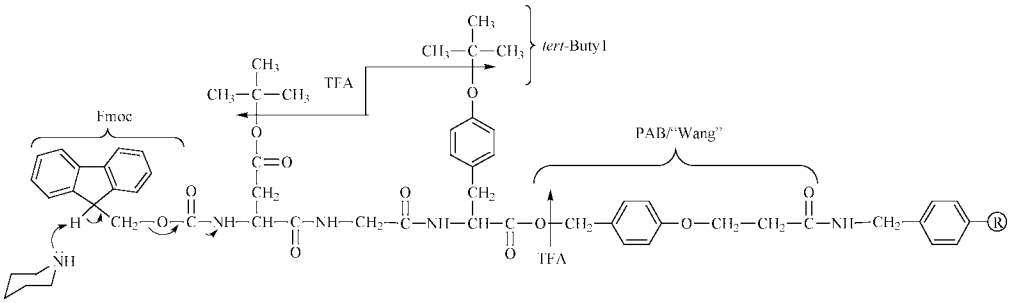

Fig. 3. A mild two-dimensional orthogonal protection scheme for solid-phase synthesis. Temporary N^{α}-amino protection is provided by the 9-fluorenylmethyloxycarbonyl (Fmoc) group, removed by a base-catalyzed elimination mechanism, typically with piperidine. Permanent *tert*-butyl-based side-chain-protecting groups and the *p*-alkoxybenzyl (PAB) ester handle linkage are both cleaved by treatment with TFA to yield the free peptide acid at the end of the synthesis. Details in text.

and *p*-thiocresol have been recommended in conjunction with a two-stage, low–high HF cleavage method that is said to provide extra control and higher purities (see section 3.4, Cleavage).

The Merrifield system is still popular today and up until the mid-1980s was the most commonly used synthetic strategy. In the last 15 years a two-dimensional orthogonal strategy based on the N^{α}-9-fluorenylmethyloxycarbonyl (Fmoc) group (26) has emerged as the method of choice for the synthesis of most research peptides (Fig. 3). The temporary Fmoc group is removed by a β-elimination mechanism with piperidine (20–50%) in *N,N*-dimethylformamide (DMF) or *N*-methylpyrollidinone (NMP) (27–30). Permanent protection is now provided by ether, ester, and urethane derivatives based on *t*-butyl alcohol, triphenylmethanol, or 9-hydroxyxanthene, which are cleaved by TFA at the same time the peptide is released from the resin. Whereas the anhydrous HF used in the final deprotection step in Boc chemistry requires a special apparatus made of all fluorocarbon (Kel F) lines and trained operators to safely cleave and isolate the peptide, the milder conditions for final cleavage in Fmoc strategies, TFA (90%), have allowed a wide variety of scientists of diverse training to now synthesize peptides by the solid-phase method. Once again, scavengers are necessary to remove reactive carbocations during final TFA cleavage. The scavenger cocktails are covered in the section on cleavage.

A three-dimensional orthogonal protecting scheme for the synthesis of lactams is illustrated in Figure 4. The side chains of aspartic acid and lysine are protected with ester and urethane derivatives, respectively, of allyl alcohol. The allyl-based protecting groups may be cleaved under neutral conditions mediated by Pd(0) while the fully protected peptide is still attached to the resin. The lactam ring may then be formed taking advantage of the psuedo-dilution effect of the peptide–resin. Fmoc removal followed by final TFA cleavage from the 5-(4-aminomethyl-3,5-dimethoxyphenoxy)valeric acid (PAL) handle results in the side chain-to-side chain cyclic peptide with a C-terminal amide.

Side-chain–protecting groups keep reactive side chains from coupling with the next incoming activated amino acid and thus forming a branch point in the

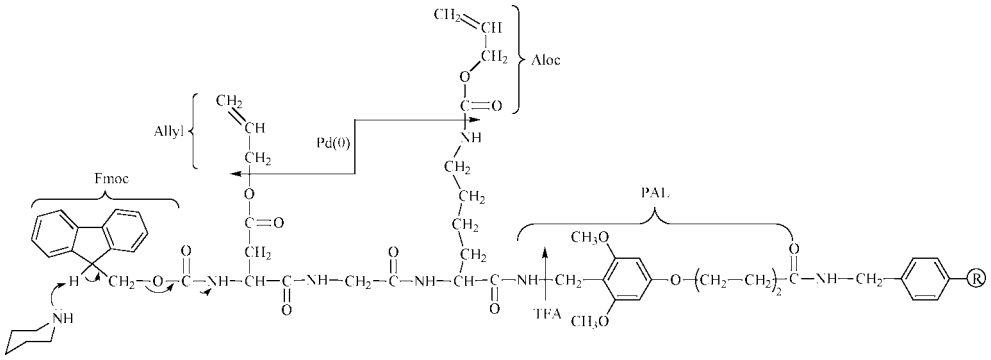

Fig. 4. A mild three-dimensional orthogonal protection scheme for side chain-to-side chain cyclization strategies. The allyl alcohol based side-chain protection of Asp and Lys are removed with Pd(0) without affecting the temporary Fmoc protection or the permanent peptide–PAL handle linkage. The lactam bond between Asp and Lys can now be formed on resin, followed by sequential treatment with piperidine to remove the Fmoc group and TFA to cleave the peptide from the PAL handle to yield the side chain-to-side chain cyclic C-terminal amide peptide.

peptide, they protect sensitive residues from degradation during synthesis, and they can greatly increase the solubility of certain residues in the common solvents used in peptide synthesis. Because the occurrence of many of the degradation side reactions are sequence-dependent, for the synthesis of research peptides in which process development is often not an option, a maximal protecting group strategy is recommended in which all trifunctional amino acids are protected. The recommended protecting groups for each trifunctional amino acid that are commercially available and compatible with either Boc or Fmoc chemistries are listed in Tables 2 and 3, respectively. These permanent side-chain–protecting groups are cleaved at the same time as the peptide–resin linkage is cleaved.

For the synthesis of cyclic peptides, either lactams (58,59) (Fig. 4) or multiple disulfide-containing (60) peptides, and for the synthesis of protected fragments, permanent protecting groups must be selected whose cleavage mechanism is orthogonal to that used to remove the N^{α}-protecting group and to that used to cleave the peptide–resin linker. If on-resin cyclization is to be attempted, the orthogonal protecting group does not have to be stable to the final cleavage/deprotection conditions. All that is necessary is that the orthogonal side chain group can be removed without affecting the N^{α}-protection, the other permanent side-chain–protected amino acids, and the peptide-linker bond. Table 4 summarizes the commercially available amino acid derivatives for both Boc and Fmoc chemistries with side-chain protection that is cleavable by mechanisms orthogonal to either acidolysis and/or piperidine treatment.

The standard methodology of SPPS involves attachment of the first amino acid to the resin via the C^{α}-carboxyl. Synthesis then proceeds in the C → N direction. The majority of anchoring linkages have been designed to provide C-terminal ester or amide linkages to provide upon cleavage, respectively, peptide acids or amides (Table 5). The original linker used by Merrifield was a benzyl ester formed by the reaction between the first protected amino acid and chloromethyl groups on

Table 2. Recommended Commercially Available Side-chain–Protected Amino Acids Compatible with Boc Chemistry and Removed by HF During Final Deprotection/Cleavage[a]

Amino acid and protecting group	Abbreviation	Stability	Reference	Structure
Arginine				
Mesitylene-2-sulfonyl	Arg(Mts)	TFA Piperidine Pd(0) Hydrazine	31–33	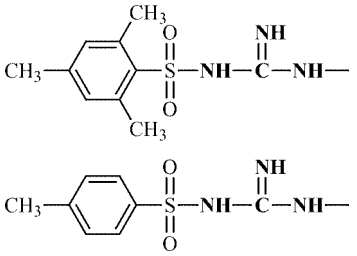
4-Toluenesulfonyl	Arg(Tos)	TFA Piperidine Pd(0) Hydrazine	31	
Aspartic/glutamic				
Cyclohexyl	Asp/Glu(OcHex)	TFA Piperidine Pd(0) Hydrazine	31,32,34–36	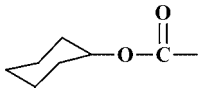
Asparagine/glutamine				
9-Xanthenyl	Asn/Gln(Xan)[b]	Piperidine Pd(0) Hydrazine	8,31,37,38	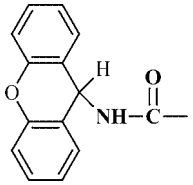

Table 2. (Continued)

Amino acid and protecting group	Abbreviation	Stability	Reference	Structure
Cysteine 4-Methylbenzyl	Cys(Meb)	TFA Piperidine	7,31,39,46	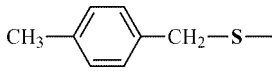
Histidine Benzyloxymethyl	His(Bom)	TFA Piperidine Pd(0) Hydrazine	31,36,41	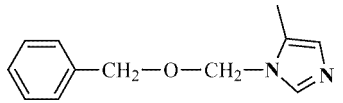
Lysine 2-Chlorobenzyloxycarbonyl	Lys(2-ClZ)	TFA Piperidine Pd(0) Hydrazine	2,31,36,39	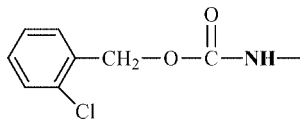
Methionine Sulfoxide	Met(O)	TFA Piperidine Pd(0) Hydrazine	2,31,40,42–44	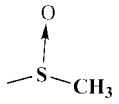

Serine/threonine Benzyl	Ser/Thr(Bzl)	TFA Piperidine Pd(0) Hydrazine	32,36	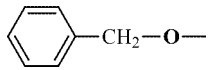
Tryptophan Formyl	Trp(CHO)	TFA Piperidine Pd(0) Hydrazine	2,31,32	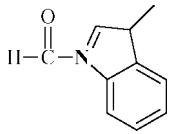
Cyclohexyloxycarbonyl	Trp(Hoc)	TFA Piperidine Pd(0) Hydrazine	45	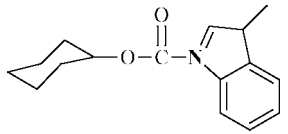
Tyrosine 2,6-Dichlorobenzyl	Tyr(Cl_2-Bzl)	TFA Piperidine Pd(0) Hydrazine	31,32,36,39	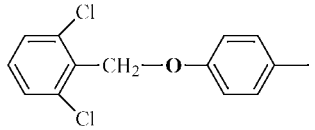

[a] The boldfaced atoms and structures to the right are the functional group being protected.
[b] The Xan group is removed by TFA during subsequent deprotection steps. Xan prevents dehydration of Asn/Gln during coupling and greatly increases the solubility of these residues.

Table 3. Recommended Commercially Available Side-chain–Protected Amino Acids Compatible with Fmoc Chemistry and Removed by TFA During Final Deprotection/Cleavage[a]

Amino acid and protecting group	Abbreviation	Stability	Reference	Structure
Arginine 2,2,4,6,7-Pentamethyldihydrobenzofuran-5-sulfonyl	Arg(Pbf)	Piperidine Pd(0) Hydrazine	46,47	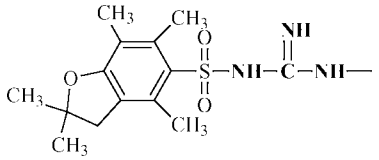
Aspartic/glutamic *tert*-Butyl	Asp/Glu(O-*t*-Bu)	Piperidine Pd(0) Hydrazine	2,48	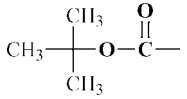
Asparagine/glutamine Triphenylmethyl	Asn/Gln(Trt)	Piperidine Pd(0) Hydrazine	49	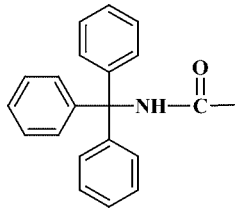

Cysteine				
Triphenylmethyl	Cys(Trt)	Piperidine Pd(0) Hydrazine	2,50–52	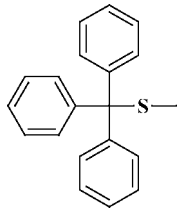
9-Xanthenyl	Cys(Xan)[b]	Piperidine Pd(0) Hydrazine	53	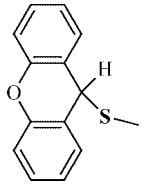
Histidine				
Triphenylmethyl	His(Trt)	Piperidine Pd(0) Hydrazine	11	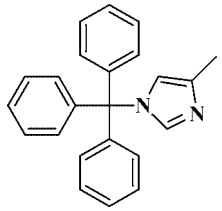

Table 3. (Continued)

Amino acid and protecting group	Abbreviation	Stability	Reference	Structure
Lysine *tert*-Butyloxycarbonyl	Lys(Boc)	Piperidine Pd(0) Hydrazine	2,51	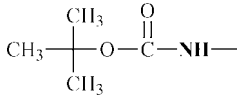
Serine/threonine *tert*-Butyl	Ser/Thr(*t*-Bu)	Piperidine Pd(0) Hydrazine	51,54,55	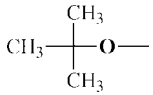
Tryptophan *tert*-Butyloxycarbonyl	Trp(Boc)	Piperidine Pd(0) Hydrazine	47,56,57	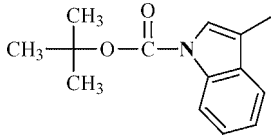
Tyrosine *tert*-Butyl	Tyr(*t*-Bu)	Piperidine Pd(0) Hydrazine	51,54,55	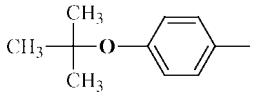

[a] The boldfaced atoms and structures to the right are the functional group being protected.
[b] The Xan group can be removed from Cys with 1% TFA without affecting the peptide–resin linkage (53).

Table 4. Commercially Available Amino Acids with Side-chain Protection That Is Cleavable by Mechanisms Orthogonal to Either Acidolysis and/or Piperidine Treatment[a]

Amino acid and protecting group	Abbreviation	Stability	Cleavage	Reference	Structure
Aspartic/glutamic					
Allyl	Asp/Glu(OAl)	TFA HF Piperidine Hydrazine	Pd(0)	52,62,63	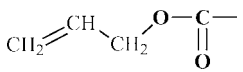
4-{*N*-[1-(4,4-Dimethyl-2,6-dioxocyclohexylidene)-3-methylbutyl]-amino}-benzyl	Asp/Glu(ODmab)	TFA Piperidine Pd(0)	Hydrazine	64	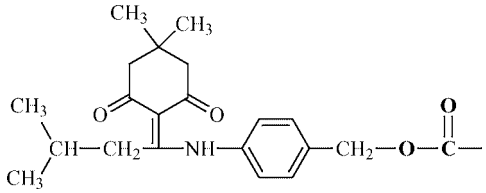
Fluorenylmethyl	Asp/Glu(OFm)	TFA HF Pd(0) Hydrazine	Piperidine	65	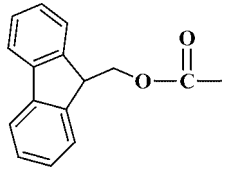
Cysteine					
Acetamidomethyl	Cys(Acm)	HF TFA Piperidine Hydrazine	I_2 Hg(II) $Tl(Tfa)_3$	2,60,66,67	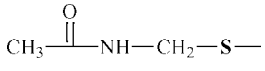

Table 4. (Continued)

Amino acid and protecting group	Abbreviation	Stability	Cleavage	Reference	Structure
tert-Butysulfenyl	Cys(S-*t*-Bu)	TFA Piperidine Pd(0) Hydrazine	Thiols Phosphines	68,69	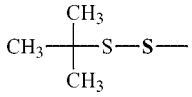
Lysine					
Allyloxycarbonyl	Lys(Aloc)	HF TFA Piperidine Hydrazine	Pd(0)	63	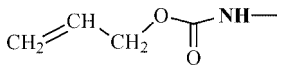
4,4-Dimethyl-2,6-dioxocyclohex-1-ylidene–ethyl	Lys(Dde)	TFA Piperidine Pd(0)	Hydrazine	70–73	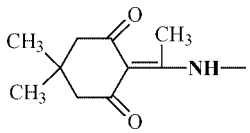

[a]The boldfaced atoms and structures to the right are the functional group being protected. For a more comprehensive review of orthogonal protecting groups see Reference 61.

Table 5. Resin Linkers and Handles[a]

Linker/handle	Cleavage conditions	Resulting C-terminus	Reference	Structure
4-Chloromethyl resin	HF	Acid	8,74	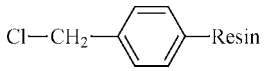
4-Hydroxymethylphenylacetic acid (PAM)	HF	Acid	75,76	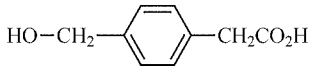
9-(Hydroxymethyl)-2-fluoreneacetic acid (HMFA)	Piperidine	Acid	67,77,78	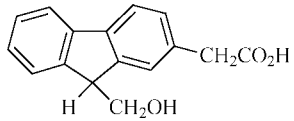
4-Nitrobenzophenone oxime resin	HOPip AA^{-} $^{+}$N(n-Bu)$_4$ AA-NH$_2$	Acid[b] Amide	80–82	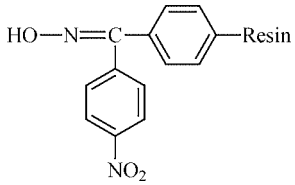
α-Bromophenacyl	$h\nu$ (350 nm)	Acid	83	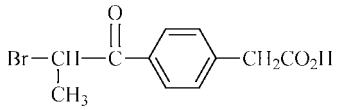

Table 5. (Continued)

Linker/handle	Cleavage conditions	Resulting C-terminus	Reference	Structure
3-(4-Hydroxymethylphenoxy)propionic acid (PAB) (Wang)	TFA	Acid	84–86	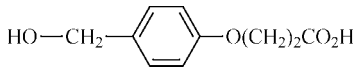
4-(2′,4′-Dimethoxyphenylhydroxymethyl)-phenoxymethyl resin	Dilute TFA	Acid	87	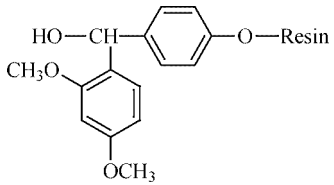
2-Chlorotrityl chloride resin	TFA, HOAc	Acid	88,89	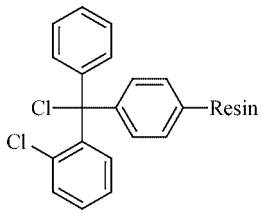
5-(4-Hydroxymethyl-3,5-dimethoxyphenoxy)valeric acid (HAL)	Dilute TFA	Acid	90	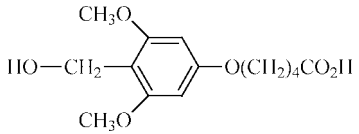
Hydroxy–crotonyl–aminomethyl resin (HYCRAM)	Pd(0)	Acid	91–93	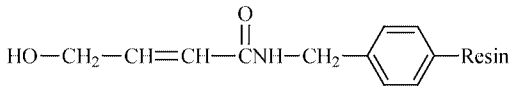

3-Nitro-4-hydroxymethylbenzoic acid (ONb)	*hν* (350 nm)	Acid	22,94–96	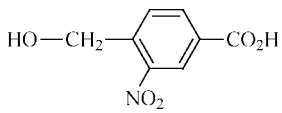
4-(2′-Aminoethyl)-2-methoxy-5-nitro–phenoxypropionic acid	*hν* (350 nm)	Amide	97	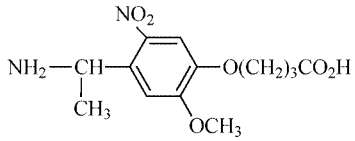
4-Methylbenzhydrylamine resin (MBHA)	HF	Amide	98,99	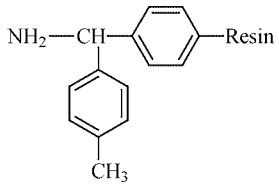
4-(2′,4′-Dimethoxyphenylaminomethyl)phenoxymethyl resin (Rink)	Dilute TFA	Amide	87	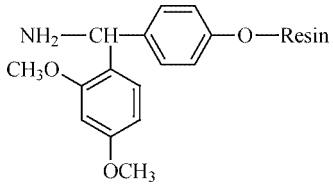
5-(4-Aminomethyl-3,5-dimethoxyphenoxy)valeric acid (PAL)	TFA	Amide	100,101	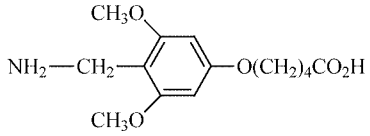

Table 5. (Continued)

Linker/handle	Cleavage conditions	Resulting C-terminus	Reference	Structure
5-(9-Aminoxanthen-3-oxy)valeric acid (XAL)	Dilute TFA	Amide	13,102, 103	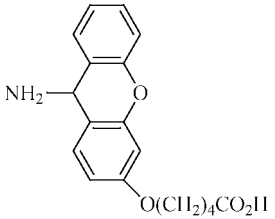
3-Nitro-4-aminomethylbenzoic acid (Nonb)	$h\nu$ (350 nm)	Amide	104	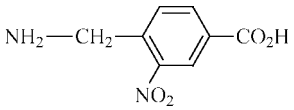
4-(4-Fmoc–aminomethyl-3,5-diethoxy–phenoxy)butyric acid (BAL)	TFA	Amide	105	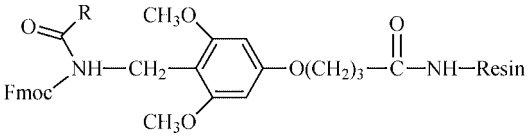
4-(α-Mercaptobenzyl)phenylacetic acid	HF	Thioester	106–108	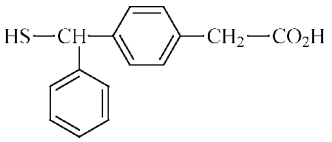

[a] Structural diagrams are oriented so that the resin or point of attachment to support is on the far right, and the site for anchoring the C-terminal amino acid residue is on the far left. Benzyl ester linkages may also be cleaved by a range of nucleophiles to create acids, esters, or other derivatives. Consult References 7,9, and 20 for further examples.

[b] Cleavage by aminolysis results in 0.6–2% racemization (79).

polystyrene resin (Table 5). The simple benzyl ester linkage was found to be slowly cleaved by TFA and has now been replaced by the phenylacetamidomethyl (PAM) ester handle (Fig. 2) which is stable to TFA but readily cleaved by HF. The preferred loading technique for ester linkages is to attach the first amino-acid to the handle in solution forming a "preformed handle." The preformed handle may be purified in solution before coupling to an amino-functionalized resin. The preformed handle strategy gives one greater control over the loading in that the formation of the amide bond between the handle and the resin can easily be driven to completion (75,76). For synthesizing peptide acids by Fmoc chemistries, *p*-alkoxybenzyl esters (PAB), "Wang resins" (Fig. 3, Table 5), are the preferred handles. Both PAM and Wang resins preloaded with the first amino acid are now commercially available at low cost and high purity from a variety of vendors (see Appendix). Finally, for a detailed discussion of side reactions that can occur when forming the ester bond between the first amino acid and either a handle- or a resin-bound hydroxyl group, see Reference. 20 (pp. 129–132).

The recommended linker for synthesizing C-terminal amides compatible with Boc chemistries is the MBHA linker (Table 5). For Fmoc chemistries either the PAL (Fig. 4) or the Rink handles are recommended (Table 5).

Many other handles exist that are cleavable by orthogonal mechanisms for the synthesis of protected peptide fragments; these are also summarized in Table 5. A novel strategy for the synthesis of cyclic peptides on resin is to attach the peptide to the resin by a backbone nitrogen rather that the C^{α}-carboxyl. The N- and C-termini then remain free for further functionalization such as cyclization, esterification, or thioester formation. This backbone amide linker (BAL) is listed in Table 5. Other strategies such as attaching the peptide to the resin via the side chain of trifunctional amino acids and more comprehensive listings of linkers and handles are covered in References 9,12, and 109–111.

Procedures

Deprotection/Coupling Cycle. Tables 6 and 7 show representative deprotection/coupling cycles for Boc- and Fmoc-based syntheses, respectively. When

Table 6. General Boc Chemistry SPPS[a]

Step	Description	Solvents/chemicals	Time[b], min
1.	Deprotection	20–50% TFA in DCM or NMP	1 + 30
2.	Wash	DCM or NMP	4 × 2
3.	Neutralization	5% DIEA in DMF or NMP	2 × 2
4.	Wash	DMF or NMP	4 × 2
5.	Activation and coupling[c,d,e]	Selection from Table 8	
6.	Wash	DMF or NMP	4 × 2

[a] Boc–Asn and Boc–Gln are side-chain–protected.
[b] Times are for batchwise synthesis. If a flow apparatus is used, the time is the combined times of a step, eg, 2 × 2 min = 4 min of flow.
[c] When double coupling, steps 1 through 4 are omitted between couplings.
[d] When capping, the coupling reagents of Table 8 are replaced with acetic anhydride/DIEA (10 equiv each), and steps 1 through 4 are omitted as when double coupling.
[e] Steps 3 and 5, neutralization and coupling, may be combined into one step (112–116).

Table 7. General Fmoc Chemistry SPPS[a]

Step	Description	Solvents/chemicals	Time[b], min
1.	Wash	DMF or NMP	3 × 1
2.	Deprotection	Piperidine/DMF or NMP (1:4)	1 + 20
3.	Wash	DMF or NMP	3 × 1
4.	Activation and coupling[c,d]	Selection from Table 8	
5.	Wash	DMF or NMP	3 × 1

[a] Fmoc–Asn and Fmoc–Gln are side-chain–protected.
[b] Times are for batchwise synthesis. If a flow apparatus is used, the time is the combined times of a step, eg, 3 × 1 min = 3 min of flow.
[c] When double coupling, steps 1 through 3 are omitted between couplings.
[d] When capping, the coupling reagents of Table 8 are replaced with acetic anhydride/DIEA (10 equiv each), and steps 1 through 3 are omitted as when double coupling.

double coupling or capping, the deprotection step is skipped and the protocol is repeated, starting at the wash step before the activation and coupling steps.

The recommended coupling reagents and their respective protocols are listed in Table 8. The structures of the coupling reagents are shown in Figure 5. Each lab has a preference for coupling reagent, reaction time of each step, and solvents (DCM, DMF, or NMP) used. Each coupling reagent has certain limitations. *N,N′*-Diisopropylcarbodiimide (DIPCDI) activation in DMF or NMP is a slow process that takes about 1 h to reach completion. In DCM the reaction is instantaneous (117). Thus, preactivation in a separate vessel while deprotection is occurring is often done with carbodiimide activation in DMF or NMP. Activated arginine derivatives undergo a slow side reaction, where the guanido group attacks the activated C^{α}-carboxyl to form a six-membered ring. The amino acid is then no longer able to couple. This side reaction does not affect the purity of the peptide, it only nonproductively consumes the activated arginine residue. Thus, long preactivation of arginine by carbodiimides is not recommended to avoid the loss of the activated amino acid before it can couple to the free amino group of the peptide–resin. The reagents benzotriazol-1-yl-oxy-tris(dimethylamino)phosphonium hexafluorophosphate (BOP), 2-(1*H*-benzotriazol-1-yl)-1,1,3,3-tetramethyluronium hexafluorophosphate (HBTU), and *O*-(7-azabenzotriazol-1-yl)-1,1,3,3-tetramethyluronium hexafluorophosphate (HATU) must contain excess *N*-methylmorpholine (NMM) or *N,N*-diisopropylethylamine (DIEA) for efficient coupling (118–124). The excess tertiary amines present in these coupling cocktails (Table 8, entries 2–4) will racemize cysteine (125). Either the DIPCDI or the pentafluorophenyl active ester protocols are recommended for coupling this amino acid. The BOP reagent releases the carcinogen hexamethylphosphoramide, so the waste stream from this reagent must be handled with care. Excess unreacted HBTU and HATU can cap unreacted amino groups (126,127); preactivation should always be done in a separate vessel and the amino acid derivative should always be present in slight excess to these two coupling reagents. Because of this side reaction, HBTU and HATU are not recommended as reagents for on-resin cyclizations. Pentafluorophenyl esters (*O*Pfp) couple slowly as compared to the other methods, addition of HOBt can increase the reaction rate (128,129).

The coupling times listed in Table 8 are only approximate, and for manual syntheses the actual length of the coupling step is determined by monitoring for unreacted amino groups by the sensitive ninhydrin test.

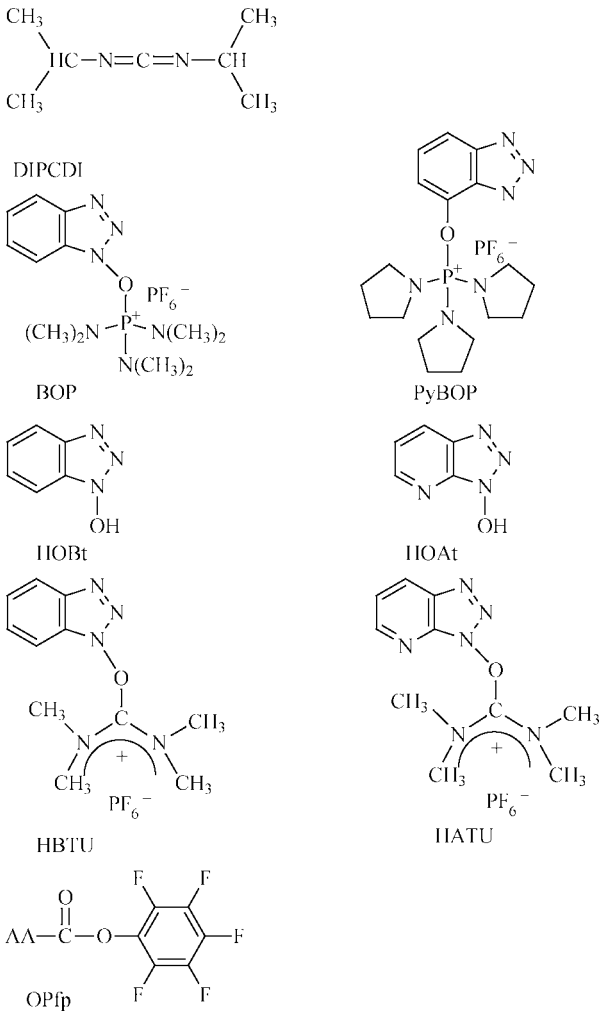

Fig. 5. Structures of coupling reagents of Table 8.

Many other side reactions that can occur during coupling have been documented and are listed in the more comprehensive reviews (5–8, 10–20). However, if one uses the protected amino acids listed in Tables 2–4 and the deprotection/coupling protocols of Tables 6–8, these other side reactions generally are not a problem during chain elongation.

Monitoring. A key assumption in solid-phase procedures is that coupling reactions can be made to go to completion (Table 1). A number of qualitative and quantitative methods of monitoring these steps exist, including some with a possibility of "real-time" feedback based on the kinetics of appearance or disappearance of soluble chromophores measured in a flow-through system. Most accurate and meaningful are qualitative and quantitative tests for the presence of unreacted amines after a coupling step. Such tests should ideally be negative before proceeding to the next deprotection/coupling cycle.

The most widely used qualitative test for monitoring unreacted amines is the ninhydrin test (130). For monitoring imines (secondary amines) such as proline,

Table 8. Coupling Protocols for SPPS

Entry	Solvents/chemicals	Time[a], min
1.	Protected amino acid (4 equiv) in DMF or NMP	5
	DIPCDI (4 equiv)/HOBt (4 equiv) in DMF[b,c]	60
2.	Protected-amino acid (4 equiv) in DMF or NMP	5
	BOP or PyBOP (3 equiv)/NMM (4.5 equiv)/HOBt (3 equiv) in DMF or NMP[b]	20
3.	Protected amino acid (4 equiv) in DMF or NMP	5
	HBTU (3.6 equiv)/DIEA (7.2 equiv)/HOBt (4 equiv) in DMF[d]	20
4.	Protected amino acid (4 equiv) in DMF or NMP	5
	HATU (3.6 equiv)/DIEA (7.2 equiv)/HOAt (4 equiv) in DMF[d]	20[e]
5.	Protected amino acid pentafluorophenyl ester (4 equiv) in DMF or NMP	60

[a]The first line in the second column is the preactivation time, and the second line is the coupling time. Entry 5 is the coupling time only.

[b]The reagents can be added directly to the reaction vessel without preactivation, eg, during on-resin cyclizations to form a lactam.

[c]Earlier references on the carbodiimide method of activation use *N,N′*-dicyclohexylcarbodiimide (DCC) as the coupling reagent. DCC can cause severe dermatitis when handled, and the urea by-product is prone to precipitate in the lines of automated synthesizers. DCC is no longer recommended for use in solid-phase synthesis.

[d]Preactivation in a separate vessel is required to avoid capping the N^{α}-amino group.

[e]Coupling times as short as 1 min have been recommended with the reagents of entry 4 (115,116).

the isatin test is used (131). These tests, which are carried out on an aliquot of peptide–resin, are easy, reliable, and require only a few minutes to run, making it possible to make a quick decision on how to proceed. A highly accurate quantitative version of the ninhydrin test has been described (132). The ninhydrin test is not amenable to automation, however. Other monitoring techniques exist that are nondestructive and may be carried out on the whole batch of resin. These tests are time consuming and not widely used.

As an alternative to monitoring unreacted N^{α}-amino groups, soluble reactants and coproducts can be analyzed. Continuous measurement of electrical conductivity can be used to evaluate Fmoc coupling and Fmoc deprotection efficiencies (133–135). The progress of Fmoc chemistry can be evaluated by observing the decrease of absorbance at 300 nm when Fmoc amino acids are taken up during coupling, and by the increase in absorbance at 300 nm when the Fmoc group is released with piperidine (136). Software on modern peptide synthesizers can evaluate the kinetics of these deprotection/coupling steps and lengthen reaction times if necessary.

Continuous flow monitoring is inherently insensitive for direct judgment of reaction end points. In a typical coupling procedure with a fourfold excess of amino acid, absorbance drops from 4.00 to 3.05 or 3.01 units with 95 or 99% coupling, respectively. It is difficult to distinguish the approximate 1% difference between 3.05 and 3.01 accurately. In contrast, the 400% difference between 0.05 and 0.01 is easily measured when monitoring unreacted N^{α}-amino groups.

An essential, although time-consuming, way to monitor the course of solid-phase synthesis is total hydrolysis of aliquots of the peptide–resin removed after

Table 9. Preview in the Sequential Degradation of a Hypothetical Peptide Made by Solid-Phase Synthesis[a]

	Edman cycle	%	1	2	3	4
Correct	A-B-C-D-E-F-resin	90	A	B	C	D
Des(A)	B-C-D-E-F-resin	0.4	**B**	**C**	**D**	**E**
Des(B)	A-C-D-E-F-resin	0.4	A	**C**	**D**	**E**
Des(C)	A-B-D-E-F-resin	0.2	A	B	**D**	**E**
Des(D)	A-B-C-E-F-resin	9.0	A	B	C	**E**
Preview[b], %			0.4	0.8	1.0	10

[a] Refs. 138–140.
[b] With respect to expected residue.

certain synthetic steps. The technique of internal reference amino acids (IRAA) is often used to measure yields and chain retention accurately (11,101,137).

Invasive monitoring of both synthetic efficiency and amino acid composition of peptide–resins can be achieved by a powerful quantitative variation of the Edman sequential degradation, called "preview analysis" (138–140). To illustrate preview analysis (Table 9), assume that the desired sequence A-B-C-D-E has been assembled on 90% of the peptide–resins, that deletions of A, B, and C have occurred at 0.4, 0.4, and 0.2%, respectively, and that due to a significant error at the step to incorporate D, 9% of the chains lack this latter residue. After one cycle of Edman degradation, the residue B is quantitatively determined by sensitive analytical techniques at 0.4% of the expected A, even though B should only be viewed in the second cycle. Thus the 0.4% preview of B reflects that amount of deletion of A. The second cycle of Edman degradation in Table 9 shows the amplification effect inherent in the method, because now 0.8% preview of C is noted. It is difficult to ascribe a low degree of deletion to specific positions in the chain, but an average deletion can be assumed because the precision increases with each Edman step. In fact, the average level of deletions in a typical synthesis is $<0.3\%$ per step. The fourth degradation of the example (Table 9) illustrates the dramatic jump in preview reflecting a failure in the corresponding stage of the synthesis. Because this level is large, the specific location of the deletion can be identified.

Recently, on-resin mass spectrometry (MS) via the MALDI (matrix-assisted laser desorption/ionization) technique has been developed. This method can be used as a semi-on-line monitoring technique during SPPS (141). An especially elegant approach for on-resin MS is to use the photolabile α-methylphenacyl ester linker (Table 5, α-bromophenacyl entry), which is cleaved directly upon laser photolysis and MALDI ionization (142,143).

Resins. The solid-phase support (Resin, Fig. 1) is a well-solvated polymeric matrix in which the peptide chains are attached throughout a resin bead. The polymeric backbone is a flexible superstructure through which reagents and solvents can easily flow and once swollen has the physical properties of a gel (144,145). This is in contrast to the common perception that solid-phase chemistry only occurs on the surface of each polymer bead. Because of the permeable nature of the polymers, reaction rates approach but are slightly slower than that found in solution. Commercially available polymers have functional group loadings typically in the 0.2–1.0 mmol/g range. As an example of the distribution

of peptide chains within a polymer, polystyrene contains approximately 10 mmol/g phenyl groups. Thus, a polystyrene resin with an aminomethyl substitution of 0.5 mmol/g contains a functional group on about every 20th phenyl ring. By the end of the synthesis a resin may easily double in mass and volume but will remain a well-solvated gel in the common solvents used in SPPS. This increase in size does not appreciably affect reaction rates, and couplings generally continue to proceed to completion (144).

Polymeric supports must be compatible with either of the two modes of SPPS. The first is the batchwise method, where the reactions are agitated by mechanical means such as shaking, vortexing, or bubbling with an inert gas such as nitrogen. Reagents are removed by filtration either with suction or with nitrogen pressure. The second mode is the continuous-flow method. In this mode reagents and solvents are pumped through columns packed with resins. Resins for use in continuous-flow SPPS must have sufficient mechanical stability to be stable to the back pressures that develop during synthesis.

Two polymeric supports have classically been used in batchwise SPPS. The first is polystyrene polymer cross–linked with 1% of 1,3-divinyl benzene. A typical dry bead has a diameter of 50 μm that swells five- to sixfold in DCM or DMF (144). The second was developed on the basis of the idea that the polymeric backbone should be of similar chemical composition, a polyamide, as the peptide backbone (11). Thus, copolymerized dimethylacrylamide, *N,N*'-bisacryloylethylenediamine, and acryloylsarcosine methyl ester, or polyamide resin, was developed (146). Polyamide supports are commercially known as Pepsyn resin. Many other supports have been developed that are compatible with batchwise SPPS and are summarized in the more comprehensive reviews (7,10–20,109).

The original supports designed to withstand the high flow rates and resulting back pressures of continuous-flow SPPS are low density, highly permeable inorganic matrices that have polyamide embedded within. These matrices include polyamide–kieselguhr (Pepsyn K) (147) and polyamide–Polyhipe (148). These polyamide-embedded resins have now been largely replaced by polyethylene glycol–polystyrene graft supports that have superior swelling properties in a range of solvents and have excellent physical and mechanical properties for both batchwise and continuous-flow SPPS (13,149–154). These graft polymers are commercially available as PEG-PS, TentaGel (Rapp Polymere GmbH, Tübingen, Germany), and ArgoGel (Argonant, Foster City, Calif.)

Other resins compatible with both batchwise and continuous-flow SPPS are poly(*N*-[2-(4-hydroxyphenyl)ethyl]acrylamide) (core Q) (155), polyethylene glycol dimethylacrylamide (PEGA) resins (156,157), and cross–linked ethoxylate acrylate resin (CLEAR). CLEAR has excellent swelling properties in a wide range of polar and nonpolar solvents ranging from water to DCM (158).

Cleavage. Upon completion of chain assembly the peptide must be cleaved from the resin. In standard Boc and Fmoc chemistries cleavages simultaneously remove side-chain–protecting groups as the peptide is liberated from the resin by acidolytic conditions. A variety of unwanted side reactions can occur during cleavage, so careful attention to detail is necessary to successfully complete this step in a synthesis. Detailed discussions of the fine points of cleavage are covered in the reviews (5–8,10–20).

Fmoc chemistries utilize the moderate-strength acid TFA to cleave the PAB ester and either Rink or PAL amide linkages. TFA simultaneously cleaves the

Table 10. Recommended Cocktails for Final Cleavage of the Peptide–Resin Linker and the Permanent Side-Chain–Protecting Groups Used in Fmoc-Based Synthesis[a]

Cocktail	Ratio of ingredients, v/v	Reference
Reagent K	TFA/phenol/thioanisole/ethanedithiol/water, 82.5:5:5:2.5:5	165,166
Reagent R	TFA/thioanisole/ethanedithiol/anisole, 90:5:3:2	101
Reagent B	TFA/phenol/water/triisopropylsilane, 88:5:5:2	166,167

[a]The peptide–resin is swollen in the cocktail, approximately 5 mL/g resin, for 1–2 h. The cleavage solution is then added to 10 volumes of ice-cold diethyl ether to precipitate the peptide. The crude peptide is then isolated by centrifugation to form a pellet that is washed with cold ether. After washing, the pellet may be dissolved, and the peptide purified by preparative reversed–phase HPLC.

side-chain–protecting groups listed in Table 3. In TFA the cleaved *tert*-butyl groups exist either as cations or *tert*-butyl trifluoroacetate (159–162). The trityl, 9-xanthenyl, and Pbf groups also exist as cations. Alkylation of Trp, Met, and to a lesser degree Cys and Tyr by these reactive species is prevented by including scavengers in the reaction mixture (47,163,164). Table 10 contains three cocktails that effectively scavenge reactive intermediates and also help prevent oxidation of Met to Met(O) and oxidation of Trp by ozone generated in the reaction mixture from dissolved oxygen (165,168). Once again the choice of cocktail is a preference of each lab.

Final cleavage in Boc-based syntheses is usually achieved with anhydrous HF. HF cleaves both the PAM and MBHA handles along with the side-chain–protecting groups listed in Table 2 (31). HF cleavage procedures require an all-fluorocarbon apparatus, since this strong acid will dissolve glassware. Just as in the Fmoc TFA procedure, HF cleavages must contain carbonium ion scavengers. The standard cleavage conditions are HF-anisole (9:1) at 0°C for 1 h (8). To deprotect Trp(CHO) and Met(O), a two-stage "low–high HF" procedure is used in which low HF concentrations of 20–25% in the presence of 4-thiocresol and dimethyl sulfide first deprotect these two residues and others as well. Final cleavage from the resin is then achieved by increasing the HF concentration to near that found in the standard procedure. This low–high procedure is said to give better control and better product purities than the standard procedure (31).

Purification. Reversed phase HPLC is the standard method for purification of synthetic peptides. This technique can generally remove the accumulated low level systematic by-products present in the crude peptide isolated after cleavage. The homogeneity of purified peptides should be checked by at least two orthogonal techniques, either, analytical reversed-phase or ion-exchange HPLC, or capillary zone electrophoresis (169). Mass spectrometry must also be used to confirm that the molecular ion of the isolated product has the correct mass. Amino acid analysis is used to confirm the correct amino acid composition. Sequencing information either by automated Edman degradation or by mass spectrometry techniques may also be done, although sequence analysis is not routinely required.

Side Reactions.

Solvents and Reagents. To assure that each deprotection/coupling cycle is completed with the necessary high fidelities illustrated in Table 1, all solvents and reagents must be of the highest grade available. In Fmoc-based syntheses,

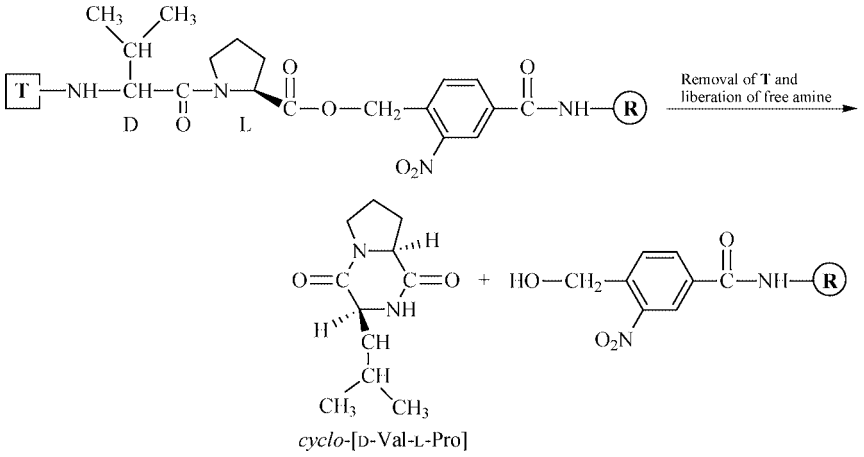

Fig. 6. Formation of a diketopiperazine from a D-valyl-L-proline sequence anchored as an *o*-nitrobenzyl ester. The example shown is designed to accentuate the potential problem, in that susceptible amino acid residues and a very good leaving group toward intramolecular aminolysis were both chosen. In this example, the level of diketopiperazine formation depended significantly on the N^{α}-amino-protecting group used, with >75% side reaction occurring in 2 min under Fmoc removal conditions and ~40% shortly after neutralizataion following Boc removal (22). See References 7,170, and 171 for additional information on mechanistic details regarding diketopiperazine formation, and References 105,112, and 171–173 for coupling protocols that mitigate the problem.

low levels of contaminating secondary amines found either in the DMF (dimethylamine) or in the DIEA used during an activation/coupling step can prematurely deprotect the Fmoc group. The highest purity, "peptide synthesis grade," of these reagents should always be purchased; old reagents should not be used in syntheses. Secondary amines can be detected with the ninhydrin test.

Diketopiperazine Formation during Attempted Incorporation of Third Amino Acid. The free N^{α}-amino group of an anchored dipeptide is poised for acid- or base-catalyzed intramolecular attack upon the C-terminal carbonyl (Fig. 6). The formation and release of the six-membered-ring diketopiperazine from the resin is kinetically favorable for residues that can form *cis*-peptide bonds, for example, Gly, Pro, *N*-methylamino acids, and D-amino acids in either of the dipeptide residues. A hydroxymethyl group remains on the resin. Diketopiperazine formation is also a problem when the third amino acid is added to a BAL-anchored (Table 5) sequence (105) or to an activated leaving group such as the *O*-nitrobenzyloxy handle (22). However, for most syntheses this problem can be adequately handled.

Succinimide Formation and $\alpha \rightarrow \beta$ Rearrangement, Particularly at Asn–Gly Sequences. Asn- and to a lesser extent Asp-containing peptides can cyclize to form a succinimide derivative (Fig. 7). The formation of the five-membered succinimide ring is kinetically favorable. The ring can open to yield either α- or β-Asp peptides. The Asn–Gly sequence has the greatest tendency to rearrange (174). This rearrangement can be a significant problem, especially if a peptide is left to stand for too long in dilute acid solutions, such as the aqueous

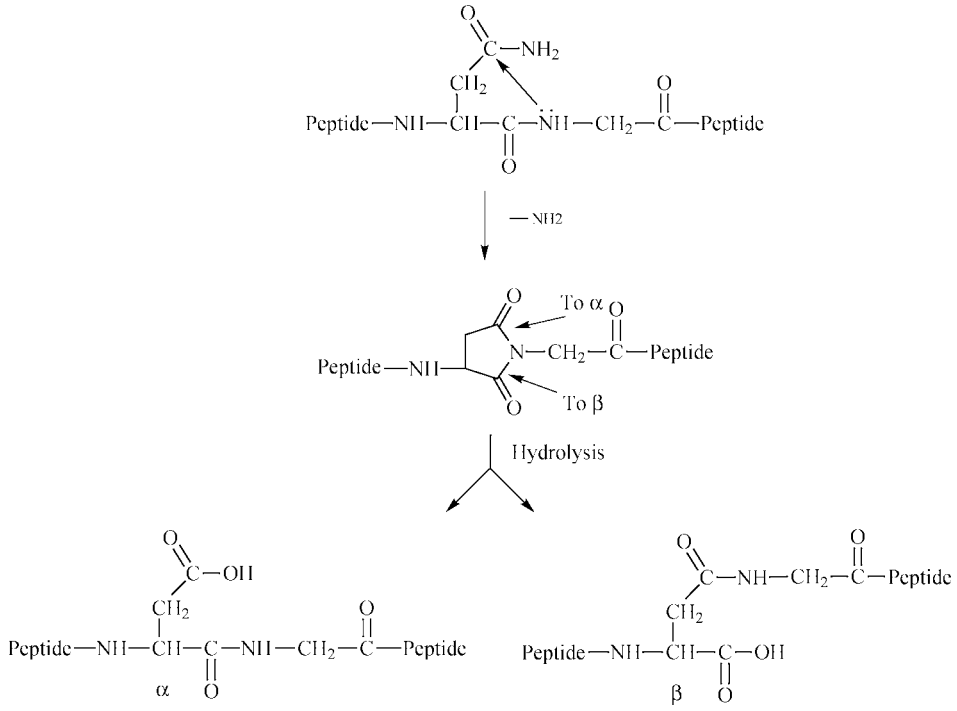

Fig. 7. Succinimide formation at the Asn–Gly sequence. The ultimate ratio of α/β peptides is determined by the thermodynamic stability of each sequence.

0.1% TFA commonly used for purification by preparative reversed-phase HPLC (174–176), or even if stored with residual acid in the solid state (177).

Acid-Sensitive Side Chains and Bonds. Trp is very sensitive to acidic conditions and to a lesser extent so is Tyr. Both can easily react with carbocations and activated molecular oxygen species. To avoid repeated exposure to acid, multiple-Trp–containing peptides are best synthesized by Fmoc strategies. Use of one of the cleavage cocktails listed in Table 10 during final cleavage is essential to avoid degradation of Trp and Tyr residues. Finally, the Asp—Pro bond is acid-labile, and Fmoc chemistries are recommended for peptides that contain this sequence (178).

Problems with Methionine and Cysteine. Sulfur-containing amino acids are susceptible to oxidation and alkylation. The cocktails of Table 10 will protect these residues during cleavage. Met is very susceptible to oxidation to methionine sulfoxide, Met(O), while standing in acidic solutions that contain dissolved oxygen. Low levels of this side reaction are very hard to avoid during HPLC purification of peptides that contain this residue. C-terminal-esterified Cys residues can be racemized by repeated piperidine deprotection treatments during Fmoc SPPS (179,180). This side reaction is manageable if the protecting groups of Table 3 are used. Alternatively, attachment of C-terminal Cys residues to the XAL handle (Table 5) via the side chain followed by chain elongation has been shown to prevent racemization (181). The use of either Trt or Xan side-chain protection also diminishes the formation of 3-(1-piperidinyl)alanine by-products (Fig. 8) that can be a serious side reaction with C-terminal Cys during Fmoc SPPS (181,182).

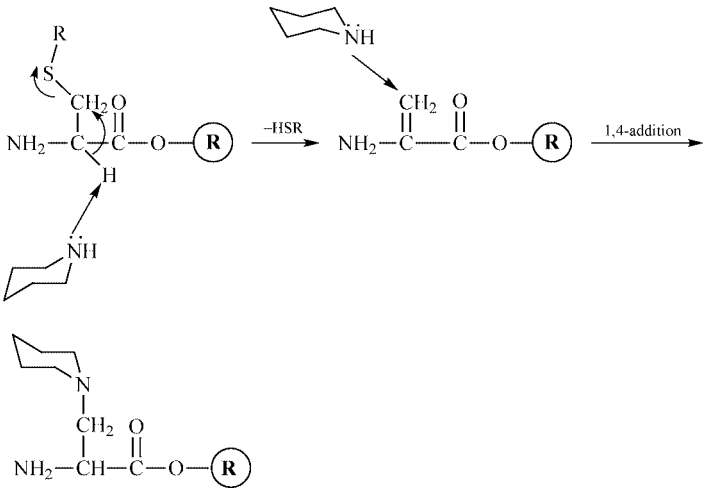

Fig. 8. Base–catalyzed elimination of C-terminal Cys residues attached to the resin via an ester linkage. 1,4-Addition of piperidine results in the formation of a 3-piperidinylalanine derivative, which can undergo chain elongation in subsequent cycles.

Prognosis

Solid-phase synthesis has evolved to where even the nonspecialist can easily make peptides of 50 amino acids or more in length. It is important to remember that each synthetic procedure has limitations, and that even in the hands of highly experienced workers, sequences will arise that defy facile preparation.

This article has touched on the key issues of chain assembly, cleavage, and purification. More challenging issues such as modification by phosphorylation (183–185), glycosylation, prenylation, and sulfation, are covered in References 20 and 186. The appendix contains strategies for finding synthesis apparatus, amino acid derivatives, resins, handles, and chemical reagents on the Internet. Research continues in other challenging areas such as disulfide bond formation, lactam cyclization, combinatorial methods, and improved reagents, handles, and resins. Finally, there is the exciting area of chemical ligation, where peptide fragments synthesized by the solid-phase method are chemoselectively condensed together to form proteins, of both natural and designed sequences (187–190). With the increasing number of peptide and protein targets identified by genomic sequencing, improvements in synthesis, and especially purification and isolation are needed to accelerate research in the field of proteomics (191–193). Thus, even now 45 years after the introduction of SPPS by Merrifield, much challenging and exciting work remains to be done.

Appendix

Solid-phase Peptide Synthesis and the Internet. The Internet contains many sites of interest for the peptide chemist. Since Internet addresses tend to regularly change, we have chosen to list terms that one can use in a search

engine rather than addresses. One should search the term contained in the quotation marks to find the specific site or topic of interest. Combining various parts of the terms in quotations while searching can make a search more accurate.

Peptide Societies. The first three societies have sites in English. The last three are in the native language of the respective country.

(1) "American Peptide Society"
(2) "Australian Peptide Society"
(3) "European Peptide Society"—The European Peptide Society Web site contains the best links to manufacturers of automated synthesizers and reagents for SPPS at the time of publication of this review
(4) "Chinese Peptide Society"
(5) "Japanese Peptide Society"
(6) "Korean Peptide Society"

General SPPS Information.

(1) "ABRF Peptide Synthesis Research Group"—This Association of Biomolecular Resource Facilities (ABRF) Web site contains summaries of difficult peptide syntheses attempted by its members. This is a good resource to see how various procedures actually work when used by practicing peptide chemists.
(2) "NRC peptide synthesis database"—This database, run by the National Research Council of Canada, contains a wealth of information about amino acid derivatives.

Consumables and Automated/Manual Synthesizers. Many manufactures of protected amino acids, resins, coupling agents, and automated/manual synthesizers exist.

(1) "Fmoc amino acids," "Boc amino acids," or "protected amino acids"—Trying either of these phrases will lead to the majority of the commercial amino acid vendors. Many of these vendors also sell resins and coupling reagents.
(2) "Solid-phase resins"—To find manufactures of resins for solid-phase synthesis
(3) "Solid-phase coupling reagents" or "peptide coupling reagents"—To find commercial sources for the coupling reagents of Figure 5
(4) "Solid-phase synthesis vessels," "Solid-phase synthesis glassware," "peptide synthesis vessels," or "combinatorial chemistry glassware"—To find reaction vessels for manual SPPS
(5) "Peptide synthesizers" or "Solid-phase synthesizers"—To find automated SPPS machines
(6) "HF apparatus"—This term will find the special all-fluoropolymer apparatus necessary for final cleavage with HF.

BIBLIOGRAPHY

"Polypeptide Synthesis, Solid-Phase Method," in *EPST* 1st ed., Suppl. Vol. 1, pp. 492–510, by M. Manning, Medical College of Ohio at Toledo; "Polypeptide Synthesis, Solid-Phase Method," in *EPSE* 2nd ed., Vol. 12, pp. 811–858, by George Barany, Nancy Kneib-Cordonier, Daniel G. Mullen, University of Minnesota.

1. F. M. Finn and K. Hofmann, in H. Neurath and R. L. Hill, eds. *The Proteins*, Vol. 2, Academic Press, New York, 1976, pp. 105–253.
2. M. Bodanszky and A. Bodanszky, *The Practice of Peptide Synthesis*, Springer-Verlag, Berlin, 1984.
3. M. Goodman, A. Felix, L. Moroder, and C. Toniolo, eds., *Synthesis of Peptides and Peptidomimetics* (Houben-Wey E22: Methods of Organic Chemistry), Georg Thieme Verlag, Stuttgart, 2002.
4. B. Merrifield, *Science* **232**, 341–347 (1986).
5. B. W. Erickson and B. W. Merrifield, in H. Neurath and R. L. Hill, eds., *The Proteins*, Vol. 2, Academic Press, New York, 1976, pp. 255–527.
6. C. Birr, *Aspects of the Merrifield Peptide Synthesis*, Springer-Verlag, Heidelberg, 1978.
7. G. Barany and R. B. Merrifield, in E. Gross and J. Meienhofer, eds., *The Peptides*, Vol. 2, Academic Press, New York, 1979, pp. 1–284.
8. J. M. Stewart and J. D. Young, *Solid Phase Peptide Synthesis*, 2nd ed., Pierce Chemical Co., Rockford, Ill., 1984.
9. G. Barany, N. Kneib-Cordonier, and D. G. Mullen, *Int. J. Pept. Protein Res.* **30**, 705–739 (1987).
10. S. B. H. Kent, *Annu. Rev. Biochem.* **57**, 957–990 (1988).
11. E. Atherton and R. C. Sheppard, *Solid Phase Peptide Synthesis: A Practical Approach*, IRL Press, Oxford, 1989.
12. G. B. Fields and R. L. Noble, *Int. J. Pept. Protein Res.* **35**, 161–214 (1990).
13. G. Barany and F. Albericio, in K. North, ed., *Biotechnology International 1990/1991*, Century Press Ltd., London, 1991, pp. 155–163.
14. G. B. Fields, Z. Tian, and G. Barany, in G. A. Grant, ed., *Synthetic Peptides: A User's Guide*, W. H. Freeman and Co., New York, 1992, pp. 77–183.
15. B. Gutte, ed., *Peptides: Synthesis, Structures, and Applications*, Academic Press, Orlando, Fla., 1995.
16. G. B. Fields, ed., *Solid-phase Peptide Synthesis*, Academic Press, Orlando, Fla., 1997.
17. P. Lloyd-Williams, F. Albericio, and E. Giralt, eds., *Chemical Approaches to the Synthesis of Peptides and Proteins*, CRC Press LLC, Boca Raton, Fla., 1997.
18. W. C. Chan and P. D. White, eds., *Fmoc Solid Phase Peptide Synthesis—A Practical Approach*, Oxford University Press, Oxford, 2000.
19. S. A. Kates and F. Albericio, eds., *Solid-Phase Peptide Synthesis. A Practical Guide*, Marcel Dekker, New York, 2000.
20. G. B. Fields, J. L. Lauer-Fields, R. Liu, and G. Barany, in G. A. Grant, ed., *Synthetic Peptides. A User's Guide*, Oxford University Press, New York, 2002, pp. 93–219.
21. G. Barany and R. B. Merrifield, *J. Am. Chem. Soc.* **99**, 7363–7365 (1977).
22. G. Barany and F. Albericio, *J. Am. Chem. Soc.* **107**, 4936–4942 (1985).
23. L. A. Carpino, *J. Am. Chem. Soc.* **79**, 4427–4431 (1957).
24. F. C. McKay and N. F. Albertson, *J. Am. Chem. Soc.* **79**, 4686–4690 (1957).
25. G. W. Anderson and A. C. McGregor, *J. Am. Chem. Soc.* **79**, 6180–6183 (1957).
26. L. A. Carpino and G. Y. Han, *J. Org. Chem.* **37**, 3404–3409 (1972).
27. E. Atherton, H. Fox, D. Harkiss, C. J. Logan, R. C. Sheppard, and B. J. Williams, *J. Chem. Soc., Chem. Commun*. 537–539 (1978).
28. C.-D. Chang, A. M. Felix, M. H. Jimenez, and J. Meienhofer, *Int. J. Pept. Protein Res.* **15**, 485–494 (1980).
29. G. B. Fields and C. G. Fields, *J. Am. Chem. Soc.* **113**, 4202–4207 (1991).

30. J. Meienhofer, M. Waki, E. P. Heimer, T. J. Lambros, R. C. Makofske, and C.-D. Chang, *Int. J. Pept. Protein Res.* **13**, 35–42 (1979).
31. J. P. Tam and R. B. Merrifield, in S. Udenfriend and J. Meienhofer, eds., *The Peptides*, Vol. 9, Academic Press, New York, 1987, pp. 185–248.
32. H. Yajima, N. Fujii, S. Funakoshi, T. Watanabe, E. Murayama, and A. Otaka, *Tetrahedron* **44**, 805–819 (1988).
33. H. Yajima, M. Takeyama, J. Kanaki, and K. Mitani, *J. Chem. Soc., Chem. Commun*. 482–483 (1978).
34. J. P. Tam, M. W. Riemen, and R. B. Merrifield, *Pept. Res.* **1**, 6–18 (1988).
35. B. Penke and G. K. Toth, in G. Jung and E. Bayer, eds., *Peptides 1988*, Walter de Gruyter and Co., Berlin, 1989, pp. 67–69.
36. Y. Kiso, M. Yoshida, T. Tatsumi, T. Kimura, Y. Fujiwara, and K. Akaji, *Chem. Pharm. Bull.* **37**, 3432–3434 (1989).
37. L. C. Dorman, D. A. Nelson, and R. C. L. Chow, in S. Lande, ed., *Progress in Peptide Research*, Vol. 2, Gordon and Breach, New York, 1972, pp. 65–68.
38. Y. Han, N. A. Sole, J. Tejbrant, and G. Barany, *Pept. Res.* **9**, 166–173 (1996).
39. B. W. Erickson and R. B. Merrifield, *J. Am. Chem. Soc.* **95**, 3757–3763 (1973).
40. N. Fujii, A. Otaka, S. Funakoshi, K. Bessho, T. Watanabe, K. Akaji, and H. Yajima, *Chem. Pharm. Bull.* **35**, 2339–2347 (1987).
41. T. Brown, J. H. Jones, and J. D. Richards, *J. Chem. Soc. Perkin Trans.* **I**, 1553–1561 (1982).
42. R. A. Houghten and C. H. Li, *Anal. Biochem.* **98**, 36–46 (1979).
43. W. Beck and G. Jung, *Lett. Pept. Sci.* **1**, 31–37 (1994).
44. T. Ferrer, E. Nicolas, and E. Giralt, *Lett. Pept. Sci.* **6**, 165–172 (1999).
45. Y. Nishiuchi, H. Nishio, T. Inui, T. Kimura, and S. Sakakibara, *Tetrahedron Lett.* **37**, 7529–7532 (1996).
46. L. A. Carpino, H. Shroff, S. A. Triolo, E. S. M. E. Mansour, H. Wenschuh, and F. Albericio, *Tetrahedron Lett.* **34**, 7829–7832 (1993).
47. C. G. Fields and G. B. Fields, *Tetrahedron Lett.* **34**, 6661–6664 (1993).
48. C.-D. Chang, M. Waki, M. Ahmad, J. Meienhofer, E. O. Lundell, and J. D. Haug, *Int. J. Pept. Protein Res.* **15**, 59–66 (1980).
49. P. Sieber and B. Riniker, *Tetrahedron Lett.* **32**, 739–742 (1991).
50. I. Photaki, J. Taylor-Papadimitriou, C. Sakarellos, P. Mazarakis, and L. Zervas, *J. Chem. Soc. Perkin Trans.* **1**, 2683–2687 (1970).
51. J. Meienhofer, in G. C. Barrett, ed., *Chemistry and Biochemistry of the Amino Acids*, Chapman & Hall, London, 1985, pp. 297–337.
52. T. W. Greene, *Protective Groups in Organic Synthesis*, John Wiley & Sons, Inc., New York, 1991.
53. Y. Han and G. Barany, *J. Org. Chem.* **62**, 3841–3848 (1997).
54. A. Loffet, N. Galeotti, P. Jouin, and B. Castro, *Tetrahedron Lett.* **30**, 6859–6860 (1989).
55. G. Lajoie, A. Crivici, and J. G. Adamson, *Synthesis* 571–572 (1990).
56. P. White, in J. A. Smith and J. E. Rivier, eds., *Peptides: Chemistry and Biology*, Escom, Leiden, 1992, pp. 537–538.
57. B. Riniker, A. Floersheimer, H. Fretz, P. Sieber, and B. Kamber, *Tetrahedron* **49**, 9307–9320 (1993).
58. S. A. Kates, N. A. Sole, F. Albericio, and G. Barany, C. Basava and G. M. Anantharamaiah, eds., *Peptides: Design, Synthesis, and Biological Activity*, Birkaeuser, Boston, 1994, pp. 39–58.
59. C. Blackburn and S. A. Kates, *Methods Enzymol.* **289**, 175–198 (1997).
60. D. Andreu, F. Albericio, N. A. Sole, M. C. Munson, M. Ferrer, and G. Barany, *Methods Mol. Biol.* **35**, 91–169 (1994).
61. F. Albericio, *Biopolymers* **55**, 123–139 (2000).
62. P. J. Belshaw, S. Mzengeza, and G. A. Lajoie, *Synth. Commun.* **20**, 3157–3160 (1990).

63. M. H. Lyttle and D. Hudson, in J. A. Smith and J. E. Rivier, eds., *Peptides: Chemistry and Biology*, Escom, Leiden, 1992, pp. 583–584.
64. W. C. Chan, B. W. Bycroft, D. J. Evans, and P. D. White, *J. Chem. Soc., Chem. Commun*. 2209–2210 (1995).
65. F. Albericio, E. Nicolas, J. Rizo, M. Ruiz-Gayo, E. Pedroso, and E. Giralt, *Synthesis* 119–122 (1990).
66. D. F. Veber, J. D. Milkowski, S. L. Varga, R. G. Denkewalter, and R. Hirschmann, *J. Am. Chem. Soc.* **94**, 5456–5461 (1972).
67. S. Sakakibara, *Biopolymers* **51**, 279–296 (1999).
68. E. Atherton, M. Pinori, and R. C. Sheppard, *J. Chem. Soc., Perkin Trans.* **1**, 2057–2064 (1985).
69. S. Romani, L. Moroder, W. Goehring, R. Scharf, E. Wuensch, Y. A. Barde, and H. Thoenen, *Int. J. Pept. Protein Res.* **29**, 107–117 (1987).
70. B. W. Bycroft, W. C. Chan, S. R. Chharbra, and N. D. Hone, *J. Chem. Soc., Chem. Commun*. 778–779 (1993).
71. G. B. Bloomberg, D. Askin, A. R. Gargaro, and M. J. A. Tanner, *Tetrahedron Lett.* **34**, 4709–4712 (1993).
72. C. G. Fields, C. M. Lovdahl, A. J. Miles, V. L. M. Hagen, and G. B. Fields, *Biopolymers* **33**, 1695–1707 (1993).
73. B. Rohwedder, Y. Mutti, P. Dumy, and M. Mutter, *Tetrahedron Lett.* **39**, 1175–1178 (1998).
74. B. Gutte and R. B. Merrifield, *J. Biol. Chem.* **246**, 1922–1941 (1971).
75. A. R. Mitchell, S. B. H. Kent, M. Engelhard, and R. B. Merrifield, *J. Org. Chem.* **43**, 2845–2852 (1978).
76. J. P. Tam, S. B. H. Kent, T. W. Wong, and R. B. Merrifield, *Synthesis* 955–957 (1979).
77. M. Mutter and D. Bellof, *Helv. Chim. Acta* **67**, 2009–2016 (1984).
78. Y. Liu, S. Ding, J. Chu, and A. M. Felix, *Int. J. Pept. Protein Res.* **35**, 95–98 (1990).
79. W. F. DeGrado and E. T. Kaiser, *J. Org. Chem.* **45**, 1295–1300 (1980).
80. W. F. DeGrado and E. T. Kaiser, *J. Org. Chem.* **47**, 3258–3261 (1982).
81. M. A. Findeis and E. T. Kaiser, *J. Org. Chem.* **54**, 3478–3482 (1989).
82. R. B. Scarr and M. A. Findeis, *Pept. Res.* **3**, 238–241 (1990).
83. S.-S. Wang, *J. Org. Chem.* **41**, 3258–3261 (1976).
84. S.-S. Wang, *J. Am. Chem. Soc.* **95**, 1328–1333 (1973).
85. R. C. Sheppard and B. J. Williams, *Int. J. Pept. Protein Res.* **20**, 451–454 (1982).
86. F. Albericio and G. Barany, *Int. J. Pept. Protein Res.* **26**, 92–97 (1985).
87. H. Rink, *Tetrahedron Lett.* **28**, 3787–3790 (1987).
88. K. Barlos, D. Gatos, J. Kallitsis, G. Papaphotiu, P. Sotiriu, W. Yao, and W. Schaefer, *Tetrahedron Lett.* **30**, 3943–3946 (1989).
89. K. Barlos, O. Chatzi, D. Gatos, and G. Stavropoulos, *Int. J. Pept. Protein Res.* **37**, 513–520 (1991).
90. F. Albericio and G. Barany, *Tetrahedron Lett.* **32**, 1015–1018 (1991).
91. H. Kunz and B. Dombo, *Angew. Chem.* **100**, 732–734 (1988).
92. F. Guibe, O. Dangles, G. Balavoine, and A. Loffet, *Tetrahedron Lett.* **30**, 2641–2644 (1989).
93. P. Lloyd-Williams, G. Jou, F. Albericio, and E. Giralt, *Tetrahedron Lett.* **32**, 4207–4210 (1991).
94. D. H. Rich and S. K. Gurwara, *J. Am. Chem. Soc.* **97**, 1575–1579 (1975).
95. E. Giralt, F. Albericio, E. Pedroso, C. Granier, and J. Van Rietschoten, *Tetrahedron* **38**, 1193–1208 (1982).
96. N. Kneib-Cordonier, F. Albericio, and G. Barany, *Int. J. Pept. Protein Res.* **35**, 527–538 (1990).
97. C. P. Holmes and D. G. Jones, *J. Org. Chem.* **60**, 2318–2319 (1995).
98. G. R. Matsueda and J. M. Stewart, *Peptides* **2**, 45–50 (1981).

99. S. A. Gaehde and G. R. Matsueda, *Int. J. Pept. Protein Res.* **18**, 451–458 (1981).
100. F. Albericio and G. Barany, *Int. J. Pept. Protein Res.* **30**, 177–205 (1987).
101. F. Albericio, N. Kneib-Cordonier, S. Biancalana, L. Gera, R. I. Masada, D. Hudson, and G. Barany, *J. Org. Chem.* **55**, 3730–3743 (1990).
102. Y. Han, S. L. Bontems, P. Hegyes, M. C. Munson, C. A. Minor, S. A. Kates , F. Albericio, and G. Barany, *J. Org. Chem.* **61**, 6326–6339 (1996).
103. P. Sieber, *Tetrahedron Lett.* **28**, 2107–2110 (1987).
104. R. P. Hammer, F. Albericio, L. Gera, and G. Barany, *Int. J. Pept. Protein Res.* **36**, 31–45 (1990).
105. K. J. Jensen, J. Alsina, M. F. Songster, J. Vagner, F. Albericio, and G. Barany, *J. Am. Chem. Soc.* **120**, 5441–5452 (1998).
106. L. E. Canne, S. M. Walker, and S. B. H. Kent, *Tetrahedron Lett.* **36**, 1217–1220 (1995).
107. J. Blake and C. H. Li, *Proc. Natl. Acad. Sci. USA* **78**, 4055–4058 (1981).
108. D. Yamashiro and C. H. Li, *Int. J. Pept. Protein Res.* **31**, 322–334 (1988).
109. G. Barany and M. Kempe, in A. W. Czarnik and S. H. DeWitt, eds., *A Practical Guide to Combinatorial Chemistry*, American Chemical Society, Washington, DC, 1997, pp. 51–97.
110. M. F. Songster and G. Barany, *Methods Enzymol.* **289**, 126–174 (1997).
111. C. Blackburn, in S. A. Kates and F. Albericio, eds., *Solid-Phase Peptide Synthesis. A Practical Guide*, Marcel Dekker, New York, 2000, pp. 197–273.
112. K. Suzuki, K. Nitta, and N. Endo, *Chem. Pharm. Bull.* **23**, 222–224 (1975).
113. M. Schnolzer, P. Alewood, A. Jones, D. Alewood, and S. B. Kent, *Int. J. Pept. Protein Res.* **40**, 180–193 (1992).
114. J. Sueiras-Diaz and J. Horton, *Tetrahedron Lett.* **33**, 2721–2724 (1992).
115. P. Alewood, D. Alewood, L. Miranda, S. Love, W. Meutermans, and D. Wilson, *Methods Enzymol.* **289**, 14–29 (1997).
116. L. P. Miranda and P. F. Alewood, *Proc. Natl. Acad. Sci. USA* **96**, 1181–1186 (1999).
117. D. H. Rich and J. Singh, in E. Gross and J. Meienhofer, eds., *The Peptides*, Vol. 1, Academic Press, New York, 1979, pp. 241–261.
118. V. Dourtoglou, B. Gross, V. Lambropoulou, and C. Zioudrou, *Synthesis* 572–574 (1984).
119. A. Fournier, C. T. Wang, and A. M. Felix, *Int. J. Pept. Protein Res.* **31**, 86–97 (1988).
120. D. Ambrosius, M. Casaretto, R. Gerardy-Schahn, D. Saunders, D. Brandenburg, and H. Zahn, *Biol. Chem. Hoppe-Seyler* **370**, 217–227 (1989).
121. R. Seyer, A. Aumelas, A. Caraty, P. Rivaille, and B. Castro, *Int. J. Pept. Protein Res.* **35**, 465–472 (1990).
122. C. G. Fields, D. H. Lloyd, R. L. MacDonald, K. M. Otteson, and R. L. Noble, *Pept. Res.* **4**, 95–101 (1991).
123. G. E. Reid and R. J. Simpson, *Anal. Biochem.* **200**, 301–309 (1992).
124. L. Carpino, A. El-Faham, C. A. Minor, and F. Albericio, *J. Chem. Soc., Chem. Commun*. 201–203 (1994).
125. Y. Han, F. Albericio, and G. Barany, *J. Org. Chem.* **62**, 4307–4312 (1997).
126. H. Gausepohl, U. Pieles, and R. W. Frank, in J. A. Smith and J. E. Rivier, eds., *Peptides: Chemistry and Biology*, Escom, Leiden, 1992, pp. 523–524.
127. S. C. Story and J. V. Aldrich, *Int. J. Pept. Protein Res.* **39**, 87–92 (1992).
128. E. Atherton, L. R. Cameron, and R. C. Sheppard, *Tetrahedron* **44**, 843–857 (1988).
129. D. Hudson, *Pept. Res.* **3**, 51–55 (1990).
130. E. Kaiser, R. L. Colescott, C. D. Bossinger, and P. I. Cook, *Anal. Biochem.* **34**, 595–598 (1970).
131. E. Kaiser, C. D. Bossinger, R. L. Colescott, and D. B. Olsen, *Anal. Chim. Acta* **118**, 149–151 (1980).
132. V. K. Sarin, S. B. H. Kent, J. P. Tam, and R. B. Merrifield, *Anal. Biochem.* **117**, 147–157 (1981).

133. C. S. Nielsen, P. H. Hansen, A. Lihme, and P. M. H. Heegaard, *J. Biochem. Biophys. Methods* **20**, 69–80 (1989).
134. J. Fox, R. Newton, P. Heegard, and C. Schafer-Nielsen, in R. Epton, ed., *Innovation and Perspectives in Solid Phase Synthesis*, Solid Phase Conference Coordination, Ltd., Birmingham, U.K., 1990, pp. 141–153.
135. N. V. McFerran, B. Walker, C. D. McGurk, and F. C. Scott, *Int. J. Pept. Protein Res.* **37**, 382–387 (1991).
136. R. Frank and H. Gausepohl, in H. Tschesche, ed., *Modern Methods in Protein Chemistry*, Vol. 3, Walter de Gruyter and Co., Berlin, 1988, pp. 41–60.
137. G. R. Matsueda and E. Haber, *Anal. Biochem.* **104**, 215–227 (1980).
138. G. W. Tregear, J. Van Rietschoten, R. Sauer, H. D. Niall, H. T. Keutmann, and J. T. Potts, Jr., *Biochemistry* **16**, 2817–2823 (1977).
139. G. R. Matsueda, E. Haber, and M. N. Margolies, *Biochemistry* **20**, 2571–2580 (1981).
140. S. B. H. Kent, M. Riemen, M. LeDoux, and R. B. Merrifield, in M. Elzinga, ed., *Methods in Protein Sequence Analysis*, Humana Press, Clifton, NJ, 1982, pp. 205–213.
141. G. Talbo, J. D. Wade, N. Dawson, M. Manoussios, and G. W. Tregear, *Lett. Pept. Sci.* **4**, 121–127 (1997).
142. B. J. Egner, M. Cardno, and M. Bradley, *J. Chem. Soc., Chem. Commun*. 2163–2164 (1995).
143. M. C. Fitzgerald, K. Harris, C. G. Shevlin, and G. Siuzdak, *Bioorg. Med. Chem. Lett.* **6**, 979–982 (1996).
144. V. K. Sarin, S. B. H. Kent, and R. B. Merrifield, *J. Am. Chem. Soc.* **102**, 5463–5470 (1980).
145. D. Live and S. B. H. Kent, in J. E. Mark and J. Lal, eds., *Elastomers and Rubber Elasticity*, American Chemical Society, Washington, DC, 1982, pp. 501–515.
146. R. Arshady, E. Atherton, D. L. J. Clive, and R. C. Sheppard, *J. Chem. Soc., Perkin Trans.* **I**, 529–537 (1981).
147. E. Atherton, E. Brown, R. C. Sheppard, and A. Rosevear, *J. Chem. Soc., Chem. Commun*. 1151–1152 (1981).
148. P. W. Small and D. C. Sherrington, *J. Chem. Soc., Chem. Commun*. 1589–1591 (1989).
149. H. Hellermann, H. W. Lucas, J. Maul, V. N. R. Pillai, M. Mutter, *Makromol. Chem.* **184**, 2603–2617 (1983).
150. E. Bayer and W. Rapp, in W. Voelter, E. Bayer, Y. A. Ovchinnikov and V. T. Ivanov, eds., *Chemistry of Peptides and Proteins*, Vol. 3, Walter de Gruyter & Co., Berlin, 1986, pp. 3–8.
151. S. Zalipsky, J. L. Chang, F. Albericio, and G. Barany, *React. Polym.* **22**, 243–258 (1994).
152. G. Barany, F. Albericio, S. A. Kates, and M. Kempe, in J. M. Harris and S. Zalipsky, eds., *Poly(ethylene) glycol: Chemistry and Biological Applications* (ACS Symposium Series 680), American Chemical Society Books, Washington, DC, 1997, pp. 239–264.
153. S. A. Kates, B. F. McGuinness, C. Blackburn, G. W. Griffin, N. A. Sole, G. Barany, and F. Albericio, *Biopolymers* **47**, 365–380 (1999).
154. O. W. Gooding, S. Baudart, T. L. Deegan, K. Heisler, J. W. Labadie, W. S. Newcomb, J. A. Porco, Jr., and P. Van Eikeren, *J. Comb. Chem.* **1**, 113–122 (1999).
155. R. Epton, D. A. Wellings, and A. Williams, *React. Polym.* **6**, 143–157 (1987).
156. M. Meldal, *Tetrahedron Lett.* **33**, 3077–3080 (1992).
157. M. Renil, M. Ferreras, J. M. Delaisse, N. T. Foged, and M. Meldal, *J. Pept. Sci.* **4**, 195–210 (1998).
158. M. Kempe and G. Barany, *J. Am. Chem. Soc.* **118**, 7083–7093 (1996).
159. E. Jaeger, P. Thamm, S. Knof, E. Wuensch, M. Low, and L. Kisfaludy, *Hoppe-Seyler's Z. Physiol. Chem.* **359**, 1617–1628 (1978).
160. M. Low, L. Kisfaludy, E. Jaeger, P. Thamm, S. Knof, and E. Wuensch, *Hoppe-Seyler's Z. Physiol. Chem.* **359**, 1637–1642 (1978).

161. B. F. Lundt, N. L. Johansen, A. Voelund, and J. Markussen, *Int. J. Pept. Protein Res.* **12**, 258–268 (1978).
162. Y. Masui, N. Chino, and S. Sakakibara, *Bull. Chem. Soc. Jpn.* **53**, 464–468 (1980).
163. J. L. Harrison, G. M. Petrie, R. L. Noble, H. S. Beilan, and S. N. McCurdy, in T. E. Hugli, ed., *Techniques in Protein Chemistry*, Academic Press, San Diego, Calif., 1989, pp. 506–516.
164. H. Choi and J. V. Aldrich, *Int. J. Pept. Protein Res.* **42**, 58–63 (1993).
165. D. S. King, C. G. Fields, and G. B. Fields, *Int. J. Pept. Protein Res.* **36**, 255–266 (1990).
166. R. J. Van Abel, Y.-Q. Tang, V. S. V. Rao, C. H. Dobbs, D. Tran, G. Barany, and M. E. Selsted, *Int. J. Pept. Protein Res.* **45**, 401–409 (1995).
167. N. A. Sole' and G. Barany, *J. Org. Chem.* **57**, 5399–5403 (1992).
168. C. A. Guy and G. B. Fields, *Methods Enzymol.* **289**, 67–83 (1997).
169. J. S. McMurray, in S. A. Kates and F. Albericio, eds., *Solid-Phase Synthesis. A Practical Guide*, Marcel Dekker, Inc., New York, 2000, pp. 735–749.
170. B. F. Gisin and R. B. Merrifield, *J. Am. Chem. Soc.* **94**, 3102–3106 (1972).
171. E. Pedroso, A. Grandas, X. De las Heras, R. Eritja, and E. Giralt, *Tetrahedron Lett.* **27**, 743–746 (1986).
172. M. Gairi, P. Lloyd-Williams, F. Albericio, and E. Giralt, *Tetrahedron Lett.* **31**, 7363–7366 (1990).
173. M. Ueki and M. Amemiya, *Tetrahedron Lett.* **28**, 6617–6620 (1987).
174. R. C. Stephenson and S. Clarke, *J. Biol. Chem.* **264**, 6164–6170 (1989).
175. K. Patel and R. T. Borchardt, *Pharm. Res.* **7**, 703–711 (1990).
176. K. Patel and R. T. Borchardt, *Pharm. Res.* **7**, 787–793 (1990).
177. P. B. W. Ten Kortenaar, B. M. M. Hendrix, and J. W. Van Nispen, *Int. J. Pept. Protein Res.* **36**, 231–235 (1990).
178. C. R. Wu, J. D. Wade, and G. W. Tregear, *Int. J. Pept. Protein Res.* **31**, 47–57 (1988).
179. J. D. Wade, J. Bedford, R. C. Sheppard, and G. W. Tregear, *Pept. Res.* **4**, 194–199 (1991).
180. Y. Fujiwara, K. Akaji, and Y. Kiso, *Chem. Pharm. Bull.* **42**, 724–726 (1994).
181. G. Barany, Y. Han, B. Hargittai, R. Liu, and J. T. Varkey, *Biopolymers* **71**, 651–664 (2004).
182. J. Lukszo, D. Patterson, F. Albericio, and S. A. Kates, *Lett. Pept. Sci.* **3**, 157–166 (1996).
183. L. F. Bonewald, L. Bibbs, S. A. Kates, A. Khatri, J. S. McMurray, K. F. Medzihradszky, and S. T. Weintraub, *J. Pept. Res.* **53**, 161–169 (1999).
184. J. S. McMurray, D. R. I. V. Coleman, W. Wang, and M. L. Campbell, *Biopolymers* **60**, 3–31 (2001).
185. J. W. Perich, *Methods Enzymol.* **289**, 245–266 (1997).
186. C. Garcia-Echeverria, in S. A. Kates and F. Albericio, eds., *Solid-Phase Synthesis. A Practical Guide*, Marcel Dekker, Inc., New York, 2000, pp. 419–473.
187. T. W. Muir, P. E. Dawson, and S. B. H. Kent, *Methods Enzymol.* **289**, 266–298 (1997).
188. P. E. Dawson and S. B. H. Kent, *Annu. Rev. Biochem.* **69**, 923–960 (2000).
189. J. P. Tam, J. Xu, and K. D. Eom, *Biopolymers* **60**, 194–205 (2001).
190. S. Kent, *J. Pept. Sci.* **9**, 574–593 (2003).
191. M. Kussmann and P. Roepstorff, *Methods Mol. Biol.* **146**, 405–424 (2000).
192. U. Reineke, R. Volkmer-Engert, and J. Schneider-Mergener, *Curr. Opin. Biotechnol.* **12**, 59–64 (2001).
193. R. Frank, *Combin. Chem. High Throughput Screen.* **5**, 429–440 (2002).

GEORGE BARANY
NANCY KNEIB-CORDONIER
DANIEL G. MULLEN
The University of Minnesota

POLY(PHENYLENE ETHER). See POLYETHERS, AROMATIC.

POLY(*p*-PHENYLENEVINYLENE). See Volume 7.

POLYPHOSPHAZENES. See Volume 7.

POLYPROPYLENE. See PROPYLENE POLYMERS.

POLYSACCHARIDES

Introduction

Polysaccharides are naturally occurring polymers in which the repeat unit consists of monosaccharides linked through glycosidic linkages by a condensation type reaction; the example of cellulose is given in Figure 1. They exist in plants, animals, or microbial worlds where their roles as energy storage or structural materials or as source of biological activity are recognized. Many general books published can be taken into consideration (1–13).

Monosaccharides are most readily obtained from natural sources; in that respect D-glucose plays a central role in the biochemistry of carbohydrates.

In addition, because of the presence of —OH groups, natural polysaccharides may be modified by controlled chemical reaction to give derivatives with new specific properties; industrial derivatives are mainly obtained from cellulose (qv), starch (qv), and chitin and chitosan (qv). The presence of these —OH functional groups is also the origin of interaction with water molecules (hydrophilic character of oligo- and polysaccharides) and intra- and interchain H-bond network formation playing a role in reactivity control, swelling, or dissolution rate.

This article describes the structure of the principal polysaccharides from natural sources, some methods for their characterization, and some physical properties. Few derivatives are described and this article is extended to synthetic polymers having a sugar entity in the basic structure.

Carbohydrate Nomenclature

The international rules of carbohydrate nomenclature adopted by the International Union of Pure and Applied Chemistry and the International Union of Biochemistry have been published (14). A brief summary of the structural basis for naming oligo- and polysaccharides is given in the following.

Structure of Monosaccharides. Monosaccharides (general formula $C_n(H_2O)_n$) are the basic constitutional units of oligo- or polysaccharides. A monosaccharide is a polyhydroxycarbonyl compound classified as tetrose, pentose, hexose, etc, according to the number of carbon atoms in the molecule; a prefix indicates the nature of the carbonyl group which is an aldehyde or a ketone. Thus, aldohexose has six carbons and one end of the molecule (position 1) has an aldehydic group with a reducing character. If the reducing group is a ketone in the second position, a six-carbon chain is called a ketohexose (Table 1) (9,10).

Encyclopedia of Polymer Science and Technology. Copyright John Wiley & Sons, Inc. All rights reserved.

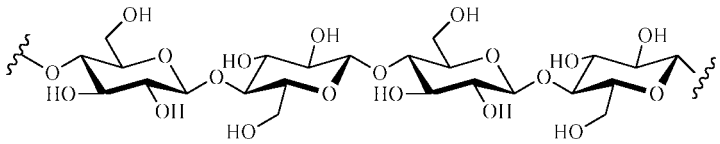

Fig. 1. Cellulosic chain formed from condensed D-glucose.

Fig. 2. The two tetrahedral representations of glyceraldehydes.

Configuration of Monosaccharides. Different representations were proposed to show the structure of the monosaccharide. The original Fischer representation allows description of different structures and especially demonstrates the chiral relation between monosaccharides, eg, that D-galactose is the C-4 epimer of D-glucose.

The chirality of monosaccharides is related to the presence of asymmetric carbon in the molecule; aldohexose contains four asymmetric carbons (see Table 1) and consequently 16 stereoisomers can be described.

The first member of the polyhydroxycarbonyl series is the aldotriose glyceraldehyde which contains one asymmetric carbon, and thus two stereoisomers. Figure 2 shows the two different molecules, which are mirror images of each other, in the tetrahedral representation with the asymmetric carbon in the center. The projection on a plane of these molecules corresponds to the Fischer representations (Fig. 3). Initially, one of the forms was found to be dextrorotary (+) and was named

Table 1. Acyclic Forms of D-Aldoses and D-Ketoses[a]

	Trioses	Tetroses	Pentoses	Hexoses
Aldoses	CHO *CHOH CH_2OH	CHO *CHOH *CHOH CH_2OH	CHO *CHOH *CHOH *CHOH CH_2OH	1. CHO 2. *CHOH 3. *CHOH 4. *CHOH 5. *CHOH 6. CH_2OH
Ketoses	CH_2OH C=O CH_2OH	CH_2OH C=O *CHOH CH_2OH	CH_2OH C=O *CHOH *CHOH CH_2OH	1. CH_2OH 2. C=O 3. *CHOH 4. *CHOH 5. *CHOH 6. CH_2OH

[a] Asterisk (*) indicates the presence of asymmetric carbons.

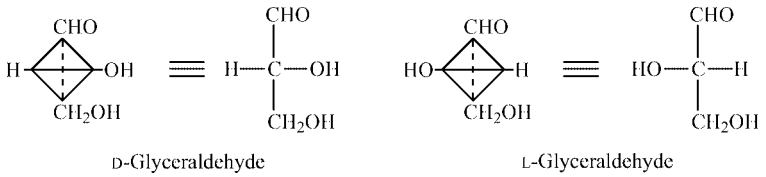

Fig. 3. Fisher projection of D- and L-glyceraldehyde.

D-glyceraldehyde; the other one was levorotary (−) and called L-glyceraldehyde. From the triose, in the Fischer representation, a series of stereoisomers are generated as indicated in Figure 4. The D-series refers to molecules in which the —OH on the last asymmetric carbon is on the right. The D- or L-identification does not mean that it is dextro (+) or levo (−) (Rosanoff convention). Physical investigation, later after Fischer, concluded that the D- and L-attribution represents the absolute configuration as demonstrated for (+)-D-glyceraldehyde. The majority of natural monosaccharides involved in polymeric systems belongs to the D-series.

Cyclic Conformation of Monosaccharides. The crystalline form of glucose was shown as cyclic (six-membered, oxygen-containing ring) from X-ray diffraction (15); infrared spectroscopy detects no carbonyl group, confirming a

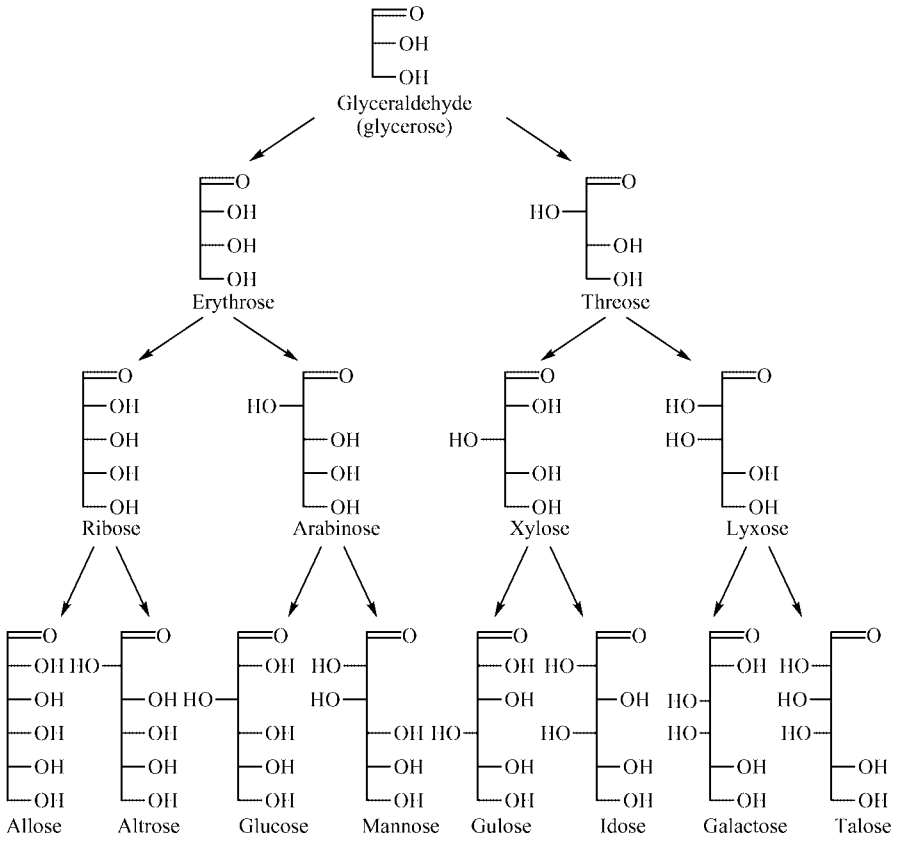

Fig. 4. Acyclic forms of D-aldoses in their Fischer projections.

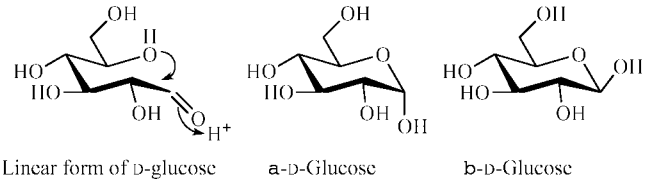

Fig. 5. Representation of the α- and β-cyclic anomers of D-glucopyranose.

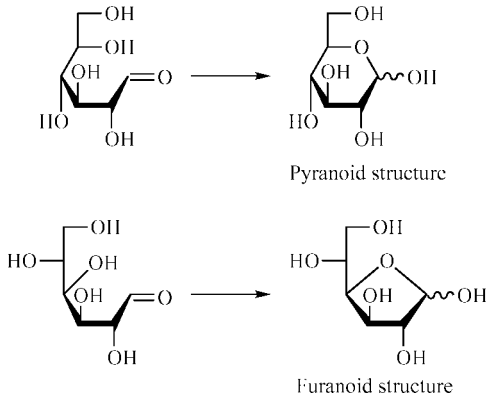

Fig. 6. Haworth representation of the cyclic forms (pyranoid and furanoid) of D-glucose.

cyclic hemiacetal structure. In the hemiacetalic form, the carbonyl carbon changes from sp^2 to sp^3 hybridization and thus becomes chiral with two anomeric forms (α and β) on carbon C-1 as shown in Figure 5. Among common hexoses, six-membered (pyranose) and/or five-membered (furanose) rings can be formed. Haworth introduced more realistic pictures of the cyclic forms (Fig. 6). The representation ~OH means that the two configurations α and β exist in equilibrium. For the D-series, the α-anomer has the hydroxyl at the anomeric center (position 1) downwards in the Haworth representation; the β-anomer is upwards.

Considering the six-membered ring, different conformations can be distinguished, taking as reference the cyclohexane. The favored conformations are chairs in the $^4C_1$ and $^1C_4$ conformations. The representation of α-D-glucose is

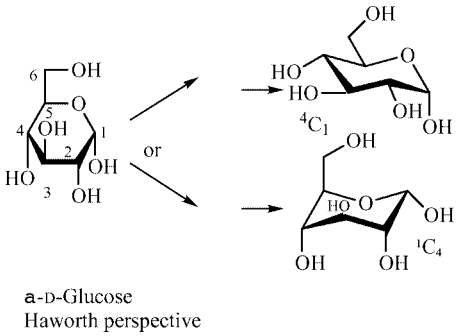

Fig. 7. Two chair conformations for α-D-glucose.

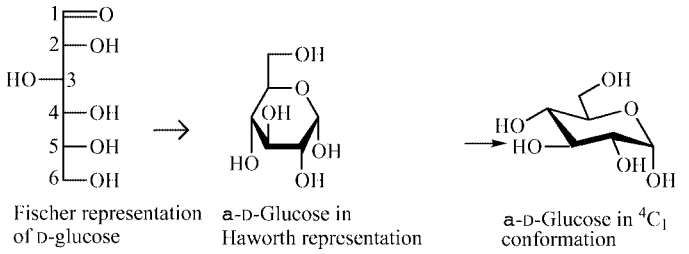

Fig. 8. The different representations for D- glucose in the α conformation for the cyclic form: (**a**) Fischer, (**b**) Haworth, (**c**) $^4C_1$ chair corresponding to the energy minimum.

given in Figure 7; the $^4C_1$ conformation, with all but the OH at C-1 in the equatorial orientation, is preferred compared with the $^1C_4$ conformation. In the α-D geometry, the anomeric hydroxyl (on C-1) is axial but it is equatorial in the β-D conformer.

For D-aldopyranose in general, the conformation $^4C_1$ is usually preferred. A summary of the different representations of D-glucose and the most probable conformation of α-D-glucose are given in Figure 8.

Mutarotation in Solution. In solution, equilibrium exists between the linear conformation and the two anomeric forms of pyranose and furanose cyclic hemiacetal forms (Fig. 9); the percentage of each form as well as the ratio α/β is characteristic of the monosaccharide considered.

A few values of the percentage at equilibrium are given in Table 2. Because of this equilibrium the reducing nature of the sugar is maintained.

^1H NMR in D_2O allows characterization of the anomeric contents in equilibrium after a short time at 25°C; an example is given in Figure 10: the H-1

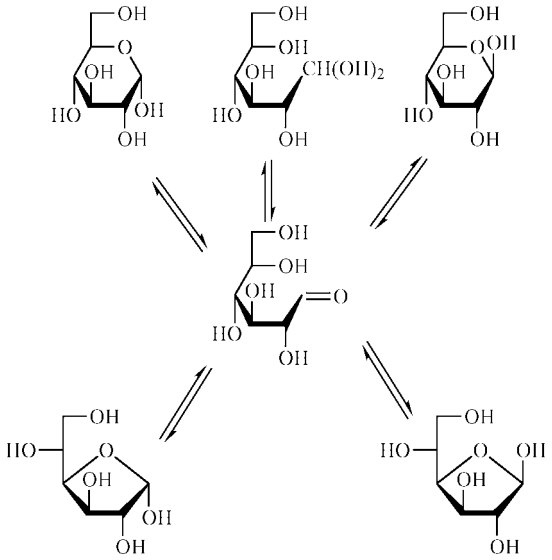

Fig. 9. Mutarotation in solution: representation of the different species in equilibrium for D-glucose (see Table 2).

Table 2. Conformation Equilibrium for Some Monosaccharides[a]

Sugar	$T_{°C}$	α-Pyran, %	β-Pyran, %	α-Furan, %	β-Furan, %	Acyclic, %
Arabinose	31	60	35.5	2.5	2	0.03
Glucose	31	38	62	—	0.14	0.02
Galactose	31	30	64	2.5	3.5	0.02

[a]Reference 10.

signal corresponding to the α-anomer is located at 5.12 ppm with a narrow doublet ($J = 3.7$ Hz) but the signal for the β-anomer is located 0.6 ppm upfield with a coupling constant $J = 7.9$ Hz. ^{13}C NMR also allows identification of the equilibrium in solution; in addition, no C=O signal is seen, confirming the cyclic configuration. The NMR characteristics given for D-glucose in water are recalled in Table 3 (16,17).

From this example, it is shown that the coupling constants and the location of the signals allow identification of the nature of the sugar and its configuration (16–19). The NMR technique is one of the most powerful tools for characterizing monosaccharides but also for establishing the structure of polysaccharides. The anomeric equilibrium only affects the reducing end of the chain; for a high molar mass, the spectrum is not perturbed by this effect and only one series of signals appears.

Uronic Acid and Other Monosaccharides. Formation of a uronoside requires the oxidation of the primary hydroxyl group of a hexopyranoside. This type of unit is very important in many natural polysaccharides such as alginates, pectins, or some hemicelluloses. Some important monosaccharides are represented in Figure 11.

Some chemical or enzymic methods are recognized to allow the specific oxidation of primary hydroxyls in the C-6 position. The TEMPO method applied to polysaccharides was used to oxidize the *N*-acetylglucoamine unit in hyaluronan (20); galactose oxidase was used to modify the galactose side groups in galactomannan (21,22).

Table 3. NMR Spectrum Characteristics of D-Glucose in D_2O

	H-1	H-2	H-3	H-4	H-5	H-6	H-6′
δ (ppm)							
α	5.09	3.41	3.61	3.29	3.72	3.72	3.63
β[a]	4.51	3.13	3.37	3.30	3.35	3.75	3.60
J (Hz)							
α	3.6	9.5	9.5	9.5		2.8	5.7, 12.8
β	7.8	9.5	9.5	9.5		2.8	5.7, 12.8
	C-1	C-2	C-3	C-4	C-5	C-6	
δ (ppm)							
α	92.9	72.5	73.8	70.6	72.3	61.6	
β[b]	96.7	75.1	76.7	70.6	76.8	61.7	

[a]Measured at 400 MHz in D_2O at 296 K relative to acetone (2.12 ppm) 16.
[b]Given in Table 1, Ref. 17.

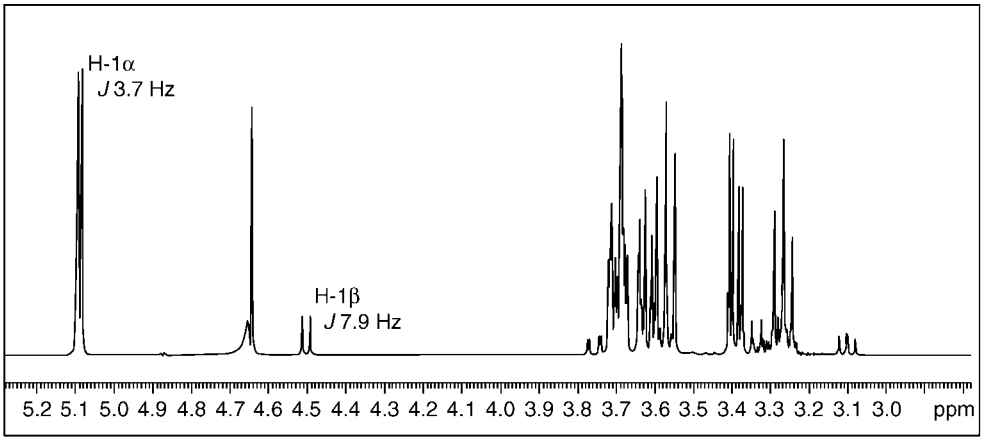

(**a**)

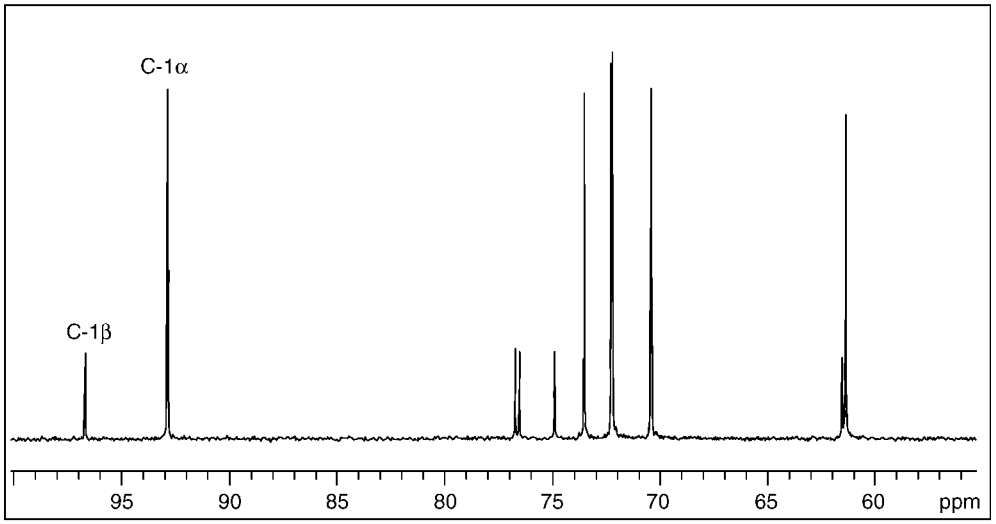

(**b**)

Fig. 10. ^{1}H and ^{13}C NMR spectra for D-glucose after a short time in D_2O at 25°C at 400 and 100 MHz respectively (low content of β-form).

Important monosaccharides are the amino sugars which have an amino group at any position other than anomeric carbon: 2-amino-2-deoxy-D-glucose or D-glucosamine also called chitosamine is the monomeric unit constitutive of chitosan, the polymer obtained by deacetylation of chitin which is based on the *N*-acetyl derivative of D-glucosamine (see Fig. 11). The sugar 2-amino-2-deoxy-D-galactose is found in dermatan and chondroïtin sulfate, constituents of mammalian tissues and cartilage.

Oligosaccharides. These oligomers result from partial acid or enzymatic hydrolysis of polysaccharides and they are prepared for structural analysis of polysaccharides. Few disaccharides exist naturally, or are produced by enzymes;

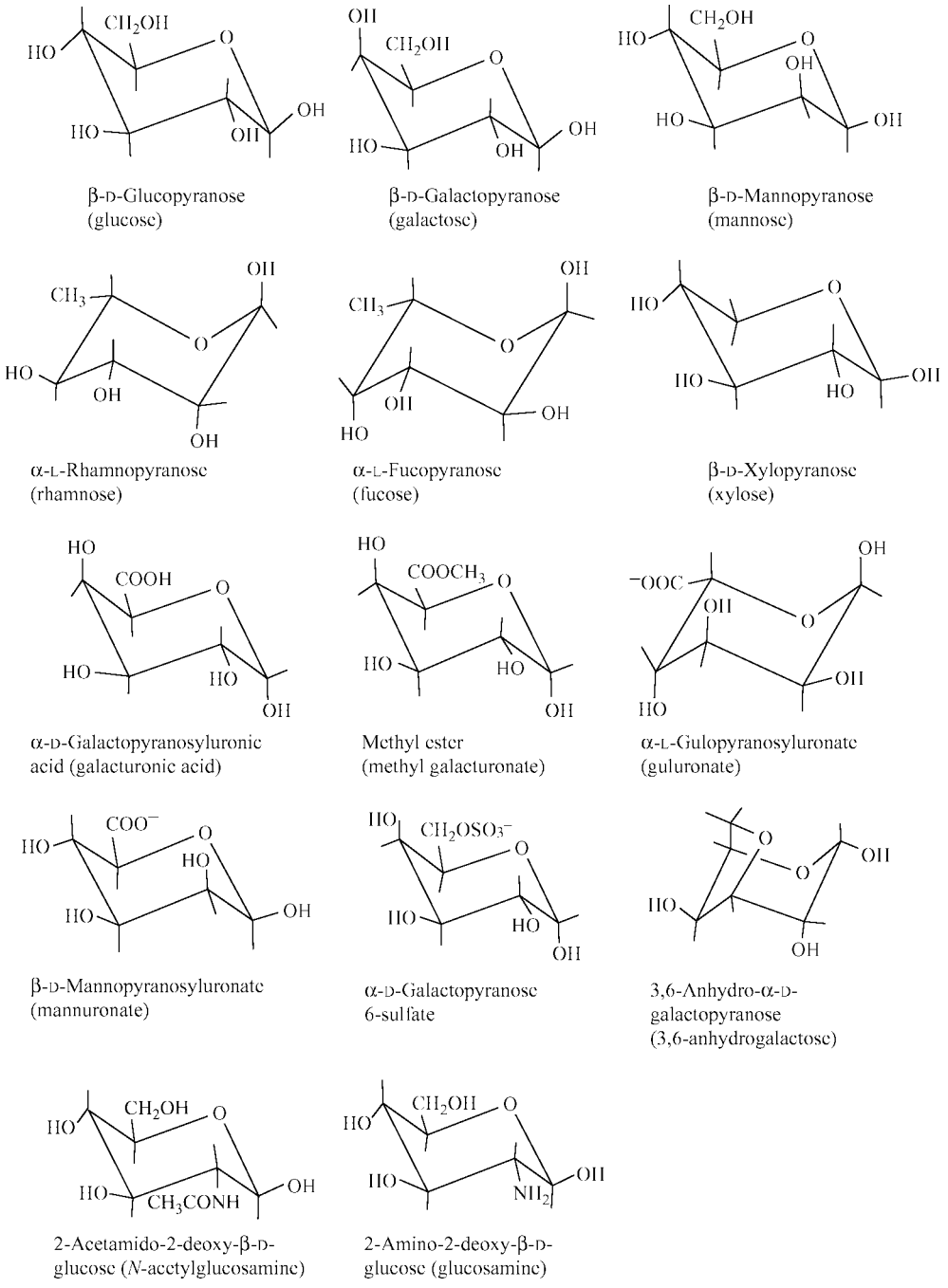

Fig. 11. Representation of some monosaccharides involved in most of the polysaccharides.

the linkage between two monosaccharides is an acetal bond also called an osidic bond. The acetal bond imparts a nonreducing character to the anomeric carbon. For common di- or trisaccharides, trivial names are normally used instead of systematic names. The nonreducing elements of an oligosaccharide are designated by the suffix -yl. In the case of nonreducing disaccharides the monomers are listed in alphabetical order.

Examples of reducing disaccharides are such as lactose and maltose. Lactose occurs in milk of mammals and is named systematically as β-D-galactopyranosyl-(1→4)-D-glucopyranose or 4-*O*-β-D-galactopyranosyl-D-glucopyranose and abbreviated Gal*p*-β-(1→4)-Glc (the italic *p* indicates the pyranoid form). Maltose, obtained by hydrolysis of amylose, is named (4-*O*-α-D-glucopyranosyl-D-glucose or α-D-glucopyranose-(1→4)-D-glucose). The -ose suffix in the systematic name denotes a reducing disaccharide, eg, one with one anomeric carbon in a hemiacetal form. Sucrose or saccharose is a nonreducing disaccharide. It is extracted from sugarbeet or sugar cane, is named β-D-fructofuranosyl-α-D-glucopyranoside, and abbreviated as β-D-Fru*f*-(2↔1)-α-D-Glc*p*. The biosynthesis and structure of disaccharides are developed in Reference 11. The -ide suffix denotes a nonreducing disaccharide wherein both anomeric carbons are in the acetal linkage.

In Figure 13, the ^{13}C NMR spectra of cellobiose (β-D-Glc*p*-(1→4)-D-Glc) (Fig. 12**a**) and maltose (α-D-Glc*p*-(1→4)-D-Glc) (Fig. 12**b**) are given; the anomeric equilibrium of D-glucose at the reducing end is demonstrated (23); the signals corresponding to the C-1 of the nonreducing D-glucose (indicated as ′) are located at a different chemical shift depending on the anomeric configuration: C-1′β is at 105.3 ppm (cellobiose) but C-1′α is at 102.5 ppm (maltose) (in D_2O at 60°C). NMR spectroscopy data are given in the literature for mono- and oligosaccharides (16–19).

Cyclodextrins (qv) represents a series of cyclic α-(1→4)-linked D-glucopyranose oligomers obtained by enzymic degradation of starch using a cyclodextrin glucotransferase (11). The most common cyclodextrins are called α, β, γ cyclodextrins with 6, 7, 8 sugars respectively resulting in intrasaccharide α-1,4-glycosidic bonds.

They have a toroïdal structure with hydrophilic exteriors and a hydrophobic cavity in which hydrophobic organic compounds can be trapped.

They are used to stabilize vitamins against temperature or increase solubility of pharmaceutical products. They also show an interesting selectivity in relation with the dimensions of the cavities (Fig. 13).

Fructosans are oligomers or polymers of β-D-fructofuranose and belong to the inulin-type ((2→1)-β-linked) or to the phlein-type (2→6 linked); inulin oligomers are found in Jerusalem artichoke or dahlia tubers where they are carbohydrate reserves. They are usually low molecular weight polymers (degree of polymerization, DP $\leq$ 50). The high yield in fructosans in Jerusalem artichoke may be considered as a source of fructose for the food industry. The juice extracted from grounded tubers was isolated and studied by liquid chromatography (HPLC). The oligosaccharide distribution was obtained by size exclusion chromatography (SEC) and by normal-phase HPLC (24–29). After separation of the different constituents and NMR analysis, it is concluded that the juice consists of an oligomer series formed of oligo-β-fructofuranosyl units (2→1) ended by one α-D-glucopyranosyl unit (Fig. 14).

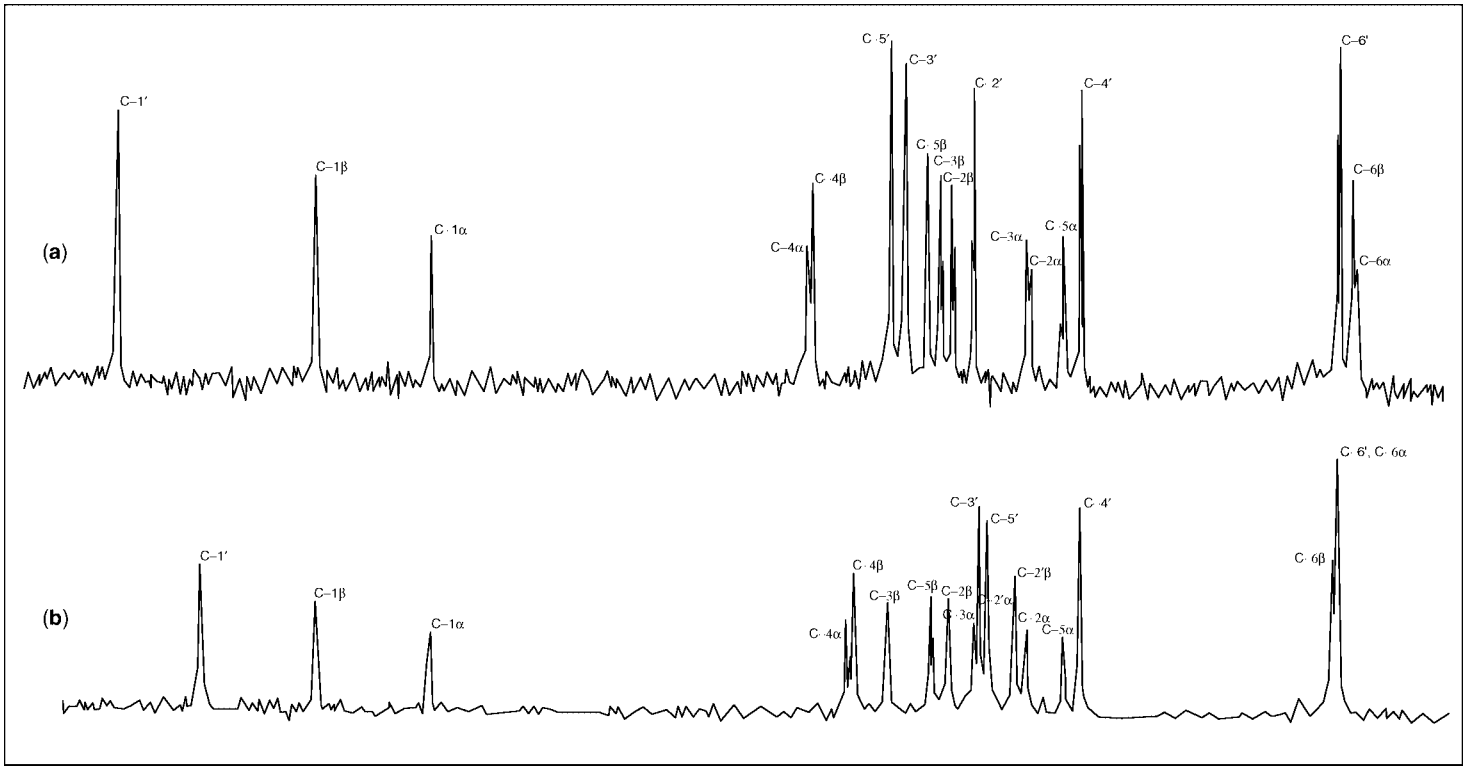

Fig. 12. ^{13}C NMR of (**a**) cellobiose and (**b**) maltose at 60°C in D_2O at 62.86 MHz. The anomeric equilibrium is clearly observed on the C-1 position. Reproduced from Ref. 23, with the permission of John Wiley & Sons (Copyright 2003).

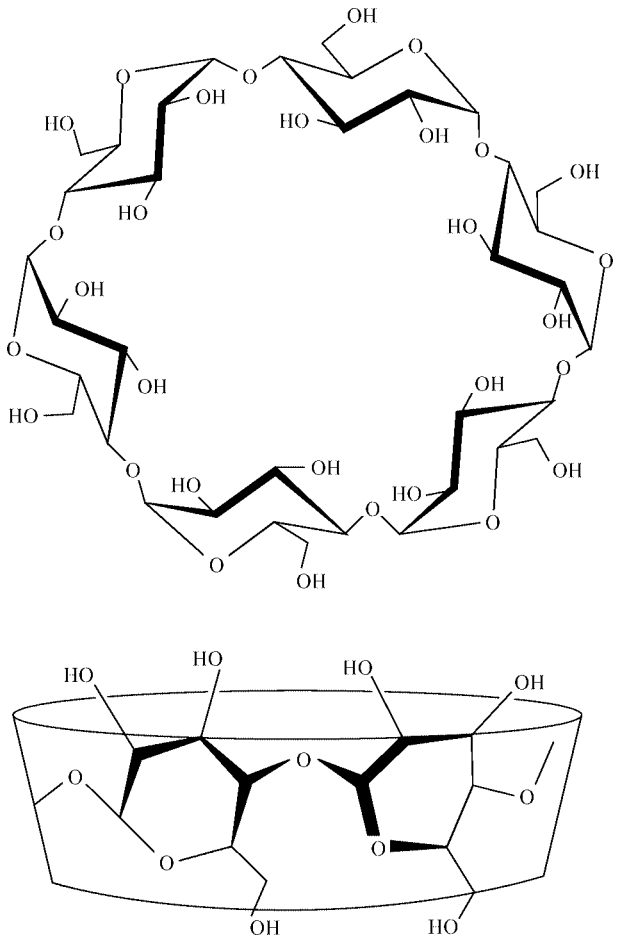

Fig. 13. Representation of the α-cyclodextrin (six glucose units) in the cyclic and toroidal forms showing the hydrophobic cavity and the hydrophilic faces.

Oligosaccharins. It has been demonstrated that specific oligosaccharides are used to control biological processes in plant. Albersheim who was a pioneer in this work recognized that specific oligosaccharide components of plant cell walls (named oligosaccharins) can have biochemical activity which results in regulatory response (30). α-(1→4)-linked D-galacturonic acid oligosaccharides obtained from pectins have regulatory effects on plant growth and development.

In connection with the biological activity of mono- and oligosaccharides, it is important to mention plant lectins: lectins are proteins possessing at least one noncatalytic domain which binds reversibly to specific mono- and oligosaccharides (31,32); lectins are carbohydrate-binding (glyco)proteins of nonimmune origin capable of specific recognition of carbohydrates and reversible binding to them, without altering their covalent structure. Many of plant-based food ingredients contain lectins, some with striking biological activities.

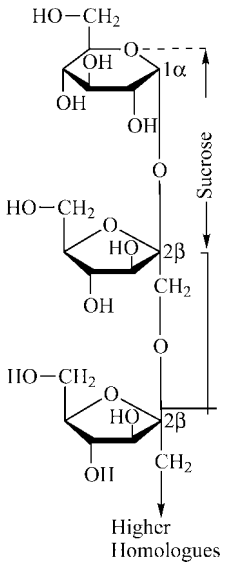

Fig. 14. Fructans, as reserve polysaccharides, from the inulin-type like in Jerusalem artichoke.

Glycans. The generic name for polysaccharides is glycan using the suffix "an." The names of polysaccharides should be D-glucan, or D-mannan for homopolymers constituted of D-glucose or D-mannose respectively. Certain historic names have been retained such as cellulose (β-(1→4)-D-glucan) or amylose (α-(1→4)-D-glucan). The homopolymers are also named homoglycans, whereas polysaccharides composed of two or more monosaccharides are named heteroglycans. An example is given with the bacterial polysaccharide called Fucogel® based on a trisaccharide repeating unit:

$$3)\alpha\text{−L−Fuc}p\text{−}(1\rightarrow3)\text{−}\alpha\text{−D−Gal}p\text{−}(1\rightarrow3)\text{−}\alpha\text{−D−Gal}p\text{A−}(1\rightarrow$$

in which the sequence, the name of the constitutive sugars, the type of bonds, and the configuration are all given (33). A labile acetyl substituent was located on the Gal*p*A unit.

Single words such as xylans or mannans may also be used to refer to related groups of polysaccharides without implying that they are homopolymers. The name xylan is used for arabinoxylan and glucuronoarabinoxylan, heterogeneous polysaccharides found in plants. The term mannan is used for glucomannan, galactomannan, and galactoglucomannan.

The extract from a natural source is often a mixture of different polymers, especially from plant sources; the extract must be fractionated but each fraction still contains molecules with minor structural features (partial acetylation or length of side chains). The fraction is polydisperse in molecular structure; the difference in local structure is also termed the microstructure.

Bacterial polysaccharides produced by a specific strain are usually perfectly homogeneous; the only difference between molecules being in the DP (or the

molecular weight); the sample is characterized by the *polydispersity index*, which is defined as the ratio between the mass-average molar mass (M_w) and the number-average molar mass (M_n) (34) (see MOLECULAR WEIGHT DETERMINATION).

Molecular Modeling

The physical and biological properties of macromolecules depend on their three-dimensional structures. Knowledge of the different stable conformations is required to better understand and to predict their behavior in different environments. This knowledge is also important to control and modify the role played by these macromolecules in recognition and interaction processes. Conformational data can be obtained by both experimental and computational methods. Experimental studies give data that are often incomplete, dependant on conformational equilibra or specific for a frozen state. An alternative method is molecular modeling where results depend unfortunately on human decisions. However, conjunction, these two approaches lead to a good understanding of the three-dimensional arrangements of the studied molecule.

Monosaccharides. Most of the monosaccharides exist as pyranose rings. The most stable conformation of such six-membered ring systems is usually one of the chair forms (C). In principle the pyranoid ring can also adopt energetically less favorable conformations. Six different skew conformers (S) separated by six different boat conformers can be identified on the pseudorotational itinerary (35). Three puckering parameters define unambiguously the position of the individual forms of the pyranoid ring on the conformational sphere (Fig. 15), Q is the maximum puckering amplitude, the parameters θ and ϕ are angles in the range $0^\circ < \theta < 180^\circ$ and $0^\circ < \phi < 360^\circ$, and can be thought as polar and azimutal angles for a sphere of radius Q. The two poles $\phi = 0^\circ$ and 180° represent the energy wheels of the chair conformations; $^1C_4$ and $^4C_1$.

All 12 flexible forms are located at the equator. In unsubstituted cyclohexane, the two chair forms are the prominent species. Substitution of heteroatom in the ring and addition of hydroxyls or other exocyclic substituents further stabilize or destabilize ring conformers in reference to cyclohexane. As a general rule, the equatorial position of bulky substituents would be preferred because of 1, 3 *syn–diaxial* interaction that causes steric clashes. The $^4C_1$ of glucopyranose having all ring substituents in the equatorial position is preferred to the $^1C_4$ conformer in which all the substituents are in axial orientation. However, at high temperature conformational transition to this form can arise spontaneously as demonstrated by the formation of levoglucosan (1,6-anhydro-β-D-glucopyranose). Besides, the α-L-iduronate ring, which is a constituent of the glycosaminoglycans (heparin, heparan sulfate, and dermatan sulfate), shows conformational mobility. Three forms, namely $^1C_4$, $^2S_0$, and $^4C_1$, of this ring have been suggested to be responsible for the biological activities of these compounds.

Very important furanose molecules (five-membered rings) are commonly found in nature. For example, D-ribose and D-deoxyribose are found as the building units of nucleic acids, and fructose is a constituent of sucrose. These rings are not planar, either one (envelope form) or two (twist form) atoms are out of the plane containing the others. The different envelope and twist conformations

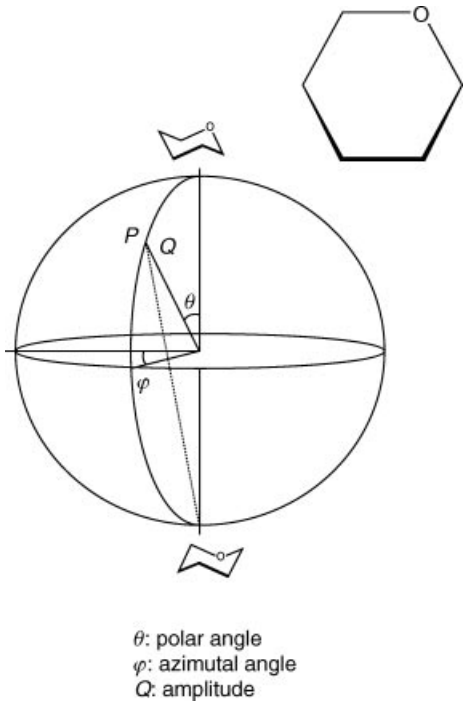

Fig. 15. Pseudorotation sphere of pyranoid rings.

are of similar energy, and the barrier to their interconversion is small, therefore mixtures of different conformations are expected in solution. The different conformations of the furanoid ring are described by a pseudorotation circle (Fig. 16). Two puckering parameters are needed to define a conformation for those rings, the puckering amplitude ν and the phase angle P (35).

Several low energy conformations are accessible for the primary hydroxyl exocyclic groups. The energies of the different ring conformations are affected by the orientations of the hydroxymethyl group. This group usually exists in three staggered positions called *gauche–gauche*, *gauche–trans*, and *trans–gauche* (Fig. 17).

In this terminology, the torsion angle ω(O-5—C-5—C-6—O-6) is stated first, followed by the torsion angle ω'(C-4—C-5—C-6—O-6). It is known from crystallographic studies, NMR measurements, and theoretical calculations that the conformational equilibrium around the C-5—C-6 bond in aldopyranoses depends significantly upon the configuration at C-4. For the "gluco" configuration (O-4 equatorial) the *trans–gauche* is high in energy and the remaining two conformations are almost equally populated, while the *trans–gauche* and *gauche–trans* positions are preferred for those having a "galacto" configuration (36).

The secondary hydroxyl groups undergo almost free rotational transitions. All these hydroxyl groups can participate in the creation of hydrogen bonds. As a result of the many possible orientations of such groups, prediction of the hydrogen bonding network is a difficult task. Most carbohydrates offer an exceptionally

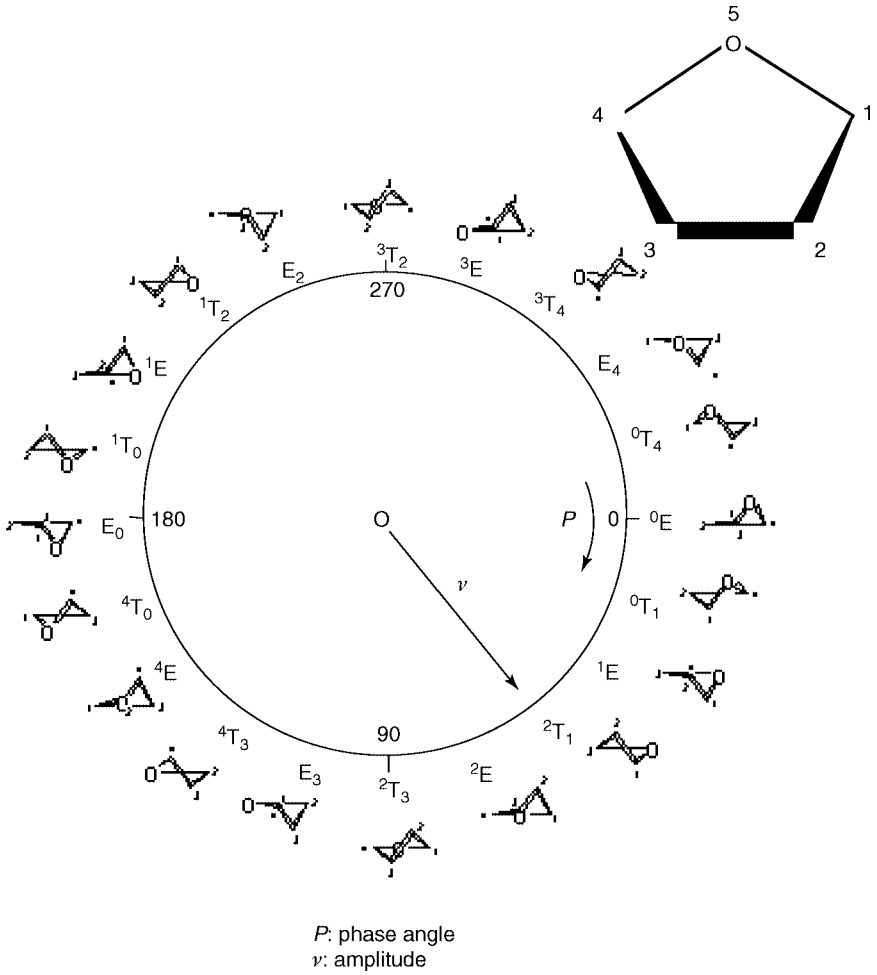

Fig. 16. Pseudorotation wheel of furanoid rings.

high ratio of hydroxyl groups per saccharide residue. Such a hydrogen-bonding potential is satisfied by association with neighboring carbohydrate molecules, glycoproteins, or surrounding water molecules.

Anomeric Effect. The anomeric effect describes the axial preference for an electronegative substituent of the pyranose ring adjacent to the ring oxygen, whereas the exo-anomeric effect describes the rotational preference of the glycosidic C-1—O bonds (37). These stereoelectronic effects are of general importance for all molecules having two heteroatoms linked to a tetrahedral center. Survey of X-ray crystallographic data reveals that these effects have geometrical consequences. The most obvious feature of the experimental data on both the α and β configuration is a marked difference in the molecular geometry around the acetal group. By way of example, in the axial configuration one observes a general shortening of the C-1—O-5 bond, a lengthening of the C—O-*X* bond (for a 1→*X* linkage), and an increase in the O-5—C-1—O-*X* bond angle value. Molecular orbital

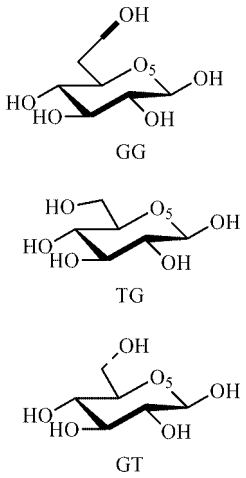

Fig. 17. The staggered orientations of the hydroxymethyl group. GG = *gauche–gauche*; GT = *gauche–trans*; TG = *trans–gauche*.

theory accounts for these observations. The magnitude of the anomeric effect varies with the nature of the electronegative group, the polarity of the solvent, and the location of the other substituents in the molecule.

The exo-anomeric effect influences the rotations around the glycosidic C-1—O bond and is therefore important in determining the relative orientations of saccharide units in carbohydrate chains. The exo-anomeric effect is a balance between electronic and steric effects. The three staggered orientations for rotation about the glycosidic bond are not equivalent; the exo-anomeric effect causes preference for the +*synclinal* orientation of the aglycone group in the α series and −*synclinal* for the β series (see Fig. 18 for the definition of the torsion angle domains).

Disaccharides. Monosaccharides can be condensed to produce oligomeric structures through glycosidic bond formation. Water is eliminated between the anomeric hydroxyl and any one of the hydroxyls of a second monosaccharide or oligosaccharide. The glycosidic linkage is constituted by two bonds, the glycosidic C-1—O-*X* and the aglycone O-*X*—C-*X*. In the case of (1→6) linkages between two pyranosic units, three bonds connect the successive sugar rings.

The low energy conformers of a disaccharide can be estimated using molecular mechanics. The conformational parameters that occur for a simple disaccharide are as follows:

OH rotation	7 torsion angles
CH_2 OH rotation	2 torsions
Aglycone rotation	1 torsion
Glycosidic bond	2 torsions
Puckering	6 variables

If we assume three minima that should be explored for each variable, there are 3^{18} combinations to consider, far beyond the available computer resources.

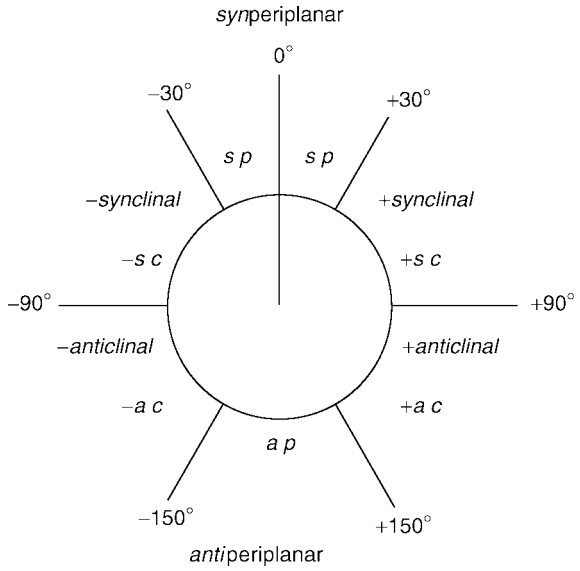

Fig. 18. Definition of angle domains.

It is therefore important to recognize that the global shape of a disaccharide depends mainly on rotations around the glycosidic linkages, because the flexibility of the pyranose ring is rather limited and the different orientations of the pendant groups do not participate in the description of the backbone trajectories. The relative orientations of saccharide units are therefore expressed in terms of the glycosidic linkage torsional angles Φ and Ψ which have the definition $\Phi =$ O-5—C-1—O-X—C′-X and $\Psi =$ C-1—O-X—C′-X—C′-$(X + 1)$ for a $(1\rightarrow X)$ linkage. The Φ,Ψ space is then explored in a systematic fashion. Both torsions are sequentially rotated in small increments over the full 360° range. At each point on the grid, energy contributions calculated from the force field in use are evaluated. It is then possible to represent the energies of all the conformations available as a contour map in the Φ,Ψ space. These contour maps enable graphical description of energy change as related to the relative orientation of the monosaccharides; this is a three-dimensional cross section of the complex conformational space of disaccharides. They indicate the shape and position of minima, the routes for interconversion between conformers, and the heights of the transitional barriers. Among the many different methodologies for calculating contour maps, adiabatic procedures are now widely accepted. In such procedures, the strain produced by steric interactions inherent from rotation of monosaccharide residues is relieved by the inclusion of bond length and angle adjustment in the form of minimization, with respect to all degrees of freedom of the system (except Φ,Ψ), at each point of the space. However, as minimization will only lead to conformations "downhill" from the starting structure, the torsional dimension where most conformational variation occurs is limited to only one orientational well. It is possible that rotation of pendant groups over torsional barriers could produce lower energy conformations at that point in Φ,Ψ space. Ideally at each point in Φ,Ψ space investigation of all possible combinations of pendant group orientations is required. Adiabatic

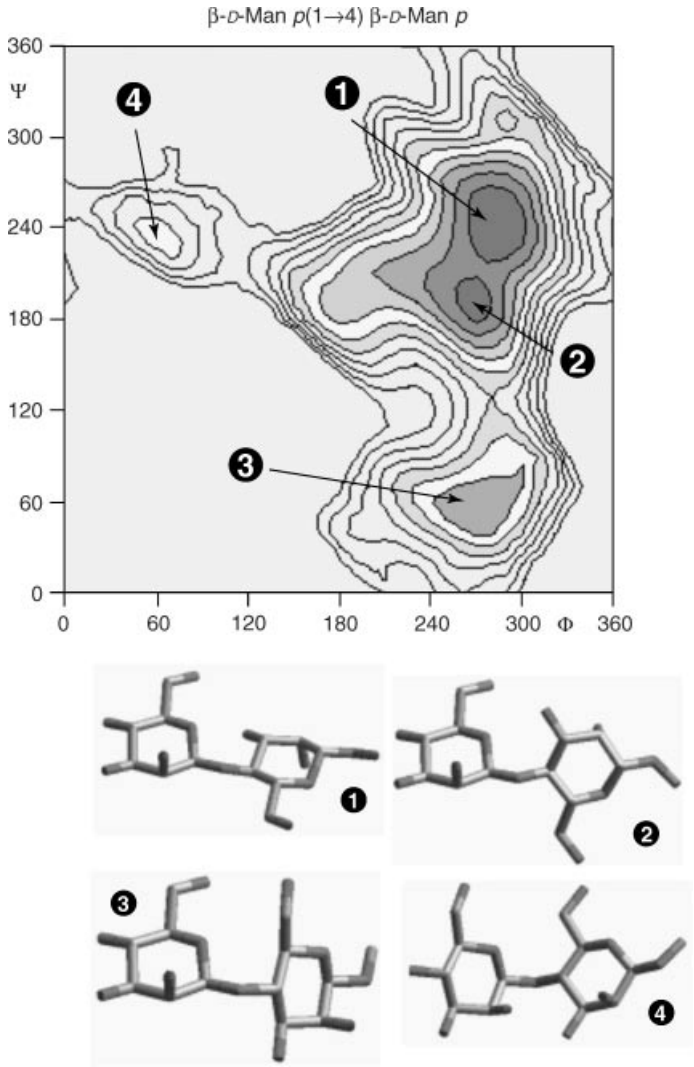

Fig. 19. The potential energy surface of mannobiose.

maps attempt to represent the lowest energy of all possible pendant group orientations at each point in the Φ,Ψ space. An example of an adiabatic map is given in Figure 19.

Solvation. It is important to recognize that most procedures are designed to treat molecules in the isolated state. Omission of the effect of the environment from the calculation results in a neglect of the fraction of the energy contribution that arises from these interactions.

Several different approaches have been proposed to treat solvation effects (38). In the simplest one, the effect of the solvent is achieved by increasing the dielectric constant for calculations of electrostatic interactions or by the use of a distance-dependant dielectric constant. Another possible way is to explicitly

include a limited number of solvent molecules in the calculation. By way of example, in aqueous solution the potential importance of hydrogen bonding and the great strength and directionality of hydrogen bonds requires explicit consideration of the water molecules surrounding the solute. An example obtained on maltose–water interaction is given in Reference 39. To account for such a solvent effect, molecular dynamics with the inclusion of explicit water molecules around the carbohydrate can be used. An alternative approach is to treat the solvent as a dielectric continuum. The conformational free energy of a given conformer in a particular solvent may be described as arising from the contribution of the energy of the isolated state and the solvation free energy. The latter is evaluated from the continuum model and is partitioned into cavity, electrostatic, and dispersion contributions.

Probing Potential Energy Surfaces. The accuracy of the predicted potential energy surfaces has to be evaluated. Indeed, many observable properties of oligosaccharides can be calculated and have been shown to be sensitive to the details of the conformational energy surface. Many crystal structure determinations of carbohydrates, nucleosides, and nucleotides are available in the Cambridge Crystallographic Database. X-ray analysis gives the best data for the conformation of an oligosaccharide. Precise atomic coordinates are provided, along with an explicitly defined environment. Comparisons with crystal structures are among the most precise test of modeling available for carbohydrate molecules, provided that packing forces are taken into account. These surveys of crystalline conformations are indicative of the structural variations and the conformational flexibility that the glycosidic linkages exhibit in the solid state.

In solution, the method of choice to study the three-dimensional structure of saccharides is NMR, through the parameters represented by chemical shifts, coupling constants, nuclear Overhauser effects (nOe), and also relaxation time measurements. Although the conformational dependence of the carbon chemical shifts is far from understood, coupling constants can be used to evaluate the magnitude of the torsion angles, and nOe measurements can provide estimations of distances between protons located in rather close proximity. In addition, relaxation time measurements give information on the mobility and the behavior of molecules in solution.

Three bond coupling constants provide a source of information with regards to torsional angles about the bonds. They can be interpreted by trigonometric formulas with suitable parameters derived from empirical studies on model compounds. $^{3}J_{\mathrm{H-H}}$ coupling constants allow the extraction of information about the sugar ring pucker. For the exocyclic group of pyranose, the vicinal coupling constants between H-5 and H-6 define the torsional angle about C-5—C-6, provided that the stereospecific assignment of the two H-6 protons is possible. The relative magnitudes of the coupling constants, $^{3}J_{\mathrm{H5-H6}}$ and $^{3}J_{\mathrm{H5-H6'}}$ can be used to determine the distribution of conformers about the ω angle in the case of (1→6)-linked pyranoses. As for the torsional angles Φ and Ψ about the glycosidic linkage, only heteronuclear coupling constants $^{3}J_{\mathrm{C-H}}$ and $^{1}J_{\mathrm{C-H}}$ can be used, and empirical trigonometric formulas relating $^{3}J_{\mathrm{C-H}}$ to torsional angles have been proposed. The angular dependence that incorporates the solvent effects of $^{1}J_{\mathrm{C-H}}$ have been established in α- and β-oligosaccharides (40,41).

The nOe data may be obtained by either one- or two-dimensional methods. These through-space effects may be used to estimate internuclear distances. However, nOe cross-peak volumes are inversely proportional to the sixth power of the distance between the correlated protons only in the case of rigid spherical molecules whose tumbling is isotropic. The simplest method that has been proposed for the interpretation of nOe-derived distance data is the "isolated spin pair approximation." The matrix treatment is more rigorous, although relying also on several approximations. A set of equations describing the cross-relaxation pathways of all the protons in the molecule is cast into a matrix form and solved.

All these NMR parameters represent average values, because of the acknowledged flexibility of carbohydrates and of all the rapidly interconverting conformations accessible to the molecule on the NMR time scale. This means that a straightforward interpretation of experimental data leads only to the definition of a "virtual conformation" without real physical meaning. Conformational averaging based on the abundances of the predicted structures gives averaged values which can be compared safely to the experimental ones.

The Disordered State of Polysaccharides. The polysaccharide chains in solution tend to adopt a more or less coiled structure. Such a dissolved coil would fluctuate between local and overall conformations. Polysaccharides are able to assume an enormous variety of spatial arrangements around the glycosidic linkages because these molecules have extensive conformational freedom; they may sample a large part of the space around the glycosidic and aglycone bonds. Theoretical polysaccharide models are based on studies of the relative abundance of the various conformations, of a given polysaccharide, in conjunction with the statistical theory of polymer chain conformation (42). Possible interactions between residues of the polysaccharide chain that are not nearest neighbors in the primary sequence of the polymer are ignored.

The Monte Carlo sample then reflects the number of conformations of polymer molecules. This means that observable parameters describing the solution behavior of polysaccharides are averages of the properties of individual conformations. This approach yields properties corresponding to the equilibrium state of the chain. Results refer to a model for an unperturbed chain that ignores the consequences of the long range excluded volume effect, because only nearest-neighbor interactions are accounted for in the computation of the Φ,Ψ surfaces.

Given a sufficient Monte Carlo sample of unperturbed polysaccharide chains, it is possible to assess many mean properties of the polymer in question simply by computing unweighted arithmetic averages over the chains of the sample. For example, the mean-square end-to-end distance, the average square radius of gyration, the mean persistence length, and dipole moment, are all average geometric properties readily computed from a knowledge of the coordinates of the atoms or atomic groups making up the Monte Carlo sample.

Models of polymer chain extension were first used to compare the effect of the glycosidic linkage geometry of simple polysaccharide chains, eg cellulose and amylose (43). Both polymers are 1,4-linked glucans; the only difference is in the anomeric configuration on the C-1 atom of the monomeric unit, α for amylose and β for cellulose. The calculated data show a remarkable pseudohelical chain

trajectory of the amylosic chains, the characteristic ratio of 5 denotes a moderately compact chain configuration. This behavior seems to be the consequence of the glycosidic bond geometry because changing this geometry from the α to the β configuration has a dramatic effect on the character of the chain trajectory. Relative to amylose, the cellulosic characteristic ratio of 100 is an increase of a factor of 20. This reflects the extended character of the cellulosic chains. Investigation of the solvent effects on those two representative polysaccharides has also been carried out (44). In good concordance with the experimentally observed solvent dependence, significant changes in the unperturbed chain dimensions were found; the characteristic ratio is larger in water than in vacuum for amylose, whereas for cellulose it is smaller.

The answer to the question of how reliable is the predicted conformational behavior of the polysaccharide chains lies again in the comparison of theoretically and experimentally measured properties. A few examples were analyzed (chitin, chitosan, hyaluronan, galactomannan) and the local stiffness of the chain reflected by the persistence length L_p has been compared with the value obtained experimentally using multidetection SEC (45–47).

Molecular Structure

The polymer may be linear (such as hyaluronan) (Fig. 20**a**) or branched with a long side chain (as in xanthan) (Fig. 20**b**) or with many short chains or monosaccharide side groups (as in galactomannan) (Fig. 20**c**) or branched with side chains themselves branched giving rise to a tree-like structure (as in amylopectin) (Fig. 20**d**).

The determination of the structure is a very difficult task especially in heteroglycans. The structure must be established on a pure sample isolated from its natural source with a minimum degradation.

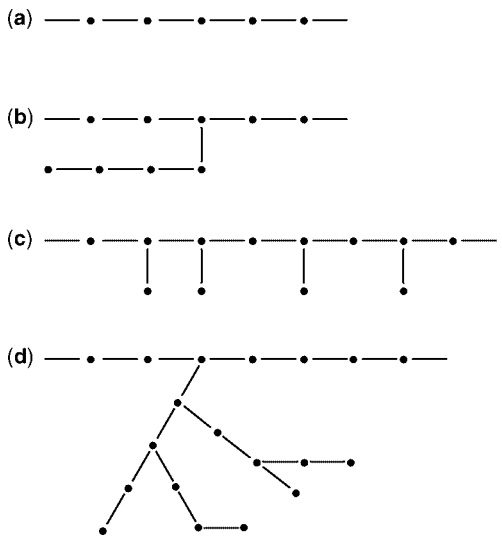

Fig. 20. Structural patterns of polymer chains.

Considering the repeat unit of a polysaccharide represented by the scheme,

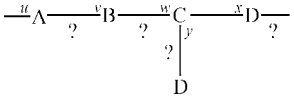

the answers to the different following questions are required:

(1) What is the nature and relative proportion of the A, B, C, D monosaccharides involved in this oligomer, including ring size and their configuration (D- or L-)?
(2) At which positions (u, v, x) are A, B, D engaged in the osidic linkage and what is the anomeric geometry (α or β) of each glycosidic linkage ?
(3) Unit C is substituted at w and y positions but which position corresponds to the attachment of the side chain and which to the main chain linkage?
(4) Which is the exact sequence of the four sugars in the repeat unit?

The general methods are reviewed in many books (3) and in this article only general overview will be given.

If there are any substituents on the rings as is frequent in plant or bacterial polysaccharides (acetyl, pyruvyl, succinyl groups), they must be located on a specific position, but often they are labile in acidic or mainly basic conditions and the structure determination becomes even more difficult.

Extraction–Purification. Purification of polymeric molecules is often easier than for small molecules. It is relatively easy to separate small (impurities) from large molecules on solubility criteria, gel filtration, or by dialysis.

If the polymer is water soluble as in exocellular bacterial polysaccharides, it is often a polyelectrolyte (containing uronic acid); it can be precipitated using a nonsolvent such as ethanol or 2-propanol (in a ratio around 1:1 water/alcohol) after clarification of the extract by filtration and addition of monovalent salt excess to exchange the multivalent counterions. The presence of bivalent counterions left in the sample will prevent resolubilization after drying. For a strongly interacting polymer with calcium (such as pectin) the use of oxalate as chelating agent is useful.

Before extraction of polysaccharides from plants or woods, it is recommended

(1) to extract these materials with organic solvents (toluene, chloroform, methanol, etc) to remove pigments, waxes, or oils;
(2) then, to eliminate Lignin (qv), a highly cross-lilnked polyaromatic compound, by chemical treatment (chlorite, ozone, sulfite, etc).

For neutral polymers (cellulose being excluded), extraction can be performed using DMSO (48), *N*-methylmorpholine *N*-oxide (49), NaOH, or KOH at different concentrations. Over pH 12, alcoholate is formed on the —OH groups, increasing the solubility of polysaccharides. When hemicelluloses have to be extracted from a plant source, KOH 24% or NaOH 18% are often used; these hydroxides produce

swelling of the cellulosic matrix by rupturing hydrogen-bonding associations, allowing better diffusion of other polymers (50).

The extract may contain different polysaccharides and it is useful to resolubilize this material after first purification and to perform SEC in addition to ion-exchange chromatography before establishment of the structure. This allows separation of fractions with different average molecular weights and different average charge densities.

NMR Spectroscopy. The structure can be established as mentioned before using ^{1}H and ^{13}C NMR; many examples are given in the literature. NMR is very useful especially for analyzing polysaccharides with a regular structure. Figure 21 shows the NMR analysis of a bacterial polysaccharide (hyaluronan) based on a 2 sugars repeat unit. On the ^{1}H NMR spectrum, the two anomeric C-1 are identified as well as the acetyl of the *N*-acetyl-D-glucosamine unit. On the ^{13}C NMR spectrum, two different C=O appear in the range of 175 ppm due to the carboxylic group and to the acetyl group. The attribution of all the signals was given by Haxaire (51). NMR is also useful for estimating the population of substituents, the number of sugars in the repeat units, and to determining the anomery as well as the position of linkage and the sequence.

Composition. The most usual method to determine the composition of a polysaccharide (nature of the sugar units) is the complete hydrolysis by heating in acidic conditions (1 *M* H_2SO_4 followed by neutralization with barium carbonate, or with 2 *M* trifluoroacetic acid, which is volatile and easily eliminated after reaction) (52,53). Nevertheless, no recommendation can be proposed a priori; especially, for heteropolysaccharides, the rate of hydrolysis of the osidic linkage depends on the sugars involved: glycosidic bonds of deoxysugars and furanose sugars (like arabinose and fructose) are more labile whereas the glycosidic bond of the uronic moiety is more stable. In the latter case, it is better to reduce the polymer before hydrolysis (54,55). Methanolysis is sometimes preferred to simple acid hydrolysis, leading to methyl-glycoside derivatives (56).

Quantitative determinations of sugars are achieved by liquid chromatography (HPLC) or gas chromatography (GC). HPLC has the advantage of utilizing sugars directly but each sugar can give two or more peaks corresponding to the anomeric equilibrium; an example of HPLC chromatogram obtained on C18-μ Bondapak on maltodextrins is given in Figure 22. The peaks corresponding to DP = 4–6 show the anomeric equilibrium (26).

Reduction of the saccharide gives alditols and only one peak per sugar. The same occurs in GC; but, in addition, as sugars are not volatile, they must be transformed into alditol acetates by reduction and peracetylation to get a single peak per sugar in GC (57).

Methylation. Methylation involves the complete conversion of all free hydroxyl groups in a polysaccharide into methoxyl groups ($-OH \rightarrow -OCH_3$). The most used method is the Hakomori procedure using DMSO, sodium hydride, and methyl iodide (58). To give significant results, methylation must be perfectly completed; then, total hydrolysis yields monomeric units with different degrees of methylation. The position of nonetherified —OH indicates the position of the glycosidic bond. Thus, a tetra-*O*-methylhexose is representative of a terminal unit (nonreducing end). In a linear oligo- or polysaccharide, the fraction of these units can be used to estimate the number-average degree of polymerization.

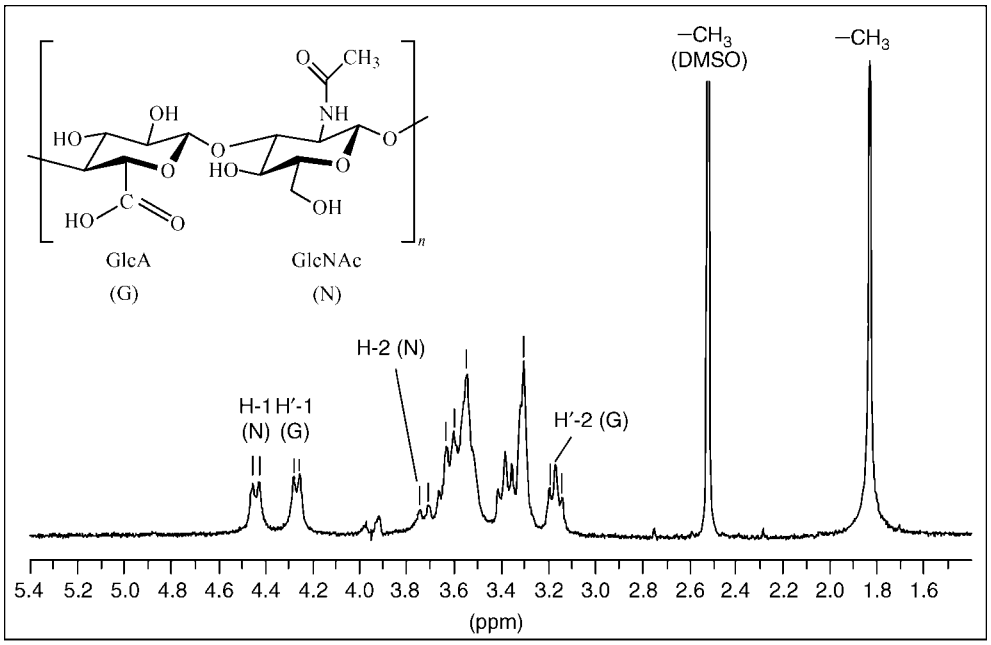

(**a**)

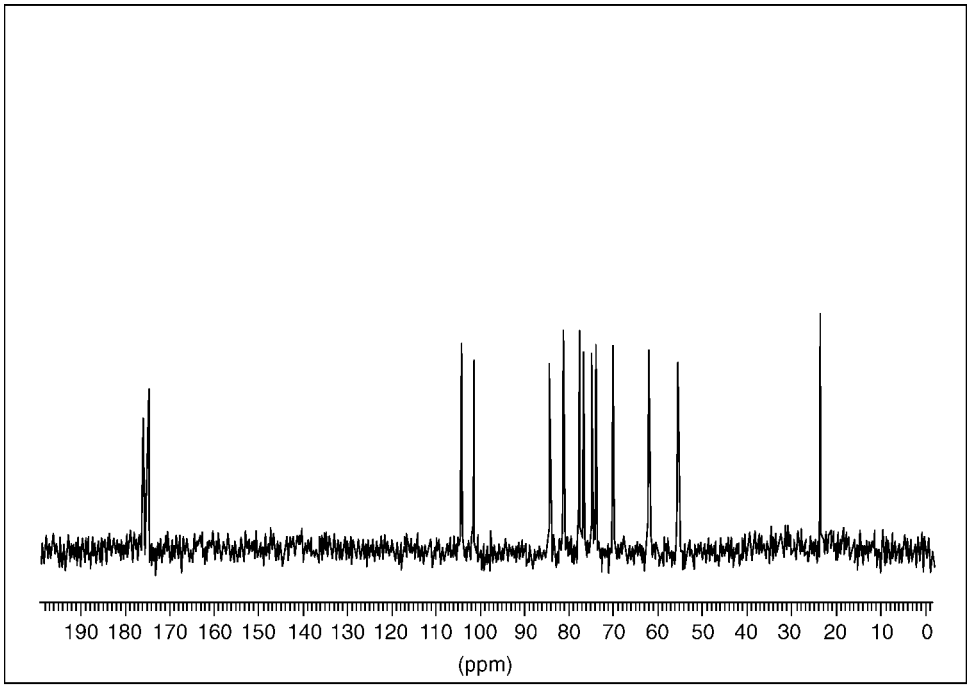

(**b**)

Fig. 21. (**a**) ^{1}H and (**b**) ^{13}C NMR spectra for hyaluronan in D_2O at 85°C in the presence of DMSO as standard at 300 and 75 MHz respectively (51).

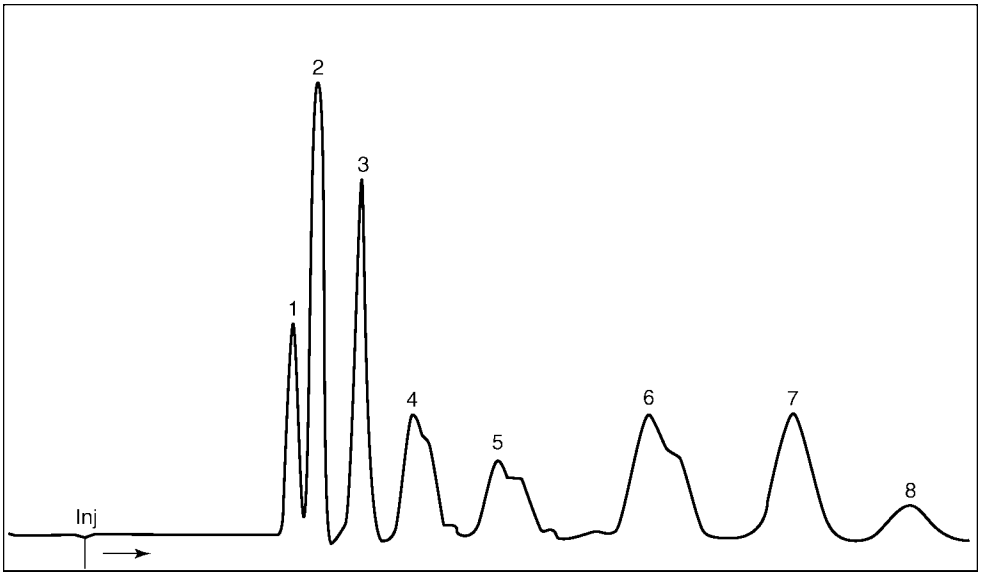

Fig. 22. Separation of maltodextrins (the degree of polymerization is indicated by the number over the peaks) by gel permeation chromatography on Biogel P-2 ($T = 15°C$; eluent: water). Anomeric equilibrium is shown under peaks 4–6. Reproduced from Ref. 26, by courtesy of Marcel Dekker, Inc. (Copyright 2003).

A tri-*O*-methylhexose is an in-chain unit; di-*O*-methylhexose indicates the existence of a branched point. The partially methylated sugars can be fractionated by HPLC. This technique allowed determination of the distribution of methyl substituents in methylcellulose (59); Figure 23 shows the chromatogram obtained for partially methylated glucose after total hydrolysis of the methylcellulose. Eight modified D-glucose derivatives are obtained including unsubstituted glucose.

Usually, the methylated sugars are derivatized to alditol acetates and separated by GC combined with mass spectroscopy (60–63).

Partial Acid and Enzymic Hydrolysis. Partial hydrolysis with acid under mild conditions gives a mixture of oligosaccharides. Homoglycan gives a series of homologous oligomers, whereas heteroglycan gives a series of products depending on the relative acid labilities of the different glycosidic bonds. The fragments permit the sequencing of the monosaccharide residues in the polysaccharides.

Establishment of the polysaccharide structure can be obtained by the use of specific enzymes. The most developed studies concern the amylopectin molecular structure using α- and β-amylase and debranching enzymes (isoamylase, pullulanase, glucoamylase). These enzymes hydrolyze specifically the $\alpha(1\rightarrow6)$ and/or $\alpha(1\rightarrow4)$ linkages, allowing separation of the side chains. The different sizes of side chains in amylopectins were separated by SEC (64,65). Endo- and exoglycanases specific for the cellulose ($\beta(1\rightarrow4)$ linkage) were also investigated; a cocktail of these types of enzymes is also used to disrupt the plant cell walls. Bacteriophages possess a highly specific endoglycanase for a single glycosidic bond in each repeat unit of the corresponding bacterial polysaccharide, thus giving a single oligosaccharide motive in good yield, identified as the repeat unit, easier to characterize (66).

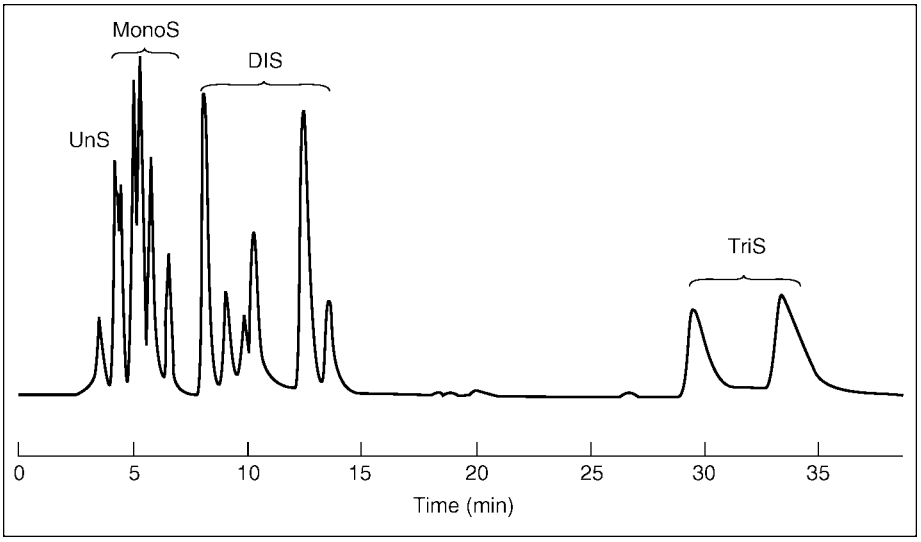

Fig. 23. HPLC analysis of methycellulose (DS = 1.7) after total hydrolysis on a Nucleosil C18 reverse-phase column. Eluent: water; ambient temperature. Reproduced from Ref. 59, with permission from Elsevier (Copyright 2003).

Molecular Weight Determination. Whenever the polysaccharide is perfectly water soluble it is easy to perform SEC; but the polyhydroxyl nature of polysaccharides causes specific problems: owing to the large number of —OH groups in the molecules, cooperative interaction may form aggregates; the associated molecules are connected by a network of H-bonds, often created by the conditions of isolation and drying of the pure polysaccharide. The presence of aggregates disturbs the chromatogram which becomes difficult to interpret.

In addition, when uronic acid or pyruvic acid substituents are present, the polysaccharide becomes a polyelectrolyte (see POLYELECTROLYTES). It is necessary to shield the polymer from electrostatic interactions; this implies that the polymer has to be solubilized in the presence of an external 1–1 electrolyte (67–70). A multidetection experimental device in which a complete molecular weight distribution can be obtained without any calibration has been developed (71).

Another important parameter is the intrinsic viscosity $[\eta]$ (expressed in mL/g). It is obtained by extrapolation to zero polymer concentration of the reduced viscosity (η_{red}) of the polymeric solution plotted as a function of the polymer concentration C (g/mL) in accordance with the Huggins relation:

$$\eta_{red} = (\eta - \eta_0)/\eta_0 C = [\eta] + k'[\eta]^2 C \quad (1)$$

in which η is the viscosity of the polymer solution, η_0 is the viscosity of the solvent, and k' is the Huggins constant. There is a relative relation between the intrinsic viscosity and the molecular weight of the polymer following the Mark–Houwink relationship:

$$[\eta] = K M_v^a \quad (2)$$

Table 4. Mark–Houwink Parameters for Cellulose and Some Cellulosic Derivatives and for Starch and Starch Derivatives

Polymer	Solvent	T, °C	K, 10^{-3} mL/g	a	Reference
Cellulose	Cupriethylenediamine	25	10.1	0.9	92
Cellulose	Cupriethylenediamine	25	7.62	0.936	72
Cellulose nitrate	Tetrahydrofuran	25	1.32	1.01	73
Cellulose acetate	acetone	30	16.0	0.82	74
Cellulose acetate butyrate	acetone	25	13.7	0.85	75
Cellulose triacetate	acetone	25	14.9	0.82	76
Sodium carboxymethylcellulose	Aqueous NaCl (0.1 M)	25	12.3	0.91	77
Methylcellulose	Water	25	316	0.55	78
Methylcellulose	Water	20	280	0.55	79
Amylose	Dimethyl sulfoxide	25	15.1	0.70	80
Amylose	Dimethyl sulfoxide	25	30.6	0.64	81
Amylose	Water	20	13.2	0.68	82
Amylose	Aqueous KOH (0.15 M)	25	8.36	0.77	80
Amylose triacetate	Chloroform	30	1.06	0.92	83

in which M_v is the viscometric average molecular weight; K and a are two parameters depending on the polymer, the solvent, and the temperature. Some values are given in Table 4.

Plant Polysaccharides

Polysaccharides from the biomass consist largely of renewable polymers which have been used for a long time in many industrial applications. The main polysaccharides concerned are cellulose (qv) and starch (qv) (84).

Cellulose is the main structural polymer in wood (representing around 50% of the dried matter) or agricultural resources (normally between 35 and 75% of the dried matter depending on the source; in the case of cotton (qv), values are between 90 and 99%) (85–88). Cellulose is found in a very organized fibrous structure. In contrast, starch constitutes the reserve polysaccharide organized in a granular structure. Both of these polymers are semicrystalline polymers (qv) based respectively on β-(1→4)-D-glucose and α-(1→4), α-(1→6)-D-glucose (89,90).

Derivatization may be used to extend the domains of application for these natural polymers; nevertheless, their relative lack of solubility and their high degree of organization lead usually to heterogeneous chemical modifications. Heterogeneity of the substitution gives bad reproducibility of the samples, depending also on the sources of polymers. Because of this problem, a large variety of parameters relating the degree of substitution and molecular weight to the physical properties can be found in the literature.

The supramolecular structure of the initial materials is a very important point. The swelling and/or dissolution in different conditions depend on the morphology of the native substrate. Cellulose in cellulosic fibers and

amylose/amylopectin in starch granules are tightly packed in a more or less regular organization, depending on their source but also on the presence of other additional components. Thus, the accessibility of the reactive groups (—OH) depends on this supramolecular structure in addition to the degree of crystallinity (diffusion control of the reactants) and on the intra- or interchain H-bonds modulating the —OH reactivity. This is why cellulose and starch are not thermoplastic materials but in presence of water playing the role of plasticizer; especially starch becomes thermoplastic. Only a complete destructuration passing through a solution state avoids a memory effect of the original state of organization and attainment of regular chemical modification.

The two main characteristics of cellulose and starch derivatives are the distribution in molecular weight (the weight average DP_w or M_w) in addition to the degree of substitution represented by DS (DS is the average number of substituents per glucose unit; $0 < DS < 3$).

Cellulose and Cellulose Derivatives. The solubilization of cellulose to determine its molecular weight is delicate; one of the most powerful solvents is cupriethylenediamine for which the Mark–Houwink parameters relating the intrinsic viscosity to the molecular weight ($[\eta] = KM^a$) have been determined (see Table 4). Some authors previously prepared cellulose derivatives (nitrocellulose or cellulose tricarbanilate) to determine the molecular weight and molecular weight distribution, assuming no polymer degradation (72–83,91,92).

Cellulose derivatives are the most important derivatives obtained from natural sources. Chemical modifications of cellulose are very useful to enhance solubility in organic or aqueous solvents or to obtain new thermoplastic materials. The main derivatives are described in Table 5.

In designing derivatives for various properties and applications the degree of substitution is a very important parameter, as well as the chemical structure of the substituent. Recent studies have been done in selective cellulose functionalization obtaining regioselectively substituted esters and ethers (93–97).

Table 5. Main Substituents in Cellulose Derivatives

Product	Functional group (R=)[a]	DS[b]	MS[c]
Cellulose nitrate	—NO_2	1.8–2.8	
Cellulose acetate	—$C(O)CH_3$	0.6–3.0	
Carboxymethylcellulose	—CH_2COONa	0.5–2.9	
Methylcellulose	—CH_3	0.4–3.0	
Hydroxyethycellulose	—$[CH_2CH_2O]_x$ H ($x = 1, 2, 3, \ldots$)	0.8–1.2	1.7–3.0
Hydroxypropylcellulose	—$[CH_2CH(CH_3)O]_x$H ($x = 1, 2, \ldots$)		<4.6
Ethylcellulose	—CH_2CH_3	0.5–4.6	

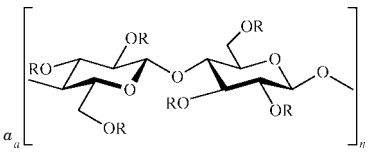

[b] $0 < DS < 3$ is the degree of substitution.

[c] MS is the molar substitution (gives the average number of monomoles of reactant added to one anhydroglucose unit).

Among the large variety of cellulose derivatives, two main groups of products are prepared: cellulose esters and cellulose ethers. Worldwide, around 1.4×10^6 t/year of cellulosic dissolving pulp is used in the production of cellulose esters, whereas 5.4×10^5 t/year is used in the production of cellulose ethers (98).

Cellulose ethers (qv) are obtained by substitution of hydroxyl groups by ether groups, and depending on the substituent they can be soluble in water or organic solvents. Carboxymethylcellulose (CMC) is the ether of cellulose of largest production. Approximately 300,000 t/year is produced each year. It is a water-soluble polymer in the sodium salt form and when DS is larger than 0.5. It is produced by reaction of the alkalicellulose with sodium chloroacetate or reaction with sodium in liquid nitrogen in the presence of chloroacetic acid (99–101). On a laboratory scale, soluble CMC with DS varying from 0.5 up to 3 has been produced. Typical raw materials for cellulose-ether production are wood pulp or cotton linters. Cotton linters are used for the production of high viscosity ethers because of their higher DP. CMC sodium salt is a white, odorless, and nontoxic solid. Viscosities range in aqueous solution from 10 to over 50,000 mPa·s (=cP) for 2% aqueous solutions. The DS of commercial samples may be between 0.3 and 1.2 although clear and fiber-free CMC solutions require a minimum DS value of about 0.5. The majority of commercial products have a DS between 0.65 and 0.85. Most CMC solutions are highly pseudoplastic (102,103).

Methylcellulose (MC) is produced, as in the case of CMC, by the Williamson synthesis, ie, by reaction of alkali cellulose with methyl chloride. World annual production is around 80,000 t/year (98). Other hydroxyalkyl derivatives or mixed ethers such as hydroxyethylmethylcellulose, hydroxypropylmethylcellulose, hydroxybutylmethylcellulose, ethylmethylcellulose, and carboxymethylmethylcellulose have similar properties to MC.

MC is a white to slightly off-white, essentially odorless and tasteless powder. The solubility of MC varies as a function of DS. In fact, commercial MC is divided into two types of products according to DS. MC with a degree of substitution between 1.4 and 2.0 are soluble in cold water, whereas lower substituted materials are soluble in dilute alkali. MC is also soluble in ethanol, acetone, ethyl acetate, benzene, and toluene for higher DS. Just as in the case of CMC, viscosity values of MC vary as a function of (average) molecular weight. Apparent viscosity at 2% and 20°C can vary between 10 and 19,000 mPa·s (=cP) in a range of average molar mass between 13,000 and 140,000. MC and its derivatives form gels at specific temperatures when heated (104).

The mechanism of gelation is related to the distribution of substituents along the chain; two steps in the gelation mechanism have been demonstrated. The first step of gelation is the formation of a clear gel related to the existence of blocks of highly substituted glucose units (105–108). The second step is the phase separation giving a turbid gel when temperature is larger than 60°C. Below their gel point, solutions of MCs exhibit pseudoplastic rheology, but appear to be Newtonian at low shear rates. MCs have excellent water retention properties.

The two main types of commercial hydroxyalkylcelluloses are hydroxyethylcellulose (HEC) and hydroxypropylcellulose (HPC). HEC is produced in larger amount with around 60,000 t/year, but investments are planned in order to increase the capacities of HPC, in future years. HEC and HPC are synthesized by reaction of alkali cellulose with ethylene oxide or propylene oxide respectively in a

slurry process in an organic medium. In the case of HPC it is possible to use liquid propylene oxide as a medium of reaction; after etherification the crude product is purified by washing with hot water (109–111).

HEC is available in a wide range of viscosities (from 10 to 100,000 mPa·s (=cP) in 2% aqueous solution at ambient temperature). It is soluble in cold and hot water or some mixtures of water and water-miscible organic solvents. The nonionic chemical structure and its solubility in both cold and hot water are the main advantages for the utilization of HEC. HPC has a thermal gel point like MC and it is thermoplastic. Because of its high level of substitution (molar substitution about 4) and its remarkable hydrophobic character it is soluble in a number of organic solvents as well as water.

Many general books develop the structure and reactivity of cellulosic materials and the preparation of their derivatives (112–115).

Starch and Starch Derivatives. The starch granule dimensions depend on the sources as well as the composition and degree of crystallinity. The molecular structure of the principal component in the starch granules consists of a linear (1→4)-D-glucose chain, amylose. Amylose is a flexible polymer having a relatively low thickening power; its molecular weight seems to remain relatively low (less than 1 million). The second major component is a highly grafted polymer, amylopectin. It is a very compact molecule with a very high molecular weight (10–100 millions have been cited in the literature). Also, in some materials a third component is a slightly grafted amylose called the intermediate material (116,117).

The main techniques to characterize starch molecules consist of iodine or butanol complex formation to estimate the fraction of linear amylose (118). A colored complex is formed with iodine; its wavelength of absorption is characteristic of the length of the helicoïdal segments involved in the complex formed with iodine. This technique has been examined by Salemis (119). The second important characteristic is the molecular weight or better, the molecular weight distribution. It is often difficult to solubilize starch in aqueous solution. In one SEC investigation of starch in aqueous systems containing KOH (120), it was shown that amylopectin has a low solubility. SEC studies were also done in DMSO (121,122). The determination of the molecular weights can be performed using the empirical relation relating the intrinsic viscosity to the viscometric average molecular weight. Some parameters are given in Table 4.

Nowadays, starch is used in industry as native starch (world production: (10–12) $\times$ 10^6 t/year), gelatinized starch, modified starch (7 $\times$ 10^6 t/year), or as partially or totally degraded starch ((16,17) $\times$ 10^6 t/year), (98). First, the characteristics of the products depend on the parent starch sample.

The hydroxyl groups of starch can be derivatized as esters or ethers, as in the case of cellulose. Table 6 gives the main substituents for starch.

Starch esters are synthesized by reaction of a carboxylic acid or an acyl chloride or an acid anhydride with the hydroxyl groups of amylose or amylopectin chains. As in the case of cellulose derivatives, there are organic and inorganic esters depending on the origin of the substituent.

Acetate of starch is the most important ester of starch industrially produced. Commercial products are traditionally low substituted derivatives (DS $<$ 0.3) (123–125). In this range of DS it is possible to derivatize preserving the granule

Table 6. Main Substitutents in Starch Derivatives

Product	Functional group	DS	MS
Starch acetate	$-C(O)CH_3$	0.04–3.0	
Starch phosphate	$-OPO_3HNa$	0.02–0.25	
Hydroxyethylated starch	$-[CH_2CH_2O]_xH$ ($x = 1, 2, 3, \ldots$)		0.05–1.25
Hydroxypropylated starch	$-[CH_2CH(CH_3)O]_xH$ ($x = 1, 2, \ldots$)		0.1–1.0
Quaternary ammonium starch esters	$-OCH_2CH(OH)CH_2N(CH_3)_3Cl$ and others	0.1–0.7	
Starch alkenylsuccinates	$-OC(O)CH_2CH_2C(O)ONa$	0.02	

structure, to purify by washing with water, and to recover by centrifugation or filtration. The acetylating agent is commonly acetic anhydride in aqueous medium in the presence of dilute sodium hydroxide. Derivatization eases the formation and stability of colloidal dispersions of starch and the adjustment of the colloidal properties to the requirements of the application. Products obtained have high purity and low ash content. The principal uses are in food (paste clarity and viscosity stability) and the pharmaceutical and textile industry (warp sizing, finishing operations). Other higher acetylated starches are those obtained with a DS of 2–3 (126,127). Their characteristics of solubility and thermoplasticity permit their utilization as materials. Nevertheless, this type of material has not been developed commercially because they could not compete with similar cellulose derivatives in terms of strength and cost. The glass transition (T_g) stabilizes around 150°C. These polymers have been proposed to prepare hydrophobic thermoplastic materials or to coat hydrophilic films (128–130). Even up to DS $\sim$ 3, the polymers remain biodegradable (129).

Syntheses of longer chain organic esters (C_3–C_{18}) have been carried out on a laboratory scale, but have not yet been industrially produced because at present they are not profitable (125,130–133).

Starch can be etherified by reaction of an alkyl halide or an epoxy in alkaline medium. Depending on the substituent it is possible to obtain anionic, hydroxyalkyl, and cationic products.

The two main types of hydroxyalkyl ethers industrially produced are hydroxyethyl starch and hydroxypropyl starch. These compounds are synthesized by reaction of ethylene oxide or propylene oxide respectively with starch under alkaline conditions (134).

Low MS hydroxyalkyl starch products (MS < 0.1) are prepared by reaction of the epoxy in an aqueous and alkaline starch slurry. A salt such as sodium sulfate is often added to protect the starch from swelling so that relatively high levels of caustic can be added to increase the reaction efficiency. In this case usual temperatures are between 25 and 50°C. If the temperature is increased and the salt eliminated, it is possible to do the reaction in a starch solution and obtain higher molar substitutions.

High MS hydroxyalkyl products are prepared by reaction of the epoxy in alcohol slurry and alkaline conditions. The alcohols typically used are methanol, ethanol, and 2-propanol. Another possibility is to combine starch with a low level

of moisture (5–15%) with ethylene or propylene oxide under pressure in presence of an alkaline catalyst. In this process the starch retains its granular form.

Low MS hydroxyalkyl starches are very similar in appearance to unmodified starch. Nevertheless, there are two main differences in their properties owing to the presence of hydroxyalkyl groups. On one hand, these groups weaken the hydrogen bonding between starch molecules and facilitate the reduction of pasting temperature. On the other hand, when the product is solubilized, retrogradation of the starch chains is inhibited, resulting in a more fluid paste with improved clarity, viscosity stability, freeze–thaw stability, and cohesiveness. Although the substituted starch paste thickens when it cools, reheating will return it to its original hot viscosity and clarity.

When the MS increases the pasting temperature decreases, until the product is soluble in cold water. These products have excellent viscosity stability over a wide range of conditions. The viscosity of high MS hydroethyl starch solution is quite stable to shear changes, changes in pH, and enzymatic attack. Salts have little effect on these products.

Hydroxyethyl starch is used in papermaking, textile manufacturing, medical and pharmaceutical industries. Hydroxypropyl starch is used in the food industry, textile and paper products, building materials, cosmetics, and pharmaceuticals (134).

Cationic starches are obtained by reaction of starch with reagents containing amino, imino, ammonium, sulfonium groups. The two main types of commercial products are the tertiary amino and quaternary ammonium starch ethers (135).

Quaternary Ammonium Starch Ethers. Among the reagents that can add quaternary ammonium groups to starch probably the most popular is 2,3-epoxypropyltrimethylammonium chloride. Ethers of this type with different DS have been prepared and tested for their role in adsorption on calcium carbonate in relation with the mechanisms of dispersion and flocculation of small particles (136).

Cross-linking. Starch polymer chains can be cross-linked with difunctional reagents to form diethers or diesters. These derivatives are distinguished from starch ethers and starch esters because the properties obtained by the cross-linking of starch are specific. In general terms cross-linking reinforces granule integrity, modifies the water retention capacity, and provides higher mechanical resistance and improves film properties.

Cross-linking is employed when a stable, high viscosity starch paste is needed, and particularly when the dispersion is to be subjected to high temperature, high shear, and/or low pH (137).

Hemicelluloses. Hemicelluloses constitute a series of polysaccharides associated with cellulose in plants. In wood, in addition to lignin and cellulose, hemicelluloses represent around 25% by weight (138). Some structures are given in Figure 24. The composition of hemicelluloses depends on the source: deciduous trees (hardwoods) have mainly glucuronoxylan; coniferous trees (softwoods) yield more glucomannans, *O*-acetylgalactoglucomannans, and xylans having both arabinofuranosyl and 4-*O*-CH_3-galacturonic side chains. Some softwoods also have significant amounts of arabinogalactan (eg in larch wood) (138).

Hemicelluloses from annual plants (cereals crops) are mainly of the xylan type; mixed-linked β-1,3-1,4 glucans are also found. The structure has been

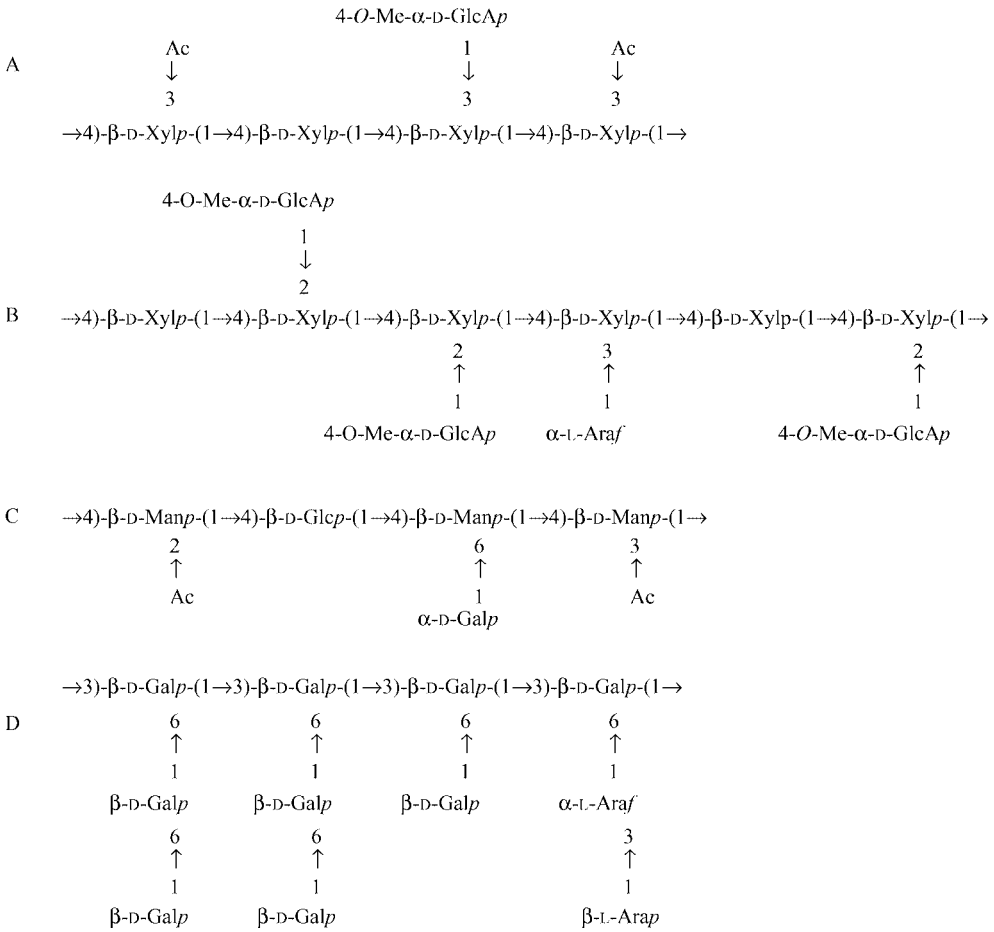

Fig. 24. Partial chemical structure of some hemicelluloses: **A** = *O*-acetyl-(4-*O*-methylglucurono)xylan from hardwood; **B** = arabino-(4-*O*-methylglucurono)xylan from softwood; **C** = *O*-acetyl-galactoglucomannan; **D** = arabinogalactan from larch wood (138).

reviewed (138) and it is clear that they represent a large variety of molecules. There are no important applications for hemicelluloses extracted from plants.

Galactomannans and Glucomannans. Galactomannans are neutral polysaccharides isolated from seeds (carob, guar, locust bean, tara, etc) (140). The main chain is made of →4-β-D-Man-(1 (M) with different degrees of substitution on *O*-6 with α-D-galactopyranosyl units (G) (Fig. 25). The structure is easily determined by ^{1}H NMR.

The solubility of the galactomannan depends on the ratio M/G and on the distribution of galactose units along the mannan chain; the larger the galactose content, the higher the solubility in water. The ratio M/G varies from 1:1 to 1:5 in *Mimosa scrabella* to locust bean gum respectively. In addition, the rheological properties of solutions depend on M/G because of an increase of loose interchain interactions when G content increases (141–144).

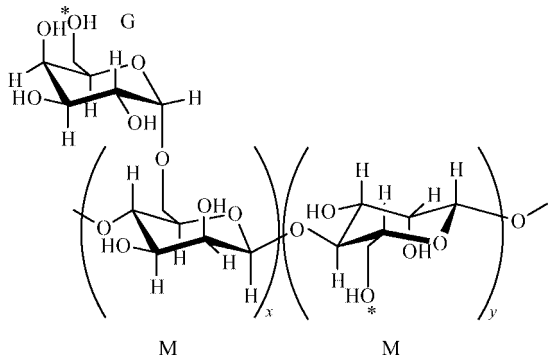

Fig. 25. Representation of the galactomannan structure. ∗ represents the C-6 position where —OH can be specifically modified.

Cooperative interactions may be stabilized between xanthan and galactomannan depending on the conformation of xanthan (helical or coiled). Two types of gels can be identified: one around 20°C involving disordered xanthan and galactomannan whatever its content in galactose; the second one, around 60°C, engages helical xanthan and it is the usual gel identified when these two polymers are mixed (145–152). Molecular modeling was applied for the determination of the persistence length of a galactomannan model for which M/G $\approx$ 1 (47); the value predicted as a function of the DP is given in Figure 26. The role of the microstructure of the polymer (random or blockwise distribution of galactose, content of galactose) was also analzsed by molecular modeling (153).

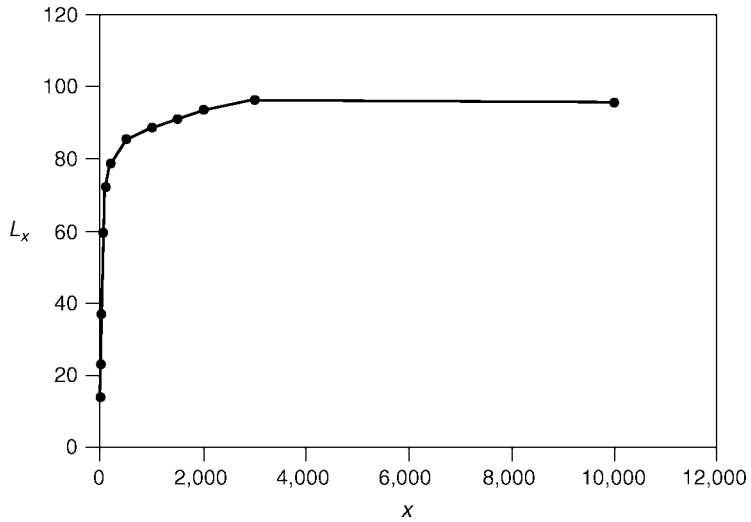

Fig. 26. Persistence length of galactomannan (for G/M = 1) as a function of the degree of polymerization x. L_∞ is equal to 9.6 nm. Reproduced from Ref. 47, with permission from Elsevier (Copyright 2003).

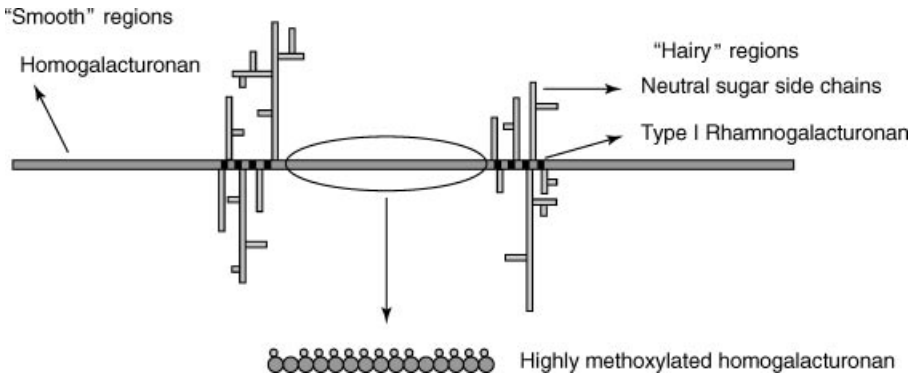

Fig. 27. Schematic representation of the pectin structure. Reproduced from Ref. 157 with the permission from American Chemical Society. (Copyright 2003).

Glucomannans are also obtained from seeds or roots; the structure is a random arrangement of $\rightarrow$4)-β-Glc-(1 and $\rightarrow$4)-β-Man-(1. The ratio Glc/Man depends on the source and varies from 1:1 in Iris bulbs to 1:5 in certain gymnosperms. Konjac glucomannan has been developed mainly in Japan for food applications (154,155).

Pectins. Pectins are located in the middle lamella and primary cell walls of plant tissues. They are extracted from apple skins and citrus peels. Pectins consist primarily of 1,4-linked α-D-galacturonic units or their methyl esters with some interruption by a rhamnogalacturonan region kinking the linear polygalacturonic backbone (156). They also contain branched chains composed of neutral sugars such as galactose or arabinose. These neutral sugars amount to 10–15% of the pectic dried weight and are concentrated in blocks (called the hairy region; Fig. 27) (157).

In nature, they occur often with different degrees of esterification (DE) around 70%. Because of enzymic degradation, they can have a lower DE; in that case (if DE $<$ 50%), they are insolubilized by calcium cross-linkage. Extraction requires the use of chelating agent.

The interaction between calcium ions and carboxyl groups of the pectins forms gels; the interaction with calcium is very cooperative owing to the stereochemistry of the 1,4-linked monomeric units, leading to the formation of a polar cavity that can be occupied by calcium or related cations. The mechanism of interaction is described by the egg-box model. A series of galacturonic acid oligomers was investigated to test the minimum carboxylic group necessary to get a stable junction (158–160). A two-step process leads to gelation: first dimer formation followed by aggregation forming junction zones (161–163).

The ability to gel can be determined from the dependence of viscosity as a function of counterions added (164). At a given concentration, the critical amount of cations at the gel point is directly related to the distribution of carboxyl groups along the chain (Fig. 28).

It is shown that the divalent counterions form gels with a sequence of affinity Ba $>$ Sr $>$ Ca, but Mg does not form gels nor dimers. The interaction with counterions as well as change in conformation have been identified by X rays (165) and by circular dichroism (162).

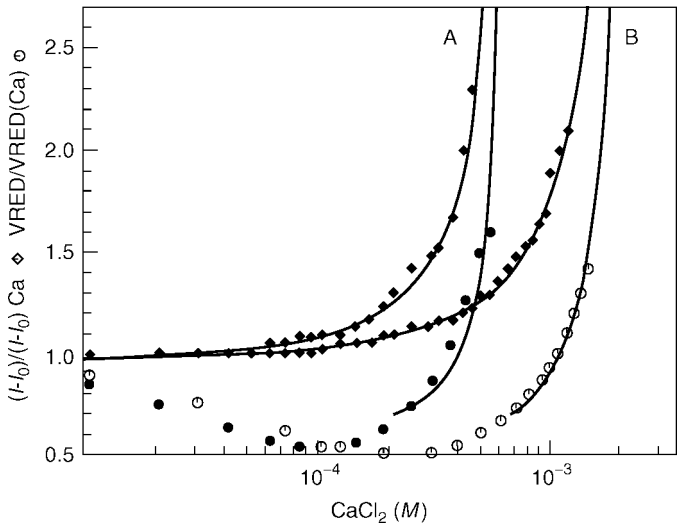

Fig. 28. Change in reduced viscosity and scattered light during addition of $CaCl_2$ to pectins (polymer concentration: 0.2 g/L; 5×10^{-3} *M* $CaCl_2$). Role of the carboxyl groups distribution: (**a**) DE = 30% blockwise distribution obtained by pectinesterase hydrolysis; (**b**) DE = 30% random distribution obtained by alkaline hydrolysis. Reproduced from Ref. 164, with permission from John Wiley & Sons, Inc., on behalf of the Society of Chemical Industry (Copyright SCI 2003).

There are different categories of pectins: HM pectins (high methoxyl; DE > 50%) form gels in acid conditions and in the presence of sucrose to decrease the water activity. The gelation is based on H-bond association and is thermoreversible. Only, LM pectins (low methoxyl; DE < 50%) form gels in presence of calcium.

HM pectins can be extracted by water, mineral acids, or bases. LM pectins immobilized *in situ* via metallic ions need a sequestering agent to displace the counterions. Alkaline treatment also has a role in the deesterification. Different treatments were compared on sugar beet and potato pulps. HM pectins are naturally occurring in sugar beet pulp; they were extracted in alkaline conditions (50 m*M* NaOH, pH 12) and precipitated with ethanol after neutralization to pH 6.5–7. A pretreatment of the plant material is necessary to inactivate enzymes (water at 85°C, 20 min). On the contrary, for potato pulp containing an LM pectin the extraction is performed in acid conditions (pH 3.5 in presence of 0.75% hexametaphosphate, 75°C, 1 h). The pectins are precipitated at pH 2 with HCl. The precipitate is redispersed in water with NaOH up to pH 6.5–7 and reprecipitated by ethanol. Potato pulp was also extracted in alkaline conditions with hexametaphosphate, precipitated at pH 2, redispersed in water to pH 6.5–7, and precipitated by ethanol as previously. The LM pectins obtained in alkaline conditions have a higher gelling ability due to deesterification and partial deacetylation (166,167).

Seaweed Polysaccharides

Algae are an important sources of polysaccharides with different structures. Among the different groups of algae, green algae (Chlorophycea), red algae

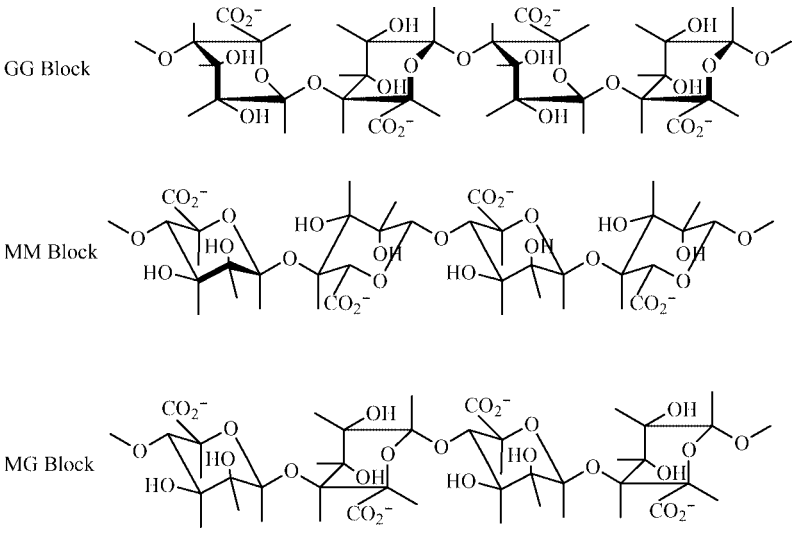

Fig. 29. Structure of alginate consisting of guluronic (G) and mannuronic (M) blocks or MG blocks.

(Rhodophycea), and brown algae (Phaeophycea), only the last two series are used on an industrial scale (168). Many different polysaccharides may be extracted but alginates and carrageenans are the more developed especially as physical gel formers (169). Fucoidans also are now under investigation because of the importance of sulfated polysaccharides for biological applications (170,171).

Alginates. Alginates are linear copolymers of α-L-guluronate (G) and α-D-mannuronate (M) (Fig. 29). They are also called polyuronides and are extracted from brown algae. Their gelling properties derive from the cooperative binding of divalent cations on the G blocks in the egg-box model (similar to that proposed in LM pectins).

Alginates behave as polyelectrolytes in the presence of monovalent counterions, and in 0.1 *M* NaCl, the intrinsic viscosity allows determination of the average molar mass (172).

Mechanical properties of calcium alginate gels are related to the ratio M/G and also to the distribution of the G units along the chain and to the molar mass of the polymer (173). Alginate is often used for encapsulation of pharmaceuticals, bacteria, or yeasts in biotechnological processes. The beads of gel are formed by a dripping technique; drops of alginate solution falling in 1 *N* $CaCl_2$ solution form beads which are washed in water after a few hours maturation. Smaller and more regular particles can be obtained by emulsification (174,175); the porosity of these gels is smaller than for that obtained by the dripping method.

Agarose and Carrageenans. These polysaccharides represented a family of alternating (AB) type copolymers with different degrees of sulfation; agarose is the neutral polymer form. They are extracted from red algae. Their structures are given in Figure 30. They consist of alternating (1→3)-β-D-galactose and (1→4)-α-(3,6)anhydro-D-galactose or (1→4)-α-(3,6)anhydro-L-galactose (in agarose).

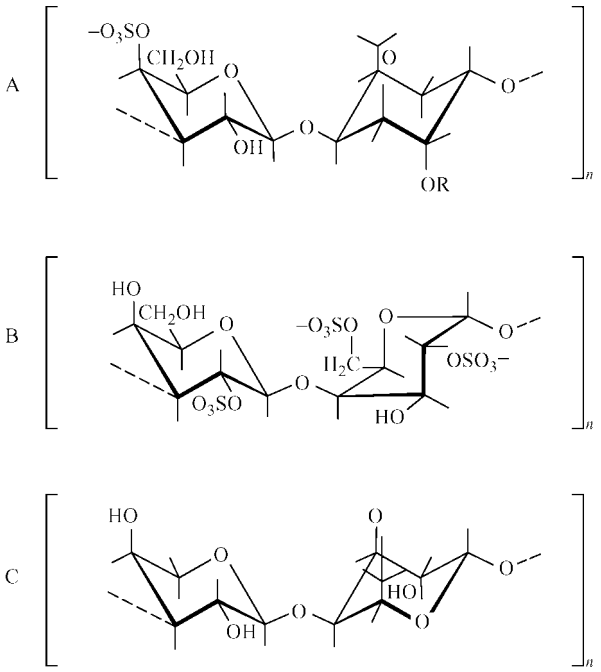

Fig. 30. Structure of red algae polysaccharides. (**A**) R = H in κ-carrageenan; R = SO_3^- in ι-carrageenan; (**B**) λcarrageenan; (**C**) agarose.

Agarose, κ-carrageenans, and ι-carrageenans are recognized as gelling polymers; the conditions of gelation as well as the mechanism of gelation have been abundantly discussed in the literature. The gels are thermoreversible based on H-bond stabilized conformations. Gelation is based on the formation of double helices which associate forming an aggregate or a junction zone which is the basis of the network formation; a two-step gelation process has been demonstrated clearly. Gelation and melting of the gel present a hysteresis in temperature directly related with the degree of aggregation of double helices and to the charge density of the polymers (176–178). The rigidity of the gels follows the same trend. A sequence of solubility has been established : Agarose $<$ κ-carrageenan $<$ ι-carrageenan $<$ λ-carrageenan following the order of sulfate density: No sulfate $<$ 1 sulfate $<$ 2 sulfates $<$ 3 sulfates The stiffness of the gels formed in presence of K^+ counterions varies in the following order: Agarose $>$ κ-carrageenan $>$ ι-carrageenan The polymer λ-carrageenan never forms gels or helical conformation.

For charged polysaccharides, the formation of double helices and gelation depends on the ionic concentration, nature of electrolyte, and temperature. A phase diagram relating the total ionic concentration and the inverse of the temperature for conformational change ($T_m{}^{-1}$) has been established for each of them. For κ-carrageenan, the ionic selectivity among monovalent cations is very important (179,180); the sequence is as follows:

$$Rb^+ > K^+, Cs^+ > Na^+ > Li^+, NH_4^+ > R_4N^+$$

The mechanical properties of the gels formed in the presence of different counterions follow the same order: Rb-carrageenan gel has a higher modulus and a higher melting temperature than those of Na-carrageenan gel. The molecular weight also plays a role on the elastic modulus which increases up to a limit around $M \sim 250{,}000$ (181). The mechanism of gelation in two steps is described in Reference 182.

In the series of anions, a characteristic behavior was observed with I^-; it stabilizes the double helix but prevents gelation (180).

Microbial Polysaccharides

Fungi and bacteria are sources of polysaccharides and especially of exopolysaccharides which can be produced in culture media on an industrial scale. They are a source of new additives for cosmetic or food applications but also for biological activity. Many of them are now in development; a review will be published in the second edition of Reference 12. Many of these polysaccharides are water soluble and able to compete with natural polysaccharides as described before (alginates, carrageenans, galacto- and glucomannans, chitosans, pectins, etc) especially in the domain of food additives. Many books discuss their applications (183–187).

The best examples of fungal polysaccharides are the $\beta(1\rightarrow3)$ glucans with a few $\beta(1\rightarrow6)$ glucose units as side groups. They often form a triple helical conformation with a tendency to give physical gel. There have been studies on scleroglucan, lentinan, schizophillan, etc (139,188,189). Because they are neutral, solubility depends on the fraction of side glucose units and their distribution.

Bacterial polysaccharides represent a large variety of polymers biosynthesized by bacteria. Their chemical structures and also their physical properties in solution or in the solid state may vary widely. They often contain uronic acid and then become polyelectrolytes (190). Many new polysaccharides have been developed from bacteria for industrial purposes. Exocellular polysaccharides are produced on a large scale by the usual techniques of microbiology and fermentation. This procedure allows good control of the characteristics of the polymers and allows purification of the polysaccharides more easily than from other natural sources (191–194). Extension of such production also allows reducing the price and extends the range of applications. A good example remains the hyaluronan previously produced by extraction from animal sources but in which some fraction of proteins remained. Bacterial hyaluronan can be prepared in a very pure form (195).

In general, polysaccharides are especially important in the domain of water-soluble polymers; they play an important role as thickening, gelling, emulsifying, hydrating, film forming, and suspending polymers. Especially important is the fact that some polysaccharides give physical gels in well-defined thermodynamic conditions. They constitute a very important class of materials in food, cosmetics, or pharmaceutical applications.

Specific methods for the purification of the polysaccharides have been developed. They are usually isolated in their sodium salt forms by precipitation from aqueous solution with ethanol or 2-propanol. This step is the most important one to get reproducible experimental characteristics. In fact, because of the presence

of many —OH groups in the molecule, the polysaccharides have a tendency to form cooperative intra- and interchain H-bonds, causing some insolubility or at least the presence of aggregates when solutions are prepared. Because of their stereoregularity, they are often able to form helical conformations in solution. Their ordered conformation has a semirigid character and its stability depends on temperature and ionic concentration if the polysaccharide structure contains uronic acid unit or ionic substituents; an example is given for succinoglycan (196,197).

Details of the chemical structure of bacterial polysaccharides have been given previously (198,199). In the following, the main industrial bacterial polysaccharides (xanthan, succinoglycan, gellan) are described briefly.

Succinoglycans are produced by many soil bacteria of the species *Pseudomonas*, *Rhizobium*, *Agrobacterium*, and *Alcaligenes*. These polysaccharides have a general chemical structure based on an height sugar repeat unit (D-glucode/D-galactose ratio equals 7:1); this structure is given in Figure 31.

Different substituents are also present in the molecule such as acetyl, succinyl, and pyruvyl groups, depending on the strain and on the conditions of fermentation and/or isolation (200–203). The content in substituents is easily determined by ^{1}H NMR in the presence of an internal standard to calibrate the signals and get a quantitative determination.

Succinoglycan, whatever its origin, is water soluble and, being stereoregular, it adopts a single-chain helical conformation at least in dilute solution. As shown by different techniques, the conformational transition is reversible and very cooperative at least in the presence of some salt excess. The stability of the ordered conformation depends on the salt concentration in solution as is usual for charged polysaccharides. On the two sides of the transition, the stiffness is completely different. In the helical conformation, the chain behaves as a semirigid chain having an intrinsic persistence length (L_p) estimated to be 35 nm and becoming more flexible at higher temperature in the coiled conformation with $L_p \sim 5$ nm. The persistence length in the helical conformation has been confirmed by AFM from the analysis of chain curvature (204).

The rheological behavior in dilute and semidilute solution is quite usual and typical of viscoelastic systems (197).

Xanthan was the first bacterial polysaccharide produced by the strain *Xanthomonas campestris* and developed on a large scale. The chemical structure of xanthan is recalled in Figure 31; it was confirmed by NMR. The ^{13}C spectrum allows identification of the different sugar units as well as the substituents (205). ^{1}H allows quantification of the yield in substituents. Xanthan is a semirigid polymer for which, in the native conformation, a persistence length around 40 nm was found (206–208). It has been demonstrated that when the native form is heated to coil conformation (with a much lower stiffness) and renatured by cooling, the conformation is changed. Xanthan has many industrial applications due to its suspending character (stabilizer of solid suspensions or foams), its pseudoplastic and thickening properties, good stability of the rheological properties as a function of pH, temperature, and salt concentration, and also its ability to be cross-linked and gelled. It is used in paints and coatings, cosmetics, ceramics, etc. In Figure 32 the rheological behavior characteristic for these semirigid polysaccharides is shown. The dependence of the viscosity as a function of shear rate and polymer concentration demonstrates the existence of a Newtonian plateau for low shear

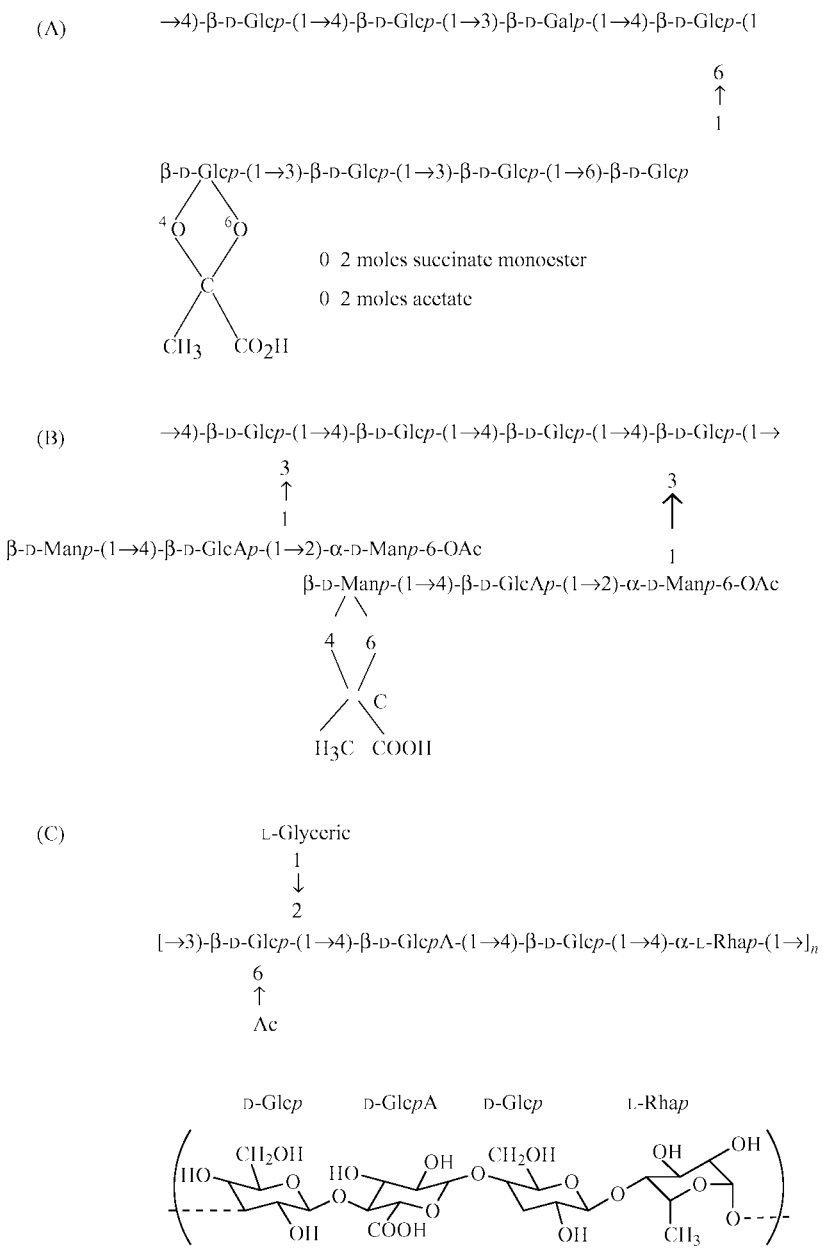

Fig. 31. Examples of some bacterial polysaccharide structures: (**A**) succinoglycan; (**B**) xanthan; (**C**) gellan in the native form and after deacylation.

rate followed by a decrease of the viscosity due to the viscoelastic character of the solution (209).

Gellan is produced by the bacteria *Sphingomonas elodea* (210). The native gellan as produced by the bacteria contains two additional substituents (acetyl and L-glyceryl) compared to the commercial polymer named Gelrite® (Fig. 31).

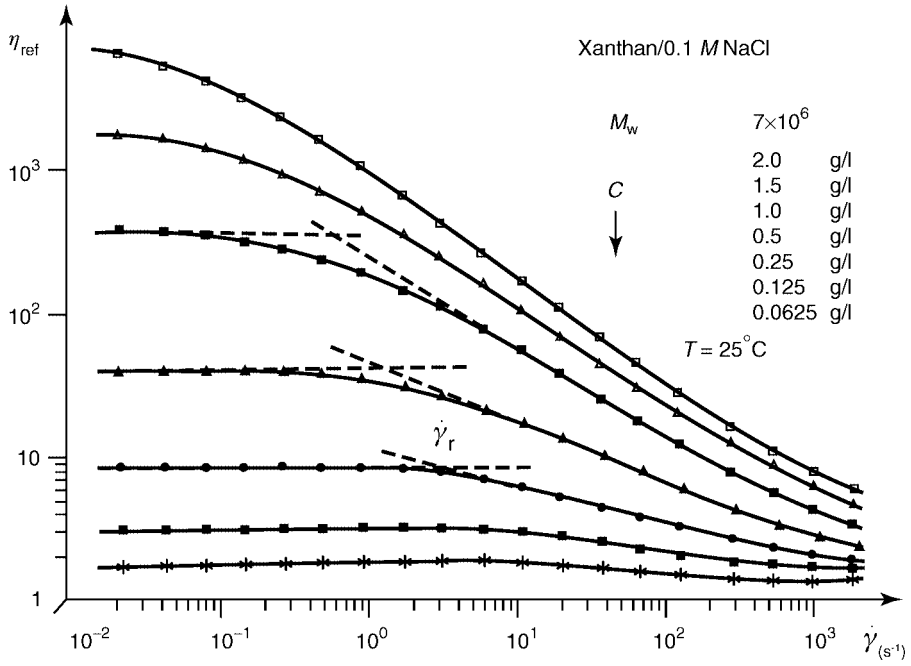

Fig. 32. Relative viscosity–shear rate curves for xanthan at different polymer concentration. Solvent: 0.1 *M* NaCl; $T = 25^\circ C$; $M_w = 7 \times 10^6$. Reproduced from Ref. 209, with the permission from Springer-Verlag GmBh & Co. (Copyright 2003).

The native gellan gives highly viscous solutions with a loose gel-like behavior. After deacylation, gellan gives a strong and rigid gel; a comparison between the native and deacylated gellan has been done (211,212). The chemical structures of the repeat units of the native and deacylated gellans are easily controlled by ^1H NMR.

The mechanism of gelation of deacylated gellan was examined and shown as a two-step process similar to the mechanism proposed for κ-carrageenan (182,213). Deacylated gellan adopts an ordered double-helix conformation in salt excess and the temperature for conformational change T_m increases when the salt concentration increases as is usual for stereoregular Polyelectrolytes (qv). The helical conformation is more stable in the presence of divalent counterions but no ionic selectivity appears among monovalent counterions (Li, Na, K, TMA) on one side and among divalent counterions (Ca, Mg) on the other side (212). When the salt and polysaccharide concentrations increase, the double helices interact to give a physical gel with strong ionic selectivity. The sequence of selectivity is

$$K^+ > Na^+ > Li^+$$

K^+ promotes gel formation and gives the higher elastic modulus.

Many new bacterial polysaccharides are now under development when they have specific physical behavior.

Mammalian Polysaccharides

Two homopolysaccharides are found in animals: glycogen and chitin. The others are heteroglycans based on disaccharide repeat units (they are also named glycosaminoglycans).

Glycogen. It is a storage polysaccharide able to produce D-glucose depending on the nutritional level. It is a highly branched neutral polysaccharide, analogue to amylopectin but more highly branched; thus, its solubility in water is larger.

Chitin. It is found in bacteria, fungi (such as *Aspergillus niger*), and crustaceans but only crustaceans are important commercial sources (see CHITIN AND CHITOSAN). Especially crab or shrimp shells are the main sources of chitin; *in situ* chitin is embedded in calcium carbonate and proteins. Chitin is a linear polymer made of $\rightarrow$4(β-D-*N*-acetyl-D-glucosamine)-1. Treatment of shells with acid and alkali allows isolation of chitin partially deacetylated. When chitan in decetylated to about 50% of the free amine form it is refered to as chitosan. Chitin is the renewable polysaccharide of most importance in quantity produced per year after cellulose. It has found many applications, at least on laboratory scale in food, medical, cosmetic applications in which their original structure is appreciated. After partial deacetylation, the polymer becomes soluble in acidic conditions by protonation of the amino group in C-2 position; the intrinsic pK of the $-NH_2$ groups is around 6 (214,215). Methods for characterizing chitosans with different degrees of acetylation (DA) have been re-examined using infrared spectroscopy and NMR (216–218). The molar mass distribution was examined by SEC (219). This polymer is the only natural water soluble polycation; it may be used for flocculation in water purification. It is recognized for its mucoadhesive properties. Unlike cellulose or starch, chitosan is able to be chemically modified on the specific C-2 position of the glucosamine unit. Several derivatives have been prepared. Alkylation gives alkylchitosans (220,221), amphiphilic polymers which are good thickeners. Carboxymethylation gives an anionic polymer (222) and quaternization of $-NH_2$ gives a cationic polymer (223,224). Grafted cyclodextrin–chitosan has also been prepared (225,226). Another original property of chitosan is its chelating properties; a specific complex is formed with Cu^{2+} and its structure has been proposed (227,228). The applications and biochemical properties of chitosan have been reviewed in two books (229,230).

Proteoglycans. They are carbohydrate–protein polymers in which many long polysaccharide chains are covalently linked to the protein core. The percentage of protein is low. They are also classified as glycoproteins, but the name proteoglycan is now preferred to the historical term mucopolysaccharide. These polymers are widely distributed in connective tissue, cartilage, tendon, or synovial fluid. Carbohydrate components (with an alternating structure $(AB)_n$ divided into six groups) based on disaccharide repeat units (Table 7) are joined to the protein core in different ways by a N- or O-glycosidic linkage. Depending on their composition, glycoaminoglycans are known as hyaluronan, chondroïtin sulfate (in 4- or 6-position), dermatan sulfate, heparin, heparan sulfate, and keratan sulfate. Much research is in progress on these biopolymers; a review on the structure, properties, medical and biological applications of hyaluronan has been published (231).

Table 7. Disaccharide Units Constitutive of Proteoglycans

Basic disaccharide unit	Common names
GlcNAcβ1,4-GlcAβ1,3	Hyaluronic acid
GalNAc(6 or 4-SO_3^-)β1,4-GlcAβ1,3	Chondroitin sulfate
GalNAc(4-SO_3^-)β1,4-L-IduAα1,3	Dermatan sulfate
GlcNSO$_3$(6-So_3^-)α1,4-L-IduAα1,4	Heparin
GlcNSO$_3\beta$1,4-L-IduAα1,4	Heparan sulfate
GlcNAc(6-SO_3^-)β1,3Gal(6-SO_3^-)β1,4	Keratan sulfate

Glycoconjugates

Glycoconjugates, eg glycoproteins and glycolipids, are biopolymers; the name indicates that the carbohydrate is the minor component. In the glycoconjugates, oligosaccharide moieties consist of up to 20 monomers. They are basic components of all the cell membranes. Thus, certain oligosaccharides can be associated with degenerative cell growth and can be used in cancer diagnostics as so-called tumor-associated antigens.

Glycoproteins. They are proteins containing one or several oligosaccharide side chains. The linkages are N- or O-glycosidic linkages or by ethanolamine phosphate. The *O*-glycoproteins seem to be more involved in the stabilization and protection of protein structures rather than as signaling molecules in cell communication.

Glycolipids. They are amphiphilic molecules of low molecular weight. The lipophilic part consists of 1,2-di-*O*-diacylglycerol or *N*-acylsphingosin; the hydrophilic part is a phosphate group and/or a carbohydrate moiety. There are many glycolipids with different covalent structures with specific biological roles.

Another series of glycoconjugates (but usually not joined in this classification) is represented by natural plant gums such as Arabic gum which is recognized as very specific to stabilize emulsion. In these polymers, the glycosidic part is the most important in weight fraction compared to the protein fraction.

Glycopolymers

Under this term we refer to synthetic polymers in which at least one of the monomers engaged contains a saccharidic unit.

The extensive participation of saccharides in recognition processes has sparked the synthesis of new polymeric materials expected to have sophisticated functions similar to or even superior to natural glycoconjugates. Numerous synthetic polymers carrying various kinds of saccharide residues as information elements have therefore been developed. It has been shown that such glycoconjugates may have enhanced binding capacity with lectins based on a polymer sugar-cluster effect whereas the monomeric carbohydrate derivatives exhibit only weak affinity to the same lectins (232–235). These “glycopolymers” have thus diverse potential uses, such as multivalent inhibitors of cell or virus binding, cell-specific culture substrata, artificial antigens, targeted drug delivery systems. The

term "glycopolymers" was first introduced by Roy and co-workers (236) as a replacement for "pseudo-polysaccharide" previously used, to designate water-soluble as well as insoluble polymers bearing covalently bound carbohydrates. In the following, the term *glycopolymer* refers to synthetic (or natural) linear polymers possessing sugar moieties as pendant or terminal groups irrespective of whether they are water soluble or not. Glycopolymers can be obtained by polymerization of sugar-carrying monomers. An alternative synthetic method consists of the chemical modification of preformed polymers using carbohydrate-containing agents. Nevertheless, both strategies generally rely on the same carbohydrate precursors.

In accordance with the great attention that these glycoconjugates have attracted for the last 10 years, several reviews on the synthesis and biological functions of these macromolecules have been published (237–243). In fact, the selection and design of a glycopolymer for a given application is a challenging task because of the inherent diversity of structures and to the impact of the latter and solution conformation of the sugar-containing polymers on their biorecognition. Here in is considered glycopolymers with an emphasis on their structures, their physicochemical and biological properties, and their applications.

Synthesis Strategy. Polymer chemistry offers the possibility to prepare glycopolymers with custom-designed properties since several groups with specific properties can be easily introduced along the polymer chain, as shown in the scheme:

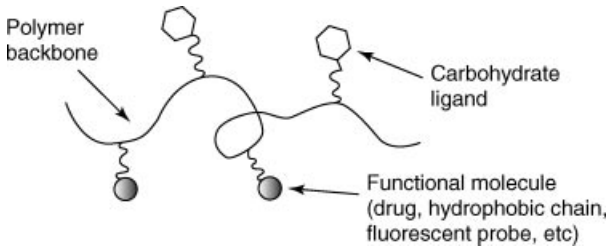

Indeed, besides the saccharide moieties which are expected to act, in most cases, as recognition signals, various molecules such as hydrophobic chains, fluorescent probes, and drugs can be used to modulate the solution properties of the polymer, label the cells, or deliver a given drug on site. In addition, the polymer backbone can be adjusted to confer desired physical or biological properties.

The most commonly used strategies for the syntheses of such glycopolymers involve direct homopolymerization of sugar-bearing monomers or copolymerization of the latter with one or two other monomers. The next most used strategy involves chemical modification of preformed polymers with suitably functionalized carbohydrate residues. Generally, both methodologies require the same glycosynthons and several methods leading to activated carbohydrate derivatives suitable to be covalently linked to either a preformed polymer or a polymerizable anchor have been described. These methods belong to five main categories, discussed below and depicted in Figures 33–37.

The first one relies on standard glycosylation chemistry, providing *O*-, *C*-, or S-glycosides having, for example, alkene, styrene or amine groups in the aglycon portion (Fig. 33) (236,244–255) The intermediate amine-containing glycoside can be used in graft copolymerizations or acryloylated to give a monomer precursor.

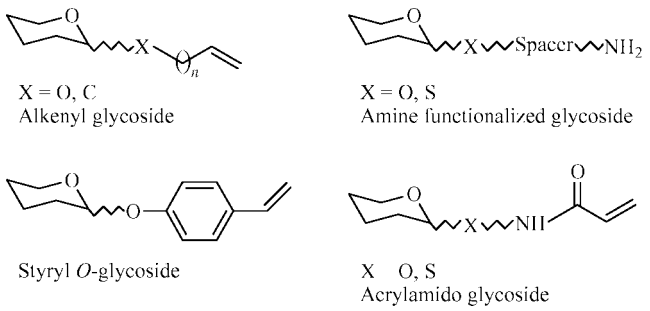

Fig. 33. Examples of glycosynthons obtained by standard glycosylation reactions.

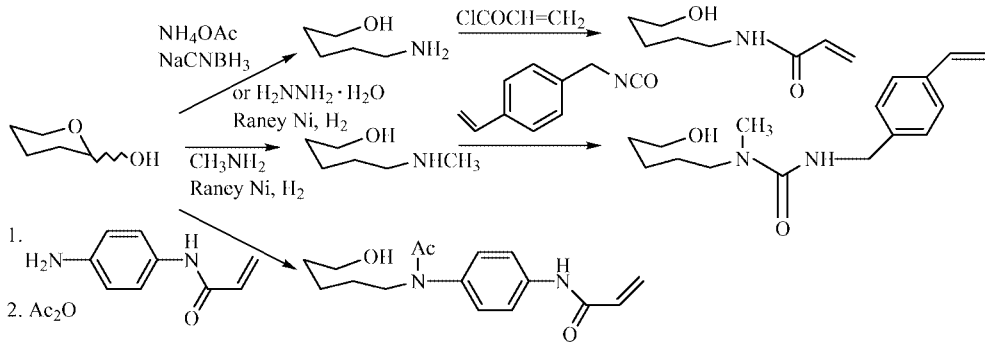

Fig. 34. Synthetic routes to carbohydrate monomers based on the reductive amination reaction.

The second approach is based on the reductive amination of the saccharide (lactose, maltose, *N*-acetylchitooligosaccharides, etc) by ammonium acetate, hydrazine, *N*-methylamine, or 4-acrylamidobenzylamine, followed by N-acryloylation (256,257), addition of 4-vinylbenzyl isocyanate (258) or N-acetylation (259,260) (Fig. 34).

This method is quite easy and rapid; however, it leads to an altered saccharide, the reducing sugar being transformed into a linear polyol amine derivative. Therefore, it is rather applied to oligosaccharides since at least, the terminal sugar is preserved.

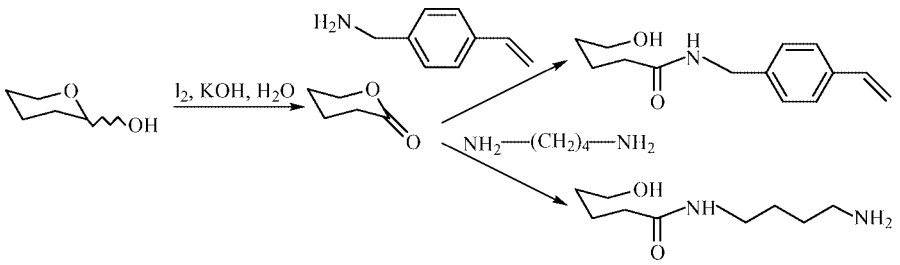

Fig. 35. Preparation of suitable glycosynthons for polymer synthesis from carbohydrate lactones.

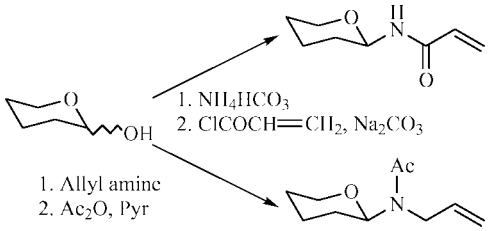

Fig. 36. Synthetic routes to polymerizable glycosylamides.

In the third approach, the reducing end of the carbohydrate (maltose, lactose, maltotriose, etc) is oxidized by hypoiodite and then, the resulting lactone can be condensed with *p*-vinylbenzylamine (261) or 1,4-diaminobutane (262) (Fig. 35). For the same reasons as those described above, this reaction is rather applied to oligosaccharides.

In the fourth approach, the carbohydrate can be reversibly converted into a glycosylamine by treatment with an ammonium salt (263,264) or an aliphatic amine (265,266). However, these derivatives are quite unstable in slightly acidic medium or neutral medium. They are further stabilized by acylation with, for example, anhydride acetic (265), *p*-vinylbenzoyl chloride (267), acryloyl chloride (263), or chloroacetic anhydride, followed by ammonolysis (268) (Fig. 36). The N-linked structure of these glycosynthons is distinct from the open chain structure of the carbohydrate derivatives described above. This method may be useful to introduce complex oligosaccharides.

These different methodologies generally provide unprotected activated glycosynthons. Carbohydrate hydroxyl or amine residues at positions other than the anomeric center can also be used to introduce functional groups for direct or graft polymerization. These carbohydrate precursors can be fully protected or unprotected. However, in the former case, the resulting glycopolymers must undergo a final deprotection step of the carbohydrate moieties under the usual conditions. Some examples of these glycosynthons such as *N*-methacryloylglycylglycylgalactosamine (MA-GG-GalN) (269,270), diacetone glucofuranose acrylate (271), *p*-vinylbenzylether (272) are given in Figure 37.

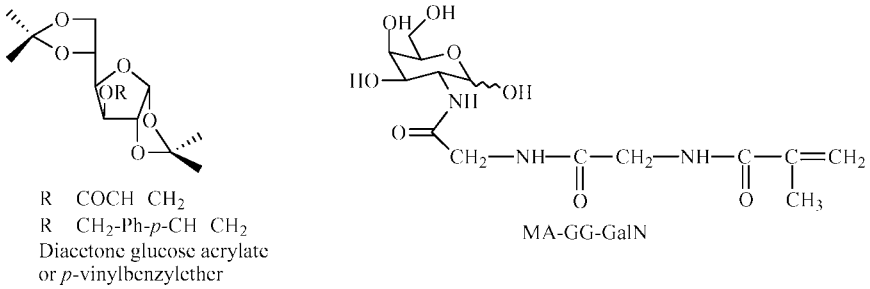

Fig. 37. Examples of carbohydrates monomers bearing a polymerizable group at a position other than the anomeric center.

In this last approach, although it has been shown in some cases that the carbohydrate–protein interaction remains efficient (269,270), the carbohydrate modification at a position other than the anomeric center may decrease its affinity toward the protein.

Glycopolymer Syntheses by Homo- or Copolymerization. The radical polymerization of *N*-acryloylated carbohydrate precursors with acrylamide and/or acrylamide derivatives with specific properties is likely one of the most commonly used strategies for the syntheses of glycopolymers. Indeed, this is a versatile method which can be easily and efficiently performed in aqueous solution from unprotected sugar-carrying monomers. Moreover, it generally leads to water-soluble derivatives. This method has been extensively used for the preparation of sialic acid bearing polyacrylamides as inhibitors of influenza virus adhesion (251–253,273). Several custom-designed glycopolymers made of two or more components were also synthesized according to this methodology. Various applications of such copolymers have been envisaged as discussed in the following section.

Numerous carbohydrate styrene monomers such as (*p*-vinylbenzamido)-β-lactose and *N*-(*p*-vinylbenzyl)-4-*O*-β-D-galactopyranosyl-D-gluconamide have been homopolymerized (or copolymerized) in an organic solvent (dimethyl sulfoxide) using 2,2′-azobisisobutyronitrile (261,267). The resulting polystyrenes, having amphiphilic structures, were shown to have strong affinity toward specific lectins. Moreover, the hydrophobic effect of the styrene moiety allowed preparation of polymeric nanospheres with a polystyrene core and a glycopolymer corona. These nanospheres were synthesized by free radical copolymerization in a polar solvent (ethanol/water mixture) of styrene with a hydrophilic carbohydrate macromonomer such as the glucosyloxyethyl methacrylate macromonomer (Fig. 38) (274). The concanvalin A lectin recognized the glucose on the nanospheres with a better binding activity than with the monomeric glucose.

Living polymerization techniques have been successfully used for the synthesis of glycopolymers with controlled molecular weights and molecular weight

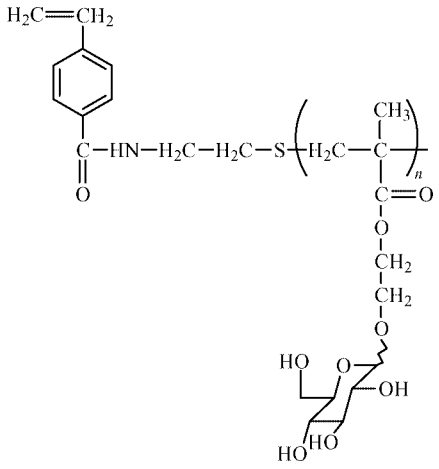

Fig. 38. Structure of the glucosyloxyethyl methacrylate (GEMA) macromonomer.

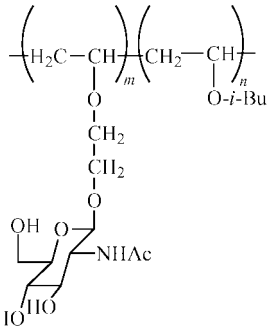

Fig. 39. Example of an amphiphilic block copolymer obtained by living cationic polymerization.

distributions. They have also served for the preparation of well-defined block copolymers. These methods are based on "living" radical polymerizations such as nitroxide-controlled polymerization (271,275) and atom transfer radical polymerization (276), living cationic (277–279) or anionic (280) polymeriation (see LIVING POLYMERIZATION, CATIONIC; ANIONIC POLYMERIZATION; CARBOCATIONIC POLYMERIZATION). Thus these polymerization strategies allowed preparation of new amphiphilic block copolymers, the hydrophilic segment having pendant sugar moieties (see Fig. 39). However, one of the drawbacks of the approach is that it involves protected carbohydrate monomers and thus, a final deprotection step of the glycopolymer is necessary.

An alternative method developed by Kiessling and co-workers is ring-opening metathesis polymerization (ROMP) (281–285). A significant advantage of this strategy is that living polymerization can be performed from unprotected carbohydrate monomers including, for example, sulfated sugar-carrying monomers. Moreover, besides the possibility of preparing block copolymers, specific endlabels can be introduced. However, although the molecular weight distribution of glycopolymers obtained by the ROMP strategy is narrower than polymers prepared through classical radical polymerization approaches, the control of molecular weights remains difficult.

Glycopolymer Syntheses by Reactions on Preformed Polymers. Compared to the methodologies based on polymerizations of sugar-carrying monomers, the chemical modification of preformed polymers using carbohydrate-containing reagents is generally advantageous as it requires fewer reaction steps and it allows easy control of the number of sugars along the polymeric chain. Moreover, large quantities of preformed polymers can be synthesized with the desired molecular weight. Therefore, the same polymer backbone can be used to prepare glycopolymers with different carbohydrate contents and/or carbohydrate residues. Of course, the preformed polymers must have reactive functionalities such as amine, carboxylic acid, or alcohol groups. These polymers may be activated or not. For instance, polyacrylates with *p*-nitrophenyl (249,268) or succinimidyl esters (252,255) react at room temperature with carbohydrate amines in aprotic polar solvents (DMSO or DMF) to give glycopolymers after the quenching of excess active esters with sodium hydroxide, ammonia, or ethanolamine.

Carbohydrate amines also react with polymers possessing pendant hydroxyl groups partially functionalized with *p*-nitrophenyl carbonate groups (286). Maleic anhydride copolymers have the advantage of being directly modified by carbohydrate amines under mild conditions. This method allowed efficient preparation of various glycopolymers useful for solid-phase assays or new drug delivery systems (262,287–289). Various carbohydrate derivatives have also been grafted to natural polymers such as chitosan. The free amine group at the C-2 position of the glucosamine unit can easily react with aldehydes which allows preparation of a wide variety of compounds such as L-fucose-, D-fucose-, D-mannose-branched chitosan (290), cyclodextrin-grafted chitosans (225,291,292), and a sialic acid dendron-grafted chitosan (293).

Moreover, the pendant carbohydrate chains of synthetic glycopolymers have been shown to be further elongated by enzymatic reactions. Thus, by this approach, Nishimura and co-workers have been able to prepare a glycopolymer having a sialyloligosaccharide using glycosyl transferases and transglycosidases (294). More recently, this strategy allowed the selective modification of a glycopolymer possessing both lactose and mannose residues (254). Indeed, using a galactosyl transferase, a galactose unit could be introduced specifically on the pendant lactose moieties.

Role of Glycopolymer Structure. The properties of glycopolymers of course depend on the nature of the pendant saccharide chain as a biorecognizable element, but also on the whole chemical structure. Indeed, the latter influences conformation, charge, biodegradability, etc, which are important parameters for the glycopolymer functions. For example, glycosylated polystyrenes have been shown to exhibit strong binding affinities to lectins, viruses, and cells (267,295,296) The strong binding affinity has been attributed to the characteristic conformations based on the amphiphilic structure of glycopolystyrenes. Indeed, the hydrophobic main chain tends to form a hydrophobic core that is sheltered from water, and hence the saccharide chains gather on the outside of the polymer in water. In addition, as mentioned above, the hydrophobic effect of the styrene moiety allowed preparation of original polymeric nanospheres having a polystyrene core and a glycopolymer corona. Furthermore, the significant enhancement of protein–carbohydrate interactions due to hydrophobic associations in water has been well evidenced by Kopecek and co-workers (269) who have synthesized glycopolymers with photoresponsive benzospiropyran side chains. Upon irradiation by UV light, benzospiropyrans change to a red colored polar (zwitterionic) merocyanine form. On exposure to visible light, merocyanine converts back to the nonpolar (hydrophobic) spiro form. Thus, under visible light, the photoresponsive glycopolymers show a high lectin binding due to contraction of the polymer chains, which tends to increase the probability of formation of clustered saccharide chains. After irradiation, the binding decreases as a result of the expansion of polymer chains.

The flexibility of glycopolymers may also have a large influence on their biorecognition. In the case of flexible glycopolymers, the increased content of carbohydrate side chains generally increases biorecognition. This is not confirmed at all in the case of rigid ones. Indeed, rigid cylindrical phenyl isocyanide (PPI) glycopolymers have been shown to exhibit little specific interactions with lectins (297). In these systems, the saccharide arrays are crowded too thickly to be accessible or to be induced-fit to the binding sites. The decrease of saccharide density

by insertion of comonomer units into the rigid PPI glycopolymer backbone was found to increase the binding affinity to the lectin.

Applications of Glycopolymers. Most applications of glycopolymers arise from the specific molecular and cell recognition of saccharides. Therefore, many bio- and immunochemical properties have been demonstrated for a large number of glycopolymers. The synthesis of sugar-based hydrogels from carbohydrate monomers and cross-linking agents or by covalent attachment of carbohydrates to commercially available affinity supports made of agarose, cellulose, or polyacrylamide allowed preparation of new bioaffinity supports (298–300). The latter have been used for the purification of antibodies, enzymes, lectins, and myeloma proteins. Sugar-based hydrogels also show potential as substrates for cell growth. Indeed, the replacement of agar, used in culture plates, by hydrogels containing specific sugars may enhance the adhesion of cells. Such properties have also been evidenced by a lactose-carrying styrene homopolymer (301,302). The latter has been shown to be adsorbed on the surface of glass culture dishes and the resulting polymer-coated dishes have been found to be useful for hepatic cell cultures.

Moreover, glycopolymers have been shown to constitute very sensitive coating antigens in solid-phase enzyme-linked immunosorbent assays (ELISA). In comparison to protein glycoconjugates, glycopolymers offer several advantages such as lower cost productions and improved thermal and biological stabilities. Therefore, many examples of applications of glycopolymers in the detection of carbohydrate-binding proteins including serodiagnosis of bacterial antigens have been reported. These have been summarized in several reviews (240–242).

Glycopolymers can also be advantageously used to inhibit cell adhesion. Typical examples are polymers bearing pendant α-sialoside groups which show potent anti-influenza activity (249,251–253,268,273,303). Indeed, it is now well established that human infections by influenza viruses are mediated by the binding of the viral membrane protein hemagglutinin (hyaluronan) to sialosides on cell surface glycolipids and glycoproteins. The inhibitory properties of such glycopolymers illustrate the value of cooperative polyvalent interaction in the design of potent inhibitors of viral adherence to the host cell.

Glycopolymers also show promising properties as drug-targeting delivery agents. One of the most successful polymer–drug–saccharide conjugate systems reported are the *N*-(2-hydroxypropyl)methacrylamide (HMPA) copolymer–adriamycin (ADR)–sugar conjugates, in which both ADR and sugar were attached to a polymer backbone via lysosomally cleavable oligopeptide spacers (304). The conjugates containing galactosamine moieties were reported to accumulate in the liver selectively (305). Other glycopolymers such as lactose-carrying styrene polymers were also found to be very efficient liver-specific targeting materials (306).

Besides these fields of applications, Wulff and co-workers (307,308) investigated the potential ability of glycopolymers to modify surface properties. Thus, they copolymerized several isopropylidene-protected vinyl sugars with styrene, methyl methacrylate, and acrylonitrile. After eliminating the isopropylidene protecting groups from the copolymer surfaces by acid hydrolysis, these surfaces were shown to become hydrophilic with improved dyeability and surface conductivity.

Synthesis of Oligo- and Polysaccharides

The chemical synthesis of oligosaccharides or their analogues is well developed now; nevertheless, it is a difficult task. Protection of labile groups of the —OH position which are not engaged in an osidic linkage is needed. Then, reaction with specific groups of the anomeric and nonanomeric position must be done with a control of the stereochemistry of the anomeric position. Oligosaccharides in which glycosidic oxygen atoms are replaced by sulfur atoms can be routinely synthesized by iterative or convergent approaches (309,310) and these nonnatural compounds are not hydrolyzed by various glycosidases (311,312).

Polysaccharides having a regular structure were first obtained by polymerization of anhydrosugars or step-by-step elongation. For synthesis of irregular structures, a step-by-step elongation by polycondensation is the usual method at least to produce the repeating unit which is then polymerized. These routes have been discussed previously in the review of Kochetkov (313).

A different but interesting approach comes from the enzymatic polymerization of the corresponding mono- or disaccharide precursors with controlled structure.

Synthesis of Regular Polysaccharides. The first attempt at such synthesis appears with the work of Haq and Whelan in 1956 (314); they proposed, without success, the polycondensation of 2,3,4,-ti-*O*-acetyl-α-D-glucosyl bromide in the presence of Ag_2O and $CaSO_4$ to get a (1–6)-β-D-glucan. Other negative attempts have been published (313).

The most fruitful results came with the synthesis of polysaccharides by polymerization of anhydrosugars. Schuerch (315–317) investigated the mechanism of cationic polymerization in solution of 1,6-anhydro-hexopyranoses wherein the 2,3,4 positions were protected by benzyl groups. He got high molecular weight (1,6)-α-D-glucan and the benzyl groups were easily removed at the end of polymerization. The 1,4; 1,3; 1,2 anhydrosugar polymerizations were also performed with less success. However, (1–3)-α-D-glucopyranans and (1–3)-α-D-mannopyranans were obtained with high stereoregularity. These results are discussed in the review by Kochetkov (313).

Chemoenzymatic Synthesis. Original oligosaccharides bifunctionalized with fluorescent entities were synthetized in the presence of a mutant of *Humicola insolens* endoglucanase (318). Hemithiocellodextrins with degree of polymerization from 4 to 14 were synthetized in the presence of a cellulase in buffer/organic solvent (319).

Homopolymers were also obtained with mutant of Barley (1,3)-β-D-glucan endohydrolase producing (1,3)-β-D-glucan and with mutant of cellulase producing β-(1$\rightarrow$4)-oligo- and polysaccharides (320,321).

A very active research is lead by the Kobayashi group in Japan; in a recent review, cellulose, chitin, and xylan syntheses were described using Enzymatic Polymerization (qv) (322).

Hydrolases were most often used as catalyst forming the glycosidic bonds *in vitro*. Recently, synthetic polysaccharides were synthetized using other enzymes such as glycosyltransferase, phosphorylases, oxidoreductases, and lipases (323).

Copolymers may also be produced using combinations of chemically modified mono- or disaccharides and enzymatic condensation. Such a route has been proposed to prepare an artificial hyaluronan, GlucA-β-(1→3) GlucNAc oxazoline monomer reacting with hyaluronidase (324).

BIBLIOGRAPHY

"Polysaccharides" in *EPST* 1st ed., Vol. 11, pp. 396–424, by R. L. Whistler, Purdue University; "Polysaccharides" in *EPSE* 2nd ed., Vol. 13, pp. 87–147, by G. G. S. Dutton, University of British Columbia.

1. W. Pigman and D. Horton, *The Carbohydrates, Chemistry and Biochemistry.*, 2nd ed., Academic Press, New York, Vol. IA, 1972; Vol. IB, 1980; Vols. IIA and IIB, 1970.
2. G. O. Aspinall, *The Polysaccharides*, Academic Press, New York, Vol. 1, 1982; Vol. 2, 1983; Vol. 3, 1985.
3. *Methods in Carbohydrates Chemistry*, John Wiley & Sons, Inc., New York, Vols. I to X, 1962 to 1994.
4. J. Lehmann, *Carbohydrates. Structure and Biology*, Georg-Thieme Verlag, Stuttgart, 1998.
5. T. K. Lindhorst, *Essentials of Carbohydrate Chemistry and Biochemistry*, Wiley-VCH, Weinheim, 2000.
6. B. Ernst, G. W. Hart, and P. Sinay, *Carbohydrates in Chemistry and Biology*, Part I, Wiley-VCH, Weinheim, Vols. 1 and 2: Chemistry of Saccharides, 2000.
7. *Advances in Carbohydrate Chemistry*, Academic Press, New York, Vols. 1 to 23, 1945 to 1968.
8. *Advances in Carbohydrate Chemistry and Biochemistry*, Academic Press, New York, Vols. 24 to 57, 1969 to 2001.
9. R. D. Guthrie and J. Honeyman, *An Introduction to the Chemistry of Carbohydrates*, Clarendon Press, Oxford, 1964.
10. P. Collins and R. Ferrier, *Monosaccharides: Their Chemistry and Their Role in Natural Products*, John Wiley & Sons, Inc., New York, 1998.
11. F. A. Loewus, and W. Tanner, *Encyclopedia of Plant Physiology (New series), Volume 13A: Plant Carbohydrates I. Intracellular Carbohydrates*, Springer-Verlag, Berlin, 1982.
12. S. Dumitriu, *Polysaccharides: Structural Diversity and Functional Versatility*, Marcel Dekker, New York, 1998.
13. S. Dumitriu, *Polysaccharides in Medical Applications*, Marcel Dekker, New York, 1996.
14. *Eur. J. Biochem.* **21**, 455 (1971); *Biochemistry* **10**, 3983 (1971); *Pure Appl. Chem.* **54**, 1518 (1982); *Pure Appl. Chem.* **55**, 1269 (1983); *Pure Appl. Chem.* **68**, 1919 (1996); *Carbohydr. Res.* **297**, 1–92 (1997).
15. G. A. Jeffrey, *Carbohydr. Res.* **28**, 233 (1973).
16. K. Bock and H. Thogersen, *Annu. Reports NMR Spectrosc.* **13**, 1 (1982).
17. K. Bock and C. Pedersen, *Advances in Carbohydrate Chemistry and Biochemistry*, Vol. 41, Academic Press, New York, 1983, p. 27.
18. A. De Bruyn, J. Carbohydr, *Chem.* **10**, 159 (1991).
19. K. Bock, C. Pedersen, and H. Pedersen, *Advances in Carbohydrate Chemistry and Biochemistry*, Vol. 42, Academic Press, New York, 1984, p. 193.
20. B. Jiang, E. Drouet, M. Milas, and M. Rinaudo, *Carbohydr. Res.* **327**, 455 (2000).
21. E. Frollini, W. F. Reed, M. Milas, and M. Rinaudo, *Carbohydr. Polym.* **27**, 129 (1995).

22. M. R. Sierakowski, M. Milas, J. Desbrières, and M. Rinaudo, *Carbohydr. Polym.* **42**, 51 (2000).
23. M. Vincendon, M. Vignon, A. Heyraud, and M. Rinaudo, *Biopolymers* **18**, 167–185 (1979).
24. A. Heyraud and M. Rinaudo, *J. Chromatogr.* **166**, 149 (1978).
25. A. Heyraud and M. Rinaudo, *J. Liquid Chromatogr.* **4**, 175 (1981).
26. A. Heyraud and M. Rinaudo, *J. Liquid Chromatogr.* **3**, 721–739 (1980).
27. A. Heyraud and M. Rinaudo, *J. Appl. Polym. Sci., Appl. Polym. Symp.* **45**, 203 (1990).
28. A. Heyraud and M. Rinaudo, in R. B. Friedman, ed., *Biotechnology of Amylodextrin Oligosaccharides* (ACS Symposium Series 458) American Chemical Society, Washington, D.C., 1991, p. 171.
29. A. Heyraud, M. Rinaudo, and F. R. Taravel, *Carbohydr. Res.* **128**, 311 (1984).
30. P. Albersheim, *Acc. Chem. Res.* **25**, 77 (1992).
31. W. J. Peumans and E. J. M. Van Damme, *Plant Physiol.* **109**, 347 (1995).
32. E. J. M. Van Damme, W. J. Peumans, A. Psusztai, and S. Bardocz, *Handbook of Plant Lectins: Properties and Biomedical Applications*, John Wiley & Sons, Inc., New York, 1998.
33. U.S. Pat. 9623057 (1996), F. M. B. Paul, D. F. Perry, and P. F. Monsan (to Bioeurope).
34. *IUPAC Macromolecular Division, Pure Appl. Chem.* **61**, 211 (1989).
35. D. Cremer and J. A. Pople, *J. Am. Chem. Soc.* **97**, 1354 (1975).
36. K. Bock and J. O. Duus, *J. Carbohydr. Chem.* **13**, 513 (1994).
37. I. Tvaroska and T. Bleha, *Adv Comp. Chem. Biochem.* **47**, 45 (1989).
38. M. Orozco, C. Alhambra, X. Barril, J. M. Lopez, M. A. Busquets, and F. J. Luque, *J. Mol. Model.* **2**, 1 (1996).
39. C. Fringant, I. Tvaroska, K. Mazeau, M. Rinaudo, and J. Desbrieres, *Carbohydr. Res.* **278**, 27 (1995).
40. I. Tvaroska and F. R. Taravel, *Carbohydr. Res.* **221**, 83 (1991).
41. I. Tvaroska and F. R. Taravel, *J. Biomol. NMR.* **2**, 421 (1992).
42. P. J. Flory, *Statistical Mechanics of Chain Molecules*, Wiley-Interscience, New York, 1969.
43. B. A. Burton and D. A. Brant, *Biopolymers* **22**, 1769 (1983).
44. R. Urbani and A. Cesaro, *Polymer* **32**, 3013 (1991).
45. K. Mazeau, S. Perez, and M. Rinaudo, *J. Carbohydr. Chem.* **19**, 1269 (2000).
46. K. Haxaire, I. Braccini, M. Milas, M. Rinaudo, and S. Perez, *Glycobiology* **10**, 587 (2000).
47. C. L. O. Petkowicz, M. Rinaudo, M. Milas, K. Mazeau, T. Bresolin, F. Reicher, and J. L. M. S. Ganter, *Food Hydrocolloids* **13**, 263–266 (1999).
48. H. O. Bouveng and B. Lindberg, *Meth. Carbohydr. Biochem.* **5**, 147 (1965).
49. J. P. Joseleau, G. Chambat, B. Chumpitazi-Hermoza, *Carbohydr. Res.* **90**, 339 (1981).
50. J. O. Warwicker, and H-Swelling, in N. M. Bikales and L. Segal, eds., *Cellulose and Cellulose Derivatives*, Part IV, Wiley-Interscience, New York, 1971, p. 325.
51. K. Haxaire, PhD dissertation, Joseph Fourier University, Grenoble, France, 2000.
52. P. Albersheim, D. J. Nevins, P. D. English, and A. Karr, *Carbohydr. Res.* **5**, 340 (1967).
53. I. Morrison, *Phytochemistry* **27**, 1097 (1988).
54. R. L. Taylor, and H. E. Conrad, *Biochemistry* **11**, 1383 (1972).
55. A. Anderson, and B. A. Stone, *Carbohydr. Polym.* **5**, 115 (1985).
56. M. F. Chaplin, *Anal. Biochem.* **123**, 336 (1982).
57. A. B. Blakeney, P. J. Harris, R. J. Henry, and B. A. Stone, *Carbohydr. Res.* **113**, 291 (1983).
58. S. Hakomori, *J. Biochem. (Tokyo)* **55**, 205 (1964).
59. M. Hirrien, J. Desbrières, and M. Rinaudo, *Carbohydr. Polym.* **331**, 243–252 (1996).

60. H. Bjorndal, B. Lingberg, and S. Svensson, *Carbohydr. Res.* **5**, 433 (1967).
61. D. J. Harvey, *Mass Spectrom Rev* **18**, 349 (1999).
62. V. N. Reinhold, B. B. Reinhold, and S. Chan, in B. L. Karger, W. S. Hancok, eds., *Methods in Enzymology*, Vol. 271, Academic Press, New York, 1996, p. 377.
63. J. A. McCloskey, *Methods in Enzymmology, Vol. 193: Mass Spectrometry*, Academic Press, New York, 1990.
64. S. Hizukuri, Y. Takeda, and M. Yasuda, *Carbohydr. Res.* **94**, 205 (1981).
65. S. Hizukuri, *Carbohydr. Res.* **141**, 295 (1985).
66. M. Beurret, and J. P. Joseleau, *Carbohydr. Res.* **157**, 27 (1986).
67. M. Rinaudo and J. Desbrières, *Eur. Polym. J.* **16**, 849 (1980).
68. C. Rochas, A. Domard, and M. Rinaudo, *Eur. Polym. J.* **16**, 135 (1980).
69. M. Rinaudo, J. Desbrières, and C. Rochas, J. Liquid, *Chromatogr.* **4**, 1297 (1981).
70. J. Desbrières, J. Mazet, and M. Rinaudo, *Eur. Polym. J.* **18**, 269 (1982).
71. B. Tinland, J. Mazet, and M. Rinaudo, *Makromol. Chem. Rapid Commun.* **9**, 69 (1988).
72. M. Rinaudo, *La Papeterie* **5**, 479 (1968).
73. J. P. Merle, PhD dissertation, Joseph Fourier University, Grenoble, France, 1968.
74. V. M. Golubev, and S. Y. Frenkel, *Vysokomol. Soedin A* **49**, 1847 (1967).
75. J. W. Tamblyn, D. R. Morey, and R. H. Wagner, *Ind. Eng. Chem* **37**, 573 (1945).
76. W. J. B. Badgley, and H. Mark, *J. Phys. Colloid Chem.* **51**, 58 (1947).
77. G. Sitaramaiah, and D. A. I. Goring, *J. Polym. Sci.* **58**, 1107 (1962).
78. W. B. Neely, *J. Polym. Sci. A.* **1**, 311 (1963).
79. K. Uda and G. Meyerhoff, *Makromol. Chem* **47**, 168 (1961).
80. W. Banks and C. T. Greenwood, *Polymer* **10**, 257 (1969).
81. W. W. Everett and J. F. Foster, *J. Am. Chem. Soc.* **81**, 5459 (1959).
82. W. Burchard, *Makromol. Chem.* **64**, 110 (1963).
83. J. M. G. Cowie, *J. Polym. Sci.* **49**, 455 (1961).
84. M. Rinaudo, J. Reguant, in E. Frollini, A. Leao, L. H. Capparelli Mattoso, eds., *Natural Polymers and Agrofibers Composites*, Embrapa Instrumentacao Agropecuaria, Brazil, 2000, pp. 15–39.
85. D. N. S. Hon, in S. Dimitriu, ed., *Polysaccharides in Medicinal Applications*, Marcel Dekker, Sherbrooke, Canada, 1996, p. 87.
86. R. M. Rowell, A. R. Sanadi, D. F. Caulfield, and R. E. Jacobson, in A. L. Leao, F. X. Carvalho, and E. Frollini, eds., *Lignocellulosic-Plastics-Composites*, USP, UNESP, Sao Paulo, 1997, p. 23.
87. R. A. Young, in A. L. Leao, F. X. Carvalho, and E. Frollini, eds., *Lignocellulosic-Plastics-Composites*, USP, UNESP, Sao Paulo, 1997, p. 1.
88. D. Klemm, B. Philipp, T. Heinze, U. Heinze, and W. Wagenknecht, *Comprehensive Cellulose Chemistry. Functionalization of Cellulose*, Wiley-VCH, Weinheim, 1998.
89. J. Sugiyama, J. R. Voung, and H. Chanzy, *Macromolecules* **24**, 4168 (1991).
90. W. Herbert and H. Chanzy, *Starch* **48**, 185 (1996).
91. N. M. Bikales and L. Segal, *Cellulose and Cellulose Derivatives, Part V*, Wiley-Interscience, New York, 1971.
92. M. Marx, *Makromol. Chem.* **16**, 157 (1955).
93. P. Mischnick, in Ref. 97, p. 118.
94. D. Klemm, T. Heinze, B. Philipp, and W. Wagenknecht, *Acta Polym.* **48**, 277 (1997).
95. D. Klemm, A. Stein, T. Heinze, B. Philipp, and W. Wagenknecht, Cellulose in J. C. Salamone, ed., *Polymeric Materials Encyclopedia*, Vol. 2, CRC Press, Boca Raton, Fla., 1996, p. 1043.
96. T. J. Heinze and W. G. Glasser, in Ref. 97, p. 2.
97. T. J. Heinze and W. G. Glasser, eds., *Cellulose Derivatives: Modification, Characterization, and Nanostructures* (ACS Symposium Series No. 688), American Chemical Society, Washington, D.C., 1998.

98. J. Engelhardt, *Carbohydr Europe* **12**, 5 (1995).
99. G. Hudry-Clergeon, PhD dissertation, Joseph Fourier University, Grenoble, France, 1965.
100. M. Milas, PhD dissertation, Joseph Fourier University, Grenoble, France, 1974.
101. M. Rinaudo, and G. Hudry-Clergeon, *J. Chim. Phys.* **64**, 1746 (1967).
102. C. Barba, D. Montané, M. Rinaudo, X. Farriol, *Cellulose* **9**, 319 (2002).
103. C. Barba, D. Montané, X. Farriol, J. Desbrières, and M. Rinaudo, *Cellulose* **9**, 327 (2002).
104. E. K. Just and T. G. Majewicz, in H. F. Mark, N. M. Bikales, C. G. Overberger, and G. Menges, eds., *Encyclopedia of Polymer Science and Engineering*, Vol. 3, John Wiley & Sons, Inc., New York, 1985, p. 226.
105. J. Desbrieres, M. Hirrien, and M. Rinaudo, *Carbohydr. Polym.* **37**, 145 (1998).
106. J. Desbrières, M. Hirrien, and M. Rinaudo, in Ref. 97, p. 332.
107. M. Vigouret, M. Rinaudo, and J. Desbrieres, *J. Chim. Phys.* **93**, 858 (1996).
108. M. Hirrien, C. Chevillard, J. Desbrières, M. A. Axelos, and M. Rinaudo, *Polymer* **39**, 6251 (1998).
109. L. Brandt, in W. Gerhartz, ed., *Ullmann's Encyclopedia of Industrial Chemistry*, Vol. A5, VCH, Manheim, 1986, p. 461.
110. G. K. Greminger, in *Encyclopedia of Chemical Technology*, Vol. 5, John Wiley & Sons, Inc., New York, 1979, p. 143.
111. E. K. Just, and T. G. Majewicz, in H. Mark, D. F. Othmer, C. G. Overberger, and G. T. Seaborg, eds., *Encyclopedia of Polymer Science and Engineering*, Vol. 3, John Wiley & Sons, Inc., New York, 1985, p. 226.
112. R. Malcolm Brown Jr., *Cellulose and Other Natural Polymer Systems: Biogenesis, Structure and Degradation*, Plenum Press, New York, 1982.
113. J. F. Kennedy, G. O. Phillips, P. O. Williams, and L. Piculell, *Cellulose and Cellulose Derivatives: Physico-Chemical Aspects and Industrial Applications*, Woodhead Publishing Ltd., Cambridge, England, 1995.
114. R. D. Gilbert, *Cellulosic Polymers: Blends and Composites.*, Hanser, Munich, 1994.
115. T. L. Vigo, in H. F. Mark, N. M. Bikales, C. G. Overberger, and G. Menges, eds., *Encyclopedia of Polymer Science and Technology*, Vol. 3, John Wiley & Sons, Inc., New York, 1985, p. 124.
116. H. Zoebelein, ed., *Dictionary of Renewable Resources*, VCH Verlagsgeselshaft, Weinheim, 1997, p. 262.
117. R. L. Whistler and E. F. Paschall, *Starch: Chemistry and Technology*, Academic Press, New York, Volume 1: Fundamental Aspects, 1965; Volume 2: Industrial Aspects, 1967.
118. J. M. Bayley and W. J. Welan, *J. Biol. Chem.* **236**, 969 (1961).
119. Ph. Salemis, PhD dissertation, Joseph Fourier University, Grenoble, France, 1984.
120. Y. Chen, C. Fringant, and M. Rinaudo, *Carbohydr. Polym.* **33**, 73 (1997).
121. P. Salemis and M. Rinaudo, *Polym. Bull.* **12**, 283 (1984).
122. P. Salemis and M. Rinaudo, *Polym. Bull.* **11**, 397 (1984).
123. W. Jarowenko, in O. B. Wurzburg, ed., *Modified Starches: Properties and Uses*, CRC Press, Boca Raton, Fla., 1986, p. 55.
124. J. N. BeMiller, in H. F. Mark, N. M. Bikales, C. G. Overberger, and G. Menges, eds., *Encyclopedia of Polymer Science and Engineering*, Vol. 3, John Wiley & Sons, Inc., New York, 1985, p. 226.
125. J. A. Aburto, PhD dissertation, Institut National Polytechnique, Toulouse, France, 1998.
126. C. Fringant, PhD dissertation, Joseph Fourier University, Grenoble, France, 1996.
127. C. Fringant, J. Desbrieres, and M. Rinaudo, *Polymer* **37**, 2663 (1996).
128. C. Fringant, J. Desbrieres, M. Milas, M. Rinaudo, C. Joly, and M. Escoubes, *Int. J. Biol. Macromol.* **18**, 281 (1996).

129. C. Fringant, M. Rinaudo, N. Gontard, S. Guilbert, and A. Derradji, *Starch* **50**, 292 (1998).
130. C. Fringant, M. Rinaudo, M-F. Foray, and M. Bardet, *Carbohydr. Polym.* **35**, 97 (1998).
131. A. D. Sagar and E. W. Merrill, *J. Appl. Polym. Sci.* **58**, 1647 (1995).
132. I. W. Wolff, D. W. Olds, and G. E. Hilbert, *Ind. Eng. Chem.* **43**(4), 911 (1951).
133. I. W. Wolff, D. W. Olds, and G. E. Hilbert, *Ind. Eng. Chem.* **49**(8), 1247 (1957).
134. J. V. Tuschhoff, in O. B. Wurzburg, ed., *Modified Starches: Properties and Uses*, CRC Press, Boca Raton, Fla., 1986, p. 90.
135. D. B. Solarek, Cationic starches in O. B. Wurzburg, ed., *Modified Starches: Properties and Uses*, CRC Press, Boca Raton, Fla., 1986, p. 114.
136. M. Rinaudo and C. Noik, *Polym. Bull.* **9**, 543 (1983).
137. O. B. Wurzburg, in A. M. Stephen, ed., *Modified Starches in Food Polysaccharides*, Marcel Dekker, Rondebosch, South Africa, 1995, p. 1.
138. K. Shimizu, in D. N. S. Hon and N. Shiraishi, eds., *Wood and Cellulosic Chemistry*, Marcel Dekker, New York, 1990, p. 67.
139. B. A. Stone and A. E. Clarke, *Chemistry and Biology of (1→3)-β-Glucans*, La Trobe University Press, Australia, 1992.
140. J. S. G. Reid, *Cell wall storage carbohydrates in seeds. Adv. Botanical Res.* **11**, 125 (1985).
141. J. Ganter, M. Milas, and M. Rinaudo, *Carbohydr. Polym.* **17**, 171 (1992).
142. V. P. Kapoor, M. Milas, F. R. Taravel, and M. Rinaudo, *Carbohydr. Polym.* **25**, 79 (1994).
143. V. P. Kapoor, M. Milas, F. R. Taravel, and M. Rinaudo, *Food Hydrocolloids* **10**, 167 (1996).
144. V. P. Kapoor, F. R. Taravel, J. P. Joseleau, M. Milas, H. Chanzy, and M. Rinaudo, *Carbohydr. Res.* **306**, 231 (1998).
145. L. Lopes, C. T. Andrade, M. Milas, and M. Rinaudo, *Carbohydr. Polym.* **17**, 121 (1992).
146. T. M. Bresolin, P. C. Sander, F. Reicher, M. R. Sierakowski, M. Rinaudo, and J. L. Ganter, *Carbohydr. Polym.* **33**, 131 (1997).
147. M. Rinaudo, M. Milas, T. Bresolin, and J. Ganter, *Polym. Prepr.* **39**, 1680 (1998).
148. T. Bresolin, M. Milas, M. Rinaudo, and M. Ganter, *Int. J. Biol. Macromol.* **23**, 263 (1998).
149. M. Rinaudo, M. Milas, T. Bresolin, and J. Ganter, *Macromol. Chem. Phys., Macromol. Symp.* **140**, 115 (1999).
150. T. Bresolin, M. Milas, M. Rinaudo, F. Reicher, and J. Ganter, *Int. J. Biol. Macromol.* **26**, 225 (1999).
151. F. M. Goycoolea, M. Milas, and M. Rinaudo, in G. O. Phillips, P. A. Williams, eds., *Gums and Stabilizers for the Food Industry, 10*, The Royal Society of Chemistry, Cambridge, UK, 2000, p. 229.
152. F. M. Goycoolea, M. Milas, and M. Rinaudo, *Int. J. Biol. Macromol.* **29**, 181 (2001).
153. C. L. O. Petkowicz, F. Reicher, K. Mazeau, *Carbohydr. Polym.* **37**, 25 (1998).
154. K. Nishinari, P. A. Williams, G. O. Phillips, *Food Hydrocolloids* **6**, 199 (1992).
155. L. Huang, S. Kobayashi, and K. Nishinari, *Trans. Mater. Res. Soc. Jpn* **26**, 597 (2001).
156. J. Visser, A. G. J. Voragen, *Pectins and Pectinases, Progress in Biotechnology*, Vol. 14, Elsevier, Amsterdam, 1996.
157. M-C. Ralet, J-F. Thibault, *Biomacromolecules* **3**, 917–925 (2002).
158. G. Ravanat and M. Rinaudo, *Biopolymers* **19**, 2209 (1980).
159. M. Rinaudo, G. Ravanat, and M. Vincendon, *Makromol. Chem.* **181**, 1059 (1980).
160. R. Kohn and B. Larsen, *Acta Chem. Scand.* **26**, 2455 (1972).
161. J. F. Thibault and M. Rinaudo, *Biopolymers* **24**, 2131 (1985).
162. J. F. Thibault and M. Rinaudo, in M. L. Fishman and J. J. Jen, eds., *Chemistry and Function of Pectins* (ACS Symposium Series 310) American Chemical Society, Washington, D.C., 1986, p. 61.

163. J. F. Thibault and M. Rinaudo, *Biopolymers* **25**, 455 (1986).
164. J. F. Thibault and M. Rinaudo, *Br. Polym. J.* **17**, 181–184 (1985).
165. E. D. T. Atkins, D. H. Isaac, I. A. Nieduszynski, C. F. Phelps, and J. K. Seehan, *Polymer* **15**, 263 (1974).
166. T. Turquois, M. Rinaudo, F. R. Taravel, and A. Heyraud, *Food Hydrocolloids* **13**, 255 (1999).
167. T. Turquois, M. Rinaudo, F. R. Taravel, and A. Heyraud, in K. Nishinari, ed., *Hydrocolloids 1: Physical Chemistry and Industrial Application of Gels, Polysaccharides and Proteins*, Elsevier, Amsterdam, 2000, p. 229.
168. A. Heyraud, M. Rinaudo, and C. Rochas, in I. Akatsuka, ed., *Introduction to Applied Phycology*, SPB Academic Publishing, The Hague, The Netherlands, 1989, p. 59.
169. M. Rinaudo, *J. Intell. Mater. Syst. Struct.* **4**, 210 (1993).
170. S. Mabeau, B. Kloarec, J. P. Joseleau, *Phytochemistry* **29**, 2441 (1990).
171. R. Daniel, O. Berteau, J. Jozefonvicz, and N. Goasdone, *Carbohydr. Res.* **322**, 291 (1999).
172. M. Rinaudo and D. Graebling, *Polym. Bull.* **15**, 253 (1986).
173. A. Martinsen, G. Skjaak-Break, O. Smidsrod, *Biotechnol Bioeng.* **33**, 79 (1989).
174. G. Fundueanu, E. Esposito, D. Mihai, A. Carpov, J. Desbrières, M. Rinaudo and C. Nastruzzi, *Int. J. Pharm.* **170**, 11 (1998).
175. G. Fundueanu, C. Nastruzzi, A. Carpov, J. Desbrières, and M. Rinaudo, *Biomaterials* **20**, 1427 (1999).
176. C. Rochas, M. Rinaudo, and M. Vincendon, *Biopolymers* **19**, 2165 (1980).
177. C. Rochas and M. Rinaudo, *Biopolymers* **19**, 1675 (1980).
178. C. Rochas and M. Rinaudo, *Carbohydr. Res.* **105**, 227 (1982).
179. M. Rinaudo, C. Rochas, and B. Michels, *J. Chim. Phys.* **80**, 305 (1983).
180. M. Ciancia, M. Milas, and M. Rinaudo, *Int. J. Biol. Macromol.* **20**, 35 (1997).
181. C. Rochas, M. Rinaudo, and S. Landry, *Carbohydr. Polym.* **10**, 115 (1989).
182. C. Rochas and M. Rinaudo, *Biopolymers* **23**, 735 (1984).
183. A. M. Stephen, *Food Polysaccharides and Their Applications*, Marcel Dekker, New York, 1995.
184. A. L. Branen, P. M. Davidson, and S. Salminen, *Food Additives*, Marcel Dekker, New York, 1990.
185. E. Dickinson, *Food Polymers, Gels and Colloids*, The Royal Society of Chemistry, Cambridge, UK, 1991.
186. G. Doxastakis and V. Kiosseoglou, *Novel Macromolecules in Food Systems. Developments in Food Science 41*, Elsevier Science B. V., Amsterdam, 2000.
187. A. Nussinovitch, *Hydrocolloid Applications. Gum Technology in the Food and Other Industries*, Blackie Academic & Professional, London, 1997.
188. M. Rinaudo and M. Vincendon, *Carbohydr. Polym.* **2**, 135 (1982).
189. S. Bo, M. Milas, and M. Rinaudo, *Int. J. Biol. Macromol.* **9**, 153 (1987).
190. V. J. Morris, Bacterial Polysaccharides, in A. M. Stephen, ed., *Food Polysaccharides and Their Applications*, Marcel Dekker, New York, 1995, p. 341.
191. I. W. Sutherland, in V. Crescenzi, I. C. M. Dea, S. Paoletti, S. S. Stivala and I. W. Sutherland, eds., *Biomedical and Biotechnological Advances in Industrial Polysaccharides*, Gordon and Breach Science Publishers, London, 1989, p. 123.
192. M. Yalpani and P. A. Sanford, in M. Yalpani, ed., *Industrial Polysaccharides: Genetic Engineering, Structure/Property Relations and Applications*, Elsevier, Amsterdam, 1987, p. 311.
193. K. Jann and B. Jann, in S. Dimitriu, ed., *Polysaccharides: Structural Diversity and Functional Versatility*, Marcel Dekker, New York, 1998, p. 211.
194. A. Morin, in S. Dimitriu, ed., *Polysaccharides: Structural Diversity and Functional Versatility*, Marcel Dekker, New York, 1998, p. 275.

195. N. Berriaud, M. Milas, and M. Rinaudo, in S. Dumitriu, ed., *Polysaccharides: Structural Diversity and Functional Versatility*, Marcel Dekker, New York, 1998, p. 313.
196. G. Gravanis, M. Milas, M. Rinaudo, and A. J. Clarke-Sturman, *Int. J. Biol. Macromol.* **12**, 195 (1990).
197. G. Gravanis, M. Milas, M. Rinaudo, and A. J. Clarke-Sturman, *Int. J. Biol. Macromol.* **12**, 201 (1990).
198. B. Lindberg, in S. Dimitriu, ed., *Polysaccharides: Structural Diversity and Functional Versatility*, Marcel Dekker, New York, 1998, p. 237.
199. L. Kenne and B. Lindberg, in G. O. Aspinall, ed., *The Polysaccharides*, Vol. 2, Academic Press, New York, 1983, p. 287.
200. B. Courtois, J. Courtois, A. Heyraud, and M. Rinaudo, *J. Gen. Appl. Microbiol.* **32**, 519 (1986).
201. A. Heyraud, M. Rinaudo, and B. Courtois, *Int. J. Biol. Macromol.* **8**, 85 (1986).
202. K. P. Hebbar, B. Gueniot, A. Heyraud, P. Colin-Morel, T. Heulin, J. Balandreau, and M. Rinaudo, *Appl. Microbiol. Biotechnol.* **38**, 248 (1992).
203. A. Boutebba, M. Milas, and M. Rinaudo, *Bipolymers* **42**, 811 (1997).
204. E. Balnois, S. Stoll, K. J. Wilkinson, J. Buffle, M. Rinaudo, and M. Milas, *Macromolecules* **33**, 7440 (2000).
205. M. Rinaudo, M. Milas, F. Lambert, and M. Vincendon, *Macromolecules* **16**, 816 (1983).
206. L. Chazeau, M. Milas, and M. Rinaudo, *Int. J. Polym. Anal. Charact.* **2**, 21 (1995).
207. M. Milas, W. F. Reed, and S. Prinz, *Int. J. Biol. Macromol.* **18**, 21 (1996).
208. M. Rinaudo, in J. Kahovec, ed., *Macromolecules*, VSP, Zeist, the Netherlands, 1992, p. 207.
209. M. Milas, M. Rinaudo, and B. Tinland, *Polym. Bull.* **14**, 157–164 (1985).
210. M. Milas, X. Shi, and M. Rinaudo, *Biopolymers* **30**, 451 (1990).
211. F. Mazen, M. Milas, and M. Rinaudo, *Int. J. Biol. Macromol.* **26**, 109 (1999).
212. M. Rinaudo and M. Milas, in G. Doxastakis and V. Kiosseoglou, eds., *Novel Macromolecules in Food Systems*, Elsevier, Amsterdam, 2000, p. 239.
213. M. Milas and M. Rinaudo, *Carbohydr. Polym.* **30**, 177 (1996).
214. M. Rinaudo, G. Pavlov, and J. Desbrieres, *Int. J. Polym. Anal. Charact.* **5**, 267 (1999).
215. M. Rinaudo, G. Pavlov, and J. Desbrieres, *Polymer* **40**, 7029 (1999).
216. L. Heux, J. Brugnerotto, J. Desbrières, M. F. Versali, and M. Rinaudo, *Biomacromolecules* **1**, 746 (2000).
217. J. Brugnerotto, J. Lizardi, F. M. Goycoolea, W. Arguelles-Monal, J. Desbrières, and M. Rinaudo, *Polymer* **42**, 3569 (2001).
218. J. Brugnerotto, J. Desbrieres, L. Heux, K. Mazeau, and M. Rinaudo *Macromol. Symp.* **168**, 1–20 (2001).
219. J. Brugnerotto, J. Desbrieres, G. Roberts, and M. Rinaudo, *Polymer* **42**, 9921 (2001).
220. J. Desbrieres, C. Martinez, and M. Rinaudo, *Int. J. Biol. Macromol.* **19**, 21 (1996).
221. O. E. Philippova, E. V. Volkov, N. L. Sitnikova, A. Khokhlov, J. Desbrieres, and M. Rinaudo, *Biomacromolecules* **2**, 483 (2001).
222. M. Rinaudo, L. D. Pham, C. Gey, and M. Milas, *Int. J. Biol. Macromol.* **14**, 122 (1992).
223. A. Domard, C. Gey, M. Rinaudo, and C. Terrassin, *Int. J. Biol. Macromol.* **9**, 233 (1987).
224. Pham Le Dung, M. Milas, M. Rinaudo, and J. Desbrieres, *Carbohydr. Polym.* **24**, 209 (1994).
225. R. Auzely-Velty and M. Rinaudo, *Macromolecules* **34**, 3574 (2001).
226. R. Auzely-Velty and M. Rinaudo, *Macromolecules* **35**, 7955 (2002).
227. R. A. A. Muzzarelli, *Natural Chelating Polymers*, Pergamon Press, Oxford, England, U.K., 1973.
228. M. Rhazi, J. Desbrières, A. Tolaimate, M. Rinaudo, P. Vottero, and A. Alagui, *Polymer* **43**, 1267 (2002).

229. R. A. A. Muzzarelli and C. Muzzarelli, *Chitosan in Pharmacy and Chemistry*, ATEC Edizioni, Italy, 2002.
230. R. A. A. Muzzarelli, *Chitin Enzymology 2001*, ATEC Edizioni, Italy, 2001.
231. J. F. Kennedy, G. O. Phillips, and P. A. Williams, *Hyaluronan*, Woodhead Publishing Ltd., Cambridge, U.K., 2002. Volume 1: Chemical, Biomedical and Biological Aspects; Volume 2: Biomedical, Medical and Clinical Aspects.
232. S. I. Nishimura, K. Matsuoka, and K. Kurita, *Macromolecules* **23**, 4182 (1990).
233. S. I. Nishimura, K. Matsuoka, T. Furuike, S. Ishii, K. Kurita, and K. M. Nishimura, *Macromolecules* **24**, 4236 (1991).
234. R. Roy, R. A. Pon, F. D. Tropper, and F. O. Andersson, *J. Chem. Soc., Chem. Commun.* 264 (1993).
235. X. Zeng, T. Murata, H. Kawagishi, T. Usui, and K. Kobayashi, *Carbohydr. Res.* **312**, 209 (1998).
236. R. Roy, F. D. Tropper, and A. Romanowska, *Bioconjugate Chem.* **3**, 256 (1992).
237. G. Magnusson, A. Ya. Chernyak, J. Kihlberg, and L. O. Kononov, in Y. C. Lee and R. T. Lee, eds., *Neoglycoconjugates: Preparation and Applications*, Academic Press, San Diego, 1994, p. 53.
238. F. D. Tropper, A. Romanowska, and R. Roy, in Y. C. Lee, R. T. Lee, eds., *Methods in Enzymology*, Vol. 242, Academic Press, San Diego, 1994, p. 257.
239. M. Okada, *Prog. Polym. Sci.* **26**, 67 (2001).
240. R. Roy, in G. J. Boons, ed., *Carbohydrate Chemistry*, Thomson Science, London, 1998, chap. 1.
241. R. Roy, *Top. Curr. Chem.* **187**, 241 (1997).
242. R. Roy, *Trends Glycosci. Glycotechnol.* **8**, 79 (1996).
243. N. V. Bovin and H. J. Gabius, *Chem. Soc. Rev.* **24**, 413 (1995).
244. V. Horejsi, P. Smolek, and J. Kocourek, *Biochim. Biophys. Acta* **538**, 293 (1978).
245. N. K. Kochetkov, *Pure Appl. Chem.* **56**, 923 (1986).
246. R. Roy, C. A. Laferrière, A. Gamian, and H. J. Jennings, *J. Carbohydr. Chem.* **6**, 161 (1987).
247. S. I. Nishimura, T. Furuike, and K. Matsuoka, *Methods Enzymol.* **242**, 235 (1994).
248. K. Kobayashi, T. Akaike, T. Usui, *Methods Enzymol.* **242**, 226 (1994).
249. N. E. Byramova, L. V. Mochalova, I. M. Belyanchikov, M. N. Matrosovich, and N. V. Bovin, *J. Carbohydr. Chem.* **10**, 691 (1991).
250. R. Roy, F. D. Tropper, and A. Romanowska, *J. Chem. Soc., Chem. Commun.* 1611 (1992).
251. R. Roy, F. O. Andersson, G. Harms, S. Kelm, and R. Schauer, *Angew. Chem. Int. Ed. Engl.* **31**, 1478 (1992).
252. G. B. Sigal, M. Mammen, G. Dahmann, and G. M. Whitesides, *J. Am. Chem. Soc.* **118**, 3789 (1996).
253. T. Furuike, S. Aiba, T. Suzuki, T. Takahashi, Y. Suzuki, K. Yamada, and S. I. Nishimura, *J. Chem. Soc., Perkin Trans.* **1**, 3000 (2000).
254. J. Li, S. Zacharek, X. Chen, J. Wang, W. Zhang, A. Janczuk, and P. G. Wang, *Biorg. Med. Chem.* **7**, 1549 (1999).
255. M. G. Baek, and R. Roy, *Biomacromolecules* **1**, 768 (2000).
256. J. Klein, and A. H. Begli, *Makromol. Chem.* **190**, 2527 (1989).
257. M. E. Wilson, S. Najdi, J. M. Krochta, Y. L. Hsieh, and M. J. Kurth, *Macromolecules* **31**, 4486 (1998).
258. W. J. Zhou, M. J. Kurth, Y. L. Hsieh, and J. M. Krochta, *Macromolecules* **32**, 5507 (1999).
259. E. Kallin, in Y. C. Lee and R. T. Lee, eds., *Neoglycoconjugates: Preparation and Applications*, Academic Press, San Diego, 1994, p. 199.

260. A. Ya. Chernyak, A. Weintraub, T. Norberg, and E. Kallin, *Glycoconjugate, J.* **7**, 111 (1990).
261. K. Kobayashi, H. Sumitomo, and Y. Ina, *Polym. J.* **17**, 567 (1985).
262. R. Auzély-Velty, M. Cristea, and M. Rinaudo, *Biomacromolecules* **3**, 998 (2002).
263. E. Kallin, *Methods Enzymol.* **242**, 221 (1994).
264. A. Lubineau, J. Augé, and B. Drouillat, *Carbohydr. Res.* **266**, 211 (1995).
265. W. Spevak, F. Dasgupta, C. J. Hobbs, and J. O. Nagy, *J. Org. Chem.* **61**, 3417 (1996).
266. D. H. Charych, J. O. Nagy, W. Spevak, and M. D. Benarski, *Science* **261**, 585 (1993).
267. K. Kobayashi, A. Tsuchida, T. Usui, and T. Akaike, *Macromolecules* **30**, 2016 (1997).
268. A. B. Tuzikov, A. S. Gambaryan, L. R. Juneja, and N. V. Bovin, *J. Carbohydr. Chem.* **19**, 1191 (2000).
269. R. C. Rathi, P. Kopeckova, and J. Kopecek, *Macromol. Chem. Phys.* **198**, 1165 (1997).
270. A. David, P. Kopeckova, A. Rubinstein, and J. Kopecek, *Bioconjugate Chem.* **12**, 890 (2001).
271. K. Ohno, Y. Izu, S. Yamamoto, T. Miyamoto, and T. Fukuda, *Macromol. Chem. Phys.* **200**, 1619 (1999).
272. Y. Z. Liang, Z. C. Li, G. Q. Chen, and F. M. Li, *Polym. Int.* **48**, 739 (1999).
273. R. Roy, M. G. Baek, and K. Rittenhouse-Olson, *J. Am. Chem. Soc.* **123**, 1809 (2001).
274. T. Serizawa, S. Yasunaga, and M. Akashi, *Biomacromolecules* **2**, 469 (2001).
275. K. Ohno, Y. Tsuji, T. Miyamoto, T. Fukuda, M. Goto, K. Kobayashi, and T. Akaike, *Macromolecules* **31**, 1064 (1998).
276. K. Ohno, Y. Tsuji, T. Miyamoto, and T. Fukuda, *J. Polym. Sci., Part A: Polym. Chem.* **36**, 2473 (1998).
277. K. Yamada, K. Yamaoka, M. Minoda, and T. Miyamoto, *J. Polym. Sci., Part A: Polym. Chem.* **35**, 255 (1997).
278. K. Yamada, M. Minoda, and T. Miyamoto, *J. Polym. Sci., Part A: Polym. Chem.* **35**, 751 (1997).
279. K. Yamada, M. Minoda, and T. Miyamoto, *Macromolecules* **32**, 3553 (1999).
280. Y. Z. Liang, Z. C. Li, G. Q. Chen, and F. M. Li, *Polym. Int.* **48**, 739 (1999).
281. M. Kanai, K. H. Mortell, and L. L. Kiessling, *J. Am. Chem. Soc.* **119**, 9931 (1997).
282. D. D. Manning, L. E. Strong, X. Hu, P. J. Beck, and L. L. Kiessling, *Tetrahedron* **53**, 11937 (1997).
283. D. D. Manning, X. Hu, P. J. Beck, and L. L. Kiessling, *J. Am. Chem. Soc.* **119**, 3161 (1997).
284. N. L. Pohl and L. L. Kiessling, *Synthesis*, 1515 (1999).
285. E. J. Gordon, J. E. Gestwicki, L. E. Strong, and L. L. Kiessling, *Chem. Biol.* **7**, 9 (2000).
286. M. C. Garcia-Oteiza, M. Sanchez-Chaves, and F. Arranz, *Macromol. Chem. Phys.* **198**, 2237 (1997).
287. A. Satoh, T. Kojima, T. Koyama, H. Ogawa, and I. Matsumoto, *Anal. Biochem.* **260**, 96 (1998).
288. A. Satoh, E. Fukui, S. Yoshino, M. Shinoda, K. Kojima, and I. Matsumoto, *Anal. Biochem.* **275**, 231 (1999).
289. D. Cade, R. Auzély-Velty, T. Delair, T. Hamaide, and M. Rinaudo, in preparation.
290. M. Morimoto, H. Saimoto, H. Usui, Y. Okamto, S. Minami, and Y. Shigemasa, *Biomacromolecules* **2**, 1133 (2001).
291. F. Tanida, T. Tojima, H. Katsura, S. M. Han, N. Nishi, S. Tokura, N. Sakairi, H. Seino, and K. Hamada, *Polymer* **39**, 5261 (1998).
292. T. Tojima, H. Katsura, S. M. Han, F. Tanida, N. Nishi, S. Tokura, and N. Sakairi, *J. Polym. Sci., Part A: Polym. Chem.* **36**, 1965 (1998).
293. H. Sashiwa, Y. Shigemasa, and R. Roy, *Macromolecules* **33**, 6913 (2000).
294. S. I. Nishimura, K. B. Lee, K. Matsuoka, and Y. C. Lee, *Biochem. Biophys. Res. Commun.* **199**, 249 (1994).

295. K. Kobayashi, A. Kobayashi, S. Tobe, and T. Akaike, in Y. C. Lee, ed., *Neoglycoconjugates*, Academic Press, San Diego, 1994, p. 261.
296. A. Tsuchida, S. Akimoto, T. Usui, and K. Kobayashi, *J. Biochem.* **123**, 715 (1998).
297. T. Hasegawa, S. Kondoh, K. Matsuura, and K. Kobayashi, *Macromolecules* **32**, 6595 (1999).
298. G. R. Gray, *Anal. Chem.* **52**, 9R (1980).
299. J. H. Pazur, *Adv. Carbohydr. Chem. Biochem.* **39**, 405 (1981).
300. R. L. Schnaar, *Anal. Biochem.* **143**, 1 (1984).
301. A. Kobayashi and T. Akaike, *Makromol. Chem., Rapid Commun.* **7**, 645 (1986).
302. C. S. Cho, M. Goto, K. Kobayashi, and T. Akaike, *J. Biomater. Sci., Polym. Edn.* **7**, 1097 (1996).
303. H. Kamitakahara, T. Suzuki, N. Nishigori, Y. Suzuki, O. Kanie, C. H. Wong, *Angew. Chem., Int. ed.* **37**, 1524 (1998).
304. R. Duncan, I. C. Hume, P. Kopeckova, K. Ulbrich, J. Strohalm, and J. Kopecek, *J. Controlled Release* **10**, 51 (1989).
305. L. W. Seymour, R. Duncan, V. Chytry, J. Strohalm, K. Ulbrich, and J. Kopecek, *J. Controlled Release* **16**, 255 (1991).
306. M. Goto, H. Yura, C. W. Chang, A. Kobayashi, T. Shinoda, A. Maeda, S. Kojima, K. Kobayashi, and T. Akaike, *J. Controlled Release* **28**, 223 (1994).
307. G. Wulff, H. Schmidt, and L. Zhu, *Macomol. Chem. Phys.* **200**, 774 (1999).
308. G. Wulff, L. Zhu, and H. Schmidt, *Macromolecules* **30**, 4533 (1997).
309. C. Schou, G. Rasmussen, M. Schulein, B. Henrissat, and H. Driguez, *J. Carbohydr. Res* **12**, 743 (1993).
310. F. Ratajczak, L. Greffe, S. Cottaz, and H. Driguez, *Synlett* **9**, 1253 (2003).
311. H. Driguez, *ChemBioChem* **2**, 311 (2001).
312. X. Robert, R. Haser, T. E. Gottschalk, H. Driguez, B. Svensson, and N. Aghajari, *Structure* **11**, 973 (2003).
313. N. K. Kochetkov, *Tetrahedron* **43**, 2389 (1987).
314. S. Haq and W. J. Whelan, *J. Chem. Soc.* 4543 (1956).
315. C. Schuerch, J. Zachoval, and B. Versuovic, *Chem. Listy* **66**, 1124 (1972).
316. C. Schuerch, *Acc. Chem. Res.* **6**, 184 (1973).
317. C. Schuerch, *Adv. Carbohydr. Chem. Biochem.* **39**, 157 (1981).
318. V. Boyer, S. Fort, T. P. Frandsen, M. Schülein, S. Cottaz and H. Driguez, *Chem. Eur. J.* **8**, 1389 (2002).
319. V. Moreau and H. Driguez, *J. Chem. Soc., Perkin Trans.* **1**, 525 (1996).
320. M. Hrmova, T. Imai, S. J. Rutten, J. K. Fairweather, L. Pelosi, V. Bulone, H. Driguez, and G. B. Fincher, *J. Biol. Chem.* **30**, 102 (2002).
321. S. Fort, V. Boyer, L. Greffe, G. J. Davies, O. Moroz, L. Christiansen, M. Schülein, S. Cottaz, and H. Driguez, *J. Am. Chem. Soc.* **122**, 5429 (2000).
322. S. Kobayashi, J. Sakamoto, and S. Kimura, *Prog. Polym. Sci.* **26**, 1525 (2001).
323. S. Kobayashi, H. Uyama, and S. Kimura, *Chem. Rev.* **101**, 3793 (2001).
324. S. Kobayashi, H. Morii, R. Itoh, S. Kimura, and M. Ohmae, *J. Am. Chem. Soc.* **123**, 11825 (2001).

M. RINAUDO
R. AUZELY
K. MAZEAU
Centre de Recherches sur les Macromolécules Végétales,
Affiliated with Joseph Fourier University

POLYSILANES. See Volume 7.

POLYSULFIDES. See Volume 3.

POLYSULFONES. See Volume 4.

POLYTETRAFLUORETHYLENE. See PERFLUORINATED POLYMERS.

POLYTRIACETYLENE. See DIACETYLENE AND TRIACETYLENE POLYME.

POLY(TRIMETHYLENE TEREPHTHALATE). See Volume 3.

POLYURETHANES. See Volume 4.

POLY(VINYL ACETATE). See VINYL ACETATE POLYMERS.

POLY(VINYL ALCOHOL). See VINYL ALCOHOL POLYMERS.

POLYVINYLCARBAZOLE. See VINYLCARBAZOLE POLYMERS.

POLY(VINYL CHLORIDE). See VINYL CHLORIDE POLYMERS.

POLY(VINYL ETHER). See VINYL ETHER POLYMERS.

POLY(VINYL FLUORIDE). See VINYL FLUORIDE POLYMERS.

POLY(VINYLIDENE CHLORIDE). See VINYLIDENE CHLORIDE POLYMERS.

POLY(VINYLIDENE FLUORIDE). See VINYLIDENE FLUORIDE POLYMERS.

POLYVINYLPYRROLIDINONE. See VINYL AMIDE POLYMERS.

POM. See POLYOXYMETHYLENE.

POSS NANOCOMPOSITES. See THERMOSETS.

PRESSURE-SENSITIVE ADHESIVES. See Volume 4.

PROCESSING, MODELING

Introduction

A *model* is a quantitative abstraction of a physical process, in which the description of the process is represented by the solution to a set of mathematical equations (1,2). The model equations represent the behavior of the real process to the extent that the equations embody an accurate description of the underlying physical and physicochemical phenomena. The mathematical formulation enables the model to be used for a variety of purposes, including design, control, and exploration of operating strategies; the effects of changes in process variables and material properties can be inferred from the model without extensive experimentation. Mathematical models have long been used for these purposes in the chemical and petrochemical industries, and computer-aided design and computer-aided manufacturing (CAD/CAM) have been taking on growing importance in some polymer processing operations.

The essential elements of any model of a physical process are threefold: the geometry, the relevant laws of physical conservation (mass, momentum, and energy), and the specific constitutive relations. In polymer processing applications, the last of these could include the stress-deformation equations for the material being processed (the material rheology) and the kinetic equations for phase change. The mathematical complexity of a model depends on the process and the type of information required. Qualitative information can often be obtained from a model that greatly simplifies the physical phenomena to obtain mathematical simplicity and consists only of one or more algebraic equations, for example, whereas structural predictions typically require the consideration of details of stress and flow fields and hence the solution of nonlinear partial differential or integral equations. Advances in computing technology have made the latter goal possible for some processing applications (3,4).

The term *computer model* is often employed as a consequence of the extensive use of computing technology in conjunction with mathematical models. This terminology is unfortunate, because it confuses modeling and simulation. The equations describing the physical phenomenon make up the model and incorporate the full understanding of the process. The model is independent of the means that are used to solve the equations, which might be analytical or numerical, with or without the use of computers. Application of the model to simulate some specific situation requires the choice of a solution technique; numerical artifacts associated with the solution method could introduce errors that are not inherent in the physical assumptions on which the model is based. Comparison of the predictions of a model with experiments requires careful separation of the effects of modeling assumptions and numerical techniques.

Polymer processing operations include polymerization reactors; devices for mixing, conveying, and extruding molten polymer or polymer solutions; and devices for forming shaped objects in the liquid state and post-forming solid-state operations. The modeling of chemical reactors to predict conversions and product distributions is a mature art (5). Efforts in this field have focused on process control and the conditions leading to instabilities and "runaway" reactions.

Encyclopedia of Polymer Science and Technology. Copyright John Wiley & Sons, Inc. All rights reserved.

Polymerization reactors form a subset of the subject of reaction engineering, distinguished only by the need to know the details of the specific reaction pathways and kinetics, and perhaps the dependence of viscosity on conversion. Polymerization reactions and reactors, including reaction injection molding, are treated elsewhere, and this article is concerned only with the modeling of the mechanics and structure development in mixing, conveying, extrusion, and forming processes.

Rheology

Models of the mechanics of polymer processing operations can be categorized by the rheological description used. Low molecular weight liquids are Newtonian, which means that the stress at any point in a deformation field is a linear function of the instantaneous rate of strain and is independent of any prior history; the stress in an incompressible Newtonian liquid is characterized by a single material parameter, the viscosity (η), which can be temperature- and pressure-dependent but is independent of the deformation rate:

$$\boldsymbol{\sigma} = -p\boldsymbol{I} + \boldsymbol{\tau} \tag{1}$$

$$\boldsymbol{\tau} = \eta[\nabla v + (\nabla v)^{\mathrm{T}}] \tag{2}$$

Here, $\boldsymbol{\sigma}$ is the total stress, p the isotropic pressure, $\boldsymbol{I}$ the identity (unit) tensor, and $\boldsymbol{\tau}$ the extra stress (ie, the stress in excess of the isotropic pressure). ∇ is the gradient differential operator, and v is the velocity vector; $^{\mathrm{T}}$ denotes the transpose of a tensor. For a one-dimensional flow with a single velocity component v, in which v varies in a single spatial direction y that is transverse to the flow direction, equation 2 simplifies to the familiar form

$$\tau = \eta \, \mathrm{d}v/\mathrm{d}y \tag{3}$$

When the flow is isothermal and the liquid has a viscosity that can be taken to be independent of pressure (ie, η is constant over the entire flow field), substitution of equations 1 and 2 into the balance of linear momentum leads to the Navier–Stokes equations, which have been the subject of intense study in classical fluid mechanics for more than a century.

In contrast, the stress in a macromolecular liquid depends in a nonlinear manner on the entire history of deformation. The nonlinearity is manifested by phenomena such as the strain-rate dependence of the shear viscosity, strain hardening in extension, and the transverse normal stresses in shear flow that cause extrudate swell. The dependence on history is demonstrated by the transient buildup and relaxation of stresses following changes in flow variables, and by the existence of the dynamic storage modulus (G') in oscillatory shearing. There have been many routes to the development of appropriate stress constitutive equations for use in processing flows of polymeric liquids (6–8), including general continuum mechanics formulations and molecular and quasi-molecular theories. No constitutive theory developed to date is adequate for quantitative predictions in all processing flows, in some cases because the complexity of the equation prevents

efficient calculation in complex flow geometries, but some stress equations have been useful in particular classes of flows.

Purely viscous constitutive equations, which account for some of the nonlinearity in shear but not for any of the history dependence, are commonly used in process models when the deformation is such that the history dependence is expected to be unimportant. The stress in an incompressible, purely viscous liquid is of the form given in equation 2, but the viscosity is a function of one or more invariant measures of the strength of the deformation rate tensor, $[\nabla v + (\nabla v)^{\mathrm{T}}]$. [An invariant of a tensor is a quantity that has the same value regardless of the coordinate system that is used. The second invariant of the deformation rate tensor, often denoted II_{D}, is a three-dimensional generalization of $2(\mathrm{d}v/\mathrm{d}y)^2$, where $\mathrm{d}v/\mathrm{d}y$ is the strain rate in a one-dimensional shear flow, and so the viscosity is often taken to be a specific function–a power law, for example–of $(\frac{1}{2}\mathrm{II}_{\mathrm{D}})^{\frac{1}{2}}$.]

The dependence of the stress on the strain-deformation history of macromolecular liquids can be incorporated in two ways. The stress constitutive equation can be formulated as a differential equation, in which the extra stress $\boldsymbol{\tau}$ is the solution of an equation that is typically of the general form

$$\mathbf{A}(\boldsymbol{\tau}/G)\cdot\frac{\boldsymbol{\tau}}{G}+\lambda\frac{\mathcal{D}(\boldsymbol{\tau}/G)}{\mathcal{D}t}=\lambda[\nabla v+(\nabla v)^{T}] \tag{4}$$

Here, $\mathbf{A}(\boldsymbol{\tau}/G)$ is a nonlinear tensor function of the extra stress; the simplest such form is a Maxwell liquid, in which $\mathbf{A}$ is equal to the unit tensor and the first term in equation 4 simply becomes $\boldsymbol{\tau}/G$. λ is the time constant for stress relaxation, and G is the shear modulus, which is a material property; the shear viscosity η is equal to the product λG. $\mathcal{D}/\mathcal{D}t$ denotes a nonlinear time derivative that accounts for the invariance of the physical quantities under changes of the frame of reference of the observer; $\mathcal{D}/\mathcal{D}t$ contains terms of the form $\boldsymbol{\tau}\cdot\nabla\boldsymbol{v}$, but the precise form depends on the particular constitutive theory. Equations of this type follow from transient-network theories, which are based in part on concepts embedded in the theory of rubber-like elasticity. Equations of this type also follow from "tube" or "reptation" theories, in which the chain in an entangled melt or concentrated solution is envisioned as being restricted to an imaginary tube made up of the constraints imposed by the surrounding chains, which restrict chain motion that is transverse to the molecular backbone. (Differential equation forms for tube models usually require mathematical approximations that are not contained in the basic model.) The relaxation time and shear modulus depend on the deformation rate or stress in some theories, whereas in others they depend on a dynamical scalar or tensor variable characterizing the structural state of the melt or solution. If the spectrum of relaxation modes characterizing the linear viscoelastic response is to be included, the stress is comprised of a sum of terms,

$$\boldsymbol{\tau}=\sum\boldsymbol{\tau}_i \tag{5}$$

where each term in the sum satisfies an equation of the form of equation 4, with a spectrum of material parameters $\{\lambda_i, G_i\}$. The values of the spectral parameters in the limit of vanishingly small deformations are obtained from classical linear viscoelastic experiments.

The stress constitutive equation can also be formulated as an integral over the history of the deformation. The most common form used for simulations is

$$\tau(t) = \int_{-\infty}^{t} m(t-t')\, h(\mathrm{I_C}, \mathrm{II_C})\, \mathbf{C}^{-1}(t,t')\, dt' \tag{6}$$

Here, $\mathbf{C}^{-1}$ is the Finger measure of strain and $m(t)$ is a memory function that can be determined from the linear viscoelastic response; $m(t)$ can be expressed in terms of the spectral parameters $\{\lambda_i, G_i\}$ and is usually taken to be a sum of exponentials. $h(\mathrm{I_C}, \mathrm{II_C})$ is a nonlinear "damping" function that depends on the first and second invariants of the Finger strain. Other strain measures may also be used, and the popular K-BKZ model includes a small second term proportional to the Cauchy strain measure **C**. The time–strain separability indicated by the product of the functions m and h fails experimentally at very short times (9). As with the differential equation forms, constitutive models of the general form of equation 6 follow from general continuum mechanics formulations, from transient-network formulations, and from tube theories. There is sometimes a one-to-one equivalence between a differential and integral equation formulation, but in general only approximate equivalences can be developed. Most tube models are naturally formulated as integral equations.

There are advantages and disadvantages to both differential and integral constitutive equations. Differential equations adapt naturally to the numerical methods commonly used for the solution of the momentum and energy equations, which are in differential form, and most process modeling has been carried out using differential stress constitutive equations. It is often important to include the relaxation spectrum in process calculations, however, and each term in the spectrum (eq. 5) requires an additional nonlinear partial differential equation in the solution set, which greatly increases the magnitude of the computational problem. The entire spectrum enters naturally in the integral formulation through the memory function $m(t)$, but it now becomes necessary to track the history of the strain with great accuracy along material element paths on a computational grid that cannot be laid out to ensure that particle paths pass through the spatial nodes.

Finally, there are some constitutive models that cannot be expressed in closed form as differential or integral equations, but require the solution of a Fokker–Plank equation (or an equivalent set of stochastic differential equations) for the orientation distribution of chain segments in order to compute the stress (Reference 4, pp. 338 ff; Reference 10 and references therein). This technique may become more useful as computing power increases, but to date it has been used only for viscometric flows and a few very simple non-viscometric geometries.

Classification

Classifications of viscoelastic flows are useful for analysis, mainly in determining conditions under which a viscoelastic constitutive equation that accounts for fluid memory can be replaced by a much simpler purely viscous equation.

The broadest classification scheme that has been found to be useful in modeling is based on the Deborah number (11–13), which is loosely defined as the ratio of the fluid time scale to the time scale of the process. Small Deborah numbers correspond to situations in which stress transients occur rapidly compared to the total processing time; hence the "memory" of the fluid is short and can be neglected. Large Deborah number flows take place over a time scale in which stress transients cannot be neglected, and a viscoelastic description like that in equation 4 or 6 is essential. The significance of this classification is apparent in a linear viscoelastic frequency sweep, where the Deborah number is the product of the relaxation time λ and the frequency ω; for $\lambda\omega \ll 1$ the loss modulus G'' dominates and the response is that of a viscous liquid, whereas for $\lambda\omega \gg 1$ the storage modulus G' dominates and the response is closer to that of an elastic solid. The fluid time scale is unambiguous for polymeric liquids described by constitutive equations such as equation 4; if the spectrum of relaxation times is required, as with equation 5 or 6, an average or maximum relaxation time would be used, and there is some ambiguity in the choice. There is frequently ambiguity in the choice of the process time scale; the residence time is the obvious choice in a unidirectional flow, but the selection is not clear in more complex flow fields.

The concept of strong and weak flows (14) is one attempt to quantify the Deborah number concept unambiguously. This classification is based on the notion that shearing flows are an ineffective (weak) means of stretching polymer molecules, whereas extensional flows can be effective (strong) in elongating molecules. The physical basis for the concept is rooted in the coil-stretch transition; a macromolecule modeled by a Rouse chain with a maximum relaxation time λ_m will be stretched out in an elongational flow with stretch rate Γ when $\lambda_m\Gamma > \frac{1}{2}$. (The "upper convected" Maxwell model is the continuum equivalent of a fluid made up of Rouse chains, and the stresses in an elongational flow for this fluid model become unbounded when $\lambda_m\Gamma > \frac{1}{2}$.) Let $\boldsymbol{L}$ be the velocity gradient, $\boldsymbol{L} = \nabla v$, and α an eigenvalue of the matrix $\lambda_m\boldsymbol{L} - \frac{1}{2}\boldsymbol{I}$. A flow is strong if any eigenvalue α has a positive real part, in which case a Rouse chain will become fully extended if the time in the flow is large relative to a relaxation time; this is equivalent to the condition $\lambda_m\Gamma > \frac{1}{2}$ for pure extension. A processing flow can be strong in some regions and weak in others according to this classification.

Classification in terms of stress level has not been widely used, but stress level is an important factor in process modeling. It is well known that process behavior in confined flows changes dramatically when the wall stress in highly entangled melts or concentrated solutions is comparable in magnitude to the shear modulus, which is essentially equal to the plateau value of the storage modulus. Flow instabilities like melt fracture (15) are observed, for example, and there is an apparent failure of adhesion between the melt and the metal surface (15). Low stresses are those for which $\|\tau\|/G_p' \leq 1$, where $\|\tau\|$ denotes the magnitude of the stress tensor and G_p' is the plateau modulus. This ratio is equivalent to what is often called the recoverable shear and is proportional in channel flow to a dimensionless group known as the Weissenberg number, $We = \lambda v/d$, where λ is a characteristic relaxation time, v is the average velocity, and d is the diameter or thickness of the channel. As discussed subsequently, the appropriate formulation of wall boundary conditions for model equations is uncertain outside the low stress regime.

Flows must also be classified on the basis of whether the melt is isotropic or anisotropic at rest, and whether the material is homogeneous or heterogeneous. Liquid crystalline polymers are anisotropic at rest and heterogeneous in the melt, containing highly oriented "domains" over micrometer-length scales. Even elementary flows of liquid crystalline polymers have not been successfully modeled, because the continuum rheology is incompletely understood. Highly filled fiber composites are heterogeneous and usually anisotropic in the melt even at rest because of the absence of Brownian restoring forces. Modeling of shaping flows for these systems is primitive, except in some idealized situations, because of the need to account for nonlocal interactions in the rheology. The only well-developed art is for homogeneous polymers that are isotropic at rest.

Numerical Methods

The equations describing polymer processing operations are usually coupled, nonlinear partial-differential or partial-differential-integral equations in which two or three spatial directions and perhaps time appear as independent variables. Fully three-dimensional problems can usually be solved only for purely viscous liquids, and substantial simplification is usually required even for two-dimensional problems of viscoelastic liquids because of limitations of computer speed and memory. In some situations the geometry provides simplifications that lead to closed-form analytical solutions, but these are rare, and numerical methods are usually required in order to obtain process information. Numerical methods relevant to polymer processing flows are discussed in (3,4,16,17). The following three broad classes of numerical methods are in common use:

Finite difference methods are the traditional approach to the numerical solution of partial differential equations. The spatial regime is divided into a grid, as shown in Figure 1. Partial derivatives are approximated by differences; the derivative $\partial u/\partial x$ at grid point (i,j) might be approximated as $[u_{i,j} - u_{i-1,j}]/h$, for example. The partial differential equations are thus reduced to a set of algebraic equations for the values of the dependent variables at the grid points. Iterative

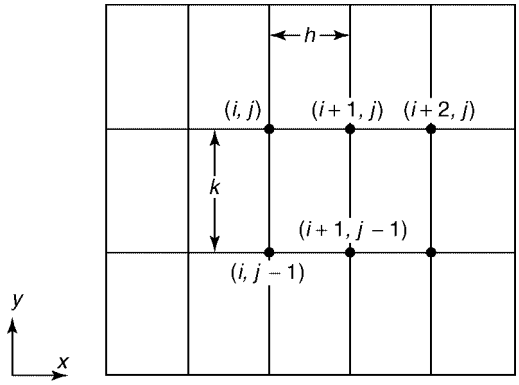

Fig. 1. Finite difference grid.

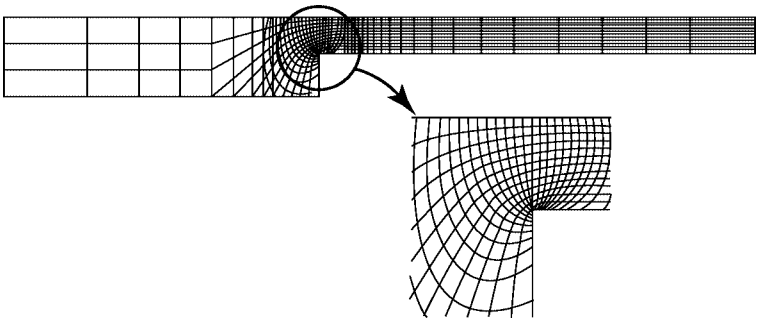

Fig. 2. Finite element grid.

methods are usually required, because the equations are generally nonlinear. Finite difference methods are used infrequently for numerical simulation of viscoelastic flows because of a perceived lack of versatility. Programming is difficult unless the grid spacing is uniform, but accurate approximation of derivatives requires closer spacing of grid points in regions of rapid change of the dependent variables than in regions of little change; nonuniform spacing can be introduced, usually through coordinate transformations, but the techniques for doing so have not been widely adopted for viscoelastic simulation. Finite difference methods are difficult to apply to complex shapes, especially with curved boundaries, although this limitation too can be overcome. Finite difference is the approach of choice for flow problems when inertial effects are significant, but this is rarely the case in polymer processing.

Finite element methods are used in most commercial simulation programs for polymer processing. In this approach the spatial regime is broken up into small elements, usually of triangular or quadrilateral shape, as shown in Figure 2. The solution is approximated over each element in terms of simple functions, usually linear or quadratic, with unknown coefficients that must then be evaluated. The Galerkin method of weighted residuals is the most common method for evaluating the unknown coefficients; in this method, weighted averages of the equations, using the approximating functions themselves as weighting functions, are required to be zero. The approximation leads to a set of algebraic equations for the coefficients that are usually nonlinear and must be solved iteratively. The finite element method is adaptable to complex shapes, and the element size can be easily changed throughout the regime to account for different rates of change of dependent variables.

The Galerkin finite element method has a rigorous foundation for the type of equation set that usually arises in creeping isothermal flow of Newtonian fluids and in steady heat conduction, where the differential operator is elliptic and "self-adjoint," but the method is commonly used for other flows as well. Inertial terms in the momentum equation, and the convective flow terms in the energy equation, which are important even in the absence of inertia, cause the system to be non-self-adjoint, however, whereas the equations describing viscoelastic flow are non–self-adjoint even for creeping flow; the operator for viscoelastic flow can sometimes change from elliptic to hyperbolic in a part of the flow domain. Hence, the standard tools may sometimes fail. "Streamline upwinding" and "discrete Galerkin"

methods are sometimes used for the convective terms. Some codes, particularly those that include heat transfer in the metallic surfaces, use hybrid methods in which some parts of the problem are solved using finite elements and others using finite differences.

Boundary element methods can be applied to a limited class of problems in which Green's theorem equating volume and surface integrals can be exploited; this usually requires that the differential operator in the equations be the Laplacian. The differential equations can be partially integrated and converted to a set of equations in which the dependent variables enter only through integrals along the boundary. In such a case the computational problem is substantially reduced; instead of approximations over a two-dimensional area, for example, approximation is required only along a one-dimensional boundary curve. The method of approximation along the boundary is usually similar to that used in finite element methods, hence the name boundary element. The boundary element method has been adapted to the solution of several transient and free-surface processing problems, as well as to the calculation of the orientation of rodlike suspensions in Newtonian fluids, but general-purpose codes are not widely available.

Continuous Low Deborah Number Processes

The most successful process modeling has been carried out on continuous low Deborah number processes (18–20). This category includes calendaring, the metering region in melt extrusion, and many coating operations. The fluid deformation in these flow fields is closely approximated by combined drag- and pressure-driven flow between nearly parallel surfaces, and the lubrication approximation (21,22), developed by Reynolds for the analysis of lubrication flows, is applicable as a first approximation. The lubrication approximation is broadly based on the assumption that the flow between nearly parallel surfaces is locally the same as the fully developed flow between parallel walls, for which exact solutions to flow problems exist. (The isothermal lubrication flow of a Newtonian fluid would have a locally parabolic velocity profile, for example, but with the length scale defining the parabola changing slowly with position in the flow.) The lubrication equations are sometimes integrated across the gap in flows in which there are two primary flow directions and a narrow gap in the transverse direction, leading to a set of equations for local gap-averaged velocities and the pressure distribution; this averaged formulation is sometimes referred to as the Hele–Shaw approximation.

The flow of a viscoelastic liquid between infinite parallel walls is a viscometric flow, or a flow with constant stretch history. The velocity profile for a fluid that is isotropic at rest is determined in such a flow only by the shear viscosity, although the stress distribution depends on the viscoelastic parameters. A nearly parallel flow for which the Deborah number is low, and stress growth and relaxation is not important, can be treated as though the local flow were that between infinite parallel walls; in that case the viscoelasticity is not important for determining the flow field and the process can be analyzed with the lubrication or Hele-Shaw equations as though the polymer were purely viscous. Effects attributable to the viscoelastic parameters (eg, interface movement in co-extrusion)

can then be determined using the computed flow field. The main complicating factors in such a calculation are the correct incorporation of the energy balance equation, since the temperature field is generally developing throughout the flow, and the pressure dependence of the viscosity. Calculation of velocity and temperature distributions, residence times, and pressure drops is straightforward; some closed-form analytical solutions are available for simple processing geometries, and some commercially available computer codes can routinely handle two- and three-dimensional nonisothermal creeping flows of inelastic liquids. Good heat transfer coefficient data are limited, however, and little attention has been paid to the effect of high pressure on physical properties (22).

The procedure outlined above has long been the standard approach. The simulation of coating thickness in blade coating, for which experimental data are available for a range of liquids of increasing viscoelasticity, is a good example of the application and limitation of these approximations. The process geometry is shown schematically in Figure 3, together with a finite element mesh used for computation. Data for the coating thickness as a function of gap spacing are

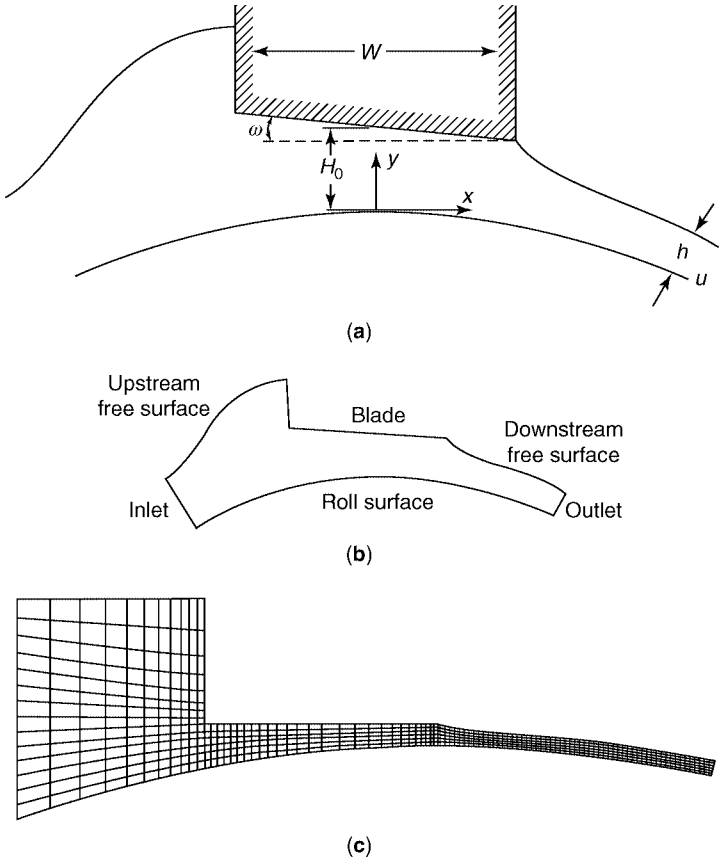

Fig. 3. (**a**) Blade coating; (**b**) surfaces requiring boundary conditions; and (**c**) finite-element mesh used in calculations. From Ref. 23. Courtesy of the American Institute of Chemical Engineers.

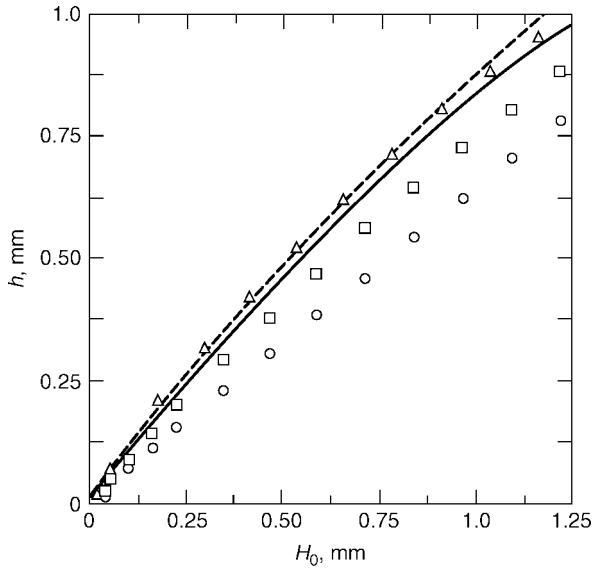

Fig. 4. Coating thickness as a function of gap thickness for a blade angle of 10°, showing agreement between lubrication theory (——), finite element calculations (– – –), and experimental data for aqueous solutions of 1.25% carboxymethylcellulose and (△, 0%; □, 0.005%; ○, 0.020%) polyacrylamide. From Ref. 24. Courtesy of the American Institute of Chemical Engineers.

shown in Figure 4 for three shear-thinning polymer solutions: an aqueous solution of 1.25% carboxymethylcellulose, and the same solution with an additional 0.005% and 0.02% of a high molecular weight polyacrylamide; all three liquids have nearly the same shear viscosity functions, with a power-law index of 0.6 in the power-law region, but the polyacrylamide solutions are more viscoelastic. The solid line is the lubrication approximation to the flow. The dashed line is a finite-element numerical solution of the full two-dimensional purely viscous equations without the nearly parallel approximation. The lubrication approximation is acceptable for small gap spacings but deviates systematically from the numerical solution of the full equation set for larger spacings. The solution to the purely viscous equations agrees well with the data for the least elastic solution, but deviates substantially for the most elastic liquid; the coating flow with the latter is clearly not a low Deborah number process.

Periodic Low Deborah Number Processes

Mold filling, which is a repetitive transient process, can often be treated as a low Deborah number process when the fill time is long relative to a characteristic time for stress relaxation, so that only purely viscous rheology need be considered. The fluids are usually of very high viscosity, and the characteristic gap size is usually small; inertial effects are thus usually negligible compared with viscous stresses. The transient terms in the momentum balance are inertial, so the

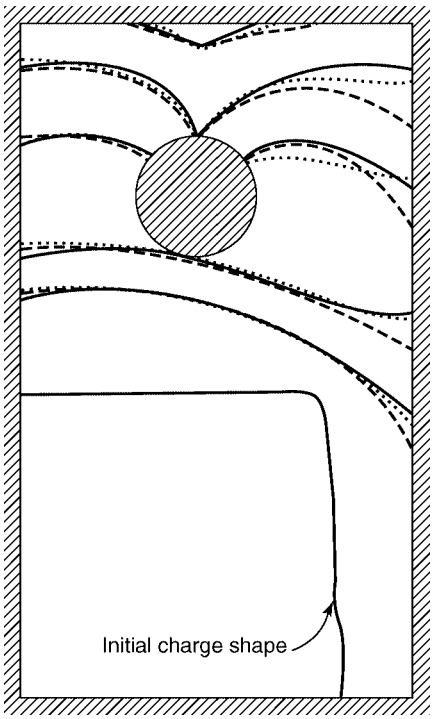

Fig. 5. Experimental and computed front movement during filling of a compression mold with a silicone liquid. (——) experimental; (– – –) predicted (FEM); (-----) predicted (BEM). Reproduced from Ref. 27. Courtesy of the Society of Plastics Engineers.

momentum equation becomes quasi-static if inertial effects can be neglected. Mold filling under these conditions is simulated by solving the steady-state momentum equation for an inelastic liquid, with the front movement calculated at each time step from the normal velocity at the front. The numerical methods used for continuous processes can thus be applied, with (conceptually) minor modification to follow the moving front (24–26). Special techniques must be implemented to follow temperature transients and any solidified regions.

Fill rates and front movements are usually well described by Hele-Shaw calculations for purely viscous fluids. Simulations of isothermal mold filling of a silicone oil in a compression mold using both finite element (FEM) and boundary element (BEM) methods are shown in Figure 5, together with experimental front locations. Simulation of front movement in the injection molding of polypropylene with a series of short shots, including the development of the weld line, is shown in Figure 6. The polypropylene was treated as a purely viscous power-law fluid with temperature-dependent physical properties, using a hybrid finite element-finite difference technique to solve the Hele-Shaw equations.

Details of the kinematics within the mold, which would be required for the computation of stress distributions, require solution of the full (quasi-static) momentum equation with an appropriate stress constitutive equation. This can be done routinely for purely viscous fluids for flows with two velocity components

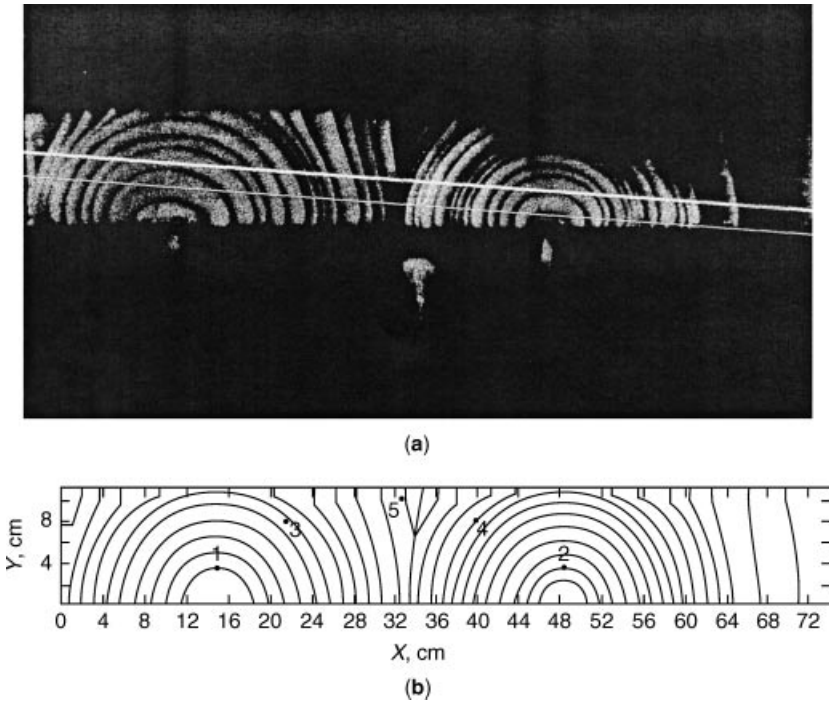

Fig. 6. Filling of a double-gated injection mold with polypropylene. (**a**) Experiment using a series of short shots; and (**b**) simulation. +++++++ = Computed weld line. Reproduced from Ref. 28. Courtesy of Elsevier Science Publishers.

(two-dimensional or axisymmetrical) and for three-dimensional flows in relatively simple mold geometries. Complex geometries can be addressed by linking together Hele-Shaw solutions in regimes where the transverse velocity component can be neglected with full three-dimensional calculations in other portions of the mold. The three-dimensional flow near a moving front is rarely treated, although the "fountain flow" near the front can be approximated by neglecting the larger of the two radii of curvature of the front. A typical calculation of the flow near the front is shown in Figure 7; numerous studies modeling these kinematics indicate that the agreement with experiments on front movement is very good, and that the computed flow field is insensitive to the particular choice of constitutive equation, although the stress field is not. The implication of this observation for mold filling is quite important, since low Deborah number computations, in which viscoelasticity can be neglected, are much simpler than computations with viscoelastic constitutive equations. In many mold filling applications the flow field can be computed first, treating the melt as purely viscous, and the viscoelastic stress computed afterward. Since stress and orientation are linked in noncrystalline polymers through the stress-optical law, such a decoupled approximation is efficient in computing molecular orientation distributions.

The computational problem is considerably more difficult if solidification is to be taken into account. The assumption is often made that solidification is instantaneous at a specified temperature. Some modeling studies have been carried

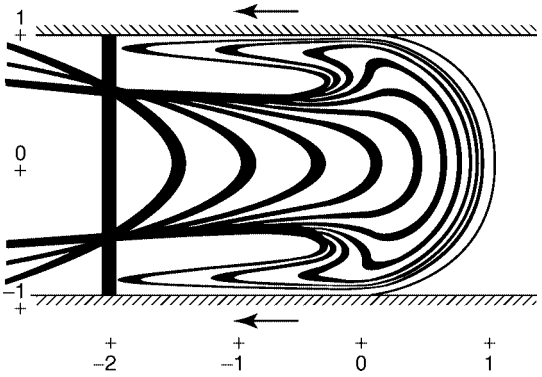

Fig. 7. Calculated tracer line formation as a function of time during mold filling. Reproduced from Ref. 29. Courtesy of the American Institute of Chemical Engineers.

out in which crystallization kinetics are included in the mass and energy balances in order to estimate the degree of crystallization and the morphology when the motion is frozen. Most such studies have used quiescent crystallization data. A reliable theory of crystallization rates during deformation at very high stress levels is still a subject of research (30,31), as is a complete theory of the rheology of the crystal/melt mixture, and commercial codes do not address this issue. The ultimate goal is the prediction of stress and morphology following molding (32).

Free-Surface Processes

The modeling of polyester fiber spinning from the melt is well developed for take-up speeds below about 4,000 m/min, where crystallinity is low (33); commercial and in-house computer codes have long been available for the prediction of temperature and diameter profiles along the spinline and the radial birefringence distribution (through a stress-optical coefficient) at take-up, and they have been used widely to analyze process performance and to evaluate modifications. The major challenge has been the incorporation of crystallization, which is an important factor in the spinning of nylon at all take-up speeds and of polyesters at high speeds. Spinline models that account for stress-induced crystallization and the effect of the crystalline phase on the rheology (34) are now available .

Most spinline models are based on thin-filament equations, in which the essentially elongational character of the deformation is exploited and the conservation and constitutive equations are averaged over the diameter or, in a mathematically equivalent process, expanded in a small scaling parameter. The thin-filament approximation is similar in approach to the lubrication approximation for confined flows, but the low Deborah number assumption need not be made. It is straightforward to include a solution of the energy equation that incorporates the radial dependence of temperature in this formalism. (There is a region near the point of extrusion where the melt undergoes a transition from the shear flow in the spinnerette to the extensional flow on the spinline, and the thin-filament approximation cannot apply in this region. Finite-element solutions of the flow

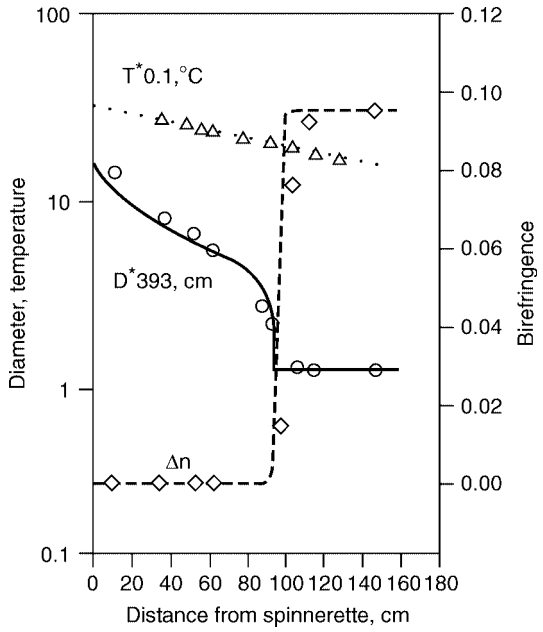

Fig. 8. Comparison of model calculations of diameter attentuation, birefringence, and temperature profiles with pilot plant data for melt spinning of 0.65 IV poly(ethylene terphthalate) at a take-up speed of 5947 m/min. Reproduced from Ref. 33. Courtesy of the Society of Rheology.

in the transition region indicate that the thin-filament equations become valid within a few spinneret diameters.) Full two-dimensional axisymmetric models are available but add little additional physical understanding. Most spinline models assume that the polymer is a Newtonian fluid, but differential viscoelastic models are easily incorporated and there is no reason to use the Newtonian approximation when rheological data are available. A comparison of the prediction of diameter attenuation, birefringence, and mean temperature profiles for high-speed spinning of poly(ethylene terephthalate) with pilot plant spinning data is shown in Figure 8. The viscoelastic model incorporates stress-induced crystallization and successfully captures the rapid diameter attenuation and increase in birefringence at the onset of crystallization. Predictions of the temperature profile and the final stress level tend to be insensitive to stress constitutive assumptions, despite the sensitivity of the diameter attenuation profile to the constitutive assumptions. Limited dynamic simulations to study disturbance propagation through spinlines have been less successful, probably because of inadequate treatment of the solidification process (35).

The proper representation of macroscopic transport properties, particularly the heat transfer coefficient, is a major problem in the predictive modeling of spinning and other free-surface processing flows. Heat transfer coefficients are typically obtained from experiments on nondeforming wires, and the extension to a deforming surface with a variable cross section is not obvious. Data obtained on real spinlines require either infrared or intrusive contact temperature

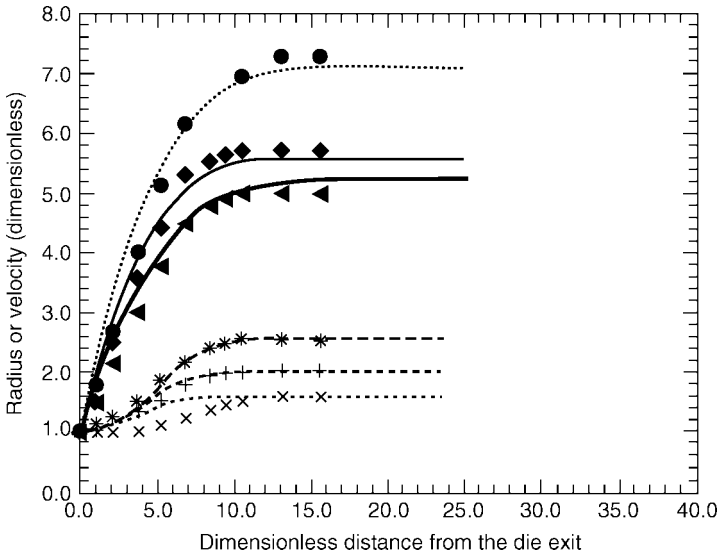

Fig. 9. Comparison of model calculations of bubble radius and film velocity with blown film data for a low density polyethylene, 3.84-cm radius × 0.8-mm thickness die, 4.1-kg/hr throughput. Data of Tas. Experiment 12: inflation pressure = 118 Pa, take-up force = 7.6 N, × radius, (- - - -) predicted radius, ● velocity, (·····) predicted velocity; experiment 15: 108 Pa, 7.7 N, + radius, (– – –) predicted radius, ◆ velocity, (——) predicted velocity; experiment 18: 95 Pa, 6.8 N, ∗ radius, (- - -) predicted radius, ◀ velocity, (———) predicted velocity. Reproduced from Ref. 38. Courtesy of the Society of Rheology.

measurements, neither of which is reliable for the accurate determination of a heat transfer coefficient. Model calculations indicate that the diameter attenuation is highly sensitive to the heat transfer coefficient; small uncertainties can mask other factors and make extrapolation to new processing conditions questionable.

The blown film process is kinematically similar to fiber spinning, and thin-sheet equations analogous to the thin-filament equations have been employed in process modeling (36–38). As with the thin-filament equations, temperature variation in the film thickness direction can be incorporated in a straightforward way. Figure 9 compares bubble radius and velocity profile data from three experiments on a blown film line with a thin-sheet calculation that incorporates a viscoelastic constitutive equation, a transverse temperature variation, and a crystallization model (38). The calculation was based on an empirical heat transfer coefficient that is not formulated in terms of scalable dimensionless groups. The operating characteristics of film lines depend on details of the placement of cooling air, but this feature cannot be incorporated into existing blown film models without a better understanding of the heat transfer.

Modeling of the blown film process illustrates characteristics that are very different from those of fiber spinning, even with primitive representations of the heat transfer (37). These differences are a consequence of the hoop stress in the bubble. Multiple steady states are computed for fixed operating conditions, for example, and steady axisymmetric bubbles can vanish suddenly following small changes in operating parameters; both phenomena are seen in practice. The

models also show important differences in the stability characteristics of the two processes.

Numerics

The numerical realization of a model requires the availability of algorithms that can solve the model equations accurately. Modeling of the detailed flow and stress fields in confined geometries has been limited historically by the fact that iterative numerical algorithms for solving the momentum and continuity equations together with the nonlinear constitutive equations typically fail to converge to a solution above a critical value of the recoverable shear or Weissenberg number. This convergence failure, which is often called the "high Weissenberg number problem," appears to be a numerical artifact of the techniques in use, which propagate the large stresses generated near corners, lips, and other areas of stress concentration into the bulk and degenerate the solution quality; precise identification of the cause is difficult, because the strength of the stress singularity near a corner is an outstanding mathematical problem for the flow of most viscoelastic fluids, for which only partial solutions have been obtained (Reference 4, pp. 68 ff).

Stress constitutive equations with the structure of equation 4 are hyperbolic when the flow field is specified. Experience in areas where hyperbolic equations commonly arise, such as compressible gas dynamics, has guided the development of special techniques, including operator decompositions and "upwinding," that are implemented in some available computer codes. Use of these methods has extended the range over which convergence can be obtained to the lower end of practical processing conditions. Reviews can be found in References 4,16, and 17. A simulation that is representative of the state of the art of computations for highly viscoelastic melts is shown in Figure 10. Calculated isochromatic fringes, which are contours of the principal stress $[(\tau_{xx} - \tau_{yy})^2 + {\tau_{xy}}^2]^{\frac{1}{2}}$, are superposed on the

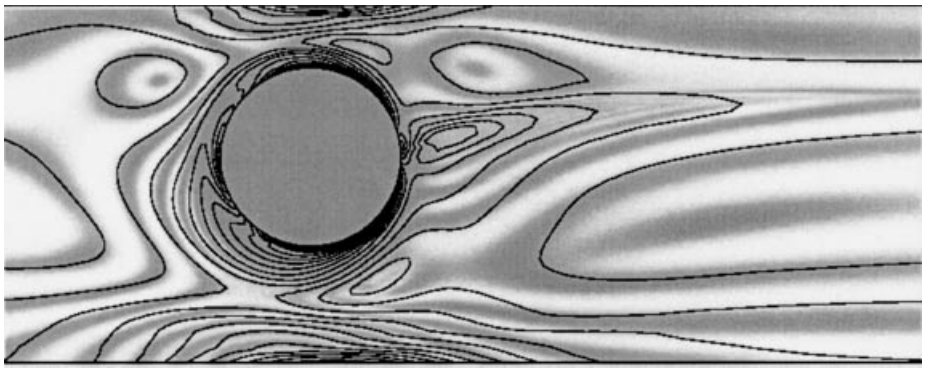

Fig. 10. Isochromatic fringe patterns for flow of a low density polyethylene ($M_w = 1.55 \times 10^5$, $M_w/M_n = 11.9$) past an offset cylinder of diameter 2.5 mm in a plane channel at 190°C with a mean upstream velocity of 8.53 mm/s. The mean relaxation time of the melt is 1.5 s. From Ref. 39. Courtesy of Elsevier Science Publishers.

experimental fringes at 190°C for the flow of a low density polyethylene through a planar region containing an offset cylindrical insert. Characteristic Deborah numbers based on mean residence times for flow in the small and large gaps were, respectively, 0.7 and 11.5, indicating the likelihood of strong elastic effects. The constitutive equation, which was fit to linear viscoelastic and steady shear data, is a special form of equations 4 and 5 often used for simulations known as the Phan–Thien/Tanner equation, with four terms in the linear viscoelastic spectrum. The computations are in qualitative agreement with the experiments and show the development of an asymmetric wake in which the stresses are very high downstream of the aft stagnation point. The experimental wake extends farther in the downstream direction than the calculated wake. The fringes appear to be more densely packed in the lower upstream region close to the cylinder in the experiments than in the calculations, indicating that the experimental stress gradients were stronger than the computed gradients.

Boundaries

The tradition in fluid mechanics, dating to the mid-nineteenth century, has been that a fluid adheres to a solid boundary during flow, and that the fluid at the boundary therefore takes on the velocity of the solid. This "no-slip" condition has been used routinely in the modeling of polymer flows, despite occasional hints in the processing literature as early as the 1960s that there might be "slip" at the wall. It is now generally accepted that the composition and state of the boundary affect the flow (15); the properties of a polymer extrudate can be controlled by changing the materials of construction of the metal die-face, for example, thus establishing that the boundary is not simply a passive element in the flow field. Figure 11 shows flow curves for a linear low density polyethylene extruded through two

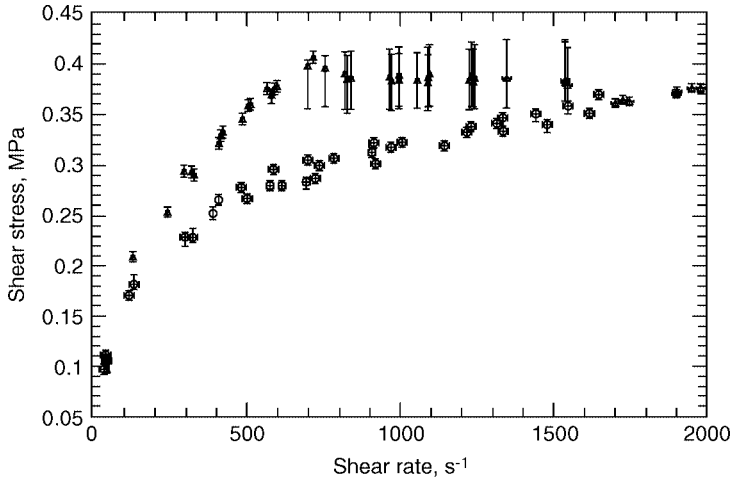

Fig. 11. Flow curves for a linear low density polyethylene ($M_w = 114{,}000$, $M_n/M_w = 3.9$) at 200°C in identical 1 × 20 mm 304 stainless steel (△) and CDA-464 naval brass (○) capillaries. Reproduced from Ref. 40. Courtesy of the Society of Rheology.

geometrically identical capillaries, one constructed of 304 stainless steel and the other of CDA-464 naval brass (40). The data for the steel capillary show the range of pressure fluctuations in the "spurt" regime. The polymer extruded through the brass capillary experienced significantly lower stresses at the same throughput ("apparent slip") and was free of surface defects that appeared on the extrudate from the steel die at a stress just above 0.17 MPa.

Most experimental evidence indicates that deviations from the no-slip condition are unimportant up to a wall stress of the order of 0.2 MPa (29 psi). Since the plateau modulus of most polymers at processing conditions is of the same order, this observation suggests that no-slip can be used with confidence under conditions where $\|\tau\|/G_p' < 1$. The appropriate boundary condition at higher stresses is not known, although some data indicate that the tangential velocity at the wall is proportional to a power of the wall shear stress; the slip law proposed by Navier in the early nineteenth century assumes a power of unity. It is not straightforward to impose a slip boundary condition in a numerical code and simultaneously satisfy mass conservation at a sharp corner, however. Slip conditions have therefore been implemented only sparingly. The range of convergence of numerical schemes is extended when a slip condition is used, since the high stresses that degenerate the solution are moderated. The effect of wall slip in complex geometries is relatively unexplored. Analytical solutions for flow of shear-thinning inelastic liquids between converging planes using a Navier slip law indicate substantial departure from the expected radial streamline pattern (41), which, as discussed subsequently, could have a large impact on the stability of die entry flows.

Mixing

Mixing in polymer melt processing takes place in the laminar regime. Laminar mixing, which is related to the theory of chaotic dynamical systems, has been intensely studied since the late 1980s (42), and techniques have been developed for visualizing the evolution of apparent disorder in strictly deterministic systems. Application to the simulation of continuous mixers for immiscible materials with viscosities of comparable magnitude requires the use of an efficient mapping procedure for tracking fluid elements as they progress through the three-dimensional flow (43), where the local kinematics and pressure profile are calculated with a finite-element solution. A simulation of a cross section of identical black-and-white inelastic shear-thinning Carreau-Yasuda fluids with a power-law exponent of 0.1 following laminar flow through a static mixer is shown in Figure 12. Simulations of this type can be used in principle to optimize mixer design, but they have been limited to inelastic fluids with identical viscosity functions and no interfacial tension.

Droplet breakup and coalescence are the primary physical processes in the mixing of liquids with very different viscosities. Computational tools for the breakup of individual Newtonian droplets are well developed; Figure 13 shows a boundary element calculation of the sequence of shapes of a polydimethylsiloxane droplet in a polyisobutylene of nearly the same viscosity, together with experimental data. Computational tools for breakup with viscoelastic constitutive

Fig. 12. Simulation of the mixing pattern for two identical shear-thinning inelastic liquids in a static mixer after passing six blades oriented at 140°. Reproduced from Ref. 44. Similar images for Newtonian liquids may be found in Ref. 45.

equations are not well developed. Emulsion models for the rheology of immiscible blends with a dispersed droplet phase do an excellent job of describing the linear viscoelasticity, and models for nonlinear deformations of blends based on an understanding of droplet dynamics are under development (47).

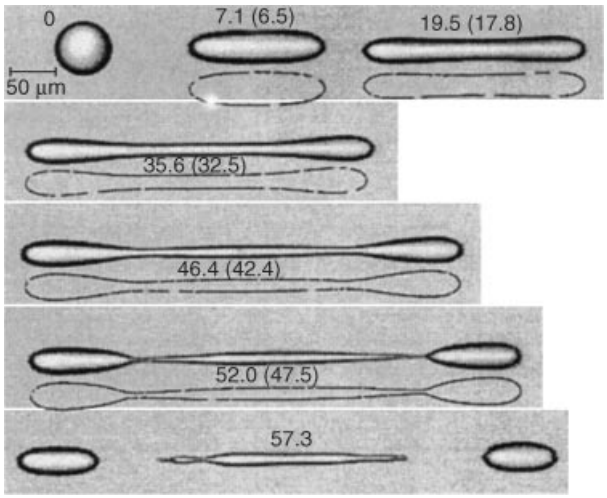

Fig. 13. Deformation and breakup of a polydimethylsiloxane droplet in a polyisobutylene of nearly the same viscosity; viscosity $\approx$ 100 Pa · s, interfacial tension $\approx$ 2.4 mN/m. Images are experimental data and profiles are simulations using slightly adjusted parameters to ensure a good fit at pinch-off. Numbers are experimental total strain (time multiplied by shear rate), whereas numbers in parentheses are computed total strain for the same droplet shape. Reproduced from Ref. 46. Courtesy of the Society of Rheology.

Stability and Sensitivity

Polymer processes are subject to a variety of instabilities that limit throughput or degrade product quality. Dynamic models are routinely used in engineering applications to study conditions under which stable operation cannot be maintained, and idealized models of some polymer process have been employed to gain insight into operability. The most common technique for studying process stability is linear stability theory (48), in which the dynamical response to infinitesimal disturbances is obtained by solution of a set of approximate linear equations through an eigenvalue analysis. Complex flows can be analyzed through the eigenvalues of a matrix that arises in the course of a finite element solution. If infinitesimal disturbances die out, the steady mode of operation is stable; if infinitesimal disturbances grow, the steady mode of operation cannot be maintained (since no process can be kept free of infinitesimal disturbances), and the system is unstable. Linear stability theory establishes absolute instability but only relative stability; a process that is unstable to infinitesimal disturbances is unstable to all disturbances, but a process that is stable to infinitesimal disturbances might still be unstable to some finite disturbances.

Dynamic modeling has been quite successful in describing the onset of a flow instability known as draw resonance, which occurs in fiber spinning and extrusion coating (1,19,33). Draw resonance is characterized by regular oscillations in the fiber diameter or coating thickness, with a period that is slightly greater than the residence time in the melt zone. Some subtleties associated with the role of heat-transfer mechanisms remain, and the effect of the spinneret flow (as transmitted through the initial conditions used in the thin-filament equations) has not been completely quantified, but the mechanism is well understood and the models have been very useful in discriminating between the effects of rheology, cooling, gravitational forces, and inertia. Dynamic modeling to describe the propagation of disturbances through a melt spinline under stable spinning conditions is much less well developed (35).

Spinline failure appears to occur through a cohesive mechanism, which has received little theoretical attention (49,50). A simple scaling model that predicts a critical value of the recoverable strain as a function of stretch rate captures the qualitative features of the limited data on melt failure in extension (50,51).

The blown film process undergoes a variety of processing instabilities. Modeling of these is less advanced than for fiber spinning, in large measure because of the sensitivity to details of the heat-transfer mechanisms and the treatment of the solidification region. A draw resonance-like instability is predicted to occur under some conditions (37). One striking result predicted by the dynamic model is that the process stability is highly sensitive to the manner in which process control is effected; under some conditions, a bubble controlled by air-flow adjustment to maintain a constant diameter is predicted to be stable, whereas the same bubble controlled by a feedback system utilizing the internal pressure is predicted to be unstable.

Melt extrusion is characterized by at least two distinct instabilities that cause surface defects, generally known as melt fracture, or gross melt fracture, and sharkskin, or sharkskin melt fracture (15). Sharkskin, a high frequency,

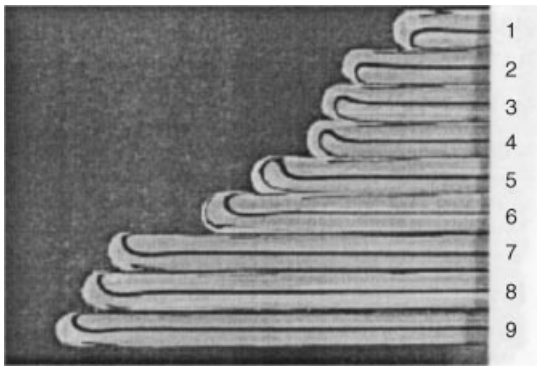

Fig. 14. Short shots with two-color injection molding of a filled polypropylene compound. Reproduced from Ref. 55. Courtesy of the Society of Rheology.

small-amplitude surface distortion, appears to occur only in highly entangled linear polymers and is believed to be associated with a material failure resulting from the stress concentration at the die exit. Melt fracture, in which the distortions may be regular or irregular, typically occurs when the wall shear stress is comparable to the plateau modulus (recoverable shear of order unity) and appears to originate in the die land or at the die entry. There have been numerous linear stability analyses of fully developed pressure-driven viscoelastic flow in long slits and capillaries; the general conclusion has been that the flow is stable to infinitesimal disturbances in the absence of inertia, but a linear instability may exist for some constitutive equations (52). A weakly nonlinear ("subcritical") instability has been reported (53,54). Whether model calculations can predict the instability that is observed in the actual process remains an open question.

Flow mark surface defects on injection-molded parts were first reported in the early 1960s and have been considered by some authors to be an indication of wall slip in the neighborhood of the advancing front (15). Figure 14 shows a series of short shots of injection molding of a filled polypropylene compound in which a thin strip of black polymer was placed along the centerline. With stable fountain flow, as shown in Figure 7, the black polymer will coat both mold surfaces. Instead, the black strip is first carried to the bottom of the mold, then to the top. A swirling flow near the melt front is predicted by linear stability theory combined with a finite element analysis for one of two constitutive equations studied (55). It thus remains an open question as to whether an instability in the neighborhood of the front is the cause of the flow marks, although this is the likely mechanism.

Interface stability in co-extrusion has been the subject of extensive analysis. There is an elastic driving force for encapsulation caused by the second normal stress difference (56), but this is probably not an important mechanism in most coprocessing instabilities. Linear growth of interfacial disturbances followed by dramatic "breaking wave" patterns is observed experimentally. Interfacial instabilities in creeping multilayer flows have been studied for several simple constitutive equations (57–59). Instability modes can be traced to differences in viscosity and normal stresses across the interface, and relative layer thickness is important.

Aside from the examples cited here, the experimental literature on viscoelastic flow instabilities in the absence of inertia has emphasized dilute polymer solutions. These stability studies include the flow between rotating concentric cylinders, torsional cone-and-plate flow, flow in a "lid-driven" cavity, stagnation flow, and flow past a cylinder in a channel, all of which have been analyzed for simple constitutive equations (60). It is likely that these phenomena have relevance to polymer melt processing, but direct connections have not been made. The common feature of these inertialess "elastic" instabilities seems to be the coexistence of normal stresses and curved streamlines, and the experimental and theoretical onsets of instabilities for this class of flows correlate with a criterion of the form $\lambda U/(\Re H)^{\frac{1}{2}} > M_{\text{crit}}$ (61,62). λ is a mean relaxation time, U the characteristic velocity, H the length scale defining the shear rate, and $\Re$ the length scale defining the curvature of the streamlines. M_{crit} is a constant characteristic of the specific flow. The critical value can be interpreted as the geometric mean of the Deborah and Weissenberg numbers. Substantial streamline curvature predicted in converging flow of shear-thinning fluids with wall slip (41) suggests a possible die entry mechanism for melt fracture.

Anisotropic Materials

Anisotropic materials, such as liquid crystalline polymers and fiber-filled melts, present special difficulties because of the incomplete state of development of constitutive models that account for the spatial distribution of the orientation and stress fields. In nearly all cases the constitutive equations are derived from microscopic theories of the orientation of rodlike elements, and the statistical mechanics requires a closure approximation that expresses the fourth moment of the orientation distribution in terms of the second moment (63,64). The closure approximation can affect the details of the evolution of the orientation distribution. The models for both types of anisotropic liquids are very similar in structure, differing in the way in which structural interactions are incorporated. Liquid crystalline polymer models incorporate interaction potentials between neighboring rigid molecules and include Brownian forces. Simulations using continuum models of liquid crystalline polymers in simple geometries show orientational structures and layering in rectilinear shear flows, but they are unable to replicate the complex defect-driven textures characteristic of real nematic polymers, where the correlation lengths for nematic order are independent of the geometric scale of the system (63,65,66). Models for fiber-filled systems are based on theories for noninteracting and slightly interacting non-Brownian rods, and they do not rigorously account for coordinated fiber motions; the latter are dealt with empirically by introducing an apparent diffusion term with a coupling coefficient that correlates with the product of fiber aspect ratio and volume fraction (67). Simulations of both liquid crystalline polymer and fiber-filled systems often assume that the flow field can be calculated independently of the orientation distribution, but full coupling is usually required to obtain even qualitatively correct flow and orientation field solutions to the constitutive and field equations (63,64,68,69).

BIBLIOGRAPHY

"Processing, Modeling" in *EPSE* 2nd ed., Vol. 13, pp. 425–444, by Morton M. Denn, Lawrence Berkeley Laboratory and University of California at Berkeley.

1. M. M. Denn, *Process Modeling*, Longman, New York, 1986.
2. R. Aris, *Modelling Techniques*, Pitman, London, 1978.
3. C. L. Tucker III, *Fundamentals of Computer Modeling for Polymer Processing*, Hanser, Munich, 1989.
4. R. G. Owens and T. N. Phillips, *Computational Rheology*, Imperial College Press, London, 2002.
5. M. Tirrell, R. Galvan, and R. L. Lawrence, in J. J. Carberry and A. Varma, eds., *Chemical Reaction and Reactor Engineering*, Marcel Dekker, New York, 1987.
6. R. B. Bird, R. C. Armstrong, O. Hassager, and C. F. Curtis, *Dynamics of Polymeric Liquids*, 2nd ed., John Wiley & Sons, Inc., New York, 1987 (Vol. 1: Fluid Mechanics; Vol. 2: Kinetic Theory).
7. R. G. Larson, *Constitutive Equations for Polymer Melts and Solutions*, Butterworths, Boston 1988.
8. T. C. B. McLeish, *Adv. Phys.* **51**, 1379 (2002).
9. M. T. Islam, J. Sanchez-Reyes, and L. A. Archer, *J. Rheol.* **45**, 61 (2001).
10. A. Lozinski, C. Chauviere, J. Fang, and R. G. Owens, *J. Rheol.* **47**, 535 (2003).
11. M. Reiner, *Phys. Today* **17**, 62 (1969). Reprinted in M. Reiner, *Selected Papers on Rheology*, Elsevier, Amsterdam, 1975.
12. A. B. Metzner, J. L. White, and M. M. Denn, *Chem. Eng. Prog.* **60**(12), 81 (1966).
13. A. B. Metzner, J. L. White, and M. M. Denn, *AIChE J.* **22**, 209 (1966).
14. R. I. Tanner, *Engineering Rheology*, 2nd ed., Oxford University Press, Oxford, 2002, p. 221.
15. M. M. Denn, *Ann. Rev. Fluid Mech.* **33**, 265 (2001).
16. F. P. T. Baaijens, *J. Non-Newtonian Fluid Mech.* **79**, 361 (1998).
17. R. Keunings, in D. Binding and K. Walters, eds., *Annual Rheology Reviews 2003*, British Society of Rheology, Aberystwyth, Wales, 2003.
18. J. R. A. Pearson and S. Richardson, eds., *Computational Analysis of Polymer Processing*, Elsevier Applied Science Publishers, Ltd., London, 1983.
19. J. R. A. Pearson, *Mechanics of Polymer Processing*, Elsevier Applied Science Publishers, Ltd., London, 1985.
20. J. F. Agassant, P. Avenas, J. P. Sergent, and P. Carreau, *Polymer Processing, Principles and Modeling*, Hanser, Munich, 1991.
21. M. M. Denn, *Process Fluid Mechanics*, Prentice-Hall, Englewood Cliffs, N.J., 1980, Chapt. 13.
22. G. Hay, M. E. Mackay, K. M. Awati, and Y. Park *Y, J. Rheol.* **43**, 1099 (1999).
23. T. M. Sullivan, S. Middleman, and R. Keunings, *AIChE J.* **33**, 2047 (1987).
24. M. J. Crochet, F. Dupret, and V. Verleye, in S. G. Advani, ed., *Flow and Rheology in Polymer Composites Manufacture*, Elsevier, Amsterdam, 1994.
25. M. R. Kamal, W. Frydrychowicz, and L. Ansari, in M. R. Tant, J. W. Connell, and H. L. N. McManus, eds., *High-Temperature Properties and Applications of Polymeric Materials*, American Chemical Society, Washington, D.C., 1995.
26. W. Michaeli, S. Hoffman, M. Kratz, and K. Webelhasu, *Int. Polym. Processing* **XVI**, 398 (2001).
27. T. A. Osswald and C. L. Tucker III, *Polym. Eng. Sci.* **28**, 413 (1988).
28. C. A. Hieber and S. F. Shen, *J. Non-Newtonian Fluid Mech.* **7**, 1 (1980).
29. D. J. Coyle, J. W. Blake, and C. W. Macosko, *AIChE J.* **33**, 1168 (1987).
30. G. Eder and H. Janeschitz-Kriegl, in H. E. H. Meijer, ed., *Processing of Polymers*, (Vol. 18 of R. W. Cahn, P. Haasen, and E. J. Kramer, eds., Materials Science and Technology), VCH, Weinheim, Germany, 1997.

31. A. K. Doufas, I. S. Dairanieh, and A. J. McHugh, *J. Rheol.* **43**, 85 (1999).
32. T. Huang and M. R. Kamal, *Polym. Eng. Sci.* **40**, 1796 (2000).
33. M. M. Denn, in Ref. 18, p. 179.
34. A. K. Doufas and A. J. McHugh, *J. Rheol.* **45**, 403 (2001).
35. B. M. Devereux and M. M. Denn, *Ind. Eng. Chem. Res.* **33**, 2384 (1994).
36. C. J. S. Petrie, in Ref. 18, p. 217.
37. J. J. Cain and M. M. Denn, *Polym. Eng. Sci.* **28**, 1527 (1988).
38. I. A. Muslet and M. R. Kamal, *J. Rheol.* (in press).
39. F. P. T. Baaijens, S. H. A. Selen, H. P. W. Baaijens, G. W. M. Peters, and H. E. H. Meijer, *J. Non-Newtonian Fluid Mech.* **68**, 173 (1997).
40. V. G. Ghanta, B. L. Riise, and M. M. Denn, *J. Rheol.* **43**, 435 (1999).
41. Y. M. Joshi and M. M. Denn, *J. Non-Newtonian Fluid Mech.* **114**, 185 (2003).
42. J. M. Ottino, *The Kinematics of Mixing: Stretching, Chaos, and Transport*, Cambridge University Press, Cambridge, 1989.
43. P. G. M. Kruijt, O. S. Galaktionov, P. D. Anderson, G. W. M. Peters, and H. E. H. Meijer, *AIChE J.* **47**, 1005 (2001).
44. O. S. Galaktionov, *Optimzation of Distributive Mixing*, Technische Universteit Eindhoven, Eindhoven, 2002.
45. O. S. Galaktionov, P. D. Anderson, G. W. M. Peters, and H. E. H. Meijer, *Can. J. Chem. Eng.* **80**, 604 (2002).
46. V. Cristini, S. Guido, A. Alfani, J. Blawzdziewicz, and M. Loewenberg, *J. Rheol.* **47**, 1283 (2003).
47. C. L. Tucker III and P. Moldenaers, *Ann. Rev. Fluid Mech.* **34**, 177 (2002).
48. M. M. Denn, *Stability of Reaction and Transport Processes*, Prentice-Hall, Englewood Cliffs, N.J., 1975.
49. A. Ya. Malkin and C. J. S. Petrie, *J. Rheol.* **41**, 1 (1997).
50. Y. M. Joshi and M. M. Denn, in D. Binding and K. Walters, eds., *Annual Rheology Reviews 2004*, British Society of Rheology, Aberystwyth, Wales, 2004.
51. Y. M. Joshi and M. M. Denn, *J. Rheol.* **47**, 291 (2003).
52. A. M. Grillet, A. C. B. Bogaerds, G. W. M. Peters, and F. P. T. Baaijens, *J. Non-Newtonian Fluid Mech.* **103**, 221 (2002).
53. K. Atalik and R. Keunings, *J. Non-Newtonian Fluid Mech.* **102**, 299 (2002).
54. B. Meulenbroek, C. Storm, V. Bertola, C. Wagner, D. Bonn, W. van Saarloos, *Phys. Rev. Lett.* **90**, 024502 (2003).
55. A. M. Grillet, A. C. B. Bogaerds, G. W. M. Peters, and F. P. T. Baaijens, *J. Rheol.* **46**, 651 (2002).
56. B. Debbaut and J. Dooley, *J. Rheol.* **43**, 1525 (1999).
57. H. K. Ganpule and B. Khomami, *J. Non-Newtonian Fluid Mech.* **81**, 27–69 (1999).
58. Y. Y. Renardy, M. Renardy, *J. Non-Newtonian Fluid Mech.* **81**, 215–234 (1999).
59. B. Khomami and K. C. Su, *J. Non-Newtonian Fluid Mech.* **91**, 59–84 (2000).
60. E. S. G. Shaqfeh, *Ann. Rev. Fluid Mech.* **28**, 129 (1996).
61. G. H. McKinley, P. Pakdel, and A. Öztekin, *J. Non-Newtonian Fluid Mech.* **67**, 19 (1996).
62. G. H. McKinley, in M. J. Adams, R. A. Mashelkar, J. R. A. Pearson, and A. R. Rennie, eds., *Dynamics of Complex Fluids*, Imperial College Press and the Royal Society, London, 1998.
63. A. D. Rey and M. M. Denn, *Ann. Rev. Fluid Mech.* **34**, 233 (2002).
64. B. E. VerWeyst and C. L. Tucker III, *Can J. Chem. Eng.* **80**, 1093 (2002).
65. R. Kupferman, M. N. Kawaguchi, and M. M. Denn, *J. Non-Newtonian Fluid Mech.* **91**, 255 (2000).
66. G. Sgalari, L. G. Leal, and E. Meiburg, *J. Rheol.* **47**, 1417 (2003).
67. N. Phan-Tien, X.-J. Fan, R. I. Tanner, and R. Zheng, *J. Non-Newtonian Fluid Mech.* **103**, 251 (2002).

68. G. G. Lipscomb, M. M. Denn, D. U. Hur, and D. V. Boger, *J. Non-Newtonian Fluid Mech.* **26**, 297 (1988).
69. C. L. Tucker. III *J. Non-Newtonian Fluid Mech.* **39**, 239 (1991).

MORTON DENN
The Levich Institute,
City College of the City University of New York

PROPYLENE POLYMERS

Introduction

The stereospecific polymerization of propylene by Giulio Natta in 1954 is one of the most commercially significant scientific breakthroughs in polymer chemistry. Natta's discovery that a Ziegler catalyst could be used to produce highly isotactic polypropylene led to the first commercial processes for the production of this polymer by Montecatini in Italy and Hercules in the United States in 1957. The attractive properties and relatively low cost of polypropylene produced using this technology led to its rapid commercial acceptance. Consequently, Karl Ziegler and Giulio Natta were awarded the Nobel Prize in Chemistry in 1963. The commercial potential of olefin polymerization was recognized by many of the leading companies, leading to a tremendous amount of activity and the invention of a number of competing technologies in the early 1950s. These technologies were not economically competitive with those based on Ziegler–Natta catalysts. However, the competing claims of a number of companies led to a massive patent interference in the United States that continued for almost 30 years, eventually resulting in the award of a U.S. patent for the composition of matter of crystalline polypropylene to Hogan and Banks of Phillips Petroleum in 1983. Continued interest in olefin polymerization led to the invention of the supported high yield, high stereoregularity catalyst systems by Montedison and Mitsui Petrochemical. This led to the development of a number of low cost polymerization processes, spurring a dramatic increase in production capacity. Today, these catalyst systems are used to produce polypropylene in every major region of the world. The use of homogeneous organometallic (metallocene) olefin polymerization catalysts has led to the development of a number of unique propylene polymers. Currently, these polymers are produced in relatively limited amounts for a number of specialty applications.

Polypropylene is one of the most widely used polymers in the world because of the widespread availability and low cost of monomer, low manufacturing cost, and attractive polymer properties. These properties can be modified to be suitable for a wide variety of applications. Polypropylene can be processed by almost all commercial fabrication techniques. Approximately 30,000,000 ton was consumed worldwide in 2001.

Encyclopedia of Polymer Science and Technology. Copyright John Wiley & Sons, Inc. All rights reserved.

Table 1. Physical Properties of Propylene

Property	Value	Reference
Molecular weight	42.078	1
Boiling point at 101.3 kPa[a], °C	−47.7	3
Melting point, °C	−185.3	3
Critical temperature, °C	92	1
Critical pressure, MPa[b]	4.65	1
Critical density, g/mL	0.233	2
Critical compressibility	0.275	3
Dipole moment, 10^{-30} C·m[c]	1.3	3
Refractive index, n_D	1.3567	3
Explosion limit, % by volume in air		
Lower	2.4	1
Upper	11.1	1
Autoignition temperature, °C	224	1
Solubility in water (at 20°C, 101.3 kPa[a]), mL gas/100 mL	44.6	3

[a] To convert kPa to mm Hg, multiply by 7.5.
[b] To convert MPa to atm, multiply by 9.87.
[c] To convert C·m to D, divide by 3.336 x 10^{-30}.

Monomer

Properties. Propylene is an olefin hydrocarbon that is a gas under ambient conditions but is normally stored as a liquid under pressure. The physical properties of propylene are given in Table 1. Thermodynamic properties are widely reported in the literature. Vapor–liquid equilibria of mixtures of propylene with other hydrocarbons and hydrogen are accurately represented by correlations for hydrocarbon mixtures, such as the Chao–Seader correlation.

The reactivity of propylene is a result of the olefinic double bond in $H_2C{=}CHCH_2$, which gives rise to addition reactions. Consequently, propylene is used in the synthesis of many industrially important compounds, including propylene oxide, acrylonitrile, cumene, and isopropyl alcohol. The consumption of propylene in the production of polymers, however, is greater than the total for all other chemicals. Propylene is also used in alkylating feedstocks for gasoline.

Manufacture. The major commercial sources of propylene are processes for the cracking of hydrocarbons. Initially, these processes were designed for the manufacture of other products, and propylene was considered an undesirable by-product. Now, propylene is often an equally desirable co-product. Ethylene is produced by the steam cracking of hydrocarbons at high temperatures and very short residence times. The two most common feedstocks are naphtha and ethane. This process produces a variety of by-products; the ratio of ethylene to by-products is dependent on the type hydrocarbon feedstock and the reaction conditions. Propylene production is higher when naphtha is used as a feedstock rather than ethane. Catalytic cracking of hydrocarbons is often used to increase the production of gasoline in oil refining. Increasing consumption of gasoline in the United States has led refiners to increase the severity of the cracking process, resulting in an increase of the production of propylene as a by-product. Consequently, the ratio of

Table 2. Recommended Maximum Limits of Impurities in Propylene Used in Polymerization[a]

Impurity	Maximum limit
Acetylene, ppm vol	5
Methylacetylene, ppm vol	3
Propadiene, ppm vol	5
Butadiene, ppm vol	50
Green Oils (C6-C12), ppm vol	20
Oxygen, ppm vol	2
CO, ppm vol	0.03
CO_2, ppm vol	5
COS, ppm vol	0.02
Total sulphur, ppm wt	1
Methanol, ppm vol	5
Isopropanol, ppm vol	15
Water, ppm wt	2
Arsine, ppm vol	0.03
Phosphine, ppm vol	0.03
Ammonia, ppm wt	5

[a]Source: Basell.

propylene isolated from refineries to propylene from steam cracking is greater in the United States than in Western Europe and other parts of the world. The propylene isolated from the cracking processes is purified by distillation to remove propane and other impurities. Propylene is commercially available as chemical grade (approximately 95% propylene) and polymerization grade (>99.5% propylene) where propane is the major impurity. However, the suitability of propylene as polymerization monomer is dependent on the levels of trace impurities rather than on the propane content. Commonly occurring impurities are acetylenes, dienes, CO, COS, water, and alcohols. These impurities affect the activity and stereospecificity of propylene polymerization catalysts. Typical limits for the level of impurities acceptable in polymerization grade propylene are given in Table 2.

Propylene is also produced by the metathesis of butene and ethylene. Usually, this process is installed as an addition in a refinery or steam cracking facility to increase the production of propylene. The first commercial metathesis process for the production of propylene was developed by Phillips, and is now licensed by ABB Lummus.

The relative abundance of propane and other light hydrocarbons in certain locations has increased interest in the production of propylene by the catalytic dehydrogenation of propane. Currently only a few propane dehydrogenation plants are operating, producing a small fraction of the world supply of propylene; however, it is anticipated that propane dehydrogenation will be the major source of propylene in the Middle East. The two major processes available are the Catofin process originally developed by Houdry and now licensed by ABB Lummus and the Oleflex process licensed by UOP. Natural gas can be used as the feedstock for the production of propylene by adding a Lurgi MTP process facility to a conventional methanol plant.

Transportation, Storage, and Handling. Propylene is stored and transported as a liquid under pressure The preferred method of transporting propylene is through pipelines. Commercial quantities of propylene are also shipped by tanker and rail. The most extensive pipeline system for the transportation of propylene is in the Gulf Coast region of the United States. This pipeline system is also connected to a series of underground brine caverns used for propylene storage. Pressure vessels are also used for the storage of propylene.

Propylene is a flammable gas under normal ambient conditions and is not hazardous at low concentrations, but is an asphyxiant, which is a concern in closed environments. Direct contact with liquid propylene can cause skin burns from freezing. Fire or explosion is the greatest potential hazard associated with the storage and handling of propylene. Care must be exercised to avoid creating an explosive atmosphere when disconnecting lines and unloading vessels containing propylene. Explosions of vapor clouds formed from large leaks of liquid or gaseous propylene are the greatest potential hazard. The fire and explosion hazards associated with propylene are similar to those of propane and liquified petroleum gas (LPG).

Molecular Structure

The unique feature of propylene polymerization, versus ethylene polymerization, is the symmetry of the monomer insertion into the growing polymer chain. It is the presence of the methyl group in the propylene monomer that is responsible for this difference. This gives the monomer insertion an orientation (the monomer has a "head" and a "tail") and a stereochemical configuration with respect to the other units in the chain backbone. Regularity with respect to monomer orientation is termed the *regiospecificity* of the polymerization. Regularity of the methyl group placement relative to the other methyl groups along the chain backbone is termed the *stereospecificity* of the polymerization. The three limiting classifications of stereospecificity in polypropylene (PP) are illustrated in Figure 1. In isotactic polypropylene (iPP), all of the methyl groups have the same configuration with respect to the polymer backbone. In syndiotactic polypropylene (sPP), the methyl groups have an alternating configuration. Atactic polypropylene (aPP) has a random configuration. An additional configuration, hemi-isotactic polypropylene, is discussed elsewhere (4). iPP is overwhelmingly the most commercially significant form of PP. In practice, the degree of stereoregularity (and tacticity microstructure) can vary considerably within these general classifications. For the specific case of isotactic polymerization, Figure 2 shows three idealized limiting sample microstructures. Figure 2**a** shows a case where an isolated stereo error is immediately corrected along the growing chain. Figure 2**b** shows a case where a stereo error is propagated along the growing chain, and Figure 2**c** shows an iPP/aPP multiblock structure (5–7). Figure 2**a** is most common. Further discussions of stereo defects are available in the literature (4–22). In general terms, stereoregularity (or stereospecificity) refers to the content of defects that disrupt the regular placement of methyl groups. The intrachain defect content can also vary widely between chains (interchain distribution) (23) for different catalyst systems. The

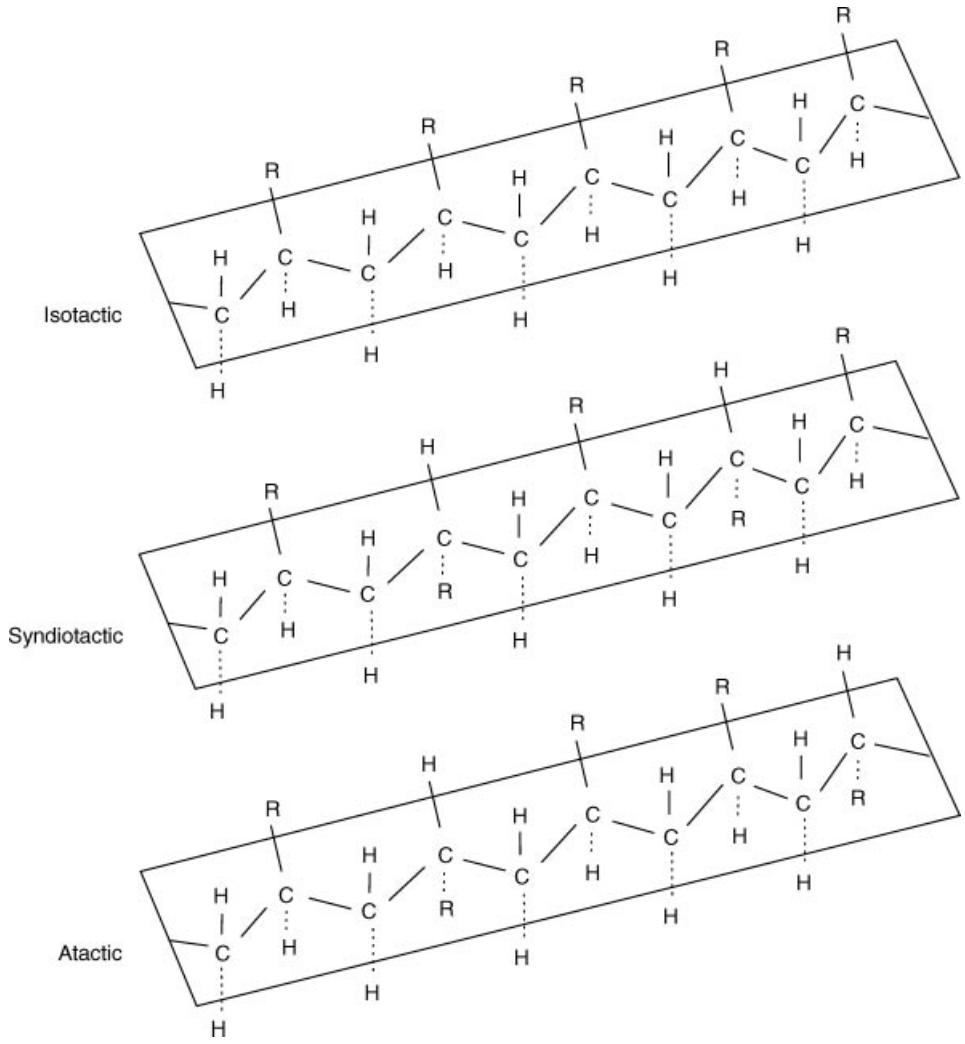

Fig. 1. Polypropylene stereochemical configurations: (**a**) isotactic; (**b**) syndiotactic; (**c**) atactic.

control of stereoregularity by catalyst and polymerization process is a critical determinant of PP properties.

Kinetic arguments suggest that iPP polymerization shows a strong preference for primary "head-to-tail" insertion of monomer into the growing chain (24–26). Regioirregular insertion of monomer renders the active site kinetically dormant (24–30), and its incorporation in the growing polymer chain occurs infrequently. With Ziegler–Natta polymerization catalysts, regio misinsertion errors are generally not present in the isotactic fraction (30). Metallocene polymerization catalysts can show appreciable levels of regio misinsertion errors in chains of high stereospecificity (4,27,31–41) (see METALLOCENES; SINGLE-SITE CATALYSTS).

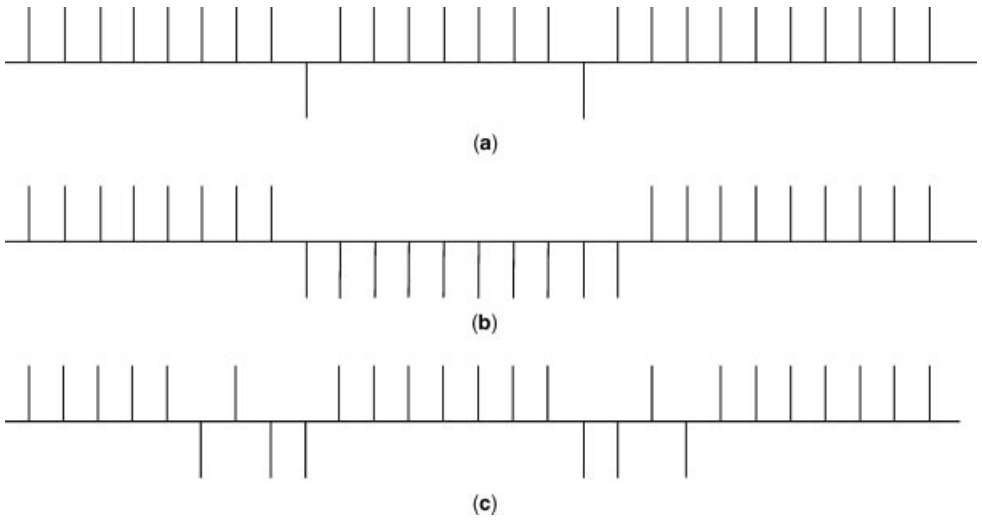

Fig. 2. Sample tacticity microstructures in isotactic polymerization: (**a**) isolated stereo error is corrected in growing chain; (**b**) stereo error is propagated in growing chain; (**c**) an iPP/aPP multi-block structure.

The stereo- and regioregularity of PP is best characterized by solution ^{13}C NMR spectra (42). These spectra can also provide information on the polymerization mechanism (4,7,9,11,12,14–22,30), and have been modeled in terms of the interchain tacticity distribution (14,43–45). Infrared spectroscopy (IR) has also been used to characterize the stereospecificity of iPP. Commonly the ratio of the 998 and 973 cm^{-1} band absorbance is used (46,47). The result is sensitive to thermal history (46). Solvent fractionation techniques are commonly used in industrial practice. These methods are based on the fact that chains with varying stereospecificity have different crystallinity and solubility in hydrocarbon solvents. In nominally isotactic PP, the atactic fractions of the interchain tacticity distribution are soluble, whereas the isotactic fractions are not. The isotactic index suggested by Natta represents the percentage of polymer insoluble in boiling *n*-heptane (48). Other procedures require preliminary total dissolution of the polymer in high boiling hydrocarbons such as xylene, and subsequent cooling in order to separate the precipitated crystalline portion (an example is ASTM D5492-94). The insoluble fraction is a measure of the stereospecificity. Often the term *stereoblock* is used to refer to fractions of the interchain distribution of intermediate solubility. Related solvent fractionation techniques include preparative and analytical temperature rising elution fractionation (TREF) (49). The use of pulsed proton solid-state NMR has been demonstrated as an alternative to solubility measurements of stereoregularity (50). Other secondary measurements which probe melting and/or crystallinity behavior can also be applied.

In addition to tacticity, important additional parameters of the PP chain which influence properties include the molecular weight, polydispersity, and composition and comonomer distribution in blends and copolymers. PP, like all synthetic and most natural polymers, consists of a distribution of macromolecules of different lengths. Therefore, the polymers exhibit a molecular weight

distribution. The number-average molecular weight (M_n) is determined by gel-permeation chromatography (GPC), more generally referred to as size-exclusion chromatography (51). Because of the strength of the GPC technique, the older techniques of osmometry (52,53), cryoscopy (54), and ebulliometry (54) are less commonly used today. For PP, the GPC method typically utilizes high temperatures (135–145°C) in solvents such as *o*-dichlorobenzene and trichlorobenzene. The weight-average molecular weight (M_w) can be obtained by light scattering (55) and GPC. Higher moments of the molecular weight distribution can also be obtained by GPC. The viscosity-average molecular weight M_v can be obtained by measurement of the solution intrinsic viscosity $[\eta]_0$ (52). M_v and $[\eta]_0$ are related by the Mark–Houwink equation:

$$[\eta]_0 = K \cdot (\mathrm{M}_v)^a$$

Generally, values of M_v lie between M_n and M_w values. Values of the constant K and exponent a are determined by calibration with homogeneous fractions of known molecular weight for specific solvent/temperature conditions. In practice, for polypropylene, homogeneous fractions are not available and values for some moment of the molecular weight distribution (M_n or M_w) are used in equation 1 on an empirical basis to determine K and a. This allows for the correlation of viscosity to molecular weight, though corrections need to be applied for samples with polydispersity much different from the correlation standards (56). Representative values using M_w from relatively narrow polydispersity fractions in decalin at 135°C are $K = 2.38 \times 10^{-4}$, $a = 0.725$ (57) and $K = 1.0$–1.10×10^{-4}, $a = 0.80$ (58,59), and in tetralin at 135°C are $\mathrm{K} = 9.42 \times 10^{-5}$, $a = 0.784$ (60). A common industrial measure of molecular weight is the melt-flow rate (MFR) (ASTM D1238), which is related to the melt viscosity. The MFR technique measures the amount of molten polymer extruded by a standardized apparatus in 10 min. Higher MFR values are obtained for lower molecular weight polymer. The breadth of the molecular weight distribution (polydispersity) has a large effect on polymer properties. The polydispersity is commonly characterized by the ratio M_w/M_n as measured by GPC or by semiempirical correlation of the dynamic melt oscillitory shear behavior of the polymer (61). This ratio has a value of 1 for macromolecules of equal molecular weight (monodisperse) and increases with increasing polydispersity. Rheological measurements, including the steady-state compliance, can be very sensitive to higher moment components (62) important in flow processes.

The molecular structure of PP can be further modified by the introduction of comonomers during the polymerization process, most commonly ethylene or butene. This comonomer incorporation greatly expands the property range of PP. Table 3 illustrates the broad range of copolymer microstructures possible for the specific case of propylene–ethylene copolymerization. Similar to the case of stereoregular defects in PP homopolymer, comonomer defects introduced into "random" PP copolymers (PP-RACO) can show an interchain composition distribution depending on the catalyst and process. In some cases it can be advantageous, in terms of quality and the process conditions, to achieve a homogeneous distribution of the comonomer molecules. Metallocene catalysts show a greater tendency for homogeneous comonomer incorporation (4). In this case, each chain, regardless of length, contains the same percentage of comonomer. Impact-modified

Table 3. Propylene–Ethylene Copolymerization Microstructure

Microstructure[a]	Products
PPPPPPPPPPPPPPP (PP)	Homopolymer polypropylene
PPPEPPPPPPPPEPPP (PP-RACO)	Polypropylene randomly modified with ethylene
PPPPPPPP + EPEPEP (PP-EPR)	Impact-resistant polypropylene
PPPPP + EPEP + EEEE (PP-EPR + PE)	Impact-resistant polypropylene (with polyethylene
EPEPPEEPEPEPEPE (EPR)	Ethylene–propylene rubber (elastomer)
EEEPEEEEEEEEPEEE (PE-RACO)	Polyethylene randomly modified with propylene
EEEEEEEEEEEEEEE (PE)	Homopolymer polyethyle

[a] P= propylene, E= ethylene.

"copolymers" (PP-EPR) are better described as polymer blends or alloys. The composition of the PP-EPR formulations varies over a wide range in industrial practice. However, a typical formulation would contain 60–90% homopolymer (or PP-RACO) and 10–40% ethylene–propylene copolymer rubber (EPR) with ethylene concentration of 30–60%. The EPR component has a lower glass-transition temperature (T_g), lower crystallinity, and typically exists as a separate phase. PP-EPR formulations were first produced by mechanical blending of two components. Today they are commonly synthesized directly in a multistage process to obtain better economics, and often better distribution of the elastomeric phase in the polypropylene matrix and thus better quality. In some cases polyethylene is present as a third phase. The characterization of PP copolymers is often complicated by the multiplicity of structural species present. An in-depth characterization requires knowledge of the distributions of molecular weight and composition. Different solvent fractionation techniques are combined, and each fraction is analyzed. Composition is most frequently determined by solution ^{13}C NMR, by IR, or inferred from secondary measurements which probe melting behavior, crystallinity, or glass-transition temperature.

Morphology

Crystallography and Polymorphism. The stereochemistry of PP plays a critical role governing the packing of chains in the crystalline regions of the morphology (qv). Figure 3 shows the wide-angle X-ray scattering (WAXS) patterns of iPP, sPP, and aPP (23). The regular molecular structure of iPP and sPP readily enables crystallization of the chains, leading to well-defined crystalline reflections differing in unit cell symmetry. aPP lacks a regular molecular structure, and does not crystallize. This leads to a very broad and diffuse scattering from X-rays. The iPP chain adopts a helical conformation in the crystalline unit cell, as shown in Figure 4 (63). The helix repeats itself after three monomeric units, with an identity period of 0.65 nm. Four helical arrangements are possible by right- or left-handed rotation about the central axis with unique (non-identical) "up" and "down" inclinations independent of the handedness (23,64,65). The dominant

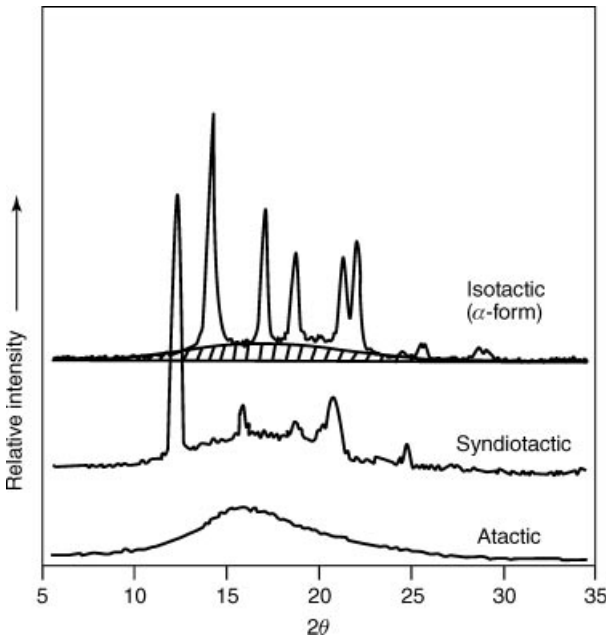

Fig. 3. Wide-angle X-ray scattering (WAXS) patterns of iPP, sPP, and aPP. The shaded region illustrates the separation of crystalline and amorphous scattering contributions. Adapted from Ref. 23.

crystallographic form for iPP is the α-form. The elementary unit cell of α-form iPP is monoclinic, containing 4 chains and 12 monomeric units with specific packing of helical arrangements. Crystallographic densities are generally in the range of 0.936–0.946 gm/cm^3. Representative cell constants are given in Table 4, and have been reviewed elsewhere (23). The helical conformation of sPP differs from that of iPP, and has an identity period of 0.74 nm. The elementary unit cell of the most stable crystallographic form of sPP is orthorhombic, containing 4 chains and 16 monomeric units with specific packing of helical arrangements (23,64,66–69). The crystallographic density is 0.930 gm/cm^3. Representative cell constants are given in Table 4 (69).

Table 4. Unit Cell Constants of Polypropylene

Cell constants	Isotactic[a]	Syndiotactic[b]
Unit cell	monoclinic	orthorhombic
a, nm	0.664	1.45
b, nm	2.084	1.12
c, nm	0.651	0.74
β	99.0°	90°

[a]Averages from literature compilation of $P2_1/c$ space group symmetry refinements (23).
[b]From Ref. 69.

Both iPP and sPP exhibit polymorphism, which is the tendency to crystallize into different crystallographic forms depending on crystallization conditions. In iPP, the dominant form is the α-form. Other forms include the β-, γ-, and mesomorphic (smectic) forms. All of these crystalline forms maintain the same helical conformation with 0.65 nm repeat distance, but differ in unit cell symmetry, interchain packing, and structural disorder. The mesomorphic form is formed by rapid quenching conditions, and has important property implications, particularly in film and fiber applications. Crystallographically, the mesomorphic form has disordered interchain packing relative to the other polymorphic unit cell symmetries (65,70,71). The mesomorphic form converts rapidly to the α-form on heating (23). Formation of the β-form results from the addition of specific nucleators and additives, specific crystallization conditions, crystallization under controlled temperature gradients, and in some cases crystallization under shear (20). The β-form has lower unit cell density, higher rate of crystallization, and lower apparent melting point relative to the α-form which

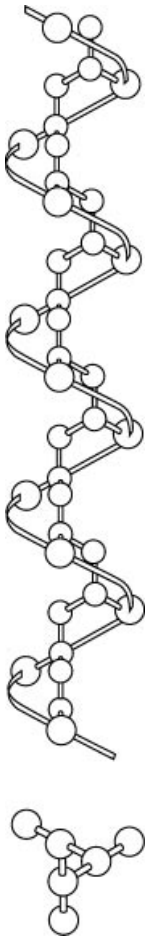

Fig. 4. Chain conformation of isotactic polypropylene (iPP).

is due, in-part, to its unique crystallography (64,72,73). The γ-form is rarely observed in pure form in commercially significant homopolymer from Ziegler–Natta catalysts under typical processing conditions. A variety of conditions for γ-form formation are outlined below (23). The γ-form occurs in low molecular weight fractions, homopolymer from some homogeneous (metallocene) catalysts (74–76), random copolymers, random copolymer and metallocene homopolymer at high crystallization temperature (76), samples with high stereoblock content, and homopolymer crystallized at high pressure (77). Crystal structure refinements suggest that γ-form iPP has nonparallel chains (64,65,78–81), a conclusion not previously cited in polymeric crystal structure. Because of its importance, further discussion of iPP morphology is restricted to the α-form of iPP.

sPP also exhibits polymorphism (23,64,66–69,82,83). Polymorphism is related to both the intrachain conformation and interchain packing. Crystallization at lower temperature can lead to defect structures relative to the unit cell symmetry of the dominant form (66–68,84–86). Other unit cell variations are formed from sPP with low syndiospecificity (87,88), as-polymerized sPP (89–92), sPP copolymers (92), oriented sPP (23,87,93), sPP crystallized at low temperature (94,95), and nonhelical structures associated with cold drawing (87,96) and exposure of cold drawn samples to solvent vapor (97).

Crystallinity. The degree of crystallininity varies between 0 for a completely amorphous material (such as aPP) and 1 for a completely crystalline material. As with most semicrystalline polymers (qv), the degree of crystallinity plays a critical role in determining properties of PP. Commonly measured properties such as modulus, yield stress, oxygen and moisture barrier resistance, and hardness, to name a few, all increase with increasing crystallinity. In iPP (and sPP) tacticity is a critical factor influencing the crystallinity (23,47,98). This is due to the role of stereo defects in disrupting the length of the crystallizable isotactic sequences. Details of the interchain tacticity distribution affect not only the crystallinity at room temperature, but also the partial melting behavior (and hence crystallinity) at elevated temperature, influencing hot drawing characteristics. Solvent fractionation techniques, which separate the interchain tacticity distribution of the whole iPP homopolymer into fractions of varying tacticity, show that the lower tacticity fractions have lower crystallinity (47). With metallocene catalysts (4,18,30), PP chain microstructure can now be varied continuously with decreasing isospecific sequencing from iPP (stiff thermoplastic) to aPP (very low modulus lacking dimensional integrity) to sPP (stiff thermoplastic) correlating to changes of either isotactic or syndiotactic crystallinity. The crystallinity of sPP is less than that of iPP with currently available catalysts. In addition to tacticity, crystallinity generally increases with decreasing molecular weight (increased chain mobility), and is promoted by slower cooling rates from the melt. It should be emphasized that the crystalline fraction of perfectly isotactic PP is still much less than unity because of the long-chain nature. Copolymerization (PP-RACO in Table 3) is also used to modify the polymer crystallinity in a controlled manner. In this case, the comonomer is the source of irregularity in the polypropylene chain. The introduction of comonomer decreases crystallinity, reduces stiffness and melting temperature, and increases impact resistance (99).

The degree of crystallinity is determined by a number of analytical techniques based on different criteria (see CRYSTALLINITY DETERMINATION). The most widely used are fractional solubilization (previously discussed), density determination, X-ray diffraction, and thermal analysis. The density of iPP in the α-form varies between the limit of 100% amorphous (ρ_a=0.850 to 0.855 g/cm^3) and 100% crystalline (ρ_c=0.936 to 0.946 g/cm^3) (20). In this way, the measured mass density ρ gives a measure of the crystallinity. Values of ρ are most often measured by the density gradient technique (ASTM D1505-85). Similarly, dilatometric methods are used to measure variations of density as a function of temperature (100). X-ray diffraction (101) is also widely used to determine PP crystallinity. Figure 3 shows the contributions of the crystalline scattering and amorphous scattering in the unoriented pattern of the α-form of iPP. The shaded region represents the area attributable to the noncrystalline fraction. From the relationship of the peak area to the total area, crystallinity can be evaluated by a number of numerical means (101). Orientation complicates the analysis (101). Differential scanning calorimetry (DSC) provides useful information on PP structure by the determination of related parameters, such as transition temperature, heat of fusion, crystallization temperature, and others. The crystalline fraction is given by the ratio of the measured heat of fusion to the value for 100% crystalline material (see THERMODYNAMIC PROPERTIES OF POLYMERS). The shape of the melting curve gives information on the melting distribution.

Lamellar and Spherulitic Morphology. The crystal habit of iPP quiescently crystallized from the melt, like other semicrystalline homopolymers, is that of folded chain lamellae (Fig. 5). The lamellar thickness ($\langle l_c \rangle$) increases with increasing crystallization temperature, and is generally in the range of 5–20 nm for iPP. iPP in the α-form exhibits a tendency, unique among semicrystalline polymers, to form a "cross-hatched" pattern (23,64). Radial lathlike lamellae coexist with "cross-hatched" tangential lamellae oriented nearly orthogonal to the radial direction. This homoepitaxy (102–107) is related to the relatively modest mismatch between the c- and a-axis unit cell parameters (Table 4), and the detailed molecular aspects have been reviewed (64). Spherulites are larger scale aggregates made up of the smaller scale lamellar building blocks. Depending on the

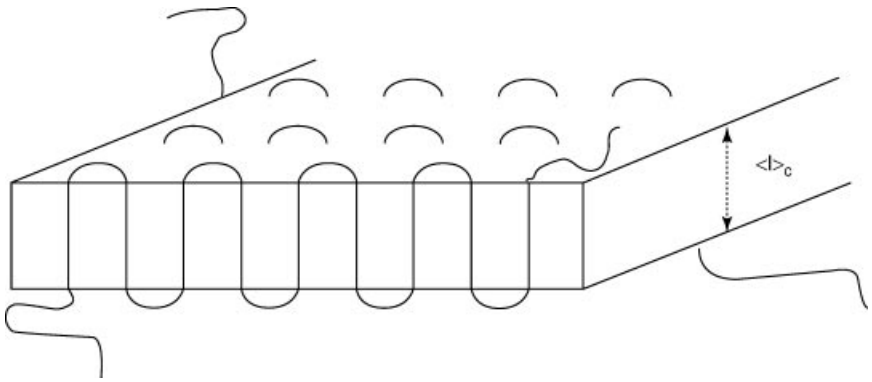

Fig. 5. Schematic of chain-folded lamellar structure in semicrystalline polymers.

crystallization conditions, the dimensions of spherulites can vary from a few micrometers to 100 μm, or larger. In the α-form of iPP, there is a strong link between lamellar and spherulitic morphologies. The α-form iPP spherulites have been classified according to different optical characteristics in cross-polarized light (106,108,109). The optical characteristic is highly sensitive to crystallization temperature and resin type, and has been linked to the lamellar morphology through the balance of cross-hatched radial and tangential lamellae (23,103,104,106,109,110). Optical and mechanical properties depend on the dimension and number of spherulites, which can be modified with nucleating agents that act as crystallization centers. Optical properties (such as clarity) improve with decreasing spherulite size. The borders among spherulites can represent weak zones (111), with large spherulites adversely affecting properties such as impact. Unlike iPP, pronounced cross-hatched lamellar morphologies in bulk crystallized material appears limited in sPP (112,113). As with iPP, well-developed small-angle X-ray (SAXS) long spacings, characteristic of well-developed lamellar morphologies, are observed for sPP of high syndiospecificity (113–116). In general terms, spherulite formation in as-polymerized metallocene based sPP tends to be more restricted than in iPP (117–119), and the spherulite-scale morphologies are generally smaller than in iPP in bulk-crystallized specimens. Spherulitic growth rate measurements have been summarized (120), with rates lower than those of Ziegler–Natta iPP (113). Unique morphologies (relative to iPP) are observed in sPP with special preparation procedures, including a transition from single-crystal like entities to spherulitic structures on cooling (68,117–119).

Macromorphology and Processing Relationships. Other morphologies in iPP include the macroscopic phase morphologies in multiphase structures such as rubber-modified iPP (an example being PP-EPR in Table 3), and additional morphologies associated with the specific method of polymer processing. Unique morphologies and structure/processing relationships are associated with fiber, film, and injection molding processes to name a few. In parts formed by the injection molding process, pronounced morphological gradients exist in a processed part which can be crudely partitioned into highly oriented skin layers (near the mold surface) and less oriented core layers (near the part center). These layers can approach macroscopic dimensions ($\sim$mm) depending on the part geometry, resin, and molding conditions. The properties of moldings can often be correlated to the orientation and crystallinity of the part (23,121). A literature review of more detailed aspects of the morphology of iPP injection moldings is available (23). In mixtures of iPP homopolymer and EPR (PP-EPR in Table 3), the two components are generally immiscible in the melt. In the solid state, the rubber has low glass-transition temperature (T_g) and imparts impact resistance to the blend. The effectiveness of the rubber phase as an impact modifier depends critically on the dispersion (particle size). The dispersion is a complex function of (*1*) matrix and rubber phase composition, (*2*) viscosity ratio of matrix and dispersed phases, (*3*) compounding history, and (*4*) melt deformation history during fabrication of the final processed part (23). In impact-modified copolymers for injection molding applications, the dimension of the dispersed rubber phase in the core (reduced melt deformation) is typically on the order of 0.5–2 μm in formulations with optimal impact performance. Near the surface of moldings (high melt deformation), highly anisotropic dispersed phase morphologies can be observed

depending on blend composition. Generally rubber phase dispersion worsens (increased phase size) with increasing melt temperature and melt time prior to molding due to coalescence.

High speed melt spinning of fibers represents another of the most common processing methods for iPP. The final morphology results from the complex interrelationships of polymer structure (polydispersity, molecular weight, tacticity) and processing conditions (melt temperature, melt throughput, spinnerette design, spin speed, cooling rate). For high spinning speeds, the orientation of melt-spun fibers greatly exceeds that of injection-molded parts. The orientation of crystalline regions is greater than the non crystalline regions (122). As the spinning speed increases, orientation increases. The orientation can be further increased with post-spinning drawing operations (122). As with unoriented material, the as-spun fiber shows alternating crystalline and amorphous regions on lamellar size scales (10–30 nm), but generally smaller than hot-drawn articles. This periodicity is highly oriented along the fiber axis, and characterized by a high fraction of tie molecules (the same chain passing through several crystalline regions).

Drawn film, and more specifically biaxially oriented polypropylene (BOPP) film, is another of the most common fabrication methods (see FILMS, MANUFACTURE; FILMS, ORIENTATION). During BOPP film formation, a cast sheet of iPP is drawn below the melting point in two directions. This drawing process creates a film of useful dimension while imparting desired properties such as barrier and stiffness. These properties are related to the imposed orientation during drawing. During unidirectional drawing of semicrystalline polymers at elevated temperature, the initial spherulitic morphology of the cast sheet is transformed to an oriented fibrillar morphology (122–125). The yielding process, during which the lamellar crystallites are disrupted, is strongly correlated to the crystallinity at the draw temperature. As with melt-spun fibers, the orientation of the crystalline regions is greater than that of the noncrystalline regions (122). Orientation is generally much higher than in injection moldings. For BOPP, the molecular orientation is dominated by the transverse orientation stage for sequentially oriented film (126), and tends to be planar (126,127) for both sequential and simultaneous oriented film. Generally, the lamellar crystals in the initial as-cast sheet are highly disrupted in the final BOPP film.

Polymerization Particle Morphology. Morphological control of as-polymerized polymer particles influences the polymerization process. Aspects of the particle morphology include the shape, size, size distribution, and porosity. Control of particle morphology is also a critical concern to technologies which utilize the as-polymerized particle in subsequent polymerization processes (128). Because of the replication phenomenon (129–137), the morphological characteristics are strictly dependent on the catalyst. The catalyst reproduces its shape in the polymer on an obviously greater scale according to its activity. The activity is the quantity of polymer produced by a unit of catalyst.

The replication phenomenon of iPP polymerization from magnesium chloride supported Ziegler–Natta catalysts is illustrated in Figure 6. The polymer particle has the same shape as the catalyst particle, although its diameter is approximately 20–100 times larger. The growth of the polymer particle during polymerization has been extensively modeled (129–137). In the multigrain model (131–135,137), the

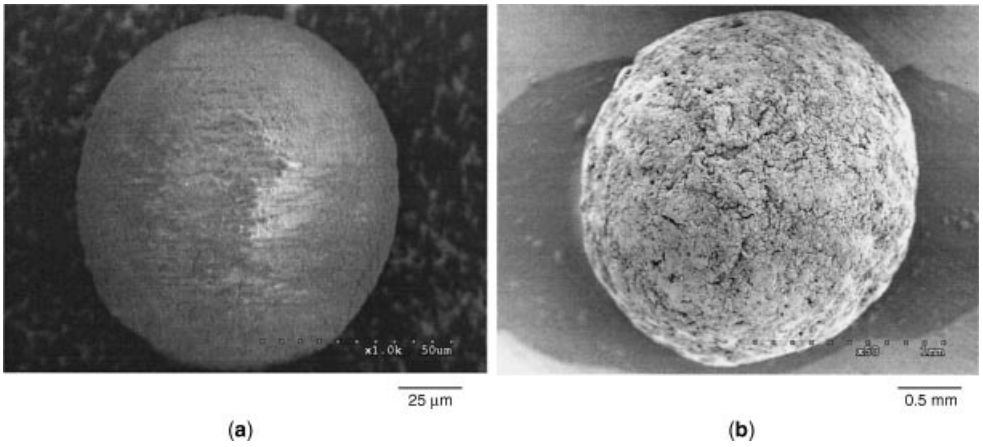

Fig. 6. Ziegler–Natta catalyst particle (**a**) and corresponding polymer particle (**b**).

catalyst undergoes fragmentation into microparticles evenly distributed within the macroscopic particle due to forces exerted by the growing polymer layers. In Ziegler–Natta catalysts, fragmentation occurs at very low polymer yields (137–139), which provides a large active surface from the beginning of polymerization. The growth of the macroparticle results from the cumulative uniform expansion of microparticle layers. Although the actual morphology of Ziegler–Natta polymerized particles shows a more complicated hierarchy than the "two-level" approach of the multigrain model, a key feature is the replication of the porous spherical catalyst morphology into a porous spherical polymer particle during polymerization. In practice, a careful morphological analysis of the polymerization particle requires, beyond microscopic investigations, analyses of particle size distribution (ASTM D1921-96), poured bulk density (ASTM D1895-96, Method A), and pourability (ASTM D1895-96, Method A).

Thermodynamic Properties

Melting. The melting point of α-form iPP is strongly influenced by the stereoregularity (19,23,47,99,140–144) and regioregularity (4,33,34,145,146). Melting point increases with improved regularity. T_m^0 is the theoretical equilibrium melting point of a perfect and infinitely large crystal. This value exceeds experimentally observed melting points because of kinetic effects leading to small crystal size (23) (Fig. 5). The value of T_m^0 is sensitive to stereoregularity. However, the value for 100% isotactic material is not expected to differ significantly from that of highly isotactic commercial materials (23). For highly regular materials, literature summaries of T_m^0 suggest that values of 185–188°C seem reasonable (23), though there remains disagreement in the literature (147). Melting points in the 160–168°C range are typical for commercial homopolymer samples under normal analysis conditions. Introduction of comonomer (ethylene, butene, and higher α-olefins) reduces the melting point, and can vanish at intermediate compositions

as the material approaches an amorphous rubber (Table 3). Literature summaries of the heat of fusion of 100% crystalline material, ΔH^0, generally lie in the range of 148–209 J/g (23). The most often applied values are clustered around 165 J/g (77,140,148,149) and 209 J/g (150,151).

As with iPP, the melting point of sPP is highly sensitive to stereoregularity. While comparison of T_m^0 for 100% syndiotactic sPP is ambigous, with current catalysts and in current commercial sPP materials, the observed melting point is generally less than that of Ziegler–Natta iPP under practical crystallization conditions when compared at comparable stereospecificity (23). This difference is often of the order of 10–15°C. Introduction of comonomer also reduces the melting point of sPP. Syndiospecific copolymerization with butene has the unique feature of being crystalline at all compositions because of the similarity of crystal structures of sPP and syndiotactic polybutene (152). Literature summaries of ΔH^0 lie in the range of 105–190 J/gm (23). Values in the lower end of this range agree with extrapolated heats of fusion versus density (23) and X-ray crystallinity (116).

Glass-Transition Temperature. The value of the glass transition (qv) temperature (T_g) is dependent on the crystallinity of the polymer, the molecular weight, and the measurement techniques used. DSC measurements of T_g for high molecular weight aPP and sPP are generally similar and usually close to 0°C. The DSC glass-transition temperature in highly stereospecific iPP is often difficult to distinguish because of the high crystallinity. Transition temperatures are generally in the range of −13 to 0°C. Other techniques, such as dynamic mechanical analysis, are often more sensitive to the T_g of iPP. Copolymerization with ethylene reduces the glass-transition temperature. Figure 7 shows DSC measured T_g values of propylene/ethylene copolymers prepared with an aspecific catalyst. In this case, all samples are noncrystalline and not affected by crystallinity. A similar trend is generally observed for isospecific and syndiospecific catalysts as well. Copolymerization with butene is less effective at lowering the T_g.

Heat Capacity and Thermal Expansion. Extensive tabulations of the extrapolated heat capacities of crystalline and amorphous iPP as a function of temperature are available (147). The specific volume (153) and heat capacity (154) of iPP in the melt as a function of temperature and pressure, and typical thermal expansion coefficients in the solid state as a function of temperature (151) are also reported.

Chemical Properties

iPP is soluble in high boiling aliphatic and aromatic hydrocarbons at high temperature. sPP shows solubility at lower temperature and in lower boiling hydrocarbons. aPP shows the highest solubility of the three forms. Extensive chemical resistance data is available for iPP (155). The high chemical resistance of iPP results in exceptional stain resistance, and has led to the use of iPP in automobile batteries (156). iPP has outstanding resistance to water and other inorganic environments (155). iPP resists most strong mineral acids and bases, but like other polyolefins is subject to attack by oxidizing agents including 98% sulfuric acid and 30% hydrochloric acid at high temperature (∼100°C), and fuming nitric acid (ambient temperature) (155). Inorganic chemicals produce little or no effect over

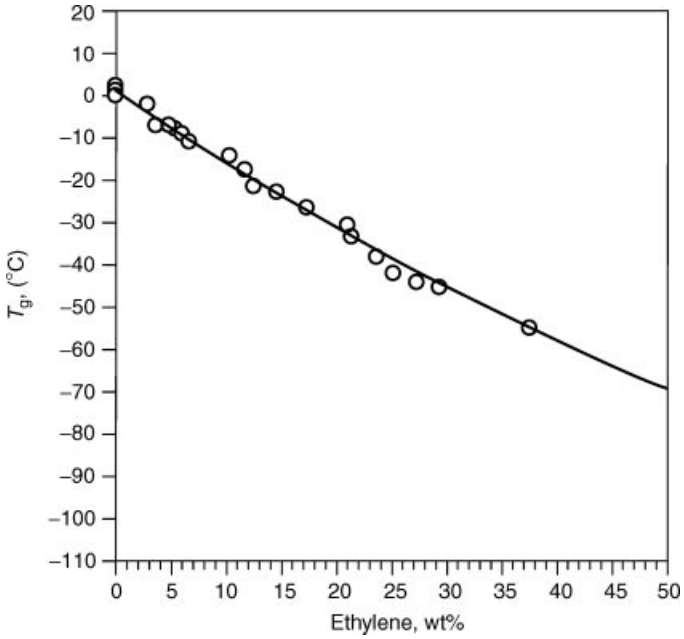

Fig. 7. Glass-transition temperature (T_g) versus ethylene concentration in propylene–ethylene random copolymer using aspecific catalyst (no crystallinity). Values were determined by differential scanning calorimetry (DSC).

a period of 6 months at temperatures up to 120°C (155). For organic media, absorption is greater for higher temperatures and decreased polarity, and is higher in copolymers than in homopolymer.

PP reacts with oxygen in several ways, causing chain scission and brittleness that is associated with the loss in molecular weight. This action is promoted by high temperatures, light, or mechanical stress. A wide variety of stabilization packages are added for protection, depending on the application (157).

The reactivity of iPP can also be usefully exploited. For example, treatment with peroxides has led to controlled rheology resins (61,158,159) with reduced molecular weight and narrow polydispersity relative to as-polymerized product from Ziegler–Natta catalysts. For a fixed final melt-flow rate (MFR), lower precursor MFR gives narrower polydispersity. These resins are used in some fiber-spinning and injection-molding applications. The creation of radical sites along the polymer backbone, most often through peroxide-based initiation, is also an essential condition for many functionalization/grafting chemistries. The functionalization chemistry of post-polymerized iPP has been extensively reviewed (160). The focus has been on the incorporation of polar functional groups into the polymer chain and/or the graft polymerization of monomers which are generally incompatible with Ziegler–Natta catalysts. The incorporation of polar functionality has been sought to improve paintability, printability, and metal adhesion characteristics (important to coatings); to act as coupling agents in composites such as glass-reinforced iPP; to improve oxygen barrier resistance; and to act as compatibilizers in polymer alloys. Recent advancements in metallocene and

related transition metal catalysts are showing promise for the direct copolymerization of polar monomers with ethylene and propylene (161). Other chemical modifications include plasma and acid treatment technologies.

Radiation chemistry of PP has been extensively reviewed (162). Under suitable conditions, radiation treatment can lead to desirable branching reactions (163) with rheological characteristics favorable for thermoforming, foaming, blow molding, and extrusion coating. Resistance to radiation sterilization is an important requirement in some medical applications, and requires specialized formulation and stabilization packages.

Physical Properties

A vast number of PP grades are sold in the United States, including homopolymers with varying molecular weight (melt-flow rate) and tacticity, filled grades, grades with varying stabilization packages, and grades which incorporate comonomers with varying architecture (Table 3). The basic categories of iPP polymers are homopolymers, random copolymers, impact or heterophasic copolymers, and filled polymers. A number of grades are approved for food contact (164). Many polymers carry a UL94 flammability class HB rating (164), and some specialized formulations have improved ratings. Additional specialty grades include nucleated polymers for improved clarity and mechanical properties, radiation-resistant formulations, chemically visbroken "controlled rheology" grades (61,158,159), high melt strength grades, and a large number of formulations with specialized additive functions including slip agents, antiblocking agents, antistats, and pigments to name a few (157). Standardized test methods such as ASTM or ISO are used in commercial specifications. The properties that distinguish iPP from high density polyethylene are high heat distortion temperature, stiffness, hardness, and lower density.

Properties of various homopolymer grades are given in Table 5. In this table, polymer molecular weight and polydispersity is tailored to give the best processing characteristics for each fabrication process. The polymers shown in Table 5 are produced by direct polymerization. Higher melt flow grades, and "controlled rheology" grades with narrow polydispersity, can be important in other applications, including fibers. Narrow polydispersity resins can also be produced by metallocene catalysts (4). These catalysts can also produce iPP with a narrow interchain tacticity distribution and low levels of extractables. High crystallinity (tacticity) grades, and high polydispersity grades, provide additional stiffness and higher heat distortion temperature in injection molding applications (23,120,166,167). Properties of selected random copolymer grades are given in Table 6. These copolymers have ethylene as the comonomer, although butene copolymerization is also possible. The stiffness of these polymers is lower than that of homopolymers. The impact resistance is improved, particularly at refrigeration temperatures. Clarity is also enhanced. The low melting point allows the use of some copolymer grades as sealant layers in PP films. Properties of impact-resistant, or heterophasic, copolymers are given in Table 7. Much of this class of material is used in injection-molding applications,

Table 5. Properties of Polypropylene Homopolymers[a]

Melt flow, (g/10 min) (ASTM D1238)	Tensile strength,[b] Mpa[c] (ASTM D638)	Elongation,[b] % (ASTM D638)	Flexural modulus 1% secant, Mpa[c] (ASTM D790A)	Deflection tempeature at 455 kPa,[d] °C (ASTM D648)	Notched Izod Impact at 23°C, J/m[e] (ASTM D256A)	Rockwell hardness, *R* (ASTM D785A)	Products/Applications
0.5	33	13	1200	96	81	86	Extrusion, sheet, profiles
4	34	12	1400	93	39	86	Injection molding, general-purpose
12	34	10	1400	92	35	88	Injection molding, general-purpose
22	36	10	1500	93	34	93	Injection molding, general-purpose, thin wall
35	32	12	1200	95	32	89	Controlled rheology injection molding, thin-wall

[a] Ref. 165.
[b] At yield.
[c] To convert Mpa to psi, multiply by 145.
[d] To convert kPa to psi, multiply by 0.145.
[e] To convert J/m to ft·lbf/in., divide by 53.38.

Table 6. Properties of Polypropylene Random Copolymers[a,b]

Melt flow, (g/10 min) (ASTM D1238)	Tensile strength,[c] Mpa[d] (ASTM D638)	Elongation,[c] % (ASTM D638)	Flexural modulus 1% secant, Mpa[d] (ASTM D790A)	Deflection tempeature at 455 kPa,[e] °C (ASTM D648)	Notched Izod Impact at 23°C, J/m[f] (ASTM D256A)	Products/Applications
2	28	13	940	79	330	High clarity blow molding, extrusion, thermoforming
6.5	28	13	920	76	56	High clarity cast film
11	30	13	1000	84	66	High clarity injection molding and injection-stretch blow molding
35	28	13	940	83	140	Controlled rheology high clarity injection molding

[a] Ref. 165
[b] Based on ethylene comonomer.
[c] At yield.
[d] To convert Mpa to psi, multiply by 145.
[e] To convert kPa to psi, multiply by 0.145.
[f] To convert J/m to ft·lbf/in, divide by 53.38.

Table 7. Properties of Polypropylene Impact Copolymers[a,b]

Melt flow, (g/10 min) (ASTM D1238)	Tensile strength,[c] Mpa[d] (ASTM D638)	Elongation,[c] % (ASTM D638)	Flexural modulus 1% secant, Mpa[d] (ASTM D790A)	Deflection tempeature at 455 kPa,[e] °C (ASTM D648)	Notched Izod Impact at 23°C, J/m[f] (ASTM D256A)	Products/Applications
0.45	27	11	1100	88	No break	Extrusion
2	27	9	1200	90	270	Injection molding medium impact
4	27	8	1200	90	110	Injection molding medium impact
35	27	6	1400	100	70	High flow injection molding and thin-wall medium impact
50	26	6	1200	107	42	High flow injection molding and thin-wall medium impact
4	21	8	1000	81	No break	Extrusion and injection molding high impact
8	26	8	1200	87	100	Blush-resistant injection molding medium impact
22	24	7	1000	83	100	Blush-resistant controlled rheology injection molding medium impact
12	22	8	900	82	340	Blush-resistant injection molding high impact

[a] Ref. 165
[b] Based on ethylene comonomer.
[c] At yield.
[d] To convert Mpa to psi, multiply by 145.
[e] To convert kPa to psi, multiply by 0.145.
[f] To convert J/m to ft·lbf/in, divide by 53.38.

providing impact resistance well below 0°C. Copolymers containing high flexible product. Mineral fillers, such as talc or calcium carbonate, and other reinforcements such as glass fiber or mica, increase the stiffness and heat-distortion temperature. Some properties of mineral-filled iPP are given in Table 8. Filled formulations based on impact copolymers (PP-EPR) are also common.

Catalysts for Polymerization

$TiCl_3$-Based Catalyst. Isotactic polypropylene was first synthesized by Natta in 1954 by employing a system consisting of $TiCl_4$ and $Al(C_2H_5)_3$ activator (169–174). It was based on Ziegler's catalyst system (175), which was used for the polymerization of ethylene. Only 30–40% of the polypropylene produced by Natta's catalyst had the typical characteristics of isotactic polypropylene; for example, it was insoluble in boiling heptane and had a melting point of about 165°C. The remaining product was atactic with poor structural uniformity and a rubbery consistency. Natta quickly realized that the polymer isotacticity was directly connected to the uniformity of the catalyst surface. Thus for the polymerization of propylene, he employed solid crystalline $TiCl_3$ (obtained by the reduction of $TiCl_4$) (176) with $Al(C_2H_5)_2Cl$ or $Al(C_2H_5)_3$ and obtained a higher percentage of isotactic product (see ZIEGLER-NATTA CATALYSTS).

The various $TiCl_3$ structural forms, α, β, γ, and δ, were identified in subsequent studies (177); the δ-form, in combination with $Al(C_2H_5)_2Cl$, gave the best results. The high polymer isotacticity (ca 90%) permitted a scaled-up industrial process by Montecatini, which had supported Natta's research at the Politechnic in Milan. This first plant (and subsequent others) contained a large section for the separation of the undesirable atactic fraction from the isotactic fraction and a section for the removal of catalyst residues that affected product quality. Substantial progress was achieved in a short time (178,179).

Hercules discovered the role of hydrogen as a molecular weight regulator (180). Esso improved performance by using $AlCl_3$ in $TiCl_3$ solid solution instead of pure $TiCl_3$ (181). Mitsubishi increased isotacticity to 92–94% by adding an electron donor, such as carboxylic acid ester, to the $TiCl_3$ (182).

The treatment of the $TiCl_3$ produced from the reaction between $TiCl_4$ and $Al(C_2H_5)_2Cl$, first with the electron donor, diisoamyl ether, and then with $TiCl_4$, gave a highly stereospecific catalyst. This catalyst system was four to five times more active than δ-$TiCl_3$ (183) and capable of producing a polymer with narrow particle size distribution. This system can be referred to as the second-generation catalyst (Table 9). However, the catalyst yield was still insufficient to reduce catalyst residues enough to eliminate the deashing step in the production process.

In the meantime it was established that only a small percentage of the titanium on the catalyst was actually active. The active titanium was located on the lateral faces and edges, and along the crystal defects (184). This led to the realization that much of the catalyst mass acted as the support (185). Decisive progress could be achieved by depositing the active Ti on a support whose residues, unlike those of $TiCl_3$ would not be detrimental to polymer properties.

$MgCl_2$-Supported Catalysts. Magnesium chloride, in the active form as a support (186,187), increases catalyst yield and allows for the simplification of the

Table 8. Properties of Filled Homopolymer[a]

Melt flow, (g/10 min) (ASTM D1238)	Tensile strength,[b] Mpa[c] (ASTM D638)	Elongation,[b] % (ASTM D638)	Flexural modulus 1% secant, Mpa[c] (ASTM D790A)	Deflection tempeature at 455 kPa,[d] °C (ASTM D648)	Notched Izod Impact at 23°C, J/m[e] (ASTM D256A)	Rockwell hardness, *R* (ASTM D785A)	Products/Applications
4	34	12	1400	93	39	86	Injection molding homopolymer, general-purpose
3	83	—	4500	157	85	—	20% glass filled homopolymer
4	31	4	1900[f]	109	37	84	20% talc filled homopolymer
4	29	4	2900[f]	125	27	94	40% talc filled homopolymer
4	30	7	1500[f]	96	37	89	20% calcium carbonate filled homopolymer

[a] Ref. 168.
[b] At yield.
[c] To convert Mpa to psi, multiply by 145.
[d] To convert kPa to psi, multiply by 0.145.
[e] To convert J/m to ft·lbf/in, divide by 53.38.
[f] Tangent method.

Table 9. Different Ziegler–Natta Catalyst Generations—Composition, Performance, Morphology and Process Requirements

Generation	Composition	Productivity, kg of PP/g of catalyst	Isotactic index	Morphology control	Process requirements
1	δ-$TiCl_3 \cdot 0.33AlCl_3$ + $AlEt_2Cl$	0.8–1.2	90–94	Not possible	Deashing and atactic removal
2	δ-$TiCl_3$ + $AlEt_2Cl$	3–5 (10–15)	94–97	Possible	Deashing
3	$TiCl_4$/ester/$MgCl_2$ + AlR_3/ester	5–10 (15–30)	90–95	Possible	Atactic removal
4	$TiCl_4$/diester/$MgCl_2$ + $AlEt_3$/silane	10–25 (30–60)	95–99	Possible	None
5	$TiCl_4$/diether/$MgCl_2$ + $AlEt_3$	25–35 (70–120)	95–99	Possible	None

[a] Polymerization productivity: hexane slurry, 70°C, 0.7 MPa, 4 h, with hydrogen for molecular weight control. Values in parentheses are polymerizations performed in liquid propylene at 70°C for 2 h with hydrogen.
[b] Only possible with alkyl aluminum reduced $TiCl_3$ to produce a catalyst within a 200–300 μm size.

polymerization process in hydrocarbon slurry with the elimination of the costly deashing step. This discovery and further improvements led to the development of the superactive, third-generation catalysts (188–193) (Table 9). Better yield, higher stereospecificity, and morphology control resulted in simplified processes in which the monomer is the polymerization medium.

Other catalyst systems that are usually soluble in the reaction medium are of high scientific importance but not used industrially. Among these is the system consisting of the product of the reaction of AlR_2Cl and $Al_2R_2Cl_4$ with vanadium compounds. This system is utilized in the production of syndiotactic polypropylene at very low temperature (194,195).

Isotactic polypropylene has been obtained, although with very low yields, from Ti and Zr benzyl compounds (196) and allylic derivatives (197).

Other highly active catalyst systems are based on single-site catalyst, for example (η-$^5C_5H_5)_2M(CH_3)_2$; (M = Ti, Zr). These systems will be discussed in more detail in the Homogeneous Catalyst section.

Heterogeneous Catalyst Preparation.

$TiCl_3$-Based Catalysts. First-generation catalysts are prepared by the reduction of $TiCl_4$ with metallic aluminum in aromatic solvent between 100 and 200°C (198,199). A solid solution with the composition of $AlCl_3 \cdot 3TiCl_3$ (200) is formed. Milling converts the crystalline $TiCl_3$ from the α- to the δ-form, increasing its surface area and radically improving its performance (201); $Al(C_2H_5)_2Cl$ is the best activator. Hydrogen and $Zn(C_2H_5)_2$ are the molecular weight regulators, but diethyl zinc is rarely used. Typical performance for this type of catalyst is reported in Table 9. Milling produces a catalyst, and thus a polymer, with broad particle size distribution.

A second-generation catalyst (183) is prepared by reducing $TiCl_4$ with $Al(C_2H_5)_2Cl$ in a hydrocarbon at 0°C. The $3TiCl_3 \cdot AlCl_3$ product with surface area

around 1 m^2/g thus obtained is washed at 35°C with diisoamyl ether to remove most of the $AlCl_3$. The product is then treated with $TiCl_4$ at 65°C and washed with hydrocarbons. The catalyst has a high surface area (up to 150 m^2/g). In polymerization with $Al(C_2H_5)_2Cl$ and hydrogen, it gives the average performance shown in Table 9. The polymer has regular shaped, compact particles and narrow particle size distribution, with an average diameter around 300–400 μm. Catalyst activity is maintained by storage under refrigeration.

$MgCl_2$-Supported Catalysts. The scientific and patent literature reports several methods for the preparation of the $MgCl_2$-supported catalysts of third and superactive third generations. They can be classified as follows:

(1) Catalysts obtained by milling mixtures of anhydrous $MgCl_2$ with an electron donor and a titanium compound (186,187)
(2) Catalysts obtained by milling anhydrous $MgCl_2$ with an electron donor and treated with a titanium compound ($TiCl_4$) above 80°C, followed by washing with hydrocarbons (188–192)
(3) Catalysts obtained by treatment of "active" $MgCl_2$ with an electron donor and a titanium compound ($TiCl_4$) under conditions similar to those of the previous case (202)

The second method gives the average results reported in Table 9 with regard to third-generation catalysts. In practice, anhydrous $MgCl_2$ and an aromatic ester, usually ethyl benzoate (EB) in molar ratios between 2 and 15, are shaken in a vibrating mill containing steel spheres for 20–100 h. The $MgCl_2$ is activated; that is, it is converted from the crystalline ordered form to the disordered δ-form while the crystallite size is reduced.

The product is treated twice with an excess of $TiCl_4$ between 80 and 130°C, washed repeatedly with hydrocarbons, and dried. During the treatment with $TiCl_4$, the base is partially extracted, and $TiCl_4$ enters the support. The final composition of the solid includes 0.5–3.0 wt% Ti and 5–15% EB; the remainder is $MgCl_2$. The surface area is in excess of 100 m^2/g. The active or δ-form of $MgCl_2$ resembles the δ-form of $TiCl_3$ (203). It can also be obtained by direct contact of anhydrous $MgCl_2$ with Lewis base or by chlorination of magnesium organic compounds (188–192). The degree of activation can be determined by X-ray diffraction (203), where the passage from α to δ gives rise to a widening and lowering of the diffraction peaks. The active form, because of the corners, edges, and surface defects of the crystallites, binds the titanium compound strongly, and repeated washing or treatment under vacuum cannot remove it. This strong binding is attributed to the closeness of the Mg and Ti ionic radii (204) and to the similarity among the crystallographic forms of their halogens. The Ti atoms located in exposed sites give rise to polymerization active centers (205–208). Magnesium chloride may easily interact with electron donors, probably affecting the stereospecificity of the active site. It can be easily transformed into particles with controlled morphology because of the low melting point of its adducts with alcohols or water. These catalysts are used with aluminum trialkyl alone or in blends with chlorinated aluminum alkyls and with a second electron donor, which can be equal to or different from that contained in the solid catalyst.

Heterogeneous Catalyst Evaluation. To evaluate a catalyst system, the following characteristics must be known: yield or productivity, which is the amount of polymer produced per unit of total catalyst or single component; the polymerization kinetics, or yield development with time; stereospecificity; sensitivity to the molecular weight regulator; the molecular weight distribution of the polymer produced; the microtacticity of the resulting polymer; ability to copolymerize; and the final polymer morphology.

To forecast the behavior of a catalyst system in an industrial continuous polymerization, these characteristics should be determined within a wide range of conditions; eg, temperature, concentration, and ratios of the various components (activator, external donor, solid catalyst, etc). A laboratory batch-scale test can provide most of this information. A small, simple reactor suitable for these studies is shown in Figure 8. The polymerization can be carried out in a hydrocarbon or liquid propylene. In some cases the polymerization test can be performed in the gas phase, provided the reactor is prepared with a suitable heat transfer and catalyst dispersing bed (eg, a salt bed).

The stainless steel reactor is provided with a jacket for temperature control in the range $\pm 0.5^{\circ}C$ using a steam and chilled water mixture. The reactor contents are agitated by a magnetic stirrer (500–900 rpm). The consumption of the propylene is followed by weighing the vessel from time to time or through gas flow meters.

A test using hexane as diluent is the simplest to perform because it does not require the safety measures required for tests in liquid propylene. It can be carried out as follows.

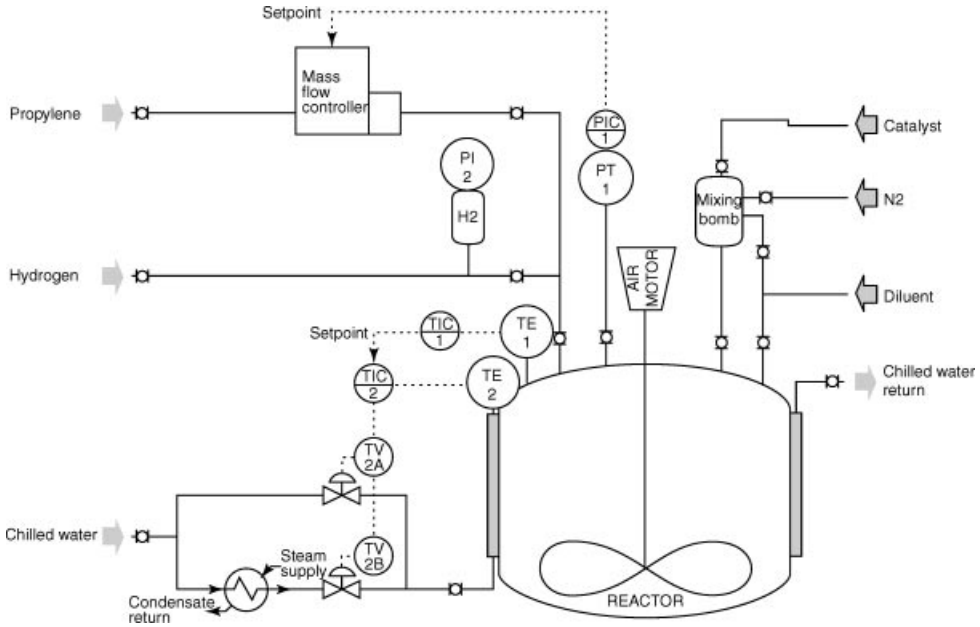

Fig. 8. Lab-scale polymerization reactor.

The reactor is kept under nitrogen at 40–50°C to exclude oxygen and moisture. Anhydrous, deaerated hexane is introduced followed by a fixed amount of catalyst. The reactor is closed and heated to 60–70°C, and hydrogen and propylene are fed at the desired concentrations. These feeds are maintained for a certain time. Data on the polymerization kinetics are obtained from the mass of propylene fed over time. At the end of the test the temperature is reduced, the reactor degassed, and the slurry (hexane/polypropylene) discharged from the reactor (either through a dip tube or a bottom valve). The polymer is separated from the hexane by filtration or by evaporation. The polymer is dried at 60°C under nitrogen, weighed, and analyzed.

Typical graphs follow which represent the performance of a superactive, third-generation catalyst system as a function of processing variables. The activity is expressed as kilograms polymer per gram catalyst, and the isotacticity as polymer percentage residue from a boiling heptane extraction in a modified Soxhlet extractor for 12 h.

Figure 9 shows the trend of activity for polymerizations in hexane with a propylene concentration of 14% at 70°C; Figure 10 shows the isotactic index.

Polymerization temperature, as reported in Figure 11, influences performance; an increase from 50 to 80°C increases both activity and isotacticity.

Isotacticity should be between 94 and 98% to meet various application requirements. The ratio between aluminum and electron donor controls stereospecificity. At very high levels of electron donor the activity will be reduced, as shown in Figure 12 (209).

The aluminum compound alkylates the transition metal and can act as a transfer agent. It also removes impurities from the reaction medium (eg, water, CO_2, alcohols), thereby avoiding catalyst poisoning. In addition, aluminum alkyl reduces the transition metal to lower valence, thus affecting its activity (210). In the case of supported catalysts, aluminum alkyl plays a fundamental role by complexing the electron donors (204).

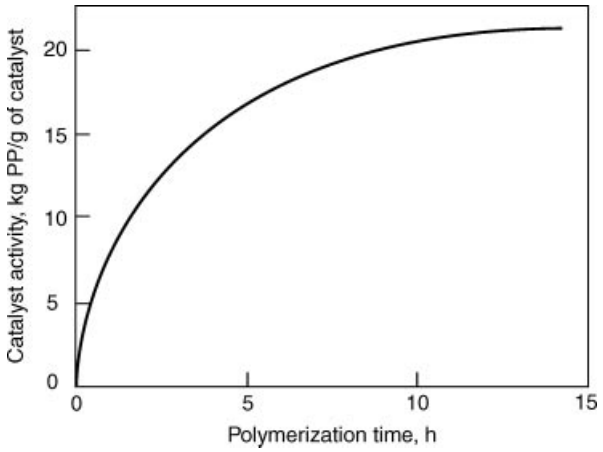

Fig. 9. Activity vs polymerization time.

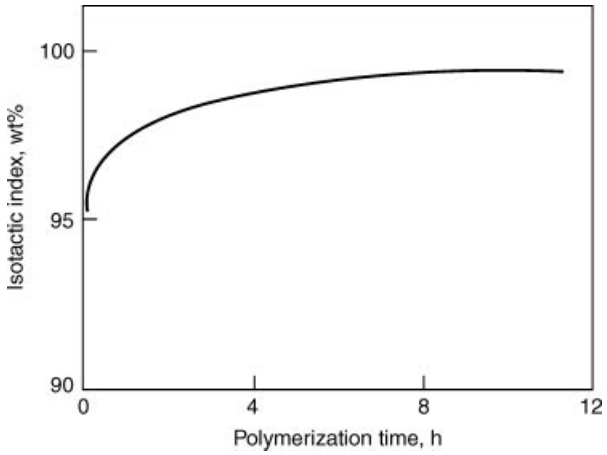

Fig. 10. Isotactic index vs polymerization time.

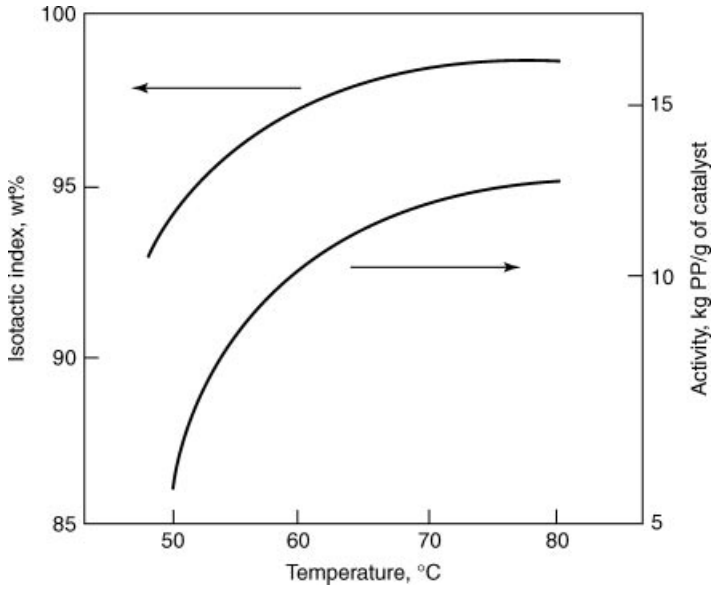

Fig. 11. Activity and isotactic index vs polymerization temperature.

Polymerization Reaction Mechanisms

The rate R_p of the primary propagation step of monomer to polymer in Ziegler–Natta catalysis is represented by

$$R_p = k_p[C^*][M]$$

where k_p is the propagation constant, [C*] the concentration of active sites, and [M] the monomer concentration.

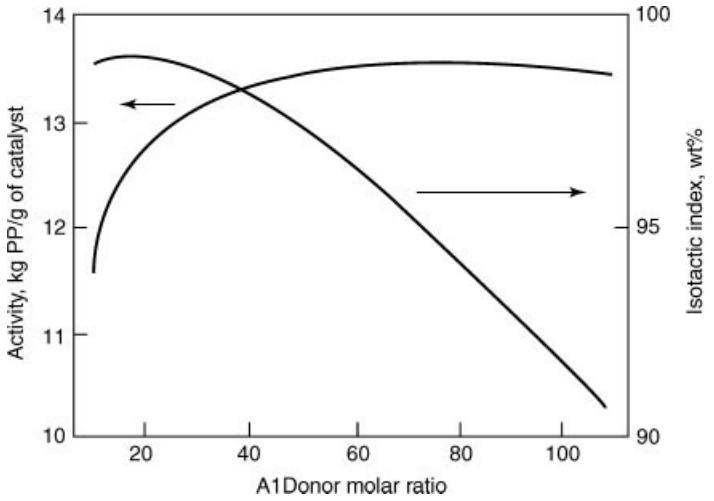

Fig. 12. Activity and isotactic index vs Al:donor ratio.

The global polymerization rate changes with time. A period of increasing rate is usually followed by a decline and eventually by a stationary state. The rate decay is often attributed to the change in concentration of active sites in the context of the above noted expression. The initial increase may be due to the progressive activation of new active centers. The deactivation, particularly evident in supported catalysts (211,212), is attributed to variations in both number and chemical nature of the centers (213).

Global polymerization rate and rate of primary propagation are affected by the catalyst system and polymerization conditions (203,214). Effects are due to the chemical and physical structure of the catalyst as well as to the nature of the activator. Important parameters include the ratio between catalyst and activator, and their concentrations, hydrogen concentration, temperature, stirring rate, and type and amount of Lewis base. The effects vary with the polymerization medium; ie, diluent or the monomer in liquid or gas phase (215–218).

The complexity of the catalyst systems and their heterogeneous nature make an accurate analysis of the parameters associated with the primary propagation step difficult. This is one reason why literature analyses are rarely in agreement; also, the data are obtained by methods and under conditions that are rarely comparable. A typical example is the determination of the concentration of the active sites and the propagation constant, which can be carried out by various methods (chemical, radiochemical) that are not completely reliable. Nonetheless the parameters are valuable in determining catalyst potential and performance.

The same uncertainty is involved in the determination of the activation energy of the propagation reaction and the average lifetime of the polymer chain. A value of 23 kJ/mol (5.5 kcal/mol) for $TiCl_3$-based catalysts is reported for the former (219). For the latter, values of 360–600 s (220) and 160 s (219) for $TiCl_3$-based catalysts are reported at 70°C and 5 s (221) for $MgCl_2$-supported catalysts at 45°C.

A short time after the discovery of Ziegler–Natta catalysts, it was suggested (222,223) that chain propagation occurred by monomer insertion into a Ti–carbon

bond of the catalyst. This bond was considered to be polarized, with a weak negative charge on the carbon atom; this hypothesis is still widely supported today. It was confirmed by IR analysis of chain terminal groups (224) as well as by ^{13}C enriched aluminum alkyls (225).

In an attempt to provide a model to explain the growth of the polymer chain satisfactorily, several hypotheses have been suggested. In Boor's book on Ziegler–Natta catalysis (179), he exhaustively reviewed the literature and addressed four mechanisms for chain growth. The four mechanisms are based on the description of the center where chain growth takes place:

(1) transition metal–carbon bond,
(2) activator metal–carbon bond,
(3) bound radical center, and
(4) bound anion center.

Of these four, the majority of the research tends to support the transition metal–carbon center model, as the mechanistic scheme of choice. Using a homogeneous catalyst (Cp_2TiEt_2) as a model, Breslow and Newburg proposed that polymerization growth occurred at the Ti—C center. Somewhat later, Cossee extended this concept into a more elaborate mechanism for supported catalysts, which he substantiated with molecular orbital calculations (see Ref. 179, Chapt. 13).

According to this widely accepted model (226–230) for the surface site and surface coordination environment, the active site is a titanium atom with octahedral shape and a vacant position (the other positions being occupied by an alkyl group derived from the alkylation by the aluminum alkyl and the remaining chloride atoms). In total the active site is made up of four ligands, which, in the case of $TiCl_3$, are chlorine atoms, the alkyl group, and the vacant site.

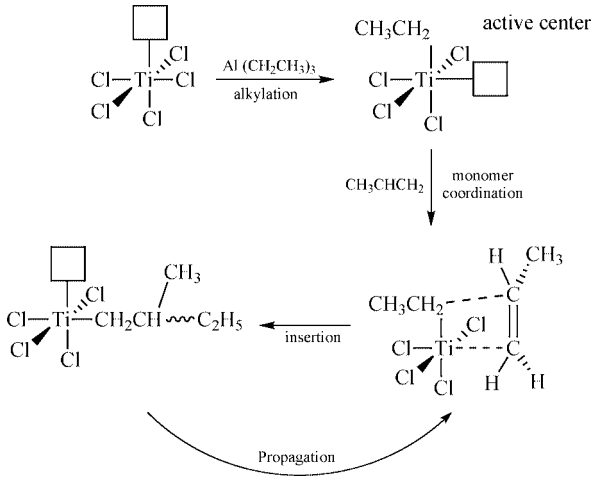

Monomer insertion occurs through a first step of monomer coordination to the transition metal, with formation of a π-complex, subsequent weakening of

the Ti—C bond, and finally insertion of the monomer coordinated between the transition metal and the C atom. Because the two positions are not equivalent in the crystal lattice of the catalyst, the vacancy and the growing chain exchange positions. These phases are repeated at the insertion of each monomer unit. On the basis of molecular orbital theory, a semiquantitative interpretation of the mechanism was provided by assuming weakening of the metal–carbon bond during olefin complexation in the case of metal ions with 0–3 d-electrons (as in Ti, V, Cr), and with more difficulty when the number of d-electrons is greater. This mechanism is called monometallic; it requires only the participation of the transition metal, attributing to the aluminum compound the role of forming the active center by alkylating the titanium atom. The aluminum compound is also involved, as demonstrated by the different effects that various aluminum alkyls have on the performance of these catalyst systems.

Some researchers believe that the active metal (aluminum) directly participates in directing of the incoming monomer, in which case this system would be considered a bi metallic site. However, Boor makes a convincing argument that because of the size of the polypropylene helix, there is no room at the active site for the aluminum to participate. The titanium site occupies roughly 0.16 nm^2 (diameter $\sim$0.45 nm) and the cross-sectional area of a polypropylene helix is about 0.35 nm^2 (diameter $\sim$0.7 nm). This would eliminate the titanium and aluminum from sharing a common chloride bridge and thus preclude aluminum from directly participating in directing the incoming monomer (179). It has been suggested that the effect the different aluminum alkyls have on polymer microstructure and molecular weight is due to the way in which the alkyl aluminum sets up the titanium chloride surface. These differences in polymer microtacticity and molecular weight could be due to the fact that the activator may be generating different isotactic sites.

The basic concept of monomer insertion has now been discussed and for the polymerization of ethylene this simple description of a monometallic, transition metal–carbon centered active site would be sufficient to describe the polymerization. However, with α-olefins the matter of stereo- and regio-chemistry must be addressed and will be done in the next section.

Stereo- and Regiochemistry of Monomer Insertion. For substituted α-olefins a number of issues concerning monomer coordination/insertion must be considered. The way in which the monomer inserts itself into the polymer chain determines the microstructure of the polymer and subsequently the properties. Does the methyl group on the propylene end up towards the chain or away? What is the position of the methyl group on the propylene molecule with respect to coordination site of the metal and the polymer chain, cis versus trans? The way in which the propylene molecule may be inserted in the polymer chain by various mechanisms can give rise to complex phenomena of structural and steric isomerism.

Two possible regio-insertion mechanisms for α-olefins exist—primary and secondary. In a primary insertion the unsubstituted end (methylene group) of the monomer attaches to titanium center. This is also known as a 1,2-insertion. In a secondary insertion the substituted end of the monomer attaches the titanium. This is also called a 2,1-insertion.

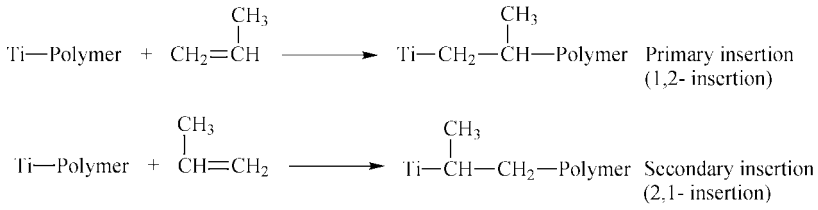

The experimental evidence indicates that for the production of isotactic polypropylene the primary insertion mechanism is predominant. This is substantiated via end group analysis by the presence of isopropyl groups as the end groups after chain transfer by hydrogen. The regioselectivity of Ziegler–Natta catalysts is very high as have been proved by NMR analyses (231,232). Syndiotactic polypropylene can be prepared by the low temperature polymerization of propylene using a vanadium catalyst. In this case the secondary insertion mechanism is operative (233,234).

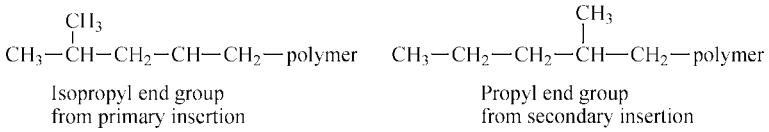

For stereoregular insertion there are two modes to consider—cis insertion and trans insertion. For both isotactic and syndiotactic production, the cis mechanism has been determined to be in operation. This was established by polymerizing with *cis*-, and *trans*-1-deuteriopropylene or related monomers. The expected stereochemistry was demonstrated when deuteriopropylene was polymerized. The cis monomers produce *erythro* monomer units whereas the trans monomer yields the *threo* units when *cis*- and *trans*-1-d-propylene is polymerized. In some cases the nomenclature appearing in the literature can be confusing and contradictory, but all indicate cis insertion. To be specific, as defined below, stereochemical structures from cis and trans addition to the double bond of *cis*-(1-d_1) and *trans*-(1-d_1)-propylene to isotactic polypropylene are as follows (229):

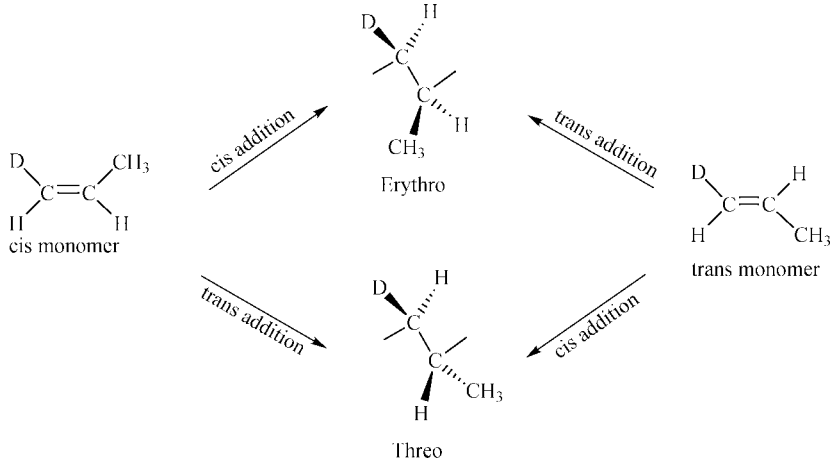

Two potential mechanisms have been proposed as governing factors regulating the stereochemistry of the isotactic insertion, the first being the asymmetric structure of the active site (enantiomeric site control) and the second being the asymmetric carbon atom of the last chain-inserted monomer unit (chain end control). It has been proved experimentally that the regulating factor is the active center (enantiomeric site control) because the steric order is transferred also through ethylene units and because an occasional error is not perpetuated in the chains (231,232). This mechanism is valid for Ziegler–Natta catalysts and many (if not most) homogeneous metallocene catalysts. In addition it has been shown (235–240) how, in the polymerization of racemic α-olefins, a mixture of optically active polymer can be obtained with an asymmetric catalyst.

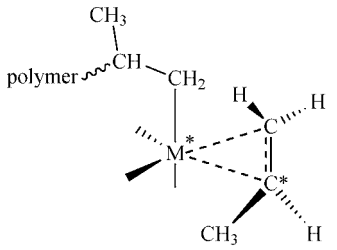

Chiral centers in the propagation step

Examination of the crystalline structure of the catalyst components reveals the asymmetric structure of the active center. In $TiCl_3$ six chlorine atoms at the vertices of an octahedron surround each titanium atom. These six chlorine atoms are then chelated, by pairs, to three other titanium atoms. This creates two enantiomorphic structures.

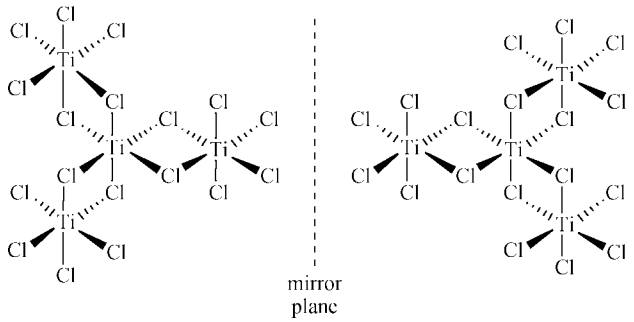

The next section will discuss some of the concepts associated with models for the catalytic sites.

Ziegler–Natta Active Site Models

An important characteristic of a polymerization catalyst is its morphology or structural architecture. Titanium chloride exhibits four different crystalline modifications: α, β, γ and δ forms depending upon the method of preparation. In each

case the titanium atom is octahedrally coordinated, except at various defects and edges. The violet α-form, and the γ and δ forms consist of regular stacking of Cl—Ti—Cl layers containing titanium atoms between two layers of chloride ions. The α-$TiCl_3$ form, which will be discussed, is hexagonally close packed.

Stereospecific behavior of the catalyst site is related to the chirality of the surface sites of the solid $TiCl_3$. Models by Corradini can explain a number of observations—the type of tacticity errors along a predominantly isotactic chain, stereospecificity of the initiation reaction, and the maintenance of isotacticity after the insertion of ethylene monomer in the chain (241). Furthermore, since violet $TiCl_3$ and $MgCl_2$ solid-state crystal structures are similar, Corradini's model relates well to both $TiCl_3$ and $MgCl_2$-supported catalysts.

The structure of titanium trichloride and other Ziegler–Natta catalysts consisting of transition metal halides (VCl_3, $CrCl_3$, etc) is comprised of layers of close-packed chlorine atoms. The crystalline modifications are based on the different ways in which the layers are stacked on top of one another. Within each layer the metal atoms reside in an ordered arrangement. The metal atoms occupy two thirds of the octahedral positions. The adjacent metal atoms, which are bridged by two chlorine atoms, have opposite chirality. The chirality of these metal atoms is designated Λ and Δ according to the International Union of Pure and Applied Chemistry (IUPAC) nomenclature (242). In the $MgCl_2$ structure there are no vacancies in the lattice and every octahedral position is occupied by a magnesium atom; however, it can be seen that the gross structures of $TiCl_3$ and $MgCl_2$ are similar. This similarity in structure between $TiCl_3$ and $MgCl_2$ is what makes magnesium chloride a suitable substrate for the deposition of titanium chloride to form active sites. It was determined early on that only a small portion of the titanium on $TiCl_3$ catalysts was active; the rest was essentially acting as a support. The bulk of the titanium chloride was the culprit in causing polymer instability and degradation problems. When using $MgCl_2$ as a support the yield of polymer per weight of catalyst is much greater. Along with the fact that the magnesium chloride is practically inert, this produced a polymer that was inherently more stable.

A diagram of the $TiCl_3$ structure of the (110) cut and the (100) cut of $MgCl_2$ is shown in Figure 13; the chloride atoms are omitted for clarity.

Magnesium chloride can be treated either chemically or physically (ball milling) to achieve activation. Activated $MgCl_2$ has a very disordered structure, which consists of very small lamellae. In the bulk, magnesium atoms are coordinated to six chlorine atoms, but at the lateral edges or cleaved surfaces the coordination is with 4 or 5 chorine atoms. These lateral cuts correspond to the (110) and (100) faces respectively for magnesium chloride. Upon treatment of activated $MgCl_2$ with $TiCl_4$, the bridged dinuclear Ti_2Cl_8 species coordinate on the (100) surface while the single $TiCl_4$ species usually prefer the (110) faces. Treatment of the catalyst by aluminum alkyls will reduce the Ti_2Cl_8 to Ti_2Cl_6 species and alkylate the titanium. This will generate both $TiCl_3$ and Ti_2Cl_6 species on the $MgCl_2$ support. The placement of these Ti_2Cl_6 units on the (100) lateral surface of $MgCl_2$ produces sites very similar to those on the (110) surface of $TiCl_3$ catalysts. These Ti_2Cl_6 sites are chiral and stereospecific. Coordination of the $TiCl_4$ species on the (110) faces and reduction by aluminum alkyls produce $TiCl_3$ sites, which lack chirality and are nonstereospecific producing sites for propylene polymerization. In Figure 14, is shown both the $TiCl_3$ catalyst and $MgCl_2/TiCl_4$ catalyst after

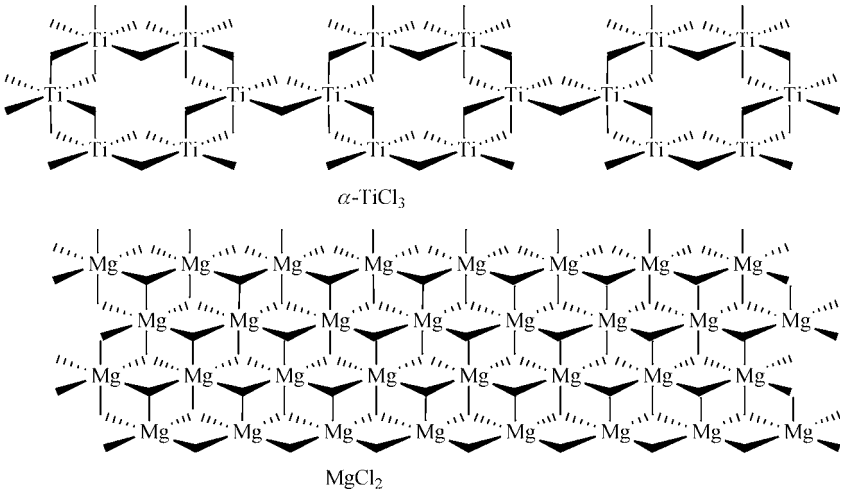

Fig. 13. Comparison of the structures of α-$TiCl_3$ and $MgCl_2$.

reduction with AlR_3. Now with the basics of the active centers and structures described, the details of the polymerization mechanism can be discussed.

As mentioned previously, a two-stage reaction mechanism for the polymerization of propylene was proposed which consists of a coordination stage of the olefin then followed by an insertion step of the monomer into the Ti–polymer bond. Although this picture (Fig. 15) reveals the basic mechanism of monomer coordination and then insertion, it does not provide any insight into the mechanism for stereocontrol of the propylene monomer. This is addressed by chirality considerations.

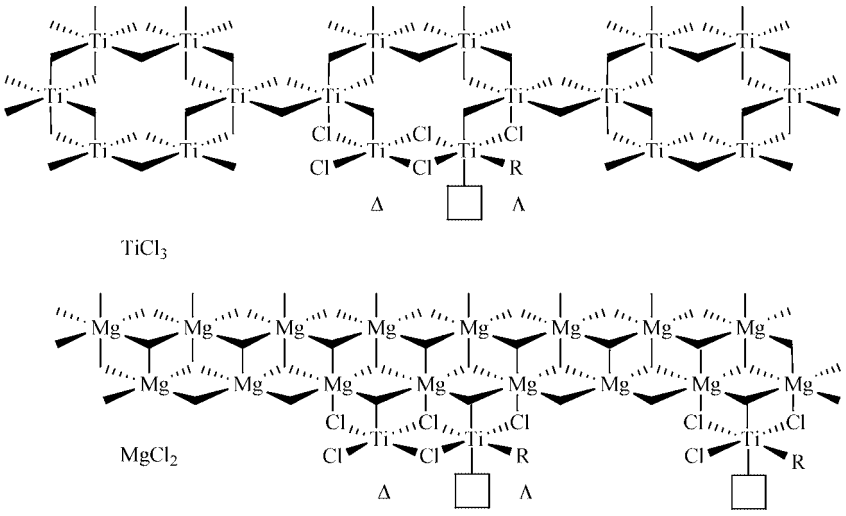

Fig. 14. Crystal structures of α-$TiCl_3$ and $MgCl_2$ with Ti_2Cl_6 clusters. Chlorine atoms are shown at the catalyst sites, and substrate chlorine atoms are omitted for clarity.

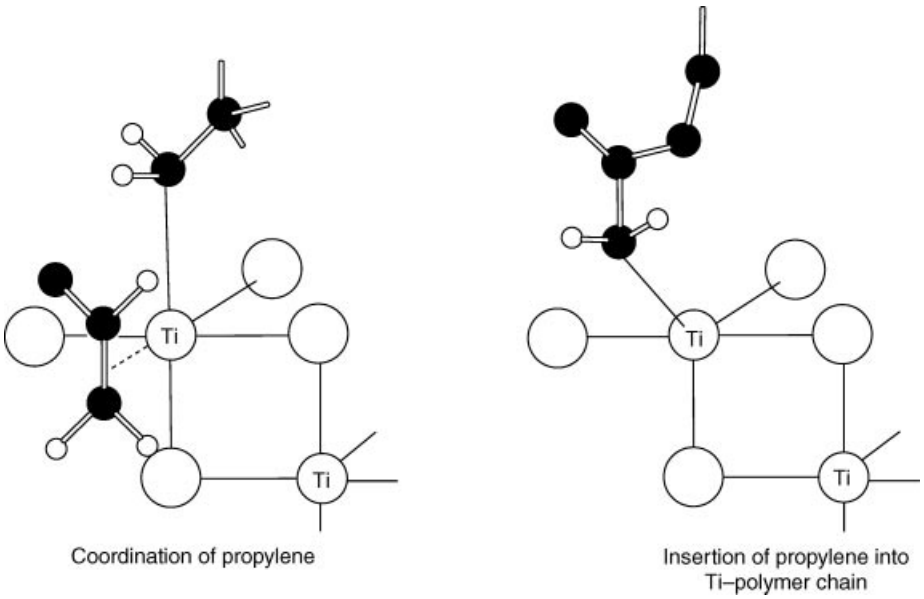

Fig. 15. Propylene coordination to titanium and then insertion of propylene into the Ti–polymer bond.

As discussed previously the active sites on $TiCl_3$-based catalysts or $MgCl_2$-supported catalysts are chiral. In all, there are three elements of chirality that are considered with respect to the polymerization of α-olefins and stereospecificity of the polymer:

(1) α or δ chirality of the titanium atoms
(2) The *si* or *re* chirality of the coordinated propylene monomer
(3) The chirality of the tertiary carbon atoms of the growing polymer chain

For this discussion the bridged dimers of Ti_2Cl_6 on the lateral face of a $MgCl_2$ crystal will be considered. If Figure 16 (below) is studied in detail, it can be seen that at one of titanium atoms of the Ti_2Cl_6 cluster there are two positions that are available to the growing polymer chain and the coordinating monomer. One position can be considered outside or away from the bulk of the crystal and the other can be considered inside, or towards the bulk of the crystal lattice. These two positions are not sterically equivalent. Through computer modeling calculations, Corradini and co-workers demonstrated that the most favorable energy position for the growing chain was at the inside position (241).

If the most favorable energetic position for the chain is at the inward position, then the monomer must occupy the outside location. For the Λ titanium site, the *si* outward coordination of propylene is favored (*re* for the outward Δ titanium site). In this model the production of stereospecific polypropylene can be explained.

For syndiotactic propagation it was proved that the steric control of the insertion comes from the last inserted monomer unit, whose hindrance affects the

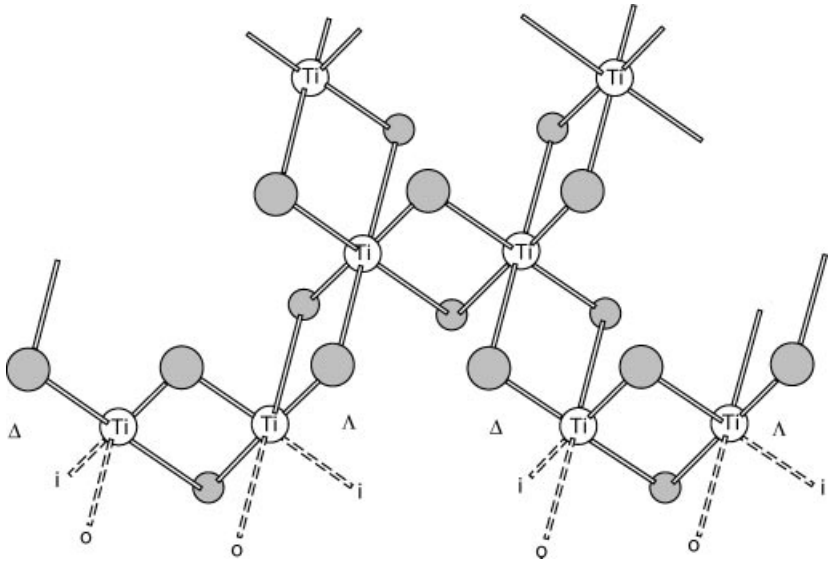

Fig. 16. Inward and outward positions available for occupation by the monomer and polymer chain.

insertion of the subsequent unit in such a way as to prevent a monomer molecule with the same configuration of the previous molecule from entering (243,244). Recall that syndiotactic polymerization from Ziegler–Natta vanadium catalysts differs from this isotactic polymerization monomer insertion. For the vanadium syndiotactic catalysts secondary or 2,1-insertion is operative (233,234). More recently developed homogeneous syndiotactic catalysts follow 1,2-insertion.

Summarizing, isotactic and syndiotactic propagation highlights the catalyst site as the entity controlling stereoregularity for iPP and the last monomer unit of growing chain for syndiotactic propagation with vanadium catalysts. The monomer insertion type is primary (1,2) for isotactic and secondary (2,1) for this latter syndiotactic catalyst.

Electron Donors

There are two classifications of electron donors, internal and external. Electron donors are thus named for their ability to act as Lewis bases and donate electrons to Lewis acid sites. For the $TiCl_3$ type catalyst, the electron donors are traditionally referred to as just donors and are generally amines, esters, ethers, alcohols, etc. Their roles range from modifying the catalyst site and structure of the $TiCl_3$ substrate to complexing with the alkyl aluminum either during catalyst preparation or catalyst activation.

For $MgCl_2$-supported catalysts (the third- and fourth-generation types; see Table 9 the electron donors are classified as internal and external based on their sequence of addition during catalyst preparation or during activation, respectively. For the preparation of the $MgCl_2$-supported catalyst an electron donor is added

during the process of adding the $TiCl_4$ (titanation of the support) to the activated $MgCl_2$-support; this is referred to as the *internal donor*. At the stage of activation of the $MgCl_2$-supported catalyst, another donor is added during the addition of the alkyl aluminum; this donor is referred to as the *external donor*. For the third-generation $MgCl_2$-supported catalyst, the internal donors are usually phthalates and the external donors are alkyl alkoxy silanes. For the fifth-generation type catalysts, the internal donors are diethers and the external donor (alkyl alkoxy silane) may or may not be used. In most cases electron donors are used to increase the activity and stereospecificity of the catalyst system.

Donors work in a variety of ways and the roles of both internal and external donors as they relate to the $MgCl_2$-supported catalysts will be discussed in this section. As mentioned previously, $MgCl_2$ can be activated through mechanical or chemical means. The process of activating magnesium chloride through mechanical means can be achieved by ball milling. This process usually involves co-milling the magnesium chloride with a Lewis base (233). The preparation of the catalyst is followed by treatment of the activated magnesium chloride with $TiCl_4$ and heat. The subsequent treatment of the $MgCl_2$/internal donor support with $TiCl_4$ usually removes some to the internal donor. In other cases the activated $MgCl_2$-support can be treated with $TiCl_4$ and the Lewis base at the same time, and then given a heat treatment. The internal donor helps structurally stabilize the activated magnesium chloride, prepare sites for the $TiCl_4$, and possibly block certain sites on the $MgCl_2$ surface, thus making them unavailable for titanium chloride.

Whereas third-generation Ziegler–Natta catalysts use an ester (ethyl benzoate, EB) as internal donors and another ester as the external donor (methyl *para*-toluate, MPT), the fourth-generation catalysts use a phthalate (usually di-iso-butylphthalate, DIBP) as the internal donor and an alkyl alkoxy silane (eg phenyl triethoxy silane, PES) as an external donor (233). In both cases the internal and external donors play similar roles. The internal donors stabilize the $MgCl_2$ support and set up positions for the $TiCl_4$ complex. The purpose of employing an external donor in both the third- and fourth-generation catalyst systems is that without them, the stereospecificity of the catalyst would be very poor for the polymerization of propylene. This is due to the fact that activation of the catalyst with the alkyl aluminum extracts a portion of the internal donor out of the catalyst. The external donor is added during the activation of the catalyst for the purpose of occupying the site left vacant by the extracted internal donor (233).

From the discovery of the high yield $MgCl_2$-supported catalysts it was apparent that the presence of both an internal and external donor was a necessary condition for a highly active, highly stereospecific catalyst. Soon after, it was learned that an interrelationship existed between the two donors and, furthermore, specific donor pairs gave optimum results. However, with the advent of the fifth-generation catalysts, those employing diethers, there was no need for the addition of an external silane donor (234). These catalysts, $MgCl_2/TiCl_4$/diether, did not lose the internal donor during activation with the alkyl aluminum and consequently maintained relatively good stereocontrol and excellent activities (2 to 3 times that of the conventional $MgCl_2$-supported/phthalate catalysts) (245,246) (see Table 9). Interestingly enough, these diether donors can also be used as external donors in the more traditional $MgCl_2$-supported/phthalate/$TiCl_4$ catalyst systems and they produce the same type of homopolymer. This supports the theory that there is a phthalate/external donor exchange during activation where

the external donor (diether) occupies the site left vacant by the phthalate, very similar to the phthalate/alkoxy silane exchange. In general the following model best describes the interactions between the internal and external donors with the catalyst and activator (246,247):

(1)

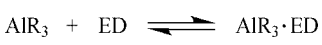
(2)

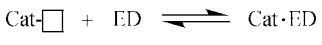
(3)

(4)

(5)

As previously mentioned, the alkyl activator will extract internal donor from the catalyst; therefore equilibrium 1 is always present even in the absence of an external donor. Depending upon the location of the titanium site on the magnesium chloride support, the free site (Cat-□) could be isospecific or aspecific. Equilibrium 2 is also present because of the propensity of the external donor and AlR_3 to form acid/base adducts. These $ED{\cdot}AlR_3$ adducts may also form exchange products (248). In fact, these exchange products are important because they reduce the concentration of free external donor present in the system, which also acts as a poison. In the presence of excess aluminum, there should be very little free external donor present in the system; therefore equilibrium 3, (the interaction of catalyst with free external donor) can be neglected. For the external donor to interact with the free titanium site there are two possibilities—through the $ED{\cdot}AlR_3$ complex (equilibrium 4) and through the $ED{\cdot}AlR_3$ complex initially as a carrier for the ED (equilibrium 5). In equilibrium 5, the $ED{\cdot}AlR_3$ complex releases the ED to the vacant titanium site. Experimental results indicate equilibrium 5 as the most likely case. The alkyl aluminum activates the titanium and removes the internal donor but does not participate in the actual stereochemical regulation of the polymerization of propylene (246).

To recap, there are two types of donors, internal and external. For the third-generation catalysts the internal/external pair is an ester/ester pair, while for the fourth-generation it is the phthalate/alkoxy silane pair. The fifth-generation Ziegler–Natta catalysts are comprised of an internal donor, which is a diether compound and may be used with or without the additional external donor (see Table 9).

There has been a large effort towards elucidating the roles of the external donor in the polymerization of propylene. Some of this work has centered on the

structural considerations of the external donor. Since the $MgCl_2/TiCl_4$/phthalate–alkoxy silane/AlR_3 catalyst system is the most widely used commercial catalyst system for polymerization of propylene, the focus in the next section will be on the alkoxy silane as the external donor.

Structural Considerations of Electron Donors. The most effective alkoxy silanes used in the polymerization of propylene give the greatest activity along with the highest selectivity. These types of silanes are of the general formula $R^1R^2Si(OR)_2$ and $R^1Si(OR)_3$, with R = methoxy or ethoxy (any larger alkoxy group is ineffective). Early on, $PhSi(OEt)_3$ was used; however, the more effective silanes for catalyst performance are those that contain methoxy groups (R = OMe). Interestingly enough, silanes with only one alkoxy group were poor performers, producing polypropylene with low isotacticity. The best activity/selectivity balance was found for silanes having two methoxy groups and two alkyl groups (R^1 and R^2) that are relatively large—in other words, sterically bulky. The importance of steric volume was investigated by Okano and co-workers (249). They correlated silane molecular volume and electron density (calculated by molecular modeling) with polymerization performance (activity) and stereocontrol (isotactic index). In their study they found a straight-line correlation with silane volume and isotacticity. Both Okano's group and Härkönen (250) found a decrease in atactic polymer formation with an increase in electron density.

In addition to affecting polymer stereoregularity and catalyst activity, silane donors influence other aspects of propylene polymerization. It was also found that external silane donors influenced molecular weight of the polymer via the use of hydrogen as a chain-transfer agent. When using hydrogen to decrease the molecular weight of the polymer, there was also an increase in activity when using an external alkoxy silane with the $MgCl_2/TiCl_4$/phthalate ester catalyst system (251–254). While hydrogen is used as a molecular weight control agent, this level of control varies from external donor to external donor. In some cases, under the same hydrogen charge, two different donors will give polypropylene with two very different molecular weights (255). These differences between donors in molecular weight control are not unlike the differences observed in stereocontrol. Some donors are better at stereocontrol than others. The general observation is that donors with good stereocontrol or high selectivity (usually those containing bulky hydrocarbon groups) are usually poor at effectively using hydrogen to lower the molecular weight of the polymer. Donors with poor regio- or stereocontrol exhibit good hydrogen response. Chadwick and co-workers have explained this phenomenon by the process of chain transfer after a regioirregular insertion of propylene (256). With a 2,1-insertion it is harder for the next propylene unit to insert into the $Ti{-}CH(CH_3)CH_2$–polymer bond; however, there is a probability of hydrogen inserting to affect a chain transfer. Therefore those donors with low regio-control permit more 2,1-insertions, thus making chain transfer with hydrogen easier. Donors with good regio- control make far fewer 2,1-insertions, thus denying an easy path and an opportunity towards chain transfer with hydrogen.

Molecular Weight and Molecular Weight Distribution Effects of Electron Donors. The production of broad molecular weight distributed polypropylene is a function of the multiplicity of active centers, which differ in stereo- and regiospecificity, and the propagation rate. Lewis bases in general, and external alkoxy silane donors in particular can influence the molecular weight

distribution of polypropylene by associating with these multiple active centers (245,257,258). The regio- and stereoselectivity of the external donors affects the molecular weight distribution of the polymer indirectly. Normally the atactic fraction of polypropylene has a lower molecular weight. This is in part due to regioirregular insertions of the monomer, which in turn leads to the easier pathway of hydrogen complexation and subsequent chain transfer (259). It has been shown that the different fractions of homopolypropylene separated by temperature rising elution fractionation (TREF) not only differ in microtacticity but also by molecular weight (245). For the $MgCl_2/TiCl_4$/diether based catalyst, Chadwick and co-workers found that the higher temperature eluting fractions also had higher molecular weights. Not unexpectedly, each fraction from TREF exhibited a narrow molecular weight distribution (259).

Microtacticity Considerations. In the early days of Ziegler–Natta polymerization of propylene, two concerns were activity of the catalyst and the stereospecificity of the polymer. Stereospecificity or stereoregularity of the polymer was measured by the amount of insolubles produced versus the amount of solubles. However, another important feature affecting the performance of polypropylene is the microtacticity of the polymer chain. Nowadays, with the aid of TREF and ^{13}C NMR spectroscopy, the overall stereospecificity of polypropylene can be further defined by observing stereoirregular and regioirregular insertions. The type and quantity of these disruptions in the chain lead to differences in the physical properties and processing performances.

Chadwick and co-workers demonstrated that the quantities of the three major fractions derived from TREF vary with different donors (256). The fraction of polymer that elutes from 26 to 95°C, normally referred to as the *stereoblock fraction*, can vary from as little as 4% up to 21% by weight of the total polypropylene sample (260). The differences in homopolymer made with two different donors can be seen by looking at the *mmmm* pentads, via ^{13}C NMR spectroscopy, of the TREF fraction eluting from 96 to 125°C.

In summary, donors, both internal and external (alkoxy silanes and diethers), affect catalyst performance and polypropylene properties in the following ways:

(1) The internal donors restrict the placement of titanium on the (110) face of $MgCl_2$.
(2) The internal donors shift the equilibrium between the aspecific monomeric species ($TiCl_3$) to the stereospecific dimeric species (Ti_2Cl_6) on the (100) face of the $MgCl_2$.
(3) The external donors transform nonstereospecific sites into isospecific sites by blocking open coordination sites near the titanium active centers.
(4) External donors control the path of the incoming monomer to varying degrees:
    a. Little control produces stereo- and regioirregularities that result in microtacticity changes; this in turn affects crystallinity and thus the solubles levels.
    b. Lack of monomer insertion control also affects regioirregular insertions (2,1-insertions), which leads to chain transfer by hydrogen and lower molecular weight.

Metallocenes

Metallocene catalysts for the polymerizations of olefins have been known since early 1957 when Natta and co-workers first reacted triethyl aluminum ($AlEt_3$) and bis(cyclopentadienyl) titanium dichloride $(\eta^5\text{-}C_5H_5)_2TiCl_2$ to form a complex that polymerized ethylene. The structure of this complex was described and the polymerization results reported. With ethylene they reported to have made 7 g of crystalline polyethylene in about 8 h at 95°C with 40 atm ethylene pressure in *n*-heptane. Later in the same year, Breslow and co-workers repeated Natta's experiments. They found that the blue complex described by Natta was a somewhat poor catalyst (in agreement with Natta's findings), but discovered that small amounts of oxygen in the ethylene boosted polymerization activity. When compared to the heterogeneous Ziegler–Natta catalyst system, these metallocene catalysts were poor with respect to polymerization activity. They were used essentially for mechanistic studies because of their simplicity and ease of structure elucidation.

In 1975 Kaminsky found that a slight amount of water added to a mixture of biscyclopentadienyl titanium dimethyl and trimethyl aluminum rapidly polymerized ethylene. Eventually it was determined that the addition of water produced methylaluminoxane (MAO), which was responsible for the boost in activity (261). Although these Cp_2MX_2/MAO catalyst systems rapidly polymerized ethylene and copolymerized other monomers with ethylene, they were less effective for the polymerization of propylene. There were several critical shortcomings with these early metallocene catalysts toward the polymerization of propylene: low activity, poor stereospecificity, and low molecular weight polypropylene production.

Because these metallocene catalysts are discrete, single molecules, their structures can easily be determined by X-ray crystallography. This allows the catalyst chemist to begin the process of relating the structure of the metallocene catalyst to polymer properties (molecular weight, stereoregularity, stereospecificity, etc) and polymerization activity. This ability to relate catalyst structure to polymer properties allows the process of elucidating polymerization mechanisms and designing catalysts to tailor make polymers and copolymers. This is a big advantage over the traditional Ziegler–Natta catalysts, which contain multiple sites (see METALLOCENES; SINGLE-SITE CATALYSTS).

General Description of Structures. A brief description of metallocene catalyst structures is necessary before going any further in discussions concerning these systems. In their most basic form these metallocenes consist of a Group IV metal (M= Ti, Zr, Hf), two π-bonded cyclopentadienyl rings, and two sigma-bonded groups (these rings are also referred to as carbocyclic π-ligands while all the groups attached to the metal are generally referred to as ligands). Because of the nature of the π-bonding between the metal atom and the carbocyclic π-ligands, there is free rotation of these ring groups about their metal-to-ring centroid axes. This free rotation makes these metallocenes nonstereorigid and produces atactic polypropylene.

A bridged metallocene contains a linking unit (usually CH_2, $-CH_2CH_2-$, or SiR_2) between the two carbocyclic ligands. These bridged metallocenes are stereorigid, but will not necessarily produce stereospecific polypropylene.

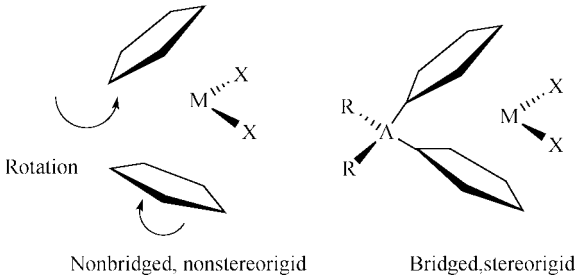

Nonbridged, nonstereorigid Bridged,stereorigid

Furthermore, these bridged metallocenes can become more complicated structurally with more substitutions on the carbocyclic π-ligands. In fact, the more complicated bridged metallocenes are of commercial interest because they provide for the production of isotactic and syndiotactic forms of polypropylene at high molecular weights. Because of the carbocyclic π-ligand's complexity, catalyst stereochemistry will be addressed in the next few paragraphs.

Bridged metallocenes can be further classified based on their stereochemistry. Using an ethylene-bridged bis-indenyl metallocene ($CH_2CH_2[Ind]_2MX_2$) as an example, one can follow the spatial relationships between the ligands and their effects on monomer insertion mechanisms and polymer properties. The $CH_2CH_2[Ind]_2MX_2$ metallocene can exist in two forms, *mesomeric* and *racemic* (*meso* and *rac*). The *meso*-$CH_2CH_2[Ind]_2MX_2$ catalyst has a mirror plane and is nonstereospecific in the polymerization of propylene; it is designated as C_s-symmetric. The *rac*-$CH_2CH_2[Ind]_2MX_2$ catalyst has a nonsuperimposable mirror image and, to a certain degree, each enantiomer is a stereospecific catalyst site; it is labeled as C_2-symmetric.

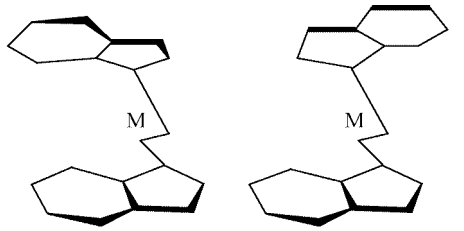

meso-$CH_2CH_2[Ind]MX_2$ C_s-symmetric *rac*-$CH_2CH_2[Ind]MX_2$ C_2-symmetric

Finally, two other structural types of metallocenes need to be mentioned. One type consists of carbocyclic π-ligands, which are not identical but each possessing a plane of symmetry (orthogonal to the ring plane). These types of metallocenes are labeled as C_s-symmetric. The other type of metallocene contains two nonidentical carbocyclic ligands, one symmetrical and one asymmetrical. These types of

metallocenes are labeled as C_1-symmetric.

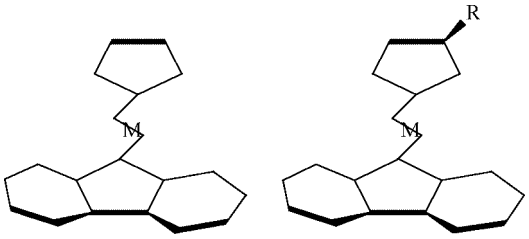

C_s-symmetric C_1-symmetric

Implications of Metallocene Catalyst Structure on Polypropylene Structure. The previous section gave a brief description of the various types of metallocenes. In this section a general relationship between metallocene structure and type of polypropylene produced will be made. It is important to note that these are generalizations. While the stereochemistry of the metallocene plays an important role in mechanism of monomer insertion and ultimately the stereo- and regiospecificity of the polymer, the substituents and location of the substituents on the carbocyclic π-ligands also effect the microstructure of the polymer.

In general, metallocenes that are either bridged or nonbridged *and* posses C_{2v} symmetry (eg, Cp_2TiCl_2 or $Me_2Si[fluorenyl]_2ZrCl_2$) will produce atactic polypropylene. This is because these types of catalysts have low stereocontrol. The only stereocontrol mechanism operating in these systems is chain end control from the polymer. Consequently the polymer is predominately atactic at normal polymerization temperatures. In fact, these metallocenes are the best source for producing high molecular weight, high atactic polypropylene (very low to almost zero crystalline polymer).

To produce highly isotactic polypropylene the metallocene catalyst should be a bridged chiral metallocene (preferably containing zirconium) having C_2 symmetry with some alkyl substitution in the ring (262). However, with the right substitution others have shown that a C_1-symmetric metallocene can also produce highly isotactic polypropylene with high T_m (161°C) (263).

Early metallocenes were less than desirable polypropylene catalysts because they produced polymer with low stereocontrol and low molecular weight. Recently there has been much progress in making high molecular weight, high stereo- and regioregular polypropylene with relatively high melting points. In general, all these metallocenes are structurally complicated and the reader should refer to references cited.

Advantages of Metallocenes. Because they are discreet molecules, one of the important features of metallocenes is that their structures are easily deduced. This allows almost direct correlation between the catalyst's structure and the microstructure of the polymer produced. This fact allows for a rather rapid evolution of focused catalyst design to tailor polymer properties to specific needs. For example, one of the early successful metallocenes used in the isospecific polymerization of propylene was $[Et(Ind)_2]ZrCl_2$. By structurally characterizing this compound and making some changes in the bridging group, a new metallocene was prepared $[Me_2Si(Ind)_2ZrCl_2]$ which produced a higher molecular

Table 10. Evolution of the Carbocyclic π-ligands and the Effect on Polypropylene Properties[a]

Metallocene	kg PP/mmol Zr·hr	MW, g/mol	Melting point, °C	Isotacticity,% mmmm pentads
$[Et(Ind)_2]ZrCl_2$	188	24,000	132	78.5
$[MeSi_2(Ind)_2]ZrCl_2$	190	36,000	137	81.7
$[MeSi_2(2\text{-}Me\text{-}4,6\text{-}iPr_2(Ind)_2]ZrCl_2$	245	213,000	150	88.6
$[MeSi_2(2\text{-}Me\text{-}4\text{-}PhInd)_2]ZrCl_2$	755	729,000	157	95.2

[a]Bulk polymerization in 1 L of liquid propylene at 70°C, Al/Zr = 15,000 using MAO as activator.

weight polypropylene with high isotacticity and, consequently, a higher melting point. The evolution of the carbocyclic ligand and subsequent improvement in isotactic polypropylene properties can be seen in Table 10.

From the standpoint of monomer insertion control, judicious choice of groups and location on the carbocyclic π-ligand produce polypropylene with higher isotacticity, greater molecular weight, and higher melting points.

Polymer Property Advantages. Metallocene catalysts, through variation of catalyst structure, can produce a broad spectrum of polymer microstructures leading to a very wide property envelope which is potentially accessible. Because of the defined molecular structure of the catalyst, once a catalyst is chosen for a given application, the properties can be precisely controlled.

Some of the property advantages and types of polypropylene and copolymers of propylene that can be realized with metallocenes are as follows:

(1) Highly tunable tacticity microstructure (isotactic, syndiotactic, atactic, isoblock/stereoblock, regiospecific microstructures)
(2) Narrow molecular weight distribution
(3) Absence of oligomers and extractables
(4) Improved melting point/extractable balance
(5) Narrow interchain composition distribution in copolymers
(6) Polypropylene with vinyl end groups
(7) Polymerization of expanded comonomer types (including dienes and cycloolefins)

Activators/Cocatalysts. As in conventional Ziegler–Natta catalysts, metallocene catalysts must be activated before polymerization of olefins can proceed. Methyl aluminoxane (MAO) has been the activator of choice since its discovery by Kaminsky in 1975 (261). MAO is prepared by the controlled hydrolysis of trimethyl aluminum. The product is a relatively difficult species to characterize. It consists of oligomers, both linear and cyclic. The composition of the numerous oligomer structures varies depending upon the preparation methods, concentration of the reactants, temperature, and time. The two simplified linear and cyclic oligomeric alumoxane structures (with a general alleyl group) are shown in Figure 17.

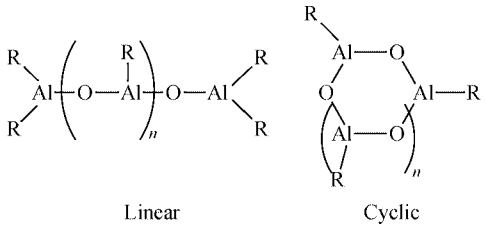

Fig. 17. Aluminoxane oligomer structures, linear and cyclic.

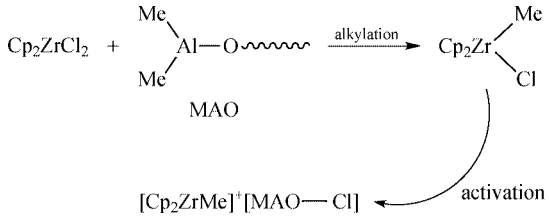

Fig. 18. Aluminoxane activating Cp_2ZrCl_2.

The role of MAO in the activation of a metallocene is essentially the same as in the traditional Ziegler–Natta catalyst that is to alkylate the halogenated metal center. The MAO forms a cationic complex with the metallocene and a dispersed anionic charge on the aluminoxane. An excess of MAO will lead to dialkylation of the metallocene metal center. One of the main disadvantages of aluminoxane activators is the high aluminum concentration level needed; typical AlZr ratios are over 1000:1. The basic mechanism for the alkylation and activation of a Cp_2ZrCl_2 is shown in Figure 18.

Other cocatalysts can be used to activate single-site catalysts. Some other typical activators, in addition to other alumoxanes, include tetraphenylborate $[(C_6H_5)_4B^-]$, tetra(perfluorophenyl)borate $[(C_6F_5)_4B^-]$, and carborane $(C_2B_9H_{12}^-)$.

Supportation of Single-Site Catalysts. Without the ability to support single-site catalysts, the commercial use of these systems would be eliminated in the numerous bulk and gas-phase polymerization facilities used today. In essence, they would be restricted to a limited number of slurry processes. The strategy of supporting a single-site catalyst for an industrial process is much the same as that for the heterogeneous Ziegler–Natta catalysts. The target is a morphologically uniform catalyst particle that is easy to feed into a slurry, bulk-monomer, or gas-phase process, which produces a polymer that is roughly the same shape as the catalyst particle but that is 20 to 200 times in volume. In addition the catalyst particle should be robust and not easily fractured during polymerization. Fracturing of the polymer particle during polymerization produces fines that foul the process.

There are a number of materials suitable for supporting single-site or metallocene catalysts. These are inorganic oxides, metal halides, and polymers. Among the inorganic oxides, silica or silica gels have been the supports most widely used because of their wide range of particle sizes, porosities, etc. More about

silica supports will be discussed later. Other types of supports, which will not be discussed in detail, are the other types of inorganic oxides such as aluminas (zeolites type materials), MgO, etc. However, it should be noted that zeolites have shown some promise as supports because of their ordered structures and precisely known pore sizes. Other support materials are polymers which include polystyrene, derivatized polystyrenes, polysiloxanes, and various polyolefins (porous types of polyethylene and polypropylene) and copolymers. The following discussions will be predominately focused on silica gel since it is the most widely used support for metallocenes.

There are essentially three methods in which to make a supported-metallocene catalyst:

(1) Supporting the metallocene, then treating with an activator
(2) Supporting the activator, then treating with the metallocene
(3) Preparing the metallocene/activator complex in solution, then treating the support with the complex

Supporting the Metallocene, then Treating with the Activator. Because of their method of preparation, silicas have a high concentration of surface hydroxyl groups and complexed water. Normally both hydroxyl groups and water will promote decomposition of a metallocene or metallocene/activator complex. Therefore it is necessary to remove the water either by thermal or chemical dehydration. Full dehydration of silica can occur at 150°C. At this point the silica gel will have a surface that is fully hydroxylated. Even these hydroxyl groups can decompose some types of metallocenes. In most cases the silica gel can be further dehydrated at 400°C (see Fig. 19).

Much work has been reported in the literature on the preparation of silica at various temperatures and under various conditions. Needless to say, the calcination conditions play a large part in preparing the silica support for the metallocene.

As far as the actual mechanism of how the metallocene is supported, various theories abound. However, the metallocene can be "connected" in two ways to

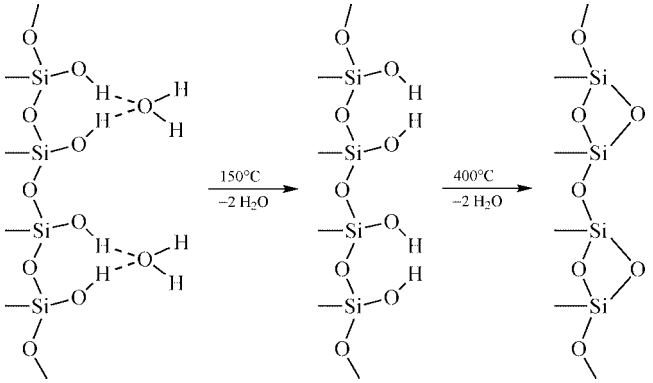

Fig. 19. The steps to the dehydration of silica gel.

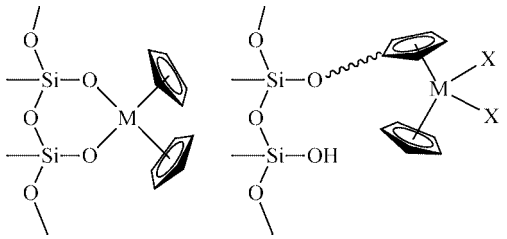

Fig. 20. Methods of attachment of a metallocene to silica.

the support: (*1*) through bonding to the metal and the oxygen of the Si—O to create the Si—O—Metal complex, or (*2*) by connection of the metallocene to the support via a linkage through the carbocyclic ligand moiety (Fig. 20). Tethering the metallocene to the support through the ring system is the method of choice, but requires preparing specialized carbocyclic ligands, which have spacers with groups that are able to react with residual OH groups on the silica. In this case it is necessary to have some remaining hydroxyl groups on the silica.

Supporting the Activator, then treating with the Metallocene. Supporting the alumoxane on the silica support first and then treating with the metallocene was one of the first methods used for supporting metallocenes. Many methods of silica treatment, prior to contacting with the MAO, have been reported. In addition, treatment of the silica gel with solutions of MAO at various temperatures and pressures, heating with dry MAO, etc, have been reported. All of these methods have advantages and disadvantages depending on the metallocene, monomers polymerized, and polymerization conditions used.

Supporting the Metallocene/Activator Complex. The last method to discuss is the supportation of the Metallocene/MAO complex. In this method the metallocene and the MAO are reacted in solution to form a complex. The silica is then treated with the metallocene/MAO solution. The solvent is then evaporated from the silica support to leave a dry, free-flowing catalyst. In some cases the support is held under low pressure while treated with the metallocene/MAO solution to assist in the impregnation of the catalyst complex into the pores of the silica. Other methods have been developed which improve the impregnation of the metallocene/MAO complex into the interstitial pores of the support. Concentrating the catalytic complex into the interior of the support rather than on the surface improves flowability of the supported catalyst system, decreases fouling, and improves the final polymer morphology. While much is known about the structure of the single-site catalyst and the properties of the resulting polymers, much of this changes upon supportation.

Commercialization Aspects of Metallocene/Single-Site Catalysts. While metallocenes have been known to polymerize olefins since the 1950s, only in the last 10 years have they been introduced commercially. Exxon introduced its first generation metallocene in 1989 for the limited production of polyethylene. This was a homogeneous catalyst used in solution. Other companies have followed with their own metallocene catalyst technologies, which are supported and are used in solution, gas phase, and supercondensed phases and processes.

Table 11. Metallocene/Single–Site Technologies

Company	Technology Name	Type of Polymer
Exxon/Mobil	Univation (Exxpol/Unipol)	iPP, impact co-PP (commercial)
Basell	Metocene	iPP, impact co-PP (in development)
Dow	INSPiRE	iPP (in development)
Borealis	Borecene	iPP, impact co-PP (commercial)
JPC/Mitsubishi	Proprietary use[a]	iPP, impact co-PP (in development)
TotalFina	Proprietary use[a]	iPP (commercial)
Mitsui	Proprietary use[a]	sPP (in development)
Chisso	Proprietary use[a]	iPP, sPP (in development)
BP Amoco	Proprietary use[a]	EPP (in development)

[a]Implies that technology is not commercially available, but the polymer may be commercially available.

The nonsupported metallocenes are used only in solution processes. The strategies for market penetration run from targeting commodities to specialty grades.

In the infancy of metallocene catalysis, many companies spent considerable research dollars on metallocene preparations and understanding the structure of the metallocene in relation to the polymer properties. In addition to these research dollars, large expenditures were also made to establish strong patent positions. In an effort to recoup these expenses for this budding technology, to be competitive, and to fill voids in their technology portfolios, many have established cooperative alliances or have consolidated.

At the time of this writing a number of metallocene/single-site catalyst technologies are available with which to produce polypropylene (see Table 11). Metallocene-based polypropylenes are commercially available and even catalyst licenses are available (264).

Manufacturing Processes

The first commercial processes for the production of polypropylene were batch polymerization processes using $TiCl_3$ catalysts activated by $Al(C_2H_5)_2Cl$ in a hydrocarbon medium. The hydrocarbon, usually hexane or kerosene, maintained the isotactic polypropylene in suspension and dissolved the undesirable atactic fraction. After polymerization, the suspension is treated with alcohol to deactivate and solubilize the catalyst residues, and filtered to separate the residues and atactic fraction from the desirable polymer, which is then dried. The alcohol and diluent are recovered by multiple distillations, and the atactic fraction is sold as a by-product. As the demand for polypropylene increased, these batch polymerization processes were rapidly replaced by continuous ones, such as the Hercules process shown in Figure 21. In this process, typical of those used throughout the 1960s and 1970s, a suspension of $TiCl_3$ catalyst in $Al(C_2H_5)_2Cl$ and kerosene diluent is continuously fed to the first of a series of continuous stirred overflow reactors. Monomer is fed to the first reactors and allowed to react out in the later ones, obviating the requirement for monomer recycle. Typical polymerization temperatures were in the range of 55–70°C and maximum pressures as high as 0.5 MPa (75 psig).

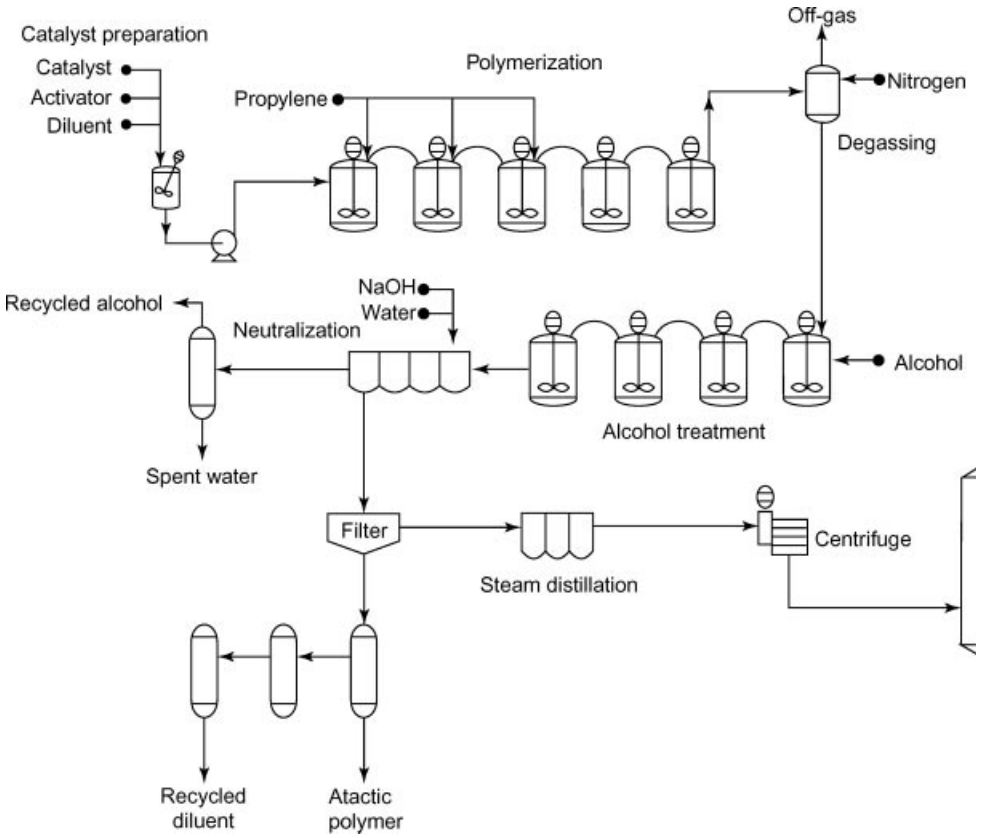

Fig. 21. Hercules slurry process for polypropylene.

Other similar processes, such as Montedison's, operated at pressures as high as 1.3 MPa (200 psig) with monomer recycle (265). Hydrogen is added to the reactors as required to achieve the desired polymer molecular weight (266). Following polymerization, the slurry is contacted with isopropyl alcohol, then aqueous caustic to decompose and neutralize catalyst residues. The aqueous phase containing the alcohol and catalyst residues is separated from hydrocarbon, polymer slurry phase. The suspended isotactic polymer is separated from the diluent containing the atactic polymer by continuous filtration or centrifugation, then dried. The alcohol and kerosene are each purified by a series of distillations, then recycled. Atactic polymer is dried using a thin-film evaporator and sold as by-product. The aqueous stream containing catalyst residues is treated prior to disposal of wastewater and inorganic solids. The products available from this technology were limited to homopolymers with relatively high molecular weights (MFR$<$ 15 dg/min), random copolymers containing low amounts of ethylene, and impact-resistant copolymers of high molecular weight and low rubber content. Excessive production of soluble polymer causing fouling of heat-transfer surfaces, was the primary cause of this limitation, more so than the loss of monomer to the production of less valuable by products. This limitation, and the high energy cost of recycling

diluent and alcohol, led to the development of processes that eliminated the need for diluent.

Polymerization in liquid monomer was pioneered by Rexall Drug and Chemical and Phillips Petroleum. In the Rexall process, liquid propylene is polymerized in a stirred reactor to form a polymer slurry. This suspension is transferred to a cyclone to separate the polymer from gaseous monomer under atmospheric pressure. The gaseous monomer is then compressed, condensed and recycled to the polymerizer (267). In the Phillips process, polymerization occurs in loop reactors, increasing the ratio of available heat-transfer surface to reactor volume (268). In both of these processes, high catalyst residues necessitate post-reactor treatment of the polymer.

Gas-phase polymerization of propylene was pioneered by BASF, who developed the Novolen process, using stirred-bed reactors (269). Unreacted monomer is condensed and recycled to the polymerizer, providing effective removal of the heat of reaction. As in the early liquid-phase systems, post-reactor treatment of the polymer is required to remove catalyst residues (270). The high content of atactic polymer in the final product limits its usefulness in many markets.

In the 1970s, Solvay introduced an advanced $TiCl_3$ catalyst with high activity and stereoregularity (271). The level of atactic polymer was sufficiently low so that its removal from the product was not required. When this catalyst was used in liquid monomer processes, residues were sufficiently reduced so that simplified systems for post-reactor treatment were acceptable. Montedison and Mitsui Petrochemical introduced $MgCl_2$-supported high yield catalysts in 1975 (272). Use of these catalyst systems reduced the level of corrosive catalyst residues to the extent that neutralization or removal from the polymer was not required. Stereospecificity, however, was insufficient to eliminate the requirement for removal of the atactic polymer fraction. These catalysts were used in the Montedison high yield slurry process, which does not contain the sections required for alcohol treatment, neutralization, and diluent purification in older slurry processes (265).

Current Processes. Introduction of high yield, high stereoregularity catalysts by Montedison and Mitsui in 1983 enabled the development of processes in which removal of catalyst and atactic polymer is unnecessary. This enabled the widespread use of processes in which monomer is the polymerization medium replacing slurry processes using an inert diluent. Investment and operating costs were dramatically reduced because of the elimination of the sections of the plant required for handling and purifying diluent and alcohol, removing catalyst and separating atactic polymer. Consequently, many companies invested in new plants either increasing capacity or replacing plants using the older, now obsolete processes. Almost all of the plants built in the past 15 years use one of the simplified processes. Moreover, the production capacity of a newer plant using these processes is often many times greater than those of earlier plants. Single line production capacities of 250 kt/y are no longer unusual, and plants with higher production capacities have been announced. The most widely used processes are Spheripol, licensed by Basell; Unipol, licensed by Univation; and Novolen, licensed by Novolen Gmbh.

The Spheripol process consists of one or more loop reactors for production of homopolymer and random copolymer, and one or more fluid bed gas-phase reactors for the production of the rubber phase for impact-resistant copolymers (Fig. 22).

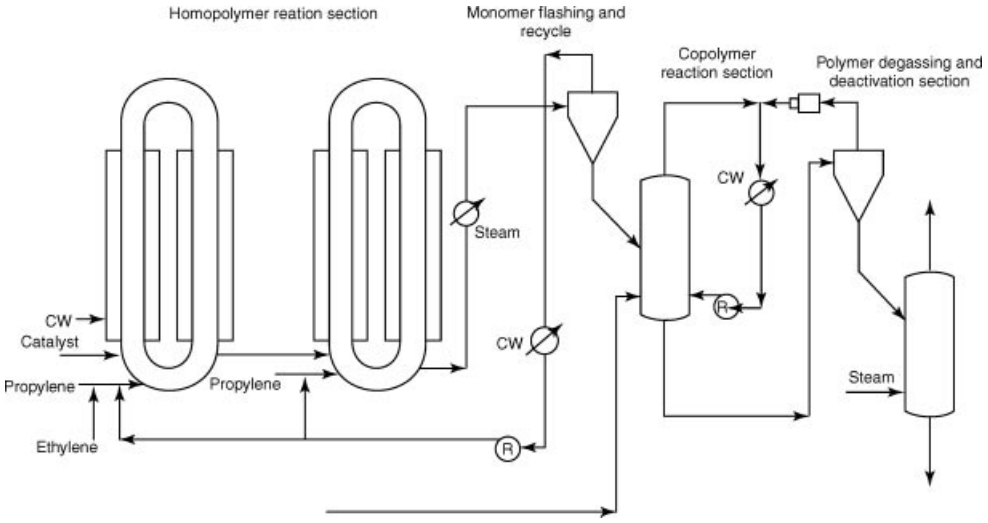

Fig. 22. Spheripol process

When producing impact-resistant copolymers, monomer and catalyst components are fed to the loop reactor for homopolymerization. The use of spherical form catalyst, with a narrow particle size distribution, coupled with high liquid velocities, minimizes reactor fouling maintaining effective heat transfer and enabling specific outputs in excess of 400 kg PP/h·m^3. After polymerization in the loop reactors, the polymer is separated from the liquid monomer by flashing at a pressure sufficient to allow condensation and recycle of the liquid monomer without recompression. The polymer is then transferred to the gas-phase reactors for the production of the rubber phase of impact-resistant copolymers. Ethylene and propylene are fed to the fluid bed reactor to produce ethylene–propylene rubber of the desired composition. Unreacted monomer is recycled and cooled using an external heat exchanger. The polymer is then separated from the unreacted monomer at a pressure slightly above 1 atm, and then contacted with steam for complete removal of residual monomer and termination of polymerization (273).

Liquid monomer is polymerized in continuous stirred tank reactors in a number of processes. The Hypol process, developed by Mitsui Petrochemical, uses a cascaded series of stirred reactors for homopolymerization, followed by fluidized bed gas-phase reactors for copolymerization (274). El Paso (now Huntsman) converted the Rexall liquid monomer process to use high yield catalysts eliminating the sections required for deashing and removal of atactic material (275). Shell (now Basell) developed the LIPP process to produce homopolymers and random copolymers, using their high yield catalysts.

The Unipol PP process developed by Union Carbide (now Dow) and licensed by Univation, uses a large gas phase fluidized bed reactor for the production of homopolymer and random copolymer. A second, smaller fluidized bed reactor is used in series to produce the rubber required for impact copolymers. The heat of reaction is removed by cooling the monomer through an external heat exchanger (Fig. 23). The heat removal capacity of this heat exchanger and, consequently, the

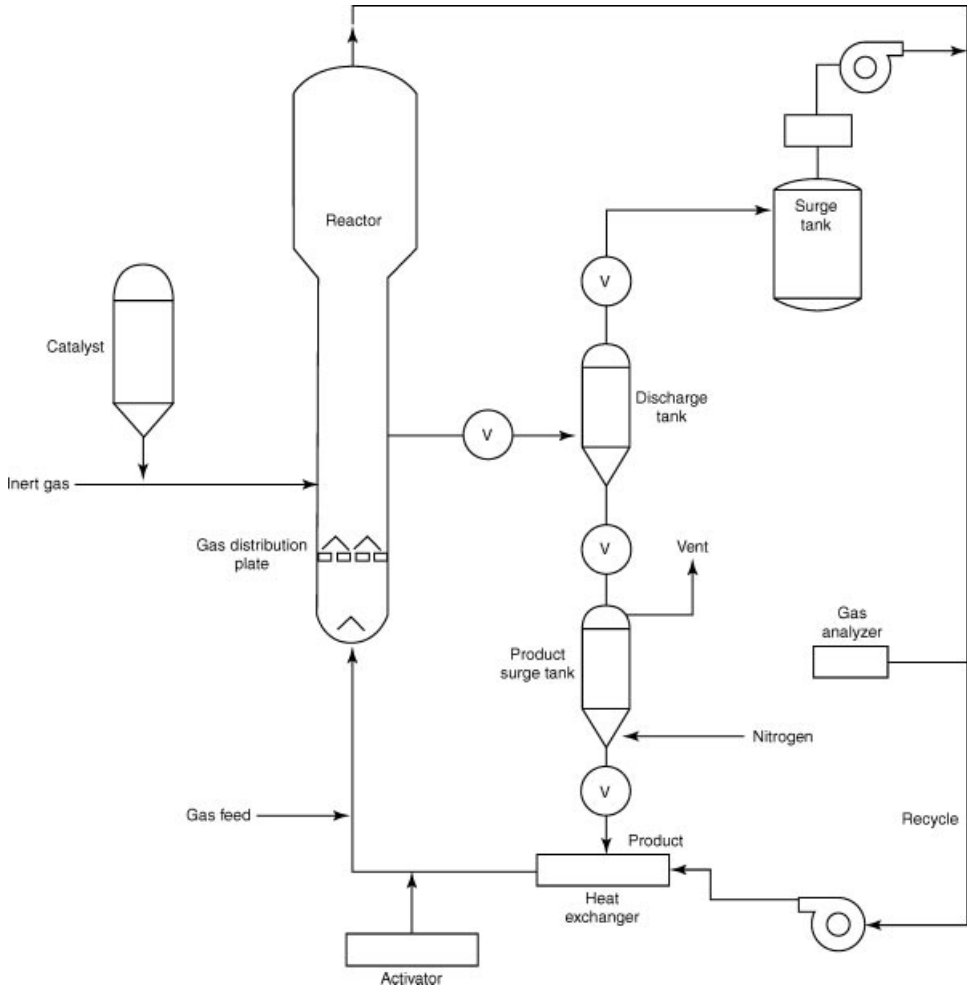

Fig. 23. The Unipol process.

production capacity of the plant is increased by facilitating condensation of hydrocarbon. This "condensing mode" technology has enabled this process to be used in very large single line polymerization plants (patent). Use of high yield catalysts in the Novolen process (Fig. 24), developed by BASF and licensed by Novolen Gmbh, has eliminated the problems associated with the use of first-generation catalysts. These catalysts enable the plants to achieve high capacity and improve product quality by minimizing catalyst residues and atactic polymer. This process uses a single vertical stirred bed reactor for the production of homopolymer and random copolymer and a second, similar reactor for the production of impact copolymers. Amoco (now BP) developed a horizontal stirred bed gas-phase reactor that acts as a series of polymerization stages in a single reactor vessel. This facilitates the production of homopolymers with broad molecular weight distribution. As in other processes, a second reactor can be used in series for the production of impact

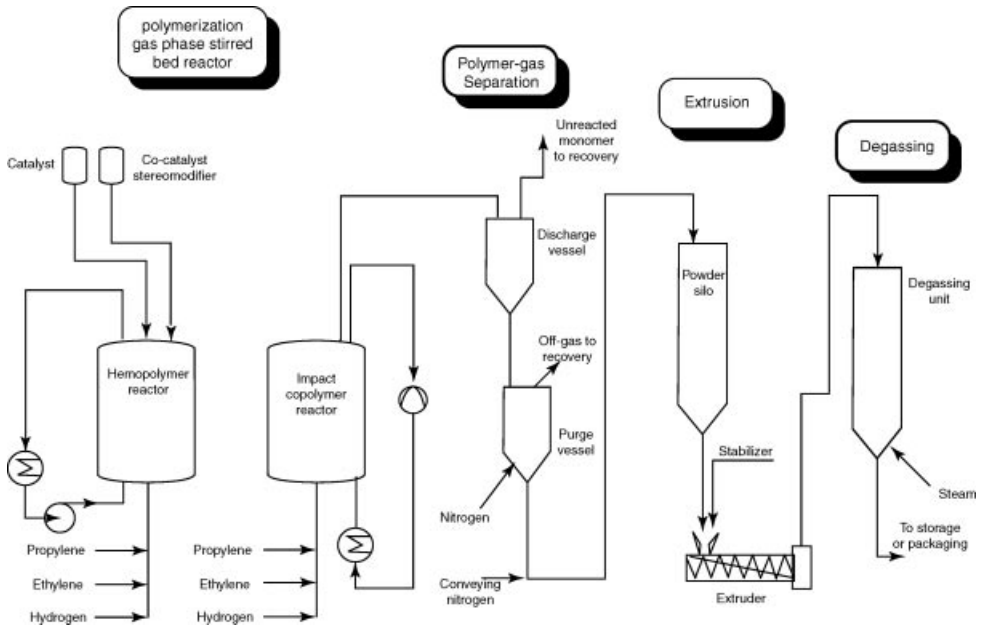

Fig. 24. The Novolen process.

copolymers. Basell produces specialty propylene copolymers in the multistage gas-phase Catalloy process (276).

The Borstar PP process developed by Borealis can operate at temperatures above the critical temperature of the reaction medium. This process uses a loop reactor and gas-phase reactor in series for the production of homopolymer. Additional gas-phase reactors are required for the production of impact copolymers. The first commercial scale plant using this process started in 2000. Basell has announced the development of the Spherizone process using a recirculating gas-phase reactor (Covezzi paper). The reactor contains two zones that can be operated under different conditions, enabling the production of multiphase specialty copolymers in a single reactor. This reactor was first used in a commercial scale plant in 2002.

Processing

PP structure can be tailored for use in most polymer processing technologies. The physical and mechanical properties of PP in the end use product are a function of both the molecular structure and the processing conditions. The most commonly used processes for iPP are discussed in the following.

Injection Molding. In the injection molding (qv) process, molten polymer is injected into a cold mold cavity. During mold filling, the melt is oriented by a combination of shear and elongational flow (277). Crystallization partially freezes in this orientation history. Injection-molded iPP articles are made from homopolymers, random and impact copolymers, and filled polymers. Melt flow rates lower

than 4 dg/min and as high as 100 dg/min in some impact copolymers can be used, depending on the mold geometry, part thickness, and cycle time desired. Processing conditions vary over a wide range because of the differences in polymer types. Since iPP melts exhibit shear-thinning properties, high injection pressures and high shear rates are used to promote the filling of the mold. Higher melt flow (lower molecular weight) polymers provide more uniform flow and low cycle times in parts with thin sections. Lower melt flow (higher molecular weight) polymers are employed when toughness is required, and can be used in parts that have thicker cross sections. Melt temperature varies with the melt-flow rate of the polymer and the mold shape. Higher temperatures reduce the melt viscosity and facilitate mold filling; however, the cycle time is increased. Melt temperatures as low as 200°C can be used with high melt-flow polymers; higher melt temperatures are required with low melt-flow polymers. Mold temperatures typically range from 20 to 50°C. Lower mold temperatures reduce the cycle time, but may produce a rough or low gloss surface. Orientation is an important determinant of properties and related to the skin layer thickness (see MORPHOLOGY). Melt temperature, melt-flow rate (MFR), polydispersity, and proximity to the mold gate influence skin thickness (120,278–286). Lower values result from higher melt temperature and MFR, and lower polydispersity. Regions far from the gate also have lower values. Molds should be designed to minimize localized stresses and ensure mold filling. When nonuniform wall thickness is required, it should decrease gradually in the flow direction. Like all crystalline thermoplastics, iPP is sensitive to failure at notches, and smooth radii are recommended at all sharp angles, corners, or ribs. Mold shrinkage varies with thickness from 1 to 2.5%. Thicker sections shrink more than thinner sections.

Fiber.

Melt Spinning. Melt spinning produces a broad range of iPP fibers, ranging from short staple fiber to continuous filament (CF) or bulked/textured continuous filaments (BCF) (see OLEFIN FIBERS). The tex per filament of the as-spun filaments, where tex is the mass of fiber (g) per 1000 m of length, is typically in the range of 0.14–7.78 tex (1.3–70 dpf). The lower end of this range corresponds to fine filaments of ∼15-μm diameter. Noncircular cross sections can be used to modify fiber appearance.

Melt spinning of iPP typically involves forcing molten polymer through a spinnerette (a collection of small-diameter orifices) and collecting it, typically on a take-up reel, some distance from the spinnerette at a velocity exceeding the orifice velocity. The tension provided by the take-up reel (melt drawing) provides partial orientation which greatly influences the final properties of the fiber. Yarns are collections of individual filaments, and can range from monofilaments to several thousand filaments depending on the process. Spinning speeds can approach 3000 m/min or higher in some cases. The iPP melt expands upon exiting the holes, a phenomenon known as *extrudate die swell* (287). The diameter of the extruded filament just after the die plate can typically increase on the order of 30–100% relative to the spinnerette hole depending on resin structure (melt flow rate, polydispersity). The swelling increases as the size of the die holes is reduced. This factor, and most often more importantly the maximum sustainable spin speed, determines the minimum diameter of melt-spun iPP fibers. During the spinning process, a fluid element experiences an acceleration (increase of velocity), decreasing temperature

due to a high rate of cooling, and decreasing diameter with increasing distance along the spin line (288). Large vertical air-cooling chambers, or chimneys, as high as 15 m can be required to cool the molten filament and allow adequate time for crystallization under the applied extensional force. Short spin processes generally use low spinning speeds to minimize the space required for quenching.

Fiber properties depend on the complex interrelationship of polymer structure (polydispersity, molecular weight, tacticity), processing conditions (melt temperature, melt throughput, spinnerette design, spin speed, cooling rate), and equipment design. Both material and processing variables influence the die swell, extensional melt rheology, maximum spin speed, crystallization/nucleation characteristics along the spin-line, and fiber orientation. Controlled rheology resins with narrow polydispersity are often used to improve the balance of spinning performance and fiber properties. Metallocene iPP resins have been introduced as an alternative technology (289,290). The tenacity (ultimate stress) of individual as-spun filaments is generally in the range of 0.088–0.353 N/tex (1–4 g/den). Break elongation decreases and tenacity increases with increasing spin speed due to increasing orientation. Post-drawing of filaments in the solid state below the polymer melting point, either via in-line continuous or off-line batch processes, further increases the tenacity of the fibers by improving fiber orientation. Drawing is generally carried out at temperatures exceeding 70°C, with draw ratios in the 2–10 range. The drawability is a function of the starting morphology, polymer structure, draw rate, and draw temperature. The ultimate tenacity of perfectly oriented iPP fibers has been estimated to be 1.32 N/tex (15 g/den) (121), though most commercial drawn fibers have tenacities of 0.353–0.794 N/tex (4–9 g/den). A heat setting, or annealing process below the polymer melting point, can minimize fiber shrinkage.

Melt Blowing. The melt-blowing process uses very high melt-flow rate (low molecular weight) iPP, sometimes in excess of 400–1500 dg/min. These melt-flow rates are much higher than for melt-spinning operations. The flow of molten, low viscosity polymer, extruded through a small die is disrupted by high velocity hot air. A large volume of cooling air fed near the die exit quenches the fibers and deposits them on a collecting screen as a mat of entangled fibers. Processing conditions and polymer structure can be varied to alter the filament diameter, characteristics of the collected mat, and undesirable large "shots," or polymer particles. Very fine fibers, less than 5 μm in diameter, can be produced. The fiber entanglement is sufficient to maintain the integrity of the web, and thermal bonding is not necessary. Fabrics produced by this process are very soft because of the small fiber diameter. Because the fibers are not highly oriented or bonded, meltblown fabrics usually have low tensile strength. Meltblown fabrics have improved barrier properties to aqueous liquids relative to spun-bonded fabrics.

Spun Bonded Fabrics. Spun bonded fabrics are produced by depositing extruded, spun filaments onto a collecting belt in a uniform randomized manner, followed by thermal bonding of the filaments. Polymers with melt-flow rates above 20 dg/min and narrow polydispersity improve stability during fiber formation and adequate melt throughput. The fibers are separated during the web-laying process by air jets and the collecting belt is usually perforated to prevent the air stream from deflecting and carrying the fibers in an uncontrolled manner. Thermal bonding, using heated embossing rolls or hot needles, imparts strength to the web

by fusing some of the fibers. This process can be combined with the melt-blowing process to produce soft, multilayer fabrics with good tensile properties. In these multilayer structures the meltblown fabric provides barrier resistance and the spun bonded fabric imparts strength.

Slit and Split Films. Thick industrial-grade yarns are often produced by slitting films, providing a less expensive alternative to direct extrusion. Cast film is slit in the machine direction by parallel rotary knives. The resulting tape can then be cold drawn in an oven below the polymer melting point, in a manner similar to drawn melt spun fibers, to produce the final fiber. Draw ratios of 4–11 are common. Higher draw ratios produce higher tenacity. The width of the slit tapes depends on the spacing between knives and the draw ratio. Knife spacings as low as 1 mm are sometimes used to produce textile fibers, although spacings of 10–35 mm are more common. Tapes produced by slitting a fully drawn film are wider than those oriented after slitting because of the physical limitations on minimum knife spacing. An alternative approach is to directly extrude the tapes prior to drawing. The tapes are annealed to minimize shrinkage. Fibers from split or fibrillated films are formed by the drawing of polypropylene film to the degree that it splits into numerous fiber-like interconnected tapes. In some processes the draw-induced splitting is mechanically augmented by gears, rollers, or gas jets (291).

Film.

Cast Film. The first commercial iPP films were produced by extrusion casting. Polymer is extruded through a slit or a tubular die and quenched by cooling on chill rolls or in a water bath. Cast film is not highly oriented and consequently does not have the stiffness of oriented films. Resins are typical iPP homopolymer or random copolymers. Random copolymers have improved clarity, and somewhat improved impact resistance. Rapid quenching often results in conversion to the mesomorphic form, which can be advantageous for film clarity. This tendency is greater in random copolymers than in homopolymer. High chill roll temperatures can result in hazy films, while chill roll temperatures which are too low (below the dew point of the ambient air) can result in water condensation on the film. Additives such as antiblock and slip agents are often added for improved handling of the film rolls.

Biaxially Oriented Polypropylene. Orientation improves the strength of iPP films. Biaxially oriented polypropylene (BOPP) films have higher strength and stiffness than cast films and consequently can often be used in much thinner gauges. Homopolymers are used almost exclusively to provide maximum stiffness and water-vapor barrier. Oriented films are produced by the tenter frame and tubular blown or double bubble methods. Most of the newly installed capacity has utilized the tenter frame process, taking advantage of the economics of the large, high capacity units available. The trend is to ever increasing line speeds, with 300 m/min not uncommon. In the tenter frame process, iPP is melt extruded through a slot die to form a sheet after quenching onto a cast roll. The cast sheet is heated to a temperature below the melting point, and drawn. In the case of sequential orientation, the softened cast sheet is drawn by a series of rolls to the desired draw ratio in the machine (longitudinal) direction, and subsequently clamped by a series of clips and conveyed into a tenter oven where it is subsequently drawn in the transverse direction to the desired draw ratio by the divergent chain clips. In the bubble process, a tube is extruded, quenched, and radially expanded by

inflation with air to provide transverse orientation. Axial orientation is provided by extension in the machine direction through a series of nip rolls. The tube is then flattened and slit into flat film. Orientation in both processes is provided by stretching below the melting point. The drawing process is strongly correlated to the crystallinity at the draw temperature which is closely related to the stereoregularity of the resin. Generally there is a trade-off between processability and final film mechanical and barrier properties. Heat aging under slight tension at a temperature above the orientation temperature but below the melting point minimizes subsequent shrinkage. Opaque films are produced by introducing microvoids into the film during the orientation by introducing small particles during extrustion. During orientation, microvoids are created as the polymer expands from the inelastic solid. Untreated oriented iPP films are not easily heat sealed. Consequently, lower melting random copolymers and terpolymers are often coextruded with the homopolymer to form a heat sealing layer.

Blow Molding. Low melt flow polymers are used in blow molding (qv) to provide the melt strength required to maintain stability of the parison, ie, a molten, thick-walled tube of melt. High density polyethylene has been more commonly used to form large parts because of its greater stability; however, a number of improved polypropylene grades are suitable for these applications (292). In extrusion blow molding, the extruded parison hangs freely before entering the mold, and low melt temperatures (between 205 and 215°C) are preferred. In injection blow molding, a preform is injection-molded on a steel rod, transferred to a blow molding mold, and blown. Consequently, the melt strength requirements of extrusion molding is alleviated to some extent, and higher melt temperatures can be used. Injection stretch blow molding produces a biaxially oriented part with higher stiffness, lower temperature impact strength, and greater clarity. The parison is cooled after it is formed by extrusion or injection molding, reheated to the desired orientation temperature, mechanically stretched, and then formed into the desired shape by blowing. Random copolymers of intermediate melt-flow rate (~10 MFR) have improved processing characteristics.

Extrusion and Thermoforming. iPP is extruded into sheet, usually for subsequent stamping or thermoforming (qv), or into pipes and profiles (see EXTRUSION). Low melt flow rate resins are used to provide the melt strength required to maintain uniformity. The choice of resin can often be dictated by subsequent forming operations. High melt strength polymers, produced by post-polymerization modification of conventional iPP, improve uniformity. Care must be taken for profiles of complicated geometry due to dimensional changes on crystallization, and variable cooling rate for regions differing in thickness. Good mixing of the melt during the extrusion process is important. Melt temperatures which are too high can promote degradation, leading to loss of properties, discoloration, and *plate out* which is the migration of additives and/or low molecular weight polymer to the surface of the sheet or profile. Lower temperatures reduce throughput and uniformity and lead to higher levels of orientation detrimental to subsequent forming.

In the thermoforming process, the sheet is extruded either in-line or off-line and formed, either in melt phase or solid phase, into a part of desired shape. Sheet uniformity is important. Historically, iPP has not been used in conventional melt-phase thermoforming equipment because of its narrow forming temperature range and the tendency of the melt to sag. Controlling the sag is particularly important

for large parts or multiple cavities. The introduction of newer iPP grades with higher melt strength and improved sag resistance has increased the use of iPP in conventional melt-phase thermoforming equipment (293). Processes such as Shell's solid-phase pressure forming (294) were developed to overcome problems associated with melt forming. The iPP article is formed at temperatures close to but below the crystalline melting point, by stretching the sheet into the mold cavity with a shaped plug. The part is forced against the mold surface by cold air to obtain the desired shape. Manufacturers of thermoforming equipment have also modified their processes to effectively utilize iPP (295).

Stabilization. Polypropylene is subject to attack by oxygen, radiation, and excessive heat causing a loss of molecular weight and physical properties. Stabilizers are added to the polymer to minimize these effects. Small quantities of hindered phenolic antioxidants (qv) are added in the polymerization plant, usually in the drying section, to protect the polymer against degradation (qv) during short-term storage. Typically 2,6-di-*tert*-butyl-*p*-cresol (BHT) and octadecyl 3,5-di(*tert*-butyl-4-hydroxy)hydrocinnamate (Irganox 1076) are used. The bulk of the stabilizer is added during pelletization or fabrication to protect the polymer during processing or in the final application. Typical stabilization formulations include a hindered phenolic antioxidant, possibly with a thiodipropionate synergist, a phosphite to provide high temperature melt stabilization, and an acid scavenger such as calcium stearate or dihydrotalcite (296). Hindered phenols limit the propagation of alkyl radicals and the resulting chain scission. Thiodipropionic acid esters act to decompose peroxides formed by polypropylene oxidation. More importantly, the sulfonic acid intermediate of thiodipropionate oxidation acts as a scavenger for the free radicals formed by the decompositon of phenols, increasing the effectiveness of the phenolic antioxidant (297). Phosphites also act to decompose peroxides and are most effective at the temperatures usually encountered in processing. The acid scavenger acts to prevent the reactions between hindered phenols and metal chlorides that can form colored titanium phenolates, as well as minimize equipment corrosion. Protection against ultraviolet radiation is usually provided by a hindered amine light stabilizer (HALS), such as Tinuvin 770 (see UV STABILIZERS). Stabilization (qv) of polypropylene has been reviewed (157).

Economic Aspects

Polypropylene consumption continues to increase more rapidly than the economy and most other thermoplastics. Although the comparative growth in polypropylene consumption has slowed from that in the 1970s and 1980s, the relative share of polypropylene use in North America has increased from 17% to 20% of all thermoplastics during the 1990s (298). The annual increase in consumption of polypropylene in North America averaged about 7% through the same period (299). Consumption in Western Europe has also increased at a similar rate. Growth in Japan has been much slower than in other countries, in part because of the protracted Japanese recession in the late 1990s, but also because of competition from the emerging economies in East Asia. The rapid growth of the Asia/Pacific region has been the major economic story of the past decade, and the growth in polypropylene consumption and production has been phenomenal. This region is

Table 12. World Consumption of Polypropylene, 10^3 ton[a,b]

Country	1994	1995	1996	1997	1998	1999	2000	2001
United States	4145	4220	4654	5063	5412	6350	6439	7317
Canada	293	358	379	368	361			
Mexico	236	219	227	285	310			
Brazil	374	527	537	584	612	687		
Western Europe	5030	4979	5440	5766	6278	6795	6976	7360
Japan	2080	2219	2365	2439	2268	2298	2756	2734
China					3100	3535	4230	
India					763	931	1026	1194

[a] Ref. 300.
[b] U.S. consumption in 2002 was 7748×10^3 t (301).

now the world's largest market for polypropylene, accounting for almost 40% of supply and demand (302). China has developed as one the world's major markets for polypropylene and other thermoplastics, and is the leading importer of plastics, despite a significant increase in its production capacity. World consumption data for polypropylene are listed in Table 12. Malaysia, South Korea, India, and Thailand have joined Taiwan as significant producers, with the construction of modern, world-scale manufacturing plants. Brazil, the largest market in Latin America, has also grown at a rapid pace.

This increase in consumption has, however, been more than matched by a larger increase in production capacity, fostering a situation of oversupply and low capacity utilization. New plants often have production capacities of 250 kt/y to capitalize on the economy of large-scale facilities. In North America, where refinery propylene is the source for most monomer, the decision to invest in polypropylene capacity is often related to the need to market propylene. Arco Products (now part of BP) and Tosco (now owned by Phillips) both decided to produce polypropylene as the most cost-effective way to eliminate regulatory problems caused by excess propylene production at their refineries. Arco/Tosco capacity increased by 23% from 1998 to 2001; however, consumption only increased by 17% over the same period. Capacity utilization dropped to the lowest levels since 1989. Producers' profit margins have decreased dramatically as the polymer prices have fallen relative to the cost of production. These profit margins are highly dependent upon the difference between the price of polymer and the price of propylene monomer. Monomer prices are related to oil prices; however, polymer prices are related to supply and demand. This difference has decreased consistently through the past decade, as some producers have been willing to supply at the lower prices. It has been estimated that a significant number of producers have been operating at a loss (303). Consequently, producers reduced capacity by closing or idling plants. Table 13 gives world production data, and Table 14 gives world capacity information and Table 15 gives U.S. production and capacity for the years 2000–2002. The 4% decrease in polypropylene capacity in 2002 is unprecedented in North America. Excess capacity and low profit margins characterize the polypropylene industry throughout the world, not just in North America, as the industry has become globalized. The market situation in Asia can dramatically affect prices in North America and Europe as imports into that region increase or decrease.

Table 13. World Production of Polypropylene, 10^3 ton[a]

Country	1994	1995	1996	1997	1998	1999
United States	4326	4939	5438	6041	6270	7026
Canada	258	329	320	320	322	
Mexico	170	227	210	196		
Brazil	535	557	590	636	707	767
Western Europe						
Japan[b]	2248	2488	2683	2788	2597	2678

[a] Ref. 300.
[b] 2001 production in Japan, 2760×10^3 t (302).

Table 14. World Capacity of Polypropylene, 10^3 ton[a]

Country	1994	1995	1996	1997	1998	1999[b]
United States	4644	5433	5911	6453	7001	7732
Canada	324					324
Mexico	249					220
Brazil		796	778	755	785	912
Western Europe						8166
Japan		2454				3063
China		841	888	1257	1423	1503
South Korea	1705	1696	2025	2175	2620	
India	161	349	490	745	791	
Taiwan	460	469	479	489	798	
Thailand	310	359	580	800	1088	

[a] Ref. 300.
[b] For countries other than U.S., Ref. 304.

Table 15. United States Production and Capacity of Polypropylene, 10^3 ton, for 2000–2002[a]

	2000	2001	2002
Production	7138	7226	7690
Capacity	8117	8620	8241

[a] Ref. 301.

To combat the decrease in profitability major producers have chosen to reduce costs through mergers. Royal Dutch/Shell and BASF have merged their polyolefin activities, formerly Montell, Elenac and Targor, to form Basell, which is the world's largest producer of polypropylene. This company contains facilities that were once part of BASF, Hercules, Hoechst, ICI, Montedison, and Shell. Borealis, one of the largest European producers and the result of a merger between the polyolefin businesses of Statoil and Neste, acquired PCD and OMV, two smaller producers. Major mergers of large petroleum companies, such as Exxon and Mobil (ExxonMobil), BP, Amoco and ARCO (BP), and Total, Elf Aquitane and Fina (TotalFina) have also resulted in the combination of their polymer operations. The Dow Chemical Co. purchased Union Carbide, combining the polypropylene businesses of the two companies. Japanese producers affiliated with Mitsui have

Table 16. Distribution of Polypropylene by Principal North American Market, 10^3ton

Market	1994	1995	1996	1997	1998	1999	2000	2001	(Growth)	2002	(Growth)
Transportation	281	342	329	352	378	334	337	323	(0.051)	345	(0.053)
Packaging	922	1036	1104	1182	1270	1614	1586	1578	0.089	1851	0.096
Building and construction	115	0	0	0	0	171	179	159	0.066	168	0.065
Electrical/electronic	147	162	180	193	207	185	155	156	0.038	164	0.039
Furniture and furnishings	766	866	937	1003	1078	834	913	829	0.034	923	0.041
Consumer and institutional	1091	1215	1283	1373	1476	1538	1497	1510	0.075	1661	0.077
All other	892	904	1200	1285	1381	1784	1771	1784	0.104	1878	0.099
Exports	297	332	463	565	489	539	629	856	0.016	758	0.004
Total	*4511*	*4857*	*5497*	*5952*	*6278*	*7000*	*7067*	*7317*	*0.068*	*7748*	*0.068*

Table 17. Consumption of Polypropylene by Use in North America, 10^3 ton

USe	1994	1995	1996	1997	1998	1999	2000	2001
Injection molding	1498	1665	1765	1655	1818	2108	2068	2158
Appliances	120	129	142	116	134	150	113	118
Consumer products	598	539	611	695	768	923	898	938
Rigid packaging	390	438	484	545	609	674	712	795
Transportation	229	281	262	185	215	251	259	244
Other	162	278	266	109	93	110	86	63
Blow molding	75	80	78	78	81	84	66	81
Extrusion	1834	2048	2184	2209	2382	2546	2587	2478
Film	420	488	514	525	548	598	609	601
Sheet	72	108	104	108	116	141	150	196
Fiber	1275	1391	1505	1499	1645	1729	1732	1593
All other	67	60	63	77	73	77	96	88
Other End Use	806	732	1006	1446	1508	1724	1718	1744
Total	*4214*	*4525*	*5034*	*5387*	*5789*	*6461*	*6439*	*6461*

merged operations to form Grand Polymers and those affiliated with Mitsubishi have formed Japan Polychem. Mitsui and Sumituomo have announced a merger of their chemicals businesses, and included polypropylene. At the end of 2001, the largest producers of polypropylene in order of capacity are Basell, BP, Atofina, ExxonMobil, and Dow Chemical (305). In Europe, the largest producers are Basell, Borealis, Atofina, Sabic, and BP, respectively.

The principal market applications of polypropylene in North America are shown in Table 16. The use of polypropylene in packaging has grown more rapidly than other areas because of its increased use in injection-molded containers and packaging films. The consumer and institutional products sector is the largest market for polypropylene. This sector is the most diverse and includes nonwoven polypropylene fabrics in baby diapers as well as injection-molded toys and houseware. This market has also grown considerably in the past decade. The consumption of polypropylene in furniture and furnishings, which includes carpet fiber, continues to be one of the major applications, but is growing more slowly than overall consumption. The use of polypropylene in transportation, primarily automobiles, is not growing as fast as other areas. Consumption of polypropylene in injection-molded transportation applications has declined in recent years, as shown in Table 17. Polypropylene is most commonly extruded into fibers or films, or injection molded. Other fabrication processes are not used as frequently.

BIBLIOGRAPHY

"Propylene Polymers" in *EPST* 1st ed., Vol. 11, pp. 597–619, by J. L. Jezl, Avisun Corp., and E. M. Honeycutt, Patchogue Plymouth Co.; in *EPSE* 2nd ed., Vol. 13, pp. 464–531, by Richard B. Lieberman, Himont Research and Development Center, and Pier Camillo Barbe, Himont Italia, Centro Recerche Guilio Natta, Italy.

1. G. L. Yaws, *Physical Properties*, McGraw-Hill Inc., New York, (1977).
2. R. W. Gallant, *Physical Properties of Hydrocarbons*, Vol. 1, Gulf Publishing Co., Houston, Tex., (1968).

3. R. C. Reid, J. M. Prausnitz, and T. K. Sherwood, *The Properties of Gases and Liquids*, 3rd ed., McGraw-Hill Inc., New York, (1977).
4. H. H. Brintzinger, D. Fischer, R. Mulhaupt, B. Rieger, and R. M. Waymouth, *Angew. Chem., Int. Ed. Engl.* **34**, 1143 (1995).
5. G. H. Llinas, S.-H. Dong, D. T. Mallin, M. D. Rausch, Y.-G. Lin, H. H. Winter, and J. C. W. Chien, *Macromolecules* **25**, 1242 (1992).
6. E. Hauptman, R. M. Waymouth, and J. W. Ziller, *J. Am. Chem. Soc.* **117**, 11586 (1995).
7. W. J. Gauthier, J. F. Corrigan, N. J. Taylor, and S. Collins, *Macromolecules* **28**, 3771 (1995).
8. E. A. Youngman and J. Boor, *Macromol. Rev.* **2**, 33 (1967).
9. A. Zambelli and C. Tosi, *Adv. Polym. Sci.* **32**, 15 (1974).
10. C. Wolfsgruber, G. Zannoni, E. Rigamonti, and A. Zambelli, *Makromol. Chem.* **176**, 2765 (1975).
11. A. Zambelli, P. Locatelli, G. Zannoni, and F. A. Bovey, *Macromolecules* **11**, 923 (1978).
12. F. C. Shilling and A. E. Tonelli, *Macromolecules* **13**, 270 (1980).
13. Y. Doi, T. Suzuki, and T. Keii, *Makromol. Chem. Rapid Commun.* **2**, 293 (1981).
14. S. N. Zhu, X. Z. Yang, and R. Chûjô, *Polym. J.* **15**, 859 (1983).
15. J. A. Ewen, *J. Am. Chem. Soc.* **106**, 6355 (1984).
16. R. Paukkeri, T. Väänänen, and A. Lehtinen, *Polymer* **34**, 2488 (1993).
17. M. Farina, G. DiSilvestro, and P. Sozzani, *Macromolecules* **26**, 946 (1993).
18. V. K. Gupta, S. Satish, and I. S. Bhardwaj, *J. Macromol. Sci., Rev. Macromol. Chem. Phys.* **34**, 439 (1994).
19. R. Paukkeri, E. Iiskola, A. Lehtinen, and H. Salminen, *Polymer* **35**, 2636 (1994).
20. V. Busico, P. Corradini, R. DeBiasio, L. Landriani, and A. L. Segre, *Macromolecules* **27**, 4521 (1994).
21. M. Farina, G. DiSilvestro, and A. Terragni, *Macromol. Chem. Phys.* **196**, 353 (1995).
22. M. D. Bruce and R. M. Waymouth, *Macromolecules* **31**, 2707 (1998).
23. R. A. Phillips and M. D. Wolkowicz, in E. P. Moore Jr., ed., *Polypropylene Handbook*, Hanser, Munich, 1996.
24. V. Busico, R. Cipullo, and P. Corradini, *Makromol. Chem.* **194**, 1079 (1993).
25. V. Busico, R. Cipullo, and P. Corradini, *Makromol. Chem., Rapid Commun.* **14**, 97 (1993).
26. V. Busico, R. Cipullo, J. C. Chadwick, J. F. Modder, and O. Sudmeijer, *Macromolecules* **27**, 7538 (1994).
27. T. Tsutsui, N. Kashiwa, and A. Mizuno, *Makromol. Chem., Rapid Commun.* **11**, 565 (1990).
28. J. C. Chadwick, A. Miedema, and O. Sudmeijer, *Macromol. Chem. Phys.* **195**, 167 (1994).
29. J. C. Chadwick, G. M. M. van Kessel, and O. Sudmeijer, *Macromol. Chem. Phys.* **196**, 1431 (1995).
30. E. Albizzati, U. Giannini, G. Collina, L. Noristi, and L. Resconi, in E. P. Moore Jr., ed., *Polypropylene Handbook*, Hanser, Munich, 1996.
31. K. Soga, T. Shiono, S. Takemura, and W. Kaminsky, *Makromol. Chem. Rapid Commun.* **8**, 305 (1987).
32. A. Grassi, A. Zambelli, J. L. Resconi, E. Albizzati, and R. Mazzocchi, *Macromolecules* **21**, 617 (1988).
33. A. Toyota, T. Tsutsui, and N. Kashiwa, *J. Mol. Catal.* **56**, 237 (1989).
34. T. Tsutsui, N. Ishimaru, A. Mizumo, A. Toyota, and N. Kashiwa, *Polymer* **30**, 1350 (1989).
35. H. N. Cheng and J. A. Ewen, *Makromol. Chem.* **190**, 1931 (1989).
36. W. Roll, H.-H. Brintzinger, B. Rieger, and R. Zolk, *Angew. Chem., Int. Ed. Engl.* **29**, 279 (1990).

37. B. Rieger, X. Mu, D. T. Mallin, M. D. Rausch, and J. C. W. Chien, *Macromolecules* **23**, 3559 (1990).
38. J. C. W. Chien and R. Sugimoto, *J. Polym. Sci., Polym. Chem. Ed.* **29**, 459 (1991).
39. D. Fischer and R. Mulhaupt, *Macromol. Chem. Phys.* **195**, 1433 (1994).
40. U. Stehling, J. Diebold, R. Kirsten, W. Roll, H. H. Brintzinger, S. Jungling, R. Mulhaupt and F. Langhauser, *Organometallics* **13**, 964 (1994).
41. L. Resconi, A. Fait, F. Piemontesi, M. Colonnesi, H. Rychlicki, and R. Zeigler, *Macromolecules* **28**, 6667 (1995).
42. F. A. Bovey, *High Resolution NMR of Macromolecules*, Academic Press, Inc., New York, 1972.
43. R. Chûjô, Y. Kogure, and T. Väänänen, *Polymer* **35**, 339 (1994).
44. M. Härkönen, J. V. Seppälä, R. Chûjô, and Y. Kogure, *Polymer* **36**, 1499 (1995).
45. Y. Doi, *Makromol. Chem., Rapid Commun.* **3**, 635 (1982).
46. D. R. Burfield and P. S. T. Loi, *J. Appl. Polym. Sci.* **36**, 279 (1988).
47. R. Paukkeri and A. Lehtinen, *Polymer* **34**, 4075 (1993).
48. G. Natta, G. Mazzanti, G. Crespi, and G. Moraglio, *Chim. Ind.* **39**, 275 (1957).
49. J. B. P. Soares and A. E. Hamielec, *Polymer* **36**, 1639 (1995).
50. U. S. Pat. 5,302,897 (Apr. 12, 1994), R. L. Dechene, T. B. Smith, S. A. Marino, J. Tache, and A. Roy (to Auburn International).
51. M. G. Styring and A. E. Hamielec in A. R. Cooper, ed., *Determination of Molecular Weight*, John Wiley & Sons, Inc., New York, 1989.
52. P. J. Flory, *Principles of Polymer Chemistry*, Cornell University Press, Ithaca, N.Y., 1953.
53. H. Coll, in A. R. Cooper, ed., *Determination of Molecular Weight*, John Wiley & Sons, Inc., New York, 1989.
54. A. R. Cooper, in A. R. Cooper, ed., *Determination of Molecular Weight*, John Wiley & Sons, Inc., New York, 1989.
55. B. Chu, in A. R. Cooper, ed., *Determination of Molecular Weight*, John Wiley & Sons, Inc., New York, 1989.
56. M. Kurata and Y. Tsunashima, in J. Brandrup, E. H. Immergut, and E. A. Grulke, eds., *Polymer Handbook*, 4th ed., John Wiley & Sons, Inc., New York, 1999.
57. Th. G. Scholte, N. L. J. Meijerink, H. M. Schoffeleers, and A. M. G. Brands, *J. Appl. Polym. Sci.* **29**, 3763 (1984).
58. I. Pasquon, *Pure Appl. Chem.* **15**, 465 (1967).
59. J. B. Kinsinger and R. E. Hughes, *J. Phys. Chem.* **63**, 2002 (1959).
60. P. Parrini, F. Sebastiano, and G. Messina, *Makromol. Chem.* **38**, 27 (1960).
61. G. Zeichner and P. Patel, *2nd World Congress of Chemical Engineering*, Montreal, P. Q., Canada, 1981.
62. W. W. Graessley, *The Entanglement Concept in Polymer Rheology*, Advance Polymer Science Series 16, Springer-Verlag, New York, 1974.
63. G. Natta and P. Corradini, *del Nuovo Cimento* **XV**, 40 (1960).
64. B. Lotz, J. C. Wittmann, and A. J. Lovinger, *Polymer* **37**, 4979 (1996).
65. S. Bruckner, S. V. Meille, V. Petraccone, and B. Pirozzi, *Prog. Polym. Sci.* **16**, 361 (1991).
66. A. J. Lovinger, B. Lotz, D. D. Davis, and F. J. Padden Jr., *Macromolecules* **26**, 3494 (1993).
67. C. DeRosa and P. Corradini, *Macromolecules* **26**, 5711 (1993).
68. A. J. Lovinger, B. Lotz, D. D. Davis, and M. Schumacher, *Macromolecules* **27**, 6603 (1994).
69. W. Stocker, M. Schumacher, S. Graff, J. Lang, J. C. Wittmann, A. J. Lovinger, and B. Lotz, *Macromolecules* **27**, 6948 (1994).

70. P. Corradini, V. Petraccone, C. DeRosa, and G. Guerra, *Macromolecules* **19**, 2699 (1986).
71. P. Corradini, C. DeRosa, G. Guerra, and V. Petraccone, *Polym. Commun.* **30**, 281 (1989).
72. S. V. Meille, D. R. Ferro, S. Bruckner, A. J. Lovinger, and F. J. Padden, *Macromolecules* **27**, 2615 (1994).
73. D. L. Dorset, M. P. McCourt, S. Kopp, M. Schumacher, T. Okihara, and B. Lotz, *Polymer* **39**, 6331 (1998).
74. B. Rieger, X. Mu, D. T. Mallin, M. D. Rausch, and J. C. W. Chien, *Macromolecules* **23**, 3559 (1990).
75. D. Fischer and R. Mulhaupt, *Macromol. Chem. Phys.* **195**, 1433 (1994).
76. R. Thomann, C. Wang, J. Kressler, and R. Mulhaupt, *Macromolecules* **29**, 8425 (1996).
77. K. Mezghani and P. J. Phillips, *Polymer* **39**, 3735 (1998).
78. S. Bruckner and S. V. Meille, *Nature* **340**, 455 (1989).
79. S. V. Meille, S. Bruckner, and W. Porzio, *Macromolecules* **23**, 4114 (1990).
80. B. Lotz, S. Graff, C. Staupe, and J. C. Wittmann, *Polymer* **32**, 2902 (1991).
81. D. R. Ferro, S. Bruckner, S. V. Meille, and M. Ragazzi, *Macromolecules* **25**, 5231 (1992).
82. A. J. Lovinger and B. Lotz, *J. Polym. Sci., Part B: Polym. Phys.* **35**, 2523 (1997).
83. I. Rodriguez-Arnold, Z. Bu, and S. Z. D. Cheng, *J. Macromol. Sci., Rev. Macromol. Chem. Phys. C* **35**, 117 (1995).
84. P. Sozzani, R. Simonutti, and M. Galimberti, *Macromolecules* **26**, 5782 (1993).
85. A. Marigo, C. Marega, and R. Zannetti, *Macromol. Rapid Commun.* **15**, 225 (1994).
86. C. DeRosa, F. Auriemma, and V. Vinti, *Macromolecules* **30**, 4137 (1997).
87. C. DeRosa, F. Auriemma, and V. Vinti, *Macromolecules* **31**, 7430 (1998).
88. C. DeRosa, F. Auriemma, V. Vinti, and M. Galimberti, *Macromolecules* **31**, 6206 (1998).
89. F. Auriemma, R. H. Lewis, H. W. Spiess, and C. DeRosa, *Macromol. Chem. Phys.* **196**, 4011 (1995).
90. F. Auriemma, R. Born, H. W. Spiess, C. DeRosa, and P. Corradini, *Macromolecules* **28**, 6902 (1995).
91. F. Auriemma, C. DeRosa, O. Ruiz de Ballesteros, and P. Corradini, *Macromolecules* **30**, 6586 (1997).
92. C. DeRosa, F. Auriemma, V. Vinti, A. Grassi, and M. Galimberti, *Polymer* **39**, 6219 (1998).
93. J. Loos, A. M. Schauwienold, S. Yan, J. Petermann, and W. Kaminsky, *Polym. Bull.* **38**, 185 (1997).
94. T. Nakaoki, Y. Ohira, H. Hayashi, and F. Horii, *Macromolecules* **31**, 2705 (1998).
95. Y. Ohira, F. Horii, and T. Nakaoki, *Macromolecules* **33**, 5566 (2000).
96. G. Natta, M. Peraldo, and A. Allegra, *Makromol. Chem.* **75**, 215 (1964).
97. Y. Chatani, H. Maruymama, T. Asanuma, and T. Shiomura, *J. Polym. Sci., Polym. Phys.* **29**, 1649 (1991).
98. D. R. Burfield, P. S. T. Loi, Y. Doi, and J. Majzik, *J. Appl. Polym. Sci.* **41**, 1095 (1990).
99. D. S. Davis, *J. Plast. Film Sheeting* **8**, 101 (1992).
100. J. H. Griffith and B. G. Ranby, *J. Polym. Sci.* **XXXVIII**, 107 (1959).
101. F. J. Baltá-Calleja and C. G. Vonk, *X-ray Scattering of Synthetic Polymers*, Elsevier, Amsterdam, 1989.
102. F. J. Padden Jr. and H. D. Keith, *J. Appl. Phys.* **37**, 4013 (1966).
103. F. L. Binsbergen and B. G. M. deLange, *Polymer* **9**, 23 (1968).
104. F. J. Padden Jr. and H. D. Keith, *J. Appl. Phys.* **44**, 1217 (1973).
105. A. J. Lovinger, *J. Polym. Sci., Polym. Phys. Ed.* **21**, 97 (1983).
106. D. R. Norton and A. Keller, *Polymer* **26**, 704 (1985).
107. B. Lotz and J. C. Wittmann, *J. Polym. Sci., Polym. Phys. Ed.* **24**, 1541 (1986).
108. F. J. Padden and H. D. Keith, *J. Appl. Phys.* **30**, 1479 (1959).

109. J. Varga, *J. Mater. Sci.* **27**, 2557 (1992).
110. H. Awaya, *Polymer* **29**, 591 (1988).
111. A. Lustiger, C. N. Marzinsky, and R. R. Mueller, *J. Polym. Sci., Part B: Polym. Phys.* **36**, 2047 (1998).
112. M. Schumacher, A. J. Lovinger, P. Agarwal, J. C. Wittmann, and B. Lotz, *Macromolecules* **27**, 6956 (1994).
113. A. Galambos, M. Wolkowicz, and R. Zeigler, in E. J. Vandenberg and J. C. Salamone, eds., *Catalysis in Polymer Synthesis*, ACS Symposium Series, **496**, 1991.
114. Z-G. Wang, R. A. Phillips, and B. S. Hsiao, *J. Polym. Sci., Part B: Polym. Phys.* **39**, 1876 (2001).
115. J. Schmidtke, G. Strobl, and T. Thurn-Albrecht, *Macromolecules* **30**, 5804 (1997).
116. P. Supaphol, J. E. Spruiell, and J. S. Lin, *Polym. Int.* **49**, 1473 (2000).
117. A. J. Lovinger, D. D. Davis, and B. Lotz, *Macromolecules* **24**, 552 (1991).
118. J. Rodriquez-Arnold, A. Zhang, S. Z. D. Cheng, A. J. Lovinger, E. T. Hsieh, P. Chu, T. W. Johnson, K. G. Honnell, R. G. Geerts, S. J. Palackal, G. R. Hawley, and M. B. Welch, *Polymer* **35**, 1884 (1994).
119. J. Kressler, in J. Karger-Kocsis, ed., *Polypropylene an A-Z Reference*, Kluwer Academic Publishers, Dordrecht, the Netherlands, 142, 1999.
120. P. Supaphol and J. E. Spruiell, *Polymer* **41**, 1205 (2000).
121. R. Phillips, G. Hebert, J. News, and M. Wolkowicz, *Polym. Eng. Sci.* **34**, 1731 (1994).
122. R. J. Samuels, *Structured Polymer Properties: The Identification, Interpretation, and Application of Crystalline Polymer Structure*, John Wiley & Sons, Inc., New York, 1974.
123. A. Peterlin, *Polym. Eng. Sci.* **17**, 183 (1977).
124. A. Peterlin, *Colloid Polym. Sci.* **265**, 357 (1987).
125. M. F. Butler, A. M. Donald, and A. J. Ryan, *Polymer* **39**, 39 (1998).
126. I. Karacan, A. K. Taraiya, D. I. Bower, and I. M. Ward, *Polymer* **34**, 2692 (1993).
127. M. Cakmak, J. E. Spruiell, J. L. White, and J. S. Lin, *Polym. Eng. Sci.* **27**, 893 (1987).
128. P. Galli, *Macromol. Symp.* **78**, 269 (1994).
129. R. Galvan and M. Tirrell, *Chem. Eng. Sci.* **41**, 2385 (1986).
130. W. R. Schmeal and J. R. Street, *AIChE J.* **17**, 1188 (1971).
131. E. J. Nagel, V. A. Kirillov, and W. H. Ray, *Ind. Eng. Chem., Prod. Res. Dev.* **19**, 372 (1980).
132. S. Floyd, K. Y. Choi, T. W. Taylor, and W. H. Ray, *J. Appl. Polym. Sci.* **32**, 2935 (1986).
133. M. A. Ferrero and M. G. Chiovetta, *Polym. Eng. Sci.* **27**, 1436 (1987).
134. M. A. Ferrero and M. G. Chiovetta, *Polym. Eng. Sci.* **31**, 904 (1991).
135. R. A. Hutchinson, C. M. Chen, and W. H. Ray, *J. Appl. Polym. Sci.* **44**, 1389 (1992).
136. E. L. Hoel, C. Cozewith, and G. D. Byrne, *AIChE J.* **40**, 1669 (1994).
137. T. F. McKenna, J. Dupuy, and R. Spitz, *J. Appl. Polym. Sci.* **57**, 3731 (1995).
138. L. Noristi, E. Marchetti, G. Baruzzi, and P. Sgarzi, *J. Polym. Sci., Polym. Chem. Ed.* **32**, 3047 (1994).
139. M. A. Ferrero, E. Koffi, R. Sommer, and W. C. Conner, *J. Polym. Sci., Polym. Chem. Ed.* **30**, 2131 (1992).
140. E. Martuscelli, M. Pracella, and A. Zambelli, *J. Polym. Sci., Polym. Phys. Ed.* **18**, 619 (1980).
141. B. Wunderlich, *Macromolecular Physics*, Vol. 3, Academic Press, Inc., New York, 1980.
142. E. Martuscelli, M. Pracella, and L. Crispino, *Polymer* **24**, 693 (1983).
143. J. J. Janimak, S. Z. D. Cheng, A. Zhang, and E. T. Hsieh, *Polymer* **33**, 729 (1992).
144. R. Paukkeri and A. Lehtinen, *Polymer* **34**, 4083 (1993).
145. K. D. Hungenberg, J. Kerth, F. Langhauser, B. Marczinke, and R. Schlund, in G. Fink, R. Mulhaupt, and H. H. Brintzinger, eds., *Ziegler Catalysts*, Springer-Verlag, Berlin, 1995, p. 363.

146. J. C. Haylock, R. A. Phillips, and M. D. Wolkowicz, in J. Scheirs and W. Kaminsky, eds., *Metallocene-Based Polyolefins: Preparation, Properties and Technology*, Vol. 2, John Wiley & Sons, Inc., New York, 2000, p. 333.
147. J. Xu, S. Srinivas, and H. Marand, *Macromolecules* **31**, 8230 (1998).
148. U. Gauer and B. Wunderlich, *J. Chem. Phys. Ref. Data* **10**, 1051 (1981).
149. E. B. Bond, J. E. Spruiell, and J. S. Lin, *J. Polym. Sci., Part B: Polym. Phys.* **37**, 3050 (1999).
150. H. S. Bu, S. Z. D. Cheng, and B. Wunderlich, *Makromol. Chem. Rapid Commun.* **9**, 75 (1988).
151. F. Bai, F. Li, B. H. Calhoun, R. P. Quirk, and S. Z. D. Cheng, in J. Brandrup, E. H. Immergut, E. A. Grulke, eds., *Polymer Handbook*, 4th ed., John Wiley & Sons, Inc., New York, 1999.
152. C. DeRosa, G. Talarico, L. Caporaso, F. Auriemma, M. Galimberti, and O. Fusco, *Macromolecules* **31**, 9109 (1998).
153. Y. Z. Wang, W. J. Chia, K. H. Hsieh, and H. C. Tseng, *J. Appl. Polym. Sci.* **44**, 1731 (1992).
154. K. H. Hsieh and Y. Z. Wang, *Polym. Eng. Sci.* **30**, 476 (1990).
155. *Pro-fax® Polypropylene Chemical Resistance*, Montell Polyolefins Technical Bulletin TL-101, 1996.
156. D. DelDuca and E. P. Moore Jr., in E. P. Moore Jr., ed., *Polypropylene Handbook*, Hanser, Munich, 1996.
157. R. F. Becker, L. P. J. Burton, and S. E. Amos, in E. P. Moore Jr., ed., *Polypropylene Handbook*, Hanser, Munich, 1996.
158. T. S. Dziemianowicz and W. W. Cox, *SPE ANTEC 85* 540 (1985).
159. M. Gahleitner, J. Wolfschwenger, C. Bachner, K. Bernreitner, and W. Neißl, *J. Appl. Polym. Sci.* **61**, 649 (1996).
160. T. Simonazzi, A. DeNicola, M. Aglietto, and G. Ruggeri, in S. Laggarwal, and W. Russo, eds., *Comprehensive Polymer Science, 1st suppl*. Pergamon Press, Oxford, 1992.
161. B. Löfgren and J. Seppälä, in J. Scheirs and W. Kaminsky, eds., *Metallocene-Based Polyolefins: Preparation, Properties and Technology*, Vol. 2, John Wiley & Sons, Inc., New York, 2000, p. 143.
162. D. O. Geymer, in M. Dole, ed., *The Radiation Chemistry of Macromolecules*, Vol. 2, Academic Press, Inc., New York, 1973.
163. A. J. DeNicola, A. F. Galambos, and M. D. Wolkowicz, *ACS PMSE Polym. Prep.* **67**, 106 (1992).
164. C. E. Ruiz and R. T. LeNoir, in E. P. Moore Jr., ed., *Polypropylene Handbook*, Hanser, Munich, 1996.
165. Montell Polyolefins Resin Data Sheets, 1996. Adapted.
166. R. B. Lieberman and D. DelDuca, *Proc. SPE Retec: Polyolefins* **VIII**, 21 (1993); *Plast. World* **4**, 4 (1989).
167. U. S. Pat. 5,173,540 (Dec. 22, 1992), J. Saito and A. Sampei (to Chisso Corp.).
168. Basell Polyolefins Resin Data Sheets, 2000. Adapted.
169. U. S. Pat. 3,112,200 (Nov. 26, 1963) (to Montecatini).
170. U. S. Pat. 3,112,301 (Nov. 26, 1963) (to Montecatini).
171. G. Natta, *Atti Accad. Naz. Lincei Rend. Classe Sci. Fis. Mat. Nat. Sez 3a* **84**, 61 (1955).
172. G. Natta, P. Pino, P. Corradini, F. Danusso, E. Mantica, and G. Moraglio, *J. Am. Chem. Soc.* **77**, 1708 (1955).
173. G. Natta, *J. Polym. Sci.* **16**, 143 (1955).
174. G. Natta, *Angew. Chem.* **76**, 430 (1955).
175. Belg. Pat. 533,362 (Nov. 16, 1953) (to Karl Ziegler).
176. W. Klemm and E. Krose, *Z. Anorg. Chem.* **253**, 209 (1947).
177. G. Natta, P. Corrandini, and G. Allegra, *J. Polym. Sci.* **51**, 399 (1961).

178. M. Sittig, *Polyolefin Production Processes*, Noyes Data Co., Park Ridge, N.J., 1976.
179. J. Boor, *Ziegler–Natta Catalysts and Polymerization*, Academic Press, Inc., New York, 1979.
180. U. S. Pat. 3,051,690 (July 29, 1955) (to Hercules).
181. U. S. Pat. 3,128,252 (Aug. 15, 1956) (to Esso Research and Engineering Co.).
182. Brit. Pat. 1,092,390 (Apr. 27, 1966) (to Mitsubishi).
183. Ger. Offen. 2,213,086 (Oct. 5, 1972) (to Solvay & Cie).
184. L. A. M. Rodriguez and H. M. VanLooy, *J. Polym. Sci., Part A1* **4**, 1971 (1966).
185. N. B. Chumaevskii, *Makromol. Chem.* **177**, 747 (1976).
186. Brit. Pat. 1,286,867 (Nov. 26, 1969) (Montecatini).
187. Belg. Pat. 785,332 (June 23, 1972) (Montedison).
188. Ger. Offen. 2,643,143 (Nov. 21, 1975) (Montedison and Mitsui Petrochemical Ind.).
189. Ger. Offen. 2,735,672 (Aug. 9, 1976) (Montedison).
190. Ger. Offen. 2,822,783 (May 25, 1977) (Montedison).
191. Ger. Offen. 2,828,887 (July 4, 1977) (Montedison).
192. Eur. Pat. 29,232 (Nov. 24, 1979) (Montedison).
193. P. Galli, In *IUPAC International Symposium on Macromolecules*, Florence, Italy, IUPAC, 1980.
194. G. Natta, I. Pasquon, and A. Zambelli, *J. Am. Chem. Soc.* **84**, 1488 (1962).
195. A. Zambelli, and co-workers, *J. Polym. Sci., Part C* **16**, 2485 (1967).
196. U. Giannini, U. Zucchini, and E. Albizzati, *J. Polym. Sci., Part B* **8**, 405 (1970).
197. D. G. H. Ballard, *Adv. Catal.* **23**, 263 (1973).
198. U. S. Pat. 3,023,513 (May 1, 1962) (Esso Research and Engineering Co.).
199. U. S. Pat. 3,424,774 (Jan. 28, 1969) (Esso Research and Engineering Co.).
200. E. Tornquist and co–workers, *J. Catal.* **8**, 189 (1967).
201. Z. W. Wilchinsky, R. W. Looney, and E. Tornquist, *J. Catal.* **28**, 351 (1973).
202. Brit. Pat. 2,000,514 (July 3, 1978) (Montedison).
203. P. C. Barbe, G. Cecchin, and L. Noristi, eds. *Advances in Polymer Science*, Vol. 81, Springer-Verlag, Berlin, 1–81, 1987.
204. K. Soga and co–workers, *Polym. J.* **5**(2), 128 (1973).
205. E. Suzuki and co–workers, *Makromol. Chem.* **180**, 2275 (1979).
206. U. Giannini, *Makromol. Chem. Suppl.* **5**, 216 (1981).
207. N. Kashiwa, and J. Yoshitake, *Makromol. Chem. Rapid Commun.* **3**, 211–214 (1982).
208. P. C. Barbe and co–workers, *Makromol. Chem., Rapid Commun.* **4**, 249–252 (1983).
209. G. DiDrusco and R. Rinaldi, *Hydrocarbon Process* **63**(11), 113 (1984).
210. N. Kashiwa and J. Yoshitake, *Makromol. Chem.* **185**, 1133–1138 (1984).
211. R. Spitz, J. L. Lacombe, and A. Guyot, *J. Polym. Sci., Polym. Chem. Ed.* **22**, 2641 (1984).
212. R. Spitz, J. L. Lacombe, and A. Guyot, *J. Polym. Sci., Chem. Ed.* **22**, 2625 (1984).
213. T. Keii, *Kinetics of Ziegler–Natta Polymerization*, Kodanska, Chapman and Hall, London, 1972.
214. I. Pasquon and U. Giannini, in J. R. Anderson and M. Boudart, eds. *Catalysts, Science and Technology*, Springer-Verlag, Berlin, 1984.
215. K. Y. Choi and W. H. Ray, *J. Appl. Polym. Sci.* **30**, 1065 (1985).
216. N. F. Brockmeier, and J. B. Rogan, *Ind. Eng. Chem. Prod. Res. Dev.* **24**, 278 (1985).
217. T. Keii and co–workers, *Makromol. Chem.* **183**, 2285–2304 (1982).
218. Y. Doi and co–workers, *Ind. Eng. Chem. Prod. Res. Dev.* **21**, 580 (1982).
219. V. A. Zakharov, G. D. Bukatov, and Y. I. Yermakov, *Polym. Sci. Technol. Coord. Polym.* **19**, 267 (1983).
220. G. Natta and I. Pasquon, *Adv. Catal.* **11**, 1–65 (1959).
221. N. M. Chirkov, *Proceedings of the IUPAC International Macromolecules Symposium*, Bucharest, Romania, IUPAC, 1969.

222. C. D. Nentizescu, C. Huch, and A. Huch, *Angew. Chem.* **68**, 438 (1956).
223. D. B. Ludlum, A. W. Anderson, and C. E. Ashby, *J. Am. Chem. Soc.* **80**, 1380 (1958).
224. G. Natta and co–workers, *Chim. Ind. Milan* **38**, 124 (1956).
225. A. Zambelli and co–workers, *Macromolecules* **13**, 798 (1980).
226. P. Cossee, *Tetrahedron Lett.* **17**, 12 (1960).
227. P. Cossee, *Proceedings of the International Congress on Coordination Chemistry*, 1961, p. 241.
228. P. Cossee, *J. Catal.* **3**, 80–88 (1964).
229. T. Miyazawa and Y. Ideguchi, *J. Polym. Sci. Polym. Lett.* **1**, 389 (1963); A. Zambelli, M. G. Giongo, and G. Natta, *D. Makromol. Chem.* **112**, 183 (1968); A. Zambelli and C. Tosi, *Adv. Polym. Sci.* **15**, 32 (1974).
230. E. J. Arlman and P. Cossee, *J. Catal.* **3**, 99 (1964).
231. A. Zambelli, P. Locatelli, and E. Rigamonti, *Macromolecules* **12**, 156 (1979).
232. A. Zambelli, *NMR Basic Principles and Progress*, Springer, Berlin, 1971, p. 101.
233. P. C. Barbé, L. Noristi, and G. Baruzzi, *Makromol. Chem.* **193**, 229–241 (1992).
234. U. S. Pat. 4,971,937 (to HIMONT).
235. P. Pino and co–workers, in J. C. W. Chein, ed., *Coordination Polymerization*, 1975, Academic Press, Inc.: New York. p. 25.
236. P. Pino, *Adv. Polym. Sci.* **4**, 393 (1965).
237. P. Pino and G. P. Lorenzi, *Chim. Ind. Milan* **42**, 712 (1960).
238. P. Pino and co–workers, *J. Am. Chem. Soc.* **84**, 1487 (1962).
239. P. Pino, F. Ciardelli, and G. P. Lorenzi, *J. Polym. Sci., Part C* **4**, 21 (1963).
240. P. Pino and co–workers, in *Proceedings of the International Symposium Transition Metal Catalyzed Polymerization—Unsolved Problems*, Midland, Mich., 1981.
241. P. Corradini, V. Barone, and R. Fusco, *Gazzetta Chimica Italiana* **113**, 601–607 (1983).
242. P. Corradini, V. Busico, and G. Guerra, in S. G. Allen, ed. *Comprehensive Polymer Science*, Pergamon Press, New York, 1988, p. 29–48.
243. A. Zambelli, in J. C. W. Chien, ed., *Coordination Polymerization*, Academic Press, Inc., New York. p. 15, 1975.
244. P. Locatelli, A. Immirzi, and A. Zambelli, *Makromol. Chem.* **176**, 1121 (1975).
245. G. Morini and co–workers, *Macromolecules* **29**, 5770–5776 (1996).
246. M. C. Sacchi and co–workers, *Macromolecules* **29**, 3341–3345 (1996).
247. L. Noristi, P. C. Barbé, and G. Baruzzi, *Makromol. Chem.* **192**, 1115–1127 (1991).
248. E. Iiskola, P. Sormunen, and T. Garoff, W. Kaminsky and H. Sinn, eds., *Transition Metals and Organometallics as Catalysts for Olefin Polymerization*, Springer-Verlag, Berlin, 1988, pp. 113–122.
249. T. Okano and co–workers, *Stud. Surf. Sci. Catal. Olefin Polym*. 1990. p. 177–183.
250. M. Härkönen, L. Kuutti, and J. V. Seppälä, *Makromol. Chem.* **193**, 1413–1421 (1992).
251. R. Spitz and co–workers, *Makromol. Chem.* **190**, 717–723 (1989).
252. I. W. Parsons and T. M. Al-Turki, *Polymer Commun.* **30**(3), 72–73 (1989).
253. M. Kioka and N. Kashiwa, *J. Macromol. Sci. Chem. A* **28**, 865–873 (1991).
254. K. Imaoka and co–workers, *J. Mol. Catal.* **82**, 37–44 (1993).
255. J. C. Chadwick, A. Miedema, and O. Sudmeijer, *Macromol. Chem. Phys.* **195**, 167–172 (1994).
256. J. C. Chadwick in *Polyolefins 2000 International Conference on Polyolefins Society of Plastics Engineers*. Society of Plastics Engineers, Houston, Tex., 2000.
257. E. Albizzati and co–workers, *Macromol. Symp.* **89**, 73–89 (1995).
258. K. Soga, T. Shinon, and Y. Doi, *Makromol. Chem.* **189**, 1531 (1988).
259. J. C. Chadwick and co–workers, *Macromol. Chem. Phys.* **197**, 2501–2510 (1996).
260. J. C. Chadwick, *Macromol. Symp*., 2001.

261. W. Kaminsky, *Rapra Rev. Rep.* **10**, 1–135 (1999).
262. W. Spaleck and co–workers, *Organometallics* **13**, 954–963 (1994).
263. S. Miyake, Y. Okumura, and S. Inazawa, *Macromolecules* **28**, 3074–3079 (1995).
264. H. R. Blum, in *MetCon 2000, Polymers in Transition "Platforms in Single-Site Catalysis"*, Houston, Tex., 2000.
265. G. DiDrusco and R. Rinaldi, *Hydrocarbon Process.* **60**(5), 153 (May 1981).
266. U. S. Pat. 3,051,690 (July 29, 1955), E. J. Vandenberg (to Hercules Powder Co.).
267. Brit. Pat. 1,044,811 (Apr. 9, 1962) (to Rexall Drug and Chemical Co.).
268. U.S. Pat. 3,476,729 (Nov. 4, 1969), D. E. Smith, R. M. Keeler, and E. Guenther (to Phillips Petroleum).
269. J. F. Ross and W. A. Bowles, *Ind. Eng. Chem. Prod. Res. Dev.* **24**, 149 (1985).
270. *Oil Gas J.* **68**, 64 (1970).
271. Ger. Offen. 2,213,086 (Oct. 5, 1972), J. P. Hermans (to Solvay & Cie SA).
272. Ger. Offen. 2,643,143 (Nov. 21, 1975) (to Montedison and Mitsui Petrochemical); Ger. Offen. 2,735,672 (Aug. 9, 1976), U. Giannini, E. Albizzati, and S. Parodi (to Montedison and Mitsui Petrochemical); Ger. Offen. 2,822,783 (May 25, 1977), U. Scata, L. Luciani, and P. C. Barbe (to Montedison); U. S. Pat 4,069,169 (Jan. 17, 1978), N. Kashiwa and A. Toyota (to Mitsui Petrochemcial).
273. G. DiDrusco and R. Rinaldi, *Hydrocarbon Process.* **63**(11), 116 (Nov. 1984).
274. *Hydrocarbon Process* **72**(3), 204 (1993).
275. C. Cipriani and C. A. Trishman Jr., *Chem. Eng.* **80**, (Apr. 20, 1981).
276. *Plast. World* **51**(6), 12 (1993).
277. Z. Tadmor and C. G. Gogos, *Principles of Polymer Processing*, John Wiley & Sons, Inc., New York, 1979.
278. M. R. Kantz and H. D. Newman Jr., F. H. Stigale, *J. Appl. Polym. Sci.* **16**, 1249 (1972).
279. D. R. Fitchmun and Z. Mencik, *J. Polym. Sci., Polym. Phys. Ed.* **11**, 951 (1973).
280. M. Fujiyama, H. Awaya, and S. Kimura, *J. Appl. Polym. Sci.* **21**, 3291 (1977).
281. M. Fujiyama and S. Kimura, *J. Appl. Polym. Sci.* **22**, 1225 (1978).
282. M. Fujiyama and K. Azuma, *J. Appl. Polym. Sci.* **23**, 2807 (1979).
283. S. S. Katti and J. M. Schultz, *Polym. Eng. Sci.* **22**, 1001 (1982).
284. M. Fujiyama and T. Wakino, *J. Appl. Polym. Sci.* **43**, 57 (1991).
285. M. Fujiyama and T. Wakino, *J. Appl. Polym. Sci.* **43**, 97 (1991).
286. M. Fujiyama, *Int. Polym. Proc.* **8**, 245 (1993).
287. P. Ramanini, *Rheol. Acta* **21**, 699 (1982).
288. V. Bansal and R. L. Shambaugh, *Polym. Eng. Sci.* **36**, 2785 (1996).
289. A. Winter, *SPO '97 Proc*. 1 (1997).
290. J. J. McAlpin, C. Y. Cheng, D. A. Plank, and G. A. Stahl, *INSIGHT '95 Proc*. (1995).
291. A. Ahmed, *Polypropylene Fibers-Science and Technology*, Elsevier, Amsterdam, 1982.
292. J. R. Beren and C. Capellman, paper presented at *SAE International Congress*, 1994.
293. K. E. McHugh and K. Ogale, *SPE ANTEC '90* 452 (1990).
294. J. Foster, in *Modern Plastics Encyclopedia 1983-1984*, Vol. 60 (10A), McGraw-Hill, New York, 1983, p. 328.
295. K. T. Johansson, *Proc. SPE Retec: Polyolefins* **8**, 334 (1993).
296. S. Al-Malaika and G. Scott, in N. S. Allen, ed., *Degradation and Stabilization of Polyolefins*, Applied Science Publishers Ltd., London, 1983, p. 247.
297. C. Armstrong, M. J. Husbands, and G. Scott, *Eur. Polym. J.* **15**, 241 (1979).
298. Society of the Plastics Industry, *Facts and Figures 1999*.
299. A. H. Tullo, *Chem. Eng. News* **79**, 12–14 (Feb. 5, 2001).

300. Mod. Plast. 22–29 (Feb. 2002); 44–49 (Feb. 2001); 48–79 (Feb. 2000); 72–80 (Jan. 1999); 74–82 (Jan. 1998); 56, 76–84 (Jan. 1997); 54, 70–78 (Jan. 1996); 63–68 (Jan. 1995).
301. American Plastics Council Plastics Industry Producers' Statistics Group, as compiled by VERIS Consulting, LLC.
302. *Asia Chem. News* 14–21 (June 11, 2001).
303. *Mod. Plast.* 54 (Jan. 1999).
304. Chemical Market Resources Inc., *CMR Polym. Tracker* **5**, 25 (Apr. 2000).
305. *Mod. Plast.* 22–29 (Feb. 2002).

RICHARD LIEBERMAN
Basell R&D Center
CONSTANTINE STEWART

PROTEIN FOLDING. See Volume 7.

PSA. See PRESSURE SENSITIVE ADHESIVES.

PULTRUSION. See COMPOSITES, FABRICATIOIN.

PVC. See VINYL CHLORIDE POLYMERS.

PVDC. See VINYLIDENE CHLORIDE POLYMERS.

PVF. See VINYL FLUORIDE POLYMERS.

PVK. See VINYLCARBAZOLE POLYMERS.

PVP. See VINYL AMIDE POLYMERS.

RADICAL POLYMERIZATION

Introduction

Free radical polymerization is one of the most studied chemical processes. This is not surprising, because free radical polymerization is carried out on a large industrial scale; the world production of polymers by this method is in the range of 100 million tons per year. This enormous production corresponds to nearly 50% of all synthetic polymers. The importance of free radical polymerization is likely to increase in the coming years as new controlled/living radical polymerization techniques find industrial applications. Free radical polymerization has been known for more than 60 years. As far back as the 1950s, the basic theory and comprehension of radical polymerization was established (1–5). It included the thorough understanding of the mechanism of the process, encompassing the chemistry and kinetics of the elementary reactions involved, with the determination of the corresponding absolute rate constants, the structure, and concentrations of the growing species, as well as a correlation of the structure of the involved reagents and their reactivities. Similar to other chain reactions, the radical polymerization process may be subdivided into initiation, propagation, transfer, and termination steps as depicted in Scheme 1. The radicals necessary to initiate the chain process have to be generated *in situ* in most cases.

A multitude of monomers can be used in radical polymerization and it is impossible to list them all. The fundamental feature of the vast majority of monomers in question is the vinylic double bond. Thus the simplest monomer is ethylene, which, however, can only be polymerized under high pressure and high temperature to the commercially very important low density polyethylene. Common monomers are monosubstituted or unsymmetrically (1,1-) disubstituted ethylenes, $CH_2{=}CHR$ or $CH_2{=}CRR'$. The substituents R and R′ determine the properties of resulting polymers and also the kinetic and thermodynamic

Encyclopedia of Polymer Science and Technology. Copyright John Wiley & Sons, Inc. All rights reserved.

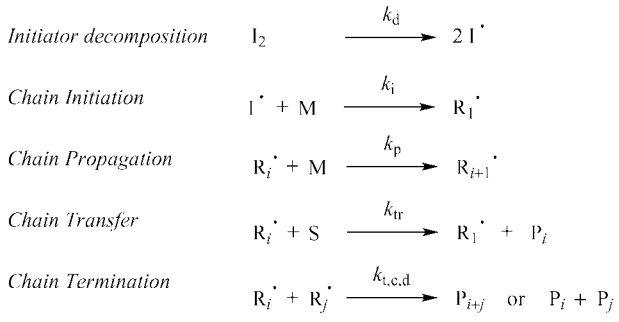

(Where $R_i^{\cdot}$ is a radical of chain length i, I_2 is the initiator, M is the monomer, S is a transfer agent, and P is polymer)

Scheme 1.

polymerizability of monomers. Polymerizable monomers under radical conditions include styrene and its substitution products, dienes, mono- and disubstituted ethylene derivatives, such as vinyl acetate, acrylonitrile, (meth)acrylates, (meth)acrylamides, and vinyl chloride, and a variety of halogenated alkenes. Carbon–heteroatom (N,O) double bonds only rarely polymerize via radical polymerization (eg, CF_3—CHO (6)).

The essential polymerization step is a repetitive free radical addition to the monomer double bonds, forming chains of carbon atoms constructed of units —(—CH_2—CHR—)— or —(—CH_2—CRR′—)— linked together predominantly head-to-tail (the substituted carbon atom is denoted as the head). Since the free radical is essentially sp^2 hybridized, very limited control of tacticity is observed, with many monosubstituted monomers providing atactic polymers and disubstituted like methacrylates showing (thermodynamic) preference for syndiotacticity.

Monomers with exocyclic double bond can polymerize via ring-opening polymerization and incorporate heteroatoms to the backbone. The systematic study of ring-opening polymerization started in the 1950s (7). Ring-opening polymerization has several characteristic features, and it can produce a wide variety of polymers, many of which have found important industrial applications (8,9). A characteristic feature of ring-opening polymerization is the smaller volume shrinkage of cyclic monomers during polymerization in comparison with vinyl monomers (10). Consequently, cyclic monomers are better as adhesives, curing resins, and molding and filling materials. Vinyl monomers show volume shrinkage about two times larger than the shrinkage of cyclic monomers of identical molecular weight. This is due to the compact structures of cyclic monomers and the compensation of the closeness of monomer molecules by ring opening during polymerization.

Most cyclic monomers polymerize ionically, but there are several monomers undergoing radical ring-opening polymerization (RROP). The copolymerization of radically polymerizable cyclic monomers with common vinyl monomers can add functions to common vinyl polymers. Scheme 2 illustrates the typical patterns of RROP, depicting vinyl-substituted cyclic and *exo*-methylene-substituted monomers. The radical species formed by the radical addition to the double bond undergoes ring opening to form a propagating radical species. RROP is commonly

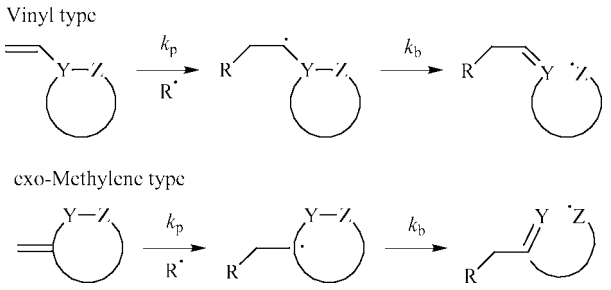

Scheme 2.

accompanied by so-called vinyl polymerization without ring opening of the cyclic structure.

Although fewer monomers undergo RROP than cationic, anionic, and coordination ring-opening polymerizations, novel monomers undergoing RROP are steadily being developed, some of which were recently examined as monomers for living radical polymerization (11). RROP can provide a wide variety of functional polymers with industrially promising radical polymerization.

1,6-Dienes having vinylic double bonds that are not polymerizable can form polymers consisting of repeat units made up of five- or six-membered rings. Such processes are called cyclopolymerization (qv), and typically the intramolecular cyclization followed by intermolecular addition of the cyclized radicals (see Scheme 3) is orders of magnitudes faster than individual propagation via the carbon–carbon double bonds (12–15).

Typical cyclopolymerizable monomers include N-substituted dimethylacrylamides where the nonpolymerizability of the N,N-disubstituted methylacrylamido group results in the generation of five-membered cyclic structures involving head–head linkages. In cases where one of the carbon–carbon double bonds is severely sterically hindered, cyclopolymerization (qv) may not occur and a linear polymer with pendant double bonds is formed (16). Other examples of monomers that undergo cyclopolymerization are 4-(*N,N*-diallylamino)pyridine, 5,6-di-*O*-isopropylidene-D-mannitol, 1,5-hexadiene, *N*-methyl-*N*-methallyl-2-(methoxycarbonyl)-allyl amine, and dipropargyl compounds (13). One of the most efficient ways to achieve structural control in radical polymerization is via cyclopolymerization. For example, the free radical cyclopolymerization of a diacryloyl monomer involving a chiral template results in the generation of stereogenic centers and four different stereoisomers (17).

Another essential component of free radical polymerization systems are initiators which should provide initiating free radicals via homolytic cleavage of covalent bonds, redox reaction, photochemical or other stimuli. In addition, various

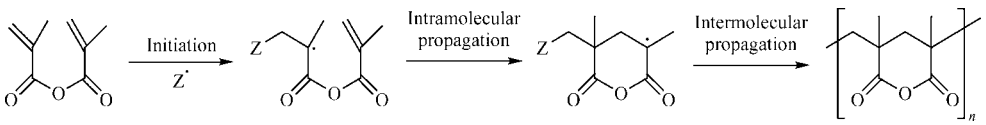

Scheme 3.

compounds which can regulate molecular weights (transfer agents) or rates (retarders/inhibitors) can be used. Free radical polymerizations tolerate many protic impurities such as water or alcohols but require absence of oxygen, which act as a powerful inhibitor. Various solvents can be used which should not (unless desired) participate in transfer.

Initiation

The initiation process constitutes the first reaction step in free radical polymerization, leading to the generation of (primary) radicals. The kinetics of the initiation process, ie its rate and effectiveness, are of fundamental importance in both theoretical studies and commercial applications. Commercial procedures mainly rely on the formation of primary radicals via thermal decomposition processes using azo- and peroxy-type compounds. Investigative kinetic studies are—to a large extent—carried out using photoinitiators, which decompose upon irradiation with UV or visible light. The main reason for this choice is the possibility to define exact start and end times of the initiation and subsequently the polymerization process.

The decomposition scheme (eq. 1) describing the generation of radicals is common to both thermal and photoinitiators.

$$\text{Initiator} \xrightarrow[h\nu,\,\Delta]{k_d} I_1^{\cdot} + I_2^{\cdot} \tag{1}$$

The measurable decrease of the initiator concentration [I] in a polymerizing systems with time is given by

$$-\frac{d[I]}{dt} = k_d[I] \tag{2}$$

Integration of equation 2 leads to equation 3, an expression which describes the decreasing initiator concentration as a function of time.

$$[I] = [I]_0\, e^{-k_d t} \tag{3}$$

However, the rate of the formation of initiating primary radicals is of greater interest in kinetic studies. The rate of generation of radicals that are capable of initiating the polymerization process, R_d, is described via the following general first-order rate law:

$$R_d = \frac{d[I^{\bullet}]}{dt} = -2f\frac{d[I]}{dt} = 2fk_d[I] \tag{4}$$

where k_d corresponds to the rate coefficient of initiator decomposition and f denotes the initiator efficiency (see below). It should be noted that in the case of photoinitiation, k_d is a composite of various variables.

In order to initiate the polymerization process via reaction with a monomer unit, the generated primary radicals, $I_1^{\bullet}$ and $I_2^{\bullet}$, have to leave the solvent cage that surrounds them. The ability of the primary radicals to leave the solvent cage

unreacted and to start the polymerization process is quantified by the initiator efficiency f, with theoretical values between zero and unity. Not all generated primary free radicals initiate polymer growth. Shortly after decomposition, the free radicals are very close to each other and recombination can occur. In addition, they can also react in alternative ways before they can react with a monomer unit. An efficiency of zero corresponds to no initiation taking place, whereas $f = 1$ indicates that every generated primary radical escapes the solvent cage and subsequently initiates polymerization. Typical values of f are between 0.5 and 0.8, depending on the viscosity of the reaction medium, indicating that the escaping process is diffusion controlled. It should be noted that in the case of an unsymmetrical initiator molecule, $I_1^\bullet$ and $I_2^\bullet$ do not necessarily display the same reactivity toward the monomer unit (18–20). Hence, the initiation process may be described by equations 5 and 6:

$$I_1^\bullet + M \xrightarrow{k_i^{(1)}} R_1^\bullet \tag{5}$$

$$I_2^\bullet + M \xrightarrow{k_i^{(2)}} R_1^\bullet \tag{6}$$

where $I_1^\bullet$ and $I_2^\bullet$ represent initiator fragment 1 and 2, respectively, M indicates a monomer unit, $R_1^\bullet$ corresponds to a macroradical of chain length 1, and $k_i^{(1)}$ and $k_i^{(2)}$ refer to the individual initiation rate coefficient of the respective fragments. The rate of initiation, R_i, is given by equation 7:

$$R_i = \frac{d[R_1^\bullet]}{dt} = -\frac{d[I_1^\bullet]}{dt} - \frac{d[I_2^\bullet]}{dt} = k_i^{(1)}[M][I_1^\bullet] + k_i^{(2)}[M][I_2^\bullet] \tag{7}$$

Because $[I_1^\bullet] = [I_2^\bullet] = [I^\bullet]/2$, the rate coefficient of initiation, k_i, is a composite of the individual rate coefficients of initiation for the initiator fragments $I_1^\bullet$ and $I_2^\bullet$.

$$R_i = k_i[M][I^\bullet] \quad \text{with} \quad k_i = \frac{k_i^{(1)} + k_i^{(2)}}{2} \tag{8}$$

Thermal Initiation. Thermally decomposing initiators (mainly) fall into two classes: azo- and peroxy-type molecules. The general structures of azo- and peroxy-initiators are represented by **1** and **2** respectively.

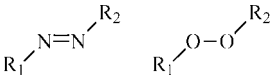

1 **2**

An important quantity of a thermal initiator is its *half-life* $t_{1/2}$ (at a certain temperature), given by equation 9. The half-life is the time period during which half of the initiator molecules initially present is decomposed.

$$t_{1/2} = \frac{\ln 2}{k_d} \tag{9}$$

There are initiators available for virtually any desired decomposition rate in a given solvent (or monomer) at a given temperature. Initiators are often characterized by the temperature at which their half-life is 10 h. These temperatures range from 20 to 120°C, depending on the structure of the initiator. Extensive data on initiator decomposition rates and their activation parameters can be found in the *Polymer Handbook* (21). In the following, the basic features of thermal initiation systems are discussed.

Azoinitiators. This widely used class of thermally decomposing initiators generates both carbon- and oxygen-centered radicals by either C—N (dialkyl diazenes) or O—N (dialkyl hyponitrites) bond scission driven by the expulsion of a stable nitrogen molecule (22–25). Dialkyl diazenes are generally used at higher temperatures than dialkyl hyponitrites. Most of the azoinitiators generate two identical radical species upon fragmentation. The most common azoinitiators are 2,2′-azobisisobutyronitrile (AIBN, **3**), dimethyl 2,2′-azobisisobutyrate (**4**), 1,1′-azobis(1-cyclohexanecarbonitrile) (**5**), and 2,2′-azobis-2,4-dimethylvaleronitrile (**6**). Both the delocalization of the free electron in the generated radical (22,23) and the steric demand of the leaving radical (24) significantly affect the decomposition rate coefficient k_d: The more the free electron in the resulting radical is delocalized and the bulkier the leaving radical, the larger is k_d. The choice of the solvent, however, has comparatively little effect on the rate of azoinitiator decomposition (26).

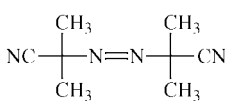

3

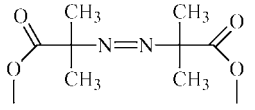

4

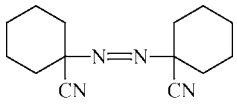

5

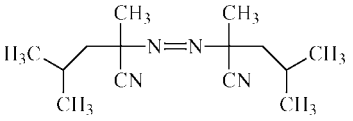

6

The concept of azoinitiators has been extended toward the generation of macroazo-initiators for the synthesis of block copolymers. The development of techniques for block copolymer preparation was especially important before the advent of living free radical polymerization processes such as reversible addition–fragmentation chain transfer (RAFT) polymerization or atom transfer radical polymerization (ATRP). Macroazoinitiators are low molecular weight polymers containing one or more —N=N— units (27–32). Usually, the macroazo-initiator is prepared by a technique other than free radical polymerization, ie polycondensation of low molecular weight azoinitiators with suitable end groups. A typical example of such a strategy is the polycondensation of 2,2-azobis(2-cyanopropanol) with isocyanate functionalized prepolymer. The generated polymer can subsequently be used to initiate the free-radical polymerization of styrene. The rate of macroazo-initiator decomposition may be different from the parent initiator, but still follows first-order kinetics (32). Macroazo-initiators have also been used in conjunction with (NMP) (nitroxide-mediated polymerization) and ATRP for the

synthesis of block copolymers (29,33). It is interesting to note that polymers containing azo-moieties along the backbone have been reported to be biodegradable (34).

Peroxide-Based Initiators. The use of peroxides as thermally decomposing initiators is—especially in an industrial context—more widely spread than the use of azoinitiators (35,36). Peroxy compounds range from alkyl, acyl, and peresters to inorganic peroxides (26,37). The most employed peroxides are di-*tert*-butyl peroxide (**7**), benzoyl peroxide (**8**), di-*tert*-butyl peroxalate (**9**), cumene hydroperoxide (**10**), and di-*n*-propyl peroxydicarbonate (**11**). The primary—oxygen-centered—radicals that are generated by organic peroxide decay may undergo further reactions such as β-scission, which leads to the formation of secondary radicals. A common reaction pathway is the expulsion of carbon dioxide from the generated primary radicals originating from acyl peroxides. For example, the decomposition of benzoyl peroxide leads to the formation of benzoyloxy and phenyl radicals. The mechanism of peroxide decomposition is still under investigation, especially in the case of alkyl peroxyesters. Peresters may decompose—depending on their structure—by either a concerted two-bond scission or a one-bond homolysis of the oxygen–oxygen bond (38). The one-bond homolysis results in the formation of acyloxy and alkoxy radicals, whereas the concerted two-bond fragmentation generates alkyl and alkoxy radicals plus carbon dioxide.

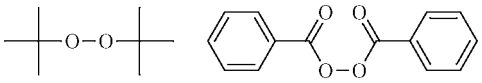

7

8

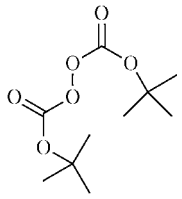

9

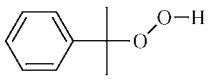

10

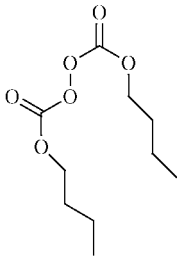

11

The rate of peroxide decomposition is strongly dependent on the structure of the molecule in question. The rate of decomposition for diacyl peroxides and peresters increases when going from aryl to primary alkyl to secondary alkyl to tertiary alkyl substituents (39). In the case of peresters, the structure of the molecule governs both the rate of fragmentation and the above mentioned mode

of fragmentation (ie one-bond homolysis vs concerted two-bond cleavage). Experimental data indicate that the rate of decomposition increases when going from primary to secondary to tertiary carbons connected to the $(CO)O_2$ moiety in the perester. The concerted mechanism is favored in the case of secondary and tertiary carbons (38,40,41). Because of the strong dependence of the rate of decomposition on the peroxide structure, a wide variety of decomposition rates exists for a given temperature. The general guideline is that dialkyl peroxides and hydroperoxides are mostly used at elevated temperatures, whereas dialkyl peroxydicarbonates are best suited for lower temperatures. The solvent in which the decomposition is carried out affects the rate to much larger extent than for azoinitiators. For example, the decomposition rate coefficient for the diacyl peroxide bis(3,5,5-trimethylhexanoyl)peroxide increases by a factor of 7 when going from pentadecane to acetonitrile (at 150 MPa and 80°C) (42). The rate of diacyl peroxide and peroxy ester decomposition has also been studied in supercritical CO_2 and—contrary to the above—no significant change in decomposition rate compared to *n*-heptane as solvent has been observed (43).

Photoinitiation. An attractive alternative to thermally decomposing initiators are photoinitiators that decay upon irradiation with UV or visible light (44–48). The use of photoinitiators is (in most cases) restricted to applications involving accurate kinetic measurements, whereas their usage in industrial processes is very limited because of the technical problems associated with the uniform irradiation of large reaction volumes. Some exceptions are applications involving coatings and surface polymerizations. The main advantage of photoinitiators used in polymerizing systems is the possibility to define exact start and end points of the polymerization process via the duration of the irradiation period. In addition, the rate of (most) photoinitiator decomposition is almost independent of the reaction temperature, but depends strongly on the (UV) light intensity. However, weak temperature dependencies of the primary quantum yield (see below) have long been known for the photoinduced decomposition of azoalkanes (23). The weak dependence of the rate of decomposition on the reaction medium temperature is due to the large amount of energy which is deposited into the initiator molecules via the light source. This energy exceeds the thermal energy of the surrounding medium by orders of magnitude. An ideal photoinitiator for a specific polymerization may be defined via the following criteria:

(1) The photoinitiator should decompose upon irradiation with the (UV) light source; eg, an absorption should coincide with the radiation wavelength. The monomer(s) used in the specific polymerization process should not absorb light at the selected wavelength.
(2) The efficiency of the initiator should be high, preferably close to one; ie, all radicals generated should start growing chains.
(3) At best, there should be only one type of free radical species that is formed upon laser irradiation.

On the basis of the mechanism by which initiating radicals are formed, photoinitiators are generally divided into two classes: Type I photoinitiators undergo a unimolecular bond cleavage upon irradiation to yield free radicals. Type II

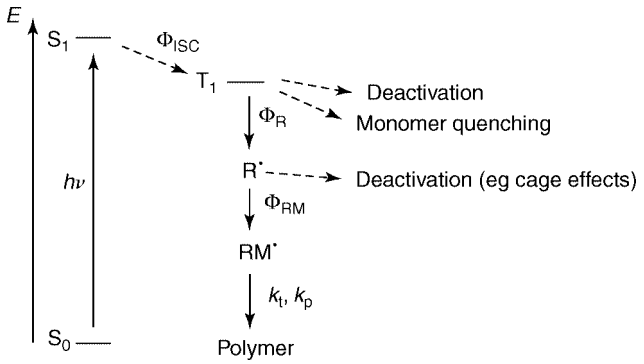

Fig. 1. Simplified Jablonski diagram of the photochemically initiated acetophenone type initiator decomposition.

photoinitiators undergo a bimolecular reaction where the excited state of the photoinitiator interacts with a second molecule (a co-initiator) to generate free radicals. However, visible light photoinitiators belong almost exclusively to the Type II class of photoinitiators. Within the Type I initiator class, there are several structural variations. The most widely used class are photoinitiators containing a benzoyl group as the effective initiating moiety (acetophenone type). Their general formula and primary decomposition products are given in equation 10.

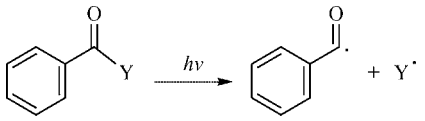

(10)

It is a standard practice to show the processes that can take place upon irradiation (ie assuming that each photoinitiator molecule absorbs a certain dose of energy) in a so-called Jablonski diagram. Such a diagram is a simplified illustration of the relative positions of the electronic energy levels of a molecule.

Upon (UV) irradiation, the molecule is converted from its (singlet) ground state to its first excited state. The Jablonski diagram given in Fig. 1 shows that there is more than one possibility to deactivate an excited initiator molecule. This multitude of deactivation modes is quantified in the quantum yield for the primary free radical production, Φ. Φ is composed of three parts, which can be assigned to the reactions shown in Scheme 4.

The quantum yield for intersystem crossing (Ib) is rather high for ketones (49), so that to a good approximation Φ_{ISC} can be set to one. Thus, the overall

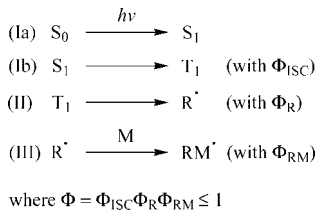

Scheme 4.

quantum yield of the initiation process depends only on Φ_R and Φ_{RM}. From the T_1 triplet state, parallel reactions can lead to a decrease in the quantum yield Φ_R. In free radical polymerizations these reactions are deactivation by molecular oxygen and deactivation by the monomer (50). This is one of the reasons why the monomer mixture should be thoroughly degassed prior to the polymerization process. The longer the lifetime of the triplet state, the higher the chances that deactivation processes can reduce the quantum yield. For example, 2,2-dimethyl-2-phenylacetophenone (DMPA) has a rather short-lived T_1 state [$\tau < 0.1$ ns (51), whereas the respective value for 1,1-dimethoxy-1-hydroxyacetophenone (Darocur 1173) is close to 20 ns (52)], which results in a high Φ_R value. The quantum yield of the third reaction, which leads to the formation of macroradicals, has been termed *initiator efficiency*, $f \equiv \Phi_{RM}$. The initiator efficiency is influenced by the ability of the radicals formed by the laser pulse to diffuse from the solvent cage to the reaction site and its definition is analogous to the definition of the efficiency factor for thermally decomposing initiators. This process has been termed *cage effect*. The initiator efficiency of the typical acetophenone initiator DMPA (at 30°C and ambient pressure) is close to 0.4 (53). However, the situation for most acetophenone-type initiators is more complex than for a photoinitiator which yields only a single type of free radical, $R^\bullet$, upon irradiation. It is generally accepted that most acetophenone-type initiators (eg, DMPA, Darocur 1173, or benzoin) decompose into two radical species, $R_1^\bullet$ and $R_2^\bullet$, as detailed in equation 10. Generally, both species are distinctly different in their character. The carbonyl radical is very efficient in terms of starting macromolecular growth, whereas the second radical is often not [for the example of DMPA, the methoxy-type radical is only involved in termination steps (54)]. Initial radicals that come from a common initiator molecule, but have clearly different efficiencies, may be termed "effective" and "ineffective" (primary) initial radicals, respectively. The sum of both radical concentrations is termed "overall" radical concentration and is two times ρ, with ρ being the concentration of primary radicals that are capable of starting macromolecular growth. The concentration of effective and ineffective initial radicals is the same and equal to ρ. The occurrence of primary radicals with markedly different reactivities may have serious consequences for the polymerization kinetics.

Another widely used structural variation of class I photoinitiators are azoinitiators, which are also employed as thermal initiators. However, their mechanism of photodecomposition is markedly different from acetophenone-type initiators. Equation 11 shows the UV-induced decomposition of the widely used azoinitiator 2,2′-azobisisobutyronitrile (AIBN).

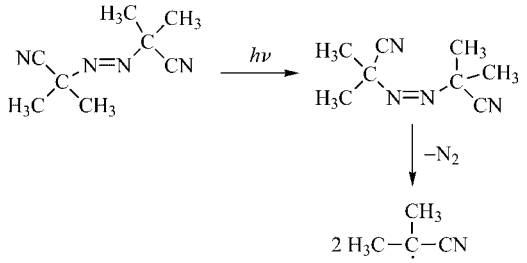

(11)

Upon irradiation by laser light, the initiator molecule changes its stereochemical configuration from the trans to the cis isomer. This cis/trans isomerism becomes of importance if azoinitiators are employed in pulsed laser experiments: The time at which the laser pulse hits the reaction mixture is no longer identical with the generation of the primary radicals. The time delay is usually in the order of microseconds and may be observed in time-resolved pulsed laser experiments.

It is possible to calculate the effective primary free radical concentration ρ generated by monochromatic irradiation of a reaction mixture containing a photoinitiator. The radical concentration ρ, which is generated by a specific number of absorbed photons, is given by equation 12:

$$\rho = 2\Phi \frac{n_{\text{abs}}}{V} \tag{12}$$

where Φ is the primary quantum yield (see above), n_{abs} is the number of absorbed photons, and V is the irradiated volume. According to Beer–Lambert's law, the number of absorbed photons may be calculated by equation 13:

$$n_{\text{abs}} = \frac{E_{\text{p}}}{E_{\lambda}}(1 - 10^{-\varepsilon c d}) \tag{13}$$

where E_{p} is the energy deposited, E_{λ} is the energy of 1 mole of photons at the irradiation wavelength λ, ε is the molar absorption coefficient of the initiator molecule at the laser wavelength λ, c is the photoinitiator concentration, and d is the optical path length.

The rate of photochemical initiation is given by the product of the intensity of absorbed light (in moles of light quanta per liter and second) and the primary quantum yield. A good survey on different photoinitiators and their photodecomposition by UV light was given by Gruber (55).

Self-Initiated Polymerization. Free radical polymerizations can also be initiated by the monomer itself or peroxy compounds that are formed via exposure of the reaction mixture to molecular oxygen. The processes (mainly) take place at high temperatures. However, under very pure conditions in exhaustively purified reaction vessels, most monomers do not tend to polymerize spontaneously by increasing the temperature. Styrene is one of the rare monomers that—also in its purest state—does exhibit initiation processes without additionally added initiator. The self-initiation of styrene has been studied in great detail with respect to its kinetics and mechanism (56–58). The underlying reaction is a self-Diels–Alder cycloaddition of two styrene moieties as shown in equation 14:

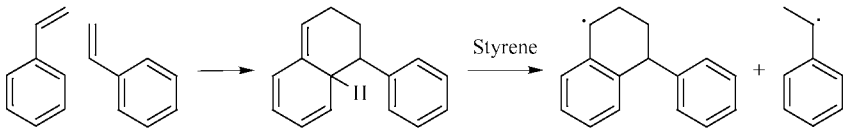

(14)

The self-initiated bulk polymerization of styrene has a substantial activation energy: a 50% monomer conversion needs 400 days at 29°C, but only 4 h at 127°C. However, the produced polystyrene is very pure because of the absence of

initiators and other additives. Methyl methacrylate was also thought to undergo self-initiated polymerization, but increasing evidence indicates that this may not be the case (59–64). It should be noted that certain pairs of monomers undergo spontaneous copolymerization without the addition of a thermal initiator. Examples include maleic anhydride/styrene (65) and acrylonitrile/styrene (66,67). The mechanism of initiation of such copolymerization is still unclear, but pathways analogous to that operative in styrene homopolymerizations but with acrylonitrile acting as the dienophile in the formation of the Diels–Alder adduct is debated. Other postulated mechanisms for spontaneous initiation include hydrogen atom transfer between the solvent and charge-transfer complex (68) and electron transfer followed by proton transfer to yield macroradicals (69).

Redox-Initiated Polymerization. Redox-initiating systems are very often used, especially in aqueous media. However, the redox initiation can also be carried out in organic media. These systems consist of a reducing and oxidizing agent (70,71). Redox initiators very often form only one radical (eg, classic Fenton system of ferrous salts and hydrogen peroxide or other peroxides) which, by eliminating cage termination, increases initiation efficiency:

$$Fe^{2+} + RO{-}OR \rightarrow Fe^{3+} + RO^- + RO^{\bullet} \quad (15)$$

Commercially important is also the use of ceric salts, which can reduce alcohols to alkoxy radicals and enable grafting from cellulose and other surfaces with OH groups.

Some redox systems provide two radicals such as persulfates with thiosulfates and metabisulfates:

$$S_2O_8^{2-} + S_2O_3^{2-} \longrightarrow SO_4^{\bullet -} + SO_4^{2-} + S_2O_3^{\bullet -} \quad (16)$$

$$S_2O_8^{2-} + S_2O_5^{2-} \longrightarrow SO_4^{\bullet -} + SO_4^{2-} + S_2O_5^{\bullet -} \quad (17)$$

The electrostatic repulsion between radical anions also reduces the probability of cage termination.

Transition metals in redox initiation usually act as reducing agents but may also act as oxidants:

$$Co^{3+} + {}^-OH \rightarrow Co^{2+} + {}^{\bullet}OH \quad (18)$$

There are also several nonaqueous redox systems which proceed by either outer- or inner-sphere electron transfer (OSET or ISET). As already stated before, aromatic amines accelerate decomposition of peroxides by electron transfer and formation of peroxide radical anions as depicted in equation 19:

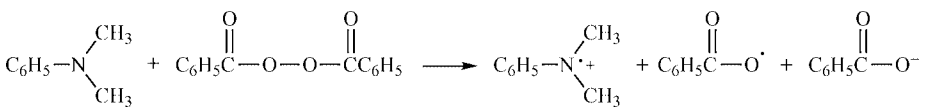

(19)

Trialkylboron derivatives are also powerful reducing agents and their interaction with benzoyl peroxide allows to initiate radical polymerization at very low temperatures, approximately −50°C. A similar low temperature redox-initiating system consists of trialkylboron derivatives and oxygen.

Another class of redox-initiating systems involves transition metal complexes which either alone provide radicals by homolytic cleavage or react with organic halides. The latter system applied under reversible conditions forms the basis of ATRP, one of the most powerful controlled/living radical polymerization systems (*vide infra*).

Some transition metal chelates, such as Mn(II), Co(II), Ce(IV), Fe(III), or Cu(II) acetylacetonates, initiate polymerization of alkenes at wide temperature range 25–100°C, depending on monomer and solvent, which both can affect the stability of the complexes.

The reaction of transition metal complexes with alkyl halides may occur via OSET or ISET, depending on the redox potential of the components and also on the coordination sphere of the transition metal compound. The saturated coordination sphere favors OSET or requires ligand dissociation. The open coordination sphere enables ISET process, as in ATRP. The most common alkyl halides used in this process are polyhalogenated methanes (CBr_4, CCl_4, $HCCl_3$) and also halogenated esters (CCl_3CO_2R, $ClCH_2CO_2R$), sulfonyl halides, *N*-haloamines, or *N*-haloureas.

$$Mt^0 + Cl{-}CCl_3 \rightarrow Mt^{I}Cl^- + {}^{\bullet}CCl_3 \qquad (20)$$

Low oxidation state transition metal complexes include $Mo(CO)_6$, and $Ni(P(OR)_3)_4$, and $Ni(CO)_4$; more recently many Cu(I) complexes with bi-, tri-, and tetradentate N-ligands and Fe(II), Ni(II), and Ru(II) complexes with phosphine ligand as well as CO, Cp, and other ligands have been reported.

Other Methods of Initiation. Apart from the above-mentioned methods of initiating free radical polymerizations, there are several more alternatives which can be selected from, if required for the specific application. These techniques include (*1*) ionizing irradiation, (*2*) plasma initiation, (*3*) electroinitiation, and (*4*) ultrasonic initiation.

(1) Radioactive sources and ionizing particles (such as γ-irradiation (72), electrons (73), neutrons, and α-particles) are used to initiate free radical polymerization processes. The interaction of these radiations with matter are—compared to the interactions of less energetic irradiation (such as UV or visible light)—much more complex. High energy radiation applied to vinylic monomers usually results in the formation of anions, cations, and primary free radicals. These species may then initiate chain growth. Whether this growth is of the free radical type depends largely on the reaction conditions. Ionic chain initiation is predominant at low reaction temperatures, because the formed ions tend to dissociate into free radicals at higher reaction temperatures. High-energy-radiation-initiated free radical polymerizations are less applied in scientific and commercial applications, which is mainly due to the complex initiation mechanism and the safety issues associated with the usage of this type of irradiation.

(2) When a gaseous monomer under low pressure is exposed to a high voltage electric discharge, plasma polymerization may occur (74). The plasma consists of ionized molecules. A large number of monomers undergo plasma polymerization and form high molecular weight products. The polymerization process appears to be rather complicated but seems to involve both ionic and free radical species. Plasma polymerization is especially attractive for the generation of thin polymer films for a variety of applications (75).

(3) Electroinitiation—which is not to be confused with initiation by an electron beam—is done by direct electrolysis of the reaction mixture. The reaction mixture usually contains an organic solvent, the monomer, and an inorganic compound that allows to conduct the current or participates in the ionization process itself (76). The polymerization proceeds via either free radicals or ions, depending on the reaction conditions and the substances present in the reaction mixture.

(4) Sonication—the application of high intensity ultrasound—produces high concentrations of $H^{\bullet}$ and $OH^{\bullet}$ radicals in water, which can lead to polymerization of aqueous monomer solutions. Free radicals are also produced in organic solvents and vinyl monomers, however, to a lesser extent than in water. Most of the physical and chemical effects caused by ultrasound are due to the process of cavitation, or the formation and collapse of microscopic bubbles as the sound wave passes through the liquid. Although the origin of chemical effects has been attributed to electrical discharge processes, the most widely accepted theory assumes the generation of very large temperatures and pressures during an adiabatic bubble collapse (77–79).

Initiator-Derived Radical/Monomer Reactions. An initiator-derived radical (also called a primary radical) can undergo a multitude of reactions including hydrogen abstraction (from the solvent, the monomer, or already present polymer), tail/head addition to the monomer, fragmentation, and/or primary radical termination. Which of these reactions primarily occurs depends on the structure of the generated radicals, the monomer, and to some extent the solvent and the general reaction conditions (ie pressure and temperature). The reaction pathways of the primary radicals may be studied via the nitroxide trapping technique and for some initiator/monomer systems these have been successfully mapped out (80–82). For example, the specificity of reaction with styrene monomer is found to decrease in the series cyanoisopropyl ~ methyl ~ *tert*-butoxy > phenyl > benzoyloxy. While cyanoisopropyl (83), *tert*-butoxy, and methyl radicals almost exclusively afford tail addition, (84), phenyl radicals give tail addition and 1% aromatic substitution (84). Benzoyloxy radicals have been reported to undergo head addition, tail addition, and aromatic substitution (84,85). Interestingly, in methyl methacrylate free radical polymerizations, the same radicals display a very different order of reactivity. Here, the regiospecificity decreases in the order cyanoisopropyl ~ methyl > phenyl > benzoyloxy > *tert*-butoxy. Methyl and cyanoisopropyl radicals almost exclusively yield tail addition. Phenyl and benzoyloxy radicals also tend to react with the double bond, whereas hydrogen abstraction is very minor (86,87). *tert*-Butoxy radicals react with methyl methacrylate via 63% tail addition

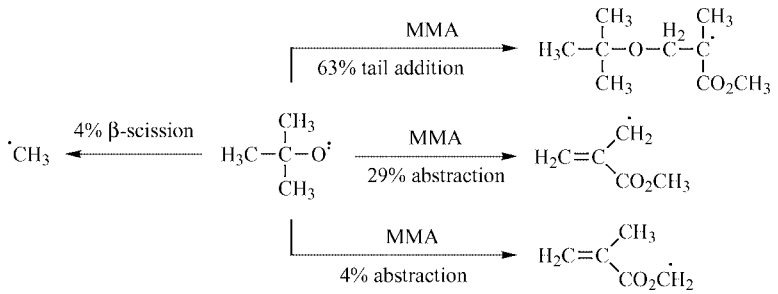

Scheme 5.

(88) and hydrogen abstraction mainly from the α-methyl group or the ester methyl group (see Scheme 5) (88,89).

Inspection of Scheme 5 indicates that a significant proportion of the poly(methyl methacrylate) chains will have an olefinic end group, when *tert*-butyl peroxide is employed as free radical initiator. Such chains may themselves undergo reaction in the polymerization, leading to a variation in the desired product properties. It is thus mandatory to carefully match the monomer with the initiator to achieve the required end group functionalities.

Some initiators generate two types of radicals upon fragmentation, which greatly differ in their reactivity and/or reactions toward the monomer units. Such initiators include the above-discussed photoinitiators, such as DMPA or benzoin, but also encompass acyl phosphine oxides and the thermal iniferter phenylazotriphenylmethane. The reactivity differences between the individual radicals can be quite dramatic. It has been proposed that the acetal-type radical generated by DMPA decomposition is not involved in initiation reactions at all, while its counter benzoyl radical is very effective in initiating macromolecular growth (18). Similarly, the addition rates to vinyl monomers of (2,4,6-trimethyl benzoyl)diphenylphosphine oxide derived radicals have been found to differ greatly (90–92). The carbon-centered radicals add to vinyl monomers about 2 orders of magnitude slower than the phosphorus-centered ones.

Initiator Efficiency. A prerequisite for primary radical/monomer reactions is the successful escape of the generated radicals from their "solvent cage". If the formed radicals remain inside the cage, they may undergo reactions with themselves. Potential 'in-cage' reactions are the main reason for initiator efficiencies, f, being below unity ($0.3 < f < 0.8$, typically) (93). In-cage reactions include radical recombination or disproportionation. If the initiator is regenerated by an in-cage reaction, the initiator efficiency is not affected, but the rate of initiator decomposition is reduced. The importance of reactions within the solvent cage strongly depends on the rate of diffusion of the generated radicals away from each other. Therefore, both the size and the reactivity of the primary radicals as well as the medium's microviscosity determine the initiator efficiency. As increasing monomer-to-polymer conversion goes hand in hand with a large increase in system viscosity, the likelihood of in-cage reaction will increase with monomer conversion (94,95). The species generated by reactions within the solvent cage can be reactive under the polymerization conditions or they may have detrimental effects on the polymer properties. For example, cyanoisopropyl radicals formed by

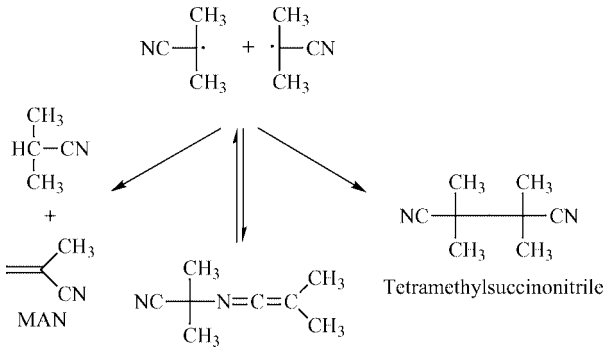

Scheme 6.

the fragmentation of AIBN can react to yield methacrylonitrile, which undergoes copolymerization and will be incorporated in the final polymer (83,96). In addition, the toxic tetramethylsuccinonitrile is generated (97). The in-cage reaction pathways of primary cyanoisopropyl radicals generated from AIBN are depicted in Scheme 6.

These reactions are almost exclusively taking place within the solvent cage when styrene monomer is present. In the absence of monomer, however, with only a solvent present (eg, benzene), close to half of the products are formed outside the solvent cage, indicating that the addition of the cyanoisopropyl radicals to the monomer units is effectively competing with self-reactions of the primary radicals (94).

The efficiency of peroxide initiators is affected by the mode of their fragmentation. Concerted decomposition results in an alkoxy and in an acyloxy radical, whose recombination will not affect the initiator efficiency (38). Such processes have also been termed 'cage-return' reactions. However, concerted two-bond scission yields alkyl and alkoxy radicals, which—when coupled inside the cage—lead to a lower f value. Experimental investigations into the initiator efficiency can be carried out via radical trapping techniques (98), infrared spectroscopy (99), and product or polymer-end-group analysis via NMR (94). Measurements of the temperature dependency of the initiator efficiency are extremely scarce; however, it has been found that in the AIBN-initiated bulk free radical polymerization of styrene at 100 MPa, f increases by approximately a factor of 1.5 when going from 40 to 80°C (99). The same study indicated that the initiator efficiency decreases when the reaction pressure is increased (f decreases by close to one third when going from ambient pressure to 200 MPa bar at 70°C).

As mentioned earlier, initiation efficiency is much higher in the redox process since in many systems only one radical is generated. However, with transition metals, the radicals may be formed reversibly either by abstracting back halogen or by formation of organometallic species.

Propagation

The propagation step in free radical polymerization has been in the center of scientific interest within the last decade, because of the advent of novel methods for the

accurate determination of propagation rate coefficients. The addition of a macroradical to a monomer unit can be described via the following rate law expression:

$$-\frac{\mathrm{d[M]}}{\mathrm{d}t} = \sum_i k_\mathrm{p}^i[\mathrm{R}_i^\bullet][\mathrm{M}] \tag{21}$$

with $k_\mathrm{p}{}^i$ being the propagation rate coefficient of a macroradical with chain length i, R_i, [M] the monomer concentration, and [R_i] the free radical concentration. It is generally accepted that the propagation reaction is chemically controlled up to high monomer conversions, ie high viscosities of the reaction medium. This implies that the propagation rate coefficient is independent of monomer conversions up to 80%. The chemical control of the propagation step is impressively demonstrated when comparing the average collision frequency of 10^{12} s^{-1} in the liquid phase at room temperature (100) to the frequency of successful propagation reactions (typically close to 10^3 s^{-1}). These numbers indicate that (approximately) only every 10^9th collision leads to a successful addition of a monomer unit to a macroradical. The propagation rate coefficient given in equation 21 carries the index i (representing the chain length of the growing chain), because it is beyond doubt that k_p is a chain-length-dependent rate coefficient. This is especially true for the first few addition steps, which proceed at a markedly increased rate compared to long-chain propagation. In the case of methyl methacrylate, for example, the first propagation step at 60°C is approximately 16 times faster than the long-chain propagation (101–106). The difference in the polymerization of monosubstituted monomers may be smaller (107). Nevertheless, recent evidence points toward a chain length dependence of the product of k_p and the monomer concentration [M], up to chain lengths of hundreds of monomer units (108–111). Unfortunately, to this date, there is no method to determine k_p independently of the monomer concentration. It is thus quite possible that the apparent chain length dependence of k_p reflects a structuring of the monomer concentration at the propagating chain end.

For most free radical polymerizations, the propagation step is fast (see below) and exothermic. The thermodynamics of free radical polymerization propagation have been reviewed by a few authors including Busfield (112), Sawada (113), and Allen and Patrick (114). Heats of free radical polymerization have been commonly determined from calorimetric data using standard thermochemical techniques. Entropies of polymerization are more scarce. It should be noted that the addition of radicals to vinyl monomers is—at least in principle—a reversible process. Depropagation is favored entropically and its importance increases with increasing temperature. Details about depropagation reactions can be found in the relevant subsection.

The propagating radical has been studied in great detail via electron spin resonance (ESR) spectroscopy. The monomers under ESR investigation include styrene and substituted styrenes (115–117), acrylic esters (118,119), methacrylic esters (120–124), vinyl chloride (125), α-substituted acrylic esters, and other monomers (115,121). In the overwhelming majority of cases, free radical propagation proceeds in a regioselective way to afford a polymer chain almost exclusively consisting of head–tail linkages. For mono- and 1,1-substituted monomers, it is usual to call the less substituted side the 'tail' and the more substituted side the

'head.' For more complex monomer substitution patterns (such as 1,2-di-, tri-, and tetrasubstituted monomers), the above definition is less stringent and the terms 'head' and 'tail' are used more arbitrarily. A terminology has been suggested for polymerization *regioselectivity*, where head–tail linkages are called *isoregic*, head–head linkages *syndioregic*, and tail–tail linkages *aregic* (126). Despite the high regiospecificity of the propagation step, it is in general not stereospecific, because of an addition of the very shallow pyramidal propagating radical center to an almost planar vinyl double bond.

For the formation of high molecular weight polymer, the propagation step must be sufficiently fast to compete with other elemental reactions such as transfer and termination. In fact, range of factors may prevent fast propagation, as discussed below.

Free radical propagation is poorly stereocontrolled, with nearly equal proportion of meso and racemic dyads in polymerization of monosubstituted alkenes and a preference for syndiotactic placement for disubstituted monomers such as methacrylates ($rr = 0.62$, $mm = 0.04$). The sequence distribution follows a first-order Markov model with a slight deviation from Bernoulian statistics. However, for very bulky substituents, as in polymerization of triphenylmethyl methacrylate, the preference for isotacticity was observed ($mm = 0.64$, $rr = 0.12$). Recently, complexation with Lewis acids and acidic solvents enabled to enhance stereocontrol in polymerization of vinyl esters and acrylamides, and to a smaller degree in polymerization of methacrylates (127–129).

Complexation with Lewis acids has also been used to alter sequences in copolymerization and prepare alternating copolymers in systems which usually provide very small tendency for alternation like styrene/methyl methacrylate ($r_S \sim r_{MMA} \sim 0.5$) (130,131).

Monomer Structure and Reactivity: Electronic and Entropic Effects. The absolute value of the propagation rate coefficient is governed by the nature of the monomer unit and the reactivity of the propagating radical. Both entropic and electronic factors influence the absolute value of the propagation rate coefficient and its activation parameters, E_A and A. It is important to note that the reactivity of the propagating radical and the reactivity of the monomer units correlate reciprocally. For example, methacrylates are several times more reactive then acrylates but polyacrylate radicals are significantly more reactive than poly(methacrylate) radicals. For polymerization and chain growth to take place, it is mandatory that the free macroradical lives long enough to survive the above-mentioned 10^9 ineffective collisions. The addition of the monomer in a propagation reaction has to take place before any possible decomposition reaction or other side reaction. For example, acetone cannot be polymerized at ambient reaction conditions—besides thermodynamic reasons, which make the polymerization unfavorable, because the associated free radicals quickly decompose into methyl free radicals and a ketone.

The substituent that is introduced into the ethene molecule to facilitate polymerization via activation of the double bond and stabilization of the propagating radical, respectively, has also the effect of adding steric hindrance to the propagation step. A mechanistic model has been proposed for the propagation of sterically hindered monomers (132). In such a model the propagating radical and the monomer attain the maximum overlap of the π-electrons and the unpaired electron at a certain angle between the C_α—C_β bonds of the monomer and the

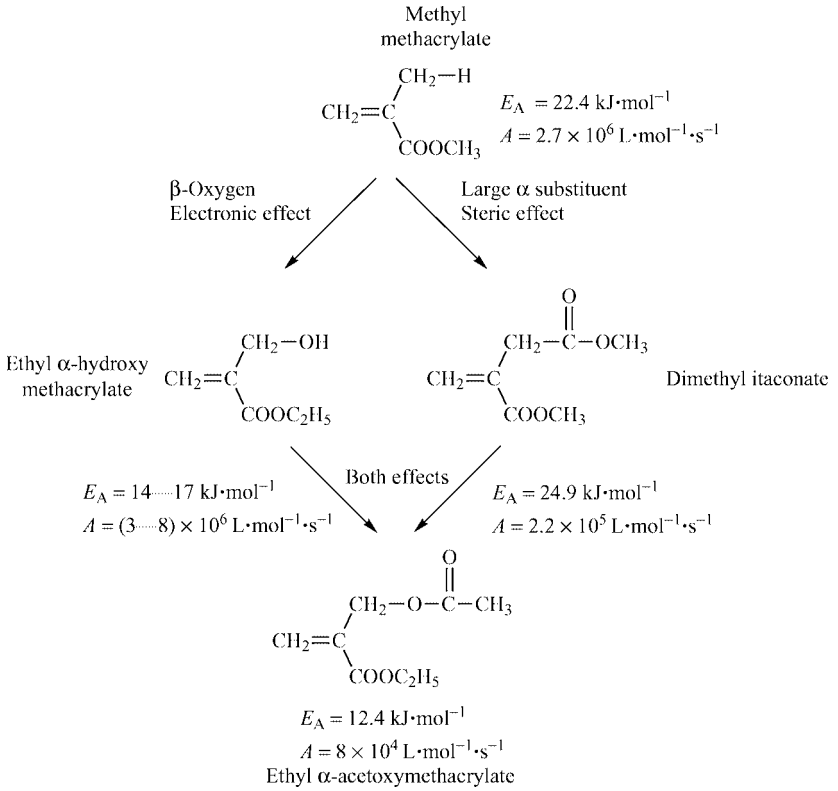

Scheme 7.

propagating radical. If the propagation reaction is sterically hindered, the bond formation is energetically not suppressed, but the probability that the radical and the monomer approach each other such that bond formation can occur is decreased. It is thus evident that it is close to impossible to completely separate enthalpic from entropic effects.

An attempt to separate individual contributions using different monomers is illustrated in Scheme 7. While electronic effects should be reflected in the activation energy E_A, steric effects are associated with the preexponential factor A. When going from methyl methacrylate to dimethyl itaconate (133), a substantial decrease in the preexponential factor of about one order of magnitude is observed (r.h.s. of Scheme 7). This decrease is due to the sterically more demanding nature of the propagating dimethyl itaconate radical. When going from methyl methacrylate to ethyl α-hydroxy methacrylate (EHMA), the preexponential factor remains unchanged, but the activation energy is reduced due to the electronic effect of the additional β-oxygen atom (l.h.s. of Scheme 7). Both effects may be combined in one monomer (ethyl α-acetoxymethacrylate, EAMA, bottom of Scheme 7), with a resulting decrease in the activation energy and the preexponential factor.

This illustrates the effect of different contributions (ie steric and electronic) to the activation parameters using different monomers.

Table 1. Activation Parameters for the Propagation Step for Various Monomers, Obtained via PLP–SEC[a]

Monomer	E_A, kJ · mol^{-1}	A, L · mol^{-1} · s^{-1}	k_p at 60°C, L · mol^{-1} · s^{-1}
Methyl methacrylate	22.3	2.65×10^6	833
Ethyl methacrylate	23.4	4.07×10^6	873
Butyl methacrylate	22.9	3.80×10^6	976
Isodecyl methacrylate	20.8	2.19×10^6	1,590
Dodecyl methacrylate	21.0	2.51×10^6	1,280
2-Ethylhexyl methacrylate	20.4	1.87×10^6	1,190
Cyclohexyl methacrylate	22.3	4.88×10^6	1,560
Glycidyl methacrylate	21.9	4.41×10^6	1,620
Hydroxyethyl methacrylate	21.9	8.89×10^6	3,270
Hydroxypropyl methacrylate	20.8	3.51×10^6	1,900
Isobornyl methacrylate	22.5	4.28×10^6	1,290
3-[Tris(trimethylsilyloxy)silyl]propyl methacrylate[b]	19.9	1.44×10^6	1,092
Dimethyl itaconate[c]	24.9	2.20×10^5	27
Dicyclohexyl itaconate[d]	22.0	1.74×10^4	6
Methyl acrylate[e]	13.9	3.61×10^6	24,000
Butyl acrylate	17.4	1.8×10^7	33,700
Dodecyl acrylate[e]	15.8	1.09×10^7	36,400
Styrene	32.5	4.27×10^7	341
p-CH_3-Styrene	32.4	2.84×10^7	236
p-Cl-Styrene	32.1	4.48×10^7	415
p-F-Styrene	32.0	3.50×10^7	336
Vinyl acetate	20.4	1.49×10^7	9,460

[a] From Ref. 134, unless otherwise indicated.
[b] Ref. 136.
[c] Ref. 133.
[d] Ref. 135.
[e] Experiments carried out at 10 MPa (100 bar).

The propagation rate coefficients of similar monomers are also similar, which allows them to be arranged in groups or families. This is the case for structurally similar monomers such as acrylates or methacrylates. The homologous series of acrylates with increasing ester groups, such as methyl, ethyl, butyl, and dodecyl acrylate, have approximately the same k_p value as do the corresponding methacrylate systems. The propagation rate coefficients and Arrhenius parameters [determined via the pulsed laser polymerization–size exclusion chromatography (PLP–SEC) method] for these and additional monomers are given in Table 1 (data taken from References 134 and 137).

The propagation rate coefficient for most monomers is pressure dependent with negative activation volumes; ie, an increase in pressure leads to an increased k_p value. Typical activation volumes $\Delta V^{\#}$ (cm^3 · mol^{-1}) for the propagation step for some common monomers are as follows: −11.7 (methyl acrylate) (138), −11.7 (dodecyl acrylate) (138), −16.7 (methyl methacrylate) (139), −16.0 (butyl methacrylate) (140), and −16.5 (dodecyl methacrylate) (140).

It should be noted that the termination rate coefficient is unexpectedly decreasing with increasing pressure, owing to viscosity effects. The opposite behavior of k_p and k_t with respect to an increase in pressure results in markedly increased overall polymerization rates at higher reaction pressures.

Effect of the Reaction Medium. Since the transition state in propagation is relatively nonpolar and the propagation reaction is chemically controlled (up to high monomer conversions of ~80%), there is weak solvent influence on the propagation rate coefficients. Extensive studies have been carried out, which mainly confirm this small influence of the solvent on the propagation rate coefficient (141–143). Larger effects in solvents have only been observed for specific monomers, eg, EHMA (144), vinyl acetate (145), vinyl benzoate (146), or specific solvents like supercritical CO_2 (147–151). Furthermore, the k_p values for the polymerizations of methacrylic acid and acrylic acid in water are significantly affected by the monomer concentrations (152–154). In the case of the solvent effects on EHMA, where k_p falls between 580 $L \cdot mol^{-1} \cdot s^{-1}$ (tetrahydrofuran) and 1860 $L \cdot mol^{-1} \cdot s^{-1}$ (xylene), it was proposed that the solvent is playing a specific role in the transition state of the reaction by possibly affecting the geometry of the transition state via specific interactions. This suspicion is underpinned by the observation that the solvent also affects both the activation energy and the preexponential factor. However, it should always be kept in mind that any existing technique to assess the propagation rate coefficient is only capable of measuring the product of k_p and the monomer concentration. Results obtained from free radical polymerizations carried out in supercritical CO_2 suggest that the actual monomer concentration at the reaction site is somewhat different from the solution concentration; ie, a structuring of the solution occurs. Since at present there is no methodology to separate the propagation rate coefficient from the monomer concentration, these interpretations are somewhat speculative.

Effects of solvents on the tacticity of the generated polymeric material have been reported (155). When fluoroalcohols were used as solvents, the stereochemistry of the polymerizations of some vinyl esters was affected to varying extents, depending on the structure of the acyl group of the monomer (156–159).

It has been shown that for conversion exceeding 80%, the propagation reaction becomes diffusion controlled, which leads to a marked decrease of k_p. For example, in the case of the bulk free radical polymerization of methyl methacrylate, both the propagation rate coefficient and the initiator efficiency decrease significantly at high monomer conversion in a highly viscous regime (160–162). However, exact measurements in this highly viscous reaction regime are extremely difficult to carry out and thus reliable data are scarce.

Transfer

The measured average molecular weights, eg, obtained from molecular weight distributions, of macromolecules generated by free radical polymerization processes are often lower than those predicted by accounting for initiation, propagation, and termination processes. This experimental observation can be attributed to chain stopping events via chain transfer reactions (163,164). The transfer reaction can be described via equations 22 and 23.

$$R_i^{\bullet} + T{-}X \xrightarrow{k_{tr}} P_i{-}X + T^{\bullet} \quad (22)$$

$$T^{\bullet} + M \xrightarrow{k_i} R_1^{\bullet} \quad (23)$$

The propagating macroradical of chain length i, R_i, abstracts a weakly bonded atom X (eg, a hydrogen or halogen atom) from the transfer agent TX. A dead polymer chain with X attached to the end group is generated, as well as a new small free radical ($T^{\bullet}$), which can in turn react with a monomer unit. The transfer agent may be the monomer itself, the initiator, the solvent, or any other deliberately added transfer agent. The transfer reaction does not change the free radical concentration—at least in its ideal form—but transfers the radical center from one end of the growing polymer chain to another molecule. The overall rate of polymerization hence remains unchanged. The kinetic chain length, which describes the amount of monomer units that are polymerized by one radical during its lifetime between initiation and termination, remains unaltered. However, the transfer process relocates the radical center from one molecule to another and enables the radical site to polymerize more than one molecule to completion. Hence, the actual physical chain length, ie the degree of polymerization, of the produced polymer is reduced and concomitantly the number of polymer molecules increases (see Figure 2).

The decrease in the degree of polymerization should not be confused with the effect of a decrease of monomer concentrations and increase of initiator concentration, which also leads to an effective reduction of the kinetic chain length. It should be noted that an increase in the initiator concentration is always associated with a considerable increase in the rate of polymerization according to equation 56, which may lead to a loss over the control of the polymerization.

The fragments of the chain transfer agent (T and X) are incorporated into the polymer chain as end groups instead of the end groups otherwise resulting from the initiation and termination process. A transfer reaction can therefore be used to introduce specific end groups into the polymeric material. This technique is however limited by the fact that the degree of polymerization is strongly decreased

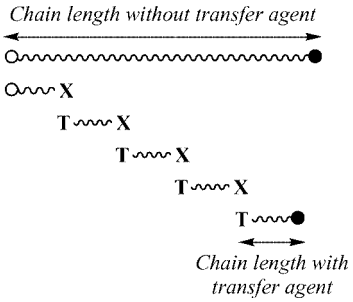

Fig. 2. Schematic description of chain transfer: ○ denotes the initiator-derived end group, ● denotes the end group generated by the termination process. Additional transfer-agent-derived end groups (T and X) are incorporated into the polymeric material by the transfer mechanism and the chain length of the polymer is reduced.

when using a transfer agent and that an efficiency of 100% regarding the end group introduction can never be achieved—even with very effectively transferring compounds—because the bimolecular termination reaction is always present in free radical polymerization.

The chain transfer reaction is mainly used in industrial processes to effectively reduce the molecular weight of the generated polymer. This procedure prevents the significant increase of the viscosity, which is related to the weight-average degree of polymerization. This facilitates the heat transfer inside the reactor and the processing of the final polymeric material. It should be kept in mind that conventional chain transfer agents are consumed according to equations 22 and 23 during the reaction. However, there are catalytic chain transfer agents based on transition metal complexes [eg, Co(II)] that are capable of effectively transferring the radical center without being consumed. Such agents were discovered in the late 1970s and are now commonly used in industrial applications (see below).

The rate of the transfer reaction is described by the consumption of the transfer agent TX, expressed by the following equation:

$$-\frac{\mathrm{d[TX]}}{\mathrm{d}t} = k_{\mathrm{tr}}[\mathrm{R}^{\bullet}][\mathrm{TX}] \tag{24}$$

where k_{tr} is the transfer rate coefficient, [TX] is the concentration of the transfer agent, and [$\mathrm{R}^{\bullet}$] is the free radical concentration. The transfer rate coefficient is often reported as a ratio with the propagation rate coefficient k_{p}. The resulting quantity is called the transfer coefficient, C:

$$C = \frac{k_{\mathrm{tr}}}{k_{\mathrm{p}}} \tag{25}$$

The transfer coefficient C is, in principle, not constant, since it is dependent on the same external parameters as the propagation rate coefficient (ie chain length, temperature, pressure, etc). However, C is also often denoted the chain transfer constant. The chain transfer coefficient C describes the effectiveness of the transferring compound to reduce the degree of polymerization. Its value depends on structural features of the attacking radical and the transfer agent. A chain transfer coefficient of one has been called optimal, because the transfer agent/monomer ratio will remain constant throughout the polymerization (165). The degree of polymerization therefore stays constant up to high conversions and the polydispersity of the product remains at the theoretical value of close to 2. If $C \gg 1$, the transfer agent will be consumed rapidly during the polymerization and the molecular weight will increase with conversion. A small value of the transfer coefficient ($C \ll 1$), on the other hand, will lead to a decrease of the molecular weight, accordingly. In both cases, a broadening of the molecular weight distribution with conversion occurs.

The ideal chain transfer reaction does not alter the overall rate of polymerization, R_{p}. However, if the chain transfer reaction has a measurable effect on R_{p}, this rate depends on the size of the propagation, reinitiation, and transfer rate coefficients. That is, the free radical which is newly formed by the transfer

step is not always of the equal activity to that which is lost. Four cases can be distinguished:

(1) $k_p \gg k_{tr}$ and $k_{ri} \approx k_p$ leads to 'ideal' chain transfer, decreasing molecular weights, and no measurable effect on R_p.
(2) $k_p \ll k_{tr}$ and $k_{ri} \approx k_p$ leads to telomerization (166), a large decreasing effect on molecular weights, and no measurable effect on R_p.
(3) $k_p \gg k_{tr}$ and $k_{ri} < k_p$ leads to retardation (167), a decrease in molecular weights, and a decrease in R_p.
(4) Finally, $k_p \ll k_{tr}$ and $k_{ri} < k_p$ results in degradative chain transfer (168), a large decrease in molecular weights, and a large decrease in R_p.

It can thus be easily inferred that chain transfer may alter the properties of the polymeric product in an undesirable way, or—in contrast—may be used advantageously to specifically reduce the molecular weights obtained in a specific polymerization process or to introduce specific end groups. The first case discussed above (which refers to the kinetic concept of chain transfer) is assumed for the derivation of the Mayo equation, which is frequently used to derive chain transfer rate coefficients. This specific case does not alter the overall rate of the polymerization system, because it does not change the overall free radical concentration, but rather influences the molecular weight distribution.

There are at least two basic mechanisms for chain transfer: (*1*) atom or group transfer and (*2*) addition–fragmentation (169). The two mechanisms differ mainly in the nature of the intermediate that is formed by the two participating molecules. The atom transfer mechanism—the most common mechanism—proceeds via an S–2 mechanism (substitution, homolytic, bimolecular) as depicted in equation 26.

$$R_i^{\cdot} + X{-}Y \longrightarrow \left[R_i \cdots X \cdots Y\right]^{\cdot \ddagger} \longrightarrow R_i{-}X + Y^{\cdot} \tag{26}$$

The intermediate of this reaction is identical with the activated complex at the transition state (170), and hence is destabilized and immediately decomposes into the final products (see Figure 3**a**).

Tedder (171) suggested guidelines to predict qualitatively the rate and outcome of radical transfer processes:

(1) When there is little polarity in the transition state, the relative rates of the atom transfer by a specific radical will correlate with the strengths of the bonds being broken.
(2) The strength of the bond being formed is important for the absolute rate of the transfer event.
(3) The steric strain released or incurred when going from the reactants to the products is especially important for endothermic or thermoneutral reactions.
(4) Nucleophilic radicals will preferably attack electron-rich sites, and electrophilic radicals will attack electron-poor sites. For example, transfer coefficient for nucleophilic trialkylamine with partially positively charged

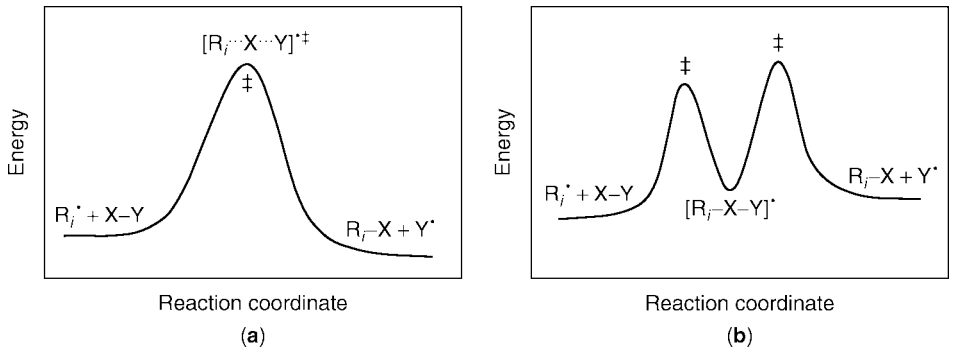

Fig. 3. Schematic representations of the energy profile along the reaction coordinate for (**a**), atom or group transfer and (**b**) addition–fragmentation transfer.

β-hydrogens is over 1000 times higher with electrophilic polyacrylonitrile and polyacrylate radicals rather than with polystyrene radicals. On the other hand, in dimethyl formamide, the electrophilic $FeCl_3$ with partially negatively charged Cl atoms transfers 15 times faster with nucleophilic polystyrene radicals than with polyacrylonitrile radicals (172).

The addition–fragmentation mechanism, on the other hand, proceeds via the formation of a relatively stable intermediate, as depicted in equations 27 and 28, with k_β being the rate coefficient of the addition reaction and $k_{-\beta}$ the rate coefficient of the fragmentation. The corresponding energy profile along the reaction coordinate is outlined in Figure 3**b**. The absolute depth of the sink may vary according to the stability of the intermediate. The reactivity of the transfer agent, toward the propagating species and the properties of the intermediate radical—especially its stability—are both important to characterize the overall transfer reaction. If the fragmentation rate coefficient is small, ie the intermediate exhibits a significant lifetime, it is possible that it reacts via different pathway other than fragmentation. Depending on the structure of the intermediate radical, reversible and irreversible bimolecular termination reactions may occur, leading to inhibition and/or retardation. If the intermediate radical adds on to monomer, ie initiates polymerization, the compound is not a transfer agent, but rather a comonomer and a branching agent.

$$R_i^{\bullet} + X{-}Y \xrightarrow{k_\beta} [R_i{-}X{-}Y]^{\bullet} \tag{27}$$

$$[R_i{-}X{-}Y]^{\bullet} \xrightarrow{k_{-\beta}} R_i{-}X + Y^{\bullet} \tag{28}$$

Transfer to Monomer. The only transfer reaction that cannot be avoided is transfer to monomer. Thus, the maximum molecular weight that can be reached under a given set of reaction conditions is limited by the transfer-to-monomer reaction, assuming the absence of all other transfer events. Fortunately, the transfer-to-monomer rate coefficients in free radical polymerization are usually

rather low, approximately between 3×10^{-5} and 20×10^{-5} $L \cdot mol^{-1} \cdot s^{-1}$. It is important to be aware that the transfer-to-monomer reaction cannot be suppressed by a decrease in monomer concentration, because the number-average degree of polymerization is independent of the monomer concentration for the transfer-to-monomer step. This is, because the transfer-to-monomer effect is governed by the ratio of the transfer rate to propagation rate and both the denominator and numerator of this ratio contain the monomer concentration, which consequently cancels out. (This is illustrated in eq. 91). However, the activation energies for propagation and transfer to monomer differ for most of the common monomers. Thus, a decrease in the temperature normally lowers the monomer transfer coefficient C_M. Table 2 gives the transfer-to-monomer constants C_M for some common monomers.

Table 2. Transfer Coefficients to-Monomers, C_M, at 60°C[a]

Monomer	T,°C	C_M (10^{-5})
Acrylamide	60	6.0[b]
Acrylonitrile	60	3.3–10.2[c]
1-Butene	60	73
Butyl acrylate	60	3.33–12.5
o-Chlorostyrene	50	2.5–2.8
Ethyl acrylate	60	5.79
Ethylene	60	4–42[d]
	110	11–90
	130	16–112
Methacrylonitrile	60	58.1
Methyl acrylate	60	0.36–3.25[e]
Methyl methacrylate	0	1.28–1.48
	30	1.17–2.6
	50	5.15[f]
	100	3.8
α-Methylstyrene	50	412[f]
Styrene	25	3.5[g]
	60	7.8–8.7
	90	15–16.5
Vinyl acetate	0	5.0–9.6
	25	9.0–107
	40	12.9–13.2
	60	18[h]
Vinyl chloride	60	108–160
Vinylidene chloride	60	380[i]

[a] Data From Ref. 173, unless other reference is noted.
[b] Ref. 174.
[c] Ref. 175.
[d] Ref. 176.
[e] Ref. 177.
[f] Ref. 178.
[g] Ref. 179.
[h] Ref. 180.
[i] Ref. 181.

The transfer-to-monomer reaction mostly proceeds via an abstraction of a hydrogen atom; however, it is often not clear which hydrogen is involved. This abstraction mechanism is reasonable for monomers with aliphatic hydrogens (eg, methyl methacrylate, vinyl acetate), but different mechanisms seem to be operational when only vinylic and/or aromatic hydrogens are present. The transfer to monomer in the free radical ethylene polymerization, for instance, also involves hydrogen atom transfer from the radical to the monomer (182). Although this hydrogen transfer (see eq. 29), is thermoneutral—reactants and products are the same—it is disfavored—due to the high strength of the vinylic hydrogen–carbon bond that has to be broken—over the endothermic hydrogen abstraction reaction depicted in equation 30.

$$CH_3{-}CH_2^{\bullet} + CH_2{=}CH_2 \rightarrow CH_2{=}CH_2 + CH_3{-}CH_2^{\bullet} \quad (29)$$

$$CH_3{-}CH_2^{\bullet} + CH_2{=}CH_2 \rightarrow CH_3{-}CH_3 + CH_2{=}CH^{\bullet} \quad (30)$$

The transfer to styrene monomer is unlikely to proceed via a direct hydrogen abstraction, because the chain transfer coefficient is higher than that of ethylbenzene with its weaker bound hydrogen atoms. The transfer step rather involves the abstraction of a weakly bound hydrogen of the Diels–Alder adduct (see eq. 14), formed by two styrene molecules (183).

The chain transfer to vinyl chloride monomer involves a chlorine atom transfer reaction, following a head-to-head addition of a monomer molecule to the growing macroradical (184–186). The head-to-head addition leads to a highly unstable radical that stabilizes itself via a chlorine abstraction. This reaction pathway (eq. 31) accounts for C_M being much greater than for other commercially important monomers.

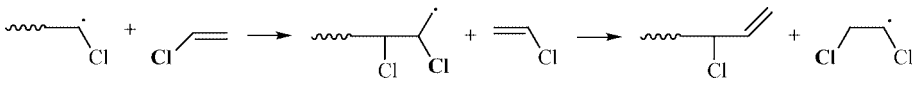

(31)

Allylic compounds ($CH_2{=}CHCH_2X$) are usually reluctant to undergo homopolymerization, because of the activation of the allylic hydrogen atom toward abstraction. The generated allylic radical is highly stabilized both by the substituent X and by delocalization of the free electrons into the double bond. These radicals add to monomer very slowly and perform side reactions that in turn lead to retardation.

Transfer to Initiator. In most polymerization systems the transfer reaction to the initiator is also unavoidable. However, this form of chain transfer is to some extent controllable via the choice of the employed initiator. In addition, the effects on the overall polymerization kinetics and on the molecular weight distribution are small if low concentrations of initiator are employed. Typical transfer-to-initiator constants C_I are presented in Table 3.

A special case of chain transfer to initiator is the reaction involving thiurams. The photosensitizers tetraalkylthiuram disulfides can either be cleaved

Table 3. Transfer Coefficients to Initiators, C_I, at 60°C[a]

	C_I		
Initiator	Styrene	Methyl acrylate	Methyl methacrylate
2,2′-Azobis(isobutyronitrile)	0.09–0.14[b]	—	0.02[c]
tert-Butyl peroxide	0.00023–0.0006[d]	0.00047[e] (65°C)	0.0001[f] (20°C)
2-Butanone peroxide	0.46 (50°C)	0.05 (65°C)	0.0025–0.00698 (65°C)
tert-Butyl hydroperoxide	0.035	0.01	—
Ethyl peroxide	0.00066	—	—
2,2′-Azobis(2,4,4-trimethyl valeronitrile)	0.59 (25°C)	—	—
Benzoyl peroxide	0.101[g]	0.0246[e]	0.02[h]

[a] Data from Ref. 173, unless other reference is noted.
[b] Ref. 187.
[c] Ref. 188.
[d] Ref. 189.
[e] Ref. 177.
[f] Ref. 190.
[g] Ref. 191.
[h] Ref. 192.

photochemically to initiate polymerization or exhibit a transfer reaction via group abstraction with another macroradical, as depicted in Scheme 8. The resulting thiyl radical can either initiate macromolecular growth or terminate a growing chain to give a polymer chain with $R_2NC(S)S-$ groups at both ends (193,194). Under the photoirradiating conditions this termination reaction is reversible, leading to an equilibrium of propagating and dormant radicals. This equilibrium can effectively reduce the free radical concentration and hence bimolecular termination reactions. The tetraalkylthiuram disulfides are known as *iniferters* (195,196) and they function as initiator, transfer agent, and terminator simultaneously.

Transfer to Transfer Agents and Solvents. In contrast to transfer to monomer and initiator, the transfer to a solvent molecule is of considerable importance, because solvents are used in high concentrations in most industrial

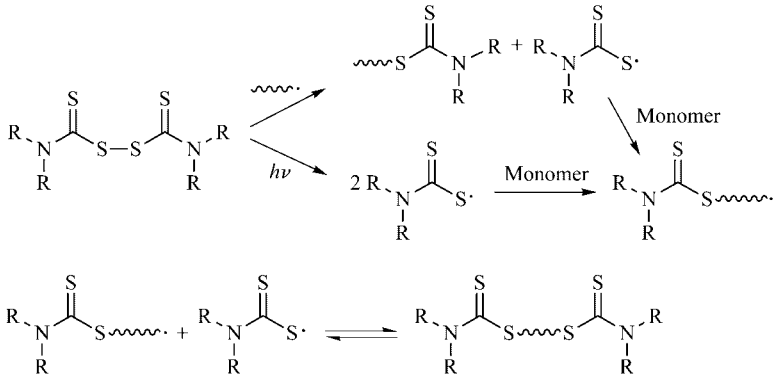

Scheme 8.

polymerization processes. Many organic solvents exhibit transfer coefficients similar to those found for common monomers and their significant transfer effect can be largely attributed to their usage in high concentrations. There are a few solvents that show significantly higher transfer coefficients, such as carbon tetrachloride. In the case when the transfer coefficient of a solvent is too high, it may not be used as a solvent but rather as a modifier, ie a 'conventional' chain transfer agent. Chain transfer agents with chain transfer coefficients greater than one are very useful, as they can be employed in low concentrations. Every solvent that contains abstractable hydrogen atoms is capable of acting as a chain transfer agent. However, most of the common solvents show only minor transfer activity as can be seen in Table 4. The transfer reaction is strongly dependent on the nature of the propagating radical. The very reactive vinyl acetate radical, for example, has a much higher tendency to transfer than the relatively low reactive methyl methacrylate radical. However, many transfer agents exhibit significant retardation when used in vinyl acetate polymerization (203). The factors influencing the reactivity in hydrogen atom abstraction reactions are discussed above in general terms. The transfer of aromatic compounds may involve the addition of the growing radical to the aromatic system, generating a cyclohexadienyl radical adduct, which in turn may restore its aromaticity via the transfer of a hydrogen to another macroradical. A solvent can also be deliberately used to introduce specific end groups into the polymeric chain if its transfer coefficient for the specific system is moderate. The compound then serves as both solvent and transfer agent, and side reactions may hence be suppressed (204).

Thiols. There are various thiols (R—SH) that are used as chain transfer agents and they are employed in many different free radical polymerization processes (205). A considerable disadvantage of these transfer agents is their often very unpleasant odor. The general transfer process of these compounds is depicted in equations 32 and 33.

(32)

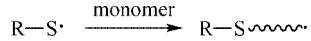

(33)

The vast majority of the generated polymeric material possesses a thioether end group. The chain transfer coefficients of some thiols in styrene and methyl methacrylate polymerizations are given in Table 4. It should be noted that the value of the chain transfer coefficient is dependent on the polymerization system, ie monomer, temperature, pressure, etc. However, the tabulated values are guidelines for the transfer ability of the transfer agents in other monomer systems. A number of functional thiols have been used to prepare end-functional polymeric material. These were used as starting materials for block (206,207) and graft (208) copolymers for the application as emulsifier, thermoplastic elastomers, compatibilizer, and adhesives. Thiols react more rapidly with nucleophilic than electrophilic radicals. Hence, thiols have a greater transfer coefficient with styrene and vinyl esters than with acrylates and methacrylates. Aromatic thiols have a higher transfer ability; however, they exhibit more retardation. The thiyl

Table 4. Transfer Coefficients to Solvents and Additives, C_T, at 60°C[a]

	C_T (10^{-4})	
Transfer agent	Styrene	Methyl methacrylate
2-Aminoethanthiol hydochloride	—	1,100[b]
2-Butanone	4.98	0.45
Acetaldehyde	8.5	6.5
Acetic acid	2.22 (40°C)	0.24 (80°C)
Acetone	0.32[c]	0.195
Acetonitrile	0.44	—
Aniline	2.0	4.2
Benzaldehyde	4.5–5.5	0.86–2.5
Benzene	0.018–0.04	0.04–0.83
Benzenesulfonyl chloride	4,330	5
Benzenethiol	—	27,000
Carbon tetrabromide	2,500,000[d]	1,500–2,700
Carbon tetrachloride	69–148	0.5–20.11
Chloroform	0.41[c]	0.45–1.77
Copper(II) chloride	10^8	2×10^7
Cumene	0.8–3.88	1.9–2.56
Cyclohexane	0.024–0.063	0.1–0.2 (80°C)
Diethyldisulfide	45 (99°C)	1.3
Dibenzyldisulfide	100	63
Diphenyldisulfide	1,500	110
Ethyl acetate	15.5	0.1–0.46
Ethyl ether	5.64	—
Ethyl iodoacetate	8,000	—
Ethyl bromoacetate	430	—
Ethyl tribromoacetate	100,000	—
Ethyl trichloroacetate	100	—
Heptane	0.42	1.8 (50°C)
Iron(III) chloride	5,360,000	4,000
2-Propanol	3.05	0.583
Methanol	0.296–0.74	0.2
Mercaptoacetic acid methyl ester	14,000[e]	3,000[e]
N,*N*-Dibenzylhydroxylamine	5,000	—
N,*N*-Dimethyl acetamide	4.6	—
N,*N*-Dimethyl formamide	4.0	—
n-Butyl alchol	1.6	0.394
n-Butanethiol	220,000	6,600
n-Dodecanethiol	150,000	9700–12300[f]
Pentaphenylethane	20,000	—
Phenyl ether	7.86	9.13
Pyridine	0.6	0.176 (70°C)
Tetraethylthiuram	3,200[g]	—
Tetrahydrofurane	0.5 (50°C)	—
Toluene	0.105–2.05	0.17–0.45
Trichlorotoluene	57.5	
Triethylamine	1.4–7.5	8.3
Water	0.006–0.31	

[a] Data from Ref. 173, unless other reference is noted.
[b] Ref. 197.
[c] Ref. 198.
[d] Ref. 199.
[e] Ref. 200.
[f] Ref. 201.
[g] Ref. 202.

radical produced by the transfer reaction of a thiol is electrophilic and, when used in copolymerizations, will more likely react with electron-rich monomers.

A wide range of functional thiols, eg, mercaptoethanol ($OHCH_2CH_2SH$) and thioglycolic acid ($OH(CO)CH_2SH$), have been used to produce monofunctional polymers (165,209,210).

Sulfides. A wide range of various disulfides have been employed as chain transfer agents: dialkyl disulfides (211), diaryl disulfides (212,213), diaroyl disulfides (214), and xanthogens (215). The reaction of these compounds leads to the incorporation of sulfur-containing end groups at both ends of the polymer, as shown in equations 34 and 35. They therefore have found some applications in the preparation of telechelic polymers.

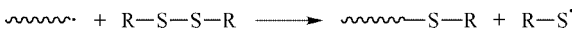

(34)

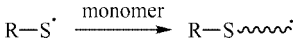

(35)

The transfer coefficients of disulfides are extremely low for styrene and methyl methacrylate (see Table 4), but are close to one for the vinyl acetate polymerization. In general the xanthogens and thiurams have higher chain transfer ability, which has been attributed to the iniferter mechanism described above. Monosulfides have lower transfer coefficients in comparison to disulfides. This may reflect steric factors and the relative strength of the C—S bond, which is significantly stronger than the S—S bond.

Catalytic Chain Transfer. A highly useful variant of chain transfer was discovered in the 1970–1980s in the Soviet Union (216). A number of reviews have been published in recent years (217–221) on this synthetic method which has acquired the nomenclature of either catalytic chain transfer (CCT) or special chain transfer (SCT). The most commonly adopted catalysts are based on low spin cobalt macrocycles, although other metal-containing complexes have also been suggested in the patent and scientific literature. Some typical catalyst structures are shown as **12** and **13**.

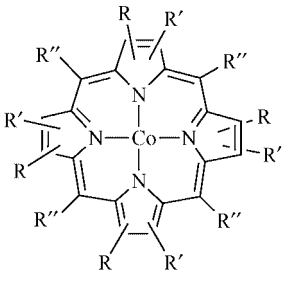

Cobalt(II)Porphyrins

12

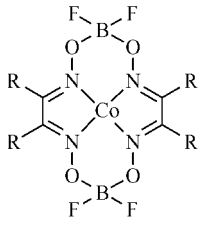

Cobaloximes

13

Some of the highest chain transfer constants ever measured have been reported for COBF (**14**), as shown below:

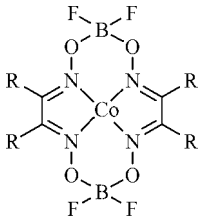

COBF: R = Methyl
COPhBF: R = Phenyl

14

Monomer	C_s (10^{-3}) at 60°C
Methyl methacrylate	28.1 (222)
tert-Butyl methacrylate	15.1 (222)
Dimethyl itaconate	9.5 (222)
Styrene	9.0 (223)

These high transfer values would only be of curiosity value for synthetic purposes if a conventional chain transfer mechanism was operative. However, these cobalt complexes appear to catalyze transfer to monomer and they do not get incorporated into the polymer chains, nor do they get consumed in the transfer reaction. A catalytic cycle involving methyl methacrylate as the monomer is thought to be a good representation of the mechanism. The cobalt complex abstracts a β-hydrogen from a growing radical (creating terminal unsaturation) and a cobalt hydride, which then reinitiates a monomer unit via hydrogen-atom addition or insertion into the double bond (eqs. 36 and 37).

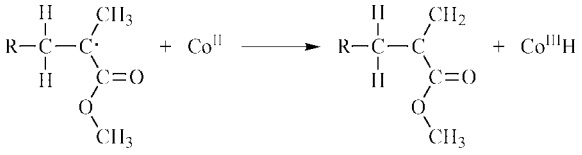

(36)

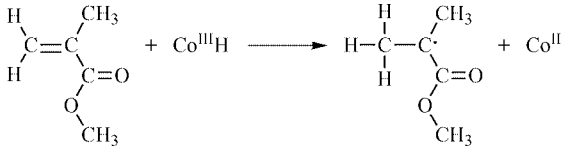

(37)

An interesting variation of this reaction (224,225), termed *catalytic chain transfer isomerization*, has been described whereby transfer occurs from a radical with a β-CH_2OH group, as shown in Scheme 9. A keto–enol isomerization occurs and an aldehyde end group results.

Catalytic chain transfer is most efficient for tertiary propagating radicals such as methyl methacrylate. When secondary radicals are involved, such as

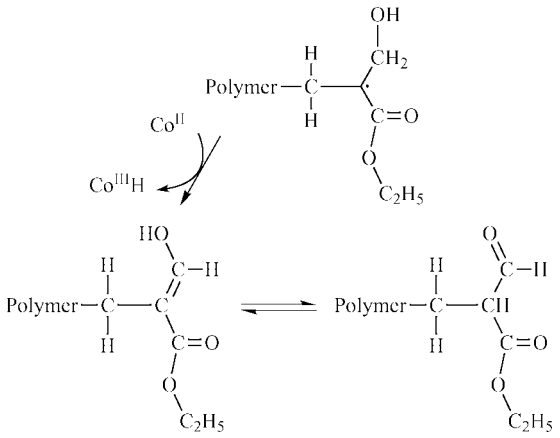

Scheme 9.

acrylates or styrene, the efficiency of the reaction is diminished. It is now thought that this is primarily caused by cobalt–carbon bonding acting as a significant side-reaction, effectively removing some active catalyst from the reacting system (226). This cobalt–carbon bonding has been observed directly in methyl acrylate polymerization using MALDI (227) (see MASS SPECTROMETRY).

There remains some minor unsolved mechanistic mysteries in the CCT reaction. The rate constant for transfer in methacrylates is similar to those for radical–radical termination reactions; these are known to be diffusion controlled. This has lead to speculation that the CCT reaction is also diffusion controlled (229) and there is some evidence to support this. However, this evidence is not absolute and the most prudent analysis is that the CCT reaction of methacrylates falls in a regime where both features of diffusion and chemical control can be observed dependent on the reaction conditions. Hopefully further experimental work will allow clarification of this situation.

The CCT reaction has attained commercial utility as it is ideal for synthesizing low molecular weight polymers with terminal unsaturation. The resultant macromonomers can be used as either chain transfer agents (useful for making block structures) or polymerizable monomers, useful in the synthesis of comb- and star-type molecules. The reaction is tolerant of many functionalities and of water, making it amenable to emulsion reactions.

Alkyl Halides. Transfer to alkyl halides depends on structures of both alkyl group and halogen, but also on the polymeric radicals. Thus, nucleophilic radicals (styrene) react faster with alkyl halides than electrophilic radicals (acrylates). Hence, the C values with styrene and vinyl acetate are higher than those with acrylic monomers.

The halogen abstraction ability decreases according to I > Br > Cl. For example, in styrene polymerization, transfer coefficient for iodoacetates is $C = 0.8$, for bromoacetates $C = 0.043$, but only $C = 0.0001$ for chloroacetates. The C value increases with number of halogens, for example for dibromoacetates $C = 0.27$ and $C > 10$ for tribromoacetates. Among the most often use alkyl halides are halomethanes and aforementioned halogenated esters. Both of them—including

chloroform, carbon tetrachloride, carbon tetrabromide, bromotrichloromethane—have widely been used in the preparation of telomers. The application of effective transfer agents in very high concentrations leads to so-called telomerization, ie the exclusive formation of oligomeric (dimeric, trimeric, etc) species. The kinetics of such telomerization is far from simple, because of the disparate radical reactivities displayed by the very short—halogen-substituted—radicals involved: The shorter radicals show a smaller reactivity toward propagation and transfer reactions than do the longer ones. In the case of carbon tetrachloride mediated polymerizations, this has been attributed to the stabilizing effect of the CCl_3 end group (229–231). The chain length dependence of the chain transfer coefficient most likely reflects a variation of both k_p and k_{tr} with the length of the macroradical. However, common techniques for the determination of C do not allow for the separation of such effects.

The perhalomethanes react in the chain transfer process (as shown in eq. 38) to give a perhaloalkyl radical, which in turn is capable of initiating the polymerization.

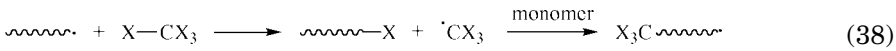

(38)

With hydrohalomethanes, two pathways for the transfer step may be envisaged: halogen- or hydrogen-atom abstraction. For chloroform the hydrogen transfer is favored because of the relative bond strengths, especially for electrophilic radicals.

Very fast transfer which results in the inhibition occurs with transition metal halides such as $FeCl_3$ and $CuCl_2$. In dimethyl formamide at 60°C transfer coefficients for $CuCl_2$ decrease in the order, styrene ($C = 10{,}000$) > MMA ($C = 2000$) > acrylonitrile ($C = 100$). $FeCl_3$ is less efficient transfer agent and C values decrease in the following order: vinyl acetate ($C = 626$) > styrene ($C = 536$) > vinyl chloride ($C = 85$) > MMA ($C = 4$) and acrylonitrile ($C = 2$) (232). Ligands which solubilize transition metal halides provide additional possibility for tuning transfer coefficients. Moreover, the resulting lower oxidation state transition metal compounds can activate the alkyl halides, resulting from the transfer process. Such a reversible activation/deactivation is used for ATRP.

Atom Transfer Radical Polymerization. ATRP is one of the most successful controlled/living radical polymerization (CRP) systems, in addition to NMP and degenerative transfer processes, such as RAFT (5,233,234). The key feature of all of them is the dynamic equilibration between the active radicals and various types of dormant species (see LIVING RADICAL POLYMERIZATION).

Mechanistically, these systems are quite similar to conventional radical polymerizations. Polymeric radicals grow and terminate with similar rate constants. The main difference is how the radicals are generated. They are generated slowly and irreversibly in the conventional processes through dissociation of peroxides or diazo compounds which typically have a half-life in the range of 10 h. Propagation is rapid with an approximate frequency of monomer addition of ∼1 ms. This means that within 1 s, a polymer chain with the chain length P ∼ 1000 is typically formed. Within approximately the same time, chains terminate by either

coupling or disproportionation. During such a short time, it is not possible to perform any kind of macromolecular engineering by adding another monomer, functionalizing reagent, etc. In controlled/living reactions, however, the radical formation is reversible. Similar values for the equilibrium constants during initiation and propagation ensure that the initiator is consumed at the early stages of the polymerization, generating chains which slowly and continuously grow, as in a living process. Perhaps the most important difference between the two approaches is the lifetime of the propagating chains, which is extended from ~1 s to more than 1 h. The second major difference is the dramatic increase in the initiation rate, which enables simultaneous growth of all the polymer, chains. Both parameters allow various macromolecular engineering techniques to be applied, such as making well-defined star polymers, block and grafts, end functional polymers, and many other well-defined, materials.

Termination processes cannot be avoided in CRPs. Since termination is a bimolecular process, increasing the polymerization rate increases the concentration of radicals and enhances the termination process. Termination also becomes more significant for longer chains and at higher conversion. However, this process is somehow self-tuned, since termination is chain length dependent. Polymers prepared by CRPs will never have 100% functionality and 100% blocking efficiency. For monomers with low values of rate constants of radical propagation (k_p), such as dienes, styrenes, and methacrylates, it is necessary to slow down the polymerization rate to avoid excessive termination; for those with high k_p value, such as acrylates, this is less important. Since propagating species are free radicals, chemo-, regio-, and stereoselectivities are similar to those found in conventional radical polymerizations. This means that similar reactivity ratios, similar sensitivity to transfer reagents, and similar tacticities are observed.

Each of the controlled/living radical polymerization systems has some limitations and some special advantages, and it is expected that each technique may find special areas where it would be best suited synthetically. For example, NMP carried out in the presence of bulky nitroxides cannot be applied to the polymerization of methacrylates owing to fast β-hydrogen abstraction. ATRP cannot yet be used for the polymerization of acidic monomers, which can protonate the ligands and complex with copper. RAFT is very slow for the synthesis of low molecular weight polymers because of retardation effects, and may provide branching owing to trapping of growing radicals by the intermediate radicals. At the same time, each technique has some special advantages. Terminal alkoxyamines may act as additional stabilizers for some polymers. ATRP enables the synthesis of special block copolymers by utilizing a halogen exchange and has an inexpensive halogen at the chain end. RAFT can be applied to the polymerization of some less reactive monomers, such as vinyl acetate.

A successful ATRP (and any controlled/living radical polymerization process) should meet three requirements: initiator should be consumed at the early stages of polymerization to form polymers with degrees of polymerization predetermined by the ratio of the concentrations of converted monomer to the introduced initiator ($DP = \Delta[M]/[I]_0$); the number of monomer molecules added during one activation step should be small, resulting in polymers with low polydispersities; the contribution of chain breaking reactions (transfer and termination) should be negligible to yield polymers with high degrees of end functionalities, and allow the synthesis

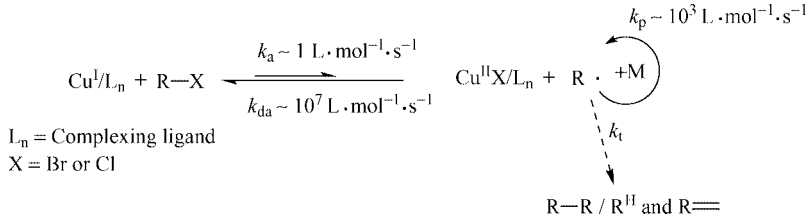

Scheme 10.

of block copolymers. In order to reach these three goals, it is necessary to select appropriate reagents and appropriate reaction conditions.

ATRP is based on the reversible transfer of an atom or group from a dormant polymer chain (R-X) to a transition metal (M_t^n/Ligand) to form a radical ($R^\bullet$), which can initiate the polymerization, and a metal halide whose oxidation state has increased by one (X—M_t^{n+1}/Ligand); the transferred atom or group is covalently bound to the transition metal. A catalytic system employing copper(I) halides (M_t^n/Ligand) complexed with substituted 2,2′-bipyridines (bpy) was successful for polymerization of styrenes, various (meth)acrylates, acrylamides, acrylonitrile, and other monomers (235–238). Other metal centers have been used, such as ruthenium, nickel, iron, and other transition-metal-based systems. Copper salts with various anions and polydentate complexing ligands were used, such as substituted bpys, pyridines, and linear polyamines. The rate constants of the exchange process, propagation and termination shown in Scheme 10 relate to styrene polymerization catalyzed by CuBr/2bpy and initiated by 1-phenylethyl bromide at 110°C.

According to this general ATRP scheme (Scheme 10), the rate of polymerization is given by the following equation:

$$R_p = k_p[M][RX]_0 k_a[Cu^I]/(k_{da}[X—Cu^{II}]) \quad (39)$$

Thus, the rate of polymerization is internally first order in monomer, externally first order with respect to initiator and activator, Cu(I), and negative first order with respect to deactivator, XCu^{II}. However, the kinetics may be more complex because of the formation of XCu^{II} species via the persistent radical effect. The actual kinetics depend on many factors, including the solubility of activator and deactivator, their possible interactions, and variations of their structures and reactivities with concentrations and composition of the reaction medium. It should also be noted that the contribution of persistent radical effect at the initial stages might be affected by the mixing method, solubility of the metal compound and ligand, etc (239–242).

One of the most important parameters in ATRP is the dynamics of exchange, and especially the relative rate of deactivation. If the deactivation process is slow in comparison with propagation, then a classic redox initiation process operates, leading to conventional, and not controlled, radical polymerization. Polydispersities in ATRP are defined by the following equation, when the contribution of chain

breaking reactions is small and initiation is complete:

$$M_w/M_n = 1 + \{(k_p[RX]_0)/(k_{da}[X - Cu^{II}])\}(2/p - 1) \quad (40)$$

Thus, polydispersities decrease with conversion, p, the rate constant of deactivation, k_{da}, and also the concentration of deactivator, $[XCu^{II}]$. They, however, increase with the propagation rate constant k_p and the concentration of initiator, $[RX]_0$. This means that more uniform polymers are obtained at higher conversions, when the concentration of deactivator in solution is high and the concentration of initiator is low. Also, more uniform polymers are formed when the deactivator is very reactive and monomer propagates slowly (styrene rather than acrylate). Polydispersities can also be expressed as a function of the reaction time t (243):

$$M_w/M_n = 1 + 1/(2k_a[Cu^I]t) \quad (41)$$

The most important benefit of living polymerizations is that they allow preparation of new macromolecules with precisely designed and controlled compositions (homopolymers, random, periodic, block, graft, and gradient copolymers), topologies (linear, star, comb, (hyper)branched, networks, etc), and functionalities placed at different parts of macromolecules or various combinations of these. Some of the possibilities are outlined below (244,245).

The advent of controlled/living radical polymerization enables preparation of many new materials such as well-defined components of coatings (with narrow molecular weight distribution, precisely controlled functionalities, and reduced volatile organic compounds), nonionic surfactants, polar thermoplastic elastomers, entirely water-soluble block copolymers (potentially for crystal engineering), gels and hydrogels, lubricants and additives, surface modifiers, hybrids with natural and inorganic polymers, various biomaterials and electronic materials. Extensive discussion of more detailed aspects, such as the monomers, initiators, catalysts, and media, can be found in Reference 5.

Addition–Fragmentation Chain Transfer. The addition–fragmentation chain transfer process is induced by the addition of a growing radical to a simple organic compound with a reactive double bond. The general structure of the addition–fragmentation chain transfer agents and the transfer process is depicted in equation 42: A is part of the activated double bond, Z is both the activating group for the double bond and the stabilizing group for the intermediate radical, and B and the leaving group R are connected to each other by a weak single bond. The propagating radical adds to the activated double bond with the rate coefficient k_β, and an intermediate radical is formed. This intermediate radical in turn fragments with the rate coefficient $k_{-\beta}$ via generation of a new double bond and a small radical. The success of the transfer process is dependent on three factors: (*1*) the reactivity of the double bond toward radical addition must be similar or higher to that of the polymerizing monomer double bond, (*2*) the leaving ability of the released moiety R must be substantial, and (*3*) the reactivity of the expelled radical $R^\bullet$ toward reinitiation of the polymerization process has to be high (246,247).

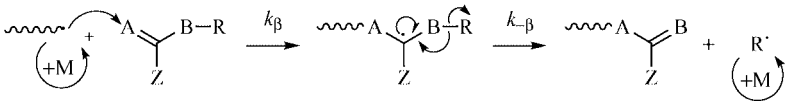

(42)

Several different types of addition–fragmentation chain transfer agents may be envisaged, when considering different types of atoms and/or groups for A, B, Z, and R in the general structure given in equation 42. The first class (A = B = CH_2) represents the allylic compounds, which include the allylic sulfides (R = SR) (248–250), allylic peroxides (R = OOR) (251,252), allylic bromides (R = Br) (248,253,254), allylic sulfones (R = S(O)R) (248,253), allylic phosphonates (R = $P(O)(OR)_2$) (248,253), and allylic stannanes (R = SnR) (248,253). The other two classes are the vinyl ethers (A = CH_2 and B = O) (248,255) and the thiocarbonyl compounds (A = S and B = O) (256,257). R is any good homolytic leaving group and *Z* can be varied to give optimum transfer coefficients. The addition–fragmentation chain transfer coefficients of the various compounds are very high compared to common transfer agents with *C* values in the order of one and above (0.2–20) (246) depending on the structure of the transferring compound and the reacting radical.

The addition–fragmentation chain transfer is a versatile process being applicable to a wide range of monomers (styrene, acrylates, methacrylates) to introduce functionalized end groups (246,258). End functional polymers—the type of end group may be governed by the chosen transfer agent and its different A, B, Z, and R groups—are very useful for building block, graft, and network polymer structures (259–261).

Methyl methacrylate macromonomers act as a chain transfer agent by an addition–fragmentation mechanism as depicted in equation 43. By that, an olefinic group is installed at the end of the polymer chain. These products are themselves macromonomers that can react in the same way during the polymerization. In the acrylate polymerizations these macromonomers are readily copolymerized, hence leading to branching (262). The polymerization of methacrylates in the presence of methacrylate macromonomers will produce new macromonomers, which are in turn participating in the described addition–fragmentation mechanism. This reversible addition–fragmentation process gives rise to living behavior, as described in the next section.

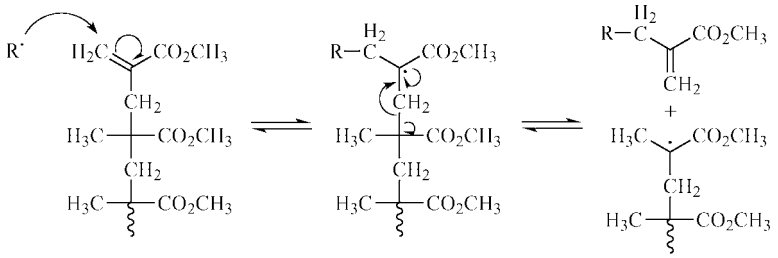

(43)

Reversible Addition–Fragmentation Chain Transfer. The RAFT represents a process for performing living free radical polymerization. Many simple organic compounds possessing a thiocarbonylthio (S=C–S) moiety are employed

as mediating agents which exhibit a great effectiveness and versatility toward controlling the free radical polymerization. The general scheme of these dithio-compounds is depicted as structure **15**. The ability of a RAFT agent to control the polymerization activity is governed by two characteristic groups, the Z and R groups, also denoted as the 'stabilizing' and the 'leaving' group.

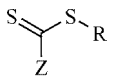

15

Different substituents as Z and R groups lead to a wide array of different RAFT agents: (*1*) dithioesters (Z = phenyl, methyl, etc), (*2*) trithiocarbonates (Z = S—R), (*3*) xanthates (Z = O—R), and (*4*) dithiocarbamates (Z = NR_2). A controlled polymerization involving xanthates is referred to as MADIX (263,264). The RAFT polymerization is performed by adding a chosen quantity of an appropriate RAFT agent to a conventional free radical polymerization mixture. The process yields polymers of predetermined chain length and narrow polydispersity. Polydispersities indices of less than 1.1 can be usually achieved under optimal conditions. The RAFT process generates polymeric material with active thiocarbonylthio end groups, which can be used for chain extensions and/or further chemical reactions, to yield complex polymeric architectures. Polymeric structures ranging from star and comb polymers to block copolymers can be prepared with relative ease for a variety of monomers (265–272).

The mechanism of the living free radical RAFT polymerization with dithio compounds involves two important equilibrium reactions that are superimposed on a conventional free radical polymerization (see Scheme 11). As in conventional free radical polymerization, initiation leads to the formation of propagating chains. In the early stages of the polymerization the macroradicals react with the initial RAFT agent (species 1 in Scheme 11), generating the intermediate radical (species 2 in Scheme 11), followed by the decomposition of these species by formation of polymeric RAFT agent (species 3 in Scheme 11) and the leaving group radical. The first equilibrium reaction may be simplified by an overall transfer step involving the initial RAFT agent as transfer agent. The leaving group radical $R^{\bullet}$ initiates in turn a new polymeric chain with the rate coefficient $k_{p,1}$ by reaction with monomer and leads to macromolecular chain growth of the free radicals with the propagation rate coefficient k_p. The reaction step (IV) constitutes the core of the RAFT process and has been termed the main or core equilibrium. The addition reaction proceeds with a rate coefficient k_β, whereas the formed intermediate—the macro-RAFT radical (species 4 in Scheme 11)—fragments proceed with the rate coefficient $k_{-\beta}$. Finally, the reaction step (V) considers the termination reactions of the linear macroradicals, which proceed with a chain-length-averaged termination rate coefficient $\langle k_t \rangle$.

The equilibrium between the active propagating species ($P_n^{\bullet}$ and $P_m^{\bullet}$) and the dormant polymeric RAFT agent (species 3 in Scheme 11) provides an equal probability for all chains to grow. Because of the reversible nature of the transfer reaction, the transfer agent (ie the polymeric RAFT agent) is not consumed and the active dithio groups are incorporated into the final polymeric material (273). Each

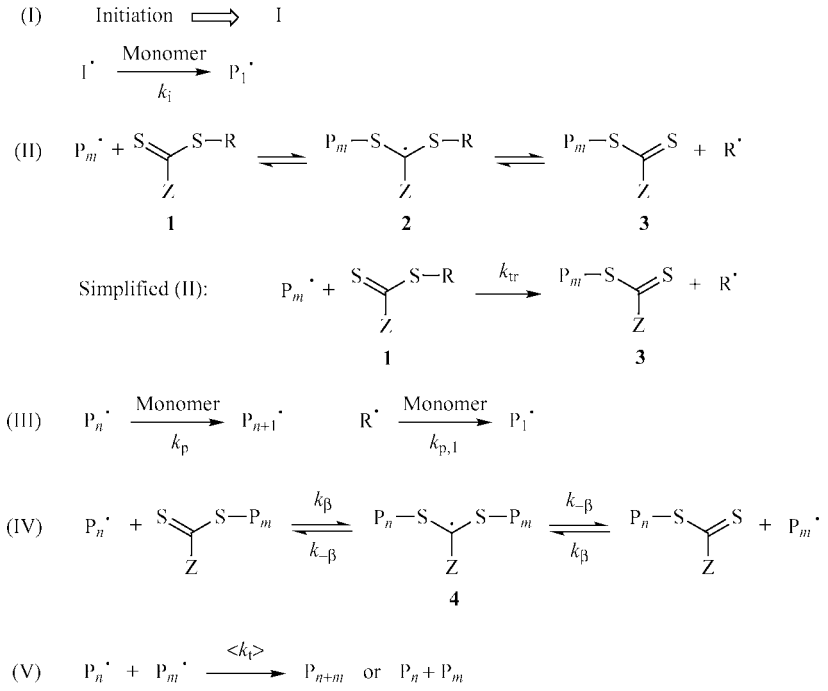

Scheme 11.

RAFT agent molecule is transformed into the end group of one polymer chain. Hence, the final chain lengths of the polymeric material can easily be controlled via varying the ratio of RAFT agent concentration to conversion. It should be noted that the free radical concentration—at least in principle—is not reduced in the RAFT process. Hence, the overall rate of polymerization is unchanged in an ideal RAFT polymerization compared to a conventional free radical polymerization.

A successful RAFT process is, on the one hand, dependent on the effective addition of the growing radical to the RAFT agent compound. On the other hand, the leaving and reinitiating ability of the leaving group also governs the effectiveness of the transfer step. This very effective transfer reaction—which has to be competitive with the propagation step—is illustrated by the large transfer coefficients for the simplified preequilibrium: transfer coefficients of more than 5000 in styrene polymerization can be observed for some dithiobenzoates (274). The transfer step is strongly enhanced when the RAFT agent possesses a well-stabilizing Z group (eg, phenyl). The stabilizing ability of the Z group, however, leads to relatively stable RAFT intermediate radicals, causing rate retardation, that is, a decrease in the overall rate of polymerization up to high conversions with increasing initial RAFT agent concentration. This kinetic phenomenon may be explained either by intermediate radicals with very long lifetimes (275) or by reversible (276–278) and/or irreversible (279) termination of this species. The different leaving abilities of various R groups sometimes affect the preequilibrium and leads to inhibition phenomenon, that is, a time period without any polymerization activity at early

Table 5. Transfer-to-Polymer Constants, C_P[a]

Polymer	T,°C	C_P (10^{-4})
Poly-1,3-butadiene	50	11
Polyacrylonitrile	50	4.7
Polyethylene	175	108.4
Poly(methyl methacrylate)	50	0.22–1.5
Poly(*N*,*N*-dimethyl acrylamide)	50	0.61
Polystyrene	50	1.9–16.6
Poly(vinyl acetate)	50	0.06–10.2

[a]Data from Ref. 173.

reactions times, dependent in extent on the initial RAFT agent concentration (280).

Transfer to Polymer. At higher monomer conversion, transfer processes to the formed polymer are becoming significant. Interestingly, the transfer-to-polymer rate constants are considerably higher (approximately by a factor of 10) than those observed for the corresponding monomer. Transfer to polymer is resulting in so-called long-chain branching if the reaction takes place intermolecularly (281). In the case of intramolecular transfer to polymer, the reaction is described as 'backbiting,' leading to short-chain branching, as observed in ethylene polymerizations. The length of the branched side chains generated via backbiting is usually smaller than five carbons. Typical values for the transfer-to-polymer constants C_P of some common monomers are collected in Table 5.

Transfer coefficients to polymers are not as readily determined as other transfer coefficients because the process does not necessarily lead to a reduction of the molecular weight. Polymerization in the presence of polymer yields a mixture of the polymer initially present and the new polymer formed, and thus the decrease in the molecular weight cannot be accurately evaluated. However, chain transfer coefficients to polymers are accessible via the structural investigations of the generated branched macromolecules, eg, via NMR (282,283). As NMR measurements of branching rely on the determination of the branching points on the polymeric backbone, a quantitative distinction between long- and short-chain branching is a major analytical problem. The determination of the number of end groups per polymeric chain is another viable technique to quantify the branching of macromolecules (284). For some polymers, the value of C_P depends on the polymer molecular weight. This may account for the wide range of values for C_P in the literature.

Detailed structural analysis of poly(vinyl acetate) has revealed that hydrogen abstraction from the acetyl group is the predominant chain transfer mechanism (285). Abstraction from the methine hydrogen of the main chain leads to a small amount of branching (286,287).

Mid-chain radicals may be formed by intermolecular abstraction of a tertiary hydrogen atom from the polyacrylate main chain. This pathway is favored under the conditions of low monomer and high polymer concentration such as during emulsion polymerization, where the particles consist of large amount of polymer and small amount of polymer (288–290) and at high conversion during solution/bulk polymerization (281). It has been proposed that this process and

the consequent formation of branches may contribute to the early onset of the gel effect in the polymerization of acrylates.

The presence of long-chain branches in low density polyethylene accounts for the difference in properties (eg, better melt strength, greater toughness) when compared to completely linear polyethylene chains. The long-chain branching can be routinely detected by determining the end group—ie methyl—content of the polyethylene via infrared spectroscopy (291,292). Other studies involve NMR (293–295) and SEC (size exclusion chromatography) (296,297). The extent of long-chain branching is known to be strongly dependent on the reactor design and the reaction conditions employed.

Termination

The radical–radical termination reaction in free radical polymerization is the most complex reaction in the polymerization process (298,299). Its termination rate coefficient k_t is influenced by a multitude of different factors, which are not easily separated. Only within the last 15 years new methods have become available that allow for an accurate measurement of this rate coefficient. The scatter of the termination rate coefficients given in the *Polymer Handbook* (173) reported for the same monomer at the same reaction temperature is a direct manifestation of the influence of these various parameters on k_t. This appreciable disagreement is partly explainable by the frequent use of incorrect values for the propagation rate coefficient k_p, which is always needed to determine k_t from the coupled form of the two coefficients. However, the situation has improved greatly with the invention of the PLP–SEC method.

Combination vs Disproportionation. There are two modes of termination: one is the direct coupling (combination) of two free macroradicals to give a dead polymer chain of chain length $i + j$, with the rate coefficient $k_{t,c}$. The other mode is the so-called disproportionation, where a hydrogen atom is transferred from one of the radical chain ends to another radical, yielding two stabilized polymer chains, of which one carries a double bond. This reaction is associated with the rate coefficient $k_{t,d}$. The process is illustrated in equation 44 using polyethylene macroradicals as the example. It is important to notice that—in the case of macroradicals derived from other monomers—in principle any β-hydrogen may be abstracted.

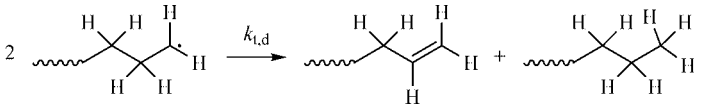

(44)

The reactions between carbon-centered radicals generally give a mixture of disproportionation and combination. Which termination mode dominates depends largely on the structure of the monomer unit, and to a lesser extent on the reaction temperature, pressure, and solvent (300). Disproportionation is (slightly) favored at higher reaction temperatures. The reasons for this behavior have yet

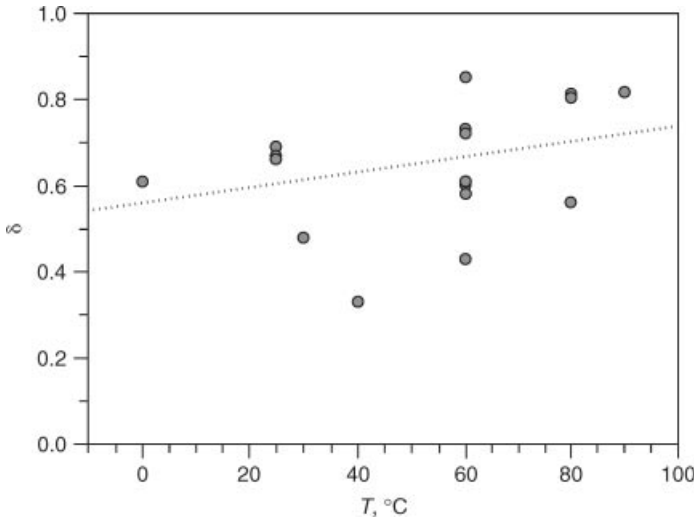

Fig. 4. Temperature dependence of the contribution of disproportionation to the overall termination process, δ, for a methyl methacrylate polymerization at ambient pressure (selected references: Refs. 305–308).

to be clarified, but there is some evidence pointing toward a different temperature dependence of the corresponding preexponential factors in the Arrhenius expression for $k_{t,c}$ and $k_{t,d}$. Combination and disproportionation should be considered as two different reactions with two distinct transition states; this is supported by theoretical studies (301–304). However, the observed effects are small and associated with a large experimental scatter, as indicated in Figure 4, showing the temperature dependence of the contribution of disproportionation to the overall termination process, δ, defined according to equation 45, for a methyl methacrylate polymerization at ambient pressure.

$$\delta = \frac{k_{t,d}}{k_{t,d} + k_{t,c}} \tag{45}$$

For a given series of radicals, δ increases with the number of β-hydrogen atoms. However, there is no direct relationship and it is clear that a number of other factors are involved (300,309). In addition, it is generally observed that the importance of disproportionation increases with increasing substitution at the radical center. Steric effects play a very important role as demonstrated by the self-reaction of cumyl radicals **16** and of the *tert*-butyl-substituted equivalent **17**. The termination reaction of radical **16** shows predominantly combination, whereas radical **17** gives predominantly disproportionation, although there are less β-hydrogen atoms. This finding may imply that the combination reaction is more suppressed by the steric hindrance than the disproportionation reaction. The statistical effect that favors disproportionation when more β-hydrogen atoms are available is hence to be considered less pronounced than the steric effect (310). The steric crowding can lead in extreme cases to persistent radicals

(eg, di-*tert*-butyl methyl radical (311) and triisopropylmethyl radical (312)) that are relatively reluctant to undergo radical–radical reactions.

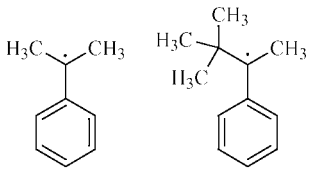

16 17

The increase of δ with polar solvents is attributed to the fact that the transition state of disproportionation has polar character while that for combination is neutral (304).

It should be noted that the mode of termination has no influence on the kinetics of the free radical polymerization process. However, the generated molecular weight distributions are strongly influenced by the termination mode and it is hence vital to the understanding of structure–property relationships. Since some methods for the determination of the termination rate coefficient rely on the analysis of the full molecular weight distributions, it is mandatory to have reliable data on the termination mode of a specific monomer. In addition, the termination mode governs the end groups of the generated polymer (one initiator derived end group with disproportionation and two with combination). Table 6 gives data on combination–disproportionation modes for various monomers at ambient pressure and various temperatures.

The dead polymer chains generated via disproportionation carry an unsaturated end group which may be reactive during polymerization. Copolymerization of these macromonomers is a possible mechanism for the formation of long-chain

Table 6. Contribution of Disproportionation to the Overall Termination, δ, for Different Monomers

Monomer	T,°C	δ	Reference
Acrylonitirile	10–90	0	313–315
Butyl methacrylate	80	0.54	316
Dicyclohexyl itaconate	25	0.8–1.0	294,317
Ethyl methacrylate	80	0.42	316
Methacrylonitrile	25	0.65	318
Methyl acrylate	−34	∼0.25	317
Methyl methacrylate	0	0.61	308
	25	0.67	305
	60	0.73	305
	90	0.81	319
α-Methylstyrene	55	0.091	320
Styrene	20–50	0.17	321
	30	0.14	322,323
	50	0.2	322
	60	0.1–0.2	83
	90	0.054	319

branches (316,324). A comprehensive review of the literature known data on combination vs termination modes for various monomers and model systems can be found in Reference 325. However, unequivocal numbers for α are not yet available for most of the polymerization systems and in most cases there is only a qualitative agreement between different literature values. Despite these discrepancies four different generalizations can be made:

(1) Termination of polymerizations involving vinyl monomers involves predominantly combination.
(2) Termination of polymerizations involving α-methylvinyl monomers always exhibit a significant contribution of disproportionation.
(3) The hydrogen atoms of the α-methyl group are much more prone to abstraction during the disproportionation reaction than the methylene hydrogens.
(4) Within a series of vinyl or α-methylvinyl monomers, δ apparently decreases according to the radical-stabilizing ability of the substituent.

Kinetic Aspects of the Termination Reaction. It is generally accepted that the termination rate coefficient depends on the following factors and experimental parameters: (*1*) the system viscosity, (*2*) the chain length of the terminating free macroradicals, (*3*) the temperature, (*4*) the pressure, and (*5*) the monomer-to-polymer conversion.

The rate law expression for the termination step that describes the variation of the free radical concentration with time reads (326)

$$-\frac{\mathrm{d}[\mathrm{R}^\bullet]}{\mathrm{d}t} = \sum_i \sum_j 2k_\mathrm{t}^{i,j}[\mathrm{R}_i^\bullet][\mathrm{R}_j^\bullet] \tag{46}$$

The indices i and j indicate the individual chain lengths of the terminating macroradicals. There has been considerable confusion in the past on whether to incorporate the factor 2 from the rate law expression into the termination rate coefficient. The factor 2 is necessary if the rate law describes the rate of the loss of macroradicals; however, it is unnecessary if only termination events are considered. Nevertheless, the IUPAC ruling on this is clear; termination rate coefficients are to be reported without the incorporated factor 2. All termination rate coefficients given in this article are in accordance with the IUPAC guideline.

Because of the above-mentioned chain length dependence of the termination rate coefficient (327) and its strong dependence on the monomer conversion, it is rather difficult to report tabulated values for k_t. However, it is possible to give a chain-length-averaged k_t value for a specific monomer conversion, $\langle k_\mathrm{t} \rangle$. It is important to note that for many of the reported chain-length-averaged k_t values, it is unclear to which chain length region they correspond. Since most measurements of the termination rate coefficient have been carried out at low monomer conversion, it is sensible to report k_t values for the low conversion regime (see below for a discussion of high conversion k_t data).

Average termination rate coefficients have been reported over several orders of magnitude, ranging from approximately 50 to 10^9 L $\cdot$ mol^{-1} $\cdot$ s^{-1} (173). This impressive range may be explained by a shift in the rate-determining step when

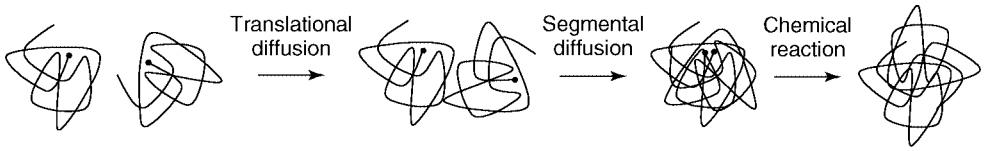

Scheme 12.

going from one monomer to another. The termination reaction can be broken down into a three-stage process (328–330), as can be seen in Scheme 12:

(1) The translational (ie center of mass) diffusion of the individual macroradical coils toward each other through the reaction medium.
(2) The so-called segmental diffusion of the radical chain ends toward each other. This segmental diffusion process brings the chain ends into a position that enables them to react.
(3) The chemical reaction of the two radicals which yields the polymeric product(s).

The slowest reaction step—in a sequence of reaction steps—will always determine the rate of the overall reaction according to equation 47, which describes the inverse overall termination rate coefficient as the sum of the inverse rate coefficients of the individual reaction steps:

$$\frac{1}{k_t} = \frac{1}{k_{TD}} + \frac{1}{k_{SD}} + \frac{1}{k_R} \tag{47}$$

with k_{TD} being the rate coefficient for the translational diffusion, k_{SD} the rate coefficient for the segmental diffusion, and k_R the rate coefficient for the chemical reaction of radical–radical recombination. Because of the extremely fast reaction rate of the radical combination/disproportionation reaction (ie strictly speaking the termination itself) with k_R being in the order of 10^{10} L · mol^{-1} · s^{-1}, the center of mass and segmental diffusion steps are (in almost all the cases) the rate-determining steps. At low monomer conversions, the rate-determining step for reasonably high molecular weight macroradicals (of length 50 or above) is believed to be almost exclusively segmental diffusion. Typical examples for high k_t monomers are methyl methacrylate and styrene, ie, $\langle k_t \rangle \approx 10^8$ L · mol^{-1} · s^{-1}. Differences in the (average) termination rate coefficients that can be observed when comparing different monomers are most likely due to differences in segmental diffusion coefficients. However, lower values of k_t, as observed for example for dodecyl methacrylate, ie $\langle k_t \rangle \approx 10^6$ L · mol^{-1} · s^{-1}, have been attributed to the sterically demanding substituents, leading to a (partly) chemically controlled termination process (331). For reported ultralow k_t monomers, such as the fumarates (332,333) or itaconates (135,334) with $\langle k_t \rangle < 500$ L · mol^{-1} · s^{-1}, a chemically controlled termination process may also be envisaged, but evidence for this hypothesis is nonexistent and other explanations can by no means be ruled out.

As indicated above, the termination reaction for most common monomers is believed to be segmental diffusion controlled at low and intermediate monomer

conversions and center of mass diffusion controlled at high conversion. If the diffusion controlled nature of the termination reaction is accepted, this has the immediate consequence that the termination rate coefficient should be chain length dependent. However, the chain length dependence of k_t is markedly different for the two diffusion mechanisms.

The chain length dependence of k_t is normally quantified by the following equations: A macroscopic—ie experimental—k_t value may be obtained by the following averaging procedure (335):

$$\langle k_t \rangle = \frac{\sum_i \sum_j k_t^{i,j} [R_i^\bullet][R_j^\bullet]}{\left(\sum_i [R_i^\bullet]\right)^2} \tag{48}$$

The microscopic k_t value $k_t{}^{i,j}$ corresponds to the individual termination rate coefficient involving two free macroradicals with the chain length i and j. The averaging procedure is advantageous because the chain length distribution of the macroradicals in free radical polymerization is normally highly disperse. The individual termination rate coefficient $k_t{}^{i,j}$ may be described via the following equation:

$$k_t^{i,j} = k_t^0 (\bar{i,j})^{-\alpha} \tag{49}$$

with $\bar{i,j}$ denoting some average [eg, the harmonic (336) or the geometric (337) mean] of the two chain lengths i and j involved and α being a positive constant. As a consequence, the problem of determining k_t is not solved by the evaluation of one specific value but comprises the evaluation of an entire functional dependence. The chain length dependence of the macroscopic $\langle k_t \rangle$ is consequently often expressed via the following power law:

$$\langle k_t \rangle = k_t^0 \bar{P}_n^{-\alpha} \tag{50}$$

This power law correlates the average value of the termination rate coefficient $\langle k_t \rangle$ with the number-average degree of polymerization, $\bar{P}_n$. The chain length dependence of k_t is now easily described and quantified by the exponent α in equation 50.

If center of mass diffusion is the rate-determining step in the termination reaction, an exponent of 0.5–0.6 results, depending on the thermodynamic quality of the solvent. This result can be explained by considering the translational diffusion properties of the polymer coil. The diffusion coefficient D of the polymer coil is inversely proportional to its hydrodynamic radius. If the hydrodynamic radius is equated with the radius of gyration $\langle s^2 \rangle^{0.5}$, it can be inferred that for a theta solution $\langle s^2 \rangle \propto i$ and for an athermic solution $\langle s^2 \rangle \propto i^{1.176}$ (338). This leads directly to the chain length dependence of the diffusion coefficient of $D \propto i^{-0.5}$ for theta solutions and $D \propto i^{-0.59}$ for athermic solutions. According to various theories for diffusion controlled reactions, the diffusion coefficient is directly proportional to the termination rate coefficient. The majority of these models is based on the work by Smoluchowski (339), which describes the rate coefficient for a diffusion

controlled reaction (see eq. 51):

$$k_t^{i,j} = 2p\pi(D_i + D_j)\sigma N_A \tag{51}$$

in which p is the spin multiplicity, σ is the capture radius of the reaction, and N_A is the Avogadro's number.

The segmental diffusion coefficient is generally chain length independent. However, a slight chain length dependence of the termination rate coefficient of close to $\alpha = 0.16$ is predicted for athermic solvents, owing to thermodynamic shielding effects of the chain. The chain shields its own reactive center owing to its size from the second chain, which displays a similar shielding effect. The exponent of -0.167 has been confirmed in various theoretical studies applying the scaling theory (336,340), as well as in chain statistical simulations (341). The chain length dependence of k_t is almost negligible in theta solvents for the segmental diffusion controlled regime, with α being close to 0.05.

Experimentally, evidence has been gathered for both exponents, ie 0.1–0.2 for segmental diffusion and 0.5–0.6 for center of mass diffusion, depending on the size of the macroradicals undergoing termination. Consequently, the chain length dependence of the termination rate coefficient is best described by a step function featuring two (main) domains of different chain length dependencies, as depicted in Figure 5.

Domain A is associated with center of mass diffusion controlled termination, owing to the small size of the macroradicals (ie, $\alpha \approx 0.5$–0.6), whereas domain B is controlled by segmental diffusion processes (ie, $\alpha \approx 0.05$–0.16). Domain C represents an intermediate region associated with the change in mechanism. These numbers have been confirmed experimentally by various research groups in the past (18,342–347) and the general shape of the curve could be confirmed in recent work (348,349). Styrene and methyl methacrylate have been studied particularly extensively with respect to the chain length dependence of the termination rate coefficient in the segmental diffusion region. These chain length dependencies

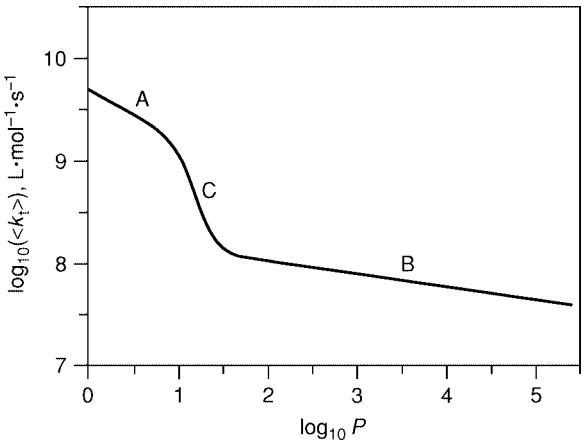

Fig. 5. General step function for the termination rate coefficient as a function of the chain length of terminating macroradicals. For details see text.

Table 7. Activation Parameters of the Termination Step for Various Acrylates and Methacrylates

Monomer	E_A, kJ · mol^{-1}	$\Delta V^{\#}$, cm^3 · mol^{-1}	log(k_t), L · mol^{-1} · s^{-1}	Reference
Methyl acrylate	8.0 (100 MPa)	16.0 (30°C)	8.13	350
Butyl acrylate	6.0 (100 MPa)	16.0 (40°C)	7.55	351
Dodecyl acrylate	3.0 (100 MPa)	20.0 (40°C)	6.38	350
Methyl methacrylate	6.0 (100 MPa)	15.0[a] (40°C)	7.39	352,353
Butyl methacrylate	—	—	6.70	352,353
Dodecyl methacrylate	—	10.8 (30°C)	6.22	

[a]This activation volume is pressure dependent; the value is valid for the pressure range from 100 to 150 MPa. To convert MPa to bar, multiply by 10.

may be described by the following (345):

$$\text{MMA } (25^\circ\text{C}): \langle k_t \rangle_i = 7.56 \times 10^7 \times i^{-0.18} \quad \text{Styrene } (25^\circ\text{C}): \langle k_t \rangle_i = 1.21 \times 10^8 \times i^{-0.16}$$

where $\langle k_t \rangle_i$ denotes the average experimental termination rate coefficient for a mean chain length i.

Although the termination rate coefficient of a particular monomer is influenced by the system viscosity and the chain lengths of the terminating free macroradicals, it is important to notice that the pressure and, to a lesser extent, the reaction temperature have a significant effect on its value. Especially the reaction pressure influences the absolute value of the termination rate to a far greater extent than the change in k_t associated with its chain length dependence. Table 7 gives activation energies and activation volumes for selected acrylate and methacrylate termination rate coefficients along with its value at 100 MPa and 40°C at low monomer conversions. The numbers given in Table 7 were mainly derived from single pluse–pulsed laser polymerization (SP–PLP) experiments.

Inspection of Table 7 shows that the activation energies are rather low and between 3 and 8 kJ · mol^{-1}. This observation is consistent with the diffusion (either segmental or translational) controlled nature of the termination reaction. Strictly speaking, these activation energies correspond to the temperature dependence of the inverse system viscosity. Up to this date, there is no data on the activation energy of the actual termination reaction itself. However, it is very likely that the termination reaction itself has a close to zero activation energy. This conclusion may be deduced from the activation parameters observed for small radical termination (354,355). It is interesting to note that the activation volume of the termination reaction is positive, ie the value of k_t is reduced at higher reaction pressures. The activation volumes of a given reaction is defined by

$$\frac{\mathrm{d}\ \ln k}{\mathrm{d}p} = -\frac{\Delta V^{\#}}{RT} \tag{52}$$

where $\Delta V^{\#}$ is the activation volume and p is the pressure.

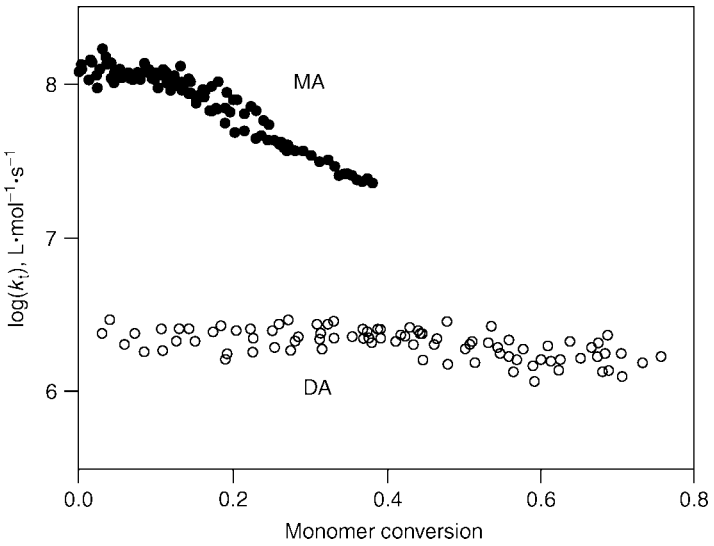

Fig. 6. Termination rate coefficients in bulk methyl acrylate (MA) and dodecyl acrylate (DA) homopolymerizations as a function of monomer conversion. The reaction conditions were 40°C and 100 MPa.

This experimental observation can also be correlated with the pressure dependency of the viscosity. The reaction medium tends to be more viscous at higher reaction pressures, thus slowing the rate of termination; ie, the activation volume of the termination rate coefficient is very close to the corresponding activation volume that characterizes the pressure dependence of the inverse of the monomer viscosity (356). It is important to note that the pressure dependencies of the termination and propagation rate coefficients display opposite behavior, ie allowing for increased rates of polymerization at elevated pressures.

As has been indicated above, the termination rate coefficient is—depending on the monomer in question—strongly dependent on the overall monomer conversion. The conversion dependencies of the (average) termination rate coefficient have been reported for several monomers, with most measurements being done via the SP–PLP technique, which allows to point-wise probe the kinetics of the polymerization reaction up to high overall monomer conversions. A typical k_t vs monomer conversion dependence is given in Figure 6 for the example of methyl acrylate and dodecyl acrylate. The data are taken from Reference 331.

Inspection of Figure 6 shows that both monomers behave very differently. While in the case of methyl acrylate different regions for the change of the termination rate coefficient with conversion can be identified, dodecyl acrylate exhibits a constant (average) k_t value up to high conversions. The different regions in the methyl acrylate k_t vs conversion dependence may be attributed to segmental diffusion (0 to ∼15%), followed by translational diffusion and the onset of the so-called gel effect, which is characterized by a strong autoacceleration of the reaction (see below). At very high monomer conversions, the reaction medium is highly viscous and the macroradicals are no longer capable of movement via translational diffusion. Instead, the addition of new monomer units to the chain end results in

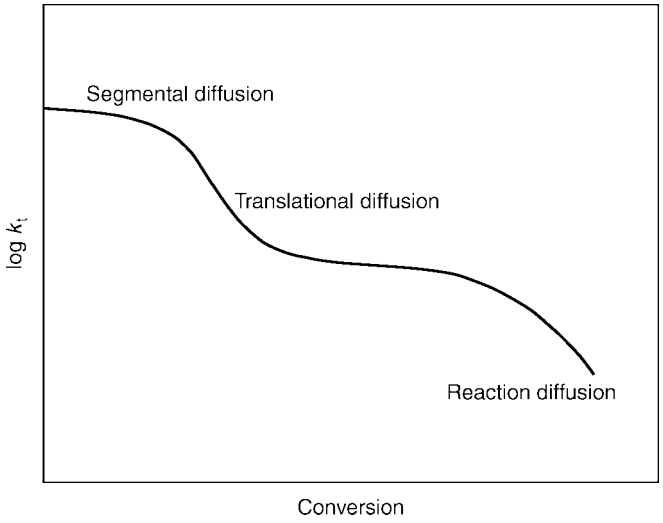

Fig. 7. Schematic dependence of the (average) termination rate coefficient on the overall monomer conversion, indicating different regimes of reaction control.

a change in the position of the radical chain end. This process has been termed reaction diffusion or propagation diffusion. Buback has introduced a model for the above-described dependence of the termination rate on the monomer conversion, which considers segmental, translational, and reaction diffusion processes (357). This model has been extremely successful in describing a large set of data up to high monomer conversions (358–360). In the case of dodecyl acrylate, the segmental diffusion region seems to extend to high monomer conversions, although the system viscosity changes by orders of magnitude when going from 0 to 80% conversion. However, in a monomer behaving like dodecyl acrylate, it has not been conclusively clarified up to this point (*1*) whether the entire conversion range is in the segmental or translational diffusion controlled regime and (*2*) what the exact cause for a nonchanging (average) termination rate coefficient is.

Figure 7 shows the three different regimes of the termination rate coefficient in general, which can be described as follows:

(1) Low conversion: this regime—prior to the onset of the gel effect—is characterized by highly mobile propagating species. Segmental diffusion is the rate-determining step for the termination reaction.
(2) Medium-to-high conversion: The diffusion mechanism of the propagating radicals becomes complex after the onset of the gel effect. Large chains become immobile; however, the chain ends may move by reptation or reaction diffusion. Monomer and short species may still be highly mobile in the polymerizing system. Translational center-of-mass diffusion may become the rate-determining step for radical–radical termination.
(3) Very high conversion: The polymerizing system becomes a glassy matrix. Reaction diffusion is the only remaining pathway for radical movement.

The precise conversion ranges are determined by the nature of the monomer, the molecular weight of the polymer that is produced, and the solvent. For bulk polymerizations, these regimes are (a) typically <10–20%, (b) between 15 and 90%, and (c) >90%. When using a solvent and/or chain transfer agents to reduce the molecular weight of the polymer, the initial regime (a) can be extended and (c) may not even occur.

It has been observed that the average k_t value slightly increases up to 5–10% of conversion and then starts to decrease (361–364). An explanation for such behavior was first offered by North and Reed who assumed faster segmental diffusion to be responsible (328). The initial increase of k_t with increasing monomer conversion has also been associated with a change in solvent quality: k_t increases when going from a good to a poor solvent, because of either diminishing coil sizes (which increases the segmental diffusion coefficient) or decreasing repulsions between macroradicals. This behavior of k_t has not only been observed experimentally, but is also predicted theoretically (365,366).

The conversion dependence of the termination rate coefficient is linked to the above-mentioned autoacceleration effect of the polymerization (367,368), which can be observed with some monomers at increased conversion, eg, methyl methacrylate (369), styrene (370), vinyl acetate (371), and methyl acrylate (372). Also known as the 'Trommsdorff,' 'Norrish–Smith,' or 'Norrish-Trommsdorff' effect, this effect can cause problems within both an industrial and scientific context ranging from a product mixture to reactor explosion, owing to its exothermic nature (373,374). It is important not to confuse the gel effect with the autoacceleration that is observed when a polymerization is carried out under nonisothermal conditions, so that the reaction temperature increases with increasing monomer conversion, owing to the exothermic nature of the polymerization reaction. The gel effect is observed under isothermal reaction conditions. The cause of the gel effect has been debated over 50 years and various theories have emerged which can explain all or part of the experimental data (excellent reviews on the topic can be found in References 375 and 376). In theory, any given model that links the termination rate coefficient to the increasingly difficult diffusion of macroradicals through the reaction mixture as the monomer conversion increases and thus accounts for a decrease in the termination rate, is capable of explaining the gel effect, without introducing a drastic change in the physical chemistry of the polymerizing system. The debate does not so much focus on the fact that the termination reaction becomes increasingly hindered as the mobility of the polymer chains decreases, than on the details of exactly what type of mobility is important. The main explanation for the gel effect that is offered concentrates on the formation of chain entanglements that hinders the diffusion of the macroradicals, thus causing a decrease in the rate of termination.

Primary Radical Termination. Primary radical termination refers to the bimolecular reaction between a propagating radical and a primary, initiator-derived radical. This process leads to lower rates of initiation and propagation, thus causing a deviation from the predictions of classical kinetics (377). In analogy with the termination reactions between propagating radicals, primary radical termination can also occur by either combination or disproportionation. It has been shown that primary radical termination between cyanoisopropyl radicals and polystyryl radicals occurs mainly via combination at 98°C with extremely

high AIBN concentrations, generating polymeric material with degree of polymerizations of 10 and below (378). Primary radical termination in conventional AIBN- or benzoyl peroxide-initiated polymerizations occurs only to a significant extent when high initiator or low monomer concentrations are used. Hence, the effect of primary radical termination becomes more pronounced at high conversions and high dilutions (319,379–381). Even under experimental conditions that would favor the primary radical termination reaction, more than 85% of the termination events occur between two macroradicals in AIBN-initiated styrene polymerization at 100°C (83). In conventional bulk polymerizations of the same system under conventional conditions (ie initiator concentration in the order of 10^{-2} mol · L^{-1}) less than 2% of the end groups in the generated polymeric material are due to primary radical termination events. When using BPO as initiator, approximately 8% of the end groups have been formed through transfer or termination with primary radicals (85).

Many industrial photopolymerization processes exploit unusually high initiation rates in order to achieve a rapid cure and a high final degree of conversion. These conditions favor primary radical termination reactions (380,382). Certain primary radical fragments derived from photoinitiators exhibit a relatively high stability and show reluctance to initiate polymerization. This is often observed with benzoin and benzoin ethers that fragment upon UV irradiation into an initiating species (the benzoyl fragment) and an inhibiting species (the benzyl alcohol fragment in the case of benzoin, and the acetal fragment in the case of benzoin ethers) (19,20,54,383). A manifestation of such a photoinitiator nonideality has been reported for 2,2-dimethoxy-2-phenylacetophenone- (DMPA-) and benzoin-initiated SP–PLPs of various monomers (18). A decrease in monomer conversion per single laser pulse with increasing photoinitiator concentrations was observed. MALDI-TOF investigations of benzoin and DMPA photoinitiated polymer show that the two radical fragments generated upon pulsed laser irradiation show markedly different reactivity toward methyl methacrylate: whereas the benzoyl fragment—common to both DMPA and benzoin—clearly participates in the initiation process, the acetal and benzyl alcohol fragments cannot be identified as end groups in the polymer (384). Another example of how comparatively low rates of addition of primary radicals to monomer may lead to higher rates of primary radical termination is the polymerization of hindered monomers, eg, fumarates and itaconates, initiated by AIBN (379,385).

Rate of Polymerization

Stationary Polymerization. A stationary polymerization system is characterized by a constant free radical concentration as given by equation 53:

$$\frac{d[R^{\bullet}]}{dt} = 0 \tag{53}$$

In the past it has been a standard practice to derive a simple but general expression for the rate of polymerization, R_p. This expression correlates the rate of polymerization with the initiator and monomer concentrations on one side and the

kinetic rate coefficients k_d, k_p, and k_t on the other side. Although this expression contains many approximations, it is surprisingly successful in describing the experimental reality. Detailed kinetic studies have revealed the shortcomings of this equation. However, it remains the basis of standard free radical polymerization kinetics. The approximations that are made in its derivation are

(1) chain length and conversion independent rate coefficients k_t and k_p;
(2) instantaneous establishment of a steady-state free radical concentration;
(3) assumption that monomer is only consumed by chain propagation and not via the initiation process or chain transfer. This assumption allows to equate the rate of the loss of monomer with the rate of polymerization;
(4) all reactions are irreversible;
(5) the effective concentration of initiator-derived free radicals is constant throughout the polymerization.

The core of the derivation for the rate of polymerization expression is the assumption that the rate of initiation equals the rate of termination, equation 46 in its simplified form. This assumption is mandatory for the establishment of a constant free radical concentration (eq. 54).

$$2fk_d[\mathrm{I}] = 2k_t[\mathrm{R}^\bullet][\mathrm{R}^\bullet] \tag{54}$$

Rearrangement of equation 54 and insertion into the simplified form of equation 21

$$R_p = -\frac{d[\mathrm{M}]}{dt} = k_p[\mathrm{M}][\mathrm{R}^\bullet] \tag{55}$$

yields the final expression for the rate of polymerization, R_p:

$$R_p = -\frac{d[\mathrm{M}]}{dt} = k_p\left(f\frac{k_d}{k_t}\right)^{0.5}[\mathrm{M}][\mathrm{I}]^{0.5} \tag{56}$$

Equation 56 indicates a first-order dependence of the rate of polymerization on the monomer concentration and a square-root dependence on the concentration of the initiator. These dependencies have been confirmed for the example of many polymerizing systems. It should be pointed out that deviations from equation 56 (such as chain-length-dependent rate coefficients or primary radical termination) are manifest in a change in the exponents associated with the initiator and monomer concentrations (386,387). The rate of polymerization will scale with a weaker than square-root dependence on [I] and a stronger than linear dependence on [M]. Extreme dilution of monomer can also change the exponents of monomer and initiator concentration. Equation 56 is easily integrated to yield an expression which directly correlates the monomer conversion with the observed kinetic rate coefficient k_{obs}.

$$\ln\left(\frac{1}{1-p}\right) = k_{obs}t \quad \text{where} \quad k_{obs} = k_p\left(f\frac{k_d}{k_t}[I]\right)^{0.5} \tag{57}$$

where p is the conversion of monomer to polymer. The temperature dependence of the polymerization rate is given by the temperature dependencies of the individual rate coefficients. Each rate coefficient follows its own Arrhenius law, $k = A\ \exp(-E_A/RT)$, where A is the preexponential factor and E_A denotes the activation energy. The overall activation energy of the rate of polymerization, $E_A^{R_p}$, equals the sum of the weighted activation energies of the elementary reactions, propagation (E_A^p), initiation (E_A^i), and termination (E_A^t).

$$E_A^{R_p} = E_A^p + \frac{1}{2}E_A^i - \frac{1}{2}E_A^t \tag{58}$$

Activation energies for commonly used thermal decomposing initiators, E_A^i, are in the order of 120–150 kJ · mol^{-1}. The E_A^p values for most common monomers lie within the range of 20–40 kJ · mol^{-1}, and E_A^t is generally in the range of 4–10 kJ · mol^{-1}. Hence, typical values for overall activation energies for the rate of polymerization initiated by a thermally decomposing initiator are close to 80 kJ · mol^{-1}. This corresponds to a two- or threefold increase in rate for a 10°C temperature increase. Photochemical polymerization rates have a much lower activation energy of about 20 kJ · mol^{-1}, according to close to zero activation energy of the photoinitiation process.

Dead-End Polymerization. To reach a steady state in free radical polymerization it is important that the initiator concentration is constant over a significant time span to ensure a constant rate of initiation. However, the initiator decomposes according to equation 3 and its concentration unavoidably decreases. This can often be neglected when the decomposition rate of the initiator is very small in comparison with the rate of polymerization. To perform a steady-state experiment an appropriate initiator should be chosen with a rate coefficient of decomposition, k_d (at the given temperature), that ensures a maximum decrease in initiator concentration of no more than 10% over the entire reaction time. Especially for fast decomposing initiators or very long reaction times the decreasing initiator concentration has to be accounted for. If all initiator molecules are decomposed before the end of polymerization, the reaction ceases. This experimental conditions are referred to as *dead-end polymerization* (388–391). However, the polymerization can be reinitiated by adding new initiator. Insertion of equation 3 in equation 56, separation of the variables, and integration from $[M]_0$ to [M] and from $t = 0$ to $t = t$ yields

$$-\ln\frac{[M]}{[M]_0} = -\ln(1-p) = 2k_p\left(\frac{f[I]_0}{k_d k_t}\right)^{0.5}(1-e^{-k_d t/2}) \tag{59}$$

where p is the monomer-to-polymer conversion and is defined by $p = ([M]_0-[M])/[M]_0$. At long reaction times ($t \to \infty$), the monomer concentration and conversion reach the limiting values of $[M]_\infty$ and p_∞.

$$-\ln\frac{[M]_\infty}{[M]_0} = -\ln(1-p_\infty) = 2k_p\left(\frac{f[I]_0}{k_d k_t}\right)^{0.5} \quad (60)$$

The example for polymerizations of styrene using AIBN at 60°C shows how the maximum conversion depends on the concentration of the initiator (k_p = 341 $L\cdot mol^{-1}\cdot s^{-1}$, $k_t = 5\times10^7$ $L\cdot mol^{-1}\cdot s^{-1}$, $k_d = 1.35\cdot10^{-5}$ s^{-1}, $f = 0.5$):

$[AIBN] = 0.001$ mol $\cdot$ L^{-1}	$p_\infty = 44.4\%$
$[AIBN] = 0.01$ mol $\cdot$ L^{-1}	$p_\infty = 84.4\%$
$[AIBN] = 0.1$ mol $\cdot$ L^{-1}	$p_\infty = 99.7\%$

A higher initiator concentration results in a higher polymer yield. However, the molecular weight of the polymer produced decreases at the same time.

Nonstationary (Instationary) Polymerization. Especially at the beginning and at the end of the polymerization process the steady-state principle does not hold. The generation of new free radicals by the initiator decay exceeds their consumption via termination events at early reaction times (preeffect) (392). After the initiation process ceases, the free radical concentration decreases according to the termination rate law expression (aftereffect) (393). Consequently, the rate of polymerization is not constant over the entire time period of the polymerization (394–396). Measurement of the polymerization rate in the pre- and aftereffect regions allows for the determination of the coupled form of termination and propagation rate coefficients, k_p/k_t, whereas in the steady-state region, they can only be accessed as the ratio k_p^2/k_t. The individual propagation and termination rate coefficients can be calculated by combining the above two ratios. The determination of k_p/k_t and k_p^2/k_t via the pre- and aftereffects and stationary polymerization experiments, respectively, has long been the only possibility to determine propagation and termination rate coefficients. However, recent studies reveal that serious problems were associated with this approach, owing to the chain length dependence of k_t, (397), which was not accounted for. This may be the reason for the large discrepancies observed when comparing values for k_p and k_t from different sources. The situation has improved drastically by the invention of the pulsed laser polymerization (PLP) method, which has been introduced in the late 1980s. This improvement is impressively demonstrated when comparing recent data for the propagation rate coefficient in styrene homopolymerizations with earlier data (see Figure 8).

Although the steady state is reached within a couple of seconds after starting the initiation process, the generation of free radicals exceeds their loss by termination (ie the preeffect) in this period. Therefore, the concentration of free radicals $[R^\bullet]$ is not constant but a function of time. The rate of free radical production is the rate of initiation minus the rate of termination, as given by equation 61:

$$\frac{d[R^\bullet]}{dt} = R_i - 2k_t[R^\bullet]^2 \quad (61)$$

Assuming a constant rate of initiation, integration leads to

$$[R^\bullet] = [R^\bullet]_S \tanh\left[(2k_t R_i)^{0.5} t\right] \quad (62)$$

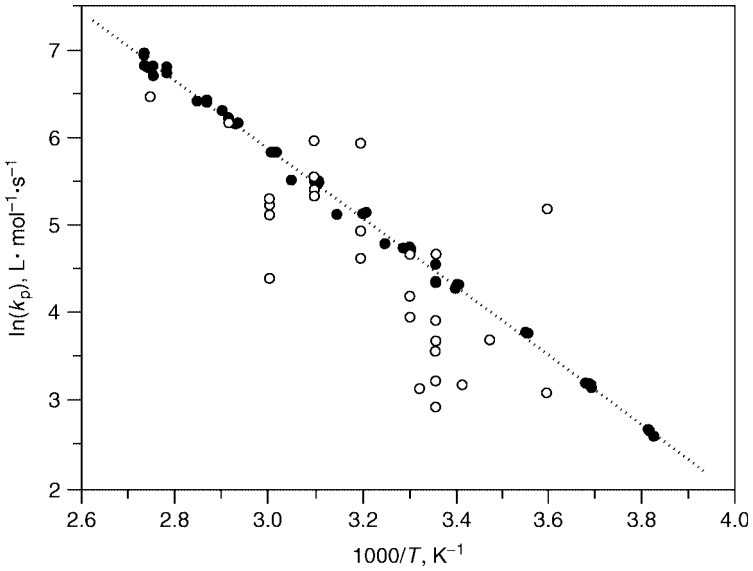

Fig. 8. Comparison of propagation rate coefficients for bulk styrene homopolymerizations from two generations: PLP–SEC data from an IUPAC benchmark publication (Ref. 398 (●), and data compiled from Ref. 399 (○).

where $[R^{\bullet}]_S$ represents the steady-state free radical concentration. The example for polymerizations of styrene using 10^{-3} mol · L^{-1} AIBN at 60°C shows how fast the steady state is reached: $k_p = 341$ L · mol^{-1} · s^{-1}, $k_t = 5 \cdot 10^7$ L · mol^{-1} · s^{-1}, $k_d = 1.35 \cdot 10^{-5}$ s^{-1}, $f = 0.5$ (see Figure 9). The polymerization can be considered to proceed in a steady state after approximately 3 s.

After stopping the initiation process no new free radicals are available and the concentration decreases according to a second-order rate law. Integration of

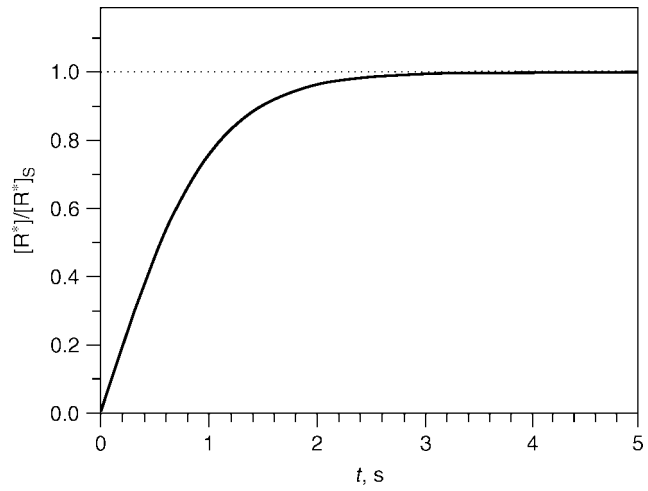

Fig. 9. Increase of the radical concentration in a conventional AIBN-initiated bulk polymerization of styrene. For kinetic parameters see text.

equation 61 with $R_i = 0$ yields the concentration of free radicals as a function of time in the so-called aftereffect region:

$$[R^\bullet]^{-1} - [R^\bullet]_S^{-1} = 2k_t t \tag{63}$$

Insertion into the rate law of propagation (eq. 54)—assuming that the rate of loss of monomer equals the rate of polymerization, R_p—gives

$$R_p = \frac{k_p[M]}{2k_t t + [R^\bullet]_S^{-1}} \tag{64}$$

which contains the individual rate coefficients k_p and k_t in a combination different from that obtained via steady-state experiments. Thus, the ratio k_p/k_t is accessible by equation 64 via the measurement of the polymerization rate in the aftereffect region.

Pseudostationary Polymerization. Conversions in the pre- and after–effect regions are rather low, making it experimentally challenging to determine them accurately. To overcome this problem a structured continuous initiation profile is chosen by which the system is facing pre- and aftereffects in sequences. This can be achieved by using a photo-polymerizable system, which is exposed to a succession of light and dark periods, leading to a *pseudostationary* state, which provides a continuous polymerization of a system being in a non-steady state (400,401). It is characterized by a constant mean free radical concentration, averaged over one cycle period, but a permanently changing actual concentration of the reactive intermediates. While the technique was introduced by using a rotating sector (402–404)—where light periods are considerably long, ie about 1/4 of the whole cycle time t_0—the technique improved by using a pulsed laser as light source (51,405–407). The extremely short duration of the laser flash—in the order of nanoseconds—allows to assume an instantaneous formation of free radicals. Strictly speaking, instantaneous radical generation is equivalent to neglecting the preeffect and termination during the laser pulse, respectively. Figure 10 shows a typical time profile of the free radical concentration in a pulsed laser experiment.

The maximum free radical concentration $[R_+^\bullet]$ is reached immediately after the laser pulse has been applied. It is the sum of the radical concentration formed at each laser flash, ρ, and the amount of free radicals still in the system, which are produced by former pulses, $[R_-^\bullet]$. This value is identical to the minimum free radical concentration in the polymerizing system. Radical formation during the dark time is neglected. Assuming that termination is not dependent on the chain length, the rate law for termination can be written as

$$-\frac{d[R^\bullet]}{dt} = 2k_t[R^\bullet]^2 \tag{65}$$

Integration of equation 65 over the whole pulse period t_0 yields

$$[R_-^\bullet]^{-1} - [R_+^\bullet]^{-1} = 2k_t t_0 \tag{66}$$

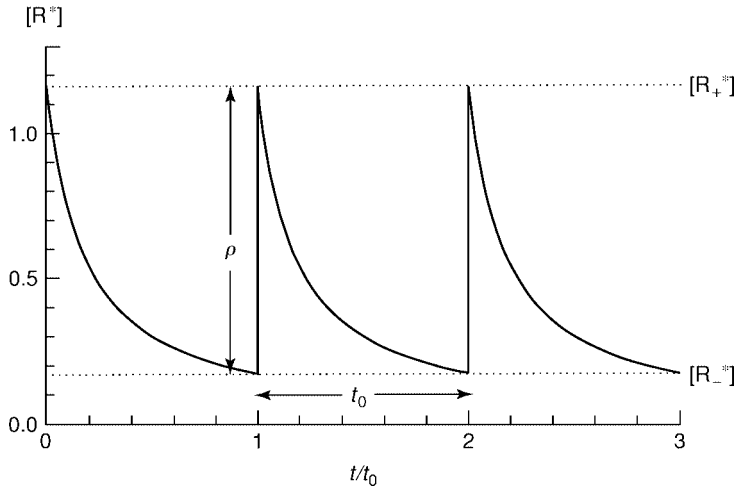

Fig. 10. Typical radical concentration profile generated by the pulsing action of laser on a reaction mixture of photoinitiator and monomer. The maximum free radical concentration $[R_+^\bullet]$ is reached immediately after the laser pulse has been applied. It is the sum of the radical concentration formed at each laser flash, ρ, and the amount of free radicals still in the system produced by former pulses, $[R_-^\bullet]$.

The pseudostationary state is defined by the exact compensation of the loss of free radicals during the dark period via termination by the radical formation of the laser pulse.

$$\rho = [R_+^\bullet] - [R_-^\bullet] \tag{67}$$

Combination of equations 66 and 67 leads to

$$[R_+^\bullet] = \rho\left[\frac{1}{2} \pm \left(\frac{1}{4} + \frac{1}{2\rho k_t t_0}\right)^{0.5}\right] \tag{68}$$

The free radical concentration at any moment during the pulse period is

$$[R^\bullet] = \left(\frac{1}{[R_+^\bullet]} + 2k_t t\right)^{-1} = \frac{[R_+^\bullet]}{1 + 2[R_+^\bullet]k_t t} \tag{69}$$

Averaging over the whole pulse period leads to a mean value for the free radical concentration

$$[\bar{R}^\bullet] = \frac{1}{t_0}\int_0^{t_0} \frac{[R_+^\bullet]}{1 + 2[R_+^\bullet]k_t t}\, dt = \frac{1}{2k_t t_0}\ln(1 + 2[R_+^\bullet]k_t t_0) \tag{70}$$

By insertion of equations 68 and 70 in equation 55, the expression for the polymerization rate in pseudostationary PLPs is obtained.

$$R_p = \frac{k_p[M]}{2k_t t_0} \ln \left\{ 1 + \rho k_t t_0 \left[1 + \left(1 + \frac{2}{\rho k_t t_0} \right)^{0.5} \right] \right\} \quad (71)$$

This expression contains the ratio of k_p/k_t, which is typically derived from nonstationary polymerizations. The measurement of the rate of polymerization under pseudostationary conditions may hence allow for the determination of the ratio of k_p/k_t (408). However, the major advantage of pseudostationary polymerization does not lie within the possibility to separate the ratio of k_p^2/k_t into its individual components, but to generate structured chain length distributions. These structured distributions allow for the accurate determination of the propagation and termination rate coefficients.

A special case of the PLP is the SP–PLP technique (409,410). The equations needed to analyze the monomer conversion vs time traces obtained from SP–PLP experiments are easily derived. Integration of the rate law expression for termination, assuming a chain length independent, average termination rate coefficient k_t (eq. 65), yields

$$[R^\bullet] = \left(2k_t t + \frac{1}{[R_+^\bullet]} \right)^{-1} \quad (72)$$

Substitution of equation 72 into the rate law expression for the propagation step (eq. 55) and subsequent integration yields the change in relative monomer concentration after a single laser pulse:

$$\frac{[M]}{[M]_0} = (2k_t[R_+^\bullet]t + 1)^{-k_p/2k_t} \quad (73)$$

Expression 73 can be fitted to time-resolved monomer conversion vs time traces obtained from SP–PLP experiments (see below), with the two fit variables being $k_t[R_+^\bullet]$ and k_p/k_t. With knowledge of the primary free radical concentration $[R_+^\bullet]$, it is possible to determine k_t and k_p from a single conversion vs time trace. Unfortunately, in reality, $[R_+^\bullet]$ is often not known (because of insufficient knowledge about initiator efficiencies) and k_t can only be assessed via knowledge of the propagation rate coefficient from independent experiments (eg, PLP–SEC). However, in recent studies the accurate determination of primary radical concentrations produced by a laser flash have been reported in nonpolymerizing systems (411,412), giving promising results for future work.

The Chain Length Distribution

The kinetic rate coefficients of the various steps involved in the polymerization reaction are controlling the rate of polymerization, R_p, and the overall free radical concentration. Keeping in mind that the polymerization is a chain mechanism leading to macromolecules, it is self-evident that the same kinetic parameters may be employed to calculate the sizes of polymeric intermediates and the polymer generated. For this purpose it is necessary to solve the complete set of

coupled differential equations, one equation for each chain length plus one for the initiation step.

The rate law for the concentration change of a macroradical with chain length i can be written as

$$\frac{\mathrm{d}[\mathrm{R}_i^\bullet]}{\mathrm{d}t} = k_\mathrm{p}^{i-1}[\mathrm{M}][\mathrm{R}_{i-1}^\bullet] - \left(k_\mathrm{p}^i[\mathrm{M}] + k_\mathrm{tr}^\mathrm{M}[\mathrm{M}] + \sum_k k_\mathrm{tr}^{\mathrm{T}_k}[\mathrm{T}_k] + 2\sum_{j=1}^{\infty} k_\mathrm{t}^{i,j}[\mathrm{R}_j^\bullet] \right)[\mathrm{R}_i^\bullet] \tag{74}$$

This rate law reflects a polymerization process during which a free radical with chain length i is solely formed by a propagation step from the free radical with chain length $i - 1$. The free macroradical has then the possibility to grow either by reaction with a monomer molecule M, giving a chain length of $i + 1$, or it can undergo a transfer reaction with the monomer or any other transferring molecule T_k (eg, transfer agent, solvent, initiator, polymer). Alternatively, it may be terminated by another free radical. The analytical solution of this problem is obviously very difficult. However, numerical solutions of this set of equations became possible because the rapid increase in computer power and simulations of chain length distributions of polymers are of increasing importance for academic and industrial applications (413).

The chain length distribution of a polymer is defined as the fraction of molecules x_P that contains P basic monomer units. It should be noted that the degree of polymerization P is equivalent to the chain length i. The living macroradicals by which the dead polymer is generated through any chain-stopping event show a chain length distribution, too. Both distributions are closely related to each other and the chain length distribution of the dead polymer can be calculated via the derivative of the distribution of the living macroradicals.

Like any other distribution function, the chain length distribution is described by its statistical moments, which are defined as

$$m^{(k)} = \sum_{P=1}^{\infty} P^k x_P \tag{75}$$

By combination of such moments one can easily calculate mean values for the degree of polymerization, $\bar{P}$, which characterize the chain length distribution. The distribution is only fully described if all moments are known. However, in practice there are two mean values calculated by the first three statistical moments, which are extensively used: the number-average degree of polymerization, $\bar{P}_\mathrm{n}$, and the weight-average degree of polymerization, $\bar{P}_\mathrm{w}$.

$$\bar{P}_\mathrm{n} = \frac{m^{(1)}}{m^{(0)}} = \frac{\sum_{P=1}^{\infty} P x_P}{\sum_{P=1}^{\infty} x_P} \quad \bar{P}_\mathrm{w} = \frac{m^{(2)}}{m^{(1)}} = \frac{\sum_{P=1}^{\infty} P^2 x_P}{\sum_{P=1}^{\infty} P x_P} \tag{76}$$

Stationary Polymerization.

Average Degree of Polymerization. To calculate the number-average degree of polymerization, $\bar{P}_\mathrm{n}$, of a polymer produced by a steady-state polymerization,

it is mandatory to know how many propagation steps occur before the chain reaction is stopped. A distinction has to be made between the term 'chain' used in a molecular sense and 'chain' used as a kinetic concept. The kinetic chain length ν, assuming that every radical $I^{\bullet}$ initiates polymerization, is defined as

$$\nu = \frac{\text{Total number of polymerized monomer unit}}{\text{Total number of initiation step}} = \int_0^t \frac{d[M]}{dt} dt \Big/ \int_0^t \frac{d[M]}{dt} dt \tag{77}$$

In a system that has reached the steady state, the integrands of equation 77 may be constant over a significant time span. By substituting equations 4 and 21—with the assumption of chain-length-independent rate coefficients—equation 77 can therefore be rewritten as

$$\nu = \frac{R_p}{R_d} = \frac{k_p[R^{\bullet}][M]}{2fk_d[I]} \tag{78}$$

Elimination of $[R^{\bullet}]$ by means of equation 54 leads to an expression for the kinetic chain length ν that shows the dependence of the different kinetic parameters. One important characteristic of the free radical polymerization is hereby well illustrated: The sizes of the macromolecules produced are inversely proportional to the square root of initiator concentration. Increasing the initiator concentration leads to smaller size polymer molecules.

$$\nu = \frac{k_p[M]}{2\left(fk_dk_t[I]\right)^{0.5}} \tag{79}$$

Disregarding any transfer effect as a first approximation correlates the kinetic chain length with the number-average degree of polymerization, $\bar{P}_n$. In the case of termination by disproportionation one polymer molecule is produced per every kinetic chain

$$\bar{P}_n = \nu \tag{80}$$

Termination by combination leads to one polymer molecule per two kinetic chains, reflecting the combination mechanism.

$$\bar{P}_n = 2\nu \tag{81}$$

Any mixture of both mechanisms can be described by using the value δ (see eq. 45), the contribution of disproportionation to the overall termination process.

$$\bar{P}_n = \frac{2}{1+\delta}\nu \tag{82}$$

The mean kinetic chain length can be experimentally determined by using marked initiator molecules, eg, ^{14}C radiolabeled (414). By these means the number

of initiator fragments per weight of polymer can be measured, and therefore the number of monomer units polymerized by each initiator step may be calculated. This represents one method to determine the mode of termination. With the values for the AIBN-initiated styrene polymerization (10^{-3} mol · L^{-1} AIBN at 60°C, k_p = 341 L · mol^{-1} · s^{-1}, $k_t = 5 \times 10^7$ L · mol^{-1} · s^{-1}, $k_d = 1.35 \times 10^{-5}$ s^{-1}, $f = 0.5$) the average kinetic chain length is about 3500 and it will take approximately 1.2 s to be finished.

Without changing the free radical concentration, 'normal' chain transfer processes remain hidden in any experiment measuring the rate of polymerization alone. The kinetic chain length is also unaffected by the transfer process, because the growing free radical center generated by the initiation step stays alive after any chain transfer event, although more than one polymer chain is produced. For this reason, equation 82 does not hold true any longer if chain transfer reactions are taken into account. In many kinetic measurements based on the analysis of the molecular weight distributions, transfer processes are neglected and are seen as disturbing factors. However, determination of the chain length distribution of a polymer remains the only possibility to measure the rate coefficients for transfer processes.

Taking chain transfer into account, the number-average degree of polymerization, $\bar{P}_n$, can be described as

$$\bar{P}_n = \frac{\text{Total number of polymerized monomer units}}{\text{Half the number of formed end groups}} \tag{83}$$

The various reactions within the polymerization process generate different amounts of end groups per initiation step:

Initiation	1 end group
Propagation	0 end groups
Transfer	2 end groups
Termination by disproportionation	1 end group
Termination by combination	0 end groups

Again the steady state with its general approximations is assumed in which the concentrations of the reactants, such as the monomer, free radicals, and transfer agent, do not vary with time. Hence, in equation 83 the number of polymerized monomer units can be substituted with the rate of polymerization and the numbers of end groups by the rate of their formation.

$$\bar{P}_n = \frac{R_p}{(1/2)(R_i + R_{t,d} + 2R_{tr})} \tag{84}$$

Insertion of the simplified rate laws of the different processes

$$\textit{Initiation} \quad R_i = 2fk_d[I] = 2(k_{t,d} + k_{t,c})[R^\bullet]^2 \tag{85}$$

$$Propagation \quad R_p = k_p[M][R^\bullet] \tag{86}$$

$$Termination \ (disproportionation) \quad R_{t,d} = 2k_{t,d}[R^\bullet]^2 \tag{87}$$

$$Chain\ transfer \quad R_{tr} = \sum_k k_{tr}^{T_k}[T_k][R^\bullet] + k_{tr}^{M}[M][R^\bullet] \tag{88}$$

and subsequent inversion leads to

$$\frac{1}{\bar{P}_n} = \frac{2k_{t,d} + k_{t,c}}{k_p^2[M]^2}R_p + \frac{k_{tr}^{M}}{k_p} + \sum_k \frac{k_{tr}^{T_k}}{k_p}\frac{[T_k]}{[M]} \tag{89}$$

$[T_k]$ is the concentration of any molecule that is capable of taking part in a chain transfer reaction, including solvent S, initiator I, polymer P, and added chain transfer agent T. It is usual to define chain transfer coefficients C for the different molecules:

$$C_M = \frac{k_{tr}^{M}}{k_p}\ C_S = \frac{k_{tr}^{S}}{k_p}\ C_I = \frac{k_{tr}^{I}}{k_p}\ C_P = \frac{k_{tr}^{P}}{k_p}\ C_T = \frac{k_{tr}^{T}}{k_p} \tag{90}$$

Thus, equation 89 becomes

$$\frac{1}{\bar{P}_n} = \frac{2k_{t,d} + k_{t,c}}{k_p^2[M]^2}R_p + C_M + C_S\frac{[S]}{[M]} + C_I\frac{[I]}{[M]} + C_P\frac{[P]}{[M]} + C_T\frac{[T]}{[M]} \tag{91}$$

This equation gives the fundamental correlation of the number-average degree of polymerization with the rate of polymerization and the various chain transfer coefficients. Equation 91 constitutes the basis for determining the various chain transfer coefficients.

Performing a polymerization experiment with only low conversion of monomer to polymer, the concentration of polymer is often too low to show significant chain transfer. The same holds true for the initiator, which is mainly used in the range of low concentrations. Without addition of solvent and additional chain transfer agent, equation 91 reads after introduction of equation 45

$$\frac{1}{\bar{P}_n} = \frac{(1+\delta)k_t}{k_p^2[M]^2}R_p + C_M \tag{92}$$

Hence, a plot of the inverse number-average degree of polymerization, $\bar{P}_n$ against the rate of polymerization, R_p, (the rate of polymerization can easily be varied by the concentration of the initiator) yields the monomer chain transfer coefficient C_M as intercept and the ratio $(1+\delta)k_t/(k_p^2[M]^2)$ as slope of a linear plot. The value of C_M entails an inevitable limit for the maximum number-average degree of polymerization, $\bar{P}_n^{max}$. The value for $\bar{P}_n$ is increased by lowering the rate of polymerization R_p according to equation 92. The limit is reached when R_p becomes zero.

$$\lim_{R_p \to 0} \left(\frac{1}{\bar{P}_n} \right) = C_M \tag{93}$$

Hence, the maximum number-average degree of polymerization, $\bar{P}_n^{max}$, which is feasible is given by

$$\bar{P}_n^{max} = C_M^{-1} \tag{94}$$

Methyl methacrylate, for instance, has a monomer chain transfer coefficient of about $C_M = 5 \times 10^{-5}$ at 60°C, leading to a maximal mean chain length of about 20,000, whereas in a free radical polymerization of vinyl acetate with a monomer chain transfer coefficient of $C_M = 2 \times 10^{-4}$ at 60°C, the limit is already reached at a number-average degree of polymerization of 5000.

The Full Chain Length Distribution. So far, only the average degree of polymerization has been considered. To calculate the distribution function itself for a steady-state polymerization it is convenient to choose a statistical approach based on kinetic parameters. A probability factor α of propagation is defined as the probability that a radical will propagate rather than terminate. The factor α is the ratio of the rate of propagation over the sum of the rates of all possible reactions the macroradical can undergo.

$$\alpha = \frac{R_p}{R_p + R_{tr} + R_t} \tag{95}$$

Firstly, we assume that termination is solely by disproportionation and that the propagation probability factor is equal for each chain length. The probability for the occurrence of a polymer chain—hence its distribution function—with the length P is given by the probability of $P - 1$ propagation steps and the probability of one chain-stopping event (termination *or* transfer).

$$x_{P,d} = \alpha^{P-1}(1 - \alpha) \tag{96}$$

The molecular weight averages can be evaluated by calculating the moments of this distribution function by insertion of equation 96 into equation 75,

$$m^{(0)} = \sum_{P=1}^{\infty} x_{P,d} = 1 \tag{97}$$

$$m^{(1)} = \sum_{P=1}^{\infty} P x_{P,d} = (1 - \alpha)^{-1} \tag{98}$$

$$m^{(2)} = \sum_{P=1}^{\infty} P^2 x_{P,d} = (1 + \alpha)(1 - \alpha)^{-2} \tag{99}$$

and subsequent insertion into equation 76.

$$\bar{P}_{n,d} = m^{(1)}/m^{(0)} = (1-\alpha)^{-1} \quad \bar{P}_{w,d} = m^{(2)}/m^{(1)} = (1+\alpha)(1-\alpha)^{-1} \tag{100}$$

The ratio of the weight-average and the number-average degree of polymerization, $\bar{P}_w/\bar{P}_n$, describes the polydispersity of a chain length distribution. It becomes unity if all chains have the same length—called a monodisperse distribution—and values greater than one, if the distribution exhibits a broader shape.

$$\frac{\bar{P}_{w,d}}{\bar{P}_{n,d}} = \frac{m^{(2)}m^{(0)}}{m^{(1)}m^{(1)}} = 1+\alpha \tag{101}$$

It should be noted that the propagation step must be highly favored over chain-stopping events to produce polymer with a significant chain length and the value of α must be near to one. Hence, equation 101 shows that for a chain length distribution of a polymer produced in a stationary experiment, where chain-stopping events are termination by disproportionation or transfer, the polydispersity becomes nearly 2. This holds true for chain length distributions which are controlled by termination via disproportionation and also for distributions where chain transfer is the dominant chain-stopping event. It should be kept in mind that this theoretical value for the polydispersity is valid for an instantaneous chain length distribution. The polydispersities in real polymerizing systems are always higher than the theoretical value, because of changes in the concentration of the participating compounds (ie initiator, monomer, transfer agent), which lead to an overlay of a multitude of different chain length distributions.

Expressions may also be derived for the chain length distribution produced, when the termination process is by combination. The expression for the probability of the occurrence of a chain with the chain length P is now given by the contributions of two chains with the chain length n and m, which form the desired molecule by combination. Hence, the auxiliary condition $n + m = P$ must be valid:

$$x_{P,c} = \sum_{n=1}^{P-1} \alpha^{n-1}(1-\alpha)\alpha^{m-1}(1-\alpha) = (P-1)\alpha^{P-2}(1-\alpha)^2 \tag{102}$$

Evaluating the moments of this distribution function by insertion of equation 102 into equation 75 as above

$$m^{(0)} = \sum_{P=1}^{\infty} x_{P,c} = 1 \tag{103}$$

$$m^{(1)} = \sum_{P=1}^{\infty} P x_{P,c} = 2(1-\alpha)^{-1} \tag{104}$$

$$m^{(2)} = \sum_{P=1}^{\infty} P^2 x_{P,c} = (4+2\alpha)(1-\alpha)^{-2} \tag{105}$$

leads to

$$\bar{P}_{n,c} = m^{(1)}/m^{(0)} = 2(1-\alpha)^{-1}\ \bar{P}_{w,c} = m^{(2)}/m^{(1)} = (2+\alpha)(1-\alpha)^{-1} \tag{106}$$

The breadth of the distribution is therefore given by

$$\frac{\bar{P}_{w,c}}{\bar{P}_{n,c}} = \frac{m^{(2)}m^{(0)}}{m^{(1)}m^{(1)}} = 1 + \frac{\alpha}{2} \tag{107}$$

Keeping in mind that α has a value close to one, equation 107 leads to a polydispersity of 1.5 for a polymer produced in a polymerization process where termination is by combination. The corresponding chain length distribution is somewhat narrower than that generated by disproportionation, because of the statistical coupling of two chains with different sizes.

Almost every polymerization system shows both disproportionation and combination modes. In order to combine the two modes the general expression for the polydispersity of any given termination-controlled chain length distributions reads

$$\frac{\bar{P}_w}{\bar{P}_n} = \frac{1}{2}(3-\delta)(1+\delta) \tag{108}$$

Because the value of α is close two one, the expression $\ln(\alpha) \approx \alpha - 1$ does hold true, leading to $\alpha \approx \exp[-(1-\alpha)]$. With this correlation in mind the combination of equation 96 with the l.h.s of equation 100 gives

$$x_P = \frac{1}{\bar{P}_n}\alpha^{P-1} \approx \frac{1}{\bar{P}_n}\exp\left[-\frac{(P-1)}{\bar{P}_n}\right] \approx \frac{1}{\bar{P}_n}\exp\left(-\frac{P}{\bar{P}_n}\right) \tag{109}$$

with the factor $(P-1)$ substituted by P, because the chain length P is assumed to be much larger than 1, ie $P \gg 1$. Equation 109 demonstrates that the chain length distribution of the polymer formed by disproportionation or chain transfer follows an exponential function in the limit of infinite chain length.

The same calculation procedure, starting with equation 102, also leads to an exponential expression for the chain length distribution for termination by combination.

$$x_P = \frac{4P}{\bar{P}_n^2}\exp\left(-\frac{2P}{\bar{P}_n}\right) \tag{110}$$

However, equation 110 has the independent variable, the chain length P, in the preexponential factor, giving the chain length distribution of the polymer formed by combination a different shape.

Evaluation of equation 95 immediately leads to

$$\alpha = \frac{k_p[M]}{k_p[M] + 2(fk_dk_t[I])^{0.5} + k_{tr}[T]} \tag{111}$$

All derived distribution functions and average degrees of polymerization may now be expressed via the kinetic coefficients.

Nonstationary (Instationary) Polymerization. Calculation of chain length distributions of a polymer formed via a nonstationary polymerization (also sometimes denoted as instationary polymerization) is reasonable only if the nonstationary process is not linked to another polymerization process, eg, the pre- and aftereffect of a steady-state polymerization. One possibility to perform such an uncoupled nonstationary polymerization is the so-called single pulse experiment. A single laser pulse produces a free radical concentration ρ; the polymerization process is started, and no new free radicals are generated. The kinetic equations for such an experiment can be solved analytically, even if a chain-length-dependent termination rate coefficient is assumed. This is the case, because in such an experiment all macroradicals have the same chain length—within a narrow Poisson distribution and neglecting chain transfer—at any given time.

The free radical concentration formed by the laser pulse, ρ, decays according to the termination rate law expression.

$$-\frac{\mathrm{d}[\mathrm{R}^\bullet]}{\mathrm{d}t} = 2k_\mathrm{t}[\mathrm{R}^\bullet]^2 \tag{112}$$

Assuming a perfect correlation of time and the degree of polymerization, $P = k_\mathrm{p}[\mathrm{M}]t$, the average frequency of the propagation steps, and the postulated law for the chain length dependence of k_t, $k_\mathrm{t} = k_\mathrm{t}^0 P^{-\alpha}$, equation 112 can be written as

$$-\frac{\mathrm{d}[\mathrm{R}^\bullet]}{\mathrm{d}t} = 2k_\mathrm{t}^0(k_\mathrm{p}[\mathrm{M}])^{-\alpha}t^{-\alpha}[\mathrm{R}^\bullet]^2 \tag{113}$$

Solving this differential equation yields the concentration of free radicals as function of time, where ρ is the free radical concentration at $t = 0$:

$$[\mathrm{R}^\bullet]_\mathrm{t} = \left\{\frac{1}{\rho} + \frac{2k_\mathrm{t}^0(k_\mathrm{p}[\mathrm{M}])^{-\alpha}}{1-\alpha}t^{1-\alpha}\right\}^{-1} \tag{114}$$

The termination process by disproportionation transforms the living macroradicals into dead polymer chains with exactly the same chain length. This transformation process can be written as

$$-\frac{\mathrm{d}[\mathrm{R}^\bullet]_\mathrm{t}}{\mathrm{d}t} = [\mathrm{P}_P]k_\mathrm{p}[\mathrm{M}] \tag{115}$$

because the loss of free radicals must equal the generation of dead polymer. The factor $k_\mathrm{p}[\mathrm{M}]$ allows for the transformation of time to chain length. The concentration of dead polymer with chain length P, $[\mathrm{P}_P]$, is the chain length distribution in terms of concentrations. Division of $[\mathrm{P}_P]$ by the free radical concentration at the beginning, ρ, according to $x_{P,\mathrm{d}} = [\mathrm{P}_P]/\rho$ with $\sum[\mathrm{P}_P] = \rho$), insertion of equations 113, 114, and 115, and rearrangement yields the number chain length distribution for a single pulse experiment with termination by disproportionation.

$$x_{P,\mathrm{d}} = \frac{2k_\mathrm{t}^0\rho}{k_\mathrm{p}[\mathrm{M}]}P^{-\alpha}\left\{1+\frac{2k_\mathrm{t}^0\rho}{(1-\alpha)k_\mathrm{p}[\mathrm{M}]}P^{1-\alpha}\right\}^{-2} \tag{116}$$

The combination process gives a dead polymer chain with exactly double the chain length of the living macroradical, because all macroradicals have the same size at any given time. The transformation process from time to chain length therefore reads

$$-\frac{\mathrm{d}[\mathrm{R}^\bullet]_t}{\mathrm{d}t} = 4[\mathrm{P}_{2P}]k_\mathrm{p}[\mathrm{M}] \tag{117}$$

Because two free radicals are leading to one dead polymer, $\sum[\mathrm{P}_{2P}] = \rho/2$ must hold true. With this in mind and insertion of equations 113, 114, and 117 and subsequent rearrangement gives the number chain length distribution for a single pulse experiment with termination by combination.

$$x_{P,c} = \frac{2k_\mathrm{t}^0\rho}{4k_\mathrm{p}[\mathrm{M}]}\left(\frac{P}{2}\right)^{-\alpha}\left\{1+\frac{2k_\mathrm{t}^0\rho}{(1-\alpha)k_\mathrm{p}[\mathrm{M}]}\left(\frac{P}{2}\right)^{1-\alpha}\right\}^{-2} \tag{118}$$

According to the different termination modes the overall number chain length distribution can be calculated via

$$x_P = \frac{2}{1+\delta}[\delta x_{P,\mathrm{d}} + (1-\delta)x_{P,\mathrm{c}}] \tag{119}$$

with δ being the contribution of disproportionation to the overall termination process.

Pseudostationary Polymerization. Throughout many decades the pseudostationary polymerization was carried out—mainly with a rotating sector—to measure a different ratio of the individual rate coefficients k_p and k_t as that obtained from steady-state experiments. The rate of polymerization was the only measured value, and the chain length distribution of the polymer produced during such an experiment was not evaluated, mainly because of the lack of suitable analytical techniques. The invention and improvement of SEC paved the way for detailed investigations of the chain length distribution formed throughout a pseudostationary polymerization experiment (415). This improvement eventually lead to the invention of the PLP–SEC method (416), which turned out to be the best improvement in polymerization kinetic measurements long since. This technique allows for the direct measurement of the individual propagation rate coefficient k_p (133,417).

The principle of the pulsed laser technique is simple but ingenious. A monomer/photoinitiator mixture is irradiated by a pulsed laser beam. Each laser flash generates free radicals which initiate a polymerization process. No new free radicals are formed during the dark time periods. All growing macroradicals formed by one specific laser pulse have the same chain length within a narrow Poisson distribution. As the free radical concentration decreases owing to termination processes, the rate of termination decreases according to equation 46, too.

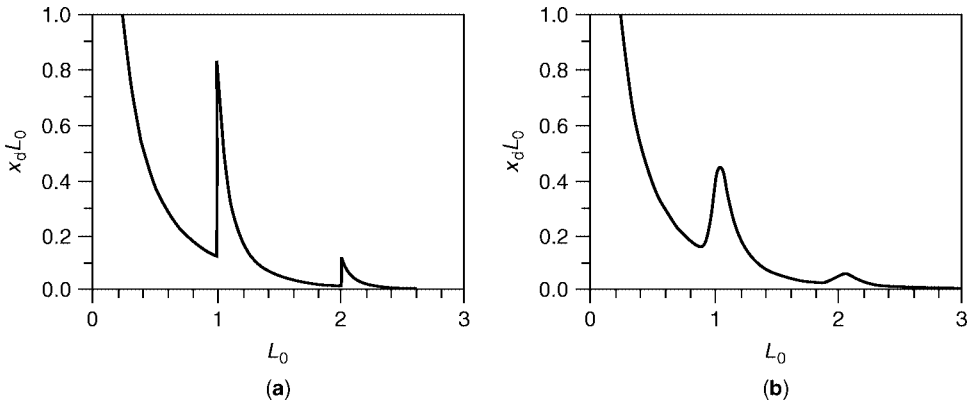

Fig. 11. Simulated and normalized number distribution for a pulsed laser experiment, with termination exclusively via disproportionation (**a**) without and (**b**) with Poisson broadening.

After the dark period, t_0, the next laser flash irradiates the system and instantaneously increases the free radical concentration. Hence, the termination rate is suddenly highly increased, too, leading to a significant amount of dead polymer with the chain length L_0 being the chain length of a macroradical that grew for one dark time period, t_0. Taking into account that the radicals have a certain probability to survive the laser flash and to terminate at any later pulse, the relative concentration of polymer with the chain length $2L_0$, $3L_0$, and so on, is increased, too. The described polymerization conditions therefore produce a well-structured chain length distribution with additional peaks at the chain length of L_0 and its multiples (see Figure 11). The radicals which are formed at the laser pulse are very small. The mode of termination is therefore not overly important for the formation of the additional peaks of the chain length distribution.

Assuming a low conversion of monomer to polymer, the monomer concentration can be expected to be constant. The propagation rate coefficient and the monomer concentration can therefore be combined into a new rate coefficient, $\tilde{k_p} = k_p[M]$, which is associated with the following first-order rate law:

$$R_p = \tilde{k}_p[R^\bullet] \quad \text{with} \quad \tilde{k}_p = k_p[M] \tag{120}$$

The average time span between two first-order reaction steps, τ, is given by

$$\tau = k^{-1} \tag{121}$$

with k being the first-order rate coefficient. Insertion of equation 120 into equation 121 yields the time of an average propagation step τ_p, assuming the monomer concentration is constant.

$$\tau_p = \frac{1}{\tilde{k}_p} = \frac{1}{k_p[M]} \tag{122}$$

The chain length $L_{0,n}$ of a macroradical that grows n laser periods, nt_0, is now easily correlated with the propagation rate coefficient k_p.

$$L_{0,n} = nk_p[M]t_0 \tag{123}$$

The evaluation of the additional peaks occurring in the chain length distribution of a PLP experiment and the corresponding values of $L_{0,n}$ by means of SEC enables the calculation of k_p, because the monomer concentration and the laser frequency are known.

Because of the statistical process of the chain growth, the macroradicals produced by the same laser pulse do not exhibit the same chain length at any given time, but rather show a narrow Poisson distribution with L being the mean value.

$$x_P = e^{-L}\frac{L^P}{P!} \tag{124}$$

The theoretical chain length distribution is therefore subject to a broadening, losing its discontinuities (see Figure 11**b**). It turned out that the inflection point on the low molecular weight side of the additional peak is in most cases the best measure for the real value of L_0 (418). Only at the so-called high termination limit, where the free radical concentration produced by each laser pulse is extremely high, the maximum of the additional peak may be a better choice (419). However, second or higher points of inflection can often be evaluated, even when there is no peak maximum visible. In addition, because of being a point of second order, the inflection point is less affected by baseline errors occurring during the SEC.

Analytical solutions for the chain length distribution generated by PLP (415, 416,420,421) are very complex, even in their simplest form, assuming no Poisson distribution, no transfer, and no initiation process during the dark time period. The chain length distribution for assuming a strict coupling of time and degree of polymerization for termination by disproportionation can be written as

$$x_{P,d}^{(n)} = \rho\left\{\frac{\tilde{C}}{L_0}\left[1+\frac{\tilde{C}}{L_0}(P-nL_0)\right]^{-2}(1+\tilde{C})^{-n}\right\} \tag{125}$$

where

$$0 \le P \le L_0 \quad \text{for} \quad n = 0$$

$$nL_0 < P \le (n+1)L_0 \quad \text{for} \quad n = 1,\ 2,\ 3\ldots$$

with the definitions

$$\tilde{C} = C\frac{[R_+{}^\bullet]}{\rho} \tag{126}$$

$$C = 2\rho k_t t_0 \tag{127}$$

$$L_0 = k_p[M]t_0 \tag{128}$$

Especially the value C is of importance, because it governs the overall shape of the chain length distribution. A typical value of C is 0.5–10, whereas higher values of C yield more pronounced first additional peaks (high termination limit). The shape of a PLP distribution can be (in principle) held constant by balancing the product of the laser period t_0 and the free radical concentration produced by each laser pulse, ρ, to give constant values of C. It should be noted that the extra peaks are sharper greater the value for L_0.

The expression for the chain length distribution for termination by combination reads

$$x_{P,\mathrm{c}}^{(n)} = \rho\left[n(1+\tilde{C})^{-n+1}\frac{\hat{x}_{P-(n-1)L_0,\mathrm{c}}}{\rho} + (n+1)(1+\tilde{C})^{-n}\frac{\hat{x}_{P-nL_0,\mathrm{c}}}{\rho}\right] \tag{129}$$

with

$$\hat{x}_{P,\mathrm{c}} = \frac{\rho}{2}\frac{C}{2L_0}\left(1+\tilde{C}\frac{P}{2L_0}\right)^{-2} \tag{130}$$

The statistical moments of the chain length distribution in the long-chain limit can be calculated by insertion of equations 125 and 129 into equation 75.

For termination by disproportionation,

$$m_{\mathrm{d}}^{(0)} = \rho \tag{131}$$

$$m_{\mathrm{d}}^{(1)} = \rho\left[L_0\frac{\ln(1+\tilde{C})}{C}\right] \tag{132}$$

$$m_{\mathrm{d}}^{(2)} = \rho\left(2L_0\frac{L_0}{C}\right) \tag{133}$$

For termination by combination,

$$m_{\mathrm{c}}^{(0)} = \frac{\rho}{2} \tag{134}$$

$$m_{\mathrm{c}}^{(1)} = \rho\left[L_0\frac{\ln(1+\tilde{C})}{C}\right] \tag{135}$$

$$m_{\mathrm{c}}^{(2)} = \rho\left(3L_0\frac{L_0}{C}\right) \tag{136}$$

The number- and weight-average degrees of polymerization can be calculated via combination of these moments according to equation 76. For termination by disproportionation,

$$\bar{P}_{\mathrm{n,d}} = L_0\frac{\ln(1+\tilde{C})}{C} \tag{137}$$

$$\bar{P}_{\mathrm{w,d}} = 2L_0\frac{1}{\ln(1+\tilde{C})} \tag{138}$$

For termination by combination,

$$\bar{P}_{n,c} = 2L_0 \frac{\ln(1+\tilde{C})}{C} \tag{139}$$

$$\bar{P}_{w,d} = 3L_0 \frac{1}{\ln(1+\tilde{C})} \tag{140}$$

The polydispersity of the chain length distribution of a polymer produced via a pulsed laser experiment for disproportionation reads

$$\frac{\bar{P}_{w,d}}{\bar{P}_{n,d}} = 2\frac{C}{[\ln(1+\tilde{C})]^2} \tag{141}$$

and for combination

$$\frac{\bar{P}_{w,c}}{\bar{P}_{n,c}} = \frac{3}{2}\frac{C}{[\ln(1+\tilde{C})]^2} \tag{142}$$

As can be easily seen, the breadth of the PLP distribution is not only dependent on the termination mode, as this is the case for steady-state experiments. The polydispersity is additionally controlled by the polymerization conditions like initiator concentration and laser intensity, which both influence the value of the free radical concentration which is produced at each laser flash, ρ. The polydispersity is also different for different pulse periods, t_0.

Thermodynamics

Especially at elevated temperatures the propagation step can no longer be considered irreversible. The propagation step is in fact reversible, leading to a thermodynamic equilibrium. This equilibrium can be described by the magnitude of the free energy difference ΔG_p between the polymer and the monomer. The polymerization process is thermodynamically favored if ΔG_p is negative. The value of the free energy difference is given by the fundamental equation

$$\Delta G_p = \Delta H_p - T\Delta S_p \tag{143}$$

For long polymer chains the enthalpy and entropy changes in the propagation reaction are effectively those of the overall polymerization reaction (113,422). The polymerization enthalpies ΔH_p of most free radical polymerizations are negative, with typical values of -30 to -100 kJ $\cdot$ mol^{-1} as can be seen in Table 8.

The values for the polymerization entropies are negative, too, reflecting the loss of degrees of freedom of the monomer becoming a part of the polymer chain. Typical values for the polymerization entropies are -100 to -120 J $\cdot$ K^{-1} $\cdot$ mol^{-1} (see Table 8). Hence, the two terms on the r.h.s. of equation 143 are antagonistic. Under normal temperature conditions, the exothermicity of the reaction exceeds the entropic term and ΔG_p becomes negative. However, at elevated temperatures

Table 8. Standard Polymerization Enthalpies ΔH_p^0 and Polymerization Entropies ΔS_p^0 of Various Monomers for the Reaction of Liquid Monomers to Condensed Polymers[a]

Monomer	$-\Delta H_p^0$, kJ · mol^{-1}	$-\Delta S_p^0$, J · K^{-1} · mol^{-1}
α-Methylstyrene	35	110
α-Vinylnaphthalene	36	—
Acetone	0	—
Acrylamide	79	—
Acrylonitrile	76	109
Methyl acrylate	78	—
Methyl methacrylate	54	112
Styrene	70	105
Sulfur, S_8	−19	−31
Tetrafluoroethylene	138.1	112
Vinyl acetate	89	—
Vinyl chloride	108.8	—
Vinylidene chloride	60	106

[a] Data from Ref. 173.

the entropic term becomes significantly larger and finally equals the enthalpic term at the so-called ceiling temperature T_c.

$$T_c = \frac{\Delta H_p}{\Delta S_p} \tag{144}$$

At this temperature the free energy difference is zero and no polymerization process occurs—the system is in equilibrium (423). A few systems are known in which both the enthalpy and the entropy changes of the polymerization reaction are positive. The polymerization of sulfur of the eight-membered ring conformation is one example (424–426): the entropy increases because the S_8 ring is rigid and the ring-opening reaction makes additional conformations available. It follows from equation 143 that in such cases there exists a floor temperature with polymerization possible only above a certain temperature.

The kinetic interpretation of the thermodynamic effects describes the propagation reaction as reversible with a propagation and depropagation step (113,427):

$$R_i^{\cdot} + M \xrightarrow{k_p} R_{i+1}^{\cdot} \tag{145}$$

$$R_{i+1}^{\cdot} \xrightarrow{k_{dp}} R_i^{\cdot} + M \tag{146}$$

The rate coefficient of depropagation is written as k_{dp}. The activation energy of the depropagation reaction, $E_{A,dp}$, is generally much higher than that of the propagation reaction, $E_{A,p}$, the difference being equal to the enthalpy change of

the polymerization reaction:

$$E_{A,p} - E_{A,dp} = \Delta H_p \tag{147}$$

For many typical free radical polymerization systems and conditions, depropagation does not occur to any appreciable extent. However, for some 1,1-disubstituted ethylene monomers, it is possible to polymerize at conditions where the effects of the reverse reaction cannot be neglected. The classical example of such a monomer is α-methylstyrene, with a low ceiling temperature of around 60°C for bulk polymerization, arising from its relatively low heat of polymerization (Table 8), and the equilibrium monomer concentrations are correspondingly high (0.76 mol $\cdot$ L^{-1} at 0°C) (427). Methacrylate and styrene monomers also exhibit depropagation, although at much higher temperatures (220 and 310°C, respectively, for bulk polymerizations). The depropagation process lowers the rate of polymerization according to

$$R_p = k_p[M][R^\bullet] - k_{dp}[R^\bullet] = \left(k_p - \frac{k_{dp}}{[M]}\right)[M][R^\bullet] = k_p^{eff}[M][R^\bullet] \tag{148}$$

The effective rate coefficient of propagation is therefore defined as

$$k_p^{eff} = k_p - \frac{k_{dp}}{[M]} \tag{149}$$

The depropagation effect is inversely proportional to the monomer concentration, because it is part of the thermodynamic equilibrium. The effective propagation rate coefficient can be determined via the PLP–SEC method. Figure 12

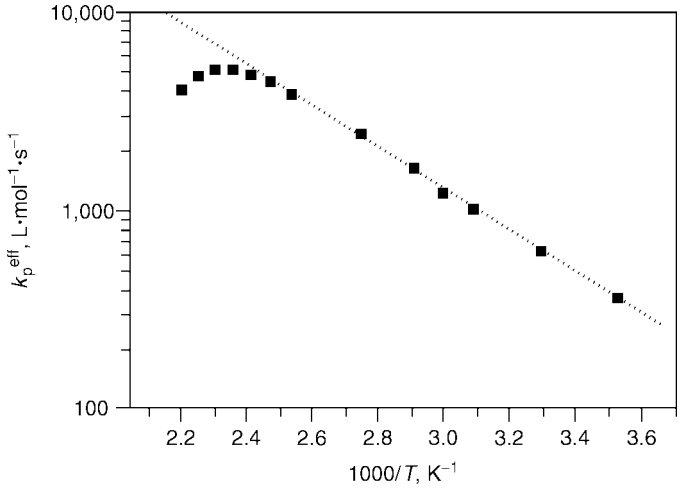

Fig. 12. Temperature dependence of the effective propagation rate coefficient k_p^{eff} observed in the bulk polymerization of dodecyl methacrylate. The data are taken from Ref. 429.

shows the deviation of k_p^{eff} from the linear slope of an Arrhenius plot at higher temperatures, where depropagation becomes important (429).

At the ceiling temperature, the effective rate coefficient becomes zero, that is, k_{dp} equals $k_p[M]$. Using this and equation 147 leads to

$$T_c = \frac{\Delta H_p}{R \ln(A_p/A_{dp}) + R \ln[M]} \tag{150}$$

when introducing Arrhenius relations for k_p and k_{dp} with A_p and A_{dp} being the frequency factors for the propagation and depropagation reactions. Comparison of equations 144 and 150 shows that

$$\Delta S_p = R \ln(A_p/A_{dp}) + R \ln[M] = \Delta S_p^0 + R \ln[M] \tag{151}$$

where ΔS_0^p is the standard entropy change for $[M] = 1 \text{ mol} \cdot L^{-1}$, so that

$$T_c = \frac{\Delta H_p}{\Delta S_p^0 + R \ln[M]} \tag{152}$$

The considerations leading to equation 152 enable the *ceiling temperature* to be defined as the temperature above which no polymerization to high polymers can occur, with monomer at the specified concentration [M]. It should therefore be kept in mind that the ceiling temperature is a function of the monomer concentration. It is determined by thermodynamic parameters and is independent of the mechanism, eg, whether ionic or free-radical. The applicability of the above relations depends on depropagation being the exact reverse of propagation. Hence, the observation of a ceiling temperature requires the presence of active centers. In their absence polymers can exist without change at temperatures well above their ceiling temperatures. When active centers are present there exists an equilibrium concentration of monomer given by equation 152. The introduction of active centers, eg, via UV radiation and/or high temperatures, and subsequent depropagation is one pathway for the degradation of polymers. By adding stabilizers these radicals can be trapped and the depropagation may hence be suppressed.

With many monomers the equilibrium monomer concentrations at ambient temperatures are too small to be measured directly since the ceiling temperatures are relatively high. However, they may be obtained via extrapolation (430). Some of the deviations from simple kinetic behavior at high temperatures recorded in the older literature can be explained by the occurrence of depropagation. Use of the effective monomer concentration, defined as the total concentration minus the equilibrium concentration, removes the discrepancies.

The thermodynamic definition of the equilibrium constant K reads

$$\Delta G_p = -RT \ln K \tag{153}$$

whereas the kinetic expression for K is the ratio of the rate coefficients of the forward reaction to the rate coefficient of the backward reaction. This can be set equal to the thermodynamically definition of K (eq. 153). If the degree of polymerization

is very large, the concentrations of growing chains i and $i + 1$ can be considered nearly identical, which leads to

$$K = \frac{\overrightarrow{k}}{\overleftarrow{k}} = \frac{k_p}{k_{dp}} = \frac{[R_{i+1}^{\bullet}]}{[R_i^{\bullet}][M]_e} \approx \frac{1}{[M]_e} \tag{154}$$

where $[M]_e$ is the equilibrium monomer concentration (eg, 10^{-6} mol$^{-1} \cdot$ L^{-1} for styrene at 25°C). By combining equations 149 and 154 it can be seen that when the monomer concentration equals the equilibrium monomer concentration, the effective propagation rate coefficient k_p^{eff} becomes zero, which is the definition for the ceiling temperature. This implies that there exists a specific ceiling temperature for every given monomer concentration. The maximum ceiling temperature is reached for the bulk polymerization system. It has been recently demonstrated that effective molecular weight control in copolymerizations may be achieved by the judicious selection of monomers which display a low ceiling temperature (431).

Equilibrium concentrations and ceiling temperatures are additionally influenced by the pressure. According to the Clausius–Clapeyron equation, a change in the molar volume change $\Delta V_c = V_p - V_m$ at the ceiling temperature generally leads to

$$\frac{dT_c}{dp} = T_c \frac{\Delta V_c}{\Delta H_p} \tag{155}$$

The polymer usually has the smaller molar volume with respect to monomer units, ΔV being therefore negative, eg, -14.7 cm$^3 \cdot$ mol^{-1} for α-methylstyrene (432). This leads, together with a negative reaction enthalpy, to a positive pressure dependence of the ceiling temperature. The T_c value, for instance, of α-methylstyrene rises from 60°C at 0.1 MPa (1 bar) over 131°C at 421 MPa to 171°C at 648 MPa. With increasing pressure, however, the melting points of the monomers are also raised, and polymerizations of crystalline monomers are far from being easy.

Inhibition and Retardation

Since the polymerization reaction should proceed under controlled reaction conditions it is undesirable that polymerization activity is induced during the monomer preparation, storage, or purification. However, premature radical formation from the pure monomer and from impurities or contaminants can easily lead to unwanted polymerization. If a substance can quantitatively scavenge these initiating radicals the propagation reaction is effectively suppressed (167,433). When this scavenger compound is consumed by reaction with the generated radicals, the polymerization proceeds with the same rate as without any additives. These additives are consequently denoted as *inhibitors*. The *inhibition period*, ie the time span that is necessary for the complete consumption of the scavenger molecules, is often measured to calculate the initiation rate (see Figure 13**b**). A *retarder* is a substance that

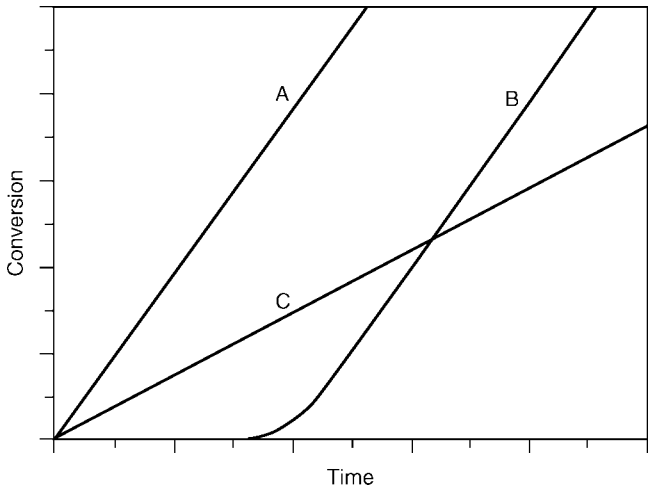

Fig. 13. Typical conversion versus time profiles for conventional free radical polymerization (A) with addition of inhibitor (B) and retarder (C).

decreases the overall polymerization rate without any induction period, and is not completely consumed throughout the polymerization (see Figure 13**c**). The distinction between inhibition and retardation is not always clear. However, both effects are based on the concept of effectively preventing the generated radicals from initiating polymerization. Two general cases can be identified:

(1) The scavenger molecule reacts with the initiator-derived—or very small polymeric—radical to form a relatively stable radical that by itself is not capable of initiating polymerization. However, this radical may be active toward other radicals in the system and may hence terminate irreversibly or reversibly via radical–radical reactions.
(2) The scavenger molecule is by itself a radical and reacts with any other radicals in the system to generate nonreactive products. Because of the stability of the radical compounds employed for such inhibition/retardation reactions, the generated bond is very weak and may homolytically cleave at elevated temperatures to give back the radical reactants. This reaction behavior is exploited in the living free radical polymerization technique using nitroxides as mediators (434,435).

Stable free radicals are frequently employed as inhibitors (436,437). The most commonly used species are nitroxides, eg, 2,2,6,6-tetramethylpiperidine-1-oxyl (TEMPO) **18**. They are far too stable to be able to initiate polymerization, but they are reactive enough to undergo reaction with other free radicals (438). Nitroxides are very efficient inhibitors, being capable of producing induction periods when present in concentrations of less than 10^{-4} mol $\cdot$ L^{-1}. Nitroxides, such as TEMPO, react with carbon-centered radicals at close to diffusion controlled reaction rates (439–441). The stoichiometry between the number of the chains

terminated and the number of the nitroxide molecules consumed is 1:1, making these compounds very useful for quantitative measurements of free radical concentrations (81,82,442). The coupling process of the nitroxide with the propagating radical is reversible, especially at elevated temperatures. This equilibrium enables a living free radical polymerization by capping the reactive chain ends. The free radical concentration is therefore extremely decreased, suppressing the termination process. Temporarily uncapped free radicals are adding monomers, leading to a very slow, but controlled polymerization process (435,443,444). Recent review articles on nitroxide-mediated living free radical polymerization are References 434 and 445.

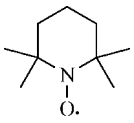

18

Another commonly used stable radical is 1,3,5-triphenylverdazyl **19** (446, 447). It is less thermally stable than TEMPO. Both TEMPO and the verdazyl radical do not react with oxygen-centered radicals or oxygen. If an initiator generates an oxygen-centered radical the nitroxide will capture the carbon-centered radical that is generated via the first addition step involving a monomer. Galvinoxyl **20** and 1,3-bisdiphenylene-2-phenylallyl (or Koelsch's) radical **21** can also be used as inhibitors. Diphenylpicrylhydrazyl **22** is used much less frequently because of its complicated reaction mode of inhibition (448).

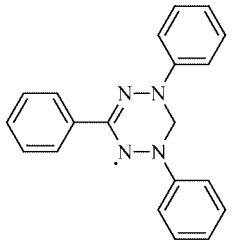

19

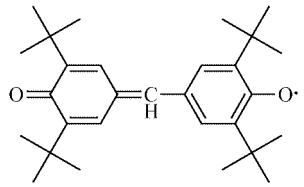

20

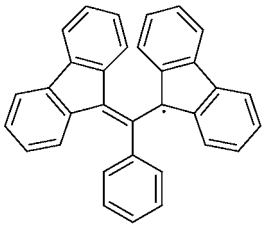

21

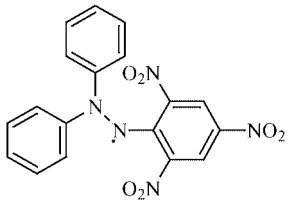

22

The overall polymerization rate decreases with increasing concentration of retarder. An induction period as with inhibitors is not observed. The rate retarding

reactions can be considered very similar to the inhibition reactions; however, the reactivity of retarding agents toward radicals present in the polymerization mixture is smaller than that of inhibitors, and the compounds are therefore consumed slower, not depleting during the polymerization. Some retarder-derived radicals may even reinitiate the polymerization slowly—therefore constituting a comonomer—again leading to decreased polymerization rates. This slow reinitiation rate of the retarder-derived radicals effectively increases their concentration in the polymerization mixture, hence leading to an increased probability of termination reactions and other side reactions. In some cases it is very difficult to completely identify the real reason for rate retardation, because of the coupled nature of all the different reactions involved.

The most common retarders—denoted as *stabilizers*, because of their application in stabilizing monomers during their storage—are substituted phenols (eg, *p*-methoxyphenol, 2,6-di-*tert*-butyl-4-methyl phenol, used as stabilizer for styrene) (449). They readily undergo subtraction of the weakly bonded phenolic hydrogen to yield low reactive phenoxy radicals. The retardation ability of these compounds is strongly dependent on the type of monomers, since the phenoxy radicals may add on to monomer molecules with very different rates, hence acting as a transfer agent with a slow reinitiation rate. Phenols react slowly with electrophilic radicals and essentially do not inhibit polymerization of acrylates and methacrylates in the absence of oxygen (450,451).

Benzoquinone, which also may be employed as retarder (used as stabilizer for methyl methacrylate), gives a phenoxy radical as a result of a rapid addition of the radicals present in the system to the C=O double bond. The addition is facilitated by aromatic stabilization (452–454). The relative reactivities of alkyl- and methoxy-substituted benzoquinones have been correlated to their redox potentials and steric factors of the substituents (455,456). Industrially, hydroquinone is often added to monomers, although hydroquinone itself acts neither as an inhibitor nor as a retarding agent. However, if oxygen or peroxides are present in the system, the hydroquinone will be oxidized to quinone. Hydoquinone therefore acts in two ways: it reduces the peroxides that may initiate the polymerization and acts as an inhibitor in its oxidized quinone form.

A further important class of retarders, generally less effective than quinones, are the aromatic nitro compounds. They show very different effectiveness toward the retardation of different monomer types: the polymerization of vinyl acetate is inhibited, the styrene polymerization is retarded, but there is nearly no influence on the polymerization rate of acrylates and methacrylates. The effectiveness, however, increases with the number of nitro groups per molecule.

Transition metal [eg, Fe(III), Cu(II), Ce(IV), Hg(II), and Ag(I)] salts such as halides or pseudohalides are also employed as inhibitors (457). The reaction mechanism involves the effective electron transfer (redox process) or a ligand transfer mechanism. The carbon carrying the unpaired electron is converted to a σ-bonded carbon or ionic species. In nonaqueous systems the most used retarder is iron(III) chloride which shows no reinitiation abilities, hence being considered as an ideal inhibitor or retarder (205). The Fe(III) is reduced to Fe(II) during the reaction. This Fe(II) formation can be monitored by UV/vis spectroscopy to investigate the reaction rate. Equation 156 shows the reaction scheme for the retarding reaction involving ferric chloride.

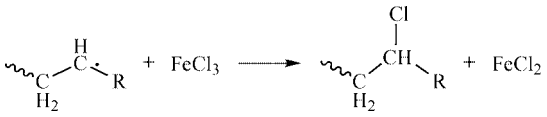

(156)

$CuCl_2$ is an even more powerful inhibitor/transfer agent than $FeCl_3$. It reacts with growing polystyrene radicals 20 times faster ($C = 10{,}000$ vs 500) and with poly(methyl methacrylate) radicals 50 times faster ($C = 2000$ vs 4) (458). In the presence of a suitable ligand the resulting alkyl halides can react reversibly with Cu(I) species and establish an atom transfer equilibrium, which is at the essence of ATRP.

One of the most well-known retarders of free radical polymerization is molecular oxygen (459,460). Because of the diradical character of oxygen it reacts readily with carbon-centered radicals present in the polymerization system via an addition process to yield peroxy radicals. These peroxy radicals may reinitiate the polymerization, effectively incorporating the molecular oxygen into the polymeric chain, so that oxygen is a potential comonomer. In many cases the reinitiation reaction is slower than the propagation and oxygen acts as a retarder. The generated polyperoxides may act subsequently as initiator (461–463). Consequently, the kinetics of polymerizations performed in presence of oxygen may be complex.

Interestingly, the polymerization rates of vinyl esters are remarkably retarded by small amounts of styrene. The highly reactive vinyl ester radicals readily react with the activated styrene monomer, which results in a relatively stable benzyl-type styrene radical. The vinyl ester monomer molecule is not activated enough for the addition of the styrene radicals and the reaction ceases (464).

Buckminsterfullerene (C_{60}) has attracted much interest, not only because of its structure and physical properties, but also because of its reaction behavior in radical polymerization systems. C_{60} reacts rapidly with radicals to yield ESR-detectable radical species $C_{60}^{\bullet}$ (465). C_{60} was found to act as an effective inhibitor in vinyl acetate polymerization and all consumed C_{60} molecules were incorporated into the polymeric chains during the polymerization. The relation between the induction period and the initiation rate revealed that one C_{60} molecule can trap 15 radicals (466). The rate of polymerization of styrene and methyl methacrylate is also significantly retarded in the presence of C_{60} (467–471). The average number of C_{60} molecules incorporated in the polymer chains increases when increasing the C_{60} concentration, maybe because of coupling of polymer–$C_{60}^{\bullet}$ to give polymer–C_{60}–C_{60}–polymer (472).

The kinetics of the retardation effect for a stationary polymerization can be analyzed by adding an additional reaction to the basic scheme of polymerization, including initiation, propagation, and termination (473,474).

$$R_i^{\cdot} + Q \xrightarrow{k_Q} P_i + Q^{\cdot} \tag{157}$$

where Q is the retarder or inhibitor and k_Q is the rate coefficient of the retardation reaction.

The kinetics is simplified by assuming that the generated radical $Q^{\bullet}$ does neither reinitiate nor show any transfer behavior. The steady-state assumption—which is only a very rough approximation until all inhibitor is consumed (475)—can now be written as

$$-\frac{d[R^{\bullet}]}{dt} = R_i - 2k_t[R^{\bullet}]^2 - k_Q[R^{\bullet}][Q] = 0 \tag{158}$$

which yields in combination with equation 55 (again assuming that the rate of the loss of monomer, $-d[M]/dt$, equals the rate of polymerization, R_p)

$$R_i - \frac{2k_t R_p^2}{k_p^2[M]^2} - \frac{k_Q R_p[Q]}{k_p[M]} = 0 \tag{159}$$

The ratio of the rate coefficients for retardation, k_Q, and propagation, k_p, is often referred to as the inhibition constant, $z = k_Q/k_p$, which reflects the ability of a molecule to cause inhibition. Table 9 gives selected values for the inhibitor constants of some inhibitors in conjunction with a specific monomer.

If the inhibition constant is large ($z \gg 1$), the second term of the l.h.s. of equation 159 will become much smaller than the third one. In this case, the rate of inhibition is much larger than the rate of termination. Equation 159 then reads

$$R_p = \frac{k_p[M]R_i}{k_Q[Q]} \tag{160}$$

Table 9. Inhibition Constants *z* of Various Inhibitors to Selected Monomers at 50°C[a]

Inhibitor	Monomer	*z*
Nitrobenzene	Methyl acrylate	0.00464
	Styrene	0.326
	Vinyl acetate	11.2
1,3,5-Trinitrobenzene	Methyl acrylate	0.204
	Styrene	64.2
	Vinyl acetate	404
Chloranil	Methyl methacrylate (44°C)	0.26
	Styrene	2,040
Oxygen	Methyl methacrylate	33,000
	Styrene	14,600
Phenol	Methyl acrylate	0.0002
	Vinyl acetate	0.012
TEMPO	Styrene	335,712
$CuCl_2$	Styrene	10,000
	Methyl methacrylate	2,000
$FeCl_3$	Styrene	536
	Methyl methacrylate	4

[a] Data from Ref. 173.

Equation 160 shows that the polymerization rate is inversely proportional to the inhibitor concentration. It should be kept in mind that the inhibitor concentration will decrease during the reaction. Each free radical generated by the initiation process will consume one inhibitor molecule. If the inhibitor concentration finally becomes sufficiently low, propagation can become competitive with the inhibition reaction.

Dividing the rate law for the loss of inhibitor, $-\mathrm{d[Q]}/\mathrm{d}t, = k_\mathrm{Q}[\mathrm{R}^\bullet][\mathrm{Q}]$, by the rate law of propagation, $-\mathrm{d[M]}/\mathrm{d}t, = k_\mathrm{p}[\mathrm{R}^\bullet][\mathrm{M}]$, leads to

$$\frac{\mathrm{d[Q]}}{\mathrm{d[M]}} = \frac{z[\mathrm{Q}]}{[\mathrm{M}]} \tag{161}$$

and subsequent integration with $[\mathrm{Q}]_0$ and $[\mathrm{M}]_0$ being the concentration of inhibitor and monomer at the beginning of the reaction.

$$\ln\left(\frac{[\mathrm{Q}]}{[\mathrm{Q}]_0}\right) = z \ln\left(\frac{[\mathrm{M}]}{[\mathrm{M}]_0}\right) \tag{162}$$

It is apparent from equation 162 that if z is large, the monomer conversion remains nearly zero until the inhibitor is consumed.

Experimental Methods

The aim of most kinetic experimental methods has always been to determine accurate values for the individual rate coefficients that govern the free radical polymerization process, especially k_t, k_p, and k_tr. Up to the late 1980s termination and propagation rate coefficients were accessible only in their coupled form, $k_\mathrm{p}/k_\mathrm{t}^{0.5}$, or individually via combination with pseudo flickering techniques like the rotating sector or spatially intermittent polymerization methods in combination with stationary polymerization measurements. The only exception has been the direct determination of the propagation rate coefficient via the measurement of the steady-state free radical concentration by ESR experiments in combination with rate measurements. However, the detection of such low free radical concentrations (typically close to 10^{-8} mol $\cdot$ L^{-1}) has always been subject to large uncertainties, leading to a large scatter in the values for the rate coefficients. The situation has dramatically improved with the invention of the PLP technique in the late 1980s. Since then, this technique (and its spin-offs like SP–PLP) has been extensively used to collate propagation and termination rate coefficients for various homo- and copolymerizations. Today, the PLP method is almost exclusively used to determine propagation and termination rate coefficients and has been recommended by the IUPAC for the measurement of propagation rate coefficients. In contrast, the methods available for the determination of the chain transfer rate coefficient have not changed significantly over the last decades. It should, however, be mentioned that the interpretation of the transfer controlled molecular weight distributions generated in stationary free radical polymerizations has been somewhat refined with the introduction of the Clay–Gilbert method.

Methods for the Measurement of k_d.

Direct Measurement of the Initiator Concentration as a Function of Time. The rate coefficients of initiator decomposition, k_d, can be assessed by various methods. A straightforward approach is to directly assess the thermal decay of the initiator via the measurement of its concentration as a function of the reaction time by equation 3. The concentration can be measured via any quantity it is directly proportional to, eg, a spectroscopic infrared absorption that can be easily followed with reaction time. The connectivity of the initiator concentration and the intensity of the absorption (at a specific wavelength) is given by Beer–Lambert's law. Infrared spectroscopy has been used extensively in the past to study the decay of organic peroxides in various reaction media (including supercritical CO_2). Organic peroxides are widely used to initiate polymerizations, and knowledge about their rate of decomposition at various temperatures and their mechanism of decomposition are vital for optimizing polymerization processes (476,477).

Dead-End Polymerization. *Dead-end polymerization* refers to a polymerization process where the initiator concentration significantly decreases to a very low value during the polymerization. The measurement of the conversion of monomer to polymer, p, according to such an experiment, allows to determine the rate coefficient of initiator decomposition, k_d, and the calculation of the efficiency factor f.

Dividing equation 59 by equation 60, rearranging, and subsequently taking the logarithms of both sides yields

$$-\ln\left[1-\frac{\ln(1-p)}{\ln(1-p_\infty)}\right]=\frac{k_d t}{2} \tag{163}$$

The value of k_d can now easily be evaluated from a slope of a plot of the l.h.s. of equation 163 against the polymerization time t. If the ratio of $k_p{}^2/k_t$ is known by other studies, a value for the frequency factor f can be estimated by insertion into equation 56 or equation 60.

Methods for the Measurement of k_p.

Pulsed Laser Polymerization–Size Exclusion Chromatography. The careful determination of the chain length distribution of the polymer produced via a pseudostationary pulsed laser experiment allows to obtain accurate values for the propagation rate coefficient k_p. The polymerizable system—containing monomer and photoinitiator, occasionally solvent and transfer agents—is irradiated by a pulsed laser beam and the chain length distribution formed is subsequently analyzed by SEC. The determination of the additional peaks and its points of inflection on the low molecular side, respectively, gives a value for $L_{0,n}$ which can easily be inserted into equation 123.

$$L_{0,n}=nk_p[\mathrm{M}]t_0 \tag{123}$$

The propagation rate coefficient k_p is now available because the monomer concentration [M] and the time interval between laser pulses, t_0, are known. This method has developed into the IUPAC recommended method for k_p determination (398,478,479).

Prior to the PLP experiment the monomer should be purified to remove the stabilizer, which is added to most of the commercially available monomers. This can be achieved by either distillation or column chromatography. Both methods have different advantages: distillation removes small amounts of polymer dissolved in the monomer, but many inhibitors are very volatile and distillation does not completely remove them. However, PLP experiments without cleaning the monomer were reported and have shown the robustness of this method. Photoinitiators are added in typical concentrations of millimoles per liter. Degassing the samples by a number of freeze–pump–thaw cycles on a high vacuum line or purging with inert gases like nitrogen or argon makes sure that the dissolved oxygen, which disturbs the kinetic measurements by an inhibition effect, is removed.

For a successful PLP experiment, care must be taken to ensure a homogeneous intensity profile over the whole optical cross section of the reaction cell so as to produce homogenous reaction conditions. In addition, absorption of the laser light by initiator and monomer molecules should be accounted for. Accurate temperature control is necessary to dissipate the heat of reaction and any possible temperature increase induced by absorbed laser energy. Typical laser sources are pulsed Nd/YAG solid-state lasers (355 or 532 nm) or XeF excimer lasers (351 nm) with a pulse energy up to 80 mJ per pulse and a pulse width of 5–20 ns. Laser repetition rates between 100 and 0.1 Hz have been used in the past. The value of ρ (ie the free radical concentration generated by each laser pulse) can be varied by the initiator concentration and the laser pulse energy. Samples are exposed to pulsed laser irradiation to allow for a maximum conversion of monomer to polymer of about 1–3%, with typical pulsing times between 1 min and 5 h.

It should be noted that a pulsed lamp or even a rotating sector in combination with a continuous lamp as a pulsed radiation source leads to well-structured molecular weight distributions, allowing for the determination of k_p. However, optimum results are obtained by the use of a pulsed laser.

After the monomer solution has been irradiated, the produced polymer is analyzed by a SEC system, which is calibrated by narrow polymer standards or by absolute molecular weight detection methods. The values of $L_{0,n}$ can easily be determined by differentiating the chain length distribution. The use of different types of distributions (size exclusion, mass, or number distribution) leads to slightly different values for k_p. Figure 14 shows a typically data sheet for styrene bulk polymerization. It should be noted that the obtained k_p value is slightly dependent on the type of molecular weight distribution (ie size exclusions, weight, or number distribution) that is used for the data analysis (480).

Electron Spin Resonance Spectroscopy—Stationary Polymerization. The experimental determination of k_p data usually proceeds via the IUPAC recommended PLP–SEC procedure (see above). However, under certain circumstances, k_p data are also available by direct determination of the concentration of propagating free radicals via ESR spectroscopy, accompanied by the measurement of the overall polymerization rate (481) (see ELECTRON SPIN RESONANCE). The calculation of k_p then proceeds via either the differential (eq. 55) or the integrated form of the propagation rate law expression:

$$\ln\frac{[M]_1}{[M]_2} = k_p[R^\bullet](t_1 - t_2) \tag{164}$$

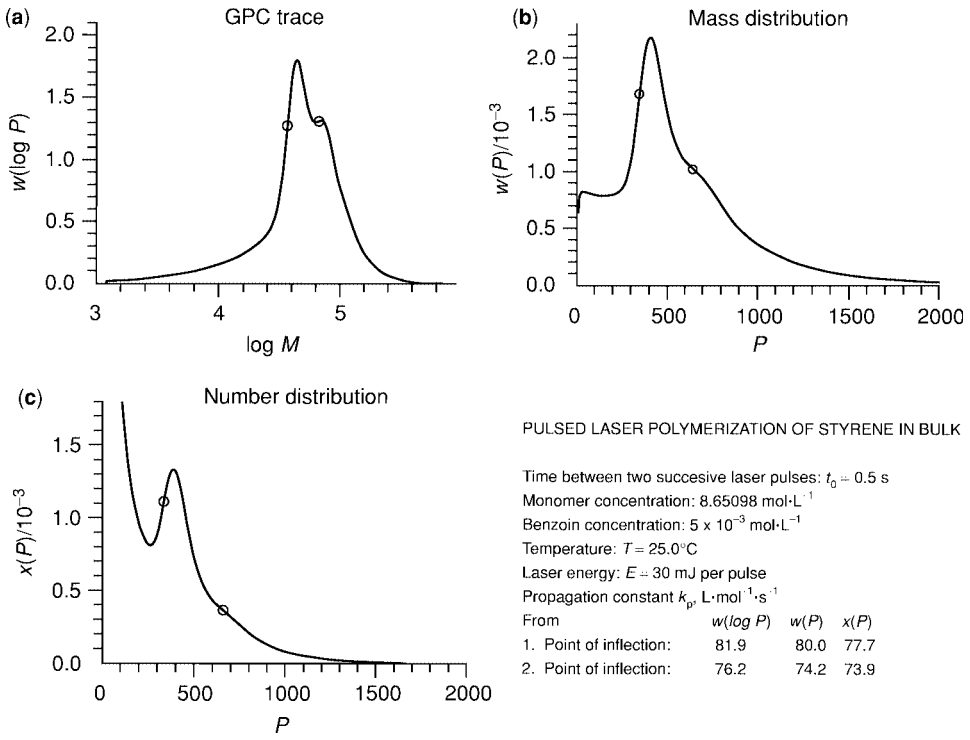

Fig. 14. Typical data sheet detailing the outcome of a successful PLP–SEC experiment for a styrene bulk polymerization at 25°C.

where $[M]_1$ and $[M]_2$ are the monomer concentrations at the reaction times t_1 and t_2, respectively. The determination of the monomer conversion at various reaction times can proceed via independent experiments (under the same experimental conditions as the ESR measurements) using, eg, NMR spectroscopy, infrared spectroscopy, gravimetry, or chromatographic methods.

Inspection of the existing literature indicates that k_p values derived from ESR are in poor agreement with k_p data from PLP–SEC measurement (482–485). Only a few recent studies indicate a somewhat better agreement (117,120), which is partly due to a significant increase in the quality of the ESR signals by using optimized ESR cavities and spectrometers (482). The studies indicating better agreement seem to have been carried out under specific experimental conditions, allowing for a reliable measurement of the long chain limit of the propagation rate coefficient. These studies indicate that particular attention needs to be paid to the size of the steady-state free radical concentration, which should be in an intermediate range. The type of initiator also seems to be important as is the fact that the only free radical in the system is the propagating species. This point is of special importance in photochemically induced polymerizations where, in addition to the photoinitiator, the monomer may also be excited. Additionally, the experimental conditions must be such that the majority of propagating radicals are of sufficiently large size to avoid determination of untypically high propagation rate coefficients,

which are known to occur with free radicals of short chain length. Because of this limitation, studies into higher k_p monomers may be advantageous (unless polymerization rates become too fast to precisely determine monomer conversion vs time profiles). Moreover, it should be checked that high molecular weight material is indeed produced. A specific problem of ESR spectroscopy is the calibration of the spectrometer. Usually, calibration proceeds via the measurement of the signal of a known concentration of a stable radical (eg TEMPO) in the same medium as the polymerization is carried out. The calibration may be the most serious drawback of the ESR method for k_p determination, since (*1*) it is very likely that the two different radicals, ie the radical used for calibration purposes and the propagating radical, are not comparable in terms of their detector signal, and (*2*) the calibration is—strictly speaking—only valid for the hypothetical case of 0% conversion and is immediately invalidated as the polymerization process changes the bulk viscosity of the reaction medium. It should also be noted that—similar to the PLP–SEC technique—only the product of the propagation rate coefficient and the monomer concentration is the measured quantity. Up to this date, no technique exists that allows the direct measurement of k_p.

Because these problems, the ESR technique remains problematic for the reliable determination of propagation rate coefficients and may only be applicable in very specific cases. However, the ESR technique also has the indisputable advantage of actually probing the propagating radicals directly and—in contrast to the PLP–SEC method—does not rely on the interpretation of secondary data material such as a molecular weight distribution. Valuable insight into the polymerization process, particularly at high conversions, has been deduced from ESR spectra recorded at different monomer conversions.

It should be briefly mentioned that the ESR technique may (via equation 65) also be applied toward the measurement of termination rate coefficients. There are several publications reporting on the k_t measurements via ESR. However, these measurements are associated with same problems as the k_p determinations (see for example References 161,486,487).

Quenched Instationary Polymerization Systems. Quenched instationary polymerization systems (QUIPS) (488,489) are characterized by the complete deactivation of all radicals by reaction with an inhibitor after a certain time. A photopolymerizable mixture passes through a capillary system, is irradiated at a specific location, and polymerizes in the capillary during a well-defined dark period until it drops into a quenching bath. The parameters determining the type of QUIPS are the duration of the initiation period (t_L) and an eventual following dark period (t_D). The method is based on the intentional limitation of the maximum active chain length $L_{act,max}$ the radicals can achieve. For this purpose all radicals present at a certain time in the system are deactivated by reaction with an inhibitor. Therefore, the kinetic scheme for the free radical polymerization is extended by the quench reaction with the rate constant k_q. A number of stable free radicals are known which fulfill the conditions of an extremely fast and efficient quench reaction (for instance nitroxyl radicals below 100°C). It is essential that the products of the quench reaction are stable and are not mediators for consecutive reactions. Experimental conditions can be chosen to ensure that the quench reaction is complete within the time span necessary for an ordinary propagation step, namely $1/(k_p[M])$. Under these conditions the radical spectrum present at

the beginning of (the short) quench period is immediately converted into inactive products.

Measuring the chain length distribution by SEC reveals a structured shape which allows to determine k_p in accordance to the same equation 123 used in PLP–SEC, which relates the active lifetime of a growing macroradical with its maximum active chain length. Recently, Vana and co-workers (135) modified the QUIPS technique in an attempt to make it applicable to hindered monomer systems. The original QUIPS method was changed into a batch operation; ie, a multipulse sequence of laser pulses was applied to the reaction mixture to effect a high primary radical concentration. Subsequently, the reaction mixture was quenched after a quenching time, t_q, by rapid mixing with an inhibitor containing solution. The propagation rate coefficient (at varying temperatures) can be assessed via the maximum of the formed polymer distribution, L_{max}. In addition, the multipulse quenched instationary polymerization also allows for easy access to termination rate coefficients k_t. The novel strategy has so far been successfully applied to the hindered monomer dicyclohexyl itaconate.

Methods for the Measurement of k_{tr}. The evaluation procedures and theoretical basis for the determination of transfer coefficients C have been extended and perfected over the past decade and a great number of transfer coefficients have been determined by various research groups [see for example References 490 and 491 or the multiple entries in the *Polymer Handbook* (492)]. The transfer coefficient is defined by equation 90 as the ratio of the transfer rate coefficient k_{tr} to the propagation rate coefficient k_p.

$$C = \frac{k_{tr}}{k_p} \tag{165}$$

The classical procedure for transfer coefficient measurement (to the monomer itself, any other added substance, or deliberately added transfer agent, such as a thiol or a catalytic chain transfer agent) has always been the Mayo method (493). However, Gilbert and co-workers recently introduced the chain length distribution (CLD) method (494) as an alternative way to determine transfer coefficients. The Mayo and CLD methods in themselves also provide different choices of data analysis. Both methods have been carefully compared and thoroughly discussed with the conclusion that both are theoretically equivalent (201).

In terms of applied experimental procedures, there are only two conceptually different methods available. The first one is the conventional or classical polymerization via thermal polymerization experiments, with specific amounts of thermally decaying initiator being present in the reaction mixture. Various groups have used this technique to determine transfer coefficients, as the impressive collection of data in Reference 492 indicates. Kukulj and co-workers (178), for example, investigated the transfer-to-monomer constant of methyl methacrylate, styrene, and α-methylstyrene at 50°C using thermal polymerization. To generate a sufficiently low radical flux to achieve transfer-dominated reaction conditions, the stock solution of the initiator in monomer is successively diluted. This gives a series of solutions with decreasing initiator concentrations, yielding increasing molecular weights upon polymerization. In many cases and when the initiator

concentrations are chosen correctly, a limiting molecular weight is reached which may then be used to determine the transfer to monomer constant via either the Mayo or the CLD method.

A second and more recent experimental technique became possible with the advent of pulsed laser systems: PLP in combination with subsequent SEC of the resulting polymer is the standard and IUPAC recommended technique for the determination of propagation rate coefficients k_p (398). However, several research groups have used PLP to determine transfer rate constants to a range of chain-transfer agents. For example, Hutchinson and co-workers (495) determined the transfer coefficients for transfer to *n*-dodecyl mercaptan in methyl methacrylate, styrene, ethyl methacrylate, and butyl methacrylate homopolymerizations in the temperature range between 20 and 80°C. By adding sufficient transfer agent, these authors were able to generate transfer-dominated conditions, as seen by the loss of the PLP characteristics in the molecular weight distributions obtained by SEC analysis of the polymers. In addition, Buback and co-workers (496) designed a method to determine the value of the propagation rate coefficient k_p and the transfer-to-monomer rate coefficient k_{tr}^M from a single PLP experiment. Packages of high frequency pulses separated with long dark time intervals give rise to two polymer distributions. This procedure has been termed the 'rail-road' experiment, because of the characteristic pulse profile of the light source that resembles the sound patterns generated by a moving train. The polymer produced during the high frequency pulse packages may be used to determine k_p, while the polymer produced in the longer dark time may be used to determine C_M (413,496).

PLP, however, is normally not the method of choice for measuring transfer-to-monomer rate coefficients via the CLD method, because the CLD method requires termination to be an unimportant or even absent route of radical chain stoppage as compared to transfer to monomer. In addition, the CLD method is, like the Mayo method, derived for steady-state polymerizations. Moreover, the radical flux must be low enough so that transfer, rather than termination, is the main chain-stopping event, so that the polymerization is truly transfer dominated. PLP is essentially used as a flickering termination rate technique, ie as a technique that makes essential use of effective termination. PLP, can however, be made applicable for studying even transfer to monomer, if combined with a rotating reactor/cuvette assembly (179). This assembly permits time efficient experiments with very long pulse periods and thus enables high molecular weight material to be produced at very low radical concentrations or termination rates, respectively. The rotating reactor/cuvette allows for acceptable polymerization rates even for slowly propagating monomers such as styrene.

The mathematical methods used to analyze molecular weight distributions generated in transfer-controlled free radical polymerization experiments, ie the Mayo and CLD methods, are discussed below.

The Mayo Method. The overall chain transfer coefficient C is defined as the ratio of the chain transfer and propagation rate coefficients, k_{tr}/k_p. For example, C_T is the ratio of the rate coefficient for chain transfer to the chain transfer agent T, and the rate coefficient for propagation. It is a measure for the reactivity of a chain transfer agent. The higher the value of C_T, the lower the concentration of the chain transfer agent required for a particular molecular weight reduction. This effect on the molecular weight of the polymer is quantitatively described by

the Mayo equation 91, which expresses the reciprocal of $\bar{P}_n$, the number-average degree of polymerization, as a function of the rates of chain growths and chain-stopping events. Neglecting chain transfer to solvent, initiator, and polymer—this assumption is nearly fulfilled in bulk polymerizations at low overall monomer conversions—equation 91 reads after insertion of equation 45.

$$\frac{1}{\bar{P}_n} = \frac{(1+\delta)k_t}{k_p^2[M]^2}R_p + C_M + C_T\frac{[T]}{[M]} \tag{166}$$

The usual procedure for measuring the chain transfer coefficient C_T—henceforth referred to as the Mayo procedure—involves the determination of the average degree of polymerization for a range of [T]/[M] values and plotting the data as $(\bar{P}_n)^{-1}$ vs [T]/[M], ie, a so-called Mayo plot. The value of C_T is then determined as the straight-line slope of this plot. This procedure assumes that the intercept is independent of the variation of [T]/[M]. However, the chain-length-dependent termination rate coefficient implies that the first term on the r.h.s. of equation 166 is in general not a constant, and therefore a Mayo plot is not necessarily linear. This is a principal weakness of the Mayo method. However, in practice, this effect does not seem to be significant, which suggests that in systems with added chain transfer agent, the first term on the r.h.s. of equation 166 generally makes a negligible contribution to $(\bar{P}_n)^{-1}$.

CLD Method. The transfer process shifts the chain length distribution generated by the polymerization process to lower molecular weights. The Mayo method, described above, relies on the accurate determination of the number-average degree of polymerization, $\bar{P}_n$. Especially if the chain length distribution shows considerable amounts of low molecular weight material, the application of the Mayo method is problematic. In the cases when SEC is chosen to measure the number-average degree of polymerization, $\bar{P}_n$, baseline errors in the low molecular weight region show a significant influence on its value.

To overcome this problem, Gilbert and co-workers introduced a method which puts more emphasis on the high molecular weight region of the polymer chain length distribution (497).

The general rate law for the polymerization process reads

$$\frac{d[R_i^\bullet]}{dt} = k_p[M][R_{i-1}^\bullet] - \left(k_p[M] + k_{tr}^M[M] + k_{tr}^T[T] + 2\sum_{j=1}^{\infty}k_t^{i,j}[R_j^\bullet]\right)[R_i^\bullet] \tag{167}$$

Introducing the steady-state principle, $d[R^\bullet]/dt = 0$, yields an recursive expression for the concentration of macroradicals with chain length i.

$$[R_i^\bullet] = \left(1 + \frac{k_{tr}^M[M] + k_{tr}^T[T] + 2\sum_{j=1}^{\infty}k_t^{i,j}[R_j^\bullet]}{k_p[M]}\right)^{-1}[R_{i-1}^\bullet] \tag{168}$$

A repeated substitution leads to an expression of this free radical concentration as a function of the concentration of radicals being composed of one monomeric unit, $[R_1^\bullet]$.

$$[R_i^\bullet] = \left(1 + \frac{k_{tr}^M[M] + k_{tr}^T[T] + 2\sum_{j=1}^{\infty} k_t^{i,j}[R_j^\bullet]}{k_p[M]}\right)^{1-i} [R_1^\bullet] \tag{169}$$

The rate law for radicals of chain length one, $[R_1^\bullet]$, combines the rate of formation of these radicals via the initiation process, R_i, the rate of their formation by transfer, and the rate of their loss by propagation, transfer, and termination events.

$$\frac{d[R_1^\bullet]}{dt} = R_i + \left(k_{tr}^M[M] + k_{tr}^T[T]\right)\mu_0 - \left(k_p[M] + k_{tr}^T[T] + 2\sum_{j=1}^{\infty} k_t^{i,j}[R_j^\bullet]\right)[R_1^\bullet] \tag{170}$$

where $\mu_0 \equiv \sum_{i=1}^{\infty} [R_i^\bullet]$ is the overall free radical concentration.

Introducing the steady-state assumption and inserting equation 170 into equation 169 leads to

$$[R_i^\bullet] = \left(\frac{R_i + k_{tr}^M[M]\mu_0 + k_{tr}^T[T]\mu_0}{k_p[M]}\right)\left(1 + \frac{k_{tr}^M[M] + k_{tr}^T[T] + 2\sum_{j=1}^{\infty} k_t^{i,j}[R_j^\bullet]}{k_p[M]}\right)^{-i} \tag{171}$$

If transfer and termination events are much less probable than propagation, ie $k_{tr} \ll k_p$, and $2\sum_{j=1}^{\infty} k_t^{i,j}[R_j^\bullet] \ll k_p[M]$, the r.h.s. of equation 171 can be rewritten as a progression with only two terms, using $e^x \cong 1 + x$,

$$[R_i^\bullet] \propto \exp\left(-\frac{k_{tr}^M[M] + k_{tr}^T[T] + 2\sum_{j=1}^{\infty} k_t^{i,j}[R_i^\bullet]}{k_p[M]} i\right) \tag{172}$$

For transfer-dominated systems the shape of the polymer distribution is the same as that of the free radical distribution, $[R_i^\bullet] \sim [P_P]$, keeping in mind that the chain length i equals the degree of polymerization, P. It turns out that this situation is in fact more general: Clay and Gilbert (497) have shown that for partly termination controlled distributions also, the following equation holds true, in which the slope of the logarithmic number distribution ($x_p \equiv [P_p]/\sum_{P=0}^{\infty}[P_P]$) is correlated with the kinetic parameters:

$$\frac{d\ \ln x_P}{dP} = -\frac{k_{tr}^M[M] + k_{tr}^T[T] + 2\sum_{j=1}^{\infty} k_t^{i,j}[R_j^\bullet]}{k_p[M]} \tag{173}$$

Equation 173 indicates that a semilogarithmic number distribution should be linear, as can be seen in Figure 15.

A plot of the slopes of semilogarithmic number distributions, $d\ \ln\ x_P/dP$, against the ratio of the transfer agent-to-monomer concentration, [T]/[M], allows

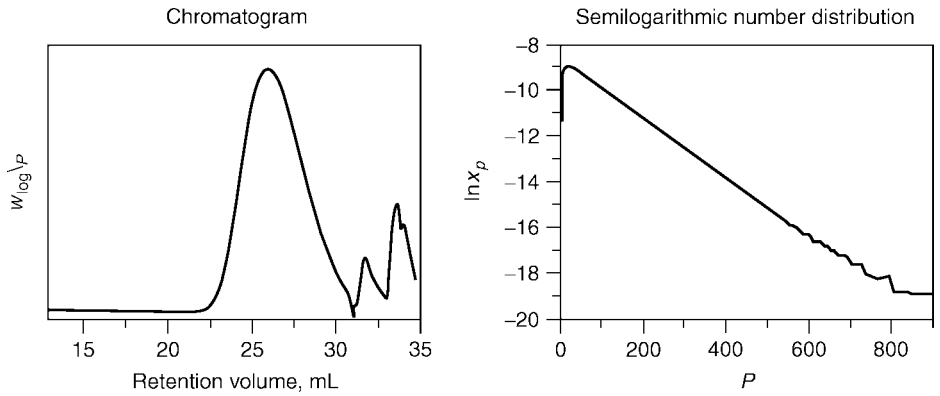

Fig. 15. Transformation of a gel permeation chromatography (GPC) trace of a stationary styrene bulk polymerization at 25°C with carbon tetrachloride as transfer agent, into a semilogarithmic number distribution according to equation 173.

to calculate the transfer coefficient $C = k_{tr}/k_p$. It should be kept in mind that because of the chain length dependent termination process, equation 173 is only valid in the long chain limit. However, reasonable results are achieved at lower molecular weights as well. This method has been studied extensively in the last few years (201) and is now frequently used as an alternative to the classical Mayo method. Although it was recently shown that both methods are in essence the same (498), there may be situations which makes the CLD method preferable over the Mayo method.

As mentioned earlier, the number-average degree of polymerization, $\bar{P}_n$, is associated with a certain degree of error. This is a difficulty of the Mayo method, which therefore encounters problems with low molecular weight polymers. Another situation when the CLD procedure is more advantageous than the Mayo method, is when one must analyze a contaminated polymer sample. A contamination (of an arbitrary nature) may alter the molecular weight distribution and will therefore significantly change the molecular weight averages, rendering the Mayo procedure useless. However, if a region in the molecular weight distribution can be identified in which the distribution is less affected by the contaminant, this region can still be used in the CLD procedure. The CLD procedure is also expected to be more robust when one has systematic errors in the SEC calibration, because then the obtained molecular weight averages will not be accurate, but the systematic error in values of x_P can be expected to cancel out to some extent when the slope of a ln x_P plot is taken.

Methods for the Measurement of k_t.

Single Pulse–Pulsed Laser Polymerization. Applying PLP in conjunction with infrared or near-infrared spectroscopic measurement of monomer conversion induced by a single laser pulse (SP–PLP) allows for the determination of the ratio of termination to propagation rate coefficients, k_t/k_p, in wide ranges of temperature, T, pressure, p, and monomer conversion. The SP–PLP technique was pioneered in the 1980s by Buback and co-workers (409). The monomer conversion induced by a single laser pulse, typically of 20 ns width, is measured by on-line

IR/NIR spectroscopy, with a time resolution of microseconds. The distribution, of free radical chain lengths after a single laser pulse is close with a Poisson distribution, with chain length being linearly correlated with time, unless chain transfer interferes. As a consequence, SP–PLP experiments may provide access to investigations into the chain length dependence of k_t. SP–PLP has first been used for studies into ethene kinetics and subsequently to measure free radical termination of methyl acrylate, butyl acrylate, and dodecyl acrylate (350,351). Because of the high academic and technical interest in detailed k_t studies on slowly propagating monomers, the technique has also been applied to methyl methacrylate (353), butyl methacrylate, and dodecyl methacrylate and various acrylate/methacrylate binary and ternary comonomer systems (499). Figure 16 shows the spectroscopically measured relative monomer concentration vs time profile of a methyl acrylate/dodecyl acrylate copolymerization at equimolar amounts of both monomers in the reaction mixture. The relative change in overall monomer concentration induced by the single laser pulse in this particular experiment is 1% after about 600 ms. Equation 73 has been used to evaluate the kinetic trace. The difference between measured and fitted data is illustrated by plotting the residuals (*res*) in the lower part of the figure, indicating the excellent applicability of equation 73 to represent the kinetic data.

The majority of SP–PLP experiments reported in the literature have been carried out under high pressure to increase the conversion per single pulse. 'True' single pulse experiments can readily be carried out for the acrylates (eg, methyl acrylate, butyl acrylate, or dodecyl acrylate). However, for slowly propagating monomers like methyl methacrylate and styrene, the signal-to-noise ratio of a 'true' single pulse experiment is too poor to allow a meaningful kinetic analysis of the monomer conversion vs time trace. Nevertheless, slowly propagating monomers may be studied by enhancing the signal-to-noise ratio by co-adding a larger number of individual SP–PLP signals recorded under virtually the same conditions, with only a minor decrease in both monomer and photoinitiator concentration between 'true' single pulse experiments. As the concentration of free radicals originating from the previous pulse decays to a very low level and as small primary radicals are generated by each pulse, the range of chain length covered during successively recorded individual concentration vs time traces is identical. The number of co-added signals is limited by the requirement of deriving k_t/k_p for a small range of monomer conversion extending over no more than about 2% to stay close to the intention of 'pointwise' probing the kinetics. To effectively probe the kinetics of a given monomer, a minimum of 0.001% monomer conversion per single laser pulse is required for a sufficient signal-to-noise ratio after approximately 100 co-additions of single pulse signals. A particular strength of the SP–PLP technique is that it offers the possibility to probe the conversion dependence of the termination rate coefficient. At present, the technique is limited to studying monomers with a $\ln(k_t/k_p)$ of less or close to approximately 10, otherwise the resulting conversion per single pulse is insufficient to be detected even with co-addition of true single pulses. In the past and again recently, the SP–PLP technique has been used for investigations into the chain length dependence of the termination rate coefficient. Since all chains grow linearly with time upon initiation with a laser pulse, the time-resolved monomer conversion vs time signal contains information about the chain length dependence of k_t. The linear

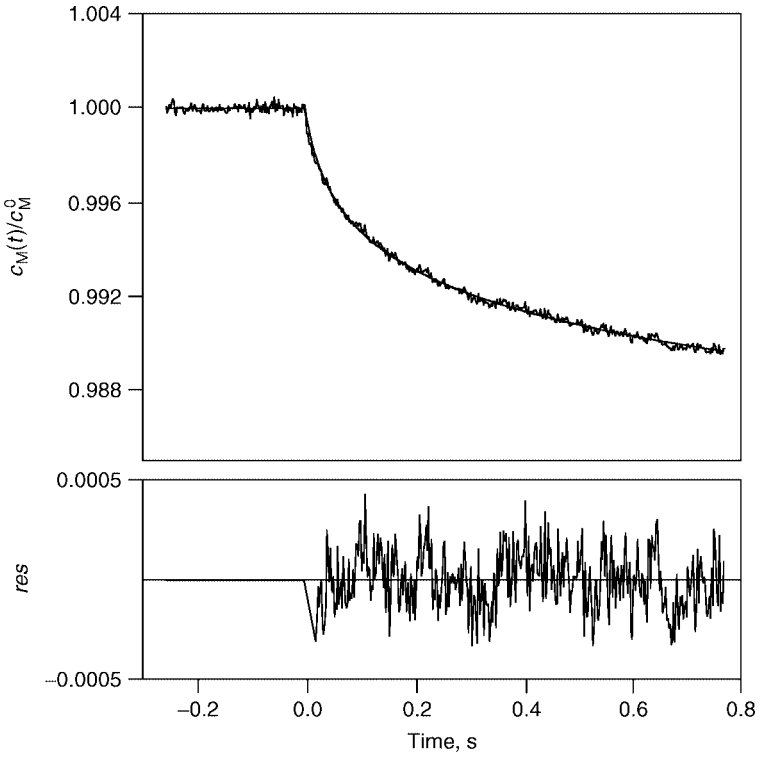

Fig. 16. Monomer concentration vs time trace of a methyl methacrylate/dodecyl acrylate copolymerization at equimolar amounts of both monomers measured in a reaction mixture at 40°C, 100 MPa, and 5 wt% polymer concentration. The difference between measured and fitted data (eq. 73) is illustrated by plotting the residuals (*res*) in the lower part of the figure. Reprinted with friendly permission by the American Chemical Society.

chain growth–time relation is, however, valid only if chain transfer, does not interfere. Early investigations into $k_t^{i,i}$ using the SP–PLP technique were carried out on ethylene (500,501), whereas more recent data are available for styrene, methyl acrylate, butyl acrylate, and dodecyl acrylate (18). It should be mentioned that the SP–PLP equipment requires a relatively high level of technical expertise to be successfully operated. Furthermore, the related equipment costs are high. However, to this date it probably remains the most powerful tool for detailed investigations into the termination rate coefficient.

The CLD Method. The shape of the chain length distribution of a polymer is directly governed by the kinetic parameters of the polymerization process by which the distribution is generated. It is therefore self-evident to try to extract these parameters from such a distribution, which is convincingly realized by measuring k_p by PLP or determining the chain transfer coefficient C via the Mayo or CLD method. Determining the rate coefficient of termination, k_t, via the evaluation of the chain length distributions is possible only in combination with polymerization rate measurements. However, these methods also allow for the determination of the chain length dependence of k_t. The chain length dependence of the termination

rate coefficient should always be taken into account if reasonable results are to be achieved.

The termination rate coefficient is strictly speaking not a constant, but is proven to vary with the chain length of the two radicals involved in the termination process (342).

$$k_t^{i,j} \propto F(i,j) \tag{174}$$

where $k_t{}^{i,j}$ is the rate constant of termination between radical chains of length i and j. $F(i,j)$ is usually represented by a power law of the type

$$F(i,j) = (\bar{i,j})^{-\alpha} \tag{175}$$

with $\bar{i,j}$ denoting some average [eg, the harmonic (336) or the geometric (337) mean] of the two chain lengths i and j involved and α a positive constant. As a consequence, the problem of determining k_t is not solved by the evaluation of one specific value but rather comprises the evaluation of an entire functional dependence.

Most of the methods employed to deduce k_t and k_p are based on the assumption of a chain-length-independent termination rate coefficient and yield k_p and k_t in some combination (k_p/k_t or $k_p{}^2/k_t$, respectively). In the past, before k_p could be determined directly, the usual procedure was to use two different ratios of k_p and k_t and to split them into their individual components via combination. In view of the chain length dependence of k_t it is clear that any (single) experiment aiming at the determination of k_t will render only an average value $\bar{k_t}$, which is defined by the method used and the experimental conditions chosen (eg, monomer and initiator concentration, type of initiation). Combination of k_p/k_t and $k_p{}^2/k_t$ ratios, which are invariably taken from different experiments, therefore always involves averages of k_t, which are not consistent with each other.

Any serious approach aimed at the determination of k_t should therefore avoid the shortcomings outlined above. This implies that one should (*1*) preferentially refer to single point measurements, (*2*) avoid combinations of two different ratios of k_p and k_t, (*3*) take advantage of the possibility of determining k_p directly (eg by PLP–SEC), and (*4*) make sure that the average of k_t is a fair replicate of the true average of k_t, $\langle k_t \rangle$ (see eq. 48), which is operative in the respective experiment.

With these premises fulfilled it is possible to treat a k_t value originating from an experiment dealing with reactions between radicals of different chain lengths, as an average $\bar{k_t}$ specific for the experimental conditions chosen. Assuming this average $\bar{k_t}$ to be physically correct, a power law of the form

$$\bar{k_t} = k_t^0 \nu'^{-\alpha} \tag{176}$$

with the same exponent α as in equation 175 will be obtained. In order to establish the correct chain length dependence of k_t, the averages of k_t have to be correlated with a quantity characteristic of the population of terminating radicals in each experiment. The best solution to this problem appeared to chose a quantity ν' which marks the number-average chain length of the radicals at the moment

of their termination. ν', which is proportional to the number-average degree of polymerization, $\bar{P}_n$, of the polymer formed

$$\nu' = \bar{P}_n(1+\delta)/2 \tag{177}$$

thus in itself is independent of the mode of termination (combination or disproportionation). The preexponential factor in equation 176, k_t^0, is not to be confused with the termination rate coefficient of two radicals of chain length one, but is rather a proportionality factor with no physical meaning associated with it.

Two successful approaches, designed for systems with negligible chain-transfer, are (*1*) the analysis of the second moment of the chain length distribution, represented by the product of the rate of polymerization, R_p, and the weight-average degree of polymerization, $\bar{P}_w$, and (*2*) the formal solution for $\bar{k}_t$ of the rate equation for polymerization with periodic laser pulses. Both methods were originally derived for chain-length-independent termination (502,503). In both cases additional quantities have to be known: Apart from k_p, the quantity δ (contribution of disproportionation to overall termination) must be available in the first case and the quantity ρ (the concentration of new radicals formed in each laser pulse) in the second (implicitly the knowledge of δ is necessary, too).

The two averages of k_t, $\bar{k}_t^m$ and $\bar{k}_t*$, are calculated as follows:

(1) $\bar{k}_t^m$ from the product of rate of polymerization, R_p, and weight-average degree of polymerization, $\bar{P}_w$ (which represents the second moment of the chain length distribution per time)

$$\bar{P}_w R_p = \frac{k_p^2}{2\bar{k}_t^m}[M]^2(3-\delta) \tag{178}$$

(2) $\bar{k}_t*$ from the rate of polymerization under the same conditions given by

$$R_p = \frac{k_p[M]}{2\bar{k}_t^* t_0} \ln\left\{1+\rho\bar{k}_t^* t_0\left[1+\left(1+\frac{2}{\rho\bar{k}_t^* t_0}\right)^{0.5}\right]\right\} \tag{179}$$

As indicated above, both equations were originally developed for chain-length-independent termination; their use in the context of chain length dependence, however, is permissible only if the k_t data obtained are explicitly treated as averages.

The quantity ρ can be determined as follows. In systems with negligible chain transfer the following relation holds:

$$\rho = \frac{2R_p t_0}{\bar{P}_n(1+\delta)} \tag{180}$$

Once $\bar{P}_n$ is known, ρ can be calculated for a given δ. A reasonable estimate of δ is sufficient because δ never appears as an isolated factor in the calculation [either as $(3-\delta)$ or as $(1+\delta)$]. However, errors in δ do not significantly influence

absolute values of k_t. The values for α, representing the chain length dependence of k_t, remain nearly unchanged.

The polymerization is performed via a PLP–SEC experiment, which allows to control the number-average degree of polymerization easily by choosing different laser frequencies and gives the exact chain length distribution of the produced polymer. The value of the propagation rate coefficient k_p can be obtained by the same experiment. Measuring the rate of polymerization, R_p, by determining the conversion of the polymer produced per time, and the number- and weight-average degrees of polymerization, $\bar{P}_n$ and $\bar{P}_w$, allow to calculate the absolute values of average k_t according to equations 178 and 179. Insertion into equation 176 gives values of α, which is a measure for the chain length dependence of the termination rate coefficient for macroradicals of sufficiently large size [according to region B in Figure 5].

Another method to measure the chain length dependence of k_t via evaluation of the chain length distribution of the polymer formed in a single pulse experiment uses equation 181 to measure model independent values of the termination rate coefficient k_t at any given chain length (504,505).

$$k_t^{i,i} = \frac{V k_p [M] x_{2P}}{\left(\int_0^\infty x_{2P}\, dP - \int_0^P x_{2P}\, dP\right)^2} = \frac{V k_p [M] x_{2P}}{\left(\int_P^\infty x_{2P}\, dP\right)^2} \tag{181}$$

where x_{2P} is the differential number distribution for termination by combination and V is an arbitrary volume.

There are two uncertainties in this development which prevent a direct application of equation 181. The first one is the quantity V, which plays the role of a scaling factor, and the second refers to the fact that the integration of x_{2P} cannot be carried out to infinity in practice, because of the effect of chain transfer in the high molecular weight region. This implies that some maximal chain length, P_{max}, has to be introduced which corresponds to a specific residual radical concentration $[R^\bullet]_{res}$ present at the moment at which integration is stopped. The calibration problem as a whole might be solved by estimating values for $[R^\bullet]_0$ as well as for $[R^\bullet]_{res}$. They may be calculated via $k_t^{1,1}$ from the Smoluchowski equation or from literature data and by combination with average $\bar{k}_t$ data linking $[R^\bullet]_0$ and $[R^\bullet]_0$ or alternatively from SP–PLP traces.

The chain length dependence of k_t can also be assessed by fitting a chain length distribution obtained from a single pulse experiment to the theoretical distribution given by equation 119 (506). However, with this method it is also not possible to measure absolute termination rate coefficients, because of unknown absolute scaling factors.

Stationary Polymerization Methods. The determination of the kinetic rate coefficients k_t and k_p in their coupled form k_p^2/k_t has long proceeded via measurement of the rate of polymerization and the calculation of the k_p^2/k_t via equation 56. With the advent of pulsed laser techniques that allow to obtain much more accurate and detailed information about the kinetic rate coefficients (such as chain length dependencies), these techniques became less important. Nevertheless, measurements of the rate of polymerization are still widely performed and are

especially used for systems where the novel techniques are not applicable. This is especially true for measurements of the termination rate coefficient k_t, where rate of polymerization measurements, in combination with independent experiments for the k_p determination, are sometimes the only possibility to get an estimate for k_t. However, it should always be kept in mind that the determination of termination rate coefficients from stationary polymerization experiments yields only an average and approximate value for k_t, as has been outlined above. The polymerization rate can be measured via any quantity that it is directly proportional to. Possible quantities are the density (dilatometry), the refractive index (refractrometry), the heat of polymerization (calorimetry), the polymer mass (gravimetry), or a spectral absorption (IR/NIR and NMR spectroscopy).

The two most common methods are dilatometry and spectroscopic methods. Dilatometry has the advantages of being easy to perform and having low equipment costs. This technique utilizes the volume change that occurs upon polymerization to follow monomer conversion vs time. It is well applicable to free radical polymerization, because of the large difference in the densities of polymer and monomer. For example, the density of methyl methacrylate changes by approximately 22% when going from its monomeric to its polymeric form. The density changes in other polymerizing systems are of the same order of magnitude. The density change is followed in a volume calibrated dilatometer. In modern dilatometers the volume change is followed via the computer controlled observation of the meniscus of a solvent in a capillary on top of the reaction mixture. It is important that the solvent does not mix with the reaction mixture.

The spectroscopic measurement of the rate of polymerization is inherently more elegant than any other of the above-mentioned methods, since it directly probes the reaction mixture on a molecular level and does not rely on the interpretation of a secondary quantity. In addition to providing the rate of polymerization, spectroscopic methods provide real-time insight into the reaction process. The major disadvantage of spectroscopic methods is the relatively large price of, eg, NMR or FTIR spectrometers. Kinetic spectroscopic measurements normally proceed via the recording of a part of the spectrum where a spectroscopic absorption is directly associated with the monomer in the reaction mixture. Care has to be taken that during the course of the reaction no formed product displays an absorption in the same frequency region as the monomeric species. This requirement is met for most monomers in kinetic ^{1}H NMR spectroscopic investigations, where the vinylic absorption(s) can be easily used to probe the progress of the reaction (507). However, NMR spectroscopic investigations are limited in their time resolution. For faster proceeding reactions, NIR/FTIR spectroscopy has been successfully performed to follow free radical acrylate and methacrylate polymerizations, using the first overtone of the C—H stretching vibration on the double bond at roughly 6200 cm^{-1} (351).

Using Living Free Radical Polymerization for k_t Determination. Living free radical polymerization presents—at least in theory—an ideal tool for investigations into chain-length-dependent termination rate coefficients, since in living systems the monomer conversion and the molecular weight, ie the chain length of the growing polymer, are closely interlinked. With increasing reaction time, ie monomer conversion, the terminating polymer chains increase linearly in length. If termination events are occurring, it should be possible to extract information

about the chain length dependence of the termination rate coefficients from rate of polymerization measurements. Thus, the use of a living free radical polymerization system is similar to the time-resolved SP–PLPs described above. In some living free radical polymerization systems, however, the concentration of propagating radicals is greatly reduced, thus almost completely suppressing termination events from occurring. A typical example of such systems are NMP (434) and ATRP (508,509). The RAFT process (268,269), however, makes use of repeated reversible transfer events during the polymerization without, changing, at least in principle the free radical concentration so as to induce an equilibrium of dormant and living chains. In such an 'ideal' living RAFT system—in which no rate retardation effects and other kinetic phenomena occur that may alter the radical concentration, the overall rate of polymerization, R_p, and the rate of the individual reaction steps remain unaltered. The specific characteristics of the RAFT process thus allow for undisturbed investigations into the termination reaction of free radical polymerizations. Because the termination reaction is present throughout the polymerization, RAFT is a suitable tool to study radical–radical termination events. A study of the chain length dependence of an average termination rate coefficient for the termination reaction of two radicals with (approximately) the same chain length i, $\bar{k}_t^{i,i}$, is therefore possible.

The basis of the RAFT k_t method (as mentioned above) is the direct determination of R_p as a function of time throughout a free radical polymerization.

$$\bar{k}_t(t) = \frac{k_p^2}{[R_p(t)]^2}(2fk_d)[I]_0 e^{-k_d t}\left[[M]_0 - \int_0^t R_p(t)\,dt\right]^2 \tag{182}$$

Equation 182 gives $\bar{k}_t$ as a function of time during a free radical polymerization when considering the concentration changes of the participating reagents. It should be noted that this expression assumes steady-state conditions.

When using a RAFT polymerization, the terminating radicals are considered to be approximately of the same chain length—ideally Poisson-distributed—at every single instant in time. The time axis may hence easily be converted to a chain length axis following the simple procedure of calculating the conversion vs time data from the measured polymerization rate and assuming that the chain length of the polymer chains increases linearly with conversion. The chain length P may therefore be calculated as a function of time by

$$P(t) = \frac{\int_0^t R_p(t)\,dt}{[RAFT]_0} \tag{183}$$

with the initial RAFT agent concentration $[RAFT]_0$. The termination rate coefficient is now accessible by measuring the polymerization rate as a function of time in a RAFT-agent-mediated polymerization to ensure that all terminating chains have the same chain length. This task may be carried out by isothermal differential scanning calorimetry, which directly determines the polymerization rate by monitoring the reaction heat. The chain length dependence *and* the absolute value of k_t are therefore accessed via *one* experiment. This very novel procedure has to

this date been used to successfully determine chain-length-dependent termination rate coefficient of styrene (510). The main advantage of this novel RAFT-based technique for k_t determination is its simplicity in combination with the enormous amount of information that is obtained: A single polymerization rate measurement yields the conversion dependence, the chain length dependence, and the absolute value of k_t. It should be noted that it is very important to choose the RAFT agent carefully and the selected RAFT agent/monomer system must not show any retardation and inhibition phenomena. In addition, the technique is suited only for monomers that polymerize fairly rapidly in order to allow for a precise measurement of the polymerization rate.

Determining the Mode of Termination: Disproportionation vs Combination. Several experimental approaches have been taken to determine the mode of chain termination in free radical polymerization. These have been extensively reviewed by Moad and Solomon (511,512). In the case of termination by disproportionation, a chain is generated with one initiator fragment, whereas in the case of combination, a chain with two initiator fragments is formed. The determination of the ratio of number of end groups to the number of monomer units consumed by the polymerization process allows for the calculation of δ, via the additional knowledge of the number-average degree of polymerization, $\bar{P}_n$. Unfortunately, identification and quantification of chain ends are not simple as they give only small signals (relative to the rest of the polymer chain) in a spectroscopic analysis. This can be overcome to some extent by isotopic labeling of the initiator end groups by ^{14}C or by using initiator fragments containing fluorine or phosphorus as NMR-sensitive molecules. Other complications in the analysis include isolating the long-chain termination process from other chain-stopping mechanisms such as chain transfer and primary radical termination. Because of these experimental difficulties, there remains considerable uncertainty in existing termination mode measurements and there is a large scatter in the obtained results. The application of soft ionizing mass spectrometry techniques, such as the matrix-assisted laser desorption ionization time-of-flight mass spectroscopy and electrospray ionizaton, to the problem of end group analysis of polymers brought some promising results to this field of polymerization kinetics (317,319).

BIBLIOGRAPHY

"Free-Radical Polymerization" in *EPST 1st ed.*, Vol. 7, pp. 361–431, by G. C. Eastmond, University of Liverpool; "Radical Polymerization" in *EPST 2nd ed.*, Vol. 13, pp. 708–867, by C. H. Bamford, University of Liverpool.

1. C. Walling, *Free Radicals in Solution*, John Wiley & Sons, Inc., New York, 1957.
2. C. H. Bamford, W. G. Barb, A. D. Jenkins, and P. F. Onyon, *The Kinetics of Vinyl Polymerization by Radical Mechanisms*, Academic Press, New York, 1958.
3. H. S. Bagdasarian, *Theory of Radical Polymerization*, Izd. Akademii Nauk, Moscow, 1959.
4. G. Moad and D. H. Solomon, *The Chemistry of Free Radical Polymerization*, Elsevier, Oxford, U.K., 1995.
5. K. Matyjaszewski and T. P. Davis, *Handbook of Radical Polymerization*, Wiley-Interscience, Hoboken, N.J., 2002.
6. W. K. Busfield and R. W. Humphrey, *J. Polym. Sci., Polym. Chem.* **8**, 2923 (1970).

7. K. J. Ivin and T. Saegusa, *Ring-Opening Polymerization*, Elsevier Applied Science, London, 1984, Chapt. 1.
8. F. Sanda and T. Endo, *J. Polym. Sci., Polym. Chem.* **39**, 265 (2000).
9. T. Endo, T. Yokozawa, and W. J. Mijs, eds., *New Methods in Polymer Synthesis*, Plenum, New York, 1992, p. 155.
10. T. Takata and T. Endo, in R. K. Sadhir and R. M. Luck, eds., *Expanding Monomers: Synthesis, Characterization, and Application*, CRC Press, Boca Raton, Fla., 1992; Chapt. 3.
11. I. S. Chung and K. Matyjaszewski, *Macromolecules*, **36**, 2995 (2003).
12. T. Kodaira, *Progr. Polym. Sci.* **25**, 627 (2000).
13. G. B. Butler, *J. Polym. Sci., Polym. Chem.* **38**, 3451 (2000).
14. K. Yokota, T. Kakuchi, T. Uesaka, and M. Obata, *Acta Polym.* **48**, 459 (1997).
15. L. J. Mathias, *Trends Polym. Sci.* **4**, 330 (1996).
16. B. Yamada, M. Azukizawa, and T. Hirayama, *Polym. Bull.* **43**, 457 (2000).
17. G. Wulff and B. Kuhneweg, *J. Org. Chem.* **62**, 5785 (1997).
18. M. Buback, M. Busch, and C. Kowollik, *Macromol. Theory Simul.* **9**, 442 (2000).
19. R. Kuhlmann and W. Schnabel, *Polymer* **18**, 1163 (1977).
20. J. Hutchison, M. C. Lamber, and A. Ledwith, *Polymer* **14**, 250 (1973).
21. K. W. Dixon, in Ref. 173, p. II/1.
22. P. S. Engel, *Chem. Rev.* **80**, 99 (1980).
23. E. M. Y. Quinga and G. D. Mendenhall, *J. Org. Chem.* **50**, 2836 (1985).
24. M. Minamii and B. Yamada, in J. C. Salamone, ed., Polymeric Materials Encyclopedia, CRC Press, Boca Raton, Fla., 1996, p. 432.
25. C. S. Sheppard, *Encycl. Polym. Sci. Eng.* **2**, 143 (1985).
26. K. W. Dixon, in Ref. 173, p. II/12.
27. O. Nuyken, C. Scherer, A. Baindl, A. R. Brenner, U. Dahn, R. Gartner, S. Kaiser-Rohrich, R. Kollefrath, P. Matusche, and B. Voit, *Prog. Polym. Sci.* **22**, 93 (1997).
28. A. Ueda and S. Nagai, *J. Polym. Sci., Polym. Chem.* **24**, 405 (1986).
29. E. Yoshida and S. Tanimoto, *Macromolecules* **30**, 4018 (1997).
30. A. Ueda and S. Nagai, *J. Polym. Sci., Polym. Chem.* **22**, 1611 (1984).
31. H. Inoue, A. Ueda, and S. Nagai, *J. Polym. Sci., Polym. Chem.* **26**, 1077 (1988).
32. T. Cheikhalard, V. Massardier, L. Tighzert, and J. P. Pascault, *J. Appl. Polym. Sci.* **70**, 613 (1998).
33. H.-J. Paik, M. Teodorescu, J. Xia, and K. Matyjaszewski, *Macromolecules* **32**, 7023 (1999).
34. S. H. Soozandehfar, J. L. Bragger, G. P. Martin, and A. W. Lloyd, *Int. J. Pharm.* **198**, 71 (2000).
35. P. A. Callais, in D. Satas and A. A. Tracton, eds., Coatings Technology Handbook, 2nd ed., Marcel Dekker, New York, 2001, p 581.
36. C. S. Sheppard, *Encycl. Polym. Sci. Eng.* **11**, 1 (1987).
37. G. Moad and D. H. Solomon, in G. C. Eastmond, A. Ledwith, S. Russo, and P. Sigwalt, eds., *Comprehensive Polymer Science*, Pergamon, London, 1989, p. 97.
38. M. Buback, in K. Matyjaszewski, ed., *Controlled/Living Radical Polymerization* (ACS Symposium Series 768), American Chemical Society, Washington, D.C., 2000, p. 39.
39. G. Moad and D. H. Solomon, *The Chemistry of Free Radical Polymerization*, Pergamon, Oxford, 1995, p. 67.
40. M. Buback, S. Klingbeil, J. Sandmann, M.-B. Sderra, H.-P. Voegele, H. Wackerbarth, and L. Wittkowski, *Phys. Chem.* **210**, 199 (1999).
41. M. Buback and J. Sandmann, *Phys. Chem.* **214**, 583 (2000).
42. M. Buback and C. Hinton, *Phys. Chem.* **199**, 229 (1997).

43. Y. L. Barner, Ph.D. dissertation, University of Göttingen, Göttingen, 1997.
44. J. P. Fouassier, *J. Photopolym. Sci. Tec.* **3**, 1 (1990).
45. J. P. Fouassier, *Prog. Org. Coat.* **18**, 229 (1990).
46. J. P. Fouassier, *Recent Res. Dev. Photochem. Photobiol.* **4**, 51 (2000).
47. Y. Yagci, *Macromol. Symp.* **161**, 19 (2000).
48. H. F. Gruber, *Prog. Polym. Sci.* **17**, 953 (1992).
49. N. J. Turro, *Macromolecular Photochemistry*, Benjamin-Cummings, Redwood City, Calif., 1978.
50. N. S. Allen, ed., *Photopolymerization and Photoimaging Science and Technology*, Elsevier Science Publisher Ltd., New York, 1989.
51. J. P. Fouassier, P. Jacques, D. J. Lougnot, and T. Pilot, *Polym. Photochem.* **5**, 57 (1984).
52. J. Eichler, C. P. Herz, I. Naito, and W. Schnabel, *J. Photochem.* **12**, 225 (1980).
53. C. J. Groenenboom, H. J. Hageman, T. Overeem, and A. J. M. Weber, *Makromol. Chem.* **183**, 281 (1982).
54. H. Fischer, R. Baer, R. Hany, I. Verhoolen, and M. J. Walbiner, *Chem. Soc. Perkin Trans. 2* 787 (1990).
55. H. F. Gruber, *Prog. Polym. Sci.* **17**, 953 (1992).
56. O. F. Olaj, H. F. Kauffmann, and J. W. Breitenbach, *Makromol. Chem.* **178**, 2707 (1977).
57. O. F. Olaj, H. F. Kauffmann, J. W. Breitenbach, and H. Bieringer, *J. Polym. Sci., Polym. Lett. Ed.* **15**, 229 (1977).
58. H. F. Kauffmann, O. F. Olaj, and J. W. Breitenbach, *Makromol. Chem.* **177**, 939 (1976).
59. R. S. Lehrle and A. Shortland, *Eur. Polym. J.* **24**, 425 (1988).
60. E. Brand, M. Stickler, and G. Meyerhoff, *Makromol. Chem.* **181**, 913 (1980).
61. J. Lingnau, M. Stickler, and G. Meyerhoff, *Eur. Polym. J.* **16**, 785 (1980).
62. M. Stickler and G. Meyerhoff, *Makromol. Chem.* **181**, 131 (1980).
63. M. Stickler and G. Meyerhoff, *Polymer* **22**, 928 (1981).
64. M. Stickler, *Makromol. Chem.* **184**, 2563 (1983).
65. L. Eberson and O. Persson, *Acta Chem. Scand.* **53**, 680 (1999).
66. D. Liu, A. B. Padias, and J. H. K. Hall, *Macromolecules* **28**, 622 (1995).
67. D. L. Hasha, D. B. Priddy, P. R. Rudolf, E. J. Stark, M. D. Potter, and F. V. Damme, *Macromolecules* **25**, 3046 (1992).
68. M. Matsuda and K. Abe, *J. Polym. Sci., Polym. Chem.* **6**, 1441 (1968).
69. T. Sato, M. Abe, and T. Otsu, *J. Macromol. Sci., A: Chem.* **15**, 367 (1981).
70. A. S. Sarac, *Prog. Polym. Sci.* **24**, 1149 (1999).
71. C. H. Bamford, in G. Allen, S. L. Aggarwal, and S. Russo, eds., *Comprehensive Polymer Science*, Vol. **3**, Pergamon, Oxford, 1989, p. 123.
72. L. Barner, J. F. Quinn, P. Vana, C. Barner-Kowollik, and T. P. Davis, *Eur. Polym. J.* **39**, 449 (2003).
73. J. I. M. Botman, A. T. A. Derksen, A. M. van Herk, M. Jung, F.-D. Kuchta, L. G. Manders, C. J. Timmermans, and M. J. A. de Voigt, *Nucl. Instrum. Methods Phys. Res., Sect. B* **139**, 490 (1998).
74. H. V. Boenig, in J. I. Kroschumtz, ed., *Encyclopedia of Polymer Science and Engineering*, Vol. **11**, Wiley-Interscience, New York, 1988, pp. 248–261.
75. F. F. Shi, *Surf. Coat. Technol.* **82**, 1 (1996).
76. T. F. Otero and M. A. Mugarz, *Makromol. Chem.* **188**, 2885 (1987).
77. I. Reetz, Y. Yagci, and M. K. Mishra, *Turk. Plast. Eng.* **48**, 31 (1998).
78. G. J. Price, D. J. Norris, and P. J. West, *Macromolecules* **25**, 6447 (1992).
79. M. W. A. Kuijpers, D. van Eck, M. F. Kemmere, and J. T. F. Keurentjes, *Science* **298** 1969 (2002).

80. T. Nakamura, W. K. Busfield, I. D. Jenkins, E. Rizzardo, and S. H. Thang, *Polymer* **40**, 1395 (1999).
81. W. K. Busfield, I. D. Jenkins, and P. V. Le, *J. Polym. Sci., Polym. Chem.* **36**, 2169 (1998).
82. T. Nakamura, W. K. Busfield, I. D. Jenkins, E. Rizzardo, S. H. Thang, and S. Suyama, *J. Org. Chem.* **62**, 5578 (1997).
83. G. Moad, D. H. Solomon, S. R. Johns, and R. I. Willing, *Macromolecules* **17**, 1094 (1984).
84. G. Moad, E. Rizzardo, and D. H. Solomon, *Macromolecules* **15**, 909 (1982).
85. G. Moad, D. H. Solomon, S. R. Johns, and R. I. Willing, *Macromolecules* **15**, 1188 (1982).
86. G. Moad, E. Rizzardo, and D. H. Solomon, *Aust. J. Chem.* **36**, 1573 (1983).
87. G. Moad, E. Rizzardo, and D. H. Solomon, *Polym. Bull.* **12**, 471 (1984).
88. P. G. Griffiths, E. Rizzardo, and D. H. Solomon, *J. Macromol. Sci., A: Chem.* **17**, 45 (1982).
89. T. Sato and T. Otsu, *Makromol. Chem.* **178**, 1941 (1977).
90. A. Kajiwara, Y. Konishi, Y. Morishima, W. Schnabel, K. Kuwata, and M. Kamachi, *Macromolecules* **26**, 1656 (1993).
91. M. Kamachi, A. Kajiwara, K. Saegusa, and Y. Morishima, *Macromolecules* **26**, 7369 (1993).
92. M. Kamachi, K. Kuwata, T. Sumiyoshi, and W. Schnabel, *J. Chem. Soc., Perkin Trans. 2* 961 (1988).
93. G. Odian, *Principles of Polymer Science*, 3rd ed., John Wiley & Sons, Inc., New York, 1991, p. 234.
94. G. Moad, E. Rizzardo, D. H. Solomon, S. R. Johns, and R. I. Willing, *Makromol. Chem., Rapid Commun.* **5**, 793 (1984).
95. D. S. Achilias and C. Kiparissides, *Macromolecules* **25**, 3739 (1992).
96. W. H. Starnes Jr., I. M. Plitz, F. C. Schilling, G. M. Villacorta, G. S. Park, and A. H. Saremi, *Macromolecules* **17**, 2507 (1984).
97. H. Ishiwate, T. Inoue, and K. Yoshihira, *J. Chromatogr.* **370**, 275 (1986).
98. A. Matsumoto and K. Mizuta, *Macromolecules* **27**, 5863 (1994).
99. M. Buback, B. Huckestein, F.-D. Kuchta, G. T. Russell, and E. Schmid, *Macromol. Chem. Phys.* **195**, 2117 (1994).
100. J. Samios and T. Dorfmüller, *J. Chem. Phys.* **76**, 5463 (1982).
101. A. A. Gridnev and S. D. Ittel, *Macromolecules* **29**, 5864 (1996).
102. J. P. A. Heuts, R. G. Gilbert, and L. Radom, *Macromolecules* **28**, 8771 (1995).
103. M. Deady, A. W. H. Mau, G. Moad, and T. H. Spurling, *Makromol. Chem.* **194**, 1691 (1993).
104. P. B. Zetterlund, W. K. Busfield, and I. D. Jenkins, *Macromolecules* **32**, 8041 (1999).
105. D. A. Shipp, T. A. Smith, D. H. Solomon, and G. Moad, *Macromol. Rapid Commun.* **16**, 837 (1995).
106. G. Moad, E. Rizzardo, D. H. Solomon, and A. L. J. Bechwith, *Polym. Bull.* **29**, 1691 (1993).
107. P. Zeterlund, W. K. Busfield, and I. D. Jenkins, *Macromolecules* **32**, 8041 (1999).
108. O. F. Olaj, P. Vana, A. Kornherr, and G. Zifferer, *Macromol. Rapid Commun.* **19**, 913 (2000).
109. O. F. Olaj, P. Vana, and M. Zoder, *Macromolecules* **35**, 1208 (2002).
110. P. B. Zetterlund, W. K. Busfield, and I. D. Jenkins, *Macromolecules* **35**, 7232 (2002).
111. A. Kajiwara and M. Kamachi, *Polym. Prepr. (Am. Chem. Soc., Div. Polym. Chem.)* **43**, 144 (2002).

112. W. K. Busfield, in J. Brandup and E. H. Immergut, eds., Polymer Handbook, 3rd ed., John Wiley & Sons, Inc., New York, 1987, p. 555.
113. H. Sawada, *J. Macromol. Sci., C: Rev. Macromol. Chem.* **3**, 313 (1969).
114. P. E. M. Allen and C. R. Patrick, *Kinetics and Mechanism of Polymerization Reactions*, Ellis Horwood, Chichester, U.K., 1974.
115. B. Yamada, D. G. Westmoreland, S. Kobatake, and O. Konosu, *Prog. Polym. Sci.* **24**, 565 (1999).
116. M. Kamachi and A. Kajiwara, *Macromol. Chem. Phys.* **198**, 787 (1997).
117. M. P. Tonge, A. Kajiwara, M. Kamachi, and R. G. Gilbert, *Polymer* **39**, 2305 (1998).
118. M. Azukizawa, B. Yamada, D. J. T. Hill, and P. J. Pomery, *Macromol. Chem. Phys.* **195**, 774 (2000).
119. B. Yamada, M. Azukizawa, H. Yamazoe, D. J. T. Hill, and P. J. Pomery, *Polymer* **41**, 5661 (2000).
120. M. Buback, C. Kowollik, M. Kamachi, and A. Kajiwara, *Macromolecules* **31**, 7208 (1998).
121. M. Kamachi, *Adv. Polym. Sci.* **82**, 207 (1987).
122. A. Matsumoto and B. Giese, *Macromolecules* **29**, 3758 (1996).
123. M. Spichty, B. Giese, A. Matsumoto, H. Fischer, and G. Gescheidt, *Macromolecules* **34**, 723 (2001).
124. M. P. Tonge, R. J. Pacce, and R. G. Gilbert, *Macromol. Chem. Phys.* **1995**, 1144 (1994).
125. A. Kajiwara and M. Kamachi, *Macromol. Chem. Phys.* **201**, 2165 (2000).
126. F. A. Bovey, *Chain Structure and Conformation of Macromolecules*, John Wiley & Sons, Inc., New York, 1982.
127. Y. Okamoto, S. Habaue, Y. Isobe, and T. Nakano, *Macromol. Symp.* **183**, 83 (2002).
128. Y. Isobe, D. Fujioka, S. Habaue, and Y. Okamoto, *J. Am. Chem. Soc.* **123**, 7180 (2001).
129. A. Matsumoto, in Ref. 5, pp. 691–773.
130. H. Hirai, *J. Polym. Sci., Macromol. Rev.* **11**, 47 (1976).
131. B. Kirci, J.-F. Lutz, and K. Matyjaszewski, *Macromolecules* **35**, 2448 (2002).
132. H. Azuma, Y. Katagiri, and S. Yamabe, *J. Polym. Sci., Polym. Chem.* **34**, 1407 (1996).
133. L. H. Yee, M. L. Coote, T. P. Davis, and R. P. Chaplin, *J. Polym. Sci., Polym. Chem.* **38**, 2192 (2000).
134. S. Beuermann and M. Buback, *Prog. Polym. Sci.* **27**, 191 (2002).
135. P. Vana, L. H. Yee, and T. P. Davis, *Macromolecules* **35**, 3008 (2002).
136. L. M. Muratore, M. L. Coote, and T. P. Davis, *Polymer* **41**, 1441 (2000).
137. A. M. van Herk, *Macromol. Theory Simul.* **9**, 433 (2000).
138. M. Buback, C. H. Kurz, and C. Schmaltz, *Macromol. Chem. Phys.* **199**, 1721 (1998).
139. S. Beuermann, M. Buback, and G. T. Russell, *Macromol. Rapid Commun.* **15**, 351 (1994).
140. M. Buback, U. Geers, C. H. Kurz, and J. Heyne, *Macromol. Chem. Phys.* **198**, 3451 (1997).
141. O. F. Olaj and I. Schnöll-Bitai, *Monatsh. Chem.* **130**, 731 (1999).
142. M. D. Zammit, T. P. Davis, G. D. Willett, and K. F. O'Driscoll, *J. Polym. Chem., Polym. Chem.* **35**, 2311 (1997).
143. M. L. Coote, T. P. Davis, B. Klumperman, and M. J. Monteiro, *J. Macromol. Sci., C: Rev. Macromol. Chem. Phys.* **38**, 567 (1998).
144. D. A. Morrison and T. P. Davis, *Macromol. Chem. Phys.* **201**, 2128 (2000).

145. M. Kamachi, *Adv. Polym. Sci.* **38**, 56 (1981).
146. T. F. McKenna and A. Villanueva, *J. Polym. Sci., Polym. Chem.* **37**, 589 (1999).
147. S. Beuermann, M. Buback, C. Schmaltz, and F.-D. Kuchta, *Macromol. Chem. Phys.* **199**, 1209 (1998).
148. S. Beuermann, M. Buback, C. Isemer, and A. Wahl, *Macromol. Rapid Commun.* **20**, 26 (1999).
149. M. A. Quadir, J. M. DeSimone, A. M. van Herk, and A. L. German, *Macromolecules* **31**, 6481 (1998).
150. A. M. van Herk, B. G. Manders, D. A. Canelas, M. A. Quadir, and J. M. DeSimone, *Macromolecules* **30**, 4780 (1997).
151. S. Beuermann, M. Buback, and C. Schmaltz, *Macromolecules* **31**, 8069 (1998).
152. F.-D. Kuchta, A. M. van Herk, and A. L. German, *Macromolecules* **33**, 3641 (2000).
153. S. Beuermann, D. A. Paquet Jr., J. H. McMinn, and R. A. Hutchinson, *Macromolecules* **30**, 194 (1997).
154. C. Bunyakan, L. Armanet, and D. Hunkeler, *Polymer* **40**, 6225 (1999).
155. T. Nakano, A. Matsuda, and Y. Okamoto, *Polym. J.* **28**, 556 (1996).
156. K. Isobe, K. Yamada, T. Nakano, and Y. Okamoto, *Macromolecules* **32**, 5979 (1999).
157. K. Yamada, T. Nakano, and Y. Okamoto, *J. Polym. Sci., Polym. Chem.* **37**, 2677 (1999).
158. K. Yamada, T. Nakano, and Y. Okamoto, *Macromolecules* **31**, 7598 (1998).
159. Y. Okamoto, K. Yamada, and T. Nakano, in Ref. 234, vol. 268, p. 57.
160. J. Shen, Y. Tian, G. Wang, and M. Yang, *Makromol. Chem.* **192**, 2269 (1991).
161. T. G. Carswell, D. J. T. Hill, D. I. Londero, J. H. O'Donnell, P. J. Pomery, and C. L. Winzor, *Polymer* **33**, 137 (1992).
162. J. Shen, G. Wang, Y. Zheng, and M. Yang, *Makromol. Chem. Symp.* **63**, 105 (1992).
163. M. Farina, *Makromol. Chem., Macromol. Symp.* **10/11**, 255 (1987).
164. C. A. Barson, in G. C. Eastmond, A. Ledwith, S. Russo, and P. Sigwalt, eds., *Comprehensive Polymer Science*, Pergamon, London, 1989, p. 171ff.
165. T. Corner, *Adv. Polym. Sci.* **62**, 95 (1984).
166. B. Boutevin, *J. Polym. Sci., Polym. Chem.* **38**, 3235 (2000).
167. Y. Yagci and M. K. Mishra, *Plast. Eng. (New York)* **48**, 15 (1998).
168. J. Ugelstad, *J. Macromol. Sci., A: Chem.* **11**, 1281 (1977).
169. G. F. Meijs, E. Rizzardo, and T. P. T. Le, *Polym. Int.* **26**, 239 (1991).
170. J. P. A. Heuts, Sudarko, and R. G. Gilbert, *Macromol. Symp.* **111**, 147 (1996).
171. J. M. Tedder, *Angew. Chem., Int. Ed. Engl.* **21**, 401 (1982).
172. W. I. Bengough and W. H. Fairservice, *Trans. Faraday Soc.* **67**, 414 (1971).
173. A. Brandrup, E. H. Immergut, and E. A. Grulke, eds., Polymer Handbook, 4th ed., John Wiley & Sons, Inc., New York, 1999, p. II/77.
174. C. F. Jasso, E. Mendizabal, and M. E. Hernandez, *Rev. Plast. Mod.* **62**, 823 (1991).
175. I. Capek, *Collect. Czech. Chem. Commun.* **51**, 2546 (1986).
176. B. Erussalimsky, N. Tumarkin, F. Duntoff, S. Lyubetzky, and A. Goldenberg, *Makromol. Chem.* **104**, 288 (1967).
177. V. Mahadevan and M. Santhappa, *Makromol. Chem.* **16**, 119 (1955).
178. D. Kukulj, T. P. Davis, and R. G. Gilbert, *Macromolecules* **31**, 994 (1998).
179. H. Kapfenstein-Doak, C. Barner-Kowollik, T. P. Davis, and J. Schweer, *Macromolecules* **34**, 2822 (2001).
180. S. P. Potnis and A. M. Deshpande, *Makromol. Chem.* **153**, 139 (1972).
181. K. Matsuo, G. W. Nelb, R. G. Nelb, and W. H. Stockmayer, *Macromolecules* **10**, 654 (1977).
182. J. P. A. Heuts, A. Pross, and L. Radom, *J. Phys. Chem.* **100**, 17087 (1996).

183. W. A. Pryor and J. H. Coco, *Macromolecules* **3**, 500 (1970).
184. A. Rigo, G. Palma, and G. Talamini, *Makromol. Chem.* **153**, 219 (1972).
185. G. S. Park and M. Saleem, *Polym Bull. (Berlin)* **1**, 409 (1979).
186. W. H. Starnes, F. C. Schilling, K. B. Abbas, R. E. Cais, and F. A. Bovey, *Macromolecules* **12**, 556 (1979).
187. J. G. Braks and R. Y. M. Huang, *J. Appl. Polym. Sci.* **22**, 3111 (1978).
188. G. Ayrey and A. C. Haynes, *Makromol. Chem.* **175**, 1463 (1974).
189. W. A. Pryor, A. Lee, and C. E. Witt, *J. Am. Chem. Soc.* **86**, 4229 (1964).
190. I. M. Bel'govskii, L. S. Sakhonenko, and N. S. Enikolopyan, *Vysokomolekul. Soedin.* **8**, 369 (1966).
191. J. A. May and W. B. Smith, *J. Phys. Chem.* **72**, 216 (1968).
192. S. Henrici-Olive and S. Olive, *Fortschr. Hochpolym. Forsch.* **2**, 496 (1961).
193. T. Otsu and M. Yoshida, *Makromol. Chem. Rapid Commun.* **29**, 127 (1982).
194. T. Otsu and A. Matsumoto, *Adv. Polym Sci.* **136**, 75 (1998).
195. C. P. R. Nair and G. Clouet, *J. Macromol. Sci., C: Rev. Macromol. Chem. Phys.* **31**, 311 (1991).
196. T. Otsu, *J. Polym. Sci., Polym. Chem.* **38**, 2121 (2000).
197. C. P. R. Nair, M. C. Richou, P. Chaumont, and G. Clouet, *Eur. Polym. J.* **26**, 811 (1990).
198. N. Y. Kaloforov and E. Borsig, *J. Polym. Sci., Polym. Chem.* **11**, 2665 (1973).
199. G. Gleixner, J. W. Breitenbach, and O. F. Olaj, *Makromol. Chem.* **178**, 2249 (1977).
200. L. Businelli, H. Deleuze, Y. Gnanou, and B. Maillard, *Macromol. Chem. Phys.* **201**, 1833 (2000).
201. J. P. A. Heuts, T. P. Davis, and G. T. Russell, *Macromolecules* **32**, 6019 (1999).
202. C. P. R. Nair, G. Clouet, and P. Chaumont, *J. Polym. Sci., Polym. Chem.* **27**, 1795 (1989).
203. J. T. Clarke, R. O. Howard, and W. H. Stockmayer, *Makromol. Chem.* **44**, 427 (1961).
204. S. Collins and S. Rimmer, *Polym. Prepr. (Am. Chem. Soc., Div. Polym. Chem.)* **43**, 1085 (2002).
205. A. H. Krause, *Rubber Age* **75**, 217 (1954).
206. B. Boutevin, J.-M. Lusinchi, Y. Pietrasanta, and J.-J. Robin, *Eur. Polym. J.* **30**, 615 (1994).
207. B. Boutevin, A. El Idrissi, and J. P. Parisi, *Makromol. Chem.* **191**, 445 (1990).
208. P. Gregor, D. Dolar, and G. K. Hoesche, *J. Am. Chem. Soc.* **77**, 3675 (1995).
209. B. Boutevin, J. M. Lusinchi, Y. Pietrasanta, and J. J. Robin, *Eur. Polym. J.* **30**, 615 (1994).
210. A. Bechkok, M. Belbachir, B. Guyot, and B. Boutevin, *Eur. Polym. J.* **35**, 413 (1998).
211. W. A. Pryor and T. L. Pickering, *J. Am. Chem. Soc.* **84**, 2705 (1962).
212. A. J. Costanza, R. J. Coleman, R. M. Pierson, C. S. Marvel, and C. J. King, *J. Polym. Sci.* **17**, 319 (1955).
213. T. Otsu, Y. Kinoshita, and M. Imoto, *Makromol. Chem.* **79**, 225 (1964).
214. K. Tsuda and T. Otsu, *Bull. Chem. Soc. Jpn.* **39**, 2206 (1966).
215. T. Otsu and K. Nayatani, *Makromol. Chem.* **73**, 225 (1958).
216. N. S. Enikolopyan, B. R. Smirnov, G. V. Ponomarev, and I. M. Belgovski, *J. Polym. Sci., Polym. Chem.* **19**, 879 (1981).
217. A. A. Gridnev, *J. Polym. Sci., Polym. Chem.* **38**, 1753 (2000).
218. A. A. Gridnev and S. D. Ittel, *Chem. Rev.* **101**, 3611 (2001).
219. T. P. Davis, D. Kukulj, D. M. Haddleton, and D. R. Morsley, *Trends Polym. Sci.* **3**, 365 (1995).

220. T. P. Davis, D. M. Haddleton, and S. N. Richards, *J. Macromol. Sci., C: Rev. Macromol. Chem. Phys.* **34**, 243 (1994).
221. J. P. A. Heuts, G. E. Roberts, and J. D. Biasutti, *Aust. J. Chem.* **55**, 381 (2002).
222. G. E. Roberts, T. P. Davis, J. P. A. Heuts, and G. E. Ball, *Macromolecules* **35**, 9954 (2002).
223. G. E. Roberts, J. P. A. Heuts, and T. P. Davis, *J. Polym. Sci., Polym. Chem.* **41**, 752 (2003).
224. D. A. Morrison, L. Eadie, and T. P. Davis, *Macromolecules* **34**, 7967 (2001).
225. T. P. Davis, M. D. Zammit, J. P. A. Heuts, and K. Moody, *Chem. Commun.* **21**, 2383 (1998).
226. J. P. A. Heuts, D. J. Forster, T. P. Davis, B. Yamada, H. Yamazoe, and M. Azukizawa, *Macromolecules* **32**, 2511 (1999).
227. G. E. Roberts, J. P. A. Heuts, and T. P. Davis, *Macromolecules* **33**, 7765 (2000).
228. G. E. Roberts, J. P. A. Heuts, T. P. Davis, and G. T. Russell, *J. Polym. Sci., Polym. Chem.* **40**, 782 (2002).
229. W. Kirkham and J. Robb, *Trans. Faraday Soc.* **57**, 1757 (1961).
230. J. Robb and E. Senogles, *Trans. Faraday Soc.* **58**, 708 (1962).
231. C. M. Starks, *Free Radical Telomerization*, Academic Press, New York, 1974.
232. W. I. Bengough and N. M. Chawdry, *J. Chem. Soc.* 1807 (1972).
233. K. Matyjaszewski, ed., *Controlled Radical Polymerization*, Vol. **685**, American Chemical Society, Washington, D.C., 1998.
234. K. Matyjaszewski, ed., *Controlled/Living Radical Polymerization: Progress in ATRP, NMP, and RAFT*, Vol. **768**, American Chemical Society, Washington, D.C., 2000.
235. J. S. Wang and K. Matyjaszewski, *J. Am. Chem. Soc.* **117**, 5614 (1995).
236. M. Kato, M. Kamigaito, and M. Sawamoto, and T. Higashimura, *Macromolecules* **28**, 1721 (1995).
237. K. Matyjaszewski and J. Xia, *Chem. Rev.* **101**, 2921 (2001).
238. M. Kamigaito, T. Ando, and M. Sawamoto, *Chem. Rev.* **101**, 3689 (2001).
239. J.-S. Wang and K. Matyjaszewski, *Macromolecules* **28**, 7901 (1995).
240. K. Matyjaszewski, T. E. Patten, and J. Xia, *J. Am. Chem. Soc.* **119**, 674 (1997).
241. T. E. Patten, J. Xia, T. Abernathy, and K. Matyjaszewski, *Science* **272**, 866 (1996).
242. T. E. Patten and K. Matyjaszewski, *Acc. Chem. Res.* **32**, 895 (1999).
243. C. Yoshikawa, A. Goto, and T. Fukuda, *Macromolecules* **36**, 908 (2003).
244. T. E. Patten and K. Matyjaszewski, *Adv. Mater.* **10**, 901 (1998).
245. K. A. Davis and K. Matyjaszewski, *Adv. Polym. Sci.* **159**, 2 (2002).
246. E. Rizzardo, G. F. Meijs, and S. H. Thang, *Macromol. Symp.* **98**, 101 (1995).
247. E. Rizzardo, Y.-K. Chong, R. A. Evans, G. Moad, and S. H. Thang, *Macromol. Symp.* **111**, 1 (1996).
248. WO 8804304 (1988), E. Rizzardo, G. F. Meijs, and S. T. Thang (to CSIRO).
249. G. F. Meijs, E. Rizzardo, and S. T. Thang, *Macromolecules* **21**, 3122 (1988).
250. G. F. Meijs, T. C. Morton, E. Rizzardo, and S. T. Thang, *Macromolecules* **24**, 3689 (1991).
251. WO 9106535 (1990), E. Rizzardo, G. F. Meijs, and S. T. Thang (to CSIRO).
252. G. F. Meijs, E. Rizzardo, and S. T. Thang, *Polym. Prepr. (Am. Chem. Soc. Div. Polym. Chem.)* **33**, 893 (1992).
253. G. F. Meijs, E. Rizzardo, and S. T. Thang, *Polym. Bull.* **24**, 501 (1990).
254. B. Yamada and T. Otsu, *Makromol. Chem., Rapid Commun.* **11**, 513 (1990).
255. G. F. Meijs and E. Rizzardo, *Makromol. Chem., Rapid Commun.* **9**, 547 (1988).
256. G. F. Meijs and E. Rizzardo, *Polym. Bull. (Berlin)* **26**, 291 (1991).
257. G. F. Meijs, E. Rizzardo, T. P. T. Le, and Y.-C. Chen, *Makromol. Chem.* **193**, 369 (1992).
258. D. Colombani and P. Chaumont, *Prog. Polym. Sci.* **21**, 439 (1996).

259. J. McGrath, *Pure. Appl. Chem.* **55**, 1573 (1983).
260. P. V. Caeter, *Trends. Polym. Sci.* **3**, 227 (1995).
261. H. A. Nguyen and E. Marechal, *J. Macromol. Sci., C: Rev. Macromol. Chem. Phys.* **28**, 187 (1988).
262. U.S. Pat. 6,100,350 (2000), L. Wilzcek and E. F. McCord (to CSIRO and E. I. du Pont de Nemours & Co., Inc.).
263. D. Charmot, P. Corpart, H. Adam, S. Z. Zard, T. Biadatti, and G. Bouhadir, *Macromol. Symp.* **150**, 23 (2000).
264. WO 9858974 (1998), P. Corpart, D. Charmot, T. Biadatti, S. Z. Zard, and D. Michelet (to Rhone Poulene Chimie).
265. M. Stenzel-Rosenbaum, T. P. Davis, A. G. Fane, and V. Chen, *J. Polym. Sci., Polym. Chem.* **39**, 2777 (2001).
266. M. Stenzel, *Aust. J. Chem.* **55**, 239 (2002).
267. M. H. Stenzel-Rosenbaum, T. P. Davis, A. G. Fane, and V. Chen, *Angew. Chem. Int. Ed.* **40**, 3428 (2001).
268. J. Chiefari, Y. K. Chong, F. Ercole, J. Krstina, J. Jeffery, T. P. T. Le, R. T. A. Mayadunne, G. F. Meijs, C. L. Moad, G. Moad, E. Rizzardo, and S. H. Thang, *Macromolecules* **31**, 5559 (1998).
269. R. T. A. Mayadunne, E. Rizzardo, J. Chiefari, Y. K. Chong, G. Moad, and S. H. Thang, *Macromolecules* **32**, 6977 (1999).
270. G. Moad, J. Chiefari, Y. K. Chong, J. Krstina, R. T. A. Mayadunne, A. Postma, E. Rizzardo, and S. H. Thang, *Polym. Int.* **49**, 993 (2000).
271. Y. K. Chong, T. P. T. Le, G. Moad, E. Rizzardo, and S. H. Thang, *Macromolecules* **32** 2071 (1999).
272. S. Qin, H. G. Borner, K. Matyjaszewski, and S. S. Sheiko, *Polym. Prepr. (Am. Chem. Soc., Div. Polym. Chem.)* **43**, 237 (2002).
273. P. Vana, L. Albertin, L. Barner, T. P. Davis, and C. Barner-Kowollik, *J. Polym. Sci., Polym. Chem.* **40**, 4032 (2002).
274. A. Goto, K. Sato, Y. Tsujii, T. Fukuda, G. Moad, E. Rizzardo, and S. H. Thang, *Macromolecules* **34**, 402 (2001).
275. C. Barner-Kowollik, J. F. Quinn, T. L. U. Nguyen, J. P. A. Heuts, and T. P. Davis, *Macromolecules* **34**, 7849 (2001).
276. C. Barner-Kowollik, P. Vana, J. F. Quinn, and T. P. Davis, *J. Polym. Sci., Polym. Chem.* **40**, 1058 (2002).
277. P. Vana, J. F. Quinn, T. P. Davis, and C. Barner-Kowollik, *Aust. J. Chem.* **55**, 425 (2002).
278. P. Vana, T. P. Davis, and C. Barner-Kowollik, *Polym. Prepr. (Am. Chem. Soc., Div. Polym. Chem.)* **43**, 321 (2002).
279. M. J. Monteiro and H. de Brouwer, *Macromolecules* **34**, 349 (2001).
280. S. Perrier, C. Barner-Kowollik, J. F. Quinn, P. Vana, and T. P. Davis, *Macromolecules* **35**, 8300 (2002).
281. H. Tobita and K. Hatanaka, *J. Polym. Sci., Polym. Phys.* **33**, 841 (1995).
282. D. Britton, F. Heatley, and P. A. Lovell, *Macromolecules* **34**, 817 (2001).
283. D. Britton, F. Heatley, and P. A. Lovell, *Macromolecules* **31**, 2828 (1998).
284. J. C. Bevington, B. J. Hunt, and C. A. Barson, *Macromol. Symp.* **111**, 293 (1996).
285. W. H. McDowell and W. O. Kenyon, *J. Am. Chem. Soc.* **62**, 415 (1940).
286. N. M. Ahmad, D. Britton, F. Heatley, and P. A. Lovell, *Macromol. Symp.* **143**, 231 (1999).
287. K. Hatada, Y. Terawaki, T. Kitayama, M. Kamachi, and M. Tamaki, *Polym. Bull.* **4**, 451 (1981).
288. A. Ghielmi, S. Florentino, G. Storti, M. Mazzotti, and M. Morbidelli, *J. Polym. Sci., Polym. Chem.* **35**, 827 (1997).

289. C. Plessis, G. Arzamendi, J. M. Alberdi, M. Agnely, J. R. Leiza, and J. M. Asua, *Macromolecules* **34**, 6138 (2001).
290. H. Tobita, *Polymer* **35**, 3023 (1994).
291. A. H. Wilbourn, *J. Polym Sci.* **34**, 569 (1959).
292. T. Usami and S. Takayama, *Polym. J.* **16**, 731 (1984).
293. P. M. Cotts, Z. Guan, E. McCord, and S. McLain, *Macromolecules* **33**, 6945 (2000).
294. A. Jurkiewicz, N. W. Eilerts, and E. T. Hsieh, *J. Polym. Sci., Polym. Chem.* **38**, 1210 (2000).
295. I. Ando, M. Kobayashi, M. Kanekiyo, S. Kuroki, S. Ando, S. Matsukawa, H. Kurosu, H. Yasunaga, and S. Amiya, in T. Tanaka, ed., *Experimental Methods in Polymer Science*, Academic Press, New York, 2000, pp. 261–493.
296. A. M. Striegel and M. R. Krejsa, *J. Polym. Sci., Polym. Phys.* **38**, 3120 (2000).
297. T. Housaki, K. Satoh, K. Nishikida, and M. Morimoto, *Makromol. Chem., Rapid Commun.* **9**, 525 (1988).
298. M. Buback, M. Egorov, R. G. Gilbert, V. Kaminsky, O. F. Olaj, G. T. Russell, P. Vana, and G. Zifferer, *Macromol. Chem. Phys.* **203**, 2570 (2003).
299. E. L. Madruga, *Rev. Plast. Mod.* **74**, 151 (1997).
300. M. J. Gibian and R. C. Corley, *Chem. Rev.* **73**, 441 (1973).
301. S. W. Benson, *Acc. Chem. Res.* **19**, 335 (1986).
302. J. J. Dannenberg and B. Baer, *J. Am. Chem. Soc.* **109**, 292 (1987).
303. M. Imoto, S. Sakai, and T. Ouchi, *J. Chem. Soc. Jpn.* **1**, 97 (1985).
304. T. Minato, S. Yamabe, H. Fujimoto, and K. Fukui, *Bull. Chem. Soc. Jpn.* **51**, 1 (1978).
305. C. H. Bamford, G. C. Eastmond, and D. Whittle, *Polymer* **10**, 771 (1969).
306. G. Ayrey and A. C. Haynes, *Eur. Polym J.* **9**, 1029 (1973).
307. C. H. Bamford, R. W. Dyson, and G. C. Eastmond, *J. Polym. Sci., Part C* **16**, 2425 (1967).
308. J. C. Bevington, H. W. Melville, and R. P. Taylor, *J. Polym. Sci.* **14**, 463 (1954)
309. C. Ruechardt, *Top. Curr. Chem.* **88**, 1 (1980).
310. G. Fraenkel and M. J. Geckle, *J. Chem. Soc., Chem. Commun.* 55 (1980).
311. D. Griller and K. U. Ingold, *Acc. Chem. Res.* **9**, 13 (1976).
312. D. Griller and P. R. Marriott, *Int. J. Chem. Kinet.* **11**, 1163 (1979).
313. J. C. Bevington and D. E. Eaves, *Trans. Faraday. Soc.* **55**, 1777 (1959).
314. B. E. Bailey and A. D. Jenkins, *Trans. Faraday Soc.* **56**, 903 (1960).
315. C. H. Bamford, A. D. Jenkins, and R. Johnston, *Trans. Faraday Soc.* **55**, 179 (1959).
316. S. Bizilj, D. P. Kelly, A. K. Serelis, D. H. Solomon, and K. E. White, *Aust. J. Chem.* **38**, 1657 (1985).
317. P. Vana, T. P. Davis, and C. Barner-Kowollik, *Aust. J. Chem.* **55**, 315 (2002).
318. C. H. Bamford, R. W. Dyson, and G. C. Eastmond, *Polymer* **10**, 885 (1969).
319. M. D. Zammit, T. P. Davis, D. M. Haddleton, and K. G. Suddaby, *Macromolecules* **30** 1915 (1997).
320. R. C. Neuman Jr. and M. J. Amrich Jr., *J. Org. Chem.* **45**, 4629 (1980).
321. O. F. Olaj, J. W. Breitenbach, and B. Wolf, *Monatsh. Chem.* **95**, 1646 (1964).
322. K. C. Berger and G. Meyerhoff, *Makromol. Chem.* **176**, 1983 (1975).
323. K. C. Berger, *Makromol. Chem.* **176**, 3575 (1975).
324. P. Cacioli, D. G. Wawthorne, R. L. Laslett, E. Rizzardo, and D. H. Solomon, *J. Macromol. Sci., A: Chem.* **23**, 839 (1986).
325. Ref. 39, pp. 217.
326. G. T. Russell, *Aust. J. Chem.* **55**, 399 (2002).
327. G. T. Russell, R. G. Gilbert, and D. H. Napper, *Macromolecules* **25**, 2459 (1992).
328. A. M. North and G. A. Reed, *J. Polym. Sci., Part A* **1**, 1311 (1963).

329. S. W. Benson and A. M. North, *J. Am. Chem. Soc.* **84**, 935 (1962).
330. A. M. North and G. A. Reed, *Trans. Faraday Soc.* **57**, 859 (1961).
331. M. Buback and C. Kowollik, *Macromolecules* **32**, 1445 (1999).
332. A. Matsumoto and T. Otsu, *Macromol. Symp.* **98**, 139 (1995).
333. A. Matsumoto and T. Otsu, *Proc. Jpn. Acad. B* **70**, 43 (1994).
334. P. Vana, L. H. Yee, C. Barner-Kowollik, J. P. A. Heuts, and T. P. Davis, *Macromolecules* **35**, 1651 (2002).
335. H. K. Mahabadi and K. F. O'Driscoll, *J. Polym. Sci., Polym. Chem.* **15**, 283 (1977).
336. A. R. Khokhlov, *Makromol. Chem., Rapid Commun.* **2**, 633 (1981).
337. T. Yasukawa and K. Murakami, *Polymer* **12**, 1423 (1980).
338. J. C. Le Guillou and J. Zinn-Justin, *Phys. Rev., B: Condens. Matter* **21**, 3976 (1980).
339. M. Smoluchowski, *Z. Physik. Chem.* **92**, 129 (1917).
340. B. Friedman and B. O'Shaughnessy, *Macromolecules* **26**, 5726 (1993).
341. O. F. Olaj and G. Zifferer, *Makromol. Chem.* **189**, 1097 (1988).
342. H. K. Mahabadi, *Macromolecules* **18**, 1319 (1985).
343. O. F. Olaj, P. Vana, A. Kornherr, and G. Zifferer, *Macromol. Chem. Phys.* **200**, 2031 (1999).
344. O. F. Olaj and P. Vana, *J. Polym. Sci., Polym. Chem.* **38**, 697 (2000).
345. O. F. Olaj, M. Zoder, and P. Vana, *Macromolecules* **34**, 441 (2001).
346. O. F. Olaj and P. Vana, *Macromol. Rapid. Commun.* **19**, 533 (1998).
347. O. F. Olaj and P. Vana, *Macromol. Rapid. Commun.* **19**, 433 (1998).
348. P. Vana, T. P. Davis, and C. Barner-Kowollik, *Macromol. Rapid Commun.* **23**, 952 (2002).
349. J. B. L. De Kock, A. M. Van Herk, and A. L. German, *J. Macromol. Sci., C: Polym. Rev.* **41**, 199 (2001).
350. C. H. Kurz, Ph.D. dissertation, University of Göttingen, Göttingen, 1995.
351. S. Beuermann, M. Buback, and C. Schmaltz, *Ind. Eng. Chem. Res.* **38**, 3338 (1999).
352. C. Kowollik, Ph. D. dissertation, University of Göttingen, Göttingen, 1999.
353. M. Buback and C. Kowollik, *Macromolecules* **31**, 3211 (1998).
354. A. J. L. Beckwith, D. Griller, and J. P. Lorand, in H. Fischer, ed. *Landolt–Börnstein, Numerical Data and Functional Relationships in Science and Technology* (New Series Vol. 13), Springer-Verlag, Berlin, 1984, Pt. a, Chapt. 1.
355. H. Fischer and H. Paul, *Acc. Chem. Res.* **20**, 200 (1987).
356. M. Buback and F.-D. Kuchta, *Macromol. Chem. Phys.* **198**, 1445 (1997).
357. M. Buback, *Makromol. Chem.* **191**, 1575 (1990).
358. M. Buback and J. Schweer, *Z. Phys. Chem.* **161**, 153 (1989).
359. M. Buback, B. Degener, and B. Huckestein, *Makromol. Chem., Rapid Commun.* **10**, 311 (1989).
360. M. Buback and B. Degener, *Makromol. Chem.* **194**, 2875 (1993).
361. J. P. Fischer, J. Mücke, and G. V. Schulz, *Ber. Buns. Phys. Chem.* **73**, 154 (1969).
362. W. A. Ludwico and S. L. Rosen, *J. Appl. Polym. Sci.* **19**, 757 (1975).
363. W. A. Ludwico and S. L. Rosen, *J. Polym. Sci., Polym. Chem.* **14**, 2121 (1976).
364. J. Dionisio, H. K. Mahabadi, and K. O'Driscoll, *J. Polym. Sci., Polym. Chem.* **17**, 1891 (1979).
365. K. Horie, I. Mita, and H. Kambe, *Polym. J.* **4**, 341 (1973).
366. K. Ito, *J. Polym. Sci, Polym. Chem. Ed.* **10**, 3159 (1972).
367. R. Z. Radicevic and D. M. Stoiljkov, *Hemijska Ind.* **53**, 336 (1999).
368. G. A. O'Neil and J. M. Torkelson, *Trends. Polym. Sci.* **5**, 349 (1997).
369. G. A. O'Neil and J. M. Torkelson, *Macromolecules* **32**, 411 (1999).
370. H. Yamazoe, P. B. Zetterlund, B. Yamada, D. J. T. Hill, and P. J. Pomery, *Macromol. Chem. Phys.* **202**, 824 (2001).

371. K. E. Miller, E. L. Burch, F. D. Lewis, and J. M. Torkelson, *J. Polym. Sci., Polym. Phys.* **32**, 2625 (1994).
372. B. Subrahmanyam, S. D. Baruah, M. Rahman, N. C. Laskar, and R. K. Mazumder, *Polymer* **35**, 862 (1994).
373. R. G. W. Norrish and R. R. Smith, *Nature* **150**, 336 (1942).
374. E. Trommsdorf, H. Köhle, and P. Lagally, *Makromol. Chem.* **1**, 169 (1948).
375. G. A. O'Neil, M. B. Wisnudel, and J. M. Torkelson, *Macromolecules* **29**, 7477 (1996).
376. J. Gao and A. Penlidis, *J. Macromol. Sci., C: Rev. Macromol. Chem. Phys.* **36**, 199 (1996).
377. G. David, J.-J. Robin, and B. Boutevin, *J. Polym. Sci., Polym. Chem.* **39**, 2740 (2001).
378. W. Konter, B. Bomer, K.-H. Kohler, and W. Heitz, *Makromol. Chem.* **182**, 2619 (1981).
379. M. Yoshioka and T. Otsu, *Macromolecules* **25**, 559 (1992).
380. M. D. Goodner and C. N. Bowman, *Macromolecules* **32**, 6552 (1999).
381. R. Guerrero Santos, P. R. Chaumont, J. E. Herz, and G. J. Beinert, *Eur. Polym. J.* **30**, 851 (1994).
382. M. D. Goodner and C. N. Bowman, *Chem. Eng. Sci.* **57**, 887 (2002).
383. N. T. Lipscomb and Y. Tarshiani, *J. Polym. Sci., Polym. Chem.* **26**, 529 (1988).
384. C. Barner-Kowollik, P. Vana, and T. P. Davis, *J. Polym. Sci., Polym. Chem.* **40**, 675 (2002).
385. T. Sato, S. Inui, H. Tanaka, T. Ota, M. Kamachi, and K. Tanaka, *J. Polym. Sci., Polym. Chem.* **25**, 637 (1987).
386. G. T. Russell, *Macromol. Theory Simul.* **4**, 519 (1995).
387. F. Tudos and T. Foldes-Berezsnich, *Magy. Kem. Foly.* **88**, 213 (1982).
388. G. David, B. Boutevin, J.-J. Robin, C. Loubat, and N. Zydowicz, *Polym. Int.* **51**, 800 (2002).
389. M. G. Joshi and F. Rodriguez, *J. Polym. Sci., Polym. Chem.* **26**, 819 (1988).
390. D. J. T. Hill and J. H. O'Donnell, *J. Chem. Educ.* **61**, 881 (1984).
391. E. Senogles and L. A. Woolf, *J. Chem. Educ.* **44**, 157 (1967).
392. C. H. Bamford, *Eur. Polym. J.* **29**, 313 (1993).
393. A. Bratus, A. Turovki, Y. Medvedevskikh, E. Zagladko, and G. Zaikov, *J. Appl. Polym. Sci.* **83**, 1892 (2002).
394. C. H. Bamford, *Eur. Polym. J.* **33**, 487 (1997).
395. H. Tobita, *Macromolecules* **29**, 3073 (1996).
396. C. H. Bamford, *Eur. Polym. J.* **30**, 1127 (1994).
397. O. F. Olaj, A. Kornherr, and G. Zifferer, *Macromol. Theory Simul.* **9**, 131 (2000).
398. M. Buback, R. G. Gilbert, R. A. Hutchinson, B. Klumperman, F.-D. Kuchta, G. B. Manders, K. F. O'Driscoll, G. T. Russell, and J. Schweer, *Macromol. Chem. Phys.* **196**, 3267 (1995).
399. A. Brandrup, E. H. Immergut, and E. A. Grulke, *Polymer Handbook*, Wiley-Interscience, New York, 1998.
400. G. M. Burnett and H. W. Melville, *Nature* **156**, 661 (1945).
401. O. F. Olaj and G. Zifferer, *Macromol. Symp.* **111**, 209 (1996).
402. H. W. Melville, *Proc. R. Soc. London, Ser. A* **163**, 511 (1937).
403. G. Gans and D. Duesentrieb, *Enth. J. Polym. Res.* **206**, 503 (1954).
404. P. D. Bartlett and C. G. Swain, *J. Am. Chem. Soc.* **67**, 2273 (1945).
405. M. L. Coote, M. D. Zammit, and T. P. Davis, *Trends. Polym. Sci.* **4**, 189 (1996).
406. T. P. Davis, *J. Photochem. Photobiol. A* **77**, 1 (1994).
407. O. F. Olaj, I. Bitai, H. Kauffmann, and G. Gleixner, *Österr. Chem.-Ztg.* **84**, 264 (1983).

408. O. F. Olaj, I. Bitai, and G. Gleixner, *Makromol. Chem.* **186**, 2569 (1985).
409. M. Buback, H. Hippler, J. Schweer, and H. P. Voegele, *Makromol. Chem. Rapid Commun.* **7**, 261 (1986).
410. M. Buback, B. Huckestein, and U. Leinhos, *Makromol. Chem. Rapid Commun.* **8**, 473 (1987).
411. G. Moad, D. A. Shipp, T. A. Smith, and D. H. Solomon, *J. Phys. Chem. A* **103**, 6580 (1999).
412. G. Moad, D. A. Shipp, T. A. Smith, and D. H. Solomon, *Macromolecules* **30**, 7627 (1997).
413. M. Wulkow, *Macromol. Theory Simul.* **5**, 393 (1996).
414. J. C. Bevington, J. H. Bradbury, and G. M. Burnett, *J. Polym. Sci.* **12**, 469 (1954).
415. O. F. Olaj, I. Bitai, and F. Hinkelmann, *Makromol. Chem.* **188**, 1689 (1987).
416. A. P. Aleksandrov, V. N. Genkin, M. S. Kitai, I. M. Smirnova, and V. V. Sokolov, *Kvantovaya Elektron. (Moscow)* **4**, 976 (1977).
417. A. M. Van Herk , *J. Macromol. Sci., C: Rev. Macromol. Chem. Phys.* **37**, 633 (1997).
418. O. F. Olaj and G. Zifferer, *Makromol. Chem. Theory Simul.* **1**, 71 (1992).
419. J. Sarnecki and J. Schweer, *Macromolecules* **28**, 4080 (1995).
420. A. Kornherr, G. Zifferer, and O. F. Olaj, *Macromol. Theory Simul.* **8**, 260 (1999).
421. A. V. Evseev and A. N. Nikitin, *Laser Chem.* **16**, 83 (1995).
422. D. G. Hawthorne and D. H. Solomon, *J. Polym. Sci., Polym. Symp.* **55**, 211 (1976).
423. E. W. Merrill, *Plast. Eng.* **33**, 13 (1996).
424. F. Fairbrother, G. Gee, and G. T. Merrall, *J. Polym. Sci.* **16**, 459 (1955).
425. A. V. Tobolsky, *Polym. Prepr. (Am. Chem. Soc., Div. Polym. Chem.)* **11**, 165 (1970).
426. R. Steudel, S. Passlack-Stephan, and G. Holdt, *Z. Anorg. Allg. Chem.* **517**, 7 (1984).
427. H. Sawada, *Encycl. Polym. Sci. Eng.* **4**, 719 (1985).
428. H. W. McCormick, *J. Polym. Sci.* **25**, 488 (1957).
429. R. A. Hutchinson, D. A. Paquet, S. Beuermann, and J. H. McMinn, *Ind. Eng. Chem. Res.* **37**, 3567 (1998).
430. F. S. Dainton and K. J. Ivin, *Quart. Revs (London)* **12**, 61 (1958).
431. C. Barner-Kowollik and T. P. Davis, *Macromol. Theory Simul.* **10**, 255 (2001).
432. T. Mitani, Y. Ogo, and T. Imoto, *Rev. Phys. Chem. Soc. Jpn.* **42**, 25 (1972).
433. F. Tudos and T. Foldes-Berezsnich, *Prog. Polym. Sci.* **14**, 717 (1989).
434. C. J. Hawker, A. W. Bosman, and E. Harth, *Chem. Rev.* **101**, 3661 (2001).
435. M. K. Georges, R. P. N. Veregin, P. M. Kazmaier, and G. K. Hamer, *Macromolecules* **26**, 2987 (1993).
436. J. Fossey, D. Lefort, and J. Sorba, *Free Radicals in Organic Chemistry*, John Wiley & Sons, Inc., Chichester, U.K., 1995, p. 36.
437. J. C. Bevington and B. J. Hunt, *J. Polym. Mater.* **19**, 113 (2002).
438. G. Moad, E. Rizzardo, and D. H. Solomon, *Polym. Bull.* **6**, 589 (1982).
439. G. Moad and E. Rizzardo, *Macromolecules* **28**, 8722 (1995).
440. A. L. J. Beckwith, V. W. Bowry, and G. Moad, *J. Org. Chem.* **53**, 1632 (1988).
441. K. Platkowski and K.-H. Reichert, *Chem.-Ing.-Tech.* **71**, 493 (1999).
442. W. G. Skene, T. J. Connolly, and J. C. Scaiano, *Int. J. Chem. Kinet.* **32**, 238 (2000).
443. G. Moad, E. Rizzardo, and D. H. Solomon, *Macromolecules* **15**, 909 (1982).
444. U.S. Pat. 4,581,429 (1986), D. H. Solomon, E. Rizzardo, and P. Cacioli.
445. M. K. Georges, *Polym. Mater. Sci. Eng.* **80**, 283 (1999).
446. B. Yamada, H. Tanaka, K. Konishi, and T. Otsu, *J. Macromol. Sci., A: Pure Appl. Chem.* **31**, 351 (1994).
447. M. Kinoshita and Y. Miura, *Makromol. Chem.* **124**, 211 (1969).
448. K. Vassilev, S. Ivanov, and S. Tanielyan, *Oxid. Commun.* **22**, 387 (1999).

449. F. Lartigue-Peyrou, *Ind. Chem. Libr.* **8**, 489 (1996).
450. K. S. Bagdasarian and Z. A. Sinitsina, *J. Polym. Sci., Polym. Chem.* **52**, 31 (1961).
451. S. C. Barton, R. A. Bird, and K. E. Russell, *Can. J. Chem.* **41**, 2737 (1963).
452. T. Zytowski and H. Fischer, *J. Am. Chem. Soc.* **119**, 12869 (1997).
453. T. L. Simandi, A. Rockenbauer, and L. I. Simandi, *Eur. Polym. J.* **31**, 555 (1995).
454. T. L. Simandi and A. Rockenbauer, *Eur. Polym. J.* **27**, 523 (1991).
455. T. L. Simandi, A. Rockenbauer, and F. Tudos, *Eur. Polym. J.* **25**, 501 (1989).
456. T. L. Simandi and F. Tudos, *Eur. Polym. J.* **21**, 865 (1985).
457. C. H. Bamford, *Polym. Prepr. (Am. Chem. Soc., Div. Polym. Chem.)* **8**, 26 (1967).
458. W. I. Bengough and W. H. Fairservice, *Trans. Faraday Soc.* **67**, 414 (1971).
459. H. D. Bruyn, R. G. Gilbert, and B. S. Hawkett, *Polymer* **41**, 8633 (2000).
460. K. Kishore and V. A. Bhanu, *J. Polym. Sci., Polym. Chem.* **26**, 2831 (1988).
461. R. P. Singh, S. M. Desai, S. Sivaram, and K. Kishore, *Macromol. Chem. Phys.* **203**, 2163 (2002).
462. A. K. Nanda and K. Kishore, *J. Appl. Polym. Sci.* **86**, 2108 (2002).
463. A. K. Nanda and K. Kishore, *Macromolecules* **35**, 6505 (2002).
464. F. Tudos and T. Berezsnich-Foldes, *Magy. Kem. Folyoirat* **72**, 11 (1966).
465. P. J. Krusic, E. Wasserman, P. N. Keizer, J. R. Morton, and K. F. Preston, *Science* **254**, 1183 (1991).
466. M. Seno, M. Maeda, and T. Sato, *J. Polym. Sci., Polym. Chem.* **38**, 2572 (2000).
467. K. E. Geckeler and S. Samal, *Fullerene Sci. Technol.* **9**, 17 (2001).
468. S. Mehrotra, A. Nigam, and R. Malhotra, *Chem. Commun.* 463 (1997).
469. N. Arsalani and K. E. Geckeler, *Fullerene Sci. Technol.* **4**, 897 (1996).
470. D. Stewart and C. T. Imrie, *Chem. Commun.* 1383 (1996).
471. Y. Chen and K.-C. Lin, *J. Polym. Sci., Polym. Chem.* **37**, 2969 (1999).
472. Y.-P. Sun, G. E. Lawson, C. E. Bunker, R. A. Johnson, B. Ma, C. Farmer, J. E. Riggs, and A. Kitaygorodskiy, *Macromolecules* **29**, 8441 (1996).
473. M. D. Goldfein, G. P. Gladyshev, and A. V. Trubnikov, *Polym. Yearb.* **13**, 163 (1996).
474. G. C. Eastmond, in C. H. Bamford and C. F. H. Tipper, eds., *Comprehensive Chemical Kinetics, Volume 14A: Free-Radical Polymerisation*, Elsevier, Amsterdam, 1976, p. 125.
475. P. E. M. Allen and C. R. Patrick, *Kinetics and Mechanisms of Polymerization Reactions*, John Wiley & Sons, New York, 1974.
476. M. Buback and C. Hinton, *Z. Phys. Chem.* **193**, 61 (1996).
477. M. Buback and H. Lendle, *Z. Naturforsch.* **36a**, 1371 (1981).
478. S. Beuermann, M. Buback, T. P. Davis, R. G. Gilbert, R. A. Hutchinson, O. F. Olaj, G. T. Russell, J. Schweer, and A. M. van Herk, *Macromol. Chem. Phys.* **198**, 1545 (1997).
479. S. Beuermann, M. Buback, T. P. Davis, R. G. Gilbert, R. A. Hutchinson, A. Kajiwara, B. Klumperman, and G. T. Russell, *Macromol. Chem. Phys.* **201**, 1355 (2000).
480. R. A. Hutchinson, M. T. Aronson, and J. R. Richards, *Macromolecules* **26**, 6410 (1993).
481. S. E. Bresler, E. N. Kozbekov, V. N. Fomichev, and V. N. Shadrin, *Makromol. Chem.* **157**, 167 (1972).
482. A. Kajiwara and M. Kamachi, *Macromolecules* **29**, 2378 (1996).
483. M. Buback, L.-H. Gracia-Rubio, R. G. Gilbert, D. H. Napper, J. Guillot, A. E. Hamielec, D. Hill, K. F. O'Driscoll, O. F. Olaj, J. Shen, D. Solomon, G. Moad, M. Stickler, M. Tirrell, and M. A. Winnik, *J. Polym. Sci., Polym. Lett.* **26**, 293 (1988).
484. H. P. Aleksandrov, V. N. Genkin, M. S. Kital, J. Smirovna, and V. V. Sokolov, *Kvantovaya Elektron. (Moscow)* **4**, 976 (1977).

485. T. P. Davis, K. F. O'Driscoll, M. C. Pinton, and M. A. Winnik, *Macromolecules* **22**, 2785 (1989).
486. J. Shen, G. Wang, Y. Zheng, and M. Yang, *Macromol. Chem., Macromol. Symp.* **63**, 105 (1992).
487. J. Shen, Y. Tian, Y. Zeng, and Z. Qiu, *Makromol. Chem., Rapid Commun.* **8**, 615 (1987).
488. I. Schnöll-Bitai, *Macromol. Rapid Commun.* **20**, 162 (1999).
489. I. Schnöll-Bitai, *Macromol. Theory Simul.* **9**, 230 (2000).
490. L. V. Karmilova, G. V. Ponomarev, B. R. Smirnov, and I. M. Belgovskii, *Russ. Chem. Rev.* **53**, 132 (1984).
491. T. P. Davis, D. Kukulj, D. M. Haddleton, and D. R. Maloney, *Trends Polym. Sci.* **3**, 365 (1995).
492. Ref. 173, p. II/97.
493. F. R. Mayo, *J. Am. Chem. Soc.* **65**, 2324 (1943).
494. D. I. Christie and R. G. Gilbert, *Macromol. Chem. Phys.* **197**, 403 (1996). Erratum: *Macromol. Chem. Phys.* **198**, 663 (1997).
495. R. A. Hutchinson, D. A. Paquet Jr., and J. H. McMinn, *Macromolecules* **28**, 5655 (1995).
496. M. Buback and R. A. Lämmel, *Macromol. Theory Simul.* **6**, 145 (1997).
497. P. A. Clay and R. G. Gilbert, *Macromolecules* **28**, 552 (1995).
498. J. P. A. Heuts and T. P. Davis, *Macromolecules* **32**, 6019 (1999).
499. M. Buback and C. Kowollik, *Macromol. Chem. Phys.* **200**, 1764 (1999).
500. M. Buback and J. Schweer, *Makromol. Chem. Rapid Commun.* **9**, 699 (1988).
501. M. Buback and J. Schweer, *Makromol. Chem. Rapid Commun.* **9**, 145 (1988).
502. O. F. Olaj, I. Bitai, and G. Gleixner, *Makromol. Chem.* **186**, 2569 (1985).
503. O. F. Olaj and G. Zifferer, *Eur. Polym. J.* **25**, 961 (1985).
504. J. B. L. de Kock, Ph.D. dissertation, Technical University Eindhoven, Eindhoven, 1999.
505. J. B. L. deKock, B. Klumperman, A. M. van Herk, and A. L. German, *Macromolecules* **30**, 6743 (1997).
506. O. F. Olaj, P. Vana, A. Kornherr and G. Zifferer, *Macromol. Chem. Phys.* **200**, 2031 (1999).
507. C. Barner-Kowollik, J. P. A. Heuts, and T. P. Davis, *J. Polym. Sci., Polym. Chem.* **39**, 656 (2000).
508. J. S. Wang and K. Matyjaszewski, *J. Am. Chem. Soc.* **117**, 5614 (1995).
509. D. M. Haddleton, M. C. Crossman, B. H. Dana, D. J. Duncalf, A. M. Heming, D. Kukulj, and A. J. Shooter, *Macromolecules* **32**, 2110 (1999).
510. P. Vana, T. P. Davis, and C. Barner-Kowollik, *Macromol. Rapid Commun.* **23**, 952 (2002).
511. G. Moad, and D. H. Solomon, in G. Moad and D. H. Solomon, eds., *Azo and Peroxy Initiators*, Vol. **3**, Pergamon Press, London, 1989, p. 97.
512. G. Moad, and D. H. Solomon, in G. Moad and D. H. Solomon, eds., *Chemistry of Bimolecular Termination*, Vol. **3**, Pergamon Press, London, 1989, p. 147.

PHILIPP VANA
University of Göttingen
CHRISTOPHER BARNER-KOWOLLIK
THOMAS P. DAVIS
The University of New South Wales
KRZYSZTOF MATYJASZEWSKI
Carnegie Mellon University

RAMAN SPECTROSCOPY. See VIBRATIONAL SPECTROSCOPY.

RAYON. See CELLULOSIC FIBERS, REGENERATED.

REACTIVE POLYMERS. See POLYMER-SUPPORTED REAGENTS.

RECYCLING, PLASTICS. See Volume 7.

REINFORCEMENT. See Volume 4.

RELEASE AGENTS. See Volume 4.

RHEOLOGICAL MEASUREMENTS

Rheology is the science of the deformation and flow of matter. It is concerned with the response of materials to applied stress. That response may be irreversible viscous flow, reversible elastic deformation, or a combination of the two. Control of rheology is essential for the manufacture and handling of numerous materials and products, eg, foods, cosmetics, rubber, plastics, paints, inks, and drilling muds. Before control can be achieved, there must be an understanding of rheology and an ability to measure rheological properties.

Deformation is the relative displacement of points of a body. It can be divided into two types: flow and elasticity. Flow is irreversible deformation; when the stress is removed, the material does not revert to its original form. This means that work is converted to heat. Elasticity is reversible deformation; the deformed body recovers its original shape, and the applied work is largely recoverable. Viscoelastic materials show both flow and elasticity.

This article is concerned with rheological measurements on both liquids and solids and the principles on which they are based. The flow properties of a liquid are defined by its resistance to flow, ie, viscosity, and may be measured by determining the rate of flow through a capillary, the resistance to flow when the fluid is sheared between two surfaces, or the rate of motion of an object or ball moving through the fluid. The mechanical properties of an elastic solid may be studied by applying a stress and measuring the deformation or strain. Many solids, such as polymers, undergo flow in addition to recoverable elastic deformation. Furthermore, a number of liquids show elastic as well as flow behavior. These materials are viscoelastic, and additional techniques beyond those indicated for solids and liquids are needed for complete characterization. Examples of such methods are the measurement of response to sinusoidal oscillatory motion; the measurement of flow with time after application of stress, ie, creep; and the measurement

Encyclopedia of Polymer Science and Technology. Copyright John Wiley & Sons, Inc. All rights reserved.

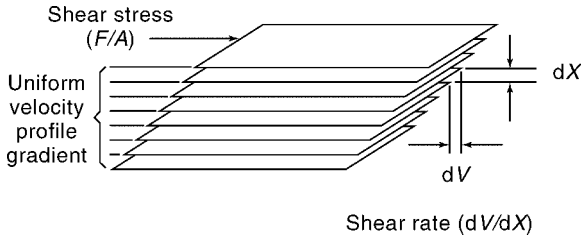

Fig. 1. Laminar flow in simple shear. $F/A = \eta\ \mathrm{d}V/\mathrm{d}X$, where F is the force acting on area A, V the velocity and X the thickness of the layer, and η the coefficient of viscosity or the Newtonian viscosity.

of the rate and degree of recovery after removal of stress, ie, creep recovery or recoil.

In addition to viscometers, optical devices such as microscopes and cameras can be used for defining and solving flow problems as well as characterizing materials (1–3). Optical techniques allow the investigator to determine the physical structure of the material and visualize its flow processes.

Viscosity

A liquid is a material that continues to deform as long as it is subjected to a tensile and/or shear stress. The latter is a force applied tangentially to the material. In a liquid, shear stress produces a sliding of one infinitesimal layer over another, resulting in a stack-of-cards type of flow (Fig. 1).

For a liquid under shear, the rate of deformation or shear rate is a function of the shearing stress. The original exposition of this relationship is Newton's law, which states that the ratio of the stress to the shear rate is a constant, ie, the viscosity. Under Newton's law, viscosity is independent of shear rate. This is true for ideal or Newtonian liquids, but the viscosities of many liquids, particularly a number of those of interest to industry, are not independent of shear rate. These non-Newtonian liquids may be classified according to their viscosity behavior as a function of shear rate. Many exhibit shear thinning, whereas others give shear thickening. Some liquids at rest appear to behave like solids until the shear stress exceeds a certain value, called the yield stress, after which they flow readily.

Some commonly observed types of flow behavior are shown in Figure 2, in which the shear stress is plotted against shear rate. These plots are called flow curves and are frequently used to express the rheological behavior of liquids. Newtonian flow is shown by a straight line, and shear thinning and thickening by curves. Yield stresses, τ_0, are shown by intercepts on the stress (y) axis. It should be pointed out that the existence of yield stresses is controversial; they may be artifacts resulting from high Newtonian viscosity at low shear rates (4). However, in many dispersed systems, particularly where severe flocculation occurs, this viscosity is so high that the material would take years to flow. Therefore, in practice, there are true yield stresses. This parameter can be quite useful in characterizing materials. Additional information on yield is available (5–8).

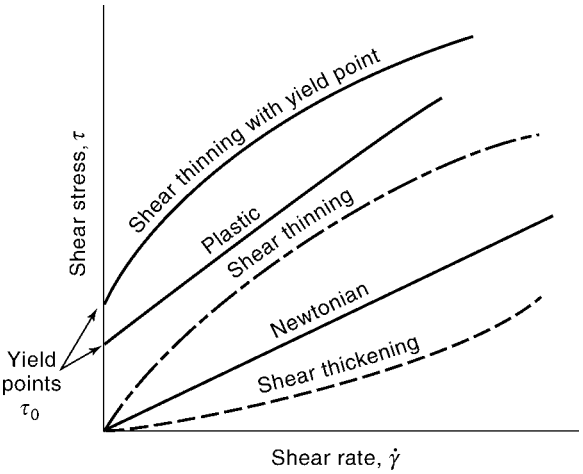

Fig. 2. Flow curves (shear stress vs shear rate) for different types of flow behavior.

Viscosity is equal to the slope of the flow curve, $\eta = d\tau/d\dot{\gamma}$. The quantity $\tau/\dot{\gamma}$ is the viscosity η for a Newtonian liquid and the apparent viscosity η_a for a non-Newtonian liquid. The kinematic viscosity is the viscosity coefficient divided by the density, $\nu = \eta/\rho$. The fluidity is the reciprocal of the viscosity, $\phi = 1/\eta$. The common units for viscosity, dyne seconds per square centimeter ((dyn·s)/cm^2) or grams per centimeter second ((g/(cm·s)), called poise, which is usually expressed as centipoise (cP), have been replaced by the SI units of pascal seconds, ie, Pa·s and mPa·s, where 1 mPa = 1 cP. In the same manner the shear stress units of dynes per square centimeter, dyn/cm^2, have been replaced by Pascals, where 10 dyn/cm^2 = 1 Pa, and newtons per square meter, where 1 N/m^2 = 1 Pa. Shear rate is $\Delta V/\Delta X$, or length/time/length, so that values are given as per second (s^{-1}) in both systems. The SI units for kinematic viscosity are square centimeters per second (cm^2/s), ie, Stokes (St), and square millimeters per second (mm^2/s), ie, centistokes (cSt). Information is available for the official Society of Rheology nomenclature and units for a wide range of rheological parameters (9).

Flow Models. Many flow models have been proposed (8,10), which are useful for the treatment of experimental data or for describing flow behavior (Table 1). However, it is likely that no given model fits the rheological behavior of a material over an extended shear rate range. Nevertheless, these models are useful for summarizing rheological data and are frequently encountered in the literature.

Of the models listed in Table 1, the Newtonian is the simplest. It fits water, solvents, and many polymer solutions over a wide strain rate range. The plastic or Bingham body model predicts constant plastic viscosity above a yield stress. This model works for a number of dispersions, including some pigment pastes. Yield stress, τ_0, and plastic (Bingham) viscosity, $\eta_p = (\tau - \tau_0)\dot{\gamma}$, may be determined from the intercept and the slope beyond the intercept, respectively, of a shear stress vs shear rate plot.

The other models can be applied to non-Newtonian materials where time-dependent effects are absent. This situation encompasses many technically important materials from polymer solutions to lattices, pigment slurries, and polymer

Table 1. Flow Equations for Flow Models

Flow model	Flow equation
Newtonian	$\tau = \eta\dot{\gamma}$
Plastic (Bingham) body	$\tau - \tau_0 = \eta\dot{\gamma}$
Power law	$\tau = k\lvert\dot{\gamma}\rvert^n$
Power law with yield value	$\tau - \tau_0 = k\lvert\dot{\gamma}\rvert^n$
Casson fluid	$\tau^{1/2} - {\tau_0}^{1/2} = {\eta_\infty}^{1/2}\ \dot{\gamma}\rvert^{1/2}$
Williamson	$\eta = \eta_\infty + \frac{(\eta_0 - \eta_\infty)}{1 + \frac{[r]}{r_m}}$
Cross	$\eta = \eta_\infty + \frac{(\eta_0 - \eta_\infty)}{1 + \alpha\dot{\gamma}^n}$

melts. At high shear rates most of these materials tend to a Newtonian viscosity limit. At low shear rates they tend either to a yield point or to a low shear Newtonian limiting viscosity. At intermediate shear rates, the power law or the Casson model is a useful approximation.

The power law, $\tau = k\dot{\gamma}^n$, is widely used as a model for non-Newtonian fluids. It holds for many solutions and can describe Newtonian, shear-thinning, and shear-thickening behavior, depending on the power factor, n, also called the flow behavior index. For a Newtonian fluid, $n = 1$ and the equation reduces to the Newtonian model. If n is less than 1, the fluid is shear thinning; if it is greater than 1, the fluid is shear thickening. A test of whether the power law applies and a means of determining n is to plot the log shear stress vs the log shear rate. If the plot is linear, the power law applies. The value of n, which is the reciprocal of the slope of the line, can be used as a measure of the degree of shear thinning or shear thickening. Dividing the power law equation through by $\dot{\gamma}$ gives an expression in terms of viscosity, $\eta = k'\dot{\gamma}^{n-1}$.

The power law model can be extended by including the yield value $\tau - \tau_0 = k\dot{\gamma}^n$, which is called the Herschel–Bulkley model, or by adding the Newtonian limiting viscosity η_∞. The latter is done in the Sisko model, $\eta_\infty + k\dot{\gamma}^{n-1}$. These two models, along with the Newtonian, Bingham, and Casson models, are often included in data-fitting software supplied for the newer computer-driven viscometers.

Another model is the Casson equation (11), which is useful in establishing the flow characteristics of inks, paints, and other dispersions. An early form of this expression (eq. 1) was modified (12) to give equation 2.

$$\tau^{1/2} = k_0 + k_1\dot{\gamma}^{1/2} \tag{1}$$

$$\eta^{1/2} = \eta_\infty^{1/2} + \tau_0^{1/2}\dot{\gamma}^{-1/2} \tag{2}$$

The square root of viscosity is plotted against the reciprocal of the square root of shear rate (Fig. 3). The square of the slope is τ_0, the yield stress; the square of the intercept is η_∞, the viscosity at infinite shear rate. No material actually experiences an infinite shear rate, but η_∞ is a good representation of the condition

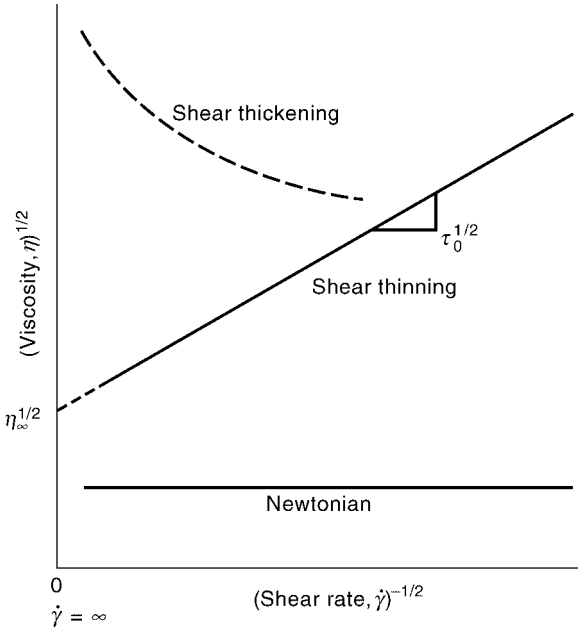

Fig. 3. Examples of Casson plots: (viscosity)$^{1/2}$ vs (shear rate)$^{-1/2}$. The Casson equation is $\eta^{1/2} = {\eta_\infty}^{1/2} + {\tau_0}^{1/2}\dot{\gamma}^{-1/2}$.

where all rheological structure has been broken down. The Casson yield stress τ_0 is somewhat different from the yield stress discussed earlier in that there may or may not be an intercept on the shear stress–shear rate curve for the material. If there is an intercept, then the Casson yield stress is quite close to that value. If there is no intercept, but the material is shear thinning, a Casson plot gives a value for τ_0 that is indicative of the degree of shear thinning.

The Williamson equation is useful for modeling shear-thinning fluids over a wide range of shear rates (13). It makes provision for limiting low and high shear Newtonian viscosity behavior (eq. 3), where τ is the absolute value of the shear stress and τ_m is the shear stress at which the viscosity is the mean of the viscosity limits η_0 and η_∞, ie, at $\eta = (\eta_0 + \eta)_\infty/2$.

$$\eta = \eta_\infty + \frac{\eta_0 - \eta_\infty}{1 + (|\tau|/\tau_m)} \tag{3}$$

The Cross equation assumes that a shear-thinning fluid has high and low shear-limiting viscosity (14) (eq. 4), where α and n are constants.

$$\eta = \eta_\infty + \frac{\eta_0 - \eta_\infty}{1 + \alpha\dot{\gamma}^n} \tag{4}$$

The value for n is often given as 2/3, but polymer melts have shown a wide range of values. The constant α is associated with rupture of the linkages in the structure

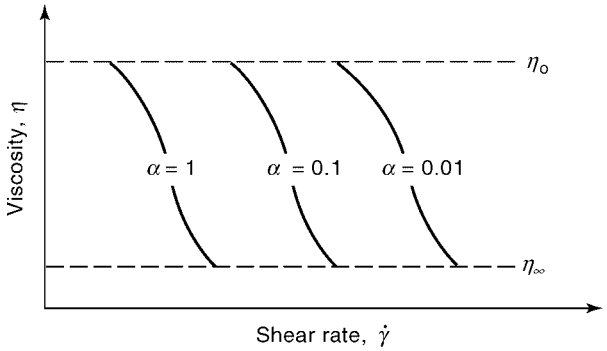

Fig. 4. Graphic representations (viscosity vs shear rate) of Cross model with different values for α.

of the fluid. The effect of different values of α, ie, at the same values of η_0 and η_∞, is shown in Figure 4. As α increases, breakdown occurs at lower and lower shear rates.

Thixotropy and Other Time Effects. In addition to the nonideal behavior described, many fluids exhibit time-dependent effects. Some fluids increase in viscosity (*rheopexy*) or decrease in viscosity (*thixotropy*) with time when sheared at a constant shear rate. These effects can occur in fluids with or without yield values. Rheopexy is a rare phenomenon, but thixotropic fluids are common. Examples of thixotropic materials are starch pastes, gelatin, mayonnaise, drilling muds, and latex paints. The thixotropic effect is shown in Figure 5, where the curves are for a specimen exposed first to increasing and then to decreasing shear rates. Because of the decrease in viscosity with time as well as shear rate, the up-and-down flow curves do not superimpose. Instead, they form a hysteresis loop, often called a thixotropic loop. Because flow curves for thixotropic or rheopectic liquids depend on the shear history of the sample, different curves for the same material can be obtained, depending on the experimental procedure.

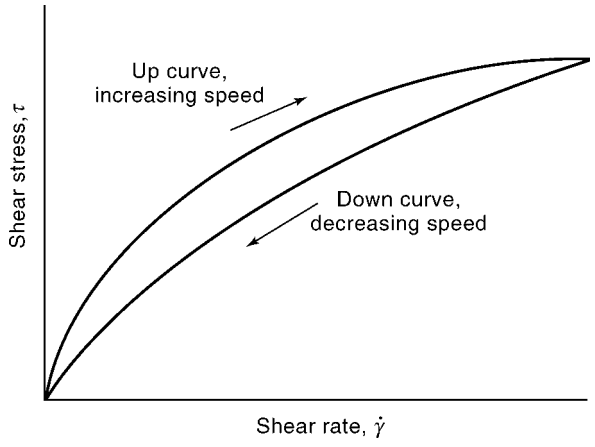

Fig. 5. Flow curves (up and down) for a thixotropic material: hysteresis loop.

Experimentally, it is sometimes difficult to detect differences between a shear-thinning liquid in which the viscosity decreases with increasing shear, and a thixotropic material in which the viscosity decreases with time, because of the combined shear and time effects that occur during a series of measurements. This is especially true if only a few data points are collected. In addition, most materials that are thixotropic are also shear thinning. In fact, one definition of a thixotropic fluid limits it to materials whose viscosity is a function of both shear rate and time (8).

Viscosity–time measurements during or after shearing can be used to show time-dependent effects. The plots in Figure 6 (15) are representative of the results of such measurements on a thixotropic material. On shearing at a given shear rate, the viscosity drops sharply at first, but the rate of change continually decreases until a constant or nearly constant level is reached. This is sometimes referred to as the sheared state. Changing to a higher shear rate causes a a further drop in viscosity. When the shear rate is reduced, the viscosity increases quickly at first, and then increases more slowly. A good example of this is the behavior of latex house paint. The shearing plot represents the brushing action, whereas the recovery plot shows what happens when the brushing stops. The thixotropic behavior allows the paint to be easily brushed to a thin film and gives a short period of time for the brush marks to level; then the viscosity increase prevents running and sagging.

Causes of time-dependent behavior include irreversible changes such as cross-linking, coagulation, degradation, and mechanical instability, and reversible changes involving the breaking and re-forming of colloidal aggregations and networks. Models of time-dependent behavior are less satisfactory and more controversial than those of shear-dependent behavior. Few comprehensive investigations of the viscosity–shear–time profiles of thixotropic and rheopectic materials have

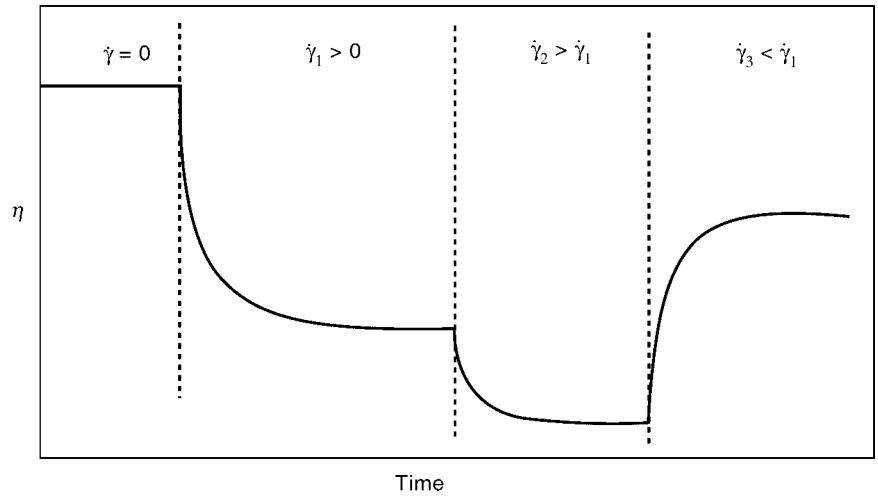

Fig. 6. Viscosity–time effects for a thixotropic material at rest ($\dot{\gamma} = 0$), at some shear rate, $\dot{\gamma}$, at an increased shear rate, and then at a lower shear rate.

been published, but there are sources that contain good discussions of thixotropy (15–17). Rheopexy has also been described (18,19).

Time-dependent effects are measured by determining the decay of shear stress as a function of time at one or more constant shear rates (20). Sequential increases in shear rate followed by equilibration allows the shear stress to reach a maximum value and then decrease exponentially toward an equilibrium level. The peak shear stress, which is obtained by extrapolating the curve to zero time, and the equilibrium shear stress are indicative of the viscosity–shear behavior of unsheared and sheared material, respectively. The stress–decay curves are indicative of the time-dependent behavior. A rate constant for the relaxation process can be determined at each shear rate. In addition, zero-time and equilibrium shear stress values can be used to construct a hysteresis loop that is similar to that shown in Figure 5, but unlike that plot, is independent of acceleration and time of shear.

Another method is the step-shear test (15), which uses controlled shearing and the recovery behavior shown in Figure 6 to characterize the material. In this method, a high shear rate ($\sim 10^4$ s^{-1}) is applied to the specimen until the viscosity falls to an equilibrium value. The shear rate then is reduced to a low value (~ 1 s^{-1}), allowing the structure to re-form and the viscosity to recover. The data can be analyzed in a number of ways. The time it takes to achieve 50% viscosity recovery or some other fraction of the original value can be used to indicate the rate of recovery. Comparisons can be made based on these times or on the time needed to reach a given viscosity. Equation 5 has been fit to the recovery curve, where $\eta\,(t)$ is the viscosity as a function of time, t; $\eta_{t=0}$, the sheared-out viscosity at recovery time zero; $\eta_{t=\infty}$, the infinite time recovered viscosity; and τ, a time constant describing the recovery rate.

$$\eta(t) = \eta_{t=0} + (\eta_{t=\infty} - \eta_{t=0})(1 - e^{-t/\tau}) \tag{5}$$

Another method for estimating thixotropy involves the hysteresis of the thixotropic loop. The area of the thixotropic loop is calculated or measured, which works well with printing inks (1). In a variation of this method, the up curve on an undisturbed sample is determined. The sample is then sheared at high shear (>2000 s^{-1}) for 30–60 s, followed by determination of the down curve (21). The data are plotted as Casson–Asbeck plots, $\eta^{1/2}$ vs $\dot{\gamma}^{-1/2}$ (12), as shown in Figure 7. Such plots are best used for comparison and ranking, but a measure of the degree of thixotropy can be gained by determining the angle formed by the two lines or the area of the triangle formed by the lines and a vertical line through a given value for $\dot{\gamma}^{-1/2}$. Additional methods for determining the degree of thixotropy have been described (7).

Results from measurements of time-dependent effects depend on the sample history and experimental conditions and should be considered approximate. For example, the state of an unsheared or undisturbed sample is a function of its previous shear history and the length of time since it underwent shear. The area of a thixotropic loop depends on the shear range covered, the rate of shear acceleration, and the length of time at the highest shear rate. However, measurements of

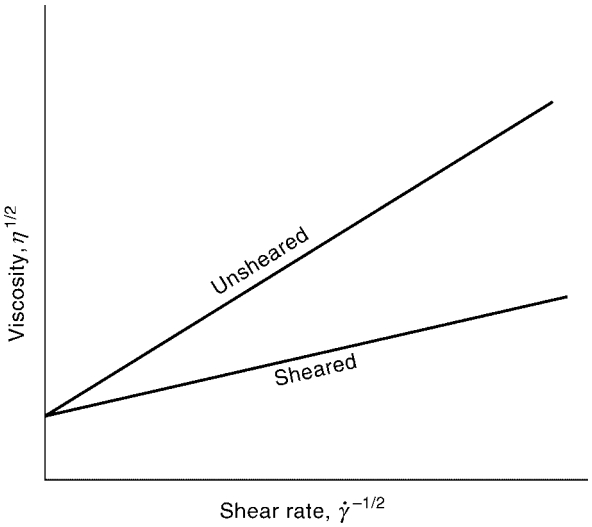

Fig. 7. Casson plots of sheared and unsheared paints. The degree of divergence of the lines is used to estimate thixotropy.

time-dependent behavior can be useful in evaluating and comparing a number of industrial products and in solving flow problems.

Effect of Temperature. In addition to being often dependent on parameters such as shear stress, shear rate, and time, viscosity is highly sensitive to changes in temperature. Most materials decrease in viscosity as temperature increases. The dependence is logarithmic and can be substantial, up to 10% change/°C. This has important implications for processing and handling of materials and for viscosity measurement.

A common expression relating viscosity to temperature is the Arrhenius equation, $\eta = A \times e^{B/T}$ or $\eta = A \times 10^{B/T}$, where A and B are constants characteristic of the polymer or other material, and T is the absolute temperature. Estimation of the viscosity of a polymer at a given temperature requires a knowledge of the viscosity at two other temperatures. This knowledge allows calculation of the constants A and B and subsequent determination of viscosities at other, intermediate temperatures.

The Arrhenius equation may also be expressed in logarithmic form (eq. 6):

$$\log \eta = \log A + B/T \tag{6}$$

For two temperatures (viscosity known at one), this expression may be written as follows (eq. 7):

$$\log(\eta_1/\eta_2) = B\left(\frac{1}{T_1} - \frac{1}{T_2}\right) \tag{7}$$

In practice, plots of $\log \eta$ vs $1/T$ tend to be straight lines over a considerable range of values. Such plots may be used to predict viscosity at one temperature

from viscosities at other temperatures. Likewise, previously measured viscosity–temperature curves for commerical products are often used to ensure meaningful viscosity data for quality assurance even where temperature control is not possilbe.

The Arrhenius equation holds for many solutions and for polymer melts well above their glass-transition temperatures. For polymers closer to their T_g and for concentrated polymer and oligomer solutions, the Williams–Landel–Ferry (WLF) equation (22) works better (23,24). With a proper choice of reference temperature T_s, the ratio of the viscosity to the viscosity at the reference temperature can be expressed as a single universal equation (eq. 8):

$$\log(\eta/\eta_s) = \frac{-8.86(T - T_s)}{101.6 + (T - T_s)} \tag{8}$$

Because T_s is often defined as $T_g + 50$ K, the equation thus becomes

$$\log(\eta/\eta T_g) = \frac{-17.4(T - T_g)}{51.6 + (T - T_g)}$$

In general, the WLF equation holds over the temperature range T_g to $(T_g + 100^\circ\text{C})$.

Dilute Polymer Solutions. The measurement of dilute solution viscosities of polymers is widely used for polymer characterization. Very low concentrations reduce intermolecular interactions and allow measurement of polymer–solvent interactions. These measurements are usually made in capillary viscometers, some of which have provisions for direct dilution of the polymer solution. The key viscosity parameter for polymer characterization is the limiting viscosity number or intrinsic viscosity, $[\eta]$. It is calculated by extrapolation of the viscosity number (reduced viscosity) or the logarithmic viscosity number (inherent viscosity) to zero concentration.

The *viscosity ratio* or *relative viscosity*, η_{rel}, is the ratio of the viscosity of the polymer solution to the viscosity of the pure solvent. In capillary viscometer measurements, the relative viscosity (dimensionless) is the ratio of the flow time for the solution t to the flow time for the solvent t_0 (Table 2). The specific (sp) viscosity (dimensionless) is also defined in Table 2, as is the viscosity number or reduced (red) viscosity, which has the units of cubic meters per kilogram (m^3/kg) or deciliters per gram (dL/g). The logarithmic viscosity number or inherent (inh) viscosity likewise has the units m^3/kg or dL/g. For η_{red} and η_{inh}, c, the concentration of polymer, is expressed in convenient units, traditionally g/100 cm^3 but kg/m^3 in SI units. The viscosity number and logarithmic viscosity number vary with concentration, but each can be extrapolated (Fig. 8) to zero concentration to give the limiting viscosity number (intrinsic viscosity) (Table 2). Usually, measurements at four or five concentrations are needed.

The specific viscosity can also be represented by (25)

$$\eta_{sp} = [\eta]c + k_1[\eta]^2 c^3$$

Table 2. Viscosity Expressions

Common name	Recommended name	Definition	Common units
Relative viscosity	Viscosity ratio	$\eta_{rel} = t/t_0 = \eta/\eta_0$	None
Specific viscosity		$\eta_{sp} = (\eta - \eta_0)/\eta_0 = \eta_{rel}^{-1}$	None
Reduced viscosity	Viscosity number	$\eta_{red} = \eta_{sp}/c = \left(\eta_{rel}^{-1}\right)\Big/c$	dL/g
Inherent viscosity	Logarithmic viscosity number	$\eta_{inh} = (\ln \eta_{rel})/c$	dL/g
Intrinsic viscosity	Limiting viscosity number	$[\eta] = \text{limit}_{c\to 0} \frac{\eta_{rel}}{c} = \text{limit}_{c\to 0} \frac{\ln \eta_{rel}}{c}$	dL/g

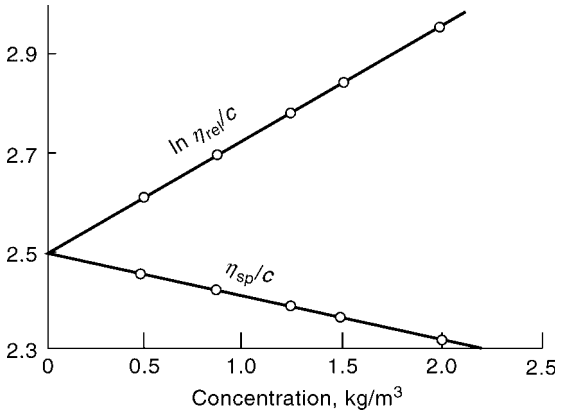

Fig. 8. Plots of viscosity number ($\eta_{rel} = \eta_{sp}/c$) and the logarithmic viscosity number ($\eta_{inh} = \eta_{rel}/c$) vs concentration. Extrapolations to zero concentration give the limiting viscosity number $[\eta]$.

which becomes the Huggins equation (26)

$$\eta_{sp}/c = [\eta](1 - k_h[\eta]c)$$

where k_h is the Huggins viscosity constant, the most commonly used dilute solution viscosity number or index. It is easily determined from the slope of a plot of η_{sp}/c vs c such as the lower plot in Figure 8. The Huggins constant can be thought of as a measure of the "goodness" of the solvent for the polymer with values around 0.3 in good solvents and 0.5–1 in theta solvents. A large number of Huggins constants can be found in Reference 25 along with constants for another semiempirical equation relating viscosity and concentration, that of Schulz and Blaschke (27).

The Huggins equation and Huggins constants can be used to determine values for $[\eta]$ (28,29). The latter gives an equation

$$[\eta] = (1 + 4k_h\eta_{sp})^{1/2} - 1/2k_hc$$

that can be used for single-point determinations (calculations from a single viscosity measurement at a known concentration). The general validity of single-point methods has been questioned, however (30). An even simpler but equally useful method is to approximate $[\eta]$ by the logarithmic viscosity number of a single sufficiently dilute solution: $[\eta]\eta_{inh} = (\ln \eta_{rel})/c$, where c = 1–2 kg/m^3 or 0.1–0.2 g/100 cm^3.

The limiting viscosity number depends on the polymer, solvent, and temperature, but under a given set of conditions it is related to the molecular weight by the Mark–Houwink relation, $[\eta] = KM^a$, where K and a are constants and M is the molecular weight of the polymer. Tables of K and a are available for a large number of polymers and solvents (31,32). Excellent summaries of equations, techniques, and references relating to the viscosity of dilute polymer solutions are also available (33,34), as is information on dilute polymer solutions that are shear thinning (35).

Concentrated Polymer Solutions. Knowledge of the viscosity behavior of concentrated solutions (36–38) is important to the manufacture and application of caulks, adhesives, inks, paints, and varnishes. It is also useful for designing and controlling polymer manufacturing processes, fiber spinning, and film casting. Viscosity behavior can be investigated by a variety of methods, including the use of simple capillary viscometers, extrusion rheometers, and rotational viscometers. Unlike dilute solutions, concentrated polymer solutions show a vast amount of interaction between the macromolecules. The degree of interaction is governed by the concentration, the characteristics of the chains, and the nature of the solvent. A convenient measure of concentration is the dimensionless reduced concentration $\tilde{c}$, which is the product of the concentration and the limiting viscosity number (intrinsic viscosity) $[\eta]$ (36). The transition from dilute to concentrated solutions occurs at a critical concentration c_c and corresponds to c values of several units. In addition, at a critical molecular weight, where $M > M_c$ and $c > c_c$, a fluctuating entanglement network forms. For a concentrated solution, properties above and below M_c may be quite different. For example, the dependence of viscosity on molecular weight, which is much greater in concentrated than in dilute solutions, changes from a value on the order of unity below M_c to one of 3.4–3.5 above M_c (37,39,40). That is, $\eta = KM$ below M_c and $\eta = KM^{3.4-3.5}$ above M_c. Viscosity in these expressions should be the zero-shear viscosity η_0, but because the relationships hold for low shear measurements in many cases, the notation remains in the more general form η.

The break point above which entanglement occurs varies widely with molecular structure; a range of 3,800–36,000 molecular weight has been shown (41). In highly concentrated oligomeric solutions such as high solids organic coatings (volume fraction > 0.7), high dependencies of viscosity on molecular weight occur even at low molecular weights (42–44). This is probably on account of hydrogen bonding that causes the stringing together of short chains or the formation of a loose network, thereby increasing the effective chain length. Something similar to

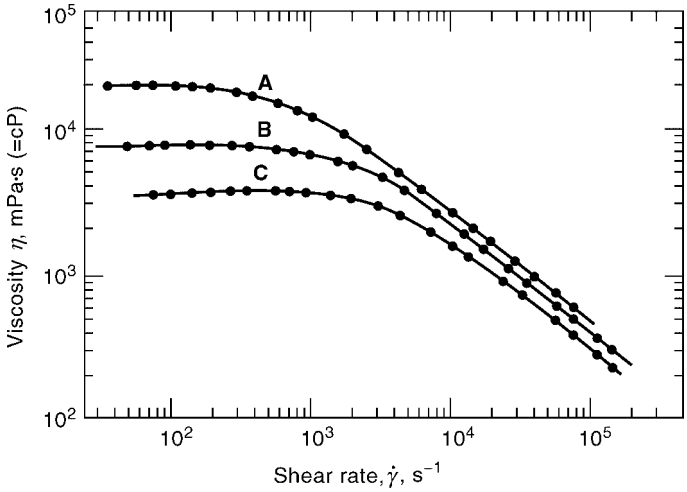

Fig. 9. Viscosity vs shear rate for solutions of a styrene–butadiene–styrene block copolymer (46). (**A**) Cyclohexanone, where $c = 0.248$ g/cm^3; (**B**) *o*-xylene, where $c = 0.246$ g/cm^3; (**C**) toluene, where $c = 0.248$ g/cm^3. Courtesy of the Society of Plastics Engineers, Inc.

this has been seen with the formation of viscosity-building needle-like structures by low molecular weight materials (45).

Depending on the concentration, the solvent, and the shear rate of measurement, concentrated polymer solutions may give wide ranges of viscosity and appear to be Newtonian or non-Newtonian. This is illustrated in Figure 9, where solutions of a styrene–butadiene–styrene block copolymer are Newtonian and viscous at low shear rates, but become shear thinning at high shear rates, dropping to relatively low viscosities beyond 10^5 s^{-1} (46). The shear rate at which the break in behavior occurs depends on the concentration and on the solvent.

Melt Viscosity. The study of the viscosity of polymer melts (47–62) is important for the manufacturer who must supply suitable materials and for the fabrication engineer who must select polymers and fabrication methods. Thus, melt viscosity as a function of temperature, pressure, rate of flow, and polymer molecular weight and structure is of considerable practical importance. Polymer melts exhibit elastic as well as viscous properties. This is evident in the swell of the polymer melt upon emergence from an extrusion die, a behavior that results from the recovery of stored elastic energy plus normal stress effects. Theoretical developments include a constitutive equation that correctly captures nonlinear behavior in both elongation and shear (63,64).

A number of experimental methods have been applied to measure the melt viscosity of polymers (53–55,65), but capillary extrusion techniques probably are generally preferred. Rotational methods are also used, and some permit the measurement of normal stress effects resulting from elasticity as well as of viscosity. Slit rheometers can also be used to measure normal stress (66). Oscillatory shear measurements are useful for measuring the elasticity of polymer melts (57,58). Controlled stress methods have also been applied (59). Squeeze film flow has also been proposed as a geometry suitable for processibility testing of polymer melts

(60). Nonlinear viscoelastic behavior is found in many molten plastics. Theoretical (67) as well as practical approaches address this issue, including a sliding plate normal-thrust rheometer (68,69).

Polymer melts show a low shear rate Newtonian limit and a region of diminishing viscosity with increasing shear rate. Although it is likely that a high shear rate Newtonian region exists, this has generally not been observed experimentally because of the effects of heat generation and polymer degradation at high shear rates.

The limiting low shear or zero-shear viscosity η_0 of the molten polymer can be related to its weight-average molecular weight M_w by the same relations noted for concentrated solutions: $\eta_0 = KM_w$ for low molecular weight and $\eta_0 = KM_w^{3.5}$ for high molecular weight.

The transition between two forms of behavior occurs at a critical molecular weight M_c, which corresponds to a critical chain length, Z_c. The transition is clearly shown in Figure 10, which is a plot of Newtonian viscosity vs chain length in terms of carbon atoms for a series of molten polyethylenes (34). This transition is thought to be related to chain fluctuations in the polymer melt in such a way that the motion changes from displacement of whole chains to restricted motion called *reptation*, ie, wiggly, snake-like motion within the tight tube formed by the matrix of neighboring chains (70–73). Polymer entanglement and reptation

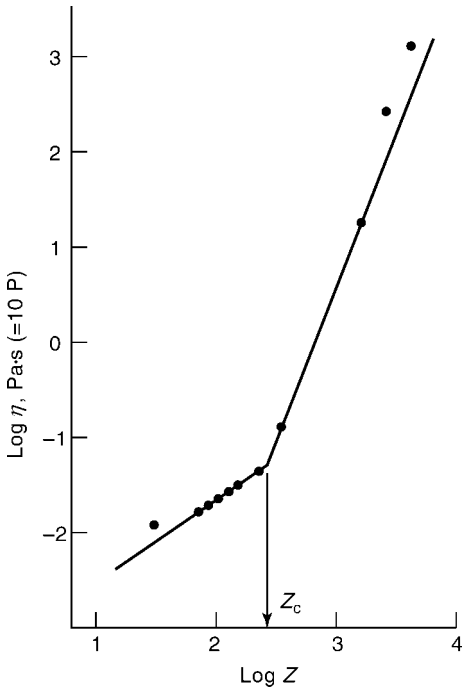

Fig. 10. Newtonian viscosity vs chain length in terms of the number of carbon atoms for a series of molten polyethylenes. To convert Pa·s to P, multiply by 10. Courtesy of Springer Verlag.

have considerable influences on melt rheology, particularly on viscoelasticity, with many consequences for the molding and extrusion of plastics.

The viscosity–molecular weight relationships noted above hold for narrow molecular weight distribution polymers. For polymers having broad molecular weight distributions, viscosity depends on a molecular weight average between M_w and the next higher average M_z (z average), approaching M_z as the distribution broadens. Branching can have a considerable effect, reducing or increasing the viscosity depending on the ratio of the length of the branch to the entanglement length (74). The flow curve for a polymer melt can be predicted from the molecular weight distribution (75) and, under some circumstances, a molecular weight distribution can be determined from the flow curve (76,77). As might be expected, fillers also have an effect on melt viscosity (78).

The dependence of viscosity on temperature is critical to the handling of molten polymers in molding, extrusion, and other manufacturing processes. In fact, the drop in viscosity with increasing temperature makes these operations possible. Therefore, viscosity–temperature relationships are important. Data for many polymers can be found in the literature (47–56). The behavior of others can be determined by viscosity measurements over a range of temperatures. Viscosity–stress master curves are useful in the prediction of viscosity at a given temperature (79). The viscosity–stress curves shown in Figure 11 (47) are approximately superimposable by shifting at constant stress.

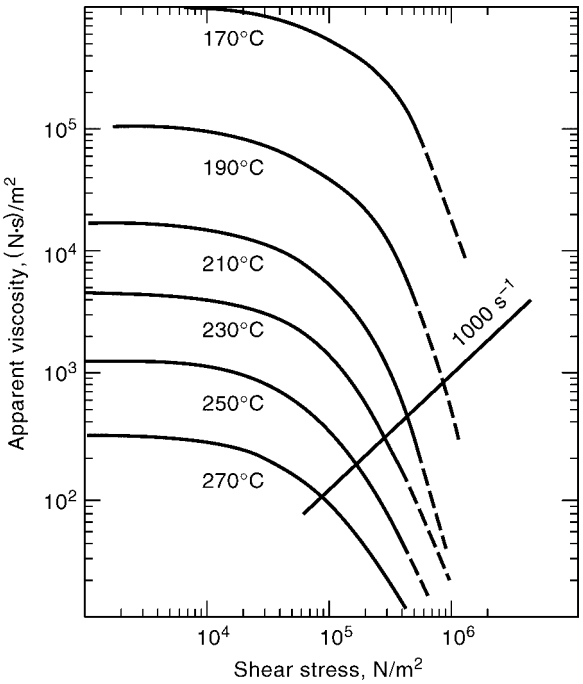

Fig. 11. Viscosity at different temperatures measured by a capillary viscometer: injection-molding grade of poly(methyl methacrylate) (47). To convert N/m^2 to psi, multiply by 145; to convert $(N \cdot s)/m^2$ to $(dyn \cdot s)/cm^2$(P), multiply by 10.

The temperature dependence of melt viscosity at temperatures considerably above T_g approximates an exponential function of the Arrhenius type. However, near the glass transition the viscosity temperature relationship for many polymers is in better agreement with the WLF treatment (22).

Melt viscosity is also affected by pressure (47,80,81). The compression of a melt reduces the free volume and therefore raises the viscosity. For example, the viscosity of low density polyethylene increases by a factor of roughly 10 over a static pressure range of 34–170 MPa (5,000–25,000 psi).

Dispersed Systems. Many fluids of commercial and biological importance are dispersed systems, such as solids suspended in liquids (dispersions) and liquid–liquid suspensions (emulsions). Examples of the former include inks, paints, pigment slurries, and concrete; examples of the latter include mayonnaise, butter, margarine, oil-and-vinegar salad dressing, and milk. Dispersion of a solid or liquid in a liquid affects the viscosity. In many cases Newtonian flow behavior is transformed into non-Newtonian flow behavior. Shear thinning results from the ability of the solid particles or liquid droplets to come together to form network structures when at rest or under low shear. With increasing shear the interlinked structure gradually breaks down, and the resistance to flow decreases. The viscosity of a dispersed system depends on hydrodynamic interactions between particles or droplets and the liquid, particle–particle interactions (bumping), and interparticle attractions that promote the formation of aggregates, flocs, and networks.

Emulsions have not been studied as thoroughly as dispersions, probably because of the greater complexity of the former. Emulsions tend to be unstable, and frequently droplets begin to coalesce soon after the emulsion forms. Thus the emulsion is continually changing. In addition, droplets may change shape under shear or when packed tightly together. This makes it difficult to apply theories developed for solid spheres or other well-defined geometries of shape.

Detailed treatments of the rheology of various dispersed systems are available (82–88), as are reviews of the viscous, elastic, and yield behavior of dispersions (89–92), of the flow properties of concentrated suspensions (90,93–99), and of viscoelastic properties (100–102).

The viscosities of dilute dispersions have received considerable theoretical and experimental treatment, partly because of the similarity between polymer solutions and small particle dispersions at low concentration. Nondeformable spherical particles are usually assumed in the cases of molecules and particles. The key viscosity quantity for dispersions is the relative viscosity or viscosity ratio, η_{rel}.

$$\eta_{rel} = \frac{\eta}{\eta_0} = \frac{\text{Dispersion viscosity}}{\text{Viscosity of liquid}} \tag{9}$$

This is because the effect of the dispersed solid, rather than the dispersing medium, is usually more significant. However, the latter should not be ignored. Many industrial problems involving unacceptably high viscosities in dispersed systems are solved by substituting solvents of lower viscosity.

The relative viscosity of a dilute dispersion of rigid spherical particles is given by $\eta_{rel} = 1 + a\phi$, where a is equal to $[\eta]$, the limiting viscosity number (intrinsic viscosity) in terms of volume concentration, and ϕ is the volume fraction. Einstein has shown that, provided that the particle concentration is low enough and certain

other conditions are met, $[\eta] = 2.5$, and the viscosity equation is then $\eta_{rel} = 1 + 2.5\phi$. This expression is usually called the Einstein equation.

For higher ($\phi > 0.05$) concentrations where particle–particle interactions are noticeable, the viscosity is higher than that predicted by the Einstein equation. The viscosity–concentration equation becomes equation 10, where b and c are additional constants (103).

$$\eta_{rel} = 1 + 2.5\phi + b\phi^2 + c\phi^3 + \cdots \tag{10}$$

The deviation from the Einstein equation at higher concentrations is represented in Figure 12, which is typical of many systems (104,105). The relative viscosity tends to infinity as the concentration approaches the limiting volume fraction of close packing ϕ_m ($\phi = \sim 0.7$). Equation 10 has been modified (106,107) to take this into account, and the expression for η_{rel} becomes (eq. 11)

$$\eta_{rel} = \frac{1 + 2.5\phi + b\phi^2 + c\phi^3 + \cdots}{1 - (\phi_m/\phi)} \tag{11}$$

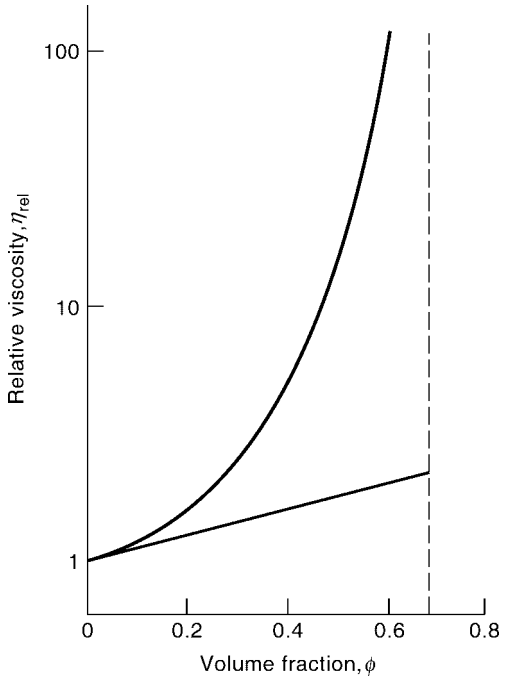

Fig. 12. Relative viscosity vs volume fraction for a typical dispersion (curved line), where the solid straight line represents the Einstein relationship $[\eta] = 2.5$, and the dashed line is an approximate value for the limiting volume fraction ϕ_m.

Another model that has been successful in fitting much data is the Krieger–Dougherty equation (eq. 12) (8,108):

$$\eta_{\mathrm{rel}} = \left(1 - \frac{\phi}{\phi_{\mathrm{m}}}\right)^{-[\eta]\phi_{\mathrm{m}}} \tag{12}$$

Factors other than concentration affect the viscosity of dispersions. A dispersion of nonspherical particles tends to be more viscous than predicted if the Brownian motion is great enough to maintain a random orientation of the particles. However, at low temperatures or high solvent viscosities, the Brownian motion is small and the particle alignment in flow (streamlining) results in unexpectedly lower viscosities. This is a form of shear thinning.

If the dispersion particles are attracted to each other, they tend to flocculate and form a structure. At low concentrations the particles form open aggregates, which give a fractal structure (109,110). At higher concentrations a network structure results, which can be so pronounced that the mixture has a yield point and behaves like a solid when at rest. Shearing breaks up this structure, and viscosity decreases.

If the volume concentration of the solid in the dispersion is high enough, shearing may produce an increase rather than a decrease in viscosity. Such behavior, called *shear thickening* (8,16,111–114) or *dilatancy*, is common in dispersions of certain pigments and other powders. These dispersions are closely packed, but are usually shear thinning up to moderate shear rates, ie, a few hundred to a few thousand per second. Higher shear introduces irregularities in the packing, with bridging effects occurring between the particles. The overall packing loosens, which implies that the total space between particles increases. The liquid is not able to fill this space and can no longer wet all the particles. Much of the lubricating effect of the liquid is therefore lost, and internal friction rises, producing a high viscosity. This is true dilatancy, and the volume actually increases. Shear thickening can also occur in dilute suspensions (115). In such cases there is no volume expansion; instead there is buildup of particle aggregates which ultimately produces a network that behaves like a gel.

Because emulsions are different from dispersions, different viscosity–concentration relationships must be used (82,103). In an emulsion the droplets are not rigid, and viscosity can vary over a wide range. Several equations have been proposed to account for this. An extension of the Einstein equation includes a factor that allows for the effect of variations in fluid circulation within the droplets and subsequent distortion of flow patterns (116,117).

Extensional Viscosity. In addition to the shear viscosity η, two other rheological constants can be defined for fluids: the bulk viscosity, K, and the extensional or elongational viscosity, η_{e} (36,52,53,118–125). The bulk viscosity relates the hydrostatic pressure to the rate of deformation of volume, whereas the extensional viscosity relates the tensile stress to the rate of extensional deformation of the fluid. Extensional viscosity is important in a number of industrial processes and problems (36,118,126–128). Shear properties alone are insufficient for the characterization of many fluids, particularly polymer melts (119,125,129,130).

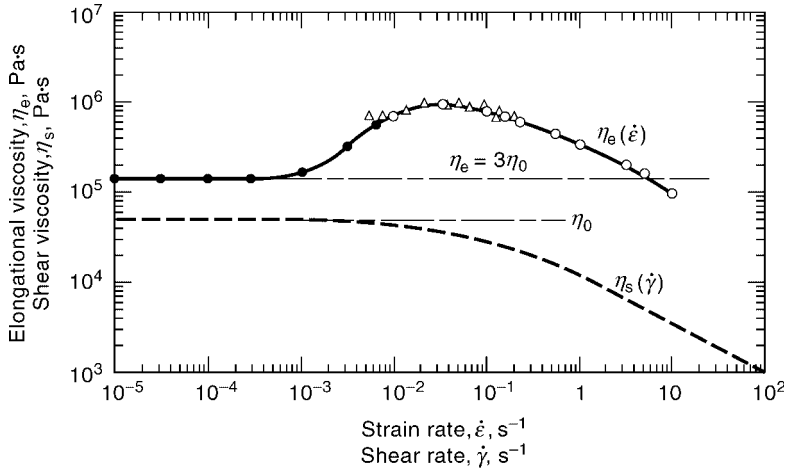

Fig. 13. Shear viscosity, η_s, and extensional viscosity, η_e, as a function of deformation rate of a low density polyethylene (LDPE) at 150°C (129). To convert Pa·s to P, multiply by 10. Courtesy of *Rheologica Acta*.

Extensional flows occur when fluid deformation is the result of a stretching motion. Extensional viscosity is related to the stress required for the stretching. This stress is necessary to increase the normalized distance between two material entities in the same plane when the separation is s and the relative velocity is ds/dt. The deformation rate is the extensional strain rate, which is given by equation 13 (126):

$$\dot{\varepsilon} = \frac{1}{s}\frac{ds}{dt} \tag{13}$$

Unlike shear viscosity, extensional viscosity has no meaning unless the type of deformation is specified. The three types of extensional viscosity identified and measured are uniaxial or simple, biaxial, and pure shear. Uniaxial viscosity is the only one used to characterize fluids. It has been employed mainly in the study of polymer melts, but also for other fluids. For a Newtonian fluid, the uniaxial extensional viscosity is three times the shear viscosity: $(\eta_e)_{uni} = 3\eta$. This is confirmed at very low shear rates in Figure 13, which provides a typical example of the extensional viscosity behavior of a polymer (129). The two other extensional viscosities are used to study elastomers in the form of films or sheets. Uniaxial and biaxial extensions are important in industry (118,125–128,130,132), the former for the spinning of textile fibers and roller spattering of paints, and the latter for blow molding, vacuum forming, film blowing, and foam processes.

Electrorheological Behavior. Electrorheological (ER) fluids are colloidal suspensions whose properties change strongly and reversibly upon application of an electric field. When an electric field is applied to an ER fluid, it responds by forming fibrous or chain structures parallel to the applied field. These structures greatly increase the viscosity of the fluid, by a factor of 10^5 in some cases. At low

shear stress the material behaves like a solid. The material has a yield stress, above which it will flow, but with a high viscosity.

A parameter used to characterize ER fluids is the Mason number, M_a, which describes the ratio of viscous to electrical forces, and is given by equation 14, where ε is the solvent dielectric constant; η_0, the solvent viscosity; $\dot{\gamma}$, the strain or shear rate; β, the effective polarizability of the particles; and E, the electric field (133).

$$M_a = \frac{24\pi\varepsilon\eta_0\dot{\gamma}}{(\beta E)^2} \tag{14}$$

A considerable literature on ER fluids and their measurement has developed: a selection of reviews and papers is given in References 134–163. There is an analogous magnetorheological (MR) effect where suspensions filled with magnetic particles show reversible changes in their rheological behavior when subjected to a magnetic field (163–168). Measurements on ER and MR fluids are made with viscometers modified to allow the the application of electric or magnetic fields.

Elasticity and Viscoelasticity

Elastic deformation is a function of stress and is expressed in terms of relative displacement or strain. Strain may be expressed in terms of relative change in volume, length, or other measurement, depending on the nature of the stress. An ideal elastic body (169,170) is a material for which the strain is proportional to the stress (Hooke's law) with immediate recovery to the original volume and shape when the stress is released. The relationship between the stress σ and strain ε may be written as $\sigma = K\varepsilon$, where K is a proportionality constant called the modulus of elasticity. For a homogeneous, isotropic, Hookean solid, three moduli may be defined. Young's modulus, E, relates tensile stress to tensile strain. The shear modulus, G, relates shear stress to shear strain, ie, $G = \tau/\gamma$. The bulk modulus B relates hydrostatic pressure to the change in volume. Another elastic constant needed for complete specification of behavior in tension is Poisson's ratio, μ, which relates change in volume to change in shape. Incompressible solids and polymer melts have $\mu = 0.5$, but for most solid materials, $\mu < 0.5$. For isotropic, Hookean materials, Young's modulus is related to the shear modulus by $E = 2G(1 + \mu)$. If μ is 0.5, Young's modulus is three times the shear modulus. Values for the various moduli and Poisson's ratio for some representative materials are given in Table 3.

Materials such as metals are nearly elastic and show almost no flow or viscous component. Polymers and many of their solutions are both viscous and elastic, and both types of deformation must be taken into account to explain their behavior (see VISCOELASTICITY).

Mechanical Behavior of Materials. Different kinds of materials respond differently when they undergo mechanical stress. For purely viscous behavior, stress is relieved by viscous flow and is independent of strain. For purely elastic behavior, there is a direct dependence of stress on strain and the ratio of the two is the modulus E (or G).

Table 3. Measured Values of Elastic Constants at Small Extensions and 25°C[a]

Material	Young's modulus, E, GPa[b]	Proportionality limit[c] % extension	Shear modulus, G, GPa[b]	Poisson's ratio, μ	Bulk modulus, B, GPa[b]
Vitreous silica	70.0	3	30.5	0.14	37.4
Mild steel	200–220	2.5	76–83	0.29	160.0
Brass	80–100	2	26–38	0.25–0.4	61
Constantan	163	2	61	0.33	160.0
Nickel	200–220	2	78–80	0.30	170.0
Tin	39–55		17–20	0.33	52
Silver	60–80	2	24–28	0.38	100
Granite	ca 30	0.5	ca 10	ca 0.3	ca 30
Gelatin gel[d]	2×10^{-4}	10		0.50	
Dry wood					
Axial piece	4–18	1			
Radial piece	~1	1			
Silk thread	6.4	1			
Natural rubber	8.6×10^{-4}	400–600	2.9×10^{-4}	0.49	0.019
Hard rubber	0.36	3			
Phenolic resin, mineral-filled	2.4	2			
Nylon	0.31	3			
Polyethylene	0.010	2			

[a] Ref. 20.
[b] To convert GPa to psi, multiply by 145,000.
[c] Values are approximate.
[d] 80% H_2O.

The response of different materials to a constant stress applied at time $t = t_0$ followed by removal of that stress at $t = t_1$, ie, creep and recovery, is shown in Figure 14 (171). For an elastic material (Fig. 14**a**), the resulting strain is instantaneous and constant until the stress is removed, at which time the material recovers and the strain immediately drops back to zero. In the case of the viscous fluid (Fig. 14**b**), the strain increases linearly with time. When the load is removed, the strain does not recover but remains constant. Deformation is permanent. The

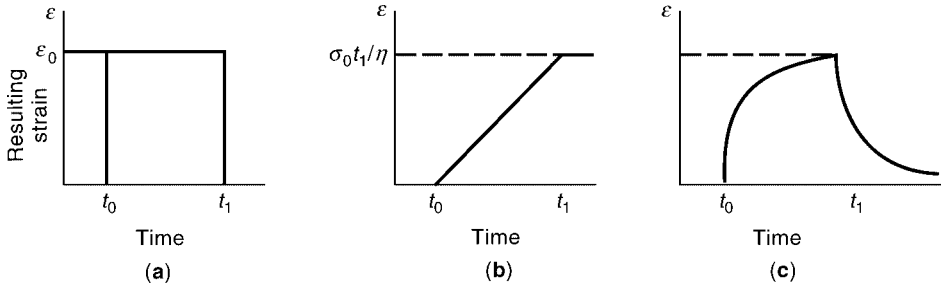

Fig. 14. Response (strain) of different idealized materials to an instantaneous application of a stress at time $t = t_0$: (**a**) elastic, (**b**) viscous, and (**c**) viscoelastic.

response of the viscoelastic material (Fig. 14**c**) draws from both kinds of behavior. An initial instantaneous (elastic) strain is followed by a time-dependent strain. When the stress is removed, the initial strain recovery is elastic, but full recovery is delayed to longer times by the viscous component.

Mechanical Models. Because the complex rheological behavior of viscoelastic bodies is difficult to visualize, mechanical models are often used. In these models the viscous response to applied stress is assumed to be that of a Newtonian fluid and is represented by a dashpot, ie, a piston operating in a cylinder of Newtonian fluid. The elastic response is idealized as an ideal elastic (Hookean) solid and is represented by a spring. The dashpot represents the dissipation of energy in the form of heat, whereas the spring represents a system that stores energy. Mechanical behavior of materials may be approximated by combinations of springs and dashpots. These models, which are largely being replaced by mathematical (integral and differential) models, have been covered in detail elsewhere (8,10,20,103,171,172).

Whether a viscoelastic material behaves as a viscous liquid or an elastic solid depends on the relation between the time scale of the experiment and the time required for the system to respond to stress or deformation. Although the concept of a single relaxation time is generally inapplicable to real materials, a *mean characteristic time* can be defined as the time required for a stress to decay to 1/*e* of its elastic response to a step change in strain. The ratio of this characteristic time to the time scale of the experiment, t_e, is called the Deborah number. A material at a high Deborah number responds elastically, whereas that at a low Deborah number exhibits viscous behavior: at $t_e \ll \lambda$, it behaves like an elastic solid; at 0 $t_e > \lambda$, like a viscous liquid. These effects can be seen in geological strata, where rock has flowed to relieve the stresses imposed by geological events. The time scale is long, and the material appears to be viscous.

Dynamic Behavior. Knowledge of the response of materials to stress–strain, creep, and stress–relaxation measurements are useful to define material properties. The dynamic response of viscoelastic materials to cyclic stresses or strains is also important, partly because cyclic motion occurs in many processing operations and applications, and partly because so much rheological information can be gained from dynamic measurements. By subjecting a specimen to oscillatory stress and determining the response, both the elastic and viscous or damping characteristics can be obtained. Elastic materials store energy, whereas liquids dissipate it as heat. This dissipation results in highly damped motion. Viscoelastic materials exhibit both elastic and damping behavior. The latter causes the deformation to be out of phase with the stress applied in the dynamic measurement.

A sinusoidal stress applied to an ideal elastic material produces a sinusoidal strain proportional to the stress amplitude and in phase with it. For ideal viscous materials the stress and strain are out of phase by 90°. Figure 15 gives an example of a stress–strain diagram for a sinusoidal stress applied to a real material. The amplitude of the deformation (strain) in response to the stress is proportional to that of the stress, but lags behind the strain curve by some angle δ between 0 and 90°, depending on the elastic/viscous characteristic of the material. This behavior is usually analyzed by the use of complex variables to represent stress and strain. These variables, complex stress and complex strain, ie, τ^* and γ^*, respectively, are

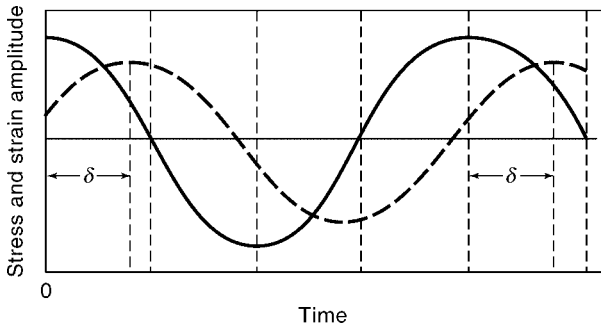

Fig. 15. Viscoelastic material: stress (—) and strain (---) amplitudes vs time where δ is the phase angle that defines the lag of the strain behind the stress.

vectors in complex planes. They can be resolved into real (in phase) and imaginary (90° out of phase) components.

The complex stress is $\tau^* = \tau' + i\tau''$, which is the sum of a real part of the stress and an imaginary part; the complex strain is $\gamma^* = \gamma' + i\gamma''$, where i is the operator $\sqrt{-1}$ that signifies the rotation of 90° between τ' and τ' and γ' and γ''. The shear modulus can also be represented by a complex variable, ie, the complex dynamic modulus G^*, which is the ratio of the complex stress and complex strain: $G^* = \tau^*/\gamma^*$. The dynamic modulus can also be resolved into two components or vectors (G' and G'): $G^* = G' + iG''$, where equation 15 holds, and where $G' = G^* \cos\delta$ and $G' = G^* \sin\delta$.

$$G^* = [(G')^2 + (G'')^2]^{-1} \tag{15}$$

The parameter G' is called the storage modulus. It is in phase with the real components of γ^* and τ^* and is a measure of elasticity. It is associated with the energy stored in elastic deformation and is approximately equal to the elastic modulus determined in creep and stress–relaxation experiments when measured at appropriate timescales, ie, $G'(\omega)G(t)$ when $t = 1/\omega$. The value of G' is high when a polymer is in its glassy state, but drops with increasing temperature as the polymer goes through the glass transition and becomes soft and rubbery (Fig. 16). If the polymer is cross-linked, the storage modulus does not drop so far after the glass transition. The exact level depends on the degree of cross-linking. For viscoelastic melts it is common practice to associate G' with the ability of a melt to recover from a deformation. However, this has been shown to be invalid in some cases, and an association with the stiffness of the melt is preferred (173).

G' is called the loss modulus. It arises from the out-of-phase components of γ^* and τ^* and is associated with viscous energy dissipation, ie, damping. The ratio of G'' and G' gives another measure of damping, the dissipation factor or loss tangent (often just called tan δ), which is the ratio of energy dissipated to energy stored (eq. 16).

$$\tan\delta = G''/G' \tag{16}$$

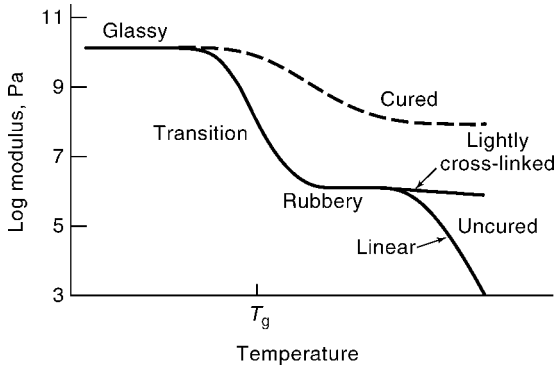

Fig. 16. Generalized modulus–temperature curves for polymeric materials, showing the high modulus glassy state, glass-transition regions for cured and uncured polymers, plateau regions for cross-linked polymers, and the drop-off in modulus for a linear polymer.

Plots of loss modulus or tan δ vs temperature for polymers give peaks at energy absorbing transitions, such as the glass transition and low temperature secondary transitions (Fig. 17). Such plots are useful for characterizing polymers and products made from them.

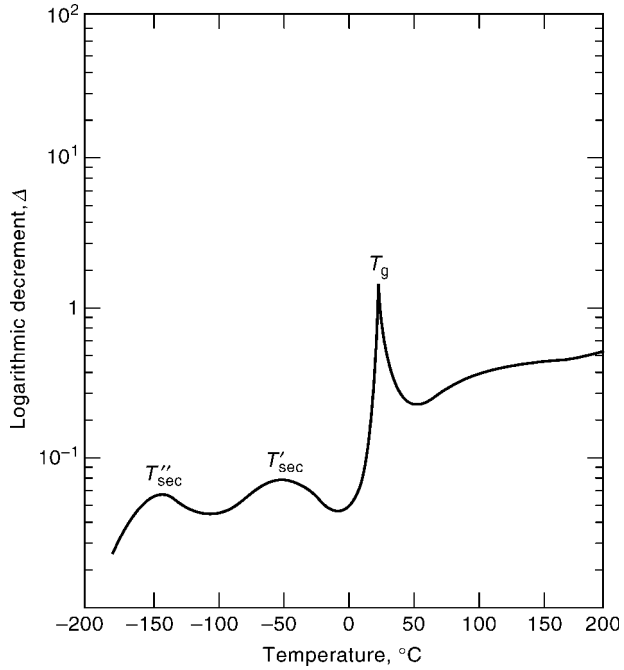

Fig. 17. Logarithmic decrement (related to tan δ and loss modulus) vs temperature for a fluorocarbon dibenzoxazole (174). After drying up to 200°C, the experiment was conducted at 200 → −180 → 200°C: $\Delta T/\Delta t = \pm 1.5$°C/min in a helium atmosphere. The T_g gives a sharp damping peak, whereas the secondary glassy state transitions, T_{sec}, are very broad.

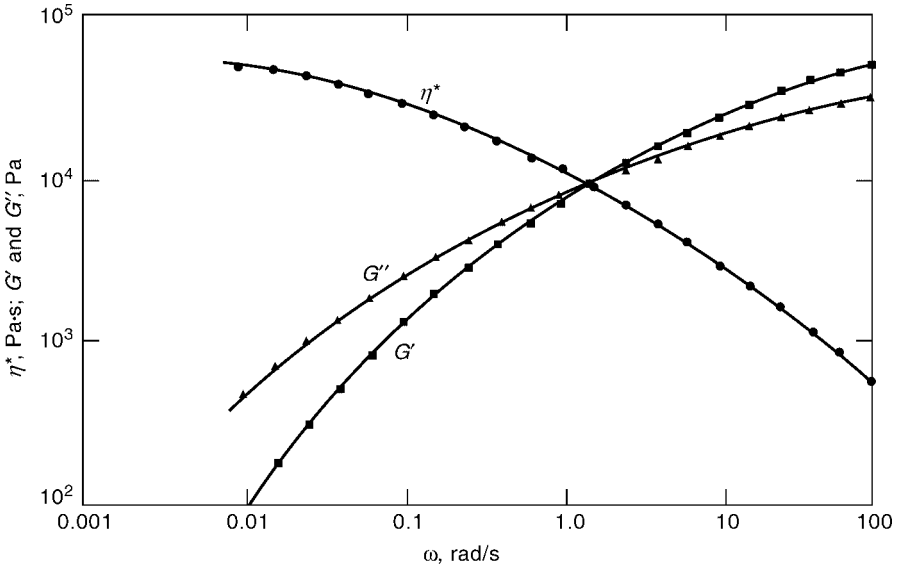

Fig. 18. Dynamic viscoelastic properties of a low density polyethylene (LDPE) at 150°C: complex dynamic viscosity η^*, storage modulus G', and loss modulus G' vs angular velocity, ω. To convert Pa·s to P, multiply by 10; to convert Pa to dyn/cm^2, multiply by 10. Courtesy of Rheometric Scientific.

A viscoelastic material also possesses a complex dynamic viscosity, $\eta^* = \eta' + i\eta''$, and it can be shown that $\eta^* = G^*/i\omega$; $\eta' = G'/\omega$; and $\eta'' = G'/\omega$, where ω is the angular frequency. The parameter η^* is useful for many viscoelastic fluids in that a plot of its absolute value η^* vs angular frequency in rad/s is often numerically similar to a plot of shear viscosity η vs shear rate. This correspondence is known as the Cox–Merz empirical relationship (175,176). The parameter η' is called the dynamic viscosity and is related to G', the loss modulus; the parameter η'' does not deal with viscosity, but is a measure of elasticity.

The significance of G', G', tan δ, η', and η'' is that they can be determined experimentally and used to characterize real materials. These parameters depend on frequency and temperature, and this dependence can be used to define behavior. For example, viscoelastic fluids are often characterized by log–log plots of one or more of these quantities vs the angular frequency ω, as shown in Figure 18, which illustrates the behavior of a polymer melt (177,178).

Normal Stress (Weissenberg Effect). Many viscoelastic fluids flow in a direction normal (perpendicular) to the direction of shear stress in steady-state shear (20,106). Examples of the effect include flour dough climbing up a beater, polymer solutions climbing up the inner cylinder in a concentric cylinder viscometer, and paints forcing apart the cone and plate of a cone–plate viscometer. The normal stress effect has been put to practical use in certain screwless extruders designed in a cone–plate or plate–plate configuration, where the polymer enters at the periphery and exits at the axis.

The two normal stress functions, $N_1(\dot{\gamma})$ and $N_2(\dot{\gamma})$, are referred to as the first and second normal stress differences, respectively. The former is positive

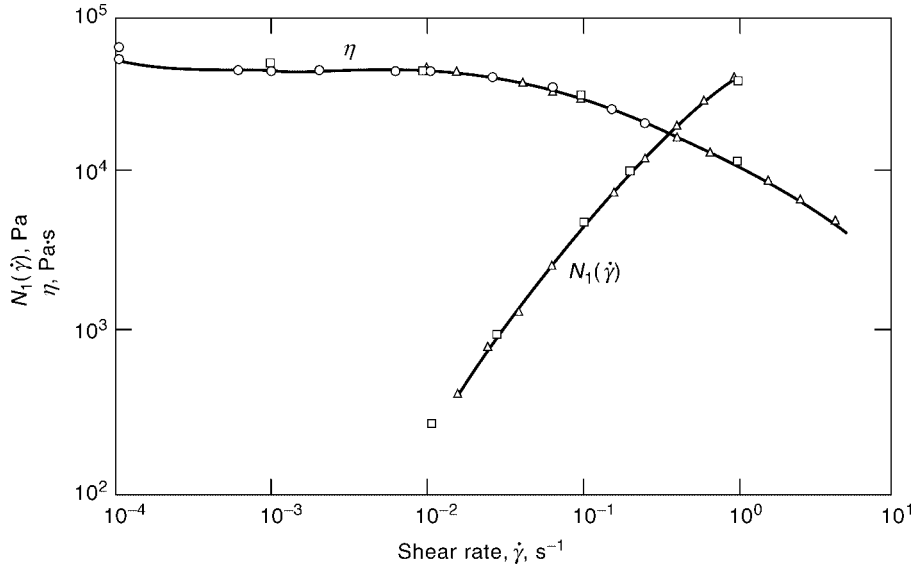

Fig. 19. Shear viscosity η and first normal stress difference $N_1(\dot{\gamma})$ vs shear rate $\dot{\gamma}$ for a low density polyethylene at 150°C (177,178), where ○ parallel plate; Δ cone and plate; and □: Weissenberg rheogoniometer. To convert Pa to dyn/cm^2, multiply by 10; to convert Pa·s to P, multiply by 10. Courtesy of *Rheometric Scientific*.

and increases with increasing shear rate, as shown in Figure 19 (177,178), which describes the steady-shear behavior of the polymer melt in Figure 18. The stress function $N_2(\dot{\gamma})$ is smaller in absolute value than $N_1(\dot{\gamma})$ and is sometimes negative. The first normal stress difference is a useful quantity, as it often gives a good quantitative measure of viscoelasticity. It can be determined from the normal force, which is measurable with several commercial rotational viscometers. In highly elastic liquids it is common for $N_1(\dot{\gamma})$ to be considerably larger than the shear stress.

Description of normal stress measurements on a practical but complex material, paint, is available (179). Other publications (180–183) give the results of investigations of normal stress differences for a variety of materials. These papers and their references form a useful introduction to the measurement of normal stress differences.

Viscometers

To solve a flow problem or characterize a given fluid, an instrument must be carefully selected. Many commercial viscometers are available with a variety of geometries for wide viscosity ranges and shear rates (8,20,53,54). Rarely is it necessary to construct an instrument. However, in choosing a commercial viscometer a number of criteria must be considered. Of great importance is the nature of the material to be tested, its viscosity, its elasticity, the temperature dependence of its viscosity, and other variables. The degree of accuracy and precision required, and

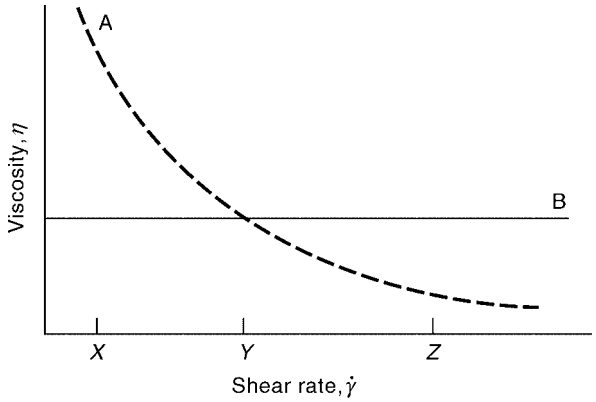

Fig. 20. Viscosity vs shear rate curves for two fluids, showing the fallacy of a single-point measurement. Fluid A would appear to be more viscous than fluid B if measured only at point X, of the same viscosity if measured at point Y, and less viscous if measured only at point Z.

whether the measurements are for quality control or research, must be considered. The viscometer must be matched to the materials and processes of interest; otherwise, the results may be misleading.

Most early viscometers, many of which have been incorporated into standard industrial tests, give single-point measurements. Instead of describing viscosity or shear stress over a range of shear rates, only a single point on the flow curve is produced; the rest of the curve is unknown. This is not a problem with Newtonian liquids because viscosity is independent of shear rate, but it can be misleading in the case of non-Newtonian materials, as shown in Figure 20, where the viscosity profiles of two fluids cross each other. Measurements carried out at the shear rate corresponding to the intersection would indicate that the two materials are identical, even though a simple examination, such as shaking or pouring, would show that they are not. A non-Newtonian fluid cannot be adequately characterized by a single-point measurement, and multipoint measurement techniques are strongly recommended.

Temperature control is also important. Viscosity is highly dependent on temperature; accurate, precise measurements can be made only if the temperature is carefully controlled. More errors are made and more disagreements over viscosity results arise because of incorrect or drifting temperature than for any other reason. Good temperature control can be achieved with commercial baths or circulators equipped with thermostats. Unfortunately, this is impossible with some viscometers. Others lose temperature control because of heat generation at high shear rates, especially with high viscosity materials. Such a temperature increase causes an apparent loss of viscosity under shear. A natural but erroneous conclusion would be that the material is thixotropic or shear thinning.

Viscometers may be separated into three main types: capillary, rotational, and moving body. There are other kinds, usually designed for special applications. For example, it has been reported that the viscosity of volumes of liquid in the nanoliter range can be measured by monitoring the shape of a droplet while it is

suspended in a medium with an extensional or shear field (184). For any given type of viscometer there is usually a choice of several different instruments. The choice depends on the particular requirements of the investigator and the price range.

Capillary Viscometers. Capillary flow measurement is a popular method for measuring viscosity (20,171,172); it is also the oldest. A liquid drains or is forced through a fine-bore tube, and the viscosity is determined from the measured flow, applied pressure, and tube dimensions. The basic equation is the Hagen–Poiseuille expression (eq. 17), where η is the viscosity, r the radius of the capillary, Δp the pressure drop through the capillary, V the volume of liquid that flows in time t, and L the length of the capillary.

$$\eta = \frac{\pi r^4 \Delta p t}{8VL} \tag{17}$$

Steady-state, laminar, isothermal flow is assumed. For a given viscometer with similar fluids and a constant pressure drop, the equation reduces to $\eta = Kt$ or, more commonly, $\nu = \eta/\rho = Ct$, where ρ is the density, ν the kinematic viscosity, and C a constant. Therefore, viscosity can be determined by multiplying the efflux time by a suitable constant.

Capillary viscometers are useful for measuring precise viscosities of a large number of fluids, ranging from dilute polymer solutions to polymer melts. Shear rates vary widely and depend on the instruments and the liquid being studied. The shear rate at the capillary wall for a Newtonian fluid may be calculated from equation 18, where Q is the volumetric flow rate and r the radius of the capillary; the shear stress at the wall is $\tau_w = r\Delta p/2L$.

$$\dot{\gamma}_w = \frac{4Q\pi}{r^3} \tag{18}$$

Absolute viscosities are difficult to measure with capillary viscometers, but viscosities relative to some standard fluid of known viscosity, such as water, are readily determined. The viscometer is calibrated with the reference fluid, and viscosities of other fluids relative to the reference sample are determined from their flow times.

For highly accurate work, corrections must be made for kinetic energy losses, incomplete drainage, turbulence, and possible surface tension and heat effects (20). The largest correction for liquids is that resulting from loss of effective pressure because of the appreciable kinetic energy of the issuing stream. The next most important correction for liquids and the largest for polymer melts is that for energy loss resulting from end effects, ie, viscous resistance caused by velocity gradients as the liquid enters and leaves the capillary (171,172,185). When the terms for these two correction factors are incorporated into the viscosity equation, it is changed to equation 19, where t is the time of flow and B and C are instrument constants generated from measurements of fluids of known viscosity.

$$\nu = \eta/\rho = Ct - B/t \tag{19}$$

These corrections are rarely used in industrial applications because the Poiseuille equation adequately expresses the flow. However, corrections are absolutely necessary for determining even approximate viscosities when using short capillary devices, such as orifice viscometers. Use of a long capillary (>10 dia) and long efflux times (>300 s) minimizes the need for corrections. The ASTM standards D3835 and D5099 describe experimental procedures for using capillary rheometers to measure rheological properties of polymers and rubbers under process conditions.

The glass capillary viscometer is widely used to measure the viscosity of Newtonian fluids. The driving force is usually the hydrostatic head of the test liquid. Kinematic viscosity is measured directly, and most of the viscometers are limited to low viscosity fluids, approx 0.4–16,000 mm^2/s. However, external pressure can be applied to many glass viscometers to increase the range of measurement and enable the study of non-Newtonian behavior. Glass capillary viscometers are low shear stress instruments: 1–15 Pa or 10–150 dyn/cm^2 if operated by gravity only. The rate of shear can be as high as 20,000 s^{-1} based on a 200–800 s efflux time.

The basic design is that of the Ostwald viscometer: a U-tube with two reservoir bulbs separated by a capillary, as shown in Figure 21**a**. The liquid is added to the viscometer, pulled into the upper reservoir by suction, and then allowed to drain by gravity back into the lower reservoir. The time that it takes for the liquid to pass between two etched marks, one above and one below the upper reservoir, is a measure of the viscosity. In U-tube viscometers, the effective pressure head and therefore the flow time depend on the volume of liquid in the instrument. Hence, the conditions must be the same for each measurement.

The original Ostwald viscometer has been modified in many ways, and a number of different versions are on the market (Table 4) (20). Most are available with a wide choice of capillary diameters and therefore a number of viscosity ranges. A number of viscometers are described in ASTM D445, which also lists detailed recommendations on dimensions and methods of use.

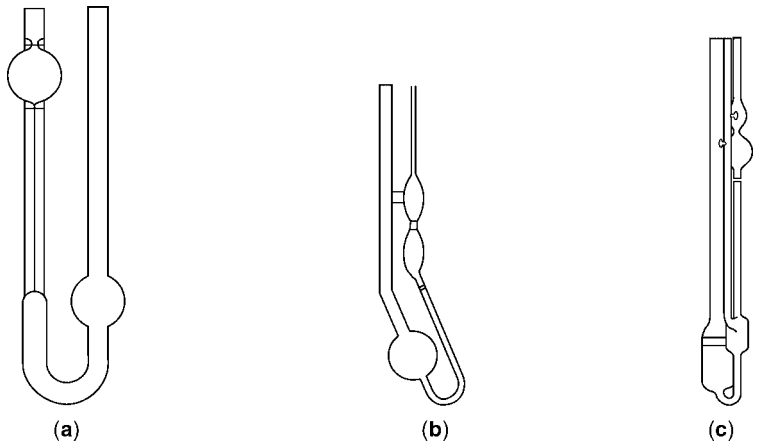

Fig. 21. (**a**) Ostwald glass capillary viscometer, (**b**) Cannon–Fenske viscometer, and (**c**) Ubbelohde viscometer.

Table 4. Glass Capillary Viscometers[a]

Approximate constant, C[b]	Viscosity range, mm^2/s	Capillary diameters, mm					
		Cannon–Fenske	Ubbelohde	FitzSimons	SIL[c]	Atlantic	Zeitfuchs
0.003	0.6–3.0	0.31 ± 0.02		0.43 ± 0.01	0.41 ± 0.02	0.41–0.42	0.28
0.005	1.0–5.0	0.42				0.47 ± 0.01	
0.01	2.0–10	0.63	0.58 ± 0.02	0.61	0.61	0.56	0.38
0.03	6–30	0.78	0.77	0.81 ± 0.03	0.73	0.74 ± 0.02	0.50
0.05	10–50		0.87		0.91	0.84	
0.1	20–100	1.02	1.10 ± 0.03	1.05	1.14 ± 0.03	1.00	0.67
0.3	60–300	1.26	1.43	1.32 ± 0.04	1.50	1.31 ± 0.02	0.88
0.5	100–500	1.48	1.64		1.71	1.48	
1	200–1,000	1.88	1.95	1.96	2.03	1.77 ± 0.03	1.20
3	600–3,000	2.20 ± 0.05	2.67 ± 0.04		2.80	2.34	1.42
5	1,000–5,000	3.10	3.06		3.06	2.65 ± 0.04	
10	2,000–10,000	4.0	3.62		3.79 ± 0.04		1.93
30	6,000–30,000						2.52
100	(2–10) × 10^4						3.06

[a] Ref. 21.
[b] Constant for equation $\nu = Ct$, where ν = kinematic viscosity in mm^2/s.
[c] Standard Inspection Laboratories.

The Cannon–Fenske viscometer (Fig. 21**b**) is excellent for general use. A long capillary and small upper reservoir result in a small kinetic energy correction; the large diameter of the lower reservoir minimizes head errors. Because the upper and lower bulbs lie on the same vertical axis, variations in the head are minimal even if the viscometer is used in positions that are not perfectly vertical. A reverse-flow Cannon–Fenske viscometer is used for opaque liquids. In this type of viscometer the liquid flows upward past the timing marks, rather than downward as in the normal direct-flow instrument. Thus the position of the meniscus is not obscured by the film of liquid on the glass wall.

The Ubbelohde viscometer is shown in Figure 21**c**. It is particularly useful for measurements at several different concentrations, as flow times are not a function of volume, and therefore dilutions can be made in the viscometer. Modifications include the Cannon-Ubbelohde, semi-micro, and dilution viscometers. The Ubbelohde viscometer is also called a suspended-level viscometer because the liquid emerging from the lower end of the capillary flows down only the walls of the reservoir directly below it. Therefore, the lower liquid level always coincides with the lower end of the capillary, and the volume initially added to the instrument need not be precisely measured. This also eliminates the temperature correction for glass expansion necessary for Cannon–Fenske viscometers.

For accurate and precise measurement the glass capillary must be clean. The viscometer must be cleaned thoroughly after each series of operations. Samples being tested and cleaning solvents should be filtered to remove particles that can clog the capillary.

All glass capillary viscometers should be calibrated carefully (20). The standard method is to determine the efflux time of distilled water at 20°C. Unfortunately, because of its low viscosity, water can be used only to standardize small capillary instruments. However, a calibrated viscometer can be used to determine the viscosity of a higher viscosity liquid, such as a mineral oil. This oil can then be used to calibrate a viscometer with a larger capillary. Another method is to calibrate directly with two or more certified standard oils differing in viscosity by a factor of approximately 5. Such oils are useful for calibrating virtually all types of viscometers. Because viscosity is temperature-dependent, particularly in the case of standard oils, temperature control must be extremely good for accurate calibration.

In recent years several commercial capillary viscometers that allow automation have been developed. For example, the time of flow is measured by the interruption of a light beam focused on a photoelectric cell. Such a device can be attached to an existing viscometer to facilitate measurements and improve precision. Some completely automatic instruments control the temperature, fill the viscometer, take several readings (sometimes with dilutions), as well as clean, rinse, and dry the viscometer before the next filling. The instrument prints efflux times and in some cases can be programmed to print viscosities. Manufacturers of automated viscosity systems include Cannon, Schott, Design Scientific, and Lauda; Wescan supplies timer and photocell combinations. An inexpensive timer is based on light pipes and an electronic stopwatch (186). Cannon Instrument Co. supplies a wide range of glass capillary viscometers, temperature baths, viscosity standards, and related equipment.

Orifice viscometers, also called efflux or cup viscometers, are commonly used to measure and control flow properties in the manufacture, processing, and application of inks, paints, adhesives, and lubricating oils. Their design answered the need for simple, easy-to-operate viscometers in areas where precision and accuracy are not particularly important. In these situations knowledge of a true viscosity is unnecessary, and the efflux time of a fixed volume of liquid is a sufficient indication of the fluidity of the material. Examples of orifice viscometers include the Ford, Zahn, and Shell cups used for paints and inks and the Saybolt Universal and Furol instruments used for oils (Table 5).

Orifice viscometers usually have extremely short capillaries. The typical orifice viscometer is a cup with a hole in the bottom. The cup is filled, and the time required for the liquid to flow out is measured. The hydrostatic head decreases as the liquid flows, and there is a large kinetic energy effect. Flow analysis shows that the flow does not follow the Hagen–Poiseuille law, and efflux times are not related to viscosities in any simple manner. Therefore, it is better not to convert efflux times to viscosities except during calibration with standard oils. Efflux times should be accepted as arbitrary measures of viscosity and noted in terms of the viscometer being used, ie, Saybolt seconds, Ford seconds, etc. The precision of orifice viscometers is poor because of the lack of temperature control, wear during use, and variations in manufacture. However, they are widely used in industry because they are inexpensive, robust, and easy to use. Some of these instruments have the added convenience of being capable of dipping into or remaining in the material to be tested. Dip cups determine approximate or relative viscosities in resin reactors, ink reservoirs, paint dip tanks, adhesive mixing tanks, etc. These are applications where the limitations of orifice cups are unimportant.

Orifice viscometers should not be used for setting product specifications, for which better precision is required. Because they are designed for Newtonian and near-Newtonian fluids, they should not be used with thixotropic or highly shear-thinning materials; such fluids should be characterized by using multispeed rotational viscometers.

Some orifice viscometers, such as the Shell dip cup and the European ISO cup, which resembles a Ford cup with a capillary, have long capillaries. These cups need smaller kinetic energy corrections and give better precision than the corresponding short-capillary viscometers. However, they are still not precision instruments, and should be used only for control purposes.

If it is necessary to calculate kinematic viscosities from efflux times, such as in a calibration procedure, equation 20 should be used, where t is the efflux time and k and K are constants characteristic of the particular viscosity cup (see Table 5) (187–189,192).

$$\nu = kt - K/t \tag{20}$$

In most cases it is sufficient to be able to convert from one viscometer value to another or to approximate kinematic viscosities with the help of charts or tables; literature from manufacturers is useful.

Linear equations of the type $\nu = ct–C$, where c and C are constants, relate kinematic viscosity to efflux time over limited time ranges. This is based on the fact that, for many viscometers, portions of the viscosity–time curves can be taken

Table 5. Some Orifice Viscometers Used in Industry

Viscometer[a]	Orifice length, mm	Orifice diameter, cm	Viscosity range, mm^2/s (= cSt)	Approximate constants[b]		Main applications
				k	K	
DIN[c] No. 4		0.40	60–460	4.67	570	Paints, varnishes
Fisher[d] No. 2		0.4	35–230	2.32	200	Paints
Ford[e,f]						
No. 2		0.25	30–120	1.30 (for $40 < t < 100$ s)	1000	Paints, varnishes
No. 3		0.34	50–250	2.30 (for $30 < t < 100$ s)	800	Paints, varnishes
No. 4		0.41	70–400	3.70	400	Paints, varnishes
ISO[g]						
No. 3	20 ± 0.05	0.30	10–45	0.443	200	Paints, inks
No. 4	20 ± 0.05	0.40	30–160	1.37	200	Paints, inks
No. 6	20 ± 0.05	0.60	200–700	6.90	570	Paints, inks
Redwood (U.K.) No. 1	10 ± 0.05	0.16	1–500	0.264 (for $40 < t < 85$ s) 0.247 (for $85 < t < 200$ s)	190	Petroleum products
Redwood No. 2	50 ± 0.2	0.38	500–5000	2.6	40	Petroleum products
Saybolt Universal[h]	12.2	0.18	1–200	0.226 (for $t <$ 1000 s)	195	Petroleum products
Saybolt Furol[h]	12.2	0.32	200–4000			Petroleum products
Shell[f,i]						
No. 1	25	0.18	4–20	0.19	48	Inks
No. 2	25	0.24	10–60	0.55	46	Inks
No. 3	25	0.31	30–150	1.50	37	Paints, inks
No. 4	25	0.38	70–300	3.45	14	Paints, inks
No. 5	25	0.46	125–500	6.5	42	Inks
No. 6	25	0.58	320–1500	16.2	34	

Table 5. (Continued)

Viscometer[a]	Orifice length, mm	Orifice diameter, cm	Viscosity range, mm^2/s (= cSt)	Approximate constants[b]		Main applications
				k	K	
Zahn[e,f]						
No. 1		0.20	20–100	0.80 (for $40 < t < 100$ s)	400	Varnishes
No. 2		0.27	50–300	2.93	500	Paints, inks
No. 3		0.38	100–1000	10.7	1800	Paints, inks
No. 4		0.43	200–1500	14.0	1200	Paints bodied
No. 5		0.53	400–2000	23.3	200	Paints

[a] No thermostat; Viscosity unit = s, unless otherwise noted.
[b] Constants k and K are based on $\nu = kt - K/t$, in mm^2/s (=cSt). Unless otherwise noted, constants hold for $20 < t < 100$ s.
[c] DIN (Deutsche Normen) cup constants from DIN Standard 53211.
[d] Fisher cup constants based on data from only two cups.
[e] Ford and Zahn cup constants (192).
[f] Linear equations for Ford, Shell, and Zahn cups (187).
[g] ISO cup constants are from ISO International Standard 2431.
[h] Thermostatted, Viscosity units = s/60 mL.
[i] Based on data from manufacturers of Shell cups (187) (Norcross Corp.).

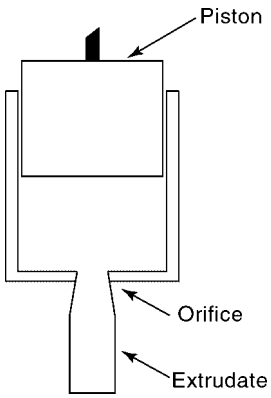

Fig. 22. Piston cylinder capillary viscometer (53)

as straight lines over moderate time ranges. Linear equations, which are simpler to use in determining and applying correction factors after calibration, must be applied carefully as they do not represent the true viscosity–time relation. Linear equation constants have been given (187) and are used in ASTM D4212.

Pressure-driven piston cylinder capillary viscometers, ie, extrusion rheometers (Fig. 22), are used primarily to measure the melt viscosity of polymers and other viscous materials (20,51,53–55). A reservoir is connected to a capillary tube, and molten polymer or another material is extruded through the capillary by means of a piston to which a constant force is applied. Viscosity can be determined from the volumetric flow rate and the pressure drop along the capillary. The basic method and test conditions for a number of thermoplastics are described in ASTM D1238. Melt viscoelasticity can influence the results (190).

Polymer melts are frequently non-Newtonian. In this case the earlier expression given for the shear rate at the capillary wall does not hold. A correction factor $(3n + 1)/4n$, called the Rabinowitsch correction, must be applied in such a way that equation 21 applies, where $\dot{\gamma}_{\mathrm{tw}}$ is the true shear rate at the wall and n is a power law factor (eq. 22) determined from the slope of a log–log plot of the true shear stress at the wall, τ_{tw}, vs $\dot{\gamma}_{\mathrm{w}}$. For a Newtonian liquid, $n = 1$. A true apparent viscosity, η_{t}, can be calculated from equation 23.

$$\dot{\gamma}_{\mathrm{tw}} = \frac{(3n+1)\dot{\gamma}_{\mathrm{w}}}{4n} \tag{21}$$

$$n = \frac{\mathrm{d}\log \tau_{\mathrm{tw}}}{\mathrm{d}\log \dot{\gamma}_{\mathrm{w}}} \tag{22}$$

$$\eta_t = \frac{\tau_{\mathrm{tw}}}{\dot{\gamma}_{\mathrm{tw}}} \tag{23}$$

An even more important correction for polymer melts is that for end effects. Entrance and exit effects cause pressure drops that interfere with an accurate determination of the pressure gradient, $\Delta p/L$, needed for viscosity determination

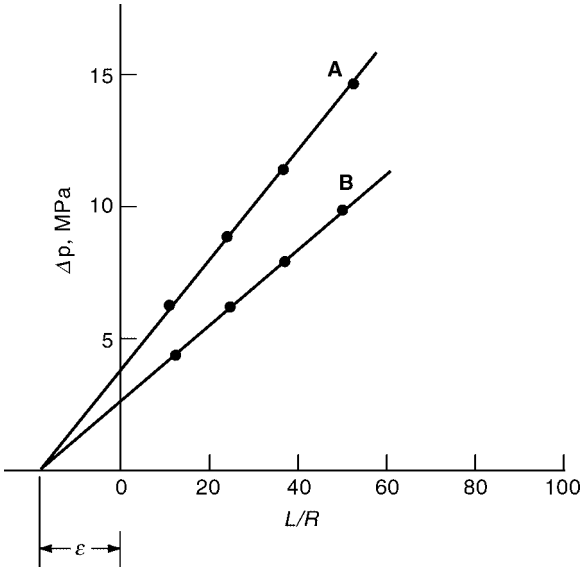

Fig. 23. Bagley plot of pressure, p, drop along a capillary versus capillary aspect ratio, L/R, at (**A**), $\dot{\gamma} = 590\ s^{-1}$ and (**B**), $\dot{\gamma} = 295\ s^{-1}$. To convert MPa to psi, multiply by 145.

using the Hagen–Poiseuille equation. It has been assumed (185) that the effective length of the capillary is greater than the actual length, and the shear stress at the wall has been corrected as equation 24, where R is the capillary radius, L is the actual length, and E is an empirical parameter obtained by extrapolating a plot of Δp versus the capillary aspect ratio, L/R, to zero pressure drop at constant shear rate, $\dot{\gamma}$, for capillaries of different length, as shown in Figure 23 (171).

$$\tau_w^c = \frac{R\Delta\,p}{2(L+ER)} \tag{24}$$

A number of instruments are based on the extrusion principle, including slit flow and normal capillary flow (Table 6). These instruments are useful when large numbers of quality control or other melt viscosity test measurements are needed for batches of a single material or similar materials. When melt viscosities of a wide range of materials must be measured, rotational viscometers are preferable. Extrusion rheometers have been applied to other materials with some success with adhesives and coatings (8,191).

Rotational Viscometers. Rotational viscometers consist of two basic parts separated by the fluid being tested (20,171,172,187,192–197). The parts may be concentric cylinders (cup and bob), plates, a low angle cone and a plate, or a disk, paddle, or rotor in a cylinder. Rotation of one part against the other produces a shearing action on the fluid. The torque required to produce a given angular velocity or the angular velocity resulting from a given torque is a measure of the viscosity. Rotational viscometers are more versatile than capillary viscometers. They can be used with a wide range of materials because opacity, settling, and non-Newtonian behavior do not cause difficulties. Viscosities over a range of

Table 6. Selected Extrusion Rheometers

Manufacturer	Instrument	Temperature range, °C	Maximum force, kN	Comments
Benz www.benztesters.com	Melt Flow Index	100–350		
Bohlin www.bohlin.com	Rosand RH2100	RT–500	20	Single bore
	Rosand RH2200	RT–500	20	Twin bore
	Rosand RH7-D	RT–500	50	
	Rosand RH10-D	RT–500	100	
Burrell www.burrellsci.com	Burrell-Severs Model A-120	RT	100 psi	
Ceast www.ceast.com	Melt Flow Quick Index	100–400		
	Melt Flow Modular	30–400		
	RheoIndex	30–450		
	Melt Flow Tester			Motorized control for piston lifting and motion
	Rheologic 1000	50–450	10	
	Rheologic 2500	50–450	25	Shear rate to 3.4×10^6 for all three
	Rheologic 5000-Twin	50–450	50	
Dynisco www.dynisco.com	Capillary Rheometer LCR7000/7001/7002	to 430	5–15	
	Melt Flow Indexer LMI D4001-4004	40–425		
Goettfert www.goettfert.com	Rheograph 200			Single or twin
	Rheograph 6000		60	Triple bore
	Rheo-Tester 500		5	
	Rheo-Tester 1000		15	
	Rheo-Tester 2000		20	
	Melt Flow Indexer MP			
	Melt Flow Indexer MP-DE			
Magna Projects www.magna-projects.com	Eta 2100/BFR 2100	RT–450	66	Shear rate to 2×10^6 Single or twin

Table 6. (Continued)

Manufacturer	Instrument	Temperature range, °C	Maximum force, kN	Comments
Anton Paar www.anton-paar.com	HVA 6	−20–80		Shear rate to 10^6 Viscosity 1–10^4 mPa·s
RheoTest www.rheotest.de	Rheotest LK	0–80		Viscosity range 1–10^5 mPa·s
SDLAtlas www.sdatlas. com	F255 Digital Melt Flow Indexer			Formerly Atlas MF-12
Shimadzu Scientific www.shimadzu.com	Capillary Rheometer CFT-500D/100D	(RT + 20)–400		Viscosity range 800–10^9 mPa·s
Thermo Electron (Haake)	RheoCap S20	450 max	20	Single bore
www.thermo. com	RheoCapT100	500 max	100	Twin bore

shear rates and as a function of time can be measured. Therefore, they are useful for characterizing shear thinning and time-dependent behavior.

Since the 1990s rotational viscometers have been developed that have integrated computers for operation and control of the instrument as well as for data collection, reduction, and storage. The combination of a computer, modern electronics, and feedback loops provides great flexibility and control. For example, pulses from the computer coupled with feedback from the viscometer can give precise oscillatory motion as well as shear viscosity measurement at constant stress or speed; only simple hardware is involved. Such instruments are useful for rheological measurements and studying the structure of dispersions and formulated products. These new instruments are versatile, easy to use, and allow the collection, analysis, and comparison of large amounts of data in a short time.

The mechanical parts of computer-controlled viscometers can be simple and should not become obsolete for many years. The complexity is in the software, and this is where changes will have to be made to keep the instrument up to date. Some manufacturers are offering new, updated software free for a period of several years after the instrument is purchased.

Rotational viscometers often were not considered for highly accurate measurements because of problems with gap and end effects. However, corrections can be made, and very accurate measurements are possible. Operating under steady-state conditions, they can closely approximate industrial process conditions such as stirring, dispersing, pumping, and metering. They are widely used for routine evaluations and quality control measurements. The commercial instruments are effective over a wide range of viscosities and shear rates (Table 7).

Table 7. Selected Rotational Viscometers

Manufacturer	Viscometer	Viscosity range, mPa·s (= cP)	Shear rate, s^{-1}	Maximum torque, mNm	Temperature range, °C
ATS RheoSystems www.atsrheosystems.com	Dynalyser	$0.1–10^{12}$	$0–2 \times 10^5$	200	−180 to 550
	Stresstech Stresstech HR Viscoanalyser Viscoanalyser DSR Viscotech	Configurable to above levels			
Bohlin Instruments www.bohlin.com	Gemini	to 10^{12}	to 10^5	200	−150 to 550
www.bohlinusa.com	C-VOR	$10^{-1}–10^{11}$	$10^{-1}–10^4$	200	−150 to 550
	CVO			100	
	CS				
	CSR 10		$10^{-3}–10^4$		−25 to 300
	V88	$5–10^7$	$5–2 \times 10^4$	10	−35 to 150
C. W. Brabender www.cwbrabender.com	ATR Plasti-Corder	$1–10^5$	Low shear		
	Intelli-Torque Plasti-Corder				
Brookfield Engineering Co. www.brookfieldengineering.com	DV spindle series	$1–10^9$	Low shear		No control
	R/S Rheometer	$1–10^7$	$0–5 \times 10^3$		−20 to 200
	YR-1 Yield Stress				
	Wells-Brookfield cone/plate	$5–10^9$	0.1–200		−20 to 100
	Cap 1000	$25–10^6$	One speed		5 to 235
	Cap 2000	$10–10^6$	$10–2 \times 10^4$		5 to 235
	KU-1 Stormer-type	100–5000			

Table 7. (Continued)

Manufacturer	Viscometer	Viscosity range, mPa·s (= cP)	Shear rate, s^{-1}	Maximum torque, mNm	Temperature range, °C
Coesfeld Material Test GmbH ww.coesfeld.com	Visco-Mix	$10–10^8$			
	Rheosyst	$1–10^9$			
Fann Instrument Co. www.fann.com	Model 35		$5–10^3$		
	Model 35/SR12		12 speeds		
Fluid Dynamics, Inc. www.fluiddynamics.com	T2SR	$0.01–5 \times 10^6$			−20 to 400
GBC Scientific Equipment www.gbsci.com	MFR 2100 Micro Fourier Viscometer		0.01–1000	45	
Grace Instrument Co. www.graceinstrument.com	M3500	$0.5–5 \times 10^6$	0.003–3254		
OFI Testing Equipment, Inc. www.ofite.com	Model 900		0.01–1700		
Anton Paar www.anton-paar.com	Physica MCR 150			150	−150 to 600
www.paarphysica.com	Physica MCR 300			150	−150 to 600
	Physica MCR 500	$1–10^{12}$		200	−150 to 600
	Rheolab MC 1	$1–10^{10}$	$0.1–10^5$		−40 to 300
	SVM 300 Stabinger				−40 to 100
	DV-P Series	$1–10^7$			−10 to 100
RheoTec Messtechnik GmbH www.rheotec.de	Rheometer RC-1	$1–10^6$	$0.9–4 \times 10^3$	50	−20 to 180
	Rheometer RC-20	$1–3 \times 10^6$	$0.9–4 \times 10^3$	50	−20 to 180
	Rheometer RC-CPS	$10–10^8$	up to 4800	50	−20 to 250
Rheotest Mendigen GmbH www.rheotest.de	Rheotest RN	$1–3 \times 10^9$	$0.04–2 \times 10^4$	160	−30 to 200
	Rheotest RV 2.1	$1–4 \times 10^8$	0.02–1300		−60 to 300

TA Instruments www.tainst.com	Ares		200	−150 to 600
	Ares-RDA		200	−150 to 600
	Ares-RFS		100	−150 to 250
	Ares-LS1		200	−150 to 600
	Ares-LS2		200	−150 to 250
	AR 2000 CS		200	−150 to 600
	AR 2000 CR		200	−150 to 600
	AR 1000		100	−150 to 400
	AR 550/QCR		50	−150 to 400
Thermo-Electron Corp. www.thermo.com	Haake 550 Concentric cylinder	$1–10^6$	30	−20 to 100
	Haake 550 Cone/plate	$1–10^6$	30	−20 to 100
	Haake Viscotester			No control
	1+	1.5–330		
	2+	$30–4 \times 10^5$		
	Haake Viscotester 6/7	$3–2 \times 10^6$		
	Haake Viscotester 01/02	1.5–330		

The equations and methods for determining viscosity vary greatly with the type of instrument, but in many cases calculations may be greatly simplified by calibration of the viscometer with a standard fluid, the viscosity of which is known for the conditions involved. General procedures for calibration measurement are given in ASTM D2196. The constant thus obtained is used with stress and shear rate terms to determine viscosity by equation 25, where the stress term may be torque, load, or deflection, and the shear rate may be in rpm, revolutions per second (rps), or s^{-1}.

$$\eta = K(\text{stress term}/\text{shear rate term}) \tag{25}$$

Constants and factors are often supplied by the manufacturer. Separate constants may be given for converting the stress and shear rate terms to the correct quantities and units.

A constant is often determined from measurements with a Newtonian oil, particularly when the calibrations are supplied by the manufacturer. This constant is valid only for Newtonian specimens; if used with non-Newtonian fluids, it gives a viscosity based on an inaccurate shear rate. However, for relative measurements this value can be useful. Employment of an instrument constant can save a great deal of time and effort and increase accuracy because end and edge effects, slippage, turbulent interferences, etc, are included.

The earliest and probably the most common type of rotational viscometer is the coaxial or concentric cylinder instrument. It consists of two cylinders, one within the other (cup and bob), keeping the specimen between them, as shown in Figure 24. The first practical rotational viscometer consisted of a rotating cup with an inner cylinder supported by a torsion wire. In variations of this design the inner cylinder rotates. Instruments of both types are useful for a variety of applications.

The relationship between viscosity, angular velocity, and torque for a Newtonian fluid in a concentric cylinder viscometer is given by the Margules equation (eq. 26) (20,172), where M is the torque on the inner cylinder, h the length of the inner cylinder, Ω the relative angular velocity of the cylinder in radians per second, R_i the radius of the inner cylinder wall, R_o the radius of the outer cylinder wall, and k an instrument constant.

$$\eta = \left(\frac{M}{\Omega 4\pi h}\right)\left(\frac{1}{R_i^2} - \frac{1}{R_o^2}\right) = \frac{kM}{\Omega} \tag{26}$$

Therefore, the viscosity can be determined from the torque and angular velocity. However, the viscosity is usually calculated from the shear rate and shear stress, which can be obtained from the Margules equation. The shear rate is given by equation 27, where r is any given radius.

$$\dot{\gamma} = \frac{(2\Omega/r^2)\left(R_i^2 R_o^2\right)}{R_o^2 - R_i^2} \tag{27}$$

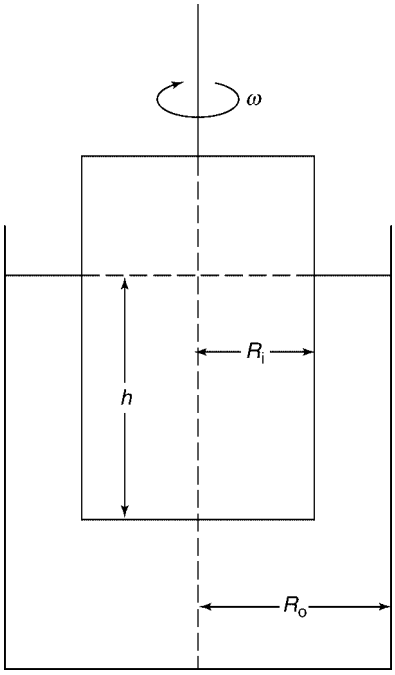

Fig. 24. Concentric cylinder viscometer. R_i and R_o are the radii of the inner and outer cylinder, respectively, and ω is the relative angular velocity.

The shear stress is given by equation 28:

$$\tau = \frac{M}{2\pi r^2 h} \tag{28}$$

The shear rate and shear stress can be calculated for any radius r from these equations. In most cases the radius used is R_i because the shear stress and shear rate of interest are at the inner, torque-sensing cylinder. Thus equations 27 and 28 become

$$\dot{\gamma} = \frac{2\Omega R_o^2}{R_o^2 - R_i^2} \text{ and } \tau = \frac{\mathrm{M}}{2\pi R_i^2 h}$$

The viscosity of a Newtonian fluid may be determined from the Margules equation or from the slope of a shear stress–shear rate plot. Non-Newtonian fluids give intercepts and curves with such plots. Viscosities can be calculated, but accurate values depend on including correction factors for yield points and shear thinning, ie, shear rate corrections, in the above equations (20). The shear rate correction may be minimized by using a very small gap size; in other words, the ratio of the inner to outer radius should be as close to unity as possible. In practical terms this means maintaining a ratio of 0.95, which is impossible with many sensors used with commercial rotational viscometers. With highly shear thinning materials even this is insufficient, and corrections must be made regardless of the

gap size. However, with viscosity–shear rate curves, although correction shifts each point by a rather large amount, the corrected curve itself is only slightly different from the uncorrected curve (198).

In addition to non-Newtonian flow, the main correction necessary for concentric cylinder measurements is that on account of end effects. Because the inner cylinder is not infinitely long, there is drag on the ends as well as on the face of the cylinder. The correction appears as an addition, h_0, to the length, h. The correction is best determined by measuring the angular velocity and torque at several values of h, that is, at various depths of immersion. The data are plotted as M/Ω vs h, and extrapolation is made to a value of h_0 at $M/\Omega = 0$. The quantity $(h + h_0)$ is substituted for h in the various equations.

In a cone–plate viscometer (Fig. 25), a low angle ($\leq 3^\circ$) cone rotates against a flat plate with the fluid sample between them. The cone–plate instrument is a simple, straightforward device that is easy to use and extremely easy to clean. It is well-suited to routine work because measurements are rapid and no tedious calculations are necessary. With careful calibration and good temperature control it can be a very effective research and problem-solving tool. Heated instruments can be used for melt viscosity measurements.

In most rotational viscometers the rate of shear varies with the distance from a wall or the axis of rotation. However, in a cone–plate viscometer the rate of shear across the conical gap is essentially constant because the linear velocity and the gap between the cone and the plate both increase with increasing distance from the axis. No tedious correction calculations are required for non-Newtonian fluids. The relevant equations for viscosity, shear stress, and shear rate at small angles α of Newtonian fluids are equations 29, 30, and 31, respectively, where M is the torque, R_c the radius of the cone, v the linear velocity, and r the distance from the axis.

$$\eta = \frac{3\alpha M}{2R_c^3} \tag{29}$$

$$\tau = \frac{3M}{2\pi R_c^3} \tag{30}$$

$$\dot{\gamma} = \frac{\mathrm{d}\,v}{\mathrm{d}\,r} = \frac{\Omega}{\alpha} \tag{31}$$

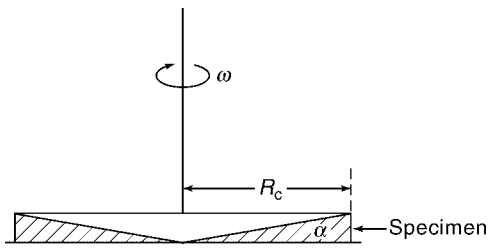

Fig. 25. Cone–plate viscometer. R_c is the radius of the cone, α is the angle between cone and plate, and ω is the relative angular velocity.

Cone–plate geometry has several advantages over concentric cylinder geometry, including a smaller sample size, a homogeneous shear rate, and easy conversion of data. Disadvantages include the need for precise adjustment of the gap (done automatically in many viscometers), including resetting when the temperature is changed, specimen drying, solvent evaporation, slinging of material from the gap, and the possibility of viscous heating, particularly at high shear rates. The last problem is compounded by the fact that temperature control with commercial instruments is not always as good as it should be.

In parallel plate viscometers (195) the gap width is usually larger and can be varied freely. This is an advantage when measuring suspensions or dispersions with large particles or with a tendency to fly out of the gap. The wide gap means that there is less sensitivity to temperature changes. Therefore, resetting is usually not necessary and temperature scans are much easier to run than with a cone–plate viscometer. However, with the plate–plate instrument, the velocity, and therefore the shear rate, varies with the distance from the center of the plate. This makes viscosity data more difficult to evaluate.

The maximum shear rate (at the plate rim) is given by equation 32, where R_p is the radius of the plate and h the distance between the two plates.

$$\dot{\gamma}_\mathrm{m} = \frac{\Omega R_\mathrm{p}}{h} \tag{32}$$

The viscosity is given by equation 33, where M is the torque.

$$\eta = \frac{3M}{2\pi R_p^3 \dot{\gamma}_\mathrm{m}} \left(1 + 3\frac{\mathrm{d}\ln M}{\mathrm{d}\ln\dot{\gamma}}\right) \tag{33}$$

A dynamic viscometer is a special type of rotational viscometer used for characterizing viscoelastic fluids. It measures elastic as well as viscous behavior by determining the response to both steady-state and oscillatory shear. The geometry may be cone–plate, parallel plates, or concentric cylinders; parallel plates have several advantages, as noted above.

Many rotational viscometers operate by controlling the rotational speed and, therefore, the shear rate. The shear stress varies uncontrollably as the viscosity changes. Often, before the structure is determined by viscosity measurement, it is destroyed by the shearing action. Yield behavior is difficult to measure. In addition, many flow processes, such as flow under gravity, settling, and film leveling, are stress-driven rather than rate-driven.

An instrument where the shear stress and rate of stress change, rather than the rotational speed, are controlled offers advantages. A few such instruments have existed for many years, eg, the Stormer; others have been developed more recently (199–205). A typical instrument consists of a drag cup motor, a frictionless air-bearing torque shaft, sensors for measuring angular deflection and velocity, and a rotating bob and fixed cup or parallel plates (201–204). The rotating shaft must be suspended in a frictionless manner to permit measurements at very low stresses.

Controlled stress viscometers are useful for determining the presence and the value of a yield stress. The structure can be established from creep measurements, and the elasticity from the amount of recovery after creep. The viscosity can be determined at very low shear rates, often in a Newtonian region. This zero-shear viscosity, η_0, is related directly to the molecular weight of polymer melts and concentrated polymer solutions.

Yield stresses are determined with the help of a vaned cylinder acting as sensor (206), which is attached to a stress rheometer (207). The sensor has four to eight thin blades centered around the cylindrical shaft. The instrument is immersed in the material, and a stress is applied. If the stress is below the yield stress, the material deforms elastically (small strain), but does not yield. When the applied stress exceeds the yield stress, the material flows and the sensor rotates continuously. Usually, a series of measurements are carried out at successively higher stresses, as shown in Figure 26 (207). The yield behavior is seen as a large strain over a short period of time. The torque for yielding is between the last nonyield torque value and the one that produced continuous rotation. Subsequent tests are performed with smaller torque increments to narrow the range for the yield stress. Details of the method and the equation relating yield stress to torque are available (207). Controlled stress techniques are used to determine yield stresses and other flow properties for polymer melts (59) as well as for solutions and dispersions.

Some rotational viscometers employ a disk as the inner member or bob, eg, the Brookfield and Mooney viscometers; others use paddles (a geometry of the Stormer). These nonstandard geometries are difficult to analyze, particularly for an infinite bath, as is usually employed with the Brookfield and the Stormer. The Brookfield disk has been analyzed for Newtonian and non-Newtonian fluids and shear rate corrections have been developed (21). Other nonstandard geometries are best handled by determining instrument constants by calibration with standard fluids.

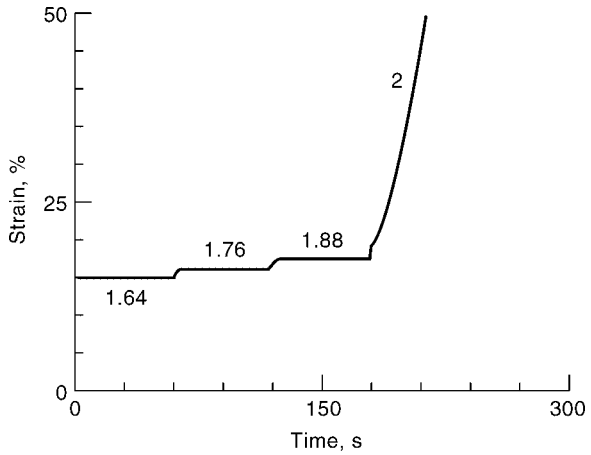

Fig. 26. Measurements of yield stress with a vane device and Rheometrics controlled stress rheometer. The torque required to cause yielding is between 1.88 and 2 mN·m as indicated on the curve. To convert mN·m to dyn·cm, multiply by 10^4. Courtesy of the Society of Rheology.

Information on selected commercial rotational viscometers can be found in Table 7. Pictures and more detailed descriptions are available on the relevant Web sites. Great changes have been made in commercial instruments, particularly in their integration with computers, but a recent paper may point to even greater changes in the future (208). Rheometers generally require actuators to stress specimens and sensors to record the response. However, sensors contribute considerably to the cost and complexity of instruments. A possible alternative to sensors is self-sensing, a technique that involves using knowledge of the actuator's behavior to estimate force or position. Torque or force is self-sensed in some commercial rheometers, but they still need position sensors to measure motion. Since it is possible to self-sense motion of electromagnetic actuators, it should be possible to construct a rheometer having no sensors. Such a rheometer could be small, simple, and inexpensive. To prove their point the authors built a rheometer that fit that description.

Moving Body Viscometers. In moving body viscometers, the motion of a ball, bubble, plate, needle, or rod through a material is monitored. A number of commercial moving body viscometers are listed in Table 8.

Falling ball viscometers are based on Stokes' law, which relates the viscosity of a Newtonian fluid to the velocity of the falling sphere. If a sphere is allowed to fall freely through a fluid, it accelerates until the viscous force is exactly the same as the gravitational force. The Stokes' equation relating viscosity to the fall of a solid body through a liquid may be written as equation 34, where r is the radius of the sphere; d_s and d_l are the density of the sphere and the liquid, respectively; g is the gravitational force; and v is the velocity of the sphere.

$$\eta = \frac{2r^2 g(\mathrm{d_s} - \mathrm{d_l})}{9v} \tag{34}$$

Viscometers of the falling ball type can be used over an extremely wide viscosity range, but are usually employed for fairly viscous materials because small balls and small differences in density are needed to obtain a suitably slow rate of fall in a low viscosity fluid. The devices are limited to measurements of Newtonian fluids because no practical formula has been developed for non-Newtonian materials. They had been considered as instruments for routine viscosity measurements rather than highly accurate work, but more recent designs (209–211) have changed this. The technique has proved to be useful in the study of suspensions, including those that are opaque and concentrated. The cylinder is jacketed for temperature control to within 0.1°C. Optical techniques are used for clear solutions and X-rays for opaque suspensions. A high speed video system is used for recording data.

The speed at which a sphere rolls down a cylindrical tube filled with a fluid or down an angled plate covered with a film of the fluid also gives a measure of viscosity. For the cylindrical tube geometry, equation 35 a generalized form of the Stokes' equation, is used for any given instrument, where v is the translational velocity of the rolling sphere and k is the instrument constant determined by calibration with standard fluids.

Table 8. Selected Commercial Moving Body Viscometers

Manufacturer	Viscometer	Viscosity range, mPa·s	Temperature range, °C	Comments
Cargille Laboratories, Inc. www.cargille.com	Bubble Tubes	~10–1000	RT or water bath	Viscosity range is nonlinear
Kimble Kontes www.kimble-kontes.com	Bubble Tubes			
Anton Paar www.anton-paar.com	Rolling Ball AMVn		10–100	
The Paint Research Association www.pra.org.uk	Bubble Tubes			
RheoTec Messtechnik GmbH www.rheotec.de	Falling Ball KF 10	$500–7\times10^7$		Hoeppler type
RheoTest Mendingen GmbH www.rheotest.de	Falling Ball	$0.6–7\times10^4$	−60 to 150	
	Hoeppler KF 3.2			
	Ball Pressure Hoeppler KD 3.1	$1–10^9$	−30 to 200	
	Ball Pressure Hoeppler KO 2.2	$10^4–10^{12}$	−60 to 120	
Stony Brook Scientific, Ltd. www.stonybrooksci.com	Falling Needle DV-100	$1–10^8$	0–100	HTV-100 to 350C
	Falling Needle FNV-200	$0.5–2.4\times10^6$	−40 to 150	Shear rate 10^{-4} to 10^4
Testing Machines, Inc. (TMI) www.testingmachines.com	Laray Falling Rod			Also yield value
Thermo-Electron Corp. www.thermo.com	Haake Falling Ball	$0.5–10^5$	−20–120	Hoeppler type

$$\eta = \frac{k(d_s - d_l)}{v} \tag{35}$$

The technique of determining viscosity from the velocity of a rolling ball on an inclined plate or panel has been used largely for following the flow, drying, and curing of paints and other coatings (212–215), but can also be used for other materials. The system can be calibrated with standard oils or other fluids of known

viscosity. The geometry is ill-defined because the ball often slides and rolls, but the technique is useful. Rolling ball methods based on an inclined plane or an inclined path leading to a horizontal test specimen have been employed to determine the tack of pressure-sensitive adhesives (ASTM D3121) (216–218). The reciprocal of the distance rolled by the ball is considered to be proportional to the tackiness of the adhesive.

Under a broad definition of a moving body, certain other viscometers can be considered to be of this type, including the band, falling rod, falling needle, sliding plate, and bubble tube viscometers. The band viscometer includes an arrangement of parallel plates, the basic geometry used to define shear viscosity. The band, which is a strip of Mylar film, is sandwiched between two fixed plates. The fluid is placed between the band and the plates, and the band is pulled through the fluid. For a given gap and force on the band, the speed of the band is a measure of viscosity.

The falling rod viscometer, though similar to the band viscometer, is based on the movement of a rod rather than a plate through the fluid (219–222). It is a form of a falling coaxial cylinder viscometer. Initially, this device was used for semiempirical studies of materials such as bitumens and rosins. In the 1990s, the Laray falling rod viscometer became a standard test instrument in the ink industry (ASTM D4040), and more recent versions of the falling rod viscometer are capable of precise measurements of polymer melts and solutions (223). In the falling needle viscometer (224,225) (ASTM D5478), the moving body is a glass or stainless steel needle that falls vertically through the fluid. The viscous properties and density of the fluid are derived from the velocity of the needle.

The sliding plate rheometer has been in use for some time, but new types were developed in the 1990s (226–230). The well-defined simple shear deformation generated by this technique is useful for the characterization of polymer melts and concentrated solutions. Of particular interest is the fact that it can cause a high degree of molecular stretching. The sliding plate rheometer is useful for the characterization of polymer slip at solid boundaries and the determination of the effectiveness of processing aids (231,232).

Viscosity can also be determined from the rising rate of an air bubble through a liquid. This simple technique is widely used for routine viscosity measurements of Newtonian polymer solutions. A bubble tube vicometer consists of a glass tube of a certain size to which liquid is added until a small air space remains at the top. The tube is then capped. When it is inverted, the air bubble rises through the liquid. The rise time may be taken as a measure of viscosity or matched to that of a member of a series of standards (ASTM D1545).

Other Viscometers. A number of other viscometers are built for specific research or product applications. In one type of design, vibrational techniques are used to measure viscosity. The A&D Weighing SV-10 (233), the Automation Products Dynatrol (234), and the Nametre (235) are all based on this principle. The SV-10 and the Nametre measure viscosity by monitoring the power required to maintain torsional vibrations in their sensors, two small, thin circular plates for the SV-10 and a small stainless steel rod with a bulb at the end for the Nametre. The Dynatrol determines viscosity by measuring the amplitude of vibration of an immersed flexural member. Because the rate of shear is not easily determined or changed, these instruments are best used for controlling or studying

processes in which viscosity changes with time or temperature. In such cases they can be useful because wide ranges of viscosity can be measured without changing sensors (for example, 10^{-1}–10^{6} mPa·s for the Nametre). Special versions of the Dynatrol and Nametre devices are employed for in-line process control for many polymeric solution-based products because of their insensitivity to stirring and flow, wide viscosity ranges, simplicity of design, and ability to be controlled from and transmit data to a remote point.

The Vilastic VE system (236) is based on controlled oscillatory flow in a cylindrical tube. Measurements are performed using oscillatory flow generated at a selected frequency in a precision measurement tube. Viscosity, elasticity, and storage and loss moduli are calculated from data obtained from sensors that monitor the pressure drop across the tube and volume through the tube.

Extensional Viscosity Measurement Techniques

All three types of extensional viscosity can be measured (119,121): uniaxial, biaxial, and pure shear. Only a few commercial instruments are available, however, and most measurements are made with improvised equipment. Extensional viscosity of polymer melts can be estimated from converging flow (entrance pressure) or from a melt strength drawdown test (237) as well as measured with techniques described below.

Most uniaxial measurement techniques involve extending a strand or cylindrical rod of the material and measuring the force required. To measure fluids, the fluid is extruded from a spinnerette nozzle and allowed to fall under gravity. It is then extended by being rolled up on a rotating drum (119,127,238–241). The generated force is measured by the deflection of the nozzle or tube as the latter is pulled by the filament of fluid or at the take-up roller. This method has been the basis for home-built viscometers and a commercial instrument (238,241).

Another type of experiment involves a fluid filament being drawn upward against gravity from a reservoir of the fluid (119,242,243), a phenomenon often called the tubeless siphon. The maximum height of the siphon is a measure of the spinnability and extensional viscosity of the fluid. More quantitative measures of stress, strain, and strain rate can be determined from the pressure difference and filament diameter. A more recent technique involves monitoring the stretching of a fluid filament as it is extended (244–251). The basic design is called a filament stretching rheometer (FSR). With a commercial version, the CaBER (Capillary Breakup Extensional Rheometer (252), a specimen is placed between two parallel plates, and then the upper plate is raised to form a filament. A laser micrometer measures the midpoint diameter of the filament as it thins. The filament breakup time, deformation rate, and extensional viscosity can be calculated from the decrease in diameter with time. All of these methods are limited to spinnable fluids under small total strains and strain rates. High strain rates tend to break the column or filament.

There is another technique that can be used with low viscosity (100 mPa·s) nonspinnable fluids and which allows high strain rates ($>10^{3}$ s^{-1}). A modified opposing jets device (253) is employed that consists of opposing nozzles through which the fluid is sucked or blown out. Extensional viscosity is determined from

the force required to keep the nozzles at a fixed distance apart as a function of flow rate. A wide range of fluids can be investigated, and the high strain rates obtainable make it possible to study industrial processes and the effects of low concentrations of additives. A commercial instrument based on this device was on the market for a few years and has been used for some interesting research (254–258).

A sliding plate rheometer (simple shear) can be used to study the response of polymeric liquids to extension-like deformations involving larger strains and strain rates than can be employed in most uniaxial extensional measurements (68,226,230). The technique requires knowledge of both shear stress and the first normal stress difference, $N_1(\dot{\gamma})$, but has considerable potential for characterizing extensional behavior under conditions closely related to those in industrial processes.

Flow entering an orifice from a larger tube produces both shear and extensional deformation of the fluid (259). Although both shear and extensional effects are present, the pressure across the orifice is often dominated by extensional effects. This has been used as the basis for an extensional viscosity attachment for the Vilastic VE tube viscometer (236,260).

A method for measuring the uniaxial extensional viscosity of polymer solids and melts uses a tensile tester in a liquid oil bath to remove effects of gravity and provide temperature control; cylindrical rods are used as specimens (261,262). The rod extruder may be part of the apparatus and may be combined with a device for clamping the extruded material (263). However, most of the more recent versions use prepared rods, which are placed in the apparatus and heated to soften or melt the polymer (121,129,264–266). A constant stress or a constant strain rate is applied, and the resultant extensional strain rate or stress, respectively, is measured. Similar techniques are used to study biaxial extension (119).

In another elongational rheometer (264), the specimen is suspended on the end of a flexible tape, which is wound onto a wheel turned by a servo-controlled torque motor. This design is the basis for the Göttfert Rheostrain instrument. One device for melts and solids is an add-on fixture for rotational rheometers. The SER testing platform (267) incorporates dual wind-up drums and can be used for tensile, tear, peel, and friction testing as well as for elongational viscosity measurements.

The Rheometric Melt Elongational Rheometer (RME) (Fig. 27) is designed for high elongations of polymer melts (268–270). It uses a small ($\sim$1 g) compression-molded specimen which it supports on a stream of inert gas and holds in place with a rotary clamping device. The specimen is heated to the test temperature (up to 350°C) by electric heaters and extended by the motion of metal belts. Three sets of belts are available to provide different ranges of extensional strain rates: 10^{-3}–10^{-1} s^{-1}, $3 \times 10^{-3} - 3 \times 10^{-1}$ s^{-1}, and $10^{-2} - 1$ s^{-1}. The force generated by the specimen is measured by a spring-type transducer.

An FSR similar to those becoming popular for measuring the extensional viscosity of fluids has been constructed and applied to polymer melts (271). The FSR results were compared to those obtained from RMEs and agreement was good. Advantages of the FSR include the ability to make measurements on less viscous fluids than with the RME and the use of a smaller size specimen. In addition, the FSR measures all parameters online and very little post-processing of data is

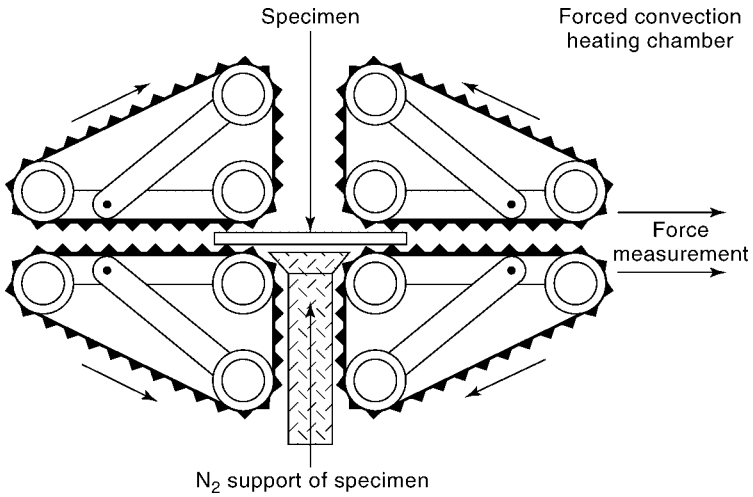

Fig. 27. Diagram of the Rheometric Melt Elongational Rheometer for elongational viscosity measurements on polymer melts. Courtesy of Rheometric Scientific.

necessary. In the RME, a measure of strain during an experiment usually requires observation from a videotape or similar (270).

Biaxial extensional viscosity can be measured by several methods. The most common is bubble inflation, in which a thin polymer sheet is inflated with an inert gas or liquid (272–274). Another method involves stretching a polymer sheet using eight rotating clamps placed in an octagonal pattern (275). A complex servo control system is required to coordinate the motion of the clamps. In a newer technique, displacement is measured as the material is squeezed between two disks having lubricated surfaces (lubricated squeezing flow) (276–285). A commercial instrument based on this technique, the MARS-III Multifunction Axial Rheometer System, has been developed (280). The specimen is a disk 1–4 cm in diameter and 1–2 cm in thickness. A variety of deformation modes that emulate industrial processes are provided: deformation under constant load, constant strain rate, or constant velocity, or in a step mode for stress relaxation. After deformation the specimen can be monitored for elastic recovery. The temperature ranges are 20–250°C in oil and 20–400°C in air. The viscosity range is $10^4 - 10^{10}$ Pa·s, with strain rates of $2 \times 10^{-5} - 20\ s^{-1}$. The instrument is computer controlled and data collection is as automatic as the operator wishes.

Extensional viscosity that results purely from shear deformation seems to be of less interest, but has been measured (126). The rheology of several different polymer melts in terms of shear viscosity and uniaxial and biaxial extensional viscosity has been compared (279). Additional information on the measurement of extensional viscosity is also available (123,286–289).

Viscoelastic Measurement. A number of methods measure the various quantities that describe viscoelastic behavior. Some require expensive commercial rheometers, others depend on custom-made research instruments, and a few require only simple devices. Even qualitative observations can be useful in the case of polymer melts, paints, and resins, where elasticity may indicate an inferior batch

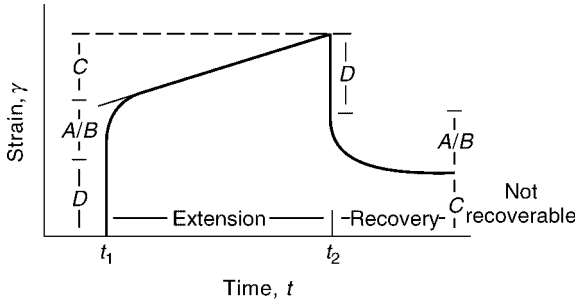

Fig. 28. Typical creep curve for a viscoelastic material. Stress applied at time t_1 and removed at t_2.

or unusable formulation. For example, the extrusion swell of a material from a syringe can be observed with a microscope. The Weissenberg effect is seen in the separation of a cone and plate during viscosity measurements or the climbing of a resin up the stirrer shaft during polymerization or mixing.

Creep experiments are among the simplest for describing viscoelastic behavior. They involve the measurement of deformation as a function of time after a given load has been applied. Such measurements may be made on specimens in tension, compression, or shear. Many more sophisticated devices exist, including tensile testers. The data are usually presented in the form of a strain–time curve (Figs. 14 and 28). Most materials undergo initial elastic deformation followed by a slow increase in strain with time. After the stress is removed, elastic deformation is recovered, but viscous deformation is not. Creep measurements are useful for evaluating the behavior of structural materials, fasteners, gaskets, pipe, and other articles that are subject to loading while in use. Creep measurements can also be carried out on fluids and are useful for measuring low shear viscosity and elasticity and for estimating and comparing structures, particularly in dispersions such as paints and inks.

Figure 28 is representative of creep and recovery curves for viscoelastic fluids. Such a curve is obtained when a stress is placed on the specimen and the deformation is monitored as a function of time. During the experiment the stress is removed, and the specimen, if it can, is free to recover. The slope of the linear portion of the creep curve gives the shear rate, and the viscosity is the applied stress divided by the slope. A steep slope indicates a low viscosity, and a gradual slope a high viscosity. The recovery part of Figure 28 shows that the specimen was viscoelastic because relaxation took place and some of the strain was recovered. A purely viscous material would not have shown any recovery, as shown in Figure 14**b**.

In a stress–relaxation test the deformation is held constant, and the resulting stress is measured as a function of time. Deformation produces an initial stress that decays with time in the case of viscoelastic materials. In an experiment the sample is rapidly deformed, and the resulting force measured as a function of time. The data may be plotted as stress, stress/initial stress, or modulus. A stress–relaxation curve for a lightly cross-linked rubber is shown in Figure 29 (290).

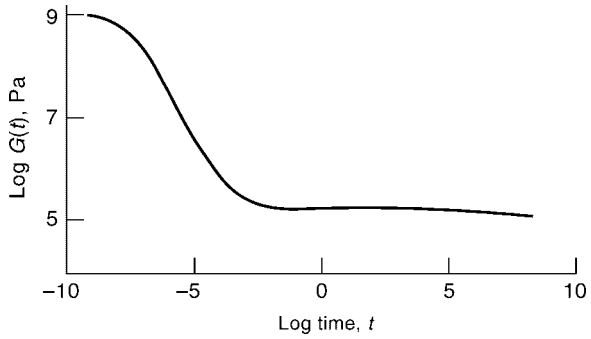

Fig. 29. Stress–relaxation curve for a lightly vulcanized rubber (290). To convert Pa to dyn/cm^2, multiply by 10.

The stress–relaxation process is governed by a number of different molecular motions. To resolve them, the thermally stimulated creep (TSCr) method was developed, which consists of the following steps:

(1) The specimen is subjected to a given stress at a temperature T for a time t, both chosen to allow complete orientation of the mobile units that one wishes to consider.
(2) The temperature is then lowered to $T_0 \ll T$, where any molecular motion is completely hindered; then the stress is removed.
(3) The specimen is subsequently heated at a controlled rate. The mobile units reorient according to the available relaxation modes. The strain, its time derivative, and the temperature are recorded versus time. By running a series of experiments at different orientation temperatures and plotting the time derivative of the strain rate observed on heating versus the temperature, various relaxational processes are revealed as peaks (291).

In a similar fashion, thermally stimulated current spectrometry (TSC) makes use of an applied d-c potential that acts as the stress to orient dipoles. The temperature is then lowered to trap these dipoles, and small electrical currents are measured during heating as the dipoles relax. The resulting relaxation maps have been related to G' and G' curves obtained by dynamic mechanical analysis (292–294). This technique, long carried out only in laboratory-built instruments, is available as a commercial TSC spectrometer from Thermold Partners LP, formerly Solomat Instruments (295).

Penetration and indentation tests have long been used to characterize viscoelastic materials such as asphalt, rubber, plastics, and coatings. The basic test consists of pressing an indentor of prescribed geometry against the test surface. Most instruments have an indenting tip, eg, cone, needle, or hemisphere, attached to a short rod that is held vertically. The load is controlled at some constant value, and the time of indentation is specified; the size or depth of the indentation is measured. Most instruments make use of a probe geometry which gives an increasing area of contact as penetration proceeds. In this way, at some depth of penetration, the resisting force can become sufficient to balance the applied force on the

indentor. Unfortunately, many geometries, eg, diamonds, pyramids, and cones, do not permit the calculation of basic viscoelastic quantities from the results. Penetrometers of this type include the Pfund, Rockwell, Tukon, and Buchholz testers, used to measure indentation hardness which is dependent on modulus.

The Rheo-Tex rheometer is an inexpensive, automated instrument using load cell technology to measure indentation and creep. Available software calculates hardness/softness, brittleness, plasticity, and tensile strength. This instrument is particularly valuable for measurements on foods and personal care products.

Other penetrometer–indentometers include transducers to sense the position and movement of the probe and microprocessors for temperature control and data collection and reduction. These instruments are used mainly to measure softening points, which are not glass transitions but are usually close to those values. Because a softening point is indicative of behavior under load, it is often more useful for predicting performance than the T_g. Penetrometer–indentometers can also be used to measure indentation hardness, creep, creep recovery, and modulus. Examples of such instruments include the TA Instruments, Mettler, Perkin-Elmer, Seiko, and Shimadzu thermomechanical analyzers (TMAs). They can be used to generate modulus and modulus–temperature data from indentation–time plots by applying the Hertz equation (eq. 36) (170,296), where E is the elastic or Young's modulus, μ the Poisson's ratio, r the radius of the hemispherical indentor, P the force on the indentor (mass load $\times$ g), h the indentation, and H_k the indentation hardness.

$$\frac{E}{1-\mu^2} = \frac{3}{4r^{1/2}} \frac{P}{h^{3/2}} = H_k \tag{36}$$

Because the indentation varies with time, the modulus must be specified for a certain indentation time, eg, a 10-s modulus. The Hertz equation holds only for purely elastic materials. However, it has been applied to viscoelastic materials, including polymers and coatings, with excellent results (296–303). Indentation hardness vs temperature curves are shown in Figure 30 (296–298).

A fully automated microscale indentor known as the Nano Indentor is available from Nano Instruments (304–306). Used with the Berkovich diamond indentor, this system has load and displacement resolutions of 0.3 N and 0.16 nm, respectively. Multiple indentations can be made on one specimen with spatial accuracy of better than $\pm$200 nm using a computer-controlled sample manipulation table. This allows spatial mapping of mechanical properties. Hardness and elastic modulus are typically measured (306,307) but time-dependent phenomena such as creep and adhesive strength can also be monitored.

Indentation is not usually thought of as a method for measuring viscoelastic properties, but the technique can be useful particularly for measurements of coatings on rigid substrates. Modern instrumentation, as described above, allows for precise, computer-controlled loading and unloading of force. The Mettler TMA, Perkin-Elmer's DMA, and the Nano Indentor have modes by which periodic and very short indentation creep measurements can be made while the specimen is being heated, thereby allowing estimates of the changes in modulus with temperature. A more quantitative technique is called modulus profiling, which uses a modified TMA instrument to measure tensile compliance, a measurement closely

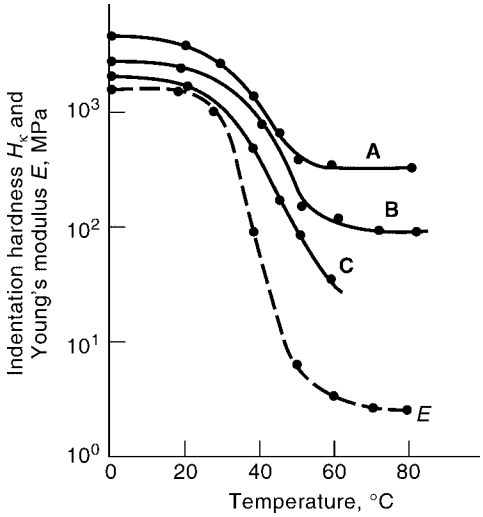

Fig. 30. Indentation hardness H_k at (**A**) 19 μm; (**B**) 47 μm; and (**C**) 108 μm thickness, and Young's modulus, E, of a free film (as functions of temperature) of an acrylic coating (296). These results show the dependence of thickness that occurs with thin films. To convert MPa to psi, multiply by 145. Courtesy of *Farbe & Lack*.

related to the inverse of the tensile modulus (308). The instrument can be used to profile or map tensile properties of a polymer specimen to show spatial variations resulting from processing inhomogeneities or aging phenomena such as oxidation.

The most widely used instrument for measuring the viscoelastic properties of solids is the tensile tester or stress–strain instrument, which extends a sample at constant rate and records the stress. Creep and stress–relaxation can also be measured. Numerous commercial instruments of various sizes and capacities are available. They vary greatly in terms of automation, from manually operated to completely computer controlled. Some have temperature chambers, which allow measurements over a range of temperatures. Manufacturers include Applied Test Systems, Benz, Com-Ten Industries, Custom Scientific, Detroit Testing Machine, Dillon Force Measuremet, Dynatek, GRC Instruments, Instron, MTS, Monsanto,, SATEC Systems, Inc., Shimadzu, Thwing-Albert, and Tinius Olsen.

A typical stress–strain curve generated by a tensile tester is shown in Figure 31. Creep and stress–relaxation results are essentially the same as those described above. Regarding stress–strain diagrams and from the standpoint of measuring viscoelastic properties, the early part of the curve, ie, the region of small deformations, is usually of the most interest. At small strains, stress is proportional to strain; therefore, the modulus is constant. At higher stresses and corresponding strains, a point is reached where the modulus depends on strain. Eventually, irreversible changes take place, resulting in rupture. These forms of behavior are shown in Figure 31. The linear relationship between stress and strain is shown in the region between the start of the experiment and point A. The latter is the yield point common to many materials, in which the specimen yields with no increase or with a decrease in stress. At higher levels the sample breaks at break point B. The tensile strength b and elongation at break d are important

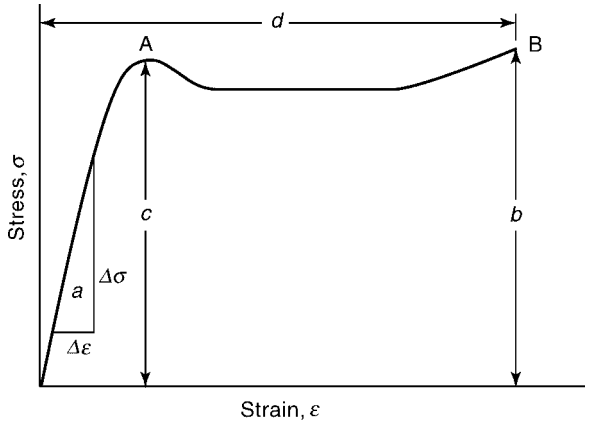

Fig. 31. Typical stress–strain curve. Point A is the yield point of the material; the sample breaks at point B. Mechanical properties are identified as follows: $a = \Delta\sigma/\Delta\varepsilon$, modulus; $b =$ tensile strength; $c =$ yield strength; $d =$ elongation at break. The toughness or work to break is the area under the curve.

mechanical properties, used to characterize plastics, paint films, and many other materials. For more information on tensile testing, consult ASTM methods D2370, D638M, and D882 as well as more recent literature (309–313).

Measurement of the propagation of ultrasonic acoustic waves has been found useful for determining the viscoelastic properties of thin films of adhesives. In this method, the specimen is clamped between transmitting and receiving transducers. The change in pulse shape between successive reverberation of the pulse is dependent on the viscoelastic properties of the transmitting material. Modulus values can be calculated (314,315).

Dynamic Measurements. Dynamic methods are required for investigating the response of a material to rapid processes, studying fluids, or examining a solid as it passes through a transition region. Such techniques impart cyclic motion to a specimen and measure the resultant response. Dynamic techniques are used to determine storage and loss moduli, G' and G', respectively, and the loss tangent, tan δ. In addition, the frequency dependence of these moduli can provide insight into polymer architecture (316,317). Some instruments are sensitive enough for the study of liquids and can be used to measure the dynamic viscosity η'. Measurements are made as a function of temperature, time, or frequency, and results can be used to determine transitions and chemical reactions as well as the properties noted above. Dynamic mechanical techniques for solids can be grouped into free vibrations and forced vibrations. Dynamic techniques have been described in detail (290,298,302,313,318–328). A number of instruments are listed in Table 9. Related ASTM standards are listed in Table 10.

Free-vibration instruments subject a specimen to a displacement and allow it to vibrate freely. The oscillations are monitored for frequency and damping characteristics as they disappear. The displacement is repeated again and again as the specimen is heated or cooled. The results are used to calculate storage and loss modulus data. The torsional pendulum and torsional braid analyzer (TBA) are examples of free-vibration instruments.

Table 9. Selected Dynamic Mechanical Analyzers

Manufacturer	Analyzer	Frequency Range, Hz	Approximate modulus range, Pa·s	Maximum temperature range, °C	Comments
Bohlin Instruments/ Malvern www.bohlin.com; www.bohlinusa.com	Bohlin VOR	10^{-4}–10			
Imass, Inc. www.imass.com	Autovibron/Rheovibron	3.5–110	10^{5}–10^{11}		Good for minor transitions
Metravib Instruments www.metravib.com	VA2000, 3000, 4000	0.001–1000			
Perkin Elmer www.perkinelmer.com	Diamond DMA	0.01–100	10^{3}–10^{12}		Multifrequency Fourier transform method
	Diamond TMA (DMA mode)	0.001–1			
Seiko Instruments www.sii-kgk.com/en/	DMS 6100		10^{5}–10^{12}		
TA Instruments www.tainst.com	Ares	10^{-5}–500			Diverse materials: solids to polymer melts
	Ares-RDA	10^{-5}–500			
	Ares-RFS	10^{-5}–200			Good to characterize fluid structure
	Ares-LS1	10^{-5}–200			
	Ares-LS2	10^{-5}–500			
	RSA III	2.5×10^{-5}–80	10^{3}–3×10^{12}	−150–600	Controlled strain
	Q800	0.01–200	10^{3}–3×10^{12}	−150–600	Controlled stress

Table 10. Selected ASTM Standards on Dynamic Mechanical Analysis

Designation	Title
D4092-01	Standard Terminology: Plastics: Dynamic Mechanical Properties
D4473-03	Standard Test Method for Plastics: Dynamic Mechanical Properties: Cure Behavior
D5279-01	Standard Test Method for Plastics: Dynamic Mechanical Properties: In Torsion
D5024-01	Standard Test Method for Plastics: Dynamic Mechanical Properties: In Compression
D5023-01	Standard Test Method for Plastics: Dynamic Mechanical Properties: In Flexure (Three-Point Bending)
D5026-01	Standard Test Method for Plastics: Dynamic Mechanical Properties: In Tension
D4440-01	Standard Test Method for Plastics: Dynamic Mechanical Properties: Melt Rheology
E1640-99	Standard Test Method for Assignment of the Glass Transition Temperature by Dynamic Mechanical Analysis
D6382-99	Standard Practice for Dynamic Mechanical Analysis and Thermogravimetry of Roofing and Waterproofing Membrane Material

The torsional pendulum is a simple apparatus for making dynamic tests in the frequency range of 0.1–10 Hz. The specimen is rigidly clamped at its lower end, and the upper end is clamped to an inertia bar or disk that is free to rotate. The suspension wire supporting the system is passed over a pulley, and the weight is counterbalanced to prevent tensile stresses on the specimen. The experiment is begun by setting the inertia member into free oscillation, and the natural frequency and decay of these oscillations are measured. The storage modulus, G', is calculated from the square of the frequency, and the loss tangent, tan δ, from the logarithmic decrement of the sample. The logarithmic decrement is the natural logarithm of the ratio of two successive amplitudes.

A TBA is a torsional pendulum with which a composite specimen instead of a free film is used (318,322,323). The specimen is prepared by soaking a multifilamented glass braid in a polymer solution and, after mounting the specimen in the apparatus, removing the solvent by heating. Measurements are similar to those with the torsional pendulum. Rigidity and damping values are calculated. The former is proportional to G'; the latter, to tan δ.

With both instruments, data can be plotted as a function of time or temperature to give dynamic mechanical spectra. An example is shown in Figure 32, where rigidity and damping from TBA experiments are shown as functions of temperature for a styrene–butadiene–styrene radial block copolymer (329). Such spectra are particularly useful for the study of polymers, including the identification of physical transitions and the onset and kinetics of cross-linking (323,330) or embrittlement (329), as well as for measuring various viscoelastic parameters. The

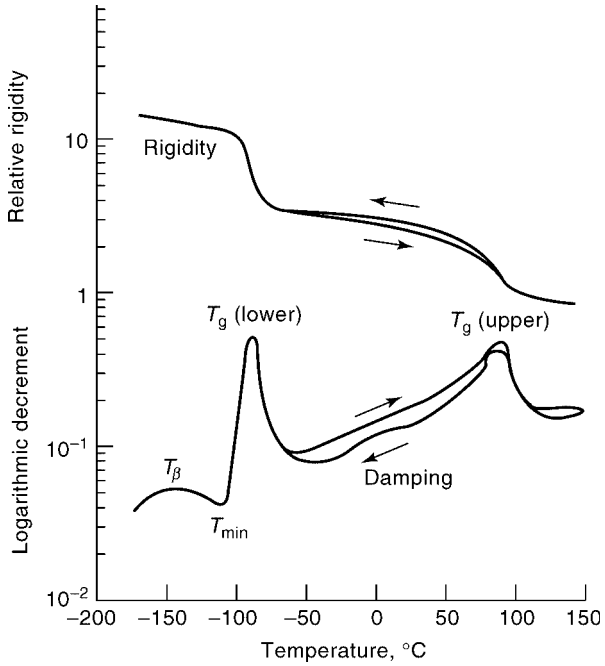

Fig. 32. Thermal mechanical behavior of a styrene–butadiene–styrene block copolymer in nitrogen at −180 to 150°C (329). Courtesy of the Federation of Societies for Coatings Technology.

curves in Figure 32 show that the material has two glass-transition temperatures, each indicated by a downturn in the rigidity curve and a damping peak. The material is glassy (high modulus) below the lower T_g, rubbery or leathery (moderate modulus) between the two transitions, and almost fluid (low modulus) above the upper T_g. Knowledge of such characteristics is important for predicting behavior under processing or use conditions.

Forced-vibration instruments drive specimens at specific frequencies and determine the response, usually over a range of temperatures. Storage and loss moduli or related parameters are determined. Series of modulus–temperature curves can be generated by making measurements at several different frequencies. Because thermal and mechanical transitions are functions of frequency as well as temperature, data from such curves can be used to calculate activation energies of transitions. In addition, frequencies can be chosen to represent or approximate polymer processing effects and use conditions.

Probably the most common modes of operation are the double cantilever and the tensile mode. In double cantilever, the specimen is held at its ends and driven by a vibrating drive shaft which is clamped to the center of the specimen. In tensile mode the specimen is also clamped at both ends but is driven along the axis between the clamps as one of them is part of the vibrating shaft. With most instruments, several frequencies can be monitored at the same time, as shown in the modulus and tan δ plots of Figure 33. A typical modulus range is $10^3 - 10^{11}$ N/m^2 ($10^4 - 10^{12}$ dyn/cm^2).

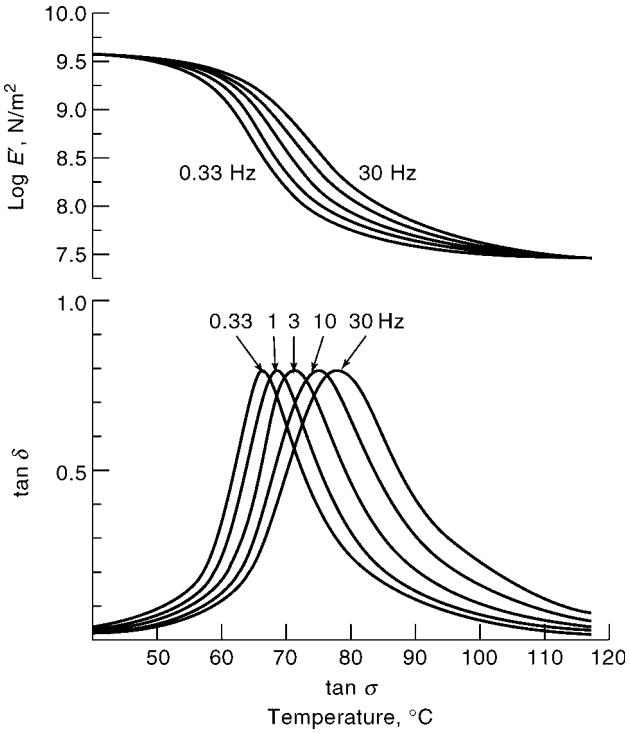

Fig. 33. Multifrequency modulus and tan δ vs temperature plots. To convert N/m^2 to psi, multiply by 1.45×10^4.

Fluids. The methods described above were designed for solid specimens, although some can be used for fluids if a solid support or carrier is used. The fluid must be highly viscoelastic for data to register, and absolute modulus values are difficult to determine because of the presence of the support. Different instrumentation is needed for the determination of meaningful modulus values over wide viscosity and elasticity ranges. Viscoelastic fluids can be characterized with a number of the rotational viscometers described previously. However, instead of constant rotational motion in one direction, a sinusoidal oscillatory motion must be used. Some oscillatory instruments can act as both dynamic viscometers and dynamic mechanical testing devices. They are capable of making measurements on solids, melts, and relatively concentrated solutions and dispersions. Viscoelasticity can also be determined by a controlled stress rheometer. The shape of a creep curve can show that a fluid is viscoelastic, and the amount of recovery after the stress is removed gives a measure of elasticity.

Time–Temperature Superposition and Master Curves. Because the modulus of a viscoelastic material varies with time and temperature, measurements must be made over wide ranges of these variables for full characterization. This is often impossible, particularly for very long and very short times. Even if it were possible, the amount of experimental work involved would be prohibitive. Therefore, techniques have been developed to determine modulus values

and curves at times or temperatures not attainable experimentally. A series of stress–relaxation, indentation, or modulus curves measured at different temperatures can be shifted on a log time axis to give a single modulus time master curve that covers a wide time range. A creep–compliance–time master curve can be constructed in the same fashion, as can a similar curve by using the families of modulus curves at different frequencies, such as those in Figure 33, generated by dynamic mechanical instruments with multiplexing capabilities. These curves can be shifted to a single modulus–frequency master curve because time and temperature have equivalent effects on modulus and other viscoelastic quantities (171,319,320,325–328).

The shift factor required to superimpose a set of data for an amorphous polymer is described mathematically by the WLF equation (eq. 8) (22), which becomes

$$\log a_T = \frac{-17.4(T - T_g)}{51.6 + (T - T_g)}$$

where a_T is the shift factor, the amount of horizontal shift of the timescale. Figure 34 shows the preparation of a modulus master curve from experimentally measured stress–relaxation curves at various temperatures (331).

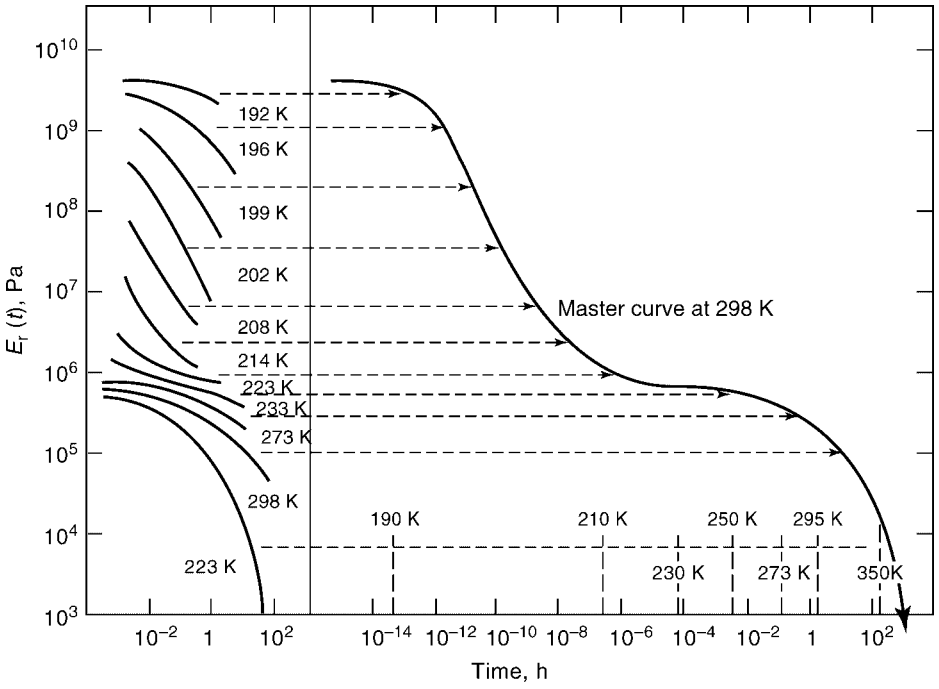

Fig. 34. Illustration of the time–temperature superposition principle as based on stress–relaxation data for polyisobutylene (331,332). To convert Pa to dyn/cm^2, multiply by 10. Courtesy of International Textbook Co., Ltd.

Master curves can also be constructed for crystalline polymers, but the shift factor is usually not the same as the one calculated from the WLF equation. An additional vertical shift factor is usually required. This factor is a function of temperature, partly because the modulus changes as the degree of crystallinity changes with temperature. Because crystallinity is dependent on aging and thermal history, vertical factors and crystalline polymer master curves tend to have poor reproducibility.

Master curves can be used to predict creep resistance, embrittlement, and other property changes over time at a given temperature, or the time it takes for the modulus or some other parameter to reach a critical value. For example, a rubber hose may burst or crack if its modulus exceeds a certain level, or an elastomeric mount may fail if creep is excessive. The time it takes to reach the critical value at a given temperature can be deduced from the master curve. Frequency-based master curves can be used to predict impact behavior or the damping ability of materials being considered for sound or vibration deadening. The theory, construction, and use of master curves have been discussed (171,290,320,326,327,331,332).

There also is interest in applying the principle of superposition to and developing master curves for polymer solutions. A recent paper (333) describes success in doing so. Measurements of shear viscosity, viscoelasticity, and extensional viscosity were carried out on solutions of polyisobutylene in a solvent consisting of a mixture of polybutene oil and dekalin. Eight solutions were tested, ranging in concentration from 0 to 2.5%. The results showed that both time–temperature and time–concentration superposition held for shear flows. By means of time–concentration superposition, a single master curve could be generated from the various flow curves. A single master curve was not possible for extension dominated flows. Instead, three curves were found, one for each of three concentration regimes, 0–0.1%, 0.25–1.5%, and 2.5%.

Practical Rheology

A common problem in rheology is that technologists in charge of research and development, quality control, and problem-solving are rarely trained in rheology, and rheologists are rarely trained in the technology of the product or process. The technologist may use flow to describe effects that are not connected with rheology in the way that a trained rheologist would interpret them. For example, a paint technologist may describe a paint as having poor flow, meaning that the surface has imperfections or defects. However, the same sample may flow easily in a rheological sense during application and cure. The solution of the problem may not involve a change in viscosity, and a small amount of a surfactant may improve the surface appearance of the paint film.

A good working rule in the correlation of viscosity measurements with processing conditions is to select and compare viscosities of materials at the shear rate that corresponds to the process in question. However, problems are encountered with high shear processes. For example, a viscometer with a sufficiently high shear rate may not be available. High shear rates can give heating effects, slip, and erroneous viscosity values. These difficulties can be solved by careful

extrapolation from lower shear measurements; Casson plots and other viscosity models can be useful.

Often, a simple ordering of good and poor materials can provide insight into the desired range of viscosity required for satisfactory processing. This strategy assumes that the viscosity of the material is the significant controlling parameter in the process, an assumption that should always be tested. Often, other factors have an equal or even greater influence on the system. For example, in the case of thin films and surfaces, the surface tension and physics of wetting can play a role equal to that of viscosity.

Few processes involve a single shear rate or set of mechanical conditions. Typical processes involve low, intermediate, and high shear regions or sections or stages. For example, a paint or coating may be pumped (intermediate shear rate), be sprayed (high shear rate), coalesce, and flow to form a uniform film (intermediate to low shear rate) and sag or run under gravity (low shear rate) during application. Thus a complete rheological evaluation of a material to determine its processing characteristics requires consideration of the viscosity of the material over an extended shear rate range. A given material may process well at low or intermediate shear rates, but fail completely at higher shear rates.

Additional complications can occur if the mode of deformation of the material in the process differs from that of the measurement method. Most fluid rheology measurements are made under shear. If the material is extended, broken into droplets, or drawn into filaments, the extensional viscosity may be a more appropriate quantity for correlation with performance. This is the case in the parting nip of a roller in which filamenting paint can cause roller spatter if the extensional viscosity exceeds certain limits (127). In many cases shear stress is the key factor rather than shear rate, and controlled stress measurements are necessary.

These examples indicate that the correlation of rheological measurements with product and process performance requires study, knowledge, and hard work (3,8,103,172,187,193,194,334). Extensive applications of rheological measurements have been made to food products (19,103,282,284,335–340), lubricants (341–344), adhesives (216–218,345–349), paints (8,17,21,42–45,127,128, 179,188–190,195,214,215,324,350–359), printing inks (1,190,219,222,360–362), rubber (334,363–366), polymers and plastics (47,171,226–232,289,314–323,325–328,367–370), sealants (371), foams (372–376), slurry fuels (377) and other slurries (378,379), cosmetics (103,380), concentrated suspensions (381–389), crude oil (390,391), and powders and granular material (392–395). Careful rheological measurements and a thorough knowledge of the literature should enable the investigator to meet most rheological challenges.

BIBLIOGRAPHY

"Rheological Measurements" in *EPSE* 2nd ed., Vol. 14, pp. 454–541, by C. K. Schoff, PPG Industries, Ic.

1. H. Green, *Industrial Rheology and Rheological Structures*, John Wiley & Sons, Inc., New York, 1949.
2. M. Van Dyke, *An Album of Fluid Motion*, The Parabolic Press, Stanford, Calif., 1982.

3. D. V. Boger and K. Walters, *Rheological Phenomena in Focus*, Elsevier Science Publishing Co., Inc., New York, 1993.
4. H. A. Barnes and K. Walters, *Rheol. Acta* **24**, 323 (1985).
5. C. W. Macosko, in R. J. Goldstein, ed., *Fluid Mechanics Measurements*, Hemisphere Publishing Corp., New York, 1983, p. 423.
6. T. C. Papanastasiou, *J. Rheol.* **31**, 385 (1987).
7. E. A. Collins, C. H. Chen, and J. P. Padolewski, *J. Rheol.* **32**, 163 (1988).
8. R. Eley, in J. Koleske, ed., *Paint Testing Manual: Gardner-Sward Handbook*, 14th ed., ASTM, Philadelphia, 1995, p. 333.
9. J. M. Dealy, *J. Rheol.* **39**, 253 (1995).
10. M. Rosen, *Polym. Plast. Technol. Eng.* **12**(1), 1 (1979).
11. N. Casson, in C. C. Mills, ed., *Rheology of Disperse Systems*, Pergamon Press, New York, 1959, p. 84.
12. W. K. Asbeck, *Off. Dig. Fed. Soc. Paint Technol.* **33**(432), 65 (1961).
13. R. V. Williamson, *Ind. Eng. Chem.* **21**(11), (1929).
14. M. M. Cross, *J. Colloid Sci.* **20**, 417 (1965).
15. Ref. 8, p. 341.
16. W. H. Bauer and E. A. Collins, in F. R. Eirich, ed., *Rheology*, Vol. 4, Academic Press, Inc., New York, 1967, p. 423.
17. O. C. C. Lin, *J. Appl. Polym. Sci.* **19**, 199 (1975).
18. R. Roscoe, in J. J. Hermans, ed., *Flow Properties of Disperse Systems*, North-Holland Publishing Co., Amsterdam, the Netherlands, 1953, p. 1.
19. G. W. Scott Blair, *Elementary Rheology*, Academic Press, Inc., New York, 1969.
20. J. R. Van Wazer, J. W. Lyons, K. Y. Kim, and R. E. Colwell, *Viscosity and Flow Measurement, A Laboratory Handbook of Rheology*, Wiley-Interscience, New York, 1963.
21. P. E. Pierce, *J. Paint Technol.* **43**(557), 35 (1971).
22. M. L. Williams, R. F. Landel, and J. D. Ferry, *J. Am. Chem. Soc.* **77**, 3701 (1955).
23. Z. W. Wicks Jr., G. F. Jacobs, I.-C. Lin, E. H. Urruti, and L. G. Fitzgerald, *J. Coat. Technol.* **57**(725), 51 (1985).
24. Z. W. Wicks Jr., F. N. Jones, and S. P. Pappas, *Organic Coatings: Science and Technology*, Vol. II, John Wiley & Sons, Inc., New York, 1994, p. 13.
25. C. K. Schoff, in J. Brandrup, E. H. Immergut and E. A. Grulke, eds., *Polymer Handbook*, 4th ed., Wiley-Interscience, New York, 1999, p. VII/265.
26. M. L. Huggins, *J. Am. Chem. Soc.* **64**, 2716 (1942).
27. G. V. Schulz and F. Blaschke, *J. Prakt. Chem.* **158**, 130 (1941); *J. Prakt. Chem.* **159**, 146 (1941).
28. P. M. Reilly, B. M. E. van der Hoff, and M. Ziogas, *J. Appl. Polym. Sci.* **24**, 2087 (1979).
29. M. M. Rafi'ee Fanood and M. H. George, *Polymer* **28**, 2244 (1987).
30. K. K. Chee, *J. Appl. Polym. Sci.* **34**, 891 (1987).
31. M. Kurata and Y. Tsunashima, in J. Brandrup, E. H. Immergut, and E. A. Grulke, eds., *Polymer Handbook*, 4th ed., Wiley-Interscience, New York, 1999, p. VII/1.
32. S. H. Aharoni, *J. Appl. Polym. Sci.* **21**, 1323 (1977).
33. J. F. Rabek, *Experimental Methods in Polymer Chemistry*, Wiley-Interscience, New York, 1980.
34. M. Bohdanecky and J. Kovar, *Viscosity of Polymer Solutions*, Elsevier, Amsterdam, the Netherlands, 1982.
35. V. N. Kalashnikov, *J. Rheol.* **38**, 1385 (1994).
36. G. V. Vinogradov and A. Ya. Malkin, *Rheology of Polymers*, Springer-Verlag, New York, 1980.
37. T. G. Fox, S. Gratch, and S. Loshaek, in F. R. Eirich, ed., *Rheology*, Vol. 1, Academic Press, Inc., New York, 1956, p. 431.
38. G. Berry and T. G. Fox, *Adv. Polym. Sci.* **5**, 261 (1968).

39. H. Fujita and Y. Einaga, *Rheol. Acta* **25**, 487 (1986).
40. W. Thimm, C. Friedrich, M. Marth, and J. Honerkamp, *J. Rheol.* **43**, 1663 (1999).
41. W. W. Graessley, in J. E. Mark, ed., *Physical Properties of Polymers*, American Chemical Society, Washington, D.C., 1984, Chapt. 3, p. 97.
42. C. K. Schoff, *Prog. Org. Coat.* **4**, 189 (1976); *Am. Chem. Soc. Div. Polym. Mater. Sci. Eng. Prepr.* **55**, 8 (1986).
43. C. K. Schoff, in *Proceedings of the 14th Waterborne and Higher-Solids Coatings Symposium*, New Orleans, La., Feb. 1987, p. 252.
44. M. A. Sherwin, J. V. Koleski, and R. A. Taller, *J. Coatings Technol.* **53**(683), 35 (1981).
45. R. Buter, in G. D. Parfitt and A. V. Patsis, eds., in *Proceedings of the Fifth International Conference on Organic Coatings Science and Technology*, Athens, Greece, 1979, Technomics Publishing Co., Westport, Conn., 1981, p. 12.
46. D. R. Paul, J. E. St. Lawrence, and J. H. Troell, *Polym. Eng. Sci.* **10**, 70 (1970).
47. F. N. Cogswell, *Polymer Melt Rheology*, Halsted Press, a division of John Wiley & Sons, Inc., New York, 1981, p. 40.
48. G. Pezzin, *Materie Plastiche ed Elastomeri*, Aug. 1962; translated and reprinted as *Application Series, PC-12*, Instron Corp., Canton, Mass., 1972.
49. R. A. Mendelson, in N. M. Bikales, ed., *Encyclopedia of Polymer Science and Technology*, Vol. 8, Wiley-Interscience, New York, 1968, pp. 587–620.
50. J. L. White, in K. Walters, ed., *Rheometry: Industrial Applications*, Research Studies Press, a division of John Wiley & Sons, Inc., New York, 1980, pp. 209–280.
51. J. M. Dealy and K. F. Wissbrun, *Melt Rheology and Its Role in Plastics Processing*, Van Nostrand Reinhold Co., Inc., New York, 1990.
52. J. Meissner, *Makromol. Chem. Macromol. Symp.* **56**, 25 (1992).
53. J. M. Dealy, *Rheometers for Molten Plastics*, Society of Plastics Engineers and Van Nostrand Reinhold Co., Inc., New York, 1982.
54. J. M. Dealy and T. O. Broadhead, *Polym. Eng. Sci.* **33**, 1513 (1993).
55. W. Gleissle, *Rheology* **4**, 13 (1994).
56. R. Hingmann and B. L. Marzinke, *J. Rheol.* **38**, 573 (1994).
57. B. Maxwell and M. Nguyen, *Polym. Eng. Sci.* **19**, 1140 (1979).
58. B. Maxwell, in C. D. Craver, ed., *Polymer Characterization*, American Chemical Society, Washington, D.C., 1983, p. 149.
59. P. J. Hansen and M. C. Williams, *Polym. Eng. Sci.* **27**, 586 (1987).
60. H. T. Pham and E. Meinecke, *J. Appl. Polym. Sci.* **53**, 257, 265 (1994).
61. N. J. Inkson, T. C. B. McLeish, O. G. Harlen, and D. J. Groves, *J. Rheol.* **43**, 873 (1999).
62. Suneel, R. S. Graham, and T. C. B. McLeish, *Appl. Rheol.* **13**, 19 (2003).
63. T. C. B. McLeish and R. G. Larson, *J. Rheol.* **42**, 81 (1998).
64. W. M. H. Verbeeten, G. W. M. Peters, and H. W. Spiess, *J. Rheol.* **45**, 823 (2001).
65. J. M. Maia, O. S. Carneiro, A. V. Machado, and J. A. Covas, *Appl. Rheol.* **12**, 18 (2002).
66. G. Hay and M. E. Mackay, *J. Rheol.* **43**, 1099 (1999).
67. D. von Dusschoten, M. Wilhelm, and H. W. Spiess, *J. Rheol.* **45**, 1319 (2001).
68. J. G. Oakley and A. J. Giacomin, *Polym. Eng. Sci.* **34**, 580 (1994).
69. F. Koran and J. M. Dealy, *J. Rheol.* **43**, 1279 (1999).
70. S. F. Edwards, *Proc. Phys. Soc., London* **92**, 9 (1967); P. Doi and S. Edwards, *J. Chem. Soc., Faraday Trans. 2* **74**, 1789 (1978).
71. P.-G. de Gennes, *J. Chem. Phys.* **55**, 572 (1971); *Phys. Today* **36**(6), 33 (June 1983).
72. J. Maddox, *Nature* **330**, 11 (1987).
73. J. des Cloizeaux, *Macromolecules* **23**, 4678 (1990).
74. W. W. Graessley, *Acc. Chem. Res.* **10**, 332 (1977).
75. S. H. Wasserman and W. W. Graessley, *J. Rheol.* **36**, 543 (1992).
76. W. H. Tuminello, *Polym. Eng. Sci.* **26**, 1339 (1986); A. Ya. Malkin and A. E. Teishev, *Polym. Eng. Sci.* **31**, 1590 (1992).

77. S. H. Wasserman, *J. Rheol.* **39**, 601 (1995).
78. M. I. Aranguren and co-workers, *J. Rheol.* **36**, 1165 (1992).
79. R. A. Mendelson, *Polym. Eng. Sci.* **8**, 235 (1968); *Polym. Eng. Sci.* **16**, 690 (1976).
80. P. D. Driscoll and D. G. Bogue, *J. Appl. Polym. Sci.* **39**, 1755 (1990).
81. S. E. Kadijk and B. H. A. A. Van Den Brule, *Polym. Eng. Sci.* **34**, 1535 (1994).
82. H. L. Frisch and R. Simha, in F. R. Eirich, ed., *Rheology*, Vol. 1, Academic Press, Inc., New York, 1956, p. 525.
83. I. M. Krieger, in R. Buscall, T. Corner, and I. F. Stageman, eds., *Polymer Colloids*, Elsevier Science Publishing Co., Inc., New York, 1986.
84. J. Mewis and P. D'Haene, *Macromol. Chem. Macromol. Symp.* **68**, 213 (1993).
85. S. M. Jogun and C. F. Zukoski, *J. Rheol.* **43**, 847 (1999).
86. J.-D. Lee, J.-H. So, and S.-M. Yang, *J. Rheol.* **43**, 1117 (1999).
87. M. K. Lyon, D. W. Mead, R. E. Elliott, and L. G. Leal, *J. Rheol.* **45**, 881 (2001).
88. A. Sierou and J. F. Brady, *J. Rheol.* **46**, 1031 (2002).
89. J. Mewis, in G. Astarita and co-workers, eds., *Rheology*, Vol. 1, Plenum Press, New York, 1980, p. 149.
90. A. B. Metzner, *J. Rheol.* **29**, 739 (1985).
91. C. Ancey and H. Jorrot, *J. Rheol.* **45**, 297 (2001).
92. I. Zhu, N. Sun, K. Papadopoulos, and D. DeKee, *J. Rheol.* **45**, 1105 (2001).
93. W. B. Russel, *J. Rheol.* **24**, 287 (1980).
94. S. C. Tsai, D. Botts, and J. Plouff, *J. Rheol.* **36**, 1291 (1992).
95. Lj. Djaković, I. Šefer, and T. Djaković, *J. Disp. Sci. Technol.* **13**, 697 (1992).
96. W. B. Russel and P. R. Sperry, *Progr. Org. Coatings* **23**, 305 (1994).
97. T. Shikata and D. S. Pearson, *J. Rheol.* **38**, 601 (1994).
98. J. Persello, A. Magnin, J. Chung, J. M. Piau, and B. Cabanc, *J. Rheol.* **38**, 1845 (1994).
99. N. Phan-Thien, *J. Rheol.* **39**, 679 (1995).
100. T. A. Strivens, *Colloid Polym. Sci.* **261**, 74 (1983).
101. E. Windhab, *Rheology* **2**, 102 (1992).
102. T. Tadros, *Chem. Ind. (London)*, 907 (Dec. 7, 1992).
103. P. Sherman, *Industrial Rheology*, Academic Press, Inc., New York, 1970.
104. D. Quemeda, *Rheol. Acta* **16**, 82 (1977).
105. N. L. Ackermann and H. T. Shen, *AIChE J.* **25**, 237 (1979).
106. M. Mooney, *J. Colloid Sci.* **6**, 162 (1951).
107. D. C.-H. Cheng, *Chem. Ind. (London)*, 408 (May 17, 1980).
108. I. M. Krieger and T. J. Dougherty, *Trans. Soc. Rheol.* **3**, 137 (1959).
109. T. A. Witten and M. F. Cates, *Science* **232**, 1607 (1986).
110. L. M. Sander, *Nature* **322**, 789 (1986).
111. T. A. Strivens, *J. Colloid Interface Sci.* **57**, 476 (1976).
112. W. H. Boersma, J. Laven, and H. N. Stein, *AIChE J.* **36**, 321 (1990); *J. Rheol.* **39**, 841 (1995).
113. A. A. Catherall, J. R. Melrose, and R. C. Ball, *J. Rheol.* **44**, 1 (2000).
114. J. Mewis and G. Biebaut, *J. Rheol.* **45**, 799 (2001).
115. E. P. Vrahoponlu and A. J. McHugh, *J. Non-Newtonian Fluid Mech.* **25**, 157 (1987).
116. G. I. Taylor, *Proc. R. Soc. Lond., Ser. A* **138**, 41 (1932).
117. Ref. 101, p. 137.
118. J. W. Hill and J. A. Cuculo, *J. Macromol. Sci. C: Rev. Macromol. Chem.* **14**, 107 (1976).
119. J. Ferguson and N. E. Hudson, in R. A. Pethrick, ed., *Polymer Yearbook 2*, Harwood Academic Publishers, London, 1985, p. 155.
120. J. M. Dealy, *Polym. Eng. Sci.* **11**, 433 (1971).
121. J. Meissner, *Polym. Eng. Sci.* **27**, 537 (1987).
122. J. Ferguson and K. Walters, *Chem. Br.* **24**(1), 39 (1988).

123. K. Walters, in P. Moldenaers and R. Keunings, eds., *Theor. Appl. Rheol.*, Vol. 1, Elsevier, Amsterdam, the Netherlands, 1992, p. 16.
124. J. Ferguson and N. E. Hudson, *Int. J. Polym. Mater.* **20**(3–4), 181 (1993).
125. M. Takahashi, T. Isaki, T. Takagawa, and T. Masuda, *J. Rheol.* **37**, 827 (1993).
126. C. D. Denson, *Polym. Eng. Sci.* **13**, 125 (1973).
127. J. E. Glass, *J. Coatings Technol.* **50**(641), 56, 72 (1978); D. A. Soules, R. H. Fernando, and J. E. Glass, *J. Rheol.* **32**, 181, 199 (1988).
128. D. F. Massouda, *J. Coatings Technol.* **57**(722), 27 (1985).
129. H. M. Laun and H. Munstedt, *Rheol. Acta* **17**, 415 (1978).
130. K. F. Wissbrun, *Chemtracts: Macromol. Chem.* **1**(2), 131 (1990).
131. S. Catrei, C. W. Macosko, and H. H. Winter, *J. Rheol.* **25**, 433 (1981).
132. J. L. White, *Appl. Polym. Symp.* **33**, 31 (1978).
133. L. Marshall, C. F. Zukoski, and J. Goodwin, *J. Chem. Soc., Faraday Trans.* **185**, 2785 (1989).
134. W. Winslow, *J. Appl. Phys.* **20**, 1137 (1949).
135. H. Aldersey-Williams, *New Scientist* **125**(178), 37 (Mar. 17, 1990).
136. N. Webb, *Chem. Br.* **26**, 338 (1990).
137. T. C. B. McLeish, T. Jordan, and M. T. Shaw, *J. Rheol.* **35**, 427 (1991).
138. D. L. Hontsock, R. F. Novak, and G. J. Chaundy, *J. Rheol.* **35**, 1305 (1991).
139. W. S. Yen and P. J. Achorn, *J. Rheol.* **35**, 1375 (1991).
140. H. Conrad, A. F. Sprecher, Y. Choi, and Y. Chen, *J. Rheol.* **35**, 1393 (1991).
141. W. A. Bullough, *Endeavor.* **14**(4), 165 (1991).
142. T. C. Halsey, *Science* **258**, 761 (1992).
143. R. T. Bonnecaze and J.-F. Brady, *J. Rheol.* **36**, 73 (1992).
144. T. C. Halsey, J. E. Martin, and D. Adolf, *Phys. Rev. Lett.* **68**, 1519 (1992).
145. T. C. Jordan, M. T. Shaw, and T. C. B. McLeish, *J. Rheol.* **36**, 441 (1992).
146. F. E. Filisko, *Chem. Ind. (London)* (10), 370 (May 18, 1992); *J. Rheol.* **34**, 539 (1990); *J. Rheol.* **35**, 399 (1991).
147. H. Block, *CHEMTECH* **22**, 368 (1992).
148. D. R. Gamota, A. S. Wineman, and F. E. Filisko, *J. Rheol.* **37**, 919 (1993).
149. Z. Lon and R. D. Ervin, *J. Rheol.* **37**, 55 (1993).
150. K. M. Blackwood and H. Block, *Trends Polym. Sci.* **1**(4), 98 (1993).
151. C. F. Zukoski, *Annu. Rev. Mater. Sci.* **23**, 45 (1993).
152. T. C. Halsey, *Adv. Mater.* **5**(10), 711 (1993).
153. E. Westkämper and J. Meschke, *Rheology* **3**, 243 (1993).
154. Y. Otsubo and K. Edamura, *J. Rheol.* **38**, 1721 (1994).
155. B. Abu-Jdayil and P. O. Brunn, *Rheology* **4**, 187 (1994).
156. A. Inoue and S. Maniwa, *J. Appl. Polym. Sci.* **55**, 113 (1995).
157. H. Conrad, Y. Li, and Y. Chen, *J. Rheol.* **39**, 1041 (1995).
158. P. J. Rankin and D. J. Klingenberg, *J. Rheol.* **42**, 639 (1998).
159. H. Onihara, Y. Hosoi, K. Tajiri, Y. Ishibashi, M. Doi, and A. Inoue, *J. Rheol.* **43**, 125 (1999).
160. S.-H. Chu and S. J. Lee, *J. Rheol.* **44**, 105 (2000).
161. B. D. Chin and O. O. Park, *J. Rheol.* **44**, 397 (2000).
162. B. Liu and M. T. Shaw, *J. Rheol.* **45**, 641 (2001).
163. H. P. Gavin, *J. Rheol.* **45**, 983 (2001).
164. J. Rabinow, *AIEE Trans.* **67**, 1308 (1948).
165. H. Janocha and B. Rech, *Rheology* **3**, 39 (1993); **4**, 198 (1994).
166. G. J. Besseris, I. F. Miller, and D. B. Yeates, *J. Rheol.* **43**, 591 (1999).
167. Y. M. Shkel and D. J. Klingenberg, *J. Rheol.* **45**, 351 (2001).
168. P. Kuzhir, G. Bossis, and V. Bashtovoi, *J. Rheol.* **47**, 1373, 1385 (2003).

169. C. Zener, *Elasticity and Anelasticity of Metals*, University of Chicago Press, Chicago, Ill., 1948.
170. S. P. Timoshenko and J. N. Goodier, *Theory of Elasticity*, 3rd ed., McGraw-Hill Book Co., Inc., New York, 1969.
171. J. R. Fried, *Polymer Science and Technology*, Prentice Hall Inc., Englewood Cliffs, N.J., 1995.
172. J. Ferguson and Z. Kemblowski, *Applied Fluid Rheology*, Elsevier Science Publishing Co., Inc., New York, 1991.
173. Y. P. Khanna and K. R. Slusarz, *Polym. Eng. Sci.* **33**, 122 (1993).
174. J. K. Gillham and C. K. Schoff, *J. Appl. Polym. Sci.* **20**, 1875 (1976).
175. W. P. Cox and E. H. Merz, *J. Polym. Sci.* **28**, 619 (1958).
176. W. Geissle and B. Hochstein, *J. Rheol.* **47**, 897 (2003).
177. J. Starita, in G. Astarita and co-workers, eds., *Rheology*, Vol. 2, Plenum Press, New York, 1980, p. 229. J. Starita, *Rheometrics System Four*, Rheometrics, Inc., Union, N.J., 1980.
178. J. Meissner, *J. Appl. Polym. Sci.* **16**, 2877 (1972), Weissenberg Rheogoniometer data.
179. O. C. C. Lin, *CHEMTECH* **5**(1), 51 (1975).
180. A. S. Lodge, T. S. R. Al-Hadithi, and K. Walters, *Rheol. Acta* **26**, 516 (1987).
181. A. Ait-Kadi, L. Choplin, and P. J. Carreau, *Polym. Eng. Sci.* **29**, 1265 (1989).
182. G. A. Nuñez, G. S. Ribeiro, M. S. Arncy, J. Feng, and D. D. Joseph, *J. Rheol.* **38**, 1251 (1994).
183. D. Hadjistamov, *Rheology* **5**, 29 (1995).
184. Y. T. Hu and A. Lips, *J. Rheol.* **45**, 1453 (2001).
185. E. B. Bagley, *J. Appl. Phys.* **28**, 624 (1957).
186. R. J. Gardner and P. C. Senanayake, *Rev. Sci. Instrum.* **57**, 3129 (1986).
187. T. C. Patton, *Paint Flow and Pigment Dispersion*, 2nd ed., John Wiley & Sons, Inc., New York, 1979.
188. M. Euverard, *The Efflux Type Viscosity Cup*, Scientific Section, National Paint, Varnish and Lacquer Association, Washington, D.C., 1948.
189. M. Euverard, *ASTM Bull.* **162**, 67 (Oct. 1950).
190. W. Gleissle, *Rheology* **4**, 138 (1994).
191. D. Hadjistamov and F. Gutekunst, *Rheology* **4**, 29 (1994).
192. P. E. Pierce, *J. Paint Technol.* **41**(533), 383 (1969).
193. K. Walters, ed., *Rheometry: Industrial Applications*, Research Studies Press, a division of John Wiley & Sons, Inc., New York, 1980.
194. R. W. Whorlow, *Rheological Techniques*, Halsted Press, a division of John Wiley & Sons, Inc., New York, 1980.
195. T. A. Strivens, in R. Lambourne, ed., *Paint and Surface Coatings*, Ellis Horwood Ltd., Chichester, U.K., 1987, Chapt. 14, p. 547.
196. P. Toepke, *Rheology* **1**, 102 (1991).
197. M. Breuker, *Rheology* **1**, 179 (1991).
198. R. E. Smith, *J. Rheol.* **28**, 155 (1984).
199. S. S. Davis, J. J. Deer, and B. J. Warburton, *Phys. Educ.* **2**, 1 (1968); *J. Pharm. Pharmacol.* **20**, 836 (1968).
200. T. E. R. Jones, J. M. Davies, and H. A. Barnes, in B. Mena, A. Garcia-Rejon, and C. Rangel-Nafnile, eds., *Proceedings of the IX International Congress of Rheology*, Vol. 4, Univ. Nacional Autonoma de Mexico, Mexico City, Mexico, 1984, p. 45.
201. L. Bohlin, *News Bohlin Rheol.* **2**, 6 (1986).
202. A. J. P. Franck, *J. Rheol.* **29**, 833 (1985).
203. A. J. P. Franck, in *Proceedings of the XI International Congress on Rheology*, Brussels, Belgium, Aug. 1992, p. 982.

204. M. Schmidt and A. J. P. Franck, *Rheology* **4**, 23 (1994).
205. T. S. Wilson, *Appl. Rheol. Meas. Newsl.* **3**(1), 3 (Mar. 1994).
206. Q. D. Nguyen and D. V. Boger, *J. Rheol.* **27**, 331 (1983); *J. Rheol.* **29**, 335 (1985); *Rheol. Acta* **26**, 508 (1987).
207. A. S. Yoshimure, R. K. Prud'homme, H. M. Princen, and A. D. Kiss, *J. Rheol.* **31**, 699 (1987).
208. B. Hanson, M. Levesley and J. Fisher, *Appl. Rheol.* **13**, 242 (2003).
209. L. A. Mondy, A. L. Graham, A. Majumdar, and L. E. Bryant Jr., *Int. J. Multiphase Flow* **12**, 497 (1986).
210. A. L. Graham and co-workers, *Appl. Phys. Lett.* **50**, 127 (1987).
211. B. J. Briscoe, P. F. Luckham, and S. R. Ren, *Colloids Surf.* **62**, 153 (1992).
212. A. Quach and C. M. Hansen, *J. Paint Technol.* **46**(592), 40 (1974).
213. W. Goring, N. Dingerdissen, and C. Hartmann, *Farbe Lack* **83**, 270 (1977).
214. C. K. Schoff, *Rheology*, Federation of Societies for Coatings Technology, Blue Bell, Pa., 1991, p. 38.
215. C. K. Schoff, in *Proceedings of the 5th Annual ESD Adv. Coatings Conference*, Dearborn, Mich., Nov. 1995, p. 77.
216. J. Johnston, *Adhes. Age* **26**, 34 (1983).
217. F. Urushizuki, H. Yamaguchi, and H. Mizumachi, *J. Adhes. Soc. Jpn.* **20**, 195 (1984).
218. H. Mizumachi and T. Saito, *J. Adhes.* **20**, 83 (1986).
219. R. Bassemir, *Am. Inkmaker* **39**(4), 24 (1961).
220. J. Mewis, in Ref. 193, p. 324.
221. G. Pangalos and J. M. Dealy, *J. Oil Colour Chem. Assoc.* **68**(3), 59 (1985).
222. G. Pangalos, J. M. Dealy, and M. B. Lyre, *J. Rheol.* **29**, 471 (1985).
223. K. K. Chee, K. Sato, and A. Rudin, *J. Appl. Polym. Sci.* **20**, 1467 (1976).
224. N. A. Park and T. F. Irvine Jr., *Rev. Sci. Instrum.* **59**, 2051 (1988); *Am. Lab.* **21**(12), 8 (Dec. 1989).
225. N. A. Park and T. F. Irvine, in M. K. Sharma, ed., *Surface Phenomena and Additives in Water-Based Coatings and Printing Technology*, Plenum Press, New York, 1991, p. 241.
226. J. M. Dealy and S. S. Soong, *J. Rheol.* **28**, 355 (1984).
227. S. R. Doshi and J. M. Dealy, *J. Rheol.* **31**, 563 (1987).
228. J. M. Dealy and A. J. Giacomin, in A. A. Collyer and D. W. Clegg, eds., *Rheological Measurement*, Elsevier Applied Science, New York, 1988.
229. A. J. Giacomin, T. Samurkas, and J. M. Dealy, *Polym. Eng. Sci.* **29**, 499 (1989).
230. N. R. Demarquette and J. M. Dealy, *J. Rheol.* **36**, 1007 (1992).
231. S. G. Hatzikiriakos and J. M. Dealy, *J. Rheol.* **35**, 497 (1991); *Int. Polym. Process.* **8**, 36 (1993).
232. I. B. Kazatchov, S. G. Hatzikiriakos, and C. W. Stewart, *Polym. Eng. Sci.* **35**, 1864 (1995).
233. www.andveighing.com, A&D Company, Ltd.
234. www.dynatrolusa.com, Dynatrol Division of Automated Products, Inc.
235. www.nametre.com, Nametre.
236. www.vilastic.com, Vilastic Scientific, Inc.
237. H. M. Laun and H. Schuch, *J. Rheol.* **33**, 119 (1989).
238. J. Ferguson and M. K. H. El-Tawashi, in Ref. 151, p. 257.
239. C. A. Moore and J. R. A. Pearson, *Rheol. Acta* **14**, 436 (1975).
240. K. M. Baid and A. B. Metzner, *Trans. Soc. Rheol.* **21**, 237 (1977).
241. D. M. Jones, K. Walters, and P. R. Williams, *Rheol. Acta* **26**, 20 (1987).
242. F. D. Martischius, *Rheol. Acta* **21**, 288, 311 (1982).
243. K. K. K. Chao and M. C. Williams, *J. Rheol.* **27**, 451 (1983).
244. T. Sridhar and co-workers, *J. Non-Newtonian Fluid Mech.* **40**, 271 (1991).

245. V. Tirtaatmadja and T. Sridhar, *J. Rheol.* **37**, 1081 (1993).
246. M. Stelter and co-workers, *J. Rheol.* **44**, 595 (2000).
247. S. Anna and co-workers, *J. Rheol.* **45**, 83 (2001).
248. S. Anna and G. H. McKinley, *J. Rheol.* **45**, 115 (2001).
249. G. H. McKinley and T. Sridhar, *Ann. Rev. Fluid Mech.* **34**, 375 (2002).
250. M. Stelter and co-workers, *J. Rheol.* **46**, 507 (2002).
251. X. Ye, R. G. Larson, C. Pattamaprom, and T. Sridhar, *J. Rheol.* **47**, 445 (2003).
252. www.thermo.com, Thermo Haake, Thermo Electron Corp.
253. G. G. Fuller, C. A. Cathey, B. Hubbard, and B. F. Zembroski, *J. Rheol.* **31**, 235 (1987).
254. M. R. Anklam, G. G. Warr, and R. K. Prud'homme, *J. Rheol.* **38**, 797 (1994); R. K. Prud'homme and G. G. Warr, *Langmuir* **10**, 3419 (1994).
255. M. E. Mackay, A. M. Dajan, H. Wippel, H. Janeschitz-Kriegl, and M. Lipp, *J. Rheol.* **39**, 1 (1995).
256. S. A. McGlashan, V. T. O'Brien, K. Awati, and M. E. Mackay, *Rheol. Acta* **37**, 214 (1998).
257. S. A. McGlashan and M. E. Mackay, *J. Non-Newtonian Fluid Mech.* **85**, 213 (1999).
258. V. T. O'Brien and M. E. Mackay, *J. Rheol.* **46**, 557 (2002).
259. D. D. Valle, P. A. Tanguy and P. J. Carreau, *J. Non-Newtonian Fluid Mech.* **94**, 1 (2000).
260. Extensional Viscosity and Elasticity of Fluids, Technical Note, Vilastic Scientific, Inc., 2001. Available at www.vilastic.com.
261. R. L. Ballman, *Rheol. Acta* **4**, 137 (1965).
262. F. N. Cogswell, *Rheol. Acta* **8**, 187 (1969).
263. J. Meissner, *Rheol. Acta* **8**, 78 (1969).
264. H. Munstedt, *J. Rheol.* **20**, 211 (1976).
265. H. Munstedt, *J. Rheol.* **23**, 421 (1979).
266. A. Franck and J. Meissner, *Rheol. Acta* **23**, 117 (1984).
267. www.xinst.com, Xpansion Instruments LLC.
268. J. Meissner and J. Hostettler, *Rheol. Acta* **33**, 1 (1994).
269. A. D. Gotsis and M. A. Odriozola, *J. Rheol.* **44**, 1205 (2000).
270. J. S. Schulze, T. P. Lodge, C. W. Macosko, and co-workers, *Rheol. Acta* **40**, 457 (2001).
271. A. Bach, H. K. Rasmussen and O. Hassager, *J. Rheol.* **47**, 429 (2003).
272. C. D. Denson and J. R. Gallo, *Polym. Eng. Sci.* **11**, 174 (1971).
273. D. D. Joye, G. W. Poehlein, and C. D. Denson, *Trans. Soc. Rheol.* **16**, 421 (1972).
274. J. M. Maerker and W. R. Schowalter, *Rheol. Acta* **13**, 627 (1974).
275. J. Meissner, T. Raible, and S. E. Stephenson, *J. Rheol.* **25**, 1, 673 (1981).
276. S. H. Chatraei, C. W. Macosko, and H. H. Winter, *J. Rheol.* **25**, 433 (1981).
277. A. C. Papanastasiou, L. E. Scriven, and C. W. Macosko, *J. Rheol.* **27**, 387 (1983).
278. P. R. Soskey and H. H. Winter, *J. Rheol.* **29**, 493 (1985).
279. S. A. Kahn, R. K. Prud-homme, and R. G. Larson, *Rheol. Acta* **26**, 144 (1987).
280. T. C. Hsu and I. R. Harrison, *Polym. Eng. Sci.* **31**, 223 (1991).
281. M. Takahashi, T. Isaki, T. Takagawa, and T. Masuda, *J. Rheol.* **37**, 827 (1993).
282. H. Huang and J. L. Kokini, *J. Rheol.* **37**, 879 (1993).
283. H. C. Kim, A. Pendse, and J. R. Collier, *J. Rheol.* **38**, 831 (1994).
284. K. Wikström, L. Bohlin, and A.-C. Eliasson, *Rheology* **4**, 192 (1994).
285. N. Golshan Ebrahimi, M. Takahashi, O. Araki, and T. Masuda, *Acta Polym.* **46**, 267 (1995); *J. Rheol.* **39**, 1385 (1995).
286. R. K. Gupta and T. Sridhar, in A. A. Collyer and D. W. Clegg, eds., *Rheological Measurement*, Elsevier Applied Science, New York, 1988, p. 211.
287. T. Sridhar, in Y. L. Yeow and P. H. T. Uhlherr, eds., *Proceedings of the 5th National Conference on Rheology*, Australia Society of Rheology, Melbourne, Australia, 1990, p. 1.
288. B. H. Bersted, *Polym. Eng. Sci.* **33**, 1079 (1993).

289. J. Meissner, *Rheology* **5**, 120 (1995).
290. J. D. Ferry, *Viscoelastic Properties of Polymers*, 2nd ed., John Wiley & Sons, Inc., New York, 1970.
291. J. C. Monpagens, D. G. Chatain, C. Lacabanne, and P. G. Gautier, *J. Polym. Sci., Polym. Phys. Ed.* **15**, 767 (1977).
292. A. Matthiesen and co-workers, *Amer. Lab.* **23**(1), 44 (Jan. 1991).
293. C. M. Neag, J. P. Ibar, J. R. Saffell, and P. Denning, *J. Coatings Technol.* **65**(826), 37 (1993).
294. J. P. Ibar, P. Denning, T. Thomas, A. Bernes, C. de Goys, J. R. Saffell, P. Jones, and C. Lacabanne, *Polymer Characterization: Physical Property, Spectroscopic, and Chromatographic Methods*, American Chemical Society, Washington, D.C., 1990, p. 167.
295. Technical data, Thermold Partners L.P., Stamford, Conn., 1995.
296. A. Zosel, *Farbe Lack* **82**, 15 (1976).
297. A. Zosel, *Farbe Lack* **80**, 1130 (1974); *Farbe Lack* **83**, 804 (1977).
298. A. Zosel, *Progr. Org. Coat.* **8**, 47 (1980).
299. A. G. Epprecht, *Farbe Lack* **80**, 505 (1974); *Farbe Lack* **82**, 685 (1976).
300. R. L. J. Morris, *J. Oil Colour Chem. Assoc.* **53**, 761 (1970).
301. K. T. Gillen, *J. Appl. Polym. Sci.* **22**, 1291 (1978).
302. D. J. Skrovanek and C. K. Schoff, *Progr. Org. Coat.* **16**, 135 (1988).
303. C. K. Schoff and P. Kamarchik, in A. T. Riga and C. M. Neag, eds., *Materials Characterization by Thermomechanical Analysis* (ASTM STP 1136), ASTM, Philadelphia, Pa., 1991, p. 138.
304. G. M. Pharr and W. C. Oliver, *Mater. Res. Soc. Bull.* **17**, 28 (1992).
305. W. C. Oliver, *Mater. Res. Soc. Bull.* **11**, 15 (1986).
306. M. F. Doerner and W. D. Nix, *J. Mater. Res.* **1**, 601 (1986).
307. W. C. Oliver and G. M. Pharr, *J. Mater. Res.* **7**, 1564 (1992).
308. K. T. Gillen, R. L. Clough, and C. A. Quintana, *Polym. Degrad. Stab.* **17**, 31 (1987).
309. L. W. Hill, *Progr. Org. Coatings* **5**, 277 (1977).
310. A. Toussaint and L. D'Hont, *J. Oil Col. Chem. Assoc.* **64**, 302 (1981).
311. L. W. Hill, *Mechanical Properties of Coatings*, Federation of Societies for Coatings Technology, Philadelphia, Pa., 1987.
312. Z. W. Wicks Jr., F. N. Jones, and S. P. Pappas, *Organic Coatings Science and Technology*, Vol. II, John Wiley & Sons Inc., New York, 1994, chapt. 24, p. 105.
313. L. W. Hill, in J. V. Koleske, ed., *Paint Testing Manual: Gardner-Sward Handbook*, 14th ed., ASTM, Philadelphia, 1995, p. 534.
314. R. E. Challis, R. P. Cocker, A. K. Holmes, and T. Alper, *J. Appl. Polym. Sci.* **44**, 65 (1992).
315. A. W. Chow and J. L. Bellin, *Polym. Eng. Sci.* **32**, 182 (1992).
316. J. R. Dargan, J. S. Williams and D. N. Lewis, *J. Rheol.* **43**, 1141 (1999).
317. F. Prochazka, D. Durand and T. Nicolai, *J. Rheol.* **43**, 1511 (1999).
318. J. B. Enns and J. K. Gillham, *Computer Applications in Applied Polymer Science*, American Chemical Society, Washington, D.C., 1982, chapt. 20.
319. T. Alfrey Jr., *Mechanical Behavior of High Polymers*, Wiley-Interscience, New York, 1984.
320. J. J. Aklonis, W. J. MacKnight, and M. Shen, *Introduction to Polymer Viscoelasticity*, Wiley-Interscience, New York, 1972.
321. R. F. Boyer, *Am. Chem. Soc. Org. Coat. Plast. Div. Prepr.* **44**, 491 (1981).
322. J. K. Gillham, *AIChE J.* **20**, 1066 (1974).
323. J. K. Gillham, *Developments in Polymer Characterization-3*, Applied Science Publishers, London, 1982, Chapt. 5.
324. S. Ikeda, *Progr. Org. Coat.* **1**, 205 (1972–1973).

325. N. G. McCrum, B. E. Read, and G. Williams, *Anelastic and Dielectric Effects in Polymer Solids*, John Wiley & Sons, Inc., New York, 1967.
326. L. E. Nielson, *Mechanical Properties of Polymers and Composites*, vols. **1** and **2**, Marcel Dekker, Inc., New York, 1974.
327. A. V. Toblosky, *Properties and Structures of Polymers*, John Wiley & Sons, Inc., New York, 1960.
328. I. M. Ward, *Mechanical Properties of Solid Polymers*, John Wiley & Sons, Inc., New York, 1971.
329. C. K. Schoff, *J. Coatings Technol.* **49**(633), 62 (1977).
330. J. K. Gillham, *Polym. Eng. Sci.* **26**, 1429 (1986).
331. J. M. G. Cowie, *Polymers: Chemistry and Physics of Modern Materials*, International Textbook Co., Ltd., Aylesbury, U.K., 1973, p. 236.
332. E. Catsiff and A. V. Tobolsky, *J. Colloid Sci.* **10**, 375 (1955).
333. A. J. Nogueiro and J. M. Maia, *Appl. Rheol.* **13**, 87 (2003).
334. J. W. White, *Rubber Chem. Technol.* **42**, 257 (1960).
335. C. Gallegos and M. Berjano, *J. Rheol.* **36**, 465 (1992).
336. K. Seethamraju and M. Bhattacharya, *J. Rheol.* **38**, 1029 (1994).
337. D. Jaros and H. Rohm, *Rheology* **4**, 77 (1994).
338. H.-D. Tscheuschner, *Rheology* **4**, 83 (1994).
339. V. Breton, J. Korolczak, J.-H. Doublier, and J. F. Maingonnat, *Rheology* **5**, 24 (1995).
340. E. Kuhn, *Rheology* **2**, 252 (1992).
341. P. M. Cann and H. A. Spikes, *Lubric. Eng.* **48**, 335 (1992).
342. S. M. Goh, M. N. Charalambides, and J. G. Williams, *J. Rheol.* **47**, 701 (2003).
343. R. Mas and A. Magnin, *J. Rheol.* **38**, 889 (1994).
344. E. Kuhn, *Rheology* **4**, 129 (1994).
345. P. R. Steiner, *J. Adhesion* **16**, 279 (1984).
346. G. Schmitt, J. Wiley, and J. Gotro, *Polym. Eng. Sci.* **29**, 329 (1989).
347. S. Vleeshouwers, A. M. Jamieson, and R. Simha, *Polym. Eng. Sci.* **29**, 662 (1989).
348. M. H. Pahl and D. Hesekamp, *Rheology* **3**, 97 (1993).
349. N. R. Manoj, P. P. De, D. K. Tripathy, and S. K. De, *J. Adhesion Sci. Technol.* **7**, 363 (1993).
350. T. C. Patton, *J. Paint Technol.* **38**, 656 (1966).
351. A. Quach and P. E. Pierce, *J. Paint Technol.* **45**(586), 69 (1973).
352. P. A. Sanford, J. E. Pittsley, P. R. Watson, K. A. Burton, M. C. Cadmus, and A. Jeanes, *J. Appl. Polym. Sci.* **22**, 701 (1978).
353. R. E. Smith, *J. Coat. Technol.* **54**(694), 21 (1982).
354. M. Osterhold and M. Bruecker, *Rheology* **1**, 230 (1991).
355. M. Breucker, *Rheology* **3**, 48 (1993).
356. M. Osterhold and Y. Jäger, *Rheology* **3**, 250 (1993).
357. N. Leskovsek, L. Tusar, and M. Tusar, *Rheology* **5**, 140 (1995).
358. J. E. Glass and R. K. Prud'homme, in S. F. Kistler and S. M. Schweitzer, eds., *Liquid Film Coating*, Chapman & Hall, London, 1996, p. 137.
359. M. Osterhold, *Eur. Coat. J.* **2000**, 206 (2000).
360. Y.-H. Zang, J. S. Aspler, M. Y. Boluk, and L. H. DeGrâce, *J. Rheol.* **35**, 345 (1991).
361. T. Hartford, *Am. Inkmaker* **72**(11), 42 (1994).
362. M. Fernández and co-workers, *J. Rheol.* **42**, 239 (1998).
363. Y.-H. Zang, R. Muller, and D. Froelich, *J. Rheol.* **30**, 1165 (1986).
364. J. L. White, M. H. Han, N. Nakajima, and R. Brzoskowski, *J. Rheol.* **35**, 167 (1991).
365. M. H. Wagner and J. Schaeffer, *J. Rheol.* **37**, 643 (1993).
366. A. Roychoudhury and S. K. De, *J. Appl. Polym. Sci.* **50**, 811 (1993).
367. D. J. Plazek, *Macromolecules* **16**, 1469 (1983); *Polym. Eng. Sci.* **24**, 111 (1984); *J. Rheol.* **36**, 1671 (1992).

368. T. S. Chow, *J. Mater. Sci.* **25**, 957 (1990); *Polymer* **32**, 29 (1991); *J. Rheol.* **36**, 1707 (1992); *Adv. Polym. Sci.* **103**, 149 (1992).
369. P. J. Halley and M. E. Mackay, *J. Rheol.* **38**, 1 (1994); *High Perform. Polym.* **6**, 405 (1994).
370. G. Sanz, *J. Appl. Polym. Sci.* **55**, 75 (1995).
371. E. A. Collins, C. H. Chen, and J. P. Padolewski, *J. Rheol.* **32**, 163 (1988); *J. Rheol.* **36**, 117, 131 (1992).
372. A. M. Kraynik and M. G. Hansen, *J. Rheol.* **31**, 175 (1987).
373. D. Weaire and T.-L. Fu, *J. Rheol.* **32**, 271 (1988).
374. E. Mora, L. D. Artavia, and C. W. Macosko, *J. Rheol.* **35**, 921 (1991).
375. A. M. Kraynik, D. A. Reinelt, and H. M. Prince, *J. Rheol.* **35**, 1235 (1991).
376. T. Okuzono, K. Kawasaki, and T. Nagai, *J. Rheol.* **37**, 571 (1993).
377. S.-F. Lin and R. S. Brodkey, *J. Rheol.* **29**, 147 (1985).
378. R. J. Mannheimer, *J. Rheol.* **35**, 113 (1991).
379. M. K. Agarwala, B. R. Patterson, and P. E. Clark, *J. Rheol.* **36**, 319 (1992).
380. D. Holland, *Rheology* **2**, 108 (1991).
381. A. J. Poslinski, M. E. Ryan, R. K. Gupta, S. G. Seshardi, and F. L. Frechette, *J. Rheol.* **32**, 703 (1988).
382. Y.-S. Lin, T.-J. Liu, and N.-J. Chu, *J. Appl. Polym. Sci.* **42**, 1767 (1991).
383. S. Pricl and G. Torriano, *Rheology* **1**, 223 (1991).
384. S. C. Tsai, D. Botts, and J. Plouff, *J. Rheol.* **36**, 1291 (1992).
385. J. Schröder, *Rheology* **2**, 40 (1992).
386. S. A. Khan and N. J. Zoeller, *J. Rheol.* **37**, 1225 (1993).
387. D. M. Kalyon, *CHEMTECH* **25**(5), 22 (May 1995).
388. R. L. Hoffman, *J. Rheol.* **42**, 111 (1998).
389. P. Pignon, A. Magnin and J.-M. Piau, *J. Rheol.* **42**, 1349 (1998).
390. L. T. Wardhaugh and D. V. Boger, *AIChE J.* **37**, 871 (1991).
391. L. E. Sanchez and J. L. Zakin, *Ind. Eng. Chem. Res.* **33**, 3256 (1994).
392. R. Jackson, *J. Rheol.* **30**, 907 (1986).
393. P. K. Haff, *J. Rheol.* **30**, 931 (1986).
394. R. Ocone and G. Astarita, *J. Rheol.* **37**, 727 (1993).
395. Y. Tomita, H. Ikeuchi, S. Kuchii, and K. Funatsu, *J. Rheol.* **38**, 231 (1994).

GENERAL REFERENCES

References 8,10,19,20,36,47,53,54,103,171,179,187,193–195,290,319,320,325–328, and 331 are good general references.

Reference 20, although out of date, is the single-most useful reference in this area. References 42 and 53 are good references for viscometers in general.

H. A. Barnes, J. F. Hutton, and K. Walters, *An Introduction to Rheology*, Elsevier Applied Science, New York, 1989.

B. D. Coleman, H. Markovitz, and W. Noll, *Viscometric Flow of Non-Newtonian Fluids*, Springer-Verlag, New York, 1966.

A. A. Collyer, ed., *Techniques in Rheological Measurement*, Chapman and Hall, New York, 1993.

A. A. Collyer and D. W. Clegg, eds., *Rheological Measurement*, Elsevier Applied Science, New York, 1988.

A. Dinsdale and R. Moore, *Viscometry and Its Measurement*, The Institute of Physics and the Physical Society, Reinhold Publishing Corp., New York, 1963.

F. R. Eirich, ed., *Rheology: Theory and Application*, vols. **1–5**, Academic Press, Inc., New York, 1956–1970.

A. G. Fredrickson, *Principles and Applications of Rheology*, Prentice-Hall, Inc., Englewood Cliffs, N.J., 1964.
C. W. Macosko, ed., *Rheology: Principles, Measurements, and Applications*, VCH Publishers, Inc., New York, 1994. An excellent text and reference.
T. G. Mezger, *The Rheology Handbook*, Vincentz Verlag, Hannover, 2002. An excellent resource for users and potential purchasers of rotational and oscillatory rheometers.
M. Reiner, *Deformation, Strain and Flow*, 2nd ed., Interscience Publishers, New York, 1960.
M. Rosen, *Polym. Plast. Technol. Eng.* **12**(1), (1979). A very useful, practical review.
S. Ross and I. D. Morrison, *Colloidal Systems and Interfaces*, John Wiley & Sons, Inc., New York, 1988.
W. R. Schowalter, *Mechanics of Non-Newtonian Fluids*, Pergamon Press, New York, 1977.
K. Walters, *Rheometry*, Halsted Press, a division of John Wiley & Sons, Inc., New York, 1975.
There are a number of excellent journals that cover or include rheological studies. Two particularly useful ones are the *Journal of Rheology* (free with membership in the Society of Rheology, see www.rheology.org/sor/) and *Applied Rheology* (www.ar.ethz.ch), which provides an excellent combination of papers, new equipment descriptions, announcements, abstracts of dissertations and papers, and other information. Other useful journals include *Rheologica Acta, Polymer Engineering and Science*, and the *Journal of Applied Polymer Science*.

CLIFFORD K. SCHOFF
PETER KAMARCHIK JR.
Schoff Associates

RIGID-ROD POLYMERS. See Volume 7.

RIM. See THERMOSETS.

RING OPENING POLYMERIZATION

Introduction

Poly(ε-caprolactone) and polylactides are synthetic polymers with quite unusual properties of biodegradability and biocompatibility. They have thus great potential as biomaterials and environmentally friendly thermoplastics. This explains why attention was paid quite early to the macromolecular engineering of these aliphatic polyesters (1). For this purpose, living, or at least controlled, polymerization is a prerequisite, which nowadays is met whenever the ring opening polymerization (ROP) of lactones, lactides, and glycolide (Fig. 1) proceeds through a coordination–insertion mechanism. Then, aliphatic polyesters can be prepared with a predictable degree of polymerization, a narrow molecular weight

Encyclopedia of Polymer Science and Technology. Copyright John Wiley & Sons, Inc. All rights reserved.

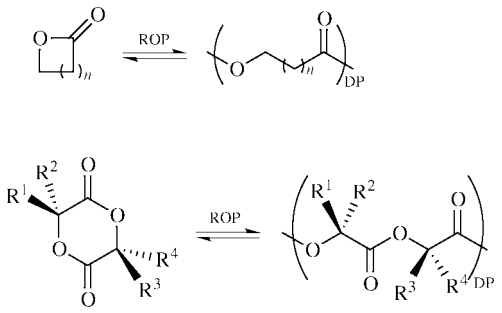

Fig. 1. Ring opening polymerization of unsubstituted lactones, lactides, and glycolide. $n = 1$: β-propionolactone (β-PL); $n = 2$: γ-butyrolactone (γ-BL); $n = 3$: δ-valerolactone (δ-VL); $n = 4$: ε-caprolactone (ε-CL); DP = degree of polymerization. $R^1 = R^2 = R^3 = R^4 = H$: glycolide; $R^1 = R^4 = CH_3$ and $R^2 = R^3 = H$: L-lactide (L-LA); $R^1 = R^4 = H$ and $R^2 = R^3 = CH_3$: D-lactide (D-LA); $R^1 = R^3 = CH_3$ and $R^2 = R^4 = H$: *meso*-lactide (*meso*-LA); D-LA/L-LA = 50/50: *racemic*-lactide (D,L-LA).

distribution, and well-defined end groups at one or both ends. Synthesis of block and graft copolymers of lactones and lactides has also been reported. In all these instances, lactones of different ring sizes, substituted or not by functional groups, have been involved (2).

The first reports on ROP mainly dealt with anionic and cationic polymerization of lactones, with formation of aliphatic polyesters of low molecular weight as a result of detrimental side reactions. Indeed, anionic propagating species are known for their propensity for transesterification reactions (Fig. 2). Whenever intramolecular, these reactions decrease the molecular weight and form low molecular weight cyclics. Intermolecular reactions are responsible for a Poisson distribution of the chain length. Moreover, the basicity of anionic species can account for proton transfer reactions, such as epimerization of the chiral center of poly(LA) units. A first strategy proposed to suppress, or at least reduce, the extent of the side reactions is the use of bulky ligands able to protect the ester groups in the chains against nucleophilic attack by the propagating species. For example, Lin and co-workers reported on the controlled ROP of L-LA by a mixed-ligand lithium aggregate prepared by reaction of 2,2′-ethylidene-bis(4,6-di-*tert*-butylphenol) and *n*-butyl lithium. The lithium alkoxide which is formed

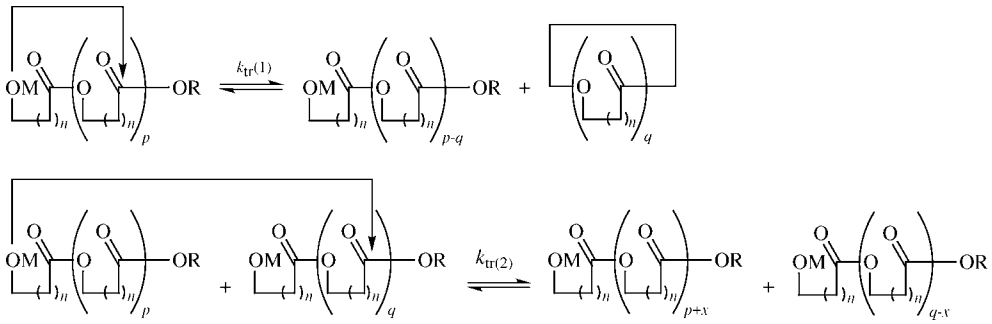

Fig. 2. Intramolecular and intermolecular transesterification reactions.

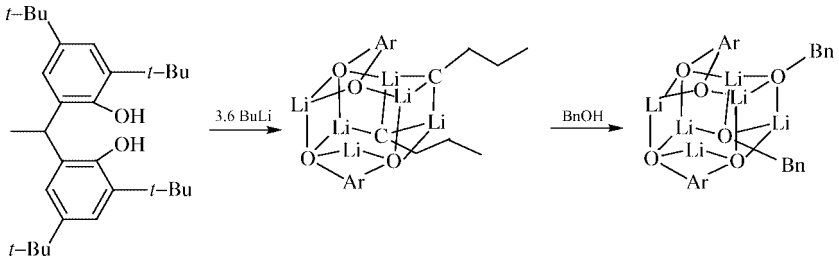

Fig. 3. Synthesis of mixed lithium–ligand aggregate, for the controlled ROP of L-LA.

further reacts with benzyl alcohol (Fig. 3) (3). Polydispersity of poly(L-LA) is then low (∼1.1) and M_n is predetermined by the monomer/initiator molar ratio. Nevertheless, the more general and powerful strategy consists in using active species of lower basicity and nucleophilicity, ie, organometallics derived from metals with d orbitals of favorable energy such as Al, Sn, Y, Nd, Yb, Sm, La, Fe, Zn, Zr, Ti, and Mg. Kricheldorf and co-workers studied the kinetics of the intramolecular transesterification reactions when poly(ε-CL) is exposed to a series of metal alkoxides. $(C_4H_9)_3SnOR$ and $(C_4H_9)_2Sn(OCH_3)_2$ turned out to be very active transesterification reagents. In contrast, no cyclic was formed at 150°C within 4 days, when $Al(O\text{-}i\text{-}C_3H_7)_3$ was the initiator (4). An intermediate behavior was reported for $Ti(O\text{-}i\text{-}C_3H_7)_4$ and $Zr(O\text{-}n\text{-}C_3H_7)_4$. Penczek and co-workers determined experimentally two selectivity factors, $\beta = k_p/k_{tr(1)}$ and $\gamma = k_p/k_{tr(2)}$, where $k_{tr(1)}$ and $k_{tr(2)}$ stand for the rate constant for the unimolecular and bimolecular transfer reactions, respectively, and k_p is the propagation rate constant (5). The most crowded and least reactive species expectedly shows a higher selectivity, as illustrated by this order of reactivity: $Al(O\text{-}i\text{-}C_3H_7)_3 < Ti(O\text{-}i\text{-}C_3H_7)_4 < Fe(OR)_3 < (C_2H_2)_5AlOR < La(OR)_3 < (C_4H_9)_3SnOR < (C_4H_9)_2Sn(OCH_3)_2 < Sm(OR)_3 < K^+ {}^- OR$.

Living/Controlled ROP Initiated or Catalyzed by Organometallics

Alkoxides of some metals with d-orbitals, including Al and Sn, are efficient initiators for ROP of ε-CL and LA, which proceeds according to a *coordination–insertion* mechanism (Fig. 4). The very first step is the coordination of the alkoxide (ROM) to the carbonyl of the monomer. As a result of this nucleophilic attack, the acyl–oxygen bond of the monomer is cleaved with the simultaneous insertion into the metal–alkoxide bond. This mechanism is supported by ^1H NMR analysis of oligomer end groups, ie, an OR-containing ester as the α end group and a hydroxyl ω end group that results from the hydrolysis of the propagating alkoxide. The energy of each transition state, TS1 and TS2 (Fig. 4), and thus the electronic and steric properties of the monomer, decides which step is rate-determining (6). The reactivity of the initiator also depends on how electronic and steric effects are combined (6). For instance, a lower energy for the LUMO orbital of the alkoxide results in a more electrophilic initiator and a faster ROP. Instead of being preformed, the alkoxide can be formed *in situ* by the reaction of a metal derivative, eg, tin octanoate and alkyl Al, with an alcohol. Whenever the alcohol is used in

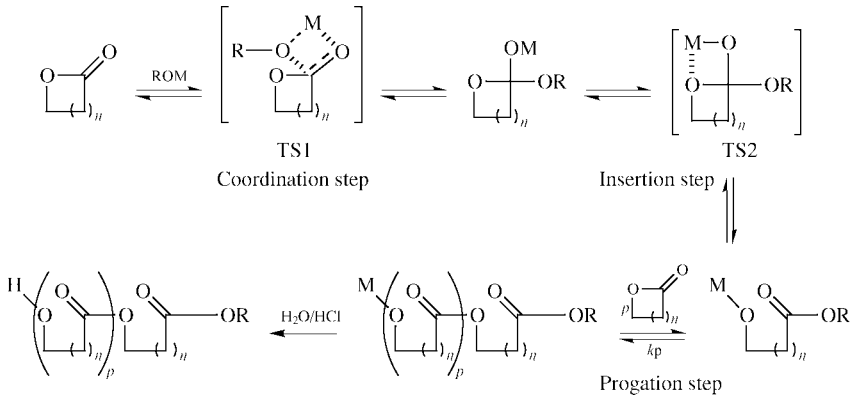

Fig. 4. The coordination–insertion mechanism for ROP of lactones and lactides.

excess and it participates in a fast exchange with the *in situ*–formed alkoxide, the metal derivative is rather a catalyst than the actual initiator. This "catalytic" system has the advantage of decreasing the extent of the polyester contamination by metal residues. The structure of the α end group is then dictated by the alcohol.

Aluminum Alkoxides. Aluminum alkoxides [$R_{3-n}Al(OR)_n$] are widely used as initiators for the macromolecular engineering of polylactones and polylactides (1,5), particularly Al trialkoxides [$Al(OR)_3$] and dialkyl Al alkoxides [R'_2AlOR]. Transesterification reactions are minimized and a good control is imparted to ROP, as assessed by a high γ value (for instance, 100 for ROP of L-LA in THF at 80°C) (7). Many experimental data reported in the literature confirm indeed that the molecular weight can be predicted from the monomer/initiator molar ratio and that the molecular weight distribution is narrow, in line with a fast initiation compared with propagation.

Except for γ-BL (8), high molecular weight polyesters can be prepared in the presence of Al alkoxides (9). This type of initiator can also polymerize other cyclic monomers, such as adipic anhydride and trimethylene carbonate, reviewing which is however beyond the scope of this review (9).

Because aluminum alkoxides can be prepared by reaction of trialkyl aluminum with an alcohol, the large variety of alcohols available offers a large choice for the structure of the α end group, including polymerizable end groups of the methacrylate and the norbornenyl types (10–13). These hydrophobic macromonomers can be copolymerized with hydrophilic comonomers, such as 2-hydroxyethylmethacrylate (HEMA), with formation of amphiphilic diblock copolymers (14). In case of α,ω-acrylate PCL (or PLA), formation of amphiphilic polymer network can be envisioned. In apolar solvents, aluminum alkoxides tend to self-associate (5), which may influence the polymerization course. For instance, $Al(O\text{-}i\text{-}C_3H_7)_3$ exists in toluene and benzene as a mixture of tetrameric (A_4) and trimeric (A_3) species in equilibrium (Fig. 5) (15,16). Only the trimers are active in ROP of ε-CL in toluene at 0°C (17), which explains that the average number of alkoxides active per Al is not 3.0 but rather close to 1.0 (16). This average number actually depends on the position of the A4 <=> A3 equilibrium in relation to the experimental conditions (solvent, temperature, and monomer).

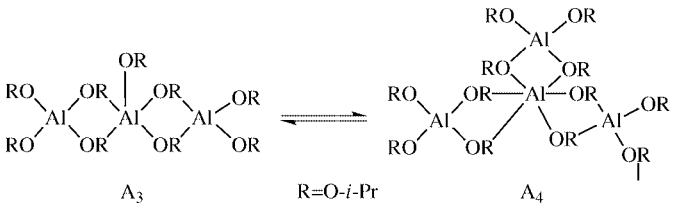

Fig. 5. Equilibrium between tetramers and trimers of $Al(O\text{-}i\text{-}C_3H_7)_3$.

Additives that coordinate to Al perturb the polymerization kinetics in toluene. For instance, THF and cyclohexanone compete ε-CL for coordination to aluminum (18), which decreases the propagation rate and may even inhibit polymerization. In contrast, kinetics is faster upon addition of a Lewis base, such as 4-picoline (19), because the coordination of this Lewis base onto the Al atom polarizes the metal–alkoxide bond and facilitates the monomer insertion. Although the reactivity of the active sites is increased, the extent of transesterification reactions is reduced, more likely for steric reasons.

Preparation of polyester free from toxic metallic residues is a prerequisite for biomedical applications. Because the metal extraction is time-consuming, it is worth decreasing the amount of initiator by using an alcohol as co-initiator. The molecular weight is then predetermined by the monomer/(alcohol + alkoxide) molar ratio. The apparent propagation rate increases first with the excess of alcohol up to a certain value, beyond which the kinetics becomes slower (20).

ROP has been initiated by well-defined single-site aluminum alkoxides modified by bulky ligands (21), eg, tetraphenylporphyrin (22), 2-2′-ethylidenebis(4,6-di-*tert*-butylphenol) (23,24), SALEN (25), and SALBINAP (26) (Fig. 6). The 5-Cl-SALEN (27,28) and HAPENOMe (28,29), ligands are efficient to promote ROP of LA at room temperature in dichloromethane. Interestingly enough, chiral ligands can induce stereoselective ROP of LA. Spassky and co-workers reported that (*R*)-(SalBinap)AlOMe polymerizes D-LA 20 times faster than L-LA (26). Similarly, the bulk poylmerization of L-LA is 14 times faster than that of D-LA when initiated by (*R*,*R*)-(SALEN)AlO-*i*-C_3H_7 (30). Long isotactic sequences are shown by ^{13}C NMR analysis of poly(LA), which then exhibits a tapered stereoblock microstructure. This stereocontrol is important because it directly influences the thermal properties of poly(LA). As an example, ROP of *rac*-LA initiated by (*rac*)-SALENAlO-*i*-C_3H_7 (30) or by achiral complexes (31) results in a polymer with a high melting temperature ($\sim$185°C) owing to the cocrystallization of poly(L-LA) and poly(D-LA) sequences. ROP of *meso*-LA initiated by (*R*)-(SALBINAP)AlO-*i*-C_3H_7 results in syndiotactic PLA (32), whereas *rac*-(SALBINAP)AlOR polymerizes *meso*- and *rac*-LA into heterotactic poly(LA) (33) and formation of isotactic stereoblocks (34), respectively. An exchange mechanism has been proposed to account for the poly(LA) microstructure prepared from *meso*-LA (33).

Tin. Tin octoate, $Sn(O(O)CCH(C_2H_5)C_4H_9)_2$, abbreviated further as $Sn(Oct)_2$, is one of the more widely used promoter of the ROP of lactones and lactides, owing to its acceptance as a food additive by the American Food and Drug Administration (FDA). $Sn(Oct)_2$ is used at the industrial scale for the

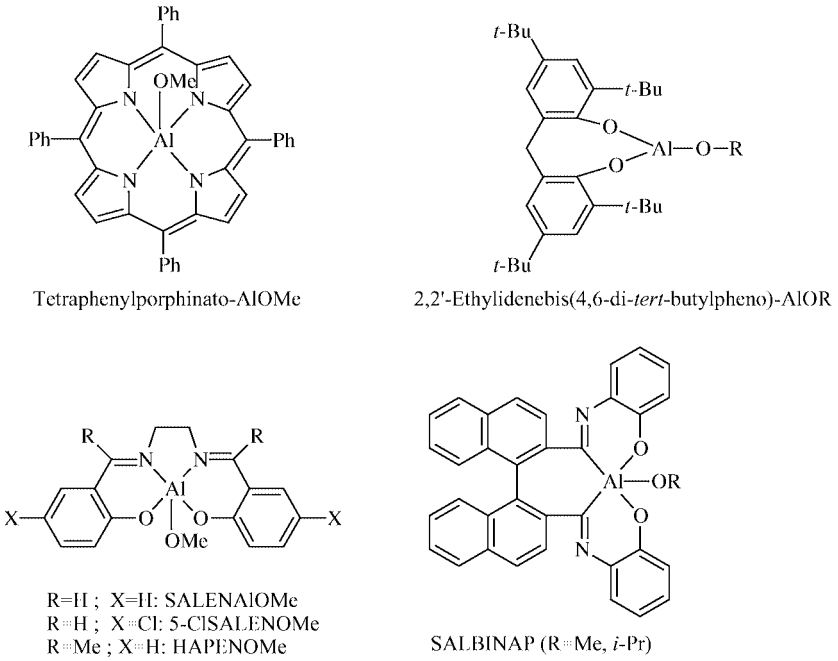

Fig. 6. Single-site aluminum alkoxides.

polymerization of LA by Cargill. Its activity depends on the availability of a protic co-initiator, either contaminating water and/or octanoic acid (35), or an alcohol added on purpose. Molecular weight in the 10^2–10^4 range is easily controlled by the monomer/alcohol molar ratio (35).

Although different mechanisms were proposed in the past in order to account for the role of $Sn(Oct)_2$ (36), it is now accepted that the active species are tin(II) alkoxides formed *in situ* by reaction of $Sn(Oct)_2$ with either adventitious water and hydroxy acids, or with an alcohol co-initiator as schematized by equations 1 and/or 2. The classical coordination–insertion mechanism shown in Figure 4 would thus be operative. Kricheldorf and co-workers pointed out that $Sn(Oct)_2$ initiators is a complex dynamic system that responds to changes of the reaction conditions (37). When the bulk polymerization of ε-CL is carried out at high temperature (180°C), the reaction of $Sn(Oct)_2$ with an alcohol is more complex and leads to a variety of compounds that contain tin–oxygen bonds (eg, tin hydroxides, stannoxanes, lactate complexes) and are liable to initiate the polymerization (37).

$$Sn(Oct)_2 + ROH \rightleftharpoons OCT\text{—}Sn\text{—}OR + Oct\text{—}H \quad (1)$$

$$Oct\text{—}Sn\text{—}OR + ROH \rightleftharpoons Sn(OR)_2 + Oct\text{—}H \quad (2)$$

Whenever water coexists with the $ROH/Sn(Oct)_2$ initiating system, it converts propagating tin(II) alkoxides into dormant hydroxyl end-capped chains and stannous hydroxide, which is less reactive than stannous alkoxide. The accordingly decreased concentration in the active propagating species accounts for a

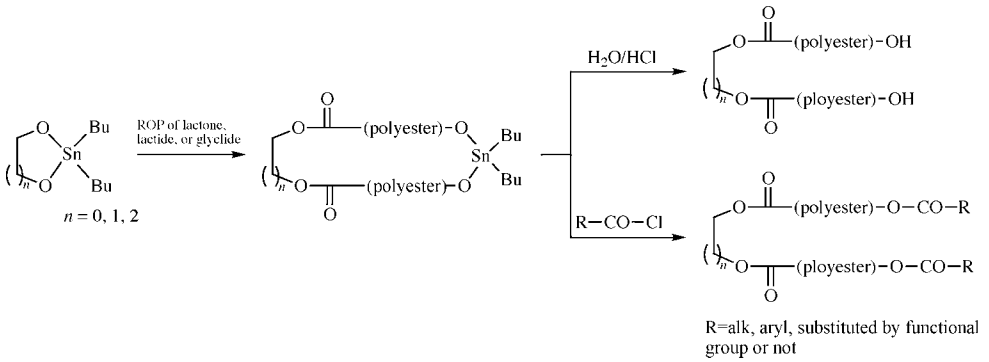

Fig. 7. ROP initiated by cyclic tin(IV) alkoxides.

slower polymerization. Because reaction is equilibrated, the molecular weight is not affected by water (38). The same general mechanism holds for dibutyltin dicarboxylates (39). The use of stannous(II) trifluoromethane sulfonate has also been reported for the ROP of ε-CL at low temperature (0°C) (40,41).

Tin alkoxides have also been preformed and used as ROP initiators. Alkyl-substituted tin(IV) alkoxides are more commonly used than the tin(II) counterparts. Compared with tin monoalkoxide (R'_3SnOR), tin(IV) dialkoxides (R'_2SnOR_2) are preferred because of a higher reactivity (42). Cyclic tin(II) alkoxides deserve interest because they form macrocyclic polyesters, which are precursors of telechelics, upon ring opening by acidic hydrolysis or reaction with acid chlorides (Fig. 7).

One drawback of tin(IV) alkoxides compared with aluminum alkoxides, is the broader molecular weight distribution of the formed polyesters. For instance, polydispersity of PCL is in the range of 1.4 and higher. Several phenomena contribute to this effect depending on the structure of the alkoxide, the monomer and the experimental conditions: (43) (*1*) slow initiation, (*2*) slow equilibrium between differently aggregated species, and (*3*) transesterification reactions (44). As a rule, tin alkoxides, are efficient transesterification catalysts and they are less selective in ROP than aluminum alkoxides, in agreement with the lower γ values (43). Nevertheless, the molecular weight is still predetermined by the monomer/initiator molar ratio. The control of ROP mediated by tin(IV) alkoxides is maintained in environmentally friendly supercritical carbon dioxide (45). The extraction of monomer and tin residues by this supercritical fluid is a further advantage, particularly for the production of biomedical-grade aliphatic polyesters.

ROP of ε-CL or LA initiated by tin(II) butoxide is living and proceeds through the previously mentioned coordination–insertion mechanism (35,43). This very good control results from the very low extent of intermolecular transesterification reactions, as witnessed by the very high value of γ (125 for ROP of L-LA in THF at 80°C). The higher reactivity of tin(II) alkoxides ($Sn(OR)_2$) compared with tin(IV) alkoxides ($((C_4H_9)_2Sn(OR)_2$) is consistent with the lower steric hindrance of tin at the benefit of the monomer coordination and with the positive induction effect of the R (butyl) groups, which decreases reactivity toward nucleophiles. The higher reactivity of tin(II) dialkoxides compared with aluminum trialkoxides results from

the difference in the ionic radii of the two metals and the accordingly stronger polarization of the tin–oxygen bond.

Rare Earth Metals. A large variety of rare earth derivatives have been used to initiate ROP of lactones and lactides (46). Their usually high reactivity must be emphasized, as exemplified by the polymerization of a low-strained lactone, ω-pentadecalactone, by $Y(O\text{-}i\text{-}C_3H_7)_3$ (47) Similarly, β-BL is polymerized by $Y(OCH_2CH_2OMe)$ at room temperature (48), in contrast to the long reaction time and high temperature required when aluminum-based initiators are used.

Several divalent lanthanide derivatives, eg, SmI_2, SmI_2/Sm (48), $SmCp_2$ (49), $Sm(OAr)_2(THF)_3$, $[(C_6H_5)Sm(\mu\text{-}OAr)]_2$, $(C_5H_9C_9H_6)_2Yb(THF)_2$(II) (50), promote ROP with a poor control. Trivalent lanthanide halides (LnX_3) are not very active initiators (51). For instance, ROP of ε-CL requires long reaction times (16–40 h) and temperature higher than 100°C. LnX_3 is actually a catalyst, which activates lactones by coordination to the carbonyl group, ROP being then initiated by traces of water or nucleophilic impurities. $LnCpX_2$ and $LnCp_2X$, are more active, such that the polymerization temperature can be decreased to 50-60°C. It is worth noting that a mixture of propylene oxide and LnX_3 initiates ROP at 30°C, as result of the *in situ* formation of a lanthanide alkoxide by ring opening of propylene oxide by LnX_3 (51). Halo-bridges/Sm(III) complexes ($[Sm(\mu\text{-}X)(N(SiMe_3)_2)_2(THF)]_2$) and non-halo-bridged Sm(III) complexes ($SmCp_3$, $Sm(N(C_6H_5)_3)_3$, $Sm(N(SiMe_3)_2)_3$) promote ROP at room temperature in less than 1 h without the assistance of a cocatalyst. The polydispersity index is rather high (~2.0 and higher) even though "livingness" has been supported by synthesis of block copolymer) (48). Recently, Greiner and co-workers have shown that bimetallic $[Sm_2I(NP(C_6H_5)_3)_5(DME)]$ is an effective initiator for ROP of ε-CL and δ-VL in toluene (52). At 0°C, the molecular weight distribution is narrow (PDI ~ 1.2), which indicates a fast initiation compared with propagation and transesterification reactions if any. The experimental molecular weight agrees with the theoretical value on the assumption that two chains are initiated per complex molecule. From the analysis of the chain end groups by ^{1}H NMR, the *in situ* formation of samarium alkoxides is supposed to result from the addition of the bridged nitrogen atom to the carbonyl group of the lactone, followed by the cleavage of the endocyclic acyl–oxygen bond (Fig. 8) (52).

$Y(CF_3CO_2)_3/Al(O\text{-}i\text{-}Bu)_3$ also leads to the formation of poly(ε-CL), poly(DL-LA) (53), and block copolymers (54) with a rather good control of the molecular parameters. The mechanism remains however an open question.

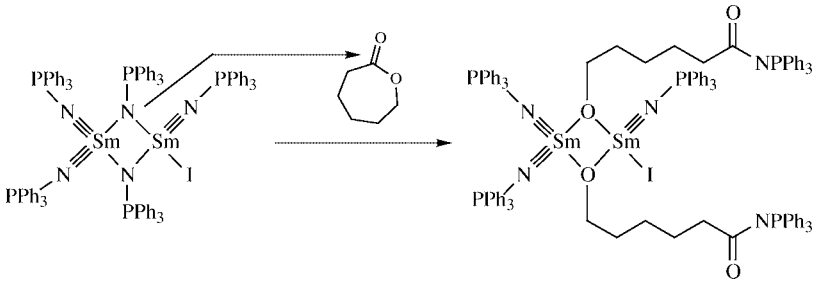

Fig. 8. Mechanism of ROP initiated by $Sm_2I(NP(C_6H_5)_3)_5(DME)$.

Yasuda and co-workers have reported on ROP of ε-CL and δ-VL initiated $Cp_2SmMe(THF)$ and $[SmHCp_2]_2$ with an efficiency of ~60%. Very high molecular weight polyester with very low polydispersity ($M_n > 75000$ and $M_w/M_n < 1.08$) is accordingly formed (55). Reaction of $Cp_2SmMe(THF)$ with the lactone would form *in situ* the actual initiator, ie, $Cp_2SmO(CH_2)_x{-}C(=O)Me$ (x = 4, 5). A difunctional initiator, $Cp_2SmO(CH_2)_xOSm_2Cp$, is proposed to be formed as result of the reaction of $[SmHCp_2]_2$ with the monomer, including β-PL (55).

Monomeric lanthanide alkoxides are generally unstable, unless they are stabilized by bulky substituents (20). Spassky and co-workers have shown that clustered lanthanide alkoxides $Ln_5(\mu\text{-}O)(O\text{-}i\text{-}C_3H_7)_{13}$ can initiate ROP of DL-lactide in dichloromethane (56). The following order of reactivity (La ≫ Sm ≫ Yb) has been reported. Low polydispersity is seen even at high conversion and long reaction time, except in case of lanthane because of exceedingly high reactivity and low selectivity. ROP of ε-CL is more complex, and transesterification reactions can occur before the monomer conversion is complete.

Samarium, neodynium, and yttrium isopropoxide have been used in combination with benzyl alcohol, which is a transfer agent, for the ε-CL polymerization. The catalytic activity is higher compared with aluminum and zirconium counterparts. The apparent propagation rate constant first increases with the alcohol/metal molar ratio up to an optimum value, and then decreases according to an egg-shaped curve (20,57). Once again, the use of a catalytic amount of lanthanide alkoxides is a valuable strategy to decrease the polyester contamination by metallic residues.

Soum and co-workers reported on experimental conditions such that $La(O\text{-}i\text{-}C_3H_7)_3$ is a dimer or a trimer or a mixture of both, in equilibrium with nonassociated species. The number of active isopropoxy per La however depends on the monomer and the $[monomer]_0/[initiator]_0$ molar ratio (58). Propagating poly(δ-valerolactone) chains are aggregated in contrast to the poly(ε-caprolactone) active ones.

In order to overcome the drawbacks associated to the clustering of Y isopropoxide. Feijen and co-workers initiated ROP of ε-CL and LA by converting *in situ* the inactive tris(2,6-di-*tert*-butylphenoxy) yttrium precursor into the active monomolecular Y alkoxide by reaction with 3 equivalents of 2-propanol (Fig. 9) (59). A well-defined kinetics is then observed, being first-order in both the monomer and the initiator (60). The propagation rate constant for LA in dichloromethane at 22°C is $1.92 \times 10^3\ L \cdot mol^{-1} \cdot min^{-1}$, which is an exceptionally high activity. This strategy was improved further by Jérôme and co-workers, who substituted the commercially available tris(bis(trimethylsilyl)amido) yttrium ($Y[N(SiMe_3)_2]_3$) for the Y phenoxide, whose synthesis is time consuming (61).

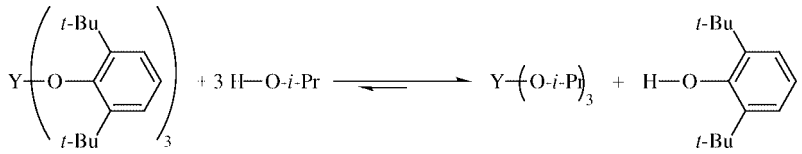

Fig. 9. *In situ* formation of $Y(O\text{-}i\text{-}C_3H_7)_3$ from Y triphenoxide.

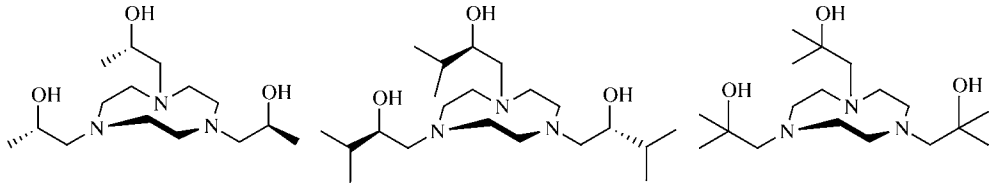

Fig. 10. Multidentate amines used by Hillmyer and co-workers as yttrium ligands.

The rapid exchange between the *in situ*–formed yttrium alkoxide and the alcohol allows the average number of the initiated chains to be controlled by the excess of alcohol with respect to Y. At a molar excess of 50, all the alcohol molecules participate to the exchange and thus to the initiation of ε-CL polymerization at 20°C. In addition to M_n, which can be predicted from the monomer/alcohol molar ratio, the molecular weight distribution is narrow even at high monomer conversion. The same strategy has been extended to the preparation of neodynium alkoxides from tris(bis(trimethylsilyl)amido) neodynium ($Nd[N(SiMe_3)_2]_3$) (62).

Multinuclear complexes of Y alkoxide have been synthesized with multidentate amines and they have shown high activity in ROP (Fig. 10) (63,64). Although the polymerization of ε-CL can be controlled, the polydispersity is rather high ($1.5 < PDI < 1.7$), and parasitic aggregation and clustering can be the source of complexity.

Mononuclear complexes have also been considered as controllable single-site catalysts, as illustrated in Figure 11 (21). In contrast to the poor efficiency of an arylimidinate ligand (65), $(EA)_2YO\text{-}i\text{-}C_3H_7$ and $(EA)_2NdO\text{-}i\text{-}C_3H_7$ (where EA stands for ethylacetoacetate) are more promising initiators of ROP of ε-CL and DL-LA (66). The polydispersity index is then rather low ($1.1 < M_w/M_n < 1.5$), and the polymerization kinetics is first order in monomer and in initiator, thus not perturbed by aggregation. An interesting alternative may be found in the addition of $Nd(O\text{-}i\text{-}C_3H_7)_3$ by a donor adduct, ie, 1,10-phenanthroline, 2,2′-bipyridyl, and 18-crown-6, because then M_w/M_n of PCL is as low as 1.05–1.10 (66).

Titanium. $Ti(O\text{-}n\text{-}C_4H_9)_4$ was tested as an initiator by Kricheldorf and co-workers (4). In order to restrict transesterification reactions, bulky ligands were associated to titanium, as illustrated by mono(cyclopentadienyl)titanium

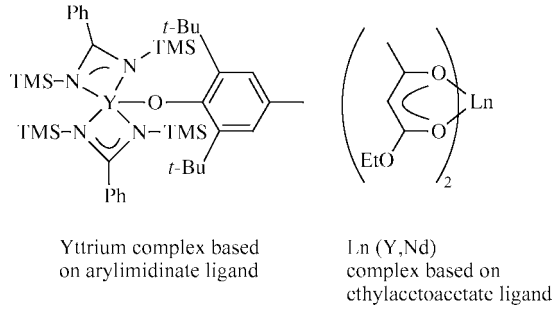

Fig. 11. Well-defined mononuclear lanthanide complexes used in ROP of ε-CL and LA.

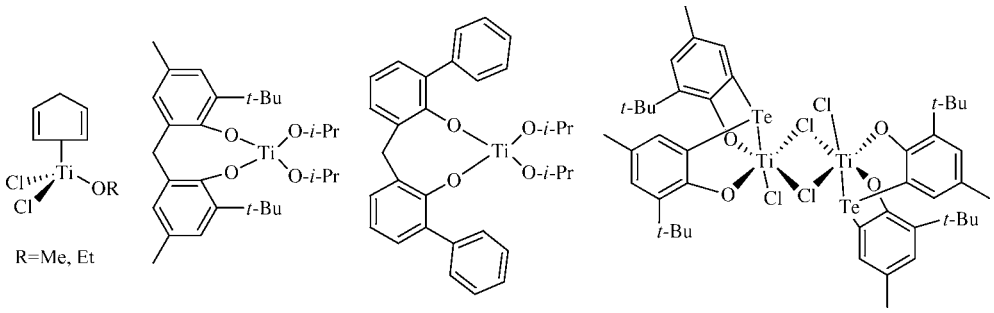

Fig. 12. Examples of titanium alkoxide complexes used as ROP initiators.

complexes (67), titanium dialkoxides ligated by bulky bis(phenoxides) (68), and titanium complexes with chalcogen-bridged chelating diaryloxo ligands (69) (Fig. 12).

Miscellaneous Metals. With the purpose of producing aliphatic polyesters free from toxic metallic residues, Kricheldorf and co-workers screened a large series of bioresorbable salts that could be active in the ROP of LA at 180°C (70,71). Na^+, K^+, Mg^{2+}, Ca^{2+}, Zn^{2+}, and Fe^{2+} were considered as cations, andchloride, iodide, oxide, hydroxide, carbonate, acetate and higher fatty acids, lactate, tartrate, citrate, α-amino acids and peptides as anions. Zinc lactate gave the best results (70,71).

Although strong Lewis acid metal halogenides are known catalysts for cationic ROP, zinc dichloride can initiate ROP of ε-CL, according to a coordination–insertion mechanism in which the alkyl–oxygen bond of the monomer is cleaved (Fig. 13) (72). The mechanism was assessed by computational calculations, analysis of the two chain-ends by ^{1}H NMR, and agreement between M_n and the monomer/zinc dichloride molar ratio. Zinc carboxylates are ROP promoters in the presence of alcohols (71,73). Similarly to tin octanoate, zinc alkoxide is formed, which is the real initiator (72,74). Side formation of octanoate ester end groups is kinetically less favorable compared with the tin counterpart (73).

Zinc alkoxides have also been prepared by reaction of diethylzinc with alcohols. $Zn(O\text{-}n\text{-}C_4H_9)_2$ was studied by Kricheldorf (4). $C_2H_5ZnO(CH_2)_2Br$ and $Zn(O(CH_2)_2Br)_2$ were used by Jérôme and co-workers for the controlled ROP of ε-CL (75). Well-defined single-site zinc-based catalysts, $[(BDI\text{-}1)ZnO\text{-}i\text{-}C_3H_7)]_2$ (Fig. 14), convert β-BL and β-VL into high molecular weight poly(3-hydroxyalkanoates) (76). Moreover, ROP of (*S*,*S*-LA, *rac*-LA, and *meso*-LA leads to isotactic, heterotactic, and syndiotactic PLAs, respectively (77–79).

Only few reports deal with iron-containing catalysts/initiators (80–84). Iron monocarboxylate derivatives mediate bulk polymerization of L-LA at high temperature (170–200°C) with formation of high molecular PLLA (~150,000). An iron alkoxide is proposed to be formed by ring opening of one monomer and to initiate ROP (84). Recently, Hillmyer and co-workers have shown that the structure of $Fe_5(\mu_5\text{-}O)(OC_2H_5)_{13}$ is similar to that of clustered yttrium alkoxide and that ROP of LA can be controlled in toluene at 70°C (85). $Fe_2(OCH(C_6H_5)_2)_6$ initiates ROP of LA and ε-CL and imparts a good control to the polymerization (86). A first order in both the monomer and the initiator is the rule. The mononuclear

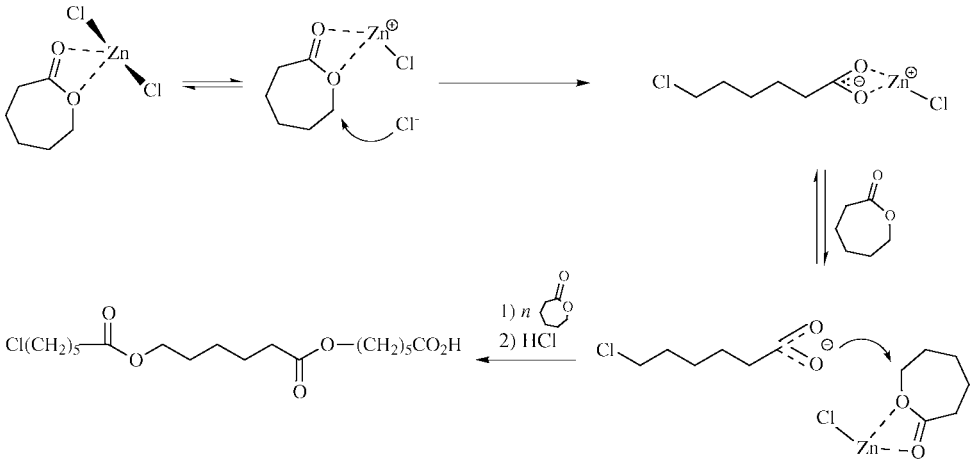

Fig. 13. Initiation of ROP of ε-CL by zinc dichloride.

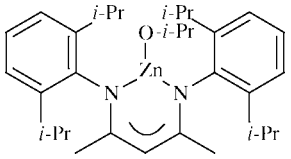

Fig. 14. Single-site zinc-based alkoxide.

$L_2Fe(OCHC_6H_5)_2$ (L stands for *N*,*N*-bis(trimethylsilyl)benzamidinate) (Fig. 15) is also an effective initiator. The polydispersity of poly(ε-CL) and poly(LA) is however rather high ($1.5 < M_w/M_n < 1.9$), and the order in iron alkoxide is fractional (0.5), which points to an aggregation phenomenon. In this case, the bulky ligand makes the kinetics more complex and 50 times slower (86).

Although commercially available and highly active in ROP of ε-CL and L-LA, calcium methoxide is of limited interest because of its low solubility and aggregation (87). Feijen and co-workers used however successfully the strategy implemented for lanthanide alkoxides. The $(THF)_2Ca[N(SiMe_3)_2]_2$ precursor was indeed reacted with isopropanol with *in situ* formation of Ca isopropoxide. ROP of ε-CL and L-LA is then controlled at room temperature as testified by the agreement between theoretical and experimental M_n and low M_w/M_n(<1.3). Poly(ε-CL)-*b*-poly(L-LA) was also synthesized with success, racemization was not observed during ROP of L-LA, and the kinetics was second order in monomer (88).

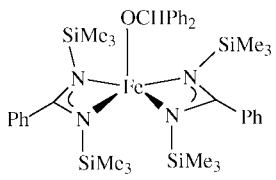

Fig. 15. Structure of $L_2Fe(OCH(C_6H_5))_2$, where L = bis(trimethylsilyl)benzamidinate.

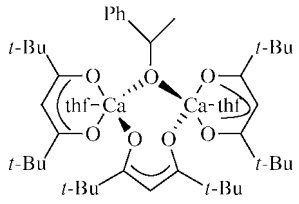

Fig. 16. Structure of $[(THF)Ca(tmhd)]_2[\mu\text{-}OCH(Me)Ph](\mu\text{-}thmd)$.

A bimetallic catalyst $[(THF)Ca(tmhd)]_2[\mu\text{-}OCH(CH_3)C_6H_5](\mu\text{-}thmd)$ (where thmd stands for 2,2,6,6-tetramethylheptane-3,5-dione) (Fig. 16), was prepared by the same authors who observed an induction period of time for ROP of ε-CL and LA and a first order in LA up to high conversion. Added with isopropanol, $[(THF)Ca(tmhd)]_2[\mu\text{-}N(Si(Me)_3)_2Ph](\mu\text{-}thmd)$ releases the parent alkoxide which initiates the controlled ROP of ε-CL and LA, no induction period is observed and the apparent propagation rate of ROP of LA ($0.125\ min^{-1}$) is 4.4 times higher compared with the preformed compound. Remarkably, ROP is much faster when initiated by β-diketonate calcium alkoxides than by aluminum, yttrium and tin alkoxides.

Zirconium derivatives are 10 times less toxic than tin counterparts. Zr-containing drugs and cosmetics are accepted by the Food and Drug Administration (89). Kasperczyk and co-workers (co)polymerized LA and CL by $Zr(acac)_4$ in the 100–150°C range (89,90). Because Zr complexes usually aggregate (coordination number = 6) (20), Hamaide and co-workers added benzyl alcohol to $Zr(O\text{-}n\text{-}C_3H_7)_4$ (20,57). M_n was determined by the monomer/alcohol molar ratio, M_w/M_n was low and, in contrast to aluminum alkoxides, the propagation rate decreased regularly with increasing benzyl alcohol/Zr molar ratio.

Kricheldorf and co-workers paid attention to germanium alkoxides because of less toxicity and higher reactivity in transesterification than tin alkoxides (91). However, ROP of ε-CL required higher temperature [140°C for $Ge(OC_2H_5)_4$], the content of cyclics was low (less than 1 mol% at 120°C), and the molecular weight distribution broad. It must be pointed out that spirocyclic germanium-based alkoxides are soluble and can initiate ROP of ε-CL at 140°C, which is not the case for tin, zirconium, and titanium analogues. The use of magnesium alkoxides as initiators or catalysts was scarcely reported (77,92,93). Initiation by $Mg(OC_2H_5)_2$ was briefly discussed by Kricheldorf and co-workers.

Heterogeneous ROP. Grafting of metal alkoxides onto solid supports is a valuable strategy to produce polyesters free from metallic residues. These heterogeneous initiators/catalysts can be used in batch production and their easy recycling/reactivation is promising for continuous processes (57).

Hamaide and co-workers grafted metal alkoxides (eg Al, Nd, Y, Sm, Zr) onto silica and alumina (57,94). Nevertheless, the alcohol that is released in the reaction medium can react with the silanol groups of silica and form water. Therefore, part of the active species can be lost by hydrolysis. In case of alumina, Al—O—R species can be additionnally formed and participate in the polymerization.

Jérôme and co-workers tackled this problem by using an Y alkoxide precursor, ie $Y[N(SiMe_3)_2]_3$ (95). The Y triamide was first reacted with one or two equivalent(s) of isopropanol with formation of mixed yttrium alkoxide/amide. The

unreacted amide functions were then used to graft the Y alkoxide to the support. This method is free from side reactions, quite reproducible, and allows to vary the average number of alkoxides per Y (1 or 2). The grafted alkoxide can participate in a fast exchange with an alcohol added on purpose in the polymerization medium, at 40°C. Chains are detached from the support by methanolysis, which restores the Y alkoxides at the surface of the support. Starting with Y amide, rather than with preformed Y alkoxide known for fast association in solution, has the advantage of grafting, well-defined monomolecular species to the support.

Enzymatic Ring Opening Polymerization

Enzymatic Polymerization (qv) is an alternative technique for producing metal-free polyesters. Some lipases are known to catalyze (trans)esterification reactions. A first report on the enzymatic bulk ROP of ε-CL in organic solvents was published in 1993 (96,97). At the time being, many lactones with the ring size from 4 up to 17 have been polymerized by lipases (98), either in organic solvents or in more environmentally friendly supercritical carbon dioxide (99). ROP of γ-BL, which is usually a problem by traditional techniques, is oligomerized in the presence of porcine pancreas and *Pseudomonas capacia* (100). As a rule, large-size lactones react faster than the smaller ones (73), which is the reverse of what is observed for chemical ROP. Actually, the rate-determining step in enzymatic polymerization is the formation of a lactone–lipase complex (Fig. 17), which is more favorable for more hydrophobic large-size lactones (73). The catalytic site of lipases is a hydroxyl-containing serine residue (73). ROP takes place according to an "activated monomer" mechanism (Fig. 17) (73). The key step is the reaction of lipase with the lactone with formation of an acyl–enzyme intermediate, which further reacts with water, alcohols, or hydroxyl end-capped chains during either the initiation or the propagation step. Moreover, a second mechanism, which should also be taken into account, relies on the activation of the polyester chain-end either by direct activation of carboxylic acid end groups by lipase (Fig. 18) (101) or by transesterification of an inner ester group by lipase (Fig. 19) (102).

By tuning the monomer/initiator molar ratio, M_n ranging from 10^3 up to 10^5 can be prepared (98,103), Unfortunately, the control imparted to ROP in not as

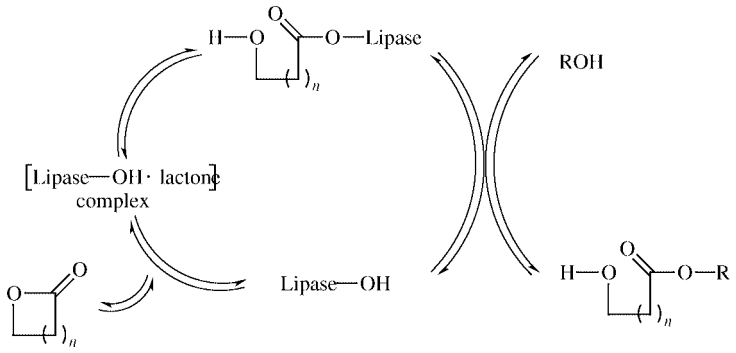

Fig. 17. Mechanism of enzymatic ROP catalyzed by lipases.

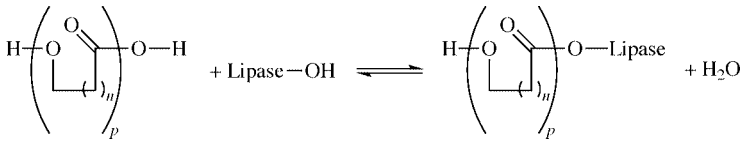

Fig. 18. Activation of polyester chain-ends by lipases.

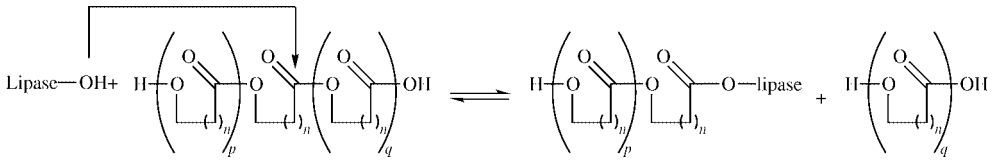

Fig. 19. Intra-chain activation of polyesters by lipases.

good as the one obtained by chemical ROP, with M_w/M_n higher than 2 (98). One advantage of the enzymatic route is to be found in the optical activity of lipases, which opens up a new route to stereoselective ROP. For example, the enantioselective ROP of racemic α-methyl-β-propiolactone by *Pseudonomas capacia* lipase produces an (*S*)-enriched polyester with an enantiomeric excess of 50% (103). More recently, isotactic (*S*)-enriched poly(4-methyl-ε-CL) and poly(4-ethyl-ε-CL) with an enantiomeric purity higher than 95% have been prepared by enantioselective ROP of the racemic mixture, in the presence of lipase Novozym-435. Optically active (*R*)-4-methyl-ε-CL and (*R*)-4-ethyl-ε-CL, which remain unreacted after ROP completion, have been isolated and further polymerized by tin octoate into isotactic (*S*)-enriched poly(4-methyl-ε-CL) and poly(4-ethyl-ε-CL), respectively (104).

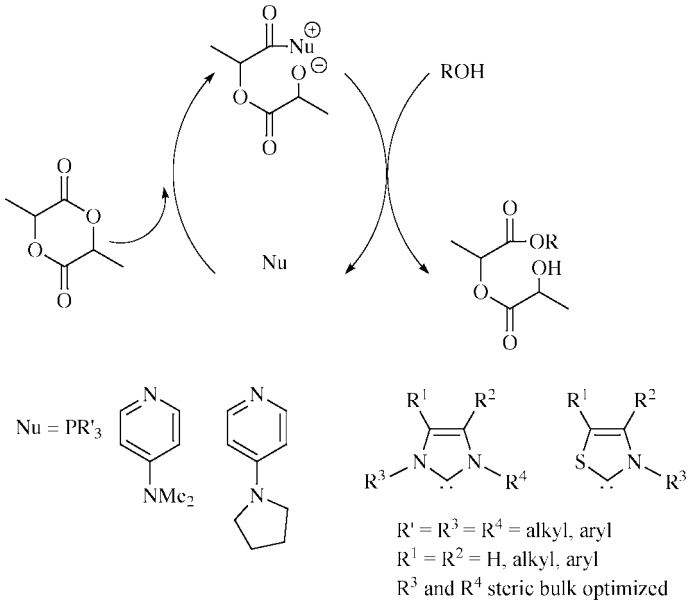

Fig. 20. Mechanism of all-organic ROP promoted by nucleophilic catalysts.

"All Organic" Ring Opening Polymerization

Last but not least, metal-free polyesters can be prepared by using all-organic initiators. Endo showed that a mixture of alcohol and $HCl \cdot C_2H_5O$ is a cationic catalyst for the controlled ROP of ε-CL and δ-VL (105). One limitation of this system is that low M_n chains are usually prepared, ie, M_n lower than 15,000 for poly(ε-CL) (106). Poly(δ-VL) is an exception, with M_n up to 50,000.

The use of nucleophilic catalyst is also promising (Fig. 20). Indeed, ROP of LA initiated by alcohols is catalyzed by phosphines (107), tertiary amines (eg, 4-dimethylaminopyridine, 4-pyrrolidinopyridine) (108), *N*-imidazolium (109) and thiazaolium (110) carbenes. The mechanism would be similar to the one reported for biocatalysis: activation of the monomer by the nucleophilic attack of the carbonyl by the catalyst, with formation of an intermediate that reacts further with an alcohol, polymeric or not. *N*-heterocyclic carbenes can be generated *in situ* from the corresponding imidazolium and thiazolium salts (110), whereas changing the substituents of these compounds is a tool for tuning their reactivity (110). This promising process could be more widely used in the future.

BIBLIOGRAPHY

"Living Polymer Systems, Epoxides and Lactones" in *EPSE* 2nd ed., Suppl. Vol., pp. 412–420, by Shohei Inoue and Takuzo Aida, University of Tokyo.

1. D. Mecerreyes and R. Jérôme, *Macromol. Chem. Phys.* **200**, 2581–2590 (1999).
2. X. Lou, Ch. Detrembleur, and R. Jérôme, *Macromol. Rapid Commun.* **24**, 161–172 (2003).
3. B. T. Ko and C. C. Lin, *J. Am. Chem. Soc.* **123**, 7973–7977 (2001).
4. H. R. Kricheldorf, M. Berl, and N. Schnargl, *Macromolecules* **21**, 286–293 (1988).
5. S. Penczek, A. Duda, and J. Libiszowski, *Macromol. Symp.* **128**, 241–254 (1998).
6. H. von Schenck, M. Ryner, A. Ch. Albertsson, and M. Svensson, *Macromolecules* **35**, 1556–1562 (2002).
7. J. Baran, A. Duda, A. Kowalski, R. Szymanski, and S. Penczek, *Macromol. Symp.* **123**, 93 (1997).
8. A. Duda, S. Penczek, Ph. Dubois, D. Mecerreyes, and R. Jérôme, *Macromol. Chem. Phys.* **197**, 1273–1283 (1996).
9. D. Mecerreyes, R. Jérôme, and Ph. Dubois, *Advances in Polymer Science* **147**, 1–59 (1999).
10. J. L. Eguiburu, M. J. Fernandez-Berridi, F. P. Cossio, and J. S. Roman, *Macromolecules* **32**, 8252 (1999).
11. J. L. Eguiburu, M. J. Fernandez-Berridi, and J. San Roman, *Polymer* **41**, 6439 (2000).
12. Ph. Dubois, N. Ropson, R. Jérôme, and Ph. Teyssié, *Macromolecules* **29**, 1965–1975 (1996).
13. I. Barakat, Ph. Dubois, Ch. Grandfils, and R. Jérôme, *J. Polym. Sci., Polym. Chem.* **34**, 497–502 (1996).
14. I. Barakat, Ph. Dubois, Ch. Granfils, and R. Jérôme, *J. Polym. Sci., Polym. Chem.* **37**, 1401–2411 (1999).
15. A. Duda and S. Penczek, *Macromol. Rapid Commun.* **16**, 67–76 (1995).
16. N. Ropson, Ph. Dubois, R. Jérôme, and Ph. Teyssié, *Macromolecules* **28**, 7589–7598 (1995).
17. N. Ropson, Ph. Dubois, R. Jérôme, and Ph. Teyssié, *Macromolecules* **27**, 5950–5956 (1994).

18. J. P. Latere Dwan'Isa, Ph. Lecomte, Ph. Dubois, and R. Jérôme, *Macromolecules* **36**, 2609–2615 (2003).
19. Ph. Degée, Ph. Dubois, R. Jérôme, S. F. Jacobsen, and G. Hans, *Macromol. Symp.* **144**, 289–302 (1999).
20. Miola, Ch. Delaite, Th. Hamaide, and R. Spitz, *Macromol. Chem. Phys.* **200**, 1771–1778 (1999).
21. B. J. O'Keefe, M. A. Hillmyer, and W. B. Tolman, *J. Chem. Soc., Dalton Trans*. 2215–2224 (2001).
22. M. Endo, T. Aida, and S. Inoue, *Macromolecules* **20**, 2982–2988 (1987).
23. B. T. Ko and C. C. Lin, *Macromolecules* **32**, 8296–8300 (1999).
24. I. Taden, H.-C. Kang, W. Massa, T. P. Spaniol, and J. Okuda, *Eur. J. Inorg. Chem*. 441–445 (2000).
25. M. Wisniewski, A. Le Borgne, and N. Spassky, *Macromol. Chem. Phys.* **198**, 1227–1238 (1997).
26. N. Spassky, M. Wisniewski, C. Pluta, and A. Le Borgne, *Macromol. Chem. Phys.* **197**, 2627–2637 (1996).
27. P. A. Cameron, D. Jhurry, V. C. Gibson, A. J. P. White, D. J. Williams, and S. Williams, *Macromol. Rapid. Commun.* **20**, 616–618 (1999).
28. D. Jhurry, A. Bhaw-Luximon, and N. Spassky, *Macromol. Symp.* **175**, 67–79 (2001).
29. A. Bhaw-Luximon, D. Jhurry, and N. Spassky, *Polym. Bull.* **44**, 31–38 (2000).
30. Z. Zhong, P. J. Dijkstra, and J. Feijen, *Angew. Chem., Int. Ed.* **41**, 4510–4513 (2002).
31. N. Nomura, R. Ishii, M. Akakura, and K. Aoi, *J. Am. Chem. Soc.* **124**, 5938–5939 (2002).
32. T. M. Ovitt and G. W. Coates, *J. Am. Chem. Soc.* **121**, 4072–4073 (1999).
33. T. M. Ovitt and G. W. Coates, *J. Am. Chem. Soc.* **124**, 1316–1326 (2002).
34. T. M. Ovitt and G. W. Coates, *J. Polym. Sci., Polym. Chem.* **38**, 4686–4692 (2000).
35. A. Duda, S. Penczek, A. Kowalski, and J. Libszowski, *Macromol. Symp.* **153**, 41–53 (2000).
36. A. Kowalski, A. Duda, and S. Penczek, *Macromolecules* **33**, 7359–7370 (2000).
37. H. R. Kricheldorf, I. Kreiser-Saunders, and A. Stricker, *Macromolecules* **33**, 702–709 (2000).
38. R. F. Storey and J. W. Sherman, *Macromolecules* **35**, 1504–1512 (2002).
39. H. R. Kricheldorf, A. Stricker, and D. Langanke, *Macromol. Chem. Phys.* **202**, 2963–2970 (2001).
40. M. Möller, R. Kange, and J. L. Hedrick, *J. Polym. Sci., Polym. Chem.* **38**, 2067–2074 (2000).
41. M. Möller, F. Nederbery, L. S. Lim, R. Kange, C. J. Hawker, J. L. Hedrick, G. Yuedung, R. Shah, and N. L. Abbott, *J. Polym. Sci., Polym. Chem.* **39**, 3529–3528 (2001).
42. H. R. Kricheldorf, M. V. Sumbel, and I. Kreiser-Saunders, *Macromolecules* **24**, 1944 (1991).
43. A. Kowalski, J. Libiszowski, A. Duda, and S. Penczek, *Macromolecules* **33**, 1964–1971 (2000).
44. H. R. Kricheldorf, A. Stricker, and D. Langanke, *Macromol. Chem. Phys.* **202**, 2525–2534 (2001).
45. F. Stassin, O. Halleux, and R. Jérôme, *Macromolecules* **34**, 775 (2001).
46. A. Le Borgne, Ch. Pluta, and N. Spassky, *Macromol. Rapid Commun.* **15**, 955–960 (1994).
47. Z. Zhong, P. J. Dijkstra, and J. Feijen, *Macromol. Chem. Phys.* **201**, 1329–1333 (2000).
48. S. Agarwal, C. Mast, K. Dehnicke, and A. Greiner, *Macromol. Rapid. Commun.* **21**, 195–212 (2000).
49. W. J. Evans and H. Katsumata, *Macromolecules* **27**, 2330–2332 (1994).
50. D. Cui, T. Tang, J. Cheng, N. Hu, W. Chen, and B. Huang, *J. Organomet. Chem.* **650**, 84–90 (2002).

51. Y. Shen, Z. Shen, J. Shen, Y. Zhang, and K. Yao, *Macromolecules* **29**, 3441–3446 (1996).
52. P. Ravi, T. Gröb, K. Dehicke, and A. Greiner, *Macromolecules* **34**, 8649–8653 (2001).
53. J. Zhang, Z. Gan, Z. Zhong, and X. Jing, *Polym. Int.* **45**, 60–66 (1998).
54. Z. Zhang, D. Yu, F. Meng, Z. Gan, and X. Jing, *Polym. J.* **31**, 633–636 (1999).
55. M. Yamashita, Y. Takemoto, E. Ihara, and H. Yasuda, *Macromolecules* **29**, 1798–1806 (1996).
56. V. Simic, N. Spassky, and G. H. Hubert-Pjalzgraf, *Macromolecules* **30**, 7338–7340 (1997).
57. Ch. Miola-Delaite, E. Colomb, and Th. Hamaide, *Macromol. Symp.* **153**, 275–286 (2000).
58. M. Save, M. Schappacher, and A. Soum, *Macromol. Chem. Phys.* **203**, 889–899 (2002).
59. W. M. Stevels, M. J. K. Ankoné, P. J. Dijkstra, and J. Feijen, *Macromolecules* **29**, 3332–3333 (1996).
60. W. M. Stevels, M. J. K. Ankoné, P. J. Dijkstra, and J. Feijen, *Macromolecules* **29**, 6132–2138 (1996).
61. E. Martin, Ph. Dubois, and R. Jérôme, *Macromolecules* **33**, 1530–1535 (2000).
62. K. Tortosa, T. Hamaide, C. Boisson, and R. Spitz, *Macromol. Chem. Phys.* **202**, 1156–1160 (2001).
63. B. M. Chamberlain, Y. Sun, J. R. Hagadorn, E. W. Hemmesch, V. G. Young Jr., M. Pink, M. A. Hillmyer, and W. B. Tolman, *Macromolecules* **32**, 2400–2402 (1999).
64. B. M. Chamberlain, B. A. Jazdsewski, M. Pink, M. A. Hillmyer, and W. B. Tolman, *Macromolecules* **33**, 3970–3977 (2000).
65. K. B. Aubrecht, K. Chang, M. A. Hillmyer, and W. B. Tolman, *J. Polym. Sci., Polym. Chem.* **39**, 284–293 (2001).
66. Y. Shen, Z. Shen, Y. Zhang, and K. Yao, *Macromolecules* **29**, 8289–8295 (1996).
67. J. Okuda and I. L. Rushkin, *Macromolecules* **26**, 5530–5532 (1993).
68. D. Takeuchi, T. Nakamara, and T. Aida, *Macromolecules* **33**, 725–729 (2000).
69. Y. Takashima, Y. Nakayama, K. Watanabe, T. Itono, N. Ueyama, A. Nakamura, H. Yasuda, A. Harada, and J. Okuda, *Macromolecules* **35**, 7538–7544 (2002).
70. H. R. Kricheldorf, I. Kreiser-Saunders, and D. O. Damrau, *Macromol. Symp.* **159**, 247–257 (2000).
71. H. R. Kricheldorf, I. Kreiser-Sanders, and D. O. Damrau, *Macromol. Symp.* **144**, 269–276 (1999).
72. G. Abraham, A. Gallardo, A. E. Lozano, and J. San Roman, *J. Polym. Sci., Polym. Chem.* **38**, 1355 (2000).
73. A. Duda, A. Kowalski, S. Penczek, H. Uyama, and S. Kobayashi, *Macromolecules* **35**, 4266–4270 (2002).
74. J. Libiszowski, A. Kowalski, A. Duda, and S. Penczek, *Macromol. Chem. Phys.* **203**, 1694–1701 (2002).
75. I. Barakat, Ph. Dubois, R. Jérôme, and Ph. Teyssié, *Macromolecules* **24**, 6542–6545 (1991).
76. L. R. Rieth, D. R. Moore, E. B. Lobkovsky, and G. W. Coates, *J. Am. Chem. Soc.* **124**, 15239–15248 (2002).
77. B. M. Chamberlain, M. Cheng, D. R. Moore, T. M. Ovitt, E. Lobkowsky, and G. W. Coates, *J. Am. Chem. Soc.* **123**, 3229–3238 (2001).
78. M. Cheng, A. B. Attygalle, E. B. Lobovsky, and G. W. Coates, *J. Am. Chem. Soc.* **121**, 11583–11584 (1999).
79. M. Cheng, T. M. Ovitt, Ph. D. Hustad, and G. W. Coates, *ACS Polym. Preprints* **40**, 542–543 (1999).
80. P. Dobrzynski, J. Kasperczyk, H. Janeczek, and M. Bero, *Polymer* **43**, 2595–2601 (2002).
81. S. Penczek, A. Duda, R. Szymanski, and T. Biela, *Macromol. Symp.* **153**, 1–15 (2000).

82. S. Penczek, A. Duda, and R. Szymanski, *Macromol. Symp.* **132**, 441–449 (1998).
83. J. Baran, A. Duda, A. Kowalski, R. Szymanski, and S. Penczek, *Macromol. Symp.* **123**, 93–101 (1997).
84. M. Stolt and A. Sodergard, *Macromolecules* **32**, 6412–6417 (1999).
85. B. J. O'Keefe, S. M. Monnier, M. A. Hillmyer, and W. B. Tolman, *J. Am. Chem. Soc.* **123**, 339–340 (2001).
86. B. J. O'Keefe, L. E. Breyfogle, M. A. Hillmyer, and W. B. Tolman, *J. Am. Chem. Soc.* **124**, 4384–4393 (2002).
87. Z. Zhong, M. J. K. Ankone, P. J. Dijkstra, Ch. Birg, M. Westerhausen, and J. Feijen, *Polym. Bull.* **46**, 51–57 (2001).
88. Z. Zhong, P. J. Dijkstra, Ch. Birg, M. Westerhausen, and J. Feijen, *Macromolecules* **34**, 3863–3868 (2001).
89. M. Bero, P. Dobrzynski, and J. Kasperczyk, *Polym. Bull.* **42**, 131–139 (1999).
90. P. Dobrynski, J. Kasperczyk, H. Janeczek, and M. Bero, *Macromolecules* **34**, 5090–5098 (2001).
91. H. R. Kricheldorf and D. Langanke, *Polymer* **43**, 1973–1977 (2002).
92. M. H. Chisolm, J. C. Huffman, and K. Phomphrai, *J. Chem. Soc., Dalton Trans*. 222–224 (2001).
93. M. H. Chisolm, N. W. Eilerts, J. C. Huffman, S. S. Iyer, M. Pacold, and K. Phomphrai, *J. Am. Chem. Soc.* **123**, 11845–11854 (2000).
94. Ch. Miola, Th. Hamaide, and R. Spitz, *Polymer* **38**, 5667–5676 (1997).
95. E. Martin, Ph. Dubois, and R. Jérôme, *J. Polym. Sci., Polym. Chem.* **41**, 569–578 (2003).
96. H. Uyama and S. Kobayashi, *Chem. Lett*. 1149–1150 (1993).
97. D. Knani, A. L. Gutman, and D. H. Kohn, *J. Polym. Chem. Polym. Chem. Ed.* **31**, 1221 (1993).
98. S. Kobayashi, H. Uyama, and S. Kimura, *Chem. Rev.* **101**, 3793–3818 (2001).
99. T. Nakaoki, M. Kitoh, and R. A. Gross, *ACS Polym. Preprints* **44**(2), 633–634 (2003).
100. G. A. R. Nobes, R. J. Kazlauskas, and R. H. Marchessault, *Macromolecules* **29**, 4829–4833 (1996).
101. Y. Mei, A. Kumar, and R. Gross, *Macromolecules* **36**, 5530–5536 (2003).
102. M. Bankova, A. Kumar, G. Impallomeni, A. Ballistreri, and R. A. Gross, *Macromolecules* **35**, 6858–6866 (2002).
103. Y. Y. Svirkin, J. Xu, R. A. Gross, D. L. Kaplan, and G. Swift, *Macromolecules* **29**, 4591–4597 (1996).
104. T. F. Al-Azemi, L. Kondaveti, and K. S. Bisht, *ACS Polym. Preprints* **44**(2), 597–598 (2003).
105. Y. Shibasaki, H. Sanada, M. Hokoi, F. Sanda, and T. Endo, *Macromolecules* **33**, 4316 (2000).
106. X. Lou, Ch. Detrembleur, and R. Jérôme, *Macromolecules* **35**, 1190–1195 (2002).
107. M. Myers, E. F. Connor, Th. Glauser, A. Mock, G. Nyce, and J. L. Hedrick, *J. Polym. Sci., Polym. Chem.* **40**, 844–851 (2002).
108. F. Nederberg, E. F. Connor, M. Möller, Th. Glauser, and J. L. Hedrick, *Angew. Chem. Int. Ed.* **40**, 2712–2715 (2001).
109. E. F. Connor, G. W. Nyce, M. Myers, A. Möck, and J. L. Hedrick, *J. Am. Chem. Soc.* **124**, 914–915 (2002).
110. G. W. Nyce, Th. Glauser, E. F. Connor, A. Möck, R. M. Waymouth, and J. L. Hedrick, *J. Am. Chem. Soc.* **125**, 3046–3056 (2003).

PH. LECOMTE
R. JÉRÔME
University of Liège

RNA. See POLYNUCLEOTIDES.

ROTATIONAL MOLDING

Introduction

Rotational molding (also referred to as *rotomolding* or *rotational casting*) is a unique molding process. The heating, shaping, and cooling of the plastic all takes place inside the mold, with no application of pressure. This method dates back to the early 1900s. Today the rotational molding industry is one of the fastest growing segments of the plastics industry, with an annual growth of 10%. This is largely due to the efforts of the Association of Rotational Molders (ARM), an international organization that includes molders, equipment suppliers, professional consultants, and design firms, and the Society of Plastics Engineers (SPE), who have recently formed a rotomolding division.

Initially only vinyl plastisols were used for rotational molding; however, in the early 1960s, polyethylenes, the first polyolefin powders, were employed (1). This created the opportunity for molders to enter markets where vinyl products could not compete. In the early 1970s cross-linkable and modified polyethylenes opened up more new areas, especially in the large-tank market. In the mid-1970s, linear low density polyethylene, a major development in resins, was formulated. In the 1980s nylon, polypropylene, and polycarbonate were introduced for rotational molding applications. The 1990s saw rotolining resins, materials that bonded to metal, and one-step foam resin systems that provided for a finished part with a rotomolded outer skin and a foam-filled core. The year 2000 ushered in single-site catalyst resins, some known as metallocenes as well as numerous compounders providing blends of resins for very specific end use requirements. Most resin is used as a ground powder, ranging in particle size from 20 to 120 mesh (125–840 μm). Liquids and small-diameter micropellets can also be rotomolded. Rotational molding provides a more uniform wall thickness, for both single- and double-wall construction, than other methods. Thick corners impart strength. Inserts, ribs, and undercuts are easily included (2,3).

The range of designs is limitless. The ARM organization has published a design manual for rotational molding (4). This was the first publication to address the design guidelines required in the rotational molding industry. Since that time, numerous books have been published on rotomolding (5).

Molds and tooling costs are lower than those of other processing methods, since channels for cooling water and resistance to a clamping force are not required. Different articles and colors may be molded on the same machine and in the same cycle. Quick mold changes are possible when several short production runs are required. Large, hollow products are conveniently made by rotomolding. The largest article molded to date is an 85-m^3 tank. Trimming can be eliminated since very little flash is produced. Rotomolded parts are comparatively stress-free. Corner sections are thicker than with other processes, which increases strength.

Encyclopedia of Polymer Science and Technology. Copyright John Wiley & Sons, Inc. All rights reserved.

Undercuts, intricate contours, molded-in inserts, and double-wall construction are routinely included; wall thicknesses are uniform.

Process

In most rotomolding operations the molds or cavities are filled with a certain amount of powder or liquid (charging the molds); the mold halves are pressed together by bolts or clamps, placed in a heated oven, and rotated biaxially. During heating the resin melts, fuses, and densifies into the shape of the mold. The molds are moved into a cooling chamber, where they are slowly cooled by air and water. After removal from the cooling chamber, the molds are opened and the finished articles are released.

Many rotomolded parts are produced in the color of the plastic. For colored parts, suppliers provide a compounded colored resin; however, many molders blend a dry color into the resin—for this operation, addition and dispersion are critical. New developments in liquid colors allow for use at both the compounder and rotomolder. Nylon and polycarbonate may require drying before molding. Although scrap or regrind is not produced in large quantities, only a small percentage of regrind should be used with the virgin resin.

The particle size of the resin is extremely important; 500-μm (35-mesh) powder is the standard of the industry, although coarser or finer grinds may be employed.

Wall distribution is determined by the rotation ratio. The fewer rpms in a certain ratio, the more uniform the wall thickness. Resin, molds, and final application must be taken into consideration to establish the most efficient cycle.

Equipment. The equipment used in rotational molding is simple; many variations are available. The most common type is the so-called carousel type (Fig. 1). This machine consists of a heating station or oven, a cooling station (frequently an enclosed chamber), and a loading and unloading station. A carousel has three to six spindles or arms where the mold or molds are mounted. Most carousels have the freedom to revolve in a complete circle. The spindles are mounted on a central hub and driven by variable motor drives. New control systems allow each arm to operate independently in movement and control of oven temperature and time. Microprocessors are incorporated in the control system. Computer simulation software can be utilized in prototyping and manufacturing.

The ovens are usually fired with natural gas and equipped with blowers to distribute the heat throughout the chamber. Some ovens can be heated by oil or propane gas, but natural gas is preferred. A new composite mold technology is also available to produce rotomolded parts. This is done without an oven as heating and cooling takes place inside the mold.

A fan provides forced air to the cooling station for the initial cooling, whereas a water system cools the molds and products. A spray mist is used for even cooling. The cooling station may or may not be enclosed.

In an open-flame machine a mold is rotated on a single axis over an open flame. After the article is formed, the excess resin is discarded and the flame is turned off to allow for air-cooling. This process requires a longer cycle time, but the equipment is less expensive.

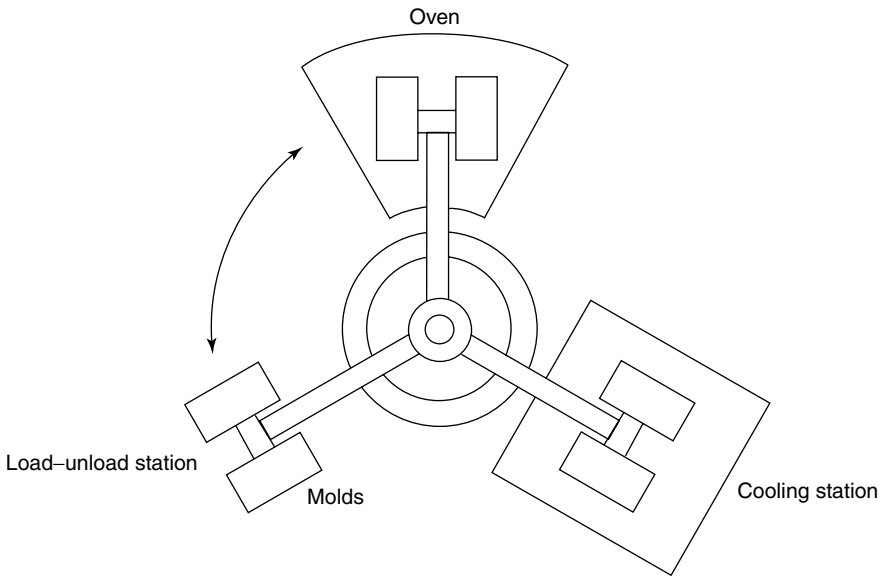

Fig. 1. Carousel-type machine.

The shuttle-type machine (Fig. 2) is used for large products, such as tanks. A frame for holding a mold is mounted on a movable bed. The drive motors for turning the mold biaxially are incorporated in the bed, which is on a track that allows the mold and bed to move into and out of the oven. After the heating cycle is completed, the mold is moved into the cooling station, which is not enclosed, Another bed with a mold is moved into the oven from the opposite end. (Some shuttle machines will use a movable oven.)

The clamshell type of rotational molder utilizes an enclosed area that serves as both the oven and the cooling station (Fig. 3). This machine employs only one arm; heating, cooling, and loading–unloading stations are all in the same location.

Rock and roll machines are commonly used for kayaks and canoes. These machines do not rotate biaxially but will rock back and forth while spinning on

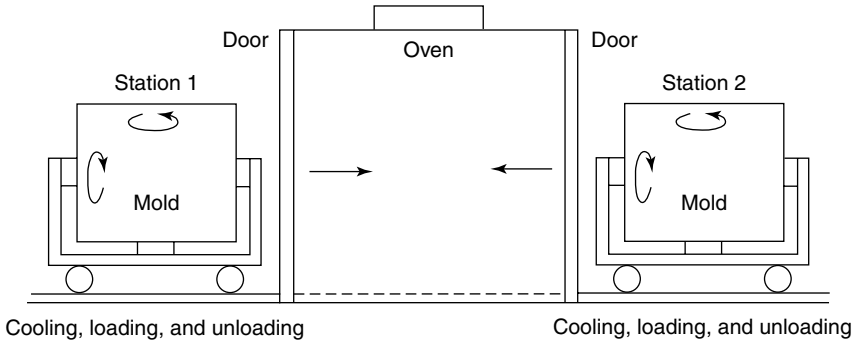

Fig. 2. Shuttle-type machine.

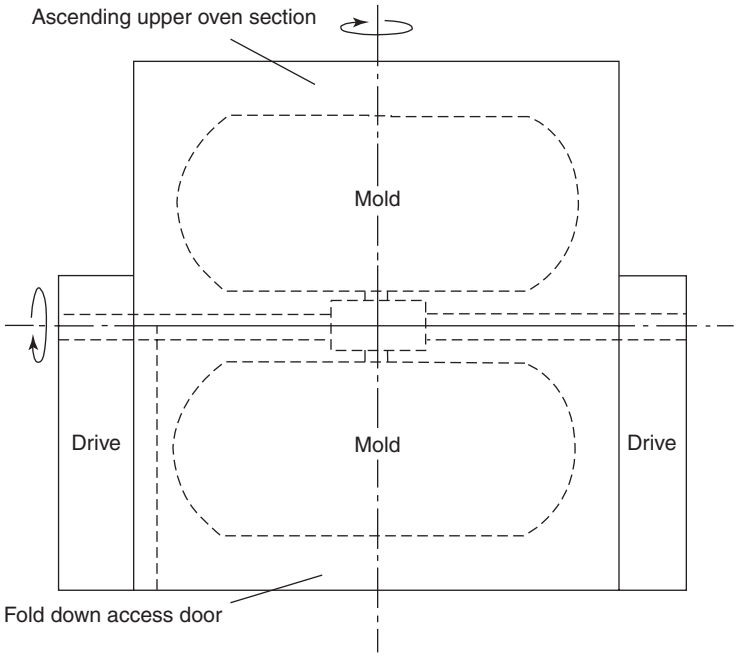

Fig. 3. Clamshell-type machine.

the longest axis. This can be accomplished over an open flame or a variation, which uses a rocking oven.

Machine maintenance is of extreme importance. A weekly inspection, as well as a good inventory of spare parts, is necessary in case of breakdowns. Filling devices can be automated but are usually manually operated. This requires an accurate weighing device and a container for each of the resins. Robotic systems for loading/unloading of powder and parts are now making their way into this industry. Some resins, such as nylons, require a nitrogen atmosphere. The nitrogen is introduced through a channel in the spindle and connected to the mold with rotary hoses.

Molds. The molds used in rotational molding are among the easiest and least expensive to fabricate; two-piece molds are standard, but three-piece molds are sometimes required to remove the finished products. Molds can be as simple as a sphere, or complex, with undercuts, ribs, and tapers. Design considerations include heat transfer, mounting, parting lines, clamping mechanisms, venting, and material stability. Mold makers commonly use 2-D and 3-D electronic files to design new molds.

Cast aluminum is the most widely used mold material. Small to medium articles are molded with a cast mold. Cast aluminum has good heat transfer, and is cost-effective when several moldings of the same article are required. Cast molds can be porous, however, and are easily damaged. Sheet-metal molds are normally used for larger parts. They are easy to fabricate; frequently the sections of the molds only have to be welded together. Sheet-metal molds are cost-effective for large articles. Other molds, such as electroformed nickel molds, give a product

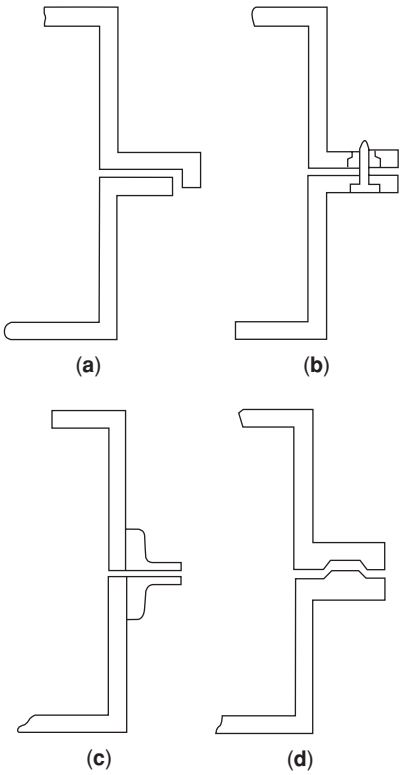

Fig. 4. Parting lines (**a**) stepped, (**b**) pin and bushing, (**c**) fabricated, and (**d**) tongue and groove.

with very fine detail. Vapor-formed nickel molds also give good detail but are more expensive.

Parting Lines. Each mold must have two or more sections, requiring good parting lines (Fig. 4) for a close fit and minimum flash.

Mounting. The molds are mounted on the spindle or the arm of a rotational molding machine. Large sheet-metal molds are easily mounted by bolts or simple clamping systems. Several small to medium aluminum molds can be mounted on spindle or arm. A part commonly known as a spider is used to mount several cast aluminum molds. The spider consists of several arms or mounting legs where each mold is attached, normally by bolts. A central mounting location is attached to the spindle by bolts. The spider allows two or three dozen cast molds to be mounted on one central structure. The entire spider, or just one or two cast molds, can be removed or mounted efficiently. The spider or a single, large sheet-metal mold may be removed easily with a forklift or crane. This is important, since the rotomolding industry normally requires short production runs of a variety of parts. Figure 5 shows molds mounted on a straight arm and an offset arm.

Clamping Systems. The most common clamping system for small to medium molds is that of spring-loaded clamps, which are welded onto the sections of a mold. As the molds get larger, nuts and threaded bolts are normally used; they are installed and removed with an air gun (impact wrench).

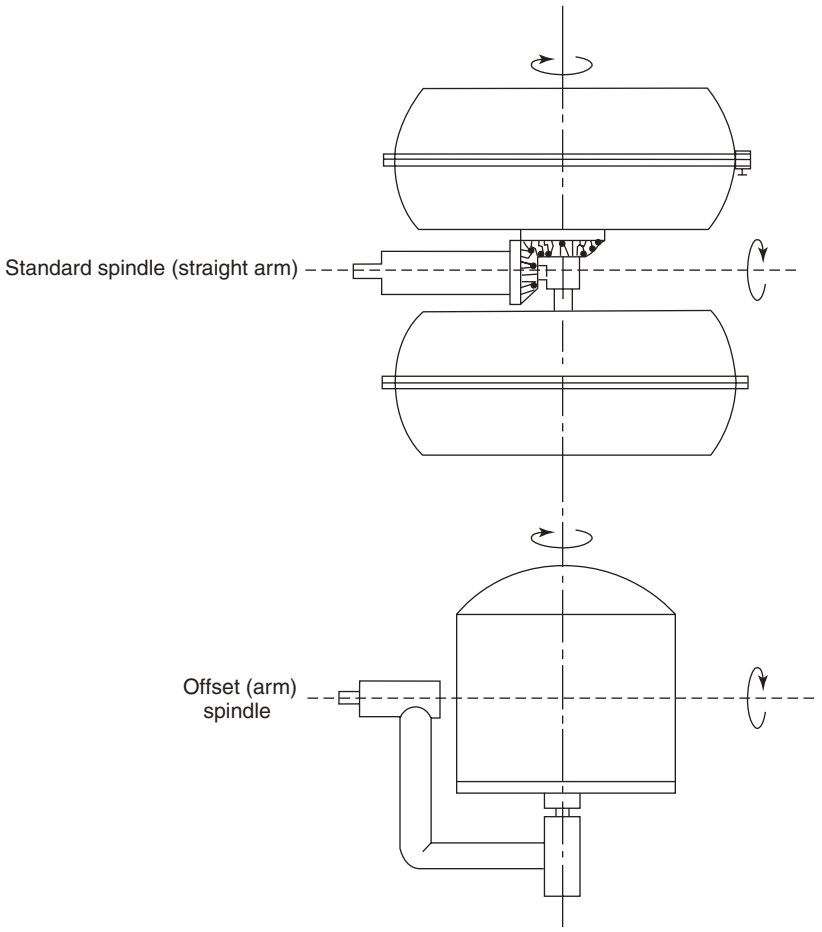

Fig. 5. Mold mountings.

Venting System. Most rotational molds require a venting system to remove the gas that develops in the heating cycle. Depending on the mold size, vents range from 3 to 50 mm in diameter. A 12.5-mm-i.d. tube is used for an article of 0.76-m^3 volume.

Since vents leave a hole in the molded parts, correct placement is essential. They should be located in an area that may be cut out of the finished product or where a patch does not impair appearance. Vents must also be so located as to prevent water from entering the product while it is in the cooling cycle, because this may leave a water-track mark on the inside of the hot article. Improper venting can cause problems, such as blow holes in the parting line.

Mold Release. Since most rotational molds are designed with little or no draft angle, they must be treated with a release agent. Molds are usually cleaned with a solvent and a lightly abrasive cloth to remove foreign particles from the surface. A light coating of release agent is applied and baked on to ensure adhesion. The amount of release agent required depends on the resins to

be used. After the initial application, several hundred articles can be molded before the mold is stripped and another coating is applied; during this time touch-up may be required. Sandblasting is also used to remove resin buildup before reapplying the mold release. A more effective release agent is usually applied to the parting line to facilitate demolding. Teflon provides for a permanent-release coating but care must be taken not to damage it, as it is normally very thin.

Special Molds. Some molds may require a complicated design, inserts, and special machining. Alignment pins may be used to ensure a perfect fit. If a rotomolded article contains a large section where no resin buildup is desired, the mold can be shielded with an insulating material such as Teflon.

Regular maintenance prolongs the useful life of the mold. For cleaning, nonabrasive tools should be used. Steel molds should be oiled to prevent rusting.

Secondary Operations. Secondary operations may be required, such as automatic or manual drilling. Additional fittings can be added by spin welding. Sections may be joined by hot-bar, hot-gas, or ultrasonic welding. Flame treatment before painting provides a surface for adhesion. As in all plastic processing methods, secondary operations are time-consuming and should be kept to a minimum. Automatic computer-driven 3–5-axis routers are now commonplace for secondary operations. Decorating, labeling, and graphics have become an important area for parts that are rotomolded. Graphics, labels, and colors can be molded in or applied afterwards.

Resins

In the early days of rotational molding only vinyl plastisols were used. The first polyethylene for rotomolding was produced in the 1960s. Today polyethylene is the principal material for the industry. The distribution of resin use in rotational molding is indicated below (6).

85%	Polyethylene
10%	Fluorocarbons
	Polycarbonate
	Nylon
	Poly(vinyl chloride)
	Polypropylenes
5%	ABS
	Acetals
	Acrylics
	Cellulosics
	Epoxies
	Phenolics
	Polybutylenes
	Polyesters
	Polystyrenes
	Polyurethanes
	Silicones

A rotomolding resin requires good flow, which is measured by the melt index. The higher the melt index, the better the flow. Most rotomolding resins have melt indexes between 3 and 20. The melt index is also an approximate measure of molecular weight or chain length. A resin with a high index has shorter chains and a lower molecular weight; a low index indicates longer chains and a higher molecular weight. Molecular weight distribution is also important. The narrower the distribution, the more uniform the melt properties.

Polyethylene. Linear low density polyethylenes (LLDPE) are the most widely used materials for rotational molding. Large pellets cannot be used and must be reduced to a smaller particle size to promote heat transfer from the mold to the powder. This also improves the flow of the particles during melting to prevent the deleterious effect of oxidation. This size reduction is done by the resin supplier, a custom grinder compounder, or the molder on mechanical grinding mills. Some resins, such as nylon, are supplied as small pellets and can be molded without grinding (see ETHYLENE POLYMERS, LLDPE).

The molecular weight distribution of a polyethylene for rotational molding should be very narrow, allowing for uniform melting of the particles during the molding cycle. Polyethylenes are easily ground to 500 μm (35 mesh) at high rates, yielding acceptable powder at nominal upcharge. They are thermally stable, and with stabilization can be molded in high temperature, high speed rotational-molding equipment without oxidation. Excellent low temperature physical properties, such as impact strength, allow use in a broad temperature range.

Polyethylenes are inexpensive and available in a wide range of densities and melt indexes for a wide variety of applications. Ultraviolet stability or outdoor life is significantly improved by the addition of pigment or UV stabilizer. Most polyethylene resins meet FDA food additive regulations, except for some specialized cross-linkable polyethylenes and some resins with certain UV stabilizers. The high dielectric strength of polyethylenes makes them suitable for electrical applications. Density and melt indexes (2.0–20 g/10 min) are the main criteria for selecting a polyethylene for a particular application (Table 1).

Polyethylene is classified by density. Type I has a density of up to 0.925 and is called low density (LDPE). Type II has a density range from 0.926 to 0.940 and is called medium density (LMDPE); most LLDPEs fall into this range. Type III has a range from 0.941 to 0.969 and is classified as high density copolymer (HDPE). Type IV is above 0.960 and is classified as high density homopolymer; it is not used in rotational molding.

LDPE is flexible and tough, easy to process, and has excellent chemical resistance. LLDPE and LMDPE have better mechanical properties than LDPE, higher stiffness, excellent low temperature impact strength, and excellent environmental stress crack resistance. HDPE is the stiffest polyethylene, with excellent chemical resistance and good processability. XLPE contains a cross-linking agent that reacts with the resin during the molding cycle, similar to a thermoset. This reaction improves the toughness and stress-crack resistance of the rotomolded product.

Ethylene vinyl acetate copolymer (EVA) is a low density polyethylene copolymer with excellent low temperature impact properties. The higher the level of vinyl acetate, the greater the flexibility of the material. Colorants, flame retardants, and foaming and antistatic agents may be added to polyethylene for specialty applications. Comparisons with other resins are given in Table 2.

Table 1. Molding Properties of Polyethylenes

Resin	Advantages	Disadvantages
LDPE	Flexibility	No stiffness
	Excellent warp resistance	No ESCR[a]
	Uniform shrinkage	
	FDA accepted	
BVA	Flexibility	No stiffness
	Excellent cold temp. impact	No ESCR[a]
	Uniform shrinkage	
	FDA accepted	
LLDPE–LHDPE	Excellent ESCR[a]	Less stiff than HDPE
	Good warp resistance	Lower heat deflection
	More stiffness than LDPE	
	FDA accepted	
HDPE	Excellent stiffness	Low ESCR[a]
	FDA accepted	Warpage and shrinkage are not consistent
	Good impart strength	
	Higher heat deflection	
XLPE	Excellent impact	Not accepted by FDA
	Excellent ESCR[a]	Longer molding cycle

[a]Environmental stress-crack resistance.

Table 2. Resins Used for Rotomolding

Resin	Advantages	Disadvantages
Polyethylene	Low cost, ease of moldability	Lower impact strength than other types
Polycarbonate	Clarity, toughness	Tendency to absorb moisture, harder to mold than PE
Nylon	Excellent impact strength	High cost, harder to mold than PE
	High heat resistance	
Poly(vinyl chloride)	Flexibility, paintability	Greater cost than PE, stiffness

Poly(vinyl chloride). Poly(vinyl chloride) can be molded in liquid or powdered form. The liquid plastisols are fluid suspensions of fine particle-sized resins in a plasticizing liquid. PVC compounds are easily processed. They can be formulated to produce articles ranging from flexible to semirigid, with durometer hardness of 60 Shore A to 65 Shore D (see VINYL CHLORIDE POLYMERS).

Molded plastisols possess outstanding chemical resistance. Plastisol systems for rotational molding are usually formulated to a Brookfield viscosity of 1000–4000 mPa·s (=cP) to provide high mold detail reproduction. Plastisols have excellent fluorescent pigment retention, which eliminates pigment bleeding. This can be an advantage in rotomolding when bright colors are required.

Nylon. Nylon has excellent tensile strength, stiffness, impact strength, and high heat resistance, and properties are maintained at elevated temperatures; chemical resistance is excellent (see POLYAMIDES, PLASTICS).

Table 3. Less Important Resins Used in Rotomolding

Resin	Advantages	Disadvantages
ABS	Good dimensional stability, low temp. impact strength	Hard to mold
Acetals	Very rigid, good chemical resistance	Hard to mold, high cost
Acrylics	Good clarity	Low impact strength
Cellulosics	Good chemical resistance, impact strength, and clarity	Hard to mold
Epoxies	Good electrical properties and chemical resistance	Hard to mold
Fluorocarbons	Good thermal properties, excellent chemical resistance	Hard to mold
Phenolics	Good at high temp.	Hard to mold, low impact strength
Polybutylenes	Good abrasion properties, long-term water resistance	Hard to mold
Polypropylene	Good chemical resistance	Low impact strength
Polystyrenes	Good electrical properties and clarity	Low impact strength
Polyurethanes	Good insulating properties and abrasinn resistance	Hard to mold
Styrene acrylonitrile (SAN)	Good chemical resistance and clarity	Hard to mold
Silicones	Good moisture resistance, excellent, chemical resistance	Hard to mold, high cost

Polycarbonate. Polycarbonates (qv) provide resins with excellent mechanical properties, including stiffness, tensile strength, creep resistance, and the highest heat resistance of all rigid plastics.

Other Resins. Many other resins have been processed by rotational molding. In most cases their disadvantages outweigh their advantages. Disadvantages include high cost, poor impact strength, and low flowability (Table 3).

Applications

Almost any type of part or product can be produced by rotational molding. Rotomolding has fewer limitations than any other plastic processing method. It is used for tanks, ranging in size from 19 L to 88 m^3. Rotomolded tanks are utilized in the agricultural, chemical, and recreational vehicle industries. Rotomolded containers are used for packaging and material handling. Rotational molding is used for portable toilets, battery cases, light globes, vacuum cleaner and scrubber housings, toys, and garbage containers. Rotomolded kayaks, canoes, boats, and playground equipment are commonplace.

Economic Aspects

Compared with blow molding, rotational molding offers lower equipment and mold costs and broad design parameters. Blow molding, however, provides a quicker

Table 4. Plastics Processing[a]

	Rotomolding	Blow Molding	Thermoforming
Equipment cost	2	3	1
Mold cost	1	3	2
Cycle time	3	1	2
Design limits	1	3	2
Materials available	1	3	2

[a] 1 = lowest costs; 3 = highest costs.

cycle and can be used with more resins. Compared with thermoforming, rotational molding offers cheaper mold cost and more design freedom. Thermoforming equipment is cheaper, cycles are shorter, and the resin selection is wider. Table 4 compares these processes. Rotomolding resins are priced slightly higher than most other resins because of higher stabilizer requirements. Grinding costs are 11–15 cents/kg. Rotomolding machine prices range from $80,000 for a small machine up to $800,000. Grinding systems are $50,000 to $100,000.

Safety

Rotational molding is a reasonably safe industry. Most resins used are nonhazardous. Some resins may cause mild irritation; suppliers provide safety information on their handling and use. Most resins used for rotational molding are ground to 500 μm (35 mesh), and appropriate procedures should be followed to prevent a dust explosion and fire. A rotomolder is a relatively safe piece of processing equipment; fans are enclosed with guards; spindles and arms operate at a low speed. The oven is equipped with a temperature control.

BIBLIOGRAPHY

"Rotational Molding" in *EPSE* 2nd ed., Vol. 14, pp. 659–670, by Philip T. Dodge, Quantum Chemical Company, USI Division.

1. *USI Chemicals, Petrothene Polyolefins, A Processing Guide*, National Distillers, Cincinnoti, Ohio, 1971.
2. P. B. Brains, *Basic Principles of Rotational Molding*, New York, 1971.
3. *Engineering Design Handbook, Rotational Molding of Plastic Powders*, U.S. Army Material Command, Alexandria, Va., 1975.
4. G. Beall, *The Engineers' Guide to Designing Rotationally Molded Plastic Parts*, Association of Rotational Molders, Chicago, Ill., 1982.
5. R. Crawford, *Rotational Moulding of Plastics*, John Wiley & Sons, Inc., New York, 1992; P. Mooney, *Analysis of the North American Rotational Molding Business*, 1995; R. Crawford, *Rotational Moulding of Plastics*, 2nd ed., John Wiley & Sons, Inc., New York, 1997; P. Mooney, *The Recent Pace and Growth in North American Rotational Molding*, 1997; G. Beall, *Rotational Molding*, Hanser/Gardner, 1998; P. Mooney, *The New Economics of Rotational Molding*, 1999; P. Nugent, *Rotational Molding: A Practical Guide*, 2001; P. Mooney, *New Market Dynamics in Rotomolding*, 2003.

6. P. T. Dodge, *Materials for Rotational Molding*, Plastics Design Forum, Denever, Colo. 1984;

GENERAL REFERENCES

Association of Rotational Molders Library, www.Rotomolding.org.
Society of Plastics Engineers, Rotomolding Division. www.rotomolding.net.

PHILLIP T. DODGE
STEVE ANDRZEJEWSKI
DUANE MAHAN
Equistar Chemicals, LP, Lyondell Chemical Co.

RUBBER CHEMICALS

Introduction

Rubber processing chemicals are used extensively to impart performance and processability to rubber and the products made thereof. These chemicals are typically organic compounds but several inorganic materials are also included under the umbrella of rubber chemicals. The rubber compound is described as a mixture of one or more rubber polymers (elastomers) with a combination of one or more of fillers, oils, and rubber chemicals (see RUBBER COMPOUNDING). The compound, once vulcanized, provides technologically useful properties, such as may be applied to tires, hoses, belts, tracks, and a variety of mechanical goods.

Vulcanization systems and antidegradants are the two dominant classes of rubber chemicals, given that the largest class of rubbers used in industry (the so-called general-purpose rubbers) require cross-linking by sulfur or other curative to provide meaningful performance, and require protection from oxygen and ozone to provide meaningful service lifetimes (see ANTIOXIDANTS).

The present article reviews several recent developments in the field of rubber chemicals of particular interest to practitioners. These topics include

(1) non-nitrosamine curatives as a response to health concerns and legislation
(2) reversion-resistance curatives to enhance product durability and support higher temperature cures
(3) silica-to-rubber coupling agents to support expanded use of silica filler
(4) nonstaining and persistent antidegradants for enhanced performance

Non-Nitrosamine Curatives

General-purpose rubbers are those made from the monomers isoprene, 1,4-butadiene, and styrene. Each isoprene and butadiene unit contributes one

Encyclopedia of Polymer Science and Technology. Copyright John Wiley & Sons, Inc. All rights reserved.

carbon–carbon double bond to the final structure, plus a number of allylic hydrogen sites, which are the reactive centers for sulfur vulcanization. In sulfur vulcanization, polymer chains are connected by covalent bonds (cross-linked) of sulfur atoms or chains of sulfur atoms attached to the allylic positions of individual chains. The chemical components necessary for this process include the polymer(s) with allylic hydrogens, elemental sulfur or a source of sulfur, plus chemical promoters called accelerators and activators. In current practice, the curative promoter package typically employs a primary accelerator, one or more secondary accelerators, and zinc oxide and fatty acid (or a zinc fatty acid salt) activator. Several excellent reviews have been written detailing the chemistry involved between these ingredients and the influence they have on the development of final vulcanizate properties (1–9).

The benefits of an optimized sulfur vulcanization system are several: economical, good kinetics, and good performance. *Economical* in that sulfur is very inexpensive, and typical accelerators and activators are also low cost commodity chemicals. *Good kinetics* in that rapid cross-linking is achievable in a matter of a few minutes at usual curing temperatures of 130–180°C but that the rubber compound can withstand many minutes at processing temperatures often in the range of curing temperatures (ie, 100–140°C) before the onset of cross-linking.

The undesirable premature cross-linking of polymer chains in the processing step is called scorch; the ability of the vulcanization system to withstand the heat of processing without premature cross-linking is called scorch safety. This attribute of delayed action (scorch safety) with fast cure is unique to accelerated sulfur vulcanization, and allows for safe and rapid mixing and fabrication of rubber compounds and parts coupled with rapid cure.

Good performance derives from the structure of the cross-links as a blend of sulfur chain lengths, from one sulfur atom (monosulfidic) to two (disulfidic) to three or more, up to eight and more (polysulfidic). The differing chain lengths impart differing physical characteristics: shorter chain impart heat stability and resistance to permanent set, longer chain lengths impart tear resistance. The ratio of sulfur to primary accelerator controls cross-link length distribution, and thus can be used to tailor physical properties, even as the concentration of curatives controls cross-link density, itself a dominant contributor to compound properties such as modulus, strength, hardness, and abrasion resistance.

Figure 1 illustrates the curing process as measured by a rheometer. The rheometer follows the development of cure state as a function of time. Vulcanization characteristics such as minimum torque M_L (a measure of compound green viscosity), onset of cure (T1 pt rise), M_H (a measure of maximum cure state reached), and T90% cure (time required to reach 90% cure state) are valuable properties defining cure behavior. Likewise the rheometer cure profile can be broken into three regions of interest, an estimate of scorch safety, an idea of what the cure state development looks like during the cross-linking phase, and how the cross-linked vulcanizate network matures with additional heat.

Primary Accelerators. The primary accelerator of choice is a mercaptobenzothiazole sulfenamide of general chemical structure (**1**). Specific examples of this class are listed in Tables 1 and 2.

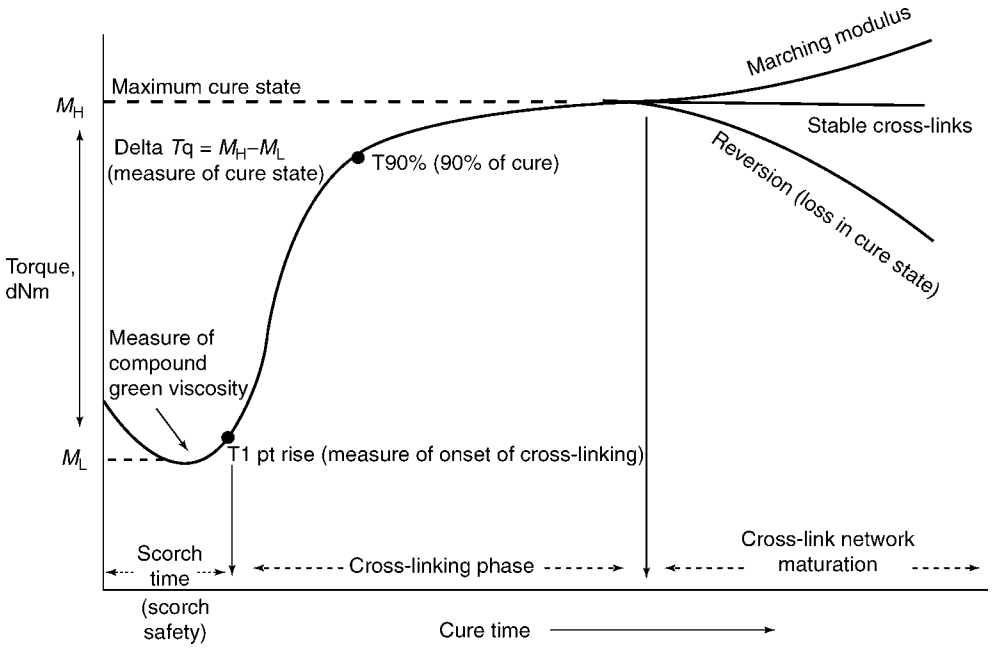

Fig. 1. Example of rheometer cure curve illustrating major cure attributes. To convert dNm to in lb, multiply by 0.885.

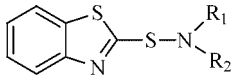

1

The sulfenamide S—N bond strength controls the scorch safety and cure rate. The more labile this bond, the more readily the active cure promoter mercaptobenzothiazole is released at the onset of the cross-linking process. A family of sulfenamides has been developed to span a range of cure rates. Common historical members of this class are shown in Table 3, arranged from fast curing to

Table 1. Nitrosamine-Generating Sulfenamides

Chemical name	Abbreviation	Chemical structure
4-Morpholinyl-2-benzothiazole disulfide	MBSS	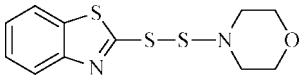
N-Oxydiethylene benzothiazole-2-sulfenamide	MBS	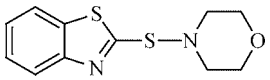
N,*N*-Diisopropylbenzothiazole-2-sulfenamide	DIBS	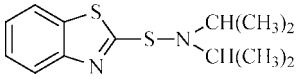

Table 2. Non-Nitrosamine-Generating Sulfenamides and Sulfenimides

Chemical name	Abbreviation	Chemical structure
N-Cyclohexyl benzothiazole-2-sulfenamide	CBS	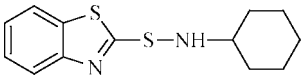
N-tert-Butyl-2-benzothiazole sulfenamide	TBBS	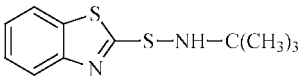
N-Dicyclohexyl-2-benzothiazole sulfenamide	DCBS	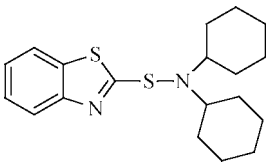
N-tert-Butyl-2-benzothiazole sulfenimide	TBSI	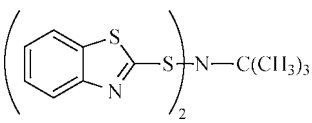

slow, based on primary amines of weakening base strength (ie, a to b to c) and/or increasing steric hindrance (ie, c to d to e) (10).

German legislation targeting elimination of stable and volatile nitrosamines as by-products of vulcanization became effective in September 1988 as the "Technical Rules for Hazardous Materials TRGS 552" (11,12). It recognized 11 nitrosamines as carcinogenic and set industry limits to exposure. Nitrosamines are potent carcinogens in laboratory animal testing, and are suspect human carcinogens. The amines released from sulfenamide accelerators in the necessary early step of vulcanization can combine with nitrogen oxides (NO_x) in the atmosphere to produce nitrosamines. Primary amines form unstable nitrosamines that immediately decompose and do not constitute a health risk, whereas secondary amines produce stable nitrosamines by this process, $(R\text{-})_2\text{—N—N=O}$). The

Table 3. Sulfenamide Structure Influence or Cure Rate and Scorch Safety

CBS > TBBS > MBS > DIBS > DCBS				
a	b	c	d	e
Fastest cure rate least scorch safety →				Slowest cure rate most scorch safety
a	b	c	d	e
CBS	TBBS	MBS	DIBS	DCBS
Cyclohexlyamine Base strength pK_a 10.7	*t*-Butylamine Base strength pK_a 10.5	Morpholine Base strength pK_a 8.3	Diisopropylamine Base strength pK_a 11.0	Dicyclohexylamine Base strength pK_a 11.3
			Steric hindrance predominates	Steric hindrance predominates

Table 4. Comparison of sulfenamide cure properties normalized to MBS[a,b]

	Cure time (T90%)	Scorch time
Nitrosamine-generating		
MBS	100	100
MBSS	27% shorter	45% shorter
DIBS	7% longer	10% longer
Non-nitrosamine alternatives		
CBS	27% shorter	29% shorter
TBBS	15% shorter	22% shorter
DCBS	31% longer	30% longer

[a]Base compound: SBR, 50; polyisoprene, 50; N299 carbon black, 50; naphthenic oil, 28; stearic acid, 1; ZnO, 3; antioxidant, 1; sulfur, 1.75; sulfenamides at an equal molar level (4.74 mmol).
[b]Samples tested at 150°C.

immediate effect of the legislation was thus to target for elimination from vulcanization systems of all sulfenamides made from secondary amines able to form 1 of the 11 listed nitrosamines. The accelerators given in Table 1, MBS and MBSS (derived from morpholine) and DIBS (derived from diisopropyl amine), had to be replaced at least for European markets.

Compromise cure systems based on the faster and slower curing "non-nitrosamine" sulfenamides listed in Table 2 have been recommended as alternatives (12–14). The sulfenimide variant *N-tert*-butyl-2-benzothiazole sulfenimide (TBSI) was also produced to satisfy this need (15). As with DCBS the large steric hindrance associated with the sulfenimide slowed the reaction kinetics, resulting in slower cures and extended scorch safety.

Table 4 (16) makes a comparison of cure properties for the sulfenamides listed in Tables 1 and 2 relative to MBS. No exact replacements are available for MBS, MBSS, and DIBS, but DCBS can serve as an alternative for MBS and DIBS and CBS and TBBS can serve as alternatives for MBSS. Proper adjustments in sulfur and sulfenamide levels can provide similar cure performance. CBS and TBBS also satisfy the need in providing rapid curing kinetics where required. Additional scorch protection, if needed, can be obtained by application of the widely used scorch inhibitor *N*-(cyclohexylthio)phthalimide (17).

Secondary Accelerators. Even bigger changes have come to the secondary curative segment. Three classes of chemicals served historically as secondary accelerators, useful in low levels to speed up sulfenamide cures: the thiuram (**2**) and dithiocarbamate (**3**) types, and the guanidine type (**4**). Specific examples for these classes are listed in Tables 5 and 6.

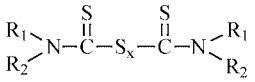

2

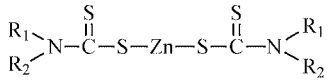

3

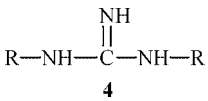

4

Table 5. Nitrosamine-Generating Thiurams

Chemical name	Abbreviation	Chemical structure
Tetramethylthiuram disulfide	TMTD	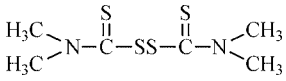
Tetramethylthiuram monosulfide	TMTM	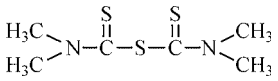

Two workhorse members of the thiuram class, particularly active in cure rate as well as economical, are TMTD and TMTM (R= methyl, $x = 2$ and 1, respectively, in **2**). Both TMTD and TMTM are stable nitrosamine generators, as they liberate the secondary amine, dimethyl amine, during vulcanization (12,13). Replacements for these rubber chemicals has been a target of considerable technical effort in the rubber industry. Several candidates have emerged, each with its own attributes. None is a direct substitute for either TMTD or TMTM but several have proven

Table 6. Low or Non-Nitrosamine-Generating Thiurams, Dithiocarbamates, and Guanidines

Chemical name	Abbreviation	Chemical structure
N,*N*,*N*′,*N*′-Tetraisobutylthiuram disulfide	IBT	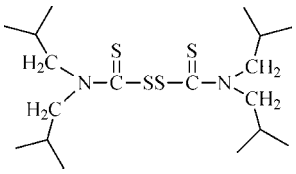
N,*N*,*N*′,*N*′-Tetraisobutylthiuram monosulfide	IBM	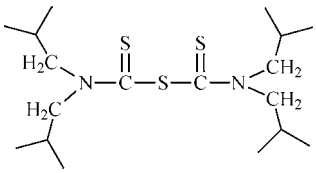
Tetrabenzylthiuram disulfide	TBzTD	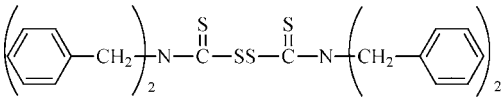
Zinc dibenzyldithiocarbamate	ZBEC	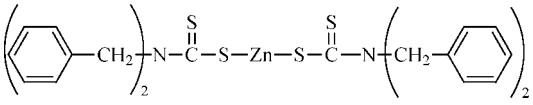
Diphenylguanidine	DPG	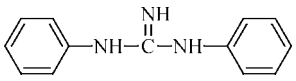
Di-*o*-tolylguanidine	DOPG	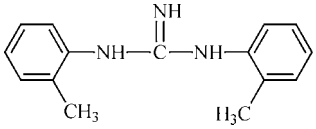

Table 7. Comparison of Cure Properties Relative to TMTD[a] of Non-Nitrosamine Secondary Accelerator Alternatives[b,c]

	Cure time (T90%)	Scorch time
TBzTD (eq molar, 0.67 phr)	18% longer	33% longer
IBT (eq molar, 0.47 phr)	18% longer	33% longer
ZBzDC (eq molar, 0.76 phr)	6% longer	Equal

[a] At an equal molar level (0.30 phr).
[b] Base compound: SBR, 50; Polyisoprene, 50; N299 carbon black, 50; naphthenic oil, 28; stearic acid, 1; ZnO, 3; antioxidant, 1; sulfur, 1.75; sulfenamides at an equal molar level (4.74 mmol).
[c] Samples tested at 150°C.

useful in non-nitrosamine cure packages. Cure properties of likely replacements are compared to TMTD in Table 7 (16).

As secondary curatives, both TBzTD and IBT provide slightly longer cure times but have the advantage of prolonging scorch safety. A much closer match to TMTD is ZBzDC in both cure time and scorch time. When used at equal molar concentrations, significantly more weight of the non-nitrosamine replacements are required versus TMTD.

TBzTD and ZBzTD do, in fact, generate stable nitrosamines from the secondary amine dibenzyl amine; however, this nitrosamine is nonvolatile and is not readily released from the vulcanized product into the atmosphere. It is also considered noncarcinogenic (18). Therefore, these materials are considered non-nitrosamine in usage. IBT likewise generates a stable nitrosamine but its level has been claimed to be 100 times less than TMTD (19).

Sulfur Donors. A fourth class of sulfur vulcanization chemicals has been affected by the move to non-nitrosamine generators: the sulfur donors. These are organic chemicals which have a relatively high level by weight of sulfur atoms that are able to be donated in the vulcanization process to create sulfur cross-links. Elemental sulfur is the material of choice as a source of the sulfur atoms which create these cross-links, but some articles cannot tolerate free sulfur for requirements of color, solubility, or performance.

With regard to solubility, compounds which require a very high cure state may require more sulfur than can be supplied as elemental sulfur. Sulfur has a solubility limit of about 1 part per hundred rubber at room temperature (20) and at higher levels will "bloom," that is, crystallize out of solution onto the rubber compound surface, where it can be detrimental to processing, particularly to "tack," the ability of rubber to stick to itself or other rubber component in the building of a composite product. So-called insoluble sulfur has been developed as an alternative form of elemental sulfur: it has a polymerized long-chain structure ($-S_x-$) as opposed to crystalline sulfur (S_8 rings) (21,22). Insoluble sulfur can be substituted for crystalline sulfur and can be used at levels well above the solubility limits without bloom, in theory. In practice, however, insoluble sulfur will revert to soluble sulfur at the temperatures often attained in mixing and shaping rubber components, and thus can result in bloom in processing (23). Suffice it to say that some alternative forms for sulfur are sometimes needed for processing.

Table 8. Nitrosamine-Generating Sulfur Donors

Chemical name	Abbreviation	Chemical structure
4,4′-Dithiodimorpholine	DTDM	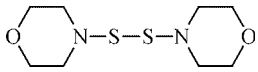
4-Morpholinyl-2-benzothiazole disulfide	MBSS	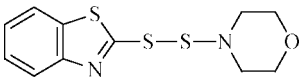
N-Oxydiethylenethiocarbamoyl-*N*′-oxydiethylenesulfenamide	OTOS	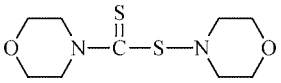
Tetramethylthiuram disulfide	TMTD	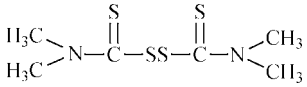

Likewise, for performance, sometimes a sulfur donor is needed as well. Elemental sulfur gives rise to variable cross-link lengths, regulated to some extent by sulfur-to-accelerator ratio. In some applications, particularly those which require very high temperature and or oxidative stability, one may need a preponderance of cross-links of very low rank, mostly monosulfidic. For this purpose, organic sulfur donors may be useful (24).

Four conventional sulfur donor curatives employed historically are all nitrosamine generators, derived from either morpholine or dimethylamine, as shown in Table 8. The industry has developed non-nitrosamine substitutes, as shown in Table 9. As discussed earlier, TBzTD is used primarily as a secondary accelerator to further accelerate cure while offering good scorch protection. Similarly, IBT performs like TBzTD. CLD appears to be as active as DTDM in donating sulfur evidenced by its ability to generate the same cure state as DTDM when used at equal available sulfur levels. CLD however can introduce more scorch. These attributes are illustrated in Table 10 (16). TESPT has found value as a sulfur donor in what has been described as an equilibrium cure, or EC for short (25). The concept relies on the slow release of sulfur from TESPT during the curing process to control the reversion process illustrated in the rheometer chart of Figure 1. Rhenocure® SDT/S is a thiophosphite and thus not amine-based. It can be used where high levels of short cross-links of the mono- and di-type are desirable for long-term heat age stability (26). The Vultac® class of Table 9 has found uses in diene rubbers as partial or total replacement for sulfur (27). Benefits claimed include improvements in aging properties and promoting covulcanization of blends. Table 10 illustrates the sulfur-donating ability of the Vultac® class by showing Vultac® 7 provides a similar cure state as sulfur when used as a total replacement. One drawback is the introduction of scorch.

The rubber chemist has reacted vigorously to the challenge of eliminating volatile nitrosamine-generating chemicals in the workplace, even though many had been fixtures of the sulfur vulcanization process. Non-nitrosamine primary and secondary accelerators and sulfur donors are now available and used extensively.

Table 9. Non-Nitrosamine Sulfur Donors

Chemical name	Abbreviation	Chemical structure
Tetrabenzylthiuram disulfide	TBzTD	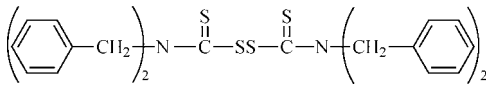
N,*N*,*N*′,*N*′-Tetraisobutylthiuram disulfide	IBT	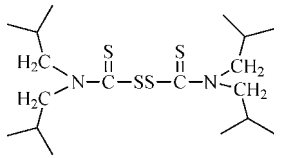
Caprolactam disulfide	CLD	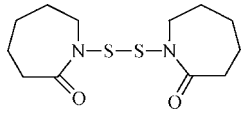
Bis-(3-triethoxysilylpropyl)tetrasulfane	TESPT	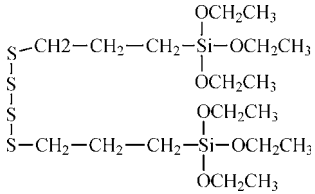
Bis-(*O*,*O*-di-2-ethylhexyl-thiophosphoryl)polysulfide	Rhenocure® SDT/S	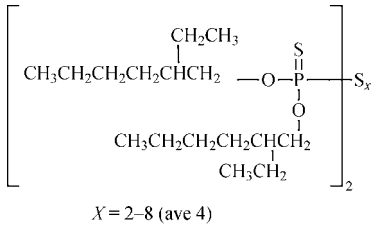 *X* = 2–8 (ave 4)
Alkylphenol disulfide oligmer	Vultac®	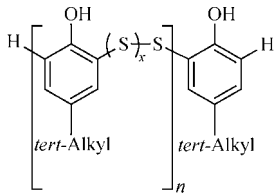

Table 10. Activity of Sulfur Donors Versus Free Sulfur Compared Using a Rheometer Cure Trace[a,b]

Sulfur donor	Sulfur	DTDM	CLD	Vultac® 7
Sulfur donor, phr	1.0	3.7	4.5	3.3
Available sulfur, phr	1.0	1.0	1.0	1.0
Delta *T*q , dNm (cure state)	19.2	26.4	26.6	19.6
T90%, min	21.7	36.3	19.7	21.5
T1 pt rise, min	9.0	12.3	5.7	4.0

[a] Base compound: SBR, 50; polyisoprene, 50; N299 carbon black, 50; naphthenic oil, 28; stearic acid, 1; ZnO, 3; antioxidant, 1; CBS, 1.25.
[b] Samples tested at 150°C.

Reversion-Resistance Curatives

Concomitant with the several benefits of sulfur vulcanization described above are certain deficiencies owing to the complexity of the formation of, and instability of, the sulfur cross-link system. Reversion is defined as the anaerobic (nonoxidative) degradation of sulfur-cured vulcanizates which results in a loss of compound performance. This phenomenon is generally associated with loss in cross-link density via thermal degradation of sulfur cross-links caused by heat and/or extraneous accelerator fragments (28,29). It occurs during overcure conditions, elevated cure temperatures (30), and severe service conditions (31). Reversion is most pronounced for natural rubber, which tend to lose cross-links and soften with heat and aging, whereas synthetics (polybutadiene, styrene-butadiene copolymers (qv)) tend to add cross-links and harden with heat and aging (see BUTADIENE POLYMERS).

Overcure, elevated cure temperatures, and severe service are all growing trends industrially, particularly for large tires as are used in over-the-highway trucks, off-the -road equipment, and aircraft tires, all of which also use a lot of natural rubber. Manufacturing efficiencies promote higher temperature cure conditions for better throughput. Tires are cured from heat applied at the outside (mold) and inside (bladder) surfaces. For tires with thick rubber cross sections, and given the poor thermal conductivity of rubber, a temperature gradient is produced from surfaces to interior. The surfaces may see significantly more total heat history than the interior. This may be so even allowing for slow cooling of the interior and continued cure of the inside after the tire is removed from the mold. Cure systems are tailored for individual components to try to balance the cure profile across the cross section, but a given thick tread may still be subjected to a broad range of heat inputs, so that only a portion of that one component will be optimally cured while a portion will be overcured. (No portion can be undercured without generating a useable product. Indeed, cure conditions are set so as to require all portions of the tire to achieve a minimum acceptable level of cure.) Tires, like other rubber goods, perform to ever higher levels: mileage, service life, and service conditions. Still, high operating temperatures and loads may impart reversion. Thus, there has been a growing interest in chemicals which inhibit the tendency to reversion of sulfur-cured natural rubber.

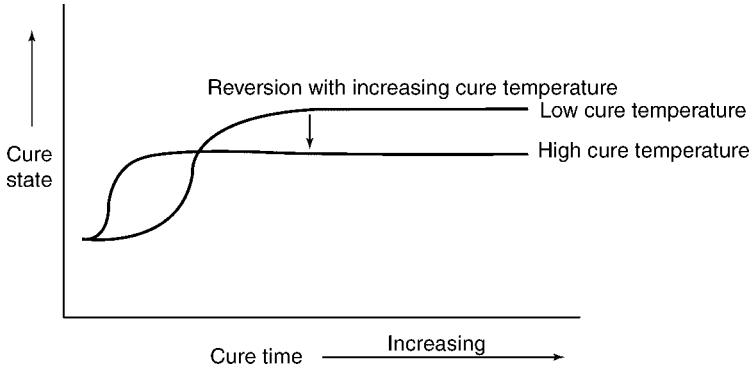

Fig. 2. Reversion during cross-link formation.

Reversion can occur during cross-link formation (high temperature cure) and after cross-link formation (overcure or in service). These are shown pictorially in Figures 2 and 3.

For processes which contribute to reversion seen during cross-link formation, several pathways can be envisioned contributing to loss in ultimate cure state development. As Figure 4 shows, these pathways most likely involve desulfuration or decomposition of intermediate polythio-sulfurating species or the polythio-benzothiazole cross-link precursor formed by the heat of the curing process. This decomposition pathway effectively reduces the concentration of active cross-linking agents resulting in lower cross-link density. Also at very high temperatures as cross-links are forming, they may, in a similar manner, be immediately desulfurated and decomposed.

In the development of maximum cure state, the initial cross-link structure, which may be high in polysulfides, goes through a rearrangement process in which the Zn-accelerator complexes, which promote curing, extrude sulfur from the initial cross-links and reutilize the extruded sulfur to form additional cross-links (29). After the maximum cure state is established with a desired proportion of polysulfide, disulfide, and monosulfide cross-links for compound performance, the network cross-link structures will continue to evolve with additional heat introduced

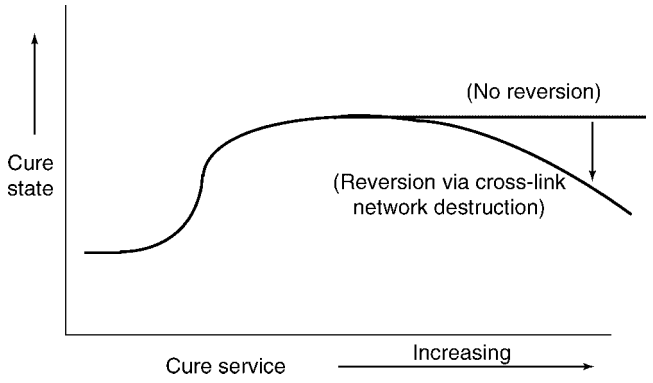

Fig. 3. Reversion after cross-link formation.

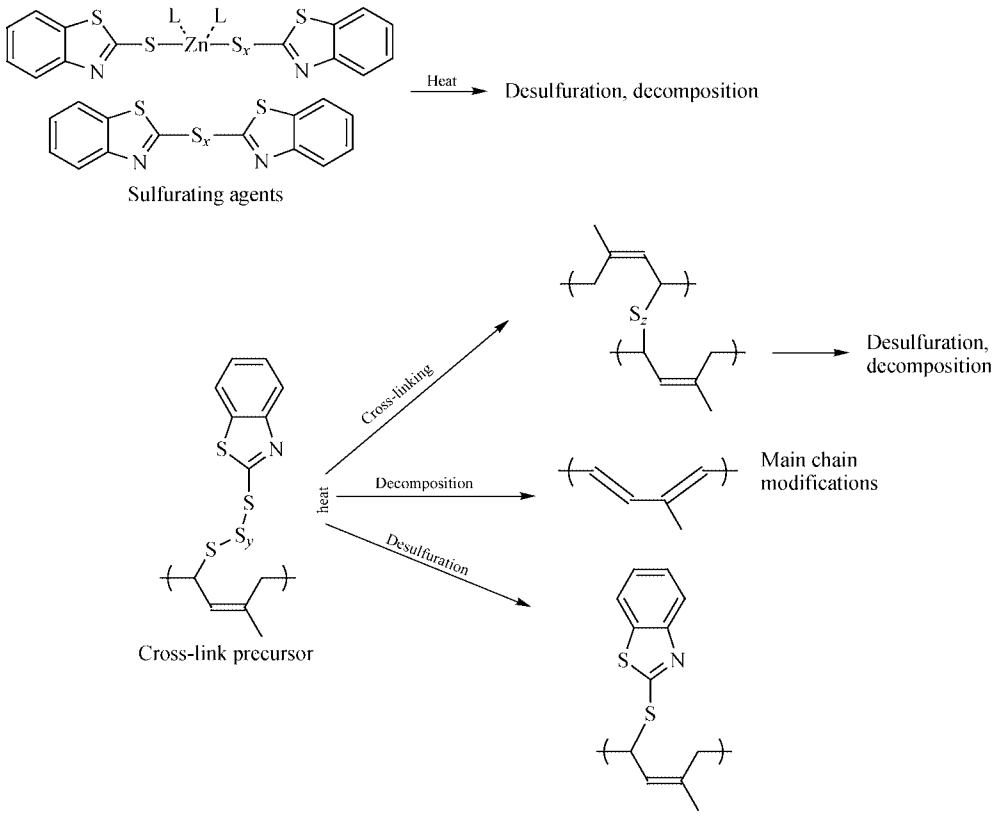

Fig. 4. Reversion pathways during cross-link Formation.

during an overcure situation (30) or during the service life of the compound (31). Figure 5 shows that this reversion process involves loss of polysulfide cross-links with the formation of more mono and disulfide types and finally decomposition of the mono and disulfidic types yielding modifications in the polymer backbone. Modifications would include carbon–carbon double bond rearrangement, growth of diene and triene structures, and isomerization of existing double bonds. For

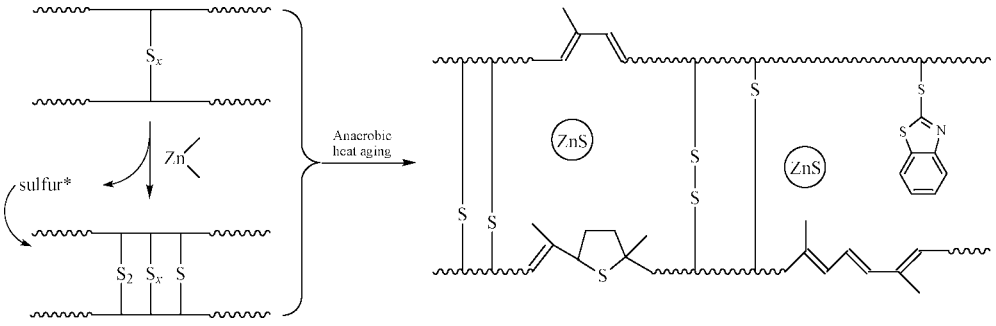

Fig. 5. Cross-link network maturation and reversion with heat from curing or high temperature service.

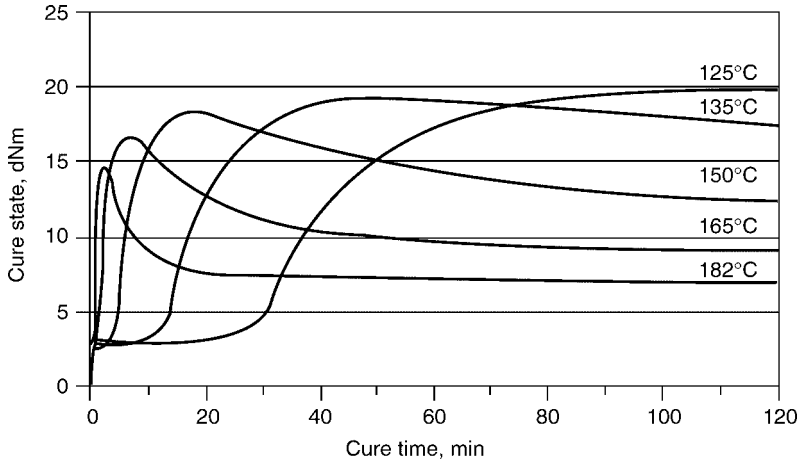

Fig. 6. Effect of temperature on cure rate and cure state. Base compound: NR, 100; N347 carbon black, 50; naphthenic oil, 8; stearic acid, 1; ZnO, 3; antioxidant, 0.75; sulfur, 3; TBBS, 0.75. To convert dNm to in lb, multiply by 0.885.

natural rubber, this results in creation of some trans double bonds in the otherwise all-cis structure. Additionally, unproductive (nonload bearing) cyclic sulfides increase in number in reversion: sulfur attached by both of its valences to neighboring segments of the same polymer chain. Zinc sulfide is produced as a stable but inactive by-product of both vulcanization and reversion. All these changes are followed by a drop in cross-link density (32–35).

The effect of cure temperature on the cure kinetics and cure state profile of a simple carbon black filled, sulfenamide/sulfur cured natural rubber compound is shown in Figure 6 (16). As shown in the growth of the cure state, an article which would require 110 min to cure to its maximum cure state at 125°C can be cured at 135°C in 50 min, at 150°C in 18 min, at 165°C in about 7 min, and at 182°C in about 3 min. However, the maximum state of cure achieved keeps dropping as cure temperature increases.

The same process continues beyond "optimum" or maximum cure state if cure is allowed to continue ("overcure"). Again, as seen in Figure 6, the cure state now drops from the maximum to attain a lower plateau. This decline is faster and more pronounced as cure temperature increases. The window of time for near-optimum cure narrows, and the regime of overcure grows.

Physical manifestations of reversion, beyond loss in cure state, include

(1) loss in resilience
(2) greater heat buildup
(3) loss in abrasion resistanec
(4) loss in wire adhesion
(5) initial increase then large loss in tear and fatigue resistance
(6) loss in modulus and hardness
(7) loss in tensile strength

How much of the decay in properties is due to cis–trans isomerization, cyclic sulfides, growth of dienes, reduction in sulfur rank, and reduction in total cross-link density is a subject of ongoing research, but all processes likely contribute.

Because of the large demands put on rubber compounds to address issues of increased productivity via high cure temperatures or increased service temperatures brought about by overloads and high speeds, reversion-resistance chemicals are now becoming part of the compounder's arsenal to combat reversion issues.

Reversion-resistance chemicals operate by one of two mechanisms:

(1) Relink polymer chains to maintain cross-link density. These may be via sulfur or non-sulfur covalent bonding.
(2) Form heat stable cross-links that are more resistant to scission than conventional sulfur cross-links. These may or may not contain sulfur.

Several rubber chemicals have been developed to inhibit or compensate for sulfur cross-link reversion. Several of these are shown in Table 11.

MPBM operates under the mechanism of forming heat-stable cross-links. It has been reported that the network structures formed with MPBM are not prone to revert (36,37) and offer heat resistance during high temperature curing and overcure. Detailed mechanistic studies have found the major reactions occurring during vulcanization in sulfur-containing systems to be 1,2-cross-linking of the imide double bond across polymer chains generating a heat-stable carbon–carbon cross-link. Additional reactions included homopolymerization, copolymerization giving multiple cross-links, and Michael addition reactions with 2-mercaptobenzothiazole and amines derived from sulfenamide curatives as well as other extraneous sulfur species formed during cure (38).

BCI-MX also provides its heat-resistant performance by the formation of carbon–carbon cross-links but does it by the mechanism of relinking polymer chains to maintain cross-link density (38,39). The relinking mechanism takes place only during reversion when sulfur cross-links are broken and in their place cyclic sulfides, dienes, and trienes are formed along the polymer backbone (16,35). The structural differences of BCI-MX from MPBM prevent it from undergoing the reactions discussed about MPBM. Instead, the citraconimide group undergoes a Diels–Alder addition reaction with these chain modifications to relink polymer chains and compensate for the lost, reverted, sulfur cross-links (39–41). For BCI-MX to be effective, some initial reversion must take place. This is nicely illustrated in Figure 7 (16) which shows the reversion characteristics of BCI-MX versus the same compound with no BCI-MX added.

As discussed earlier, TESPT functions as a reversion-resistant chemical by the slow release of sulfur to compensate for cross-links lost (25). It has also been found that TESPT leads to higher levels of monosulfidic cross-links (42), which yields improved reversion (thermal aging) resistance (43,44).

Both HTS and BDTCH can be classified as proceeding through the mechanism, which forms heat-stable cross-links that are more resistant to scission. The cross-link has been referred to as a hybrid cross-link in which a hexylmethylene dithio group $-S_n-[(CH_2)_6-S_x]_k-$ is the bridging group between two polymer chains (45–49). In this scheme, k is presumed to be small. At high sulfur

Table 11. Anti-Reversion Agents

Chemical name	Abbreviation	Chemical structure
N-*N*′-*m*-phenylenedimaleimide	MPBM	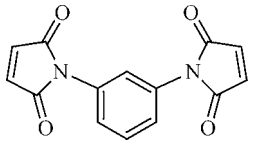
1,3-Bis(citraconimidomethyl) benzene	BCI-MX	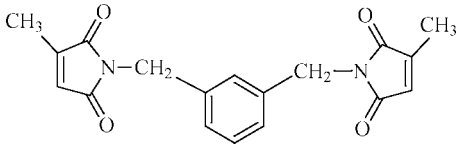
Bis(3-triethoxysilylpropyl)tetrasulfane	TESPT	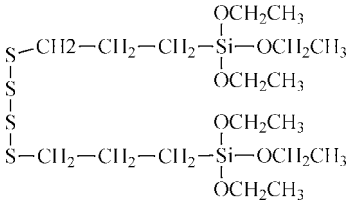
Hexamethylene bis-thiosulfate disodium salt dihydrate	HTS	$NaO_3SS(CH_2)_6SSO_3Na\ 2\ H_2O$
Mixture of zinc salts of aliphatic and aromatic carboxylic acids	Activator® 73	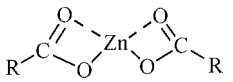 R = aliphatic–aromatic mix
1,6-Bis(*N*,*N*-dibenzylthiocarbamyldithio)hexane	BDTCH	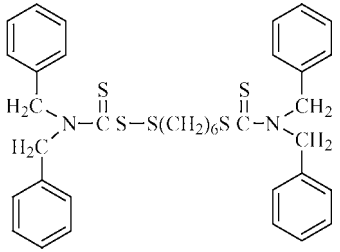
Trifunctional acrylate coagent	Sartomer SR534	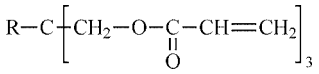

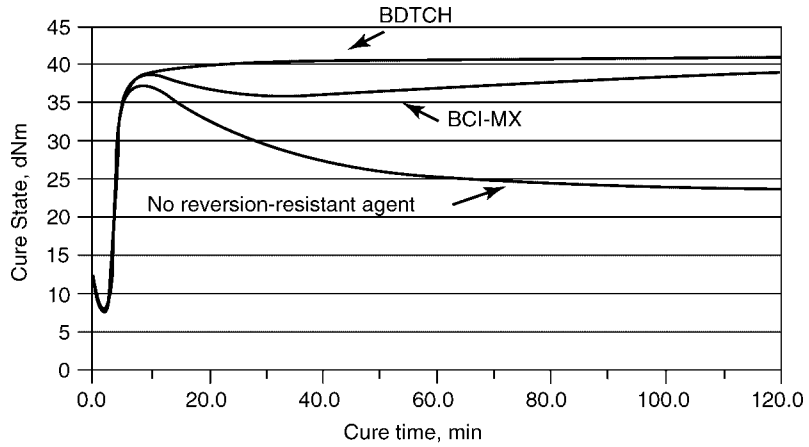

Fig. 7. Example of reversion-resistant agent effect on reversion (cure temperature 165°C). Base compound: NR, 100; N347 carbon black, 50; naphthenic oil, 8; stearic acid, 1; ZnO, 3; antioxidant, 0.75; sulfur, 3; TBBS, 0.75. To convert dNm to in lb, multiply by 0.885.

levels both n and x would be greater than 1. As reversion proceeds, the number of n and x sulfur atoms would be reduced to one resulting in a hybrid cross-link with monosulfide linkages for thermal stability and the hexylmethylene bridge to add flexibility to the cross-link for improved tear and fatigue properties. Figure 7 illustrates the reversion-resistant capabilities the hybrid cross-link can offer.

Since Activator 73 A is a mixture of zinc salts of linear aliphatic and aromatic carboxylic acids (50), it would be expected that the mechanism of action would be similar to zinc stearate, which can extract sulfur from polysulfidic cross-links and reuse that sulfur to generate more cross-links (51). Ultimately this would result in a network structure high in monosulfidic content (42).

Trifunctional acrylates, such as Sartomer SR534, have been found to provide reversion-resistant protection (52). Test results of the three trifunctional acrylate and methacrylate monomers, pentaerythritol triacrylate, trimethylolpropane trimethacrylate, and trimethylolpropane triacrylate, versus BCI-MX prove interesting (53). Rheometer traces of cure development and reversion characteristics with these trifunctional monomers duplicated BCI-MX behavior even to the point of having initial reversion chemistry occurring before they became active. This would suggest these materials operate by the same mechanism as BCI-MX.

To conclude this section, the rubber chemist has vigorously pursued materials and means to inhibit and counteract the tendency to reversion, so as to permit higher temperature cures, buttress rubber goods against overcure, and permit increasingly greater operating conditions and service lifetimes.

Silica-to-Rubber Coupling Agents

Rubber must be cross-linked to be technologically useful, hence the emphasis historically and in the two sections above, on chemicals to facilitate and optimize this process. However, even cured rubber is practically of little value unless the rubber

is reinforced by a particulate filler (see FILLERS). Cured, unfilled ("gum") rubber has very low tensile strength, and poor tear and abrasion resistance. Contrast a pencil eraser or a rubber band to a tire tread or transmission belt, for example. The early tires and rubber goods were "filled" with inert fillers such as zinc oxide. The discovery about a century ago that carbon black (qv) greatly enhanced rubber performance began the evolution of tough durable goods made from rubber. It turns out that very few other substances reinforce rubber as does carbon black. None do at the same cost. Hence, even today, carbon black is the dominant reinforcing filler for rubber, even as talc, calcium carbonate, kaolin clay, and other lower cost, nonreinforcing fillers retain uses in selected nontire applications.

The characteristics shared by reinforcing fillers are few but vital:

(1) Small hard particles, with diameters upon ultimate dispersion below micron size
(2) Ability of said particles to disperse in the rubber medium
(3) Ability of said particles to interact with themselves, so as to produce an independent filler network, which interpenetrates with and synergistically supports the polymer network. This attribute is called "filler/filler interaction."
(4) Ability of said particles to interact with the polymer matrix. This attribute is called "polymer/filler interaction."

Carbon Black. Carbon black (qv) has all of these characteristics. Carbon black is amorphous elemental carbon with a graphitic-like microcrystalline substructure (54). The furnace process rubber grades come in a range of particle and aggregate sizes and shapes, with reinforcing grades in the 10–100 nm ultimate particle diameters. Carbon black disperses very well in general-purpose rubbers, with which it shares an organic chemical nature. It has a strong self-affinity; once a sufficient loading is achieved in a rubber matrix, it imparts electrical conductivity to the composite via the filler network, for example. This filler network is also responsible for the enhanced low strain dynamic stiffness of filled rubber, and the loss (recoverable upon relaxation) of this stiffness with strain. This phenomenon is called the Payne effect (55). Finally, and most importantly, carbon black has a strong affinity to general-purpose rubbers, as a function of attributes built into the carbon black in its manufacture ("surface activity") and the unsaturated organic structures of the polymers, such as carbon–carbon double bonds, and styrene units.

Much has been written on the nature of the carbon black/rubber interaction, which is still not fully understood (selected references include References 56–59). One thing is clear: carbon black has a strong affinity to general-purpose rubbers. It is manifest in the simple experiment called "bound rubber" or "insoluble polymer" measurement. A sample of uncured rubber, which may or may not be devoid of rubber chemical additives, is admixed with an amount of reinforcing carbon black. The composite is then immersed in a solvent in which the polymer is soluble. Whereas all, or all save any gelled portion, of the unfilled rubber dissolves in the solvent, the same polymer, as a carbon black filled composition, produces only a portion of soluble polymer. For a typical recipe containing 30–50 parts by weight

of carbon black per hundred parts rubber, a typical value for the nondissolved or bound polymer might be 20–40%. Empirically, the quantity of bound rubber correlates with abrasion resistance, or tread wear for a (subsequently cured) tire tread compound (60). Bound rubber cannot be measured on cured rubber, of course; all but a fraction of a percent will be bound in that case, regardless of the type or amount of filler. But the phenomenon of polymer/filler interaction, measured in the uncured state, carries forward to the cured compound and product, in many toughness and resilience related properties.

The search for alternative reinforcing fillers to carbon black has continued for decades, and has recently produced one material which offers in selected applications, even greater performance: precipitated silica.

Silica. Silica (a mineral with a repeat unit of SiO_2) is, in its crystalline form, as quartz and sand/sandstone, the most abundant compound on the earth's crust. Synthetic silica can be produced by a fumed process via silicon tetrachloride, $SiCl_4$, or aqueous process, via sodium silicate, itself made from natural silica. The product of the aqueous process is precipitated in an amorphous form, which provides two of the attributes of a reinforcing filler: small particle size and high degree of self-affinity or networking. The self-affinity is due to hydrogen bonding between surface silanol groups (Si—OH), which are present in large amount (5–7 per nm^2) on the surface. Fumed silica has much fewer surface silanol groups. A representation of the silica surface is given in Figure 8.

In the early 1990s, a new generation of precipitated silicas was developed: the so-called highly dispersable silicas (HDS) (61–65). This class provides another vital attribute of a reinforcing filler for rubber: easy dispersability at high loadings to submicron sizes.

The remaining attribute, polymer/filler interaction, is inherently missing from silica but can be provided by the use of a specific class of rubber chemicals, the silica-to-rubber coupling agents. Silica-to-rubber coupling agents have been known since the 1960s, and had permitted limited use of silica filler, much of this in nonblack mechanical goods and shoe soles. Use in tires was restricted to low levels in skim compounds for wire adhesion and treads for cut resistance. A good review of the state of the technology in the mid-1970s is given by Wagner (66).

With the advent of HDS, the ability to disperse silica to levels equal to that of carbon black is now possible for the creation of highly silica-filled rubber compounds. Thus, there has been a revolution in growing use of silica in place of carbon black in tires since the early 1990s, requiring growing use of specific coupling agents, whose number and chemistries have also expanded in this time period. A description of this class of rubber chemicals follows.

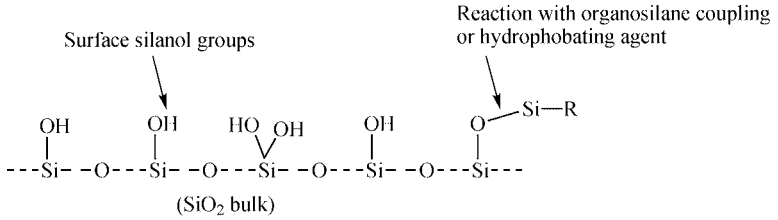

Fig. 8. Silica surface chemistry.

The predominant chemical class of silica-to-rubber coupling agents are the functionalized silane esters of general structure **5** (where typically R = Me, Et, $n = 3$; R″ = propylene [—$(CH_2)_3$—]; and X is a variable function). Many of these were developed in the mid-1970s (67).

$$(RO)_n(R,)3-n—Si—R"—X$$

5

The most commonly used silane coupling agents (qv) for rubber are shown in Table 12.

All Silane Coupling Agents (qv) work by a twofold bonding mechanism (68–70):

(1) The silane ester moiety hydrolyzes because of heat and moisture present on the surface of the silica (RO—Si → HO—Si) and the then-formed silanol condenses with a silanol group on the silica surface to produce a siloxane bond linking coupling agent to silica (—Si—O—Si—).

(2) The functional group (X above) on the other end of the coupling agent reacts directly either with the polymer chain or with the vulcanization system so as to provide a covalent bond between the coupling agent (already attached to silica) and the polymer.

Step 1, reaction with silica, occurs in the mixing (with heat) of the silica, rubber, and coupling agent. The polymer is as yet uncured and not bonded to the filler. This step is called *hydrophobation*: the hydrophilic silanol containing surface is converted to a hydrophobic organic modified surface. The silica loses much of its self-affinity by this process, rendering it more compatible with rubber. The Payne effect is reduced and may be nearly eliminated if hydrophobation is thorough.

Step 2, reaction with polymer, occurs in the vulcanization step (with heat, after curatives have been added in a *lower* temperature stage addition). Figure 9 shows the two-step coupling mechanism in the general case.

A subclass of silane rubber chemicals exists in which the "X" function of structure **5** is replaced by an inert alkyl group, creating a silica-reactive but non-coupling process aid, of the general formula **6** (where R′ = C1—C18 *n*-alkyl). These materials can be very effective in reducing compound viscosity and the Payne effect (71) but do not themselves provide cured compound reinforcement. A selected series of alkyl silanes is shown in Table 13. Alkyl silanes may be used in conjunction with coupling agent silanes to balance processability and cured performance.

$$(RO)_3\text{-Si-R'}$$

6

The nature of function "X" is dependent on the nature of the cure system. Historically, the methacrylate function was used for peroxide-cured rubber and the mercapto function was first used for sulfur-cured rubber (see *a* and *b* in Table 12). Definitive studies of the role of coupling bonds on physical properties

Table 12. Selected Organofunctional Silane Coupling Agents for Silica-Filled Rubber

Chemical name	Formula	CAS no.	Flash point, °C	Supplier (trade name)	Polymer application(s)
Chloro					Polychloroprene
3-Chloropropyltriethoxysilane	$Cl(CH_2)_3Si(OCH_2CH_3)_3$	[5089-70-3]	N/A	Degussa (Si 230)	
Amino					Polyamide, epoxy, acrylic
γ-Aminopropyltriethoxysilane	$H_2N(CH_2)_3Si(OCH_2CH_3)_3$	[919-30-2]	96	GE Silicones (A-1100) Degussa (VP Si 251)	
γ-Aminopropyltrimethoxysilane	$H_2N(CH_2)_3Si(OCH_3)_3$	[13822-56-5]	82	GE Silicones (A-1110)	
N-β-(Aminoethyl)-γ-aminopropylmethyldimethyoxysilane	$H_2N(CH_2)_2NH(CH_2)_3SiCH_3(OCH_3)_3$	[3069-29-2]	>93	GE Silicones (A-2120)	
Vinyl					Polyolefin, SBR, BR, NR (peroxide cure)
Vinyltriethoxysilane	$CH_2{=}CHSi(OCH_2CH_3)_3$	[78-08-0]	44	GE Silicones (A-151) Degussa (VP Si 225)	
Vinyltrimethoxysilane	$CH_2{=}CHSi(OCH_3)_3$	[2768-02-7]	28	GE Silicones (A-171)	
Epoxy					Acrylic, nitrile, polyurethane, SBR
γ-Glycidoxypropyltrimethoxysilane	$CH_2CH(O)CH_2O(CH_2)_3Si(OCH_3)_3$	[2530-83-8]	110	GE Silicones (A-187)	
Methacryloxy					Butyl, polyolefin, SBR, BR, NR (peroxide)

γ-Methacryloxypropyltrimethoxysilane[a]	$CH_2=C(CH_3)CO_2(CH_2)_3Si(OCH_3)_3$	[2530-85-0]	108	GE Silicones (A-174) Degussa (VP Si 123)	
Sulfur					Nitrile, SBR, BR, NR (sulfur cure)
γ-Mercaptopropyltrimethoxysilane[b]	$HS(CH_3)_3Si(OCH_3)_3$	[4420-74-0]	88	GE Silicones (A-189) Degussa (VP Si 163)	
Bis-(triethoxysilylpropyl)tetrasulfide[c]	$[(CH_3CH_2O)_3Si(CH_2)_3]_2S_4$	[40372-72-3]	104	GE Silicones (A-1289) Degussa (Si 69)	
Bis-(triethoxysilylpropyl)disulfide[d]	$[(CH_3CH_2O)_3Si(CH_2)_3]_2S_2$	[56706-10-6]	75	GE Silicones (A-1589) Degussa (Si 266, Si 75)	
3-Octanoylthio-1-propyltriethoxysilane[e]	$CH_3(CH_2)_6(C=O)S(CH_2)_3Si(OCH_2CH_3)_3$	N/A	N/A	GE Silicones (NXT)	
Thiocyanato					SBR, BR, NR (sulfur cure)
3-Thiocyanatopropyltriethoxysilane	$N=C=S(CH_2)_3Si(OCH_2CH_3)_3$	[34708-08-2]	N/A	Degussa (Si 264)	
Miscellaneous					Polyurethane, phenolic, urea-formaldehyde
γ-Ureidopropyltrimethoxysilane	$H_2N(C=O)NH(CH_2)_3Si(OCH_3)_3$	[23843-64-3]	99	GE Silicones (A-1524)	
γ-Isocyanatopropyltriethoxysilane	$O=C=N(CH_2)_3Si(OCH_2CH_3)_3$	[24801-88-5]	77	GE Silicones (A-1310)	

[a]MAS.
[b]MPTMS.
[c]TESPT.
[d]TESPD.
[e]NXT.

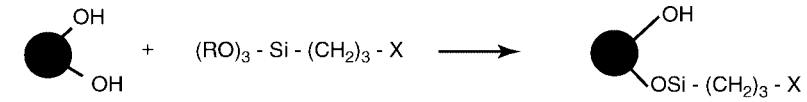

Silane ester reaction with silica silanol surface function during mixing

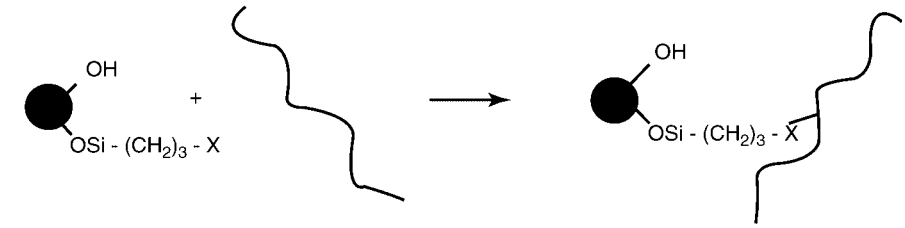

Silane functional end reaction with polymer chain during vulcanization

Fig. 9. Silane coupling chemistry.

and tire performance of silica-filled tire rubber compounds was done by Wagner using these two coupling agents (72).

Several other silanes were originally used to adhere rubber to glass substrates as well as applied to various rubbers with mineral fillers such as clays. Some of these are given in Table 12 as well.

Despite the performance benefits of mercaptosilane, serious drawbacks limited its use in tires: a strong and bad odor, plus a large reduction in scorch safety, resulting in inability to process the rubber. The mercapto group was simply too reactive to the rubber, when combined with sulfur and curatives. Cross-linking would initiate in mixing or extrusion.

Table 13. Selected Alkyl Silane (Silane Ester) Hydrophobating Agents for Silica-Filled Rubber

Chemical name	Formula	CAS no.	Flash point, °C	Supplier (trade name)
Methyltriethoxysilane	$CH_3Si(OCH_2CH_3)_3$	[2031-67-6]	29	GE Silicones (A-162)
Propyltriethoxysilane	$CH_3(CH_2)_2Si(OCH_2CH_3)_3$	[2550-02-9]	N/A	Degussa (VP Si 203)
Octyltriethoxysilane	$CH_3(CH_2)_7Si(OCH_2CH_3)_3$	[2943-75-1]	41	GE Silicones (A-137) Degussa (VP Si 208)
Methyltrimethoxysilane	$CH_3Si(OCH_3)_3$	[1185-55-3]	12	GE Silicones (A-1630)
Hexadecyltriethoxysilane	$CH_3(CH_2)_{15}Si(OCH_2CH_3)_3$	[16415-13-7]	N/A	Degussa (VP Si 216)

In the 1970s, the first step change improvement in coupling agents for sulfur-cured rubber, as used in tires, came with the development of the tetrasulfide silane, TESPT (see *c* in Table 12) (67,68). Now, the mercaptan function was protected in the form of a polysulfide. To generate the active mercaptan, a sulfur–sulfur bond cleavage was needed. By analogy to the generation with scorch safety of mercaptobenzothiazole (MBT) by the cleavage of the disulfide MBTS, the tetrasulfide silane imparted scorch safety yet retained polymer reactivity of the mercaptosilane.

TESPT remained the industry standard coupling agent for sulfur cured rubber into the 1990s. With the development of HDS came expanded applications for silica-based compounds, particularly in high performance passenger tire treads which needed a combination of tread wear, low rolling resistance, and good wet traction (73). This combination of performance attributes can be simultaneously optimized to unique levels with silica. Recipes with 50–100 phr silica were now permissible and desirable.

As silica technology expanded to meet market performance targets, certain processing deficiencies grew in importance, and remedies through materials development emerged and continue to do so presently.

First, it became apparent that highly silica-filled compounds, even using HDS, required longer mixing times and processed worse than their carbon black counterparts (extrusion, tire building). It became clear that TESPT itself did not have sufficient scorch safety for all operating conditions; the middle sulfur–sulfur bonds in the polysulfide bridge are relatively weak and can be broken, liberating elemental sulfur to impart scorch. TESPT is a known sulfur donor curative, after all. So, the market for TESPD expanded (see *c* and *d* in Table 12). The stronger sulfur–sulfur bonds in TESPD provided extra processability in production while retaining necessary polymer reactivity.

The newest sulfur silane coupling agent, NXT (see *e* in Table 12) (74,75) carries this approach even further. A substituted carbonyl group is used to protect a mercaptosilane during processing and reaction at the silanol end with the silica (**7**), deprotection occurs during cure, catalyzed by curatives, to release active mercaptan function (**8**), which, through reactions with the vulcanization system, bonds to polymer (**9**), as shown below.

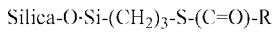

7

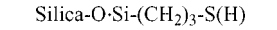

8

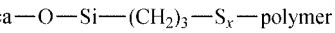

9

The rubber chemist has recognized and reacted to the growing trend to employ silica as reinforcing filler for rubber with development of multiple silane ester coupling agents and alkyl silane process aids for improved processability and performance.

Nonstaining and Persistent Antidegradants

General-purpose rubbers are susceptible to degradation by atmospheric oxygen (O_2) and ozone (O_3).

Chemical antioxidants (qv) act to preserve rubber from degradation by molecular oxygen. This degradation is manifest in hardening (cross-linking) for polybutadiene and SBR and initial softening (chain scission) than hardening for polyisoprene rubber (natural or synthetic). All rubbers lose tensile strength and cut and tear resistance due to oxidation as well. Antioxidants inhibit the free-radical autoxidation cyclic chain reaction process via several mechanistic pathways. The primary antioxidants scavenge polymer carbon and hydroperoxy radicals by donation of an active hydrogen. Secondary antioxidants decompose hydroperoxides. A review is available, with attendant references to the historical development of antidegradants and their mechanisms of action in rubber (76). Autoxidation and antioxidant mechanisms have also been reviewed (77,78).

The hydrogen-bonded intermediate complex of a hindered phenolic antioxidant with a stable aminoxyl radical (TEMPO), used as a model for a hydrocarbon oxidant, has been isolated and its structure determined, as confirmation of the radical scavenging mechanism (79).

The principal classes of primary antioxidants for rubber remain the phenolics (nonblack articles) and amines (black-filled articles). Among the amine types are the substituted diphenylamines, *para*-phenylenediamines (PPD, (**10**), where R,R′ = alkyl or aryl), and polymeric trimethyl-dihydroquinoline (TMQ). Representative phenolic antioxidants are given in Table 14, and selected amine antidegradants are given in Table 15. The majority of tire and mechanical goods made from general-purpose rubbers are protected by the phenolic and amine antioxidants.

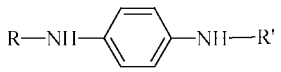

10

Macroscopically, ozonation leads to cracking of the rubber surface and ultimate product failure. A polar mechanism was proposed by Criegee for ozonation of unsaturated hydrocarbon rubbers, with addition of ozone to the carbon–carbon double bond followed by decomposition of the intermediate ozonide leading to cleavage of the polymer chain (80). Polymers without carbon bond unsaturation in the backbone do not crack in the presence of ozone. Zhang recently proposed a free-radical mechanism and attributed PPD antiozonant activity to its low ionization potential and ability to quench polymer radicals (81).

The PPD class of antidegradants provides by far the best antiozonant protection (for a review of antiozonants, see Reference 82). PPDs inhibit ozone degradation of rubber by multiple mechanisms (76,83–85):

(1) Migration to the surface of the rubber article
(2) Competitive reaction with and scavenging of ozone at the surface

Table 14. Representative Phenolic Antioxidants Used in Rubber

Chemical name	Structure	CAS no.	Supplier (trade name)
a. Styrenated phenol	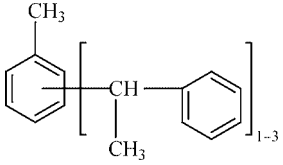	[61788-44-1]	Akcros Chemical (Akcrostab C53-P) Flexsys (Montaclere SPH) Great Lakes Chemical (Anox G2) Goodyear Chemical (Wingstay S) Harwick Standard (Antioxidant SP) PMS Specialties (Prodox 120) RT Vanderbilt (Wingstay S) Sovereign Chemical (AO 47) Sumitomo Chemical (Sumilizer S) Crompton Uniroyal (Naugard SP)
b. Alkylated hindered phenol	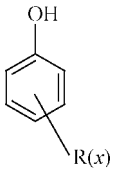 $x = 1, 2, 3$		Akrochem (Antioxidant 32, 33, 43) CP Hall (Stabiwhite Powder 49-454) Goodyear Chemical (Wingstay C, T) Great Lakes Chemical (Anox T) Inspec Fine Chemicals (Ionol K65, J65) RT Vanderbilt (Wingstay C, T)
c. Polybutylated bisphenol A	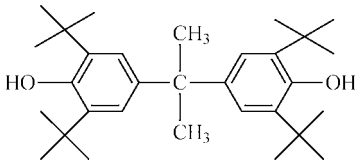	[68610-51-5]	BF Goodrich (Goodrite Superlite) RT Vanderbilt (Agerite Superlite) Sumitomo Chemical (Sumilizer NW)

Table 14. (Continued)

Chemical name	Structure	CAS no.	Supplier (trade name)
d. 2,2′-Methylene-bis-(4-methyl-6-*t*-butylphenol)	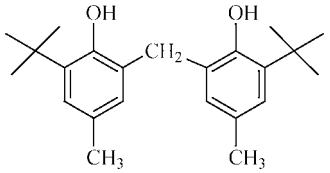	[119-47-1]	Akrochem (Antioxidant 235) Ashland Chemical (Ashland AO 46) Bayer Corp. (Vulkanox BKF) CP Hall (Cyanox 2246) Chemetall (Naftonox 2246) Cytec Industries (Cyanox 2246) Great Lakes Chemical (Lowinox 22M46) Harwick Standard (Stangard PC) PMC Specialties (CAO-5) RT Vanderbilt (Vanox MBPC) Raschig (Ralox 46) Sumitomo Chemical (Sumilizer MDP-S)
e. Butylated reaction product of *p*-cresol and dicyclopentadiene	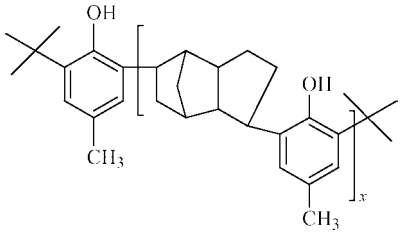	[68610-51-5]	Akrochem (Antioxidant 12) Ashland Chemical (Ashland AO CL) Goodyear Chemical (Wingstay L) Great Lakes Chemical (Lowinox CPL) PMC Specialties (Ralox LC LC) Raschig (Ralox LC) RT Vanderbilt (Wingstay L) Sovereign Chemical (AOL 600)
f. Mixed methylenic bridged adducts of alkylated phenol and dicyclopentadiene	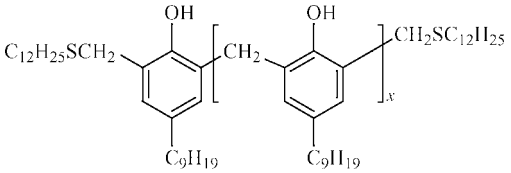		Goodyear Chemical (Wingstay K) RT Vanderbilt (Wingstay K)

g. Tetrakis methylene (3,5-di-*t*-butyl-4-hydroxyhydro

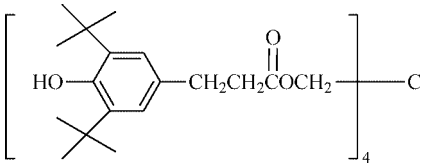

[6683-19-8]

Akrochem (Antioxidant 1010)
Ashland Chemical (Ashland AO 610)
Akcros Chemicals (Lankromark LE373)
Ciba Specialty Chemicals (Irganox 1010)
Dover Chemical (Dovernox 10)
Great Lakes Chemical (Anox 20)
Mayzo, Inc. (BNX 1010)
PMC Specialties (Prodox 1010)
Raschig (Ralox 630)
Sumitomo Chemical (Sumilizer BP-101)

h. 1,3,5-Trimethyl-2,4,6-tris (3,5-di-*tert*-butyl-4-hydroxybenzyl)benzene

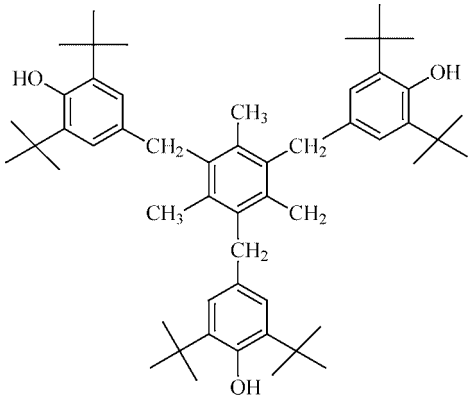

[1708-70-2]

Albemarle Corp. (Ethanox 330)
Ciba Specialty Chemicals (Irganox 1330)

Table 15. Representative Amine Antidegradants Used in Rubber

Chemical name (abbreviation)	Structure	CAS no.	Supplier (trade name)
a. *para*-Styrenated diphenylamine	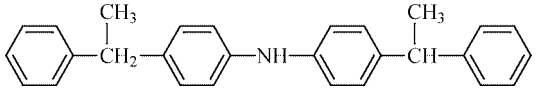	[68442-68-2]	Akrochem (Antioxidant POSDA) Goodyear Chemical (Wingstay 29) RT Vanderbilt (Wingstay 29)
b. Octylated diphenylamine (ODPA)	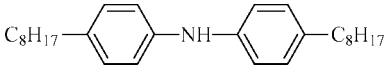	[68411-46-1]	Akrochem (Antioxidant S) BF Goodrich (Goodrite Stalite S) Bayer (Vulkanox OCD/SG) Crompton Uniroyal (Octamine) Flexsys (Permanox ODPA) Harwick Standard (Stangard ODP) RT Vanderbilt (Vanox 12)

c. 2,2,4-Trimethyl-1,2-dihydro quinoline, polymerized (TMQ)	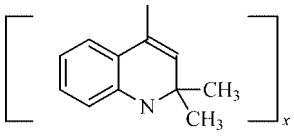	26780-96-1	Ashland Chemical (Ashland AO TQ-T) Bayer (Vulkanox HS/LG) BF Goodrich (Goodrite MA, Resin D) Chemetall (Naftonox TMQ) Crompton Uniroyal (Naugard Q) Flexsys (Flectol TMQ) Great Lakes Chemical (Anox HB, HPG) PMC Specialties (Ralox TMQ) RT Vanderbilt (Agerite Resin D) Raschig (Ralox TMQ) Sovereign Chemical (Pilnox TDQ) Sumitomo Chemical (Antigene RD-G) Struktol (Struktol TMQ)
d. Mixed diaryl-*p*-phenylenediamine (DPPD)	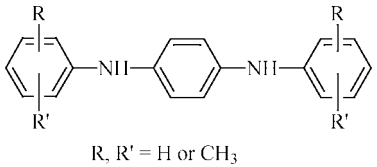 R, R' = H or CH_3	[68953-84-4]	Akrochem (Antiozonant MPD-100) Bayer (Vulkanox 3100) Goodyear Chemical (Wingstay 100, 200) Crompton Uniroyal (Novazone AS) RT Vanderbilt (Wingstay 100)

Table 15. (Continued)

Chemical name (abbreviation)	Structure	CAS no.	Supplier (trade name)
e. *N,N′*-Bis(1,4-dimethylpentyl)-*p*-phenylendiamine (77PD)	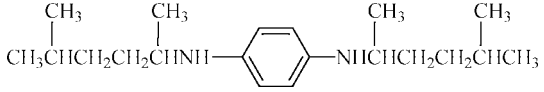	[3081-14-9]	CP Hall (UOP 788) Crompton Uniroyal (Flexzone 4L) Flexsys (Santoflex 77PD) UOP (UOP 788)
f. *N*-(1,3-Dimethylbutyl)-*N′*-phenyl-*p*-phenylenediamine (6-PPD)	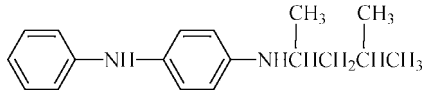	[61931-82-6] [793-24-8]	Akrochem (Antiozonant PD-2) CP Hall (UOP 588) Chemetall (Naftonox 6PPD) Crompton Uniroyal (Flexzone 7L, 7P) Duslo Sala (Dusantox 6PPD) Bayer (Vulkanox 4020) Flexsys (Santoflex 6PPD) RT Vanderbilt (Antozite 67P) Sovereign Chemical (Dusantox 6PPD) Struktol (Struktol 6PPD) Sumitomo Chemical (Antigene 6C) UOP (UOP 588)

g. Benzenamine, *N*-[4-(1,3-dimethyl (butyl)imino]-2,5-cyclohexadien-1-ylidene (6-QDI)	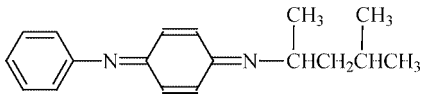	[52870-46-9]	Flexsys (Q-Flex QDI)
h. 2,4,6-Tris(*N*-1,4-dimethyl-pentyl-*p*-phenylenediamino)-1,3,5-triazine (TAPDT)	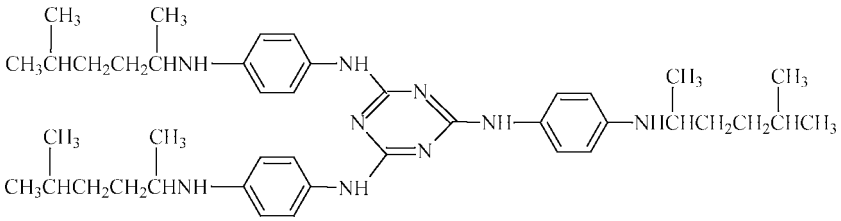		Crompton Uniroyal (Durazone 37)

(3) Formation, through its reaction products with ozone, of a protective film at the rubber surface

(4) Increase in the critical stress of the rubber article. The critical stress is the applied static stress at which ozone cracking appears on the surface of a rubber article exposed to ozone.

N-(1,3-dimethylbutyl)-*N*′-phenyl-*p*-phenylenediamine; abbreviated 6-PPD, is a particularly versatile chemical offering a blend of antioxidant and antiozonant behavior combined with good rubber solubility and modest volatility, although other PPDs have applications as well. The diaryl PPDs have limited rubber solubility but lower volatility than 6-PPD. They provide excellent antioxidant protection and decent persistence with diminished antiozonant protection.

All PPDs are highly staining and discoloring. This behavior is not necessarily a problem in carbon black filled articles, but restricts usage in colored goods—or even tires with colored components.

Two long-standing deficiencies with the PPD antidegradants, lack of persistence and discoloration/staining, have been addressed, respectively, in recent additions to the field: 6-QDI, a dehydrogenated PPD, and TAPDT, a trimeric, high MW form of PPD.

6-QDI (*N*-(1,3-dimethylbutyl)-*N*′-phenyl-*p*-quinonediimine, Table 15) offers improved persistence because of its partial immobilization and binding to the polymer matrix during mixing (86,87). As an efficient radical trap, 6-QDI acts as a chemical peptizer to reduce natural rubber chain length and viscosity in mixing by capping cleaved polymer chain end radicals. 6-QDI still provides chemical antidegradant protection similarly to its hydrogenated parent, 6-PPD, and is considered to be produced *in situ* from 6-PPD as part of the latter's mechanism of action in the cured rubber compound, as shown in equation 1 (88,89). 6-QDI is also reported to preserve sulfur network rank stability better than 6-PPD and impart improved abrasion resistance to a natural rubber tread compound relative to PPD and TMQ antidegradants (90).

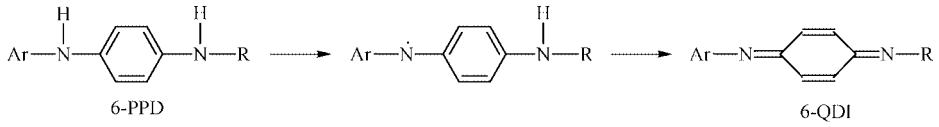

(1)

TAPDT [2,4,6-tris-(*N*-1,4-dimethylpentyl-*p*-phenylenediamino)-1,3,5-triazine, Table 15 provides reduced discoloration as a result of its increased molecular size which imparts reduced mobility in the rubber matrix (91). Discoloration results from bloom of ozonation by-products of the antidegradant to the rubber surface. PPD containing compounds will stain adjacent compounds in a composite structure because of migration of the PPD. An example is a black sidewall protected by PPD staining the white sidewall of a tire. TAPDT does not

migrate like the monomeric PPDs. TAPDT gives excellent static ozone protection, flex resistance, as well as antioxidant behavior, but does not provide the same level of dynamic ozone protection (protection to product under stress, such as in cyclic flexing) as the monomeric PPDs (91). Blends of TAPDT and 6-PPD have been shown to give excellent overall protection and durability (91).

A new partially graftable, aminic PPD of unspecified structure was recently presented as another means to nonstaining antidegradant protection for rubber (92).

In summary, the field of rubber chemicals is both mature and ever evolving. Recent advances and changes have been prompted by environmental concerns, the move to higher efficiency cures and processing, the pursuit of more durable rubber products, and the growth of silica as a reinforcing filler.

BIBLIOGRAPHY

"Rubber Chemicals" in *EPST* 1st ed., Vol. 12, pp. 256–280, by F. W. Shaver, The B. F. Goodrich Co.; "Rubber Chemicals" in *EPSE* 2nd ed., Vol. 14, pp. 716–762, by J. A. Kuczkowski, The Goodyear Tire & Rubber Co.

1. P. Ghosh, S. Katare, P. Patkar, J. M. Caruthers, V. Venkatasubramanian, and K. A. Walker, *Rubber Chem. Technol.* **76**, 592 (2003).
2. M. R. Krejsa and J. L. Koenig, *Rubber Chem. Technol.* **66**, 376 (1993).
3. M. Akiba and A. S. Hashim, *Prog. Polym. Sci.* **22**, 475 (1997).
4. M. A. Faith, *Rubber World* **208**(5), 15 (1993).
5. M. A. Faith, *Rubber World* **209**(1), 22 (1993).
6. M. A. Faith, *Rubber World* **209**(3), 17 (1993).
7. M. A. Faith, *Rubber World* **209**(5), 18 (1994).
8. M. A. Faith, *Rubber World* **210**(1), 24 (1994).
9. A. V. Chapman and M. Porter, in A. D. Roberts, ed., *Natural Rubber Science and Technology*, Oxford University Press, New York, 1988, pp. 512–620.
10. J. O. Harris and C. D. Trivette Jr., in G. Alliger and I. J. Sjothum, eds., *Vulcanization of Elastomers*, Robert E. Krieger Publishing Co., New York, 1978, pp. 174–178.
11. R. H Schuster, Hannover, Sowie F. Nabholz and M. Gmünder, *Kautschuk Gummi Kunststoffe* **43**(2), 95 (1990).
12. W. Hoffmann, *GAK* **43**, 562 (1990).
13. W. Hofmann and J. Diederichsen, *Int. Polym. Sci. Technol.* **21**(8), T/23 (1994).
14. K. M. Davies, D. G. Lloyd, and A. Orband, *Kautschuk Gummi Kunststoffe* **42**(2), 120 (1989).
15. C. J. Hann, A. B. Sullivan, B. C. Host, and G. H. Kuhls Jr., *Rubber Chem. Technol.* **67**(1), 76 (1994).
16. R. M. D'Sidocky, *The Goodyear Tire & Rubber Co*., unpublished results, 2004.
17. R. I. Keib, A. B. Sullivan, and C. D. Trivette, *Rubber Chem. Technol.* **43**, 1188 (1970).
18. D. B. Seeberger, Rubber Division, ACS, Detroit, Mich., Paper No. 70, Oct. 1989.
19. D. W. Chasar, *Rubber World* **22**(5), 26 (2002).
20. B. H. To and A. D. Hoog, *Rubber Plast. News* Sept. 23, 14 (2002).
21. A. A. Kuznetsov and O. A. Kulikova, *Prog. Rubber Plast. Technol.* **16**, 255 (2000).

22. F. Cataldo, *Die Angewandte Makromolekulare Chemie* **249**, 137 (1997).
23. Y. B. Aziz and C. Hepburn, *J. Rubber Res. Inst., Malaysia* **27**(2), 57 (1979).
24. R. N. Datta, *Rapra Rev. Rep.* **12**(12), 1 (2002).
25. S. Wolff, Rubber Division, ACS, Las Vegas, Nev., Paper No. 30, May 1980.
26. A. Johansson and T. Frueh, Rubber Division, ACS, Cleveland, Ohio, Paper No. 106, Oct. 1997.
27. Thio & Fine Chemicals, Vultac Rubber Chemicals. Available at http://www.Atofinachemicals.com/Products.
28. P. M. Lewis, in G. Scott, ed., *Developments in Polymer Stabilization*, Elsevier Applied Science Publishers, New York, 1987, pp. 105–191.
29. P. J. Nieuwenhuizen, J. Reedijk, M. Van Duin, and W. J. McGill, *Rubber Chem. Technol.* **70**, 368 (1997).
30. C. T. Loo, *Polymer* **15**, 357 (1974).
31. J. I. Cunneen and R. M. Russell, *J. Rubber Res. Inst., Malaysia* **22**, 300 (1969).
32. M. Mori, Rubber Division, ACS, San Francisco, Calif., Paper No. 4, Apr. 2003.
33. C. H. Chen, J. L. Koenig, J. R. Shelton, and E. A Collins, *Rubber Chem. Technol.* **54**, 734 (1981).
34. E. J. Blackman and E. B. McCall, *Rubber Chem. Technol.* **43**, 651 (1970).
35. N. J. Morrison and M. Porter, *Rubber Chem. Technol.* **57**(1), 63 (1984).
36. L. M. Volchenok, A. D. Leiken, and E. A. Dzyura, *Int. Polym. Sci. Technol.* **21**(7), T/44 (1994).
37. U.S. Pat. 5,616, 279 (Apr. 1, 1997), R.M. D'Sidocky and N.A. Maly (to The Goodyear Tire & Rubber Co.).
38. R. N. Datta, A. G. Talma, and A. H. M. Schotman, *Rubber Chem. Technol.* **71**, 1073 (1998).
39. A. G. Talma, R. N. Datta, A. H. M. Schotman, and W. H. Helt, Rubber Division, ACS, Cleveland, Ohio, Paper No. 64, Oct 1995.
40. R. N. Datta and N. M. Huntink, *Kautschuk Gummi Kunststoffe* **55**, 350 (2002).
41. A. H. M. Schotman, P. J. C. Van Haeren, H. I. M. Weber, F. G. H. Van Wijk, J. W. Hofstraat, A. G. Talma, A. Steenbergen, and R. N. Datta, *Rubber Chem. Technol.* **69**, 727 (1996).
42. R. N. Datta, *Plast. Recycling Technol.* **19**(3), 143 (2003).
43. P. M. Lewis, *N. R. Technol.* **17**(4), 57 (1986).
44. D. S. Campbell and A. V. Chapman, *J. Natl. Rubber Res.* **5**, 246 (1990).
45. G. Anthoine, E. R. Lynch, D. E. Mauer, and P. G. Moniotte, Rubber Division, ACS, Indianaipolis, Ind., Paper No. 51, Spring 1984.
46. D. G. Lloyd, *Int. Polym. Sci. Technol.* **15**(9), T/1 (1988).
47. F. Ignatz-Hoover, *Rubber World* **214**(5), 19 (1996).
48. J. Hahn, P. Palloch, E. Walter, and N. Thelen, Rubber Division, ACS, Providence, R.I., Paper No. 35, Apr. 2001.
49. T. Kleiner, J. Neilsen, H. J. Weidenhaupt, W. Jeske, and H. Buding, *Rubber Plast. News* **14**, 14 (Jan. 2002).
50. *Rubber Handbook*, Struktol, Ohio, p. 58. Available at http://www.struktol.com/rubber.asp.
51. A. V. Chapman, *Phosphorus, Sulfur, and Silicon*, Vol. 59, Gordon and Breach Science Publishers, United Kingdom, 1991, pp. 271–274.
52. *New Sartomer Products Bull.* **3**(14) (Nov. 2003).
53. E. J. Blok, M. L. Kralevich, and J. E. Varner, *Rubber Chem. Technol.* **73**(1), 114 (2000).
54. D. T. Norman, in R. Ohm, ed., *The Vanderbilt Rubber Handbook*, 13th ed., 1990, p. 397.

55. A. R. Payne, *Rubber Plast. Age* **963**, (Aug. 1961).
56. A. I. Medalia, *Rubber Chem. Technol.* **51**, 437–523 (1978), and references cited therein.
57. E. Papirer, A. Voet, and P. H. Given, *Rubber Chem. Technol.* **42**, 1200 (1969).
58. J. LeBras and E. Papirer, *Rubber Chem. Technol.* **52**, 43 (1979).
59. J. A. Belmont and J. M. Funt, *Kautsch Gummi Kunststoffe* **44**, 1135 (1991).
60. G. R. Cotten and E. M. Dannenberg, *Tire Sci. Technol.* **2**, 211 (1974).
61. U.S. Pat. 5,089,554 (Feb. 18, 1992), F. Bomo, Y. Chevallier, P. Lamy, and J.-C. Morawski, (to Rhone-Poulenc Industries).
62. P. Cochet, P. Barruel, L. Barriquand, J. Grobert, E. Prat, and Y. Bomal, *Rubber World* **210**(3), 20 (1994).
63. P. Cochet, L. Barriquand, Y. Bomal, and S. Touzet, Rubber Division, ACS, Cleveland, Ohio, Paper No. 74, Oct. 1995.
64. S. Wolff, U. Gorl, M.-J. Wang, and W. Wolff, presentation at *Tyretech '93*, Basel, Oct. 1993.
65. U. Gorl, R. Bausch, H. Esch, and R. Kuhlman, in *DIK German Rubber Conference 1994*, Stuttgart, June 1994.
66. M. P. Wagner, *Rubber Chem. Technol.* **49**, 703 (1976).
67. F. Thurn and S. Wolff, *Kautsch Gummi Kunststoffe* **28**, 733 (1975).
68. S. Wolff, *Rubber Chem. Technol.* **55**, 967 (1982).
69. S. Wolff, *Tire Sci. Technol.* **15**, 276 (1987).
70. U. Gorl, A. Hunsche, A. Mueller, and H. G. Koban, *Rubber Chem. Technol.* **70**, 608 (1997).
71. L. Ladouce-Stelandre, Y. Bomal, P. Cochet, and J. Ramier, *Tire Technol. Int*. (2003). Annual Review 36.
72. M. P. Wagner, *Rubber Chem. Technol.* **47**, 697 (1974).
73. B. Schwaiger and A. Blume, *Rubber World* **222**(1), 32 (Apr. 2000), and references cited therein.
74. P. Joshi, R. Cruse, R. Pickwell, K. Weller, M. Hofstetter, E. Pohl, M. Stout, and F. Osterholtz, *Rubber Plast. News* **30** (Sept. 9, 2002).
75. P. Joshi, R. Cruse, R. Pickwell, K. Weller, W. Sloan, M. Hofstetter, M. Stout, and F. Osterholtz, *Tire Technol. Int*. (2003). Annual Review 44.
76. J. Kuczkowski, Rubber Division, ACS, Cleveland, Ohio, Paper No. 83, Oct. 2003.
77. J. R. Shelton, *Rubber Chem. Technol.* **45**, 359 (1972).
78. J. A. Howard, *Rubber Chem. Technol.* **47**, 976 (1974).
79. B. Ahrens, M. Davidson, V. Forsyth, M. Mahon, A. Johnson, S. Mason, R. Price, and P. Raithby, *J. Am. Chem. Soc.* **123**, 9164 (2001).
80. R. Criegee, A. Kerckow, and H. Zinke, *Berichte* **88**, 1878 (1955).
81. J.-M. Zhang, Rubber Division, ACS, Cleveland, Ohio, Paper No. 99, Oct. 2003.
82. R. Ohm, *Rubber World* **208**(5), 18 (Aug. 1993).
83. W. L. Cox, *Rubber Chem. Technol.* **32**, 364 (1959).
84. E. R. Erickson, R. A. Bernstein, E. L. Hill, and P. Kosy, *Rubber Chem. Technol.* **32**, 1062 (1959).
85. R. P. Lattimer, E. R. Hooser, R. W. Layer, and C. K. Rhee, *Rubber Chem. Technol.* **56**, 431 (1983).
86. F. Ignatz-Hoover, Rubber Division, ACS, Pittsburgh, Pa., Paper No. 141, Oct. 2002.
87. F. Ignatz-Hoover and B To, Rubber Division, ACS, Cleveland, Ohio, Paper No. 98, Oct. 2003.
88. M. E. Cain, I. R. Gelling, G. T. Knight, and P. M. Lewis, *Rubber Ind.* **216** (1975).

89. I. R. Gelling and G. T. Knight, *Plast. Rubber Process.* **83** (Sept. 1977).
90. F. Ignatz-Hoover and B. To, Rubber Division, ACS, Cleveland, Ohio, Paper No. 119, Oct. 2003.
91. S. W. Hong and C.-Y. Lin, *Rubber World* **222**(5), 36 (Aug. 2000).
92. C. Fagouri and J. Fay, Rubber Division, ACS, Cleveland, Ohio, Paper No. 101, Oct. 2003.

MARTIN P. COHEN
RICHARD M. D'SIDOCKY
The Goodyear Tire & Rubber Company

RUBBER COMPOUNDING

Introduction

Rubber compounding is the complex, multidisiplinary science of selecting and blending the appropriate combination of elastomers and other ingredients to meet the performance, manufacturing, environmental, and cost requirements for rubber goods made and used in commerce. There is a wide variety of elastomers and ingredients that are available in making rubber goods, which include all of the following types of products: tires, innertubes, retreaded tires, footwear, rubber rolls, hoses, belts, weatherstripping, O-rings, seals, diaphragms, tubing, rubber and latex gloves, ball bladders, medical devices, bumpers, and numerous other products. This is a review of the basic materials used in designing many common types of rubber products. The development of the combination of materials contained in a usable rubber compound involve many disciplines that include chemistry, physics, mathematics, and polymer science. In many cases, classical scientific methods can predict the interaction effects and estimate the properties expected from rubber compounds. However, discovery and development of new materials that modify the rubber compound to produce new, useful, and beneficial properties are appearing regularly. Also, environmental concerns are creating an interest in utilizing recycled rubber products into new rubber compounds.

Compounding Hierarchy

Compounding is a term that has evolved within the plastics and rubber industry and in many respects is a misnomer for the material science of modifying a polymer or polymer blend through addition of other materials to achieve a set of mechanical properties for a specific service application. Compounding is therefore a highly

Encyclopedia of Polymer Science and Technology. Copyright John Wiley & Sons, Inc. All rights reserved.

complex science involving many traditional disiplines such as organic chemistry, polymer chemistry, materials physics, mathematics, and engineering mechanics.

There are some excellent reviews and discussion papers on the science of rubber compounding (1–8). The purpose of this discussion is to provide an introductory overview of the range of materials used by the materials scientist in compounding elastomers. In designing or making the selection of ingredients for use in a rubber article, the technologist relies upon published literature, experimental work, competitive benchmark information, and various information sources such as raw material supplier data, technical documents, and reports. Raw materials for a compound are generally selected in the following order:

(1) polymer (natural or synthetic rubber)
(2) fillers or reinforcing agent
(3) antioxidants and antiozonants
(4) plasticizers or oils
(5) bonding agent or adhesive (if needed)
(6) tackifer (if needed)
(7) vulcanization system [curing agent, accelerator(s), or coagent]

Performance requirements of the final product often dictate which specific type of elastomer can be used. The expected usable life for the product is controlled by many factors such as end-customer needs, competitive situation in the marketplace, safety, and reliability. Rubber products are almost always used as a functional part of another system. For example, tires, hoses, belts, O-rings, and numerous rubber components are used in manufacturing automobiles and trucks. The overall life of the vehicle as well as its performance level often relates to the service life or quality level of the rubber parts.

Elastomers Used in Rubber Compounding

Elastomers can be divided into two general categories, natural rubber and synthetic rubbers. Synthetic elastomers in turn are either termed *general purpose rubbers* (GPR) or *special purpose rubbers*. Natural rubber is generally obtained from southeast Asia or Africa. Synthetic rubbers are produced from monomers obtained from the cracking and refining of petroleum. The most common monomers are styrene, butadiene, isoprene, isobutylene, ethylene, propylene, and acrylonitrile. There are monomers for specialty elastomers which include acrylics, chlorosulfonated polyethylene, chlorinated polyethylene, epichlorohydrin, ethylene–acrylic, ethylene–octene rubber, ethylene–propylene rubber, fluoroelastomers, polynorbornene, polysulfides, silicone rubber, thermoplastic elastomers, urethanes, and ethylene–vinyl acetate.

Elastomers can be classified by their heat resistance and resistance to swelling (Fig. 1). The Society of Automotive Engineers (SAE) has developed a specification, SAE J200 (9), for classifying special-purpose elastomers by swelling in a special oil denoted IRM 903, which replaced ASTM (American Society for Testing and Materials) Number 3 (10). Properties for evaluating elastomers include

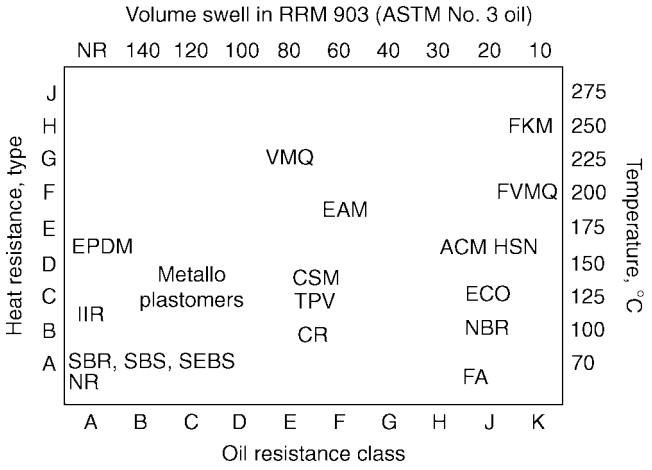

Fig. 1. SAE J200 classification systems for IRM 903 (ASTM No. 3) oil, where, for volume swell, NR = no requirement. Polymer abbreviations are defined in Table 1 (9,10).

hardness, tensile strength, change in tensile strength, elongation, and change in volume, tensile strength, and hardness after exposure to IRM 903 oil. However, probably the most effective classification system has been published by the International Standards Organization in specification ISO 1629 (11). Polymers containing residual unsaturation such as polybutadiene have abbreviations ending in —R (eg, BR), methylene containing polymers ending in —M (eg, ethylene propylene diene monomer, EPDM), silicone rubbers ending in —Q, oxygenates ending in —O, and urethanes ending in —U. A list of International Institute of Synthetic Rubber Producers (IISRP) abbreviations are shown in Table 1 (12). Table 2 displays typical general physical properties for a selection of the different types of elastomers including specifc gravity, hardness, tensile strength, and ratings for resilience, compression set, and permeability.

Natural Rubber. Natural Rubber is a biological homopolymer of isoprene and has the general structure illustrated in equation 1. The principal producing countries are Malaysia, Indonesia, Thailand, India, China, and Sri Lanka (see RUBBER, NATURAL). New sources are also being developed. To obtain natural rubber (NR), the Hevea brasiliensis tree is tapped for its sap. An off-white sap is collected and is coagulated by the addition of a strong acid such as sulfuric acid. The tapped latex consists of between 30% and 35% rubber, 60% aqueous serum, and 5 to 10% of other constituents such as fatty acids, amino acids and proteins, starches, sterols, esters, and salts. Some of the nonrubber substances, such as lipids, carotenoid pigments, sterols, triglycerides, glygolipids, and phospholipids, can influence the final properties of rubber such as compounded vulcanization characteristics and classical mechanical properties. Natural rubber is predominantly of the cis structure though the trans isomer, or *Gutta Percha*, can be found in latex tapped from the trees of the genus *Dichopsis*.

There are several systems that define the quality and uniformity of natural rubber. One system of grading natural rubber is based on form and visual observation of color and cleanliness. This is known as the International Natural Rubber Specification. The principal types and grades presented in Table 3 (13).

Table 1. IUPAC Nomenclature for Selected Elastomers[a]

AU	Polyester urethane
BR	Polybutadiene
BIIR	Brominated isobutylene–isoprene (bromobutyl)
CIIR	Chlorinated isobutylene–isoprene (chlorobutyl)
CPE	Chlorinated polyethylene
CR	Chloroprene rubber
CSM	Chlorosulfonyl polyethylene
EAM	Ethylene–vinyl acetate coploymer
EPDM	Terpolymer of ethylene, propylene, and a diene with a residual unsaturated portion in the chain
EPM	Ethylene–propylene copolymer
EU	Polyether urethane
HNBR	Hydrogenated acrylonitrile–butadiene rubber (highly saturated nitrile rubber)
IIR	Isobutylene–isoprene rubber
IR	Synthetic polyisoprene
NBR	Acrylonitrile–butadiene rubber
SBR	Styrene–butadiene rubber
E-SBR	Emulsion styrene–butadiene rubber
S-SBR	Solution styrene–butadiene rubber
X-NBR	Carboxylated nitrile–butadiene rubber
X-SBR	Carboxylated styrene–butadiene rubber
YSBR	Block copolymers of styrene and butadiene

[a] From Ref. 12.

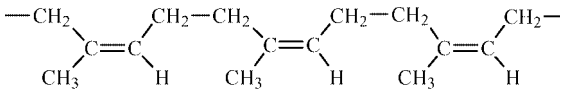

cis-Polyisoprene (1)

Malaysian and Indonesian natural rubber growers have established a system based on technical characteristics. A summary of the standard technical specification scheme shown in Table 4 for natural rubber can be found in ISO 2000 (14,15). In addition to the solid form of natural rubber, it is available as a suspension in water and is known as latex. Synthetic rubbers are also available in latex form. Latex has become an important commodity used in the manufacture of dipped goods for pharmaceutical applications. The principal uses of natural rubber are as follows: tires and tire retreading, 70%; latex (eg, gloves), 12%; mechanical goods, 9%; load-bearing components, 4%; and other, 5%.

Styrene–Butadiene Rubber. Styrene–butadiene rubber (SBR) is made by either an emulsion or solution process (eq. 2). The classification systems for emulsion SBR is shown in Table 5. In the emulsion process, it is more difficult to control polymer microstructure and the final product is not as pure as the solution form. However it tends to show a higher tensile strength and tear strength, and is easier to process. It is used in applications such as tire treads, sidewalls, bead

Table 2. Physical Properties of Elastomers[a]

Elastomer[b]	Specific gravity	Hardness Shore A	Tensile strength,[c] MPa[d]	Elongation,[c] %	Resilience[e]	Compression set[e]	Impermeability to gases[e]
NR	0.93	30–100	27.6	750	E	G	F
Polyisoprene	0.92	30–100	24.1	750	E	F	F
SBR	0.94	35–100	20.7	600	G	G	F
Butyl	0.92	30–90	17.2	700	P–F	P–F	E
Polybutadiene	0.91	45–80	17.2	500	E	F	F
EPDM	0.86	30–90	20.7	600	G	G	F
Chloroprene	1.23	35–95	20.7	600	G–E	F–G	F–G
Nitrile	1.00	30–100	20.7	600	F–G	G	G
Thiokol	1.25–1.35	20–80	10.3	450	P–F	P–F	E
Urethane	1.02–1.25	55–100	55.2	750	F–E	G–E	P–F
Silicone	0.98–1.60	25–90	10.3	800	F–G	G–E	P–F
CSM	1.12–1.28	40–95	20.7	600	F–G	F	G
Acrylic	1.09	40–90	13.8	400	F–G	G	F–G
Fluorocarbon	1.85	55–95	20.7	450	F	G–E	G–E
Epichlorohydrin	1.27–1.36	40–90	17.2	400	F–G	F	E
Chlorinated PE	1.16–1.25	45–95	24.1	600	F–G	F–G	G
Cross-linked PE	0.92	90+	20.7	500	P	F	G

[a] Ref. 7.
[b] NR = natural rubber; SBR = styrene–butadiene rubber; EPDM = ethylene–propylene–diene monomer; CSM = chlorosulfonated polyethylene; and PE = polyethylene.
[c] Maximum value at room temperature.
[d] To convert MPa to psi, multiply by 145.
[e] E = excellent; G = good; F = fair, and P = poor.

Table 3. Selected Categories of Visually Inspected Natural Rubber[a]

Type	Grade	Description
1	Ribbed smoked sheet	Coagulated sheets, dried and smoked latex. Five grades are available
2	White and pale crepe	Coagulated natural rubber latex milled to produce a crepe
3	Estate brown crepe	Fresh lump and other high quality scrap generated on the plantation
4	Compo crepe	Lump, tree scrapes, and smoked sheet cuttings milled to a crepe
5	Thin brown crepe	Unsmoked sheet, wet slab, lump, and other scrap from estates and small holdings
6	Thick blanket crepe	Wet slab, lump, and unsmoked sheets milled to give a crepe
7	Flat bark crepe	All types of scrap natural rubber including earth scrap
8	Pure smoked blanket crepe	Milled smoked rubber derived exclusively from ribbed smoked sheet

[a]Ref. 13.

Table 4. Technically Specified Rubbers Defined by ISO 2000[a]

	Grade					
	TSR CV	TSR L	TSR S	TSR 10	TSR 20	TSR 50
Dirt content, %wt max	0.05	0.05	0.05	0.1	0.2	0.5
Ash content, %wt max	0.6	0.6	0.5	0.75	1	1.5
Nitrogen content, %wt max	0.6	0.6	0.5	0.6	0.6	0.6
Volatile matter, %wt max	0.8	0.8	0.8	0.8	0.8	0.8
Initial Wallace plasticity $P_{0,min}$		30	30	30	30	30
Plasticity retention index, min	60	60	60	50	40	30
Color, max (lovibond units)		6				
Mooney viscosity	60 ± 5					

[a]Ref. 15.

Table 5. Classification of Emulsion Polymerized Synthetic Elastomers by IISRP[a]

Series	Description
1000	Hot, nonpigmented emulsion SBR; polymerized above 38°C
1500	Cold, nonpigmented emulsion SBR; polymerized below 10°C
1600	Cold, nonpigmented emulsion SBR; carbon black/oil master batch/14 phr oil max
1700	Oil extended cold emulsion SBR
1800	Cold, nonpigmented emulsion SBR; carbon black/oil master batch. More than 14 phr oil
1900	Emulsion resin rubber master batches

[a]Ref. 12.

Table 6. IISRP Classification of Solution Polymerized Stereo Polymers[a]

Category	Butadiene and copolymers	Isoprene and copolymers	Butadiene, isoprene, and styrene copolymers
Dry polymer	1200–1249	2200–2249	2250–2599
Oil extended	1250–1299	2250–2299	
Black master batch	1300–1349	2300–2349	
Oil-black master batch	1350–1399	2350–2399	
Latex	1400–1449	2400–2449	
Miscellaneous	1450–1499	2450–2499	

[a]Ref. 12.

wire insulation, ply and breaker compounds of bias tires, conveyor belt covers, and other industrial products not requiring oil resistance.

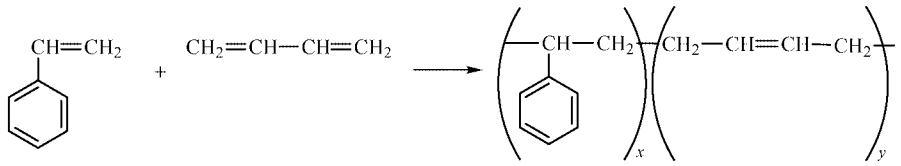

Styrene Butadiene (2)

Solution SBR is classified as shown in Table 6. The principal use of solution polymerized SBR is in the tire industry as a major component of passenger and light truck tire treads (see STYRENE-BUTADIENE COPOLYMERS). It is also finding application in radial medium truck tire drive axle tire tread, aircraft, farm tire treads, and large, off-the-road tires. It can replace emulsion SBR in ply compounds and even in sidewalls where a lower modulus is required. SBR uses in North America are tires, 75%; automotive mechanical goods, 8%; and other, 17% (14). Important properties of SBR are relatively low cost, good physical properties with the proper reinforcing agent, good abrasion, and skid resistance. A deficiency of SBR is its tendency to have fairly high heat generation (hysteresis).

Polybutadiene. The many forms that can result from the polymerization of butadiene, depending on the catalysts used, include high cis, medium cis, low cis, trans, and high vinyl polybutadiene (BR) as illustrated in equation 3 (see BUTADIENE POLYMERS). The property of polybutadiene of most interest to the rubber compounder is abrasion resistance coupled with good resilience (14). The polymer has very high rebound and low heat-generation values. With a few exceptions, such as the core of solid golf balls, the polymer is blended with other polymers to take advantage of its excellent abrasion resistance and hysteretic properties. Table 7 illustrates the effect the cataysts system has on polymer microstructure.

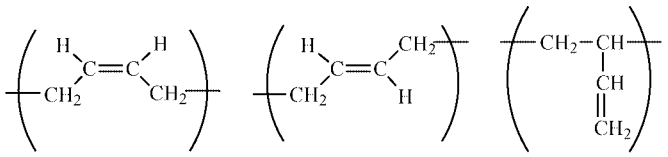

cis-1,4-Polybutadiene *trans*-1,4-Polybutadiene Vinyl-1,2-polybutadiene (3)

Table 7. Microstructure of Commercially Available Polybutadiene

	Typical expected microstructure		
Catalyst	Cis, %	Trans, %	Vinyl, %
	(levels to ± 1%)		
Li	35	55	10
Ti	92–94	2–4	4
Co	96	2	2
Nd	98	1	1
Ni	96–98	0–1	2–4

Ethylene–Propylene Rubber. Ethylene and propylene can be copolymerized to produce a wide range of elastomeric and thermoplastic polymers. Often a third monomer such as dicyclopentadiene, hexadiene, or ethylidene norbornene, illustrated in equation 4, is incorporated at between 2 and 12% into the polymer backbone, and therefore leads to the designation ethylene–propylene–diene monomer (EPDM) rubber (see ETHYLENE-PROPYLENE ELASTOMERS). The diene monomer introduces sites of unsaturation in the polymer that allow vulcanization by conventional sulfur curatives (16). At high levels of a third monomer, it is possible to achieve cure rates that are equivalent to conventional rubbers such as

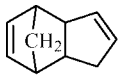

Dicyclopentadiene (DCPD)

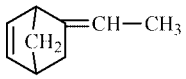

Ethylidene norbornene (ENB)

$H_2C{=}CH{-}CH_2{-}CH{=}CH{-}CH_3$ 1,4 -Hexadiene (1,4 -HD) (4)

SBR and BR. Ethylene–propylene rubber (EPR) is typically vulcanized using a peroxide-based cure system.

Variation of the ethylene–propylene ratio changes the viscoelastic properties of the rubber. The hardness can be varied widely by the filler and plasticizer level. In addition, EPDM can be highly extended with black and nonblack fillers, and oils. At high levels of fillers, EPDM can display very good resistance to swelling by the IRM 903 oil. The principal properties of EPR and EPDM are excellent weathering, good heat and water resistance, electrical insulation, and low temperature brittleness. As a result, EPDM is used in a wide variety of rubber goods. EPR elastomers are used in applications such as roofing, 20%; plastic modification, thermoplastic olefins (TPOs) and thermoplastic vulcanizates (TPVs), 17%; weather stripping, 15%; hoses and belts, 14%; oil viscosity modification, 10%; wire and cable, 6%; molded goods, 5%; tires, 3%; carpet backing, 2%; and other, 9% (14). EPR and EPDM have been made by either solution or emulsion polymerization processes and by gas-phase polymerization using metallocene catalysts.

Butyl and Halobutyl Rubber. Butyl rubber is made by the copolymerization of isobutylene with 1–3% isoprene (eq. 5), which is added to provide sites for curing. It is designated IIR because of these monomers. Halogenation of butyl rubber with bromine or chlorine increases the reaction rate for vulcanization (eq. 6). It is estimated that of the 200,000 kt of butyl (IIR) and halobutyl (HIIR) rubber manufactured in North America, over 90% is used in tire applications. The halogenated polymer is used in the innerliner of tubeless tires.

Isobutylene Isoprene Butyl (5)

Butyl rubber is used to make innertubes and curing bladders (see BUTYL RUBBER). Butyl polymers are about eight times more resistant to air permeability compared to natural rubber and have excellent resistance to heat, steam, and water. This accounts for its use in gaskets and diaphragms for hot water and steam services. In addition, butyl rubber can be compounded to have low resilience properties and has found use in high damping mounts for engines, motors, and similar devices (6,17,18).

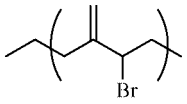

Most common isomer of bromobutyl (or chlorobutyl) rubber (6)

Special-Purpose Elastomers. Polychloroprene and polysulfide rubber were the first synthetic specialty elastomers discovered. Since their invention in the 1930s the total number of classes of synthetic rubbers has grown to almost 30. Table 1 has listed standard acronyms by the International Institute of Synthetic Rubber Producers (12).

Chloroprene Elastomers. Polychloroprene is made by polymerizing 2-chloro-1,3-butadiene (eq. 7). The elastomer is largely composed of the trans isomer. There are three major polymer types: the G-type, the W-type, and the T-type.

(1) G-types are made by using a sulfur-modified process. G-type polymers possess excellent processing and dynamic properties, and are thus used in applications such as V-belts. However, they have poorer aging properties than W-types. They contain sulfur and tetramethylthiaram disulfide (TMTD) and they can be cured with only a metal oxide.

(2) W-types use no sulfur modification. The W-type polymers tend to be used in applications requiring better aging, such as rolls and mechanical goods (see CHLOROPRENE POLYMERS). W-type polychloroprenes require an organic accelerator.

(3) T-types are similar to W-type polychloroprenes but contain a high level of gel, which in this instance offers improvements in processing. They find use where fast, uniform extrusions and calendering is required.

Polychloroprene is made from one of two starting materials, acetylene or butadiene. Acetylene can be dimerized and then chloronated to form chloroprene. Alternatively, when adequate butadiene is available, this can be directly halogenated (eqs. 7 and 8). In either case, the chloroprene product can then be polymerized to polychloroprene. Essentially a butadiene elastomer with chlorine present in the backbone,the polymer exhibits excellent tensile strength and low hysteresis, much like natural rubber. Tensile strength properties up to 28 MPa are possible with the proper reinforcing system (see FILLERS). The polarity imparted by the chlorine atom improves the oil and solvent resistance approaching those of nitrile polymers. The polymer can be protected with *para*-phenylenediamine antiozonants to give ozone resistance, and heat aging is also good. As a result, chloroprene elastomers are used in a wide variety of applications needing a balance of such properties.

Principal uses include automotive V-belts, industrial and hydraulic hoses, specialty roofing, heels and soles in footwear, wire covering, and a wide variety of coated fabric uses, eg, rafts. Polychloroprene elastomers are also used extensively in adhesives. It is estimated that about 77,000 ton of polychloroprene are used each year in the United States (4,7,19).

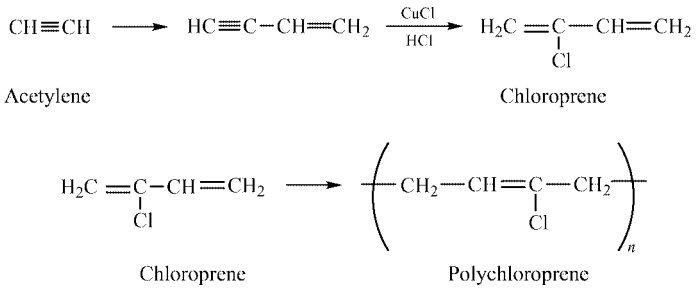

(7)

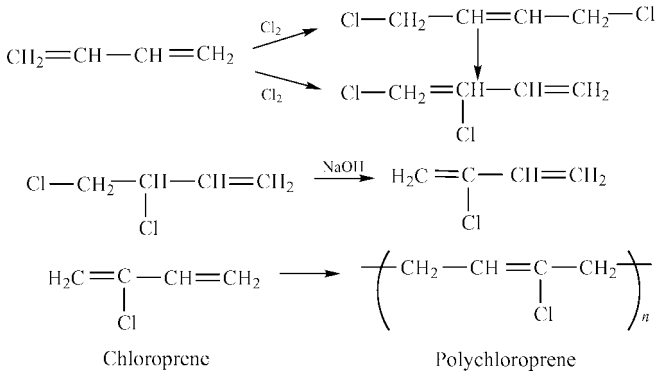

(8)

Chlorinated Polyethylene. Under pressure, polyethylene can be chlorinated to produce a polymer having a halogenated monomer content varying from 25 to 42%. The polymer requires the incorporation of carbon black and minerals for achieving good physical properties. The polymers handle like conventional polymers and can be mixed and processed on conventional rubber equipment. Chlorinated polyethylene (CPE) has excellent ozone, oil, and heat resistance, and as a result chlorinated polyethylene has replaced chloroprene elastomers. CPE has a lower specific gravity than chloroprene compounds and produces compounds that are similar to CR in properties but with lower costs. Also, because of high levels of chlorine, the flame resistance of compounds of CPE are high.

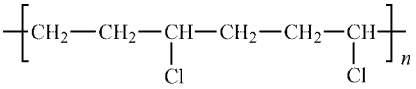

Chlorinated polyethylene (9)

An estimated 18 kt of these elastomers is used per year. The main uses of CPE are in construction, automotive, and electrical applications. These include power steering hose, electrical cords used in low voltage applications (extension cords, ignition wire), pond liners, and as a plastic modifier to improve impact modification.

Chlorosulfonated Polyethylene. This elastomer is made by the simultaneous chlorination and chlorosulfonation of polyethylene in an inert solvent. The resulting polymer is an odorless, colorless chip that is mixed and processed on conventional rubber equipment (2). The polymer (eq. 10) typically contains between 20 and 40% chlorine and 1% sulfur (see ETHYLENE POLYMERS, CHLOROSULFONATED). The polymer requires compounding with normal fillers to produce useful properties. Chlorosulfonated polyethylene (CSM) excels in resistance to attack by oxygen, ozone, corrosive chemicals, and oil, and in addition has very good electrical properties. The physical properties and abrasion resistance are also good. Light-colored articles made from CSM have excellent color-fastness. Because of the presence of chlorine atoms, this elastomer also shows good flame resistance.

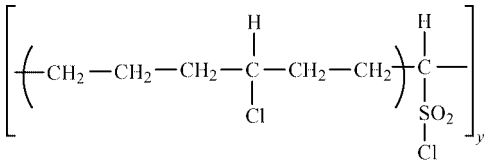

Chlorosulphonated polyethylene (10)

CSM is extensively used in construction and electrical applications. This includes roofing membranes, automotive ignition boots and wires, roll compounds, and some automotive hoses requiring good heat and oil resistance, eg, air conditioning and power steering hoses. It is also used in nuclear power plants because of its excellent resistance to radiation degradation. Chlorosulfonated polyethylene is sold under the trade name Hypalon.

Fluoroelastomers. Fluoroelastomers were introduced to the rubber industry in the late 1950s. They were made by modification of Teflon polymers and designed to have excellent heat and chemical resistance, but remain elastomeric in nature. With the increasing demand in the automotive and industrial market for improved reliability and longer in-service life, fluoroelastomers have made significant inroads into these applications (see FLUOROCARBON ELASTOMERS). Compared to all other elastomers, fluoroelastomers excel in heat, chemical, flame, weathering, fuel, and ozone resistance. In addition, oil, oxygen, and water resistance are very good. Fluoroelastomers, however, are attacked by amines and some highly polar solvents. Abrasion resistance and low temperature properties are adequate for most applications.

Seals and gaskets in the marine, oilfield, and chemical processing industries employ fluoroelastomers. In addition, many hoses in the automotive and chemical industry are made entirely of fluoroelastomer compounds or have a veneer of the fluoroelastomer as a barrier exposed to the harsh environment.

Epichlorohydrin. Commercial polyester elastomers include both the homopolymer and the copolymer of epichlorohydrin with ethylene oxide. The very polar chloromethyl group creates basic resistance to oil for these polymers, and they have been extensively used in fuel lines; however, the desire for lower fuel permeation is causing a search to be made for other polymers (20). Epichlorohydrin (ECO) has excellent resistance to fuel and oil swell. The ECOs show a volume swell of 35% at room temperature compared to 70% for a medium ACN–nitrile rubber in ASTM Reference Fuel C. The copolymer has a low temperature brittle point of −40°C; and the homopolymer, −15°C. An interesting property of these elastomers is a stable dynamic performance over a wide temperature range; however, the electrical properties are only average.

The principal uses of ECO are in automotive applications; eg, for fuel line and fuel vapor recirculation. There are also some downhole seal applications where ECO is used.

Nitrile and Acrylic Rubber. Nitrile rubbers are made by the emulsion copolymerization of acrylonitrile (9–50%) and butadiene (21) and are abbreviated NBR (eq. 11). The ratio of acrylonitrile (ACN) to butadiene has a direct effect on the properties and the nature of the polymers. As the ACN content increases, the oil resistance of the polymer increases (14). As the butadiene content increases, the low temperature properties of the polymer are improved. Nitrile rubber is much like SBR in its physical properties. It can be compounded for physical strength and abrasion resistance using traditional fillers such as carbon black, silica, and reinforcing clays. The primary benefit of the polymer is its oil and solvent resistance. At a medium ACN content of 34% the volume swell in IRM 903 oil at 70°C is typically 25–30%. Nitrile rubber can be processed on conventional rubber equipment and can be compression, transfer, or injection molded. It can also be extruded easily. Nitrile rubber compounds have good abrasion and water resistance. They can have compression set properties as low as 25% with the selection of a proper cure system. The temperature range for the elastomers is from −30 to 125°C. The compounds are also plasticized using polar ester plasticizers.

Applications requiring good oil resistance and moderate heat aging are the principal uses of nitrile rubber compounds. The automotive industry has been the primary consumer of nitrile rubber based products with hoses, fuel lines, and

numerous O-rings and seals representing typical applications. In addition many rolls in the printing industry are made from nitrile rubber. However, fluoroelastomers, silicone, epichlorohydrin, and acrylic elastomers have been replacing nitrile rubber for better durability and longer service life.

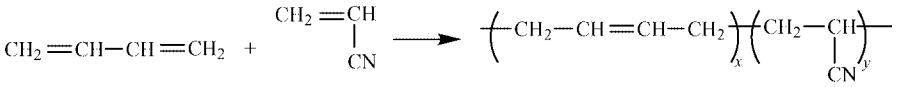

Nitrile elastomers (11)

For compounding of nitrile elastomers, reference should be made to model formulations for a range of applications where such polymers are used (22). Hydrogenation of nitrile rubber improves the aging properties of the oil-resistant backbone. The polymers are available with acrylonitrile contents from 17 to 50% and residual double-bond unsaturation from 2 to 20% (eq. 12). In addition to outstanding oil resistance and improved aging properties, the abrasion resistance of the polymers is very good. The basic polymer is quite polar, giving inherent resistance to swelling in oils or gasoline, but can be affected by ketones, halogenated solvents and oils, and oxygenated solvents. They have a service range from −45 to 149°C. Hydrogenated nitrile rubber (HSN or HNBR) compounds compete with FKM, FVMQ, ECO, ACM, and high ACN content nitrile rubbers. Major applications include automotive timing belts, blow-out preventors, drill pipe protectors, and numerous oil and fuel pump components.

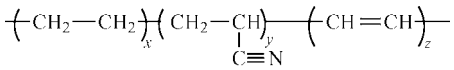

Hydrogenated NBR
y 17–50%
z = 1–15% (12)

Acrylic elastomers possess good oil and heat resistance. They are made by polymerizing monomeric acid esters of ethyl or butyl acrylate and methoxyethyl acrylate or ethoxyethyl acrylate. They can be polymerized in emulsion, suspension, or solution systems (8). The polyacrylates are inherently tacky and soft. They require compounding with carbon black or mineral fillers for achieving useful properties. Their main properties are a temperature performance range of −40 to 175°C. They have good resistance to oils, oxidation, ozone, aliphatic solvents, sunlight, and weathering, and exhibit low permeability to gases. The tensile strength is usually 7 to 14 MPa (1000–2000 psi). Compounds can be fabricated with Shore A hardness values ranging from 40 to 90.

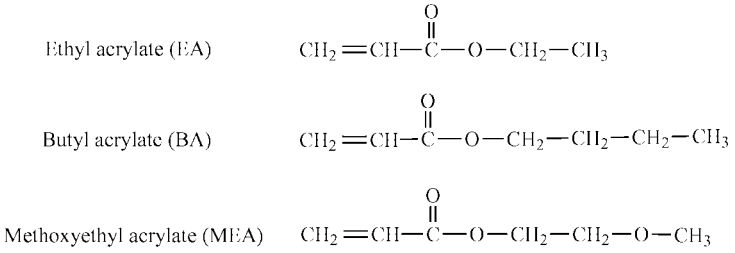

(13)

The major monomers used in in polyacrylates are shown in equation 13. It is estimated that 9000 ton of these elastomers are used annually in the United States, principally in automotive applications requiring both oil and heat resistance. These include transmission, valve stem, crankshaft, pinion, and oilpan gaskets and seals. In addition, hoses, tubing, rolls, and belts are made from acrylic polymers (2,7).

Other Special Polymers. There are a variety of other polymers which, though when compared to the general-purpose polymers such as SBR, are used in low quantities but still merit discussion. These include elastomers such as polysulfides, silicone rubbers, and polyurethanes. Each are considered in turn.

Polysulfides. Polysulfides are also called Thiokol's (T) after the company that originally made them. They were discovered in 1927 (see POLYSULFIDES). Thiokol elastomers have low tensile strength and tear strength properties. However, they have good resistance to both aliphatic and aromatic solvents at room temperature and at slightly elevated temperatures. It is estimated that 1.4 to1.6 kt are used annually in the United States. The primary use of polysulfide elastomers are in seals, gaskets, rolls, and diaphragms where solvent resistance and low permeability are required.

Silicones. Silicone elastomers have a siloxane (—Si—O—Si—) backbone with methyl, vinyl, or phenyl groups attached. The elastomers are designated by their chemical composition as follows: methyl silicone (MQ), methyl vinyl silicone (VMQ), methyl phenyl silicone (PMQ), methyl phenyl vinyl silicone (PVMQ), and fluorovinyl methyl silicone (FVMQ). Silicone elastomers possess good resistance to heat aging. The siloxane backbone imparts resistance to oxygen, ozone, UV light, and to some polar fluids. However, the tensile strength of these elastomers is usually low. They also have low abrasion resistance and tear strength (see SILICONES). By fluorinating the silicone polymer it is possible to improve the solvent, fuel, and oil resistance of this already heat-resistant class of elastomers. The resulting polymers are especially useful in select automotive seals and gaskets, military, and oilfield equipment parts. Fluorosilicones (FVMQ) have excellent low temperature flexibility properties coupled with good oil, fuel, and solvent resistance and excellent aging properties. The materials are compounded and reinforced with fine particle fillers such as silica. The materials are mixed and processed on especially clean equipment and are peroxide-cured. The primary uses of these elastomers are in O-rings, shaft seals, wire and cable, and electrical connectors.

Urethanes. Urethane elastomers are prepared by the reaction of an isocyanate molecule with a high molecular weight ester or ether molecule. The result

is either an elastomeric rubber form or a liquid prepolymer that can be vulcanized with an amine or a hydroxyl molecule (see POLYURETHANES). Urethanes are processed as rubber-like elastomers, cast systems, or thermoplastic elastomers. The elastomer form is mixed and processed on conventional rubber mills and internal mixers, and can be compression, transfer, or injection molded. The liquid prepolymers are cast using automatic metered casting machines, and the thermoplastic pellets are processed like all thermoplastic materials on traditional plastic equipment. The unique property of polyurethane is high abrasion resistance and moderately high Shore A (75–95) hardness. In addition, tear strength, tensile strength, and resistance to swelling by many oils is very high. The main deficiencies of the urethanes are their resistance to heat over 100°C and that shear and sliding abrasion tend to make the polymers soft and gummy. It is estimated that close to 68,000 ton of these rubbers are used per year in the United States if all forms are included. Uses include sport wheels (roller blades, ski wheels); printing, paper, and steel processing rolls; gears; pump liners; appliance components; and solid industrial tires.

Vinyl Acetate–Ethylene Copolymers. Vinyl Acetate–Ethylene copolymers would also fall into this category. In these random copolymers, the ratio of ethylene to vinyl acetate (EVA) is varied from 30 to 60%. As the vinyl acetate content increases, the oil and heat resistance increases. With higher ethylene content the physical strength, tensile, and tear increases. The polymers are cured with peroxides. The main properties of these elastomers include heat resistance, moderate oil and solvent resistance, low compression set, good weather resistance, high damping, and excellent ozone resistance, and they can be easily colored (see VINYL ACETATE POLYMERS). Applications include automotive electrical system components, eg, ignition cable, footwear, weather stripping, and miscellaneous O-rings and seals for industrial applications.

Fillers for Rubber

Fillers (qv) are particulate materials added to improve the physical properties and optimize the cost of the rubber compound (see FILLERS). All particulate fillers increase the hardness and stiffness of rubber compounds. The chemical composition and its effect on rubber compound physical properties typically classify fillers into three broad categories: nonreinforcing, semireinforcing or extending, and reinforcing fillers. Reinforcing fillers improve the physical properties of the rubber vulcanizate, while some fillers simply act as diluents or extenders. Improvements in rubber compound physical properties are directly related to the filler particle size, whereby the smaller particulate fillers impart greater reinforcement. Particle-size distribution and particle shape also have significant effects on composite reinforcement. Filler structure ranges from precise geometrical forms, such as spheres or hexagonal plates, to irregular masses. A particle with a high aspect ratio has higher reinforcement than a more spherical one. Fillers having a broad particle-size distribution have better packing in the rubber matrix and provide lower viscosity than that provided by an equal volume of the filler with a narrow particle-size distribution. The properties of particulate-filled elastomers are determined by the properties of the components, by the shape of the filler phase, by the morphology of the system, and by the polymer-filler interfacial interactions.

A wide variety of particulate fillers are used in the rubber industry. Carbon black is the filler of choice. All grades, with the exceptions of N880 and N990 thermal blacks, reinforce rubber with the finest particle-size carbon blacks imparting the highest degree of reinforcement based upon improved abrasion resistance, tear strength, tensile strength, and stiffness. A number of mineral fillers are used in the rubber industry to extend and/or reinforce elastomers. They include carbonates, clays, silicas, silicates, and talc. However, when compared to carbon black, the use of nonblack fillers by the tire and rubber industry is limited.

Carbon Black. This is the primary reinforcing filler used in the rubber industry. Carbon black can be made by three processes: the furnace process, the thermal process, and the channel process. Over 97% of black is made by the furnace process (see CARBON BLACK).

The furnace process involves spray injection of a low end fraction of crude oil into a heated chamber. The temperature, shape of the injectors of the oil, rate of injection, shape of the reactor, and other factors are controlled to produce carbon black fillers of different particle sizes and structures. The particle size and structure control and the reinforcing character of carbon black are the bases of their classification system (Table 8). There are approximately 30 common grades of carbon black used in the rubber industry. There are also numerous specialty grades produced for use in plastics, conductive applications, and proprietary grades produced for use in tires and other special-purpose products (14).

Carbon black primarily owes its reinforcing character to the size and shape of the aggregate structure; for example see Figure 2. An aggregate consists of primary particles essentially spherical in shape that are chemically bonded (fused) to one another. The two most important properties of carbon black are surface area and structure. Surface area depends inversely upon the size of the primary particles, and is one measure of the area available for physical interaction with an elastomer. The structure of carbon black depends upon the size and grouping of these primary particles in the aggregate. The more the primary particles in the aggregate, the higher is the structure of the carbon black due to the more complex shape and void volume (porosity). Surface activity refers to the strength of the carbon black/rubber interaction either from nonbonded physical interactions or chemisorption. The small (2–3%) but significant amount of noncarbon atoms, such as hydrogen, oxygen, and sulfur, that are present on the carbon black surface results in surface activity differences. During mechanical mixing with polymers, it is desirable to minimize the presence of agglomerates, which are physically

Table 8. Tire and Industrial Products Carbon Black Categories[a]

Type	ASTM designation	Particle size, nm	Application
SAF	N110	11–19	Tires
ISAF	N220	20–25	Tires
HAF	N330	26–30	Tires
FF	N475	31–39	Industrial products
FEF	N550	40–48	Tires, industrial products
GPF	N660	49–60	Tires, industrial products
SRF	N762	61–100	Industrial products

[a]Ref. 14.

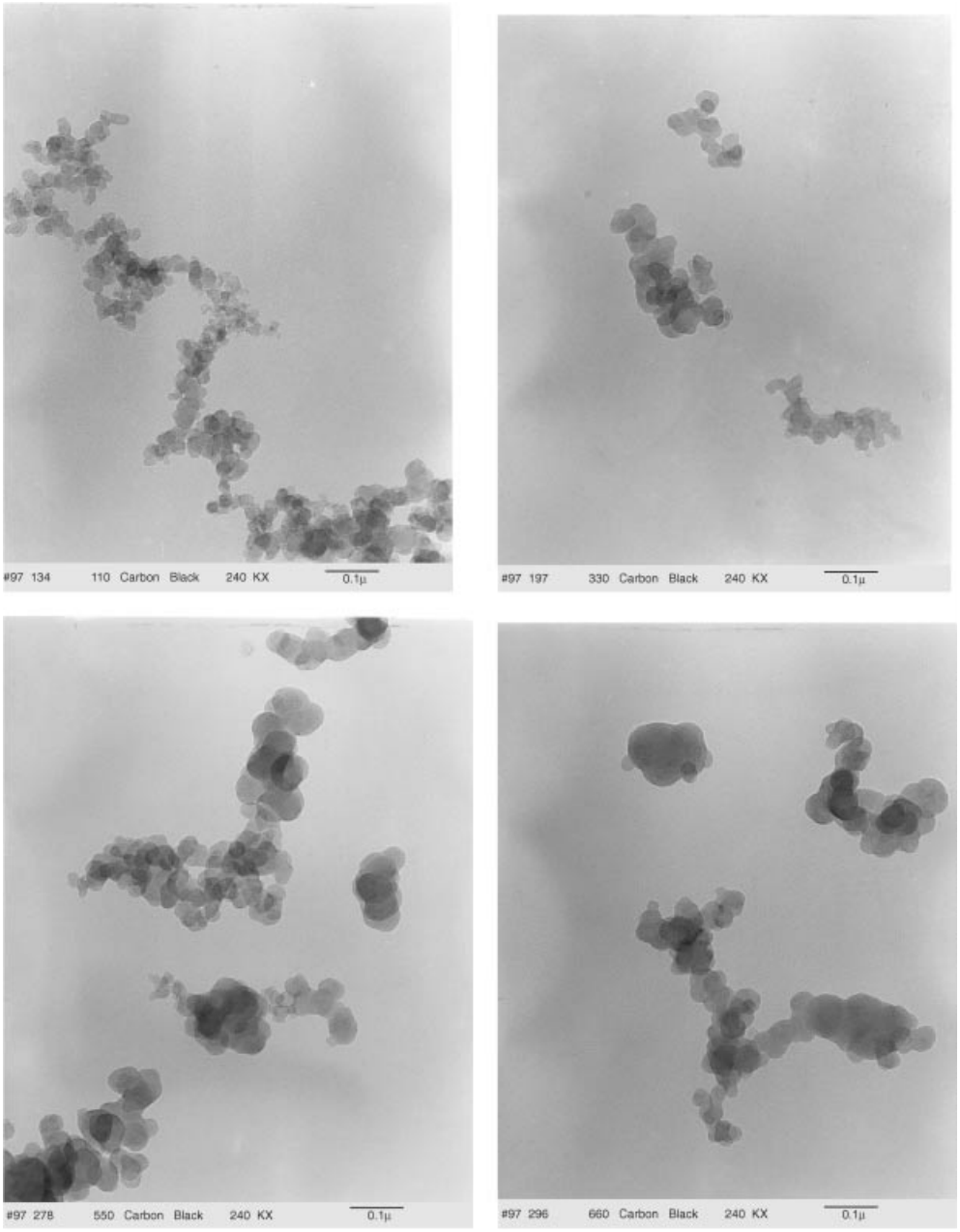

Fig. 2. Electron micrographs illustrating particle structure of carbon blacks N110, N330, N550, and N660.

associated aggregates. Aggregate structures are not thought to be broken down into primary particles by simple mechanical processes such as mixing, milling, etc.

The structure of the carbon black is determined by dibutyl phthalate (DBP) absorption and the surface area is estimated by nitrogen or CTAB absorption (Table 9).

Table 9. Common Commercial Grades of Carbon Black[a]

ASTM Designation	Iodine number	DBP	Compressed DBP	CTAB	Nitrogen absorption	Tint strength
N110	145	113	98	126	143	124
N115	160	113	96	128	145	123
N121	121	132	112	121	132	121
N220	121	114	100	111	119	115
N231	121	92	86	108	117	117
N234	120	125	100	119	126	124
N299	108	125	105	104	108	113
N326	82	72	69	83	84	112
N330	82	102	88	82	83	103
N339	90	120	101	93	96	110
N347	90	124	100	87	90	103
N351	68	120	97	73	73	100
N375	90	114	97	96	100	115
N472	250	178	114	145	270	
N550	43	121	88	42	42	
N630	36	78	62	35	38	
N660	36	90	75	36	35	
N762	27	65	57	29	36	
N772	30	65	58	33	29	
N990		43	40	9	6	
N991		35	38	8	7	

[a]Refs. 14,23.

Carbon blacks are also classified into reinforcing, semireinforcing, and extender blacks. The furnace blacks from N100 through N300 are considered reinforcing blacks based on the increase in tensile strength observed when they are incorporated into rubber. They are sometimes referred to as *hard blacks*, and are used in treads, black sidewalls, casings, and breaker compounds of radial passenger and truck tires. In addition, they are commonly used in the covers of belts, a few select hose compounds, and other rubber goods requiring high tensile strength, tear strength, modulus, and good abrasion resistance.

The N500 through N700 series carbon blacks are considered semi-reinforcing blacks. These are used widely in bias and radial tire casings, innerliners, beads, squeeges, and other tire components not requiring the ultimate in strength and abrasion. They are also used in matting, roofing, curing bladders, and innertubes.The N900 series thermal blacks are viewed as extender blacks because of the limited reinforcement they provide for the rubber compound. All semi-reinforcing carbon blacks are often referred to as *soft blacks*.

Mineral Fillers. Mineral fillers are naturally occurring materials that are mined and are ground to a specified particle size (24,25). Grinding may be done dry using mechanical mills. For a finer product the ore is ground wet. Wet grinding may be autogenous where the ore grinds by attrition with itself or a grinding media may be employed. Additional processing may include a combination of steps. They include (*1*) separation of fine and coarse particles by use of screens, by air or water flotation, or by centrifugal filtration (*2*) removal of impurities by washing,

heat treatment, magnetic separation, or chemical treatment and/or (*3*) surface treatment with a variety of chemicals to improve the compatibility with the rubber matrix.

Calcium carbonate is usually derived from a naturally occurring source, such as calcite or whiting, by wet grinding. Precipitated and synthetic calcium carbonates are available in high purity; typically have a higher surface area, finer particle size, and narrower particle-size distribution; and thus a higher degree of reinforcement. Kaolin clay, a hydrated aluminum silicate, is one of the most abundant silicate minerals. Depending upon the type of processing, kaolin can be categorized as air-floated, water-washed, calcined, or surface-treated. Kaolin has the finest particle-size range of any naturally occurring mineral. Silicas are categorized as naturally occurring such as crystalline and diatomaceous earth, or as synthetic silicas which include precipitated silica, pyrogenic (fumed) silica, and silica gel. Crystalline silica is an inert, abrasive, large particle obtained from grinding sand or quartz. Diatomaceous earth or dolomite is obtained from sedimentary rocks and often contains up to 30% organic matter and inorganic impurities such as sand, clay, and soluble salts. Precipitated and pyrogenic silicas are high surface areas, fine-particle reinforcing fillers (see Fig. 3). Talc is a hydrated magnesium silicate with a morphology and purity varying according to the mining location.

Among the nonblack fillers, the highest hardness is provided by rod-shaped or plate-like particles, which can orient parallel during processing, compared to spherical particles of similar diameter. Uses of clay in rubber produces compounds with high hardness values. Clay is further classified as a hard clay if it reinforces rubber also imparting high modulus, tensile strength, and resistance to abrasion, or as a soft clay if it produces a compound with lower physical properties. Of the spherical particulate fillers, precipitated silicas, surface-treated clays, and calcium silicates also produce high hardness and high modulus compounds (see Fig. 4). The highest tensile strengths are produced in rubber compounds by using precipitated silicas. Calcium silicate and surface-modified clay also afford high tensile strength compounds, followed by use of zinc oxide, carbonates, and hard

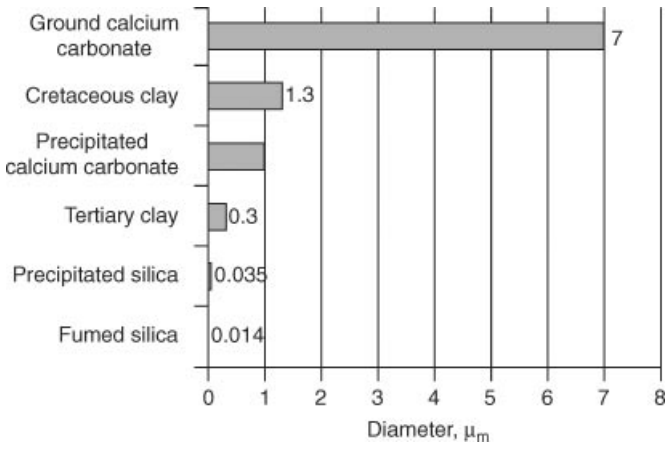

Fig. 3. Median particle diameters of nonblack fillers.

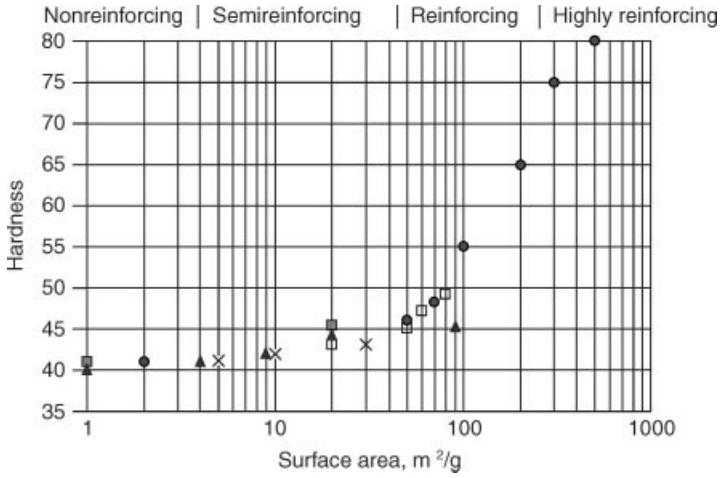

Fig. 4. Reinforcing effect on hardness of nonblack fillers with different surface areas. ● Silica, ■ talc, ▲ calcium carbonate, × soft clay, □ hard clay.

clay. No other nonblack filler approaches the precipitated silicas for imparting abrasion resistance.

Calcium Carbonate. Calcium carbonate ($CaCO_3$) is also known as whiting, limestone, marble, chalk, or calcite. It has been ground and added to rubber compounds to reduce cost and to impart hardness and opacity to rubber articles. Particle sizes range from 2 to 80 μm for dry-ground product and from 0.5 to 11 μm for wet-ground product. The chemical composition and crystalline nature depend on the limestone deposit that is mined, for example chalk or marble, and the color of the deposit.

Important applications of calcium carbonate in the rubber industry include use in electrical wire and cable insulation where the low moisture content and natural insulating properties make it a preferred filler, in the production of articles where low cost and smooth surface appearance are desired, such as footwear, and in extruded hoses and automotive sealing parts.

Clay. Kaolin clay, also called kaolinite or China clay, is hydrous aluminum silicate [$Al_2Si_2O_5(OH)_4$] consisting of platelets with alternating layers of silica and alumina in the structure. The weathering of granite forms fine particles of clay. Clay deposits are classified as primary, secondary, and tertiary. Primary deposits are mixtures of clay and granite found where they were originally weathered, and contain only 40 to 50% particles less than 2 μm in diameter. Secondary deposits form when fine particles from primary deposits flow and are deposited in a new location. Tertiary deposits are the most important commercial deposits because of their fine particle size, with >80% of the particles being less than 2 μm in diameter. Their high purity results when water carries the fine particles of a secondary deposit to a new location.

Clay can be generally divided into soft and hard clays on the basis of their producing softer and harder rubber compounds at a given loading level. There are several processes for producing clay for rubber reinforcement from the mined form: (*1*) Air-floated clay, in which the ore is milled to break up lumps and air

classified, is the least expensive form of clay and imparts moderate reinforcement. (*2*) Water-washed clay involves gravity separation of impurities, bleaching, magnetic separation to improve color properties, and centrifuging to produce the desired particle size range to impart higher reinforcement by the control of pH, color, and particle size. (*3*) Delaminated kaolin uses chemical and/or mechanical means to break apart the platelet structure of the clay, which further increases the available surface area and reinforcement properties. (*4*) Metakaolin is partially calcined by heat treating to 600°C. (*5*) Calcined clay is formed by heating to 1000°C, which produces a very white, high surface area mineral with an inert surface.

Clays are used as a filler for many rubber goods. The natural air-floated and water-washed clays are considered semi-reinforcing fillers for most rubber compounds. They are used in large volumes by the footwear, mat, industrial tire, and mechanical goods manufacturers. In addition, a small amount of clay is used by the tire industry in innerliners and white sidewalls, using the clay as an extender filler in low to medium dynamic stress applications. Clays are also used as partitioning agents in slab dips and antitacks. Clays were formerly used as fillers for bias tire carcasses; however, radial tires require better flex fatigue resistance than clay can impart.

Talc. Talc [$Mg_3Si_4O_{10}(OH)_2$] is a platelet form of magnesium silicate with a high aspect ratio. Platelets can orient in the extrusion process, thus providing rubber extrudates with smooth surfaces that can be extruded at high rates. It is commonly used in compounds, which have critical surface appearance such as exterior automotive components or consumer goods.

Talc is used in tires in white sidewall compounds to provide a smooth appearance to the buffed sidewall. The large platelets of talc provide a barrier to gas and moisture permeability in compounds, which allows talc to be used in applications such as hydraulic and automotive hoses, barrier films, and tire innerliners.

Synthetic Fillers. Synthetic fillers are generally manufactured by precipitation of soluble materials under carefully controlled conditions to provide tailored properties. They may be found as colloidal particles which may be spherical, ellipsoid, rod, or tube shaped; as aggregates which are covalently bonded groupings of individual particles, or as agglomerates that are loosely held associations of aggregates physically interacting. Reinforcement properties are a function of the colloidal particle size and shape, the aggregate dimensions and morphology, and the ability of agglomerates to break down during mixing. Additionally, the composition and surface chemistry of the filler plays a significant role.

Precipitated Calcium Carbonate. Precipitated calcium carbonate is formed by dissolving limestone and precipitating $CaCO_3$ as very fine particles using carbon dioxide (Aroganite Process) or sodium carbonate (Solvay Process). Typical particle sizes range from 0.02 to 2 μm. Most commercially available precipitated calcium carbonate is spherical colloidal particles or aggregates consisting of a few spherical particles. Additional shapes and aggregates of varying morphology are possible and provide increased reinforcement. Precipitated calcium carbonate is used as a semi-reinforcing filler in shoe products and industrial rubber goods, particularly when resistance to alkali solutions is needed. The low moisture content and good reinforcement allow precipitated calcium carbonate to be used in wire and cable insulation applications.

Metal Oxides. Zinc oxide, which is formed from the burning of zinc metal, was the first nonblack filler used for reinforcement of rubber compounds. Although zinc oxide and magnesium oxide are still used as a reinforcing filler in some specialty compounds, particularly those that require heat resistance, their role in rubber compounding in the last several decades is that of an activator for the sulfur cure system or as curatives for chloroprene rubber compounds.

The rutile form of titanium dioxide (TiO_2) is an important filler for white and colored rubber articles. The ability of the titanium dioxide particle to scatter light provides high whiteness and opacity to rubber, which gives the filler particle the ability to cover background colors. The anatase crystalline form of titanium dioxide is also used.

Silicates. Amorphous silicates are precipitated from aqueous blends of soluble silicate, typically sodium silicate, and soluble salts of other metals. The most important types for reinforcement of elastomers are aluminosilicates with mixed Al_2O_3 and SiO_2 structures, magnesium aluminosilicates, and calcium silicates. The silicates have surface areas and resultant reinforcement which span the range from the highest surface area clays (ca 30 m^2/g) to the lower end of the precipitated silicas (ca 100 m^2/g).

Silica. Because of its small particle size and complex aggregate structure (see Fig. 5), precipitated silica imparts the highest degree of reinforcement to rubber among all of the nonblack particulate fillers. The main uses of silica are in the treads of passenger and truck tires for traction and low rolling resistance, in the treads of off-the-road tires for improved chunking and tear resistance, and as a component of the bonding system for adhering brass and zinc-plated steel cord to rubber. Silica is used in shoe soles for its resistance to wear and tearing, its nonscuffing characteristics, and to obtain compounds with light color. It is used to improve the tear strength and resistance to flex fatigue (cracking, cut-growth) and heat aging in a wide variety of manufactured rubber goods including conveyor and power transmission belts, hoses, motor and dock mounts, bumper pads, and rubber rolls. For comparative purposes, some properties of silica and their applications are illustrated in Tables 10 and 11.

The reaction of a bifunctional organosilane with precipitated silica involves the hydrophobation of the alkoxy group of the silane with a surface silanol group of the silica, followed by reaction of the sulfur-containing function of the silane with an olefin group of the elastomer to afford a covalently bonded structure. This silane-coupled silica is useful in improving the abrasion resistance of silicas to levels of carbon blacks, and promoted their use in the treads of radial passenger tires.

For comparative purposes, the effects of nonblack fillers, both natural rubber and SBR compounds, are shown in Tables (12) and (13). For example it illustates

Table 10. Properties of Commercial Amorphous Silica[a]

	Colloidal silica	Precipitated silica	Pyrogenic silica	Silica gels
SiO_2	15–50	85–95	98–99	96.5–99.5
Weight loss at 105°C	50–80	4–7	0.5–2.5	
Particle size, nm	4–60	5–50	5–50	1–100

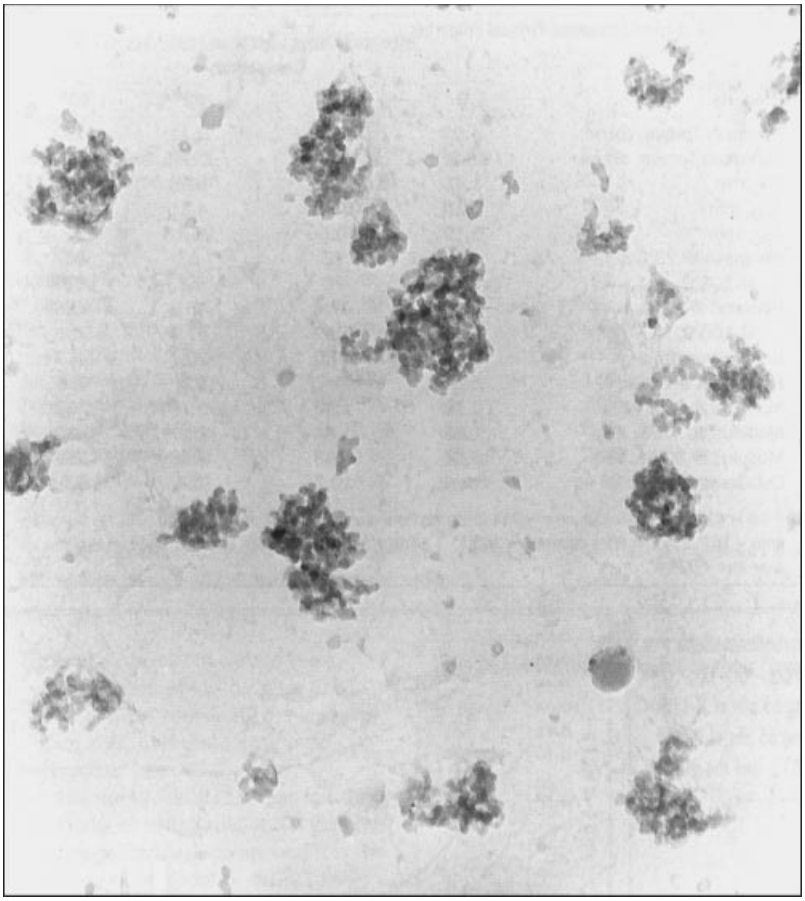

Fig. 5. Transmission electron micrograph of precipitated silica showing aggregate structure (27).

Table 11. Application of Amorphous Silica by Partical Size and Form

	Surface area, m^2/gm		
	90–130	130–180	180 –220
Conventional	Tire casing; Non-tire internal and external components	Tire treads; tire casings and non-tire products external components	Tire treads and non-tire external components for abrasion resistance
Semi highly dispersible	Tire casing; non-tire products external components	Tire treads; tire casings	Tire treads
Highly dispersible	Tire casings; tire treads	Tire treads	High performance tire treads

how tensile can vary from 11 MPa for ground whiting or calcium carbonate filled NR to 25 MPa for HiSil 233 or silica-filled compounds.

Surface Treatment. Carbon black remains the particulate filler of choice for rubber articles since the inherent reinforcing effect of the nonblack fillers in hydrocarbon elastomers is not comparable. This is primarily due to the nonbonded interactions established between the particulate filler and polymer functionality (28). Surface chemistry plays an important role in the interaction of the nonblack fillers and the polymer with contributions ranging from electrostatic interactions to covalent bonding to the polymer backbone. However, surface chemistry also strongly affects the interaction of the nonblack filler with other chemicals in the rubber compound, particularly active metal oxides, curatives, and antidegradants.

Both surface morphology and surface chemistry play an important role in the interaction of a filler with coupling agents. For example, the dipole-induced dipole interactions between the polar groups such as siloxane and silanol on the surface of silicas to the nonpolar groups (methyl, alkenyl, aryl) of hydrocarbon elastomers are weak compared to the dipole–dipole interactions resulting from hydrogen bonding between surface silanol groups in silica aggregates. In addition, the dispersive forces between a nonpolar molecule and silica are low, while those between a nonpolar molecule and carbon black are high. Thus, materials to improve the compatibility between hydrocarbon elastomers and mineral fillers are of considerable interest. Organosilane coupling agents have been successfully utilized to further increase the physical properties of a number of nonblack fillers including calcium silicate, clays, mica, silica, and talc. Clays pretreated with an amino-functional or mercapto-functional silanes, and silicas pretreated with the mercapto-functional or tetrasulfide-containing silanes are commercially available. A manual of commercial coupling agents to promote adhesion between polymers and various substrates is available (29). The reaction of a bifunctional organosilane with a silica or silicate particulate filler involves the hydrophobation of the alkoxy group of the silane with a surface silanol group of the silica or silicate, followed by reaction of the sulfur-containing function of the silane with an olefin group of the elastomer to afford a covalently bonded structure (see Fig. 6).

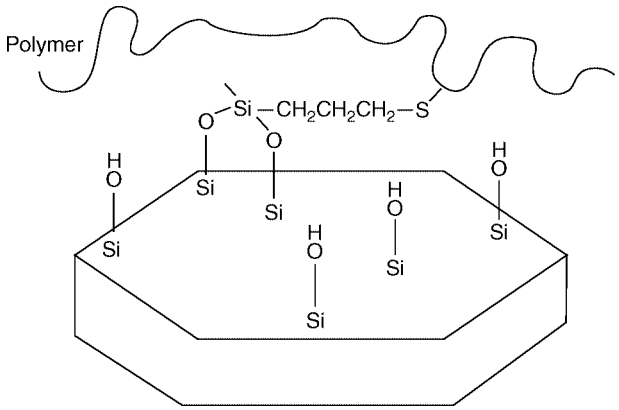

Fig. 6. Illustration of silane coupling of polymer to a silicate surface.

Table 12. Effects of nonblack Fillers on Natural Rubber Properties[a,b]

Filler loading	Volume, parts	Mooney viscosity	Optimum cure (at 141°C), min	Modulus (at 300%), MPa[c]	Tensile strength, MPa[c]	Elongation, %	Hardness, shore A	NBS abrasion, ASTM D1630	Rebound, %
Pure gum		21	15	2.1	24.2	680	43		81.2
Barytes	30	27	20	2.1	15.0	640	49	22.1	80.5
	50	24	20	2.1	11.5	610	56	19.4	
Ground whiting	30	32	20	2.1	15.0	640	50	24.1	81.5
	50	43	15	1.9	10.7	590	57	21.6	
Soft clay	30	35	25	7.2	17.9	500	49	44.4	81.5
	50	41	25	12.4	16.4	390	58	36.4	
Hard clay	30	29	25	9.2	19.9	500	55	54.4	68.2
	50	31	25	14.9	18.4	370	64	43.8	
Purecal U	30	37	15	5.0	19.0	580	53	42.2	75.9
	50	46	15	6.1	14.9	540	57	31.8	
Calcene TM	30	32	15	3.7	19.2	640	48	50.0	70.5
	50	42	15	5.1	16.6	610	58	39.6	
Zinc oxide	30	22	20	5.2	21.8	600	55	54.1	73.1
	50	23	20	5.5	15.4	550	64	48.1	
Zeolex	20	23	10	3.5	22.6	660	49	51.4	
	30	65	10	5.3	19.3	600	53	46.0	67.3
	40	62	10	7.9	18.0	540	64	39.4	
Silene EF[d]	20	47	10	4.0	24.8	670	52	59.7	
	30	51	10	5.2	20.1	610	61	48.9	67.3
	40	56	10	7.9	17.4	540	67	45.6	
HiSil 233[e]	20	64	10	5.6	27.2	640	58	57.2	77.5
	30	81	10	9.2	25.3	590	73	60.9	65.9
	40	89	10	13.0	23.9	500	78	79.6	53.9

[a] Ref. 7.

[b] Recipe, in parts by wt: smoked sheets, 100.00; zinc oxide, 5.00; filler, as indicated; nondiscoloring antioxidant, 1.00; MBTS, 1.00; TMTD, 0.10; sulfure, 2.75; stearic acid, 3.00.

[c] To convert MPa to psi, multiply by 145.

[d] Silene EF stocks contain 2.4, 3.8, and 5.0 parts of diethylene glycol, respectively.

[e] In addition to the 1 part of MBTS shown in recipe, the 20 vol HiSil 233 stock contains 0.25 parts TMTD and 0.5 parts triethanolamine; the 30 vol stock contains 0.5 parts TMTD and 2 parts triethanolamine; and the 40 vol stock contains 0.5 parts TMTD and 3 parts triethanolamine.

Table 13. Effect of Nonblack Fillers on the Properties of SBR[a,b]

Filler loading	Volume, parts	Mooney viscosity	Optimum cure (at 141°C), min	Modulus (at 300%), MPa[c]	Tensile strength, MPa[c]	Elongation, %	Hardness, shore A	NBS abrasion, ASTM D1630
Pure gum		26	45	0.6	1.4	680	30	13.3
Barytes	30	37	45	1.6	3.8	620	46	15.2
	50	48	45	2.3	3.8	530	54	15.3
Ground whiting	30	40	45	1.2	4.0	620	48	16.5
	50	47	45	1.4	5.0	680	50	15.7
Soft clay	30	42	90	2.1	9.0	1080	42	28.8
	50	51	90	2.8	7.0	1130	46	33.5
Hard clay	30	41	90	2.8	11.4	890	50	34.2
	50	42	90	3.5	10.1	960	51	37.2
Calcene TM	30	45	45	1.6	12.6	860	45	26.6
	50	61	45	1.9	11.9	830	49	16.0
Purecal U	30	46	45	1.7	14.0	710	45	27.7
	50	65	45	2.5	15.2	680	52	27.3
Zinc oxide	30	28	45	1.4	14.5	840	45	30.7
	50	39	45	2.1	14.9	760	54	25.6
Zeolex	20	50	30	2.1	14.0	680	47	34.1
	30	62	30	3.3	16.2	670	53	33.7
	40	79	30	4.2	14.0	620	56	32.1
Silene EF[d]	20	58	15	5.4	14.1	520	56	34.2
	30	72	15	5.3	15.9	570	60	42.0
	40	77	15	6.6	15.0	510	63	46.7
HiSil 233[e]	20	53	60	4.0	18.7	610	51	48.7
	30	81	30	5.8	23.5	610	56	45.9
	40	112	30	7.7	21.9	560	67	40.3

[a]Ref. 7.

[b]Recipe, in parts by wt: SBR 1502, 100.0; zinc oxide, 5.00; filler, as indicated; nondiscoloring antioxidant, 1.00; MBTS, 1.50; TMTD, 0.10; sulfur, 3.00; Cumar MH 2.5, 15.00; stearic acid, 1.00.

[c]To convert MPa to psi, multiply by 145.

[d]Silene EF stocks contain 2.4, 3.8, and 5.0 parts of diethylene glycol, respectively.

[e]The HiSil 233 stocks contain 2.3, 3.5, and 4.8 parts of diethylene glycol, respectively. The 30 vol stock contains 1.2 parts MBTS and 0.15 parts TMTD instead of the combination in the recipe; the 20 and 40 vol stocks contain 1.5 parts MBTS and 0.1 parts TMTD.

Silane-modified clays have found broad acceptance in a wide variety of rubber goods. The silane serves as a bridge between the organic rubber molecule and the inorganic filler particle. The result is a filler with higher reinforcing properties than regular clay. However, the dynamic properties and the degree of reinforcing improvement usually does not permit their use as a carbon black substitute or replacement.

Silane-modified silicas are used in tire tread compounds to reduce rolling resistance, increase wear resistance, and improve wet and snow traction properties.

Reclaim Rubber. Reclaimed and recycled rubber is considered as a filler in this discussion. The process of reclaiming rubber by chemical digestion has been in use since the late 1800s. Early processes involved the treatment of the rubber cord mix with acid. Acids attack cotton, rayon, and nylon. The acid treatment was used to remove the reinforcing components. The rubber was ground and treated. It was then washed, steam devulcanized, and shaped so it could then be reincorporated into new rubber compounds. An improvement on this technique was the use of alkali digestion. The principal benefit of using reclaim is its lower cost compared to new polymers. Reclaim typically sells for 20–30% of the cost of its nonreclaimed counterparts. Reclaimed rubber also imparts some desirable improvements in processing such as lower nerve, seen when milled or extruded components tend to snap back or develop distortions, than new polymers. As a result, compounds containing reclaim have a much lower die swell and faster extrusion rates. It also increases calendering rates and improves flow and mold filling. One of the shortcomings of reclaim is that it lowers the green strength and tensile strength of the compounds in which it is used. Reclaim is in fact a mixture of rubber, carbon black, oil, zinc oxide, stearic acid, and other compounding ingredients used in the original compounds. The levels of reclaim used are generally 15 to 25 phr, about half of which is rubber and the other half compounding ingredients. In some low performance requirement rubber products, such as mats, much higher levels can be used.

Reclaim can be used in many tire applications such as internal casings components and innerliner compounds, sidewalls, chafers, and rubber used in bead components. The introduction of radial tires changed the property needs for compounds used in tire manufacturing and reduced the volume of reclaim. Butyl reclaim made from tubes is used in the innerliner of both bias and radial tire compounds and some reclaim is used in low speed bias tires. There is a fairly large volume of some high quality rubbers such as natural rubber and butyl being reclaimed and used in some solid tires and other mechanical goods to extend the compound without having too adverse of an effect on the product. Ground rubber has replaced reclaim in many tire applications including treads, innerliners, subtreads, and bead components. It is also used in mechanical goods, footwear, solid tires, mats, and retreads. Cryogenic and wet-ground rubbers which are of smaller particle size can be used at moderately high levels and still allow compounds to be processible. A comprehensive discussion on reclaim and recycled elestomers is available (31).

Steam digestion of silicone rubber produces a silicone reclaim, used to reduce the cost of silicone compounds. It has been widely used by silicone automobile ignition systems. The resulting compounds have excellent aging characteristics and still possess outstanding electrical properties.

Antidegradants

Good aging properties of rubber compounds are essential for providing required service life of rubber products. The type of elastomer used is the principal factor in considering aging properties. In general, the more saturated the backbone of the elastomer, the better is the aging properties. For example, EPDM and butyl rubbers are quite stable when compared to more unsaturated polymers such as polyisoprene, sytrene-butadiene rubber, and polybutadiene. Unsaturated polymers are susceptible to oxidation thermally or by reaction with ozone; thus antioxidants and antiozonants are needed to extend the useful service lives of products made with these elastomers. The factors affecting the aging of general-purpose rubber having conventional sulfur and accelerator systems are as follows (6,32,33).

Oxygen. Addition of only 1 to 2% of oxygen is sufficient to cause deterioration of properties for most general-purpose elastomers. Oxidation proceeds by free-radical mechanisms and leads to chain scissioning and cross-linking (34). In the chain scission reaction, free radicals attack the unsaturated polymer backbone causing chain breaking, which results in softening and weakening. This is the primary effect observed for oxidation of natural rubber and butyl rubber. Brittle stocks result from attack at cross-links, resulting in formation of new cross-links. This is a predominant reaction with SBR, neoprene, nitrile, and EPDM rubbers. A drop in ultimate elongation is the most sensitive physical criterion for the aging measurement regardless of mechanism, and is a favored method compared to measurement of tensile loss for cured compounds. In synthetic rubber production (SBR, in particular), viscosity increases with aging and can affect processing if not prevented.

Heat. As expected, heat accelerates oxidation. Therefore, the effects described previously are observed earlier in product use and are more severe as the service temperature of the product is increased. Because oxidation is a chemical reaction, a temperature increase of 10°C almost doubles the rate of oxidation.

Flexing. Flex cracking is a common mode of fatigue failure in rubber compounds. Flex cracking involves not only a mechanical fatigue but also oxidation that is accelerated by heat generated during the flexing cycle. The higher the rate of flexing, the greater is the heat generation, and the worse is the fatigue life of the compound or product.

Ozone. Although ozone concentration in the atmosphere is only a few parts per hundred million (pphm), it rapidly reacts with an elastomer's carbon–carbon double bonds, particularly the backbone unsaturations, causing cracking of the rubber products. This reaction is especially accelerated by stress (stretching and bending) of the elastomer. For every rubber compound, there is a critical elongation below which cracks do not form. Usually, this is in the range of 5–10% elongation. Ozone reacts with double bonds so rapidly that it cannot diffuse into the rubber and therefore all action is at the surface. Thus, surface-protective agents are most useful against ozone attack. For example, waxes that bloom to the surface of rubber to form an inert film are used effectively for static protection (34). Effective antiozonants protect rubber surfaces initially by a sacrificial reaction with ozone, and then by the formation of a protective surface layer on the ruber surface by the reaction products called ozonides (7,14) which are formed in reaction with ozone, but which can also further react to protect the rubber. Certain polymers

also provide good ozone protection. The use of 40–50 parts of a low diene rubber, such as brominated isobutylene-*co*-*p*-methylstyrene, chlorobutyl, or EPDM, in natural rubber, polybutadiene or SBR compounds significantly increases ozone resistance.

Light. Ultraviolet (UV) light promotes free-radical oxidation at the rubber surface causing discoloration and formation of a brittle film of oxidized rubber. This skin cracks in random directions to form a pattern called crazing but can be minimized by the addition of carbon black fillers or UV stabilizers. Carbon black filled rubber compounds are more resistant to UV light than are gum (unfilled) or light-colored stocks containing mineral fillers. Nonblack compounds require use of larger quantities of nonstaining antioxidants which should continually bloom to the product surface as the UV stabilizers on the surface are depleted.

Sulfur. Low sulfur compounds and *efficient vulcanized* (EV) sulfur-accelerated systems have better aging resistance. Normally, the oxidation rate increases with the amount of sulfur used in the cure. The increased rate may be due to activation of adjacent C—H groups by high levels of combined sulfur. Saturated sulfides are more inert to oxidation than allylic sulfides. Polysulfidic cross-links impart excessive hardening of SBR as compared to more stable monosulfidic cross-links.

Metals. Transition-metal ions, such as iron, copper, manganese, and cobalt, when present even in small amounts, catalyze rubber oxidative reactions by affecting the breakdown of peroxides in such a way as to accelerate further attack by oxygen. Natural rubber vulcanizates are especially affected. Therefore, these metals and their soluble salts, such as oleates and stearates, should be avoided.

Selection of Proper Antidegradant. Because the various antioxidants function by different mechanisms, an antioxidant under one condition may become an oxidation promoter in a different condition. Therefore, an antioxidant should be carefully selected depending on service requirements. Most antioxidants are either amines, phenols, or phosphates. The following are some important properties in the selection of proper antidegradant that should be considered.

Persistence in Service (Volatility, Leachability, etc). Volatility is related to molecular weight, and type of antioxidant molecule. In general, the higher the molecular weight, the less the volatility (37). The type of molecule also has an effect. For example, hindered phenols have higher volatility than amine types of the same molecular weight. Volatility is also important from the standpoint of loss of antioxidant during service and depends on surface exposed, temperature of service, flexing, etc. Comparative loss studies for amine and phenolic-type antioxidants have been done (17). Rubber testing is affected by the volatility of antidegradants and widely varying results are obtained depending on whether open or closed aging chambers are used.

Solubility. Another desirable property of an antidegradant is its high solubility in rubber, but poor solubility in water and solvents that come in contact with rubber. Poor solubility in the rubber means that only small quantities of antioxidants can be dissolved without producing a bloom, a migration to the surface. As an example, *N*-isopropy-*N*′-phenyl-*p*-phenylenediamine (IPPD) has limited use because of its poor solubility in, for example, natural rubber (less than 2.0 phr). On the other hand, phenolic and phosphite antioxidants have high solubility and

bloom is not a concern. Solubility of antiozonants in rubber is especially important because their effectiveness depends on the use of small amounts, ie 2 to 5 phr, which must be soluble in the rubber but which also must migrate to the rubber surface in sufficient concentrations to establish a protective layer.

Protection Against Flex Cracking. Most antioxidants including waxes provide oxidation protection under static conditions. However, most of them are not effective in rubber products subjected to dynamic flexing, such as sidewall compounds in tires. The best dynamic protection is provided by *N*-alkyl-*N*′-phenyl-*p*-phenylenediamines.

Stability. In order to have maximum effectiveness over long periods of time, an antioxidant should be stable upon exposure to heat, light, oxygen, water, etc. Many antioxidants, especially in the presence of an impurity when exposed to light and oxygen, are subject to oxidation reactions with the development of colored species. Alkylated diphenylamines are least susceptible and the *p*-phenylenediamine derivatives the most susceptible to direct oxidation.

Physical Form. Physical form is an important characteristic. Compounders prefer solid, free-flowing, nondusty materials, whereas polymer manufacturers prefer materials that are liquid. Less desirable forms are semicrystalline materials which may stratify during storage. Also, substances to be avoided are highly viscous liquids and low melting resins which may solidify upon storage.

Staining Properties. For rubbers containing carbon black, discoloration is not generally a problem and the more potent staining amine antioxidants are used. For white or light-colored rubber products, nonstaining antidegradants are required. Functional classes of nonstaining antioxidants include substituted monophenols, hindered bisphenols and thiobisphenols, substituted hydroquinones, organic phosphites, and thioesters. Triphenyl phosphine, substituted thioureas and isothioureas, thiosemicarbazides, esters of dithiocarbamates, lactams, and olefinic and enamine compounds are reported to be nonstaining antiozonants. Approaches to completely replace the para-phenylenediamine antiozonants with a non-discoloring antiozonant have had only limited success leading to the development of new classes of nonstaining antiozonants (30).

Metal Deactivation. Compounds capable of forming coordination complexes with metal ions are needed for this purpose. A chelating agent such as ethylene–diaminetetraacetic acid (EDTA) is a good example.

Condition of Use. The selection of suitable antioxidants is highly dependent on the conditions under which the rubber product is to be used. It is difficult to find a single material that meets all requirements of a product. Consequently, quite often, blends of antioxidants are used. Table 14 provides a summary of characteristics of commercially important antidegradants (7).

Antioxidant Types. Commercially available antioxidants may be divided into three general classes: secondary amines, phenolics, and phosphites. In general, the amines are more active than the phenolics which in turn are more active than the phosphites. Amine antioxidants, however, often cause staining problems and are therefore used mainly in black-colored compounds. The phenolics and phosphites are relatively nonstaining and are normally used in light-colored elastomer formulas. Many antioxidants in these classes are volatile to some extent at elevated temperatures and almost all antioxidants are readily extracted from their vulcanizates by the proper solvent. These disadvantages have become more

Table 14. Antidegradants[a]

Type	Example (trade name)	Staining	Resistance[b] to				
			Oxygen	Heat	Flexing	Metal catalysis	Ozone
Hindered phenols	2,6-Di-*t*-butyl-*p*-cresol (CAO-1)	None to slight	F	F	F–P	P	P
Hindered bisphenols	2,2′-Methylenebis-(4-methyl-6-*t*-butylphenol) (Antioxidant 2246)	None to slight	G–F	G–F	F–P	G	P
Hindered thiobisphenols	4,4′-Thiobis(6-*tert*-butyl-*m*-cresol) (Santowhite Crystals)	Slight	G–F	G–F	F–P	F	P
Hydroquinones	2,5-Di(*tert*-amyl)hydroquinone (Santovar A)	None to slight	G–F	F	F–P	P	P
Phosphites	Tri(mixed mono- and dinonylphenyl)-phosphite (Polygard)	None to slight	G–F	F	F–P	P	P
Diphenylamines	Octylated diphenylamine (Cyanox 8)	Slight to moderate	G–F	G–F	F	P	P
Naphthylamines	Phenyl-α-naphthylamine (Akrochem PANA)	Moderate	G	G	G–F	F	P
Quinolines	Polymerized 2,2,4-trimethyl-1,2-dihydroquinoline (AgeRite Resin D)	Slight to moderate	G	E	F	P	F–P
Carbonylamines condensation products	Reaction product of diphenyl-amine/acetone (BLE-25)	Considerable	G	E	E–G	P	F–P
para-Phenylene-diamines	Mixed diaryl-*p*-phenylenediamines (Wingstay 100)	Considerable to severe	E–G	E–G	E–G	E	E–G

[a] Ref. 7.
[b] E = excellent, G = good, F = fair, and P = poor.

pronounced as performance requirements for rubber products have been increased. Higher operating temperatures and the need for improved oxidation resistance under conditions of repeated extraction have accelerated the search for new techniques for polymer stabilization. Seals, gaskets, and hoses are some examples where high temperatures and solvent extraction can combine to deplete a rubber product of its antioxidant and thus lead to its oxidative deterioration faster (38,39).

Techniques for providing increased protection against oxidation under severe temperature and solvent extraction conditions include the use of polymer-bound antioxidants. Chemical attachment of the antioxidant molecule to the polymer backbone eliminates volatility and extraction by making the antioxidant essentially infinite in molecular weight after curing. Two general methods of accomplishing this attachment have been used:

(1) functionalized macromolecules react with antioxidant molecules to provide the bound antioxidant, and
(2) antioxidant molecules containing polymerizable functional groups may be copolymerized with conventional monomers during polymer production.

Test Methods. The most common methods used for determining the efficiency of antioxidants in vulcanized elastomers involve accelerated aging tests rather than oxygen absorption experiments. The standard tests involve aging dumbbell specimens cut from tensile strength test sheets under varying conditions of time, temperature, and oxygen content. They are as follows:

(1) air oven (ASTM D573) at 70°C for 1, 3, 5, 7, and 14 days, or in a test tube (ASTM D865) to eliminate cross-contamination (40,41);
(2) oxygen pressure (oxygen bomb, ASTM D572) of 2 MPa (300 psi) at 70°C for 2, 48, 72, and 96 h (42); and
(3) air pressure heat test (air bomb, ASTM D454) at 126°C, and at 80 psi of air for 3, 5, 8, 12, 20, and 30 h (43).

Because of the simplicity of the first test method, most of the comparisons are made using this technique. The effects of the aging process are usually measured on tensile properties such as breaking strength, elongation, and stress (modulus) at 300% elongation. In general, one day of oven aging at 70°C corresponds to one year of shelf aging (a minimum requirement for rubber products), whereas the oxygen and air bomb methods are more drastic. By varying the amounts, types, or combinations of antioxidants, the relative effectiveness of these materials against oxygen deterioration can be determined.

Processing Agents

To improve processing and to plasticize the rubber compound, numerous processing agents have been used over the years, such as petroleum and ester plasticizers, resins and tars, liquid rubber peptizers, peptizers, fatty acids and derivatives from

Table 15. Benefits Through Use of Processing Aids[a]

Operation	Benefit of processing aids	Controlling materials parameters
Mixing	Faster filler incorporation	Reduced viscosity
	Better dispersion	Hydrophobation reaction in silica compounds
	Reduced viscosity	
	Improved release	Homogenization
	Lower dump temperature	
	Reduce mix times	
Processing	Faster and easier calendering and extrusion	Rheological properties
	Improved release	Viscosity
	Less energy consumption	Green strength
		Tack, bloom
Curing and molding	Faster cavity fill at lower operating pressure	Scorch resistance
	Reduced stress in molded parts through easy cavity fill	Rheological properties
	Shorter cycle times	Clean
	Improved release	Mold

[a]Refs. 6,7 and 44.

vegetable oils, and polyethylene and hydrocarbon waxes. Benefits from the use of plasticizers are illustrated in Table 15 (6).

Petroleum plasticizers are the most universally used plasticizers for all rubber compounds. They improve flow and processing properties and also reduce the cost of the final compound. Aromatic process oils are the most common plasticizer for general-purpose rubbers. Naphthenic process oils are used where a minimum of discoloring or staining is required. Paraffinic process oils are used in the low polarity rubbers where high loadings and good solubility are required to avoid bleeding and maximize the plasticizing action.

Ester plasticizers are used in highly polar elastomers, such as neoprene and nitrile rubber, to improve low or high temperature performance or impart particular oil or solvent resistance to a compound. From 5 to 40 phr are commonly used (see PLASTICIZERS). Resins and tars are added to impart tack, soften the compound, improve flow, and in some cases improve filler dispersion, as is the case with organic resins in mineral-filled SBR. Resinous substances are also used as processing agents for homogenizing elastomer blends.

Stearic acid is used in many compounds as a cure activator and in addition may serve as a processing agent to improve mill and processing equipment release properties. Thus stearic acid may be the most widely used processing agent in the rubber industry. Stearic acid is typically used at 1 to 3 phr, and may also be added as a zinc salt (ie, zinc stearate). Because of its low molecular weight it has limited solubility in many elastomers. The term *stearate* often refers to a fatty acid mixture containing palmitates and small quantities of other fatty acids such as oleic acid and linoleaic acid.

Processing agents can be prepared by blending fatty acids, zinc, and calcium soaps into waxes, such as myricyl palmitate, to overcome solubility limitations of individual products. The result is a blend of organic fatty acids, usually in paste form, which serves to improve processing. In some cases, processing agents contain blends of fatty-acid chemicals and an ester-type plasticizer. This makes the processing agent more effective in highly polar elastomers such as nitrile rubber.

Table 16 illustrates how specific classes of processing aids may be used depending on the need. For example, should the rubber technologist encounter difficulties in the product-building operation, tackifiers can be used to assist in ensuring that the respective components in the product will come together in an efficient manner. Further upstream in mixing, peptizers, dispersion aids, or homogenizing agents can be varied to give the desired throughput and compound quality at the mixers. A comphensive review of processing aids has been prepared (44).

Vulcanization

Vulcanization is a chemical process where sulfur or other materials form cross-links in the elastomer and thereby improve the polymer's mechanical properties. In many instances, not all of the desired properties reach an optimum level simultaneously. The task is to achieve a balance of the most important property requirements through design of the cure system and time–temperature cure cycle so as to attain the necessary compound mechanical properties. Frequently, the curing equipment available, such as presses or autoclaves, do not allow the curing conditions to be varied as desired, and so a cure system compatible with the existing equipment must be designed and also meet the compound performance requirements.

Measuring Vulcanization. The formation of a three-dimensional cross-linked structure during vulcanization increases the stiffness (modulus) of the compound. Therefore, following the modulus increase versus cure time provides a continuous picture of the vulcanization process. Oscillating disk rheometers (ODR) and moving die rheometers (MDR) provide useful methods (45,46). In these tests, a preweighed sample of uncured rubber is placed into a preheated cavity containing a conical rotor. The cavity is closed and the rotor is set to oscillate within the rubber sample. As vulcanization proceeds, the compound's resistance to rotor movement increases and this resistance is followed as a function of time, thereby generating a continuous profile of cure behavior. A cure curve, shown in Figure 7, provides information on scorch safety or cure induction time, cure rate, state of cure or stiffness developed, optimum cure time or time when modulus no longer increases significantly, and reversion or the tendency of the compound to degrade upon overcure.

Sulfur vulcanization is a complex reaction during which both the number (density) and type (structure) of cross-links are continuously evolving as the reaction proceeds. The chemical structures formed at any given time during cure may favor one set of properties such as tear strength while not being optimum for others such as hysteresis and compression set. A cure system designed to minimize these trade-offs is always an objective of the rubber technologist (47).

For example, modulus or stiffness increase as the number of cross-links increase because the three-dimensional structure which forms becomes more

Table 16. Operations Using Processing Aid, Types, Examples, and Function[a]

Processing operation	Processing aid	Examples	Function
Mixing	Chemical peptizer	2,2′-Dibenzamididiphenyl-disulfide	Reduces polymer viscosity by chain scission; reduces molecular weight
		Pentachlorothiophenol	
	Physical peptizer	Zinc soaps	Reduces polymer viscosity by internal chain lubrication
	Dispersing agent	Mineral oils	Improves filler dispersion; reduces mixing time; reduces mixing energy
		Fatty acid esters	
		Metal soaps	
		Fatty alcohols	
	Homogenizing agent	Resin blends	Improves polymer blend compatibility; improves compound uniformity
Mixing extruding	Lubrication agent	Mineral oils	Improves compound flow and release
		Metal soaps	
		Fatty acid esters	
		Fatty acid amides	
	Fatty acids		
	Softening agent	Mineral oils	Lower hardness
	Plasticizer	Aromatic di and tri esters	Improves product performance at low and high temperatures
		Aliphatic di esters	
		Alkyl and alkylether monoesters	
Building product assembly	Tackifier	Hydrocarbon resins	Improves green tack; use hydrocarbon resins in summer, phenolics in winter, or as temperature varies
		Phenolic resins	
Curing	Stiffening agent	High styrene resin—rubber	Increased hardness
		Masterbatches	
		Phenolic resins	
		trans-polyoctenamer	
	Mold release agent	Organosilicones	Easier product release from mold; decreased mold contamination
		Fatty acid esters	
		Metal soaps	
		Fatty acid amides	

[a] Refs. 6,7, and 44.

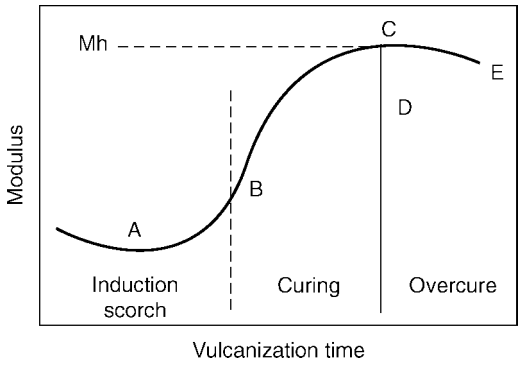

Fig. 7. Cure curve from oscillating disk rheometer where **A** represents scorch safety, **B** cure rate, **C** state of cure, **D** optimum cure, and **E** reversion.

resistant to deformation under load, thereby requiring greater force to reach a given elongation. With overcure, cross-link structure either degrades and modulus drops as in the case of natural rubber, or it continues to build, resulting in a *marching modulus* as in the case of SBR.

Tensile strength, tear strength, and fatigue resistance frequently pass through a maximum as cure state or cross-link network evolution progresses. These ultimate properties are highly dependent on the presence of flaws in the material. As cross-linking proceeds and modulus builds, any applied load acting on a flaw (from poor dispersion, small nicks or tears, localized overcure due to inhomogeneity, etc) concentrates the stresses at the flaw and provides a mechanism for tensile failure and tear propagation or poor fatigue life (Fig. 8). Permanent set and low hysteresis properties depend on minimizing the viscous or plastic component of modulus. Because cross-linking increases elasticity, a high state of cure typically provides the best compression set and heat buildup properties.

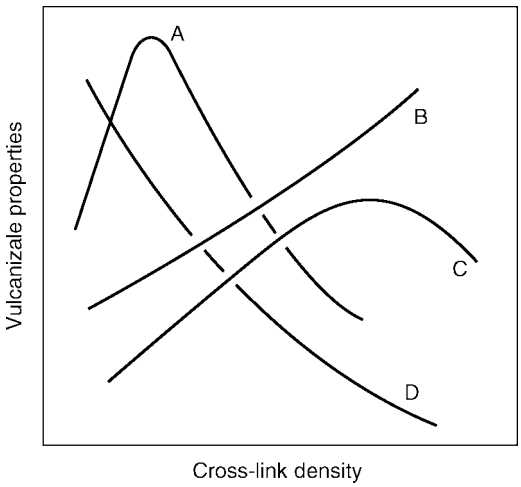

Fig. 8. Effect of cross-link density where **A** represents tear strength, fatigue life, and toughness; **B**, elastic recovery and stiffness; **C**, tensile strength; and **D**, hysteresis, permanent set, and friction coefficient.

Heat resistance is influenced by both the type and extent of cure. The greater the strength of the chemical bonds in the cross-link, the better is the compound's heat resistance. Peroxide cure systems, which result in carbon–carbon bonds, show good heat resistance because of more thermally stable, short, cross-links. This is an important factor in designing the desired cure system.

Cross-link density has only a minor effect on some compound properties such as thermal conductivity, electrical properties, and low temperature brittleness. Another cure system consideration is the compound scorch behavior. Prior to vulcanization, rubber is plastic-like and can be processed into desired shapes such as tires, hoses, belts, or other articles. The time available to accomplish this processing depends largely on the cure system and is referred to as the scorch time. If a compound cures prematurely during the processing step, it is usually scraped. Therefore, a key requirement of the vulcanization step is to minimize premature vulcanization or scorch (Fig. 7).

Vulcanizing Agents. Sulfur is the most common vulcanizing agent for the widely used diene-containing elastomers, such as natural rubber, SBR, and polybutadiene. Rubbermakers' sulfur is a rhombic form existing as a cyclic or eight-member ring structure. Insoluble sulfur is an amorphous polymeric form with molecular weights of 100,000–300,000. Because this material is insoluble in rubber, it resists migration to the surface prior to cure and this bloom-free attribute contributes to maintaining better building tack and better component-to-component adhesion (48,49). Sulfur-containing chemicals such as dimorpholinyl disulfide (DTDM) and tetramethylthiuram disulfide (TMTD) are not only effective accelerators, but they can also be used as sulfur donors. As such, they are effective in controlling sulfur cross-link length to form primarily mono- and disulfide cross-links. These short cross-links are more thermally stable than conventional sulfur curing and thereby provide better heat and set resistance. However, these accelerators are potentially nitrosamine-generating species, and research continues to replace them.

Peroxides are probably the most common materials used after sulfur because of their ability to cross-link a variety of diene- and nondiene-containing elastomers, and their ability to produce thermally stable carbon–carbon cross-links. Carbon–carbon bonds are inherently stronger than the carbon–sulfur bonds developed with sulfur vulcanization (49). Peroxides decompose when heated to produce active free radicals, which in turn react with the rubber to produce cross-links. The rate of peroxide cure is controlled by temperature and selection of the specific peroxide, based on half-life considerations (see INITIATORS, FREE-RADICAL). Although some chemicals, such as bismaleimides, triallyl isocyanurate, and diallyl phthalate, act as coagents in peroxide cures, they are not vulcanization accelerators. Instead, they act to improve cross-link efficiency (cross-linking vs scission), but not rate of cross-link formation.

Halogen-containing elastomers such as polychloroprene, chlorosulfonated polyethylene, and brominated isobutylene-*co*-*p*-methylstyrene are cross-linked by their reaction with metal oxides, typically zinc oxide. The metal oxide reacts with halogen groups in the polymer to produce an active intermediate which then reacts further to produce carbon–carbon bonds. Zinc chloride is liberated as a by-product and it serves as an autocatalyst for this reaction. Magnesium oxide is typically used with zinc oxide to control the cure rate and minimize premature cross-linking (scorch).

Two commercially important, high performance elastomers which are not normally sulfur-cured are the fluoroelastomers (FKM) and the polyacrylates (ACM). Polyacrylates typically contain a small percent of a reactive monomer designed to react with amine curatives such as hexamethylene–diamine carbamate (Diak #1). Because the type and level of reactive monomer varies with ACM type, it is important to match the curative type to the particular ACM in question. Sulfur and sulfur-bearing materials can be used as cure retarders; they also serve as age resistors (50). Fluoroelastomer cure systems typically utilize amines as the primary cross-linking agent and metal oxides as acid acceptors.

Other examples of difunctional compounds used for curing are epoxy resins for nitrile rubber, quinone dioximes for butyl rubber, and phenolic resins for butyl rubber, EPDM, and some EPDM-based thermoplastic elastomers (TPEs). The cross-linking mechanism involves a condensation reaction between each of the two curative difunctional groups with the polymer chain to form a three-dimensional network. Because only carbon–carbon linkages result, thermal stability and permanent set resistance are excellent, often approaching those of peroxide curing. A summary of the advantages and disadvantages of each of the various cross-linking agents appears in Table 17.

Rubber Vulcanization Chemicals. The vulcanization systems consist of the following components; the vulcanizing agent such as sulfur, the accelerator to activate the sulfur, a retarder to help control the rate of vulcanization, and an activator such as zinc oxide and stearic acid.

Accelerators. During sulfur vulcanization of rubber, accelerators serve to control time to onset of vulcanization, rate of vulcanization, and number and type of sulfur cross-links that form. These factors in turn play a significant role in determining the performance properties of the vulcanizate.There are seven principal classes of accelerators which include thiazoles, sulfenamides, guanidines, carbamates, thiurams, xanthates, and phosphates (Fig. 9). There are also miscellaneous accelerators that do not fit into these categories. In addition, blends of several accelerators are prepared which are designed as cure packages for a specific applications. Choosing the best cure system requires extensive knowledge of each accelerator type and its applicability in each elastomer. Table 18 shows a simplified comparison of the scorch and cure rate attributes for the five most widely used classes of accelerators used in the high volume diene-based elastomers.

Table 17. Vulcanization Agents

Accelerator Class	Elastomer	Advantages	Disadvantages
Sulfur	Dienes	Versatile	Heat and compression set resistance
Sulfur donors			
Peroxides	Saturated polymers	Heat and compression set resistance	Cure rate control
	Dienes		
Resins	Primarily butyl-based polymers	Heat resistance	Slow cure rate
Metal oxides	Halogenated polymers	Preferred for CR, CSM	Water resistance

Table 18. Accelerated Sulfur Vulcanization

Accelerator class	Example	Abbreviation	Scorch safety	Cure rate	Expected sulfur cross-link length
None present	Sulfur only	—	—	Slow	S4–S8
Guanidines	Diphenyl guanidine	DPG	Moderate	Moderate	S2–S4
Mercapto-benzothioazoles	Mercaoptobenzothiazole	MBT	Moderate	Moderate	S2–S4
	Mercaptobenzothiazole Disulfide	MBTS	Moderate	Moderate	S2–S4
Sulfenamides	Cyclohexyl-2-benzothiazole-sulfenamide	CBS	Long	Fast	S2–S4
	tert-Butyl-2-benzothiazole-sulfenamide	TBBS	Long	Fast	S2–S4
Thiurams	Tetramethylthiuram disulfide	TMTD	Short	Very fast	S2
Dithiocarbamates	Zinc dimethyldithiocarbamate	ZDMC	Very short	Very fast	S2

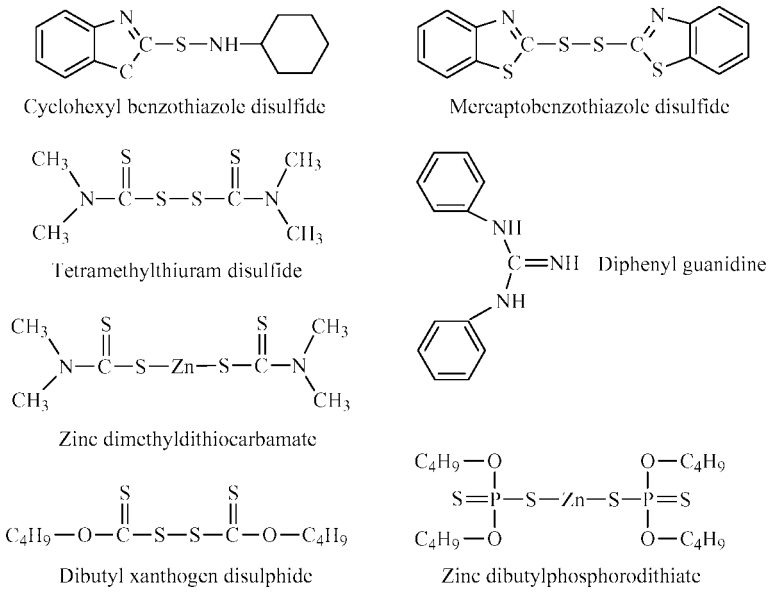

Fig. 9. Structure of a selection of accelerators.

Although differences in accelerator response do occur from one rubber type to another because of inherent differences in their molecular structures, the guidelines in Figure 10 serve as an overview of the principal accelerators and their performance (see RUBBER CHEMICALS).

It is common practice in the rubber industry for a compounder to use combinations of several accelerators in developing a cure system. Typically, these cure systems comprise a primary accelerator and one or more secondary types. Primary accelerators are generally the thiazole and sulfenamide classes; the secondary accelerators are the thiurams, dithiocarbamates, guanidines, and to a much lesser extent, certain amines and the dialkylphosphorodithioates (32). Typically, secondary accelerators are more basic than the primary or major accelerator.

The role of activators in the mechanism of vulcanization is as follows. The soluble zinc salt forms a complex with the accelerator and sulfur termed the

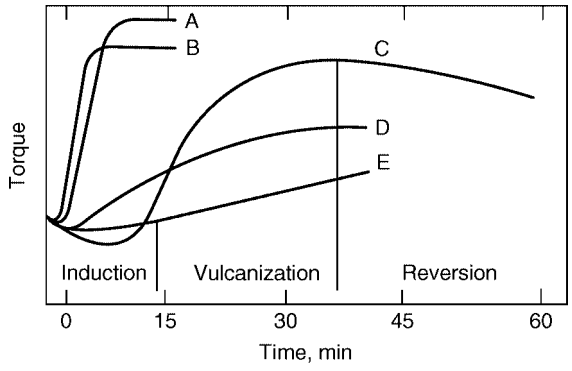

Fig. 10. Cure characteristics of accelerators: **A**, thiurams; **B**, dithiocarbamates; **C**, sulfenamides; **D**, thiazoles; **E**, guanidines. The induction period represents scorch time.

sulfurating agent (eq. 14). The sulfurating agent

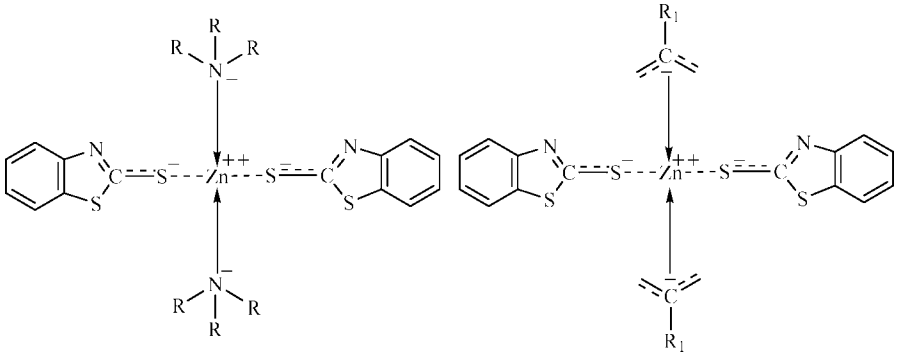

(14)

is stabilized by amine from the accelerator or COO— ligands. This complex then reacts with a diene elastomer to form a rubber–sulfur–accelerator cross-link cursor while also liberating the zinc ion. For simplicity the vulcanization mechanism leading to completion of the sulfur cross-link to another rubber diene segment can be illustrated in the schematic in equation (15) (50). As a general rule the sulfenamides exhibit faster cure rate than the thiazoles. If secondary accelerators are used, dithiocarbamates give the fastest cure followed by the thiurams, then the guanidines.

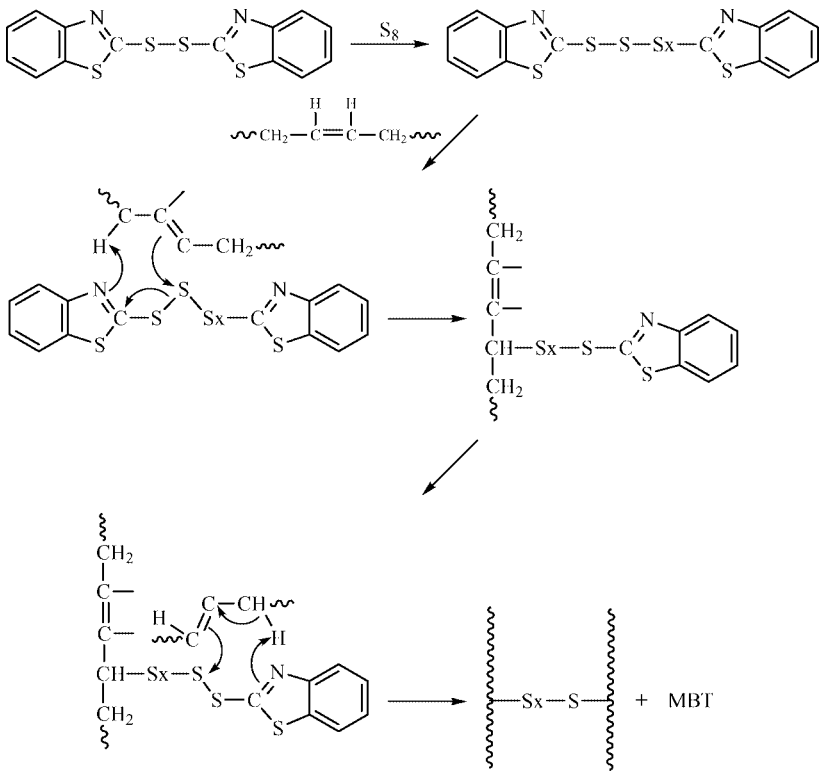

(15)

Comprehensive reviews on the mechanism of vulcanization, roll of the sulfurating complex, metal oxide vulcanization, etc, are available (50,51).

Activators. *Activators* are chemicals that increase the rate of vulcanization by reacting first with the accelerators to form rubber-soluble complexes. These complexes then react with the sulfur to form sulfurating agents (eqs. 14,15). The most common activators are combinations of zinc oxide and stearic acid. Other fatty acids used include lauric, and oleic, acids. Soluble zinc salts of fatty acid such as zinc 2-ethylhexanoate are also used, and these rubber-soluble activators are effective in natural rubber to produce low set, low creep compounds used in load-bearing applications. Weak amines and amino alcohols have also been used as activators in combination with the metal oxides. Natural rubber usually contains sufficient levels of naturally occurring fatty acids to solubilize the zinc salt. However, if these fatty acids are first extracted by acetone, the resultant "clean" natural rubber exhibits a much lower state of cure. Therefore, to ensure consistent cure rate, fatty acids are usually added. Synthetic rubbers, especially the solution polymerized elastomers, do not contain fatty acids and require their addition to the cure system.

Sulfenamide accelerators generally require lower levels of fatty acid because they release an amine during the vulcanization process which acts to solubilize the zinc. Guanidines and similar amine accelerators also serve to both activate and accelerate vulcanization. A study of the effect of stearic acid and zinc oxide on a sulfenamide-accelerated, sulfur-cured natural rubber compound showed the need for both zinc and fatty acid activators is presented in Figure 11 (52).

Retarders. The purpose of vulcanization retarders is to delay the initial onset of cure in order to allow sufficient time to process the unvulcanized rubber. Several main classes of materials are used commercially such as organic acids and anhydrides, cyclohexylthiophthalimide (Santogard PVI), and a sulfenamide

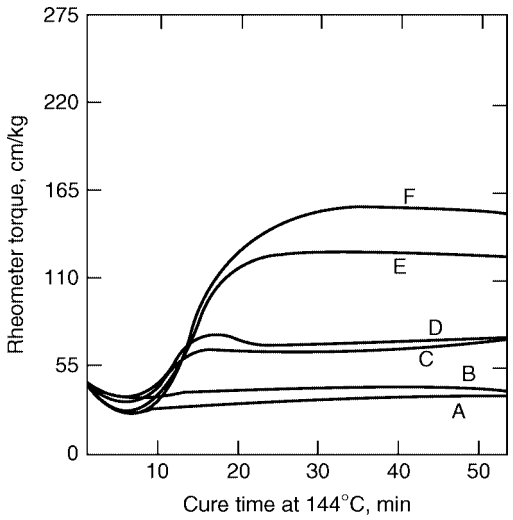

Fig. 11. Effect of activators on cure rate, where **A** is 2.5 phr sulfur, **B** sulfur plus stearic acid (2 phr) plus zinc oxide (5 phr), **C** sulfur plus TBBS (0.6 phr), **D** sulfur plus stearic acid, **E** sulfur plus TBBS plus ZnO, **F** sulfur plus TBBS plus stearic acid plus ZnO.

(Vulkalent E). Examples of organic acid retarders include phthalic anhydride, benzoic acid, and salicylic acids. These materials are thought to function by reaction with basic components present as accelerator fragments, from other basic compounding ingredients, and from impurities. These basic moieties, which would normally serve to accelerate vulcanization and produce a higher state of cure, are neutralized by the acid retarders. Therefore, they are effective in delaying the initial onset of cure. However, some retarders also lower the rate of vulcanization and in many cases detract from the final mechanical properties (22).

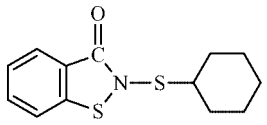

N -(cyclohexylthio) phthalimide (16)

The thiophthalimide (CTP) and sulfenamide classes of retarders differ from the organic acid types by their ability to retard scorch (onset of vulcanization) without significantly affecting cure rate or performance properties. Much has been published on the mechanism of CTP retardation. It functions particularly well with sulfenamide-accelerated diene polymers, typically those used in the tire industry. During the initial stages of vulcanization, sulfenamides decompose to form mercaptobenzothiazole (MBT) and an amine. The MBT that is formed reacts with additional sulfenamide to complete the vulcanization process. If the MBT initially formed is removed as soon as it forms, vulcanization does not occur. It is the role of CTP to *temporarily* remove MBT as it is formed. The retardation effect is linear with CTP concentration and allows for excellent control of scorch behavior.

Cure System Design. There are three generally recognized classifications for sulfur vulcanization: conventional, efficient (EV) cures, and semiefficient (semi-EV) cures. These differ primarily in the type of sulfur cross-links that form as shown in Figure 12, which in turn significantly influences the vulcanizate properties (33). The term *efficient* refers to the number of sulfur atoms per cross-link (32).

Conventional cure systems use relatively high levels (2.5 phr and higher) of sulfur combined with lower levels of accelerator(s). These typically provide high initial physical properties, tensile strength, tear strength, and good initial fatigue resistance, but with a greater tendency to lose these properties after heat aging.

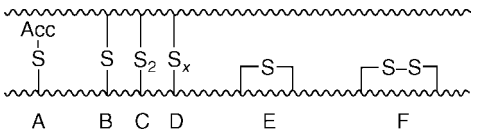

Fig. 12. Sulfur-based cure system designs where conventional systems are polysulfidic, EV systems are mono- to disulfidic, and semi-EV are di- to polysulfidic. **A** is pendent sulfide group terminated with accelerator residue, **B** monosulfidic cross-link, **C** disulfidic cross-link, **D** polysulfidic cross-link ($x > 20$), **E** cyclic monosulfidic cross-link, **F** cyclic polysulfidic cross-link, and Acc accelerator residue.

In contrast, EV cure systems employ much lower levels of free sulfur (0.1 to 1.0 phr) or they use sulfur donors such as TMTD or DTDM combined with higher accelerator levels. The short mono- and disulfide cross-links that form often do not exhibit the physical properties afforded by the conventional systems, but they better retain properties after aging. Semi-EV cures represent a compromise between conventional and EV cures. Although semi-EV cures do yield polysulfide cross-links, they tend to minimize formation of inefficient moieties such as sulfur bridging with itself, accelerator-terminated sulfur linkages, etc. This cleaner usage of sulfur is the reason for their affording a compromise properties between conventional and EV cures.

The reason for the greater loss in properties with conventional cure systems can be understood by examining cross-link bond strengths. Polysulfide bond strengths are significantly lower than are the bond strengths from the shorter cross-links obtained with EV cure systems. The relatively unstable S_x bonds break and rearrange to form mono- and disulfide linkages plus non-cross-linking cyclic and accelerator-terminated fragments. These reactions are observed as changes in properties with increased aging severity. However, conventional systems in natural rubber do provide better flex life than EV cures, and this is one of the limitations of EV curing. The short monosulfide bonds are less able to rearrange to relieve localized stresses which can build during flexing, whereas the longer S_x bonds can rearrange. This ability for stress relief is thought to be one mechanism for the superior flex life of conventional cures. If natural rubber compounds are subjected to thermal aging plus fatigue, the conventional systems perform no better than EV systems. The compromise obtained by using semi-EV systems involves the balance between heat aging and flex life.

Table 19 illustrates formulas for conventional, semi-EV, and EV cure systems in a simple, carbon black-filled natural rubber compound cured to optimum cure (t90).

All three systems give similar tensile strength, elongation, and hardness properties. Conventional and semi-EV systems tend to display better hysteresis (heat buildup) as measured by tangent delta and unaged fatigue resistance.

Table 19. Cure System Classification

Material	Conventional cure system, phr	Semi-EV (semiefficient vulcanization system, phr	EV (efficient vulcanization system), phr
Natural rubber	100	100	100
N330 Carbon Black	50	50	50
ZnO	4	4	4
Stearic acid	1	1	1
6PPD[a]	1	1	1
Sulfur	2.5	1.5	0.15
CBS[b]	0.5	1	2
TMTD[c]			2.5

[a] 6PPD = *N*-1,3-Dimethylbutyl-*N*′-phenyl-*p*-phenylene diamine.
[b] CBS = Cyclohexyl-2-benzothiazole-sulfenamide.
[c] TMTD = Tetramethylthiuram disulfide.

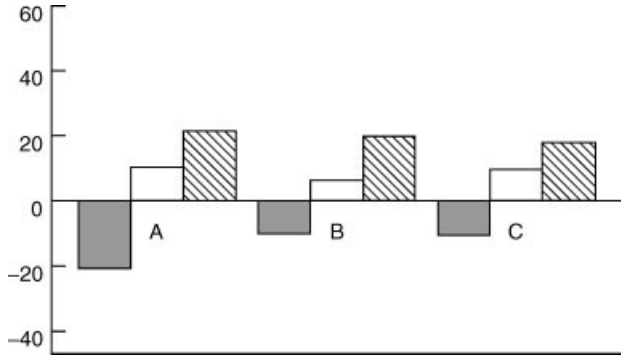

Fig. 13. Aging properties of cured natural rubber. **A** conventional cure system, **B** semi-EV, **C** EV system, ■ tensile strength loss (%), □ fatigue life, and ◥ hardness change.

Figure 13 summarizes properties obtained after heat aging these compounds at 70°C. Both EV and semi-EV systems are superior in tensile strength and hardness retention. Loss of fatigue resistance is greatest for the conventional cure. These observations illustrate the importance of achieving the necessary cross-link structures for an optimum balance of properties. These illustrations are for compounds subjected to ideal or t90 cure conditions at a relatively mild temperature of 140°C. Extremely high cure temperatures, such as those used in injection molding, can be expected to alter these results, but not the overall trends.

In a study of how cross-link structure of a conventionally cured compound changes as a function of cure time, it was observed that total cross-links decrease rapidly past optimum cure (reversion) and that most of the cross-links lost are the S_x types as cure progresses (7). Cure temperature affects cross-link density; there is a dramatic decrease in cross-link density as cure temperature increases. This is a serious concern for the compounder charged with increasing productivity by going to higher temperature, shorter cure cycles. Although plant efficiencies might improve, compound performance is likely to deteriorate.

Cure Systems of Butyl Rubber and EPDM. Regular (nonhalogenated) butyl rubber is a copolymer of isobutylene with a small percentage of isoprene which provides cross-linking sites. Because the level of unsaturation is low relative to that of natural rubber BR, or SBR, cure system design generally requires higher levels of fast accelerators such as the dithiocarbamates and thiurams. Examples of typical butyl rubber cure systems, their attributes, and principal applications have been reviewed (18). Use of conventional and semi-EV techniques can be used in butyl rubber as shown in Table 20 (4).

EPDM is a terpolymer of ethylene, propylene, and a small amount of an unsaturated diene as a third monomer to provide a cure site. Unlike the elastomers previously discussed, the unsaturation in EPDM is not in the main chain, but it is pendent to the chain. Peroxide-based cure systems afford better aging resistance and low compression set. A comparison of a sulfur-based cure to two different peroxides in EPDM is shown in Table 21 (4). Initial properties for these three compounds are reasonably close. However, after air aging, the advantages of peroxide curing are apparent. Most dramatic is the improved compression set

Table 20. Conventional and Semi-EV Cure Systems for Butyl Rubber (in PHR)[a,b]

Ingredient	Semi-EV	Conventional
Sulfur	0.5	2.0
TMTD	1.0	1.0
MBT		0.5
DTDM	1.2	
TBBS	0.5	
Mooney scorch at 121°C t15, min	36.2	18.5
Rheometer at 165°C t90, min	21.0	21.8
Cured to t90 at 165°C		
Hardness, Shore A	68	68
300% modulus, MPa	5.5	7.1
Ultimate tensile, MPa	11.0	11.3
Ultimate elongation, %	600	510
Heat age resistance, 70 h at 121°C		
Retained tensile, %	76	57
Compression set, %	56	81

[a] Ref. 7.
[b] Master batch: butyl polymer, 100 phr; GPF carbon black grade N660, 70 phr; paraffinic oil, 25 phr; zinc oxide, 5 phr.

obtained by the highly stable C—C cross-links developed with peroxides. Other advantages include ability to achieve high transparency or nondiscoloring and very low creep or stress relaxation. Disadvantages limiting the use of peroxides include poor hot tensile and tear strengths, slow cure rate, a tendency for scorch problems, and somewhat more difficult storage and handling problems in the factory.

Effect of Other Compounding Ingredients on Vulcanization. Other ingredients besides the elastomer and the cure system itself influence cure and scorch behavior. Usually the effect of a material on compound vulcanization is dependent upon the pH of the material. Ingredients which are basic in nature tend to accelerate the rate of both scorch and cure, whereas acidic materials exhibit the opposite effect. Reviews of the effect of antidegradants, fillers, process oils, and plasticizers are available (6,14,32,33).

Amine-type antioxidants or antiozonants such as the *p*-phenylenediamines (PPD) can decrease scorch time. As the PPD degrades and liberates free amine, scorch time decreases and cure rate is increased.

Nonblack fillers such as the precipitated silicas can reduce both rate and state of cure because of their strong physical interactions with the polar activator and accelerator chemicals. Neutral fillers such as calcium carbonate (whiting) and clays have little or no effect on the cure properties. Carbon black effects are small.

General Strategy (Statistical Techniques). Often statistically designed experiments are used to optimize curative levels (53). By using properly designed experiments, ie, balanced and/or orthogonal arrays of curative levels, regression analyses can be performed which quantify the effect of each ingredient, and combination of ingredients (interactions), on the properties of interest. From this, an optimum balance of properties is obtained much more efficiently than via the traditional approach of linearly varying one ingredient at a time. It is encouraged

Table 21. Peroxide Versus Sulfur Cured EPDM[a]

Product	Sulfur	Di-cup	Vul-cup
Nordel[b] 1040	100	100	100
HAF black, phr	50	50	50
ZnO, phr	5.0	5.0	5.0
Stearic acid, phr	1.0		
Sulfur, phr	1.5		
TMTM,[c] phr	1.5		
MBT,[d] phr	0.5		
40KE, phr		6.5	
			4.1
TMQ,[e] phr	0.5	0.5	0.5
Cure temperature, °C	160	171	177
Cure time, min	20	20	20
Original Properties			
Modulus, MPa[f]			
100%	2.2	1.8	1.9
200%	6.2	5	5.4
Tensile strength, MPa[f]	17.9	17.2	18.1
Elongation, %	400	375	375
Hardness, points	68	62	60
Air-Aged, 70 h at 150°C			
Modulus, MPa[f]			
100%	5.38	1.7	2.1
200%	12.8	4.7	5.2
Tensile strength, MPa[f]	15	17.4	16.8
Elongation, %	220	400	350
Hardness, points	78	58	60
Compression set, %	77	21	19

[a] Ref. 7.
[b] E. I. du Pont de Nemours & Co., Inc.
[c] TMTM = tetramethylthiuram monosulfide.
[d] MBT = 2-mercaptobenzothiazole.
[e] TMQ = polymerized trimethyldihydroquinoline.
[f] To convert MPa to psi, multiply by 145.

that this technique be used for solving problems in cure system design or any problem involving optimizing combinations of materials and identifying interactions between materials.

Tire Compounding

The pneumatic tire consists of two basic areas: the tread area which is responsible for ground contact, and the casing which is responsible for supporting load and transmitting power to the tread area. Each of these areas has several components with different properties which serve specific and unique functions, and all of which must interact for maximum performance (8,54). The role of the rubber compounds which are used in these basic components is threefold: (*1*) to provide the contact area between the vehicle and the surface; (*2*) to provide the cohesive

material that holds the tire together such that it acts as an integral unit; and, (*3*) to provide protection for the ultimate strength bearing components, ie, the textile, steel beads, and steel or fabric breakers or belts in radial tires.

Tire Component Parts. Desired properties in the components of a radial steel belted passenger car (PC) tire are as follows. The tread is designed and compounded for abrasion resistance, traction, low rolling resistance, vehicle handling characteristics, and protection of the casing from road hazards and obstacles. Often it is divided into two subcomponents to maximize performance: the outer tread for surface contact and the undertread for tying into the casing while reducing tire rolling resistance through decreased hysteresis.

The steel belt, which provides strength and protection for the ply or plies, is encased in a compound that must possess adhesion to the steel which provides stress transfer from the very rigid steel to the considerably more flexible tread, sidewall, and textile carcass components. The wedge compound is formulated to reduce belt-edge sheer stresses while tying the belt to the carcass and reducing hysteresis.

The casing ply coat compound functions are similar to the steel breaker compound. Normally in the steel belted passenger car tire, the ply is a textile cord of polyester or nylon fabrics which are soft and flexible. The truck radial steel tire normally uses a steel cord ply. Earthmover tires are of two basic constructions, ie, radial using steel and bias using textiles. The sidewall compound is formulated to protect the ply and must possess resistance to weathering, ozone, abrasion, and tearing while providing excellent flex fatigue resistance. The innerliner compound must provide good air-permeation resistance and resist moist, hot-air aging.

The apex (often referred to as bead filler) compound must be formulated for dynamic stiffness to facilitate stress distribution and provide good car-handling properties. The bead insulation compound must possess good adhesion to this most important component for enclosing the plies of the tire and holding the tire to the rim. The chafer or rim strip compound protects the plies from rim abrasion and seals the tire to the rim.

There are many ways to measure these properties, some of which are proprietary. However, most laboratory tests are standardized by the American Society for Testing Materials (ASTM). Many of them are interactive to various degrees. The rate and state of vulcanization is especially important to consider for components of heavier and thicker tires. The heat used to vulcanize the tire in a mold under pressure requires time to penetrate from both sides, of the larger tire to the innermost portions. Securing a balanced state of cure, ie, the maximizing of physical properties in all the components, results in the innermost components having a faster rate of cure. The peripheral compounds should have a cure system which holds its physical properties well when overcured. Most tire companies utilize their own physical and chemical laboratories in addition to extensive tire-testing facilities which include laboratory and field vehicle tests. These facilities are augmented by the availability of private commercial companies which operate worldwide.

Materials. Tire compounds contain the following generalized ingredients in the approximate proportions noted. Industry practice is to formulate starting with 100 parts per hundred weight of the rubber (phr). Table 22 offers examples for various treads.

Table 22. General Composition of Tire Tread Compounds by Application[a]

Compound	Material	Standard, phr	High performance, phr	Low rolling resistance, phr	Radial medium truck, phr
Polymer	NR			0–40	60–100
	SBR	50–100	0–100	60–100	0–30
	BR	0–50			0–40
Carbon black grades	N100 Series	N100 Series			N100 Series
	N200 Series	N200 Series	N200 Series	N200 Series	N200 Series
	N300 Series	N300 Series	N300 Series	N300 Series	
Carbon black loading		70–80	70- 85	40–65	45–60
Oil		30–60	25–45	0–30	0–20
Antioxidants, antiozonants		1–2	1–2	1–2	1–3
Sulfur		1	1	1	1
Accelerator		1–2	1–2	1–2	1–2
Stearic acid		1–2	1–2	1–2	1–2
ZnO		3	3	3	3

[a]Ref. 7.

There may be as many as 15 different compounds in a single tire. Each compound typically uses between 8 and 12 ingredients. There are approximately 1000 different chemicals or materials used in the tire compounding field. Thus, the potential combinations are extremely high. In addition, interactions between materials are encountered and must be controlled. For example, premixing of certain vulcanization ingredients must be avoided because of their reactions with each other and formation of end products that do not give the desired rate and state (number of elastomer cross-links) of cure in the finished tire. Interactions are not limited to the 8 to 12 ingredients within a single formula, but may also occur between the compounds of adjacent components, in preassembly of components for tire building, in storage of green (uncured) tires, in vulcanization of the tire, in warehousing, and during operation of the tire through its service life.

Migration of chemicals from adjoining compounds, in addition to preferential absorption of various materials into each other, makes knowledge of the chemistry and physics of materials most important in realizing specific, highly varying properties in the different compounds and components necessary to maximize tire performance and optimize cost. Some interactions of materials are desired. For example, without migration of resins at compound component interfaces, adhesion of one component to another is significantly weakened and intercomponent separation is enhanced. Solubility parameters of materials are important in processing of compounds and components. A material used in excess of this parameter can bloom (diffuse to the surface of the component) and render it difficult in final tire assembly or inhibit the desired migration of other ingredients and weaken component interfacial adhesion.

Tire Elastomers. For the mechanical strength requirements of tires, NR is better than SBR or BR and offers excellent tread chipping/chunking resistance with low tire running temperatures and improved rolling resistance. Although more difficult to mix and process, it is very good in downstream processes such as extruding, calendering, and tire building. Although good in chip/chunk-type wear and in severe stress wear, it is usually faster wearing in nominal passenger and truck over-the-road tires. It offers better ice traction and excellent flexibility in extreme low temperature service (ie, less than 40°C). It is by far the preferred rubber for wire belt and textile ply/breaker coat compounds.

SBR is by far the preferred polymer for passenger car tire treads, mainly owing to its good wear and traction. It is also the least expensive polymer when produced by the emulsion (water-based) process which is the most commonly used. In the 1980s, specialty solution polymerized SBRs (SSBR) were introduced. These rubbers, using hydrocarbon solvent such as hexane as media and special catalytic systems, were found to offer increased capabilities for compounders to improve rolling resistance for decreased fuel consumption while maintaining high levels of wear and traction. The specialty SSBRs accomplish this through control of the styrene–butadiene polymer backbone structure, coupling of polymers, and addition of reactive chemical units at the polymer ends. Not all of these changes are used in the same specialty polymer, but coupled polymers are common and can significantly affect polymer molecular weights; ie, larger (higher molecular weights) branched polymers which are more difficult to produce, are more expensive, and have some deficiencies in processing. Many of these polymers are available in the

oil/black master batch (premixed blends) as is the emulsion SBR. SBR, whether emulsion or solution, is still not as resilient as NR or BR which limits applications in tires.

BR can be produced in both emulsion and hydrocarbon solution processes. It is the butadiene part of SBR that is controlled in specialty SSBRs. Originally polybutadiene found its niche in tires by offering excellent over-the-road wear characteristics because of its high cis, high linearity structure. This offers resilience (low hysteresis) and excellent flex fatigue resistance along with excellent wear and could only be achieved in the more expensive solvent process. BR is more difficult to process in the factory, particularly in milling operations. It does not possess the excellent tack of NR and makes tire building more difficult. BR is also very low in resistance to tearing.

Halobutyl rubber (HIIR) is used in innerliner and white sidewalls, and sometimes in treads to improve winter traction properties. This class of polymer offers marked improvements in tire-air retention owing to lower air permeability as well as excellent age resistance and flex fatigue life. Both the chlorine and bromine versions of isobutylene isoprene rubber (IIR) are used to improve co-vulcanization with the other commodity tire rubbers. It is an almost saturated polymer with few sites (1–2%) available for conventional sulfur curing. IIR offers high hysteresis at nominal tire operating temperatures and thus acts as a superior cushioning rubber. It is the preferred rubber for tire curing press bladders. A new isobutylene polymer modified with *p*-methylstyrene and subsequently brominated is available which offers a fully saturated backbone to resist aging while improving compatibility with tire commodity rubbers. Use of such polymers may allow improvement in a broad range of tire performance parameters.

EPR has a fully saturated backbone and has only unsaturation points available for vulcanization cross-linking in very small percentages of the pendent diene modifier (EPDM). It is an excellent aging compound with high flex fatigue life even when heavily loaded with fillers and is utilized in PC tire white sidewalls.

It is common to use more than one type of rubber within a given compound. An example of this is the truck tire sidewall which must not only possess high strength but must also have excellent aging and flex fatigue life in order to survive multiple retreading, ie, vulcanizing a new tread to the worn original tire casing. The original casing of a radial truck tire, if properly maintained, can last for a million miles, while the original tread on this casing can deliver 100,000 to 300,000 miles. In passenger car tires, as many as four different polymers may be used for the tread compound totaling 100 phr; eg, 25 phr emulsion SBR, 25 phr SSBR, 30 phr BR, and 20 phr NR. If solution polymerized SBR categories can be considered as falling with a 10°C T_g range increments, there are at least nine groups of specialty SSBRs that are commercially available. In addition some large vertically interated, tire companies are producing for their own captive use. Natural rubber can be purchased in several grades. SBR also comes in different grades and is available in oil and oil/carbon black master batches (oil and/or carbon black added to the rubber at the rubber producers) which may use a different SBR (usually higher molecular weight) than if it were produced without master batching. The use of different materials within a single grouping is commonly encountered, ie, the use of two or more elastomers making up the 100 parts total as mentioned above.

Table 23. Carbon Blacks and Their Applications in Tires

		Tire components						
Series	Tire types	Tread	Sidewall	Ply breaker	Apex	Chafer	Bead	Liner
N100	Truck	+				+		
N200	Most	+				+		
N300	Most	+	+	+	+	+	+	
N500	Most			+			+	+
N600	Most			+			+	+
N700	Most			+				

Tire Compound Filler Reinforcement. The popular carbon blacks for tires and their application patterns are shown in Table 23. In tires, carbon black is important because of the high flex fatigue and tear strength requirements of this product. Poor dispersion may result in premature cracking in both treads and sidewalls. In off-the-road tires, poor dispersion could result in excessive chipping, chunk-outs, and cutting of tread material, causing a significant loss in treadwear in addition to tread "base-of-lug" cracking which can lead to loss of an entire lug. Because of demands for improved fuel consumption through reduced rolling resistance, a new series of carbon blacks referred to as low hysteresis or LH, which are N220 or N300 series, have emerged. Basically these series of carbon blacks have a wider size range in both the primary particles and primary aggregates in addition to a more chemically active surface area.

Second in tonnage for tire use, silica's utilization has been increasing in spite of higher per kilogram cost because of increased compound tear strength and contribution to improvement in tire traction performance, and lower rolling resistance. Silica as a tire reinforcing filler was first introduced in earthmover tire treads owing to its ability to improve tear resistance and lower tire operating temperatures. These properties are of utmost importance in off-the-road tires, which function at high operating temperatures and encounter rocks that may cut and tear out large chunks of tread under high traction and torque conditions. With demand for improved rolling resistance, silica usage has expanded into other tire lines. This expansion has also been boosted by the introduction of a silane coupling agent, which forms a chemical bond between the silica and the rubber resulting in improved treadwear. With the use of the bifunctional silane coupling agent silica treads are equal in wear to some carbon blacks while still offering an improvement in rolling resistance. Silane use slightly reduces tear, but this is acceptable in most applications. Silica has also found applications in wire breaker coat compounds, where it stabilizes the copper sulfide bonding layer to the brass-coated steel cable, thus improving adhesion.

Reinforcement and stiffness of a compound can also be achieved with the use of reactive resins. Resins consisting of two-component systems of resorcinol or resorcinol condensation products and a methylene donor, such as hexamethoxymethylmelamine (HMMM) or hexamethyltetramine (HMT), are the most popular in tires. These materials can be prereacted and added to the formula, or for more effective results they can react *in situ*; ie, they can be added separately into the formula and react when the tire is vulcanized.

Softeners, Extenders, and Plasticizers. Other materials can affect the properties of rubber such as softeners, extenders, and Plasticizers (qv). In tires the most popular of these are petroleum oils. They are utilized for controlling green compound viscosity and vulcanized compound hardness. The term *extender* is used to denote their use to allow for increased use of reinforcing fillers as the oils are significantly less expensive than are the rubbers. These materials also act as processing aids. The term *plasticizer* is used to denote their ability to act as an internal lubricant for processing purposes as well as for improving low temperature flexibility in the vulcanized product. The synthetic phthalates are the most effective in meeting low temperature flexibility while also serving as softeners. Cost limits their application.

The petroleum oils are of three basic types: aromatic, naphthenic, and paraffinic. Naphthenic oil does not contain high levels of polynuclear aromatics and is therefore less hysteretic. Because of these considerations the naphthenic oil is gaining in usage at the expense of aromatics. Paraffinic oil is only used in very limited quantities in tire compounds. The petroleum oils are more specific to certain rubbers and therefore require compounding considerations for full optimized usage. All three softeners migrate from one compound to another, and this must be considered when compounding for a set range of stiffness (modulus) gradiations in the tire components designed to alleviate stress.

(1) *Processing aids*. Petroleum oils are processing aids as well as functioning as softeners, extenders, and plasticizers.

(2) *Peptizers* are materials used rather extensively in natural rubber (NR) compounds. When added to NR in premastication, they cleave or break the molecular backbone resulting in lower molecular weights which allows for easier processing. However, there has been a move to reduce usage in order to maximize strength. Some tire companies have gone to mixing variations which are more expensive to preserve molecular weight.

(3) *Other processing aids* utilized in tires are vegetable oils (fatty acids, fatty acid esters, alcohols, and metal salts of these oils), naturally occurring resins such as pine tar, and hydrocarbon resins.

The main benefits of processing aids are as follows: (*1*) improving incorporation of fillers; (*2*) reducing mixing energies; (*3*) reducing internal friction for ease of milling, extruding, and calendering; (*4*) compatibilizing the different rubbers for improved processing as well as for better adhesion of one compound to a different compound in the vulcanized tire (compatibilizers have gained markedly in usage because of polarity differences of blended polymers); and (*5*) providing improved green tack (tackifiers) for better tire building.There is a definite trend in the industry to develop multifunctional materials with value-added properties.

Vulcanization System Components. Tire compounds are almost exclusively cured (cross-linked) with sulfur. Sulfenamides, thiazoles, thiurams, guanidine, and carbamates are the most popular choices to accelerate curing. Efficient vulcanization (EV), semiefficient (semi-EV), and the conventional curing systems

are all used, sometimes in the same tire for different compounds and components. They are also varied depending on the elastomer or elastomer blend used within a given compound, such as a compound using a blend of NR and SBR which uses a more efficient cure system than NR alone may require.

Zinc oxide and stearic acid are used to activate the curing system as well as to preserve cured properties when overcuring, which is curing beyond the point of time and temperature at which maximum properties are obtained.

Overcuring is encountered to some degree in all compounds of any thickness because of the slow conduction of heat through rubber. Earthmover tires may have tire shoulder gauges in excess of 0.3 m (12 in.). The outside and inside of the tire are overcured to obtain a satisfactory state-of-cure in internal components. Even though heat is being conducted to the midpoint of the tire shoulder from both sides it can take many hours to reach the same temperature as the plies and that portion of rubber next to the mold. Although the earthmover tire epitomizes this phenomena, it is an excellent example of the problem of maximizing cured properties which change rather dramatically with state-of-cure. The properties of tear strength, resilience, modulus, tensile strength, elongation, and cut growth (fatigue) are significantly affected by state-of-cure. Of course many factors are involved in effecting the desired end goal of an optimized state-of-cure: the mold, the temperatures and media to effect the temperatures, the pressures, etc. Thus knowledge and understanding of engineering and physics, particularly thermodynamics, in addition to the chemistry of rubber and material reactions, are required.

An important consideration of any vulcanization system is scorch resistance. Scorch time is that period after heat has been applied until a significant change in compound stiffness occurs indicating that cross-linking of the polymer has initiated. As the rubber compound is hot when the accelerators and sulfur are added, it appears that the scorch period starts immediately. As the compound is processed through the factory to form tire components, it is heated and is subject to premature vulcanization (scarch) if heat is excessive (scorch). Scorched compounds are more difficult to process to their finished component.

To assist in control of the onset of vulcanization, a retarder or prevulcanization inhibiter (PVI) is used. Retardation of the onset of cure does not mean that the rate of cure is slowed; in fact, cure rate may actually be increased. Rather, there is an extension to the induction period prior to cure.

Compound Formulating. Generally two basic approaches are used to formulate for achieving desired tire performance: the use of known relationships of materials used in a given compound to a specific performance parameter, and computing relationships of materials to physical properties and in turn estimating the effect on a given performance parameter. Using physical properties relating to performance parameters facilitates development of regression equations to predict performance for laboratory screening of potential improvements. Many of these relationships are well established. The two main categories of measurement criteria are either classical mechanical or dynamic mechanical properties.

Mechanical Strength. Strength is measured in the laboratory with tests of stretch, compression, and torque in both uncured and cured compounds. Uncured or so-called green compounds are measured to assess processing

characteristics. An example is plasticity of the green compound at a given temperature and torque to predict the ease or difficulty of milling, extruding, and calendering to secure a given profile and, or gauge of a component for subsequent tire building. Cured compounds are tested for mechanical or physical properties to relate them to a specific tire parameter. Both green and cured properties are run after mixing of a formula to assure its correctness before subsequent processing for given components. Testing is also conducted on the final component before tire building in some cases.

Some tests, while undergoing deformation, are usually referred to as static, in that they are performed at slow speeds or low cycles. Examples of these tests are stretch modulus, ultimate tensile strength, and elongation to break, ie, a measure of total energy capabilities or rupture phenomena. Dynamic properties are measured by continuous cycles of varying deformation (tension, compression, or shear), at varying frequencies which can be set close to that which a component would experience in a tire. These properties are more correlative to many tire performance parameters.

Aged and Fatigued Properties. Tire compounds are subjected to static and dynamic aging throughout their entire life cycle. Static aging begins even in the green (uncured) state with exposure to oxygen, ozone, light, heat, and humidity. In the tire factory, these effects can be minimized to the point where they barely exist. Factory tire compounders are assigned to tire plants to assure the integrity of their compounds throughout the production cycle. Even as tires are warehoused they are protected by regulations and procedures followed by the material's technologist or compounders. It is when tires are applied to the vehicle that this natural phenomenon of aging becomes most important.

Heat has a detrimental effect on rubber compounds. For example, the tensile strength of a tire compound at 150°C may only be 50% of its room temperature maximum. Furthermore, most of the strength properties, such as tear strength and modulus, are similarly affected. When a tire is heated up through use and allowed to cool again to ambient temperature, it loses some of its original strength and is subject to attack by ozone. This can sever molecular chains and leads to cracking at points of deflection. Finally, flex fatigue resistance diminishes markedly upon aging and repeated cycling because of chemical changes in the compound when heated by rolling and working. Low tire inflation means more work and more heat adding to degradation by a power factor.

Wire cords are particularly subject to degradation of their adhesion values by moisture. To combat this, halogenated butyl (HIIR) use is essential in tire innerliners because of its property of low air and water vapor diffusion rates. Moisture is present in most air pumps and many tires are mounted with water left in the tire on mounting. For these reasons, tires and tire compounds are tested extensively at simulated aging conditions in the laboratory and on test vehicles before they are sold to the customer.

Test Methods

Because of the long-range elasticity of soft rubber vulcanizates and the various special conditions under which they are degraded in use, special test methods

have been developed which in many respects are unlike those used for wood, metals, and hard plastics. The American Society for Testing and Materials (ASTM), through its Committee D11 on Rubber and Rubber-like Materials, is constantly developing and promulgating new and improved methods for testing rubber and rubber products.

Test methods to characterize rubber compounds fall into four general catagories.

(1) Rheological characterization, which would include measurement of compound viscosity using a Mooney Viscometer, indicating ease of processing, vulcanization and curing kinetics, and rheological information obtained from a capillary rheometer.
(2) Classical mechanical properties such as tensile strength, tear strength, peel adhesion, hardness, and aged properties.
(3) Dyanamic mechanical properties such as storage modulus and loss modulus obtained in tension, compression, and shear. A range of associated terms may be calculated from this data which in turn can be used to estimate final product performance parameters.
(4) Secondary properties which might include properties such as permeability, fatigue resistance, rebound, and heat buildup.

The test protocol followed in a development program will depend on the nature of the final product under development. However, as a minimum, based curing properties, processing properties, and basic mechanical properties are required for decisions regarding selection of a compound formula to be used in a product such as a hose or belt.

Summary

The science of rubber compounding is among the most complex disiplines in industrial chemistry. The role of the modern materials scientist in the tire and rubber industry is to use materials to improve current products and develop new technology products. Four major factors govern this development process:

(1) *Quality*. The product must meet the design expectations and be trouble-free.
(2) *Performance*. The product must meet the customer's expectations.
(3) *Environmental*. Products must be in compliance with regulatory requirements and present minimum concern with regard to disposal.
(4) *Cost*. The product or system of which the rubber part is a component must provide value to the customer.

In meeting these objectives, the disipline of rubber compounding has evolved from an "art" 50 years ago to a highly complex science.

BIBLIOGRAPHY

1. J. E. Mark, B. Erman, and F. R. Eirich, *Science and Technology of Rubber*, Academic Press, San Diego, 1994.
2. K. C. Baranwal and H. L. Stephens, *Basic Elastomer Technology, Rubber Division*, American Chemical Society, Washington, D.C., 2001.
3. J. S. Dick, *Rubber Technology, Compounding and Testing for Performance*, Hanser, Cincinnati. 2001.
4. M. Morton, *Rubber Technology*, Van Nostrand Reinhold, New York, 1987.
5. F. W. Barlow, *Rubber Compounding*, 2nd ed., Marcel Dekker, Inc., New York, 1993.
6. M. B. Rodgers, *Rubber Compounding, Chemistry and Applications*, Marcel Dekker, Inc., New York, in press.
7. W. Klingensmith, *Kirk-Othmer Encyclopedia of Chemical Technology*, 4th ed., Vol. 21, John Wiley & Sons, Inc., New York, 1997, pp. 481–562.
8. M. B. Rodgers, *Encyclopedia of Materials: Science and Technology*, Elsevier Science, Ltd., London, 2001, pp. 8237–8242.
9. Classification System for Rubber Materials (SAE J200), Society of Automotive Engineers, Warrendale, Pa., 2000.
10. Standard Test Method for Rubber Property—Effect of Liquids (ASTM D471-79) 1979. ASTM D5964-96, Standard Practice for Rubber IRM 902 and Replacement Oils for ASTM No. 2 and ASTM No. 3 Oils.
11. Rubbers and Laticies—Nomenclature (ISO 1629), International Standards Organization, 1995.
12. *The Synthetic Rubber Manual*, 14th ed., International Institute of Synthetic Rubber Producers, Inc., Houston, 1999.
13. *The Green Book, International Standards of Quality and Packaging for Natural Rubber Grades*, The Rubber Manufacturers Association, Inc., Washington, D.C., 1979.
14. W. W. Barbin and M. B. Rodgers, in J. E. Mark, B. Erman, and F. R. Eirich, eds., *Science and Technology of Rubber*, Academic Press, Inc., New York, 1994.
15. ISO 2000 (1989). Rubber, Raw Natural—Specification.
16. *The Vanderbilt Rubber Handbook*, 13th ed., RT Vanderbilt Co., Inc., Norwalk, Conn., 1990.
17. W. H. Waddell, in M. B. Rodgers, *Butyl Rubbers, In, Rubber Compounding, Chemistry & Applications*, Marcel Dekker, Inc., New York, in press.
18. E. N. Kresge, R. H. Schatz, and H. C. Wang, *Encyclopedia of Polymer Science and Engineering*, 2nd ed. Vol. 8, John Wiley & Sons, Inc., New York, 1987, pp. 423–435.
19. R. P. Kane, *The Vanderbilt Rubber Handbook*, 13th ed., RT Vanderbilt Com., Inc., Norwalk, Conn., 1990, pp. 156–165.
20. D. L. Hertz, *The Vanderbilt Rubber Handbook*, 13th ed., RT Vanderbilt Co., Inc., Norwalk, Conn., 1990, pp. 223–244.
21. M. S. Jones, in K. C. Baranwal and H. L. Stephens eds., *Basic Elastomer Technology*, Rubber Division, American Chemical Society, Washington, D.C., 2001, pp. 358–369.
22. J. R. Dunn and R. G. Vara, *Rubber Chem. Technol.* **56**, 557–574 (1982).
23. ASTM D1765-82. Standard Classification System for Carbon Black Used in Rubber Products, 1982.
24. H. S. Katz and J. V. Milewski, *Handbook of Fillers and Plastics*, Van Nostrand Reinhold Co., New York, 1987.

25. W. H. Waddell and L. R. Evans, in J. Dick, ed., *Rubber Compounding and Testing for Performance*, Hanser Publishers, Cincinnati, 2000.
26. T. G. Florea, *Elastomerics* **118**, 22 (1986).
27. W. H. Waddell, P. A. Beauregard, and L. R. Evans, *Tire Technol. Int*. 24–36 (1995).
28. M. Rigby, E. B. Smith, W. A. Wakeman, and G. C. Maitl, *The Forces Between Molecules*, Clarendon Press, Oxford, 1986.
29. T. H. Ferrigno, *The Couplant Index*, Intertech Corp., Portland, Maine, 1993.
30. W. H. Waddell, *Rubber Chemistry and Technology, Rubber Rev.* **71**, 590–618 (1998).
31. W. Klinensmith and M. B. Rodgers, *Rubber Compounding, Chemistry and Applications*, Marcel Dekker, Inc., New York, 2004, pp. 1–50.
32. S. W. Hong, in *International Tire Exhibition and Conference (ITEC)*, Paper 19A, Akron, Ohio, 2000.
33. S. W. Hong, C. Y. Lin, in *International Tire Exhibition and Conference (ITEC)*, Pusan, Korea, 2001.
34. J. R. Shelton and W. L. Hawkins, ed. *Polymer Stabilization*, John Wiley & Sons, Inc., New York, 1972.
35. L. D. Loan, R. W. Murray, and P. R. Story, *J. IRI* **2**, 73 (1968).
36. J. R. Dunn, *Rubber Chem. Technol.* **34**, 686 (1961).
37. R. B. Spacht, W. S. Hollinshead, H. L. Bullard, and D. C. Willis, *Rubber Chem. Technol.* **38**, 134 (1965).
38. H. Long, *Basic Compounding and Processing of Rubber*, Rubber Division, American Chemical Society, Washington, D.C., 1985.
39. J. A. Kuczkowski, J. G. Gillick, Rubber Chem. Technol., Vol. 57, p. 621, 1984.
40. Standard Test Method for Rubber—Deterioration In An Air Oven (ASTM D573-81).
41. Standard Test Method for Rubber—Deterioration By Heating In Air (Test Tube Enclosure) (ASTM D865-81).
42. Standard Test Method for Rubber—Deterioration By Heat And Oxygen (ASTM D572-81).
43. Standard Test Method for Rubber—Deterioration By And Air Pressure (ASTM D454-82).
44. Rubber Handbook, Technical Bulletin, Struktol Company of America, 2001.
45. Standard Test Method for Rubber Property—Vulcanization Characteristics Using Oscillating Disk Curemeter (ASTM D2084-81).
46. Standard Test Method for Rubber Property—Vulcanization Using A Rotorless Cure Meter (ASTM D5289-95).
47. W. F. Helt, B. H. To, and W. W. Paris, *Rubber World* **204**(5), 18–24 (1991).
48. J. A. Brydson, *Rubber Chemistry*, Applied Science Publishers, Ltd., London, 1978.
49. W. W. Paris, *Education Symposium*, Rubber Division, American Chemical Society, Akron, Ohio, 1982.
50. L. Batemen, C. G. Moore, M. Porter, and B. Saville, *The Chemistry and Physics of Rubber-Like Substances*, MRPRA, Oxford, 1963, pp. 449–561.
51. A. D. Roberts, *Natural Rubber Science and Technology*, Oxford University Press, New York, 1988.
52. M. Studabaker, *Vulcanization of Hydrocarbon Rubbers*, Phillips Chemical Co., 1970.
53. G. P. Box, W. G. Hunter, and J. S. Hunger, *Statistics for Experimenters*, John Wiley & Sons, Inc., New York, 1978.

54. F. J. Kovac, M. B. Rodgers, in J. E. Mark, B. Erman, F. R. Eirich, ed., *Science and Technology of Rubber*, Academic Press, Inc., New York, 1994, pp. 675–718.

BRENDAN RODGERS
WALTER H. WADDELL
ExxonMobil Chemical Company
WILLIAM KLINGENSMITH
Akron Rubber Consulting

RUBBER, GUAYULE

Introduction

Natural rubber (*cis*-1,4-polyisoprene [9003-31-0]) is a vital, strategic, and irreplaceable raw material used in enormous quantities by the commercial, medical, transportation, and defense industries (1) (see RUBBER, NATURAL). At least 40,000 different products and over 400 medical devices contain natural rubber (2). Primarily due to its molecular structure and high molecular weight (>1 million g/mol), natural rubber has excellent performance properties, such as elasticity, resilience, heat dispersion, abrasion resistance and cold-malleability, which cannot easily be mimicked by artificially produced polymers derived from petroleum. Demand for natural rubber has increased throughout the last century, despite competition from synthetic rubber, and currently constitutes 40–45% of the total amount of natural and synthetic rubber used (1,3,4). Temperate-zone regions, including the United States and Europe are wholly dependent upon imports from tropical countries. At present, almost all commercial natural rubber comes from a single tropical plant, *Hevea brasiliensis* Müll. Arg. [the Brazilian rubber tree (5) referred to as "Hevea" in this article], mostly from plantation-grown, clonal trees, made by grafting clonal buds onto seedling rootstocks. Global dependence on this single species for natural rubber is risky because *H. brasiliensis* cultivars have very little genetic variability. This lack of genetic diversity leaves the crop susceptible to pathogenic attack and failure (6,7). Disease is the primary cause of the current dearth of production in South America, and global rubber production could essentially be destroyed by the introduction of South American leaf blight into southeast Asia. Asia currently supplies over 90% of the world demand for Hevea natural rubber (1). Despite steadily increasing demand, largely fueled by the developing automotive industry in China, Hevea acreage has diminished in recent years as growers change to palm oil and other higher value crops, and a shortage of natural rubber is expected in the near future. Moreover, Hevea has strict climatic requirements, limiting its cultivation to specific tropical regions. Natural rubber prices are directly tied to labor costs which increase as the rubber-producing countries develop; latex production is labor-intensive since it is tapped by hand following incisions in the bark of the trees (5,8). In addition, in 2002, the

Encyclopedia of Polymer Science and Technology. Copyright John Wiley & Sons, Inc. All rights reserved.

three principal rubber-producing countries, Thailand, Malaysia, and Indonesia, formed an (Organization of Petroleum Exporting Countries) OPEC-like rubber triumvirate. The immediate goal of the triumvirate, which controls 70% of global production, is to reduce rubber production by 4% and exports by 10%, and drive up natural rubber prices.

The United States is the largest single natural rubber consumer in the world, using about 18% of the global supply of 6.8 million metric tons for its commercial, medical, transportation, and defense industries (1,2,9,10). The United States imports, at a cost approaching $2 billion, about 1.2 million metric tons of raw natural rubber for manufacturing products worth billions of dollars, in addition to its enormous finished goods imports (over $8 billion, containing 349,000 metric tons of rubber) (1,2,9,11). Unlike fossil fuel, the United States has no domestic source of natural rubber to buffer or ameliorate the effects of the triumvirate's decisions, and prices are expected to increase in double digits for several years to come.

Quite apart from the issue of security of supply, another fundamental problem with Hevea rubber concerns the worldwide occurrence of life-threatening, IgE-mediated, latex allergy caused by the proteins in Hevea latex and latex products. Complete protein removal cannot be easily or cheaply achieved, or proven, and, when attempted, negatively impacts latex product performance (3,12). This has led to the ongoing effort to commercially produce hypoallergenic latex from domestically-grown guayule employing the best lines from the U.S. Department of Agriculture (USDA) and university plant-breeding programs.

Although over 2500 plants are known to produce natural rubber, few synthesize commercial quality or quantities (13,14). A notable exception is guayule (*Parthenium argentatum* Gray), a species classified in the Class Angiospermae, the Subclass Dicotyledonae, the Superorder Asteridae, the Order Asterales, the Family Asteraceae (Compositae), the Subfamily Asteroidae, and the Tribe Helianthae. Guayule is a woody shrub native to the Chihuahuan Desert of northern Mexico and the Big Bend region of Texas. Guayule produces linear, high molecular weight natural rubber that can have physical properties and applications equivalent to those of Hevea rubber (15,16). Guayule rubber can be extracted as a solid bulk polymer (17) or as a latex (18–21). Guayule also is one of very few rubber-producing plants to have ever been used commercially for rubber production (22,23). Although guayule rubber was commercially produced in the early part of the last century (22,23), more recent efforts to reinstate production have not led to commercial success because the production costs of bulk rubber were too high to permit direct competition with Hevea rubber (24). Guayule commercialization has been revitalized in recent years by use of the plant to produce hypoallergenic latex, a higher value rubber raw material (25–30).

Biology and Biosynthesis

Natural rubber is a secondary product, compartmentalized in cytosolic rubber particles, which is not recatabolized during the life of the plant. Rubber particles are often made in laticifers, as in Hevea (5,8), but guayule produces them in generalized bark parenchyma cells (31,32). The rubber particles probably originate

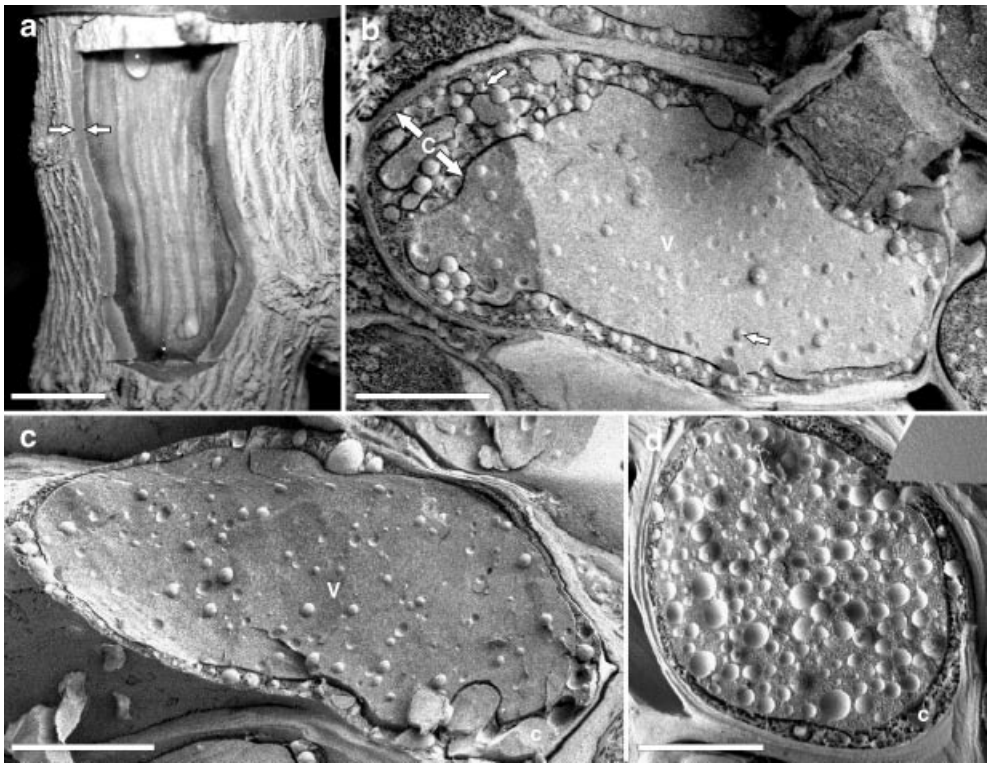

Fig. 1. (**a**) Guayule stem segment (line O-16-1, large, older stem) showing the region where the excised tissue piece for SEM study was taken. The cells containing the rubber particles are located in the tissue indicated between the two arrows, just beneath the bark. (**b–d**) Cryo scanning electron micrographs of rubber-containing cells showing cells from (**b**) young tissue containing rubber particles in the cytosol as well as in the vacuoles, (**c**) maturing cells from medium-sized stems showing an increasing accumulation of rubber particles in the large central vacuole and rubber particles compressed into a single layer in the much-diminished, surrounding cytosol, and (**d**) mature cells from large-sized stems showing a central vacuole filled with rubber particles, and a single layer of rubber particles in the remaining cytosol. Cells are from the following lines: O16-1 (**b**); AZ101 (**c**); N9-5 (**d**). C, cytosol; cw, cell wall(s); V, vacuole. Magnification bars: (**a**) 5 mm; (**b–d**) 10 μm. Photograph from Ref. 33.

in the rough endoplasmic reticulum, but little is known about ontogeny or development. In guayule, as tissues age and the cytosol fills with particles, the rubber particles also move from the cytosolic compartment to fill the vacuole (Fig. 1). As in all rubber-producing plant species investigated to date, rubber is synthesized in guayule by an enzyme called rubber transferase (*cis*-prenyl transferase, EC 2.5.1.20). Although soluble rubber transferases have been reported (34; and see literature reviews in References 35 and 36), rubber polymerization is catalyzed by a rubber particle-bound enzyme (35–41); the earlier reports can be explained by the role of the soluble enzymes in the synthesis of allylic pyrophosphate (allylic-PP) initiator molecules. The membrane-bound rubber transferase is associated with the monolayer biomembrane surrounding the rubber

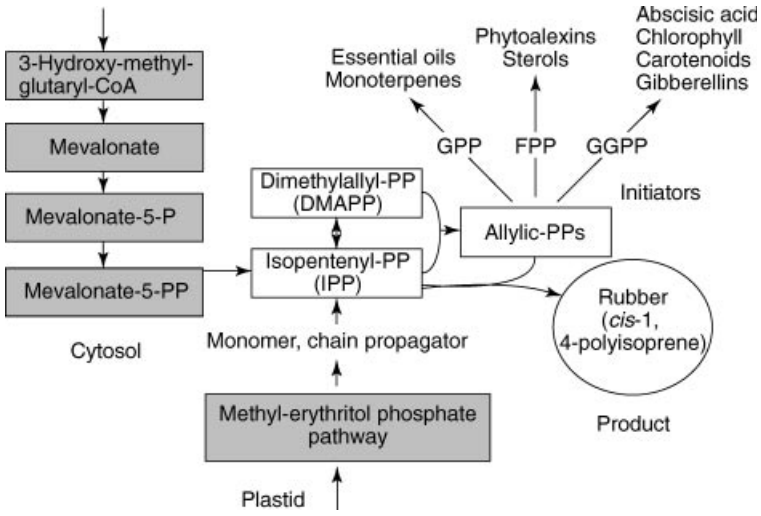

Fig. 2. A section of the isoprenoid pathway illustrating the branch to rubber biosynthesis. Rubber (the product) is synthesized in the cytosol from one molecule of allylic pyrophosphate (the initiator) and many molecules of isopentenyl pyrophosphate (the monomer). Isopentenyl pyrophosphate is produced by the cytosolic mevalonate pathway and by the plastidic methyl-erythritol pathway, as indicated by the shaded boxes. GPP, geranyl pyrophosphate; FPP, farnesyl pyrophosphate; GGPP, geranylgeranyl pyrophosphate.

particles (32,35–44). Rubber transferase produces the rubber polymer (*cis*-1,4-polyisoprene) from isoprene monomers, which it links, chain-like, to an allylic-PP initiator molecule. The rubber polymer grows as more isoprene units are added to the chain. Each rubber transferase is capable of producing many rubber polymers in series, but the eventual polymer molecular weight may vary depending upon substrate concentration, and also varies considerably among species (2,9,45–47). In all rubber-producing species so far investigated, including guayule, rubber transferase requires an allylic-PP substrate (produced by soluble *trans* prenyl transferases) to initiate polymer formation, and a divalent cation, such as Mg^{2+} or Mn^{2+}, as cofactor (35,39–41,48,49). The initiator normally used *in vivo* by rubber transferase appears to be the C_{15} farnesyl pyrophosphate (FPP) (48), although rubber transferases are able to accept a wide range of allylic-PP's as initiating substrate (38,39,45,50), and Mg^{2+} is the *in vivo* cofactor (49). The substrates for rubber biosynthesis, isopentenyl pyrophosphate (IPP) (the monomer) and its allylic pyrophosphate (APP) catabolites (the initiators), are synthesized from carbohydrates via acetyl-coenzyme A, 3-hydroxy-3-methylglutaryl-coenzyme A reductase, and mevalonate (Fig. 2) (51). The plastid-localized deoxy-xylulose/methyl-erythritol phosphate pathway also produces IPP (52,53), but it is not yet known if this contributes to the cytosolic IPP pool from which the rubber polymers are synthesized.

Rubber biosynthesis is an unusual enzymological reaction in that the rubber transferase can accept any one of a number of APPs as the initiating molecule (38,39,45,50). However, the identity of the initiating molecule affects the IPP condensation reaction rate as the rubber molecule polymerizes (Fig. 3). In nonlimiting

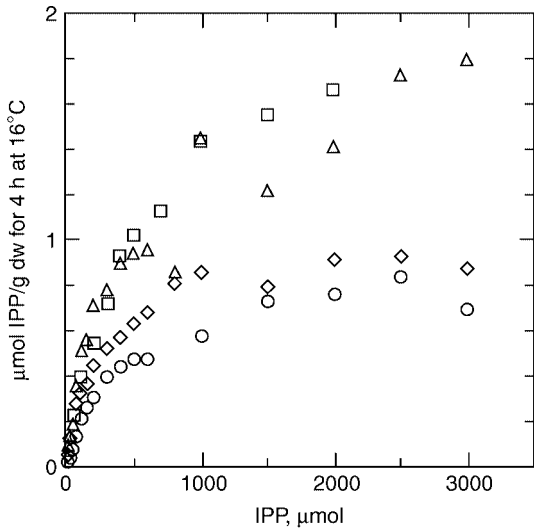

Fig. 3. Dependence of IPP incorporation rate by rubber transferase on IPP concentration in 20 μM allylic pyrophosphate initiator: ○ DMAPP, △ GPP, □ FPP, ◇ GGPP. Data from Ref. 54.

APP concentrations, the longer the initiator, up to the FPP, the higher the rate of IPP incorporation into rubber by the guayule rubber transferase (45,54). In this species, the C_{20} initiator geranylgeranyl pyrophosphate (GGPP) leads to a slower IPP polymerization rate with only the C_5 dimethyl allyl pyrophosphate (DMAPP) giving a slower rate. It is noteworthy that the lower IPP incorporation rate in the presence of GGPP as the initiator is not due to a decrease in the affinity of the rubber transferase for IPP as compared to the affinity in the presence of GGPP or FPP. In fact the IPP affinity is actually greatest in GGPP (Table 1).

Kinetic analysis of the dependence of IPP incorporation on APP concentration (Fig. 4, Table 1) has indicated that multiple binding constants are involved in the reaction, and led to the interpretation that the rubber transferase active site contains a nonspecific hydrophobic binding region which traverses the particle monolayer membrane and with which the growing rubber molecule interacts

Table 1. Substrate Binding Constants for IPP in the Presence of Different APP-Initiating Substrates and the Different APPs[a,b]

Initiator	Size (Number of Carbons)	K_m^{IPP}, μM	K_m^{APP}, μM
DMAPP	5	400	3.52
GPP	10	400	0.50
FPP	15	370	0.02
GGPP	20	240	0.02

[a] Reactions were performed for IPP (isopentenyl pyrophosphate) in the presence of 20 μM APP (allylic pyrophosphate) initiator and for the APPs in the presence of 1 mM IPP.
[b] Apparent K_m's were calculated from log plots of $v/(V_{max} - v)$ against substnrate concentration [S].

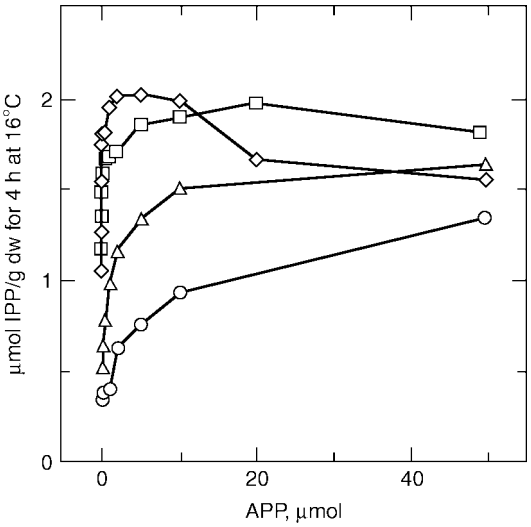

Fig. 4. Dependence of IPP incorporation rate on allylic pyrophosphate initiator concentration in 1 m*M* IPP: ○ DMAPP, △ GPP, □ FPP, ◇ GGPP. Data from Ref. 54.

until the rubber core is reached (2,9). Because DMAPP is an effective initiator of rubber biosynthesis, the specific allylic pyrophosphate binding site probably recognizes the allylic carbon and pyrophosphate and specifically binds via an amino acid/magnesium ion/pyrophosphate bridge in a manner comparable to other prenyl transferases [aspartate being the amino acid employed there (55–57)]. The rubber transferase presumably binds the same small portion of the larger allylic pyrophosphate molecules. A nonspecific hydrophobic binding region may account for the higher binding affinity of the larger allylic pyrophosphate initiators, and the greater this hydrophobic interaction between the allylic pyrophosphate and the binding site, the higher the overall affinity of the enzyme for the substrate.

The binding affinity of the guayule rubber transferase for the different APPs varies considerably. The K_m^{FPP} and K_m^{GGPP} are much lower than the K_m^{GPP} or K_m^{DMAPP} (Table 1). The guayule rubber transferase also exhibits strong negative cooperativity for the FPP and GGPP (Fig. 5). Thus, when a new rubber molecule is initiated by FPP (or GGPP) it becomes much more difficult for another initiator to bind. This directly inhibits the chain transfer reaction and allows the rubber molecule to continue to grow. This property of the guayule rubber transferase may be why the rubber produced during the summertime still appears to be of high molecular weight even though the overall rate of synthesis is slow at that time of year. Of course, *in vivo* it is unlikely that the plastid-produced GGPP initiates rubber biosynthesis, whereas FPP is produced in the cytosol and shares this compartment with the rubber particle-bound rubber transferase.

Rubber biosynthesis in guayule is under strong environmental control, the rubber transferase being induced at the onset of winter (Fig. 6) (40,58–67). The substrate synthesis pathway also appears to be induced at this time (65). In the wintertime, the guayule plant is essentially dormant and can afford to use

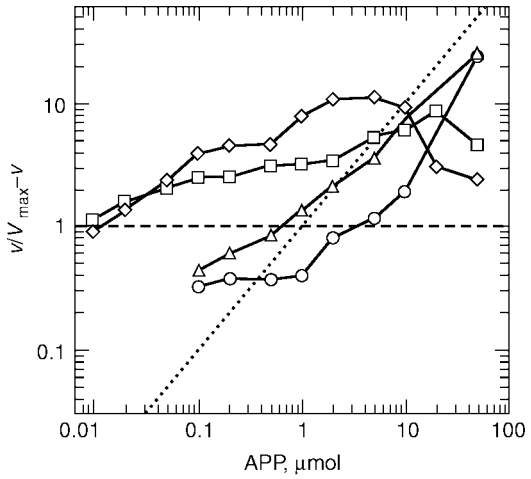

Fig. 5. Hill plot of IPP incorporation rate as a function of allylic pyrophosphate initiator concentration in 1 m*M* IPP: ◯ DMAPP, △ GPP, □ FPP, ◇ GGPP. The diagonal dashed line indicates a gradient of 1. The intercept of the data lines with the horizontal dashed line indicates K_m^{APP}. Data from Ref. 54.

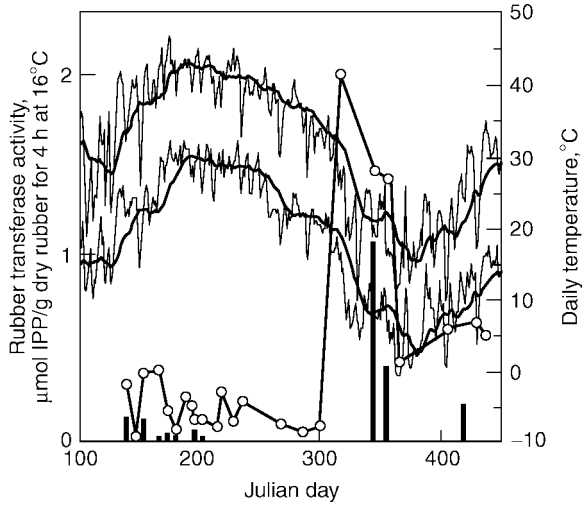

Fig. 6. Rubber transferase activity in rubber particles purified from two lines of field-grown, five-year-old guayule throughout one year. The activity for line 11591 (open circles) and line 593 (filled bars) was determined in 80 μM IPP in rubber particles purified from whole branches. The maximum and minimum daily temperatures also are plotted (light lines), as well as moving averages of both temperature sets (dark lines, data smoothed over 21 days). Data from Ref. 58.

large quantities of photoassimilate to make a compartmentalized secondary product, which it cannot recatabolize. During the summertime, when guayule is rapidly growing and is dependent on the isoprenoid pathway to fuel developmental processes (Fig. 2), the unique kinetic properties of the guayule rubber transferase

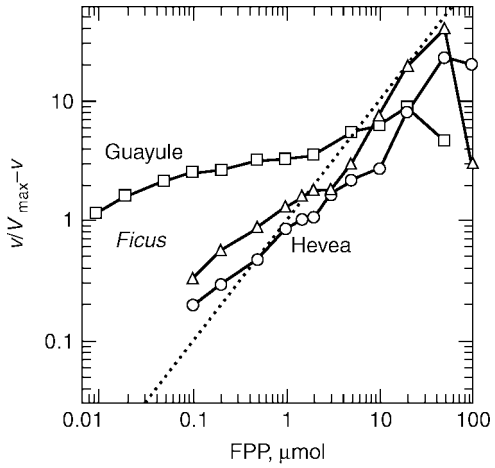

Fig. 7. Hill plot of IPP incorporation rate (5 mM IPP) as a function of FPP concentration for guayule (□), *Ficus* (△) and Hevea (◯). Data from Ref. 47.

appear to allow rubber production without adversely affecting plant growth and development. The high rubber transferase K_m^{IPP}, which is at least 10-fold greater than known competing enzymes in the cytosol, ensures that rubber can only be made when IPP is not required for vital reactions (40,000 isoprenoid metabolites have been identified in higher plants as a group). However, the K_m^{FPP} is smaller than reported K_m^{FPP}'s for other FPP-utilizing enzymes, meaning that rubber transferase can compete successfully for FPP in the presence of cytosolic FPP-requiring enzymes. Substrate deficits are avoided, in this case, because FPP negative cooperativity ensures that rubber biosynthesis does not deplete the FPP pool to the detriment of plant growth and development. It is interesting that the rubber transferases from two laticiferous rubber-producing species (Hevea and *Ficus elastica*) evince much less FPP negative cooperativity than the guayule transferase (Fig. 7) (47,54). This may reflect the disparate location of rubber production in the three species. *F. elastica* and Hevea both synthesize rubber in laticifers; multinucleate systems anatomically separate from the rest of the plant. Thus, production in laticifers depends on a flow of photoassimilate to the laticifer, which then regulates the rate of rubber biosynthesis. If something goes amiss with regulation, rubber biosynthesis may cease but the tree lives on (eg, tapping panel dryness) (68,69). In contrast, guayule makes its rubber in generalized bark parenchyma cells, which may make the process of rubber biosynthesis more dependent on developmental processes.

Even though FPP negative cooperativity plays a role in the regulation of rubber molecular weight in guayule (47,54), outside the concentration range through which the negative cooperativity operates (0.1 to 2.0 μM FPP) rubber molecular weight *in vivo* is highly dependent upon the concentration and ratio of IPP and FPP (2,9,45–47). The initiator concentration seems to be the critical parameter and, as substrate concentrations increase, while maintaining a constant IPP:FPP substrate ratio, the rubber molecular weight produced by the guayule rubber transferase decreases (47,54). Increasing IPP concentrations will increase the

molecular weight of the polymer, but only if FPP is limiting or at a concentration at which negative cooperativity is operating.

Production

Cultivation. Guayule agronomy is well understood (70–74), and so will not be covered in this article. In general terms, guayule likes alkaline, well-drained soil, hot summers, and cold winters without snow cover or serious frosts. Stands can be established using transplants or by direct seeding (75–78). As a crop, guayule has many environmental advantages, requiring relatively little water and fertilizer, and no pesticide. Major advances have been made within the last five years in the development of new, improved germplasm. The time to harvest was generally considered to be from 3 to 5 years, but with the latest germplasm releases this time has been reduced to harvesting in 2 to 3 years (79).

Harvesting. The guayule research carried out in the 1980s demonstrated that guayule can be harvested effectively by pollarding as well as by digging the entire shrub (80). The advanced lines from the plant breeding programs have been selected for their ability to regrow after pollarding, in addition to high rubber yield and biomass (79). Thus, the current commercialization effort is based on farming guayule as a perennial crop harvested biennially using pollarding (cutting the shrub about 10 cm above the soil). The plants regrow rubber-containing branches and can be harvested again in two years, avoiding costs associated with crop replacement. However, once a stand begins to decline, or when new, improved lines warrant its replacement, the entire stand would be dug so that the rubber latex could be extracted from the roots as well as from the above-ground branches.

Processing. Guayule produces its rubber in the form of membrane-bound rubber particles suspended in the aqueous cytosol and vacuole of the bark parenchyma cells (Fig. 1). There is no laticifer system that would allow tapping, as with Hevea, even if this were a cost-effective procedure. Whether processing guayule for latex or dry rubber, it is necessary to rupture the latex-bearing cells.

Latex. To produce guayule latex, the rubber particles must be removed intact from the parenchyma cells while maintaining an aqueous suspension (18,19,21,81,82). Thus, the shrub must remain in a hydrated condition through harvest, shipping, and storage until homogenized in an alkaline aqueous extraction medium. The rubber particles, which have a specific gravity of slightly less than 1, can then be purified from the homogenate using a series of centrifugation steps and/or flotation with alginate creaming agents (82). This process results in an artificially-produced natural rubber latex from which the cytoplasmic components have been removed. Throughout this process it is important to prevent coagulation or degradation of the rubber particles. Coagulation within the plant is highly tied to tissue hydration level (83), beginning after 10% of the defoliated branch water is lost, leading to almost complete coagulation after 50% water loss. Rubber particle coagulation is distinct from degradation, a temperature dependent process that can destroy the latex fraction in hydrated and dehydrated shrub

as well as in shrub homogenate. At high temperatures (40°C) commonly experienced in the southwestern United States during the summer, the extractable latex rapidly declines, in this case primarily through degradation. This effect is clearly demonstrated by a large increase in polydispersity of the rubber in the extractable latex, especially in the smallest and youngest branches, with values as high as 4 being reached (12) (a value of 1 indicates a monodispersed sample). This is probably caused by some cells in the harvested branches dying before others allowing some rubber particle membrane damage, which in turn allows access to, and degradation of, the rubber polymers. Severely damaged or destroyed rubber particles would not show up in this analysis because they would no longer be extractable in the latex fraction. The rubber particle size distribution appears unaltered during the degradative process although the number of particles declines.

These parameters still leave reasonable windows of operation for farmers and processors. Losses in baled and tarped shrub brought out of the direct summer heat are much less, and the latex content is quite stable over two weeks (12,83).

The guayule shrub must be wet-ground in an aqueous, alkaline medium to extract the latex. Grinding protocols must be optimized for each grinding system, with the goal of disrupting every rubber-containing cell without damaging the rubber particles themselves. Inefficient grinding and extraction will greatly impact profitability (19,81,82). Woody material can then be filtered away from the homogenate. The filtered homogenate is then clarified to reduce the substantial component of fine solids that cannot be filtered away from the rubber particles because of their similar size.

Ammoniated homogenate appears to provide a stable environment for latex, without refrigeration, provided that the pH is kept basic (eg, pH 10) and the concentration of rubber particles is at least 5 mg/ml (84). The latex concentration and polymer molecular weight remains stable for 20 weeks before significant degradation occurs. Interestingly, the polymer polydispersity varies little even while the polymers are being degraded after 20 weeks of storage, indicating a uniform degradation process throughout the homogenate. Degradation does not appear to generate the mixture of small and large polymers seen in harvested branches over time.

The latex can be separated from the clarified homogenate and purified and concentrated using continuous flow centrifugation, and/or creaming agents (82), purified and concentrated. Purified latex (in 0.2% NH_4OH, 0.1% Na_2SO_3, and 0.05% ammonium alginate) appears to be stable for months.

In summary, guayule latex is stable within the living plant, the ammoniated homogenate, and in purified form, and is unstable in harvested shrub. This means that, as in the dairy and fresh vegetable industries, harvesting must be coordinated with processing, to minimize the delay between shrub harvest and homogenization. Unavoidable post-grinding delays in a latex extraction and purification process are unlikely to cause serious latex losses.

Dry Rubber. Typically, the plant material is coarsely ground and then subject to compression and shear forces (17,85,86). Dry bulk guayule rubber has been produced by two basic methods: flotation (87,88) and solvent extraction (17,88). Flotation processing was in common use during the early part of the 20th century.

Ground shrub was mixed with a dilute caustic solution that coagulated the rubber and resin (extractable low molecular weight secondary metabolites) as solid particles called "worms". The worms were skimmed from the surface, deresinated with an acetone wash, dried, and compressed into bales. Alternatively, the deresinated rubber was dissolved in a nonpolar solvent such as hexane. Antioxidant was added to the hexane cement prior to filtration and desolventization. The weaknesses of flotation processing included the rate-limiting nature of the deresination step and the need to dispose of large volumes of caustic flotation medium.

Solvent extraction addresses the need to remove nonrubber resinous components from the rubber product. Evaluated at the USDA Northern Regional Research Center (89), sequential extraction involves deresination with a polar organic solvent, followed by rubber removal with a nonpolar hydrocarbon solvent. In the USDA study, defoliated ground shrub was extracted with acetone to remove resin. The deresinated shrub was then extracted with hexane at 60°C in a semibatch continuous countercurrent operation. An oilseed extractor was used at a shrub feed rate of 12 kg/h. Rubber recoveries were as high as 88%. The performance properties of the rubber product were not determined, however.

Sequential extraction does not accommodate an important constraint on the quality of the rubber product: unlike Hevea, cultivated guayule does not produce rubber that meets established product specifications (17,90). The process would have to incorporate an additional operation for the selective recovery of the high molecular weight fraction of the rubber polymer.

In simultaneous extraction, the grounded shrub is initially extracted with a rubber solvent to produce a dilute solution, or miscella, of rubber and resin. The rubber solvent may have a single component such as xylene, or it may be a mixed system such as the acetone–pentane azeotrope. A polar solvent such as methanol or acetone is then added to the miscella to coagulate the high molecular weight rubber fraction. At Texas A&M University, a continuous countercurrent extractor with a nameplate capacity of 900 kg of shrub per 24 hours yielded 270 kg of rubber product (91). The majority of the rubber was extracted with xylene or toluene at 100–125°C. Methanol was the precipitating medium. Under these conditions, rubber recovery was 92% based on whole shrub analysis. Between 1988 and 1990, the Bridgestone/Firestone prototype processing facility in Sacaton, Ariz, produced a total of 8.8 ton of rubber product, of which 5.4 ton met the release specifications described below in Table 2 (92). The Bridgestone/Firestone process employed simultaneous extraction using either the acetone–pentane azeotrope or an equivalent mixture of acetone and hexane, although the primary extraction medium was actually recycled rubber-resin miscella. Extraction was carried out at 50°C. Acetone was the precipitating/fractionating medium. The processing facility had a feed rate capacity of 990 kg fresh weight per hour. Table 3 summarizes the composition and plasticity properties of several batches from a typical production lot.

Latex Properties

Rubber Particle Structure and Composition. Rubber particles are surrounded by a monolayer membrane (32,43,44), the lipid and protein composition

Table 2. Acceptance Specifications for Guayule Rubber

Property	Modifed Grade 20 NR	Modified FEMA
Dirt, %	≤0.10	≤0.20
Ash, %	≤1.00	≤1.25
Volatile matter, %	≤0.80	≤1.50
Nitrogen, %	[a]	[a]
Copper, %	≤0.0008	≤0.0008
Manganese, %	≤0.0015	≤0.0020
Acetone extract, %	≤4.0[b]	≤4.0[b]
Wallace plasticity, P_0	≥35	≥30
Plasticity retention, PRI	≥40	≥40

[a]No specification.
[b]Corrected for antioxidant content.

Table 3. Properties of Guayule Rubber from the Bridgestone/Firestone Prototype Processing Facility

Property	Performance
Dirt, %	0.01 ± 0.00
Ash, %	0.5 ± 0.1
Volatile matter, %	0.6 ± 0.2
Copper, %	0.0005 ± 0.0002
Manganese, %	0.0014 ± 0.0004
Acetone extract, %[a]	3.2 ± 0.8
Antioxidant, %[b]	0.9 ± 0.3
Wallace plasticity, P_0	38 ± 3
Plasticity retention, PRI	60 ± 6

[a]Excluding antioxidant.
[b]Santoflex 134.

of which is species-specific (43). As can be seen (Fig. 8) guayule rubber particles contain relatively few different proteins compared with Hevea. The figure indicates that latices from *F. elastica*, guayule, and *Helianthus annuus* (sunflower) contain far fewer potential allergy-causing epitopes than either Hevea or *Taraxacum kok-saghyz* (Russian dandelion).

Guayule latex not only contains few proteins compared with Hevea but also contains very little protein, ranging from 0.2 to 4% of the amount in Hevea latex (Table 4) (3,12,93). Animal and human trials, including western blot analysis, ELISA (enzyme-linked immunosorbent assay), skin-prick tests, and *in vivo* RAST (radioallergosorbent) assays demonstrated that guayule proteins do not cross-react with anti-Hevea latex protein antibodies at concentrations of up to 1000× the amount of protein sufficient to cause a response with Hevea proteins (94–96). Reciprocal tests in mice showed that guayule latex antibodies do not cross-react with Hevea latex proteins (96). Thus, Hevea latex allergy can be circumvented using rubber products made from guayule latex. The low protein content of guayule latex, and the hydrophobic nature of these proteins, makes it unlikely that large-scale use of guayule latex products will induce a widespread guayule latex allergy in its turn.

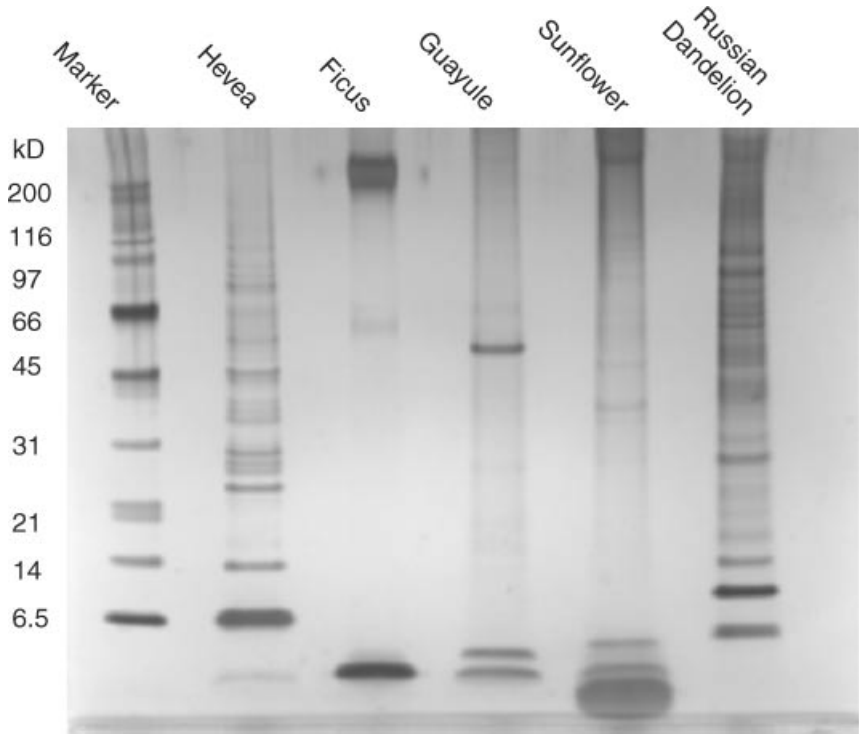

Fig. 8. The protein profiles of washed rubber particles from several different rubber-producing species, separated on a 4–12% SDS PAGE gel. From Ref. 12.

The lipid composition of rubber particles also differs among species (43). Guayule particles contain a rather ordinary complement of fatty acids in contrast to the unusual, but disparate, membrane compositions in Hevea (high in furanoid fatty acid) and *Ficus elastica* (high in long-chain fatty acids). The guayule particle composition may reflect their origin in bark parenchyma cells—a much less specialized cell type than the laticifers producing the rubber particles in Hevea and *F. elastica*.

Rubber Particle Size. The guayule rubber particle mean diameter (1.4 μm) is larger than that of *Hevea* (1.0 μm), and the distribution is broader (Fig. 9) (12,42,97). The absence of a well-known minor subset of *Hevea* particles of 0.1–0.2 μm may reflect their resistance to creaming in the ammonium alginate used to purify the latex tested here.

Rheology. Latex purified from guayule and Hevea was concentrated to the maximum possible degree using ammonium alginate creaming agent and centrifugation. The maximum rubber particle concentration approximated 550–600 mg/ml dry rubber content (DRC) for Hevea and 400–450 mg/ml for guayule. These numbers reflect the concentration at which the latex undergoes a phase shift and gels to a reversibly aggregated semisolid (similar to whipped cream). The Hevea and guayule gelled latices have to be thoroughly remixed in additional suspension medium before the latex particles will fully resuspend. Viscosity of the two

Table 4. Protein Content of Latex from *Parthenium argentatum* and *Hevea brasiliensis*, Determined Using a Modified Micro-BCA Assay[a]

Treatment	Commercial latex, μg protein/g dw rubber	Purified rubber particles (not commercially available), μg protein/g dw rubber
Guayule		
Low ammonia (2%)	0.10 ± 0.10[b]	
Hevea		
Buffered (nonammoniated)	4.28 ± 1.90	0.61 ± 0.01
	3.75 ± 0.31	
High ammonia (6%)	4.33 ± 0.33	0.13 ± 0.10
		0.38 ± 0.08
		0.10 ± 0.04
Low ammonia (2%)	3.21 ± 0.27	0.05 ± 0.01
		0.24 ± 0.03
		0.11 ± 0.02
		0.10 ± 0.02
Enzymatically deproteinized	3.29 ± 0.50	0.07 ± 0.04
		0.17 ± 0.14
		0.22 ± 0.07
		0.05 ± 0.01
		0.03 ± 0.003

[a]From Ref. 17.
[b]The guayule latex value is a mean of 20 latex samples prepared throughout a year from bimonthly harvests of different lines. Each value in the mean was itself a mean of four protein determinations. All Hevea latex determinations are the mean of 4 assays $\pm$ s.e. Hevea latex samples were obtained from CentroTrade, Virginia Beach, Va, although the enzymatically deproteinized material is Allotex from Tillotson Rubber Co.

latices was investigated using flow temperature ramps, over a temperature range in which the particular latex did not coagulate (97). At any particular temperature and concentration, guayule latex was more viscous than Hevea latex. In addition, the tendency for the latex to coagulate increased with increasing temperature and with increasing particle concentration. Guayule latex also was more sensitive to temperature than Hevea latex, with respect to coagulation (97). In both latices, latex viscosity increased with increasing rubber particle concentration, but declined with increasing temperature at all concentrations. This effect was fully reversible over all the experimental temperature ranges used (97). The difference between the two species was dramatically illustrated when the viscosity of their latices was plotted as a function of rubber particle concentration, at several selected temperatures (Fig. 10). Intrinsic latex differences clearly override the concentration effects. Temperature effects are large only at the highest concentration of Hevea latex.

The underlying causes of these differences in latex rheology are not clear but may partially relate to the particle size, the particle size distribution, and/or to the considerable differences in the biochemical components of the monolayer biomembrane that surrounds the different rubber particles (43).

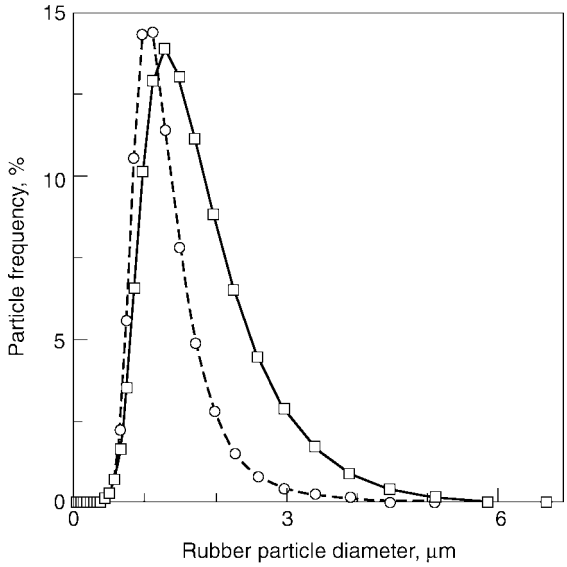

Fig. 9. Particle size distribution of rubber particles purified from guayule stem bark and Hevea latex. Measurements were made on rubber particles in aqueous suspension using a Horiba LA-900 Laser Light Scattering Particle Size Distribution Analyzer. —○—, Hevea; —□—, Guayule. Data from Ref. 12.

For example, the rubber particles are not of a single size, but are a distribution of particle sizes existing in both latices (Fig. 9). The smaller particles mixed with the larger ones would have a large effect on viscosity by impeding the flow of the larger particles and leading to gel formation at a lower concentration. The differing viscosities and packing densities of the two latices suggest that smaller particles play a pronounced role in the low gel point and high viscosity of the guayule latex.

Differences in the molecular weight of the rubber contained within the rubber particles (see References 12, 14, and 42, and Table 5) seem less likely to play a role since the particles were intact in this study.

Rubber Polymer Molecular Weight

When molecular characteristics of THF-dissolved purified rubber particles were determined, the 18-angle light-scattering analysis indicated a single peak for both Hevea and guayule rubber (Fig. 11) although the change in amplitude as the angle increased indicated some interspecific differences. The molecular weight distribution derived from the light-scattering data coupled with refractive index data indicate that guayule latex contains uniformly high molecular weight rubber (Fig. 12). This appears, at first sight, to conflict with published reports of a broad bimodal distribution in this species (98). However, these bimodal rubber peaks were found in rubber solvent extracted from guayule shrub. Rubber from purified rubber particles that coagulated during particle purification (suggesting

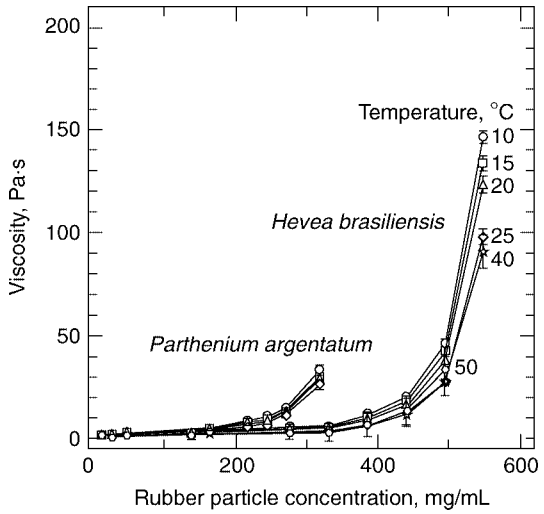

Fig. 10. Viscosity of purified latex from guayule and Hevea, as a function of rubber particle concentration. Each point is the mean ± s.e. of the data from four flow temperature ramps at one of six selected temperatures. Rheological measurements were made using a Texas Instruments AR 500 Advanced Rheometer, plate to plate, 40-mm diameter steel sensor, with solvent trap. Data from Ref. 97. To convert Pa · s to P, multiply by 10.

that the particle membranes had been damaged prior to separation) was of a substantially lower molecular weight (M_p) of about 87,000. This suggests that the polymer in these damaged rubber particles had been degraded in the plant. Thus, it seems that healthy, intact rubber particles consistently contain high molecular weight rubber, but the entire plant also contains degraded rubber in dying and

Table 5. Molecular Weight parameters determined for tetrahydrafuran (THF)-solubilized rubber from different latex samples

Sample	M_n, g/mol	M_w, g/mol	M_z, g/mol	M_w/M_n	r_z,[a] nm	RMS/Molar mass
Guayule						
May-harvested AZ R2 stems						
	954,600	1,266,000	1,628,000	1.33	88.4	0.54
	1,005,000	1,336,000	1,732,000	1.33	91.0	0.58
	845,800	1,124,000	1,467,000	1.33	84.1	0.58
	1,122,000	1,426,000	1,745,000	1.27	83.2	0.61
October-harvested AZ R2 stems						
	816,600	1,146,000	1,522,000	1.40	82.6	0.58
	824,600	1,062,000	1,365,000	1.29	79.5	0.56
Roots and stem bases						
	665,000	1,040,000	1,420,000	1.57	46.3	0.28
Hevea						
	1,210,000	1,650,000	2,040,000	1.36	55.3	0.20

[a]root mear square radius.

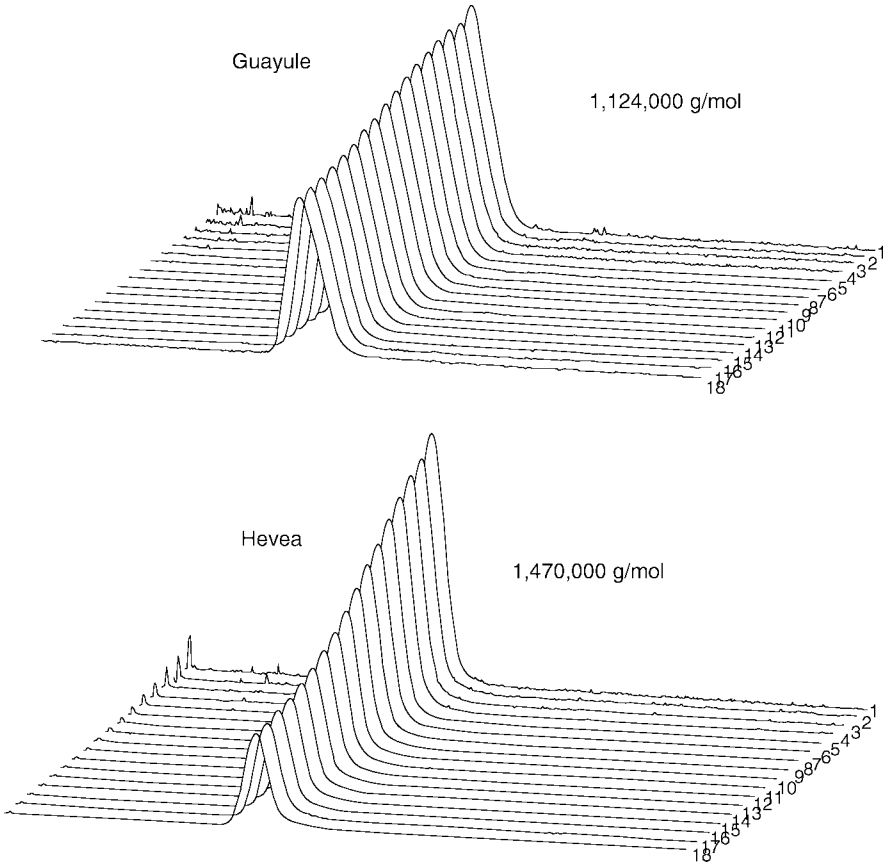

Fig. 11. Light scattering profiles for Hevea and guayule latex rubber gathered from 18 different angles of Wyatt Technology Corporation DAWN DSP Laser Photometer, analyzing rubber passed through an Agilent Technologies HP 1100 HPLC, with 2 P-gel columns in series.

dead cells. Solvent extraction removes all of the rubber in the plant, not just the rubber from the healthy particles obtained through latex extraction. Solvent extraction of fresh, healthy, shrub, under conditions designed to minimize thermal and oxidative degradation, yielded high molecular weight rubber with a unimodal distribution (99), suggesting that intact healthy shrub contains very little low molecular weight rubber. Thus, reported broad bimodal distributions probably reflect a combination of polymer degradation during processing and extraction, and poor quality shrub.

In data generated from purified latex (Table 5), the molecular weight of the guayule latex rubber is consistent over season. Also, rubber molecular weight was not affected by the presence of leaves during extraction (84). The sample of Hevea rubber measured appears to be of a higher molecular weight than the guayule samples. However, the guayule stem latex is of a sufficiently high molecular weight to consistently generate high quality products (3,100).

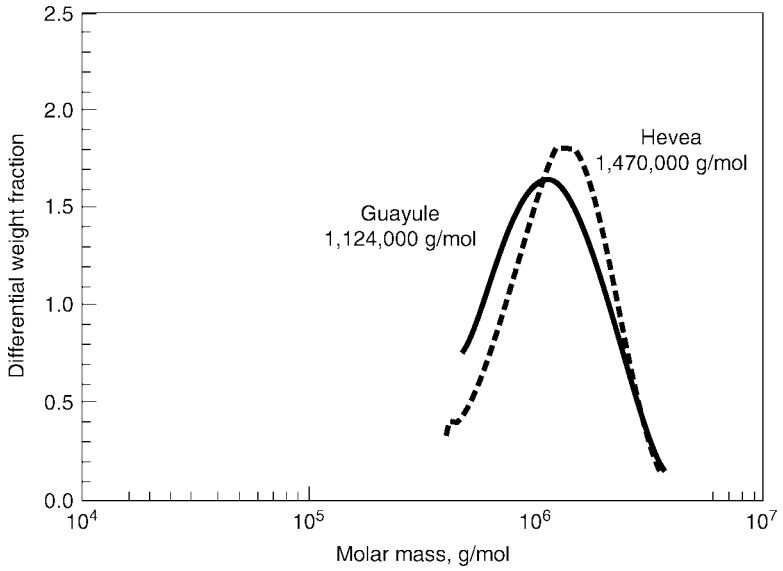

Fig. 12. Molecular weight distributions of rubber from purified latex of guayule and Hevea, determined using an Agilent Technologies HP 1100 HPLC, 2 P-gel columns in series, with an HP1047 RI Detector, and a Wyatt Technology Corporation DAWN DSP Laser Photometer.

Modern guayule is farmed as a biennial crop with repeated harvests of the same plants. The high molecular weight rubber present in the root and stem base latex sample [Table 5 (12)] indicates that the high yielding, last harvest of shrub, when a stand is dug in order to replant a new line, also will be of high quality. Film tests of latex purified from stems and roots confirmed high performance characteristics (unpublished data).

The RMS (root mean square measurement of the molecular radius) versus the molar mass gives an indication of polymer molecular shape and branching, where a value of 1 indicates an unbranched, rod shaped molecule; 0.5 a random coil; 0.3 a spherical structure; and 0.1 a highly branched molecule. Guayule stem rubber seems to form a random coil with few branch points, whereas Hevea rubber appears to be a more compact and branched polymer [Table 5 (12)]. Guayule latex rubber from the roots and stem bases seems more like the Hevea rubber in shape than the stem latex rubber, but it is not known whether this is a reflection of its location or of its greater age.

Dry Rubber. The microstructure of the guayule rubber polymer has been studied in detail (100). Although similar to Hevea rubber in many respects, guayule rubber has lower green strength and an enhanced crystallizability. The higher green strength of Hevea rubber has been ascribed to the formation of cross-linked polymer gel (101) through reactive substituents such as epoxides, amines, and carbonyl groups naturally present in the polymer (102–104). Guayule rubber contains few such reactive substituents. As a result, guayule rubber has a lower viscosity and a shorter stress relaxation time (105). Mixing operations produce a more rapid dispersion of fillers and compounding ingredients in guayule rubber

(106). Compared with higher purity or deproteinized Hevea rubber, guayule rubber has a higher propensity for strain-induced crystallization (107,108). This behavior is ascribed to the presence of higher levels of nonrubber impurities in guayule rubber.

Among these nonrubber impurities, those extractable with polar organic solvents such as acetone are collectively known as resin. Guayule resin is a complex mixture of low molecular weight secondary metabolites such as terpenes, sesquiterpenes, and fatty acid triglycerides (109). It is these latter components that have been implicated as contributors to the degradative effect that resin has on guayule rubber (110). As a consequence, reducing the resin content of bulk guayule rubber has been an important goal of process development efforts.

The sulfur vulcanization properties of guayule rubber reflect the low level of reactive substituents. Because of natural vulcanization activators not present in guayule rubber, Hevea rubber has a higher cure rate and attains a higher level of cross-linking (111,112). However, adjusting the cure system can reduce these performance differences (112).

Technical Specifications. The guayule rubber produced by Bridgestone/Firestone, Inc., and accepted for testing by the Department of Defense met either one of two specifications (Table 2) (113). These were derived from the ASTM specification for grade 20 natural rubber (114) or a modified Federal Emergency Management Agency (FEMA) specification (115) established for guayule rubber itself.

Applications

Latex. The physical properties of guayule latex differ from those of Hevea latex, and a Hevea compounding recipe will generate a guayule latex film with poor performance characteristics (116). However, successful compounding formulations, with excellent physical properties, were developed by the Akron Rubber Development Laboratory, Akron, Ohio (Harry Bader, unpublished results). Guayule latex prototype medical products were then manufactured (Akron Rubber Development Laboratory, Akron, Ohio), including surgical gloves, examination gloves, household gloves, industrial gloves, miniature gloves, surgical tubing, assorted surgical balloons, condoms, and children's balloons. Even after four years of storage, films from condoms and examination gloves were proved to provide an effective barrier to the transmission of human viruses (100). No signs of film deterioration have yet been observed (now seven years post-manufacture). Also, when stabbed with an 18 gauge hypodermic needle against a styrofoam backing, a smaller hole was left in guayule latex glove films than in unchlorinated, powdered Hevea or nitrile films (3). For the new Hevea glove film and the nitrile films, the holes on the inner glove surface were only slightly smaller than the needle diameter. However, it was interesting to note that almost all films were left with holes considerably smaller than the needle diameter when the narrower 25 gauge needle was used. The relatively large holes in the thinnest nitrile gloves indicate that this film lacked sufficient strength to stretch around the needle as it penetrated the film. The old Hevea glove films used in this study were of a similar age as that of the guayule gloves but, unlike the guayule gloves, had noticeably deteriorated.

Research by Apex Medical Technologies, San Diego, Calif, in collaboration with Yulex Corp, has led to a report that a novel cure process creates even better performance properties in guayule latex films than synthetic polyisoprene films (3,117). The guayule latex films have essentially the same tensile strength as those obtained from Hevea latex under similar processing conditions. Guayule latex films exceed ASTM standards for surgical gloves and are 33% stronger than synthetic polyisoprene latex films produced under similar conditions. They are considerably stronger than enzymatically deproteinized Hevea latex films made from enzyme-treated but unwashed latex (see Table 4). Also, the deproteinized latex was unstable and, especially when purified, prone to coagulation. Synthetic polyisoprene and deproteinized Hevea latex films are generally expected to become more common in the nonallergenic latex medical products market. The films were cured via an organic peroxide post-vulcanization system, where anaerobic conditions are used to affect a total cure without concurrent polymer degradation. The prevulcanization step normally used with traditional sulfur-cured Hevea materials is not necessary, which represents a considerable cost savings in manufacturing. Total curing can now be accomplished in less than five minutes (3).

The organic peroxide curing system was used to cure films made from latex extracted from different guayule lines and plant parts as well as from Hevea samples. Performance parameters (Table 6) indicate that good quality films can be made from different guayule lines, and from stem latex and latex extracted from the roots and stem bases.

Nonetheless, it is clear that guayule latex rubber differs from Hevea latex rubber. It seems possible to compensate for undesirable differences by the astute application of rubber chemistry and judicious selection of compounding methods and ingredients. However, some of these unique differences may prove advantageous. For example, of potential product relevance, the rubber particle cores of raw guayule latex retain malleability at $-196^{\circ}C$, independent of purification procedure and line or tissue age (33). Raw latex from Hevea is brittle at this temperature and currently available Hevea latex products are considered malleable only to about $-50^{\circ}C$. Low temperature malleable polymeric materials are especially desired by the aerospace industry, for high value gaskets, seals, tires, bags, tubing, and numerous other products, and many other applications await the development of such materials. Although the underlying causes of the low temperature malleability are not yet understood, compounded guayule latex may be able to serve such applications.

Dry Rubber. Because of its enhanced crystallizability, guayule rubber can exhibit superior failure properties in unfilled rubber compositions. As a double network, an elastomer cured a second time while in a deformed state guayule rubber exhibits substantially better fatigue resistance than deproteinized Hevea rubber (118). When compounded with carbon black, guayule rubber and Hevea rubber behave similarly (119). In tread and wire skim stocks, the compounding and performance behavior of guayule rubber was comparable to that of Hevea rubber (Tables 7, 8) (120).

Recent evaluations of guayule rubber in finished rubber goods have focused on military applications. Guayule rubber has been evaluated in tank track pads (121,122), in aircraft tires (123–125), and in light truck tires (126). The performance of rebuilt aircraft tires built with guayule rubber was comparable to the

Table 6. Some Performance Characteristics of Latex Films Cured With an Organic Peroxide Post-Vulcanization System

Plant	Sample[a]	500% Modulus, MPa	% Elongation at break	% Swell
Guayule, line AZR2	Stem	1.89	738	85.4
	Roots + stem bases	1.55	8.52	86.3
Guayule, line Cal-6	Stem	2.34	712	80.0
	Roots + stem bases	1.64	908	85.2
Hevea	High protein	1.95	816	87.7
	Low protein	2.55	732	82.9

[a] All samples were adjusted to 0.05% ammonium alginate before making the films. The soluble proteins were removed from a sample of high protein Hevea (normal) latex by several cycles of creaming to generate the low protein Hevea sample. The guayule latex samples also contain no soluble protein.

performance of those containing Hevea rubber (123,124). However, new aircraft tires fabricated either from 100% guayule rubber or from a 50:50 blend of guayule rubber and NR did not pass all dynamic testing requirements. Guayule rubber was not a direct drop-in replacement for NR in this application (125). Comparative performance tests have been run on light truck tires containing 100% guayule rubber or a 50–50 blend of guayule and Hevea rubbers, with guayule rubber or the guayule–Hevea rubber blend being substituted in all component stocks normally containing Hevea rubber. Commercial tires served as controls. Overall, the performance of the tires containing guayule rubber was comparable to that of the controls (126).

Commercialization Update. High quality guayule latex rubber and bulk rubber can both be produced from guayule, but the economics of latex production

Table 7. Guayule Rubber (GR) Performance in a Steel Belt Skim Compound Relative to a Hevea Rubber (NR) Control (NR Performance = 100)

Property	NR	GR[a]
Cure time	100	85
Maximum rheometer torque	100	107
50% Modulus	100	119
Tensile strength	100	102
Aged retention, %	40	46
Elongation, %	100	108
Aged retention, %	32	35
Tear strength 23°C	100	100
100°C	100	133
Steel cord adhesion	100	95
Rubber coverage, %	95	95
Aged retention, %	67	69
Aged coverage, %	40	50
Stock–stock adhesion	100	82
Aged retention, %	45	56

[a] Plasticity = 29, PRI = 73, volatiles = 0.33%, ash = 0.38%.

Table 8. Guayule Rubber (GR) Performance in a Tread Compound Relative to a Hevea Rubber (NR) Control (NR Performance = 100)

Property	NR	GR[a]
Cure time	100	98
Maximum rheometer torque	100	108
50% Modulus	100	118
Tensile strength	100	113
Aged retention, %	77	96
Elongation, %	100	98
Aged retention, %	76	86
Tear strength 23°C	100	92
100°C	100	100
Pico abrasion	100	109
Rebound, % 23°C	100	109
100°C	100	104
Aged coverage, %	40	50
Stock-stock adhesion	100	100
Aged retention, %	61	53

[a]Plasticity = 29, PRI = 73, volatiles = 0.33%, ash = 0.38%.

favor commercialization based upon hypoallergenic latex as the primary product. The solvent-based extraction process proved too expensive to produce guayule rubber commercially competitive with the low cost of Hevea bulk rubber. The water-based latex extraction process not only is cheaper than the solvent-based process but produces guayule rubber in the higher value latex form. In addition, the low protein, hypoallergenic properties of the guayule latex allow market entry into the hypoallergenic medical products market where high priced synthetic polymers are the principal competitors, and Hevea latex products are less usable because of Type I latex allergy. The exclusive licenses to the USDA's guayule latex process (19) and product patents (21) were awarded to Yulex Corp in 1997. Yulex has identified over 75 commercial farms in southern Arizona and the desert southwest United States with the interest and established infrastructure to grow guayule. The company has developed large-scale commercial processes for producing, harvesting, cleaning, and conditioning guayule seed for transplant operations, and currently maintains seed banks for the advanced lines (from the plant breeding programs) to plant several thousand hectares. Yulex Corp began operation of their first commercial pilot latex bioprocessing facility (750 ton shrub per year) in 2003, and moved guayule farming from an experimental industrial crop into main-stream agriculture. In addition, Yulex has entered into product development agreements with several major medical device manufacturers. Yulex may be reached at www.yulex.com for additional information.

Implications of Commercial Guayule Production. Domestic rubber production will safeguard natural rubber supplies to the United States and provide hypoallergenic latex products safe for use by patients suffering from Type I latex allergy. Economic value to rural America is harder to assess, but domestic guayule farmland is rapidly expanding. Much of the acreage will be on currently retired farmlands, enhancing its impact on rural economies. Ten-fold increases

in production capacity are planned in 2004 (7500 ton/y) and 2005 (75,000 ton/y). These production facilities will be located in the guayule-growing region enhancing the positive impact on rural development. Improved guayule lines will enhance profitability for the farmers and processors.

As the guayule crop expands, a vast quantity of bagasse will be generated as a by-product of latex production. The United States already produces large agricultural surpluses and large volumes of agricultural wastes, which has led to extensive research into biobased products and biofuels to profitably consume these resources, and supplement and eventually supplant synthetic petroleum-derived products and fuels (127,128). A harvest of 1,000,000 acres of guayule would generate approximately 5,000,000 t of biomass composed of 500,000 ton of rubber, 500,000 ton of resin, and 4,000,000 ton of lignocellulosic bagasse.

The natural resins present in native guayule have been extensively studied and include mono-, sesqui-, di-, and triterpene groups, as well as other secondary metabolites (108). Unfractionated guayule resin has shown considerable promise in the areas of wood preservation (in marine and terrestrial environments) (129) and insect antifeedents (termite resistance) (130–132). These resins also show promise as a biobased renewable replacement for petroleum-based monomers and oligomers in adhesives and coatings. Additional profitable uses for the resins include a natural, low toxicity replacement for creosote in wood treatment and for prevention of termite attack. Resin/lignin products, such as additives for phenol formaldehyde resins, may also prove possible.

Guayule bagasse has shown promise in the manufacture of particleboard and ceiling tiles, especially because it contains sufficient low molecular weight rubber and resin components to provide a natural adhesive. Additional potential uses for guayule bagasse and fiber, before or after resin extraction, include their use in building materials (108,133,134).

Residual guayule bagasse also shows promise as a feedstock for the production of biofuels. The energy content of the bagasse from the latex extraction process is equivalent to 5×10^{12} Btu or 62,500,000 gallons of ethanol. California currently uses 2 billion gallons of gasohol per annum containing 200 million gallons of ethanol. The bagasse from 10 million acres of guayule processed per year, if all converted to ethanol through fractionation and fermentation, could meet projected western annual needs for 600 million gallons ethanol (135), while greatly reducing transportation costs of corn ethanol from the mid-western states. The bagasse could also be used to generate energy via gasification or the production of pyrolysate oils, or through combustion.

Conclusions

New rubber-producing crops face substantial barriers they must overcome before they can successfully enter the commercial arena (133–143). Decades of guayule research have allowed guayule to overcome these barriers and reenter the commercial arena. Researchers have investigated a plethora of approaches seeking ways

to best exploit and consume the crop (144), and research into new applications and uses for the latex and the resins and lignocellulosic coproducts is continuing. Guayule latex can be used to make high quality medical products (3,98) and substitute for latex from *H. brasiliensis*. However, latex characterization has also revealed novel properties that affect manufacturing processes and product quality (3,96,99,117,144). Some of these properties may lead to natural rubber products superior to those currently available. Continuing research on novel polymers and properties, and on utilization of the coproducts and bagasse, will not only increase the profitability but will allow conversion of the entire guayule crop to a plethora of products, while essentially eliminating the negative environmental impact of agricultural waste. Thus, guayule is positioned as a model industrial crop feeding a new generation of biorefineries capable of producing a wide range of bioproducts and biofuels.

BIBLIOGRAPHY

1. H. Mooibroek and K. Cornish, *Appl. Microbiol. Biotechnol.* **53**, 355 (2000).
2. K. Cornish, *Nat. Prod. Rep.* **18**, 1 (2000).
3. K. Cornish, J. L. Brichta, P. C. Yu, D. F. Wood, M. W. McGlothlin, and J. A. Martin, *Agro Food Ind. Hi-Tech* **12**, 27 (2001).
4. M. S. Reisch, *Chem. Eng. News* 11 (Aug. 14 1995).
5. J. d'Auzac, J.-L. Jacob, and H. Chrestin, eds., *Physiology of Rubber Tree Latex*, CRC Press, Boca Raton, Fla., 1989.
6. P. Besse, M. Seguin, P. Lebrun, C. Lanaud, *Genome* **36**, 1049–1057 (1993).
7. W. Davis, *Fortune* Aug. 4, 1997, p. 86.
8. M. R. Sethuraj and N. M. Mathew, eds., *Natural Rubber: Biology, Cultivation and Technology*, Elsevier, Amsterdam, 1992.
9. K. Cornish, *Phytochemistry* **57**, 1123 (2001).
10. International Rubber Study Group, York House, Empire Way, Wembley, U.K.
11. U.S. Department of Commerce, Office of Trade and Economic Analysis. Data on Web.
12. K. Cornish, J. L. Brichta, M. H. Chapman, D. J. Scott, J. E. Van Fleet, D. F. Wood, and W. Xie, in *Proceedings of the 5th International Latex Conference*, Akron, Ohio, July 30–31, 2002, pp. 1–15.
13. J. E. Bowers, *Natural Rubber-Producing Plants for the United States*, National Agricultural Library, Beltsville, Md., 1990.
14. C. L. Swanson, R. A. Buchanan, and F. H. Otey, *J. Appl. Polym. Sci.* **23**, 743–748 (1979).
15. F. A. Eagle, *Rubber Chem. Technol.* **54**, 662 (1981).
16. W. W. Schloman, Jr. and J. P. Wagner, in J. W. Whitworth and E. E. Whitehead, eds., *Guayule Natural Rubber*, GAMC/USDA-CSRS, Tucson, Ariz., 1991, p. 287.
17. J. P. Wagner and W. W. Schloman, Jr., in J. W. Whitworth and E. E. Whitehead, eds., *Guayule Natural Rubber*, GAMC/USDA-CSRS, Tucson, Ariz., 1991, pp. 261–286.
18. E. P. Jones, *Ind. Eng. Chem.* **40**, 864 (1948).
19. U.S. Pat. 5,580,942 (1996), K. Cornish (to Yulex Corp.).
20. W. W. Schloman, Jr., F. Wyzgoski, D. McIntyre, K. Cornish, and D. J. Siler, *Rubber Chem. Technol.* **69**, 215 (1996).

21. U.S. Pat. 5,717,050 (1998), K. Cornish (to Yulex Corp.).
22. J. Bonner, in J. W. Whitworth and E. E. Whitehead, eds., *Guayule Natural Rubber*, GAMC/USDA-CSRS, Tucson, Ariz., 1991, pp. 1–16.
23. D. T. Ray, T. A. Coffelt and D. A. Dierig, *Ind. Crops Prod*. (in press).
24. N. G. Wright, S. Fansler, R. D. Lacewell, in J. W. Whitworth and E. E. Whitehead, eds., *Guayule Natural Rubber*, GAMC/USDA-CSRS, Tucson, Ariz., 1991, pp. 352–367.
25. J. E. Slater, *J. E., N. Engl. J. Med.* **320**, 1126 (1989).
26. C. Morales, A. Bascomba, J. Carrieira, and A. Sastre, *Clin. Exp. Allergy* **19**, 425 (1989).
27. V. J. Tomazic, T. J. Withrow, B. R. Fisher, and S. F. Dillard, *Clin. Immunol. Immunopathol.* **64**, 89 (1992).
28. G. Pailhories, *Clin. Rev. Allergy* **11**, 391 (1993).
29. D. R. Ownby, H. E. Ownby, J. A. McCullough, and A. W. Shafer, *J. Allergy Clin. Immunol.* **93**, 282 (1994).
30. L. E. Larsen, *1998. Lab. Med.* **29**, 278 (1998).
31. R. A. Backhaus, *Isr. J. Bot.* **34**, 283 (1985).
32. D. F. Wood and K. Cornish, *Int. J. Plant Sci.* **161**, 435 (2000).
33. K. Cornish and D. F. Wood, *J. Polym. Env.* **10**, 155 (2002).
34. B. L. Archer, B. G. Audley, E. G. Cockbain, G. P. McSweeney, *Biochem. J.* **89**, 565 (1963).
35. K. Cornish, *Eur. J. Biochem.* **218**, 267 (1993).
36. K. Cornish and D. J. Siler, *Plant Physiol. Biochem.* **34**, 377 (1996).
37. J. Berndt, US Government Research Report AD-601729, Vol. 1, 1963.
38. F. Lynen, J. J. Rubber *Res., Inst. Malaya* **21**, 389 (1969).
39. B. L. Archer and B. G. Audley, *Bot. J. Linn. Soc.* **94**, 181 (1987).
40. S. Madhavan, G. A. Greenblatt, M. A. Foster, C. R. Benedict, *Plant Physiol.* **89**, 506 (1989).
41. K. Cornish and R. A. Backhaus, *Phytochemistry* **29**, 3809 (1990).
42. K. Cornish, D. J. Siler, O. K. Grosjean and N. Goodman, *J. Nat. Rubber Res.* **8**, 275 (1993).
43. D. J. Siler, M. Goodrich-Tanrikulu, K. Cornish, A. E. Stafford, T. A. Mckeon, *Plant Physiol. Biochem.* **35**, 281 (1997).
44. K. Cornish, D. F. Wood, and J. J. Windle, *Planta* **210**, 85 (1999).
45. K. Cornish and D. J. Siler, *J. Plant Physiol.* **147**, 301 (1995).
46. J. Castillón and K. Cornish, *Phytochemistry* **51**, 43 (1999).
47. K. Cornish, J. Castillón, and D. J. Scott, *Biomacromolecules* **1**, 632 (2000).
48. Y. Tanaka, E. Aik-Hwee, N. Ohya, N. Nishiyama, J. Tangpakdee, S. Kawahara, R. Wititsuwannakul, *Phytochemistry* **41**, 1501 (1996).
49. D. J. Scott, B. M. T. da Costa, S. C. Espy, J. D. Keasling, and K. Cornish, *Phytochemistry* **64**, 121 (2003).
50. K. Cornish, J. Castillón, and M. H. Chapman, in A. Steinbüchel, ed., *Biochemical Principles and Mechanisms of Biosynthesis and Biodegradation of Polymers*, Wiley-VCH-Verlag, Weinheim, Germany, 1999, p. 316.
51. J. Chappell, *Annu. Rev. Plant Physiol. Plant Mol. Biol.* **46**, 521 (1995).
52. M. Rohmer, M. Knani, P. Simonin, B. Sutter, and H. Sahm, *Biochem. J.* **295**, 517 (1993).
53. W. Eisenreich, M. Schwarz, A. Cartayrade, D. Arigoni, M. H. Zenk, A. Bacher, *Chem. Biol.* **5**, 221 (1998).
54. K. Cornish and D. J. Scott, *Ind. Crops Prod*. (in press).
55. S. Y. Chang, P. C. Tsai, C. S. Tseng, and P. H. Liang, *Protein Expr. Purif.* **23**, 432 (2003).

56. L. C. Tarshis, M. Yan, C. D. Poulter, and J. C. Sacchettini, *Biochemistry* **33**, 10871 (1994).
57. A. Chen, P. A. Koon, and C. D. Poulter, *Protein Sci.* **3**, 600 (1994).
58. K. Cornish and R. A. Backhaus, *Ind. Crops Prod.* **17**, 83 (2003).
59. J. Bonner, *Bot. Gaz.* **105**, 233 (1943).
60. M. G. Gilliland and J. van Staden, *South Afr. J. Plant Soil* **3**, 21 (1986).
61. R. A. Goss, C. R. Benedict, J. H. Keithly, C. L. Nessler, and R. D. Stipanovic, *Plant Physiol.* **74**, 534 (1984).
62. R. W. Downes and M. L. Tonnet, *Aust. J. Agric. Res.* **36**, 285 (1985).
63. M. R. Appleton and J. van *Staden, J. Plant Physiol.* **134**, 524 (1989).
64. M. R. Appleton and J. van *Staden, Bioresource Technol.* **35**, 147 (1991).
65. W. Ji, C. R. Benedict, and M. A. Foster, *Plant Physiol.* **103**, 535 (1993).
66. D. Sundar and A. R. Reddy, *Photosynthetica* **38**, 421 (2000).
67. D. Sundar and A. R. Reddy, *J. Plant Physiol.* **158**, 1291 (2001).
68. R. Krishnakumar, S. Sreelatha, M. Thomas, J. Gopalakrishnan, J. Jacob, and M. R. Sethuraj, *Indian J. Nat. Rubber Res.* **11**, 92 (1999).
69. R. Krishnakumar, K. Cornish, and J. Jacob, *J. Rubber Res.* **4**, 131 (2001).
70. M. A. Foster and J. Moore, in J. W. Whitworth and E. E. Whitehead, eds., *Guayule Natural Rubber*, GAMC/USDA-CSRS, Tucson, Ariz., 1991, p. 107.
71. F. S. Nakayama, D. A. Bucks, C. L. Gonzalez, and M. A. Foster, in J. W. Whitworth and E. E. Whitehead, eds., *Guayule Natural Rubber*, GAMC/USDA-CSRS, Tucson, Ariz., 1991, p. 145.
72. J. D. Mikhail, S. M. Alcorn, J. W. Whitworth, in J. W. Whitworth and E. E. Whitehead, eds., *Guayule Natural Rubber*, GAMC/USDA-CSRS, Tucson, Ariz., 1991, p. 173.
73. F. S. Nakayama, in J. W. Whitworth and E. E. Whitehead, eds., *Guayule Natural Rubber*, GAMC/USDA-CSRS, Tucson, Ariz., 1991, p. 217.
74. M. A. Foster, *Ind. Crops Prod*. (in press).
75. M. A. Foster and J. Moore, *J. Prod. Agric.* **5**, 163 (1992).
76. M. A. Foster, L. G. Kleine, and J. Moore, *J. Am. Oil Chem. Soc.* **70**, 1239 (1993).
77. M. A. Foster, J. L. Fowler, L. G. Kleine, and N. Puppala, *Ind. Crops Prod.* **9**, 93 (1999).
78. M. A. Foster, J. L. Fowler, L. G. Kleine, M. M. Grote, and N. Puppala, *Ind. Crops Prod.* **15**, 23 (2002).
79. D. T. Ray, D. A. Dierig, A. E. Thompson, and T. A. Coffelt, *Crop Sci.* **39**, 300 (1999).
80. W. Coates, in J. W. Whitworth and E. E. Whitehead, eds., *Guayule Natural Rubber*, GAMC/USDA-CSRS, Tucson, Ariz., 1991, p. 241.
81. K. Cornish, M. H. Chapman, F. S. Nakayama, S. H. Vinyard, and L. C. Whitehand, *Ind. Crops Prod.* **10**, 121 (1999).
82. K. Cornish and J. L. Brichta, in J. Janick, ed., *Trends in New Crops and New Uses, Proceedings of the 5th National Symposium on New Crops and New Uses: Strength in Diversity*, Atlanta, Ga., Nov. 10–13, 2001, ASHS Press, Alexandria, Va., 2002, p. 214.
83. K. Cornish and M. H. Chapman, *Ind. Crops Prod.* **12**, 25 (2000).
84. K. Cornish, J. E. Van Fleet, M. H. Chapman, J. L. Brichta, and B. E. Knuckles, *Ind. Crops Prod*. (in press).
85. *Guayule: An Alternative Source of Natural Rubber*, National Academy of Sciences, Washington, D.C., 1977.
86. D. McIntyre, H. L. Stephens, W. W. Schloman, Jr., and A. K. Bhowmick, in A. K. Bhowmick and H. L. Stephens, eds., *Handbook of Elastomers*, 2nd ed., Marcel Dekker, Inc., New York, 2000, pp. 1–27.

87. E. Campos López, E. Neavez Camacho, and R. Maldonado *García, Guayule: Reencuentro en el desierto*, Centro de Investigación en Quimica Aplicada, Saltillo, Mexico, 1978, p. 375.
88. W. W. Schloman, Jr., *Ind. Crops Prod*. (in press).
89. G. E. Hamerstrand and R. R. Montgomery, *Rubber Chem. Technol.* **57**, 344 (1984).
90. W. W. Schloman, Jr., D. T. Ray, and W. Coates, in *Seventh Annual Conference of the Guayule Rubber Society*, Annapolis, Md., 1987.
91. J. P. Wagner and D. G. Parma, *Polym. Plast. Technol. Eng.* **27**, 335 (1988).
92. W. M. Cole, A. S. Hilton, W. W. Schloman, Jr., J. B. Compton, and J. A. Dembek, Jr., Guayule Rubber Project: Final Report Prepared Under Contract No. 53-3142-7-6005, Bridgestone/Firestone, Inc., Akron, Ohio, 1991, pp. 68–182.
93. D. J. Siler and K. Cornish, *Anal. Biochem.* **229**, 278 (1995).
94. D. J. Siler and K. Cornish, *Ind. Crops Prod.* **2**, 307 (1994).
95. A. B. Carey, K. Cornish, P. J. Schrank, B. Ward, and R. A. Simon, *Ann. Allergy Asthma Immunol.* **74**, 317 (1995).
96. D. J. Siler, K. Cornish, and R. G. Hamilton, *J. Allergy Clin. Immunol.* **98**, 895 (1996).
97. K. Cornish and J. L. Brichta, *J. Polym. Env.* **10**, 13 (2002).
98. R. A. Backhaus and F. S. Nakayama, *Rubb. Chem. Technol.* **61**, 78 (1988).
99. W. W. Schloman, Jr., D. J. Garrot, Jr., and D. T. Ray, *J. Agric. Food Chem.* **34**, 683 (1986).
100. K. Cornish and C. D. Lytle, *J. Biomed. Mat. Res.* **47**, 434 (1999).
101. W. S. E. Fernando and M. C. S. Perera, *Kautsch. Gummi Kunstst.* **40**, 1149 (1987).
102. J. L. Angulo-Sanchez, L. L. Jimenez-Valdez, and E. Campos-Lopez, *J. Appl. Polym. Sci.* **26**, 1511 (1981).
103. A. Subramaniam, *J. Rubber Res. Inst. Malaya.* **25**, 61 (1977).
104. A. Subramaniam and W. W. Suin, *J. Nat. Rubb. Res.* **1**, 58 (1986).
105. S. Montes and J. L. White, *Rubber Chem. Technol.* **55**, 1354 (1982).
106. M. A. Ponce and R. R. Ramirez, *Rubber Chem. Technol.* **54**, 211 (1981).
107. S. Choi and C. M. Roland, *Rubber Chem. Technol.* **69**, 591 (1996).
108. S. Choi and C. M. Roland, *Rubber Chem. Technol.* **70**, 202 (1997).
109. W. W. Schloman, Jr., R. A. Hively, A. Krishen, and A. M. Andrews, *J. Agric. Food Chem.* **31**, 873 (1983).
110. R. W. Keller, D. S. Winkler, and H. L. Stephens, *Rubber Chem. Technol.* **54**, 115 (1981).
111. D. S. Winkler, H. J. Schostarez, and H. L. Stephens, *Rubber Chem. Technol.* **50**(5), 981 (1977).
112. L. F. Ramos de Valle, *Rubber Chem. Technol.* **54**(1), 24 (1981).
113. W. M. Cole, A. S. Hilton, W. W. Schloman, Jr., J. B. Compton, and J. A. Dembek, Jr., Guayule Rubber Project: Final Report Prepared Under Contract No. 53-3142-7-6005, Bridgestone/Firestone, Inc., Akron, Ohio, 1991, p. 210.
114. *ASTM D2227-88, Annual Book of ASTM Standards*, Vol. 9.01, ASTM, Philadelphia, 1989, p. 408.
115. FEMA, National Stockpile Purchase Specification, Rubber—Parthenium (Guayule), U. S. Dept. of Commerce Report P-48C-R, 1984.
116. W. W. Schloman, Jr., F. Wyzgoski, D. McIntyre, K. Cornish, and D. J. Siler, *Rubber Chem. Technol.* **69**, 215 (1996).
117. M. W. McGlothlin, in *Proceedings of the 4th International Latex Conference*, Akron, Ohio, July 31–Aug 1, 2001. Rubber and Plastics News, Vol. 18, Crain Communications Akron, Ohio.

118. P. G. Santangelo and C. M. Roland, *Rubber Chem. Technol.* **76**, 892 (2003).
119. P. G. Santangelo and C. M. Roland, *Rubber Chem. Technol.* **74**, 69 (2001).
120. J. K. Valaitis, W. J. Kern, W. W. Schloman, Jr., W. M. Cole, and A. S. Hilton, in H. H. Naqvi, A. Estilai, and I. P. Ting, eds., *Proceedings: The First International Conference on New Industrial Crops and Products, Office of Arid Land Studies*, University of Arizona, Tucson, Ariz., 1992, p. 131. (1992).
121. G. N. Avgeropoulos, T. Maistros, and J. Patt, U. S. Dept. of Defense Report No. TACOM-TR-12651, 1982.
122. P. Touchet, in R. E. Singler, and C. A. Byrne, eds., *Elastomer and Rubber Technology, Sagamore Army Material Research Conference Proceedings*, Vol. 32, U.S. Government Printing Office, Washington, D.C., 1987, p. 535.
123. M. K. Morris, *El Guayulero* **6**(1,2), 13 (1984).
124. W. E. Detweiler, *El Guayulero* **6**(3), 13 (1984).
125. L. T. Lukich, *Final Report–U. S. Navy/USDA Guayule Program*, Goodyear Tire & Rubber Co., Akron, Ohio, p. 13, 1992.
126. W. Lucas, *Summary Test Report for the Guayule Tire Evaluation of the M1028, Commercial Utility Cargo Vehicle*, U.S. Army Yuma Proving Ground, Yuma, Ariz., 1996, pp. 1–5.
127. C. J. Campbell and J. H. Laherrere, *Sci. Am*. 78 (1998).
128. R. Monastersky, *Sci. News* **154**, 278 (1998).
129. F. S. Nakayama, S. H. Vinyard, P. Chow, D. S. Bajwa, J. A. Youngquist, J. H. Muehl, and A. M. Krzysik, *Ind. Crops Prod.* **14**, 105 (2001).
130. J. D. Bultman, S.-L. Chen, and W. W. Schloman, Jr., *Ind. Crops Prod.* **8**, 133 (1998).
131. J. D. Bultman, R. L. Gilbertson, J. Adaskaveg, T. L. Amburgey, S. V. Parikh, and C. A. Bailey, *Bioresource Technol.* **35**, 1997 (1991).
132. C. Gutierrez, A. Gonzalez-Coloma, and J. J. Hoffman, *Ind. Crops Prod.* **10**, 35 (1999).
133. P. Chow, F. S. Nakayama, J. A. Youngquist, J. H. Muehl, and A. M. Krzysik, The International Research Group on Wood Preservation IRG/WP 02-40225, 2002.
134. U.S. Pat. nos. 60/203,813 and 09/828,634 (2002), F. S. Nakayama, J. A. Youngquist, and P. Chow.
135. S. S. Kelley, Department of Energy/National Renewable Energy Laboratory, Golden, Clo., personal communication, 2001.
136. Council for Agricultural Science and Technology, Development of New Crops: Needs, Procedures, Strategies, and Options, Report No. 102, Council for Agricultural Science and Technology, Ames, Iowa, 1984.
137. Council for Agricultural Science and Technology, Genetic Engineering in Food and Agriculture, Report No. 110, Council for Agricultural Science and Technology, Ames, Iowa, 1986.
138. Council for Agricultural Science and Technology, *Diversifying U.S. Crop Production*, Issue Paper No. 6, Council for Agricultural Science and Technology, Ames, Iowa, 1996.
139. Critical Agricultural Materials Act (1984).
140. J. Harsch, *New Industrial Uses, New Market for U.S. Crops: Status of Technology and Commercial Adoption*, USDA, Cooperative State Research Service, Office of Agricultural Materials, 1993.
141. G. D. Jolliff, in *Grain Legumes as Alternative Crops, A Symposium Sponsored by The Center for Alternative Crops and Products*, University of Minnesota, St. Paul, Minn., 1987, p. 7.
142. G. D. Jolliff and S. S. Snapp, *J. Prod. Agric.* **1**, 83 (1988).

143. G. D. Jolliff, *J. Prod. Agric.* **2**, 6 (1989).
144. D. McIntyre, H. L. Stephens, W. W. Schloman, Jr. in A. K. Bhowick and H. L. Stephens, eds., *Handbook of Elastomers*, Marcel Dekker, Inc., New York, 2000, p. 1.

KATRINA CORNISH
United States Department of Agriculture,
Agricultural Research Service,
Western Regional Research Center
WILLIAM W. SCHLOMAN JR.
Department of Chemistry, University of Akron

SCANNING FORCE MICROSCOPY

Introduction

Synthetic polymers, as well as biopolymers, exhibit a rich and very complex structural and morphological hierarchy on multiple length scales, spanning the size range from monomer residue units comprising the polymer chains to higher order micro- or macroscale structures, such as fibers or spherulites. Since the performance of polymeric materials is intimately related to this hierarchy, the structural and morphological analysis of polymers has played a central role in polymer science and technology. With the continual striving toward the mesoscopic and nanoscopic size regime in modern technology, high resolution analysis tools gain increasing importance.

Following the Nobel prize winning invention of the scanning tunneling microscope (STM) (1,2), the well-developed and established family of microscopy techniques in the field of polymer science, such as polarized optical microscopy (OM) (3) and various electron microscopies (4), was enriched by a range of newly developed scanning proximity probe microscopy techniques in the late 1980s (5). Among these techniques, scanning force microscopy (SFM) in particular has successfully complemented the traditional techniques for studying simultaneously polymer morphology *and* surface properties.

Compared to STM, which is inherently limited to conducting samples or ultrathin samples on conducting substrates, SFM is generally applicable to a much broader range of materials, including insulators, such as polymers. SFM, which includes the originally developed atomic force microscopy (AFM) (5), can be considered to be a unique technique in the sense that it yields topographical information in 3-D with, in the optimized case, (sub-)nanometer spatial resolution over lateral length scales of >100 μm to nanometers. In addition, material-specific

Encyclopedia of Polymer Science and Technology. Copyright John Wiley & Sons, Inc. All rights reserved.

contrast can also be obtained based on, eg, adhesion, friction, or elasticity differences, thus enabling high resolution mapping of composition in heterogeneous systems.

It is clear that SFM has been quickly established as an important research tool in academia in the field of polymers; at the same time its huge potential has been realized in industry, where it finds increasing application in research and development laboratories. The range of applications reaches from unraveling structure–property relationships, as well as long-standing, unresolved issues, such as polymer crystallization, polymer morphology and its relation to processing and mechanical properties, to the analysis of novel polymer architectures and substrate-supported assemblies. It includes studies of the behavior of macromolecules in confinement, compositional mapping for applications in the biomedical sector, as well as in polymer surface modification and elucidation of failure mechanisms, and more recently real-time studies of *dynamic* processes at the relevant length scale. In addition to a still needed standardization and definition of protocols in the industrial environment, the development and improvement of new SFM modes, in particular local thermal analysis (6) and chemically sensitive imaging (7), pose challenges for the near future. The impact of SFM can undoubtedly be expected to further grow for polymer science and technology.

Considering the rapid increase in the number of SFM-related publications in the field of polymers, it is necessary to focus on key areas and make a narrow selection of the discussed material. The author would like to offer his apologies to those authors who consider possible omissions as negligence by the author. Whenever possible and appropriate, references to the many excellent reviews on particular topics have been included.

In this contribution, the basic concepts and modes of SFM, as well as some rudimentary theory, are introduced and only briefly reviewed in order to provide a self-supporting basis for the discussion of selected areas of application of SFM on polymers. The study of the morphology and hierarchical ordering of polymers by SFM is reviewed, starting from the visualization of single macromolecules, chain packing, and surface crystal structures. The imaging of lamellar crystals, hedrites, and spherulites by SFM approaches is discussed, followed by investigations on effects of deformation and processing, as well as studies on morphology of latex particles and fibers. A second central section is devoted to the mapping of surface properties and composition via the spatially resolved measurement of forces and surface mechanical properties. Finally, structure development and dynamic processes, including polymer crystallization, followed in real-time by SFM are discussed.

Within the numerous proximal probe techniques developed in the years following the breakthrough inventions of the STM (1) and AFM (5), scanning force microscopy (8) represents a family of scanning probe techniques that rely in their contrast mechanism on various forces between probe tip and sample (9–12) (see ATOMIC FORCE MICROSCOPY). In order to provide a basis for an understanding and appreciation of the SFM work on polymers (13–18), as presented in this review, the basic principles of SFM, as well as selected imaging modes, are briefly discussed.

SFM and Its Imaging Modes

In scanning probe microscopy (SPM), a scanned probe is utilized to collect highly localized information of sample surface properties via the corresponding physical quantities. Typically, the proximal probe and the sample specimen are in (near) contact and the corresponding information is collected, while probe and sample are mutually displaced laterally by suitable transducers (Fig. 1). The probe microscopy techniques belonging to the family of SFM discussed below comprise, among others, contact, intermittent contact, and force modulation modes. These modes are of central importance to provide information on, eg, topography (quantitative surface profile), composition in heterogeneous systems, elasticity, and other mechanical properties of polymeric materials on length scales between $\sim$100 μm and the mesoscopic and nanoscopic size regime. In most of the SFM modes, topography and additional properties can be probed simultaneously, which allows one to make important correlations of structure and local physical properties. Complicated sample preparation, such as replication techniques needed for transmission electron microscopy (TEM), can often be circumvented and experiments can be carried out in a wide range of media (gas, vacuum, liquids) and experimental conditions. For other specialized SFM techniques the reader is referred to the corresponding literature (8–20).

Contact Mode SFM. The different SFM techniques have many basic features in common, which will be introduced in this first section on contact mode SFM. In *contact mode* SFM a sharp probe tip, which is attached to a cantilever

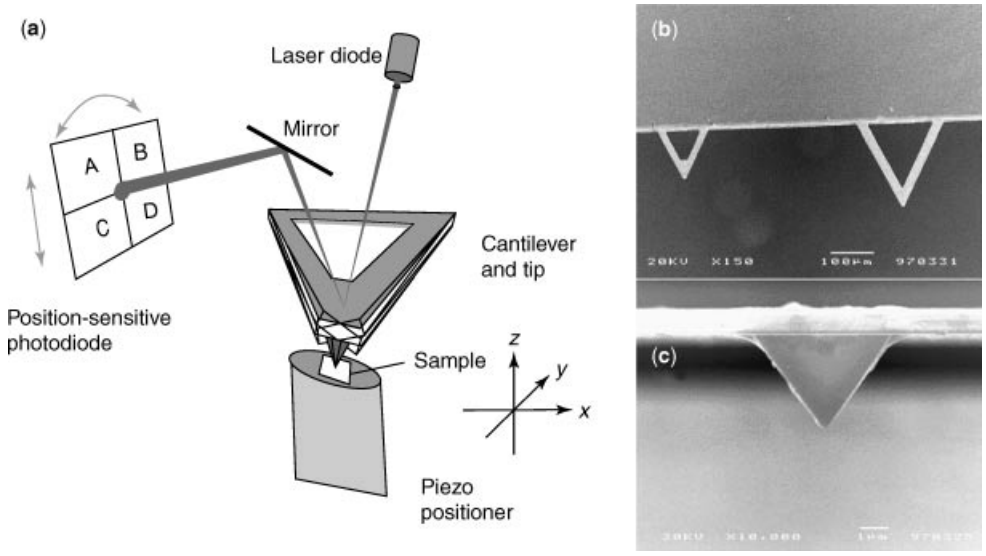

Fig. 1. (**a**) Schematic diagram of contact mode SFM and SEM images of (**b**) V-shaped SFM cantilevers and (**c**) tip. The basic elements of transducer (piezo positioner), cantilever and tip assembly, and ultra-sensitive force detection system (optical beam deflection/photodiode detector) are common for all SFM techniques, while details may differ. Adapted with permission from Ref. 21.

(typical spring constant k of 1.0–0.1 N/m), is brought into contact with the sample surface (Fig. 1) (21). While the probe is scanned across the sample surface, or likewise the sample is scanned under this probe, the deflection of the cantilever is measured.

SFM cantilevers and tips are often made of silicon or silicon nitride; SFM tips possess radii of curvature at the apex between few and several tens to hundreds of nanometers (Fig. 1). A piezoelectric transducer is used in order to position the sample accurately. Depending on the scanner type (piezo tube length and design) the maximum scan sizes vary between ca 1 μm and several hundred micrometers, with an accuracy of positioning in the best cases of $\sim$0.01 nm. The cantilever deflection is typically monitored by an optical beam deflection technique (Fig. 1**a**). Other possibilities to measure the deflection include STM, piezoresistive, capacitance, or interferrometric detection schemes (22). In the optical beam deflection setup, laser light is reflected off the end of the cantilever and is collected by a position-sensitive photodiode. For instance, a 4-quadrant photodiode can simultaneously measure deflections in vertical (surface normal) and horizontal (lateral) direction (Fig. 1**a**).

In the so-called constant height mode the deflection of the cantilever is measured in order to obtain the surface profile or topography of the specimen. The deflection of the cantilever is a result of the repulsive and attractive interactions between the atoms of the tip and the atoms of the sample surface. In the more commonly used constant force mode, a feedback loop holds a preset deflection of the cantilever constant by adjusting the sample height (z). A graphic representation of the adjustment of specimen height z yields an isoforce surface, which represents the sample topography. These data correspond to the true profile *only* if variations in local sample compliance are negligible (23,24). On the basis of an accurate calibration, SFM thus becomes an instrument for metrology, which includes the quantitative determination of surface roughness as well (25).

SFM experiments are often performed in ambient conditions, although the presence of a contamination layer (typically water) gives rise to sometimes significant capillary forces (26). In addition to measurements in air, experiments can be performed in other gases, in liquids, or under (high) vacuum. The problem of capillary forces can be easily eliminated by performing measurements in liquids utilizing a liquid cell (27). Contact mode SFM imaging is typically difficult or impossible on very rough samples, samples with high adhesion, such as adhesives, as well as most types of liquids (28). Highly viscous liquids, such as polymer melts, can be imaged in some cases even with *contact mode* SFM (see section Structure Development and Dynamic Processes in Real Time). In addition, the lateral forces between tip and sample may lead to modification or destruction of delicate polymer specimens (29,30).

The true lateral resolution for imaging is limited by the shape (aspect ratio) and the radius of curvature of the tip (31–34). Imaging artifacts, which are inherent to microscopic techniques, are well known and can be identified as such by systematic variations of relative scan angles, scan velocities (comprising scan rate and scan size), respective imaging forces, and a thorough tip shape analysis (35).

The data, in imaging applications most importantly the surface profile or topography (height), can be displayed graphically using a color scale to indicate the

height of each point observed. A significant difference between SFM and scanning electron microscopy (SEM) for imaging surface topography is that SFM provides a *quantitative* surface profile with excellent lateral and vertical resolution. In addition, contact mode SFM has been used to measure both repulsive and attractive forces between sample and surface with a high accuracy (force spectroscopy), as well as (lateral) friction forces, as will be discussed in the sections under Normal Forces and Lateral Forces, respectively.

Intermittent Contact Mode SFM. Intermittent contact mode SFM, also called tapping mode SFM, has been developed to reduce shear forces (36), which can cause sample deformation or even destruction of soft samples in contact mode SFM (for a recent review see Ref. 19). In addition, this mode can be useful to probe adhesive or surface mechanical properties, and thus achieve contrast between different materials. Intermittent contact mode SFM uses an oscillating cantilever/tip assembly to minimize contact time and contact forces, and to especially eliminate shear forces between tip and sample surface. This mode relies on a similar setup as contact mode SFM. However, in intermittent contact mode (in air) a stiffer cantilever is used (k = 20–80 N/m). This cantilever is excited to vibrate near its resonance frequency by an excitation piezo. Close to a sample surface, the vibration is damped as a result of tip sample interactions. The original amplitude A_0 is hence reduced to A, depending sharply on the distance to the surface (Fig. 2**c**). The

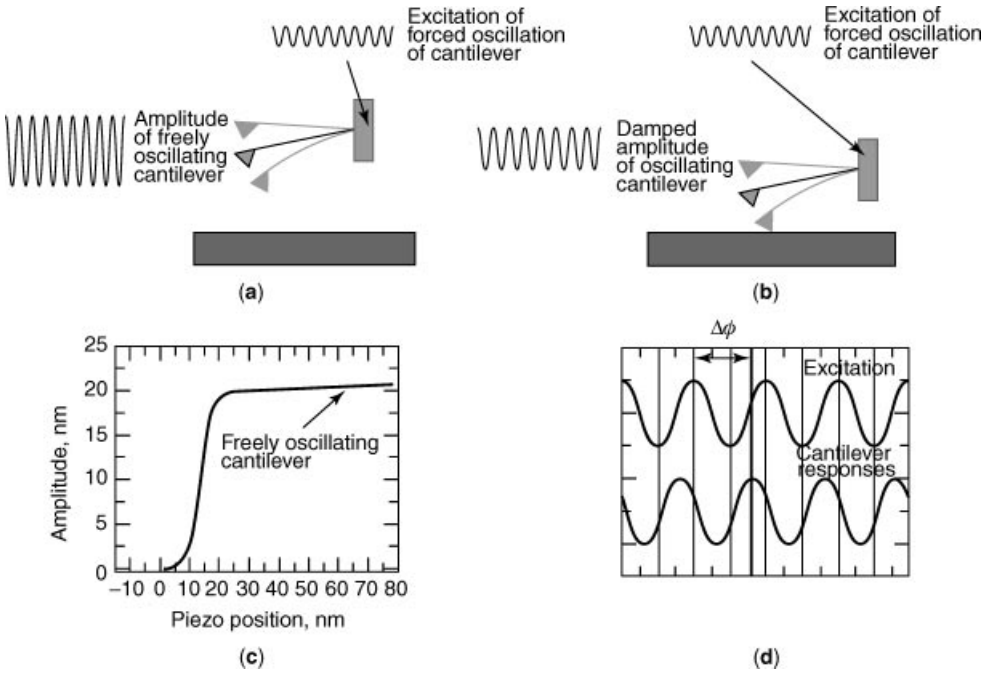

Fig. 2. Schematic of intermittent contact mode SFM: (**a**) cantilever vibrating freely in air vs (**b**) damped oscillation due to interactions with the surface; (**c**) amplitude vs displacement dependence showing the steep decrease of the amplitude as function of distance; (**d**) phase angle shift $\Delta\phi$ between excitation signal and cantilever response owing to interactions of the tip with the surface.

feedback loop uses the amplitude as control variable and holds a certain amplitude damping constant, while the sample is raster-scanned. Typically, high A/A_0 ratios are chosen in order to keep the contact time and peak forces during one cycle of oscillation to a minimum (intermittent contact) (37–41).

Anomalous height data may be observed in intermittent contact mode SFM owing to various reasons. Reduced heights may be observed because of flattening of soft matter as a result of forces exerted by the probe tip (42), as well as owing to the effect of attractive forces (43–45). The corresponding force gradient near the imaged surface changes the effective spring constant of the oscillating cantilever, and this change in effective spring constant causes a shift of the amplitude vs frequency curve of the cantilever and thus a change in the acquired amplitude. As the tip is scanned over a heterogeneous surface, the induced force is dynamically changing owing to perturbations from the different phases present (46,47). Anomalously increased heights can also be observed when certain surface areas damp the oscillation of the probe tip much stronger than other areas. Since the feedback loop holds a predefined amplitude constant by adjusting the sample position in z direction, this leads to an often significant overestimate of the "true" height (48).

The phase relation of the excitation piezo and the vibration of the cantilever in time yields often highly useful information on the interaction of tip and sample surface (Fig. 2**d**) (49). The phase angle shift $\Delta\phi$ between excitation oscillation and forced oscillation of the cantilever can be described by a simple harmonic (50–52), but also more complicated anharmonic (19), treatment of a forced oscillator. The phase angle shift can be used to obtain contrast due to different surface characteristics related to materials properties (intermittent contact mode SFM *phase* imaging) (49). These properties include, depending on the operation conditions, differences in adhesion (53) or differences in Young's modulus (50–52,54,55). Hence the amorphous and crystalline phases in semicrystalline polymers can be clearly differentiated, as well as different phases in polymer blends or filled systems.

Force Modulation Mode SFM. Force modulation mode (FMM) SFM is a contact mode technique that allows one to resolve lateral differences in modulus (56,57). In FMM SFM, the cantilever is excited by a bimorph to oscillate at a frequency of tens of kilohertz, while it scans the surface in contact mode. By monitoring the oscillation amplitude, the elastic modulus of the surface can be mapped with high resolution. Depending on the corresponding moduli, the contrast in the amplitude image reveals high modulus (ie, large amplitude) and low modulus (ie, lower amplitude) areas (Fig. 3) (58).

Recently, the use of frequency-dependent FMM SFM has been described, where selective contrast can be achieved in heterogeneous systems (59,60). A practical limitation for the approach in the field of polymers is the fact that shear forces, similar to contact mode, may cause severe sample damage or distortion of the underlying morphology.

Further Relevant Modes of SFM. In addition to the standard modes of SFM, there exists a plethora of different modes, which found their niche applications. Instead of treating all these modes in detail, the most relevant modes in light of the work reviewed in the following sections will be very briefly mentioned.

Laterally resolved imaging of adhesion and modulus in contact mode SFM is becoming increasingly important, for instance, in the current strive for mesoscale

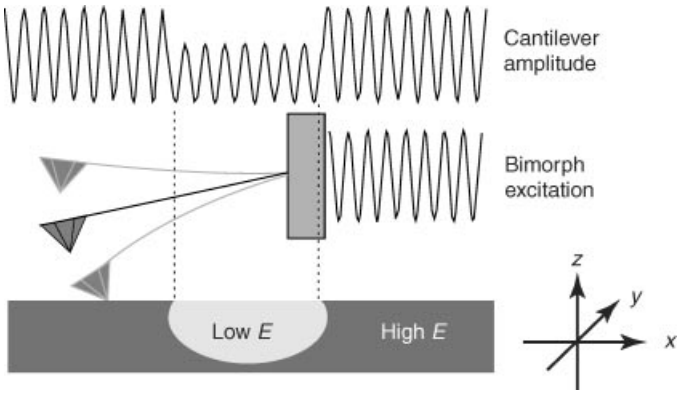

Fig. 3. Schematic of FMM SFM. The cantilever is excited by a bimorph during a contact mode SFM scan. The cantilever amplitude depends on the local modulus of the underlying material.

and nanometer-scale structured or patterned polymers, as well as for biopolymers and polymers in biomedical applications. In these techniques (61–63), described first by Mizes and co-workers for polymers (64), force–displacement (f-d) curves (see section under Normal Forces) are recorded for each pixel and the pull-off force, as a measure for adhesion, and the indentation part of the loading curve, to extract/fit the elastic modulus, are evaluated for each pixel. In particular for adhesion mapping, the use of chemically functionalized SFM probe tips (7,65) has been shown to be a suitable approach to map chemical composition and functional group distributions down to the sub-50-nm scale (see section Mapping of Surface Properties and Composition) (66).

The slow data acquisition rates of this useful approach have been overcome in the so-called pulsed force mode SFM technique developed by Marti and co-workers (67). In this mode, the sample is modulated sinusoidally ($\sim$1 kHz) during a conventional contact mode SFM scan with an amplitude, which is just large enough to overcome the adhesive interactions. Hence the tip contacts, indents, and breaks free from the surface with a frequency of $\sim$1 kHz during scanning. Instead of recording the complete f-d curve, only the four points are captured, ie, the baseline, the maximum repulsive force, the maximum adhesion force, and a point that can be used with the maximum repulsive force to define the slope in the loading regime as a measure of stiffness, respectively. Thus, the simultaneous mapping of sample topography, pull-off forces, *and* stiffness at useful scan rates becomes possible.

Other SFM methods, including scanning thermal imaging (68), electrochemical (69), and noncontact mode SFM (19) have been recently reviewed.

Force Measurements

The basis for the SFM methodologies are by definition forces between the probe tip and the sample surface of interest. Consequently, SFM techniques can be directly used to qualitatively and quantitatively measure these forces, often with high precision and, depending on the range of the corresponding forces (70), with high

lateral resolution. The discussion of the measurement of these forces and some rudimentary theory has been divided into two sections dealing with forces in the surface normal direction and lateral forces, respectively.

Normal Forces. In the treatment of normal forces, a differentiation into the measurement of adhesive forces, related to, eg, surface chemistry, quantification of entropic and enthalpic forces, dealing with single polymer chain properties, and finally indentation measurements, yielding surface mechanical properties, has been made.

Adhesive Forces. Forces that give rise to adhesion (qv) at polymer surfaces include, depending on the material and medium, electrostatic forces, electrostatic double layer forces, hydrogen bonding, dipolar interactions, van der Waals interactions, as well as steric forces and bridging forces (70). In suitable experimental setups, all these interactions can be probed, often down to a molecular level. In a typical *force spectroscopy* experiment, the force between (modified) probe tip and polymer is measured by monitoring the deflection of the cantilever as a function of sample/piezo position, while the tip is brought periodically in and out of contact with the sample surface. The measured cantilever deflection Δz can be converted to the corresponding force F, by applying Hooke's law, if the spring constant of the lever k is known.

$$F = k\Delta z \tag{1}$$

In Figure 4 the corresponding movements of piezo (sample) and cantilever deflection are schematically depicted. The resulting f-d plot (force curve) is shown in Figure 5. The interpretation of force curves has been discussed in detail by Burnham and co-workers (71) and by Cappella and Dietler (72).

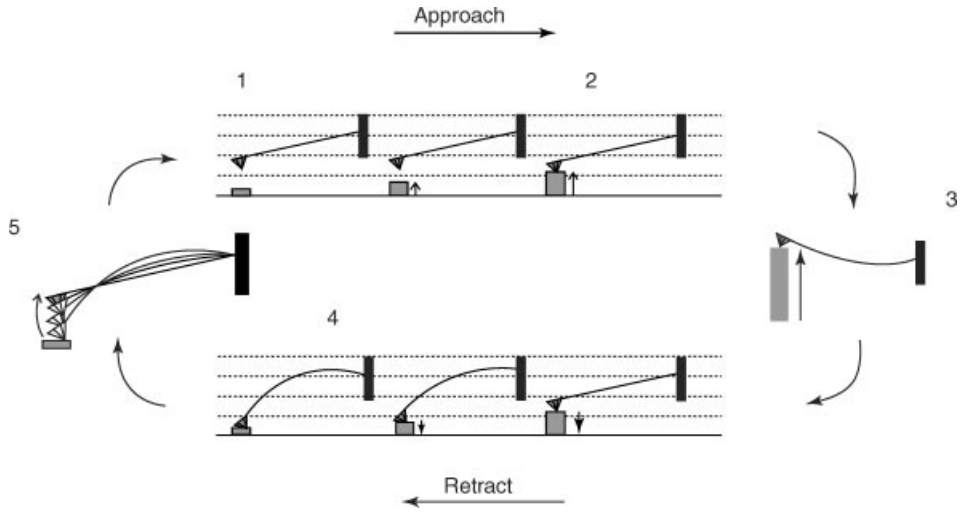

Fig. 4. Measurement of force–distance curves (schematic representation). The sample is approaching the tip (1); at some distance the gradient of the force overcomes the cantilever spring constant and the tip jumps into contact (2); further movement up causes a deflection of the cantilever (3), during the retraction the tip sticks usually much longer (4) and snaps off, when the spring constant overcomes the force gradient (5). Adapted with permission from Ref. 21.

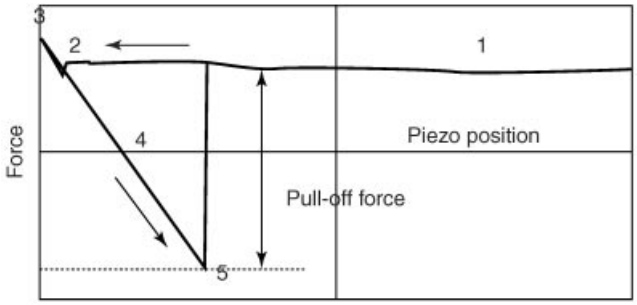

Fig. 5. Force–displacement plot. Adapted with permission from Ref. 21.

The adhesion between tip and sample is characterized by the so-called pull-off or pull-out force (Fig. 5) (73). A quantitative determination of forces requires a thorough calibration of the cantilever spring constant. Despite the large number of different methods (74–77), an accurate quantitative and nondestructive calibration remains difficult. The resolution limit for an optical detection system and spring constants used in experiments on typical commercial SFMs has been estimated to be in the order of 10^{-11} N (78). Depending on the detection system, the force constant, the stiffness, and the resonance frequency of the cantilever, even smaller forces are in principle measurable (79).

The pull-off forces obtained in f-d measurements can be related to the work of adhesion and the respective surface free energies utilizing, eg, (continuum) contact mechanics theories, such as the Johnson–Kendall–Roberts (JKR) theory (80). In particular for monomolecular model systems (65), but also polymers, this approach has yielded a satisfactory description of the experimental data, despite the fact that the contacting bodies are treated as purely elastic (81).

For the idealized geometry of a sphere with radius R interacting with a flat planar surface, the JKR theory predicts that the contact area is a function of R, the moduli of the sphere and surface material (through the reduced modulus K), the work of adhesion W_{12} and load L.

$$A = \pi\left(R/K\left(L + 3\pi R W_{12} + \sqrt{\left[6\pi R W_{12} L + (3\pi R W_{12})^2\right]}\right)\right)^{2/3} \tag{2}$$

where K is written as function of Young's moduli E_i and Poisson's number ν_i as

$$K = 4/3\left[\left(1-\nu_1^2\right)/E_1 + \left(1-\nu_2^2\right)/E_2\right]^{-1} \tag{3}$$

On the basis of equation 2 the force can be expressed for the situation at pull-off $F_{\text{pull-off}}$, ie, minimum contact area, as

$$F_{\text{pull-off}} = -3/2\,\pi R W_{12} \tag{4}$$

The work of adhesion (surface energy per unit area) W_{12} is a function of the surface free energies of the tip (γ_1), the sample γ_2, and the corresponding interfacial free energy γ_{12} (eq. 5). If the experiment is carried out in a medium, the

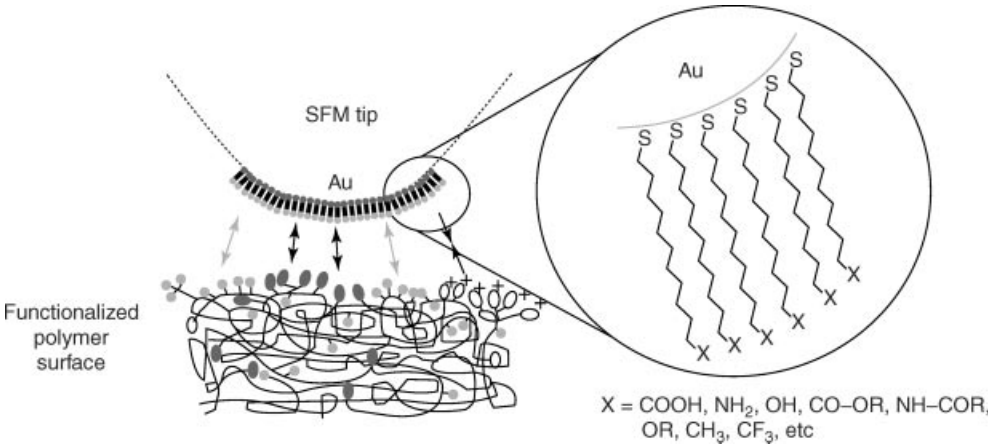

Fig. 6. Schematic of chemically modified SFM tip interacting with a functionalized polymer surface. The tip is coated with a thin layer of gold, which has been modified with a self-assembled monolayer of ω-functionalized alkanethiols. The wide range of functional groups that can be incorporated in these monolayers allows one to tune the chemical character of the tip; thus, by tuning the tip's surface free energy, the type and strength of the interactions with functional groups at the polymer surface can be controlled over a broad range. Adapted with permission from Ref. 21.

γ_i refer to the surface free energy for the surface i in contact with the corresponding medium.

$$W_{12} = \gamma_1 + \gamma_2 - \gamma_{12} \tag{5}$$

In the methodology termed chemical force microscopy (CFM), differences in long- and short-range forces are exploited for imaging under improved force conditions (82,83) or "chemical imaging" (7,65). This is achieved (*1*) via the control of the tip chemical composition by selective deposition of various materials or preferably the assembly of a functionalized monolayer (Fig. 6) (84), thus via control of γ_{tip}, and (*2*) via the control of the medium (7,65,66). Consequently, by correlating the pull-off forces extracted in laterally resolved f-d measurements with surface energies based on equations 4 and 5, it is possible to discriminate between different materials and material with different surface energies (7,53,64–66,85).

The correlation of pull-off forces with the cosine of contact angles measured with water clearly showed the applicability of this approach for various polar polymers (66,85). For apolar polymers, for example, the Lifshitz theory can be successfully applied to predict the "chemical" contrast. Feldman and co-workers demonstrated this powerful quantitative approach for different polymers probed with gold-coated and silicon oxide coated tips in perfluorodecalin (86), in which the dispersive van der Waals interactions are selectively amplified (see section Surface Forces and Energies).

Entropic and Enthalpic Elasticity. In recent years, SFM approaches and complementary force-sensing approaches, such as biomembrane probe and laser optical trap techniques, have been perfected to an extent that the study of individual (bio)macromolecules have become feasible as routine experiments in many

laboratories. In the field of polymer science, single molecule studies are particularly intriguing since statistical factors, such as molecular weight distribution, diverse morphologies, and interchain interactions can be ignored.

In particular, the measurement of the elasticity of single polymer chains by the SFM-based approach termed single molecule force spectroscopy (SMFS) (87, 88) is of importance in this context. SMFS has helped to shed light onto a number of interesting phenomena, including protein unfolding (89), DNA unzipping (90), force-induced conformational transitions in individual polymer chains (91), as well as the mentioned single-polymer chain elasticity (92).

In SMFS, f-d curves are recorded analogously to the experiment described in the section under Adhesive Forces on samples exposing isolated polymer molecules in a suitable medium (93–96). The measured intramolecular force vs extension characteristics of single polymer molecules include entropic and enthalpic elasticity, described well by the (modified) freely jointed chain (FJC) model or wormlike chain model (WLC) (87,88), as well as specific structural changes along the stretched polymer chain. In addition, the intermolecular forces may reflect the unbinding and desorption processes in which the interaction is transmitted through the surrounding medium. These interactions include the rupture of covalent chemical bonds and the unbinding of all kinds of intermolecular aggregates based on noncovalent binding interactions. Examples of the successful application of the FJC model are, for example, oligonucleotides (97), polydimethylsiloxane (PDMS) (98), and poly(methacrylic acid) (PMAA) (Fig. 7) (99).

Deviations of the force extension curves from FJC or WLC behavior, for example the kink in the force profile shown in Figure 8, often indicate conformational and configurational transitions along the polymer chain. As shown in Figure 8, Li and co-workers detected a force-induced chair-twist boat conformational transition, which cannot be measured by conventional methods, for α-(1,4)-linked polysaccharides (95).

Recent evidence based on SMFS experiments on collagen suggested that energy dissipation in the form of "hidden length" plays an important role in the stability of bone and thus led to an improved understanding of osteoporosis (100).

Indentation Measurements. Indentation force measurements utilize the indentation part of a f-d curve (compare Figs. 4 and 5). In the case of a noncompliant sample surface, the SFM tip does not indent significantly the sample, and hence the deflection vs piezo position curve in the contact region has a slope of 1.0. For compliant samples, the slope is <1.0 (Fig. 9) and can be used to obtain the elastic modulus of the sample by fitting the measured indentation to a suitable model. Knowledge of the tip shape/geometry and elastic constants of the tip is required to obtain the desired materials properties.

There have been many different approaches discussed in the corresponding literature. Hertz theory (see section Lateral Forces) is among the often used theories. For instance, Radmacher and co-workers used this theory to estimate the elasticity of lysozyme molecules on mica (102).

Van Landingham and co-workers reviewed the state of the art in nanoindentation of polymers (101,103) including a summary of the most common analyses of load-indentation data. Chief among these methods is an analysis of indentation load-penetration curves according to the Oliver–Pharr method (104). This method is based on relationships developed by Sneddon for the penetration of a

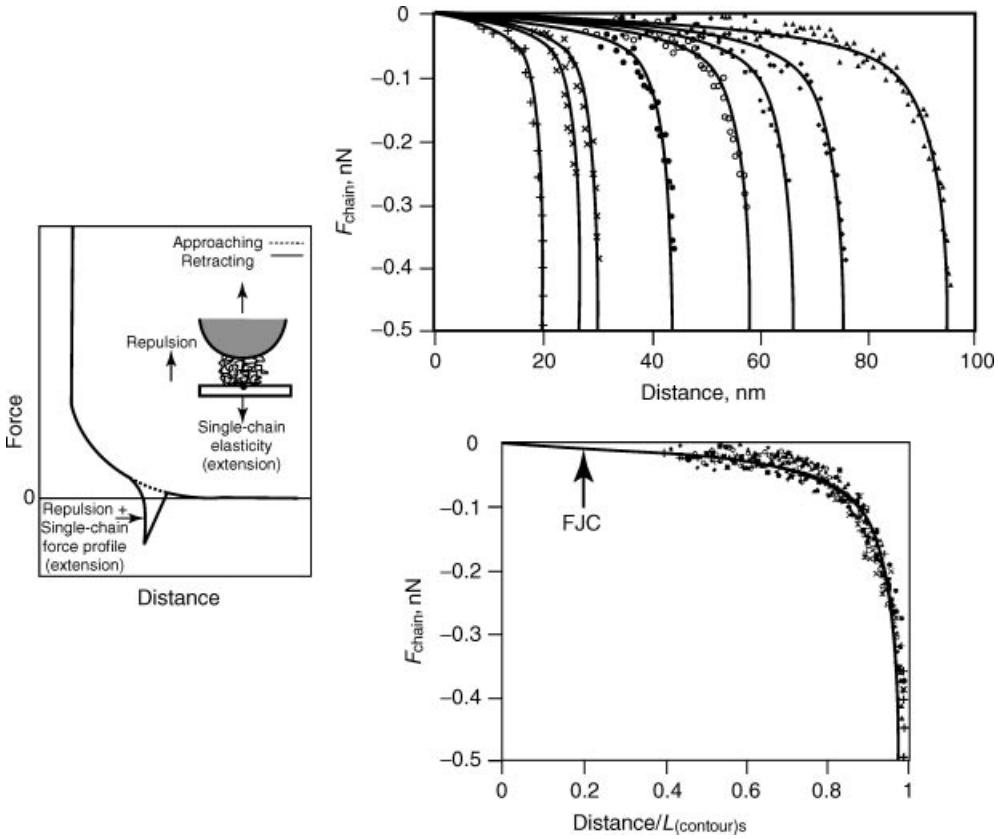

Fig. 7. (Left) Force–distance curve measured with PMAA in demineralized water; (Top right) Experimental data of several force versus distance experiments (each peak corresponds to a single experiment) for single chains of PMAA fit to the FJC model. (Bottom right) Master curve of experimental data for stretching single chains of PMAA compared to FJC model. $L_{(contour)s}$ denotes the contour length. Reprinted with permission from Ref. 99. Copyright (1999) American Chemical Society.

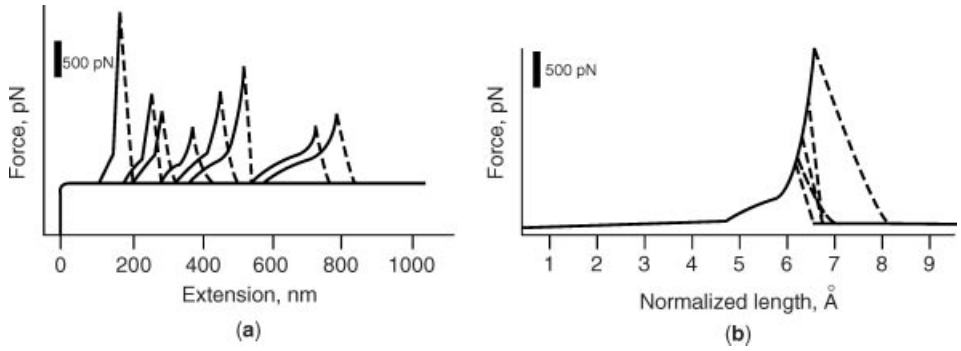

Fig. 8. (**a**). Force-extension curves of carboxymethylated amylose in buffer. (**b**). Superposition of different curves via normalization showed that single molecules of one class are indeed observed. Reprinted from Ref. 95. Copyright (1999), with permission from Elsevier.

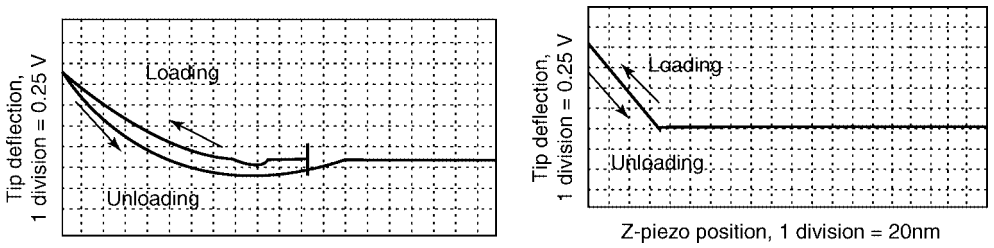

Fig. 9. Force–displacement curves measured on polybutadiene before (left) and after cross-linking (right). Reprinted in part with permission from Ref. 101. Copyright (2000). American Chemical Society.

flat elastic half space by different probes with particular axisymmetric shapes (eg, a flat-ended cylindrical punch, a paraboloid of revolution, or a cone) (105). For details on the experimental procedures and analysis, including pitfalls, the reader is referred to the mentioned review (101). In practice it is found that the application of these methods to polymers often leads to overestimates of moduli compared to bulk measurements. This deviation and other effects have been largely attributed to neglected *viscoelastic* effects (106).

Lateral Forces. Lateral or friction forces can be measured simultaneously with the topography in constant force mode in *contact mode* SFM (for a review see Ref. 107). In order to maximize the sensitivity of friction force measurements, the sample is scanned typically at an angle of 90° with respect to the long axis of the cantilever. The torsion of the cantilever around its long axis is measured with a 4-quadrant photodiode (see Fig. 1). Quantitative nanotribology by friction force microscopy (FFM) requires consideration of the dependence of the photodiode output signal on laser alignment and accurate calibration (107) of the lateral force spring constant and the photodiode response. In many cases, when qualitative materials contrast is needed, FFM is a rapid and straightforward method for compositional mapping.

The corresponding output of the (lateral) photodiode signal is shown in Figure 10. The so-called friction loop (108) displayed allows one to calculate the

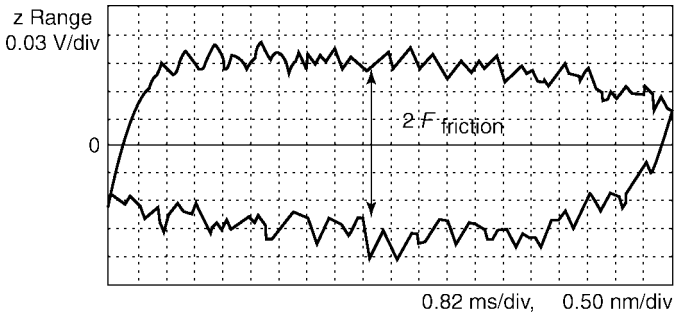

Fig. 10. Friction loop (friction force vs scanned distance plot) measured perpendicular to the polymer chain direction of oriented PE with a —CF_3 modified tip. The photodiode output signal in volts is directly proportional to the friction force range. Adapted with permission from Ref. 21.

friction force from the difference of the trace and retrace line multiplied by 0.5. In order to improve the statistics and exclude artifacts related to coupling of topography into the friction image, the mean friction forces are calculated typically from the corresponding difference image of complete scans acquired simultaneously for both relative scan directions (trace and retrace).

The understanding of the fundamentals of interfacial friction has been emerging in the last decades, and is in part based on measurements with the surface forces apparatus (109,110). In particular, friction was shown to be related to adhesion hysteresis rather than adhesion itself (110).

An early description of friction, Amontons' law, which describes the macroscopic friction between rough surfaces, gives a relation between friction force F_{friction} and applied load L (eq. 6).

$$F_{\text{friction}} = \mu L \tag{6}$$

where μ represents the friction coefficient. For presumed multiasperity contacts, this behavior is often observed also in SFM-based nanotribology. The equation has been modified to account for adhesion that is observed at zero load (111).

$$F_{\text{friction}} = \alpha L + F(0) \tag{7}$$

with constants α and $F(0)$ being related to the chemical composition of the interface.

For a single asperity contact the friction force F_{friction} is proportional to contact area A (eq. 8).

$$F_{\text{friction}} = \tau A \tag{8}$$

where τ denotes the interfacial shear strength (112).

Since friction forces are proportional to the tip–sample contact area for single asperity contacts, it is important to consider how the two contacting surfaces will be deformed during scanning in FFM. The simplest approach to describe the contact mechanics of two interacting bodies was derived by Hertz (113,114). In the Hertz theory only elastic deformations of the contacting surfaces are considered, and thus the adhesion is neglected. If adhesive interactions are considered as well, the already mentioned JKR theory of contact mechanics (80) can be successfully applied to estimate the contact area as a function of normal loading force (eq. 2). However, since friction forces are related to energy dissipation, these forces may depend on factors other than surface free energy or mechanical properties. Examples include polymer specimens with orientational order on various length scales (molecular, lamellar) or systems, which possess differences in conformational order. In these cases, FFM images may reveal subtle details of molecular scale organization (see section Lamellar Crystals). For a concise treatment of nanometer-scale friction measurements see also Reference 22.

Morphology of Semicrystalline Polymers

The hierarchical ordering of polymers from the molecular to the micrometer scale and the underlying morphology can nowadays be routinely addressed by SFM for countless polymer systems (115). Owing to the often important

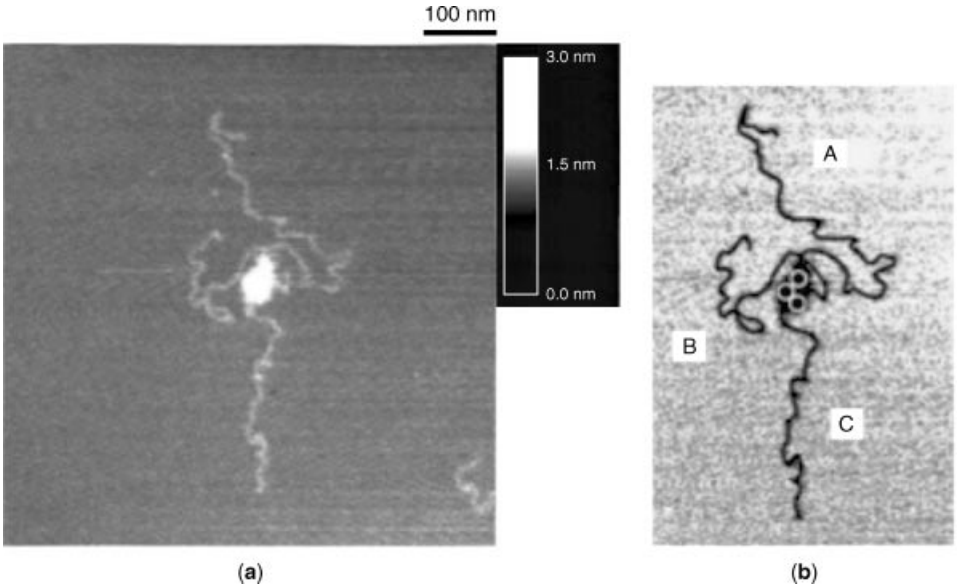

Fig. 11. (**a**) SFM image of a PS-*b*-PMMA monolayer deposited on mica (left). (**b**) Schematic representation of a possible molecular conformation. Reprinted with permission from Ref. 116. Copyright (1996) American Chemical Society.

relation of molecular or supramolecular organization and properties, this area of SFM on polymers is vital for many practical applications (see MORPHOLOGY; SEMICRYSTALLINE POLYMERS).

Single Macromolecules. The high resolution imaging capabilities of intermittent contact mode SFM allowed several groups to image and analyze the contour, ie, the shape and conformation, of *individual* adsorbed polymer molecules for selected systems. The first example of a successful imaging of the conformation of a flexible polymer was reported by Kumaki and co-workers, who studied a monolayer of polystyrene-block-poly(methyl methacrylate) (PS-*b*-PMMA) on mica (Fig. 11) (116). The interplay of interactions between the polymer segments with each other and the substrate were carefully adjusted to avoid the typically observed coiling of polymer chains on substrates. The structure of individual macromolecules was further studied for various shape-persistent polymers, including "hairy rods" (117), worm-like brushes (118), monodendron-jacketed chains (119), as well as biomacromolecules, including DNA (120). In a recent review (121), Sheiko and Möller provided a complete overview on the developments in this area that leads from structural analysis of the adsorbed macromolecules in 2-D confinement to controlled motility on the surface. In particular, the data reported by Sheiko and co-workers for individual molecular brushes showed the arrangement of the PMMA backbone and the pendant poly(*n*-butyl acrylate) side chains resolved to submolecular detail, which demonstrates the vast potential of SFM in these applications (Fig. 12) (121).

Further examples of imaging of individual macromolecules using SFM comprise dendrimers (122–125) and physisorbed or chemisorbed polymer chains (126,127). Owing to the softness of the macromolecules, as well as to tip

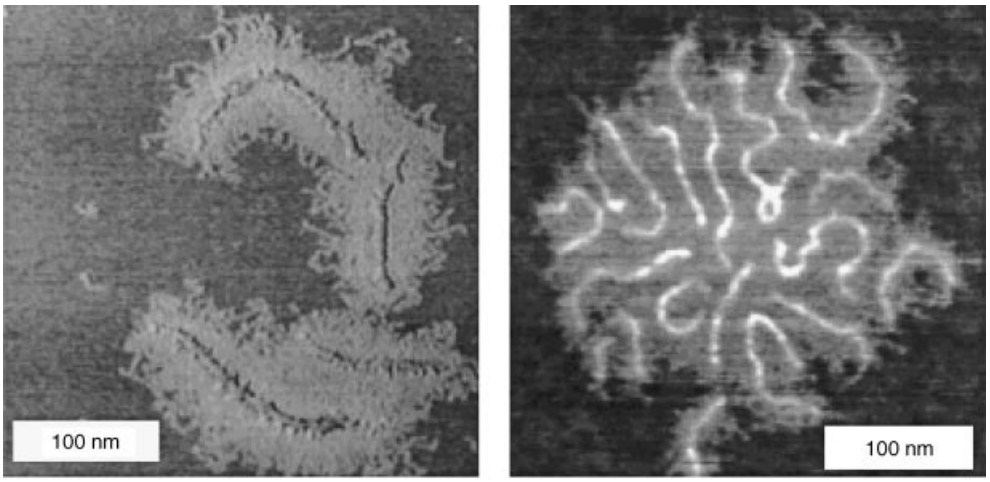

Fig. 12. PMMA molecular brushes with poly(*n*-butyl acrylate) side chains of different degrees of polymerization: (**a**) $n = 52$ and (**b**) $n = 10$. Reprinted with permission from Ref. 121 Copyright (2001) American Chemical Society.

convolution effects (34) and thus limited spatial resolution (33), the *true* resolution of SFM does not allow one in general to resolve submolecular structural details of the studied macromolecules.

Chain Packing and Crystal Structures. The chain packing and the submolecular arrangement of repeat units and pendant side groups of macromolecules in crystalline domains of polymers can be visualized using contact mode SFM. The resolution is in most cases not *true* resolution, since the area of the contact area (1 − few nm^2) exceeds the molecular scale and must be considered *lattice resolution* instead. The first example of molecularly resolved structures of a polymer dates back to 1988, when Marti and co-workers reported on an SFM study on a polydiacetylene film (128). Examples for resolved chain packing and polymer crystal structure determination at the surface of semicrystalline polymers include poly(tetrafluoroethylene) (PTFE) (129,130), polyethylene (PE) (131–133), polypropylene (PP) (134,135), poly(ethylene oxide) (PEO) (136), aramids (137,138), and poly(oxy methylene) (POM) (139).

In Figure 13, a typical high resolution contact mode SFM scan of uniaxially oriented POM is shown together with the corresponding 2-D fast Fourier transform filtered image (139). Since the polymer chain direction is in this particular case known a priori, the observed periodicities can be related to the well-established hexagonal crystal structure of POM in a straightforward manner. Uniaxially oriented or epitaxially crystallized specimens thus help in the analysis of the data, as has been discussed in recent review articles (140,141).

In most cases the surface crystal structures observed correspond to the structures found by diffraction techniques in the bulk (21,140). For isotactic PP, the groups of Lotz (142) and Vancso (143) succeeded to determine the handedness of the PP helices exposed at the specimen surface based on the arrangement of the methyl groups.

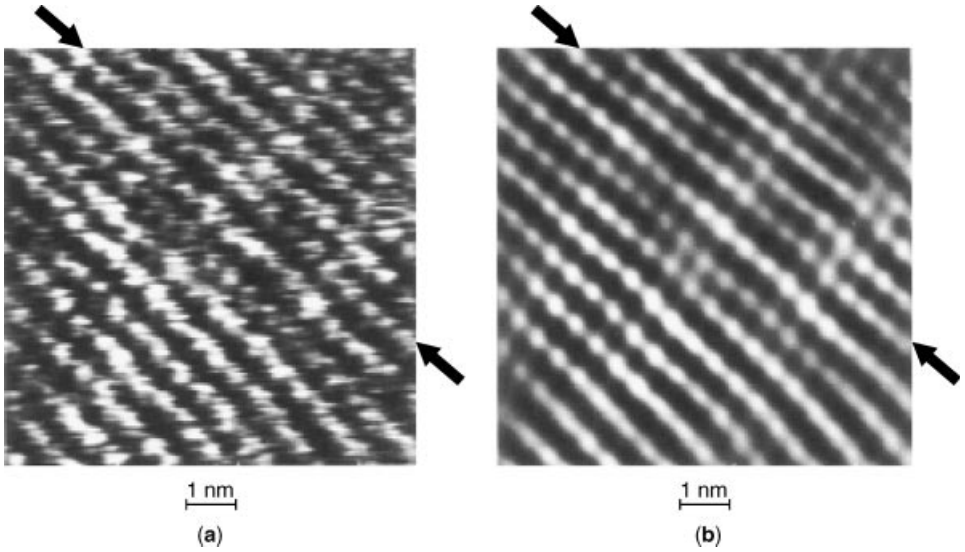

Fig. 13. Contact mode SFM height image of POM with molecular (lattice) resolution: (**a**) raw data; (**b**) image obtained from Fourier reconstruction. The arrow indicates the polymer chain direction (image size 7×7 nm^2). Reprinted with permission from Ref. 139. Copyright (1992). American Chemical Society.

Besides the identification of the local polymorphic structure of the crystallized polymer, it is possible in some cases to detect new (minority) crystal structures. For aramid fibers, previously not detected, but predicted, crystal structures have been identified based on SFM data obtained on cleaved fibers (137). Noteworthy are also the studies by Lotz and co-workers who elucidated the frustrated crystal structure of β-PP with the help of SFM images with methyl group resolution (144). Finally, the mechanism of friction reduction on oriented PTFE films has been confirmed using SFM measurements with molecular resolution (145,146).

Lamellar Crystals. Chain-folded lamellar crystals are regarded as the intermediate hierarchical level in polymer morphology between macromolecule and higher order multicrystal aggregates, such as spherulites. Because of the central importance of lamellae in the field of polymer crystallization and the relation of polymer crystallization to, eg, mechanical properties, lamellae have been widely studied by SFM in all important imaging modes.

Solution-grown single lamellar crystals of, eg, PEO (147), POM (148), PE (149,150), syndiotactic PP, poly(dimethyl silane) (151), poly(4-methyl-pentene) (152), and poly[(*R*)-3-hydroxybutyrate] (153) deposited onto solid substrates have been studied by SFM. The habit and thickness of the lamellae in flat-on projection are directly accessible and in addition to these data, which have previously been typically provided by TEM in conjunction with shadow evaporation techniques (4), more subtle details of domain boundaries and fold direction orientation have been revealed. In Figure 14, the habit of a collapsed PE lamellae is depicted, as well as the anisotropic lateral force recorded in the different fold sectors (154).

Friction anisotropy in different sectors of lamellar crystals (154), which is thought to be related to the orientation of the folds at the fold surface, has also

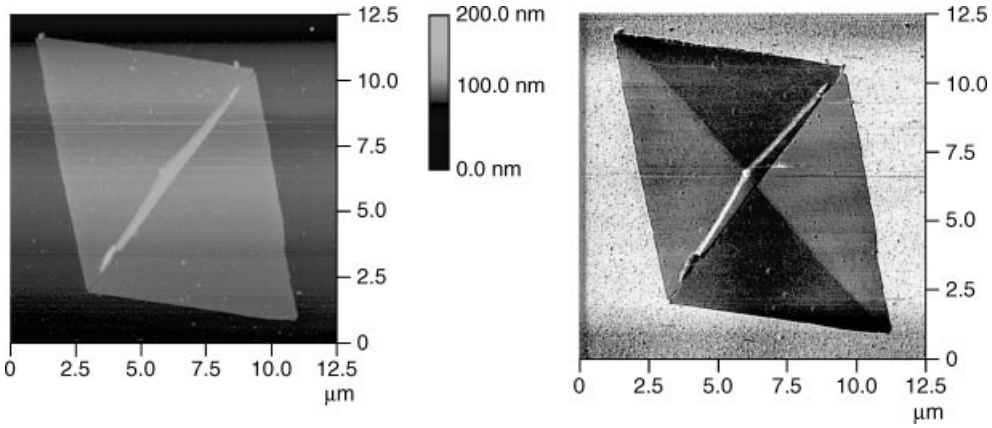

Fig. 14. Contact mode SFM height image of single lamellar crystal of PE deposited on mica (left) and friction image of the same PE lamella (right; friction forces increase from dark to bright contrast). Reprinted in part with permission from Ref. 154. Copyright (1999) American Chemical Society.

been reported for solution-grown lamellae of POM (115), various PEs (155,156) and poly(4-methyl-pentene) (152). For lamellae of poly(dimethyl silane) (151), molecular resolution SFM data provided direct evidence for an arrangement of the polymer chains consistent with an adjacent reentry model.

Crystallization from the melt also results in chain-folded lamellar crystals and for numerous polymers single lamellae have been studied by SFM approaches. Since typical lamellar thicknesses, depending on the polymer and the crystallization temperature, are in a range of 10 nm to several tens of nanometers, the finite size of the SFM probe tip leads to convoluted data, if lamellae are viewed edge-on (33). Among the countless examples are isotactic PS (157,158), PEO (159,160), PP (161–163), PE (164), polycarbonate (PC) (165), etc.

The determination of lamellar thicknesses (161) has been discussed in detail by Trifonova and co-workers (162). The cross-sectional analyses of contact mode SFM images acquired on permanganate-etched specimens of isotactic PP (100% β-modification) are shown in Figure 15.

From a thorough analysis the corresponding distribution of lamellar thicknesses can be directly accessed. In addition, the mechanism of lamellar branching via the action of screw dislocations (166,167), which eventually leads to a spherical envelope of spherulites (see section Multilamellar Crystals, Hedrites, and Spherulites), could be confirmed.

Lamellar thicknesses were also studied by Marand and co-workers, who reported on lamellar thickening of bisphenol A PC (168). The SFM data showed clearly that the most probable lamellar thickness shifts toward higher values with annealing time and provided support for the feasibility of isothermal lamellar thickening in this polymer, as also inferred by differential scanning calorimetry.

While contact mode SFM allowed several groups to image semicrystalline polymers at this level of resolution, intermittent contact mode phase imaging provides in many cases superior differentiation between the amorphous and the crystalline phase because of its stiffness-based contrast (169). For isotactic PP the

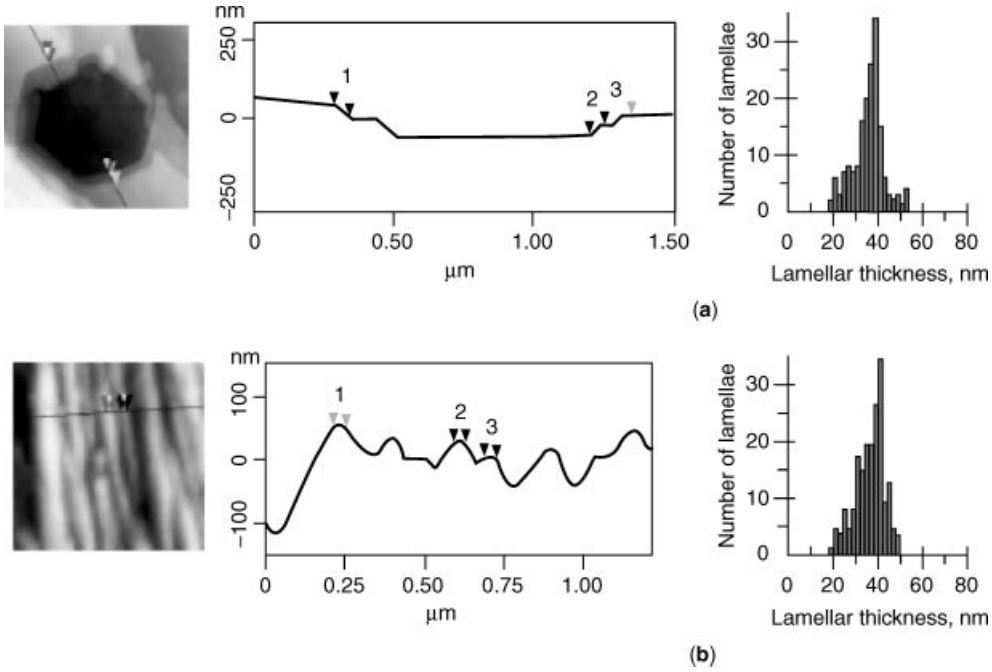

Fig. 15. CM-SFM images of β-iPP lamellae (crystallized isothermally in a thick film at 140°C for 1 h and subsequently exposed to $KMnO_4$ etching) viewed in flat-on projection (top) and in edge-on projection (bottom) together with corresponding section analyses and histograms of lamellar thicknesses. Reprinted with permission from Ref. 162. Copyright (1998) Springer-Verlag.

crystallization from the melt produces, depending on the crystallization temperature, and regio and stereo defect concentrations, the α modification of isotactic PP. This polymorph can be identified owing to the typical cross-hatched arrangement of the lamellae with an angle of 80.4° (170,171), as depicted in Figure 16 (172).

SFM studies of low crystallinity thermoplastic polyolefin elastomers based on polyethylene–alkene copolymers or stereoblock polypropylenes highlighted the importance of the crystalline regions as physical cross-links in these systems (173, 174). Even though crystallinity was very low in these materials, SFM provided sufficient contrast to interrogate the size and distribution of crystallites in the as-prepared and deformed materials (175). As will be discussed in the section under Polymer Crystallization, the crystallization process in such materials was also imaged in real time (176).

Multilamellar Crystals, Hedrites, and Spherulites. Upon crystallization from the quiescent melt (or concentrated solution), polymers exhibit higher order supramolecular structures, including stacks of lamellae, hedrites, and finally spherulites (167). Hedrites (177) are entities composed of multiple lamellar crystals and as such correspond to intermediate stages of spherulitic growth. SFM in various modes was used to determine spherulite sizes and details of lamellar arrangement within spherulites for a wide variety of polymers and polymer processing conditions. SFM data acquired at free surfaces, at the surface of microtomed

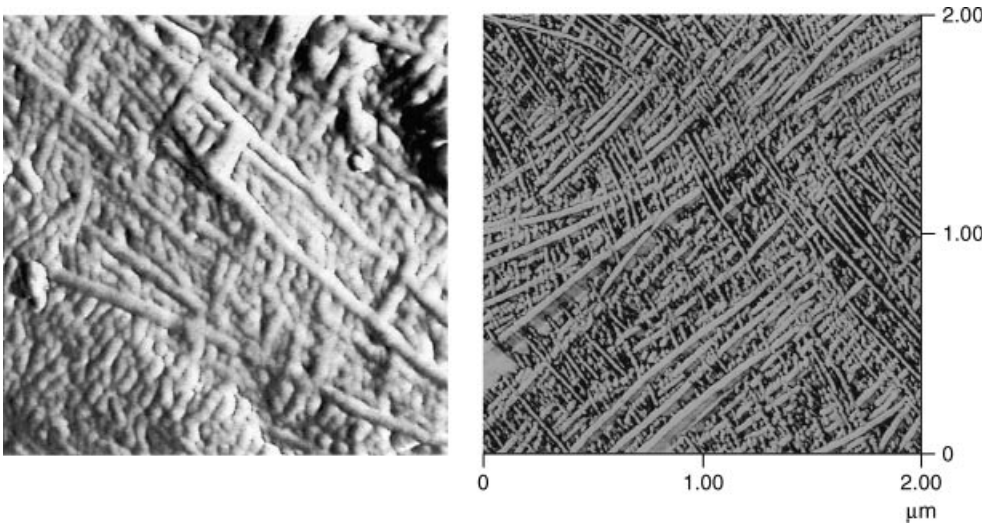

Fig. 16. (Left) Contact mode SFM deflection image of cross-hatched morphology found at the surface of melt-crystallized isotactic PP (image size 1.0 μm^2). Reprinted with permission from Ref. 161. Copyright (1993) Springer-Verlag. (Right) Intermittent contact mode SFM phase image of isotactic PP in film of the heptane insoluble fraction of elastomeric PP. Courtesy of H. Schönherr, R. M. Waymouth, and C. W. Frank (172).

specimen exposing the bulk morphology, as well as at the surface of thin and ultrathin films of crystallized films, were reported.

Harron and co-workers reported on the crystallization of PC films induced by solvent using both *ex situ* contact and intermittent contact SFM (165). The growth of spherulites was followed in ultrathin films for different exposure times to butyl acetate vapor and the growth rates were quantitatively determined.

Viswanathan and Marr complemented SFM studies with small-angle light scattering to confirm the quantitative spherulite sizes obtained in contact mode SFM measurements in high density PE films (178). In addition, individual PE lamellae were resolved.

Figure 17 shows two typical examples of well-developed spherulites of PP grown from the quiescent melt under isothermal conditions.

Banded spherulites, eg in PE (179,180), poly(vinylidene fluoride) (PVDF) (181), or polyhydroxyalkanoates (182), have also been studied in detail. The periodic bands detected in optical microscopy correspond typically to periodic corrugations along the radial direction of the spherulite. Particularly interesting is the case of PVDF (181). On the basis of a careful analysis it was found that the slopes of the observed multilayer terraces of lamellar crystals are retained in each half of a banded spherulite. This evidence confirmed the macroscopic selection of one-handedness in the formation of spiral terraces in each growth direction of the sheaf at the center of banded spherulites of PVDF (181).

In addition to the characterization of the morphology formed as a result of different thermal history, the role of interfaces and shear in transcrystallization (Fig. 18) (164,183) and thin films (184), as well the confinement effects of ultrathin films (185,186) on polymer crystallization, have been addressed by SFM approaches.

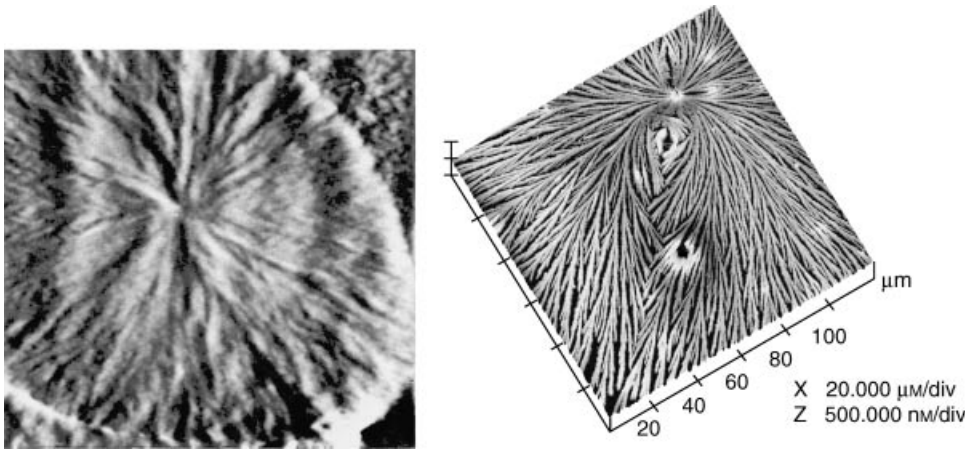

Fig. 17. (Left) Contact mode SFM deflection image of spherulite observed at the surface of melt-crystallized isotactic PP (image size, 15 μm^2). Reprinted with permission from Ref. 161. Copyright (1993). Springer-Verlag. (Right) Intermittent contact mode SFM height image of 2-D spherulite observed in a 200 nm-thick film of elastomeric PP. Courtesy of H.-Schönherr, R. M. Waymouth, and C. W. Frank (172).

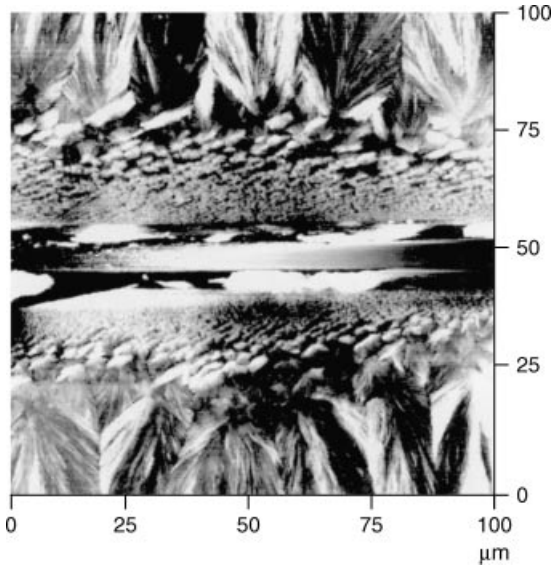

Fig. 18. SFM image of the α,β-cylindritic columnar morphology of transcrystallized isotactic PP induced by pulling of a carbon fiber. On the basis of these observations, Vancso and co-workers concluded that the lamellar growth occurs during epitaxial crystallization on bundles of extended isotactic PP chains, which form during shearing of the polymer matrix by fiber pull. Reprinted with permission from Ref. 183. Copyright (1997) Steinkopff Verlag.

Fibers, Latex Particles, and Polymer Processing. In addition to the typical morphologies displayed by semicrystalline polymers, the morphologies formed or present in polymers used in important applications or subjected to various processes, namely fibers (141) and latex particles (187), were investigated by SFM.

The mapping of fiber surface morphologies (188), as well as internal structures of fibers exposed, eg, by microtoming, and the determination of fiber diameters for very thin fibers (136,189) are among the versatile applications of SFM. Various types of oriented PEs have been investigated by SFM, revealing the fibers and their corresponding fine structure with great detail. For instance, the microfibrillar architecture of PE fibers was visualized by Magonov and co-workers (190). The fibrillar morphology of the uniaxially oriented material was found to be parallel to the orientation direction. In addition, microfibrils with diameters between 20 and 90 nm were also found parallel to this direction.

In a different study, gel-drawn ultrahigh molecular weight PE was analyzed by SFM. The images showed different well-defined levels of the underlying fibrillar morphology (132). These include bundles of microfibrils (diameter between 4 and 7 μm), microfibrils (diameter between 0.2 and 1.2 μm), nanofibrils, and regular chain patterns on the molecular level (Fig. 19).

In drawn thin films of PE, shish-kebab crystals have been investigated by Miles and co-workers (191). Using contact mode SFM at minimized forces in liquid, the arrangement of the lamellae and the polymer molecules comprising the lamellae were resolved in molecular detail. Similar morphologies were also observed for poly(1-butene) (192), as well as many processed polymers, because of orientation effects during the production process (193,194).

The deformation mechanisms in various polyolefins have been studied in great detail. Kravchenko and co-workers have reported on the deformation behavior of elastomeric PP, for which the orientation and deformation of lamellae during tensile testing could be followed with high resolution using intermittent contact mode SFM (175).

The development of a quasi-single crystal texture during plastic deformation of high density PE has been elucidated based on a combination of high resolution contact mode SFM and X-ray scattering techniques. In particular, the absence of a block-like long period comprising crystalline lamellae and amorphous regions, as well as the presence of different crystal facets at the surface of microtomed specimens, was observed (133).

The process of latex assembly in thin films and drying of latex-based paints has attracted tremendous attention, and many SFM studies have been published (187,195,196). Patel and co-workers analyzed latex films composed of hard and soft latex particles and showed by following the distribution of the hard latex beads for different compositions that voids in the film interior were responsible for the observed transition of transparency to turbidity (197).

Juhue and Lang investigated the effect of surfactant post-added to surfactant-free poly(butyl methacrylate) latex dispersions on film formation. The particle ordering and packing was determined by SFM, which allowed these authors to determine the optimal surfactant concentration corresponding to fully covered latex particles (198).

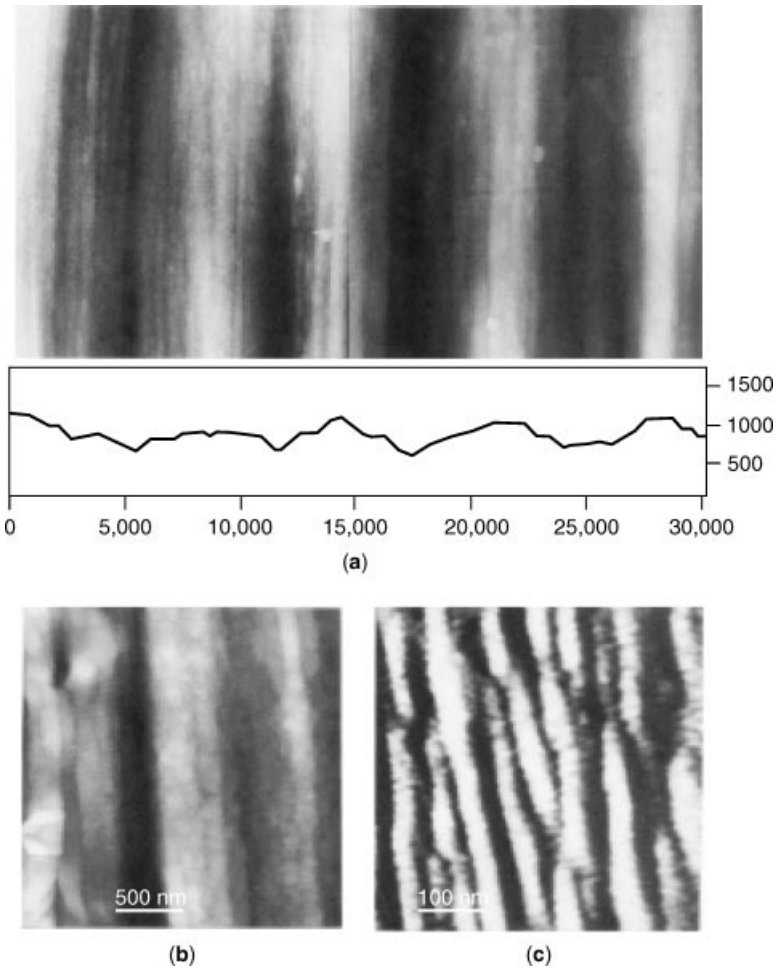

Fig. 19. SFM images obtained from the neck region of gel-drawn PE with a draw ratio of $\lambda = 10$. (**a**) 30 μm $\times$ 15 μm section with a horizontal profile showing bundles of microfibrils, (**b**) 3.3 μm $\times$ 3.3 μm, and (**c**) 0.8 μm $\times$ 0.8 μm SFM scans displaying microfibrils and nanofibrils, respectively. Reprinted with permission from Ref. 132. Copyright (1993) American Chemical Society.

Butt and Geharz reported on the morphology of individual latex particles adsorbed on mica (199). Homogeneous and composite latex particles, made of different amounts of poly(butyl acrylate) and PMMA yielding different viscoelastic properties and different morphologies, were studied (Fig. 20). The latex particle shape was shown to depend on the original latex morphology and viscoelastic properties. The packing of the particles during adsorption and subsequent drying was concluded to be determined by capillary forces, while the particle deformation was caused by interfacial forces.

The analysis of oriented morphologies resulting from polymer processing was already mentioned above. In addition to the characterization of the fibrillar

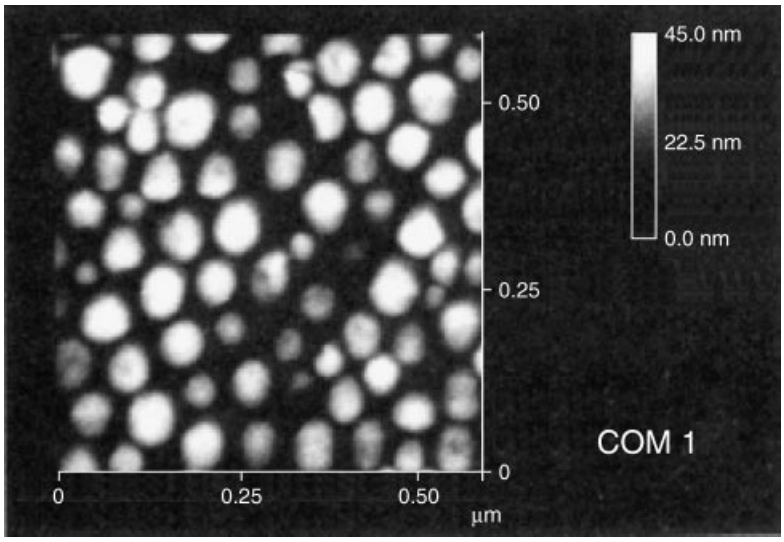

Fig. 20. Contact mode SFM image of dried composite latex particles of *n*-butyl acrylate and methyl methacrylate on mica. Reprinted in part with permission from Ref. 199. Copyright (1996) American Chemical Society.

arrangement in processed polymer, SFM is useful to analyze changes in surface morphology and roughness owing to surface treatments. For example, Vancso and co-workers reported on a SFM study of the surface morphology of commercial polymer films. The effects of flame-treatment of HDPE, corona treatment, and metallization of PP have been unraveled. The thickness and orientation of the exposed lamellae were determined (194).

The roughness analyses of blown PE films yielded useful insight into the origin of optical properties (200). The results showed that the haze is related predominantly to surface roughness and can be reduced by changing the processing conditions. In full agreement with WAXS (wide-angle X-ray scattering) studies, the SFM images unveiled lamellar features, which were oriented predominantly in the transverse direction.

The effects of surface treatments on roughness and more importantly surface energy have been addressed by various groups (see also section Mapping of Surface Properties and Composition). The roughening of PP owing to plasma treatment (201,202) and oxyfluorination (203,204), as well as the surface erosion of LDPE during chromic acid oxidation, have been described (205). Surface roughness can be estimated based on quantitative image analysis procedures (25) and can often be coupled to important mechanical properties (206).

Mapping of Surface Properties and Composition

In addition to a quantitative determination of the surface topography, SFM has proven to be a unique approach to simultaneously map surface properties with high spatial resolution. The resulting maps are particularly useful

to characterize intrinsically heterogeneous systems, such as polymer blends, microphase-separated block copolymers, particulate-filled polymers, but also chemically modified polymers, where a heterogeneous distribution of, for instance, surface functional groups, is not a priori expected (see SURFACE PROPERTIES; SURFACE ANALYSIS).

Surface Forces and Energies.

Miscellaneous Forces. Force measurements on polymer surfaces or between chemically modified SFM tips and polymer surfaces yielded important insight into fundamental force vs separation distance relationships for, eg, polymer colloidal particles (207), mechanochemical behavior of individual macromolecules (see section Entropic and Enthalpic Elasticity) (87–96,99), but also adhesion information directly relevant for practical applications, such as electrochemically controlled adhesion (208) or toner particle–rubber interactions relevant for xerographic applications (209,210).

For example, Segeren and co-workers used SFM cantilevers that were functionalized directly with a toner particle to study the adhesion between particle and different rubbers (Fig. 21) (211). Hodges and co-workers utilized a similar approach to investigate the particle size dependence of forces between polystyrene particles in water (212,213).

Typical forces present in polymeric systems, such as bridging forces and steric forces, play an important role in many applications and have been successfully interrogated by SFM. Briggs studied bridging and steric forces between zirconia spheres coated with poly(acrylic acid) (214), while the groups of Butt and Rühe measured steric forces of polymer brushes as a function of solvent quality and temperature (215). Upon tip–sample approach, exponentially decaying repulsive forces were observed and when the temperature was increased, a linear increase of the decay length, eg, for PS in cyclohexane resulted. These results confirm that the observed repulsion is of entropic origin. Measurements of forces on polymer surfaces in liquids have also been reviewed by Hodges (207).

As mentioned in the section under Normal Forces, van der Waals interactions in different media between SFM probes and apolar polymers have been successfully described using the Lifshitz theory (86). As shown in Figure 22 (left), various polymers can be differentiated clearly in force measurements. For polymers containing polar groups, a correlation of adhesive forces and the cosine of the water contact angle have been predicted and observed (66,85,204). An obvious requirement for reliable force data are flat substrates (205,217,218).

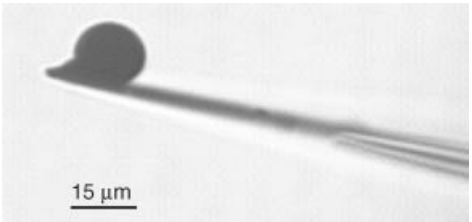

Fig. 21. Optical microscopy image of a colloidal force probe. Adapted with permission from Ref. 211. Copyright (2002) Materials Science VSP International Science Publishers/Brill Academic Publishers, Zeist.

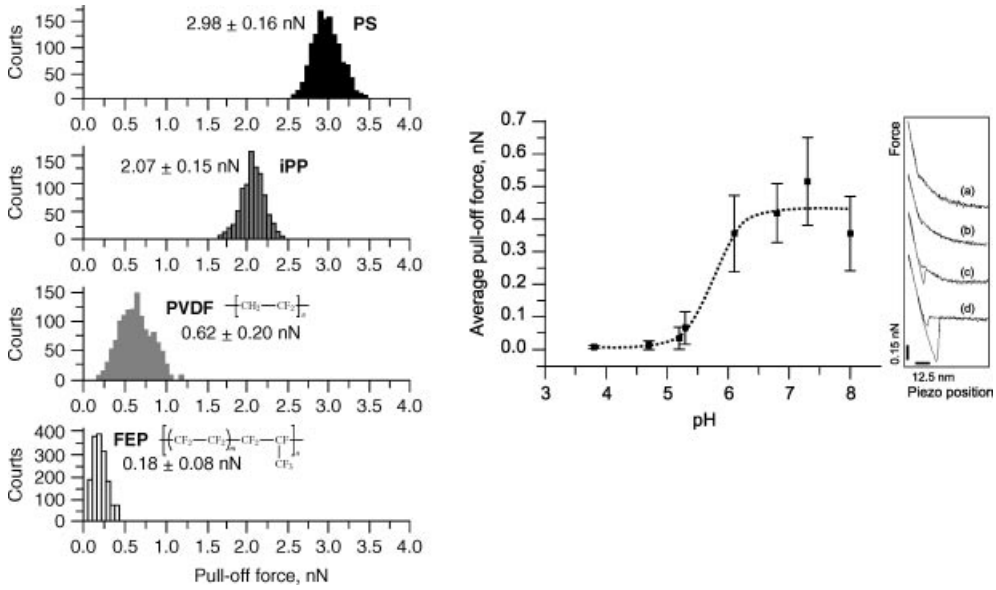

Fig. 22. Pull-off force histograms recorded with a SiO_x probe on PS, isotactic PP, PVDF, and poly-(tetrafluoroethylene-*co*-hexafluoropropylene) (FEP), respectively, in perfluorodecaline (left) and force titration of plasma-polymerized allylamine films as measured in buffer using hydroxyl-terminated SFM tips together with representative f-d curves (right). The f-d curves display (depending on the pH of the buffered aqueous solution) (**a**) exclusively repulsive (pH 4.7), (**b**), (**c**) repulsive and attractive (pH 5.3 and 6.2, respectively), or (**d**) exclusively adhesive interactions (pH 6.8). Reprinted in part with permission from Ref. 86 (left). Copyright (1998) American Chemical Society, and Ref. 216 (right). Copyright (2000) American Chemical Society.

The interaction between hydrophobic tips and protein adherence resistant tri(ethylene glycol)-containing self-assembled monolayers on gold has been studied in electrolyte solution in order to unravel the type of (repulsive) force that is experienced by hydrophobic probes (219). This force is thought to play an important role in the resistance of these films to protein adsorption. In related work, force measurements were utilized to elucidate the factors that govern selective deposition of polyamines on acid and oligoethylene oxide surfaces (220). The data suggested that although PEO derivatives are known as protein-deposition-resistant, certain hydrophobic polyelectrolytes are attracted to the ethylene glycol surface under certain pH conditions.

A particularly powerful approach for the study of surface functional groups in polymers is the so-called method of force titration, introduced originally for monolayer systems (7,66,216,221–223). Force titration refers to the measurement of pull-off forces as a function of pH on polymers comprising ionizable functional groups. For instance, for plasma polymerized allylamine films, the force titration behavior (Fig. 22, right) was found to agree with the presence of primary amino groups in a locally hydrophobic environment based on the observed shift in force pK_a ($\sim$5.7) with respect to solution pK_a ($\sim$10.5) (216).

In addition to forces in the surface normal direction, lateral, ie, friction, forces have been utilized to detect area-selective deposition of polyelectrolytes (224), to

record glass-transition temperatures of various polymers (225–228), to probe the relaxation behavior and viscoelasticity in the surface-near region (229–231), and to obtain information on molecular orientation based on anisotropic friction forces (145,152,155,156,232).

Compositional Mapping by Chemical Force Microscopy. As introduced in the section under Adhesive Forces, CFM is an SFM-based technique, which allows one to determine and map the distribution of chemically distinct functional groups at surfaces. Owing to the small contact area between sample and the (functionalized) tip, this mapping can be performed, depending on the modulus, down to the sub-50-nm level for typical polymers (66). The chemical contrast is achieved by exploiting the spatial or temporal variations of the relevant forces in quantitative measurements of the pull-off and/or friction forces between the tip and selected areas on the surface of interest (compare Fig. 6).

While originally developed for highly ordered monolayers systems (65), this approach is in particular promising for high resolution studies of functional group distributions in surface-treated polymers, such as oxidized polyolefins. In addition to chemically sensitive imaging, the control of tip–sample interactions by means of tip functionalization has been exploited by various authors to improve the imaging forces and thus force contrast (233,234).

The first example for the study of polymer surfaces by adhesion force mapping is the report by Mizes and co-workers, who studied PC with a conventional Si_3N_4 tip (Fig. 23) (64).

Flatness of the polymer surface to be analyzed is a prerequirement since rough surfaces lead to geometrical variations in contact areas, which interfere with the detection of specific interactions, as discussed by various authors (205, 217,218).

van der Vegte and co-workers studied microphase-separated block copolymers using CFM and reported that chemically specific contrast allowed them to differentiate between the two microphases exposed at the surface of microtomed

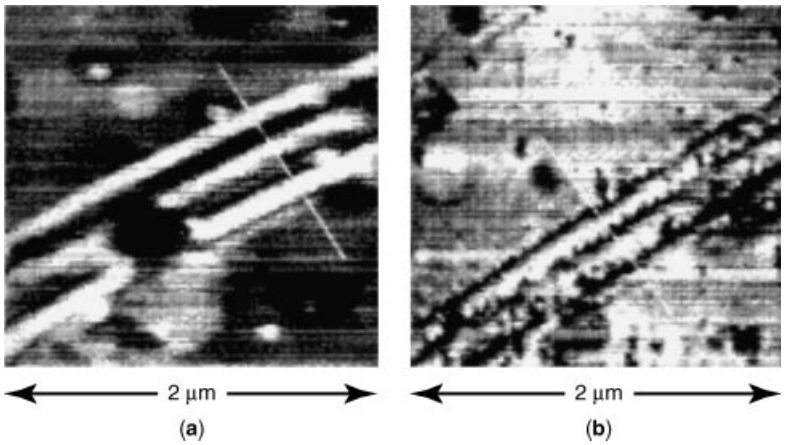

Fig. 23. (**a**) Topography of an undoped PC film. (**b**) Spatial variation in adhesion over approximately the same area. The adhesion ranges from 0.76 to 3.63 mdyn. Reprinted with permission from Ref. 64. Copyright (1991) by the American Institute of Physics.

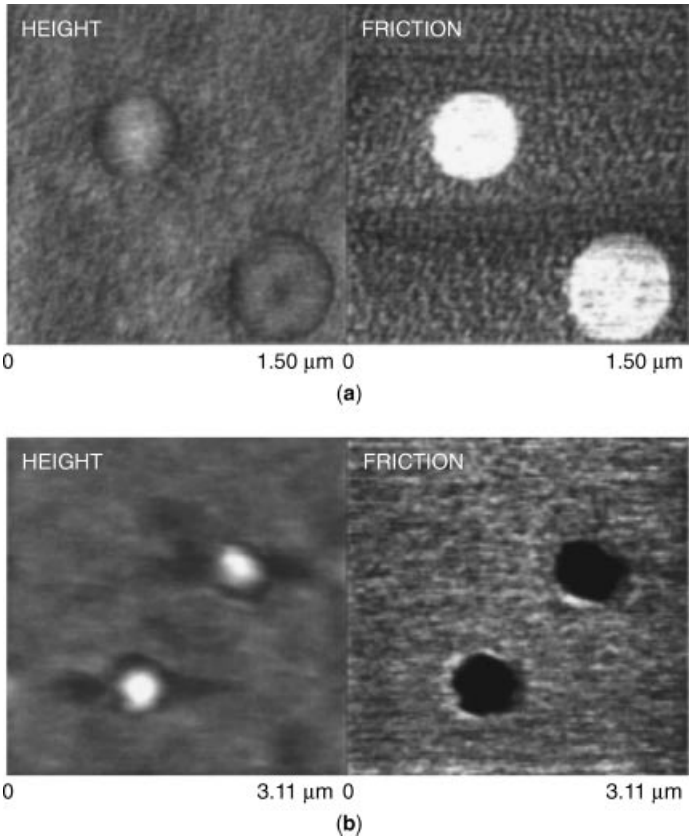

Fig. 24. SFM height (left) and friction (right) images of a spin-cast PS/PMMA polymer blend (PS/PMMA, 1:10 w/w), obtained with (**a**) gold-coated and (**b**) SiO_x tips under perfluorodecalin. Reprinted with permission from Ref. 86. Copyright (1998) American Chemical Society.

films (235). Sinniah and co-workers (236) showed that functionalized SFM tips can be utilized to differentiate polyamide-rich regions from poly(ethylene glycol)-rich regions in a blocky segmented copolymer in water. In this particular case, the friction forces observed with the more hydrophobic methoxy-terminated tips on the polyamide-rich domains exceeded the forces measured on the PEG-rich domains, while for amide-terminated tips, the contrast was significantly reduced.

Feldmann and co-workers studied phase-separated blends of PS and PMMA with gold-coated and silicon oxide coated tips in perfluorodecalin (Fig. 24) (86), where the contrast is dominated by the selectively amplified dispersive van der Waals interactions. The gold-coated tip experiences higher friction forces on the PS compared to PMMA, while the silicon oxide terminated tip shows an inverted contrast.

For the analysis of polar polymer films, the correlation between pull-off forces and surface free energies can be utilized (see section Normal Forces). Ionizable functional groups, such as carboxylic acid groups in oxyfluorinated isotactic PP

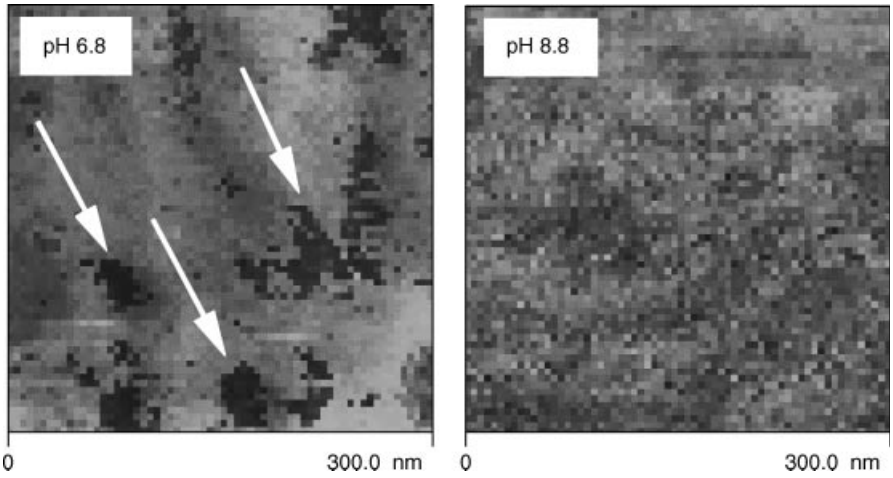

Fig. 25. Pull-off force images of oxyfluorinated isotactic iPP (γ = 39.6 mN/m) at pH 6.8 (left) and pH 8.8 (right). Dark color indicates high adhesion (-0.3 nN for pH 6.8, $\approx$0 nN for pH 8.8), bright color indicates low adhesion (0 nN for pH 6.8 and 8.8). The arrows indicate areas of high pull-off forces, which were attributed to areas with the most hydrophobic character, ie, lower density of polar —COOH and —OH functional groups introduced by the oxyfluorination. Reprinted in part with permission from Ref. 66. Copyright (2000) American Chemical Society.

films (203), have been force-titrated (221,222), and the spatially different response of the films to changes in pH have been used to map the functional group distribution in pull-off force measurements with $<$50 nm resolution (Fig. 25) (66).

Related observations were reported for plasma-polymerized allylamine films on oxidized silicon and for plasma-modified PP (216,223). On the basis of the force titration behavior (Fig. 22, right) the heterogeneous distribution of pull-off forces at pH values close to the force pK_a was related to variations in local hydrophilicity and hence amino group content.

In a pulsed force mode CFM study on poly(ethylene imine), Möhwald and co-workers showed that electrostatic and hydrophobic forces were responsible for the adhesion contrast in this system (237). pH-dependent measurements were thus exploited for chemical imaging. Recently, Vezenov and co-workers presented a systematic study in which the factors contributing to the measured forces in polymers have been discussed in detail (238).

Nysten and co-workers reported on the CFM mapping of the distribution of process stabilizers, UV-light stabilizers and antioxidants in stabilized polypropylene films as a function of aging time (239,240). Differences in the pull-off forces between the additives and PP allowed a submicrometer imaging of the lateral distribution of the additives present on the surface and a clear differentiation between antioxidants and UV-light stabilizers.

CFM using hydroxy- or methyl-terminated tips has also been used to investigate the frictional properties of PS films exhibiting different degrees of oxidation, ranging between 0 and 20 at% by X-ray photoelectron spectroscopy (241,242). A linear increase in the coefficient of friction with increasing surface oxygen level

and water contact angle was observed. The use of chemically modified tips allowed Ton-That and co-workers to differentiate the constituent phases of a PS/PMMA blend in laterally resolved CFM measurements.

Eaton and co-workers reported on force-mapping a phase-separated blend (218,243) of PMMA and poly(dodecyl methacrylate) (PDDMA). Using unmodified silicon nitride probes, the PDDMA-rich domains, which exhibited higher adhesion, could be differentiated from the PMMA-rich domains.

Finally, Nie and co-workers reported an increase in surface energy of mechanically scratched structures on biaxially oriented PP based on adhesion mapping and friction force imaging data using a conventional Si_3N_4 (244).

Surface Mechanical Properties. Phases within heterogeneous polymer systems, such as blends, block copolymers, or particulate-filled systems, can be routinely differentiated owing to image contrast arising from differences in surface mechanical properties (19). In addition, the arrangement of polymer architectures in ultrathin films, such as films formed by block copolymer micelle adsorption (39) or phase-separated blends on chemically structured surfaces (245,246), can be elucidated. For contact mode SFM, friction force measurements, as well as adhesion and indentation mapping, provide materials contrast. In intermittent contact mode, the use of the phase angle shift is particularly useful when differences in compliance exist. Finally, force modulation and pulsed force modes also provide stiffness-based contrast. Since the literature in this area is so abundant, only illustrative examples will be discussed in the following.

Bar and co-workers studied blends of poly(styrene)-*block*-poly(ethene-*co*-but-1-ene)-*block*-poly(styrene) with different PPs and resolved macrophase separation, as well as microphase separation, from size ranges of 15 μm down to 15 nm by intermittent contact mode SFM phase imaging (51). The heights and phase angle shifts determined were found to depend crucially on the operation conditions (169), as also shown in a companion paper (52). Using frequency sweep intermittent contact mode SFM, Bar and co-workers further showed in experiments on PS and PDMS that the phase angle shift obeys a harmonic approximation (53). The underlying features of intermittent contact mode SFM, eg with the sometimes observed tip bistability near the surface (247), and in particular the phase angle shift, have also been addressed in detail by various authors (19,37–41,169,248). The use of active control to tune the quality factor of the oscillating cantilever has been reported to yield optimized stable experimental conditions in the attractive force regime (249).

The elastic and viscoelastic properties of blends of PP and ethylene–propylene (EP) were investigated with the force modulation technique by Nysten and co-workers (250,251). In addition to a mapping of the distribution of the rubbery nodules of EP at the surface, the subsurface distribution of these nodules could be estimated. While the FMM data yielded qualitative data, more recent indentation mapping based on f-d curves allowed Nysten and co-workers to obtain quantitative information of the surface elastic modulus (252).

Tsukruk and co-workers evaluated different classic models of elastic contacts, including Sneddon's, Hertz, and JKR model, to probe the micromechanical properties of elastic polymeric materials (253). A close agreement between absolute values of elastic moduli and bulk data has been observed. With typically available cantilevers with stiffnesses in the range of 0.1–50 N/m, materials moduli

between 1 MPa and several GPa can be probed. The lateral resolution for mapping of moduli has been reported to be better than 100 nm.

van Landingham and co-workers mapped polymer heterogeneity by intermittent contact mode phase imaging and nanoscale indentation measurements for thin film blends of PS and PB (polybutadiene) as a function of annealing time (101). These authors observed that the phase contrast decreased with increasing annealing time because thermal oxidation causes cross-linking in PB, and hence a change in compliance of the PB region. The phases were identified using indentation data (Fig. 9). Similar observations were reported for blends of PMMA and PB (254).

Gracias and Somorjai reported on the determination of the elastic modulus, hardness, and friction of PE and PP using SFM tips with large radii (255). Higher values of modulus and hardness of the polymer surfaces were found to be correlated with the degree of crystallinity of the polymers. The frictional response was dominated by the deformation component of the friction, ie, the yield strength, the elastic modulus, and the pressure dependence of the shear strength.

Du and co-workers (256) analyzed SFM force indentation curves according to the method by Oliver and Pharr (104). For PS and PC thin films, good agreement between theory and experiment required the introduction of a correction factor that accounts for the asymmetry to the SFM indentation (256).

Microphase-separated block copolymer films have been investigated by numerous authors (257,258). van den Berg and co-workers reported on the film structures of poly(styrene-*block* butadiene-*block*-styrene) (SBS) triblock copolymers of PB and PS (259). In particular, the effect of film thickness on the observed morphology was unraveled for this system.

Using FMM SFM, Chen and Thomas investigated the surface and internal fracture surface morphologies of different block copolymers (58). Compared to the height images, the elasticity images were found to exhibit improved contrast and spatial resolution of the respective block copolymer domain structure.

The microphase separation and morphological transitions at the surface of acrylic block copolymers has been studied by Leclere and co-workers, who took advantage of the significant difference in local mechanical properties to obtain clear image contrast (260). The dependence of image contrast has been discussed by Pickering and Vancso, who analyzed the image contrast observed in films of commercial triblock copolymers of PS and isoprene (55). The image contrast was also analyzed by Bar and co-workers in related polymer systems (50–52).

As mentioned above, SFM approaches have also found widespread application in the analysis of block copolymer morphologies found in confinement. Magerle and co-workers showed, on the basis of SFM data and simulations, that the phase behavior at interfaces (261) and in thin films (interphases) (262) can be understood in terms of surface reconstructions analogous to those of classic, inorganic crystals. In Figure 26, thin triblock copolymer films of SBS on silicon are shown, which display a rich variety of morphologies depending on the local film thickness (263).

Owing to the different mechanical properties, filler particles can be in most cases differentiated from the polymeric matrix in SFM. Examples include carbon black or silica-filled rubbers, carbon-black-filled polymer blends or salt-loaded block copolymer micelles. For the latter case, Spatz and co-workers demonstrated

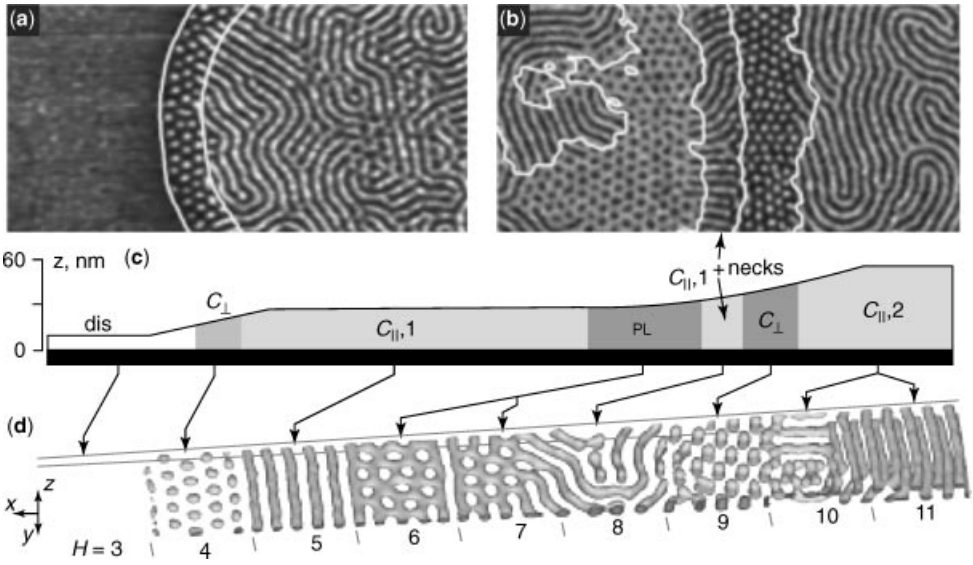

Fig. 26. (**a**,**b**) Intermittent contact mode SFM phase images of thin SBS films on silicon substrates after annealing in chloroform vapor. (**c**) Schematic height profile of the phase images shown in (**a**,**b**). (**d**) MesoDyn computer simulation of a $A_3B_{12}A_3$ block copolymer film in one large simulation box with from left to right increasing film thickness. Reprinted with permission from Ref. 263. Copyright (2002) by the American Physical Society.

that intermittent contact mode can differentiate $HAuCl_4$ loaded and unloaded block copolymer micelles with a mean diameter of 18 nm owing to stiffness differences (39).

The distributions of filler particles in carbon-black- and silica-filled elastomers were detected by intermittent contact mode SFM phase imaging, as well as adhesion mapping by Trifonova and co-workers (264). In the detailed particle size analysis evidence for the observation of primary filler particles was found.

Similarly, Leclere and co-workers utilized FFM to differentiate carbon black from PE and PS in filled blends (265). Carbon black was identified owing to the low friction forces compared to the blend. Ganter and co-workers showed that SFM measurements can provide information about the local distribution of the filler particles, as well as about the morphology of filler modified 1,4-BR/SBR blends (266).

The areas of tribology and lubrication are intimately linked to surface mechanical properties and the analysis thereof. The pioneering work in this area regarding lubrication of computer hard drives with perfluoropolyethers has been carried out by Mate and co-workers (267,268). These authors showed for instance that friction and topography are coupled on nontextured discs, whereas strongly textured discs do not show this effect. It was also shown that perfluoropolyether lubricant films substantially reduce the magnitude and variation of the frictional forces as measured by SFM. On the basis of noncontact mode SFM approaches the disjoining pressure of lubricants on oxidized silicon surfaces was successfully determined (269).

The surface viscoelastic properties of various polymers were studied by Takahara and co-workers (270). The effect of molecular weight on the surface dynamic viscoelastic properties for PS films and the measurement of surface relaxation processes were, for instance, reported (271).

Gladfelter and co-workers probed polymer viscoelastic relaxations with temperature-controlled FFM (272,273). The dependence of the mean value of the friction force on temperature was reported to be correlated to the glass-to-rubber transition and/or secondary relaxation mechanisms in films of PMMA, poly(ethylene terephthalate) (PET), and PS. Viscoelastic mechanical losses were thought to be the dominant contribution to friction, which were found to obey the time–temperature superposition principle. Interestingly, the surface T_g's and values for the activation energy measured for the β-relaxation at the surface were lower than those of the bulk material.

Structure Development and Processes in Real Time

SFM methodologies have been applied predominantly as static imaging and analysis techniques in polymer science and technology. However, recently the potential of the approaches for real-time studies, in particular for the investigation of phase transitions, has been realized. Owing to great importance of an improved fundamental understanding of crystallization and crystallinity in semicrystalline polymers, this section deals with this topic in more detail than the other real-time applications of SFM in the field of polymers.

Polymer Crystallization. In 1997, Miles and co-workers reported on the *in situ* study of polymer crystallization in poly(hydroxy butyrate) at ambient temperatures (274). This work of the Miles group, together with the groundbreaking work of Pearce and Vancso (152,275), who established SFM studies of polymer crystallization at elevated temperatures, initiated a rapid development in this area (276,277). Polymer crystallization can be followed in real time at the nanometer, ie, lamellar, level with this approach, also named hot-stage SFM, and central novel observations were made. The work by the groups of Miles and Vancso established that lamellar growth in spherulites does not proceed with linear growth rates when visualized at the level of individual lamellae. Instead, individual lamellae may remain dormant for some time before growing very rapidly (274–276) (see CRYSTALLIZATION KINETICS).

To date, numerous studies on different polymers have been reported, including poly(hydroxy butyrate) (274,276), PEO (275,277–280), PEO–PMMA blends (281), PE (282–284), poly(ε-caprolactone) (PCL) (285,286), poly(propylene oxide) (287), syndiotactic PP (288), and elastomeric PP (176). As an example, the different stages of development in the hedritic crystallization of PCL are shown in Figure 27.

Although SFM is traditionally an intrinsically slow imaging technique, a wealth of growth rate data has been obtained on the lamellar level. Furthermore, recent developments in the area of high speed SPM (289–291) show that real-time SFM at elevated temperatures possesses the potential to develop into an indispensable microscopic tool for the quantitative investigation of polymer phase transitions and other processes at elevated temperatures and as such may help to develop better theories of, eg, polymer crystallization.

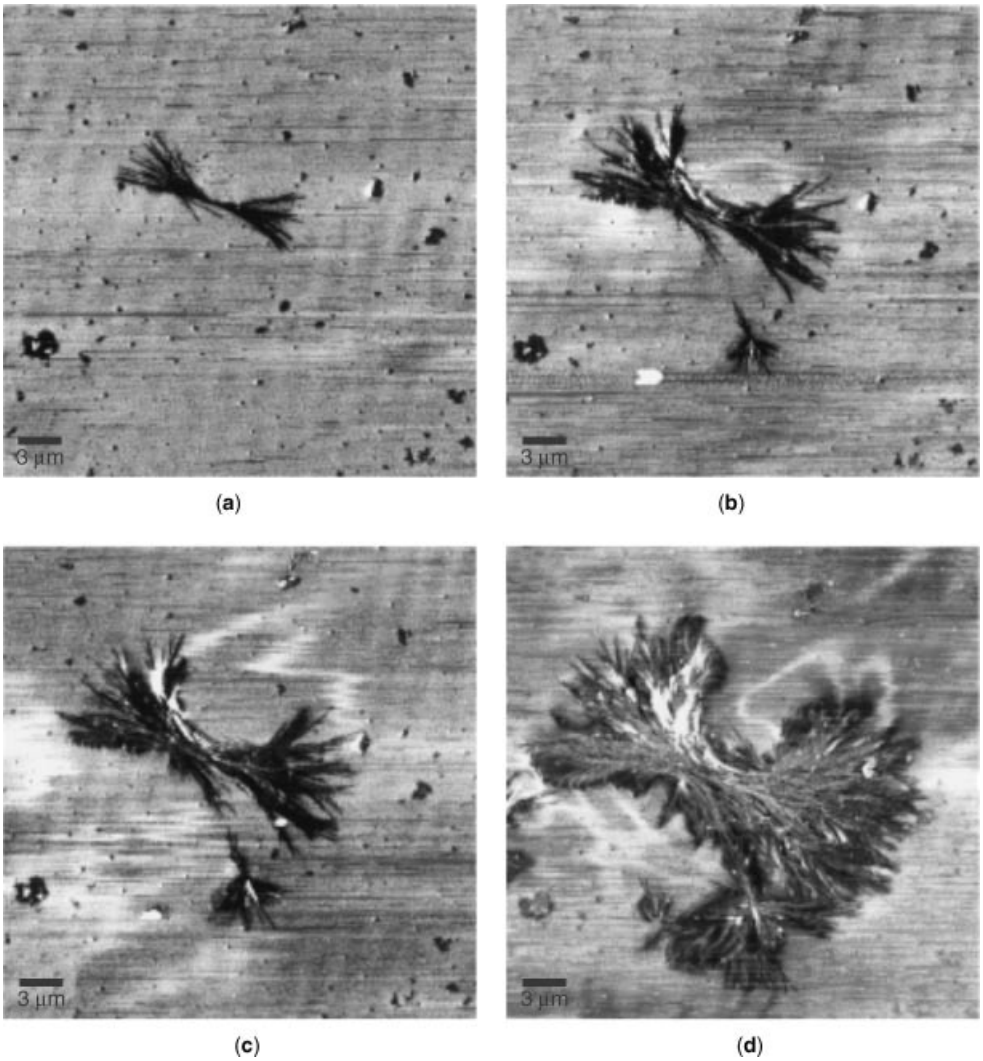

Fig. 27. Four steps in the development of hedrite of PCL as monitored by hot-stage SFM. Reprinted from Ref. 286. Copyright (2000), with permission from Elsevier.

In particular, in the area of nucleation and crystallization of polymers one can anticipate in the near future significant improvements in quantitative real-space investigation on processes occurring at the nanometer level. To date, the nucleation of polymer lamellae from the melt has been observed in some systems (176); however, the limited spatial resolution allowed only to observe the presence and not the shape/precise dimensions of stable, metastable, or unstable nuclei.

The first report of visualization of nuclei in polymer melts by SFM was published by Lei and co-workers (Fig. 28) (292). Subsequently, the observation of stable, unstable, and metastable nuclei has been reported for isotactic PP sequences of stereoblock PP (176).

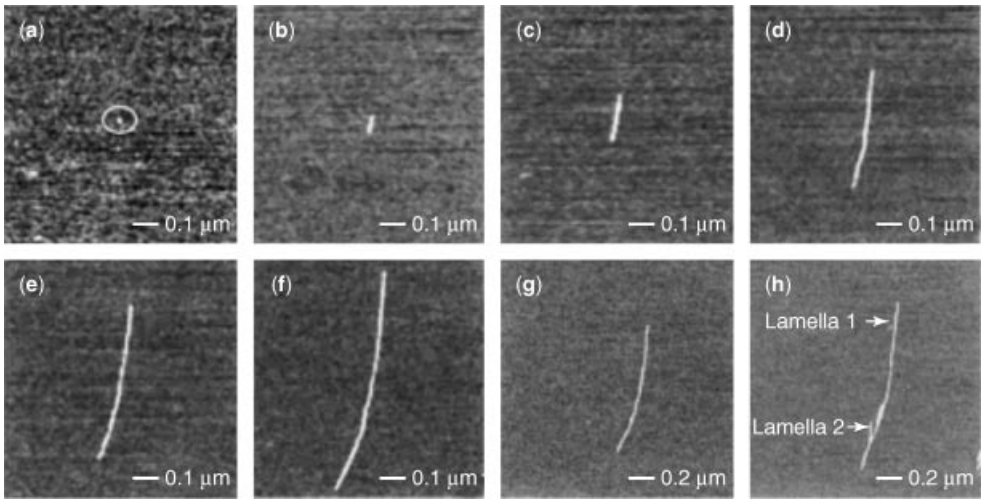

Fig. 28. Nuclei and growing lamellar crystals of poly(bisphenol A octane ether) observed by hot-state SFM. Reprinted in part with permission from Ref. 292. Copyright (2002) American Chemical Society.

Zhou and co-workers investigated the crystallization of individual lamellar crystals of syndiotactic PP from the melt and observed different lamellar thicknesses in different fold sectors (288). In addition, the effect of annealing and the melting behavior was followed in real time.

The crystallization of PEO was also unveiled at the level of individual lamellae in ultrathin films (278–280). It was observed that although lamellar growth rates were retarded in films thinner than 200 nm because of interfacial interactions, SFM provided the same qualitative and quantitative information as typically applied bulk characterization techniques on lamellar growth rates, lamellar thicknesses, and melting points. The Hoffman–Weeks extrapolation, the Gibbs–Thompson equation, and the Hoffman–Lauritzen theory were applied and the results compared favorably to the corresponding bulk data.

The nucleation process of nucleation agents added on purpose to polymer melts, as well as the effects of shear on polymer crystallization, are still not well understood. SFM can provide insight into the underlying processes as shown by Beekmans and co-workers, who investigated the transcrystallization of PCL on PTFE fibers using hot-stage SFM (293), and Hobbs and co-workers who studied the crystallization of sheared PE melts (283,284). In the latter studies, shish-kebab structures, nucleated on oriented backbones, were detected in the melt and could be followed in real time (Fig. 29).

More recently, new developments of hot-stage instrumentation have allowed several groups to study phase transitions in polymers at higher temperatures, thus establishing this approach as generic approach for the investigation of polymers relevant for a wide range of applications (294).

Various Dynamic Processes. The hot-stage approach has also found widespread use in studies on melting and annealing of single lamellae on solid substrates (295), as well as the fundamental mechanisms of melting in

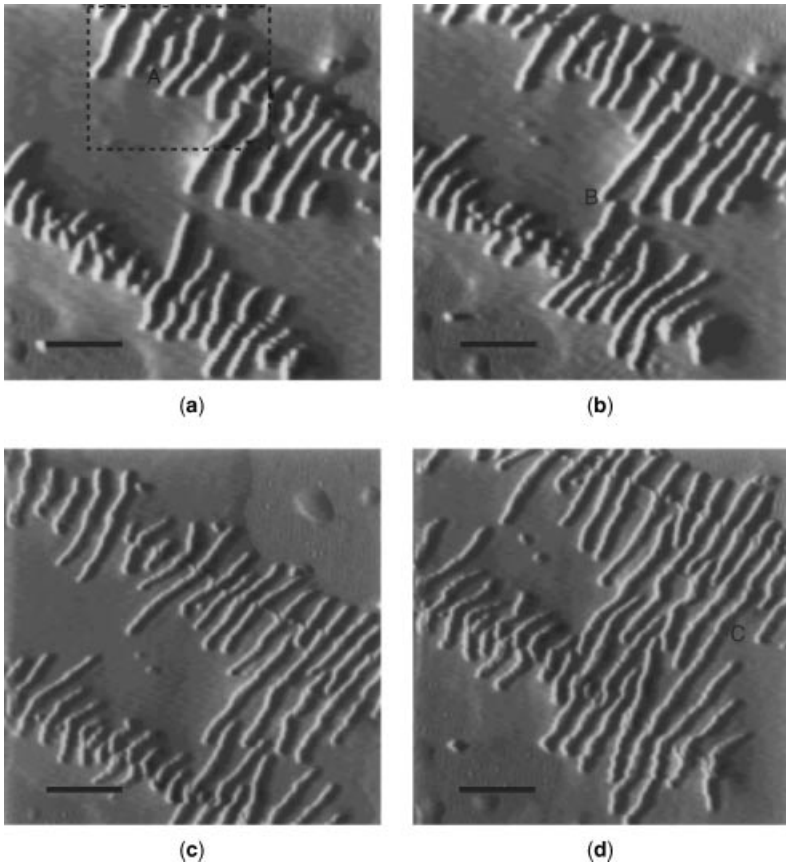

Fig. 29. Crystallization of shish-kebab-type lamellae observed by hot-state SFM in sheared melts of PE. This series of tapping mode SFM amplitude images shows the growth of lamellae from the oriented backbone. (**a**) Taken at 132.5°C; (**b**) taken at 132.3°C; (**c**) taken at 132°C; (**d**) taken at 131°C. The scale bars represent 300 nm. Reprinted with permission from Ref. 283. Copyright (2001) American Chemical Society.

melt-crystallized polymers (296–298). These studies complement the efforts reviewed in the previous section and although the character of the experiments is fundamental, there is a considerable practical significance of the results.

Further examples for real-time studies, which are becoming increasingly more important, target (surface) glass-transition temperatures (225–228), and thermotropic transitions in liquid crystalline polymers both at high and low temperatures (299–301). The analysis of temperature-dependent dynamical–mechanical surface properties has already been mentioned in the section under Surface Mechanical Properties (229–231,270–273).

The surface-glass-transition temperatures found by, eg, SFM approaches in polymers are usually lower than the corresponding values measured in the bulk. This effect has been attributed to an increased mobility of the macromolecules near or at the polymer–air interface. In very thin substrate-supported thin films, interfacial energy effects stemming from the substrate–polymer interface were

found to be important and can in some circumstances lead to an *increase* in T_g. Nealey and co-workers analyzed the dependence of T_g on interfacial energy and film thickness by various methods, including local thermal analysis using SFM-based scanning thermal microscopy (302).

The structure and phase transitions of polydiethylsiloxane were investigated with SFM at temperatures between 300 and 268 K. At room temperature, layers of polydiethylsiloxane are shown to be a mixture in both amorphous and mesomorphic states, while for a temperature of 273 K all material converts into the mesomorphic state (299).

Conformational changes of polymers as a result of stimulation by external stimuli, such as applied potential, changes in solvent or swelling agent, temperature, or irradiation with a suitable wavelength, have been investigated on different length scales in real time. The electrochemically induced response of organometallic polymers was shown to reversibly affect the adhesive properties (208). Ultrathin films composed of chemisorbed poly(ferrocenyl silane) showed fully reversible changes in film thickness, as shown in a recent electrochemical SFM study (303). Very recent work also highlighted the capabilities of SFM to follow the collapse of single polymer chains and the motility of adsorbed macromolecules in real time (121).

Dewetting (304–306) and phase separation phenomena are also amenable to *in situ* real-time SFM studies. As shown by Jacobs and co-workers, the dewetting of PS on an oxidized silicon wafer can be followed *in situ* at elevated temperatures. These observations are useful to develop a better understanding for film stability necessary in many modern applications of polymer ultrathin films in miniaturized electronic and microfluidic device applications.

Finally, SFM has also found widespread application in biology-related polymer science; in particular, the behavior of biopolymers in liquid medium has been studied *in situ*. These studies include the biodegradation of such polymers (307,308) and the crystallization of proteins (309,310).

Outlook: The Future of SFM on Polymers

The examples discussed in this article show that in less than two decades after its invention, SFM has already become an indispensable tool for many materials and polymer scientists for the characterization of polymers. The applications range from conventional surface topography and morphology imaging, mapping of composition and properties to a quantitative estimation of vital surface properties and real-time analysis of important processes.

The immense potential of SFM has been realized in industry, where it finds increasing application in research and development laboratories. It is fair to say that for both bulk and specialty polymers, such as coatings, SFM more than complements the traditional techniques of OM, SEM, and TEM. Despite this success, the standardization of procedures and a clear definition of protocols in the industrial environment are only beginning to emerge. The same is true for establishing routine measurements of various properties in a truly *quantitative* manner.

Together with the mentioned technical developments and improvements of SFM instrumentation (289–291), the anticipated development of new modes and

contrast mechanisms, as well as an improved theoretical understanding of the fundamental physics, the hitherto rapid development will likely continue and fully establish SFM and related approaches as routine technique in polymer science and technology. The expectations, eg, for chemical mapping, localized thermal analysis, and high resolution artifact free imaging are high, considering the recent introduction of functionalized carbon-nanotube probe tips as ultimate probes (311–313) and the progress in the area of scanning thermal microscopy. The many applications of polymers in the biomedical sector, as well as in ultrathin films in miniaturized electronic and microfluidic devices, underline the importance for nanometer-scale metrology and accurate characterization of polymer properties in confinement and constrained geometries. SFM techniques will therefore play an important role in the development of vital future technologies, and hence the impact of SFM can faithfully be expected to further grow in modern polymer science and technology.

BIBLIOGRAPHY

1. G. Binnig and H. Rohrer, *Helv. Phys. Acta* **55**, 726 (1982).
2. G. Binnig, H. Rohrer, C. Gerber, and E. Weibel, *Appl. Phys. Lett.* **40**, 178 (1982).
3. D. A. Hemsley, *Applied Polymer Light Microscopy*, Elsevier Applied Science, London, 1989.
4. L. C. Sawyer and D. T. Grubb, *Polymer Microscopy*, 2nd ed., Chapman and Hall, London, 1996.
5. G. Binnig, C. F. Quate, and C. Gerber, *Phys. Rev. Lett.* **56**, 930 (1986).
6. J. M. Bouton, G. Lepalec, P. Nardin, M. O. Rigo, and D. Rondot, *Rev. Gen. Therm.* **31**, 24 (1992).
7. A. Noy, D. V. Vezenov, and C. M. Lieber, *Annu. Rev. Mater. Sci.* **27**, 381 (1997).
8. R. J. Colton, A. Engel, J. E. Frommer, H. E. Gaub, A. A. Gewirth, R. Guckenberger, J. Rabe, W. M. Heckl, and B. Parkinson, *Procedures in Scanning Probe Microscopies*, John Wiley & Sons, Inc., New York, 1998.
9. D. Sarid, *Scanning Force Microscopy, with Applications to Electric, Magnetic and Atomic Forces*, Oxford University Press, Oxford, 1991.
10. J. Frommer, *Angew. Chem., Int. Ed. Engl.* **31**, 1298 (1992).
11. R. Wiesendanger, *Scanning Probe Microscopy and Spectroscopy, Methods and Applications*, Cambridge University Press, Cambridge, UK, 1994.
12. S. N. Magonov and M.-H. Whangbo, *Surface Analysis with STM and AFM*, VCH, Weinheim, 1996.
13. M. C. Goh, in I. Prigogine and S. A. Rice, eds., *Advances in Chemical Physics*, Vol. XCI, John Wiley & Sons, Inc., New York, 1995.
14. M. J. Miles, in S. J. Spells, ed., *Characterization of Solid Polymers*, Chapman and Hall, New York, 1994, Chapt. 2, pp. 17–55.
15. S. N. Magonov and D. H. Reneker, *Annu. Rev. Mater. Sci.* **27**, 175 (1997).
16. V. V. Tsukruk and D. H. Reneker, *Polymer* **36**, 1791 (1995).
17. S. S. Sheiko, *Adv. Polym. Sci.* **151**, 61 (2000).
18. D. A. Schiraldi and J. C. Poler, in H. F. Mark, N. Bikales, C. G. Overberger, G. Menges, and J. I. Kroschwitz, eds., *Encyclopedia of Polymer Science and Technology*, 3rd ed., Vol. 1, John Wiley & Sons, Inc., New York, 2002.
19. R. García and R. Pérez, *Surf. Sci. Rep.* **47**, 197 (2002).
20. M. Fujihira, *Annu. Rev. Mater. Sci.* **29**, 353 (1999).

21. H. Schönherr, Ph.D. dissertation, University of Twente, the Netherlands, 1999.
22. E. Meyer, R. M. Overney, K. Dransfeld, and T. Gyalog, *Nanoscience: Friction and Rheology on the Nanometer Scale*, World Scientific, Singapore, 1998.
23. N. A. Burnham, *Appl. Phys. Lett.* **63**, 114 (1993).
24. A. L. Weisenhorn, M. Khorsandi, S. Kasas, V. Gotzos, and H.-J. Butt, *Nanotechnology* **4**, 106 (1993).
25. T. R. Thomas, *Rough Surfaces*, 2nd ed., Imperial College Press, London, 1999.
26. M. Binggeli and C. M. Mate, *Appl. Phys. Lett.* **65**, 415 (1994).
27. A. L. Weisenhorn, P. K. Hansma, T. R. Albrecht, and C. F. Quate, *Appl. Phys. Lett.* **54**, 2651 (1989).
28. T. Pompe, A. Fery, and S. Herminghaus, *Langmuir* **14**, 2585 (1998).
29. T. Albrecht, M. Dovek, C. Lang, P. Grütter, C. Quate, S. Kuan, C. Frank, and F. Pease, *J. Appl. Phys.* **64**, 1178 (1988).
30. J. P. Pickering and G. J. Vancso, *Appl. Surf. Sci.* **148**, 147 (1999).
31. S. S. Sheiko, M. Möller, E. M. C. M. Reuvekamp, and H. W. Zandbergen, *Phys. Rev. B* **48**, 5675 (1993).
32. T. P. Weihs, Z. Nawaz, S. P. Jarvis, and J. B. Pethica, *Appl. Phys. Lett.* **59**, 3536 (1991).
33. D. L. Wilson, P. Dalal, K. S. Kump, W. Benard, P. Xue, R. E. Marchant, and S. J. Eppell, *J. Vac. Sci. Technol, B* **14**, 2407 (1996).
34. P. Markiewicz and M. C. Goh, *Langmuir* **10**, 5 (1994).
35. K. A. Ramirez-Aguilar and K. L. Rowlen, *Langmuir* **14**, 2562 (1998).
36. Q. Zhong, D. Inniss, K. Kjoller, and V. B. Elings, *Surf. Sci.* **290**, L688 (1993).
37. J. P. Spatz, S. Sheiko, M. Möller, R. G. Winkler, P. Reineker, and O. Marti, *Nanotechnology* **6**, 40 (1995).
38. N. A. Burnham, O. P. Behrend, F. Oulevey, G. Gremaud, P.-J. Gallo, D. Gourdon, E. Dupas, A. J. Kulik, H. M. Pollock, and G. A. D. Briggs, *Nanotechnology* **8**, 67 (1997).
39. J. P. Spatz, S. Sheiko, M. Möller, R. G. Winkler, P. Reineker, and O. Marti, *Langmuir* **13**, 4699 (1997).
40. R. G. Winkler, J. P. Spatz, S. Sheiko, M. Möller, P. Reineker, and O. Marti, *Phys. Rev. B* **54**, 8908 (1996).
41. J. Tamayo and R. Garcia, *Langmuir* **12**, 4430 (1996).
42. T. C. Marsh, J. Vesenka, and E. Henderson, *Nucleic Acids Res.* **23**, 697 (1995).
43. A. Kuhle, A. H. Sorensen, and J. Bohr, *J. Appl. Phys.* **81**, 6562 (1997).
44. W. Mahoney, D. M. Schaefer, A. Patil, R. P. Andres, and R. Reifenberger, *Surf. Sci.* **316**, 383 (1994).
45. M. Rasa, B. W. M. Kuipers, and A. P. Philipse, *J. Colloid Interface Sci.* **250**, 303 (2002).
46. S. J. T. Van Noort, K. O. Van der Werf, B. G. De Grooth, N. F. Van Hulst, and J. Greve, *Ultramicroscopy* **69**, 117 (1997).
47. Y. Ebenstein, E. Nahum, and U. Banin, *Nano Lett.* **2**, 945 (2002).
48. H. Schönherr and C. W. Frank, *Macromolecules* **36**, 1199 (2003).
49. M.-H. Whangbo, S. N. Magonov, and H. Bengel, *Probe Microsc.* **1**, 23 (1997).
50. G. Bar, Y. Thomann, and M.-H. Whangbo, *Langmuir* **14**, 1219 (1998).
51. G. Bar, Y. Thomann, R. Brandsch, H.-J. Cantow, and M.-H. Whangbo, *Langmuir* **13**, 3807 (1997).
52. G. Bar, R. Brandsch, and M.-H. Whangbo, *Langmuir* **14**, 7343 (1997).
53. A. Noy, C. H. Sanders, D. V. Vezenov, S. S. Wong, and C. M. Lieber, *Langmuir* **14**, 1508 (1998).
54. Ph. Leclère, R. Lazzaroni, J. L. Brédas, J. M. Yu, Ph. Dubois, and R. Jérôme *Langmuir* **12**, 4317 (1996).
55. J. P. Pickering and G. J. Vancso, *Polym. Bull.* **40**, 549 (1996).
56. P. Maivald, H.-J. Butt, S. A. C. Gould, C. B. Prater, B. Drake, J. A. Gurley, V. B. Elings, and P. K. Hansma, *Nanotechnology* **2**, 103 (1991).

57. L.-F. Chi, M. Anders, H. Fuchs, R. R. Johnston, and H. Ringsdorf, *Science* **259**, 213 (1993).
58. J. T. Chen and E. L. Thomas, *J. Mater. Sci.* **31**, 2531 (1996).
59. B. Anczykowski, D. Krüger, K. L. Babcock, and H. Fuchs, *Ultramicroscopy* **66**, 251 (1996).
60. J. S. Jourdan, S. J. Cruchon-Dupeyrat, Y. Huan, P. K. Kuo, and G.-Y. Liu, *Langmuir* **15**, 6495 (1999).
61. S. A. Joyce, J. E. Houston, and T. A. Michalske, *Appl. Phys. Lett.* **60**, 1175 (1992).
62. K. O. van der Werf, C. A. J. Putman, B. G. de Grooth, and J. Greve, *Appl. Phys. Lett.* **65**, 1195 (1994).
63. D. R. Baselt and J. D. Baldeschwieler, *J. Appl. Phys.* **76**, 33 (1994).
64. H. A. Mizes, K.-G. Loh, R. J. D. Miller, S. K. Ahuja, and E. F. Grabowski, *Appl. Phys. Lett.* **59**, 2901 (1991).
65. C. D. Frisbie, L. F. Rozsnyai, A. Noy, M. S. Wrighton, and C. M. Lieber, *Science* **265**, 2071 (1994).
66. H. Schönherr, Z. Hruska, and G. J. Vancso, *Macromolecules* **33**, 4532 (2000).
67. H. U. Krotil, T. Stifter, H. Waschipky, K. Weishaupt, S. Hild, and O. Marti, *Surf. Interface Anal.* **27**, 336 (1999).
68. A. Majumdar, *Annu. Rev. Mater. Sci.* **29**, 505 (1999).
69. A. A. Gewirth and B. K. Niece, *Chem. Rev.* **97**, 1129 (1997).
70. J. N. Israelachvili, *Intermolecular and Surface Forces*, 2nd ed., Academic Press, London, 1991.
71. N. A. Burnham, R. J. Colton, and H. M. Pollock, *Nanotechnology* **4**, 64 (1993).
72. B. Cappella and G. Dietler, *Surf. Sci. Rep.* **34**, 1 (1999).
73. A. L. Weisenhorn, P. Maivald, H.-J. Butt, and P. K. Hansma, *Phys. Rev. B* **45**, 11226 (1992).
74. J. P. Cleveland, S. Manne, D. Bocek, and P. K. Hansma, *Rev. Sci. Instrum.* **64**, 403 (1993).
75. J. L. Hutter and J. Bechhoefer, *Rev. Sci. Instrum* **64**, 1868 (1993).
76. J. E. Sader, I. Larson, P. Mulvaney, and L. R. White, *Rev. Sci. Instrum.* **66**, 3789 (1995).
77. M. Tortonese and M. Kirk, *Proc. SPIE* **3009**, 53 (1997).
78. C. A. J. Putman, B. D. deGrooth, N. F. van Hulst, and J. Greve, *J. Appl. Phys.* **72**, 6 (1992).
79. M. B. Viani, T. E. Schäffer, G. T. Paloczi, L. I. Pietrasanta, B. L. Smith, J. B. Thompson, M. Richter, M. Rief, H. E. Gaub, K. W. Plaxco, A. N. Cleland, H. G. Hansma, and P. K. Hansma, *Rev. Sci. Instrum.* **70**, 4300 (1999).
80. K. L. Johnson, K. Kendall, and A. D. Roberts, *Proc. R. Soc. London, Ser. A* **324**, 301 (1971).
81. K. L. Johnson, in V. V. Tsukruk and K. J. Wahl, eds., *Microstructure and Microtribology of Polymer Surfaces*, (ACS Symposium Series, Vol. 741), American Chemical Society, Washington, D.C., 1999, pp. 24–41.
82. R. L. Alley, K. Komvopoulos, and R. T. Howe, *J. Appl. Phys.* **76**, 5731 (1994).
83. L. Howald, R. Lüthi, E. Meyer, P. Güthner, and H.-J. Güntherodt, *Z. Phys. B* **93**, 267 (1994).
84. P. E. Laibinis and G. M. Whitesides, *J. Am. Chem. Soc.* **114**, 1990 (1992).
85. H. Schönherr and G. J. Vancso, *Polym. Prepr.* **39**, 1177 (1998).
86. K. Feldmann, T. Tervoort, P. Smith, and N. D. Spencer, *Langmuir* **14**, 372 (1998).
87. T. Hugel and M. Seitz, *Macromol. Rapid Commun.* **22**, 989 (2001).
88. A. Janshoff, M. Neitzert, Y. Oberdörfer, and H. Fuchs, *Angew. Chem., Int. Ed.* **39**, 3212 (2000).
89. M. Rief, M. Gautel, F. Oesterhelt, J. Fernandez, and H. Gaub, *Science* **276**, 1109 (1997).
90. M. Rief, H. Clausen-Schaumann, and H. Gaub, *Nat. Struct. Biol.* **6**, 346 (1999).

91. P. Marszalek, Y. Pang, H. Li, J. Yazal, A. Oberhauser, and J. Fernandez, *Proc. Natl. Acad. Sci. U.S.A.* **96**, 7894 (1999).
92. H. Li, B. Liu, X. Zhang, C. Gao, J. Shen, and G. Zou, *Langmuir* **15**, 2120 (1999).
93. H. Li, M. Rief, F. Oesterhelt, and H. E. Gaub, *Adv. Mater.* **3**, 316 (1998).
94. T. Hugel, M. Grosholz, H. Clausen-Schaumann, A. Pfau, H. E. Gaub, and M. Seitz, *Macromolecules* **34**, 1039 (2001).
95. H. Li, M. Rief, F. Oesterhelt, H. E. Gaub, X. Zhang, and J. Shen, *Chem. Phys. Lett.* **305**, 197 (1999).
96. W. Zhang, S. Zou, C. Wang, and X. Zhang, *J. Phys. Chem. B* **104**, 10258 (2000).
97. G. U. Lee, L. A. Chrisey, and R. J. Colton, *Science* **266**, 771 (1994).
98. T. J. Senden, J.-M. di Meglio, and P. Auroy, *Eur. Phys. J. B* **3**, 211 (1998).
99. C. Ortiz and G. Hadziioannou, *Macromolecules* **32**, 780 (1999).
100. J. B. Thompson, J. H. Kindt, B. Drake, H. G. Hansma, D. E. Morse, and P. K. Hansma, *Nature* **414**, 773 (2001).
101. D. Raghavan, M. van Landingham, X. Gu, and T. Nguyen, *Langmuir* **16**, 9448 (2000).
102. M. Radmacher, M. Fritz, J. Cleveland, D. A. Walters, and P. K. Hansma, *Langmuir* **10**, 3809 (1994).
103. M. R. van Landingham, J. S. Villarrubia, W. F. Guthrie, and G. F. Meyers, in V. V. Tsukruk and N. D. Spencer, eds., *Scanning Probe Microscopy of Polymers*, (ACS Symposium Series, Vol. 694), American Chemical Society, Washington, D.C., 2001, p. 15.
104. W. C. Oliver and G. M. Pharr, *J. Mater. Res.* **7**, 1564 (1992).
105. I. N. Sneddon, *Int. J. Eng. Sci.* **3**, 47 (1965).
106. J. P. Aime, Z. Elkaakour, C. Odin, T. Bouhacina, D. Michel, M. J. Curely, and A. Dautant, *Appl. Phys. Lett.* **76**, 754 (1994).
107. R. W. Carpick and M. Salmeron, *Chem. Rev.* **97**, 1163 (1997).
108. R. M. Overney, H. Takano, M. Fujihira, W. Paulus, and H. Ringsdorf, *Phys. Rev. Lett.* **72**, 3546 (1994).
109. I. L. Singer and H. M. Pollock, eds., *Fundamentals of Friction*, Kluwer, Dordrecht, the Netherlands, 1992.
110. B. Bushan, J. N. Israelachvili, and U. Landman, *Nature* **374**, 607 (1995).
111. B. J. Briscoe and D. C. B. Evans, *Proc. R. Soc., Ser. A* **380**, 389 (1982).
112. F. P. Bowden and D. Tabor, *Friction and Lubrication of Solids*, Part II, Oxford University Press, Oxford, 1964.
113. H. Hertz, *Reine Angew. Math.* **92**, 156 (1881).
114. S. P. Timoshenko and J. N. Goodier, *Theory of Elasticity*, McGraw-Hill, Inc., New York, 1970.
115. G. J. Vancso, R. Nisman, D. Snétivy, H. Schönherr, P. Smith, C. Ng, and H. Yang, *Colloids Surf., A: Physicochem. Eng. Aspects* **87**, 263 (1994).
116. J. Kumaki, Y. Nishikawa, and T. Hashimoto, *J. Am. Chem. Soc.* **118**, 3321 (1996).
117. P. Samorí, C. Ecker, I. Gössl, P. A. J. de Witte, J. J. L. M. Cornelissen, G. A. Metselaar, M. B. J. Otten, A. E. Rowan, R. J. M. Nolte, and J. P. Rabe, *Macromolecules* **35**, 5290 (2002).
118. H. G. Börner, K. Beers, K. Matyjaszewski, S. S. Sheiko, and M. Möller, *Macromolecules* **34**, 4375 (2001).
119. V. Percec, C.-H. Ahn, G. Ungar, D. J. P. Yeardley, M. Möller, and S. S. Sheiko, *Nature* **161**, 391 (1998).
120. C. Rivetti, M. Guthold, and C. Bustamante, *J. Mol. Biol.* **264**, 919 (1996).
121. S. S. Sheiko and M. Möller, *Chem. Rev.* **101**, 4099 (2001).
122. S. S. Sheiko, G. Eckert, G. Ignateva, A. M. Muzafarov, J. Spickermann, H. J. Rader, and M. Möller, *Macromol. Rapid Commun.* **17**, 283 (1996).
123. J. Li, L. T. Piehler, D. Qin, J. R. Baker Jr., D. A. Tomalia, and D. J. Meier, *Langmuir* **16**, 5613 (2000).

124. B.-H. Huisman, H. Schönherr, W. T. S. Huch, A. Friggeri, H. van Manen, E. Menozzi, G. J. Vancso, F. C. J. M. Van Veggel, and D. N. Reinhoudt, *Angew. Chem., Int. Ed.* **38**, 2248 (1999).
125. S. Loi, U.-M. Wiesler, H.-J. Butt, and K. Müllen, *J. Chem. Soc., Chem. Commun.* 1169 (2000).
126. A. Pfau, W. Schrepp, and D. Horn, *Langmuir* **15**, 3219 (1999).
127. E. Uchida and Y. Ikada, *Macromolecules* **30**, 5464 (1997).
128. O. Marti, H. O. Ribi, B. Drake, T. R. Albrecht, C. F. Quate, and P. K. Hansma, *Science* **239**, 50 (1988).
129. S. N. Magonov, S. Kempf, M. Kimmig, and H. J. Cantow, *Polym. Bull.* **26**, 715 (1991).
130. H. Hansma, F. Montamedi, P. Smith, P. K. Hansma, and J. C. Wittman, *Polymer* **33**, 647 (1992).
131. D. Snetivy, H. Yang, and G. J. Vancso, *J. Mater. Chem.* **2**, 891 (1992).
132. S. N. Magonov, S. S. Sheiko, R. A. C. Debliek, and M. Möller, *Macromolecules* **26**, 1380 (1993).
133. H. Schönherr, G. J. Vancso, and A. S. Argon, *Polymer* **36**, 2115 (1995).
134. B. Lotz, J. C. Wittmann, W. Stocker, S. N. Magonov, and H. J. Cantow, *Polym. Bull.* **26**, 209 (1991).
135. D. Snétivy, J. E. Guillett, and G. J. Vancso, *Polym. Commun* **34**, 429 (1993).
136. R. Jaeger, H. Schönherr, and G. J. Vancso, *Macromolecules* **29**, 7634 (1996).
137. D. Snétivy, G. J. Vancso, and G. C. Rutledge, *Macromolecules* **25**, 7037 (1992).
138. B. H. Glomm, M. C. Grob, P. Neuenschwander, U. W. Suter D. D. Snétivy, and G. J. Vancso, *Polymer* **35**, 878 (1994).
139. D. Snétivy and G. J. Vancso, *Macromolecules* **25**, 3320 (1992).
140. W. Stocker, A. J. Lovinger, M. Schumacher, S. Graff, J. C. Wittmann, and B. Lotz, in V. V. Tsukruk and N. D. Spencer, eds., *Scanning Probe Microscopy of Polymers*, (ACS Symposium Series, Vol. 694), American Chemical Society, Washington, D.C., 2001, pp. 53–66.
141. G. J. Vancso, D. Snétivy, and H. Schönherr, in V. V. Tsukruk and N. D. Spencer, eds., *Scanning Probe Microscopy of Polymers*, (ACS Symposium Series, Vol. 694), American Chemical Society, Washington, D.C., 2001, pp. 67–93.
142. W. Stocker, S. N. Magonov, H. J. Cantow, J. C. Wittmann, and B. Lotz, *Macromolecules* **26**, 5915 (1993).
143. D. Snétivy and G. J. Vancso, *Polymer* **35**, 461 (1994).
144. W. Stocker, M. Schumacher, S. Graff, A. Thierry, J. C. Wittmann, and B. Lotz, *Macromolecules* **31**, 807 (1998).
145. G. J. Vancso, S. Förster, and H. Leist, *Macromolecules* **29**, 2158 (1996).
146. H. Schönherr and G. J. Vancso, *Polymer* **39**, 5705 (1998).
147. D. Snétivy and G. J. Vancso, *Polymer* **33**, 432 (1992).
148. R. Nisman, P. Smith, and G. J. Vancso, *Langmuir* **10**, 1667 (1994).
149. R. Patil, S.-J. Kim, E. Smith, D. H. Reneker, and A. L. Weisenhorn, *Polym. Commun.* **31**, 455 (1990).
150. R. Patil and D. H. Reneker, *Polymer* **35**, 1909 (1994).
151. R. D. Boyd and J. P. S. Badyal, *Adv. Mater.* **9**, 895 (1997).
152. R. Pearce and G. J. Vancso, *Polymer* **39**, 6743 (1998).
153. T. Murase, T. Iwata, and Y. Doi, *Macromol. Biosci.* **1**, 275 (2001).
154. G. J. Vancso and H. Schönherr, in V. V. Tsukruk and K. J. Wahl, eds., *Microstructure and Microtribology of Polymer Surfaces*, (ACS Symposium Series, Vol. 741), American Chemical Society, Washington, D.C., 1999, pp. 317–335.
155. P. F. Smith, R. Nisman, C. Ng, and G. J. Vancso, *Polym. Bull.* **33**, 459 (1994).
156. T. Kajiyama, I. Ohki, and A. Takahara, *Macromolecules* **28**, 4768 (1995).

157. S. J. Sutton, K. Izumi, H. Miyaji, K. Fukao, and Y. Miyamoto, *Polymer* **37**, 5529 (1996).
158. K. Taguchi, Y. Miyamoto, H. Miyaji, and K. Izumi, *Macromolecules* **36**, 5208 (2003).
159. M. Motomatsu, H.-Y. Nie, W. Mizutani, and H. Tokumoto, *Polym. Commun.* **37**, 183 (1996).
160. H. Schönherr, L. E. Bailey, and C. W. Frank, *Langmuir* **18**, 490 (2002).
161. H. Schönherr, D. Snétivy, and G. J. Vancso, *Polym. Bull.* **30**, 567 (1993).
162. D. Trifonova, J. Varga, and G. J. Vancso, *Polym. Bull.* **41**, 341 (1998).
163. D. Trifonova-van Haeringen, J. Varga, G. W. Ehrenstein, and G. J. Vancso, *J. Polym. Sci., Part B: Polym. Phys.* **38**, 672 (2000).
164. Z. Bartczak, A. S. Argon, R. E. Cohen, and T. Kowalewski, *Polymer* **40**, 2367 (1999).
165. H. R. Harron, R. G. Pritchard, B. C. Cope, and D. T. Goddard, *J. Polym. Sci., Part B: Polym. Phys.* **34**, 173 (1996).
166. D. C. Bassett, *Macromol. Symp.* **143**, 11 (1999).
167. D. C. Bassett, *Principles of Polymer Morphology*, Cambridge University Press, Cambridge U.K., 1981.
168. A. Alizadeh, S. Sohn, J. Quinn, H. Marand, L. C. Shank, and H. D. Iler, *Macromolecules* **34**, 4066 (2001).
169. S. N. Magonov, V. Elings, and M.-H. Whangbo, *Surf. Sci.* **372**, L385 (1997).
170. B. Lotz and J. C. Wittmann, *J. Polym. Sci., Part B: Polym. Phys.* **24**, 1541 (1986).
171. R. H. Olley and D. C. Bassett, *Polymer* **30**, 399 (1989).
172. H. Schönherr, R. M. Waymouth, and C. W. Frank, unpublished data, 2001.
173. S. Bensason, J. Minick, A. Moet, S. Chum, A. Hiltner, and E. Baer, *J. Polym. Sci., Part B: Polym. Phys.* **34**, 1301 (1996).
174. H. Schönherr, W. Wiyatno, J. Pople, C. W. Frank, G. G. Fuller, A. P. Gast, and R. M. Waymouth, *Macromolecules* **35**, 2654 (2002).
175. R. L. Kravchenko, B. B. Sauer, R. S. McLean, M. Y. Keating, P. M. Cotts, and Y. H. Kim, *Macromolecules* **33**, 11 (2000).
176. H. Schönherr, R. M. Waymouth, and C. W. Frank, *Macromolecules* **36**, 2412 (2003).
177. P. H. Geil, *Polymer Single Crystals*, Wiley-Interscience, New York, 1963, Chapt. 3.
178. R. Viswanathan and D. W. M. Marr, *Langmuir* **12**, 1084 (1996).
179. J. J. Janimak, L. Markey, and G. C. Stevens, *Polymer* **42**, 4675 (2001).
180. S. Sasaki, Y. Sakaki, A. Takahara, and T. Kajiyama, *Polymer* **43**, 3441 (2002).
181. A. Toda, T. Arita, M. Hikosaka, J. K. Hobbs, and M. J. Miles, *J. Macromol. Sci.-Phys., B* **42**, 753 (2003).
182. J. Xu, B. H. Guo, G. Q. Chen, and Z. M. Zhang, *J. Polym. Sci., Part B: Polym. Phys.* **41**, 2128 (2003).
183. G. J. Vancso, G. Liu, J. Karger-Kocsis, and J. Varga, *Colloid Polym. Sci.* **275**, 181 (1997).
184. A. Tracz, J. Jeszka, I. Kucinska, J.-P. Chapel, and G. Boiteux, *Macromol. Symp.* **169**, 129 (2001).
185. O. Mellbring, S. H. Oiseth, A. Krozer, J. Lausmaa, and T. Hjertberg, *Macromolecules* **34**, 7496 (2001).
186. B. B. Sauer, R. S. McLean, and R. R. Thomas, *Polym. Int.* **49**, 449 (2000).
187. Y. Wang, D. Juhue, M. A. Winnik, O. M. Leung, and M. C. Goh, *Langmuir* **8**, 760 (1992).
188. J. Hautojarvi and A. Leijala, *J. Appl. Polym. Sci.* **74**, 1242 (1999).
189. R. Jaeger, M. M. Bergshoef, C. Martín i Batlle, H. Schönherr, and G. J. Vancso, *Macromol. Symp.* **127**, 141 (1998).
190. S. N. Magonov, K. Qvarnstrom, V. Elings, and H. J. Cantow, *Polym. Bull.* **25**, 689 (1991).
191. K. D. Jandt, M. Bukh, M. J. Miles, and J. Petermann, *Polymer* **35**, 2458 (1994).

192. M. J. Miles, K. D. Jandt, T. J. McMaster, and R. L. Williamson, *Colloids Surf., A: Physicochem. Eng. Aspects* **87**, 235 (1994).
193. J. Hautojarvi and H. Niemi, *Text. Res. J.* **70**, 820 (2000).
194. G. J. Vancso, T. D. Allston, I. Chun, L. S. Johansson, G. Liu, and P. F. Smith, *Int. J. Polym. Anal. Charact.* **3**, 89 (1996).
195. M. P. Goh, D. Juhue, O. M. Leung, Y. Wang, and M. A. Winnik, *Langmuir* **9**, 1319 (1993).
196. H.-J. Butt, R. Kuropka, and B. Christensen, *Colloid Polym. Sci.* **272**, 1218 (1994).
197. A. A. Patel, J. Feng, M. A. Winnik, G. J. Vancso, and C. B. Dittman, *McBain, Polymer* **37**, 5577 (1996).
198. D. Juhue and J. Lang, *Langmuir* **9**, 7902 (1993).
199. H.-J. Butt and B. Gerharz, *Langmuir* **11**, 4735 (1996).
200. P. F. Smith, I. Chun, G. Liu, D. Dimitrievich, J. Rasburn, and G. J. Vancso, *Polym. Eng. Sci.* **36**, 2129 (1996).
201. M. C. Coen, G. Dietler, S. Kasas, and P. Groning, *Appl. Surf. Sci.* **103**, 27 (1996).
202. M. D. Duca, C. L. Plosceanu, and T. Pop, *Polym. Degrad. Stab.* **61**, 65 (1998).
203. Z. Hruska and X. Lepot, *J. Fluorine Chem.* **105**, 87 (2000).
204. H. Schönherr, Z. Hruska, and G. J. Vancso, *Macromolecules* **31**, 3679 (1998).
205. H. Schönherr and G. J. Vancso, *J. Polym. Sci., Part B: Polym. Phys.* **36**, 2486 (1998).
206. T. Ogawa, H. Mukai, and S. Osawa, *J. Appl. Polym. Sci.* **71**, 243 (1999).
207. C. S. Hodges, *Adv. Colloid Interface Sci.* **99**, 13 (2002).
208. J. E. Hudson and H. D. Abruna, *J. Am. Chem. Soc.* **118**, 6303 (1996).
209. L. H. G. J. Segeren, Ph.D. dissertation, University of Twente, the Netherlands, 2002.
210. L. H. G. J. Segeren, B. Siebum, F. G. Karssenberg, J. W. A. van den Berg, and G. J. Vancso, *J. Adhes. Sci. Technol.* **16**, 793 (2002).
211. L. H. G. J. Segeren, F. G. Karssenberg, J. P. Pickering, J. W. A. van den Berg, and G. J. Vancso, in K. L. Mittal, ed., *Particles on Surfaces 7: Detection, Adhesion and Removal*, Materials Science VSP International Science Publishers/Brill Academic Publishers, Zeist, 2002, pp. 197–217.
212. C. S. Hodges, J. A. S. Cleaver, M. Ghadiri, R. Jones, and H. M. Pollock, *Langmuir* **18**, 5741 (2002).
213. W. A. Ducker, T. J. Senden, and R. M. Pashley, *Nature* **353**, 239 (1991).
214. S. Briggs, *Langmuir* **11**, 156 (1995).
215. H.-J. Butt, M. Kappl, H. Mueller, R. Raiteri, W. Meyer, and J. Rühe, *Langmuir* **15**, 2559 (1999).
216. H. Schönherr, M. T. van Os, R. Förch, R. B. Timmons, W. Knoll, and G. J. Vancso, *Chem. Mater.* **12**, 3689 (2000).
217. R. McKendry, M. E. Theoclitou, C. Abbell, and T. Rayment, *Langmuir* **14**, 2846 (1998).
218. P. Eaton, J. R. Smith, P. Graham, J. D. Smart, T. G. Nevell, and J. Tsibouklis, *Langmuir* **18**, 3387 (2002).
219. C. Dicke and G. Hahner, *J. Phys. Chem. B* **106**, 4450 (2002).
220. X. Jiang, C. Ortiz, and P. T. Hammond, *Langmuir* **18**, 1131 (2002).
221. D. V. Vezenov, A. Noy, L. F. Rozsnyai, and C. M. Lieber, *J. Am. Chem. Soc.* **119**, 2006 (1997).
222. E. W. van der Vegte and G. Hadziioannou, *J. Phys. Chem.* **101**, 9563 (1997).
223. H. Schönherr, M. T. van Os, Z. Hruska, J. Kurdi, R. Förch, F. Arefi-Khonsari, W. Knoll, and G. J. Vancso, *J. Chem. Soc., Chem. Commun*. 1303 (2000).
224. M. A. Hempenius, N. S. M. Robins, M. Péter, E. S. Kooij, and G. J. Vancso, *Langmuir* **18**, 7629 (2002).
225. S. Ge, Y. Pu, W. Zhang, M. Rafailovich, J. Sokolov, C. Buenviaje, R. Buckmaster, and R. M. Overney, *Phys. Rev. Lett.* **85**, 2340 (2000).

226. F. Dinelli, C. Buenviaje, and R. M. Overney, *J. Chem. Phys.* **113**, 2043 (2000).
227. O. K. C. Tsui, X. P. Wang, J. Y. L. Ho, T. K. Ng, and X. Xiao, *Macromolecules* **33**, 4198 (2000).
228. R. M. Overney, C. Buenviaje, R. Luginbuhl, and F. Dinelli, *J. Therm. Anal. Calorimetry* **59**, 205 (2000).
229. N. Satomi, A. Takahara, and T. Kajiyama, *Macromolecules* **32**, 4474 (1999).
230. R. H. Schmidt, G. Haugstad, and W. L. Gladfelter, *Langmuir* **15**, 317 (1999).
231. F. Ouveley, N. A. Burnham, G. Gremaud, A. J. Kulik, H. M. Pollock, A. Hammiche, M. Reading, M. Song, and D. J. Hourston, *Polymer* **41**, 3087 (2000).
232. H. Schönherr and G. J. Vancso, *Macromolecules* **30**, 6391 (1997).
233. S. Akari, W. Schrepp, and D. Horn, *Langmuir* **12**, 857 (1996).
234. S. Akari, W. Schrepp, and D. Horn, *Ber. Bunsen-Ges. Phys. Chem.* **100**, 1014 (1996).
235. M. P. L. Werts, E. W. van der Vegte, V. Grayer, E. Esselink, C. Tsitsilianis, and G. Hadziioannou, *Adv. Mater.* **10**, 452 (1998).
236. S. K. Sinniah, A. B. Steel, C. J. Miller, and J. E. Reutt-Robey, *J. Am. Chem. Soc.* **118**, 8925 (1996).
237. M. Schneider, M. Zhu, G. Papastavrou, S. Akari, and *H. Möhwald, Langmuir* **18**, 602 (2002).
238. D. V. Vezenov, A. V. Zhuk, G. M. Whitesides, and C. M. Lieber, *J. Am. Chem. Soc.* **124**, 10578 (2002).
239. C. Poleunis, P. Bertrand, and B. Nysten, *Langmuir* **17**, 6351 (2001).
240. A. S. Duwez and B. Nysten, *Langmuir* **17**, 8287 (2001).
241. C. Ton-That, P. A. Campell, and R. H. Bradely, *Langmuir* **16**, 5054 (2000).
242. C. Ton-That, D. O. H. Tear, and R. H. Bradely, *Chem. Mater.* **12**, 2106 (2000).
243. P. J. Eaton, P. Graham, J. R. Smith, J. D. Smart, T. G. Nevill, and J. Tsibouklis, *Langmuir* **16**, 7887 (2000).
244. H. Y. Nie, M. J. Walzak, B. Berno, and N. S. McIntyre, *Langmuir* **15**, 6484 (1999).
245. J. Heier, E. J. Kramer, S. Walheim, and G. Krausch, *Macromolecules* **30**, 6610 (1997).
246. M. Boltau, S. Walheim, J. Mlynek, G. Krausch, and U. Steiner, *Nature* **391**, 87 (1998).
247. P. Gleyzes, P. K. Kuo, and A. C. Boccara, *Appl. Phys. Lett.* **58**, 2989 (1991).
248. B. Anczykowski, D. Krüger, and H. Fuchs, *Phys. Rev. B* **53**, 15485 (1996).
249. R. Garcia and T. R. Rodriguez, *Appl. Phys. Lett.* **82**, 4821 (2003).
250. B. Nysten, R. Legras, and J.-L. Costa, *J. Appl. Phys.* **78**, 5953 (1995).
251. E. Tomasetti, B. Nysten, and R. Legras, *Nanotechnology* **9**, 305 (1998).
252. B. Nysten, C. Meerman, and E. Tomasetti, in V. V. Tsukruk and K. J. Wahl, eds., *Microstructure and Microtribology of Polymer Surfaces*, (ACS Symposium Series, Vol. 741), American Chemical Society, Washington, D.C., 1999, pp. 304–316.
253. S. A. Chizhik, Z. Huang, V. V. Gorbunov, N. K. Myshkin, and V. V. Tsukruk, *Langmuir* **14**, 2606 (1998).
254. D. Raghavan, M. van Landingham, X. Gu, and T. Nguyen, *Langmuir* **16**, 9448 (2000).
255. D. H. Gracias and G. A. Somorjai, *Macromolecules* **31**, 1269 (1998).
256. B. Y. Du, O. K. C. Tsui, Q. L. Zhang, and T. B. He, *Langmuir* **17**, 3286 (2001).
257. B. K. Annis, D. W. Noid, B. G. Sumpter, J. R. Reffner, and B. Wunderlich, *Makromol. Rapid Commun.* **13**, 169 (1992).
258. W. Stocker, B. Bickmann, S. N. Magnonv, H. J. Cantow, B. Lotz, J. C. Wittmann, and M. Möller, *Ultramicroscopy* **28**, 1141 (1992).
259. M. A. van Dijk and R. van den Berg, *Macromolecules* **28**, 6773 (1995).
260. P. Leclere, J. L. Bredas, G. Moineau, M. Minet, P. Dubois, R. Jerome, and R. Lazzaroni, in V. V. Tsukruk and K. J. Wahl, eds., *Microstructure and Microtribology of Polymer Surfaces*, (ACS Symposium Series, Vol. 741), American Chemical Society, Washington, D.C., 1999, pp. 356–368.

261. N. Rehse, A. Knoll, M. Konrad, R. Magerle, and G. Krausch, *Phys. Rev. Lett.* **87**, 035505 (2001).
262. R. Magerle, *Phys. Rev. Lett.* **85**, 2749 (2000).
263. A. Knoll, A. Horvat, K. S. Lyakhova, G. Krausch, G. J. A. Sevink, A. V. Zvelindovsky, and R. Magerle, *Phys. Rev. Lett.* **89**, 035501 (2002).
264. D. Trifonova, H. Schönherr, L. van der Does, P. J. P. Janssen, J. W. M. Noordermeer, and G. J. Vancso, *Rubber Chem. Technol.* **72**, 862 (1999).
265. P. Leclere, R. Lazzaroni, F. Gubbels, M. de Vos, R. Deltour, R. Jerome, and J. L. Bredas, in V. V. Tsukruk and N. D. Spencer, eds., *Scanning Probe Microscopy of Polymers*, (ACS Symposium Series, Vol. 694), American Chemical Society, Washington, D.C., 2001, pp. 129–140.
266. M. Ganter, R. Brandsch, Y. Thomann, T. Malner, and G. Bar, *Kautsch. Gummi Kunst.* **52**, 717 (1999).
267. C. M. Mate, *IBM J. Res. Dev.* **39**, 617 (1995).
268. C. M. Mate, *Surf. Coat. Technol.* **62**, 373 (1993).
269. H. I. Kim, C. M. Mate, K. A. Hannibal, and S. S. Perry, *Phys. Rev. Lett.* **82**, 3496 (1999).
270. T. Kajiyama, K. Tanaka, S. R. Ge, and A. Takahara, *Prog. Surf. Sci.* **52**, 1 (1996).
271. K. Tanaka, A. Taura, S. R. Ge, A. Takahara, and T. Kajiyama, *Macromolecules* **29**, 3040 (1996).
272. J. A. Hammerschmidt, B. Moasser, W. L. Gladfelter, G. Haugstad, and R. R. Jones, *Macromolecules* **29**, 8996 (1996).
273. J. A. Hammerschmidt, W. L. Gladfelter, and G. Haugstad, *Macromolecules* **32**, 3360 (1999).
274. T. J. McMaster, J. K. Hobbs, P. J. Barham, and M. J. Miles, *Probe Microsc.* **1**, 43 (1997).
275. R. Pearce and G. J. Vancso, *Macromolecules* **30**, 5843 (1997).
276. J. K. Hobbs, T. J. McMaster, M. J. Miles, and P. J. Barham, *Polymer* **39**, 2437 (1998).
277. J. M. Schultz and M. J. Miles, *J. Polym. Sci., Part B: Polym. Phys.* **36**, 2311 (1998).
278. H. Schönherr, L. E. Bailey, and C. W. Frank, *Langmuir* **18**, 490 (2002).
279. H. Schönherr and C. W. Frank, *Macromolecules* **36**, 1188 (2003).
280. H. Schönherr and C. W. Frank, *Macromolecules* **36**, 1199 (2003).
281. R. Pearce and G. J. Vancso, *J. Polym. Sci., Part B: Polym. Phys.* **36**, 2643 (1998).
282. Y. K. Godovsky and S. N. Magonov, *Langmuir* **16**, 3549 (2000).
283. J. K. Hobbs and M. J. Miles, *Macromolecules* **34**, 353 (2001).
284. J. K. Hobbs, A. D. L. Humphris, and M. J. Miles, *Macromolecules* **34**, 5508 (2001).
285. G. J. Vancso, L. G. M. Beekmans, R. Pearce, D. Trifonova, and J. Varga, *J. Macromol. Sci. Phys. B* **38**, 491 (1999).
286. L. G. M. Beekmans and G. J. Vancso, *Polymer* **41**, 8975 (2000).
287. L. G. M. Beekmans, M. A. Hempenius, and G. J. Vancso, *Eur. Polym. J.* **40**, 893–903 (2004).
288. W. Zhou, S. Z. D. Cheng, S. Putthanarat, R. K. Eby, D. H. Reneker, B. Lotz, S. N. Magonov, E. T. Hsieh, R. G. Geerts, S. J. Palackal, G. R. Hawley, and M. B. Welch, *Macromolecules* **33**, 6861 (2000).
289. T. Sulchek, R. Hsieh, J. D. Adams, G. G. Yaralioglu, S. C. Minne, C. F. Quate, J. P. Cleveland, A. Atalar, and D. M. Adderton, *Appl. Phys. Lett.* **76**, 1473 (2000).
290. T. Sulchek, R. Hsieh, J. D. Adams, S. C. Minne, C. F. Quate, and D. M. Adderton, *Rev. Sci. Instrum.* **71**, 2097 (2000).
291. A. D. L. Humphris, J. K. Hobbs, and M. J. Miles, *Appl. Phys. Lett.* **83**, 6 (2003).
292. Y.-G. Lei, C.-M. Chan, J.-X. Li, K.-M. Ng, Y. Wang, Y. Jiang, and L. Li, *Macromolecules* **35**, 6751 (2002).

293. L. G. M. Beekmans, R. A. L. Beekmans, and G. J. Vancso, *Macromolecules* **35**, 9383 (2002).
294. D. A. Ivanov, Z. Amalou, and S. N. Magonov, *Macromolecules* **34**, 8944 (2001).
295. A. K. Winkel, J. K. Hobbs, and M. J. Miles, *Polymer* **41**, 8791 (2000).
296. L. G. M. Beekmans, D. W. van der Meer, and G. J. Vancso, *Polymer* **43**, 1887 (2002).
297. Y. Jiang, X. G. Jin, C. C. Han, L. Li, Y. Wang, and C. M. Chan, *Langmuir* **19**, 8010 (2003).
298. M. Fujita and Y. Doi, *Biomacromolecules* **4**, 1307 (2003).
299. S. N. Magonov, V. Elings, and V. S. Papkov, *Polymer* **38**, 297 (1997).
300. Y. K. Godovsky, V. S. Papkov, and S. N. Magonov, *Macromolecules* **34**, 976 (2001).
301. M. Debowski and G. J. Vancso, *Probe Microsc.* **2**, 11 (2000).
302. D. S. Fryer, R. D. Peters, E. J. Kim, J. E. Tomaszewski, J. J. dePablo, P. F. Nealey, C. C. White, and W. L. Wu, *Macromolecules* **34**, 5627 (2001).
303. M. Péter, M. A. Hempenius, R. G. H. Lammertink, and G. J. Vancso, *Macromol. Symp.* **167**, 285 (2001).
304. R. Seemann, S. Herminghaus, and K. Jacobs, *Phys. Rev. Lett.* **86**, 5534 (2001).
305. C. Neto, K. Jacobs, R. Seemann, R. Blossey, J. Becker, and G. Grün, *J. Phys.: Condens. Matter* **15**, 3355 (2003).
306. J. Becker, G. Grün, R. Seemann, H. Mantz, K. Jacobs, K. R. Mecke, and R. Blossey, *Nat. Mater.* **2**, 59 (2003).
307. M. C. Davies, K. M. Shakesheff, A. G. Shard, A. Domb, C. J. Roberts, S. J. B. Tendler, and P. M. Williams, *Macromolecules* **29**, 2205 (1996).
308. Y. Kikkawa, T. Murase, H. Abe, T. Iwata, Y. Inoue, and Y. Doi, *Macromol. Biosci.* **2**, 189 (2002).
309. S. D. Durbin and G. Feher, *Annu. Rev. Phys. Chem.* **47**, 171 (1996).
310. A. McPherson, A. J. Malkin, and Y. G. Kuznetsov, *Annu Rev. Biophys. Biomol. Struct.* **29**, 361 (2000).
311. H. J. Dai, J. H. Hafner, A. G. Rinzler, D. T. Colbert, and R. E. Smalley, *Nature* **384**, 147 (1996).
312. S. S. Wong, E. Joselevich, A. T. Woolley, C. L. Cheung, and C. M. Lieber, *Nature* **394**, 52 (1998).
313. C. V. Nguyen, R. M. D. Stevens, J. Barber, J. Han, M. Meyyappan, M. I. Sanchez, C. Larson, and W. D. Hinsberg, *Appl. Phys. Lett.* **81**, 901 (2002).

HOLGER SCHÖNHERR
University of Twente

Nomenclature

T_g	glass-transition temperature
Δz	cantilever deflection
F	force
k	spring constant
R	tip radius
K	reduced modulus
L	load
$F_{pull-off}$	pull-off force

W_{12}	work of adhesion (surface energy per unit area)
γ	surface free energies
E	Young's modulus
ν	Poisson's number
F_{friction}	friction force
μ	friction coefficient
τ	interfacial shear strength
λ	draw ratio
A	amplitude
$\Delta\phi$	phase angle shift

SCATTERING. See LASER LIGHT SCATTERING.

SCRATCH BEHAVIOR OF POLYMERS

Introduction

Abrasion and wear is a long existing deteriorating phenomenon occurring when two moving surfaces are in intimate contact. Although the history of systematic study of abrasion and wear can be dated back more than 70 years (see Ref. 1, and references therein), the actual processes involved in abrasion and wear are still not clearly understood. It is generally believed that asperity interactions between two surfaces are responsible for such occurrence. Mechanisms involved include adhesion, shearing, fatigue, microcutting, and surface smearing. The resulting damage features will vary with materials properties, compounded by changes with sliding conditions. The situation for polymers is particularly complicated because of their viscoelastic–viscoplastic nature, leading to wear features that alter with the history of wear and time of observation. In addition, those circumstances that result in abrasion and wear often involve multiple asperities, which render studying into the science behind this phenomenon difficult. Since abrasion and wear can be considered as multiple asperities making multiple, repeated scratches on the contact surfaces, a simplified situation where a stylus is used to scratch a polymer surface is often examined to gain insight into this complex process.

Apart from the macroscopic wear behavior that traditional tribology is concerned with, research on micro/nanotribology has gained pace recently to develop crucial understanding of nanoscale surface wear and interfacial mechanical phenomena on a small scale. This trend is driven by both the industrial needs of miniaturization and the desire to understand engineering material-to-material contact damage phenomena based on fundamental science.

Compared to other materials, polymers are more susceptible to scratches and abrasion because they are relatively soft. Yet, polymers and polymer matrix

Encyclopedia of Polymer Science and Technology. Copyright John Wiley & Sons, Inc. All rights reserved.

composites have increasingly been chosen for microelectronic packaging, coatings, aerospace, automotive, food packaging, and biomedical applications because of their adequate strength, lightness, versatility, ease of processing, and low cost. In many cases, they will be subjected to wear or scratch at loads, resulting in surface damages at various scales. Thus, there is a strong need to improve scratch and wear resistance in plastics.

Significant research and developmental efforts have been placed to characterize and improve abrasion and wear resistance of polymers (2–5). However, advances in fundamental knowledge on abrasion and wear are limited mainly because of the complexity of the available test methods, such as the Taber abrasion test. No direct correlation between the applied loading conditions and the observed abrasion damage can be made. As a result, no definitive relationship between material parameters and abrasion resistance can be established.

It is believed that the first step to the understanding of abrasion and wear resistance is to fundamentally understand the scratch behavior of polymers. Since abrasion and wear usually involve repetitive damage on the same location of the polymer surface, it smears the damage mechanisms. As a result, no definitive information can be obtained to identify the exact sequence of events and process(es) leading to the surface damage of the polymer. On the other hand, it is possible to create controlled surface damage on polymers using a single- or multiple-pass scratch process from which the mechanics related to the generation of surface damage is understood and the corresponding surface damage can be characterized to make fundamental correlations between mechanics and materials science of scratch of polymers (6,7).

The objective of this article is to highlight the importance of understanding scratch behavior of polymers by giving readers an up-to-date knowledge in this field of research. The theoretical framework concerning interfacial contacts will be introduced, and the experimental aspects in terms of methodology and quantitative measures summarized. Various factors influence the scratch behavior of polymers in different ways which will be discussed.

Theoretical Background

Even a surface that appears to be flat on a millimeter scale may in fact be rough with micrometer scale asperities on it. Friction and the resulting energy dissipation are thus due to the interaction between the asperities of the different surfaces when they touch each other. It is the real contact area that affects the friction opposing the action of motion and the real area of contact may be therefore a few orders of magnitude smaller than the apparent area of contact. A brief summary on the development of theoretical models for friction is given by Meyer and co-workers (8).

Theory of Contact.

Bowden and Tabor Model. In 1950, Bowden and Tabor (1) presented a simple model for friction on a micrometer scale. They proposed a contact model based on adhesion and shearing that take place at the interfaces of asperity surfaces during translational motion. Based on this model, the energy loss in the friction mechanism is due to plastic deformation of the asperities at the surfaces

on contact. The model assumes that friction F_f is proportional to both the real area of contact, A_R and a mean lateral force per unit area, the so-called shear strength σ. The real area of contact is the area of asperities that are deformed by the normal load and is independent of nominal contact area. Thus, the friction force does not depend on the apparent area of contact. When the normal applied force F_N, is large, F_f takes the form of

$$F_f = \frac{\sigma}{p_m^*} F_N \tag{1}$$

$$A_R = \frac{F_N}{p_m^*} \tag{2}$$

with $p_m{}^*$ being the yield stress of the asperity, which can be smaller than the yield stress of the bulk materials due to the asperity's small size.

Hertzian Model. Hertz described in a general form a contact phenomenon between two spheres of radii R and R', respectively, where the deformation mechanism is totally elastic. $R' \to \infty$, if one of the objects in contact is a plane. Based on his analysis and for symmetry reasons, the area of contact between the sphere and the plane is a circle and its area is

$$A_R = \pi (DR)^{2/3} (F_N)^{2/3} \tag{3}$$

where R is the radius of the sphere, and D is the inverse "plane stress modulus," which is composed of the elastic moduli and Poisson's ratios of both the sphere and the plane. One should note that based on equations 1 and 2, the result in equation 3 suggests $A_R \propto (F_N)^{2/3}$. Assuming the shear strength σ is independent of the load, it leads to a conclusion that $F_f \propto (F_N)^{2/3}$, which contradicts the Amonton's law.

The JKR Model. Since adhesion will surely come into play when the two surfaces are in intimate contact, Johnson and co-workers (9) extended the Hertzian model to include terms due to surface tension γ. The real area of contact is related to normal force by

$$A_R(F_N) = (DR)^{2/3} \left(F_N + 3\pi\gamma R + \sqrt{6\pi\gamma R F_N + (3\pi\gamma R)^2} \right)^{2/3} \tag{4}$$

From equation 4, A_R is finite when F_N is zero and equals

$$A_R(0) = \pi (6\pi D\gamma R^2)^{2/3} \tag{5}$$

Hence, a negative load is required to break the contact. In addition, in the limit of zero surface tension, ie $\gamma \to 0$ and also when the external applied load is large compared to γR, the JKR model coincides asymptotically with the Hertzian model. A comparison at the point of asperities in contact is given in Figure 1.

The Greenwood and Williamson Model. Since a real surface consists of multiple asperities of different heights, a model that takes such a factor into consideration is required. Greenwood and Williamson (10) considered a surface with a random distribution of asperity heights. In this model, every asperity has the same

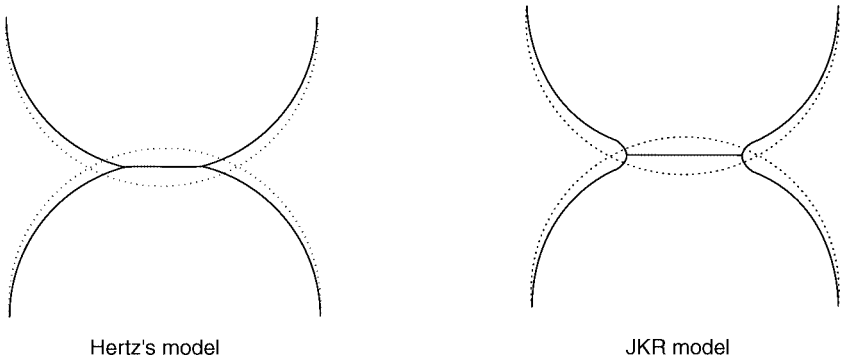

Fig. 1. A comparison of asperities in contact based on the Hertzian model and the JKR model.

radius of curvature β at the summit, and is pressed against a plane (Fig. 2). A probabilistic approach is used to take the height distribution of asperities into account when calculating A_R. The separation between the reference plane in the rough surface and that of the smooth surface is denoted d. We consider the deformation of an asperity with height z; then $w = z - d$ is the "penetration depth" of this asperity. Using Hertz's theory of a total elastic contact, the final form of A_R is related to F_N:

$$A_R = \frac{4\sqrt{\pi}}{3} D F_N \sqrt{\frac{\beta}{\sigma}} \tag{6}$$

Thus, the real contact area is proportional to the load and independent of the nominal contact area.

Theory of Sliding Contact. Based on Hertzian contact model, Hamilton and Goodman (11), which was later elaborated by Hamilton (12), presented the scratch process as a combination of an indentation process and a sliding process. Figure 3 shows the schematic of the scratch process in this model. At the contact surface, where $z = 0$,

$$\sigma_z = \frac{3P}{2\pi a^3}(a^2 - x^2 - y^2)^{1/2} \tag{7}$$

$$\tau_{zx} = \frac{3Q}{2\pi a^3}(a^2 - x^2 - y^2)^{1/2} \qquad x^2 + y^2 \leq a^2 \tag{8}$$

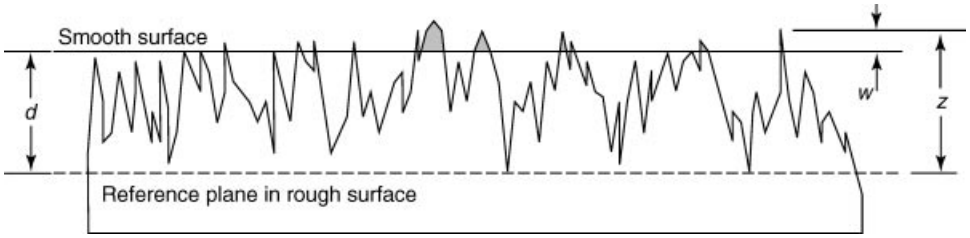

Fig. 2. The Greenwood–Williamson model.

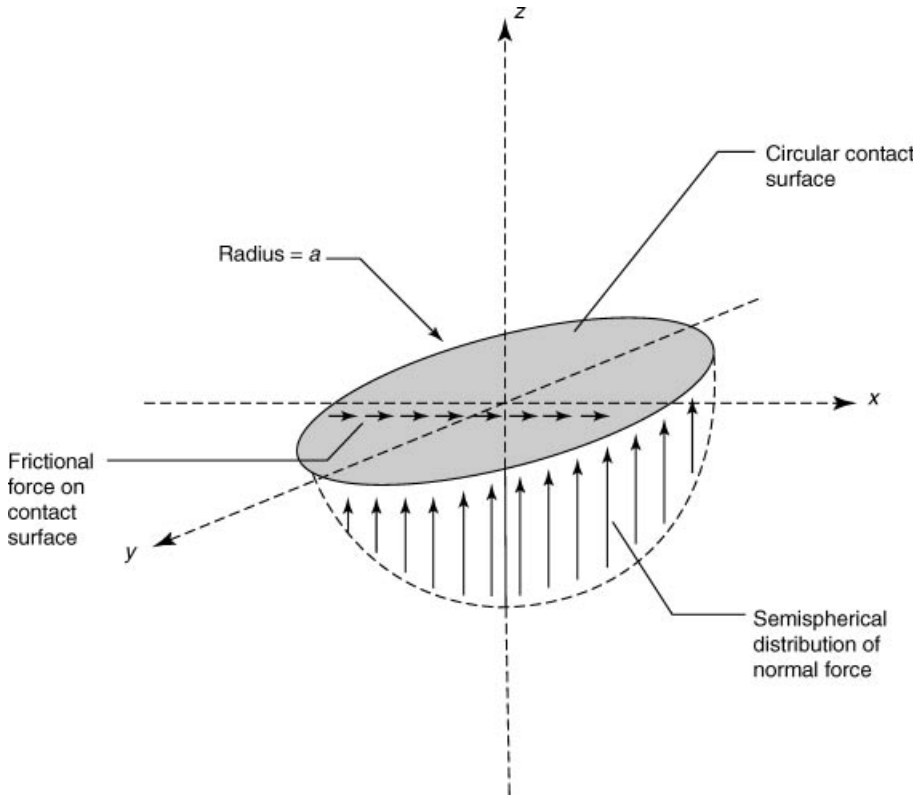

Fig. 3. The Hamilton and Goodman model.

where P and Q are the total normal load in the z-direction and the total frictional force in the x-direction, respectively. Equations 7 and 8 give the normal stress and frictional stress distribution. The maximum tensile stress during the scratch process, which occurs on the circumference of the circle of contact, is

$$\sigma_x = \frac{3P}{2\pi a^3}\left(\frac{1-2v}{3} + \frac{4+v}{8}\pi\mu\right) \tag{9}$$

The existence of friction adds a compressive stress to the front edge of the contact and intensifies the tensile stress at the back edge.

Similarly, Sackfield and Hills (13–15), based on Hertzian contact model, derived mathematical expression for elliptical contacts. In addition, a number of models have been developed recently, mostly based on JRK models (16–18). Furthermore, Ford (19) has derived an analytical model on multiasperity against smooth surface based on a model developed for narrow slider and a single asperity and the Greenwood–Williamson model. All these efforts are exerted, aiming at giving a mechanics-based understanding of the scratch process and potentially help us to correlate scratch conditions, materials properties, and scratch features observed.

Methodology

To assess the scratch behavior of polymers, scratch tests are performed. A compendium of the use of various instruments and methods applied is given in Reference (20). Although different setups have been used for scratch studies, the basic principle relies on the use of a stylus to scratch a surface (2,3,21–43). The stylus can be made of materials ranging from diamond and sapphire, to tool steel, and silicon nitrite for the case of AFM tips. It also comes with a variety of geometries including conical tips with different included angles, spherical tips of different radii, and Berkovich tip. In addition, the observation length scale and controlled experimental parameters are instrument specific.

Individual scratch is often done with a constant loading rate (which includes constant load) and constant scratch rate. The scale of damage of interest varies from macroscopic features to those of nanometer scale. This renders comparisons between studies difficult. The recent concerted industry–university effort (6,7,44) has led to the development of a scratch test method and universal scratch testing equipment to facilitate good scratch test practices and fundamental study of scratch behavior of polymers. Figure 4 presents the scratch tester that was developed. It aims to provide reasonable capability to vary experimental conditions for capturing the essential scratch characteristic of the materials with reliable and reproducible results. One unique feature of the tester is its ability to alter scratch load and velocity at a linear rate. This feature is found to be useful in understanding scratch behavior of polymers, to be presented in later sections.

Since scratches exist on the surface of the materials, different surface morphology evaluation tools and techniques are employed to quantify the severity of scratch damages. The instruments used for such quantification include

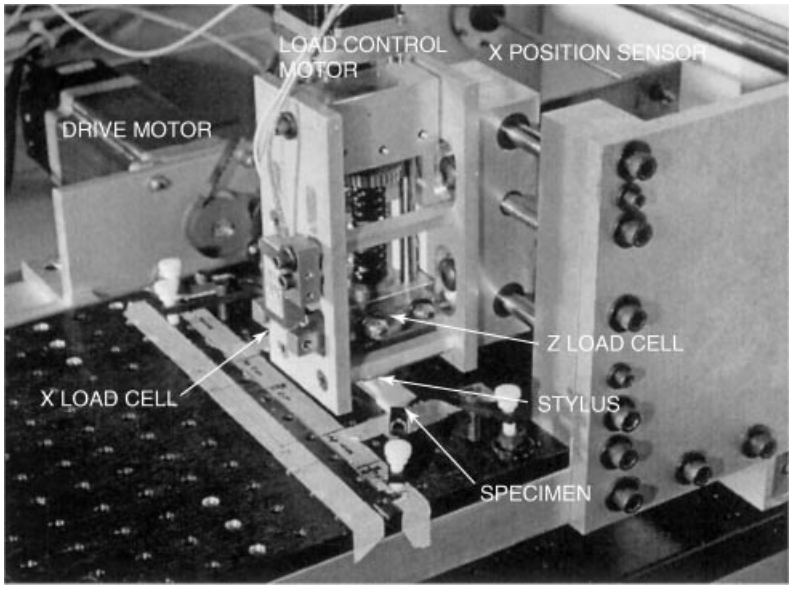

Fig. 4. Custom-made scratch tester in PTC, Texas A&M University.

atomic force microscope (22–24,45–48), optical microscope (22,30,37), scanning electron microscope (38,49), laser confocal microscope (30), Raman spectroscope (39), white-light interferometer (3,22), cross profilometer (50), tribometer (51), ellipsometer (39), and scanner (37,52,53). Each of these equipments examines certain aspects of scratch damages, inter alia scratch surface topology and resulted light reflectivity. With such a wide range of equipments being utilized, a variety of scratch resistance measures were devised.

Scratch Hardness. One of the more commonly used scratch resistance measures is the so-called scratch hardness (10,21,54). This is a concept borrowed from static indentation HARDNESS. Like indentation hardness, scratch hardness is often a measure of force experienced by the sample per unit area. The frequently used definitions for scratch hardness, H_S, and ploughing hardness, H_P, are given in Reference (10):

$$H_S = \frac{\text{Applied Normal Load}}{\text{Apparent Load Bearing Area}} \tag{10}$$

$$H_P = \frac{\text{Tangential Load Measured}}{\text{Apparent Load Bearing Area}} \tag{11}$$

The magnitude of force applied normally and the tangential force exerted on the samples can be measured accurately by force sensors. The definition of contact/load-bearing area is however controversial. When a scratch groove is formed, three kinds of deformation can be differentiated (36): the elastic deformation inside the groove; the elastic deflection of the surface responsible for the vertical displacement of the edge of the contact; and the plastic deformation, which results in the remaining groove, and the pile-up pads. This renders the estimation of true contact area difficult. Figure 5 is a schematic diagram of the scratch process. Assuming that the sample undergoes totally plastic deformation when being scratched, only the front half of the indenter will be supported by the sample. In this case, two definitions of contact area can be devised. First, an apparent scratch contact area, similar to that in the indentation process, is the projected area of the half-cone supported by the sample, as line-shaded in Figure 5**a** and 5**c** for equations 10 and 11, respectively. Second, a true contact area equals to the front half of the indenter curved surface in contact with the sample (line-shaded in Fig. 5**b**).

The issues of defining and measuring contact area become complicated when the viscoelastic–viscoplastic nature of polymer is taken into consideration. As shown in Figure 5**b**, the geometry of the scratch groove that formed during the scratch process (the dash lines) would be different from that of the residual groove that remains after the indenter is removed (the solid lines). Such deviation arises because viscoelastic recovery occurs in polymers (4,55,56). Both the apparent and true contact areas are difficult to define and measure in this case. This is because the materials behind the indenter will recover to support the indenter. Yet the amount of viscoelastic recovery is time-dependent (57,58) and it is not necessary to be isotropic in nature. In addition, if pile-ups exist, materials will be push forward and to the sides of the groove by the indenter to rise above the original sample surface. These materials might provide extra support for the indenter. Moreover,

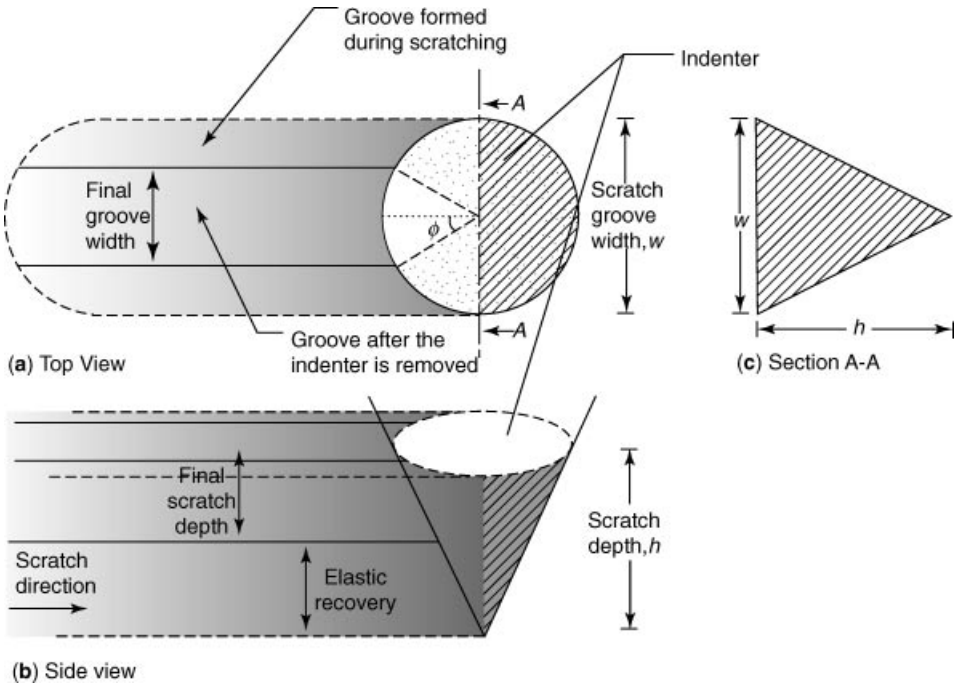

Fig. 5. Schematic diagram showing the scratch process showing difference in groove gemoetry during and after the scratch process.

because of the wide variety of scratch mechanisms that can be involved during the scratch process, the amount of materials supporting the indenter is changing even when the scratch condition is kept constant. These factors contribute to the uncertainties of the actual contact area and render an accurate estimation difficult, subjective, and ambiguous. Under the same line of argument, the use of cross-sectional scratch profiles for surface damage quantification (22,43,52,53,57, 58) suffers from the similar shortcomings mentioned above.

Scratch Visibility. As polymer coatings are frequently used as protective and decorative coatings, another way to quantify scratch resistance and surface damage would be to measure scratch visibility (2,3,28,29,59–62). It has been shown that the use of light reflectivity measure for identification of crack formation and differentiating subtle changes in scratch damage severity is more effective than visual observation by optical or scanning electron microscopy (59). In most cases, a light source is shone on the scratched surface and the reflected light signals are collected and quantified using digital image analyzing software to give a measure of intensity or gloss of the surface. The intensity collected is generally on a per pixel basis. Some types of integration are required in order to find the total intensity/reflectivity of the scratched surface and a comparison to its initial condition.

While some software has generated a measure of gloss or grey scale level, which can be used as a measure of scratch visibility (60,61), others prefer to develop scratch visibility measure after manipulation of data captured by computer.

This is normally done to highlight certain aspects of the scratch properties of the materials. For example, a percentage change of brightness or grey scale is often used for assessing scratch visibility of mineral-filled polyolefin composites (3,5,28,29). This is because the inclusion of mineral fillers might facilitate the light scattering when the sample is being scratched. Such effect of light scattering can be better represented by the manipulated measures than by the raw data generated by the software. In another study (2), by measuring intensity of reflected light using polarized light source and changing the orientation of the scratch with respect to the light source, the importance of different stress whitening mechanisms at a variety of scratch rate was studied. Effort has been made to develop more sophisticated light reflectivity measurements in order to better correlate experimental results with human impression on scratch visibility (62).

Effect of Sliding Conditions

From the equations presented in under Theoretical Background, it can be derived that materials properties, such as modulus and yield strength, and any modifications that might affect them will influence the scratch behavior of polymers. The unique characteristics of polymers make research in polymer scratch particularly challenging. First, as mentioned in the previous section, polymers are viscoelastic–viscoplastic in nature. This makes polymer properties very sensitive to test conditions, especially temperature and strain rate (21,34,56,63,64).

Second, it has been suggested by various authors that the surface properties of polymers might be different from those of the bulk owing to differences in molecular dynamics (66–68). Such differences propagate from the surface over a very short distance. A lower surface glass-transition temperature could result in variation of surface friction with scratching rate and temperature (68–70). Results to date suggest that behaviors of polymers in nanoscale are different from those in the micro- and macroscale. An example is the observation that nanoscale surface coefficient of friction is lower than that of the bulk, owing to the reduction of real area of contact and subsequent effects caused by such reduction when very low loads were being applied to the polymer (24,63–65,71–74). Thus, scratch properties obtained from bulk polymers might not be the same as their nanoscale surface scratch properties.

With these complications in mind, research in this area has blossomed rapidly. Two main foci of research in this area are on (*1*) how external conditions (such as levels of loadings, the use of different indenters, and scratch rate) and (*2*) intrinsic materials properties (such as modulus and crystallinity) affect the tribological behaviors of the polymers. Apart from examining the scratch resistance of polymers, a closely related quantity which is of interest would be changes in coefficient of friction. Studies relating mechanical properties (3–5,9,36,71,75,76), deformation patterns (18,33,63,71,77–81), fabrication process (3,5,35,72,77,82–86) with respect to experimental parameters, such as temperature (18), loading effect (24,71,72,87–96), indenter geometry (21,33,75,82,95,97), and scratch velocity (21,56,57,59,64,65,96,98) have been carried out. In addition, scratch maps for different polymers have been produced (32,33), and various scratch resistance properties estimated (33,37,56,58,59,99).

Scratch Mechanisms. We have considered how external and intrinsic factors influence the scratch resistance of polymers. Here a brief summary on scratch mechanisms is given.

External parameters interact with intrinsic materials properties by varying the stress distribution on the surface and subsurface of the samples. Based on stress distribution, different deformation mechanisms will operate (12). By scratching crystallized poly(ethylene terephthalate), polypropylene, acetate, and gelatin with blunt spherical styli, Ni and Faou (38) identified three possible operating processes when two surfaces are brought into relative motion: (*1*) interfacial slip accompanied with interfacial shear; (*2*) subsurface shear; and (*3*) interfacial shearing and tensile loading in the vicinity of an asperity, which may initiate crack formation (ploughing effect). Associated with these processes are four types of scratch morphologies: (*1*) with deformation bands inside a scratch that are convex with respect to the sliding direction; (*2*) with deformation bands inside a scratch that are concave with respect to the sliding direction; (*3*) with the removal of the top coating; and (*4*) with featureless clear track with shoulders on both sides (Fig. 6).

Type 1 deformation bands (displacement of materials) correspond to ductile materials being squeezed in front of the styli by shear stress (von Mises shear stress being maximum at the surface). Thus, it is a result of surface shear yielding developed by the compressive shear stress in front of the moving stylus. Type 2 concave bands (surface crack) for brittle materials are due to tensile failure arisen by tangential force. Type 3 delamination occurs as coating delaminates under the compressive stress ahead of the stylus and removed under tensile cracking. Thus, the severity depends on tangential force. Type 4 plastic ploughing is due to normal loading and occurs when normal loading and frictional coefficient are low, giving low frictional force. This is due to indentation and friction generated during sliding. This more ductile type of deformation associated with shallower grooves formed at lighter loads might also be the result of lower strain rate experienced

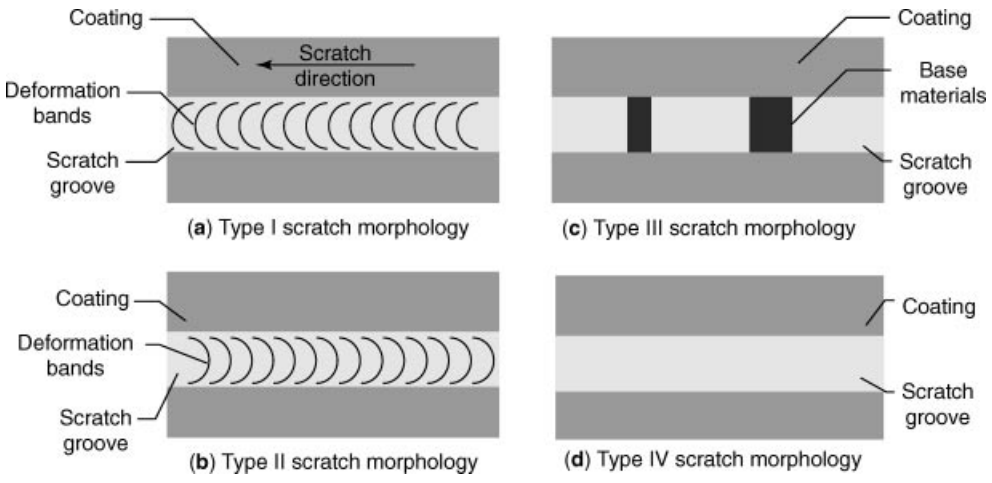

Fig. 6. Schematic diagram shwoing the different types of scratch morphologies.

by the materials because of indenter geometry effect (98). At low normal and tangential force, type 4 prevails. As tangential load increase, we have type 1 and then type 2 domination. In addition, materials properties play an important role in how polymers react to increasing scratch loads. The scratch mechanism governs the measured scratch resistance in terms of amount of materials removed and scratch visibility (58,61,62,100).

Effect of Experimental Conditions.

Magnitude of Loading. One of the most thoroughly studied parameters is the effect of applied load on scratch behavior of polymers (4,32,34,101). An increase in loading will increase severity of scratch damages inflicted on polymer surface (24). In general, the wear rate and the scratch roughness change only slightly when the sample undergoes elastic and plastic deformations. Depending on materials properties, polymers might recover elastically without scratch marks left after being scratched below a critical load owing to its high elasticity and viscoelasticity (96). When the first fracture event occurs there is a sudden increase in both the wear rate and the scratch roughness. This is due to a characteristic change in fracture feature when cracks are involved.

Under a linear load increase condition, abrupt changes in frictional force and coefficient of friction normally indicate the initiation of fracture (78), changes in scratch pattern formed on the scratched surface, and changes in deformation mode of the polymer (54,63,64,71,77–81). Because of the effect of loading on deformation mode, critical loading is often used as an indicator of scratch resistance. There are also situations where the fluctuations in loading curves were associated with stick–slip phenomenon and crack growth (102). In the case of stick–slip motion, both true force and true scratch velocity experienced by the polymer will change with scratch distance (103).

Frictional behavior affects the stress magnitude and distribution when the polymer is being scratched. Thus, it is important to investigate how frictional force and coefficient of friction respond to applied load at various loading scales. According to Amonton's law, the frictional force is proportional to normal load applied. While it is expected for frictional force to increase with applied load, the coefficient of friction, μ, is not constant with normal loadings for both polymeric and nonpolymeric materials when light load is applied to produce nanoscratch (24,63–65,72,74). Thus the general observation of having constant coefficient of friction in macroscale does not apply to nanoscale (63,104). It is the case for polystyrene (63). Its μ first increases with applied load, and then becomes constant for nanofriction. It was found that for the μ increasing regime, a scratch pattern was formed with opening and propagation of cracks. Yet at constant μ regions, wear marks and debris due to buckling are observed. Thus, a change in surface deformation mode exists.

Microfriction in many cases is lower than macrofriction (65,74). This phenomenon is suggested to be due to a reduction in real area of contact and the degree of wear arises from increased hardness and modulus of elasticity with micro/nanoscratch. In addition, the small apparent area of contact reduces the number of particles trapped at the interface, and thus minimizes the "ploughing" contribution to the friction force (73,74).

It should be noted that three types of loads have been utilized for polymer scratch. They are dead load, constant load, and linear-load-increase cases. The

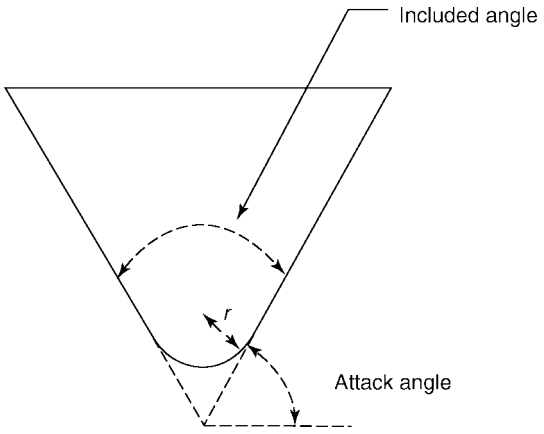

Fig. 7. Schematic diagram showing the gemoetry of a conical indenter.

constant-load and linear-load-increase tests are performed with a good control of the load applied during the scratch test (6). The test results as well as scratch damage exerted are reproducible and reliable. However, the dead-load test, eg, the Ford Five-Finger test, usually leads to jumping and oscillation of the load exerted on the indenter head during scratch. As a result, inconsistency in test results usually ensues.

Effect of Indenter Geometry. An indenter for scratch test can come with various shapes: Vickers, Berkovich, spherical, conical, and wedge-shaped. In the case of conical indenter, two geometric parameters describe the shape of a conical indenter, ie, the included/attack angle and the radius of the tip (Fig. 7). It is observed that different deformation modes are operating at different cone angle regimes. Such changes can be related to changes in contact pressure with a different sharpness of indenter (33). Briscoe and Tabor (102) found that the use of a sharper indenter will give a higher contact pressure with the same applied load. The frictional force increases with increasing contact pressure in a linear fashion for both low and high molecular weight polymers. In addition, an increase in contact pressure might cause a reduction in free volume. This will affect the surface T_g, and thus the general surface property of the polymers (105). Therefore, the indenter geometry influences the stress distribution on the surface of the sample.

In general, deformation becomes more severe as attack angle increases (97). As the attack angle increases, the deformation mode changes from elastic to ironing, ductile ploughing, ductile machining, cracking, and finally to brittle machining. Since the deformation mode changes with the attack angle, it is reasonable to observe that scratch behavior and the coefficient of friction of materials change when the attack angle is altered (21,33,82). Similar effects were observed for changes in tip radius (64,75). The difference between maximum shear stress in front of a stylus and the maximum tensile stress behind is crucial to determine the deformation mechanism during scratching (38).

Based on the relationship between deformation mode and the attack angle, the coefficient of friction during scratch can be estimated (34). However, the quality of fit will be strain-rate-dependent and it is also affected by the classification of deformation mode (82).

Effect of Scratch Velocity and Temperature. Another frequently investigated experimental parameter on the effect of scratch behavior of materials is the scratching rate or the scanning velocity. Since polymers are viscoelastic–viscoplastic in nature, the importance of scratching rate lies in its ability to change the strain and strain rate at the interface of the sample and the indenter and thus alters the deformation mode. The relationship between velocity and coefficient of fiction will depend on the relaxation state of the surface concerned, especially for nanoscratch (21,56,57,63–65). It was shown that rate and temperature interplay to affect nanotribological behavior of polymer films (57).

To explain the scratch rate and temperature dependence of polymer scratch properties, Gauthier and Schirrer (57) proposed a four-volume model, which divides the materials interacting with the tip mainly into two zones. The first zone is the surface and subsurface region in the proximity of the indenter, which is a very thin layer that undergoes extremely high shear strain at a high strain rate and adhesive slipping, with local strain rate equals the tip velocity divided by the width of groove. The second zone is a larger and deeper volume beneath the tip where viscoelastic–viscoplastic yielding occurs. Since the contact area might change with tip speed, an increase in tip speed changes the strain rate (56). Thus, the contact area changes with strain rate. Provided the initial mean strain is no more than a few percent, a transition from viscoplastic scratching to viscoelastic grooving takes place with increasing strain rate. In addition, strain hardening might occur (33). This may further complicate the scratching process.

When temperature is increased, the indenter penetrates deeper into the material and the contact area between the indenter and the specimen increases owing to thermally induced softening of the polymer. This may lead to an increase in the friction force. The increase in temperature may also lead to an increase in the contribution of viscous energy loss to the friction of the polymer, which is strongly dependent on temperature and strain rate (18). Similarly, an increase in scratch velocity that accompanies the high grooving forces will produce a substantial frictional heat exchange at the contact. Such heat may facilitate the permanent displacement of the material (21,98). In addition, scratch behavior correlates with molecular relaxation and surface molecular state of the materials (45,63). When a stick–slip phenomenon is involved in the scratch process, the scratch rate and temperature influence the amplitude, period, and average horizontal force of the process (18). Thus, how the surface and immediate subsurface zone responds to changes in strain and temperature will influence the scratch properties of polymers. This also explains why contradictory results on strain rates and temperature dependence arises with different materials as each of them might respond to such changes differently (38,57,106).

Because of the reason mentioned above, scratch patterns formed were observed to depend on velocity, temperature, and storage modulus (107). Temperature and scratch rate also affect the amount of elastic recovery displayed after scratch is formed (96). In addition, the scratch rate effect might be coupled with cone angle effect to complicate the scratch phenomenon (108).

Effect of Environmental Conditions. Apart from temperature, other environmental factors can also be crucial in terms of affecting coefficient of friction (64),

scratch visibility, and polymer self-healing ability (99). Humidity alters the materials yield stress, thus affecting the mode of deformation the materials undergo (38). Coefficient of friction might increase with increasing humidity because of increasing meniscus force on one hand, and decreases because of the formation of water film, which acts as lubricant, on the other (65).

Effect of Materials Properties

Notwithstanding the importance of experimental parameters, materials characteristics play a crucial role. Modulus and yield strength impact on the size of deformation zone, amount of recovery, and mode of deformation (4,36,109). For example, the deformations shown on polycarbonate and epoxy are different (109,110). Also, depending on modulus and yield strength of polymers, the radius of contact zone, the penetration depth, and plastic zone size will vary (4). In addition, modulus and yield strength will affect the coefficient of friction, scratch hardness, and scratch visibility (3,5,9,35,71,75,76,111). One factor that closely influences the modulus of the polymer is its molecular weight and molecular weight distribution, which may affect polymer ductility and crystallinity, and thus microhardness (112). Therefore, molecular weight and molecular weight distribution will impact on both scratch resistance and deformation (41,113). Similarly, cross-link density will have an effect on scratch phenomena observed (60,109). Treatments on polymer and its fabrication process affect the nanotribological behavior of the polymer film. The effects of surface treatments and fabrication processes, such as plasma treatment (82–85), hydrogen content (86), and use of filler and additive (2,3,5,29,35,77,104) on scratch resistance have been studied. Work looking at how rheology (75) and chain length (111,114) affects scratch resistance of polymers has also been performed.

Processing and fabrication techniques impact on the intrinsic properties of the polymers, and thus influences the polymer scratch properties. Blending, in general, will affect the mechanical properties of polymers and thus the scratch resistance and deformation mode of the blend (35,111). In some cases, certain constituents might preferentially segregate to the surface (35,87). It has been shown that glass-transition temperature on the surface of the blend may vary significantly depending on its composition (115). As the constituents in polymer blend might have very different mechanical properties, scratch deformation mode might change with composition (77).

Fillers are very often added to engineer the mechanical strength of polymers. The use of rigid filler will increase modulus, and thus the polymer will be more prone to tensile cracking, whereas the use of rubber for blending will lower modulus and the scratch depth will increase (4). With the use of different types of rigid fillers, scratch pattern and deformation mechanism might be different (2,3,28,29,104). The role of rigid fillers on scratch resistance of polymer blends will also depend on other additives in the blends, such as rubber modifiers (116), nucleating agent (5), and lubricants (3). If continuous fiber is used as reinforcement, the orientation of fiber will need to be taken into account when assessing polymer scratch resistance (106,117). Lubricants are normally added to reduce surface

friction, and thus have the possibility of reducing severity of scratch damage (5). Yet, its effect on polymer scratch resistance is not necessarily positive because the application of such lubricants might reduce flow resistance of materials and thus increase penetration depth (34). And, the efficiency of lubricants will depend on the scratch rate and cone angle of indenter (34).

Finally, processing condition, such as processing temperature (80,118) and surface treatment (84), will influence the scratch properties of polymers owing to changes in the structure and morphology of polymers. An example would be the existence of skin–core structure in injection-molded samples, giving rise to variation in scratch resistance as scratch depth changes (80). Also, whether the polymer is uniaxially or biaxially stretched will change the polymer scratch properties as a result of alteration of crystallinity (76). In addition, the use of solvent either to swell the polymer surface (35,82) or for film casting (118) influences molecular arrangement on the surface and thus impact on scratch properties of polymers.

Future Work

Scratch damages inflicted on polymer surface have important consequences on the appearance and mechanical performance of the materials. Scratches, in a lot of situations, are precursors of wear and abrasion (119,120). Scratch phenomena impact on the use of polymers in automobiles, microelectronics, food packaging, and coatings. The complexity involved in research of scratch behavior of polymers has been highlighted in this article. Many factors have been considered for their influence on the subject concerned. Very often the factors that affect scratch interact with each other and are difficult to isolate the effect of individual factors. This renders the interpretation of experimental results difficult and thus explains the frequently observed contradictory results in the literature.

While researchers in this field seek to establish the relationships between scratch performance and various controlled parameters, a diversity of techniques and equipment have been used in order to examine phenomena in different scales of interest. This means that it is often difficult, if not impossible, to compare results from different studies. With these challenges in mind, the summary of research findings presented in this article gives at most phenomenological accounts of the scratch behavior of polymers under the influences of a combination of factors, with the correlation among these factors being largely unknown. These studies have provided useful insight in how different polymers respond when they are being scratched. However, in order to better predict polymer scratch properties and design scratch-resistant polymers/parts, a more fundamental understanding of the physics behind the scratch phenomena is required. The general approach toward this goal is described below.

First, in the hope of improving comparability of results among tests on different polymers, a unified testing standard in examining the scratch resistance of polymers has been proposed (44). In addition, a universal scratch test machine is developed (6). The test standard and the scratch machine were introduced to provide a standardized way to investigate scratch behavior of polymers, which is versatile enough to accommodate different testing needs in the

micro- and macroscales. Tests using such machine were carried out with satisfactory results, ensuring good reliability and repeatability, thus generating data that can be compared meaningfully (6,7). One of the distinctive features for these sets of studies is the use of linear load increase test during the course of the experiments. It is shown in our studies that various stages of scratch deformation modes can be observed and correlated to the applied load in a quantitative fashion, and thus useful insight can be gained with such setup.

Second, the more extensive use of finite element analysis (FEA) is encouraged. It is difficult to separate the influence of different factors on surface properties of polymers in real experiments. Using FEA, the effect of individual material and mechanics factor or the correlation between multiple factors can be evaluated with other parameters being held constant in a well-controlled manner. Thus, results obtained from this route can be used to supplement experimental findings. This helps us better understand the impact of individual factors and, more importantly, it also helps to develop scratch deformation theory since a more mechanistic approach rather than a phenomenological approach is applied in FEA.

Finally, in order to better understand the science of scratch phenomenon, we may start off with the simplest case of all, ie, scratch formed by single asperity with shallow scratch groove. Such scratch experiments have been made possible with the invert of atomic force microscopes and depth sensing devices, such as nanoindenter. Two reasons have prompted the rapid growth of result in nanoscratch: First, scratch properties with very shallow scratch depth is expected to be different from those with depth because of the difference in molecular conformation between the surface and the bulk (109). Second, macroscopic scratches and wear might begin with scratches in nanoscale. The observations of nanoscale scratch under single asperity condition can thus suggest mechanisms on formation of surface damage and the subsequent wear properties of polymers.

With all the strategies listed above, we hope that as our understanding on scratch behavior of polymers accumulates, a more complete formulation of theoretical framework on surface deformation and damage phenomena can be developed. Only when such framework relating all relevant materials parameters and mechanics with deformation mechanism is available, can we establish predictive model that is useful for polymer engineering and design of scratch-resistant polymers.

BIBLIOGRAPHY

1. F. P. Bowden and D. Tabor, *The Friction and Lubrication of Solids*, Oxford University Press, London, 1964.
2. J. Chu, L. Rumao, and B. Coleman, *Polym. Eng. Sci.* **38**, 1906 (1998).
3. J. Chu, C. Xiang, H.-J. Sue, and R. D. Hollis, *Polym. Eng. Sci.* **40**, 944 (2000).
4. C. Xiang, H.-J. Sue, J. Chu and B. Coleman, *J. Polym. Sci. Polym. Phys. Ed.* **39**(1), 47 (2001).
5. C. Xiang, H.-J. Sue, J. Chu, and K. Masuda, *Polym. Eng. Sci.* **41**(1), 23 (2001).
6. M. Wong, G. T. Lim, A. Moyse, J. N. Reddy, and H.-J. Sue, *Wear* **256**, 1214.

7. M. Wong, G. T. Lim, A. Moyse, F. Lee, and H.-J. Sue, *J. Mater. Sci.* **39**, 3293 (2004).
8. E. Meyer, R. M. Overney, K. Dransfeld, and T. Gyalog, *Nanoscience: Friction and Rheology on the Nanometer Scale*, World Scientific Publishing Co. Pte. Ltd., Singapore, 1998, Chapts. 1–4.
9. K. L. Johnson, K. Kendall, and D. Robert, *Proc. R. Soc. London Ser. A* **324**, 301 (1971).
10. J. A. Greenwood and J. B. P. Williamson, *Proc. R. Soc. London Ser. A* **A295**, 300 (1966).
11. G. M. Hamilton and L. E. Goodman, *J. Appl. Mech.* **33**, 371 (1966).
12. G. M. Hamilton, *Proc. Inst. Mech. Eng.* **197C**, 53 (1983).
13. A. Sackfield and D. A. Hills, *J. Strain Anal.* **18**(2), 101 (1983).
14. A. Sackfield and D. A. Hills, *J. Strain Anal.* **18**(2), 107 (1983).
15. A. Sackfield and D. A. Hills, *J. Strain Anal.* **18**(2), 195 (1983).
16. J. A. Williams, *Tribol. Int.* **29**, 675 (1996).
17. J. C. M. Li, *Mater. Sci. Eng., A* **317**, 197 (2001).
18. S. L. Zhang and J. M. Valentine, *Tribol. Lett.* **12**(4), 195 (2002).
19. I. J. Ford, *J. Phys. D: Appl. Phys.* **26**, 2219 (1993).
20. G. T. Lim, M.-H. Wong, H.-J. Sue, J. N. Reddy, and A. Moyse, unpublished data, Oct. 2003.
21. B. J. Briscoe, A. Delfino, and E. Pelillo, *Wear* **225–229**, 319 (1999).
22. A. Krupicka, M. Johansson, and A. Hult, *Prog. Org. Coat.* **46**, 32 (2003).
23. B. J. Briscoe, E. Pelillo, F. Ragazzi, and S. K. Sinha, *Polymer* **39**, 2161 (1998).
24. B. Y. Du, M. R. Vanlandingham, Q. L. Zhang, and T. B. He, *J. Mater. Res.* **16**(5), 1487 (2001).
25. P. R. J. Guevin, *J. Coat. Technol.* **67**(840), 61 (1995).
26. T. Triplett, *Ind. Paint Powder* **72**(4), 34 (1996).
27. J. R. Grasmeder, in *Polypropylene, the International Conference*, Institute of Polymer, 1994, pp. 98–108.
28. J. Chu, *43rd International SAMPE Symposium*, 1998, p. 1149.
29. R. S. Kody and D. C. Martin, *Polym. Eng. Sci.* **36**, 298 (1996).
30. A. Chanda, D. Basu, A. Dasgupta, S. Chattopadhyay, and A. K. Mukhopadhyay, *J. Mater. Sci. Lett.* **16**, 1647 (1997).
31. F. Ramsteiner, T. Jaworek, M. Weber, and S. Forster, *Polym. Test.* **22**, 439 (2003).
32. B. J. Briscoe, P. D. Evans, E. Pelillo, and S. K. Sinha, *Wear* **200**, 137 (1996).
33. B. J. Briscoe, E. Pelillo, and S. K. Sinha, *Polym. Eng. Sci.* **36**, 2996 (1996).
34. B. J. Briscoe, P. D. Evans, S. K. Biswas, and S. K. Sinha, *Tribol. Intern.* **29**(2), 93 (1996).
35. B. H. Stuart and B. J. Briscoe, *Polymer* **37**, 3819 (1996).
36. V. Jardret, H. Zahouani, J. L. Loubet, and T. G. Mathia, *Wear* **218**, 8 (1998).
37. P. Z. Wang, I. M. Hutchings, S. J. Duncan, and L. Jenkins, in *SAE Transactions*, (1999-01-0243), 1999, p. 134.
38. B. Y. Ni and A. L. Faou, *J. Mater. Sci.* **31**, 3955 (1996).
39. S. R. Kim, J. S. Song, Y. J. Choi, and J. H. Kim, *Mater. Res. Soc. Symp.—Proc.* **504**, 265 (1997).
40. L. Lin, G. S. Blackman and R. R. Matheson, *Polym. Prep. (Am. Chem. Soc. Div. Polym. Chem.)* **39**, 1224 (1998).
41. A. C.-M. Yang and T. W. Wu, *J. Mater. Sci.* **28**, 955 (1993).
42. E. Hamada and R. Kaneko, *Ultramicroscopy* **42–44**(Part A), 184 (1992).
43. Y. C. Han, S. Schmitt, and K. Friedrich, *Appl. Composite Mater.* **6**(1), 1 (1999).

44. ASTM X10-399, Evaluation of Scratch Resistance of Polymeric Coatings and Plastics Using an Instrumented Scratch Machine, submitted.
45. P. Bertrand-Lambotte, *Thin Solid Films* **420–421**, 281 (2002).
46. T. Li, Q. Chen, L. S. Schadler, R. W. Siegel, J. Mendel, and G. C. Irvin Jr., *Polym. Composite* **23**, 1076 (2002).
47. A. Khurshudov and K. Kato, *J. Vac. Sci. Technol. B* **13**, 1938 (1995).
48. G. S. Blackman, L. Lin, and R. R. Matheson, *Polym. Prep. (Am. Chem. Soc. Div. Polym. Chem.)* **39**, 1218 (1998).
49. V. N. Zhitomirsky, I. Grimberg, M. C. Joseph, R. L. Boxman, B. Z. Weiss, A. Matthews, and S. Goldsmith, *Surf. Coat. Tech.* **108–109**(1–3), 160 (1998).
50. V. D. Jardret and W. C. Oliver, *Mater. Res. Soc. Symp.—Proc.* **594**, 251 (2000).
51. M. Belin and J. M. Martin, *Wear* **156**(1), 151 (1992).
52. M. Kotaki, M.-H. Wong, C. Xiang and H.-J. Sue, in *ANTEC 2002*, Vol. 2, Society of Plastics Engineers, Nashville, Tenn., 2002, p. 1535.
53. G. T. Lim, M. Wong, A. Moyse, J. N. Reddy, and H.-J. Sue, in *SPE International Conference on Polyolefins*, 2003, pp. 577–584.
54. T. W. Wu, *J. Mater. Res.* **6**(2), 407 (1991).
55. J. Jing, P. N. Henriksen, and H. Wang, *J. Mater. Sci.* **30**, 5700 (1995).
56. C. Gauthier, S. Lafaye, and R. Schirrer, *Tribol. Int.* **34**, 469 (2001).
57. C. Gauthier and R. Schirrer, *J. Mater. Sci.* **35**, 2121 (2000).
58. F. N. Jones, W.-D. Shen, S. M. Smith, S.-H. Huang, and R. A. Ryntz, *Prog. Org. Coatings* **34**, 119 (1998).
59. B. J. Briscoe, E. Pelillo, and S. K. Sinha, *Polym. Int.* **43**, 359 (1997).
60. J. Lange, A. Luisier, E. Schedin, G. Ekstrand, and A. Hult, *J. Mater. Process. Technol.* **86**, 300 (1999).
61. Y. Hara, T. Mori, and T. Fujitani, *Prog. Org. Coatings* **40**, 39 (2000).
62. I. M. Hutchungs, P. Z. Wang, and G. C. Parry, *Surf. Coatings Technol.* **165**, 186 (2003).
63. T. Aoike, H. Uehara, T. Yamanobe, and T. Komoto, *Langmuir* **17**, 2153 (2001).
64. R. Consiglio, N. X. Randall, B. Bellation, and J. von Stebut, *Thin Solid Films* **332**, 151 (1998).
65. B. Bhushan and S. Sundararajan, *Acta Mater.* **46**, 3793 (1998).
66. H. R. Brown and T. P. Russell, *Macromolecules* **29**, 798 (1996).
67. J. L. Keddie, R. A. L. Jones, and R. A. Cory, *Europhys. Lett.* **27**, 59 (1994).
68. T. Kajiyama, K. Tanaka, and A. Takahara, *Macromolecules* **30**, 280 (1997).
69. T. Kajiyama, K. Tanaka, N. Satomi, and A. Takahara, *Macromolecules* **31**, 5150 (1998).
70. J. A. Hammerschmidt and W. L. Gladfelter, *Macromolecules* **32**, 3360 (1999).
71. M. P. deBoer, J. C. Nelson and W. W. Gerberich, *J. Mater. Res.* **13**(4), 1002 (1998).
72. V. N. Koinkar and B. Bhushan, *J. Appl. Phys.* **81**(6), 2472 (1997).
73. B. Bhushan, J. N. Israelachvili, and U. Landman, *Nature* **374**, 607 (1995).
74. B. Bhushan and A. V. Kulkarni, *Thin Solid Films* **278**, 49 (1996).
75. J. L. Bucaille, E. Felder, and G. Hochstetter, *Wear* **249**, 422 (2001).
76. B. D. Beake and G. J. Leggett, *Polymer* **43**, 319 (2002).
77. A. C.-M. Yang and T. W. Wu, *J. Polym. Sci., Part B: Polym. Phys.* **35**, 1295 (1997).
78. L. Lin, G. S. Blackman, and R. R. Matheson, *Mater. Sci. Eng. A* **317**, 163 (2001).
79. S. J. Bull, *Tribol. Int.* **30**, 491 (1997).
80. C. Pistor and K. Friedrich, *J. Appl. Polym. Sci.* **66**, 1985 (1997).
81. C. Buenviaje, S.-R. Ge, M. Rafailovich, J. Sokolov, J. M. Drake, and R. M. Overney, *Langmuir* **15**, 6446 (1999).

82. B. H. Stuart, *Polym. Testing* **16**, 517 (1997).
83. F. Benítez, E. Martínez, M. Galán, J. Serrat, and J. Esteve, *Surf. Coatings Technol.* **125**, 383 (2000).
84. S. Dahl, D. Rats, J. von Stebut, L. Martinu, and J. E. Klemberg-Sapieha, *Thin Solid Films* **355–356**, 290 (1999).
85. M. H. Blees, G. B. Winkelman, A. R. Balkenende, and J. M. J. den Toonder, *Thin Solid Films* **359**, 1 (2000).
86. A. Wienss, G. Persch-Schuy, M. Voggelgesang, and U. Hartmann, *Appl. Phys. Lett.* **75**(8), 1077 (1999).
87. W. Brostow, B. Bujard, P. E. Cassidy, H. E. Hagg, and P. E. Montemarini, *Mat. Res. Innovat.* **6**, 7–12 (2002).
88. T. Miyamoto, R. Kaneko, and S. Miyake, *J. Vac. Sci. Technol., B* **9**, 1338 (1991).
89. E. Hamada and R. Kaneko, J. Phys. *D: Appl. Phys.* **25**, A53 (1992).
90. B. Bhushan, V. N. Koinkar, and J. Ruan, in M. Sarikaya, H. K. Wickramasinghe, and M. Isaacson, eds., *Determining Nanoscale Physical Properties of Materials by Microscopy and Spectroscopy*, Vol. 332, Materials Research Society, Pittsburgh, 1994, p. 93.
91. B. Bhushan and V. N. Koinkar, *J. Appl. Phys.* **75**, 5741 (1994).
92. B. Bhushan and V. N. Koinkar, *Wear* **180**, 9 (1995).
93. B. Bhushan and V. N. Koinkar, *Wear* **181–183**, 360 (1995).
94. B. Bhushan and V. N. Koinkar, *Surf. Coatings Technol.* **76–77**, 655 (1995).
95. B. Bhushan, *Proc. Inst. Mech. Eng., Part J: J. Eng. Tribol.* **212**, 1 (1998).
96. S. L. Zhang, A. H. Tsuo, and J. C. M. Li, *J. Polym. Sci., Part A: Polym Phys.* **40**, 1530 (2002).
97. B. J. Briscoe, *Tribol. Int.* **31**(1–3), 121 (1998).
98. M. Bonne, B. J. Briscoe, S. Manimaaran, and A. Allan, *Wear* **254**, 55 (2003).
99. U. Schulz, V. Wachtendorf, T. Klimmasch, and P. Alers, *Prog. Org. Coatings* **42**, 38 (2001).
100. L. Lin, G. S. Blackman, and R. R. Matheson, *Prog. Org. Coatings* **40**, 85 (2000).
101. B. J. Briscoe, P. Enrico, and S. K. Sinha, *Polym. Eng. Sci.* **36**, 2996 (1996).
102. B. J. Briscoe and D. Tabor, *J. Adhesion* **9**, 145 (1978).
103. S. L. Zhang and J. C. M. Li, *Mater. Sci. Eng. A* **344**, 182 (2003).
104. B. Bhushan, and V. N. Koinkar, *Tribol. Trans.* **38**, 119 (1995).
105. D. H. Gracias, D. Zhang, L. Lianos, W. Ibach, Y. R. Shen, and G. A. Somorjai, *Chem. Phys.* **245**, 277 (1999).
106. P. B. Mody, T.-W. Chou, and K. Friedrich, *J. Mater. Sci.* **23**, 4319 (1988).
107. R. H. Schmidt, G. Haugstad and W. L. Gladfelter, *Langmuir* **15**, 317 (1999).
108. B. J. Briscoe, S. K. Biswas, S. K. Sinha, and S. S. Panesar, *Tribol. Int.* **26**(3), 183 (1993).
109. J. S. S. Wong, H.-J. Sue, K.-Y. Zeng, R. K. Y. Li, and Y.-W. Mai, *Acta Mater.* **52**, 431 (2004).
110. E. Hamada and R. Kaneko, *J. Phys. D: Appl. Phys.* **25**, A53 (1992).
111. A. Dasari, J. Rohrmann, and R. D. K. Misra, *Macromol. Mater. Eng.* **287**, 889 (2002).
112. C. Vanderdonckt, M. Krumova, F. J. Baltá Calleja, H. G. Zachmann, and S. Fakirov, *Colloid Polym. Sci.* **276**, 138 (1998).
113. A. Dasari, S. J. Duncan, and R. D. K. Misra, *Mater. Sci. Technol.* **19**, 239 (2003).
114. A. Dasari, S. J. Duncan, and R. D. K. Misra, *Mater. Sci. Technol.* **18**, 1227 (2002).
115. Y. Terada, M. Harada, T. Ikehara, and T. Nishi, *J. Appl. Phys.* **87**, 2803 (2000).
116. H.-X. Tang and D. C. Martin, *J. Mater. Sci.* **38**, 803 (2003).
117. K. Friedrich, K. Varadi, T. Goda, and H. Giertzsch, *J. Mater. Sci.* **37**, 3497 (2002).
118. B. J. Briscoe and P. S. Thomas, *Tribol. Trans.* **38**, 382 (1995).

119. R. Kaneko and E. Hamada, *Wear* **162–164**, 370 (1993).
120. M. J. Adams, A. Allan, B. J. Briscoe, P. J. Doyle, D. M. Gorman, and S. A. Johnson, *Wear* **251**, 1579 (2001).

JANET S. S. WONG
University of Illinois
HUNG-JUE SUE
Texas A&M University

SELF ASSEMBLY. See MOLECULAR SELF ASSEMBLY.

SEMICRYSTALLINE POLYMERS. See Volume 8.

SHAPE-MEMORY POLYMERS. See Volume 4.

SILANE COUPLING AGENTS. See Volume 8.

SILICONES

Introduction

Silicones are a class of polymers having the formula $(R_mSi(O)_{4-m/2})_n$, where $m =$ 1–3 and $n \geq 2$. The most common are the polydimethylsiloxanes (PDMS).

Silicones and silanes are the subject of many reviews (1–8). Commercial products include fluids, filled fluids and gums, greases, resins, and rubber (1,2). Various forms of silicones and examples of applications are listed in Table 1.

The designations M, D, T, and Q, respectively, are used for mono-, di-, tri-, and quaternary coordination of oxygen around silicon in silicones. A T group can also be written as $CH_3SiO_{3/2}$; a Q group as SiO_2. When groups other than methyl are present, these groups are indicated with a superscript, eg, D^{Vi} represents a methyl vinyl siloxy group $(CH_3)CHCHSiO$. Resins are often referred to as M_xQ, M_xT, M_xD_y T_zQ, etc. This common shorthand notation for silicones is depicted in Figure 1.

History of Silicones. Although silicon is quite abundant in nature, there are no natural forms of organosilicon. The first covalent compound of silicon, SiF_4, was made in 1771 (9). Berzelius, in 1823, was the first to make amorphous silicon by potassium reduction of SiF_4; he also found that the combination of SiO_2, CuO, and C had greater hardness than SiO_2 alone. In 1896 Morrison made silicon metal by the reaction of SiO_2 and C in an electric arc furnace, a process by which metallurgical-grade silicon has been produced commercially since the 1990s. Ironically, in 1900, Oswalt announced, "elementary silicon has no application or any interesting properties" (10). Six years later, in what would prove to

Encyclopedia of Polymer Science and Technology. Copyright John Wiley & Sons, Inc. All rights reserved.

Table 1. Silicone Products and Their Uses

Commercial product	Use
Fluids: heat-stable liquids	Lubricants, water repellents, defoamers, release agents, surfactants
Filled fluids and gums	Valve lubricants, moistureproof sealants for electrical connectors, pressure-sensitive adhesives, personal care products
Grease: fluid and carbon black or soap	Nonflow lubricants, polishes
Resins: cross-linked materials	Electrical insulation, lubricant and paint additives, release formulations, water repellents
Rubbers: fluids or gums and surface-treated fillers; elastic with good tensile strength	Electrical insulation, medical devices, seals, textile coatings, foams

be an important discovery, Vigreaux treated Na_2SiF_6 with copper at 1000°C to give Cu_xSi, a key intermediate in the modern preparation of methylchlorosilanes. Alkoxy silanes were first prepared in the mid-1800s (11,12).

Kipping is considered the father of organosilicon chemistry. He employed Grignard reagents to make compounds of the general class $R_{4-x}SiCl_x$ (13,14). Kipping reportedly remarked that the polymers obtained from the hydrolysis of chlorosilanes were "omnipresent nuisances" (15). In the 1930s Stock made significant contributions by carrying out gas-phase reactions to prepare silicon hydrides and compounds having Si—Si bonds (16).

The beginning of the silicone industry has been well documented (15,17). In 1930 Corning Glass made the first deliberate effort to find a use for silicones, and in 1939 the company began the etherless methyl Grignard process as a method for making methyl silicones. One of the first commercial products, DC 4, was composed of silica in PDMS fluid. It was used in high altitude aircraft applications. Another early product was DC 990A resin, $C_6H_5(C_2H_5)Si(OH)_2$, which when cross-linked

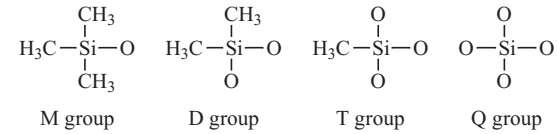

For example:

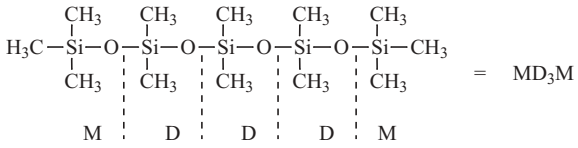

Fig. 1. Widely accepted abbreviations used for silicone groups.

at high temperature had good dielectric strength, low dielectric loss, and good thermal stability.

In 1940 Rochow discovered the direct process, also called the methylchlorosilane (MCS) process, in which methyl chloride is passed over a bed of silicon and copper at high temperature (250–300°C) to produce a mixture of methylchlorosilanes, including the industrially important dichlorodimethylsilane [75-78-5], $(CH_3)_2SiCl_2$. Working independently, Müller made a similar discovery in Germany. Consequently, the process is frequently called the Rochow process and sometimes the Rochow–Müller reaction. These discoveries were followed by two key publications describing the work that marked the beginning of the commercial silicone industry (18,19). Production increased rapidly with the need for silicones in World War II. In 1943 the Dow Corning Corp. was formed in Midland, Michigan, as a joint venture between Corning Glass and Dow Chemical. In 1947 GE opened a plant for the manufacture of silicones in Waterford, New York, and in 1949 Union Carbide opened a silicone manufacturing plant in Tonawanda, New York.

Chemistry

The chemistry of silicones has been described in many textbooks (1,20,21).

Direct Process. Passing methyl chloride vapors through a bed of copper and silicon at temperatures near 300°C yields a mixture of methylchlorosilanes. The efficiency of this process is critically dependent on reactor design and chemistry. Optimization of the fluidized-bed reactor is a critical part of the industrial process (22). The rate of methylchlorosilane (MCS) production and selectivity for dichlorodimethylsilane are significantly affected by trace elements in the catalyst bed; very pure copper and silicon give poor rate and selectivity (23–25).

Much of the early work on the direct process was devoted to understanding the structure of the active catalyst. Many reports have suggested that Cu_3Si, or eta-phase, is a key catalytic species in the MCS reaction (9,26–29). Reactions employing Cu_3Si and Cu_5Si have been shown to be good models for the direct process (30). Copper transfer appears to be the first step in the MCS process (31). There is strong evidence to support the intermediacy of a silylene in the Cu-catalyzed direct process (32).

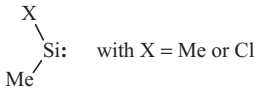

with X = Me or Cl

In a single-crystal study of the surface interaction of Si with various forms of copper as models of the direct process (33), the highest selectivity obtained was for a mixture of 82% Cu and 18% Cu_2O, similar to the selectivity obtained in a fluidized-bed reactor (34). Other surface studies have shown that silicon is efficiently removed from the Cu–Si phase when the ratio of Me to Cl is about 1:1 (35).

In one of the first comprehensive studies on the effect of trace elements on the direct process (34), the importance of zinc and tin and other trace elements as

promoters was recognized. The effects of three promoters and their synergy have been investigated empirically (23). The results show that the reaction rate of the direct process decreases as a function of catalyst bed composition in the following order: SiCuZnSn > aged SiCu > SiCuAlSn > SiCuZn > SiCuAl > fresh SiCu > SiCuZn. The selectivity for the formation of $(CH_3)_2SiCl_2$ also depends on catalyst composition and decreases in the following way: SiCuZnSn > SiCuAlSn SiCuZn > aged SiCu > SiCuSn > SiCuAl > fresh SiCu. This study concluded that zinc functions as a methylating agent. Aluminum and tin are synergistic promotors of rate and selectivity, and it appears that aluminum modifies the alloy properties of CuZnAlSi. Finally, tin and zinc have a synergistic effect. The effect of aluminum on alloying properties has been discussed (36). Aluminum affects reactivity and selectivity while calcium affects only reactivity (37). Additional promoters include phosphorus, which acts as a strong selectivity enhancer (38–40), boron (41), and alkali metal halides (42). Optimization methods have been applied to the complex mixture of promoters used in the direct process (43).

Zinc and tin surface enrichment appears to be essential for high activity and reactivity. Additives that impede silicon and/or zinc surface enrichment have a negative impact on rate. Lead is an example of such a catalyst poison for this reason (44). Considerable fundamental work remains to be done to understand the direct process at the molecular level.

Not surprisingly, the particle size and composition of the silicon used in the direct process are important parameters. Optimum silicon particle size for the fluidized-bed process is above 10 μm. Particles must also have low oxygen content (45). An interesting approach to optimizing the interaction of metal catalysts with the silicon surface is the pregrinding of silicon with at least one of the metals used to catalyze the reaction (46). The elemental composition of the silicon input is critical to its performance in the direct process. Phosphorus can be added as a promoter or may be present as a component of the silicon (47). Significant effort has been made to improve the reactivity of silicon by a water granulation method during the production of silicon (48).

Alternatives to the methyl chloride based direct process have been reviewed (49). Direct-process chemistry has been used to make phenyl and ethyl silicones. For example, chlorobenzene can be used in place of methyl chloride to make phenylchlorosilanes (15). Phenylchlorosilanes can also be produced by the reaction of benzene, $HSiCl_3$, and BCl_3 (17,49). Ethylsilicones have been made primarily in the former Soviet Union, where the direct process is carried out with ethyl chloride in place of methyl chloride (50). Vinyl chloride can also be used in the direct process to produce vinylchlorosilanes (49). Vinylchlorosilanes can also be made by reaction of vinyl chloride with $HSiCl_3$ (51) or by platinum-catalyzed hydrosilylation of acetylene with $HSiCl_3$ (52,53).

Some new direct-process-like reactions have been described. The reaction between methanol and Cu/Si gives $(CH_3O)_3SiH$ (eq. 1), and the reaction of methanol over Si/B gives $(CH_3O)_4Si$ (54–56).

$$3\ CH_3OH + Si \xrightarrow[\text{High boiling solvents}]{250^\circ C} HSi(OCH_3)_3 + H_2 \qquad (1)$$

The reaction of alcohols other than methanol with silicon sources has been examined under direct-process conditions as a method to make alkyl silicates (57). The use of HCl in the MCS reaction gas stream increases CH_3Cl_2SiH without decreasing the total combined yield of $(CH_3)_2SiCl_2$ and CH_3Cl_2SiH; no significant undesirable $SiCl_4$ or $HSiCl_3$ forms (58–60). Similar results are obtained by using hydrogen in place of HCl (61). Hydrogen in the direct process stream enriches SiH monomers, but promoters normally used in the direct process usually retard SiH monomer formation. Zinc is particularly deleterious to CH_3HSiCl_2 formation (62,63). Other forms of the direct process include the reaction of dimethyl ether and methyl halide over Si/Cu to give $(CH_3)_2Si(OCH_3)_2$ (64,65). More recently, the reaction of $(CH_3)_2NH$ and silicon to give $((CH_3)_2N)_3SiH$ has been reported (66).

Methylchlorodisilanes are by-products of the direct-process. Commonly referred to as "residue," these are formed at a level of about 4% of the total $(CH_3)_2SiCl_2$ produced (In 1994 $(CH_3)_2SiCl_2$ production was about 30,000 ton/year). Disilanes are key constituents of the residue, and novel reactions forming Si—Cl bonds have been described (67–69). Commercially, disilanes are redistributed to recover methylchlorosilane monomers (70). Some chemical reactions of direct-process disilanes are shown in Figure 2. Cleavage of Si—Si bonds with HCl has also been described and is practiced industrially (68).

A significant use of direct-process waste can be realized by C_6H_5—Si bond formation via silylative decarbonylation (eq. 2) (74,75). A novel route to C_6H_5—Si bond formation has also been described (eq. 2) (76).

Cleavage reactions:

$$Cl_2CH_3Si{-}SiCl(CH_3)_2 + HCl \xrightarrow{(C_4H_9)_3NHCl} Cl_2CH_3SiH + Cl_2Si(CH_3)_2 \quad \text{(i)}$$

Disproportionation:

$$n\ Cl_2CH_3Si{-}SiCl(CH_3)_2 \xrightarrow{\text{Base catalyst}} n\ CH_3SiCl_3 + \left(\begin{array}{c}|\\ Si\\ |\\ Cl\end{array}\right)_n \quad \text{(ii)}$$

Si—C bond forming reactions:

$$Cl_2CH_3Si{-}SiCl(CH_3)_2 + R{-}C{\equiv}C{-}R \xrightarrow{Pt} Cl_2(CH_3)_2Si{-}RC{=}CR{-}SiCl_2CH_3 \quad \text{(iii)}$$

$$Cl(CH_3)_2Si{-}Si(CH_3)_2Cl + H_2C{=}CH_2 \longrightarrow Cl(CH_3)_2Si{-}CH_2CH_2{-}Si(CH_3)_2Cl \quad \text{(iv)}$$

$$ArCOCl + Cl_2CH_3Si{-}SiCl(CH_3)_2 \xrightarrow{Pd} ArSiCl(CH_3)_2 + Cl_3SiCl(CH_3)_2 + CO \quad \text{(v)}$$

Redistribution:

$$Me(Me_2Si)_6Me \xrightarrow{AlCl_3} (Me_3Si)_3SiSiMe_2SiMe_3 \xleftarrow{AlCl_3} Me(Me_3Si)_2SiSiMe(SiMe_3)_2 \quad \text{(vi)}$$

Fig. 2. Chemistry of direct-process residue methylchlorodisilanes. The reactions are discussed in detail in the following references: (i) 71, (ii) 67,68, (iii) 72, (iv) 73, (v) 74,75, and (vi) 69.

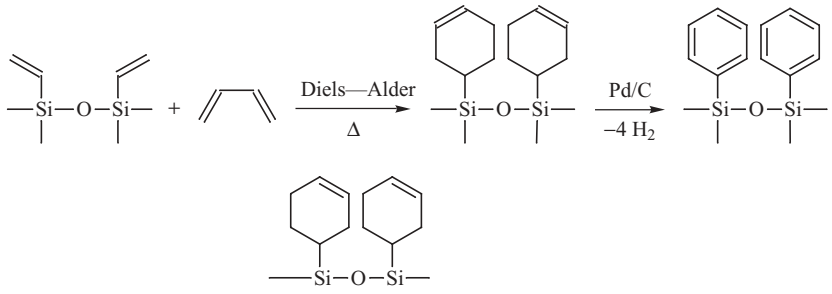

(2)

Synthesis of Silicone Monomers and Intermediates.

Hydrosilylation Products. In addition to the direct process and Grignard chemistries, a very important reaction for formation of Si—C bonds is the hydrosilylation reaction, which involves the addition of Si—H across an olefinic double bond (eq. 3).

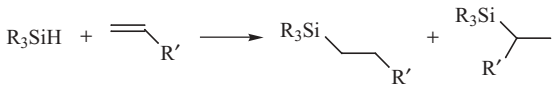

(3)

This reaction has been used for the formation of a wide variety of organofunctionalized silicones and for cross-linking silicone polymers by addition cure (77–83).

Recent examples that have utilized the hydrosilylation reaction to prepare very unique organosiloxanes are shown in equations 4 and 5. Equation 4 depicts the hydrosilylation of phenylacetylene to provide beta-vinyl silicones (84,85) and is a convenient route to high refractive index silicones.

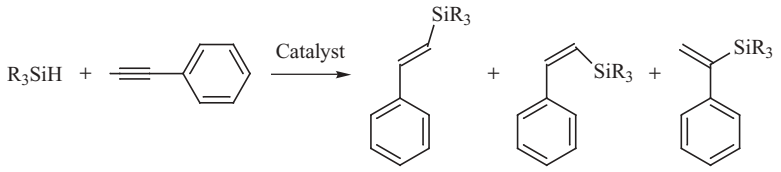

(4)

Hydrosilylation reactions have also been used as the key step (86) in the synthesis of dendritic siloxanes (eq. 5).

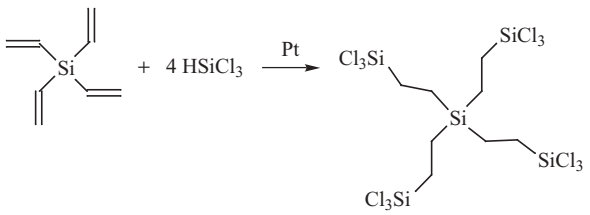

(5)

Alkoxysilanes. Alkoxysilanes are important intermediates in the manufacture of silicone-based materials. The prevalent method for forming the silyl ether linkage is alcoholysis of Si—Cl bonds (eq. 6. Removal of the concurrently formed HCl is typically accomplished by addition of tertiary amines (87,88). Often NaOR is used instead of the corresponding alcohol to give the less corrosive and more easily removed NaCl as by-product (89,90). Use of alkyl orthoformates represents an alternative to alcohols or metal alkoxides (eq. 7) (91–93).

$$RSiCl_3 + 3\ R'OH \rightarrow RSi(OR')_3 + 3\ HCl \tag{6}$$

$$R_3SiCl + HC(OR')_3 \rightarrow R_3SiOR' + R'Cl + HCOOR' \tag{7}$$

Silyl ethers can also efficiently be prepared starting from Si—H bonds. Silanes containing one or more Si—H functional groups react with alcohols in the presence of a catalyst (eq. 8). Typical catalysts include bases (eg KOH, NaOH, KOR, NaOR, amines), strong acids, metals (colloidal copper), and metal complexes of Fe, Co, Ru, Rh, Pd, Ir, and Pt (94). Recently, a highly efficient catalyst (Ph_3PCuH) was reported to affect alcoholysis of hydrosilanes under mild conditions while also tolerating unsaturated alcohols (95). Tris-pentafluorophenylboron is also a very effective catalyst for silylation of alcohols with hydrosilanes (96).

$$R_{4-n}SiH_n + n\ R'OH \xrightarrow{\text{Catalyst}} R_{4-n}Si(OR')_n + n\ H_2 \tag{8}$$

Alkoxysilanes can also be prepared by exchange of an existing alkoxy group with another one (eq. 9). Generally, alkoxy exchange requires a catalyst such as a mineral or organic acid (97), Lewis acid (alkyl titanate) (98), or strong base.

$$R_{4-n}Si(OR')_n + n\ R''OH \xrightarrow{\text{Catalyst}} R_{4-n}Si(OR'')_n + n\ R'OH \tag{9}$$

Acetoxysilanes. A very important functional group in silicone chemistry is the acetoxysilane group. It is widely used during the manufacture of single-component moisture-curable room-temperature-vulcanizable sealants. These acetoxy-stopped polymers hydrolyze more readily than the corresponding alkoxy-stopped silicones and release acetic acid during cure. Acetoxy-functionalized silicones are generally prepared by the acylation of a chlorosilane via addition of sodium acetate, acetic anhydride, or acetic acid (99,100).

It is also possible to synthesize acyloxysilanes by reacting triorganohydridosilanes with carboxylic acids (eq. 10) in the presence of strong acids, aluminum, or nickel complexes as catalysts (101).

$$R_3SiH + R'COOH \xrightarrow{\text{Catalyst}} R_3Si{-}O{-}\underset{\underset{O}{\|}}{C}{-}R' + H_2 \tag{10}$$

Polymerization

The manufacture of polydimethylsiloxane polymers is a multistep process. The hydrolysis of the chlorosilanes obtained from the direct process yields a mixture of cyclic and linear silanol-stopped oligomers, referred to as hydrolysate (eq. 11). In some cases, chloro-stopped polymers can also be obtained (102).

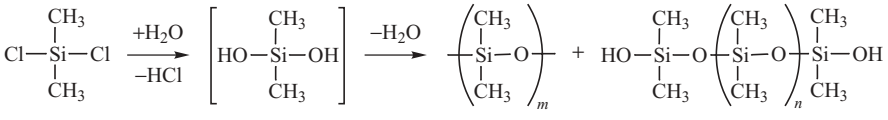

(11)

The ratio of cyclic to linear oligomers, as well as the chain length of the linear siloxanes, is controlled by the conditions of hydrolysis, such as the ratio of chlorosilane to water, temperature, contact time, and solvents (1). Commercially, hydrolysis of dichlorodimethylsilane is carried out by either a batch or continuous process (1,2,103,104). In a typical industrial operation, dichlorodimethylsilane is mixed with 22 wt% azeotropic aqueous hydrochloric acid in a continuous reactor. The resulting mixture of hydrolysate and 32 wt% hydrochloric acid is separated by means of a decanter. After separation, the anhydrous hydrogen chloride is converted by reaction with methanol to methyl chloride, which is then reused in the direct process. The hydrolysate is washed to remove residual acid, then neutralized, dried, and filtered (105). The typical yield of cyclic oligomers is between 35 and 50%. The mixture of cyclic oligomers consists mainly of tetramer and pentamer. Only a small amount of cyclic trimer is formed.

The complete conversion of the dichlorodimethylsilane to only linear oligomers is also possible in a continuous hydrolysis operation (106). In this process, the cyclics are separated from linear oligomers by a stripping process and are mixed again with dichlorodimethylsilane. This mixture undergoes equilibration to chloro-terminated oligomers and is subsequently hydrolyzed. The silanol-stopped linear oligomers are directly used in the manufacture of silicone polymers.

Dichlorodimethylsilane can also be converted into siloxane silanol-stopped oligomers by a methanolysis process (eq. 12).

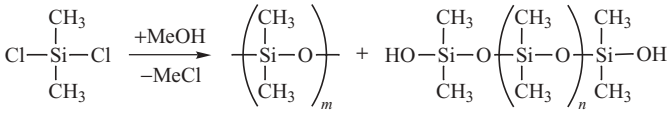

(12)

In contrast to hydrolysis technology, the methanolysis process allows for the one-step synthesis of organosiloxane oligomers and methyl chloride without formation of hydrochloric acid (104,107). The continuous methanolysis can also yield quantitatively linear silanol-stopped oligomers by recycle of the cyclic fraction into the hydrolysis loop.

If the linear fraction of siloxane oligomers is used directly in the manufacture of silicone polymers, extremely pure (greater than 99.99%) dichlorodimethylsilane is required. A high content of trichloromethylsilane can produce significant

amounts of trifunctional units and considerably affect the physical properties of the final products. If such high purity dichlorodimethylsilane is not utilized, an additional step, called cracking, must be included in the production scheme (108). In the cracking process, the hydrolyzate is depolymerized in the presence of strong base or acids to yield cyclic monomers, primarily octamethylcyclotetrasiloxane (D_4) and decamethylcyclopentasiloxane (D_5), which are distilled from the reaction mixture. The trifunctional by-products remain in the pot and are periodically removed.

Polycondensation. The linear fraction of hydrolysate, dimethyloligosiloxane-α,ω-diols having a viscosity of 10–100 mPa (=cP), is converted further to silicone fluids and high molecular weight gums by polycondensation of the silanol end groups (eq. 13). Polycondensation is an equilibrium process. In spite of the relatively high equilibrium constant for this reaction ($K_{eq@35^\circ C} = 860 \pm 90$), water removal is required to obtain high molecular weight siloxane polymers (109).

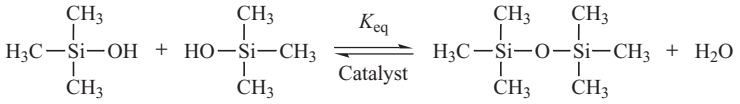

(13)

Although the low molecular weight silanols such as trimethylsilanol and dimethylsilanediol undergo condensation thermally, the higher molecular weight oligomers are much more stable and their polycondensation must be catalyzed. Many catalytic systems capable of promoting polycondensation of siloxanediols have been described in patents and open literature (1,110–117). These catalysts include strong acids such as HCl, HBr, H_2SO_4, $HClO_4$, and CF_3SO_3H; phosphonitrilic chlorides such as $(Cl_3\ PN(PCl_2N)_nPCl_3)^+PCl_6^-$; oxygen-containing chlorophosphazenes such as $Cl_3PN(PCl_2N)_nP(OH)Cl_2$; strong bases such as KOH, NaOH, and $(CH_3)_4NOH$; as well as amines, amine salts of carboxylic acids, ion exchange resins, and clays activated with mineral acids. The most selective, efficient and extensively used in industry are phosphonitrilic chlorides (112–114) and oxygen-containing chlorophosphazenes (115–117).

The first mechanistic studies of silanol polycondensation on the monomer level were carried out in the 1950s (118–120). The proposed mechanism of the acid-catalyzed condensation involves the protonation of the silanol group and subsequent nucleophilic substitution at the silicone (eq. 14).

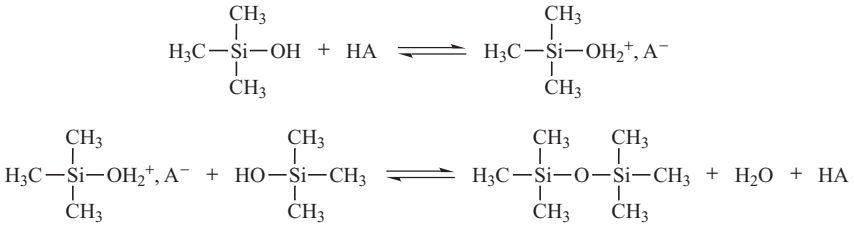

(14)

In the condensation catalyzed by a strong base the rate-determining step is the attack of silanolate anion on the silicon atom in the silanol end group (118,119). Because of the high acidity of silanol (110), the alkali metal base (MtOH) is usually transformed into the silanolate anion (eq. 15).

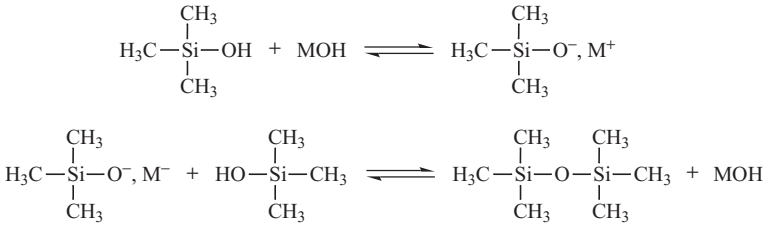

(15)

Early studies of the condensation reaction on the monomer level did not give the full picture of this process and only in the 1980s the polycondensation of siloxanols was studied by using oligomeric model compounds (121,122). These studies revealed that in the presence of strong protic acids three processes must be considered: linear condensation, cyclization, and disproportionation (eq. 16). The relative contributions from these processes strongly depend on the reaction conditions, such as type of solvent, substrate, water concentration, and acidity of catalyst (121–124). It was also discovered that in acid–base inert solvents, such as methylene chloride, another silanol group provides the basic assistance required for the condensation process. This phenomenon, called intra–inter catalysis, controls the linear-to-cyclic products ratio, which is constant at a wide range of substrate concentrations (121).

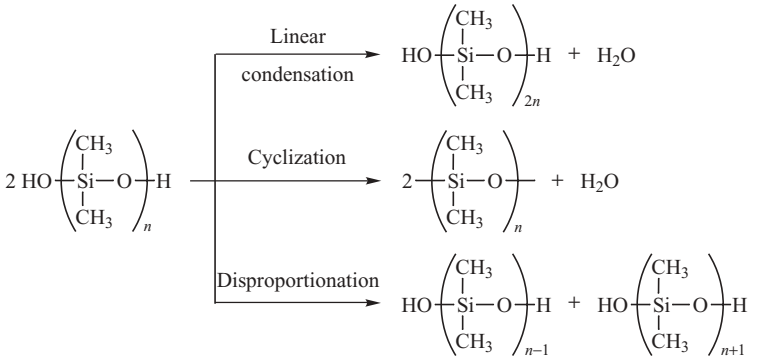

(16)

The behavior of oligosiloxanediols in the presence of strong bases is different. The contribution to the overall process of the disproportionation reaction, involving a migration of the ultimate siloxane unit between siloxane molecules, is much greater and may even completely dominate the polycondensation reaction (125). The reactivity enhancement of the siloxane bond adjacent to the silanolate anion can be understood in terms of $n(0) \rightarrow \sigma*(SiO)$ conjugation.

Ring-Opening Polymerization. Ring-opening polymerization of cyclic oligodiorganosiloxanes is an alternative to the polycondensation method of manufacturing siloxane polymers. Commercially, the polymerization of unstrained D_4 is the most important (1,102,110). In the presence of catalysts such as strong acids or bases, D_4 undergoes equilibrium polymerization, which results in a mixture of high molecular weight polymer and low molecular weight cyclic oligomers (eq. 17). The molecular weight of the polymer is easily controlled by the amount of chainstropper added and can be varied from very low molecular weight to very high molecular weight.

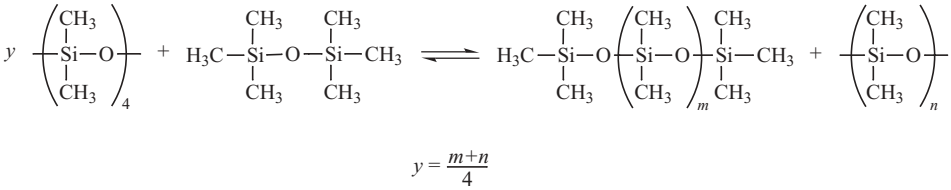

$$y = \frac{m+n}{4}$$

(17)

The position of the equilibrium depends on a number of factors, such as concentration of siloxane units and the nature of substituents on the silicon, but is independent of the starting ratio of linear to cyclics or the polymerization conditions (126,127). For a bulk polymerization of dimethylsiloxane, the equilibrium concentration of cyclic oligomers is approximately 18 wt% (128). The equilibrium mixture of cyclosiloxanes is composed of a continuous population to at least D_{400}, but D_4, D_5, and D_6 make up over 95 wt% of the total cyclic fraction (129).

The ring-opening polymerization of D_4 is controlled by entropy, because thermodynamically all bonds in the monomer and polymer are approximately the same (1,110,130). The molar cyclization equilibrium constants of dimethylsiloxane rings have been predicted by the Jacobseon–Stockmayer theory (131). The ring–chain equilibrium for siloxane polymers has been studied in detail and is the subject of several reviews (127,128,132–135). The equilibrium constant for the formation of each cyclic is approximately equal to the equilibrium concentration of this cyclic, $K_n \sim [(SiR_2O)_n]_{eq}$. The total concentration of cyclic oligomers at equilibrium is thus independent of the initial monomer concentration. As a consequence, the amount of linear polymer decreases until the critical dilution point is reached, at which point only cyclic products are formed.

Anionic Polymerization of Cyclic Siloxanes. The anionic polymerization of cyclosiloxanes can be carried out in the presence of a wide variety of strong bases such as hydroxides, alcoholates, or silanolates of alkali metals (1,102,110). Commercially, the most important catalyst is potassium silanolate (98). The activity of the alkali metal hydroxides increases in the following sequence: LiOH < NaOH < KOH < CsOH, which is also the order in which the degree of ionization of their ion pair increases (136). Another important class of catalysts is tetraalkylammonium and tetraalkylphosphonium hydroxides, and silanolates (137–139). These catalysts undergo thermal degradation when the polymer is heated above the catalyst decomposition temperature (typically >150°C), producing volatile

by-products and the neutral, thermally stable polymer. Recently, a new class of super-strong phosphazene bases such as $[(N(CH_3)_2)_3P{=}N{-})_3P{=}N(t\text{-}C_4H_9)]$ have been reported (140–142). The phosphazene bases allow for the synthesis of high molecular weight polysiloxanes, using extremely low catalyst levels with short reaction times and over a wide range of temperatures.

Anionic polymerization is widely used in the silicone industry for the manufacture of silicone polymers. The anionic polymerization of cyclic siloxanes can be conducted in a single-batch reactor or in a continuously stirred reactor (143,144). The viscosity of the polymer and type of end groups are easily controlled by the amount of added water or triorganosilyl chain-terminating groups.

The mechanism of anionic polymerization of cyclosiloxanes has been the subject of several studies (145,146). The first kinetic analysis in this area was carried out in the early 1950s (147). In the general scheme of this process, the propagation/depropagation step involves the nucleophilic attack of the silanolate anion on the silicon, which results in the cleavage of the siloxane bond and formation of the new silanolate active center (eq. 18).

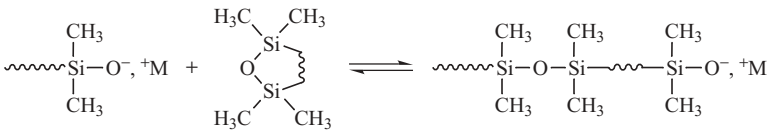

(18)

The kinetics of this process is strongly affected by an association phenomenon. It has been known that the active center is the silanolate ion pair, which is in equilibrium with a dormant ion pair complex (148,149). The polymerization of cyclosiloxanes in the presence of potassium silanolate shows the kinetic order 0.5 with respect to the initiator, which suggests the principal role of dimer complex (150).

The synthesis of new, high performance materials requires the synthesis of well-defined, narrow molecular weight distribution, cyclic-free, homo-, and copolymers. This can be accomplished by the kinetically controlled polymerization of the strained monomers, hexaalkylcyclotrisiloxanes. In the presence of the proper initiator and under the right reaction conditions, the polymerization of hexamethylcyclotrisiloxane (D_3) can proceed as a classical living polymerization. The most frequently used initiator, lithium silanolate, provides fast and quantitative initiation and a propagation that is free of depolymerization or chain-scrambling processes (151–153). However, the rate of D_3 polymerization in the presence of lithium silanolate is slow. To accelerate the polymerization process, a cation-interacting solvent such as tetrahydrofuran (THF) is commonly employed (154,155). Nucleophilic additives such as hexamethylphosphoric triamide (HMPT) or dimethyl sulfoxide (DMSO), as well as chelating agents such as cryptates, can also be used (156–161). These additives interact strongly with the lithium cation and convert the intimate ion pair into a more reactive, separated one.

Cationic Polymerization of Cyclic Siloxanes. The cationic polymerization of cyclic siloxanes is often a preferred method for the synthesis of siloxane polymers. This process, which can be performed at relatively low temperature, can

be applied to the synthesis of polysiloxanes having base-sensitive substituents such as Si—H, and the catalyst can be easily deactivated. The first high molecular weight siloxane polymer was prepared by the cationic ring-opening polymerization of D_4 in the presence of sulfuric acid (162). Since that time many catalytic systems have been reported in patents and open literature. These include strong protic acids such as CF_3SO_3H (triflic acid), $HClO_4$, H_2SO_4, aryl- and alkylsulfonic acids, heterogeneous catalysts such as ion-exchange resins, acid-treated graphite, and acid-treated clays, as well as some Lewis acids such as $SnCl_4$ (1,110,163–172). Polymerization in the presence of Lewis acids is a subject of controversy. Strong protic acids such as $HSnCl_5$, the product of the reaction of Lewis acid with water or other protic impurities, are proposed in most cases as the true catalyst (173). However, it has been reported that some nonprotic systems such as ethylboron sesquitriflate (174) and antimony chloride – acid chloride pairs (175) are able to initiate polymerization of cyclotrisiloxane. Also, electron-deficient organosilicone reagents such as trimethylsilyl triflate (176,177) and $Me_3SiH/(C_6H_5)_3C^+B(C_6F_5)_4^-$ (178) have been proven effective as initiators for cationic ring-opening polymerization of cyclosiloxanes.

Despite a long history of commercial application and in-depth studies (110,163,178–184), the mechanism of cationic polymerization of cyclic siloxanes is not as well understood as the anionic process. Several unusual kinetic results have been observed, such as the apparent negative order in the monomer concentration, negative activation energy, or a strong effect of water on the kinetics of polymerization (171,182–185). The proposed complex mechanism of acid-catalyzed polymerization consists of four processes: initiation-ring opening, step growth by homo- and heterofunctional condensation, chain propagation by direct monomer addition, and end group interconversion. Hydrogen bond association plays a crucial role in this process (148,185,186). The cationic ring-opening polymerization initiated by the electrophilic trialkylsilyl species proceeds by the simpler addition mechanism, which involves a single "long-lived" oxonium ion end group (178).

Emulsion Polymerization. Even though siloxane bond formation is an equilibrium process, it is possible to form siloxane polymers by polycondensation or ring-opening polymerization in aqueous emulsions (187–189). D_4 can be converted into high molecular weight polymer by emulsion polymerization in the presence of dodecylbenzenesulfonic acid (DBSA), which acts as both emulsifying surfactant and catalyst (190). It is also possible to obtain high molecular weight polymers by polycondensation of α,ω-dihydroxy-stopped oligosiloxanes in an aqueous emulsion employing DBSA (191) or benzyldimethyldodecylammonium hydroxide (BDDOH) (192) as the surface-active catalyst. The polycondensation involves the reaction of a complex of silanol and two molecules of DBSA with another silanol end group (193). The anionic emulsion polymerization of D_4 in the presence of BDDOH as a surface-active catalyst has been reported (192,194) and a reaction scheme proposed, which involves a quaternary ammonium silanolate as an active species.

Radiation-Induced Polymerization. In 1956 it was discovered that D_3 can be polymerized in the solid state by γ-irradiation (195). Since that time a number of papers have reported radiation-induced polymerization of D_3 and D_4 in the solid state (196,197). The first successful radiation-induced polymerization of cyclic siloxanes in the liquid state (198) and later work (199) showed that the polymerization of cyclic siloxanes induced by γ-irradiation has a cationic nature.

The polymerization is initiated by a cleavage of Si—C bond and formation of silylenium cation.

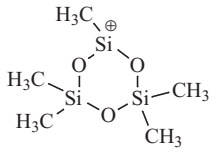

The γ-irradiation-induced polymerization requires an extremely high purity reaction system. Trace amounts of water can terminate a cationic reaction and inhibit polymerization. Organic bases such as ammonia and trimethylamine also inhibit polymerization. The γ-irradiation-induced polymerization of rigorously dried D_4 exhibits a square-root dependence of the rate on the dose rate as predicted by the Hayashi–Williams equation for completely pure systems (200).

Plasma Polymerization. Plasma polymerization as a method for modifying surfaces of materials has been known for at least 25 years. The need for well-defined, thin polymer films for applications in optics, electronics, or biomedicine stimulated the development of plasma-induced polymerization but to date, relatively few large-scale applications exist. However, in recent years increased awareness of energy consumption and hazardous waste disposal concerns have stimulated the interest in this technique as a method for manufacturing or depositing polymers on various substrates (201). The special interest that has developed in organosilicon monomers may be because many of these monomers are generally volatile, nontoxic, nonflammable, and relatively inexpensive. Also, plasma-polymerized organosilicone films have a natural chemical affinity for adhesion to single-crystal silicon, and the properties of these films can be varied widely by the choice of monomer and polymerization parameters (202). The mechanism of plasma polymerization is still not well understood as of this writing and differs substantially from the conventional ring-opening polymerization of cyclic monomers. The dissociation and ionization of organosilicone monomers by low energy electron impact is the dominant source of radical fragments and a variety of ion–molecules and ion–radicals. In the case of hexamethyldisiloxane, extension of the monomer molecule by one dimethylsiloxane unit and elimination of the trimethylsilylium ion, $(CH_3)_3Si^+$, was proposed as a crucial step in the polymer film formation. The building of Si—C—Si links also plays an important role in the polymerization. Cyclic monomers such as D_4 polymerize via the formation of a network of siloxane chains and rings. The resulting films are usually hard and scratch-resistant but often show considerable stress (203). Such films can be used as corrosion-resistant coatings on metals or as membranes in gas sensor devices (204,205). The plasma polymerization of tetramethyldisiloxane was recently employed to deposit scratch-resistant and antifogging films on transparent polycarbonate substrates (206) and more generally when the formation of silicone films with uniform thickness and without any dust interference was required.

Silicone Network Formation. Silicone rubber has a three-dimensional network structure consisting of cross-linked polydiorganosiloxane chains. Three reaction types are generally employed for the formation of silicone networks (207): peroxide-induced free-radical processes, hydrosilylation addition reactions, and

condensation reactions. Silicones have also been cross-linked using radiation to produce free radicals or to induce photoinitiated reactions.

Peroxide Cure. The use of peroxide catalysts at elevated temperatures is one of the most common methods for the preparation of silicone networks (208). Typical peroxides include acyl derivatives such as dibenzoyl (209), bis-*p*-chlorobenzoyl, and bis-2,4-dichlorobenzoylperoxides; arylalkyl derivatives such as dicumyl peroxide; and dialkyl derivatives such as di-*t*-butyl peroxide and 2,5-dimethyl-2,5-di-*t*-butylperoxyhexane. The amount and type of peroxide used determine the cure temperature of the composition as well as its ultimate properties. Diaroyl peroxides can be used with either PDMS or with vinylmethylpolysiloxanes. Bis-2,4-dichlorobenzoyl peroxide has the highest rate of decomposition and the lowest decomposition temperature. Cross-linking by peroxides is initiated by the generation of free radicals via homolytic cleavage of the peroxide at elevated temperatures. The peroxy radicals can abstract hydrogen atoms from methyl groups, forming ethylenic linkages between siloxane chains (210). Model studies have confirmed the formation of $SiCH_2CH_2Si$ as the predominant cross-linking reaction (211).

$$\begin{aligned} \mathrm{ArOOAr} &\longrightarrow 2\,\mathrm{ArO}\cdot \\ \mathrm{ArO}\cdot + \mathrm{CH_3SiR_3} &\longrightarrow \mathrm{ArO} + \cdot\mathrm{CH_2SiR_3} \\ 2\cdot\mathrm{CH_2SiR_3} &\longrightarrow \mathrm{R_3SiCH_2CH_2SiR_3} \end{aligned} \qquad (19)$$

The cross-linking of vinyl containing polydimethylpolysiloxanes can be achieved using alkylaryl or dialkyl peroxides (1,212). A radical can be formed at either the methyl or vinyl site; it is generally agreed that the reaction through the vinyl group is energetically favored. Several mechanisms have been proposed to explain the reaction. One suggestion is that the radical is first formed on a methyl group that can then attack either a methyl group or a vinyl group (213). Another proposal is that the cross-link occurs primarily through the vinyl group (214). The first step is addition of the peroxy radical to the vinyl moiety (215). The resultant radical can then attack either another vinyl group or a methyl group. Termination can occur by coupling or by hydrogen abstraction from adjacent peroxide molecules. Rheometric studies indicate that methylvinylsilicone resins do undergo cross-linking via the methyl groups but at a slower rate than through the vinyl groups (216).

Hydrosilylation. *Hydrosilylation*, the reaction between a silicone hydride group and an olefin to form an alkylenic linkage, is extremely important for the formation of silicone networks (77,83,217–219). Cross-linking and network formation occur by reaction of multifunctional silicon hydride groups with multifunctional silicone olefinic groups. Typically, vinyl groups attached to silicon are employed; however, there are reports of network formation by reaction of multifunctional silicone hydride polymers with hexenyl-terminated siloxanes (220). No by-products aside from Pt residue are produced by this type of curing and no shrinkage is observed. Addition of the hydride to the olefin may be either Markovnikoff or anti-Markovnikoff, depending upon the choice of the silicone–olefin group and catalyst. With silicon-bound vinyl groups, the reaction produces 95% of the β-addition product.

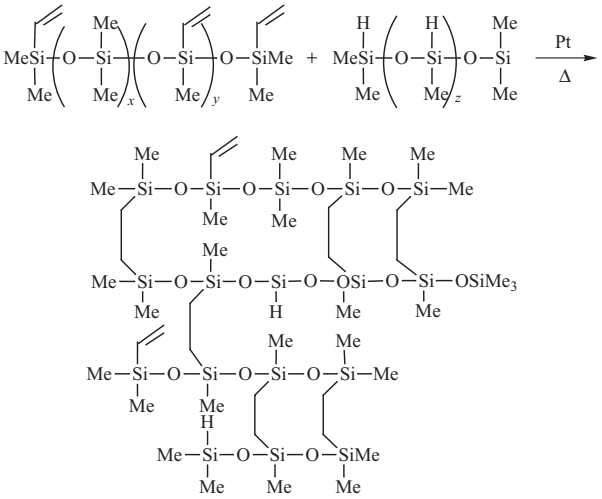

(20)

Hydrosilylation is generally catalyzed by Group 8–10 (VIII) metal complexes or supported metal catalysts. Platinum complexes are the most widely used, although rhodium(I) complexes have also been reported (83). Typical industrial catalysts include soluble platinum species such as the platinum–divinyltetramethyldisiloxane complex (Karstedt's catalyst) (221). These catalysts exhibit high turnover rates and are useful in concentrations as low as 1–2 ppm.

Side reactions or postcuring reactions are possible in the formation of silicone networks. In most cases, the silicon-bound hydride is in stoichiometric excess to enhance reaction rates. Disproportionation reactions involving terminal hydride groups have been reported (222). A major side reaction consumes Si—H to give redistributed siloxane in the resulting polymers and gaseous silane as a by-product.

Excess silicon hydride may undergo hydrolysis. The silanol thus formed can then condense with another hydride, resulting in networks with a higher crosslink density (223–225). Isomerization of a terminal olefin to a less reactive internal olefin has been noted (222). Vinylsilane/hydride interchange reactions have been observed particularly when less active catalysts are employed (217).

$$R_3SiH + R'_3SiCH{=}CH_2 \rightleftharpoons R'_3SiH + R_3SiCH{=}CH_2 \quad (21)$$

Several mechanisms have been proposed for the platinum-catalyzed homogeneous hydrosilylation reaction. The most commonly invoked mechanism, proposed by Chalk and Harrod in 1965, consists of elementary steps similar to homogeneous hydrogenation, oxidative addition, migratory insertion, and reductive elimination (226). However, this mechanism fails to describe the induction period or the presence of colloidal species at the end of the reaction. Lewis proposed an alternative mechanism based on the intermediacy of colloids that were detected by transmission electron microscopy after evaporation of catalytically active solutions (227,228).

More recently, extended X-ray absorption fine structure (EXAFS) has been used to identify the actual catalytic species in both model systems and networks (229). At the completion of the hydrosilylation reaction, the state of the platinum

species is dependent upon the reaction conditions. With a stoichiometric excess of olefin, a mononuclear platinum species containing six platinum–carbon bonds, such as platinum coordinated to three olefin groups, is obtained. However, in the presence of high silicon hydride concentrations or in reactions employing poorly coordinating olefins such as hexenes, the platinum product is multinuclear and contains platinum–silicon bonds. Upon addition of the deficient reagent (olefin or silicon hydride), the platinum products can interconvert to the catalytically active form. Colloids have been found in a postmortem analysis of hydrosilylation reactions upon evaporation or destabilization of the reactant solutions. EXAFS analysis of solutions frozen during model reactions of cross-linking systems (functional siloxane monomers) showed that regardless of reactant stoichiometry, the platinum intermediates during the catalytic portion of the reaction were mononuclear and contained both platinum–silicon and platinum–carbon bonds. A mechanism was therefore proposed that incorporates the Chalk–Harrod postulate with the addition of exchange and hydrosilylation of the ligands on the platinum during the induction period, and a pathway to colloid formation at the end of the reaction. Ab initio calculations reported on the platinum-catalyzed hydrosilylation of ethylene support the Chalk–Harrod mechanistic steps of oxidative addition, migratory insertion, and reductive elimination during the catalytic cycle (230).

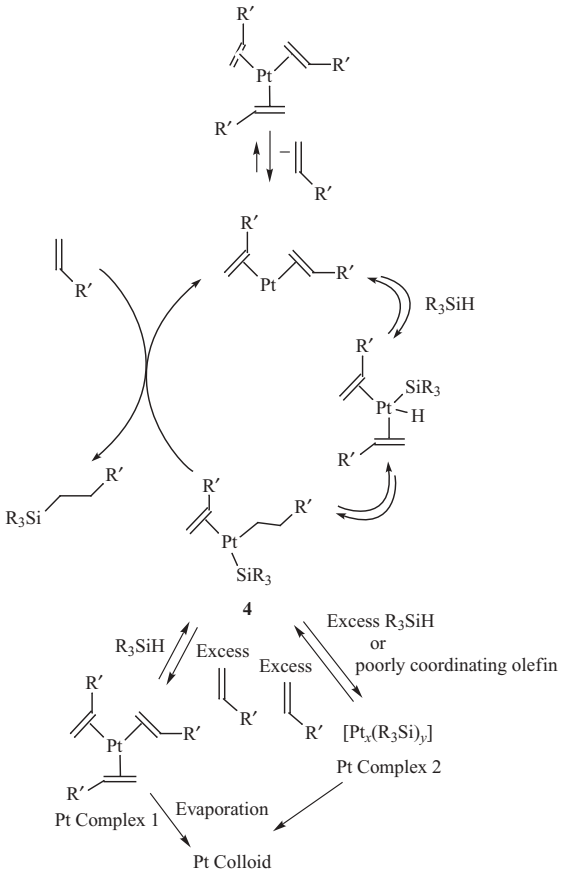

Catalyst inhibitors are often included in formulations to increase the pot life of these systems. An ideal silicone addition cure composition would combine instant cure at elevated temperature with infinite pot life at ambient conditions. Unfortunately, real systems always deviate from this ideal situation. One mechanism of inhibition consists of equilibrium between the inhibitor (I) and catalyst ligands (L) (231).

$$PtL_n + x\ I = PtL_{n-x}I_x + x\ L_n \tag{22}$$

Hydrosilylation with inhibited complexes is generally less rapid than with platinum(0) olefin compounds. Complexing ligands such as phosphines and amines are excellent inhibitors but often form complexes so stable that they act as poisons and prevent cure even at elevated temperatures. Unsaturated organic compounds such as acetylenic alcohols, acetylene dicarboxylates, maleates, fumarates, and eneynes are preferred inhibitors (231–242). Steffanut and coworkers (243) have reported the use of platinum(0) complexes with electron-deficient olefinic ligands as hydrosilylation catalysts. Some of these complexes are self-inhibiting. Platinum–fumarate or maleate complexes formed from the reaction of platinum(0) compounds with dimethyl fumarate or dimethyl maleate must undergo reduction of the fumarate or maleate ligand with silicon hydride, prior to becoming active hydrosilylation catalysts (244). An alternative inhibition strategy is to encapsulate the platinum catalysts with cyclodextrin, thermoplastics, or silicones (245–247).

Condensation Cure. The condensation of silanol groups to form siloxanes is an extremely important industrial reaction and may be represented in its simplest form as follows:

$$R_3SiOH + R'_3SiOH \rightarrow R_3SiOSiR'_3 + H_2O \tag{23}$$

Unfortunately, because self-condensation of silanols on the same silicone can occur readily, the controlled reaction of disilanol or trisilanol compounds with telechelic silanol polymers to form a three-dimensional network is not feasible. Instead, networks are derived from reactions of telechelic polymers with crosslinkers containing reactive groups such as alkoxysilanes, acyloxysilanes, silicon hydrides, or ketoximinosilanes, as in the reactions 24–27 (207). The choice of the cross-linking agent depends on the specific product characteristics desired.

$$R_3SiOH + R'_3Si(OCH_3) \rightarrow R_3SiOSiR'_3 + CH_3OH \tag{24}$$

$$R_3SiOH + R'_3Si(OOCCH_3) \rightarrow R_3SiOSiR'_3 + CH_3COOH \tag{25}$$

$$R_3SiOH + R'_3SiH \rightarrow R_3SiOSiR'_3 + H_2 \tag{26}$$

$$R_3SiOH + R'_3Si(ON{=}\underset{\displaystyle CH_3}{\overset{\displaystyle |}{C}}{-}CH_2CH_3) \longrightarrow R_3SiOSiR'_3 + HO{=}N{-}\underset{\displaystyle CH_3}{\overset{\displaystyle |}{C}}{-}CH_2CH_3 \tag{27}$$

Condensation catalysts include acids and bases, as well as organic complexes of metals. Both tin(II) and tin(IV) complexes with oxygen-donor ligands are

extremely useful. It has been suggested that the tin(IV) catalyst is converted to its active form by partial hydrolysis followed by reaction with the hydrolyzable silane to yield a tin–silanolate species (eqs. 28 and 29) (248,249).

$$R_2Sn(OCOR')_2 + H_2O \rightarrow R_2Sn(OCOR')OH + R'COOH \quad (28)$$

$$R_2Sn(OCOR')OH + Si(OR')_4 \rightarrow R_2Sn(OCOR')(OSiR')_3 + R'OH \quad (29)$$

The organotin silanolate reacts with the PDMS diol by either attack on the SiOC bond or by silanolysis of the SnOC bond (248,249). Other metal catalysts include chelated salts of titanium and tetraalkoxytitanates, which have also been shown to form silanolate species similar to those postulated for tin catalysts (250, 251). Formation of a cross-linked matrix involves a combination of the three steps in equations 30–32.

$$R'_3Si(OR) + H_2O \rightarrow R'_3SiOH + ROH \quad (30)$$

$$R_3SiOH + R'_3SiOH \rightarrow R_3SiOSiR'_3 + H_2O \quad (31)$$

$$R'_3Si(OR) + R'_3SiOH \rightarrow R'_3SiOSiR'_3 + ROH \quad (32)$$

The role of water in condensation cross-linking is dependent upon whether the material is a one- or two-component curing system (252). One-component systems do not cure until they are exposed to water. Two-component systems usually contain water in one of the components and begin to cure as soon as the components are mixed. Other work suggests that tin(II) catalysts can function in the absence of water (253). Studies of the relative rates of hydrolysis and condensation of multifunctional silanes, $R_xSi(OR)_{4-x}$, in the presence of acidic or basic catalysis have shown that the first Si—OR group hydrolyzes much more rapidly than subsequent groups (254). Silanol–silanol condensation is much slower than silanol–alkoxysilane condensation, even if the alkoxysilane is monofunctional, thus suggesting that in the presence of a cross-linker, chain extension will not occur to a significant extent (255–258).

Condensation cure can also be carried out in emulsions (259–271). In this case, the cross-linker and PDMS are emulsified using anionic, cationic, or nonionic surfactants in water, and a condensation catalyst such as dibutyltin dilaurate is added. The formulation can also be cured without a tin-catalyst if self-catalytic hydrolyzable silanes are included (265). The polymer can then undergo cross-linking, forming a continuous film when the water is evaporated.

High Energy Radiation Cure. Silicones can be vulcanized by high energy radiation examples of which include γ-irradiation, X-ray, and electron beam. High energy radiation interacts with shell electrons of atoms of the silicone materials and induces ionization. The generated radical cations and free radicals initiate chemical reactions that lead to cross-linking (272). The properties of silicones cross-linked by high energy irradiation are indistinguishable from those vulcanized with peroxides (273). But silicone rubber cross-linked by γ-irradiation

does, however, have two advantages: better resistance to aging in humid environments and greater hydrolytic stability at elevated temperatures because the compositions are catalyst-free (274). Radiation cure of methylvinyl silicone rubber is a random cross-linking process with no differentiation between methyl and vinyl groups (275). Substitution of phenyl for methyl groups on the siloxane chain increases the radiation resistance. Silicone hydride groups are highly sensitive to radiation (276).

Photoinitated Radiation Cure. Attachment of reactive functional groups such as mercaptans, acrylates, and oxiranes to a polysiloxane backbone can be used to render a silicone susceptible to curing by lower energy electromagnetic radiation such as ultraviolet (UV) or low energy electron beam (EB) (277). Thiols can be added across an olefin using an aromatic ketone as the photoinitiator (EB) (278,279). Unfortunately, the odor associated with thiols has limited the commercial acceptance of this technology. Two systems, which are widely used in the industry for silicone release and protective coatings, are silicones containing pendent acrylate groups (free-radical cure mechanism) and oxirane or vinyl ether functional siloxanes (acid-catalyzed). The acrylate functional polysiloxanes are prepared by allowing epoxy-functional siloxanes to react with acrylic acid or from the esterification of siloxane containing alcohol groups with acrylic acid (280–283). Cross-linking occurs upon the generation of free radicals by EB irradiation of the silicone matrix or by UV-initiated decomposition of benzophenone-based photoinitiators. The most important limitation of this process is sensitivity to oxygen. The typical industrial coating line requires oxygen levels below 50 ppm.

Silicones functionalized with oxiranes or vinyl ether groups can be cured by UV irradiation in the presence of diaryliodonium or sulfonium salts containing triflate, PF_6, or SbF_6 counterions (284–290). Decomposition of the onium salt under UV irradiation leads to the formation of strong acid that initiates very rapid polymerization of oxiranes or vinyl ether groups (291–293). Recently, a new class of onium salts prepared with the tetrakis(pentafluorophenyl)borate (TPFB) anion has been introduced as a UV photoinitiator (294–296). The presence of the large, weakly nucleophilic TPFB anion improves the solubility of the iodonium salts in the siloxane matrix and increases the reactivity of the formed acid (297,298). The cationic polymerization of oxiranes and vinyl ethers is not sensitive to the presence of oxygen and can be carried out under ambient conditions. Cycloaliphatic epoxies are highly reactive in the ring-opening polymerization reaction initiated by strong acids and so the typical commercial system is based on polysiloxanes with pendent cyclohexeneoxide moieties. Such polymers are readily prepared by the hydrosilylation of 4-vinylcyclohexeneoxide with hydrogen functional polysiloxane in the presence of catalytic amount of platinum or rhodium (299) (eq. 38).

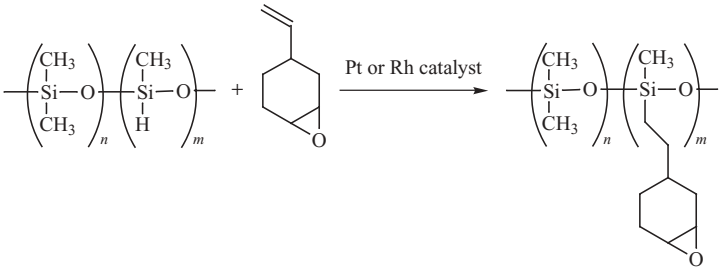

(33)

Formation of a siloxane network via hydrosilylation can also be initiated by a free-radical mechanism (300–302). A photochemical route makes use of photosensitizers such as peresters to generate radicals in the system. Unfortunately, the reaction is quite sluggish. Several complexes of platinum such as (η-cyclopentadienyl)trialkylplatinum(IV) compounds have been found to be photoactive. The mixture of silicone polymer containing alkenyl functional groups with silicon hydride cross-linker materials and a catalytic amount of a cyclopentadienylplatinum(IV) compound is stable in the dark. Under UV radiation, however, the platinum complex undergoes rapid decomposition with release of platinum species that catalyze rapid hydrosilylation and network formation (303–308). Other UV-active hydrosilylation catalyst precursors include (acetylacetonate)Pt(CH_3)$_3$ (309), (acetylacetonate)$_2$Pt (310–312), platinum triazene compounds (313,314), and other sytems (315,316).

Characterization of Silicone Networks. The cross-linking of silicones as a function of time can be monitored using a variety of techniques such as infrared spectroscopy, dynamic mechanical analysis, dielectric spectroscopy, ultrasound, differential scanning calorimetry, and thermomechanical analysis (317–324). Infrared spectroscopy is especially useful with addition cure systems because the disappearance of the SiH peak in the starting silicone hydride can be readily monitored. Dynamic mechanical analysis has been used to study the critical time for gelation of a PDMS network (317). Fourier-transform infrared dichroism has been used to investigate the molecular orientation of PDMS networks. In a study of the isothermal dielectric properties of condensation-cured networks at room temperature as a function of catalyst concentration during cure, the effect of catalyst concentration was reflected in the value of the loss factor (318). The gel point of an addition-cured network can be determined using ultrasound techniques (320). A step-like increase in the longitudinal wave velocity is exhibited at the sol–gel transition point. Differential scanning calorimetry has been used with hydrosilylation-cured systems to determine rates of conversion and to develop a kinetic model for the rubber injection-molding process (322).

In addition to the above techniques, inverse gas chromatography, swelling experiments, tensile tests, mechanical analyses, dynamic light scattering, and small-angle neutron scattering have been used to determine the cross-link density of cured networks (325–332). Solid-state ^{29}Si NMR and chemical degradation methods have been used to characterize cured networks structurally (333). ^{1}H and ^{2}H NMR and spin echo experiments have been used to study the dynamics of cured silicone networks (334–338). Stress relaxation experiments have been employed to examine the chemistry of vulcanized silicone networks (339).

Model Networks. Construction of model networks allows development of quantitative structure property relationships and provides the ability to test the accuracy of the theories of rubber elasticity (340–343). By definition, model networks have controlled molecular weight between cross-links, controlled cross-link functionality, and controlled molecular weight distribution of cross-linked chains. Silicones cross-linked by either condensation or addition reactions are ideally suited for these studies because all of the above parameters can be controlled. A typical condensation-cured model network consists of an α,ω-polydimethylsiloxanediol, tetraethoxysilane (or alkyltrimethoxysilane), and a

tin-cure catalyst (344). A typical addition-cure model is composed of α,ω-vinylpolydimethylsiloxane, $M^H{}_4Q$, and a platinum-cure catalyst (345–347).

Using both condensation-cured and addition-cured model systems, it has been shown that the modulus depends on the molecular weight of the polymer and that the modulus at rupture increases with increased junction functionality (348). However, if a bimodal distribution of chain lengths is employed, an anomalously high modulus at high extensions is observed. Finite extensibility of the short chains has been proposed as the origin of this upturn in the stress–strain curve. Calculations have been performed on the effect of including a trimodal distribution of chain lengths on ultimate properties. The study concluded that incorporation of very long chains into a bimodal network of long and short chains could lead to elastomers with improved properties (349). Monte Carlo simulations of the elastic behavior of PDMS networks have been performed (350,351).

The effect of pendent chains on the mechanical properties of model PDMS has been studied. It was found that the loss modulus of these networks was a function of the concentration and molecular weight of the dangling chains. The elastic properties of networks with pendent chains were found to be lower than those that were completely cross-linked (352).

Monodisperse model networks have been prepared using prepolymers with polydispersivities close to 1.0. Equilibrium tensile measurements on such networks prepared from fractionated PDMS show single-curve elastic moduli of all the networks (353,354). Simulations of the effect of molecular weight distribution on the equilibrium modulus indicated that with increasing polydispersity, the affine structure factor is found to decrease. Low extents of reaction were observed for the more monodisperse systems. The observed low extent of reaction is due to the reduced number of cross-links with increased molecular weight of chains in the system (355). Dynamic mechanical measurements have been reported for networks prepared by telechelic condensation of monodisperse PDMS with tetraethoxysilane (356). The tensile and swelling behaviors of PDMS networks of high junction functionality have been determined using hydride-terminated and hydride on chain siloxane reactions with vinyl-stopped PDMS (357). In an examination of the mechanical behavior and swelling properties of networks prepared by cross-linking fractionated vinylmethylpolydimethylsiloxane with pentamethylcyclopentasiloxane (358), the dynamic mechanical properties measured were in good agreement with the swelling rates. It has been found that a lowering of the elastic modulus increases broadness of the molecular weight distribution of networks (359). There is a good correlation between theoretical predictions and the experimental value of the tensile modulus for monodisperse networks prepared from vinyl-terminated silicones and $M^H{}_4Q$ (333).

Filled Silicone Networks. Few applications use silicone elastomers in the unfilled state. The addition of fillers results in a severalfold improvement in properties. Fillers can be broadly categorized as reinforcing and nonreinforcing (or semireinforcing). Reinforcing fillers increase tensile strength, tear strength, and abrasion resistance, whereas nonreinforcing fillers are used as additives for reducing cost, improving heat stability, imparting color, and for increasing electrical conductivity (360).

Nonreinforcing fillers include calcium carbonate, clays, silicates, and aluminates. They are primarily used as extending fillers; that is, they serve the purpose

of reducing cost per unit volume. Pigment-grade oxides, especially ferric oxides, are used as fillers and stabilizers for high temperature compounds used in oxidizing environments. Other fillers such as fumed titania, alumina, and zirconia find applications for extended heat stability, for imparting color, and for improving the electrical conductivity of the formulation. Although carbon black is the most common reinforcing filler for other vulcanized rubber/elastomeric applications, it is not commonly used as a reinforcing filler in silicones. Instead, it finds applications in improving electrical conductivity and pigmentation (361).

Fillers that are used for providing reinforcement include finely divided silicas prepared by vapor-phase hydrolysis or oxidation of chlorosilanes, dehydrated silica gels, precipitated silicas, diatomaceous silicas, and finely ground high assay natural silicas (362–366). The size, structure, and surface chemistry of the filler all play important roles in determining the final degree of reinforcement (367–369). The most important criteria for reinforcement are the availability of sufficient surface area and a strong van der Waals or hydrogen-bonding interaction between the polymer and the filler (a covalent linkage is not essential) (370,371). Fillers made by the fumed process have typical surface areas around 200 m^2/g and provide the maximum reinforcement. Several comparative studies of the effectiveness of fumed versus precipitated silica show that for fumed silicas, interaction with siloxane occurs by randomly distributed silanols, whereas for precipitated silica, a more complex structure is involved probably involving short chains of polysilicic acid. (365,372,373).

Several properties of the filler are important to the compounder (374). Properties that are frequently reported by fumed silica manufacturers include surface area, the acidity of the filler, nitrogen adsorption, oil absorption, and particle size distribution (375,376). Adsorption techniques provide a measure of the surface area of the filler, whereas oil absorption is an indication of the structure of the filler (377). Measurement of the silanol concentration is critical, and some techniques that are commonly used in the industry to estimate this parameter include methyl red absorption and methanol wettability tests (367,368,373). Other techniques to characterize fillers include weight loss, various spectroscopies, such as diffuse reflectance infrared spectroscopy (DRIFT), inverse gas chromatography (IGC), and photoacoustic IR, NMR, Raman, and surface forces apparatus (372,378–385).

Structuring refers to the formation of an elastic mass before cure that impedes normal processing operations such as molding and extrusion. Intensive working may be required to restore plasticity. Plasticity and process aids are therefore incorporated as monomeric or oligomeric organosilicon compounds. Alternatively, the silanol concentration on the silica surface can be controlled by filler treatment to prevent structuring (386,387). Reaction of the silica particles with hot vapors of chlorosilanes, low molecular weight cyclic siloxanes, and hexamethyldisilazane (HMDZ) are some of the commonly used filler treatments in the industry (361,388). It has been proposed that pretreatment of the filler reduces the strength of silica–silica and silica–polymer interactions (389).

Polymer–filler interactions have been studied by deuterium NMR spectroscopy. In unstrained networks, two regions of local chain mobility were identified, that within the absorption layer and that outside. In a uniaxially strained sample, the chains were immobilized near the filler surface. Chain order is increased in filled systems relative to unfilled systems (390). Molecular orientation

in stretched networks was also studied using Fourier transform infrared dichroism. Filler introduction led to an increase in orientation, which was attributed to a higher microscopic strain in the elastomeric network (391).

The final mechanical properties of the elastomer compound are a function of the concentration of the reinforcing filler in the formulation. In the small strain limit, Einstein relationships have been proposed for changes in viscosity and modulus as a function of volume fraction of the filler (392,393). Although these relationships work well for spherical and low structure fillers, they do not correctly predict the final properties of systems filled with high structure nonspherical particles. The high structure of the filler leads to a system that is not free draining, resulting in an augmentation of the filler concentration caused by the rubber trapped in the internal void space (occluded rubber) (394–397). An empirical modification to the Einstein relationship for modulus has been proposed (398). However, these relationships do not account for the secondary agglomeration that results in highly non-Newtonian and thixotropic behavior (399–405). The reasons for improvement in the failure properties of these systems are not well understood (405,407,408). Some mechanisms that have been proposed include the ability of a filled system to increase energy dissipation at the tip of the crack through viscoelastic processes, and the ability of the dispersed particles in cooperatively arresting or deflecting the growth of cracks, thereby delaying the onset of catastrophic failure. Results of tensile, IR dichroism, and birefringence experiments show strong upturns in the stress with increasing elongation while segmental–orientation–strain properties remain linear. The upturn in the stress results from limited extensibility of the chains. A model based on Monte Carlo calculations shows strong differences between stress and orientation effects (409). A phenomenon often discussed in connection with filler reinforcement is stress softening, which probably arises because of the progressive detachment, or breaking, of network chains attached to filler particles (410).

Fillers have also been shown to influence abrasive wear of silicone rubbers. The wear rates increase slowly with filler concentration until a critical volume fraction is reached, after which wear rates increase significantly with increasing filler loading. A model, which included the stress concentration induced by the filler, showed a positive correlation between the wear rate and the damage zone volume (411).

A good dispersion of the filler particles is essential for ensuring satisfactory ultimate properties (412–418). The first processing step involves the initial incorporation of the filler in the polymer matrix, and is limited primarily by the wettability of the filler. The next step involves a fracture of the aggregates and their uniform dispersion under shear. Heat treatment is often used to promote wetting and improve polymer–filler interactions (419). Dispersion is measured in terms of the remaining agglomerates, which cause premature failure in tensile testing and other ultimate properties. A trend in obtaining uniform dispersions is *in situ* precipitation of silica by catalytic hydrolysis of tetraethyl orthosilicate (TEOS) in a preformed silicone matrix using sol-gel techniques (420). Dynamic mechanical losses in addition-cured PDMS networks containing *in situ* precipitation of silica indicated that the glass-transition temperature showed only a slight dependence on the presence of the filler particles but the filler reduced both the degree and rate of crystallization for the *in situ* filled networks (421).

Properties and Uses

Silicone properties and uses have been discussed extensively (1,422–425).

Silicone Fluids. Silicone fluids are used as damping fluids, dielectric fluids, polishes, cosmetic and personal care additives, textile finishes, hydraulic fluids, paint additives, photocopy fuser oils, and heat-transfer oils. Polydimethylsiloxane oils are manufactured by the equilibrium polymerization of cyclic or linear dimethylsilicone precursors. Monofunctional organo-silane end groups, typically trimethylsilyl (M), are used, and the ratio of end group to chain units (D), ie, the ratio M/D, controls the ultimate average molecular weight and viscosity (162). Low viscosity fluids, $<10^5$ cSt, are generally prepared by acid-catalyzed equilibration. The reaction can be run continuously or in a glass-lined batch reactor at temperatures up to 180°C. Solid-acidified montmorillonite (Filtrol) or sulfuric acid on carbon catalysts are removed by filtration, and the end products are stripped under high vacuum and temperature to remove residual low molecular weight cyclic or linear siloxanes (426).

High molecular weight ($>10^6$ cSt) silicone oils and gums are prepared by base-catalyzed, ring-opening polymerization of cyclicdiorganosiloxanes, such as D_4, or by condensation polymerization of silanol-terminated PDMS. Both methods are practiced commercially. Potassium silanoate, prepared from HO–(D_n)–OH and KOH, or transient catalysts such as tetramethylammonium or tetrabutylphosphonium hydroxide, are used in the ring-opening polymerization method (147,427,428). The potassium silanoate is quenched at the end of the reaction, eg, with phosphoric acid. The transient catalysts can be decomposed at temperatures >150°C. Condensation polymerization also requires a catalyst, eg, linear phosphonitrilic chlorides (LPNC) (112–115). Ultimate molecular weight is controlled by the removal of water. LPNC catalysts can be deactivated thermally or by the addition of bases such as hexamethyldisilazane.

The physical properties of PDMS fluids have been extensively studied (1,429–431). The properties of a typical 50 cSt silicone oil (the silicone industry commonly uses centistokes, cSt, as a measure of the viscosity of a silicone polymer where 1 cSt = 1 mm^2/s) are presented in Table 2. Linear silicone fluids have low melting points and second-order (glass) transition temperatures. High molecular weight PDMS has a T_m of −51°C and a T_g of −86°C (432). The low intermolecular forces in silicones also lead to low boiling points, low activation energies for viscous flow, high compressibility, and generally Newtonian flow behavior. High molecular weight polymers (M_w > 35,000) exhibit non-Newtonian flow, especially at high shear rates. This same phenomenon also results in a material having relatively poor physical properties at high molecular weight.

Unlike the linear analogues, cyclic dimethylsiloxanes are low melting solids and the T_m generally decreases with increasing ring size. Physical properties for a series of M-stopped oligomers, MD_xM, and cyclic compounds, D_x, are listed in Table 3.

Many of the applications for silicone oils are derived from the wide temperature range over which they can be used. Addition of a small amount of phenylsiloxane in the form of diphenyl or phenymethylsiloxy groups, and/or incorporation of a slight amount of branching, suppresses the T_m of the dimethylsilicones and can reduce the pour points to as low as −100°C (433,434). Methylsilicone oils are

Table 2. Typical Silicone Fluid Properties[a]

Property	Value
Physical	
η at 25°C, mm^2/s(=cSt)	50
Viscosity-temperature coefficient	0.59
Density, g/mL	0.963
Refractive index	1.402
Pour point, °C	−55
Surface tension at 25°C, mN/m (=dyn/cm)	20.8
Thermal expansion, $cm^3/cm^3/°C$	0.00106
Max. volatiles at 150°C, %	0.5
Specific heat	0.36
Electrical	
Dielectric strength, V/min	35,000
ε at 60 Hz	2.72
Dissipation factor	0.0001
Volume resistivity, $\Omega \cdot$ cm	1×10^{14}
Service temperature (continuous), °C	150
Max. temperature in air, °C	200
Max. temperature in N_2, °C	300

[a]Refs. 1 and 430.

stable in air at 150°C for extremely long periods of time (435) and undergo only slow degradation up to 200°C. In vacuum or inert atmospheres, dimethylsilicone oil can be heated to 300°C for a limited amount of time (436). The thermal properties of silicones are important for medical applications (437). Heat-resistant silicone fluids have increasing amounts of phenyl-containing substituents. High molecular weight methylphenylsilicones can be used in air at temperatures up to 250°C for several hundred hours and can withstand brief exposures up to 450°C in the presence of inert gases (438). Table 4 compares silicone polymers with equivalent petroleum-based materials and demonstrates the wide range of temperature over which they can be used.

Dimethylsilicone fluids decompose via two principal mechanisms: retrocyclization to low volatile cyclic siloxanes such as D_3 and D_4, and thermal oxidation of the alkyl side chains to give formaldehyde, CO_2, water, and T groups (430). The retrocyclization process is catalyzed by acids or bases and can occur at temperatures above 140°C. Catalytic acidic or basic sites on glassware and metallic containers are often the source of degradation of PDMS fluids. Heating in air to 200–250°C causes thermal oxidation of PDMS, and the cross-linking from T and Q group formation ultimately results in gellation. Stabilizers such as *p*-aminophenol, naphthols, metal acetonylacetonates, and iron octoate are commonly used to improve thermal stability (439–443).

For higher molecular weight PDMS ($M_n > 2500$), the number-average molecular weight is related to the bulk viscosity by the following formula (the viscosity units are in cSt):

$$\log(\text{viscosity}) = 1.00 + 0.0123(M_n)^{1/2} \quad (34)$$

Table 3. Properties of MD_xM and D_x[a]

Compound	CAS registry number	MDT formula	Melting point, °C	Boiling point, °C	Density d^{20}, g/mL	Refractive index, n_D^{20}	Viscosity (n) at 25°C, mm^2/s (=cSt)	Flash point, °C
Hexamethyldisiloxane	[107-46-0]	MM	−67	99.5	0.7636	1.3774	0.65	−9
Octamethyltrisiloxane	[107-51-7]	MDM	−80	153	0.8200	1.3840	1.04	37
Decamethyltetrasiloxane	[141-62-8]	MD_2M	−76	194	0.8536	1.3895	1.53	70
Dodecamethylpentasiloxane	[141-63-9]	MD_3M	−80	229	0.8755	1.3925	2.06	94
Tetradecamethylhexasiloxane	[107-52-8]	MD_4M	−59	245	0.8910	1.3948	2.63	118
Hexadecamethylheptasiloxane	[541-01-5]	MD_5M	−78	270	0.9012	1.3965	3.24	133
Octadecamethyloctasiloxane	[556-69-4]	MD_6M	−63	290	0.9099	1.3970	3.88	144
Eicosamethylnonasiloxane	[2652-13-3]	MD_7M		307.5	0.9180	1.3980	4.58	159
Hexamethylcyclotrisiloxane	[541-05-9]	D_3	64.5	134				
Octamethylcyclotetrasiloxane	[556-67-2]	D_4	17.5	175.8	0.9561	1.3968	2.30	69
Decamethylcyclopentasiloxane	[541-02-6]	D_5	−44	210	0.9593	1.3982	3.87	
Dodecamethylcyclohexasiloxane	[540-97-6]	D_6	−3	245	0.9672	1.4015	6.62	
1,3,5,7,11,13-Heptaethylcycloheptasiloxane	[17909-36-3]	D_7	−32	154[b]	0.9730	1.4040	9.57	
Hexadecamethylcyclooctasiloxane	[556-68-3]	D_8	31.5	290	1.1770[c]	1.4060	13.23	

[a] Ref. 430.
[b] At 2.7 kPa (20 nm Hg).
[c] Crystals.

Table 4. Viscosity of Silicone Oil vs. Petroleum Oil

Temperature, °C	Silicone η, mm^2/s (=cSt)	Petroleum η, mm^2/s (=cSt)
100	40	11
38	100	100
−18	350	11,000
−37	660	230,000
−57	1560	Solid

The number-average molecular weight of dimethylsiloxane can also be determined from the intrinsic viscosity (dL/g) (extrapolated to zero viscosity) in toluene or methyl ethyl ketone according to equations 35 and 36 (444,445):

$$\underset{\text{Toluene}}{[\eta] = 2\times10^{-4}(M_n)^{0.66}} \quad \underset{\text{Methylethylketone}}{[\eta] = 8\times10^{-4}(M_n)^{0.5}} \tag{35}$$

$$\log(\eta + b) = a \log T + c$$
$$\text{VTC} = \eta_{38c} - \eta_{99c} \tag{36}$$

Compared to petroleum-based fluids, silicone oils show relatively small changes in viscosity as a function of temperature (1,430). A common measure of the viscosity change with temperature is the viscosity–temperature coefficient (VTC). Typical dimethylsilicone VTC is 0.6 or less. Phenylsilicones are slightly higher. Organic oils are typically 0.8 or greater. The viscosity–temperature curves are depicted in Figure 3, where a, b, and c are constants.

Figure 4 shows viscosity–temperature curves for a series of silicone oils from 20 to 10,000 cSt, an SAE 10 petroleum oil, and a diester-based oil (368). Silicones with phenyl, trifluoropropyl, or larger alkyl groups show larger viscosity changes with increasing temperature than dimethylsilicone oils. Low molecular weight silicone oils ($< 1000\ mm^2$) exhibit Newtonian flow behavior and undergo only small changes in viscosity under shearing conditions (446). Higher viscosity PDMS fluids shear thin at higher shear rates. The fluids are stable to shear stress, however, and recover to their original viscosity after being passed through small capillaries under pressure. Figure 4 shows the effect of shear rate on viscosity for a series of PDMS fluids of different molecular weights.

Many of the unique properties of silicone oils are associated with the surface effects of dimethylsiloxanes. Silicones impart water repellency to fabrics, act as antifoaming agents (447), as release liners for adhesive labels, and as polishes and waxes (448). Dimethylsilicone oils can spread onto many solid and liquid surfaces to form films of molecular dimensions (449,450). This phenomenon is greatly affected by even small changes in the chemical structure of siloxane in the siloxane polymer. Increasing the size of the alkyl substituent from methyl to ethyl dramatically reduces the film-forming ability of the polymer (449). Phenyl-substituted silicones are spread onto water or solid surfaces more slowly than PDMS (451).

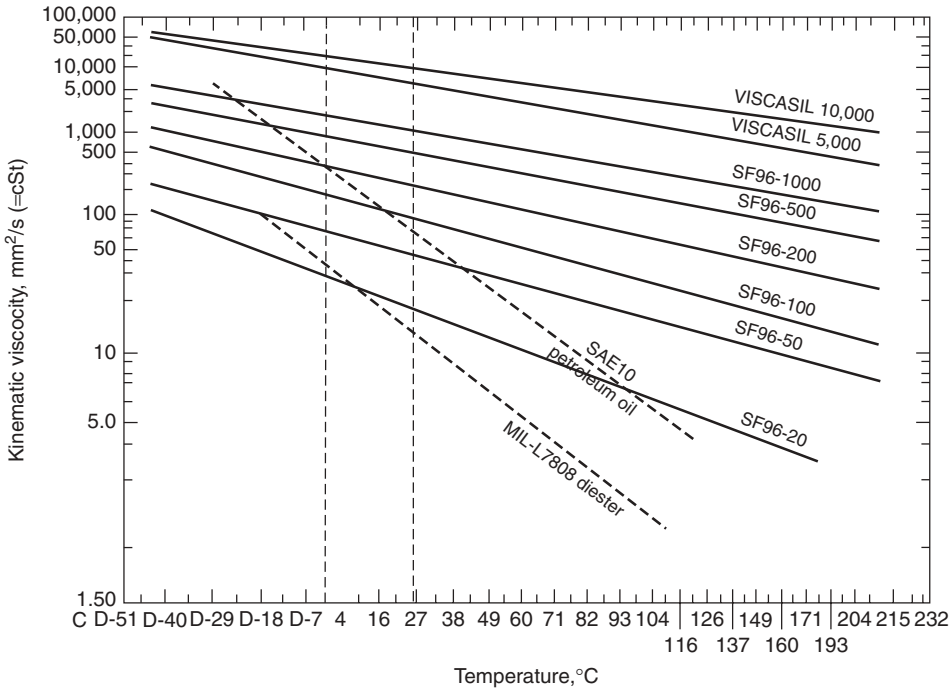

Fig. 3. Kinematic viscosity–temperature relationship of dimethylsilicone fluids.

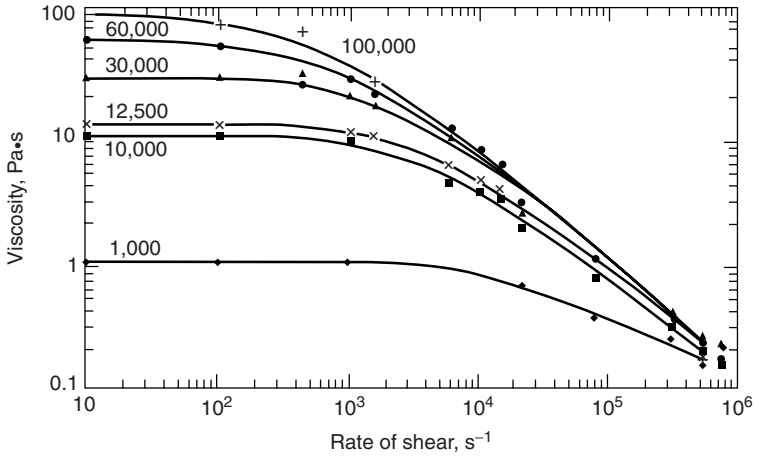

Fig. 4. Shear rate vs viscosity for PDMS. Numbers on curves indicate molecular weights. To convert Pa·s to P, multiply by 10.

Dimethylsilicone polymers are often described as having a combination of silicate and paraffin structures. The orientation of the polymer chains onto surfaces, physically, by chemical affinity, or bonding, can contribute to the observed surface properties. The surface tension of hexamethyldisiloxane, MM, is 15.7 mN/m

(dyn/cm). Increasing incorporation of D-units (MD_xM) increases the value to about 20 dyn/cm for higher viscosity fluids. Silicone fluids are characterized by their hydrophobicity (resistance to water), and the contact angle between PDMS and water is between 100° and 110°. Carefully deposited dimethysilicone on soda lime glass has a contact angle of about 60° at room temperature; the angle increases with increasing temperature to about 100° at 390°C and then decreases at the decomposition temperature (1).

Gases are very soluble in dimethylsilicone polymers, and PDMS is permeable to water vapor. The solubility of air, nitrogen, and carbon dioxide at 101.3 kPa (1 atm) is 0.17, 0.19, and 1.00 cm^3/cm^3, respectively (452). About 250–300 ppb of water can dissolve in dimethylsiloxane at 25°C and 95% relative humidity (453). The water solubility of silanol-terminated oligomers increases with decreasing molecular weight; the lowest silicone monomer, dimethylsilanediol, is water-miscible. Silicone oils are soluble in nonpolar organic solvents such as benzene, toluene, dimethyl ether, chloroform, methyl ethyl ketone, methylene chloride, or kerosene. Incorporation of phenyl and especially trifluoropropyl or β-cyanoethyl groups onto the polymer decreases the solubility of siloxane in nonpolar organic solvents (446). These derivatives are slightly soluble in acetone, ethanol, and butanol, and relatively immiscible in methanol, ethylene glycol, and water. Exposure to strong acids or bases leads to reequilibration of the polymer.

Silicone fluids have good dielectric properties, loss factor, specific resistance, and dielectric strength at normal operating conditions, and the properties vary only slightly with temperature (1,430,454). These properties in combination with relatively low flammability have led to the use of silicones in transformers and other large electrical appliances (455). The dielectric constant of a 1000-cSt oil is 2.8 at 30°C and 2.6 at 100°C. The loss factor is low, 1.2×10^{-4} at 20°C, and varies irregularly with frequency. Specific resistance is $4 \times 10^{15}\ \Omega \cdot$ cm at 20°C and decreases with increasing temperature or with exposure to moisture. The dielectric strength is 120 kV/cm (20°C, 50 cP, 6 kV/s).

Silicone oils are good hydrodynamic lubricants but have generally poor frictional lubricating properties (456–458). The latter can be improved by incorporating chlorophenyl groups into the polymer side chains (459). For steel on steel, the coefficient of friction is about 0.3–0.5. The load-bearing capacity of PDMS (Almen–Wieland machine) is only 50–150 kg, compared with ∼1000 kg for polychlorophenylmethylsiloxane and up to 2000 kg for mineral oil.

The thermal conductivity of dimethylsilicone with viscosities >100 cSt is 15.5 J/(s · cm · °C) (3.7×10^{-4} $cal^{-1} \cdot cm^{-1} \cdot °C^{-1}$), and is roughly constant with increasing viscosity (460). The specific heat is 1.55–1.70 J/(g · °C) (0.37–0.41 cal/(g · °C) over the 20–200°C range and is practically independent of viscosity. Thermal expansion of PDMS is ∼0.1/°C (460).

Liquid silicone oils are highly compressible and remain liquid over pressure ranges where normal paraffin oils have already solidified (461). This property, combined with a wide temperature use range, is the reason for silicone use in a large number of hydraulic applications. The adiabatic compressibility of 1000-cSt dimethylsilicone oils is ∼1000 Pa^{-1} (100 cm^2/dyn). This value decreases slightly with increasing viscosity, similar to paraffin oils. PDMS oils can withstand pressures greater than 3.4 GPa (35,000 kg/cm^2) even though they are compressed by >30%.

Dimethylsilicone fluids are transparent to visible light and microwave but absorb UV radiation at wavelengths below 280 nm (462). Siloxanes absorb strongly in the infrared between 1000 and 1100 cm^{-1} (Si—O stretching), 1300 and 1350 cm^{-1} (Si—C stretching), and 2950 and 3000 cm^{-1} (C—H stretching) (463). The speed of sound in PDMS is 987.3 m/s for a 1000-cSt fluid at 30°C and decreases with increasing temperature (464). Methylsilicone fluids are cross-linked when exposed to gamma ray or electron beam irradiation (465). Polymers containing aromatic substituents are more resistant than dimethylsilicone polymers.

Silicone Heat-Cured Rubber. Silicone elastomers are made by vulcanizing high molecular weight ($>5 \times 10^5$ gm/mol) linear PDMS polymer, often called gum. Fillers are used in these formulations to increase strength through reinforcement. Extending fillers and various additives, eg, antioxidants, adhesion promoters, and pigments, can be used to obtain certain properties (1,466).

Peroxides are typical vulcanizing agents and the mechanism of cure involves free-radical abstraction of a proton from a silicon methyl group, followed by dimerization of the methyl radicals to form ethylene cross-links (eq. 19) (219,467,468). Higher cure speed can be obtained with a mixture of peroxides (469). Vinyl-containing polymers are often used to control the cross-linking reaction and to accelerate the cure rate. Commonly used peroxides include di-*tert*-butyl peroxide [110-05-4], benzoyl peroxide [94-36-0], di(*p*-cumyl) peroxide, and di(*p*-chlorophenyl) peroxide. The choice of peroxide is based on the desired cure temperature and rate. Table 5 lists some common peroxide curing agents, typical cure temperatures, and some recommended processing conditions.

Recent work on peroxide curing agents (470) suggests that bis-peroxides such as that shown below are especially efficient agents for curing silicone rubber.

Table 5. Cure Agents for Silicone Rubber[a]

Curing agent	Commercial name	Activation temperature, °C	Application
Active paste[b] composition			
Di(2,4-dichlorobenzoyl) peroxide	Cadox TS-50 or Luperco CST	104–132	Hot-air vulcanizing
Benzoyl peroxide	Cadox BS or Luperco AST	116–138	Molding, steam curing
Active powder composition			
Dicumyl peroxide[c]	DI-CUP 40C	154–177	Molding thick sections, bonding, steam curing
2,5-Di(*t*-butylperoxy)-2,5-dimethylhexane[d]	Varox, Luperco 101XL, or Luperco 101[e]	166–182	Molding thick sections, bonding, steam curing

[a] Ref. 460.
[b] 50% active paste composition.
[c] 40% active powder composition.
[d] 50% active powder composition.
[e] 100% active liquid.

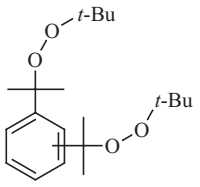

Unlike natural rubber, silicone rubber does not stress-crystallize when elongated, which leads to relatively poor physical properties. Unfilled silicone rubber has only a 0.35-MPa (50-psi) tensile stress at break; thus, silicone rubber must be compounded with 10–25 wt% reinforcing fillers, typically fumed silica, to improve the final rubber product properties (471–474). Other common fillers include precipitated silica, titanium dioxide, calcium carbonate, magnesium oxide, and ferric oxide. Pigments and colorants are also used. The addition of fillers to the gum stock can result in structuring during storage, which decreases the workability of the material. To prevent structuring, the filler is often treated with agents such as hexamethyldisilazane to reduce surface hydroxyl functionality, or with processing aids such as silanol functional silicone oils, diphenylsilanediol, or dimethylpinacoyloxysilane, (361,475).

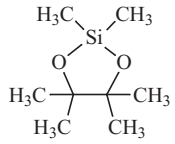

The processing methods for silicone rubber are similar to those used for natural rubber (1,476–478). Polymer gum stock and fillers are compounded in a dough or Banbury-type mixer. Catalysts are added and additional compounding is completed on water-cooled roll mills. For small batches, the entire process can be carried out on a two-roll mill.

Heat-cured silicone rubber is commercially available in several forms: as gum stock, reinforced gum, or partially filled gum. These compounds can be uncatalyzed, catalyzed, or can contain catalyst dispersions. Catalyzed compounds are ready for use without additional processing. Silicone rubber is often freshened, ie, the compound is freshly worked on a rubber mill until it is a smooth continuous sheet. The freshening process eliminates the structuring problems associated with polymer–filler interactions. Rubber can be extruded on wire and cured in place (479).

It is common practice in the silicone rubber industry to prepare specific or custom mixtures of polymer, fillers, and cure catalysts for particular applications. The number of potential combinations is enormous. Improved properties of the rubber can be achieved if a premix of some of the inputs is performed. A premixing process for fumed silica, for example, involves the breaking down of gum particles into a fine dispersion in a bed of fumed silica. As the process continues, fumed silica coats the gum surface preventing reagglomeration of these particles (480).

In general, the mixture is selected to achieve some special operating or processing requirement, and the formulations are classified accordingly. Table 6 lists some of the commercially important types of silicone rubbers.

Table 6. Properties of Different Classes of Silicone Rubbers[a]

Class	Hardness, durometer	Tensile strength, MPa[b]	Elongation, %	Compression set,[c] %	Useful temperature range, °C		Tear strength, J/cm^2[d]
					Min.	Max.	
General purpose	40–80	4.8–7.0	100–400	15–50	−60	260	0.9
Low compression set	50–80	4.8–7.0	80–400	10–15	−60	260	0.9
Extreme low temperature	25–80	5.5–10.3	150–600	20–50	−100	260	3.1
Extreme high temperature	40–80	4.8–7.6	200–500	10–40	−60	315	
Wire and cable	50–80	4.1–10.3	100–500	20–50	−100	260	
Solvent-resistant	50–60	5.8–7.0	170–225	20–30	−68	232	1.3
High strength flame retardant	40–50	9.6–11.0	500–700				2.8–3.8

[a] Refs. 481–483.
[b] To convert MPa to psi, multiply by 145.
[c] At 150°C, 22 h.
[d] To convert J/cm^2 to lbf/in., multiply by 57.1.

Silicone rubber is most commonly fabricated by compression-molding of catalyzed formulated gum compounds at 100–180°C under 5.5–10.3 MPa (800–1500 psi) pressure. Mold release compounds are usually employed. Under these conditions the rubber is cured in a few minutes. Extrusion processing is used in the manufacture of tubes, rods, wire and cable insulation, and continuous profiles. Initial properties, so-called green strength, are obtained by curing in hot air or steam tunnels from 276 to 690 kPa (40–100 psi) at 300–450°C for several minutes. Final physical properties are achieved by postcuring in air or steam, typically for 30–90 min. When silicone rubber must be bonded to other surfaces, eg, metals, plastics, or ceramics, primers are used. Silicate or titanate esters from the hydrolysis of tetraethoxysilane or tetraethoxyltitanium are often used as primers. Silicone-rubber coated textiles and glass cloth are made by initially dissolving gum stock in solvent and applying the rubber by dip coating. The fabric is then dried and the rubber cured in heated towers. Tubes and hose can be formed on mandrels from this fabric into complex shapes. Foamed or sponge silicone rubber can be made by incorporating chemical blowing agents into the rubber stock, which typically eliminate nitrogen or carbon dioxide under the thermal curing conditions. Sponge silicone rubber made in this way has a closed cell structure and densities of 0.4–1.0 g/cm^3.

Vulcanized silicone rubber is characterized by its wide temperature use range (−50 to >200°C), excellent electrical properties, and resistance to air oxidation and weathering conditions (484). Improvements in properties such as heat aging can be achieved by *in situ* treatment of the filler during rubber manufacture (480). Silicone rubber is also extremely permeable to gases and water vapor. The mechanical properties of silicone rubber are generally inferior to most organic (butyl)

Table 7. Properties of Silicone Gums[a]

Type	CAS registry number	Density, d^{25}, g/cm^3	T_g, °C	ASTM D926 Williams Plasticity
$(CH_3)_2SiO$	[9016-00-6]	0.98	−123	95–125
$CH_3(C_3H_5)SiO$	[9005-12-3]	0.98	−113	135–180
$CH_3(CF_3CH_2CH_2)SiO$	[25791-89-3]	1.25	−65	

[a] Refs. 482,485.

Table 8. Permeability of Silicone Elastomers[a]

Type	CAS registry number	Temperature, °C	Gas	Permeability, nmol/(m · s · kPa)[b]
Dimethylsilicone	[63148-62-9]	25	CO_2	180
MDnM		25	O_2	35
		25	Air	19.6
		30	Butane	0.89
		70	Butane	0.76
Fluorosilicones	[63148-56-1]	26	CO_2	35
$MD_nD_n^{(CH_2CH_2CF_3)}M$		26	O_2	5.8
Nitrilesilicone	[70775-91-6]	31	CO_2	105
$MD_nD_n^{(CH_2CH_2CN)}M$		31	O_2	17.8

[a] Refs. 486–488.
[b] To convert nmol/(m·s·kPa) to (cm^3·cm)/(s·cm^2·mm Hg), multiply by 3×10^{-8}.

rubbers at room temperature. Tables 7–9 list some typical physical properties for vulcanized silicone rubber. Silicone rubber can be made with varying degrees of hardness. Shore A values from 20 to 90 are typical; the best physical properties are generally obtained with values from 50 to 70. The properties of silicone vary with temperature (483). The Young's modulus drops from 10^5 to 2×10^2 MPa (14.5×10^4 to 2.9×10^4 psi) over a temperature range from −50°C to room temperature and is then fairly constant till 260°C. Tensile strength at break decreases from 6.9 MPa (1000 psi) at 0°C to 2.1 MPa (300 psi) at 300°C. Typical elongation at break values range from 300 to 700%, depending on the composition.

The compression set of silicone rubber is similar to organic types of rubber at low (0–50°C) temperatures, ranging from 5 to 15% (489). Above 50°C, silicone

Table 9. Electrical Properties of Typical Silicone Rubber[a]

Property	Value
Volume resistivity,[b] Ω · cm	$1 \times 10^{14} - 1 \times 10^{16}$
Electric strength, V/25.4 μm (=V/mil)	400 – 700
Dielectric constant, 60 Hz	2.95 – 4.00
Power factor, 60 Hz	0.001 – 0.01
Surface resistance, Ω	$3.0 \times 10^{13} - 4.5 \times 10^{14}$
Dielectric loss factor, tan δ	$5 \times 10^{-4} - 4 \times 10^{-3}$

[a] Ref. 57.
[b] Ref. 81.

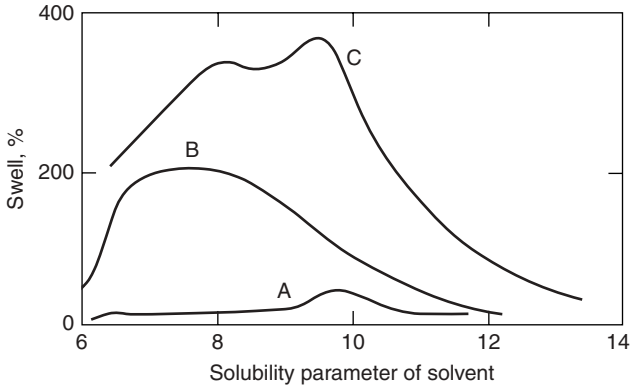

Fig. 5. Swelling of silicone rubber by solvents (493). A, fluorosilicones (methyl trifluoropropyl silicones); B, dimethylsilicone; C, methyl(phenyl)silicone.

rubber is superior, but compression set increases with time and temperature. Improvements in the compression set of silicone rubber are achieved with *in situ* treatment of the filler (490). Silicone rubber is more tear-sensitive than butyl rubber, and the degree of sensitivity is a function of filler size and dispersion, cross-link density, and curing conditions. The electrical properties of silicone rubber (491,492) are generally superior to organic rubbers and are retained over a temperature range from −50 to 250°C (76). Typical electrical values for a heat-cured silicone rubber are shown in Table (9).

Silicone rubber film is 10–20 times more permeable to gases and water vapor than organic rubber (489). The water permeability of silicone rubber is $\sim 14 \times 10^6$ mol/m^2: s · Pa, which means that silicone rubber can absorb about 35 mg of water per square centimeter of surface area after a 7-day exposure (486). Table (7) shows the permeability of silicone to common gases. Organic solvents can diffuse into and swell silicone rubber, significantly decreasing the physical properties of the material. The degree of swelling depends on the solubility parameters of the solvent and the rubber, as illustrated in Figure 5.

Solvent-resistant rubber based on either trifluoropropylmethylsiloxane or β-cyanoethylmethylsiloxane has been developed for special applications, eg as fuel tank sealants, where the material will be exposed to aggressive solvents. Those based on trifluoropropylmethylsiloxane are more important commercially. Pure water has little effect on silicone; however, long exposures in the presence of acid or base catalysts causes degradation and reversion of the rubber to a sticky gum (483,494). Prolonged exposure to temperatures above 300°C in air causes the rubber to stiffen and ultimately to become brittle (483). As with silicone oil, the principal chemical pathways of degradation are retrocyclization and oxidation of the polymer alkyl groups. Heating in air at 125°C causes a decrease in elongation and an increase in hardness, but no important changes in tensile properties are observed.

Silicone rubber burns with a high char yield, and the residual material is nonconducting silicon dioxide. The limiting oxygen index for a typical rubber formulation is about 20. Flame-retardant versions are available with oxygen index

values as high as 40–50 (481). In general, silicone rubber is not resistant to gamma or electron beam radiation and undergoes cross-linking, which leads to embrittlement (495). Increasing levels of phenyl-containing silicone in the rubber improves the radiation resistance (496).

Silicone Liquid-Injection-Molding Rubber. An increasingly important processing technique for silicone rubber is liquid injection molding. These materials are also referred to as liquid silicone rubber (LSR). Unlike heat-cured rubber, which is typically compression-molded from high viscosity gum compounds, liquid-injection-molded (LIM) rubber is made from low viscosity starting materials, 1000–20,000 mPa · s (=cP), and is cured in molds similar to those used for plastic injection molding. The principal advantages of LIM include rapid cycle times and the ability to fill complex mold shapes because of the low viscosity of the inputs. Rubber parts can be cured in 10–40 s using low molding pressures, approx. 2–20 MPa (300–3000 psi), and low curing temperatures, typically 150–260°C (497). LIM processing is increasingly being used for applications such as electrical connectors, O-ring seals, computer keypads, baby bottle nipples, valves, electrical components, health care products, and sporting equipment such as goggles and scuba masks.

Silicone LIM rubber is made from a two-component polymer system. One part (Part B) contains a linear polydimethylsiloxane polymer with pendent Si—H functionality, reinforcing fillers such as fumed silica, extending fillers, pigments, and stabilizers. The second part (Part A) contains linear PDMS with terminal and pendent vinyl groups; reinforcing and extending fillers; a platinum hydrosilylation catalyst; and a catalyst inhibitor, commonly olefins, alkynes, amines, or phosphines. Incorporation of trifluoropropylsilyl groups is possible if solvent resistance is desired (498).

After the components are mixed and heated, the catalyst initiates the cross-linking reaction by addition of the Si—H group to the double bond (eq. 37). Latent cure catalysts have been developed that allow the formulation of one-component products (499). These systems work by incorporation of platinum ligands that deactivate the platinum hydrosilylation catalysts at room temperature. When heated to temperatures above 100°C, these catalysts become active (see also Silicone Network Formation).

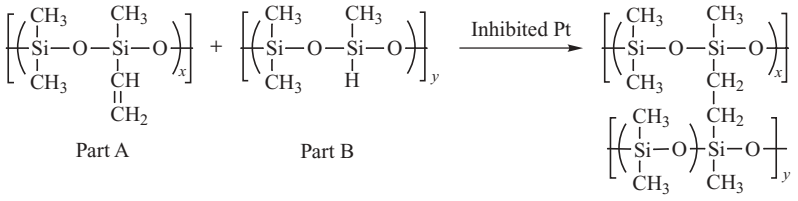

(37)

Cured silicone LIM rubber can be fabricated with physical properties equivalent to heat-cured rubber (500). Shore A hardness can range from 30 to 70, depending on formulations. Typical physical properties include tensile strengths as high as 9.7 MPa (1400 psi), elongations at break of 500–775%, and tear strengths

>30 N/mm (180 lb/in.). Compression sets of less than 10% can be achieved if the material is baked after processing.

New applications for LIM are being developed because of advances in uncured rheological properties, property improvements achieved from fillers, and advances in molding and processing (501). The rheological properties of the uncured LIM can vary from manufacturer to manufacturer (497). Fillers can enhance or degrade the thermal stability of the cured LIM (502). The final properties of LIM materials can be tailored. These properties include adhesion, hardness, green strength, elongation, and tensile strength. In addition, the precured viscosity, rheological properties, and cure speed can be modified (503). Finally, improvements in mold design (504) processing conditions (505), and advances in mold filling simulations have greatly improved the utilization of LIM materials.

Foam Rubber. Flexible foamed silicone rubber can be fabricated with flame retardancy greatly superior to that of the urethane-type foam. A self-blowing, low to medium density (80–240 kg/cm^3, 5–15 lb/ft^3) silicone foamed rubber can be prepared using polymers similar to those used in LIM products (506–509). Two components are mixed at room temperature: one part contains PDMS with pendent SiH functionality and fillers, and the other consists of terminal and pendant vinyl-containing PDMS, reinforcing and extending fillers, a platinum hydrosilylation catalyst and inhibitor, water, alcohol, and an emulsifying agent. Typical time for foam formation is less than 20 min.

Two chemical reactions occur simultaneously when the components are mixed. One is the platinum-catalyzed reaction of hydroxyl groups from water or alcohol with polymer SiH to give hydrogen gas (eq. 38). This reaction is the source of the blowing agent that forms the foam. The second reaction is the cross-linking of SiH and Si–vinyl, which increases the polymer viscosity ultimately leading to gelation and curing to give an elastomer. Proper control of the kinetics of these two reactions is critical to achieving foam having good physical properties. Emulsion-derived foam is possible as well (510).

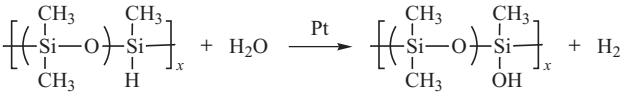

(38)

Silicone foam thus formed has an open cell structure and is a relatively poor insulating material. Cell size can be controlled by the selection of fillers, which serve as bubble nucleating sites (511). The addition of quartz and other fillers (512) greatly improves the flame retardancy of the foam; char yields of >65% can be achieved. Cone calorimetry, UL 94, and other measurements have shown the excellent flammability properties of silicone foam (513). Because of its excellent flammability characteristics, silicone foam is used in building and construction fire-stop systems and as pipe insulation in power plants, in transportation systems as carpet underlay, and in seating. Typical physical properties of silicone foam are listed in Table (10).

Silicone Resins. Silicone resins are an unusual class of organosiloxane polymers. Unlike linear polysiloxanes, the typical silicone resin has a highly

Table 10. Physical and Flammability Properties of Silicone Foam Rubber[a]

Property	Value
Density, kg/m^3	80–240
Tensile strength, MPa[b]	0.52
Elongation, %	90
Thermal conductivity, W/(m · K)	0.06
Operating temperature range, °C	−60 to 205
Limiting oxygen index	30
UL-94 flammability (3.2 mm thick)	V-0
Flame spread index (ASTM E162)	16
Smoke density flaming (ASTM E662)	18
Smoke density smoldering (ASTM E662)	9
Verticle burn (FAA 25.853)	Compliant

[a]Ref. 514.
[b]To convert MPa to psi, multiply by 145.

branched molecular structure. The most unique, and perhaps most useful, characteristics of these materials are their solubility in organic solvents and apparent miscibility in other polymers, including silicones. The incongruity between solubility and three-dimensional structure is caused by low molecular weight (M_n < 10,000 g/mol) and broad polydispersivity of most silicone resins.

A wide variety of organosilicone resins containing a combination of M, D, T, and/or Q groups have been prepared and many are commercially manufactured. In addition, resins containing hydrosilation-reactive SiH and SiVi groups or other functionalities, including OH and phenyl groups, are known. Three classes of silicone resins are most widely used in the silicone industry: MQ, TD, and T resins.

MQ Resins. These resins are composed of clusters of quadrafunctional silicate Q groups end-capped with monofunctional trimethylsiloxy M groups. The structure of an MQ resin molecule is defined by three characterization parameters: M/Q ratio, molecular weight, and %OH. Standard analytical techniques have been used to quantify these parameters, including ^{29}Si NMR to determine M/Q ratio, GPC for molecular weight, and FIIR for %OH (515). Most commercially useful MQ resins have an M/Q ratio between 0.6 and 1. Ratios lower than 0.6 result in insoluble solids, whereas those greater than 1 produce liquids (516). Molecular weight is related to M/Q ratio; higher molecular weights are associated with lower M/Q ratios. Typical molecular weights are M_n = 10,000 g /mol for a resin with an M/Q of 0.6, and M_n = 2000 g/mol for an M/Q of 1.0 (416,515). The silanol content (% OH by weight) of these resins, typically ranging between 0 and 3%, is process-dependent. An IR study indicates that OH groups are intramolecularly associated through hydrogen bonding (516). A computer-generated molecular structure of a common commercially prepared MQ resin has been reported (517). This structure, shown in Figure 6, consists of a chain of silicate clusters end-capped with trimethylsiloxy groups.

MQ resins are commercially manufactured by one of two processes: the ethyl silicate or the sodium silicate process. In the ethyl silicate process, the resins are prepared by cohydrolysis of tetraethoxysilane and trimethylchlorosilane in the

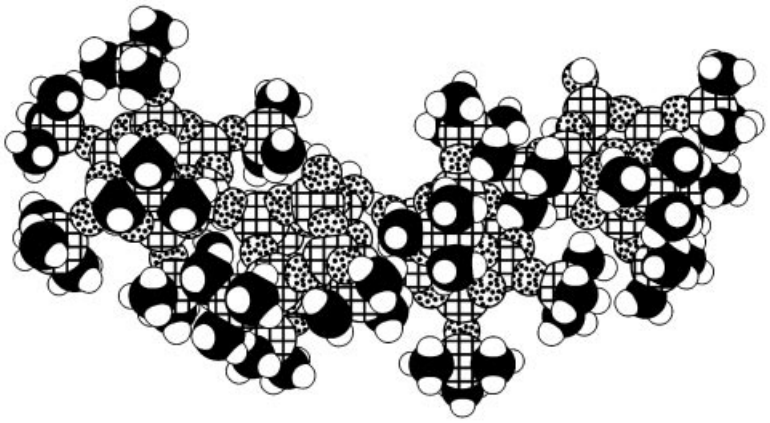

Fig. 6. Molecular structure of a typical MQ resin, $[M_{0.62}Q^{OH}{}_{0.17}Q_{0.83}]_{32}$: ○, H; ●, C; ⊕, Si; and ⊙, O.

presence of an aromatic solvent (eq. 39). This process is versatile and reproducible; it can be used to prepare soluble MQ resins with M/Q ratios ranging from 0.6 to 4 (518,519). The products of these reactions typically contain high levels of residual alkoxysilane groups.

$$Si(OCH_2CH_3)_4 + (CH_3)_3SiCl \xrightarrow{H_2O,\ solvent} [M_xQ]_y\ resin \qquad (39)$$

A more economical route to MQ resin uses inexpensive sodium silicate and trimethylchlorosilane (eq. 40) (520). The sodium silicate process is initiated by acidifying an aqueous sodium silicate solution to pH 2. The resulting hydrosol quickly builds molecular weight. The rate of this increase is moderated by the addition of an alcohol such as 2-propanol. The hydrosol is subsequently silylated by the addition of trimethylchlorosilane. This process, which is kinetically sensitive and limited to synthesizing M/Q ratios of 1 or less, is preferred when high OH (> 1%) MQ resins are required (521).

$$\left[(SiO_2)(Na_2O)_{0.3}\right]_{5.5}(aq) + HCl \xrightarrow{2\text{-Propanol}} \underset{hydrosol}{Stabilized\ silicate} \xrightarrow[2.\ Strip/filter]{1.\ (CH_3)_3SiCl} M_{0.7}Q\ resin \qquad (40)$$

Both the ethyl and sodium silicate processes can be modified by substituting SiH- or SiVi-functional chlorosilanes or combinations of chlorosilanes to produce hydrosilation-reactive MQ resins (521,522).

The most prominent use of MQ resins is as the tackifying agent for silicone pressure-sensitive adhesives (PSA) (523–525). The other main component of silicone PSA is a silicone gum. This mixture of MQ resin and silicone gum is applied to a tape backing such as polytetrafluoroethylene (PTFE) or poly(ethylene

terephthalate) (PET) and cured in the presence of a peroxide catalyst to provide an adhesive tape. MQ resins are also commonly used as control-release additives for silicone paper release products, as reinforcing agents for liquid-injection-moldable silicones, in masonry sealants, and in leather/textile water-repellent coatings (523,526–530). An additional use of MQ resins is as a surfactant. MQ resins are commercially attractive for use in defoaming applications as well as for stabilizing frothed urethane for high density carpet backing. Virtually every use for MQ resins is as a blend with a PDMS. These blends have been characterized as interpenetrating networks (517,531,532). MQ resin/PDMS blends are microphase-separated. One phase is PDMS-rich and has a glass-transition temperature of -107°C. This T_g does not change with changes in the blend ratio. The other phase is an MQ resin/PDMS-miscible phase, the T_g of which varies linearly from -100 to 200°C as the composition of the blend is changed from 30 to 90% MQ resin (517). These unique viscoelastic properties contribute to the versatility of silicone products containing MQ resin.

TD Resins. The other important class of silicone resins is TD resins. These materials are simply prepared by cohydrolyzing mixtures of chlorosilanes in organic solvents (eq. 41, where R is typically CH_3 or C_6H_5 (533). TD resins with T > 60 mol% T are substantially less soluble in PDMS than are MQ resins.

$$x\,\mathrm{RSiCl_3} + y\,\mathrm{R'_2SiCl_2} \xrightarrow[\text{Solvent}]{\mathrm{H_2O}} \mathrm{T}_x\mathrm{D}_y\,\text{resin} \tag{41}$$

A variety of liquid and solid resins can be prepared by varying the T/D ratio. Commercial TD resins are available containing from 5 to 95% T groups. Mixtures of methyl and phenylchlorosilanes are also frequently used. Some TD resins are modified by the addition of catalysts to reduce the silanol content, thereby increasing the molecular weight. Contrary to MQ resins, which are very stable, TD resins are unstable toward silanol condensation reactions.

TD resins are used as protective coatings, electrical coatings, saturants, laminates, and water repellents (1). TD resins are also useful in high performance paints. Compositions high in silanol content are utilized in reactive formulations. Low silanol TD resins are used as a nonreactive additive to alkyd paint formulations. Attractive features of TD resin-based protective coatings include superior, UV-resistant weatherability and excellent high and low temperature properties. Silicone electrical coatings are preferred when good dielectric insulation is required over a broad temperature range. TD resins are also used to saturate glass or Kevlar fabrics. After curing, these flexible composites are used in a variety of applications. TD resin-based water repellents are used chiefly with siliceous substrates. Some typical TD silicone resin properties are as follows: dielectric strength = 68,000 V/mm; dielectric constant = 2.9 at 60 Hz and 25°C; dissipation factor = 0.006 at 60 Hz and 25°C; surface resistivity = 1×10^{14} Ω/in.^{2}; and volume resistivity = 1×10^{14} Ω · cm.

T Resins. T resins have been historically called silsesquioxanes. Crystalline polyhedral silsesquioxanes can be synthesized by hydrolytic condensation of $RSiCl_3$ (eq. 42), where R = *c*-C_6H_{11} (534–538).

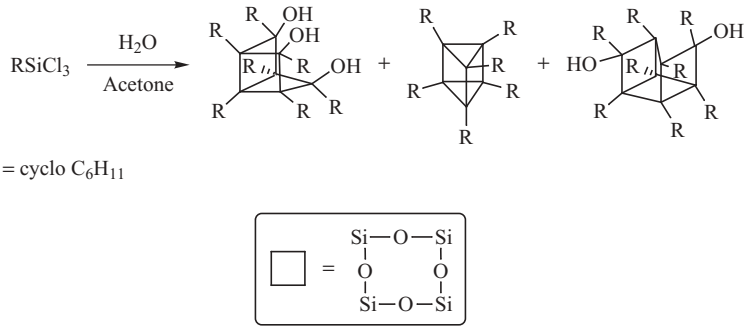

(42)

These cage structures can be derivatized with heteroatoms (539) to form catalysts or organic ligands that can act as precursors to hybrid organic/inorganic materials (540) or ligands (536).

A unique, amorphous T resin particle has been reported (541). This material, known by the trade name Tospearl (Tospearl is a trademark of the General Electric Co.), is a spherical resin particle made by the controlled, base-catalyzed hydrolysis and condensation of $CH_3Si(OCH_3)_3$ (eq. 43).

$$CH_3Si(OCH_3)_3 + H_2O \xrightarrow{NH_3} [CH_3Si(O_{3/2})]_r \quad (43)$$

Highly cross-linked spheres with an average particle size from 0.5 to 12.0 μm have been produced. Extremely narrow particle size distributions are possible. The particle size and degree of monodispersivity are controlled by kinetic factors during the hydrolysis. Applications for Tospearl powders include wear resistance, antiblocking properties, light-diffusion control, and lubrication (542).

T resins are also an important component of silicone powder coatings. T resins useful in powder coatings are obtained by the hydrolysis of $MeSiCl_3$ or the cohydrolysis of CH_3SiCl_3 and $C_6H_5SiCl_3$. These silicone formulations provide high temperature (service temperatures >800°F) and impact resistance (543,544) in solvent-free coatings.

Another key application for silsesquioxanes is in electronic insulating films having ultralow dielectric constants (< 2.7) (545–548). A solution of T resins in organic solvents is synthesized by cohydrolysis of $MeSiCl_3$ and $HSiCl_3$ in the presence of a nonpolar solvent, a polar solvent (alcohol), and a phase transfer catalyst (547). The resulting polymer has a caged structure with essentially no hydroxyl or alkoxy substituents. A film with a low dielectric constant is prepared by spin coating the organic solution of resin onto an integrated circuit device, followed by thermal curing at about 450°C. Films, having thicknesses of about 1.0 μm and low levels of internal stress, insulate the individual circuit elements of the integrated circuit.

Organosilicone Coating Products. Silicone products are used in a large variety of coating applications; most prominent among these are silicone pressure-sensitive adhesives (PSA), plastic hardcoats, and paper release coatings (523–525).

Pressure-Sensitive Adhesives. Silicone PSAs are used primarily in specialty tape applications that require the superior properties of silicones, including resistance to harsh chemical environments and temperature extremes (523–525). Silicone PSAs are also used in applications requiring long service life, electrical insulation, and protection from moisture. Another distinct advantage of silicone PSAs is their ability to wet low surface energy tape substrates such as PTFE.

Silicone PSAs are blends or interpenetrating networks (IPNs) composed of a tackifying MQ resin cured in a cross-linked polysiloxane network. The synthesis and structure of MQ resins have been described above. The polysiloxane network is traditionally derived by free-radical cross-linking of a high molecular weight PDMS polymer or gum using a peroxide catalyst, such as benzoyl peroxide or 2,4-dichlorobenzoyl peroxide. The curing reaction is performed immediately after the PSA has been coated onto a tape substrate, such as PET, PTFE, or Kapton. Uncured PSAs are supplied as a solution in an organic solvent. Some silicone PSAs also incorporate phenyl groups in the gum portion of the adhesive to increase the application temperature.

Another important aspect of the chemistry of silicone PSAs is the molecular interaction between the tackifying MQ resin and the PDMS network. For optimal adhesive properties it is important that some covalent bonding exists between the resin and the PDMS. This bonding is usually achieved by promoting a silanol condensation reaction between residual OH groups on the resin and on the end caps of the PDMS. The condensation reaction can occur either during blending of the PSA components or during processing of the tape. Studies of the viscoelastic properties of cured silicone PSAs indicate that these materials are microphase-separated (517,531,532). The adhesive properties of PSAs are a function of the unique rheological properties of the MQ resin/PDMS blends.

The key adhesive properties of a silicone PSA are tack, peel adhesion, and cohesive strength (lap shear). The required balance of these properties is controlled by several factors. A PSA composition rich in MQ resin usually favors low tack and high peel adhesion and cohesive strength values. A high cross-link density or a larger number of covalent bonds between the MQ resin and the PDMS network favors high cohesive strength at the expense of tack and peel adhesion. Low peel adhesion is observed when uncured cyclic or linear silicones are present. Other PSA properties important to the tape manufacturer, ie, viscosity, solvent content, cure time, and temperature, are typically controlled by varying the type and amount of organic solvent and peroxide cure catalyst. Primers are also frequently used to promote adhesion of the PSA to the tape backing.

One advance in silicone PSA chemistry is the use of Pt-catalyzed hydrosilylation reactions as the method of cure (549,550). Advantages of hydrosilylation-cured silicone PSAs include lowering the level of solvent, lowering cure temperatures, increasing line speeds, and the ability to be used with a broader range of tape backings. In this technology, lower molecular weight polymers containing hydrosilylation-reactive SiH and SiVi groups are substituted for the traditional OH-end-capped PDMS gum. A Pt catalyst and inhibitor are used instead of a peroxide (549,550).

There are several important, specialized applications for silicone PSA tapes. Platers tape mask selected areas of parts during etching or plating operations. Masking tapes are also used as protective coatings against high temperatures,

radiation, harsh chemical environments, or moisture. These tapes are used frequently in the manufacture of printed circuit boards (551). Splicing tapes are used to join plastic films. Silicone PSAs are often used to splice low surface energy materials or to provide high cohesive strengths at extreme temperatures. Plasma or flame spray tapes are used to protect selected metal surfaces during sandblasting or flame spraying operations. Silicone PSAs are particularly useful as the adhesive for electrical insulating tapes. A common application is as a wire wrap in motor coils. Silicone PSAs are also used in medical applications, notably as an adhesive for bandages and transdermal drug delivery systems (552).

Paper Release Coatings. Paper release coatings are a fast-growing segment of silicone technology. These materials are used in label systems in which the silicone coating is part of the disposable paper liner. The role of the silicone is to provide a low surface energy interface between the liner and PSAs. Silicone release coated substrates provide both protection for the adhesive during coating, handling, and storage, and subsequent easy release of the substrate from the adhesive surface immediately prior to use (553). The process of converting paper to a release liner involves in-line coating in which cross-linkable silicone polymers are applied to the substrate and then cured either thermally or via radiation. The dominant product form is a thermally cured solventless paper release coating comprised of a vinyl-terminated PDMS, an SiH-containing cross-linker, a Pt hydrosilylation catalyst, and a cure inhibitor. Vinyl-terminated polymer chains are more reactive than D-vinyl groups, resulting in faster cure (554). Hydrosilylation inhibitors are used to ensure that the siloxane formulation does not cure prior to deposition, thereby providing a bath-life sufficient for industrial processes. Typical hydrosilylation inhibitors are alkynols or alkyl maleates. Control release additives are frequently used in paper release coatings to increase the force required to remove the liner from the adhesive label (555). These additives are usually MQ resins that function by changing the viscoelastic properties of the coating. It is also preferred that these resins contain reactive Si–vinyl groups that cross-link into the silicone network. Ideal curing conditions involve temperatures of 150°C or lower and line speeds up to 460 m/min. Key properties for release coatings are cure speed, integrity of cure, and stable release values.

The need for faster line speeds, which result in increased productivity, and lower temperatures for thermally sensitive substrates is driving the technology of silicone paper release coatings. Advances include faster thermal curing and radiation-curable paper coatings. Substitution of 5-hexenyl groups for vinyl groups has been reported to increase the cure rate of thermal paper release coatings (556,557). However, the industry is rapidly evolving toward the use of UV-curable products. These coatings use silicone polymers and control release resin additives that are substituted with functional groups that can be cross-linked using photoinitiated catalysts (epoxides) or groups that can be directly photocured (acrylates, vinyl ethers) (277,558,559). An alternative to UV light for curing silicone release coatings is EB processing, although the initial capital investment for this technology is higher (297).

Typical substrates for silicone release coatings are supercalendered kraft paper, glassines, and thermally sensitive films such as polyethylene and polypropylene. Paper is currently the most widely used substrate, although thermally sensitive films are a growing market segment. One challenge with films is adhesion of

the cured silicone to the substrate. Typically, an adhesion promotor is required in addition to the cross-linkable silicone polymers to ensure anchorage of the cured silicone to the substrate.

Fiber Finishing Applications. Because of their unique properties, silicones have been used in both textile and hair care applications for decades. For textiles, early interest focused on water repellency (560–563), but now they are used in a wide variety of applications on fabrics derived from both natural and synthetic fibers, woven and nonwoven (264,562). For example, because of their low surface energy and extreme flexibility, silicones are among the best fabric softeners used in textile finishing. Silicone-treated fabric exhibits lower interfiber friction (565) that can lead to wrinkling benefits (durable press and wrinkle recovery). Fabric strength (566,567) and abrasion resistance (566,568,569) are other properties improved with some silicone treatments. Fabrics made from wool and other fiber types have been made shrink-resistant with certain silicone treatments (570–572). Silicones functionalized with polyether groups can impart hydrophilicity as well as softness or enhanced crease resistance to polyester and other fabrics (573–576).

Treated textile is typically rated by various ASTM or AATCC methods or by trained panelists. Standard methods exist for assessing tear strength, tensile strength, fiber friction, wettability, wrinkle recover angle, durable press rating, abrasion resistance, etc. (566,577–581). Panelists are often used to evaluate benefits such as softening, antiwrinkling, or stain removal.

For textile applications, silicones can be classified as nonreactive, conventional, reactive, or organoreactive (578,581). Polydimethylsiloxane fluids are typical nonreactive silicones. They can provide useful tactile and physical properties, but not durability. Conventional reactive silicones include SiH or SiOH polymers. These types, often having structures that give rise to three-dimensional networks upon curing, have been widely studied for durable water repellency and softening. Organoreactive silicones are substituted with groups that are capable of reacting directly with fibers. Textile finishes derived from these types of silicones, typical examples of which include silanol endcapped aminosilicones and epoxysilicones, can also provide durable benefits.

Softening is one of the most common target benefits achieved with silicone treatments (562,577,582–588). Softening benefits can be significant with silicone levels of 0.1% by weight on fabric. Aminosilicones are typically among the best softeners, providing the best feel (566,589). Studies have shown that silicone softeners can provide good durability and enhanced wrinkle recovery with a higher retention of mechanical properties when compared with traditional organic cationic softeners (578). Finishes can be hydrophobic or hydrophilic. Epoxy-substituted silicone materials modified with polyether groups, known for many years, can provide durable hydrophilic softening (590). Microemulsion technology has been applied, particularly with amino-functional silicones to improve fabric penetration and overall softening properties (591). Performance achieved with aminosilicones has been compared with that resulting from treatment with silanol polymers in the presence of alkoxy silane cross-linkers on cotton (578).

One recent study evaluated the softening benefits of aminosilicones on cotton as a function of pH and type of amino group (592). It was found that, in terms of softening, there is an optimum degree of polymer substitution as well as extent

to which the amino groups should be ionized. Electrostatic interactions between protonated amines and cotton are the primary driving force of attraction, but significant repulsive forces result from a high charge density. Computer simulations suggested that the primary amine contributes much more to the interaction energy than does the secondary amine within aminoethylaminopropyl-substituted polymers.

Wrinkle resistance and recovery are two key benefits for which silicones are widely studied (567). For example, it was found that silk and silk/wool blends exhibited improved wrinkle recovery when treated with a cationic microemulsion of an aminosilicone (580). Silicones are often added to durable press/shrinkage resistance treatments, and have been used in combination with a range of currently available cellulose cross-linking systems to both enhance the overall durable press benefits and counteract the strength loss associated with cross-linking (593,594). Silanol-terminated polymers were found to increase the durable press rating with glyoxal treatments (595,596). Treatment with aminosilicone polymers results in better durable press, retention of strength, and abrasion resistance when used with dimethyloldihydroxyethyleneurea (DMDHEU) cross-linking systems in some cases (597), although yellowing of white fabric can be a problem (568). Others have described the use of a durable hydrophilic silicone (polyether substituted) finish to impart hydrophilic softness and durable press properties (598,599). Durable press treatments for cellulosic-based textiles have also been patented where the silicone cross-links the cellulose fibers in the presence of an acid or base catalyst (600). It has also been claimed that certain silicone treatments improve wrinkle resistance and reduce the loss of tear strength when used with formaldehyde (601,602). Many other wrinkle-reducing compositions including silicone have been patented (584–586,603–608). While covalent bonding between organofunctional silicone and fiber surfaces is often invoked in the literature as a way of explaining durable benefits, it is rarely backed up with unambiguous evidence. An IR method for characterizing ester linkages to cotton has recently been described (609).

Silicone lubricants have also been studied as cotton processing aids (610). One study found an effective lubrication system containing a 1% loading by weight of a cationic silicone emulsion (611).

There are obvious links between silicone treatments for textiles and those for hair. Indeed, silicones have been used extensively in hair care products for 50 years, primarily in shampoos and conditioners (612–616). Aminofunctional silicones make hair feel soft and are thus outstanding for hair conditioning. Aminosilicones are effective because of their high pK_a and the fact that untreated hair has an isoelectric point of approx. pH 3 (617). Polyether-substituted silicones impart hydrophilicity and can be useful in compatibilizing different components of a formulation. They are also light conditioners and have antistatic characteristics. Phenyl silicones provide shine and luster. Alkyl-substituted silicone give hair volume and manageability. Silicone resins are substantive and also add volume as well as set retention. High molecular weight PDMS provides good dry feel properties and combing. These materials can be used alone or in combination.

Room Temperature Vulcanizable (RTV) Silicones. One-component, moisture-curable, room-temperature vulcanizable (RTV) silicones represent one of the largest-volume and commercially most successful silicone technologies. When exposed to atmospheric moisture, RTV silicones undergo hydrolysis and

condensation reactions and cure into high strength elastomers. Sealants and adhesives are the chief uses of RTV silicones. The rate of cure of these products is dependent on temperature and humidity. In the uncured state, in the absence of moisture, one-part products have a shelf life of 6 months to several years. The cured elastomers have excellent primerless adhesion to substrates as varied as glass, metals, wood, masonry, and plastics. Additional benefits include excellent weatherability, durability, electrical insulation, chemical resistance, stability at high temperatures, and flexibility at low temperatures. RTV products having a wide range of viscosities, from low viscosity self-leveling potting compositions to high viscosity thixotropic pastes, are commercially available. One of the few disadvantages of RTV systems is a slow rate of cure, often requiring more than 7 days in low humidities to achieve optimum properties. The cure speed can be increased by raising the temperature or by using a two-part formulation that includes water in one of the parts. Water can also be provided by the *in situ* reaction of carbonyl compounds with primary amines in a two-part formulation (618,619). Although two-part sealant formulations are exceedingly simple (silanol polymer, fillers, and alkoxysilane cross-linker; separate cure catalyst) and have long shelf lives, consumer demand has driven the development of more complex, but also more convenient, one-part formulations.

RTV Silicone Chemistry. There are two basic cure chemistries operative in RTV silicones: those based on rapidly hydrolyzing groups (acetoxy, ketoxime) and those requiring catalysts to promote hydrolysis (alkoxy-based systems) cure systems. Acetoxy-based RTV silicones were first commercialized in the early 1960s (620,621). The general chemical reactions of these first-generation products are shown in Figure 7.

In the first reaction, a multifunctional acetoxysilane cross-linker, such as methyltriacetoxysilane, reacts with a silanol-terminated PDMS, which releases acetic acid and forms a polymer containing multiple, hydrolytically unstable acetoxysilane end groups. This polymer plus fillers and other additives are compounded under anhydrous conditions and packaged as a one-part system. When exposed to atmospheric moisture, this functionalized polymer hydrolyzes, releasing more acetic acid and producing diolfunctionalized polymer end groups. This

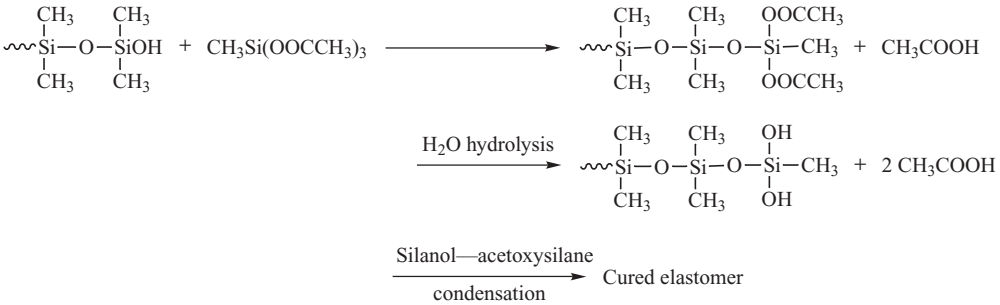

Fig. 7. Basic chemistry of acetoxy-based RTV silicones. The reactions for curing methoxy-based RTV silicones are the same; in that case, the methoxy group (OCH_3) replaces acetoxy ($OOCCH_3$), and methanol (CH_3OH), rather than acetic acid (CH_3COOH), is formed.

intermediate then undergoes self-condensation reactions, resulting in a silicone rubber. Tin(IV)-derived catalysts are frequently used to accelerate the cure of these products. Acetoxy-based RTV silicones have the advantage of having a long shelf life in the uncured state and rapid cure on exposure to moisture; however, their commercial applications are limited by the odor and corrosive nature of acetic acid.

Methoxy-based RTV silicones were introduced commercially in the late 1960s to overcome the deficiencies of their acetoxy predecessors (622). The reactions involved in curing of methoxy-based RTV silicones are similar to their acetoxy analogues.

The principal differences are that methoxy-based cross-linkers such as methyltrimethoxysilane do not spontaneously react with silanol-end-capped PDMS, and methoxysilane-terminated PDMS does not react with atmospheric moisture under neutral pH conditions. Catalysts are thus required for both of these reactions. Amines, Ti and Al complexes, and ammonium carboxylate salts are well-practiced end-capping catalysts (623–626). More recently, novel reagents such as tetralkylammonium fluorides and phosphate esters have been reported (627,628). Tin- and titanium-based catalysts are chiefly used as moisture cure catalysts (623,624,629–635). Unfortunately, these catalysts often promote undesirable siloxane redistribution reactions, which lead to instability of these RTV silicones in the uncured state. Methanol, released during the capping process, also functions in tandem with these cure catalysts in destabilizing compositions via siloxane redistribution reactions (636). Two strategies are used to overcome these side reactions and prepare commercially useful methoxy-based RTV silicones. In the first, an end-capping catalyst based on ammonium formate salts and Ti- and Sn-based cure catalysts containing specific ligands are employed. The ligands of interest are typically either hindered branched alkoxides (631–634), β-diketonates (623,630,635,637), or similar functional groups (638,639), which kinetically or thermodynamically stabilize the metal ions against alkoxy exchange reactions. As a result, these compounds have been found to be poor siloxane redistribution catalysts, and therefore are useful catalysts in RTV silicones having shelf lives of $\geq$ 6 months. In the second strategy, one-part RTV silicones with a higher degree of stability are achieved by removing methanol either physically or with methanol scavengers such as hexamethyldisilazane (629) or cyclic alkoxyaminosilanes (640,641). The latter react with methanol *in situ* to form products that also function as adhesion promoters.

RTV Silicone Compositions, Properties, and Applications. A typical commercial RTV silicone is a blend of a PDMS, end-capped with OH groups or alkoxysilanes. The compositions typically contain excess cross-linking silane, reinforcing fillers, plasticizing oils, adhesion-promoting silanes, a cure catalyst, and other optional additives. The key properties are the tensile strength and adhesion of the cured elastomer, the shelf life and thixotropic behavior of the uncured product, and the cure rate. The tensile strength of an RTV silicone is a function of the cross-link density of the silicone elastomer and the amount and type of reinforcing filler. Useful fillers include high surface area, silane-treated fumed silica (hexamethyldisilazane or D_4 are often used as treating agents), and calcium carbonate. The latter filler is either derived from natural sources or prepared synthetically (precipitated $CaCO_3$) and commonly treated with organic surface modifiers, such

Table 11. Typical RTV Silicone Properties

Property	Value
Density, g/cm^3	1.07
Hardness, Shore A	30–35
Tensile strength, MPa[a]	2.55–3.24
Elongation, %	375–450
Service temperature, continuous, °C	200–260
Max. temperature, short periods, °C	260–315
Dielectric strength, kV/mm	19.7

[a] To convert MPa to kgf/cm^2, multiply by 10.2.

as stearic acid. Plasticizing fluids are usually trimethylsiloxy-end-capped PDMS fluids, which are used to improve thixotropy and adhesion. The outstanding adhesive properties of RTV silicones are affected by almost every ingredient of the composition. Adhesion promoters, typically trialkoxy- or dialkoxy-substituted functional silanes, are frequently used to enhance adhesion to difficult substrates such as glass, metals, and plastics. Examples include γ-aminopropyltrimethoxysilane, β-cyanoethyltriethoxysilane, and γ-glycidoxypropyltrimethoxysilane. Other additives used in RTV silicones are iron and rare-earth oxides for improved high temperature stability, platinum for flame retardancy, fungicides for high humidity applications, and a variety of pigments. One-part silicone RTV silicones are sold in three primary markets: household consumer products, construction products, and industrial adhesives. Noncorrosive RTV silicones using methoxy-based cure chemistry are useful as electronic potting compositions. Typical RTV silicone properties are given in Table (11).

Analysis and Testing of Silicones

The unique chemical, physical, and spectroscopic properties of organosilicon compounds are reflected in the analytical methodology used for the detection, quantification, and characterization of these compounds. Several thorough, up-to-date reviews dealing with analytical methods applied to silicones have been published (642–645).

Chemical Analysis. The presence of silicones in a sample can be ascertained qualitatively by burning a small amount of the sample on the tip of a spatula. Silicones burn with a characteristic sparkly flame and emit a white sooty smoke on combustion. A white ashen residue is often deposited as well. If this residue dissolves and becomes volatile when heated with hydrofluoric acid, it is most likely a siliceous residue (646). Quantitative measurement of total silicon in a sample is often accomplished indirectly, by converting the species to silica or silicate, followed by determination of the heteropoly blue silicomolybdate, which absorbs at 800 nm, using atomic spectroscopy or UV spectroscopy (647–650). Pyrolysis GC with mass spectroscopic detection of the pyrolysate is a particularly sensitive tool for identifying silicones (651,652). This technique relies on the pyrolytic conversion of silicones to cyclics, predominantly to D_3 [541-05-9], which is readily detected and quantified (eq. 44).

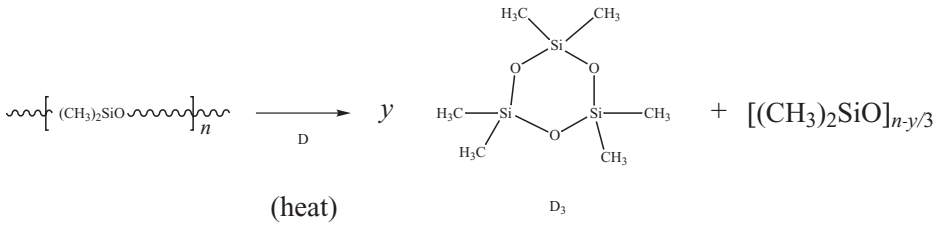

(44)

Functional groups in silicone monomers and polymers are characterized by chemical reactivity. For example, chlorosilanes are hydrolyzed, and the halogen is quantified by titration with alkali or silver nitrate (653). Other types of halogen substitution may require more drastic methods of decomposition. Silicon hydride is assayed by determining the hydrogen evolved after base-catalyzed hydrolysis or alcoholysis (654). Silanol concentration can be calculated by measuring the methane evolved with methyl Grignard reagent.

The structural architecture of silicone polymers, such as the number of D, T, and Q sites and the number and type of cross-link sites, can be determined by a degradative analysis technique in which the polymer is allowed to react with a large excess of a capping agent, such as hexamethyldisiloxane, in the presence of a suitable equilibration catalyst (655). Triflic acid is often used as a catalyst because it promotes the depolymerization process at ambient temperature (eq. 45).

$$\underset{\text{M}}{[(CH_3)_3SiO]_m}\,\underset{\text{D}}{[(CH_3)_2SiO_2]_n}\,\underset{\text{T}}{[CH_3SiO_3]_o}\,\underset{\text{Q}}{[SiO_4]_p} + (CH_3)_3SiOSi(CH_3)_3 \longrightarrow$$
$$n\,(CH_3)_2Si[OSi(CH_3)_3]_2 + o\,CH_3Si[OSi(CH_3)_3]_3 + p\,Si[OSi(CH_3)_3]_4$$

$$\underset{\text{M}}{[(CH_3)_3SiO]_m}\,\underset{\text{D}}{[(CH_3)_2SiO_2]_n}\,\underset{\text{T}}{[CH_3SiO_3]_o}\,\underset{\text{Q}}{[SiO_4]_p} + Si(OC_2H_5)_4 \xrightarrow[\text{or } KOC_2H_5]{KOH}$$
$$m\,(CH_3)_3SiOC_2H_5 + n\,(CH_3)_2Si(OC_2H_5)_2 + o\,CH_3Si(OC_2H_5)_3$$

(45)

Instrumental Methods. A variety of spectroscopic techniques are available for the characterization of silicones. The analysis of bulk samples of silicone oils and related compounds can be accomplished via standard techniques; descriptions of these techniques and literature references relevant to silicone analysis are summarized in Table (12).

However, full characterization of functionalized siloxanes, particularly those containing high degrees of polymerization, can be difficult. Therefore, separation techniques coupled with various detection devices are typically employed. Supercritical fluid chromatography is effective for the separation of silicone oligomers that have molecular weights less than 3000 Da (688,689). Time-of-flight secondary ion mass spectrometry (TOF-SIMS) is applicable up to 10,000 Da (660).

A number of techniques have been developed for the trace analysis of silicones in environmental and biological samples. In these analyses, care must be taken to avoid contamination of the samples because of the ubiquitous presence of silicones, particularly in a laboratory environment. Stopcock grease, pump oil, soap, tubing,

Table 12. Spectroscopic Methods for Analysis of Silicones

Technique	Information provided	Reference
Mass spectrometry	Identification, structural information, molecular weight information, and quantification; information is dependent on the mode of ionization; particularly useful when combined with a chromatographic separation technique, such as in GC–MS, HPLC–MS, and pyrolysis GC–MS	651,652, 656,657, 657–662
IR/UV spectroscopy	Identification, structural information, quantification, and functional group identification; can be employed as detectors in chromatographic separations	663–672
NMR[a]	Detailed structural information; molecular weights can be determined by end group analysis; solid-state cp-mas techniques can be used to characterize solid samples and cross-linked elastomers	673–681
Atomic spectrometric methods (AA/emission)	Quantitatively detects total silicon in the sample; sensitivities in the ppb range are possible; particularly useful when used in combination with chromatographic separation devices; can be used to detect trace elemental contaminants in silicones	682–687

[a] Of particular interest are ^{1}H, ^{13}C, and ^{29}Si nuclei.

septa, o-rings, and labels are just some examples of sources of silicone in the laboratory. Depending on the method of detection, interference from inorganic silicate can also be problematic; hence, non-silica-based vessels are often used in these determinations. Particularly difficult are silicon-specific analyses such as those involving atomic spectrometric techniques where ppb levels of silicon are present.

Silicones have been extracted from environmental samples with solvents such as hexane, diethyl ether, methyl isobutylketone, ethyl acetate, and THF, using either sequential or Soxhlet techniques (690–695). Silicones of a wide range of molecular weights and polarities are soluble in THF. This feature, coupled with its volatility and miscibility with water, makes THF an excellent solvent for the extraction of silicones from wet samples, ie, soils and sediments. Trace levels of silicones extracted from environmental samples have been measured by a number of techniques, including atomic absorption spectroscopy (AA), inductively coupled plasma-atomic emission spectroscopy (ICP-AES), pyrolysis GC–MS, as well as ^{1}H and ^{29}Si NMR spectroscopy (674,684,692,696–700). The use of separation techniques, such as gel permeation and high pressure liquid chromatography interfaced with sensitive, silicon-specific AA or ICP detectors, has been particularly advantageous for the analysis of silicones in environmental extracts (685,701–704).

Determination of Physical Properties. Common properties of silicone polymers, such as refractive index, density, and viscosity, are measured using

conventional techniques (705). Molecular weights can be determined by standard methods, provided suitable reference standards are available. Empirical viscosity/molecular weight correlations are also useful as a simple means of obtaining approximate molecular weights (706). End group analysis by suitable spectroscopic or chemical methods can give reliable number-average molecular weight data. Long-chain branching in silicone polymers can be ascertained chemically, by determining the ratio of branch sites to end groups using degradation methods (655,656), or instrumentally, by measuring molecular size–viscosity relationships, for example, using a GPC instrument coupled to a differential viscometry or light-scattering detector (707,708). The level of cross-linking in silicone polymers, quantified in terms of the average molecular weight of strands between cross-links, is often measured by solvent swelling or modulus measurements, which are related to the combined effects of physical and chemical cross-links (709,710). Chemical cross-links can be quantified by NMR techniques or by degradative analysis to determine actual concentrations of T and Q cross-link sites (655).

Thermal stability, highly significant in silicone evaluation, is monitored by thermogravimetric analysis (TGA), differential scanning calorimetry (DSC), or dynamic mechanical analysis (DMA). Because environmental factors and chemical neutrality affect performance at high temperatures, oven-aging tests on finished products are frequently required. Measurement of weight loss on heat aging is frequently more sensitive than direct chemical methods for detecting the presence of trace amounts of strong acid or base, which reduce polymer stability.

A great variety of analytical techniques have been applied to silicone processing and quality control. In the early days of commercial production, the composition of chlorosilane intermediate mixtures was determined by analytical distillation and weight determination of fractions, supplemented by wet analysis of hydrolyzable chlorine and specific gravity measurements. These methods have largely been supplanted by GC and GC–MS methods. Gas chromatography is also used to monitor alkoxysilanes, acyloxysilanes, and the lower boiling point linear and cyclic siloxanes. On-line (in-process) monitoring of continuous and semicontinuous processes employs these and other relevant techniques.

Quality control testing of silicones utilizes a combination of physical and chemical measurements to ensure satisfactory product performance and processibility. For example, in addition to the usual physical properties of cured elastomers, the plasticity of heat-cured rubber and the extrusion rate of RTV elastomers under standard conditions are important to the customer. Where the silicone application involves surface activity, a use test is frequently the only reliable indicator of performance. For example, the performance of an antifoaming agent can be tested by measuring the foam reduction when the silicone emulsion is added to an agitated standard detergent solution. The product data sheets and technical bulletins from commercial silicone producers can be consulted for more information.

Properties of silicone fluids can be determined by a number of ASTM tests that were developed for the petroleum industry. ASTM D2225 describes methods of testing silicone fluids. ASTM tests typically used for determining standard physical properties are as follows: flash point, D92 and D93; pour point, D97; specific gravity, D1298; viscosity, D445; refractive index, D1807; and volume resistivity, D1169.

Health and Environmental Aspects

Few materials of commercial importance possess a range of applications as diverse as silicones. The widespread acceptance of silicones has given rise to remarkable growth of these materials since their first commercial production in the mid-1940s. In 1950, approximately 10^3 t of silicones was produced. By 1965, production amounted to 1.4×10^4 t and in 1999, production reached an estimated 3.5×10^5 tons in the United States alone (711). More recently, silicones have found increasing use in personal care products, such as deodorants, shampoos, and cosmetics. As a result of their widespread use and remarkable inertness toward light, heat, and chemical agents, an understanding of the environmental fate and distribution of silicones is important. Several reviews dealing with this subject are available (712–715), including a recently published comprehensive overview of environmental fate and effects of silicones (716).

Some examples of biological applications of silicones are biofouling release coatings, oil spill containment, and vitreous humor substitutes. Silicone elastomer coatings have been developed as nontoxic alternatives to toxic antifouling paints for ship hulls and power plant intakes (717–720). Solutions containing silicone have been developed to encapsulate and solidify oil slicks for easy removal (721,722). Silicone vitreous substitutes are used after retinal attachment surgery (723–725).

Organosilicones have been detected in terrestrial, aquatic, and atmospheric environments (Table 13).

Table 13. Silicones in Environmental Samples

Location	Silicone, ppm[a]	Organic silicone, pp[b]	Reference
Nagara River[c] sediment	0.3–5.8	2–54.2	697
Dye factory	41–6290	0–1150	
Sewage plant sludge	144	10.2	
Night soil plant	34.3		
Domestic wastewater treatment plant		2.4–4.9	
Blue Plains[d] wastewater treatment plant		4	726
Sludge	89–104		726,727
Filter cake	26–46		726
Potomac River[d]	0.46–3.07		727
Delaware Bay	0.1–1.56	34	727
Chesapeake Bay	0–36.1	30	727,728
Bight[e] wastewater treatment plant	0.48		729
Hudson River[e] sediment	10–350		730

[a] Wt Si/dry wt.
[b] Aquatic samples.
[c] Japan.
[d] Washington, D.C.
[e] New York.

The highest concentrations of environmental silicones are found in the sludges of wastewater treatment plants and upstream of process plants. Much lower levels are found in water or sediment samples except at certain point sources, such as in effluents of dyeing factories and other industries that employ silicones in their processes. In general, levels of organosilicones in sludges and sediments have been found to correlate with the total organic content of these media as determined by pyrolysis weight losses. This implies a migratory aptitude similar to that of other organic pollutants. For example, analysis of undisturbed, ^{210}Pb-dated sediment taken from Puget Sound in Washington indicates the presence of organosilicone in a 15-year-old sludge but not in a 60-year-old sample (731,732). This result suggests that silicones do not migrate appreciably of their own accord but follow sediment movement. Another study of the geochronology of sedimentary siloxanes was conducted in the Ala Wai Canal in Hawaii. The cores, dated using ^{210}Pb and ^{137}Cs measurements, showed the highest concentration of silicone in the most contemporary sediments. The study also found spikes in silicone concentration that could be traced to storm events (733).

Silicones have been detected in water from various rivers and in effluent from wastewater treatment facilities. They are barely detectable in water from municipal treatment facilities. Water solubility (S) of silicones has been found to correlate with the octanol–water partition coefficients (K_{OW}) for a series of trimethylsilyl-capped siloxane oligomers of various molecular weights according to equation 46 (734).

$$\text{Log } K_{OW} = 3.047 - 1.148 \log S \tag{46}$$

This expression can be used to predict solubilities from the octanol–water partition coefficients. Solubility and K_{OW} data for four oligomeric siloxanes are listed in Table 14.

The rapid drop in solubility and increase in K_{OW} with increasing molecular weight are evident from these data.

Because of their hydrophobic nature, silicones entering the aquatic environment should be significantly absorbed by sediment or migrate to the air–water interface. Silicones have been measured in the aqueous surface microlayer at two estuarian locations and have been found to be comparable to levels measured in bulk (732). Volatile surface siloxanes become airborne by evaporation, and higher molecular weight species are dispersed as aerosols.

Silicone contamination has been implicated as a cause of failure in telephone switching systems and other devices that contain relay switch contacts

Table 14. Effect of Siloxane Molecular Weight on Water Solubility and Octanol–Water Partition Coefficient

Molecular weight	Solubility in H_2O, ppm	$\log K_{ow}$
1,200	1.6	2.86
6,000	0.56	3.26
25,000	0.17	3.83
56,000	0.076	4.25

(735). Analysis of airborne particulates near telephone switching stations showed the presence of silicones at these locations. Where the indoor use of silicones is intentionally minimized, outdoor levels were found to be higher than inside concentrations (736). Samples of particulates taken at two New Jersey office buildings revealed silicone levels that were considerably higher indoors than outdoors. In these cases, indoor silicone aerosols are believed to be generated primarily by photocopiers, which use silicone fuser oils.

Airborne organic silicon has been detected in samples collected at Barrow, Alaska (737). Organosilicone levels corresponding to an airborne concentration of 8 ng/m^3 were detected. As a comparison, these samples were determined to hold approximately 20 ng/m^3 of phthalate-based plasticizers. Two pathways have been proposed for the removal of atmospheric organosilicones: degradation resulting from a reaction with OH radicals and wet deposition from the gas phase by incorporation into areosols (738).

Knowledge of the transformation of silicones under various environmental conditions is key to understanding the fate of these materials. Model studies predict that a large fraction of silicones entering the environment through wastewater treatment systems, ie, municipal treatment plants or septic systems, will ultimately be deposited on soils as a result of absorption or of sludge amendment (739,740). The chemistry of silicones on soils is thus an important factor in assessing the overall environmental impact of these materials. The accumulation of silicone in sediments has been observed in freshwater and marine sites heavily impacted by wastewater discharge. The concentrations ranged from 0.6 ± 0.1 ppm to 78 ± 20 ppm, which were still below the "no observable effect concentration" for the sediment organisms (741).

Silicone fluids degrade when exposed to soils (694,742–744). The rate of degradation depends on soil type and moisture content. Degradation is slow but observable on moist soils and becomes quite rapid when the available moisture content of the soil drops below 5% (745). The products of soil-induced abiotic degradation are typically silanol-terminated monomers and oligomers. Dimethylsilanediol, the simplest monomeric unit derived from silicone hydrolysis, is an important degradation product of abiotic silicone degradation. This compound is produced when silicones are exposed to soils and sediments even when the overall extent of polymer degradation is small, indicating a possible kinetic preference for its formation. As a polar, water-soluble species, dimethylsilanediol exhibits environmental distribution properties drastically different from the silicones from which it is derived (746). In organic solvents, dimethylsilanediol undergoes rapid self-condensation producing oligomeric products, whereas in dilute (<400 ppm) aqueous solution (eq. 47), it is the major constituent among the water-soluble oligomeric silanols (747). Therefore, (**1**) is expected to be the principal waterborne silicone species found in most environmental samples.

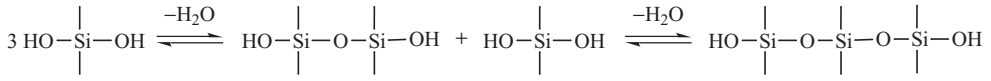

(47)

Irradiation of water-soluble silicon species such as dimethylsilanediol with artificial sunlight (xenon arc lamp) in the presence of environmentally significant levels of nitrate led to their rapid disappearance ($t_{1/2}$ = 4–9 days) (748). Silicate was determined to be the ultimate photodegradation product. Transformation of the soluble silicones to silicate under these conditions was complete in about 35 days. Irradiation of an emulsified high molecular weight silicone fluid [degree of polymerization (DP) = 50] resulted in negligible (1.7%) conversion to silicate in the same time period. Degradation did not occur in the dark or in the absence of nitrate. Nitrate is thought to act in this system by providing a source of photochemically generated hydroxyl radicals (eq. 48). Oxidative attack of these reactive species on the silicon–carbon bonds leads eventually to silicate and CO_2.

$$NO_3^- + H_2O \rightarrow NO_2 + HO^\bullet + HO^- \quad (48)$$

Water-soluble silanols such as dimethylsilanediol were found to undergo successive oxidative demethylations with tropospheric UV irradiation in the presence of suitable chromophores, such as nitrogen oxides (749). The water-soluble methylated silicones did not promote diatom (*Navicula pelliculosa*) growth but the demethylated photoproducts did. The sequence of soil-induced degradation of silicones to water-soluble species, followed by light-induced conversion to silicate, suggests a pathway, conceptually at least, for the mineralization of silicones.

Polydimethylsiloxane does not biodegrade at an observable rate under normal conditions of environmental exposure. For example, a ^{14}C-labeled 300-cSt PDMS fluid showed no evidence of biodegradation when exposed to activated sludge over a period of 70 days (750). In a similar microbiological screening study, silicones were found to be inert to all applied cultural conditions (751). However, when ^{14}C-labeled PDMS was applied to soil and allowed to degrade to low molecular weight species, the degradation products were further degraded to silicate and $^{14}CO_2$, presumably via a biotic pathway (752). This degradation has been observed both in the laboratory and in the field (694,753,754). ^{14}C-dimethylsilanediol is biodegraded on soils at a rate of $\approx$1% per month (755). The rate of $^{14}CO_2$ production can be increased an order of magnitude by the addition of certain carbon sources, such as 2-propanol and methylsulfone, to the medium. Thus, by a combination of abiotic, soil-mediated degradation and biotic or light-induced conversion of the degradation products, silicones can undergo complete mineralization in the environment (756). The rates at which this mineralization occurs depend on the conditions of environmental exposure.

Economic Aspects

Silicone polymers continue to be an important article of commerce globally. The industry grew at an average annual rate of 6–8% during the 1990s. The total global markets for silicone/silane materials totaled nearly $6.7 billion in 1998. The world capacity for silicones as of 1999 has been estimated at about 1.7 billion pounds (757). The silicones industry is a global enterprise with Dow Corning, General Electric, and SKW/Goldschmidt being the major producers of silanes. Table 15 lists the approximate sales of the principal producers for 1991 and 1998 (757).

Table 15. Total Silicone/Silane Sales of Principal Producers for 1991 and 1998

	Sales, $ millions	
Company	1991	1998[a]
Dow Corning	1850	2400
General Electric	750	1215
Shin-Etsu	750	600
Wacker Chemie	675	870
Rhodia	460	400
Degussa/SKW	—	670
Crompton	—	400
Others	465	134

[a]Ref. 757.

The recent merger of Degussa with SKW/Goldschmidt created a new global player similar in size to Shin-Etsu. This was part of a flurry of consolidation activities in the industry during the latter part of the 1990s. Also, joining forces during the period were GE and Bayer, Witco and Crompton-Knowles, and Hüls and Degussa.

BIBLIOGRAPHY

"Silicones" in *EPST* 1st ed., Vol. 12, pp. 464–569, by H. K. Lictenwalner and M. M. Sprung, General Electric Co.; "Silicones" in *EPSE* 2nd ed., Vol. 15, pp. 204–308, by B. Hardman and A. Torkelson, General Electric Co.

1. W. Noll, *Chemistry and Technology of Silicones*, Academic Press, Inc., New York, 1978.
2. E. G. Rochow, *Silicon & Silicones*, Springer-Verlag, Berlin, 1987.
3. D. Hunter, *Chem. Week* 24 (Feb. 19, 1992).
4. A. I. Gorbunfov, A. P. Belyi, and G. G. Filippov, *Rus. Chem. Rev.* **43**, 291 (1974).
5. A. D. Petrov, B. F. Mironov, V. A. Ponomarenko, and E. A. Chernyshev, *Synthesis of Organosilicon Monomers*, Consultants Bureau, New York, 1964, p. 36.
6. J. M. Zeigler and F. W. G. Fearon, eds., *Silicon-Based Polymer Science* (ACS Advances in Chemistry, Series 224), American Chemical Society, Washington, D.C., 1990.
7. F. O. Stark, J. R. Falender, and A. P. Wright, in G. Wilkinson, F. G. A. Stone, and E. W. Abel, eds., *Comprehensive Organometallic Chemistry*, Pergamon Press, Oxford, U.K., 1982, Chapt. "9.3", p. 305.
8. C. Eaborn and R. W. Bott, in A. G. MacDiarmid, ed., *The Bond to Carbon*, Vol. **I**, Part 1, Marcel Dekker, Inc., New York, 1968, p. 105.
9. R. J. H. Voorhoeve, *Organohalosilanes: Precursors to Silicones*, Elsevier, New York, 1967.
10. R. R. McGregor, *Silicones and Their Uses*, McGraw-Hill Book Co., Inc., New York, 1954.
11. A. Ladenburg, *Ann. Chem.* **164**, 300 (1872).
12. J. J. Ebelman, *Compt. Rend.* **19**, 398 (1844).
13. F. S. Kipping, *Proc. Chem. Soc.* **20**, 15 (1904).
14. See also W. Dilthey, *Chem. Ber.* **37**, 1139 (1904).
15. H. A. Liebhafsky, *Silicones under the Monogram*, John Wiley and Sons, Inc., New York, 1978.

16. A. Stock, *Hydrides of Boron and Silicon*, Cornell University Press, Ithaca, N.Y., 1933, p. 20.
17. E. L. Warrick, *Forty Years of Firsts*, McGraw Hill Book Co., Inc., New York, 1990.
18. E. G. Rochow and W. Gilliam, *J. Am. Chem. Soc.* **63**, 798 (1941).
19. J. F. Hyde and R. DeLong, *J. Am. Chem. Soc.* **63**, 1194 (1941).
20. V. Chvalovsky, in B. J. Aylett, ed., *Organometallic Derivatives of the Main Group Elements*, Butterworths, London, 1975.
21. T. C. Kendrick, B. Parbhoo, and J. W. White, in S. Patai and Z. Rappoport, eds., *The Silicon-Heteroatom Bond*, John Wiley and Sons, Ltd., Chichester, U.K., 1989, Chapt. "3".
22. J. H. Alvarez, J. Cervantes, A. F. Aguilera, and K. M. Lewis, in H. A. Oeye, ed., *Silicon for Chemical Industry V*, Norwegian University of Science and Technology, Trondheim, Norway, 2000, pp. 215–226.
23. L. D. Gasper-Galvin, D. G. Rethwisch, D. M. Sevenich, and H. B. Fridrich, in K. M. Lewis and D. G. Rethwisch, eds., *Catalyzed Direct Reactions of Silicon*, Elsevier, Amsterdam, the Netherlands, 1993, p. 279.
24. L. N. Lewis, in Z. Rappoport and Y. Apeloig, eds., *The Chemistry of Organic Silicon Compounds*, Vol. **2**, John Wiley & Sons, Inc., 1998, p. 1581.
25. C. S. Kuivila, R. H. Zapp, O. K. Wilding, and C. A. Hall, in H. A. Oeye, ed., *Silicon for Chemical Industry III, Norwegian University of Science and Technology*, Trondheim, Norway, 1996, p. 227.
26. B. Imelik and P. Trambonze, *Bull. Soc. Chim. Fr.* **238**, 680 (1954).
27. V. S. Fikhtengolts and A. I. Klebansky, *J. Gen. Chem. (USSR)* **27**, 2535 (1957).
28. I. Klebansky and V. S. Fikhtengolts, *J. Gen. Chem. (USSR)* **26**, 2795 (1956).
29. T. C. Frank, K. B. Kester, and J. L. Falconer, *J. Catal.* **91**, 44 (1985).
30. N. Floquet, S. Yilmaz, and J. L. Falconer, *J. Catal.* **148**, 348 (1994).
31. T. Glasson, J. C. Bertolini, and P. Colin, in H. A. Oeye, ed., *Silicon for Chemical Industry IV*, Norwegian University of Science and Technology, Trondheim, Norway, 1998, p. 227.
32. M. Okamoto, S. Onodera, T. Okano, E. Suzuki, and Y. Ono, in H. A. Oeye, ed., *Silicon for Chemical Industry III*, Norwegian University of Science and Technology, Trondheim, Norway, 1996, p. 239.
33. M. Mazurek and J. Chojnowski, *Macromolecules* **11**, 347 (1978).
34. W. J. Ward, A. Ritzer, K. M. Carroll, and J. W. Flock, *J. Catal.* **100**, 240 (1986).
35. J. Han, S. I. Gheyas, D. R. Strongin, B. J. Hinch, and A. P. Wright, *Catal. Lett.* **68**, 147 (2000).
36. G. Laroze, J. L. Plaque, G. Weber, and B. Gillot, in H. A. Oeye and H. Rong, eds., *Silicon for Chemical Industry*, Geironger, Norway, 1992, p. 151.
37. K. H. Brookes, M. R. H. Siddiqui, H. M. Rong, R. W. Joyner, and G. J. Hutchings, *Appl. Catal. A: Gen.* **206**, 257 (2001).
38. U.S. Pat. 4,602,101 (1986), R. L. Halm, O. K. Wilding, and R. H. Zapp (to Dow Corning).
39. W. J. Ward, L. N. Lewis, and J. M. Bablin, in H. A. Oeye, ed., *Silicon for Chemical Industry V, Norwegian University of Science and Technology*, Trondheim, Norway, 2000, p. 309.
40. U.S. Pat. 6,005,130 (1999), L. N. Lewis and J. M. Bablin (to General Electric).
41. Eur. Pat. EP 893,448 (1999), T. Nakanishi, T. Inukai, K. Tsukioka, H. Nakayama, and Y. Satoh (to Shin-Etsu).
42. H. Ehrich, D. Born, J. Richter-Mendau, and H. Lieske, *Appl. Organomet. Chem.* **12**, 257 (1998).
43. C. K. Cho and K. D. Han, *Kongop Hwahak* **9**, 394 (1998).
44. K. M. Lewis, D. McLeod, and B. Kanner, in J. W. Ward, ed., *Catalysis*, Elsevier, Amsterdam, the Netherlands, 1988, p. 415.

45. Jpn. Pat. JP 2,000,297,092 (2000), M. Aramata, A. Ohori, K. Furuya, S. Ueno, N. Shinohara, and T. Inukai (to Shin-Etsu).
46. U.S. Pat. 6,057,469 (2000), T. Margaria and F. Meoni (to Pechiney Electrometallurgie).
47. WO 9,960,001 (1999), T. Margaria, M. S. Steiner, and R. Armbrust (to General Electric Bayer and Pechiney Electrometallurgie).
48. J. P. Kohane and O. K. Wilding, in H. A. Oeye, ed., *Silicon for Chemical Industry III*, Norwegian University of Science and Technology, Trondheim, Norway, 1996, p. 275.
49. B. Kanner and K. M. Lewis, in K. M. Lewis and D. G. Rethwisch, eds., *Catalyzed Direct Reactions of Silicon*, Elsevier, Amsterdam, the Netherlands, 1993, p. 1.
50. V. M. Mikhaylov and V. N. Penskii, *Production of Monomer and Polymer Organosilicon Compounds* (English transl., No. AD-779129), NTIS, U.S. Dept. of Commerce, Springfield, Va., p. 18.
51. V. F. Mironov, *Coll. Czech. Chem. Commun.* **25**, 2167 (1960).
52. Ger. Offen. DE 2001303 19710722 (1971), S. Nitzsche, I. Bauer, W. Graf, and N. Zeller; CA 75, 88752.
53. H. Watanabe, M. Asami, and Y. Nagai, *J. Organomet. Chem.* **195**, 363 (1980).
54. U.S. Pat. 4,727,173 (1988), F. D. Mendicino (to Union Carbide); U.S. Pat. 2,473,260 (1949), E. G. Rochow (to General Electric).
55. U.S. Pat. 4,778,910 (1988), J. O. Stoffer, J. F. Montle, and N. L. D. Somasivi (to Lopata Research & Development Corp.).
56. F. D. Mendicino, H. E. Bartrug, D. J. Boley, P. J. Burns, T. E. Childress, P. J. Collins, N. G. Delong, H. D. Furbee, J. E. Goldsmith, K. W. Hartman, L. G. Hawkins, T. L. Hays, J. W. Heintzman, M. A. Hershman, M. C. Houston, T. G. Hurley, C. S. Knoop, J. P. Kuch, S. Magri, E. E. Malson, W. D. Mercer, S. Miller, L. G. Moody, J. L. McIntyre, S. W. Nichols, R. L. Ocheltree, P. H. Paugh, R. L. Pitrolo, M. R. Powell, T. A. Reed, J. S. Ritschler, C. L. Schilling, J. W. Smith, B. A. Snider, D. M. Wilcox, and J. T. Williams, in H. A. Oeye, ed., *Silicon for Chemical Industry IV*, Norwegian University of Science and Technology, Trondheim, Norway, 1998, p. 275.
57. R. J. Ayen and J. H. Burk, *Mater. Res. Soc. Symp. Proc.* **73**, 801 (1986).
58. U.S. Pat. 4,966,986 (1990), R. L. Halm and R. H. Zapp (to Dow Corning).
59. U.S. Pat. 4,962,220 (1990), R. L. Halm and R. H. Zapp (to Dow Corning).
60. DE 19,817,775 (1999), W. Kalchauer, H. Straussberger, and W. Streckel (to Wacker-Chemie).
61. U.S. Pat. 4,965,388 (1990), R. L. Halm, R. H. Zapp, and R. D. Streu (to Dow Corning).
62. U.S. Pat. 4,973,725 (1990), K. Lewis (to Union Carbide).
63. K. M. Lewis, R. A. Cameron, J. M. Larnerd, and B. Kanner, in *Xth International Symposium on Organosilicon Chemistry*, Poznan, Poland, 1993, p. 78.
64. U.S. Pat. 4,088,669 (1978), J. R. Malek, J. L. Speier, and A. P. Wright (to Dow Corning).
65. U.S. Pat. 4,593,114 (1986), K. M. Lewis, B. Kanner (to Union Carbide).
66. U.S. Pat. 4,255,348 (1981), B. Kanner and W. B. Herdle (to Union Carbide).
67. M. Kumada and K. Tamao, *Adv. Organomet. Chem.* **6**, 19 (1968).
68. E. Hengge, *Topics Curr. Chem.* **51**, 1 (1974).
69. M. Ishikawa, J. Iyoda, H. Ikeda, K. Kotake, T. Hasimoto and M. Kumada, *J. Am. Chem. Soc.* **103**, 4845 (1981).
70. U.S. Pat. 6,013,824 (2000), L. H. Wood (to Dow Corning).
71. R. Calas, J. Dunogues, G. Deleris, and N. Duffaut, *J. Organomet. Chem.* **225**, 117 (1982).
72. K. Tamao, T. Hayashi, and M. Kumada, *J. Organomet. Chem.* **114**, C9 (1976).
73. T. Hayashi, T. Kobayaski, A. Kawamoto, H. Tamashira, and M. Tanaka, *Organometallics* **9**, 280 (1990).
74. J. D. Rich, *J. Am. Chem. Soc.* **111**, 5886 (1989).

75. J. D. Rich, *Organometallics* **8**, 2609 (1989).
76. J. Stein, K. X. Lettko, J. A. King, and R. E. Colborn, *J. Appl. Polym. Sci.* **51**, 815 (1994).
77. I. Ojima, in S. Patai and Z. Rappoport, eds., *The Chemistry of Organic Silicon Compounds*, John Wiley & Sons, Inc., New York, 1989.
78. D. A. Armitage, in Ref. 7, Vol. 2, p. 117.
79. J. L. Speier, *Adv. Organomet. Chem.* **17**, 407 (1979).
80. J. F. Harrod, A. J. Chalk, in I. Wender and P. Pino, eds., *Organic Synthesis via Metal Carbonyls*, John Wiley & Sons, Inc., New York, 1977, p. 673.
81. E. Lukevics, Z. V. Belyakov, M. G. Pomerantseva, and M. G. Voronkov, *J. Organomet. Chem. Library* **5**, 1–179 (1977).
82. A. J. Chalk, J. F. Harrod, *J. Am. Chem. Soc.* **87**, 16 (1965).
83. B. Marciniec, *Comprehensive Handbook on Hydrosilylation*, Pergamon Press, Oxford U.K., 1992.
84. Z. M. Michalska, K. Strzelec, and J. W. Sobczak, *J. Mol. Catal., Part A: Chem* **156**, 91–102 (2000).
85. U.S. Pat. 5,539,137 (1996), L. N. Lewis (to General Electric).
86. D. Seyferth, D. Y. Son, A. L. Reingold, and R. L. Ostrander, *Organometallics* **13**, 2682 (1994).
87. H. J. Emeleus and R. R. Robinson, *J. Chem. Soc.* 1592 (1947).
88. R. A. Benkeser, H. Landesmann, and D. J. Foster, *J. Am. Chem. Soc.* **74**, 648 (1952).
89. K. C. Frisch and P. D. Shroff, *J. Am. Chem. Soc.* **75**, 1249 (1953).
90. H. Gilman, A. G. Brook, and L. S. Miller, *J. Am. Chem. Soc.* **75**, 3757 (1953).
91. L. M. Shorr, *J. Am. Chem. Soc.* **76**, 1390 (1954).
92. H.-R. Grüniger and G. Calzaferri, *Helv. Chim. Acta* **62**, 2547 (1979).
93. U. Herzog, N. Schulze, K. Trommer, and G. Roewer, *J. Organomet. Chem.* **547**, 133 (1997).
94. E. Lukevics and M. Dzintara, *J. Organomet. Chem.* **295**, 265 (1985).
95. C. Lorenz and U. Schubert, *Chem. Ber.* **128**, 1267 (1995).
96. J. Blackwell, W. E. Piers, K. Foster, and V. H. Beck, *J. Org. Chem.* **64**, 4887 (1999).
97. D. J. Oostendorp, G. L. Bertrand, and J. O. Stoffer, *J. Adhes. Sci. Technol.* **1**, 171 (1992).
98. M. D. Curran, T. E. Gedris, and A. E. Stiegman, *Chem. Mater.* **10**, 1604 (1998).
99. U.S. Pat. 6,084,116 (2000), M. Horn (to Degussa Huels Aktiengesellschaft).
100. U.S. Pat. 5,387,706 (1995), T. E. Rasmussen (to Dow Corning).
101. N. F. Orlov, R. A. Bogatkin, Z. I. Sergeeva, and M. G. Voronkov, *J. Gen. Chem. (USSR)* **32**, 2526 (1962).
102. C. Burkhardt, in G. Koerner, M. Schulze, and J. Weis, eds., *Silicones Chemistry and Technology*, Vulkan, Essen, 1991.
103. R. Gutoff, *Ind. Eng. Chem.* **49**, 1807 (1957).
104. U.S. Pat. 4,366,324 (1982), K. Habata, K. Ichikawa, and M. Shimizu (to Shin-Etsu).
105. U.S. Pat. 4,609,751 (1986), A. L. Hajjar (to General Electric).
106. U.S. Pat. 3,595,896 (1971) (to Wacker-Chemie GmbH).
107. U.S. Pat. 4,108,882 (1978), L. G. Mahone (to Dow Corning).
108. GB 843,273 (1960), A. N. Pines (to Union Carbide).
109. L. Wilczek, *J. Chojnowski, Makromol. Chem.* **184**, 77 (1983).
110. M. G. Voronkov, V. P. Mileshkevich, Yu. A. Yuzhelevskii, *The Siloxane Bond*, Consultants Bureau, New York, 1970.
111. J. J. Lebrun and H. Porte, in G. Allen, J. C. Bevington, G. C. Eastmond, A. Ledwith, S. Russ, and P. Sigwalt, eds., *Comprehensive Polymer Science*, Vol. **5**, Pergamon Press, Oxford, U.K., 1989.
112. U.S. Pat. 3,839,388 (1974), W. Hechtl, S. Nitzsche, and E. Wohlfarth (to Wacker-Chemie).

113. U.S. Pat. 4,739,026 (1988), M. Riederer and M. Piechler (to Wacker-Chemie).
114. U.S. Pat. 5,210,131 (1993), J. Gilson and J. de la Crol Habimana (to Dow Corning).
115. U.S. Pat. 5,403,909 (1995), S. Rubinsztajn (to General Electric).
116. U.S. Pat. 6,136,996 (2000), S. Rubinsztajn, P. P. Anderson, and D. P. Thompson (to General Electric).
117. U.S. Pat. 4,994,490 (1999), B. Deubzer and C. Herzing (to Wacker-Chemie).
118. W. T. Grubb, *J. Am. Chem. Soc.* **76**, 3408 (1954).
119. Z. Lasocki and S. Chrzczonowicz, *J. Polym. Sci.* **59**, 259 (1962).
120. Z. Lasocki and S. Chrzczonowicz, *Bull. Acad. Polon. Sci., Ser. Sci. Chim.* **9**, 519 (1961).
121. J. Chojnowski, S. Rubinsztajn, and L. Wilczek, *J. Chem. Soc., Chem. Commun.* **69** (1984).
122. J. Chojnowski, S. Rubinsztajn, and L. Wilczek, *Macromolecules* **20**, 2345 (1987).
123. M. Cypryk, S. Rubinsztajn, and J. Chojnowski, *J. Organomet. Chem.* **446**, 91 (1993).
124. S. Rubinsztajn, M. Cypryk, and J. Chojnowski, *Macromolecules* **26**, 5389 (1993).
125. J. Chojnowski, K. Kazimierski, S. Rubinsztajn, and W. Stanczyk, *Makromol. Chem.* **187**, 2345 (1986).
126. P. V. Wright and J. A. Semlyen, *Polymer* **10**, 462 (1969).
127. J. A. Semlyen, in J. A. Semlyen, ed., *Cyclic Polymers*, Elsevier, London, 1986.
128. J. B. Carmichael, *Rubber Chem. Technol.* **40**, 1084 (1967).
129. J. F. Brown and G. M. F. Slusarczuk, *J. Am. Chem. Soc.* **87**, 931 (1965).
130. T. C. Kendrick, B. Parbhoo, and J. W. White, in S. Patai and Z. Rappoport, eds., *The Silicon-Heteroatom Bond*, John Wiley & Sons, Inc., Chichester, U.K., 1989, Chapt. "3".
131. H. Jacobsen and W. H. Stockmayer, *J. Phys. Chem.* **18**, 1600 (1950).
132. J. Carmichael and J. Heffel, *J. Phys. Chem.* **69**, 2218 (1965).
133. J. Carmichael and R. Winger, *J. Polym. Sci. A* **3**, 971 (1965).
134. J. Semlyen and P. Winger, *Polymer* **10**, 543 (1969).
135. J. A. Semlyen, in S. J. Clarson and J. A. Semlyen, eds., *Siloxane Polymers*, Ellis Horwood and Prentice Hall, Englewood Cliffs, N.J., 1993, p. 135.
136. D. T. Hurd and R. C. Osthoff, *J. Am. Chem. Soc.* **76**, 249 (1954).
137. U.S. Pat. 3,041,362 (1962), R. L. Merker and W. A. Piccoli (to Dow Corning).
138. A. R. Gilbert and S. W. Kantor, *J. Polym. Sci.* **40**, 35 (1959).
139. U.S. Pat. 5,089,450 (1992), I. Watanuki, N. Kodana, and M. Sato (to Shin-Etsu).
140. A. Molenberg and M. Moeller, *Macromol. Rapid Commun.* **16**, 449 (1995).
141. P. C. Hupfield and R. G. Taylor, *J. Inorg. Organomet. Polym.* **9**, 17 (1999).
142. U.S. Pat. 6,054,548 (2000), J. Currie, P. Griffith, W. Herron, and R. Taylor (to Dow Corning).
143. U.S. Pat. 4,250,290 (1981), L. P. Petersen (to General Electric).
144. U.S. Pat. 4,128,568 (1978), W. Buchner, B. Degan, L. Fries, J. Helmut, R. Mundil, and K. H. Rudolph (to Bayer AG).
145. P. V. Wright, in K. J. Ivin and T. Seagusa, eds., *Ring Opening Polymerization*, Elsevier, London, 1984, p. 1055.
146. J. Chojnowski, in S. J. Clarson and J. A. Semlyen, eds., *Siloxane Polymers*, Ellis Horwood and Prentice Hall, Englewood Cliffs, N.J., 1993.
147. W. T. Grubb and R. C. Osthoff, *J. Am. Chem. Soc.* **77**, 1405 (1955).
148. J. Chojnowski and M. Mazurek, *Makromol. Chem.* **176**, 2999 (1975).
149. M. Mazurek and J. Chojnowski, *Macromolecules* **11**, 347 (1978).
150. M. Shinohara, *J. Am. Chem. Soc.* **14**, 1209 (1973).
151. M. Szwarc, *Carboanions, Living Polymers and Electron Transfer Processes*, John Wiley & Sons, Inc., New York, 1968.
152. U.S. Pat. 3,337,497 (1967), E. E. Bostick (to General Electric).

153. M. Cypryk, K. Kazmierski, W. Fortuniak, and J. Chojnowski, *Macromolecules* **33**, 1536 (2000).
154. U. Maschke and T. Wagner, *Macromol. Chem.* **193**, 2453 (1992).
155. J. G. Zilliox, J. E. Roovers, and S. Bywater, *Macromolecules* **8**, 573 (1975).
156. Y. Gnanou and P. Rempp, *Makromol. Chem.* **189**, 1997 (1988).
157. Yu. A. Yuzhelevskii, E. G. Kagan, and N. N. Fedoseeva, *Dokl. Akad. Nauk SSSR* **190**, 647 (1970).
158. W. H. Dickstein and C. P. Lillya, *Macromolecules* **22**, 3882 (1989).
159. L. C. Lee and O. K. Johannson, *J. Polym. Sci., Polym. Chem. Ed.* **14**, 729 (1976).
160. T. Suzuki, *Polymer* **30**, 333 (1989).
161. S. Boileau, in J. E. McGrath, ed., *Anionic Polymerization* (ACS Symposium Series 166), American Chemical Society, Washington, D.C., 1981.
162. W. Patnode and D. F. Wilcock, *J. Am. Chem. Soc.* **68**, 358 (1946).
163. J. Chojnowski, M. Mazurek, M. Scibiorek, and L. Wilczek, *Makromol. Chem.* **175**, 3299 (1974).
164. U.S. Pat. 5,241,032 (1993), K. Kobayashi and Y. Yamamoto (to Dow Corning Toray Silicone Co.).
165. K. A. Andrianov, M. I. Shkolnik, V. M. Kopylow, and N. N. Bravina, *Vysokomol. Soed. B* **16**, 893 (1974).
166. U.S. Pat. 5,206,330 (1993), K. Kobayashi, N. Ida, and S. Mori (to Shin-Etsu).
167. U.S. Pat. 3,297,725 (1967), G. Dieckelmann and W. Gundel (to Deutsche Hydrierwerke).
168. V. N. Gruber and L. S. Mukhina, *Vysokomol. Soed.* **3**, 174 (1961).
169. M. T. Bryk, N. N. Bagley, and O. D. Kurilenko, *Vysokomol. Soed. A* **17**, 1034 (1975).
170. U.S. Pat. 3,853,933 (1974), G. R. Siciliano (to General Electric).
171. U.S. Pat. 3,853,934 (1974), G. R. Siciliano (to General Electric).
172. U.S. Pat. 2,389,477 (1945), J. G. E. Wright and J. Marsden (to General Electric).
173. T. C. Kendrick, *J. Chem. Soc.* 2027 (1965).
174. E. Jordan, L. Lestel, S. Boileau, H. Charadame, and A. Gandini, *Makromol. Chem.* **190**, 267 (1989).
175. P. Sigwalt, C. Gobin, P. Nicol, M. Moreau, and M. Masure, *Macromol. Chem., Macromol. Symp.* **42/43**, 229 (1991).
176. A. Jallouli and J. C. Saam, *J. Inorg. Organomet. Polym.* **6**, 179 (1998).
177. U.S. Pat. 5,830,969 (1998), A. Jallouli and J. C. Saam (to Dow Corning).
178. Q. Wang, H. Zang, G. K. S. Prakash, T. E. Hogen-Esch, and G. A. Olah, *Macromolecules* **29**, 6691 (1996).
179. J. J. Lebrun, G. Sauvet, and P. Sigwalt, *Makromol. Chem., Rapid Commun.* **3**, 757 (1982).
180. J. Chojnowski, S. Rubinsztajn, and L. Wilczek, *L'Actualite Chimique* **3**, 56 (1986).
181. J. Chojnowski, M. Scibiorek, and J. Kowalski, *Makromol. Chem.* **178**, 1351 (1976).
182. L. Wilczek and J. Chojnowski, *Macromolecules* **14**, 9 (1981).
183. G. Sauvet, J. J. Lebrun, and P. Sigwalt, in E. J. Goethals, ed., *Cationic Polymerization and Related Processes*, Academic Press, Inc., London, 1984.
184. J. Chojnowski, L. Wilczek, and S. Rubinsztajn, in E. J. Goethals, ed., *Cationic Polymerization and Related Processes*, Academic Press, Inc., London, 1984.
185. P. Sigwalt, M. Masure, M. Moreau, and R. Bischoff, *Macromol. Chem., Macromol. Symp.* **73**, 147 (1993).
186. L. Wilczek and J. Chojnowski, *Makromol. Chem.* **180**, 117 (1979).
187. U.S. Pat. 3,294,725 (1966), D. E. Findlay and D. R. Weyenberg (to Dow Corning).
188. U.S. Pat. 4,288,356 (1981), D. J. Huebner and D. R. Weyenberg (to Dow Corning).
189. U.S. Pat. 4,999,398 (1991), D. Graiver and O. Tanaka (to Dow Corning).
190. D. E. Findlay, D. R. Weyenberg, and J. Cekada Jr., *J. Polym. Sci. C* **27**, 27 (1969).

191. U.S. Pat. 4,244,849 (1981), J. C. Saam (to Dow Corning).
192. M. Barrere, C. Maitre, F. Gaanachaud and P. Hemery, *Macromol. Symp.* **151**, 359 (2000).
193. J. C. Saam and D. J. Huebner, *J. Polym. Sci., Polym. Chem. Ed.* **20**, 3351 (1982).
194. A. De Gunzbourg, J. C. Favier, and P. Hemery, *Polym. Int.* **35**, 179 (1994).
195. E. J. Lawton, W. T. Grubb, and J. S. Baldwin, *J. Polym. Sci.* **19**, 455 (1956).
196. C. J. Wolf and A. C. Stewart, *J. Phys. Chem.* **66**, 1119 (1962).
197. A. S. Chawla and L. E. St. Pierre, *Adv. Chem. Ser.* **91**, 229 (1969).
198. A. S. Chawla and L. E. St. Pierre, *J. Appl. Polym. Sci.* **16**, 1887 (1972).
199. D. M. Naylor, V. T. Stannett, A. Deffieux, and P. Sigwalt, *J. Polym. Sci., Polym. Lett.* **24**, 319 (1986).
200. D. M. Naylor, V. T. Stannett, A. Deffieux, and P. Sigwalt, *Polymer* **31**, 954 (1990).
201. W. J. Van Ooij, and S. Guo, *Polym. Prep.* **38**, 1031 (1997).
202. A. M. Wrobel and M. R. Wertheimer, in R. d'Agostino, ed., *Plasma Deposition, Treatment and Etching of Polymers*, Academic Press, Inc., San Diego, Calif., 1990.
203. C. Rau and W. Kulisch, *Thin Solid Films* **249**, 28 (1994).
204. D. L. Cho and H. Yasuda, *J. Appl. Polym. Sci., Appl. Polym. Symp.* **42**, 327 (1988).
205. N. Inagaki and Y. Hashimoto, *J. Appl. Polym. Sci., Appl. Polym. Symp.* **42**, 221 (1988).
206. D. Huang, R.-Y. Tsai, and F. C. Ho, *Proc. SPIE-Int. Soc. Opt. Eng. (Display Devices and Systems)* **82**, 2892 (1996).
207. D. R. Thomas, in S. J. Clarson and J. A. Semlyen, eds., *PTR*, Prentice Hall, Englewood Cliffs, N.J., 1993.
208. "Organic Peroxides," *Modern Plastics Encyclopedia*, Vol. **62**, No. 13, McGraw-Hill, Book Co., Inc., New York, 1993, p. 256.
209. U.S. Pat. 2,448,565 (1948), G. Wright and C. S. Oliver (to General Electric).
210. M. L. Dunham, D. L. Bailey, and R. M. Miner, *Ind. Eng. Chem.* **49**, 1373 (1957).
211. S. W. Kantor, in *Abstracts, ACS 130th Meeting*, American Chemical Society, Washington, D.C., Sept. 1956.
212. U.S. Pat. 2,445,794 (1948), J. Marsden (to General Electric).
213. R. J. Cush and H. W. Winnan, in A. Whelan and K. S. Lee, eds., *Developments in Rubber Technology*, Vol. **2**, Applied Science Publishers, Ltd., London, 1981.
214. D. Wrobel, in G. Koerner, M. Schulze, and J. Weis, eds., *Silicones, Chemistry and Technology*, Vulkan-Verlag, Germany, 1991.
215. K. E. Polmanteer, *Rubber Chem. Technol.* **61**, 489 (1988).
216. J. B. Class and R. P. Grasso, *Rubber Chem. Technol.* **66**, 605 (1993).
217. J. L. Speier, *Adv. Organomet. Chem.* **17**, 407 (1979).
218. J. P. Collman and L. S. Hegedus, *Principles and Application of Organotransition Metal Chemistry*, University Science Books, Stanford, Calif., 1980.
219. M. A. Brook, *Silicon in Organic, Organometallic and Polymer Chemistry*, John Wiley & Sons, Inc., New York, 2000.
220. U.S. Pat. 5,281,656 (Jan. 25, 1994), L. Thayler, D. Jones, and E. Groenhof (to Dow Corning).
221. L. N. Lewis, J. Stein, Y. Gao, R. E. Colborn, and G. Hutchins, *Platinum Met. Rev.* **41**, 66 (1997).
222. C. W. Macosko and J. C. Saam, *Polym. Bull.* **18**, 463 (1987).
223. X. Quan, *Polym. Eng. Sci.* **29**, 1419 (1989).
224. A. M. Podoba, E. A. Goldovski, and A. A. Dortsov, *Int. Polym. Sci. Technol.* **14**, T/42 (1987).
225. A. V. Gorshov, Y. M. Kopylov, A. A. Donstov, and L. Z. Khazen, *Int. Polym. Sci. Technol.* **13**, T/26 (1986).
226. A. J. Chalk and J. F. Harrod, *J. Am. Chem. Soc.* **87**, 16 (1965).

227. L. N. Lewis and N. J. Lewis, *J. Am. Chem. Soc.* **108**, 7228 (1986).
228. L. N. Lewis, *J. Am. Chem. Soc.* **112**, 5998 (1990).
229. J. Stein, L. N. Lewis, Y. Gao, and R. A. Scott, *J. Am. Chem. Soc.* **121**, 3693 (1999).
230. S. Sakaki, N. Mizoe, M. Sugimoto, and Y. Musashi, *Coord. Chem. Rev.* **190–192**, 933 (1999).
231. U.S. Pat. 5,331,075 (1994), C. A. Sumpter, L. N. Lewis, and W. B. Lawrence (to General Electric).
232. U.S. Pat. 4,603,168 (1986), S. Sasaki and Y. Hamada (to Toray Silicones).
233. U.S. Pat. 4,490,488 (1984), R. J. Cush (to Dow Corning).
234. U.S. Pat. 3,445,420 (1969), G. J. Kookootsedes and E. P. Plueddemann (to Dow Corning).
235. U.S. Pat. 4,336,364 (1982), M. T. Maxson (to Dow Corning).
236. U.S. Pat. 4,347,346 (1982), R. P. Eckberg (to General Electric).
237. U.S. Pat. 4,256,870 (1981), R. P. Eckberg (to General Electric).
238. U.S. Pat. 4,783,552 (1988), P. Y. K. Lo, L. E. Thayer, and A. P. Wright (to Dow Corning).
239. U.S. Pat. 4,465,818 (1984), A. Shirahata and S. Shosaku (to Toray Silicones).
240. U.S. Pat. 4,472,563 (1987), G. Chandra, P. Y. K. Lo, and Y. A. Peters (to Dow Corning).
241. U.S. Pat. 5,122,585 (1992), C. A. Sumpter and L. N. Lewis (to General Electric).
242. U.S. Pat. 5,206,329 (1993), C. A. Sumpter, L. N. Lewis, and S. J. Danishefsky (to General Electric).
243. P. Steffanut, J. Osborn, and A. DeCian, *J. Fisher, Chem. Eur. J.* **4**, 2008 (1998).
244. L. N. Lewis, J. Stein, R. Colborn, Y. Gao, and J. Dong, *J. Organomet. Chem.* **521**, 221 (1996).
245. U.S. Pat. 5,025,073 (1991), L. N. Lewis and C. Sumpter (to General Electric).
246. U.S. Pat. 5,015,691 (1991), L. N. Lewis and T. C. Chang (to General Electric.).
247. U.S. Pat. 5,254,656 (1993), C. J. Bilgrien and B. A. Witucki (to Dow Corning).
248. V. V. Severnyi, R. M. Minas'yan, I. A. Makarenko, N. M. Bizyuakova, *Vysokomoh Soedin. Ser. A (Eng. Ed.)* **18**, 1464 (1976).
249. F. W. Van der Weij, *Makromol. Chem.* **181**, 2541 (1980).
250. A. L. Suvorov, T. G. Khonina, A. V. Kozlov, and N. A. Kochneva, *Russ. J. Gen. Chem.* **68**, 589 (1998).
251. X. Zhou, S. Hu, N. E. Shephard, and D. Ahn, *Polym. Prepr.* **42**, 255 (2001).
252. V. V. Severnyi, *Kauch. Rezina* **4**, 14 (1998).
253. U.S. Pat. 5,504,176 (1996), H. Fujiki (to Shin-Etsu).
254. K. A. Smith, *J. Org. Chem.* **51**, 3827 (1986).
255. X. W. He, J. M. Widmaier, J. E. Herz, and G. C. Meyer, *Eur. Polym. J.* **24**, 1145 (1988).
256. M. A. Sharef and J. E. Mark, *Makromol. Chem.* **190**, 495 (1989).
257. S. J. Clarson, Z. Wang, and J. E. Mark, *Eur. Polym. J.* **26**, 621 (1990).
258. M. Guibergia-Pierron and G. Sauvet, *Eur. Polym. J.* **28**, 29 (1992).
259. J. C. Saam, D. Graiver, and M. Baile, *Rubber Chem. Technol.* **54**, 976 (1981).
260. D. Graiver, D. J. Huebner, and J. C. Saam, *Rubber Chem. Technol.* **56**, 918 (1983).
261. S. B. Smith and J. Waterborne, *Coatings* **10**, 13 (1983).
262. D. T. Liles and H. V. Lefler, *Proc. Water-borne, Higher Solids, Powder Coat. Symp.* **18**, 161 (1991).
263. D. W. McCarthy and J. E. Mark, *Rubber Chem. Technol.* **71**, 906 (1998).
264. D. W. McCarthy and J. E. Mark, *Rubber Chem. Technol.* **71**, 928 (1998).
265. U.S. Pat. 5,674,937 (1997), D. T. Berg and E. J. Joffre (to Dow Corning).
266. J. Stein, T. M. Leonard, and J. F. Smith, *J. Appl. Polym. Sci.* **47**, 667 (1993).
267. U.S. Pat. 5,034,455 (1991), J. Stein and T. M. Leonard (to General Electric).
268. U.S. Pat. 4,877,828 (1989), J. Stein and T. M. Leonard (to General Electric).
269. U.S. Pat. 5,861,451 (1999), R. T. Schroeder, A. J. Tselepsis, and A. T. F. Wolf (to Dow Corning).

270. U.S. Pat. 5,807,921 (1998), M. P. L. Hill, A. J. Tselepsis, and A. T. F. Wolf (to Dow Corning).
271. U.S. Pat. 5,321,075 (1994), D. T. Liles (to Dow Corning).
272. R. S. Davidson, in J. P. Fouassier and J. F. Rabek, eds., *Radiation Curing in Polymer Science and Technology*, Vol. **I**, Elsevier Publishers, Ltd., U.K., 1993.
273. A. Vokal, P. Kourim, J. Sussmilchova, M. Heidingsfeldova, and B. Kopecky, *Radiat. Phys. Chem.* **28**, 497 (1986).
274. E. L. Warrick, *Ind. Eng. Chem.* **47**, 2388 (1955).
275. W. Ming-Jun, D. Cong, M. Zue-Teh, and D. Lianj-Chang, in *International Conference on Radiation Processing for Plastics and Rubber*, Canterbury, U.K., Mar. 28–30, 1984.
276. J. F. Zack, E. L. Warrick, and Knoll, *J. Chem. Eng. Data* **6**, 279 (1961).
277. R. P. Eckberg, in D. Satas, ed., *Advances in Pressure Sensitive Adhesives*, Satas & Associates, Warwick, R.I., 1992.
278. U.S. Pat. 4,052,529 (1977), G. N. Bokerman, J. A. Calquhoun, and D. J. Gordon (to Dow Corning).
279. U.S. Pat. 4,303,484 (1981), M. Takamizawa, F. Annaka, Y. Takasaki, and H. Aoki (to Shin- Etsu).
280. U.S. Pat. 4,348,454 (1982), R. P. Eckberg (to General Electric).
281. U.S. Pat. 4,293,678 (1981), R. G. Carter (to Union Carbide).
282. U.S. Pat. 4,908,274 (1990), J. Jachman, C. Weitemeyer, and D. Wewers (to Goldschmidt AG).
283. U.S. Pat. 4,963,438 (1990), C. Weitemeyer, D. Wewers, and J. Jachman (to Goldschmidt AG).
284. R. P. Eckberg, *UV Cure of Epoxysilicones, Radiation Curing in Polymer Science and Technology*, Vol. **IV**, Elsevier Publishers, Ltd., U.K., 1993.
285. J. V. Crivello and J. H. W. Lam, *J. Polym. Sci.* **17**, 977 (1979).
286. J. V. Crivello, *CHEMTECH* **10**, 624 (1980).
287. U.S. Pat. 4,279,717 (1981), R. P. Eckberg (to General Electric).
288. U.S. Pat. 4,421,904 (1983), R. P. Eckberg and R. W. LaRochelle (to General Electric).
289. R. P. Eckberg, K. D. Riding, M. E. Grenoble, and S. M. John, *Adhesive Age* 24 (1989).
290. U.S. Pat. 5,650,453 (1997), E. P. Eckberg and M. J. O'Brien (to General Electric).
291. J. V. Crivello, *Latest Developments in the Chemistry of Onium Salts*, Vol. **II**, Elsevier Publishers, Ltd., U.K., 1993.
292. J. V. Crivello and J. L. Lee, *J. Polym. Sci., Part A: Polym. Chem. Ed.* **27**, 3951 (1989).
293. J. P. Fouassier, D. Burr, and J. V. Crivello, *J. Macromol. Sci., Pure Appl. Chem. A* **31**, 677 (1994).
294. F. Castellanos, J. P. Fouassier, C. Priou, and J. Cavezzan, *J. Appl. Polym. Sci.* **60**, 705 (1996).
295. U.S. Pat. 5,340,898 (1994), J. Cavezzan and C. Priou (to Rhone-Poulenc Chimie).
296. U.S. Pat. 5,468,902 (1995), F. Castellanos, J. Cavezzan, J.-P. Fouasser, and C. Priou (to Rhone-Poulenc Chimie).
297. S. R. Kerr, *Adhesive Age* **41**, 26 (1998).
298. U.S. Pat. 5,703,137 (1997), C. Priou and K. Stuart (to Rhone-Poulenc Chimie).
299. U.S. Pat. 5,258,480 (1993), R. P. Eckberg and R. F. Agars (to General Electric).
300. U.S. Pat. 4,064,027 (1977), G. A. L. Gant (to Dow Corning).
301. U.S. Pat. 4,335,035 (1982), M. Hatanka and A. Kurita (to Toshiba Silicone Co.).
302. U.S. Pat. 4,435,259 (1984), M. Chang (to Pitney Bowes).
303. U.S. Pat. 6,150,546 (2000), M. D. Butts (to General Electric).
304. U.S. Pat. 6,127,446 (2000), M. D. Butts (to General Electric).

305. U.S. Pat. 4,916,169 (1990), L. D. Boardman (to 3M).
306. U.S. Pat. 4,510,094 (1985), P. J. Drahnak (to 3M).
307. U.S. Pat. 4,600,484 (1986), P. J. Drahnak (to 3M).
308. L. D. Boardman, *Organometallics* **11**, 4194 (1992).
309. T. Mayer, D. Burget, G. Mignini, and J. P. Fouassier, *J. Polym. Sci., Part A: Polym. Chem.* **34**, 3141 (1996).
310. B. E. Fry and D. C. Neckers, *Macromolecules* **29**, 5306 (1996).
311. F. D. Lewis and G. D. Salvi, *Inorg. Chem.* **34**, 3182 (1995).
312. Eur. Pat. EP 398,701 A2 (1990), J. D. Oxman (to 3M).
313. T. Lippert, B. Deubzer, J. Weis, and A. Wokaun, *Radiat. Phys. Chem.* **47**, 889 (1996).
314. U.S. Pat. 5,496,961 (1996), J. Dauth (to Wacker-Chemie).
315. U.S. Pat. 5,714,524 (1998), O. Hara (to Three Bond Co.).
316. Eur. Pat. EP 832,936 A1 (1997), H. Fujiki (to Shin-Etsu).
317. S. K. Venkataraman, L. Coyne, F. Chambon, M. Gottlieb, and H. H. Winter, *Polymer* **30**, 2222 (1989).
318. X. Xu and V. Galiatsatos, *Makromol. Chem., Macromol. Symp.* **76**, 137 (1993).
319. C. P. Wong, *J. Mater. Res.* **5**, 795 (1990).
320. A. Shefer, M. Gottlieb, and G. Gorodetsky, *Isr. J. Technol.* **24**, 673 (1988).
321. A. Shefer, G. Gorodetsky, and M. Gottlieb, *Mater. Res. Soc. Symp. Proc.* **177**, 31 (1990).
322. G. L. Batch, C. W. Macosko, and D. N. Kemp, *Rubber Chem. Technol.* **64**, 218 (1990).
323. E. M. Barrall, M. A. Flandera, and J. A. Logan, *Thermochim. Acta* **5**, 415 (1973).
324. L. Bokobza, B. Desbat, and T. Buffeteau, *Mikrochim. Acta Suppl.* **14**, 407 (1997).
325. Z. Tan, R. Jaeger, and G. J. Vancso, *Polymer* **35**, 3230 (1994).
326. V. K. Soni and R. S. Stein, *Macromolecules* **23**, 5257 (1990).
327. A. N. Gent, G. L. Lium, and M. Mazurek, *J. Polym. Sci., Part B: Polym. Phys.* **32**, 271 (1994).
328. A. L. Andrady, M. A. Lloente, and J. E. Mark, *Polym. Bull.* **26**, 357 (1991).
329. S. Venkatraman, *J. Appl. Polym. Sci.* **48**, 1383 (1993).
330. A. N. Falcao, J. Skov Pederson, and K. Mortensen, *Macromolecules* **26**, 5350 (1993).
331. H. Oikawa and K. Murakami, *Macromolecules* **24**, 1117 (1991).
332. R. Stein, V. Soni, and H. Yang, *Adv. Elastomers Rubber Elasticity (Proc. Symp.)* 379 (1986).
333. S. L. Bontems, J. Stein, and M. A. Zumbrum, *J. Polym. Sci., Part A: Polym. Chem.* **31**, 2697 (1993).
334. G. Simon and H. Schneider, *Makromol. Chem., Macromol. Symp.* **52**, 233 (1991).
335. M. G. Brereton, *Macromolecules* **24**, 6160 (1991).
336. P. Sotta and B. Deloche, *J. Chem. Phys.* **100**, 4591 (1994).
337. A. Lapp, M. Daoud, G. Jannink, and B. Farago, *J. Non-Cryst. Solids* **172–174**, 862 (1994).
338. L. Garrido, J. Mark, J. Ackerman, and R. Kinsey, *J. Polym. Sci., Part B: Polym. Phys.* **26**, 2367 (1988).
339. J. Stein and L. Prutzman, *J. Appl. Polym. Sci.* **36**, 511 (1988).
340. V. Galiatsatos and J. E. Mark, in J. D. Zeigler and F. G. W. Fearon, eds., *Advances in Silicon-Based Polymer Science*, ACS Publishing, Washington, D.C., 1990.
341. V. Galiatsatos and J. E. Mark, *Macromolecules* **20**, 2631 (1987).
342. S. J. Clarson, V. Galiatsatos, and J. E. Mark, *Macromolecules* **23**, 1504 (1990).
343. J. E. Mark, *Adv. Polym. Sci.* **44**, 1 (1982).
344. J. E. Mark and M. A. Llorente, *J. Am. Chem. Soc.* **102**, 632 (1980).
345. M. V. Valles and C. W. Macosko, *Macromolecules* **12**, 673 (1979).
346. M. A. Llorente and J. E. Mark, *Macromolecules* **13**, 681 (1980).

347. K. O. Meyers and E. W. Merrill, *Elastom. Rubber Elastic.* **193**, 329 (1982).
348. J. E. Mark, *Acc. Chem. Res.* **27**, 271 (1994).
349. B. Erman and J. E. Mark, *Macromolecules* **31**, 3099 (1998).
350. R. Stepto and D. Taylor, *J. Chem Soc., Faraday Trans.* **91**, 2639 (1995).
351. R. Stepto and D. Taylor, *Macromol. Symp. 93 (Polym. Networks 94)* 261 (1995).
352. M. Villar and E. Valles, *Macromolecules* **29**, 4081 (1996).
353. J. E. Mark, and J. L. Sullivan, *J. Chem. Phys.* **66**, 1006 (1977).
354. J. E. Mark, *Makromol. Chem. Suppl.* **2**, 87 (1979).
355. E. Castner and V. Galiatsatos, *Comput. Polym. Sci.* **4**, 41 (1994).
356. R. Kosfeld, M. Hess, and D. Hansen, *Polym. Bull.* **3**, 603 (1980).
357. K. O. Meyers, M. L. Bye, and E. W. Merrill, *Macromolecules* **13**, 1045 (1980).
358. N. Rennar, *Kautsch. Gummi Kunstst.* **6**, 480 (1989).
359. K. H. Schimmel and G. Heinrich, *Colloid Polym. Sci.* **269**, 1003 (1991).
360. A. I. Medalia and G. Kraus, in J. E. Mark, B. Erman, and F. R. Eirich, eds., *Reinforcement of Elastomers by Particulate Fillers in Science and Technology of Rubber*, Academic Press, Inc., San Diego, Calif., 1994.
361. U.S. Pat. 2,938,009 (1960), G. R. Lucas (to General Electric).
362. B. B. Boonstra, H. Cochrane, and E. M. Dannenberg, *Rubber Chem. Technol.* **48**, 448 (1975).
363. M. P. Wagner, *Rubber Chem. Technol.* **49**, 703 (1976).
364. E. L. Warrick, O. R. Pierce, and K. E. Polmanteer, *Rubber Chem. Technol.* **52**, 437 (1979).
365. G. Berrod, A. Vidal, E. Papirer, and J. B. Donnet, *J. Appl. Polym. Sci.* **26**, 833 (1981).
366. H. L. Chapman, M. A. Lutz, and K. E. Polmanteer, *Rubber Chem. Technol.* **58**, 953 (1985).
367. R. K. Iler, *The Chemistry of Silica*, John Wiley & Sons, Inc., New York, 1979.
368. H. E. Bergna, L. E. Firment, and D. G. Swartzfager, *Adv. Chem. Ser.* **234**, 561 (1994).
369. M. I. Aranguren, E. Mora, and C. W. Macosko, *J. Saam, Rubber Chem. Technol.* **67**, 820 (1994).
370. M. Morton, J. C. Healy, and R. L. Denecour, in *Proc. 5th Int. Rubber Conf.* (1967), p. 175.
371. M. Morton, *Adv. Chem. Ser.* **99**, 490 (1971).
372. A. Burneau and O. Barres, *Langmuir* **6**, 1364 (1990).
373. M. Zaborski, A. Vidal, G. Ligner, H. Balard, E. Papirer, and A. Burneau, *Langmuir* **5**, 447 (1989).
374. H. Cochrane and C. S. Lin, *Rubber Chem. Technol.* **66**, 48 (1993).
375. J. Janzen and G. Krauss, *Rubber Chem. Technol.* **44**, 1287 (1971).
376. J. Janzen, *Rubber Chem. Technol.* **55**, 669 (1982).
377. A. I. Medallia, R. R. Juengel, and J. M. Collins, in A. Whelan and K. S. Lee, eds., *Improving the Performance of Rubber Products*, Applied Science Publishers, Barking, Essex, U.K., 1979, Chapt. "5".
378. M. I. Aranguren, C. W. Macosoko, B. Thakkar, and M. Tirrell, *Mater. Res. Soc. Symp. Proc.* **170**, 303 (1990).
379. M. L. Hair, *ACS Symp. Ser.* **137**, 1 (1980).
380. A. M. Vidal and E. Papirer, *Adv. Chem. Ser.* **234**, 245 (1994).
381. M. Zumbrum, *J. Adhes.* **46**, 181 (1994).
382. G. E. Maciel, C. E. Bronnimann, R. C. Zeigler, I. Chuang, D. R. Kinney, and E. A. Keiter, *Adv. Chem. Ser.* **234**, 269 (1994).
383. L. Garrido, J. L. Ackerman, and J. E. Mark, *Mater Res. Soc. Symp. Proc.* **171**, 65 (1990).
384. A. Burneau, B. Humbert, O. Barres, J. P. Gallas, and J. C. Lavalley, *Adv. Chem. Ser.* **234**, 199 (1994).

385. G. Vigil, Z. Xu, S. Steinberg, and J. Israelachvili, *J. Colloid Interface Sci.* **165**, 367 (1994).
386. E. M. Dannenburg, *Rubber Chem. Technol.* **48**, 410 (1975).
387. S. K. Mandal and D. K. Basu, *Rubber Chem. Technol.* **67**, 672 (1994).
388. M. T. Maxson and C. L. Lee, *Rubber Chem. Technol.* **55**, 233 (1982).
389. H. Cochrane and C. Lin, *Rubber Chem. Technol.* **66**, 58 (1993).
390. V. M. Litvinov and H. Spiess, *Makromol. Chem.* **193** (1992).
391. L. Bokobza, B. Desbat, and T. Buffeteau, *Mikrochim. Acta Suppl.* **14**, 407 (1997).
392. E. Guth, R. Simha, and O. Gold, *Kolloid-Z.* **74**, 266 (1936).
393. E. Guth and O. Gold, *Phys. Rev.* **53**, 322 (1938).
394. F. Bueche, *J. Appl. Polym. Sci.* **5**, 271 (1961).
395. L. Mullins and N. R. Tobin, *J. Appl. Polym. Sci.* **9**, 2993 (1965).
396. A. I. Medalia, *J. Colloid Interface Sci.* **32**, 115 (1970).
397. G. Krauss, *J. Polym. Sci., Part B: Polym. Phys.* **8**, 601 (1970).
398. S. Wolff and J. B. Donnet, *Rubber Chem. Technol.* **63**, 32 (1990).
399. A. R. Payne, *J. Appl. Polym. Sci.* **7**, 873 (1965).
400. A. R. Payne, in G. Krauss, ed., *Reinforcement of Elastomers*, Wiley-Interscience, New York, 1965.
401. A. I. Medalia, *Rubber Chem. Technol.* **46**, 877 (1973).
402. G. Krauss, *J. Appl. Polym. Sci., Appl. Polym. Symp.* **39**, 75 (1984).
403. N. Nagata, T. Kobatake, H. Watanabe, A. Ueda, A. Yoshioka, *Rubber Chem. Technol.* **60**, 837 (1987).
404. F. T. Tsutsumi, M. Sakakibara, and N. Oshima, *Rubber Chem. Technol.* **63**, 8 (1990).
405. A. I. Medallia, *Rubber Chem. Technol.* **64**, 481 (1991).
406. M. I. Aranguren, E. Mora, J. V. DeGroot, and J. C. W. Macosko, *J. Rheol.* **36**, 1165 (1992).
407. B. B. Boonstra, H. Cochrane, and E. M. Dannenberg, *Rubber Chem. Technol.* **48**, 558 (1975).
408. A. Voet, J. C. Morawski, and J. B. Donnet, *Rubber Chem. Technol.* **50**, 342 (1977).
409. L. Bokobza and B. Erman, *Macromolecules* **33**, 8858 (2000).
410. L. Mullins, *Rubber Chem. Technol.* **42**, 339 (1969).
411. A. Yang, J. Ayala, and J. Scott, *J. Mater. Sci.* **26**, 2523 (1991).
412. C. R. Herd, G. C. McDonald, and W. M. Hess, *Rubber Chem. Technol.* **65**, 107 (1992).
413. G. C. McDonald and W. M. Hess, *Rubber Chem. Technol.* **50**, 842 (1977).
414. B. B. Boonstra and A. I. Medalia, *Rubber Age (N.Y.)* **93**, 82 (1963).
415. S. Shiga and M. Furuta, *Rubber Chem. Technol.* **58**, 1 (1985).
416. W. H. Hess, *Rubber Chem. Technol.* **64**, 386 (1991).
417. F. Bohin and I. Manas-Zloczower, *Rubber Chem. Technol.* **67**, 602 (1994).
418. Y. Li, M. J. Wang, T. Zhang, F. Zhang, and X. Fu, *Rubber Chem. Technol.* **67**, 693 (1994).
419. A. M. Gessler, *Rubber Age* **101**, 54 (1969).
420. J. E. Mark, S. Wang, P. Xu, and J. Wen, *Mater. Res. Symp. Proc.* **274**, 77 (1992).
421. M. Sharaf, A. Kloczkowski, and J. Mark, *Rubber Chem. Technol.* **68**, 600 (1995).
422. H. W. Post, *Silicones and Other Organosilicon Compounds*, Reinhold Publishing Corp., New York, 1949.
423. M. G. Voronkov, V. P. Mileshkevich, and Y. A. Yufhelevskii, *The Siloxane Bond*, Consultants Bureau, New York, 1978.
424. O. K. Johannson and C. L. Lee, in K. C. Frisch, ed., *Cyclic Monomers*, Wiley-Interscience, New York, 1972, p. 459.
425. S. J. Clarson and J. A. Semlyen, *Siloxane Polymers*, Prentice Hall, Engelwood Cliffs, N.J., 1993.
426. U.S. Pat. 2,504,388 (1949), O. A. Braley and C. L. Moyle (to Dow Corning).

427. DE 872,087 (1953), W. H. Daudt and J. F. Hyde (to Dow Corning).
428. U.S. Pat. 2,766,220 (1956), S. W. Kantor (to General Electric).
429. J. E. McGrath and J. S. Riffle, *Silicon Compounds, Register and Review*, No. S-5, Petrach Systems, Inc., Bristol, Pa., 1982, p. 62.
430. R. N. Meals and F. M. Lewis, *Silicones*, Reinhold Publishing Corp., New York, 1959.
431. S. J. Clarson, *New J. Chem.* **17**, 711 (1993).
432. M. Varma-Nair, J. P. Wesson, and B. Wunderlich, *J. Thermal Anal.* **35**, 1919 (1989).
433. K. E. Polmanteer and M. J. Hunter, *J. Appl. Polym. Sci.* **1**, 3 (1959).
434. A. Provatas, J. Matisons, S. Clarke, D. Graiver, and W. Lomas, *Macromolecules* **33**, 9156 (2000).
435. W. J. Chatterton and J. L. Goudie, in *Conference Record of IEEE International Symposium on Electrical Insulation*, IEEE, Piscataway, N.J., 2000, pp. 412–416.
436. C. M. Murphy and D. C. Smith, *Ind. Eng. Chem.* **42**, 2462 (1950).
437. J. Martin-Gil, F. J. Martin-Gil, A. I. De Andres-Santos, M. C. Ramos-Sanchez, M. T. Barrio-Arredondo, N. Chebib-Abuchala, *J. Anal. Appl. Pyrolysis* **42**, 151 (1997).
438. M. V. Sobolevskii, D. V. Nazarova, L. A. Chistyakova and V. V. Kirillina, *Plast. Massy* **3**, 13 (1962).
439. U.S. Pat. 2,389,804, R. R. McGregor and E. L. Warrick (to Dow Corning).
440. U.S. Pat. 2,389,806 (1945), R. R. McGregor and E. L. Warrick (to Dow Corning).
441. U.S. Pat. 2,465,296 (1949), J. Swiss (to Westinghouse).
442. H. R. Baker, R. E. Kagarise, J. G. O'Rear, and P. J. Sneigoski, *J. Chem. Eng. Data* **11**, 110 (1966).
443. U.S. Pat. 3,865,784 (1975), R. S. Neale and A. N. Oines (to Union Carbide).
444. J. Barry, *J. Appl. Phys.* **17**, 1020 (1946).
445. P. J. Flory, L. Mandelkern, J. B. Kisinger, and W. B. Schultz, *J. Am. Chem. Soc.* **74**, 3364 (1952).
446. A. J. Barry and H. N. Heck, in F. G. A. Stone and W. A. G. Graham, eds., *Inorganic Polymers*, Academic Press, Inc., New York, 1962.
447. V. Bergeron, P. Cooper, C. Fischer, J. Giermanska-Kahn, D. Langevin, and A. Pouchelon, *Colloids Surf., A* **122**, 103 (1997).
448. G. Schmaucks, R. Wagner, and R. Wersig, *J. Organomet. Chem.* **446**, 9 (1993).
449. W. Noll, *Kolloid-Z.* **211**, 98 (1966).
450. H. W. Fox, P. W. Taylor, and W. A. Zisman, *Ind. Eng. Chem.* **38**, 1401 (1947).
451. H. Ruether, C. Maass, and G. Reichel, *Plaste Kautschuk* **7**, 171 (1960).
452. P. Cannon, L. E. St. Pierre, and A. A. Miller, *J. Chem. Eng. Data* **5**, 236 (1960).
453. G. E. Vogel and F. O. Stark, *J. Chem. Eng. Data* **9**, 599 (1964).
454. E. B. Baker, A. J. Barry, and M. J. Hunter, *Ind. Eng. Chem.* **38**, 1117 (1946).
455. R. R. Buch, *J. Fire Saf.* **17**, 1 (1991).
456. C. C. Currie and M. C. Hommel, *Ind. Eng. Chem.* **42**, 2452 (1950).
457. G. Grand and C. C. Currie, *Mech. Eng.* **73**, 311 (1951).
458. D. H. Demby, S. J. Stoklosa and A. Gross, *Chem. Ind.* **48**, 183 (1993).
459. U.S. Pat. 2,599,984 (1952), H. J. Fletcher and M. J. Hunter (to Dow Corning).
460. R. R. McGregor, *Silicones*, McGraw-Hill Book Co., Inc., New York, 1954.
461. P. W. Bridgeman, *Proc. Am. Acad. Arts Sci.* **77**, 129 (1947).
462. Y. Isreli, J. Lacoste and J. Cavezzan, *Polym. Degrad. Stab.* **37**, 201 (1992).
463. E. D. Lipp, *Appl. Spectrosc.* **45**, 477 (1991).
464. A. Weissler, *J. Am. Chem. Soc.* **71**, 93 (1949).
465. F. Clark, *Insulating Materials for Design and Engineering Practice*, John Wiley & Sons, Inc., New York, 1962.
466. S. Fordham, *Silicones*, Philosophical Library, New York, 1960.
467. A. M. Bueche, *J. Polym. Sci.* **15**, 105 (1955).
468. M. L. Dunham, D. L. Bailey and R. Y. Mixer, *Ind. Eng. Chem.* **49**, 1373 (1957).

469. Eur. Pat. EP 767,218 (1997), H. Muller (to Dow Corning).
470. J. B. Class and R. P. Grasso, *Gummi, Fasern, Kunstst.* **49**, 218 (1996).
471. B. B. Boonstra, H. Cochrane, and E. M. Dannenberg, *Rubber Chem. Technol.* **48**, 448 (1975).
472. E. L. Warrick, O. R. Pierce and K. E. Polmanteer, *Rubber Chem. Technol.* **52**, 437 (1979).
473. G. Berrod, A. Vidal, E. Papirer and J. B. Donnet, *J. Appl. Polym. Sci.* **26**, 833 (1981).
474. A. M. Bueche, *J. Polym. Sci.* **25**, 139 (1957).
475. U.S. Pat. 3,635,743 (1972), A. H. Smith (to General Electric).
476. U.S. Pat. 2,448,756 (1948), M. C. Agens (to General Electric).
477. R. A. Labine, *Chem. Eng.* **67**, 102 (1960).
478. W. J. Bobear, in M. Morton, ed., *Rubber Technology*, 2nd ed., D. Van Nostrand Co., New York, 1973.
479. Eur. Pat. EP 1,006,164 (2000), K. Bab and K. Ota (to Dow Corning).
480. N. Singh, J. Anostario, A. Tate, and R. Dean, *Polym. Prep. (Am. Chem. Soc., Div. Polym. Chem.)* **39**, 518 (1998).
481. W. Lynch, *Handbook of Silicone Rubber Fabrication*, D. Van Nostrand Co., New York, 1978.
482. J. Brandrup, E. H. Immergut, eds., *Polymer Handbook*, Wiley-Interscience, New York, 1967.
483. F. M. Lewis, *Rubber Chem. Technol.* **35**, 1222 (1962).
484. Eur. Pat. EP 1,048,693 (2000), J. A. Osaheni, E. R. Evans, and J. E. Doin (to General Electric).
485. K. E. Polmanteer and M. J. Hunter, *J. Appl. Polym. Sci.* **1**, 3 (1959).
486. J. A. Barrie and B. Platt, *Polymer* **4**, 303 (1963).
487. R. M. Barrier, J. A. Barrie, and N. K. Raman, *Rubber Chem. Technol.* **36**, 642, (1963).
488. C. J. Major and K. Kammermeyer, *Mod. Plast.* **39**, 135 (1962).
489. C. W. Roush and S. A. Bailey Jr., *Rubber Age* **84**, 75 (1958).
490. Eur. Pat. EP 731,131 (1996), N. Meguriya and T. Yoshida (to Shin-Etsu).
491. T. G. Gustavsson and S. M. Gubanski, *IEEE Conf. Publ.* **4**, 4.46 (1999).
492. Y. Koshino, I. Nakajima, and I. Umeda, *Proc. Int. Symp. Electr. Insul. Mater.* **2**, 465 (1998).
493. K. B. Yerrick and H. N. Beck, *Rubber Chem. Technol.* **37**, 261 (1964).
494. R. Harrington, *Rubber Age* **84**, 798 (1959).
495. D. J. Fischer, R. G. Chaffee, and V. Flegel, *Rubber Age* **87**, 59 (1960).
496. S. D. Gehman and G. C. Gregson, *Rubber Rev.* **33**, 1429 (1960).
497. W. J. Schulz, C. A. Fairbank, J. V. DeGroot, and M. D. Fisher, *Rubber World* **215**, 29–33 (1996).
498. S. Narayan-Sarathy, R. H. Neilson, and D. W. Smith, *Polym. Prepr. (Am. Chem. Soc., Div. Polym. Chem.)* **39**, 609 (1998).
499. U.S. Pat. 4,418,157 (1983), F. J. Modic (to General Electric).
500. E. Gerlach, *Kautsch. Gummi Kunstst.* **52**, 110 (1999).
501. K. Pohmer, G. Schmidt, H. Steinberger, T. Bruendl, and T. Schmidt, *Kunstst. Plast. Eur.* **87**, 46 (1997).
502. S. A. Visser, *J. Appl. Polym. Sci.* **63**, 1805 (1997).
503. B. Vanwert, Bernard and S. W. Wilson, National Electronic Packaging and Production Conference-Proceedings of the Technical Program, Vol. **2**, Reed Exhibition Companiesy, Norwalk, Conn., (1996), pp. 797–804.
504. V. J. Johnson, *Rubber World* **220**, 19 (1999).
505. E. Haberstroh, E. Henze, and C. Ronnewinkel, *Kunststoffe* **89**, 68 (1999).
506. U.S. Pat. 4,026,843 (1977), R. E. Kittle (to Dow Corning).
507. U.S. Pat. 4,851,452 (1989), D. C. Gross, L. N. Lewis, and C. L. Haig (to General Electric).

508. U.S. Pat. 4,879,317 (1989), K. A. Smith and C. L. Haig (to General Electric).
509. U.S. Pat. 4,555,529 (1985), C.-L. Lee, M. T. Maxson, and J. A. Rabe (to Dow Corning).
510. J. G. Hilborn, M. A. Della, C. J. G. Plummer, J. L. Hedrick, and R. D. Miller, *Polym. Prepr. (Am. Chem. Soc., Div. Polym. Chem.)* **37**, 773 (1996).
511. U.S. Pat. 6,096,792 (2000), H. Iijima, M. Sawada, and I. Iida (to Toshiba Silicone Co.).
512. U.S. Pat. 6,084,002 (2000), W. R. Nicholson, L. J. Rapson, and K. L. Shephard (to Dow Corning).
513. F.-Y. Hshieh and C. J. Julien, *Proc. Int. Conf. Fire Saf.* **26**, 99 (1998).
514. A. L. Smith, ed., *The Analytical Chemistry of Silicones*, John Wiley & Sons, Inc., New York, 1991.
515. J. H. Wengrovius, T. B. Burnell, M. A. Zumbrum, and J. T. Bendler, in *Abstracts, XXIIth Organosilicon Symposium*, Troy, N.Y., Mar. 1994.
516. J. H. Wengrovius, T. B. Burnell, and M. A. Zumbrum, in *Abstracts, Xth International Symposium on Organosilicon Chemistry*, Poznan, Poland, Aug. 1993.
517. J. H. Wengrovius, T. B. Burnell, M. A. Zumbrum, and M. A. Krenceski, *Polym. Prepr. (Am. Chem. Soc., Div. Polym. Chem)* **39**, 512 (1998).
518. W. Huang and Y. Huang, *J. Appl. Polym. Sci.* **70**, 1753 (1998).
519. W. Huang and Y. Huang, *Chin. J. Polym. Sci.* **17**, 429 (1999).
520. U.S. Pat. 2,676,182 (1954), W. H. Daudt and L. J. Tyler (to Dow Corning).
521. U.S. Pat. 4,707,531 (1987), A. Shirahata (to Toray Silicones).
522. U.S. Pat. 5,124,212 (1992), C. Lee and M. A. Lutz (to Dow Corning).
523. L. A. Sobieski and T. J. Tangney, in D. Satas, ed., *Handbook of Pressure Sensitive Adhesive Technology*, 2nd ed., Van Nostrand Reinhold, New York, 1989, p. 508.
524. D. Satas, *Handbook of Pressure Sensitive Adhesive Technology*, 3rd ed., Loughborough Univeristy, Loughborough Leic, UK, 1999.
525. D. F. Merrill, *SAMPE Q.* **16**, 40 (1985).
526. U.S. Pat. 3,527,659 (1970), J. W. Keil (to Dow Corning).
527. U.S. Pat. 4,611,042 (1986), S. A. Rivers-Farrell and A. P. Wright (to Dow Corning).
528. U.S. Pat. 4,529,758 (1985), F. J. Traver (to General Electric).
529. U.S. Pat. 2,672,455 (1954), C. C. Currie (to Dow Corning).
530. U.S. Pat. 2,678,893 (1954), T. A. Kauppi (to Dow Corning).
531. B. C. Copley, *Org. Coat. Appl. Polym. Sci. Proc.* **48**, 121 (1983).
532. B. C. Copley, in L. H. Lee, ed., *Polymer Science and Technology*, Plenum Press, New York, 1984, p. 257.
533. U.S. Pat. 2,842,522 (1958), C. L. Frye (to Dow Corning).
534. J. F. Brown and L. H. Vogt, *J. Am. Chem. Soc.* **87**, 4313 (1965).
535. F. J. Feher, D. A. Newman and J. F. Walzer, *J. Am. Chem. Soc.* **111**, 1741 (1989).
536. F. J. Feher and T. A. Budzichowski, *Polyhedron* **14**, 3239 (1995).
537. F. J. Feher, D. Soulivong and F. Nguyen, *J. Chem. Soc., Chem. Commun.* 1279 (1998).
538. U.S. Pat. 5,047,492 (1991), R. Weidner, N. Zeller, B. Deubzer, and V. Frey (to Wacker-Chemie).
539. F. J. Feher, D. Soulivong, F. Nguyen and J. W. Ziller, *Angew. Chem. Int. Ed.* **37**, 2663 (1998).
540. F. J. Feher, D. Soulivong, and A. G. Eklund, *J. Chem. Soc., Chem. Commun.* 339 (1998).
541. U.S. Pat. 4,528,390 (1985), H. Kimura (to Toshiba Silicone).
542. R. J. Perry, *CHEMTECH* **29**(2), 39 (1999).
543. J. D. Greene, T. Laubender, and W. Goblmeier, *Eur. Coat. J.* **9**, 626 (1998).
544. D. Walter, and T. Goblmeier, *Paint Ink Int.* **9**(3), 2 (1996).
545. U.S. Pat. 6,020,410 (2000), N. P. Hacker, T. Krajewski, S. P. Lefferts, and G. Davis (to Allied Signal).

546. U.S. Pat. 6,043,330 (2000), N. P. Hacker, L. K. Figge, and S. P. Lefferts (to Allied Signal).
547. U.S. Pat. 6,143,855 (2000), N. P. Hacker, S. P. Lefferts, and L. K. Figge (to Allied Signal).
548. U.S. Pat. 6,177,199 (2001), N. P. Hacker, S. P. Lefferts, and L. K. Figge (to Allied Signal).
549. S. B. Lin, *Int. J. Adhes.* **14**(3), 185 (1994).
550. S. B. Lin, *Adhesives Age* **39**(8), 14 (1996).
551. R. Clark, *Handbook of Printed Circuit Manufacturing*, Van Nostrand Reinhold, New York, 1985.
552. S. Huie, P. F. Schmit, and J. S. Warren, *Adhesives Age* **28**, 30 (1985).
553. R. S. Kerr, *Adhesives Age* **39**, 26 (1996).
554. R. P. Eckberg, in *TAPPI Proceedings—1987 Polymers, Laminations and Coatings Conference*, Tappi Press, Atlanta, Ga., 1987, p. 21.
555. G. V. Gordon, S. V. Perz, R. L. Tabler, J. L. Stasser, M. J. Owen, and J. S. Tonge, *Adhesives Age* **41**, 35 (1998).
556. U.S. Pat. 4,609,574 (1986), J. R. Keryk, P. Y. K. Lo, and L. E. Thayer (to Dow Corning).
557. Eur. Pat. EP 523,660 (1993), C. Herzig, B. Deubzer, and D. Huettner, (to Wacker-Chemie).
558. L. Abdellah, B. Boutevin, and B. Youssef, *Prog. Org. Coat.* **23**, 201 (1994).
559. C. Priou, A. Soldat, J. Cavezzan, F. Castellanos, and J. P. Fouassier, *J. Coat. Technol.* **67**, 71 (1995).
560. E. B. Higgins, in J. L. Moilliet, ed., *Waterproofing and Water-Repellency*, Elsevier Publishing Co., New York, 1963, p. 188.
561. C. Morosan, A. Grigoriu, G. Nagy, M. Marcu, D. Giurgiu, and M. Cazacu, *Industria Textila* **45**, 164 (1994).
562. I. Holme, *Tinctoria* **94**, 27 (1997).
563. U.S. Pat. 6,165,560 (2000), J. P. Deyoung, J. B. McClain, and T. J. Romack (to Micell Technologies).
564. M. Messner, in N. Auner and J. Weis, eds., *Organosilicon Chemistry*, Vol. **4**, Wiley-VCH, New York, 2000, p. 639.
565. S. J. Moon and T. J. Kang, *Text. Res. J.* **70**, 1063 (2000).
566. M. M. Joyner, *Text. Chem. Color.* **18**, 34 (1986).
567. K. P. S. Cheng and C. M. Wong, *Text. Asia* **29**, 55 (1998).
568. J. D. Turner, *Text. Chem. Color.* **20**, 36 (1988).
569. Eur. Pat. EP 930,342 (2000), M. Messner and H. Rautschek (to Hüls Aktiengesellschaft).
570. T. J. Kang and M. S. Kim, *Text. Res. J.* **71**, 295 (2001).
571. G. B. Guise and G. N. Freeland, *Text. Res. J.* 701 (1989).
572. Jpn. Pat. JP 3,069,304 (2000), E. Yamazaki and E. Mitsuke (to Nikka Chem. Ind. Co., Ltd).
573. A. J. Sabia, *Text. Chem. Color.* **26**, 13 (1994).
574. Jpn. Pat. JP 11,158,287 (1999), S. Masami and K. Kiochi (to Dow Corning Toray Silicone).
575. U.S. Pat. 6,136,215 (2000), K. E. Zimmermann and M. W. Skinner (to Dow Corning).
576. U.S. Pat. 6,171,515 (2001), M. J. Evans, H. E. Griffin, R. Kemp, L. D. Kennan, and K. E. Zimmerman (to Dow Corning).
577. U.S. Pat. 5,445,652 (1995), D. L. Connell, K. M. Huddlestone, and A. Szpala (to Precision Processes Textiles).
578. K. O. Jang and K. Yeh, *Text. Res. J.* **63**, 557 (1993).
579. A. J. Sabia, *Text. Chem. Color.* **27**, 79 (1995).
580. J. D. Leeder, M. Shi-ying, and A. M. Pearce, *Text. Asia* 59 (1992).

581. A. J. Sabia and R. B. Metzler, *Nonwovens Ind.* **14**, 16 (1983).
582. A. Bereck, D. Riegel, B. Weber, J. Mosel, J. Bindl, P. Habereder, K. G. Huhn, H.-J. Lautenschlager, and G. Preiner, *Textilveredlung* **32**, 138 (1997).
583. R. L. Barker and K. M. Vohs, in *Book of Papers, 1996 International Conference and Exhibition (AATCC)*, Atlanta, Ga., 1986, p. 23.
584. U.S. Pat. 5,824,814 (1998), S. E. Cray and M. J. Evans (to Dow Corning).
585. Eur. Pat. EP 770725 (1997), H. Ishikawa, T. Naganawa, and I. Ona (to Dow Corning Toray Silicone).
586. Jpn. Pat. JP 2,000,110,077 (2000), N. Shuichi, Y. Jun, F. Toshikatsu, and M. Takehiko (to Lion Corp.).
587. Jpn. Pat. JP 2,000,110,076 (2000), N. Shuichi, Y. Jun, F. Toshikatsu, M. Takehiko, and H. Emiko (to Lion Corp.).
588. Jpn. Pat. JP 2,000,110,075 (2000), N. Shuichi, Y. Jun, F. Toshikatsu, M. Takehiko, and H. Emiko (to Lion Corp).
589. Eur. Pat. EP 803,527 (1997), A. Czech, G. J. Murphy, and C. L. Schilling (to inventors).
590. A. J. Sabia and R. B. Metzler, *Text. Ind.* **590**, 55 (1983).
591. M. M. Joyner, *Am. Dye. Rep.* **77**, 36 (1988).
592. M. W. Skinner, C. Qian, S. Grigoras, D. J. Halloran, and B. L. Zimmerman, *Text. Res. J.* **69**, 935 (1999).
593. C. M. Welch, and J. G. Peters, *Text. Chem. Color. Am. Dyest. Rep.* **1**, 55 (1999).
594. U.S. Pat. 5,310,418 (1994), A. M. Czech (to Union Carbide Chem and Plastics Technology Co.).
595. C. M. Welch, *Text. Chem. Color.* **16**, 265 (1984).
596. C. M. Welch, *Text. Res. J.* **53**, 181 (1983).
597. U.S. Pat. 6,102,973 (2000), R. A. Morales (to inventor).
598. U.S. Pat. 5,158,575 (1992), A. M. Czech (to Union Carbide).
599. U.S. Pat. 5,252,233 (1993), A. M. Czech (to Union Carbide).
600. U.S. Pat. 4,549,880 (1985), J. E. Hendrix, J. Y. Daniels, and T. M. White (to Spring Industries, Inc.).
601. U.S. Pat. 5,885,303 (1999), G. L. Payet (to American Laundry Machinery, Inc.).
602. WO 0,019,003 (2000), G. L. Payet (to American Textile Solutions, Inc.).
603. WO 0,015,748 (2000), R. J. Carsweell, A. N. Jarvis, A. L. Killey, W. Mooney, A. P. Parker, E. J. Peckham, and Z. Shen (to Unilever).
604. WO 0,008,249 (2000), M. Altmann, E. D. Brock, B. A. J. Hubesch, R. Mermelstein, M. M. Peffly, T. M. Torgerson, C. L. M. Vermote, and R. A. Woo (to Procter and Gamble Co.).
605. WO 9,955,953 (1999), T. Trinh, J. W. Smith, and R. E. Bolich Jr. (to Procter and Gamble Co.).
606. WO 9,955,952 (1999), T. Trinh, J. W. Smith, R. E. Bolich Jr., E. D. Brock, M. M. Peffly, J. B. Tordil, P. M. Torgerson, and M. W. Altmann (to Procter and Gamble Co.).
607. U.S. Pat. 5,798,107 (1998), J. P. Cappel, A. M. Vogel, E. H. Wahl, and T. C. Ward (to Procter and Gamble Co.).
608. U.S. Pat. 5,254,134 (1993), T. H. Chu and Z. Z. Zhao (to inventor).
609. C. Q. Yang, *Text. Res. J.* **71**, 201 (2001).
610. P. Hao, L. C. Wadsworth, and H. Suh, *Tappi J.* **81**, 187 (1998).
611. T. A. Calamari Jr., D. P. Thibodeaux, H. H. Perkins, and J. M. Hemstreet, *Am. Dye. Rep.* **80**, 28 (1991).
612. M. D. Berthiaume, in E. D. Goddard, J. V. Gruber, eds., *Principles of Polymer Science and Technology in Cosmetics and Personal Care*, Marcel Dekker, New York, 1999, p. 275.
613. E. S. Abrutyn, in R. Schueller, P. Romanowski, eds., *Conditioning Agents for Hair and Skin*, Vol. **21**, Marcel Dekker, New York, 1999, Chapt. "8", p. 167.

614. A. J. O'Lenick Jr., in R. Schueller, P. Romanowski, eds., *Conditioning Agents for Hair and Skin*, Vol. **21**, Marcel Dekker, New York, 1999, Chapt. "9", p. 201.
615. M. D. Berthiaume and A. D. Baum, *J. Soc. Cosmet. Chem.* **48**, 1 (1997).
616. M. D. Berthiaume, *Cosmet. Sci. Technol. Ser.* **22**, 275 (1999).
617. C. R. Robbins, *Chemical and Physical Behavior of Human Hair*, 2nd ed. Springer-Verlag, New York, 1988, pp. 140–141.
618. U.S. Pat. 5,482,992 (1996), T. Kimura, K. Miyoshi, and M. Arai (to Shin-Etsu Chemical Co.).
619. U.S. Pat. 5,502,096 (1996), T. Kimura and M. Arai (to Shin-Etsu Chemical Co.).
620. U.S. Pat. 3,133,891 (1964), L. Ceyzeriat (to Rhône-Poulenc).
621. U.S. Pat. 3,035,016 (1962), L. B. Bruner (to Dow Corning).
622. U.S. Pat. 3,127,363 (1964), S. Nitzsche and W. Manfred (to Wacker-Chemie).
623. U.S. Pat. 3,334,067 (1967), D. R. Weyenberg (to Dow Corning).
624. U.S. Pat. 3,542,901 (1970), K. G. Cooper and P. R. A. Hansen (to Midland Silicones, Ltd.).
625. U.S. Pat. 4,515,932 (1985), R. K. Chung (to General Electric).
626. U.S. Pat. 4,489,199 (1994), J. H. Wengrovius (to General Electric).
627. U.S. Pat. 5,674,963 (1997), R. Friebe (to Bayer AG).
628. U.S. Pat. 5,728,794 (1998), R. Friebe and K.-H. Sockel (to Bayer AG).
629. U.S. Pat. 4,395,526 (1983), M. A. White, R. A. Smith, M. D. Beers, R. T. Swiger, and G. M. Lucas (to General Electric).
630. U.S. Pat. 5,489,479 (1996), G. M. Lucas and J. H. Wengrovius (to General Electric).
631. U.S. Pat. 5,698,653 (1997), G. M. Lucas and J. H. Wengrovius (to General Electric).
632. U.S. Pat. 5,733,996 (1998), F. DeBuyl and P. Leempoel (to Dow Corning SA).
633. U.S. Pat. 5,908,909 (1999), F. DeBuyl and P. Leempoel (to Dow Corning SA).
634. U.S. Pat. 5,840,794 (1998), R. A. Palmer (to Dow Corning).
635. U.S. Pat. 4,788,170 (1988), J. H. Wengrovius (to General Electric).
636. J. H. Wengrovius, V. M. VanValkenburgh, and J. F. Smith, paper presented at *XXV Organosilicon Symposium*, Los Angeles, Calif., Apr. 1992.
637. U.S. Pat. 4,863,992 (1989), J. H. Wengrovius, J. E. Hallgren, J. Stein, and G. M. Lucas (to General Electric).
638. U.S. Pat. 6,162,756 (2000), R. Friebe, H. Sattlegger, K.-H. Sockel, W. Weber, and A. Wilms (to Bayer AG).
639. U.S. Pat. 4,667,007 (1987), J. H. Wengrovius and T. P. Lockhart (to General Electric).
640. U.S. Pat. 5,777,144 (1998), S. Rubinsztajn, G. M. Lucas, and B. P. Bayly (to General Electric).
641. U.S. Pat. 5,962,559 (1999), G. M. Lucas, S. Rubinsztajn and B. P. Bayly (to General Electric).
642. J. D. Winefordner and I. M. Kolthoff, in A. Lee Smith, ed., *The Analytical Chemistry of Silicones*, Vol. **12**, John Wiley & Sons, Inc., New York, 1991.
643. T. V. Kirillova, O. P. Trokhachenova, R. R. Tarasyants, and S. M. Chernykh, *Zh. Anal. Khim.* **47**, 159 (1992).
644. B. B. Hardman and A. Torkelson, in J. I. Kroschwitz, ed., *Encyclopedia of Polymer Science and Engineering*, 2nd ed., Vol. **15**, John Wiley & Sons, Inc., New York, 1989, p. 291.
645. B. A. Čavić-Vlasak, M. Thompson, and D. C. Smith, *Analyst* **121**, 53R (1996).
646. M. C. Angelotti, in A. Lee Smith, ed., *The Analytical Chemistry of Silicones*, Vol. **12**, John Wiley & Sons, Inc., New York, 1991, Chapt. "3", p. 47.
647. A. L. Smith and R. D. Parker, in A. Lee Smith, ed., *The Analytical Chemistry of Silicones*, Vol. **12**, John Wiley & Sons, Inc., New York 1991, Chapt. "4", p. 71.
648. H. J. Horner, J. E. Weiler, and N. C. Angelotti, *Anal. Chem.* **32**, 858 (1960).
649. W. G. Doeden, E. M. Kushibab, and A. C. Ingala, *J. Am. Oil Chem. Soc.* **57**, 73 (1980).

650. D. A. McCamey, D. P. Ianelli, L. J. Bryson, and T. M. Thorpe, *Anal. Chim. Acta* **188**, 119 (1986).
651. J. A. Moore, in A. Lee Smith, ed., *The Analytical Chemistry of Silicones*, Vol. **12**, John Wiley & Sons, Inc., New York, 1991, Chapt. "13", p. 427.
652. S. Fujimoto, H. Ontani, and S. Buge, *Z. Anal. Chem.* **331**, 342 (1988).
653. M. D. Gaul and N. C. Agnelotti, in A. Lee Smith, ed., *The Analytical Chemistry of Silicones*, Vol. **12**, John Wiley & Sons, Inc., New York, 1991, Chapt. "8", p. 205.
654. M. D. Gaul and N. C. Agnelotti, in A. Lee Smith, ed., *The Analytical Chemistry of Silicones*, Vol. **12**, John Wiley & Sons, Inc., New York, 1991, Chapt. "8", p. 197.
655. M. A. Buese, F. L. Keohan, and S. A. Swint, *J. Polym. Sci., Part A: Polym. Chem. Ed.* **29**, 303 (1991).
656. P. J. Garner and R. C. Smith, in *Pittsburgh Conference and Exposition*, Abstract No. 969, New Orleans, La., 1985.
657. J. D. Pinkston, G. Owens, L. Burkes, T. Delaney, D. Millington, and D. Malyby, *Anal. Chem.* **60**, 962 (1988).
658. W. VanderHeuvel, J. Smith, R. Firestone, and J. Beck, *Anal. Lett.* **5**, 285 (1972).
659. M. Vincenti, E. Pellizetti, A. Guarino, and S. Costanzi, *Anal. Chem.* **64**, 1879 (1992).
660. B. Hagenhoff, A. Benninghoven, H. Barthel, and W. Zoller, *Anal. Chem.* **63**, 2466 (1991).
661. X. Dong, A. Proctor, and D. M. Hercules, *Macromolecules* **30**, 63 (1997).
662. K. Käppler, U. Scheim, F. Keidel, and U. Just, *Fresunius J. Anal. Chem.* **345**, 21 (1996).
663. E. D. Lipp and A. Lee Smith, in A. Lee Smith, ed., *The Analytical Chemistry of Silicones*, Vol. **12**, John Wiley & Sons, Inc., New York 1991, Chapt. "11", p. 305.
664. P. R. Griffiths and J. A. Haseth, *Fourier Transform Infrared Spectroscopy*, John Wiley & Sons, Inc., New York, 1986.
665. A. L. Smith, *Applied Infrared Spectroscopy*, John Wiley & Sons, Inc., New York, 1979.
666. J. D. Ingle Jr. and S. R. Crouch, *Spectrochemical Analysis*, Prentice Hall, Old Tappan, N.H., 1988.
667. P. R. Griffiths, S. L. Pentony Jr., A. Giorgetti, and K. H. Shafer, *Anal. Chem.* **58**, 1349A (1986).
668. A. L. Smith, in J. R. Durig, ed., *Chemical, Biological and Industrial Applications of Infrared Spectroscopy*, John Wiley & Sons, Inc., New York, 1985.
669. E. Kohn and M. E. Chisum, *ACS Symp. Ser.* **352**, 169 (1987).
670. P. J. Madec and E. Marechal, *J. Polym. Sci., Polym. Phys. Ed.* **18**, 2417 (1980).
671. E. D. Lipp, *Appl. Spectrosc. Rev.* **27**, 385 (1992).
672. S. Wacholz, U. Just, F. Keidel, H. Geißler, and K. Käppler, *J. Chromatogr. A* **693**, 89 (1995).
673. R. B. Taylor, B. Parbhoo, and D. M. Fillmore, in A. Lee Smith, ed., *The Analytical Chemistry of Silicones*, Vol. **12**, John Wiley & Sons, Inc., New York, 1991, Chapt. "12", p. 347.
674. E. A. Williams, *Polym. Prepr. (Am. Chem. Soc., Div. Polym. Chem.)* **31**, 119 (1990).
675. P. Fux, *Analyst* **115**, 179 (1990).
676. J. F. Hampton, C. W. Lacefield, and J. F. Hyde, *Inorg. Chem.* **4**, 1659 (1965).
677. E. A. Williams, in S. Patai and Z. Rappoport, eds., *The Chemistry of Organic Silicon Compounds*, John Wiley & Sons, London, 1989, Chapt. "8".
678. P. J. Kanyha and S. Brey, in *22nd Congr. AMPERE Magn. Reson. Relat. Phenom. Proc.*, 1984, p. 341.
679. E. A. Williams, in G. A. Webb, ed., *Annual Reports on NMR Spectroscopy*, Vol. **15**, Academic, Press Inc., London, 1983, p. 235.
680. K. Beshah, J. E. Mark, and J. L. Ackerman, *J. Polym. Sci., Part B: Polym. Phys.* **24**, 1207 (1986).

681. J. Brus and J. Dybal, *Polymer* **41**, 5269 (2000).
682. K. Beshah, J. E. Mark, and J. L. Ackerman, *Macromolecules* **19**, 2194 (1986).
683. N. W. Lytle, in A. Lee Smith, ed., *The Analytical Chemistry of Silicones*, Vol. **12**, John Wiley & Sons, Inc., New York, 1991, Chapt. "14", p. 471.
684. R. Pellenbarg, A. C. Siglio, and A. Hattori, *Marine Estuarine Geochem., Proc. Symp.* 121 (1985).
685. N. Watanabe, H. Nagase, and Y. Ose, *Sci. Total Environ.* **73**, 1 (1988).
686. R. Grümping, D. Mikolajczak, and A. V. Hirner, *Fresenius J. Anal. Chem.* **361**, 133 (1998).
687. R. Grümping and A. V. Hirner, *Fresenius J. Anal. Chem.* **363**, 347 (1999).
688. P. L. Desbène, B. Yver, and B. Desmazières, *J. Chromatogr. A* **813**, 121 (1998).
689. U. Just, D. J. Jones, R. H. Auerbach, G. Davidson, and K. Käppler, *J. Biochem. Biophys. Methods* **43**, 209 (2000).
690. R. B. Annelin and C. L. Frye, *Sci. Total Environ.* **83**, 1 (1989).
691. G. E. Batley and J. W. Hayes, *Aust. J. Mar. Freshwater Res.* **42**, 287 (1991).
692. R. Pellenbarg, *Environ. Sci. Technol.* **13**, 565 (1979).
693. R. R. Buch and D. N. Ingebrigtson, *Environ. Sci. Technol.* **13**, 676 (1979).
694. J. C. Carpenter, J. A. Cella, and S. B. Dorn, *Environ. Sci. Technol.* **29**, 864 (1995).
695. R. G. Lehmann, *Environ. Toxicol. Chem.* **12**, 1851 (1993).
696. C. Anderson, K. Hochgeshwender, and W. R. Weidmann, *Chemosphere* **16**, 10 (1987).
697. N. Watanabe, H. Nagase, T. Nakamura, E. Watanabe, and T. Ose, *Sci. Total Environ.* **35**, 91 (1984).
698. C. J. Weschler, *Atmos. Environ.* **15**, 1365 (1981).
699. C. J. Weschler, *Sci. Total Environ.* **73**, 53 (1988).
700. R. E. Pellenbarg, *Appl. Organomet. Chem.* **5**, 107 (1991).
701. R. M. Cassidy, M. T. Hurteau, J. P. Mislan, and R. W. Ashley, *J. Chromatogr. Sci.* **14**, 444 (1976).
702. W. R. Biggs and J. C. Fetzer, *Anal. Chem.* **61**, 236 (1989).
703. K. H. Forbes, J. F. Vecchiarelli, P. C. Uden, and R. M. Barnes, *Anal. Chem.* **62**, 2033 (1990).
704. S. B. Dorn and E. M. Skelley-Frame, *Analyst* **119**, 1687 (1994).
705. O. L. Flaningam and N. R. Langley, in A. Lee Smith, ed., *The Analytical Chemistry of Silicones*, Vol. **12**, John Wiley & Sons, Inc., New York, 1991, Chapt. "7", p. 135.
706. M. Kurata and Y. Tsunashima, in J. Brandrup, E. H. Immergut, eds., *Polymer Handbook*, 3rd ed., John Wiley & Sons, Inc., New York, 1989.
707. E. E. Drott and R. A. Mendelson, *J. Polym. Sci., Part A-2* **8**, 1361, 1373 (1970).
708. F. M. Mirabella and L. Wild, *Polym. Mater. Sci. Eng.* **59**, 7 (1988).
709. N. R. Langley and J. D. Ferry, *Macromolecules* **1**, 353 (1968).
710. K. O. Meyers, M. L. Bye, and E. W. Merrill, *Macromolecules* **13**, 1045 (1980).
711. M. Smart, E. Anderson, and M. Yoneyama, *Silicones, Chemical Economics Handbook*, 583.0100E, SRI International, Menlo Park, Calif., Sept. 2000, p. 22.
712. E. F. C. Griessbach and R. G. Lehmann, *Chemosphere* **38**, 1461 (1999).
713. C. L. Frye, *Sci. Total Environ.* **73**, 17 (1988).
714. C. W. Lentz, *Ind. Res. Dev.* **22**, 139 (1980).
715. A. Opperhuizen, G. M. Asyee, and J. R. Parson, *Comm. Eur. Communities, EUR (Eur 11350 Org. Micropollut. Aquat. Environ.)* 176–183 (1988).
716. G. Chandra, ed., *The Handbook of Environmental Chemistry*, Vol. **3**, Part H, Springer-Verlag, Berlin, 1997.
717. K. Truby, C. Wood, J. Stein, J. Cella, J. Carpenter, C. Kavanagh, G. Swain, D. Wiebe, D. Lapota, A. Meyer, E. Holm, D. Wendt, C. Smith, and J. Montemarano, *Biofouling* **15**, 141 (2000).
718. D. Wiebe, J. Connor, G. Dolderer, and R. Riha, *Mater. Perform.* **36**, 26 (1997).

719. H. R. Bleile and S. Rodgers, in D. Brezinski, T. J. Miranda, eds., *Federation Series on Coatings Technology*, Federation of Societies for Coating Technology, Philadelphia, Pa., 1989.
720. D. W. Goupil, V. A. DePalma, and R. E. Baier, in *Proc. 9th Ann. Conf. Marine Technol. Soc.*, 1973, p. 445.
721. E. Pelletier and R. Siron, *Environ. Toxicol. Chem.* **18**, 813 (1999).
722. J. Pardos, E. Pelletier, R. Siron, and D. Delille, *Environ. Toxicol. Chem.* **18**, 819 (1999).
723. G. G. Giordano and M. F. Refojo, *Prog. Polym. Sci.* **23**, 509 (1998).
724. M. RoldanPallares, J. L. D. Sanz, S. AwadElSusi, and M. F. Refojo, *Arch. Ophthalmol.* **117**, 197 (1999).
725. C. J. Flaxel, S. M. Mitchell, and G. W. Aylward, *Eye* **14**, 834 (2000).
726. R. Pellenbarg, A. C. Siglio, and A. Hattori, *Marine Estuarian Geochem.* 121 (1985).
727. R. Pellenbarg, *Environ. Sci. Technol.* **13**, 565 (1979).
728. R. Pellenbarg, *Mar. Pollut. Bull.* **13**, 427 (1982).
729. R. Pellenbarg, *Mar. Pollut. Bull.* **10**, 267 (1979).
730. W. Balz, J. A. Cella, J. C. Carpenter, S. B. Dorn, and E. Skelly-Frame, in *Abstracts of the 205th ACS Meeting*, Denver, Colo., 1992, American Chemical Society, Washington, D.C., 1992, p. 17.
731. R. Pellenbarg, *Sci. Total Environ.* **73**, 11 (1988).
732. R. E. Pellenbarg and D. E. Tevault, *Environ. Sci. Technol.* **20**, 743 (1986).
733. R. E. Pellenbarg, E. C. DeCarlo, M. E. Boyle, and R. A. Lamontagne, *Appl. Organomet. Chem.* **11**, 345 (1997).
734. N. Watanabe, T. Nakamura, and E. Watanabe, *Sci. Total Environ.* **38**, 167 (1984).
735. N. M. Kitchen and C. A. Russell, *Electr. Contacts, Proc. Annu. Holm Semin.* **21**, 79 (1975).
736. C. J. Weschler, *Sci. Total Environ.* **73**, 53 (1988).
737. C. J. Weschler, *Atmos. Environ.* **15**, 1365 (1981).
738. E. C. Tuazon, S. M. Aschmann, and R. Atkinson, *Environ. Sci. Technol.* **34**, 1970 (2000).
739. *Fed. Regist.* **58**, 9257 (1993).
740. N. J. Fendinger, D. C. Mcavoy, W. S. Eckhoff, and B. B. Price, *Environ. Sci. Technol.* **31**, 1555 (1997).
741. D. E. Powell, R. B. Annelin, and R. H. Gallavan, *Environ. Sci. Technol.* **33**, 3706 (1999).
742. R. R. Buch and D. N. Ingebrigtson, *Environ. Sci. Technol.* **13**, 676 (1979).
743. R. G. Lehmann, S. Varaprath, and C. L. Frye, *Environ. Toxicol. Chem.* **13**, 1061 (1994).
744. U. B. Singh, S. C. Gupta, G. N. Flerchinger, J. F. Moncrief, R. G. Lehmann, N. J. Fendinger, S. J. Traina, and T. J. Logan, *Environ. Sci. Technol.* **34**, 266 (2000).
745. R. G. Lehmann, J. R. Miller, S. Xu, U. B. Singh, and C. F. Reece, *Environ. Sci. Technol.* **32**, 1260 (1998).
746. J. A. Cella and J. C. Carpenter, in *XXVII Organosilicon Symposium*, Abstract No. B-8, Troy, N.Y., 1994.
747. J. Spivack, in *XXVII Organosilicon Symposium*, Troy, N.Y., 1994.
748. C. Anderson, K. Hochgeshwender, H. Weidemann, and R. Wilmes, *Chemosphere* **16**, 2567 (1987).
749. R. R. Buch, T. H. Lane, R. B. Annelin and C. L. Frye, *Environ. Toxicol. Chem.* **3**, 215 (1984).
750. E. J. Hobbs, M. L. Keplinger and J. C. Calandra, *Environ. Res.* **15**, 229 (1975).
751. R. F. Sharp and H. O. W. Eggins, *Int. Biodeter. Bull.* **6**, 19 (1970).
752. R. G. Lehmann, S. Varaprath and C. L. Frye, *Environ. Toxicol. Chem.* **13**, 1753 (1994).
753. R. G. Lehmann, J. R. Miller and H. P. Collins, *Water, Air, Soil Pollut.* **106**, 111 (1998).
754. R. G. Lehmann, J. R. Miller, and G. E. Kozerski, *Chemosphere* **41**, 743 (2000).
755. C. L. Sabourin, J. C. Carpenter, T. K. Leib, and J. L. Spivack, *Appl. Environ. Microbiol.* **62**, 4352 (1996).

756. C. L. Sabourin, J. C. Carpenter, T. K. Leib, and J. L. Spivack, *Environ. Toxicol. Chem.* **18**, 1913 (1999).
757. Ref. 711, p. 5.

MATTHEW BUTTS
JAMES CELLA
CHRISTINA DARKANGELO WOOD
GREGORY GILLETTE
RACHID KERBOUA
JOHN LEMAN
LARRY LEWIS
SLAWOMIR RUBINSZTAJN
FLORIAN SCHATTENMANN
JUDITH STEIN
DENYCE WICHT
GE Global Research Center
SURESH RAJARAMAN
JEFFREY WENGROVIUS
GE Silicones

SILK

Introduction

Silks can be defined as externally spun fibrous protein secretions. Of all the natural fibers, silks represent the only ones that are spun. Silk fibers have been used in textiles for thousands of years, owing to their unique visual luster, tactile properties, and durability. These fibers are remarkable materials displaying unusual mechanical properties. Strong, extensible, and mechanically compressible, silks display interesting electromagnetic responses, particularly in the UV range for insect entrapment; form liquid crystalline phases related to processing; and exhibit piezoelectric properties (1). Silks were used in optical instruments as late as the mid-1900s because of their fine diameter and high strength and stability over a range of temperatures. Spider silks are reportedly used in the South Pacific for gill nets, dip nets, and fishing lures, as well as in weaving and ceremonial dress (1).

Types of Silk

Silks are synthesized by a variety of organisms, including silkworms, spiders, scorpions, mites, and flies. Few of these silks have been characterized. Silks differ in properties, composition, and morphology, depending on the source. Silkworm cocoon silk from *Bombyx mori* is the most well characterized, owing to the extensive use of these fibers in the textile industry for over 5000 years in a practice originating in China. The dragline silk from the orb-weaving spider, *Nephila clavipes*, is

Encyclopedia of Polymer Science and Technology. Copyright John Wiley & Sons, Inc. All rights reserved.

Table 1. Function and Location of Spider Silk Glands[a]

Silk	Gland	Function
Dragline	Major ampullate	Orb web frame and radii construction, safety line
Viscid	Flagelliform	Prey capture
Glue-like	Aggregate	Prey capture, attachment
Minor ampullate	Minor ampullate	Orb web frame construction
Cocoon	Cylindrical	Reproduction
Wrapping	Aciniform	Wrapping captured prey attachment to environmental
Attachment	Piriform	Substrates

[a]Ref. 3.

the most well characterized of the different spider silks. Spider silk has not been domesticated for textile applications because spiders are more difficult to raise in large numbers owing to their solitary and predatory nature. Unlike the cocoon silk from the silkworm, orb webs are not reelable as a single fiber.

Silkworm Cocoon Silk. The cocoon silk from *B. mori* contains two structural fibroin filaments coated with a family of glue-like sericin proteins, resulting in a single thread having a diameter of 10 to 25 μm. Wild silkworms generally have larger-diameter threads, ranging up to 65 μm and displaying a variety of different cross-sectional morphologies. The life cycle of *B. mori* runs for 55 to 60 days, and the organism passes through a series of developmental stages or molts. Silk production occurs during cocoon formation around day 26 in the cycle during the fifth larval instar just before molt to the pupa. The silkworm passes through four different metamorphosizing phases: egg or embryo, larva, pupa, and moth (adult). Smaller quantities of silk are produced at all larval stages except during molts.

Spider Silk. Spider silks function in prey capture, reproduction, and as vibration receptors, safety lines, and dispersion tools. Spider silks are synthesized in glands located in the abdomen and spun through a series of orifices (spinnerettes). The types and nature of the various silks are diverse and depend on the type of spider (2). Some general categories of silks and the glands responsible for their production are listed in Table 1.

Structure

Composition. Table 2 summarizes the amino acid composition of various silk proteins. The silkworm cocoon silk contains two structural proteins, the fibroin heavy chain (mol. wt. ca 350,000) and fibroin light chain (mol. wt. ca 25,000), plus the family of sericin proteins (mol wt 20,000–310,000) to hold the fibroin chains together in the final cocoon fiber and accessory proteins. Other silks, such as the caddis fly and aquatic midge, which spin silks underwater to form sheltered tubes, have also been characterized and consist of a family of proteins having high cysteine content and running from low to very high ($>10^6$) molecular weights (4). Some silkworm silks from wild strains have been reported to contain up to 95% alanine (1).

The consensus crystalline amino acid repeat in the *B. mori* silkworm cocoon silk fibroin heavy chain is the 59mer: GAGAGSGAAG[SGAGAG]$_8$Y. More detailed

Table 2. Amino Acid Composition of Silks

		B. mori		*P. c. ricini*[a]	*N. clavipes*
Amino acid	Abbreviation	Fibroin	Sericin	Fibroin	Dragline
Glycine	G	42.9	13.5	33.2	37.1
Alanine	A	30.0	5.8	48.4	21.1
Serine	S	12.2	34.0	5.5	4.5
Tyrosine	Y	4.8	3.6	4.5	
Aspartic acid–asparagine	D, N	1.9	14.6	2.7	2.5
Arginine	R	0.5	3.1	1.7	7.6
Histidine	H	0.2	1.4	1.7	0.5
Glutamic acid–glutamine	E, Q	1.4	6.2	0.7	9.2
Lysine	K	0.4	3.5	0.2	0.5
Valine	V	2.5	2.9	0.4	1.8
Leucine	L	0.6	0.7	0.3	3.8
Isoleucine	I	0.6	0.7	0.4	0.9
Phenylalanine	F	0.7	0.4	0.2	0.7
Proline	P	0.5	0.6	0.4	4.3
Threonine	T	0.9	8.8	0.5	1.7
Methionine	M	0.1	0.1	Trace	0.4
Cysteine	C	Trace	0.1	Trace	0.3
Tryptophan	W			0.6	2.9

[a]Philosamia cynthia ricini = wild–type silkworm silk.

analysis of these repeats indicates that the fibroin contains alternate arrays of repeating GAGAGS and GAGAGY. Valine or tyrosine replacements for alanine exist in the second repeat (5). These core repeats are surrounded by homogenous nonrepetitive amorphous domains. The repetitive structures in the protein are thought to be the result of genetic level continuous unequal crossovers or genetic recombination events during evolution.

The spider dragline silk from the principal ampullate gland contains at least one protein, called MaSp1, for major ampullate silk protein, previously termed spidroin 1; molecular weight is around 275,000 (6). It remains unclear whether additional proteins play a significant role in the dragline silk fiber. There is no sericin or glue-like protein associated with the dragline fiber. MaSp1 contains amino acid repeats considerably shorter than those found in the silkworm fibroin and not as highly conserved. The repeats contain polyalanine domains consisting of six to nine residues, and a 15-amino acid region showing a GGX repeat motif, where X = alanine, tyrosine, leucine, or glutamine (6,7).

Secondary Structure. The silkworm cocoon and spider dragline silks are characterized as an antiparallel β-pleated sheet wherein the polymer chain axis is parallel to the fiber axis. Other silks are known to form α-helical (bees, wasps, ants) or cross- β-sheet (many insects) structures. The cross- β-sheets are characterized by a polymer chain axis perpendicular to the fiber axis and a higher serine content. Most silks assume a range of different secondary structures during processing from soluble protein in the glands to insoluble spun fibers (see PROTEIN FOLDING).

The crystalline structure of silk was first described in the 1950s as an antiparallel, hydrogen-bonded β-sheet based on the characterization of *B. mori*

fibroin (8), and further modifications to this early model have been made over the years (9,10). Two crystalline forms for silk have been characterized on the basis of X-ray diffraction and ^{13}C-cross-polarization/magic-angle spinning (CP/MAS) NMR spectroscopy. The random coil or silk I, ie, the prespun pseudocrystalline form of silk present in the gland in a water-soluble state, is predominant in the gland; silk II, ie, the spun form of silk which is insoluble in water, becomes predominant once the protein is spun into fiber (9,11). The unit cell parameters in the silk II structure are 940 pm (a, interchain), 697 pm (b, fiber axis), and 920 pm (c, intersheet). The chains run antiparallel with interchain hydrogen bonds roughly perpendicular to the chain axis between carbonyl and amine groups. Van der Waal forces stabilize intersheet interactions owing to the predominance of short side-chain amino acids (glycine, alanine, serine) in these crystalline regions. Solid-state ^{13}C NMR studies of *N. clavipes* dragline silk have concluded that the polyalanine runs in the MaSp1 are in a β-sheet conformation (12).

The structure of silk I remains incompletely understood. This structure is unstable and upon shearing, drawing, heating, spinning, or exposure in an electric field or exposure to polar solvents, such as methanol or acetone, converts to silk II. The change in unit cell dimensions during the transition from silk I to silk II during fiber spinning is most significant in the intersheet plane, where an 18.3% decrease in distance occurs between overlying sheets (13). This change results in the exclusion of water, thus reducing solubility of the protein. Silk II is more energetically stable than silk I and the energy barrier for the transition is low, whereas the return barrier is high and considered essentially irreversible (1,14). Because the instability or metastable nature of the silk I conformation leads to difficulty in obtaining an orientated sample for fiber diffraction analysis and detailed structural characterization, different models have been proposed to describe the silk I structure (14,15).

Crystallinity. Generally, spider dragline and silkworm cocoon silks are considered semicrystalline materials having less crystalline flexible chains reinforced by strong stiff crystals (3). The orb web fibers are Composite Materials (qv) in the sense that they are composed of crystalline regions immersed in less crystalline regions, which have estimates of 30–50% crystallinity (3,16). Earlier studies by X-ray diffraction analysis indicated 62–65% crystallinity in cocoon silk fibroin from the silkworm, 50–63% in wild-type silkworm cocoons, and lesser amounts in spider silk (17).

Structure of the Spider Orb Web. The construction of the orb web is a feat of engineering involving material tailoring, optimization of material interfaces, and conservation of resources to promote survival of the spider (2,3). In addition, the web absorbs water from the atmosphere, and ingestion by the spider may provide a significant contribution to water intake needs (18). Around 70% of the energy is dissipated through viscoelastic processes upon impact by a flying insect into the web (3). Thus the web balances stiffness and strength against extensibility, both to keep the web from breaking and the insect from being ejected from the web by elastic recoil (3). The ability to dissipate the kinetic energy of a flying insect impacting the web is based on the hysteresis of radial threads and also aerodynamic damping by the web (18,19). Some orb webs appear to be at least in part recycled by ingestion as a conservation tool, and some of the amino acids are reused in new webs.

Processing

***In Vivo* Processing.** Silks are synthesized in specialized glands within the organism. Initially, some degree of self-organization or assembly occurs as a result of protein–protein interactions among the crystalline repeats in the protein chains (13). In the spider gland, changes in physiological conditions such as pH and salt concentrations accompany the processing and, presumably, help maintain solubility, despite increasing protein concentration during passage through the various regions of the gland (1). In silkworm there are three distinct regions to the glands and two sets of these organs feeding into one final thread (20,21). The fibroin is synthesized in the posterior region of the gland and the protein moves by peristalsis to the middle region of the gland where it is stored as a viscous aqueous solution until needed for spinning. The protein concentration is 12–15% in the posterior region of the gland where fibroin chain synthesis occurs, increases to around 20–30% in the middle region of the gland where the fibroin is stored and sericin is synthesized, and is significantly higher in the anterior region of the gland where spinning is initiated (20). The two lobes of the gland join just before the spinnerettes in the anterior region and the fiber is spun into air. Aside from binding together the fibroin chains in the final spun fiber, sericin in this process may function in plasticization to ease the flow through the spinneret, as a reservoir for divalent cations, or as a water-holding medium to promote plasticization of the fiber after spinning.

Rheological experiments indicate that crystallinity in the fiber correlates positively with shear and draw rates, and an extrusion rate of around 50 cm/min was found to be a minimum threshold for the appearance of birefringence and the conversion of the soluble silk solution in the gland to the β-sheet found in the spun fiber (20,22). In the posterior region of the gland, 0.4–0.8 mm in diameter, the silk solution is optically featureless; a range of secondary structures are present, including random coil and silk I; and the shear rate is low. In the middle region of the gland, the diameter is 1.2–2.5 mm, streaming birefringence is observed, and the shear rate is also low. In the anterior region of the gland, the diameter is narrow (0.05–0.3 mm), the shear rate is high, water appears to be actively transported out of the gland, the pH decreases, and active ion exchange occurs. Viscosity also increases but presumably decreases prior to spinning as a result of the liquid crystalline phase. At this point the characteristic silk II structure forms. In the pair of major ampullate glands in the spider, which are the location of dragline protein synthesis, a similar process occurs as summarized for the silkworm. This gland is smaller, however, and there is no sericin contribution in the middle region of the gland. A lyotropic nematic liquid crystalline phase of the protein forms prior to spinning in both the spider and the silkworm, as well as in many of the different glands of the spider responsible for the different silks (23). Recent studies also suggest that silk fibroin forms into micelles and then gel states in the gland as a mode to optimize protein concentration within the aqueous processing environment (24,25).

Commercial and Artificial Processing. Commercially, silkworm cocoons are extracted in hot soapy water to remove the sticky sericin protein. The remaining fibroin or structural silk is reeled onto spools, yielding approximately 300–1200 m of usable thread per cocoon. These threads can be dyed or modified

for textile applications. Production levels of silk textiles in 1992 were 67,000 t worldwide. The highest levels were in China, at 30,000 t, followed by Japan, at 17,000 t, and other Asian and Oceanian countries, at 14,000 t (26). Less than 3000 t are produced annually in each of eastern Europe, western Europe, and Latin America; almost no production exists in North America, the Middle East, or Africa. The 1993 projections were for a continued worldwide increase in silk textile production to 75,000 t by 1997 and 90,000 t by 2002 (26).

Most solvents used to solubilize globular proteins do not suffice for silks owing to extensive hydrogen bonding and van der Waals interactions, and the exclusion of water from the intersheet regions. Silks are insoluble in water, dilute acids and alkali, and most organic solvents; they are resistant to most proteolytic enzymes (6,27). Silkworm fibroin can be solubilized by first degumming or removing the sericin using boiling soap solution or boiling dilute sodium bicarbonate solution, followed by immersion of the fibroin in high concentration salt solutions such as lithium bromide, lithium thiocyanate, or calcium chloride. These salt solutions can also be used to solubilize spider silk, as can high concentrations of propionic acid–hydrochloric acid mixtures and formic acid (6). After solubilization in these aggressive solvents, dialysis into water or buffers can be used to remove the salts or acids, although premature reprecipitation is a common problem. Ternary-phase diagrams of silk, water, and chaotropic salt for processing windows have been published (28,29) for native silkworm silks and for genetically engineered versions of silkworm silk.

Films or membranes of silkworm silk have been produced by air-drying aqueous solutions prepared from the concentrated salts, followed by dialysis (11,30). The films, which are water-soluble, generally contain silk in the silk I conformation with a significant content of random coil. Many different treatments have been used to modify these films to decrease their water solubility by converting silk I to silk II in a process found useful for enzyme entrapment (30). Silk membranes have also been cast from fibroin solutions and characterized for permeation properties. Oxygen and water vapor transmission rates were dependent on the exposure conditions to methanol to facilitate the conversion to silk II (31). Thin monolayer films have been formed from solubilized silkworm silk using Langmuir techniques to facilitate structural characterization of the protein (32). Resolubilized silkworm cocoon silk has been spun into fibers (33), as have recombinant silkworm silks (34).

Recent studies have included the formation of electrospun nanometer-diameter fibers, hydrogels, and 3D porous scaffolds prepared from these proteins (35–37).

Properties

Mechanical Properties. The mechanical properties of silks are an intriguing combination of high strength, extensibility, and compressibility (Table 3).

Resistance to axial compressive deformation is another interesting property of the silk fibers. Based on microscopic evaluations of knotted single fibers, no evidence of kink-band failure on the compressive side of a knot curve has been observed (38,40). Synthetic high performance fibers fail by this mode even at relatively low strain levels. This is a principal limitation of synthetic fibers in some structural applications.

Table 3. Mechanical Properties of Silks and Other Fibers[a]

Fiber	Elongation, %	Modulus, GPa[b]	Strength, GPa[b]	Energy to break, J/kg[c]
Fibroins				
B. mori	15–35	5	0.6	7×10^4
Other silkworms	12–50	2–4	0.1–0.6	$(3–6) \times 10^4$
Draglines				
N. clavipes				
Quasistatic[d]	9–11	22–60	1.1–2.9	$(3.7–12) \times 10^4$
High strain[e]	10	20		
Other spiders	10–39	2–24	0.2–1.8	$(1–10) \times 10^4$
Other fibers				
Nylon	18–26	3	0.5	8×10^4
Cotton	5–7	6–11	0.3–0.7	$(5–15) \times 10^3$
Kevlar	4	100	4	3×10^4
Steel	8	200	2	2×10^3

[a]Refs. 1,27,38, and 39.
[b]1 GPa = $10^{:9}$ N/m^2. To convert GPa to psi, multiply by 145,000.
[c]To convert J to cal, divide by 4.184.
[d]Instron tensile test rates of 10%/s.
[e]Rates of >500,000%s.

Fibers. *B. mori* cocoon silk ranges from 10 to 25 μm in diameter; dragline silk from *N. clavipes* from 2.5 to 4.5 μm in diameter. Web fibers from some spiders have diameters as low as 0.01 μm. A silking rate of ~1 cm/s is considered equivalent to natural spinning rates for the spider (20). Some spider silks have been observed to supercontact up to around 50% when unconstrained and exposed to high moisture; other silks such as the silkworm cocoon silk do not contract under similar experimental conditions (41). A skin core has been reported using light microscopy and electron microscopy. However, more recent data using dragline silk from *N. clavipes* refute this finding (42).

Thermal Properties. Spider dragline silk was thermally stable to about 230°C based on thermal gravimetric analysis (TGA) (38). Two thermal transitions were observed by dynamic mechanical analysis (DMA), one at −75°C, presumed to represent localized mobility in the noncrystalline regions of the silk fiber, and the other at 210°C, indicative of a partial melt or a glass transition. Data from thermal studies on *B. mori* silkworm cocoon silk indicate a glass-transition temperature, T_g, of 175°C and stability to ~250°C (37). The T_g for wild silkworm cocoon silks was slightly higher, from 160 to 210°C.

Genetic Engineering

An understanding of the genetics of silk production in silkworms and spiders should help in developing processes for higher levels of silk expression generated by recombinant deoxyribonucleic acid (DNA) methods. The ability of the silkworm to produce large amounts of protein, around 300 μg of fibroin per epithelial cell lining the silk producing gland, has generated a great amount of interest from molecular biologists and developmental biologists in elucidating the genetic

regulation of this system. Genetically engineered or recombinant DNA silkworm and spider silks have been produced using either native genes or synthetic genes (34,43,44) (see GENETIC METHODS OF POLYMER SYNTHESIS). It is interesting to note that studies of variations in native silkworm populations indicate differences in sizes of the crystalline-encoding domains resulting from a high degree of polymorphism in length and organization of the fibroin gene and thus the encoded proteins (45,46). A significant degree of variation in protein size, apparently, can be tolerated in native populations of silkworms and, possibly, spiders. Owing to the highly repetitive nature of the genes and the encoded proteins, the deletion or addition of repeats has little impact on secondary structure and functional performance within a certain window of sizes.

Applications

Because of the advent of improved analytical techniques, together with the tools of biotechnology, a new generation of products is envisioned with silk. The ability to tailor polymer structure to a precise degree leads to interesting possibilities in the control of macroscopic functional properties of fibers, membranes, and coatings, as well as improved control of processing windows. Biotechnology offers the tools with which to solve limitations in spider silk production that have not been overcome with traditional domestication and breeding approaches, such as those used successfully with the silkworm. This is of interest because of the variety of silk structures available and the higher modulus and strength as compared to silkworm silk.

Hybrid silk fibers containing synthetic fiber cores having silk coextruded or grafted have been synthesized. Cosmetics and consumer products, such as hair replacements and shampoos containing silk, have also been marketed. Sutures (qv), biomaterials for tissue repairs, wound coatings, artificial tendons, bone repair, and related needs may be possible applications, since immunological responses to the silks are controllable (see TISSUE ENGINEERING). It is also reasonable to speculate on the use of silk webbing for tissue cell growth, nerve cell growth, and brain repair applications such as temporary scaffolding during regrowth and reinfusion after surgery. Cell culture Petri plates having genetically engineered silkworm silks containing cell binding or adhesive domains have already been produced and are sold commercially. These recombinant silks are stable during injection molding with polystyrene. The demonstration of fiber spinning from resolubilized silkworm silk provides further opportunities in material fabrication using native and genetically engineered silk proteins.

BIBLIOGRAPHY

"Silk" in *EPST* 1st ed., Vol. 12, pp. 578–585, by W. G. Wolfgang, Philadelphia College of Textiles and Science; in *EPSE* 2nd ed., Vol. 15, pp. 309–317, by C. D. Livengood, North Carolina State University.

1. D. L. Kaplan, W. W. Adams, B. Farmer, and C. Viney, eds., *Silks: Materials Science and Biotechnology*, Vol. 544, American Chemical Society, Washington, D.C., 1994, pp. 1–370.

2. M. W. Denny, in J. F. V. Vincent and J. D. Currey, eds., *Mechanical Properties of Biological Materials*, Cambridge University Press, New York, 1980, p. 247.
3. J. M. Gosline, M. E. DeMont, and M. W. Denny, *Endeavour* **10**, 37 (1986).
4. S. T. Case, J. Powers, R. Hamilton, and M. J. Burton, in Ref. 1, p. 80.
5. C. Z. Zhou, F. Confalonieri, N. Medina, Y. Zivanovic, C. Esnault, T. Yang, M. Jacquet, J. Janin, M. Duguet, R. Perasso, and Z. G. Li, *Nucl. Acids Res.* **28**, 2413–2419 (2000).
6. C. M. Mello, K. Senecal, B. Yeung, P. Vouros, and D. L. Kaplan, in Ref. 1, p. 67.
7. C. Y. Hayashi and R. V. Lewis, *Science* **287**, 1477–1479 (2000).
8. R. E. Marsh, R. B. Corey, and L. Pauling, *Biochim. Biophys. Acta* **16**, 1 (1955).
9. R. D. B. Fraser and T. P. MacRae, *Conformation in Fibrous Proteins*, Academic Press, Inc., New York, 1973.
10. F. Colonna–Cesari, S. Premilat, and B. Lotz, *J. Mol. Biol.* **95**, 71 (1975).
11. T. Asakura, A. Kuzuhara, R. Tabeta, and H. Saito, *Macromolecules* **18**, 1841 (1985).
12. A. Simmons, C. Michal, and L. W. Jelinski, *Science* **271**, 84 (1996).
13. D. L. Kaplan, S. Fossey, C. M. Mello, S. Arcidiacono, K. Senecal, W. Muller, S. Stockwell, R. Beckwitt, C. Viney, and K. Kerkam, *Mater. Res. Soc. Bull.* 41–47 (Oct. 1992).
14. S. A. Fossey, G. Nemethy, and H. Scheraga, *Biopolymers* **3**, 1529 (1991).
15. B. Lotz and H. D. Keith, *J. Mol. Biol.* **61**, 201 (1971).
16. C. Viney, K. Kerkam, L. Gilland, D. L. Kaplan, and S. Fossey, in E. B. Sirota, D. Weitz, T. Witten, and J. Israelachvili, eds., *Complex Fluids*, Vol. 248, Materials Research Society, Pittsburgh, Penn., 1992, pp. 89–98.
17. J. O. Warwicker, *J. Mol. Biol.* **2**, 350 (1960).
18. D. T. Edmonds and F. Vollrath, *Proc. R. Soc. London, B* **248**, 145 (1992).
19. L. H. Lin, D. T. Edmonds, and F. Vollrath, *Nature* **273**, 146 (1995).
20. J. Magoshi, Y. Magoshi, and S. Nakamura, in Ref. 1, p. 292.
21. E. K. Tillinghast and M. A. Townley, in Ref. 1, p. 29.
22. E. Ilzuka, *J. Appl. Polym. Sci. Japan* **41**, 163 (1985).
23. K. Kerkam, C. Viney, D. L. Kaplan, and S. J. Lombardi, *Nature* **349**, 596–598 (1991).
24. H.-J. Jin and D. L. Kaplan, *Nature* **410**, 541–548 (2003).
25. Bini, D. Kinight, and D. L. Kaplan, *J. Mol. Biol.* **335**, 27–40 (2004).
26. Technical data, The Freedonia Group, Inc., New York, 1993.
27. D. L. Kaplan and co-workers, in D. Byrom ed., *Biomaterials: Novel Materials from Biological Sources*, Stockton Press, New York, 1991, p. 1.
28. J. P. Anderson, M. Stephen-Hassard, and D. C. Martin, in Ref. 1, p. 137.
29. C. Viney, A. E. Huber, D. L. Dunaway, K. Kerkam, and S. T. Case, in Ref. 1, p. 120.
30. M. Demura and T. Asakura, *J. Membr. Sci.* **59**, 39 (1991).
31. N. Minoura, M. Tsukada, and M. Nagura, *Biomaterials* **11**, 430 (1990).
32. W. S. Muller, L. A. Samuelson, S. A. Fossey, and D. L. Kaplan, *Langmuir* **9**, 1857 (1993).
33. PCT W093/15244 (Aug. 5, 1993), R. Lock (to E. I. du Pont de Nemours & Co., Inc.).
34. J. Cappello, *Trends Biotechnol.* **8**, 309–311 (1990).
35. H.-J. Jin, S. V. Fridrikh, G. C. Rutledge, and D. L. Kaplan, *Biomacromolecules* **3**, 1233–1239 (2002).
36. R. Nazarov, H.-J. Jin, and D. L. Kaplan, *Biomacromolecules* (in press).
37. U.-J. Kim, J. Park, C. Li, H.-J. Jin, R. Valluzzi, and D. L. Kaplan, *Biomacromolecules* (in press)
38. P. Cunniff, S. Fossey, J. Song, M. Auerbach, D. L. Kaplan, R. Eby, W. Adams, and D. Vezzie, *Polym. Adv. Technol.* **5**, 401 (1994).
39. P. D. Calvert, in *Encyclopedia of Materials Science and Engineering*, Pergamon Press, Oxford, U.K., 1988, p. 334.
40. D. V. Mahoney, D. L. Vezie, R. K. Eby, W. W. Adams, and D. L. Kaplan, in Ref. 1, p. 196.
41. R. W. Work, *J. Arachnol.* **9**, 299 (1981).
42. S. Nakamura, J. Magoshi, and Y. Magoshi, in Ref. 1, p. 211.

43. Y. Suzuki and Y. Oshima, *Cold Spring Harbor Symp. Quantum. Biol.* **42**, 947 (1977).
44. J. P. Prince, K. P. McGrath, C. M. DiGirolamo, and D. L. Kaplan, *Biochemistry* **34**, 10879 (1995).
45. K. U. Sprague, M. B. Roth, R. F. Manning, and L. P. Gage, *Cell* **17**, 407 (1979).
46. L. P. Gage and R. F. Manning, *J. Biol. Chem.* **255**, 9444 (1980).

DAVID L. KAPLAN
Tufts University

SINGLE-SITE CATALYSTS. See Volume 4.

SMART MATERIALS, MICROGELS. See Volume 8.

SOLID-STATE EXTRUSION

Introduction

Solid-state extrusion (SSE) is one of the well-known methods used for attaining a high oriented state of polymers (1–4). It enables the production of fibers, films, pipes, shapes, including those of large cross section and of various configurations—all possessing high strain–stress characteristics. SSE is based on deformation at temperatures just below the polymer melting temperature, or for amorphous polymers just above the glass-transition temperature. The deformation is mainly by extrusion (qv) through conical or slit dies, it is used for shape forming and structure modification of polymer materials of different nature, such as homopolymers, polymer blends, filled polymer composites, etc (4–10).

For the production of high modulus high density polyethylene (HDPE), polytetrafluoroethylene (PTFE) and other polymers the solid-state extrusion is frequently used at the first stage of a two-step drawing process (11–16). The polymer is first drawn up to the limiting draw ratio at a fast rate and subsequently slowly superdrawn at a temperature that depends on the morphology. Extrusion draw ratio (EDR for short; it is defined as the ratio of die entrance to exit cross-sectional areas), pressure, extrusion rate, temperature, and die geometry are the parameters that effectively influence the process of the high oriented polymer production, the polymer structure and properties.

This article gives a brief information on different SSE methods and their influence on structure and properties of polymer materials. Attention is primarily paid to the most known methods, such as plunger extrusion and hydrostatic extrusion. Two new methods of SSE implementation are analyzed in brief, which, in contrast to the conventional ones, are based on polymer simple shear, not drawing. Lately, they have been of high interest in view of the production of nanostructural metallic materials (17) and are now known as methods of severe plastic deformation (SPD).

Encyclopedia of Polymer Science and Technology. Copyright John Wiley & Sons, Inc. All rights reserved.

The treatment by the scheme of simple shear under pressure results in the intensive refinement of metal crystallites with the formation of ultrafine grain substructures possessing unique properties (17). SPD of polymer materials has become the subject of investigation recently. The investigation results show that simple shear considerably affects the structure and properties of polymers (18,19). In contrast to the conventional SSE, the solid-state extrusion based on simple shear does not result in final changes of billet shape and dimensions. That is why, the problems relating to the conventional SSE are included in the section "Extrusion with Changes in Billet Shape", while the SPD methods for polymers and a brief analysis of the experimental results are given in the section "Extrusion Based on Simple Shear".

Extrusion with Changes in Billet Shape

The SSE process based on changes in polymer-billet shape is, first of all, characterized by the EDR value. The limited EDR value is determined by polymer type, molecular weight and morphology. For example, for HDPE it may reach more than 40 (1). For polyoxymethylene (POM), polypropylene (PP), PTFE the maximum values of draw ratio equal 10, 6, and 4 (20–22), respectively. For polymethylmethacrylate (PMMA), polystyrene (PS), polycarbonate (PC), and other amorphous polymers they are even lower (21,23). The extruded specimens are highly oriented and possess improved mechanical properties. In the case of semicrystalline polymers, the extrusion results in a considerable increase of tensile modulus and strength (1,2). With amorphous polymers, a considerable increase of plasticity is observed alongside with increase of tensile moduli (21,23).

Extrusion Methods. There exist two approaches to SSE implementation. These are the methods of plunger and hydrostatic extrusion. The first investigations by using the plunger extrusion were made on polyethylene. Extrudates were produced by melt crystallization under pressure and by orientation in a capillary rheometer of the Instron type (1,24–26). Moreover, the crystallization of polymer took place at die entrance and in the rheometer cylinder. Such a technique made it possible to produce short transparent and strong fibers of less than 1 mm diameter or films of similar characteristics.

In more recent experiments, the polymer billet was formed prior to SSE. The extrusion process was implemented with both the capillary rheometer and by using a high pressure chamber and a pressing equipment (6–8,25,27), thus the potential applications of the method have become wider. Figure 1**a** is a schematic showing the process of plunger extrusion, which is the most frequently applied in practice. The polymer is extruded by a rod through the die of conical shape. With the dies of different deforming-channel sections (such as slot, round, square, screw ones) it is possible to produce high oriented fibers or films, to change the shape and to draw the polymer billet for having shapes of improved physical and mechanical properties.

For the structural modification of polymers the method of solid-state coextrusion (SSCE) is used (28,29). This is a technique for polymers which is difficult to draw, or if the highest draw is desired. The polymer to be drawn is extruded within a second more ductile polymer (within a sandwich arrangement). The process has

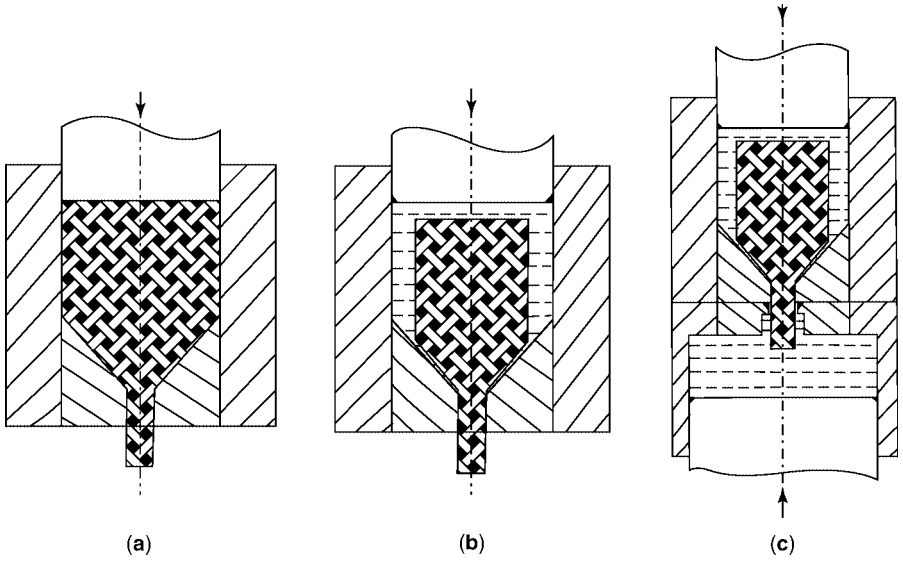

Fig. 1. Schematic representation of plunger extrusion (**a**), hydrostatic extrusion (**b**), and hydrostatic extrusion with backpressure (**c**).

been used for the extrusion of films (split-billet coextrusion) and fibers (concentric-billet coextrusion). In particular, the SSCE technique was used for the production of highly oriented films of semicrystalline polyamides (28), poly(vinylidene fluoride) (30,31), HDPE (25,28,29), poly(L-lactic acid) (32), and amorphous PS (29) and poly(ethylene terephtalate) (PET) (33). This technique makes it possible to coextrude polymers of different molecular weights at temperatures much lower than the melting temperature and to produce superthin films of high strength characteristics.

In the process of hydrostatic extrusion, the polymer billet is forced by a compressed liquid through a narrowing die. The high pressure develops due to rod travel, as shown in Figure 1**a** and 1**b**, or is generated by a high pressure compressor (the so-called "compressor version of the hydrostatic extrusion"). This processing method prevails over the plunger extrusion since there is no friction of the billet material on the channel walls in the high pressure chamber, and the friction between the polymer and the die is low because of liquid penetration into the gap. Besides, in the hydrostatic extrusion the effect of material plasticization is largely realized at the expense of high pressure action (26), so brittle polymers can be deformed as well (21,23). If necessary to increase polymer ductility, the deformation with backpressure is carried out (Fig. 1**c**) (26). The first investigation of the hydrostatic-extrusion process as well as of the structure and properties of extrudates were done approximately at the same time, as for the plunger extrusion (34–36), and they were being actively developed later on (20–23,25,37,38).

For SSE, monolithic or powder billets are used. In the latter case, the polymer powder is compacted, heated to the temperature close to the melting temperature and then extruded. The extrudates of ultra high molecular weight polyethylene (UHMWPE) (8), polymerization-filled polyethylene composites (7,9)

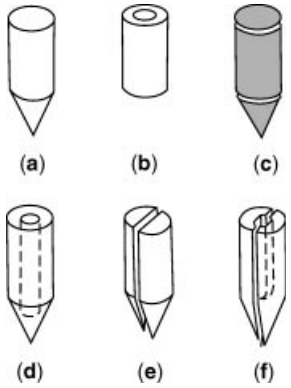

Fig. 2. Billets for SSE (**a, b, c**) and shells for SSCE (**d, e, f,**): (**a**) solid plug, (**b**) pipe billet, (**c**) powder billet, (**d**) concentric shell, (**e**) full width shell, and (**f**) half width shell.

of polyetherketone (39), polyarylate (40) have been produced in this way. With the plunger extrusion of a powder billet, high EDR values are attained at temperatures much lower than in the case when a monolithic sample is deformed. The powder billet is also used for the production of high oriented polymers by the SSCE method and twostep drawing process (12,13).

Polymer-billet geometry is defined by SSE scheme. In Figure 2, there are some variants of billets for the plunger (**a**–**f**) and hydrostatic (**a**, **b**) extrusion to be used in the described SSE techniques. The hydrostatic extrusion is of a lesser potential application as it is necessary to protect the compacted powder from liquid penetration and to seal the billet in the die to prevent liquid from leakage under pressure rise (coextrusion).

Extrusion Conditions. For a brief and clear presentation of the subject matter we make use of the approach of system analysis to represent SSE as a system having inputs and outputs, and set forth the relationships. The input variables $\{X\}$ are parameters controllable for the purpose of affecting the output variables $\{Y\}$. In the case of SSE, with a predetermined material of the billet, the former parameters are: the extrusion draw ratio, die geometry, velocity of plunger motion for the plunger extrusion, and plunger hydroextrusion; pressure in chamber in the case of compressor version of the hydroextrusion; backpressure or drag force applied to the extruded product; temperature of chamber and die heating; structure of billet material; dimensions and geometry of the billet; and lubricant and fluid (for hydroextrusion).

In SSE, the output variables are: extrusion pressure, velocity of product exiting, value of extrudate swell, degree of deformation and strain rate, and structure and properties of the processed material.

The Normal Solid-State Extrusion Process and Its Violations. The normal course of SSE is characterized by a nonstationary stage at the beginning of the process and a constant velocity of product exiting during the rest of the process. In this case, the extrudate has a regular cylindrical shape with smooth surface having no visible defects.

In the case of plunger extrusion, at the stationary stage of the normal process the velocity of the exiting extrudate υ_e is described by the relation $\upsilon_e = R\upsilon_p$,

where υ_p is the velocity of plunger motion, R is the extrusion draw ratio. For the plunger version of the hydrostatic extrusion $\upsilon_e = R\upsilon_p\, S_p/S_b$, where S_b is the cross-sectional area of the billet, S_p is the cross-sectional area of the plunger. For the compressor version of the hydrostatic extrusion, at the stationary stage of the process the velocity of extrudate existing is determined by the value of pressure (a move detailed explanation is given below).

The normal course of SSE is only realized at a definite range of input parameters. Outside the range there occurs some disturbances in the normal process: a discontinuous movement of the extrudate without an essential change of its shape (the stick-slip effect); the unstable flow of the polymer in the paraxial zone of the extrudate resulting in polymer turbidity; the pulsating flow with a considerable deformation of extrudate shape; and the occurrence of spiral-like cracks on its surface.

The above defects are due to different reasons. In the article (41), the stick-slip effect is related to self-excited oscillations initiated by the dependence of static friction–stress between the billet and the die at the time when they are in contact. The latter is connected with the viscoelastic properties of the rough billet surface and by lubricant squeezing out from the region of contact. Ward and co-workers (1) explain the stick-slip effect by the heating of billet during the deformation. The pulsatory flow is assumed to be due to a competition between the viscosity and high elasticity of polymers (42).

In accordance with different physical causes of interruption in the normal course of SSE (eg 41,42), criteria have been obtained and the boundaries of the input-variable range have been determined for the normal regime of the process. For example, for the stick-slip effect the lower bound of the velocity of plunger motion has been determined in (41). The upper bound of the velocity region of normal process has been derived in (42) based on the Weissenberg (Debora) criterion.

In (41,44), different engineering approaches to stick-slip effect elimination have been proposed. The most effective are the application of a tractive force to the front end of the product being extruded.

Extrusion Pressure. The characteristic feature of the plot of extrusion pressure P vs the logarithm of extrusion draw ratio $\ln R$ is that it is convex to the axis of $\ln R$ (Fig. 3). In the case of the hydrostatic extrusion of metals, the dependence is practically linear (44). This difference is because with polymers there is a more intensive strain hardening, strain rate, and pressure hardening as compared to metals. At a qualitative level this is shown as follows.

As the work of plastic deformation is equal to that of external forces, it follows, in the first approximation, that the hydrostatic-extrusion pressure P can be determined by the formula (45):

$$P = \int_0^{\varepsilon^* + \ln R} \sigma_s(\varepsilon, \dot{\bar{\varepsilon}}, \bar{p}, \bar{T})\, \mathrm{d}\varepsilon \qquad (1)$$

where $\sigma_s(\varepsilon, \dot{\bar{\varepsilon}}, \bar{p}, \bar{T})$ is the strain resistance of polymer, ε is the strain, $\dot{\bar{\varepsilon}}$, $\bar{p}$, $\overline{T}$ are values of the strain rate, pressure, and temperature averaged with respect to the volume of deformation center, respectively; ε^* is the strain induced by the entrance

and exit zones of the die (it depends on the value of die cone angle and does not depend on the extrusion ratio).

By double differentiation of relation 1 we have

$$\frac{\mathrm{d}^2P}{\mathrm{d}(\ln R)^2} = \left(\frac{\partial\sigma_s}{\partial\varepsilon} + \frac{\partial\sigma_s}{\partial\dot{\bar{\varepsilon}}}\frac{\mathrm{d}\dot{\bar{\varepsilon}}}{\mathrm{d}(\ln R)} + \frac{\partial\sigma_s}{\partial\bar{p}}\frac{\mathrm{d}\bar{p}}{\mathrm{d}(\ln R)}\right)\Bigg|_{\varepsilon^*+\ln R} + \\ + \int_0^{\varepsilon^*+\ln R} \frac{\mathrm{d}}{\mathrm{d}(\ln R)}\left(\frac{\partial\sigma_s}{\partial\dot{\bar{\varepsilon}}}\frac{\mathrm{d}\dot{\bar{\varepsilon}}}{\mathrm{d}(\ln R)} + \frac{\partial\sigma_s}{\partial\bar{p}}\frac{\mathrm{d}\bar{p}}{\mathrm{d}(\ln R)}\right)\mathrm{d}\varepsilon \tag{2}$$

In view of polymer strain, velocity, and pressure hardening, all the derivatives of σ_s in the righthand part of relation (2) are positive. Besides, the average values of the strain rate and pressure at the center of deformation are increasing with extrusion draw ratio, ie the derivatives of $\dot{\bar{\varepsilon}}$ and $\bar{p}$ with respect to ln R are also positive. It follows that the right-hand part of relation (2) and, thus, the second derivative of P with respect to ln R are also positive, hence we have the convex plot of function $P = P(\ln R)$ with respect to the axis of R. According to (2), more intensive the effects, the higher the strain, strain rate and, stress hardening of the material.

On the dependence of extrusion pressure on die cone angle 2β there is a minimum (Fig. 3**b**). This is because of the competition of two factors that affect the extrusion pressure: contact friction and additional deformation ε^* at the input and output from the conical part of the die. The first and the second factor become significant with a decrease or an increase in cone angle, respectively.

In view of the fact that the polymer strain resistance depends much on strain rate and temperature, in plunger extrusion and plunger version of hydrostatic extrusion the extrusion pressure increases with the velocity of plunger motion

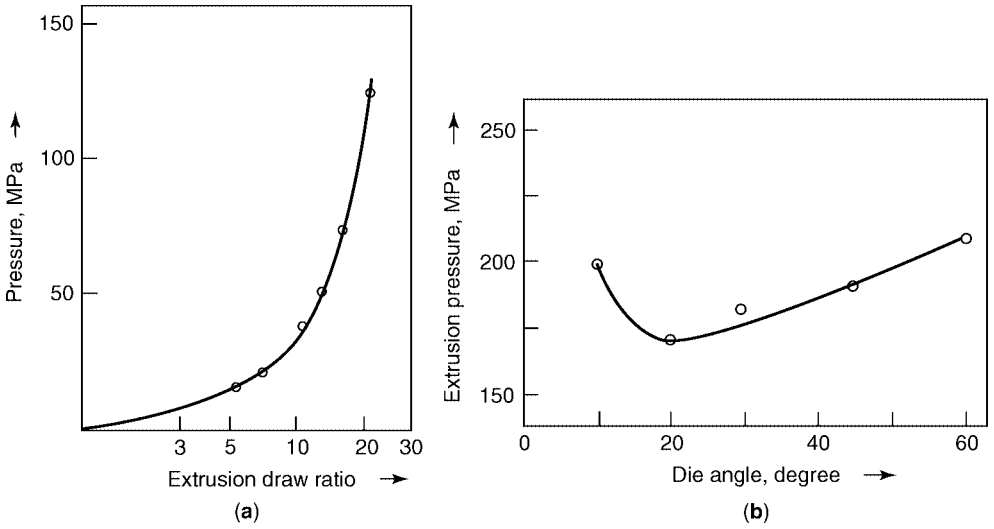

Fig. 3. Typical graphs of extrusion pressure versus extrusion draw ratio (log scale) (**a**) and die angle (**b**). (**a**) Rigidex SOLPE, $2\alpha = 30^\circ$ (43). (**b**) High density polyethylene, EDR = 6.75 (38).

and decreases with temperature rise. For the compressor version of the hydrostatic extrusion, pressure in the chamber determines the velocity of extrudate exiting.

The above-mentioned dependences of SSE pressure on input parameters can be taken into account within the framework of mechanical models of the process. In the most detailed ones (20), the relationships for calculation of pressure have been derived with a rather good agreement between theory and experiment. The value of extrusion pressure can be estimated, in a first approximation, by formula (1), where $\varepsilon^* = (\pi/2)\tan(\beta/2)$ (46). The $\sigma_s(\varepsilon)$ dependence should be experimentally determined with the average, in deformation center, temperature and rate of deformation. It is easy to show that the latter is approximately equal to $\dot{\varepsilon} = \frac{2v_e}{d_e} R^{\frac{3}{2}} \tan\beta$ where d_e is the diameter of the extrudate.

The Velocity of Extrudate Exiting. It has been already pointed that the rate of extrusion is an output variable only in the case of the compressor version of hydrostatic extrusion. For the plunger processes, under the normal flow, the rate of extrusion is an independent quantity. If the working fluid is pumped to the chamber by a compressor, and in the chamber there is a control valve for releasing unnecessary liquid, then it is possible to maintain the extrusion pressure at a preset level. In this case, the velocity of product exiting depends on pressure and temperature. According to theoretical estimates, and to experiment (38), the extrusion rate exponentially increases with pressure.

The Swelling of Extrudates. In the case of SSE, a phenomenon of extrudate swelling at the die exit is observed. Taking it into account, the quantities of the actual extrusion draw ratio $R_d = S_b/S_e$ and the nominal extrusion draw ratio $R_n = S_b/S_d$ are introduced, where S_e is the area of the extrudate cross section, S_d is the area of the die exit. Parameter R_a correlates with the EDR value.

This phenomenon is related to a partial relaxation of viscoelastic strain in polymer during the extrusion. Its value is determined by both the polymer characteristic properties and the SSE conditions (1,5,23). With an increase in EDR value the swelling diminishes sometimes close to zero, the same as was observed for the linear polyethylene with $M_W = 1 \times 10^5$ (1). A considerable swelling is characteristic of semicrystalline polymers possessing high molecular weight, as well as of amorphous polymers. To reduce the swelling, the use is made of dies with a longer calibrating zone.

Peculiarities of the Mechanics of Powder Extrusion. Mathematical modeling of the SSE process by the method of continuum mechanics is based on defining equations relating the components of stress and strain tensors. Among them is the yield condition. For the isotropic monolithic materials it is in the Tresca, Mizes or Hill form (47).

The mathematical description of the powder billet SSE cannot rely on the above conditions of plasticity, as they do not take the change in density of the extruded sample into account. Nor the conditions of plasticity used to model the compaction of metal powders are suitable for this case (48). They imply that with the increase in hydrostatic pressure the relative density of powder material tends to unity. However, in the case of hydrostatic compaction of polymer powders, the relative density of compacts tends to a value less than unity, which is typical of the polymer. The reason is in difference of compaction mechanisms for the metal and polymer powders.

For polymers, the compaction proceeds in two stages. The first stage consists in shear and turning of some particles relatively each other. They experience high elastic strain resulting in the increase of the area of real contact and forces of the interparticle friction. The second stage of compaction is mainly conditioned by high elastic–plastic straining of the particles that fill the free volume. After releasing the external pressure the polymer material decreases its density as the elastic deformation is reversible.

A condition of plasticity has been proposed (49) that makes allowance for a changing of the density of powder polymer during the deformation under pressure. It was the basis for the elaborated SSE theory to predict the density of extrudates (50). It follows, in particular, that during the SSE a nonmonotonic dependence of the density of extrudates on the extrusion ratio is possible. The presence of the effect has been verified experimentally.

Deformation Mechanism. The deformation mechanism has been studied in more detail for the case of semicrystalline polymers, polyethylene, in particular (1,2). There exist a number of models explaining the evolution of polymer structure at high draws. The models can be subdivided into two categories (2), namely, the microfiber plus the tie molecule model, as proposed by Peterlin and co-workers and the extended chain model, which is similar to Ward's crystalline bridge model.

According to the Peterlin's model (51,52), the starting material consists of the packed lamellae with chain folds, while the completely extruded one consists of oriented microfibrils. In the lamellar structure, within the lamella there is a macromolecule that forms folds in direction normal to chain axis. In the fibrillar structure, the macromolecule is within the microfiber, but already in direction parallel to chain axis. Microfibers consist of crystal blocks and noncrystalline regions connected by taut tie molecules. Under drawing, the lamellar structure changes to the fibrillar one at the expense of shearing, rotation, chain tilt, and slip processes taking place in lamella. The axial modulus is proportional to the number of load-bearing tie molecules that cross the noncrystalline regions to connect adjacent crystalline blocks along the microfiber.

Ward's model (53,54) provides the presence of "crystalline bridges" formed from groups of crystallized taut intrafibrillar tie molecules between the crystallites. This morophology consists of fibrillar stacks of crystallites, linked by intercrystalline bridges, or of a continuous crystal containing disordered regions. In either case, the crystalline phase is essentially continuous in the crystallographic *c*-direction. The degree of continuity increases with EDR. This model is intermediate between a lamellar and an extended-chain structure (2).

The results of the electron-microscopy investigations of the oriented polyethylene suggest several consecutive stages of the deformation mechanism (2). At the first stage, lamellae move rigidly apart with the strain accommodated almost entirely by the interlamellae amorphous layer. At the second stage, the tie chains become highly extended and slip initiates in the crystalline lamellae. After this, strain-induced crystallization of the oriented amorphous fibers occurs. At the third stage, the blocks of crystal are pulled out of the lamellae; as block shear continues, the portion of lamellae that is below a critical size decrystallizes and contributes to strain softening. Finally, both the blocks form the crystal shear process and the strain-induced crystallization become aligned along the tensile axis.

The SSE process of semicrystalline polymers is highly influenced by their molecular weight. Extrusions of bulk crystallized polyethylene of high molecular weight proceed at slower rates and lower maximum EDR than lower molecular weight grades (2). The deformation resistance imposed by the higher degree of entanglement between molecular chains tends to inhibit high elongation.

Properties. The SSE of polymers results in the formation of a structural state possessing high anisotropy of properties, in particular, the strain–stress characteristics, thermal expansion, thermal conductivity, and gas permeability. This anisotropy is closely connected with orientation of chains and reconstruction of structure in crystalline and amorphous regions. For example, for semicrystalline thermoplastics, already at a comparatively low extrusion ratio, the chains in the crystalline phase turn out to be almost completely oriented in the direction of deformation. In the amorphous region, the chain organization is less perfect, but the degree of orientation continuously increases during the drawing. It depends on many factors: structure organization and molecular weight of the polymer, billet type, degree of drawing, and conditions of the extrusion process.

Semicrystalline Polymers. Extrusion of semicrystalline polymers, in particular polyolefins, essentially influences their mechanical properties. The SSE can increase ten-fold their tensile modulus, as compared to the starting material. Solid plugs of HDPE deformed to EDR = 40 have tensile modulus of about 70 GPa (1). For low density polyethylene (LDPE) the limit draw ratio is less than 9 (55), which can be the result of difficulties in generation of a metastable ductile monoclinic form. As a result, the tensile modulus reaches a value of less than 1 GPa (55). The maximum value of the tensile modulus of the extruded PP is 17 GPa (34). Increase in yield strength and tensile strength occurs simultaneously with the increase of tensile modulus (22,26,56). With EDR increasing, the elongation decreases.

For equal EDR values, the values of tensile modulus and tensile strength are, as a rule, the higher, the lower the extrusion temperature (1,55,57). For these magnitudes, the dependences on die angle have been determined. For HDPE, they are extreme with a maximum in the range $2\beta = 15$–30° (58).

At compression, the effect of extrusion draw on the strain–stress characteristics of samples is not so pronounced (22). As shown (22), for PP, the increase in the modulus of elasticity and yield strength occurs under compression in a direction normal to that of extrusion. In the case of a load applied along the extrudate axis, there is a decrease in the above characteristics, as compared to the initial material.

The mechanical properties of other semicrystalline polymers similarly depend on the conditions of deformation process (4,59,60). The thermal properties of semicrystalline polymers subjected to SSE have a highly pronounced anisotropy. Thus, the measurements of thermal conductivity of linear polyethylene done in a wide temperature range in directions parallel ($K^{\parallel}$) and normal ($K^{\perp}$) to the direction of extrusion, have shown that $K^{\parallel} > K^{\perp}$ (1,61). With EDR increase, the $K^{\parallel}/K^{\perp}$ ratio increases significantly.

Upon heating the extrudates there occurs a recovery of shape (dimensions) due to thermal shrinkage (1,56,62). The larger the EDR, the more stable the dimensions of the oriented samples in a wide temperature range. In superdrawn samples of linear polyethylene, a noticeable shrinkage occurs practically near the

melting temperature of the material (1). The beginning of the shrinkage process depends on the extrusion temperature: the lower the SSE temperature, the earlier begins the shrinkage. The value of the maximum shrinkage stresses increases with increasing EDR and decreasing extrusion temperature (62).

The extrusion of powder billets ensures a considerable improvement of some physical and mechanical characteristics (5). It is used in the case of materials for which the solid plug method is not efficient enough, eg UHMPE and PTFE (9,63). For PTFE, the maximum value of the so attained flexural modulus at 24°C is 20 GPa at an EDR 40 (64).

As compared to the SSE method, the SSCE makes it possible to realize considerably higher extrusion ratios with semicrystalline polymers. Coextrusion is widely used in a two-stage draw technique for drawing of powders (12,13,65) and single-crystal aggregates of polymers grown from dilute solutions (66). For example, a two-stage draw technique was successfully applied to the superdrawing of PTFE virgin powder (13). The films, compression-molded from powder below the melting temperature T_m, were initially coextruded with draws till EDR of 20. These extrudates were further drawn by a second-stage pin draw in the temperature range 300–370°C that covers the T_m. For this, a small portion of the extrudate, gripped at both ends, was rapidly heated by contacting it with the surface of a hot metal cylinder. Then, the extrudate was quickly elongated to the desired length. During elongation, the contacted area of the extrudate was continuously moved from one end to another end at a rate of ~1 m/min to heat and elongate a new sample portion successively. The maximum total draw ratio was 160. The maximum tensile modulus and strength achieved in this work were 102 and 1.4 GPa, respectively.

The aggregates of the solution-grown crystal mats of UHMPE and ultrahigh molecular polypropylene (UHMPP) are ductile to a draw ratio of 350 and 80, respectively. Tensile drawing and a combination of SSCE followed by tensile drawing give the highest and most efficient draw for mats of UHMPE and UHMPP. The tensile modulus of UHMPE of molecular weight $M_W = 8 \times 10^6$ for the limiting draw ratio reaches 230 GPa, and tensile strength—5.4 GPa. For UHMPP of $M_W = 8 \times 10^6$ these values are 36 and 2.5 GPa.

In article (15), films of atactic poly(acrylonitrile) were initially drawn uniaxially, by SSCE to EDR = 16, followed by tensile draw at different temperatures. For this polymer the highest tensile-modulus value was 28.5 GPa and strength—1.6GPa.

Amorphous Polymers. As compared to semicrystalline polymers, the SSE exerts a lower effect on tensile modulus and tensile strength of linear amorphous polymers. It has been shown (23) that the room-temperature hydrostatic extrusion of PMMA gives an increase in the above parameters only by dozens of percent. A similar result has been attained during the three-point bending tests of the extruded PC (23).

The hydrostatic extrusion under elevated temperatures, when higher EDR values are attained, results in a significant effect. In the case of SSE at a temperature of 120°C with the EDR = 6, the tensile modulus and strength of high impact polystyrene become twice as large and equal to 3.8 GPa and 57 MPa, respectively. In the extrudates, the plasticity characteristics (elongation at break, impact strength) are higher than in the initial samples and there is a more than a

twofold increase with the EDR and extrusion temperature (23). During the extrusion of a powder billet, eg polyarylate (40), there occurs a simultaneous increase in the strength and plasticity properties as well.

In article (67), where the peculiarities of SSCE of the atactic PS were studied, it is shown that the chain orientation and extension increase with EDR and molecular weight. For a sample of molecular weight 6×10^5 it was possible to achieve a maximum EDR of 27 by multiple draw steps. For the lowest molecular weight PS, the resulting films were brittle. The highest molecular weight sample, 1.8×10^6, on the other hand, was drawable only to a EDR of 7. The results suggest (2) that in the amorphous polymer, chain entanglements provide the necessary intermolecular network, which facilitates molecular extension and the concomitant orientation. For very high molecular weight, the high viscosity prevents relaxation of the elongated chain. For low molecular weight samples the entanglement network is vastly reduced, and the resulting extensive chain slippage leads to less efficient orientation and extension.

In the case of cross-linked polymers (eg epoxy polymers), the SSE induces the increase in microhardness, tensile modulus, yield stress, and strength (68). Moreover, depending on EDR value these parameters are changing because of the competition between the processes of orientational hardening and mechanical destruction. SSE influences the structure and properties of polymers based on interpenetrating polymer networks similarly (68).

Extrusion Based on Simple Shear

Equal Channel Angular Extrusion. In this technique (69), a billet is extruded through a die containing two channels, equal in cross section, intersecting at an angle Φ (Fig. 4**a**). During extrusion the billet undergoes severe shear deformation but retains the same cross-sectional geometry so that it is possible to repeat extrusion for a number of passes. Between two consequent passes it is possible to rotate the billet around its longitudinal axis, creating different equal channel angular extrusion (ECAE) routes (69). Another factor that significantly affects the microstructural development is the channel-intersection angle, which determines the shear strain Γ from an individual pass (69).

$$\Gamma = 2\cot\left(\frac{\Phi}{2}\right) \tag{3}$$

Smaller Φ will result in higher shear strain from each pass. Usually Φ is equal to 90°–120°

Already in one of the first articles dealing with ECAE application to modify linear LDPE (LLDPE) structure (18) it has been shown that this technique is efficient in orienting the lamellar structure of semicrystalline polymers. Upon four ECAE passes the string-like lamellar bundles in LLDPE are composed of many well-aligned crystal lamellae. The sheaf-like crystal lamellar bundles tend to orient approximately along the extrusion direction. Signs of fragmented crystal lamellae are also observed.

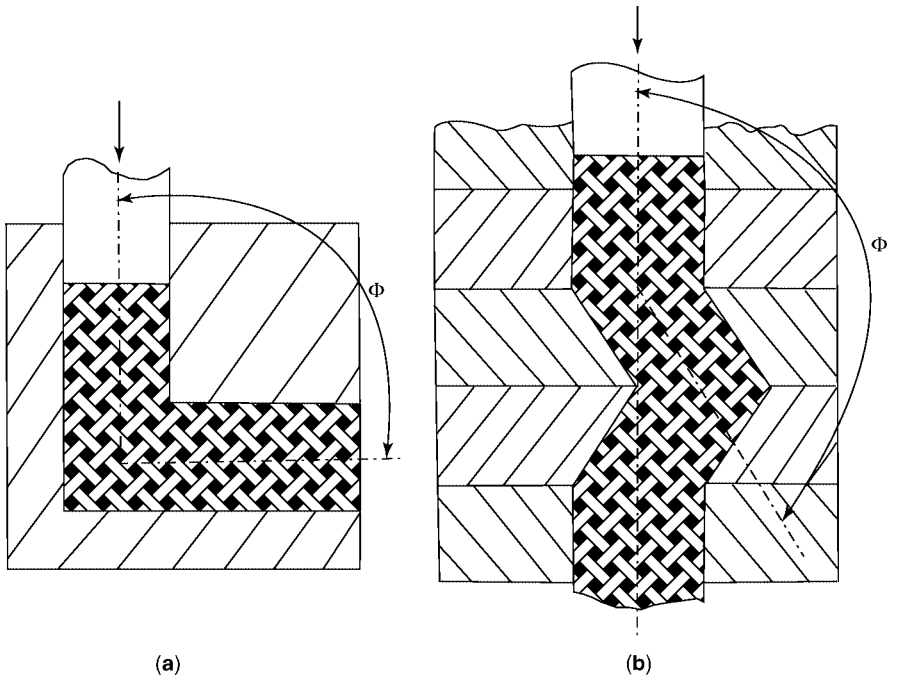

Fig. 4. Schematic representation of equal channel angular extrusion (**a**) and equal channel multiple by angular extrusion (**b**).

The large strain plastic deformation induced by ECAE, not only generates a high degree of molecular orientation but also gives better molecular packing. As a result, the polymer extrudates can exhibit improved rigidity, strength, barrier properties, and impact resistance (19). In particular, the samples of one-pass extruded PC cut along the extrusion direction have flexural modulus and critical stress-intensity factor K_{LC} values that are higher than those of the annealed PC by 15 and 40%, respectively.

The above technique has been developed into a method of equal channel multiple-angular extrusion (ECMAE) (70). It is based on forcing a polymer billet through several pairs of channels having equal cross section. The channels can intersect with each other at different angles and in different planes as well (Fig. 4**b**). A special feature of the ECMAE is that in an extrusion cycle with relatively low angles of the channel intersection (meaning that in each zone the deformation is low), the total deformation value per cycle is comparable with or exceeds the same for ECAE. At the same time, the implementation of any ECMAE scheme is accompanied by the change in shear direction including to the opposite one in a sequential zone.

ECMAE controls the deformation process more effectively and the expected result is attained quicker as compared to ECAE. The ECMAE equipment ensures the increase in manycycle extrusion output, a decrease in single deformation intensities for polymers of low plasticity, a possibility of providing a strict alternation of intensity values and shear directions for a guided structure forming. This has

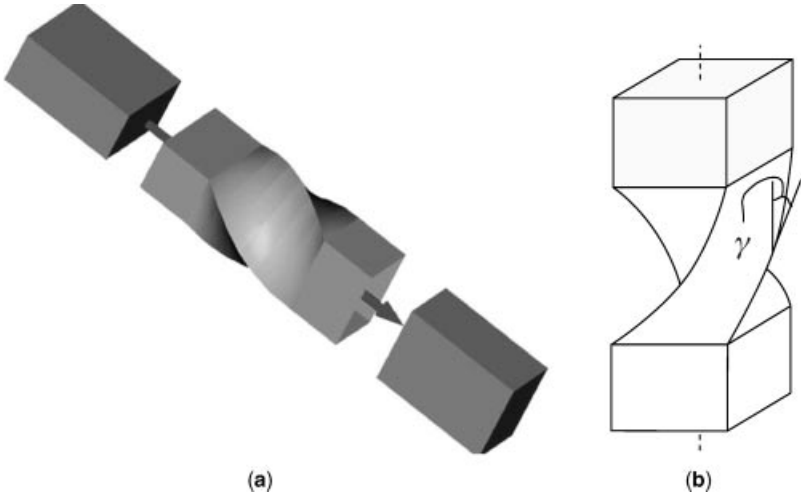

Fig. 5. Schematic presentation of the twist extrusion process (**a**) and of twist channel (**b**).

been confirmed by our experiments done on LDPE, HDPE, PTFE, nylon-6, and PC (71).

Twist Extrusion. In this technique, a billet is extruded through a die with a twist channel (Fig. 5) (72). The angle γ between the twist line and the direction of extrusion changes along the vertical axis of the die, furthermore, it is equal to zero on its starting and ending points.

The above properties of the channel geometry guarantee that the extrusion does not change the form of the workpiece, which allows to accumulate severe plastic deformations by iteratively extruding the workpiece through the die. Figure 5 shows a twist channel with a rectangular cross section. Generally, the cross section can be quite arbitrary, which allows one to use twist extrusion for obtaining not only semimanufactured article, but also prism-shaped end products. Note that by extruding on a mandrel, it is possible to get products with an inner channel.

The main factor that significantly affects the microstructural development is angle γ, which determines the shear strain Γ from an individual pass (72):

$$\Gamma = 2\tan\gamma \tag{4}$$

Another factor that significantly affects the microstructural development is the route of billet deformation consisting of a successive use of dies having the right-handed and left-handed screw channel.

The results of our WAXS investigations of LDPE and HDPE subjected to twist extrusion show that there are changes in the intensities of corresponding diffraction peaks reflection from planes (110) and (200), as compared to starting materials. The same changes have been found in the corresponding diffraction peaks of nylon-6. Several passes of twist extrusion result in the accumulation of plastic deformation in the samples affecting the level of their mechanical properties, microhardness, in particular. In the case of the LDPE, the increase in the number of cycles results in 1.5 times increase of microhardness.

Applications

Solid-state extrusion has various commercial applications. This method is used for the production of polyethylene ultrahigh-modulus fibers known under the trade name Tenflor (2). High-modulus ribbons and tapes produced from polyolefins by SSE are used as strappings and electrical insulation. In pipe production, the SSE makes it possible to manufacture biaxially oriented products possessing necessary properties in both the axial and tangential as well as radial directions (4). Owing to the suppression of cold flow (73), it is recommended to use fluoropolymer extrudates as efficient seals in structures operating in corrosive media. The thermal-shrinkage thermoplastics rods produced by SSE find their use as clamps in locking devices (74), as well as in various engineering structures (75).

BIBLIOGRAPHY

"Solid State Extrusion" in *EPSE* 2nd ed., Vol. 15, pp. 346–362, by Roger S. Porter, University of Massachusetts and Anagnostis E. Zachariades, IBM Corporation.

1. A. Ciferri and I. M. Ward, eds., *Ultra-High Modulus Polymers* Apllied Science Publishers, London, 1979.
2. R. S. Porter and L.-H. Wang, *J.M.S.-Rev. Macromol. Chem. Phys. C* **35**(1), 63 (1995).
3. I. M. Ward, P. D. Coates, and M. M. Dumoulin, *Solid Phase Processing of Polymers*, Hanser Gardner Publ., Cincinnati, 2000.
4. N. S. Yenikolopyan, B. I. Beresnev, G. D. Myasnikov, E. V. Prut, S. A. Tsygankov, A. N. Kryuchkov, and N. V. Shishkova, *Dokl. Akad. Nauk SSSR* **291**, 368 (1986) (in Russian).
5. Y. D. Wang, M. Cakmak, and F. W. Harris, *J. Appl. Polym. Sci.* **56**, 837 (1995).
6. V. A. Beloshenko, V. G. Slobodina, V. G. Grinev, and E. V. Prut, *Polym. Sci. B* **36**, 845 (1994).
7. V. A. Beloshenko, G. V. Kozlov, V. G. Slobodina, E. V. Prut, and V. G. Grinev, *Polym. Sci. B* **37**, 316 (1995).
8. G. V. Kozlov, V. A. Beloshenko, V. G. Slobodina, and E. V. Prut, *Polym. Sci. B* **38**, 251 (1996).
9. V. A. Beloshenko, G. V. Kozlov, V. N. Varyukhin, and V. G. Slobodina, *Acta Polym.* **48**, 181 (1997).
10. V. A. Beloshenko, Ya. E. Beygelzimer, and V. N. Varyukhin, *Polymer* **41**, 3837 (2000).
11. G. Hadziioannou, L. H. Wang, R. S. Stein, and R. S. Porter, *Macromolecules* **15**, 880 (1982).
12. T. Kanamoto, T. Ohama, K. Tanaka, M. Takeda, and R. S. Porter, *Polymer* **28**, 1517 (1987).
13. R. Endo and T. Kanamoto, *J. Polym. Sci. B* **39**, 1995 (2001).
14. L. H. Wang, S. Ottani, and R. S. Porter, *Polymer* **32**, 1776 (1991).
15. D. Sawai, A. Yamane, H. Takahashi, T. Kanamoto, M. Ito, and R. S. Porter, *J. Polym. Sci. B* **36**, 629 (1998).
16. D. Sawai, A. Yamane, T. Kameda, T. Kanamoto, M. Ito, H. Yamazaki, and K. Hisatani, *Macromolecules* **32**, 5622 (1999).
17. Y. T. Zhu, T. G. Langdon, R. S. Mishra, S. L. Semiatin, M. J. Saran, and T. C. Lowe, eds., *Ultrafine Grained Materials II. Proceedings of a Symposium, held during the 2002 TMS Annual Meeting I Seattle, Washington*, Feb. 17–21, 2002.
18. H.-J. Sue and C. K.-Y. Li, *J. Mater. Sci. Lett.* **17**, 853 (1998).
19. C. K.-Y. Li, Z.-Y. Xia, and H.-J. Sue, *Polymer* **41**, 6285 (2000).

20. P. D. Coates and I. M. Ward, *J. Polym. Sci. B* **16**, 2031 (1978).
21. B. I. Beresnev, N. S. Yenikolopov, S. A. Tsygankov, and N. V. Shishkova, *Dokl. Akad. Nauk USSR B* **4**, 47 (1985) (in Russian).
22. S. A. Tsygankov, N. V. Shishkova, and B. I. Beresnev, *Fizika i Techn.Vysok. Davlenii* **26**, 74 (1987) (in Russian).
23. N. Inoue, T. Nakayama, and T. Ariyama, *J. Macromol. Sci. B* **19**, 543–563 (1981).
24. J. H. Southern, N. E. Weeks, and R. S. Porter, *Macromol. Chem.* **102**, 19 (1972).
25. N. J. Capiati, S. Kojima, W. G. Perkins, and R. S. Porter, *J. Mater. Sci.* **13**, 334 (1977).
26. S. B. Ainbinder, E. L. Tyunina, and K. I. Tsyrule, *Properties of Polymers in Different Stressed States*, Khimiya, Moscow, 1981 (in Russian).
27. A. N. Kryuchkov, A. O. Baranov, I. Ya. Dorfman, N. A. Yerina, E. V. Prut, and N. S. Yenikolopyan, *Vysokomolek. Soedin. A* **26**, 1993 (1984).
28. A. E. Zachariades and R. S. Porter, *J. Appl. Polym. Sci.* **24**, 1371 (1979).
29. A. E. Zachariades, E. S. Sherman, and R. S. Porter, *J. Appl. Polym. Sci.* **24**, 2137 (1979).
30. K. Nakamura, M. Nagai, T. Kanamoto, Y. Takahashi, and T. Furukawa, *J. Polym. Sci. B* **39**, 1371 (2001).
31. M. Nagai, K. Nakamura, H. Uehara, T. Kanamoto, Y. Takahashi, and T. Furukawa, *J. Polym. Sci. B* **37**, 2549 (1999).
32. D. Sawai, K. Takahashi, A. Sasashige, T. Kanamoto, and S.-H. Hyon, *Macromolecules* **36**, 3601 (2003).
33. J. R. Pereira and R. S. Porter, *J. Polym. Sci. Polym. Phys. Ed.* **21**, 1133, 1147 (1983).
34. T. W. Williams, *J. Mater. Sci.* **8**, 59 (1973).
35. K. Imada, T. Yamamoto, K. Shigematsu, and M. Takayanagi, *J. Mater. Sci.* **6**, 537 (1971).
36. K. Imada and M. Takayanagi, *Int. J. Polym. Mater.* **2**, 71 (1993).
37. A. G. Gibson and I. M. Ward, *J. Mater. Sci.* **14**, 1838 (1979).
38. R. Gupta and P. G. McCormick, *J. Mater. Sci.* **15**, 619 (1980).
39. RU Pat. 2,083,369 (1997) V. A. Beloshenko, V. G. Slobodina, A. A. Askadskii, K. P. Bichko, A. V. Samoryadov, S. N. Salazkin, and V. V. Shaposhnikova.
40. RU Pat. 2105670 (1998), V. A. Beloshenko, G. B. Shustov, V. G. Slobodina, G. V. Kozlov, V. N. Varyukhin, K. B. Temiraev, and M. A. Gazaev.
41. Y. E. Beygelzimer and A. P. Getmansky, *Fizika i Tekhn. Vysok. Davlenii* **3**, 86 (1981) (in Russian).
42. I. Y. Dorfman, A. N. Kryuchkov, E. V. Prut, and N. S. Enikolopyan, *Dokl. Akad. Nauk SSSR* **278**(1), 141–144 (1984) (in Russian).
43. P. D. Coates, A. G. Gibson, and I. M. Ward, *J. Mater. Sci.* **15**, 359 (1980).
44. H. L. D. Pugh, ed., *The Mechanical Behaviour of Materials under Pressure* Vol. 2, Elsevier Publ. Comp. Lim., Amsterdam, 1970.
45. W. Johnson and P. B. Mellor, *Engineering Plasticity*, Van Nostrand Reinhold Co., London, 1973.
46. N. A. Kulesko, Y. A. Palant, Y. E. Beygelzimer, and A. P. Getmanskiy, *Dokl. Akad. Nauk USSR* (6), 441 (1979) (in Ukrainian).
47. R. Hill, *The Mathematical Theory of Plasticity*, Clarendon Press, Oxford, 1998.
48. A. Zavaliangos and A. Laptev, eds., *Recent Development in Computer Modeling of Powder Metallurgy Processes*, IOS Press, Amsterdam, 2001.
49. Y. E. Beygelzimer, V. A. Beloshenko, and E. V. Prut, *J. Polym. Sci. B* **37**, 573 (1995).
50. V. A. Beloshenko, Y. E. Beygelzimer, V. N. Varyukhin, and V. G. Grinev, *Mech. Composit. Mater.* **35**, 71 (1999).
51. A. Peterlin, *J. Polym. Sci. C* **15**, 427 (1966).
52. G. Meinel and A. Peterlin, *J. Polym. Sci. B* **5**, 613 (1967).
53. J. Clements, R. Jakeways, and I. M. Ward, *Polymer* **19**, 639 (1978).
54. A. G. Gibson, G. R. Davies, and I. M. Ward, *Polymer* **19**, 683 (1978).

55. S. A. Tsygankov, N. N. Shishkova, and B. I. Beresnev, *Fizika i Techn. Vysok. Davlenii* **17**, 77 (1984) (in Russian).
56. S. A. Tsygankov, N. N. Shishkova, and B. I. Beresnev, *Fizika i Techn. Vysok. Davlenii* **19**, 57 (1985) (in Russian).
57. P. S. Hope, A. G. Gibson, and I. M. Ward, *J. Polym. Sci., Polym. Phys. Ed. B* **18**, 1243 (1980).
58. W. G. Perkins and R. S. Porter, *J. Mater. Sci.* **17**, 1700 (1982).
59. B. S. Kim and R. S. Porter, *Macromolecules* **18**, 1214 (1985).
60. D. J. Mitchell and R. S. Porter, *Macromolecules* **18**, 1218 (1985).
61. S. Burgess and D. Greig, *J. Phys. C* **8**, 1637 (1975).
62. P. V. Zamotaev and V. A. Beloshenko, *Zh. Prikl. Khim.* **67**, 1863 (1994) (in Russian).
63. A. E. Zachariades, M. P. C. Watts, T. Kanamoto, and R. S. Porter, *J. Polym. Sci. Polym. Lett. Ed.* **17**, 487 (1979).
64. H. Okuyama, T. Kanamoto, and R. S. Porter, *J. Mater. Sci.* **29**, 6485 (1994).
65. D. Sawai and T. Kanamoto, *Polym. J.* **32**, 895 (2000).
66. T. Kanamoto, A. Tsuruta, K. Tanaka, M. Takeda, and M. Takeda, *Polymer J.* **16**, 75 (1984).
67. B. Appelt and R. S. Porter, *Maromolecules* **20**, 21 (1981).
68. V. A. Beloshenko, A. A. Askadskii, and V. N. Varyukhin, *Usp. Khim.* **67**, 1044 (1998) (in Russian).
69. V. Segal, *Mater. Sci. Eng. A* **338**, 331 (2002).
70. UA Pat. 58015A (2003) E. A. Medvedskaya, N. I. Matrosov, A. B. Dugadko, V. Z. Spuskanyuk, V. A. Beloshenko, and B. A. Shevchenko.
71. V. A. Beloshenko, Y. E. Beygelzimer, V. N. Varyukhin, and Yu. V. Voznyak, *Polym. Sci. B* (in press).
72. Y. E. Beygelzimer, D. V. Orlov, and V. N. Varyukhin, in Y. T. Zhu, T. G. Langdon, R. S. Mishra, S. L. Semiatin, M. J. Saran, and T. C. Lowe, eds., *Ultrafine Grained Materials II. Proceedings of a Symposium, held during the 2002 TMS Annual Meeting I Seattle*, Washington, February 17–21, 2002, p. 297.
73. G. D. Myasnikov and S. A. Tsigankov, *Plast. Massy* (2), 34 (1985) (in Russian).
74. RU Pat. 2059549 (1996), V. A. Beloshenko, Yu. N. Yermoshkin, V. I. Zaika, and V. G. Slobodina.
75. UA Pat. 20049A (1997), V. A. Beloshenko, L. O. Chigorin, and V. N. Varyukhin.

Y. E. BEYGELZIMER
V. A. BELOSHENKO
Donetsk Physics and Technology,
Institute of the National Academy of Sciences of Ukraine

SOLUTION POLYMERIZATION.

See BULK AND SOLUTION POLYMERIZATION.

STABILIZATION.

See Volume 4.

STARCH.

See ARTICLE ONLINE.

STATISTICAL THERMODYNAMICS.

See Volume 8.

STRESS RELAXATION.

See VISCOELASTICITY.

STRUCTURAL REPRESENTATION OF POLYMERS.
See Volume 8.

STYRENE–BUTADIENE COPOLYMERS . See Volume 4.

STYRENE POLYMERS . See Volume 4.

SULFUR–CONTAINING POLYMERS . See Volume 4.

SUPERABSORBENT POLYMERS. See Volume 8.

SURFACE ANALYSIS

Introduction

The surface properties of polymers are important in many applications and they are dependent on the structure and composition of the outermost molecular layers. The surface layer thickness involved is typically of the order of a few nanometers. Understanding surface structure–property relationships therefore requires analytical techniques which have this degree of surface sensitivity (or specificity). Two techniques stand out: X-ray photoelectron spectroscopy (XPS) (1), also known as ESCA (electron spectroscopy for chemical analysis), and secondary ion mass spectrometry (SIMS) (2). The information provided by these methods is highly complementary and they are frequently used in combination. This article describes the physical bases and analytical capabilities of XPS and SIMS and illustrates their application in polymer surface characterization (3).

X-ray Photoelectron Spectroscopy

Physical Basis. In XPS, the sample inside a high vacuum system (pressure $<10^{-5}$ Pa or 10^{-7} torr) is irradiated with soft X rays, usually Mg Kα (1253.6 eV) or Al Kα (1486.6 eV). The primary event is photoemission of a core electron, but relaxation processes also lead to emission of Auger electrons or photons, as shown in Figure 1. The emitted electrons are collected by an electrostatic energy analyzer and detected as a function of kinetic energy E_K, producing a spectrum such as illustrated in Figure 2.

The intense, narrow peaks are due to photoelectrons emitted from core orbitals (eg C 1s). The binding energies of these electrons are given by the equation

$$E_B = h\nu - E_K - \phi \quad (1)$$

Encyclopedia of Polymer Science and Technology. Copyright John Wiley & Sons, Inc. All rights reserved.

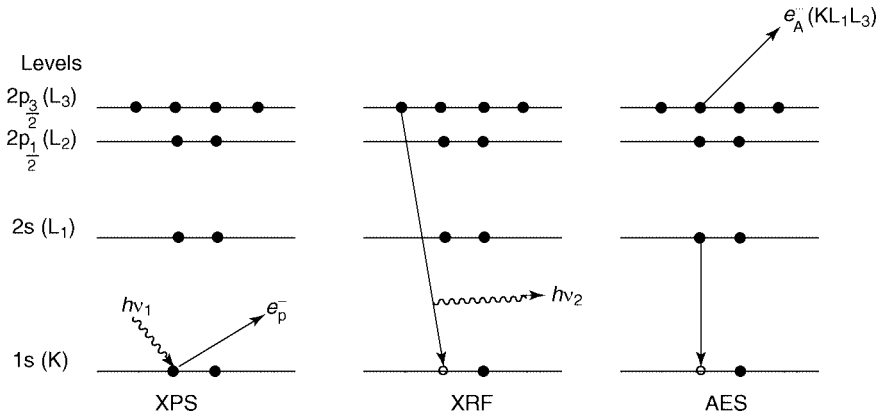

Fig. 1. Photoemission and subsequent relaxation processes (X-ray fluoresence and Auger electron emission) in XPS.

where $h\nu$ is the X-ray photon energy and ϕ is a catch-all term which includes the spectrometer work function. Core level binding energies are highly characteristic and allow the identification of all elements except H and He. The peak intensities are proportional to the number of atoms within the sampled volume and the

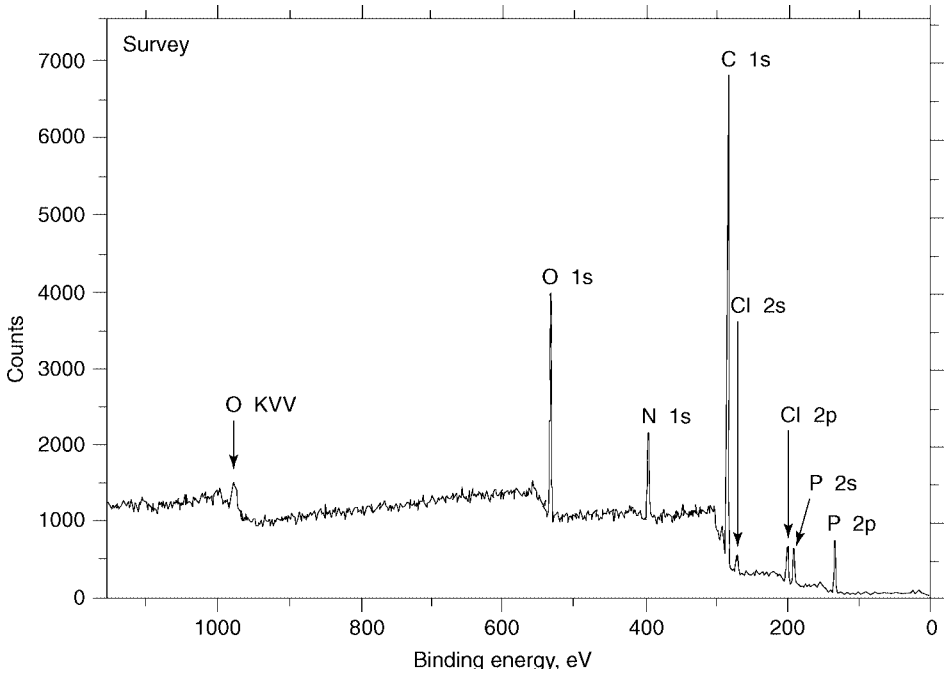

Fig. 2. XPS survey scan of poly(phenoxyphosphazene), containing C, O, N, and P, excited by monochromatic Al Kα radiation. Note the presence of Cl impurity from a synthesis intermediate. Reproduced from Ref. 6, by permission of Cambridge University Press.

surface composition can be calculated from

$$C_A = I_A S_A \Big/ \sum_n (I_n S_n) \tag{2}$$

where C_A is usually expressed as atomic% (of all elements determined, hydrogen excluded). The n elements give measured intensities (peak areas) of I_A–I_n and the peaks are associated with relative sensitivity factors S_A–S_n. When the photoemission cross sections (σ) for the most intense core levels of each atom are compared, it is found that the variation across the periodic table is about a factor of 100, if Li and Be are excluded. The cross section is the most important parameter influencing the relative sensitivity factor. Hence, XPS does not suffer unduly from inherent sensitivity effects and detection limits are 0.1 at% or better with modern instruments.

Close to zero binding energy (BE) an envelope of much lower intensity peaks, the valence band, is due to photoemission from the molecular orbitals.

The other broader peaks (appearing in series) are due to Auger electrons. The energy of an Auger electron is given approximately by

$$E_{ABC} = E_A - E_B - E_C^* - \phi \tag{3}$$

where E_A is the BE of the photoionized level A, E_B the BE of the level B from which an electron moves to fill the hole created, and $E_C{}^*$ the BE of the level C from which the Auger electron is emitted (the * indicates that level C is in the presence of a hole in level B, so $E_C{}^*$ is not the same as E_C, the ground state BE) (Fig. 1). These kinetic energy values are also element characteristic, although not all elements produce strong Auger signals under typical XPS conditions, and they are obviously independent of the exciting photon energy.

The exciting photons can penetrate many micrometers into a polymer, but the photoemitted electrons can only travel a short distance (a few nanometers) from their point of origin before they lose energy and, therefore, no longer satisfy equation 1. These inelastically scattered electrons give rise to the spectral background which increases in intensity with decreasing kinetic energy. To a first approximation, the inelastic mean free path (ie, the mean distance traveled by an electron between inelastic collisions), λ, is the parameter which determines the information (or sampling) depth of XPS. On the basis of the assumption that electron attenuation follows an exponential (Beer–Lambert) law, the vertical sampling depth below the surface from which 95% of the observed signal originates is given by

$$d = 3\lambda \sin\theta \tag{4}$$

where d and θ are defined in Figure 3. λ is a function of kinetic energy, according to a power law of the form $\lambda \propto E^x$ where, typically, $0.5 < x < 1$. Based on data appropriate for poly(methyl methacrylate), Table 1 provides a guide to sampling depths in polymer surface analysis. For flat surfaces the variation of sampling depth with θ (the "take-off" angle) provides a means of non-destructive depth profiling, as illustrated in Figure 4.

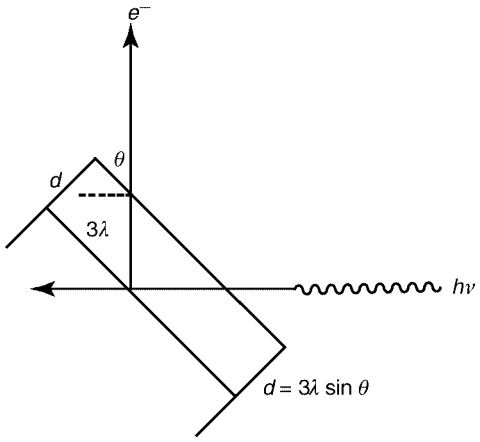

Fig. 3. Angular dependence of the (vertical) sampling depth in XPS.

Instrumental Aspects. The soft X-ray sources used in XPS are Mg K$\alpha_{1,2}$ and Al K$\alpha_{1,2}$ as noted above. These unresolved doublet lines have half-widths of 0.70 and 0.85 eV respectively, and so the Mg source is preferred on resolution grounds. However, Al Kα radiation can be monochromated by Bragg reflection from quartz crystals, reducing the half-width to <0.30 eV. Using bent crystals the beam can also be focused, which increases the flux density and compensates for intensity lost by monochromation. A further advantage of monochromation is that the high energy Bremsstralung radiation and lower intensity satellite lines are removed, resulting in a cleaner XPS spectrum.

Insulating samples, such as most polymers, tend to charge positively when irradiated with X rays because of electron emission. When a nonmonochromated source is used, a sufficient flux of low energy electrons is generated from various metal surfaces within the instrument to return to the sample surface and compensate such charging, leading to a stable surface potential which is usually just a few volts positive. This is not the case with monochromated sources and an external source of low energy electrons has to be supplied from a "flood gun."

Table 1. XPS Sampling Depths as a Function of Core Level Kinetic Energy and Take-Off Angle (Measured from the Surface Plane)

			Sampling depth (95% signal), nm					
	Kinetic energy, eV		Mg Kα			Al Kα		
Core level	Mg Kα	Al Kα	10°	45°	90°	10°	45°	90°
F 1s	568	801	0.8	3.4	4.8	1.1	4.5	6.3
O 1s	723	956	1	4.1	5.8	1.3	5.2	7.3
N 1s	852	1185	1.1	4.7	6.6	1.4	5.7	8
C 1s	967	1200	1.3	5.2	7.3	1.5	6.2	8.7
Si 2p	1152	1385	1.5	5.9	8.4	1.7	6.9	9.7

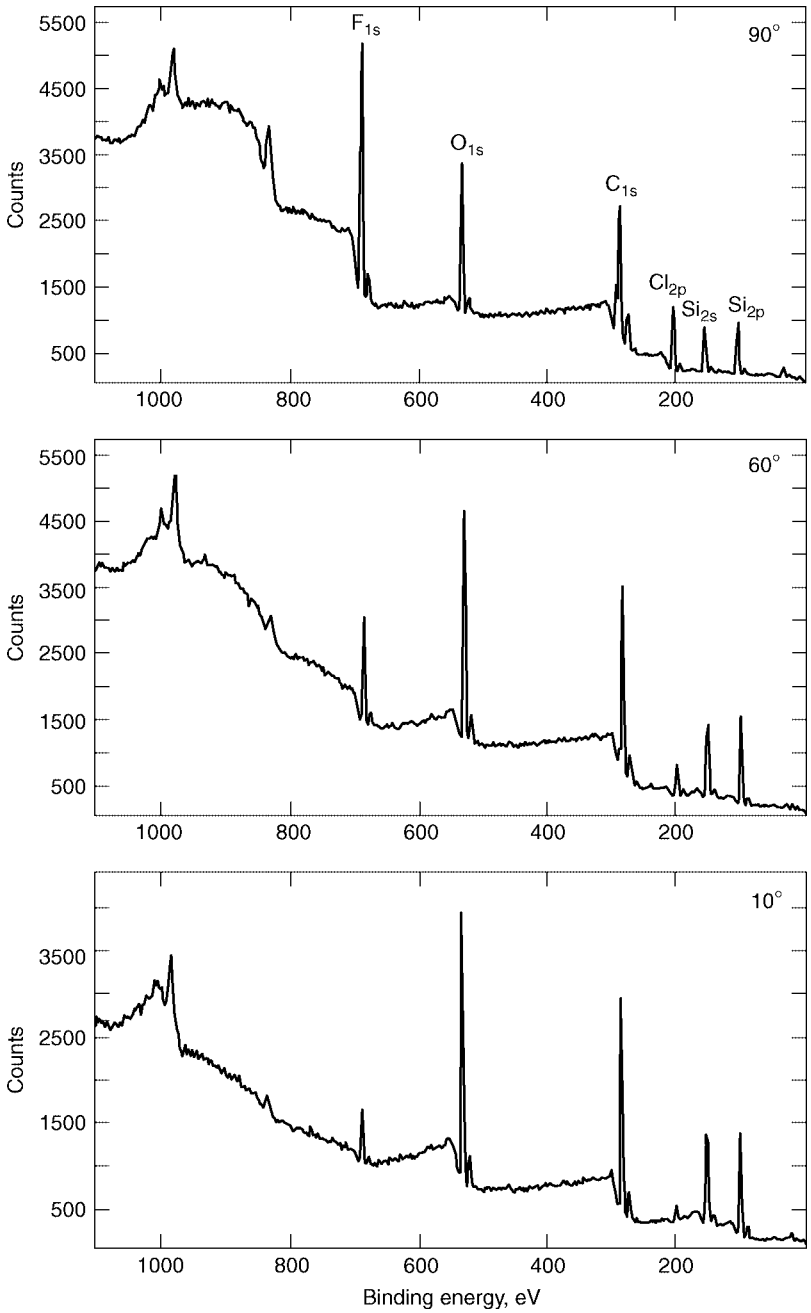

Fig. 4. Spectra from the surface of a molded plaque of poly(ethylenechlorotrifluoroethylene) contaminated with polydimethlysiloxane (silicone) taken at take-off angles of 90°, 60°, and 10° with respect to the surface. Note the rapid attenuation of the substrate signals (F 1s, Cl 2p) with increasing surface sensitivity (decreasing take-off angle). Reproduced from Ref. 3, by permission of Cambridge University Press.

There are no particular problems in handling polymeric materials in the vacuum required by the technique since any outgassing is usually slow, although high additive level rubber formulations are an exception. In such cases, cooling the sample during examination overcomes the problem. Radiation damage is also minor in most situations, and is further reduced when the X rays are monochromated, but it cannot be ignored. Two situations stand out: long acquisition times during multi-element imaging or high resolution studies of low intensity peaks; studies of thin films on high photoelectron cross-section substrates, including most metals (damage by electrons traveling through the film).

During the last 10 years there have been several approaches to providing high spatial resolution in XPS for imaging and local area analysis. One involves the production of a scanning X-ray microprobe, others achieve parallel imaging with broad area illumination and sophisticated electron optics (microscopy). In all cases the spatial resolution is inherently <10 μm, the actual resolution usually being limited by the counting statistics. For microscopy, the energy analyzer is used to preselect the energy (window) corresponding to a core level peak of interest and an image of intensity distribution from a chosen field of view acquired. A similar image is recorded at an appropriate background energy. The peak-background image is computed to realize the intensity distribution corresponding most closely to the chosen peak. Microanalysis simply involves recording spectra as normal from an area defined either by beam position and raster size (microprobe) or by apertures in the electron optics (microscope).

XPS Spectral Features and Information

Core Levels. Core level BEs are sufficiently unique to allow unambiguous element identification (see for instance the difference in BEs of the core levels in Table 1). However, all core level BEs are subject to relatively small variations, depending on the chemical environment, referred to as chemical shifts. The chemical shift range is usually <10 eV and, since peak half-widths are of the order of 1 eV, the dynamic range is low (compared to the somewhat related NMR case). An example is given in Figure 5.

The charge-potential model is a simple model that relates the core level BE to atomic charge:

$$E_i = E_i^0 - kq_i = eV_i \quad \text{where} \quad V_i = \sum q_i / r_{ij} \; (i \# j) \tag{5}$$

where E_i is the BE of the particular core level on atom i, $E_\mathrm{i}{}^0$ is a reference energy, k is a constant, q_i is the charge on atom i, and V_i sums the potential at atom i due to point charges on atoms j.

For two atoms (i) in different chemical environments, equation 5 gives

$$\Delta E_i = k\Delta q_i + e\Delta V_i \tag{6}$$

In molecular solids, atoms j are essentially the atoms bound to atom i and ΔV_i is relatively small; thus electronegativity effects will dominate Δq_i. An increase in positive charge is therefore accompanied by an increase in BE. The major

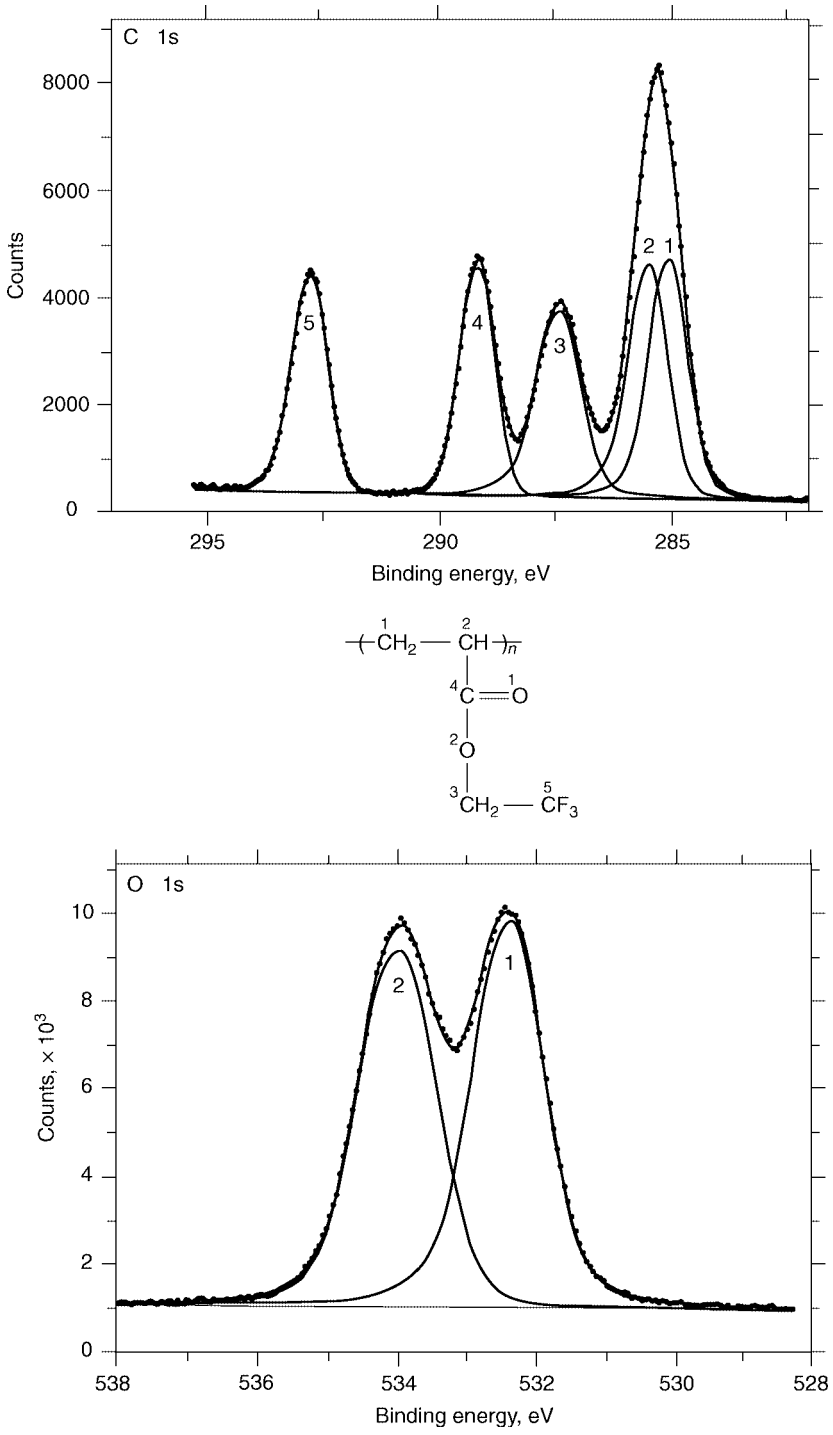

Fig. 5. High resolution C 1s and O 1s spectra from poly(trifluoroethylacrylate). Reproduced from Ref. 4, by permission of SurfaceSpectra.

simplification of equation 6 is that it ignores final state effects. The measured BE is actually the difference between the final and initial state energies, and so any chemical shift must involve consideration of both of these. The core hole of the final state has a polarizing effect on surrounding electrons, both interatomic (on atom i) and extraatomic (on atoms j). The electronic response is referred to as relaxation. Again, in molecular solids, relaxation energies are fairly constant, so initial state (particularly electronegativity) effects tend to dominate, as seen in Figure 5.

As this example illustrates, the low chemical shift dynamic range means that the components representing different functional groups overlap, sometimes severely. To accurately measure their BEs and relative intensities the components need to be resolved by curve-fitting, and this, in turn, demands some understanding of peak shape, which is variable. The underlying peak shape is a mixed Gaussian–Lorentzian (Voigt) function where the G–L ratio is determined by the experimental parameters. Additionally, when the energy resolution is very high, high BE asymmetry may be observed. This is particularly true of the C 1s peak which is affected by vibrational fine structure (due to the C—H stretch mode). A database of high energy resolution spectra of over 100 pure homopolymers (from which Figure 5 is taken) provides a great deal of information on this subject and collates data on chemical shifts for all the important core levels in polymer spectra (4,5).

As noted above, BEs from insulators are affected by surface charging. For equation 6 to be meaningful any two spectra need to be compared in the absence of this variable. This is done by referencing all measurements to a peak of known BE, usually the position of the C 1s component from aliphatic hydrocarbon (common to many polymers) assigned to 285 eV.

Shake-Up Satellites. Shake-up satellites may be observed on the low kinetic energy (high BE) side of intense core level peaks. They occur when valence electron reorganization (relaxation), following photoemission from a core level, results in the excitation of a valence electron to a higher unoccupied level. Conjugated and, especially, aromatic systems show shake-up satellites with intensities of 5–10% of the main peak, usually separated by $<$10 eV. Two transitions are important: from the two filled orbitals $b_{1\pi}$ and $a_{2\pi}$ to the unoccupied $b^*_{2\pi}$ orbital (ie $\pi \rightarrow \pi^*$). When the separation of these orbitals is small, the shake-up satellites can overlap the chemically shifted core level components, as illustrated in Figure 6. Atoms directly attached to unsaturated centers will also show shake-up satellites in their spectra (eg Cl in polychlorostyrene).

Valence Bands. Photoemission from the molecular orbitals gives rise to the valence band in the $\sim$0–20 eV BE region. Cross sections for these orbitals are typically a factor of 20–50 times lower than for the main core levels (eg C 1s). The valence band envelope is a sensitive function of polymer structure and so it can provide "fingerprint" information in situations where the core level spectra are inadequate. An example is given in Figure 7 for hydrocarbon polymers whose C 1s spectra are virtually identical, even at the highest energy resolution. Valence band spectra can be sensitive to the various types of isomerism, to geometrical conformation and tacticity, and even to degree of crystallization.

Functional Group Labeling (Derivatization). Core level chemical shifts are often ambiguous because of the small dynamic range (see Refs. 4 and 5). Particularly in the case of multifunctional surfaces, often the result of treatments carried

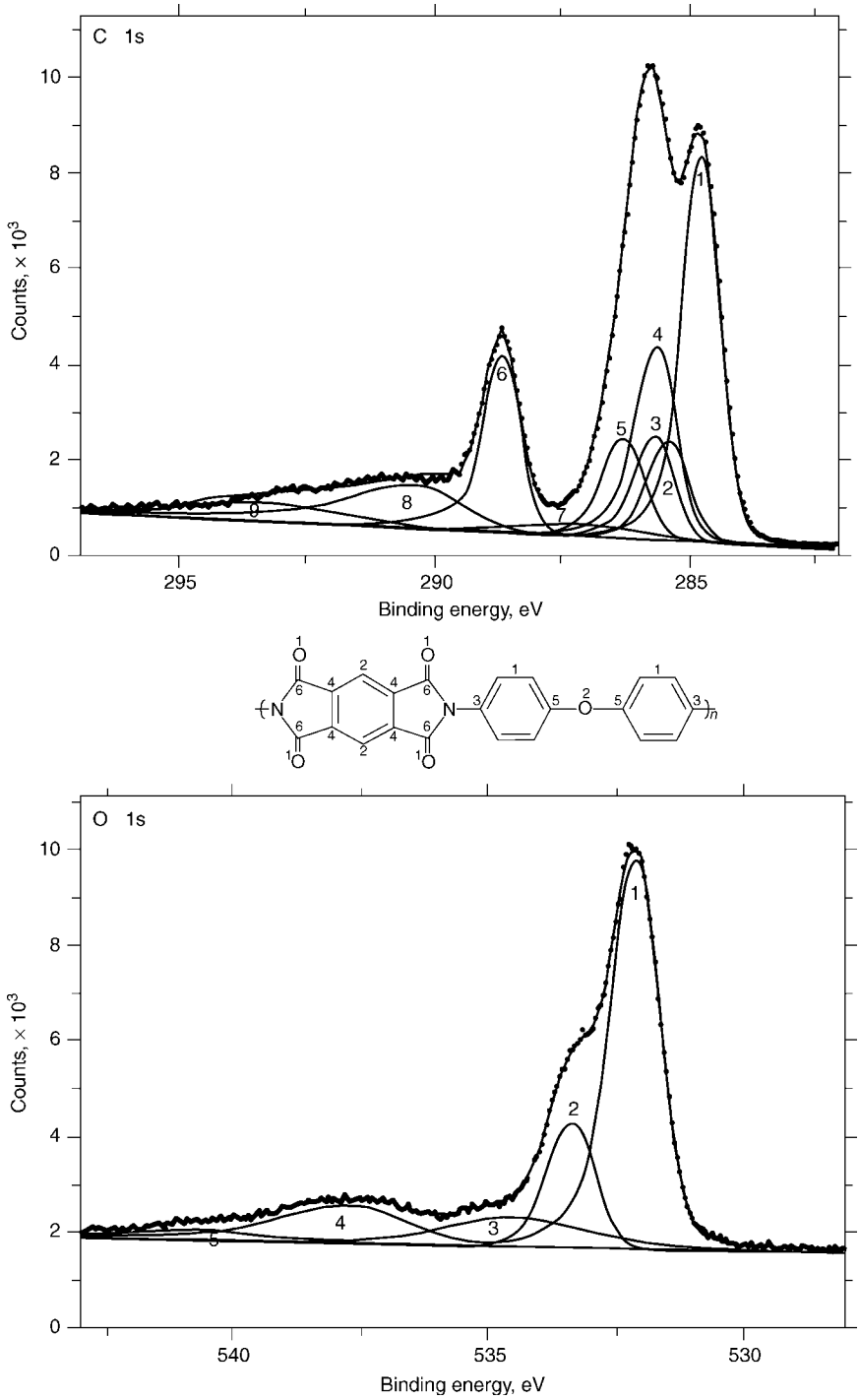

Fig. 6. Shake-up satellites in the C 1s (components 7–9) and O 1s (components 3–5) spectra of the poly(ether imide) Kapton HM. Reproduced from Ref. 3, by permission of Cambridge University Press, based on original data from Ref. 5.

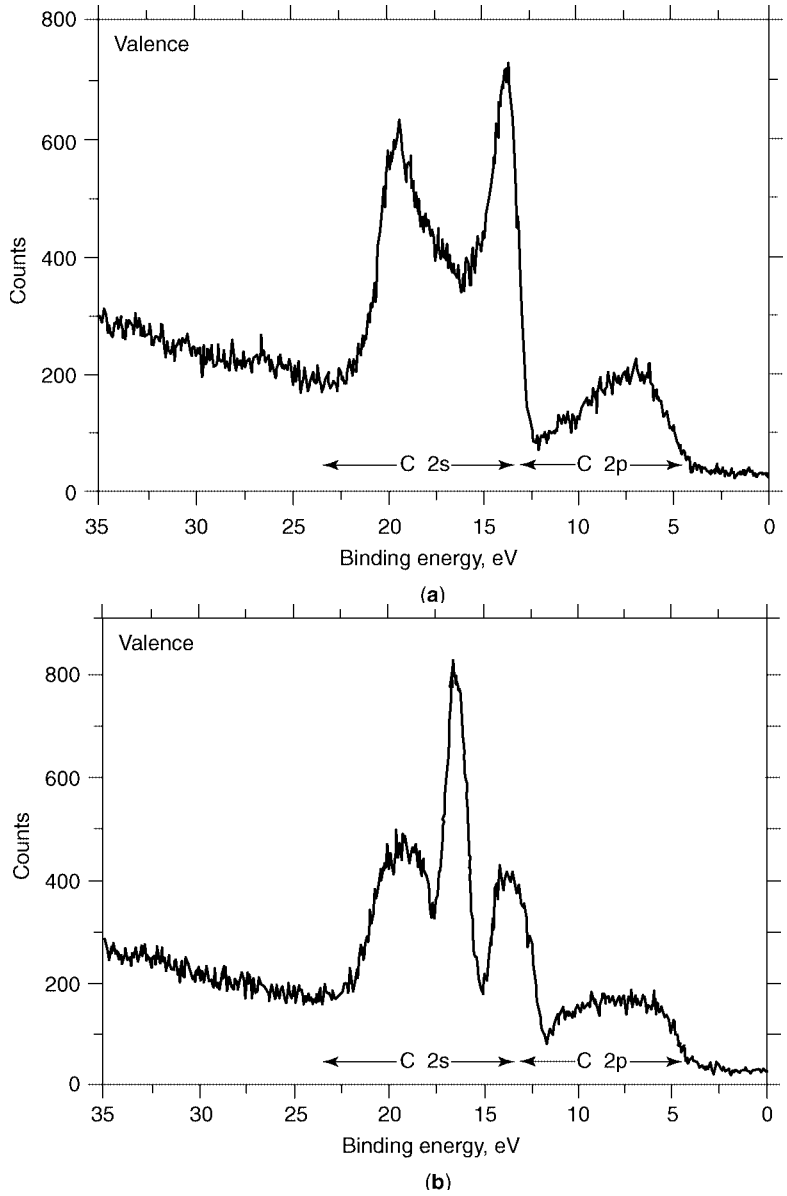

Fig. 7. Valence band spectra of (**a**) high density polyethylene, (**b**) polypropylene, and (**c**) poly(but-1-ene). Reproduced from Ref. 3, by permission of Cambridge University Press, based on original data from Ref. 5.

off to modify surface properties (eg adhesion), significant problems of functional group identification are encountered. A strategy for overcoming this problem is that of derivatization, whereby the surface is exposed to a agent which reacts specifically with one functional group and labels it with a distinctive element. An example is the reaction of surface alcohol (—OH) groups with trifluoroacetic anhydride to generate trifluoroacetate groups which can be quantified either from the

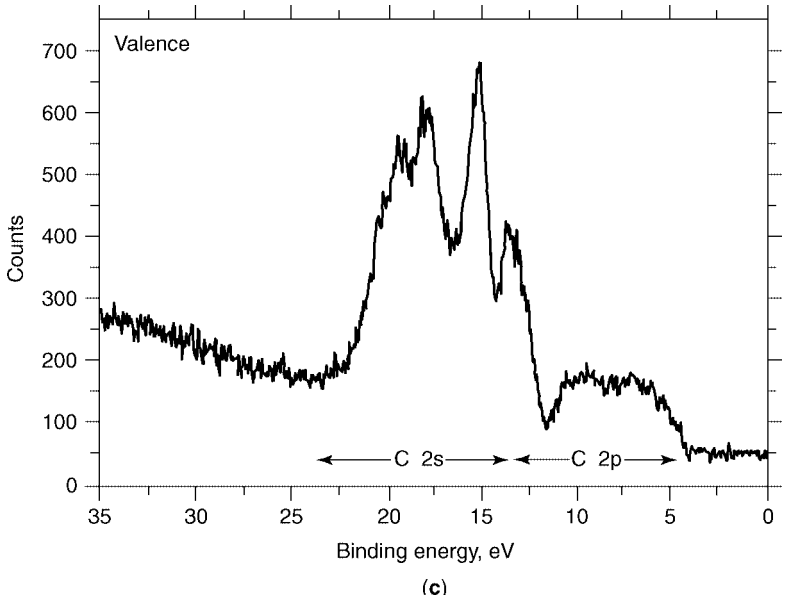

Fig. 7. (Continued)

F peak or the C 1s(CF_3) component. However, these reactions rarely proceed to completion within the XPS sampling depth and they can lead to surface reorganization, even when solvents are avoided. In recent times this approach has lost favor as the problems have become clear.

Secondary Ion Mass Spectrometry

Physical Basis. In SIMS, the sample in ultrahigh vacuum ($<10^{-7}$ Pa) is bombarded with energetic ions (typically 8–25 keV depending on the source, see below). These penetrate below the surface to a distance of several nanometers while transferring their energy to the material. In the immediate vicinity of the primary ion track, where the energy density is highest, many bonds are broken and atoms are set in motion. Secondary and higher generation collisions set up a collision cascade radiating from the impact point. Isomerization of the original translational energy also leads to electronic and vibrational excitation. As a result of the collision cascade, fragments of the material close to the surface can be desorbed (sputtered) into the vacuum. These fragments range in size from single atoms to large assemblies. Most of the sputtered material is neutral but about 1% is charged (positively or negatively). These secondary ions, the vast majority being singly charged, can be extracted into a mass spectrometer for mass analysis.

As with gas-phase organic mass spectrometry, SIMS spectra are information-rich and provide fingerprints. However, the processes leading to the spectra (both positive and negative ion spectra are utilized) are not well understood. The charged fragments can be formed directly in the collision cascade; or by ion/electron attachment, electron impact, and ion–molecule reactions in the selvedge (the affected region near the surface which may have some characteristics of a plasma); or

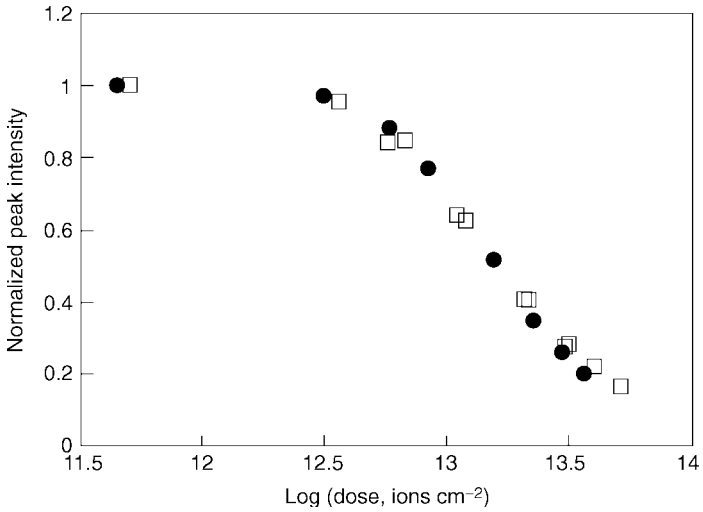

Fig. 8. Relative intensities of diagnostic fragments from PMMA ($+m/z$ 126 and $-m/z$ 185) as a function of primary ion dose (using 8 keV Cs^+). Individual spectra were acquired with a dose of $<5 \times 10^{11}$ ions cm^{-2}. ● m/z −185, □ m/z + 126. Reproduced from Ref. 6.

by unimolecular decomposition of fragments with high internal energies in the vacuum.

For the study of organic materials, in particular, it is essential to limit the primary ion dose, so that the spectrum is representative of undamaged material (the static SIMS regime). The aim is to ensure that no part of the surface receives more than one primary ion impact (affecting an area of order 10 nm in diameter) during the analysis. By measuring spectra as a function of primary ion dose it is possible to determine the "static SIMS limit," ie, the dose above which the spectra are dose-dependent (6). Figure 8 illustrates such data for poly(methyl methacrylate), a representative polymer (the origins of the chosen fragments are described under SIMS Polymer Spectra). Under the conditions used the static SIMS limit is a primary ion dose of about 3×10^{12} ions cm^{-2}.

There are very few studies which relate to the SIMS information depth for polymers, but the consensus view is that this is of the order of 1 nm. Atomic fragments may emerge from somewhat deeper below the surface but large molecular species arise only from the uppermost molecular layer or two.

Instrumental Aspects. The early developments of static SIMS (largely driven by polymer surface analysis requirements in terms of practical application) were carried out with noble gas ion sources and quadrupole mass analyzers (QMS). The latter had the benefits of compactness, ready availability, and relatively straightforward adaptability to SIMS use in UHV systems. Although all the essential features of polymer surface analysis were introduced using this technology, the QMS has major limitations for static SIMS. Firstly, it is a serial device, so that only one mass at a time can be detected. Secondly, it has a limited mass range (<1000 Da) and the transmission (ie, sensitivity) decreases with mass (by at least m^{-1}). Thirdly, it is only possible to achieve a uniform mass resolution

($m/\Delta m$) over this range of about unity. These limitations led to the introduction of energy-compensating time-of-flight (ToF) mass analyzers.

In ToF-SIMS the primary ion beam is pulsed, producing primary ion "packets" of about 1 ns duration. The secondary ions are accelerated over a short distance to typically 3 keV energy and injected into the ToF analyzer. In a linear ToF this is simply a field free tube in which the ions of different mass travel with different velocities and separate, to arrive at a detector sequentially. The flight time is related to the square root of the mass, so the "time spectrum" can be converted to a mass spectrum by suitable calibration. The mass analysis, which takes <200 μs, is carried out between primary ion pulses. The spectrum is therefore acquired in parallel and the ion dose is minimized. The secondary ions leave the surface with an energy distribution which, while only a few percent of the energy after acceleration, is enough to degrade the mass resolution. Different ToF designs compensate for this initial energy distribution in different ways, but modern instruments achieve $m/\Delta m$ of 10,000 or more. The mass range is theoretically infinite, but in practice the difficulty of registering the arrival of very large slow ions gives an upper limit of about 10 kDa. For most polymer surface studies an upper mass of 2 kDa is more than sufficient and over this range the transmission is independent of mass. Overall, the ToF approach has a 10^4 increase in sensitivity compared to a QMS.

The pulsed nature of ToF-SIMS provides a further benefit for the analysis of insulating materials. These charge up under positive ion bombardment and stabilizing the surface potential is essential, otherwise secondary ion detection is rapidly curtailed. In ToF-SIMS this is efficiently achieved by irradiating the sample with a broad flood of low energy (typically 20 eV) electrons between each primary ion pulse. This is especially important during high spatial resolution imaging (which is virtually impossible with a QMS because the ion beam current density is much higher and continuous). Because of all these advantages, ToF-SIMS is the preferred method for polymer surface analysis and during the last decade the QMS approach has been eclipsed.

A variety of ion sources are used in ToF-SIMS. Electron impact sources are used to produce Ar^+, Xe^+, and $SF_5{}^+$. Surface ionization sources produce Cs^+. Both of these types of source are used mainly for spectroscopy where spatial resolution is not important (although beam diameters of a few tens of micrometers are used). Liquid metal ion sources produce Ga^+, In^+, and, most recently, $Au^+/Au_2{}^+/Au_3{}^+$. These sources allow the production of highly focused beams with diameters down to 30 nm. There is an advantage to using high mass primary ions since the efficiency of production of large organic fragments (ie, the secondary ion yield divided by the primary ion dose) increases significantly with primary ion mass at any given ion energy.

An important aspect of imaging by ToF-SIMS is the ability to store (in memory) the whole spectrum for each pixel in the scanned array. This large data set, called a raw data file, can then be interrogated retrospectively. Two smaller data files are first created: one in which all the spectral intensity is summed for each pixel to generate a total intensity image and another in which the spectra from each pixel are summed to generate a total or average spectrum. The intensity variation in the total image is due to both topography effects (as in SEM) and major compositional differences. Regions of interest can be studied by selecting a

number of pixels and the spectrum from them recreated—retrospective microanalysis. From the total spectrum, peaks of interest can be selected (singly or collectively) and the intensity in all pixels displayed—retrospective chemical imaging or mapping. Thus two scans over the field of view to collect both positive and negative ion raw data files capture all the available information.

SIMS Spectral Features and Information

Modern, high mass resolution, ToF-SIMS instruments make detection of elements relatively easy. With the standard isotopic mass defined for $^{12}C = 12.0000$, all the elemental isotopes from ^{16}O (15.9949) upwards have masses slightly below the nominal unit mass. Organic fragments, being largely composed of carbon and hydrogen ($^{1}H = 1.0078$), have exact masses which are slightly above the nominal unit mass. Thus, for example, the single isotope of Mn^+ ($^{55}Mn = 54.9380$) would have a serious interference with a common hydrocarbon fragment, of the same nominal mass, $C_4H_7^+$ (exact mass = 55.0548). However, with a mass resolution of only 1500 (defined as $m/\Delta m$, where Δm is the full width at half maximum peak intensity) these two peaks are completely resolved. Modern instruments can usually deliver a mass resolution well above this figure, even for insulating samples which pose some problems because of surface texture or shape, and $m/\Delta m$ of >3000 would be expected. Hence the identification of elemental species is usually straightforward. Peaks due to metallic species are usually most intense in the positive ion spectrum with the alkali and alkaline earth-metals having particularly high positive ion yields. However, the expected pattern of intensities for multi-isotope metallic species can be distorted by the formation of hydrogen-attachment ions such that $^{n+1}Me^+$ overlaps $[^nMe + H]^+$ (these peaks are unlikely to be resolved). These points are illustrated in Figure 9. The major Zn isotopes are conveniently separated by two mass units so that the relative importance of the H-attachment ions can easily be observed.

Hydrogen is detected with high yield with both polarities but most other elements of interest for polymer surface analysis are detected in the negative ion spectrum. Carbon is detected as C^-, but the accompanying CH^- is always more intense. Similarly, oxygen is detected as O^- and OH^-. The relative intensity ratio OH^-/O^- is much more variable (structure-dependent) than CH^-/C^-. The halogens give very high negative ion yields. When present in high concentration and with the appropriate structural proximity they may be observed as addition fragments X_2^- and X_3^-. Nitrogen is not usually detected as an elemental peak at m/z 14 but rather as a combination ion, CN^- and additionally CNO^- if the structure is appropriate. Oxidized nitrogen functions produce NO_2^- and NO_3^-. Sulfur is detected as S^- (interfering O_2^- can usually be neglected) and SH^-. Oxidized sulfur appears as SO_x^- (x = 1–4) and SO_4H^-. Phosphorus is usually present in the oxidized state and detected as PO_2^- and PO_3^-.

SIMS Polymer Spectra

The interpretation of polymer spectra has been the subject of a significant body of literature and most of this has been summarized by Briggs (3). *The Static SIMS*

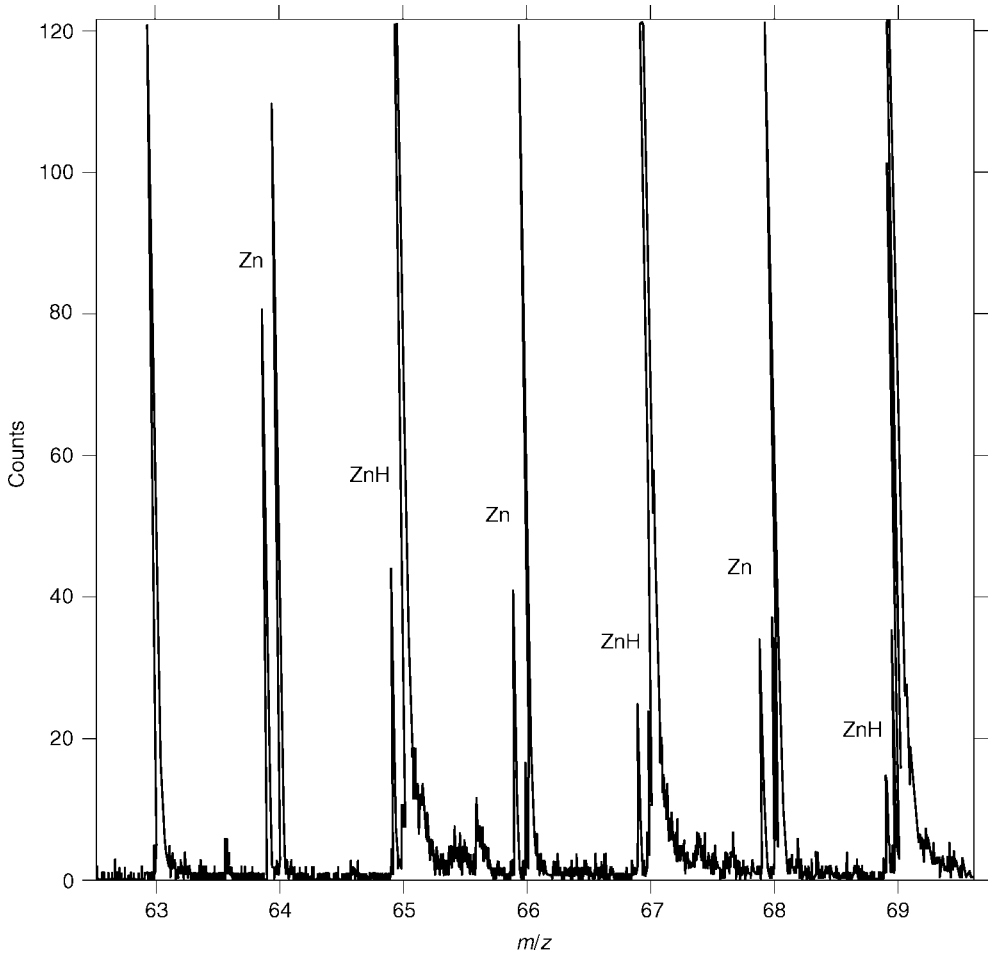

Fig. 9. Part of the positive ion ToF-SIMS spectrum from a polystyrene film sample. The most intense peaks (mostly expanded off scale) are $C_xH_y^+$ fragments from the polymer. The presence of zinc is revealed by the the mass resolved peaks at below unit mass representing the Zn^+ isotopes at nominal *m/z* 64 (47%), 66 (28%), and 68 (19%) together with an equivalent pattern for ZnH^+. Reproduced from Ref. 3, by permission of Cambridge University Press.

Library (7) contains ToF-SIMS spectra of some 200 reference polymers together with the structures of characteristic fragments. The following is, therefore, intended only to illustrate some general principles, which can be exemplified in detail using these two sources. Earlier original references, almost always involving unit-mass resolution quadrupole data, are given in Reference 3.

Hydrocarbon Polymers. Figure 10 shows the positive ion spectrum from high density polyethylene (HDPE), $(CH_2CH_2)_n$. Each cluster of peaks is due to $C_nH_m^+$ where $m = n,\ldots, 2n + 1$. For more complex aliphatic hydrocarbon polymers with pendant groups the smooth decrease in intensity of the clusters from C_2 is interrupted, and the relative intensities of the ions within each cluster

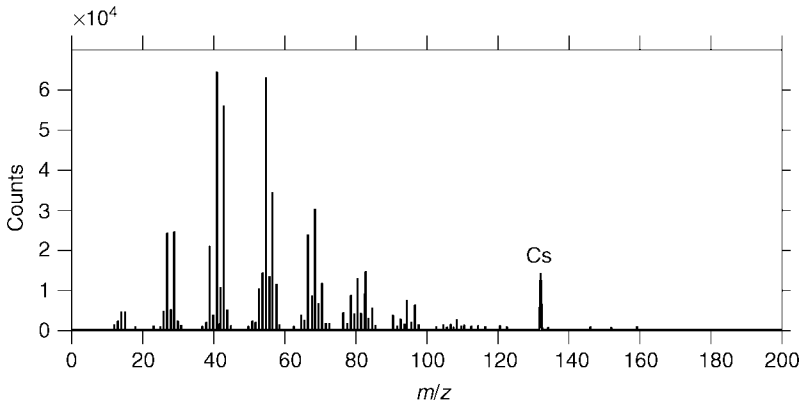

Fig. 10. Positive ion ToF-SIMS spectrum from HDPE. Reproduced from Ref. 2, by permission of SurfaceSpectra.

changes, as certain alkyl ions with methyl substituents are resonance-stabilized. Unsaturated aliphatic hydrocarbon polymer spectra are additionally characterized by a general weighting of intensity within each C_nH_m cluster toward lower values of m compared with saturated analogues.

The positive ion spectra of aromatic hydrocarbon polymers are exemplified by that of polystyrene in Figure 11. Compared to the aliphatic hydrocarbon spectra the $C_nH_m{}^+$clusters extend to much higher masses and have much lower m/n ratios as expected from the higher degree of unsaturation. Most of the prominent peaks are due to cyclic and polycyclic hydrocarbon ions, with the cyclic tropyllium ion $C_7H_7{}^+$ (m/z 91) being the most diagnostic. The negative ion spectra of all hydrocarbon polymers are very simple. C_1 and C_2 clusters dominate and above C_4 (aliphatic) or C_6 (aromatic) clusters the spectra are very weak. The $C^-/CH_2{}^-$ (m/z 12/14) intensity ratio is significantly higher for aromatic hydrocarbons compared with aliphatic hydrocarbons (saturated or unsaturated).

Aromatic Polymers. In addition to hydrocarbon polymers containing styrene, aromatic polymers comprise a large class of polymers. Attachment of heteroatoms to the phenyl ring, either in-chain or in a pendant group, leads to characteristic ions. Thus ring-substituted styrene polymers give substituted tropyllium ions, $C_7H_6X^+$ (eg X = OH, F, Cl, Br), and aromatic polyethers give $C_6H_5O^-$.

In-Chain Functionality. In the spectra of hydrocarbon polymers there is no obvious manifestation of the repeat unit chemistry. Introduction of in-chain functionality changes the situation. Figure 12 shows the positive ion spectrum of nylon-6 (polycaprolactam), $[(CH_2)_5CONH]_n$, where the amide function interrupts a hydrocarbon backbone. In addition to mainly hydrocarbon fragments at low mass, a prominent series of peaks appears due to multiple repeat unit fragments $[n\mathrm{M} + \mathrm{H}]^+$ where M is the repeat unit mass (113 amu). This behavior is much more typical of polymer spectra with multiple repeat unit fragments visible in either positive or negative ion spectra, or both, depending on the specific chemistry and opportunity for large stable fragment ion formation. [The relative intensity of these high mass ions is somewhat unusual in this case but they can be dramatically enhanced by the use of a polyatomic primary ion, such as $SF_5{}^+$.]

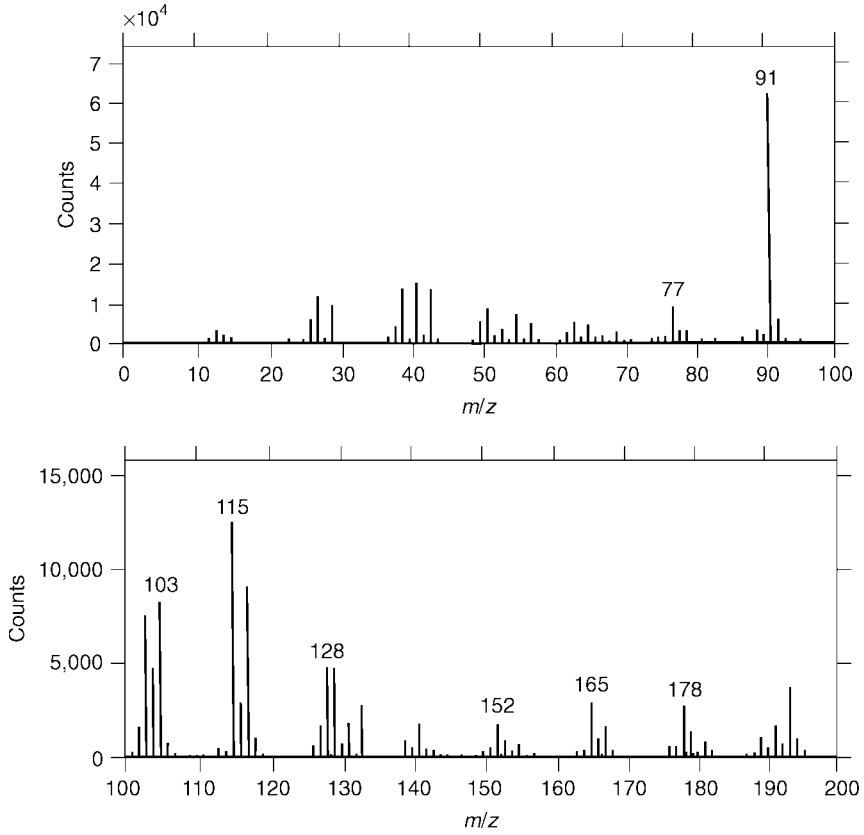

Fig. 11. Positive ion TOF-SIMS spectrum from polystyrene in the mass range m/z = 0–200. Reproduced from Ref. 3, by permission of Cambridge University Press.

Main-chain oxygen functionalized polymers also behave in this way. Thus, linear polyethers give series such as $[n\mathrm{M} + \mathrm{H}]^+$and $[n\mathrm{M} + \mathrm{OH}]^-$. In-chain polyesters either of the poly(lactone), $(\mathrm{R{-}COO})_n$, or the poly(diacid-diol), $(\mathrm{R_1COOR_2COO})_n$, types give series such as $[n\mathrm{M} + \mathrm{H}]^+$ and $[n\mathrm{M}{-}\mathrm{OH}]^-$, with probable $\mathrm{R{-}C{\equiv}O^+}$ structures, and $[n\mathrm{M} + \mathrm{H}]^-$ and $[n\mathrm{M} + \mathrm{OH}]^-$, with probable $\mathrm{R{-}COO^-}$ structures. Of course, there are many other ions formed by fragmentation at other points in the chain.

Side-Chain Functionality. Several classes of polymers consist of a hydrocarbon backbone with an oxygen-containing side chain. Collectively, they can be grouped into vinyl and acrylic polymers. Vinyl polymers have the general structure $(\mathrm{CH_2CHX})_n$. In poly(vinyl ethers) X = —OR, in poly(vinyl ketones) X = —C(=O)R, and in poly(vinyl carboxylates) X = —OC(=O)R. These polymers give positive ion spectra with hydrocarbon contributions from the backbone and from the side chain R group if this has a significant number of carbon atoms (especially if linear). Repeat unit ions are observed for the ethers but the dominant ions for the other polymers tend to be side-chain fragments, especially $\mathrm{R{-}C{\equiv}O^+}$. In the negative

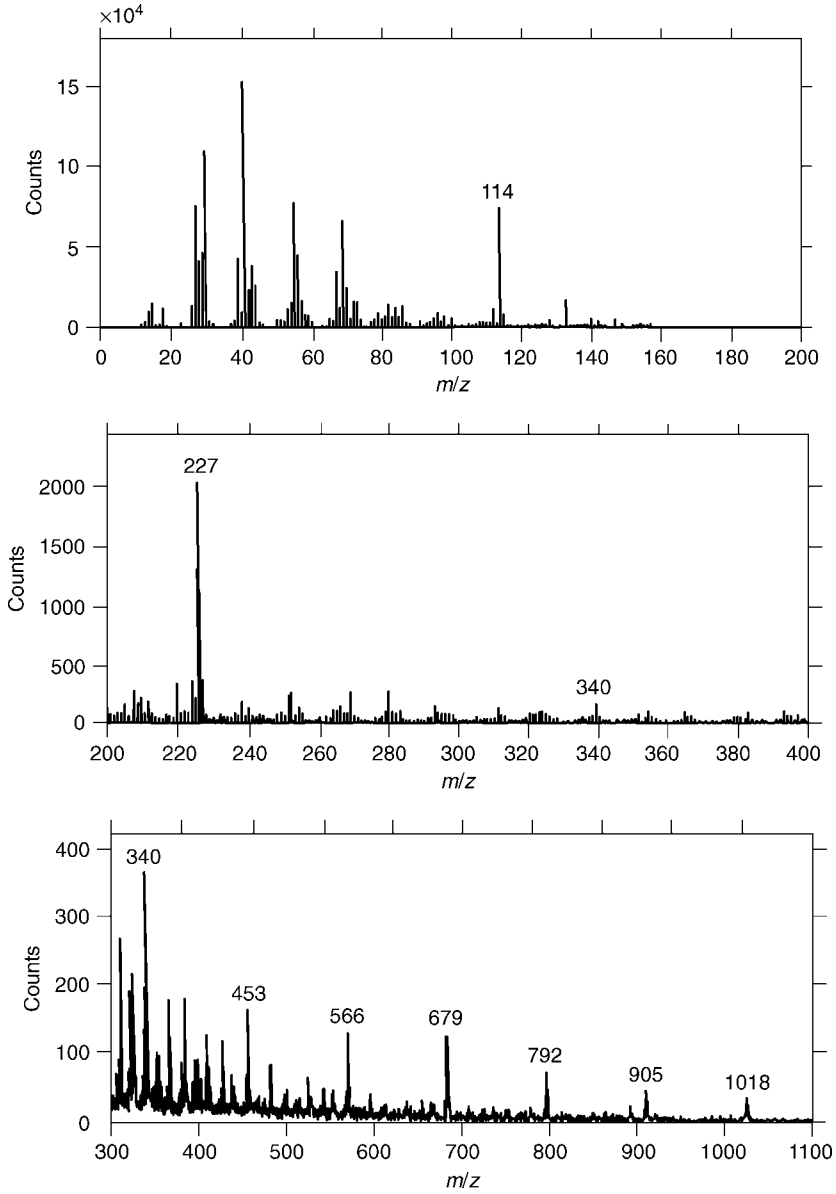

Fig. 12. Positive ion TOF-SIMS spectrum from nylon-6 (polycaprolactam). Highlighted peaks represent multiple repeat unit fragments $[n\mathrm{M}+\mathrm{H}]^+$ from $n = 1$ (m/z 114) to $n = 9$ (m/z 1018). Reproduced from Ref. 3, by permission of Cambridge University Press.

ion spectra, repeat unit ions are seen for the ketones, RO^- dominates in the case of the ethers, and RCOO^- dominates in the case of carboxylates.

Acrylic polymers are based on esters of acrylic acid and methacrylic acid and copolymers are very common. Figure 13 shows the positive ion spectrum of poly(methyl methacrylate) (PMMA). Compared with the other oxygen-containing side-chain polymers discussed above, the spectrum appears to be influenced to a

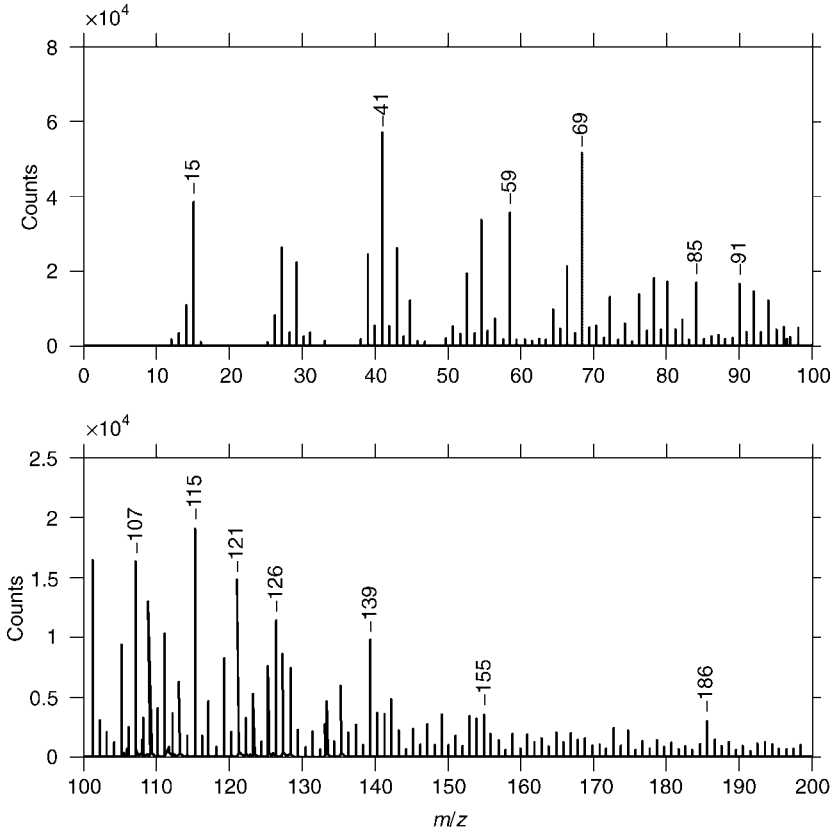

Fig. 13. Positive ion TOF-SIMS spectrum from poly(methyl methacrylate) (PMMA) in the mass range $m/z = 0$–200. Reproduced from Ref. 6.

greater extent by hydrocarbon fragments from the backbone. However, at high mass resolution, most peaks are seen to be multicomponent, often with a hydrocarbon component, but frequently due only to oxygen-containing fragments—some examples are illustrated in Figure 14. Interesting repeat unit fragments are even-mass radical cations (eg m/z 126, 154, 196, 200); these appear as essentially single-component peaks as illustrated by m/z 126 in Figure 14. With higher methacrylates (R larger than CH_3) the positive ion spectrum becomes more hydrocarbon-like. The common diagnostic ion is the methacryloyl ion at m/z 69:

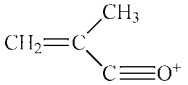

The negative ion spectrum of PMMA is shown in Figure 15. With the absence of "hydrocarbon noise" this is a much simpler spectrum and the pattern of peaks clearly reflects the repeat unit mass of 100 amu. Negative ion peaks characteristic of all methacrylates, because the side-chain alkyl group (R) has been lost, are at m/z 85, 109, 125, and 139. Specific ions having one or more intact side chains have the generic formulae: $[M+55]^-$, $[2M\text{-}15]^-$, $[2M+41]^-$, $[2M+55]^-$, and $[3M\text{-}15]^-$,

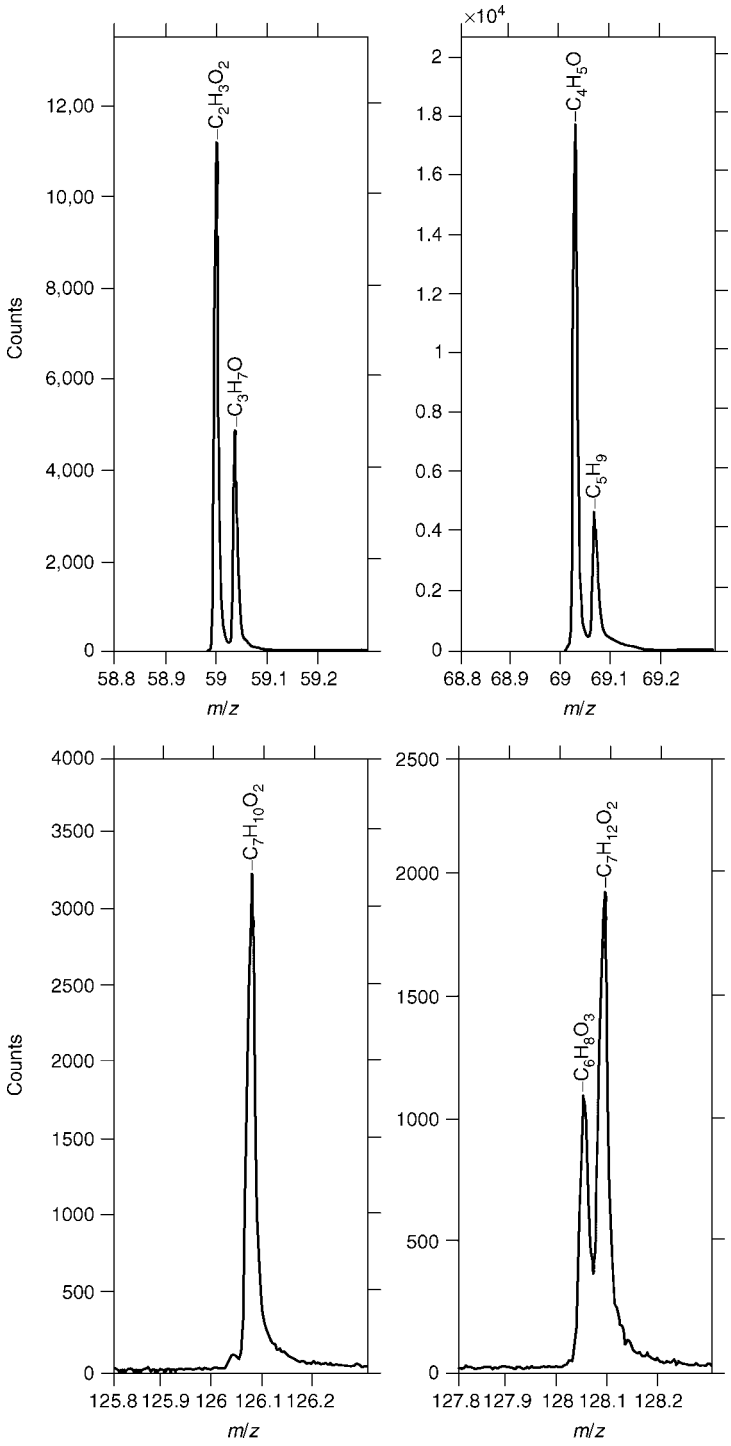

Fig. 14. High mass resolution details of some of the peaks in Figure 13. Reproduced from Ref. 6.

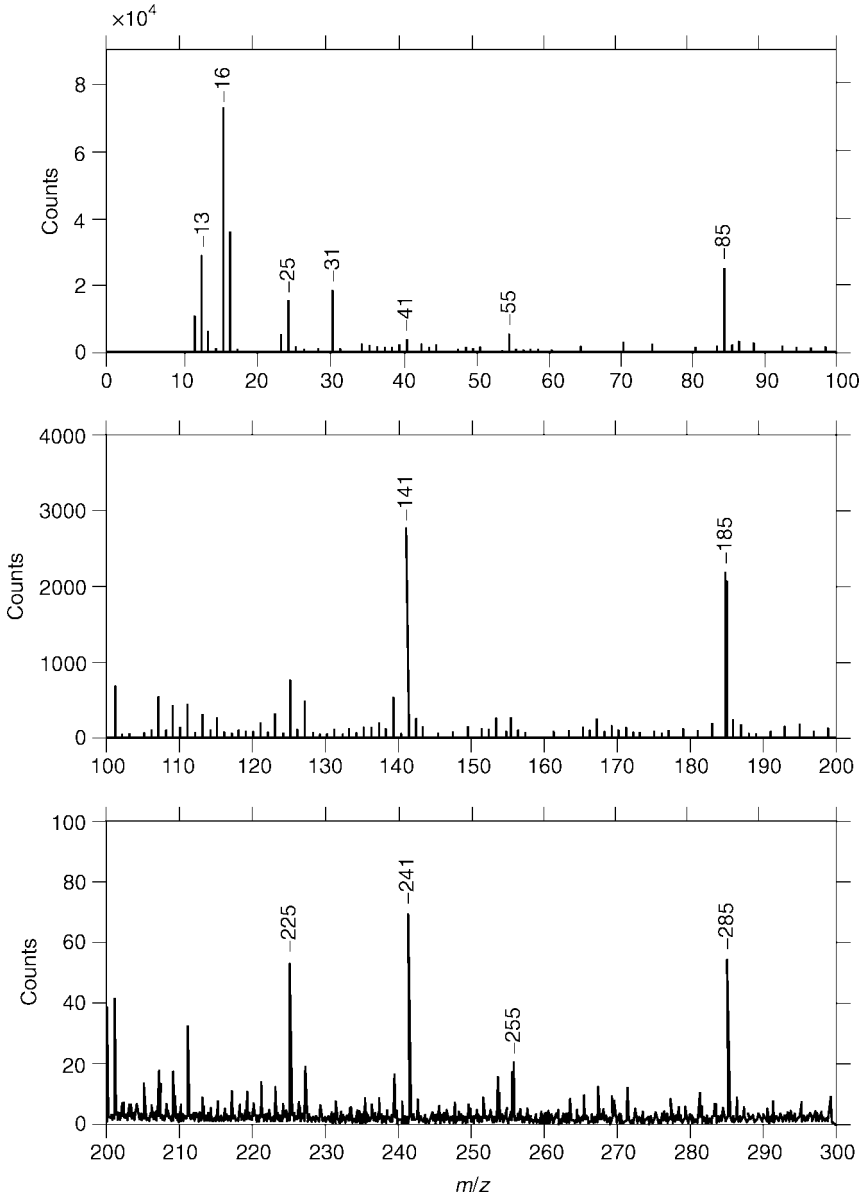

Fig. 15. Negative ion TOF-SIMS spectrum from poly(methyl methacrylate) (PMMA) in the mass range $m/z = 0$–300. Reproduced from Ref. 6.

where M is the monomer mass. In the PMMA spectrum these are at m/z 155, 185, 241, 255, and 285.

Acrylate homopolymers behave similarly, except that the repeat unit ions are much less stable. The characteristic common positive fragment is the acryloyl ion at m/z 55:

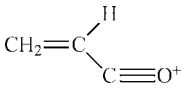

Common negative ions appear at *m/z* 65, 67, 71, and 81, while specific ions are $[M\text{-}H]^-$, $[M+13]^-$, $[M+27]^-$, $[M+39]^-$, and $[M+53]^-$.

The spectra of random acrylic copolymers display the monomer-specific features of the components together with fragment ions which reflect the linking of the different monomers in the chain. These are the equivalent of the multiple repeat unit ions from a homopolymer, but now the monomers need not be the same. In all cases the negative ion spectra are the most informative. Thus, for example, the $[2M\text{-}15]^-$ ion from a methacrylate homopolymer could appear as $[2M_1\text{-}15]^-$, $[2M_2\text{-}15]^-$, or $[M_1M_2\text{-}15]^-$, where M_1 and M_2 are the two monomers in a random copolymer.

Nitrogen-Containing Polymers. The polyamide nylon-6 has been discussed above. Other polylactams behave similarly and display a characteristic pair of peaks at $[2M+H]^+$ and $[2M\text{-}OH]^+$. Diacid–diamine polyamides, $(R_1CONHR_2)_n$, show some similarity to in-chain polyesters having dominant fragments of the type $R{-}C{\equiv}O^+$. However, since there is no equivalent of the $RCOO^-$ ion from nylons, the negative ion spectra are usually lacking in high mass molecular fragments. The characteristic peaks are simply CN^- and CNO^-. Nitrogen content is generally obvious from the positive ion spectra through the higher than normal incidence of even mass peaks (due to fragments with one, or an odd number of, N atoms).

Another important class is the polyurethanes. A common structure is:

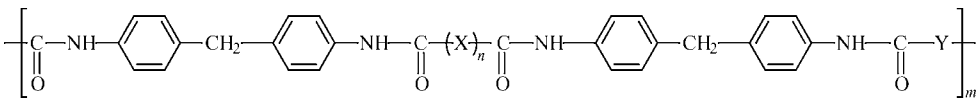

where a polyether $(X)_n$ is reacted with a diisocyanate (in this case MDI) and chain-extended with either a diamine or a diol (Y). The positive ion spectrum is principally a superposition of the polyether spectrum (discussed above) and fragments of the diisocyanate. In the case of 4,4′-methylenebis(phenylene isocyanate) (MDI), characteristic peaks are at *m/z* 106, 132, 180, and 233. The polyether can be replaced by a polyester in which case its spectrum will be a significant component of the polyurethane spectrum.

Halogen-Containing Polymers. These polymers are characterized by intense negative ions from the halogen. Aliphatic chlorine-containing polymers such as poly(vinyl chloride), $(CH_2CHCl)_n$, give positive ion spectra which at first sight resemble hydrocarbon spectra. However, at high mass resolution many peaks are seen to have additional components containing one or two Cl atoms.

Highly fluorinated polymers give an intense CF_3^+ peak at *m/z* 69, even if this group is not present in the molecule. Poly(tetrafluoroethylene), $(CF_2CF_2)_n$, gives generic fragments $C_xF_y^{+/-}$ and poly(vinylidene fluoride), $(CH_2CF_2)_n$, gives generic fragments $C_xF_yH_z^{+/-}$. An important class of lubricants are the perfluoropolyethers. These are homo- or copolymers involving the units (CF_2O), (CF_2CF_2O), and $(CF_2CF(CF_3)O)$. Complex repeat unit sequences are seen in both polarity spectra with characteristic low mass ions being CFO^+ (*m/z* 47) and CF_3O^- (*m/z* 85). Low molecular weight materials with the same repeat units are often differentiated by their end groups which give diagnostic peaks.

Silicones. Silicone rubbers and oils are usually based on polydimethylsiloxane, $(Si(CH_3)_2O)_n$. They all give spectra readily identified through the positive ions at *m/z* 28, 47, 147, 107, 221, and 281. The relative intensities of these peaks vary as a function of molecular weight, end groups, and cross-link density in the rubbers.

Organic Molecules on Surfaces

Probably the most important aspect of ToF-SIMS analysis involves the use of the technique to understand the variation in surface properties, such as wettability, adhesion, and friction, which are sensitive to submonolayer coverage of molecular species. ToF-SIMS is unique in its sensitivity and molecular speciation capability. However, unlike the situation with gas-phase organic molecule identification by electron impact mass spectrometry, there are, as yet, no well-established "rules" which allow molecular identification directly from the spectra. The situation is also complicated, in most cases, by the superposition of the spectrum of the substrate and the potential presence of more than one organic molecule.

Organic molecules usually give quasi-molecular ions of the type $[M+H]^+$ and $[M\text{-}H]^-$, where M is the molecular weight, in addition to characteristic fragments. In the case of polymer substrates, the intensity from the substrate spectrum is, typically, only high in the region *m/z* 0–200. Quasi-molecular ions are usually of higher mass, and even though their absolute intensity may be rather low, they are easily observed relative to the contribution from the substrate. An example is given in Figure 16, which shows the positive ion spectrum from the surface of pretreated (electrochemically oxidized) polypropylene. Below *m/z* 120 the spectrum is essentially due to hydrocarbon polymer fragments (compare with Fig. 10). Higher mass peaks are due to contamination and segregated additive molecules. The phosphite antioxidant Irgafos 168 gives rise to the distinctive set of peaks around *m/z* 650. Although $[M+H]^+$ for the phosphite is expected at *m/z* 647 (7), it is believed that the spectrum is mainly due to the oxidized, phosphate, product (the molecule is present to decompose hydroperoxides) which would give $[M+O+H]^+$ at *m/z* 663.

Pattern recognition is the key to organic molecule identification. Common "surface contamination" molecules fall into a relatively small number of chemical families, depending on their function, eg surfactants, lubricants, and the various types of polymer additives (plasticizers, antioxidants, etc). Thus, many surfactants are based on quaternary ammonium salts, many plasticizers are dialky phthalates, most antioxidants are di-*t*-butyl phenol derivatives, etc. The result is that each family member is likely to give a spectrum with some common fragment ions while having unique molecular ions. Alternatively, the whole spectrum may conform to a particular pattern but with components "shifted" by fixed mass intervals, eg, fatty acids which have a common hydrocarbon series in the positive ion spectrum plus molecular ions/fragments which increase in mass by 14 amu (CH_2) as the homologous series is ascended. The easiest way to recognize these patterns is to study the collections of relevant spectra, collated by function, in *The Static SIMS Library* (7).

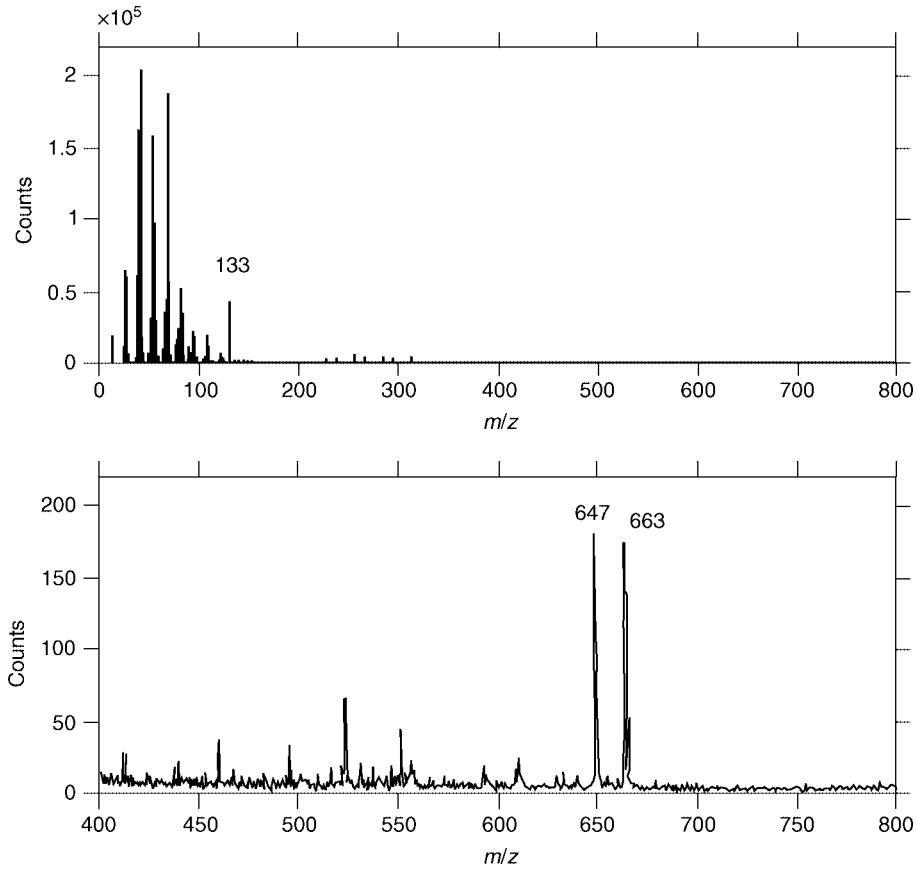

Fig. 16. Positive ion ToF-SIMS spectrum from the surface of pretreated (electrochemically oxidized) polypropylene, illustrating the typical signal noise of polymer fragments at low mass and additive molecular ions at high mass (see text). The peak at *m/z* 133 is due to primary Cs^+ ions. Reproduced from Ref. 2, by permission of SurfaceSpectra.

A number of cautionary points need to be made about pattern recognition. Firstly, some molecules are prone to cationization, that is the quasi-molecular ion may be $[M+Me]^+$ rather than, or in addition to, $[M+H]^+$, where Me is an alkali-metal ion. Sodium cationization is the most commonly encountered. Molecules containing ethylene oxide units (common amongst surfactants) are readily Na-cationized as are phthalate esters (plasticizers).

Secondly, molecules containing fatty acid residues are unlikely to be present as single components. This is because the starting materials, of natural origin, are mixtures which are not fully separated. For instance, stearates are frequently a mixture of stearate and palmitate derivatives (illustrated in Fig. 17), and saturated derivatives with C_nH_m chains may be accompanied by the unsaturated (C_nH_{m-2}) analogue.

Thirdly, the spectrum of a molecule present in a monolayer (or less) may differ from that of the molecule in multilayers. Cationization potential is one aspect of this "matrix effect". In a multilayer situation involving an *intimate* mixture of

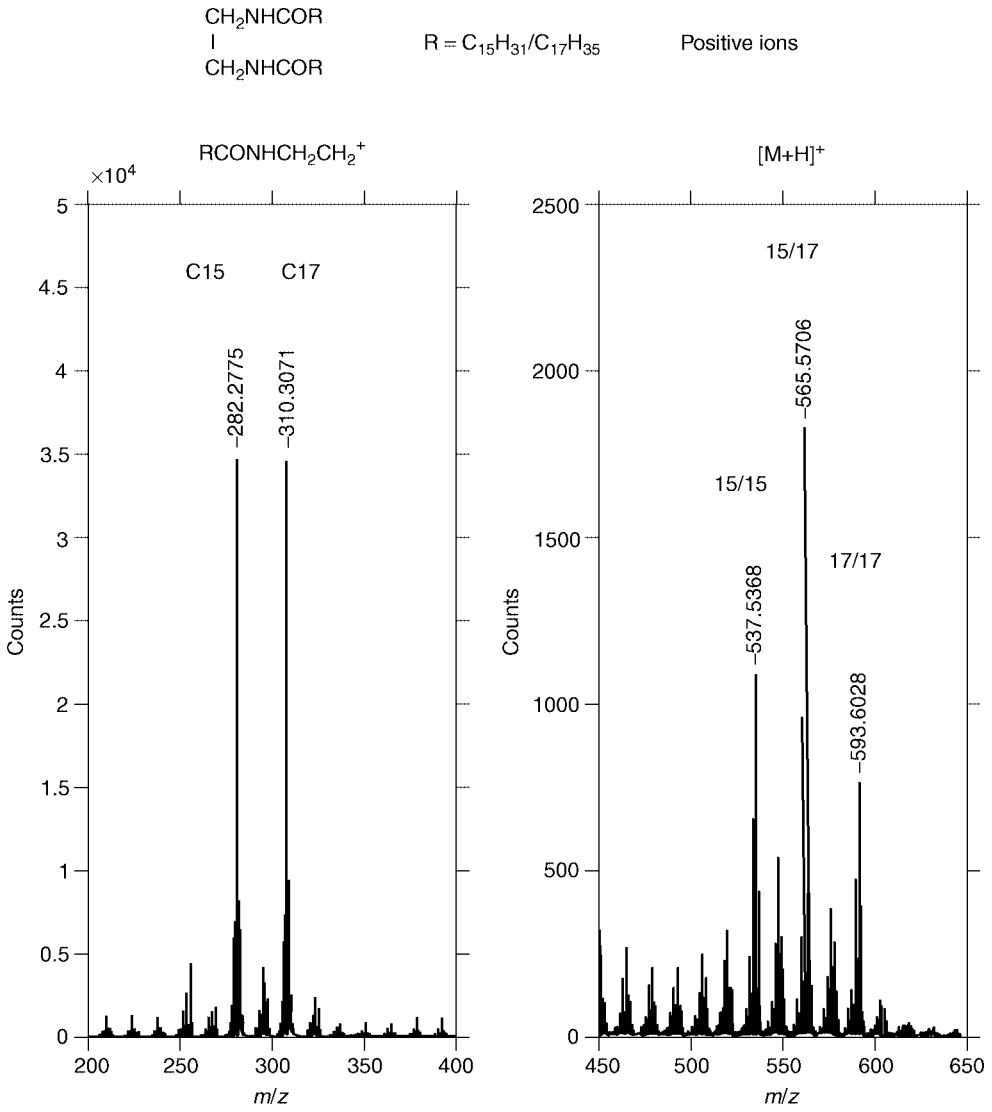

Fig. 17. Parts of the positive ion ToF-SIMS spectrum of ethylene bis-stearamide. In fact the material is a mixture of three molecules in which $C_{17}H_{35}$ and $C_{15}H_{31}$ groups are approximately equally distributed, as shown by the $RCONHCH_2CH_2^+$ fragments at *m/z* 282 and 310 (composition confirmed from accurate mass measurement). The molecular ion region accordingly has an approximately 1:2:1 triplet of peaks. [Similarly in the negative ion spectrum the $RCONH^-$ fragments give a 1:1 doublet and the $[M\text{-}H]^-$ parent ions form a 1:2:1 triplet.] Reproduced from Ref. 2, by permission of SurfaceSpectra.

two molecules, the spectra of either component may be different from that of the isolated component. This is particularly the case when one molecule is a rich source of H^+, such that the second molecule can give rise to $[M+H]^+$ ions even though it may not do so (or only weakly) when isolated.

Quantitative Aspects of SIMS

Unlike XPS, SIMS is an inherently nonquantitative technique—ie, there is no direct relationship between a peak intensity and the concentration of the species it represents. This is because secondary ion yields are strongly dependent on the chemical environment (or matrix), examples of which were noted in the previous section. Matrix effects in SIMS are most notable for yields of elemental species from inorganic matrices, but the situation is less severe for polymer matrices. Thus, relative intensities such as O^-/CH^- or F^-/CH^- correlate with XPS atomic ratios (O/C, F/C) when trends in composition are restricted to similar materials.

There have been many quantitative studies of copolymers, in which the intensities of fragments representing monomers or larger units have been correlated with composition. An early example, shown in Figure 18, concerns random hydroxyethylmethacrylate/ethylmethacrylate (HEMA/EMA) copolymers and the use of characteristic negative ions (8). Fragments at *m/z* 127 and 155 are essentially representative of HEMA and EMA monomers respectively and relative intensity plots of the form A/A+B give smooth trends (upper curves). The intensities of fragments at *m/z* 141 and 185, believed to represent HEMA–EMA linked monomers (middle curves), maximize in midrange as expected. The intensity of the fragment at *m/z* 213, representing EMA-EMA links, increases rapidly with EMA content (lower curve), also as expected. The ratio I(213)/I(155) represents the ratio of diads to singles. For a random copolymer where diad (AA) signals come from sequences B-$(A)_n$-B where $n > 2$, a statistical analysis predicts that the ratio of diads to singles (isolated A units) will be proportional to the mole fraction of A, as seen in the lower plot. The choice of fragments for such plots is not always so obvious and in many cases better results are obtained by using multivariate statistical analysis techniques which utilize the whole spectrum. This subject is discussed thoroughly in Reference 9.

The end groups of a polymer can have a marked effect on the SIMS spectra (3,10). If these are chemically distinct from the rest of the chain, because of the use of specific initiation or termination reactions, they will give rise to readily identifiable peaks. However, in all cases end groups can have a disproportionate effect on spectra because only one bond needs to be broken to produce a fragment whereas two bonds need to be broken to generate an in-chain fragment. Ratios of fragments due to end groups and in-chain fragments in homopolymer spectra depend on molecular weight, typically up to 20,000–30,000. This provides a unique method for monitoring surface average molecular weight, which can be particularly important in this range. Low molecular weight fractions of the distribution may migrate to the surface and significantly alter mechanical properties relative to the bulk polymer as well as leading to adverse surface behavior.

Application Examples

Surface Oligomer Detection and Imaging. The case of cyclic trimer (three monomers in a ring formation) on the surface of poly(ethylene terephthalate) (PET) film is interesting. The crystallization of cyclic trimer on PET surfaces

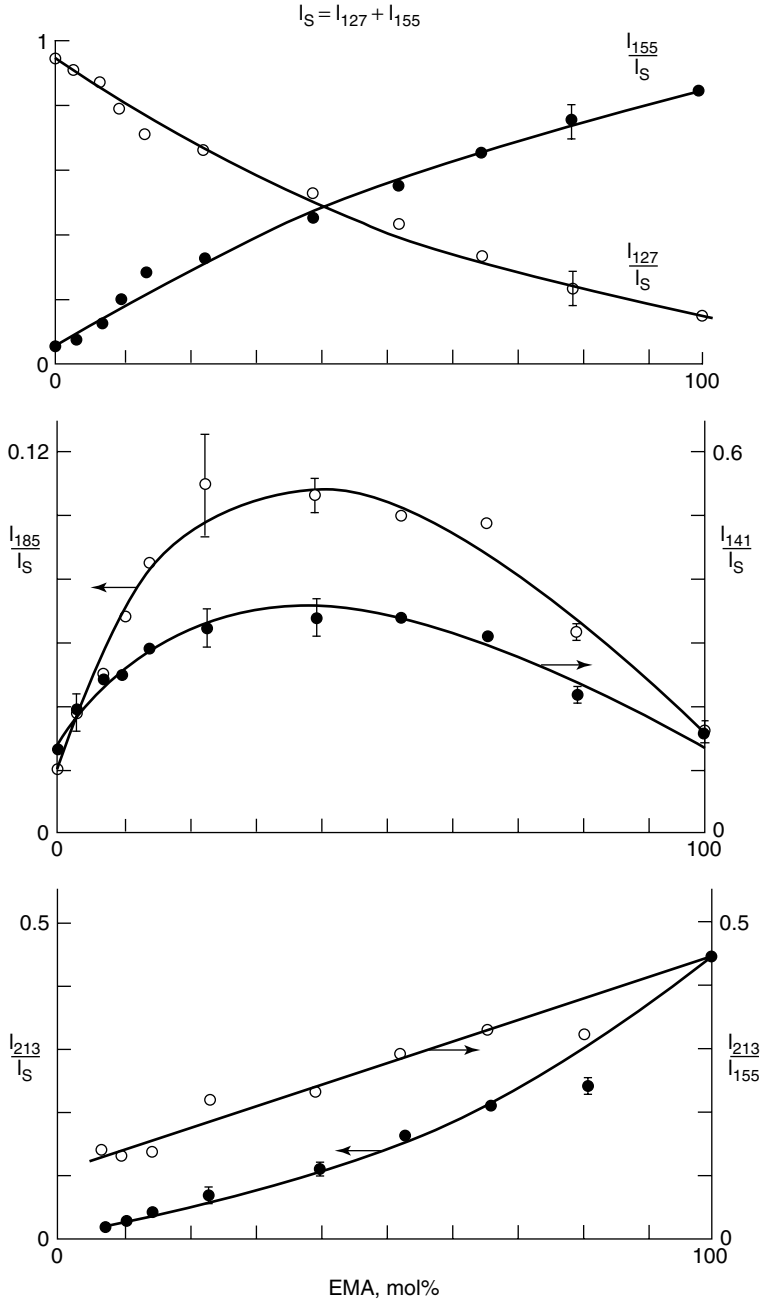

Fig. 18. Relative intensities of characteristic negative ion fragments from HEMA–EMA copolymers (see text) plotted as a function of bulk composition. Error bars in (**a**) represent the largest spread of values for any measurement, and those in (**b**) and (**c**) represent the spread of values for all repeated measurements. Reproduced from Ref. 8, by permission of Elsevier.

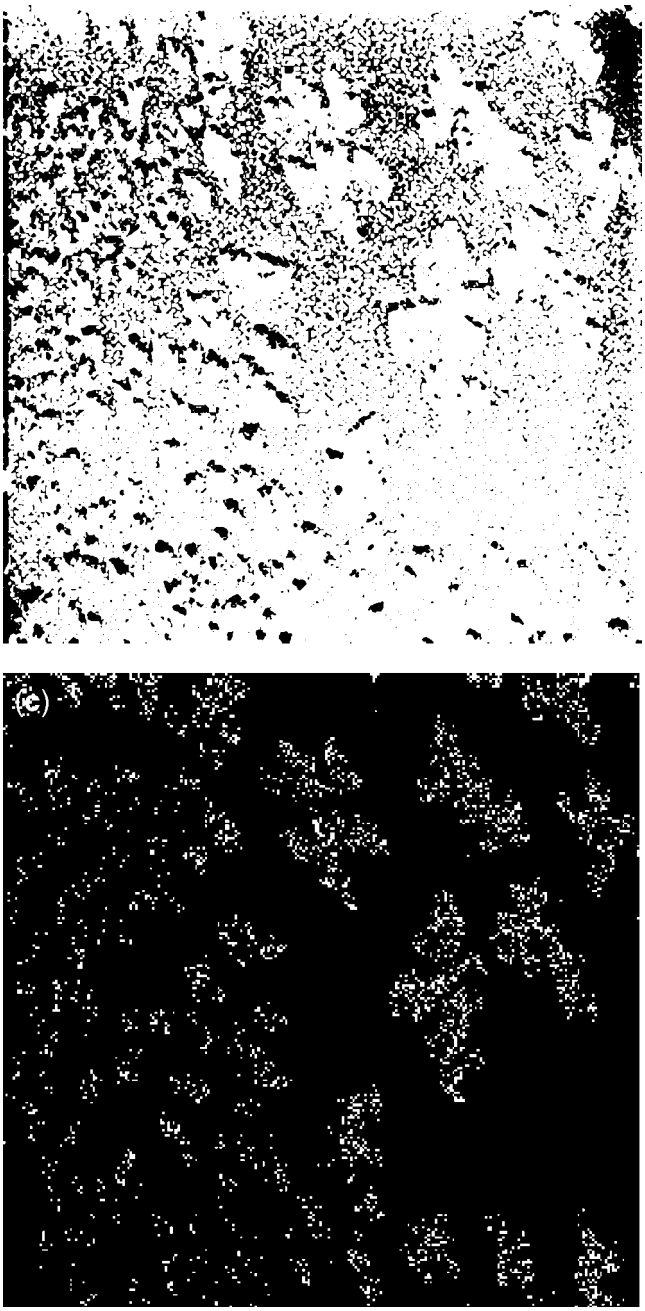

Fig. 19. (**a**) Total positive ion image of a 200 μm $\times$ 200 μm region of PET film after heating for 48 h at 170°C, showing trimer cryztallization in topographic contrast. (**b**) Spectra created retrospectively from the raw data stream of image in 1**a** for regions of approximately the same area either bounding crystals or between crystals. (**c**) Image created retrospectively from the raw data stream of image in Figure 1 using only the intensity of the *m/z* 577 peak ($C_{30}H_{25}O_{12}^{+}$ or $[M+H]^{+}$), showing the trimer crystals in chemical contrast. Adapted from Ref. 12.

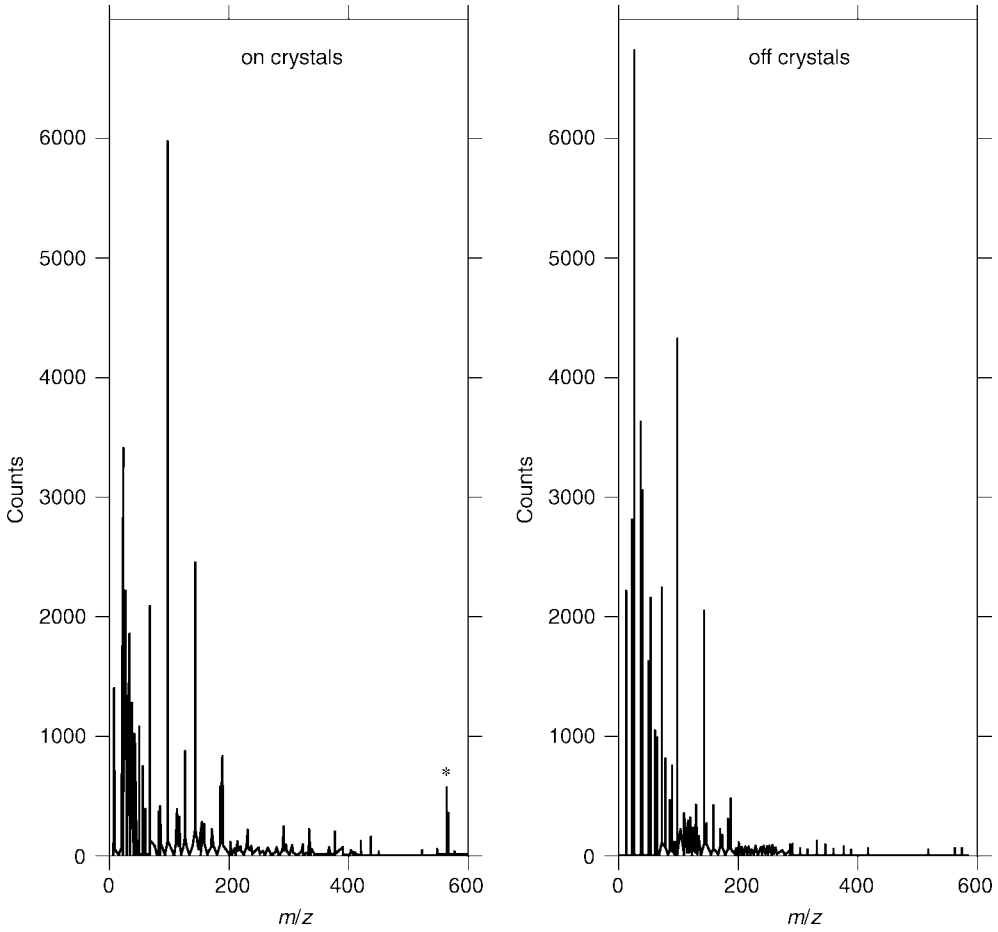

(**b**)

Fig. 19. (Contiuned)

heated to temperatures above 120°C or exposed to certain solvent vapors is well established and can be the source of problems in the wide use of this polymer in film and fiber products. The crystals were first characterized *in situ* (ie, without resort to solvent extraction from the surface) using quadrupole static SIMS (11). While the pure polymer spectrum exhibits only a weak positive ion at *m/z* 577, representing $[3M+H]^+$where M is the repeat unit mass (192 amu), this peak is around 20 times more intense (relative to the base peak at *m/z* 104) from the pure trimer crystals because it represents the molecular ion. An uncertainty remaining from the quadrupole static SIMS study was whether all the trimer on the surface was contained in the crystals, or whether amorphous trimer might also be present on the film surface between the crystals. A later ToF-SIMS imaging study was able to clarify this point (12).

Figure 19**a** shows a total positive ion image of a PET film surface after heating at 170°C for 48 h. The essentially hexagonal crystals cover a wide size range

of order 1–50 μm. From a raw data stream file containing the full spectrum at each pixel in the 256 $\times$ 256 array, it is possible to retrospectively analyze regions of the surface which are covered by the crystals and regions which appear to be bare film. This leads to the spectra shown in Figure 19**b**. The *m/z* 577/104 ratio in the intercrystalline regions is identical, within experimental error, to that of the original film surface which strongly suggests that all the trimer on the surface is crystalline. The crystals themselves are easily mapped using the *m/z* 577 trimer molecular ion (reconstructed from the raw data file) as shown in Figure 19**c**. Compared with the total ion image, which is dominated by topographic contrast, this image has higher contrast because of its chemical specificity. The study similarly confirmed that the crystals on solvent-exposed films, which have a needle-like habit quite different from those produced by heat treatment, are also due to cyclic trimer.

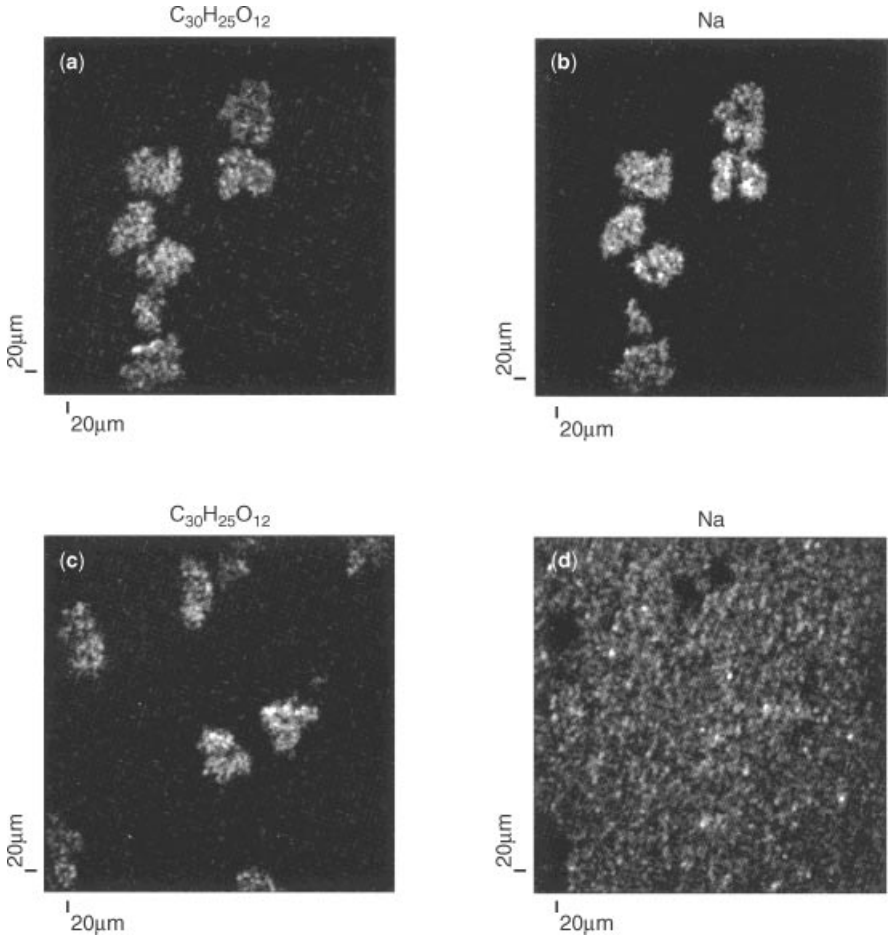

Fig. 20. Images of trimer crystals ($C_{30}H_{25}O_{12}^+$ at *m/z* 577) and sodium (Na^+ at *m/z* 23) for PET made with terephthalic acid (**a**, **b**) and dimethyl terephthalate (**c**, **d**). Both films were heated for 2 h at 180°C. Adapted from Ref. 12.

The advantage of retrospective analysis of image data files is illustrated by the behavior of sodium. This is usually present at very low levels (tens of ppm) in PET. Its appearance in the spectra after heat treatment was therefore intriguing. Figure 20 shows images from two types of PET film, one manufactured from polymer made using terephthalic acid (TA) and the other from polymer made using dimethyl terephthalate (DMT). Both films were identically treated for 2 h at 180°C. In the case of the TA polymer the sodium is clearly associated with the crystals, while in the DMT polymer case the sodium is more evenly distributed, but shows a lower than average concentration in certain crystals (12).

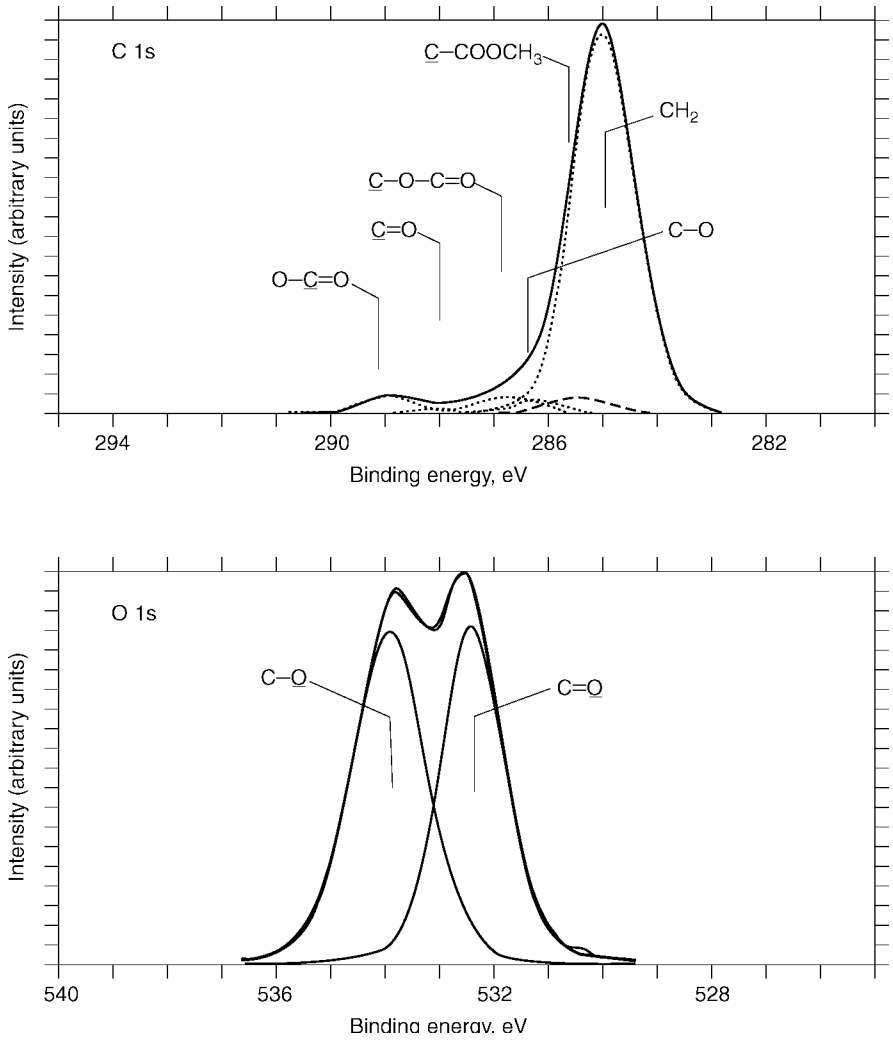

Fig. 21. C 1s and O 1s spectra from the surface of a thermally pressed poly(ethylene-*co*-methyl acrylate) film containing 23.4% methyl acrylate (45° take-off angle). Reproduced from Ref. 13.

Surface Morphology of EMA Copolymers. EMA copolymers are semicrystalline, with ethylene enrichment of the crystalline phase and methyl acrylate (MA) enrichment in the amorphous phase. They are commonly used in films and adhesives. The distribution, composition, and orientation of these phases at the surface are expected to have a major influence on the surface propereties which are critical to these applications (eg, cling, sealing, and adhesion). Galuska carried out a detailed study of a range of polymers with an MA content ranging from 6.8 to 33 wt% (13). Thermally pressed films were used.

Typical C 1s and O 1s spectra are shown in Figure 21. The ether and ketone components are due to adventitious oxidation during film pressing, so the most reliable measure of MA content is the carboxyl component. Thus, from the C 1s spectra the surface oxygen concentration due to MA could be extracted. Measurements were made as a function of take-off angle to vary the sampling depth. These results are shown in Figure 22. The interpretation of the surface morphology based on this data involves a periodic structure due to segregation of the amorphous phase into ethylene- and MA-rich layers as a result of MA clustering. Of particular interest is the behavior at the very surface (20A analysis depth correlation) where there is an abrupt change in behavior above 20% MA content.

In the ToF-SIMS positive ion spectrum the peaks characteristic of LDPE and PEMA appear but as the MA concentration increases some of the hydrocarbon peaks (eg CH_3^+, $C_5H_9^+$, $C_6H_{11}^+$, $C_7H_{13}^+$), initially with the relative intensities expected from LDPE, increase in intensity and EMA-specific ions, eg, $C_2H_3O_2^+$, are detected (high mass resolution required). Two of these ions, normalized to the nonspecific $C_2H_3^+$ ion, are plotted as a function of bulk MA content in Figure 23.

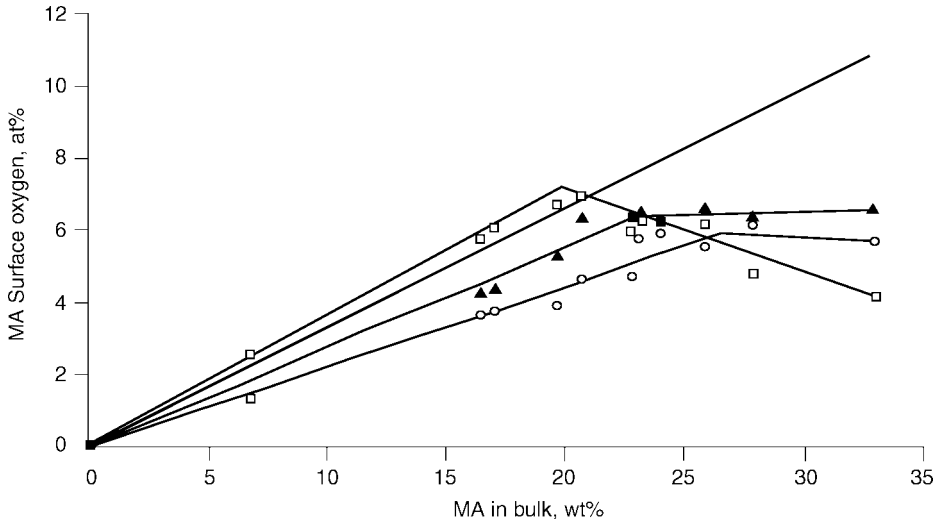

Fig. 22. Surface MA oxygen concentration vs bulk MA content for thermally pressed poly(ethylene-co-methyl acrylate) films as determined from XPS at three different take-off angles. The bold line would be obtained for a surface composition identical with the bulk. ——— Bulk Ma oxygen calibration, □ 20° Take-off angle (20 Å), ▲ 45° take-off angle (40 Å), ○ 90° take-off angle (60 Å). Reproduced from Ref. 13.

As with the XPS data for the lowest analysis depth a dramatic change occurs at about 20% bulk MA content. It is believed that ions like $C_7H_{13}^+$ represent polymer backbone with attached MA side chains, whereas the $C_2H_3O_2^+$ ion represents the side chain itself. The behavior of the two curves strongly suggests that a rearrangement of the polymer chains at the surface occurs at this critical MA concentration so that the ester side chains are preferentially orientated inwards.

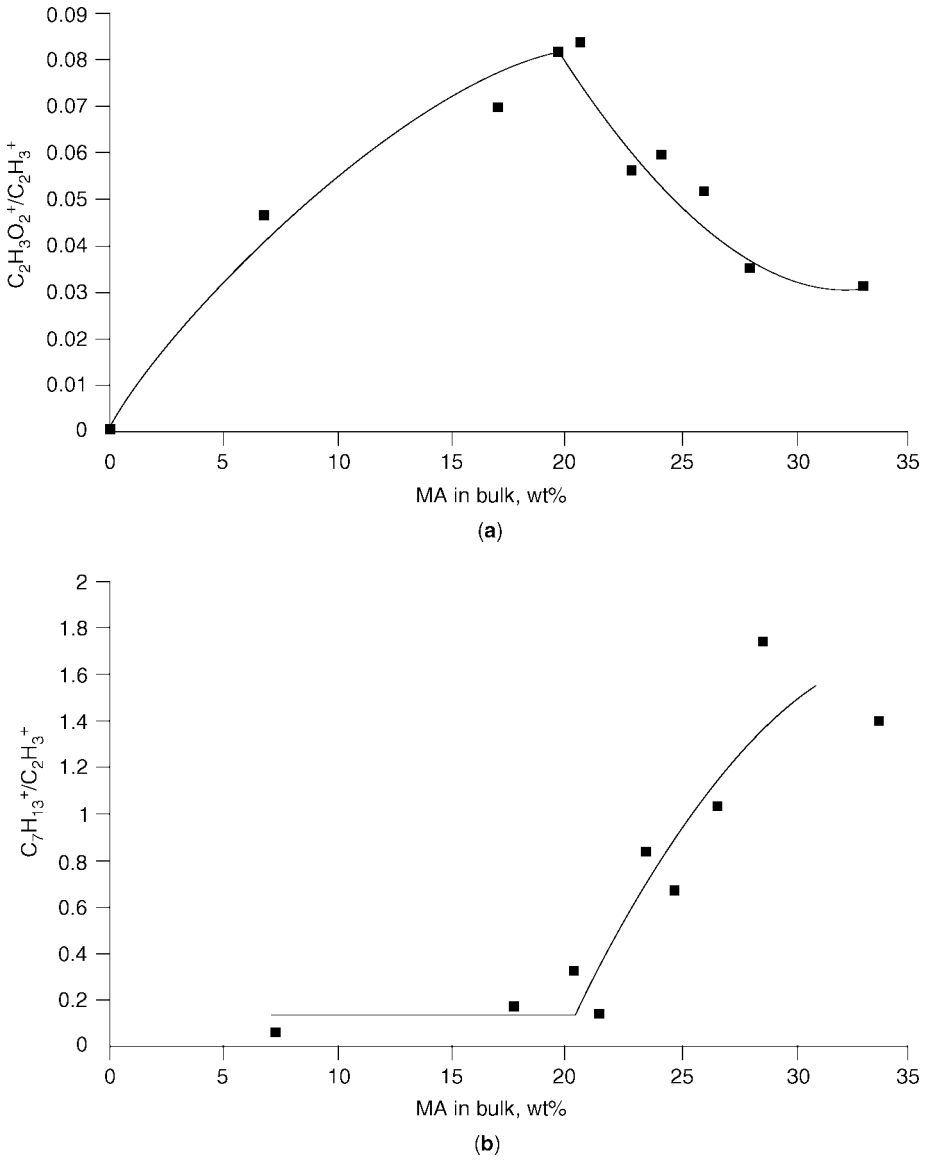

Fig. 23. ToF-SIMS intensity plot for $C_2H_3O_2^+$ (**a**) and $C_7H_{13}^+$ (**b**) (both relative to $C_2H_3^+$) as a function of bulk MA content for the thermally pressed poly(ethylene-*co*-methyl acrylate) films of Figure 22. Reproduced from Ref. 13.

BIBLIOGRAPHY

"Surface Analysis" in *EPSE* 2nd ed., Vol. 16, pp. 399–442, by D. Briggs, ICI.

1. D. Briggs and J. T. Grant, eds., *Surface Analysis by Auger and X-ray Photoelectron Spectroscopy*, SurfaceSpectra/IM Publications, Manchester, U.K., 2003.
2. J. C. Vickerman and D. Briggs, eds., *ToF-SIMS: Surface Analysis by Mass Spectrometry*, SurfaceSpectra/IM Publications, Manchester, U.K., 2001.
3. D. Briggs, *Surface Analysis of Polymers by XPS and Static SIMS*, Cambridge University Press, Cambridge, 1998.
4. G. Beamson and D. Briggs, eds., *The XPS of Polymers Database*, SurfaceSpectra, Manchester, U.K., 2000 (CD-ROM, see www.surfacespectra.com).
5. G. Beamson and D. Briggs, *High Resolution XPS of Organic Polymers*, John Wiley & Sons, Inc., Chichester, U.K., 1992.
6. D. Briggs and I. W. Fletcher, *Surf. Interface Anal*. **25**, 167 (1997).
7. The Static SIMS Library Version 3 SurfaceSpectra, Manchester, U.K., 2002 (CD-ROM, see www.surfacespectra.com).
8. D. Briggs D and B. D. Ratner, *Polym. Commun.* **29**, 6 (1988).
9. X. Vanden Eynde, in J. C. Vickerman and D. Briggs, eds., *ToF-SIMS: Surface Analysis by Mass Spectrometry*, SurfaceSpectra/IM Publications, Manchester, U.K., 2001, p. 543.
10. D. Briggs in J. C. Vickerman and D. Briggs, eds., *ToF-SIMS: Surface Analysis by Mass Spectrometry*, SurfaceSpectra/IM Publications, Manchester, U.K., 2001, p. 498.
11. D. Briggs, *Surf. Interface Anal.* **8**, 133 (1986).
12. S. Reichlmaier, S. R. Bryan and D. Briggs, *J. Vac. Sci. Technol., A* **13**, 1217 (1995).
13. A. A. Galuska, *Surf. Interface Anal.* **24**, 380 (1996).

DAVID BRIGGS
University of Nottingham, University Park

SURFACE PROPERTIES.

See Volume 4.

SUSPENSION (OR PRECIPITATION) POLYMERIZATION.

See HETEROPHASE POLYMERIZATION.

TELECHELIC POLYMERS

Introduction

Telechelic polymers are defined as macromolecules that contain two reactive end groups. A pioneering work on the synthesis functional polymers and their conversion to the final products with specific properties by reacting with functional groups may be dated back to 1947 (1). However, the concept was not fully recognized until 1960 (2). Significant contributions to the development of this class of polymeric materials are still found in the current literature. In the last decade there has been a rapid growth in the development and understanding of new controlled radical polymerizations (3). Precise control of functionality, molecular weight, and uniformity (molecular weight distribution) can now be made not only by ionic polymerization routes but also by newly developed living radical polymerization (qv) techniques. Another striking development has been achieved in the metathesis polymerization. Many new catalysts have been developed and applied to preparation of advanced materials (4–8). The range of monomers and functional groups used in the preparation of telechelic polymers has been expanded in recent years as a result of such developments.

This article describes the general techniques for the preparation of telechelics. A special emphasis has been placed on controlled radical and metathesis polymerization methods.

A polymer can be considered to be telechelic if it contains end groups that react selectively to give a bond with another molecule. Depending on the functionality, which must be distinguished from the functionality of the end group itself, telechelics can be classified as mono-, di-, tri-, and multifunctional telechelics (polytelechelics) (9). The functionality is defined as

$$f = \frac{\text{Number of functional groups}}{\text{Number of polymer chains}} \tag{1}$$

Encyclopedia of Polymer Science and Technology. Copyright John Wiley & Sons, Inc. All rights reserved.

Telechelic polymers can be used as cross-linkers, chain extenders, and precursors for block and graft copolymers. Moreover, star and hyper-branched or dendric polymers are obtained by coupling reactions of monofunctional and multifunctional telechelics with appropriate reagents. Various macromolecular architectures obtained by the reactions of telechelics are represented in Figure 1.

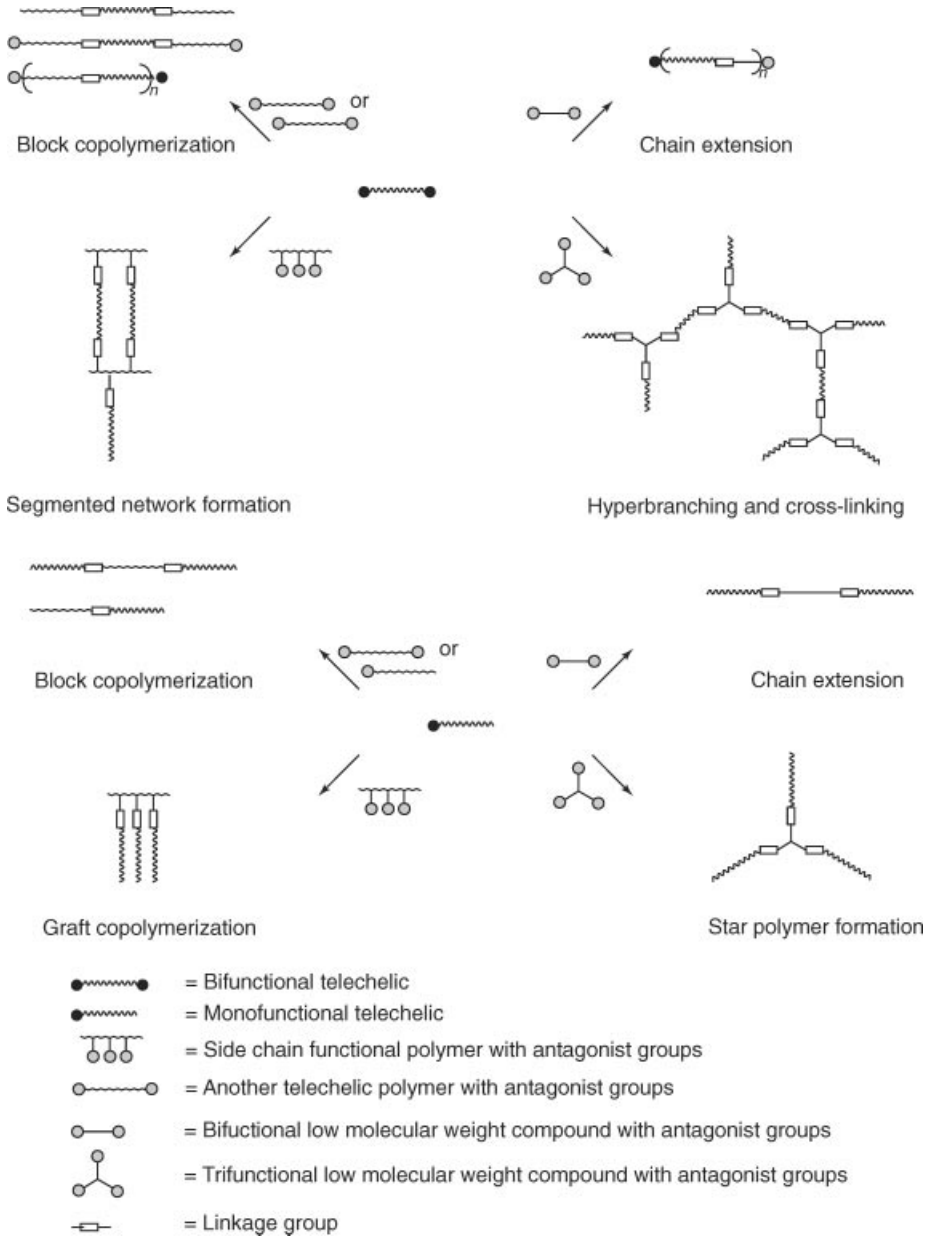

Fig. 1. Various architectures obtained by the reactions of telechelics.

The functionality of the end group itself is important. When such groups are bifunctional (eg, vinyl groups) they can participate in polymerization reactions, yielding graft copolymers or networks; such telechelic polymers are called macromolecular monomers, macromonomers, or macromers.

Industrial interest in telechelics was stimulated by the development of thermoplastic elastomers, which consist of ABA block and multiblock copolymers. Liquid telechelic polymers are the basis for reaction injection molding. Liquid telechelics that can be used for network formation offer processing advantages and may result in materials with improved properties (10).

Radical Polymerization

Free radical polymerization, is the most widely used methodology in synthetic polymer chemistry owing to its simplicity, applicability to many monomers, and relatively high tolerance to impurities and functional groups.

Conventional Radical Polymerization. Telechelics can be synthesized by radical polymerization (qv) in two ways: End groups can be controlled using a large concentration of (functional) initiator (dead-end polymerization), or polymerization can be conducted in the presence of suitable transfer agents (telomerization) (10–14).

The first method has serious limitations because well-defined end groups can be observed only if not more than one type of primary radical is formed that does not cause side reactions such as transfer. Moreover, a propagating radical will readily react with another radical, primary or macroradical, either through disproportionation or through coupling reactions (termination) (Fig. 2). The former will produce monofunctional telechelics with both a saturated and an unsaturated chain end, while only the latter will yield bifunctional telechelics.

Table 1 shows the percentage of termination by coupling (combination) for some common monomers (15).

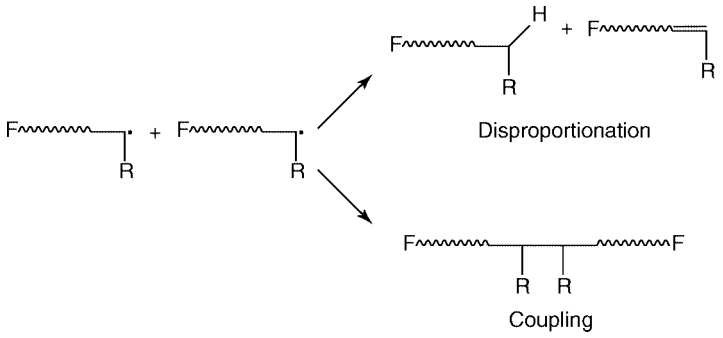

Fig. 2. Termination reactions.

Table 1. Percentage of Termination by Combination of Different Monomers at 25°C[a]

Monomer	Percent	Monomer	Percent
styrene	100	methyl methacrylate	33
p-chlorostyrene	100	ethyl methacrylate	32
p-methoxystyrene	81	*N*-butyl methacrylate	25
methyl acrylate	100	acrylonitrile	100
ethyl acrylate	100	methacrylonitrile	35

[a]Ref. 15.

Functional Initiators

Azo Initiators. In this section we report the preparation of telechelics involving thermally labile azo compounds. Upon heating, aliphatic azo compounds evolve nitrogen, thus forming two carbon-centered free radicals (see Initiators, Free-Radical).

$$R^1\text{—}N{=}N\text{—}R^2 \xrightarrow{\triangle} R^{1\cdot} + R^{2\cdot} + N_2 \qquad (2)$$

The activation energies for this reaction are, supposing R^1 and R^2 are aliphatic, between 60 and 160 $kJ \cdot mol^{-1}$. Azo groups are, therefore, a highly suitable radical source with respect to the energy required. Despite being thermally labile, azo groups are photoactive, too. Aliphatic azo groups evolve nitrogen with quantum yields as high as $\Phi = 0.44$ (AIBN 16). However, the absorbance is relatively low, being $\varepsilon = 13\ cm^2 \cdot mol^{-1}$ at $\lambda_{max} = 350$ nm (AIBN 17). In order to obtain telechelics, the initiating azo compound has to be at least bifunctional: it must carry one or more functional sites other than the azo function itself. Because of the potential variability in the chemical nature of the azo initiators it is possible to prepare telechelics with a wide variety of functional groups (Table 2).

Telechelics with certain functional groups can be prepared directly from the precursor initiators or, alternatively, via modification of the available telechelics. For instance, hydrolysis of nitrile groups yields carboxyl-terminated oligostryrene while isocyanate end groups are obtained directly from the azide telechelics or by treatment of amino-terminated polymers with phosgene (19). The functional group approach to synthesize amino telechelics causes some complications since amino compounds participate in chain-transfer reactions. Yagci and co-workers (37,38) proposed a convenient and simple synthetic route for the preparation of amino telechelics via free radical polymerization using (acyloxy) imino azoinitiator and subsequent photolysis and hydrolysis.

Table 2. Azo Initiators Used for the Synthesis of Telechelic Polymers

Structure of the initiator	Reference
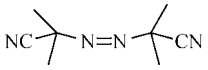	18–20
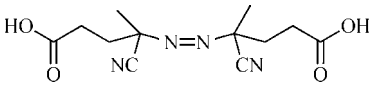	21–27
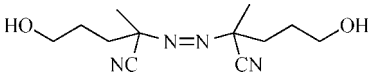	21–23,28
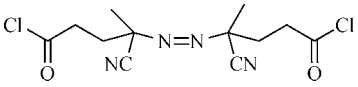	29
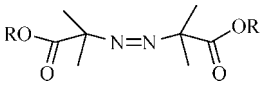	19
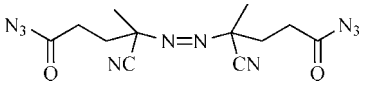	30
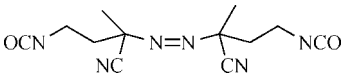	30
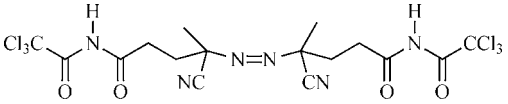	31
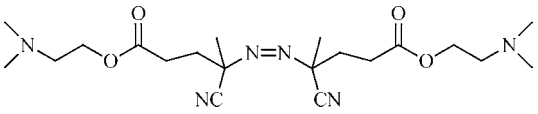	32
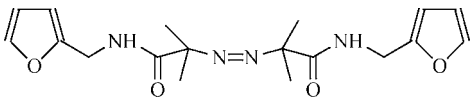	33
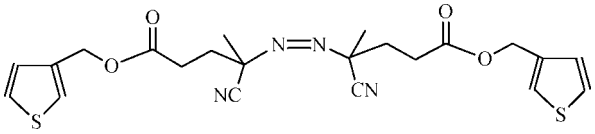	34
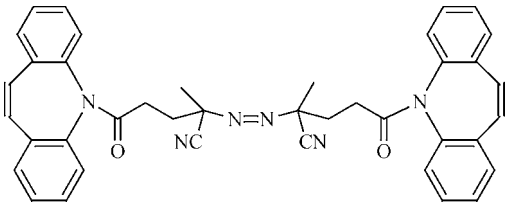	35

Table 2. (Continued)

Structure of the initiator	Reference
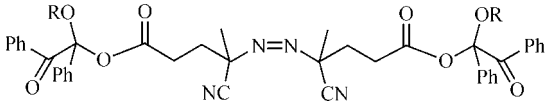	36
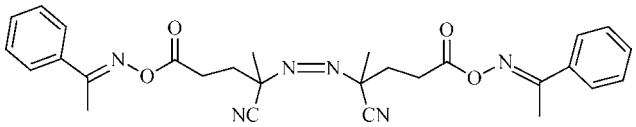	37

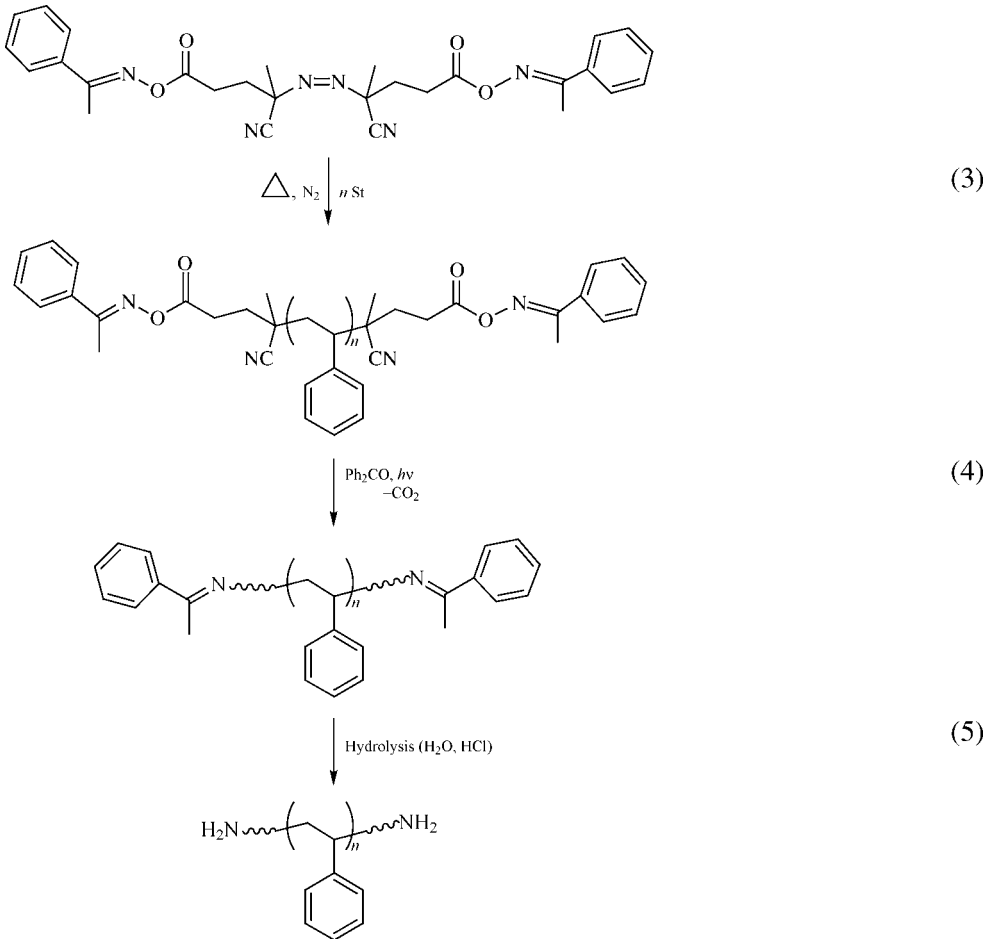

(3)

(4)

(5)

Peroxide Initiators. Hydroxyl radicals formed by a redox reaction with H_2O_2 are highly reactive, and have not been reported for the small-scale preparation of telechelics. However, the industrial preparation of hydroxy-terminated butadiene oligomers probably involves such process (39).

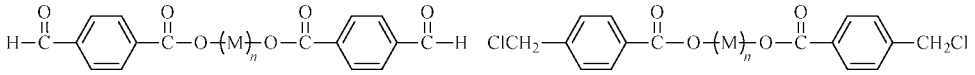

Fig. 3. Structure of telechelics obtained by functional benzoyl peroxide initiators.

Diacyl peroxide decomposition can yield two types of radicals ($RCOO^{\bullet}$, $R^{\bullet}$):

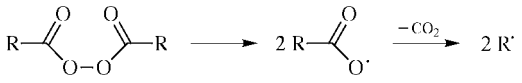

(6)

However, these peroxides have not been utilized for the preparation of telechelics. The less reactive aroyl peroxides give styryl telechelics (40). When employing benzoyl peroxides p-substituted with chloromethyl or aldehyde groups, the telechelics require no further modification before being used as prepolymers (Fig. 3).

Ethylene polymerized with diethyl peroxydicarbonate contains terminal ester groups (41). Using ^{14}C-labeled cyclohexane peroxydicarbonate, the fate of the primary radicals during the polymerization of methyl methacrylate (MMA) and styrene has been studied (42). Although this reference includes no detailed analysis of the products, it indicates that ROOCO-terminated polystyrene telechelics may be obtained by this technique. A similar method has been used for the preparation of telechelic polybutadiene (43). The carbonate end groups are easily modified into terminal hydroxyl groups by hydrolysis. Hydrogenation of the carbonate functionalized telechelic polybutadiene, followed by hydrolysis, yields hydroxy-terminated polyethylene telechelics.

Free Radical Copolymerization of Alkenes with Unsaturated Heterocyclic Compounds

Free radical ring-opening polymerizations of unsaturated heterocyclic compounds are driven by formation of a carbon–oxygen double bond at the expense of a less stable carbon–carbon double bond. By the reaction mechanism outlined in reaction 7, the seven-membered keten acetals, such as 2-methylene-1,3-dioxepane, undergo essentially complete ring opening, leading to the corresponding polyester (44–51).

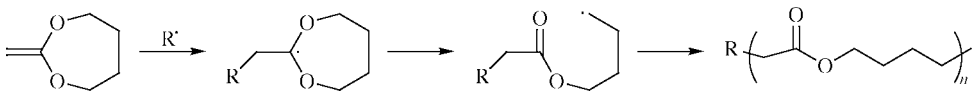

(7)

Similarly, the five-membered phenyl-substituted and nitrogen analogue monomers yield the corresponding polyester and polyamide.

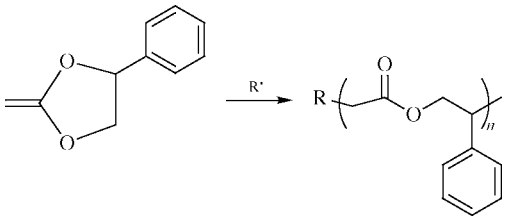

(8)

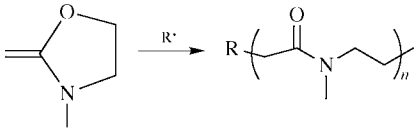

(9)

Telechelic polystyrene and polyethylene containing a hydroxyl and a carboxylic end group are obtained by copolymerizing a small quantity of 2-methylene-1,3-dioxepane with a large quantity of styrene or ethylene, and then hydrolyzing the resulting polymers (reactions 10 and 11).

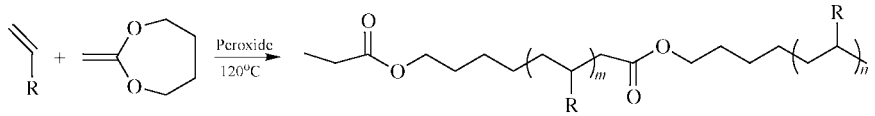

(10)

R = H or Ph

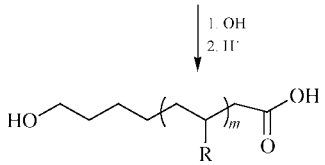

(11)

Copolymerization (qv) of common monomers with cyclic ketene thioacetals result in telechelics containing a thiol and a carboxylic acid group as chain ends.

Finally, the unsaturated spiro-*ortho*-carbonate shown in reactions 12 and 13 undergoes double ring opening during free radical copolymerization so as to introduce carbonate groups into the backbone of an addition polymer. Therefore, telechelic polystyrene containing two primary hydroxy chain ends is obtained by hydrolysis of the copolymer from styrene and the spiro monomer.

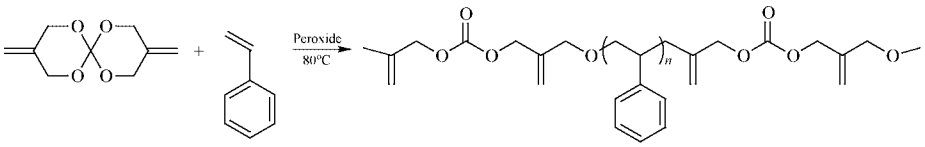

(12)

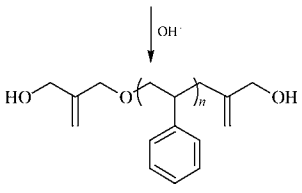

(13)

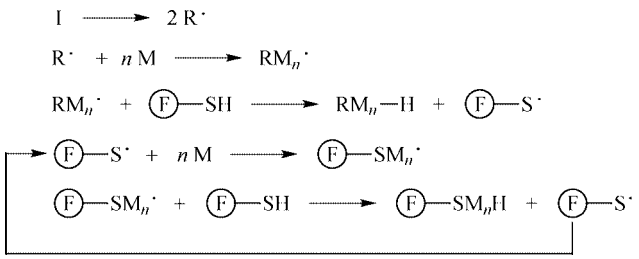

Fig. 4. Functionalization of polymers by chain transfer agents.

Transfer Techniques

Transfer Agents. In free radical polymerization, thiols are often employed as chain transfer agents. Chain transfer reactions involving thiols proceed via hydrogen atom abstraction as illustrated in Figure 4.

Consequently, these molecules do not offer any scope for introducing functionalities at both ends. However, monofunctional telechelics have been successfully prepared by using thiols. For example, Boutevin and co-workers (52,53) introduced polymerizable vinyl groups to poly(vinyl chloride) (PVC) according to that strategy. 3-Mercaptopropionic acid has been used as functional chain transfer agent producing a PVC with one carboxylic acid end group (reaction 14). This monofunctional telechelic was converted into a macromonomer according to reaction 15.

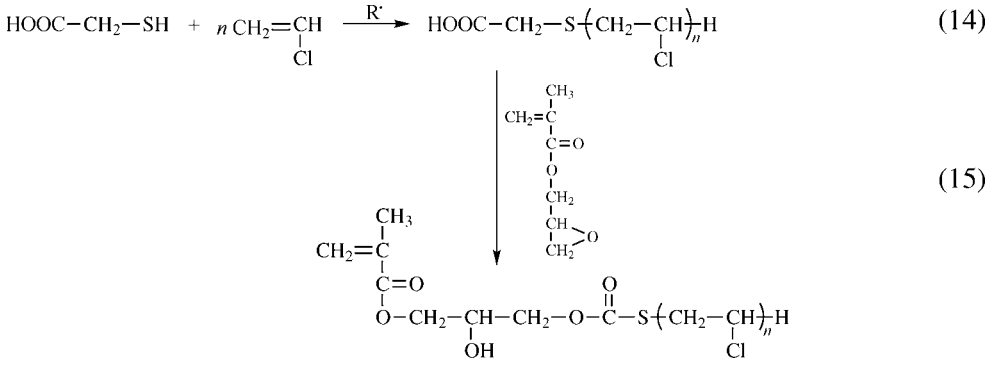

(14)

(15)

Polystyrene macromonomers (54) with molecular weight of 10^3–10^4 were also prepared. Polymerization of methacrylate or vinyl chloride in the presence of 2-mercaptoethanol (55,56) and subsequent treatment of the resulting polymer with methacrolyl chloride led to methacryl end capped polymethacrylates and PVC.

Free radical polymerization in the presence of a chain transfer agent (telogen) is often called *telomerization reaction*. Many different telogens have been reported (57); the most studied and well-documented telogen is CCl_4 (Fig. 5).

CBr_4 and CHI_3 are not suitable owing to their very high transfer constant, which yields only oligomeric materials.

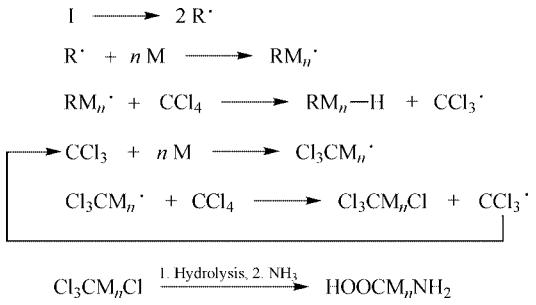

Fig. 5. Telomerization: Synthesis of α,ω-aminoacids.

Addition–Fragmentation Agents. In recent years, addition–fragmentation reactions turned out to be a versatile and exceptionally interesting tool for polymer synthesis. These reactions aim at gaining control over molecular weight and make it possible to synthesize end-functionalized polymers, often macromonomers, which may further be employed in block or graft copolymerization (58–60). The principle of addition–fragmentation type reactions can be described briefly as follows: Free radicals, macro radicals, add to olefinic double bonds of a specially designed addition–fragmentation agent. The intermediate thus produced is relatively unstable and prone to fragmentation, what mostly means β-fragmentation. In this step a new radical is generated, which initiates polymerization. As a result, a growing radical chain has been terminated and a new chain initiated (chain transfer) (61). addition–fragmentation reactions combine the advantage of high efficiency in chain transfer with the possibility of end-functionalizing the polymer. Thus, macromonomers and mono- and bifunctional polymers are prepared when functionality is introduced into one or both of the substituents R^1 and R^2, as illustrated in the example of allylic sulfides.

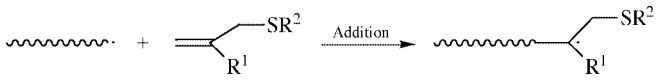

(16)

(17)

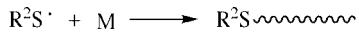

(18)

Other allylic compounds which participate in addition fragmentation reactions and yield telechelics analogous to allylic sulfides include allylic bromides, allylic phosphonate, allyl peroxides, and allylic stannane and vinyl ethers (62).

Iniferters. The peculiar behavior of thiuram disulfides in free radical polymerization was first identified by Tobolsky (63,64). These molecules can act simultaneously as an *ini*tiator, chain trans*fer* agent, and *ter*minator in a polymerization reaction and generally referred as *iniferters* by anomy to their role (65,66). Photochemically and thermally activated iniferter characteristics of thiuram disulfides

led to the derivation of telechelics. Telechelic preparation is based on the concept of locating the required function on the alkyl group of the thiuram disulfide and using it in the photo or thermal polymerization. Since end groups are introduced via initiation and transfer and common bimolecular termination between two growing chains are negligible, perfect bifunctional telechelics are available along this route.

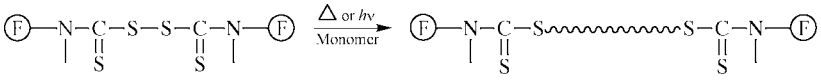

(19)

Several functional disulfides and substituted tetraphenylethylenes were also used as iniferters in free radical polymerization. Table 3 shows various functional iniferters used for deriving telechelics.

The functionalities of the telechelics prepared by iniferter method were reported to be close to 2, within experimental error. The formation of the nonfunctional polymers was claimed to be negligible because of the triple function of the iniferter.

Controlled Radical Polymerization

Accurate control of polymerization process is an important aspect for the preparation of well-defined telechelics and end-functionalized macromolecules. Such control of chain ends was traditionally accomplished using living ionic polymerization techniques. But it is well known that the ionic processes suffer from rigorous synthetic requirements and in some cases they are sensitive to the functional groups to be incorporated. As described above in detail, free radical polymerization is flexible and less sensitive to the polymerization conditions and functional groups. However, conventional free radical processes yield polydisperse polymers without control of molecular weight and chain end. Competing coupling and disproportionation steps and the inefficiency of the initiation steps lead to functionalities less than or greater than those theoretically expected. Recent developments in controlled/living radical polymerization provided the possibility to synthesize well-defined telechelic polymers with controlled functionality also with radical routes (75). As it will be shown below, all the three standard methods for controlled/living radical polymerization, namely atom transfer radical polymerization (ATRP) (76,77), stable free radical mediated polymerization (SFRP), also called as nitroxide mediated polymerization (NMP) (78), and reversible addition–fragmentation chain transfer polymerization (RAFT) (79), were used for the preparation of telechelic polymers.

Atom Transfer Radical Polymerization. Atom transfer radical polymerization (ATRP) (80,81) involves reversible homolytic cleavage of a carbon–halogen bond by a redox reaction between an organic halide (R-X) and a transition metal, such as copper(I) complexed with 2,2′-bipyridine (bpy), as illustrated in reaction 20:

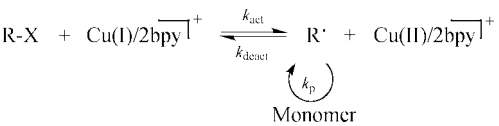

(20)

Table 3. Iniferters and End Groups

Iniferter	Monomer[a]	Functional group	Reference
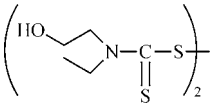	MMA	OH	67
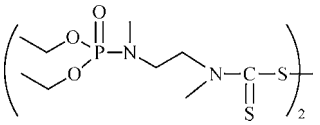	MMA, St	Phosphorylamide	68
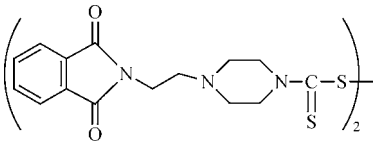	Isoprene	NH_2	69
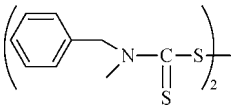	MMA, St	Phenyl	70
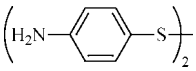	St, *t*-BA	NH_2	71
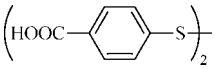	St	COOH	71
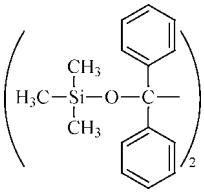	MMA	OH	72
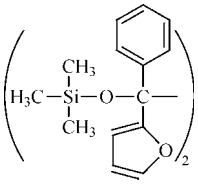	MMA, BA, STA, St	Furanyl	73
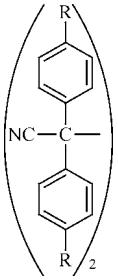	MMA	R = Cl, $C(CH_3)_3$	74

[a] MMA: methyl methacrylate, St: styrene, *t*-BA: *tert*-butyl acrylate, STA: stearyl acrylate.

Polymer functionalization by ATRP can be achieved by using functional initiators and monomers and the chemical transformation of the halogen end groups. These routes are summarized in reactions 21-23.

Through Initiator Functionality

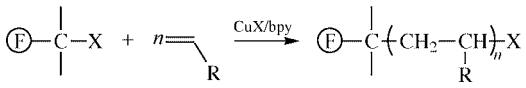

(21)

Through Monomer Functionality

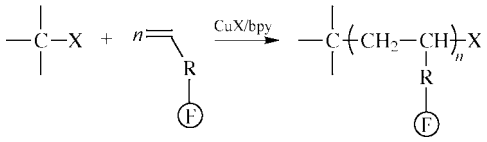

(22)

Through Chemical Reaction of Halide End Groups

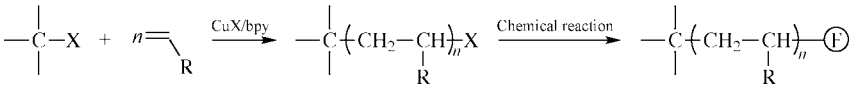

(23)

Quite a number of functional initiators were successfully used in ATRP to prepare functional styrene and acrylate type polymers (82). For this purpose initiators should be equipped with the desired functional groups as well as with a radical stabilizing group on the α-carbon atom such as aryl, carbonyl, nitrile, and multiple halogens to ensue successful ATRP. Notably, direct bonding of halogen to aryl or carbonyl group does not facilitate radical generation. In this connection, it should also be pointed out that any functionalities in the initiator should not interfere with ATRP, ie, should be inert to catalyst. The telechelic polymers prepared by using functional initiator approach in ATRP are presented in Table 4, along with the functional groups. Carboxylic acid functionalization by ATRP is rather difficult since the acid functionality poisons the catalyst. However, ATRP of MMA by using 2-bromoisobutyric acid was reported to proceed. Various protected initiators were also reported for carboxylic acid functionalization (113,114). Hydrolysis of the protecting groups yields polymers with the desired carboxylic acid functionalities.

Some other functionalities including bifunctionalities (115–117) were introduced to polymers by ATRP. Substituted aromatic and aliphatic sulfonyl chlorides were shown to be efficient initiators for ATRP and were used as initiators for the incorporation of functionalities to polystyrenes and polyacrylates (118). In these applications heterogeneous $CuCl(bpy)_3$ systems were utilized.

Obviously, ATRP leads to the formation of monofunctional telechelics since the other chain always contains halogen as a result of the fast deactivation process. These polymers could be called *heterotelechelic* since halogen is also a functional group. Therefore, α,ω-telechelics can only be prepared by transformation of the

Table 4. Monofunctional Telechelic Polymers Prepared by Using Functional Initiators in ATRP

Functional group	Polymer[a]	Reference
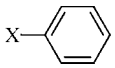		
X = H, CH_3, Br, CN, NH_2, CHO, NO_2, OCH_3	PSt, PMA	83–87
CN	PSt, PMA	88–90
	PSt, PMA, P*t*BA	
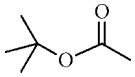	PSt, PMA	85
OH	PSt, PMA, PBA PMMA	87,91–98
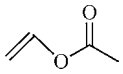	PSt	99
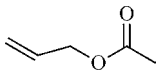	PSt, PMA	100
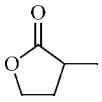	PSt, PMA	85
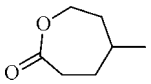		87
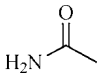	PSt	85
COOH	PMMA	101
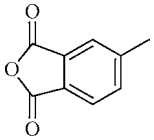	PSt	102
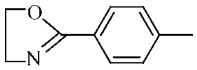	PSt	102
	PMA	103–105
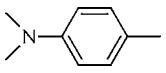	PSt	106
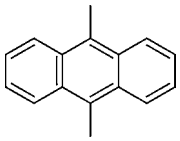	PSt	107

Table 4. (Continued)

Functional group	Polymer[a]	Reference
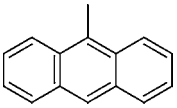	PMMA	108
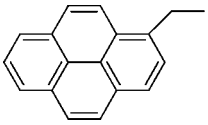	PSt	109,110
	PMMA	111
	PSt, PMMA	112

[a]PMMA: poly(methyl methacrylate), PSt: polystyrene, PBA: poly(butyl acrylate), P*t*BA: poly(*tert*-butyl acrylate), PMA: poly(methyl acrylate).

halide end group by means of nucleophilic substitution, free radical chemistry, or electrophilic addition catalyzed by Lewis acids (119). Typical example of such displacement is represented in reaction 24, which illustrates the reactions used to replace the halogens with azides and consequently leading to amino-functional telechelics (120,122).

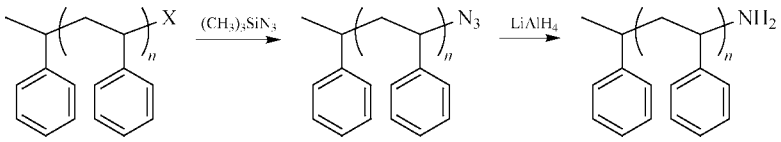

(24)

Other examples of halogen atom displacement to produce alcohol, C_{60}, epoxy, maleic anhydride, triphenylphosphine, and ketone functionalized polymers are described in the literature (123–125). The halide displacement is particularly important to prepare bifunctional hydroxy telechelics, which find application in the preparation of segmented polyester and polyurethanes (126). In such applications the first hydroxyl group can be incorporated by using hydroxy-functional initiator derivatives (127). The second hydroxyl group functionalization can then be achieved by direct displacement of halogen group with an amino alcohol or utilizing allyl alcohol. Diols can also be prepared by coupling of monohydroxy functional polymeric halides. In this connection it is noteworthy to mention the recent work (106) regarding atom transfer coupling process for the synthesis of bifunctional telechelics. Polymers monofunctionalized with aldehyde, aromatic hydroxyl, dimethyl amino groups were obtained by ATRP of styrene using functional initiators in the presence of the CuBr/bpy catalytic complex. Bifunctional

telechelics with double molecular weights as compared to the starting materials were prepared by coupling of monofunctional polymers in atom transfer radical generation conditions, in the absence of monomer, using CuBr as catalyst, tris[2-(dimethylamino)ethyl]amine (Me_6TREN) as ligand, Cu(0) as reducing agent, and toluene as solvent. The overall process is depicted in reactions 25 and 26.

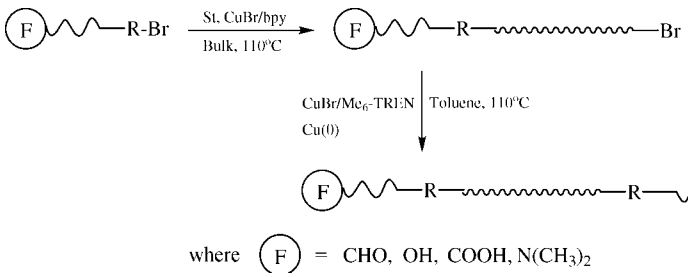

Incorporation of unsaturated end groups to polymers by ATRP is limited to certain groups. Only allyl and vinyl acetate groups were successfully incorporated (Table 4). Other polymerizable groups such as epoxides and oxazolines are not reactive toward radicals. In order to produce polymers with a more reactive unsaturated end groups such as methacrylates, a combined ATRP and catalytic chain transfer process was proposed (128). In this methodology, the catalytic chain transfer agent was added to the ATRP of MMA near to the end of polymerization, leading to the formation of ω-unsaturated PMMA macromonomer with low polydispersity and controlled molecular weight (reaction 27).

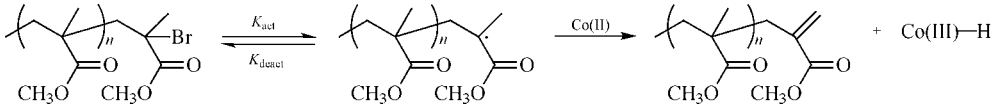

(27)

Here, the CTC agent acts as a chain transfer terminator but does not initiate new chain in the classical manner. Similarly, Haddleton and co-workers (129) used methyl(2-bromomethyl)acrylate in transition-metal-mediated controlled radical polymerization to replace the ω-halogen end group via addition–fragmentation to yield a methacrylate-based macromonomer.

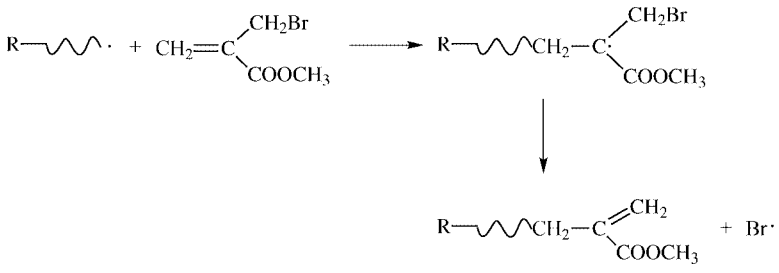

(28)

(29)

More recently, a convenient, one-pot synthesis of telechelic polymers with unsaturated end groups was developed (130). Addition of excess ethyl(2-bromomethyl)acrylate to ATRP of acrylate monomers after 80–90% conversion resulted in the formation of mono- and bifunctional polymers. The average degree of end functionality was almost quantitative ($f = 1$ for a monofunctional and $f = 2$ for a bifunctional initiator).

Nitroxide Mediated Living Radical Polymerization. Another controlled radical polymerization developed in recent years is stable free radical mediated polymerization (SFRP), also called as nitroxide mediated radical polymerization (NMP) (78,131). This type polymerization can be realized through reversible deactivation of growing radicals by stable radical such as 2,2,6,6-tetramethylpiperidinyloxy (TEMPO).

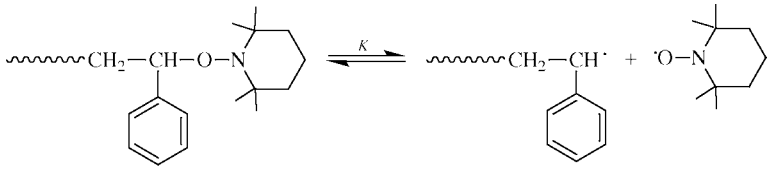

(30)

It is possible to prepare telechelic polymers by NMP procedure since it tolerates a wide variety of functional groups (78). For the synthesis of telechelics by NMP there are two general methods, ie, functional groups can be placed at the initiating chain end, F^1, or the nitroxide mediated chain end, F^2.

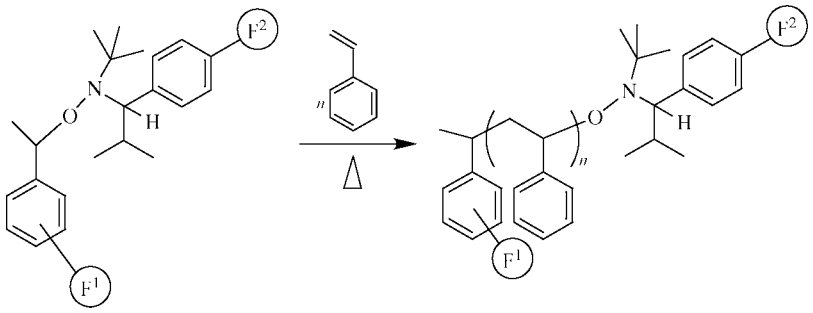

(31)

Telechelics with a variety of functional groups can essentially be prepared by using functional nitroxides (Table 5).

It was reported that high degree of functionalization, ie, greater than 95%, is possible even at molecular weights up to 50,000–75,000 by NMP method (152).

A wide variety of functional groups including polynuclear aromatic pyrene group can also be introduced by taking advantage of monoadditioin of maleic anhydrides and maleimide derivatives to alkoxy amine end group followed by elimination of mediating nitroxide radical (153). The thermal stability of the telechelics was increased as the alkoxyamine group was removed.

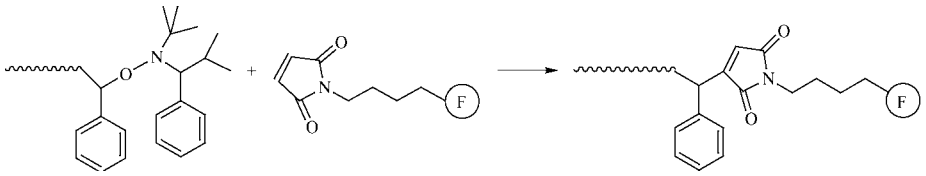

(32)

Table 5. Functional Groups Attached to Polymers by Nitroxide Mediated Living Free Radical Procedures

Functional group	Reference
OH	132–140
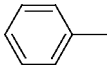	141,142
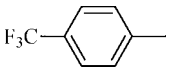	140
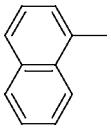	143,144
	137,144–147
CN	141,148
$PO(OR)_2$	141,149–151
$P(O)_2OH$	140
NH_2	78
COOH	78

Reversible Addition–Fragmentation Chain Transfer Polymerization. Controlled radical polymerization can also be achieved by reversible addition–fragmentation chain transfer polymerization (RAFT) (79). In this technique, after the initiation, the RAFT agents reversibly deactivate the polymer chains as the rate constant of chain transfer is faster than the rate constant of propagation (Fig. 6).

Telechelics can be prepared by RAFT process by selecting suitable RAFT agents (79).

Among the controlled radical polymerization methods discussed here, ATRP is the most applied route for the preparation of telechelics since besides the initiator functionalization, the terminal halogen produced in ATRP can easily be converted to many useful functionalities, eg by nucleophilic substitution (82).

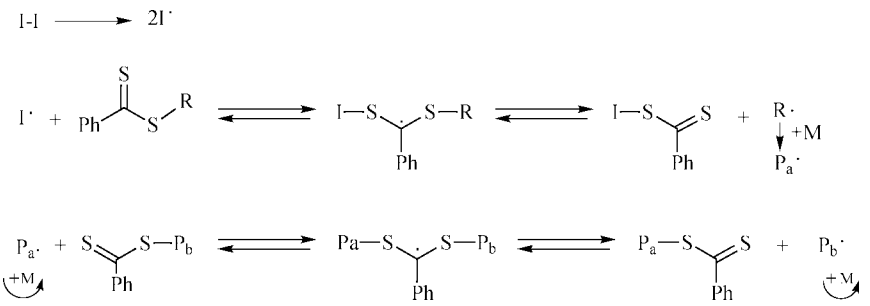

Fig. 6. Reversible addition–fragmentation chain transfer polymerization (RAFT).

Displacement of nitroxides and dihioesters is more difficult in respective NMP and RAFT processes.

Anionic Polymerization

Anionic Polymerization (qv) (154–159) and, in particular, living polymerization can be used for the synthesis of telechelics. Living polymerization is characterized by the absence of termination and transfer and, when initiation is rapid and quantitative, by narrow dispersity that can be described by a Poisson distribution, and by linear increase of molecular weight with conversion. The propagating species are carbanions or other negatively charged species. Bivalent growing chains allow the generation of two terminal end groups and the facile synthesis of telechelic polymeric materials, depending on the monomer, initiator, solvent, and termination agent (160).

Hydroxyl End Groups. Living polystyrene is terminated by the addition of oxirane, which generates hydroxylate end groups (161,162).

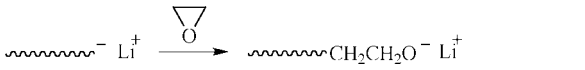

(33)

The alcoholate ion can initiate the polymerization of ethylene oxide, but the rate is low enough so that polyether formation can be avoided by quenching immediately after termination (163).

Other monomers, such as butadiene (164) and isoprene (165), have been polymerized and hydroxylated by the reaction of the corresponding living polymers with ethylene oxide. Bifunctional living polybutadiene has been generated in hexane using living oligomeric isoprene or 2,3-dimethylbutadiene as initiator (166). The hydroxyl functionality varies between 1.7 and 2.0.

Organolithium initiators with blocked hydroxyls increase the functionality of the products since one OH function is introduced with the initiator and the other one via termination, eg with oxirane (167).

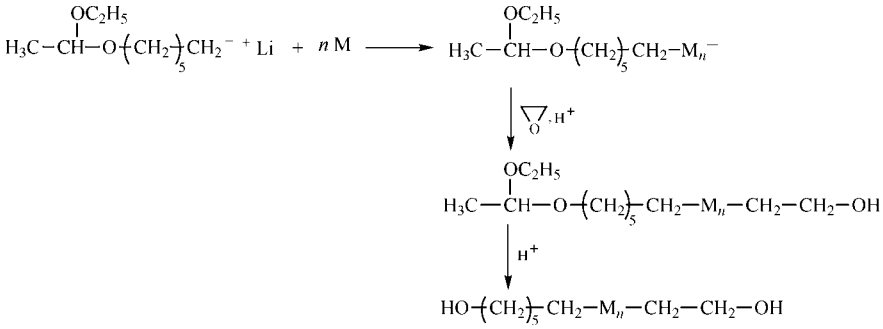

(34)

(35)

(36)

Formaldehyde can also be used as termination agent yielding OH end groups (159).

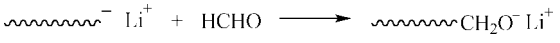

(37)

Other aldehydes and ketones lead to complications, particularly if keto–enol tautomerism is possible.

Mercapto End Groups. Living polystyrene reacts quantitatively with thiirane to form terminal mercapto groups (168). Termination with thiirane was also used for the formation of telechelic polyisoprene containing SH end groups.

Carboxyl End Groups. Termination of bifunctional living polystyrene by solid CO_2 yields polymers with carboxyl end groups (169). Because of its commercial potential, this reaction has been studied in depth. In addition to carboxyl groups (60%), dimeric ketones (30%) and trimeric carbinols (10%) are formed with gaseous CO_2 (170).

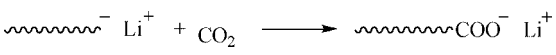

(38)

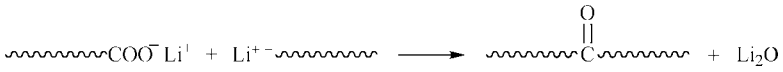

(39)

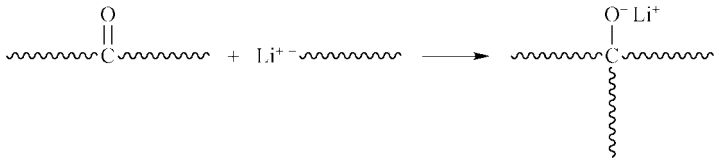

(40)

Almost quantitative carboxyl formation is observed if the polymer is converted to an intermediate Grignard (171) compound. The CO_2 is added rapidly, accompanied by a significant increase in viscosity of the monofunctional polymers and gelling of the bifunctional polymers. Yields depend on the reaction rates and on stirring efficiency. Alternatively, a anhydride can be used as termination agent (reaction 41).

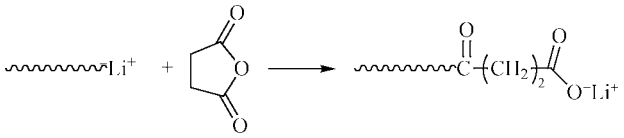

(41)

Reactions with excess phosgene give acylchloride end groups (172) but Wurtz-type side reactions can occur (173).

Halide End Groups. The most direct route for the preparation of halide terminal groups is the reaction of living polymers with a halogen, eg, chlorine (174,175) or iodine (176). Quantitative reaction is prevented by the occurrence of Wurtz coupling reactions. The percentage of halide end groups is increased by an intermediate Grignard step. For example, in this way, bromine gives an excellent yield of bromine-terminated telechelics.

A more general route employs an excess of primary α,ω-dihalides (175).

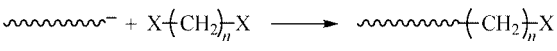

(42)

Secondary and tertiary halides lead to side reactions by β-elimination (177).

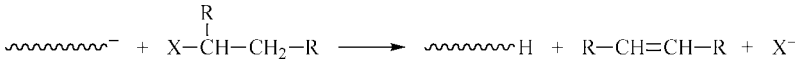

(43)

α,α-Dihaloxylene or 1,4-dihalo-2-butanone gives primary benzylic and allylic halides. Yields are increased by first converting the polymer into a Grignard salt. This process has been applied to prepare halogen-terminated telechelics from polybutadiene (178).

Amino End Groups. The polymerization of styrene initiated by potassium amide in liquid ammonia yield polymers with one primary amine group per chain (179).

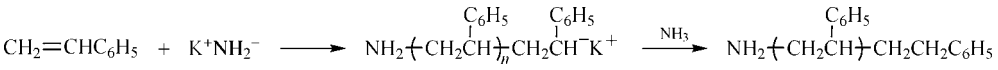

(44)

Initiators with the blocked amino groups, such as *p*-thio-*N*,*N*-bis(trimethylsilyl)aniline, have been used for anionic polymerization (Fig. 7).

Bifunctionality is achieved by coupling with dimethyldichlorosilane. The primary amine end groups are regenerated by acid hydrolysis (180).

An alternative route for the introduction of amine end groups by reaction with blocked functional terminating agents (181) is as follows:

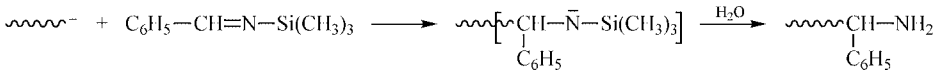

(45)

An indirect route for the introduction of amine end groups on aromatic ring has been described (182).

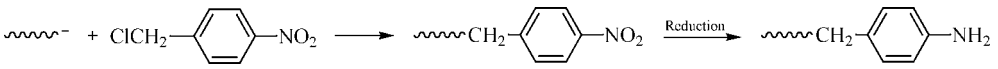

(46)

Secondary amine groups are generated by reaction with *N*-alkyl aziridines (176).

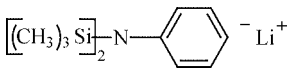

Fig. 7. Initiator with the blocked amino group.

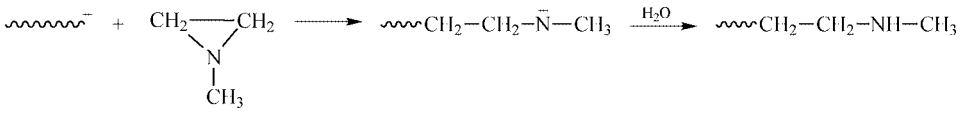

(47)

An interesting alternative is shown below (183):

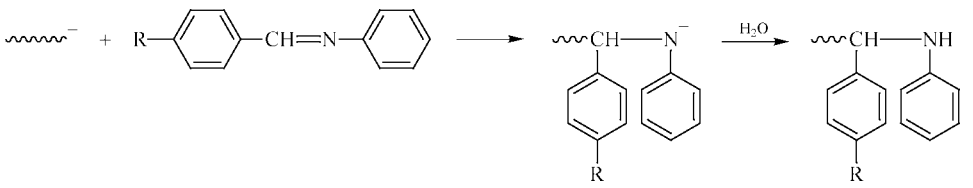

(48)

Tertiary amine terminated polymers are made by reaction with α-chloro-ω-amino-alkanes (184).

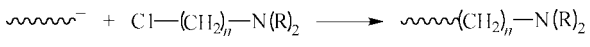

(49)

Living polybutadiene prepared with a tertiary amine functionalized alkyl lithium initiator is terminated by an α-chloro-ω-amino-alkane (185).

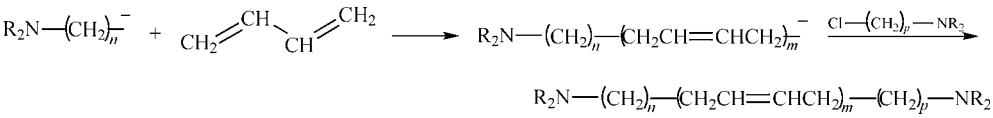

(50)

Ionic End Groups. Telechelics with quaternary ammonium end groups are prepared by quaternization of telechelic tertiary amines with organic halides (184). Unstable salts are formed by the reaction of living polymers with boron and aluminum alkyls. Only the triphenylboron derivatives are stable enough to be examined spectroscopically.

Reaction of living polymers with sulfur trioxide gives sulfonate salts. The reactivity of such salts as well as side reactions is reduced by complexation with a tertiary amine (185).

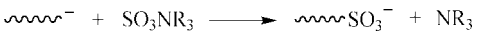

(51)

Termination of living polymers with sultones yields sulfonates. This reaction has been claimed to be quantitative in tetrahydrafuran at −78°C (186).

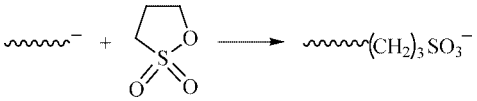

(52)

The synthesis and dilute and bulk solution properties of end-functionalized polymers with zwitterionic end groups have recently been reviewed (187). Reportedly, such polymers with different architectures (linear, block, and star copolymers) can be prepared by means of anionic polymerization. First, dimethylamine groups were introduced by using 3-dimethylaminopropyllithium as functional initiator. This group was then switched to sulfozwitterionic one by reaction with propanesultone.

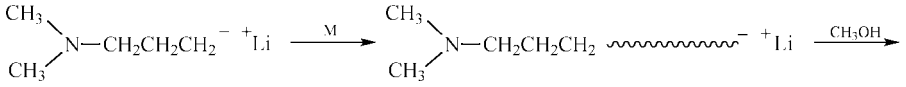

(53)

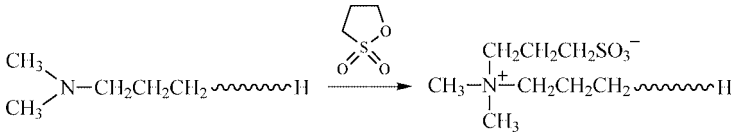

(54)

Organometallic Groups. The reaction of living polymers with $Pb(C_4H_9)_3Cl$ yields polymers containing $Pb(C_4H_9)_3$ end groups. These end groups undergo homolytic scission at the carbon–lead bond, giving terminal free radicals (188).

Dipolystyryl aluminum chloride, prepared by stoichiometric reaction of 1 mol of $AlCl_3$ and 2 mol of living polystyrene, is used together with titanium halide catalyst to synthesize styrene–ethylene block copolymers (189).

Recently, new methods for preparation of telechelic polymers with better functionalization using alkyl aluminum initiated anionic polymerization were described (190–193).

Recent Trends in Functionalization of Telechelics. As described before, the direct carboxylation of polymeric organolithium with carbon dioxide in hydrocarbon solution often results in inefficient functionalization (170). Alternatively, an *ortho*-ester functionalized alkyl chloride, namely 4-chloro-1,1,1-trimethoxy butane, was used to prepare *ortho*-ester functionalized polymers (194).

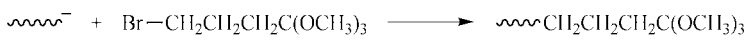

(55)

The *ortho*-ester functionalized polymers can be hydrolyzed to the corresponding carboxyl functionalized polymers. Similarly, functionalization with the oxiranes, glycidylpropyltrimethoxysilane, 3,4-epoxy-1-butene, and 1,1,1-trifluoro-2,3-epoxypropane has been investigated (195) to prepare trimethoxysilyl functionalized polymers, 1,3-diene functionalized macromonomers, and trifluoromethyl functionalized polymers, respectively. Secondary amine functionalized polymers were prepared by termination with *N*-(benzylidene)methylamine and also using an *N*-benzyl tertiary amine functionalized alkyl lithium initiator followed by hydrogenolysis of the benzyl group.

Carbocationic Techniques

The preparation of telechelics by carbocationic polymerization (qv) of vinyl monomers (196,197) has received little attention because of the high reactivity and low selectivity of growing species. The synthesis of useful telechelics requires the control of molecular weight and end groups; this was not possible until the discovery of living cationic polymerization.

Poly(alkyl vinyl ethers). The initiation of vinyl ether polymerization with $HI–I_2$ yields polymers with narrow molecular weight distribution (198–200).

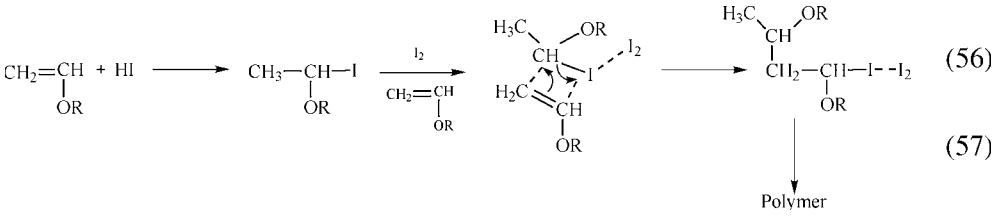

(56)

(57)

The reaction of bifunctional monomers with $HI–I_2$ gives α,ω-iodine telechelics.

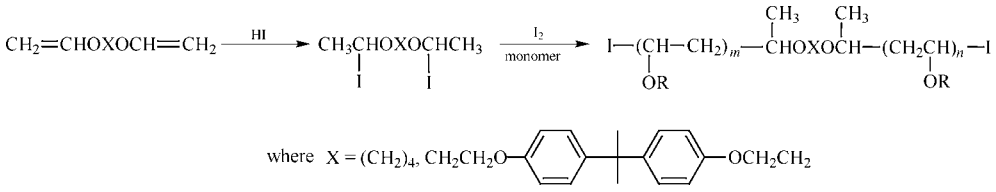

(58)

This method has been used to produce telechelics from ethyl vinyl ether (EVE), methyl vinyl ether (MVE), and hexadecyl (cetyl) vinyl ether (CVE) (201, 202).

Treatment of living poly(EVE) with mono- or diamines yields telechelics with amino end groups (201). Vinyl ether based macromonomers have been prepared by a one-pot method (203–205).

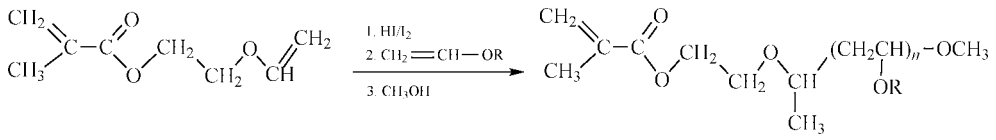

(59)

Several other functionalities were also introduced to poly(alkyl vinyl ethers) by living carbocationic polymerization (Table 6).

Polydivinylbenzene. Linear unsaturated polymers are obtained by a selective reaction between divinylbenzene (DVB) and cationic initiators such as CF_3SO_3H or CH_3COClO_4 (210–213). A sequence of protonation, propagation, and transfer steps yields telechelics with α,ω-vinyl end groups.

Table 6. Telechelic Poly(alkyl vinyl ethers)

Functionality	Polymer	Reference
Hydroxyl	Poly(2-chloroethyl vinyl ether)	206
Aldhyde	Poly(2-chloroethyl vinyl ether)	206
Malonic ester	Poly(isobutyl vinyl ether)	207
Malonic ester	Poly(methyl vinyl ether)	207
Azo	Poly(isobutyl vinyl ether)	208
Imide	Poly(isobutyl vinyl ether)	209
Amino	Poly(isobutyl vinyl ether)	209

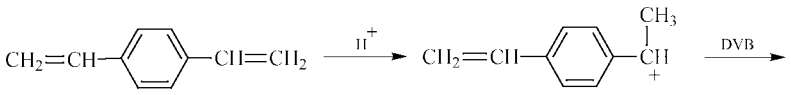
(60)

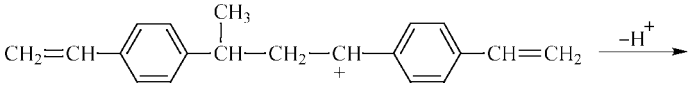
(61)

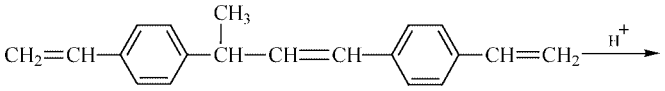
(62)

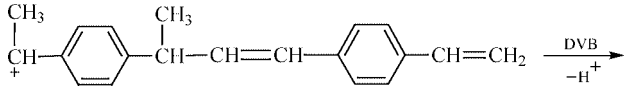
(63)

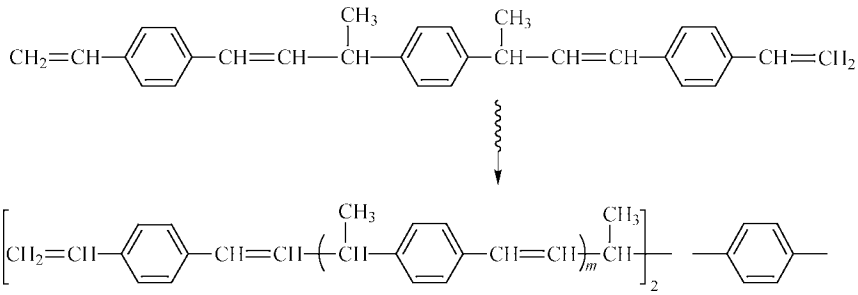
(64)

Reactions with 9-borabicyclo[3.3.1]nonane (9-BBN) and H_2O_2 yield hydroxyl-terminated telechelics (211).

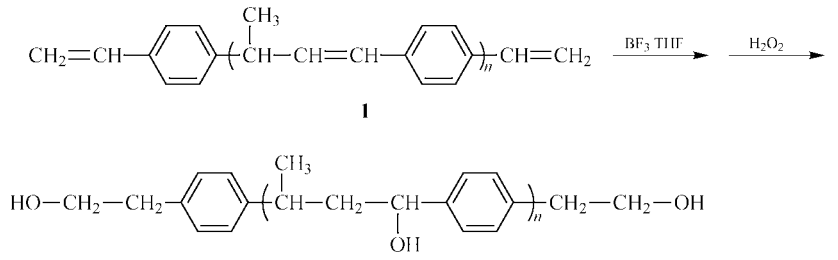

(65)

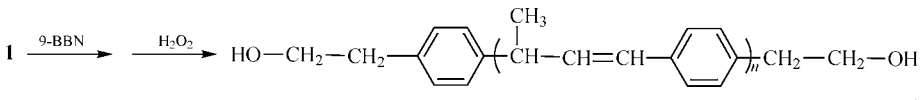

(66)

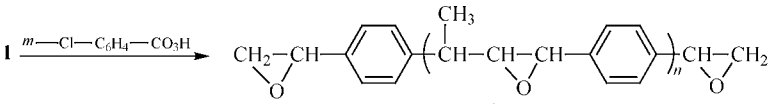

(67)

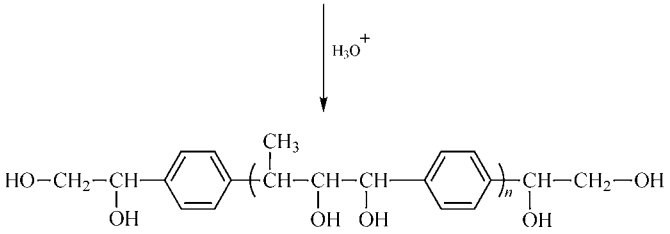

(68)

Although one keeps control over the end groups the final product may not be called a pure telechelic but a chain functionalized polymer. $\alpha\omega$-Acetoxy-poly(DVB) was synthesized from *p*-DVB, *p*-acetyl styrene, and CH_3COClO_4 in benzene at 70°C (212,213).

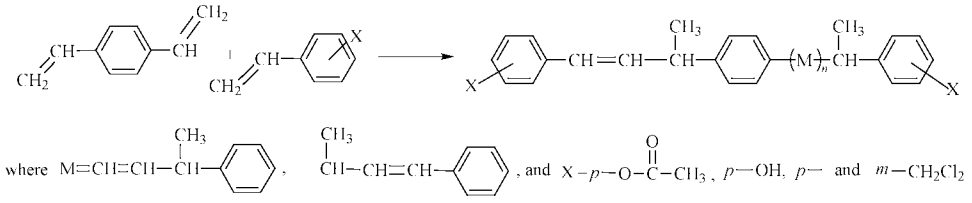

(69)

Polyisobutylene. On the basis of the reaction sequence shown in Figure 8, the conditions under which telechelics form can be predicted.

Head groups are controlled by initiation; propagation, termination, and transfer control the molecular weight and terminal groups. This method was first used for the synthesis of telechelics from isobutylene (214,215). The technique has been refined and is then called the inifer technique (216–221).

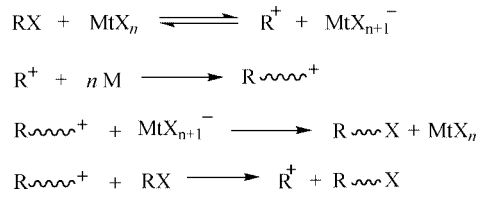

Fig. 8. Telechelics by inifer process. Here Mt is metal, M is monomer, and X is halide.

The compounds shown in Figure 9 act as both initiator and transfer agents, which led to the term inifer.

Notably, the number of functionality of the telechelics thus formed is related to the number of chloro groups present in the inifer. Preparation of telechelics by this method requires low temperatures and highly pure starting materials.

Quenching of living carbocationic polymerization also leads to *tert*-chlorine-telechelic polyisobutylenes (222). Synthesis of mono- (223–226), di- (227–235), tri- (236), and tetrafunctional (237) polyisobutylenes carrying Cl termini was reported.

The chloro end group is easily converted to olefinic or primary alcohol end groups (238–242).

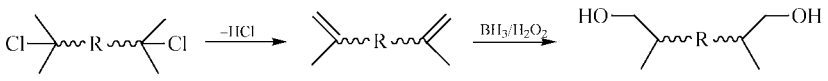

(70)

One-pot dehydrochlorination–metalation of *tert*-chloro-telechelic polyisobutylenes (PIB) by combinations of *n*- with *sec*-butyl lithium (243) and of *n*-butyl lithium with *tert*-butoxide (244) leads to terminally lithiated polyisobutylenes. Oxyethylation and reaction with CO_2 of the latter yielded primary alcohols and carboxylate termini, respectively (244).

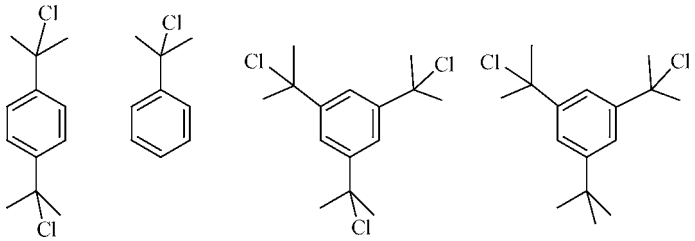

Fig. 9. Examples of inifers.

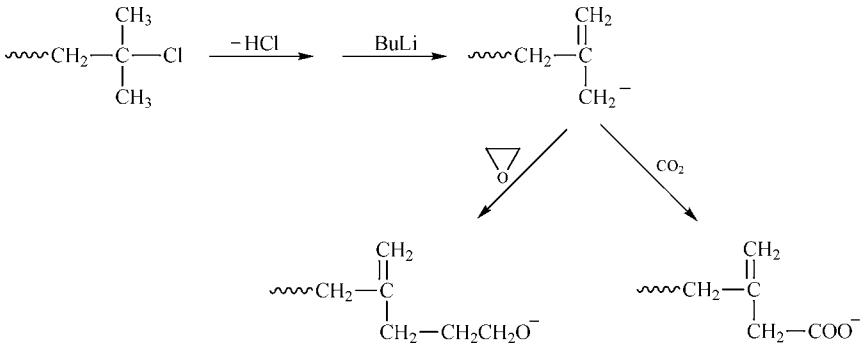

(71)

(72)

Friedel–Crafts alkylation of benzene, toluene, or phenol gives a variety of diaryl products (245):

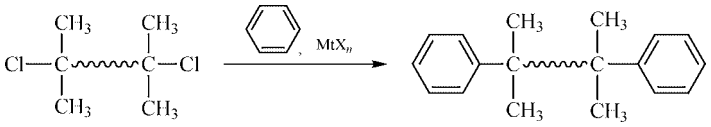

(73)

Nitration of the aromatic units followed by reduction yields an amine telechelic (245,246).

A phenol end group formed by Friedel–Crafts alkylation can be used for further derivatives (247,248).

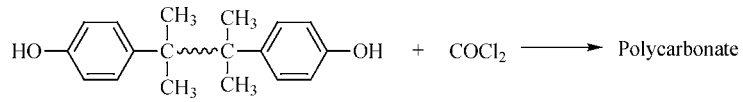

(74)

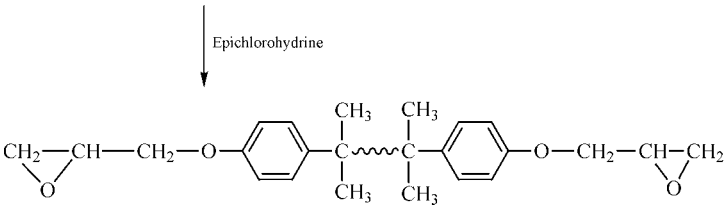

(75)

α,ω-Olefin telechelics can be converted into diepoxides and further to dialdehydes. Sulfonation of polyisobutylene with acetyl sulfate yields the corresponding sulfonate (249,250).

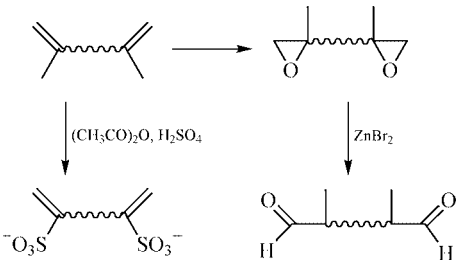

(76)

(77)

Similarly, di- and triallyl telechelic polyisobutylenes have been converted to di- and triepoxy telechelics (241,242). Hydrosilation of olefinic telechelics in the presence of suitable catalysts gives telechelics with reactive SiCl groups (251).

The hydroxy-terminated telechelics were used as starting material for numerous derivatives (252,253):

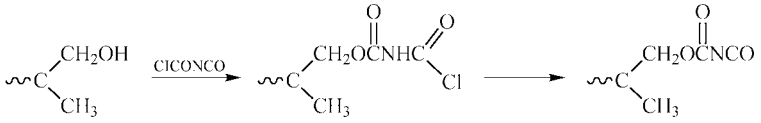

(78)

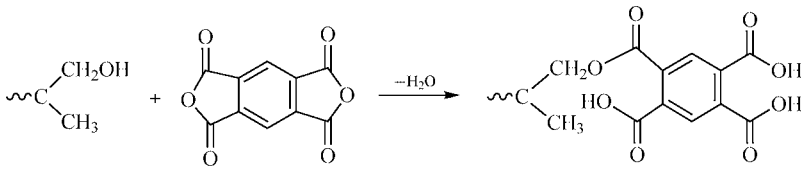

(79)

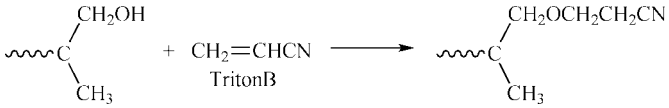

(80)

An improved Gabriel synthesis was used for amino-terminated telechelics (254).

Macromonomers can be synthesized from a hydroxy-terminated polymer by reaction with methacryloyl chloride (255).

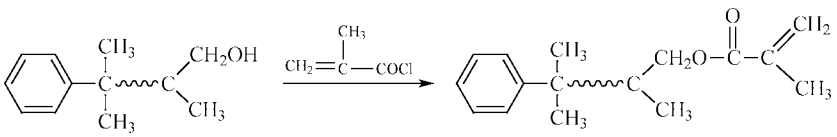

(81)

Instead of RCl, tertiary esters were used in combination with BCl_3 for the synthesis of telechelics from isobutylene. The polymerization mechanism shown in Figure 10 was suggested (256,257):

Various other initiator systems for the controlled/living polymerization of isobutylene have been reported (222). The capping reaction of living polyisobutylene with 1,1-diphenylene ethylene (DPE) results in the formation of a stable and fully ionized diarylcarbenium ion, which can be used for chain-end functionalization by quenching with appropriate nucleophiles as shown in reactions 82 and 83 (258–261).

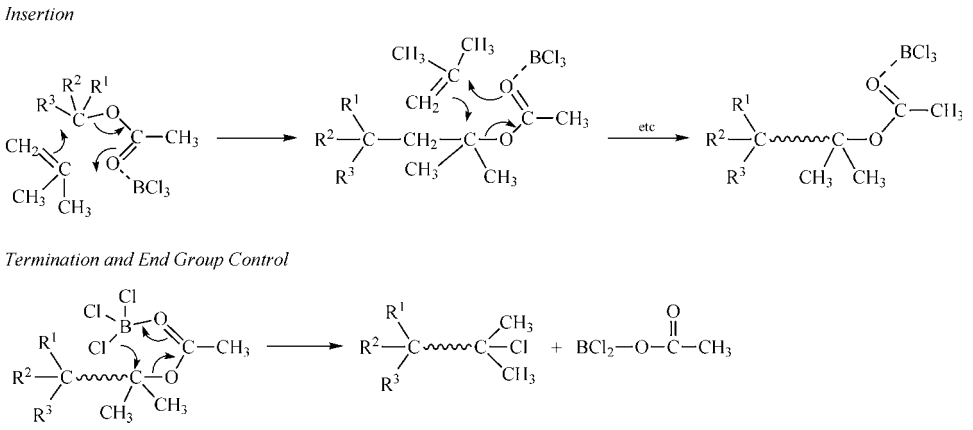

Fig. 10. Function of $(R_1R_2R_3)COOCH_3/BCl_3$ in the polymerization of isobutylene.

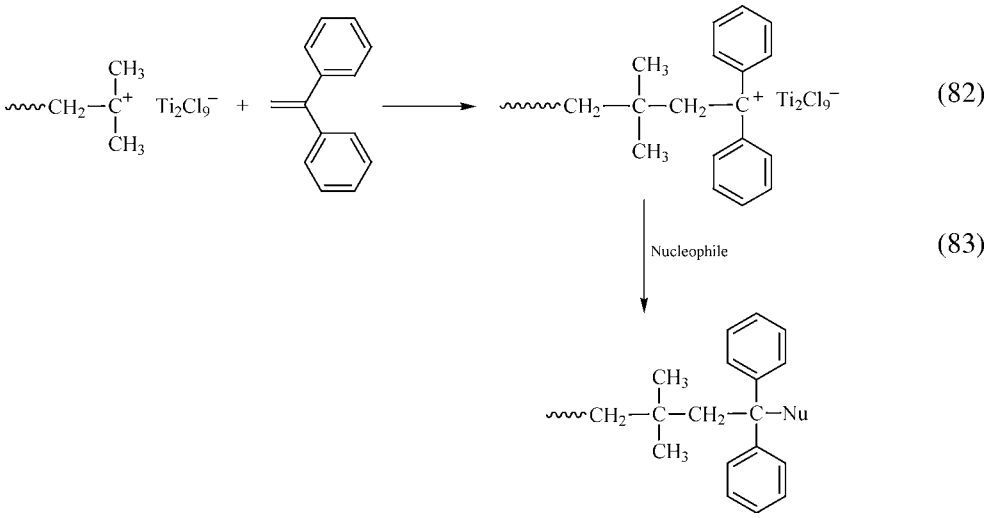

(82)

(83)

Using this strategy, a variety of chain-end functional polyisobutylenes including methoxy, amine, carbonyl, and ester end groups, have been prepared (262). By the rational combination of initiation and capping techniques, a series of α,ω-asymetrically functionalized PIBs have also been obtained (262–264). It was shown that living polyisobutylene could also be end-capped with 2-alkylfurans. Quenching the resulting cation with tributyltin hydride and methanol yielded polyisobutylene with dihydrofuran and furan functionality, respectively (265,266).

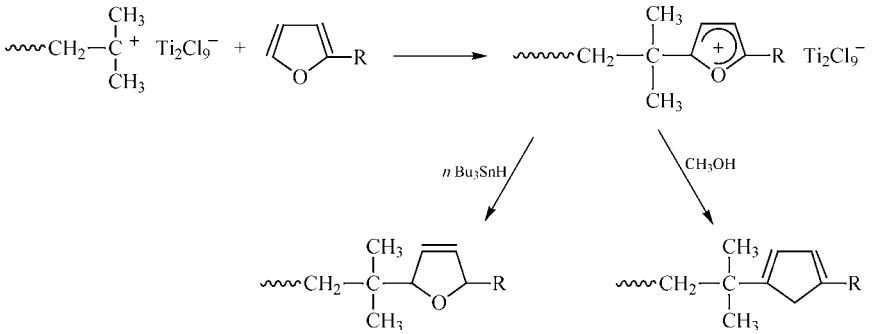

(84)

(85)

It appears that 2-alkylfurans are more suitable capping agents when subsequent functionalizations at elevated temperatures are required.

Polypinene. β-Pinene is converted into telechelics with 1,4-diisopropylchlorobenzene and BCl_3 as initiator (267).

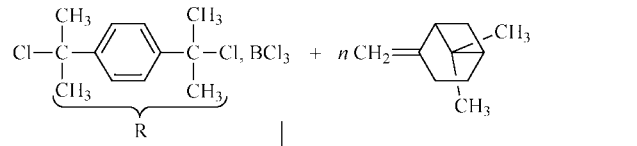

(86)

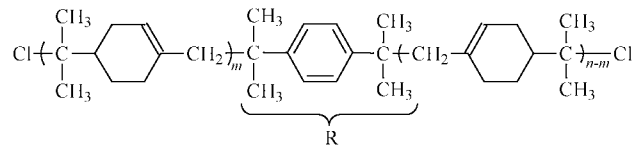

(87)

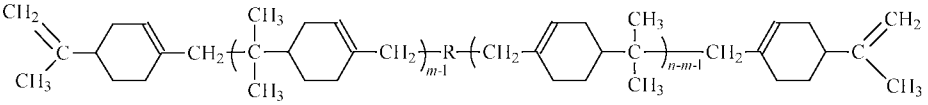

Polystyrene and Derivatives. Telechelic polystyrene, poly(2,4,6-trimethylstyrene), poly(*p*-methylstyrene), and poly(*p*-chlorostyrene) can be prepared by living carbocationic polymerization (269–271) or by inifer method (272). While end-quenching the living carbocationic polymerization gave quantitatively polymers with *sec*-benzylic termini, the dicumyl chloride/BCl_3 inifer system yielded α,ω-dichloro telechelics. Telechelics with olefine end groups were also prepared by dehydrochlorination (272,273).

Ring-Opening Polymerization

The synthesis of telechelics by ring opening has attracted great interest because of the commercial potential of the resulting compounds, such as polyether polyols. The end groups are introduced by initiation, end capping, or transfer reactions.

Cyclic Ethers.

Oxiranes. Both anionic and cationic polymerization can be used to synthesize telechelics from oxiranes. Anionic polymerization of oxirane (ethylene oxide) yields α,ω-dihydroxy poly(ethylene oxide) (274,275).

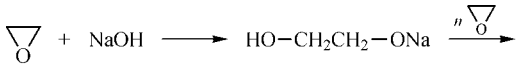

(88)

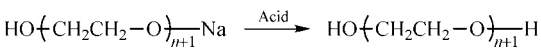

(89)

Polymerization with sodium naphthalene yields a chain with two simultaneously growing ends (276,277).

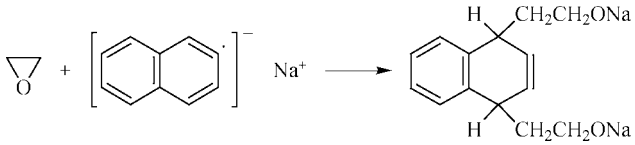

(90)

The anionic polymerization of methyl oxirane occurs predominantly by breaking of the oxygen–methylene bond, yielding terminal secondary alcohol functionality.

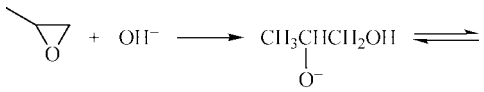

(91)

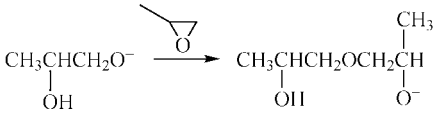

(92)

It should be mentioned that an important transfer reaction is occurring, leading to an allylic chain end:

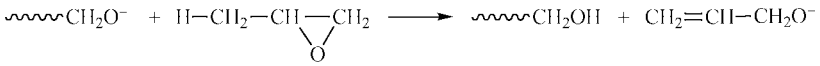

(93)

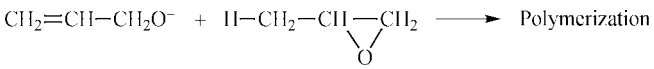

(94)

Hydroxyl end groups can be converted to various other functional groups (278). Generally, oxirane telechelics are synthesized either by one of the following methods: (*1*) end-capping of the living polymerization (termination method), (*2*) initiation of living polymerization (initiation method), and (*3*) transformation of hydroxyl end groups (279,280). Methods (*1*) and (*2*) are simple and usually afford most well-defined telechelics of a controlled degree of polymerization with a

narrow polydispersity, but critically depend on the proper combination of anionic living polymerization with an effective terminator or initiator carrying desired functionality. Suitable terminators include alkyl and acid chlorides possessing functional groups.

Termination

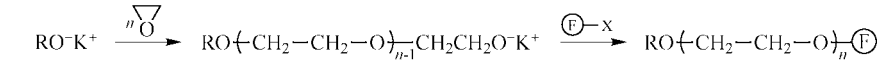

X = Cl, C(O)Cl
F = Functional group (95)

Initiation

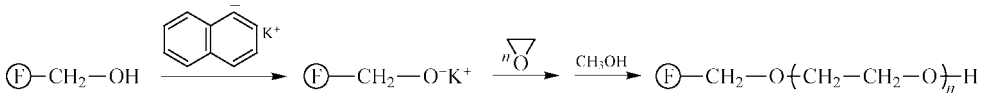

(96)

This way many poly(ethylene oxide)s with various functional groups including photo- and electroactive, and polymerizable groups were prepared (280–283). Moreover, suitable combinations of termination and initiation methods yield heterofunctional telechelics.

Although living anionic polymerization seemed to be the versatile method for the preparation of telechelic from oxiranes, with substituted oxiranes some side reactions leading to unsaturated species occur (reaction 93). An alternative initiating system based on aluminum complexes of Schiff bases was proposed for the preparation of α,ω-telechelics form differently substituted oxiranes (284–286).

The usual cationic polymerization of oxiranes cannot be used to synthesize telechelic polymers owing to a high tendency of backbiting resulting in cyclic oligomers (287). However, a process involving the addition of a hydroxyl end group to an activated (protonated) monomer has been described (287–289).

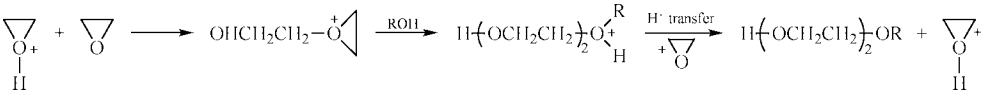

(97)

The polymer chain contains the less reactive (nucleophilic) hydroxyl end group. The driving force for this reaction comes from the protonated monomer, and no cyclic oligomers are formed. Similar results have been obtained from the polymerization of methyloxirane (290) and chloromethyloxirane in the presence of ethylene glycol (291). Photo- and azo-functional telechelics were also prepared by the so-called activated monomer polymerization (292,293).

Tetrahydrofuran. The cationic polymerization of tetrahydrofuran (THF) is living in the sense that, under certain conditions, the concentration of oxonium

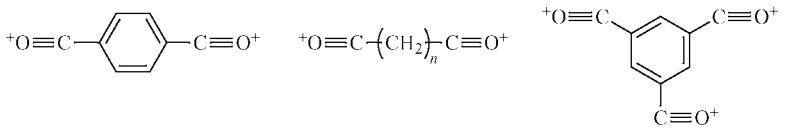

Fig. 11. Examples of bi- and trifunctional initiators with BF_4^-, PF_6^-, or SbF_6^- as counterions.

ions remains constant (294). The species is highly reactive and can be transformed into end groups by reaction with suitable nucleophiles. Polytetrahydrofuran (PTHF) with one functional end group is thus obtained after end capping of the living polymers produced with a monofunctional initiator. For the synthesis of bi- or trifunctional telechelics, initiators with corresponding functionality must be used (Fig. 11) (295,296).

Independent activity of all initiator functions of these bi- and trifunctionalized initiators has been reported. Copolymers can be formed if 10–20% of the THF is replaced by methyloxirane (297).

Anhydrides of super acids such as trifluoromethane sulfonic acid or fluorosulfonic acid yield two active ends (298,299).

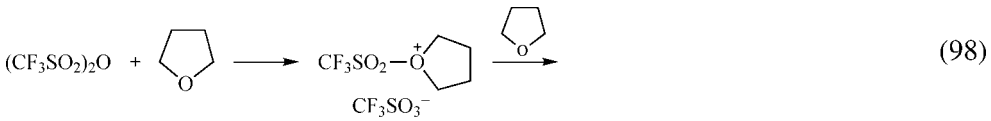

(98)

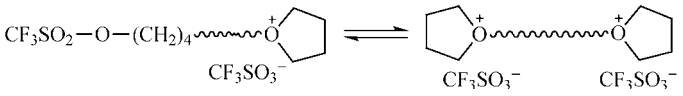

(99)

Molecular weight and functionality are controlled only at low initiator concentration because of the low solubility of the initial bisoxonium salt (299).

Because of the reversibility of the polymerization and the high reactivity of the oxonium functions, bi- and trifunctional PTHFs are not easy to use. However, addition of a nucleophile to a solution of living polymer yields telechelics that are easier to handle (300). End-capping reagents and the resulting end groups are shown in Table 7.

Table 7. End-Capping Reagents and End Groups

End-capping reagent	End group
NH_3 (liquid)	$-NH_2$
KOCN	$-NCO$
H_2S	$-SH$
$HOOC(CH_2)_2COOH$	$-COOH$
$C_2H_5NH_2$	$-NHC_2H_5$
$CH_2{=}CHCH_2NH_2$	$-NHCH_2CH{=}CH_2$
LiBr	$-Br$
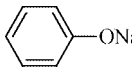	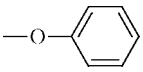

Some other functionalities such as photosensitive benzoin (301) and alkoxy pyridinium (reaction 100) (302), pyrrole (303), methacrylate groups (304) can also be introduced to PTHF by selecting suitable nucleophiles.

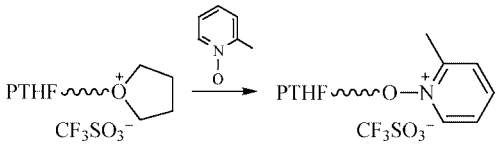

(100)

The pyridinium salt end-functionalized PTHFs can be used as polymeric initiators for photoinduced reactions. Upon photolysis the pyrdinium moiety decomposes and polymeric radicals are formed. Depending on the additives present in the system, hydroxy telechelics (305) or block copolymers (302) are thus formed.

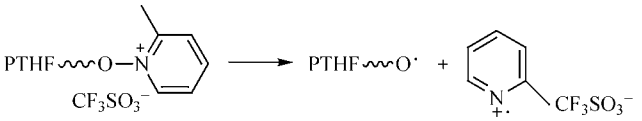

(101)

(102)

An interesting reaction is the so-called active species exchange (306).

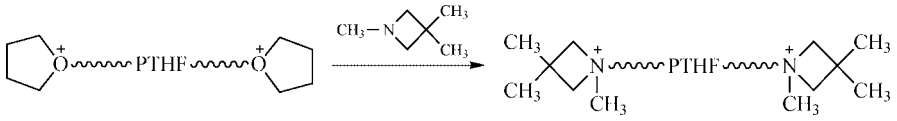

(103)

The less reactive, weak electrophilic azetidinium ions undergo ring-opening reactions with charged nucleophiles such as carboxyl ions. The reaction of PTHF with thiolane gives similar results (307).

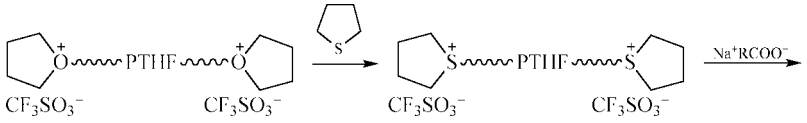

(104)

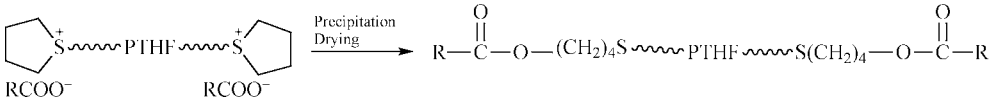

(105)

End groups have also been introduced by using a functionalized initiator (308,309).

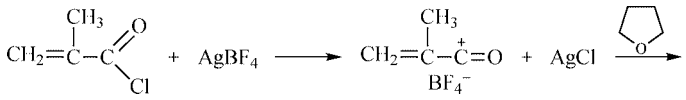

(106)

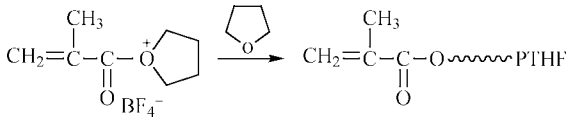

(107)

Proton-initiated polymerization of THF in the presence of carboxylic acid anhydrides gives ester-terminated end groups.

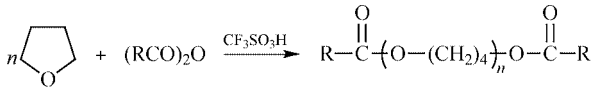

where R = CH_3, $CH{=}CH_2$, $C(CH_3){=}CH_2$ (108)

Hydrolysis results in the corresponding hydroxy-terminated PTHF.

Recently, it was shown that hydroxyl groups can be transformed *in situ* to a triflate ester in the presence of a proton trap for the initiation of the cationic ring-opening polymerization of THF. Providing that suitably functionalized hydroxyl groups are selected and the hydroxyl group is not attached to a bulky alkyl group (310), PTHF telechelics with narrow molecular weight distribution and quantitative functionalization can be obtained. Macromonomers with acrylate, methacrylate, and allyl functional groups have been successfully synthesized (311).

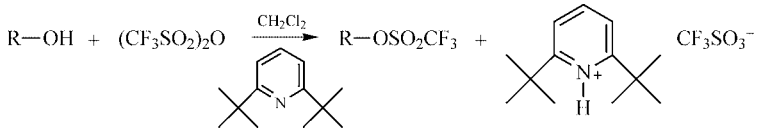

(109)

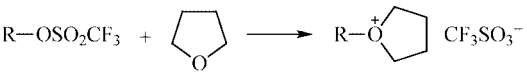

(110)

(111)

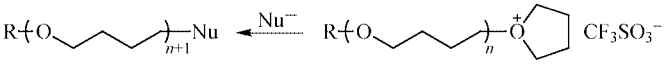

(112)

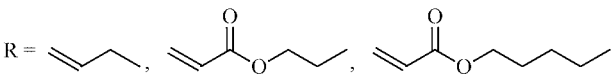

Interesting variation of end-capping reaction with *N*-phenylpyrrolidine (reaction 113) can be used to prepare mono-, bi-, and trifunctional star-shaped, telechelic PTHF having *N*-phenylpyrrolidinium salt groups as illustrated in the example of trifunctional living PTHF.

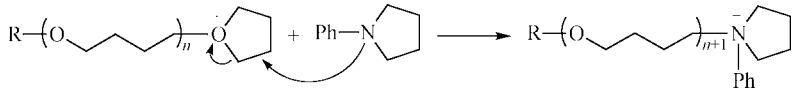

(113)

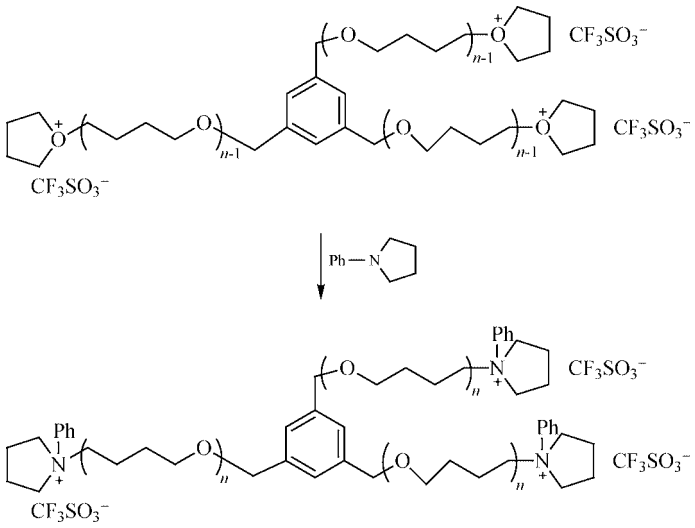

(114)

Heat treatment of the polymers carrying carboxylate anions results in a quantitative ring-opening reaction.

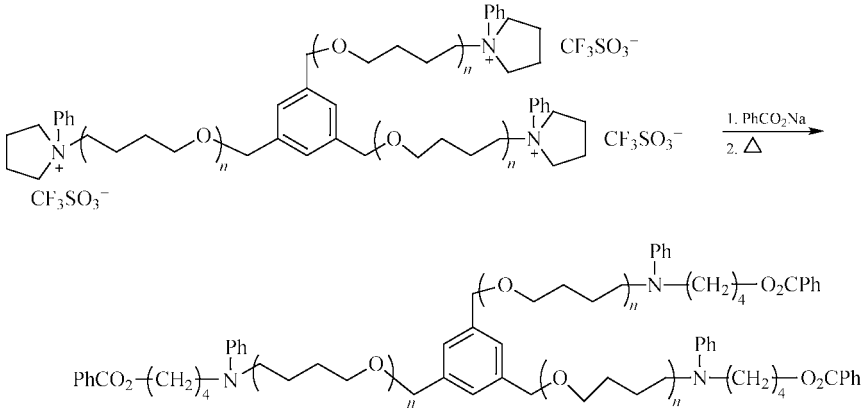

(115)

Another class of telechelic PTHFs has also been prepared, in which functional groups were located not only at the chain ends but also at the interior desired position. In this case, the *tert*-butyldimethylsilyl-protecting group was removed during the precipitation to yield α,ω-*kentro*-telechelic polymers (312).

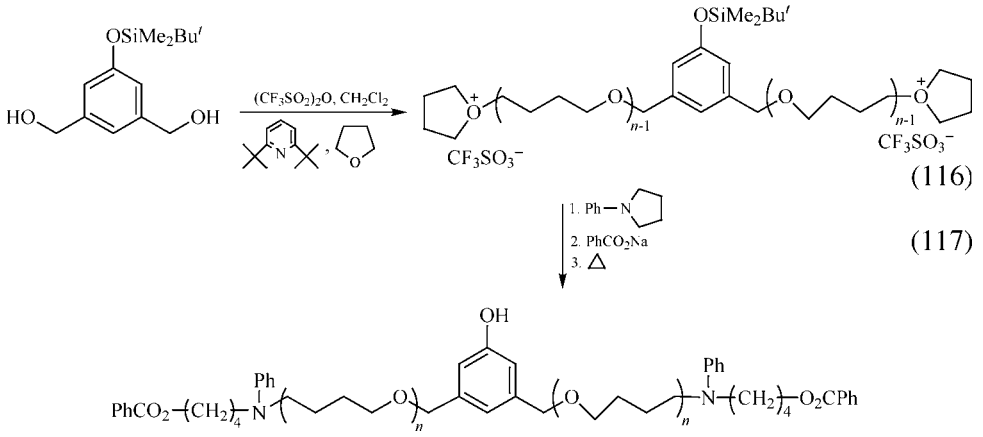

Moreover, *eso*-telechelic PTHF having pyrrolidinium salt groups at the prescribed inner positions were also prepared (313).

Cyclic polymers, having one or two functional groups, are termed as *kyklo*-telechelics with analogy to the Greek word *kyklos* (which means cyclic). Such telechelics can be prepared again by the electrostatic self-assembly and covalent fixation process as depicted in reaction (118).

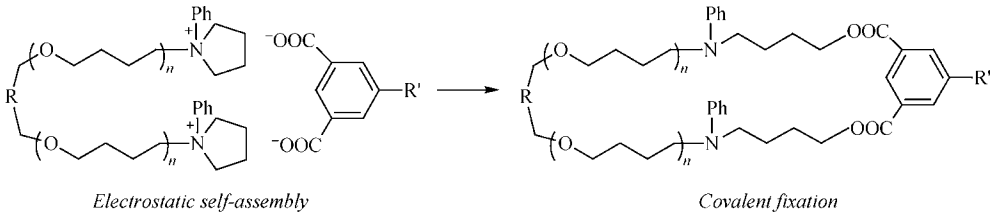

(118)

By suitably selecting R and R′ groups, various mono- and bifunctional telechelics having hydroxyl and allyl groups were prepared (314).

Cyclic Acetals. A number of cyclic acetals of varying ring size have been polymerized with cationic initiators (315); trioxane and dioxolane are the most important. Polymerization of trioxane in the presence of a transfer agent such as dimethyl formal or an anhydride yields polyoxymethylene with ether and ester end groups, respectively (316).

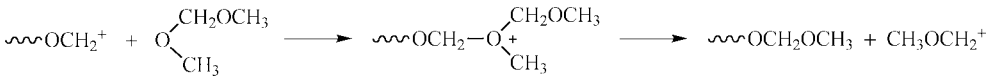

(119)

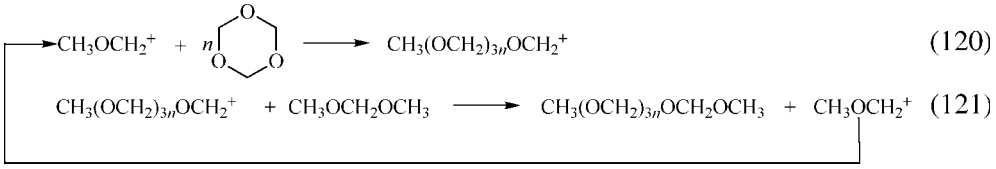

(120)

(121)

Triflic acid or anhydrides initiates polymerization of 1,3-dioxolane (DXL) and 1,3-dioxepane (DXP) (317). After transformation of the active ends into phosphonium salts, the functionality of these polymers was determined with ^{31}P NMR ($f = 2$).

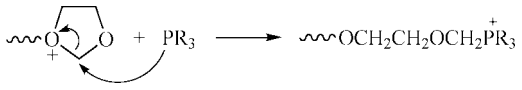

(122)

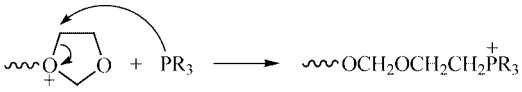

(123)

Another pathway yields a thermodynamically more stable product, but is kinetically less favorable. Because of extensive chain transfer the polymerization of DXL is not living. However, if a functionalized acetal is added to the monomer, telechelic polymers, eg α,ω-bisacrylate of poly(DXL) (318), are obtained. Similarly, addition of trimethylamine to growing poly(DXL) initiated with triethyloxonium hexafluoroantimonate yields telechelics with one trimethylammonium and one ethoxy end group (319).

An activated monomer mechanism similar to that described for oxiranes has been proposed to account for the formation of hydroxy-terminated poly(DXL) (320).

Cyclic Sulfides. The three-membered cyclic thiiranes can be polymerized cationically, anionically, or by a coordination mechanism. The four-membered cyclic thietanes can be polymerized by cationic and anionic mechanisms, but five-membered rings cannot be polymerized. Polymerization of propylenesulfide initiated with sodium naphthalene yields telechelics with naphthalene groups on both ends, if the living chain is terminated 1-chloromethylnaphthalene (321).

The propagating species in the anionic polymerization of propylene sulfide are thiolate anions, and therefore, reactions 124-126 can be used for the synthesis of α,ω-mercaptopoly(propylene sulfide)s (321,322).

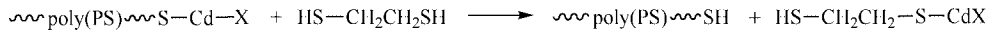

(124)

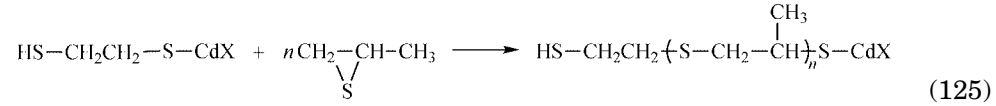

(125)

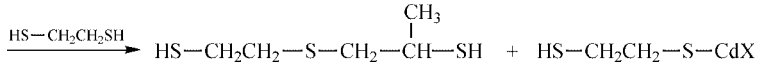

(126)

The cationic polymerization of thiiranes has not been reported as a method for the synthesis of telechelics, because of the rapid chain transfer to polymer and degradation of the active polymer to low molecular weight cyclic products (323).

Cyclic Amines. The three-membered cyclic amines and the four-membered cyclic amines can be polymerized only by cationic mechanism (324). Monofunctional initiators, such as methyl triflate (325), produce monofunctional telechelics from *t*-butylaziridine (TBA). Addition of the monomer to a bifunctional living PTHF solution (326) gives bifunctional poly(TBA). This is a method of making ABA block copolymers. The aziridinium end groups react with acrylic acids to form the corresponding esters (327).

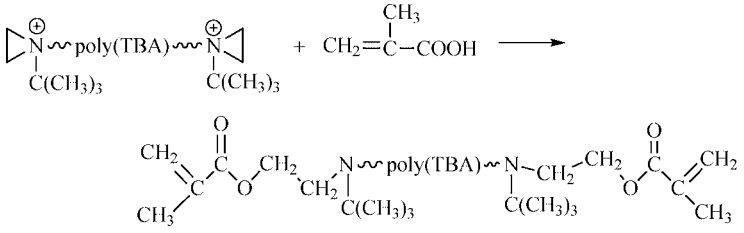

(127)

Reactions with pyrommellitic acid or with polyamines such as diethylenetriamine give cross-linked products (328).

End capping with γ-aminopropyltriethoxysilane groups yields telechelics that form networks after hydrolysis (328).

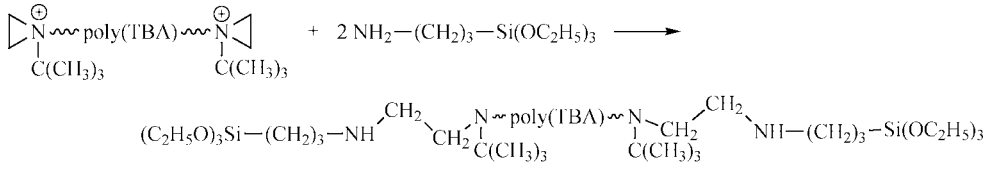

(128)

Lactones. Lactones are polymerized by anionic and cationic initiators (329). Nearly all four-, seven-, and eight-membered rings polymerize, but the five-membered rings do not, nor do many of six-membered rings (see RING-OPENING POLYMERIZATION).

The anionic initiators for the polymerization of β-lactones are usually organic bases such as tertiary amines (330). The chain transfer reactions involving a proton abstraction form the α-position and α,β-unsaturation can be avoided with α,α-disubstituted-propiolactones such as pivalactone (331–333).

Pivalactone (α,α-dimethyl-β-propiolactone) (PVL) can be converted to telechelics and used for the preparation of block copolymers (331,332). An asymmetrical telechelic is prepared from PVL (334) with cyclic amine initiators. These telechelics have α-cycloammonium and ω-carboxyl end groups.

ε-Caprolactone can be polymerized by alcoholates.

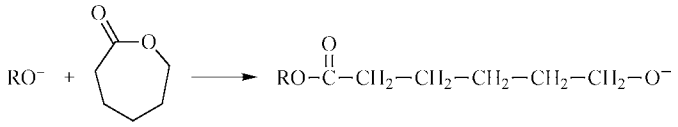

(129)

An alcoholate end group can, however, attack the ester groups of the chain, broadening the molecular weight distribution (335,336) and forming cyclic monomers. Living polymers of ε-caprolactone have been obtained with bimetallic oxoalkoxides and porphionato aluminum alcoholates (337). The selective end group functionalization of poly(ε-caprolactone) (PCL) was investigated by using aluminum alkoxides carrying functional alkoxy groups as initiators (338–341). Aluminum alkoxides carrying functional alkoxy groups (X = Br, $-CH_2N(Et)_2$, $-CH_2-CH=CH_2$, $-CH_2OC(O)C(CH_3)=CH_2$, etc) provide asymmetrical telechelic polyesters (342–344).

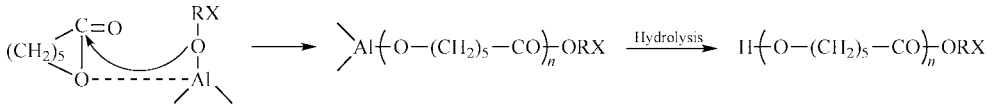

(130)

It was also shown that functional zinc alkoxides are also effective initiators for the ring-opening polymerization of ε-caprolactone under very mild conditions via a polymerization mechanism described for aluminum alkoxides (345). Tin octoate, $Sn(O(O)CCH(C_2H_5)C_4H_9)_2$, is another type of initiator to synthesize telechelics based on PCL. In particular, when it is used in conjunction with hydroxyl functional compounds or prepolymers, telechelics, linear and star-shaped block copolymers, or networks can be obtained via corresponding alkyl octoate formation (346–354). More recently, novel end-chain and mid-chain telechelics functionalized with photoactive groups of PCL were synthesized (355).

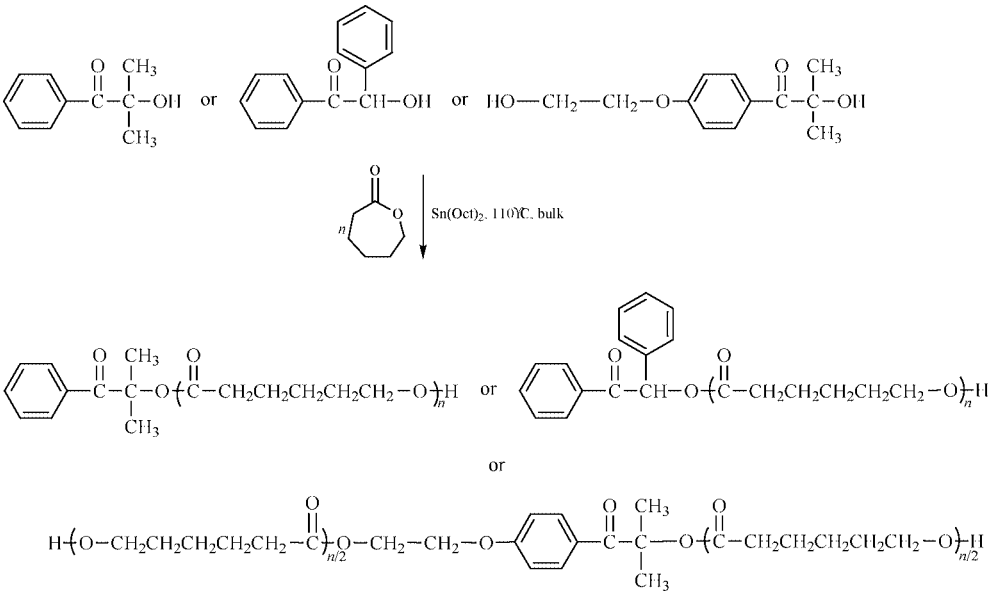

(131)

It was also reported that macromonomers based on end-functionalized PCL were prepared by different strategies using lipase enzymes as the catalysts (356–359). In the first strategy, an alcohol containing the target end-functionality initiated the ring-opening polymerization of ε-caprolactone. Alternatively, acids and esters containing the target end-functionality were added to prepolymerized ε-caprolactone. Either or both strategies yielded mono- and ditelechelics (359).

Hydroxy telechelics of PCL can be transformed to thiol functionalized polymers under mild conditions by using 2,4-dinitrophenylthioacetic acid as the protecting group (360).

ε-Caprolactone polymerization initiated with trialkyloxonium salt in combination with an alcohol (361) is easily controlled. A similar reaction has been described for cyclic ethers (288).

Siloxanes. Polysiloxanes are used as segments in block copolymers because of their low temperature flexibility, high gas permeabilities, excellent electrical properties, biocompatibility, and surface properties.

Linear polysiloxanes are prepared by anionic and cationic polymerization of cyclosiloxanes (362), such as hexamethylcyclotrisiloxane (D_3) and octamethylcylotetrasiloxane (D_4). Anionic polymerization is initiated by hydroxides, alcoholates, phenolates, silanolates, and siloxanolates. The active species is the silanolate anion.

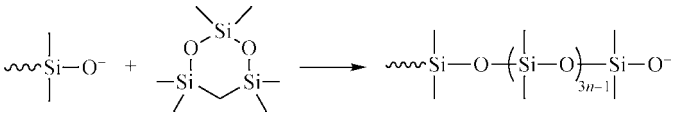

(132)

Cationic polymerization is initiated by strong protonic acids, such as sulfuric acid, trifluoromethane sulfuric acid, or trifluoroacetic acid.

Both anionic and cationic species undergo backbiting during polymerization, creating equilibrium between chains and rings (363,364).

Bifunctional polysiloxanes with a variety of end groups are obtained by using end blockers with different end groups R (365–367).

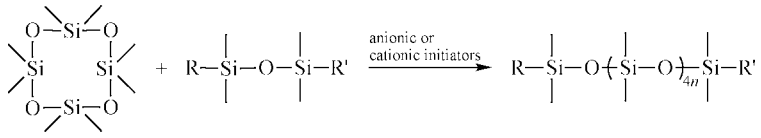

(133)

End groups include amino, dimethylamino, piperazine, carboxyl, ethylene oxide, and hydroxymethylene (Table 8).

A large number of polysiloxanes with functional end groups are commercially available (368).

The hydrosilation of unsaturated functional compounds with polysiloxanes containing Si—H end groups can also be used for the preparation of polysiloxane telechelics (369).

Table 8. Commercial Telechelic Polydimethylsiloxanes[a]

End group R	Molecular weight
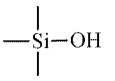	400–310,000
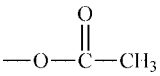	36,000
—Cl	425–600
$-N(CH_3)_2$	36–450
$-OC_2H_5$	
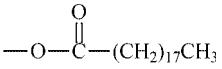	
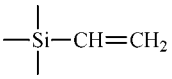	
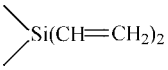	
	400–62,00
$-(CH_2)_3NH_2$	
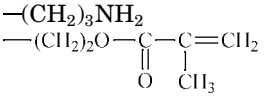	

[a] Ref. 368.

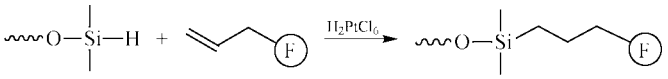

(134)

Synthesis of chain or end-functional polysiloxanes with methacrylate (370), hydroxy propyl (371), epoxy (372), benzoin (373), carboxyl ester or carboxyl amido (374), and chloromethylphenethyl (375) groups were described.

Alternatively, the chemical transformation of functional groups attached to the siloxane prepolymers by reacting with appropriate reagents provides desired functionalization. For example, electroactive pyrrole functional polysiloxanes were prepared from the corresponding amino telechelics (375).

Oxazolines. Cationic polymerization of 2-alkyl-2-oxazolines provides an excellent methodology for the easy introduction of functional end groups (376). Polymerization proceeds via oxazolinium species and functional groups can be incorporated at both initiation and termination steps by using functional initiator and nucleophile, respectively.

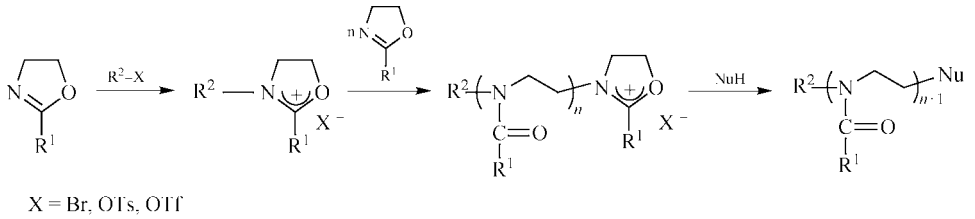

X = Br, OTs, OTf

(135)

Poly(oxazoline) telechelics with hydroxyl, amino, triphenylphosphonium, piperidine, pyrrole, styryl, acrylamide, acrylate, methacrylate, and butadiene end groups were successfully synthesized (377–387). Reaction of methyltosylate (MeOTs) with bisoxazolines gives rise to the formation of bis(oxazolinium tosylate) (387). Living polymerization of monofunctional oxazolines having propagating species at both ends can be initiated by the addition of the monomer.

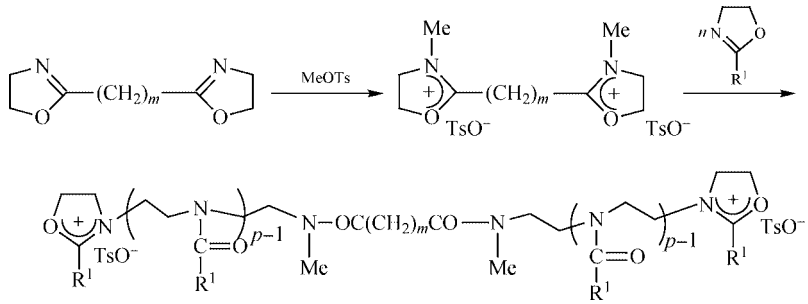

(136)

Termination of the living ends with suitable nucleophiles yields difunctional thiol, vinylbenyzl, carboxylic acid, *t*-butylmalonate, benzyl and unsaturated ester telechelics (387–389).

Metathesis Polymerization

Olefin metathesis has been of interest both industrially and academically because of its great synthetic utility (4). Mechanistically related metathesis reactions include ring opening metathesis (ROM), ring-closing metathesis (RCM), cross-metathesis (CM), acyclic diene metathesis (ADMET) polymerization, and ring-opening metathesis polymerization (ROMP) (Fig. 12) (5–8,390,391).

Acyclic Diene Metathesis Polymerization. Acyclic diene metathesis (ADMET) and the other metathesis polymerization methods are closely related to the catalyst system employed. Besides classical catalysts, Schrock-type alkylidenes and Grubbs-type carbenes can be used in ADMET polymerization.

ADMET polymerization and depolymerization methods have been used in the synthesis of telechelic oligomers. The metathesis depolymerization of 1,4-polybutadiene is accomplished in the presence or absence of a monofunctional diene by using either of the catalysts presented in Figure 13. Telechelic oligomers with terminal alkene, ester, and silyl ether and imide functional groups may be

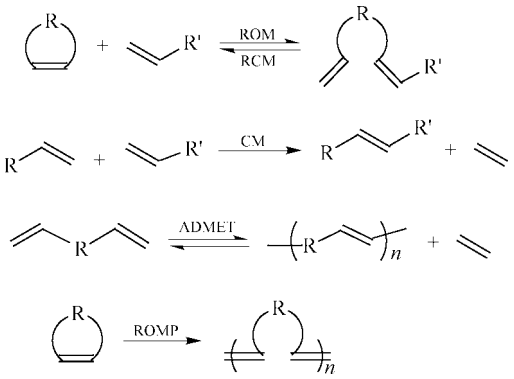

Fig. 12. Metathesis pathways.

prepared (392,393). Amine and alcohol functions are not well tolerated with the current catalysts and can be incorporated to polymers by using protecting group strategy. Telechelics with both of these types of end groups were synthesized using direct ADMET polymerization of dienes in the presence of a functional group protected α-olefin (394,395).

Ring-Opening Metathesis Polymerization. In ring-opening metathesis polymerization (ROMP), the use of functionalized acyclic alkenes as chain transfer agents not only permits the regulation of the polymer molecular weight but also opens a simple and efficient route to telechelics (4). Because of their higher reactivity, *cis*-alkenes are preferably employed for this purpose.

A broad variety of difunctional allylic olefins have been used for the synthesis of amino-, carboxyl-, and halide-terminated polybutadienes by means of the Grubbs catalyst **I** (396–398). With the same catalyst, commercially interesting hydroxy telechelic polybutadienes could be obtained by the cleavage of the acetyl end-capped polymer or the copolymer, as depicted in Figure 14 (399,400).

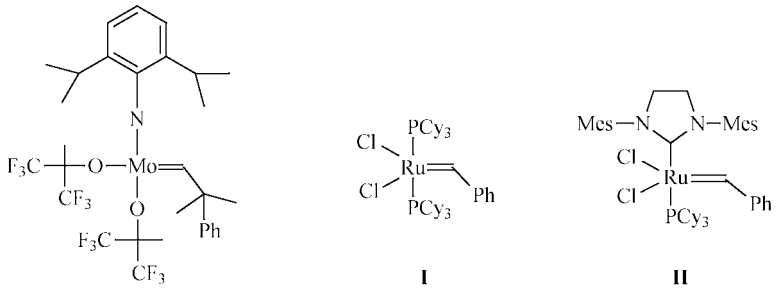

Fig. 13. Well-defined metathesis catalysts.

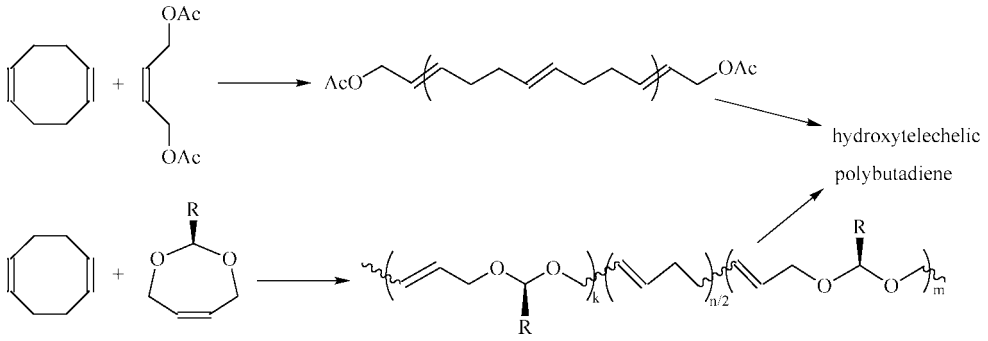

Fig. 14. Hydroxytelechelic polybutadiene by ROMP and hydrolysis.

ROMP in the presence of unprotected alcohols led to decreased yields and significant amounts of aldehyde end groups due to isomerization (399–401). However, ROMP with the addition of 1,4-bis(acetoxy)-2-butene (43) or even the related unprotected diols was performed successfully with the highly active Grubbs catalyst **II**. In the latter case, THF was added to minimize isomerization to aldehydes (401). Br- and Cl-telechelic poly(butadiene)s were employed for the synthesis of ABA triblock copolymers by subsequent grafting from the ROM polymers with methyl methacrylate (MMA) or styrene via ATRP (398). The preparation of poly(butadiene)s with cross-linkable end groups, such as epoxides or methacrylates, was reported by Grubbs and co-workers (402). Related syntheses of acetoxy end-terminated polymers with Grubbs-type catalysts were performed not only for cyclooctadiene but also for norbornene and 7-oxanorbornene derivatives (403,404).

End-functionalized poly(norbornene)s capped with one or two acetoxy or alcohol groups were prepared with the Grubbs catalyst **I** and mixed NHC/phosphine catalysts (405). Acetoxy and hydroxyl end-capped polymers were prepared by Gibson and Okada from bis(*tert*-butylester)-substituted norbornene by means of the Grubbs catalyst **I**. Subsequent hydrogenation of the hydroxy functionalized polymer gave the corresponding poly(norbornene) (406).

A further interesting approach for chain-end functionalization was reported. The treatment of a living ROM polymer Grubbs catalyst **I** with molecular oxygen led to monoaldehyde-end-capped polymers in high yields (407). With W- or Mo-based catalysts, the analogous synthetic protocol would partially lead to a coupling reaction, thereby yielding polymers with doubled molecular weight (6,407,408).

The synthesis of a homologous series of unsatured oligomeric esters by cross-metathesis of cyclopentene and MMA is reported (409,410). Ozawa and co-workers (411) reported on the polymerization of norbornene in the presence of various functionalized terminal olefins as chain-transfer agents. Mechanistic considerations let them assume that the obtained polymers each bore one vinyl end group and one functional end group.

Nomura and co-workers reported that norbornene-based macromonomers of the following structure (Fig. 15) containing ring-opened poly(norbornene) derivatives in the side chain can be prepared efficiently by the ROMP using well-defined molybdenum catalysts and subsequent end-group reactions (412,413).

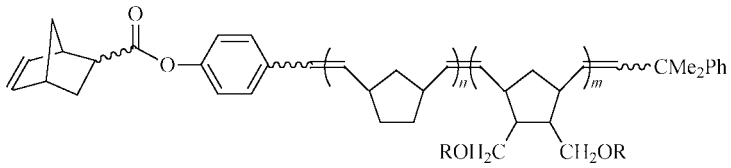

Fig. 15. Structure norbornene-based macromonomers.

Interestingly, these macromonomers were copolymerized with norbornene derivatives via ROMP to yield various macromolecular architectures (414).

ROMP approach was also applied by several groups to prepare polymers having functional groups reactive toward ATRP (398,414,415).

Chain Scission

Telechelics can also be prepared by the cleavage of high molecular weight moieties by oxidation, reduction, rearrangements, and irradiation (Table 9).

Oxidation. Treatment of PVC with ozone (416–418) gives telechelics; the attack probably starts at the vinyl double bonds.

Ozonolysis can be used as an analytical method for polymers containing carbon–carbon double bonds (438–441).

Acid, acid chlorides, and hydroxy-functionalized telechelics have been described (418). The reaction of polybutadiene with controlled amounts of ozone can be used to prepare hydroxy-terminated telechelic polybutadienes (419). The oxidative cleavage of copolymers of isobutylene with dienes has been studied

Table 9. Telechelics Prepared by Chain Scission

Structure	End group	References
—(CH$_2$—CHCl)$_n$—	COOH	416–418
	COCl	418
—(CH$_2$—CH=CH—CH$_2$)$_n$—	OH OH	419
—[CH$_2$—C(CH$_3$)$_2$]$_n$—	COOH	420–423
	COCH$_3$	424,425
	CH$_2$OH CHOHCH$_3$	426–430
—(CH$_2$—CH$_2$)$_n$—	COOH	431
—[CH$_2$—CH(C$_6$H$_5$)]$_n$—	OH	432,433
—(CH$_2$—CH$_2$—O—CH$_2$CH$_2$S$_x$)$_n$—	SH	434–436
—[(CH$_2$CH$_2$)$_n$(CH$_2$—CH)$_p$]$_q$— (CH$_3$)	OH	437

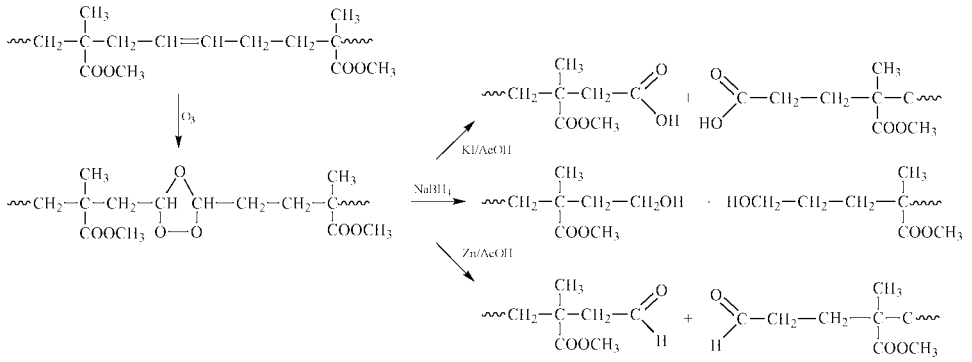

Fig. 16. Telechelic oligomers by ozonolysis.

extensively (442–444), in particular the formation of carboxyl-terminated telechelics
(424–427). Ebdon and co-workers (445–451) prepared a variety of telechelic oligomers with terminal aldehyde, hydroxyl, ketone, or carboxylic end groups by ozonolysis of suitable copolymers of MMA or St containing small amounts of C=C bonds (Fig. 16). These bonds were introduced using either a diene or acetylene as comonomer.

Polystyrene and a poly(styrene-*stat*-butadiene) have been reacted with ozone in various solvents to establish conditions necessary for the production of telechelics having high and controllable end group functionalities. Workup with sodium borohydride or Zn/acetic acid gives dihydroxy- or dialdehyde-ended oligostyrenes, respectively. Oxidative workup with SeO_2/H_2O_2 yields carboxyl end groups. Side reactions associated with the synthesis of telechelic oligostyrenes by the ozonolysis route, ie, attack of the α-position of the backbone but also of the aromatic unit, can be minimized by the use of *N*-dialkyl amides as ozone scavenger (452).

Side reactions can be avoided with a selective oxidizing agent such as ruthenium tetroxide (453) which is soluble in many solvents. It can be used in catalytic quantities in combination with another oxidizing agent, eg, peracetic acid (454). Ruthenium dioxide in combination with periodate can be used in water or in organic solvents in the presence of a phase transfer catalyst (424,425).

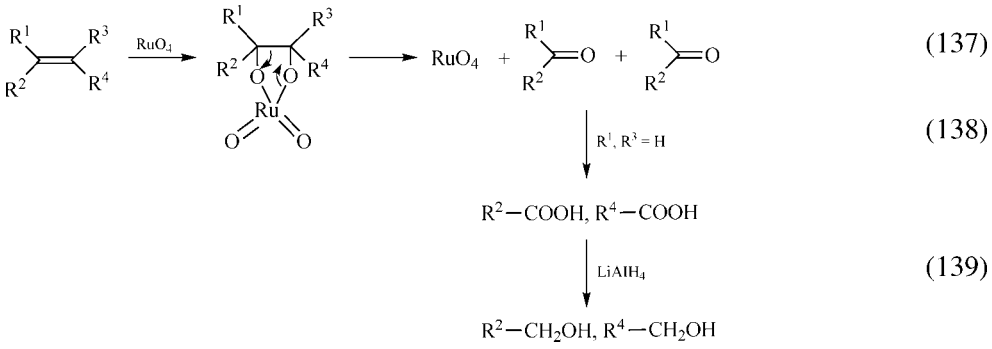

(137)

(138)

(139)

Butyl rubber yields asymmetrical α-carboxyl-ω-ketone telechelics with RuO_4, whereas poly(isobutylene-*co*-2,3-dimethylbutadiene) yields symmetrical α,ω-ketone and α,ω-carboxyl telechelics (426–429). If the incorporation of the diene is sterically specific, ideal functionalization ($f = 2$) can be obtained with these methods, provided that high molecular weight starting materials are employed (430). Cleavage of partially hydrogenated polybutadiene with RuO_4 gives α,ω-carboxypolyethylene (431).

Many other oxidizing agents can be used to cleave polymer chains. For example, fuming nitric acid cleaves polyethylene to yield carboxyl telechelic polyethylene (455–459). However, nitration of the polymer chain is a side reaction. The nitro groups can be converted to ketones without further reduction of molecular weight (460).

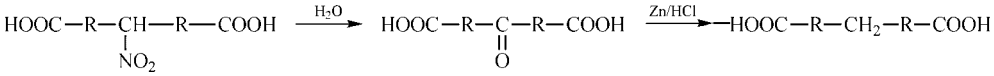

(140)

Reduction. Liquid thiokols are telechelics produced commercially by a reductive cleavage reaction (434–438).

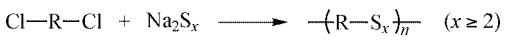

(141)

(142)

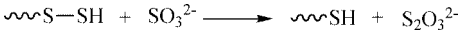

(143)

Other Degradation Methods. Ethylene–propylene telechelics with hydroxyl end groups (437) are prepared by thermal degradation followed by ozonolysis and reduction of the end group by an alkylaluminum compound. Products with molecular weights of approx 1000 with a functionality $f = 1.7$ were obtained (437).

Degradation of polyisobutylene or poly(isobutylene-*co*-isopropylene) at low temperature in the presence of a Lewis acid yields α,ω-diolefin telechelics (461).

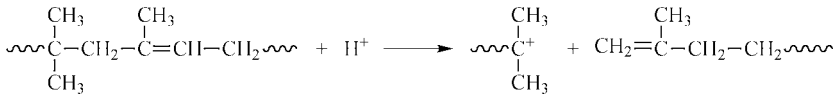

(144)

The radiolysis of polyisobutylene also gives α,ω-olefin telechelics (462).

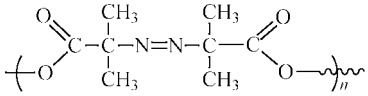

Fig. 17. Polyazoester.

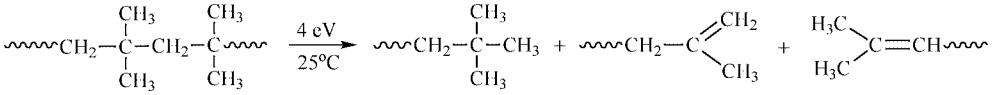

(145)

An interesting pathway to telechelics is the synthesis of polymers containing heat- or light-sensitive groups in the main chain, for example, azo groups (432, 433,463). Thus, polycondensation of AIBN with diols yields polyesters (Fig. 17).

Decomposition of the azo function in the presence of styrene yields AB block copolymers, which can be converted into α,ω-dihydroxyl polystyrene by a reductive cleavage of the ester bonds.

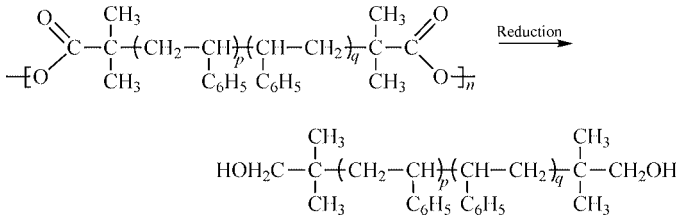

(146)

Another potential photochemical route to prepare telechelics is the photolysis of copolymers of MMA with various vinylketones. Upon irradiation these copolymers undergo chain scission almost entirely by a Norrish Type I process, giving oligomers with allylic end groups (464,465).

Step-Growth Polymerization

Step-growth polymerization is a simple method of preparing reactive oligomers (466), many of which cannot be prepared by the methods described previously. Increasing commercialization of thermoplastic elastomers, based on tri- or multiblock copolymers, has led to a growing interest in telechelics of polymers with high glass-transition temperatures, which may be used as rigid blocks. Polymers with high glass-transition temperatures are frequently prepared by a step-growth polymerization. Almost all functional groups can, in principle, be utilized for step-growth polymerization. However, side reactions such as cyclization and decarboxylation limit the molecular weight, functionality, and yield. AR^1A and BR^2B are followed to react ($x < y$),

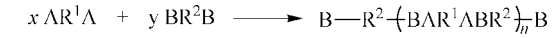

(147)

and the molecular weight of the products is given by

$$D\bar{P}_n = \frac{(1+r)}{(1+r-2rp)}$$

where DP_n is the number-average degree of polymerization, $r = (AR^1A):(BR^2B)$ with $(AR^1A) < (BR^2B)$, and p = conversion of AR^1A.

At 100% conversion of the minor reactant, the molecular weight of the product is determined by the following equation:

$$D\bar{P}_n = \frac{(1+r)}{(1-r)}$$

and the end groups are those of the major component.

This method can be applied for the preparation of α,ω-dicarboxyoligoesters, α,ω-dicarboxyoligoamides. It has also been applied to the preparation of α,ω-diphenol oligocarbonates and epoxy resins (467–472).

In an alternative method of achieving nonstoichiometry, AR^3X or BR^4X (where X represents a functional group which does not react with A or B) is added to the reaction system. At complete conversion, X forms the end groups of the polymer:

$$n\,AR^1A + n\,BR^2B + m\,BR^4X \longrightarrow XR^4B\text{—}(AR^1ABR^2B)_n\text{—}R^4X \qquad (148)$$

The latter method is also useful for preparing monofunctional telechelics. In this case a monofunctional reactant is used. For example, R^4B gives

$$n\,AR^1A + n\,BR^2B + R^4B \longrightarrow R^4\text{—}(BAR^1ABR^2)_n\text{—}B \qquad (149)$$

Nonstoichiometric Reactions. This addition of an SH group to a carbon–carbon double bond involves radical intermediates, but nevertheless exhibits the typical features of a polycondensation reaction. The end group and molecular weight are controlled by stoichiometry of the reactants (473).

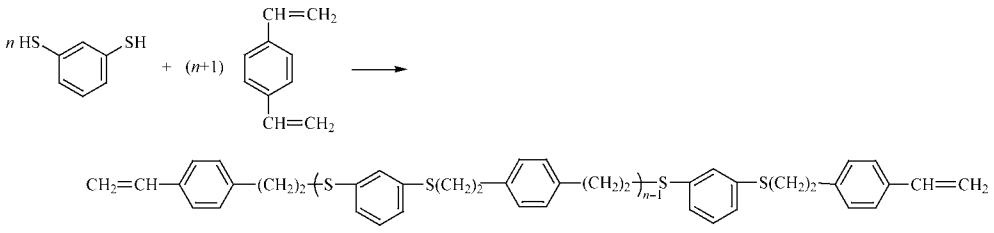

(150)

Thus an excess of the divinyl reactant yields products with olefinic end groups, whereas an excess of the dithiol component yields products with mercapto end groups. For products of molecular weight below 5000, end group analysis can be used to determine the molecular weight. Similar addition reactions have also

been carried out with triple bonds (474,475), ie using 1,4-diethynylbenzene in place of DVB.

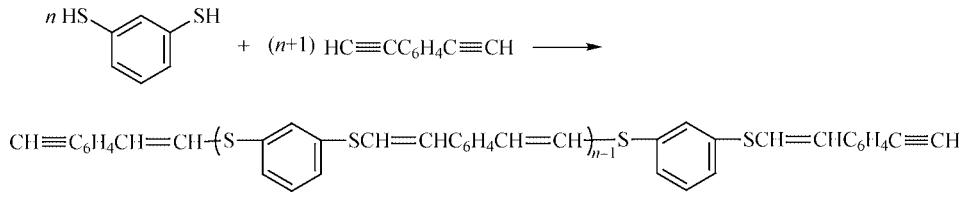

(151)

Aliphatic α,ω-dialkynes give telechelics only when the alkyne is used in excess. If the dithiol is in excess, the SH end groups react with the double bonds of the polymer backbone to produce branched or finally cross-linked products.

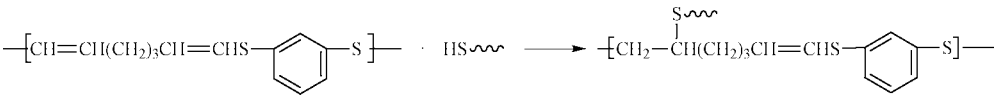

(152)

Telechelics can also be prepared by conventional polycondensation (476).

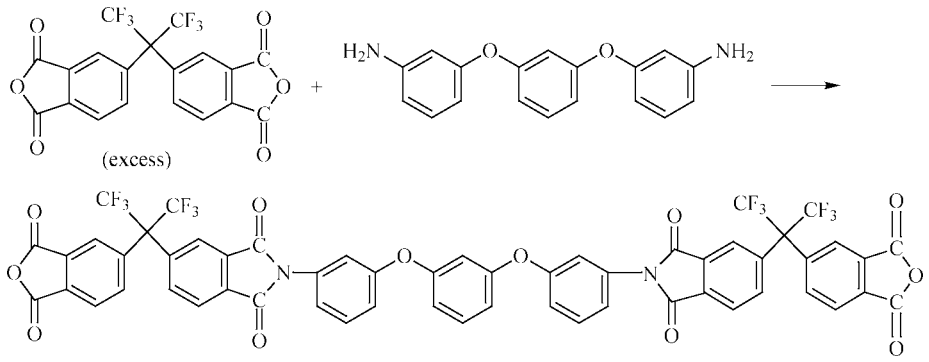

(153)

The acid anhydride end groups can subsequently be modified by reaction with substituted aromatic amines.

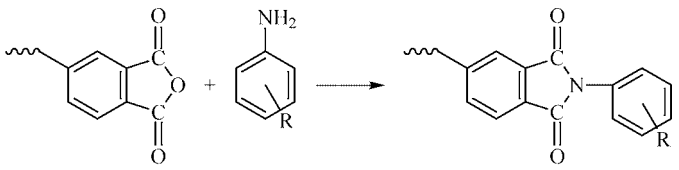

where R = — $CH{=}CH_2$, —$CH{=}CH{-}CH{=}CH_2$, or —$CH{=}CHC_6H_5$ (154)

Table 10. Reactions of Bisphenol A with *p*-Dichlorophenyl Sulfone[a]

	Molecular weight			
DP_n[b]	Theoretical	By IR	By ^1H NMR	By UV
1	670	785	680	720
2	1110	1175	1110	1110
4	2000	1950	2040	2100
7	3320	3600		3380

[a] Ref. 482.
[b] Number-average.

Other examples of telechelic synthesis by polycondensation reactions involving an excess of one of the reactants, followed by modification of the resulting end groups, have also been described (477–481).

Studies (482,483) of the polycondensation of bisphenol A and *p*-dichlorodiphenyl sulfone show that molecular weight and end groups can be controlled by using nonstoichiometric ratios of the reactants; agreement with theory is excellent (Table 10).

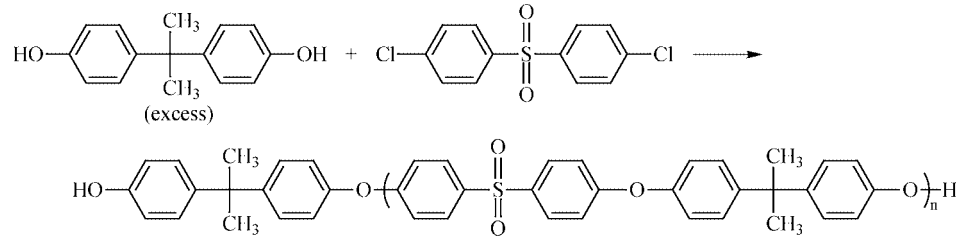

(155)

With the aid of phase-transfer catalysts, several polycondensates can be obtained under mild conditions. An example is given in reaction 156:

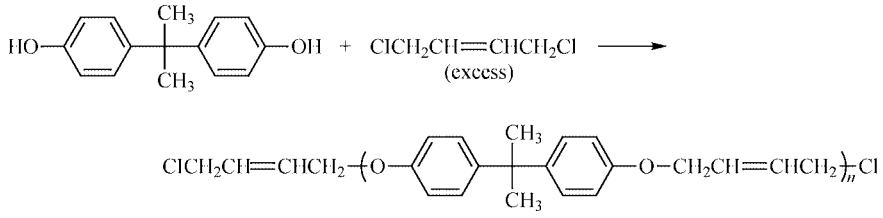

(156)

This reaction was carried out in a water–chlorobenzene mixture in the presence of NaOH and tetrabutyl ammonium hydrogen sulfate (484).

For polycondensation where a single reactant contains both functional groups, an additional reactant can achieve the necessary nonstoichiometry:

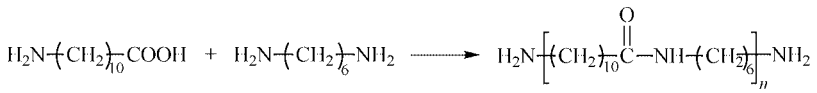

(157)

End groups and molecular weight are controlled by the diamine concentration (485). The introduction of protecting groups results in the following reactions (486):

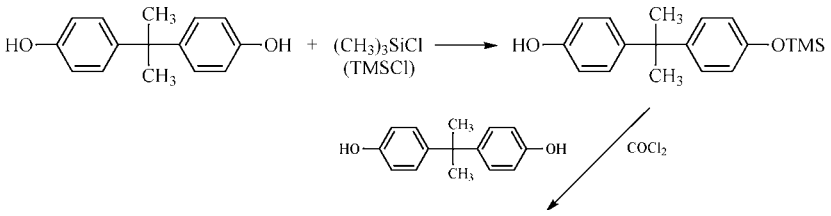

(158)

(159)

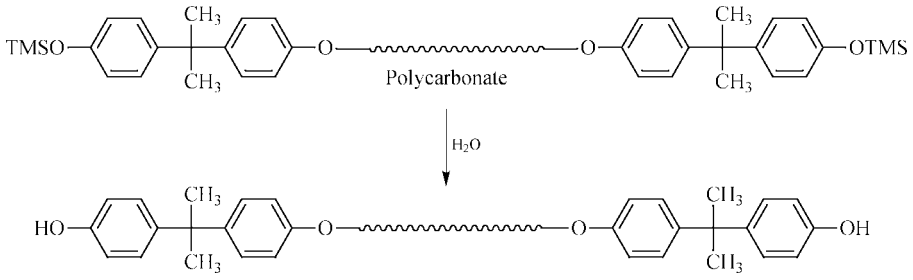

(160)

Phase-transfer catalysts have also been used for the modification of telechelics (487).

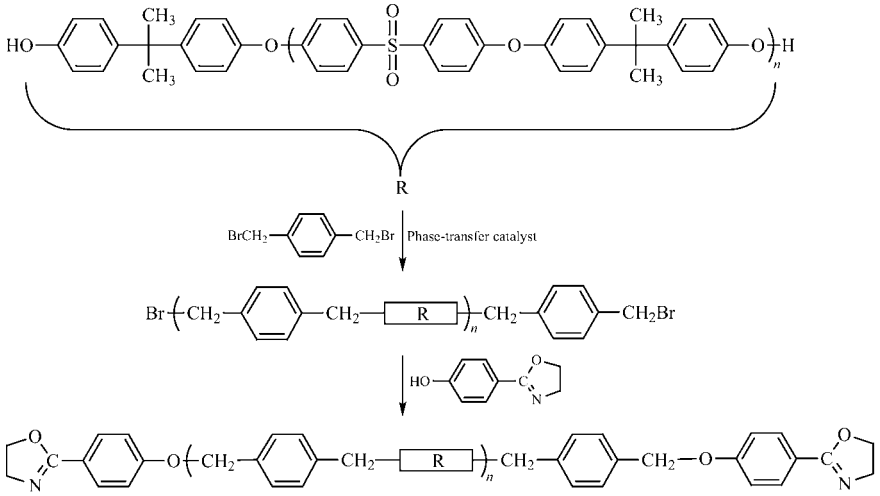

(161)

(162)

Macromonomers

Macromolecular monomers, called *macromonomers* or *macromers*, can be defined as oligomers or polymers with a polymerizable end group. Such groups may be

vinyl, acrylic, heterocyclic (ring opening polymerization), dicarboxylic, or dihydroxylic (step-growth polymerization). The increasing interest in these materials stems from the growing need for well-defined graft copolymers for which macromonomers often are ideal starting materials (488–496). The length and number of branches of the graft copolymers can be controlled by the molar mass and feed ratio of macromonomers to comonomers. In the previous sections, the synthesis of macromonomers has been described particularly when the chemistry involved is similar to that for the telechelics with other functional groups. The principal focus of the following part will be to describe well-established general approaches for the synthesis of macromonomers. For a wider view, the reader's attention should be directed to the review articles (279,280,497,498) and a book (499) solely devoted to macromonomers.

Anionic Polymerization. Anionic methods for the synthesis of macromonomers can be divided into initiation and end-capping (Table 11).

Although the initiation method is widely used, side reactions of the unsaturated head groups often lead to low functionality.

Polar monomers, such as MMA, rarely give high yields of macromonomers by straightforward anionic polymerization. However, group-transfer polymerization (517–522), which is a special case of Anionic Polymerization (qv), gives macromonomers with perfect functionality.

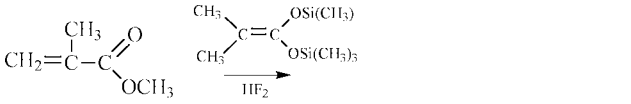

(163)

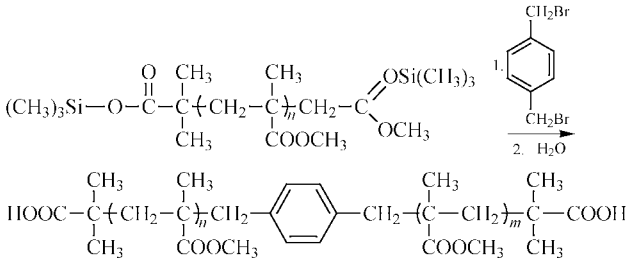

(164)

The reaction of the alcoholate of polyoxyethylene with acetylene yields a macromonomer (523).

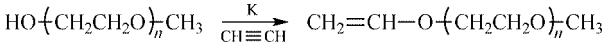

(165)

Cationic Polymerization. Both initiator and end-capping methods can be used to obtain macromonomers by cationic polymerization (see CARBOCATIONIC POLYMERIZATION). Telechelics can be made this way from PTHF (Table 12). A typical reaction is given below:

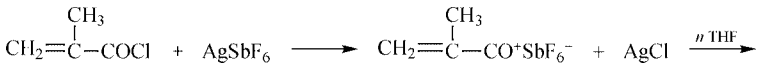

(166)

Table 11. Macromonomers by Anionic Polymerization

Initiator	References	End capping	References
Styrene			
$CH_2{=}CH_2Li$	500, 501	$CH_2{=}\underset{\displaystyle CH_3}{\overset{\displaystyle |}{C}}H{-}COCl$	488
$CH_2{=}CH_2CH_2Li$	501	$ClCH_2CH_2{-}O{-}CH{=}CH_2$	488
		$CH_2{=}CH{-}\overset{\displaystyle CH_3}{\overset{\displaystyle |}{\underset{\displaystyle CH_3}{\underset{\displaystyle |}{Si}}}}{-}CH_2Cl$	502
		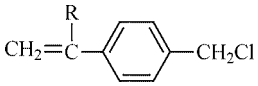	503
		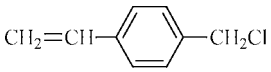	488
Methyl methacrylate			
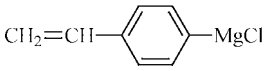	504	$CH_2{=}CH_2{-}CH_2Br$	505
		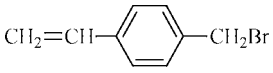	505
		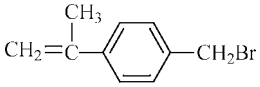	506
Ethylene oxide			
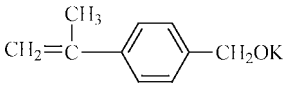	507	$CH_2{=}\underset{\displaystyle CH_3}{\overset{\displaystyle |}{C}}H{-}COCl$	507,508
	509	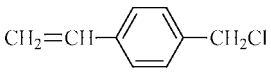	510
Vinylpyridine			
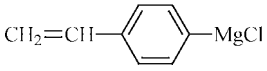	504	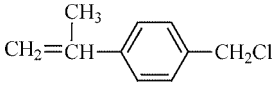	511
		$CH_2{=}\underset{\displaystyle CH_3}{\overset{\displaystyle |}{C}}H{-}COCl$	512
		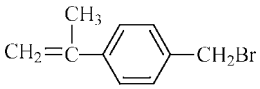	513

Table 11. (Continued)

Initiator	References	End capping	References
Hexamethylcyclo-trisiloxane		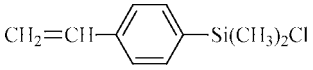	514
		$CH_2{=}CH{-}Si(CH_3)_2Cl$	515
		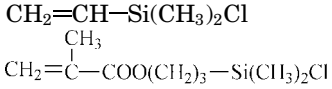	516

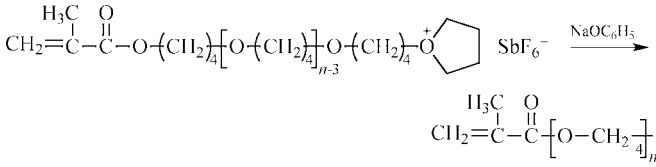

(167)

Oxiranes also polymerize under similar conditions.

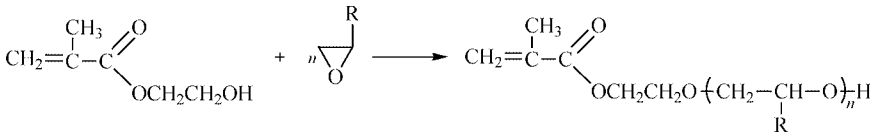

(168)

This macromonomer is sold under the trade name Blendmer (530).

Termination of the cationic ring-opening polymerization of *N-t*-butylaziridine with methacrylic acid yields macromonomers (531).

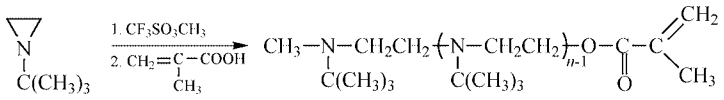

(169)

Table 12. Macromonomers from PTHF

Initiator	References	End capping	References
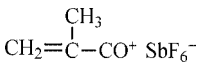	524	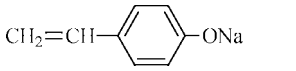	526
	525	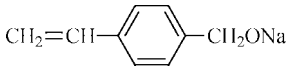	527
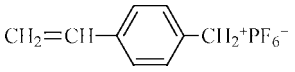	525	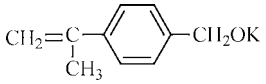	528
		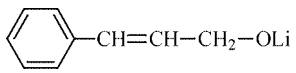	529

Macromonomers from 2-isobutylene have been prepared by the inifer method (532,533).

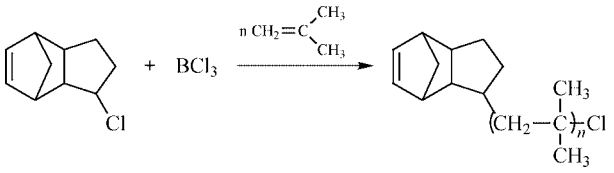

(170)

This macromonomer has been copolymerized with ethylene and propylene in the presence of Ziegler–Natta catalysts.

The living polymerization of vinyl ethers using the HI/I_2 (534,535) or the acetal/TMST method (536) can be used for macromonomer synthesis.

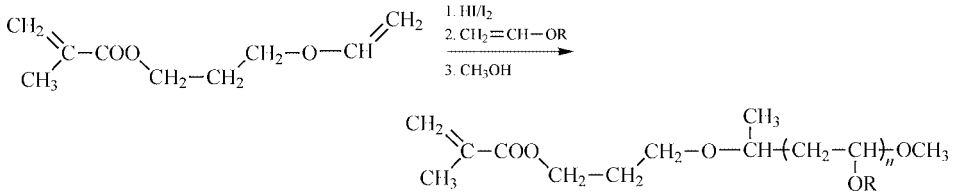

(171)

These macromonomers are characterized by narrow molecular weight distribution and excellent functionality.

Radical Polymerization. Macromonomers can also be synthesized by radical polymerization (537,538).

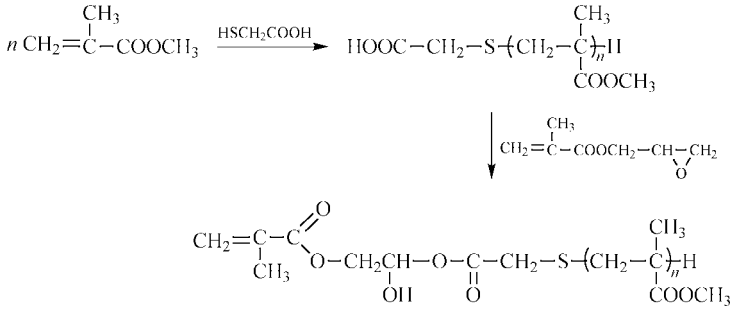

(172)

With thioglycolic acid as a chain-transfer agent, macromonomers are prepared from dimethylaminoethyl methacrylate and other acrylate and methacrylate derivatives (539). Iodoacetic acid is used as the transfer agent for polystyrene macromonomers (540).

3-Mercaptopropionic acid can be used as a transfer agent for preparing telechelics from acrylamide and *N*-vinylpyrrolidone (541).

All these reactions first lead to simple COOH-terminated (monotelechelic) polymers and are converted into macromonomers by a glycidylmethacrylate (eg reaction 172).

Other Methods. Reaction between DVB and 1,2-ethylamino ethylene in the presence of lithium amide yields macromonomers (542,543).

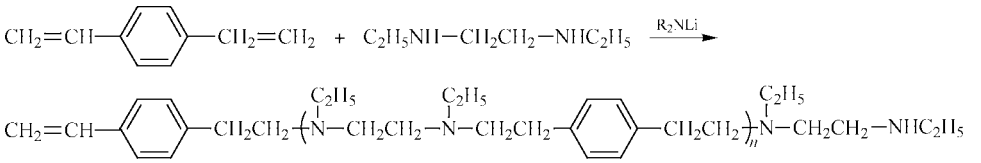

(173)

Macromonomers of poly(crown ether)s (543) and polypeptides (544) have also been prepared by this method.

The ring-opening polymerization of bicyclic oxalactams gives macromonomers (545,546).

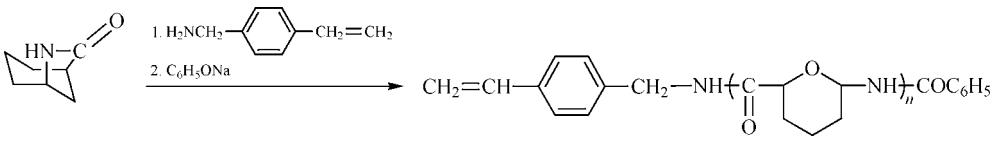

(174)

Nonpolymerizable end groups can be converted into polymerizable end groups in the presence of phase-transfer catalysts (484,547). An example of this technique is the synthesis of macromonomers from water glass (548).

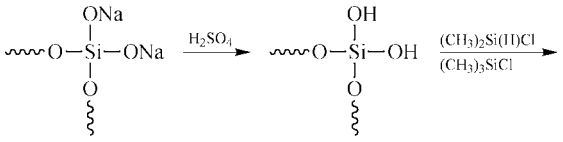

(175)

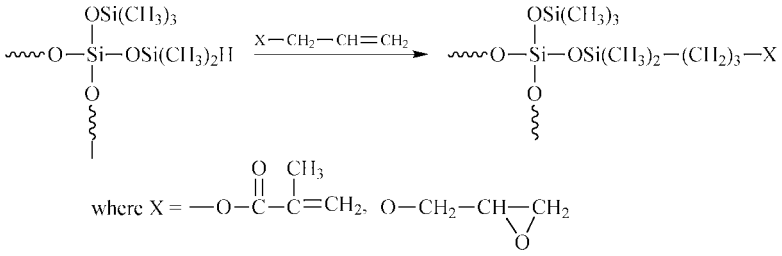

(176)

BIBLIOGRAPHY

"Telechelic Polymers" in *EPSE* 2nd ed., Vol. 16, pp. 494–532, by O. Nuyken, Universität Bayreuth and S. Pask, Bayer AG, Dormagen

1. O. Bayer, *Angew. Chem.* **59**, 257 (1947).
2. C. A. Uraneck, H. L. Hsieh, and O. G. Buck, *J. Polym. Sci.* **46**, 535 (1960).

3. K. Matyjaszewski, ed., *Controlled-Living Radical Polymerization: Progress in ATRP, NMP, and RAFT* (ACS Symposium Series, Vol. 768), American Chemical Society, Washington, D.C., 2000.
4. K. J. Ivin and I. C. Mol, *Olefin Metathesis and Methathesis Polymerization*, Academic Press, San Diego, 1996.
5. B. M. Novak, W. Risse, and R. H. Grubbs, *Adv. Polym. Sci.* **102**, 47 (1992).
6. M. R. Buchmeiser, *Chem. Rev.* **100**, 1565 (2000).
7. A. Fuerstner, *Angew. Chem., Int. Ed. Engl.* **39**, 3012 (2000).
8. U. Frenzel and O. Nuyken, *J. Polym. Sci., Polym. Chem. Ed.* **40**, 2895 (2002).
9. E. J. Goethals, ed., *Telechelic Polymers*, CRC Press, Boca Raton, Fla., 1988.
10. R. D. Athey Jr., *Prog. Org. Coat.* **7**, 289 (1979).
11. R. H. Gobran and E. M. Fettes, eds., *High Polymers, Vol. XIX: Chemical Reactions of Polymers*, Wiley-Interscience, New York, 1964, Chapt. 4.
12. D. M. French, *Rubber Chem. Technol.* **42**, 71 (1969).
13. W. Heitz, *Makromol. Chem., Macromol. Symp.* **10/11**, 297 (1987).
14. C. M. Starks, *Free Radical Telomerization*, Academic Press, New York, 1974.
15. C. H. Bamford and C. F. Tipper, *Comprehensive Chemical Kinetics, Vol. 14a: Free Radical Polymerization*, Elsevier, Amsterdam, 1976, Sect. 65.
16. P. S. Engel, D. J. Bishop, and M. A. Page, *J. Am. Chem. Soc.* **100**, 7009 (1978).
17. O. Nuyken, Diploma Thesis, TU Berlin, 1966.
18. N. D. Ghatge, S. P. Vernekar, and P. P. Wadgaonkar, *Makromol. Chem., Rapid Commun.* **4**, 307 (1983).
19. W. Konter, B. Börner, K. H. Köhler, and W. Heitz, *Makromol. Chem.* **182**, 2619 (1981).
20. W. Heitz, P. Ball, and M. Lattekamp, *Kautsch. Gummi Kunstst.* **34**, 459 (1981).
21. C. H. Bamford, A. D. Jenkins, and R. P. Wayne, *Trans. Faraday Soc.* **56**, 932 (1960).
22. C. H. Bamford and A. D. Jenkins, *Nature* **176**, 78 (1955).
23. C. H. Bamford, A. D. Jenkins, and R. Johnston, *Trans. Faraday Soc.* **55**, 179 (1959).
24. C. H. Bamford, A. D. Jenkins, and R. Johnston, *Trans. Faraday Soc.* **55**, 1451 (1959).
25. S. F. Reed, *J. Polym. Sci., Polym. Chem. Ed.* **9**, 2029 (1971).
26. S. F. Reed, *J. Polym. Sci., Polym. Chem. Ed.* **10**, 649 (1972).
27. S. F. Reed, *J. Polym. Sci., Polym. Chem. Ed.* **9**, 2147 (1971).
28. S. F. Reed, *J. Polym. Sci., Polym. Chem. Ed.* **11**, 55 (1973).
29. G. Hizal, H. Tasdemir, and Y. Yagci, *Polymer* **31**, 1803 (1990).
30. R. Walz, B. Börner, and W. Heitz, *Makromol. Chem.* **178**, 2527 (1977).
31. Y. Yagci, M. Müller, and W. Schnabel, *J. Macromol. Sci., A: Macromol. Rep* **28**, 37 (1991).
32. Y. Yagci, G. Hizal, and U. Tunca, *Polym. Commun.* **31**, 7 (1990).
33. D. Edelmann and H. Ritter, *Makromol. Chem.* **194**, 1183 (1993).
34. S. Alkan, L. Toppare, Y. Hepuzer, and Y. Yagci, *J. Polym. Sci., Part A: Polym. Chem.* **37**, 4218 (1999).
35. C. H. Bamford, A. Ledwith, and Y. Yagci, *Polymer* **19**, 354 (1978).
36. A. Onen and Y. Yagci, *J. Macromol. Sci., A: Chem.* **27**, 743 (1990).
37. A. Onen, S. Denizligil, and Y. Yagci, *Macromolecules* **28**, 5375 (1995).
38. Y. Yagci and I. Reetz, in N. P. Cheremisinoff, ed., *Handbook of Engineering Polymeric Materials*, Marcel Dekker, New York, 1997, pp. 735–753.
39. J. A. Verdol, P. W. Ryan, D. J. Carrow, and K. L. Kuncl, *Rubber Age* **98**, 57 (1966).
40. H. C. Haas, N. W. Schuler, and H. S. Kolesinski, *J. Polym. Sci., Polym. Chem. Ed.* **5**, 2964 (1967).
41. H. N. Friedlander, *J. Polym. Sci.* **58**, 455 (1962).
42. G. A. Razuvaev, L. M. Terman, and D. M. Yanovskii, *Dokl. Akad. Nauk SSSR* **161**, 614 (1965).

43. H. Schnecko, G. Degler, H. Dongowski, R. Caspary, G. Angerer, and T. S. Ng, *Angew. Makromol. Chem.* **70**, 9 (1978).
44. W. J. Bailey, P. Y. Chen, W. B. Chiao, T. Endo, L. Sidney, N. Yamamoto, K. Yonezawa, in M. Shen, ed., *Contemporary Topics in Polymer Science*, Vol. 3, Plenum Press, New York, 1979, p. 29.
45. W. J. Bailey, T. Endo, B. Gapud, Y. N. Lin, Z. Ni, C. Y. Pan, S. E. Shaffer, S. R. Wu, N. Yamazaki, and K. Yonezawa, *J. Macromol. Sci. A* **21**, 979 (1984).
46. W. J. Bailey, P. Y. Chen, S. C. Chen, W. B. Chiao, T. Endo, B. Gapud, Y. N. Lin, Z. Ni, C. Y. Pan, S. E. Shaffer, L. Sidney, S. R. Wu, N. Yamamoto, N. Yamazaki, and K. Yonezawa, *J. Macromol. Sci. A* **21**, 1611 (1984).
47. W. J. Bailey, *Polym. J.* **17**, 85 (1985).
48. W. J. Bailey, *ACS Symp. Ser.* **286**, 47 (1985).
49. W. J. Bailey, *Makromol. Chem. Suppl.* **13**, 171 (1985).
50. W. J. Bailey, B. Gapud, Y. N. Lin, Z. Ni, and S. R. Wu, *ACS Symp. Ser.* **282**, 147 (1985).
51. W. J. Bailey, P. Y. Chen, S. C. Chen, W. B. Chiao, T. Endo, B. Gapud, Y. Kuruganti, Y. N. Lin, Z. Ni, C. Y. Pan, S. E. Shaffer, L. Sidney, S. R. Wu, N. Yamamoto, K. Yonezawa, and L. L. Zhou, *Makromol. Chem., Macromol. Symp.* **6**, 81 (1986).
52. B. Boutevin, Y. Pietrasanta, M. Taha, and T. El Sarraf, *Polym. Bull.* **10**, 157 (1983).
53. B. Boutevin, Y. Pietrasanta, M. Taha, and T. El Sarraf, *Makromol. Chem.* **184**, 2401, (1983).
54. Jpn. Pat. 6 164 705 (1986), T. Tsuda, Y. Yasuda, and T. Azuma (to Tao Gosei Chemical Industry Co., Ltd.).
55. K. F. Gillman and E. Senogles, *J. Polym. Sci., Polym. Lett. Ed.* **5**, 477 (1967).
56. C. Bonardi, B. Boutevin, Y. Pietrasanta, and M. Taha, *Makromol. Chem.* **186**, 261 (1985).
57. H. A. Nguyen and E. Marechal, *J. Macromol. Sci., C: Rev. Macromol. Chem. Phys.* **28**, 187 (1988).
58. E. Rizzardo, G. F. Meijs, and S. H. Thang, *Macromol. Symp.* **98**, 101 (1995), and references cited therein.
59. D. Colombani and P. Chaumont, *Prog. Polym. Sci.* **21**, 439 (1996).
60. C. P. R. Nair, P. Chaumont, and D. Colombani, *Macromolecules* **28**, 3192 (1995).
61. P. Cacioli, D. G. Hawthorne, R. L. Laslett, E. Rizzardo, and D. H. Solomon, *J. Macromol. Sci., A: Chem.* **23**, 839 (1986).
62. Y. Yagci and I. Reetz, *React. Funct. Polym.* **42**, 255, (1999).
63. T. E. Ferington and A. V. Tobolsky, *J. Am. Chem. Soc.* **77**, 4510 (1955).
64. T. E. Ferington and A. V. Tobolsky, *J. Am. Chem. Soc.* **80**, 3215 (1958).
65. T. Otsu and M. Yoshida, *Makromol. Chem., Rapid Commun.* **3**, 127 (1982).
66. C. P. R. Nair, P. Chaumont, and G. Clouet, in M. K. Mishra, ed., *Macromolecular Design: Concept & Practice*, Polym. Front Int., Inc., New York, 1994, Chapt. 11, pp. 431–470.
67. C. P. R. Nair, G. Clouet, and P. Chaumont, *J. Polym. Sci., Part A: Polym. Chem.* **27**, 1795 (1989).
68. C. P. R. Nair and G. Clouet, *Makromol. Chem.* **190**, 1243 (1989).
69. G. Clouet and H. J. Juhl, *Macromol. Chem. Phys.* **195**, 243 (1994).
70. S. A. Haque and G. Clouet, *Macromol. Chem. Phys.* **195**, 315 (1994).
71. R. M. Pierson, A. J. Costanza, and A. H. Weinstein, *J. Polym. Sci.* **17**, 221 (1955).
72. A. Bledzki, D. Braun, and K. Titzschkau, *Makromol. Chem.* **184**, 745 (1983).
73. D. Edelmann and H. Ritter, *Macromol. Chem. Phys.* **194**, 2375 (1993).
74. D. Braun, T. Skrzek, S. Steinhauer-Beißer, H. Tretner, and H. J. Lindner, *Macromol. Chem. Phys.* **196**, 573 (1995).
75. K. Matyjaszewski, ed., *Controlled Radical Polymerization* (ACS Symposium Series, Vol. 685), American Chemical Society, Washington, D.C., 1997.

76. K. Matyjaszewski, *Chem. Rev.* **101**, 2921 (2001).
77. M. Kamigaito and M. Sawamoto, *Chem. Rev.* **101**, 3689 (2001).
78. C. J. Hawker, A. W. Bosman, and E. Harth, *Chem. Rev.* **101**, 3661 (2001).
79. J. Chiefari and E. Rizzardo, in K. Matyjaszewski, and T. P. Davis, eds., *Handbook of Radical Polymerization*, Wiley-Interscience, New York, 2002, Chapt. 12.
80. J. S. Wang and K. Matyjaszewski, *Macromolecules* **28**, 7901 (1995).
81. J. S. Wang and K. Matyjaszewski, *J. Am. Chem. Soc.* **117**, 5614 (1995).
82. V. Coessens, T. Pintauer, and K. Matyjaszewski, *Prog. Polym. Sci.* **26**, 337 (2001).
83. D. M. Haddleton and C. Waterson, *Macromolecules* **32**, 8732 (1999).
84. K. Matyjaszewski, S. Coca, Y. Nakagawa, and J. Xia, *Polym. Mater. Sci. Eng.* **76**, 147 (1997).
85. K. Matyjaszewski, V. Coessens, V. Nakagawa, Y. Xia, J. Qiu, S. G. Gaynor, S. Coca, and C. Jaseczek, *Am. Chem. Soc. Symp. Ser.* **704**, 16 (1998).
86. S. G. Gaynor and K. Matyjaszewski, *Am. Chem. Soc. Symp. Ser.* **685**, 396 (1997).
87. X. Zhang, J. Xia, and K. Matyjaszewski, *Macromolecules* **33**, 2340 (2000).
88. K. Matyjaszewski, S. M. Jo, H.-J. Paik, and S. G. Gaynor, *Macromolecules* **30**, 6398 (1997).
89. K. Matyjaszewski, M. Wei, J. Xia, and N. E. McDermott, *Macromolecules* **30**, 8161 (1997).
90. D. Mecerreyes, B. Athoff, K. A. Boduch, M. Trollsos, and J. L. Hedrick, *Macromolecules* **32**, 5175 (1999).
91. G. Moineau, M. Minet, Ph. Dubois, Ph. Teyssie, T. Senninger, and R. Jerome, *Macromolecules* **32**, 27 (1999).
92. C. J. Hawker, J. L. Hedrick, E. E. Malmström, M. Trollsos, D. Mecerreyes, G. Moineau, Ph. Dubois, and R. Jerome, *Macromolecules* **31**, 213 (1998).
93. M. Destarac, K. Matyjaszewski, and B. Boutevin, *Macromol. Chem. Phys.* **201**, 265 (2000).
94. M. Destarac, B. Boutevin, and K. Matyjaszewski, in K. Matyjaszewski, ed., *Controlled/Living Radical Polymerization* (ACS Symposium Series 768), American Chemical Society, Washington, D.C., 2000, Chapt. 17.
95. D. M. Haddleton, C. Waterson, P. J. Derrick, C. B. Jasieczek, B. Christina, and A. J. Shooter, *Chem. Commun*. 683 (1997).
96. H. Keul, A. Neumann, B. Reining, and H. Höcker, *Macromol. Symp.* **161**, 63 (2000).
97. V. Coessens and K. Matyjaszewski, *Macromol. Rapid Commun.* **20**, 66 (1999).
98. Y. Xu, C. Pan, and L. Tao, *J. Polym. Sci., Polym. Chem. Ed.* **38**, 436 (2000).
99. K. Matyjaszewski, K. L. Beers, A. Kern, and S. G. Gaynor, *J. Polym. Sci., Part A: Polym. Chem.* **36**, 823 (1998).
100. Y. Nakagawa and K. Matyjaszewski, *Polym. J. (Tokyo)* **30**, 138 (1998).
101. D. M. Haddleton, A. M. Heming, D. Kukulj, D. J. Duncalf, and A. J. Shooter, *Macromolecules* **31**, 2016 (1998).
102. H. Malz, H. Komber, D. Voigt, I. Hopfe, and J. Pionteck, *Macromol. Chem. Phys.* **200**, 642 (1999).
103. A. Kajiwara and K. Matyjaszewski, *Polym. J.* **31**, 70 (1999).
104. F. Zeng, Y. Shen, S. Zhu, and R. Pelton, *Macromolecules* **33**, 1628 (2000).
105. Y. Shen, S. Zhu, F. Zeng, and R. Pelton, *Macromol. Chem. Phys.* **201**, 1387 (2000).
106. S. Yurteri, I. Cianga, and Y. Yagci, *Macromol. Chem. Phys.* **204**, 1771 (2003).
107. K. Ohno, K. Fujimoto, Y. Tsujii, and T. Fukuda, *Polymer* **40**, 759 (1998).
108. M. Erdogan, G. Hizal, U. Tunca, D. Hayrabetyan, and O. Pekcan, *Polymer* **43**, 1925 (2002).
109. M. R. Korn and M. R. Gagne, *Chem. Commun*. 1711 (2000).
110. M. Erdogan, Y. Hepuzer, I. Cianga, Y. Yagci, and O. Pekcan, *J. Phys. Chem.* **107**, 8363, (2003).

111. S. Alkan, L. Toppare, Y. Hepuzer, and Y. Yagci, *J. Polym. Sci., Part A: Polym. Chem.* **37**, 4218 (1999).
112. D. Mecerreyes, J. A. Pompose, M. Bengoetxea, and H. Grande, *Macromolecules* **33**, 5846 (2000).
113. X. Zhang and K. Matyjaszewski, *Macromolecules* **32**, 7349 (1999).
114. X. Zhang, J. Xia, S. G. Gaynor, and K. Matyjaszewski, *Polym. Mater. Sci. Eng.* **79**, 407 (1998).
115. D. M. Haddleton and K. Ohno, *Biomacromolecules* **1**, 152 (2000).
116. D. M. Haddleton, R. Edmonds, A. M. Heming, E. J. Kelly, and D. Kukulj, *New J. Chem.* **23**, 477 (1999).
117. A. Marsh, A. Khan, D. M. Haddleton, and M. J. Hannon, *Macromolecules* **32**, 8725 (1999).
118. V. Percec, H. J. Kim, and B. Barboiu, *Macromolecules* **30**, 8526 (1997).
119. K. Matyjaszewski, Y. Nakagawa, and S. G. Gaynor, *Macromol. Rapid Commun.* **18**, 1057 (1997).
120. V. Coessens, Y. Nakagawa, and K. Matyjaszewski, *Polym. Bull.* **40**, 135 (1998).
121. V. Coessens and K. Matyjaszewski, *J. Macromol. Chem. Sci., A: Pure Appl. Chem.* **36**, 667 (1999).
122. L. Li, C. Wang, Z. Long, and S. Fu, *J. Polym. Sci., Part A: Polym. Chem.* **38**, 4519 (2000).
123. V. Coessens, J. Pyun, P. J. Miller, S. G. Gaynor, and K. Matyjaszewski, *Macromol. Rapid Commun.* **21**, 103 (2000).
124. E. G. Koulouri, J. K. Kallitsis, and G. Hadziioannou, *Macromolecules* **32**, 6242 (1999).
125. T. Ando, M. Kamigaitio, and M. Sawamoto, *Macromolecules* **31**, 6708 (1998).
126. A. K. Shim, V. Coessens, T. Pintauer, SG. Gaynor, and K. Matyjaszewski, *Polym. Prepr. (Am. Chem. Soc., Div. Polym. Chem.)* **37**, 577 (1996).
127. V. Coessens and K. Matyjaszewski, *Macromol. Rapid Commun.* **20**, 127 (1999).
128. J. Norman, S. C. Moratti, A. T. Slark, D. J. Irvine, and A. T. Jackson, *Macromolecules* **35**, 8954 (2002).
129. S. A. F. Bon, S. R. Morsley, C. Waterson, and D. M. Haddleton, *Macromolecules* **33**, 5819 (2000).
130. C. W. Bielawski, J. M. Jethmalani, and R. H. Grubbs, *Polymer* **44**, 3721 (2003).
131. M. K. Georges, R. P. N. Veregin, P. M. Kazmaier, and G. K. Hamer, *Macromolecules* **26**, 2987 (1993).
132. E. Yoshida and T. Fujii, *J. Polym. Sci., Part A: Polym. Chem.* **36**, 269 (1998).
133. W. G. Skene, S. T. Belt, T. J. Connolly, P. Hahn, and C. Scaiano, *Macromolecules* **31**, 9103 (1998).
134. C. J. Hawker, G. G. Barclay, and J. Dao, *J. Am. Chem. Soc.* **118**, 11467 (1996).
135. E. Yoshida and A. Sugita, *J. Polym. Sci., Part A: Polym. Chem.* **36**, 2059 (1998).
136. W. G. Skene, J. C. Scaiano, N. Listigovers, P. M. Kazmaier, and M. K. Georges, *Macromolecules* **33**, 5065 (2000).
137. Y. Miura, N. Nakamura, and I. Taniguchi, *Macromolecules* **34**, 447 (2001).
138. S. Marque, H. Fischer, E. Baier, and A. Studer, *J. Org. Chem.* **66**, 1146 (2001).
139. E. Harth, B. van Horn, and C. J. Hawker, *Chem. Commun.* **9**, 823 (2001).
140. K. Matyjaszewski, S. G. Gaynor, D. Greszta, D. Mardare, T. Shigemoto, and J.-S. Wang, *Macromol. Symp.* **95**, 217 (1995).
141. D. Benoit, V. Chaplinski, R. Braslau, and C. J. Hawker, *J. Am. Chem. Soc.* **121**, 3904 (1999).
142. S. Jousset and J. M. Catala, *Macromolecules* **33**, 4705 (2000).
143. T. Shigemoto and K. Matyjaszewski, *Macromol. Rapid Commun.* **17**, 347 (1996).
144. N. J. Turro, G. Lem, and I. S. Zavarine, *Macromolecules* **33**, 9782 (2000).

145. C. H. Han, M. Drache, H. Baethge, and G. Schmidt-Naake, *Macromol. Chem. Phys.* **200**, 1779 (1999).
146. R. P. N. Veregin, M. K. Georges, P. M. Kazmaier, and G. K. Hamer, *Macromolecules* **26**, 5316 (1993).
147. Y. K. Chong, F. Ercole, G. Moad, E. Rizzardo, S. H. Thang, and A. G. Anderson, *Macromolecules* **32**, 6895 (1999).
148. M. O. Zink, A. Kramer, and P. Nesvadba, *Macromolecules* **33**, 8106 (2000).
149. E. Yoshida and Y. Okada, *Bull. Chem. Soc. Jpn.* **70**, 275 (1997).
150. M. K. Georges, R. P. N. Veregin, P. M. Kazmaier, G. K. Hamer, and M. Saban, *Macromolecules* **27**, 7228 (1994).
151. D. Benoit, S. Grimaldi, S. Robin, J. P. Finet, P. Tordo, and Y. Gnanou, *J. Am. Chem. Soc.* **122**, 5929 (2000).
152. M. Rodlert, E. Harth, I. Rees, and C. J. Hawker, *J. Polym. Sci., Part A: Polym. Chem.* **38**, 4749 (2000).
153. E. Harth, C. J. Hawker, W. Fan, and R. M. Waymouth, *Macromolecules* **34**, 3856 (2001).
154. M. Szwarc, *Carbanions, Living Polymers and Electron Transfer Processes*, Wiley-Interscience, New York, 1968.
155. M. Morton, *Anionic Polymerization: Principles and Practice*, Academic Press, New York, 1983.
156. S. Bywater, *Prog. Polym. Sci.* **4**, 27 (1975).
157. M. Szwarc, *Adv. Polym. Sci.* **49**, 1 (1983).
158. R. N. Young, R. P. Quirk, and L. J. Fetters, *Adv. Polym. Sci.* **56**, 1 (1984).
159. D. H. Richards, in R. N. Haward, ed., *Development in Polymerization, 1: Ionic and Ring-Opening Polymerization and the Polymerization of Conjugatet Dienes*, Applied Science Publishers, London, 1979, p. 1.
160. D. H. Richards, G. C. Eastmond, and M. J. Stuart, in Ref. 9, pp. 33–60.
161. H. Brody, D. H. Richards, and M. Szwarc, *Chem. Ind*. 1473 (1958).
162. D. H. Richards and M. Szwarc, *Trans. Faraday Soc.* **55**, 1644 (1959).
163. E. C. Steiner, R. R. Pelletier, and R. O. Trucks, *J. Am. Chem. Soc.* **86**, 4678 (1964).
164. K. Hayashi and C. S. Marvel, *J. Polym. Sci., Part A* **2**, 2571 (1964).
165. M. Morton, L. J. Fetters, J. Inomata, D.C. Rubio, and R. N. Young, *Rubber Chem. Technol.* **49**, 303, (1976).
166. S. F. Reed, *J. Polym. Sci., Polym. Chem. Ed.* **10**, 1187 (1972).
167. D. N. Schulz, A. F. Halasa, and A. E. Oberster, *J. Polym. Sci., Polym. Chem. Ed.* **12**, 153 (1974).
168. D. H. Richards, *J. Polym. Sci., Polym. Lett. Ed.* **6**, 417 (1968).
169. M. Morton and S. L. Mikesell, *J. Macromol. Sci., A: Chem.* **7**, 1391 (1973).
170. P. Mansson, *J. Polym. Sci., Polym. Chem. Ed.* **18**, 1945 (1980).
171. F. J. Burgess and D. H. Richards, *Polymer* **17**, 1020 (1976).
172. G. Finaz, Y. Gallot, J. Parrod, and P. Rempp, *J. Polym. Sci.* **58**, 1363 (1962).
173. J. Lehmann, Ph. D. dissertation, CNRS, Strasbourgh, 1976.
174. F. J. Burgess, A. V. Cunliffe, D. H. Richards, and D. C. Sherrington, *J. Polym. Sci., Polym. Lett. Ed.* **14**, 471 (1976).
175. F. J. Burgess, A. V. Cunliffe, J. R. MacCallum, and D. H. Richards, *Polymer* **18**, 719 (1977).
176. D. H. Richards, unpublished data, 1977.
177. A. Davis, D. H. Richards, and N. F. Scilly, *Makromol. Chem.* **152**, 133 (1972).
178. F. J. Burgess, A. V. Cunliffe, J. R. MacCallum, and D. H. Richards, *Polymer* **18**, 726 (1977).
179. W. C. E. Higginson and N. S. Wooding, *J. Chem. Soc. Abstr*. 760 (1952).
180. D. N. Schulz and H. F. Halasa, *J. Polym. Sci., Polym. Chem. Ed.* **15**, 2401 (1977).

181. A. Hirao, I. Hattori, T. Sasagawa, K. Yamaguchi, S. Nakahama, and N. Yamazaki, *Makromol. Chem., Rapid Commun.* **3**, 59 (1982).
182. R. Koenig and A. Banderet, *C. R. Hebd. Seances Acad. Sci. Ger.* **252**, 2552 (1961).
183. R. Koenig, G. Riess, and A. Banderet, *Eur. Polym. J.* **3**, 723 (1967).
184. D. H. Richards, D. M. Service, and M. J. Stewart, *Br. Polym. J.* **16**, 117 (1984).
185. M. J. Stewart, Ph. D. dissertation, University of Lancaster, Lancaster, 1986.
186. C. D. Eisenbach, H. Schnecko, and W. Kern, *Makromol. Chem.* **176**, 1587 (1975).
187. N. Hadjichristidis, S. Pispas, and M. Pitsikalis, *Prog. Polym. Sci.* **24**, 875 (1999).
188. T. Souel, F. Schue, M. J. M. Abadie, and D. H. Richards, *Polymer* **18**, 1292 (1977).
189. P. Cohen, M. J. M. Abadie, F. Schue, and D. H. Richards, *Polymer* **22**, 1316 (1981).
190. H. L. Hsieh and R. P. Quirk, *Anionic Polymerization: Principles and Practical Applications*, Marcel Dekker, New York, 1996.
191. A. O. Patil, D. N. Schulz, and B. M. Novak, eds., *Functional Polymers: Modern Synthetic Methods and Novel Structures* (ACS Symposium Series, Vol. 704), American Chemical Society, Washington, D.C., 1998.
192. A. Hirao and M. Hayashi, *Acta Polym.* **50**, 219 (1999).
193. R. P. Quirk, S. H. Jang, and J. Kim, *Rubber Chem. Technol.* **69**, 444 (1996).
194. A. Hirao, H. Nagahama, T. Ishizone, and S. Nakahama, *Macromolecules* **26**, 2145 (1993).
195. R. P. Quirk, T.-H. Cheong, K. Jiang, D. L. Gomochak, T. Yoo, K. T. Andes, and R. T. Mathers, *Macromol. Symp.* **195**, 69 (2003).
196. R. D. Athey Jr., *J. Coat. Technol.* **54**, 47 (1982).
197. R. D. Athey Jr., *Prog. Org. Coat.* **7**, 289 (1979).
198. M. Miyamoto, M. Sawamoto, and T. Higashimura, *Macromolecules* **17**, 265 (1984).
199. M. Miyamoto, M. Sawamoto, and T. Higashimura, *Macromolecules* **17**, 2228 (1984).
200. T. Higashimura and M. Sawamoto, *Makromol. Chem., Suppl.* **12**, 153 (1985).
201. M. Miyamoto, M. Sawamoto, and T. Higashimura, *Macromolecules* **18**, 123 (1985).
202. M. Sawamoto and T. Higashimura, *Makromol. Chem., Macromol. Symp.* **3**, 83 (1986).
203. T. Higashimura, S. Aoshima, and M. Sawamoto, *Makromol. Chem., Macromol. Symp.* **3**, 99 (1986).
204. S. Aoshima, E. Ebara, and T. Higashimura, *Polym. Bull.* **14**, 425 (1985).
205. S. Aoshima, O. Hasegawa, and T. Higashimura, *Polym. Bull.* **14**, 417 (1985).
206. V. Heroguez, A. Deffieux, and M. Fontanille, *Makromol. Chem., Macromol. Symp.* **32**, 199 (1990).
207. M. Sawamoto, T. Enoki, and T. Higashimura, *Macromolecules* **20**, 1 (1987).
208. O. Nuyken, H. Kröner, and S. Aechtner, *Polym. Bull.* **24**, 513 (1990).
209. M. Sawamoto, S. Aoshima, and T. Higashimura, *Makromol. Chem., Macromol. Symp.* **13/14**, 513 (1988).
210. H. Hasegawa and T. Higashimura, *Macromolecules* **13**, 1350 (1980).
211. S. Aoshima and T. Higashimura, *J. Polym. Sci., Polym. Chem. Ed.* **22**, 2443 (1984).
212. T. Higashimura, S. Aoshima, and H. Hasegawa, *Macromolecules* **15**, 1221 (1982).
213. T. Higashimura and M. Sawamoto, *Adv. Polym. Sci.* **62**, 49 (1984).
214. G. Ver Strate and F. P. Baldwin, *Polym. Prepr. (Am. Chem. Soc., Div. Polym. Chem.)* **17**, 808 (1976).
215. U.S. Pat. 4 278 822 (1981), G. Ver Strate and F. P. Baldwin (to Exxon Research and Engineering Co.).
216. J. P. Kennedy and R. A. Smith, *Polym. Prepr. (Am. Chem. Soc., Div. Polym. Chem.)* **20**, 316 (1979).
217. J. P. Kennedy and R. A. Smith, *J. Polym. Sci., Polym. Chem. Ed.* **18**, 1523 (1980).
218. O. Nuyken, S. D. Pask, A. Vischer, and M. Walter, *Makromol. Chem.* **186**, 173 (1985).
219. O. Nuyken, S. D. Pask, A. Vischer, and M. Walter, *Makromol. Chem., Macromol. Symp.* **3**, 129 (1986).

220. C. V. Freyer, H. P. Mühlbauer, and O. Nuyken, *Angew. Makromol. Chem.* **145/146**, 69 (1986).
221. O. Nuyken, S. D. Pask, and A. Vischer, *Makromol. Chem.* **184**, 553 (1983).
222. J. P. Kennedy and B. Ivan, *Designed Polymers by Carbocationic Macromolecular Engineering: Theory and Practice*, Hanser Publisher, Munich, 1991, p. 169.
223. R. Faust and J. P. Kennedy, *Polym. Bull.* **15**, 317 (1986).
224. R. Faust and J. P. Kennedy, *J. Polym. Sci., Part A: Polym. Chem.* **25**, 1847 (1987).
225. M. K. Mishra and J. P. Kennedy, *J. Macromol. Sci., A: Chem.* **24**, 933 (1987).
226. R. Faust, A. Nagy, and J. P. Kennedy, *J. Macromol. Sci., A: Chem.* **24**, 595 (1987).
227. B. Ivan, M. Zsuga, F. Gruber, and J. P. Kennedy, *Polym. Prepr. (Am. Chem. Soc. Div. Poly. Chem.)* **29**(2), 33 (1988).
228. B. Ivan and J. P. Kennedy, *Macromolecules* **23**, 2880 (1990).
229. G. Kaszas, J. Puskas, and J. P. Kennedy, *Polym. Bull.* **18**, 123 (1987).
230. G. Kaszas, J. Puskas, J. P. Kennedy, and C. C. Chen, *J. Macromol. Sci., A: Chem.* **26**, 1099 (1989).
231. B. Wang, M. K. Mishra, and J. P. Kennedy, *Polym. Bull.* **17**, 213 (1987).
232. B. Wang, M. K. Mishra, and J. P. Kennedy, *Polym. Bull.* **17**, 205 (1987).
233. M. Zsuga and J. P. Kennedy, *Polym. Bull.* **21**, 5 (1989).
234. M. Zsuga, J. P. Kennedy, and T. Kelen, *J. Macromol. Sci., A: Chem.* **26**, 1305 (1989).
235. M. Zsuga, R. Faust, and J. P. Kennedy, *Polym. Bull.* **21**, 273 (1989).
236. K. J. Huang, M. Zsuga, and J. P. Kennedy, *Polym. Bull.* **19**, 43 (1988).
237. M. K. Mishra, B. Wang, and J. P. Kennedy, *Polym. Bull.* **17**, 307 (1987).
238. J. P. Kennedy, V. S. C. Chang, R. A. Smith, and B. Ivan, *Polym. Bull.* **1**, 575 (1979).
239. M. K. Mishra, B. Sar-Mishra, and J. P. Kennedy, *Polym. Bull.* **13**, 435 (1985).
240. L. Wilczek and J. P. Kennedy, *J. Polym. Sci., Part A: Polym. Chem.* **25**, 3255 (1987).
241. B. Ivan and J. P. Kennedy, *Polym. Mater. Sci. Eng.* **58**, 869 (1988).
242. B. Ivan and J. P. Kennedy, *J. Polym. Sci., Part A: Polym. Chem.* **28**, 89 (1990).
243. J. P. Kennedy, K. L. Peng, and L. Wilczek, *Polym. Bull.* **19**, 441 (1988).
244. S. Nemes, K. L. Peng, L. Wilczek, and J. P. Kennedy, *Polym. Bull.* **24**, 187 (1990).
245. J. P. Kennedy and M. Hiza, *J. Polym. Sci., Polym. Chem. Ed.* **21**, 3573 (1983).
246. B. Keszler, V. S. C. Chang, and J. P. Kennedy, *J. Macromol. Sci., A: Chem.* **21**, 315 (1984).
247. J. P. Kennedy, S. C. Guhaniyogi, and V. Percec, *Polym. Bull.* **8**, 571 (1982).
248. J. P. Kennedy, V. S. C. Chang, and W. P. Francik, *J. Polym. Sci., Polym. Chem. Ed.* **20**, 2809 (1982).
249. J. P. Kennedy and R. F. Storey, *Org. Coat. Appl. Polym. Sci. Proc.* **46**, 182 (1981).
250. J. P. Kennedy, R. F. Storey, Y. Mohajer, and G. Wilkes, in *Proceedings of the 28th IUPAC, Macromolecules Symposium*, Amherst, Mass., 1982, p. 905.
251. T. R. Fang and J. P. Kennedy, *Polym. Bull.* **10**, 82 (1983).
252. R. H. Wondraczek and J. P. Kennedy, *Polym. Bull.* **4**, 445 (1981).
253. V. Percec and J. P. Kennedy, *Polym. Bull.* **10**, 31 (1983).
254. V. Percec, S. C. Guhaniyogi, and J. P. Kennedy, *Polym. Bull.* **9**, 27 (1983).
255. J. P. Kennedy and M. Hiza, *J. Polym. Sci., Polym. Chem. Ed.* **21**, 1033 (1983).
256. A. Nagy, R. Faust, and J. P. Kennedy, *Polym. Bull.* **13**, 97 (1985).
257. Y. Yamashita, *J. Appl. Polym. Sci., Suppl.* **36**, 193 (1981).
258. Z. Fodor, S. Hadjikyriacou, D. Li, and R. Faust, *Polym. Prepr. (Am. Chem. Soc., Div. Polym. Chem.)* **35**, 492 (1994).
259. Z. Fodor, S. Hadjikyriacou, D. Li, A. Takacs, and R. Faust, *Macromol. Symp.* **95**, 57 (1995).
260. S. E. Hadjikyriacou, Z. Fodor, and R. Faust, *J. Macromol. Sci., A: Pure Appl. Chem.* **32**, 1137 (1995).
261. S. E. Hadjikyriacou and R. Faust, *Polym. Mater. Sci. Eng.* **76**, 300 (1997).

262. Y. C. Bae, S. Hadjikyriacou, H. Schlaad, and R. Faust, in J. E. Puskas, ed., *Ionic Polymerization and Related Process* (NATO Science Series), Kluwer Academic Publishers, Dordrect, the Netherlands, 1998, p. 61.
263. B. Koroskenyi and R. Faust, *Am. Chem. Soc. Symp. Ser.* **704**, 135 (1998).
264. B. Koroskenyi and R. Faust, *Polym. Prepr. (Am. Chem. Soc., Div. Polym. Chem.)* **39**, 492 (1998).
265. S. Hadjikyriacou and R. Faust, *Polym. Prepr. (Am. Chem. Soc., Div. Polym. Chem.)* **39**, 398 (1998).
266. U.S. Pat. 5 981 785 (1999), R. Faust, S. E. Hadjikyriacou, and T. Suzuki (to University of Massachusetts, Dow Corning Corp.).
267. J. P. Kennedy, T. P. Liao, S. Guhaniyogi, and V. C. Chang, *J. Polym. Sci., Polym. Chem. Ed.* **20**, 3219 (1982).
268. R. Faust and J. P. Kennedy, *Polym. Bull.* **19**, 21 (1988).
269. R. Faust and J. P. Kennedy, *Polym. Bull.* **19**, 29 (1988).
270. R. Faust and J. P. Kennedy, *Polym. Bull.* **19**, 35 (1988).
271. M. Zsuga and J. P. Kennedy, *J. Polym. Sci., Part A: Polym. Chem.* **29**, 875 (1991).
272. M. Zsuga, B. Ivan, and J. P. Kennedy, *Polym. Bull.* **21**, 281 (1989).
273. H. Hibbert and S. Z. Perry, *Can. J. Res.* **8**, 102 (1933).
274. C. C. Price and D. D. Carmelite, *J. Am. Chem. Soc.* **88**, 4039 (1969).
275. K. S. Kazanskii, A. A. Solovyanov, and S. G. Entelis, *Eur. Polym. J.* **7**, 1421 (1971).
276. I. Cabasso and A. Zilkha, *J. Macromol. Sci., A: Chem.* **8**, 1313 (1974).
277. E. J. Goethals, *Adv. Polym. Sci.* **23**, 103 (1977).
278. F. E. Bailey and J. V. Koleske, *Alkylene Oxides and Their Polymers*, Marcel Dekker, New York, 1990.
279. K. Ito, *Prog. Polym. Sci.* **23**, 581 (1998).
280. K. Ito and S. Kawaguchi, *Adv. Polym. Sci.* **142**, 129 (1999).
281. Y. Yamamoto, W. Nakao, Y. Atago, K. Ito, and Y. Yagci, *Eur. Polym. J.* **39**, 545 (2003).
282. F. Yilmaz, I. Cianga, K. Ito, T. Senyo, and Y. Yagci, *Macromol. Rapid Commun.* **24**, 316 (2003).
283. K. Ito, J. Du, T. Senyo, Y. Murakami, and Y. Yagci, in *Proceedings of International Conference on Modified Polymers*, The High Tatras, Slovak Republic, 2003.
284. C. L. Jun, A. Le Borgne, and N. Spassky, *J. Polym. Sci., Polym. Symp.* **74**, 31 (1986).
285. V. Vincens, A. Le Borgne, and N. Spassky, in E. J. Vanderberg and J. Salomone, eds., *The Role of Catalysis in Polymer Synthesis* (ACS Symposium Series, Vol. 496), American Chemical Society, Washington, D.C., 1992, Chapt. 16.
286. A. Le Borgne, V. Vincens, M. Jouglard, and N. Spassky, *Makromol. Chem., Macromol. Symp.* **73**, 37 (1993).
287. K. Brzezinska, R. Szymanski, P. Kubisa, and S. Penczek, *Makromol. Chem., Rapid Commun.* **7**, 1, (1986).
288. S. Penczek, P. Kubisa, and R. Szymanski, *Makromol. Chem., Macromol. Symp.* **3**, 203 (1986).
289. M. Wojtania, P. Kubisa, and S. Penczek, *Makromol. Chem., Macromol. Symp.* **6**, 201 (1986).
290. Y. Okamoto, *Polym. Prepr. (Am. Chem. Soc., Div. Polym. Chem.)* **25**, 264 (1984).
291. S. Penczek, P. Kubisa, and K. Matyjaszewski, *Adv. Polym. Sci.* **68/69**, 1 (1985).
292. Y. Yagci, Y. Hepuzer, A. Önen, I. E. Serhath, P. Kubisa, and T. Biedron, *Polym. Bull.* **33**, 411 (1994).
293. Y. Yagci, I. E. Serhatli, P. Kubisa, and T. Biedron, *Macromolecules* **26**, 2397 (1993).
294. E. J. Goethals and S. Penczek, in G. Allen and J. C. Bevington, eds., *Comprehensive Polymer Science*, Vol. 3, Pergamon Press, Oxford, 1989, Chapt. 45.
295. Y. Yamashita and K. Chiba, *Polym. J.* **4**, 200 (1973).
296. E. Franta, L. Reibel, J. Lehmann, and S. Penczek, *J. Polym. Sci., Polym. Symp.* **56**, 139 (1976).

297. X. Meng, H. Zhang, and X. Feng, *Gaodeng Xuexiao Huaxue Xuebao* **6**, 660 (1985).
298. S. Smith and A. J. Hubin, *J. Macromol. Sci., A: Chem.* **7**, 1399 (1973).
299. S. Smith, W. J. Schultz, and R. A. Newmark, *Am. Chem. Soc. Symp. Ser.* **59**, 13 (1977).
300. U.S. Pat. 3 824 198 (1974), S. Smith and A. J. Hubin (to Minnesota Mining and Manufacturing Co.).
301. A. Onen, Y. Yagci, and W. Schnabel, *Angew. Makromol. Chem.* **243**, 143 (1996).
302. G. Hizal, Y. Yagci, and W. Schnabel, *Polymer* **35**, 4443 (1994).
303. N. Kizilyar, L. Toppare, A. Onen, and Y. Yagci, *J. Appl. Polym. Sci.* **71**, 713 (1999).
304. I. E. Serhath, Y. Yagci, I. Tomida, M. Suzuki, and T. Endo, *J. Macromol. Sci., A: Pure Appl. Chem.* **34**, 2 (1997).
305. G. Hizal, A. Sarman, and Y. Yagci, *Polym. Bull.* **35**, 567 (1995).
306. F. D'Haese and E. J. Goethals, *Brit. Polym. J.* **20**, 103 (1988).
307. Y. Tezuka and E. J. Goethals, *Eur. Polym. J.* **18**, 991 (1982).
308. J. Sierra-Vargas, J. G. Zilliox, E. Franta, and P. Rempp, *Polym. Bull.* **3**, 83 (1980).
309. P. Dreyfuss and J. P. Kennedy, *J. Polym. Sci., Polym. Lett.* **14**, 139 (1976).
310. M. F. Dubreuil, N. G. Farcy, and E. J. Goethals, *Macromol. Rapid Commun.* **20**, 383 (1999).
311. M. F. Dubreuil and E. J. Goethals, *Macromol. Chem. Phys.* **198**, 3077 (1997).
312. H. Oike, S. Kobayashi, Y. Tezuke, and E. J. Goethals, *Macromolecules* **33**, 8898 (2000).
313. H. Oike, M. Washizuka, and Y. Tezuka, *Macromol. Rapid Commun.* **22**, 1128 (2001).
314. H. Oike, S. Kobayashi, T. Mouri, and Y. Tezuka, *Macromolecules* **34**, 2742 (2001).
315. R. C. Schulz, W. Hellermann, and J. Nienburg, in H. J. Ivin and T. Saegusa, eds., *Ring-opening Polymerization*, Elsevier Applied Science Publishers, Ltd., Barking, U.K., 1984, p. 369.
316. V. Jaacks, H. Baader, and W. Kern, *Makromol. Chem.* **83**, 56 (1965).
317. W. Chwiatkowska, P. Kubisa, and S. Penczek, *Makromol. Chem.* **183**, 753 (1982).
318. S. R. Wabraedt and E. J. Goethals, *Polym. Int.* **38**, 89 (1995).
319. P. Kubisa and S. Penczek, *Macromolecules* **10**, 1216 (1977).
320. E. J. Goethals, in Ref. 9, pp. 115–139.
321. N. Spassky, M. Sepulchre, and P. Sigwalt, in H. R. Kricheldorf, ed., *Handbook of Polymer Synthesis, Part B*, Marcel Dekker, New York, 1992, pp. 991–1011.
322. S. Boileau, G. Champetier, and P. Sigwalt, *Makromol. Chem.* **69**, 180 (1963).
323. O. Nuyken and S. Pask, in H. F. Mark, N. M. Bikales, C. G. Overberger, G. Menges, and J. I. Kroschwitz, eds., *Encyclopedia of Polymer Science and Engineering*, Vol. 16, John Wiley & Sons, Inc., New York, 1989, p. 494.
324. W. Cooper, D. R. Morgan, and R. T. Wragg, *Eur. Polym. J.* **5**, 71 (1969).
325. W. Cooper, *Br. Polym. J.* **3**, 28 (1971).
326. E. J. Goethals, in K. J. Ivin and T. Saegusa, (eds), *Ring-Opening Polymerization*, Elsevier, Amsterdam, 1984, p. 715.
327. A. Munir and E. J. Goethals, *J. Polym. Sci., Polym. Chem. Ed.* **19**, 1985 (1981).
328. M. Van de Velde and E. J. Goethals, *Makromol. Chem., Macromol. Symp.* **6**, 271 (1986).
329. D. B. Johns, R. W. Lenz, and A. Luecke, *Makromol. Chem., Macromol. Symp.* **3**, 461 (1986).
330. V. Jaacks and N. Mathes, *Makromol. Chem.* **131**, 295 (1970).
331. Br. Pat. 1 133 293 (1968), W. Bergwerf, W. M. Wagner, and A. Klootwijk.
332. U.S. Pat. 3 418 393 (1968), C. King.
333. R. W. Lenz, M. Dvor and R. Jorgensen, *Polym. Eng. Sci.* **18**, 937 (1978).
334. D. R. Wilson and R. G. Beaman, *J. Polym. Sci., Polym. Chem. Ed.* **8**, 2161 (1970).
335. K. lto, Y. Hashizuka, and Y. Yamashita, *Macromolecules* **10**, 821 (1977).
336. Y. Yamashita, *Polym. Prepr. (Am. Chem. Soc., Div. Polym. Chem.)* **21**, 51 (1980).
337. A. Hamitou, T. Ouhadi, R. Jerome, and P. Teyssie, *J. Polym. Sci., Polym. Chem. Ed.* **15**, 865 (1977).

338. Ph. Dubois, R. Jerome, and Ph. Teyssie, *Polym. Bull.* **22**, 475 (1989).
339. Ph. Dubois, R. Jerome, and Ph. Teyssie, *Makromol. Chem., Macromol. Symp.* **42/43**, 103 (1991).
340. A. Duda, Z. Florjanczyk, A. Hofman, S. Slomkowski, and S. Penczek, *Macromolecules* **23**, 1640 (1990).
341. Ph. Dubois, R. Jerome, and Ph. Teyssie, *Macromolecules* **24**, 977 (1991).
342. Ph. Dubois, Ph. Degee, R. Jerome, and Ph. Teyssie, *Macromolecules* **25**, 2614 (1992).
343. Ph. Degee, Ph. Dubois, R. Jerome, and Ph. Teyssie, *Macromolecules* **25**, 4242 (1992).
344. M. Trollsas, J. L. Hedrick, Ph. Dubois, and R. Jerome, *J. Polym. Sci., Part A: Polym. Chem.* **36**, 1345 (1998).
345. I. Barakat, Ph. Dubois, R. Jerome, and Ph. Teyssie, *Macromolecules* **24**, 6542 (1991).
346. R. F. Storey, J. S. Wiggins, and A. D. Puckett, *J. Polym. Sci., Part A: Polym. Chem.* **32**, 2345, (1994).
347. R. F. Storey, S. C. Warren, C. J. Allison, J. S. Wiggins, and A. D. Puckett, *Polymer* **34**, 4365, (1993).
348. R. F. Storey and T. P. Hickey, *Polymer* **35**, 830, (1994).
349. J. S. Riffle, W. P. Steckle Jr., K. A. White, and R. S. Ward, *Polym. Prepr. (Am. Chem. Soc., Div. Polym. Chem.)* **26**, 251 (1985).
350. Z. Guo, D. Wan, and Z. Huang, *Macromol. Rapid Commun.* **22**, 367 (2001).
351. C. Kim, S. C. Lee, I. C. Kwon, H. Chung, and S. Y. Jeong, *Macromolecules* **35**, 193 (2002).
352. Y. K. Choi, Y. H. Bae, and S. W. Kim, *Macromolecules* **31**, 8766 (1998).
353. C. A. P. Joziasse, H. Grablowitz, and A. J. Pennings, *Macromol. Chem. Phys.* **201**, 107 (2000).
354. Ph. Dobis, I. Barakat, R. Jerome, and Ph. Teyssie, *Macromolecules* **26**, 4407 (1993).
355. M. Degirmenci, G. Hizal, and Y. Yagci, *Macromolecules* **35**, 8265 (2002).
356. H. Uyama, H. Kikuchi, and S. Kobayashi, *Chem. Lett*. 1047 (1995).
357. H. Uyama, H. Kikuchi, and S. Kobayashi, *Bull. Chem. Soc. Jpn.* **70**, 1691 (1997).
358. A. Cordova, T. Iversen, K. Hult, and M. Martinelle, *Polymer* **39**, 6519 (1998).
359. A. Cordova, T. Iversen, and K. Hult, *Polymer* **40**, 6709 (1999).
360. M. Trollsas, C. J. Hawker, J. L. Hedrick, G. Carrot, and J. Hillborn, *Macromolecules* **31**, 5960 (1998).
361. E. B. Ludvig and B. G. Belenkaya, *J. Macromol. Sci. A: Chem.* **8**, 819 (1974).
362. P. V. Wright, *Makromol. Chem.* **183**, 1055 (1982).
363. S. W. Kantor, W. T. Grubb, and R. C. Osthoff, *J. Am. Chem. Soc.* **76**, 5190 (1954).
364. M. S. Beevers and J. A. Semlyen, *Polymer* **12**, 373 (1971).
365. P. M. Sormani, R. J. Minton, and J. E. McGrath, in J. E. McGrath, ed., *Ring-opening Polym-erization* (ACS Symposium Series, Vol. 286), American Chemical Society, Washington, D.C., 1985, p. 147.
366. I. Yilgor, J. S. Riffle, and J. E. McGrath, in F. W. Harris and H. J. Spinelli, eds., *Reactive Oligomers* (ACS Symposium Series, Vol. 282), American Chemical Society, Washington, D.C., 1985, p. 161.
367. I. Yilgor and J. E. MacGrath, *Adv. Polym. Sci.* **86**, 1 (1988).
368. *Silicon Compounds, Register Rev*., Petrarch Systems Inc., Bristol, Pa., 1982.
369. V. Harabagiu, M. Pintala, C. Cotzur, and B. C. Simionescu, in J. C. Salamone, ed., *The Polymeric Materials Encylopedia: Synthesis, Properties and Applications*, Vol. 4, CRC Press, Boca Raton, Fla., 1996, p. 2661.
370. G. G. Cameron and M. S. Chisholm, *Polymer* **26**, 437 (1985).
371. C. I. Simionescu, V. Harabagiu, E. Comianita, V. Hamciuc, D. Giurgiu, and B. C. Simionescu, *Eur. Polym. J.* **26**, 565 (1990).
372. V. Harabagiu, M. Pintala, C. Cotzur, B. C. Simionescu, and C. I. Simionescu, *Polym. J.* **1**, 256 (1994).

373. Y. Yagci, A. Onen, V. Harabagiu, M. Pintela, C. Cotzur, and B. C. Simionescu, *Turk. Chem. J.* **18**, 101 (1994).
374. M. Pintela, V. Harabagiu, C. Cotzur, and B. C. Simionescu, *Polym. Bull.* **32**, 173 (1994).
375. E. Kalaycioglu, L. Toppare, Y. Yagci, V. Harabagiu, M. Pintela, R. Ardelean, and B. C. Simionescu, *Synt. Met.* **97**, 7 (1998).
376. S. Kobayashi, *Prog. Polym. Sci.* **15**, 751 (1990).
377. S. Kobayashi, E. Masuda, S. Shoda, and Y. Shimano, *Macromolecules* **22**, 2878 (1989).
378. S. Kobayashi, H. Uyama, Y. Narita, and J. Ishiyama, *Macromolecules* **25**, 3232 (1992).
379. S. Kobayashi, M. Kaku, S. Sawada, and T. Saegusa, *Polym. Bull.* **13**, 447 (1985).
380. R. C. Schulz and E. Schwarzenbach, *Makromol. Chem., Macromol. Symp.* **13/14**, 495 (1988).
381. S. Kobayashi, C. Mertesdorf, T. Tanabe, and K. Matsua, *Polym. Prepr. Jpn.* **35**, 248 (1986).
382. O. Nuyken, P. Persigehl, and R. Weberskirch, *Macromol. Symp.* **177**, 163 (2002).
383. A. Cirpan, S. Alkan, L. Toppare, G. David, and Y. Yagci, *Eur. Polym. J.* **37**, 2225 (2001).
384. M. Miyamoto, K. Hayshizaki, M. Tokumizu, and T. Saegusa, *Macromolecules* **23**, 4718 (1990).
385. I.-H. Park, I.-S. Han, D.-K. Kim, and T. Saegusa, *Angew. Makromol. Chem.* **190**, 165 (1991).
386. S. Kobayashi, H. Uyama, and N. Higuchi, *Macromolecules* **23**, 54 (1990).
387. Y. Shimano, K. Sato, and S. Kobayashi, *J. Polym. Sci., Part A: Polym. Chem.* **33**, 2715 (1995).
388. G. David, V. Alupei, and B. C. Simionescu, *Eur. Polym. J.* **37**, 1353 (2001).
389. J. C. Rueda, H. Komber, J. C. Cedron, B. Voit, and G. Shevtsova, *Macromol. Chem. Phys.* **204**, 947 (2003).
390. D. S. Breslow, *Prog. Polym. Sci.* **18**, 1141 (1993).
391. J. E. Schwendeman, A. C. Church, and K. B. Wagener, *Adv. Synth. Catal.* **344**, 597 (2002).
392. J. C. Marmo and K. B. Wagener, *Macromolecules* **26**, 2137 (1993).
393. J. C. Marmo and K. B. Wagener, *Macromolecules* **28**, 2602 (1995).
394. K. R. Brzezinski and T. J. Deming, *Macromolecules* **34**, 4348 (2001).
395. J. Schwendeman, K. B. Wagener, R. Sparer, and M. E. Benz, *Polym. Prepr. (Am. Chem. Soc., Div. Polym. Chem.)* **43**, 280 (2002).
396. T. Morita, B. R. Maughan, C. W. Bielawski, and R. H. Grubbs, *Macromolecules* **33**, 6621 (2000).
397. C. Bolm, C. L. Dinter, I. Schiffers, and L. Defrere, *Synlett* **12**, 1875 (2001).
398. C. W. Bielawski, T. Morita, and R. H. Grubbs, *Macromolecules* **33**, 678 (2000).
399. M. A. Hillmyer, S. T. Nguyen, and R. H. Grubbs, *Macromolecules* **30**, 718 (1997)
400. C. Fraser, M. A. Hillmyer, E. Gutierrez, and R. H. Grubbs, *Macromolecules* **28**, 7256 (1995).
401. C. W. Bielawski, O. A. Scherman, and R. H. Grubbs, *Polymer* **42**, 4939 (2001).
402. B. R. Maughon, T. Morita, C. W. Bielawski, and R. H. Grubbs, *Macromolecules* **33**, 1929 (2000).
403. C. W. Bielawski and R. H. Grubbs, *Angew. Chem.* **112**, 3025 (2000).
404. C. W. Bielawski and R. H. Grubbs, *Angew. Chem., Int. Ed.* **39**, 2903 (2000).
405. C. W. Bielawski, D. Benitez, T. Morita, and R. H. Grubbs, *Macromolecules* **34**, 8610 (2001).
406. V. C. Gibson and T. Okada, *Macromolecules* **33**, 655 (2000).
407. S. C. G. Biagini, R. G. Davies, V. C. Gibson, M. R. Giles, E. L. Marshall, and M. North, *Polymer* **42**, 6669 (2001).
408. W. J. Feast, V. C. Gibson, E. Khosravi, E. L. Marshall, and J. P. Mitchell, *Polymer* **33**, 872 (1992).

409. W. Stüer, J. Wolf, H. Werner, P. Schwab, and M. Schulz, *Angew. Chem.* **110**, 3603 (1998).
410. W. Stüer, J. Wolf, H. Werner, P. Schwab, and M. Schulz, *Angew. Chem., Int. Ed.* **37**, 3421 (1998).
411. H. Katayama, H. Urushima, and F. J. Ozawa, *Organomet. Chem.* **606**, 16 (2000).
412. K. Nomura, S. Takahashi, and Y. Imanishi, *Polymer* **41**, 4345 (2000)
413. K. Nomura, S. Takahashi, and Y. Imanishi, *Macromolecules* **34**, 4712 (2001).
414. S. Coca, H.-J. Paik, and K. Matyjaszewski, *Macromolecules* **30**, 6513 (1997).
415. H. Katayama, F. Yonezawa, M. Nagao, and F. Ozawa, *Macromolecules* **35**, 1133 (2002).
416. A. Michel, G. Schmidt, E. Castaneda, and A. Guyot, *Angew. Makromol. Chem.* **47**, 61 (1975).
417. Y. Landler and P. Lebel, *J. Polym. Sci.* **48**, 477 (1960).
418. A. Michel, E. Castaneda, and A. Guyot, *J. Macromol. Sci. A* **12**, 227 (1978).
419. V. N. Odinokov, V. K. Ignatyuk, G. A. Tolstikov, Y. B. Monakov, A. A. Berg, A. M. Shakirova, S. R. Rafikov, and A. A. Berlin, *Bull. Acad. Sci. USSR, Div. Chem. Sci.* **25**, 1475 (1976).
420. F. P. Baldwin, G. W. Burton, K. Griesbaum, and G. Hanington, *Adv. Chem. Ser.* **91**, 448 (1969).
421. E. B. Jones and C. S. Marvel, *J. Polym. Sci.* **2**, 5313 (1964).
422. W. H. Stubbs, C. R. Gore, and C. S. Marvel, *J. Polym. Sci., Polym. Chem. Ed.* **4**, 447 (1966).
423. H. M. White and P. S. Bailey, *J. Org. Chem.* **30**, 3037 (1965).
424. P. J. Beynon, P. M. Collins, P. T. Doganges, and W. G. Overend, *J. Chem. Soc. C* **12**, 1131 (1966).
425. J. S. Orozco and H. J. Cantow, *Polym. Bull.* **12**, 203 (1984).
426. S. Wolfe, S. K. Hasan, and J. R. Campbell, *J. Chem. Soc. D: Chem. Commun*. 1420 (1970).
427. C. Guizard and H. Cheradame, *Eur. Polym. J.* **15**, 689 (1979).
428. K. B. Sharpless and D. R. Williams, *Tetrahedron Lett.* **35**, 3045 (1975).
429. C. Guizard and H. Cheradame, *Eur. Polym. J.* **17**, 121 (1981).
430. H. Cheradame, A. Gandini, H. Razzouk, and K. Bouiridah, in E. J. Goethals, ed., *Cationic Polymerization and Related Processes*, Academic Press, London, 1983, p. 355.
431. Y. Camberlin, J. P. Pascault, H. Razzouk, and H. Cheradame, *Makromol. Chem., Rapid Commun.* **2**, 323 (1981).
432. W. Heitz, C. Oppenheimer, P. S. Anand, and X. Y. Qiu, *Macromol. Chem. Phys., Suppl.* **6**, 47 (1984).
433. O. Nuyken and R. Weidner, *Adv. Polym. Sci.* **73/74**, 145 (1986).
434. E. J. Goethals, Encyclopedia of Polymer Science and Technology, Vol. 13, John Wiley & Sons, Inc., New York, 1970, p. 448.
435. U.S. Pat. 2 466 963 (1949), J. C. Patrick and H. R. Ferguson (to Thiokol Corp.).
436. Fr. Pat. 1 434 167 (1966), A. H. Weinstein, A. J. Constanza, R. J. Coleman, and G. E. Meyer (to Goodyear Tire & Rubber Co.).
437. R. A. Rhein and J. D. Ingham, *Polymer* **16**, 799 (1975).
438. J. Rehner, *Ind. Eng. Chem.* **36**, 46 (1944).
439. J. Rehner, *Ind. Eng. Chem.* **36**, 118 (1944).
440. C. S. Marvel and R. E. Light, *J. Am. Chem. Soc.* **72**, 3887 (1950).
441. D. Barnard, *J. Polym. Sci.* **22**, 213 (1956).
442. J. Rehner and P. Gray, *Ind. Eng. Chem., Anal. Ed.* **17**, 367 (1945).
443. S. G. Gallo, H. K. Wiese, and J. F. Nelson, *J. Ind. Eng. Chem.* **40**, 1277 (1948).
444. T. S. Lee, I. M. Kolthoff, and E. Johnson, *Anal. Chem.* **22**, 995 (1950).
445. C. Guizard and H. Cheradame, *Eur. Polym. J.* **15**, 689 (1979).
446. J. R. Ebdon, N. J. Flint, and P. Hodge, *Eur. Polym. J.* **25**, 759 (1989).

447. L. R. Dix, J. R. Ebdon, and P. Hodge, *Polymer* **34**, 406 (1993).
448. L. R. Dix, J. R. Ebdon, N. J. Flint, and P. Hodge, *Eur. Polym. J.* **27**, 581 (1991).
449. J. R. Ebdon and N. J. Flint, *Macromolecules* **27**, 6704 (1994).
450. J. R. Ebdon, N. J. Flint, and S. Rimmer, *Macromol. Rep. A* **32**, 603 (1995).
451. J. R. Ebdon and S. Rimmer, *J. Polym. Sci., Part A: Polym. Chem.* **35**, 3255 (1997).
452. S. Rimmer and J. R. Ebdon, *J. Polym. Sci., Part A: Polym. Chem.* **34**, 3573 (1996).
453. C. Djerassi and R. R. Engle, *J. Am. Chem. Soc.* **75**, 3838 (1953).
454. L. M. Berkowitz and P. N. Rylander, *J. Am. Chem. Soc.* **80**, 6682 (1958).
455. A. Keller and S. Sawada, *Makromol. Chem.* **74**, 190 (1964).
456. D. J. Blundell and A. Keller, *J. Polym. Sci., Polym. Phys. Ed.* **5**, 991 (1967).
457. A. Keller and Y. Udagawa, *J. Polym. Sci., Polym. Phys. Ed.* **8**, 19 (1970).
458. A. Keller and Y. Udagawa, *J. Polym. Sci., Polym. Phys. Ed.* **9**, 1793 (1971).
459. D. G. H. Ballard and J. V. Dawkins, *Eur. Polym. J.* **9**, 211 (1973).
460. L. R. Melby, *Macromolecules* **11**, 50 (1978).
461. J. P. Kennedy and R. R. Phillips, *J. Macromol. Sci., A: Chem.* **4**, 1759 (1970).
462. D. T. Turner, *J. Polym. Sci., Part A: Gen. Pap.* **2**, 1699 (1964).
463. C. Oppenheimer and W. Heitz, *Angew. Makromol. Chem.* **98**, 167 (1981).
464. S. G. Bond and J. R. Ebdon, *Polymer* **35**, 451 (1994).
465. S. G. Bond and J. R. Ebdon, *Polymer* **35**, 4079 (1994).
466. H. G. Elias, *Makromoleküle*, Hüthig und Wepf Verlag, Heidelberg, 1971, p. 574.
467. A. A. Berlin and N. G. Matveeva, *J. Polym. Sci., Part D: Macromol. Rev.* **12**, 1 (1977).
468. V. V. Korshak and S. V. Vinogradova, *Equilibrium Polycondensation*, Nauka, Moscow, 1962.
469. V. V. Korshak and S. V. Vinogradova, *Nonequilibrium Polycondensation*, Nauka, Moscow, 1972.
470. G. S. Petrov and A. N. Levin, *Thermoreactive Resins and Plastmasses*, Goskhimizdat, Moscow, 1959.
471. E. Marechal, in Ref. 9, pp. 5–32.
472. C. A. May and Y. Tanaka, eds., *Epoxy Resins—Chemistry and Technology*, Marcel Dekker, New York, 1973.
473. O. Nuyken, G. Reuschel, and F. Siebzehnrübl, *Makromol. Chem., Macromol. Symp.* **26**, 313 (1989).
474. O. Nuyken and F. Siebzehnrübl, *Makromol. Chem.* **189**, 541 (1988).
475. O. Nuyken and F. Siebzehnrübl, *Phosphorus Sulfur* **35**, 47 (1988).
476. F. W. Harris, A. Pamidimukkala, R. Gupta, S. Das, T. Wu, and G. Mock, *J. Macromol. Sci., A: Chem.* **21**, 1117 (1984).
477. J. K. Stille, *Pure Appl. Chem.* **50**, 273 (1978).
478. J. Garapon and J. K. Stille, *Macromolecules* **10**, 627 (1977).
479. J. P. Droske, U. M. Gaik, and J. K. Stille, *Macromolecules* **17**, 10 (1984).
480. J. P. Droske, J. K. Stille, and W. B. Alston, *Macromolecules* **17**, 15 (1984).
481. J. K. Stille and J. P. Droske, *J. Macromol. Sci., A: Chem.* **21**, 913 (1984).
482. A. Pourdjavadi, P. J. Madec, and A. Pourdjavadi, E. Maréchal, *Eur. Polym. J.* **20**, 305 (1984).
483. D. Gagnebien, P. J. Madec, and E. Maréchal, *Eur. Polym. J.* **21**, 273 (1985).
484. V. Percec and B. C. Auman, *Makromol. Chem.* **185**, 617 (1984).
485. P. Honore, G. Deleens, and E. Maréchal, *Eur. Polym. J.* **16**, 909 (1980).
486. E. Shchori and J. E. McGrath, *Polym. Prepr. (Am. Chem. Soc., Div. Polym. Chem.)* **20**, 634 (1979).
487. V. Percec, H. Nava, and J. M. Rodriguez-Parada, *J. Polym. Sci., Polym. Lett.* **22**, 523 (1984).
488. S. African Pat., 72,00,820 (1972), R. Milkovich and M. T. Chiang (to CPC International Inc.).

489. R. Barbucci, P. Ferruti, E. Franta, S. Ivatsuki, and P. F. Rempp, *Adv. Polym. Sci.* **58**, 1 (1984).
490. G. O. Schultz and R. Milkovich, *J. Appl. Polym. Sci.* **27**, 4773 (1982).
491. Y. Yamashita, *J. Appl. Polym., Appl. Polym. Symp.* **36**, 193 (1981).
492. P. Rempp, P. Lutz, P. Masson, and E. Franta, *Makromol. Chem., Suppl.* **8**, 3 (1984).
493. R. Asami, and M. Takaki, *Makromol. Chem. Suppl.* **12**, 163 (1985).
494. Y. Chujo and Y. Yamashita, in Ref. 9, pp. 163–180.
495. R. Milkovich, *Polym. Prepr. (Am. Chem. Soc., Div. Polym. Chem.)* **21**, 40 (1980).
496. G. O. Schulz and R. Milkovich, *J. Polym. Sci., Polym. Chem. Ed.* **22**, 1633 (1984).
497. R. S. Velichkova and D. C. Christova, *Prog. Polym. Sci.* **20**, 819 (1995).
498. Y. Yagci and L. Toppare, *Polym. Int.* **52**, 1573 (2003).
499. Y. Yamashita, ed., *Chemistry and Industry of Macromonomers*, Hüthig & Wepf Verlag, Heidelberg, 1993.
500. R. Waack and M. A. Doran, *Polymer* **2**, 365 (1961).
501. R. Waack and M. A. Doran, *J. Org. Chem.* **32**, 3395 (1967).
502. P. Chaumont, G. Beinert, J. Herz, and P. Rempp, *Eur. Polym. J.* **15**, 459 (1979).
503. R. Asami, M. Takaki, and H. Hanahata, *Macromolecules* **16**, 628 (1983).
504. G. Greber and A. Balciunas, *Makromol. Chem.* **79**, 149 (1964).
505. P. Masson, E. Franta, and P. Rempp, *Makromol. Chem., Rapid Commun.* **3**, 499 (1982).
506. P. Lutz, P. Masson, G. Beinert, and P. Rempp, *Polym. Bull.* **12**, 79 (1984).
507. P. Masson, G. Beinert, E. Franta, and P. Rempp, *Polym. Bull.* **7**, 17 (1982).
508. P. Sigwalt, *Angew. Makromol. Chem.* **94**, 161 (1981).
509. S. Kobayashi, M. Kaku, T. Mizutani, and T. Saegusa, *Polym. Bull.* **9**, 169 (1983).
510. T. Hamaide, A. Revillon, and A. Guyot, *Eur. Polym. J.* **20**, 855 (1984).
511. P. R. Rao, P. Masson, P. Lutz, G. Beinert, and P. Rempp, *Polym. Bull.* **11**, 115 (1984).
512. F. Severini, M. Pegoraro, and L. Saija, *Angew. Makromol. Chem.* **133**, 111 (1985).
513. P. R. Rao, P. Lutz, J. P. Lamps, P. Masson, and P. Rempp, *Polym. Bull.* **15**, 69 (1986).
514. Y. Kawakami, Y. Miki, T. Tsuda, R. A. N. Murthy, and Y. Yamashita, *Polym. J.* **14**, 913 (1982).
515. Y. Tezuka, A. Fukushima, and K. Imai, *Makromol. Chem.* **186**, 685 (1985).
516. G. G. Cameron and M. S. Chisholm, *Polymer* **26**, 437 (1985).
517. O. W. Webster, W. R. Hertler, D. Y. Sogah, W. B. Farnham, and T. V. Rajanbabu, *J. Am. Chem. Soc.* **105**, 5706 (1983).
518. D. Y. Sogah and O. W. Webster, *J. Polym. Sci., Polym. Lett. Ed.* **21**, 927 (1983).
519. T. H. Maugh, *Science* **222**, 259 (1983).
520. W. R. Hertler, D. Y. Sogah, O. W. Webster, and B. M. Trost, *Macromolecules* **17**, 1415 (1984).
521. O. W. Webster, W. R. Hertler, D. Y. Sogah, W. B. Farnham, and T. V. Rajanbabu, *J. Macromol. Sci., A: Chem.* **21**, 943 (1984).
522. F. Bandermann and H. D. Speikamp, *Makromol. Chem., Rapid Commun.* **6**, 335 (1985).
523. L. J. Mathias, J. B. Canterberry, and M. South, *J. Polym. Sci., Polym. Lett. Ed.* **20**, 473 (1982).
524. J. Sierra-Vargas, J. G. Zilliox, P. F. Rempp, and E. Franta, *Polym. Bull.* **3**, 83 (1980).
525. F. J. Burgess, A. V. Cunliffe, D. H. Richards, and D. Thompson, *Polymer* **19**, 334 (1978).
526. R. Asami, M. Takaki, K. Kyuda, and E. Asakura, *Polym. J.* **15**, 139 (1983).
527. R. Asami, M. Takaki, K. Kita, and E. Asakura, *Polym. Bull.* **2**, 713 (1980).
528. J. Sierra-Vargas, P. Masson, G. Beinert, P. F. Rempp, and E. Franta, *Polym. Bull.* **7**, 277 (1982).
529. M. J. M. Abadie, F. Schue, T. Souel, D. B. Hartley, and D. H. Richards, *Polymer* **23**, 445 (1982).

530. Y. Tanizaki, K. Minagawa, S. Takase, and K. Watanabe in *Proceedings of the ACS / CSJ Chemical Congress INDE*, 1979, p. 136.
531. E. J. Goethals and M. A. Vlegels, *Polym. Bull.* **4**, 521 (1981).
532. T. P. Liao and J. P. Kennedy, *Polym. Bull.* **5**, 11 (1981).
533. M. F. Farona and J. P. Kennedy, *Polym. Bull.* **11**, 359 (1984).
534. M. Miyamoto, M. Sawamoto, and T. Higashimura, *Macromolecules* **18**, 123 (1985).
535. S. Aoshima, O. Hasegawa, and T. Higashimura, *Polym. Prepr. Jpn.* **34**, 170 (1985).
536. E. J. Goethals, W. Reyntjens, and S. Lievens, *Macromol. Symp.* **132**, 57 (1998).
537. K. lto, N. Usami, and Y. Yamashita, *Macromolecules* **13**, 216 (1980).
538. Y. Yamashita, Y. Tsukahara, K. lto, K. Okada, and Y. Tajima, *Polym. Bull.* **5**, 335 (1981).
539. Y. Chujo, T. Shishino, Y. Tsukahara, and Y. Yamashita, *Polym. J.* **17**, 133 (1985).
540. Y. Yamashita, K. Ito, H. Mizuno, and K. Okada, *Polym. J.* **14**, 255 (1982).
541. M. Akashi, I. Kirikihira, and N. Miyauchi, *Angew. Makromol. Chem.* **132**, 81 (1985).
542. Y. Nitadori and T. Tsuruta, *Makromol. Chem.* **180**, 1877 (1979).
543. T. Nishimura, M. Maeda, Y. Nitadori, and T. Tsuruta, *Makromol. Chem.* **183**, 29 (1982).
544. M. Kimura, T. Egashira, T. Nishimura, M. Maeda, and S. Inoue, *Makromol. Chem.* **183**, 1393 (1982).
545. K. Hashimoto, H. Sumitomo, and M. Kawasumi, *Polym. Bull.* **11**, 121 (1984).
546. K. Hashimoto, H. Sumitomo, and M. Kawasumi, *Polym. J.* **17**, 1045 (1985).
547. V. Percec, P. L. Rinaldi, and B. C. Auman, *Polym. Bull.* **10**, 215 (1983).
548. Y. Chujo, T. Shishino, and Y. Yamashita, *Polym. J.* **16**, 495 (1984).

YUSUF YAGCI
Istanbul Technical University
OSKAR NUYKEN
VERA-MARIA GRAUBNER
Technische Universität München

TEMPLATE POLYMERIZATION

Introduction

The term "replica" polymerization for polymerization of simple vinyl monomers was first used by M. Szwarc (1) in 1954, and then displaced by "matrix" or "template" polymerization (2). Since this time, many articles and reviews have been published (3–11). The concept of template polymerization originates from natural processes such as DNA replication and the biosynthesis of proteins. As we know, the growth of living organisms is associated with very complicated processes of polymerization. Low molecular weight substrates—such as sugars, amino acids, fats, water in animals, and carbon dioxide in plants—are precursors of polymers (polypeptides, polynucleic acids, polysaccharides, etc.) (see POLYPEPTIDE SYNTHESIS; POLYNUCLEOTIDES; POLYSACCHARIDES). They are organized in tissues and are thus reproducible. In many biological reactions, such as DNA replication

Encyclopedia of Polymer Science and Technology. Copyright John Wiley & Sons, Inc. All rights reserved.

or polypeptide creation, not only are low molecular weight substrates and polymeric products present in the reaction medium, but also macromolecular compounds called matrices or templates which control the process. In spite of the fact that only nonbiological systems are discussed here, the biological processes constitute an inimitable model for template polymerization of synthetic monomers. In both cases, the process (synthetic or natural) is connected with the ability of two polymers (template- and polymer-produced—often named the daughter polymer) to form more or less stable interpolymer complexes.

Template polymerization is a particular case of a more general group of processes, such as polymerization in an organized system.

Many factors may affect the organization of monomer units during polymerization. For example, solid-state polymerization takes place when molecules of the monomer are surrounded by molecules already organized in a crystal lattice. A specific type of polymerization occurs on the surface of solids. Numerous monomers with long hydrocarbon chains can form monolayers at the gas–water interface, and are also oriented at the surface of the water. The polymerization of such organized systems leads to the preparation of polymers with peculiar morphology and properties. It is the method for polymer synthesis in ultrathin films in different form. Polymerization in the presence of minerals and clays is considered to have occurred on earth before life started. For instance, montmorillonite binds proteins so strongly that they cannot be washed out without being destroyed. Another type of polymerization of organized systems is polymerization in a liquid crystalline state.

However, in this article the term *template polymerization* will only be used for one-phase systems. The *template* is usually a linear preformed polymer added to the polymerization system.

When studying template systems, it is important to compare the template process and products of the reaction with conventional polymerization carried out under the same conditions but in a system in which the template is replaced by a low molecular nonpolymerizable analogue (blank reaction). The influence of the template on the process and on the product is usually called the *template effect* or the *chain effect* (3–6). The template effects can be expressed as follows:

(1) *Kinetic effect*: usually an enhancement of the reaction rate and changes in the kinetic equation;
(2) *Molecular effect*: the influence on the molecular weight and molecular weight distribution of the daughter polymer. In the ideal case, the degree of polymerization of the daughter polymer is the same as the degree of polymerization of the template used, which is sometimes called replication;
(3) *Effect on tacticity*: the daughter polymer may have a complementary structure to the structure of the template used;
(4) in the case of template copolymerization, the template effect deals with the change in reactivity ratios and the sequence distribution of units. This effect is very important in biological synthesis, for instance in DNA replication.

The template processes can proceed as template polycondensation, polyaddition, ring-opening polymerisation (qv), and ionic or radical polymerization (qv) (6,7) and the general rules characteristic for these processes can be applied.

Radical Template Polymerization

Much information and experimental data have been published about radical template polymerization. It is generally accepted (3–11) that template polymerization can proceed according to two different mechanisms: type I (the "zip" mechanism) or type II (the "pick-up" mechanism). In the case of type I, monomer units are connected to a template by strong forces (electrostatic, hydrogen bridges, or even covalent bonds). This is illustrated in the following scheme:

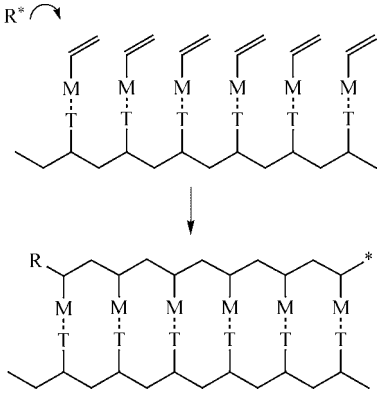

(1)

In the type II case, the monomer at the beginning of the reaction is "free" and polymerization starts outside the template. When oligoradicals reach a critical length, complexation with the template occurs, and propagation proceeds along the template by adding monomer molecules from the surrounding solution. This is illustrated in the following scheme:

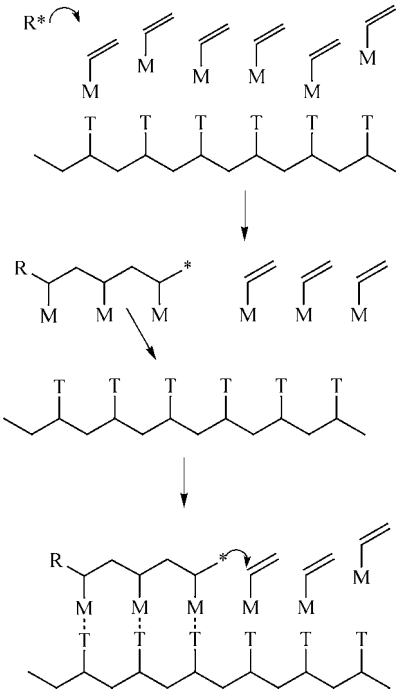

(2)

Tan and Challa (3,4) proposed using the relationship between the relative polymerization rate R_{rel} and concentration of monomer or template as a criterion for distinguishing between type I and type II template polymerization.

The most popular method is to examine the initial rate or relative rate R_{rel} as a function of base mole concentration of the template, [T], at constant monomer concentration [M].

For type I mechanism, when strong interactions exist between the monomer and the template, R_{rel} vs [T] shows a maximum for $[T] = [M]_0$.

For type II mechanism, R_{rel} increases with [T] to the critical concentration of the template, c^* (the concentration at which template macromolecules start to overlap) and then remains stable. It is worth noting that c^* (concentration in moles per volume) depends on the molecular weight of the template. The most complete kinetic model for radical-initiated template polymerization has been developed and described by Tan and Alberda van Ekenstein (12).

Typical examples of template polymerization systems are listed in Table 1.

The propagation and termination rate constants have been determined for many systems (5,12,43–46). In most cases, the propagation rate constant is lower than that for a reaction carried out in the same conditions but without a template. The termination rate constant in the template polymerization is much lower in comparison with the blank reaction. Retarded termination may be caused by retarded segmental diffusion of the template-bound radicals. This leads to the template increasing the overall rate of polymerization. Much experimental data from the literature confirm this, and it is sometimes called the *kinetic template effect*.

It has been found that for many monomer–template–solvent systems, the rate of reaction is proportional to the initiator concentration in power n and monomer concentration in power m, as in simple radical polymerization (qv). However, exponents n and m in the presence of template are different in comparison with the same system without the template.

An interesting case of template polymerization was described by Papisov and co-workers (47–49). The authors used two templates with different strengths of interaction with respect to the daughter polymer. The first template was poly(vinylpyrrolidinone) and the second, poly(ethylene glycol monolaurate). Methacrylic acid was used as a monomer.

On the basis of kinetic measurements with various concentrations and ratios of both templates, the authors found that there are conditions in which poly(methacrylic acid) molecules, in the course of growing, move from the strong, but short poly(vinylpyrrolidinone) template to the weaker template—polyethylene glycol monolaurate micelles. The circumstances of such a substitution reaction (exchange reaction) are described by the equation

$$c_1 K_1^{\varepsilon 1} = c_2 K_2^{\varepsilon^*} \tag{3}$$

where c_1 and c_2 are concentrations of template 1 [poly(vinylpyrrolidinone)] and template 2 [poly(ethylene glycol monolaurate)], K_1 and K_2 are effective strength constants for templates 1 and 2, and ε_1 and ε^* are the corresponding degrees of polymerization.

The template effect of tacticity has been shown by several authors (15,50–53). These authors found that polymerization of methyl methacrylate in the presence of isotactic poly(methyl methacrylate) proceeds as a template reaction. Extensive

Table 1. Typical Examples of Template Polymerization Systems

Monomer	Template	Solvent	Initiator	Reference
Acrylic acid	Poly(ethylene imine)	H_2O	$K_2S_2O_8$	13
N-Vinylpyrrolidinone	Poly(acrylic acid)	DMF	$K_2S_2O_8$	14
Methyl methacrylate	iso-Poly(methyl methacrylate)	DMF	TBCP[a]	15
Acrylic acid	Poly(ethylene glycol)	H_2O	$K_2S_2O_8$	16
Methacrylic acid	Poly(ethylene glycol)	H_2O	$K_2S_2O_8$	16,17
Methacrylic acid	Poly(4-vinylpyridine)		AIBN	18
Methacrylic acid	Poly(2-vinylpyridine)	DMF, DMSO, dioxane	AIBN	19–21
Methacrylic acid	Poly(vinylpyrrolidinone)	H_2O	$Na_2S_2O_8$ or UO_2SO_4 + photo.	22–24
Acrylic acid	Poly(vinyl pyrrolidinone-*co*-acrylamide)	H_2O	$K_2S_2O_8$	25
p-Styrene sulfonic acid	Polybase ionenes	H_2O/isopropyl alcohol	AIBN	26,27
Vinyl sulfonic acid	Polybase ionenes		ACA[b]	26,27
Methacrylic acid, acrylic acid	Polybase ionenes	H_2O	$K_2S_2O_8$	28
Sodium acrylate	Poly(allylamine) hydrichloride	H_2O	$K_2S_2O_8$ AIBN	29
Sodium vinyl sulfonate	Poly(allylamine) hydrichloride	H_2O	$K_2S_2O_8$	30
Acrylic acid, sodium styrenesulfonate	Chitosan	H_2O	$K_2S_2O_8$	31
N-Vinylpyridine	Poly(acrylic acid)		None	32–34
N-Vinylimidazole	Poly(methacrylic acid)	H_2O	ABIAP[c]	35–39
N-Dimethylaminoethyl methacrylate	Poly(acrylic acid)	H_2O/acetone	AIBN + UV	40
Acrylic acid	Poly(acrylic acid)	Set of solvents	AIBN	41
Monomer with uracil groups	Polymer with adenine groups	pyridine	AIBN	42

[a] Bis(*p-tert*-butyl cyclohexyl) dipercarbonate.
[b] 4,4-Azobis-4-cyanovaleric acid.
[c] 2,2′-Azobis(2-amidopropane) · 2HCl.

examination of the template polymerization process led the authors to general and important conclusions about the influence of molecular weight, the tacticity of the template, and the temperature and nature of the solvent. It was found that stereoregular poly(methyl methacrylate) can influence the microstructure of the daughter poly(methyl methacrylate).

The template molecular effect was observed by Ferguson (15), who found that the degree of polymerization of poly(acrylic acid) obtained in template polymerization onto poly(vinylpyrrolidinone) is remarkably similar to the degree of polymerization of the template. These results were surprising even to the authors, since they suggest that monomer radical propagation starts at one end of the template and continues to the other end of the templates when termination occurs. This was explained by the authors (15) in terms of the possibility of longer propagation of growing molecule in the presence of the higher molecular weight of the template and the interaction of the growing molecule with two or more template molecules.

The case described was rather exceptional, and was induced by the advantageous selection of initiator concentration. The dependence of the degree of polymerization of the template on the degree of polymerization of the daughter polymer was examined (11) for polymerization of methacrylic acid onto poly(vinylpyrrolidinone) in ethyl alcohol. In these experiments, fractions of poly(vinylpyrrolidinone) were used. The degree of polymerization of the daughter polymer can differ substantially from the degree of polymerization of the template used.

In type I template polymerization, in its most extreme case when monomer units are connected with the template by covalent bonds, the Brownian motion of the monomer units is replaced by conformational changes of the template molecules. Moreover, the distance between two monomer units is virtually independent of the overall concentration, and cannot be changed by dilution of the template solution.

For this type of polymerization, Kämmerer found (54–56) that for the oligomeric template, with an excess of azobisisobutyronitrile (AIBN), the reaction takes place according to a scheme which can be called a replication:

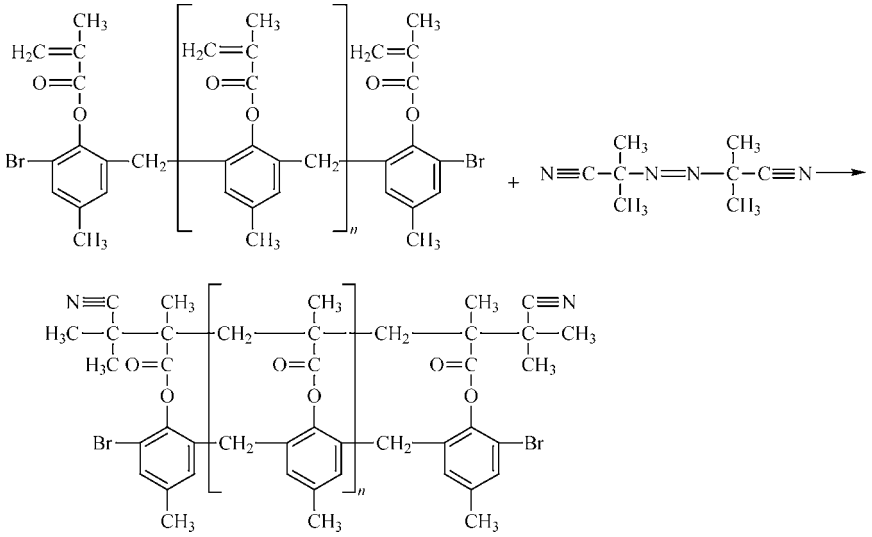

(4)

The template in this case was rather stiff, and excess of an initiator leads to termination by primary radicals. In this case the degree of polymerization of the daughter polymer was exactly the same as the degree of polymerization of the template (not taking end groups into account).

Another example is the synthesis of a ladder polymer as examined in Reference 57. Poly(vinyl alcohol) esterified by methacrylic chloride was used as a template. Polymerization can be represented by the following reaction:

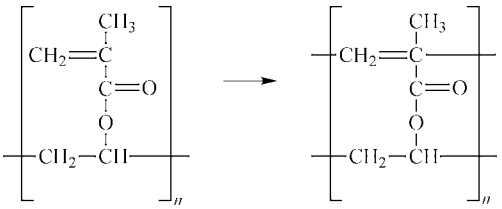

(5)

The polymerization can begin in any of the groups present and may proceed in any direction. In other words, since the reactive groups, are independent of one another and initiation occurs randomly, polymerization leads to isolated reactive groups, which are both potential cross-linking sites and breaks in the ladder structure. Cross-linking as an intermolecular reaction can be minimized by conducting the reaction at an appropriate dilution. If, however, initiation is not random but starts at one end of the template, we might expect to obtain a very regular ladder structure. Such a case was considered by Bamford (2), but has never been checked experimentally. Active radicals in multimonomer—poly(vinyl methacrylate)—can be created from $-CCl_3$ end groups, in the presence of manganese carbonyl, $Mn_2(CO)_{10}$, by irradiation with light. The radicals would be expected to initiate selectively at one end of the template according to the following reaction:

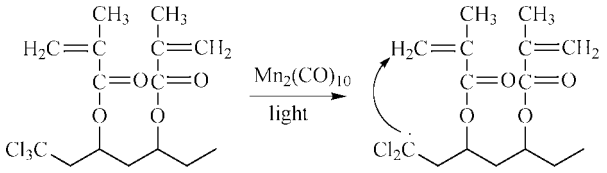

(6)

Template polymerization of multi-acrylate and multi-methacrylate with longer spacers has been studied (58–61). The reaction proceeds according to the

following scheme:

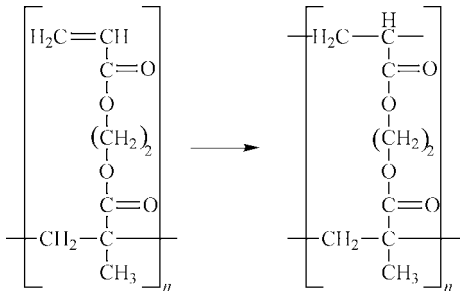

(7)

It was found that neither the average molecular weight nor the distribution of molecular weights change during polymerization, provided the molecular weight is high enough and the concentration is low (60,61). For multi-acrylates, it was found that distribution of molecular weights is the same up to more than 50% of conversion of double bonds. This means that under correct conditions, intermolecular reaction can be neglected and the polymerization proceeds as a template process. However, for high conversion and high monomer concentration, an increase of molecular weight takes place, and eventually the product becomes insoluble and cross-linked. Very similar behavior was observed for the photopolymerization of multi-methacrylate (62). The kinetics of template polymerization of multi-methacrylates, poly(2-methacryloyloxyethyl methacrylate) and poly(2-acryloyloxyethyl methacrylate), have been studied.

Template polymerization for polypeptide synthesis was reported by Ballard and Bamford (63) and described in detail in Reference 2. The substrate for the synthesis was *N*-carboxy-α-amino acid anhydride (NCA). The first step consists in the reaction of NCA with secondary amine on the end of the polypeptide template. The ring-opening process and the elimination of CO_2 then proceeds as a chain reaction. Valuable experimental material concerning the polymerization of many different *N*-carboxyanhydrides initiated by many different polypeptides (64–66) as well as by poly(vinyl pyridine) (67,68) was collected by Imanishi and co-workers.

Sugiyama and co-workers (69,70) report a very interesting template process by the ring-opening polymerization induced by radicals. The polyethylene template was connected with 2,2-diphenyl-4-methylene-1,3-dioxolane groups by the covalent bonds. The process can be illustrated by the following reaction:

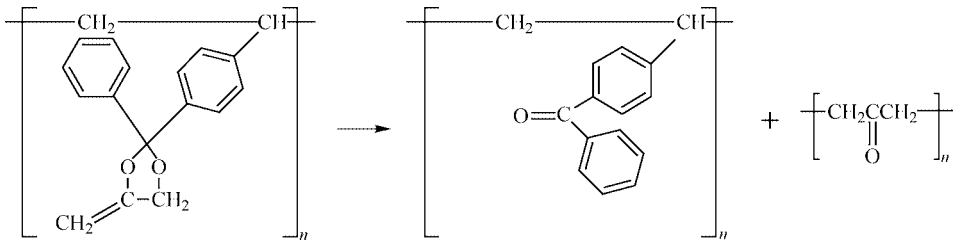

(8)

In this case the daughter polymer is not connected to the template either by hydrogen bonds or covalent bonds.

Template Radical Copolymerization

In the literature there is less information about template copolymerization than about template homopolymerization. However, the process seems to be very interesting on account of the fact that the template can influence not only the molecular weight and tacticity of the daughter polymer but also the composition and distribution of units in the copolymer macromolecule. Two different schema of template copolymerization can be considered. First, the template can be a homopolymer and one or both monomers can interact with the template. Second, the template can be a copolymer, or in the system two different templates exist. Literature in the field is not numerous.

It was found that the composition and the distribution of units in copolymerization is controlled mainly by the propagation process. From this point of view, equations have been formulated (71) concerning how the reactivity ratios depend on the template concentration and individual reactivity rate constants of monomers taking part in the template copolymerization process. However, if long critical length is necessary for the adsorption of the growing macroradical onto the template, any template effect can be destroyed (72).

It seems that the template effect can be pronounced only if interactions between at least one of the monomers is sufficiently strong. Examples of the systems in which one or both monomers were connected with the template by covalent bonds have been described (73–78). Copolymerization of multimonomers similar to the oligomers described by Kämmerer with styrene leads to semiladder copolymers, and after hydrolysis to short-block copolymers (73).

Step-Growth Template Polymerization

Template polycondensation or template polyaddition is much less elaborated than the chain template reaction. However, many cases of homo- and heteropolycondensation have been considered (11).

Strong interaction between monomers and the template is a prerequisite for the template process, while in simple polycondensation high temperature and low pressure is applied. However, in mild conditions using the direct polycondensation method it was demonstrated that terephthalic acid connected with poly(4-vinylpyridine) (79), poly(ethylene oxide) (80), poly(vinylpyrrolidinone) (81) and activated by triphenyl phosphite reacts with hexamethylenediamine, giving polyamides with high molecular weight.

Another example of template polycondensation was described by Ogata and co-workers (82–85). Polycondensation of dimethyl tartrate or dimethyl muconate with hexamethylenediamine was increased by the presence of poly(vinylpyrrolidinone) and poly(vinyl alcohol). It was also found that polysaccharides increase the polycondensation rate. It seems that hydroxyl groups play a substantial role in the absorption of monomers onto the template.

Polycondensation of various amino acids by means of triphenyl phosphite in the presence of poly(vinylpyrrolidinone) was also reported (86).

A very interesting method of polycondensation of active esters containing nucleic acid bases with diamines was described by Hattori and co-workers (87). Di-*p*-nitrophenyl methylsuccinate with thymine or theophylline was condensed with piperazine. The reaction was carried out in a pyridine/methylene chloride mixture or dimethyl formamide (DMF) in the presence of a copolymer of styrene and styrene derivatives with adenine groups as a template. The strong interaction between the complementary groups (adenine in the template and thymine in the monomer) leads to the template effect. The maximum acceleration effect was observed for copolymers with adenine content about 54% in the case of polycondensation with piperazine.

It was found that the rate of reaction differed depending on the percentage of adenine groups in the copolymer.

A template polycondensation of urea with formaldehyde in the presence of acrylic acid was published by Papisov and co-workers (88–92). The authors suggest that a complex with polyacid is formed during the reaction. The complex has a different structure than does urea–formaldehyde resin mixed with poly(acrylic acid). The reaction can be written as follows:

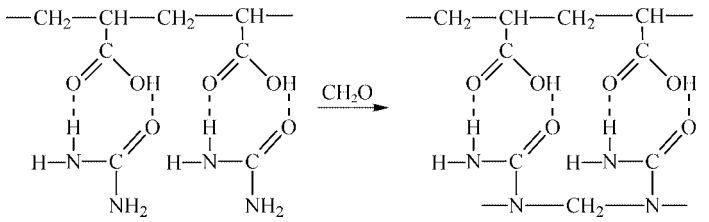

(9)

The theoretical consideration and models for a kinetic description of the template reaction in biological systems was published by Simha and co-workers (93). The model was constructed on the basis of addition reaction in order to apply to the synthesis of biological molecules, for instance DNA replication.

Potential Applications

The most promising applications of template polymerization seems to be the production of materials in which the daughter polymer and the template together form a final product, because the synthesis of polymers requiring further separation of the product from the template is not acceptable for industry. The template process can be applied in order to produce a set of new materials on the basis of ladder-type polymers, semi-adder copolymers, the properties of which are not yet well known.

Template polymerization is a convenient way to produce polycomplexes and polycomplex composites, polymer blends, and interpenetrating networks or networks with nonrandom distribution of cross-linking points.

The polycomplexes obtained by template polymerization have been used for spinning fibers (27).

The quite remarkable properties of composites obtained by template polycondensation of urea and formaldehyde are described by Papisov and co-workers (92). The structure and properties of such composites can be widely varied by changing initial composition and reacting conditions.

Rätzsch (94) reported an application of template polymerization similar in technique to photolithography. However, up to this point template polymerization has not found any industrial application.

BIBLIOGRAPHY

"Template Polymerization" in *EPSE* 2nd ed., Vol. 16, pp. 554–569, by Y. Yong Tan and G. Challa, Groningen University.

1. M. Szwarc, *J. Polym. Sci.* **13**, 317 (1954).
2. C. H. Bamford, in R. N. Haward, ed., *Developments in Polymerization*, Applied Science Publishers, London, 1979, p. 215.
3. G. Challa and Y. Y. Tan, *Pure Appl. Chem.* **53**, 627 (1981).
4. Y. Y. Tan, in G. Allen and J. C. Bevington, eds., *Comprehensive Polymer Science*, Vol. 3, Pergamon Press, Oxford, 1989, p. 245.
5. Y. Y. Tan and G. Challa, *Macromol. Chem. Macromol. Symp.* **10/11**, 215 (1987).
6. S. Polowiński, in D. Bloor, R. J. Brook, M. C. Flemings, and S. Mahajan, eds., *The Encyclopaedia of Advanced Materials*, Pergamon Press, New York, 1994, p. 2784.
7. S. Polowiński, in J. C. Salamone, ed., *Polymeric Materials Encyclopedia*, Vol. 11, CRC Press, Boca Raton, Fla., 1996, p. 8280.
8. S. Polowiński, *Template Polymerization*, ChemTec Publishers, Toronto, 1997.
9. I. M. Papisov, in J. C. Salamone, ed., *Polymeric Materials Encyclopedia*, Vol. 6, CRC Press, Boca Raton, Fla., 1996, p. 4038.
10. Y. Y. Tan, *Prog. Polym. Sci.* **19**, 561 (1994).
11. S. Polowiński, *Prog. Polym. Sci.* **27**, 537 (2003).
12. Y. Y. Tan and G. O. R. Alberda van Ekenstein, *Macromolecules* **24**, 1641 (1991).
13. J. Ferguson and S. A. O. Shah, *Eur. Polym. J.* **4**, 611 (1968).
14. V. S. Rajan and J. Ferguson, *Eur. Polym. J.* **18**, 633 (1982).
15. R. Buter, Y. Y. Tan, and G. Challa, *J. Polym. Sci., Part A-1* **10**, 1031 (1972).
16. I. M. Papisov, V. A. Kabanov, E. Osada, M. Leskano-Brito, J. Reimont, and A. N. Gvozdetskii, *Vysokomol. Soj.* **14**, 2462 (1972).
17. J. Matuszewska-Czerwik and S. Polowiński, *Eur. Polym. J.* **8**, 791 (1988).
18. K. Fujimori, G. T. Trainor, and M. J. Costigan, *J. Polym. Sci.* **22**, 2479 (1984).
19. J. Smid, Y. Y. Tan, and G. Challa, *Eur. Polym. J.* **20**, 887 (1984).
20. J. Smid, J. C. Speelman, Y. Y. Tan, and G. Challa, *Eur. Polym. J.* **21**, 2141 (1985).
21. J. Smid, Y. Y. Tan, and G. Challa, *Eur. Polym. J.* **19**, 853 (1983).
22. J. Matuszewska-Czerwik and S. Polowiński, *Eur. Polym. J.* **26**, 549 (1990).
23. J. Ferguson and S. A. O. Shah, *Eur. Polym. J.* **4**, 343 (1968).
24. N. Shavit and J. Cohen, in H. G. Elias, ed., *Polymerization in Organized Systems*, Gordon Breach, London, 1977, p. 213.
25. J. Ferguson and C. McLeod, *Eur. Polym. J.* **10**, 1083 (1974).
26. A. Blumstein, S. R. Kakivaya, and J. C. Salamone, *J. Polym. Sci., Polym. Lett. Ed.* **12**, 651 (1974).
27. A. Blumstein, S. R. Kakivaya, K. R. Shah, and D. J. Wilkins, *J. Polym. Sci., Polym. Symp.* **45**, 75 (1974).
28. E. Tsuchida and Y. Osada, *J. Polym. Sci., Polym. Chem., Ed.* **13**, 559 (1975).

29. P. Cerrai, G. D. Guerra, S. Maltini, and M. Tricoli, *Macromol Rapid Commun.* **15**, 983 (1994).
30. M. G. Cascone, L. Lazzeri, N. Barbani, C. Cristallini, and G. Polacco, *Polym. Int.* **41**, 17 (1996).
31. P. Cerrai, G. D. Guerra, M. Tricoli, S. Maltini, N. Barbani, and L. Petarca, *Macromol. Chem. Phys.* **197**, 3567 (1996).
32. K. A. Kabanov, K. V. Aliev, O. V. Kargina, T. J. Patrikeeva, and V. A. Kargin, *J. Polym. Sci., Part C* **16**, 1079 (1967).
33. V. A. Kabanov, O. V. Kargina, and V. A. Petrovskaya, *Vysokomol. Soj., Ser. A* **13**, 348 (1971).
34. V. A. Petrovskaya, V. A. Kabanov, and V. A. Kargin, *Vysokomol. Soedin, Ser. A* **12**, 1645 (1970).
35. H. T. Van de Grampel, Y. Y. Tan, and G. Challa, *Makromol. Chem. Makromol. Symp.* **21/22**, 83 (1988).
36. H. T. Van de Grampel, Y. Y. Tan, and G. Challa, *Macromolecules* **23**, 5209 (1990).
37. H. T. Van de Grampel, Y. Y. Tan, and G. Challa, *Macromolecules* **24**, 3767 (1991).
38. H. T. Van de Grampel and G. Challa, *Macromolecules* **24**, 3773 (1991).
39. H. T. Van de Grampel, Y. Y. Tan, and G. Challa, *Template. J. Polym. Sci., Polym. Chem. Ed.* **30**, 787 (1992).
40. Z. H. Ellatif, *Polym. Int.* **28**, 301 (1992).
41. A. Chapiro and J. Dulieu, *Eur. Polym. J.* **13**, 563 (1977).
42. M. Akashi, H. Takeda, Y. Inaki, and K. Takemoto, *J. Polym. Sci., Polym. Chem. Ed.* **17**, 747 (1979).
43. J. Gons, E. J. Vorekamp, and G. Challa, *J. Polym. Sci., Chem. Ed.* **15**, 1699 (1977).
44. J. Gons, E. J. Vorekamp, and G. Challa, *J. Polym. Sci., Chem. Ed.* **15**, 3031 (1977).
45. J. Matuszewska-Czerwik and S. Polowiński, *Eur. Polym. J.* **28**, 1481 (1992).
46. J. Matuszewska-Czerwik and S. Polowiński, *Eur. Polym. J.* **34**, 557 (1998).
47. I. M. Papisov, N. A. Nekrasova, V. D. Pautov, and V. A. Kabanov, *Dokl. Acad. Nauk SSSR* **214**, 861 (1974).
48. I. M. Papisov, T. I. Nedyalkova, N. K. Avramchyk, and V. A. Kabanov, *Vysokomol. Soj., A* **15**, 2003 (1973).
49. V. Baranovskii, Yu., N. N. Gnatko, A. A. Litmanowich, and J. M. Papisov, *Vysokomol. Soj.* **31**, 984 (1989).
50. R. Buter, Y. Y. Tan, and G. Challa, *J. Polym. Sci., Polym. Chem. Ed.* **11**, 989 (1973).
51. R. Buter, Y. Y. Tan, and G. Challa, *J. Polym. Sci., Polym. Chem. Ed.* **11**, 1003 (1973).
52. R. Buter, Y. Y. Tan, and G. Challa, *J. Polym. Sci., Polym. Chem. Ed.* **11**, 1013 (1973).
53. R. Buter, Y. Y. Tan, and G. Challa, *J. Polym. Sci., Polym. Chem. Ed.* **11**, 2975 (1973).
54. H. Kämmerer and A. Jung, *Makromol. Chem.* **101**, 284 (1966).
55. H. Kämmerer and S. Ozaki, *Makromol. Chem.* **91**, 1 (1966).
56. H. Kämmerer, I. Shukla, N. Önder, and G. Schurmann, *J. Polym. Sci., Polym. Symp.* **22**, 213 (1967); S. Polowiński and G. Janowska, *Eur. Polym. J.* **11**, 183 (1975).
57. R. Jantas and S. Polowiński, *J. Polym. Sci., Part A: Polym. Chem.* **24**, 1819 (1986).
58. R. Jantas, *J. Polym. Sci., Part A: Polym. Chem.* **28**, 1973 (1990).
59. R. Jantas, J. Szumilewicz, G. Strobin, and S. Polowiński, *J. Polym. Sci., Part A* **32**, 295 (1994).
60. R. Jantas, S. Polowiński, and G. Strobin, *Polym. Int.* **37**, 315 (1995).
61. A. Blasińska, S. Polowiński, and R. Jantas, *Polym. Int.* **42**, 436 (1997).
62. R. Jantas and S. Polowiński, *J. Polym. Sci., Part A: Polym. Chem.* **27**, 475 (1989).
63. D. G. H. Ballard and C. H. Bamford, *Proc. Roy. Soc. Ser. A* **236**, 384 (1956).
64. Y. Imanishi, T. Sugihara, and T. Higashimura, *Biopolymers* **12**, 1505 (1973).
65. Y. Imanishi, K. Kugimiya, and T. Higashimura, *Biopolymers* **12**, 2643 (1973).
66. Y. Imanishi, K. Kugimiya, and T. Higashimura, *Biopolymers* **13**, 1205 (1974).

67. K. Suzuoki, Y. Imanishi, and K. T. Higashimura, *Biopolymers* **7**, 925 (1969).
68. Y. Imanishi, S. Nagaoka, K. K. Suzuoki, and T. Higashimura, *Biopolymers* **12**, 181 (1973).
69. J. Sugiyama, T. Yokozawa, and T. Endo, *Macromolecules* **27**, 5536 (1994).
70. J. Sugiyama, T. Yokozawa, and T. Endo, *J. Am. Chem. Soc.* **115**, 2041 (1993).
71. S. Polowiński, *J. Polym. Sci., Polym. Chem. Ed.* **22**, 2887 (1984).
72. K. F. O'Driscoll and I. Capek, *J. Polym. Sci., Polym. Lett. Ed.* **19**, 401 (1981).
73. S. Polowiński, in *IUPAC Conference*, Budapest, Vol. 3, 1969, p. 171.
74. S. Polowiński and G. Janowska, *Eur. Polym. J.* **11**, 183 (1975).
75. S. Polowiński, *Eur. Polym. J.* **14**, 563 (1978).
76. S. Polowiński, *Polimery* **17**, 409 (1972).
77. R. Jantas, *J. Polym. Sci., Part A: Polym. Chem.* **28**, 1973 (1990).
78. R. Jantas and J. M. S. Pure, *Appl. Chem. A* **29**, 557 (1992).
79. F. Higashi, Y. Nakano, M. Goto, and H. Kakinoki, *J. Polym. Sci., Polym. Chem. Ed.* **18**, 851 (1980).
80. F. Higashi, Y. Nakano, M. Goto, and H. Kakinoki, *J. Polym. Sci., Polym. Chem. Ed.* **18**, 1099 (1980).
81. F. Higashi and Y. Taguchi, *J. Polym, Sci., Polym. Chem. Ed.* **18**, 2875 (1980).
82. N. Ogata, K. Sanui, H. Nakamura, and H. Kishi, *J. Polym. Sci., Polym. Chem. Ed.* **18**, 933 (1980).
83. N. Ogata, K. Sanui, H. Nakamura, and H. Kishi, *J. Polym. Sci., Polym. Chem. Ed.* **18**, 939 (1980).
84. N. Ogata, K. Sanui, and M. Abe, *J. Polym. Sci., Polym. Chem. Ed.* **19**, 1361 (1981).
85. N. Ogata, K. Sanui, H. Tanaka, H. Matsuto, and F. Iwaki, *J. Polym. Sci., Polym. Chem. Ed.* **19**, 2609 (1981).
86. N. Yamazaki and F. Higashi, *Adv. Polym. Sci.* **38**, 1 (1981).
87. M. Hattori, H. Nagagawa, and M. Kinoshita, *Makromol. Chem.* **181**, 2325 (1980).
88. I. M. Papisov and A. A. Litmanovich, *Adv. Polym. Sci.* **90**, 139 (1989).
89. K. I. Boliachevskaya, A. A. Litmanovich, and I. M. Papisov, *Polym. Sci. B* **37**, 424 (1995).
90. I. M. Papisov, O. E. Kuolvleva, S. V. Markov, and A. A. Litmanovich, *Eur. Polym. J.* **20**, 195 (1984).
91. A. A. Litmanovich, S. V. Markov, and I. M. Papisov, *Vysokomol. Soj.* **28**, 1271 (1986).
92. I. M. Papisov, A. A. Litmanovich, K. I. Boliachevskaya, Yu, S. Yablokov, I. A. Prokofiev, O. Ya. Litmanovich, and S. V. Markov, *Macromol. Symp.* **106**, 287 (1996).
93. R. Simha and J. M. Zimmerman, *J. Moacanin, J. Chem. Phys.* **39**, 1239 (1963).
94. M. Rätzsch, in *Abstracts 30th IUPAC Symposium on Macromolecules*, The Hague, the Netherlands, 1985, p. 37.

STEFAN POLOWIŃSKI
Technical University of Lódz

TEST METHODS.

See Volume 8.

TETRAFLUOROETHYLENE POLYMERS.

See PERFLUORINATED POLYMERS.

THERMAL ANALYSIS.

See ARTICLE ONLINE.

THERMOCHROMIC POLYMERS

Introduction

In recent years functional polymers changing their visible optical properties in response to an external stimulus have met with growing interest. According to the external stimulus which affects the optical properties, these so-called chromogenic polymers are classified as thermochromic (stimulus: temperature), photochromic (stimulus: light), electrochromic (stimulus: electric field), piezochromic (stimulus: pressure), ionochromic (stimulus: ion concentration), and biochromic (stimulus: biochemical reaction). Because of their advanced properties the demand on chromogenic polymers for future applications will become enormous. Smart windows, tunable light filters, large area displays as well as sensors, which can visualize, eg, temperature or pressure profiles, are the most important potential innovations based on chromogenic polymers. For all these applications laboratory prototypes demonstrating the effect have been presented. A few of them have already reached the readiness for marketing and certainly others will follow in the near future.

This article focuses on thermochromic polymer systems. An overview of the different types of such polymer systems is given and the origin of the thermochromic effect, their specific material properties, and potential applications are discussed. Table 1 displays the various generic types of thermochromic polymers. Following this classification, thermochromic polymer systems in which the color appears owing to a Bragg reflection on a periodic structure are discussed first. In such systems the thermochromic effect is caused by a temperature dependence of the layer periodicity. Thus the wavelength of the reflected light can only change continuously. Another inherent feature of such thermochromic systems is that the visible color depends on the viewing angle. Because of these disadvantages the potential applications of thermochromic polymer systems based on Bragg reflection are limited. The second classification is about thermochromic polymer systems varying their color or color intensity owing to temperature-dependent molecular changes of the chromophoric group. This class of thermochromic polymers can in principle switch between any user-defined colors. The third class of

Table 1. Generic Types of Thermochromic Polymers Classified by the Effect on Light Causing the Thermochromic Behavior

Effects on light	Origin	Macroscopic behavior	Polymer class
Reflection	Periodic structures	ΔI, $\Delta\lambda_{max}$	Cholesteric liquid crystalline polymers
			Crystalline colloidal arrays embedded in a gel network
			Gels
Absorption	Chromophoric groups	ΔI, $\Delta\lambda_{max}$	Conjugated polymers
			Hydrogels containing indicator dyes
Scattering	Areas with different refractive indices	$\Delta T\%$	Polymer blends exhibiting LCST[a]
			Hydrogles exhibiting LCST
			Lyotropic liquid crystalline hydrogels

[a]LCST: lower critical solution temperature.

Encyclopedia of Polymer Science and Technology. Copyright John Wiley & Sons, Inc. All rights reserved.

polymer systems reviewed are those changing their transparency with temperature by reversible switching between a transparent and a light scattering state. In the literature this subclass of thermochromic materials is generally denoted as thermotropic. The main interest in thermotropic polymer systems appears to be from their potential application in sun protecting glazing. Recently, a novel class of polymer systems changing both transparency and color with temperature has been described and will be reviewed.

Thermochromic Polymer Systems Based on Bragg Reflection

Liquid Crystalline Polymers with Thermochromic Properties. In several liquid crystalline phases a helical superstructure occurs if either a chiral compound is added or the liquid crystalline compound itself consists of a chiral molecular structure (1,2). In this way, the nematic phase, for example, transforms into the so-called cholesteric phase. Depending on structure and concentration of the chiral compound as well as on the phase type, the pitch (P) of the helical superstructure can be in the range between 100 nm and infinite. Incident light is selectively reflected, if the wavelength (λ) satisfies the Bragg condition $\lambda = nP \cos\theta$ (n stands for the mean reflective index of the liquid crystal and θ for the angle between the incident light and the orientation of the helix). In many systems the wavelength of the reflected light is in the visible region; thus these liquid crystals become intensively colored. The pitch generally changes with temperature and can be modified by applying an electric field.

Thermochromic polymer foils based on cholesteric liquid crystals are already commercially available from various manufacturers including Hallcrest Ltd., Merck KGaA, and Davis Liquid Crystals Inc. Such thermochromic sheets consist of a black backing layer, a layer of the cholesteric liquid crystal, and a protective clear polyester layer. They can indicate temperature changes ranging from a fraction of a degree to over 20°C by varying their color continuously through the entire visible region.

Chiral liquid crystalline polymers possessing thermochromic properties themselves are described in numerous publications. Besides synthetic polymers, many cellulose derivatives have been found to possess cholesteric mesophases with selective reflection in the visible wavelength region. The pentyl ether of hydroxypropyl cellulose is an example for such a cholesteric polymer (3). At room temperature it shows selective reflection at about 500 nm. With increasing temperature the wavelength of the selective reflection maximum smoothly increases, reaching 650 nm at about 80°C. For applications in information technology, those materials are of special interest which allow fixation the cholesteric order at any user-defined color (4). A fixing of the helical pitch takes place in a glassy state (5–7) as well as in cross-linked polymeric structures (3,8–12). Therefore, cholesteric polymers with a glass-transition temperature within the cholesteric phase range as well as cholesteric mixtures which are polymerizable and form cross-linked polymeric networks are suitable for this purpose. The preparation of patterned multicolor cholesteric liquid crystal polymer networks have been reported (12). The cholesteric liquid crystal polymer networks were obtained by photopolymerization of a mixture containing 20% of a chiral monoacrylate CBC

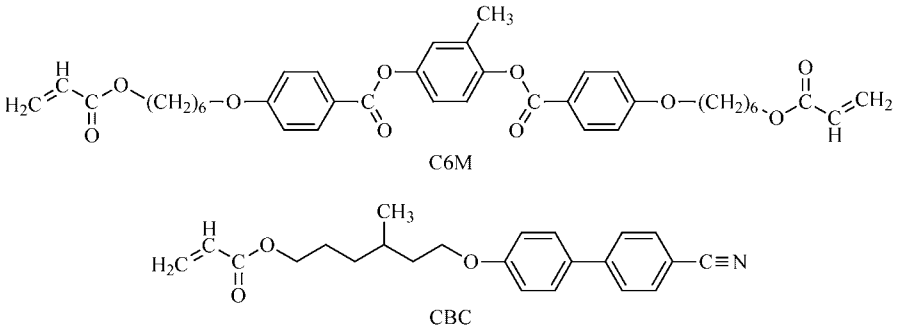

Fig. 1. Molecular structure of the acrylates C6M and CBC.

(see Fig. 1), 25% of a nonreactive commercial chiral dopant CB15 (Merck), 54% of a nonreactive commercial liquid crystal BL59 (Merck), 0.5% of a diacrylate C6M (see Fig. 1), and 0.5% Irgacure 651 photoinitiator at different temperatures. This mixture exhibits a cholesteric phase with a strong temperature dependence of the pitch. At 55°C it reflects red light, at 35°C green light, and at 30°C blue light. Thus, by performing the photopolymerization at different temperatures (55, 35, and 30°C), red, green, and blue polymer networks with a temperature-independent color were obtained. In a next step the preparation of a patterned multicolor polymer network was carried out by using masks and performing the photopolymerization step by step in different regions at different temperatures. It was concluded that by using a light source to induce patterned heating of the mixture, followed by fixing via UV-induced photopolymerization, it should be possible to produce much more complicated structures.

The formation of liquid crystalline phases with thermochromic properties in a poly(β-peptide) was reported in Reference 13. The color changes were observed by using polarizing optical microscopy. However, this method was not found to be suitable for determining thermochromism.

Thermochromic Gel Networks Based on Bragg Reflection. Polymer gel networks with thermochromic properties, based on Bragg reflection, are frequently described in the literature, whereby most of the systems are composed of a polymer and an organic solvent. It has been reported that poly-1-butene flakes swells in benzene, toluene, *o*-xylene, *m*-xylene, *p*-xylene, or tetrachloroethylene and exhibits reversible color changes with temperature between the melting point of the solvent and the sol–gel transition temperature (14). With increasing temperature the color of the poly-1-butene gels changes in the order of blue, violet, red, orange, and yellow. This thermochromic effect is explained by Bragg reflection on the microstructure of the gelled poly-1-butene. A similar behavior was observed by the same author for gelled isotactic polypropylene in benzene, toluene, and xylene (15). For example the color of a 3% isotactic polypropylene gel in benzene was found to change from blue at room temperature to yellow at about 70–80°C.

A thermochromic hydrogel based on Bragg reflection has been reported (16). The described system consists of crystalline colloidal arrays of monodisperse polystyrene spheres embedded in a poly(*N*-isopropyl acrylamide) (PNIPAM) hydrogel, which was prepared by first dispersing highly charged and monodisperse

polystyrene spheres in an aqueous solution containing the PNIPAM monomer, followed by a photochemically initiated polymerization. A temperature-dependent strong swelling or shrinking of the polymer matrix takes place. The embedded polystyrene spheres follow this volume change, causing thereby a modification of their lattice spacing and thus of their Bragg reflection wavelength. To characterize the optical properties of the novel thermochromic material, films of different layer thickness were prepared and the temperature dependence of their diffracted wavelength determined. While the bulk material is translucent because of light scattering on the colloidal particles, thin films become transparent. At room temperature 125-μm-thick hydrogel film was used to detect the thermochromic effect by absorption measurements. In this way, a continuous change of the diffracted wavelength from 704 nm at 11.7°C to 460 nm at 34.9°C was measured, which corresponds to nearly the entire visible range. However, note that the thermochromic effect is coupled with strong volume changes. An increase of the diffracted wavelength from 400 to 800 nm corresponds to a swelling in each direction by a factor of 2 and thus to an eightfold increase of the volume.

Crystalline colloidal arrays which vary the intensity of the Bragg reflection in dependence on temperature without changing the wavelength of the diffracted light have also been developed (16). Such materials were obtained by dispersing highly charged and monodisperse colloidal particles of PNIPAM with a size of 100 nm in deionized water. In water these PNIPAM colloids self-assemble and form a body-centered cubic array which diffracts light following the Bragg diffraction law. Below their lower critical solution temperature of about 32°C the PNIPAM colloids begin to swell, leading to an increase of the sphere diameter from about 100 nm above this temperature to about 300 nm at 10°C. The lattice spacing of the cubic array and thus the reflected wavelength (at a constant glancing angle between the incident light and the diffracting crystal plane) depend only on the particle density of the PNIPAM colloids. The intensity of the Bragg reflection of crystalline colloidal arrays, on the other hand, depends on the array ordering as well as on the scattering cross section of the colloidal particles, which is influenced by the particle size of the colloids. As a result the reversible swelling or shrinking of the PNIPAM colloids with temperature causes pronounced changes in the intensity of the Bragg reflection. As an example the optical properties of a crystalline colloidal array of PNIPAM colloids (diameter: 100 nm) with a lattice constant of 342 nm were reported. At 40°C the nearest neighbor sphere distance amounts to 242 nm and at the Bragg reflection wavelength nearly all incident light is reflected. On the other hand at 10°C the PNIPAM colloids are almost touching and only a weak Bragg reflection occurs.

Thermochromic Polymer Systems Based on the Absorption of Light

Conjugated Polymers. The occurrence of thermochromic properties is frequently observed in conjugated polymers (17,18) like polyacetylenes (19), polydiacetylenes (19), polythiophenes (20), and polyanilines (21). Many conjugated polymers exhibit absorption of light in the visible range as well as high reflectivity. Hence, they often are colored and show a metallic appearance. Thermochromism in conjugated polymers has its origin in changes of the conformation as they

abruptly occur at phase transitions whereby even the slightest modification of the conformational structure can cause significant color changes. Especially the planarity of the polymer backbone plays an important role. Any twisting of the chain leads to a decrease of the effective conjugation length and thus to a blue (hypsochromic) shift of the absorption in the UV–vis region. In general the color changes of conjugated polymers are reversible. However, kinetic effects can cause an irreversibility which can be useful for thermal recording (22). In Reference 23, synthesis and optical properties of a liquid crystalline polydiacetylene are described. At each of its mesogenic phase transitions a thermochromic effect was detected. That means thermochromic and mesogenic properties of the investigated polydiacetylene are coupled with one another. The structural and optical properties of poly[2′,5′-bis(hexadecyloxy)-1,4-phenylene-1,3,4-oxadiazol-2,5-diyl] have been reported in Reference 24. The polymer was found to possess liquid crystalline properties in a wide temperature range, whereby at 120°C an order–order transition from a smectic H into a smectic A phase takes place. Moreover, a thermochromic behavior was observed within the temperature range of 25–140°C. With increasing temperature the polymer changes its color continuously from yellow-green at 25°C to blue at 130°C. To characterize this thermochromic behavior in more detail, UV–vis absorption and fluorescence emission spectra were measured at different temperatures. For both, a continuous evolution with temperature was found. In contrast to the results reported in Reference 23, in Reference 24 even at the smectic H to smectic A phase transition no discontinuous change of the UV–vis and fluorescence intensities could be detected.

Another way to obtain thermochromic polymers is to incorporate a thermochromic material into a polymer matrix. Thermochromic polymers have been obtained by dispersing poly(3-alkyl thiophene)s in host polymers (25,26). Poly(3-alkyl thiophene)s belong to the group of conjugated polymers, exhibiting thermochromism according to temperature-induced changes of the conjugation of the π-electron system. The thermochromic switching temperature of the polythiophene pigments can be tailored by chemical modifications. In this way a set of pigments that visually and reversibly change colors at a prescribed temperature in the region of -35 to $+125$°C was developed. These pigments are thermally stable until more than 200°C. Commercially available paints, plastics, and rubbers were used as host polymers, whereby 0.1–1.0 wt% of the pigments were necessary to obtain a visible thermochromic effect. However, a detailed description of the chemical structure of the pigments or a list of the available switching temperatures and color changes has not been reported so far.

A thermoplastic polymer with thermochromic properties was recently presented by Seeboth et al. (27). This polymer switches on heating at a certain temperature from blue to colorless. Figure 2 displays a photograph demonstrating this thermochromic switching effect. A foil of the novel thermochromic polymer is partially heated in hot water above the switching temperature. Clearly the cool blue and the hot colorless state can be seen. So far, neither the origin of the thermochromic effect nor the composition of this thermochromic polymer has been reported.

Masterbatches of polyethylene and polypropylene containing microencapsulated thermochromic materials are already commercially available from various manufacturers. The thermochromic materials used in these microcapsules are

Fig. 2. Thermochromic switching from blue to colorless of a thermoplastic polymer foil.

composed of an electron-donating chromogenic compound, an electron acceptor, and a solvent (28). Suitable electron-donating chromogenic compounds are, for example, substituted phenylmethanes and fluorans. These so-called leuco dyes or color formers (29) are either colorless or weakly colored. However, on reaction with an electron acceptor, as for example a phenol, an opening of the lactone ring occurs. In the open ring state the conjugated π-electron system is extended, enabling color formation. By the addition of appropriate solvents the color-forming reaction becomes reversible. In the molten state these solvents function as an inhibitor of the color-forming reaction. On the other hand during the crystallization of the solvent the donating chromogenic compound reacts with the electron acceptor; thus the crystalline state becomes colored. For example a mixture of 1 wt% 2-chloro-6-diethylamino-3-methylfluoran, 5 wt% 2,2′-bis(4-hydroxyphenyl)-propane, and 94 wt% 1-hexadecanol is colorless above 48°C in the molten state and develops a vermilion color on cooling below 48°C when the crystallization of the 1-hexadecanol takes place. The reversible lactone ring opening reaction of 2-chloro-6-diethylamino-3-methylfluoran, which is the origin for this thermochromic effect, is shown in Figure 3. Although these masterbatches show excellent thermochromic switching behaviors, the use of microencapsulated thermochromic mixtures results in a variety of limitations including poor thermal and shear stability which cause difficulties in processing.

Gel Networks. In the literature a few examples of thermochromic gel networks consisting of conjugated polymers swelled in organic solvents are reported. The thermochromic effect described for these gels appears owing to changes of

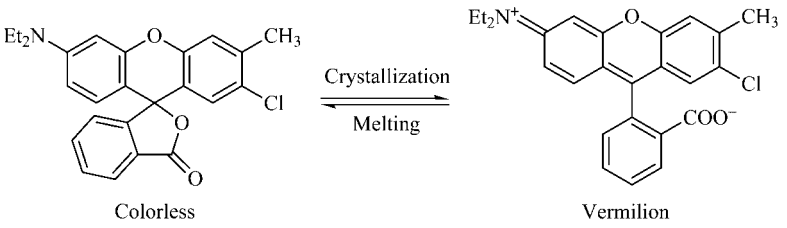

Fig. 3. Reversible lactone ring opening reaction of 2-chloro-6-diethylamino-3-methylfluoran.

the molecular structure of the polymer backbone at their respective gel–sol transition temperature. One of the reported systems consists of polydiacetylene gelled in *o*-dichlorobenzene or other gel-forming solvents (30). Upon heating above the gel–sol transition temperature reversible pronounced color changes are observed. Colors and transition temperatures could be varied by using different solvents as well as by changing the composition. A weak thermochromic effect caused by temperature-dependent molecular changes of the chromophoric group in a gel network has also been reported (31). On heating in benzene a poly[2-(3,7-dimethyloctoxy)-5-methoxy-1,4-phenylenevinylene] gel shows a gradually red to yellow color change at approximately 35°C, which corresponds to the gel–sol transition temperature. After cooling to room temperature the yellow state remains metastable. It eventually reverts after several hours to the red gel phase. The authors explained the thermochromic behavior of this system by a reduction of interchain π–π interaction at the gel to solution transition, at which the relation between aggregated and isolated chain sections abruptly changes.

The first example of a thermochromic effect of dyes embedded in a transparent hydrogel was reported by Seeboth et al. (32). The described thermochromic effect appears by the addition of suitable indicator dyes, with pK_a values between 7.0 and 9.4, to a definite poly(vinyl alcohol) (PVA)/borax/surfactant hydrogel network. With increasing temperature the used gel matrix shifts the equilibrium of the indicator dyes toward their deprotonated forms, leading thereby to gradual color changes with temperature. In dependence on the used indicator dye(s) a switching between a colorless and a colored state or between two or even more different colored states occurred. For example a gradual color change from colorless at 10°C to a deep violet at 80°C was observed for a PVA/borax/surfactant hydrogel containing the so-called Reichard betaine 2,6-diphenyl-4-(2,4,6-triphenyl-1-pyridino)-phenolate (DTPP), whose pH-sensitive equilibrium is shown in Figure 4.

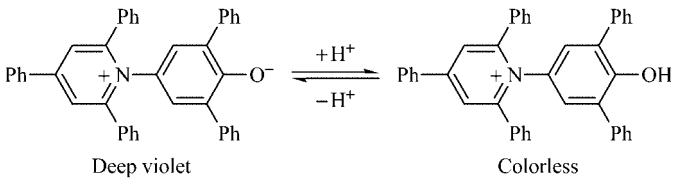

Fig. 4. Proton-transfer equilibrium between the phenol and phenolate form of the indicator dye 2,6-diphenyl-4-(2,4,6-triphenyl-1-pyridino)-phenolate.

Fig. 5. Thermochromic switching of a 3-mm-thick Cresol Red containing PVA/borax/surfactant hydrogel layer placed between two glass plates.

A Cresol Red containing PVA/borax/surfactant hydrogel on the other hand switches from yellow at 10°C to wine-red at 80°C and a Bromothymol Blue and Cresol Red containing PVA/borax/surfactant hydrogel from yellow (below 5°C) via green (between 15 and 25°C) to violet (above 60°C). A photograph displaying the thermochromic switching of the Cresol Red containing PVA/borax/surfactant hydrogel is shown in Figure 5. The 3-mm-thick layer spacing of a double-glazing assembly is filled with this thermochromic hydrogel and partially heated in a hot water bath. While the cold zone remains yellow the color in the hot zone has switched to wine-red. In order to characterize the thermochromic effect in more detail, UV–vis absorption measurements were carried out. As examples of the obtained results the UV–vis absorption spectra of the DTPP and of the Cresol Red containing PVA/borax/surfactant hydrogels measured at different temperatures are displayed in Figures 6 and 7, respectively. One absorption maximum growing continuously with increasing temperature appears in the spectra of the DTPP containing PVA/borax/surfactant hydrogel (Fig. 6). This absorption at about 550 nm is caused by the phenolate form of DTPP and its growing intensity indicates a rising phenolate concentration with increasing temperature. In Figure 7 for all temperatures two absorption maxima, one at 419 nm, which corresponds to the absorption of the phenol form of Cresol Red, and the other one at 581 nm, which corresponds to the absorption of the phenolate form of Cresol Red, are observed. With

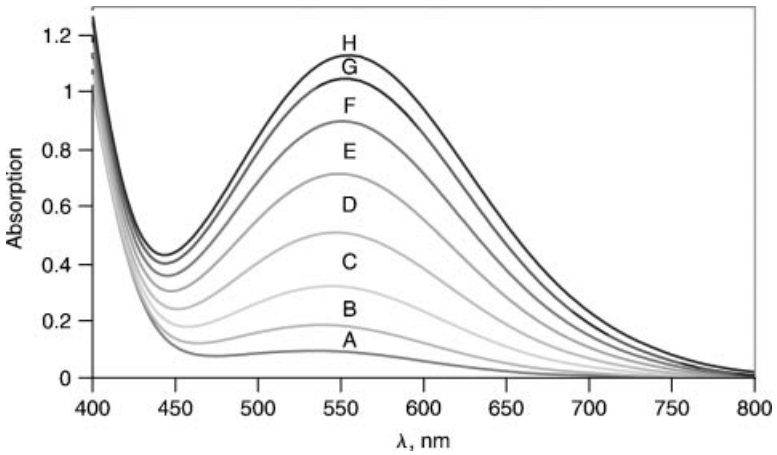

Fig. 6. Visible absorption spectra of a 2,6-diphenyl-4-(2,4,6-triphenyl-1-pyridino)-phenolate containing PVA/borax/surfactant hydrogel in dependence on temperature (d = 1 cm). — 10°C (A); — 20°C (B); — 30°C (C); — 40°C (D); — 50°C (E); — 60°C (F); — 70°C (G); — 80°C (H).

increasing temperature the intensity of the absorption band at 581 nm increases while simultaneously the intensity of the absorption band at 419 nm decreases. All spectral curves meet at an isosbestic point at 486 nm, supporting thereby the suggested model of a temperature-dependent equilibrium between two different forms of the indicator dye as the origin of the observed thermochromic effect.

In addition to the transparency another important feature of these hydrogels is that the thermochromic effect is not accompanied by volume changes. Therefore such hydrogels are applicable for smart windows, large area displays, and tunable color filters.

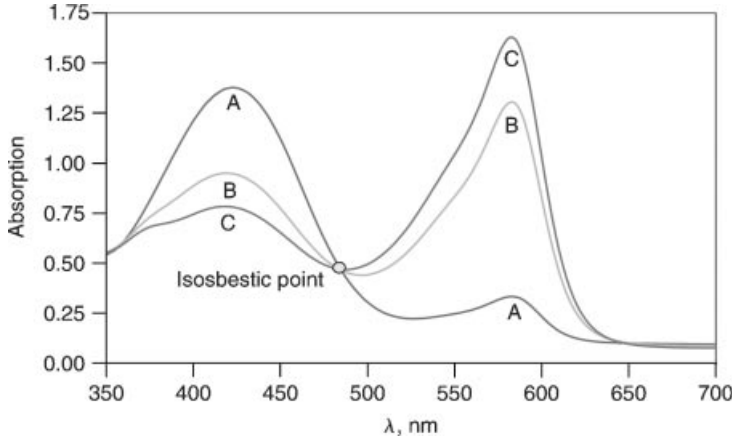

Fig. 7. UV–vis absorption spectra of a Cresol Red containing PVA/borax/surfactant hydrogel in dependence on temperature (d = 1 cm). — 16°C (A); — 60°C (B); — 80°C (C).

Transparency/Scattering Switching

Some thermotropic polymer systems switch at a certain temperature reversibly between a highly transparent and a light scattering state. Such an optical effect can be caused either by a phase transition between an isotropic and an anisotropic (liquid crystalline) state or by a phase separation process. Two different classes of thermotropic polymer materials have been extensively studied in recent years: polymer blends and polymer gels.

Thermotropic Polymer Blends. Only a few pairs of polymers are miscible with one another over the complete concentration range. There are also polymer pairs known which either mix or do not mix depending on temperature; both an increase as well as a decrease of the miscibility (qv) with increasing temperature are possible. In the phase diagrams of such polymer pairs a two-phase region appears either below a so-called upper critical solution temperature (UCST) or above a so-called lower critical solution temperature (LCST). Within a wide concentration range polymer blends of both these systems are thermotropic. Blends with an UCST in the phase diagram switch from translucent to transparent by increasing the temperature, whereas polymer blends of systems with an LCST switch in the opposite manner. For application in sun protecting glazing, a reduction of the transmission with increasing temperature is required and therefore the development of thermotropic polymer blends in recent years has focused on systems with an LCST. In 1993 Siol et al. (33) from the Roehm GmbH developed thermochromic polymer blends consisting of chlorinated rubber and polymethacrylates. Depending on the composition the transition from the transparent into the translucent state (cloud point) could be varied between 60 and 140°C. In the same year Eck et al. (34) presented polymer blends with a much better reversibility of the thermotropic switching. Moreover, cloud points between 30 and 40°C could be realized, which is the required temperature range for sun protecting glazing. These polymer blends were derived from poly(propylene oxide) and a styrene–hydroxyethyl methacrylate copolymer cross-linked with a trifunctional cyclic isocyanate. By cross-linking the copolymer in the presence of poly(propylene oxide) a semi-interpenetrating network is formed leading to an increase of the stability of the microphase separation above the cloud point and thus to a much better reversibility of the thermotropic switching. A similar cross-linked thermotropic polymer blend was developed in 1995 by BASF (35). In the first step blends of poly(propylene oxide) and a copolymer of styrene, hydroxyethyl methacrylate, and a small portion of 4-acroyloxy butyl carbonato benzophenone were prepared. However, instead of adding a cross-linking agent, radical polymerization under UV-light was used to form the semi-interpenetrating network. This method allows preparation of thermotropic coatings first and polymerization to the semi-interpenetrating network later on. In this way, the evenness of the coating surfaces and thus their optical quality could be improved. The optical properties of the two polymer blends prepared by W. Eck and by BASF respectively are presented in References 36 and 37. For a 400-μm-thick layer of the polymer blend prepared by W. Eck on glass a change of the integrated normal-hemispherical transmission from 92% at 20°C to 30% at 90°C and for a 600-μm-thick layer of the polymer blend prepared

by BASF on glass a change of the integrated normal-hemispherical transmission from 89% at 30°C to 38% at 85°C were obtained.

Thermotropic Polymer Gels. Thermotropic polymer gels can be based either on the appearance of lyotropic liquid crystalline phases or on phase separation processes. Similar to polymer blends, phase diagrams of polymer gels may also show LCST and UCST. Because of their greater practical relevance development in recent years has focused on polymer gels in which the phase separation process takes place on heating.

Since their first observation, lyotropic liquid crystalline polymers like poly(benzyl glutamate) (38,39), hydroxypropyl cellulose (40,41), and fully aromatic polyamides (42) have been extensively studied. Common properties of these polymers are their good solubility in water and the structural feature of a more or less rigid polymer backbone (stiff polymer chain). In certain concentration ranges these polymers undergo in water as well as in some organic solvents a transition from an isotropic phase to a polymer solvent system with pronounced long-range order and thus a transition from a transparent into a light scattering state.

The preparation of lyotropic liquid crystalline polymer gel networks and the determination of their thermotropic properties were reported in Reference 43. The investigated systems are poly(ethylene glycol) (PEG)/PVA/borax hydrogels, whereby the concentration of both polymers, their molecular masses, and the degree of cross-linking were varied. Within a wide range of composition the PEG was found to form lyotropic liquid crystalline domains in the PVA/borax hydrogel network as detected by microscopic observations of schlieren and radial-droplet structures between crossed polarizers. In dependence on the composition the transition from the lyotropic liquid crystalline phase into an isotropic liquid phase (clearing temperature) could be shifted between about 15 and 90°C. In all samples this transition takes place without affecting the PVA/borax hydrogel network. As a consequence of this the mechanical properties are not influenced by the optical switching process. On heating above their respective clearing temperature the transparency of the hydrogels were found to increase from below 5% to more than 70%, whereby contrast ratios of up to 85:1 were observed. This value is similar to the contrast ratios of the nematic to isotropic phase transition of thermotropic or polymer dispersed liquid crystals. The transparency versus temperature curves of some selected examples of these PEG/PVA/borax hydrogels as well as of an ethoxylated PVA/borax hydrogel are shown in Figure 8. With rising PVA concentration and increasing molecular mass of the PEG an increase of the clearing temperature and thus of the translucent to transparent switching temperature can be observed. As can be seen, the molecular mass of the PEG also influences the steepness of the transparency changes. While the samples containing PEG with a molecular mass of 20,000 change their transparency within a temperature range of a few degrees, a broadening of the switching temperature range to about 30–40°C takes place by increasing the molecular mass of the PEG to 70,000.

Phase separation processes in gel networks have been well known for a long time. In the past two decades the interest in thermotropic gel networks has rapidly increased because of their potential application in sun protecting glazing. This discussion focuses on recent developments in the preparation of thermotropic polymer gel networks based on synthetic as well as on biopolymers, the influence of

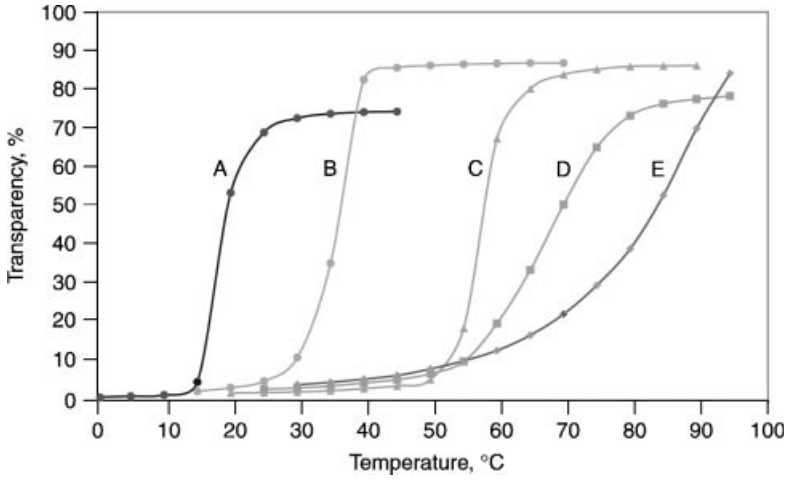

Fig. 8. Transparency versus temperature curves of (A) ethoxylated PVA 50 T; (B) 1% PEG 20 T/12% PVA 70 T; (C) 1% PEG 20 T/15% PVA 70 T; (D) 1% PEG 50 T/12% PVA 70 T; (E) 1% PEG 50 T/15% PVA 70 T.

the addition of salts on the material properties, and the construction of hybrid solar and electrically controlled light filters. Moreover, polymer gel networks which combine thermotropic and color changing properties are reviewed.

Polymer Gel Networks Based on Synthetic Polymers. Gel networks are composed of a swollen cross-linked polymeric network and a solvent. According to the nature of the cross-linker two categories—chemical and physical gels—can be distinguished. In chemical gels the cross-linker connects two polymer chains by covalent bonds. Such gels generally show a strong swelling or shrinking with temperature. Physical gels on the other hand are formed by noncovalent interactions such as ionic interaction, hydrophobic interaction, and/or hydrogen bonding between the polymer chains and a cross-linking agent. Suitable cross-linkers for this purpose are, for example, salts, polyvalent alcohols, borax, phosphonic acid derivatives, and other complex-building organic compounds. Compared with chemical gels the advantage of physical gels is that in most cases their volume does not change much with temperature, which is an essential condition, eg, for their use in sun protecting glazing.

For the preparation of thermotropic polymer gel networks mainly water-soluble polymers like poly(acrylic acid) derivatives, poly(vinyl alcohol), polyglycol, poly(vinyl acetal) resins, polyether, and cellulose derivatives have been successfully used. The first observation of a thermoresponsive volume phase transition in a nonionic hydrogel was reported by Tanaka in 1984 (44). It was found that a PNIPAM hydrogel exhibits a reversible collapse transition at about 34°C, which is accompanied by a transformation from a highly transparent into a translucent state. Hydrogels of PNIPAM or PNIPAM copolymers (45–47) are still the most frequently studied class of temperature responsive hydrogels. The optical properties of the PNIPAM hydrogel and its suitability for the construction of sun protecting glazing were investigated in Reference 48. Although the optical properties of the PNIPAM hydrogel are quite promising, the volume changes and surface

pattern formation at the transition temperature are a strong hindrance for commercial application. In 1995, a thermotropic hydrogel based on poly(methyl vinyl ether) cross-linked with methylene-bisacrylamide was presented by Chahroudi (49,50). A variation of the composition allows adjustment of the switching temperature in the range between about 10 and 65°C. This thermotropic hydrogel system is commercially available as Cloud Gel (Suntek Corp.). Investigations of the temperature dependence of the optical properties of Cloud Gel were carried out by Wilson (36) and by Wittwer et al. (51). In comparison with thermochromic polymer blends much higher contrast ratios of the transparent to translucent switching were obtained. A 1-mm-thick layer of Cloud Gel was found to change the integrated normal-hemispherical transmission in the visible range from 92% at 25°C to 6% at 50°C; just 1°C above the transition temperature a drop down of the transmission by about 65% was observed. Thermotropic hydrogels with excellent switching properties have also been developed by Seeboth et al. (52). In systems which tend to form anisotropic phases, improved switching properties of the transparent to translucent transition were found. The prepared hydrogels consist of polyalkoxides with various polyethylene/polypropylene unit ratios, which were cross-linked by the addition of salts or complex-building organic as well as inorganic compounds. These physical gels generally show no swelling or shrinking with temperature. Depending on the composition, switching temperatures ranging from room temperature to 80°C were obtained and the transparency of the translucent state could be adjusted within wide ranges. Maximum contrast ratios comparable with those of Cloud Gel were obtained. Moreover, in concentration ranges in which anisotropic phases are formed multiple transparence minima and/or maxima occur in the transmission versus temperature curves.

Polymer Gel Networks Based on Biopolymers. Biopolymers, like polysaccharides, are nontoxic and inexpensive raw materials, are available in large quantities, and compared with synthetic polymers, have the benefit of environmental compatibility. Because of these advantages, the suitability of biopolymers for the preparation of novel thermotropic hydrogels has been studied in recent years. Thermotropic hydrogels based on cellulose derivatives in combination with an amphiphilic component and various amounts of NaCl were developed by Watanabe (53). By varying the composition, thermotropic switching temperatures ranging from room temperature up to 60°C could be realized. Moreover, it was possible to modify the rate of transparency change with temperature. With one of these thermotropic hydrogels, an intelligent window a square meter in size was constructed and successfully tested under practical conditions over a period of two years. In Reference 54 thermochromic hydrogels, which are also based on cellulose derivatives, were reported. It was shown that no amphiphilic component is necessary to prevent an irreversible flocculation of suspended hydroxypropyl cellulose, if hydroxyethyl cellulose is added. Although biological decomposition is often mentioned as an advantage of biopolymers, it is also the most important hindrance for their commercial use because contact of the biopolymers with microorganism must be prevented during production and the total life time of the product.

Incorporation of Salts into Thermotropic Aqueous Polymer Systems. The addition of salts can strongly influence the material properties of aqueous polymer

systems. Even small amounts can lead to pronounced changes of the structural and macroscopic properties. Often cross-linking of the polymer chains takes place by the incorporation of the salt ions, whereby three-dimensional networks are formed. Systematic investigations of the effect of different salts on morphology, phase transition temperatures, water binding capability, as well as optical and rheological properties of thermotropic aqueous polymeric systems have been carried out by numerous authors in recent years. The influence of different salts and their concentration on the phase separation temperature of thermotropic aqueous polymer systems was studied by Alexandridis et al. (55) as well as by other authors (56–58). For all investigated systems a linear shift of the phase separation temperature dependent on the salt concentration was observed. Moreover, at a given concentration different salts were found to shift the phase separation temperatures of the aqueous polymer systems according to their salting-in or salting-out strength, which is described by the so-called Hofmeister series. Salts with a salting-in phenomena lead to an increase of the phase separation temperature, whereas salts with a salting-out phenomena have the opposite effect. The influence of LiCl on the water binding properties of an aqueous polyalkoxide system is reported in Reference 59. For four different LiCl contents the water binding properties of the investigated polyalkoxide were determined by DSC measurements. The obtained results are shown in Figure 9. Each curve consists of three linear regions. At low water contents all water is so strongly bound to the polymer that it cannot be frozen (nonfreezing bound water). Above the maximum content of nonfreezing bound water additional water is more weakly bound to the polymer. This type of water freezes at low temperature (freezing bound water). Its melting point and melting enthalpy is lower than that of pure water. Finally, at high water contents the polymer is saturated with water and additional water builds a separate phase of free water. As can be seen in Figure 9, the addition of LiCl influences the water binding properties of the polyalkoxide. Proportional to the LiCl content an increase of the non-freezing-bound water capacity of the polyalkoxide and an increase of the binding enthalpy of freezing-bound water were observed. Both results indicate that the interaction between water and polymeric system becomes stronger with increasing LiCl content. Reference 59 also reports an influence of the addition of LiCl on morphology, as well as optical and rheological properties of the investigated polyalkoxide system. As an example Figure 10 shows the temperature dependence of the optical transmission and of the dynamic viscosity of three samples with a fixed polyether/water mixing ratio of 4:1 and various LiCl contents of 0, 3, and 6 wt%. The observed changes of the optical transmission–temperature curves are caused by morphological changes through the addition of LiCl. The pronounced viscosity changes, on the other hand, show the formation of cross-linked structures, whereby in different phases gelation occurs in different LiCl concentration ranges.

Hybrid Solar and Electrically Controlled Light Filters. Compared to electrochromic glazings, smart windows based on thermotropic hydrogels have the advantages of lower costs and a much higher transparency in the clear state. However, for specific applications switching on demand is required. The construction of a hybrid solar and electrically controlled transmission changing light filter based on thermotropic hydrogels has been described (60). The described arrangement consists of a 2- or 3-mm-thick thermotropic hydrogel layer placed between

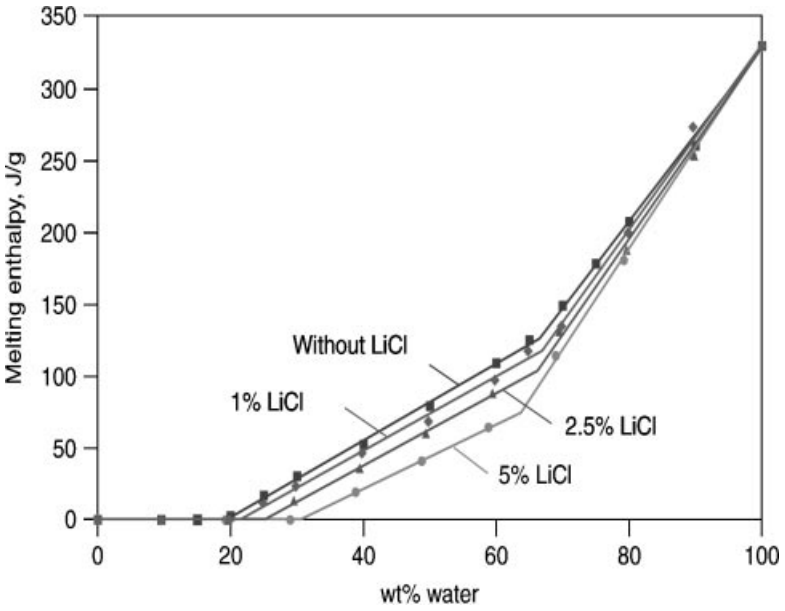

Fig. 9. Water melting enthalpy as a function of water content of polyether/LiCl/water systems.

two tin-doped indium oxide (ITO) coated glass substrates, whereby the ITO layers were placed either inside or outside the double glazing item. When heated passively by solar energy or actively by applying an electric voltage on the ITO layers the thermotropic hydrogel switches from the transparent into the light scattering state. Even for the arrangement where the ITO layers are in direct contact with the hydrogel, no electrolysis was observed under the experimental conditions. Besides the position of the ITO layers, their thickness, the applied voltage as well as the thermochromic hydrogel material used was varied and the switching times of the glazing items were determined. Figure 11 shows the transmission–time curves of one of the investigated light filters at varying applied electric voltages. As can be seen, even 133-nm-thick ITO layers which reduce the maximum transparency of the light filter by about 10% allow fast switching times in combination with high contrast ratios. An increase of the ITO layer thickness decreases the wattage, which is necessary to achieve a constant switching time. On the other hand the transparency of the glazing item is thereby also reduced. For one of the investigated glazing items a transmission change from about 62% to $\leq$ 1% and a switching time of 5 min was achieved by applying a wattage of 0.246 W/cm^2.

It was concluded that a further optimization of all components of the glazing item and especially of the layer thickness as well as the material properties of the incorporated thermotropic hydrogel will lead to a further significant reduction of the required wattage.

Gel Networks for Reversible Transparency and Color Control with Temperature. A novel class of polymer gel networks which change both their color and transparency with changing temperature has been developed (61). Starting from a

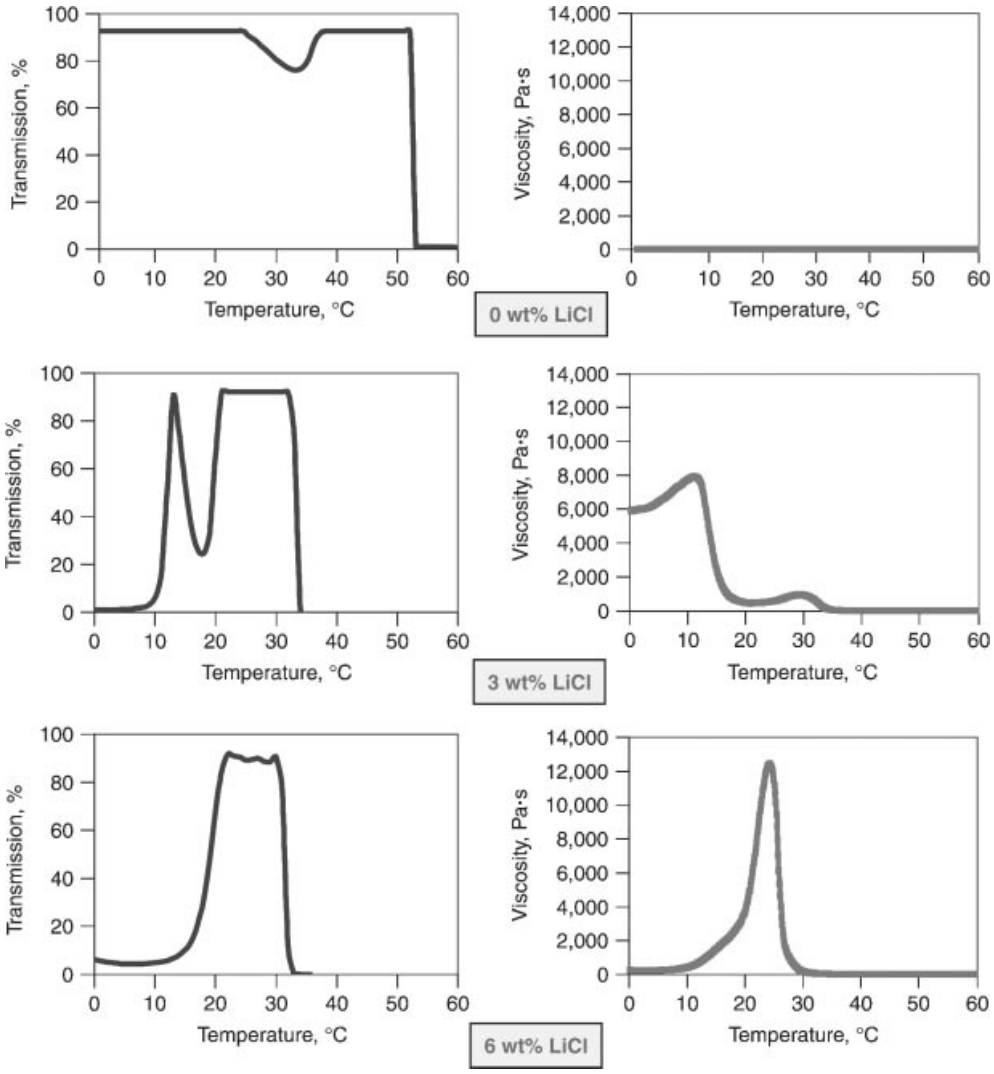

Fig. 10. Temperature dependence of the optical transmission at 600 nm ($d = 1$ cm) and of the dynamic viscosity (measuring conditions: parallel plates of 25-mm diameter, frequency: 1 rad/s) of LiCl containing aqueous polyether samples with a fixed polyether/water mixing ratio of 4:1 and various LiCl contents ranging from 0 to 6 wt%.

thermotropic hydrogel composed of a polyalkoxide and an aqueous LiCl containing buffer solution the color changing properties were obtained by adding one of the pH-sensitive indicator dyes Chlorophenol Red, Nitrazine Yellow, or Bromothymol Blue. The addition of these dyes was found to have only a slight influence on the thermotropic switching behavior of the hydrogel matrix. The switching behavior appears due to a phase separation process as is typical for such polyalkoxide/LiCl hydrogel systems. The color changing effect on the other hand has its origin in temperature-induced pH changes of the gel network similar to the effect observed

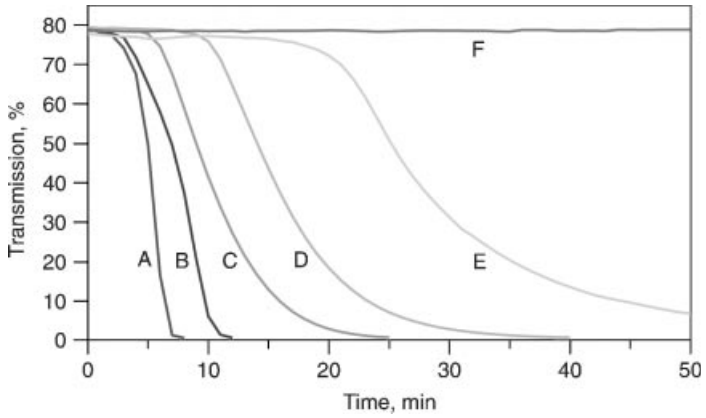

Fig. 11. Transmission versus time curves of a thermotropic gel containing light filter (12 × 15 cm) in dependence on the applied voltages; thickness of the gel layer $d = 3$ mm and thickness of the ITO layers = 133 nm. ___ 8 V/4.8 W (A); ___ 6 V/2.7 W (B); ___ 4 V/1.2 W (C); ___ 3 V/0.7 W (D); ___ 2 V/0.3 W (E); ___ 1 V/0.1 W (F).

earlier for phenol-substituted indicator dyes in a PVA/borax/surfactant gel network (32). As an example the UV–vis absorption spectra at two different temperatures and the transparency versus temperature curve of a hydrogel prepared by mixing 3.95 g polyalkoxide, 0.25 g LiCl, 0.8 g of an aqueous buffer solution (pH 10), and 0.12 g of a 2.2% aqueous solution of Bromothymol Blue are displayed in Figures 12 and 13, respectively. Both effects, the thermotropic switching at about 36°C and the temperature dependent cross over between an absorption band at $\lambda = 408$ nm and one at $\lambda = 617$ nm can be clearly seen. As a result of these effects the hydrogel changes its appearance from green transparent below 33°C, via yellow transparent until about 36°C to yellow translucent above this temperature. With increasing temperature the phenol–phenolate equilibrium of Bromothymol Blue in the polyalkoxide/LiCl/water system is shifted from the green colored phenolate form to the yellow colored phenol form. This result is in contrast to the behavior of phenol-substituted indicator dyes in a PVA/borax/surfactant gel network for which the opposite shift of the phenol–phenolate equilibrium with temperature was observed. Thus it can be concluded that the reversible color change of indicator dyes in gel systems depends on the specific composition of the gel networks. However, the origin of this effect on a molecular level is still under discussion.

Another example of a color and transparency changing gel network is reported in Reference 62. Starting from a Phenol Red containing PVA/borax/surfactant hydrogel which changes its color but not its transparency in dependence on temperature, thermotropic properties were obtained by adding small amounts of a more hydrophobic polymer. For this purpose a polyalkoxide was used. At a content of 0.8 wt% polyalkoxide thermotropic behavior based on a phase separation process was found to appear without affecting the color changing behavior very much. With further increasing polyalkoxide content the degree of the reduction of transparency with temperature is increased and the starting temperature of this process is shifted to lower temperatures. Moreover, the

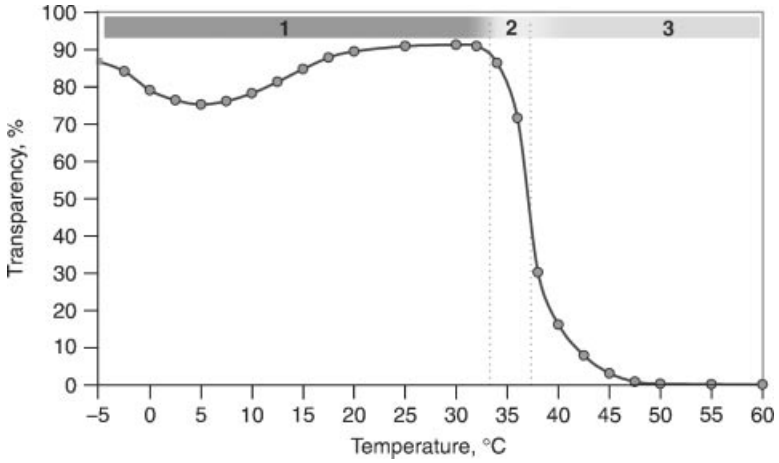

Fig. 12. Transparency versus temperature curve of a Bromothymol Blue (BB) containing hydrogel composed of a polyalkoxide and an aqueous LiCl containing buffer solution ($\lambda = 750$ nm, $d = 0.1$ cm, [BB] $= 1.9 \times 10^{-4}$ mol/L). 1 = green transparent; 2 = yellow transparent; 3 = yellow opaque.

influence of the concentration of the zwitterionic sulfobetaine surfactant on the color changing and thermotropic behavior was studied. PVA/borax/Phenol Red hydrogels containing 1.1 wt% polyalkoxide and various sulfobetaine concentrations below and above their critical micelle concentration (cmc $= 3.8 \times 10^{-3}$ mol/kg) were prepared and the UV–vis absorption spectra as well as the temperature dependence of the transparency of these hydrogels were measured. In the UV–vis absorption spectra two bands occur. The first one at $\lambda = 440$ nm corresponds

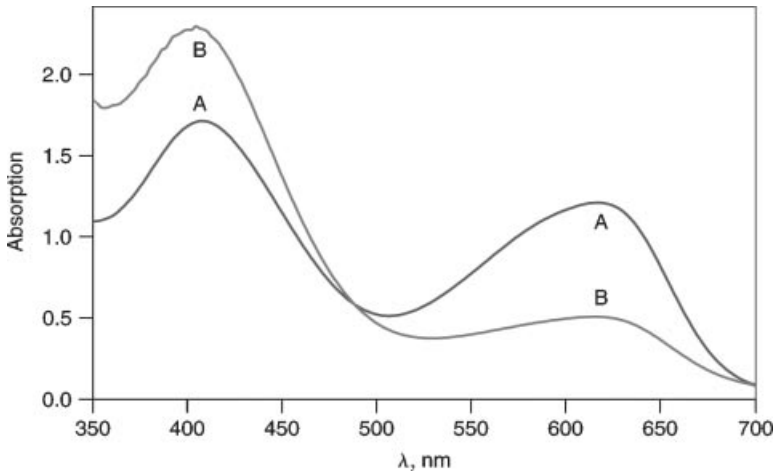

Fig. 13. UV–vis absorption spectra of a Bromothymol Blue containing hydrogel composed of a polyalkoxide and an aqueous LiCl containing buffer solution in dependence on temperature (d = 0.1 cm). —— −5°C (a); —— 38°C (b).

to the phenol form and the second one at $\lambda = 563$ nm to the phenolate form of Phenol Red. With increasing sulfobetaine concentration a decrease of the intensity of both UV–vis absorption bands occur. It is well known that above the cmc surfactants can influence the UV–vis absorption behavior of water-soluble dyes. However, here this effect takes place at the lowest sulfobetaine concentration of 2.5×10^{-3} mol/kg, which is significantly below the cmc. Also, a small but significant and reproducible influence of the surfactant concentration on thermotropic behavior is reported even below the cmc. To explain this behavior the authors suggested the formation of complexes between dye molecules and aggregates of sulfobetaine, but also discussed an interaction of the dye with single sulfobetaine molecules as an alternative model.

Application of Thermochromic Polymers

The potential applications of thermochromic material include temperature tunable light and heat radiation filters, large area displays, and temperature indicators visualizing the temperature of the surrounding medium or the temperature profile of a surface which is coated with the thermochromic material.

Materials changing their color with temperature are already used in a variety of commercial products such as textiles, toys, baby spoons, coffee pots, aquarium thermometers, novelty items, pans with a thermospot, and labels for wine bottles, indicating the proper drinking temperature (63–65). However, the commercialization of thermochromic materials is just at the beginning and certainly this market will rapidly grow in the near future. Potential industrial and processing applications are, eg, monitoring of overheating of machine parts, observation of thermal leaks, and controlling processing temperature. In the field of storage and transportation thermochromic materials with an irreversible switching could assure the observance of required temperature ranges. For example heat-sensitive materials require a storage and transportation temperature below a maximum value and for frozen food the temperature has to kept below 0°C. In medical technology skin temperature indicators might find application for diagnostic purposes. Another big market addresses security aspects. Road signs with integrated thermochromic effects could warn of icy conditions. Thermochromic coatings of heating plates, fire doors, radiators, and other parts of domestic appliances which become hot during their use could indicate that the surface is too hot to be touched. The development of thermochromic polymers suitable for all these applications is actually in progress and in some cases prototypes have already been presented.

The interest in thermotropic materials on the other hand appears more because of their optical properties than because of their ability to detect temperature changes. Such materials are optical shutters for light as well as for heat radiation. The major market for such materials arises from their potential application as functional layers in the construction of sun protecting glazing (66,67). In modern architecture glazing has become a high-tech-component with a wide range of properties and functions. Besides the classic function as viewing window glazing elements enable the use of daylight for the illumination of the building and the passive use of the solar energy for space heating. To realize these functions more and more parts of the building facade are substituted by large area view

and illumination windows, skylights, and sunroofs. In many modern buildings more than 80% of the facade area consists of glazing elements. In buildings with large glazing areas the incident solar radiation plays an important role in energy performance. While on cold days, such as during the winter, the incident solar radiation reduces the energy consumption for space heating, on hot days, such as during the summer, solar radiation causes overheating inside the buildings and thus an enormous increase of the energy consumption for space cooling. To reduce this negative effect regulation of the incident solar radiation is necessary. Today, this is achieved by mechanical optical shutters like venetian blinds, awnings, and sun blinds. An innovative solution which is under development is the use of sun protecting glazings whose optical properties can either be actively adjusted or automatically adjust themselves according to changes of the climatic conditions. Thermotropic glazing in which a functional layer of a thermotropic material is incorporated into the glazing assembly is the most promising type of sun protection glazing and closest to reaching market readiness.

As early as 1950 sun protecting glazing based on a thermotropic gel network was set up and tested in the residence of the Munich zoo for a period of about 10 years. This glazing assembly consists of a mixture of 5 wt% of poly(vinyl methyl ether) in agar-agar filled between a double glazing. However, the transmission change of the glazing assembly was insufficient for commercial use. In more recent

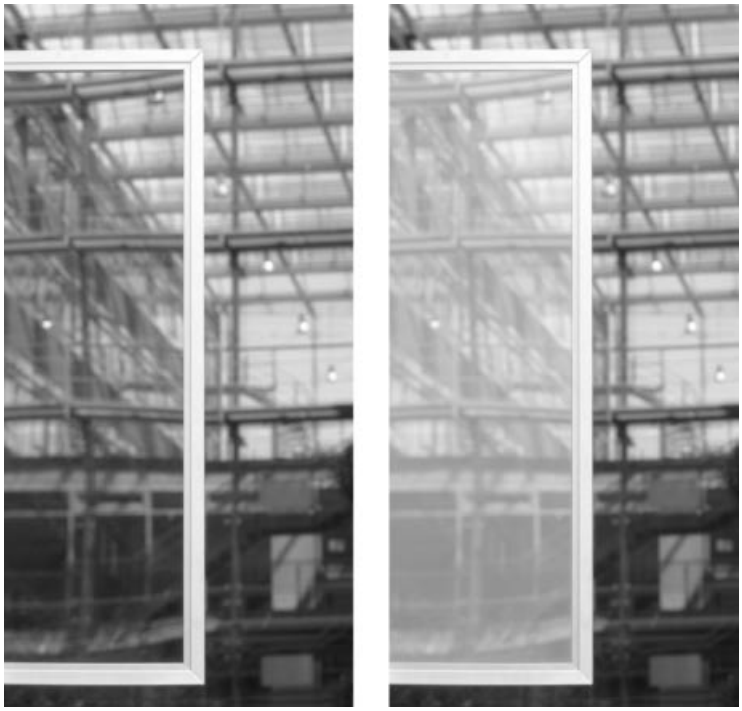

Fig. 14. Switching behavior of a sun protecting glazing (100 × 50 cm) containing a 2-mm-thick thermotropic hydrogel layer at 20°C (left side) and slightly above the switching temperature of 30°C (right side).

years advanced prototypes of sun protecting glazing based on thermotropic hydrogels with strongly improved optical properties have been presented by Chahroudi (49,50), Watanabe (53) and Seeboth (52). These glazings possess a transparency of about 90% in the transparent state and can reach a transparency of less than 10% in the translucent state. Moreover, the transparency change takes place homogeneously without the appearance of streaks. As an example, the switching of a 100 × 50 cm large prototype of a thermotropic glazing presented by Seeboth is shown in Figure 14. To commercialize thermochromic glazings based on hydrogels technology transfer from the laboratory scale to an industrial scale has to take place. Thus, for example, an automated production line for putting the polymer between the double glazing could be established.

BIBLIOGRAPHY

1. H. S. Kitzerow and C. Bahr, eds., *Chirality in Liquid Crystals*, Springer, New York, 2001.
2. K. Hiltrop, E. Figgemeier, M. Pape, and J. Partyka, in W. Kuczynski, ed., *Self-Organization in Chiral Liquid Crystals*, Scientific Publishers OWN, Poznan, Poland, 1997, p. 35.
3. T.-A. Yamagishi and P. Sixou, *Polymer* **36**, 2315 (1995).
4. N. Tamaoki, *Adv. Mater.* **13**, 1135 (2001).
5. H. Finkelmann, J. Koldehoff, and H. Ringsdorf, *Angew. Chem., Int. Ed. Engl.* **17**, 935 (1978).
6. S.-L. Tseng, G. V. Laivins, and D. G. Gray, *Macromolecules* **15**, 1262 (1982).
7. J. Watanabe, T. Nagase, H. Itoh, T. Ishi, and T. Satoh, *Mol. Cryst. Liq. Cryst.* **164**, 135 (1988).
8. T. Tsutsui and T. Tanaka, *Polymer* **21**, 1351 (1980).
9. P. J. Shannon, *Macromolecules* **17**, 1873 (1984).
10. D. J. Broer, J. Lub, and G. N. Mol, *Nature* **378**, 467 (1995).
11. M. Muller, R. Zentel, and H. Keller, *Adv. Mater.* **9**, 159 (1997).
12. R. A. M. Hikmet and R. Polesso, *Adv. Mater.* **14**, 502 (2002).
13. S. Munoz-Guerra, F. Lopez-Carrasquero, C. Aleman, M. Morillo, V. Castelletto, and I. Hamley, *Adv. Mater.* **14**, 203 (2002).
14. H. Fujimatsu, S. Ogasawara, H. Ihara, T. Takashima, K. Toyaba, and S. Kuroiwa, *Coll. Polym. Sci.* **266**, 688 (1988).
15. H. Fujimatsu and S. Kuroiwa, *Coll. Polym. Sci.* **265**, 938 (1987).
16. J. M. Weissman, H. B. Sunkara, A. S. Tse, and S. A. Asher, *Science* **274**, 959 (1996).
17. T. Skotheim, J. R. Reynolds, and R. L. Elsenbaumer, eds., *Handbook of Conducting Polymers*, 2nd ed., Marcel Dekker, New York, 1997.
18. L. Bredas and R. Silbey, eds., *Conjugated Polymers*, Kluwer, Dordrecht, the Netherlands, 1991.
19. D. N. Batchelder, *Contemp. Phys.* **29**, 3 (1988).
20. M. Leclerc, *Adv. Mater.* **11**, 1491 (1999).
21. J. G. Masters, J. M. Ginder, A. G. MacDiarmid, and A. J. Epstein, *J. Chem. Phys.* **96**, 4768 (1992).
22. N. Hirota, N. Hisamatsu, S. Maeda, H. Tsukahara, and K. Hyodo, *Synth. Met.* **80**, 67 (1996).
23. P. T. Hammond and M. F. Rubner, *Macromolecules* **30**, 5773 (1997).
24. A. F. Thünemann, S. Janietz, S. Anlauf, and A. Wedel, *J. Mater. Chem.* **10**, 2652 (2000).

25. B. L. Lucht, W. B. Euler, and O. J. Gregory, Oral Contribution POLY 307 presented at the *223rd American Chemical Society National Meeting*, Orlando, April 7–11, 2002.
26. C. Beildeck, B. L. Lucht, and W. B. Euler, *Polym. Prepr.* **42**, 211 (2001).
27. A. Seeboth, J. Kriwanek, and D. Lötzsch, Oral Contribution 2.1.3 presented at the *Polydays 2002*, Berlin, Germany, Aug. 30 to Sept. 2, 2002.
28. U.S. Pat. 4,957,949 (Sept. 18, 1990), M. Kamada, T. Maeda, T. Kobayashi, and G. Shimizu (to Matsui Shikiso Chemical Co., Ltd.).
29. R. Muthyala, ed., *Chemistry and Applications of Leuco Dyes*, Plenum Press, New York, 1997.
30. U.S. Pat. 4,439,346 (Mar. 27, 1984), G. N. Patel and D. M. Ivory (to Allied Corp.).
31. G. H. Gelnick, J. M. Warman, and E. G. J. Staring, *J. Phys. Chem.* **100**, 5485 (1996).
32. A. Seeboth, J. Kriwanek, and R. Vetter, *J. Mater. Chem.* **9**, 2277 (1999).
33. Ger. Pat. 3436477 (May 19, 1993), W. Siol, H. J. Otto, and U. Terbrack (to Röhm GmbH).
34. Ger. Pat. 4206317 (Sept. 2, 1993), W. Eck, H. J. Cantow, and V. Wittwer (to Fraunhofer-Gesellschaft zur Förderung der angewandten Forschung eV).
35. Ger. Pat. 4408156 A1 (Sept. 14, 1995), E. Jahns (to BASF AG).
36. H. R. Wilson, *SPIE* **2255**, 214 (1994).
37. H. R. Wilson, *SPIE* **2255**, 473 (1994).
38. A. E. Elliot and E. J. Ambrose, *Discuss. Faraday Soc.* **9**, 246 (1950).
39. C. Robinson, J. C. Ward, and R. B. Beevers, *Discuss. Faraday Soc.* **25**, 29 (1958).
40. R. S. Werbowji and D. G. Gray, *Macromolecules* **13**, 69 (1980).
41. L. Okrasa, J. Ulanski, P. Wojciechowski, G. Boiteux, and G. Seytre, *J. Non-Cryst. Solids* **235–237**, 658 (1998).
42. S. L. Kwolek, P. W. Morgan, J. R. Schaefgen, and J. R. Gulrich, *Macromolecules* **10**, 1390 (1977).
43. A. Seeboth and H. R. Holzbauer, *Adv. Mater.* **8**, 408 (1996).
44. T. Tanaka and Y. Hirokawa, *J. Chem. Phys.* **81**, 6379 (1984).
45. M. S. Jones, *Eur. Polym. J.* **35**, 795 (1999).
46. B. Yildiz, B. Isik, and M. Kis, *Eur. Polym. J.* **38**, 1343 (2002).
47. L. Zhu, G. Zhu, M. Li, E. Wang, R. Zhu, and X. Qi, *Eur. Polym. J.* **38**, 2503 (2002).
48. M. Zrinyi, A. Szilagyi, G. Filipcsei, J. Feher, J. Szalma, and G. Moczar, *Polym. Adv. Technol.* **12**, 501 (2001).
49. U.S. Pat. 4307942 (1981), D. Chahroudi.
50. U.S. Pat. 5404245 (1995), D. Chahroudi.
51. A. Beck, W. Körner, H. Scheller, J. Fricke, W. Platzer, and V. Wittwer, *Sol. Energy Mater. Sol. Cells* **36**, 339 (1995).
52. A. Seeboth and H.-R. Holzbauer, *Int. J. Restoration Build. Monuments* **4**, 507 (1998).
53. H. Watanabe, *Sol. Energy Mater. Sol. Cells* **54**, 203 (1998).
54. J. Schneider and A. Seeboth, *Mater. Sci. Eng. Technol.* **31**, 1 (2000).
55. P. Alexandridis and J. F. Holzwarth, *Langmuir* **13**, 6074 (1997).
56. Th. Fischer, H.-R. Holzbauer, and A. Seeboth, *Mat.-wiss. u. Werkstofftech.* **30**, 473 (1999).
57. K. Suwa, K. Yamamoto, M. Akashi, K. Takano, N. Tanaka, and S. Kunugi, *Colloid Polym. Sci.* **276**, 529 (1998).
58. H. Okamura, S. Masuda, K. Minagawa, T. Mori, and M. Tanaka, *Eur. Polym. J.* **38**, 639 (2002).
59. A. Seeboth, D. Lötzsch, and E. Potechius, *Colloid Polym. Sci.* **279**, 696 (2001).
60. Th. Fischer, R. Lange, and A. Seeboth, *Sol. Energy Mater. Sol. Cells* **64**, 321 (2000).
61. A. Seeboth, J. Kriwanek, and R. Vetter, *Adv. Mater.* **12**, 1424 (2000).

62. J. Kriwanek, R. Vetter, D. Lötzsch, and A. Seeboth, *Polym. Adv. Technol.* **14**, 79 (2003).
63. M. A. White and M. LeBlanc, *J. Chem. Educ.* **76**, 1201 (1999).
64. D. Aitken, S. M. Burkinshaw, J. Griffiths, and A. D. Towns, *Rev. Progr. Coloration* **25**, 1 (1996).
65. P. Bamfield, *Chromic Phenomena–Technological Applications of Colour Chemistry*, The Royal Society of Chemistry, Cambridge, 2001.
66. C. G. Granqvist, *Solid State Mater. Sci.* **16**, 291 (1990).
67. A. Seeboth, J. Schneider, and A. Patzak, *Sol. Energy Mater. Sol. Cells* **60**, 263 (2000).

ARNO SEEBOTH
DETLEF LÖTZSCH
Fraunhofer-Institut für Angewandte Polymerforschung

THERMODYNAMIC PROPERTIES OF POLYMERS

Introduction

The thermodynamic properties of macromolecules cover a broad field of materials science. As with any material, macromolecules are well described if two sets of information are available: structure and energetics. Each of the two information sets can be separated into a microscopic and a macroscopic part. The microscopic description deals with matter on an atomic scale and with sizes in the nanometer range, and the macroscopic description, on a phase or larger scale, with sizes larger than micrometers. The thermodynamic properties cover the macroscopic description of energetics. For full understanding, however, the connection to the microscopic description is needed, which is achieved through statistical thermodynamics (qv). Another link to the microscopic description is offered by the kinetics that can be observed macroscopically, but for its interpretation and understanding a microscopic-level model must be available.

For many years, the thermodynamic description of macromolecules lagged behind other materials because of the unique tendency of polymeric systems to assume nonequilibrium states. Most standard sources of thermodynamic data are, thus, almost devoid of polymer information (1–7). Much of the aversion to include polymer data in standard reference sources can be traced to their nonequilibrium nature. In the meantime, polymer scientists have learned to recognize equilibrium states and utilize nonequilibrium states to explore the history of samples. For a nonequilibrium sample it is possible, for example, to thermally establish how it was transferred into the solid state (determination of the thermal and mechanical history). More recently, it was discovered with the use of temperature-modulated differential scanning calorimetry (TMDSC) that within the global, nonequilibrium structure of semicrystalline polymers, locally reversible melting and crystallization processes are possible on a nanophase level (8).

Encyclopedia of Polymer Science and Technology. Copyright John Wiley & Sons, Inc. All rights reserved.

Equilibrium thermodynamic data are presented here to provide a base on which to judge the material on hand. It must always, however, be kept in mind that the actual samples analyzed are often not in equilibrium. Particularly, semicrystalline samples are not fully crystalline, do not contain perfect crystals that melt at the equilibrium melting temperature, and do not phase separate or mix when the thermodynamics are favorable (9–11). Similarly, many data must still be questioned as to their closeness to equilibrium or to the perfection of their extrapolation to equilibrium.

Basic to the thermodynamic description is the heat capacity which is defined as the partial differential $C_p = (\partial H/\partial T)_{n,p}$, where H is the enthalpy and T the temperature. The partial differential is taken at constant pressure and composition, as indicated by the subscripts p and n, respectively; A close link between microscopic and macroscopic description is possible for this fundamental property. The integral thermodynamic functions include enthalpy H entropy S, and free enthalpy G (Gibbs function). In addition, information on pressure p, volume V, and temperature T is of importance (PVT properties). The transition parameters of pure, one-component systems are seen as first-order and glass transitions. Mesophase transitions, in general, were reviewed (12) and the effect of specific interest to polymers, the conformational disorder, was described in more detail (13). The broad field of multicomponent systems is particularly troubled by nonequilibrium behavior. Polymerization thermodynamics relies on the properties of the monomers and does not have as many problems with nonequilibrium.

The instrumentation for (14) is covered mainly by calorimetry (15), thermogravimetry (16), and (17,18). Calorimetry is categorized into adiabatic calorimetry, covering the temperature range from 10 to 400 K (19–21), and differential scanning calorimetry (DSC), covering the temperature range from 200 to 1000 K (22,23). Isothermal or close-to-isothermal calorimetry includes combustion, reaction, and dissolution calorimetry (24). Much information on thermal analysis is collected in the Proceedings of the International Confederation for Thermal Analysis and Calorimetry (ICTAC) (25), and the North American Thermal Analysis Society (NATAS) (26). The broad range of literature is abstracted selectively (27). The thermal characterization of polymeric materials was described for the first time in an extensive treatise covering many types of polymers and many techniques of Thermal Analysis (qv) (28).

Heat Capacities of Solids and Liquids

Heat capacity C_p is of importance not only for the evaluation of the integral thermodynamic properties, such as enthalpy, entropy, and free enthalpy (Gibbs function), but also for the precise separation of latent heats of transition from motional energies and for the determination of glass transitions (29). Experimentally, in the low temperature region (0–100 K), heat capacity measurements are dominated by adiabatic calorimetry. Above that region, DSC has gained increasing prominence. Typical precision of measurements is now $\pm 3\%$ in the temperature range above 10 K for both solid and liquid heat capacities, although modern methods of a temperature-modulated DSC may increase the precision to levels as high as

±0.1% by eliminating heat losses through measuring the change of the calorimeter response as a function of frequency response of the calorimeter (30).

Below 10 K, the heat capacity C_p, although of interest for the theory of motion, does not contribute much to the integral H at higher temperature. It is dependent on the physical state (crystalline, semicrystalline, or amorphous), whereas the C_p of solids, from about 50 K to the glass-transition temperature T_g, is largely independent of the physical structure.

The theory of the heat capacity of solids is well established (31). The heat capacity is largely of vibrational origin and to a great extent described by the harmonic oscillator approximation. Classifying the vibrations into skeletal and group vibrations is useful. The former are of relatively low frequency, strongly coupled, and represent the intra- and intermolecular vibrations of the chain molecules. The skeletal vibrations dominate the heat capacity in the low temperature region (<100 K). All efforts to calculate the intermolecular, skeletal vibrations from crystal-structure and force-constant data were unsuccessful in the past. Heat capacity measurements still provide the best means for evaluation of the low frequency, integral vibrational spectrum. The intramolecular skeletal vibrations are somewhat higher in frequency and are accessible in their upper frequency range through isolated-chain normal-mode calculations (32). Such calculations also permit the evaluation of the numerous group vibrations. After an approximate vibrational spectrum has been established, the heat capacity at constant volume can be calculated up to, and even above, equilibrium melting temperatures of the polymeric materials. Figure 1 shows the cumulative frequency spectrum of polyoxymethylene (POM), and Figure 2 illustrates the the corresponding heat capacity contributions of the skeletal and group vibrations (**D** and **C**, respectively) as well as the total C_v (**B**) and C_p (**A**) (for theta temperatures, see Table 1).

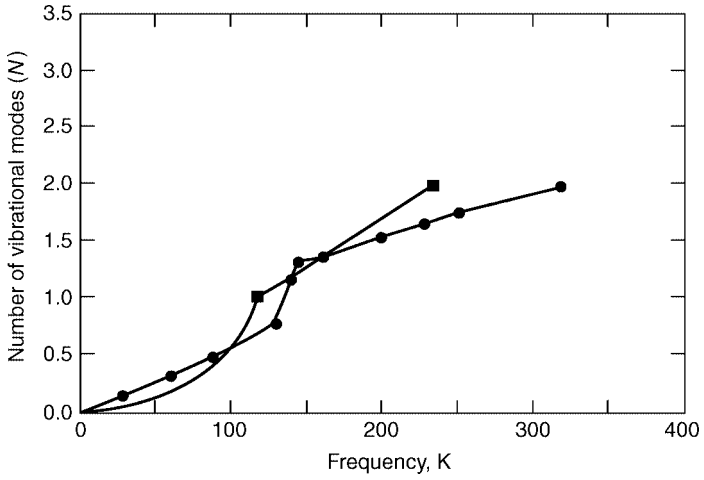

Fig. 1. Cumulative vibrational spectrum of the skeletal vibrations of polyoxymethylene (POM). ●, Experimental crystalline POM; ■, calculated with the Tarasov equation ($N = 2$).

Table 1. Thermal Properties of Linear Macromolecules[a]

	T_g	ΔC_p[b]	T_m	ΔH_f[c]	SHG[d]	S_0[e]	θ_1	θ_3	N[f]	C_p[g]
Poly(alkenes)										
Polyethylene [poly(methylene)]										
(c)	—	—	414.6	4.11	X	0	519	158	2	0.1–410
(a)	237	10.5(1)	—	—	X	3.0	519	80	2	0.1–600
Polypropylene										
(c)	—	—	460.7	8.70	X	0	714	91	7	10–460
(a)	270	19.2(2)*	—	—	X	5.2	633	78	7	10–600
Poly-1-butene										
(c)	—	—	411.2	7.00	X	0	618	93	9	10–249**
(a)	249	23.1(2)	—	—	X	6.4	618	(80)	9	249–630
Poly-1-pentene										
(c)	—	—	403.2	6.30	X	0	580	(93)	11	200–233**
(a)	233	27.0(2)	—	—	X	(0.9)	580	(80)	11	233–470
Poly-1-hexene										
(a)	223	25.1(2)	—	—	X	?	563	86	13	20–290
Polycyclopentene										
(a)	173	28.9(4)	—	—	X	?	582	88	10	10–320
Poly(4-methyl-1-pentene)										
(c)	—	—	523.2	9.96	X	0	660	(93)	14	80–303**
(a)	303	30.1(1+1)	—	—	?	?	660	?	14	303–540
Polyisobutylene										
(c)	—	—	317	12.0	X	0	850	?	10	?
(a)	200	21.3(2)	—	—	X	?	850	103	10	15–380
Poly(1-butenylene), *cis*										
(c)	—	—	284.7	9.20	X	0	589	87	8	30–171**
(a)	171	27.2(3)*	—	—	X	17.5	589	?	8	171–350
Poly(1-butenylene), *trans*										
(c)	—	—	437	3.73[h]	X	0	599	95	8	30–190**
(a)	190	28.0(3)*	—	—	X	16.2	599	?	8	190–500
Poly-1,4-(2-methyl-butadiene), *cis*										
(c)	—	—	301.2	4.35	?	0	647	(120)	1	?
(a)	200	30.9(3)	—	—	X	?	647	58	11	2–360
Poly(vinyl)s and Related Polymers										
Poly(vinyl alcohol)										
(c)	—	—	538	7.11	X	0	495	119	4	60–300**
(a)	358	?(2)	—	—	?	?	495	?	4	?
Poly(vinyl acetate)										
(a)	304	40.7(?)	—	—	X	?	600	(86)	11	80–370
Poly(vinyl fluoride)										
(c)	—	—	503.2	7.54	X	0	440	105	4	80–314**
(a)	314	17.0(2)*	—	—	X	9.4	440	?	4	480–530[i]
Poly(vinylidene fluoride)										
(c)	—	—	483.2	6.70	X	0	346	66	4	5–212**
(a)	212	21.2(2)*	—	—	X	5.1	346	?	4	450–580[i]
Polytrifluoroethylene										
(c)	—	—	495.2	5.44	X	0	315	56	4	25–280**
(a)	280	13.8(2)*	—	—	X	13	315	?	4	480–600[i]
Polytetrafluoroethylene										
(c)	—	—	605	4.10[j]	X	0	250	54	2	0.3–280[i]
(a)	200	9.4(1)	—	—	X	3.3	250	?	2	180–700

Table 1. (Continued)

	T_g	ΔC_p[b]	T_m	ΔH_f[c]	SHG[d]	S_0[e]	θ_1	θ_3	N[f]	C_p[g]
Poly(vinyl chloride)										
(a)	354	19.4(2)	—	—	X	2.4	354	45	4	5–380
Poly(vinylidene chloride)										
(c)	—	—	463	?	X	0	308	119	4	60–255**
(a)	255	?(2)	—	?		?	308	?	4	?
Poly(chlorotrifluoroethylene)										
(c)	—	—	493	5.02	X	0	215	42	4	1–325**
(a)	325	?(2)	—	—	?	?	215	?	4	?
Polystyrene										
(c)[k]	—	—	516.2	10.0	X	0	284	110	6	?
(a)	373	30.8(1+1)	—	—	X	4.4	284	48	6	0.1–600
Poly(α-methylstyrene)										
(a)	441	25.3(1+1)	—	—	X	?	450	48	9	1.4–490
Aliphatic Poly(oxide)s										
Poly(oxymethylene)										
(c)	—	—	457.2	9.79	X	0	232	117	2	0.1–390
(a)	190	28.2(2)*	—	—	X	3.4	232	?	2	190–600
Poly(oxyethylene)										
(c)	—	—	342	8.66	X	0	353	114	4	10–342
(a)	206	38.2(3)*	—	—	X	8.1	353	?	4	206–450
Poly(oxymethyleneoxyethylene)										
(c)	—	—	328	16.7	X	0	317	114	6	10–328**
(a)	209	62.1(5)*	—	—	X	27	317	?	6	209–390
Poly(oxytrimethylene)										
(c)	—	—	308	9.44	X	0	433	100	6	1.0–308
(a)	195	46.8(4)*	—	—	X	7.8	433	40	6	1.0–330
Poly(oxytetramethylene)										
(c)	—	—	330	14.4	X	0	436	90	8	5–189**
(a)	189	57.0(5)*	—	—	X	17	436	?	8	189–340
Poly(oxyoctamethylene)										
(c)	—	—	347	29.3	X	0	480	137	16	14–255**
(a)	255	83.1(9)*	—	—	X	63	480	?	16	350–360
Poly(oxymethyleneoxytetramethylene)										
(c)	—	—	296	14.3	X	0	392	122	10	10–296
(a)	189	83.8(7)*	—	—	X	15	392	?	10	189–360
Poly(oxypropylene)										
(c)	—	—	348	8.40	X	0	494	112	7	80–198**
(a)	198	32.1(3)*	—	—	X	9.4	494	?	7	198–370
Poly(acrylate)s and (methacrylate)s										
Poly(methyl acrylate)										
(a)	279	42.3(?)	—	—	X	?	552	86	11	10–500
Poly(ethyl acrylate)										
(a)	249	45.6(?)	—	—	X	?	543	89	13	90–500
Poly(*n*-butyl acrylate)										
(a)	218	45.4(?)	—	—	X	?	518	88	17	80–440
Poly(isobutyl acrylate)										
(a)	249	36.6(?)	—	—	X	?	(524)	(90)	18	230–500
Poly(methyl methacrylate)										
(c)	—	—	450	9.60	X	0	680	(140)	14	?
(a)	378	32.7(?)	—	—	X	7.1	680	67	14	0.2–550

Table 1. (Continued)

	T_g	ΔC_p[b]	T_m	ΔH_f[c]	SHG[d]	S_0[e]	θ_1	θ_3	N[f]	C_p[g]
Poly(ethyl methacrylate)										
(a)	338	31.7(?)	—	—	X	?	622	(60)	16	80–380
Poly(*n*-butyl methacrylate)										
(a)	293	27.9(?)	—	—	X	?	559	58	20	80–440
Poly(isobutyl methacrylate)										
(a)	326	39.0(?)	—	—	X	?	595	(60)	21	230–400
Polyacrylonitrile										
(a)	378	?(?)	—	—	X	?	980	62	6	60–370
Aliphatic Poly(ester)s										
Polyglycolide										
(c)	—	—	501	9.74	X	0	521	98	6	10–318**
(a)	318	31.8(2)	—	—	X	7.6	521	?	6	318–550
Poly(ethylene oxalate)										
(c)	—	—	450	23	?	0	533	?	12	?
(a)	306	56.2(4)	—	—	X	?	533	89	12	10–360
Poly(β-propiolactone)										
(c)	—	—	366	10.9	X	0	522	85	8	10–249**
(a)	249	42.9(3)	—	—	X	15.2	522	?	8	249–400
Poly(L-lactic acid)										
(c)	—	—	480	6.55	X	0	574	(52)	9	190–470**
(a)	332.5	43.8(2+1)	—	—	X	1.7	574	52	9	5.0–250
Poly(γ-butyrolactone)										
(c)	—	—	337.5	14.0	X	0	474	96	10	10–214**
(a)	214	52.0(4)	—	—	X	20.6	474	?	10	214–350
Poly(δ-valerolactone)										
(c)	—	—	331	18.8	X	0	502	101	12	10–207**
(a)	207	60.9(5)	—	—	X	32	502	?	12	207–350
Poly(ε-caprolactone)										
(c)	—	—	342.2	17.9	X	0	491	101	14	10–209**
(a)	209	67.4(6)	—	—	X	23	491	?	14	209–350
Polyundecanolactone										
(c)	—	—	365	39.5	X	0	528	105	24	10–227**
(a)	227	102.7(11)	—	—	X	68	528	?	24	227–400
Polytridecanolactone										
(c)	—	—	368	50.6	X	0	519	112	28	10–229**
(a)	229	115.8(13)	—	—	X	92	519	?	28	229–370
Polypentadecanolactone										
(c)	—	—	370.5	63.4	X	0	525	114	32	10–251**
(a)	251	124(15)	—	—	X	128	525	?	32	251–370
Poly(pivalolactone)										
(c)	—	—	513.0	14.8	X	0	585	(98)	14	150–267**
(a)	267	37.6(3)	—	—	X	16.5	585	?	14	267–550
Poly(butylene adipate)										
(c)	—	—	328.8	?	X	0	514	(108)	24	80–199**
(a)	199	140.0(?)	—	—	?	?	514	?	24	199–450
Poly(ethylene sebacate)										
(c)	—	—	356.2	31.9	X	0	514	(158)	28	120–245**
(a)	245	127.0(12)	—	—	X	(26)	514	(80)	28	245–410
Poly(dimethyl itaconate)										
(a)	377	54.2(?)	—	—	X	?	557	(67)	20	110–450

Table 1. (Continued)

	T_g	ΔC_p[b]	T_m	ΔH_f[c]	SHG[d]	S_0[e]	θ_1	θ_3	N[f]	C_p[g]
Poly(di-*n*-propyl itaconate)										
(a)	304	57.8(?)	—	—	X	?	428	(67)	28	110–410
Poly(di-*n*-heptyl itaconate)										
(a)	172[l]	45.6(?)	—	—	X	?	582	(67)	44	110–170
Poly(di-*n*-octyl itaconate)										
(a)	178[l]	99.1(?)	—	—	X	?	518	(67)	48	110–170
Poly(di-*n*-nonyl itaconate)										
(a)	187[l]	183.4(?)	—	—	X	?	589	(67)	52	110–180
Aliphatic Poly(amide)s										
Nylon 6										
(c)	—	—	533	26.0	X	0	544	(67)	14	70–313**
(a)	313	53.7(6)*	—	—	X	37	544	?	14	313–600
Nylon 11										
(c)	—	—	493	44.7	X	0	420	(67)	24	230–316**
(a)	316	68.4(11)*	—	—	X	78	420	?	24	316–550
Nylon 12										
(c)	—	—	500	48.4	X	0	455	(67)	26	230–314**
(a)	314	74.3(12)*	—	—	X	82	455	?	26	314–540
Nylon 6,6 α										
(c)	—	—	574	57.8	X	0	614	84	28	0.3–323**
(a)	323	115.5(12)*	—	—	X	77	614	?	28	323–600
Nylon 6,9										
(c)	—	—	500	69	X	0	579	(84)	34	230–331**
(a)	331	109.5(15)*	—	—	X	114	579	?	34	331–590
Nylon 6,10										
(c)	—	—	506	71.7	X	0	543	(84)	36	230–323**
(a)	323	118.0(16)*	—	—	X	120	543	?	36	323–590
Nylon 6,12										
(c)	—	—	520	80.1	X	0	533	(84)	40	230–319**
(a)	319	141.4(18)*	—	—	X	124	533	?	40	319–600
Polymethacrylamide										
(a)	?	?	—	—	X	?	523	(193)	10	60–300
Poly(amino acid)s										
Polyglycine II										
(c)	—	—	?	?	X	0	750	81	6	1.4–390**
Poly(L-alanine)										
(c)	—	—	?	?	X	0	634	58	9	1.6–390**
Poly(L-valine)										
(c)	—	—	?	?	X	0	664	65	14	2.0–390**
Poly(L-serine)										
(c)	—	—	?	?	X	0	685	(68)	10	220–390**
(a)	(400)[m]	(30.0)[m]	—	—	X	?	685	?	10	?
Poly(L-leucine)										
(c)	—	—	?	?	X	0	625	(68)	16	220–390**
Poly(L-aspartic acid) sodium salt										
(c)	—	—	?	?	X	0	597	(68)	14	220–390**
Poly(L-glutamic acid) sodium salt										
(c)	—	—	?	?	X	0	907	(68)	16	220–390**
Poly(L-phenylalanine)										
(c)	—	—	?	?	X	0	610	(68)	11	220–390**

Table 1. (Continued)

	T_g	ΔC_p[b]	T_m	ΔH_f[c]	SHG[d]	S_0[e]	θ_1	θ_3	N[f]	C_p[g]
Poly(L-tyrosine)										
(c)	—	—	?	?	X	0	729	(68)	13	220–390**
Poly(L-asparagine)										
(c)	—	—	?	?	X	0	569	(68)	12	220–390**
Poly(L-tryptophan)										
(c)	—	—	?	?	X	0	793	(68)	13	220–390**
Poly(L-proline)										
(c)	—	—	?	?	X	0	691	(68)	11	220–390**
Poly(L-lysine) hydrogen bromide										
(c)	—	—	?	?	X	0	636	(68)	20	220–390**
Poly(L-methionine)										
(c)	—	—	?	?	X	0	691	(68)	15	220–390**
(a)	(400)[m]	(61.0)[m]	—	—	X	?	691	?	15	?
Poly(L-histidine)										
(c)	—	—	?	?	X	0	808	(68)	13	220–390**
Poly(L-histidine) hydrogen chloride										
(c)	—	—	?	?	X	0	745	(68)	16	220–390**
Poly(L-arginine) hydrogen chloride										
(c)	—	—	?	?	X	0	610	(68)	23	220–390**
Phenylene Containing Polymers										
Poly(*p*-phenylene)										
(c)	—	—	>1000	?	X	0	544	(54)	3	80–300**
Poly(thio-1,4-phenylene)										
(c)	—	—	593	8.65	X	0	566	(54)	5	220–363**
(a)	363	29.2(0+1)	—	—	X	(4.2)	566	(40)	5	363–600
Poly(*p*-xylylene)										
(c)	—	—	700	10.0[n]	X	0	562	(54)	7	220–410**
(a)	286	37.6(1+1)*	—	—	?	?	562	(40)	7	(286–410)
Poly(oxy-1,4-phenylene)										
(c)	—	—	535	7.82	X	0	555	(54)	5	300–358**
(a)	358	21.4(0+1)	—	—	X	(10)	555	(40)	5	358–620
Poly(oxy-2,6-dimethyl-1,4-phenylene)										
(c)	—	—	580	5.95	X	0	564	(54)	5	80–482**
(a)	482[o]	31.9(1+1)	—	—	X	(7.5)	564	(40)	5	482–570
Poly(ethylene terephthalate)										
(c)	—	—	553	26.9	X	0	586	54	15	1.0–10
(a)	342	77.8(4+1)	—	—	X	22	586	44	15	1.0–590
Poly(trimethylene terephthalate)										
(c)	—	—	510	30.0	X	0	550	51	19	5.0–300**
(a)	315	94(5+1)	—	—	X	31.4	550	(51)	19	320–570
Poly(butylene terephthalate)										
(c)	—	—	518.2	32.0	X	0	542	(54)	19	150–310**
(a)	248[p]	107(6+1)	—	—	X	(10)	542	(40)	19	248–570
Poly(4-hydroxybenzoic acid)										
(c)	—	—	—	—[q]	X	0	823	(54)	7	170–434**
(a)	434	33.2(1+1)	—	—	X	?	823	(25)	7	—
Poly(2,6-hydroxynaphthoic acid)										
(c)	—	—	—	—[r]	X	0	640	(54)	9	170–399**
(a)	399	46.5(1+1)	—	—	X	?	640	(27)	9	399–650

Table 1. (Continued)

	T_g	ΔC_p[b]	T_m	ΔH_f[c]	SHG[d]	S_0[e]	θ_1	θ_3	N[f]	C_p[g]
Poly(ethylene-2,6-naphthalene dicarboxylate)										
(c)	—	—	610	25.0	X	0	600	(54)	17	220–390**
(a)	390	81.6(4+1)	—	—	X	(10)	600	(30)	17	390–600
Poly(4,4′-isopropylidene diphenylene carbonate)										
(c)	—	—	608.2	33.6	X	0	569	(54)	14	?
(a)	424	48.8(2+2)	—	—	X	25	569	40	14	0.4–750
Poly(oxy-1,4-phenylene-oxy-1,4-phenylene-carbonyl-1,4-phenylene)										
(c)	—	—	668.2	37.4	X	0	560	(54)	15	130–419**
(a)	419[s]	78.1(1+3)	—	—	X	(17)	560	(40)	15	419–680
Polysilylenes and Siloxanes										
Poly(dimethylsilylene)										
(c)	—	—	?	—[t]	X	0	342	(68)	8	160–490**
(a)	?	?	—	—	X	?	342	?	8	?
Poly(dipentylsilylene)										
(c)	—	—	?	—[u]	X	0	320	(68)	24	160–490**
(a)	227	71.3	—	—	X	?	320	?	24	?
Poly(dimethyl siloxane)										
(c)	—	—	219	2.75	X	0	509	68	10	8–146**
(a)	146	27.7(2)	—	—	X	3.5	509	?	10	146–340
Poly(diethyl siloxane)										
(c)	—	—	282.7	1.84[v]	X	0	480	87	14	10–135**
(a)	135	30.2(2)	—	—	X	8.4	480	?	14	135–360

[a]The glass-transition temperature is listed as T_g; ΔC_p is the change of the heat capacity at T_g for the fully amorphous sample; T_m is the equilibrium melting temperature; ΔH_f, the heat of fusion for the 100% crystalline sample; S, H, and G are the entropy, enthalpy, and Gibbs function, respectively; S_0 represents the residual entropy at absolute zero; θ_3 and θ_1 are the characteristic temperatures for the contributions of the skeletal vibrations to the heat capacity; N represents the number of skeletal vibrations per repeating unit (the total number of vibrations is given by the number of degrees of freedom = three times the number of atoms in the repeating unit); C_p denotes the heat capacity at constant pressure.

Data as of November 1994 (33); (a) represents the amorphous sample, and (c) the 100% crystalline; the mark ** represents heat capacities for a semicrystalline polymer. The continually updated full version of the data bank with tables and graphs can be accessed at the Internet over our Web page (34). The critically reviewed experimental data which provided the base for the data bank are available through References 35–44.

[b]The change in the heat capacity, listed in J/K · mol, at T_g as derived from the ATHAS recommended, experimental data. The mark * in this column indicates that the data were derived, instead, from the difference between experimental, liquid C_p and the calculated, solid C_p. The first numeral in parentheses refers to the number of small mobile beads that make up the repeating unit (such as CH_2—, O—, or $CHCH_3$—). The average increase in C_p at T_g of all listed molecules per small bead is 11.5 ± 1.7 J/K · mol. The second numeral refers to large beads (such as C_6H_4—). The increase in C_p of a large bead at T_g is double or triple that of a small bead.

[c]The melting temperature is the best estimate of the equilibrium melting temperature, and the heat of fusion in kJ/mol of repeating unit is computed for 100% crystallinity.

[d]An X in this column indicates that enthalpy, entropy, and Gibbs energy are available, on the basis of the ATHAS recommended data (34); ? indicates that the data is unknown.

[e]Residual entropy in the glassy state at zero temperature, in J/K · mol.

[f]The number of skeletal vibrational modes used in the Tarasov equation with the theta temperatures of the previous two columns. Values of theta temperatures in parentheses are estimates on the basis of data from polymers of similar backbone structure.

Table 1. (Continued)

[g] Temperature range of the ATHAS recommended experimental heat capacity data. The computations of heat capacities of solids are based on these data and are usually carried out from 0.1 to 1000 K, to provide sufficiently broad ranges of temperature for the addition schemes and for analysis of superheated polymers, as in laser ablation studies.
[h] The *trans*-PBUT has an additional condis state at lower temperature. The crystal–condis crystal transition is at 356 K, and the heat of transition is 7.8 kJ/mol (45,46).
[i] Between T_g and T_m, the C_p of the liquid cannot be extrapolated from melt since the liquid heat capacities of the fluorinated polymers are nonlinear.
[j] The PTFE has additional crystal–crystal–condis crystal transitions at 292 and 303 K; their combined heats of transition are 850 J/mol (47).
[k] For deuterated, amorphous, solid polystyrene and ring-only deuterated polystyrene, heat capacities lead to Tarasov θ_3 and θ_1 temperatures of 55, 244 K and 49, 278 K, respectively. The thermodynamic functions S, H, and G are found in Reference 48. For other data, see Reference 49.
[l] The listed glass-transition temperature has been assigned to relaxation processes of the n-alkyl side groups. The T_{gu} has been assigned to the backbone (44).
[m] The glass-transition and the ΔC_p in two amino acids PLSER and PLMET have been estimated for the main chain (50).
[n] The PPX has two lower first-order transitions, leading to condis crystals at 504 and 560 K with heats of transition of 5.0 and 1.5 kJ/mol (51).
[o] Semicrystalline PPO shows the existence of a rigid-amorphous phase which governs the thermal properties from T_g to T_m. Fusion, superheating, and annealing are directly affected by the rigid-amorphous phase (52).
[p] The glass-transition temperature of quenched PBT is 248 K, and the change in C_p at T_g is 107 J/K · mol. Semicrystalline PBT has a T_g at 310 to 325 K, and the change in C_p at 320 K is 77 J/K · mol. In addition, it shows existence of a rigid-amorphous fraction (53).
[q] The POB shows a disordering transition at 616.5 K with a heat of transition of 3.8 kJ/mol (54).
[r] The PON shows a disordering transition at 614.5 K with a heat of transition of 0.4 kJ/mol (54).
[s] Above T_g, poorly crystallized samples show a rigid–amorphous fraction that does not contribute to the increase in heat capacity at T_g (55).
[t] The PDMSi shows two small transitions. One is at 240 K with a heat of transition of 0.1 kJ/mol and the other at 432.5 K with a heat of transition of 0.56 kJ/mol is probably a transition from one crystal form to another (56).
[u] The PDPSi shows a disordering transition from condis crystal I to condis crystal II at 338.3 K with a heat of transition of 1.4 kJ/mol (56).
[v] The PDES has an additional condis state at a lower temperature. The crystal–condis crystal transition is at 206.7 K; its heat of transition is 2.72 kJ/mol (57).

The Einstein function (58) inverts frequency to heat capacity. Integrating the data of Figure 1 over all frequencies leads to the heat capacity

$$\frac{C_v}{NR} = \int_0^{\theta_{max}} \frac{(\theta/T)^2 \exp(\theta/T)}{[\exp(\theta/T) - 1]^2} \, d\theta \tag{1}$$

where T is the temperature and θ is the frequency, both expressed in kelvin ($\theta = h\nu/k$, with ν representing the frequency in Hz; h and k are Planck's and Boltzmann's constants, respectively; 1.0 Hz $= 4.799 \times 10^{-11}$ K, 1.0 cm$^{-1} = 1.4388$ K).

The integration of equation 1 is evaluated in steps for the various regions of the frequency distributions found for macromolecules. The lowest vibrational frequencies (skeletal) usually follow a quadratic function up to a frequency limit called θ_D or θ_3. This is the well-known Debye approximation (59) of the low temperature heat capacity at constant volume, C_v (**B**), which in this temperature range

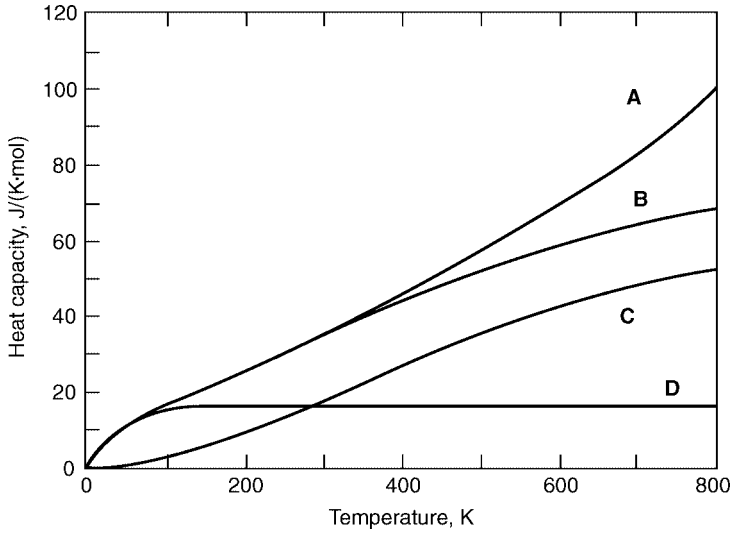

Fig. 2. Heat capacity contributions of the skeletal and group vibrations of solid polyoxymethylene, calculated by the Advanced Thermal Analysis System (ATHAS). **A**, C_p; **B**, C_v; **C**, group vibrations; **D**, skeletal vibrations. To convert J to cal, divide by 4.184.

is little different from C_p (**A**)

$$D_3\left(\frac{\theta_D}{T}\right) = \frac{C_v}{NR} = \left(\frac{12\,T^3}{\theta_3^3}\right)\int_0^{\theta_3/T} \frac{x^3 dx}{\exp(x-1)} - \frac{3\theta_D/T}{\exp(\theta_D/T)-1} \tag{2}$$

For two- or one-dimensional structures, such as are found in crystals of layer and chain molecules, the frequency distribution changes to linear and constant functions, respectively. The corresponding integrals are called the two- and one-dimensional Debye functions (60,61)

$$D_2\left(\frac{\theta_2}{T}\right) = \frac{C_v}{NR} = \left(\frac{6T^2}{\theta_2^2}\right)\int_0^{\theta_2/T} \frac{x^2 dx}{\exp(x)-1} - \frac{2\theta_2/T}{\exp(\theta_2/T)-1} \tag{3}$$

$$D_1\left(\frac{\theta_1}{T}\right) = \frac{C_v}{NR} = \left(\frac{2T}{\theta_1}\right)\int_0^{\theta_1/T} \frac{x\,dx}{\exp(x)-1} - \frac{\theta_1/T}{\exp(\theta_1/T)-1} \tag{4}$$

The N in equations 1-4 refers to the appropriate number of vibrators and x stands for $h\nu/kT = \theta/T$. The sum of all N is three times the number of atoms in a repeating unit, the number of degrees of freedom. Tarasov proposed a special combination of equations 2 and 4 for the skeletal vibrations of a linear chain (62)

$$T(\theta_3/T,\ \theta_1/T) = \frac{C_v}{NR} = D_1(\theta_1/T) - (\theta_3/\theta_1)\left[D_1\left(\frac{\theta_3}{T}\right) - D_3\left(\frac{\theta_3}{T}\right)\right] \tag{5}$$

Table 2. Group Vibration Frequencies of Polytetrafluoroethylene

	Einstein terms		Box distribution		
Normal mode	N_E	ν_E (cm^{-1})	N_b	ν_L (cm^{-1})	ν_U (cm^{-1})
ν_1 (asymmetric CF_2 stretching)	0.20	1449	0.67	1250	1440
	0.13	1256			
ν_2 (C—C stretching)			0.53	1161	1379
			0.47	1161	1229
ν_3 (symmetric CF_2 stretching)	0.17	1149	0.83	723	1154
ν_4 (CF_2 wagging)	0.20	576	0.20	630	672
			0.60	587	672
ν_5 (CF_2 rocking)	0.27	755	0.73	307	519
ν_6 (CF_2 bending)	0.13	385	0.87	283	385
ν_7 (CF_2 twisting)	0.23	294	0.77	190	289

The Tarasov equation holds for most linear macromolecules. Its limits are reached when phenylene groups are included in the backbone chain as in poly(oxy-1,4-phenylene) or poly(ethylene terephthalate) (63), or alternating heavy and light mass backbone units occur, as in poly(vinylidene fluoride) or poly(vinylidene chloride)s (64). A detailed analysis of skeletal vibration is available (32). Table 1 lists data of N, θ_1 and θ_3 for a selected number of polymers. For group vibrations, which are usually of much narrower distribution, it is sufficient to use single-frequency Einstein terms or to average over a frequency range that leads to a box-distribution function

$$B\left(\frac{\theta_U}{T}, \frac{\theta_L}{T}\right) = \frac{C_v}{NR} = \frac{\theta_U}{(\theta_U - \theta_L)}\left[D_1\left(\frac{\theta_U}{T}\right) - \frac{\theta_L}{\theta_U} D_1\left(\frac{\theta_L}{T}\right)\right] \tag{6}$$

where θ_U and θ_L are the upper and lower frequencies of the group vibrational range. Table 2 shows, as an example, the various approximated frequency regions used for the group-vibration spectrum of polytetrafluoroethylene as derived from a dispersion curve.

In the final step of computation, C_v is connected with the measured C_p. Both the thermal expansivity α and the isothermal compressibility κ must be known for this thermodynamics-based calculation

$$C_p - C_v = \alpha^2 VT/\kappa \tag{7}$$

where V represents the molar volume. Since α and κ are usually, at best, available at one temperature, the semiempirical Nernst–Lindemann expression must be utilized with modifications that account for the slow excitation of the vibrations involving the light atoms and strongly bound atoms in polymers (65,66)

$$C_p - C_v = 3RA_0 C_p T / T_m^0 \tag{8}$$

where $T_m{}^0$ is the equilibrium melting temperature and A_0 is a constant that for many polymers has a value close to 3.9×10^{-3} K · mol/J (66).

In the temperature region from above 100 K to the glass or melting transition, the intramolecular skeletal vibrations of most polymers can be evaluated after computation of the group vibrations. The intermolecular vibrations are commonly already excited at 100 K, while the remaining skeletal vibrations approach full excitation at room temperature, and then contribute a constant amount NR to the heat capacity. The values of the skeletal vibrations, N, are listed in Table 1, together with the temperature range of available experimental data. The group vibrations, as listed in Table 2 for polytetrafluoroethylene, cause another gradual increase in C_p above room temperature (note that the repeating unit is CF_2- and not C_2F_4-). It can be seen in Figure 2 that the Dulong–Petit high temperature limit for the heat capacity at constant volume, C_v, for polyoxymethylene of $12\,R = 100$ J/(K · mol) is not reached at the decomposition temperature. The highest frequencies are the CH_2 stretching vibration (as high as 4000 K).

Between the glass and melting transitions of semicrystalline macromolecules, special thermal effects can be observed. Semicrystalline macromolecules have a microphase- or nanophase-separated structure with many molecules bridging two or more phases in a nonequilibrium state. As soon as the noncrystalline portions of the molecules experience a glass transition, C_p increases. The phase boundaries result in a broadening of the glass-transition region of partially crystalline polymers beyond the high temperature end seen in noncrystalline samples due to stress transmitted into the noncrystalline phase. A detailed thermal analysis of poly(ethylene terephthalate) showed drastic changes of the relaxation energies on partial crystallization (see also Figure 11, below) (67,68). Often the increase in C_p is, in addition, less than expected from the crystallinity determined from the heat of fusion when assuming a macroscopic two-phase system (crystallinity model). The missing increase in C_p was proposed to be caused by a third phase, a rigid–amorphous nanophase, as part of the semicrystalline structure (69). In the meantime, TMDSC allowed to demonstrate that the rigid–amorphous phase RAF is produced at the same time as the crystals, and also disappears along with the crystals and may show a separate T_g below or above the melting temperature (8). In the second case, melting is retarded because of a limited mobility in the rigid noncrystalline phase (70).

Increases as well as decreases in enthalpy can also be observed between T_g and T_m in case the phase-structure changes, ie, the composition changes because of a latent heat. The change of the enthalpy is then not only caused by a heat capacity, $(\partial H/\partial T)_{n,p}$, but must be written as

$$dH = (\partial H/\partial T)_{n,p}\, dT + (\partial H/\partial T)_{T,p}\, dn \tag{9}$$

or, if the crystallinity w^c changes in a measurable way with temperature, as

$$dH/dT = C_p^{\#} = w^c C_{p,c} + (1 - w^c) C_{p,a} - \Delta H_f (dw^c/dT) \tag{10}$$

Treating dH/dT as an "apparent" heat capacity $C_p{}^{\#}$, equation 10 allows the separation of the latent heat contribution from the thermodynamic heat capacity if $C_{p,c}$ and $C_{p,a}$, the crystalline and amorphous heat capacities, are known (as well as the temperature-dependence of the heat of fusion, ΔH_f).

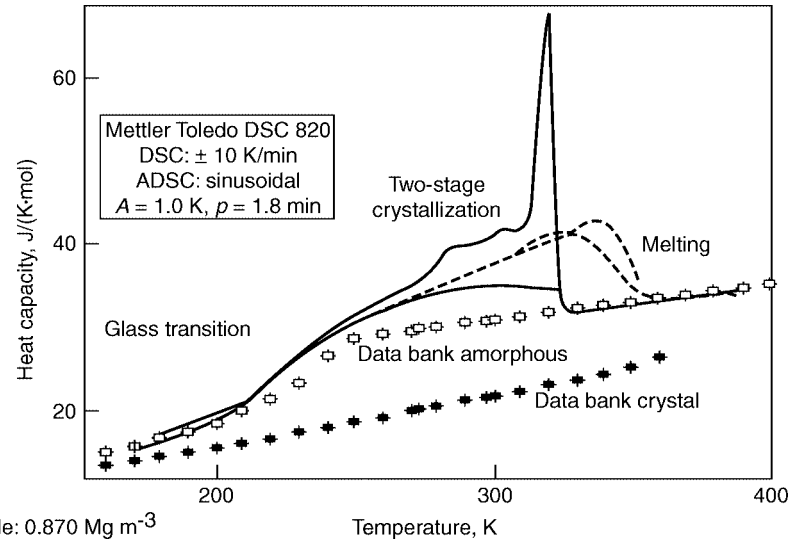

Fig. 3. Differential thermal analysis of linear low density polyethylene on cooling (continuous lines), followed by heating (broken lines), showing a high content of reversing crystallization and melting. Standard DSC: thin lines; TMDSC: thick lines. The overall supercooling contrasts the partially reversible crystallization and melting after an overall metastable, semicrystalline structure has been set up on the initial cooling. The modulation amplitude on TMDSC is given by the letter A, and the modulation period by p.

Well-known processes which can decrease or increase the enthalpy of a nonequilibrium, semicrystalline polymer on its path to higher stability are premelting (11), crystal perfection, reorganization, recrystallization (9,10), and cold crystallization (71). Recently it was found that within the metastable, global nanophase structure of semicrystalline polymers, it is also possible to observe local, reversible phase equilibria (8). Special techniques of the temperature-modulated DSC must be used to get quantitative information about the reversible equilibria. Folded-chain crystals and fringed-micellar structures show considerable reversibility in the crystallization and melting range. Figure 3 compares, as an example, TMDSC cooling and heating curves with analogous, standard DSC traces for linear low density polyethylene. The high temperature crystallization and melting mainly represents chain-folded crystals with partial reversibility. Closer toward T_g, fringed micellar crystals prevail with almost complete reversibility. More rigid macromolecules, as well as extended-chain molecules, do not exhibit such reversibility, as is shown in Figure 4, for extended-chain polyethylene (8).

The heat capacity of liquid macromolecules can be measured above the glass-transition or the melting-transition temperature. The group vibrations change little on fusion. The changes of the skeletal vibrations due to volume expansion also have little influence on heat capacity, since, once excited, the heat capacity contribution remains unchanged on lowering of the frequency. The change in volume expansion is noticed in a sizable increase in C_p at the glass transition, caused largely by a potential energy increase (hole formation). However,

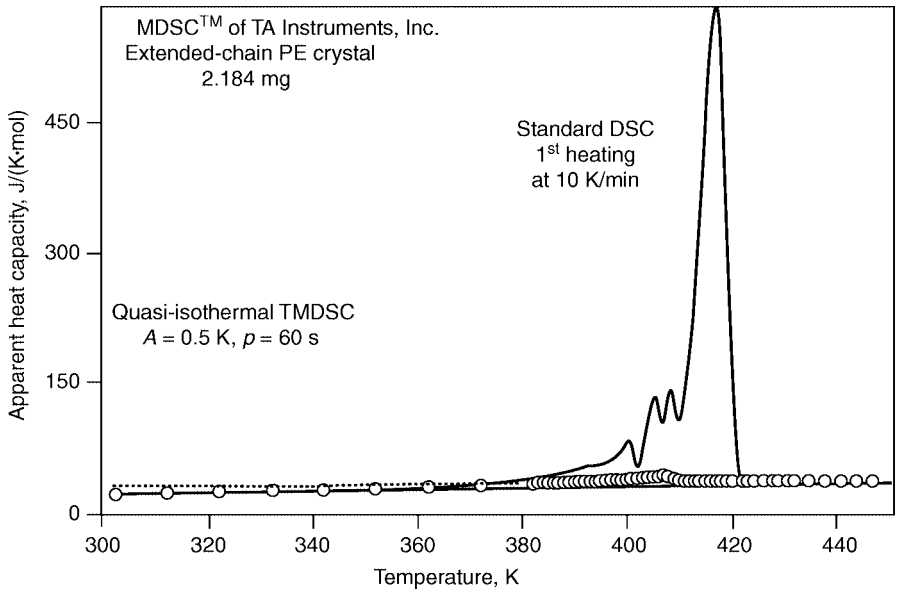

Fig. 4. Analysis of the melting of extended-chain crystals of polyethylene grown to 98% crystallinity, using high pressure crystallization (9,10,13). The standard DSC shows the sum of the latent heat and heat-capacity contributions of equations 9 and 10. The minor low temperature peaks reveal low molecular mass fractions and a small amount of remaining chain folding. The quasi-isothermal TMDSC was carried out sequentially for 20 min or longer at the temperatures indicated by the small circles. ○ 1st heating. The modulation had an amplitude A and period p. Practically no reversing melting can be seen. The small remaining reversible fraction could be accounted for quantitatively by the low molar mass portion and the remaining chain folding (8).

quantitatively, little is known about the theory of liquid heat capacity. Attempts to compute heat capacities of liquid macromolecules were based on a separation of the partition function into a vibrational part (approximated by the vibrational spectrum of the solid, as described above), a conformational part [approximated by the rotational isomers model (72) or a description using a one-dimensional Ising model (73)], and an external, configurational part (approximated by data derived from the difference in heat capacity at constant pressure and volume as given by eq. 7).

Empirically, liquid heat capacities are often observed to change linearly with temperature. They have a smaller increase with temperature than solids, and are additive with regard to their constituent groups. In case of atomic backbone repeating units, such as Se (74), O (75), or S (76), the group contribution of the heat capacity decreases with temperature. This occurs most likely because of increasing changes of vibrational modes of motion to internal rotations whose heat capacity contributions decrease with temperature from R to $R/2$. Table 3 shows the relationship between C_p and temperature T for common groups, based on an empirical addition scheme (77). An error of less than $\pm 5\%$ in the temperature range of 250–750 K is typical. References to all known liquid heat capacities and their temperature ranges are given in Table 1.

Table 3. Relationships between Liquid C_p and Temperature T for Different Structure Groups in Linear Macromolecules

Group	$C_{p,\mathrm{a}}$, J/(K · mol)
Methylene, CH_2	$0.0433\,T + 17.92$
Phenylene, C_6H_4	$0.1460\,T + 73.13$
Carboxyl, COO	$0.002441\,T + 64.32$
Carbonate, OCOO	$0.06446\,T + 84.54$
Dimethylmethylene, $C(CH_3)$	$0.2013\,T + 18.79$
Carbonyl, CO	$0.07119\,T + 32.73$
Naphthylene, C_6H_{10}	$0.2527\,T + 114.49$
Dimethylphenylene, $C_6H_2(CH_3)_2$	$0.2378\,T + 111.41$
Oxygen, O	$-0.00711\,T + 28.13$
Sulfur, S	$-0.02028\,T + 46.59$
Selenium, Se	$0.000032608\,T^2 - 0.049766\,T + 52.408$

Other Thermodynamic Functions

Enthalpy, Entropy, and Free Enthalpy. By knowing solid and liquid heat capacities of linear macromolecules, other thermodynamic functions can be obtained through the following relationships

$$H_{\mathrm{T}} - H_0 = \int_0^T C_p \, \mathrm{d}T \tag{11}$$

$$S_{\mathrm{T}} - S_0 = \int_0^T \frac{C_p}{T} \, \mathrm{d}T \tag{12}$$

$$G_{\mathrm{T}} = H_{\mathrm{T}} - TS_{\mathrm{T}} \tag{13}$$

For perfect, crystalline solids, the entropy at 0 K is zero, ${S_{\mathrm{c}}}^0 = 0$. Thus, absolute entropies can be calculated directly. Information to the available data is given in Table 1. For crystalline, linear macromolecules, the derived thermodynamic functions are reported as follows

$$\begin{array}{rc} \textit{Enthalpy}: & H^c_{\mathrm{T}} - H^c_0 \\ \textit{Entropy}: & S^c_{\mathrm{T}} \\ \textit{Free enthalpy}: & G^{\mathrm{c}}_{\mathrm{T}} - H^c_0 \end{array}$$

For amorphous solids, the residual entropy at 0 K can be calculated by equating the entropy at the equilibrium melting temperature ${T_{\mathrm{m}}}^0$

$$S^c_{T^0_{\mathrm{m}}} + \Delta S_{\mathrm{f}} = S^a_{T^0_{\mathrm{m}}} \tag{14}$$

where ΔS_f is the equilibrium entropy of fusion of fully crystalline solids. It follows that

$$S^{\mathrm{a}}_0 = S^{\mathrm{c}}_{T^0_{\mathrm{m}}} + \Delta S_f - \left(S^{\mathrm{a}}_{T^0_{\mathrm{m}}} - S^{\mathrm{a}}_0\right) = \int_0^{T^0_{\mathrm{m}}} \left(C^{\mathrm{c}}_p - C^{\mathrm{a}}_p\right) d(\ln T) + \Delta S_f \tag{15}$$

An analysis of many macromolecules indicates that the residual entropy of amorphous macromolecules at absolute zero is 2–4 J/K · mol per mobile bead, as listed in Table 1 (76,77). With the knowledge of $S_0{}^a$, the absolute entropy of amorphous solids can be calculated. The crystalline state at 0 K is chosen as a standard state for all enthalpy and free enthalpy data. The functions $(H_T{}^a - H_0{}^c)$ and $H_T{}^c - H_0{}^c)$ are directly related to the heats of fusion at temperature T

$$H_T^a - H_0^c = \left(H_T^a - H_0^a\right) + \left(H_0^a - H_0^c\right) \tag{16}$$

$$H_0^a - H_0^c = \left(H_{T_m^0}^c - H_0^c\right) + \Delta H_f - \left(H_{T_m^0}^a - H_0^a\right) \tag{17}$$

From the absolute entropy and $H_T{}^a - H_0{}^c$, the free enthalpy (Gibbs function) $G_T{}^a - H_0{}^c$ can be calculated for amorphous solids. For amorphous linear macromolecules, the reported thermodynamic functions listed in the sources for Table 1 are

Enthalpy:	$H_T^a - H_0^a$, $H_T^a - H_0^c$
Entropy:	$S_T^a - S_0^a$, S_T^a
Free enthalpy:	$G_T^a - H_0^c$

Figure 5 shows the changes of these thermodynamic functions of polyethylene with temperature.

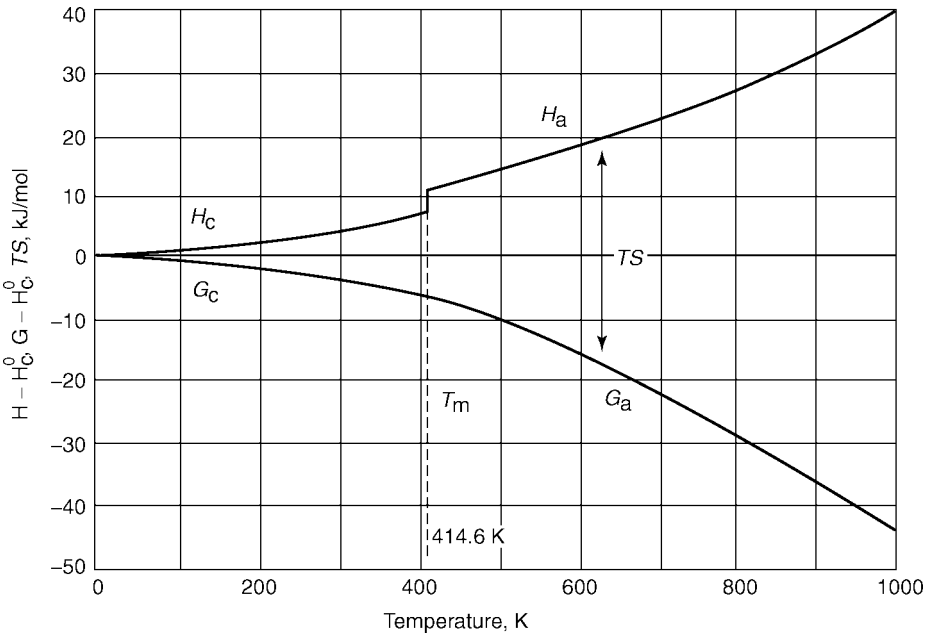

Fig. 5. Enthalpy, entropy, and free enthalpy of polyethylene as derived from heat capacities. The origin of H and G has been set arbitrarily to zero at absolute zero in temperature, and the energy equivalent TS is plotted instead of S.

Table 4. Pressure–Volume–Temperature Data of Macromolecules[a]

Polymer	Temperature range, K	Pressure, Pa $\times 10^4$	Ref.
Polyethylene, linear	414–472	0–2000	80
Polyethylene, branched	385–498	0–2000	81
Isotactic polypropylene	443–570	0–2000	82
Isotactic poly(1-butene)	406–519	0–2000	82
Poly(4-methyl-1-pentene)	508–615	0–2000	83
Polytetrafluoroethylene	603–645	0–400	84
Poly(ethylene terephthalate)	543–615	0–2000	85
Polysulfone	468–643	0–2000	86
Polystyrene	223–523	100–1800	87
Polycarbonate	303–613	100–1800	86
Polyarylate	303–613	100–1800	86
Phenoxy resin	303–573	100–1800	86

[a] To convert Pa to mm Hg, multiply with 0.0075.

Pressure, Volume, and Temperature. The pressure–volume–temperature (PVT) diagrams of linear macromolecules in different states provide another set of important thermodynamic functions, as is shown in Figure 6, for polypropylene. Using high pressure dilatometry, macromolecules have been analyzed in their liquid states, as shown in Table 4. All data can be fitted to the empirical Tait equation listed in Figure 6. Both constants of the Tait equation are exponential functions of temperature.

Empirical Tait equation:
$$v(p,T) = v_0(T)\{1 - 0.0894 \ln[1 + p/B(T)]\}$$

$v_0(T)$ = Volume at zero (atm) pressure

$B(t)$ = Tait parameter

Theoretical treatments of the equation of state are based on the lattice theory. The Simha–Somcynsky theory suggests a hole theory of polymeric liquids by determination of the reduced parameters p^*, v^*, and T^* (78,79). This statistical

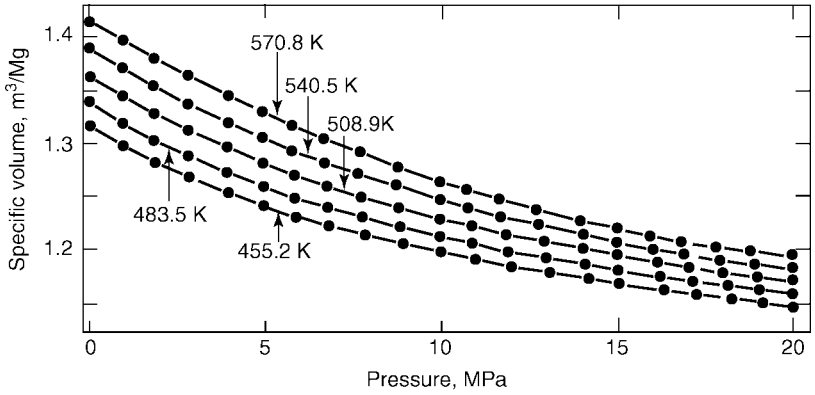

Fig. 6. Experimental (circles) and theoretical (curves) isotherms for polypropylene. The curves are based on the Simha–Somcynsky theory and show good agreement with the data ($v^* = 1.1954$ cm^3/g, $p^* = 530$ kPa, $T^* = 11{,}155$ K) (78,79).

mechanical theory describes a polymer melt as consisting of N molecules having s segments, each of which need not be identical to the chemical repeating unit. They are placed in a quasi-lattice of coordination number z, with the fraction y of the lattice sites occupied; the hole fraction is, thus, $1 - y$. Each molecule is to have $3c$ external (volume-dependent) degrees of freedom. A "square-well" approximation of the 6–12 potential is used as intersegmental potential, specified by the potential energy minimum ε^* and the hardcore volume v^* of the segment. The partitionfunction of the system contains a Boltzmann lattice–energy factor, a combinatorial factor representing the entropy of segment mixing and empty lattice sites, and a statistical-mechanical free-volume term. From the partition function, the equation of state may be calculated in the form of

$$\tilde{p}\tilde{v}/\tilde{T} = f[\tilde{v},\ \tilde{T},\ y(\tilde{v},\ \tilde{T})] \tag{18}$$

The function $y(\tilde{v},\ \tilde{T})$ is determined by the minimization of the Helmholtz free energy with respect to y.

$$(\partial \tilde{F}/\partial y)_{\tilde{v},T} = 0 \tag{19}$$

This leads to a transcendental equation for y which requires numerical solution. The equation of state and the determining equation for y are written in terms of reduced variables $\tilde{p} = p/p^*$, $\tilde{v} = v/v^*$, and $\tilde{T} = T/T^*$. The reducing parameters, p^*, v^*, and $T,^*$ contain the molecular characteristics of the system as follows (for a system of one gram of material) (88,89)

$$v^* = Nsu^* = (N_A/M)v^* \tag{20}$$

$$T^* = (z-2)s\epsilon^*/ck \tag{21}$$

$$p^* = (z-2)\epsilon^*/v^* \tag{22}$$

where N_A represents Avogadro's number, M is the molecular mass per segment, and k is the Boltzmann constant. Even though the equation of state is written in terms of reduced variables, it does not conform to a principle of corresponding states since the determining equation of y also explicitly contains the flexibility ratio $3c/s$. However, the equations of state calculated for different values of $3c/s$ are superimposable. This means that the equation of state effectively conforms to a principle of corresponding states, but it also means that the ratio $3c/s$ cannot be calculated from PVT data. Conventionally, the theoretical equation of state is evaluated by setting $3c/s = 1$ ie, the theory is formulated in terms of an effective segment having exactly one external degree of freedom. The molecular mass M_0 of this segment follows to be

$$p^*v^*/T^* = (1/3)kN_A/M_0 = R/3M_0 \tag{23}$$

where R is the gas constant. The choice $3c/s = 1$ makes T^* directly proportional to the energy parameter of the effective segment, and $M_0v^* = N_Av^*$ becomes the molar hardcore volume of the effective segment.

In order to avoid the uncertainty of the parameter c which characterizes the decrease in the external degrees of freedom, a much simpler mathematical form of the equation of state was proposed on the basis of the Ising (lattice) fluid model (88,89)

$$\tilde{\rho}^2 + \tilde{p} + \tilde{T}[\ln(1-\tilde{\rho}) + (1-1/r)\tilde{\rho}] = 0 \tag{24}$$

where $\tilde{\rho}$ is the reduced density ($\tilde{\rho} = \rho/\rho^*$), $\tilde{p}$ and $\tilde{T}$ are the same as defined above, and r is the number of lattice sites occupied by the r-mer. These equation-of-state parameters are related to the molecular mass M by

$$RT^* \ \rho^*/p^* = M/r \tag{25}$$

where R is again the gas constant.

Since r remains explicit in the reduced equation of state, a simple corresponding-state principle is not, in general, satisfied. For a polymeric liquid, however, $r \to \infty$, and the equation of state is reduced to

$$\tilde{\rho}^2 + \tilde{p} + \tilde{T}[\ln(1-\tilde{\rho}) + \tilde{\rho}] = 0 \tag{26}$$

Thus, all polymer liquids of sufficiently high molecular mass should satisfy a corresponding-state principle.

Earlier than either of the two theories mentioned above, Flory and co-workers (90,91) proposed an equation of state in a reduced form as

$$\tilde{p}\tilde{v}/\tilde{T} = \tilde{v}^{1/3}/(\tilde{v}^{1/3} - 1) - (1/\tilde{v}\tilde{T}) \tag{27}$$

Again, the reduced variables are defined as they were before: $\tilde{p} = p/p^*$, $\tilde{v} = v/v^*$, and $\tilde{T} = T/T^*$. In this theory, the reduced quantities (with an asterisk) reflect the molecular characteristics of the system.

Experimental PVT data reported so far have been described best by using the Simha-Somcynsky equation (eq. 18) (78,79), and somewhat less well by equation 27 (90,91). Equation 24 (88,89) is substantially poorer, especially at elevated pressure.

All PVT diagrams studied so far refer to polymer liquids. Substantial experimental difficulty arises in the extension to the semicrystalline state because of the nonequilibrium nature. No determined attempt at extrapolation to equilibrium data has been made to date, despite the possibility to approximate equilibrium crystal properties from unit cell parameters of X-ray data.

Transition Properties

First-Order Transitions. The principal transitions in macromolecules are those concerned with enthalpy (latent heat) and entropy changes. They are called first-order transitions according to a classification requiring the first derivative of the change in free enthalpy with respect to temperature not to be zero (92). For a single-component system (pure compound), thermodynamic equilibrium states

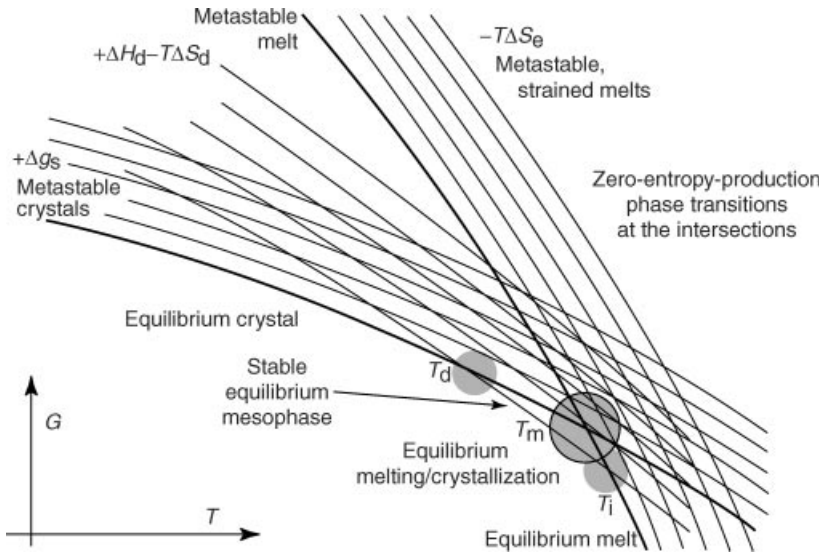

Fig. 7. Free enthalpy of equilibrium and metastable states. The solid lines represent G of the equilibrium crystal and liquid and their extrapolations beyond T_m. The G of metastable crystals and melts are largely parallel to the equilibrium states. Adding a mesophase with an intermediate entropy between liquid and solid may produce, as shown, an equilibrium mesophase between T_d, of disordering and T_i, the temperature of isotropization. Such mesophase shifts T_m into the nonequilibrium region.

are always at the lowest Gibbs energy G, as shown in Figure 7. A crystal must melt at a sharp melting temperature ${T_m}^0$. The transition shows a change in the slope of free enthalpy in going from one phase to the other. The relationship of the melting temperature to changes in enthalpy and entropy is

$$T_m^0 = \frac{\Delta H_f^0}{\Delta S_f^0} \tag{28}$$

where ${\Delta H_f}^0$ and ${\Delta S_f}^0$ are the heat and entropy of fusion, respectively.

Equilibrium crystals are defined as crystals with negligible surface effects (of infinite size) and, if any, only equilibrium defects. Complications exist, however, in the study of the transition of linear macromolecules caused by a common formation of lamellar or fibrillar crystals which are metastable and contain nonequilibrium defects (9). Therefore, even pure, one-component, crystalline macromolecules have usually a broad melting-transition range and do not approach equilibrium, although it was found recently that local equilibria may exist on the overall metastable phase structure (8). The experimental methods to approach equilibrium developed for nonpolymeric materials involving slow heating or annealing before analysis were singularly unsuccessful for macromolecules (11).

Early observations of melting transitions revealed the change of three thermodynamic functions, the degree of order (entropy), volume, and enthalpy. For the first function, a general statement about the different contributions from

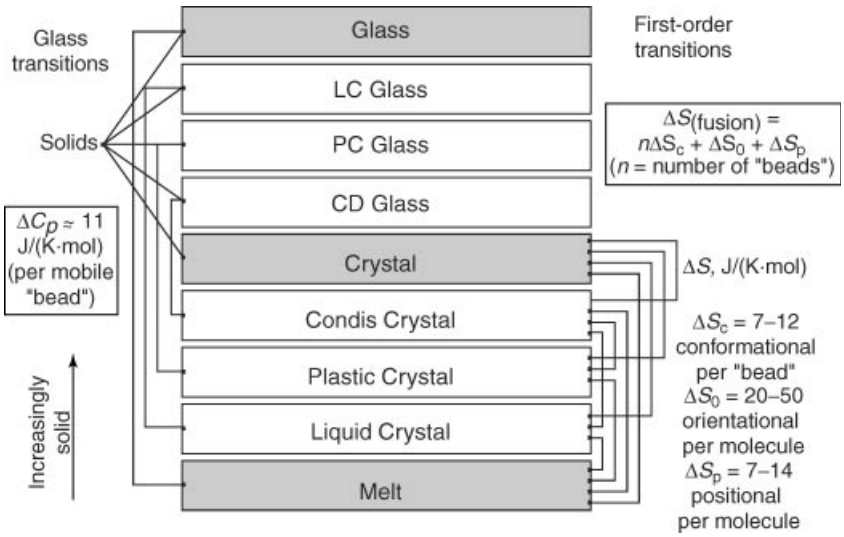

Fig. 8. Illustration of the classical condensed phases (melt, crystal and glass) and the six possible mesophases (liquid, plastic, and condis crystals and their corresponding glasses). The possible first-order transitions and their entropies of transition are marked on the right and the glass transitions and their change in heat capacity at T_g, on the left.

positional, orientational, and conformational entropy changes can be made (11). In fact, a general scheme of these entropy contributions was developed (12), as is shown in Figure 8. The most important mesophases for macromolecules are the liquid and condis crystals (13).

No such statement can be made for the volume or enthalpy changes on transition, although similar crystal structures and molecules may lead to similar changes (93). Further general observations on fusion are the lowering of ${T_m}^0$ by solvents (as a second, noncrystallizable component) and the lowering of ${T_m}^0$ for small crystals (11). The last effect has also been used to describe the fusion of small, nonequilibrium crystals as commonly found in metastable, semicrystalline polymers (11,94).

To find the equilibrium melting temperature and heat of fusion, extrapolations must be made from measurements on metastable, small crystals or on equilibrium crystals of small molecules. Only since the 1960s are crystals of extended chain macroconformation and macroscopic size available for some macromolecules. These crystals have been analyzed with respect to their melting behavior (11,95,96), which permits the discussion of equilibrium melting from both an experimental and a theoretical point of view. Although these equilibrium crystals cannot grow at ${T_m}^0$, their melting can be observed at ${T_m}^0$. Table 1 also gives a summary of all critically reviewed heats of fusion and equilibrium melting temperatures. These data deviate substantially from those expected from nonequilibrium experiments (11).

In addition to complete, one-step fusion, it is possible that some order is retained during a phase transition of the first order. In this case, mesophases are formed as shown in Figure 8. These are phases of intermediate order and mobility

(12). The entropy of fusion may be approximated by

$$\Delta S_f = \Delta S_{pos} + \Delta S_{or} T + n \Delta S_{conf} \quad (29)$$

where the three ΔS contributions are due to positional, orientational, and conformational entropy changes during the transitions. Only the last term depends on molecular size n, as also shown in Figure 8. The liquid crystals retain a small amount of orientational order because of the presence of a rod-or disk-like mesogen in the molecule; plastic crystals retain full positional order because of an almost spherical molecular shape, which permits rotation in the crystal; and condis crystals show dynamic conformational disorder in the crystal.

The phase changes of semicrystalline macromolecules that are usually not in equilibrium must make use of irreversible thermodynamics (11,97). On the other hand, even a system that is initially in equilibrium may go through a nonequilibrium transition because of kinetic restrictions, such as the superheating of crystals (98) or the more widely recognized supercooling of polymer melts on crystallization (10). The latter cases are often treated by kinetic arguments by introducing nucleation barriers (10,88,89,99).

Trying to obtain data from nonequilibrium experiments, one finds that the metastability of the system can change during the study. In order to avoid or distinguish those effects, three methods have been developed and are commonly applied for the study of nonequilibrium phase transition. The first involves the study of the transition as a function of time; the second avoids changes in the amorphous–crystalline interface by cross-linking the molecules; and the third hinders reorganization through chemical etching of the amorphous areas, producing small, equilibrium (but oligomeric) crystals, the transitions of which can be related to the small polymer crystals (11). Equilibrium transitions to be compared to the nonequilibrium measurements are listed in Table 1.

Glass Transitions. The glass-transition temperature is the main characteristic of the solid and mobile states of macromolecules with mesophase or amorphous structure. The mobile states become solid on cooling through the glass-transition temperature if crystallization does not intervene, as indicated in Figure 8. The microscopic process involved is the freezing of large-scale, molecular motion without change in structure. Since the heat capacity of the glass is always lower than that of the liquid at the same temperature, and since there is no latent heat involved, the glass transition takes superficially the appearance of a thermodynamic second-order transition (92). The freezing of molecular motion is, however, time-dependent, and, therefore, the glass transition must be called an irreversible process, and its characterization must include the time scale of the measurement. The glass transition occurs at a recognizable transition temperature because of a rather large temperature dependence of the relaxation time for large-scale molecular motion (micro-Brownian motion). Since the glass transition occurs over a larger temperature region, a characterization must involve five temperatures, as shown in Figure 9. The glass-transition temperature T_g is commonly the temperature of half-freezing, as it can be determined by heat capacity, expansion coefficient, or compressibility, as examples.

Detailed, and sometimes conflicting, theories of the glass transition, mainly applied to linear macromolecules, are discussed elsewhere (100–107). The theories

are all simplified and do not describe the glass transition fully. Their principal shortcoming is the omission of the cooperative nature of the glass transition. Unfreezing one configuration significantly helps the neighboring molecular segments to move. The frequency dependence of the glass transition cannot only be determined by mechanical analysis and dielectric measurements, but also with temperature-modulated calorimetry. A comparison of the different results is available (108,109) (see, GLASS TRANSITION).

A critical survey of over 20 macromolecules revealed that the heat capacity increase at the glass-transition temperature is about 11.3 J/K per mole of mobile units (110). The division of a repeating unit into mobile units is not fully unambiguous. However, independent motion can be expected between the different rotational isomers for mobile groups as, for example, for phenylene, carboxyl, or methylene groups. These groups are then to be counted as separate mobile units. Furthermore, the effect of a mobile unit is somewhat size-dependent. Large units seem to contribute two times or even three times the increase in heat capacity at the glass transition (76,77,111). In Table 1, the number of mobile units, assumed for the respective repeating units, is given in parentheses in column 2. Also listed are critically reviewed glass-transition temperatures and heat capacity increases at the glass-transition temperature.

The change in volume V, enthalpy H, and entropy S, as well as the derivative heat capacity C_p, and thermal expansivity α on cooling and heating are shown schematically in Figure 10. Coupling equal heating and cooling rates leads to the glass-transition behavior which is illustrated in Figure 9. It permits measurement on heating as well as on cooling. The thermodynamic quantities change almost reversibly between the values characteristic for the glass and the liquid at a temperature determined by the time scale of measurement. Different cooling and heating rates cause hysteresis effects. Shown is an endotherm after the glass transition due to slower cooling than heating.

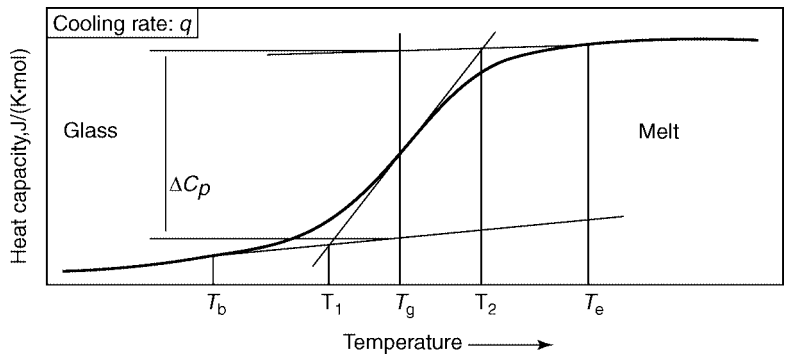

Fig. 9. Heat capacity in the glass-transition region. The first perceptible beginning of the glass transition T_b is judged by the first increase in C_p from that of the solid state; T_1 and T_2 are the extrapolated beginning and end of the glass transition. The difference between T_1 and T_2 is indicative of the broadness of the main portion of the glass transition. The glass-transition temperature T_g is chosen at half-devitrification when judged by the C_p increase. The temperature T_e is the end of glass transition; it is reached when C_p attains the value of the mobile phase. The time-scale is fixed by the cooling rate q.

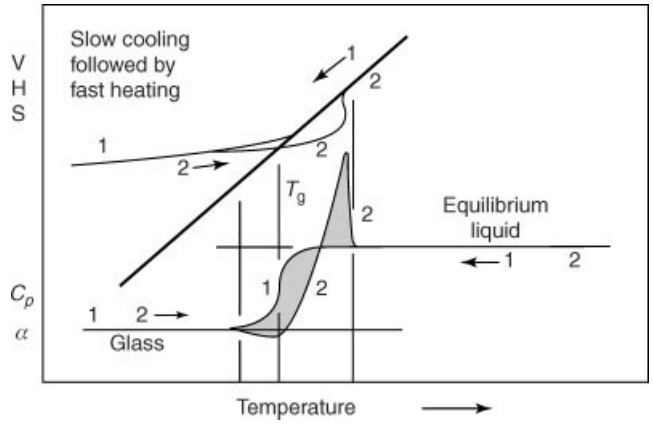

Fig. 10. Schematic drawing of the changes in volume, enthalpy, entropy, and the derivative properties (heat capacity C_p and expansivity α) on slow cooling followed by fast heating through the glass-transition region. The numeral 1 marks the response on cooling, the numeral 2, on heating. The two shaded areas are of equal magnitude and can be used to characterize the thermal history.

The glass transitions are not only affected by their previous thermal history, as demonstrated in Figure 10, but also by their mechanical (and dielectric) history. Stress, induced during sample processing such as drawing, may be frozen in on cooling through T_g. The stress introduces weak points with respect to chemical degradation. On heating into the vicinity of the glass transition, the stress causes shrinkage or deformation of the sample. Thermal analysis can detect the stress as it is released at T_g in the form of an exotherm. While exotherms induced by hysteresis decrease with increasing heating rate when a quickly cooled sample is reheated more slowly and may even turn into endotherms, the stress-related exotherms are of constant area (enthalpy) and may only broaden over a wider temperature range with increasing heating rate.

Semicrystalline samples show changes in the glass transition of the amorphous fraction which lead to a broadening of the transition range and shifts of the midpoint of the transition to higher temperature. In addition, the crystals may form a rigid–amorphous fraction, as described in the section about the heat capacities of solids and liquids at the beginning of this article on thermodynamic properties (75–77). Figure 11 illustrates the change of the glass transition of amorphous poly(ethylene terephthalate) with increasing crystallinity. The absolute levels of the heat capacity after the glass transition do not correspond to the level of crystallinity. The missing increase in heat capacity is linked to the presence of a rigid–amorphous fraction which undergoes its glass transition at a higher temperature (67), as was described above, in connection with the discussion of the heat capacity of semicrystalline structures.

Liquid Multicomponent Systems. For the description of multicomponent systems, the number of moles, N_i, or concentrations of each of the components is added to temperature and pressure as variables of state. For each extensive function of state, such as *V, U* (internal energy), *S, G, H*, C_p, and C_v (for example,

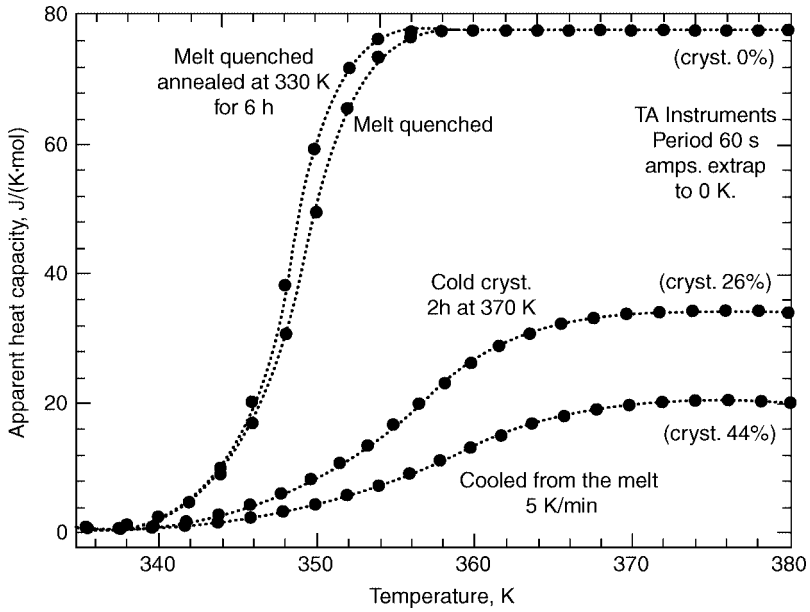

Fig. 11. Glass transitions of poly(ethylene terephthalate) with different degrees of crystallinity produced by the indicated thermal histories. The curves were measured with quasi-isothermal TMDSC at the temperatures marked by the filled circles, with modulation amplitudes extrapolated to zero and periods of 60 s (67).

for each component A, B, etc), the following derivatives can be written

$$\left(\frac{\partial X}{\partial N_{\mathrm{A}}}\right)_{T,p,N_{\mathrm{B}}} = X_{\mathrm{A}}, \left(\frac{\partial X}{\partial N_{\mathrm{B}}}\right)_{T,p,N_{\mathrm{A}}} = X_{\mathrm{B}} \tag{30}$$

The quantities X_{A}, X_{B}, etc, are called the partial molar quantities. The partial molar free enthalpy is also called the chemical potential and given the letter μ. In general, the partial molar quantities are not additive, but the following relationship can be derived between two different components (easily generalized for multicomponent systems)

$$dX = X_{\mathrm{A}}\, dN_{\mathrm{A}} + X_{\mathrm{B}}\, dN_{\mathrm{B}} \tag{31}$$

Integration of equation 29 without changing the composition gives

$$X = N_{\mathrm{A}}X_{\mathrm{A}} + N_{\mathrm{B}}X_{\mathrm{B}} \tag{32}$$

The total differential of equation 31 must be

$$dX = X_{\mathrm{A}}\, dN_{\mathrm{A}} + N_{\mathrm{A}}\, dX_{\mathrm{A}} + X_{\mathrm{B}}\, dN_{\mathrm{B}} + N_{\mathrm{B}}\, dX_{\mathrm{B}} \tag{33}$$

Comparison of the coefficients of equations 32 and 30 reveals the important equations

$$N_A\, dX_A + N_B\, dX_B = 0 \text{ or } dX_A = -\left(\frac{N_B}{N_A}\right) dX_B \tag{34}$$

which permit the calculation of the change in partial molar quantities of one component from the other.

Whether a single-phase solution or several phases are formed in a multicomponent system depends on compatibilities among the components. Generally speaking, three kinds of compatible systems are possible when dealing with macromolecules. Best known are the cases 1 and 2 which concern compatibility of small molecules with macromolecules and one macromolecule with another. The special effect introduced by the macromolecule is caused by its large molecular size, as expressed by the Flory–Huggins equations, given, below. The third kind involves the compatibility within copolymer molecules where the mixing within the molecule is fixed by the synthesis. In most cases the molecules are not altered during phase changes, unless the molecules have a dynamic structure as, for example, caused by transesterification and transamidation. As long as the sequences of repeating units of the different components within the copolymers are short, possible exothermic heats of solution are commonly insufficient to overcome the entropic driving force for mixing of the sequences between different molecules and compatibility (solubility) results, as shown in Figure 12. As the sequences get sufficiently longer, phase separation occurs and molecular segments undergo

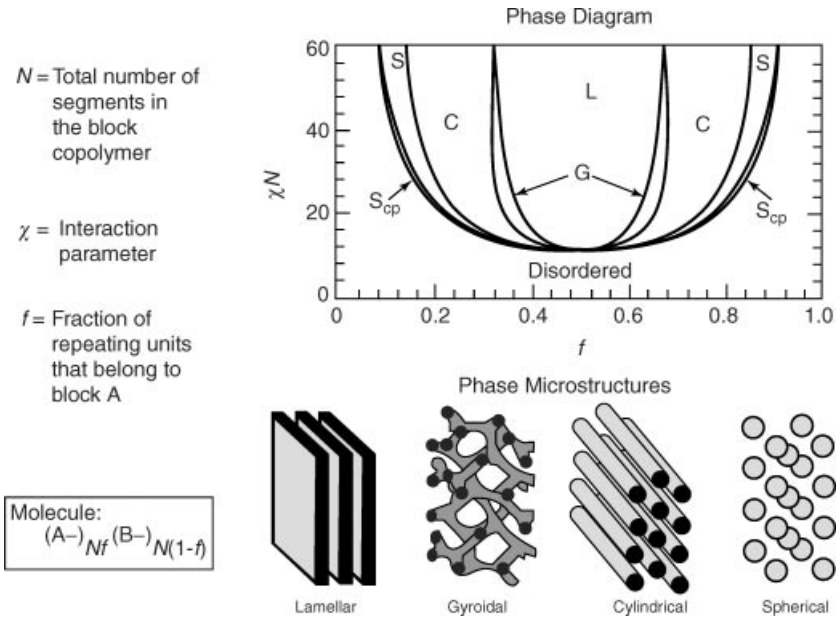

Fig. 12. Phase diagram and phase microstructures for block copolymers. The areas L, G, C, and S correspond to the structures sketched at the bottom; S_{cp} represents more complicated structures (112).

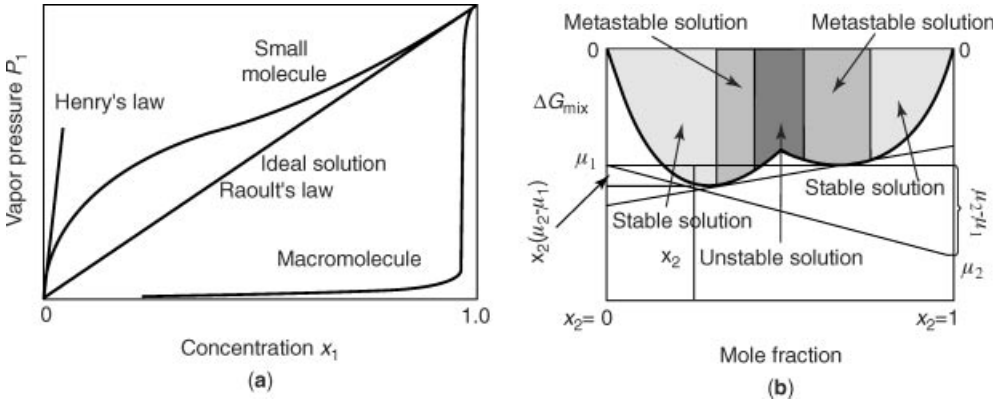

Fig. 13. Vapor pressure P_1 of and free enthalpy of mixing $[\Delta G_{mix} = \mu_1 + x_2\,(\mu_2 - \mu_1)]$ for solutions of components 1 and 2.

decoupling within the molecule, now usually called a block copolymer. Since the decoupled molecular segments must cross the phase boundary at the points of decoupling, special microphase structures arise which produce a minimum in interfacial energy, as shown in Figure 12 (112,113).

The temperature of the transition between two different phase structures is thermodynamically defined by the equality of their partial molar free enthalpies μ_1 and μ_2. Figure 13**a** illustrates the so-called ideal solution in a plot of the vapor pressure P_1 as a function of concentration in terms of the mole fraction x_1 (Raoult's law, $x_1\,P_0 = P_1$, where P_0 is the vapor pressure of the pure solvent 1). In this ideal case, only the entropy of mixing, $\Delta S_1 = -RT \ln x_1$, changes the chemical potential of the solvent, ${\mu_1}^s$, from its pure state, ${\mu_1}^0$, as expressed by

$$\mu_1^s = \mu_1^0 + RT \ln x_1 \tag{35}$$

Note that x_1 is smaller than 1, causing the positive entropy and negative contribution to the chemical potential stabilizing the solution. The vapor pressure lowering and other colligative properties are used to determine molecular masses of the solute 2.

A more quantitative treatment must also consider the change in enthalpy on mixing. The solubility parameter δ as defined as

$$\delta = (\Delta E_{vap}/V)^{1/2} \tag{36}$$

where ΔE_{vap} is the energy of evaporation to a gas at zero pressure and V is the molar volume. If there are no specific forces such as strongly polar groups, hydrogen bonds, or largely different geometries in solution and pure components, the enthalpy of mixing per unit volume is given by

$$\Delta h = v_1 v_2 (\delta_1 - \delta_2)^2 \tag{37}$$

where v_1 and v_2 are the volume fractions of the two components. Since the overall thermodynamic stability relative to the pure states must be negative for a stable

solution, the positive value of equation 37 must be overcome by the increase in entropy of mixing as shown by equation 35. Figure 13**a** displays the effect of a positive heat of mixing on the with the upper bold line. The vapor pressure of the solvent is increased and approaches the pure solute concentration ($x_1 = 0$) with the Henry's law slope which is usually accounted for by introducing an activity a_1 in place of the mole fraction x_1 ($a_1 {P_1}^0 = P_1$). For quantitative vapor pressure measurement, the approach to Raoult's law for dilute solutions is applicable, even in the presence of an enthalpy of interaction. For macromolecules, another deviation from Raoult's law must be accounted for the large size of the macromolecule. For macromolecules, a_1, the activity of the low molar mass solvent, is close to zero for most of the concentration range before it approaches Raoult's law; ie, a large mole fraction dissolves in a polymer melt without resulting in noticeable vapor pressure. Perhaps, this should not be surprising if one remembers that x_1 must be large compared to x_2 to achieve comparable masses for the two components. The Flory–Huggins equation (114–118), to be described next, will resolve this problem and describes the vapor pressure in Figure 13**a** for cases such as natural rubber dissolved in benzene.

The first step is to describe an ideal entropy of mixing for the polymer solute neglecting any interaction energy

$$\mu_2^s - \mu_2^o = RT[\ln v_2 + (1-x)(1-v_2)] \tag{38}$$

where v_2 and $v_1 = (1 - v_2)$ are the volume fractions replacing the mole fractions x_2 and x_1. This expression was derived by placing the solution on a lattice with molecules 1 occupying one unit cell each, and the macromolecules using x unit cells ($x = V_2/V_1$). Note that with $x = 1$, ie, for equal sizes of both components, the equation describing the mixing reverts back to Raoults law ($v_2 = x_2$, $v_1 = x_1$). Another, easier, derivation of equation 37 is given by Hildebrand (119). He assumes that ideal liquids have a universal free volume fraction v_f. On mixing, the molecules expand as in an ideal gas. They change from the free volumes in the pure states, $V_{f1} = V_1 v_f$ and $V_{f2} = V_2 v_f$, to the total free volume $V_{f1,2} = V_{total} v_f$, also described by equation 38. For real solutions the enthalpic contribution, as described by equation 37, must be added to equation 38. Since, however, any change in interaction will also disturb the ideal entropy of mixing, a new interaction parameter χ is defined per lattice unit cell in terms of a free enthalpy instead of an enthalpy parameter

$$\mu_2^s - \mu_2^o = RT\left[\ln v_2 + (1-x)(1-v_2) + \chi x (1-v_2)^2\right] \tag{39}$$

Figure 13**b** illustrates, then, the change of the free enthalpy of mixing by adding the appropriate chemical potentials of the components as suggested by equation 32. The interaction term χ produces the deviation in the free enthalpy of mixing which permits two concentrations to yield the same chemical potential, as indicated. These two concentrations are equally stable and may phase separate. A further increase in concentration on the left, or decrease on the right, however, still yields a decrease in chemical potential, though less than a phase separation would. This change in free enthalpy of mixing continues until the points of inflection of the curve of the free enthalpy of mixing are reached. At these points further changes in

concentrations cause an increase in free enthalpy of mixing, making the solution unstable and causing a spontaneous, spinodal decomposition into two phases.

For a multicomponent system where all components are macromolecules, a single phase is rarely found, since ΔS becomes much smaller for large molecular sizes. The positive enthalpy of mixing of equations 37 and 39, which is more closely proportional to the number of repeating units than the number of total molecules, usually overcompensates the entropy term of equations 35 and 38 and prohibits solution. Generally speaking, macromolecules are miscible in a multicomponent system only when they are of low molecular mass or are block copolymers as shown in Figure 12, because they are very similar chemically and physically, or because of specific interactions causing a negative ΔH. A large percentage of single-phase multicomponent systems that are of practical use belong to the last group. A table of many small molecule solvents of macromolecules is given in Reference 120. Compatible polymer systems are listed in References 121 and 122. An example of a phase diagram of polystyrene dissolved in acetone for two different molar masses is shown in Figure 14 (123). Because of the change of the interaction parameter of equation 39 with temperature, an upper critical solution temperature (UCST), as well as a lower critical solution temperature (LCST), is observed, with intermediate behavior at higher molar mass.

Glassy Multicomponent Systems. In the glassy states of single-phase, multicomponent systems, only a single glass transition is possible at the temperature where the large-scale motion freezes. A special observation is that a solution

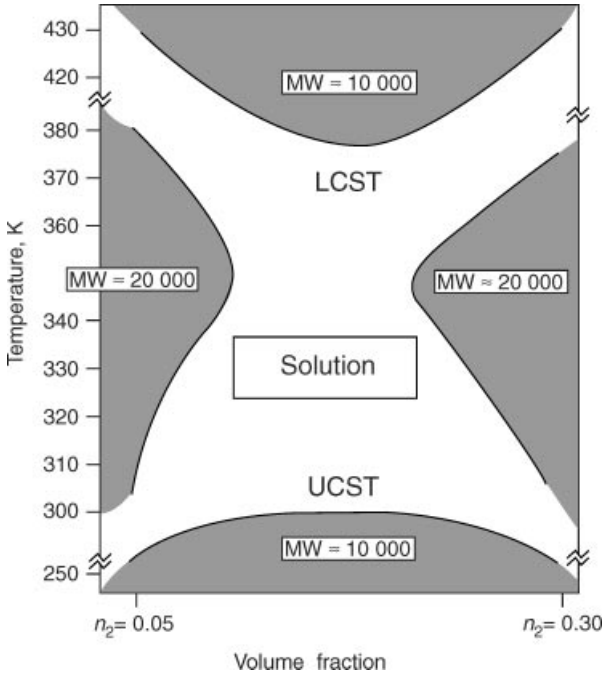

Fig. 14. Phase diagram of polystyrene in acetone, illustrating the development of an LCST and UCST by changing the molar mass.

of two small molecules or within a homogeneous copolymer system shows little change in the breadth of the glass transition, as defined in Figure 9, when compared to the pure components. If, however, one or more of the components of the solution are macromolecules, the temperature region of the glass transition is considerably broadened. This effect must be caused by the inability of the macromolecules to fully mix. Along the molecule, the arrangement of the repeating units remains unchanged on dissolution and causes nanophase regions of unmixed repeating units. Little knowledge about this effect exists beyond the experimental observation of the broadening of the glass transition (124).

The effect of composition on the glass-transition temperature $T_g(w)$ of a two-component, one-phase system has been described empirically (125) as

$$T_g(w) = wT_{g_1} + (1-w)T_{g_2} + w(1-w)K \tag{40}$$

where w is the mass fraction of component one and K is an empirical parameter chosen for good fit over the whole concentration range. Another empirical equation, the Gordon–Taylor equation, makes use of the adjustable parameter L

$$T_g(w) = [wT_{g_1} + L(1-w)T_{g_2}]/[w + L(1-w)K] \tag{41}$$

Both expressions have been linked to the conformational entropy at the glass transition (126,127). A number of additional equations have been compared to the experimental data as illustrated in Figure 15. The Gibbs–Di Marzio equation,

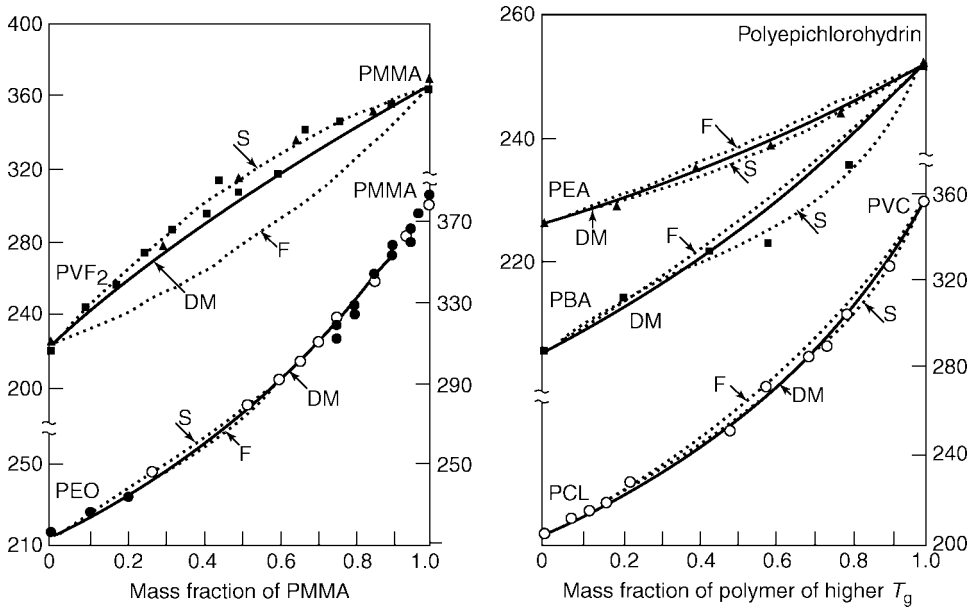

Fig. 15. Changes of the glass transition temperature for a series of polymer solutions and an effort to fit the data to equations 42 to 44. [PMMA = poly(methyl methacrylate), PVF_2 = poly(vinylidene fluoride), PEO = poly(ethylene oxide), PEA = poly(ethylene adipate), PBA = poly(butylene adipate), PVC = poly(vinyl chloride), PCL = poly(ε-caprolactone)].

abbreviated DM, is given by

$$T_g = B_1 T_{g_1} + B_2 T_{g2} \tag{42}$$

where B_1 and B_2 are the flexible bond fractions, and the Fox equation, abbreviated F, is

$$1/T_g(w) = (w/T_{g_1}) + (1-w)/T_{g_2} \tag{43}$$

Both equations are easily generalized to *PVT* equations of state assuming that the solution can be based on additivity of the homopolymer properties. The Gordon–Taylor equation, in contrast, is recovered from DM if L assumes the value $\gamma_2 w/[\gamma_1(1-w)]$ where γ represents the number of the respective flexible bonds. Finally, to add effects of specific interactions, the Gordon–Taylor equation has been expanded into a virial equation in terms of the variable w_{2c} which is the expansivity-corrected mass fraction of equation 41 [$w_{2c} = Lw_2/(w_1 + Lw_2)$]. This is the Schneider equation, S, written as

$$[T_g(w) - T_{g_1}]/[T_{g_2} - T_{g_1}] = (1+K_1)w_{2c} - (K_1+K_2)w_{2c}^2 + K_2 w_{2c}^3 \tag{44}$$

where K_1 and K_2 are the appropriate interaction constants.

Figure 15 documents that volume additivity (eq. 41) and additivity of flexible bonds (eq. 42) do not describe the data. Specific interactions as in equation 44 are needed (128). While equations 40 to 44 are often used indiscriminately for homopolymer solutions *and* copolymers, it was shown that sequence distributions in copolymers, as given by polymerization kinetics, can also be of influence on the glass transition (129,130).

Crystalline Multicomponent Systems. A multicomponent system that crystallizes with a common crystal structure is said to form mixed crystals. Formation of mixed crystals is often possible for components that crystallize in their pure state with the same crystal shapes (isomorphism). For linear macromolecules, a further condition must be fulfilled, the chain conformations of the components must match. For energy reasons, crystals usually can only be obtained with macromolecules close to their equilibrium conformations. In these conformations, close packing must be achieved with the second component, a rather rare event, although examples are known of limited solubility and cocrystallization with small molecule solvents (9).

For the more frequent case where one or more pure crystals can reach stability on cooling with the liquid solution, a eutectic phase diagram results. The free enthalpy of the pure crystal must then reach the chemical potential of its component in the solution. For equilibrium, the Flory–Huggins expression of equation 38 was used, with the free enthalpy of fusion represented by $\Delta G_f = \Delta H_f \Delta T_m / T_m{}^0$. Assuming that the molecules 2 make up the larger, macromolecular solute, one can write

$$\mu_2^s - \mu_2^0 = -\Delta G_{f_2} = -\Delta H_{f_2} \Delta T_m / T_{m_2}^0 = RT\left[\ln v_2 + (1-x)(1-v_2) + \chi x (1-v_2)^2\right] \tag{45}$$

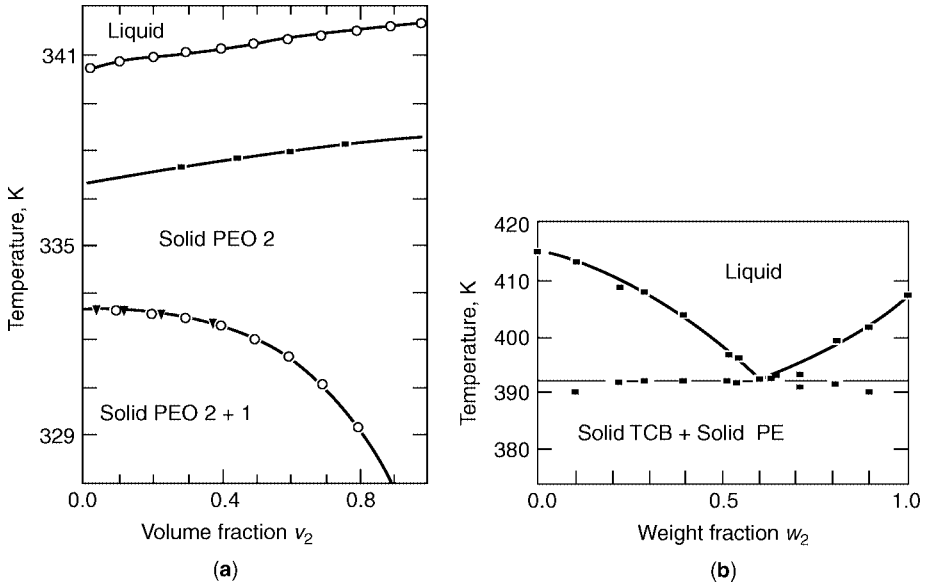

Fig. 16. (**a**) Phase diagram of poly(ethylene oxide) 3,500/100,000 mol-wt mixtures at different concentrations. The open circles represent the calculation of T_{m_2} and T_{m_1}, calculated by using the Flory–Huggins equations 46 and 47, respectively. The filled symbols represent the experimental data. (**b**) Phase diagram of polyethylene dissolved in 1,2,4,5-tetrachlorobenzene (TCB). The experimental data were obtained by melting after crystallization. The macromolecular crystals, 2, were not at equilibrium, but melted considerably lower than $T^0_{m_2}$ (see Table 1).

which can be rearranged to

$$\Delta T_{m_2} = \left[-RT^0_{m_2}/\Delta H_{f_2} \right] \left[\ln v_2 + (1-x)(1-v_2) + \chi x (1-v_2)^2 \right] \tag{46}$$

and for the smaller solvent molecule 1, an analogous expression can be derived

$$\Delta T_{m_1} = \left[-RT^0_{m_1}/\Delta H_{f_1} \right] \left[\ln v_1 + (1-\{1/x\})(1-v_1) + \chi (1-v_1)^2 \right] \tag{47}$$

Figure 16**a** is a comparison of the calculated two branches of the eutectic phase diagram for a high and a low molar mass poly(ethylene oxide). The high molarmass curve shows only a small decrease in the melting temperature with decreasing volume fraction v_2 until the logarithmic term in equation 46 forces an approach to the eutectic temperature close to the melting temperature $T^0_{m_1}$. The experimental data show a strong deviation from equation 46 for the macromolecule because of nonequilibrium effect, mainly caused by chain folding (131).

An experimental phase diagram of polyethylene dissolved in 1,2,4,5-tetrachlorobenzene (TCB) is shown in Figure 16**b** (132). Both polymer and low molar mass solvent have similar equilibrium melting temperatures. On the left-hand side of the phase diagram, the liquidus line follows equation 47, the right-hand side does not follow equation 46. Again, this indicates the usual nonequilibrium state of polymer crystals. Besides too low melting temperatures, low

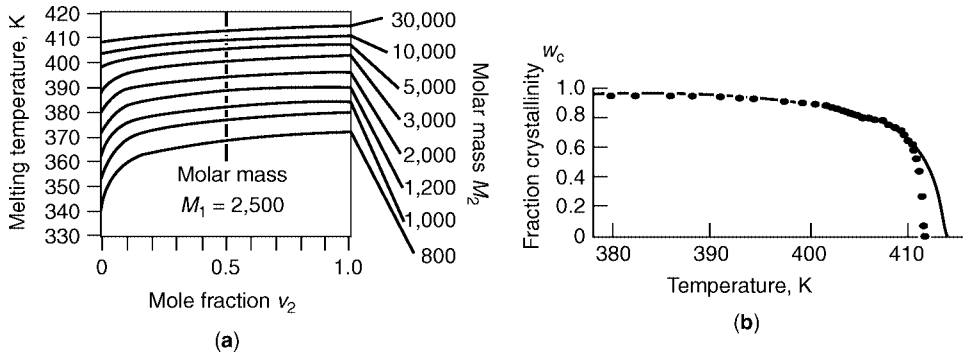

Fig. 17. (**a**) Equilibrium phase diagrams of the given molar masses of polyethylene in a low molar mass solvent of $M_1 = 2500$. (**b**) The experiments (filled circles) and the calculated crystallinities for a polyethylene of number-average molar mass of 8500 Da and a mass average molar mass of 153,300 Da.

crystallinities also are usually seen. Other complications are the presence of a rigid amorphous fraction as mentioned above in connection with the description of the pure crystals, and also the restrictions of equilibrium mixing and demixing required during melting and crystallization. If the latter processes occur too slowly, the melting or crystallization may decouple from the mixing or demixing and nonequilibrium structures may arise. An example of the change of the phase diagram because of partial decoupling of the processes during crystallization is illustrated in Figure 17. The samples were crystallized at elevated pressure to attain almost 100% crystallinity, but equilibrium, eutectically separated extended-chain crystals of the broad molar mass distribution, describable with the multicomponent form of equation 46, are seen only to the first third of melting (95). At higher temperatures, nonequilibrium mixed crystals of lower T_{m_2} are observed.

Crystallization with phase separation of random copolymers is much more complicated because usually only one component crystallizes. This component restricts the mobility of the second component to such a degree that it cannot crystallize at all. In theory, the types of phase diagrams detailed above (eutectic systems and solid solutions) should also exist for the copolymers. However, the different repeating units are connected by covalent bonds; the size effect outweighs the possible effect of demixing (11). Only local, metastable equilibrium may be achieved. The basic two-phase equilibrium theory of crystallization and melting of copolymers was developed by Flory (133). It contains the stringent condition that all crystallizable repeating units (A units) are freely available to add to crystals A. No other units can be included in the crystal of A (no isomorphism). The noncrystallizable repeating units (B units) can thus at best be located at the A crystal surface (outside the crystal proper). A general review of the earlier work is given in Reference 134. The kinetics of crystallization for copolymers is described in (135,136). Progress since then has been slow, and further work on the melting of copolymers is urgently needed. No tabular data of value can be given at present. Recent progress reports are available (137,138).

Thermodynamics of Polymer Reactions

Thermodynamics is, similarly, well suited for the description of processes which lead to changes of the molecular structure, as just seen for phase changes. A reaction with unfavorable thermodynamics expressed by a positive ΔG does not occur. However, with a negative ΔG, a reaction may still fail kinetically, while another mechanism may succeed. A typical example is the preparation of polypropylene. Although the polymerization of propylene is possible thermodynamically, it was not achieved until the work of Ziegler (139) and Natta (140), who discovered the catalyzed mechanism with favorable kinetics. Thus, much effort has been devoted to understand the kinetics of polymerization (118). Early work concentrated on predicting molecular masses and their distribution. In this section the thermodynamics of polymerization is briefly discussed. Most attention is paid to addition (chain) polymerization, but the theory is also applicable to condensation (stepwise) polymerization. The subject is extensively reviewed (141–145).

A chemical or physical reaction can only occur if there is a decrease in the free enthalpy, as discussed above. In most polymerization reactions, the entropy decreases because the polymer lacks translational and rotational motion. It has been argued that the loss of the rotational entropy is balanced by the gain of internal rotational and vibrational entropy in the polymer, and that the total loss is, therefore, equal to the translational entropy of the monomer (146). Thus, since the entropic contribution to ΔG is positive, the enthalpy of polymerization must be negative and more than compensate for the entropic term for the reaction to occur. Indeed, polymerizations are typically exothermic reactions. Polycondensations are usually acid–base type reactions that are exothermic. Addition polymerizations occur typically with the creation of two single bonds from one double bond. The bond strength of two single bonds is, however, always higher than that of one double bond; hence, those reactions are also exothermic. From the increasingly negative entropic contribution to ΔG with temperature, it follows that above a certain temperature ΔG becomes greater than zero and polymerization is no longer possible. Instead, the equilibrium of the polymerization reaction is shifted toward the monomer and a depolymerization reaction occurs. The temperature at which ΔG is zero is called the *ceiling temperature*, and is a characteristic of a polymerization reaction. It depends on the pressure of the reactant and obeys a Clausius–Clapeyron-type relation (143). Polymerizations are typically accompanied by a decrease in the system volume; thus, an increase in pressure raises the ceiling temperature. It also follows that higher pressures increase the yield of the reaction.

In some special cases, however, the polymerization is an endothermic reaction (positive ΔH) compensated by an increase in entropy. Such a case is the polymerization of elemental, eight-membered, cyclic sulfur, S_8 (147). It follows that, in such a polymerization, a minimum temperature exists below which polymerization is not possible and an inverse ceiling temperature, a floor temperature, exists. This situation can also occur in ring-opening polymerizations, where a priori predictions of the signs in ΔS and ΔH are not possible (148).

The qualitative discussion can be quantified for the prediction of the extent of a polymerization reaction.

In addition or chain polymerization, the reaction can be represented as

$$M_n^* + M_1 \rightleftarrows M_{n+1}^* \tag{48}$$

where $M_n{}^*$ is the growing chain and M_1 the monomer. The species $M_n{}^*$ and $M^*{}_{n+1}$ are indistinguishable and, therefore, the equilibrium constant is

$$K_e = \frac{\left[M_{n+1}^*\right]_e}{\left[M_n^*\right]_e [M_1]_e} \approx [M_1]_e^{-1} \tag{49}$$

The equilibrium constant K_e is equal to the free-enthalpy change $\Delta G = -RT \ln K_e$, so that

$$\ln[M_1]_e = \Delta H/(RT) - \Delta S/R \tag{50}$$

or in differential form

$$\mathrm{d}\ln[M_1]_e/\mathrm{d}T = \Delta H/(RT)^2 \tag{51}$$

where $[M_1]$ is the chemical activity of the monomer, which, in a first approximation, equals its concentration. The concentration $[M_1]_e$ is the equilibrium monomer concentration at the ceiling temperature. For the polymerization to proceed, the monomer concentration $[M_1]$ must be higher than $[M_1]_e$. For lower concentrations, depolymerization occurs.

In step polymerization, the reaction can be represented as

$$\mathrm{A} + \mathrm{B} \rightleftarrows \mathrm{C} + \mathrm{D} \tag{52}$$

where A and B are the reacting species. The species in an esterification are —OH and —COOH, and C is the resulting polymer, a polyester, and D is the by-product, H_2O. The reaction constant is $K = [\mathrm{C}][\mathrm{D}]/([\mathrm{A}][\mathrm{B}])$. For the reaction to occur, K must be smaller than the equilibrium constant K_e. This is usually forced by removing the by-product D from the system.

From the above discussion, the importance of the knowledge of ΔH and ΔS, and therefore ΔG for polymerization reactions, is obvious. The enthalpy and entropy of some polymerization reactions are given in Table 5. The experimental methods for their determination have been reviewed (141,149,150). For the determination of the entropy, the direct method is based on equation 50. From a plot of the equilibrium concentration of the monomer vs $1/T$, both ΔH and ΔS can be computed. Another method involves the estimation of ΔS from kinetic frequency factors (146).

In most cases, however, the change in enthalpy and entropy are calculated from the difference between the enthalpies (heats) of formation and entropies of formation of the products (polymer) and the reactants (monomer). Naturally, to do so, both the enthalpy and entropy of the polymer and the monomer must be known. The heat of formation of a substance which can be produced by direct reaction of its elements is the heat of the reaction, but only very few and simple substances can be formed directly from their elements. Therefore, experimentally, the heat

Table 5. Heats and Entropies of Polymerization[a]

Monomer	State[b]	ΔH, kJ/mol	ΔS, J/(K · mol)	T^c, K	Comments
Ethylene	g,g[d]	93.5	142	298	
	g,c	101.5	155 (158)[e]	298	
	g,c′	108.5 (107.5)[e]	172 (174)[e]	298	
Propylene	g,g	86.5	167	298	
	g,c′	104	191	298	syndiotactic
	g,c′	104	205	298	isotactic
	l,c	84	113 (116)[e]	298	various tacticities
	l,c′		136	298	isotactic 100% crystalline
	s,c	69		195	in *n*–butane
1–Butene	g,g	86.5	166	298	
	l,c	83.5	113 (112)[e]	298	isotactic
Isobutylene	g,c	72		298	
	g,g		172	298	
	l,c	48	112 (121)[e]	298	
Isoprene	l,c	75	101	298	
1,3-Butadiene	g,g	73		298	1,2-polymer
	g,g	78		298	1,4-polymer
	l,c	73	89 (84)[e]	298	corrected for end groups
Styrene	g,g	74.5	149	298	
	l,c	70 (68,73)[e]	104 (105,112)[e]	298	
Tetrafluoroethylene	g,g	155		298	
	g,c′	172	197	197	ΔH at 298 K
	l,c′	163 ± 17	112	197	ΔH at 298 K
Vinyl chloride	g,c	132		298	
	l,c	96		348	$\Delta H = 71$ at 298 K
Vinylidene chloride	l,c′	75.5	89	200	ΔH at 298 K
Formaldehyde	g,c′	55 (66)[e]	169 (174)[e]		298
Acetaldehyde	l,c′	64.5		298	to poly(vinyl alcohol)
	l,c	62.5		298	to poly(vinyl alcohol)
Acetone	g,g	−12		298	
	g,c	10	188		298
Trioxane	g,g	64	298		
	c′,c′	4.5 to 11.5[e]	18 ± 16	298	in various solvents
	s,c′	12.5 to 21.5[e]	42	303	ΔS at 298 K in nitrobenzene
Ethylene oxide	g,c′	140 (127.3)[e]	174	298	ΔS for 100% cryst.
Acrylic acid	l,c	67		348	
Acrylonitrile	l,c′	76.5	109	348	ΔS at 298 K
Methacrylic acid	l,c	42.5		347	$\Delta H = 64.5$ at 298 K
Methyl methacrylate	l,c	56	117	400	ΔH at 403 K
Vinyl acetate	l,c	88		348	

[a] Extracted from the extensive tables of W. K. Busfield, in Ref. 120, pp. II. 295–334.

[b] State of the monomer (first letter) and of polymer (second letter); g = gas (hypothetical for polymer), l = liquid, c = glassy condensed phase, c′ = crystalline or partially crystalline condensed phase, and s = solultion in the specified solvent.

[c] Temperature where ΔH and ΔS were measured or corrected to.

[d] The gaseous state is hypothetical; $\Delta H_{g,g}$ and $\Delta S_{g,g}$ were calculated from semiempirical schemes and correspond to the experiment only after correction with the sublimation enthalpy and entropy of the polymer.

[e] When several values are available, a second or third value is given in parentheses; for more measurements the range is indicated.

of formation of an organic substance is usually found indirectly through heats of combustion. In such an experiment, the substance is burned in an autoclave and the heat of combustion is measured. From the heat of combustion and the known heats of formation of the products, the heat of formation can be calculated. Details are given in physical chemistry textbooks (151).

The entropy of formation of a substance can be found from calorimetric measurements of the heat capacity from 0 K to the temperature of measurement, as outlined in equation 12. The entropy of formation is then simply the difference of the entropy of the substance and that of the constituent elements. The heat of formation and the entropy of various substances are given in standard thermodynamic tables at 298.15 K. It is often assumed that, at about room temperature, the heat and entropy of formation do not depend strongly on temperature; however, this is a misconception. The dependence of these quantities on temperature is evident from equations 11 and 12. The heats of formation, entropies, and other useful thermodynamic quantities are found in a number of standard data sources (1–7,152–157).

The enthalpy and entropy of formation of a compound can also be calculated with the help of various semiempirical addition schemes. In such schemes, each chemical bond is associated with a characteristic energy, transferable from one substance to another. The sum of the energy of the bonds of a compound is corrected for nonbonding interactions, such as stabilization due to resonance or destabilization due to steric hindrance, etc, to yield the heat of formation (158). In other schemes, no corrective terms are implied, but the number of the tabulated bonds is much higher. In this case, the results are more accurate (159). For the calculation of the entropy of formation, a similar method was applied, but here the entropy contributions of whole chemical groups were tabulated (160). More information on such schemes as applied to polymers and monomers is given in References 161–163. These semiempirical methods give the heat (and entropy) of formation of the compound in its gaseous state. The resulting data must be corrected by subtracting the enthalpy (and entropy) of vaporization for liquids, or of sublimation (vaporization and fusion) for solids. In Table 5 the states of the monomer and polymer are given. A gaseous polymer is, of course, hypothetical. In several cases the enthalpy and entropy of polymerization were calculated for both the polymer and monomer in the gaseous state. Correction according to the previous rules is then necessary.

BIBLIOGRAPHY

"Thermodynamic Properties" in *EPST* 1st ed., Vol. 13, pp. 788–831, by R. M. Joshi, National Chemical Laboratory, India; in *EPST* 2nd ed., Vol. 13, pp. 767–807, by B. Wunderlich, S. Z. D. Cheng, and K. Loufakis, Oak Ridge National Laboratory and The University of Tennessee, Knoxville.

1. Landolt-Boernstein, *Zahlenwerte und Funktionen*, 6th ed., Vol. 2, Parts 1–5, Springer-Verlag, Berlin, 1956–1971; continued as K. H. Hellwege, ed., *Macroscopic and Technical Properties of Matter*, neue Serie, Group IV.
2. Thermodynamics Research Center Data Project, *Selected Values of Properties of Chemical Compounds*, 4 vols., Texas A&M University, College Station, Tex., 1985.

3. American Petroleum Institute Research Project 44, *Selected Values of Properties of Hydrocarbon and Related Compounds*, Thermodynamics Research Center, Texas A&M University, College Station, Tex., 1986.
4. Y. S. Touloukian and C. Y. Ho, eds., Thermodynamical Properties of Matter, The TPRC Data Series, IFI/Plenum, New York, 1970–1979.
5. M. Kh. Karapet'yants and M. L. Karapet'yants, *Thermodynamic Constants of Inorganic and Organic Compounds* (translated by J. Sehmork) Humphrey Science Publishers, Ann Arbor, Mich., 1970.
6. I. Barin and O. Knacke, *Thermochemical Properties of Inorganic Substances*, Springer Verlag, Berlin, 1973, Suppl. 1977.
7. D. R. Lide Jr., ed. *CRC Handbook of Chemistry and Physics*, CRC Press, Boca Raton, Fla, annual editions.
8. B. Wunderlich, *Prog. Polym. Sci.* **28**, 383 (2003).
9. B. Wunderlich, *Macromolecular Physics, Vol. 1: Crystal Structure, Morphology, Defects*, Academic Press, New York, 1973.
10. B. Wunderlich, *Macromolecular Physics, Vol. 2: Crystal Nucleation, Growth, Annealing*, Academic Press, New York, 1976.
11. B. Wunderlich, *Macromolecular Physics, Vol. 3: Crystal Melting*, Academic Press, New York, 1980.
12. B. Wunderlich and J. Grebowicz, *Adv. Polym. Sci.* **60/61**, 1 (1984); see also other articles on liquid crystals in *Adv. Polym. Sci.* **59–61** (1984).
13. B. Wunderlich, M. Moeller, J. Grebowicz, and H. Baur, *Conformational Motion and Disorder in Low and High Molecular Mass Crystals*, (Advances in Polymer Science 87), Springer, Berlin, 1988.
14. W. W. Wendlandt, *Thermal Analysis*, 3rd ed., John Wiley & Sons, Inc., New York, 1986.
15. W. Hemminger and W. Höhne, *Calorimetry, Fundamentals and Practice*, Verlag Chemie, Weinheim, Germany, 1984.
16. C. J. Keattch, *An Introduction to Thermogravimetry*, Heyden and Son, London, 1975.
17. A. Weissberger and B. Rossiter, eds., *Physical Methods of Chemistry*, Vol. 1, Part V, Wiley-Interscience, New York, 1971.
18. E. Mueller, *Physikalische Methoden, Vol 3: Methoden der Organischen Chemie (Houben-Weyl)*. Part 1, G. Thieme, Stuttgart, Germany, 1955.
19. J. M. Sturtevant, in Ref. 17.
20. W. P. White, *The Modern Calorimeter*, Chemical Catalog Co., New York, 1928.
21. J. P. McCullogh, *Chemical Thermodynamics, Vol. 1: Calorimetry of Nonreacting Systems*, Plenum Press, New York, 1968.
22. B. Wunderlich, *Thermal Analysis*, Academic Press, New York, 1990.
23. G. Höhne, W. Hemminger, and H.-J. Flammersheim, *Differential Scanning Calorimetry*, Springer, Berlin, 1996, 2nd ed. 2003.
24. F. D. Rossini and H. A. Skinner, eds., *Experimental "Thermochemistry'*, Vols. 1 and 2, Interscience Publishers, New York, 1956, 1962; H. Weber, *Isothermal Calorimetry*, H. Lang and P. Lang, Bern and Frankfurt, 1973.
25. *Proceedings of the International Conferences on Thermal Analysis (and Calorimetry)* can be found under the title *Thermal Analysis*, various publications and editions., 1965, 1969, 1972, 1975, 1977, 1980, 1982, and later published in *Thermochim. Acta* **92/93** (1985), **133/135** (1988), and *J. Therm. Anal*. **40** (1993), **49** (1997), **64** (2001).
26. Proceedings of the North American Thermal Analysis Society, annual editions, since 2003 on CD-ROM.
27. Chemical Abstract Service of the Am. Chem. Soc., *Sections on Thermal Analysis*, #03B, Columbus, Ohio.
28. E. A. Turi, ed., *Thermal Characterization of Polymeric Materials*, Academic Press, New York, 1981; 2nd ed. 1997.

29. B. Wunderlich, in S. Z. D. Cheng, ed., *Handbook of Thermal Analysis and Calorimetry, Vol. 3: Applications to Polymers and Plastics*, Elsevier Science, Amsterdam, 2002, pp. 1–47.
30. J. Pak and B. Wunderlich, *Thermochim. Acta* **367/368**, 229 (2001).
31. H. Baur and B. Wunderlich, *Adv. Polym. Sci.* **7**, 151 (1970).
32. H. S. Bu, S. Z. D. Cheng, and B. Wunderlich, *J. Phys. Chem.* **91**, 4179 (1987).
33. B. Wunderlich, *Pure Appl. Chem.* **67**, 1019 (1995).
34. ATHAS Data Bank.web.utk.edu/∼athas/
35. U. Gaur, H.-C. Shu, A. Mehta, and B. Wunderlich, *J. Phys. Chem. Ref. Data* **10**, 89 (1981).
36. U. Gaur and B. Wunderlich, *J. Phys. Chem. Ref. Data* **10**, 119 (1981).
37. U. Gaur and B. Wunderlich, *J. Phys. Chem. Ref. Data* **10**, 1001 (1981).
38. U. Gaur and B. Wunderlich, *J. Phys. Chem. Ref. Data* **10**, 1051 (1981).
39. U. Gaur and B. Wunderlich, *J. Phys. Chem. Ref. Data* **11**, 313 (1982).
40. U. Gaur, S.-F. Lau, B. B. Wunderlich, and B. Wunderlich, *J. Phys. Chem. Ref. Data* **11**, 1065 (1982).
41. U. Gaur, B. B. Wunderlich, and B. Wunderlich, *J. Phys. Chem. Ref. Data* **12**, 29 (1983).
42. U. Gaur, S.-F. Lau, B. B. Wunderlich, and B. Wunderlich, *J. Phys. Chem. Ref. Data* **12**, 65 (1983).
43. U. Gaur, S.-F. Lau and B. Wunderlich, *J. Phys. Chem. Ref. Data* **12**, 91 (1983).
44. M. Varma-Nair and B. Wunderlich, *J. Phys. Chem.* **20**, 349 (1991).
45. H. S. Bu, W. Aycock, and B. Wunderlich, *Polymer* **28**, 1165 (1987).
46. J. Grebowicz, W. Aycock, and B. Wunderlich, *Polymer* **27**, 575 (1986).
47. S.-F. Lau, H. Suzuki, and B. Wunderlich, *J. Polym. Sci. Polym. Phys. Ed.* **22**, 379 (1984).
48. L. H. Judovits, Ph.D. dissertation, Rensselaer Polytechnic Institute, Troy, N.Y., 1985.
49. L. H. Judovits, R. C. Bopp, U. Gaur, and B. Wunderlich, *J. Polym. Sci., Polym. Phys. Ed.* **24**, 2725 (1986).
50. A. Xenopoulos, K. Roles, and B. Wunderlich, *Polymer* **34**, 2559 (1993).
51. D. E. Kirkpatrick and B. Wunderlich, *Makromol. Chem.* **186**, 2595 (1985).
52. S. Z. D. Cheng and B. Wunderlich, *Macromolecules* **20**, 1630 (1987).
53. S. Z. D. Cheng, R. Pan R, and B. Wunderlich, *Makromol. Chem.* **189**, 2443 (1988).
54. M.-Y. Cao, M. Varma-Nair, and B. Wunderlich, *Polym. Adv. Technol.* **1**, 151 (1990).
55. S. Z. D. Cheng, M.-Y. Cao, and B. Wunderlich, *Macromolecules* **19**, 1868 (1986).
56. M. Varma-Nair, Y. Jin, J. Cheng, and B. Wunderlich, *Macromolecules* **24**, 5442 (1991).
57. M. Varma-Nair, J. P. Wesson, and B. Wunderlich, *J. Therm. Anal.* **35**, 1913 (1989).
58. *Einstein Function Table, National Bureau of Standards Monograph 49*, National Bureau of Standards, Washington, D.C., 1962.
59. J. A. Beattie, *J. Math. Phys. (MIT)* **6**, 1 (1926–1927).
60. U. Gaur, G. Pultz, H. Wiedemeier, and B. Wunderlich, *J. Therm. Anal.* **43**, 297 (1981).
61. B. Wunderlich, *J. Chem. Phys.* **37**, 1207 (1962).
62. V. V. Tarasov, *Zh. Fiz. Khim.* **24**, 1430 (1953); **39**, 2077 (1965); *Dokl. Akad. Nauk.*, SSSR **100**, 307 (1955).
63. S. Z. D. Cheng, S. Lim, L. H. Judovits, and B. Wunderlich, *Polymer* **28**, 10 (1987).
64. K. Loufakis and B. Wunderlich, *Polymer* **26**, 1875 (1985); **27**, 563 (1986).
65. R. Pan, M. Varma, and B. Wunderlich, *J. Therm. Anal.* **35**, 955 (1989).
66. J. Grebowicz and B. Wunderlich, *J. Therm. Anal.* **30**, 227 (1985).
67. I. Okazaki and B. Wunderlich, *J. Polym. Sci., Part B: Polym. Phys.* **34**, 2941 (1996).
68. B. Wunderlich and I. Okazaki, *J. Therm. Anal.* **49**, 57 (1997).
69. H. Suzuki and B. Wunderlich, *Makromol. Chem.* **189**, 1109 (1985).
70. J. Pak, M. Pyda, and B. Wunderlich, *Macromolecules* **36**, 495 (2003).
71. B. Wunderlich, *J. Chem. Phys.* **29**, 1395 (1958).
72. K. Loufakis and B. Wunderlich, *J. Phys. Chem.* **92**, 4205 (1988).

73. M. Pyda and B. Wunderlich, *Macromolecules* **32**, 2044 (1999).
74. P. H.-C. Shu, U. Gaur, and B. Wunderlich, *J. Polym. Sci., Polym. Phys. Ed.* **18**, 449 (1980).
75. H. Suzuki and B. Wunderlich, *J. Polym. Sci., Polym. Phys. Ed.* **23**, 1671 (1985).
76. S. Z. D. Cheng, R. Pan, H. S. Bu, M.-Y. Cao, and B. Wunderlich, *Makromol. Chem.* **189**, 1579 (1988).
77. S. Z. D. Cheng and B. Wunderlich, *J. Polym. Sci., Polym. Phys. Ed.* **24**, 1755 (1986).
78. R. Simha and T. Somcynsky, *Macromolecules* **2**, 342 (1969).
79. R. Simha, *Macromolecules* **10**, 1025 (1977).
80. O. Olabisi and R. Simha, *Macromolecules* **8**, 211 (1975).
81. P. Zoller, *J. Appl. Polym. Sci.* **23**, 1051 (1979).
82. P. Zoller, *J. Appl. Polym. Sci.* **23**, 1057 (1979).
83. P. Zoller, *J. Appl. Polym. Sci.* **21**, 3129 (1977).
84. P. Zoller, *J. Appl. Polym. Sci.* **22**, 633 (1978).
85. P. Zoller and P. Bolli, *J. Macromol. Sci. Phys.* **1318**, 555 (1980).
86. P. Zoller, *J. Polym. Sci., Polym. Phys. Ed.* **20**, 1453 (1982).
87. L. D. Loomis and P. Zoller, *J. Polym. Sci., Polym. Phys. Ed.* **21**, 241 (1983).
88. I. C. Sanchez and R. H. Lacombe, *J. Polym. Sci., Polym. Lett. Ed.* **15**, 71 (1977).
89. I. C. Sanchez and R. H. Lacombe, *J. Phys. Chem.* **80**, 2352 (1976).
90. P. J. Flory, R. A. Orwoll, and A. Vrij, *J. Am. Chem. Soc.* **86**, 3507 (1964).
91. P. J. Flory, *Discuss. Faraday Chem. Soc.* **49**, 7 (1970).
92. P. Ehrenfest, *Proc. Acad. Sci. Amsterdam* **36**, 153 (1933).
93. A. R. Ubbelohde, *Melting and Crystal Structure*, Clarendon Press, Oxford, 1965; *The Molten State of Matter, Melting and Crystal Structure*, John Wiley & Sons. Inc., New York, 1978.
94. B. Wunderlich, *Polymer* **5**, 125 , 611(1964).
95. R. B. Prime and B. Wunderlich, *J. Polym. Sci. Polym. Phys. Ed.* **7**, 2073 (1969).
96. R. B. Prime, B. Wunderlich, and L. Melillo, *J. Polym. Sci., Polym. Phys. Ed.* **7**, 2091 (1969).
97. H. Baur, *Thermophysics of Polymers, Vol 1: Theory*, Springer, Berlin, 1999.
98. B. Wunderlich and E. Hellmuth, *J. Appl. Phys.* **36**, 3039 (1965).
99. J. D. Hoffman, *Polymer* **23**, 656 (1982); **24**, 3 (1983); **26**, 803, 1763 (1985).
100. G. Kanig, *Kolloid Z. Z. Polym.* **233**, 54 (1969).
101. S. E. B. Petri, in E. Baer and S. V. Radeliffe, eds., *Polymeric Materials: Relationships between Structure and Mechanical Behavior*, American Society of Metals, Metals Park, Ohio, 1974.
102. T. Somcynsky and R. Simha, *J. Appl. Phys.* **42**, 4545 (1971).
103. J. H. Gibbs and E. A. DiMarzio, *J. Chem. Phys.* **28**, 373 (1958).
104. G. Adam and J. H. Gibbs, *J. Chem. Phys.* **43**, 139 (1965).
105. B. Wunderlich, D. M. Bodily, and M. H. Kaplan, *J. Appl. Phys.* **35**, 95 (1964).
106. R. Boyer, *J. Macromol. Sci. Phys. B* **12**, 253 (1976).
107. M. C. Shen and A. Eisenberg, *Rubber Chem. Technol.* **43**, 59 (1970).
108. A. T. Riga and L. H. Judovits, eds., *Material Characterization by Dynamic and Modulated Thermal Analytical Techniques*, ASTM STP 1402, American Society for Testing and Materials, West Conshohocken, Pa., 2001.
109. S. Matsuoka, *Relaxation Phenomena in Polymers*, Hanser, Munich, 1992.
110. B. Wunderlich, *J. Phys. Chem.* **64**, 1052 (1960).
111. H. Suzuki and B. Wunderlich, *J. Polym. Sci., Polym. Phys. Ed.* **23**, 1671 (1985).
112. M. W. Matsen and F. S. Bates, *Macromolecules* **29**, 1091 (1996).
113. M. W. Matsen and F. S. Bates, *J. Chem. Phys.* **106**, 2436 (1997).
114. M. L. Huggins, *J. Phys. Chem.* **46**, 151 (1942).
115. M. L. Huggins, *Ann. N.Y. Acad. Sci.* **41**, 1 (1942).

116. M. L. Huggins, *J. Am. Chem. Soc.* **64**, 1712 (1942).
117. P. J. Flory, *J. Chem. Phys.* **10**, 51 (1942).
118. P. J. Flory, *Principles of Polymer Chemistry*, Cornell University Press, Ithaca, 1953.
119. J. H. Hildebrand, *J. Chem. Phys.* **15**, 225 (1947).
120. O. Fuchs, in J. Brandrup and E. H. Immergut, eds., *Polymer Handbook*, 3rd ed., Wiley-Interscience, 1989, pp. VII. 379–407.
121. S. Krause, in J. Brandrup and E. H. Immergut, eds., *Polymer Handbook*, 3rd ed., Wiley-Interscience, 1989, pp. VI. 347–370.
122. D. R. Paul and S. Newman, eds., *Polymer Blends*, Academic Press, New York, 1978.
123. K. S. Siow, D. Delmas, and D. Patterson, *Macromolecules* **5**, 29 (1972).
124. S.-F. Lau, J. Pathak, and B. Wunderlich, *Macromolecules* **15**, 1278 (1982).
125. E. Jenckel and R. Heusch, *Kolloid-Z* **130**, 89 (1958).
126. J. M. Gordon, G. B. Rouse, J. H. Gibbs, and W. M. Risen Jr., *J. Chem. Phys.* **66**, 4971 (1977).
127. H. A. Schneider, M.-J. Breckner and H.-J. Cantow, *Polym. Bull.* **14**, 479 (1985).
128. H. A. Schneider and E. A. DiMarzio, *Polymer* **33**, 3453 (1992).
129. H. Suzuki, N. Kamura, and Y. Nishio, *Polymer* **35**, 5555 (1994).
130. H. Suzuki and V. B. F. Mathot, *Macromolecules* **22**, 1380 (1989).
131. S. Z. D. Cheng and B. Wunderlich, *J. Polym. Sci., Polym. Phys. Ed.* **24**, 575 , 595(1986).
132. P. Smith and A. J. Pennings, *J. Materials Sci.* **11**, 1450 (1976).
133. P. J. Flory, *Trans. Faraday Soc.* **51**, 848 (1955).
134. L. Mandelkern, *Crystallization of Polymers*, McGraw-Hill, Inc., New York, 1964, Chapt. 4.
135. I. C. Sanchez and R. K. Eby, *J. Res. Natl. Stds.* **77A**, 353 (1973); *Macromolecules* **8**, 639 (1975).
136. E. Helfand and J. I. Lauritizan Jr. *Macromolecules* **6**, 631 (1973).
137. *Proceedings of the International Symposium on Polymer Crystallization in Mishima*, Japan, June 9–12, 2002, pp. 74–77, Partially printed in *J. Macromol. Sci. Part B : Phy. Ed*. **42**, (2003).
138. M. Dosiére, ed., *Crystallization of Polymers*, Kluver, Dordrecht, 1993.
139. K. Ziegler, E. Helzkamp, H. Breil, and H. Martin, *Angew. Chem.* **67**, 426 (1955).
140. G. Natta, P. Pine, P. Corradini, F. Danusso, E. Mantica, G. Mazzanti, and G. Moranglio, *J. Am. Chem. Soc.* **77**, 1708 (1955).
141. R. M. Joshi and B. T. Zwolinski, in G. E. Ham, ed., *Vinyl Polymerization*, Vol. 1, Part I, Marcel Dekker, New York, 1967, Chapt. 8.
142. P. C. Allen and C. R. Patrick, *Kinetics and Mechanisms of Polymerization Reactions*, John Wiley & Sons, Inc., New York, 1974.
143. K. J. Ivin, in A. D. Jenkins and A. Ledwith, eds., *Reactivity, Mechanism and Structure in Polymer Chemistry*, John Wiley & Sons, Inc., New York, 1974, Chapt. 4.
144. G. Odian, *Principles of Polymerization*, John Wiley & Sons, Inc., New York, 1981.
145. H. R. Allcock and F. W. Lampe, *Contemporary Polymer Chemistry*, Prentice-Hall, New Jersey, 1981.
146. F. S. Dainton and K. J. Ivin, *Q. Rev. (London)* **12**, 61 (1958).
147. A. Eisenberg and A. V. Tobolsky, *J. Polym. Sci.* **46**, 19 (1960); A. V. Tobolsky and A. Eisenberg, *J. Am. Chem. Soc.* **81**, 780 (1959).
148. H. R. Allcock, *Heteroatom Ring Systems and Polymers*, Academic Press, New York, 1967.
149. F. S. Dainton and K. J. Ivin, in H. A. Skinner, ed., *Experimental Thermochemistry*, Vol. 2, Wiley-Interscience, New York, 1962.
150. F. D. Rosini and S. Summer, eds., *Experimental Thermochemistry*, Vol. 3, Pergamon Press, Elmsford, N.Y., 1979.
151. P. W. Atkins, *Physical Chemistry*, 6th ed., Oxford University Press, Oxford, 1998.

152. K. Raznjeric, *Handbook of Thermodynamic Tables and Charts*, Hemisphere Publishing Co., McGraw-Hill Inc., New York, 1976.
153. R. H. Perry, ed., *Chemical Engineers' Handbook*, McGraw-Hill, Inc., New York, 1973.
154. R. C. Wilhoit and B. J. Zwolinski, *J. Phys. Chem. Ref. Data* **2**(suppl. 1) (1973).
155. Selected Values of Chemical Thermodynamic Properties, NBS Technical Notes 270-3 to 270-7, Institute for Basic Standards, National Bureau of Standards, Washington D.C., 1968–1973.
156. Consolidated Index of Selected Property Values: Phys. Chem. and Thermodynamics, National Academy of Sciences, National Research Council, Publ. 976, Washington, D.C., 1962.
157. J. Brandrup, E. H. Immergut, and E. A. Grulke EA, eds., *Polymer Handbook*, 4th rev. ed., John Wiley & Sons, Inc., New York, 1999.
158. L. Pauling, *The Nature of the Chemical Bond*, 3rd ed., Cornell University Press, Ithaca, N.Y., 1960.
159. J. D. Cox, *Tetrahedron* **19**, 1975 (1963).
160. G. J. Janz, *Estimation of Thermodynamic Properties of Organic Compounds*, Academic Press, New York, 1958.
161. F. S. Dainton and K. J. Ivin, *Trans. Faraday Soc.* **46**, 331 (1950).
162. R. M. Joshi, B. Zwolinski, and C. W. Hayes, *Macromolecules* **1**, 30 (1968).
163. O. E. Grikina, N. F. Stepanov, V. M. Tatevskii, and S. S. Yarovoi, *Vysokomol. Soedin A* **13**, 575 (1971).

BERNHARD WUNDERLICH
MAREK PYDA
University of Tennessee
Chemical Sciences Division of Oak Ridge National Laboratory

THERMOFORMING. See Volume 8.

THERMOSETS

Introduction

Thermosets may be defined as network-forming polymers. Unlike thermoplastic polymers, chemical reactions are involved when producing or fabricating parts. As a result of these reactions the materials cross-link and become "set," ie, they can no longer flow or dissolve. Cure most often is thermally activated, hence the term *thermoset*, but network-forming materials whose cure is light or radiation activated are also considered to be thermosets. Some thermosetting adhesives cross-link by a dual cure mechanism, ie, by either heat or light activation. In contrast to cross-linked elastomers or rubbers, the glass-transition temperature (T_g) of thermosets is generally above room temperature.

Encyclopedia of Polymer Science and Technology. Copyright John Wiley & Sons, Inc. All rights reserved.

In this article we describe the distinguishing characteristics of thermosetting materials; the more common thermosetting resins including their cure chemistry; thermoset nanocomposites; cure and properties, including cure kinetics; the development of residual stress as a result of curing; cure monitoring; and conclude with a description of selected thermoset processes.

Uncured thermosets are mixtures of small reactive molecules, often monomers. They may contain additives such as catalysts to promote or accelerate cure. Most thermosets are used in filled or reinforced form to reduce cost, modify physical properties, act as a binder for particles or fibers, reduce shrinkage during cure, or to provide or enhance flame retardance. In general, thermosets possess good dimensional stability, thermal stability, chemical resistance, and electrical properties. Because of these attributes, they find widespread use in several applications such as adhesives; primary and secondary structural members in aerospace; countertops and floors for manufacturing facilities and homes; printed circuit boards, conductive polymer elements, and encapsulation materials for electronic applications; dental materials, especially adhesives; and recreational products such as tennis racquets, bicycle frames, golf clubs, and fishing rods. Epoxy resins (qv) are probably the best-known members of the thermoset family whose members also include phenolic resins (qv), unsaturated polyester, polyurethanes (qv), dicyanate, bismaleimide, acrylate, and many others (see POLYESTERS, UNSATURATED; ISOCYANATE-DERIVED POLYMERS). Good thermoset references include Rosato (1), Prime (2), Pascault and co-workers (3), and Van Mele and co-workers (4). The first of these is process-oriented and the others are cure- and chemistry-oriented.

Characteristic Behavior of Thermosets

Thermosets are distinct from thermoplastic polymers in one major respect: their processing includes the chemical reactions of cure. As illustrated in Figure 1, cure begins by the growth and branching of chains. As the reaction proceeds, the increase in molecular weight accelerates, and eventually several chains become linked together into a network of infinite molecular weight. The abrupt and irreversible transformation from a viscous liquid to an elastic gel or rubber is called the gel point. The gel point (qv) of a chemically cross-linking system can be defined as the instant at which the weight-average molecular weight diverges to infinity (5).

Cure is illustrated schematically in Figure 1 for a material with co-reactive monomers such as an epoxy–diamine system. Reaction in the early stages of cure (**a** to **b** in Fig. 1) produces larger and branched molecules and reduces the total number of molecules. Macroscopically, the thermoset can be characterized by an increase in its viscosity η (see Fig. 2 below). As the reaction proceeds (1**b** to 1**c** in Fig. 1), the increase in molecular weight accelerates and all the chains become linked together at the gel point into a network of infinite molecular weight. The gel point coincides with the first appearance of an equilibrium (or time-independent) modulus as shown in Figure 2. Reaction continues beyond the gel point (1**c** to 1**d** in Fig. 1) to complete the network formation. Macroscopically, physical properties such as modulus build to levels characteristic of a fully developed network.

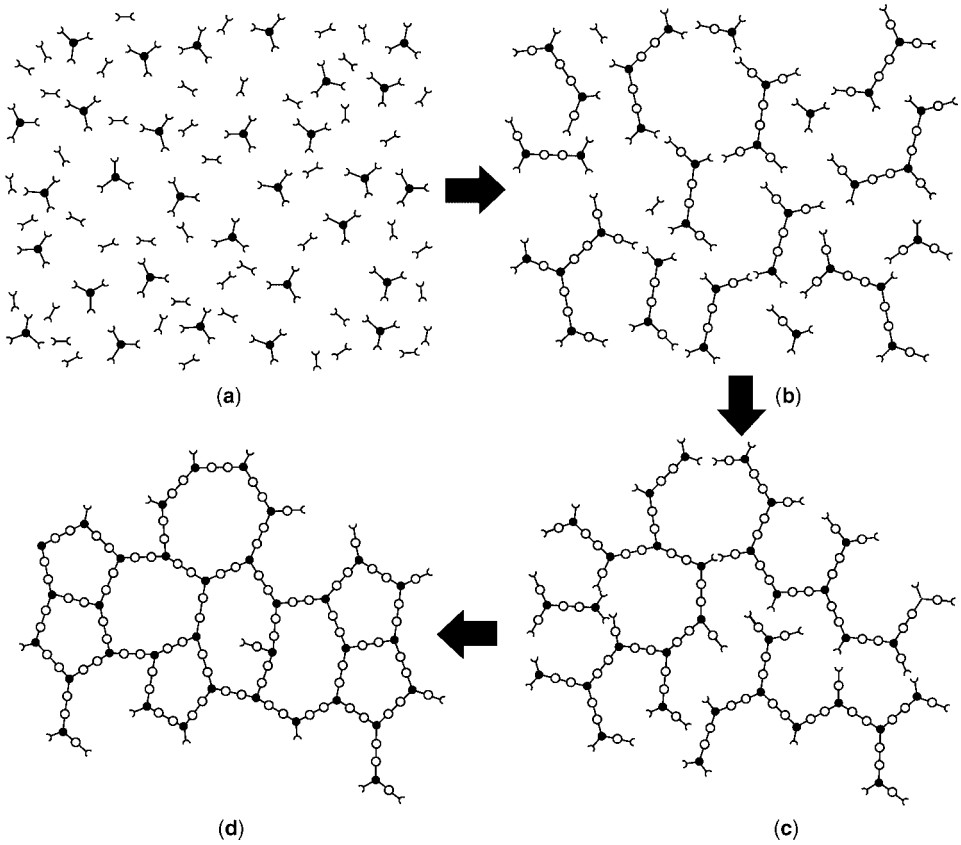

Fig. 1. Schematic, two-dimensional representation of thermoset cure. For simplicity difunctional and trifunctional co-reactants are depicted. Cure starts with A-stage monomers (**a**); proceeds via simultaneous linear growth and branching to a B-stage material below the gel point (**b**); continues with formation of a gelled but incompletely cross-linked network (**c**); and ends with the fully cured, C-stage thermoset (**d**). From Ref. 2.

Gelation is the incipient formation of a cross-linked network, and it is the most distinguishing characteristic of a thermoset. A thermoset loses its ability to flow and is no longer able to be processed above the gel point, and therefore gelation defines the upper limit of the work life. As an example, for a *Five Minute Epoxy*, which can be found in any hardware store, the "five minutes" refers to the gel point. After the two parts are mixed the user must form an adhesive joint within 5 min before the material becomes rubbery, and then keep the repaired part fixtured until cure is sufficiently complete, typically for several hours. A distinction may be drawn between the phenomenon of molecular gelation and its consequence, macroscopic gelation. Molecular gelation occurs at a well-defined stage of the chemical reaction, provided the reaction mechanism is independent of temperature and free of noncross-linking side reactions (7–9). It is dependent on the functionality, reactivity, and stoichiometry of the reactants. Macroscopic consequences of gelation include a rapid approach toward infinite viscosity and development of elastic properties not present in the pregel resin. The gel point

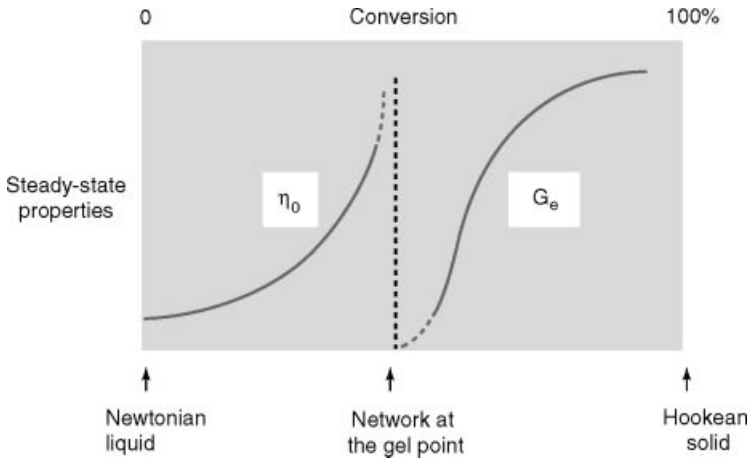

Fig. 2. Macroscopic development of rheological properties (eg, η_0 = zero-shear viscosity) and mechanical properties (eg, G_e = equilibrium shear modulus) during network formation, illustrating the approach to infinite viscosity and the first appearance of an equilibrium modulus at the gel point. From Ref. 6.

may be calculated if the chemistry is known (7,8). Molecular gelation may be detected at the point at which the reacting resin just becomes insoluble, or as the point where the mechanical loss tangent becomes frequency-independent (5–10). Macroscopic means to approximate gelation include the time to reach a specific viscosity, the $G' = G''$ crossover in a dynamic rheology measurement, and a series of frequency-independent damping peaks accompanied by a small increase in storage modulus in a dynamic mechanical measurement. Gelation in condensation or step-growth systems typically occurs between 50 and 80% conversion (degree of cure $\alpha - 0.5$–0.8). For high functionality and free-radical initiated or chain-growth systems, gelation may occur at much lower conversions. The degree of conversion at the gel point α_{gel} is constant for a given thermoset, independent of cure temperature, ie gelation is isoconversional. For this reason the time to gel versus temperature can be used to measure the activation energy for cure. Gelation does not usually inhibit cure (eg, the reaction rate remains unchanged on passing through gelation), and it cannot be detected by techniques sensitive only to the chemical reaction, such as differential scanning calorimetry (DSC). Beyond the gel point, the reaction proceeds toward the formation of one infinite network with substantial increase in cross-link density, glass-transition temperature, and ultimate physical properties.

Vitrification, a completely distinct phenomenon from gelation, may or may not occur during cure depending on the cure temperature relative to the T_g for full cure. Vitrification is glass formation due to T_g increasing from below T_{cure} to above T_{cure} as a result of the cure reaction, and is defined as the point where $T_g = T_{cure}$ (11). Vitrification can occur anywhere during the reaction to form either an ungelled glass or a gelled glass. It can be avoided by curing at or above $T_{g\infty}$, the glass-transition temperature for the fully cured network. In the glassy state, the rate of reaction will usually undergo a significant decrease and fall below the chemical reaction rate as the reaction becomes controlled by the diffusion

of reactants. It is common for complete vitrification to result in a decrease in the rate of reaction by 2–3 orders of magnitude. Unlike gelation, vitrification is reversible by heating, and chemical control of cure may be reestablished by heating to devitrify the partially cured thermoset. Vitrification may be detected by a step increase in heat capacity by modulated-temperature DSC (MTDSC) and by dynamic mechanical analysis (DMA) as a frequency-dependent transition resulting in a glassy modulus, typically >1 GPa (~150,000 psi).

Generally, the shift from chemical control to diffusion control of the reaction may be observed by a decay of the reaction rate, which is often observed when T_g reaches 10–15°C above T_{cure} (see Figs. 7 and 8). Though not common, it is possible for diffusion to control the cure kinetics prior to vitrification; it is also possible for sluggish reactions to remain under chemical control well into the glassy state (see Refs. 2–4).

Isothermal time–temperature-transformation (TTT) cure diagrams, as illustrated in Figure 3, are a useful tool for illustrating the phenomenological changes that take place during cure, such as gelation, vitrification, complete cure, and degradation (11,12). Three critical temperatures are marked on the temperature axis of the TTT cure diagram: T_{g0}, the glass transition temperature of the completely unreacted thermoset; ${}_{gel}T_g$, the temperature at which gelation and vitrification coincide; and $T_{g\infty}$, the glass-transition temperature of the fully cured network (see Table 1). In this generalized diagram, the times of gelation and the times of vitrification are plotted as functions of the cure temperature. At temperatures below T_{g0}, reaction takes place in the glassy state and is therefore slow to occur. To minimize reaction during storage, unreacted systems should be stored well below T_{g0}; 20–50°C below T_{g0}, ie deep into the glassy state, is recommended.

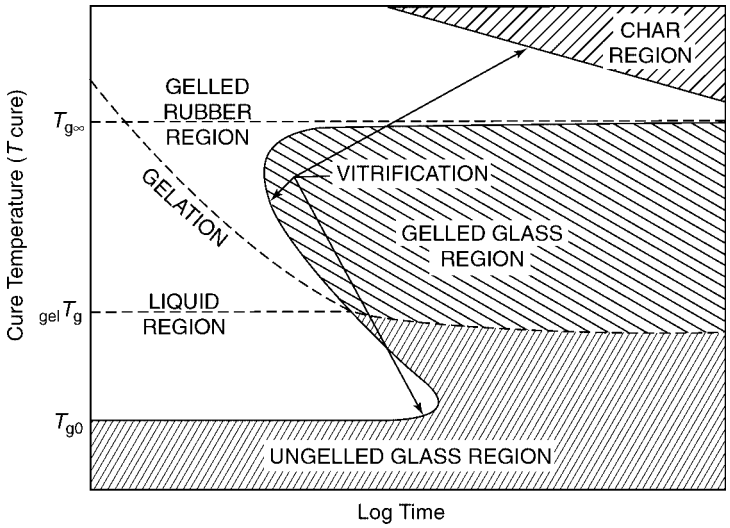

Fig. 3. Generalized time–temperature-transformation (TTT) cure diagram. A plot of the times to gelation and vitrification during isothermal cure versus temperature delineates the regions of four distinct states of matter: liquid, gelled rubber, gelled glass, and ungelled glass. From Ref. 12.

Table 1. Glossary of Characteristic Cure Parameters

α	Chemical conversion (eg, of epoxide or isocyanate groups), degree of cure
α_{gel}	α at the gel point
t_{gel}	Time to gelation, gel time
t_{vit}	Time to vitrification
T_{cure}	Cure temperature, a process parameter
T_g	Glass-transition temperature, a material property
T_{g0}	T_g for uncured thermoset with degree of conversion $\alpha = 0$
${}_{gel}T_g$	T_g for thermoset with degree of conversion α_{gel}
$T_{g\infty}$	T_g for fully cured thermoset with degree of conversion $\alpha = 1$

See the later section in this article on Adhesive Processes for comments about storing premixed and frozen adhesives. Between T_{g0} and ${}_{gel}T_g$, the liquid resin will react without gelation until its continuously rising glass-transition temperature becomes coincidental with the cure temperature, at which stage vitrification begins and the reaction may become diffusion controlled. Note that ${}_{gel}T_g$ is the temperature at which gelation and vitrification occur simultaneously.

At temperatures between ${}_{gel}T_g$ and $T_{g\infty}$, the viscous liquid changes to a viscoelastic fluid, then to a rubber, and finally to a glass. Gelation precedes vitrification, and a cross-linked rubbery network forms and grows until its glass-transition temperature coincides with the cure temperature, where the reaction may become diffusion controlled. At temperatures above $T_{g\infty}$, the network remains in the rubbery state after gelation unless other reactions occur, such as thermal degradation or oxidative cross-linking. Note that in the manufacture of carbon–carbon composites, network degradation is part of the process (see PHENOLIC RESINS). The handling and processing of thermosets are very much dependent on gelation and vitrification. For example, thermosets are often identified at three stages of cure: A, B, and C. A-stage refers to an unreacted resin; B-stage to a partially reacted and usually vitrified system, *below the gel point*, which, upon heating to devitrify, can flow and be processed and cured; and C-stage to the completely cured network. Thus, to B-stage a thermoset requires vitrification prior to gelation, and this can be accomplished by maintaining the reaction temperature below ${}_{gel}T_g$. B-staging often provides systems that are optimized for processing. In general, thermosets that need to be solid during the precure stage of processing, eg powder coatings, will be B-staged to $T_g > T_{process}$, while thermosets that need to have some flow or tack during precure processing, eg prepregs, will be B-staged to $T_g \leq T_{process}$. Prepregs are sheets of oriented fibers or fabric that are impregnated with resin and B-staged; typically several layers are laminated together under heat and pressure to fabricate a part. To avoid vitrification and achieve complete cure in a reasonable time generally necessitates cure at temperatures close to or greater than $T_{g\infty}$.

Thermosetting Resin Systems

As previously mentioned, in the uncured state, thermosetting materials are generally mixtures of small reactive molecules that form networks; catalysts, initiators and/or accelerators; and particulate, fiber-based, or nanosize fillers. There

are several families of thermosetting materials. Here we briefly review some of the more important classes both in terms of volume as well as key engineering applications.

Epoxies. Probably the best-known thermoset is epoxy (13) (see EPOXY RESINS). The largest use of epoxies is in protective coatings, with other applications including printed circuit board (PCB) laminates, electronic materials, structural composites, flooring and adhesives. The higher cost of epoxy resins vis-à-vis commodity thermosets and thermoplastics is justified by their superior properties and longer service life. Cured epoxies provide excellent mechanical strength and toughness; outstanding chemical, moisture, and corrosion resistance; good thermal, adhesive, and electrical properties; absence of volatiles and low shrinkage on cure; and good dimensional stability. Epoxy resins are characterized by a structure containing the epoxide or oxirane group (see structure **1** below). The most widely used epoxy resins are the diglycidyl ethers of bisphenol A:

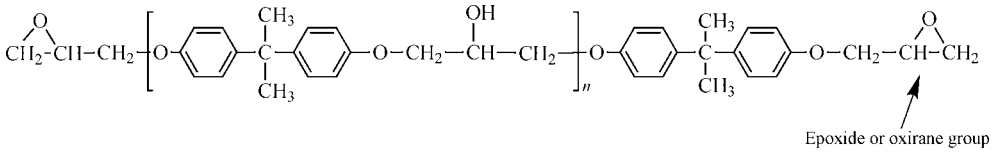

1

Others include brominated bisphenol A resins which impart fire resistance, epoxy phenol novolac (EPN) resins, bisphenol F epoxy (DGEBF) resins, epoxy cresol novolac (ECN) resins, cycloaliphatic epoxy resins, and tetraglycidyl-4,4′-diaminodiphenylmethane (TGDDM).

The number of repeat units, n, in structure **1** can be as high as 35 but is usually 0–6, 0 being the monomer. Epoxy resins can be cured by a variety of cross-linking agents known as hardeners (reactive comonomers) or by catalysts that promote homopolymerization. Common examples of homopolymerization include the anionic polymerization promoted by Lewis bases such as tertiary amines and imidizoles, and cationic polymerization promoted by Lewis acid BF_3 complexes such as boron trifluoride monoethylamine ($BF_3{\cdot}NH_2C_2H_5$). Photoinitiated cationic cure of epoxies, especially cycloaliphatic epoxies, with photoinitators such as aryldiazonium and diaryliodonium salts provide coatings and adhesives with long shelf life and near-instantaneous cure. But it is more common to cross-link epoxies with a co-reactant such as a diamine, polyamide, or acid anhydride. The low exotherm of epoxy–anhydride systems make them suitable for uses in large mass epoxy cures. Amines account for close to 50% of all epoxy curing agents. For cross-linking to occur, at least one of the reactants must be trifunctional or higher. Epoxy resins are typically difunctional, reacting through the oxirane group, although in some cases, such as homopolymerization or when epoxy is in stoichiometric excess, reaction can occur through the —OH groups.

Diamines, a well-studied co-reactant with epoxy, are tetrafunctional where each amine hydrogen can react. The reactions of primary amine and secondary amine with epoxide are illustrated in equations 1 and 2, respectively. The heat of reaction ΔH_{rxn} for epoxy–amine is ~106 kJ/mol (~25.5 kcal/mol) for reaction with

both primary amine and secondary amine (2–4). The activation energy for cure can vary from 40–125 kJ/mol (10 to 30 kcal/mol) (2–4).

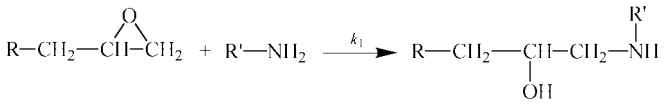

(1)

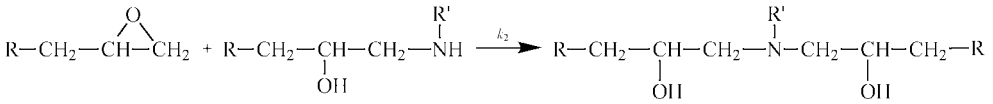

(2)

For equal reactivity of primary amine and secondary amine with epoxy $k_2/k_1 = 0.5$. But there is usually a substitution effect where the secondary amine is less reactive and $k_2/k_1 < 0.5$, often in the range of 0.40–0.45. When steric hindrance is significant, k_2/k_1 can be < 0.1.

In general, aliphatic amines are used with bisphenol A resins where room-temperature cures are desired and heat-deflection temperatures (HDT) or glass-transition temperatures (T_g) below 100°C can be tolerated. Aromatic amines can provide HDTs and T_g's up to 170°C but require curing at elevated temperatures. Anhydride cured bisphenol A systems offer long pot life, low exotherm, excellent adhesion and electrical properties, and HDT/T_g values between 125 and 170°C. A small amount of tertiary amine is frequently used to accelerate the cure reaction, which proceeds by addition esterification and addition etherification. Cycloaliphatic epoxides respond well to acidic hardeners and can have HDT/T_g values approaching 200°C. Tetraglycidyl-4,4′-diaminodiphenylmethane (TGDDM) is a tetrafunctional epoxide which is often cured with diaminodiphenylsulfone (DDS) to form high temperature, high performance epoxy systems for aerospace applications. Commercial TGDDM/DDS systems, which are typically epoxy-rich, represent materials in which secondary amine hydrogens are significantly less reactive than primary amine hydrogens and the etherification reaction of epoxide with hydroxyl is significant.

Phenolic Resins. Phenol–formaldehyde resins are employed in a wide range of applications, including commodity construction materials such as plywood to high technology applications such as honeycomb and carbon–carbon composites (see PHENOLIC RESINS). They are composed of a wide variety of structures based on the reaction products of phenols with formaldehyde. Either resole or novolac resins are formed, depending on the mole ratio of formaldehyde to phenol (F/P) and catalyst.

Resole resins are produced from an excess of formaldehyde (F/P > 1) and contain reactive methylol groups that can condense to a network structure. The cross-linking reactions in these one-part systems are exothermic and produce water and formaldehyde as volatile products, as illustrated in equation 3.

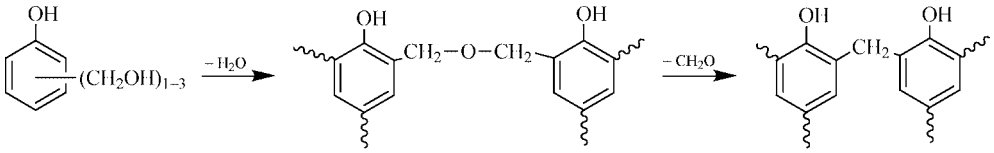

(3)

Novolac resins are produced from an excess of phenol (F/P<1) to form linear polymers, as illustrated in structure **2**, with molecular weights of 200–5000 and glass-transition temperatures of 45–70°C. In two-stage novolac systems cross-linking is accomplished by reaction with hexamethylenetetramine (hexa), which is prepared from formaldehyde and ammonia and may be considered a latent source of formaldehyde.

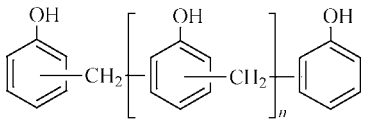

2

Amino Resins. Amino resins are the reaction product of an aldehyde with a compound containing an amino ($-NH_2$) group (see AMINO RESINS). Both urea and melamine react with formaldehyde, first by addition to form methylol compounds, and then by condensation to form cross-linked polymers through methylene bridge and methylene ether formation. The cross-linking reactions are exothermic and produce water and formaldehyde as volatile products in reactions similar to resole phenolics, illustrated in equation 3. Urea–formaldehyde and melamine–formaldehyde account for the bulk of the amino resins. Their characteristics include water solubility and unlimited colorability with dyes and pigments. Applications include decorative high pressure phenolic laminates, adhesives in the laminated wood and furniture industries, and as an additive to textile fabrics to impart wash and wear properties.

Polyester Resins. Unsaturated polyester resins consist of a linear unsaturated polyester polymer, a cross-linking monomer, activators or accelerators, and inhibitors to retard cross-linking until the resin is to be used (see POLYESTERS, UNSATURATED). Cross-linked polyesters are mainly used in glass fiber reinforced form for large structural parts. The linear unsaturated polyester is typically the condensation product of an unsaturated dibasic acid such as maleic anhydride, a glycol such as ethylene glycol, and a saturated dibasic acid such as phthalic anhydride to modify the degree of unsaturation. The most common cross-linking monomer is styrene; methyl methacrylate is added for resistance to sunlight and weathering.

Polyester resins can be cross-linked by a free-radical initiator, usually an organic peroxide. Free radicals may be formed by thermal decomposition of an initiator such as *tert*-butyl perbenzoate or benzoyl peroxide, by ultraviolet (UV) or visible light decomposition, or by chemical decomposition in ambient temperature applications utilizing activators such as dimethylaniline. Inhibitors such as hydroquinone consume free radicals initially and reaction does not proceed until the inhibitor system is completely consumed. After an induction period the free

radicals initiate exothermic cross-linking reactions involving the unsaturation in the polyester chains and the styrene monomer with gelation occurring at low levels of conversion. Reaction proceeds to form a highly cross-linked, three-dimensional network.

Allyl Resins. Allyl resins are diallyl monomers and B-staged prepolymers that can be cross-linked by free-radical polymerization through their double bonds. The allyls in widest use are diallyl phthalate (DAP) resins and diallyl isophthalate (DAIP) resins. The prepolymers can be used as the sole resin, whereas the monomers are commonly used as cross-linking agents for unsaturated polyesters; use of triallyl isocyanurate as a cross-linking monomer results in excellent high temperature properties. These resins are exceptional in their ability to maintain electrical properties under high temperature and high humidity conditions. They are also characterized by excellent dimensional stability, chemical resistance, and a chemical purity that minimizes ionic contamination. Specialty allyls have been traditionally used in eyewear applications.

Polyurethanes. Polyurethanes are produced by the reaction of a polyfunctional isocyanate with a polyol or other reactant containing two or more groups reactive with isocyanate, usually hydroxyls (see POLYURETHANES). Thermoset polyurethanes require that one reactant be trifunctional or higher and that the T_g of the cross-linked network be above room temperature. Products include rigid foams, coatings, adhesives, and binders. The reaction of an isocyanate with an alcohol, illustrated in equation 4, is exothermic and forms a urethane or carbamate linkage without the production of volatile products. Blocked isocyanates provide room temperature stable, one-component systems, such as wire and coil coatings that can be cured at high temperatures. Typically, temperatures above 120°C are required to release the blocking group and regenerate the isocyanate group. Polyurethane powder coatings, which are B-staged solid systems applied to a substrate as a dry powder, often employ blocked isocyanates. Coalescence and cure at high temperatures result in tough, durable coatings.

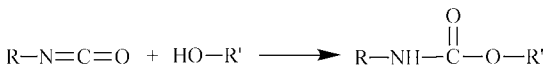

(4)

Dicyanate Resins. Bisphenol A dicyanates were commercialized in the late 1970s. The initial use was for high circuit density and high speed circuit boards (see ISOCYANATE-DERIVED POLYMERS). During initial testing, exposure to high relative humidity caused moisture stability problems. Moisture resistance was improved by blending bisphenol A dicyanates with epoxy resins to reduce the amount of ester linkages in the resulting copolymer. During the 1980s and 1990s many more new dicyanate ester monomers were developed (14), including a bicyclopentadiene containing dicyanate (Dow 71787.02) (15). The bicyclopentadiene modified cyanate exhibits excellent electrical and mechanical properties and enhanced processability. Bisphenol A dicyanates had high T_g's but were brittle and had low fracture toughness. Several approaches were developed to toughen cyanate esters including the use of core/shell rubbers (16) and thermoplastic toughening agents such as polyethersulfone, polysulfone, and polyetherimides (17).

The predominant curing pathway for cyanate ester is via cyclotrimerization using metal coordination catalysts. Three types of metal coordination catalysts are used; metal naphthenates, metal acetylacetonates (AcAc), and metal octoates. Of these, Cu AcAc and Mn octoate are the most popular. Nonylphenol is also required as a cocatalyst. Reaction 5 shows the cyclotrimerization reaction of bisphenol A dicyanate to form the triazine network structure:

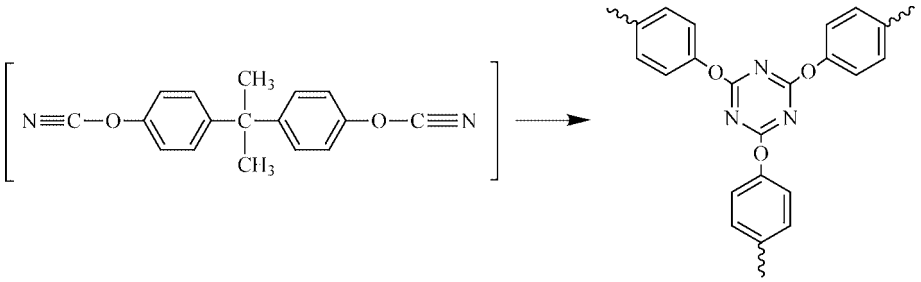

(5)

For very high T_g applications, dicyanates are cured without addition of epoxy modifiers leading to a very tight network via cyclotrimerization. The advantage of the cyanate ester family of monomers is the ability to formulate with epoxy resins. Typical resins in electronic applications are combinations of tailored epoxy monomers and oligomers along with cyanate esters.

Mitsubishi Gas Chemical pioneered the development of circuit substrates by blending bisphenol A dicyanates with epoxies and a small amount of bismaleimide. The resulting bismaleimide/triazine/epoxy (BT epoxy) laminates are the industry standard for low dielectric, high T_g chip packaging substrates. Cyanate ester networks have very high T_g's, high modulus, and low dielectric constant and have an attractive dielectric loss factor. These properties made the cyanate ester family of resins attractive for circuit packaging applications. Liquid cyanate ester monomers (bisphenol F dicyanates) have low viscosity at 25°C and exhibit good compatibility with other cyanate ester resins, epoxy resins, and bismaleimide resins (17). Blending liquid cyanate ester resins with other cyanate ester and epoxy resins provided a pathway to control the rheological properties without sacrificing the final cured performance. Liquid cyanate esters enabled the development of underfill resins for chip packaging applications, where low viscosity is required during processing. After curing, cyanate ester resins provide high T_g, low coefficient of thermal expansion, high toughness, and low moisture absorption required for underfill applications. The chemical structure of liquid bisphenol F dicyanate is shown as structure **3**:

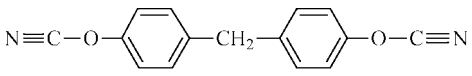

3

Dicyanate resins are versatile thermosets and have been used in a wide variety of applications. For example, RTX-366 (Hunstman Chemical) is a high molecular weight cyanate ester oligomer with excellent dielectric properties (low

dielectric constant and loss factor) along with low moisture absorption (18). RTX 366, shown in structure **4**, has been used in low outgassing and dimensionally stable, high tolerance composites for communication satellites, space antennas, microwave transparent radomes, and aircraft film adhesives.

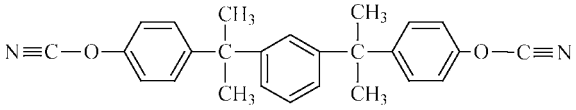

4

Additionally, cyanate ester resin blends formulated with RTX 366 have low moisture absorption, increased fracture toughness, and excellent dielectric properties, leading to use as advanced circuit board substrate materials.

Bismaleimide Resins. Polyimide resins are a class of high performance resins that have gained wide acceptance in a variety of applications (see POLYIMIDES). Bismaleimides are thermosetting polyimides that cure by addition reactions that avoid formation of volatiles. Unlike condensation polyimides which evolve volatiles during curing and are typically used as thin films, bismaleimide resins contain unsaturated double bonds which can be cured via several chemical pathways (free-radical, Michael addition, or cycloaddition, such as Diels–Alder). Thermal polymerization without the evolution of volatile byproducts enables bismaleimide resins to be used in a large number of applications from electronic materials (such as die attach adhesives), coatings, films, structural adhesives, encapsulants, and high performance fiber-reinforced composites.

Bismaleimide resins have the following generic structure (**5**):

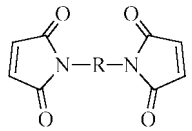

5

Depending on the desired properties, the R group can be either aliphatic or aromatic. For high T_g networks, aromatic bismaleimides are used. The most common component in bismaleimide resins is 4,4′bismaleimidodiphenylmethane (BMI) (**6**):

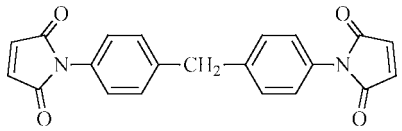

6

The BMI resin is a high melting point crystalline solid and when thermally cured, the resulting networks are very brittle. Bismaleimides are rarely used alone in the solid form. In most applications, reactive comonomers (eg vinyl and allyl

compounds, allyl phenols, aromatic amines) are used to achieve the desired final properties and processing characteristics. Commercially available resin systems are typically two-component systems. For example, the Matrimid 5292 system from Huntsman Chemical (Matrimid 5292 originally developed by Ciba Geigy) is a blend of BMI and o,o′-diallyl bisphenol A (DBA) (**7**).

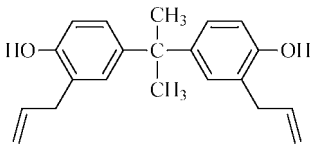

7

DBA has low viscosity and is used in place of solvents to enhance the processability and increase the toughness of the BMI composite. The DBA copolymerizes with BMI causing a decrease in the cross-link density, leading to a tougher network. BMI resins for composites are cured at temperatures in the range of 200–250°C.

Liquid BMIs with long-chain aliphatic structures between the maleimide groups are used for low modulus, low T_g, high flexibility applications. For electronic applications, BMIs have made a significant impact in die attach adhesives. Liquid BMIs can be used to formulate high performance die attach adhesives because of the ability to achieve very fast curing rates via free-radical polymerization with no void formation. Typical formulations are cured with peroxides and can have cure speeds of less than 1 min (snap cure) at curing temperatures in the range of 175–220°C. For these systems, a significant amount of the network formation is completed within seconds allowing semidconductor chips to be rapidly attached to leadframes or substrates and maintain a very high production rate at the die bonder. Additionally, the die attach formulations can be tailored to have low T_g, low modulus (to control stress and warpage during processing), low moisture absorption, and high adhesion at elevated temperatures. A potential drawback of the peroxide curing is short work life and the need to store the formulated adhesive at low temperatures to prevent slow reaction during storage. Typical work life (working time after thawing) is between 12 and 36 hours and premixed and frozen adhesives are typically stored at −40°C.

Acrylates. Acrylate-containing monomers can be used to rapidly form high cross-link density networks using free-radical initiators, radiation initiators (UV and electron beam), and Michael addition initiators. Very fast cure speed can be obtained over a wide range of formulations making this particularly useful for high speed curing of coatings and adhesives.

Typical acrylic monomers contain either the acrylate functionality (structure **8**) or the methacrylate functionality (structure **9**), where R can be aromatic or aliphatic, and also contain linear, branched, or cyclic alkanes, ethers, or esters (see ACRYLIC ESTER POLYMERS).

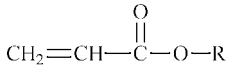

8

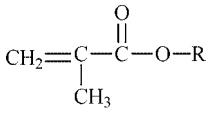

9

Free-radical curing coatings and adhesives can be formulated using temperature sensitive free-radical initiators such as peroxide and azonitrile compounds. Typical peroxide initiators are benzoyl peroxide and cumyl hydroperoxides. The most common azonitrile compound is 2,2′-azobisisobutyronitrile (AIBN). With these initiators, free radicals are generated by thermal decomposition leading to an active free radical. Once a free radical is formed it propagates to form a polymer by the following reaction pathway, where reaction 6 illustrates initiation and reaction 7 propagation:

(6)

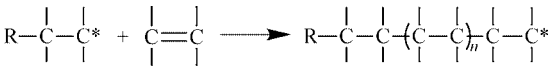

(7)

Selection of the functionality and stoichiometry of the monomers or oligomers can yield cross-linked networks with various physical and mechanical properties. For example, monomers are commercially available with mono-, di-, tri-, and multifuntionality. Choosing various ratios of di-, tri-, and multifunctional acrylate-containing monomers, the curing speed, T_g, hardness, solvent resistance, and flexibility can be tailored for a specific application. Choice of the peroxide is critical since there are a wide range of initiation temperatures. When using free-radical initiators with low cure onset temperatures, one needs to be careful with the shelf life of coatings or work life times for paste adhesives. Additionally, the free-radical curing mechanism is sensitive to oxygen inhibition. Oxygen is an effective free-radical scavenger and in order to achieve uniform curing in the thickness of the coating, oxygen must be eliminated at the surface by using an inert atmosphere (typically nitrogen) or by the addition of chemical additives that are good oxygen scavengers.

Another common curing mechanism for acrylate-containing polymers is to cure using UV light. Typical UV-cured coatings contain a free-radical-generating photoinitiator. Radicals are generated upon exposure to UV light and quickly initiate free-radical polymerization. Common photoinitators include benzophenone and the diaryl ketone derivatives including zanthone, thiozanthone, and 2-chlorothioxanthone, along with Michler's ketone, benzyl, and anthraquinone (19). Under UV irradiation, solventless coatings and adhesives can be cured extremely fast at high line speeds.

To expand the formulation toolbox, acrylates can be used as co-reactants and reactive diluents in epoxy systems cured using amines. Acrylate esters react with amine curing agents through a Michael addition reaction, resulting in a secondary

amine–acrylate adduct that can further react with epoxy resins. In this manner, highly cross-linked networks with controlled properties can be formulated.

Fast-curing coatings and adhesives using acrylate-containing monomers are used in high performance automotive primers and topcoats, concrete bridge deck coatings, industrial floorings, and specialty coatings for wood and paper. In the microelectronics industry, many photoresists use acrylate-containing monomers and oligomers. High performance die attach adhesives use a wide variety of acrylate-containing monomers, allowing solvent-free formulations, very fast curing, and control of key physical properties such as T_g and modulus.

UV curing is used in high performance coating applications, such as topcoats for flooring applications (polymer and wood flooring), coatings for metal and wood furniture, along with plastic and metal container coatings. UV curing is used extensively in the processing of photoresists in the microelectronics industry. Photodefinable soldermasks used to protect the outside surfaces of circuit boards and chip substrates make considerable use of acrylate-containing polymers.

Nanocomposites

Nanocomposites are a subset of nanotechnology. "Nano" refers to a size scale measured in nanometers (nm), or 10^{-9} m. A working definition for the nanoscale is molecules and structures with at least one dimension between 1 and 100 nm (20,21). In addition to size, shape is also a component of nanostructures, eg self-assembling nanomaterials that form nanofibers, ribbons, and molecular template structures (22,23). The benefits of using nanoscale constituents, such as clay platelets, carbon nanotubes and nanofibers, and silica-based organic hybrids, have been widely studied since the early 1990s (see NANOCOMPOSITES, POLYMER-CLAY; NANOCOMPOSITES, LAYER-BY-LAYER ASSEMBLY). Pioneering advances at Toyota research (24,25) led to a nylon-6/clay nanocomposite with remarkable property enhancements at low filler loading which stimulated further research and development. The unique combination of large interfacial area and small interparticle distances, obtained at low filler loadings, is responsible for material responses unexpected from that observed in conventional microcomposites. Nanocomposite filler loading is typically $<10\%$ and often $<5\%$ by weight as compared to 20–40% for conventional materials. The addition of nanoscale constituents provides not only reinforcement at low volume fractions but also synergism with the matrix molecules with which it shares the same size scale. Significant property enhancements are generally observed at loadings of 1–5 vol%. They include enhancements in modulus, strength, and toughness; dimensional stability at elevated temperature; decreased swellability and barrier resistance to small molecules; thermal stability and fire retardancy; and electrical and thermal conductivity. Both increases and decreases in T_g have been observed in thermoset nanocomposites.

Thermoset/Clay Nanocomposites. A number of studies have reported the processing and properties of thermoset/clay nanocomposites (26). Nanoclay materials, such as montmorillonite, are layered silicates, ie they have a lamellar structure. Elementary clay platelets consist of a 1-nm thick layer. Stacking of layers leads to a regular gap called a gallery or interlayer whose d-spacing can be measured by X-ray diffraction. The interlayer space can be penetrated by

organic cations or polar organic liquids. Exchange reactions with organic cations (eg, aminoacids or alkylammonium ions) renders the silicate surface organophilic. Such materials are referred to as *organically modified layered silicates* (OLS). To gain the property enhancements described above requires dispersion of the filler at the nanometer level, ie down to the elementary clay platelet. Two morphologies are possible: an intercalated nanocomposite in which the unreacted resin penetrates the interlayer and is subsequently cured; and an exfoliated or delaminated nanocomposite where clay layers are individually dispersed in the thermoset matrix. Intercalation leads to increased *d*-spacing and can eventually result in exfoliation. Many nanocomposite systems are a blend of intercalated and exfoliated structures. The ability to process thermoset nanocomposites depends on several compositional factors such as resin viscosity and reactivity, catalysts, and the effect of the nanoparticle itself. The filler can play a significant role in the rheology of the uncured system as well as catalyze the chemical cross-linking reactions. Organically modified layered silicates frequently catalyze the reaction so that the rate of intragallery cure exceeds extragallery cure and that in the bulk matrix. The extent and rate of cure determine gelation and ultimately the final morphology, ie intercalated or exfoliated.

Pinnavai and co-workers (27) achieved exfoliated morphologies using epoxy resins. The ability to achieve an exfoliated morphology is presumed to be due to the polarity of these systems, which promotes diffusion into the clay galleries. Subsequent to diffusion into the interlayer, it was suggested that the maximum layer expansion is obtained when the intragallery cure rate exceeds that outside the gallery, allowing exfoliation to occur before gelation freezes the morphology. It was also shown that the alkylammonium ions catalyze homopolymerization of the epoxy. The same authors (28) observed two DSC exotherms for these systems. The lower temperature and lower activation energy exotherm was attributed to cure of epoxide on the internal gallery surfaces where the acidity of the clay exchange cation was assumed to play a major role in catalyzing epoxy homopolymerization. The higher temperature peak was attributed to cure of extragallery epoxide. Miyagawa and co-workers (29) studied the thermal–mechanical properties and nanostructure of an anhydride-cured epoxy reinforced with an organoclay (OLS), natural montmorillonite modified with a ternary ammonium salt. Nanocomposites were made with clay loadings of 2.5–6.2% by weight (1.6–4.0% by volume). Following fabrication of the 2.5 wt% clay nanocomposite, the *d*-spacing was observed to expand from 1.80 to 5.84 nm, suggesting that the epoxy system was intercalated between the layers causing additional exfoliation of the clay platelets. Dynamic mechanical analysis showed a 43% increase in storage modulus at 30°C for the 6.2 wt% nanocomposite, significantly greater than that predicted from microreinforcement and nearly a 100% increase in storage modulus above T_g for the 2.5 wt% material. T_g was found to decrease linearly with increasing clay loading, with a ∼15°C decrease for 6.2 wt% clay. It was speculated that the T_g depression may be due to a stoichiometric imbalance caused by preferential adsorption of one of the resin components on the clay surface or in the clay galleries. Messersmith and Giannelis (30) prepared and cured several epoxy–organoclay nanocomposite systems. The curing reaction appeared to involve the hydroxyethyl groups of the alkylammonium ions in the galleries, which participate in the cure reaction and result in direct attachment of the polymer network to the molecularly dispersed

silicate layers. Nanocomposites exhibited a broadened but slightly higher T_g than the neat epoxy. The dynamic storage modulus of nanocomposite containing 4 vol% clay was ~58% higher in the glassy region and 450% higher in the rubbery plateau region than neat epoxy.

Phenolic resin nanocomposites have been fabricated with montmorillonite and alkyl ammonium modified montmorillonite (31,32). It was found by X-ray diffraction that the clays were intercalated by the uncured phenolic resin. The interaction between the organic modifier and the phenolic resin played an important role in determining the stable nanostructure and the final morphology. Ganguli and co-workers (33) investigated the influence of organoclay nanoparticle addition on the rheology and cure of a phenolic dicyanate system, developing cure kinetics and TTT diagrams. The organoclay (OLS) was natural montmorillonite modified with a ternary ammonium salt. While the neat system exhibited Newtonian flow, the uncured nanodispersed system exhibited pseudoplastic flow, attributed largely to resin–clay interactions. Evolution of the morphology during cure was dependent on the rate of intergallery diffusion of the prepolymer resin system and subsequent gelation and vitrification, as well as intra- and extragallery cure kinetics. An intercalated morphology was indicated. Gelation and vitrification times and activation energies for the nanocomposite systems were lower than that of the neat resins, indicating a catalytic effect of the clay on the curing reaction. It was speculated that enhanced intergallery cure kinetics may be leading to a more rapid vitrification which limits resin diffusion into the layers and subsequent exfoliation.

Silica Nanocomposites. Miyagawa and co-workers (34) studied the thermal–mechanical properties and nanostructure of epoxy–anhydride and epoxy–amine systems reinforced with silica nanoparticles at loadings of 2.5–10% by weight. Storage moduli for both systems were significantly greater than the theoretical calculation for spherical particles, which was attributed to a chain network of aggregated silica particles observed by transmission electron microscopy. Individual silica particle diameters of 15–50 nm were measured. A decrease in T_g with silica loading was observed for the epoxy–anhydride system. At higher loadings, inhomogeneous mixing was attributed to the very high viscosities due to matrix–particle interactions. The critical energy release rate and Izod impact strength increased with silica loading for homogeneous samples.

Polyhedral Oligomeric Silsesquioxane Nanocomposites. These reagents offer an opportunity for preparing molecularly dispersed nanocomposites (35). They combine a hybrid inorganic–organic composition with nanosized cage structures having dimensions of 1–3 nm, comparable to those of most polymeric segments or coils. Polyhedral oligomeric silsesquioxane (POSS) compounds contain an inner inorganic framework made up of silicon and oxygen, which is externally covered by organic substituents that can embody a range of polar structures and functional groups. For example, monofunctional and multifunctional epoxy–POSS compounds react with epoxy systems and methacryl–POSS compounds react with acrylic and vinyl ester resin systems. Lee and Lichtenhan (36) described the viscoelastic response of monofunctional epoxy–POSS/epoxy systems containing 5% and 10% by weight POSS. The cured systems were transparent. The glass-transition temperature was observed to increase (~8°C for the 10% material) and broaden with increased loading of the monofunctional POSS into

the network. Surprisingly, the instantaneous modulus was not observed to be affected by incorporation of the POSS nanoreinforcement. Experiments below T_g showed that physical aging in the glassy state was retarded, ie the time required to reach structural equilibrium was longer for POSS–epoxy than for neat epoxy. Pittman and co-workers (37) investigated the viscoelastic and mechanical properties of multifunctional epoxy–POSS/epoxy systems containing 5% and 25% by weight POSS. At sufficiently high cure temperatures, incorporation of the POSS macromer into the epoxy network broadened the glass transition but had little effect on T_g, taken as the peak in tanδ by dynamic mechanical analysis (DMA). The storage moduli at temperatures above T_g were higher than those of neat epoxy and increased with increasing POSS content, improving thermal dimensional stability. However, flexural strengths of epoxy/POSS nanocomposites were lower than that of neat epoxy. Pittman and co-workers (38) have also conducted investigations on several additional POSS/thermosetting systems, including phenolic, dicyanate, and vinyl ester. The phenolic and dicyanate systems are being examined to generate carbon–carbon materials with silica nanophases. The authors speculate that the silica-like nuclei should be effective char promoters and oxygen permeation barriers.

Carbon Nanotube and Carbon Nanofiber Nanocomposites. The discovery of single-wall carbon nanotubes (SWNT) has renewed focus on composites with SWNT, multiwalled carbon nanotube (MWNT) and carbon nanofiber (CNF) reinforcements, together referred to as 1D Nanocarbon composites (39). These constituents offer promise for new lightweight materials with incredible mechanical, electrical, and thermal properties. 1D Nanocarbon materials are envisioned as multifunctional materials, eg single materials used for structures as well as electrical and/or thermal conductors. One example is electronics in a space satellite that need to be lightweight and mechanically supported, have the excess heat dissipated, and be protected from electromagnetic interference (EMI). Other examples are structures that are also batteries and structures that store hydrogen for fuel cells.

1D Nanocarbon composites offer the capability of comparable one-dimensional and two-dimensional reinforcement as conventional carbon-fiber composites, but at much lower loadings. They also offer the unique capability of three-dimensional reinforcement, and at volume fractions less than conventional two-dimensional quasi-isotropic laminates of comparable stiffness. 1D Nanocarbon can also be added at low volume fractions to the matrix for conventional continuous fiber-reinforced composites. Enhanced properties that are envisioned include reduced residual stress by lowering the coefficient of thermal expansion and reducing cure shrinkage, and reduced hygrothermal instability and microcracking. Potential benefits include improved aging and dimensional stability. "Through thickness properties," ie properties in the thickness direction, which are heavily influenced by the matrix properties, also stand to benefit. Small additions of 1D Nanocarbon can significantly improve mechanical properties and transport properties, such as electrical and thermal conductivity, perpendicular to the continuous fiber reinforcement.

Some 1D Nanocarbon materials are already being commercialized, but significant challenges remain. While the nanoscale offers property enhancements not observed with larger reinforcing materials, it also makes dispersion and fiber

alignment more difficult. In addition continuum models may not apply on the size scale of molecules, necessitating the development of new models to guide further development.

Cure and Properties of Thermosets

The basic phenomena of cure were described in the section on characteristic behavior of thermosets. In this section we describe the cure process through the measurement of cure for actual thermoset systems. The most common analytical tools for measuring cure are differential scanning calorimetry (DSC); Fourier transform infrared (FT-IR) and Raman spectroscopy; and rheology, dynamic mechanical analysis (DMA), and dielectric analysis (DEA). Thermogravimetric analysis (TGA) provides a simple and accurate means for measuring filler content where the filler is thermally inert; for measuring cure for thermosetting systems in which a volatile component such as water is a product of the cure reaction, as is the case with many phenolics; and for measuring thermal and thermal–oxidative stability (see THERMAL ANALYSIS and VIBRATIONAL SPECTROSCOPY).

Calorimetry. Differential scanning calorimetry (DSC) measures heat flow into a material (endothermic) or out of a material (exothermic). Thermoset cure reactions are exothermic, ie heat is produced as a result of the chemical reactions. As illustrated in Figure 4, the *heat of reaction*, ΔH_{rxn}, is the total heat liberated from an uncured thermosetting system and can be measured in a DSC heating experiment. ΔH is expressed as heat per mole of reacting groups (kJ/mol or kcal/mole) or per mass of material (J/g or cal/g). The basic assumption underlying the application of DSC is that the measured heat flow dH/dt [the ordinate of a DSC measurement, measured in J/s (watts) or cal/s] is proportional to the rate of the chemical cure reaction, $d\alpha/dt$, as shown in equation 8.

$$d\alpha/dt = \frac{(dH/dt)}{\Delta H_{rxn}} \tag{8}$$

In cases such as the epoxy–amine reaction, it is further assumed that the heat of reaction for epoxy with primary amine is the same as that for the reaction of epoxy with secondary amine, and that the activation energies are the same. For systems with a symmetrical DSC exotherm these parameters are usually within a few percent of each other (2–4). As pointed out in the section on epoxy resins, there is usually a substitution effect where the secondary amine is somewhat less reactive than the primary amine, but the effect on the overall kinetics measured by DSC is not significant. In the small number of systems where steric hindrance is significant, the substitution effect is much larger, eg $k_2/k_1 < 0.2$, the DSC exotherm exhibits a high temperature shoulder or even two distinct exotherms, and an overall reaction cannot be assumed. The above assumptions have proven to be good providing that other thermal events are not occurring at the same time to interfere with measurement of the cure reaction (2–4). One example of an interfering event is the endothermic evaporation of water of condensation from some phenolic

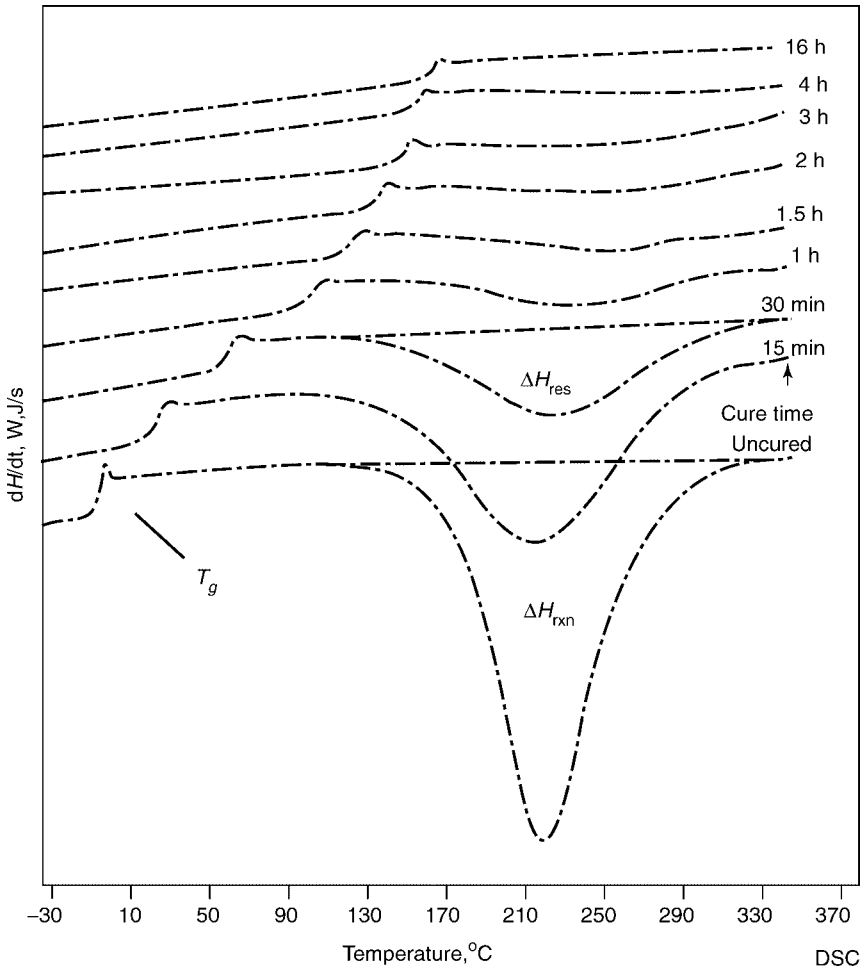

Fig. 4. A series of DSC temperature scans at 10°C/min of an epoxy–amine cured isothermally at 160°C for different times, showing T_g increasing and the residual exotherm decreasing with increasing cure times. From Ref. 40.

and amino resins, which occurs simultaneously with and as a result of the cure reaction.

In terms of a DSC measurement the conversion or degree of cure at time t, α_t, is defined as

$$\alpha_t = \frac{(\Delta H_{rxn} - \Delta H_{res})}{\Delta H_{rxn}} \tag{9}$$

where ΔH_{res} is the residual heat of reaction at time t, also illustrated in Figure 4. Sometimes the symbol x is used instead of α to denote conversion or degree of cure.

Figure 5 shows conversion vs ln(time) curves for the same epoxy for cure temperatures from 100–180°C. Conversion was calculated from equation 9. Note

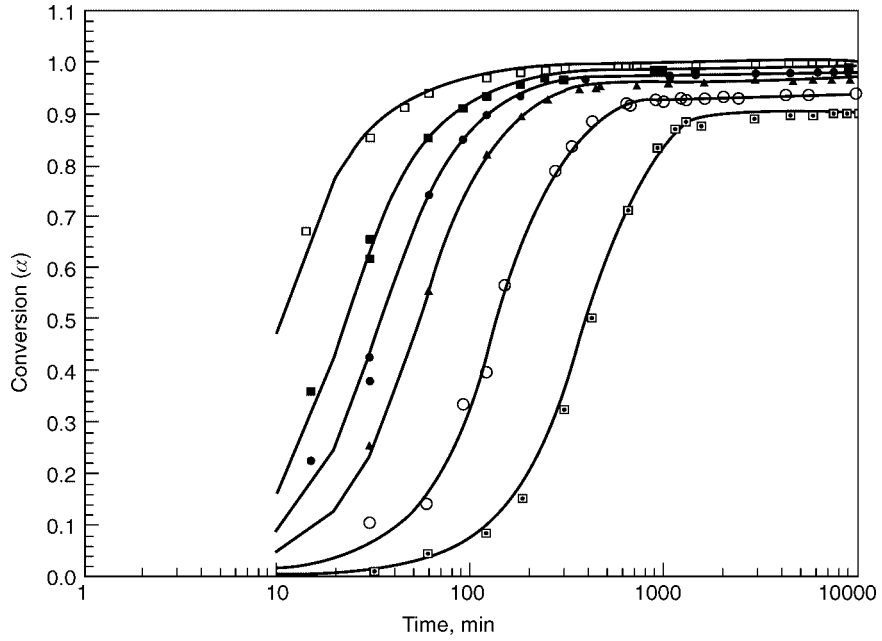

Fig. 5. Conversion versus time data for the same epoxy–amine system shown in Figure 4: ■ 100°C, ○ 120°C, ▲ 140°c, ◆ 150°C, ■ 160°C, □ 160°C. From Ref. 40.

that the curves are parallel during the first part of cure and, at the lower cure temperatures, less than 100% conversion is achieved.

As can be observed in Figure 4, there appears to be a relationship between the glass-transition temperature and conversion measured from the residual exotherm. Several workers have shown that for most thermoset systems there is indeed a unique relationship between the chemical conversion of a thermoset and its glass-transition temperature, independent of the cure temperature and thermal history (see, for example, Refs. 41–43). While a few exceptions have been noted, this appears to be the general case (see Ref. 2). Thus, measurement of T_g may be assumed equivalent to direct measurement of conversion.

Figure 6 illustrates the T_g–conversion relationship for an epoxy–amine system cured at several temperatures. All the data can be seen to collapse to a single curve and are fit to the empirical DiBenedetto equation (44,45). Excellent theoretical treatises of the T_g–conversion relationship can be found in References 41–43. As can be seen from the increasing curvature of the data in Figure 6, T_g is a more sensitive measure of cure than is conversion, as measured by ΔH_{res}, in the latter stages of cure, which are often the most critical. From the slope of the curve for the final 10% of cure [5.4°C/(% conversion)] and an ability to measure T_g to ±2°C, control of degree of cure to 0.5% from measurement of T_g is readily feasible. For thermosetting systems in which weight loss is associated with cure or for which there is no simple or unambiguous measure of cure, T_g is often the only practical means to monitor extent of cure.

The similarity of the T_g–time data in Figure 7 with the conversion–time data of Figure 5 is a consequence of the T_g–conversion relationship and illustrates

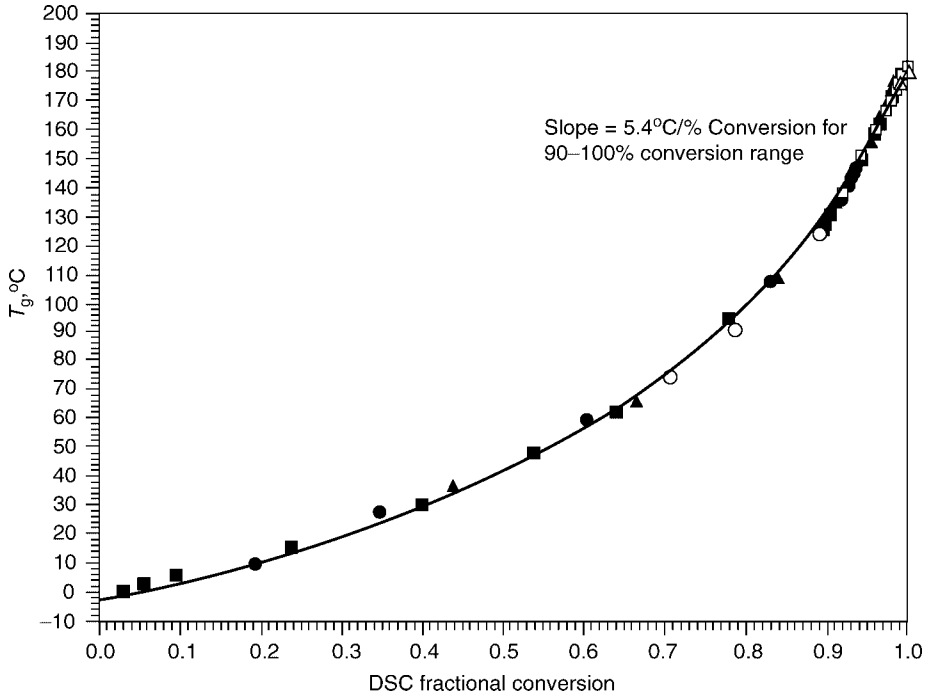

Fig. 6. Relationship for T_g and fractional conversion for the same epoxy–amine system shown in Figure 4. Different symbols represent material cured at different temperatures: ■ 100.5°C, ● 117.2°C, ▲ 139.1°C, ○ 157.1°C, □ 180.7°C, △ 200.4°C,—— DiBenedetto equation. The solid curve represents the best-fit calculation from the modified DiBenedetto equation (44, 45). From Ref. 40.

the ability to monitor cure through measurement of T_g. Figure 7 also directly illustrates vitrification, defined as T_g increasing to T_{cure} as a result of cure, and designated at each cure temperature by an arrow. Note that the progress of cure is significantly impeded shortly after vitrification, which marks the shift from chemical control to diffusion control of the reaction.

Cure Kinetics. This topic is important in two regards: the characterization of the cure behavior of a material and the design and optimization of cure processes. Cure kinetics generally fall into two categories. Aging or storage kinetics after reactants have been mixed, but prior to their use: reaction of prepregs, premixed and frozen adhesives, and powder coatings during storage fall in this category. The objective in this case is to minimize reaction. Of primary significance is cure of the thermoset after the prepreg has been formed into a structure, the resin has infused into a preform in a vacuum-assisted resin-transfer molding (VARTM) process, or the adhesive joint has been formed. Included here are the characterization, design, and optimization of cure processes, where issues such as the optimum time to apply pressure in an autoclave process, the time/temperature to reach full cure, and the increase in temperature required to reduce the cycle time by 50% are considered. Development of a kinetic equation is often needed for software that models the thermal cure process. When combined with rheological

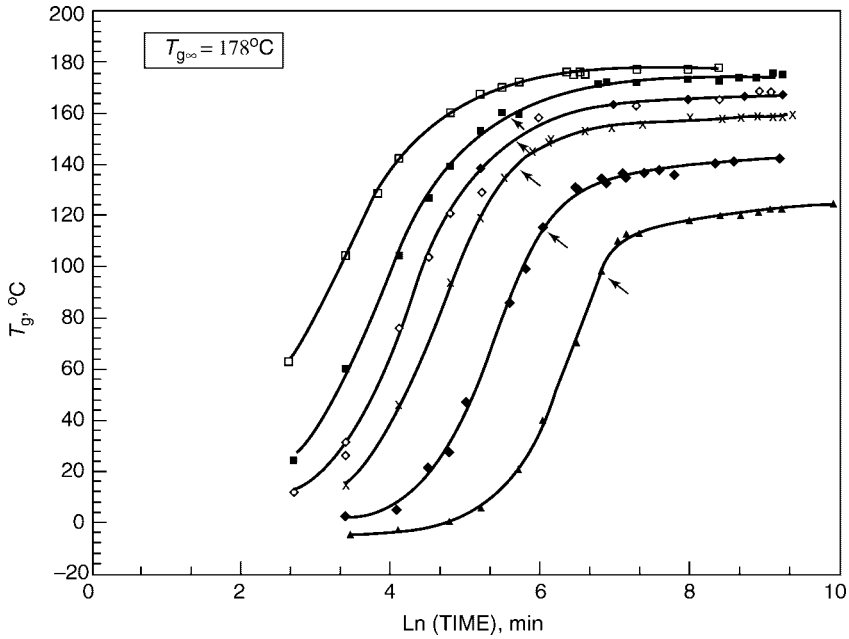

Fig. 7. T_g versus ln(time) for data at different cure temperatures: ▲ 100°C, ◆ 120°C, × 140°C, ◇ 150°C, ■ 160°C, □ 180°C. Isothermal vitrification ($T_g = T_{cure}$) at each cure temperature is designated by an arrow. Same epoxy–amine system as in Figures 4-6. From Ref. 40.

models, the flow behavior or chemorheology of the reacting system can be projected (46).

Cure kinetics is the mathematical relationship between time, temperature, and conversion. Three aspects of cure kinetics are considered: traditional kinetic analyses, model-free kinetics, and time–temperature superposition or TTS kinetics. Traditional kinetics involves models such as nth order and autocatalytic, fits conversion–time data taken at several temperatures to these models to determine reaction orders and measure rate constants, and measures the activation energy E from the Arrhenius equation. Model-free kinetics performs an isoconversional analysis on data from DSC data taken at three or more heating rates, where activation energy is allowed to vary with temperature. This methodology will not be discussed further here; those interested are referred to specific applications to thermoset cure (47,48). An assumption of TTS kinetics is that cure can be described by a single activation energy, independent of conversion and temperature, which is a good assumption for most thermosetting systems. TTS kinetics creates master cure curves by superimposing conversion–time and T_g–time curves through the T_g–conversion relationship utilizing the Arrhenius equation. It may be applied to the characterization of cure as well as to the monitoring and control of systems which cure according to complex time–temperature profiles.

Isothermal conversion–time data can be measured continuously from the beginning to the end of the reaction, or individually by scanning a series of partially cured samples. Two reliable techniques to obtain conversion–time data are isothermal DSC and spectroscopic techniques. Continuous isothermal DSC

measurements have the advantage of simultaneously measuring conversion (α) and rate of conversion ($d\alpha/dt$), which allows use of derivative forms of the rate equation such as equations 10 and 11. A disadvantage of this method is the danger of not recording the initial reaction that may take place during heating to temperature (2). Individual measurements can yield very accurate data and, in the case of DSC, give both T_g and conversion (see Fig. 4 as an example). However, they are time-consuming and since the reaction rate is not measured, integrated forms of the rate equation must be used.

Equation 10 shows the general nth-order rate equation

$$\frac{d\alpha}{dt} = k(1-\alpha)^n \tag{10}$$

where k is the rate constant and n is the reaction order. One example is the second-order reaction of an isocyanate with an alcohol to produce a polyurethane, as illustrated in equation 4. Integrated forms of this equation exist for first-order, second-order, and general nth-order reactions (2), so that either continuous or individual methods may be applied. Since there are only two unknowns, simple linear regression analysis may be used to determine values for k and n. Equation 11 shows a common autocatalytic rate equation proposed by Sourour and Kamal (49)

$$\frac{d\alpha}{dt} = (k_1 + k_2\alpha^m)(1-\alpha)^n \tag{11}$$

where k_1 is the catalyzed rate constant, attributed to impurities and/or fiber or particle surfaces; k_2 is the autocatalyzed rate constant, due to catalytic species produced by the reaction; and m and n are reaction orders. An example is the reaction of an epoxy resin with a diamine to produce an epoxy thermoset, as illustrated in equations 1 and 2. The chemistry for a stoichiometrically balanced reaction suggests that $m = 1$ and $n = 2$. For real systems, values are often close but not identical to these. In the epoxy–amine reaction the alcohol, which is also a product of the reaction, catalyzes further reaction, resulting in autocatalysis. Since there are four unknowns, nonlinear regression analysis must be employed, although k_1 can be evaluated independently as the extrapolated reaction rate at $\alpha = 0$. Autocatalytic kinetics are usually evaluated by the derivative form of the autocatalytic rate equation (eq. 11) with data collected by continuous isothermal DSC measurements. Activation energy E and preexponential factor A are measured from the Arrhenius equation:

$$k = A\exp\left(\frac{-E}{RT}\right) \tag{12}$$

where k is the rate constant, R is the gas constant (1.987 cal/K·mol $\equiv$ 8.314 J/K·mol) and T is absolute temperature. Also note that two activation energies are measured for autocatalytic cure, E_1 and E_2, corresponding to the two rate constants k_1 and k_2. Xie and co-workers (50) used this approach to investigate the effect of multiwalled carbon nanotubes (MWNT) on the cure of an epoxy–amine

system. MWNT were found to accelerate the cure with a pronounced increase in k_1 at all temperatures and a significant decrease in E_1. These authors also introduced a diffusion factor to describe the effects of vitrification on cure in the later stages. References 51–53 discuss incorporating the shift from chemical control to diffusion control upon vitrification into kinetic analyses.

For applications of TTS kinetics we consider cure reactions that can be described by a single activation energy, independent of conversion and temperature. The majority of cure reactions fall in this category, and they typically exhibit a single, symmetrical DSC exotherm. This includes epoxy–amine cure, where the primary amine–epoxy reaction and the secondary amine–epoxy reaction may have different activation energies. They are usually within a few percent of each other, and an average or overall activation energy gives a good description of the cure (see Fig. 8 below as an example). In cases where the activation energies are significantly different, the DSC exotherm will be skewed or there will be two distinct exotherms, in which case a more complex analysis of cure must be undertaken (2). Activation energies for cure are typically between 40 and 125 kJ/mol (10 and 30 kcal/mol). For an activation energy of 40 kJ/mol, an increase in temperature from 100 to 110°C will increase the rate of cure by a factor of ~2. For an activation energy of 125 kJ/mol, the increase will be a factor of 7. More detailed discussions

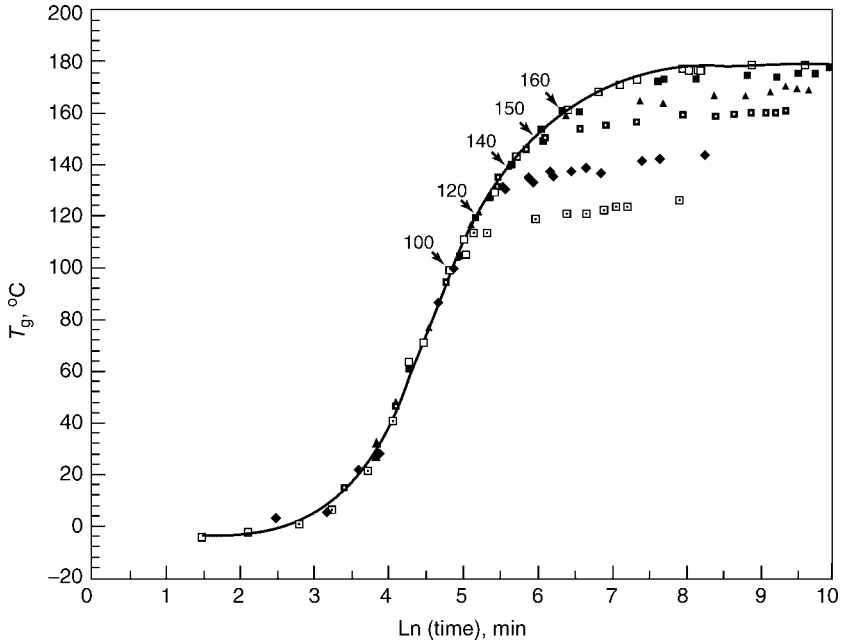

Fig. 8. Superposition of the T_g versus ln(time) data to form a master curve at 140°C by shifting each curve in Figure 7 by a constant factor [ln $(a_T) = \ln(t_{140°C}) - \ln(t_T)$] (see eq. 13) along the ln(time) axis so that its beginning section ($T_g < 90°C$) coincides with the curve for $T_{cure} = 140°C$. Isothermal vitrification points at different cure temperatures are marked by arrows. Note that vitrification points at all cure temperatures lie on the master curve, ie vitrification occurs during chemical control of the reaction: ▫ 100°C, ◆ 120°C, □ 140°C, ▲ 150°C, ■ 160°C, □ 180°C. From Ref. 40.

of kinetics, not only related to cure but also to storage life before cure and aging after cure, can be found in References 2–4.

$$a_T = \frac{t_2}{t_1} = \exp\left[\frac{E(T_1 - T_2)}{R(T_1 - T_2)}\right] \tag{13}$$

The assumption of a single or overall activation energy means that the only effect of temperature is to speed up or slow down the reaction. As illustrated in Figure 5, when E is constant conversion–time curves (or T_g–time curves through the T_g–conversion relationship; see Fig. 7) will be parallel on a ln(time) plot, allowing construction of master cure or aging curves via time–temperature superposition (2,54). Equation 13 defines the shift factor a_T, which is described by the Arrhenius equation where t is the time to constant conversion or constant T_g, E is the activation energy, and T is the absolute temperature. Master curves are useful for succinctly summarizing all of the kinetic data taken at different temperatures and for predicting behavior at times and temperatures that may be of interest but differ from those that were measured. Note the parallel nature of the curves prior to vitrification in Figures 5 and 7. Figure 8 shows the master curve from shifting the data of Figure 7 along the ln(time) axis using the measured overall activation energy of 63.5 kJ/mol (15.2 kcal/mol) (40). These data were shifted to a reference temperature of 140°C by means of equation 13. Figure 8 clearly shows the reaction under chemical control (master curve, solid line). Only the chemically controlled reaction, which follows Arrhenius kinetics, is subject to time–temperature superposition. Following vitrification, the individual curves deviate from the master curve as the reaction slows and becomes controlled by diffusion of reactants in the glassy state.

Note that in most thermoset cure processes, temperatures are high enough relative to $T_{g\infty}$ to avoid vitrification. A good example is a fast curing, two-component polyurethane used in a pultrusion process (55). Parts are made by mixing the components in-line and rapidly processing and curing. In this study conversion–time data were collected from isothermal DSC measurements. The master cure curve shown in Figure 9 was obtained by shifting these data to times at a reference temperature of 80°C by means of equation (13), using the activation energy for cure measured from multiple heating rate DSC measurements (2). To obtain additional data at high conversion but without the complication of vitrification, heat-hold-cool DSC measurements were made that simulated process cure profiles. Equivalent cure times at the same reference temperature of 80°C were calculated from the profiles by shifting individual points along the profile to times at 80°C by means of equation 13 and summing those points (2,54). The master curve was found to fit the second-order kinetic equation (eq. 10 with $n = 2$) and a complete mathematical description of cure was provided. From this kinetic equation the development of conversion along the profile shown in Figure 10 was determined. A conversion of 96.5% for the polyurethane resin cured according to this profile was estimated. The kinetic equation for cure also allowed the computation of the master curve shown in Figure 9 as "Kinetic Equation."

Modulated Temperature DSC. This is a relatively new technique with tremendous application to thermosets (4). By superimposing a sine wave on the

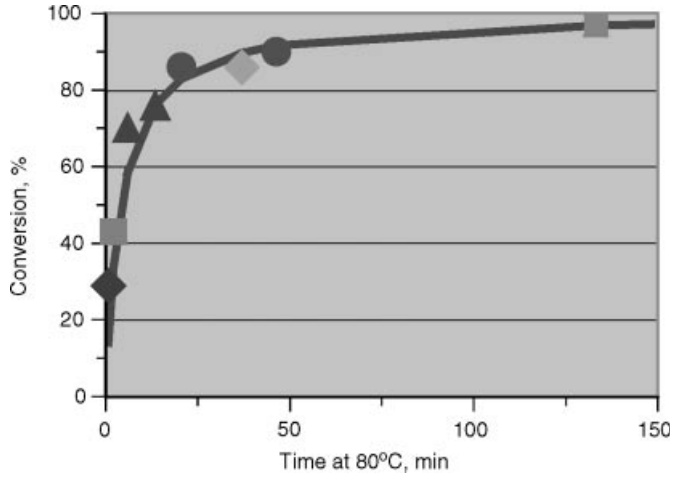

Fig. 9. Master cure curve for polyurethane pultrusion resin system. Data points from isothermal DSC and DSC simulated cure profiles were shifted to times at 80°C by means of equation 14 using the activation energy measured from multiple heating rate DSC. The solid line is calculated from the second-order kinetic equation found to fit the master curve. ◆ 30°C, ■ 45°C, ▲ 60°C, ● 80°C, ◆ 130° profile, ■ 160°C profile, ——— kinetic equation From Ref. 55.

conventional linear heating rate or isothermal temperature, reversible thermal events such as heat capacity and T_g can be separated from those that are nonreversing such as cure. Modulated temperature DSC (MTDSC) allows for the simultaneous measurement of heat capacity, heat flow, and the phase angle between heat flow and heating rate (termed *heat flow phase*). This technique has revolutionized the measurement of T_g, which is measured as a step increase in the heat capacity on heating, by eliminating nonreversing phenomena such as enthalpy relaxation and residual cure from the heat flow measurement.

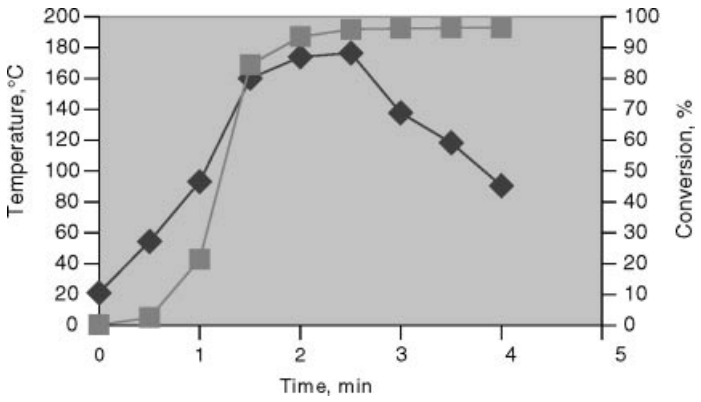

Fig. 10. Time–temperature profile for pultrusion process and development of conversion along the process. —◆— Temperature, °C, —■— conversion. From Ref. 55.

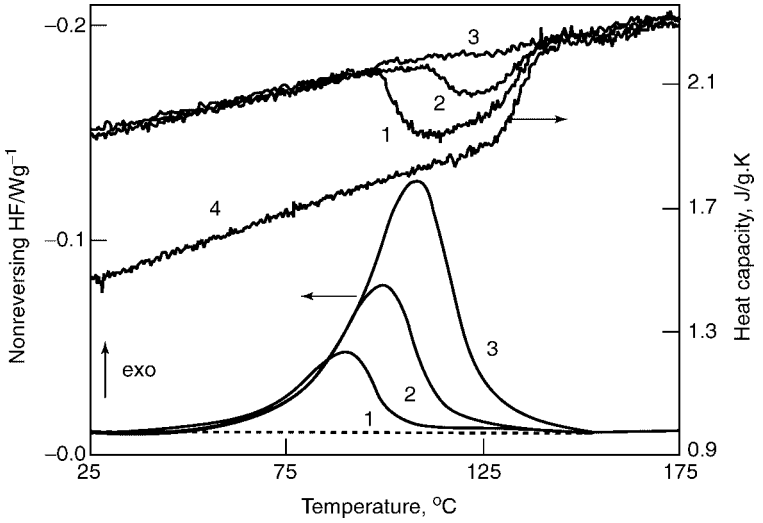

Fig. 11. Nonisothermal cure of an epoxy–anhydride at 0.2 (1), 0.4 (2), and 0.7°C/min (3), and for the fully cured material (4): nonreversing heat flow and heat capacity. From Ref. 4.

Vitrification will occur during thermoset cure when the increasing T_g becomes equal to the cure temperature. This will happen during isothermal cure if the cure temperature is below $T_{g\infty}$, the glass transition for the fully cured thermoset. It will also occur during heating providing the heating rate is sufficiently slow relative to the reaction rate. This is illustrated by the heat capacity curves in Figure 11. At a heating rate of 0.2°C/min (Curve 1), vitrification and the onset of diffusion control can be observed as a decrease in heat capacity beginning at about 100°C. The reaction remains under diffusion control as indicated by the heat capacity remaining between the upper liquid/rubber curve and the lower glassy curve until the reaction is complete, at which time the heat capacity returns to the upper liquid/rubber curve. At 0.4°C/min heating rate (Curve 2) the reaction shifts from chemical control to diffusion control at a higher temperature and over a smaller extent of reaction, and at 0.7°C/min (Curve 3) the entire reaction occurs under chemical control without vitrification.

Many thermoset systems that are brittle have been found to benefit from incorporation of rubber or thermoplastic modifiers that significantly toughen the system (56,57). In the uncured state these modifiers are compatible with the resin system, forming a homogeneous solution. The system transforms into a phase-separated structure because of the increasing molecular weight and network formation of the reacting matrix. The competition between the rates of cure and of phase separation determines the mechanism of the reaction-induced phase separation. The ability of MTDSC for real-time monitoring of reaction-induced phase separation was demonstrated with the cure of an epoxy–aniline–polyethersulfone (PES) system (4). In this case phase separation was observed as vitrification of the segregating dispersed PES-rich phase during isothermal cure at 100°C.

Combined with modeling and FT–Raman spectroscopy, MTDSC can provide specific details of cure reactions such as epoxy–amine in terms of the individual

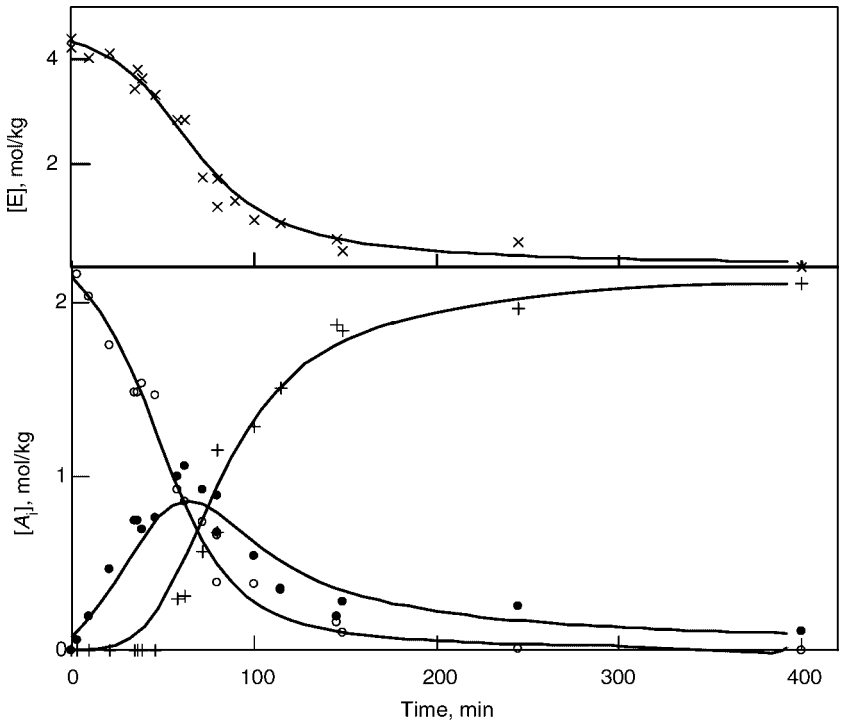

Fig. 12. Evolution of the concentration of epoxide [E] (×), primary amine [A1] (○), secondary amine [A2] (●), and tertiary amine [A3] (+) as measured by FT-Raman spectroscopy for a stoichiometric mixture of DGEBA–aniline cured at 100°C; simulation from MTDSC kinetic model (solid lines). From Ref. 58.

reactants (58). When an overall conversion can be obtained from the heat flow signal, as was shown for the epoxy–aniline system, additional information is available in the heat capacity signal where the primary and secondary amine–epoxy reactions contribute differently to the reaction heat capacity. As a result the evolution of specific reactive groups during cure can be modeled, as shown in Figure 12 where the projections from MTDSC are compared with FT–Raman measurements.

Fourier Transform Infrared and Raman Spectroscopy. These techniques are able to analyze organic and inorganic materials, including thermosets. Results are obtained by spectral interpretation, eg, band allocation to functional groups and comparison with reference spectra, or imaging such as two-dimensional mapping of functional groups (see VIBRATIONAL SPECTROSCOPY). They are capable of monitoring the cure reaction from the liquid state through gelation to the completion of conversion, and even into the glassy state with good precision, sensitivity, and temporal resolution. Determination of chemical conversion versus time and temperature can be made from measurements of functional group intensity with progress of the reaction. For the epoxy–amine reactions shown in equations 1 and 2, for example, one can measure consumption of epoxide and primary amine, production and subsequent consumption of secondary amine, and production of tertiary amine and hydroxyl, thus allowing simultaneous examination of

several kinetic processes associated with cure. Fourier transform infrared (FT-IR) and Raman spectroscopy may have advantages over other techniques such as DSC for their ability to distinguish multiple simultaneous reactions which may have different heats of reaction and activation energies.

Normal vibrations related to a change in dipole moment are infrared active. Functional reactive groups in thermosetting systems, such as epoxide, amine, and hydroxyl, typically have large dipole moments and strong infrared absorptions. Near infrared (FT-NIR) spectroscopy (12,000–4,000 cm^{-1}) has several advantages over the traditional mid-IR (MIR) spectroscopy (4000–400 cm^{-1}), including less complex absorption spectra and the transparency of glass in this region, which allows it to be used as a sample support and for the possibility of *in situ*, real-time cure monitoring, eg by fiber optic NIR spectroscopy (59). In the near-IR range, absorption bands are due to the combination and overtone of fundamental vibrations observed in the MIR region. Their absorptivities are lower, which requires NIR samples to be thicker, eg up to 1 mm or more, and which makes sample preparation simpler than that often required for MIR samples. The strongest absorption bands belong to the highest anharmonic vibrations, which involve the hydrogen atom. In epoxy resin systems, for example, only C—H, N—H, and O—H vibrations are active. As a consequence, NIR absorption spectra are less complex than their counterpart recorded in the MIR region and bands associated with reactive functional groups are better separated. In general the measurements are quantitative because of observed agreement with the Beer–Lambert Law, where absorbance has a linear dependence on concentration. Epoxide, primary amine, and secondary amine concentrations can be measured directly. Kinetic calculation allows one to determine other functional group concentrations not easily measured. The cure of epoxy model systems has been characterized by FT-NIR spectroscopy (60–66). Quantitative measurements are in good agreement with those obtained from other techniques, as illustrated in Figure 13. In this study (64) the cure of a

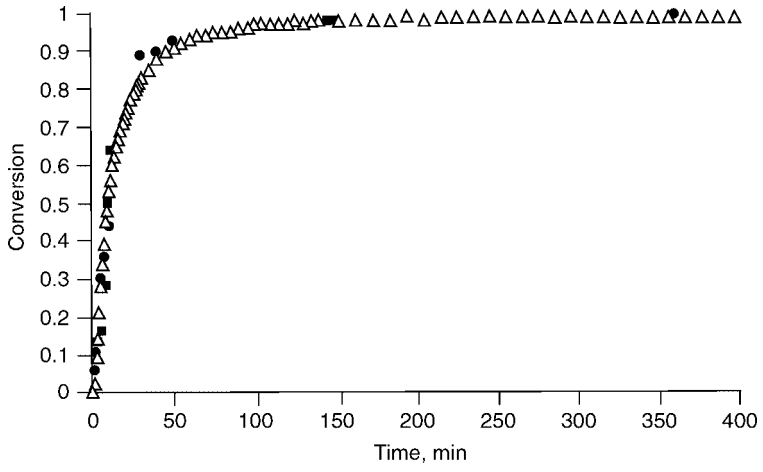

Fig. 13. Comparison of the epoxide conversion in stoichiometric DGEBA–poly(oxypropylene)triamine system at 100°C by DSC (●), SEC(□), and NIR (△). From Ref. 64.

1:1 stoichiometric epoxy–amine system at 100°C was studied by NIR, DSC, and size-exclusion chromatography (SEC, also known as gel-permeation chromatography, GPC). NIR conversion was measured from the concentration of epoxide obtained from the epoxide band at 4528 cm^{-1}, a combination of the stretching fundamental at 3050 cm^{-1} with the CH_2 deformation fundamental at 1460 cm^{-1}, as defined in equation 14.

$$\alpha_{t,NIR} = \frac{A_0 - A_t}{A_0 - A_\infty} \tag{14}$$

where A_0 represents the normalized absorbance initially, A_t the absorbance at time t, and A_∞ the absorbance at complete cure. DSC conversion was measured from the residual exotherm of samples cured for different times at 100°C (see eq. 9). SEC conversion was measured from 1% tetrahydrofuran (THF) solutions of pregel samples cured with the DSC samples. NIR band assignments for the epoxy–amine reaction can be found in References 61–63 and 67. Each functional group has at least two absorption bands. The first, located between 5100 and 4000 cm^{-1}, is assigned to a combination of fundamental vibrations. The second, located at higher wavenumbers, originates from the overtone of the fundamental vibration. Typically, epoxide, primary amine, and hydroxyl concentrations are measured from well-separated absorption bands in the combination region (5100–4000 cm^{-1}). Epoxide and primary amine as well as secondary amine can be measured from the higher wavenumber overtone region where some overlapping of absorptions occurs, often necessitating spectra to be decomposed. When the concentrations of epoxide, primary amine, and secondary amine are known, the hydroxyl and tertiary amine concentrations and the extent of etherification can be deduced from epoxy–amine chemistry and kinetic considerations (67–69). The ratio of rate constants for the epoxy–secondary amine reaction (eq. 2) to the epoxy–primary amine reaction (eq. 1) can be measured. $R = k_2/k_1 = 0.5$ for equal reactivity, which is often assumed, eg, for kinetic analyses from DSC measurements. Paz-Abuin and co-workers (65) report a simple method and R values around 0.4 for three systems but <0.2 for an epoxy–cycloaliphatic amine system. St. John and George (62) reported $R = 0.22$ for a TGDDM/DDS system and also found that the epoxy–secondary amine reaction was affected by gelation, whereas the epoxy–primary amine reaction was not.

While IR is an absorption technique that depends on a changing dipole moment, Raman is a scattering technique that depends on changing polarizability in strong covalent bonds such as C=C and C—O. Like near infrared, sample preparation is simple; water may be used as a solvent and glass as a substrate or container. The frequency range is 4000–50 cm^{-1}. In Raman spectroscopy the sample is excited with laser light. The interaction between the oscillating molecule and the incident radiation will result in both elastic Rayleigh scattering and inelastic Raman scattering. The much stronger Rayleigh scattering is filtered out and a grating disperses the Raman scattered light onto a detector to generate a spectrum. The epoxy–amine reaction has been studied by Raman spectroscopy (58,60,70).

Rheology, Dynamic Mechanical Analysis, and Dielectric Analysis. Thermosetting resins allow a wide range of processing options. When low

molecular weight monomers or oligomers are used as the starting materials, the viscosity can be very low, enabling a wide variety of application methods. Typically, with the application of heat, the low molecular weight species begin to react and increase their molecular weight. As the network builds, the viscosity increases.

Steady shearing rheological methods are good for precisely measuring the viscosity early in the curing and up to the gel point. For low viscosity monomers and oligomers, cone and plate and parallel plate geometries are typically used. Additionally, most rheometers allow precise temperature control, enabling isothermal curing studies to be conducted. If viscosity development is required over the entire conversion range, then steady shearing rheometry is not the recommended choice, since large torques will build up after the gel point and could potentially damage the torque transducers (see RHEOLOGICAL MEASUREMENTS).

Dynamic mechanical methods (typically oscillatory parallel plate rheometry) are commonly used to measure the dynamic mechanical properties from the liquid state to the solid state. By using small-amplitude oscillatory deformations (linear viscoelastic regime), the dynamic storage and loss moduli can be obtained. From these quantities, the viscosity and modulus can be calculated (71) (see DYNAMIC MECHANICAL ANALYSIS).

The dynamic moduli are obtained by applying a time varying strain:

$$\gamma = \gamma_0 \sin(\omega t) \tag{15}$$

where γ_0 is the shear strain amplitude and ω is the frequency. For small strain amplitudes the resultant stress is

$$\sigma = \sigma_0 \sin(\omega t + \delta) \tag{16}$$

where σ_0 is the shear stress amplitude and δ is the phase angle.

For small strain amplitudes, for polymers in the linear viscoelastic regime, the resultant stress is

$$\sigma = \gamma_0 [G' \sin(\omega t) + G'' \cos(\omega t)] \tag{17}$$

where $G'(\omega)$ is the dynamic storage modulus, and $G''(\omega)$ is the dynamic loss modulus. From the dynamic moduli, $G'(\omega)$ and G$''(\omega)$, the complex viscosity $\eta^*(\omega)$ can be calculated (71):

$$\eta^*(\omega) = \frac{\sqrt{[G'(\omega)]^2 + [G''(\omega)]^2}}{\omega} \tag{18}$$

In Figure 14, the complex viscosity is plotted as a function of time for an isothermal cure of an epoxy-based thermoset. The initial viscosity is low and increases rapidly at various temperatures.

In many composite applications, B-staged resins and fiber-reinforced prepregs are used. For B-staged thermoset resins, measuring the viscosity profile during nonisothermal curing provides valuable insight into the flow window, or the time when the resin is able to flow during processing. In Figure 15, the

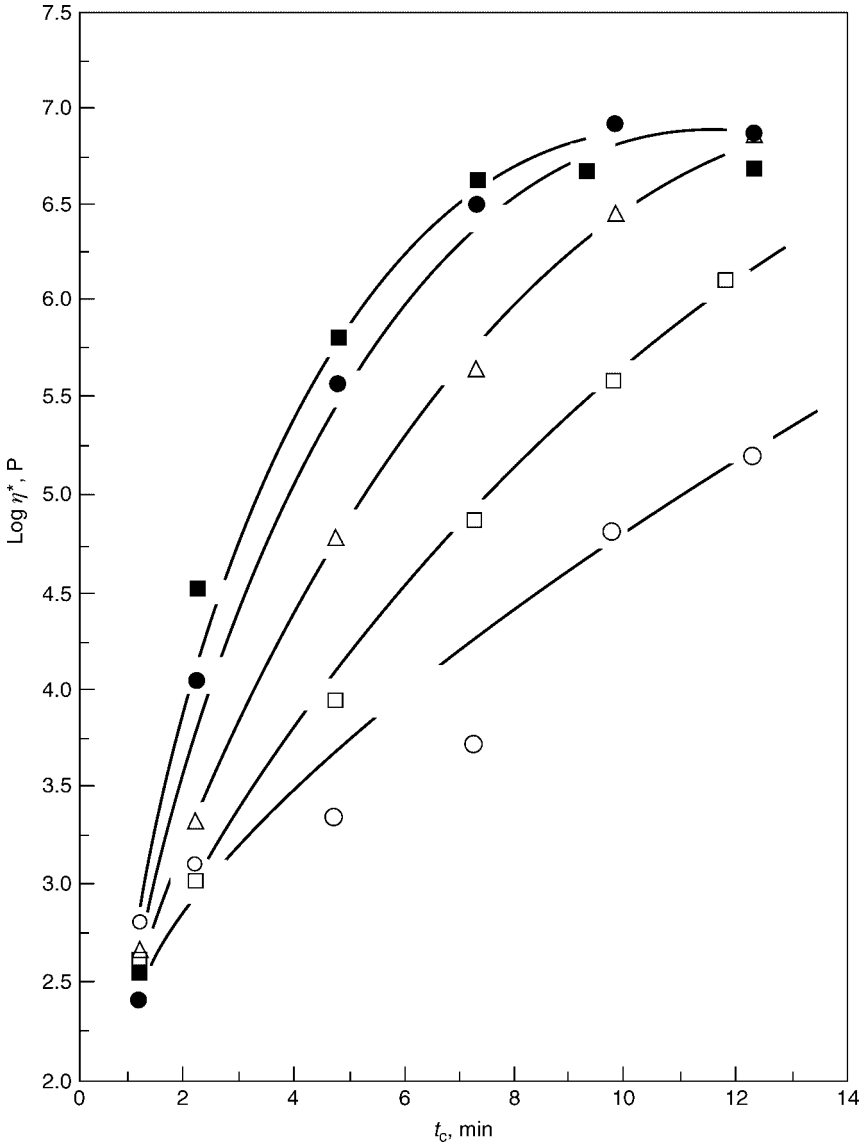

Fig. 14. Complex viscosity versus curing time for isothermal curing of epoxy resin. (1Pa·s = 10 P). ○ 123°C, □ 135°C, △ 145°C, ● 157°C, ■ 162°C. From Ref. 72.

complex viscosity and the percent conversion are plotted as a function of time for a heating rate of 9.8°C/min to 175°C. In this experiment, the rheometer run was aborted at specific time intervals, and the sample rapidly quenched and analyzed for T_g and conversion using DSC (72). The initial B-stage conversion was 23%. The viscosity rapidly decreases as the resin softens at T_g. With further heating, the viscosity reaches a minimum and then the rapid cross-linking reaction causes the viscosity to increase. During the initial softening of the resin, the conversion did not change, indicating that the temperature dependence of the

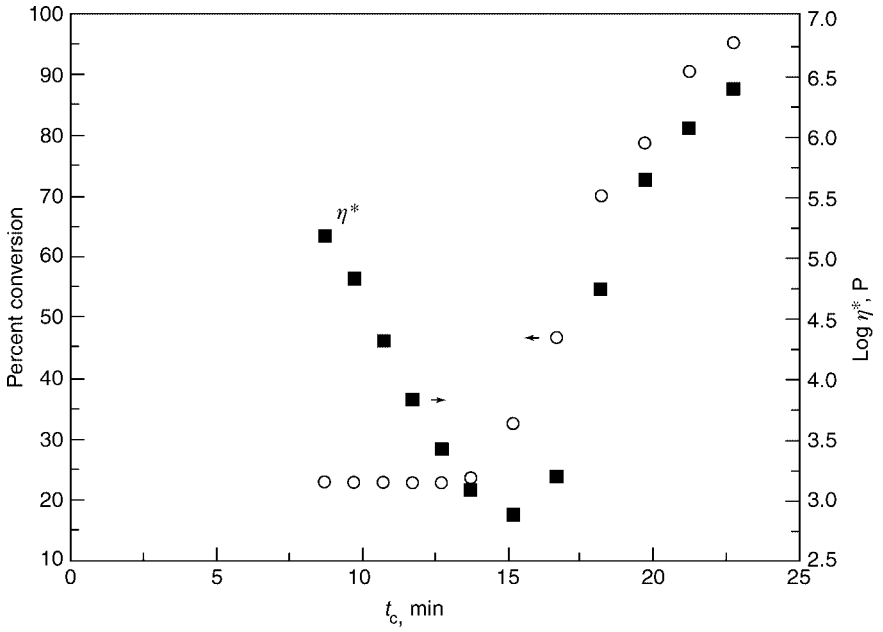

Fig. 15. Complex viscosity (■) and epoxy conversion (○) as a function of curing time for a sample heating rate of 9.8°C/min. (1Pa·s = 10 P). From Ref. 72.

viscosity is the controlling factor. When the viscosity approaches the minimum, the conversion begins to increase dramatically, indicating the onset of rapid consumption of reactive groups. The continuation of the reaction causes the viscosity to increase and ultimately leads through gelation toward full cure.

Whereas steady shear rheometry can measure the initial stages of cure up to the gel point (as illustrated in the left-hand portion of Fig. 2), dynamic mechanical analysis (DMA) can measure the cure process of unsupported thermosets from just beyond gelation to vitrification or the completion of cure, as well as the properties of cured thermosets (see the right-hand portion of Fig. 2). Oscillatory rheometry can measure viscoelastic properties during cure from the liquid state to the solid state, as illustrated in Figures 14 and 15. Figure 16 shows the 40°C isothermal cure of an epoxy resin in the shear sandwich mode, analogous to dynamic rheometry in the parallel plate mode, at frequencies from 0.1 to 100 Hz (73). The frequency-dependent increase in storage modulus to ∼1 GPa and the frequency-dependent loss peaks signify vitrification during cure. When uncured thermosets in liquid or paste form are applied to a substrate such as a metal shim (2,74), wire mesh (2,54,75–77), or glass fiber or filter media (2,12,40,78), cure can be measured from the uncured state to the completion of the reaction. Isothermal gelation and vitrification can be measured directly at several temperatures to generate TTT diagrams such as Figure 3 (12), or cure can be followed by measuring T_g versus time at several temperatures such as in Figure 7 (40,76–78). Figure 17 illustrates the wire-mesh technique which has been used in the characterization of cure of magnetic disk coating (76), powder coatings (54), and dielectric and conducting polymer thick films (77). Figure 18 shows the multifrequency DMA during

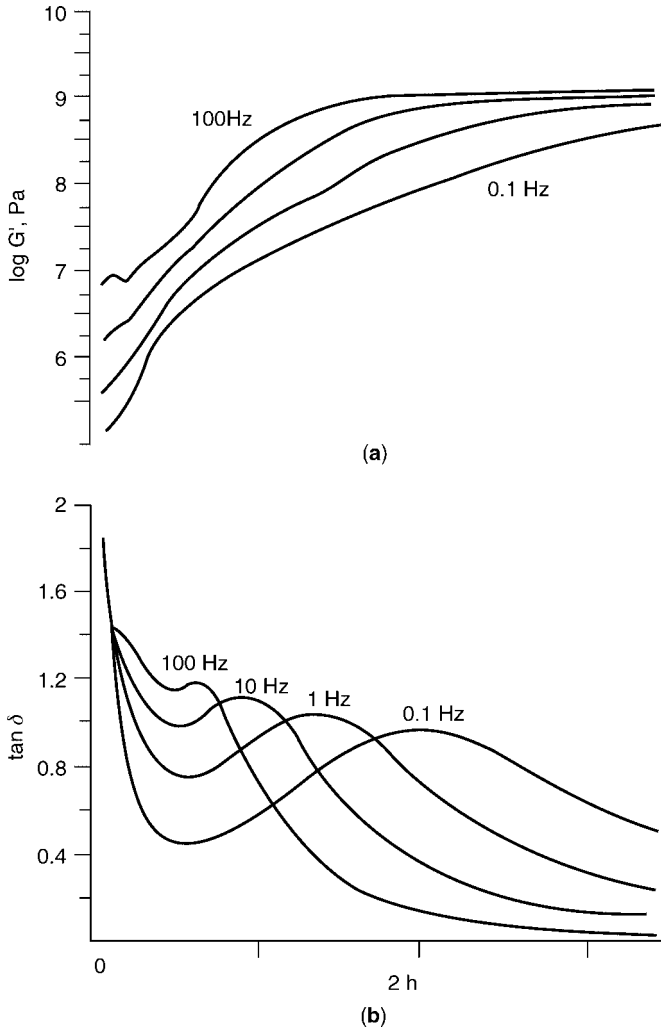

Fig. 16. Cure of epoxy resin in the shear sandwich mode at 40°C: (**a**) shear storage modulus; (**b**) tan δ. From Ref. 73.

heating of a B-staged epoxy from below T_g through the completion of cure (79). The frequency-dependent transition starting near room temperature is the glass transition of the B-staged epoxy, which gels near 140°C during heating at 2°C/min., as evidenced by the small increase in storage modulus and frequency-independent tan δ peaks.

Analogous to the dynamic mechanical measurements, dynamic dielectric measurements can also be used effectively to measure the changes in thermosetting polymers during curing. Typical dielectric measurements use two polarized electrodes. Early methods used parallel plate electrodes. More recently, interdigitated comb electrodes have proven to be more versatile for cure monitoring. All dielectric measurements are made by applying a sinusoidal voltage across the

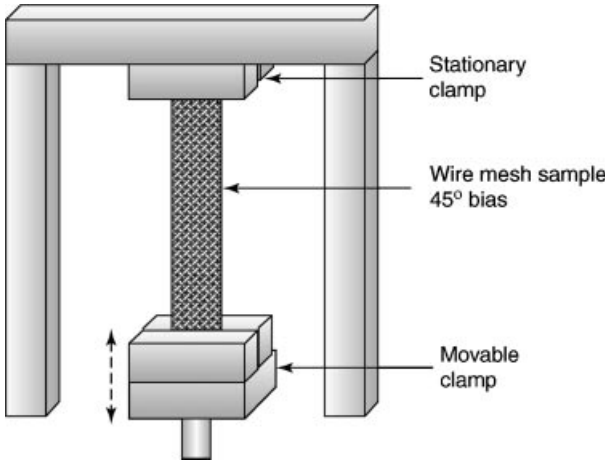

Fig. 17. Illustration of wire-mesh technique for DMA of liquid or paste materials. Tensile mode illustrated with wire-mesh cut at 45° bias to minimize shear resistance of mesh.

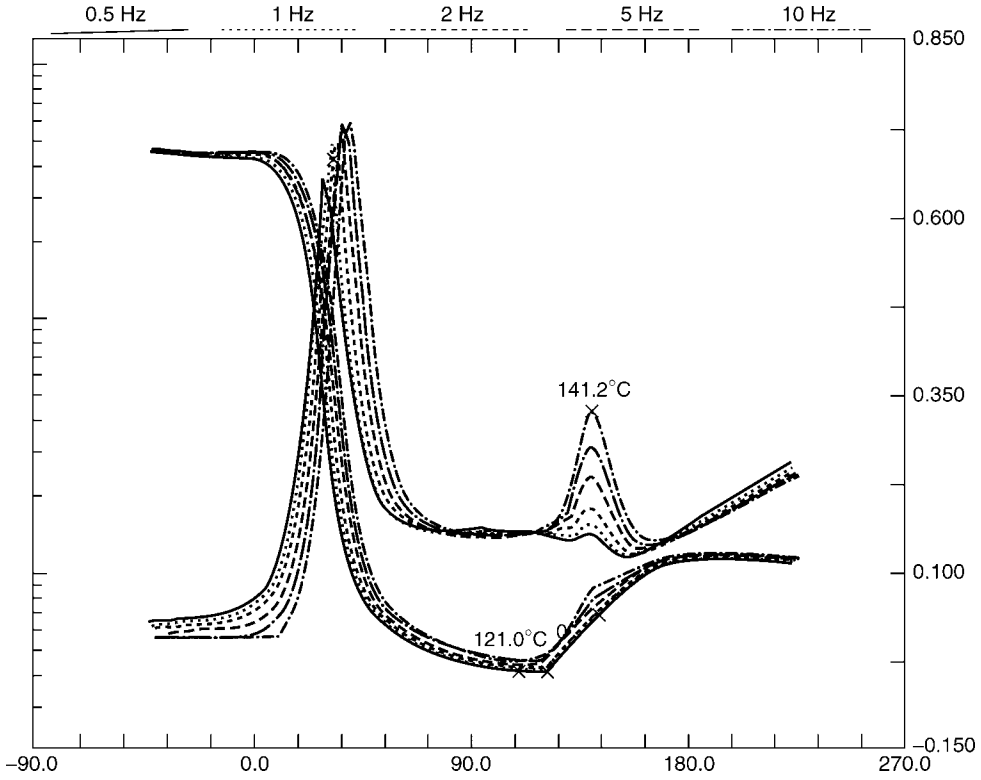

Fig. 18. Multifrequency dynamic mechanical analysis of a B-staged, fiber glass-reinforced adhesive during 2°C/min scan (68): 0.5, 1, 2, 5, 10 and 20 Hz. From Ref. 79.

material between the electrodes and measuring the in-phase and out-of-phase current. From these measurements the conductance and capacitance are obtained. The conductance is a measurement of the dissipation of energy (like the dynamic loss modulus in rheology and DMA), and the capacitance is an indication of the energy stored (analogous to the dynamic storage modulus). In the case of the dielectric measurement, the conductivity consists of two components, one arising from dipole orientation and the second arising from ionic conductivity (80).

The dielectric loss factor $\varepsilon''(\omega)$ can be expressed as

$$\varepsilon'' = \frac{\sigma}{2\pi f \varepsilon_0} + \varepsilon''_d \tag{19}$$

where σ is the ionic conductivity, f is the frequency, ε_0 is the permittivity of free space, and ε''_d is the lumped contribution from all dipoles. The ionic conductivity for a given material is controlled by the number and charge of the ionic species and, most importantly, the mobility of the ion (see DIELECTRIC RELAXATION).

For thermoset curing, there is typically a large change in segmental mobility during curing because of the stiffening of the developing cross-linked network. Measuring the dielectric loss factor as a function of time and temperature is an effective monitor of cure (80).

In Figure 19, the dielectric loss factor is plotted as a function of time for isothermal curing of an epoxy resin. Early in the curing, the viscosity is low, and thus the ionic mobility is high, leading to a large value in the loss factor. As curing proceeds, the increase in molecular weight and cross-linking cause the ionic mobility to decrease because of the tightening of the network and lower segmental mobility. The series of frequency-dependent loss peaks have been correlated with vitrification (81), analogous to those observed by DMA in Figure 16**b**. An excellent review of dielectric measurements and cure monitoring for thermosetting resins may be found in a review by Senturia and Sheppard (80).

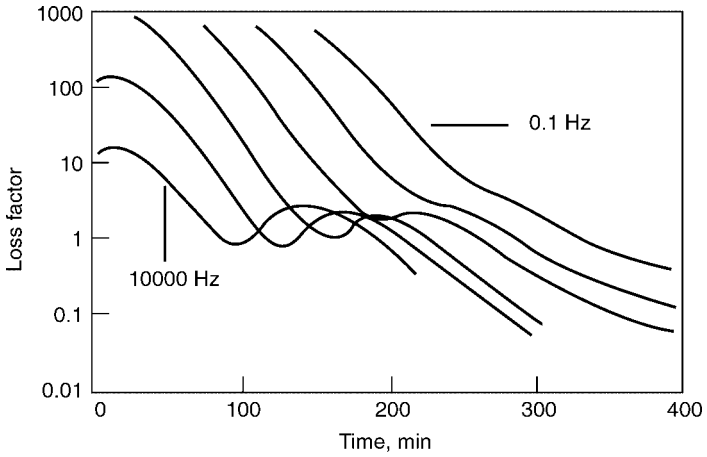

Fig. 19. Dielectric loss factor as a function of time for isothermal curing of an epoxy resin. From Ref. 82.

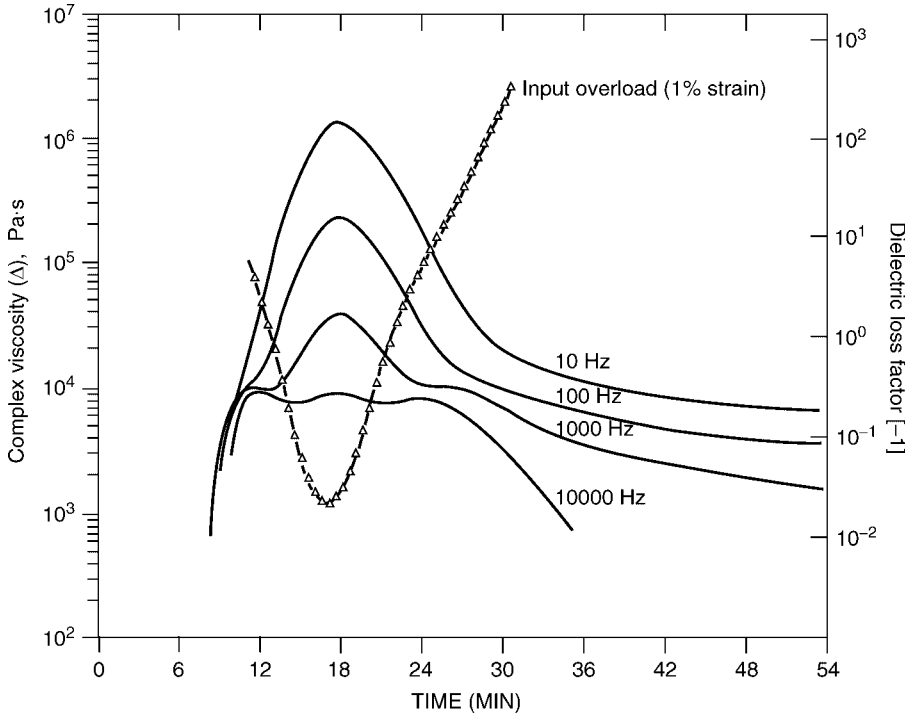

Fig. 20. Dielectric loss factor and complex viscosity plotted as a function of time for a nonisothermal ramp to the cure temperature. From Ref. 82. To convert Pa·s to p, multiply by 10.

Several important industrial applications involve the processing of B-staged prepregs in composite fabrication. Embedded dielectric cure monitors can be used to investigate the changes in the network structure during curing.

In Figure 20, the dielectric loss factor at several frequencies is plotted as a function of time for a nonisothermal ramp and hold at the cure temperature. Also in Figure 20 the complex viscosity (at 1 Hz) is plotted as a function of cure temperature. In this case, the viscosity and dielectric properties were measured simultaneously in a parallel plate rheometer (82). The figure clearly indicates increasing conductivity as the temperature exceeds the T_g of the B-staged resin and the viscosity decreases. With further curing, the viscosity goes through a minimum and then increases because of the rapid tightening of the cross-linked network. The dielectric loss factor goes through a maximum and then decreases rapidly as the cross-linking reaction proceeds. From the simultaneous measurement, the correlation of the loss factor and the complex viscosity can be established (82). Interestingly, because of the limitation of the torque sensor, the viscosity data could not be collected through the completion of the cure. The dielectric sensor is capable of measuring the continued segmental mobility change far into the reaction, giving a more complete analysis of the curing profile. In Figure 20, the final cure temperature was chosen to be lower than the T_g of the fully cured network. During cure, the T_g of the network will reach the cure temperature causing vitrification. At this

point, the reaction rate will be dramatically slowed and the resin will transition from rubbery to glassy. In Figure 20, at vitrification, the torque limit was exceeded because of the large increase in modulus at vitrification, but the temperature was held constant and dielectric data acquisition continued. One may note the continued but very slow curing reaction that continues at elevated temperatures even in the gelled glass region.

Weight Loss. Thermogravimetric analysis (TGA) measures mass flow out of a sample, ie weight loss. Weight loss in thermoset systems includes the loss of solvents and volatile products associated with cure, and degradation products associated with thermal and thermal-oxidative stability. Composition, for example, percent solids and filler content, can be measured from evaporation of solvents or complete decomposition of the resin system, respectively. For several thermosets, such as phenolic and amino resins, an integral part of cure is the formation of condensation products, such as water or formaldehyde (see eq. 3). For blocked isocyante systems, unblocking involves volatile loss and the unblocking temperature can be measured by DSC (83) and TGA (84).

Figure 21 is a TGA of a phenolic resole resin in air (85), showing 30–40% weight loss attributed to cure between 30 and 300°C and complete decomposition between 400 and 650°C. Pyrolysis in nitrogen leaves a significant residue or char. Pyrolysis of a carbon fiber phenolic composite in an inert atmosphere leads to a carbon–carbon composite where the char is the matrix (86). Analysis of the volatile products of Figure 21 by TGA coupled with mass spectroscopy (MS) showed that, in addition to water, products associated with cure included volatile starting materials such as phenol from 30 to 150°C; evolved gasses associated with the major portion of cure from 100 to 250°C, including loss of the allyl group

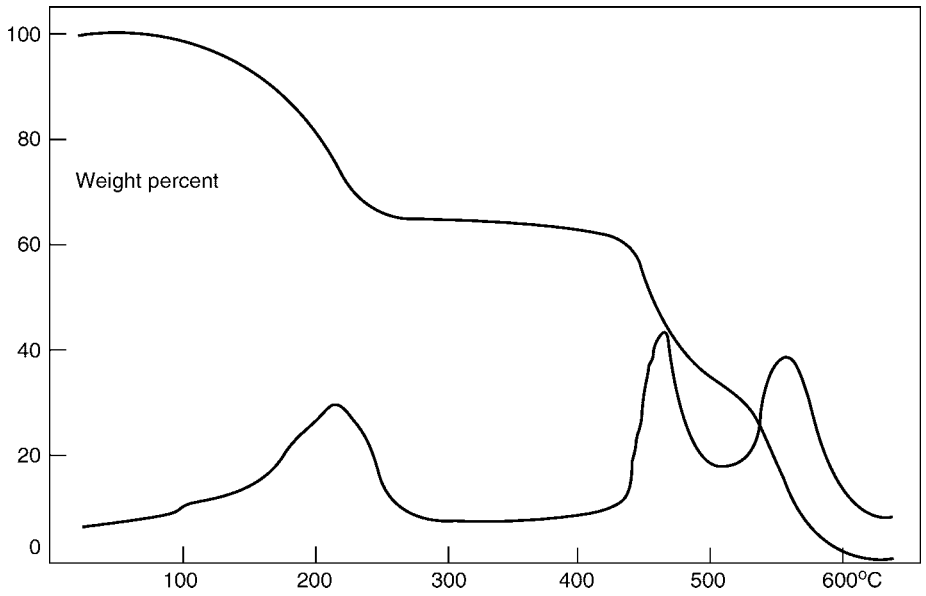

Fig. 21. Thermogravimetric analysis of phenolic resole resin, showing weight losses due to cure (30–300°C) and decomposition (400–650°C). 10°C/min in air. From Ref. 85.

from the allyl phenyl ether resin; and products associated with the latter portion of cure and/or the first stages of decomposition (200–300°C), such as methanol. It was speculated that the allyl functions as a thermally labile protecting group and its loss play a key role in cure. Decomposition was observed to occur in three steps between 400 and 650°C. The first step, accounting for ~10% of the cured polymer weight, occurred over the entire range of decomposition and consisted primarily of C_2H_4O, most likely a fragment from the decomposition of the methylene–ether bridge (see methylene–ether bridge in eq. 3). The weight loss from step 2, ~40% of the cured polymer and occurring between 400 and 500°C, consisted primarily of phenols and substituted phenols. Step 3, between 480 and 600°C and consisting primarily of CO_2, made up the remaining ~50%. The degradation products detected were consistent with a predominantly cross-linked structure which is the condensation product of 2,4,6-trimethylol phenol containing both methylene and methylene–ether cross-links. No major differences were observed between air and nitrogen pyrolyses, except that in the latter, no CO_2 is produced.

Figure 22 demonstrates the utility of TGA in measuring the uniformity of filler content within a part (87). Figure 23 shows the measurement of filler content and relative thermal stability of a series of filled molding compounds (88).

Thermal degradation of thermoset networks have been studied by TGA, often in conjunction with complementary techniques. Musto and co-workers (89) investigated the thermal oxidative stability of an epoxide–diamine (TGDDM/DDS) network and an epoxide–diamine/bismaleimide (TGDDM/DDS/BMI) interpenetrating network (IPN) system by TGA, DMA, and time-resolved FT-IR spectroscopy. Kinetics and degradation mechanisms were explored. It was found that the IPN

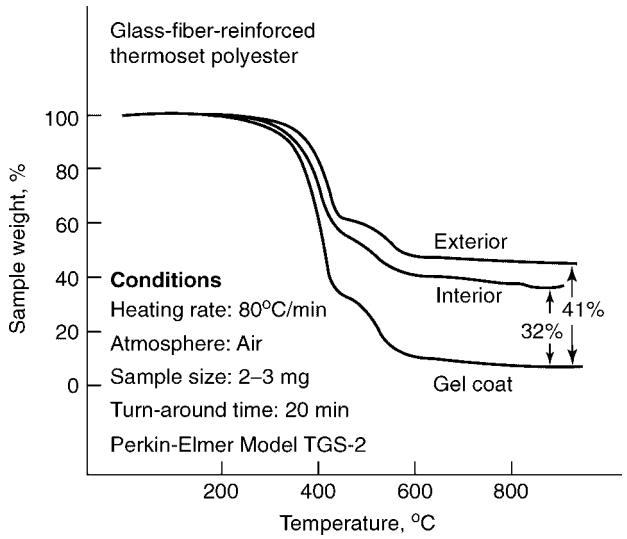

Fig. 22. TGA shows a large nonuniformity of filler content for a molded motor housing. A 9% difference was measured between the bulk ("interior") and a narrow inside ridge ("exterior"). The outer surface, which contained little or no filler, was presumed to be the gel coat. From Ref. 87.

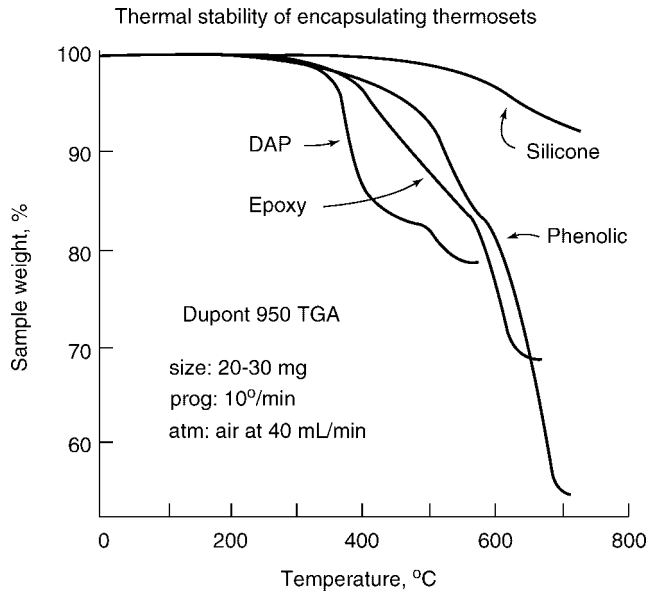

Fig. 23. TGA measurement of relative stability, used as identification tool for encapsulating compounds. Filler content is also measured. From Ref. 88.

systems were more stable than the binary epoxy–amine systems, which was attributed to the higher thermal oxidative stability of the bismaleimide.

Residual Stress

Residual stresses can lead to dimensional instability or even fracture in thermoset systems, causing reduction in part or bond efficiency or durability. Even a small amount of strain can be significant in some cases, such as the bonding of fiber-optic components where alignment is critical. Residual stresses develop within thermosetting systems cured in a geometrically constrained environment because of shrinkage that accompanies cure. Subsequent thermal cycling produces additional stresses because of thermal mismatch between the resin and the constraining environment. These stresses are often responsible for premature failures and defects observed in composite materials. In one- or two-dimensional constraining geometries, such as an adhesive bond, stresses due to shrinkage are negligible compared to thermal stresses that build on cooling through the glass transition (90,91).

Additional stresses can be induced by the process, eg, in the molding of integrated circuit (IC) devices (92). Bair and co-workers (93) defined a figure of merit for the development of stresses on an IC device as it is cooled during processing:

$$\text{residual stress} \propto (\alpha_m - \alpha_s)(E_m)(T_{anch} - T) \tag{20}$$

Residual stress is the product of three terms: the difference in expansion coefficients of the thermoset matrix and the substrate it is attached to $(\alpha_m - \alpha_s)$,

the elastic modulus of the matrix (E_m), and the difference between the anchoring temperature T_{anch} and the test or use temperature (T). T_{anch} was defined as the smallest of T_g, T_{cure}, or $T_{post-cure}$. On the basis of this relationship, means to reduce residual stress include matching of expansion coefficients by adding low expansion fillers to the thermoset matrix, reducing the thermoset modulus, eg, by incorporation of rubber modifiers, and by curing through gelation at temperatures as close to operating conditions as is feasible. Equation 20 does not consider stresses due to shrinkage.

Shuto and co-workers (94) investigated the thermal strains that develop during cure and cooling of resins for laser-diode molding. High T_g epoxy and low T_g silicone were bonded to silicon substrates at elevated temperatures and slowly cooled to room temperature. The epoxy system showed a small strain during cure (because of shrinkage) but much larger strain during cooling through T_g. The silicone system with low modulus throughout the measurement cycle exhibited negligible strain during cure or cooling. Qian and co-workers (95) modeled the thermal bending of the magnetic recording head gimbal assembly for hard disk drives with elastic theory. The bending or deflection arises from the thermal expansion coefficient difference between the ceramic slider and the stainless-steel suspension which are bonded together with a thermoset adhesive. They showed that adhesive modulus had a significant effect on slider deflection, with major deflection when the adhesive is glassy but decreasing dramatically with decreasing modulus. The same authors generalized the model to consider the adhesive as a viscoelastic solid (96). Inclusion of the measured creep compliance master curves of a low and a high modulus adhesive allowed calculation of the time dependence of the slider thermal deflection.

The effect of the cure process on the development of residual stress was investigated by Djokic and co-workers (97). The system studied was a bonded thermoset composite patch for repair or strengthening of aircraft structures. The objective was to develop optimized cure cycles to achieve a combination of minimum residual stresses and cycle time, and maximum level of cure. While reduction in cure temperature led to less residual stress, it was at the cost of increased cycle time and incomplete cure when $T_{cure} < T_{g\infty}$. Post-cure at higher temperatures tended to eliminate most of the benefit of the low temperature cure. What showed promise in meeting the objectives was a three-temperature multistep cure cycle that anchored the adhesive at moderate temperature; reduced the temperature so that T_{cure} just exceeded T_g, ie induced the onset of vitrification; and ramped at a rate that allowed T_g to increase at approximately the same rate as T_{cure}. By minimizing ($T_{cure} - T_g$) it was felt that relaxation times would be long enough to minimize relaxation of stresses that developed during the heating and high temperature portion of the cycle. This approach has some similarity to reactive thermoset processing (RTP), which is discussed in the section Thermosets and Processes, in Ref. 98.

Cure Monitoring

In situ monitoring of cure is an important and evolving part of thermoset processing, providing guidance for optimal times to adjust process parameters such as pressure and temperature and to know with confidence when cure is completed.

In some cases even more detail, such as gelation and vitrification, can be detected. Dielectric and ultrasonic methods have been used for many years to monitor thermoset processes and continue to evolve. Newer methods include fiber-optic smart sensors and fiber Bragg grating sensors. At present, only two types of microsensors are widely used in both academic research and industry to monitor cure in real time: dielectric sensors and fiber-optic sensors. Both can be embedded in multiple locations of a composite prior to cure and become part of the finished product. In addition to monitoring cure, these sensors can track the composite through its lifetime. Ultrasonic and near-infrared attenuated total reflection (NIR-ATR) contact sensors allow processes to be monitored without embedding the sensor. Fluorescence probe-label methodology is an alternative method being investigated.

Frequency-dependent dielectric measurements are a convenient sensing technique for monitoring the cure of thermosets (99). Whereas epoxy–amine systems (100–104) have been the most frequently studied, other systems such as glass/polyester prepreg (105) have also been reported. The changes in dielectric properties during cure are due to three main contributions: the decrease in ionic conductivity because of an increase in viscosity, which hinders the translational diffusion of ions; rotational diffusion of permanent dipoles in the electric field; and changes in the dipole moment because of increases in molecular weight and cross-link density and the replacement of monomer dipoles with often weaker dipoles attached to the network, eg the replacement of amine and epoxy dipoles by hydroxyl dipoles in epoxy–amine systems.

Dielectric cure monitoring generally relies on measurement of the ionic conductivity (σ in eq. 19). The conductivity during cure of epoxy–amine systems have been characterized to establish relationships between conductivity and viscosity (103,104), conductivity and T_g (104), and relationships to the conversion of epoxide (103). Recently, models were established to relate changes in the dipole component of the complex permittivity to the advancement of cure through the T_g–conversion relationship, expanding the capabilities of dielectric sensing to monitor cure (102).

Industrial applications of embedded dielectric sensors include quality assurance/quality control, process monitoring and process control applications involving thermosetting resins, composites, paints, and coatings. For industrial processes, the dielectric sensor may be either embedded (implantable) or reusable (mounted in the tool or mold cavity). In both cases, the electrode geometry is primarily two-planar interdigitated comb electrodes mounted on an inert substrate. Various sensor geometries (sensor line widths, substrates, etc) are available depending on the material being measured, tool geometry, and process type. The material being tested must come in intimate contact with the sensor, since the dielectric sensor measures the dielectric properties in the fringe fields between the fingers of the comb electrode (80). The in-process sensors monitor the dielectric loss factor (ε'', see eq. 19), which for thermoset curing is mainly driven by the mobility of the ions in the polymer. The ion viscosity is calculated from the loss factor and can be used to determine the process flow window and monitor the cure endpoint (see www.micromet.com/holometrix/micromet.htm for details on *in situ* dielectric cure monitoring).

So-called "smart composites" are being developed with embedded fiber-optic sensors, which have potential for monitoring of the composite part from the curing stage into its working life and to its ultimate end of life. This technology has

potential for several applications including aircraft structures where smart composites can lead to a reduction in maintenance, repair, and downtime of future aircraft. While fiber-reinforced composites are attractive because of their good engineering properties, these properties are strongly dependent on processing which is the most critical and costly stage in the manufacturing of composite structures. *In situ* cure monitoring opens the possibility to implement on-line control of the process, leading to transformation of the classical manufacturing stage into real smart processing, and thus to dramatic increases in quality and reliability as well as reduction in cost. Crosby and co-workers (106) describe transmission near-IR optical sensors to directly measure the degree of cure, as discussed in the section FTIR and Raman Spectroscopy. Cusano and co-workers describe an optoelectronic sensor, a low cost, on-line approach sensitive to refractive index variation, for cure monitoring (107) and optoelectronic characterization of the cure process in thermoset-based composites (108). A quantitative relationship between refractive index and DSC extent of cure was observed, demonstrating the capability of this sensor to monitor *in situ* cure kinetics. These authors indicated that future work will integrate the curing sensor with a fiber Bragg grating sensor in order to provide simultaneous monitoring of conversion, temperature, and residual stress. Murukeshan and co-workers (109) describe a fiber Bragg grating sensor system with potential to monitor cure of smart composites. Bragg grating fibers were embedded between adjacent layers of carbon fiber and graphite fiber composite plies.

Remote cure monitoring by noninvasive methods has potential advantages vis-à-vis embedded sensor techniques. Xu and Schlup (110) demonstrated the feasibility of using NIR-ATR spectroscopy as a contact sensor method with several epoxy–amine systems. A novel macrodielectric sensor was described for monitoring flow front position and cure in the resin–transfer molding (RTM) process (111). Rath and co-workers (112) describe the process monitoring of a series of compression molding compounds by ultrasonic measurements. The transducers, embedded in the compression mold, were designed to operate at elevated temperature and pressure. Both longitudinal sound velocity (related to storage modulus) and relative attenuation (related to energy loss) track the progress of cure, from devitrification of the molding compounds to completion of cure, and vitrification should that occur. Differences were observed among the molding compounds as well as effects of filler content, moisture content, and amount of hardener.

Fluorescence spectroscopy utilizing specific fluorophores as an unbound probe and/or as a label bound to the forming network shows promise for *in situ* monitoring in epoxy–amine systems (113,114). By correlation with NIR measurements, details such as onset of tertiary amine formation, point of maximum concentration of amino groups, measurement of gelation, and onset of vitrification seem plausible.

Thermoset Processes

Thermosets are reactive systems that undergo transformation from liquid to gel to rigid glassy solid, and these transformations are of necessity incorporated into the process. For thermal processes, variables are time, temperature, and pressure.

For light or radiation activated processes, variables are time, temperature, and intensity. Rheology is important because a thermoset system first needs to flow. For example, an adhesive or coating needs to flow to wet a surface and form an interface, the matrix polymer needs to flow to consolidate the prepreg layers and form a laminate, and the resin needs to flow to wet fibers and fill a mold in a pultrusion process. Speed and efficiency of these flow-related steps, which affect both cost and performance, are dependent on the rheology of the system where viscosity is decreasing with temperature but increasing with conversion. This typically results in a minimum in viscosity with process time. There is an optimal point in the process to apply pressure, which usually coincides with the minimum in viscosity (see Fig. 20). If pressure is applied too soon, resin will be squeezed out of the part; if it is applied too late, consolidation and mold filling will be incomplete. Flow-related steps must be completed prior to gelation and the part often needs to be physically supported until well past the gel point to prevent changes in dimension or weakening of an interface. This is often accomplished by fixturing an adhesively joined system or maintaining a part in a mold to allow cure to advance. While vitrification is generally to be avoided during cure, thus occurring during cooling, there are occasions when it can be incorporated into a process with advantage. For example, a novel processing scheme, referred to as reactive thermoset processing (RTP), proposes to eliminate expensive fixturing by maintaining the curing thermoset in the "just glassy" state, where the curing thermoset is dimensionally stable but still sufficiently reactive (98). RTP may also be effective in reducing residual stresses induced by the process (97).

Selection of the manufacturing process is influenced by several variables, including quantity, size, thickness, design, and cost. Thermosets are fabricated by processes using either no pressure or pressure ranging from moderate to high at temperatures of 20°C (room temperature cure) to those approaching or even exceeding 200°C. Ambient cure, especially of larger parts, often takes advantage of the exothermic heat of the cure reaction. When parts are very large, overheating can be a problem and the heat of reaction may need to be managed. Many thermoset systems incorporate fibers to enhance properties; most others incorporate fillers to modify properties or reduce cost. Contact processes refer to the assembly of fibers and resins in a mold processed and cured without pressure. Articles may be small or as large as boat hulls 25 m long or longer. Equipment may be simple or highly specialized. The most common thermal processes include open contact molding methods (hand lay-up, spraying, vacuum assisted resin-transfer molding); matched mold methods (compression molding, resin-transfer molding, reactive injection molding); and other methods (filament winding, cold press molding, pultrusion, continuous laminating, encapsulation, and e-beam).

Described below are several thermoset processes, starting with adhesive processes. The descriptions are not meant to be comprehensive, but rather they illustrate the variety of processing options that exist for thermosets (see also COMPOSITES, FABRICATION, and Ref. 1 for descriptions of additional thermoset processes).

Adhesive Processes. Most commercially available adhesive systems consist of either thermoplastic hot melt or reactive thermosetting resins. Typical thermoset adhesive formulations contain base resin monomers and oligomers, curing agents (hardeners), catalysts, adhesion promoters, and various fillers. Adhesive properties depend on the complete mixing and adequate dispersion of the

various ingredients. It is critical that solids be well dispersed. Typical solid components of adhesives are fillers, catalysts, or hardeners. Three roll mills or multishaft mixers with high speed dispersing blades are used to disperse solids into low viscosity components. The high shearing action helps break up solid agglomerates and ensure that the fillers are completely wet out and uniformly distributed in the resin. Once the fillers have been completely dispersed, additional low viscosity components can be incorporated into the formulation using double planetary or multishaft mixers in order to produce a homogeneous mixture. The high shearing action during filler wet-out and the mixing process introduces air into the formulation. The final mixing operation is typically done under vacuum to completely outgas the resin mixture. Most commercially available double planetary and multishaft mixers have the capability to apply vacuum and control temperature during the mixing operation.

For reactive chemistries, the resultant mixtures are placed in containers or syringes and frozen to well below T_{g0} to minimize cure reactions from occurring during storage. These types of adhesives are termed *premixed and frozen*. Depending on the catalyst and chemistry, the work life (the time the adhesive will retain the required processing parameters) can range from hours to days. Some adhesives are packaged in two parts. Typical home-use epoxies come packaged in a dual syringe with parts A and B. The hardener/catalyst is in one part and the resin components are in the other part. This allows a long storage life at room temperature. Once dispensed, the two-part adhesive must be thoroughly mixed and used within the required time. For most industrial adhesives, a *Five Minute Epoxy* type of formulation is not acceptable, since the work life is too short. At a minimum, the work life should be at least 8 h, allowing use over a single shift operation. Most premixed and frozen adhesives have about a 24-h work life.

When a premixed and frozen adhesive is used in production, care must be exercised during thawing to minimize voiding and separation of the adhesive from the wall of the syringe. Additionally, the environment should be controlled to minimize condensation from being incorporated into the adhesive. Rapid thawing increases the likelihood of voiding. Once the adhesive containing syringe is properly thawed, it is placed on a dispensing device. Typical dispensers include needle dispensers that deliver a prescribed amount of adhesive onto the desired surface. The adhesive is then dispensed into line, star, glob, or other patterns depending on the application.

After the adhesive is dispensed, the material is cured. Most adhesives have thermal curing reactions. The most common application is to cure the adhesive in an environmentally controlled oven (typically under nitrogen purge to minimize oxidation). Adhesives with very rapid curing are termed *snap cure* (about 1–2 min at high temperatures) or *spot cure* (approximately 10 s at high temperatures). Specifically in electronic applications, the required high manufacturing throughput requires adhesives with very fast curing speeds. Some adhesives are also B-staged to remove tackiness and give long shelf life, but under additional heating can soften, flow, and cure into a high performance network.

Very fast curing reactions can proceed after exposure to uv radiation or low wavelength visible light (blue light). Typical applications of UV cure include wood coatings (particleboard and simulated wood finishes), flexible coating for vinyl flooring, and coatings for metal surfaces (19). UV exposure is also extensively used

in photoresist technology. However, adhesive applications are often limited by the inability of light to reach the interior of the adhesive joint. Dual-cure adhesives overcome this problem, allowing the exposed adhesive at the joint edges to be cured by UV or blue light, rapidly tacking the parts to be bonded. Subsequently, the bond interior can be thermally cured without the need for expensive fixturing.

Manual Processes. A good example of manual processing is fiber glass-reinforced plastic (FRP) applications utilizing unsaturated polyester resins (see POLYESTERS, UNSATURATED). A random-chopped strand fiber glass mat is precut to fit the open-mold contour and impregnated by hand or spraying in successive plies with catalyzed polyester resin. The application of glass mat and resin at ambient temperatures is now universally employed and called the hand-lay-up or contact-molding process. The quality of the product depends on the skill of the operator in removing air and voids. Fabricated products include chemical equipment, sanitary fixtures, architectural structures, and fiber glass boats. In the spray-up technique, used for bathtub and shower applications, for example, the catalyzed resin and chopped glass fiber are laid down simultaneously on the mold surface with specialized spray equipment. The appearance of FRP products is greatly enhanced by incorporating a polyester gel coat, which may contain pigments and is usually sprayed directly onto the treated mold surface and allowed to cure. The thixotropic characteristics of gel coats need to be controlled and attention must be paid to gel-time drift caused by absorption and deactivation of the accelerator by the pigments and by thixotropic agents such as fumed silica. Resin and glass-fiber reinforcement is applied directly over the gel coat by hand-lay-up or spray-up techniques to produce a product, such as boats and bathtubs, in which the surface of the composite has a glossy appearance free of glass fibers.

Vacuum Bag and Autoclave. Articles made by hand lay-up or spray-up processes are allowed to cure without external pressure. While this is sufficient for many applications, maximum consolidation is not achieved and some porosity remains. The application of even moderate pressure can frequently overcome these drawbacks, and result in better mechanical properties, higher quality parts, and lower weight than achieved by contact molding. One way to apply moderate pressure is to enclose the wet article in the mold inside a flexible membrane or bag and apply a vacuum. Atmospheric pressure presses the bag uniformly against the wet article, generating pressures between 70–100 kPa (10–14 psi). Vacuum inside the bag also tends to degas the article, reducing its porosity. Still higher pressures can be obtained by placing the vacuum assembly in an autoclave at pressures in the range of 700–1400 kPa (~100–200 psi). The bag must be well sealed to prevent infiltration of high pressure air, steam, or water into the molded part. An initial vacuum may be used in the autoclave process to aid in gas and void removal, but the bag is usually vented to atmospheric pressure during the high temperature, high pressure portion of the cure cycle so as not to induce additional void growth from reduced pressure.

Cold Press Molding. This process is an economical method for manufacturing intermediate volumes of products, using low pressure, room temperature cure and inexpensive molds (1). Glass-fiber preform or mat is placed between the matching molds, and liquid resin is added. Gel coats may be employed and woven roving may be added for strength. The mold is closed and the resin permeates the fabric and cures, accelerated by its exothermic heat. Pressures are moderate

(140–350 kPa = 20–50 psi), and molds can be made of inexpensive metal, plaster, or reinforced thermoset. Edges need to be trimmed; ribs, bosses, and other fairly complex shapes are not easily produced.

Resin Transfer Molding. This low cost process is used to mass-produce small and mid-size parts of various shapes with two finished sides. The process requires two matched dies that are clamped together. The catalyzed resin is injected at ambient temperature into the cavity at low pressure, which allows much faster gel and cure times than open molding processes. Gel times for polyester cure are in the 3–5 min range and molding cycles can be as short as 20 min (see POLYESTERS, UNSATURATED). The size of articles that can be produced by RTM is limited by the costs of constructing molds and clamping equipment. Products can be pigmented, gel-coated, and finished. The resin systems may be modified by various types and amounts of fillers. RTM articles can include encapsulated core materials, rib formers, and structural inserts.

Vacuum-Assisted Resin-Transfer Molding. This single-sided molding process offers numerous cost advantages over traditional RTM because of lower tooling costs, room temperature processing, and scalability to large structures. Because it is a single-sided process, dimensional tolerance is less precise than with RTM. Vacuum-assisted resin-transfer molding (VARTM) is a resin infusion process in which dry reinforcement plies are placed onto a metal tool, usually aluminum, coated with a release agent. The preform is covered with a release film and multiple layers of a distribution medium. A vacuum bag is placed on top of this layered construction and a resin inlet and an outlet are positioned at opposite ends of the preform inside the vacuum bag. Vacuum is then drawn providing a driving force that promotes resin infusion first through the distribution medium and then through the fiber preform. When the laminate is completely saturated with resin, the inlet and the outlet are shut and the panel is allowed to cure either at room temperature or at higher temperatures in an oven. The VARTM process is poised for exponential growth as this manufacturing technology is inserted into major defense and commercial programs.

Compression Molding. Compression molding is a high volume, high pressure process suitable for molding complex, high strength, and fairly large articles that need excellent surface finish (1). Thermoset polyester resins, for example, sheet molding compounds (SMC) and bulk molding compounds (BMC), are commonly used. Matched molds are mounted in a hydraulic or mechanical molding press. A weighed charge of SMC or BMC, or a preform or mat treated with resin, is placed in the open mold. The two halves of the mold are closed and heat and pressure are applied. For polyesters temperatures are typically 100–160°C and pressures 1–13 MPa (150–2000 psi). Depending on thickness, size, and shape of the article, curing cycles range from <1 to about 5 min. The mold is opened and the finished product removed.

Reactive Injection Molding. *Reactive injection molding* (RIM), also known as liquid injection molding (LIM), is a process in which a mixture of two or more reactive materials is injected into a mold where the materials react to form a thermoset structure. Advantages include low cost, low pressure requirements, and flexibility in mold configuration. Conventional systems, such as isocyanate with polyol to produce a polyurethane, release little or no volatiles. The generation of substantial volatiles in the mold is obviously undesirable and has

presented a significant obstacle to phenolic-based systems, although some have been reported (see PHENOLIC RESINS). Rigid, cross-linked structural polyurethane foam systems produced by the RIM process contain a sandwich structure of solid skin and a lower density microcellular core in a single operation (see POLYURETHANES). Polyurethane structural foams utilize the smooth, hard skins as a source of impact strength, stability to heat distortion, and combustion resistance. The development of internal mold release (IMR)-based foam systems has further increased the productivity of the RIM process by reducing cleaning time and application of mold release between cycles. The metered component streams are mixed and injected into a closed mold. The chemical cure reaction begins immediately. The exothermic heat evolved vaporizes a low boiling solvent contained in the polyol component, causing the liquid mass to foam. The mixture becomes progressively more viscous, gels, and at the completion of the reaction is transformed into a rigid thermoset network. Cycle times of 1 min or less can be achieved.

Pultrusion. In pultrusion a combination of liquid resin and continuous fiber is pulled continuously through a heated die of the required shape for continuous profiles, such as structural channel, angles, rods, and sheets (1). The plastic sides and top of stepladders are common examples of pultrusion. Commonly employed resins are polyesters, epoxies, and polyurethanes. A typical process might be 3–5 min in duration where resin temperatures ramp rapidly from ambient to temperatures in excess of 150°C, hold for a short time, and ramp back down (see Fig. 10).

Continuous Lamination. Flat and corrugated, translucent to opaque panels are commonly fabricated by continuous lamination (1). A layer of liquid polyester resin is deposited on a moving belt and passed by a chopper that cuts glass fiber rovings into lengths of 35–50 mm, and deposits them in a random mat on the resin. Fibers and resin are compacted and covered with a film, such as cellophane or poly(ethylene terephthalate) and passed through squeeze rolls. The envelope may be passed through corrugators or remain flat. It next passes through an oven to cure the resin. Subsequently, the cover film is stripped, and the continuous sheet is cut into desired lengths.

E-beam Processing. Since the 1980s, the use of electron-beam (e-beam) irradiation has evolved as a promising new technology for curing thermoset composite materials. This process contrasts with traditional curing methods, such as autoclave, pultrusion, or compression molding, in which high temperature is used to initiate thermoset polymerization. In the e-beam process, a high energy electron beam is used to drive the polymerization reaction directly. To accomplish this, uncured prepreg lay-ups or resin-infused preforms are passed through a "curtain" of high energy electrons, typically on a conveyor belt system over several passes. The electron beam is generated by one of many types of accelerators, most of which operate with a beam energy of 3–10 MeV and beam power of 1–150 kW. Several hundred commercial facilities exist worldwide to provide this service, and it was envisioned that the composite community could take advantage of this infrastructure to reduce the cost of fabricating some composite components, although additional facilities dedicated to composite fabrication may also be required. Use of this reduced-temperature processing technology is seen as a potential breakthrough in lowering the costs of composite manufacturing, and it can provide additional environmental, design, and large size scale benefits (115). An excellent

summary of the history, applications, and materials involved in e-beam curing is given in Reference 116.

The primary advantage of e-beam curing is lower process temperatures, which cascades to several major benefits such as reduced tooling cost, reduced residual stress upon cool-down, and ability to co-cure or co-bond dissimilar materials (ie, materials with different coefficients of thermal expansion). Control of temperature during e-beam curing is made difficult because of the release of exothermic heat of reaction, whereas the temperature rise due to radiation input alone is significantly less than the total heat of reaction. Cure of thick parts with high dose rates can often lead to excessive temperature rise and runaway exothermic reactions. However, if radiation dose is applied slowly enough, the process temperature can be kept to a reasonably low level (50–75°C typically), and the advantages cited above can be realized. Another major benefit is extended shelf life of resin systems, which leads to less scrap. Because the resins are not thermally reactive, at least not at ambient temperature, the resins do not require freezer storage and can be stored almost indefinitely (although dark storage may be required, since UV may promote polymerization in certain resin chemistries). An additional advantage of e-beam curing is that size limitations may potentially be removed with movable, robotic methods of applying the electron beam.

Electrons accelerated to 3–10 MeV are traveling at about 99% the speed of light. Approximately 50% of the beam energy is lost in "hard collisions" that remove electrons from host atoms and thereby produce ionized species. As a result of hard collisions, polymerization can occur by free-radical or ionic mechanisms. Materials that proceed via free-radical polymerization include acrylic/methacrylic systems, maleic and fumaric polyester resins, maleimides, and thiole–ene systems. Of these systems, resins based on acrylic and methacrylic functionalities have been studied the most (116). The other major material system to be studied is that of epoxy polymerized via a cationic mechanism, which requires a diaryliodonium or triaryliodonium salt catalyst.

One of the primary technical hurdles limiting widespread application of e-beam curing to aerospace composite materials is that special resins and/or curing conditions must be developed. None of the currently qualified epoxy or bismaleimide resins used on aircraft (ie thermally cured resins) can be simply substituted into an e-beam curing process without making compositional or process modifications. E-beam curable resins that have been developed during the past decade have improved dramatically (116,117), but they still do not offer the same range of properties achieved in qualified thermally cured aerospace resins, such as toughened epoxies. Additional technical hurdles are a poor understanding of the curing process during irradiation, poor repeatability from one run to the next, lack of understanding of long-term durability and predictive capacity, and a lack of understanding of the fundamental mechanisms of cure for e-beam systems (115).

Significant additional progress will require understanding of the basic chemical mechanisms, kinetics of curing, and the development of cross-linking. Fortunately these issues have begun to receive attention in the last few years, during which several basic studies on the kinetics of e-beam curing have been published (118,119). One of the major objectives is the set-up and use of various real-time sensors in a basic research facility recently established by the University of

Dayton Research Institute in cooperation with the Air Force Research Laboratory (120,121). These sensors, which include thermal, spectroscopic, and other techniques, are enabling the generation of new knowledge, understanding, and optimization of the e-beam curing process for composite materials.

BIBLIOGRAPHY

1. D. V. Rosato, *Encyclopedia of Polymer Science and Technology*, 2nd ed., Vol. 14, John Wiley & Sons, Inc., New York, pp. 350–391.
2. R. B. Prime, in E. A. Turi, ed., *Thermal Characterization of Polymeric Materials*, Academic Press, San Diego, 1997, Chapt. 6.
3. J. P. Pascault, H. Sautereau, J. Verdu, and R. J. J. Williams, *Thermosetting Polymers*, Marcel Dekker, New York, 2001.
4. B. Van Mele, H. Rahier, G. Van Assche, and S. Swier, in M. Reading and D. J. Hourston, eds., *The Characterisation of Polymers by Modulated Temperature Differential Scanning Calorimetry*, Kluwer Academic Publishers, U.K., 2004.
5. H. H. Winter, *Polym. Eng. Sci.* **27**, 1698 (1987).
6. H. H. Winter and co-workers, in A. A. Collyer, ed., *Techniques in Rheological Measurement*, Chapman and Hall, London, 1997.
7. P. J. Flory, *J. Am. Chem. Soc.* **63**, 3083 (1941).
8. P. J. Flory, *Principles of Polymer Chemistry*, Cornell University Press, Ithaca, N.Y., 1953.
9. D. R. Miller and C. W. Macosko, *Macromolecules* **9**, 206 (1976).
10. M. Feve, *Makromol. Chem., Macromol. Symp.* **30**, 95 (1989).
11. J. K. Gillham, *Polym. Eng. Sci.* **26**, 1429 (1986).
12. J. B. Enns and J. K. Gillham, *J. Appl. Polym. Sci.* **28**, 2567 (1983).
13. C. A. May, ed., *Epoxy Resins: Chemistry and Technology*, 2nd ed., Marcel Dekker, New York, 1988.
14. D. A. Shimp, in I. Hamerton, ed., *Chemistry and Technology of Cyanate Ester Resins*, 282, Chapman and Hall, Glasgow, U.K., 1994, Chapt. 10.
15. *Plast. Technol*. 8 (1988).
16. P. C. Yang, D. Pickleman, and E. Woo, *35th Int. SAMPE Symp*. 1131 (1990).
17. D. Shimp and W. Craig, *34th Int. SAMPE Symp*. 222 (1989).
18. D. Shimp and S. Ising, *34th Int. SAMPE Symp*. 1045, (1989).
19. S. Peter Peppas, *UV Curing: Science and Technology*, Technology Marketing Corporation, Norwalk, C.T., 1980.
20. M. A. Ratner and D. Ratner, *Nanotechnology: A Gentle Introduction to the Next Big Idea*, Prentice Hall, Englewood Cliffs, N.J., 2003.
21. R. A. Vaia, T. Benson Tolle, G. F. Schmitt, D. Imeson, and R. J. Jones, *SAMPE J.* **37**(6), 24 (2001).
22. E. R. Zubarev, M. U. Pralle, E. D. Sone, and S. I. Stupp, *J. Am. Chem. Soc.* **123**, 4105 (2001).
23. J. D. Hartgerink, E. Beniash, and S. I. Stupp, *Science* **294**, 1684 (2001).
24. A. Okada, Y. Kojima, M. Kawasumi, Y. Fukushima, T. Kurauchi, and O. Kamigaito, *J. Mater. Res.* **8**, 1179 (1993).
25. Y. Kojima, A. Okada, M. Kawasumi, Y. Fukushima, T. Kurauchi, and O. Kamigaito, *J. Mater. Res.* **8**, 1185 (1993).
26. T. J. Pinnavaia and G. W. Beall, eds., *Polymer-Clay Nanocomposites*, John Wiley & Sons, Inc., New York, 2000.

27. T. Lan, P. D. Kaviratna, and T. Pinnavai, *Chem. Mater.* **7**, 2144 (1995).
28. T. Lan, P. D. Kaviratna, and T. Pinnavai, *J. Phys. Chem. Solids* **57**, 1005 (1996).
29. H. Miyagawa, M. J. Rich, and L. T. Drzal, *Proc. North Am. Therm. Anal. Conf.* **30**, 144 (2002).
30. P. B. Messersmith and E. P. Giannelis, *Chem. Mater.* **6**, 1719 (1994).
31. M. Chio, I. Chung, and J. Lee, *Chem. Mater.* **12**, 2977 (2000).
32. I. Kleba and E. Haberstroh, in *46th International SAMPE Symposium*, Long Beach, Calif., 2001.
33. S. Ganguli, D. Dean, K. Jordan, G. Price, and R. Vaia, *Polymer* **44**, 6901 (2003).
34. H. Miyagawa, M. J. Rich, and L. T. Drzal, *Proc. North Am. Therm. Anal. Conf.* **31**, CD (2003).
35. G. Z. Li, L. Wang, H. Ni, and C. U. Pittman Jr., *Inorg. Organomet. Polym.* **11**(3), 123 (2002).
36. A. Lee and J. D. Lichtenhan, *Macromolecules* **31**, 4970 (1998).
37. G. Z. Li, L. Wang, H. Toghiani, T. L. Daulton, K. Koyama, and C. U. Pittman Jr., *Macromolecules* **34**, 8686 (2001).
38. C. U. Pittman Jr., G. Z. Li, and, H. Ni, *Macromol. Symp.* **196**, 301 (2003).
39. B. Maruyama and K. Alam, *SAMPE J.* **38**(3), 59 (2002).
40. G. Wisanrakkit and J. K. Gillham, *J. Appl. Polym. Sci.* **42**, 2453 (1991).
41. J. P. Pascault and R. J. J. Williams, *J. Polym. Sci., Part B: Polym. Phys.* **28**, 85 (1990).
42. A. Hale, C. W. Macosko, and H. E. Bair, *Macromolecules* **24**, 2610 (1991).
43. R. A. Venditti and J. K. Gillham, *J. Appl. Polym. Sci.* **64**, 3 (1997).
44. L. E. Nielson, *J. Macromol. Sci.* **C3**, 69 (1969).
45. A. T. DiBenedetto, *J. Polym. Sci., Part B: Polym. Phys.* **25**, 1949 (1987).
46. C. A. May, ed., *Chemorheology of Thermosetting Polymers*, ACS Symposium Series 227, American Chemical Society, Washington, D.C., 1983.
47. N. Sbirrazzuoli and S. Vyazovkin, *Thermochim. Acta* **388**, 289 (2002).
48. N. Sbirrazzuoli, S. Vyazovkin, A. Mititelu, C. Sladic, and L. Vincent, *Macromol. Chem. Phys.* **204**, 1815 (2003).
49. S. Sourour and M. Kamal, *Thermochim. Acta* **14**, 41 (1976).
50. H. Xie, B. Liu, Z. Yuan, J. Shen, and R. Cheng, *Thermochim. Acta* (in press).
51. C. S. Chern and G. W. Poehlein, *Polym. Eng. Sci.* **27**, 788 (1987).
52. S. Matsuoka, X. Quan, H. E. Bair, and D. J. Doyle, *Macromolecules* **22**, 4093 (1989).
53. G. Wisanrakkit and J. K. Gillham, *J. Appl. Polym. Sci.* **41**, 2885 (1990).
54. C. M. Neag and R. B. Prime, *J. Coat. Technol.* **63**(797), 37 (1991).
55. R. B. Prime, C. Michalski, and C. M. Neag, *Thermochim. Acta* (submitted).
56. J. N. Sultan and F. J. McGarry, *Polym. Eng. Sci.* **13**, 29 (1973).
57. R. J. J. Williams, B. A. Rozenberg, and J.-P. Pascault, *Adv. Polym. Sci.* **128**, 95 (1997).
58. S. Swier and B. Van Mele, *J. Appl. Polym. Sci.* **91**, 2798 (2004).
59. J. Mijovic and S. Andjelic, *Polymer* **36**, 3783 (1995).
60. K. E. Chike, M. L. Myrick, R. E. Lyon, and S. M. Angel, *Appl. Spectrosc.* **47**, 1631 (1993).
61. J. Mijovic and S. Andjelic, *Macromolecules* **28**, 2787 (1995).
62. N. A. St. John and G. A. George, *Polymer* **33**, 2679 (1992).
63. J. Mijovic, S. Andjelic, C. W. Yee, F. Belluci, and L. Nicolais, *Macromolecules* **28**, 2797 (1995).
64. G. Lachenal, A. Pierre, and N. Poisson, *Micron* **27**, 329 (1996).
65. S. Paz-Abuin, A. Lopez-Quintela, M. Varela, M. P. Pellin, and P. Prendes, *Polymer* **38**, 3117 (1997).
66. L. Xu and J. R. Schlup, *J. Appl. Polym. Sci.* **67**, 895 (1998).

67. C. Billaud, M. Vandeuren, R. Legras, and V. Carlier, *Appl. Spectrosc.* **56**, 1413 (2002).
68. J. H. Fu and J. R. Schlup, *J. Appl. Polym. Sci.* **49**, 219 (1993).
69. L. Xu, J. H. Fu, and J. R. Schlup, *Ind. Eng. Chem. Res.* **35**, 963 (1996).
70. C. J. de Bakker, G. A. George, N. A. St. John, and P. M. Fredericks, *Spectrochim. Acta, Part A* **49**, 739 (1993).
71. C. Macosko, *Rheology: Principles, Measurements, and Applications*, VCH Publishers, New York, 1994.
72. B. Fuller, J. Gotro, and G. Martin, in C. Craver and T. Provder, eds., *Polymer Characterization: Physical Property, Spectroscopic, and Chromatographic Methods*, Advances in Chemistry Series 227, American Chemical Society, Washington, D.C., 1990, p. 215.
73. R. E. Wetton, P. W. Ruff, J. C. Richmond, and J. T. Neill, *Proc. North Am. Therm. Anal. Conf.* **16**, 64 (1987).
74. R. E. Wetton, in J. V. Dawkins, ed., *Developments in Polymer Characterization*, Elsevier, London, 1986, pp. 179–221.
75. S. H. Dillman, J. C. Seferis, and R. B. Prime, *Proc. North Am. Therm. Anal. Conf.* **16**, 429 (1987).
76. J. M. Burns, R. B. Prime, E. M. Barrall, and M. E. Oxsen, in K. L. Mittal, ed., *Polymers in Information Storage Technology*, Plenum Publishing Corp., New York, 1989, pp. 237–256.
77. R. B. Prime, *Polym. Eng. Sci.* **32**, 1286 (1992).
78. R. B. Prime, *J. Therm. Anal.* **31**, 1091 (1986).
79. W. J. Sichina and B. Matsumori, *Proc. North Am. Therm. Anal. Conf.* **20**, 41 (1991).
80. S. D. Senturia and N. F. Sheppard, *Epoxy Resins and Composites IV*, Advances in Polymer Science 80, Springer Verlag, Berlin, 1986, pp. 1–47.
81. N. F. Sheppard Jr., M. C. W. Coln, and S. D. Senturia, *29th Natl. SAMPE Symp. Exhib*. 1243 (1984).
82. J. Gotro and M. Yandrasits, *Polym. Eng. Sci.* **29**, 278 (1989).
83. T. Anagnostou and E. Jaul, *J. Coat. Technol.* **53**, 35 (1981).
84. P. I. Kordomenos, A. H. Dervan, and J. Kresta, *J. Coat. Technol.* **54**(687), 43 (1982).
85. R. B. Prime and B. Shushan, *Anal. Chem.* **61**, 1195 (1989).
86. J. Delmonte, *Technology of Carbon and Graphite Fiber Composites*, Van Nostrand Reinhold Co., Inc., New York, 1981.
87. B. Cassel, *Perkin-Elmer TAAS* 19 (1977). See also Ref. 2.
88. R. E. Thomas, *Motorola Semiconductor Products Division*, Phoenix, Ariz., 1974 (personal communication, R. L. Blaine, TA Instruments). See also Ref. 2.
89. P. Musto, G. Ragosta, P. Russo, and L. Mascia, *Macromol. Chem. Phys.* **202**, 3445 (2001).
90. C. Brahatheeswaran and V. B. Gupta, *Polymer* **34**, 289 (1993).
91. J. Lange, S. Toll, J. A. Manson, and A. Hult, *Polymer* **36**, 3135 (1995).
92. H. E. Bair, D. J. Boyle, A. L. Young, and K. G. Steiner, *Soc. Plast. Eng. (Proc. Annu. Tech. Conf.)* **33**, 362 (1987).
93. H. E. Bair, D. J. Boyle, J. T. Ryan, C. R. Taylor, and S. C. Tighe, *Polym. Eng. Sci.* **30**, 609 (1990).
94. Y. Shuto, H. Sato, M. Fukuda, and S. Tohno, *Elect. Comm. Japan* **81**(Part 2), 17 (1998).
95. W. Qian, W. W. Childers, R. B. Prime, T. E. Karis, and M. S. Jhon, *J. Info. Storage Proc. Syst.* **1**, 159 (1999).
96. W. Qian, W. W. Childers, R. B. Prime, T. E. Karis, and M. S. Jhon, *J. Info. Storage Proc. Syst.* **1**, 169 (1999).
97. D. Djokic, A. Johnson, A. Rogers, P. Lee-Sullivan, and N. Mrad, *Compos. Part A* **33**, 277 (2002).

98. W. V. Breitigam, R. S. Bauer, and C. A. May, *Polymer* **34**, 767 (1993).
99. D. Kranbuehl, *Processing of Composites*, Hanser, Munich, 2000, pp. 137–157.
100. S. Anjelic and J. Mijovic, *Macromolecules* **31**, 2872 (1998).
101. G. P. Johari and D. A. Washylyshyn, *J. Polym. Sci., Part B: Polym. Phys.* **38**, 122 (1999).
102. J. P. Eloundou, J. F. Gerard, J. P. Pascault, and D. Kranbuehl, *Macromol. Chem. Phys.* **203**, 1974 (2002).
103. J. P. Eloundou, J. F. Gerard, J. P. Pascault, G. Boiteux, and G. Seytre, *Angew. Makromol. Chem.* **263**, 57 (1998).
104. A. Maffezoli, A. Trivisano, M. Opalicki, J. Mijovic, and J. M. Kenny, *J. Mater. Sci.* **29**, 800 (1994).
105. H. G. Kim and D. G. Lee, *Compos. Struct.* **57**, 91 (2002).
106. P. A. Crosby, G. R. Powell, G. F. Fernando, D. N. Waters, C. M. France, and R. C. Spooncer, *Proc. SPIE* **3042**, 141 (1997).
107. A. Cusano, G. Breglio, M. Giordono, A. Calabro, A. Cutolo, and L. Nicolais, *Sens. Actuat.* **84**, 270 (2000).
108. A. Cusano, G. Breglio, M. Giordono, A. Calabro, A. Cutolo, and L. Nicolais, *J. Opt. A: Pure Appl. Opt.* **3**, 126 (2000).
109. V. M. Murukeshan, P. Y. Chan, L. S. Ong, and L. K. Seah, *Sens. Actuat.* **79**, 153 (2000).
110. L. S. Xu and J. R. Schlup, *Appl. Spectrosc.* **50**, 109 (1996).
111. A. A. Skordos, P. I. Karkanas, and I. K. Partridge, *Meas. Sci. Technol.* **11**, 25 (2000).
112. M. Rath, J. Doring, W. Stark, and G. Hinrichsen, *NDT&E Int.* **33**, 123 (2000).
113. F. Mikes, J. Gonzalez-Benito, and J. Baselga, *J. Macromol. Sci., Phys. B* **40**, 405 (2002).
114. F. Mikes, J. Baselga, and S. Paz-Abuin, *Eur. Polym. J.* **38**, 2393 (2002).
115. F. Abrams and T. Benson Tolle, *Proc. Int. SAMPE Symp.* **42**, 548 (1997).
116. D. L. Goodman and G. R. Palmese, in A. Kulshreshtha and C. Vasile, eds., *Handbook of Polymer Blends and Composites*, Rapra Technology Ltd., Shropshire, U.K., 2002.
117. B. DeFoort, F. Boursereau, J.-M. Dupillier, G. Larnac, G. Lopitaux, and X. Coqueret, *Proc. Int. SAMPE Symp*. **47** (2002).
118. R. J. Morgan, D. Li, J. L. Lu, R. Ribeiro, and S. Moon, *Proc. Int. SAMPE Symp*. **47** (2002).
119. A. Johnston, G. Palmese, K. C. Cole, L. Petrescue, J. H. Chen, and V. Lopata, *Proc. Int. SAMPE Symp*. **48** (2003).
120. D. Klosterman, R. Chartoff, T. Tong, M. Galaska, C. Theodore, and P. Hood, *Proc. Int. SAMPE Symp*. **46** (2001).
121. D. Klosterman, *Proc. Int. SAMPE Symp*. **48** (2003).

JEFFREY GOTRO
Ablestik Laboratories
R. BRUCE PRIME
IBM (retired)/Prime Thermosets.com

TISSUE ENGINEERING

Introduction

Accidents and diseases lead to devastating tissue losses and organ failures, which result in more than 8 million surgical operations each year in the United States alone (1). These problems convert to a national annual healthcare cost of approximately half trillion U.S. dollars. The state-of-the-art clinical therapies to tissue losses and organ failures can be categorized into three approaches, ie, transplantation, surgical reconstruction, and the use of prostheses. Each of these approaches has contributed to solving or alleviating the severity of these clinical problems, while all of them have serious limitations.

Organ transplantation became successful in the early 1960s because of the success of immunologic suppression in the clinical setting (2). Transplantation has saved, and is continuing to save, countless lives. This approach, however, is severely limited by the dearth of donor organs. For example, fewer than 3000 available donors are way shorter than the needs of approximately 30,000 Americans for liver transplants each year (3). Surgical reconstruction utilizes tissues harvested from the patient to rebuild a critically needed body part. The use of the patient's own tissue is advantageous in that it has a higher success rate resulting from the avoidance of immune rejection than using tissues from other sources. However, the need for second site of surgery, limited supply, inadequate size and shape, and the morbidity associated with donor site are all major concerns (4,5). In response to the shortages of needed tissues and organs, prostheses are developed to replace certain body parts for their structural and mechanical functions. There are approximately 100,000 people in the United States with transplants, while there are more than 10,000,000 with biomedical implants (6). However, the prostheses are made from artificial materials, are not biologically functional, and are therefore subject to long-term complications and rejections.

Tissue engineering is a new approach to resolve the missing tissue and organ problems. *Tissue engineering* has been defined as an interdisciplinary field that applies the principles of engineering and the life sciences toward the development of biological substitutes that restore, maintain, or improve tissue function (3). There are three strategies in tissue engineering (3,7):

(1) The use of isolated cells or cell substitutes to replace those cells that supply the needed function, including genetic or other manipulations before the cell infusion (8);
(2) The delivery of tissue-inducing substances, such as growth and differentiation factors, to targeted locations (9,10);
(3) Growing cells in three-dimensional (3-D) matrices (scaffolds) or devices, where cells can be either recruited from the host tissues *in vivo* or seeded (encapsulated) *in vitro* (3).

The advantage of the use of isolated cells is the simplicity. Cells are often directly injected into the targeted locations to avoid complex procedures and associated complications. The disadvantages include cell death and loss of function

Encyclopedia of Polymer Science and Technology. Copyright John Wiley & Sons, Inc. All rights reserved.

because cells need the right nutritional and substrate environment to grow and function. The success of using tissue-inducing substances is dependent on the economical large-scale production and purification of the bioactive molecules, and on the development of delivery systems that can deliver these molecules with the desired profiles. Certain gene therapy techniques can also be used for this approach. The above two approaches, ie, the use of isolated cells or tissue-inducing substances, are considered when the defects are very small and well contained. For engineering tissues of practical size scale and with predetermined 3-D structures, these two approaches are seriously limited. Therefore, the third approach, ie, growing cells in 3-D matrices (scaffolds) or devices, has become increasingly active.

Some of these matrices or devices are used to develop immobilized cell systems, either as implants or extracorporeal devices (11,12). The core of this technology is semipermeable membranes or matrices that have well-defined molecular weight or size cutoff (13,14). They serve as immunoprotective barriers to support cell growth and function, which allow nutrients, metabolic products, and wastes to diffuse through, but not immune cells or antibodies. These devices offer certain biological functions but are not living tissue/organ replacements (see MEMBRANE TECHNOLOGY). Some other 3-D matrices work as templates (called scaffolds) to guide cells to grow, synthesize biological molecules and extracellular matrix components, and facilitate the organization and formation of functional tissues and organs (15–17). After fulfilling the templating function, the scaffolds degrade and disappear, leaving nothing foreign to the biological system (Fig. 1). There are many additional advantages in this approach. Patient-derived cells (stem cells or differentiated cells) or future universal cell sources (nonimmunogenic) can be used so that there will be minimum complication associated with immune rejections. These cells can be expanded *in vitro* to solve the donor shortage limitations. Any tissue/organ structure can be potentially mimicked by the scaffolding design. The engineered tissues will have the capacity of growing, modeling, and remodeling in concert with dynamic changes in physiological environment of the body. In this approach, biodegradable polymers (natural or synthetic) are the materials of choice. Polymers (or macromolecules) are currently used as scaffolds for nearly every tissue type including bone and other mineralized tissues. Besides polymers, only limited inorganic materials are used for certain mineralized tissue engineering research.

Although growing cells on two-dimensional (2-D) substrates (such as petri dishes and culture plates) dates back centuries, designing 3-D scaffolds for tissue engineering is a new field, where polymer science and engineering play pivotal roles.

There are a few basic requirements that have been widely accepted for designing polymer scaffolds. First, the scaffold has to have high porosity and proper pore size. These pores allow cell seeding and migration to achieve the needed relative uniform distribution. The pores also provide the space for cell proliferation and neo tissue deposition. The pores also satisfy the needed mass transport requirements for nutrients, signaling molecules, metabolic products, and wastes. The porous structure should also allow for vascularization and innervation for sustained function of the regenerated tissues when implanted *in vivo*. High porosity is also beneficial because of the reduced polymer amount and its degradation

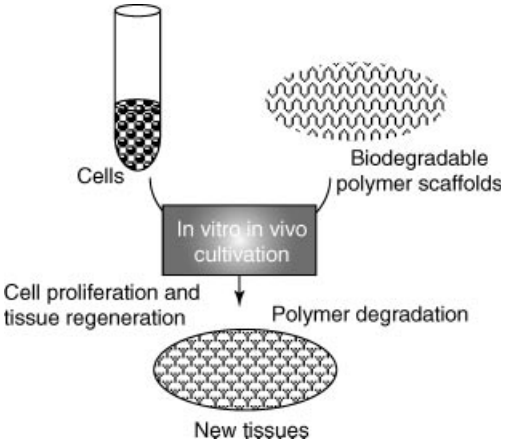

Fig. 1. Schematic diagram showing the tissue engineering concept. Scaffolding materials (temporary synthetic extracellular matrices) are designed, on which mammalian cells can grow to regenerate the needed tissue or organ in three dimensions (3-D). Because the scaffolds are biodegradable, they will resorb after fulfilling the template function and leave nothing foreign in the body.

products in the neo tissues, which can provoke unwanted inflammatory response from the host. Second, a high surface area (a.k.a. surface-to-volume ratio) is needed, which is the 3-D surface area of the porous scaffolds (not just the outside surface area). Many cell types are anchorage-dependent, ie, they can survive, grow, and function only when they are attached to an appropriate substrate. The high surface area provides cells with the sufficient area to attach, grow, and deposit neo tissue components. Third, biodegradability is generally required, and a proper degradation rate is needed to match the neo tissue formation. If the scaffold degrades too fast, it can collapse before the new tissue is formed so that it fails to serve as a 3-D guidance for the neo tissue organization. If the scaffold degrades too slowly, it remains for a prolonged time period after the neo tissue is formed and stabilized. It may hinder the new tissue replacement of the scaffold space, and may cause complications associated with long-term foreign body reactions. Fourth, the scaffold must have the needed mechanical integrity to maintain the predesigned tissue structure to serve the 3-D guidance. However, scaffolds are often not as mechanically strong as the tissues to be replaced because of the required high porosity for scaffolds. They usually serve the scaffolding purpose well as long as they can maintain the structural integrity under the cultivation or implantation conditions, while the goals are that the engineered tissues from the scaffolds are mechanically and biologically functional as their natural counterparts. Fifth, the scaffold should not be toxic to the cells (biocompatible). In addition to the polymer, the degradation products of the polymer should not be toxic to the cells, which is usually a more restricting requirement than for the polymer. Sixth, ideally the scaffold should positively interact with cells, including enhanced cell adhesion, growth, migration, and differentiated function. To achieve these positive cell–scaffold interactions, surface or bulk modifications of the

polymer structure are often employed (18–21). Even drug, protein, or gene delivery techniques are often considered in the scaffold design (22–25).

Polymers in Tissue Engineering

As discussed above, polymers play a pivotal role in tissue engineering. To fulfill the diverse needs in tissue engineering, various polymers have been exploited in tissue engineering research, including natural polymers (macromolecules), natural polymer-derived materials, synthetic polymers, and synthetic polymers made of natural monomers or modified with natural moieties. Various copolymers, polymer blends, or polymeric composite materials are also used. This section is not intended to be a complete and exhaustive review of all the polymers used in tissue engineering. Instead, some of the most frequently used polymers (macromolecules) in tissue engineering are briefly reviewed.

Polymers for Porous Scaffolds. The polymers to be discussed in this category can form stable porous structures in the solid form to serve as pre-designed 3-D scaffolds. They generally do not dissolve or melt under *in vitro* tissue culture conditions (in an aqueous tissue culture medium) or when implanted *in vivo*.

Linear Aliphatic Polyesters. Linear aliphatic polyesters are the most frequently used synthetic biodegradable polymers in tissue engineering and many other biomedical applications (26–28). These polymers degrade through hydrolysis of the ester bonds in the polymer backbone. The degradation rates and profiles differ between these polymers owing to their compositional, structural, and molecular weight differences.

Polyglycolide, also called poly(glycolic acid) (PGA), polylactide, also called poly(lactic acid) (PLA), and their copolymers, poly(lactide-*co*-glycolide), also called poly(lactic acid-*co*-glycolic acid) (PLGA), are a family of linear aliphatic polyesters called poly(α-hydroxy acids) or poly(α-hydroxy esters) (Fig. 2). These polymers can be synthesized by direct condensation of the hydroxy acid monomers (resulting in low molecular weight polymers, such as lower than 10,000) or more commonly by a ring-opening polymerization of the cyclic dimers (to achieve a higher molecular weight), from where the names of polyglycolide and polylactide stem.

Among the family of glycolic acid and lactic acid homopolymers and copolymers, PGA is the simplest in chemical structure, has many advantageous properties, and is therefore one of the most widely used scaffolding polymers (17). Because of the chain structural regularity, PGA is highly crystalline and has a high melting point of around 220°C (17). It does not dissolve in most common organic solvents. Because of its hydrophilic nature, PGA degrades rapidly in aqueous solutions or *in vivo*, and loses mechanical integrity between 2 and 4 weeks depending on the molecular weight and physical structure of the scaffolds or implants, and *in vitro* or *in vivo* conditions (17,29). It was the material used to develop the first synthetic absorbable suture, and has been processed into nonwoven fibrous fabrics as one of the most widely used scaffolds in tissue engineering today.

PLA is also widely used for scaffold fabrication because of its biodegradability. Because of the extra methyl group in PLA repeating unit in comparison to PGA, PLA is more hydrophobic. The hydrophobic methyl group reduces the molecular affinity to water and leads to a slower hydrolysis rate of PLA.

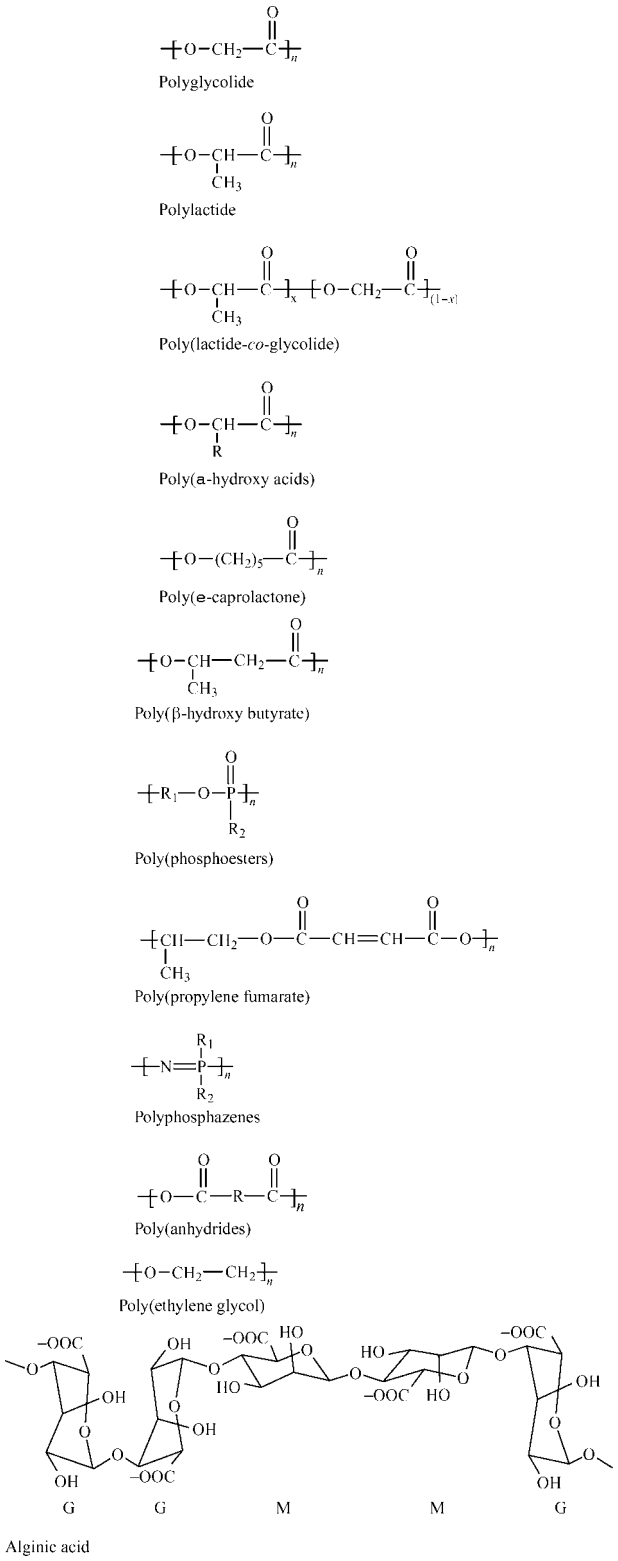

Fig. 2. Polymers frequently used as scaffolds for tissue engineering.

It takes months to years for a PLA scaffold or implant to lose mechanical integrity *in vitro* or *in vivo* (30,31). Lactic acid is a chiral molecule and exists in two stereoisomeric forms, ie, the D-lactic acid and L-lactic acid. The two stereoisomers lead to four different types of PLA: poly(D-lactic acid) (PDLA), poly(L-lactic acid) (PLLA), racemic poly(D,L-lactic acid) (PDLLA) and meso poly(D,L-lactic acid) (meso-PLA). Because of the stereoregularity, PDLA and PLLA are semicrystalline, and are less susceptible to water attack (hydrolysis), resulting in slower degradation rates. The racemic copolymer PDLLA is amorphous, and therefore more susceptible to hydrolysis, resulting in a faster degradation rate. Since L-lactic acid is the natural stereoisomer of the lactic acid in the body, PLLA is the frequently used PLA. To achieve intermediate degradation rates between PGA and PLLA, various lactic acid and glycolic acid ratios are used to synthesize PLGAs. However, there is not a linear relationship between degradation rate and lactic acid content. When lactide is copolymerized with glycolide, two distinctly different effects with regard to degradation are introduced. The first is that the lactic acid unit is more hydrophobic, contributing to a slower degradation rate. The second effect is that stereoregularity is disrupted by the different repeating units, resulting in a lower crystallinity or amorphous structure, contributing to a faster degradation rate. The resulting degradation rate is a compromise of these two factors. Theoretically, when the LA/GA ratio is higher than 50:50, these two factors are in the same direction when the amount of lactide is increased. When the LA/GA ratio is lower than 50:50, these two factors are against each other when the amount of lactide is increased. However, in a large middle range of the composition, the copolymer is amorphous and the crystallinity does not play a role. In both high and low ends of the LA/GA ratio, the crystallinity of the specific scaffold or device plays an important role on the degradation rate. In addition, high crystallinity increases modulus, yield strength, and ultimate strength of the polymers.

In addition to the biodegradability and biocompatibility, these polymers (PLA, PGA, and PLGAs) are among the few synthetic polymers approved by the Food and Drug Administration (FDA) for certain human clinical applications such as surgical sutures and some implantable devices. There is, however, some controversy around the use of these polymers for orthopedic applications. Based on a study of more than 2500 patients operated on using pins, rods, bolts, and screws made of PGA or PLA, 4.3% were affected by a clinically significant local inflammatory tissue reaction (32). Similarly, other biodegradable polyesters suited for manufacturing absorbable fixation implants appear to also elicit adverse tissue responses. These adverse tissue reactions are generally considered to result from the released acid during degradation. For polymer scaffolds with extremely high porosity used in tissue engineering applications (usually $\geq$90%) as opposed to solid implant devices used in orthopedics, the acid release (pH variation) is a less severe problem (17,30).

Polymer degradation is often categorized into bulk degradation (bulk erosion) and surface degradation (surface erosion) in the fields of biomedical engineering and biotechnology (33,34). There are actually differences between erosion and degradation. Degradation is the bond cleavage of the polymer, resulting in reduction in molecular weight of the polymer. Erosion is the mass loss process. For ideal bulk degradation, hydrolysis (or other forms of degradation) occurs in the entire polymer volume simultaneously. The length of time that polymer persists

can be altered by changing chemical composition but not by the material's size and shape. For ideal surface degradation, hydrolysis (or other forms of degradation) only occurs on the external surface of the material, ie, at the interface between the material and its immediate surrounding environments, such as medium or body fluids. Erosion rate is directly proportional to the external surface area. The length of time that polymer persists can be altered by varying the sample volume (thickness). Surface erosion is often advantageous for controlled drug delivery applications. For example, a thin slab erodes by reducing its thickness and maintaining a nearly constant surface area to achieve constant release rate.

PLA, PGA, and PLGA polymers degrade via bulk hydrolysis. However, the length of time that a polymer persists is affected by the shape and size of the material because the degradation does not occur homogeneously. Common sense would lead people to think that the surface layer degrades faster since this area is exposed to the most abundant medium or body fluids, which hydrolyze ester bonds in the polymer chains. The reality is just the opposite (35). The cleavage of ester bonds yields carboxyl and hydroxyl end groups. The produced carboxyl end groups are capable of catalyzing the hydrolysis of remaining ester bonds in the polymer chains. In the surface layer, the chains containing carboxyl end groups or the generated small acid molecules diffuse out of the device and the acidity is reduced. This autocatalysis phenomenon is enhanced by the diffusion limitations in the thick devices. In the interior, the acidity increases as ester bonds are hydrolyzed while the acidic by-products are trapped. The increased acidity further catalyzes hydrolysis, leading to heterogeneous degradation, ie, a faster degradation in the interior than on the surface.

For semicrystalline polymers such as PGA and PLLA, the degradation behavior is also related to the crystallinity and domain structures of the polymers (17). The amorphous domains are easily attacked by water molecules and degrade first. Initial mass loss occurs in the amorphous domains and causes an apparent crystallinity increase (17). As the polymer further degrades, the crystalline domains also degrade, which leads to drastic decrease in melting point and mechanical properties, and finally leads to the disintegration of the entire material (see BIODEGRADABLE POLYMERS, MEDICAL APPLICATIONS).

There are other linear aliphatic polyesters, such as poly(ε-caprolactone) (PCL) and poly(hydroxy butyrate) (PHB) (Fig. 2), which are also used in tissue engineering research and other biomedical applications. PCL has been investigated for a variety of biomedical applications. It can degrade by microorganisms, hydrolytic, enzymatic, or intracellular mechanisms under physiological conditions (36,37). PCL is a semicrystalline polymer. It has a very low glass-transition temperature of around -62°C, and thus is always in the rubbery state and has high material permeability under physiological conditions. For highly porous scaffolds, material permeability however does not contribute significantly to the scaffold permeability. Compared with PLA, PGA, and PLGA, PCL degrades at a significantly slower rate (38), which makes PCL less attractive for general tissue engineering applications but more attractive for long-term implants and controlled release applications.

Poly(hydroxy butyrate) (PHB), also called poly(β-hydroxy butyrate) or poly(hydroxy butyric acid), is the simplest member of the polyhydroxyalkanoate (PHA) polyesters (see POLY(3-HYDROXYALKANOATES)). PHB is made by

microorganisms via fermentation. It is biocompatible and biodegradable, but is highly crystalline and therefore very brittle. PHB degrades very slowly (years *in vivo*) because of the high crystallinity and hydrophobicity (39,40). PHB-based copolymers are less crystalline and mechanically more flexible, but degrade also very slowly because of the hydrophobic nature, and therefore are less popular compared to PGA, PLA, and PLGA for tissue engineering applications.

Other Important Synthetic Biodegradable Polymers. Poly(phosphoesters) (PPE) are a class of biodegradable polymers synthesized in the Leong group (Fig. 2) (41). PPE contains P(O)—O—C linkage in the polymer backbone and the pentavalent phosphorus atom allows for attachment of a pendant component. PPE degrades through hydrolysis of phosphoester bond in the PPE backbone. The variation in backbone structure and pendant side group allows for variation in structure and properties of these polymers. They have been used for controlled drug delivery and gene delivery applications (42), and are also explored for certain tissue engineering applications (43) (see CONTROLLED RELEASE TECHNOLOGY; GENE-DELIVERY POLYMERS).

Poly(propylene fumarate) (PPF) (Fig. 2) has been synthesized as a biodegradable polymer that degrades through hydrolysis of the ester bonds similar to glycolide and lactide polymers. PPF is an amorphous unsaturated polymer and has been extensively studied in the Mikos group as either a prefabricated (44) or an injectable biomaterial (45) for bone tissue engineering. Its copolymers with poly(ethylene glycol) (PEG), poly(propylene fumarate-*co*-ethylene glycol) polymers, can form hydrogels (46).

Polyphosphazenes (qv) contain a long-chain backbone of alternating phosphorus and nitrogen, with two side groups attached to each phosphorus (Fig. 2) (47). Various synthesis routes are used to prepare these polymers, allowing different side groups (R) to be attached to the backbone. These polymers can have very different properties, from degradable to nondegradable, by changes in the side groups. Polyphosphazenes are finding more and more applications in controlled drug delivery applications (48,49), and are also finding ways into the tissue engineering research (50,51).

Although polyanhydrides (qv) are attempted for use as tissue engineering scaffold (52), they are designed primarily for controlled drug delivery purposes in the Langer group (53). These polymers are very hydrophobic, and degrade through surface erosion. The surface erosion characteristic allows easy accomplishment of constant release rate for sustained drug delivery purpose. Drugs are also well protected when embedded in such polymers owing to the nearly no water penetration before the polymer erodes. Similarly, poly(ortho esters) are primarily designed for controlled drug delivery applications because of their surface erosion properties (54). Nevertheless, they have been explored for tissue engineering scaffolding applications as well (55).

Amino acids are natural nutrients. Polymers derived from amino acids may have advantageous biocompatibility, as demonstrated by PLA. However, amino acid based polymers often do not have good material properties. They are often difficult to process into 3-D structure, and possess poor mechanical properties. Tyrosine-derived polymers have been developed in the Kohn group as biodegradable polymers, which have shown certain promising properties (56), and have been used for bone tissue engineering research (57).

Nondegradable polyurethanes (qv) have been widely used for biomedical applications because of their elastic properties (58). The segmented polyurethanes allow the structural variations to achieve a range of mechanical properties. A major limitation of polyurethanes for biomedical applications is the involvement of toxic precursors (such as toluene diisocyanates) in the synthesis. Recent efforts have been on development of biodegradable polyurethanes or urethane-based polymers using less toxic diisocyanates (59). These polymers have good mechanical properties and have been explored for vascular and other tissue engineering applications (60,61). Considering the general audience in the field of polymer science and engineering, synthetic polymers and 3-D scaffold fabrications are the main foci of this article. However, it should be noted that natural polymers, such as proteins and polysaccharides, have also been used for tissue engineering applications. Collagen (qv) is a major natural extracellular matrix component (62). Collagen proteins possess triple-helix structure over a large portion of the molecules. Among the various collagen proteins the most abundant is type I collagen. Collagen has been used for various tissue regeneration applications especially for soft tissue repair (63,64). The use of collagen as a scaffolding material, however, remains challenging because of the potential pathogen transmission and immune reactions, poor handling and mechanical properties, and less controlled biodegradability (enzymatic) of the natural material from biological sources. On the other hand, collagen as a natural extracellular component has useful biological properties desired for tissue engineering applications. Yannas and colleagues have developed collagen-glycosaminoglycan (GAG) copolymers and fabricated them into scaffolds for tissue engineering (65,66). Denatured collagen (gelatin) is also processed into porous materials for tissue repair (67). Polysaccharides (qv) are another class of natural polymers, eg, alginate (68) and chitosan (69), which have been explored as tissue engineering scaffolds.

Polymers for Hydrogel Scaffolds. Hydrogels (qv) are cross-linked hydrophilic polymers that contain large amounts of water without dissolution. Hydrogels are attractive candidates for certain tissue engineering applications because of the ability to fill irregularly shaped tissue defects, allowance of minimally invasive procedures such as arthroscopic surgeries, and the ease of incorporation of cells or bioactive agents (70–75).

Among the synthetic hydrogels, PEG (Fig. 2) has been more frequently studied for tissue engineering research than other synthetic hydrogels. PEG has been extensively used in biomedical applications often to prevent protein and cell adhesion (76). This property also made PEG useful for prevention of tissue adhesions after surgery (77,78). In the tissue engineering field, PEG has been used as a model system for studies related to adhesion peptides. In such a case, the inertness of this polymer to cells and proteins is ideally utilized. PEG–diacrylamide was synthesized by the Hubbell group (79). A photopolymerization step can be performed in contact with cells, providing a means to produce scaffolds for tissue engineering. A PEG-based interpenetration network has been used for cartilage tissue engineering by Elisseeff and colleagues (80). Peptide-modified PEG materials have been used by Griffith and West groups to study relationships between cell behavior (such as adhesion, spreading, and migration) and peptide density and spacing (81–83). A major limitation of PEG hydrogel for tissue engineering scaffolds is its lack of degradability. Efforts are made to impart degradability to PEG by either

formulating copolymers with PLA or PGA, or by introducing enzyme-degradable linkages into the PEG backbone (84–86).

Alginate is the salt form of alginic acid. Alginic acid, a polysaccharide from seaweed, is a family of natural copolymers of β-D-mannuronic acid (M) and α-L-guluronic acid (G) (Fig. 2) (87,88). They have been processed into gel beads encapsulating living cells as a means of immunoprotection (89). Alginate hydrogels cross-linked using calcium sulfate ($CaSO_4$) have recently been used as cell delivery vehicles for *in vivo* tissue engineering research (74,90,91). Peptide-modified alginate has been studied to improve cell attachment (74). However, one of the major disadvantages of the use of $CaSO_4$ is that gelation kinetics is difficult to control, and the resulting structure is not uniform. Structural uniformity in tissue engineering scaffolds is necessary not only for uniform cell distribution, but also for well-controlled material properties. Mechanical properties are more consistent throughout the gel and between batches if structural uniformity can be achieved. We have developed methods to control the gelation rate so that cross-linking is allowed to take place uniformly throughout the gel to form a structurally uniform and mechanically strong alginate gel with predesigned 3-D shapes (Fig. 3**a**) (70). Cells can be uniformly incorporated into such gels (Fig. 3**b**).

Collagen, in addition to porous foam, has also been used as hydrogels for a variety of tissue repair and regeneration studies (92,93). Collagen gels have been studied as a therapeutic option for the treatment of burn patients or chronic wounds (94). Cartilage defect repair has been studied using chondrocyte–collagen gel constructs (95). Studies have also been conducted with collagen gels to deliver mesenchymal stem cells and biological agents to improve healing of ligaments and tendons (96).

Polymer Processing and 3-D Scaffolds for Tissue Engineering

In the body, tissues are organized into 3-D structures as functional organs and organ systems. Each tissue or organ has its own characteristic architecture depending on its physiological function. This architecture is also believed to provide the necessary channels for mass transport and spatial cell organization (15). Mass transport includes signaling molecules, nutritional supplies, and metabolic waste removal. Spatial cellular organization allows for cell–cell and cell–extracellular matrix interactions to occur, which are critical to physiological functions of a tissue or organ. To successfully engineer functional tissues and organs, the scaffolds have to be designed to facilitate the desired cell distribution and to guide tissue regeneration in 3-D. This section is, therefore, devoted to the 3-D pore structure and pore wall architecture of scaffolds for tissue engineering.

Textile Technologies and Traditional Fibrous Scaffolds. The textile technologies have developed over thousands of years to produce various fibrous fabrics for clothing, filtration, packaging, and many other industrial and household applications. Fibrous fabrics have excellent mechanical properties. It was natural that fibrous materials found many biomedical applications in recent years including sutures from biodegradable polymers. It was also not surprising that earlier tissue engineering scaffolds were fibrous fabrics of biodegradable polymers

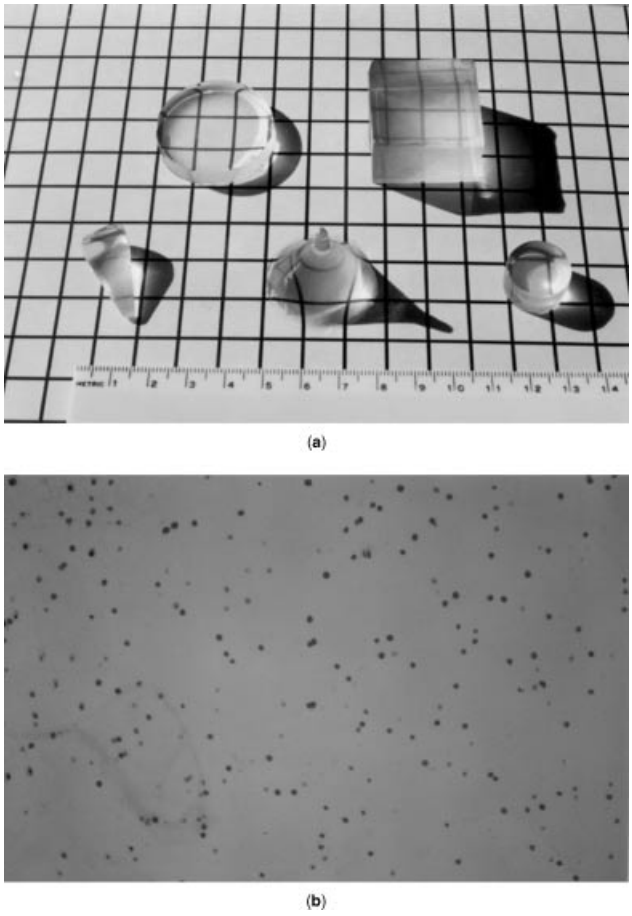

Fig. 3. Alginate hydrogels used as scaffolds for tissue engineering: (**a**) alginate gels of various molded shapes made from a slow gelation process; (**b**) MC3T3-E1 osteoblasts incorporated into slow-gelling alginate gels and cultured *in vitro* for 3 weeks, demonstrating uniform cell distribution (H&E staining, original magnification: 100×). Reprinted from Ref. 70. © 2001, by permission of Elsevier.

fabricated using textile technologies. PGA, PLA, and many other semicrystalline polymers can be processed into fibers using an extruder and these fibers can be further processed into woven, knit, or nonwoven fabrics using the textile technologies (see NONWOVENS, STAPLE FIBER).

One of such scaffolds widely used in tissue engineering research is PGA nonwoven scaffolds (Fig. 4). PGA is typically melt-spun into fibers with a diameter of around 15 μm. These fibers are then processed into nonwoven fabrics using textile technologies such as carding, needling, heat pressing, and so forth. Porosity higher than 90% can be easily achieved. These PGA nonwoven scaffolds degrade via hydrolysis both *in vitro* and *in vivo*. The mass of PGA scaffolds decrease exponentially *in vitro*, fitting well to a first-order degradation kinetics (17). The amorphous regions in the fibers degrade first presumably because of the easy access by water

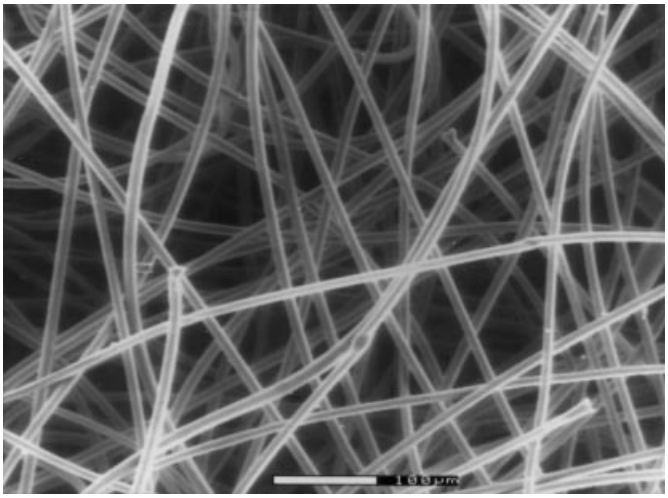

Fig. 4. SEM micrograph of a PGA nonwoven scaffold with a porosity of approximately 95% and a fiber diameter of approximately 15 μm.

molecules. The crystalline regions start to degrade soon after, leading to loss of molecular orientation in the fibers and decrease in mechanical properties. These PGA scaffolds have been used either alone or combined with other biodegradable polymers for the engineering of cartilage (97–99), tendon (100), ureter (101), intestine (102), blood vessels (103,104), heart valves (105), and other tissues.

Although PGA nonwoven scaffolds have stimulated a large wave of tissue engineering research and generated considerable excitement in the field, there are several limitations of PGA nonwoven scaffolds, such as low mechanical strength, fast degradation rate (losing mechanical properties within 2 weeks), difficulty in pore shape control, and limited fiber diameter variations. Therefore, many other processing techniques have been developed to fabricate scaffolds for desired properties in various tissue engineering applications.

Particulate-Leaching Techniques. Particulate-leaching is another technique that has been widely used to fabricate porous materials as scaffolds for tissue engineering applications. This technique was first developed by Mikos and colleagues (16), and was improved and standardized for large batch fabrications (7). This process is schematically illustrated in Figure 5, which is often called salt-leaching technique because NaCl crystals are most often used as the particles for pore generation (porogen). Briefly, salt is first ground into small particles, and the particles are then separated into different size ranges using standard sieves. The particles of desired size are added into a mold of a needed shape. A polymer solution is prepared and cast into the salt-filled mold. After the evaporation of solvent, the salt crystals are leached away using water to form the pores of the polymer foam (Fig. 6).

There is no complicated equipment needed for this technique. The process is easy to carry out and the materials used (water and salt) are economical. The technique is also versatile and can be used to fabricate foams from a variety of polymers as long as the polymer can be dissolved in a solvent that does not dissolve

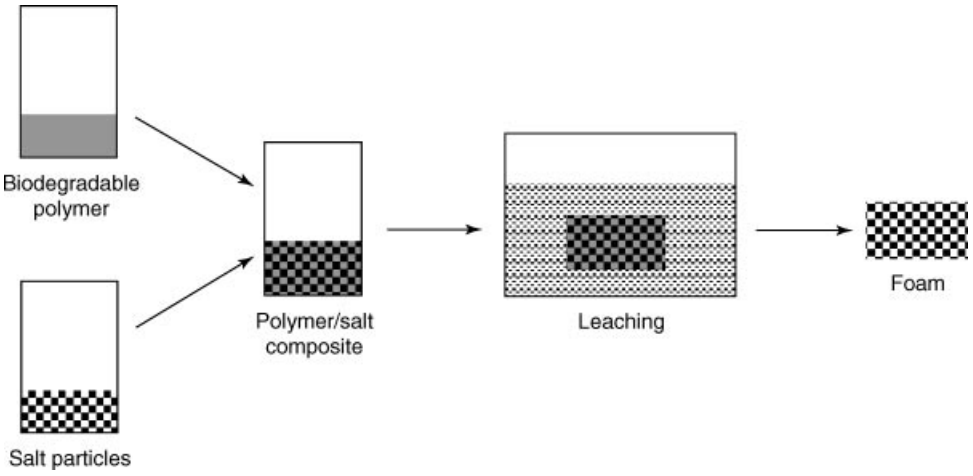

Fig. 5. Schematic illustration of the salt-leaching technique for porous foam fabrication.

the salt. The pore size can be controlled by the size of the salt crystals, and the porosity can be controlled by the salt/polymer ratio. For example, larger particle size results in larger pore size, and higher salt/polymer ratio results in higher porosity. Therefore, this technique is widely used in the tissue engineering field. However, certain critical variables such as pore shape and interpore openings are not controlled. For example, salt crystals have the characteristic cubic shape (Fig. 6). A spherical pore shape is not achievable using salt crystals. The resulting pores are often not well-connected because the polymer solution tends to penetrate between salt particles. To overcome the shortcomings of the salt-leaching

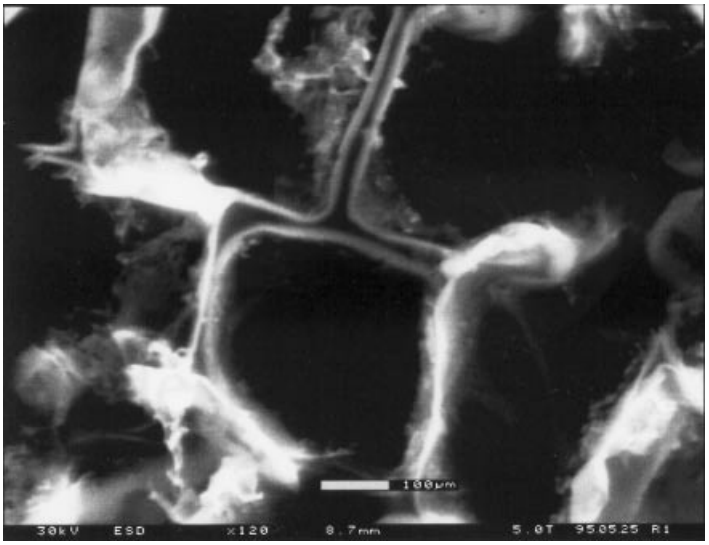

Fig. 6. SEM micrograph of a PLLA foam fabricated using the salt-leaching technique.

technique as well as the textile technologies, various other techniques have been developed to have better control over the pore structure of the scaffolds.

Phase Separation and Novel Architectures of Scaffolds. For a homogeneous multicomponent system, under certain conditions the system becomes thermodynamically unstable and tends to separate into a multiphase system in order to lower the system free energy. Controlled phase separation processes are desired for the generation of porous structures for tissue engineering scaffolding fabrication. For a polymer solution, phase separation can be induced in several different ways such as non-solvent-induced phase separation, chemically induced phase separation, and thermally induced phase separation. When phase separation occurs, a polymer solution separates into two phases, a polymer-rich phase (with a high polymer concentration) and a polymer-lean phase (with a low polymer concentration). After the solvent is removed by extraction, evaporation, or sublimation, the polymer-rich phase solidifies. Depending upon the system and phase separation conditions the resulting materials are different in physical form: powder, closed-pore foam, or open-pore foam (Fig. 7). Porous materials formed through phase separation have been utilized as membranes for filtration and separation (106). However, the pores formed through phase separation usually have diameters on the order of a few to tens of micrometers and are often not uniformly distributed, which are not suitable for tissue engineering applications.

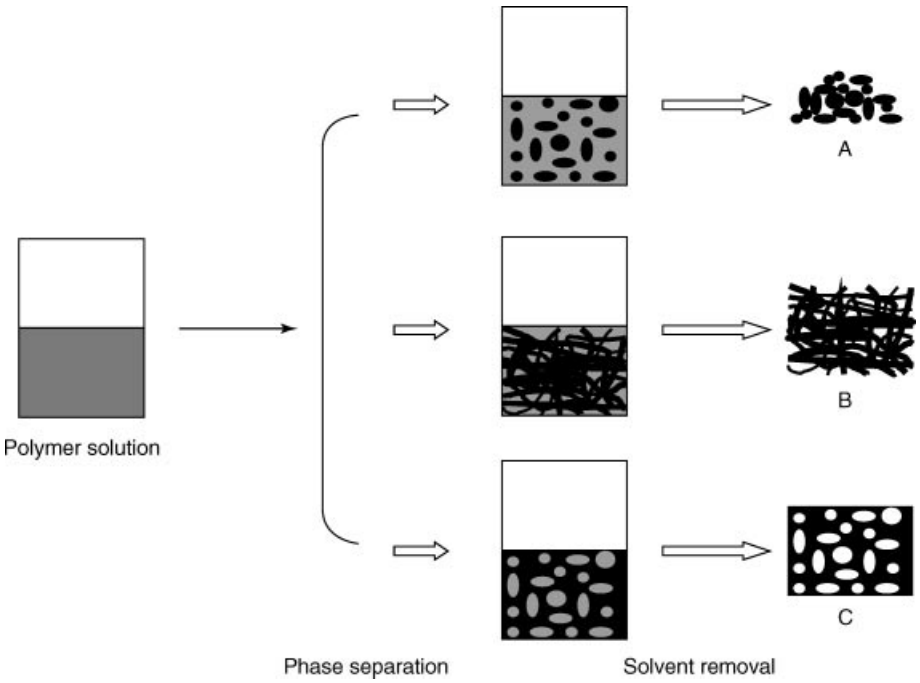

Fig. 7. Schematic illustration of phase separation processes that lead to different material forms: A, powder; B, open porous structure suitable as a scaffold for tissue engineering; and C, foam with closed pores.

As discussed earlier, a scaffold must have a pore size big enough for accommodating cells, allowing proliferation, and having room for new tissue synthesis. They also need to have high surface area to enhance cell adhesion. The pore structures should also allow for vascularization and innervation, and should facilitate diffusion of nutrients and waste materials. Thermally induced phase separation techniques have been explored in our laboratory for fabricating scaffolds to satisfy the requirements of tissue engineering. This type of phase separation is based on the thermodynamic and kinetic behavior of polymer solutions, which is a complicated process (26,107,108). The important variables are the polymer, solvent, concentration of the polymer solution, and the phase separation temperature. These variables have been manipulated to generate a variety of porous architectures for scaffold fabrication as briefly discussed below.

Solid–Liquid Phase Separation. Phase separation can be achieved by inducing solvent crystallization by decreasing the temperature of a polymer solution. This process is defined as a solid–liquid phase separation (solid-phase formation in a liquid phase). To achieve this, the crystallization temperature (freezing point) of the solvent in the polymer solution needs to be higher than the liquid–liquid phase separation temperature, or the liquid–liquid phase separation is kinetically too slow to take place before the temperature reaches the solid–liquid phase separation. When the temperature of the solution decreases and reaches the crystallization temperature, the solvent crystallizes and the polymer is expelled from the solvent crystallization front (separated from the solvent crystal lattice). After the removal of the solvent crystals (sublimation or solvent exchange), the space originally taken by the solvent crystals becomes pores. By manipulating the phase separation variables, foams with a variety of pore morphologies can be obtained. For example, PLLA and PLGA solutions have been used to fabricate interconnected pore structures as scaffolds using solid–liquid phase separation techniques (Fig. 8) (5,109). This technique can be used to fabricate scaffolds of more than one type of materials, including composite scaffold fabrication (Fig. 8**c**) (109). These interconnected pore structures also allow further modification of the pore wall surfaces after the scaffold fabrication. Bone-like apatite coating on such polymer scaffolds via a biomimetic process is such an example (20). Proteins and other bioactive molecules can also be used for such internal pore surface modifications (110).

By manipulating the phase separation conditions, various pore structures can be achieved. For example, many tissues (such as nerve, muscle, tendon, ligament, dentin, and so on) have oriented tubular or fibrous bundle architectures. To facilitate the organization and regeneration of such tissue types, a scaffold with a high porosity and an oriented array of open microtubules may be desirable. To achieve this goal, a novel phase separation technique has been developed for the creation of a parallel array of microtubules (Fig. 9) (111). In such a process, nucleation of the solvent is induced at one side of the polymer solution. The nuclei will grow in all directions until they contact with each other on this side. Then they cannot grow further in this plane, and are forced to grow along the direction perpendicular to this plane, leading to the formation of an array of parallel rod-like solvent crystals. The polymers are expelled from the solution and squeezed into thin walls surrounding these parallel solvent rods. After the removal of these rods, a parallel array of microtubules is formed as demonstrated. This oriented

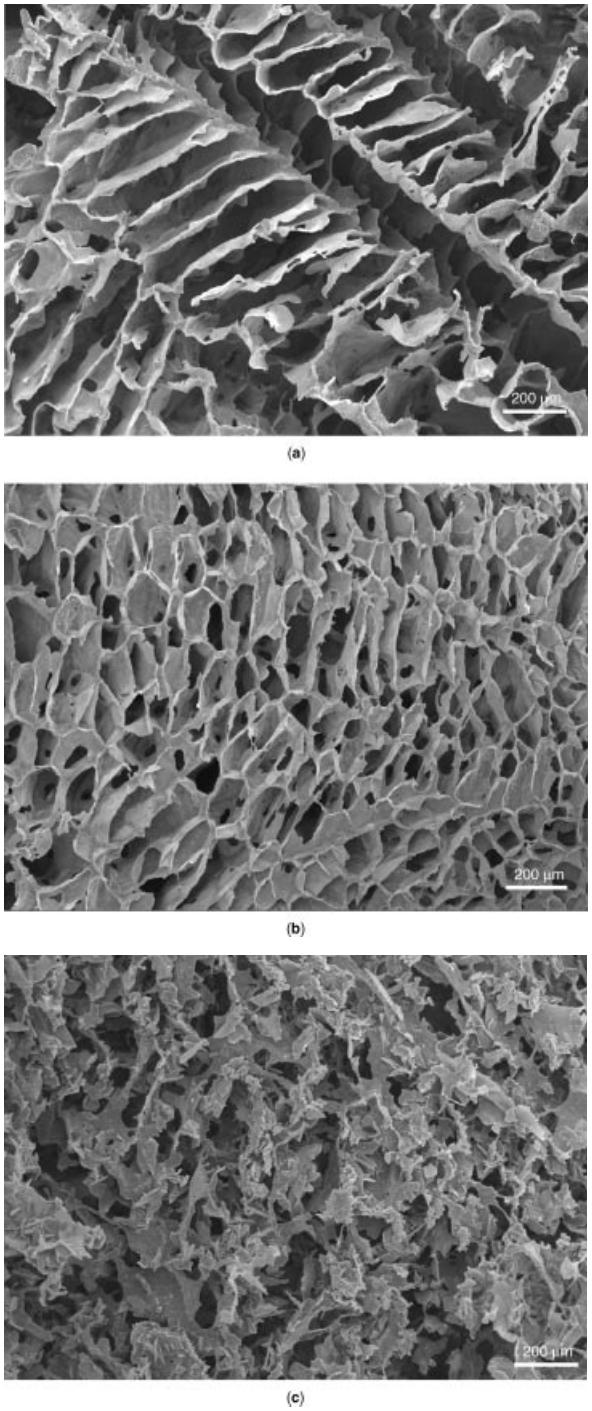

Fig. 8. SEM micrographs of polymer scaffolds fabricated using solid–liquid phase separation: (**a**) PLLA scaffold fabricated from 5% PLLA/dioxane solution (with local regular pore structure), (**b**) PLLA scaffold fabricated from 2.5% PLLA/dioxane solution (with less regular structure), (**c**) PLLA/HAP (hydroxyapatite) composite scaffold (PLLA/HAP: 50/50) fabricated from a 2.5% PLLA/dioxane solution. Reprinted from Refs. 5 and 109. © 2001, by permission of John Wiley & Sons.

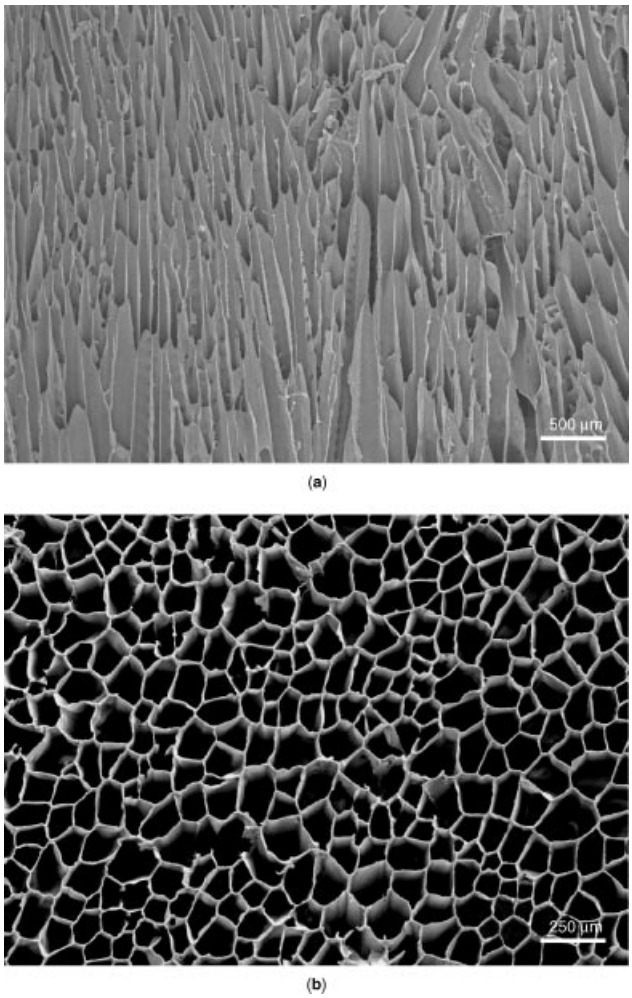

Fig. 9. SEM micrographs of a PLLA scaffold with oriented microtubular architecture prepared from 5% PLLA solution: (**a**) longitudinal section, and (**b**) cross section. From Ma and Reprinted from Ref. 111. © 2001, by permission of John Wiley & Sons.

tubular scaffold has anisotropic mechanical properties similar to fibrillar and tubular tissues, and has been shown to facilitate cell organization into oriented fibrillar or tubular tissues (Fig. 10) (111).

Liquid–Liquid Phase Separation. In contrast to solid–liquid phase separation, lowering temperature can induce liquid–liquid phase separation of a polymer solution with an upper critical solution temperature and when the crystallization temperature of the solvent is sufficiently lower than the phase separation temperature. In an equilibrium phase diagram of a polymer solution, the spinodal curve divides the liquid–liquid phase separation region into two regions: a thermodynamically metastable region (between the binodal and spinodal) and a thermodynamically unstable region (enclosed by the spinodal) (Fig. 11). Above the

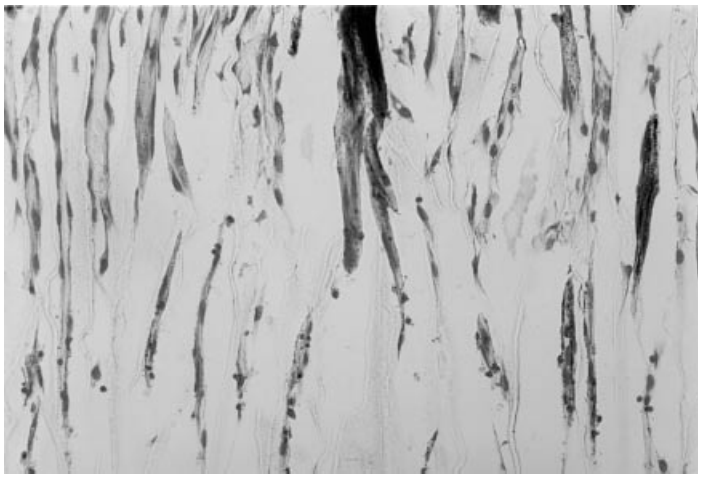

Fig. 10. MC3T3-E1 cells cultured on a PLLA scaffold with parallel open microtubular architecture for 4 weeks *in vitro*, von Kossa's silver nitrate staining. Reprinted from Ref. 111. © 2001, by permission of John Wiley & Sons.

binodal curve, the solution is homogeneous. When the temperature of the polymer solution is lowered to a point below the binodal curve, the solution is not thermodynamically stable and tends to separate into two phases, a polymer-rich phase and a polymer-lean phase, to lower the system free energy. In a solution of very low polymer concentration, when the temperature is lowered to a point in the metastable region (between binodal and spinodal), the phase separation occurs via a nucleation and growth mechanism. This process can lead to the formation of small polymer-rich domains (droplets) in a polymer-lean matrix. After the removal of the solvent, polymer powder is formed (Fig. 7**a**). When the temperature is lowered into an unstable region (spinodal region), the phase separation occurs via a spinodal decomposition mechanism. This process leads to the formation of a

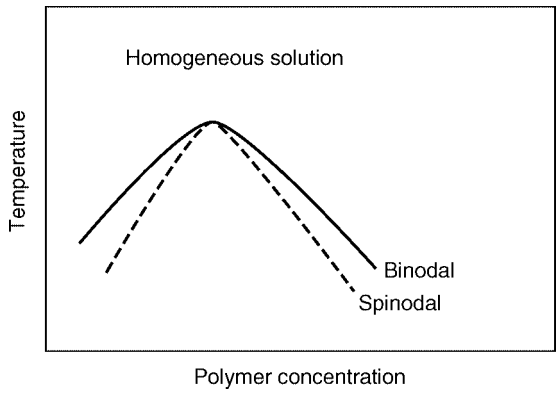

Fig. 11. Schematic equilibrium phase diagram for a polymer solution with an upper critical solution temperature.

bicontinuous structure, in which the polymer-rich and polymer-lean phases are both continuous phases. After the removal of the solvent, foam with open-pore structure is formed (Fig. 7**b**). In a solution of very high polymer concentration, when the temperature is lowered to a point in the metastable region, the phase separation leads to the formation of small solvent (polymer-lean) domains in a polymer-rich matrix. After the removal of the solvent, polymer foam of closed-pore structure is formed (Fig. 7**c**). If the polymer is crystalline, the phase separation process is more complicated (26). There is a competition between the liquid–liquid phase separation and polymer crystallization under certain conditions, making the final pore structure more complex (26,112).

Thermally induced liquid–liquid phase separation can be utilized to fabricate scaffolds for tissue engineering. For example, a solvent can be selected, where the crystallization temperature is sufficiently lower than the liquid–liquid phase separation temperature of an amorphous polymer solution. A liquid–liquid phase separation can be induced by lowering the temperature into the unstable region on the phase diagram but above the solvent crystallization temperature. For the PLA and PLGA family, a mixture of dioxane and water has been used for liquid–liquid phase separation to fabricate polymer scaffolds with interconnected pore structure (Fig. 12) (112,113).

Nanofibrous Matrix. Collagen (qv) is a major natural extracellular matrix component and possesses a fibrous structure with fiber bundles varying in diameter from 50 to 500 nm (62,114). To mimic the nanofibrous architecture of collagen and to overcome the concerns over materials from a natural source such as pathogen transmission and immune rejection, a novel phase separation technique has been developed in our laboratory to fabricate nanofibrous matrices from synthetic biodegradable polymers (112). For example, PLLA solutions are cooled to induce phase separation and gelation. The solvent is directly sublimated or first exchanged with a different solvent and then sublimated. Several solvents and solvent mixtures have been utilized to fabricate the desired nanofibrous matrices in our laboratory (Fig. 13) (112).

Three-Dimensional Pore Architecture Design. As discussed above various novel scaffolds have been developed for tissue engineering to address the critical shortage of donor tissues/organs. These scaffolds have facilitated the tissue engineering research in demonstrating the feasibility and tremendous potential of tissue engineering. However, these scaffolds are not perfect. One of the common shortcomings of these fabrication technologies is the lack of precise control of 3-D pore architecture of the scaffolds. To tackle this problem, computer-assisted-design and computer-assisted-manufacture (CAD and CAM) techniques that have been widely used in modern manufacture industry are finding ways into the field of tissue engineering (115).

These techniques were early explored by a group of materials scientists and chemical engineers at MIT (116,117). They used one of the solid free-form fabrication (a.k.a. rapid prototyping) techniques, called 3-D printing (3DP). With such a technique, complex-shaped objects can be designed using CAD softwares and directly fabricated from the generated CAD models. For example, they fabricated various structures from biodegradable polymers by ink-jet printing a binder onto sequentially laid polymer powder layers. The advantages of such a technique include the precise control of geometry and the feasibility for repeated fabrication

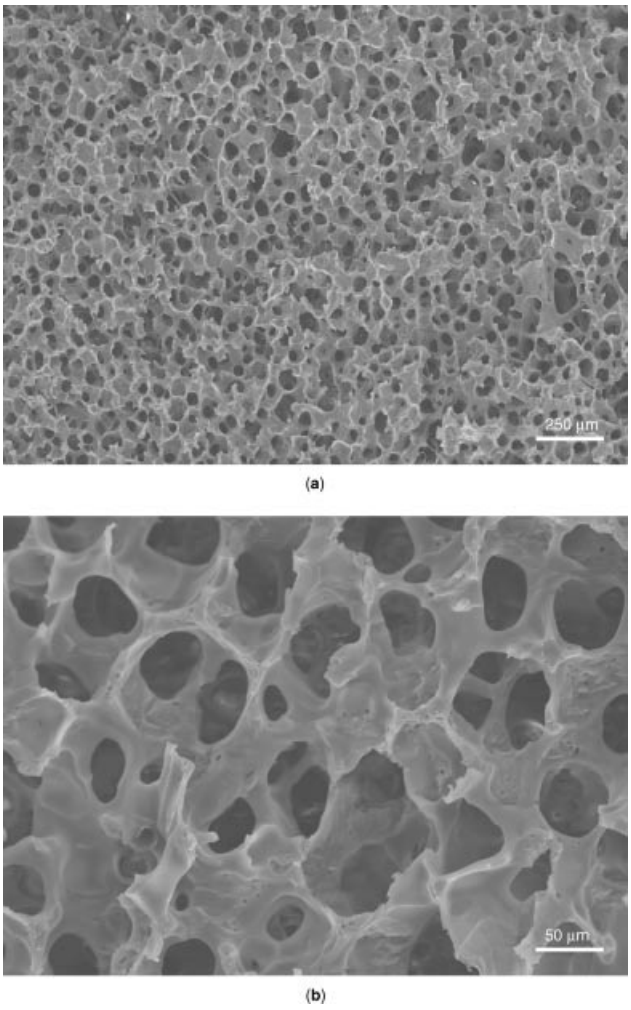

Fig. 12. SEM micrographs of a porous scaffold prepared from a 10% solution of PLGA (85/15) in a mixture of dioxane/H_2O (80/20) at two different magnifications: (**a**) low magnification and (**b**) high magnification. Reprinted from Ref. 112. © 1999, by permission of John Wiley & Sons.

of the same structure (118). However, the smallness of the powder particles and the binder drops (pixels) are limited (a few hundred micrometers). The accuracy of positioning the printing nozzle is also limited. The size of a feature (shape of a pore or architectural component) is dependent on the resolution of the pixel size and positioning control. Therefore the preciseness of the technology is seriously limited.

The anticipation of the future improvement of the resolution of such technologies has, nevertheless, maintained the research momentum in this direction. Similarly, another rapid prototyping technique, fused deposition modeling, has been used to fabricate 3-D scaffolds (119). This technique is suitable for processing thermoplastic polymers. A heated nozzle is utilized to extrude polymer

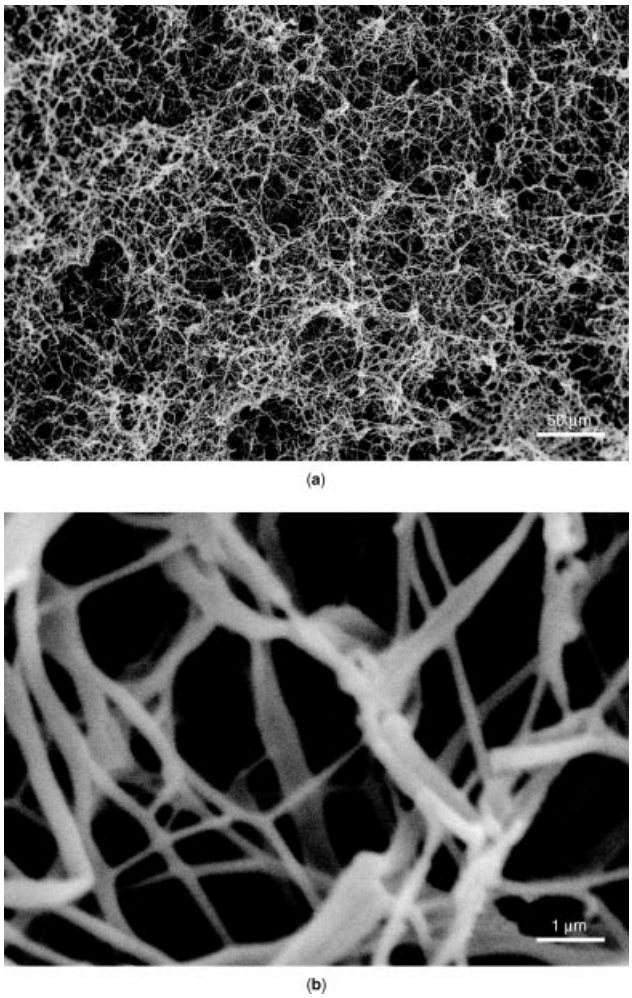

Fig. 13. SEM micrographs of a PLLA nanofibrous matrix prepared from 2.5% (w/v) PLLA/THF solution at a phase separation temperature of 8°C: (**a**) 500×; (**b**) 20,000×. Reprinted from Ref. 112. © 1999, by permission of John Wiley & Sons.

filament on to a platform. A layer is patterned by depositing the continuous polymer filament and raster in the *x–y* directions. The motion along *z* direction allows layer-by-layer integration of the 2-D patterns into 3-D structures. In our laboratory, a similar process is used to fabricate the negative replica of the scaffold. A polymer solution is cast into such a mold and solidified after the removal of the solvent. The mold is then dissolved away to form the polymer scaffold with the designed 3-D pore network (Fig. 14).

Lithography is another processing technique that is actively explored for 3-D scaffold fabrication. Stereolithographic models derived from X-ray computed tomography and CAD software were used to recreate complex anatomic structure of a human pulmonary and aortic graft. These stereolithographic models were used to generate biodegradable heart valve scaffolds by a thermal processing technique (120). Hydroxyapatite scaffolds with various pore shapes have also been fabricated

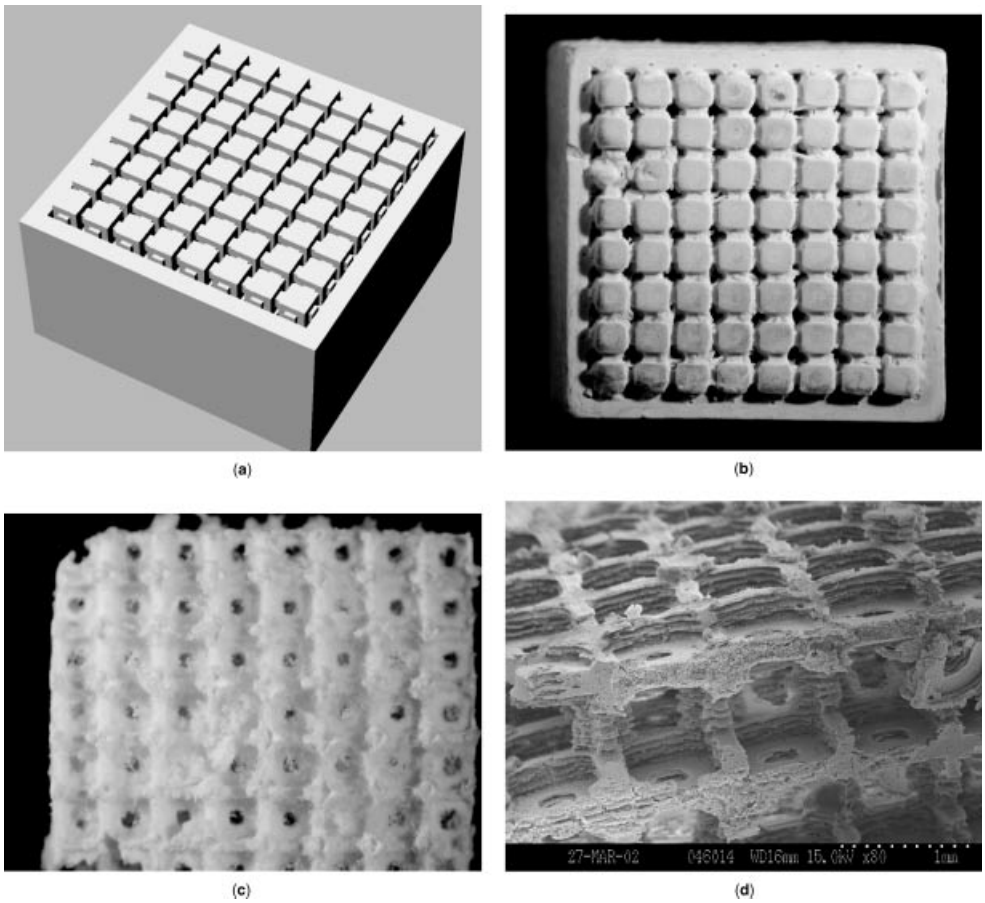

Fig. 14. Scaffold fabrication using rapid prototyped negative replica: (**a**) A computer-generated 3-D negative replica of a scaffold with a cubical pore shape; (**b**) the negative replica of the scaffold fabricated using a rapid prototyping machine; (**c**) the polymer scaffold fabricated using the negative replica; (**d**) SEM micrograph of the internal pore structure of the generated scaffold (V. J. Chen and P. X. Ma, unpublished data, 2003).

by casting ceramic slurry into molds generated using stereolithography and a subsequent sintering process (Fig. 15) (121). Lithography techniques have also been used to fabricate devices to localize cell populations in patterned configurations on rigid substrates as a potential artificial liver (122). A complex silicon structure of branched vascular channels as a model for liver fabrication has also been developed using stereolithography (123).

However, in addition to the special equipment requirements all these fabrication techniques have their inherent shortcomings such as limited material selections and inadequate resolution like the 3DP techniques discussed earlier. Furthermore, the resulting constructs have structural heterogeneity due to the "pixel assembly" nature of these fabrication processes.

In our laboratory, reversed fabrication processes have been developed to overcome these shortcomings for tissue engineering scaffold fabrications (Fig. 16)

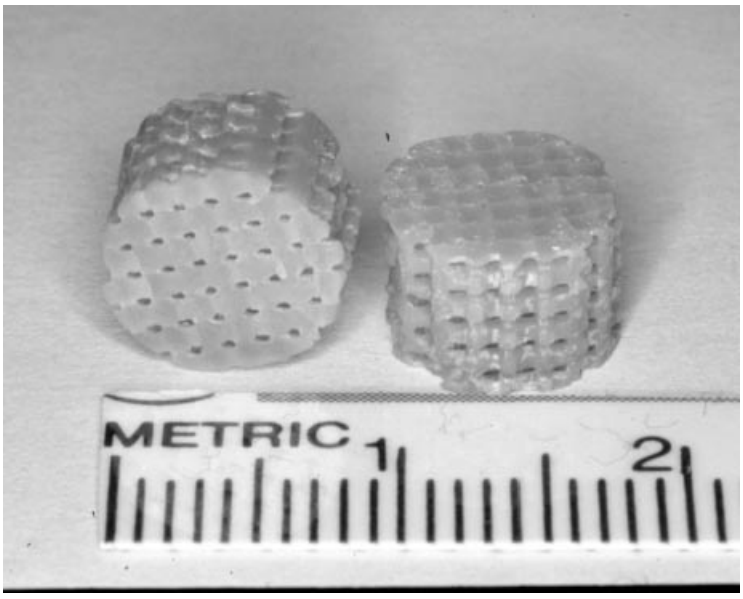

Fig. 15. Hydroxyapatite scaffolds fabricated by casting ceramic slurry into molds generated using stereolithography and a subsequent sintering process. Reprinted from Ref. 121. © 2001, by permission of Kluwer Academic Publishers.

(124). To fabricate 3-D biodegradable polymer scaffolds with well-controlled interconnected spherical pores, paraffin spheres are fabricated with a dispersion method. These paraffin spheres are then transferred into a 3-D mold of a designed shape or anatomical shape of a body part. The spheres are bonded together in the mold through a heat treatment process. A polymer solution is cast into the paraffin assembly in the mold (Note: the solvent used should not be a solvent of the paraffin spheres). After removal of the solvent through evaporation or other means, the polymer–paraffin sphere assembly is immersed in a solvent of the paraffin but not a solvent for the polymer (such as hexane for PLA or PLGA scaffolds) to dissolve the paraffin sphere assembly. In this way, an interconnected spherical pore structure is created in a predetermined shape by the mold (Fig. 17). Importantly, the generated scaffolds have homogeneous foam skeleton (platelet-like, continuous,

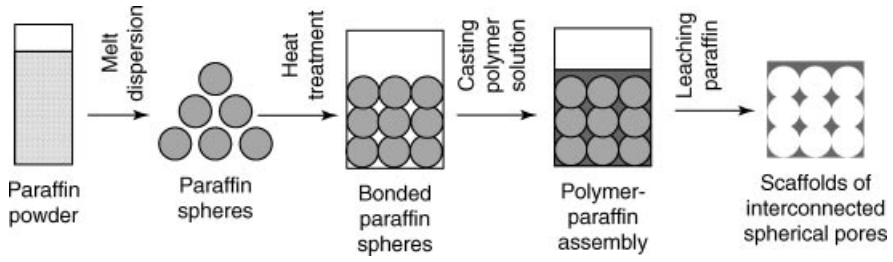

Fig. 16. Schematic fabrication processes for polymer scaffolds with interconnected spherical pores.

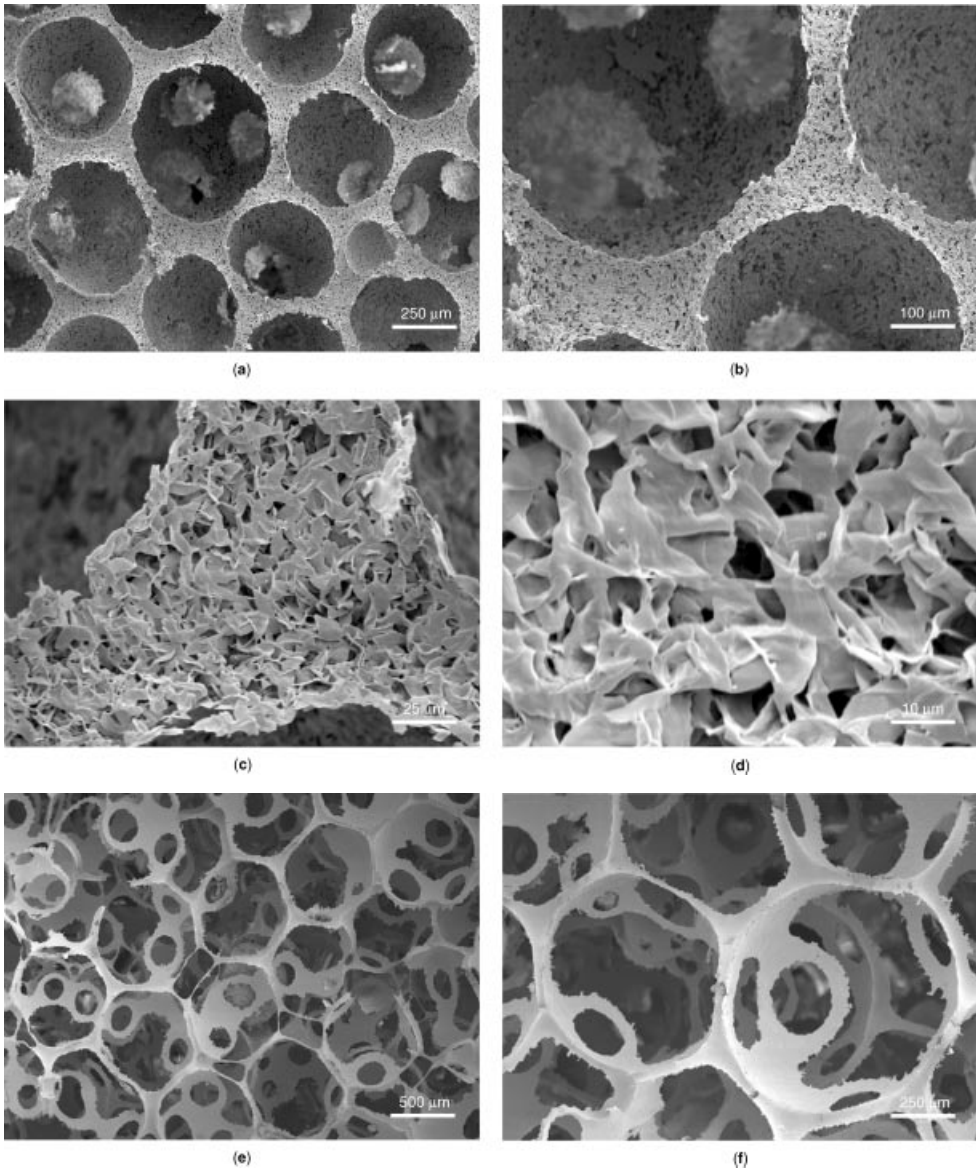

Fig. 17. SEM micrographs of polymer scaffolds [(**a**)–(**d**) PLLA; (**e**) and (**f**) PLGA85/15] with an interconnected spherical pore structure prepared using paraffin spheres (porogen): (**a**)100×, paraffin spheres: 250–420 μm; (**b**) 250×, paraffin spheres: 250–420 μm; (**c**)1000×, paraffin spheres: 250–420 μm; (**d**) 3000×, paraffin spheres: 250–420 μm; (**e**) 50×, paraffin spheres: 420–500 μm; (**f**) 100×, paraffin spheres: 420–500 μm. Reprinted from Ref. 124. © 2001, by permission of Mary Ann Liebert.

or other complex features, depending on the polymer and phase separation conditions) with homogeneous material properties, which are not easily achievable with free-forming, 3DP or lithography because of the limitation of pixel-by-pixel construction. Equally importantly, the spherical pore size is determined by the

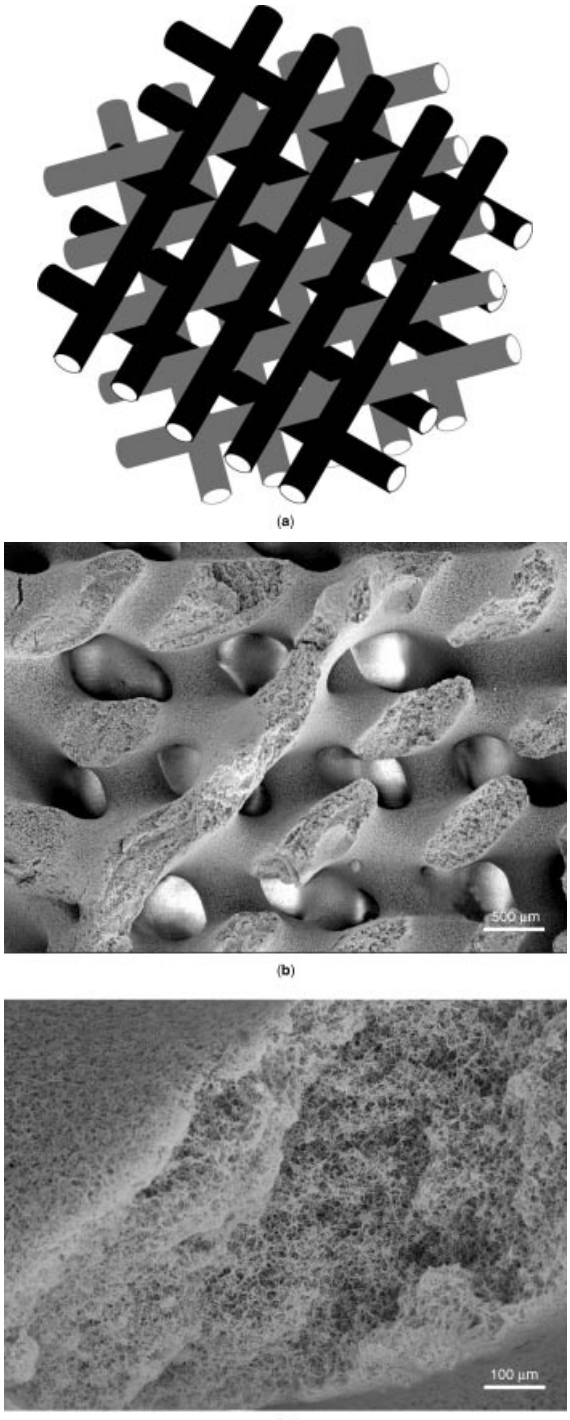

Fig. 18. PLLA nanofibrous scaffold with helicoidal tubular macropore network prepared from PLLA/THF solution and a helicoidal sugar fiber of the scaffold assembly: (**a**) schematic illustration of helicoidal sugar fiber assembly; (**b**) SEM micrograph of the scaffold at an original magnification of 35×, and (**c**) original magnification of 250×. Reprinted from Ref. 15. © 2000, by permission of John Wiley & Sons.

paraffin sphere size used, which can be controlled through paraffin sphere preparation. The features generated are significatly better than those achievable with the resolutions of the current 3-D fabrication machines. Furthermore, the interpore openings are circular and the size of these openings is adjustable through manipulating the heat treatment conditions. For example, longer heat treatment time leads to larger openings between the pores (124). Finally there is no expensive equipment investment compared to the textile technologies or rapid prototyping techniques, which allows this technology to be easily adapted in a research as well as an industrial setting.

To improve the 3-D structure of nanofibrous scaffolds for cell seeding and distribution, mass transport, vascular invasion, and tissue organization, techniques have also been developed in our laboratory to build predesigned macropore networks in nanofibrous matrices (15). For example, larger water-soluble fibers (diameters from 100 μm to 1 mm) are prepared from sugar as a geometrical porogen element, and are assembled into various 3-D structures (such as helicoidal) (Fig. 18**a**). PLLA solution is then cast into this 3-D assembly and is thermally induced to phase-separate for nanofibrous matrix formation. After the solvent removal, the sugar fiber assembly is dissolved away using water to achieve nanofibrous scaffolds with predesigned helicoidal tubular pore network (Figs. 18**b** and 18**c**). Similarly, we have combined the interconnected spherical pore network described earlier with nanofiber techniques to generate nanofibrous scaffolds with interconnected spherical macropores (Fig. 19) (125).

As discussed above, tissue engineering scaffold fabrication is a fast evolving area. Many other polymer processing techniques such as gas-foaming, emulsion freeze-drying, and so forth have also been explored (126–128). Current efforts for these techniques include overcoming the disadvantages of closed-pore structures and undesired pore size ranges.

Again this article is intended to introduce the general concepts of tissue engineering in relation to polymer science and engineering, but is not intended to be a complete and exhaustive review of the field of tissue engineering. There are

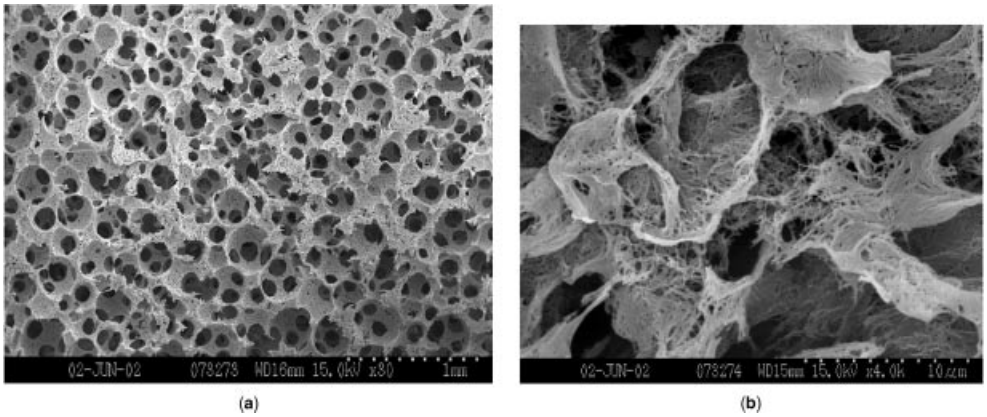

Fig. 19. SEM micrographs of nanofibrous scaffolds with interconnected spherical pore network: (**a**) original magnification 30×, (**b**) original magnification 4000×. Reprinted from Ref. 125. © 2003, by permission of John Wiley & Sons.

recently developed comprehensive books (129–131) available for further reading on various topics in tissue engineering.

BIBLIOGRAPHY

1. J. P. Vacanti and R. Langer, *Lancet* **354** (Suppl 1), SI32–SI34 (1999).
2. N. Couch, R. Wilson, E. Hager, and J. Murray, *Surgery* **59**(2), 183–188 (1966).
3. R. Langer and J. P. Vacanti, *Science* **260**, 920–926 (1993).
4. V. M. Goldberg and S. Stevenson, *Orthopedics* **17**, 809–810, 821 (1994).
5. P. X. Ma, R. Zhang, G. Xiao, and R. Franceschi, *J. Biomed. Mater. Res.* **54**, 284–293 (2001).
6. R. M. Nerem and A. Sambanis, *Tissue Eng.* **1**(1), 3–13 (1995).
7. P. X. Ma and R. Langer, in J. Morgan and M. Yarmush, eds., *Tissue Engineering Methods and Protocols*, Humana Press, Inc., Totowa, N.J., 1999, pp. 47–56.
8. L. Peterson, M. Brittberg, I. Kiviranta, E. Akerlund, and A. Lindahl, *Am. J. Sports Med.* **30**(1), 2–12 (2002).
9. J. Bloch, E. Fine, N. Bouche, A. Zurn, and P. Aebischer, *Exp. Neurol.* **172**, 425–432 (2001).
10. G. N. King, *Curr. Pharm. Biotechnol.* **2**(2), 131–142 (2001).
11. C. K. Colton, *Nat. Biotechnol.* **17**, 421–422 (1999).
12. E. S. Tzanakakis, D. J. Hess, T. D. Sielaff, and W. S. Hu, *Annu. Rev. Biomed. Eng.* **2**, 607–632 (2000).
13. H. D. Humes, W. H. Fissell, W. F. Weitzel, D. A. Buffington, A. J. Westover, S. M. MacKay, and J. M. Gutierrez,*Am. J. Kidney Dis.* **39**, 1078–1087 (2002).
14. S. Del Guerra, C. Bracci, K. Nilsson, A. Belcourt, L. Kessler, R. Lupi, L. Marselli, P. De Vos, and P. Marchetti, *Biotechnol. Bioeng.* **75**, 741–744 (2001).
15. R. Zhang and P. X. Ma, *J. Biomed. Mater. Res.* **52**, 430–438 (2000).
16. A. G. Mikos, A. J. Thorsen, L. A. Czerwonka, Y. Bao, R. Langer, D. N. Winslow, and J. P. Vacanti, *Polymer* **35**, 1068–1077 (1994).
17. P. X. Ma and R. Langer, in A. G. Mikos, K. W. Leong, M. L. Radomsky, J. A. Tamada, and M. J. Yaszemski, eds., *Polymers in Medicine and Pharmacy*, MRS, Pittsburgh, Pa., 1995 pp. 99–104.
18. J. A. Hubbell, *Curr. Opin. Biotechnol.* **10**(2), 123–129 (1999).
19. D. Barrera, E. Zylstra, P. Lansbury, and R. Langer, *J. Am. Chem. Soc.* **115**, 11010–11011 (1993).
20. R. Zhang and P. X. Ma, *J. Biomed. Mater. Res.* **45**, 285–293 (1999).
21. H. Shi and B. D. Ratner, *J. Biomed. Mater. Res.* **49**(1), 1–11 (2000).
22. H. Lee, R. A. Cusick, F. Browne, T. Ho Kim, P. X. Ma, H. Utsunomiya, R. Langer, and J. P. Vacanti, *Transplantation* **73**, 1589–1593 (2002).
23. J. Bonadio, E. Smiley, P. Patil, and S. Goldstein, *Nat. Med.* **5**, 753–759 (1999).
24. H. Lo, S. Kadiyala, S. E. Guggino, and K. W. Leong, *J. Biomed. Mater. Res.* **30**, 475–484 (1996).
25. M. H. Sheridan, L. D. Shea, M. C. Peters, and D. J. Mooney, *J. Controlled Release* **64**(1–3), 91–102 (2000).
26. R. Zhang and P. X. Ma, in A. Atala and R. Lanza, eds., *Methods of Tissue Engineering*, Academic Press, San Diego, Calif., 2001, pp. 715–724.
27. J. H. Elisseeff and Y. Yamada, in K.-U. Lewandrowski, D. L. Wise, D. J. Trantolo, J. D. Gresser, M. J. Yaszemski, and D. E. Altobelli, eds., *Tissue Engineering and Biodegradable Equivalents: Scientific and Clinical Applications*, Marcel Dekker, Inc., New York, 2002, pp. 1–23.
28. J. M. Pachence and J. Kohn, in R. P. Lanza, R. Langer, and J. Vacanti, eds., *Principles of Tissue Engineering*, Academic Press, San Diego, Calif., 2000, pp. 263–277.

29. A. Reed and D. Gilding, *Polymer* **22**, 494–498 (1981).
30. R. Zhang and P. X. Ma, *Polym. Prepr.* **41**, 1618–1619 (2000).
31. B. Eling, S. Gogolewski, and A. J. Pennings, *Polymer* **23**, 1587–1593 (1982).
32. O. M. Bostman and H. K. Pihlajamaki, *Clin. Orthop.* **371**, 216–227 (2000).
33. J. A. Tamada and R. Langer, *Proc. Nat. Acad. Sci. U.S.A.* **90**, 552–556 (1993).
34. A. Gopferich, *Biomaterials* **17**(2), 103–114 (1996).
35. S. Li, *J. Biomed. Mater. Res.* **48**, 342–353 (1999).
36. C. G. Pitt, M. M. Gratzl, G. L. Kimmel, J. Surles, and A. Schindler, *Biomaterials* **2**, 215–220 (1981).
37. S. C. Woodward, P. S. Brewer, F. Moatamed, A. Schindler, and C. G. Pitt, *J. Biomed. Mater. Res.* **19**, 437–444 (1985).
38. C. G. Pitt, in M. Chasin and R. Langer, eds., *Biodegradable Polymers as Drug Delivery Systems*, Marcel Dekker, Inc., New York, 1990, pp. 71–119.
39. S. J. Holland, A. M. Jolly, M. Yasin, and B. J. Tighe, *Biomaterials* **8**, 289–295 (1987).
40. N. D. Miller and D. F. Williams, *Biomaterials* **8**(2), 129–137 (1987).
41. M. Richards, B. I. Dahiyat, D. M. Arm, P. R. Brown, and K. W. Leong, *J. Biomed. Mater. Res.* **25**, 1151–1167 (1991).
42. J. Wang, H. Q. Mao, and K. W. Leong, *J. Am. Chem. Soc.* **123**, 9480–9481 (2001).
43. S. Wang, A. C. Wan, X. Xu, S. Gao, H. Q. Mao, K. W. Leong, and H. Yu, *Biomaterials.* **22**, 1157–1169 (2001).
44. M. S. Wolfe, D. Dean, J. E. Chen, J. P. Fisher, S. Han, C. M. Rimnac, and A. G. Mikos, *J. Biomed. Mater. Res.* **61**(1), 159–164 (2002).
45. S. J. Peter, S. T. Miller, G. Zhu, A. W. Yasko, and A. G. Mikos, *J. Biomed. Mater. Res.* **41**(1), 1–7 (1998).
46. E. Behravesh, S. Jo, K. Zygourakis, and A. G. Mikos, *Biomacromolecules* **3**, 374–381 (2002).
47. H. R. Allcock, in M. Chasin and R. Langer, eds., *Biodegradable Polymers as Drug Delivery Systems*, Marcel Dekker, Inc., New York, 1990, pp. 163–193.
48. P. Caliceti, F. M. Veronese, and S. Lora, *Int. J. Pharm.* **211**(1/2), 57–65 (2000).
49. N. N. Aldini, P. Caliceti, S. Lora, M. Fini, G. Giavaresi, M. Rocca, P. Torricelli, R. Giardino, and F. M. Veronese, *J. Orthop. Res.* **19**, 955–961 (2001).
50. A. M. Ambrosio, H. R. Allcock, D. S. Katti, and C. T. Laurencin, *Biomaterials* **23**, 1667–1672 (2002).
51. S. Cohen, M. C. Bano, L. G. Cima, H. R. Allcock, J. P. Vacanti, C. A. Vacanti, and R. Langer, *Clin. Mater.* **13**(1–4), 3–10 (1993).
52. A. K. Burkoth, J. Burdick, and K. S. Anseth, *J. Biomed. Mater. Res.* **51**, 352–359 (2000).
53. K. W. Leong, J. Kost, E. Mathiowitz, and R. Langer, *Biomaterials* **7**, 364–371 (1986).
54. U.S. Pat. 04093709 (1978), N. S. Choi and J. Heller.
55. K. P. Andriano, Y. Tabata, Y. Ikada, and J. Heller, *J. Biomed. Mater. Res.* **48**, 602–612 (1999).
56. K. James, H. Levene, J. R. Parsons, and J. Kohn, *Biomaterials* **20**, 2203–2212 (1999).
57. K. A. Hooper, N. D. Macon, and J. Kohn, *J. Biomed. Mater. Res.* **41**, 443–454 (1998).
58. H. B. Lin, W. Sun, D. F. Mosher, C. Garcia-Echeverria, K. Schaufelberger, P. I. Lelkes, and S. L. Cooper, *J. Biomed. Mater. Res.* **28**, 329–342 (1994).
59. G. A. Skarja and K. A. Woodhouse, *J. Biomater. Sci., Polym. Ed.* **12**, 851–873 (2001).
60. J. J. Guan, M. S. Sacks, E. J. Beckman, and W. R. Wagner, *J. Biomed. Mater. Res.* **61**, 493–503 (2002).
61. J. Y. Zhang, E. J. Beckman, N. P. Piesco, and S. Agarwal, *Biomaterials* **21**, 1247–1258 (2000).
62. E. D. Hay, *Cell Biology of Extracellular Matrix*, 2nd ed., Plenum Press, New York, 1991, pp. 7–44.

63. E. Bell, M. Rosenberg, P. Kemp, R. Gay, G. Green, N. Muthukumaran, and C. Nolte, *J. Biomech. Eng.* **113**(2), 113–119 (1991).
64. J. M. Pachence, *J. Biomed. Mater. Res.* **33**(1), 35–40 (1996).
65. I. V. Yannas, *J. Cell. Biochem.* **56**(2), 188–191 (1994).
66. S. M. Mueller, S. Shortkroff, T. O. Schneider, H. A. Breinan, I. V. Yannas, and M. Spector, *Biomaterials* **20**, 701–709 (1999).
67. Y. S. Choi, S. R. Hong, Y. M. Lee, K. W. Song, M. H. Park, and Y. S. Nam, *J. Biomed. Mater. Res.* **48**, 631–639 (1999).
68. L. Shapiro and S. Cohen, *Biomaterials* **18**, 583–590 (1997).
69. S. V. Madihally and H. W. Matthew, *Biomaterials* **20**, 1133–1142 (1999).
70. C. K. Kuo and P. X. Ma, *Biomaterials* **22**, 511–521 (2001).
71. J. P. Fisher, T. A. Holland, D. Dean, P. S. Engel, and A. G. Mikos, *J. Biomater. Sci., Polym. Ed.* **12**, 673–687 (2001).
72. J. H. Elisseeff, A. Lee, H. K. Kleinman, and Y. Yamada, *Ann. N.Y. Acad. Sci.* **961**, 118–122 (2002).
73. J. A. Burdick, A. J. Peterson, and K. S. Anseth, *Biomaterials* **22**, 1779–1786 (2001).
74. E. Alsberg, K. W. Anderson, A. Albeiruti, R. T. Franceschi, and D. J. Mooney, *J. Dent. Res.* **80**, 2025–2029 (2001).
75. B. K. Mann, A. S. Gobin, A. T. Tsai, R. H. Schmedlen, and J. L. West, *Biomaterials* **22**, 3045–3051 (2001).
76. N. A. Alcantar, E. S. Aydil, and J. N. Israelachvili, *J. Biomed. Mater. Res.* **51**, 343–351 (2000).
77. N. D. Winblade, I. D. Nikolic, A. S. Hoffman, and J. A. Hubbell, *Biomacromolecules* **1**, 523–533 (2000).
78. N. K. Mongia, K. S. Anseth, and N. A. Peppas, *J. Biomater. Sci., Polym. Ed.* 1055, **7**, 1055–1064.
79. D. L. Elbert and J. A. Hubbell, *Biomacromolecules* **2**, 430–441 (2001).
80. J. Elisseeff, K. Anseth, D. Sims, W. McIntosh, M. Randolph, M. Yaremchuk, and R. Langer, *Plast. Reconstr. Surg.* **104**, 1014–1022 (1999).
81. L. G. Griffith and S. Lopina, *Biomaterials* **19**, 979–986 (1998).
82. D. J. Irvine, A. M. Mayes, and L. G. Griffith, *Biomacromolecules* **2**(1), 85–94 (2001).
83. B. K. Mann and J. L. West, *J. Biomed. Mater. Res.* **60**(1), 86–93 (2002).
84. D. K. Han and J. A. Hubbell, *Macromolecules* **30**, 6077–6083 (1997).
85. A. S. Sawhney, C. P. Pathak, and J. A. Hubbell, *Macromolecules* **26**, 581–587 (1993).
86. J. L. West and J. A. Hubbell, *Macromolecules* **32**, 241–244 (1999).
87. A. Martinsen, G. Skjåk-Bræk, and O. Smidsrød, *Biotechnol. and Bioeng.* **33**, 79–89 (1989).
88. K. I. Draget, K. Ostgaard, and O. Smidsrod, *Carbohydr. Polym.* **14**, 159–178 (1991).
89. P. Aebischer, E. Buchser, J. Joseph, J. Favre, T. N. de, M. Lysaght, S. Rudnick, and M. Goddard, *Transplantation* **58**, 1275–1277 (1994).
90. A. Atala, W. Kim, K. Paige, C. Vacanti, and A. Retik, *J. Urol.* **152**(2, Ptart 2), 641–643 (1994) (discussion 644).
91. K. Paige, L. Cima, M. Yaremchuk, B. Schloo, J. Vacanti, and C. Vacanti, *Plast. Reconstr. Surg.* **97**(1), 168–178 (1996) (discussion 179–180).
92. S. Wakitani, T. Goto, S. J. Pineda, R. G. Young, J. M. Mansour, A. I. Caplan, and V. M. Goldberg, *J. Bone Joint Surg.* **76**, 579–592 (1994).
93. D. Ceballos, X. Navarro, N. Dubey, G. Wendelschafer-Crabb, W. R. Kennedy, and R. T. Tranquillo, *Exp. Neurol.* **158**, 290–300 (1999).
94. F. A. Auger, M. Rouabhia, F. Goulet, F. Berthod, V. Moulin, and L. Germain, *Med. Biol. Eng. Comput.* **36**(6), 801–812 (1998).
95. S. Kawamura, S. Wakitani, T. Kimura, A. Maeda, A. I. Caplan, K. Shino, and T. Ochi, *Acta Orthop. Scand.* **69**(1), 56–62 (1998).

96. K. A. Hildebrand, F. Jia, and S. L. Woo, *Microsc. Res. Tech.* **58**(1), 34–38 (2002).
97. C. Vacanti, R. Langer, B. Schloo, and J. Vacanti, *Plast. Reconstr. Surg* **88**, 753–759 (1991).
98. P. X. Ma, B. Schloo, D. Mooney, and R. Langer, *J. Biomed. Mater. Res.* **29**, 1587–1595 (1995).
99. L. E. Freed, R. Langer, I. Martin, N. R. Pellis, and G. Vunjak-Novakovic, *Proc. Natl. Acad. Sci. U.S.A.* **94**, 13885–13890 (1997).
100. Y. Cao, J. P. Vacanti, X. Ma, K. T. Paige, J. Upton, Z. Chowanski, B. Schloo, R. Langer, and C. A. Vacanti, *Transplant. Proc.* **26**, 3390–3392 (1994).
101. A. Atala, J. Vacanti, C. Peters, J. Mandell, A. Retik, and M. Freeman, *J. Urol.* **148**(2, Part 2), 658–662 (1992).
102. G. Organ, D. Mooney, L. Hansen, B. Schloo, and J. Vacanti, *Transplant. Proc.* **25**(1, Part 2), 998–1001 (1993).
103. T. Shinoka, D. Shum-Tim, P. X. Ma, R. E. Tanel, N. Isogai, R. Langer, J. P. Vacanti, and J. E. Mayer Jr., *J. Thorac. Cardiovasc. Surg.* **115**, 536–545 (1998) (discussion 545–536).
104. L. E. Niklason, J. Gao, W. M. Abbott, K. K. Hirschi, S. Houser, R. Marini, and R. Langer, *Science* **284**, 489–493 (1999).
105. T. Shinoka, P. X. Ma, D. Shum-Tim, C. K. Breuer, R. A. Cusick, G. Zund, R. Langer, J. P. Vacanti, and J. E. Mayer Jr., *Circulation* **94**(9, Suppl.), II164–II168 (1996).
106. R. W. Baker, *Membrane Technology and Applications*, McGraw-Hill, New York, 2000.
107. P. vandeWitte, P. J. Dijkstra, J. W. A. vandenBerg, and J. Feijen, *J. Membr. Sci.* **117**(1/2), 1–31 (1996).
108. R. Bansil, G. D. Liao, and P. Falus, *Physica A* **231**, 346–358 (1996).
109. R. Zhang and P. X. Ma, *J. Biomed. Mater. Res.* **44**, 446–455 (1999).
110. K. M. Woo, R. Zhang, H. Deng, and P. X. Ma, *Transaction of the 28th Annual Meeting of the Society for Biomaterial*, 2002, p. 605.
111. P. X. Ma and R. Zhang, *J. Biomed. Mater. Res.* **56**, 469–477 (2001).
112. P. X. Ma and R. Zhang, *J. Biomed. Mater. Res.* **46**(1), 60–72 (1999).
113. Y. S. Nam and T. G. Park, *J. Biomed. Mater. Res.* **47**(1), 8–17 (1999).
114. T. Elsdale and J. Bard, *J. Cell Biol.* **54**, 626–637 (1972).
115. S. Yang, K. F. Leong, Z. Du, and C. K. Chua, *Tissue Eng.* **8**(1), 1–11 (2002).
116. R. A. Giordano, B. M. Wu, S. W. Borland, L. G. Cima, E. M. Sachs, and M. J. Cima, *J. Biomater. Sci., Polym. Ed.* **8**(1), 63–75 (1996).
117. A. Park, B. Wu, and L. G. Griffith, *J. Biomater. Sci., Polym. Ed.* **9**(2), 89–110 (1998).
118. J. Zeltinger, J. K. Sherwood, D. A. Graham, R. Mueller, and L. G. Griffith, *Tissue Eng.* **7**, 557–572 (2001).
119. D. W. Hutmacher, T. Schantz, I. Zein, K. W. Ng, S. H. Teoh, and K. C. Tan, *J. Biomed. Mater. Res.* **55**, 203–216 (2001).
120. R. Sodian, M. Loebe, A. Hein, D. P. Martin, S. P. Hoerstrup, E. V. Potapov, H. Hausmann, T. Lueth, and R. Hetzer, *ASAIO J.* **48**(1), 12–16 (2002).
121. T.-M. G. Chu, J. W. Halloran, S. J. Hollister, and S. E. Feinberg, *J. Mater. Sci. Mater. Med.* **12**, 471–478 (2001).
122. S. N. Bhatia, U. J. Balis, M. L. Yarmush, and M. Toner, *Biotechnol. Prog.* **14**, 378–387 (1998).
123. S. Kaihara, J. Borenstein, R. Koka, S. Lalan, E. R. Ochoa, M. Ravens, H. Pien, B. Cunningham, and J. P. Vacanti, *Tissue Eng.* **6**(2), 105–117 (2000).
124. P. X. Ma and J. Choi, *Tissue Eng.* **7**(1), 23–33 (2001).
125. K. M. Woo, V. J. Chen, and P. X. Ma, *J. Biomed. Mater. Res.* (in press).
126. D. J. Mooney, D. F. Baldwin, N. P. Suh, J. P. Vacanti, and R. Langer, *Biomaterials* **17**, 1417–1422 (1996).
127. K. Whang, C. H. Thomas, K. E. Healy, and G. Nuber, *Polymer* **36**, 837–842 (1995).

128. C. M. Agrawal and R. B. Ray, *J. Biomed. Mater. Res.* **55**(2), 141–150 (2001).
129. R. P. Lanza, R. Langer, and J. Vacanti, *Principles of Tissue Engineering*, 2nd ed., Academic Press, San Diego, Calif., 2000.
130. A. Atala and R. P. Lanza, *Methods of Tissue Engineering*, Academic Press, San Diego, Calif., 2002.
131. J. R. Morgan and M. L. Yarmush, in J. M. Walker, ed., *Tissue Engineering Methods and Protocols (Methods in Molecular Medicine)*, Vol. 18. Humana Press, Inc., Totowa, N.J., 1999.

PETER X. MA
University of Michigan

TRANSITIONS AND RELAXATIONS. See VISCOELASTICITY.

TRANSPORT PROPERTIES

Introduction

Transport properties determine a polymer's ability to move through some medium or to have some penetrant medium move between its constituent segments. This definition encompasses processes with diverse driving forces such as concentration and pressure gradients, and even electrical or temperature gradients capable of motivating one component relative to another. This article emphasizes polymer transport properties under conditions of low to intermediate penetrant concentration, where extraordinary differences can exist between the diffusivities of penetrants having relatively small differences in molecular size or shape.

This article focuses on transport that proceeds by the solution-diffusion mechanism. Transport by this mechanism requires that the penetrant sorb into the polymer at a high activity interface, diffuse through the polymer, and then desorb at a low activity interface. In contrast, the pore-flow mechanism transports penetrants by convective flow through porous polymers and will not be described in this article. Detailed models exist for the solution and diffusion processes of the solution-diffusion mechanism. The differences in the sorption and transport properties of rubbery and glassy polymers are reviewed and discussed in terms of the fundamental differences between the intrinsic characteristics of these two types of polymers.

The transport properties of glassy and rubbery polymers are related to their microstructural morphology. For a penetrant to diffuse, a minimum characteristic packet of unoccupied volume is required. The penetrant diffuses by jumping through transient gaps between packets of unoccupied volume. The lifetime, size, and shape of these volume packets and the transient gaps that connect them are dependent upon the micromotions of the polymeric media. New techniques such as

Encyclopedia of Polymer Science and Technology. Copyright John Wiley & Sons, Inc. All rights reserved.

positron annihilation lifetime spectroscopy (PALS) and molecular modeling allow for elucidation of dynamic activities at the molecular scale. While a description at this length-scale offers fundamental information about the diffusion process, it is not yet possible to predict the macroscopic transport properties with sufficient accuracy for practical applications. In this regard, quantitative phenomenological models and more molecularly based treatments are complementary, and both will be considered.

Terminology

Reference Frames and Fluxes. In speaking of a diffusional flux, it is necessary to specify a reference frame from which the diffusion process is to be observed. Generally, a reference velocity such as the mass, molar, or volume average bulk velocity (v,v^*, or $v^\blacklozenge$, respectively) in the system is selected, and movement of the component of interest relative to this reference velocity is defined to be true diffusion. For practical reasons, a fixed reference frame is generally also considered to relate the mathematical treatment of this molecular scale transport process to an actual physical system with well-defined dimensions. In this case, the total flux relative to the fixed reference frame is partitioned into two parts: bulk flow and true molecular diffusion. This partitioning is necessary, because even in the absence of an externally imposed bulk flow, interdiffusion of molecules with respect to each other produces an effective bulk flow relative to fixed coordinates if the molecules have different masses (1,2).

The definitions of the mass, molar, and volume average bulk velocities are given in Table 1 along with selected mass and molar flux expressions related to each of the specified reference velocities for a binary system of components A and B. The mutual diffusion coefficient D_{AB} is the diffusivity of component A and B in the mixture as defined below. The mutual diffusion coefficients appearing in Table 1 are identical in all of the expressions and $D_{AB} = D_{BA}$.

Additional discussion of these definitions and relationships between the different reference frames and fluxes are discussed in detail elsewhere (3,4). In principle, any reference frame for analysis may be selected; however, a proper choice can reduce the mathematical difficulties. For example, in a one-dimensional diffusion process within fixed boundaries, where ideal mixing of components is a reasonable approximation, selecting the volume average frame of reference is wise because

Table 1. Average Velocities and Forms of Fick's First Law for Binary Diffusion[a]

Average velocity	Definition of average velocity	Form of Fick's first law[b]
Mass average	$v = \omega_A v_A + \omega_B v_B$	$j_i = -\rho D_{AB} \nabla\omega_i = \rho_i(v_i - v)$
Molar average	$v^* = x_A v_A + x_B v_B$	$j_i^* = -M_A C D_{AB} \nabla x_A = C_i(v_i - v^*)$
Volume average	$v^\blacklozenge = \rho_A v_A V_A/M_A + \rho_B v_B V_B/M_B$	$j_i^\blacklozenge = -D_{AB} \nabla \rho_i = \rho_i(v_i - v^\blacklozenge)$

[a] ω_i and ρ_i refer to the mass fraction and mass density of component i, respectively; ρ refers to the total solution mass density, and V_i and M_i are the molar volume and molecular weight of component i, respectively. The velocity of component i, v_i, represents the average velocity of component i relative to fixed coordinates due to both bulk and true diffusive movement.

[b] j_i and $j_i^\blacklozenge$ are the mass fluxes of the component i relative to the mass average and volume average velocities, respectively, and J_i^* is the molar flux relative to the molar average velocity.

the volume average bulk velocity as defined above is zero, and hence the fluxes viewed from both a fixed reference frame and a reference frame moving at the local volume average velocity are identical. In this case the fundamental differential equation of one-dimensional diffusion in an isotropic medium reduces to

$$\frac{\partial \rho_A}{\partial t} = \frac{\partial}{\partial z}\left(D_{AB}\frac{\partial \rho_A}{\partial z}\right) \tag{1}$$

Documented solutions for equation 1 exist for a limited number of complex concentration-dependent diffusion coefficients and boundary conditions (5).

Alternatively, for steady-state analysis involving a case with component B replaced by P, for polymer, a static reference frame and the mass average velocity as a reference velocity may be selected. The mass flux of component A (penetrant) relative to the fixed reference frame is given in general by

$$n_A = -\rho D_{AP}\frac{\partial \omega_A}{\partial z} + \omega_A(n_A + n_P) \tag{2a}$$

where n_A is the total mass flux of A relative to a fixed reference coordinate system, the first term on the right is the flux of A relative to the mass average velocity, and the last term is the flux of A due to bulk flow of fluid relative to the fixed coordinate system. However, since $n_P = 0$ in this case (since $v_P = 0$ for the membrane polymer relative to the fixed reference frame at steady state), the general expression for n_A simplifies to

$$n_A = \frac{-\rho D_{AP}}{(1-\omega_A)}\frac{\partial \omega_A}{\partial z} \tag{2b}$$

The $1/(1 - \omega_A)$ term is commonly referred to as the *frame of reference term*. For many cases of importance in polymeric systems such as in gas permeation, ω_A is relatively small, and the $1/(1 - \omega_A)$ factor can safely be neglected so that the flux relative to fixed coordinates is equal to the flux relative to moving coordinates. Even for intermediate concentrations ($0.1 < \omega_A < 0.5$), this factor may often be of second-order importance compared to difficulties in accurately determining the mutual diffusion coefficient due to strong concentration dependencies. However, not accounting for the factor $1/(1 - \omega_A)$ can lead to very significant errors in flux calculations in highly swollen systems (eg, 90–95% solvent), even if the mutual diffusion coefficient is accurately determined (6).

Mutual Diffusion Coefficients. A better appreciation of the separation of bulk and true diffusive fluxes and the significance of the mutual diffusion coefficient D_{AP} is useful prior to considering factors that determine this coefficient. Consider, for example, the transient problem of a block of polymer placed in contact with an external solvent (penetrant) phase. When a small penetrant moves into a polymer under transient conditions, most of the polymer movement, measured relative to a fixed coordinate, is thought to be due to bulk flow arising from the outward swelling of polymer segments into the region that was occupied previously by the external solvent phase (5). Because of its intrinsically high mobility, the penetrant (solvent) tends to interpose itself between the polymer segments

and invade the domain initially occupied solely by the polymer, thereby acting as the prime mover for the mixing process.

The initial invasion of the solvent effectively induces a local swelling stress. The polymer sample responds to this swelling stress and moves in a direction opposite to the invading solvent flux. This backward bulk motion thereby carries entrained solvent molecules against the direction of the simple concentration-driven diffusive flux. Unlike the steady-state membrane case, it is clearly not acceptable to assume the mass flux of polymer is zero in this situation, and some relationship between n_A and n_P must be defined. This issue becomes important for cases involving the interaction of strong swelling solvents with glassy polymers in transient sorption processes. Also in this case, a very strong concentration dependence of D_{AP} may exist, in some cases approaching a step function. In these situations, the "polymer fixed" frame of reference is often used for mathematical convenience. In this reference frame, D_{AP} is defined relative to the penetrant concentration in the unswollen polymer. On the other hand, if the polymer was not assumed to be fixed, D_{AP} would be defined relative to the concentration in the swollen polymer. D_{AP} for these two reference frames are not necessarily equal; however, diffusivities in different reference frames can be readily interconverted. A more thorough treatment of this subject is given in References 5 and 7.

However, for most cases involving gases and even low sorbing vapors or liquids, swelling of the polymer and non-Fickian complications are minimal. In these situations, solutions to equation 1, unconfused by bulk flow, provide an adequate description of the process and allow estimation of the mutual diffusion coefficient. In such cases with a constant diffusion coefficient, standard solutions of equation 1 for M_t, the amount of material sorbed (or desorbed) at time t relative to M_∞, the amount of material sorbed (or desorbed) at infinite time, can be used for this estimation of the mutual diffusion coefficient. If the initial and final concentrations in the sample of thickness ℓ are uniform and the external penetrant activity is held constant, two mathematically equivalent solutions to equation 1 are given (5):

$$\frac{M_t}{M_\infty} = 4\left[\frac{D_{AP}t}{\ell^2}\right]^{0.5}\left\{\frac{1}{\pi^{0.5}} + 2\sum_{n=1}^{\infty}(-1)^n \text{ ierfc}\left[\frac{n\ell}{2(D_{AP}t)^{0.5}}\right]\right\} \tag{3a}$$

$$\frac{M_t}{M_\infty} = 1 - \sum_{n=0}^{\infty}\frac{8}{(2n+1)^2\pi^2}\exp\left[-(2n+1)^2\pi^2\frac{D_{AP}t}{\ell^2}\right] \tag{3b}$$

On the one hand, equation 3a is generally referred to as the *short time solution* because good accuracy is achieved for values of $M_t/M_\infty \leq 0.6$ even if the infinite summation term is neglected. On the other, equation 3b is referred to as the *long time solution* because good accuracy is achieved for values of $M_t/M_\infty \geq 0.6$ if only the first term in the summation is used.

In cases where there are significant, but not extreme, concentration dependencies of the diffusion coefficient (changes in D_{AP} of up to 50–100% over the course of an experiment), an average coefficient can be used in equations 1, 2, and 3 with little loss in accuracy. For such cases, the average diffusion coefficient $\bar{D}$ is

defined as follows:

$$\bar{D} = \frac{\int_{(\omega_A)_0}^{(\omega_A)_\infty} D_{AP} d\omega_A}{(\omega_A)_\infty - (\omega_A)_0} \tag{4}$$

where $(\omega_A)_0$ and $(\omega_A)_\infty$ refer to the uniform penetrant mass fractions in the polymer at the beginning and at the end of the sorption run, respectively.

The experiment could also be run over a narrow concentration interval to determine the concentration dependence of $\bar{D}$. In this latter case, the average diffusion coefficients determined from half-time analysis are good approximations for D_{AP} over that particular concentration interval. $\bar{D}$ is calculated simply by rearrangement of equation 3a by neglecting the infinite summation terms with $M_t/M_\infty = 0.5$:

$$\bar{D} = 0.0492 \frac{\ell^2}{t_{1/2}} \tag{5}$$

where $t_{1/2}$ is the time required to achieve one-half of the mass uptake that ultimately occurs at equilibrium for the interval sorption experiment. Equation 5 applies for experiments in which the sample has two exposed faces. For a single-sided exposure the coefficient in equation 5 is replaced by 0.1968. Alternate half-time expressions for different geometries such as cylinders and spheres have been presented (5). To analyze the later stages of sorption using an average diffusion coefficient $\bar{D}$, equation 3b indicates that a plot of $\ln(1 - M_t/M_\infty)$ vs t gives a straight line with a slope equal to $\pi^2\bar{D}^2/\ell^2$.

Self vs Mutual Diffusion Coefficients. The self-diffusion coefficient $D_A{}^*$ is measured by observing the rate of diffusion of a small amount of radioactively-tagged component A in a system composed of a uniform chemical composition of untagged components A and B. Because of the essentially identical physical natures of the tagged and untagged penetrant, observing the process of interdiffusional exchange of the tagged and untagged molecules allows measurement of the true mobility of the tagged molecules with respect to the stationary solution of known concentration. By varying the concentration of A and B in the presence of a small amount of tagged component A, the concentration dependence of the diffusion coefficient of the tagged molecule can be obtained, uncomplicated by bulk-flow considerations, namely

$$D_A^* = RT\mathcal{M}_A = \frac{RT}{\zeta_A} \tag{6}$$

where $\mathcal{M}_A$ is the mobility of A, ζ_A is the molar friction coefficient, the product of the effective viscosity of the medium and the effective diameter of the penetrant (8).

In addition to pure mobility considerations, thermodynamic factors enter in determining the concentration dependence of the mutual diffusion coefficient. A single mutual diffusion coefficient exists for a given binary pair under fixed local

conditions (8). For molecules with similar sizes, shapes, and interaction potentials, the ratio of the self-diffusion coefficients of two components are related to the inverse ratio of the molar volumes, ie, $D_A{}^*/D_B{}^* = V_B/V_A$ (8). Under these conditions the individual self-diffusion coefficients may be related to the corresponding mutual diffusion coefficient D_{AB} in terms of the mole fractions of the two components and the partial derivative of the activity vs mole fraction relationship for the penetrant in the polymer at the local mole fraction of interest:

$$D_{AB} = \left(\frac{\partial \ln a_A}{\partial \ln x_A}\right)_{T,p} \left[D_B^* x_A + D_A^* x_B\right] \tag{7}$$

The activity derivative can be readily evaluated from sorption vs activity measurements. The subscripts T and p, indicating which variables are held constant, will be dropped for simplicity in the subsequent equations. Equation 7 was given earlier (4) using classical diffusion analysis for systems in which there is negligible volume change of mixing.

Although the inverse molar volume ratio relationship suggested above is probably adequate for small molecules with similar sizes, shapes, and interaction potentials, it is not clear that it applies in all cases where marked differences exist in the relative sizes of components A and B. A weight fraction based weighting of the respective $D_i{}^*$ values is probably more general. Except in the range of extremely high solvent fractions, the mobility, and hence the self-diffusion coefficient of a polymer in the presence of a low molecular weight solvent, is many orders of magnitude lower than that of the solvent. Therefore, with the reasonable approximation that $D_P{}^* = D_B{}^* \approx 0$, equation 7 can be expressed in terms of the mass fraction of component A as follows:

$$D_{AP} = D_A^* \omega_P \left(\frac{\partial \ln a_A}{\partial \ln \omega_A}\right) = D_A^* (1 - \omega_A)\left(\frac{\partial \ln a_A}{\partial \ln \omega_A}\right) \tag{8}$$

Diffusion Coefficients in Multicomponent Systems. The value of the diffusion coefficient of a species in a binary system is often not the same as the value in a multicomponent system. The diffusion coefficients can be modified in multicomponent systems as a result of added frictional forces at the atomistic scale. The multiple diffusing species interact in various complex ways that can be described using equation 9, which is derived from the so-called Stefan–Maxwell relations (4):

$$D_{im} = -\frac{n_i - x_i \sum_{j=1}^{n} n_j}{\sum_{j=1}^{n} \frac{x_i n_j - x_j n_i}{D_{ij}}} \tag{9}$$

where D_{im} is the diffusion coefficient of species "i" in the mixture, D_{ij} are the binary diffusion coefficients, x_i is the mole fraction of species "i", and n_i is the molar flux of "i". The diffusion coefficients calculated from equation 9 are used in a generalized

form of equation 2a for multicomponent diffusion:

$$n_i = -cD_{im}\nabla x_i + x_i \sum_{j=1}^{n} n_j \tag{10}$$

More detailed treatments of multicomponent diffusion are available (4,9).

Solution-Diffusion Mechanism

Small molecule transport through nonporous polymers proceeds by the solution-diffusion mechanism. This a three-step mechanism where penetrant molecules (*1*). sorb into the polymer phase from a high activity external gas or liquid phase, (*2*). diffuse across the polymer driven by a chemical potential gradient, and (*3*). desorb from the polymer phase to a low activity gas or liquid external phase. While these three general steps of the solution-diffusion mechanism are agreed upon, the specifics of sorption into and out of the polymer phase and diffusion across it are still active areas of research. As will be seen in later sections of this article, there are many ways to conceptualize the sorption and diffusion processes.

Regardless of how one conceptualizes the diffusion process, the solution-diffusion mechanism states that the flux through the polymer is proportional to a chemical potential gradient. If a chemical potential gradient does not exist, in the absence of an imposed bulk flow, no net transport of penetrant occurs through the polymer. This proportionality is stated mathematically as

$$J_A = -L\frac{\partial \mu_A}{\partial z} \tag{11}$$

where J_A is the flux of A through the polymer, μ_A is the chemical potential of penetrant A in the polymer phase, and L is the direct phenomenological transport coefficient in irreversible thermodynamics terminology. C is the concentration of A sorbed in the polymer, and $\mathcal{M}_A$, once again, is the mobility of A.

In the absence of electromotive forces, the chemical potential of a dissolved penetrant in the polymer phase is given by

$$\mu_A = \mu_A^0 + RT\ln(\gamma_A C_A) + V_A\left(p - p_A^0\right) \tag{12}$$

where ${\mu_A}^0$ is the chemical potential of the pure penetrant at the reference pressure ${p_A}^0$. Moreover, γ_A is the activity coefficient at concentration C_A, and the partial molar volume of the penetrant is V_A. The reference pressure is usually set as the pure component vapor pressure. With the knowledge that a chemical potential gradient must exist through the polymer, from inspection of equation 12 one can imagine three possible ways to affect such a gradient: (*1*) a concentration gradient across the polymer, (*2*) a pressure gradient across the polymer, or (*3*) the coexistence of both pressure and concentration gradients across the polymer. In an elegant series of articles, Paul and co-workers showed that a concentration gradient solely affects the gradient in chemical potential. The fact that no

pressure gradient exists through the membrane interior can be proved using a simple mechanical argument. In the common laboratory setup for gas separations, the membrane is supported on the low pressure side by a porous metal support. If a pressure is exerted on the upstream side of the membrane by the gas, the metal support must exert an equal and opposite pressure on the downstream side of the membrane. For this reason, the pressure inside the membrane is equal to the upstream pressure (6). By using a constant pressure through the membrane, Paul was able to rationalize the observed dependence of flux on the external pressure difference for both hydraulic permeation and pervaporation systems (10). Furthermore, Paul conducted a series of experiments using a composite membrane consisting of a stack of three to four rubber membranes to measure the concentration gradient through the membrane. It was shown that the concentration gradient determined from these measurements alone accounted for the entire chemical potential gradient (11). This result excluded the possibility of a pressure gradient inside the membrane for solution-diffusion transport processes.

With this knowledge of the physical situation, it is an easy exercise to derive Fick's Law from the more general statement of equation 11.

$$J = -L\frac{\partial \mu_A}{\partial z} = -L\frac{\partial \mu_A}{\partial C_A}\frac{\partial C_A}{\partial z} = -D_{AB}\frac{\partial C_A}{\partial z} \tag{13}$$

Since $D_{AB} = (D_A{}^* C_A/RT)(\partial \mu_A/\partial C_A)$ (5), the phenomenological coefficient L can be related back to the underlying penetrant mobility.

$$L = \frac{D_A^* C_A}{RT} = \frac{1}{\zeta_A}C_A = \mathcal{M}_A C_A \tag{14}$$

Amorphous Rubbery Polymers

Gases and Low Activity Vapors. At low concentration ($\omega_A \to 0$) and in systems where Henry's law applies ($\partial \ln a_A/\partial \ln \omega_A \to 1$), D_{AB} approaches the infinite-dilution self-diffusion coefficient $(D_A{}^*)^0$. Therefore, the mutual diffusion coefficient is a good estimator of the infinite-dilution self-diffusion coefficient for most gases in polymers at atmospheric pressure and below. Even at relatively high pressures with condensable gases and low activity vapors such as CO_2, SO_2 and propane, deviations from Henry's law can generally be described in terms of the Flory–Huggins isotherm or a similar simple expression. Therefore, self-diffusion coefficients, and thus the mobility of the penetrant, can be calculated using equations 5 and 6 or by using permeation data in conjunction with equilibrium sorption data to determine ($\partial \ln a_A/\partial \ln \omega_A$) at the appropriate ω_A value.

Rubbers are essentially high molecular weight liquids with the ability to adjust their segmental configurations rapidly over significant distances (>0.5–1 nm) and local volumes (12). Nevertheless, the rotational and translational motions of sorbed penetrants are rapid compared to the motions of the segments of the polymer (13,14). The limiting step in diffusion of such small molecules through the

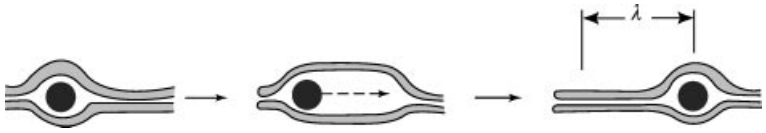

Fig. 1. Generation of a gap for the penetrant with subsequent collapse of the volume that previously housed the penetrant, emphasizing the mutual nature of the binary diffusion process.

rubber involves the generation of a sufficiently large gap for the penetrant to move into, with subsequent collapse of the sorbed cage that previously housed the penetrant (Fig. 1). This description emphasizes the mutual nature of the binary diffusion process, since both the penetrant and surrounding polymer segments tend to undergo a minute translation in their positions as a result of the event. Given the overall mass of the polymer and the small fraction of the total chain involved in a primitive diffusion jump by a small penetrant, this change is miniscule, but nonzero, even for the polymer.

In typical polyolefins, the most common moving segment is a crankshaft composed of four to five backbone carbon atoms (Fig. 2). For diene and other hydrocarbon polymers, similar cooperative motions involving several repeat units are also probably the most common types of motions observed over time scales of importance to diffusion. As expected, for penetrants such as gases that are clearly smaller than the size of the most common moving segment of the polymer, the infinite-dilution diffusion coefficient tends to show a steady drop with increasing penetrant size (Fig. 3). The tendency for diffusion coefficients of larger penetrants to approach an asymptotic plateau has been discussed (15). Branched penetrants tend to approach a lower, but still similar, asymptotic limit in a given medium. This effect suggests that larger penetrants are capable of moving in a somewhat segmental fashion as does the polymer itself. In this case, the asymptotic limit of the linear penetrants in Figure 3 presumably reflects the mobility of the more or

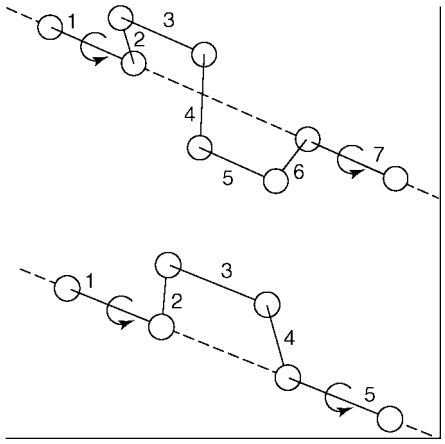

Fig. 2. The crankshaft motion requiring the simultaneous rotation of several sequential $-CH_2-$ moieties about bonds 1 and 7 or 1 and 5.

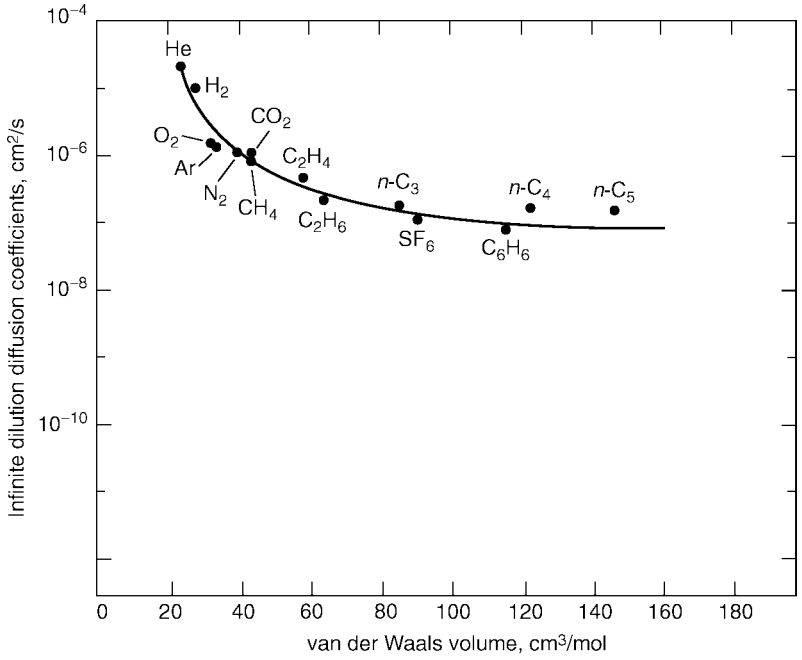

Fig. 3. Diffusion coefficients for a variety of penetrants in natural rubber at 25°C. n-C_3,n-C_4, and n-C_5 designate straight chain alkanes.

less freely orienting segments of the polymer that are themselves undergoing a self-diffusion process. Therefore, while the self-diffusion coefficient of the polymer center of mass may be orders of magnitude lower than that of intermediate-sized penetrants, segmental mobility in the polymer is still quite high. Not surprisingly, the asymptotic mobilities of penetrants in glassy polymers are orders of magnitude lower than those in the typical rubbery polymers.

Concerted movements of several adjacent segments of chain comprising the sorbed cage of a simple gaseous penetrant are believed to provide the source of the penetrant-scale hole needed for diffusion. Lennard–Jones collision diameters (σ), van der Waals volumes (b), and actual measured values of the partial molar volumes of various gases in polydimethylsiloxane (PDMS) (16) are shown in Table 2. These partial molar volumes in PDMS are close to the van der Waals volumes, very close to infinite-dilution partial molar volumes in several low molecular weight liquids (17), and are measures of the volume of the cage in which the sorbed penetrant resides at equilibrium. The occupied volume is calculated by viewing the molecule acting as a freely rotating sphere of diameter equivalent to the Lennard–Jones diameter σ. Based on these data, it is clear that only a fraction of the actual equilibrium cage volume is occupied and the remainder is in a sense "free volume" available to be shared with the neighboring polymer segments to facilitate the mutual diffusion process.

Estimates of the amounts of total free volume required for a diffusional jump of several gaseous penetrants in a copolymer of poly(vinyl chloride) and poly(vinyl acetate) have been made (18) (Table 2) (Fig. 4). Although the data in Table 2 are

Table 2. Various Molecular Volumes for Gaseous Penetrants

Volume measurement	He	N_2	O_2	CH_4	C_2H_4	CO_2
van der Waals volume b, nm^3	0.0396	0.0642	0.0529	0.0709	0.0856	0.0711
Lennard–Jones diameter σ, nm	0.258	0.368	0.343	0.382	0.422	0.400
Lennard–Jones occupied volume, nm^3	0.00899	0.0261	0.0211	0.0292	0.0393	0.0335
Partial molar volume[a] in silicone rubber (PDMS), nm^3		0.0549		0.0792	0.0940	0.0767
Free volume in sorbed state[b], nm^3		0.0288		0.0500	0.0547	0.0432
Required free volume for 0.075 diffusional jump in PVC–PVA copolymer[c], nm^3			0.299			0.690

[a] Experimental (15).
[b] Partial molar volume minus occupied volume.
[c] Ref. 17

for two different polymers, for an order of magnitude analysis they can be taken as representative of movement in typical rubbery polymers. The required free volumes for diffusional jumps are significantly greater than the penetrant volumes. Therefore, most of the free volume involved in a given jump must be supplied by a momentary fluctuation in the rubbery polymer segmental position due to a local thermal fluctuation, rather than being locally present in the equilibrium sorbed cage. This fact can be treated in several ways, eg, via Activated State Theory or Free-Volume Theory.

Activated State Theory. The diffusion process by which small molecules intermingle with a polymer can be considered a random walk of the penetrant among the segments of the polymer. Consistent with this qualitative description, the activated state theory assumes that holes covering a spectrum of different volumes and involving segments of several polymer molecules are continuously formed and destroyed because of thermal fluctuations. The rate of diffusion depends on the concentration of transient holes that are sufficiently large to accept diffusing molecules. Assuming a Boltzmann distribution, the concentration of a given size of holes decreases exponentially with the energy associated with its formation. The temperature dependence of the diffusion coefficient for the activated state theory can be expressed as

$$D = D_0 \exp\left(\frac{-\Delta E_d}{RT}\right) \tag{15a}$$

where D_0 is the preexponential factor and ΔE_d is the energy of activation for diffusion.

The indication by equation 15a that $\ln(D)$ is linearly dependent on $1/T$ has been verified for many systems well above the glass-transition temperature T_g

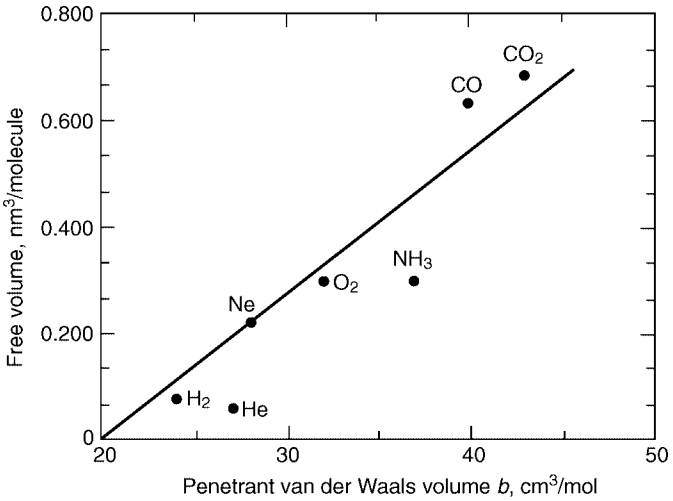

Fig. 4. Estimated required free volume for a diffusional jump for various penetrants in PVC–PVA copolymer (17).

(ie, $T > T_g > T_g + 100$ K). For penetrants smaller than the size of the primary moving segment of the polymer, the size of the molecule generally determines both the size of the required hole and the activation energy required for diffusion, as shown in Figure 5 (15). This tendency for the activation energy of diffusion for the larger penetrants to approach an asymptotic value similar to that of the activation energy of viscous flow for the uncross-linked polymer had been noted (15). This asymptotic behavior is thought to represent a similarity between the mobilities of large penetrants and the primitive segmental mobility of the polymer that participates in viscous flow (19).

The Eyring theory of rate processes (20) has been used as the basis of most theories for D_0:

$$D_0 = e\lambda^2 kT/h \exp\left(\frac{\Delta S^*}{R}\right) \tag{15b}$$

where ΔS^* is the entropy of activation and λ is the average jump length. For penetrants smaller than the average size of the jumping unit of the polymer, both the preexponential factor and activation energy increase with the size of the penetrant molecule. The actual diffusion coefficient of the penetrant decreases with penetrant size since the exponential weighting of E_d dominates the product in equation 15a.

Molecular models of the diffusion process help clarify the meaning of ΔE_d. A molecular rationalization of the value of ΔE_d in terms of the product of cohesive energy density (CED) and the volume of 1 mol of cylindrical cavities having a length λ and a diameter equal to that of a diffusing molecule, d_A, has been suggested (21). With this assumption,

$$\Delta E_d = \text{CED}\, d_A^2 \pi\lambda/4 \tag{16}$$

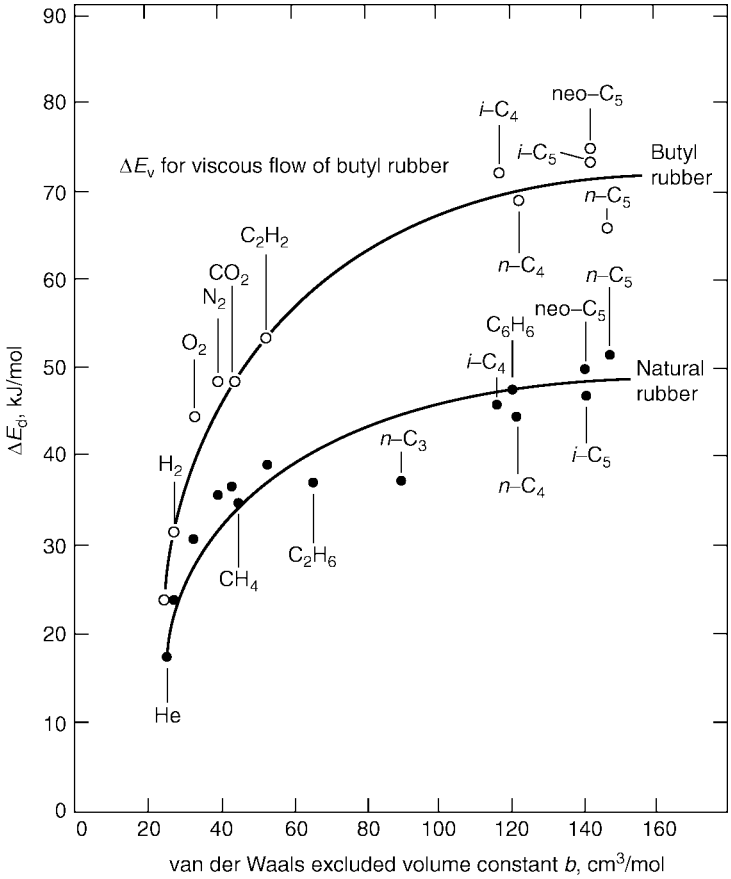

Fig. 5. Activation energy required for diffusion for various penetrants. To convert kJ/mol to kcal/mol, divide by 4.184.

An apparent diffusional jump length using such a cylindrical activation volume can be calculated. Assuming the total free volume for a diffusional jump to be equal to the activation volume, the value 0.69 nm^3 per molecule for CO_2 in Table 2 can be used to calculate $\lambda = 8.4$ nm. This seems physically unrealistic. Moreover, a large jump length (1.1 nm) would still be calculated if this same amount of free volume associated with the diffusion jump for CO_2 were converted to a spherical volume fluctuation. Even this length seems too high, since all of the activated volume may not be directly usable for a linear translation of position. Furthermore, this conceptualization of the activation energy is not in agreement with experimentally observed behaviors. Experimentally determined values of the activation energy extrapolate to zero at some value of the penetrant molecular diameter d_A greater than zero, and correlations of E_d and d_A obtained experimentally are not of the simple proportionality expected from equation 16.

To account for the experimentally observed behavior of the activation energy, a more refined picture of the diffusion jump process must be introduced. Instead of Figure 1, it may be preferable to visualize the activated volume as a bulge in a tube

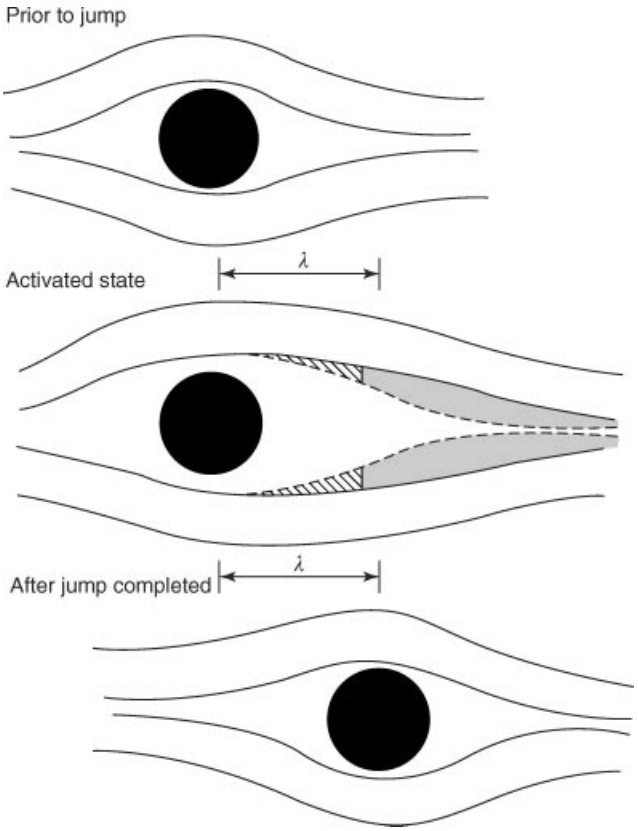

Fig. 6. Activated volume as a bulge in a tube with the openings of the bulge smaller than the penetrant diameter. ▧, Directly usable fraction of activation volume; ▩, not directly usable fraction of activation volume.

with the openings of the bulge smaller than the penetrant diameter (Fig. 6) (22). In this case, on the average, the penetrant can only execute its $\pm\lambda$ diffusional jump from the center of the bulge to one or the other side, even though the entire free volume must exist to accommodate the fact that polymer chains are not infinitely flexible, especially on the short time scale of a diffusional jump. In other words, the chains must have a considerable transition length over which the segments reapproach their original packing density; however, the volume associated with these regions is not directly usable by the penetrant in terms of $\pm\lambda$ translations of its center of mass.

These ideas were formalized mathematically by Brandt (23), who assumed that the activation energy was composed of two contributions: (*1*) an energy E_α associated with bending two initially straight chain segments away from each other to accept the penetrant molecule, and (*2*). an energy E_β needed to overcome repulsion of the bent chain segments by neighboring chains. The intermolecular energy E_α is calculated on the basis of the potential energy barrier to chain rotation, ψ_0, a measure of chain stiffness. The repulsive component E_β is calculated analogously to equation 16; however, the internal polymer pressure p_I is used instead of the

cohesive energy density. Using this framework, Brandt calculated the activation energy as follows:

$$\Delta E_d = E_\alpha + E_\beta = 18\psi_0 b_d (d_A - d_S)^2 / a_d^3 + N_A p_I d_p a_d (d_A - d_S)/2 \quad (17)$$

where N_A is Avogadro's number, b_d is the length of a backbone bond projected onto the chain axis, a_d is the length of the bent chain segments, and d_s is the initial chain spacing prior to penetrant inclusion. This conceptualization of the activation energy accounts for many of the shortcomings of equation 16. The activation energy is equal to zero when $d_A \leq d_s$, which is in accord with the nonzero extrapolations of ΔE_d versus d_A from experimental data. It is also apparent from inspection of equation 17 predicts that no simple relation should exist between the activation energy and the penetrant molecular diameter. Furthermore, equation 17 predicts that the dependence of the activation energy on the penetrant molecular diameter is weaker for flexible chain polymers, where ψ_0 is small. This model of the activation energy is the basis for more complex treatments by Pace and Daytner (24), and Dibenedetto and Paul (25).

Free-Volume Theories. The basic idea of the free-volume theories is that the mobilities of the polymer segments and the penetrant molecules in a polymer–penetrant mixture are primarily determined by the amount of free volume in the system. As originally proposed (26),

$$\mathcal{M}_A = A_d \exp\left[\frac{-B_d}{v_f}\right] \quad (18a)$$

where $\mathcal{M}_A$ is the mobility of the penetrant, v_f is the average locally available fractional free volume of the system, and A_d and B_d are empirical free-volume parameters that are assumed to be independent of penetrant concentration and temperature. The parameter A_d depends on the size and kinetic velocity of the penetrant. The parameter B_d is equivalent to the critical hole free volume necessary for a penetrant to make a diffusive jump (13). This expression was modified by arguing that crystalline material reduces the free volume in direct proportion to the amount of crystalline material present (27):

$$\mathcal{M}_A = A_d \exp\left(\frac{-B_d}{\Phi_a v_f}\right) \quad (18b)$$

where Φ_a is the amorphous volume fraction of the penetrant free polymer at zero pressure and the temperature of the system. Alternate treatments of the effects of crystallinity will be considered later in terms of a chain immobilization factor (see eq. 45).

According to free-volume theories, the diffusion coefficients of organic vapors in polymers are strongly concentration-dependent, because mobilities are extremely sensitive to changes in the average free volume of the system. A small penetrant that is unconstrained on two sides by covalently bonded neighbors introduces much more free volume into the polymer–penetrant mixture than a polymer segment of equivalent size. Increased penetrant concentration thereby alters the effective viscosity of the medium, and a significant increase in the penetrant

mobility results. The free-volume approach is simple and has evolved (28,29) into several readily useful forms. Its primary drawback lies in the difficulty of providing a precise physical definition for the parameter defined as the free volume.

The native polymer, totally devoid of penetrant, still possesses a certain distribution of free-volume packets, which wander spontaneously and randomly through the polymer. Intuitively, proponents of free-volume theory argue that a penetrant can execute a diffusive jump when a free-volume element greater than or equal to a critical size presents itself to the penetrant. In fact, the polymer chains may also execute a self-diffusive jump when a packet of sufficient size presents itself to a segment. This is the mechanism that causes the slow interdiffusion of polymer chains.

Increasing system temperature causes volume dilation, resulting in increased free volume. Thus the diffusion coefficient increases with temperature. The free-volume fraction v_f may be represented as a linear addition of several variables (28,29):

$$v_f(T,p,\varphi_1) = v_{fs}(T_s,p_s,0) + \alpha(T - T_s) - \beta(p - p_s) + \gamma\varphi_A \tag{19}$$

where v_{fs} is the fractional free volume of the pure, penetrant-free, amorphous, rubbery polymer at some reference temperature T_s, usually the glass-transition temperature, and reference pressure p_s, usually 101.3 kPa (1 atm). The penetrant volume fraction is Φ_A and the coefficients coefficients α, β, and γ are positive constants, the values of which are evaluated empirically. These coefficients characterize the effectiveness of temperature, pressure, and penetrant concentration, respectively, for changing the free volume in the amorphous phase:

$$\alpha = \left(\frac{\partial v_f}{\partial T}\right)_s \beta = \left(\frac{\partial v_f}{\partial p}\right)_s \gamma = \left(\frac{\partial v_f}{\partial \varphi_1}\right)_s \tag{20}$$

where s denotes some reference state. The free-volume thermal-expansion coefficient α can be estimated as the difference between the thermal expansion coefficient for an amorphous material above and below its glass-transition temperature. The parameter β can be related to the conventional compressibility coefficient β' by (30)

$$\frac{\beta}{1 - v_f^*} = \beta' = -\frac{1}{V}\left(\frac{\partial V}{\partial p}\right)_T \tag{21}$$

where v^*_f is the fractional free volume of the pure polymer at zero pressure. If the glass-transition temperature is used as the reference temperature, v^*_f is given by

$$v_f^* = v_{fs} + \alpha(T - T_g) + \beta p_s \tag{22}$$

Combination of equations 18 and 19 and use of the definition of mobility leads to the following expression for the polymer self-diffusion coefficient, when

the reference temperature is taken to be the glass-transition temperature:

$$D_A^* = A_d \exp\left(\frac{-B_d}{\Phi_a\{v_{fs} + \alpha[T - T_g] - \beta[p - p_s] + \gamma\varphi_A\}}\right) \tag{23}$$

Thus the self-diffusion coefficient D^*_A and its variation with concentration and temperature can be estimated if A_d, B_d, and γ are known. A correlation for γ as a function of the fractional increase in volume caused by a penetrant molecule has been developed (29). In the absence of data for a given polymer, v_{fs} and α can be approximated as the universal values of 0.025 and 4.8×10^{-4}/°C, respectively, in accordance with the theory of Williams, Landel, and Ferry (31) that interprets the glass-transition point to be an isofree volume state. This approximation is valid in the temperature range from T_g to 100°C above T_g.

In principle, each of the coefficients in equation 22 can be evaluated independently by observing the effects on $D_A{}^*$ over a sufficiently wide range of temperatures, external hydrostatic pressures, and sorbed penetrant concentrations. Hydrostatic effects on β can be decoupled from penetrant sorptive effects on γ by using a very low sorbing penetrant, such as helium in the presence of a fixed partial pressure of the penetrant of interest. On the one hand, hydrostatic pressure is expected to have a rather small effect on $D_A{}^*$ since solid polymers are only slightly compressible. On the other, increases in temperature and sorbed penetrant concentration cause large increases in the free-volume fraction v_f and in the self-diffusion coefficient $D_A{}^*$.

The permeability P is an important transport coefficient that represents the normalized molar flux N_A across a polymer film of thickness ℓ with a partial pressure driving force Δp at steady state:

$$P = \frac{N_A}{\Delta p/\ell} \tag{24}$$

Under steady-state conditions, n_P in equation 2a is zero, and for the low sorbed mass fractions typical of gases in polymers, an expression for $N_A = n_A/M_A$ can be substituted to yield

$$P = \frac{-\rho D_{AP}\ell}{M_A \Delta p}\frac{\partial \omega_A}{\partial z} \tag{25a}$$

where M_A is the molecular weight of component A. Integration between the upstream and downstream conditions gives

$$P = \frac{-1}{p_2 - p_1}\int_{\omega_{A1}}^{\omega_{A2}} \frac{-\rho D_{AP}(\omega)\, d\omega_A}{M_A} \tag{25b}$$

where ω_{A2} and ω_{A1} are the equilibrium penetrant weight fractions in the polymer at upstream (p_2) and downstream (p_2) faces. At low concentrations, D_{AP} reduces

to D_A^*. Transformation of equation 25a from mass fractions to volume fractions gives

$$P = \frac{-1}{p_2 - p_1} \int_{\varphi_{A1}}^{\varphi_{A2}} \frac{-\rho D_A^*}{M_A} \frac{d\omega_A}{d\varphi_A} d\varphi_A \tag{25c}$$

where $d\omega_A/d\varphi_A$ can be evaluated using the specific volumes of the polymer and penetrant. Substitution for D_A^* from equation 22 for the case of negligible downstream pressure yields the following expressions (32) when Henry's law applies ($\varphi_{A2} = k_A p_2$) at the upstream membrane face:

$$\ln P = \ln[RTA_d k_A] - \frac{B_d}{\Phi_a v_f^*} + \frac{p_2 B_d}{\Phi_a (v_f^*)^2}\left[-\beta + \frac{\lambda k_A}{2}\left(1 + \frac{2\beta p_2}{v_f^*}\right)\right] \tag{26}$$

Therefore, the free-volume theory permits theoretical plots of permeability as a function of temperature, penetrant pressure, and amorphous volume fraction in the rubbery polymer.

It is worth noting that in a series of articles, Vrentas and Duda (33–36) have introduced and applied a more rigorous free volume theory than the one presented above. In their approach, Vrentas and Duda include an energy factor, E_J, to the preexponential term A_d. This factor accounts for the energy required for a penetrant molecule to jump into an adjacent open hole. The exponential parameter B_d is modified to account for the molar volume of the moving polymer segment. Furthermore, Vrentas and Duda propose that only part of the total free volume is available for diffusion and is denoted by $\hat{V}_{fh}$. This concept of only a fraction of the free volume participating in diffusion is similar to the activation energy model of Brandt (see Fig. 6). The Vrentas and Duda model ultimately leads to a prediction of the thermodynamic diffusion coefficient:

$$D_T = A_{d0} \exp\left(\frac{-E_J}{RT}\right) \exp\left[\gamma_{ov}\left(w_A + \frac{w_P M_A}{M_{PJ}}\right)\frac{\hat{V}_h^*}{\hat{V}_{fh}}\right] \tag{27}$$

where w_A and w_P are mass fractions of the penetrant and polymer, respectively, and M_A and M_{PJ} are the molecular weight of the penetrant and the jumping polymer segment respectively. $\hat{V}_h^*$ is the specific volume of holes of the minimum size required for a diffusive jump. γ_{ov} is a parameter, with a value between 0.5 and 1, originally introduced by Cohen and Turnbull that accounts for the ability of a free volume hole to be available to multiple jumping segments. Although the added sophistication of this model probably captures a more accurate picture of the diffusion process, the accompanying added mathematical complexity has hindered widespread adoption of the model.

Membrane and Barrier Implications. In the case of typical rubbers, crankshaft and other related rotational motions of the repeat units are so large that little difference in diffusion coefficients exists for simple gaseous penetrants, the sizes of which differ by less than a few hundredths of a nanometer. Of course, since permeation is a solution-diffusion process, membranes or selective barriers

do not operate strictly on the basis of size selection. Under a fixed partial pressure driving force for component i, the flux through a material of given thickness ℓ is determined by the permeability, as can be seen by rearrangement of equation 24.

$$N_{\mathrm{i}} = \Delta p_{\mathrm{i}} P_{\mathrm{i}} / \ell \tag{28}$$

The permeability can be expressed as the product of a diffusivity and solubility coefficient:

$$P_{\mathrm{i}} = \bar{D}_{\mathrm{i}} \bar{S}_{\mathrm{i}} \tag{29}$$

The diffusivity and solubility coefficients in the above expression are effective averages applying across a polymer film between its upstream and downstream faces. The presence of other copermeating components can often be neglected for gases and low activity vapors permeating through rubbers (37). The average mutual diffusion coefficient $\bar{D}_i$ is given below for penetrant A in the polymer component P:

$$\bar{D}_{\mathrm{i}} = \frac{\int_{\omega_{\mathrm{A1}}}^{\omega_{\mathrm{A2}}} D_{\mathrm{AP}}\, d\omega_{\mathrm{A}}}{\omega_{\mathrm{A2}} - \omega_{\mathrm{A1}}} \tag{30}$$

When the presence of other components cannot be neglected, the system can still be treated approximately by considering the membrane in the presence of the additional component to be a new effective medium; however, this is at best a rough approximation since it neglects the bulk-flow contribution and thermodynamic influence of additional components on the flux of component A. Multicomponent thermodynamic issues are beyond the scope of this discussion, but have been treated (38).

The solubility coefficient, $\bar{S}_i$, is found from combination of equations 25b, 29 and 30 as:

$$\bar{S}_i = \frac{C_{i2} - C_{i1}}{p_{i2} - p_{i1}} \tag{31}$$

where C_{i2} and C_{i1} are the concentrations of "i" in the membrane at the upstream and downstream faces, respectively. p_{i1} and p_{i2} are the partial of "A" at the upstream and downstream faces, respectively. Under ideal conditions of fixed upstream pressure and negligible downstream pressure, the $\bar{S}_i$ parameter is equal to the secant slope of the sorption concentration vs pressure isotherm evaluated at the upstream partial pressure p_{i2} of the component

$$\bar{S}_i = \frac{C_i}{p_{i2}} \tag{32}$$

where C_i typically has units of cm^3(STP)/cm^3 polymer, and S_i can be related to the Henry's Law constant k_i in equation 26 for the gas in the polymer using partial molar volumes such as those in Table 2 in a subsequent expression (see eq. 32).

The temperature dependence of solubility coefficients are typically described in terms of van't Hoff expressions shown below (39):

$$\ln\left(\frac{S_i(T_2)}{S_i(T_1)}\right) = -\frac{\Delta H_s}{R}\left[\frac{1}{T_2} - \frac{1}{T_1}\right] \tag{33}$$

Equation 33 only applies when the solubility coefficient is independent of concentration or for solubility coefficients specified at the same concentration. The enthalpies of sorption ΔH_s are typically small and slightly negative (Fig. 7**a**). The solubilities and enthalpies of sorption of different penetrants are determined largely by their critical temperatures or other related measures of tendency to exist in a condensed phase such as normal boiling points or Lennard-Jones potential well depth $\epsilon/\bar{k}$ (Fig. 7**b**) (40).

From the dependence of permeability on both solubility and diffusivity, it is clear that two opposing factors affect the permeability as temperature is increased, namely

$$\ln\left(\frac{P(T_2)}{P(T_1)}\right) = \ln\left(\frac{D(T_2)S(T_2)}{D(T_1)S(T_1)}\right) = -\left[\frac{E_d + \Delta H_s}{R}\right]\left[\frac{1}{T_2} - \frac{1}{T_1}\right] \tag{34}$$

The positive diffusional activation energy is larger in absolute value than the negative ΔH_s, and so the overall permeability increases as temperature increases, but to a lower degree than the diffusion coefficient itself. It should be noted that the use of equation 34 is only strictly valid when the diffusion and solubility coefficients are independent of concentration.

The separation factor or permselectivity between two penetrants A and B, α_{AB}, is important in membrane separation systems. This factor is equal to the ratio of the downstream (permeate) mole fractions of component A relative to component B divided by the ratio of the upstream mole fractions of A relative to B. Under conditions of negligible downstream pressure, the permselectivity is simply equal to the ratio of the permeabilities of components A and B. In addition, since the presence of one component has a negligible effect on the permeability of the other at low pressures in rubbery materials, pure component permeabilities can often be used as good estimates of mixed-gas permeabilities:

$$\alpha_{AB} = \frac{P_A}{P_B} = \left(\frac{x_A}{x_B}\right)_1 \Big/ \left(\frac{x_A}{x_B}\right)_2 = \left(\frac{D_A}{D_B}\right)\left(\frac{S_A}{S_B}\right) \tag{35}$$

The subscripts 1 and 2 refer to downstream and upstream conditions, respectively. The ratio of the two diffusion coefficients is commonly called the diffusivity selectivity of a membrane and the ratio of the two solubilities, the solubility selectivity. A typical range of permeabilities and selectivities achievable with rubbery materials is indicated in Table 3 for several gas pairs of commercial interest. More extensive tabulations are available (41). The presence of polar groups in the polymer molecule generally leads to low diffusivity for penetrants (15); eg, the diffusivity decreases strongly on increasing the nitrile content in a series of

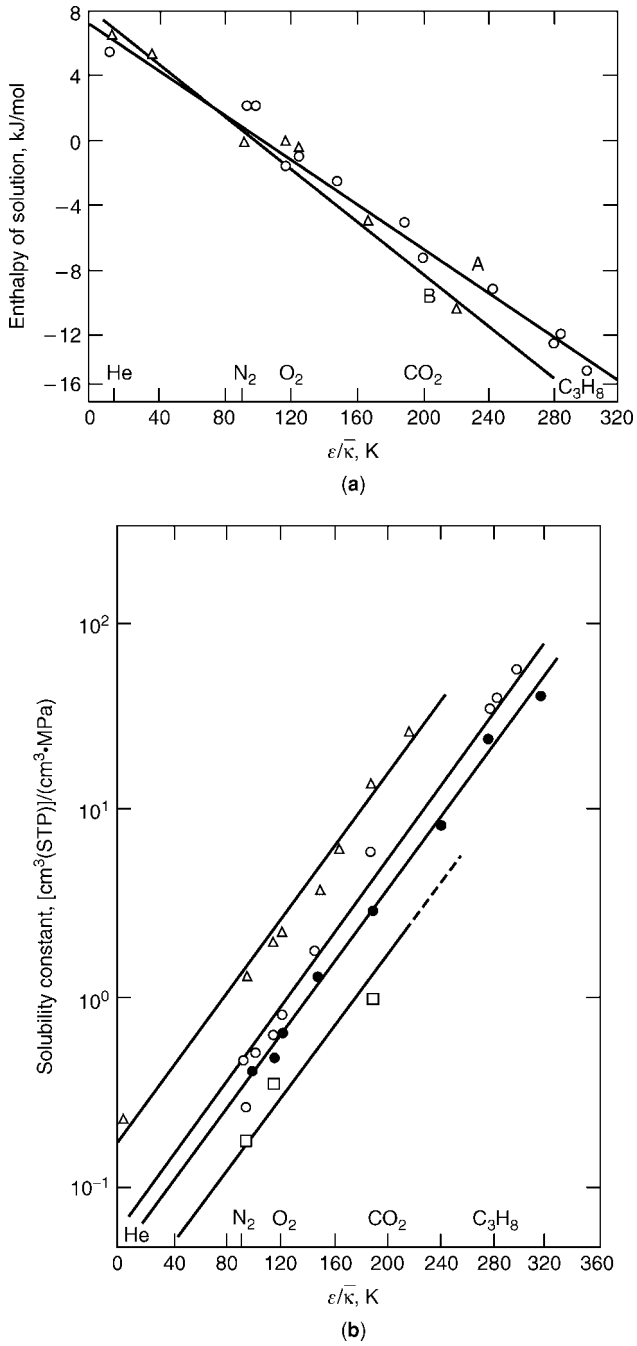

Fig. 7. (**a**) Enthalpies of solution for various gases in elastomers: A, ○, natural rubber; B, △, silicone rubber (30). To convert kJ/mol to kcal/mol, divide by 4.184. (*b*) Correlation of solubility of several gases in rubbery amorphous polymers: △, silicone rubber; ○, natural rubber; □, styrene–acrylonitrile rubber; ●, amorphous polyethylene. Temperature, 25°C (30). To convert $[cm^3(STP)]/(cm^3 \cdot MPa)$ to $[cm^3(STP)]/(cm^3 \cdot cm\ Hg)$, multiply by 1.333×10^{-3}.

Table 3. Permeabilities, Solubilities, and Diffusivities of Various Gas Pairs in Rubbery Polymers[a]

Polymer	P_{He}, mmol/(m · s · TPa)[b]	P_{He}/P_{CH}[c]	S_{He}, cm^3(STP)/(cm^3 · GPa)	S_{He}/S_{CH_4}	D_{He}, 10^{-6}cm^2/s	D_{He}/D_{CH_4}	P_{O_2}, mmol/(m · s · TPa)[b]	P_{O_2}/P_{O_2}	S_{O_2}, cm^3(STP)/(cm^3 · GPa)[c]	S_{O_2}/S_{N_2}	D_{O_2}, 10^2 cm^2/s	D_{O_2}/D_{N_2}
Natural rubber[d]	10.4	1.05	105	0.042	22	25	8.04	3.0	1125	2.0	1.6	1.5
Polyethylene[e]	1.64	1.7	54	0.048	6.8	36	0.97	3.0	473	2.1	0.46	1.44
Poly(methyl acrylate)[f]	3.55	45.1	101	0.069	7.88	650						
Poly(ethylene terephthalate)[g]	3.1	44	58	0.10	12	430	0.18	3.8	218	1.7	0.19	2.2
Polychloroprene[h]							1.34	3.42	750	2.13	0.4	1.6
Butyl rubber[i]							0.44	3.94	1200	2.19	0.081	1.8

[a] At 25°C, unless otherwise specified.
[b] To convert mmol/(m · s · TPa) to cm^3(STP)cm/(cm^2 · s · cm Hg), multiply by 2.98×10^{-10}.
[c] To convert cm^3(STP)/(cm^3 · GPa) to cm^3(STP)/(cm^3 · cm Hg), multiply by 1.333×10^{-6}.
[d] Poly(*cis*-isoprene).
[e] $\rho = 0.914$ g/mL; $\alpha = 0.57$.
[f] At 35°C.
[g] At 100°C.
[h] Neoprene.
[i] Isobutylene/isoprene (98/2) copolymer.

butadiene–acrylonitrile copolymers. The higher the nitrile content, the greater the attraction between neighboring chains. These interchain attractions are quantified by the cohesive energy density (CED). High CED tends to elevate the diffusion activation energy and hence depress the diffusivities according to equation 15b.

The diffusivity selectivities of the various rubbers in Table 3 are generally low, consistent with the large scale of segmental motions in rubbery materials relative to the penetrant sizes that must be distinguished. Besides difficulties in achieving high selectivities, rubbery materials are generally unable to be self-supporting under pressure in a high surface area hollow fiber form. This problem can be circumvented by placing a thin film of the rubber on a microporous support to make a composite membrane (42). Generally, however, the much higher selectivities of glassy polymers for separating gases make glasses the favored polymeric materials in separation applications.

For cases involving a random copolymer or a miscible blend of two amorphous rubbery polymers, the behavior is generally a volume fraction weighted average of the permeabilities of the two homopolymers. On the other hand, the transport properties of immiscible blend systems depend significantly on the relative permeabilities and the morphology of the immiscible blend.

Nonideal Transport Effects in Rubbery Polymers

Plasticization and Hydrostatic Effects. New complexity arises in the basic transport properties of a polymer at higher penetrant activities, since the local concentration of penetrant within the polymer can become quite high. At higher pressures (approaching the saturated vapor pressure), these high concentrations can occur in cases where favorable polymer–penetrant interactions promote solubility. This is common for organic vapors and even for small polar or quadrupolar molecules such as CO_2, H_2S and SO_2. *Transport plasticization* is defined as a significant increase in the diffusivity of a penetrant because of facilitation of local polymer segmental motion caused by another penetrant molecule in its neighborhood. This definition applies both to the increase in diffusivity of a penetrant caused by the presence of its own kind and increases caused by a different component. Even for pure component penetrants, a detailed fundamental analysis of this phenomenon on a molecular basis has not been achieved; however, various free-volume analyses are available (43).

Plasticization is typically an unfavorable phenomenon in separation applications because permselectivity is reduced as the diffusivity of a slower penetrant is increased. In the case of gases, plasticizing phenomena are suppressed because of hydrostatic compression in some polymers despite rather high sorption levels. Analysis in terms of the free-volume approach requires consideration of the compressibility of the rubbery matrix. In fact, exposure to the hydrostatic pressure of low solubility gases, such as helium or nitrogen, may actually compress out free volume and thereby reduce the ability of polymer segments to open gaps for movement of other segments or sorbed penetrants.

Some data (44) indicate a marked reduction in diffusivity of *n*-butane as the external pressure of helium is increased, and it was concluded that helium gas applied to silicone rubber acts only as a pressuring medium within experimental

limitations. The helium decreases the free volume of the silicone rubber and thus decreases its molecular motion. Plasticization and hydrostatic effects on the permeability of carbon dioxide, helium, nitrogen, methane, and ethylene in silicone rubber also have been studied (45). Over an extended pressure and concentration range, both compression of free volume and eventual plasticization have been observed for these different penetrants. As the amount of sorbed penetrant increases, the plasticization effect eventually overcomes the hydrostatic compression effect on the rubbery matrix for the more condensable penetrants such as carbon dioxide and ethylene.

The local solubility and diffusivity must be considered to see when true transport plasticization occurs. For this it is more useful to consider the local mutual diffusion coefficient $D_{AP}(C)$ rather than the average value assessed from equation 30. The local mutual diffusion coefficient is a measure of the ability of a penetrant to move through the membrane at a point where the local conditions are well defined in terms of the local penetrant concentration C_A, volume fraction φ_A, weight fraction ω_A, or penetrant fugacity, whichever is most convenient.

Figure 8 (45) shows the permeation data for methane, carbon dioxide, ethylene, helium, and nitrogen in silicone rubber at 35°C over a broad range of pressures. The data agree reasonably well with the data reported previously over a smaller pressure range (46). For helium and nitrogen, which have low critical temperatures, the permeability decreases with increasing pressure, while it increases with increasing pressure for carbon dioxide and ethylene, which have relatively high critical temperatures. For methane, with an intermediate critical temperature, the permeability shows negligible pressure dependence.

The sorption isotherms shown in Figure 9 (16) for each of the penetrants obey Henry's law at low pressures, and the more strongly sorbing carbon dioxide and ethylene show Flory–Huggins swelling behavior at high pressures. The lines in these plots are, in fact, modified Flory–Huggins fits to the data according to equation 36, which includes the presence of the small amount of cross-linking in the sample (47):

$$\ln\left(\frac{p}{p_0}\right) = \ln(\varphi_A) + (1-\varphi_A) + \chi(1-\varphi_A)^2 + V_A\left(\frac{v_e}{V_0}\right)\left((1-\varphi_A)^{1/3} - \frac{(1-\varphi_A)}{2}\right) \tag{36}$$

where p is the penetrant pressure, p_0 is the vapor pressure of the penetrant, V_A is the partial molar volume of the penetrant, v_e is the effective number of cross-links expressed in moles, V_0 is the volume of the penetrant-free polymer, and χ is the Flory–Huggins interaction parameter. The permeability and sorption isotherms can be used along with the following expression to calculate the local concentration-dependent mutual diffusion coefficient (48):

$$D_{AP}(C_{A_2}) = \left[\left\{P(p) + p\frac{dP}{dp}\right\}\left(\frac{dp}{dC_A}\right)\right)\Bigg|_{p2} \tag{37}$$

The Flory–Huggins expression can be used to evaluate the dp/dC_A term at the upstream pressure for conditions where Henry's law does not apply; however, only the region of Henry's law is discussed here. Figure 10 shows the local diffusion coefficient for the various penetrants as a function of local fugacity in silicone

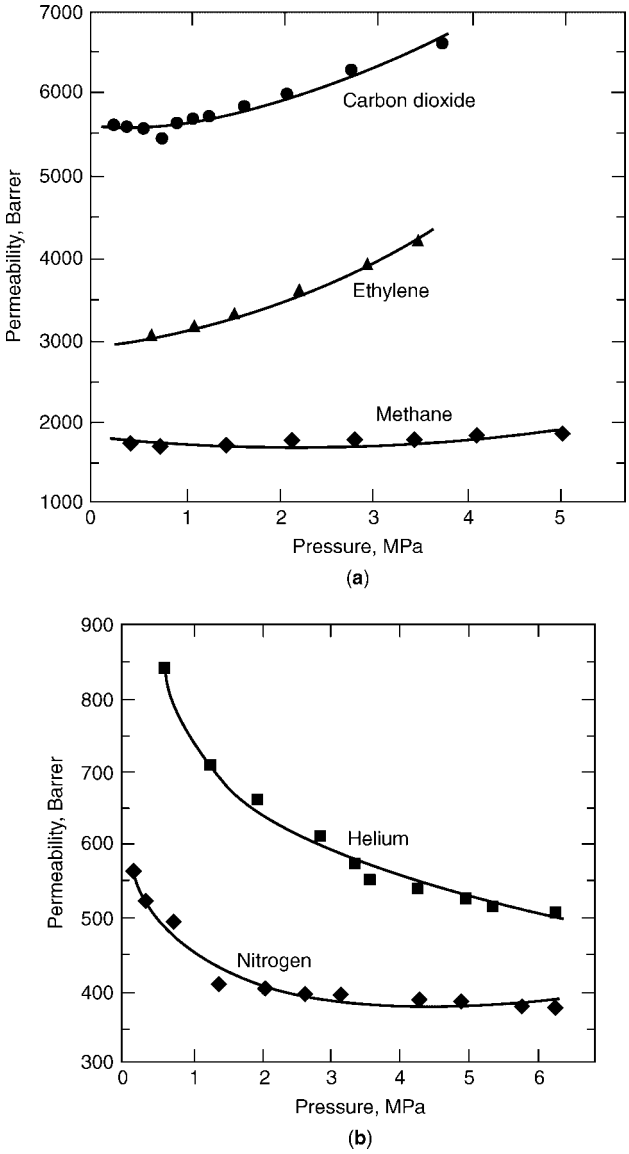

Fig. 8. Comparison of the pure-gas permeabilities of various gases in silicone rubber at 35°C. (**a**) CO_2, C_2H_4, and CH_4; (**b**) He and N_2 · 1 Barrer = 10^{-10} [cm^3(STP)cm]/($cm^2 \cdot s \cdot cm$ Hg) = 0.335 mmol/(m · s · TPa). To convert MPa to psi, multiply by 145.

rubber (45). This can be easily converted to a plot of $D_{AP}(C)$ vs C using the sorption isotherm data if desired. For carbon dioxide, the fugacity differs by as much as 22% from the pressure at the maximum pressure studied. The chemical potential difference is of course the true thermodynamic driving force for diffusion and should be used in mixed-gas calculations.

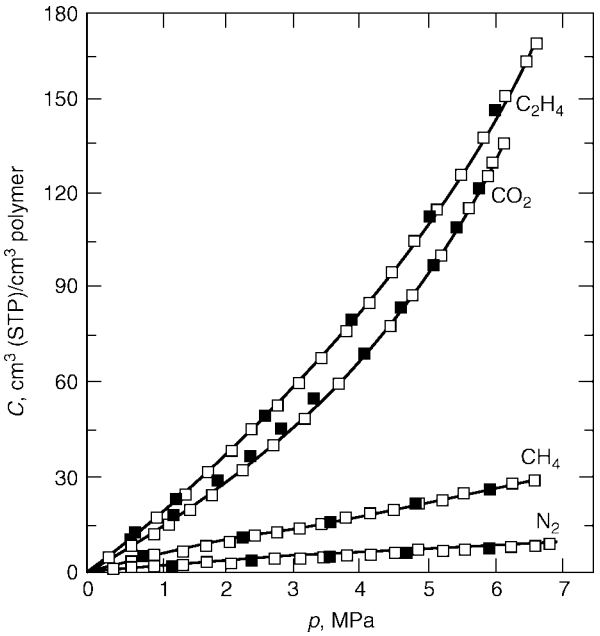

Fig. 9. Sorption isotherms for Sorption and desorption of various gases in silicone rubber at 35°C. □, Sorption; ■, desorption. To convert MPa to psia, multiply by 145.

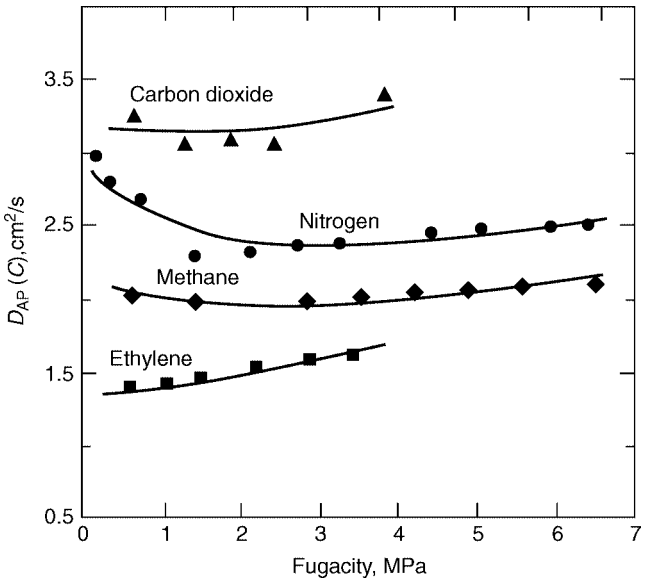

Fig. 10. The local effective diffusion coefficient of various penetrants in silicone rubber. To convert MPa to psia, multiply by 145.

The local diffusion coefficient of nitrogen decreases with increasing pressure until around 2.1 MPa (300 psia), where it levels off and slowly begins to rise with increasing pressure. These results indicate that the fractional free volume of the polymer is reduced because of nitrogen's hydrostatic pressure. At higher nitrogen pressures the solubility level is sufficient to oppose the compressive effect and cause the diffusivity to begin to increase with pressure as free volume is added by the penetrant. The results for methane and carbon dioxide show a slight decrease in diffusivity with increasing pressure, but both gases reapproach their original diffusivity at higher pressures because of their higher solubilities. Ethylene exhibits an immediate increase in diffusivity with pressure that is not surprising, given its significant solubility and the large dilation in volume with increasing ethylene pressure, shown in Figure 11 (16). Even below 0.7 MPa (100 psia), more ethylene is sorbed than nitrogen in the silicone rubber at 7 MPa (1000 psia).

The negative slope of the permeability vs pressure plot for helium and nitrogen in Figure 8**b** and the positive permeability slope for the other gases in Figure 8**a** can be explained by these two competing effects caused by the penetrant pressure. The data in Figure 11**b** show an actual compression in volume, even though a small but measurable amount of sorption was observed under these conditions. The results are believed to occur because of the low solubility of helium and high compressibility of silicone rubber. Therefore, the two competing factors that determine the volume dilation of the polymer are (*1*) the sorption of gas into the polymer that results in an increase in free volume, and (*2*) the hydrostatic pressure on the film that reduces the free volume. The second effect is usually small and is overcome for gases that have significant sorption levels. The net result of these two opposing effects determines whether the permeability (and diffusivity) will increase or decrease with increasing pressure. These two competing factors can be described quantitatively by equations 23 and 26.

The expression for the local mass diffusion flux accounting for the frame of reference term discussed in equation 2b is given below:

$$n_A = \frac{-\rho D_{AP}}{1-\omega_A}\frac{\partial \omega_A}{\partial z} \tag{38}$$

Using equations 7 and 37, the effective mutual diffusion coefficient obtained from analysis of the permeability versus pressure data can be related to the self-diffusion coefficient of the penetrant, namely

$$D_{AP} = D_A^*(1-\omega_A)\left(\frac{\partial \ln a_A}{\partial \ln \omega_A}\right) \tag{39}$$

The factor $(\partial \ln a_A/\partial \ln \omega_A)$ is available from the sorption measurements such as those in Figure 9. For the cases considered here, where Henry's law applies, this factor is simply equal to unity, whereas it is given by equation 40 for the case where curved isotherms characterized by the Flory–Huggins equation apply.

$$\left(\frac{\partial \ln a_A}{\partial \ln \omega_A}\right) = \frac{\omega_P \rho_A^2}{(\omega_A \rho_P + \omega_P \rho_A)^2}\left(1 - \frac{2\chi \omega_A \rho_P}{\omega_A \rho_P + \omega_P \rho_P}\right) \tag{40}$$

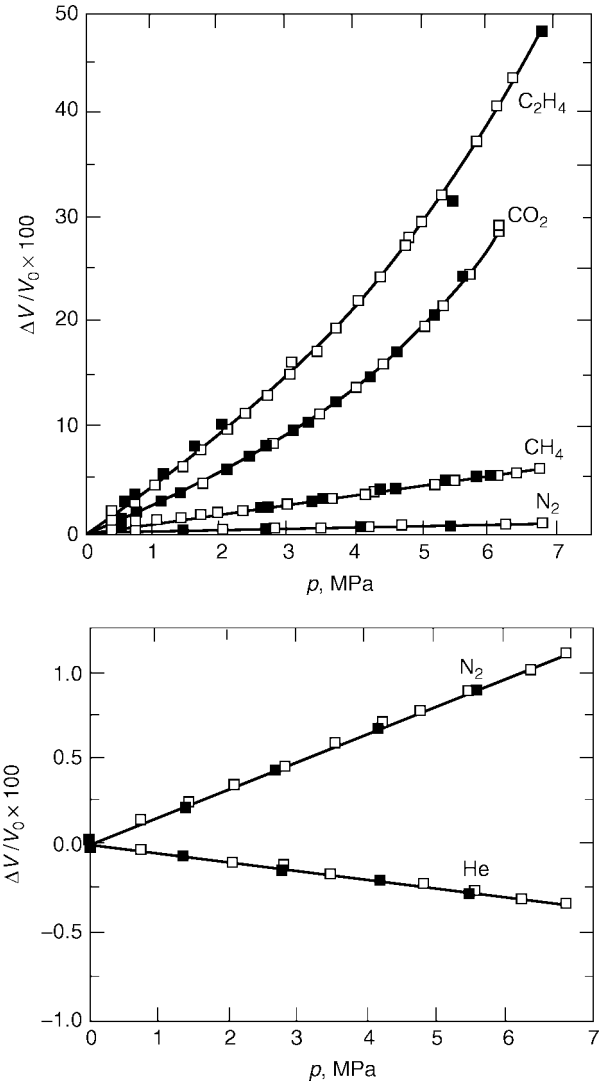

Fig. 11. Volume dilation isotherms for Sorption of various gases in silicone rubber at 35°C. □, Sorption; ■, desorption (46). To convert MPa to psia, multiply by 145.

where ρ_A and ρ_P are the mass densities of the pure penetrant and polymer, respectively.

Penetrant mobilities ($\mathcal{M}_A$) were determined as a function of local fugacity for silicone rubber (45). The mobility of nitrogen decreased with increasing pressure, but the mobility of carbon dioxide increased, suggesting that nitrogen acts predominantly as a pressurizing agent and CO_2 acts primarily as a plasticizing agent. The permeability of helium and nitrogen decreased with increasing pressure because of the reduction in free volume caused by the hydrostatic pressure of the gas. Therefore, at high pressure, these gases tend to lower the permeability of each component unless another component has sufficient solubility to overcome the

hydrostatic effect. To test this hypothesis the silicone rubber films were exposed to both a 10/90 mol% mixture and a 50/50 mol% mixture of carbon dioxide and nitrogen.

The presence of additional penetrants in the feed stream can be accounted for by the addition of a term in the free-volume equation to account for the presence of each penetrant and the applied hydrostatic pressure above $p_s = 101.3$ kPa (1 atm) as follows:

$$D_A^* = RT\mathcal{M}_A = A_d \exp\left(\frac{-B_d}{v_{fs} + \alpha[T - T_g] - \beta[p - p_s] + \gamma_1\varphi_1 + \gamma_2\varphi_2 + \cdots}\right) \tag{41}$$

The carbon dioxide permeability for both mixtures was depressed below the pure carbon dioxide values, but the carbon dioxide permeability for the 50/50 mixture did not display a decreasing tendency with pressure as was observed for the 10/90 CO_2/N_2 mixture. Therefore, at the lower nitrogen partial pressures observed in the 50/50 mixture, the impact of the hydrostatic pressure effect is reduced by the swelling effect of CO_2. Although the swelling effect of CO_2 cannot completely overcome the hydrostatic pressure effect of CO_2 nitrogen, it greatly offsets its influence.

Important extensions of the foregoing example, where hydrostatic pressure effects may be of considerable importance, involve supercritical extraction using high pressure CO_2 or ethylene for processing of foods, pharmaceuticals, and purification of polymers by removal of trace monomers (49). This topic involves greater complexity than the binary diffusion case. Moreover, the factor involving the activity coefficient derivative may become very significant near the critical point. Transport behavior in these systems, however, can be anticipated on the basis of the results shown for the pure components. Little enhancement in the self-diffusion coefficient of the penetrant in these rubbery polymers is apparent at pressures below the critical pressure; however, both carbon dioxide and ethylene begin to overcome the effects of hydrostatic pressure and to show upturns in their mobilities as the critical conditions are approached. Most of the work in the area of mass transport under supercritical conditions in polymers has been rather qualitative, but more quantitative analysis should be possible using the free-volume model.

Penetrant Clustering. Clustering may reduce the effective mobility of a penetrant such as water or methanol that can self-associate. The activated state representation of diffusion is typically used to discuss the suppressed diffusion coefficient for a clustered penetrant. If the diffusion process involves primarily jumps by monomeric, unassociated penetrants, energy must be available both to make a gap to allow the penetrant to jump into and to cause the dissociation of one of the penetrants in a local region adjacent to the gap. Therefore, higher activation energies for diffusion and, hence, lower diffusion coefficients at activities above which clustering occurs are expected if this visualization is correct. Work to document this point of view has been done for silicone rubbers (50), poly(alkyl methacrylates) (51), and hydrocarbon rubbers (52). Typical diffusion coefficients and activation energies for diffusion of water and methanol, both of which tend to cluster in hydrophobic environments, are shown for various rubbery materials

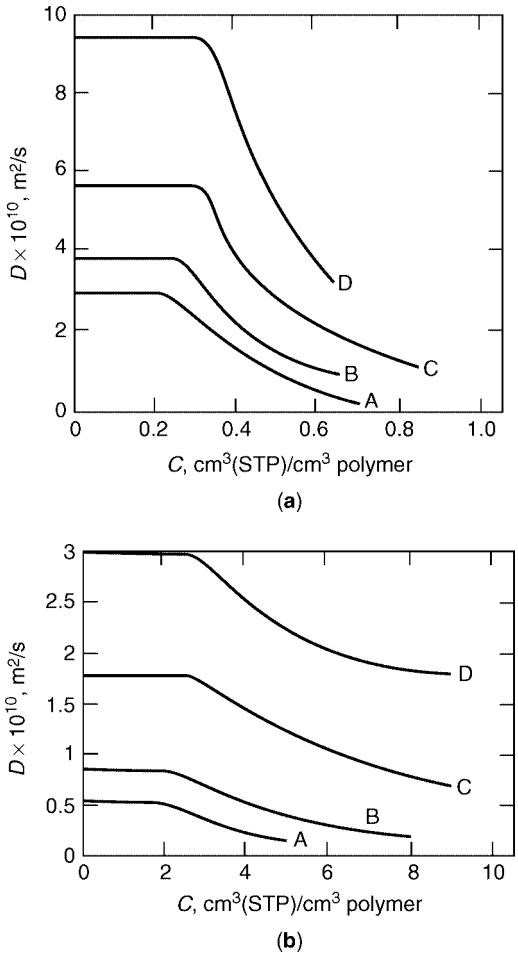

Fig. 12. (**a**) Effects of water clustering on diffusion in rubbers. Concentration dependence of the diffusion coefficient for water in Cariflex IR305: A, 37°C; B, 42°C; C, 50°C; D, 61°C. (**b**) Effects of methanol clustering on diffusion in rubbers. Concentration dependence of the diffusion coefficient for methanol in Cariflex IR305: A, 26°C; B, 31.1°C; C, 50°C; D, 60°C.

in Figures 12**a** and 12**b** (52) and in Table 4 as a function of concentration over conditions prior to and after the onset of clustering.

The sorption behavior in clustering systems is often discussed in terms of the cluster integral G_{AA} given below in terms of the partial molar volume V_A, the activity a_A, and the volume fraction of penetrant φ_A:

$$\frac{G_{AA}}{V_A} = -(1-\varphi_A)\left(\frac{\partial(a_A/\varphi_A)}{\partial a_A}\right)_{p,T} - 1 \tag{42}$$

G_{AA} may be determined from equilibrium sorption data as a function of penetrant partial pressure. Based on the theory of Zimm and Lundberg (53), the cluster function given by (φ_A G_{AA}/V_A) equals the excess number of A molecules

Table 4. Activation Energies in Clustering Systems

System	C, cm^3[STP]/cm^3 polymer	ΔE_D, kJ/mol[a]	Ref.
Water			
cis-1,4-Polyisoprene	0	42	50
	0.3	58	
	0.5	58	
Polydimethylsiloxane	0	14	48
	0.45	46	
	0.6	75	
poly(3,3,3-trifluoropropylmethylsiloxane)	0	17	
	0.7	50	48
Poly(butyl methacrylate)	0	28	49
	2	44	
	4	50	
Methanol			
Natural rubber	0	42	50
	5	54	
	8	71	
poly(3,3,3-trifluoropropylmethylsiloxane)	0	25	
	4	29	49
	8	38	

[a] To convert kJ/mol to kcal/mol, divide by 4.184.

above the number that would exist in the neighborhood of an arbitrarily chosen type A molecule if the mixing were totally random, ie, no clustering. As shown in Figure 12, the effective mutual diffusion coefficient is constant below the activity at which clustering occurs. The activity at which the cluster function deviates significantly from zero corresponds to the point at which the diffusion coefficient begins to drop significantly, and the activation energy begins to increase.

Intermediate-Size Penetrants. These penetrants are defined as molecules with sizes approaching a polymer segment, but much smaller than an entire polymer chain. The infinite-dilution mutual diffusion coefficients for increasingly large, but not macromolecular, penetrants approach the diffusion coefficient for the segment of a polymer diffusing within itself. Movement of the entire polymer molecule itself is clearly a slower and more complex concerted process than the local movement of its segments; however, the segmental mobility and the self-diffusion coefficient of the entire molecule can be related as discussed later.

For intermediate-size penetrants such as typical organic solvents, the self-diffusion coefficient of the polymer is much smaller than that for the penetrant. Consistent with this expectation, equation 8 has been found to be appropriate (36) for mass fractions of toluene as high as 85%. Therefore, for low and intermediate penetrant concentration, equation 8 should still apply as it did in the case of gases and other small penetrants.

The data in Figure 3 reflect the tendency to approach an infinite-dilution asymptotic mobility as the diameter of these intermediate-sized penetrants

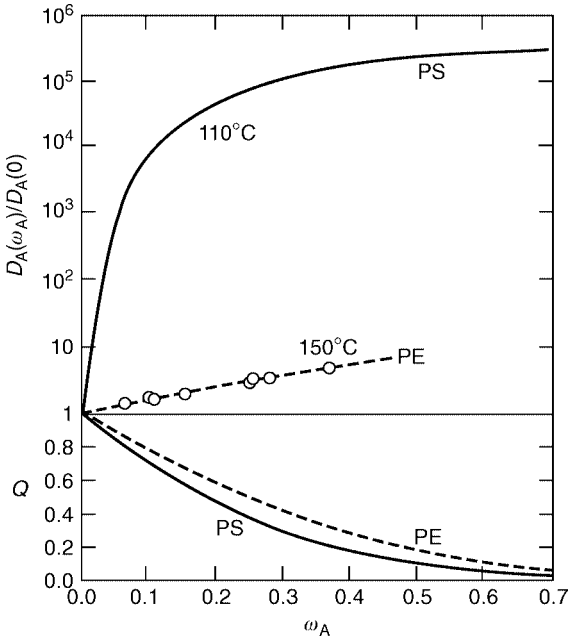

Fig. 13. Concentration dependence of the self-diffusion coefficient and the thermodynamic factor Q for the toluene–polystyrene system at 110°C and for the *o*-xylene–polyethylene system at 150°C. $Q = (1 - \omega_A)(\partial \ln a_A/\partial \ln \omega_A$. From Ref. 45.

increases (see eq. 6):

$$\lim_{\omega_A \to 0} \{D_{AP}\} = \lim_{\omega_A \to 0} RT\mathcal{M}_A(1-\omega_A)\left(\frac{\partial \ln a_A}{\partial \ln \omega_A}\right) = RT\mathcal{M}_A = \frac{RT}{\zeta_A} \tag{43}$$

Care must be used in applying such arguments when estimating practical diffusion coefficients, however, since increases in ω_1 above the infinite-dilution limit can cause significant changes in the effective mobility of the penetrant. Moreover, the $(\partial \ln a_A/\partial \ln \omega_A)$ term can deviate from unity at weight fractions as small as 10–20%, as was indicated in the case of carbon dioxide and ethylene earlier. In the case of *o*-xylene diffusion in polyethylene at 150°C, both the effects of plasticization and of the $(\partial \ln a_A/\partial \ln \omega_A)$ term on the self-diffusion coefficient have been analyzed and are shown in Figure 13 (34).

Except for supercritical extraction conditions, hydrostatic pressure effects are typically of negligible importance for simple solvent vapors diffusing in polymers, since the saturation vapor pressure is low, <101.3 kPa (1 atm), in most applications. The predictive power of the approach is indicated by the results for the mutual diffusion coefficient of toluene in a toluene–polystyrene system (Fig. 14) (35).

The rather complex behavior represented in Figure 14 was analyzed in terms of the respective contributions to the self-diffusion coefficient and the significant reduction in the thermodynamic $(1 - \omega_A)(\partial \ln a_A/\partial \ln \omega_A)$ terms in equation 39. These two constituent contributions indicate that the dramatic increases in the

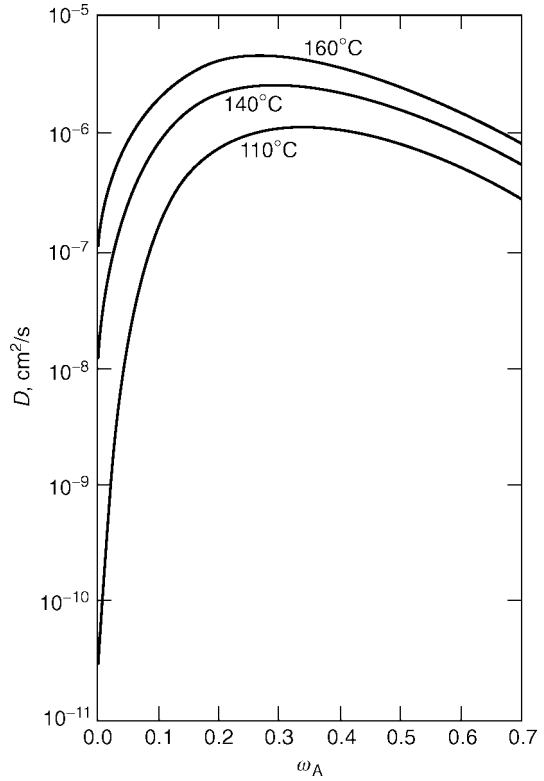

Fig. 14. Dependence of diffusivity on mass fraction for the toluene–polystyrene system.

mutual diffusion coefficient at low solvent mass fractions in the polystyrene system at 100°C is primarily due to dramatic transport plasticization-induced changes in the penetrant self-diffusion coefficient, rather than due to the thermodynamic term.

The strong temperature dependence of the infinite-dilution diffusion coefficient in the vicinity of the glass-transition temperature of the polymer ($T_g = 105$°C for polystyrene) cannot be predicted by a simple exponential expression such as the activated state model (equation 15a) unless the energy of activation is allowed to vary. Variation in the activation energy in this region, where backbone segmental motions are beginning a transition from a primarily oscillatory nature around relatively fixed positions to include large rotary crankshaft motions, is not unreasonable, but it cannot be predicted directly from the activated state theory. On the other hand, such near- T_g behavior is a natural expectation of the free-volume theory based on the Williams–Landel–Ferry (WLF) description of the effects of free volume on polymer properties.

Recent attempts to apply the free-volume approach below the glass transition have also been made (33). This sub- T_g problem often includes additional factors not related simply to Fickian transport processes, since the movements of intermediate-sized penetrants in contact with glassy polymers often induce complex time-dependent relaxations.

Semicrystalline and Cross-Linked Rubbery Polymers

Gases and Low Activity Vapors. Regions of crystallinity or points of chemical cross-linking have somewhat similar effects on the transport properties of a rubber causing restriction of swelling and suppression of long-range chain segmental motion. Semicrystalline polymers, however, are more complex than cross-linked materials because of tortuosity caused by the presence of the typically impermeable crystalline regions. Similarly, adding fillers such as glass, talc, or mica particles to an amorphous matrix prior to cross-linking can make the transport properties of the resultant material take on a semicrystalline-like character if the interfacial adhesion between the filler and matrix phase is good. Promotion of adhesion can be achieved by using interfacial wetting agents such as silanes and titanates that bond to the inorganic surface and can either chemically bond or physically interact with the elastomer matrix. In the absence of such adhesion promoters, the barrier properties may be degraded because of interfacial defects not found in semicrystalline materials under most conditions.

The effects of fillers or crystallites can be influenced considerably not only by the volume fraction of this phase, which affects the solubility of a component directly, but also by the area-to-thickness aspect ratio and orientation of the filler with respect to the direction of permeation. The orientation factor affects the apparent diffusivity by determining how the crystallites or fillers behave as tortuous impediments to penetrants. This effect is not considered in the simple free-volume analysis (eq. 18a). Since the effect of orientation can be significant, approaches which account for tortuosity and chain mobility are more desirable. Examples of materials where orientation effects are significant include phase-separated urethane–elastomer block copolymers and random copolymers of ethylene and vinyl alcohol since the two components are able to cocrystallize in the same crystal lattice. This latter copolymer is used as a barrier in which the permeability of the material can be tailored by varying the amount of the highly polar, diffusion-inhibiting (vinyl alcohol) component without strongly affecting the crystallinity.

Studies of gas sorption and transport strongly support the notion of the impenetrability of crystalline domains by even tiny gas molecules. As shown in Figure 15, the solubility coefficient ($\bar{S}_i = C_i/p_i$) of both gases and low activity vapors are essentially proportional to the volume fraction of amorphous material Φ_a and the intrinsic solubility coefficient for the totally amorphous material $\bar{S}_a$ (54), ie

$$\frac{\bar{S}}{\bar{S}_a} = \Phi_a \tag{44}$$

The effects of crystallinity on the diffusion coefficient can be more complex than this simple volumetric exclusion, since the crystallites may act not only as tortuous barriers, but also as effective restrictors of chain motion analogous to chemical cross-linking. This twofold effect has been treated (54) in terms of a tortuosity factor τ, and a chain immobilization factor β^*, both of which increase with increasing crystalline fraction. The parameters D and D_a are the diffusion

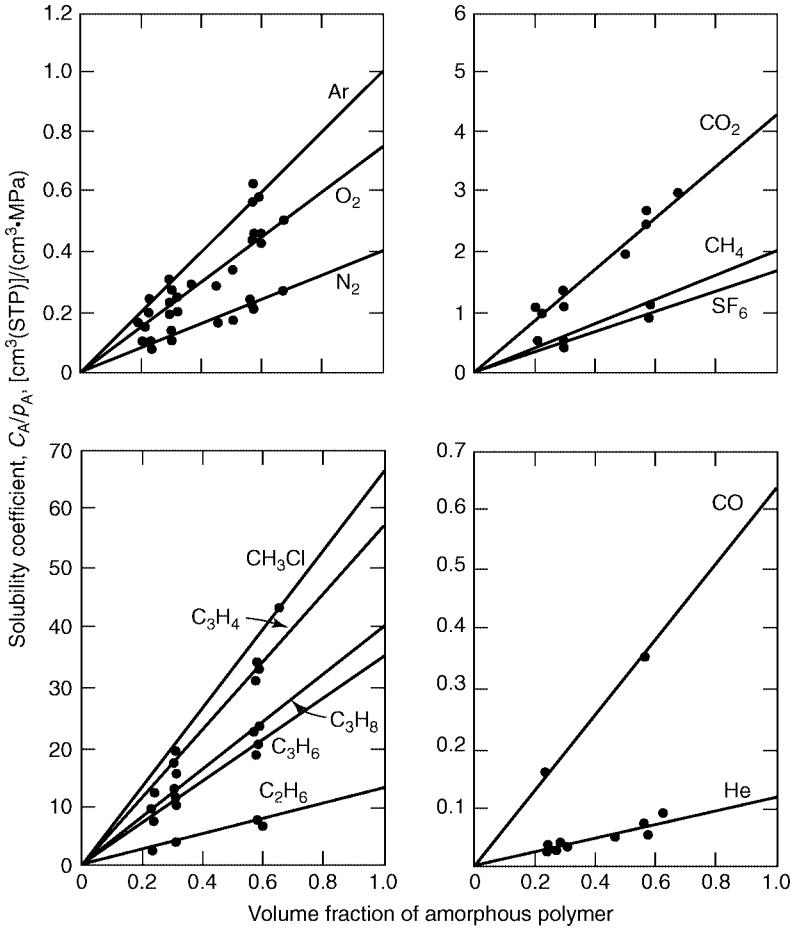

Fig. 15. Linear relationship between the infinite dilution solubility coefficient and the amorphous fraction in polyethylene at 25°C (30). To convert to [cm^3(STP)cm]/(cm^3 · MPa) to [cm^3(STP)]/(cm^3 · atm), multiply by 0.1013.

coefficients in the actual sample and in a totally amorphous sample, respectively:

$$D = \frac{D_a}{\tau\beta^*} \tag{45}$$

Chain restriction effects due to the effective cross-linking of crystallites may be negligible for helium compared to other penetrants due to the much smaller free volume required for an activated jump by helium. For example, 0.075 nm^3 is the required free volume for a jump of helium in poly(vinyl acetate) as opposed to 0.3 nm^3 for O_2 and 0.69 nm^3 for CO_2. This premise allowed estimation of the two factors in equation 45 for polyethylene (40). A 65% reduction in helium diffusivity for a 50% amorphous fraction material relative to a hypothetical branched polyethylene with no crystallinity was attributed to tortuosity. The diffusivities of the amorphous polyethylene were approximated as equivalent to

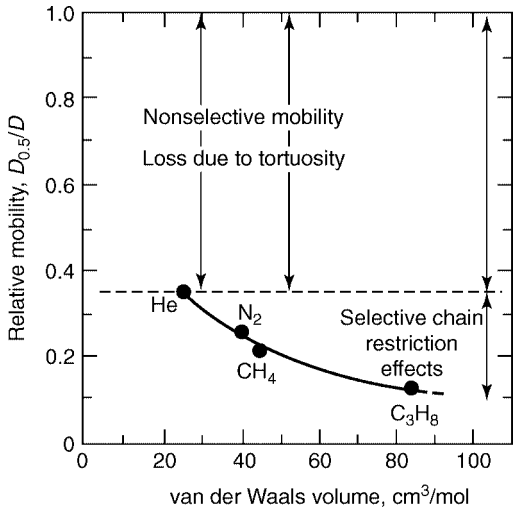

Fig. 16. Relative mobilities in semicrystalline and amorphous polyethylene for several penetrants as a function of penetrant van der Waals volume.

those of unvulcanized natural rubber. The reduction in diffusivity from simple tortuosity in polyethylene was estimated to be uniformly equal to 65% for all penetrants, and additional depressions in diffusivity relative to the amorphous reference were attributed to chain restriction effects due to the crystallites. The relative mobilities in the semicrystalline and amorphous samples are summarized in Figure 16.

In a treatment of the effects of crystallinity on transport in rubbery polymers using a modification of free-volume expressions (26), it was suggested that the introduction of crystallinity reduces the freedom of motion of amorphous chain segments between crystals. Although these ideas are physically consistent with those described above in terms of the chain immobilization factor β^*, a rather different analytical form of the diffusion coefficient is obtained.

The complementary effects of orientation and crystallinity can be treated in terms of the τ factor, since the aspect ratio and degree of orientation may alter the degree to which tortuosity influences the suppression in D. However, τ must currently be used for characterization rather than being an *a priori* predictable factor. A thorough treatment of the effect of uniaxial elongation at room temperature has been given for CO_2 diffusion in low density polyethylene (55). The effects of the orientation are complex. Prior to the onset of plastic deformation at 6% elongation, the solubility increases about 3%, and the diffusivity increases about 10%, and so a net increase of about 13% is observed in the permeability, presumably because of the introduction of free volume in the sample that dilates during the elongation. Such dilation is characteristic of materials with a Poisson ratio less than 0.5.

On the basis of increase in the sorption coefficient, it is suggested that the deformation causes dilation of the amorphous regions. At larger deformations, D falls below its original value for the unoriented crystalline material, since small increases in free volume are unable to offset the very large increase in tortuosity.

This increase in tortuosity can be anticipated as crystalline regions become more deformed by slippage and crystal lamellae rotate to adopt orientations more parallel to the film surface. Such organization makes efficient use of the lamellae as overlapping tortuous barriers capable of producing larger reductions in the effective diffusion coefficient than would be possible with spherical crystallites or even randomly oriented lamellae of equivalent volume fraction. Moreover, the alignment of chains in the amorphous regions between the plastically deformed spherulites may also act to increase the chain immobilization factor β^*.

Larger permanent deformations (up to 300% elongation), induced by either uniaxial drawing or roll processing at room temperature, reportedly produce reductions in diffusivity, solubility, and permeability (56). Larger reductions were seen for roll processing as compared to the simple drawing process, presumably due to the elimination of interfacial defects between the crystalline and amorphous phases in the rolling process.

The effects of crystalline regions on glassy materials have been found to be less extreme than for rubbery materials. For example, the chain immobilization factor affects the diffusion of different sizes of penetrants only in rubbery materials (57). This effect has been explained in terms of the low mobility of chain segments in glassy environments compared to the rubbery state. The concept of chain immobilization by crystallites loses significance in glasses, since the rigidity of the polymer backbone apparently outweighs any additional restriction on mobility imposed by crystallinity.

Although it appears in general that the assumption of impenetrability of crystalline domains is valid, poly(4-methyl-1-pentene) (PMP) may have crystals that do not fit this pattern (58). Gaps of almost 0.4 nm appear to exist between the chain segments in this material, which is consistent with the low crystal density of <0.85 g/cm^3 (Fig. 17). Contrary to the polyethylene case, these results provide provocative support for the possibility that measurable sorption does occur in the crystalline regions of this polymer. The two independent measures of crystallinity offered by X-ray and thermal analysis were found to be in good agreement.

Although the crystalline regions of PMP were found to be penetrable, the CO_2 and CH_4 permeabilities are still dependent on Φ_a, since the solubilities and diffusivities in the more structured phase were lower than in the amorphous phase. It was concluded that gases such as CO_2 and CH_4 dissolve in the crystalline regions of PMP at about 1/3 to 1/4 the extent in the amorphous phase (58). Moreover, the diffusion coefficients of CO_2 and CH_4 are about 37% and 64% lower, respectively, in the crystalline phase than the amorphous phase.

The nonzero intercept in the solubility coefficient vs amorphous fraction plot in Figure 18 (59) supports the notion that sorption occurs in the crystalline regions. Although the data provide rather strong support for the ability of small gases to penetrate the crystals of PMP, it is possible that defects at the interface between the crystalline and amorphous regions are the source of the nonzero intercept. This mechanism could also explain the tendency for the solubility associated with the crystalline phase to increase proportionally to the crystalline fraction since more interfacial defects would accompany the increasing crystalline fraction. However, it is unclear why permeation and diffusion through such regions would have lower diffusion coefficients as opposed to the amorphous phase, unless severe restriction of chain segmental mobility occurs in this region. For PMP, close to its T_g, the

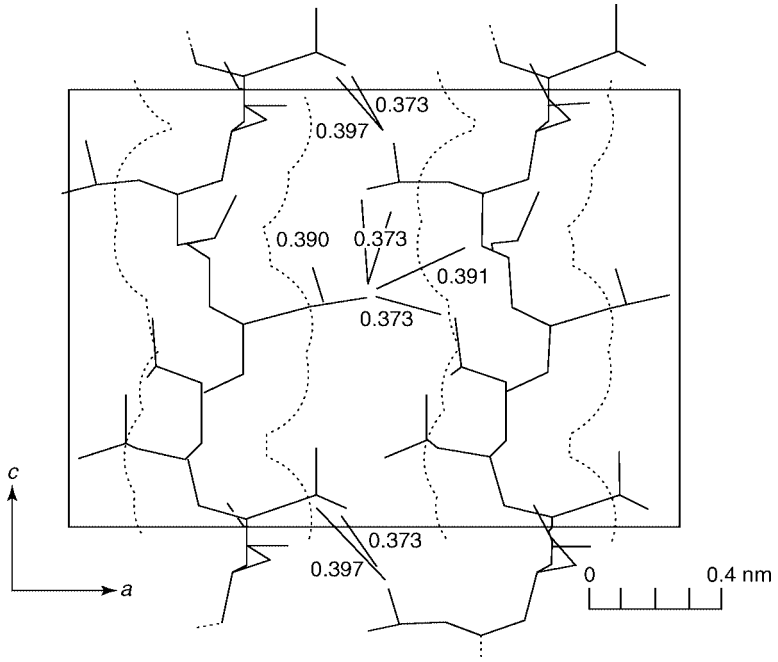

Fig. 17. Crystalline domains of poly(4-methyl-1-pentene).

concept of chain immobilization by crystallites is expected to be less significant than in the case of rubbery polyethylene because the rigidity of the glassy PMP backbone is expected to outweigh immobility imposed by neighboring crystallinity. Nevertheless, complementary proof of the important conclusions is desirable, and may be possible by consideration of the data in Table 5.

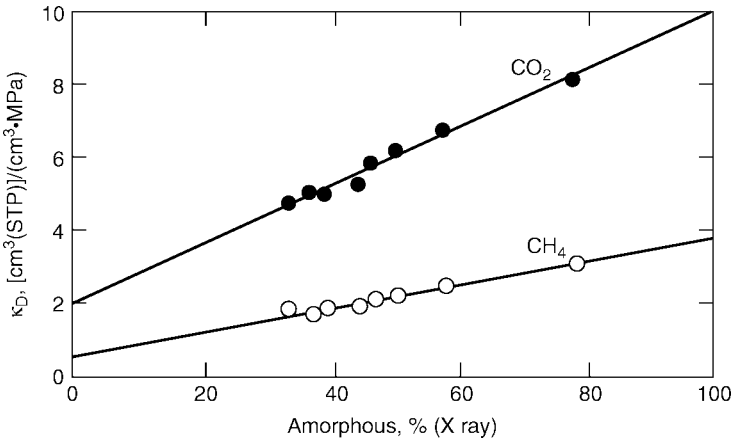

Fig. 18. Solubility coefficient vs amorphous fraction for poly(4-methyl-1-pentene). To convert [cm^3(STP)]/(cm^3 · MPa) to [cm^3(STP)]/(cm^3 · atm), multiply by 0.1013.

Table 5. Kinetic Diameters[a] of Various Penetrants[b], nm

Molecule	Diameter	Molecule	Diameter
He	0.26	C_2H_4	0.39
H_2	0.289	Xe	0.396
NO	0.317	C_3H_8	0.43
CO_2	0.33	n-C_4H_{10}	0.43
Ar	0.34	CF_2Cl_2	0.44
O_2	0.346	C_3H_6	0.45
N_2	0.364	CF_4	0.47
CO	0.376	i-C_4H_{10}	0.50
CH_4	0.38		

[a] Zeolite sieving diameters.
[b] Ref. 53

The zeolite sieving diameters in this table represent effective minimum dimensions as compared with the Lennard–Jones diameters for various penetrants. For more or less spherical penetrants such as CH_4, the two diameters agree rather well. In the case of a nonspherical molecule such as CO_2, however, restricted environments such as a zeolite can detect a minimum projected dimension that differs from the Lennard–Jones diameter characteristic of tumbling in a relatively unrestricted liquid or gaseous environment. The crystalline cage of the PMP may be acting similarly to a zeolite, and if this is the case it is anticipated that larger penetrants such as propane may, indeed, be effectively excluded from entering the crystalline region. In this case, the same type of behavior is expected for the solubility coefficient for propane in PMP as is illustrated for propane in polyethylene, ie, $\bar{S}/\bar{S}_a$ directly proportional to Φ_a and passing through the origin.

High Activity Vapor and Liquid Transport in Semicrystalline Rubbery Polymers

In considering the transport behavior of high activity vapors and liquids in semicrystalline polymers at low solubility (eg, water in polyethylene), small degrees of transport plasticization or clustering may need to be considered to generalize the $\bar{D}$ and $\bar{S}$ to include dependence on activity. Combination of these more general relations for $\bar{D}$ and $\bar{S}$ into the permeability relationship of equation 29 should approximately describe the steady-state permeability of the amorphous fraction of the material. Generally, the permeability of the crystalline fraction is assumed to be zero. Tortuosity and chain-restriction effects should be of decreasing importance as the extent of swelling increases. At high degrees of swelling (above 70% solvent fraction), frame of reference corrections must be incorporated in formulating steady-state permeability expressions.

For high solubility penetrants, great complexity is often observed in sorption–desorption kinetics or transient permeation due to time-dependent rearrangements of crystalline regions in response to swelling-induced stresses (59,60). These

are non-Fickian diffusional behaviors. Protracted approaches to equilibrium in the surface concentration may make the approach to sorption equilibrium or steady-state permeation behavior much slower than expected on the basis of the effective diffusion coefficient determined from equation 37 (5).

Using sorption–desorption kinetics, the extent of non-Fickian behavior decreases as the thickness of the film increases. Presumably, as the ratio of the time scale for diffusion to the time scale for stress-induced relaxation (ℓ^2/D) becomes large, the time-dependent relaxation occurs so rapidly (relatively) that it has a small effect on the diffusion process. In other words, in the limit where molecular-scale responses to swelling stresses are rapid compared to the rate of diffusion, the process appears to be Fickian. This is the case for totally amorphous rubbery polymers that behave as high molecular weight liquids.

Film formation protocols may cause significant nonuniformity in structure between a thin surface layer and the bulk of the film, especially when casting on a chilled roll. This effect can cause apparent thickness-dependent behavior of permeability and diffusivity parameters. Effectively, the film behaves as a laminate with different transport properties that can be treated according to a simple laminate model involving series resistances. Of course, assessment of the thickness of the surface layer must be possible for this approach to have utility. The skin layer reportedly increases in thickness as the rate of crystallization increases (61) because of contact with surfaces that promote surface nucleation. The diffusion coefficient of ethane in the 25-μm-thick surface layer of a quenched polyethylene film has been reported to be about twice as high as that in the bulk, because of favorable orientation of crystallites in this skin region of the semicrystalline film (62). In some cases, true laminate structures composed of chemically different materials are needed to obtain optimum performance in barrier applications. An example is the commercial food packaging made from ethylene–vinyl alcohol (EVOH) copolymers coextruded with polypropylene to form a laminate (63). In the dry state, the EVOH copolymers are among the best, easily processible oxygen barriers known. However, at elevated relative humidities (>80–90%), water disturbs the strong hydrogen bonds between the vinyl alcohol repeat units in the amorphous regions and reduces its barrier properties significantly. At still higher relative humidities and temperatures typical of retort conditions needed to kill microorganisms, actual disruption of crystalline domains is likely. To mitigate such problems, polypropylene layers are used to sandwich the barrier layer using multilayer coextrusion technology. This minimizes the quantity of the more expensive oxygen barrier (EVOH) but provides a package with sufficient mechanical strength.

Modeling of the transient-state transport process of water and oxygen through such a laminated barrier material also containing intermediate tie layers to promote adhesion is complex. Reported partial solutions use different physical approximations (64). Typically, the approach is to model the total amount of water, which is the major plasticizing agent transported into the barrier film through the outer polyolefin guard layer during retort, and relate this weight fraction to a new effective oxygen permeability of the partially humidified barrier layer. During subsequent cooling and drying of the container, the water is removed by back permeation out of the package into the dry storage environment over an extended period of time determined by the relative thicknesses of the outer guard layer and

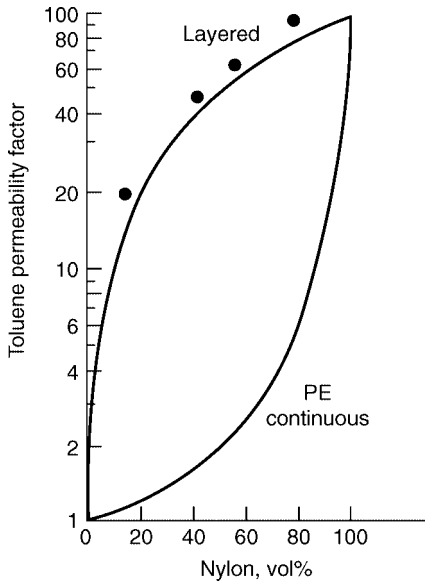

Fig. 19. Permeability of toluene in nylon–polyethylene barriers. The data (●) for a laminar blend is compared to theoretical permeabilities in a true laminate (upper curve) and in a homogeneous blend (lower curve). The permeability factor is the permeability in pure polyethylene divided by the permeability in the mixture.

the inside oxygen barrier layer. During this drying period a significant oxygen invasion can occur. Consequently, more complex structures are sometimes used to provide a desiccant material in the tie layer between the outer guard layer and the barrier layer to prevent the penetration of water into the barrier layer during the retort operations (65).

A laminar-blend technique can be used to achieve properties intermediate between those of the relatively expensive laminates formed by coextrusion and those of an inexpensive, but less effective, dispersion of a barrier component in a matrix of another material. For the laminate, the total barrier resistance is composed of the additive resistances contributed by each of the layers in the structure. For a simple dispersion of component A in a matrix of B, a volume fraction weighting of the permeabilities of the two components applies unless large aspect ratios are achieved (66). Laminar-blend technology achieves large aspect ratios by smearing out the dispersed barrier layer into thin lamellae with large area to thickness aspect ratio. Figure 19 shows the data and results of model calculations based on the two limiting cases of a true laminate or a homogeneous dispersion in comparison to the barrier properties of a laminar blend of nylon-6,6 and polyethylene for use in hydrocarbon barrier applications. The larger the aspect ratio of the primary barrier component, the closer the approach to the true multilayer laminate properties due to overlapping of the barrier lamellae (67). Such barrier-container issues involve not only a consideration of transport properties of materials, but also an economic weighing of the costs of processing and materials to achieve an optimum structure.

Glassy Polymers

Glassy polymers, polymers existing at a temperature below their T_g, are differentiated from rubbery polymers in discussions of physical properties because their responses in most experiments are quite different. Essentially all of the differences arise from the characteristic scales of the micromotions that occur at the segmental level in rubbery and glassy polymers. As noted earlier, the high molecular weight liquid-like nature of rubbers provides them with the ability to adjust their segmental configurations rapidly over significant distances by large-scale motions, such as the crankshaft example (Fig. 2); however, in the glassy state, only severely hindered torsional motions are possible.

The frequency and amplitude of torsional segmental motions increase as the temperature is raised and the glass transition is approached. Close to T_g, the frequency of torsional motions increases dramatically and gives rise to true rotational motions typical of rubbery materials. However, in glasses well below T_g, the intramolecular backbone motions occurring over time scales of seconds or microseconds are much less extensive than in rubbers and are believed to be primarily torsional oscillations (68).

A distribution of these torsional oscillations results from subtle differences in chain packing throughout the glass. The average of this distribution is sensed by most probes of the material, including spectroscopic and diffusion experiments. A corresponding cumulative distribution of average gap sizes forms spontaneously and randomly throughout the glass in response to the concerted torsional motion of repeat units. For penetrants smaller than the limiting moving segment size, the tendency of the penetrant mobility to decrease with increasing penetrant size should be clear. This visualization is in effect the basis for applying free-volume theories, discussed previously in the context of rubbery materials, to glassy polymers.

If the available gap is larger than the critical dimension of a penetrant, a diffusion jump can be taken. If the available gap is too small, a jump is precluded. The fraction of diffusion jumps available to penetrant A vs B that are actually selective is small in rubbers, unless the size difference between penetrants is very large. For glassy materials, on the other hand, the range of motions, and hence the size of transiently opening gaps, is more narrowly distributed, thereby providing a much more selective environment for penetrant diffusion. Indeed, the infinite-dilution diffusion coefficients of glassy PVC and natural rubber in Figure 20 (69) illustrate the tendency of the glass to maintain size and shape selectivity over a larger range of penetrant sizes than the rubber. The diffusivities are more strongly dependent on penetrant size in the glass. At the same time, the more highly restricted range of molecular motion possible in the glass leads to lower diffusion coefficients.

The higher diffusivity selectivities often make glasses more favorable than rubbers for small molecule permselective membranes. The lower diffusivities also favor glasses over rubbers for barrier applications. On the other hand, rubbers are used in some membranes when a very large solubility selectivity is available, such as in separating organic vapors from air. Complex non-Fickian and plasticization phenomena can occur in applications where a significant amount of penetrant is

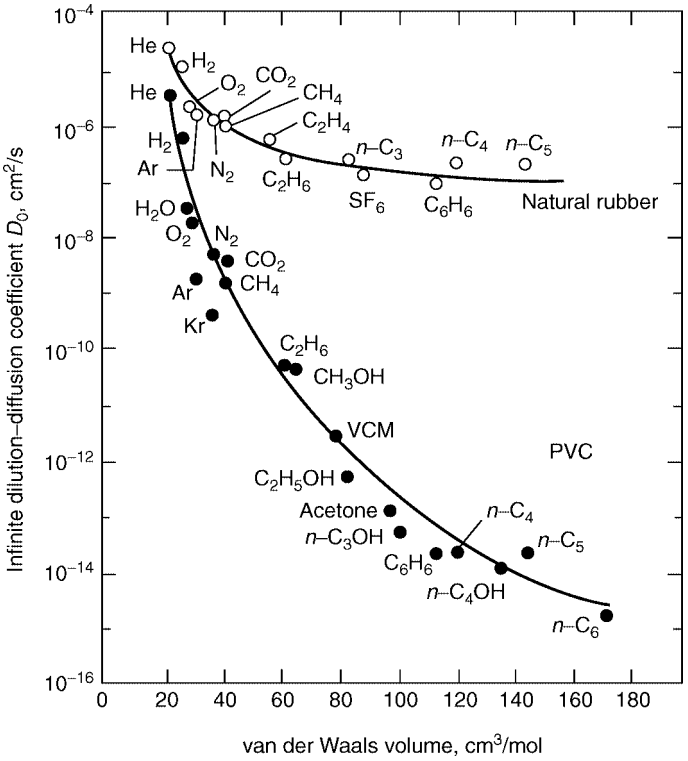

Fig. 20. Diffusion coefficients for a variety of penetrants in natural rubber at 25°C and rigid poly(vinyl chloride) at 30°C.

present in a glass. The diffusion coefficients of penetrants in glasses may increase by several orders of magnitude if the weight fraction of the penetrant reduces the T_g to the use temperature.

This plasticization phenomena can be observed in some glassy polymers exposed to high pressures of condensable gases, such as CO_2. Moreover, a pressure dependence of permeability occurs for glassy polymers prior to plasticization, whereas rubbery materials tend to have essentially pressure-independent permeabilities. The decrease in permeability of component A with increasing partial pressure of either component A or B prior to the onset of plasticization (70) shown in Figure 21 (71) is characteristic of glassy polymers.

The pressure at which plasticizing effects begin to overcome permeability depression depends primarily on the ratio of the partial pressure of the penetrant in the feed stream to the corresponding vapor pressure of the penetrant at the system temperature. As the pressure approaches the vapor pressure, solubility tends to increase rapidly, thereby inducing plasticization or clustering responses such as those already discussed for rubbery polymers. Even below the plasticization point, additional complexities not encountered with rubbery polymers are often observed in glassy materials. For example, low vapor pressure components such as water can cause depression of the permeability of other gases when water is

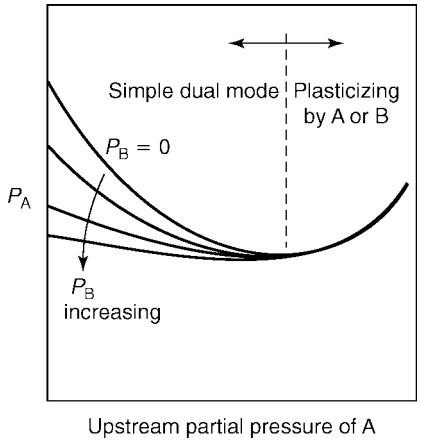

Fig. 21. Permeability of a glassy polymer to penetrant A (P_A) in the presence of varying partial pressures of penetrant B.

present at even a few hundred pascals (70). Components such as CO_2 that are only slightly supercritical can also produce a reduction in the permeability of another component if plasticization is not occurring. Although the vapor pressure of a supercritical component is not defined, a useful effective value can be obtained by extrapolation of a semi-log plot of vapor pressure versus the inverse absolute temperature to the system temperature. For instance, an effective vapor pressure of 7.3 MPa (72 atm) is obtained for CO_2 at 35°C by this method. Therefore 2 MPa (20 atm) of CO_2 should have flux depressing effects similar to only 1.6 kPa (12 torr) of water vapor having a vapor pressure of only 5.6 kPa (42 torr) at 35°C. This approach cannot be applied unambiguously to highly supercritical gases.

Sorption Models for Glassy Polymers. The sorption isotherms of glassy polymers are typically concave to the pressure axis at low pressures and tend to approach a straight line as the pressure is increased (see Fig. 22). This sorption behavior contrasts with that of a rubbery polymer, where the isotherm is typically linear at low pressures and then becomes convex to the pressure axis at high pressures, indicating the onset of plasticization or clustering. While there is general agreement in the literature on the mechanism of sorption into a rubbery polymer, there are many competing models of sorption in glassy polymers. The dual-mode model was the first successful attempt to describe sorption of small molecules in glassy polymers. The dual-mode model is still very popular today because of its simplicity and wide applicability. However, the physical basis of the dual-mode model, which rests on the concept of two dissolved penetrant populations, has never been conclusively proven. Furthermore, the parameters of the dual-mode must be measured for each system independently, and the parameters for sorption differ from those for desorption. In light of these shortcomings, multiple models have been proposed as alternatives to the dual-mode model, although none as yet enjoys the same widespread acceptance. A fairly recent review of these models is available (72). In this section, the dual-mode model, along with two alternatives, the site-distribution model and the nonequilibrium lattice fluid

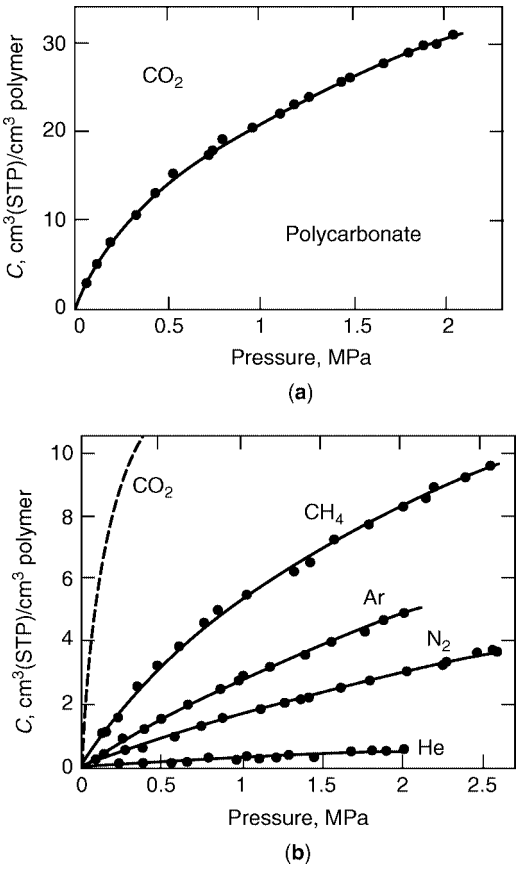

Fig. 22. Sorption isotherms for various gases in bisphenol A polycarbonate at 35°C. To convert MPa to atm, multiply by 10.

model, is presented. The two alternate models were chosen for review because they illustrate two rather different approaches. The site-distribution model is a phenomenological model based on the free-volume distribution of the glassy state, while the nonequilibrium lattice fluid model is based on nonequilibrium thermodynamics.

Dual-Mode Model. The physical basis of the dual-mode model rests on the concept of unrelaxed free volume in the glassy state. The concept of unrelaxed free volume $V_g - V_\ell$, where V_g is the specific volume of the glass and V_ℓ is the extrapolated specific volume of a hypothetical rubber, is illustrated in Figure 23 (71). The extremely long relaxation times for segmental motion in the glassy state lead to trapping of nonequilibrium chain conformations in glasses, thereby presumably permitting miniscule gaps to exist between chain segments. This results in the additional unrelaxed free volume, which causes the specific volume of a glass to be higher than the extrapolation for a hypothetical rubber.

The dual-mode sorption model considers the glassy solid to consist primarily of an equilibrium-densified matrix with a small volume fraction of uniformly

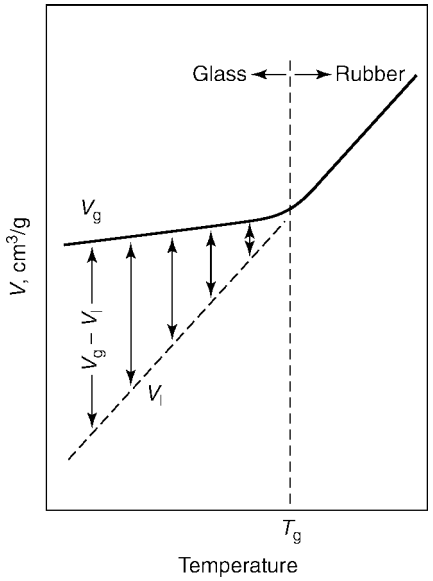

Fig. 23. Schematic representation of the unrelaxed volume, $V_g - V_\ell$, in a glassy polymer. V_g = glass specific volume; V_ℓ = equilibrium volume of densified glass. The unrelaxed volume disappears at the glass-transition temperature.

distributed molecular-scale gaps, or holes, throughout the matrix. Gaps that are smaller in size than a penetrant molecule may be locally redistributed during the sorption process in the initial exposure of the polymer to a penetrant (71). This model has proved to be very useful for interpreting a wide spectrum of phenomena including pure component and multicomponent permeation and sorption and penetrant-induced dilation in gas–glassy polymer systems. The development of the dual-mode model has been reviewed (73,74).

The dual-mode model has also been applied with some success to the sorption and transport behavior of small- and intermediate-size organic molecules in glasses (75). Above some size, however, the penetrant may be too large to be accommodated solely within individual holes, and two truly distinct environments may not actually exist for these penetrants. Even in this case, however, the concept of unrelaxed free volume remains valid, and observations of sorption and dilation behavior that apply to gases also apply qualitatively to larger penetrants up to the point of extreme plasticization where an actual glass transition occurs.

If a hypothetical equilibrium-densified glass, V_ℓ in Figure 23, is exposed to a given pressure of a penetrant, a sorption concentration C_D, characteristic of true molecular dissolution, occurs, as it does in rubbery polymers or liquids. In a nonequilibrium glass V_g, the additional volume present in the form of intersegmental gaps, or holes, provides for additional low energy berths for penetrants that do not require the energy expense of dilating the matrix as in the case of the dissolved mode (C_D) population. In this case, an additional sorption population with concentration C_H can occupy these sites in local equilibrium with the dissolved mode population. This hole-filling population is often described by a Langmuir isotherm. The dual-mode model can be written analytically up to reasonably

high pressures for a penetrant indicated by subscript A, in terms of the sum of a Henry's law expression for C_D and a Langmuir expression for C_H, namely

$$C_A = C_{D_A} + C_{H_A} \tag{46}$$

$$C_A = k_{D_A} p_A + \frac{C'_{H_A} b_A p_A}{1 + b_A p_A} \tag{47}$$

where k_{D_A} is the coefficient that characterizes sorption of the penetrant in the densified regions of the matrix and p_A is the penetrant partial pressure. The value of k_{D_A} has been correlated with the Lennard–Jones potential of the gas (76) and the free volume of the polymer (77). The b_A and C'_{H_A} parameters are the Langmuir affinity and capacity constants, respectively. Several researchers have shown that C'_{H_A} approaches zero at the glass transition in generally the same way that $V_g - V_\ell$ approaches zero (78,79). In fact, the value of C'_{H_A} has been predicted well as the product of the unrelaxed volume fraction $[(V_g - V_\ell)/V_\ell]$ and the inverse equivalent sorbed volume of penetrant molecules. The volume per molecule can be estimated with reasonable accuracy using data from gas adsorption on zeolites or activated carbons. The value of $[(V_g - V_\ell)/V_\ell]$ can be estimated using dilatometry in most cases (80).

The dual-mode model is easily extended to include gas mixtures (81). In terms of partial pressures, the expressions for mixed-gas sorption are usually written as

$$C_A = k_{D_A} p_A + \frac{C'_{H_A} b_A p_A}{1 + b_A p_A + b_B p_B} \tag{48}$$

$$C_B = k_{D_B} p_B + \frac{C'_{H_E} b_B p_B}{1 + b_A p_A + b_B p_B} \tag{49}$$

The dual-mode model thus predicts a reduction in sorption of any gas, at a fixed partial pressure, as the partial pressure of a second gas is increased. Sorption of binary mixtures of CO_2/N_2O and CO_2/CH_4 in poly(methyl methacrylate) (PMMA) is predicted to within 2% by this model. Moreover, Figure 24 shows pure and mixed-gas data (82) for the sorption of CO_2 and CH_4 in poly(phenylene oxide) (PPO). The solid lines represent dual-mode model predictions for a partial pressure of 0.5 MPa (5 atm) for each component using parameters from the pure-gas isotherm. The dual-mode sorption model provides an accurate description of the solubility of both pure and mixed-gases for these polymers over the range of partial pressures studied. The small differences between mixed-gas permeability model predictions and experimental data may be due to differences in conditioning of the polymer in single- and mixed-gas environments. These differences might also be attributable to changes in the diffusivity of mixture components due to the presence of another component; diffusivity is not as easily predicted as solubility because of potential plasticization effects for strongly sorbing penetrants. These effects appear to be less significant for equilibrium sorption coefficients than for diffusion coefficients.

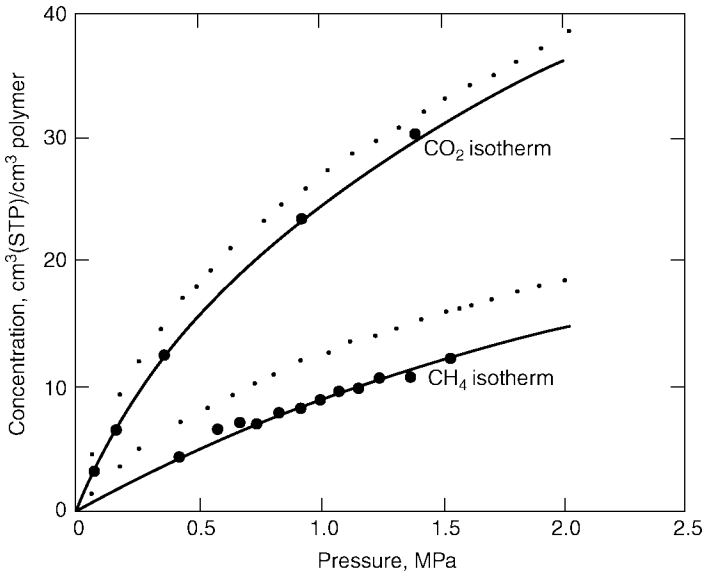

Fig. 24. Mixed-gas sorption for the PPO/CO_2/CH_4 system at 35°C. Dotted lines show pure-gas sorption and solid lines show model predictions for $p_{CO_2} = p_{CH_4} = 0.5$ MPa (5 atm) (76). To convert MPa to atm, multiply by 10.

Site-Distribution Model. In the dual-mode model, penetrants are pictured as being sorbed into either a low energy microvoid site or a high energy densified site within the glassy polymer matrix. These two idealized sorbed populations are probably an oversimplification of the actual penetrant–polymer environment. Experimental evidence to validate the assumption of two dissolved penetrant populations has been conflicting and somewhat inconclusive (44,83–85). In the site-distribution model, the glassy matrix is pictured as containing free volume distributed throughout as spherical holes. The distribution of hole volumes in the glass is assumed to be Gaussian. This Gaussian distribution of free volume throughout the polymer results in a corresponding Gaussian distribution of sorption site energies. As penetrant is dissolved into the polymer, the low energy sorption sites are preferentially occupied. As the penetrant activity is increased, higher energy sorption sites are filled. The site-distribution model uses Fermi–Dirac statistics to determine the occupancy at each energy level, where the integral of the site density times the occupancy level is the total penetrant concentration (86).

The distribution of free volume pictured in the site-distribution model is the result of volume fluctuations in the liquid polymer being frozen into the glass as the polymer is quenched below T_g. The shape of the free-volume distribution is assumed to be Gaussian and is expressed by

$$n(V_h) = \frac{1}{\sigma_v \sqrt{\pi}} \exp\left(- \frac{(V_h - V_{h0})^2}{{\sigma_v}^2} \right) \tag{50}$$

where, $\sigma_v = \sqrt{2k_B T_g V_{h0}/B}$ is the width of the distribution. V_{h0} is the average hole volume and B is the bulk modulus at the T_g. When a gas molecule of volume, V_g, is sorbed into a hole an elastic contribution, G_{el}, is made to the total Gibbs energy:

$$G_{el} = \frac{2}{3}\mu_s \frac{(V_g - V_h)}{V_h} \tag{51}$$

where, μ_s is the shear modulus. The total Gibbs energy, G, consists of this elastic contribution plus an enthalpic contribution from penetrant–polymer interactions and an entropic contribution from penetrant confinement in the sorption site. Only the elastic contribution to the Gibbs energy is assumed to vary with hole volume. Through the use of Fermi–Dirac statistics the occupancy of the sorption sites is calculated, with the total penetrant concentration equaling

$$C_A = \frac{V_{mol} N_0}{N_A} \int_{-\infty}^{\infty} \frac{1}{\sigma_G \sqrt{\pi}} \exp\left(- \frac{(G - G_0)^2}{\sigma_G^2} \right) \frac{1}{1 + \exp[(G - \mu)/RT]}\, dG \tag{52}$$

The V_{mol}/N_A prefactor is necessary to put the concentration into the common units of cc STP/cc polymer. V_{mol} equals 22,400 cc STP/mole, and N_A is Avogadro's number. G_0 is the Gibbs energy of a hole of average size V_{h0}. The chemical potential of the penetrant gas phase is given by μ. The width of the Gibbs energy distribution is given by σ_G and is related to the width of the free volume hole size distribution, σ_v. N_0 is the number of sorption sites.

The site-distribution model results in four fitting parameters: H_0, S_0, N_0, and σ_G. The parameters H_0 and S_0 are used to calculate $G_0 = H_0 - TS_0$. S_0 is the change in entropy from the gas phase to solution in a polymer. The value of S_0 in most cases is roughly equal to the change in entropy from the gas phase to the solid. The number of sorption sites, N_0, can be treated as a purely adjustable parameter but is often estimated as $6.7 \times 10^{21}/\text{cm}^3$ (86). The distribution width σ_G can be calculated from measurable quantities or treated as an adjustable parameter. Correlations do exist between the distribution width and T_g and the volume of the gas molecule, V_g (87). For high T_g polymers, more volume fluctuations exist in the liquid polymer state. When these high T_g polymers are quenched to the glassy state, the volume fluctuations are frozen and a wide distribution of sorption sites results. When large gas molecules are dissolved, there is a greater elastic strain which results in a large energy distribution.

The site-distribution model has recently been extended to mixed-gas sorption, and is able to account for competitive sorption effects (88). As with the dual-mode model, the site-distribution model allows for the prediction of mixed-gas sorption by using parameters obtained from experimentally less complicated pure-gas sorption measurements. Like the dual-mode model, the site-distribution model is phenomenological, while the dual-mode model uses the bulk specific volume V_g and extrapolated equilibrium volume V_ℓ as key parameters; the site-distribution model relies upon the bulk shear modulus μ_s as a key parameter. The use of bulk parameters to characterize sorption which occurs at the atomistic scale is questionable from a fundamental point of view; nevertheless, such models provide useful tools to describe and even predict the effect of conditioning and physical aging

on the free-volume distribution in glassy polymers. Conditioning of the polymer with a highly soluble gas such as CO_2 produces packing disruptions throughout the glass which remain after conditioning as low energy sorption sites. Physical aging, on the other hand, reduces the number of low energy sites and results in a narrower energy distribution (89). The physical insight provided by the site-distribution model and the possibility of future development into a truly predictive model are advantages which must be weighed against the added mathematical complexity.

Nonequilibrium Lattice Fluid Model. The nonequilibrium lattice fluid (NELF) model is a nonequilibrium thermodynamics approach to modeling sorption in a glassy polymer. The model pictures penetrants as a single dissolved population in a nonequilibrium glassy matrix (90). The penetrant concentration in the glassy phase is calculated by requiring that the chemical potential of the penetrant in the gaseous phase equal the chemical potential of the penetrant in the glassy phase. NELF is a modified form of the Sanchez–Lacombe (SL) lattice fluid model for a rubbery polymer. The SL lattice fluid model places polymer segments and vacancies onto a lattice (91,92). The placements of vacancies on the lattice simulate free volume in the polymer. The number of vacancies is dependent on the pressure and temperature of the system. Within this conceptual framework, the SL lattice fluid model expression for the Gibbs free energy of a pure component is (92)

$$G = rnRT^* \left\{ -\tilde{\rho} + \frac{\tilde{P}}{\tilde{\rho}} + \frac{\tilde{T}}{\tilde{\rho}} \left[(1-\tilde{\rho})\ln(1-\tilde{\rho}) + \frac{\tilde{\rho}}{r}\ln(\tilde{\rho}) \right] \right\} \tag{53}$$

In the above equation $\tilde{\rho}$, $\tilde{T}$, and $\tilde{P}$ are the reduced density, temperature, and pressure, respectively. These variables are defined as: $\tilde{\rho} = \rho/\rho^*$, $\tilde{T} = T/T^*$, and $\tilde{P} = p/P^*$. The parameters ρ^*, T^*, and P^* are obtained from the P-V-T properties of the pure component. The parameter r in equation 53 is the number of lattice sites occupied by a single molecule.

In order to extend the SL lattice fluid model to a penetrant-polymer mixture, a set of mixing rules is used to calculate ρ^*, T^*, and P^* for the mixture from the penetrant and polymer parameters. The proper set of mixing rules is given by Doghieri and Sarti (90). Using ρ^*, T^*, and P^* for a mixture of n_1 moles penetrant and n_2 moles polymer, the Gibbs free energy of the mixture is obtained from (90)

$$G = RT^*(r_1 n_1 + r_2 n_2) \left\{ -\tilde{\rho} + \frac{\tilde{P}}{\tilde{\rho}} + \frac{\tilde{T}}{\tilde{\rho}} \left[(1-\tilde{\rho})\ln(1-\tilde{\rho}) + \frac{\varphi_1}{r_1}\ln(\varphi_1\tilde{\rho}) \right] \right\} \tag{54}$$

where r_1 and r_2 are the number of lattice sites occupied by a molecule of "1" and "2," respectively, in the mixture. φ_1 is the volume fraction of penetrant in the mixture.

In the SL lattice fluid model approach, the equilibrium density is found by minimizing the Gibbs free energy. The following equilibrium conditions are enforced for the pure component and the mixture (90):

$$\left(\frac{\partial G}{\partial \rho} \right)_{T,p,n} = 0 \text{ at equilibrium for the pure component} \tag{55a}$$

$$\left(\frac{\partial G}{\partial \rho}\right)_{T,p,n_1,n_2} = 0 \text{ at equilibrium for the mixture} \tag{55b}$$

The chemical potential of the system is then calculated at values of the density which satisfy the above conditions at each temperature and pressure.

In a nonequilibrium system, the conditions for equilibrium (eqs. 55a and 55b), no longer hold. NELF bypasses the need for an equilibrium condition through the use of an internal order parameter. The order parameter characterizes the degree the system is out of equilibrium. One can imagine multiple possible choices of order parameters in the glassy state, such as the fractional free volume at the T_g (93) or simply the mixture density (94). NELF specifically makes use of the polymer partial density, ρ_2, as its order parameter. A discussion of the rationale and implications of picking an order parameter is given by Doghieri and Sarti (90). Nevertheless, with NELF the order parameter ρ_2 is related to the reduced density of the mixture by

$$\tilde{\rho} = \frac{\rho_2}{\omega_2}\frac{1}{\rho^*} \tag{56}$$

The chemical potential of the dissolved penetrant is then given as (95)

$$\frac{\mu_1}{RT} = \ln\left(\frac{\omega_1\rho_2}{\omega_2\rho_1^*}\right) - \frac{M_1P_1^*}{\rho_1^*RT_1^*}\left\{\begin{array}{c}\left[1+\left(\dfrac{T_1^*P^*}{T^*P_1^*}-1\right)\dfrac{\omega_2\rho^*}{\rho_2}\right]\ln\left(1-\dfrac{\rho_2}{\omega_2\rho^*}\right)\\ +\dfrac{T_1^*P^*}{T^*P_1^*}+\dfrac{\rho_2}{\omega_2\rho^*}\left[\dfrac{T_1^*}{T}\left(1+\dfrac{P^*}{P_1^*}-\left(\omega_2\dfrac{\rho^*}{\rho_2^*}\right)^2\dfrac{\Delta P_{12}^*}{P_1^*}\right)\right]\end{array}\right\}+1 \tag{57}$$

where ω_1 and ω_2 are the weight fractions of penetrant and polymer. ΔP^*_{12} is a binary interaction term and is assumed equal to $(\sqrt{P_1^*}-\sqrt{P_2^*})^2$ (91). The weight fraction of penetrant in the glassy phase is solved for by requiring that the chemical potential of dissolved penetrant, given by equation 57, equal the chemical potential of the penetrant in the gas phase. The chemical potential in the gas phase may be calculated using the SL lattice fluid model or an equation of state such as Peng–Robinson.

The truly impressive feature of NELF is that it is a completely predictive model of small molecule sorption in glassy polymers, if information about the polymer partial density, ρ_2, is known. Unfortunately, ρ_2 is obtained from dilatometry data, and these data exist for only a very small number of penetrant–polymer systems, which limits the general practical applicability of the model. In light of this shortcoming, two approaches have been used to make NELF more widely applicable. The first approach assumes that the polymer partial density is equal to the density of the pure polymer, $\rho_2{}^0$ (96). This approach limits NELF to low pressures, where no polymer swelling occurs; however, in this pressure range, NELF is still completely predictive. The second approach to increase the applicability of NELF introduces one or two adjustable parameters (95). In this approach, the polymer partial density is assumed to vary linearly with pressure such that

$$\rho_2 = \rho_2^0(1-kp) \tag{58}$$

where k is the swelling coefficient. If the pure polymer density is known, equation 58 is substituted into equation 57 and k is treated as an adjustable parameter. If the pure polymer density is unknown, then both ${\rho_2}^0$ and k are treated as adjustable parameters. This approach allows for the prediction of the entire isotherm from just one or two sorption measurements. Another drawback of NELF is that values of ρ^*, T^*, and P^* are required for both components. These values are available for most common penetrants (92,97). However, fewer of these values exist for polymers because they are obtained from the P-V-T behavior of the polymer above T_g. Many high performance glassy polymers of interest have extremely high glass transitions, which makes obtaining P-V-T data in the rubbery state experimentally challenging.

Transport Models for Glassy Polymers

The following three multicomponent transport models have been used to explain the depression of the permeability of a component in a mixture relative to its pure component value (Fig. 21): the Petropoulos model and the competitive sorption model, both of which assume that direct competition for diffusive pathways within the glass is negligible, and a more general permeability model in which direct competition can occur between penetrant molecules for both sorption sites and diffusion pathways. All three of the models presented here are based upon the framework of the dual-mode model. It is worth mentioning that the site-distribution model has recently been extended to account for diffusion (98) and that free volume models exist for transport in glassy polymers (99).

Simple Dual-Mode Transport Models. As a direct extension of the dual-mode sorption model, it is convenient to treat pure-gas permeability as the sum of two terms, which are characteristic of the two sorbed penetrant populations. Petropoulos first developed such an expression in terms of the chemical potential gradient of the sorbed gas (100). For the case where there is a vacuum downstream and a pressure p_{A_2} of component A upstream, the following expression results:

$$P_A = k_{D_A} D_{TD_A} + \frac{C'_{H_A} D_{TH_A}}{p_{A_2}} \ln(1 + b_A p_{A_2}) \tag{59}$$

where D_{TD_A} and D_{TH_A} are diffusion coefficients characteristic of the Henry's law (dissolved), and the Langmuir (hole-filling) populations of sorbed gas molecules. Extension of the Petropoulos model to include gas mixtures involves numerical integration of the flux equations for components A and B (101).

Taking an approach similar to that of Petropoulos, a model was developed (102) representing the flux for gas A in terms of concentration gradients rather than chemical potential gradients:

$$J_A = -D_{D_A} \frac{dC_{D_A}}{dx} - D_{H_A} \frac{dC_{H_A}}{dx} \tag{60}$$

where D_{D_A} and D_{H_A} are diffusion coefficients characteristic of Henry's law and the Langmuir populations of sorbed gas molecules. After substitution of equation 47

into equation 60, the flux expression can be integrated analytically to give the equation for pure-gas permeability, again for the condition of zero downstream pressure and an upstream pressure of p_{A_2}:

$$P_A = k_{D_A} D_{D_A} \left\{ 1 + \frac{F_A K_A}{1 + b_A p_{A_2}} \right\} \tag{61}$$

where $F_A = D_{H_A}/D_{D_A}$, $K_A = C'_{H_A} b_A / k_{D_A}$, and p_{A_2} is the upstream pressure of pure component A, with the downstream pressure assumed to be negligible. This equation represents the partial immobilization dual-mode transport model of Koros and Paul. By plotting pure-gas permeability data for component A, values of F_A, D_{D_A}, and D_{H_A} can be determined. The sorption parameters k_{D_A}, C'_{H_A}, and b_A can be determined independently in equilibrium sorption measurements, and so the parameters in either equation 59 or equation 61 can be easily determined. Therefore, by making only pure-gas sorption and permeation measurements, all of the model parameters can be determined in either of these simple dual-mode formulations of the transport expressions.

Assuming that the diffusion coefficients D_{D_i} and D_{H_i} for components in a gas mixture are unchanged from their pure-gas values, the simple expression represented above can be extended to gas mixtures. After substitution of equation 48 into equation 60, the flux equation can be analytically integrated to give the following expression for the permeability of component A in a binary mixture of gases A and B (103):

$$P_A = k_{D_A} D_{D_A} \left\{ 1 + \frac{F_A K_A}{1 + b_A p_{A_2} + b_B p_{B_2}} \right\} \tag{62}$$

Similarly, for component B,

$$P_B = k_{D_B} D_{D_B} \left\{ 1 + \frac{F_B K_B}{1 + b_A p_{A_2} + b_B p_{B_2}} \right\} \tag{63}$$

Assuming that D_{TD_i} and D_{TH_i} are constant in mixed feed situations, the Petropoulos expressions can be generalized for mixed-gas feeds; however, numerical solutions are required in this case. Equations 62 and 63 and the analogous predictions in terms of the chemical potential driving force model of Petropoulos indicate that the presence of a second gas B lowers the permeability of gas A only by reducing the sorption of gas A.

Advanced Dual-Mode Transport Models. To account for the effect of nearby gas molecules on the ability of a given gas molecule to find sites into which it might jump, Barrer proposed and developed a model that adopts a somewhat more complex description of the diffusion process in glassy materials (104). A gas molecule is capable of executing four distinct types of diffusional jumps, depending on which of the two distinct sorption environments it is diffusing from and diffusing into (104,105). Denoting the Henry's law and Langmuir

environments as D and H, respectively, the four possible jumps can be depicted as follows:

$D \rightarrow D$ (dissolved to dissolved)	$D \rightarrow H$ (dissolved to hole)
$H \rightarrow D$ (hole to dissolved)	$H \rightarrow D$ (hole to hole)

Each jump is described by a distinct primitive diffusion coefficient D_{DD}, D_{DH}, D_{HD}, or D_{HH} that is related to the average mobility of a penetrant in each of the two environments D_{D_A} and D_{H_A} as shown below:

$$D_{D_A} = D_{DD_A} + D_{DH_A}(1 - \theta_A) \tag{64}$$

$$D_{H_A} = D_{HD_A} + D_{HH_A} \tag{65}$$

where $\theta_A = C_{H_A}/C'_{H_A}$ represents the fraction of Langmuir sorption sites occupied by sorbed gas A molecules. Consequently, the model predicts that D_{D_A} decreases as the concentration of gas in the polymer increases. In effect, this model predicts a reduction in the number of diffusional pathways available to a penetrant molecule. When combined with the dual-mode sorption model for describing the fraction of filled holes, the flux equations can be integrated to give the permeability of a pure-gas A:

$$P_A = k_{D_A} D_{DD_A} + \frac{C'_{H_A} b_A (D_{HH_A} + D_{HD_A}) - k_{D_A} D_{DH_A}}{1 + b_A p_{A_2}} + 2k_{D_A} D_{DH_A} \frac{\ln(1 + b_A p_{A_2})}{b_A p_{A_2}} \tag{66}$$

Using nonlinear regression techniques to fit the pure-gas permeability vs pressure data for gas A, values for $D_{DD_A} + D_{DH_A}$, and $(D_{HH_A} + D_{HD_A})$ can be determined.

The extension of this model to mixed-gases is considerably more difficult than the extension of the simple dual-mode transport models. To include gas mixtures, the Barrer model must be modified to accurately describe the fraction of filled Langmuir sorption sites when more than one gas species is present in the polymer. To account for the presence of a second gas, the flux expressions can be rewritten using the following definition for the fraction of filled holes:

$$\theta_{total} = \frac{C_{H_A}}{C'_{H_A}} + \frac{C_{H_B}}{C'_{H_B}} \tag{67}$$

where θ_{total} represents the fraction of the total unrelaxed volume occupied by either penetrant A or B, and therefore is not available for allowing a penetrant to jump into it.

This model results in a system of nonlinear differential equations that must be solved numerically. Figure 25 (82) shows pure-gas permeability data for CO_2

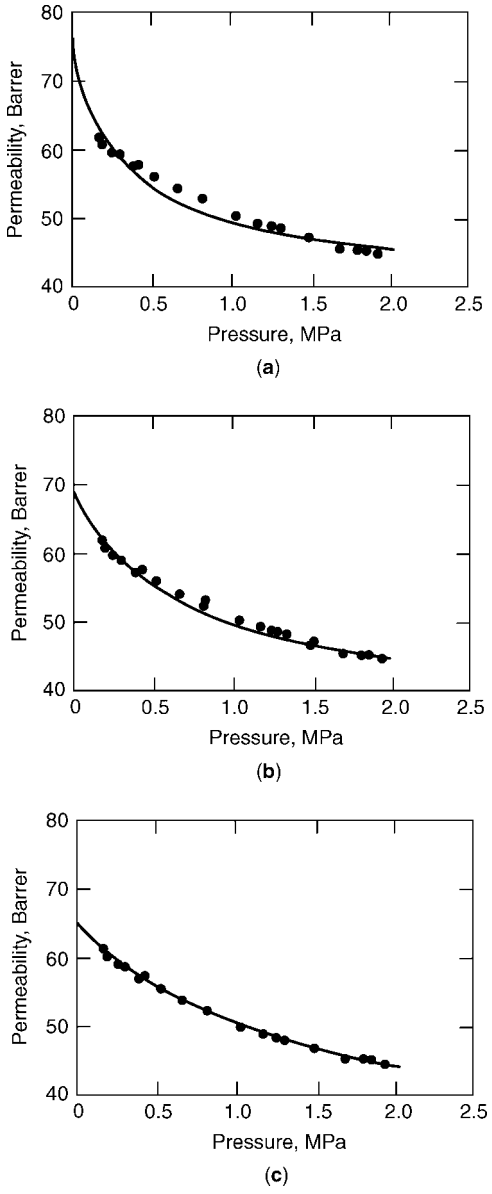

Fig. 25. Permeability of pure CO_2 in poly(phenylene oxide). The solid lines represent (**a**) the Koros and Paul, (**b**) the Petropoulos model, and (**c**) the Barrer model. To convert MPa to atm, multiply by 10.1 Barrer $= 10^{-10}$ [cm^3(STP)cm]/($cm^2 \cdot s \cdot cm$ Hg) $= 0.335$ mmol/(m · s · TPa).

in poly(phenylene oxide) along with the theoretical fits for the Petropoulos, Koros and Paul, and Barrer models, respectively. The Barrer model provides a slightly more accurate fit of the permeability data than either of the simpler models, especially in the low pressure region. This is expected because of the additional model parameter.

Figures 26 and 27 (82) show mixed-gas permeability data for an equimolar mixture of CO_2 and CH_4 in PPO along with predictions made using the Petropoulos, Koros and Paul, and Barrer models. Mixed-gas permeability is depressed relative to the pure-gas values for both components. As expected, the mixed-gas Barrer model predicts lower permeability for both components than either of the simpler models.

Below about 1 MPa (10 atm) total pressure, all three mixed-gas models give fairly accurate predictions for CO_2 permeability in the mixture. Above this pressure, however, CO_2 data lie below all model predictions. By contrast, permeability data for CH_4 in the equimolar mixture lie above all three predictions over the entire range of upstream partial pressures.

The Barrer model provides a better prediction for mixed-gas carbon dioxide permeability data, while methane permeability is predicted more accurately by the simpler model of Koros and Paul. Thus none of the models emerge as having a clear advantage over the other two in predicting PPO/CO_2/CH_4 permeability. However, several factors can be suggested as possible sources of error inherent in all of the models.

One possible discrepancy involves fugacity effects at high pressures, but fugacity effects do not fully account for the differences between permeability data and model predictions. The relative deviations of fugacity-based predictions from experimental data are somewhat smaller than those with pressure-based calculations for all three models (82).

It is unlikely that deviations from the mixed-gas sorption model are to blame for the discrepancies between mixed-gas permeability data and model predictions because the mixed-gas sorption model provides an accurate description of PPO/CO_2/CH_4 sorption. However, different conditioning effects between the equilibrium sorption and permeation conditions may introduce a significant source of error. In equilibrium sorption the polymer experiences uniform conditioning, while during permeation a conditioning profile exists through the polymer. These different conditioning histories ultimately may lead to nonnegligible differences in sorption.

From a purely practical point of view, the Koros and Paul model for mixed-gas permeability is significantly more straightforward than either the Petropoulos or Barrer model in terms of parameter calculation and comparisons between different gas–polymer systems. Although the Barrer model provides a tighter fit of pure-gas permeability data, it does not provide the more accurate prediction of mixed-gas permeability for which it was initially proposed. The inability of the more complex model to correct for the small differences between mixed-gas permeability data and the two simpler model predictions suggests that these subtle deviations may be the result of the fundamental assumptions of all three models. In terms of transition-state theory, all three of these models assume that the activated state is the same regardless of whether the penetrant was originally sorbed in a Henry's law or a Langmuir site, which leads to independent, additive fluxes through the Henry's law and Langmuir modes. This assumption is not valid if the local density around a Langmuir site is less than the density of the dissolved polymer matrix. In this case, the activated state of a penetrant sorbed in a Langmuir site will be lower in energy than that of a penetrant sorbed in a Henry's law site. Petropoulos has recently developed a more general

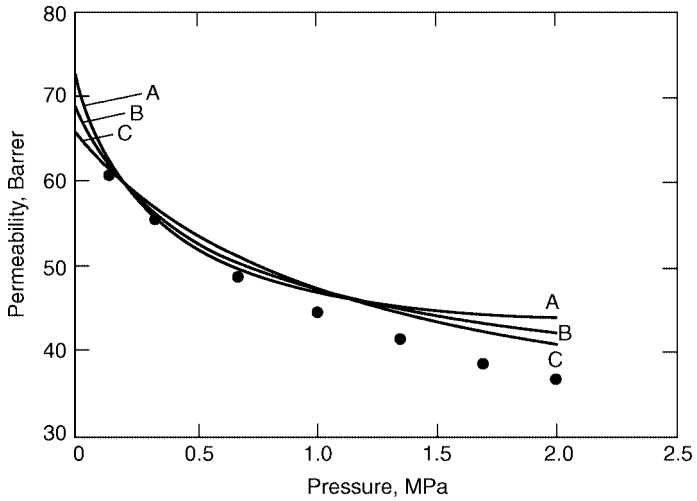

Fig. 26. CO_2 permeability for the PPO/CO_2/CH_4 system at 35°C using an equimolar gas mixture, compared with the three permeability model predictions: **A**, the Koros and Paul model; **B**, the Petropoulos model; and **C** the Barrer model. To convert MPa to atm, multiply by 10.1 Barrer $= 10^{-10}$ [cm^3(STP)cm]/($cm^2 \cdot s \cdot$ cm Hg) $= 0.335$ mmol/(m · s · TPa).

dual-mode transport model that incorporates this more complex picture of the diffusion process (106).

Another likely source of error in all three models is related to the very high solubility of CO_2 in PPO. In both the Koros and Paul and Barrer models, the characteristic diffusivity parameters are assumed constant on the

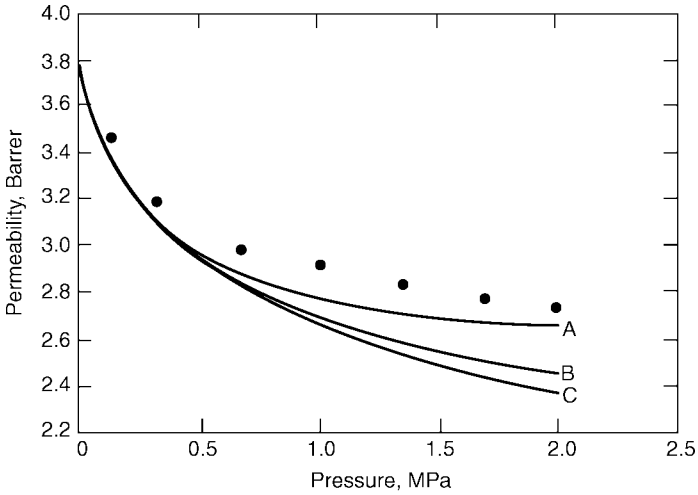

Fig. 27. CH_4 permeability for the PPO/CO_2/CH_4 system at 35°C using an equimolar gas mixture, compared with the three permeability model predictions: **A**, the Koros and Paul model; **B**, the Petropoulos model; and **C**, the Barrer model. To convert MPa to atm, multiply by 10.1 Barrer $= 10^{-10}$ [cm^3(STP)cm]/($cm^2 \cdot s \cdot$ cm Hg) $= 0.335$ mmol/(m · s · TPa).

basis of the assumption that polymer segmental mobility does not significantly change as a result of penetrant-induced dilation. This approximation ultimately breaks down and plasticization begins to dominate the behavior of the system (Fig. 21).

Polymers highly dilated with CO_2 have significantly decreased glass-transition temperatures, implying that polymer segmental motion is facilitated by high CO_2 concentration (107,108). Such increased polymer motions make it easier for gas molecules to execute diffusional jumps from one point to another in the polymer matrix. Thus, dilation may not only manifest itself in higher sorbed gas concentrations, but in increased gas diffusivity as well. As noted earlier, such changes in transport characteristics of a polymer due to high concentrations of sorbed penetrants are termed *transport plasticization*. Failure to account for this molecular-scale phenomenon is probably a significant source of the small but measurable inadequacies of the mixed-gas permeability models. The diffusivity parameters of CO_2 as determined by pure-gas sorption and permeability may, in fact, represent apparent values, which reflect the effects of CO_2 dilation. On the other hand, pure-gas diffusivity parameters for CH_4 cannot supply any information as to how much the methane diffusivity would be influenced by CO_2-induced plasticization. Thus, the mixed-gas permeability data for methane may be higher than model predictions because of increased methane diffusivity in the plasticized polymer.

Conversely, the presence of CH_4 may suppress CO_2-induced plasticization of the polymer, relative to its pure CO_2-dilated state, by compression of the free volume introduced by CO_2 sorption. It may thereby suppress CO_2 diffusivity below model predictions. Studies have also sought to refine the original idea of a constant C'_H parameter by considering plasticization-induced reductions in C'_H due to depression in the effective T_g (109).

It is most likely that the prediction of the permeability of gas mixtures containing CO_2 could be improved by accounting for the effects of CO_2-induced plasticization on transport parameters. This could be tested best at higher CO_2 pressures where such effects should be significant and, in fact, would correspond to conditions of practical importance in enhanced oil recovery operations where CO_2 and CH_4 must be separated at pressures as high as 6.9 MPa (1000 psia) and with CO_2 contents above 50%. The dual-mode transport model of Petropoulos has recently been extended to account for the effects of plasticization in both pure- and mixed-gas environments (110).

Although extensive data for mixed-gas permeation in the plasticization regime are not available, good pure-gas values are available and illustrate some important points. The permeability of CO_2 in various substituted polycarbonates shown in Figure 28 (111) increases with pressure above a certain characteristic value for each of the polymers. The shapes of the permeability curves are like the curve shown schematically in Figure 21. Plasticization occurs despite the fact that the downstream pressure is maintained at a vacuum of less than 1330 Pa (10 mm Hg). To determine when true transport plasticization occurs, the local diffusion coefficient $D_{AP}(C_A)$, which measures the ability of a penetrant to move through the membrane at a point where the local concentration of penetrant is equal to C_A, must be considered. The sorption isotherms for CO_2 in the various materials are shown in Figure 29 (111), and application of the standard

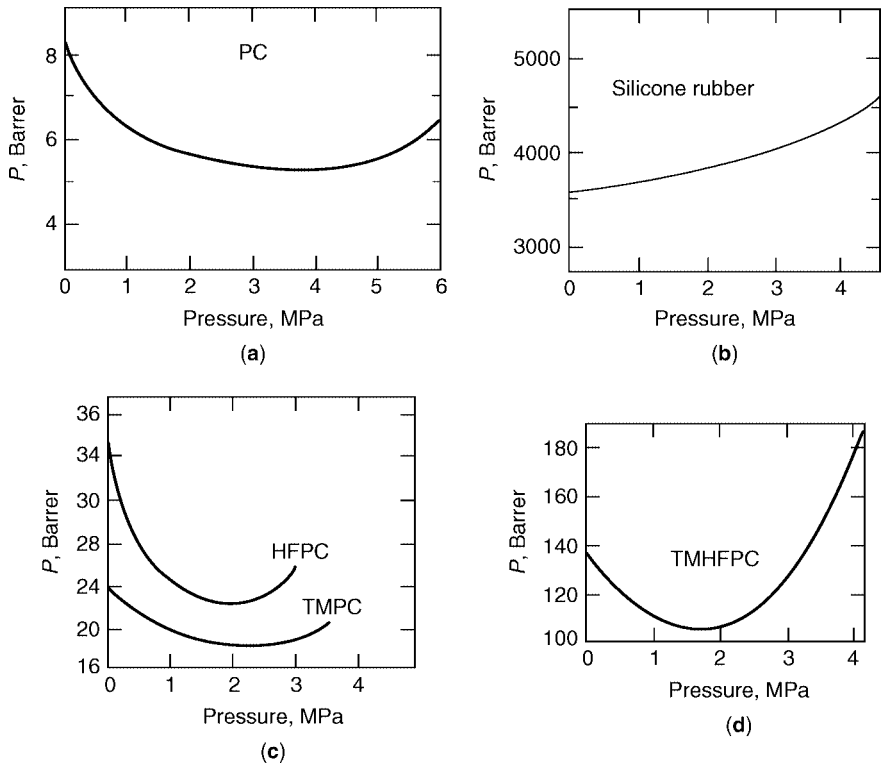

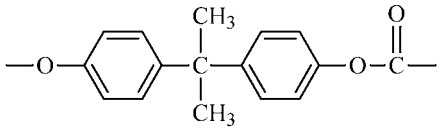

(a)

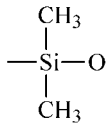

(b)

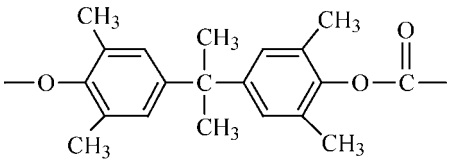

(c)

Fig. 28. Carbon dioxide permeability for (**a**) polycarbonate (PC), (**b**) silicone rubber, (**c**) tetramethylpolycarbonate (TMPC), and the fluorinated species wherein the methyls on the central carbon are fluoromethyl (CF_3) groups, ie, hexafluoropolycarbonate (HFPC) and tetramethylhexafluorocarbonate (TMHFPC). To convert MPa to psia, multiply by 145.1 Barrer = 10^{-10} [cm^3(STP)cm]/($cm^2 \cdot s \cdot cm$ Hg) = 0.335 mmol/($m \cdot s \cdot TPa$).

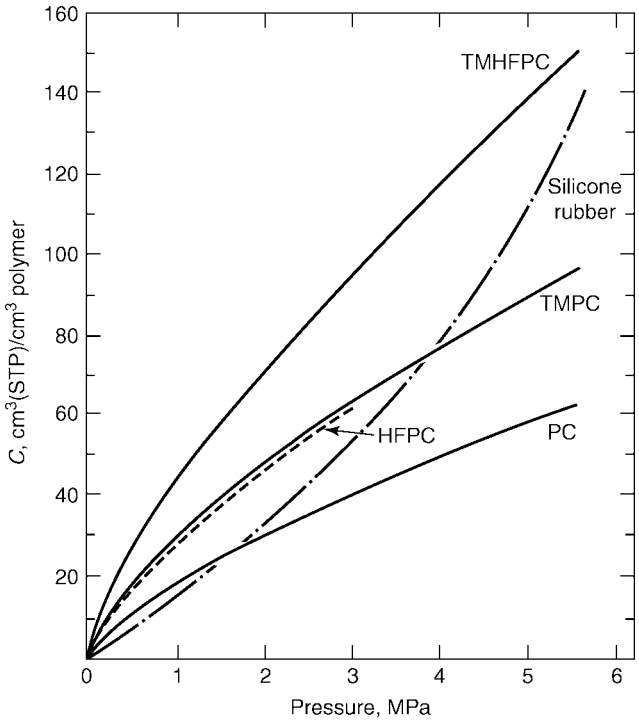

Fig. 29. Sorption isotherms of carbon dioxide in (**a**) polycarbonate (PC), (**b**) silicone rubber, (**c**) tetramethylpolycarbonate (TMPC), and the fluorinated species wherein the methyls on the central carbon are fluoromethyl (CF_3) groups, ie, hexafluoropolycarbonate (HFPC) and tetramethylhexafluorocarbonate (TMHFPC). To convert MPa to psia, multiply by 145.

formula (eq. 37) for determination of $D_{AP}(C_A)$ leads to the results shown in Figure 30 (111).

The characteristic tendency of the $D_{AP}(C_A)$ curves to rise to a plateau at intermediate concentrations does not reflect true plasticization, but instead reflects the saturation of preexisting intersegmental packing defects as considered in the dual-mode theory. The deviation upward from the plateau at higher concentrations indicates a breakdown in the constancy of the local diffusion coefficient for the normally-packed matrix and thereby signals the onset of extreme transport plasticization. Despite the markedly different thermal-transition points of the various glassy materials, it is interesting that all of them show plasticizing inflections at around 35 ± 2 cm^3 polymer. On the other hand, the local partial pressure (or fugacity) at which plasticization is reached varies greatly for the different materials, suggesting that the useful operating range for the various materials will also vary considerably. For bisphenol A polycarbonate (PC), the upturn point in local diffusion coefficient is not reached until roughly 2.76 MPa (400 psia); for tetramethylhexafluoro-bisphenol A polycarbonate (TMHFPC), the point occurs at ~0.93 MPa (135 psia) because of the much higher solubility in this open, packing-inhibited material.

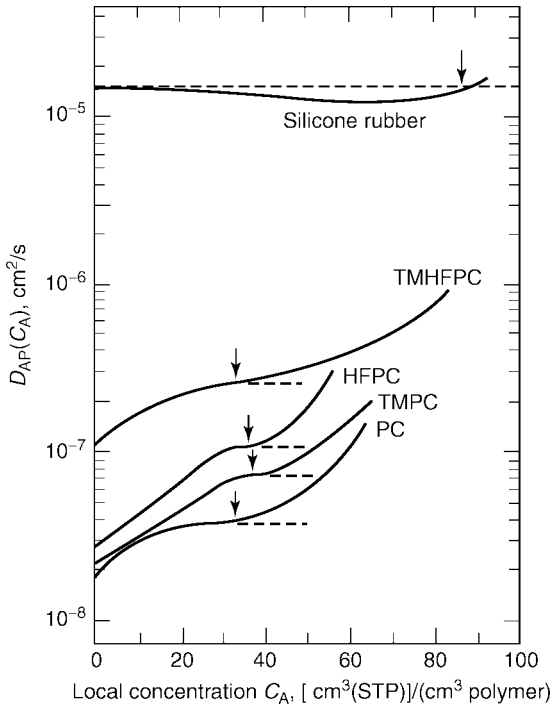

Fig. 30. Effective diffusion coefficient for carbon dioxide at 35°C. The arrows show the approximate concentration at which plasticization occurs as indicated by the upward inflection in the curve.

Measurements on PC and tetramethylbisphenol A polycarbonate (TMPC) indicate that the overall volume dilations due to sorption of 35 cm^3 (STP) CO_2/cm^3 polymer are 3.8% and 2.9%, respectively (111), suggesting that less volume dilation is required to induce plasticization in the more rigid TMPC (T_g = 198°C) than the PC (T_g = 150°C). X-ray diffraction measurements indicate higher intersegmental spacings in TMPC, than in PC (112). It may be that more dilation is needed to free a neighboring segment of the more packable PC. In addition, because of the larger sorption coefficient in TMPC, the plasticization condition is reached at a lower CO_2 pressure.

History Effects in Glassy Polymers

Penetrant-Induced Effects. History-dependent properties of glassy polymers are well documented in terms of thermal (113,114) and mechanical (115) properties. Studies have related excess enthalpy changes measured by differential scanning calorimetry to changes in small-molecule sorption (116,117). Many studies have reported penetrant-induced history-dependent (or conditioning) effects for gas and vapor sorption and transport properties in glassy polymers. The ability to display long-lived changes in sorption, diffusion, and permeation properties

Table 6. Partial Molar Volumes of CO_2 in Organic Liquids

Medium	Partial molar volume, cm^3/mol
Carbon tetrachloride	48.2
Chlorobenzene	44.6
Benzene	47.9
Acetone	44.7
Methyl acetate	44.5
Methanol	43.0
Average	*45.5*

distinguishes glassy materials from rubbery ones and is believed to arise from the long relaxation times in glasses that reflect their inhibited segmental motions (68).

If a sufficient amount of some penetrant is absorbed into a glassy polymer and then totally removed, the amount of excess volume and enthalpy of the sample will have been changed. In a real sense, the material is no longer the same, since it is now in a different nonequilibrium state. If the upstream face of a glassy film is exposed to a conditioning agent while maintaining the downstream face at vacuum, it is possible to induce a conditioning profile of excess volume and enthalpy. A complete treatment of this phenomenon is exceedingly complex, and since the excess enthalpy and excess volume of a nonequilibrium glass tend to change correspondingly, it is common to use excess volume as the primary variable for discussion. This is convenient since it allows direct monitoring of changes in sorption-induced nonequilibrium properties by dilatometry. Experiments illustrate that dilation and sorption for the glass have marked hystereses (Fig. 31) (16), whereas rubbers behave simply as equilibrium materials with no measurable hysteresis.

The essentially linear nature of the dilation response of the glass during sorption may seem surprising at first, given the marked nonlinearity of the sorption isotherm. This response, however, is consistent with the dual-mode sorption model and, in fact, is rather an important independent verification that the model has a realistic physical basis. The dual-mode viewpoint suggests that only the fraction of the total sorption associated with the actual separation of chain segments to accommodate penetrant will cause volume dilation. Since the gap-filling population in a glass contributes substantially less to dilation than the Henry's law population, the infinite-dilution partial specific volume of a penetrant is lower in the glassy polymer than in low molecular weight solvents or rubbery polymers in which no gap filling occurs.

Infinite-dilution partial molar volumes for CO_2 in various low molecular weight liquids (Table 6) are insensitive to the type of medium and decrease only slightly as interactions between the medium and CO_2 increase. This approximation may be somewhat inappropriate for highly supercritical gases such as nitrogen or methane, but for CO_2 near ambient temperature it appears valid. The average of the CO_2 partial molar volumes in the organic liquids is approximately 46 cm^3/mol. The value for CO_2 in silicone rubber determined from analysis of

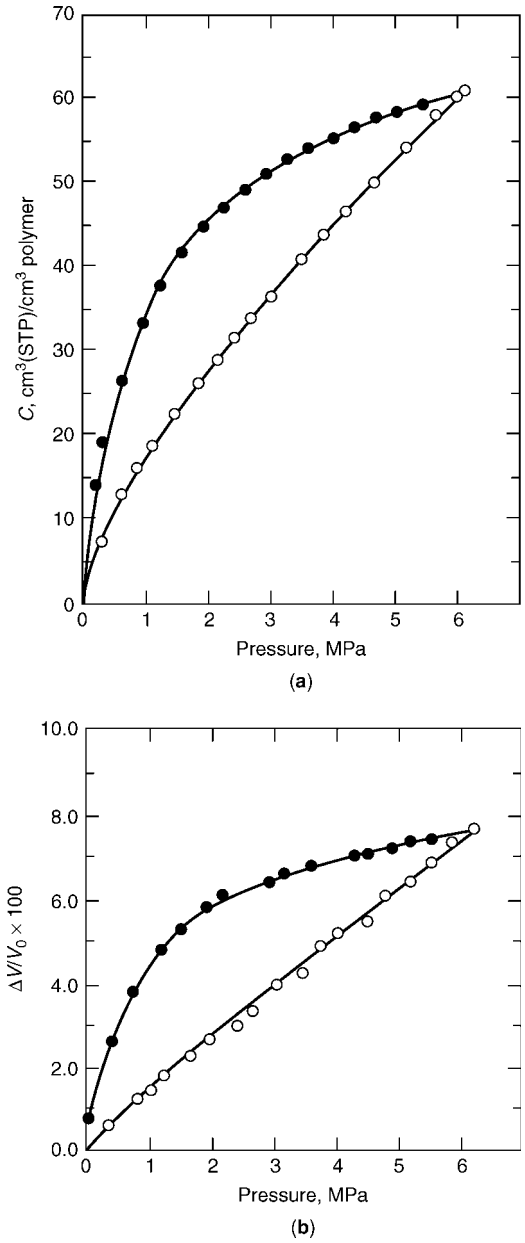

Fig. 31. (**a**) Sorption and (**b**) dilation isotherms for CO_2 in bisphenol A polycarbonate at 35°C. ○, Sorption; ●, desorption. To convert MPa to psia, multiply by 145.

sorption and dilation data is also approximately 46 cm^3/mol. In measurements (118) of the partial molar volume for CO_2 in low density polyethylene over a temperature range of 25–55°C, no strong temperature dependence is observed. The average value reported over this temperature range, 44.5 cm^3/mol, is also

in good agreement with the value in low molecular weight liquids and silicone rubber.

An impressive quantitative test of the dual-mode model is possible using partial molar volume results. Dilation of the glassy matrix is predictable using the average value of the partial molar volume from Table 6 (119) for CO_2. If the Langmuir sorption term in the dual-mode sorption model corresponds to a true hole-filling process, the volume dilation relative to V_0, the unswollen polymer volume, can be predicted using the fraction of CO_2 sorbed according to linear Henry's law sorption terms, $k_D p$. Volume dilation predictions assuming that the entire population causes dilation correspond to the dashed line in Figure 32, whereas the solid line is the prediction based on the assumption that only the Henry's law population causes the dilation. The solid line is remarkably effective for predicting dilation (120). Similar success has been demonstrated using the Henry's law prediction for other glassy polymers (118).

The effects of conditioning on subsequent sorption behavior of glasses, as well as the hystereses seen in both the dilation and mass uptake curves in Figure 31, have been studied. On total removal of the CO_2, the nonzero intercept on the volume dilation axis represents the additional excess volume introduced during sorption–desorption cycles. For this same system of CO_2 and bisphenol A polycarbonate, the experiments measuring the permeability while steadily increasing the upstream pressure, then monotonically decreasing the upstream pressure back to zero, add insight. During the experiment, the downstream face of the film is always maintained under vacuum. The CO_2 permeability in PC shown in Figure 33 (121) displays the shape typical of a dual-mode response at low pressures, followed by

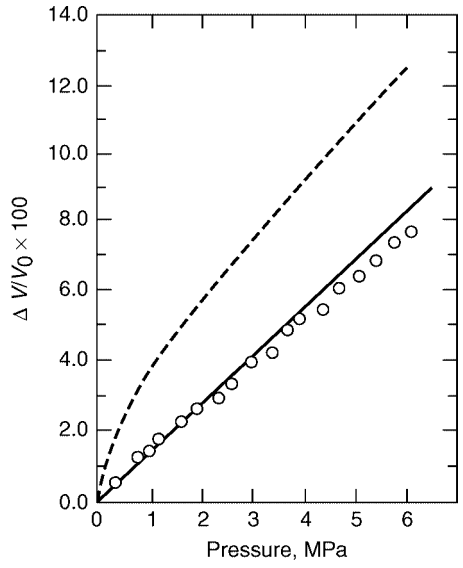

Fig. 32. Volume dilation by sorption of CO_2 in bisphenol A polycarbonate at 35°C. The dashed line is the prediction assuming that the entire population causes dilation, whereas the solid line is the prediction based on the assumption that only the Henry's law population causes the dilation. To convert MPa to psia, multiply by 145.

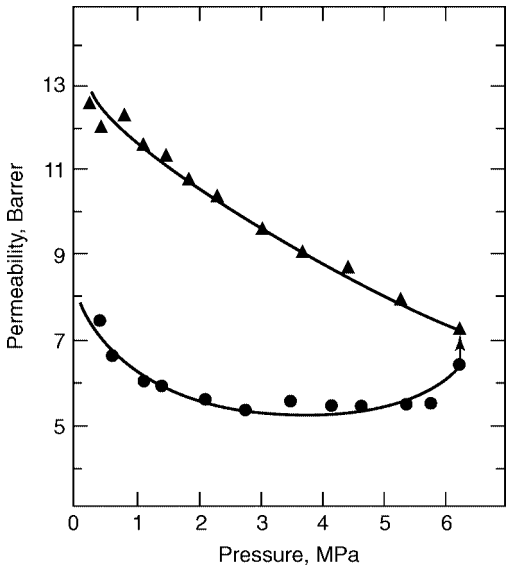

Fig. 33. Permeability of CO_2 through bisphenol A polycarbonate at 35°C illustrating the hysteretic behavior due to conditioning. ●, pressure increasing; ▲, pressure decreasing. To convert MPa to psia, multiply by 145.

plasticization at high pressures during the pressurization leg of the cycle. During depressurization, the permeability increases steadily as the pressure is reduced. The nominal time to reach steady state for the 0.127-mm sample of polycarbonate is much less than one day if simple Fickian kinetics applies; longer times were used to guarantee true equilibration because polymer relaxation effects might protract the process. The permeability at 3.4 MPa (500 psia) following the normal equilibration time (5 days) was shown to be negligibly different from the value after a 63-day equilibration time (121).

At low pressures, the permeabilities for the depressurization legs are about 100% larger than the permeability for the pressurization leg of the cycle. The increase in the permeability for the depressurization can be explained in terms of the enhanced solubility and diffusivity in the disturbed matrix. The disturbances to the matrix appear to be more subtle than those responsible for the true packing defects characterized by the C'_H parameter. In the dilated state, the disturbances can be thought of as causing a generalized reduction in the cohesive energy density of the polymer, thereby making it energetically easier to make a cavity to insert a gas molecule into a dissolved state. On total removal of the disturbing penetrant, some of these subtle disturbances may coalesce as a result of slow segmental movement to produce new packing defects of sufficient size to accommodate a penetrant.

Typically, even at high pressure the lower sorbing gases, such as nitrogen, helium, and even methane, are not able to induce the hysteretic responses (conditioning) observed with CO_2. The lower condensability, and hence lower solubility of these supercritical gases, is presumably responsible for their lack of conditioning capability. Although these low sorbing gases are not able to induce a hysteretic

response, they can maintain the disturbed matrix in an open state if the solubility is sufficiently high under the conditions used after the exposure to the primary conditioning gas (122).

Similar effects have been noted for gases using intermediate-size penetrants as the disturbing and probing agents (123–126). The use of PMMA, PVC, or polystyrene monodisperse microspheres allows study of these larger penetrants with exceedingly small diffusion coefficients. Effects consistent with the general ideas noted above are seen in these cases, but additional complexity often enters because of protracted glassy state relaxation.

Sample Dimension Dependent Effects. Recently, it has been noted that the permeability of glassy polymers decreases over time and the selectivity increases over time. Interestingly, the decreases in permeability and increases in selectivity are accelerated for thin films, on the order of a micrometer in thickness. The study of the gas transport properties in thin films is not only academic because film thicknesses of this order are often used in semiconductors, in adhesives, and in packaging. Furthermore, the skin thicknesses of asymmetric hollow fibers, the most common industrial membrane geometry, are usually 1 μm or less.

The work of Pinnau and co-workers with asymmetric films was the first to show dramatic time-dependent gas transport properties (127,128). Later, Pfromm and co-workers showed similar behavior in free-standing polyimide and polysulfone films (129). Figure 34 shows that for a 0.5-μm thick polyimide film, the N_2 permeability decreases by approximately 50% over a 6000-h period, while the He/N_2 selectivity increases by approximately 25% in the same time period. The decrease in permeability is not nearly as dramatic for the thick films. Rezac and co-workers (130) and McCaig and co-workers (131) saw similar effects in polyimide/ceramic and polycarbonate/ceramic composite membranes, respectively. Chung and Teoh observed the same effects in asymmetric hollow fiber gas separation membranes (132).

The time-dependent gas transport properties illustrated above are usually described in terms of physical aging. Physical aging is a well-known phenomenon in glassy polymers that results from their nonequilibrium nature. As already mentioned, the segmental motions of the polymer chains are severely hindered in the glassy state, but these motions are not completely excluded. The hindered segmental motions allow for the recovery of unrelaxed free volume, $V_g - V_\ell$ (see Fig. 22). The gradual approach to the equilibrium volume, V_ℓ, is called physical aging (68).

Two mechanisms are often used to describe physical aging: lattice contraction and diffusion of free volume. In the lattice-contraction mechanism, the polymer chains are pictured as uniformly moving closer together, as if the lattice spacing throughout the polymer has decreased. The kinetics of the lattice contraction are not dependent on the sample dimensions. The diffusion of free volume or holes was first proposed by Alfrey (134). In this mechanism, packets of free-volume are pictured as diffusing from the interior to the surface of the sample where they are eliminated. Since the diffusion of free-volume process is assumed to be Fickian, the loss of free volume becomes dependent on the sample dimensions.

Curro and co-workers (135) proposed that contributions from both the lattice contraction and diffusion of free volume mechanisms represented the overall volume recovery in the glass. McCaig and co-workers extended this idea to capture

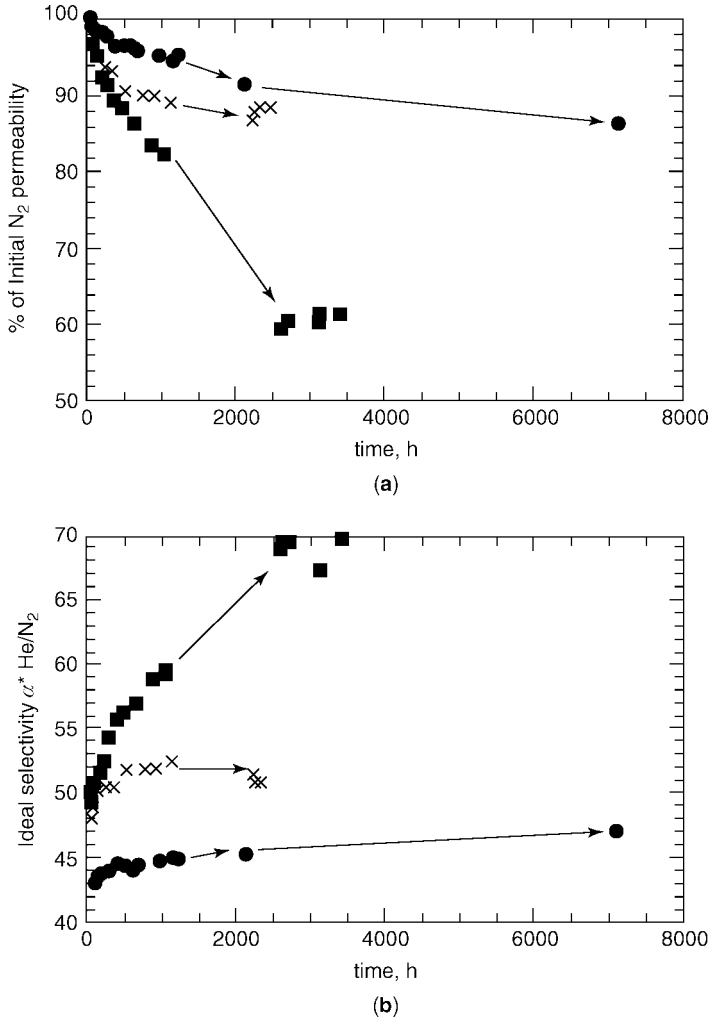

Fig. 34. (**a**) Decrease in N_2 permeability and (**b**) increase in He/N_2 selectivity for polyimide films of varying film thickness: ●, 28.45 μm; ×, 2.54 μm; and ■, 0.5 μm. Arrows indicate storage in dry air at 35°C. From Ref. 133.

the effect the free volume recovery had on the permeability of the glass (136). In this approach, the free volume is related to the permeability by the commonly used correlation:

$$P(t) = A\exp[-B/v_f(t)] \tag{68}$$

where A and B are parameters dependent on the penetrant–polymer pair and $v_f(t)$ is the time-dependent fractional free volume. The time dependence of the free volume loss from the lattice contract mechanism was modeled as a first-order exponential with time constant τ. The time dependence of the free-volume loss from the free-volume diffusion mechanism was calculated by solving the diffusion equation with a concentration-dependent diffusion coefficient. The concentration

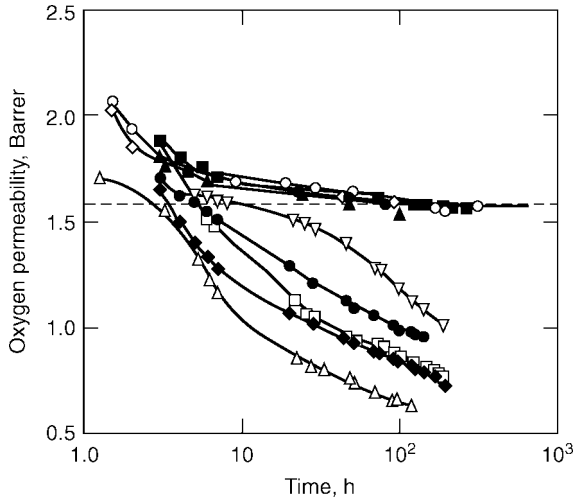

Fig. 35. Oxygen permeability decay through BPA–BnzDCA films illustrating physical aging effects for the following film thicknesses: ○, 33 μm; ■, 28 μm; ◇, 9.7 μm; ▲, 4.4 μm; ▽, 1.85 μm;, ●, 0.99 μm; □, 0.74 μm; ◆, 0.58 μm; △, 0.25 μm. Reprinted from Ref. 131 with permission from Elsevier..

dependence of the free volume diffusion coefficient was assumed to be of the form:

$$D = D_g \exp\left[-Z\left(\frac{1}{v_f(t)} - \frac{1}{v_f^g}\right)\right] \tag{69}$$

where $v^g{}_f$ is the fractional free volume of the slowly cooled glassy polymer, D_g is the diffusion coefficient when $v_f = v^g{}_f$, and Z is a material parameter. The concentration dependence of the diffusion coefficient captures the experimentally observed self-retarding nature of physical aging. The diffusion coefficient of free volume decreases as free volume is eliminated from the sample. This is the same concentration dependence seen for the diffusion coefficient with many small penetrants.

The dual-mechanism approach of McCaig and co-workers described above was able to describe the oxygen permeability decay in bisphenol. A benzophenonedicarboxylic acid (BPA–BnzDCA) films of varying thickness remarkably well. This data is illustrated in Figure 35. All films, regardless of thickness, experience an initial sharp decline in permeability. This drop is due to the lattice-contraction mechanism, which is independent of sample dimension. Only in the thin films where the half-thickness ℓ was less than 2.5 μm was a contribution from the free-volume diffusion mechanism observed.

Orientation-Induced Effects. Orientation and combined heat and orientation processing affect the transport properties of glassy polymers. Especially when crystallites are present, the effects can become surprisingly large. As noted for rubbery semicrystalline materials, the obvious improvements in barrier properties associated with organization of lamellar crystalline domains with their platelets perpendicular to the direction of penetrant flow can produce significant

Table 7. Transport Properties of Kapton H and PMDA–ODA Polyimide Films at 2 MPa

Sample	CO_2 permeability, Barrers[a]	CO_2 solubility, $cm^3(STP)/(cm^3 \cdot MPa)$[b]	CO_2 diffusivity, 10^{-10} cm^2/s	CO_2/CH_4 selectivity
Kapton H	0.3	22	11	55.0
PMDA–ODA	2.6	37	56	44.6

[a] 1 Barrer $= 10^{-10}$ $[cm^3(STP)cm]/(cm^2 \cdot s \cdot cm\ Hg) = 0.335$, $mmol/(m \cdot s \cdot TPa)$.
[b] To convert $cm^3(STP)/(cm^3 \cdot MPa)$ to $cm^3(STP)/(cm^3 \cdot atm)$, multiply by 0.1.

reductions in permeability. Simple crystallinity appears to act principally as tortuous blocking elements to increase the path length of penetrants in their random walks across the film (eqs. 18b and 45).

Depending on the aspect ratio, orientation of the crystallites can have minimal or profound effects. The results in Table 7 show roughly an order of magnitude reduction in the permeability of CO_2 in a sample of biaxially oriented Kapton polyimide as compared to a chemically identical, but essentially unoriented, sample of the same polyimide of pyromellitic dianhydride and oxydianiline (PMDA–ODA). The reductions in permeability caused by the biaxial orientation are greater for the larger CH_4 molecule as indicated by the higher permselectivity in the Kapton. X-ray scattering measurements indicate the presence of small platelet-like aggregates in the Kapton (137). The orientation of the platelets perpendicular to the direction of permeation adds significantly to the tortuosity of the Kapton samples. This is reflected in the solubility and diffusivity data in Table 7. The primary effect on permeability is due to the diffusivity component. It has been suggested that the platelet dimensions are on the order of 20 nm $\times$ 20 nm $\times$ 5 nm.

In studies of oxygen and water vapor permeability in PVC having low crystallinity (ca 3–5%) (138), the effects of biaxial orientation, draw rates, temperature of draw, and subsequent annealing temperatures have been reported. As expected, the effects of orientation are much less significant in PVC than in more highly crystalline materials in which the effectiveness of flow impediments can be influenced greatly by orientation. The oxygen and water permeability typically decrease by less than 50% with the various processing parameters, and in fact show increases in some cases.

In another study of the effects of uniaxial orientation on PVC and other essentially amorphous glasses (139), a wide range of penetrants has been considered and permeability, solubility, and diffusivity effects caused by various orientation variables have been explicitly determined (Fig. 36) (139). The orientation, measured by birefringence, leads to improved barrier properties, and appears to have an effect on both the apparent solubility coefficient $k_a = C/p$ and the apparent diffusivity determined by time-lag measurements.

One of the few studies of transport in liquid crystalline glassy polymers has yielded some interesting results (140). The liquid and more ordered nematic morphologies characteristic of these highly rigid rod-like materials is compared in Figure 37 to more flexible chained materials such as glassy poly(ethylene terephthalate) (PET), PVC, or rubbery polyethylene discussed previously.

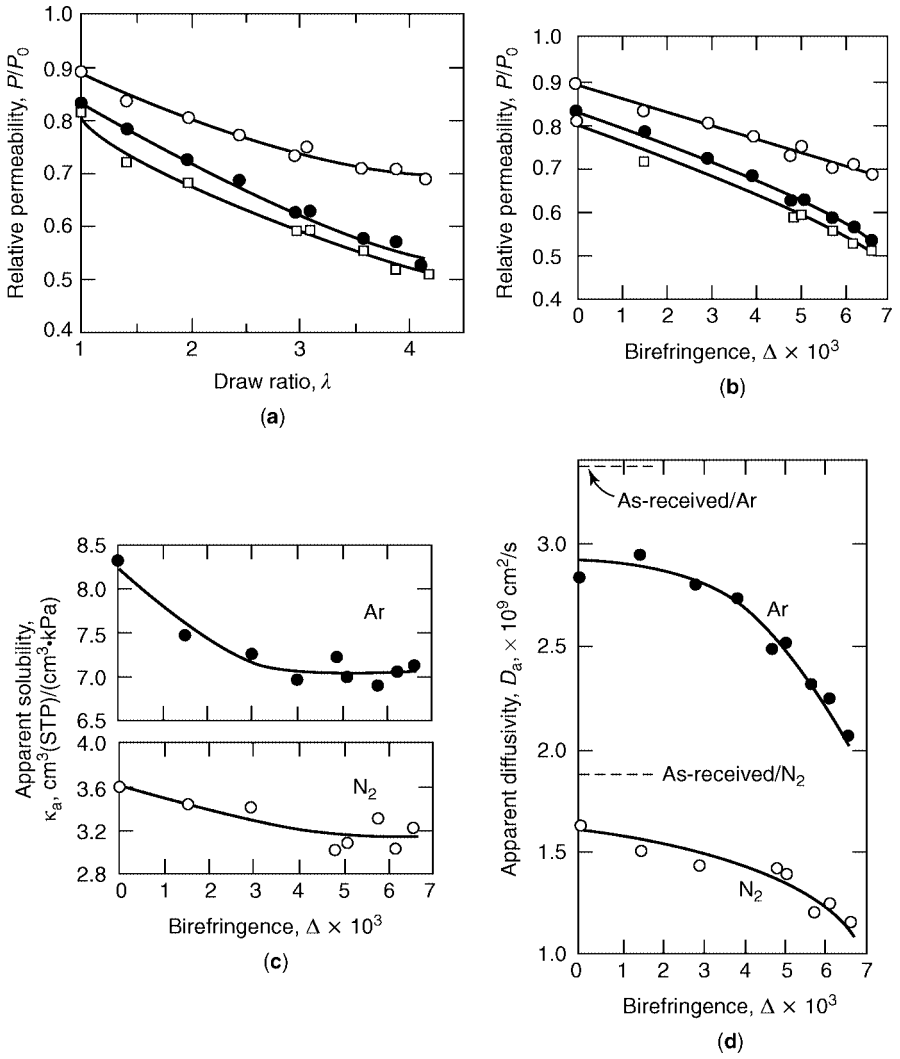

Fig. 36. Effects of uniaxial orientation on permeability at 35°C. Drawing temperature = 100°C. (**a**) Permeability, relative to "as received" value P_0 at 35°C for ○, He; ●, Ar; and □, N_2 in PVC as a function of draw ratio. (**b**) Relative permeability at 35°C for ○, He; ●, Ar; and □, N_2 as a function of birefringence. (**c**) Apparent solubility for Ar and N_2 in PVC at 35°C vs film birefringence. (**d**) Apparent diffusion coefficients for Ar and N_2 in PVC at 35°C as a function of film birefringence.

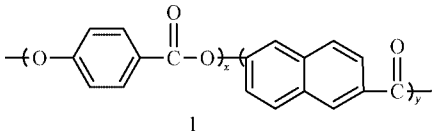

1

The liquid crystalline material with the approximate repeat unit shown as structure (**1**) above has properties that approach those of the excellent barrier

Table 8. Gas Transport Properties at 35°C of Liquid Crystalline Polymer and Polyacrylonitrile[a]

	P, 10^{-5} Barrers[b]		D_a, 10^{-10} cm^2/s		S_a, $cm^3(STP)/(cm^3 \cdot MPa)$[c]	
Gas	LCP	PAN	LCP	PAN	LCP	PAN
Helium	17,700	71,000	6,600	270	0.002	0.20
Nitrogen	3.0	2.9	1.4	0.042	0.0016	0.052
0Oxygen	47	54	7.1	0.14	0.0050	0.29
Argon	10	18	1.5	0.042	0.0054	0.33
Carbon dioxide	70	280	0.96	0.023	0.0510	9.2

[a] Ref. 116.
[b] 1 Barrer $= 10^{-10}$ $[cm^3(STP)/cm]/(cm^2 \cdot s \cdot cm\ Hg) = 0.335$ $mmol/(m \cdot s \cdot TPa)$.
[c] To convert $cm^3(STP)/(cm^3 \cdot MPa)$ to $cm^3(STP)/(cm^3 \cdot atm)$, multiply by 0.1.

polyacrylonitrile (PAN) and are much superior to those of the structurally similar, but nonliquid crystalline PET (Table 8). PAN provides a permeation barrier largely on the basis of its tremendous resistance to penetrant diffusion. The low diffusion coefficients are associated with the intersegmental polar attractions of the acrylonitrile pendent groups. The strong polar attractions produce a high cohesive energy density that in turn increases activation energy for diffusion and thereby suppresses the diffusion coefficient. Resistances to intrasegmental motion caused by the size of the acrylonitrile group are believed to be of secondary importance in suppressing diffusion compared to the strong intersegmental forces.

The rigid liquid crystal material does not have particularly strong intersegmental attractions, and although it has significant intrasegmental resistance to rotation, it is not even as rigid as the polyimide materials noted earlier. Because of the highly ordered structure of the liquid crystalline material, the extremely

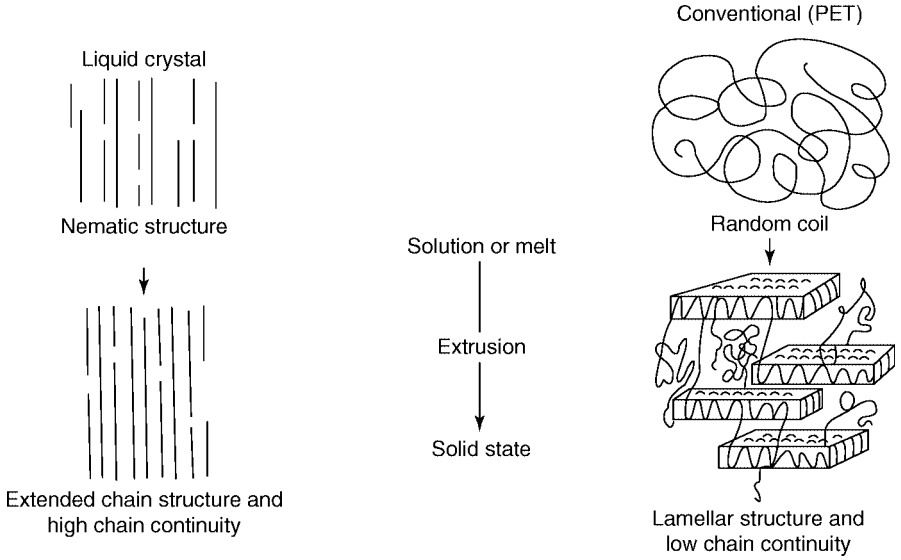

Fig. 37. Comparison of liquid crystal and conventional random coil polymer properties.

low gas solubilities reported are not surprising; however, it is surprising that the diffusivities in this highly crystalline medium are not significantly different from those of PET, which has a much lower crystalline fraction.

Non-Fickian Transport Behavior

The topic of non-Fickian transport encompasses all cases in which the simple form of the flux equation given by equation 1, with a concentration-dependent diffusion coefficient and constant-system boundary conditions, is insufficient to describe the observed time-dependent behavior of the system. This definition includes cases with position-dependent diffusion and solubility coefficients. For example, a film conditioned with a swelling agent (eg, CO_2) used to induce different properties at the upstream and downstream faces falls in this category. Another variation of this problem includes cases in which quenching or orientation produces transverse swelling stresses during the sorption kinetics process. Such position dependencies, superimposed on concentration-dependent transport coefficients, considerably complicate the response characteristics of a system. Nevertheless, mathematical analysis of the problem is possible by generalizing procedures used for the case of concentration-dependent, time-invariant coefficients if the position-dependent profile of the transport properties can be defined.

Complex concentration dependence of the sorption and diffusion coefficients can be accommodated within the framework of Fickian transport if nonisotropic variations in properties are not too serious. The use of an average diffusion coefficient and an average solubility coefficient defined over a particular range of external penetrant boundary conditions are acceptable for many practical applications.

Unlike the situation with Fickian systems, when dealing with non-Fickian systems data derived from the kinetic responses of a system cannot be readily extended to other configurations with significantly different boundary conditions or sample dimensions. By far the most difficult problems encountered in the domain of non-Fickian processes involve time-dependent changes in transport and sorption properties, ie, additional time dependence, beyond that caused by simple time variation in the local concentration. The additional time-dependent problem is the most difficult to treat because it generally involves introducing additional physical expressions. Transverse swelling stresses typify such cases (141). In this example, the additional physics are accommodated by a linear viscoelastic approximation to account for the time-dependent relaxation of stresses induced in the medium by swelling.

Another example of this class is solvent-induced crystallization (142). The effects of crystallization kinetics and rate of movement of the boundary between penetrated and unpenetrated regions have been treated. Moreover, effects of increasing impediments to diffusion caused by the increasing crystalline fraction during the same time scale as that of the solvent transport are included in the model of the system. Such models become exceedingly complex and fall outside the domain of the present discussion; however, they clearly require the input of information related to transport properties and their dependence on local conditions.

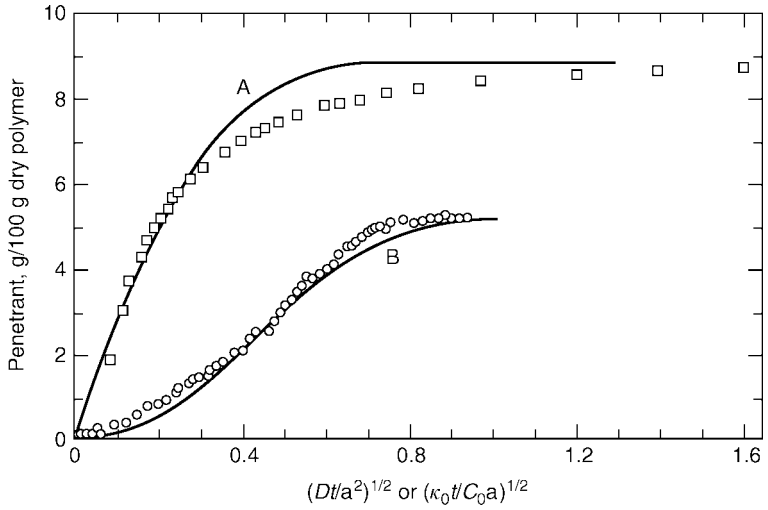

Fig. 38. Comparison of theoretical curves and experimental data for n-hexane sorption in the large- and small-diameter spheres at $P/P_0 = 0.75$ and 30°C. **A**, Fickian model, diameter = 184 μm; **B**, Case II model, diameter = 0.534 μm.

Testing samples of different macroscopic dimensions of a given material under certain conditions can bring unusual factors into play.

Indeed, entirely different responses can be observed as the time required for relaxation of stresses varies relative to the time required to change the local concentration at a point in the material. The dependence of mass absorbed M_t on time at early time in a sorption run is often used to categorize the type of transport process occurring. A simple dependence on the square root of time ($t^{0.5}$) is an indication of Fickian transport (recall eq. 3a), whereas dependence t^a, $a >$ 0.5 on is indicative of non-Fickian transport and is termed anomalous.

A limiting case of non-Fickian response in which $a = 1.0$ is typically referred to as *Case II diffusion* to differentiate it from normal Fickian (Case I) diffusion. Case I (Fickian) diffusion shows a linear increase in sorption as a function of the square root of time. By contrast, Case II kinetics are characterized by linear mass uptake with time as shown in Figure 38, where uptake of n-pentane in polystyrene at high activity (penetrant partial pressure) shows a Fickian response in small spheres and a non-Fickian response in larger diameter spheres (143). The data strongly suggest that diffusion into the small spheres is so rapid that there is insufficient time to generate a Case II concentration profile. Apparently the diffusional equilibration in the small spheres is essentially complete before the complex step concentration profile associated with Case II sorption can be established. This behavior is similar to other observations (144).

The general problem of two independent time scales for diffusive equilibration and molecular relaxation existing in a system has been considered (145). Fickian transport is obtained when the time scale of the relaxation is either effectively zero or infinite compared to the time required to establish a concentration profile in the sample. These two limits have been called the elastic and viscous Fickian diffusion limits, respectively.

The elastic limit is characteristic of samples exposed to gases or low activities of vapors that experience little segmental disruption relative to the native polymer and are able to accommodate the sorption by elastic deformation of intrasegmental bonds or slight disruption of intersegmental bonds while maintaining the essential integrity of the entanglements of interpenetrating chains in the matrix. On removal of the perturbing penetrant, the matrix is able to recover to its original condition.

The viscous limit applies when significant swelling occurs and reorganization of the entanglement network may occur sufficiently rapidly during the solvent invasion to relax any local stresses that may tend to build. In this situation, only a complex concentration-dependent diffusion coefficient is required to describe the locally changing environment through which a penetrant must move. An example of this behavior is the initial desorption of solvent from a highly swollen polymer.

Between these two limiting Fickian cases lies an important domain in which significant swelling (greater than 10% by volume) occurs. Under such conditions, the polymer deformation in response to a local swelling stress caused by a local penetrant concentration is rapid (but not infinite) as compared to the time required to produce a change in local concentration. Typical uptake behavior in such Case II situations is linear with time as shown for the large spheres in Figure 38. The chief attributes (146) of these systems are a sharp advancing boundary existing between an inner glassy core and an outer swollen rubbery shell; a swollen gel behind the advancing penetrant front close to equilibrium with the external solvent supply; and a boundary between the swollen gel and glassy core, which advances at a constant velocity.

An induction time prior to the onset of the linear uptake in mass with time is also a characteristic common in Case II systems (147). However, this behavior is somewhat difficult to discern using the gravimetric and optical methods usually employed. An induction time is consistent with the criterion for the relatively rapid polymer deformation in response to a local swelling stress compared to the time required to produce a change in concentration profile. The approach of the surface concentration to true equilibrium in such non-Fickian systems is protracted (148). A connection has been made between the effective deformation stress acting to dilate the matrix and a thermodynamically calculable osmotic swelling stress (149). Case II front movement is visualized to occur when local stresses build to a sufficient extent to allow crazing. Combining the two concepts of an induction time at the surface and an osmotically driven local dilational stress, the yielding problem has been formulated in terms of a concentration-dependent viscosity of the matrix (150).

Thus, in essence, the Case II process is initiated when a surface element of sufficient thinness experiences a significant reduction in viscosity and is able to relax some of the stresses due to the elastically deformed chains of the polymer. This relaxation of stresses allows more solvent to invade the thin element, further depressing the viscosity, and thereby autocatalytically accelerating the stress relaxation. This results in a surface concentration that exponentially approaches its equilibrium value. While this outermost element is undergoing its rapid, but not instantaneous, relaxation, the solvent that is now available to the next infinitesimally thin element invades it as has occurred in the first exposure of the surface element. The transport to this interior element is essentially instantaneous,

because of the much lower resistance to diffusive supply through the swollen gel as compared to diffusive invasion of the virgin polymer in the second element. In this case, therefore, the second element experiences significant relaxation by the time the first is approaching its equilibrium conditions with respect to the external penetrant. A third, fourth, and progressive repetition of this process leads to a negligible concentration gradient in the swollen gel behind the front, and a small and very sharp concentration gradient in some characteristically small number of volume elements ahead of the front.

Assuming the viscosity is dependent on the local penetrant volume fraction φ_A in the volume element under consideration (147),

$$\eta = \eta_0 \exp(-m\varphi_A) \tag{70}$$

where m is an empirical constant and η_0 is the viscosity of the virgin polymer containing no penetrant. This expression is, again, related to the free-volume concepts discussed in relation to equations 18a and 19 with regard to diffusion coefficients. Further treatment (147) has focused on the magnitude of the induction time for front initiation, neglecting all diffusional resistance in the gel layer behind the front and assuming an effective average diffusion coefficient $\bar{D}$ of the penetrant in the partially plasticized thin element ahead of the front. The front velocity should be proportional to the square root of the ratio of the local effective diffusivity in each of the infinitesimal volume elements preceding the relaxation front and the unplasticized viscosity of the glassy material prior to penetration, namely

$$V(T) \propto \left(\frac{D(T)}{\eta_0(T)}\right)^{0.5} \tag{71}$$

Evidence is given to support this suggestion (147). In the study, it was concluded that the relative activation energies for the effective solvent diffusion coefficient and the intrinsic viscosity of the glass were 58.6 kJ/mol (14 kcal/mol) and 167 kJ/mol (40 kcal/mol), respectively. Based on the earlier discussion of Figure 5, the infinite-dilution values of the activation energy for the diffusion coefficient and viscosity of the glass are expected to be similar. The lower activation energy for the diffusion coefficient $\bar{D}$ in the partially plasticized glass ahead of the front as compared to the viscosity of the unplasticized glass, η_0, is not surprising.

Recent theoretical and experimental work has significantly advanced the understanding of Case II transport; however, because of the general complexity of this work, a review of it is beyond the scope of this article. The interested reader is directed to the work of Petropoulos and co-workers (151), Wu and Peppas (152), Huang and Durning (153), and the references therein.

Facilitated Transport

Facilitated transport involves the coupling of a reversible chemical reaction to the mass transfer through the polymer. This type of transport is very common in biological systems, and is capable of substantially increasing the flux and selectivity of synthetic polymers. Facilitated transport still proceeds by the solution-diffusion

mechanism; however, the penetrant now has two diffusive pathways through the polymer. The penetrant can sorb into the membrane and diffuse down its chemical potential gradient, or the penetrant can complex with the carrier upon sorption and diffusion down a penetrant-carrier complex chemical potential gradient. The second pathway is only available to penetrants that complex with the carrier. The presence of a carrier usually increases the sorption of the complexing penetrant as well.

The inclusion of the complexation reaction in facilitated transport greatly increases the mathematically complexity of the flux equations at steady state. The concentration through the polymer of the penetrant, c_A, the carrier, c_c, and the penetrant–carrier complex, $c_{A–c}$, must satisfy the following continuity equations:

$$D_A \frac{d^2 c_A}{dx^2} - r_{A–c} = 0 \tag{72a}$$

$$D_c \frac{d^2 c_c}{dx^2} - r_{A–c} = 0 \tag{72b}$$

$$D_{A–c} \frac{d^2 c_{A–c}}{dx^2} + r_{A–c} = 0 \tag{72c}$$

where D_A, D_c, and $D_{A–c}$ are the diffusion coefficients of the penetrant, carrier, and penetrant-carrier complex, respectively. The net reaction rate of complexation is $r_{A–c}$. The boundary conditions for the above equations are determined from an appropriate sorption model. Cussler solved the above set of equations analytically for the two limiting cases of fast reaction and fast diffusion (154). Except for these limiting cases, numerical methods are required to determine the flux of each species.

Facilitated transport has been reported in a number of systems. One of the most common systems uses silver as a carrier for olefins (155–157). Olefins are able to complex with silver, while paraffins are not. Transport of carbon dioxide has been facilitated through the use of amine complexes (158–160). Porphyrins have been used to facilitate the transport of oxygen and increase oxygen/nitrogen selectivity (161–163). Several methods have been used for carrier inclusion in the polymer: (*1*). carriers are blended as ionic salts with the polymer, (*2*). carriers are bonded to the polymer backbone through the use of crown ethers, and (*3*). carriers are used as the exchange sites on ionic exchange membranes. Regardless of the carrier and the inclusion technique, all facilitated transport membranes still currently suffer from unstable performance. The carrier is often poisoned by contaminants in the feed stream, and in some cases the carrier simply leaches out of the membrane. These issues must be resolved before there is widespread industrial adoption of facilitated transport membranes.

Contradictory to facilitated transport, the use of scavengers attempts to inhibit transport of particular penetrants. Scavengers are adsorbents that are blended with the polymer. This technology is often used in food packaging.

Unfortunately, most of the literature on scavenging techniques is only available in patents (164–166). Scavengers typically attempt to limit transport of oxygen, water, and organoleptics. Anthraquinone and iron have been used as oxygen scavengers. Clays, molecular sieves, and other common desiccants have been used as water scavengers. Antioxidants, such as butylated hydroxytoluene (167), are often used as organoleptic scavengers.

Proton Exchange Membranes

In recent years, a great deal of research has been focused on proton exchange membranes (PEMs) for use in fuel cells. Fuel cell based vehicles are touted as a more efficient, environmentally-friendly replacement for internal combustion engines. The fuel cell harnesses energy from the chemical reaction of hydrogen and oxygen to form water. In this reaction, the cathode and anode are separated by the PEM which allows passage of protons and theoretically blocks passage of other species. The electrons produced from the reaction are routed through an external circuit to provide power.

Nafion produced by Dupont is the most commonly used PEM material. Nafion is a hydrated perfluorosulfonic acid (PFSA) polymer. The Nafion backbone is hydrophobic, while side-chain sulfonic acid groups are hydrophilic. The repeat unit of Nafion is given as structure (**2**).

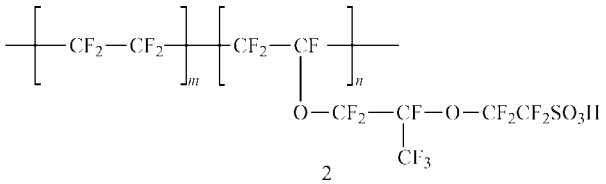

2

Hydrated Nafion is thought to have a morphology composed of a hydrophobic matrix with dispersed hydrophilic sulfonic acid clusters connected by pores (168). At low hydration levels, the pores between sulfonic acid clusters are thought to be collapsed. At high hydration, the pores become open and the sulfonic acid clusters are truly interconnected. As a result of this rather complex morphology, a great detail of debate exists in the literature about the mechanism of transport in Nafion. Models of transport based on the solution-diffusion mechanism have been proposed (169,170). These models picture Nafion as a one-phase homogenous material where transport is driven by chemical potential gradients. Alternative models, based on the pore-flow mechanism, have also been proposed for transport in Nafion (171,172). In these models, Nafion is pictured as a porous material, where transport is achieved by convective flow through pores. Neither type of model is able to describe all of the observed transport phenomena in Nafion. Recently, it has been argued that a combination of the solution-diffusion and pore-flow models may be appropriate for Nafion (173,174). At low hydration levels, solution-diffusion based transport is the dominant mode because no interconnected pores exist. At high hydration levels, pore flow based transport is dominant because now

an interconnected pore network does exist. At intermediate levels of hydration, the two mechanisms of transport are both present.

Since the scope of this article is limited to transport in dense, nonporous polymers, the rest of this discussion is limited to transport where a solution-diffusion mechanism is assumed to occur. In this regime, the flux of "A" is given by (175)

$$j_A = -D_A\left(\frac{dc_A}{dx} + z_A c_A \frac{F}{RT}\frac{d\psi}{dx}\right) \tag{73}$$

where z_A is the charge of "A", F is Faraday's constant, and ψ is the electrostatic potential. For protons, which have a charge of $z_A = 1$, the gradient in electrostatic potential is the dominant driving force, and the flux equation reduces to

$$j_{H^+} = -\frac{D_{H^+} c_{H^+} F}{RT}\frac{\Delta\psi}{L} \tag{74}$$

where L is the membrane thickness. In the literature, the flux is often reported as a current density i, which equals

$$i = Fj_A = \frac{\sigma\,\Delta\psi}{L} \tag{75}$$

where the conductivity $\sigma = D_A c_A F^2/RT$. In the case of noncharged penetrants, the charge equals zero, and equation 73 reduces to Fick's law. The above equations are exact only when the diffusion coefficient is constant, the membrane is uniformly charged, and electroosmosis effects are neglected.

Positron Annihilation Lifetime Spectroscopy

From the models of transport through both rubbery and glassy polymers given previously, it becomes apparent that knowing the free-volume distribution of the material is crucial for a microscale description of gas transport. Recently, positron annihilation lifetime spectroscopy (PALS) has been developed to probe the free volume of glassy polymers. PALS injects positrons, antielectrons, into the material where they have an extended lifetime because of interactions with the sample. The lifetime of the positronium species is on the order of a few nanoseconds and is sensitive to the electron density of the environment. This makes PALS a model-dependent technique which is capable of measuring free-volume holes that exist for 10^{-9} s or longer. PALS is able to resolve free-volume hole sizes in the range of 1–10Å;. Reviews of PALS are available (176–178).

The positron source is usually ^{22}Na, which releases a positron every 1.5 ms as it decays into ^{22}Ne. Approximately 3 ps after the positron is emitted from the source, gamma radiation of energy 1.28 MeV is released. This energy release is detected and marks the positron "birth." Once inside the sample, the positron annihilates by one of the three possible modes. The first and shortest lived mode results from the *para*-positronium, *p*-Ps, species which is formed when the positron

extracts an electron from the sample with opposite spin. The *p*-Ps species annihilates with its own electron after a lifetime of 125 ps. The lifetime of *p*-Ps is independent of the environment. The second mode of annihilation results from free positrons which have a lifetime of 100–500 ps. The third and longest lived mode results from the *ortho*-positronium, *o*-Ps, species which is formed from a positron and an extracted electron with opposing spins. The *o*-Ps decays after approximately 10^3 ps when it extracts or picks off another electron from the sample. After each annihilation event, regardless of the mode, gamma radiation of energy 0.511 MeV is released. This energy is detected and marks the "death" of the positron. The spectrum produced from these annihilation events is most commonly fit using three exponential decays. The resulting parameters are I_1, I_2, and I_3 for the intensity of each mode and the time constants τ_1, τ_2, and τ_3.

Since the behavior of the *o*-Ps species is dependent on the polymer free volume, the parameters associated with it, I_3 and τ_3, can be used to characterize the glassy structure. The probability of *o*-Ps formation and the concentration of free-volume holes are related to the intensity I_3. The time constant τ_3 is sensitive to the size of the free-volume holes. Simplistically, the time constant is short in small free-volume holes because the close proximity of the *o*-Ps to neighboring mass within the sample makes it easier for the *o*-Ps to pick off an electron. The semiempirical relationship between the time constant τ_3 and the free-volume hole radius R is given below (179).

$$\tau_3 = \frac{1}{2}\left[1 - \frac{R}{R_0} + \frac{1}{2\pi}\sin\left(\frac{2\pi R}{R_0}\right)\right]^{-1} \tag{76}$$

R_0 is equal to $R + \Delta R$ where ΔR is the electron layer thickness. The value of ΔR was found empirically and is usually assumed to equal 1.66Å;. Equation 76 assumes that the *o*-Ps resides in the center of a spherical free-volume hole, and so it follows that the hole volume V_h is equal to $4/3\pi R^3$. The fractional free volume of the material is given by (180)

$$v_\mathrm{f} = CV_\mathrm{h}I_3 \tag{77}$$

where C is a material parameter determined from the P-V-T properties of the polymer. The free volume probability-density function, $V_\mathrm{h}\,p dv_\mathrm{f}$, is given as (181)

$$V_\mathrm{h} p\, dv_\mathrm{f} = -3.32\left\{\cos\left[\frac{2\pi R}{R + 1.66}\right] - 1\right\}\frac{\alpha(\lambda)}{(R + 1.66)^2 K(R) 4\pi R^2} \tag{78}$$

where the fraction of holes between V_h and dV_h is $V_\mathrm{h}\,p dv_\mathrm{f}\,dV_\mathrm{h}$. In equation 78, $\alpha(\lambda)$ is the annihilation probability-density function. This function is obtained from a continuous fit of the positron lifetime spectra. $K(R)$ is a correction for the capture probability of *o*-Ps in different size holes. A detailed description of equation 78 is given elsewhere (182).

Because PALS is still a very new technique for characterizing glassy polymers, only a limited number of materials have been investigated which are also of interest from a gas transport standpoint (181,183–187). The most thorough

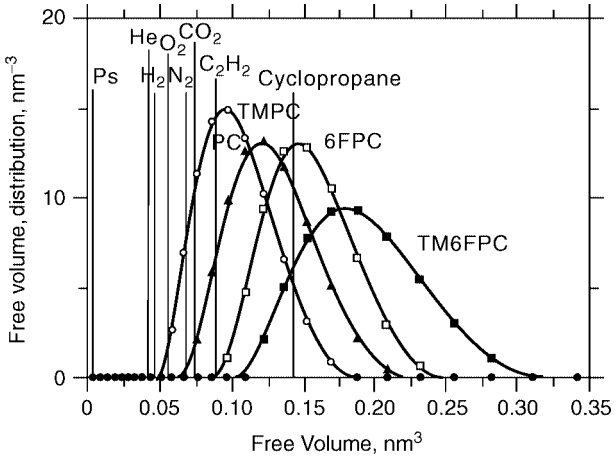

Fig. 39. Free-volume hole distributions of various polycarbonates. Dashed lines are the molecular volumes of common penetrants. Reprinted from Ref. 181. This material is used by permission of John Wiley & Sons, Inc.

study of this kind yet conducted was carried out by Shantarovich and co-workers, where positron lifetime spectra were collected for 10 glassy polymers (187). Jean and co-workers used PALS to study the same polycarbonates shown in Figure 28: PC, TMPC, HFPC, and TMHFPC (181). The distribution of free-volume hole sizes in these polymers is given in Figure 39 along with the molecular volume of common penetrants. The materials with larger average free-volume hole size also had a wider distribution of hole sizes. The diffusion coefficient of O_2 and CO_2 through these materials correlated well with the experimentally determined fractional free volume from equation 77. The ability of PALS to determine both the hole size distribution and the fractional free volume opens up a number of very interesting questions. For example, how will the transport differ in materials of the same fractional free volume but with different free-volume distributions?

Another interesting set of articles (188,189) uses PALS to investigate the behavior of the free-volume as the polymer is subjected to high pressure gases. As PC is pressurized to approximately 4.14 MPa (600 psi) by N_2, the free-volume hole radius obtained from the positron lifetime spectra increases. Continuing to increase the N_2 pressure from 4.14 MPa (600 psi) to 8.28 MPa (1200 psi) results in a decrease in the free-volume hole radius. No hysteretic effects were observed upon depressurization. This behavior was explained as plasticization and hydrostatic effects similar to those already discussed in the context of rubbery polymers. The N_2 is claimed to initially plasticize or soften the polymer resulting in larger free-volume holes. These results appear rather contrary to concepts noted with regard to the effect of pressurization on free volume in Fig. 8. As the pressure is increased more, the polymer compresses resulting in smaller free-volume holes, which is consistent with Fig. 8. A very different effect was observed when PC was exposed to high pressure CO_2. The free-volume hole size was observed to monotonically increase with CO_2. Upon depressurization, a large hysteresis was seen. After CO_2 exposure, the fractional free volume and average hole size were larger. This

behavior results from the strong conditioning effect of CO_2 that was described in a previous section.

Although PALS has been applied successfully to determine the glassy polymer microstructure, the technique has several limitations. In many low polar liquids, the positronium species forms a "bubble." This bubble results from repulsions between the electron in the positronium and electrons in the surrounding. Obviously, formation of such a bubble would affect the free-volume characterization. This bubble formation process may be possible in rubbery polymers, but is generally not thought to occur in glassy polymers (176). Inhibition or quenching effects can also affect the lifetime of the positronium species. Halogen-containing polymers can lead to inhibition effects when the positronium interacts with the halogen atom. Nitroaromatics, such as polyimides, may react with the positron causing quenching (190). Perhaps, the largest disadvantage of PALS is that it is a model-dependent technique. In this respect, characterization of free-volume distributions in polymers using PALS is analogous to obtaining the pore-size distribution of a porous material from vapor sorption–desorption experiments.

Molecular Modeling of Transport in Amorphous Polymers

The rapid increase in computing power over recent years has led to a significant body of research, which seeks to describe penetrant sorption and diffusion in amorphous polymers through the use of computer simulations. Two main goals exist for computer simulations: first, to gain a better fundamental understanding of the transport mechanism through amorphous polymers; and second, to accurately predict the transport properties (ie, the diffusion and solubility coefficients) of novel polymers. The first goal is motivated by the fact that small-molecule transport is determined by the structure of the penetrant–polymer environment on an atomistic scale. Excluding the recent use of PALS structural information on this length-scale is not accessible from traditional macroscopic transport experiments but is accessible from molecular dynamic (MD) simulations. The second goal, accurate prediction of transport properties, seeks to eliminate expensive and labor-intensive experiments. Several reviews are available on computer simulations of gas diffusion through amorphous polymers (191,192).

The starting point for all computer simulation methods is the choice of a potential energy function or force field, $\Phi(R)$. This function gives the potential energy of a system of N atoms at positions r_i. The positions of all atoms in the system are represented by the three dimensional vector $R = (r_1, r_2, \ldots, r_N)$. The force-field accounts for all bonded and nonbonded interactions between atoms in the system. Bonded interactions include bondlength and bond-angle deformations and conformational deformations. These interactions are usually described as mechanical springs with the spring constant related to experimentally known bonding energies. The nonbonded interactions include van der Waals forces and other molecular forces and are accounted for empirically by a Lennard–Jones potential. Since the nonbonded interactions include contributions from each atom pair in the system, current computational power limits the number of atoms in the system to less than 10,000 (191). Many force-field models exist and proper selection is crucial for accurate results.

Once the force-field is chosen the motion of atoms in the system is simulated using classical equations of motions:

$$\frac{du_{\mathrm{i}}(t)}{dt} = \frac{1}{m_{\mathrm{i}}} F_{\mathrm{i}}[R(t)] \tag{79a}$$

$$\frac{dr_{\mathrm{i}}(t)}{dt} = u_{\mathrm{i}}(t) \tag{79b}$$

where $u_i(t)$ is the velocity of atom i with mass m_i, at time t. The force on i, F_i, is given by

$$F_i = -\frac{\partial \Phi(R)}{\partial r_i} \tag{79c}$$

Equations 79a, 79b, and 79c are a coupled set of second-order differential equations. Methods exist to solve these equations numerically only for small timesteps. The timestep can not be greater than about 1 fs, which is about a tenth of the C—H bond oscillation time. Because such extremely small timesteps are required, an upper limit of several nanoseconds is imposed on current MD simulations (191).

The limit of MD models to at most 10,000 atoms on current workstations results in model systems that are cubic volume elements with a side length of just a few nanometers. Many approaches have been attempted to initially populate the system with atoms. The approach described by Theodorou and Suter seems to have gained the most use in recent literature (193,194). In this method the cubic volume element is filled by growing the chain one backbone bond at a time. Rotational isomeric states (RIS) theory is used to calculate the conditional probability of each conformation. As the chain is grown, the conformation angle is selected statistically to agree with the RIS information. After the chain has grown a few repeat units, it is likely to cross the boundary of the volume element. When this happens, the chain growth is continued by reentering the volume element on the opposite side. Chains grown in this manner typically achieve the overall density target, but the chain growth often results in regions of severe atomic overlap. To combat this effect, a series of static energy minimizations and dynamic simulations are carried out to equilibrate the structure. After equilibration, it is possible to get the density of the volume element to within a few percent of the experimentally determined density; however, such a high level of agreement is not currently possible for all materials because of deficiencies in the force field.

The particle trajectories from the MD simulations can be used to determine the self-diffusion coefficient using the Einstein equation:

$$D_{\mathrm{A}}^{*} = \langle |r(t) - r(0)|^2 \rangle / 6t = \frac{\lambda^2 f}{6} \tag{80}$$

where $r(t)$ is the position of a penetrant atom at time t, $r(0)$ is the initial position of the penetrant, and the angular brackets indicate an average over all penetrants in the system. The term $\langle |r(t) - r(0)|^2 \rangle$ is the mean-squared displacement of the

penetrant. f simple indicates the average frequency of a diffusional jump of length λ. The diffusion coefficient in equation 80 ideally allows one to estimate the self-diffusion coefficient in equation 6. The Einstein equation gives accurate results for rubbery polymers; however, in glassy polymers, anomalous diffusion effects act to degrade the accuracy (195). In anomalous diffusion the penetrant is not proceeding by a truly random walk from one free-volume hole to the next which is assumed by the Einstein equation. This effect results from penetrant oscillations inside the free-volume holes that occur between diffusive jumps from one hole to the next. Since the simulation time is only a few nanoseconds, these oscillations have a nonnegligible effect on the mean-squared displacement. It is important to note that this definition of anomalous diffusion is different than non-Fickian diffusion, discussed previously, which is also commonly referred to as *anomalous diffusion* in classic texts (5).

Gusev and Suter have developed a transition-state theory that is based on a Monte Carlo scheme which requires less computational power than the MD simulations and therefore is able to calculate diffusion coefficients where anomalous diffusion effects are negligible (192,196–198). In this method a three-dimensional grid is overlaid on a fully equilibrated MD volume element. A typical grid spacing is 0.03 nm (191). The insertion energy of a penetrant molecule is calculated at each grid location. In this calculation the insertion energy comes from the nonbonded contribution of the force field. The volume element is then mapped as regions of high and low packing on the basis of whether the insertion energy was high or low. This mapping allows for the identification of pathways between adjacent low energy regions. Each of these pathways is assigned a jump probability which is based on the Boltzmann distribution. This jump probability is affected by the thermal motion of the polymer atoms which is characterized by the mean-squared displacement of polymer atoms, $\langle\Delta\rangle^2$. This parameter is often gained from a short MD simulation. It should be noted that the Gusev and Suter method does not account for polymer relaxation as a result of penetrant insertion, and so this theory is only reasonable for small penetrants up to methane. With the appropriate jump probabilities, the penetrant diffusion is simulated using a Monte Carlo scheme. The insertion energy E_{ins} calculated during this process can also be used to calculate the solubility coefficient S:

$$S = \exp(-\mu_{\text{ex}}/RT) \tag{81}$$

where the excess chemical potential $\mu_{\text{ex}} = RT \ln \langle \exp(-E_{\text{ins}}/k_{\text{B}}T)\rangle$ (199). Diffusion and solubility coefficients calculated using the above techniques are usually within a factor of 3 to 5 of experimentally determined values. This degree of agreement is not accurate enough for many applications.

Molecular modeling of the type described above has been conducted on a number of polymer systems. Of these systems the great majority have been based on rubbery polymers. It is only recently that molecular simulations based on glassy polymer systems are appearing in the literature (200–206). From these studies, differences in the diffusion mechanism of rubbery and glassy polymers are starting to emerge. In both cases, the penetrant can spend relatively long periods of time (several hundred picoseconds) bouncing around inside the free-volume hole. At some point in time, a transient gap opens up because of thermally induced polymer

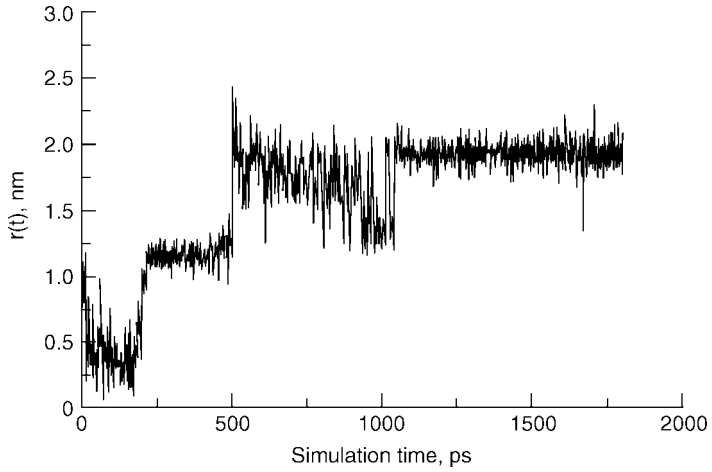

Fig. 40. H_2 diffusion through PEEK shows diffusion jumps of 5–10Å; separated by several hundred picoseconds of oscillations in free volume. Reprinted from Ref. 200, with permission from Elsevier.

motion between free-volume holes. While the gap is open, the penetrant may make a diffusive jump between holes. These jumps are usually estimated to be 5–10Å; in length (see Figs. 40 and 41). In rubbers the gaps between free-volume holes is only open for a few picoseconds, and the penetrant does not have the opportunity to make a backwards jump into the original free-volume hole. This is not the case in glassy polymers, where the channel between voids can be open for an extended period of time (several nanoseconds). This allows the penetrant molecule to jump back and forth numerous times between the two connected free-volume holes. The back-and-forth motion experienced by the penetrant in this behavior does not add to the overall diffusion coefficient (see eq. 80). This effect has been suggested

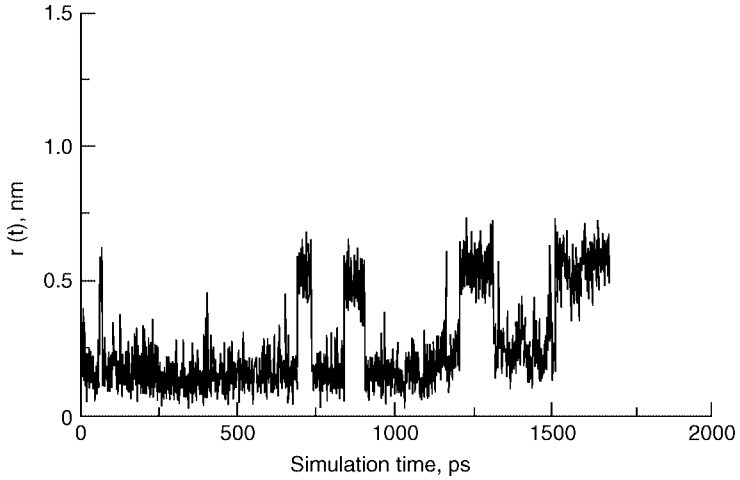

Fig. 41. N_2 diffusion through PEEK shows back-and-forth diffusion jumps that have been observed in many glassy polymers. Reprinted from Ref. 200, with permission from Elsevier.

as a contributing factor to explain why rubbery polymers exhibit much higher diffusion coefficients than glassy polymers (191), since it reduces the frequency f of a successful jump in equation 80. However, there has been recent evidence that even amorphous rubbery polymers may be significantly affected by anomalous diffusion because of alignment of the polymer chains at the nanoscale (207).

The frontier in the field of transport properties of polymers involves bridging the gap between the molecular scale penetrant–polymer environment and the macroscale solubility and diffusion coefficients. Impressive efforts to achieve this goal have already been made through the use of PALS and molecular modeling. The continued increase in computing power will allow for molecular dynamic simulations of larger volume elements for longer time periods. These improvements should cure many of the current inaccuracies inherent in molecular modeling, and allow for the first time a truly predictive method of determining polymer transport properties.

The topics discussed in this article only dealt with small-molecule diffusion through polymers. Another interesting and complex topic involves the diffusion of large polymeric penetrants through a polymeric medium. de Gennes provided a theoretical treatment of a polymer chain diffusing through a cross-linked rubber (208). In this treatment the polymer chain motion is referred to as *reptation*, since the motion of the chain is similar to that of a snake. The diffusing polymer chain is confined to a tube defined by the surrounding cross-linked matrix which restricts transverse motions. More complex treatments of reptation allow for the self-diffusion of the surrounding polymer matrix (209). The diffusion of macromolecular penetrants is of importance in a number of industrial applications including crack healing and adhesion between polymer surfaces, and in the use of polymer composites and blends.

BIBLIOGRAPHY

"Transport Properties" in *EPSE* 2nd ed., Suppl. Vol., pp. 724–802, by William J. Koros and Mark W. Hellums, University of Texas at Austin.

1. L. S. Darken, *Trans. AIME.* **174**, 184 (1948).
2. A. D. Smigelskas and E. O. Kirkendall, Technical Publication No. 2071, North-Holland, Amsterdam, The Netherlands, 1963.
3. R. B. Bird, W. E. Stewart, and E. N. Lightfoot, *Transport Phenomena*, John Wiley & Sons, Inc., New York, 1960.
4. A. L. Hines and R. N. Maddox, *Mass Transfer Fundamentals and Applications*, Prentice-Hall, Englewood Cliffs, N.J., 1985.
5. J. Crank, *The Mathematics of Diffusion*, 2nd ed., Clarendon Press, Oxford, 1975.
6. D. R. Paul, *J. Appl. Polym. Sci.* **16**, 771 (1972).
7. J. H. Petropoulos, in D. R. Paul and Y. P. Yampolskii, eds., *Polymeric Gas Separation Membranes*, CRC Press, London, 1994.
8. R. J. Bearman, *J. Phys. Chem.* **65**, 1961 (1961).
9. R. Taylor and R. Krishna, *Multicomponent Mass Transfer*, John Wiley & Sons, Inc., New York, 1993.
10. D. R. Paul and O. M. Ebra-Lima, *J. Appl. Polym. Sci.* **14**, 2201 (1970).
11. D. R. Paul and O. M. Ebra-Lima, *J. Appl. Polym. Sci.* **15**, 2199 (1971).
12. R. H. Boyd and S. M. Breitling, *Macromolecules* **7**(6), 855 (1974).

13. M. H. Cohen and D. Turnbull, *J. Chem. Phys.* **31**, 1164 (1959).
14. M. Litt, *J. Rheol.* **30**(4), 853 (1986).
15. G. J. van Amerongen, *Rubber Chem. Technol.* **24**, 109 (1951).
16. G. K. Fleming, Ph.D. dissertation, The University of Texas at Austin, Austin, Tex, 1987.
17. R. C. Reid, J. M. Prausnitz, and B. E. Poling, *The Properties of Gases and Liquids*, 4th ed., McGraw-Hill, Inc., New York, 1987.
18. C. A. Kumins and J. Roteman, *J. Polym. Sci.* **55**, 683 (1961).
19. G. J. van *Amerongen, J. Polym. Sci.* **5**, 307 (1950).
20. S. Glasstone, K. J. Laidler, and H. Eyring, *The Theory of Rate Processes*, McGraw-Hill, Inc., New York, 1941.
21. P. Meares, *J. Am. Chem. Soc.* **76**, 3415 (1954).
22. C. A. Kumins and T. K. Kwei, in G. S. Park, ed., *Diffusion in Polymers*, Academic Press, London, 1968.
23. W. W. Brandt, *J. Phys. Chem.* **63**, 1080 (1959).
24. R. J. Pace and A. Daytner, *J. Polym. Sci., Polym. Phys. Ed.* **17**(3), 437 (1979).
25. A. T. Dibenedetto and D. R. Paul, *J. Polym. Sci., Part A: Polym. Chem.* **2**(2), 1001 (1964).
26. H. Fujita, *Fortschr. Hochpolym.—Forsch* **3**, 1 (1961).
27. A. Kreitus and H. L. Frisch, *J. Polym. Sci., Polym. Phys. Ed.* **19**(5), 889 (1981).
28. S. A. Stern, S. M. Fang, and H. L. Frisch, *J. Polym. Sci., Polym. Phys. Ed.* **10**(2), p. 201 (1972).
29. S. M. Fang, S. A. Stern, and H. L. Frisch, *Chem. Eng. Sci.* **30**(8), 773 (1975).
30. S. S. Kulkarniand, S. A. Stern, *J. Polym. Sci., Polym. Phys. Ed.* **21**(3), 441 (1983).
31. M. L. Williams, R. F. Landel, and J. D. Ferry, *J. Am. Chem. Soc.* **77**, 3701 (1955).
32. S. A. Stern, J. T. Mullhaupt, and P. J. Gareis, *AIChE J.* **15**(1), 64 (1969).
33. J. S. Vrentas, H. T. Liu, and J. L. Duda, *J. Appl. Polym. Sci.* **25**(7), 1297 (1980).
34. J. L. Duda, J. S. Vrentas, S. T. Ju, and H. T. Liu, *AICHE J.* **28**(2), 279 (1982).
35. J. S. Vrentas, J. L. Duda, and M. K. Lau, *J. Appl. Polym. Sci.* **27**(10), 3987 (1982).
36. J. S. Vrentas, J. L. Duda, and L. W. Ni, *Macromolecules* **16**(2), 261 (1983).
37. N. Yi-Yan, R. M. Felder, and W. J. Koros, *J. Appl. Polym. Sci.* **25**(8), 1755 (1980).
38. E. L. Cussler, *Multicomponent Diffusion*, Elsevier, Amsterdam, The Netherlands, 1976.
39. K. Denbigh, *The Principles of Chemical Equilibrium*, 3rd ed., Cambridge University Press, Cambridge, U.K., 1971.
40. H. J. Bixler and O. J. Sweeting, in O. J. Sweeting, ed., *The Science and Technology of Polymer Films*, Vol. 2, John Wiley & Sons, Inc., New York, 1971.
41. W. J. Koros, G. K. Fleming, S. M. Jordan, T. H. Kim, and H. H. Hoehn, *Prog. Polym. Sci.* **13**(4), 339 (1988).
42. I. Pinnau, J. G. Wijmans, I. Blume, T. Kuroda, and K. V. Peinemann, *J. Membr. Sci.* **37**(1), 81 (1988).
43. H. L. Frisch and S. A. Stern, *CRC Rep.* **11**(2), 123 (1983).
44. R. A. Assink, *J. Polym. Sci., Polym. Phys. Ed.* **12**(11), 2281 (1974).
45. S. M. Jordan, Ph. D. dissertation, The University of Texas at Austin, Austin, Tex., 1988.
46. S. A. Stern, V. M. Shah, and B. J. Hardy, *J. Polym. Sci., Polym. Phys. Ed.* **25**(6), 1263 (1987).
47. P. J. Flory, *Principles of Polymer Chemistry*, Cornell University Press, Ithaca, N.Y., 1953.
48. W. J. Koros, D. R. Paul, and A. A. Rocha, *J. Polym. Sci., Polym. Phys. Ed.* **14**(4), 687 (1976).

49. S. V. Dhalewadikar, M. A. McHugh, and T. L. Guckes, *J. Appl. Polym. Sci.* **33**(2), 521 (1987).
50. J. A. Barrie and D. J. Machin, *J. Macromol. Sci. Phys.* **3**(4), 645 (1969).
51. J. A. Barrie and D. J. Machin, *Trans. Faraday Soc.* **67**(1), 244 (1971).
52. J. A. Barrie, D. Machin, and A. Nunn, *Polymer* **16**(11), 811 (1975).
53. B. H. Zimm and J. L. Lundberg, *J. Phys. Chem.* **60**, 425 (1956).
54. A. S. Michaels and H. J. Bixler, *J. Polym. Sci.* **50**, 393 (1961).
55. H. Yasuda and A. Peterlin, *J. Appl. Polym. Sci.* **18**(2), 531 (1974).
56. F. De Candia, R. Russo, V. Vittoria, and A. Peterlin, *J. Polym. Sci., Polym. Phys. Ed.* **18**(10), 2083 (1980).
57. A. S. Michaels, W. R. Vieth, and J. A. Barrie, *J. Appl. Phys.* **34**, 1 (1963).
58. A. C. Puleo, D. R. Paul, and P. K. Wong, *Polymer* **30**(7), 1357 (1989).
59. D. A. Blackadder and J. S. Keniry, *J. Appl. Polym. Sci.* **18**(3), 699 (1974).
60. D. A. Blackadder and J. S. Keniry, *J. Appl. Polym. Sci.* **17**(2), 351 (1973).
61. T. K. Kwei, H. Schonhorn, and H. L. Frisch, *J. Appl. Phys.* **38**(6), 2512 (1967).
62. R. K. Eby, *J. Appl. Phys.* **35**(9), 2720 (1964).
63. L. B. Ryder, *Plast. Eng*. 41 (1984).
64. K. Ikari and T. Sato, Paper presented at the *Ninth International Conference on Oriented Plastic Containers*, Mar. 25–27, 1985, Atlanta, Ga.
65. U.S. Pat. 4,405,667 (1983), R. C. Christensen, R. P. Genske, D. E. Kester, and W. F. Ossian, (to American Can Co.).
66. L. M. Robeson, A. Noshay, M. Matzner, and C. N. Merriam, *Angew. Makromol. Chem.* **29/30**, 47 (1973).
67. P. M. Subramanian, *Polym. Eng. Sci.* **25**(8), 483 (1985).
68. L. C. E. Struik, *Polym. Eng. Sci.* **17**(3), 165–173 (1977).
69. R. T. Chern, W. J. Koros, H. B. Hopfenberg, and V. T. Stannett, in D. R. Lloyd, ed., *Materials Science of Synthetic Membranes*, ACS Symposium Series 269, American Chemical Society, Washington, D.C., 1985.
70. D. G. Pye, H. H. Hoehn, and M. Panar, *J. Appl. Polym Sci.* **20**(2), 287 (1976).
71. R. T. Chern, W. J. Koros, E. S. Sanders, S. H. Shen, and H. B. Hopfenberg, in T. E. Whyte, ed., *Industrial Gas Seperations*, ACS Symposium Series 223, American Chemical Society, Washington, D.C., 1983.
72. T. A. Barbari and R. M. Conforti, *Polym. Adv. Technol.* **5**(11), 698 (1994).
73. W. R. Vieth, J. M. Howell, and J. H. Hsieh, *J. Membr. Sci.* **1**(2), 177 (1976).
74. H. B. Hopfenberg and V. T. Stannett, in R. N. Haward, ed., *The Physics of the Glassy State*, Applied Science Publishers, Ltd., London, U.K., 1973, Chapt. 9, p. 505.
75. V. Saxena and S. A. Stern, *J. Membr. Sci.* **12**(1), 65 (1982).
76. R. J. Pace and A. Datyner, *J. Polym. Sci., Polym. Phys. Ed.* **18**(5), 1103 (1980).
77. Y. Maeda and D. R. Paul, *J. Polym. Sci., Polym. Phys. Ed.* **25**(5), 1005 (1987).
78. W. J. Koros, G. N. Smith, and V. Stannett, *J. Appl. Polym. Sci.* **26**(1), 159 (1981).
79. K. Toi, G. Morel, and D. R. Paul, *J. Appl. Polym. Sci.* **27**(8), 2997 (1982).
80. W. J. Koros and D. R. Paul, *J. Polym. Sci., Polym. Phys. Ed.* **19**(10), 1655 (1981).
81. W. J. Koros, *J. Polym. Sci., Polym. Phys. Ed.* **18**(5), 981 (1980).
82. B. J. Story and W. J. Koros, *J. Polym. Sci., Polym. Phys. Ed.* **27**(9), 1927 (1989).
83. A. Bandis, B. J. Cauley, C. E. Inglefield, W. Y. Wen, P. T. Ingelfiend, A. A. Jones, and A. Melc'uk, *J. Polym. Sci., Polym. Phys. Ed.* **31**(4), 447 (1993).
84. E. J. Cain, W. Y. Wen, A. A. Jones, P. T. Inglefield, B. J. Cauley, and J. T. Bendler, *J. Polym. Sci., Polym. Phys. Ed.* **29**(8), 1009 (1991).
85. S. A. Stern, S. Zhou, J. L. Araux-Lara, and B. R. Ware, *J. Polym. Sci., Part C: Polym. Lett.* **27**(11), 427 (1989).
86. R. Kirchheim, *Macromolecules* **25**(25), 6952 (1992).

87. A. Gruger, P. Gotthardt, M. Ponitsch, H. G. Brion, and R. Kirchheim, *J. Polym. Sci., Polym. Phys. Ed.* **36**(3), 483 (1998).
88. P. Pekarski and R. Kirchheim, *J. Membr. Sci.* **152**(2), 251 (1999).
89. P. Pekarski, J. Hampe, I. Boehm, H. G. Brion, and R. Kirchheim, *Macromolecules* **33**(6), 2192 (2000).
90. F. Doghieri and G. C. Sarti, *Macromolecules* **29**(24), 7885 (1996).
91. I. C. Sanchez and R. H. Lacombe, *Macromolecules* **11**(6), 1145 (1978).
92. I. C. Sanchez and R. H. Lacombe, *J. Phys. Chem.* **80**(21), 2352 (1976).
93. R. G. Wissinger and M. E. Paulaitis, *Ind. Eng. Chem. Res.* **30**(5), 842 (1991).
94. D. Boudouris and C. Panayiotou, *Macromolecules* **31**(22), 7915 (1998).
95. M. Giacinti Baschetti, F. Doghieri, and G. C. Sarti, *Ind. Eng. Chem. Res.* **40**(14), 3027 (2001).
96. F. Doghieri and G. C. Sarti, *J. Membr. Sci.* **147**(1), 73 (1998).
97. I. C. Sanchez and P. A. Rodgers, *Pure Appl. Chem.* **62**(11), 2107 (1990).
98. M. Ponitsch, P. Gotthardt, A. Gruger, A. G. Brion, and R. Kirchheim, *J. Polym. Sci., Polym. Phys. Ed.* **35**(15), 2397 (1997).
99. J. S. Vrentas and C. M. Vrentas, *J. Polym. Sci., Polym. Phys. Ed.* **41**(8), 785 (2003).
100. J. H. Petropoulos, *J. Polym. Sci., Polym. Phys. Ed.* **8**(10), 1797 (1970).
101. J. H. Petropoulos, *J. Membr. Sci.* **48**(1), 79 (1990).
102. D. R. Paul and W. J. Koros, *J. Polym. Sci., Polym. Phys. Ed.* **14**(4), 675–685 (1976).
103. W. J. Koros, R. T. Chern, V. Stannett, and H. B. Hopfenberg, *J. Polym. Sci., Polym. Phys. Ed.* **19**(10), 1513 (1981).
104. R. M. Barrer, *J. Membr. Sci.* **18**, 25 (1984).
105. J. Schaefer and co-workers, *Macromolecules* **18**(3), 368 (1985).
106. J. H. Petropoulos, *J. Polym. Sci., Polym. Phys. Ed.* **27**(3), 603 (1989).
107. J. S. Chiou, J. W. Barlow, and D. R. Paul, *J. Appl. Polym. Sci.* **30**(6), 2633 (1985).
108. Y. Kamiya, T. Hirose, K. Mizoguchi, and Y. Naito, *J. Polym. Sci., Polym. Phys. Ed.* **24**, 1525 (1986).
109. J. S. Chiou and D. R. Paul, *J. Appl. Polym. Sci.* **32**(1), 2897 (1986).
110. J. H. Petropoulos, *J. Membr. Sci.* **75**, 47 (1992).
111. W. J. Koros and M. W. Hellums, Paper presented at the *Fifth International Conference on Fluid Properties and Phase Equilibria for Chemical Process Design*, Banff, Alberta, Canada, May 1989.
112. M. W. Hellums, W. J. Koros, G. R. Husk, and D. R. Paul, *J. Membr. Sci.* **46**(1), 93 (1989).
113. A. R. Berens and I. M. Hodge, *Macromolecules* **15**(3), 756 (1982).
114. S. E. B. Petrie, *J. Polym. Sci., Polym. Phys. Ed.* **10**(7), 1255 (1972).
115. W. C. Dale and C. E. Rogers, *J. Appl. Polym. Sci.* **16**(1), 21 (1972).
116. A. H. Chan and D. R. Paul, *Polym. Eng. Sci.* **20**(1), 87–94 (1980).
117. H. Hachisuka, Y. Tsujita, A. Takizawa, and T. Kinoshita, *Polymer* **29**(11), 2050 (1988).
118. T. Hirose, K. Mizoguchi, and Y. Kamiya, *J. Polym. Sci., Polym. Phys. Ed.* **24**, 2107 (1986).
119. J. Horuiti, *Sci. Pap. Inst. Phys. Chem. Res. Jpn.* **17**, 126 (1931).
120. G. K. Fleming and W. J. Koros, *Macromolecules* **19**(8), 2285 (1986).
121. S. M. Jordan, W. J. Koros, and G. K. Fleming, *J. Membr. Sci.* **30**(2), 191 (1987).
122. S. M. Jordan, W. J. Koros, and J. K. Beasley, *J. Membr. Sci.* **43**(1), 103 (1989).
123. R. W. Connelly, N. R. McCoy, W. J. Koros, H. B. Hopfenberg, and M. E. Stewart, *J. Appl. Polym. Sci.* **34**(2), 703 (1987).
124. M. E. Stewart, H. B. Hopfenberg, W. J. Koros, and N. R. McCoy, *J. Appl. Polym. Sci.* **34**(2), 721 (1987).
125. M. E. Stewart, D. L. Sorrells, N. R. McCoy, W. J. Koros, and H. B. Hopfenberg, *J. Appl. Polym. Sci.* **34**(7), 2493 (1987).

126. A. R. Berens and H. B. Hopfenberg, *J. Polym. Sci., Polym. Phys. Ed.* **17**(10), 1757 (1979).
127. I. Pinnau, M. W. Hellums, and W. J. Koros, *Polymer* **32**(14), 2612 (1991).
128. P. H. Pfromm, I. Pinnau, and W. J. Koros, *J. Appl. Polym. Sci.* **48**(12), 2161 (1993).
129. P. H. Pfromm and W. J. Koros, *Polymer* **36**(12), 2379 (1995).
130. M. E. Rezac, P. H. Pfromm, L. M. Costello, and W. J. Koros, *Ind. Eng. Chem. Res.* **32**(9), 1921 (1993).
131. M. S. McCaig and D. R. Paul, *Polymer* **41**(2), 629 (1999); **41**, 639–648 (2000).
132. T. S. Chung and S. K. Teoh, *J. Membr. Sci.* **152**(2), 175 (1999).
133. P. H. Pfromm, Ph.D. dissertation, The University of Texas at Austin, Austin, Tex, 1994.
134. T. Alfrey, G. Goldfinger, and H. Mark, *J. Appl. Phys.* **14**, 700 (1943).
135. J. G. Curro, R. R. Lagasse, and R. Simha, *Macromolecules* **15**(6), 1621 (1982).
136. M. S. McCaig, D. R. Paul, and J. W. Barlow, *Polymer* **41**(2), 639–648 (1999).
137. K. C. O'Brien, W. J. Koros, and G. R. Husk, *Polym. Eng. Sci.* **27**(3), 211 (1987).
138. T. E. Brady, S. A. Jabarin, and G. W. Miller, *Permeability of Plastic Films and Coatings to Gases, Vapors and Liquids*, Plenum Press, New York, 1974.
139. M. J. El-Hibri, and D. R. Paul, *J. Appl. Polym. Sci.* **30**(9), 3649 (1985).
140. J. S. Chiou and D. R. Paul, *J. Polym. Sci., Polym. Phys. Ed.* **25**(8), 1699 (1987).
141. J. H. Petropoulos, *J. Membr. Sci.* **17**(3), 233 (1984).
142. C. J. Durning and W. B. Russel, *Polymer* **26**(1), 119 (1985).
143. D. J. Enscore, H. B. Hopfenberg, and V. T. Stannett, *Polymer* **18**(8), 793 (1977).
144. A. R. Berens, *Polym. Prepr. (Am. Chem. Soc., Div. Polym. Chem.)* **15**(2), 203 (1974).
145. H. B. Hopfenberg and H. L. Frisch, *J. Polym. Sci., Polym. Lett. Ed.* **7**(6), 405 (1969).
146. J. T. Alfrey, E. F. Gurnee, and W. G. Lloyd, *J. Polym. Sci., Part C: Polym. Symp.* **12**, 249 (1966).
147. R. C. Lasky, E. J. Kramer, and C. Y. Hui, *Polymer* **29**(4), 673 (1988).
148. J. H. Petropoulos, *J. Polym. Sci., Polym. Phys. Ed.* **22**(11), 1885 (1984).
149. G. C. Sarti, *Polymer* **20**(7), 827 (1979).
150. N. L. Thomas and A. H. Windle, *Polymer* **23**(4), 529 (1982).
151. M. Sanopoulou, D. F. Stamatialis, and J. H. Petropoulos, *Macromolecules* **35**(3), 1012 (2002).
152. J. C. Wu and N. A. Peppas, *J. Appl. Polym. Sci.* **49**(10), 1845 (1993).
153. S. J. Huang, C. J. Durning, and B. D. Freeman, *J. Membr. Sci.* **143**, 1 (1998).
154. E. L. Cussler, *Diffusion Mass Transfer in Fluid Systems*, 2nd ed., Cambridge University Press, New York, 1997.
155. G. H. Hsiue and J. S. Yang, *J. Membr. Sci.* **82**(1/2), 117 (1993).
156. J. H. Kim, B. R. Min, H. S. Kim, J. Won, and Y. S. Kang, *J. Membr. Sci.* **212**(1/2), 283 (2003).
157. J. Muller and K.-V. Peinemann, *Desalination* **145**(1–3), 339 (2002).
158. T. Yamaguchi, C. A. Koval, R. D. Noble, and C. Bowman, *Chem. Eng. Sci.* **51**(21), 4781 (1996).
159. T. Yamaguchi, L. M. Boejte, C. A. Koval, R. D. Noble, and C. N. Bowman, *Ind. Eng. Chem. Res.* **34**(11), 4071 (1995).
160. J. D. Way, R. D. Noble, D. L. Reed, G. M. Ginley, and L. A. Jarr, *AIChE J.* **33**(3), 480 (1987).
161. T. Suzuki, H. Yasuda, H. Nishide, X. Chen, and E. Tsuchida, *J. Membr. Sci.* **112**(2), 155 (1996).
162. J. Yang and P. Huang, *Chem. Mater.* **12**(9), 2693 (2000).
163. J. P. Yang and P. C. Huang, *J. Appl. Polym. Sci.* **77**(3), 484 (2000).
164. U.S. Pat. Appl. Publ. 2001-916671 (2003), D. Tung, E. A. Sisson, and R. A. Leckonby.

165. U.S. Pat. Appl. Publ. 2001-28167 (2002), J. M. Tibbitt, G. E. Rotter, D. P. Sinclair, G. T. Brooks, and R. T. Behrends.
166. U.S. Pat. Appl. Publ. 1998-183239 (2001), C. L. Ebner and T. A. Blinka.
167. T. S. Dunn, E. E. Williams, and J. L. Williams, *J. Polym. Sci., Polym. Chem. Ed.* **20**(6), 1599 (1982).
168. W. Y. Hsu and T. D. Gierke, *J. Membr. Sci.* **13**(3), 307 (1983).
169. T. E. Springer, T. A. Zawodzinski, and S. Gottesfeld, *J. Electrochem. Soc.* **138**(8), 2334 (1991).
170. G. J. M. Janssen, *J. Electrochem. Soc.* **148**(12), A1313 (2001).
171. D. M. Bernardi and M. W. Verbrugge, *J. Electrochem. Soc.* **139**(9), 2477 (1992).
172. M. Eikerling, Y. I. Kharkats, A. A. Kornyshev, and Y. M. Volfkovich, *J. Electrochem. Soc.* **145**(8), 2684 (1998).
173. A. Z. Weber and J. Newman, *J. Electrochem. Soc.* **150**(7), A1008 (2003).
174. K. D. Kreuer, *Solid State Ionics* **97**(1–4), 1 (1997).
175. B. S. Pivovar, Y. Wang, and E. L. Cussler, *J. Membr. Sci.* **154**(2), 155 (1999).
176. G. P. Simon, *Trends Polym. Sci.* **5**(12), 394 (1997).
177. D. M. Bigg, *Polym. Eng. Sci.* **36**(6), 737 (1996).
178. Y. C. Jean, *Microchem. J.* **42**(1), 72 (1990).
179. H. Nakanishi, S. J. Wang, and Y. C. Jean, *Int. Symp. Positron Annihilation Stud. Fluids*, 292–298 (1988).
180. Y. Y. Wang, H. Nakanishi, Y. C. Jean, and T. C. Sandreczki, *J. Polym. Sci., Polym. Phys. Ed.* **28**(9), 1431 (1990).
181. Y. C. Jean, J. P. Yuan, J. Liu, Q. Deng, and H. Yang, *J. Polym. Sci., Polym. Phys. Ed.* **33**(17), 2365–2371 (1995).
182. Q. Deng and Y. C. Jean, *Macromolecules* **26**(1), 30 (1993).
183. A. Y. Alentiev, V. P. Shantarovich, T. C. Merkel, V. I. Bondar, B. D. Freeman, and Y. P. Yanpolskii, *Macromolecules* **35**(25), 9513 (2002).
184. C. Nagel, K. Guenther-Schade, D. Fritsch, T. Strunskus, and F. Faupel, *Macromolecules* **35**(6), 2071 (2002).
185. M. Mohsen, E. A. H. Gomaa, H. Schut, and A. Van Venn, *J. Appl. Polym. Sci.* **80**(7), 970 (2001).
186. Y. P. Yampolskii, A. P. Korikov, V. P. Shantarovich, K. Nagai, B. D. Freeman, T. Masuda, M. Teraguchi, and G. Kwak, *Macromolecules* **34**(6), 1788 (2001).
187. V. P. Shantarovich, I. B. Kevdina, Y. P. Yampolskii, and A. Y. Alentiev, *Macromolecules* **33**(20), 7453 (2000).
188. J. P. Yuan, H. Cao, E. W. Hellmuth, and Y. C. Jean, *J. Polym. Sci., Polym. Phys. Ed.* **36**(17), 3049 (1998).
189. X. Hong, Y. C. Jean, H. Yang, S. M. Jordan, and W. J. Koros, *Macromolecules* **29**(24), 7859 (1996).
190. Y. Ito, K. I. Okamoto, and K. Tanaka, *Journal de Physique* **4**, 241 (1993).
191. D. Hofmann, L. Fritz, J. Ulbrich, C. Schepers, and M. Bohning, *Macromol. Theory Simul.* **9**(6), 293 (2000).
192. A. A. Gusev, F. Muller-Plathe, W. F. Van Gunsteren, and U. W. Suter, *Adv. Polym. Sci.* **116**, 207 (1994).
193. D. N. Theodorou and U. W. Suter, *Macromolecules* **18**(7), 1467 (1985).
194. D. N. Theodorou and U. W. Suter, *Macromolecules* **19**(1), 139 (1986).
195. F. Mueller-Plathe, S. C. Rogers, and W. F. van *Gunsteren, Chem. Phys. Lett.* **199**(3/4), 237 (1992).
196. A. A. Gusev and U. W. Suter, *J. Comput.-Aided Mater. Des.* **1**(1), 63 (1993).
197. A. A. Gusev and U. W. Suter, *J. Chem. Phys.* **99**(3), 2228 (1993).
198. A. A. Gusev and U. W. Suter, *J. Chem. Phys.* **99**(3), 2221 (1993).

199. B. Widom, *J. Chem. Phys.* **39**(11), 2808 (1963).
200. E. Tocci, E. Bellacchio, N. Russo, and E. Drioli, *J. Membr. Sci.* **206**(1/2), 389–398 (2002).
201. M. Heuchel and D. Hofmann, *Desalination* **144**(1–3), 67 (2002).
202. D. Hofmann, L. Fritz, J. Ulbrich, and D. Paul, *Polymer* **38**(25), 6145 (1997).
203. E. Smit, M. H. V. Mulder, C. A. Smolders, H. Karrenbeld, J. Van Eerden, and D. Feil, *J. Membr. Sci.* **73**(2/3), 247 (1992).
204. R. Zhang and W. L. Mattice, *J. Membr. Sci.* **108**(1/2), 15 (1995).
205. D. Hofmann, J. Ulbrich, D. Fritsch, and D. Paul, *Polymer* **37**(21), 4773 (1996).
206. J. R. Fried, M. Sadat-Akhavi, and J. E. Mark, *J. Membr. Sci.* **149**(1), 115 (1998).
207. C. S. Chassapis, J. K. Petrou, J. H. Petropoulos, and D. N. Theodorou, *Macromolecules* **29**(10), 3615 (1996).
208. P. G. de Gennes, *Scaling Concepts in Polymer Physics*, Cornell University Press, Ithaca, N.Y., 1979.
209. W. W. Graessley, *Adv. Polym. Sci.* **47**, 67 (1982).

WILLIAM J. KOROS
WILLIAM C. MADDEN
Georgia Institute of Technology

TRIBOLOGICAL PROPERTIES OF POLYMERS.

See SCRATCH BEHAVIOR OF POLYMERS; SURFACE MECHANICAL DAMAGE AND WEAR.

ULTRASOUND-INDUCED RADICAL POLYMERIZATION

Introduction

Ultrasound comprises sound waves typically in the range of 20 kHz to approximately 500 MHz, which cause compression and expansion in a fluid. The frequency and intensity (amplitude) are the most important properties to characterize the pressure wave. The use of ultrasound can be divided into two areas: low intensity, high frequency ultrasound (2–500 MHz, 0.1–0.5 W/cm^2) and power ultrasound with a high intensity and a low frequency (20–100 kHz, $>$10 W/cm^2). The former does not alter the state of the medium through which it travels and is commonly used for nondestructive evaluation and medical diagnosis (1). This type of ultrasound cannot be used for reactions. Contrarily, power ultrasound uses the energy to create cavitations, which involve the formation, growth, and implosive collapse of microscopic bubbles in a liquid. These bubbles are generated when the "negative" pressure during the rarefaction phase of the sound wave is sufficiently large to disrupt the liquid (see Fig. 1). The implosive collapse of the bubbles can locally produce extreme temperatures and pressures (5000°C, 20 MPa) for very short times, because of compression of the gas phase inside the cavity (2,3). These hotspots can lead to irreversible changes such as the formation of excited states, bond breakage, and the generation of radicals. Power ultrasound is applied for cleaning purposes, treatment of kidney stones, plastic welding, and for chemical reactions. Table 1 summarizes the different types of ultrasound and their applications.

With respect to polymerization processes, ultrasound has significant potential as a clean and safe technology. After the production of most types of polymers, catalyst and initiator residues contaminate the product. Since ultrasound generates the radicals *in situ* (4,5), no initiator or catalyst is required to start a polymerization reaction. An additional advantage of ultrasound is the intrinsic safe

Encyclopedia of Polymer Science and Technology. Copyright John Wiley & Sons, Inc. All rights reserved.

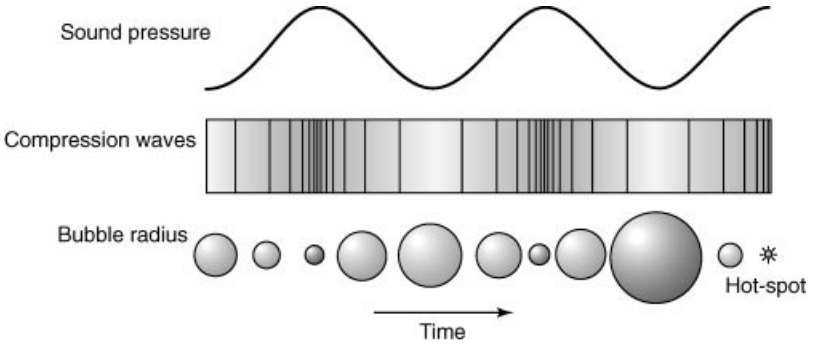

Fig. 1. Schematic representation of bubble growth and collapse in a liquid irradiated with ultrasound and the resulting hot-spot due to adiabatic compression.

operation, because turning off the electrical power supply will immediately stop the radical formation and, consequently, the polymerization reaction. Besides polymerization, polymer scission also can occur through irradiation with ultrasound (6). The rapid flow around a cavitation bubble stretches and ultimately breaks the polymer chain. At a sufficiently small chain length, typically 10^4 g/mol, further fracture of the polymer is prevented (7). In this way ultrasound-induced polymer scission provides an additional means to tune the molecular weight of the product.

In the following sections, the physical background of ultrasound-induced cavitation and radical formation is described. Subsequently, an overview of the various types of ultrasound-induced polymerizations is given, including bulk, precipitation, and emulsion polymerization. Finally, the breakage of polymer chains by cavitation is discussed.

Ultrasound Fundamentals

To understand ultrasound-induced radical polymerization, insight in the physical background of sonochemistry is a prerequisite. The rate at which ultrasound-induced reactions occur is generally determined by the collapse of the cavitation

Table 1. Overview of Different Types of Ultrasound, Including the Various Applications

Power ultrasound (20–100 kHz)	Sonophoresis (20 kHz, low power)	Therapeutic ultrasound (1 MHz, high power)	Nondestructive ultrasound (> 2 MHz, low power)
Sonochemistry	Transdermal drug delivery	Therapeutic massage	Flaw detection
Welding		Controlled release	Medical diagnoses
Cleaning			
Cell disruption			
Sterilization			
Kidney stones			

bubbles. The movement of these cavities depends on the frequency and intensity of the sound wave as well as on the physical properties of the liquid.

Ultrasound in Liquids. Sound passes through an elastic medium as a longitudinal wave, ie, a series of alternating compressions and rarefactions. This means that liquid is displaced parallel to the direction of motion of the wave. The maximum displacement velocity together with the density (ρ) and the speed of sound in the medium (v) determine the ultrasound intensity and the maximum acoustic pressure ($P_{A,max}$) (8). The variation of the acoustic pressure (P_A) as a function of time (t) at a fixed frequency (f) is described by equation 1:

$$P_A = P_{A,max} \cdot \sin(2 \cdot \pi \cdot f \cdot t) \tag{1}$$

The acoustic pressure amplitude determines the growth of a cavitation bubble and consequently the chemical effects upon collapse. The amplitude of the pressure wave can be measured with a hydrophone or can be calculated using a calorimetric method (9,10), in which it is possible to determine the ultrasound power (Q_{US}) that is transferred to the liquid. With the ultrasound power and the surface area of the ultrasound source (A_{US}), the acoustic amplitude can be calculated according to equation (2), for which the ultrasound intensity is the power input divided by the surface area of the source (11).

$$P_{A,max} = \sqrt{2 \cdot \rho \cdot v \cdot \frac{Q_{US}}{A_{US}}} \tag{2}$$

Cavitation Bubble Dynamics. Ultrasound waves in a liquid cause the molecules to oscillate around their mean position. During the positive-pressure cycle the distance between the molecules decreases, while during the negative pressure period the distance increases. At a sufficiently high intensity a critical distance between the molecules is exceeded during the negative pressure period, and a cavity is formed. Because of the presence of nuclei such as dissolved gases and solid impurities, cavities are formed at far lower sound pressures than theoretically predicted.

After the formation of a cavity, a critical acoustic pressure has to be overcome to initiate the explosive growth of this bubble. The Blake threshold pressure (P_B) describes this critical pressure [eq. 3 (12)]:

$$P_B = P_0 - P_v + \frac{4}{3} \cdot \sigma \cdot \sqrt{\frac{2}{3} \cdot \frac{\sigma}{\left(P_0 + 2 \cdot \frac{\sigma}{R_0} - P_v\right) \cdot R_0^3}} \tag{3}$$

Equation 3 assumes that the external pressure (P_0), the vapor pressure (P_v), the surface tension (σ), and the equilibrium radius of the bubble (R_0) determine the required negative pressure in the liquid to start an explosive growth of a cavity (13). The Blake threshold pressure is based on a static approach and is only valid when the surface tension dominates all dynamic effects, eg, mass transfer and viscosity.

This explosive growth is followed by an implosive collapse. During this collapse, the content of the bubble is almost adiabatically heated, which leads to local,

short-lived hot-spots in the liquid. Depending on the specific conditions, bubble wall velocities, pressures, and temperatures in the bubble can increase up to 1500 m/s, 20 MPa, and 5000 K, respectively. The influence of the medium characteristics and the physical conditions on the implosion can be calculated with a dynamic bubble model (14,15). The dynamic movement of a bubble in a sound pressure field can be described with the Rayleigh-Plesset equation (eq. 4), which includes the density of the fluid (ρ), the gas pressure, the surface tension, the equilibrium radius of the bubble, the vapor pressure, the polytropic index of the gas phase (κ), the liquid viscosity (η) and the acoustic pressure.

$$R \cdot \frac{\mathrm{d}^2}{\mathrm{d}t^2}R + \frac{3}{2} \cdot \left(\frac{\mathrm{d}}{\mathrm{d}t}R\right)^2 = \frac{1}{\rho} \cdot \left[\left(P_0 + \frac{2 \cdot \sigma}{R_0} - P_\mathrm{v}\right) \cdot \left(\frac{R_0}{R}\right)^{3^*\kappa} + P_\mathrm{v} - \frac{2 \cdot \sigma}{R} - \frac{4 \cdot \eta \cdot \frac{\mathrm{d}}{\mathrm{d}t}R}{R} - P_0 - P_A(t)\right] \quad (4)$$

By combining the Rayleigh–Plesset equation with a mass and energy balance over the bubble, the temperature and pressure in the bubble can be calculated (16,17). The model also describes the dynamic movement of the bubble wall, which results in a calculated radius of the cavitation bubble as a function of time (see Fig. 2). The explosive growth phase and the collapse phase of the bubble can clearly be distinguished. Moreover, in case dynamic effects are more important than the surface tension, the cavitation threshold can be calculated with the dynamic model, while the Blake threshold pressure cannot be used at these conditions.

Parameters Influencing Cavitation. The intrinsic rate of a polymerization reaction is determined by the initiation, propagation, and termination rate. However, only the initiation rate is influenced by ultrasound. The amount of

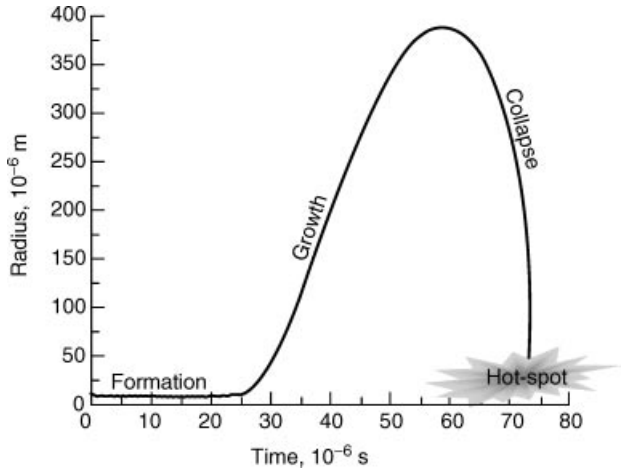

Fig. 2. Illustrative radius of a cavitation bubble as a function of time, calculated in water at ambient pressure.

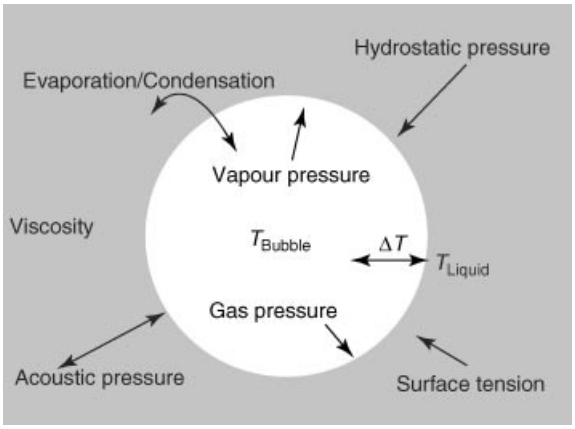

Fig. 3. Schematic representation of a bubble, including the processes and physical properties that determine the cavitation process.

radicals formed due to sonification is a function of the number of cavities created and the number of radicals that are formed per cavitation bubble. The bubble wall velocity during collapse and the hot-spot temperature determine the rate at which radicals are formed, both inside and outside a single bubble. These two parameters depend on the physical properties of the liquid as well as on the physical and chemical processes occurring around the cavity. The most important properties and processes occurring in a cavitation bubble are schematically depicted in Figure 3. The number of cavities is, for instance, determined by the impurities in the liquid, the static pressure, the ultrasound intensity, and the vapor pressure. This emphasizes that the overall radical formation rate is influenced in a complex way (18,19). In the following, the effect of the most important parameters will be discussed.

Temperature. When the reaction temperature is altered, the liquid properties will change. Although all these properties (viscosity, surface tension, sound velocity, vapor pressure, etc) have an influence on the chemical effect of cavitation, the change in vapor pressure dominates the other liquid properties. As the temperature is raised, the vapor pressure in the bubble is increased, which cushions the implosion of the cavity. This results in a lower local temperature inside the cavity at higher overall temperatures. Consequently, fewer radicals are formed per cavitation bubble. On the other hand, a higher vapor pressure can lead to easier bubble formation because of the decrease of the cavitation threshold. In most cases, however, an increase in reaction temperature will result in an overall decrease in the radical formation rate. Therefore, ultrasound-induced reactions exhibit opposite behavior as compared to common radical reactions (20).

Static Pressure. A high static pressure can prevent the formation of cavitation bubbles, as the Blake threshold pressure increases. This implies that less or no cavitations are formed at higher static pressures. To counteract this effect, a higher acoustic pressure is required, which will result in a more violent collapse of a cavitation bubble.

Viscosity. At increasing viscosities the growth and collapse of a cavitation bubble is retarded, because of the higher drag of the liquid. At a certain viscosity

the drag force becomes too high and the bubble has insufficient time to grow to a critical radius. If this radius is not reached, no collapse will occur. Additionally, the higher viscosity slows down the collapse, which makes it possible for heat to be transferred to the liquid. Because of this heat transfer, lower hot-spot temperatures are reached and subsequently less radicals are being generated.

Ultrasound Intensity. At first the radical formation rate will increase to a maximum with increasing ultrasound intensity (18). This is caused by the higher cavitation intensity per bubble and the larger number of cavitation bubbles. At too high ultrasound intensities, however, a cloud of cavitation bubbles is formed near the ultrasound source, because of which the pressure wave is no longer transmitted efficiently to the liquid. As a result, the cavitation intensity and, consequently, the radical formation rate decrease with a continued increase in intensity (18). An optimum radical formation rate with ultrasound intensity can thus be found.

Ultrasound Frequency. The frequency of ultrasound has a significant effect on the cavitation process. At very high frequencies (>1 MHz), the cavitation effect is reduced as the inertia of a cavitation bubble becomes too high to react to fast changing pressures. Most ultrasound-induced reactions are therefore carried out at frequencies between 20 and 900 kHz. The optimum ultrasound effect as a function of frequency depends on the reaction system; eg, water dissociation has an optimum frequency at approximately 500 kHz (21). For bulk polymerizations the maximum radical formation rate is obtained at 20 kHz. At this frequency the highest strain rates are produced, which results in a high radical formation rate by polymer scission (22).

Cavitation-Induced Polymerization

Generally, free-radical polymerization consists of four elementary steps: initiation, propagation, chain transfer, and termination (see RADICAL POLYMERIZATION). When ultrasound is used to initiate polymerization, radicals can be formed both from monomer and from polymer molecules. This implies that because of radical formation by polymer scission, an additional elementary step is involved in ultrasound-induced polymerization, as indicated in Figure 4.

The radicals from polymer and monomer are generated by two different mechanisms. The monomer molecules are dissociated by the high temperatures inside the hot-spot, whereas the polymer chains are fractured by the high strain rates outside the bubble (23,24). It has to be noted that the radicals are only formed in the immediate vicinity of the ultrasound source where cavitation occurs. Subsequently, these radicals are dispersed throughout the reactor. A typical ultrasound reactor used for batch polymerization is given in Figure 5. This system uses a horn to transmit the 20-kHz ultrasound vibrations to the liquid (4,5,9). To allow for comparison of different experiments, the total configuration of the reactor has to be exactly the same. This includes the flow rate of the gas, which is bubbled through the reaction mixture to create nuclei. A different ultrasound system is the plate transducer, which does not have a fixed frequency (8,13). This type of transducer is typically used for polymerizations where the optimum frequency is higher than 20 kHz, such as emulsion polymerizations. In the literature several types of ultrasound-induced polymerizations have been reported, ie, bulk,

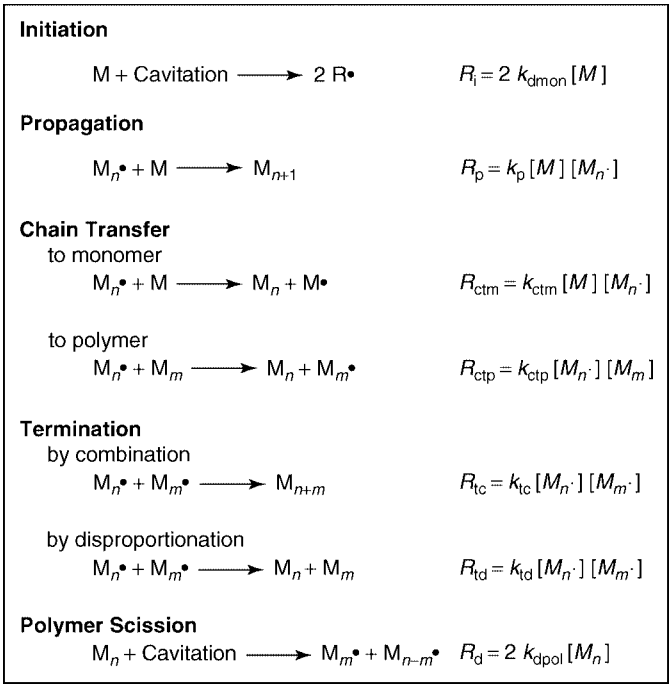

Fig. 4. Reaction mechanism of ultrasound-induced radical polymerization, assuming intrinsic polymerization and avoiding thermal initiation.

precipitation, and emulsion polymerization. Additionally, an interesting application of ultrasound polymerization is the synthesis of block copolymers.

Bulk Polymerization. Most ultrasound-induced bulk polymerizations are performed at room temperature (22). This low temperature is chosen because

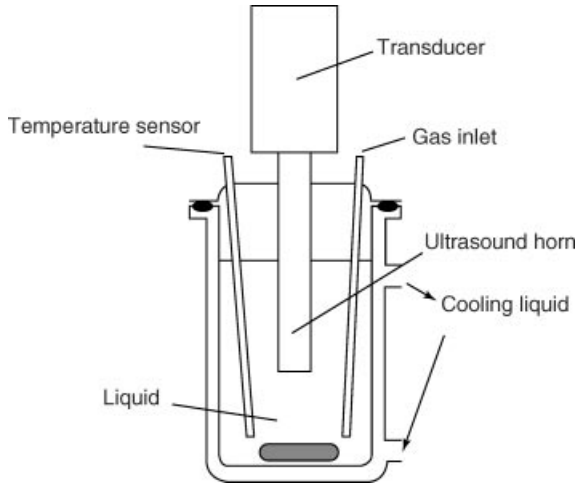

Fig. 5. Typical batch reactor of 200 mL used for ultrasound-induced polymerization reactions.

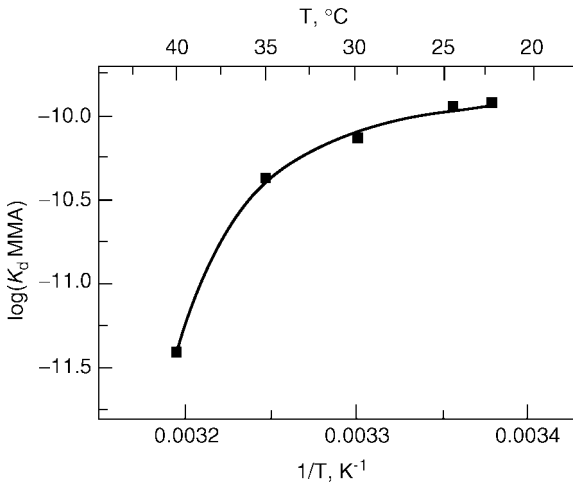

Fig. 6. Arrhenius plot for monomeric radicals generated by ultrasound in bulk MMA at an ultrasound intensity of 62 W/cm^2 (9).

radical formation induced by ultrasound appears to be more efficient at lower temperatures (9) (see also section under (Parameters Influencing Cavitation)). Figure 6 shows that at temperatures above 40°C almost no radicals are formed in methyl methacrylate (MMA) by ultrasound. In contrast to conventional thermal initiators such as potassium persulfate, ultrasound can initiate a polymerization reaction at ambient temperatures. It should be noted, however, that the propagation rate increases with an increasing temperature. Therefore, a suitable temperature in terms of propagation rate constant and radical formation rate has to be chosen to optimize ultrasound-induced polymerization. Additionally, the type of monomer is important. For example, styrene radicals will be less reactive and will probably be more stable than MMA radicals because of the conjugated system. Moreover, the aromatic ring will increase the chance for decomposition of the monomer. In literature several bulk polymerizations initiated by ultrasound have been reported; eg, the polymerization of methyl methacrylate (4,25,26), ethyl methacrylate (27), *n*-butyl methacrylate (5,23), and styrene (28).

Since the basic reaction kinetics are well known (25,29), the ultrasound-induced polymerization of MMA is the farmost studied system. Typically, the resulting molecular weight of the obtained poly(methyl methacrylate) (PMMA) is in the range of 1×10^5 to 6×10^5 g/mol. An experimental study on the ratio between radicals originating from monomer and polymer in a MMA/PMMA ($M_w = 3.5 \times 10^5$ g/mol) bulk system has revealed that the polymer chains dissolved in the reaction mixture produce far more radicals than the monomer molecules (30). According to Figure 4 the formation rate constant for monomeric and polymeric radicals is assumed to be first order in polymer and monomer concentration, respectively, from which it can be calculated that the radical formation rate constant from polymer chains is substantially higher; ie, 10^{-4}/s versus 10^{-9}/s from monomeric units. The influence of the weight percentage polymer present in the liquid on the dissociation constants for monomer and polymer is given in Figure 7.

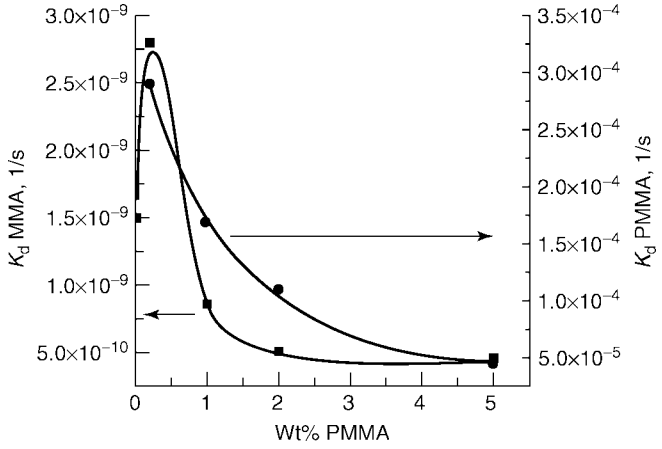

Fig. 7. Radical formation rate constants from monomer and polymer as a function of the wt% polymer dissolved at a temperature of 20°C and an ultrasound intensity of 62 W/cm^2 (30). ■ MMA; PMMA.

An important parameter during ultrasound-induced bulk polymerizations is the viscosity. As the reaction proceeds, the formed polymer chains cause a drastic increase in the viscosity, resulting in slower growth and collapse of the cavity. Since the cavitations become less effective, the radical formation rate from both monomer and polymer will decrease, as shown in Figure 7. At a conversion of approximately 20% the collapse is no longer sufficiently strong to induce hot-spot temperatures that are able to generate monomeric radicals. Moreover, the strain rates outside the collapsing bubble are not large enough to produce polymeric radicals by polymer scission (5). As a consequence, the polymerization ultimately stops at this conversion, which represents a serious drawback for the development of ultrasound-induced bulk polymerization towards industrial application.

Precipitation Polymerization. As described in the previous section, ultrasound-induced bulk polymerizations are limited to relatively low conversions, because a strong viscosity increase upon reaction hinders cavitation. To obtain higher conversions, precipitation polymerization forms a potential solution. Because the produced polymer precipitates from the reaction medium, the viscosity and consequently the radical formation rate are expected to remain virtually constant. In this perspective, liquid carbon dioxide is a suitable reaction medium, because most monomers have a high solubility in CO_2, whereas it exhibits an antisolvent effect for most polymers. Moreover, CO_2 is regarded as an environmentally friendly compound, which is nontoxic, nonflammable, and naturally abundant. Since higher pressures are required for CO_2 to act as an antisolvent (31–33), the possibility of ultrasound-induced cavitation in pressurized carbon dioxide systems has been studied (34).

During pressurization of a liquid, the Blake threshold pressure increases, which implies that higher acoustic pressures are needed to produce cavitations. Obviously, no cavitation occurs when the Blake threshold pressure exceeds the maximum acoustic pressure that can be applied with the currently available equipment. The vapor pressure of the liquid, however, can counteract the static

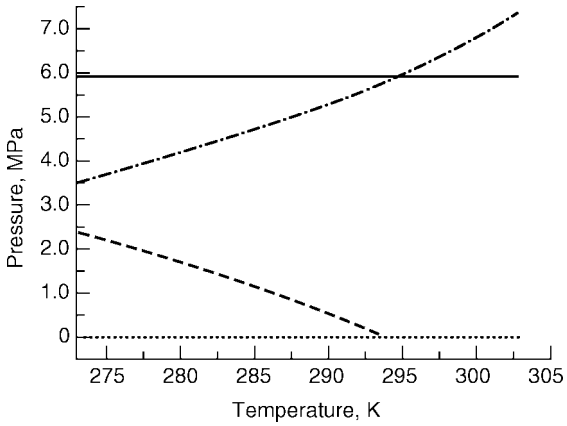

Fig. 8. Calculated Blake threshold and vapor pressure for water and carbon dioxide at 5.82 MPa (34). _____ Blake threshold H_2O; - - - - - Blake threshold CO_2; ▪ ▪ ▪ ▪ ▪ vapor pressure H_2O; – – – – – vapor pressure CO_2.

pressure. As a result of this, the Blake threshold is reduced in liquids with a high vapor pressure; eg, CO_2, ethylene and ammonia. This enables cavitation at increased static pressures (34). To illustrate this effect, Figure 8 shows the calculated Blake threshold pressure of carbon dioxide and water at 5.82 MPa as a function of temperature. The threshold curves are calculated using equation (3), in which the vapor pressure is the most important parameter, next to the hydrostatic pressure and the surface tension. For water the Blake threshold is determined only by the static pressure and the surface tension of the liquid, because of the low vapor pressure of water. As the vapor pressure does not change significantly with increasing temperature, the threshold pressure of water is virtually constant at 5.8 MPa, making cavitation impossible to occur. In the case of carbon dioxide, which condenses at a substantially higher pressure, only an acoustic pressure of 0.5 MPa is required to generate cavitation at 5.8 MPa static pressure and a temperature of 290 K.

The dynamic movement of the bubble in CO_2 has been calculated using equation 4. Initially, a small cavity with a radius of 10^{-5} m is present, which consists of argon and the corresponding vapor of the liquid phase. In the simulations, an ultrasound wave with an acoustic pressure of 1 MPa and a frequency of 20 kHz is imposed on this bubble. The variation of the radius of the bubble is shown in Figure 9. As the acoustic pressure for water at 5.82 MPa is lower than the Blake threshold pressure, almost no bubble movement is observed and no cavitation can occur. In contrast to the situation in water, carbon dioxide at 5.82 MPa allows for cavitation and the bubble exhibits a similar movement compared to water at 0.1 MPa. Moreover, the maximum temperature (585 K) and maximum bubble wall velocity (777 m/s) reached during collapse in liquid CO_2 are in the same order of magnitude as compared to water at ambient pressure (722 K and 840 m/s, respectively). To validate these simulations, cavitation experiments have been performed in pressurized CO_2–MMA systems using the radical scavenger 1,1-diphenyl-2-picrylhydrazyl (35). The radical formation rate appears to be in

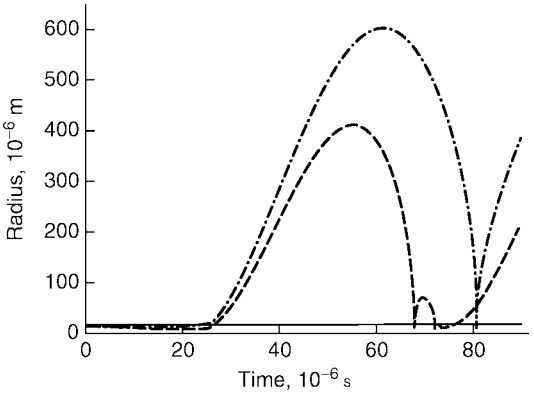

Fig. 9. Calculated radius of a cavitation bubble as a function of time in water and CO_2 (34). H_2O at 0.1 MPa; H_2O at 5.82 MPa; CO_2 at 5.82 MPa.

the order of 1.5×10^{14}/s, for which no noticeable difference occurs at varying MMA–CO_2 ratios.

Ultrasound-induced polymerizations of MMA in CO_2-expanded MMA have resulted in high molecular weight polymers (see Table 2). With respect to the initial polymerization rate, both polymerizations in CO_2 have a reaction rate in the same order of magnitude as compared to the bulk experiment at ambient pressure. Although the reaction rates are similar, the polymer produced at 0.1 and 0.7 MPa CO_2 pressure have much higher molecular weights than the reference polymer in bulk. A possible explanation for the difference in molecular weight is the fact that a precipitated polymer is not susceptible to ultrasound-induced polymer scission (see the next paragraph), whereas the dissolved polymer chains in the bulk experiment can break because of cavitation. In addition, it is possible that the precipitated polymer chains are swollen with monomer and continue to grow, while termination is not likely to occur in that particular situation.

During high pressure view-cell experiments of a solution of 4 wt% polymer in MMA at 0.7 MPa CO_2 and 20°C, a second phase (polymer phase) has clearly been observed. This illustrates the strong antisolvent effect of CO_2. Before the polymer actually precipitates, the antisolvent already causes a lower viscosity in the CO_2-expanded system as compared to the bulk system. Because CO_2 is a poor solvent for most polymers, the gyration radius of the polymer will be lower. This means fewer entanglements between polymer molecules, and subsequently a lower viscosity. Although the viscosity does not increase, so far only relatively low

Table 2. Results of Ultrasound-Induced Polymerizations of MMA at 20°C and Different CO_2 Pressures[a]

CO_2 pressure, MPa	Reaction time, min	Conversion, %	Initial polymerization rate, mol/m^{3}s	M_n, kg/mol
0	180	3.1	0.034	110
0.1	270	3.8	0.018	471
0.7	145	2.5	0.024	428

[a] Ref. 35.

conversions have been obtained, as a result of the large reactor scale compared to the ultrasound power input to the system. As soon as the reactor and ultrasound power are better scaled, it is expected that high conversions will be reached (35).

Emulsion Polymerization. The generation of radicals by ultrasound can also be applied in emulsion polymerization, which comprises a free-radical polymerization in a heterogeneous reaction system, yielding submicrometer polymer particles in a continuous aqueous phase. In literature a number of publications have appeared over the years on the application of ultrasound in emulsion polymerization (36–46). Ultrasound can be applied both for emulsification purposes as well as at higher conversions in the emulsion polymerization process (see HETEROPHASE POLYMERIZATION).

In the beginning of the polymerization, emulsification and nucleation govern the course of the process. The monomer droplets have to be small enough to provide a negligible resistance to monomer transport from the droplets through the aqueous phase to the growing polymer particles. Only in the case of sufficient emulsification, intrinsic polymerization kinetics can be assumed. This implies that in conventional emulsion polymerization, vigorous stirring is required to disperse the monomer droplets. When ultrasound is applied as an energy source for emulsification, a very uniform emulsion of small monomer droplets is obtained without additional stirring. The high implosion velocity of the cavitation bubbles ensures that the monomer droplets are well dispersed. A special case involves mini- or microemulsion polymerization. Depending on the surfactant system used and the emulsification induced by ultrasound, the monomer droplets become so small that they can serve as nucleation loci. In ordinary emulsion polymerization, the main locus of nucleation is within the monomer-swollen micelles. Typically, polymer particles produced by ultrasound-induced emulsion polymerization have a diameter of approximately 50 nm and a molecular weight of 3×10^6 g/mol (36,37).

During emulsion polymerization induced by ultrasound, the redundancy of initiator is advantageous in terms of process control and safety. Moreover, initiator residues do not contaminate the product. In contrast to ultrasound-induced bulk polymerizations, high conversions can be obtained in ultrasound-induced emulsion polymerization (38,39). Since a heterogeneous reaction system is involved, in which the polymer is insoluble in the continuous aqueous phase, the viscosity of the water phase does not increase upon reaction. The cavitation events occur in the continuous phase, producing radicals mainly from water and surfactant molecules (40). Subsequently, the oligomeric radicals enter the monomer swollen polymer particles and continue to polymerize. Examples of ultrasound-induced emulsion polymerization are described for styrene (37,39,41), MMA (36,40,42–45), *n*-butyl acrylate (46), and the copolymerization of vinyl acetate and butyl acrylate (38).

Synthesis of Block Copolymers. Anionic and living radical polymerization are the most important techniques for synthesis of block copolymers (qv) which are used in many applications where different polymers are connected to yield a material with hybrid properties (47); for instance, as compatibilizing agent between immiscible polymers (48). Alternatively, ultrasound can be used to produce these block copolymers, for which two different methods are applicable.

The first route to synthesize block copolymers by ultrasound starts with the dissolution of a homopolymer in a different monomer (49). Subsequently,

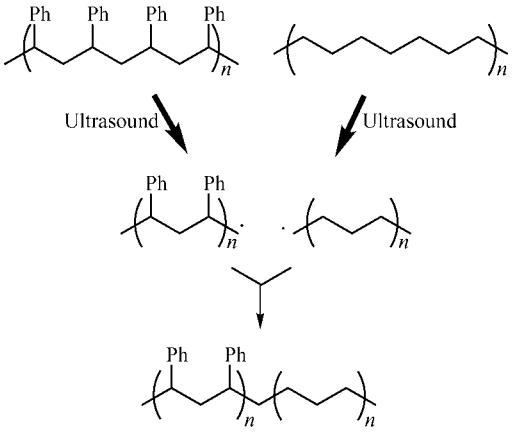

Fig. 10. The production of a block copolymer from two homo polymers with ultrasound (5).

ultrasonic scission of the polymer chains generates polymeric radicals, which initiate the polymerization reaction with the monomer present. In this way ultrasound provides the controlled formation of block copolymers, for which examples are polyethylene with acrylamide (49) and PMMA with styrene (50). Secondly, dissolving two different homopolymers in a nonreactive solvent can lead to block copolymers as well. In this case, the generated polymeric radicals have to undergo termination by cross combination (see Fig. 10) (51,52). If no cross combination occurs, the original homopolymers are reproduced again. The advantage of the second method is that block copolymers can be produced from homopolymers of which the polymer–monomer systems are immiscible. Using this approach the synthesis of the block copolymer of polystyrene and poly(methyl phenyl silane) (51) as well as the block copolymer of poly(vinyl chloride) and poly(acrylonitrile-*co*-butadiene) (52) is described.

Cavitation-Induced Polymer Scission

In terms of product properties, the molecular weight distribution is an important characteristic of polymers. In the polymer industry often a post-processing step is applied to alter the molecular weight of the polymers; eg, the peroxide-induced degradation of polypropylene (53). In this process, fracture of the polymer chain occurs at a random site. An alternative method is ultrasound-induced polymer scission, which involves a much better controlled, nonrandom process (7). This enables a relatively straightforward production of the desired molecular weight as well as the formation of block copolymers, as described in the previous section.

Mechanism. Although there is still some debate about the precise origin of scission, it has been shown that ultrasound-induced polymer breakage is a direct consequence of cavitation, because under conditions that suppress cavitation, no degradation is observed. In this nonrandom scission process the polymer is fractured at the centre of the chain (54–56). This is clearly shown in Figure 11,

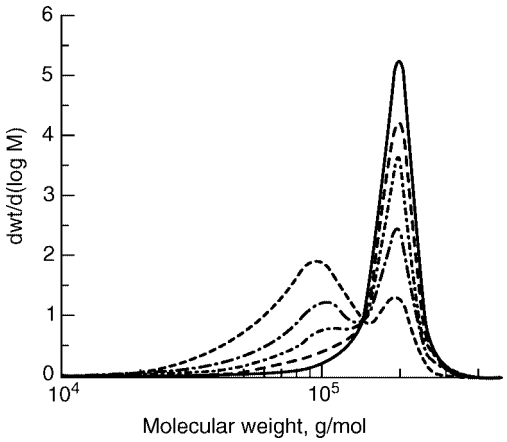

Fig. 11. Molecular weight distributions of an ultrasound-induced polymer scission experiment of PMMA with an initial M_n of 18.0×10^4 g/mol and a polydispersity of 1.05 (35). ——— 0 min; - - - - - 5 min; ——— 10 min; — — — — 20 min; • • • • • • 40 min.

in which a polymer with a peak value of 90 kg/mol is produced from the initial molecular weight distribution with a peak value of 180 kg/mol and a polydispersity of 1.05. It is often thought that the extreme temperatures inside the bubble upon implosion contribute to the degradation. However, temperature degradation implies a random process, and thus does not explain the scission at the middle of the chain. Ultrasound-induced chain fracture arises from the high strain rates on the polymer chain upon implosion. The generally accepted scission mechanism can best be described as the chain being caught in the rapid flow of solvent, as is schematically shown in Figure 12 (57). The chains are thus subjected to extremely large shear forces. Under sufficiently strong flow conditions, the solvent drag force causes extension of the coiled polymer molecule. If the drag force on the stretched polymer molecule exceeds the bond strength, scission will occur in the middle of the chain; otherwise no breakage occurs and a constant molecular weight (M_{lim}) is reached (58). This limiting molecular weight is no longer fractured as the forces acting on the chain are smaller than the force required to break a bond.

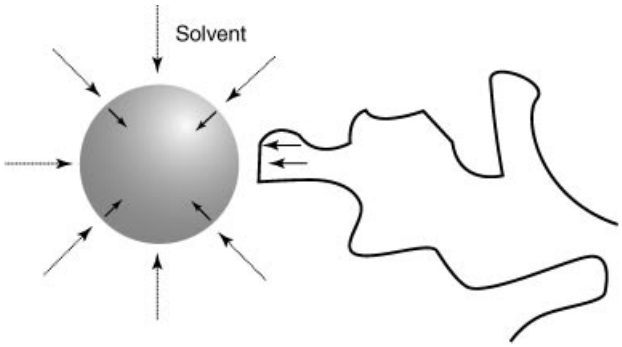

Fig. 12. Schematic presentation of the generally accepted mechanism of degradation of polymer by cavitational collapse (23).

In our view, the generally accepted mechanism of ultrasound-induced polymer scission, in which the polymer chain is uncoiled though not completely straightened near the cavitation bubble, does not explain the preferred breakage at the centre of the chain. Breakage in the middle of the chain can only occur when the polymer chain is completely stretched (59). Because of the gradient in radial solvent velocity near a cavity, a frictional force is exerted on the polymer molecule. The maximum stress will be in the centre of the polymer chain, which is in analogy with flow-induced polymer scission (60). When the bond scission probability along the chain is known from experimentally obtained molecular weight distributions, it is possible to deduce the molecular conformation of the polymer chains prior to bond rupture; ie, whether the chains are completely straightened.

Scission Kinetics. The kinetics of ultrasonic scission can be directly ascribed to the implosion velocity of the cavitation bubbles and the polymer that is fractured. The scission rate and the limiting molecular weight are thus influenced by the ultrasonic wave, the solvent properties, and the polymer structure.

The influence of ultrasound intensity, liquid viscosity, and liquid temperature on the degradation rate and limiting molecular weight have been studied by Price and West (51). A higher intensity results in a faster scission and a lower limiting molecular weight (see Fig. 13). Lower temperatures and lower viscosities have similar influences on the scission rate and M_{lim}. These three effects can be ascribed to the higher implosion velocity, which induces higher strain rates around the bubble and, therefore, lead to a lower limiting molecular weight and a higher scission rate.

The initial molecular weight of the polymer does not influence the implosion velocity of a cavity or the limiting molecular weight that is reached. However, the molecular weight has a large influence on the fracture rate of the polymer chains. The slopes of the degradation curves in Figure 14 indicate a higher scission rate for polymers with a higher initial molecular weight. This is a consequence of the higher solvent drag force on the longer chains. As a result, narrow molecular

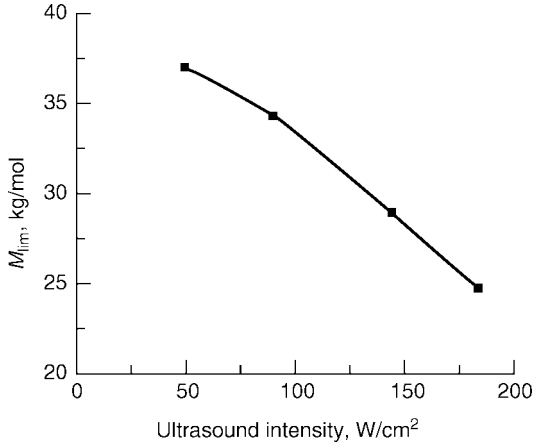

Fig. 13. Effect of ultrasound intensity on the limiting number-average molecular weight during the degradation of 0.5 wt% polystyrene in toluene at 25°C (51).

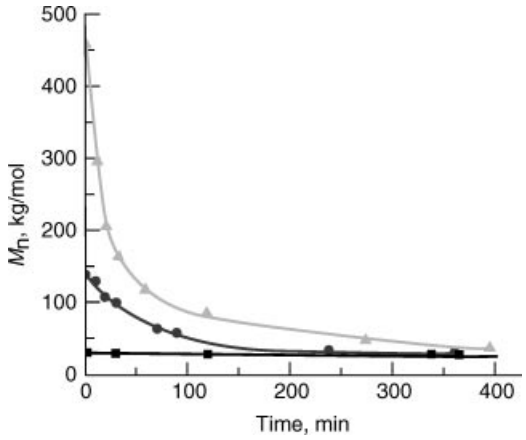

Fig. 14. Ultrasonic scission of polystyrene with different initial molecular weights in toluene (51). ■ 30 kg/mol; ● 140 kg/mol; ▲ 460 kg/mol.

weight distributions can be produced by ultrasound-induced polymer scission, because a high molecular weight polymer is fractured faster. Note that a similar limiting molecular weight is obtained for all three scission experiments shown in Figure 14 as the final conditions are equal after several breakage events of the higher molecular weight polymers.

Conclusions

The examples described in this article indicate that ultrasound is a promising technology in terms of the development of more sustainable polymer processes, because it allows for a clean and safe polymerization reaction, yielding well-defined products. Although no large-scale industrial polymerization process based on ultrasound exists as yet, commercial applications in other fields such as ultrasound cleaning and sterilization prove that ultrasound is a readily available technique and relatively simple to implement in existing equipment. Nevertheless, the application of ultrasound for polymerization purposes requires a thorough understanding of both ultrasound parameters and liquid properties, which provides a continuing challenge in physics, chemistry, and engineering.

BIBLIOGRAPHY

1. L. Kornet, A. P. Hoeks, B. J. Janssen, J. M. Willigers, and R. S. Reneman, *J. Hypertens.* **20**, 1165 (2002).
2. Y. T. Didenko and K. S. Suslick, *Nature* **407**, 877 (2002).
3. K. S. Suslick, *Sci. Am.* **260**, 80 (Feb. 1989).
4. P. Kruus and T. J. Patraboy, *J. Phys. Chem.* **89**, 3379 (1985).
5. G. J. Price, *Ultrason. Sonochem.* **3**, S229 (1996).
6. G. J. Price, *Adv. Sonochem.* **1**, 231 (1990).

7. J. Niezette and A. Linkens, *Polym.* **19**, 939 (1978).
8. T. J. Mason and J. P. Lorimer, *Applied Sonochemistry*, Wiley-VCH, Weinheim, 2002, p. 25.
9. M. W. A. Kuijpers, M. F. Kemmere, and J. T. F. Keurentjes, *Ultrasonics* **40**, 675 (2002).
10. J.-M. Löning, C. Horst, and U. Hoffmann, *Ultrason. Sonochem.* **9**, 169 (2002).
11. U. Hoffmann, C. Horst, U. Wietelmann, S. Bandelin and R. Jung, *Sonochemistry, Ullmann's Encyclopedia of Industrial Chemistry*, Wiley-VCH, Weinheim, 2003.
12. T. J. Leighton, *The Acoustic Bubble*, Academic Press, London, 1994, p. 84.
13. Y. T. Shah, A. B. Pandit, and V. S. Moholkar, *Cavitation Reaction Engineering*, Plenum, New York, 1999, p. 16.
14. S. Hilgenfeldt, M. P. Brenner, S. Grossmann, and D. Lohse, *J. Fluid Mech.* **365**, 171 (1998).
15. J. P. Lorimer and T. J. Mason, *Chem. Soc. Rev.* **16**, 239 (1987).
16. K. Yasui, *J. Acoust. Soc. Am.* **98**, 2772 (1995).
17. K. Yasui, *Ultrasonics* **36**, 575 (1998).
18. L. H. Thompson and L. K. Doraiswamy, *Ind. Eng. Chem. Res.* **38**, 1215 (1999).
19. J. M. Pestman, J. B. F. N. Engberts, and F. de Jong, *Recl. Trav. Chim. Pays-Bas* **113**, 533 (1994).
20. M. Ibisi and B. Brown, *J. Acoust. Soc. Am.* **41**, 568 (1967).
21. I. Hua and M. R. Hoffmann, *Environ. Sci. Tech.* **31**, 2237 (1997).
22. J.-L. Luche, *Synthetic Organic Chemistry*, Plenum, New York, 1998.
23. G. J. Price, P. J. West, and P. F. Smith, *Ultrason. Sonochem.* **1**, S51 (1994).
24. G. J. Price and P. F. Smith, *Polym.* **34**, 4111 (1993).
25. P. Kruus, J. A. G. Lawrie, and M. L. O'Neill, *Ultrasonics* **26**, 352 (1988).
26. G. J. Price, *Chem. Ind*. 75 (Feb. 1993).
27. N. Erolan, F. Arisan, and H. Çatalgil-Giz, *Angew. Makromol. Chem.* **226**, 53 (1995).
28. P. Kruus, *Ultrasonics* **25**, 20 (1987).
29. D. Feldman, *Polym. News* **20**, 138 (1995).
30. M. W. A. Kuijpers, M. F. Kemmere, J. T. F. Keurentjes, *Annual AIChE-meeting* 341B (Nov. 2001).
31. P. G. Jessop and W. Leitner, *Chemical Synthesis Using Supercritical Fluids*, Wiley-VCH, Weinheim, 1999.
32. M. A. Abraham and L. Moens, *Clean Solvents, Alternative Media for Chemical Reactions and Processing*, American Chemical Society, Washington, D.C., 2002.
33. K. A. Shaffer and J. M. DeSimone, *Trends Polym. Sci.* **3**, 146 (1995) .
34. M. W. A. Kuijpers, D. Van Eck, M. F. Kemmere, and J. T. F. Keurentjes, *Science* **298**, 1969 (2002).
35. M. F. Kemmere, M. W. A. Kuijpers, L. J. M. Jacobs, and J. T. F. Keurentjes, *Macromol. Symp*. (in press).
36. H. C. Chou and J. O. Stoffer, *J. Appl. Polym. Sci.* **72**, 797 (1999).
37. S. K. Ooi and S. Biggs, *Ultrason. Sonochem.* **7**, 125 (2000).
38. G. Cooper, F. Grieser, and S. Biggs, *J. Colloid Interface Sci.* **184**, 52 (1996).
39. C. Zhang, Q. Wang, H. Xia and G. Qiu, *Eur. Polym. J.* **38**, 1769 (2002).
40. H. C. Chou and J. O. Stoffer, *J. Appl. Polym. Sci.* **72**, 827 (1999).
41. S. Biggs and F. Grieser, *Macromolecules* **28**, 4877 (1995).
42. M. Bradley, M. Ashokkumar, and F. Grieser, *J. Am. Chem. Soc.* **125**, 525 (2003).
43. H. C. Chou, W. Y. Lin, and J. O. Stoffer, *Polym. Mater. Sci. Eng.* **72**, 363 (1995).
44. H. C. Chou, Y. B. Liu, O. C. Sitton, and J. O. Stoffer, *Polym. Mater. Sci. Eng.* **69**, 376 (1993).
45. Y. Liao, Q. Wang, H. Xia, X. Xu, S. M. Baxter, R. V. Slone, S. Wu, G. Swift, and D. G. Westmoreland, *Ultrason. Sonochem.* **9**, 151 (2002).

46. Q. Wang, H. Xia, Y. Liao, X. Xu, S. M. Baxter, R. V. Slone, S. Wu, G. Swift, and D. G. Westmoreland, *Polym. Int.* **50**, 1252 (2001).
47. I. W. Hamley, *Encyclopedia of Polymer Science and Technology*, 3rd ed., Vol. 1, John Wiley & Sons, Inc., New York, 2002, pp. 457–482.
48. T. J. Mason, *Sonochemistry, The Uses of Ultrasound in Chemistry*, CRC Press, Inc., Boca Raton, Fla., 1990, p. 125.
49. H. Fujiwara, J. Tanaka, and A. Horiuchi, *Polym. Bull.* **36**, 723 (1996).
50. G. Schmidt-Naake, M. Drache, and M. Weber, *Macromol. Chem. Phys.* **15**, 203 (2002).
51. G. J. Price and P. J. West, *Polym.* **37**, 3975 (1996).
52. H. Fujiwara, *Polym. Bull.* **47**, 247 (2001).
53. A. V. Machado, J. A. Covas, and M. van Duin, *J. Appl. Polym. Sci.* **81**, 58 (2001).
54. P. A. R. Glyn, B. M. E. van der Hoff, and P. M. Reilly, *J. Macromol. Sci., Chem. A* **6**, 1653 (1972).
55. B. M. E. van der Hoff and C. E. Gall, *J. Macromol. Sci. A* **11**, 1739 (1977).
56. G. Madras, S. Kumar, S. Chattopadhyay, *Polym. Degr. Stab.* **69**, 73 (2003).
57. J. R. Ebdon and G. C. Eastmond, *New Methods of Polym. Synthesis*, Blackie, Glasgow, U.K., 1995, p. 117.
58. T. Q. Nguyen, Q. Z. Liang, and H.-H. Kausch, *Polym.* **38**, 3783 (1997).
59. M. W. A. Kuijpers, P. D. Iedema, M. F. Kemmere, and J. T. F. Keurentjes, manuscript submitted.
60. A. M. Basedow and K. H. Ebert, *Adv. Polym. Sci.* **22**, 83 (1977).

MARTIJN W. A. KUIJPERS
MAARTJE F. KEMMERE
JOS T. F. KEURENTJES
Eindhoven University of Technology

URETHANE COATINGS. See Volume 8.

URETHANE POLYMERS. See Polyurethanes.

UV STABILIZERS. See Volume 8.

VEGETABLE FIBERS

Introduction

Fibers for commercial and domestic use are broadly classified as natural or synthetic. The natural fibers are vegetable, animal, or mineral in origin. Vegetable fibers, as the name implies, are derived from plants. The principal chemical component in plants is cellulose (qv), and therefore they are also referred to as cellulosic fibers. The fibers are usually bound by a natural phenolic polymer, lignin (qv), which also is frequently present in the cell wall of the fiber; thus, vegetable fibers are also often referred to as lignocellulosic fibers, except for cotton, which does not contain lignin.

Vegetable fibers are classified according to their source in plants as follows: (*1*) the bast or stem fibers, which form the fibrous bundles in the inner bark (phloem or bast) of the plant stems, are often referred to as soft fibers for textile use; (*2*) the leaf fibers, which run lengthwise through the leaves of monocotyledonous plants, are also referred to as hard fibers; and (*3*) the seed-hair fibers, the source of cotton (qv), which is the most important vegetable fiber and is discussed in another article. There are over 250,000 species of higher plants; however, only a very limited number of species have been exploited for commercial uses (less than 0.1%). The commercially important fibers are given in Table 1 (1–3).

The fibers in bast and leaf fiber plants are integral with the plant structure, providing strength and support. In bast fiber plants, the fibers are next to the outer bark in the bast or phloem and serve to strengthen the stems of these reed-like plants. The fibers are in strands running the length of the stem or between joints (Fig. 1). To separate the strands, the natural gum binding them must be removed. This operation is called *retting* (controlled rotting). For most uses, particularly for textiles, this long composite-type strand fiber is used directly; however, when such fiber strands are pulped by chemical means the strand is broken down into much shorter and finer fibers, the ultimate fibers shown in Figure 1.

Encyclopedia of Polymer Science and Technology. Copyright John Wiley & Sons, Inc. All rights reserved.

Table 1. Vegetable Fibers of Commercial Interest[a]

Commercial name	Source	Botanical name of plant	Growing area
		Bast or soft fibers	
China jute	Abutilon	*Abutilon theophrasti*	China
Flax		*Linum usitatissimum*	North and south temperate zones
Hemp		*Cannabis sativa*	All temperate zones
Jute		*Corchorus capsularis; C. olitorius*	India
Kenaf		*Hibiscus cannabinus*	India, Iran, CIS, South America
Ramie		*Boehmeria nivea*	China, Japan, United States
Roselle		*Hibiscus sabdariffa*	Brazil, Indonesia (Java)
Sunn		*Crotalaria juncea*	India
Urena	Cadillo	*Urena lobata*	Zaire, Brazil
		Leaf or hard fibers	
Abaca		*Musa textilis*	Borneo, Philippines, Sumatra
Cantala	Manila maguey	*Agave cantala*	Philippines, Indonesia
Caroa		*Neoglaziovia variegata*	Brazil
Henequen		*Agave fourcroydes*	Australia, Cuba, Mexico
Istle		*Agave* (various species)	Mexico
Mauritius		*Furcraea gigantea*	Brazil, Mauritius, Venezuela, tropics
Phormium		*Phormium tenax*	Argentina, Chile, New Zealand
Pineapple	Piña	*Ananas comasus*	Hawaii, Philippines, Indonesia, India, West Indies
Sansevieria	Bowstring hemp	*Sansevieria* (entire genus)	Africa, Asia, South America
Sisal		*Agave sisalana*	Haiti, Java, Mexico, South Africa, Brazil
		Seed-hair fibers	
Coir	Coconut husk fiber	*Cocos nucifera*	Tropics, India, Mexico
Cotton		*Gossypium* sp.	United States, Asia, Africa
Kapok		*Ceiba pentandra*	Tropics
Milkweed floss		*Chorisia* sp.	North America
		Other fibers	
Broom root	Roots	*Muhlenbergia macroura*	Mexico
Broom corn	Flower head	*Sorghum vulgare technicum*	United States
Crin vegetal	Palm leaf segments	*Chamaerops humilis*	North Africa
Palmyra palm	Palm leaf stem	*Brossus flabellifera*	India
Pissava	Palm leaf base fibers	*Attalea funifera*	Brazil
Raffia	Palm leaf segments	*Raphia raffia*	East Africa

[a]Refs. 1–3.

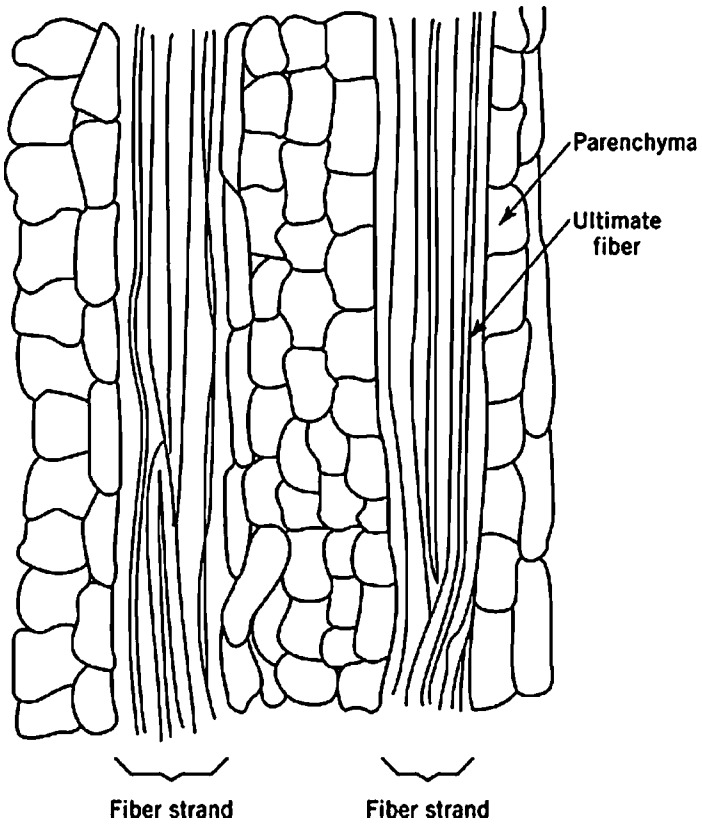

Fig. 1. Typical longitudinal section of bast fiber showing very long fiber strands composed of many ultimate fibers (see Table 3 for dimensions).

The long leaf-fibers contribute strength to the leaves of certain nonwoody, monocotyledonous plants. They extend longitudinally the full length of the leaf and are buried in tissues of a parenchymatous nature. The fibers found nearest the leaf surface are the strongest. The fibers are separated from the pulp tissue by scraping because there is little bonding between fiber and pulp; this operation is called *decortication*. Leaf fiber strands are also multicelled in structure.

Ancient humans used cordage in fishing, trapping, and transport, and in fabrics for clothing. Rope and cord making started in Paleolithic times, as seen in cave drawings. Rope, cords, and fabrics were made from reeds and grasses in ancient Egypt (400 BC). Ropes, boats, sails, and mats were made from palm leaf fibers and papyrus stalks and writing surfaces, known as papyrus, from the pith section. Jute, flax, ramie, sedges, rushes, and reeds have long been used for fabrics and baskets. Jute was cultivated in India in ancient times and used for spinning and weaving. The first true paper is believed to have been made in southeastern China in the second century AD from old rags (bast fibers) of hemp and ramie and later from the bast fiber of the mulberry tree.

Scientists at the U.S. Department of Agriculture (USDA) Northern Regional Research Center in Peoria, Illinois, carried out an extensive screening of over 500

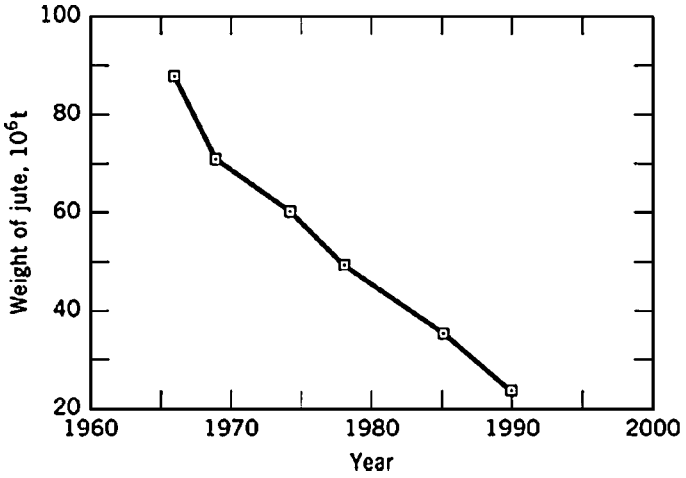

Fig. 2. Export of jute goods from India (1965–1990).

species of plants as potential sources of papermaking fibers (4–7). The species were rated for agronomic potential, chemical composition, fiber properties, and physical characteristics. The species with the greatest potential were in the genera *Hibiscus, Crotalaria, Sorghum, Cannabis, Gynerium, Lygerum,* and *Sinarundinaria*.

World markets for vegetable fibers have been steadily declining in recent years, mainly as a result of substitution with synthetic materials. Jute has traditionally been one of the principal bast fibers (tonnage basis) sold on the world market; however, the precipitous decline in jute exports by India (Fig. 2) indicates the decreasing market demand for this fiber that has been vitally important to the economies of India (West Bengal), Bangladesh, and Pakistan.

General Properties

Chemical Composition. The chemical composition of the principal commercial vegetable fibers is given in Table 2 (8,9). These compositions are for the commercial fibrous materials after processing and differ from the chemical composition of the whole plant material that is frequently cited in the literature (1,10). Chemically, cotton is the purest, containing over 90% cellulose with little or no lignin. The other fibers contain 40–75% cellulose, depending on processing. Boiled and bleached flax and degummed ramie may contain over 95% cellulose. Kenaf and jute contain higher contents of lignin, which contributes to their stiffness. Although the cellulose contents shown in Table 2 are fairly uniform, the other components, eg, hemicelluloses, pectins, extractives, and lignin vary widely without obvious pattern. These differences may characterize specific fibers.

Fiber Dimensions. Except for the seed-hair fibers, the vegetable fibers of bast or leaf origins are multicelled (Fig. 1) and are used as strands (see Table 3) (1,2,9,11). In contrast to the bast fibers, leaf fibers are not readily broken down into their ultimate cells. The ultimate cells are composites of microfibrils, which, in turn, are comprised of groups of parallel cellulose chains.

Table 2. Chemical Composition (wt %) of Vegetable Fibers[a]

Fiber	Cellulose	Hemicellulose	Pectins	Lignin	Extractives
		Bast fibers			
Flax	71.2	18.6	2.0	2.2	6.0
Hemp	74.9	17.9	0.9	3.7	3.1
Jute	71.5	13.4	0.2	13.1	1.8
Kenaf	63.0	18.0		17.0	2.0
Ramie	76.2	14.6	2.1	0.7	6.4
		Leaf fibers			
Abaca	70.1	21.8	0.6	5.7	1.8
Phormium	71.3				
Sisal	73.1	13.3	0.9	11.0	1.6
		Seed-hair fibers			
Coir	43.0	0.1		45.0	
Cotton	92.9	2.6	2.6		1.9
Kapok	64.0	23.0	23.0	13.0	

[a]Refs. 1,2,8, and 9.

Table 3. Dimensions of Ultimate Fibers and Strands[a]

	Ultimate fiber		Cell cross-section		Fiber strand	
Fiber	Length, mm	Diameter, μm	Shape	Diameter,[b] μm	Length, cm	Width, mm
			Bast fibers			
Chinese jute	2–6.5	7–33				
Flax	4–69	8–31	Polygonal	8.8–16.1	25–120	0.04–0.62
Hemp	5–55	16	Polygonal	13.1–23.6	100–400	0.5–5
Jute	0.7–6	15–25	Polygonal to oval	12.3–18.6	150–360	
Kenaf	2–11	13–33	Cylindrical		200–400	
Ramie	60–250	16–120	Hexagonal to oval	6.2–32.4	10–180	
Sunn	2–11	13–64	Irregular	13.6–24.6	108–216	
Nettle	4–70	20–70		50–50		
			Leaf fibers			
Abaca	2–12	6–40	Oval to round	14–20	150–360	0.01–0.28
Cantala				13.8–16.4		
Caroa	2–10	3–13		3.2–8.2		
Henequen	1.5–4	8.3–33.2		11.6–22.2		
Istle		9.6–16		11.2–13.4	30–75	
Mauritius	1.3–6	15–32	Cylindrical		124–210	
Phormium	2–11	5.25	Round	10.3–12.1	150–240	
Sansevieria	1–7	13–40				
Sisal	0.8–7.5	8–48	Cylindrical	11–16	60–120	0.1–0.5
			Seed-hair fibers			
Coir	0.2–1	6.24				1
Cotton	10–50	12–25	Circular elliptical		1.5–5.6	0.012–0.025
Kapok	15–30	10–30	Round		1.5–3	0.03–0.036
			Others			
Broom root					25–40	

[a]Refs. 1,2,8–11.
[b]Minor and major diameters, respectively.

Table 4. Mechanical Properties of Vegetable Fibers[a]

Fiber	Fineness, km/kg	Tensile strength,[b] km	Elongation, %	Modulus of elasticity,[c] N/tex[d]	Modulus of rupture mN/tex[d]
			Bast (soft) fibers		
Flax		24–70	2–3	18–20	8–9
Hemp	139	38–62	1–6	18–22	6–9
Jute	489	25–53	1.5	17–18	2.7–3
Kenaf	180	24	2.7		
Ramie		32–67	4.0	14–16	11
Urena	342	16	1.9		
			Leaf (hard) fibers		
Abaca	32	32–69	2–4.5		6
Cantala	58	30			
Henequen	32	20–42	3.5–5		
Istle	34	22–27	4.8		
Phormium	38	26			
Sansevieria	118	43	4.0		
Sisal	40	36–45	2–3	25–26	7–8
			Seed-hair fibers		
Coir		18	16	4.3	16
Kapok		16–30	1.2	13	10

[a]Refs. 9–12.
[b]Based on breaking length, which measures strength per unit area.
[c]Young's modulus.
[d]To convert N/tex to g · f/den, multiply by 11.33.

Physical Properties. Mechanical properties are given in Table 4 (1,11, 12). Bast and leaf fibers are stronger (higher tensile strength and modulus of elasticity) but lower in elongation (extensibility) than cotton. Vegetable fibers are stiffer but less tough than synthetic fibers. Kapok and coir are relatively low in strength; kapok is known for its buoyancy.

Among the bast textile fibers, the density is close to 1.5 g/cm^3, or that of cellulose itself, and they are denser than polyester, as shown in Table 5. Moisture regain (absorbency) is highest in jute at 14%, whereas that of polyester is below 1%. The bast fibers are typically low in elongation and recovery from stretch. Ramie fiber has a particularly high fiber length/width ratio.

Table 5. Textile-Associated Properties of Bast Fibers Compared to Polyester[a]

Property	Cotton	Flax	Hemp	Jute	Ramie	Polyester
Density, g/cm^3	1.54–1.5	1.50	1.48	1.50	1.51	1.22–1.35
Moisture regain, %	8–11	12	12	13.7	6	0.4–0.8
Fiber tenacity, mN/tex[b]	260–440	230–240	510–600	260–510	450–653	180–790
Elongation, dry, %	3–10	2.7–3.3	1.6	1.2–1.9	3.0–7.0	18–67
Recovery from 2% elongation, %	75	65		74	52	85–97
Length/width ratio	1400	1200			3000	

[a]Ref. 13.
[b]To convert N/tex to g · f/den, multiply by 11.33.

The microfibrils in vegetable fibers are spiral and parallel to one another in the cell wall. The spiral angles in flax, hemp, ramie, and other bast fibers are lower than cotton, which accounts for the low extensibility of bast fibers.

Bast Fibers

Bast fibers occur in the phloem or bark of certain plants. The bast fibers are in the form of bundles or strands that act as reinforcing elements and help the plant to remain erect (Fig. 1). The plants are harvested and the strands of bast fibers are released from the rest of the tissue by retting, common for isolation of most bast fibers. The retted material is then further processed by breaking, scutching, and hackling. A general description of the processing of bast fibers is given below with modifications for specific fibers described in the following sections.

Processing.

Harvesting and Pretreatment. At optimum maturity, the plants are pulled or mowed by hand or machine and, if necessary, threshed to remove seeds. The plants are spread out in a field to dry.

Retting. The removal of the bast fibers from bark and woody stem parts is promoted by a biological treatment called retting (rotting). This is an enzymatic or bacterial action on the pectinous matter of the stem. After retting, the bundles are dried in fields. Retting may be carried out in several ways.

Dew retting involves the action of dew, sun, and fungi on the plants spread thinly on the ground. Dew retting takes 4–6 weeks, but the action is not uniform and it tends to yield a dark-colored fiber. However, it is far less labor-intensive and less expensive than water retting. It is commonly used in regions of low water supply and accounts for 85% of the western European crop, especially in France, and also in the former Soviet Union.

Water retting involves immersion of bundles of plants in stagnant pools, rivers, ditches (dam retting), or in specially designed tanks (tank retting). The biological effect is achieved through bacterial action and takes 2–4 weeks for dam retting. In tanks with warm water (tank retting), the time is reduced to a few days. Water retting gives a more uniform product. In stream retting the plants are immersed in slow-moving streams for a longer time and the quality of the product is high.

Chemical retting involves immersion of the dried plants in a tank with a solution of chemicals, such as sodium hydroxide, sodium carbonate, soaps, or mineral acids. The fibers are loosened in a few hours, but close control is required to prevent deterioration. Chemical retting is more expensive and does not produce a superior fiber to that obtained from biological retting.

Breaking and Scutching. The dried retted stalks in bundles are passed through fluted rolls to break or reduce the woody portion into small particles, which are then separated by scutching. The scutching is done by beating with blunt wooden or metal blades by hand or mechanically.

Hackling. The bundles are hackled or combed to separate the short and long fibers. This is done by drawing the fibers through sets of pins, each set finer than the previous one. As a result the fibers are further cleaned and aligned parallel to one another.

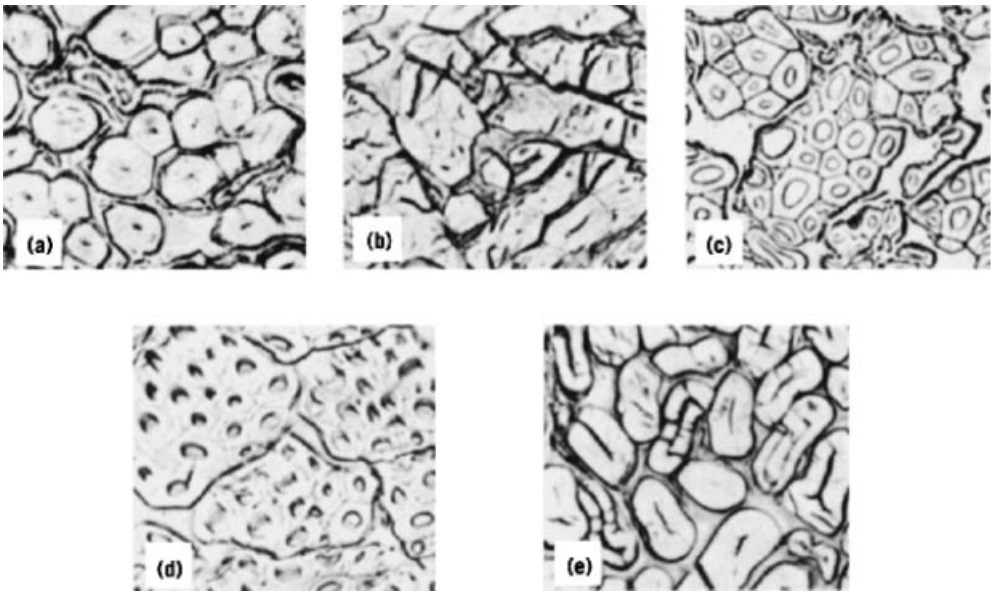

Fig. 3. Cross-sections (500×) of bast fibers: (**a**) flax; (**b**) hemp; (**c**) jute; (**d**) kenaf; and (**e**), ramie. Courtesy of the American Association of Textile Chemists and Colorists (14).

Flax. The flax fiber from the annual plant *Linum usitatissimum* (flax family, Linaceae) has been used since ancient times as the fiber for linen. The plant grows in temperate, moderately moist climates, for example, in Belgium, France, Ireland, Italy, and Russia. The plant is also cultivated for its seed, from which linseed oil is produced. A by-product of the seed plant is the tow fiber used in papermaking.

The bast fibers are dew or water retted with dew retting generally yielding a gray fiber. High quality flax fiber is produced by water (stream) retting in the river Lys in Belgium. A cross-sectional view of the flax fiber is shown in Figure 3**a**, the fibers are round to polygonal with a small lumen. The boiled, bleached fiber contains almost 100% cellulose. The flax fiber is the strongest of the vegetable fibers, even stronger than cotton. The fiber is highly absorbent, an important property for clothing, but is particularly inextensible. The most important application is in linen for clothing, fabrics, lace, and sheeting. Flax fiber is also used in canvas, threads and twines, and certain industrial applications such as fire hoses. Chemical pulping of flax provides the raw material for production of high quality currency and writing paper. Flax fiber is also commonly used in cigarette papers. Flax fibers are graded for fineness, softness, stretch, density, color, uniformity, luster, length, handle, and cleanliness.

Hemp. The source of hemp fiber is the plant *Cannabis sativa* (mulberry family, Moraceae) originating in central China. It is grown in central Asia and eastern Europe. The stem is used for fiber, the seeds for oil, and leaves and flowers for drugs, among them marijuana. The stalks grow 5–7 m tall and 6–16 mm thick. The hollow stems, smooth until the rough foliage at the top, are hand-cut and spread on the ground for dew retting for the highest quality product. Water retting

is used on sun-dried bundles from which the seeds and leaves have been removed. Strands of hemp fiber can be 2 m in length. The fibers are graded for color, luster, spinning quality, density, cleanliness, and strength.

A cross-sectional view of hemp fiber is shown in Figure 3**b**. It has a "Z" twist in contrast to the "S" twist of flax. Hemp is regarded as a substitute for flax in yarn and twine. Its earlier use in ropes has been replaced by leaf and synthetic fibers. Hemp fiber is used in Japan, China, Hungry, and Italy to make specialty papers, including cigarette paper, but bleaching is difficult. The fiber is coarser and has less flexibility than flax. There is currently interest in reintroducing hemp into the United States and Canada as an alternate fiber crop for farmers. However, this is wrought with political and legal problems because of the inability to distinguish industrial hemp from hemp plants with high narcotic content.

Jute. Jute fiber is obtained from two herbaceous annual plants, *Corchorus capsularis* (linden family, Tiliaceae) originating from Asia, and *Corchorus olitorius* originating from Africa. The former has a round seed pod, and the latter a long pod. Jute is grown mainly in India, Bangladesh, Thailand, and Nepal.

The plants are harvested by hand, dried in the field for defoliation, and water (pool) retted for periods up to a month. The depth of the retting pools is dependent on the volume of rainfall during the monsoon season in Southeast Asia. Thus, a year with less rainfall results in low water levels in the retting pools and a lower grade jute product due to contamination with sand and silt. The fibers for export are graded for color, length, fineness, strength, cleanliness, luster, softness, and uniformity. The color ranges from cream white to reddish brown, but usually the fiber has a golden luster. A cross-sectional view of the fiber is shown in Figure 3**c**. The fibers are polygonal in cross section with a wide lumen. Jute has traditionally been an important textile fiber, second only to cotton; however, jute has been steadily replaced by synthetics in the traditional high volume uses such as carpet backings and burlap (hessian) fabrics and sacks (Fig. 2). The strands are also used for twine, while kraft pulping of jute gives ultimate fibers for cigarette papers. The Indian government in cooperation with the United Nations Development Program has been involved in a significant jute diversification program to find new uses for jute in finer yarns and textiles, composites and boards, and paper products. A particularly promising outlet for jute is in molded composites with thermoplastic materials for interior automobile head, door, and trunk liners (1).

Kenaf and Roselle. These closely related bast fibers are derived from *Hibiscus cannabinus* and *Hibiscus sabdariffa* (mallow family, Malvaceae), respectively. The fibers have other local names. Kenaf is grown for production in China, Egypt, and regions of the former Soviet Union; roselle is produced in India and Thailand. Plantation-grown kenaf is capable of growing from seedlings to 5 m at maturity in 5 months. It is reported to yield about 6–10 tons of dry matter per acre, nine times the yield of wood (15,16).

The plants are hand-cut, mowed, or pulled in developing countries, while mechanized harvesting methods are under investigation in the United States. Ribboning machines are sometimes used to separate the fiber-containing bark before retting for recovery of the kenaf strands. For pulping, the kenaf is shredded or hammermilled to 57-cm pieces, washed, and screened.

A cross-sectional view of kenaf is shown in Figure 3**d**. The ultimate cells are nearly cylindrical with thick cell walls. Kenaf fibers are shorter and coarser than

those of jute. Both chemical (kraft) and mechanical pulps have been produced from kenaf, and successful demonstration runs of newsprint have been made for the Dallas Morning News, the St. Petersburg Times, and the Bakersfield Californian with a furnish of 82% kenaf chemithermomechanical pulp and 18% softwood kraft pulp. Kenaf fiber is also considered a substitute for jute and used in sacking, rope, twine, bags, and as papermaking pulp in India, Thailand, and the Balkan countries. Roselle bleached pulp is marketed in Thailand.

Ramie. The ramie fiber is located in the bark of *Boehmeria nivea*, a member of the nettle family (Urticaceae). The plant is a native of China (hence, its name China grass), where it has been used for fabrics and fishing nets for hundreds of years. It is also grown in the Philippines, Japan, Brazil, and Europe. The ramie plant grows 1–2.5 m high with stems 8–16 mm thick. The roots send up shoots on harvesting, and two to four cuttings are possible annually, depending on soil and climate.

The plant is harvested by hand sickle and, after defoliation, is stripped and scraped by hand or machine-decorticated. Because of the high gum (xylan and araban) content of up to 35%, retting is not possible. The fibers are separated chemically by boiling in an alkaline solution in open vats or under pressure, then washed, bleached with hypochlorite, neutralized, oiled to facilitate spinning, and dried.

The degummed, bleached fiber contains 96–98% cellulose. A cross-sectional view is shown in Figure 3**e**. The ramie fibers are oval-like in cross-section, with thick cell walls and a fine lumen. The cell wall constituents in the ramie fiber, like other bast fibers except flax, have a counterclockwise twist. Ramie is the longest of the vegetable fibers and has excellent luster and exceptional strength; however, it tends to be stiff and brittle. Wet strength is high and the fiber dries rapidly, an advantage in fish nets.

Traditional uses for ramie have been for heavy industrial-type fabrics such as canvas, packaging material, and upholstery. Increased production of the fiber in Asia, particularly China, has promoted the use in blended fabrics with silk, linen, and cotton which can now be found on the market.

Sunn Hemp. The stems of the herbaceous plant *Crotalaria juncea* (legume family, Fabaceae), called sunn or sunn hemp, provide a bast fiber. The plant is native to India, the chief fiber producer, and it is also grown in Bangladesh, Brazil, and Pakistan. It has a long tap root and grows to a height of up to 5 m. Harvesting is done manually by pulling or cutting. The plant is defoliated in the field, water retted, and processed similarly to jute. The white fiber is graded by color, firmness, length, strength, uniformity, and extraneous matter content. Sunn is used for canvas, paper, fishing nets, twine, and other cordage.

Urena and Abutilon. These are less important vegetable fibers of a jute-like nature. *Urena lobata* (Cadillo) of the mallow family (Malvaceae) is a perennial that grows in Zaire and Brazil to a height of 4–5 m with stems 10–18 mm in diameter. Because of a lignified base, the stems are cut 20 cm above the ground. The plants are defoliated in the field and retted similarly to jute and kenaf. The retted material is stripped and washed and, in some cases, rubbed by hand. The soft, near-white fiber is graded for luster, color, uniformity, strength, and cleanliness. It is used for sacking, cordage, and coarse textiles.

Abutilon theophrasti is a herbaceous annual plant producing a jute-like fiber. The plant is native to China and is commercially grown in China and the former

Soviet Union. Because of its association with jute in mixtures and export, it is also called China jute. The plant grows to a height of 3–6 in. with a stem diameter of 6–16 mm. After harvesting by hand and defoliation, bundles of the stems are water retted and the fiber is extracted by methods similar to those for jute. The fiber is used for twine and ropes.

Leaf (Hard) Fibers

Hard or cordage fibers are found in the fibrovascular systems of the leaves of perennial, monocotyledonous plants growing in Central America, East Africa, Indonesia, Mexico, and the Philippines. They are generally of the Agave and Musa genera. The leaf elements are harvested by cutting at the base with a sickle-like tool, and bundled for processing by hand or by machine decortication. In the latter case, the leaves are crushed, scraped, and washed. The fibers are generally coarser than the bast fibers and are graded for export according to national rules for fineness, luster, cleanliness, color, and strength.

Abaca. The abaca fiber is obtained from the leaves of the banana-like plant (same genus) *Musa textilis* (banana family, Musaceae). The fiber is also called Manila hemp from the port of its first shipment, although it has no relationship with hemp, a bast fiber. The mature plant has 12–20 stalks growing from its rhizome root system; the stalks are 2.6–6.7 m tall and 10–20 cm thick at the base. The stalk has leaf sheaths that expand into leaves 1–2.5 m long, 10–20 cm wide, and 10 mm thick at the center; the fibers are in the outermost layer. The plant produces a crop after 5 years, and 2–4 stalks can be harvested about every 6 months.

In the Philippines, the principal supplier of abaca fiber, the fibrous layer in the sheath is separated with a knife between the layers, and the strips of fiber-containing layers, called tuxies, are pulled off and cleaned by hand to remove the pulp. In Indonesia and Central America these operations are performed mechanically. Hand- and spindle-stripped fiber is graded for braids, fine textiles, and cordage; decorticated fiber is another class. A cross-sectional view is shown in Figure 4**a**. The abaca fiber has a large lumen and the presence of silicified plates is not unusual.

Abaca fiber is unique in its resistance to water, especially salt water, and it is used for marine ropes and cables, although it has been largely replaced by synthetic fibers. Abaca fiber is the strongest of the leaf fibers (Table 4), followed by sisal, phormium, and henequen; it is also the strongest among the papermaking fibers. It is used for sausage casings and it is the preferred fiber for tea bags because of its high wet strength, cleanliness, and structure that permits rapid diffusion of the tea extract.

Cantala, Manila Maguey. *Agave cantala* is a member of the agave family (Agavaceae) that includes sisal. It originated in Mexico and was transported to Indonesia and the Philippines, where it is now produced commercially. The plant grows in a moist, humid soil. The fiber is extracted in Indonesia mechanically by a decorticator (raspador) and in the Philippines by retting in seawater and cleaning by hand or with a decorticator. The cantala fiber is lighter in color than other agaves, and its strength depends on its preparation.

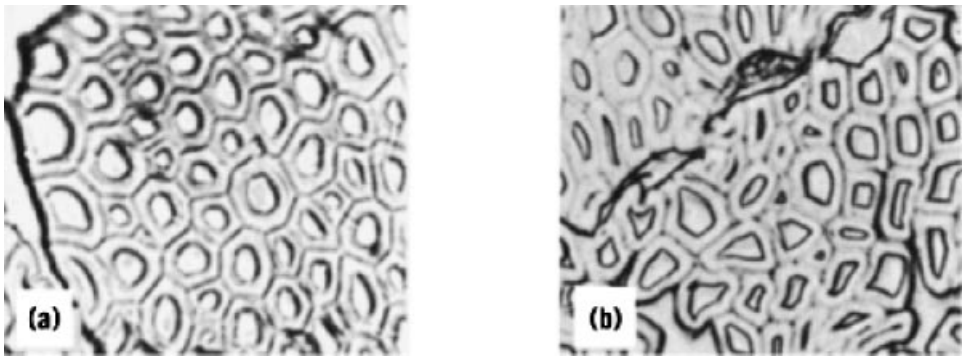

Fig. 4. Cross-sections (500×) of leaf fibers: (**a**) abaca and (**b**) sisal. Courtesy of the American Association of Textile Chemists and Colorists (14).

Caroa. Caroa is a hard leaf fiber, resembling sisal, obtained from *Neoglaziovia variegata*, a plant of the pineapple family (Bromeliaceae) growing wild in eastern and northern Brazil. The sword-shaped leaves are 1–3 m long and 2.5–5 cm wide. The fiber is extracted by hand scraping after beating or retting. The fiber is used for cordage and acoustic material.

Henequen. *Agave fourcroydes* grows in Mexico where it was first cultivated by the Mayans in the Yucatan (Yucatan Sisal). The plant produces for 20–30 years. The lower bottom leaves, which are up to 2 m long and 10–15 cm wide, are cut, machine-decorticated, and cleaned. Henequen fibers are white to yellowish red and are inferior to sisal in strength, cleanliness, texture, and length, the other grading criteria. Henequen is grown for local use in Cuba (Cuban Sisal) and El Salvador. Twines, small ropes, coarse rugs, and sacks are made commercially from henequen.

Istle. Istle is the general name for several agave species and related plants producing short, coarse, hard fibers. The commercial name is tampico. The plants from which the fibers are harvested include tula istle (*Agave lophantha*), jaumave istle (*Agave funkiana*), and palma istle (*Samuela carnerosana*). They are grown in central and northern Mexico. The fibers are recovered by hand scraping and drying; the palma istle is gummy and requires presteaming. The jaumave istle fibers closely resemble animal bristles in brushes.

Mauritius Hemp. Mauritius hemp, also called piteira, is obtained from *Furcraea gigantea,* also a member of the Agavaceae. The plant is mostly grown on the island of Mauritius, but is also harvested in Brazil and other tropical countries. The leaves are longer and heavier than those of the agaves. The fiber is extracted by mechanical decortication. It is whiter, longer, and weaker than sisal fiber. Because of its color it is used in blends.

Phormium. The *Phormium tenax* plant yields a long, light-colored, hard fiber also known as New Zealand hemp or flax, although it has none of the bast fiber characteristics. The plant is a perennial of the Agavaceae with leaves up to 4 m long and 10 cm wide. The fibers are recovered by mechanical decortication.

Sansevieria. This genus of the Agavaceae is a perennial also known as bowstring hemp from its use in bow strings. The plant is native to tropical Africa

and Asia but is widely grown, mainly as an ornamental plant. It is of minor importance as a fiber plant, even though the fiber is of high quality. The highest grade of *Samuela cylindrica* fiber is greenish yellow, very soft and fine, and compares with sisal in strength.

Sisal. The true sisal fiber from *Agave sisalana* is the most important of the leaf fibers in terms of quality and commercial use. Originating in the tropical western hemisphere, sisal has been transplanted to East Africa, Indonesia, and the Philippines. It is named after the port in the Yucatan from which it was first exported. The sisal plant leaves grow from a central bud and are 0.6–2 m long, ending in a thorn-like tip. The fibers are embedded longitudinally in the leaves, which are crushed, scraped, washed, and dried. The highest grades are further cleaned with a revolving drum. The growth of the sisal plant depends on water availability; it stores water during the wet season and consumes it during periods of drought.

A cross section of the sisal ultimate fiber is shown in Figure 4**b**. The sisal fiber is coarse and strong, but compared with the abaca fiber it is inflexible, although with a relatively high elongation under stress. It is also resistant to salt water. The principal applications are in binder and baling twine and as a raw material for pulp for products requiring high strength. A large pulp mill is operating in Brazil based on sisal.

Seed- and Fruit-Hair Fibers

The seeds and fruits of plants are often attached to hairs or fibers or encased in a husk that may be fibrous. These fibers are cellulosic-based and of commercial importance, especially cotton, the most important natural textile fiber.

Coir. This fiber, obtained from husks of the fruit of the coconut palm, *Cocos nucifera* (palm family, Arecaceae), is mainly produced in India and Sri Lanka. The fruits are broken by hand or machine, and the fiber extracted from the broken husks from which the coconut has been removed for the copra. The husks are retted in rivers, and the fiber separated by hand beating with sticks or by a decortication machine. The fibers are washed, dried, and hackled, and used in upholstery, cordage, fabrics, mats, and brushes.

Kapok. Kapok fiber is obtained from the seed pods of the kapok tree, *Ceiba pentandra*, of the Kapok tree family (Bombacaceae) which is indigenous to Africa and southeast Asia; the fiber is produced mainly in Java. The tree grows to a height of 35 m. The seeds are contained in capsules or pods that are picked and broken open with mallets. The floss is dried and the fiber is separated by hand or mechanically. A nondrying oil is produced from the seeds with properties similar to cottonseed oil. The fiber is exceedingly light, with a circular cross section, thin walls, and a wide lumen. Kapok fibers are moisture-resistant, buoyant, resilient, soft, and brittle, but not suitable for spinning. The traditional uses were in life jackets, sleeping bags, insulation, and upholstery; however, synthetics have replaced most of the applications as filling material and now kapok is mainly used for life preservers. Kapok-filled life preservers can support up to three times the weight of the preserver and do not become waterlogged.

Palm and Other Fibers

Piassava and Crin Vegetal. These palm (palm family, Arecaceae) fibers are obtained from the palm leaf base of *Attalea funifera* growing in Brazil and the palm leaf segments of *Chamaerops humilis* growing in North Africa. The former are used for cordage and brushes, the latter for stuffing.

Broom Root and Broom Corn. Broom root fiber is obtained from the root of the bunch grass, *Muhlenbergia macroura* (Poaceae), found in Mexico, where it grows 1–3 m high. The long fibers are bleached in fumes of burning sulfur before grading according to length. They are used in stiff scrubbing and scraping brushes and whisk brooms.

Broom corn is the fiber obtained from the flower head of another grass, *Sorgum vulgare technicum*, grown in the United States. The fibers are less stiff than those of the broom root and are used in brooms.

Economic Aspects

The principal bast and leaf fibers are produced in yields of 2–5%, with some exceptions such as flax (15%) and kapok (17%), on a green plant basis. The world production of several cordage (leaf) and textile (bast) fibers is given in Table 6.

Table 6. World Production (10^3 t) of Major Vegetable Fibers in 2002[a]

Fiber	Major countries		World production
Flax (fiber and tow)	China	221	647
	France	77	
	Egypt	63	
	Russia Fed.	62	
	Benelux	30	
Hemp (fiber and tow)	China	15	55
	Korea (Dem.)	13	
	Romania	8	
	Spain	7	
Jute and jute-like	India	1,875	3,107
	Bangladesh	860	
	China	136	
	Myanmar	42	
	Nepal	16	
Ramie	China	175	179
	Philippines	2	
	Brazil	1	
Sisal	Brazil	177	331
	Mexico	27	
	Kenya	25	
	Tanzania	21	
	Madagascar	15	

[a] Source: http://apps.fao.org.

Table 7. Uses of Vegetable Fibers

	Leaf fibers				Bast fibers					Seed, fruit, and other fibers		
Uses	Abaca	Cantala	Henequen	Sisal	Flax	Hemp	Jute	Kenaf	Ramie	Sunn	Kapok	Coir
Textiles and woven goods												
Fine household, clothing					X	X			X			
Coarse household					X	X	X	X	X			
Bags and sacks			X				X	X				
Thread, yarn					X	X	X		X			
Canvas, sailcloth							X	X	X	X		
Carpet backing, matting[a]	X	X	X	X	X		X	X				X
Rugs, hammocks, belting, hose		X	X	X	X		X	X	X			
Cordage and twine												
Industrial ropes	X		X			X			X	X		
Marine ropes	X					X						
Binder, baling twine		X	X	X								
Nets									X	X		
Twines[a]	X		X		X	X	X	X	X	X		
Upholstery and stuffing												
Mattresses, furniture			X	X					X		X	
Sleeping bags, life preservers											X	
Other uses												
Brooms, brushes												X
Pulp for papermaking	X			X	X	X	X	X				
Biobased composites	X			X	X		X	X				

[a] Also phormium leaf fibers.

Vegetable fiber production on the world market has dropped substantially because of periods of economic recession and synthetic fiber replacements. U.S. imports of vegetable fibers have also dropped in recent years for similar reasons (with the exception of flax wastes). The precipitous decline in jute exports from India are shown in Figure 2. Although most vegetable fibers are converted to lower cost commodity products, some of the fibers are converted into the most expensive products in their respective industries, eg, U.S. currency (paper).

Uses

Vegetable fibers have application in a broad range of fibrous products, including textiles and woven goods, cordage and twines, stuffing and upholstery materials, brushes, paper, and new biobased composites (Table 7). The uses for each of the specific fibers have been discussed in the designated sections. The traditional uses for the vegetable fibers have been eroded by substitution with synthetics on the world market. The declining uses include cordage, mats, filling material, brushes, etc. However, the unique properties of the bast fibers have allowed continued use in such specialty papers as bank notes, some writing papers, and cigarette papers.

Work at the USDA and Kenaf International (Texas) during the past decade demonstrated the potential of both growing and processing kenaf fibers for newsprint and other paper products in the United States (15). Another promising use for vegetable fibers is in the new biobased composites that are now marketed in various parts of the industrialized world (1). The vegetable fibers are mixed with thermoplastic or thermosetting resin matrices and either extrusion or compression molded into a variety of useful shapes. Such products are already utilized in the automotive industry for automobile interior door and head liners and as trunk liners. Although vegetable fibers will continue to provide indigenous populations with traditional uses, new innovative applications need to be developed to maintain international markets for the fibers.

BIBLIOGRAPHY

"Fibers, Vegetable" in *EPST* 1st ed., Vol. 6, pp. 691–712, by D. Himmelfarb, Boston Naval Shipyard; "Fibers, Vegetable" in *EPSE* 2nd ed., Vol. 7, pp. 16–34, by J. N. McGovern, University of Wisconsin-Madison.

1. R. M. Rowell and R. A. Young, eds., *Paper and Composites from Agro-Based Resources*, CRC/Lewis Publishers, Boca Raton, Fla., 1997.
2. M. Harris, ed., *Handbook of Textile Fibers*, Harris Research Laboratories, Inc., Washington, D.C., 1954.
3. *ASTM Annual Book of Standards*, Sect. 7 07 01, D 123, Tables 4-6, American Society for Testing and Materials, Philadelphia, Pa., 1983.
4. H. J. Nieschlag and co-workers, *Tappi* **43**(3), 193 (1960).
5. G. H. Nelson and co-workers, *Tappi* **44**, 319 (1961).
6. R. L. Cunningham and co-workers, *Tappi* **53**, 1697 (1970).
7. T. F. Clark and co-workers, *Tappi* **56**(3), 107 (1973).
8. L. Rebenfeld, in J. I. Kroschwitz, ed., *Encyclopedia of Polymer Science and Engineering*, 2nd ed., Vol. 6, Wiley-Interscience, New York, 1986, p. 647.
9. T. Zylinski, *Fiber Science*, Office of Technical Services, U.S. Department of Commerce, Washington, D.C., 1964, pp. 27–30.

10. F. Hamilton and B. Leopold (for Joint Textbook Committee of the Paper Industry), *Pulp and Paper Manufacture, Vol. 3: Secondary Fibers and Non-Wood Pulping*, Tappi Press, Atlanta, Ga., 1987.
11. W. Von Bergen and W. Krauss, *Textile Fiber Atlas*, American Wool Handbook Co., New York, 1942.
12. W. E. Morton and J. W. S. Hearle, *Physical Properties of Textile Fibers*, 2nd ed., John Wiley & Sons, Inc., New York, 1975, p. 284.
13. M. L. Joseph, *Introductory Textile Science*, 5th ed., Holt, Rinehart, and Winston, New York, 1986, pp. 63–80.
14. *AATCC Technical Manual*, American Association of Textile Chemists and Colorists, Research Triangle Park, N.C., 1984, pp. 87 and 88.
15. T. Sellers Jr. and N. Reichert, eds., *Kenaf Properties, Processing and Products*, Mississippi State University, Mississippi State, Miss, 1999.
16. J. Young, *Tappi* **70**(11), 81 (1987).

GENERAL REFERENCES

R. A. Young and M. Akhtar, eds., *Environmentally Friendly Technologies for the Pulp and Paper Industry*, John Wiley & Sons, Inc., New York, 1998.
L. T. Lorimer, ed., *Encyclopedia Americana*, Vol. 11, Grolier Inc., Danbury, Conn., 1992, p. 147.
J. G. Cook, *Handbook of Textile Fibers, Vol. I: Natural Fibers*, 5th ed., Merrow Publishing, Durham, N.C., 1984.
AATCC Technical Manual, Vol. 59, American Association of Textile Chemists and Colorists, Research Triangle Park, N.C., 1984.
D. M. Colling and J. E. Grayson, *Identification of Vegetable Fibres*, Chapman and Hall Ltd., London, 1982.
J. M. Dempsey, *Fiber Crops*, University Presses of Florida, Gainesville, Fla., 1975.

RAYMOND A. YOUNG
University of Wisconsin

VESICLES. See POLYMER VESICLES.

VIBRATIONAL SPECTROSCOPY. See Volume 8.

VINYL ACETAL POLYMERS. See Volume 8.

VINYL ACETATE POLYMERS

Introduction

Vinyl acetate [108-05-4] (VAc), CH_2=CHOOCCH$_3$, the ethenyl ester of acetic acid, is primarily used for the manufacture of poly(vinyl acetate) [9003-20-7] (PVAc) and vinyl acetate copolymers. Poly(vinyl acetate) homo- and copolymers are found as components in coatings, paints and sealants, binders (adhesives, nonwovens, construction products, and carpet-backing), and miscellaneous uses such as chewing

Encyclopedia of Polymer Science and Technology. Copyright John Wiley & Sons, Inc. All rights reserved.

gum and tablet coatings. Applications have grown over the years in a number of areas (1–4).

Vinyl acetate is a colorless, flammable liquid having an initially pleasant odor which quickly becomes sharp and irritating. Table 1 lists the physical properties of the monomer. Information on properties, safety, and handling of vinyl acetate has been published (5–9). The vapor pressure, heat of vaporization, vapor heat capacity, liquid heat capacity, liquid density, vapor viscosity, liquid viscosity, surface tension, vapor thermal conductivity, and liquid thermal conductivity profile over temperature ranges have also been published (10). Table 2 (11) lists the solubility information for vinyl acetate. Unlike monomers such as styrene, vinyl acetate has a significant level of solubility in water which contributes to unique polymerization behavior. Vinyl acetate forms azeotropic mixtures (Table 3) (12).

The most important chemical reaction of vinyl acetate is free-radical polymerization (13,14). The reaction is summarized as follows:

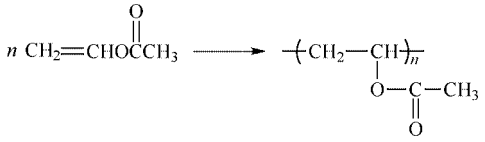

Polymerization can be initiated by organic and inorganic peroxides, azo compounds, redox systems, light, and high energy radiation. Polymerization is inhibited or strongly retarded by aromatic hydroxyl, nitro or amine compounds, and by oxygen, quinone, crotonaldehyde, copper salts, sulfur, conjugated polyolefins, and enynes. Tabulations of quantitative information, eg, polymerization-rate constants, chain-transfer constants, and activation energies for the polymerization reactions of vinyl acetate, are available (13,14). Vinyl acetate has been polymerized by bulk, suspension, solution, and emulsion methods. It copolymerizes readily with some monomers but not with others. Some reactivity ratios are presented in Table 4 for common comonomers. The Q (monomer reactivity factor) and e (electronic factor) values are 0.026 and −0.22, respectively (14).

Hydrolysis of vinyl acetate is catalyzed by acidic and basic catalysts to form acetic acid and vinyl alcohol which rapidly tautomerizes to acetaldehyde. This rate of hydrolysis of vinyl acetate is 1000 times that of its saturated analogue, ethyl acetate, in alkaline media (15). The rate of hydrolysis is minimal at pH 4.44 (16). Other chemical reactions which vinyl acetate may undergo are addition across the double bond, transesterification to other vinyl esters, and oxidation (15–21).

World production of vinyl acetate monomer was 4×10^6 t in 1999. This represented 84% of the total capacity. In 2002, North American companies produced 1654×10^3 t of vinyl acetate. See Table 5 for producers and their capacities (22). The dominant method of production in North America is by the reaction of ethylene with acetic acid and oxygen in the presence of palladium catalyst. New construction in recent years has been focused in southeast asia, although European and North American producers have expanded their plants.

Vinyl acetate's main use is as a monomer. Consumption patterns vary by world area, however. In the United States, consumption in 2002 was as follows: 82%, poly(vinyl acetates) including poly(vinyl alcohol); 8%, ethylene vinyl acetate;

Table 1. Properties and Characteristics of Vinyl Acetate

Property	Value
Formula weight	86.09
Physical state	liquid
Flammable limits in air (101.3 kPa[a]), vol %	LEL 2.6, UEL 13.4
Flash point, °C	
Tag closed cup (ASTM D56)	−8
Tag open cup (ASTM D1310)	−4
Autoignition temperature, °C	426.9
Boiling point at 101.3 kPa[a], °C	72.7
Relative evaporation rate (*n*–butyl acetate = 1)	8.9
Vapor pressure, kPa[a]	
at 60°C	64.9
40°C	29.5
20°C	11.8
Antoine equation coefficients	logP = A −[B/(T + C)]
log = base10, *T* = °C, *P* = kPa[a]	range = 10–83°C
A	7.51868
B	1452.058
C	240.588
Critical temperature, °C	246
Critical pressure, kPa[b]	3950
Color	Clear and colorless
Specific gravity, 20/20°C	0.934
Vapor density (air = 1.00)	2.97
Viscosity at 20°C	0.43 cps
Freezing point, °C	−92.8
Heat of combustion at 25°C	−495.0 kcal/mol
Heat of vaporization (1 atm)	87.6 cal/g
Heat of formation (liquid at 25°C), kJ/mol[c]	−349.4
Heat of polarization, kJ/mol[c]	89.1
Specific heat at 20°C (liquid)	0.46 cal/g °C
Odor	Not unpleasant, sweetish smell in small quantities
Reactivity	Reactive with self and variety of other chemicals; stable when property stored and inhibited
Light sensitivity	Light promotes polymerization
Electrical conductivity at 23°C	2.6 × 104 pS/m (1 S = 1 mho)
Refractive index, n_D^{20}	1.3953
Surface tension at 20°C, mN/m(= dyn/cm)	23.6
Coefficient of cubical expansion	0.00137/°C at 20°C

[a]To convert kPa to mm Hg, multiply by 7.5.
[b]To convert kPa to atm, divide by 101.3.
[c]To convert kJ/mol to kcal/mol, divide by 4.184.

Table 2. Solubilities of Vinyl Acetate[a]

Solubility of	Temperature, °C	Concentration, %
water in vinyl acetate	20	2.0–2.4
	50	2.1–2.5
vinyl acetate in water	20	0.9–1.0
	50	2
2.0 wt% solution of sodium lauryl sulfate	30	4.0
organic liquids		soluble

[a]Ref. 11.

Table 3. Azeotropes of Vinyl Acetate[a]

Second component	Azeotropic boiling point, °C	Vinyl acetate, wt%
Water	66.0	92.7
Methanol	58.9	63.4
2-Propanol	70.8	77.6
Cyclohexane	67.4	61.3
Heptane	72.0	83.5

[a]Ref. 12.

Table 4. Copolymerization Parameters of Vinyl Acetate (M_1) and Comonomers (M_2)

Comonomer (M_2)	r_1	r_2	Temperature, °C
Acrylamide	0.07	7.5	50
Acrylic acid	0.01 ± 0.003	10.0 ± 1	70
n-Butyl acrylate	0.388	5.529	50
Crotonic acid	0.33 ± 0.05	0.01 ± 0.01	68
Diethyl maleate	0.17 ± 0.01	0.043 ± 0.005	60
Ethylene	1.02 ± 0.02	0.97 ± 0.02	120
2-Ethylhexyl acrylate	0.04	7.5	60
Maleic anhydride	0.072	0.010	
Methyl acrylate	0.029 ± 0.011	6.7 ± 2.2	60
Sodium acrylate	0.01	2.0	70
Styrene	0.01 ± 0.01	55 ± 10	60
Vinyl benzoate	0.6	1.3	60
Vinyl chloride	0.6 ± 0.2	1.8 ± 0.6	40
Vinylidene chloride	0.0 ± 0.03	3.6 ± 0.5	60
Vinylidene cyanide	0.0054	0.11	45
Vinyl formate	1.41	0.68	50
Vinyl laurate	1.4	0.7	60
Vinyl pivalate	0.75 ± 0.04	0.43 ± 0.05	60
N-Vinylpyrrolidinone	0.205 ± 0.015	3.30 ± 0.15	50
Vinyl stearate	0.90	0.73	70
Vinyl Versatate VV9	0.93	0.90	60
Vinyl Versatate VV10	0.99	0.92	60

Table 5. North American Producers of Poly(vinyl acetate) and their Capacities, 10^3 t[a]

Producer	Location	Capacity
Celanese Mexicana	Cangrejera, Mexico	109
Celanese	Bay City, Tex.	288
Celanese	Clear Lake, Tex.	265
Dow Chemical	Texas City, Tex.	340
DuPont	LaPorte, Tex.	272
Millennium Petrochemicals	LaPorte, Tex.	381
Total		1654

[a]Ref. 22.

6%, ethylene–vinyl alcohol; 1%, vinyl chloride/vinyl acetate copolymer; 3%, miscellaneous. In Japan and China the major final consumption is for poly(vinyl alcohol). Half of Western Europe's consumption of vinyl acetate goes to producing poly(vinyl acetate).

Most of the applications for vinyl acetate are mature. The strongest growth areas are in ethylene–vinyl alcohol, poly(vinyl butyral), and vinyl acetate–ethylene resins. Growth of use for ethylene–vinyl alcohol is expected at 10–15%/year through 2004. Poly(vinyl butyral) is used in safety glass in automobile windshields. The U.S. market is mature for this use, but has a potential as a replacement for tempered glass in Europe. A potential market exists for side and rear automobile windows worldwide (23).

Overall growth in consumption through 2004 is forecasted as follows: United States, 3%/year; Western Europe, 2.8%/year; and Japan, 1–2% (23).

Vinyl acetate monomer is supplied in three grades, which differ in the amount of inhibitor they contain but otherwise have identical specifications. A low *p*-hydroquinone grade, containing 3–7 ppm *p*-hydroquinone, is preferred if it is expected to be used within two months of delivery. For monomer stored up to four months before polymerization, the grade containing 12–17 ppm *p*-hydroquinone is used. When indefinite storage is anticipated, a grade containing 200–300 ppm diphenylamine is supplied. Typical manufacturers' specifications are given in Table 6 (5–9).

Table 6. Typical Manufacturers' Specifications for Vinyl Acetate

Specification	Value
Vinyl acetate, wt%, min	99.8
Boiling point, °C	72.0–73.0
Acidity as acetic acid, wt%, max	0.007
Carbonyls as acetaldehyde, wt%, max	0.013
Water, wt%, max	0.04
Color, APHA system	0.5
Suspended matter	none

In storage, vinyl acetate should be kept away from ignition sources. It should be stored in a cool environment away from heat, direct sunlight, oxidizing materials, and free-radical generating chemicals to avoid rapid uncontrolled polymerization. Bulk storage should be blanketed with dry nitrogen. The monomer is actually more stable at a lower oxygen concentration (24). In the presence of oxygen, there is a tendency to form polyperoxides which could lead to polymerization. Using dry gas helps avoid the potential for hydrolysis to acetic acid and acetaldehyde. Additional information concerning the safe handling and transportation of vinyl acetate is provided in the Material Safety Data Sheet (MSDS) for vinyl acetate (5,25).

Gas chromatography is an excellent method to determine vinyl acetate and its volatile contaminants. If wet chemical techniques are used, vinyl acetate is assayed by adding excess bromide to an aliquot of material, followed by addition of excess potassium iodide and titration with standard sodium thiosulfate. Acidity is determined by direct titration in methanol solution with a standard caustic solution, aldehydes are determined by the addition of excess sodium bisulfite followed by titration with standard iodine solution, and water is determined by the Karl Fischer method. *p*-Hydroquinone and diphenylamine can be determined by standard titration techniques, or spectrophotometrically in the UV region after evaporation of vinyl acetate. Several companies describe in their product brochures empirical procedures for determining the polymerization activity of the monomer. In these tests, a given amount of monomer is polymerized under standard conditions and the rate of temperature increase or volume shrinkage and induction period are measured. Appropriate ASTM specifications and test procedures are D2190, D2191, D2193, and D2083.

The National Institute for Occupational Safety and Health (NIOSH) recommends a ceiling limit of 4 ppm for 15 min of exposure to vinyl acetate vapor. The American Conference of Governmental Industrial Hygienists (ACGIH) recommends an 8-h TLV Time Weighted Average of 10 ppm and a 15-min. short-term exposure limit of 15 ppm to its vapor. Vinyl acetate is a severe eye and skin irritant, forming blisters on the skin, and redness, swelling, or corneal burns on the eyes. The vapor is irritating to the nose and throat, and high levels of exposure may result in pulmonary edema. Nausea, headache, or weakness may result with inhalation of mists. Good industrial hygiene practices should be followed and adequate ventilation provided. Repeated or prolonged exposure should be avoided. The ACGIH has designated vinyl acetate as an A3 Animal Carcinogen. This designation refers to an agent which is carcinogenic in experimental animals at a relatively high dose. The International Agency for Research on Cancer (IARC) has evaluated vinyl acetate as a Group 2B material (26). This evaluates VAc as probably carcinogenic to humans on the basis of the sufficient evidence of the carcinogenicity of acetaldehyde in experimental animals. Both VAc and acetaldehyde were found to induce nasal tumors in rats on inhalation. VAc was also found to be genotoxic to human cells *in vitro* and to animal cells *in vivo*.

Vinyl acetate has moderate acute toxicity if ingested. The LD_{50} for oral ingestion in rats is 2.9 g/kg body weight; for absorption through the skin, the LD_{50} in rats is more than 5 mL/kg in 24 h. First-aid procedures to be followed in the event of overexposure to vinyl acetate are as follows:

Type of exposure	Treatment
Ingestion	Do not induce vomiting; drink large quantities of milk
Inhalation	Provide fresh air; keep victim warm and quiet; apply artifical respiration if necessary
Skin contact	Wash with water
Eye contact	Flush with water for 15 min; contact physician immediately

Vinyl Acetate Polymers

Properties. Poly(vinyl acetate) (PVAc) polymer resins are manufactured in a variety of molecular weights. Some physical properties of the polymer are listed in Table 7 (27–29). With increasing molecular weight, properties vary from viscous liquids to low melting solids to tough, horny materials. They are neutral, water-white to stray-colored, tasteless, odorless, and nontoxic. The resins have no sharply defined melting points but become softer with increasing temperature. Because of their solubility parameter, they are soluble in organic solvents, eg, esters, ketones, aromatics, halogenated hydrocarbons, carboxylic acids, etc, but are insoluble in the lower alcohols (excluding methanol), glycols, water, and nonpolar liquids such as ether, carbon disulfide, aliphatic hydrocarbons, oils, and fats. Alcohols, eg, ethyl, propyl, and butyl, containing 5–10 wt% water dissolve PVAc; butyl alcohol or xylene, both of which only swell the polymer at normal temperatures, dissolve it when heated. The electrical properties are strongly affected by the ability of poly(vinyl acetate) to absorb water. Whereas dried resin has a dielectric constant ϵ of 3.3 and a loss factor ϵ' of 0.08 $\pm$ 0.02 at 35°C and 60 Hz, after exposure to 100% relative humidity the numbers become 10 and 0.7, respectively (30,31).

As with many thermoplastic resins, strength properties increase with molecular weight; tensile strengths up to 50.3 MPa (7300 psi) may be obtained. The softening point, as determined by the ring-and-ball method or by the Kraemer and Sarnow method, also increases with molecular weight, as shown in Table 8 (32,33). Poly(vinyl acetate) resin is commercially available in pure, dry form as beads, granules, or lumps and is graded according to viscosity at 20°C of a 1 *M* solution in benzene (86.09 g or 1 *M* of repeating units of the resin dissolved in benzene to make 1 L). In Europe, the Fikentscher *K* value, also derived from viscosity measurements, is used to characterize commercial resins.

On cooling below room temperature, poly(vinyl acetate)s become brittle. The brittle point may be lowered by plasticization or copolymerization. When heated above room temperature and above the polymer glass-transition temperature (30°C), all viscosity grades become very flexible, and at 50°C become limp. The glass-transition temperature of PVAc is depressed by the incorporation of moisture causing the polymer to be more flexible under humid conditions. Poly(vinyl acetate) can be heated at 125°C for hours without changing, but at 150°C it gradually darkens, and at over 225°C it liberates acetic acid forming a brown insoluble resin which carbonizes at a much higher temperature. The products of thermal

Table 7. Physical Constants for Poly(vinyl acetate)

Property	Value
Absorption of water at 20°C for 24–144 h, %	3–6
Coefficient of thermal expansion, K^{-1}	
Cubic	6.7×10^{-4}
Linear, below T_g	7×10^{-5}
Above T_g	22×10^{-5}
Cohesive energy density, $(MJ/m^3)^{1/2}$ [a]	18.6–19.09
Compressibility, $cm^3/(g \cdot kPa)$ [b]	17.8×10^{-6}
Decomposition temperature, °C	150
Density, g/cm^3	
at 20°C	1.191
25°C	1.19
50°C	1.17
120°C	1.11
200°C	1.05
Dielectric constant at 2 MHz	
at 50°C	3.5
150°C	8.3
Dielectric dissipation factor, at 2 MHz, tan δ	
at 50°C	150
120°C	260
Dielectric strength, V/L	
at 30°C	0.394
6°C	0.307
Dipole moment, $C \cdot m$ [c] per monomer unit	
at 20°C	2.30
150°C	1.77
Dynamic mechanical loss peak at 100 Hz, °C	70
Elongation at break, at 20°C and 0% rh, %	10–20
Glass-transition temperature, T_g, °C	28–31
Pressure dependence, °C/100 MPa [d]	0.22
Hardness, at 20°C, Shore units	80–85
Heat capacity, at 30°C, J/g [a]	1.465
Heat distortion point, °C	50
Heat of polymerization, kJ/mol [a]	87.5
Refraction index, n_D	
at 20.7°C	1.4669
30.8°C	1.4657
52.1°C	1.4600
80°C	1.4800
142°C	
Interfacial tension, mN/m (= dyn/cm)	
at 20°C with polyethylene	14.5
20°C with polydimethylsiloxane	8.4
20°C with polyisobutylene	9.9
20°C with polystyrene	4.2

Table 7. (Continued)

Property	Value
Internal pressure, MJ/m^3 [a]	
at 0°C	255
28°C	397.8
60°C	418.7
20°C	284.7
40°C	431.3
Modulus of elasticity, GPa[d]	1.275–2.256
Notched impact strength, J/m[e]	102.4
Softening temperature, °C	35–50
Specific volume, L/kg	
at t = 100–200°C	$0.823 + (6.4 \times 10^{-4}\ t)$
t = 28°C (T_g)	0.84
Surface resistance (Ω/cm)	5×10^{11}
Surface tension, mN/m(= dyn/cm))	
at 20°C	36.5
140°C	28.6
180°C	25.9
Tensile strength, MPa[d]	29.4–49.0
Thermal conductivity, mW/(m·K)	159
Young's modulus, MPa[d]	600

[a] To convert J to cal, divide by 4.184.
[b] To convert kPa to atm, divide by 101.3.
[c] To convert C · m to debye, divide by 3.336×10^{-30}.
[d] To convert MPa to psi, multiply by 145; GPa to psi, multiply by 145,000.
[e] To convert J/m to lbf/in., divide by 53.38.

decomposition of PVAc are at 150–200°C acetic acid, and at 300–350°C aromatic compounds, ie, benzene, toluene, naphthalene, etc (34). PVAc resists oxidation and degradation by UV and visible radiation; therefore its aging qualities are excellent.

The NMR spectrum of PVAc in carbon tetrachloride solution at 110°C shows absorptions at 4.86δ (pentad) of the methine proton; 1.78δ (triad) of the methylene group; and 1.98δ, 1.96δ, and 1.94δ, which are the resonances of the acetate methyls in isotactic, heterotactic, and syndiotactic triads, respectively. Poly(vinyl acetate) produced by normal free-radical polymerization is completely atactic and noncrystalline. The NMR spectra of ethylene vinyl acetate copolymers have also been obtained (35). The IR spectra of the copolymers of vinyl acetate differ from that of the homopolymer depending on the identity of the comonomers and their proportion.

The chemical properties of PVAc are those of an aliphatic ester. Thus, acidic or basic hydrolysis produces poly(vinyl alcohol) and acetic acid or the acetate of the basic cation. Industrially, poly(vinyl alcohol) is produced by a base-catalyzed ester interchange with methanol, where methyl acetate forms in addition to the polymeric product. The chemical properties of PVAc can be modified by copolymerization. When a comonomer having a carboxylic acid group or a sulfuric acid group is used, the copolymer becomes soluble in dilute aqueous alkali or

Table 8. Softening Points and Molecular Weights of Commercial Poly(vinyl acetate)[a,b]

Grade viscosity, mPa·s (= cP)	Softening point, °C			
	Fikentsher *K* value	Kraemer and Sarnow	Ring-and-ball	Mol weight
1.5	13	65	75	11,000
2.5	19	81	90	18,000
7	32	106	116	45,000
15	42	131	139	90,000
25	38	153	163	140,000
60	58	196		300,000
100	62	230		500,000
800	79			1,500,000

[a] Refs. 32 and 33.
[b] A 1 *M* solution in benzene at 20°C.

ammonia. These copolymers also adhere better to metals than homopolymers or neutral copolymers because of the interaction between the acid groups and the metal surface. Copolymerization with monomers such as butyl acrylate can improve flexibility and provide specific adhesion to surfaces. Monomers such as *n*-methylol acrylamide copolymerized with vinyl acetate provide sites for cross-linking either during polymerization reaction or in use. Other comonomers such as vinyl Versatate (vinyl neodecanoate) reduce the potential for hydrolytic breakdown of the polymer chain by shielding the VAc group from attack.

In poly(vinyl acetate) copolymer emulsions, the properties are significantly affected by the composition of the aqueous phase and by the stabilizers and buffers used in the preparation of these materials, along with the process conditions (eg, monomer concentrations, pH, agitation, and temperature). The emulsions are milk-white liquids containing ca 55 wt% PVAc, the balance being water and small quantities of wetting agents or protective colloids. The use of poly(vinyl acetate) or copolymer emulsions eliminates the need for expensive, flammable, odorous, or toxic solvents and the need for the recovery of such solvents. They are easy to apply and the equipment is easy to clean with water, if done promptly. Emulsions also offer the advantage of high solids content with fluidity, since the viscosity of emulsions are independent of the molecular weight of the resin in the particles.

The specific gravity at 20°C for all poly(vinyl acetate) emulsions is about 1.1. There generally is a slight odor of residual monomer in standard materials, but if this is removed by some means, such as steam stripping or further reaction, the emulsions are virtually odorless. Traces of acetic acid can be neutralized with a base, eg, ammonia, sodium bicarbonate, or triethanolamine, and when the free monomer has been removed, the pH of the resulting emulsion can be adjusted to remain constant at ca 7. The product developer can choose from ingredient and process options to develop properties for the intended end use. These properties include particle size and molecular weight distributions, pH, emulsion viscosity, particle charge, environmental resistance (solvent, moisture, temperature, and

UV), film characteristics (modulus, elongation, toughness), and stability to storage, freezing, dilution, mechanical action, and compounding.

Poly(vinyl acetate) polymer and copolymer properties may be modified through the addition of plasticizers and fillers. Cross-linking agents react with copolymers of vinyl acetate containing a cross-linkable group. The material properties can be altered to allow improved flow, rigidity, and toughness. Various resins, plasticizers, thickening agents, solvents, pigments, extenders, and some dyes may be added. Plasticizers are often added to provide increased flexibility to the dried film, but these usually are not incorporated before the final formulation is made because their presence may adversely affect stability, particularly in cold weather.

When the emulsion is applied to a surface, water is lost by evaporation and absorption if the surface is porous. The particles stick together and eventually coalesce to form a tough and somewhat clear continuous coating. Clarity is often improved by the presence of plasticizer, which also enhances the film's resistance to water. This may be due to the improvement in coalescence of the films. Films from most emulsions containing poly(vinyl alcohol) as the protective colloid are likely to re-emulsify on contact with water, unless they contain relatively large quantities of plasticizer or solvent, or are costabilized with a surfactant which helps plasticize the polymer. The films are unaffected by light, oxygen, chlorine in moderation, and dilute solutions of acids, alkalies, and salts. The films are also inert to oils, fats, waxes, and greases, unless these are mostly aromatic. Some solvents, namely acetone, alcohol, ethyl acetate, benzene, and toluene, dissolve or at least swell the film. The extent of dissolution depends on the branching in the chain.

Poly(vinyl acetate) emulsion films adhere well to most surfaces that have relatively high surface energy, (eg, wood, paper, glass, and metal), and have good binding capacity for pigments (qv) and fillers (qv). The ability to bond to other surfaces may be enhanced with the use of comonomers. Ethylene copolymers have shown good adhesion to PVC. Elasticized films are strong and flexible at ordinary temperatures.

An important property of a PVAc film is its permeability to water vapor. The permeability to saturated water vapor at 40°C is 2.1 g/(h · m^2) for a film 0.025 mm thick. This allows the film to be laid down on a damp surface with trapped moisture gradually passing through the film without lifting or blistering it.

Poly(vinyl acetate) polymers are environmentally friendly because they easily biodegrade. Poly(vinyl acetate) may be hydrolyzed to poly(vinyl alcohol) which is then assimilated by naturally occurring organisms. In the use of emulsion polymers, the associated components (stabilizers, initiators, etc) should be scrutinized for their effect on the environment. Poly(vinyl acetate) is nontoxic and is approved by the U.S. Food and Drug Administration (FDA) for food applications (qv) (CFR 176.170, 175.105). Components in the emulsion polymer system which may migrate from the film into the food may impact the approval of the total package. In food applications the impact on odor and taste of residual low molecular weight components may be important in the selection of a product for use.

Polymerization Processes. Vinyl acetate has been polymerized industrially by bulk, solution, suspension, and emulsion processes (36). Perhaps 90% of the material identified as poly(vinyl acetate) or copolymers that are predominantly vinyl acetate are made by emulsion techniques. Detailed information is in

patent and scientific literature and in procedures available in the brochures from monomer producing companies (15,36).

Emulsion Polymerization. Poly(vinyl acetate)-based emulsion polymers are produced by the polymerization of an emulsified monomer through free radicals generated by an initiator system. Descriptions of the technology may be found in several references (37–41) (see HETEROPHASE POLYMERIZATION).

Recipe. An emulsion recipe, in general, contains monomer, water, protective colloid or surfactant, initiator, buffer, and perhaps a molecular weight regulator. The recipe may contain 30–70% monomer, but most commercially available emulsions contain ca 55 wt% solids, although copolymer emulsions have been commercially introduced which have greater than 70% solids content. Several monomers are copolymerized commercially with vinyl acetate in emulsion polymerization and numerous others have been copolymerized on a laboratory scale. Among the comonomers most commonly used industrially in emulsion copolymerization with vinyl acetate are ethylene, dibutyl maleate, bis(2-ethylhexyl) maleate, ethyl-, butyl-, and 2-ethylhexyl acrylates, vinyl laurate, and vinyl neodecanoate (13,15). Vinyl hydrogen maleate and vinyl hydrogen fumarate have also been used as comonomers, as have acrylic acid, maleic anhydride, and sodium ethylenesulfonate, in order to incorporate an acidic or ionic group in the polymer. The neutral comonomers are added primarily to decrease the brittle temperature of the polymer below commonly encountered ambient temperatures, since many uses of PVAc require some degree of flexibility in service. They may also improve the compatibility of the polymer with surfaces of different compositions and energies. The monomers that contain acidic groups are added primarily to make the copolymer soluble in basic media, eg, aqueous ammonia. They also help improve adhesion to metallic surfaces. Copolymerization with monomers which lower the glass-transition temperature, gives a polymer which is innately and permanently flexible. In comparison, the lowering of the brittle point accomplished by addition of plasticizers such as dibutyl phthalate, tricresyl phosphate, etc, to the preformed polymer may be lost with the migration of the plasticizer out of the film. The most efficient plasticizing comonomer on a weight or price basis is ethylene. Copolymerization of vinyl acetate with ethylene is the most significant in the adhesive market (42).

Many different combinations of surfactant and protective colloid are used in emulsion polymerizations of vinyl acetate as stabilizers. The properties of the emulsion and the polymeric film depend to a large extent on the identity and quantity of the stabilizers. The choice of stabilizer affects the mean and distribution of particle size, which affects the rheology and film formation. The stabilizer system also impacts the stability of the emulsion to mechanical shear, temperature change, and compounding. Characteristics of the coalesced resin affected by the stabilizer include tack, smoothness, opacity, water resistance, and film strength (43,44).

Poly(vinyl acetate) emulsions can be made with a surfactant alone or with a protective colloid alone, but the usual practice is to use a combination of the two. Normally, up to 3 wt% stabilizers may be included in the recipe, but when water sensitivity or tack of the wet film is desired, as in some adhesives, more may be included. The most commonly used surfactants are the anionic sulfates and sulfonates, but cationic emulsifiers and nonionics are also suitable. Indeed,

some emulsion compounding formulas require the use of cationic or nonionic surfactants for stable formulations. The most commonly used protective colloids are poly(vinyl alcohol) and hydroxyethyl cellulose, but there are many others, natural and synthetic, which are usable if not preferable for a given application.

Issues to be considered in selecting the best stabilizing system are polymeric chain branching which increases with high temperature and the presence of some stabilizers, polydispersity of the particles produced, and grafting copolymerization, which may occur because of the reaction of vinyl acetate with emulsifiers such as poly(vinyl alcohol) (45,46).

In general, the greater the quantity of stabilizers in a recipe, the smaller the particle size of the emulsion. At the higher emulsifier levels ($\geq$1 wt%) used for emulsion polymerization, the polymer forms tiny particles that do not settle but remain indefinitely suspended. Particle sizes resulting from high surface active agent to low protective colloid ratios may be 0.005–1 μm; such emulsions contain lower solids and have lower viscosities. Commercial poly(vinyl acetate) emulsions used in adhesives usually are made with higher ratios of protective colloids in the recipes and usually contain ca 55 wt% solids. Average particle sizes are 0.2–10 μm and the viscosity of the emulsion is 400–5000 mPas (= cP). These latter compositions, ie, with higher ratios of protective colloids, are occasionally described as stable dispersions rather than true emulsions (47–51). The term *latex* is also used to denote these products, particularly those with small, ie, $<$0.2 μm, particle size.

The initiators used in vinyl acetate polymerizations are the familiar free-radical types, eg, hydrogen peroxide, peroxysulfates, benzoyl peroxide, *tert*-butyl hydroperoxide, lauryl peroxide, and redox combinations. In redox combinations, reducing agents such as sodium metabisulfite, sodium formaldehyde sulfoxylate, and ascorbic acid are among those commonly used along with transition-metal salts such as ferrous sulfate. Emulsion polymerizations are usually conducted with water-soluble initiators; benzoyl peroxide has been used in emulsion polymerizations with water-soluble initiators, especially where monomer has been added continuously during the reaction. Radiation-induced initiation has been explored because the activation energy is lower (29 kJ/mol), allowing polymerization to take place at lower temperatures (52).

Buffers are frequently added to emulsion recipes and serve two main purposes. The rate of hydrolysis of vinyl acetate and some comonomers is pH-sensitive. Hydrolysis of monomer produces acetic acid, which can affect the initiator, and acetaldehyde which as a chain-transfer agent may lower the molecular weight of the polymer undesirably. The rates of decomposition of some initiators are affected by pH and the buffer is added to stabilize those rates, since decomposition of the initiator frequently changes the pH in an unbuffered system. Vinyl acetate emulsion polymerization recipes are usually buffered to pH 4–5, eg, with phosphate or acetate, but buffering at neutral pH with bicarbonate also gives excellent results. The pH of most commercially available emulsions is 4–6.

Often a chain-transfer agent is added to vinyl acetate polymerizations, whether emulsion, suspension, solution, or bulk, to control the polymer molecular weight. Aldehydes, thiols, carbon tetrachloride, etc, have been added. Some emulsion procedures call for the recipe to include a quantity of preformed PVAc emulsion, and sometimes antifoamers must be added (see FOAMS).

Process. A polymerization process may consist of simply charging all ingredients to the reactor, heating to reflux, and stirring until the reaction is over while controlling the heat removal at the reaction temperature using cooling systems. However, this simple procedure is seldom followed. Typically, only a portion of the monomer and catalyst is initially charged and the remainder is added during the course of the reaction. Better control of the rate of polymerization can be maintained in this fashion, which is particularly important in industrial-scale operations where large quantities of material are involved and heat-transfer capacity may be limited. Continuous monomer addition in emulsion polymerization usually leads to smaller particle size and a more stable dispersion. On the molecular level, monomer fed over the course of the reaction results in more branches in the polymer chain, if the monomer content of the reaction mix is held low. Consequently, the rate of monomer addition has an effect on final film properties. Copolymerizations usually must be conducted with a continuous monomer feed to obtain homogeneous polymer compositions, especially if there is a significant disparity in the reactivities of the two monomers. Emulsifiers may also be added in increments to help stabilize growing particle populations. In a Kuraray comparison of batch to semicontinuous systems (53), films from emulsions made batchwise were found to have better tensile strength than films made from semicontinuous emulsions.

Various finishing techniques are used to reduce the residual monomer in the emulsion polymer. These include raising the temperature, adding a more concentrated initiator, or using mechanical means, such as stripping. Industrially, polymerizations are carried out to over 99% conversion, and thus there is no need to reduce the unreacted monomer unless very low levels are required to meet regulatory, product, or workplace requirements. Most poly(vinyl acetate) emulsions contain less than 0.5 wt% unreacted vinyl acetate, which minimizes development of acetic acid and acetaldehyde by monomer hydrolysis on long storage. Rohm and Haas has patented an ultrafiltration (qv) process for recovering and recycling polymer emulsions from dilute wastewater (54).

All of these processes are operated in conventional glass-lined or stainless steel kettles or reactors. The pressure rating of the reactors depends on the volatility of the monomers used. In the homopolymerization of the vinyl acetate and its copolymerization with monomers of low vapor pressure, the use of vessels with a pressure rating close to atmospheric pressure is sufficient. The ethylene–vinyl acetate copolymer (EVA) processes must of necessity be operated under high pressure (42). Agitation design in these systems is important, taking into consideration the need to blend all the ingredients without zones of high concentration and remove the heat from the reaction mass while avoiding subjecting the reaction mixture to conditions of high shear which could destabilize the material. Heat removal in atmospheric pressure reactions, especially those carried out close to or higher than the boiling point of the vinyl acetate, uses reflux condensers. In vinyl acetate polymerizations where low temperatures are maintained to avoid chain transfer, which results in lowering the average molecular weight, internal coils, jackets on the reactors, and external heat exchangers are used.

Control of the process is important to ensure reproducibility of the product. Methods have been developed to control the composition of copolymers and their molecular weight (55,56). Calorimetric methods have been described to estimate

conversion and provide the basis for control of the reaction. Other properties such as density and particle size can also be monitored to gauge the reaction progress and development of the product properties (57–59). Agitator design is important in controlling particle size and can influence the kinetics, molecular weight, and coagulum formation (60).

Continuous emulsion copolymerization processes for vinyl acetate and vinyl acetate–ethylene copolymer have been reported (61–66). Cyclic variations in the number of particles, conversion, and particle-size distribution have been studied. Control of these variations based on on-line measurements and the use of preformed latex seed particles have been discussed (63,64).

Continuous polymerization systems offer the possibility of several advantages including better heat transfer and cooling capacity, reduction in downtime, more uniform products, and less raw material handling (61,62). In some continuous emulsion homopolymerization processes, materials are added continuously to a first kettle and partially polymerized, then passed into a second reactor where, with additional initiator, the reaction is concluded. Continuous emulsion copolymerizations of vinyl acetate with ethylene have been described (63–66). Recirculating loop reactors which have high heat-transfer rates have found use for the manufacture of latexes for paint applications (61).

Mini-emulsion processes have been developed where the monomer is emulsified under high energy with either a long-chain alcohol or a polymer producing very small droplets. The long-chain alcohol retards the diffusion of the monomer out of the droplets (67). Polymerization takes place primarily in the droplets, allowing the development of fine, narrow particle-size distributions (68). The proceedings of a symposium on the emulsion polymerization of vinyl acetate is available (69).

Bulk Polymerizations. In the bulk polymerization of vinyl acetate, the viscosity increases significantly as the polymer forms, making it difficult to remove heat from the process. Low molecular weight polymers have been made in this fashion. Continuous processes are known to be used for bulk polymerizations (70).

Suspension Polymerization. At very low levels of stabilizer, eg, 0.1 wt%, the polymer does not form a creamy dispersion that stays indefinitely suspended in the aqueous phase but forms small beads that settle and may be easily separated by filtration (71). This suspension or pearl polymerization process has been used to prepare polymers for adhesive and coating applications and for conversion to poly(vinyl alcohol). Products in bead form are available from several commercial suppliers of PVAc resins. Suspension polymerizations are carried out with monomer-soluble initiators predominantly, with low levels of stabilizers. Suspension copolymerization processes for the production of vinyl acetate–ethylene bead products have been described, and the properties of the copolymers determined (72). Continuous tubular polymerization of vinyl acetate in suspension (73,74) yields stable dispersions of beads with narrow particle-size distributions at high yields.

Solution Polymerization. Solution polymerization of vinyl acetate is carried out mainly as an intermediate step to the manufacture of poly(vinyl alcohol) (see VINYL ALCOHOL POLYMERS). A small amount of solution-polymerized vinyl acetate is prepared for the merchant market. When solution polymerization is carried out, the solvent acts as a chain-transfer agent and, depending on its transfer constant, has an effect on the molecular weight of the product. The rate of

polymerization is also affected by the solvent but not in the same way as the degree of polymerization. The reactivity of the solvent-derived radical plays an important part. Chain-transfer constants for solvents in vinyl acetate polymerizations have been tabulated (13). Continuous solution polymers of poly(vinyl acetate) in tubular reactors have been prepared at high yield and throughput (75,76).

Mechanisms. Because of its considerable industrial importance as well as its intrinsic interest, emulsion polymerization of vinyl acetate in the presence of surfactants has been extensively studied (77–79). The Smith-Ewart theory, which describes emulsion polymerization of monomers such as styrene, does not apply to vinyl acetate. Reasons for this are the substantial water solubility of vinyl acetate monomer, and the different reactivities of the vinyl acetate and styrene radicals; the chain transfer to monomer is much higher for vinyl acetate. The kinetics of the polymerization of vinyl acetate has been studied and mechanisms have been proposed (80–84).

Initiation. Radicals formed from the initiator species, or generated by chain transfer, initiate the dissolved monomer in the water phase as well as in the micelles (aggregates of stabilizer molecules). Homogeneous nucleation applies to moderately soluble monomers like vinyl acetate (75,79,85). In homogeneous nucleation, oligomers grow from monomers in the water phase. After reaching the solubility limit, they precipitate and partially stabilized primary particles are formed. The particles grow by absorbing and converting monomer to polymer and also by coagulation. Where PVOH is used as a protective colloid, grafting may occur onto the PVOH backbone and the growing polymer may maintain its solubility in water to a higher degree of polymerization (86). The efficiency of the initiator system may be dependent on the stabilizer used. The presence of oxygen may be inhibitory in nature, probably due to the high chain-transfer constant of the oxygen–vinyl acetate adduct (Table 9). pH is also important as the initiator efficiency may be affected, especially in redox systems.

Propagation. The rate of emulsion polymerization has been found to depend on initiator, monomer, and emulsifier concentrations. In a system of vinyl acetate, sodium lauryl sulfate, and potassium persulfate, the following relationship for the rate of polymerization has been suggested (87):

$$R_p = k_p[M]_0^{0.34}[E]_0^{0.5}[I]_0^{0.5}$$

where R_p is in g/(cm^3 of H_2O) in seconds, $[M]_0$ is the monomer concentration, $[E]_0$ the emulsifier concentration, and $[I]_0$ the initiator concentration. The polymerization rate is constant during the period when monomer conversion is between 15 and 80%. The number of particles per unit volume of aqueous phase is given by the following equation:

$$N_p = [E]_0^{0.094}[I]_0^{0.04}$$

The Smith–Ewart theory predicts $R_p = K[I]^{0.4}$. The rate of polymerization of vinyl acetate is virtually independent of emulsifier concentration, depending on the study, whereas the Smith–Ewart theory predicts the rate to be proportional to the 0.6th power of the emulsifier concentration for monomers such as styrene. This may be due to the high chain transfer to the vinyl acetate monomer. The

Table 9. Chain-Transfer Constants

Compound	$C_s \times 10^4$	°C
n-Heptane	17.0	50
Toluene	20.75	60
Methanol	6	60
Ethanol	25	60
tert-Butyl alcohol	1.3	60
Acetone	1.5	60
Acetaldehyde	530	45
Propionaldehyde	1000	60
Crotonaldehyde	1800	60
Methyl acetate	2.5	60
n-Butyl mercaptan	$(48 \pm 14) \times 10^4$	60
Acetic acid	10	60
Lauroyl peroxide	1.0×10^3	60
Oxygen–vinyl acetate adduct	2.6×10^3	60
Poly(vinyl alcohol)	3.5×10^{-3}	60
Poly(vinyl chloride)	2.1×10^{-1}	60
Polystyrene	1.5×10^{-3}	60
	1.9×10^{-3}	75
Poly(methyl methacrylate)	2.1×10^{-3}	60
	2.6×10^{-3}	75
Poly(vinyl acetate)	1.5×10^{-4}	60

resulting small radical size has higher mobility, allowing diffusion out of the particle into the aqueous phase and causing reinitiation there. This has a significant effect in lowering the molecular weight of the polymer and increasing the overall rate. At high conversions where monomer concentrations are low (due to either a low feed rate of monomer or in later stages of the reaction), the transfer to polymer becomes important, leading to branched chains. Transfer can also occur to the stabilizing species resulting in permanent incorporation into the polymer matrix. An assessment of the best values of the rate constants for propagation and termination is given below (21):

$$\textit{Propagation } k_p \text{ [L/(mol·s)]} = 3.2 \times 10^7 \exp(-3150/T)$$

$$\textit{Termination } k_t \text{ [L/(mol·s)]} = 3.7 \times 10^9 \exp(-1600/T)$$

For example, at 60°C, k_p = 2300 and k_t = 2.9 × 10^7. An estimate of kinetic chain lifetime, ie, the time from initiation to termination by reaction with another radical, is 1–2 s at 50°C and 4% per hour rate of polymerization. If there are five chain-transfer steps in the course of the kinetic chain, then a PVAc molecule forms in 0.2–0.4 s. Faster rates of conversion give shorter kinetic chain lifetimes in inverse proportion, but an increased percentage of conversion leads to longer chain lifetimes. At 75% conversion and at 60°C, the radical lifetime is ca 10 s.

Vinyl acetate polymerizes chiefly in the usual head-to-tail fashion, but some of the monomers orient head-to-head and tail-to-tail as the chain grows. The fraction of heat-to-head addition increases with temperature. For example, a 1.15 mol% head-to-head structure and a 1.86 mol% structure were determined at 15°C and 110°C, respectively (88).

In vinyl acetate polymerizations, the molecular weights of the products increase with the extent of conversion: the ratio of weight to number-average degree of polymerization also changes, becoming larger at higher conversions (89,90). The dilute solution viscosity of poly(vinyl acetate) can be related to the molecular weight by the following equations (30):

$$[\eta] = 0.0102\,M^{0.72}\text{dL/g in acetone solvent at } 30^{\circ}\text{C}$$

$$[\eta] = 0.314\,M^{0.60}\text{dL/g in methanol solvent at } 30^{\circ}\text{C}$$

These equations apply to linear polymers of $M_w/M_n = 2.0$.

Chain Transfer. At the molecular scale, vinyl acetate polymerizations are generally understood as free-radical polymerizations, but are characterized in particular by a relatively large amount of chain transfer (13). This high reactivity of the PVAc growing chain radical is attributed to its low degree of resonance stabilization. The high reactivity of the vinyl acetate radical also contributes to the high rate constant for propagation in vinyl acetate polymerization compared to styrene, the acrylates, and the methacrylates. Chain transfer to monomer is an extremely important factor controlling the molecular weight (13). Several determinations of the transfer constant to monomer C_m, ie, the ratio of rate constants of the transfer reaction and the propagation step k_{tr}/k_p, show that C_m increases from 1×10^4 to 3×10^4 from 0 to 75°C (13,91,92).

Chain transfer to monomer and to other small molecules leads to lower molecular weight products, but when polymerization occurs in the relative absence of monomer and other transfer agents, such as solvents, chain transfer to polymer becomes more important. As a result, toward the end of batch-suspension or batch-emulsion polymerization reactions, branched polymer chains tend to form. In suspension and emulsion processes where monomer is fed continuously, the products tend to be more branched than when polymerizations are carried out in the presence of a plentiful supply of monomer.

Chain transfer also occurs to the emulsifying agents, leading to their permanent incorporation into the product. Chain transfer to aldehydes, which may be formed as a result of the hydrolysis of the vinyl acetate monomer, tends to lower the molecular weight and slow the polymerization rate because of the lower activity of the radical that is formed. Thus, the presence of acetaldehyde condensates as a poly(vinyl alcohol) impurity strongly retards polymerization (93). Some of the initiators such as lauryl peroxide are also chain-transfer agents and lower the molecular weight of the product.

Investigation has shown that chain transfer to polymer occurs predominantly on the acetate methyl group in preference to the chain backbone; one estimate of the magnitude of the predominance is 40-fold (94,95). The number of branches per molecule of poly(vinyl acetate) polymerized at 60°C is ca 3, at

80% conversion. It rises rapidly thereafter and is ca 15 at 95% conversion and 1–2 $\times$ 10^4 number-average degrees of polymerization.

Grafting and Stabilizers. The degree of grafting of poly(vinyl acetate) (PVAc) on poly(vinyl alcohol) (PVA) and other stabilizers during emulsion polymerization strongly affects latex properties such as viscosity, rheology, and polymer solubility (96). The composition and structure of poly(vinyl alcohol) significantly affects the emulsion polymerization of vinyl acetate. The chain distribution of residual acetate groups in poly(vinyl alcohol) is important to successful vinyl acetate emulsion polymerization. A block-like distribution is preferred over a random distribution (97–100). The structure of poly(vinyl acetate-*co*-vinyl alcohol) emulsion particles has been determined by electron microscopy. The latex particle is formed of a great many smaller particles packed together by flocculation processes (101,102).

An extensive series of papers (103–111) have been published on the grafting of vinyl acetate and styrene on poly(vinyl alcohol) studying the effects of type and concentration of the poly(vinyl alcohol), initiator, and reaction temperature. The partially acetylated poly(vinyl alcohol) was the superior grafting base because of the attachment of the poly(vinyl acetate) segments to the polymerizing particle. The resulting latices with the anchored poly(vinyl alcohol) chains had superior stability. The methine hydrogen atom of the poly(vinyl alcohol) was proposed to be a grafting site in all cases as opposed to the acetyl groups. In mixed systems of poly(vinyl alcohol) and ethoxylated cetyl alcohol both benzene-soluble and water-soluble fractions of graft copolymer were identified, with their ratio dependent on the ratio of initially charged-to-delay fed stabilizer and the stirring speed (112).

Emulsion polymerizations of vinyl acetate in the presence of ethylene oxide- or propylene oxide-based surfactants and protective colloids also are characterized by the formation of graft copolymers of vinyl acetate on these materials. This was also observed in mixed systems of hydroxyethyl cellulose and nonylphenol ethoxylates. The oxyethylene chain groups supply the specific site of transfer (113). The concentration of insoluble (grafted) polymer decreases with increase in surfactant ratio, and R_p (max) is observed at an ethoxylation degree of 8 (114).

Porous membranes with selective permeability to organic solvents have been prepared by the extraction of latex films prepared with moderate ratios of PVA–PVAc graft copolymer fractions. The extracted films are made up of a composite of spherical cells of PVA, PVAc microgel, and PVA–PVAc graft copolymers (115).

Poly(vinyl acetate) chains are also stabilized as aqueous-soluble anionic species by complexation with a surfactant. The charge on the water-soluble species prevents their absorption into the particle (116).

The kinetics of vinyl acetate emulsion polymerization in the presence of alkyl phenyl ethoxylate surfactants of various chain lengths indicates that part of the emulsion polymerization occurs in the aqueous phase and part in the particles (117). A study of the emulsion polymerization of vinyl acetate in the presence of sodium lauryl sulfate reveals that a water-soluble poly(vinyl acetate)–sodium dodecyl sulfate polyelectrolyte complex forms, and that latex stability, polymer hydrolysis, and molecular weight are controlled by this phenomenon (118).

Problems with grafting and morphological changes in the particles are reviewed (119). Vinyl acetate has been grafted onto atactic polypropylene (120) and casein (121).

Copolymers. The effects of emulsion polymerization process type or latex and polymer properties have been studied. Vinyl acetate copolymerizes easily with a few monomers, eg, ethylene, vinyl chloride, and vinyl neodecanoate, which have reactivity ratios close to its own (see Table 4). The kinetics and the effect of process parameters on the copolymerization of vinyl acetate with ethylene have been studied (122,123). With some monomers, eg, maleic anhydride, it tends to form alternating copolymers. Other monomers with high r_2 and low r_1, eg, alkyl acrylates, tend to form copolymers much leaner in vinyl acetate than the initial charge composition with near homopolymer formed by the faster reacting comonomer. A process is required in which the faster reacting monomer is kept at a low concentration relative to the vinyl acetate, preferably by adding it over the course of the reaction. Studies have been carried out to design processes that result in copolymers which have narrow composition distributions (55,56). The morphology of the polymer particle depends on the monomer characteristic and the process. Thus, emulsion copolymerization of vinyl acetate–butyl acrylate comonomer systems by a delayed monomer addition process yields a core-shell structure particle, in which poly(butyl acrylate)-rich copolymer forms the core and vinyl acetate-rich copolymers form the shell (124).

Block copolymers of vinyl acetate with methyl methacrylate, acrylic acid, acrylonitrile, and vinyl pyrrolidinone have been prepared by copolymerization in viscous conditions, with solvents that are poor solvents for the vinyl acetate macroradical (125). Similarly, the copolymerization of vinyl acetate with methyl methacrylate is enhanced by the solvents acetonitrile and acetone and is decreased by propanol (126). Copolymers of vinyl acetate containing cyclic functional groups in the polymer chain have been prepared by copolymerization of vinyl acetate with *N*,*N*-diallylcyanamide and *N*,*N*-diallylamine (127,128).

Alternating equimolar copolymers of vinyl acetate and ethylene and alternating copolymers of vinyl acetate and acrylonitrile have been reported (129,130). Vinyl acetate and certain copolymers can be produced directly as films on certain metallic substrates by electroinitiation processes in which the substrate functions as one electrode (131).

New terpolymers of vinyl acetate with ethylene and carbon monoxide have been prepared and their uses as additives to improve the curing and flexibility of coating resins, eg, nitrocellulose, asphalt, phenolics, and polystyrene, have been described (132–134). Vinyl acetate and vinylidene cyanide form highly alternating copolymers.

The low vinyl acetate ethylene–vinyl acetate copolymers, ie, those containing 10–40 wt% vinyl acetate, are made by processes similar to those used to make low density polyethylene for which pressures are usually >103 MPa (15,000 psi). A medium, ie, 45 wt% vinyl acetate copolymer with rubber-like properties, is made by solution polymerization in *tert*-butyl alcohol at 34.5 MPa (5000 psi). The 70–95 wt% vinyl acetate emulsion copolymers are made in emulsion processes under ethylene pressures of 2.07–10.4 MPa (300–1500 psi).

Blends. Latex film properties are commonly modified through the blending of latexes, eg, a "soft" polymer is made slightly harder by blending with a "hard" latex.

Poly(ethyl methacrylate) (PEMA) yields truly compatible blends with poly(vinyl acetate) up to 20% PEMA concentration (135). Synergistic improvement in material properties was observed. Poly(ethylene oxide) forms compatible

homogeneous blends with poly(vinyl acetate) (136). The T_g of the blends and the crystallizability of the PEO depend on the composition. The miscibility window of poly(vinyl acetate) and its copolymers with alkyl acrylates can be broadened through the incorporation of acrylic acid as a third component (137). A description of compatible and incompatible blends of poly(vinyl acetate) and other copolymers has been compiled (138). Blends of poly(vinyl acetate) copolymers with urethanes can provide improved heat resistance to the product providing reduced creep rates in adhesives used for vinyl laminating (139).

Economic Aspects. In 2000, approximately 1.4×10^6 t of poly(vinyl acetate) emulsions and resins (dry content, including copolymers) were produced in North America, Western Europe, and Japan. The United States accounted for 50% of production, Western Europe accounted for 39%, Japan accounted for ca 9%, and the remainder was attributed to Canada and Mexico (140).

In general, poly(vinyl acetate) production is located close to end use industries (textile mills, adhesive plants, etc). In the United States, small-volume captive producers also contribute to the market.

In the United States, poly(vinyl acetate) consumption will follow general economic growth. Adhesives for use in packaging and construction will exhibit the largest growth. Demand for paper coatings will grow at less than GDP. Demand for PVAc copolymers for use in latex paint formulations will also grow. These formulations replace solvent-based paints that government regulations are limiting because of solvent emissions from the coatings.

Western European consumption of poly(vinyl acetate) and its copolymers is forecasted to grow at the rate of 1.5%/year. PVAc homopolymers will grow at the rate of 1%/year. Copolymers with ethylene are expected to grow at the rate of 3.4% through 2005. Redispersible powers will show the most dynamic growth increasing at the rate of 5%/year. Paint and coatings demand will decline because of substitution by acrylic-based emulsions. Japanese demand for poly(vinyl acetate) emulsions and resins should grow at the rate of 2%/year. Adhesives will be the biggest market (140).

Specifications and Standards. Typical specifications of the commercially available emulsions are tabulated in Table 10. However, there are exceptions to the ranges given. For example, most emulsions contain 55–56 wt% solids, but some are available at 46–47 wt% with viscosities of 10–15 mPa·s (= cP), and others at 59 wt% solids with viscosities of 200–4500 mPa·s. Specialty copolymer emulsions are available containing 72 wt% solids and viscosities under 2000 mPa·s (141).

Borax stability is an important property in adhesives, paper additives and resins (qv), and textile a plications where borax is a frequently encountered substance. This is a function of poly(vinyl alcohol) used for stabilization of the product. Other emulsion properties tabulated by manufacturers include tolerance to specific solvents, surface tension, minimum film-forming temperature, dilution stability, freeze–thaw stability, percent soluble polymer, and molecular weight. Properties of films cast from the emulsions are also sometimes listed, including clarity, gloss, light stability, water resistance, flexibility, heat-sealing temperature, specific gravity, and bond strength. Homopolymer resin specifications usually include viscosity grade (1.0 molar solution in toluene at 20°C), 1.5–800 mPa · s (= cP) ∼ 10%; volatiles, 1–2 wt%; acidity as acetic acid, 0.1–0.3 wt%; and

Table 10. Poly(vinyl acetate) Emulsion Specifications

Property	Range	Method
Solids, wt%	4–72	Moisture balance or oven
Viscosity, mPa · s (= cP)	200–4500	Viscometer
pH	4	pH meter
Residual monomer, % max	0.5	Titration or gas Chromatography
Particle size	0.1–3.0	
Particle charge	Neutral or negative	
Density at 25°C, g/cm^3	0.92	Pyknometer
Borax stability	Stable or unstable	Stable to borax addition
Mechanical stability	Good or excellent	Maintain stability for set period in high speed high shear blender
Freeze–thaw stability	Passes 0–5 cycles	Remains fluid after multiple cycles of freezing and thawing
Accelerated sedimentation, %	<4	Sediment after centrifuging diluted sample
Coagulum	<50 GMs on 100-mesh screen	Filter through a screen or stacked screens
T_g (glass-transition temperature), °C		DS calorimetry

softening point. Data are also given on heat-sealing temperature, tensile strength, elongation, and abrasion resistance. For alkali-soluble resins, the solubility in ammonia and its viscosity are listed (see Table 10).

Poly(vinyl acetate) and its copolymers with ethylene are available as spray-dried emulsion solids with average particle sizes of 2–20 μm; the product can be reconstituted to an emulsion by addition of water, or it can be added directly to formulations, eg, concrete. The powders may be used to raise solids of a lower solids latex. Solutions of resin in methyl and ethyl alcohol at 2–50 wt% solids are also available.

Emulsions are shipped in 19-L pails, 209-L drums, 11.0–18.9-m^3 (3000–5000 gal) tank trucks, and 38–76-m^3 (10,000–20,000 gal) railroad tank cars. During storage and handling, care should be taken not to destabilize or otherwise alter the character of the product. Storage tanks must be maintained clean and free from microbial contamination. Latices must not be put into a tank which contains a material with which it is incompatible. Routine cleaning is scheduled to remove skins or other accumulations of dried latex. Some of the large particle size latices may settle if stored for a long time and may need to be agitated to retain consistency. Latices corrode ordinary steel (qv) and must be stored in tanks with stainless steel, glass, plastic, or coated surfaces. Suitable coatings are baked phenolic, epoxy phenolic, or PVC. Storage should be at around room temperature, because excessive exposure to high or low temperatures may cause phase separation. Large shipments are insulated against cold. Precautions should be taken to avoid the formation of foam during unloading. If containers are not full during

shipment, foam may be generated because of sloshing. Containers should be closed to prevent evaporation of water, which leads to skin formation. Diaphragm pumps and screw pumps are preferred to centrifugal pumps (qv). High shear pumps such as centrifugal pumps may destabilize the latex causing the formation of grit or coagulum. In the case of colloid-protected latices, an irreversible reduction of viscosity may occur. Latices are susceptible to biocontamination, largely due to the stabilizer systems. In handling the latices, care should be taken to avoid exposure to microbial sources. Producers add microbicidal agents to protect the material against a moderate level of incident contamination. Biocontamination can result in the generation of foul odor, discoloration, and destabilization of the latex. Dry resins should be stored at or below room temperature to prevent caking.

Uses.

Adhesives. The uses of poly(vinyl acetate) adhesive are packaging and wood gluing (142,143). Table 11 (144) lists characteristics of poly(vinyl acetate) (PVAc) emulsions important to adhesive applications. PVAc copolymer adhesives are finding application in more diverse areas such as construction and adhesion to more difficult-to-bond surfaces because of the range of adhesion and the flexibility that may be built into the polymer. The emulsion form of PVAc is especially suitable for adhesives because of several properties that are peculiar to emulsion systems. The stability of PVAc emulsions allows them to accept many types of modifying additives without being damaged. For example, solvents, plasticizers, tackifying resins, and fillers can be added directly to homopolymer and copolymer emulsions without requiring pre-emulsification, unlike the elastomeric adhesive latexes. Homopolymer emulsions containing partially hydrolyzed poly(vinyl acetate) as a protective colloid can accept greater amounts of these modifying additives than any other type of emulsion without coagulating.

The stability of the emulsions further permits them to be compounded in simple liquid-blending vessels by means of agitators, eg, marine-type propellers, paddles, or turbines. The adhesives can be adapted to any type of machine application, ie, from spray guns to rollers to extruder-type devices. Different applicators are fairly specific in their viscosity requirements, as are the various substrates receiving the adhesive.

Poly(vinyl acetate) emulsions can be used in high speed gluing equipment. In contrast to aqueous solutions of natural or synthetic products which lose water slowly, the emulsions quickly lose water and invert and set rapidly into a bond.

Poly(vinyl acetate) homopolymers adhere well to porous or cellulosic surfaces, eg, wood, paper, cloth, leather, and ceramics. Homopolymer films tend to creep less than copolymer or terpolymer films. They are especially suitable in adhesives for high speed packaging operations.

Copolymers wet and adhere well to nonporous surfaces, such as plastics and metals. They form soft, flexible films, in contrast to the tough, horny films formed by homopolymers, and are more water-resistant. As the ratio of comonomer to vinyl acetate increases, the variety of plastics to which the copolymer adheres also increases. Comonomers containing functional groups often adhere to specific surfaces; for example, carboxyl-containing polymers adhere well to metals.

Plasticization, whether internal (by copolymerization) or external (with additives), is also extremely important for proper performance at the time of application. The ease of coalescence and the wetting characteristics of the polymer

Table 11. Characterization of Emulsion Polymers[a]

Compound	Properties
Emulsion	Surface tension
	Foaming tendency
	Stability (dilution, mechanical, shear, freeze–thaw, heat, bacterial)
	Compatibility (plasticizers, thickeners, pigments, extenders, coalescing agents)
	Rheological character
Polymer	T_g
	Molecular weight distribution
	Rheological behavior
	Solubility
	Infrared spectra
Film	Blocking
	Flex
	Tensile/elongation
	Hardness
	Water and chemical resistance
Adhesive	Heat seal temperature
	Bond strength (miscellaneous substrates)
	Tack
	Peel
	Creep

[a] Ref. 144.

emulsion particles are related to their softness and the chemical nature of the plasticizer.

New vinyl acetate–acrylate (VAA) emulsion copolymers stabilized with poly(vinyl alcohol) have been developed. The acrylic component of the VAAs contributes to improved compatibility with tackifiers (145).

Cross-linked polymer emulsions accept water-miscible solvents better than straight-chain emulsions. In the film state, the former resist water and organic solvents better and tend to have higher heat-sealing temperatures, which signify a greater resistance to blocking and cold flow. Straight-chain polymers can have high molecular weights, which contribute to high heat-sealing temperatures. Varying the conditions of polymerization results in either straight-chain or cross-linked polymer emulsions. The incorporation of functional monomers such as *n*-methylol acrylamide or acrylic acid into the polymer provides the ability to cross-link the product in the application either through heat, catalysis, or by a curing agent. In these cases, the polymer flows onto the substrate surface, then develops its strength on curing. Wood glues which can withstand boiling water immersion have been prepared in this fashion (146).

Tack enables an adhesive to form an immediate bond between contacting surfaces when they are brought together. It permits the alignment of an assembly and prevents the adherends from separating before the adhesive sets. Tack is differentiated into two types: (*1*) wet tack, also called grab or initial tack, is the tack of an adhesive before the liquid carrier, ie, organic solvent or water, has fully evaporated; (*2*) dry tack, also called residual tack or pressure sensitivity,

is the tack remaining after the liquid carrier has evaporated. Wet tack is often necessary in paper-converting operations. Applicators with little or no pressure on the combining section require emulsion adhesives with enough wet tack to bond strongly at the slightest touch. Emulsions containing poly(vinyl alcohol) as a protective colloid have stronger wet tack than those protected with a cellulose derivative. If more wet tack is required of the poly(vinyl alcohol)-protected adhesive, both a solvent and a plasticizer can be added and the solids content can be increased. Dry tack is needed where two nonporous surfaces are to be bonded. The nature of the adherends does not permit the water in the adhesive to escape by penetration or evaporation, and so the adhesive must dry before the adherends are joined, yet still retain enough tack to form a permanent bond. Film-to-film and film-to-foil laminations are good examples of applications requiring dry tack.

The *setting speed of an adhesive* is the time during which the bond formed by the adhesive becomes permanent. Before the setting of an emulsion adhesive can occur, inversion of the emulsion must take place; that is, it must change from a dispersion of discrete polymer particles in an aqueous continuous phase to a continuous polymer film containing discrete particles of water. The point at which the adhesive has actually set is that point at which an assembly, whether joint or lamination, can no longer be disassembled without damaging one or more of the adherends. Rapid setting speeds are necessary in many types of packaging adhesives intended for use with high speed gluing equipment. The rapid inversion possible with PVAc emulsions and their low viscosities allow them to be compounded into adhesives that not only set rapidly but also machine easily at high speeds. This machinability permits their application by practically any means, including glue guns, rollers, and spray guns.

Increases in setting speed can be achieved by increasing the dispersed phase content; that is, by increasing the amount of water-insoluble substances contained in the emulsions. This crowds the aqueous phase of the emulsion, hastening inversion and setting. Adding tackifying resins is one way to crowd the emulsion; adding plasticizers and solvents is another, but these additives mainly increase the setting speed by softening the polymer particles and hastening their coalescence. Surface-active agents also increase setting speed by helping the water in an adhesive to penetrate porous surfaces more rapidly; they can also retard it by stabilizing the emulsion. The usual way to prepare a high speed adhesive is to add both a solvent and a plasticizer to the base emulsion.

Poly(vinyl acetate) emulsions are excellent bases for water-resistant paper adhesives destined for use in manufacturing bags, tubes, and cartons. Glue-lap adhesives, which require moderate-to-high resistance to water, exemplify this type. When routine water resistance is required, a homopolymer vinyl acetate emulsion containing a cellulosic protective colloid is effective for most purposes. Next effective are emulsions containing fully hydrolyzed poly(vinyl alcohol) as a protective colloid, followed by those containing partially hydrolyzed poly(vinyl acetate).

When more than routine water resistance is required, a copolymer vinyl acetate emulsion can be used. The plasticizing comonomer in the polymer particles increases their intrinsic coalescing ability; thus, they can coalesce more readily than homopolymer particles to a film that has a higher resistance to water. This resistance to water does not extend to the organic solvents, however, which are

better resisted by homopolymer films. The soft copolymers have lower solubility parameters than homopolymers and are more readily attacked by solvents of low polarity, eg, hydrocarbons.

Despite their high resistance to water, copolymer emulsions are seldom chosen to bond paper to paper, as the less expensive homopolymer emulsions are effective enough. When copolymers are used in paper adhesives, it is done so chiefly to join coated or uncoated papers to films so as to take advantage of the lower critical surface tension required for wetting the copolymers. Because most packaging adhesives must be able to form strong paper-to-paper bonds, homopolymer vinyl acetate emulsions containing cellulosic protective colloids are always the first choice. The water resistance of any emulsion can be increased by improving its coalescence into a film either by adding solvents and plasticizers to it or by adding specific coalescing agents, eg, diethylene glycol monoethyl ether or diethylene glycol monoethyl ether acetate. Emulsions containing completely hydrolyzed poly(vinyl alcohol) can also be incorporated with cross-linking agents, which further insolubilize them. Cross-linking agents, however, can make a formulation unstable, so that it must often be used within a few hours after it has been compounded.

For any adhesive to be effective, it must first thoroughly wet the surface to be bonded; hence, it must be fluid at the time it is applied. Fluidity is not a problem with emulsion adhesives; wetting, however, can be problematic, especially when slick or coated surfaces are to be joined. An example is the manufacture of high gloss, clay-coated cartons, or the adhering of waxed papers. Copolymer emulsions tend to wet slick surfaces better than homopolymer emulsions because of the extra mobility and softness given to the polymer particles by the plasticizing comonomer. Their dried films also tend to conform better with this type of substrate. Homopolymer emulsions containing poly(vinyl alcohol) as a protective colloid wet paper surfaces well and are the first choice for paper-to-paper packaging adhesives. The setting ability of these emulsions can be increased by incorporating either nonionic wetting agents or partially hydrolyzed poly(vinyl acetate), or both. Small amounts of partially hydrolyzed poly(vinyl acetate) present in an adhesive also help it to wet lightly waxed papers.

The viscosity of an adhesive directly influences its penetration into a substrate; as the viscosity increases, the penetrating power decreases. It also determines the amount of mileage or spread that can be obtained. An optimum viscosity exists for each substrate and each set of machine conditions and must be achieved in order to manufacture an efficient adhesive. Poly(vinyl acetate) emulsions are frequently too low in viscosity to be metered efficiently or to perform well as adhesives by themselves. They must be bodied to working viscosities, eg, by adding thickeners.

Blocking and cold flow are undesirable properties. Blocking refers to dried adhesive surfaces that become sticky, causing unwanted bonding. Cold flow occurs with a polymer having a low softening point; if the temperature of the adhesive assembly warms to the softening range of the polymer, the bond slips. The temperature at which a dried adhesive film forms an instantaneous bond between two surfaces when heat is applied is its *heat-sealing temperature*. This property is closely related to the blocking temperature and to the temperature at which cold flow or creep can occur.

The heat-sealing temperature of an emulsion is related to the thermoplasticity of the poly(vinyl acetate) particles dispersed in it. Thermoplastic polymers are softened by heat; those of relatively high molecular weight or those that are cross-linked soften at higher temperatures than those of low molecular weight. In addition, poly(vinyl acetate) homopolymers soften at higher temperatures than do copolymers (with monomers that lower the glass-transition temperature) which have similar molecular weight. Another factor which affects the heat-sealing temperature of an emulsion is the amount of poly(vinyl alcohol) in it, if any, since poly(vinyl alcohol) has a high melting point. High heat-sealing temperatures, which are desirable in an emulsion adhesive because they indicate resistance to blocking and cold flow, are usually attainable with emulsions containing large amounts of poly(vinyl alcohol) as a protective colloid.

Fillers are added to emulsion adhesives to build the total solids content, to reduce penetration into a porous substrate, and to lower costs. Plasticizers are added to emulsion adhesives to modify several properties of both the emulsion and the finished adhesive film. By softening the polymer particles dispersed in the emulsion and increasing their mobility, plasticizers cause them to flow together more easily. This usually increases the viscosity of the emulsion and tends to destabilize it for faster breaking and setting speeds at the time it is applied. In addition, the increased softness and mobility help the emulsion to wet smooth, nonporous surfaces, eg, films, foils, and coated papers, thereby increasing its adhesion to them. Also, the softened polymer particles coalesce more rapidly and at a lower temperature than is possible with the unplasticized emulsion. This improved coalescence increases the water resistance of the adhesive film. Plasticizers are usually high boiling esters, eg, phthalates. Phosphate esters are useful as fire-retardant plasticizers.

Solvents are frequently used to perform several functions in emulsion adhesives. Solvents promote adhesion to solvent-sensitive surfaces, they increase the viscosity of the emulsion and intensify the tack of the wet adhesive, and they improve the coalescing properties of the film. Low boiling solvents impart only wet tack to the adhesive film, whereas high boiling solvents confer both dry and wet tack and lower the heat-sealing temperature. The solvent can impart the necessary speed to the wet adhesive but, because it evaporates, it does not cause the dried bond to creep, which often happens with a plasticized film that ages under stress. Solvents promote adhesion to solvent-sensitive adherends by softening and partially dissolving them, thus allowing the adhesive to wet or penetrate the surface or both. Because of the increasing regulatory pressure on solvent emissions, there is a need to develop these properties without volatile materials.

Tackifiers are used to increase the tackiness and the setting speed of adhesives. They increase tackiness by softening the poly(vinyl acetate) polymer in the wet and the dry adhesive film. Tackifiers are usually rosin or its derivatives or phenolic resins. Other additives frequently needed for specific application and service conditions are antifoams, biocides, wetting agents, and humectants.

Specialized copolymer latices, which are inherently and permanently tacky, are available as pressure-sensitive emulsions. They are mechanically stable and have excellent machinability. They are compatible with many other PVAc latices and, therefore, can be easily blended with other resins for modification of surface tack, peel strength, and creep.

Poly(vinyl acetate) dry resins and ethylene–vinyl acetate (EVA) copolymers are used in solvent adhesives, which can be applied by total industrial techniques, eg, brushing, knife-coating, roller-coating, spraying, or dipping. Proper allowances must be made for evaporation of solvent during or before bonding. Poly(vinyl acetate) resins and EVA copolymers containing 21–30 wt% vinyl acetate are widely used in hot-melt adhesive applications. Homopolymers are compounded with 25–35 wt% plasticizer and 25–30 wt% extender resins. These additives increase fluidity and adhesion as well as reduce cost. Ethylene–vinyl acetate resins are mixed with waxes, rubbers, and resin to make the hot-melt adhesive compound. Hot-melt adhesive application processes may be extremely rapid both in application and setting speed, cause no problems resulting from solvent or water evaporation, and provide bonds of high water resistance. The adhesive materials have indefinite shelf lives. Hot-melts are largely used in packaging, laminating, and bookbinding. For the last application, alkali-soluble copolymers are frequently used to facilitate the reclamation of scrap paper.

Film and foil adhesives based on internally plasticized copolymer adhesives have been suggested. For instance, vinyl acetate–ethylene or vinyl acetate–acrylate copolymers may be used for adhesion of films to porous surfaces. For metallic foil adhesion, copolymers containing carboxylate functionality are suggested.

Spray-dried powders find application in adhesives to build solids, increase viscosity, improve tack, and decrease drying time (147). A primary use is in joint compounds with other applications in mastics and grouts, and patching compounds (148).

Paints. Paints prepared from poly(vinyl acetate) and its copolymers form flexible, durable films with good adhesion to clean surfaces, including wood, plaster, concrete, stone, brick, cinder blocks, asbestos board, asphalt, tar paper, wallboards, aluminum, and galvanized iron (149). Adherence is also good on painted surfaces if the surfaces are free from dirt, grease, and rust. Developments in emulsion polymerization for paint latices have been reviewed (150).

Poly(vinyl acetate) latex paints are the first choice for interior use (151). Their ability to protect and decorate is reinforced by several advantages belonging exclusively to latex paints: they do not contain solvents so that physiological harm and fire hazards are eliminated; they are odorless; they are easy to apply with spray gun, roller-coater, or brush; and they dry rapidly. The paint can be thinned with water, and brushes or coaters can be cleaned with soap and tepid water. The paint is usually dry in 20 min to 2 h, and two coats may be applied the same day.

Poly(vinyl acetate) latex paints are also widely used as exterior paints. Their durability, particularly their resistance to chalking, far surpasses that of any conventional oleoresinous paints, which chalk soon after application. The good nonchalking properties of PVAc paints result from their resistance to degradation by UV light. Latex paints that are correctly formulated from quality PVAc latices develop little or no chalk, thus giving maximum tint retention, and they last a long time before repainting becomes necessary. The blister resistance of PVAc paints is another important advantage for their exterior use. Latex paint films are permeable enough to permit water vapor to penetrate them, which prevents blistering and peeling. Their film formation is not impaired if they are painted on damp surfaces or are applied under very humid conditions.

Several types of plasticizing comonomers can be copolymerized with vinyl acetate to produce latices suitable for manufacturing paints. The older, less common comonomers are the alkyl maleates and fumarates, eg, dibutyl maleate and dibutyl fumarate. Acrylic esters, eg, butyl acrylate and 2-ethylhexyl acrylate, as well as ethylene, are the most widely used comonomers in the 1990s. The chief reason for using a comonomer in vinyl acetate polymers is to increase the deformability of the paint film permanently, thus permitting it to expand and contract as the dimensions of the substrate change with changes in temperature. The plasticizing comonomer also softens the polymer particles. For a film to form from a latex paint, the polymer particles must deform and fuse to form a continuous film. This coalescing ability is directly related to the amount of comonomer present. In both interior and exterior paints, the improvement in coalescence that is obtainable by using high comonomer levels results in a general improvement in all the properties necessary for interior and exterior paints. High levels of comonomers, such as ethylene or butyl acrylate, must be added with care. If high comonomer levels are used with low molecular weight polymers, the resulting paint film suffers from excessive dirt pickup at high temperatures because it becomes soft and tacky. It is required, therefore, that high molecular weight polymers be prepared, because only with these is a sufficient amount of comonomer incorporated to give the tint retention without dirt pickup required in exterior paints.

The strength of a polymer increases with its molecular weight; consequently, the toughest paint films are formed from latex polymers having the highest molecular weights. For exterior paints, there is a federal specification of a minimum intrinsic viscosity of 0.45 dL/g. The minimum intrinsic viscosity of commercial paint polymers usually is 0.60–1.0 dL/g and above.

Special vinyl acetate copolymer paints have been developed with greatly improved resistance to blistering or peeling when immersed in water. This property allows better cleaning and use in very humid environments. These lattices exhibit the water resistance of higher priced acrylic resins (152). VAc, vinyl chloride–ethylene terpolymers have been developed which provide the exterior resistance properties of vinyl chloride with the flexibility of the ethylene for exterior paint vehicles (153).

The critical pigment volume concentration (CPVC) of vinyl acetate paints is 48–60%. Generally, the smaller and softer the polymer particles, the higher the CPVC and the greater the pigment-binding capacity of the latex. The most widely used white pigment is titanium dioxide in the form of rutile or of anastase. The color pigments used in latex paints are of two types: the organic pigments (see PIGMENTS, ORGANIC), which are usually hydrophobic, and the inorganic pigments (see PIGMENTS, INORGANIC), which are usually hydrophilic. The hydrophilic pigments are relatively easy to incorporate into water-base paints. The hydrophobic pigments are more difficult to incorporate, but this can be overcome by choosing the correct blend of surfactants for a particular pigment. The organic colorants commonly used are toluidine red, Hansa yellow, phthalocyanine blue and green, pigment green B, and carbon black, among others. Examples of acceptable inorganic colorants are iron oxide red, brown, yellow, black, and chrome oxide green. Colorants that should not be used are those that are reactive, partially water-soluble, or sensitive to pH changes.

In addition to latex and pigment, paint formulations contain dispersants and wetting agents (both surfactants), defoamers, thickeners and protective colloids, freeze–thaw stabilizers, coalescing agents, and biocides. The coalescing agents used in the paint formulations tend to be volatile. In order to reduce the odor levels and reduce solvent emissions, some paint producers are researching latex bases which require less or no solvent to aid in coalescence and yet provide a durable, glossy surface (154). Copolymers are potentially useful in meeting this requirement (155,156).

Paper. Poly(vinyl acetate) emulsions and resins have been used as the binder in coatings for paper and paperboard since 1955 (157–159). The coatings may be clear, colored, or pigmented, and are glossy, odorless, tasteless, greaseproof, nonyellowing, and heat-sealable. Conventional paper-coating equipment is used; formulations normally contain 60–65 wt% solids with a pigment-to-binder ratio of 1:5. Printing quality and ink-pick resistance are excellent. In papermaking, emulsions applied as wet-end additions to the furnish improve the strength and durability of the final product. Plasticized emulsions may be used to give the product toughness and flexibility.

Emulsions used in paper coatings must meet special requirements: the particle size must be small (ca 0.1 μm) and its distribution rather narrow. These properties provide good pigment binding efficiency and high gloss. They must have exceptionally good mechanical stability and freedom from off-sized latex particles or grit, and must exhibit no trace of dilatant flow in a pigment slurry. These properties are required for modern high speed paper-coating applications. They should also be compatible with starch and alginate natural resins frequently used as cobinders (160).

Nonwoven Binders and Textiles. The use of vinyl acetate copolymers as binding agents for nonwoven fabrics has grown rapidly. Vinyl acetate–ethylene copolymer latices have been particularly successful in part because of their low cost but also because of their excellent adhesion to a wide range of substrates, their water and alkali resistance, and their low flammability (161–164). Products made from these binders include paper towels, wipes, and personal hygiene articles. Self-cross-linking polymers are available as are polymers requiring external curing agents. Many of the self-cross-linking polymers release formaldehyde (qv) as part of the reaction. Because formaldehyde has been listed as a potential carcinogen, alternative chemistries have been developed to reduce or eliminate formaldehyde content in the products.

Poly(vinyl acetate) emulsions are widely used as textile finishes because of their low cost and good adhesion to natural and synthetic fibers. In textile piece goods finishing, dispersions diluted with water to 1–3 wt% resin are most often used to obtain a stiff or crisp hand on woven cotton fabrics. Concentrations of 2–20 wt% emulsion are recommended for bodying, stiffening, and bonding. Principal applications include the stiffening of felts. Finishes to improve snag resistance and body or hand of nylon hosiery are based on PVAc emulsions.

Poly(vinyl acetate) emulsions are used to prime-coat fabrics to improve the adhesion of subsequent coatings or to make them adhere better to plastic film. Plasticized emulsions are applied, generally by roller-coating, to the backs of finished rugs and carpets to bind the tufts in place and to impart stiffness and hand. For upholstery fabrics woven from colored yarns, PVAc emulsions

may be used to bind the tufts of pile fabrics or to prevent slippage of synthetic yarns.

The emulsion formulations are generally applied to cloth by padding from a bath and squeezing off the excess. Modifying a formulation in the pad box, eg, to increase or decrease firmness, can be easily done by adding an emulsion or softener. The alkali-soluble vinyl acetate copolymers previously mentioned can be used as warp sizes during weaving.

Concrete Additives. Poly(vinyl acetate) was first used in concrete in the 1940s as a thermoplastic polymer to strengthen the concrete matrix. In contrast to other polymers, the resistance to water permeation is low due to the hydrolysis of the poly(vinyl acetate) (165,166). Ethylene copolymers have been developed which have improved water resistance and waterproofness. The polymer can be used in the latex form or in a spray-dried form which can be preblended in with the cement (qv) in the proper proportion. The compressive and tensile strength of concrete is improved by addition of PVAc emulsions to the water before mixing. A polymer solids to total solids ratio of ca 10:90 is best. The emulsions also aid adhesion between new and old concrete when patching or resurfacing.

Other. Vinyl acetate resins are useful as antishrinking agents for glass fiber reinforced polyester molding resins (167). Poly(vinyl acetate)s are also used as binders for numerous materials, eg, fibers, leather (qv), asbestos, sawdust, sand, clay, etc, to form compositions that can be shaped with heat and pressure. Joint cements, taping compounds, caulks, and fillers are other uses.

Emulsions containing added poly(vinyl alcohol) and dichromate are used to make light-sensitive stencil screens for textile printing and ceramic decoration. The resins are used in printing inks, nitrocellulose lacquers, and special high gloss coatings. Inks made with PVAc and metallic pigments look like foil because the formulations have a high leafing power, do not induce tarnish, and contribute no unwanted color or aging.

Vinyl acetate polymers have long been used as chewing gum bases. They have been studied as controlled release agents for programmed administration of drugs and as a base for antifouling marine paints (168,169).

BIBLIOGRAPHY

"Vinyl Ester Polymers," in *EPST* 1st ed., Vol. 15, pp. 677–703, by M. K. Lindemann, Charls S. Tanner Co.; in *EPSE* 2nd ed., Vol. 17, pp. 393–445, by Wiley E. Daniels, Air Products and Chemicals.

1. C. A. Schildknecht, *Vinyl and Related Polymers*, John Wiley & Sons, Inc., New York, 1952, p. 323.
2. *Chemical Economics Handbook Marketing Research Report*, SRI International, Menlo Park, Calif., July 1993.
3. C. Sumner and J. R. Zoeller, *Chem. Ind.* **49**, 225–240 (1993).
4. *Plast. Ind. News* **41**(4), 2 (Apr. 1995).
5. *Vinyl Acetate, A Guide to Safety and Handling*, compiled by E. I. duPont de Nemours and Co., Inc., Hoechst Celanese Chemical Group, Inc., Quantum Chemical Co., and Union Carbide Corp., 1995.
6. *Vinyl Acetate*, Bulletin S-56-3, Celanese Chemical Co., New York, 1969.
7. *Vinyl Acetate Monomer F-41519*, Union Carbide Corp., New York, June 1967.

8. *Vinyl Acetate Monomer BC-6*, Borden Chemical Co., New York, 1969.
9. *Vinyl Acetate Monomer*, Air Reduction Co., New York, 1969.
10. R. W. Gallant, *Hydrocarbon Process.* **47**(10), 115 (1968).
11. S. Okamura and I. Motoyama, *J. Polym. Sci.* **58**, 221 (1962).
12. L. H. Horsley, *Azeotropic Data, II*, Advances in Chemistry Series 35, American Chemical Society, Washington, D.C., 1962.
13. M. K. Lindemann, in G. E. Ham, ed., *Vinyl Polymerization*, Vol. 1, Marcel Dekker, Inc., New York, 1967, Part 1, Chapt. 4.
14. J. Brandrup and E. H. Immergut, eds., *Polymer Handbook*, Interscience Publishers, a division of John Wiley & Sons, Inc., New York, 1966.
15. M. K. Lindemann, in N. M. Bikales, ed., *Encyclopedia of Polymer Science and Technology*, Vol. 15, John Wiley & Sons, Inc., New York, 1971, p. 636.
16. G. O. Morrison and T. P. G. Shaw, *Trans. Electrochem. Soc.* **63**, 425 (1933).
17. D. Swern and E. F. Jordan Jr., in N. Rabjohn, ed., *Organic Syntheses*, collective Vol. 4, John Wiley & Sons, Inc., New York, 1963, p. 977.
18. H. Hopff and M. A. Osman, *Tetrahedron* **24**, 2205 (1968).
19. C. F. Kohll and R. van Helden, *Rec. Trav. Chim.* **86**, 193 (1967).
20. H. E. Simmons and R. D. Smith, *J. Am. Chem. Soc.* **81**, 4256 (1959).
21. C. Walling, *Free Radicals in Solution*, John Wiley & Sons, Inc., New York, 1957, Chapt. 6.
22. *Chem. Marlet Rep.* **263**(21), 27 (May 26, 2003).
23. W. Johnson, T. Kaelin, and G. Tohi, *Chemical Economics Handbook*, SRI International, Menlo Park, Calif., March 2001.
24. L. B. Levy, *Process Safety Progr.* **12**(1), 47–48 (Jan. 1993).
25. D. W. Butcher and H. M. Sharpe, *MariChem*, 5th ed., 1984, pp. 189–192.
26. *IARC Monogr.* **63**, (Feb. 1995).
27. R. VanHelden and co-workers, *Rev. Trav. Chim.* **87**, 961 (1968).
28. *Petr. Refiner* **38**, 304 (1959).
29. H. C. Volger, *Rev. Trav. Chim.* **87**, 501 (1968).
30. D. N. Mead and R. M. Fuoss, *J. Am. Chem. Soc.* **63**, 2832 (1941).
31. S. O. Morgan and Y. A. Yager, *Ind. Eng. Chem.* **32**, 1519 (1940).
32. H. Fikentscher, *Cellul. Chem.* **13**, 71 (1932).
33. E. O. Kraemer, *Ind. Eng. Chem.* **30**, 1200 (1938).
34. A. Ballisteri and co-workers, *J. Polym. Sci. Polym. Chem. Ed.* **18**, 1147 (1980).
35. T. Okada, *Polym. J.* **9**, 121 (1977).
36. H. Bartl, in E. Muller, ed., *Methods of Organic Chemistry (Houben-Weyl), Macromolecular Materials, Part 1*, Georg Thieme Verlag, Stuttgart, Germany, 1961, pp. 905–918.
37. D. R. Bassett and A. E. Hamielec, eds., *Emulsion Polymers and Emulsion Polymerization* (ACS Symposium Series 165), American Chemical Society, Washington, D.C., 1981.
38. I. Piirma, ed., *Emulsion Polymerization*, Academic Press, New York, 1982.
39. R. D. Athey, *Emulsion Polymer Technology*, Marcel Dekker, New York, 1991.
40. Q. Wang and co-workers, *Prog. Polym. Sci.* **19**, 703–753 (1994).
41. D. C. Blackley, *Emulsion Polymerisation: Theory and Practice*, John Wiley & Sons, Inc., New York, 1975.
42. M. K. Lindemann, *Paint Manuf.* **38**(9), 30 (1968).
43. E. Levine, W. Lindlaw, and J. Vona, *J. Paint Technol.* **41**, 531 (1969).
44. C. Chellappa, *Mod. Paint Coat.* **85**(13), 28–32 (Dec. 1995).
45. A. S. Badran and co-workers, *J. Appl. Polym. Sci.* **49**(2), (1993), 187–196.
46. N. J. Earhart, *The Grafting Reactions of Poly(vinyl alcohol) During the Emulsion Copolymerization of Poly(vinyl acetate–co-butyl acrylate)*, Ph.D. dissertation.
47. Product List, Air Reduction Co., New York, 1968.

48. Elvacet Poly(Vinyl Acetate) Brochure, E. I. Du Pont de Nemours & Co., Inc., Wilmington, Del., 1968.
49. Thermoplastics Division Product Directory, Borden Chemical Co., New York, 1968.
50. Gelva Poly(Vinyl Acetate) Technical Bulletin, Publication No. 6103, Monanto Chemical Co., St. Louis, Mo., 1969.
51. E. Tromsdorff and C. E. Schildknecht, in C. E. Schildknecht, ed., *Polymer Processes*, Interscience Publishers, Inc., New York, 1956, 105–109.
52. V. T. Stannett and co-workers, *Prog. Polym. Process. 3, Radiat. Process. Polym.* 289–317 (1992).
53. T. Okaya and co-workers, *J. Appl. Polym. Sci.* **50**(5), 745–751 (1993).
54. U.S. Pat. 5,171,767 (Dec. 15, 1992), R. G. Buckley and co-workers (to Rohm and Haas).
55. J. Dimitratos and co-workers, *AIChE J.* **40**(12) (Dec. 1994).
56. A. Urretabizkaia and co-workers, *J. Polym. Sci. Part A–Polym. Chem.* **31**, 2907–2913 (1993).
57. L. M. Gugliotta and co-workers, *Polymer* **36**, 2019–2023.
58. S. Canegallo and co-workers, *J. Appl. Polym. Sci.* **47**, 961–979 (1993).
59. P. D. Gossen and J. F. Macgregor, *J. Colloid Interface Sci.* **160**(1), 24–38 (1993).
60. W. Baade and co-workers, *J. Appl. Sci.* **27**, 2249–2267 (1982).
61. P. Bataille and co-workers, *J. Appl. Polym. Sci.* **38**, 2237–2244 (1989).
62. A. Iabbadene and co-workers, *J. Appl. Polym. Sci.* **51**, 503–511 (1994).
63. U.S. Pat. 4,164,489 (Aug. 14, 1979), W. E. Lenney and W. E. Daniels (to Air Products and Chemicals, Inc.).
64. C. Kipparissides, J. F. MacGregor, and A. E. Hamiliec, *Can. J. Chem. Eng.* **58**(1), 48 (1980).
65. R. K. Greene, *Continuous Emulsion Polymerization of Vinyl Acetate*, Ph.D. dissertation, 1976.
66. U.S. Pat. 4,035,329 (Nov. 19, 1975), H. Wiest and co-workers (to Wacker Chemie, GmbH).
67. P. L. Tang, *Semicontinuous Polymerization Using Miniemulsions*, M. S. Report, 1989.
68. J. Delgado, *Miniemulsion Copolymerization of Vinyl Acetate and n-Butyl Acrylate*, Ph.D. dissertation, 1986.
69. M. S. El-Aasser and J. W. Vanderhoff, eds., *Emulsion Polymerization of Vinyl Acetate*, Applied Science Publishers, Inc., Englewood, N.J., 1981.
70. R. D. Dunlop and F. E. Reese, *Ind. Eng. Chem.* **40**, 654 (1948).
71. G. Kalfas, H. Yuan, and W. H. Ray, *Ind. Eng. Chem. Res.* **32**, 1831–1838 (1993).
72. V. T. Shiriniyan and co-workers, *Zh. Prikl. Khim. (Leningrad)* **44**, 1345 (1977).
73. K. H. Reichert and H. V. Moritz, *J. Appl. Polym. Sci., Polym. Symp.* **36**, 151 (1981).
74. H. V. Moritz and K. H. Reichert, *Chem. Eng. Tech.* **53**(5), 386 (1981).
75. J. W. Harter and W. H. Ray, *Chem. Eng. Sci.* **41**, 3083 (1986).
76. J. W. Harter and W. H. Ray, *Chem. Eng. Sci.* **41**, 3095 (1986).
77. R. G. Gilbert, *Emulsion Polymerization: A Mechanistic Approach*, Academic Press, Inc., New York, 1995.
78. E. Daniels and co-authors, eds., *Polymer Latexes: Preparation, Characterization, and Applications* (ACS Symposium Series), American Chemical Society, Washington, D.C., 1992, p. 492.
79. B. S. Casey, B. R. Morrison, and R. G. Gilbert, *Progr. Polym. Sci.* **18**, 1041–1096 (1993).
80. N. Friis and L. Nyhagen, *J. Appl. Polym. Sci.* **17**, 2311–2327 (1973).
81. A. Penlidis, J. F. MacGregor, and A. E. Hamielec, *Polym. Process Eng.* **3**(3), 185–218 (1985).
82. M. S. El-Aaser and co-workers, *J. Polym. Sci. Polym. Chem. Ed.* **21**, 2363–2382 (1983).
83. J. W. Breitenbach, H. Edelhauser, and R. Hochrainer, *Monatsh. Chem.* **99**, 625 (1968).

84. C. E. Schildknecht and I. Skeist, *Polymerization Processes*, John Wiley & Sons, Inc., New York, 1977.
85. J. Meuldijk and co-workers, *Chem. Eng. Sci.* **47**, 2603–2608 (1992).
86. C. M. Gilmore and co-workers, *J. Appl. Polym. Sci.* **48**, 1449–1460 (1993).
87. M. Nomura and K. Fujita, *Makromol. Chem. Suppl.* **10/11**, 25–42 (1985).
88. P. J. Flory and F. S. Leutner, *J. Polym. Sci.* **3**, 880 (1948); **5**, 267 (1950).
89. D. Stein, *Makromol. Chem.* **76**, 170 (1964).
90. M. Matsumoto and I. Ohyang, *J. Polym. Sci.* **46**, 441 (1960).
91. S. P. Pontis and A. M. Deshpande, *Makromol. Chem.* **125**, 48 (1969).
92. W. W. Graessley, W. C. Uy, and A. Gandhi, *Ind. Eng. Chem. Fundam.* **8**, 697 (1969).
93. V. T. Shiriniyan and co-workers, *Plast. Massy* **8**, 15 (1974).
94. S. Imoto, J. Ukida, and T. Kominami, *Kobunshi Kagaku* **14**, 101 (1957).
95. D. Stein and G. V. Schultz, *Makromol. Chem.* **52**, 249 (1962).
96. I. Gavat, V. Dimonie, and D. Donescu, *J. Polym. Sci., Polym. Symp.* **64**, 125 (1978).
97. K. Noro, *Br. Polym. J.* **2**, 128 (1970).
98. M. Shiraishi, *Br. Polym. J.* **2**, 135 (1970).
99. S. S. Mnatskanov and co-workers, *Vysokmol. Soyed.* **A14**, 4,851 (1972).
100. V. T. Shirininyan and co-workers, *Vysokmol. Soyed.* **A17**, 1,182 (1975).
101. M. Furuta, *J. Polym. Sci., Polym. Lett. Ed.* **11**, 113 (1973).
102. M. Furuta, *J. Polym. Sci., Polym. Lett. Ed.* **12**, 459 (1974).
103. H. Meissner and G. Heublein, *Acta Polym.* **34**, 379 (1983).
104. H. Meissner and co-workers, *Acta Polym.* **35**, 250 (1984).
105. G. Heublein and H. Meissner, *Acta Polym.* **35**, 744 (1984).
106. G. Heublein and H. Meissner, *Acta Polym.* **36**, 245 (1985).
107. G. Heublein and H. Meissner, *Acta Polym.* **35**, 343 (1985).
108. H. Meissner, P. Hartschansky, and G. Heublein, *Acta Polym.* **36**, 345 (1985).
109. H. Meissner, P. Hartschansky, and G. Heublein, *Acta Polym.* **36**, 699 (1985).
110. H. Meissner and G. Heublein, *Acta Polym.* **37**, 323 (1986).
111. H. Meissner and G. Heublein, *Acta Polym.* **38**, 75 (1987).
112. D. Donescu and co-workers, *J. Macromol. Sci. Chem.* **22**, 931 (1985).
113. D. Donescu, *Rev. Roum. Chem.* **24**(9), 1399 (1979).
114. D. Donescu and co-workers, *Rev. Roum. Chem.* **19**(6), 483 (1984).
115. S. Hayashi and co-workers, *J. Appl. Polym. Sci.* **27**(5), 1607 (1982).
116. V. T. Stannett, *Proc. R. Aust. Chem. Inst.* **42**, 232 (1975).
117. G. F. Lundardon, G. P. Talamini, and V. Grosso, *Eur. Polym. J.* **11**, 437 (1975).
118. P. K. Isaacs and H. A. Edelhauser, *J. Appl. Polym. Sci.* **10**, 171 (1966).
119. H. Warson, *Chem. Ind. London* **6**, 220 (1983).
120. J. Schellenberg and co-workers, *Angew. Makromol. Chem.* **130**, 99 (1985).
121. D. Mohan and co-workers, *J. Polym. Sci., Polym. Chem. Ed.* **21**, 3041 (1983).
122. P. J. Scott, A. Penlidis, and G. L. Rempel, *J. Polym. Sci., Part A: Polym. Chem.* **31**(9), 2205–2230 (1993).
123. P. J. Scott, A. Penlidis, and G. L. Rempel, *J. Polym. Sci., Part A: Polym. Chem.* **31**, 403–426 (1993).
124. J. W. Vanderhoff, *J. Polym. Sci., Polym. Lett. Ed.* **17**, 567 (1979).
125. R. B. Seymour and G. A. Stahl, *J. Macromol. Sci. Chem.* **11**(1), 53 (1977).
126. W. K. Busfield and R. B. Low, *Eur. Polym. J.* **11**, 309 (1975).
127. A. G. Sayadyan and D. A. Simonyan, *Arm. Khim. Zh.* **21**, 1041 (1968).
128. U.S. Pat. 4,260,533 (Apr. 7, 1981), J. G. Iacoviello and W. E. Daniels (to Air Products and Chemicals, Inc.).
129. T. Yatsu, S. Moriuchi, and H. Fuji, *Makromolecules* **10**, 243 (1977).
130. C. H. Chen, *J. Polym. Sci.* **14**, 2109 (1976).
131. B. Tidswell and A. W. Train, *Br. Polym. J.* **7**, 409 (1975).

132. U.S. Pat. 4,137,382 (Jan. 30, 1979), C. J. Vetters (to National Distillers and Chemical Corp.).
133. U.S. Pat. 4,172,939 (Oct. 30, 1979), G. J. Hoh (to E. I du Pont de Nemours & Co., Inc.).
134. Research Disclosure 13816, Industrial Opportunities, Ltd., Hampshire, U.K., Oct. 1975.
135. J. Y. Olayemi and M. K. Ibiyeve, *J. Appl. Polym. Sci.* **31**, 237 (1986).
136. F. Le and co-workers, *J. Polym. Eng.* **7**(2), 113 (1987).
137. R. H. Bott, J. A. Kuphal, L. M. Robeson, and D. Sagl, *J. Appl. Polym. Sci.* **58**, 1593–1605 (1995).
138. D. R. Paul and co-workers, *Polymer Blends*, Vol. 1, Academic Press, New York, 1978, pp. 71–74.
139. W. R. Furlan, *Adhesives Age* **37**(2), 20–22 (Feb. 1994).
140. N. Chinn, T. Kaelinu, and G. Toki, *Chemical Economics Handbook*, SRI International, Menlo Park, Calif., June 2001.
141. M. L. Hausman and co-workers, *Adhesives Age* **38**(11), 49–60 (Oct. 1995).
142. *Working with Vinyl Acetate Based Polymers, An Adhesives Manual*, 3rd ed., Air Products and Chemicals, Inc., Allentown, Pa., 1996.
143. R. A. Weidener, in R. L. Patrick, ed., *Treatise on Adhesion and Adhesives*, Vol. 2, Marcel Dekker, Inc., New York, 1969, Chapt. 10, pp. 432–447, 467–471.
144. I. Skeist, ed., *Handbook of Adhesives*, Van Nostrand Reinhold Co., New York, 1990, p. 468.
145. F. P. Hoenisch and M. C. Bricker, *Adhesives Age* **36**(8), 20–23 (July 1993).
146. U.S. Pat. 5,185,308 (1993), J. G. Iacoviello and D. W. Horwat (to Air Products and Chemicals, Inc.).
147. K. W. Rizzi, *Adhesives Age* **38**(8), 24–26 (July 1995).
148. I. Skeist, ed., *Handbook of Adhesives*, Van Nostrand Reinhold Co., New York, 1990, p. 472.
149. *Paint Handbook*, Air Products and Chemicals, Inc., New York, 1969.
150. H. Warson, *Polym. Paint Colour J.* **180**, 473–486 (July 1990).
151. *Am. Paint J.* **53**, 7, 58 (1968).
152. *Am. Paint/Coating J.* **66** (Nov. 13, 1978).
153. D. B. Farmer and M. H. Edser, *Chem. Ind.* 228–235 (Mar. 21, 1983).
154. *Chem. Week* **43** (Aug. 1995).
155. B. Currie, *Mod. Paint Coat.* **83**(8), 34–40 (Aug. 1993).
156. U.S. Pat. 5,346,948 (1994), F. L. Floyd and G. P. Craun (to Glidden).
157. D. K. Stinebaugh, *Tappi Notes, 1990 Blade Coating Seminar*, Tappi Press, Atlanta, Ga., 1990.
158. J. W. Ramp, *Tappi Notes, 1990 Coating Binders Short Course*, Tappi Press, Atlanta, Ga., 1990.
159. T. F. Walsh and L. A. Gaspar, TAPPI Monograph Series 37, 1975, Tappi Press, Atlanta, Ga., Chapt. 5.
160. U.S. Pat. 4,228,047 (July 31, 1981), W. E. Daniels and W. H. Pippen (to Air Products and Chemicals, Inc.).
161. J. R. Halker, *Formed Fabric Ind.* **26** (June 1976).
162. P. L. Rosamilia, *Tappi Paper Synth. Proc.* **251** (1979).
163. C. C. Chappelow, P. L. Rosamilia, and M. J. Taylor, *INDEX 81 Congress Papers*, Session 2, Washington, D.C.
164. D. A. Brighton, *Non-Wovens Yearbook*, 1982, pp. 24–29.
165. S. Chandra and Y. Ohama, *Polymers in Concrete*, CRC Press, Boca Raton, Fla., 1994.
166. L. Holloway, *Polymers and Polymer Composites in Construction*, T. Telford, London, 1990.

167. K. E. Atkins and B. W. Lipinsky, *Auk. Offentliche Jahrestagung Der. 13 Int. Tagung, Freudenstadt* **39**, 1–4 (Oct. 1976).
168. H. Leeper and H. Benson, SPE 2nd Ann. Conf., Seattle, Wash., Aug. 1976, pp. 141–149.
169. U.S. Pat. 4,143,015 (Jan. 21, 1977), E. Soeterik.

CAJETAN F. CORDEIRO
FRANCIS P. PETROCELLI
Air Products and Chemicals, Inc.

VINYL ALCOHOL POLYMERS. See Volume 8.

VINYL CHLORIDE POLYMERS. See Volume 8.

VINYL FLUORIDE POLYMERS (PVF). See Volume 4.

VINYLIDENE CHLORIDE POLYMERS. See Volume 4.

VINYLIDENE FLUORIDE POLYMERS. See Volume 4.

VISCOELASTICITY. See Volume 4.

VISCOMETRY. See RHEOLOGICAL MEASUREMENTS.

VULCANIZATION. See RUBBER COMPOUNDING.

WATER-SOLUBLE POLYMERS

Introduction

Water-soluble macromolecules represent a diverse class of polymers ranging from biopolymers that mediate life processes to synthetic polymers of immense commercial utility. In this article water-soluble polymers have been grouped into the categories biopolymers, nonionic, ionic, and associative, based on key structural features. Recently developed controlled polymerization techniques imparting important technological features to water-soluble polymers are also discussed.

General Considerations

Structure. Solution properties and ultimate performance of water-soluble polymers are determined by specific structural characteristics of the hydrated polymer chain. Primary structure depends directly on the nature of the repeating units (bond lengths, valence bond angles) effective compositions, and locations along the backbone. The polymer structure may derive from a single monomer [ie, poly(ethylene oxide) or polyacrylamide] or from multiple monomers. These units may be placed to yield random, alternating, block, graft, or more intricate architectures such as stars or dendrimers (Fig. 1). Biopolymers such as proteins and polynucleotides have multiple repeating units specifically ordered by template polymerization.

Secondary structure in water-soluble polymers is related to configuration, conformation, and intramolecular effects such as hydrogen bonding and ionic interactions. Tertiary structure involves intermolecular and water-polymer interactions; quaternary structure requires multiple chain aggregation or complexation.

Encyclopedia of Polymer Science and Technology. Copyright John Wiley & Sons, Inc. All rights reserved.

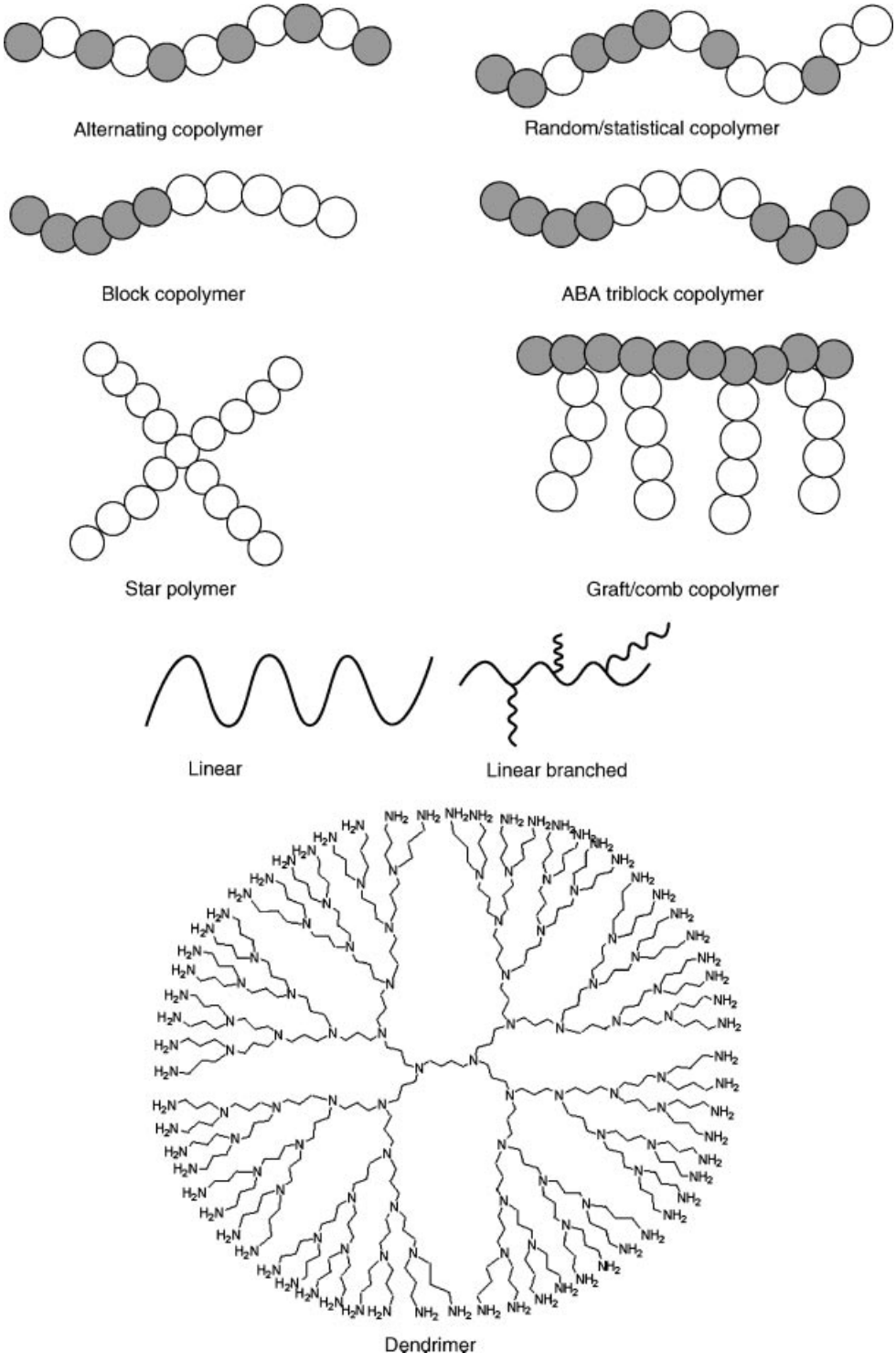

Fig. 1. Structural representation of polymer architectures (1).

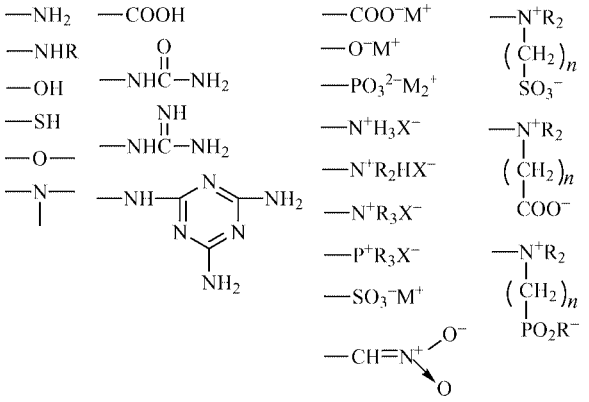

Fig. 2. Examples of functional groups imparting water solubility.

A large number of functional groups (Fig. 2) can impart water solubility in copolymers. The degree of solubility is dependent on the number, position, and frequency of these moieties. Hydration relies on interaction at polar (ionic and hydrogen bonding) sites.

Hydrodynamic Volume. Polymers are often described in terms of hydrodynamic volume (HDV) or that volume occupied by the solvated chain. HDV and molecular shape, determined from light scattering measurements, may be used along with chemical microstructure to predict rheological behavior.

Theoretical attempts to relate dimensions of polymers to chemical structure were pioneered by Flory (2). Statistical macromolecular size in solution can be modeled from first principles by considering the number and length of bonds along with valence bond angles and conformational restrictions. Excluded volume, segmental interactions, specific intramolecular interactions, and chain solvation contribute to dimensions.

Ionic interactions (repulsive or attractive) can also dramatically affect HDV. For charged polymers, ionic effects often dominate behavior, especially in aqueous solutions. Theoretical treatments for predicting polyelectrolyte dimensions and phase behavior are discussed by Barrat and Joanny (3); scaling theory for charged polymers is reviewed by Dobrynin, Colby, and Rubinstein (4).

A number of synthetic strategies may be employed to increase macromolecular coil size (HDV) for water-soluble polymers. Monomers with water-soluble moieties may be polymerized to high molecular weight. Effective bond lengths along the backbone may be increased by introducing chain stiffening-elements. These include covalent rings (polysaccharides), charge–charge repulsions (polyelectrolytes), and helical segments (nucleic acids and proteins). The shape of the solvated coil is determined by placement of charged groups, hydrophobic moieties, hydrogen bonds, chiral centers, or restrictive rings along the molecular backbone. The native shapes of globular proteins, for example, are a result of water-induced organization of strategically placed hydrophilic and hydrophobic moieties.

Polymers dissolved in water can have structures (Fig. 3) ranging from random coils to microheterogeneous polymeric vesicles. Solution behaviors of the various types are quite diverse. Water-soluble random and extended coil polymers are

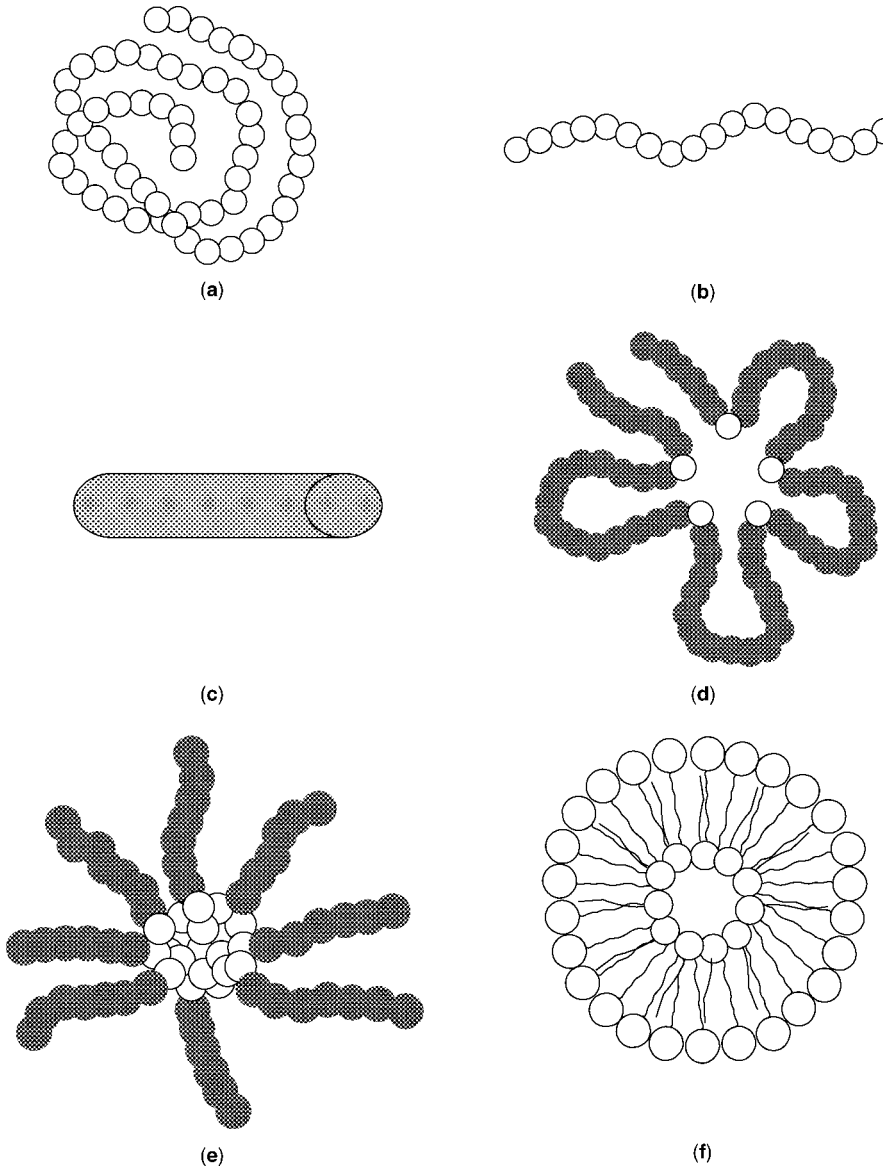

Fig. 3. Structural dependence of molecular shapes of copolymers in aqueous media. (**a**) Hydrated random coil; (**b**) hydrated extended coil; (**c**) rod-like polymer; (**d**) unimeric micelle; (**e**) multimeric micelle; (**f**) vesicle.

often used for rheology control in various applications. Extended rods in aqueous solution may exhibit lyotropic liquid crystalline behavior. Amphiphilic molecules such as hypercoils, polymeric micelles, and vesicles are used in formulation, drug delivery, and phase-transfer catalysis.

Role of Water in Solvation/Phase Behavior. Water plays an extremely important role in determining the properties and ultimate utility of polymers in solution. Solvation of polymer chains may involve simple interaction of ionic, polar,

or hydrogen-bonded hydrophilic segments of linear chains with water (Figs. 3**a** and 3**b**) or more complex solvation of amphiphilic structures (Figs. 3**d**, 3**e**, and 3**f**). For amphiphilic polymers, water structure around the hydrophobic portion of the chain is thought to be more ordered than in the bulk whereas hydrophilic portions disorder water structure. Amphiphilic macromolecules, including stimuli-responsive copolymers, have been studied in great detail and are the subject of several books and reviews (5–7). Although the precise nature of water structuring is the subject of continuing debate and extensive research, polymer solubility and phase behavior is rationalized in terms of entropy- or enthalpy-dominated events.

Some polymers such as poly(acrylic acid) or polyacrylamide precipitate from aqueous solutions when cooled (normal solubility behavior) whereas others such as poly(ethylene oxide), poly(propylene oxide), or poly(methacrylic acid) phase separate when heated (inverse solubility behavior). Solution turbidimetry is often used to obtain plots of phase-separation temperatures termed *cloud point* vs concentration for fixed solvent conditions. Changes in ionic strength, molecular weight, and addition of co-solvents or structure breakers affect the shapes of phase behavior curves. The important conclusion of such studies is that the total free energy of the polymer and water must be considered to predict phase behavior. The structure and dynamics of water surrounding polynucleotides, proteins, polysaccharides, and lipids are also major determinants of biological activity (8–10).

Viscosity and Rheology. Viscosity yields important information as to the disposition of the polymer chains in solution and is routinely used to evaluate polymers for particular applications. Dilute solution measurements can yield intrinsic viscosity $[\eta]$, which is a direct indication of the hydrodynamic volume of an isolated polymer chain. This fundamental parameter is related to molecular weight M through the Mark–Houwink–Sakurada (MHS) relationship (eq. 1):

$$[\eta] = KM^a \tag{1}$$

The parameters K and a are characteristics of a polymer chain under specific conditions of solvency and temperature. Values of a can be related to chain extension in dilute solution.

Flexible polyelectrolytes generally are more extended than nonionic polymers owing to charge–charge repulsions along the chain, particularly at low ionic strength. Estimates of $[\eta]$ under such conditions are made by the Fuoss (11) relationship (eq. 2) rather than the traditional Huggins relationship (eq. 3). η_{sp} is the specific viscosity, c is polymer concentration, B and k are characteristic constants. Alternatively, small-molecule electrolytes may be added in sufficient quantity to suppress the charge–charge interactions and equation 3 may then be used.

$$\frac{\eta_{sp}}{c} = [\eta]/(1 + B\sqrt{c}) \tag{2}$$

$$\frac{\eta_{sp}}{c} = [\eta] + kc \tag{3}$$

The MHS relationship (eq. 1) is often used in conjunction with experimentally determined values of molecular weight and intrinsic viscosity to determine chain

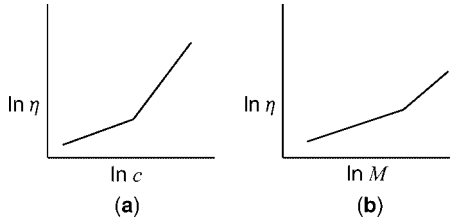

Fig. 4. Relationship between apparent viscosity and (**a**) concentration at constant molecular weight; (**b**) molecular weight at constant concentration.

stiffness indicated by values of a. Values can range from 0.5 for random coils in theta conditions to nearly 2.0 for extended rods.

In semidilute and concentrated solutions, polymer molecules are no longer isolated from one another. Chain–chain interactions at and above a critical concentration c^*, often termed the *overlap concentration*, lead to increased values of apparent viscosity η. Apparent viscosity can be related to concentration and molecular weight by equation 4, in which b and d are scaling constants.

$$\eta \propto c^b M^d \tag{4}$$

Usually plots of ln η vs ln c at constant molecular weight (Fig. 4**a**) or ln η vs ln M at constant concentration (Fig. 4**b**) are used to measure entanglement onset. Measurements are made at constant shear rate, temperature, and solvent conditions.

Rheological characteristics of aqueous solutions are dictated by molecular structure, solvation, and by inter- and intrachain associations. In many cases, segmental interactions must be accounted for in more rigorous terms than simple statistical encounters. Enthalpic interactions or entropically driven hydrophobic associations must be considered.

Rheological behavior is dependent on polymer type and can be clearly illustrated, providing appropriate interactive parameters of polymer concentration, ionic strength, pH, shear rate or shear stress, temperature, and time are taken into account. Representative plots are shown in Figure 5 for major behavioral patterns. Figure 5**a** illustrates the shear thickening (dilatant), Newtonian, and shear thinning (pseudoplastic) behavior. Figure 5**b** represents time dependence on viscosity for rheopetic and thixotropic polymers. Figure 5**c** illustrates the viscosity-concentration dependence in water for a polyelectrolyte and nonionic polymer in dilute solution.

Synthetic Methods. Water-soluble copolymers are prepared by step-growth or chain-growth mechanisms. Linear or branched systems may be formed from single monomers or from multiple monomers. Distribution of monomers, along the backbone or side chain, can be controlled in a number of ways. In nearly all cases, sequence selection is obtained by carefully controlling monomer reactivity, concentration, addition order, and reaction conditions. Most chain-growth, water-soluble polymers are prepared by classical free radical polymerization techniques.

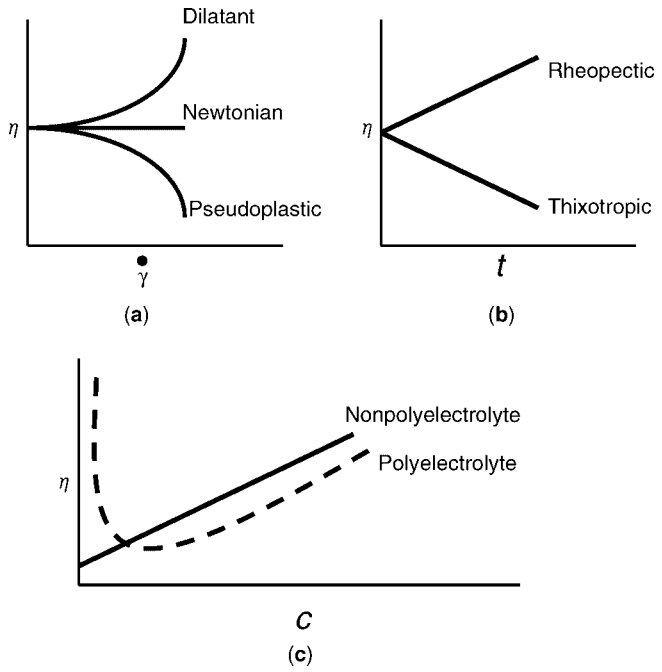

Fig. 5. Rheological characteristics of water-soluble polymers. All variables other than those on the axes are held constant. (**a**) Viscosity vs shear rate; (**b**) viscosity vs time; (**c**) viscosity vs concentrations below c^*.

Step-growth condensation reactions may be carried out in organic solvents, interfacially, in bulk, microheterogeneously, or on a solid support. Active esters are often employed in solution methods at relatively low temperatures to yield water-soluble polyesters or polyamides. Synthetic polypeptides, polynucleotides, and polysaccharides are commonly made by sequential addition of protected monomer units onto polymer supports.

Major commercial synthetic water-soluble polymers are made by chain-growth polymerization of functionalized alkenes, carbonyl monomers, or strained ring compounds, as illustrated in Figure 6. These may be initiated utilizing free

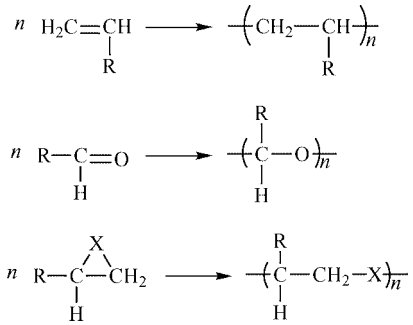

Fig. 6. Synthetic pathways to common water-soluble chain growth polymers.

radical, cationic, anionic or coordinated cationic initiators, depending on monomer structure. Of particular *commercial* interest are syntheses of water-soluble polymers in solutions, dispersions, suspensions, or emulsions. In cases where hydrophobic monomers are to be incorporated with hydrophilic species, microemulsions, or micellar polymerization methodologies are required.

During the last 10–20 years significant advances have occurred in polymer synthesis. Noteworthy is the development of less demanding living polymerization techniques, such as group transfer polymerization (GTP) (12,13) and oxyanionic polymerization (14,15). Most recently, rapid technological advances have been made in the so-called controlled/living free radical polymerizations

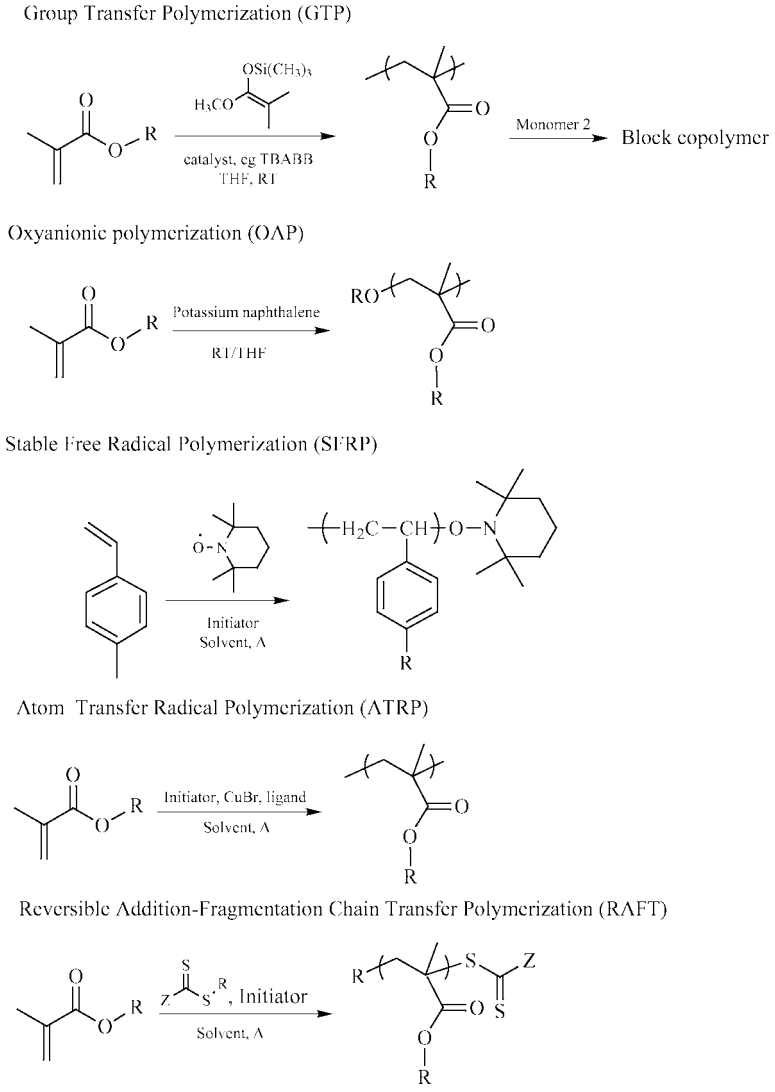

Fig. 7. Controlled or controlled/living polymerization techniques potentially applicable to synthesis of water-soluble or amphiphilic copolymers.

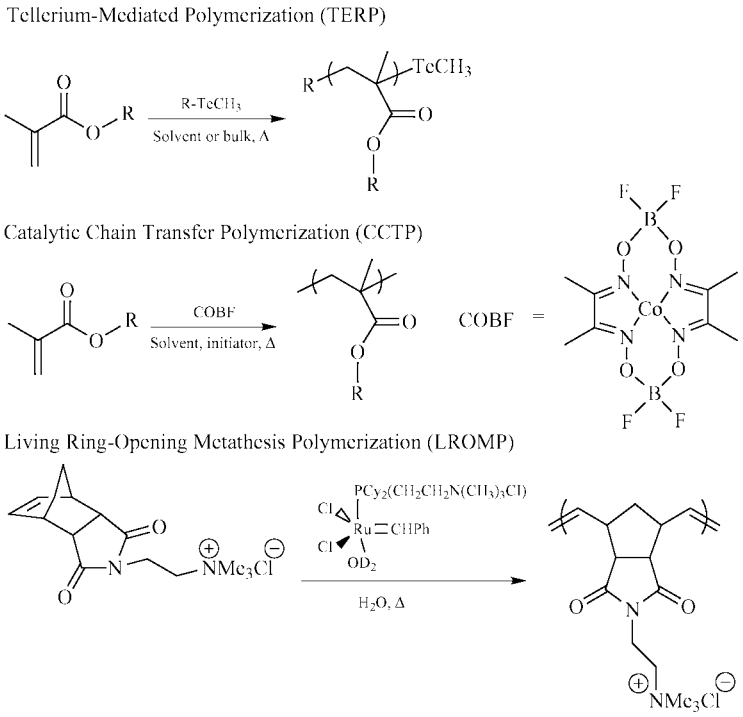

Fig. 7. (Continued)

(CLRP), such as stable free radical polymerization (SFRP) (16,17), atom transfer radical polymerization (ATRP) (18–23), reversible addition-fragmentation chain transfer (RAFT) polymerization (24–27), and tellerium-mediated radical polymerization (TERP) (28–31). Additionally, catalytic chain transfer polymerization (CCTP) (32,33) and living ring-opening metathesis polymerization (LROMP) (34–37) have also been developed. All of these techniques, to some greater or lesser degree, have been employed for the synthesis of novel water-soluble (co)polymers (Fig. 7) with much of the research having been conducted in academic research laboratories (see ANIONIC POLYMERIZATION; LIVING RADICAL POLYMERIZATION).

Whereas each of these techniques has its merits, many have severe limitations either with respect to monomer choice or reaction conditions. The most versatile of the above techniques are arguably the CLRP techniques and have received the greatest attention, to date, with respect to the preparation of novel water-soluble (co)polymers (38,39). These techniques generally exhibit the versatility associated with conventional free radical polymerizations but simultaneously bear many of the characteristics associated with living polymerizations. They are highly tolerant of functional substituents with virtually all vinylic monomers being polymerized by one, or more, of the techniques; additionally, polymerization may be conducted under a wide range of conditions (bulk, solution, dispersion, emulsion etc). Also, molecular weights can be tuned via the monomer/initiator ratio; (co)polymers with narrow molecular weight distributions are typically

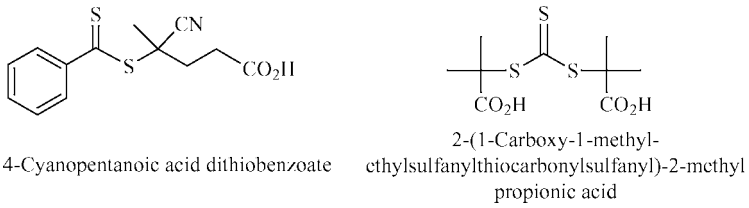

4-Cyanopentanoic acid dithiobenzoate

2-(1-Carboxy-1-methyl-ethylsulfanylthiocarbonylsulfanyl)-2-methyl propionic acid

Fig. 8. Structures of chain transfer agents CTP and CTSP.

produced and materials with complex architectures, such as blocks or stars, can be obtained (40,41). With specific reference to the preparation of water-soluble polymers, ATRP and RAFT have been the most widely examined, with RAFT being the most versatile, at least with respect to monomer choice. For example, certain species such charged (meth)acrylamido monomers can, at present, *only* be polymerized in a controlled fashion by RAFT (42–45). Key to control in RAFT polymerizations is an appropriate thiocarbonylthio compound, called a chain transfer agent (CTA). While many have proven to be effective, such as the dithioesters, trithiocarbonates, xanthates, and dithiocarbamates (38,46,47), to conduct the polymerizations directly in water requires the use of a suitable water-soluble CTA. Of those reported to date, 4-cyanopentanoic acid dithiobenzoate (CTP) has proven to be the most generally effective (46–48), with others such as 2-(1-carboxy-1-methylethylsulfanylthiocarbonylsulfanyl)-2-methylpropionic acid (CTSP) (Fig. 8) also proving particularly effective for acrylamido and methacrylamido monomers (49,50).

Naturally Occurring Polymers

A large number of water-soluble polymers are derived from biological sources. Termed *biopolymers*, this class includes polynucleotides (qv), polypeptides and polysaccharides (qv). Because these polymers perform special biological functions, they have specific microstructures and are often perfectly monodisperse. In the following section the general structural features of major biopolymer types will be reviewed as related to water solubility.

Polynucleotides.

Structure. Nucleic acids (Fig. 9) are biopolymers that carry genetic information involved in the processes of replication and protein synthesis. The primary structural units of the nucleic acids, the mononucleotides, are composed of a 5-carbon cyclic sugar with a phosphate ester at the C-5 carbon. A heterocyclic amine base (purine or pyrimidine) is attached at C-1. RNA and DNA are terpolymers with sugar phosphate backbones (3′ and 5′ position) and pendent bases on the 1′ position. Deoxyribonucleic acids (DNAs) contain the deoxyribose sugar (no hydroxyl group at the 2′ position on the sugar ring). The usual bases substituted at the 1′ position are adenine (A), guanine (G), thymine (T), and cytosine (C). Ribonucleic acids contain a ribose sugar and the principal bases A, G, C, and uracil (U).

Studies of the structure of DNA by a large number of investigators led to the proposal by Watson and Crick (51) of the classic DNA double helix. Major

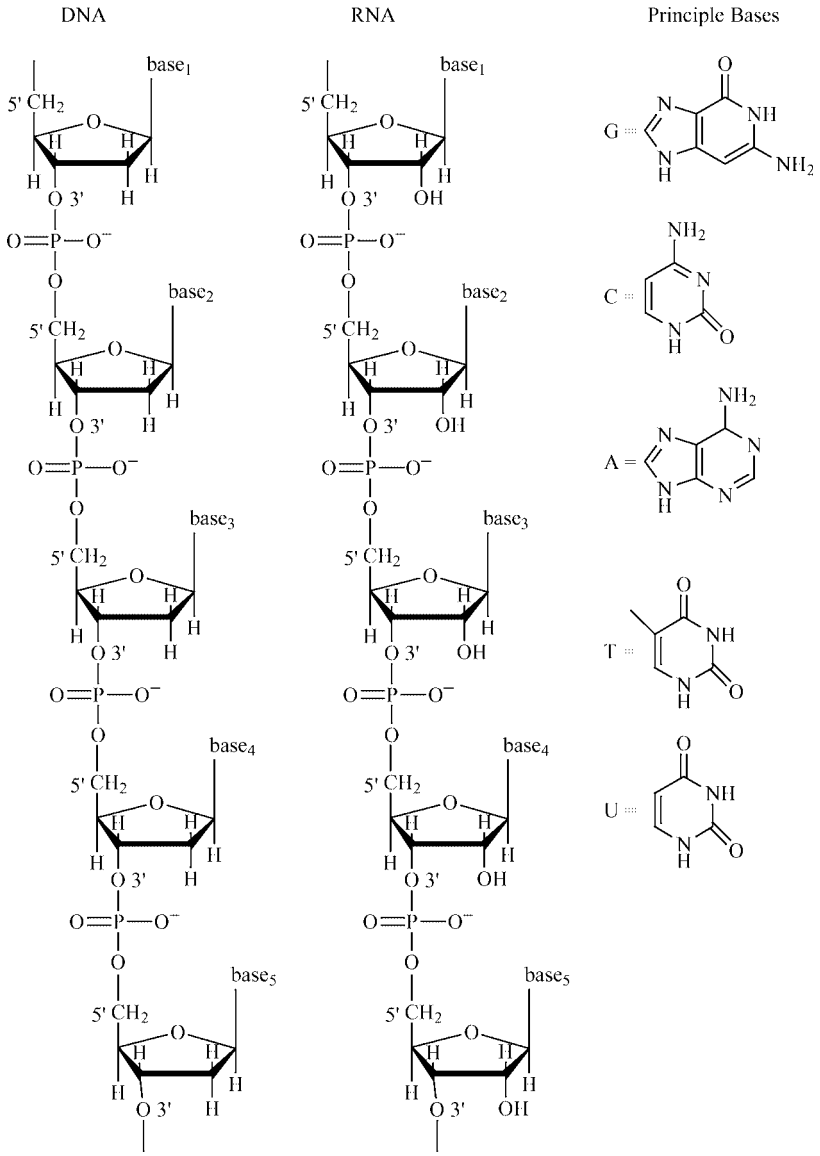

Fig. 9. Structural representations of DNA and RNA; principal bases present in nucleic acid. U,T, and C are the pyrimidines; A and G are the purines.

contributions as to base content and of X-ray structure were made by the groups of Chargaff (52) and Wilkins and co-workers (53). This proposal not only allowed explanation of DNA stability but also provided a framework for postulation of template polymerization during the replication and transcription processes.

The template synthetic process allows organization of the DNA helix into an assembly having two antiparallel strands of DNA (Fig. 10). The pendent bases on the strands are paired in such a manner that A is always paired with T and G with C. The strong hydrogen bonding of the complimentary pairs in hydrophobic

Fig. 10. DNA double-stranded helix (54).

regions orients the hydrophilic-charged phosphate groups outwardly. One negative charge per phosphate unit gives the DNA polyanionic character. The balance of hydrophilic and hydrophobic forces and the presence of divalent ions such as Mg^{2+} are also responsible for chain stability under physiological conditions. Three conformational variations of the double helix have been confirmed by X-ray diffraction—the A, B, and Z forms. Conformational variation, location of certain base-paired sequences, and specific modification (methylation for example) can lead to supercoiling, branching, and direct binding to other polynucleotides or to specific proteins. Such structural organization has major implications in gene regulation (transcription, silencing, etc).

The molecular weights of DNA, depending on the source, can be extremely large. For example, the recently sequenced human genome has been reported to have over 27,000 genes and 3 billion base pairs (55). By contrast, a simple bacterium such as *Escherichia coli* has 5 million (54) chromosomal base pairs. In addition, the latter contains cyclic DNA, called plasmids, which contain from 1000 to 10,000 base pairs. Recombinant DNA technology is routinely utilized to insert synthetic genes or genes from other species into such plasmids. The resultant recombinant DNA segments then serve as templates for synthesis of specific proteins with pharmacological, agricultural, or materials applications.

Ribonucleic acids are synthesized from the DNA template through transcription. The mononucleotides contain ribose. Unlike DNAs, RNAs are single stranded, although twisting may occur in a complementary fashion matching base pairs. RNAs are much lower in molecular weight than DNAs. The three major types—messenger RNA (mRNA), transfer RNA (tRNA), and ribosomal RNA (rRNA)—are involved in a multistep process of protein synthesis (56,57).

Beyond their well-established roles in protein synthesis, RNAs termed *ribozymes* have been shown to catalyze a number of biochemical reactions. Significantly, short hairpin sequences of RNA can hybridize with DNA to suppress (silence) gene expression (58). Alternatively, some of these short RNA sequences bind in a complementary fashion to mRNA resulting in destruction of the latter and preventing protein translation from that gene segment (58).

Synthesis. Recently, nucleic acids have been synthesized from mononucleotides, some with altered or substituted bases. Synthetic methods, along with nucleic acid sequencing methods, have allowed rapid advancement in identifying gene sequences responsible for specific protein synthesis. Kornberg and coworkers first prepared synthetic DNAs polymerized from mononucleotides using isolated enzymes, DNA polymerases (59). Likewise, RNA polymerases have been found for synthesis of oligomeric RNAs (60). DNA also can be made from RNA using reverse transcriptase enzymes. The resulting complementary DNA can be greatly amplified using the polymerase chain reaction process (PCR) (61). These are readily characterized and in many instances introduced into plasmids or other vectors for recombinant protein synthesis. Automated synthesis of single-stranded polynucleotides can be accomplished utilizing sequential protection/deprotection chemistry (62). Although entirely synthetic methods are quite slow compared to biosynthesis, designed oligonucleotides for targeting or diagnostic purposes (including micro arrays with variable sequences for rapid screening) can be readily produced. Post-reaction chemistry including ligation and PCR can then be utilized to produce significant quantities of desired oligonucleotides.

Polypeptides and Proteins. Most polypeptides and proteins are water-soluble or water-swellable. Enzymes are proteins that catalyze all chemical reactions of biological origin. Enzyme functions include oxygen transport, muscle movement, nerve response, nutrient digestion and storage, hormonal regulation, gene expression, and protein synthesis (63).

Structure. Despite the large number of functions, all proteins are similar with repeating structures along the backbone chosen from 20 amino acid monomers (Fig. 11). These polymers, the structures of which are assembled from a template coded by mRNA, are monodisperse. Each protein has a unique sequence and molecular weight. The 20 amino acids, capable of appearing in various microstructural combinations, sequence lengths, and total molecular lengths, allow assembly of a nearly unlimited number of distinct proteins with specific physical properties and behavioral characteristics.

Primary structure (covalent bond lengths and bond angles) is determined by the microstructure of the amino acid repeating units along the chain. Numerous procedures, including sequential degradation, gel electrophoresis, dye binding, and immunoassays, have been used to determine sequences (63).

Secondary structure of proteins is determined by configuration and conformation along the backbone of the polymer. The resistance to bond rotation of the C—N bond of the peptide unit, the configuration about the chiral carbon, and conformational restrictions to rotation by short-range charge–charge interactions or intramolecular hydrogen bonding play major roles in secondary structure.

The three-dimensional structure, or tertiary structure, depends strongly on primary and secondary structure with the added elements of long-range intramolecular hydrogen bonding, polar and ionic effects, and chain solvation. An

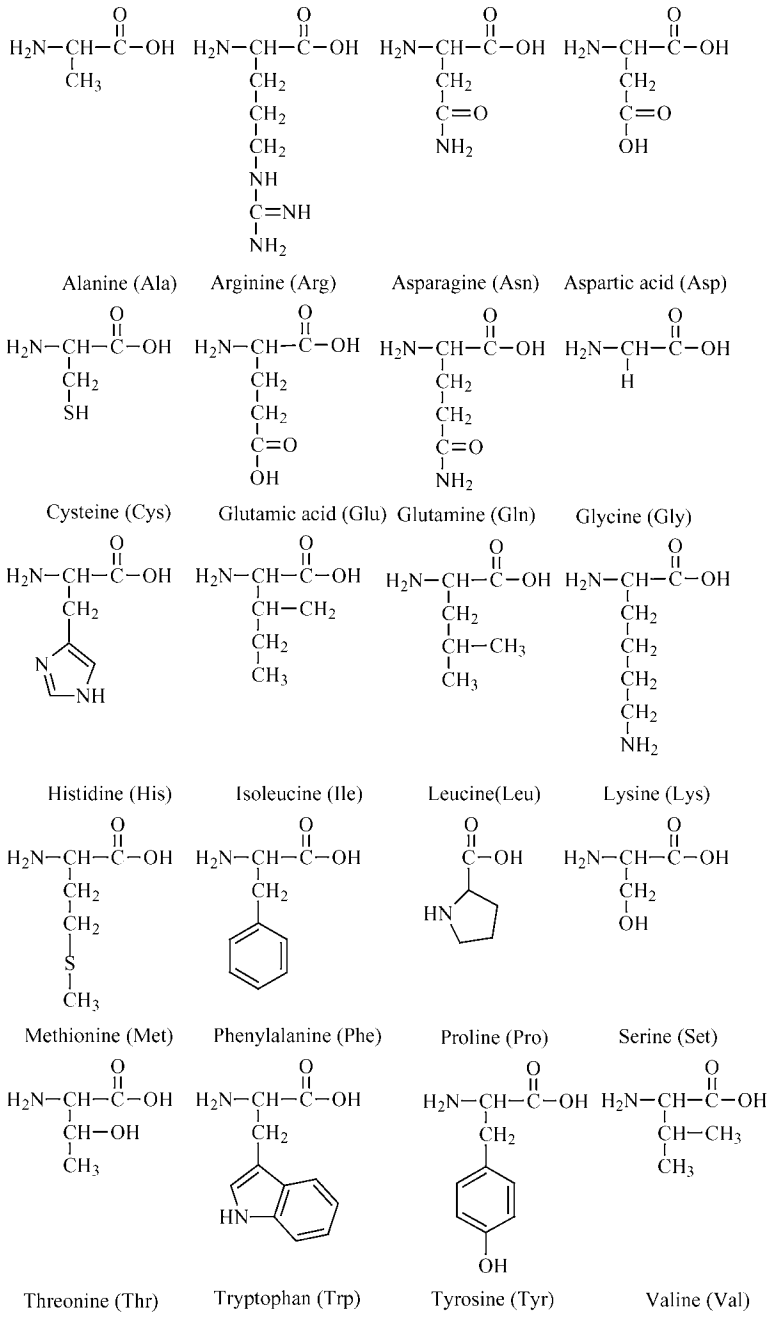

Fig. 11. Chemical structures of the 20 amino acids.

example of the three-dimensional structure of myoglobin is shown in Figure 12. The compact structure illustrates the hydrophobic interior, helical features from intramolecular hydrogen bonding and the L-amino acids, and polar external groups for hydration (see PROTEIN FOLDING).

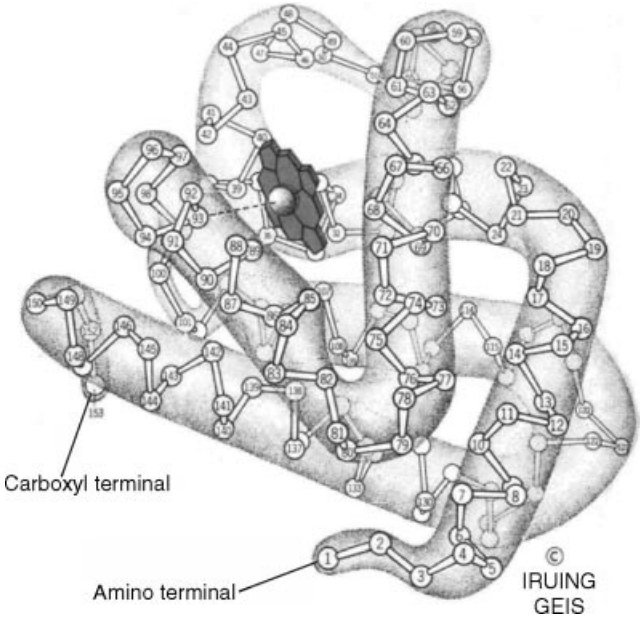

Fig. 12. Tertiary structure of myoglobin (64).

Many proteins exist in subunits of a composite structure. The organization of these subunits is termed the *quaternary structure* and is particularly important in enzyme-mediated reactions. The tertiary and quaternary structure of native protein in water can be disrupted by addition of electrolytes, alkali solutions, urea, or detergents, and by increasing temperature. The properties change markedly; eg, enzyme activity is often lost. In most cases this denaturation is not reversible. The solubilities of proteins vary considerably based on composition and conditions of ionic strength, pH, and concentration. Those with the highest density of polar groups or electrolyte character are most soluble. Therefore, solubility in water is lowest at the isoelectric point and increases with increasing basicity or acidity. A review of enzyme activity as related to protein structure is given by Fersht (65).

Protein Synthesis. Protein biosynthesis is complex, involving more than 300 macromolecules (63). Five stages can be identified involving (*1*) activation of amino acid monomers and transfer to ribosomes, (*2*) initiation of polymerization, (*3*) propagation, (*4*) termination and release, and (*5*) folding and processing. Ordering of the monomers is dictated by operation of the triplet code in which a sequence of three consecutive nucleotide units on mRNA positions a specific amino acid for polymerization.

Synthetic polypeptides can be made by sequential addition of protected amino acids onto a solid support. This procedure, pioneered by Merrifield (66,67) has been used to prepare hundreds of peptides of varying sizes and functions. A review of the technique and recent modifications are found in Reference 68.

The study of genes responsible for identifiable biological products and processes (genomics) (69) and the more ambitious study of translated proteins, their isoforms, modifications and interactions (proteomics) (70) has advanced at an incredibly fast pace during the last five years. In a very short time a number of genes

have been targeted for recombinant expression in a variety of hosts to produce a wide range of new drugs and to develop new diagnostic markers.

Commercial Use. In addition to the rapid growth of genetically engineered enzymes and hormones for medical and agricultural applications, other water-soluble proteins are isolated from biological sources in a more traditional manner for commercial application. Enzymes are used as detergent additives, for hydrolyzing polysaccharides and proteins, to isomerize various glucose and sucrose precursors, for wine and beer making, for leather tanning, and for mineral recovery. Support-bound enzymes are becoming commercially significant for large-scale substrate conversion.

Polysaccharides

Water-soluble polysaccharides are a diverse class of biological macromolecules with a wide range of structural and behavioral characteristics. More than 100 sugars and sugar derivatives comprise the monomers available for polysaccharide synthesis (63). Covalent linkages between repeating units may occur at different ring positions; linear and branched structures with single or multiple monomers may be formed (see POLYSACCHARIDES).

Industrial polysaccharides have traditionally been extracted from renewable resources in the plant and animal kingdom. Examples include starch and gums from plant seeds, pectin from fruits, and algin and carrageenan from algae. Recently, microbial sources have produced commercially useful polysaccharides such as dextran, curdlan, pullulan, xanthan, and pharmacologically active oligosaccharides.

Polysaccharides are cyclolinear or branched polymers formed by enzyme-directed step-growth condensation reactions of various activated sugar molecules (71). Some common monomer units are shown in Figure 13; other units include

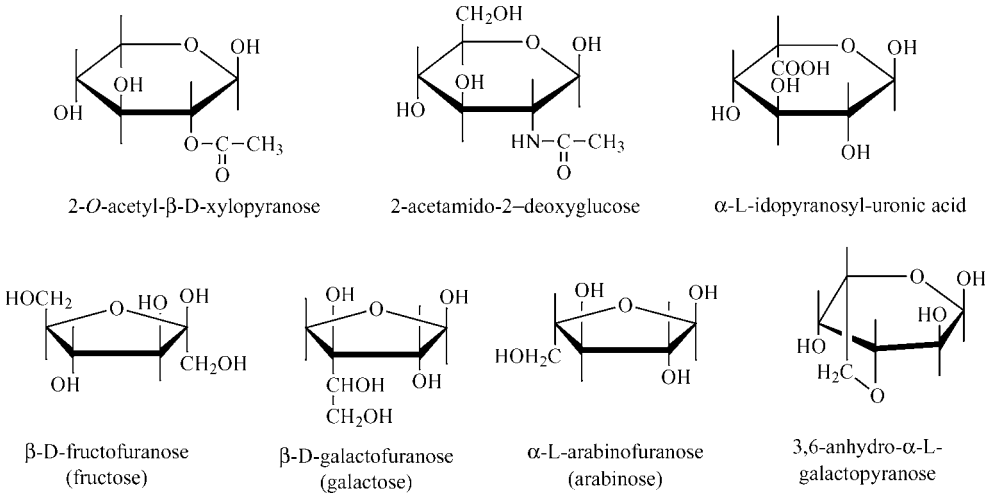

Fig. 13. Common structural units in naturally occurring polysaccharides (71).

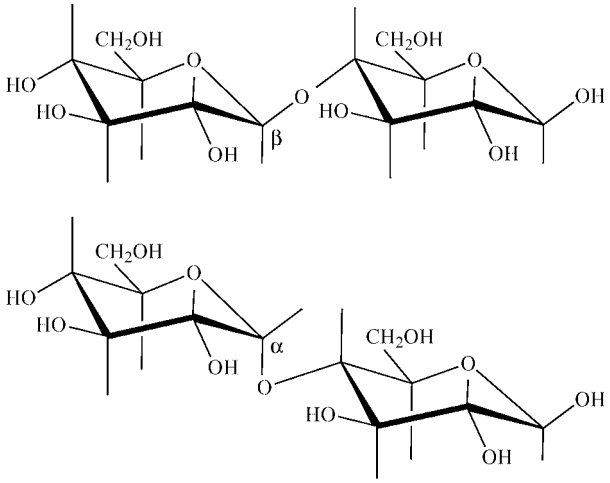

Fig. 14. Dimerization of glucopyranose units to yield α and β structures.

glycerol and other polyhydroxyalcohols, phosphate, sulfate, malonate, and pyruvate.

Aqueous solution properties, including solubility, phase behavior, and viscosity, are highly dependent on the macroscopic nature (linear, branched) of the chain as well as the chemical microstructure (polar characteristics, sequencing) of the repeating units. As with proteins, the presence of acidic or basic functionality causes pH, electrolyte, and temperature-dependent behavior. Degrees of polymerization may vary from 30 to 1×10^5. Of primary importance in the solution behavior of water-soluble polysaccharides are the configurations of asymmetric carbon atoms in the cyclic monomers and the ring conformations of the resulting covalent backbone units.

Dimerization of glycopyranose (Fig. 14) by condensation of the hydroxyl group at C-1 on one ring with C-4 on the other can lead to two isomers, depending on whether the reaction is equatorial–equatorial or axial-equatorial. The former linkage is designated β, the latter, α. Polymers formed by successive α-1 $\rightarrow$4 linkages, eg, amylose, have markedly different properties than polymers formed by successive β-1$\rightarrow$4 linkages, eg, cellulose.

Polysaccharides based on glucopyranose occur with backbones through carbons 1$\rightarrow$2, 1$\rightarrow$3, 1$\rightarrow$4, and 1$\rightarrow$6. The less-ordered structures are more water-soluble in general, with the α-1$\rightarrow$3 and the β-1$\rightarrow$6 forms exhibiting highest aqueous solubility; β structures often form strong inter- or intramolecular hydrogen bonds, making solubilization difficult.

Branched structures, especially for α linked polysaccharides, enhance solubility. Heterogeneity in types of repeating units, backbone linkages, and polar or charged functionality also imparts greater solubility. Excellent reviews of the effects of the structural conformation of monosaccharides are found in References 71 and 72.

Water-soluble polysaccharides can be classified according to structure and commercial applications. Classes include storage polysaccharides, pectins, plant gums, seed and bark mucilage, algal polysaccharides, bacterial and fungal

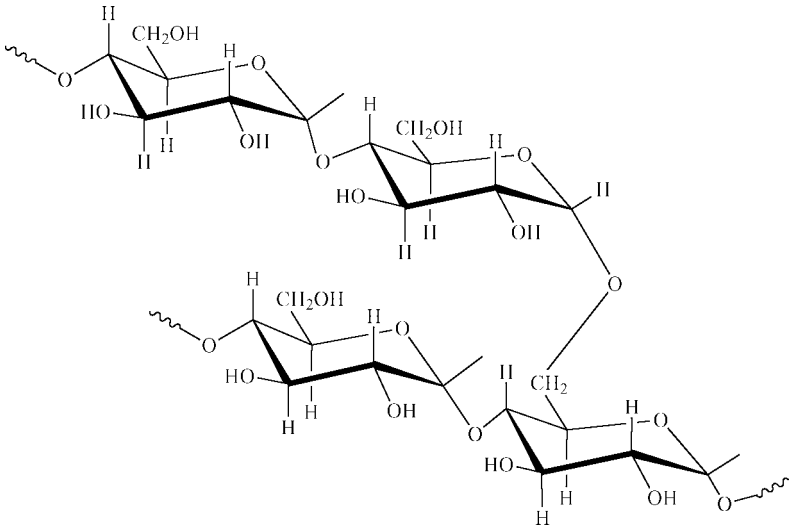

Fig. 15. Structure of amylopectin (73).

polysaccharides, mucopolysaccharides, and synthetically modified polysaccharides. For more detailed descriptions see References 72–75.

Storage Polysaccharides. *Starch and Starch Derivatives*. Amylose and amlyopectin are the major components of starch granules found in food reserves of all green plants. Commercial starch is obtained from sources such as corn, sorghum, rice, wheat, and potatoes. The compositions of the amylose and amylopectin vary with source.

Amylose is the linear polysaccharide of α-1$\rightarrow$4-D-glucopyranose having a molecular weight of $1.6 \times 10^5 - 2.6 \times 10^6$. Amylose is not water-soluble in an unmodified state but can be dispersed in water. In the solid state it is reported to exist as a left-hand six-fold helix; in solution it behaves like an extended helix (74). Shearing and heating of starch cause hydration and swelling termed *germination*. Gradually the amylose in this dispersion precipitates through association in a process called *retrogradation*.

Amylopectin (Fig. 15), the water-soluble portion of starch, is an α-1$\rightarrow$4-D-linked glucopyranose with α-1$\rightarrow$6-D-branches. Amylopectin is polydisperse with a molecular weight of $5 \times 10^7 - 4 \times 10^8$.

A number of starch derivatives (73,74) have been prepared in order to control solubility, viscosity, and phase behavior over a temperature range or under conditions of shear and added electrolytes. Major modifications include lowering molecular weight enzymatically or chemically, oxidation, forming derivatives, and cross-linking. Derivatives include starch esters, phosphates, sulfates, and ethers. Cationic, anionic, and amphoteric starches have been prepared as well as starch–graft copolymers, some with super absorbent properties.

Starch (qv) and starch derivatives have a number of applications in the food industry as viscosifiers, gelatinizers, fillers, and paste formers; in the textile and paper industries for coatings, sizing agents, rheology modifiers, and pigment binders; and in the medical area as surgical powders, absorbents, adhesives, and in pharmaceuticals.

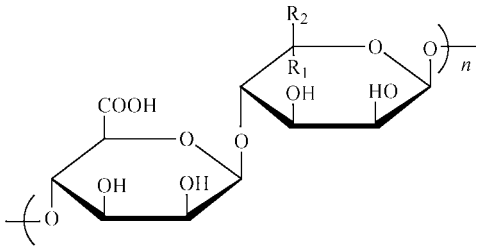

Fig. 16. Structure of β-D-mannuronic acid.

Glycogen. Glycogen is the storage polysaccharide in animals and is found in highest concentration in the liver and muscle tissues. The backbone of glycogen is α-1→4-D-linked glucopyranose units with large numbers of α-1→6-D-branch points.

Glucans. Algae form two types of storage polysaccharides. Starch type algal polysaccharides are α-D-glucans similar to those found in land plants, except they contain a small number of α-1→3-D-linkages and are of lower molecular weight (76). Laminaran is the main carbohydrate food reserve of several green seaweeds and is a β-1→3-D-linked D-glucan with β-1→6-D-branches. Other sources include fungi, yeast, flagellates, and diatoms.

Laminaran has two forms distinguished by solubility in cold water. Differences are related to the degree of 1→6 branching. Both are soluble in hot water and have molecular weights from 3500 to 5300. Laminaran has been used for surgical dusting powder and has been reported to have antitumor activity.

Algal Polysaccharide. *Alginic Acid*. Alginic acid represents the generic group of polymers (74) composed of D-mannuronic acid and L-guluronic acid extracted from brown algae (77). Alginic acid is not soluble in pure water, but easily dissolves in aqueous solutions of alkali metal hydroxides or carbonates. The structure (77) of alginic acid shown in Figure 16 is complicated with three types of segments: poly(β-1→4-D-mannuronic acid); poly(α-1→4-L-gluronic acid); and those in alternating patterns. The ionic forms of algins are polyelectrolytes with extended structures. The precise properties are determined by the structural disposition of these segments. Alginates are used as thickeners and stabilizers in the food industry, in pharmaceutical, cosmetic, and coating formulations, and as flocculants.

Sulfated Derivatives. Sulfated algal polysaccharides (78) are a class of heteropolymers with alternating α-1→3-D- and β-1→3-D- (carrageenan and furcellaran) or alternating α-1→3-L- and β-1→3-D- galactans (agar). Conformational differences have been shown between the nongelling λ carregeenan and gel-forming κ and ι forms (Fig. 17) (71). Molecular weights range from 1×10^5 to 1×10^6.

Carrageenan has diverse industrial applications including use in toothpaste, ice cream, chocolate milk, jellies, puddings, pet foods, pharmaceutical and industrial suspensions, antiulcer treatments, shampoos, creams, lotions, and oil/water and water/oil emulsions. Carrageenan reacts with denatured proteins and has been shown to exhibit properties similar to those of the animal mucopolysaccharides, such as anticoagulant activity and induction of growth of new connective tissue.

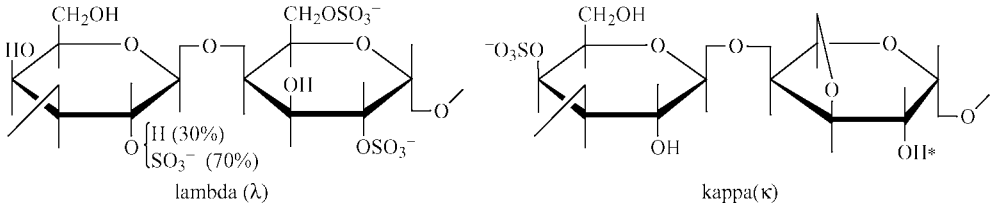

Fig. 17. λ and κ carrageenan. In ι carrageenan, OSO_3^- replaces OH^* in the κ-form (72).

Pectins. Pectins (pectic and pectinic acids or their derivatives) are gel-forming water-soluble polysaccharides found in the primary cell walls and intercellular layers in land plants. They are found in abundance in apples, sugar beets, and the rinds of citrus fruits. Pectic acids are poly(α-D-galactopyranoslyuronic acids) with varying degrees of neutralization. Pectinic acids are also galactouronglycans but with significant quantities of methyl ester groups. Pectins are soluble in water and exhibit pseudoplastic behavior. When heated at appropriate pH, in the presence of divalent electrolytes and sugars, they form spreadable gels (74). For this reason pectins are used for making jams and jellies.

Plant Gums. Plant gums or exudate gums are formed spontaneously at sites of injury to the plant. The exudate is a viscous fluid consisting of complex, highly branched polysaccharides with residues of hexuronic acid and two or more neutral sugars. Many plant gums are used commercially as thickening agents or emulsion stabilizers. Commercially important are karaya gum, gum tragacanth, gum Arabic, and gum ghatti (76).

Seed Mucilages. Guaran is a purified polysaccharide from the guar plant seed. It is a linear chain of β-1→4-linked D-mannopyranosyl units onto which is linked an α-1→6-D-galactopyranosyl unit (Fig. 18). Molecular weights are estimated to be 2.2×10^5 (79). Guaran forms high viscosity, pseudoplastic solutions at low concentrations, is nonionic, and is little affected by electrolyte addition or pH changes. Guar easily forms gels with transition metal elements or borate ions and is therefore useful in drilling, cementing, and fracturing in oil-filed applications. It has also been used as a thickener and stabilizer in the manufacture of ice cream, cheese, pet foods, and deodorant gels.

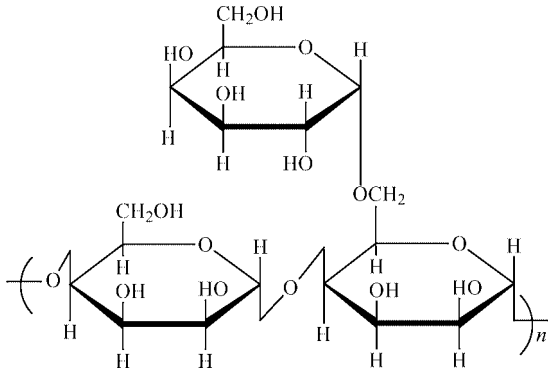

Fig. 18. Structure of guaran.

Extracellular Polysaccharides. One of the most important extracellular bacterial polysaccharides is dextran. Dextrans are high molecular weight α-1$\rightarrow$6-D-glucopyranose polymers with varying proportions of α-1$\rightarrow$4 and α-1$\rightarrow$3 branch linkages. Dextran is produced from sucrose by a number of bacteria from the family *Lactobacillaceae*. Dextran has a variety of commercial applications, including use as a plasma substitute, an anticoagulant, or in studies of cells, viruses, and proteins. Fractionated commercial dextrans are used as standards in various studies of the properties of water-soluble polymers. Dextran–graft copolymers have utility in viscosifications, superabsorbancy, and oil-field applications (80).

Bacterial and Fungal Polysaccharides. Microbes generate a large number of polysaccharides, many of which are not produced by the higher plants or animals. A large number of microbial polysaccharides are used in the food, cosmetic, and pharmaceutical industries. Particular polysaccharides, when isolated from the dried bacteria, have been shown to induce an immune response and generate antibodies in organisms exposed to them. Several of these capsular polysaccharides have been used to develop vaccines for various bacterial infections such as meningitis and typhoid fever (81).

Xanthan (qv) is an extracellular bacterial polysaccharide produced by *Xanthomonas campestris*. Xanthan is a branched polysaccharide with β-1$\rightarrow$4-D-glucopyranose units along the backbone. On every other unit the oxygen at C-3 is substituted with a trisaccharide unit. Approximately half the β-D mannose units have a pyruvic acid group linked as an acetal derivative. Molecular weight has been estimated to be 2×10^6.

The solutions are viscous as low polymer concentrations, pseudoplastics, and insensitive to salt, temperature, and pH over a wide range. Much controversy remains as to changes in the tertiary structure with changing solution conditions. Single, double, and even triple helical structures have been proposed as well as quaternary structures from side-by-side double helix dimers (72,75,82).

Other water-soluble microbial polysaccharides include the anionic polysaccharides gellan from *Pseudomonas elodea* and bacterial alginate from *Pseudomonas aeruginosa*, and the neutral polysaccharides scleroglucan, curdlan, and pullulan (72,75,76,83).

Scleroglucan and schizophyllan (Fig. 19) are examples of fungal polysaccharides (72,75,81,84). Their structures are identical except for the distribution of

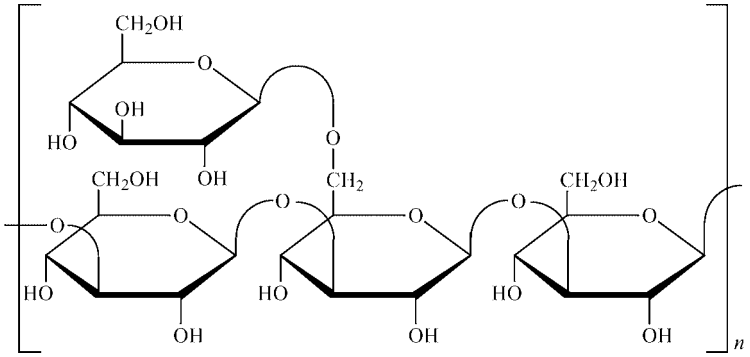

Fig. 19. Structures of scleroglucan and schizophyllan (75).

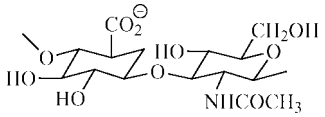

Fig. 20. Structure of hyaluronic acid.

side chains along the polymer backbone. Both are rod-like macromolecules forming triple helices in aqueous solutions. They are used industrially as viscosifiers and in polymer flooding for enhanced oil recovery. They have also been shown to exhibit specific biological activity against cancers and infections.

Mucopolysaccharides of Higher Animals. Mucopolysaccharides of higher animals are generally found in the connective tissues. They form highly viscous aqueous solutions that gel readily. These polysaccharides consist of amino sugars (D-glucuronic acid or L-iduronic acid) and may have *N*-acetyl, *O*-sulfate, or *N*-sulfate groups. Their functions include induction of calcification; control of metabolites, ions, and water; and healing of wounds. Several of these polymers are under study for medical, cosmetic, and personal care applications.

Hyaluronic acid (Fig. 20) is a regularly alternating copolymer of D-glucuronic acid and 2-acetamido-2-deoxy-D-glucose (77). It is found in most connective tissues, especially in umbilical cord, vitreous tissue, joint fluid, and skin. It is synthesized by fibroblasts in the mesenchymal tissue and also by bacteria. Hyaluronic acid binds a large amount of water in the interstitial spaces and is thought to be involved with the control of permeability and thus resistance of the tissues to infection. Hyaluronic acid is involved in the wound-healing process and is produced in large amounts at the site of the wound in the days following the injury. Hyaluronic acid also serves as a lubricant in the joints. Commercially, hyaluronic acid has application in postoperative healing in eye surgery.

Chondroitin and chondroitin sulfates (Fig. 21) are found in cartilage, skin, cornea, sclera, and bone. They show high viscosity and water retention and play a role in the connective tissue similar to that of hyaluronic acid. Sulfate groups contribute additional ion-binding capacity.

Dermatan sulfate (β-heparin) is found in the skin, lungs, tendons, spleen, brain, and heart. Dermatan sulfate exhibits high water retention and acts in a way similar to the chondroitin sulfates. It is also an anticoagulant.

Heparin (85) is found in the heart, liver, lung, spleen, muscle, kidney, and blood. It is synthesized in the mast cells and has a molecular weight of

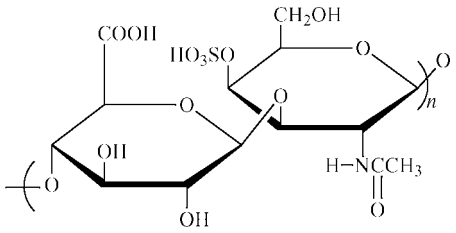

Fig. 21. Structure of chondroitin sulfate. In dermatan sulfate the —COOH group extends axially from the bottom face (77).

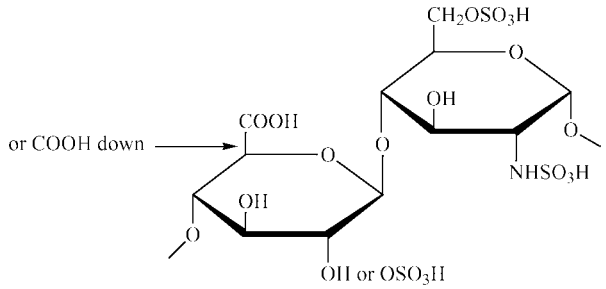

Fig. 22. Structure of heparin.

5000–25,000. Heparin is a mixture of polysaccharide chains of varying lengths and heterogeneity. It consists of 2-acetamido-2-deoxy-α-D-glucopyranosyl, α-D-glucopyranosyluronic acid, and L-iduronic acid residues containing various proportions of *O*-sulfate, *N*-sulfate, and *N*-acetyl groups (Fig. 22). It is an anticoagulant and antilipemic agent and is widely used in cardiovascular surgery and therapy.

Synthetically Modified Polysaccharides. Water solubility can be conferred on a number of naturally occurring polysaccharides by synthetic derivations producing charged or polar functionality. Two of nature's most abundant polysaccharides, cellulose and chitin, have been synthetically modified in a multitude of ways to produce polymers with significant commercial utilization (86,87).

Cellulose Derivatives. Cellulose (qv) is a β-1$\rightarrow$4-D-anhydroglucopyranose copolymer (Fig. 23) that serves as the major structural component of plants. When the cellulose molecule is extended, it is a flat ribbon with hydroxyl groups protruding laterally and is capable of forming both intra- and intermolecular hydrogen bonds. This form allows the strong interaction with neighboring chains that makes dissolution difficult. In fact, strongly interactive solvents are necessary for solubilization. Molecular weights range from 5×10^5 to 1.5×10^6, depending on the source. Water-soluble cellulose ethers can be prepared by nucleophilic substitution, ring opening, or Michael addition mechanisms (72).

Carboxymethylcellulose (CMC) is usually prepared by the reaction of cellulose with the sodium salt of chloroacetic acid in aqueous alkaline organic slurries. The extent of substitution on C-2, C-3, and C-6 is related to the degree of disruption of hydrogen bonding, steric factors, and reaction conditions (72,87). The acid form of CMC is a polyelectrolyte with limited solubility and a pK_a of 4. The monovalent metal or ammonium salts are soluble; divalent cations result in borderline solubility; multivalent cations allow gel formation. Solutions of sodium CMC are pseudoplastic for high viscosity grades with degrees of substitution (DS) of 0.9–1.2. Solutions of less uniformly substituted, high molecular weight CMC

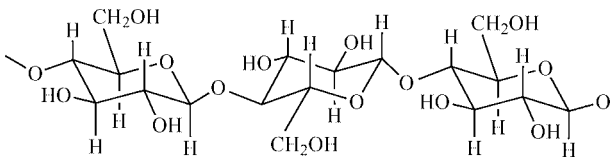

Fig. 23. Structure of cellulose.

with low DS are thixotropic; CMC is stable over the pH range 4–10 (see CELLULOSE ETHERS).

CMC is used in sizing for textile and paper applications and as a thickener, stabilizer, suspending agent, or binder in foods, pharmaceuticals, and cosmetics. CMC is a fluid loss and rheology modifier in drilling muds.

Hydroxyethylcellulose (HEC) and hydroxypropylcellulose (HPC) are prepared by nucleophilic ring opening of ethylene oxide and propylene oxide, respectively, by the hydroxyl anions on the anhydroglucose ring of cellulose. Reactions are conducted commercially in caustic aqueous slurry processes (72). Laboratory methods recently have been reported for preparation of cellulose ethers, esters, and carbamates under homogeneous reaction conditions in organic solvents (88–91). Such solvents may lead to development of new commercial processes for cellulose derivatives with more uniform substitution.

HEC is a nonionic polymer with little surface activity in solution and is compatible with a wide range of surfactants and salts. Solutions are pseudoplastic at higher molecular weights and concentrations. Molecules behave as rigid rods in dilute aqueous solution. Commercial HEC has molar substitution (MS) between 1.8 and 3.5 degree of substitution of 0.8–1.8.

HPC is more hydrophobic than HEC owing to the presence of the methyl group on the side chain. The polymer is soluble in organic solvents but phase separates from water above 45°C. In concentrated solutions, HPC exhibits lyotropic liquid cryalline behavior (61). Commercial HPC has MS values between 3.5 and 4.5 and DS values of 2.2–2.8 (72,87).

HEC is used in coatings, cements, thickeners, pharmaceuticals, oil-well fracturing, cementing, and drilling applications, and in cosmetics, inks, paper finishes, lubricants, gels, and agricultural formulations. HPC is used for warp sizing, flocculations, wetting, thickening, binding, formulation of hair sprays, cosmetics, pharmaceuticals, and personal care items.

Methylcellulose is prepared commercially by reaction of the respective methyl chloride or dimethyl sulfate with alkali cellulose with organic slurry systems, batch methods, or continuous processes (72,87). The methyl ether derivatives have a DS range from 1.5 to 2.0, the uniformity of which depends on the heterogeneity of the reaction medium and other reaction conditions. Substitution occurs preferentially at the C-6 and C-2 positions. Methylcellulose exhibits both an upper and lower critical solution temperature as signified by gel formation on heating or cooling homogeneous solutions. Uses for methyl cellulose include gelling fluids, viscosifiers, pharmaceutical coatings, and food additives.

Hydroxypropylmethylcellulose (HPMC) is one of the many mixed ethers of cellulose. It is prepared by reactions of alkali cellulose with methyl chloride and propylene oxide in a slurry process. Reaction conditions may be varied to control compositions despite the greater reactivity of methyl chloride. HPMC is an extremely effective viscosifier compared to conventional cellulose ethers. Its microheterogeneous nature, phase behavior, and interaction with surfactants allow use in food, pharmaceutical, and coatings applications (72,87).

Cellulose sulfates and phosphates are water-soluble derivatives prepared by reactions of alcohol/water/organic diluent mixtures of sulfuric or phosphoric acids. Phosphate derivatives are flame retardant but have not been commercialized (72).

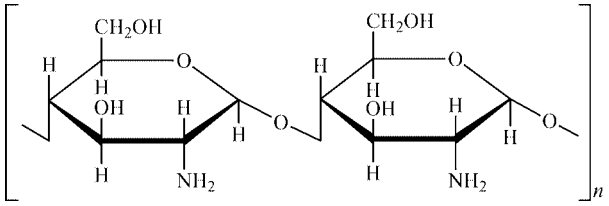

Fig. 24. Chitosan.

Chitin Derivatives and Chitosan. Chitin (92) is a water-insoluble, high molecular weight polymer of 2-acetamido-2-deoxy-D-glucopyranosyl units linked through β-1→4-D bonds. This most abundant skeletal material of invertebrates is recovered from shrimp, crab, or lobster waste materials. Fungi are also an important commercial source of chitin. Chitin may be converted to chitosan by partial or complete deacetylation. In the protonated form (Fig. 24), this cationic polyelectrolyte is water-soluble with a number of potential commercial uses including flocculation, viscosification, wound healing, medical dressing, pharmaceutical formulation, drug delivery, membrane technology, and animal nutrition.

Chitin can be derivatized (92–95) by reaction of the hydroxyl substituents on carbons 3 and 6 of the anhydroglucose ring. *N*-substituted derivatives at C-2 can be obtained from reactions on chitosan or partially deacetylated chitin. Hydroxyethylchitin and other water-soluble derivatives are useful wet-end additives in papermaking and flocculants for anionic waste streams (see CHITIN AND CHITOSAN).

Inorganic Water-Soluble Polymers

Poly(metaphosphoric acid) (96,97) (Fig. 25) is formed by controlled dehydration of NaH_2PO_4. The lower molecular weight sodium hexametaphosphate is available commercially. High molecular weight analogues can be prepared with various cations. The other widely abundant inorganic polymers, poly(silicic acid) (Fig. 26) and its sodium or potassium salts are highly branched, associated, high viscosity polymers. Aqueous solutions of silicates have been used as raw materials for centuries in window-glass formation and insulating-glass fibers (96).

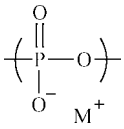

Fig. 25. Poly(phosphoric acid) salt.

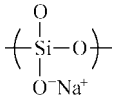

Fig. 26. Poly(silicic acid) salt.

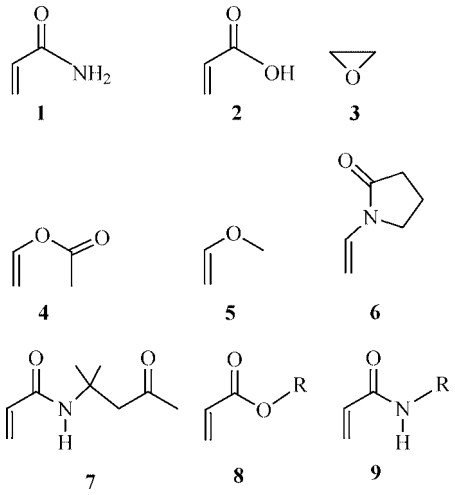

Fig. 27. Examples of uncharged monomers utilized in the synthesis of water-soluble, nonionic copolymers.

Nonionic Polymers

A number of commercially available and experimental nonionic monomers including those shown in Figure 27 have been utilized to prepare a large number of water-soluble (co)polymers. Water solubility is a result of a high concentration of polar or hydrogen-bonding functional groups on the repeating units. Major commercial polymers are based on acrylic, vinyl, oxide, or imine functionality.

Polyacrylamide. Acrylamide (AM) monomer **1** is polymerized by free-radical initiators, eg, azo compounds, redox, catalysts, light, and radiation (Fig. 28). This monomer is unique among vinyl and acrylic monomers because it can be polymerized to ultrahigh molecular weight (10^6–10^7). This extraordinary feature of acrylamide polymerization is attributed, in part, to the ease of purification of AM monomer and to the unusually high ratio of its propagation to termination rate constants (k_p/k_t). In fact, AM has the highest k_p/k_t of any free radically polymerizable monomer. Polyacrylamide (PAM) can be prepared via solution, inverse emulsion, inverse microemulsion, or precipitation techniques (98–100) (see ACRYLAMIDE POLYMERS).

Low temperature initiation, high monomer concentration, and a small amount of added 2-mercaptobenzimidazole, a radical scavenger, are reported to be the optimal reaction conditions for preparing high molecular weight, soluble polymers. High total solids concentrations usually result in intractably high solution viscosities. Inverse emulsion polymerization offers the opportunity for lowered

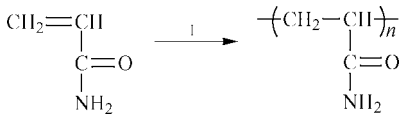

Fig. 28. Polymerization of acrylamide.

viscosities without compromising polymer molecular weights (101–103). Inverse microemulsion polymerization results in rates 10–200 times faster than conventional inverse emulsion systems (104). Precipitation polymerization can also be accomplished using a solvent (eg, *tert*-butyl alcohol) that dissolves the AM monomer but not the PAM (100).

Solution polymers are usually isolated by precipitation or dialysis/freeze drying. However, such solid products are hard to re-dissolve. Recently this problem was overcome by the discovery that water-in-oil (w/o) emulsions of polyacrylamide can be inverted by adding a water-soluble surfactant to produce an oil-in-water (o/w) emulsion. Thus a low HLB surfactant is used for polymerization and a high HLB surfactant is used for phase inversion (103). The resulting polymers re-dissolve easily. Inversion must be complete or polymer (activity) is lost.

AM is difficult to polymerize by any of the "controlled/living" polymerization techniques. However, McCormick and co-workers have recently made significant progress in this area by reporting the CLRP, via RAFT, of AM in both aqueous and organic media (47,49,50). To achieve "living" conditions, judicious choices must be made with respect to RAFT chain transfer agent (CTA) and polymerization conditions.

PAM has reported T_g values of 165 and 188°C. No matter which value is correct, it is clear that PAM remains glassy to relatively high temperatures. Although PAM is slow to dissolve, it is soluble in water in all proportions. However, PAM solution viscosities show a time dependence, attributed to intramolecular conformational changes (98). Because PAM can be polymerized to very high molecular weight, it is a highly efficient aqueous viscosifier. Solution viscosities of nonionic PAM are insensitive to changes in pH (between 1 and 10). Above pH = 10, it is subject to hydrolysis. Solutions of nonionic polyacrylamide are also tolerant of electrolytes (eg, NaCl). Viscosities increase with increasing molecular weights, according to equation 5.

$$[\eta] = 1.0 \times 10^{-2} M_w^{0.755} \text{ (water, 25°C)} \tag{5}$$

Polyacrylamides function as flocculating agents, in rheology control, and as adhesives.

Poly(acrylic acid). Poly(acrylic acid) (PAA) can be prepared by direct free-radical polymerization of **2** in aqueous solution (6) or by precipitation polymerization in benzene. Alcohols and mercaptans are commonly used chain-transfer agents for regulating polymer molecular weight. Alternatively, PAA can be prepared by hydrolysis of poly(alkyl acrylates) (6) (Fig. 29).

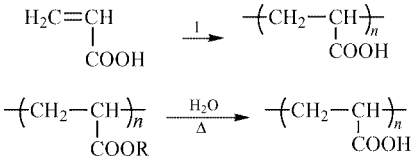

Fig. 29. Preparation of poly(acrylic acid) by direct polymerization or by hydrolysis of a polyacrylate.

Both RAFT and NMP controlled/living techniques are suitable for the direct polymerization of acrylic acid. The RAFT polymerization of AA has been reported in DMF (24,105), various alcohols (106,107), water (108), and dioxane (109) employing a variety of RAFT CTAs including dithioesters, xanthates, dithiocarbamates and trithiocarbonates. AA is also susceptible to controlled polymerization by NMP (110,111).

The T_g of PAA has been variously reported as 75, 106, and 126°C, depending on the mode of measurement. However, the highest value is probably the most accurate. Solid polymers are hard, clear, brittle materials. In aqueous solutions, viscosity increases with increasing molecular weight. PAA undergoes a number of reactions in solution, ie, hydrolysis, esterification, dehydration, and complex formation with polyethers. PAA is an excellent thickener for lattices. PAA has been used in oil recovery, as a dispersant for inorganic pigments, as a flocculant, and as an adhesive.

Poly(ethylene oxide). Poly(ethylene oxide) (PEO) is prepared by ring-opening polymerization of the ethylene oxide monomer **3** (112,113). Polymers of molecular weight greater than 1×10^5 are prepared by heterogeneous catalysis (eg, alkaline earth carbonates) in low boiling aliphatic hydrocarbons. Few of the details of the commercial manufacture have been made public (see ETHYLENE OXIDE POLYMERS).

PEO is a white free-flowing powder with commercial grades from 100,000 to 5 million molecular weight (114). It has a T_m of about 65°C and a T_g of −45 to −53°C. Above the melting point it can be processed as a thermoplastic, ie molded or extruded. However, owing to its high melt viscosity, incorporation of plasticizer is often desired. PEO resins are completely soluble in water at room temperature, but show a lower critical solution temperature (LCST) near the boiling point of water. The LCST is lowered by the addition of inorganic salts according to the following order: $PO_4^{3-} > SO_4^{2-} > F^- > Cl^- > I^- > K^+ > Na^+ > Li^+$. Aqueous solutions of high molecular weight PEO show high extensional and shear viscosities and pseudoplastic rheology.

Poly(vinyl alcohol). Poly(vinyl alcohol) (PVA) is manufactured by alcoholysis/hydrolysis of poly(vinyl acetate), which is, in turn, produced by free-radical polymerization of vinyl acetate monomer **4** (114) (Fig. 30) (see VINYL ALCOHOL POLYMERS).

Polymerization of vinyl acetate monomer can be effected by bulk, solution, or emulsion techniques. The poly(vinyl acetate) formed is then dissolved in solvent (eg, CH_3OH) and alcoholized/hydrolyzed with acidic or basic catalysts. Vinyl acetate can also be polymerized in a controlled fashion via RAFT/MADIX (115). PVA is insoluble in CH_3OH and precipitates. It is isolated by filtration, washing, and drying.

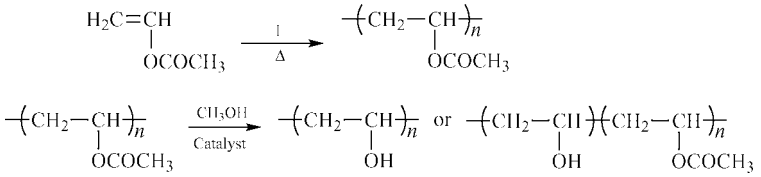

Fig. 30. Polymerization of vinyl acetate.

Properties of PVA depend on the degree of alcoholysis/hydrolysis and polymer viscosity/molecular weight. Bulk/film properties (eg, tensile strength, tear resistance, elongation, and flexibility) of PVA increase with increasing extent of alcoholysis/hydrolysis and with increasing viscosity/molecular weight. The tensile strength is exceptional compared with other water-soluble polymers. Water solubility/sensitivity is at a maximum at 88% alcoholysis/hydrolysis. Beyond that level, polymer–polymer interactions via intramolecular H-bonding become so extreme that solvation of the polymer becomes difficult.

Other noteworthy properties of PVA are its film-forming ability, its barrier, adhesive, and emulsifier properties, and its grease, oil, and solvent resistance. PVA films and coatings do not require a curing cycle because tough films can be formed by evaporation. PVA film also has remarkable gas impermeability, forming barriers to oxygen, nitrogen, carbon dioxide, hydrogen, helium, and hydrogen sulfide. However, PVA does exhibit permeability to ammonia and water vapor. Its adhesive binding strength is attributable, in part, to its film-forming ability and its high strength. PVA has surface activity as an o/w emulsifier and/or protective colloid. Oil and solvent resistance increases with extent of hydrolysis.

Poly(vinyl alcohol) is used alone or combined with extenders, pigments, etc, in the preparation of high wet-strength adhesives for paper. It is an excellent binder for textiles and sizing agent for paper and can be used to emulsify a wide range of materials including vegetable oils, mineral oils, solvents, plastics, waxes, and resins. Its emulsifying, binding, film-forming, and thickening behaviors are useful in cosmetic formulation. PVA films can also be used for making oxygen tents.

Poly(methyl vinyl ether). Methyl vinyl ether (MVE) **5** is isomeric with PPO, but is significantly more water-soluble. Indeed, it is the methyl ether derivative of poly(vinyl alcohol). MVE is readily polymerized using carbocationic methods (116–118). This also facilitates the preparation of novel MVE-based block copolymers. Purification of homo polymers and copolymers prepared by the termination of living poly(methyl vinyl ether) (PMVE) with *n*-alcohols involves a combination of solvent removal, dialysis, and freeze drying (118).

MVE can also be polymerized under alternating free radical conditions with, for example, maleic anhydride to yield poly(9-methylvinylether-alt-maleic anhydride).

The T_g of PMVE is -34°C (119) and as such exists in a rubbery state at standard temperatures and pressures. PMVE exhibits broad solubility. Common solvents include benzene, halogenated hydrocarbons, ethanol, *n*-butanol, acetone, ethylacetate, cold water, heptane and cyclohexenes. Common nonsolvents include hexane, ethylene glycol, and dioxyl ether (119). PMVE is readily soluble in water, but like many nonionic water-soluble polymers, PMVE exhibits inverse temperature water-solubility. The cloud point varies over a broad range depending on MW. For example, low molecular weight PMVE with a D_p of 19 is reported to have a cloud point of 18°C while some commercial grades have significantly higher cloud points at ca 35°C (117).

Poly(*N*-vinylpyrrolidinone). *N*-Vinylpyrrolidinone (NVP) monomer **6** polymerizes under free-radical conditions via bulk, solution, and suspension methods (Fig. 32).

Azo initiators are preferred over persulfate initiators because the latter react with the monomer. One of the curious features of this polymerization is that it has a

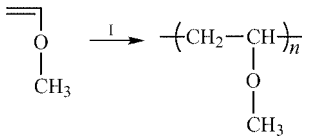

Fig. 31. Polymerization of methyl vinyl ether.

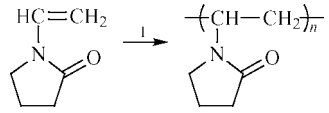

Fig. 32. Polymerization of *N*-vinylpyrrolidinone.

maximum rate of polymerization in the presence of about 1 mol of water (120,121). Presumably, a specific complex forms between the monomer and a water molecule. NVP does not polymerize to particularly high molecular weight, in part because it is difficult to purify the monomer.

The T_g of PNVP is 175°C, but this value is reduced considerably by small amounts of water. Dry-cast films of PNVP are hard and transparent. However, the presence of strong intermolecular dipole–dipole interactions causes it to have a high processing temperature. Consequently, PNVP has never found acceptance for molded parts. PNVP has interesting solution properties. It is readily soluble in water and forms complexes with a wide variety of substances, eg, iodine, polyacids, phenolics. Solutions of PNVP are stable to electrolytes. Solution viscosities increase with increasing polymer molecular weight. PNVP (bulk or solution) is also characterized by high thermal or thermohydrolytic stability and chemical resistance. PNVP is also compatible with a wide range of hydrophilic and hydrophobic resins and modifiers.

PNVP has found applications in a wide variety of industries, including medicine, pharmaceuticals, cosmetics, textiles, beverages, adhesives, and paper (121,122). For example, PNVP was an early plasma and blood volume extender. It is used extensively in pharmaceutical tablets. Its complex with iodine is a germicide. It is used as a component in cosmetics, hair shampoos, and sprays and is a stabilizing agent for beer. PNVP also exhibits excellent adhesion to glass (see *N*-Vinylamide Polymers).

Polyelectrolytes

Polyelectrolytes (qv) are polymers with charged functional groups attached along the chain. These polymers are usually classified as either polyanions (negative charges) or polycations (positive charges). Associated with the polyions are counterions or gegenions of the opposite charge in sufficient numbers to maintain electroneutrality (123).

Water-soluble polyelectrolytes exhibit a number of common traits with water-soluble nonionics. However, differences arise from the presence of charges on the macromolecular backbone and more mobile counterions electrostatically bound to

an extent determined by pK_a, solvent, and local dielectric effects. Generally, phase behavior and enhanced solubility result from increased segmental hydration and increased free energy of mixing.

The interactions between fixed charges on the polymer chain in dilute solution normally expand (repulsive) or contract (attractive) coil dimensions. Counterion binding also influences hydrodynamic volume and involves specific ion binding as well as atmospheric ion binding. Theoretical discussions of these effects can be found in References 123 and 124.

Polyelectrolytes with flexible chains and high charge density are more expanded in water than nonionic polymers, especially at low ionic strength. Determination of intrinsic viscosity is difficult in this regime (Fig. 5**c**). Electrostatic repulsions not only cause increases in hydrodynamic volume but also increases in shear sensitivity or non-Newtonian behavior.

The extent of ionization of polybases or polyacids depends on the relative base or acid strength, degree of solvation, and dielectric constant of the solvent. Poly(acrylic acid), for example, ionizes progressively in aqueous basic solution to yield a copolymer with ionized acrylate units and un-ionized acrylic acid units along the backbone; neighboring group hydrogen-bonding effects accelerate initial ionization. Eventually, however, ionization becomes more difficult owing to excessive buildup of charge along the backbone.

Polyelectrolytes have been studied extensively because molecular structures can be tailored to allow large conformational changes with pH, temperature, or added electrolytes. Molecular parameters that influence behavior include number, type, and distribution of charged repeat units on the chain, hydrophobic/hydrophilic balance, distance of charged moiety from the backbone, and counterion type. Solution properties including phase behavior, hydrodynamic volume, and binding can be altered, offering utilization in flocculation, adhesion, stabilization, compatibilization, viscosification, suspension, etc.

Anionic Polyelectrolytes. Anionic poly(acrylic acid) (PAA) can be synthesized in two ways, ie direct polymerization of **1A** (Fig. 33) or via hydrolysis of a suitable precursor polymer (6). In the direct method, salts of acrylic acid are homopolymerized or copolymerized by free-radical initiation in aqueous media. Usually the rate of polymerization of the ionic monomer is lower than the corresponding nonionic monomer, presumably owing to charge repulsion between the growing chain and the incoming ionic monomer. Direct polymerization of acrylic acid salt solutions has some commercial advantages because the nonvolatility of acrylic acid salts allows simultaneous polymerization and spray drying (or drum drying) to produce high molecular weight polymers directly. Hydrolysis (saponification) is the alternative method for producing anionic poly(acrylic acid) (Fig. 34). Hydrolysis of syndiotactic esters gives syndiotactic salt, and hydrolysis of isotactic esters gives isotactic salts.

The T_g of anionic poly(acrylic acid) [eg poly(sodium acrylate)] is substantially higher (251°C) than that of nonionic poly(acrylic acid) (102°C) because of the strong intermolecular forces due to ionomeric clustering. Physical/mechanical properties (eg, moduli) are also generally higher for salts vs free acids in the bulk phase. Atactic and syndiotactic salts of acrylic acid are water-soluble, but isotactic forms are not. Salts of poly(acrylic acid) show characteristic polyelectrolyte solution behavior (6).

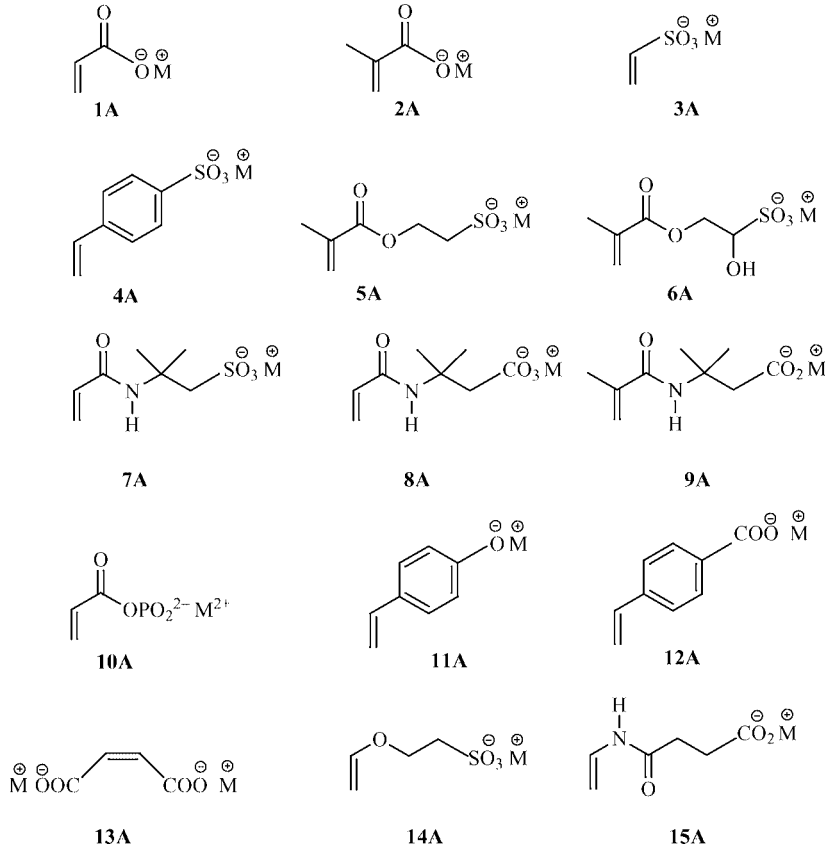

Fig. 33. Examples of monomers utilized in preparing anionic polyelectrolytes.

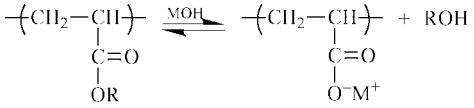

Fig. 34. Preparation of poly(acrylic acid) salts via hydrolysis of a precursors poly(alkyl acrylate).

The applications of anionic poly(acrylic acid) include use as latex thickeners, oil-field chemicals, dispersants, and flocculants. In addition, poly(acrylic acids) containing small amounts of cross-linking agents are water-swellable polymers that have found use as superabsorbents.

Poly(methacrylic acid) and Its Salts. A wide variety of methods have been used to prepare poly(methacrylic acid) (PMAA) (6) (Fig. 35). Free-radical

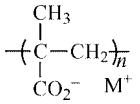

Fig. 35. Structure of poly(methacrylic acid) salt.

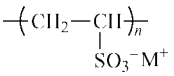

Fig. 36. Structure of poly(vinylsulfonic acid) salt.

polymerization by hydrogen peroxide, persulfate, or redox systems in aqueous solution yields atactic polymer with syndiotactic tendency. At higher pH, a higher syndiotactic content is produced. Stereoregularity can be obtained by hydrolysis of appropriate precursor polymers.

Controlled structure PMAA can be prepared by the deprotection of an appropriate precursor polymethacrylate which has itself been polymerized under living conditions. Both anionic polymerization and GTP have been used to prepare PMAA employing a variety of PMAA precursor monomers such as benzyl methacrylate (125), *tert*-butyl methacrylate (126), trimethylsilyl methacrylate (127) and 2-tetrahydropyranyl methacrylate (128,129). Removal of the protecting group yields the desired PMMA.

The sodium salt of methacrylic acid **2A** has also been polymerized directly in aqueous media via ATRP employing a PEO macro-initiator (130). Short chain, controlled structure oligomers of PMAA may also be prepared by CCTP (131).

Poly(methacrylic acid) in the nonionized form in solution has a compact conformation and low intrinsic viscosity. Upon ionization to the polyelectrolyte form, chain expansion occurs and viscosity increases. Unlike PAA, PMAA shows inverse solubility-temperature behavior. The presence of chain-stiffening methyl groups and their added hydrophobicity are responsible for the phase and viscosity behavior. Tacticity also plays an important role.

PMAA and its copolymers with acrylamide are used in viscosification and flocculation. Copolymers of MAA and its salts have been used as components of superabsorbents, coatings, adhesives, and in drilling operations.

Poly(vinylsulfonic acid) and Its Salts. Poly(vinylsulfonic acid) (PVSA) (Fig. 36) is prepared by polymerization of ethylenesulfonic acid or its sodium salt **3A** under free-radical conditions. It is purified precipitating aqueous solutions of the sodium salt form with methanol or dioxane.

The sodium and ammonium salts of PVSA are soluble in water but insoluble in organic solvents (6). The calcium salt is insoluble. Potentiometric titration studies indicate that PVSA is a strong acid that ionizes completely in water. Ion binding selectivity with alkali metals has been observed in viscosity and phase separation studies. Mark–Houwink–Sakurada (MHS) parameters of $K = 2.22$ and $\alpha = 0.65$ have been obtained for sodium PVSA in 0.5 M NaCl at 25°C.

Poly(styrenesulfonic acid) and Its Salts. Poly(styrenesulfonic acid) (PSSA) (6) (Fig. 37) may be prepared by free-radical polymerization of the monomer in solution using the free acid, sodium, or potassium salt **4A** form.

PSSA may also be prepared by sulfonation of polystyrene or by hydrolysis of poly(*n*-propyl *p*-vinylbenzenesulfonate). The latter cases allow preparation of tactic structures. Copolymers can also be prepared by free-radical copolymerization of appropriate monomers or post-reaction. Polymers are purified by precipitation of aqueous solutions with methanol, alkaline methanol, or other alcohols. Controlled structure PSSA homopolymers and block copolymers may also be prepared directly in aqueous media via RAFT using 4-cyanopentanoic acid dithiobenzoate as the CTA and V-501 as the radical source (48). NMP has been successfully

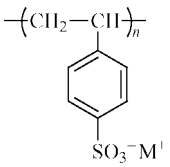

Fig. 37. Structure of poly(styrene sulfonate) salt.

employed in the preparation of near-monodisperse PSSA homo/copolymers. For example, PSSA homopolymer can be prepared in an ethylene glycol/water mixture (3:1 vol/vol) using TEMPO and sodium bisulfite/potassium persulfate as the redox initiating pair (132,133).

Atactic PSSA is soluble in water, methanol, and ethanol but insoluble in hydrocarbons. PSSA salts are insoluble in common organic solvents but soluble in water. Ultraviolet and fluorescence spectrometry measurements can yield information on features including local environment, neighboring groups, and tacticity. MHS values and solution properties are reviewed in Reference 56. Cross-linked PSSA has been used commercially as an ion-exchange resin and in heavy metal binding studies. Fractionated PSSA has been offered as a standard for aqueous gel-permeation chromatography.

Other Sulfonic Acids. Extensive development work has been conducted on acrylic sulfonate-containing monomers. 2-Sulfoethyl methacrylate (SEM) monomer **5A** has proved to be of limited commercial value owing to the hydrolytic instability of the ester linkage. However, recently well-defined homopolymers of 3-sulfopropyl methacrylate (SPMA) were prepared under aqueous RAFT conditions with 4-cyanopentanoic acid dithiobenzoate and V-501 as the CTA/initiator pair at 70°C (39). This same hydrolytic instability has been a serious problem with 3-sulfo-2-hydroxypropyl methacrylate. In contrast, 2-acrylamido-2-methylpropanesulfonic acid (AMPSA) **6A**, prepared by the reactions of SO_3 with isobutylene followed by the Ritter reaction with acrylonitrile (134), is quite hydrolytically stable.

AMPS or 2-acrylamido-2-methyl propanesulfonate **7A** is highly reactive in both homo- and copolymerizations and can be incorporated by homogeneous, solution, or emulsion polymerization techniques. With advances in CLRP, acrylamido monomers such as AMPS (specifically in its Na+ form) are now easily polymerized in a controlled manner, as homopolymers, statistical copolymers, or block copolymers. Indeed PAMPS and its copolymers may be prepared under facile conditions via RAFT, directly in water employing CTP and V-501 as the CTA/initiator pair (42,44,45). Applications include improving emulsion stability (135), flocculation (136), improving dry strength in paper (137), sludge dispersal in boiler-water treatment (138), and silt control in cooling water systems (139). Copolymers of the sodium salt of AMPS with acrylamide copolymers (140–142) and ampholytic terpolymers (143,144) have potential in oil-field applications and in superabsorbency, respectively.

Other Anionic Carboxylate Monomers. The anionic carboxylate monomers **8A** and **9A**, prepared by the Ritter reaction involving acrylonitrile or methacrylonitrile and 3,3-dimethylacrylic acid have been copolymerized in the sodium salt form to yield calcium-tolerant copolymers with utility in enhanced oil recovery (145–148). Monomer **8A**, for example, has been copolymerized with **7A**

under RAFT conditions to yield novel stimuli-responsive water-soluble polymers capable of reversible pH-induced micellization (42,44). Sodium 4-vinylbenzoate **12A** has also been polymerized under both NMP and ATRP conditions (133,149).

Other examples of specialty anionic monomers shown in Figure 33 include salts of vinylphosphonates **10A**, vinylphenolates **11A**, vinyl benzoate **12A**, maleic acid **13A**, 3-vinyloxypropane sulfonates **14A**, and *N*-vinylsuccinimidic acid **15A**.

Cationic Polyelectrolytes. Cationic polymers are a class of polyelectrolytes that derive their unique properties from the density and distribution of positive charges along a macromolecular backbone as well as molecular weight. Chain conformation and solubility depend on the extent of ionization and interaction with water. Cationic functional groups can strongly interact with suspended, negatively charged particles or oil droplets and are useful for many applications (76,150–153) including waste treatment and paper making. A number of the most common monomers utilized for preparation of cationic polyelectrolytes are shown in Figure 38.

Polymethacrylic Cationics.

Poly(2-(dimethylamino)ethyl methacrylate). 2-(Dimethylamino)ethyl methacrylate [DMAEMA, **1C** (Fig. 38)] is readily polymerized under a variety of conditions such as conventional free radical polymerization (154), living free radical polymerization, specifically ATRP and RAFT, anionic polymerization (155), group transfer polymerization (156) and oxyanionic polymerization (157,158). For example, conventional free radically prepared copolymers of **1C** with *N*-vinyl-2-pyrrolidone (159,160), *N*-phenylmaleimide (161), and ethylene (162) have been reported. While 1C is readily polymerized via both ATRP and RAFT, to date ATRP has received the most attention as a means of preparing controlled-structure homo- and copolymers of **1C** in both aqueous (163) and organic media (164,165) with Cu(I) species as the catalysts employing a variety of different ligands (166–169). It should be noted that under certain conditions **1C** may undergo a transesterification reaction when polymerized via ATRP in MeOH and MeOH/H_2O mixtures (170). It is also possible to directly polymerize quaternized versions of **1C** via aqueous or mixed H_2O/MeOH ATRP (171). **1C** has been successfully polymerized via RAFT in EtOAc with CTP and V-501 as the CTA/initiator pair (172), and also under bulk conditions with cumyl dithiobenzoate and AIBN (173).

Synthesis of Other Amine-Containing Polymethacrylates. Figure 38 shows the structures of other amine-containing methacrylic monomers. Like poly(2-dimethylamino)ethyl methacrylate) (PDMAEMA), the homopolymers of these monomers are water-soluble, albeit under somewhat more limiting conditions. The copolymerization of **2C** with methacrylic acid has been reported under conventional free radical conditions in methanol using AIBN as the initiator (174). The controlled polymerization of **2C**, **3C**, **4C**, and **5C** have been reported under GTP conditions (175–179) and oxyanionic conditions (15,180). Homopolymers of **2C** have also been prepared under ATRP conditions (181). Interestingly, **6C** can be polymerized in a controlled fashion by both oxyanionic and classical anionic techniques even though it contains a secondary amine species (180,182).

Aqueous Solution Characteristics. The behaviors of the polyamine methacrylates in aqueous media are both interesting and varied. The polymer

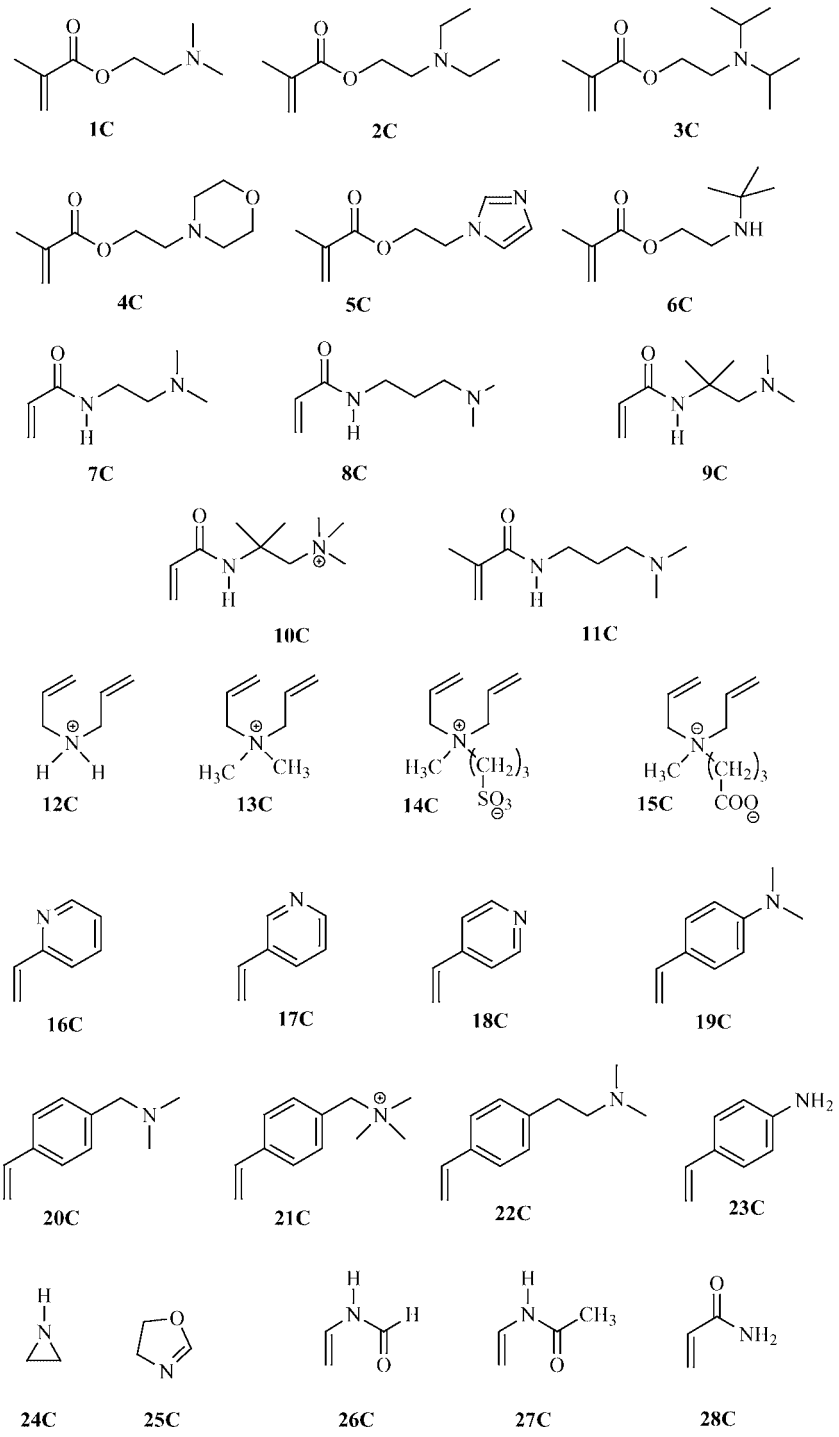

Fig. 38. Chemical structures of common amine-containing monomers (**1C–23C**) and reactive precursors (**24C–28C**) to amine-containing polymers.

from **1C** is a weak polybase which is soluble over most of the useful pH range. However, in its non ionized form, and like most nonionic water-soluble polymers, it shows inverse-temperature water-solubility. The neutral polymer has a lower critical solution temperature (LCST), or cloud-point (C_p), between ~32 and 47°C depending on its molecular weight. In its protonated form, however, it remains readily soluble up to 100°C.

The other "common" tertiary amine polymethacrylates, PDEAEMA, PDiPAEMA, and PMEMA from **2C** and **3C**, are also responsive to applied stimuli in aqueous solution. These are only soluble in aqueous media at low pH, ie under those conditions in which the tertiary amine residues are protonated and thus cationic. Under basic conditions, where the 3° amine groups are neutral both species are hydrophobic and thus phase separate. So, simply adjusting the pH of an aqueous solution for homopolymers derived from **2C** or **3C** results in phase separation. Polymers from **4C** and **1C** are soluble over the entire useful pH range, but do have an LCST in the range 34–54°C, the exact C_p being molecular weight dependent. However, the former is also susceptible to changes in electrolyte concentration. Certain salts such as sodium sulfate readily "salt out" this polymer inducing a phase change (183). These various responses to different applied stimuli have been exploited for the synthesis of novel self-assembled polymeric micelles.

Poly(meth)acrylamido Cationics. (Meth)acrylamido species are one of the most important commercial class of water-soluble monomers with wide-ranging applications. Cationic polyacrylamides are most often prepared by the normal free radical polymerization of the amine-containing monomer, and then most often in a copolymerization. For example, the protonated form of **9C** and the monomer **10C** are both readily copolymerized with **28C** to yield high molecular weight statistical copolymers in which the molar composition is virtually identical to the feed composition (184,185).

The controlled polymerization of amine-containing (meth)acrylamido monomers has, until recently, remained elusive. None of the classical living techniques can be employed and of the controlled free radical polymerization techniques only RAFT has the versatility required for this particular class of monomer. Even so, there is only one report of the controlled polymerization of an amine-containing monomer, namely *N*-[3-(dimethylamino)propyl] methacrylamide, **11C** (186). **11C** is readily homopolymerized in aqueous media (neutral pH) at 70°C using 4-cyanopentanoic acid dithiobenzoate as the RAFT CTA and V-501 as the azo initiator, at an initial molar ratio of 5/1. Under these conditions reasonable control was attained as evidenced by the molecular weight control and resulting polydispersities. Control over the RAFT polymerization of **11C** was attained by conducting the polymerizations in a buffered solution (pH = 5.0). Under these conditions possible side reactions such as monomer hydrolysis followed by aminolysis of the CTA is essentially eliminated (such side reactions have been previously shown to be significant in the homopolymerization of **28C**) (47,186).

Amine functionality can also be introduced into acrylamido polymers via post-polymerization modification of polyacrylamide from monomer **28C**. Strategies include the Mannich reaction (introduction of tertiary-amine functionality), Hofmann degradation (yields polyvinylamine residues) and transamidation reactions. The Mannich reaction is reversible; however, subsequent quaternization of the Mannich product prevents the reverse reaction (187).

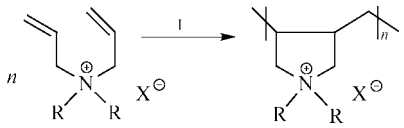

Fig. 39. Cyclopolymerization of diallyl ammonium monomers.

Polydiallylammonium Cationics. Diallyl ammonium monomers, such as **13C**–**15C** in Figure 38, can be polymerized via so-called cyclopolymerization (Fig. 39) (188).

DADMAC **13C**, for example, can be readily polymerized under these cyclopolymerization conditions to yield PolyDADMAC in which a structure composed of 5-membered *N*-heterocycles predominates. **13C** will readily polymerize at ∼35°C employing ammonium persulfate as the initiator. **13C** is readily copolymerized with other diallyl monomers, with acrylamido monomers such as **28C** or diacetone acrylamide, or quaternized **1C**. Extensive reviews of cyclopolymerization and cyclocopolymerization can be found in Reference 188. Recent examples of cyclocopolymerization with sulfobetaine (**14C**) and carboxybetaine (**15C**) diallyl ammonium monomers are given in References (188–191).

Polyvinylpyridines

2-, 3- and 4-vinylpyridines (**16C**, **17C**, and **18C**) are all readily polymerized under normal free radical conditions. Of these species, **18C** has been the most widely studied. An extensively studied derivative of **17C** is 2-methyl-5-vinylpyridine (or 6-methyl-3-vinylpyridine) and its quats (192–195). For example, 1,2-dimethyl-5-vinylpyridinium methyl sulfate is readily polymerized in aqueous solution at room temperature with common free radical initiators such as AIBN or potassium persulfate. In fact it will spontaneously polymerize at concentrations in excess of ∼75% (196).

It is also possible to prepare vinylpyridine-based (co)polymers in a controlled fashion with predetermined molecular weights and narrow molecular weight distributions. For example, the controlled polymerization of **16C** and **18C** is possible via anionic polymerization (197–201).

Also, **16C**, **17C**, and **18C** have been polymerized via nitroxide-mediated controlled radical polymerization employing a variety of different nitroxides (202–209). For example, **17C** may be polymerized under bulk or solution conditions (in ethylene glycol) employing 2,2,6,6-tetramethylpiperidin-1-oxyl (TEMPO) as the persistent free radical and benzoyl peroxide as the free radical initiator to yield controlled structure homopolymers with narrow molecular weight distributions (210). More recently, the controlled polymerization of **18C** using a β-phosphonylated nitroxide, namely *N*-*tert*-butyl-*N*-(1-diethylphosphono-2,2-dimethylpropyl) nitroxide, was reported and was shown to be extremely effective for the homopolymerization of **17C** as well as facilitating the synthesis of novel AB diblock copolymers (202).

The controlled polymerizations of **16C** and **18C** have also been reported using RAFT chemistry (211,212). Triblock copolymers of **17C** and styrene were prepared

using dibenzyl trithiocarbonate as the RAFT CTA and AIBN as the azo initiator. The RAFT polymerization of **16C** and **18C** has additionally been achieved using cumyl dithiobenzoate and AIBN as the CTA/initiator pair (212). Homopolymers of **16C** and **18C** were prepared under bulk conditions at 60°C. Excellent control over both the molecular weight and molecular weight distribution was observed with the polydispersity indices for the homopolymers all in the range 1.10–1.25. It was also shown that the corresponding AB diblock copolymers of **16C** with **18C** could be readily prepared using either homopolymer as the macro-CTA for the polymerization of the second block (212).

As well as NMP and RAFT, **16C** and **18C** have been polymerized via ATRP (213–215). For example, **18C** may be polymerized in a controlled fashion using 1-phenylethyl chloride as the initiator and CuCl/5,5,7,12,12,14-hexamethyl-1,4,8,11-tetraazamacrocyclotetradecane (Me_6[14]aneN_4) as the catalyst/ligand pair in propanol at 40°C (215).

Polymers from **16C** and **18C**, and presumably **17C**, may be hydrogenated to form the corresponding polyvinylpiperidines (6), or oxidized to the corresponding water-soluble *N*-oxide. The polyvinylpyridines may also be readily derivatized via quaternization with an appropriate alkylating agent, such as methyl iodide. The monomeric quats are readily water-soluble but can be prone to spontaneous polymerization above critical concentrations (216). The nature of the counterion can also affect the propensity of the quaternized monomers to autopolymerize.

Aqueous Solution Characteristics. The polymer from **16C** becomes water-soluble at a critical degree of ionization (protonation) of ca 30 mol% (217). In comparison, the polymer from **18C** only becomes water-soluble at an apparent degree of ionization of 70 mol%. The polymeric quats behave as strong polyelectrolytes and are readily water-soluble.

Amine-Containing Styrenic Monomers

Several amino-styrenic monomers are known; for example see **19C**–**23C** in Figure 38. The simplest of these, the primary amine species 4-vinylaniline (or 4-aminostyrene), **23C**, is susceptible to polymerization under conventional free radical conditions, as are **19C**–**22C**. For example, the UV-induced graft polymerization of **23C** from a Si surface was recently disclosed (218). These monomers tend to polymerize most effectively in aqueous media in their hydrochloride salt form. Given the reactive nature of the amine functionality in **23C** it is also a suitable precursor for the synthesis of novel amide-based styrenics (219). The controlled polymerization of **19C**, **20C**, and **22C**, under classical anionic conditions is also possible (220,221). For example, AB diblock copolymers of **22C** with styrene can be prepared at −78°C, in THF using cumyl potassium as the initiator with **22C** being polymerized first. Near-monodisperse *n*-butyl quats of **19C**, **20C**, and **22C** have also been reported. These were prepared by the post-polymerization modification of polymers from **19C**, **20C**, and **22C** with *n*-butyl bromide (220).

Homo and copolymers comprised of amine-containing styrenic monomers have also been reported by controlled free radical polymerization techniques. Both NMP and RAFT have been employed with varying degrees of success. For example, **20C** was block copolymerized with sodium 4-styrenesulfonate which was

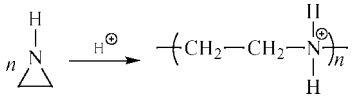

Fig. 40. Polymerization of ethyleneimine.

employed as a macro-initiator and had been prepared using TEMPO in a 3:1 ethylene glycol water mixture at 120°C with potassium persulfate as the initiator (133). More recently, McCormick and co-workers reported the synthesis of novel diamine AB diblock copolymers comprised of **21C** with the protonated form of **20C** (48). These were prepared directly in aqueous media using CTP as the RAFT CTA and V-501 as the azo initiator. Well defined block copolymers were obtained with excellent control over the molar mass and molar mass distribution. Also, new RAFT-synthesized AB diblock copolymers of *N*,*N*-dimethylacrylamide and **20C** have been reported (222). This work demonstrated the importance of blocking order in RAFT polymerizations when the two comonomers are from different monomer families. While highly efficient blocking was achieved when *N*,*N*-dimethylacrylamide was polymerized first, very poor crossover efficiencies were seen in the case of the styrenic-based macro-CTA.

Aqueous Solution Characteristics. The amine monomers tend to be water-soluble only in their protonated or quaternized forms. For example, homopolymers from **19C** are water-soluble at pH's below ~5.3; above this value they are hydrophobic and phase separate. This behavior is completely reversible and has been exploited by several researchers for the preparation of reversible pH-induced supramolecular nanoassemblies (48).

Poly(ethylene imine). Poly(ethylene amine) (PEI) is the simplest polybase. It can be prepared directly via the acid-catalyzed polymerization of ethyleneimine (aziridine, **24C**) (Fig. 40). **24C** may be prepared via a number of routes with ethanolamine being a convenient precursor (223). The cationic polymerization of **24C** is very rapid due to the release of the ring strain associated with the monomer. However, the synthesis of PEI under these conditions leads to highly branched structures due to chain transfer reactions involving the —NH— species in the polymer backbone. Cyclic products can also be produced under these conditions. Copolymerization with an appropriate comonomer can reduce the degree of chain branching (224).

The polymerization of suitable precursor monomers, with subsequent conversion to PEI, is the only route to truly linear products. The most common precursors studied are the substituted oxazolines (Fig. 41), with the 2-substituted-2-oxazolines **25C** being the most thoroughly investigated (225).

Polyvinylamine. Along with PEI, polyvinylamine (PVAm) prepared from **26C** is the simplest polybase, and is related to PEI in a similar manner to the

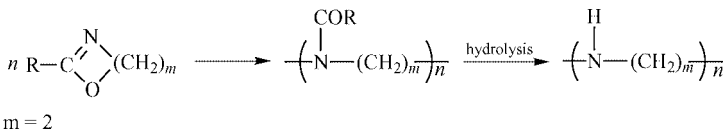

Fig. 41. Polymerization of substituted oxaolines.

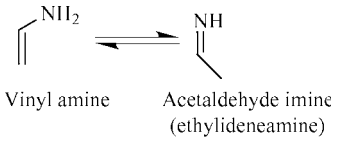

Fig. 42. Vinylamine tautomerization.

relationship between PVOH and PEO, ie as constitutional isomers. Also like PVOH, PVAm cannot be prepared by the direct polymerization of the vinyl amine monomer because it very readily tautomerizes to acetaldehyde imine (Fig. 42).

As such, PVAm must be prepared by indirect methods employing protected monomers which, once polymerized, can be converted to PVAm. The most common employed precursors are the *N*-vinylamides (eg **26C** and **27C**) which after polymerization may be converted to PVAm via hydrolysis. For example, suitable precursors include poly(*N*-vinylacetamide) (PNVA) (226) and poly(*N*-vinylformamide) (PNVF) (227). PNVF is more readily hydrolyzed than other *N*-vinylamides. It is also possible to prepare PVAm via the Hofmann degradation of polyacrylamide prepared from **28C** (228). These precursor polymers are typically prepared using normal free radical polymerization chemistries and as such have broad molecular weight distributions. Recent advances in controlled radical polymerization methodologies, and especially the RAFT technology, should facilitate the synthesis of controlled-structure near-monodisperse PVAm. For example, it is now possible to polymerize **28C** in a controlled fashion under RAFT conditions (49,50). There is also at least one report detailing the RAFT polymerization of **26C** (229).

Miscellaneous Cationic Monomers

While the most common, amine-based species are not the only type of cationic monomers/polymers. There are several other functional species capable of yielding cationic species, namely the sulfonium (230), phosphonium (231,232), and pyrylium (233) species. Several examples of such species are shown in Figure 43.

For example, the statistical free radical polymerizations of **32C** and **33C** with *N*-isopropyl acrylamide were successfully conducted in DMSO employing AIBN at 50°C (234,235). This yielded readily water-soluble copolymers with a thermosensitive component. Such copolymers are also interesting since they can exhibit antibacterial properties against *Escherichia coli* and *Staphylococcus aureus* (234,236,237). Novel water-soluble sulfonium monomers such as **31C** can be polymerized and used as precursor polymers for the synthesis of light-emitting polymers such as poly(2,5-bis(trimethylsilyl)-1,4-phenylenevinylene (238).

Polyzwitterions. Amphoteric water-soluble polymers are polymeric systems containing both anionic and cationic charges. Such polyzwitterions may be subdivided into two major families, the *polyampholytes* and the *polybetaines* (239). Each of these groups may be further subdivided into specific types of each (see below). Figure 44 shows a number of monomers which have been used in pairs (cationic with anionic) to form polyampholytes.

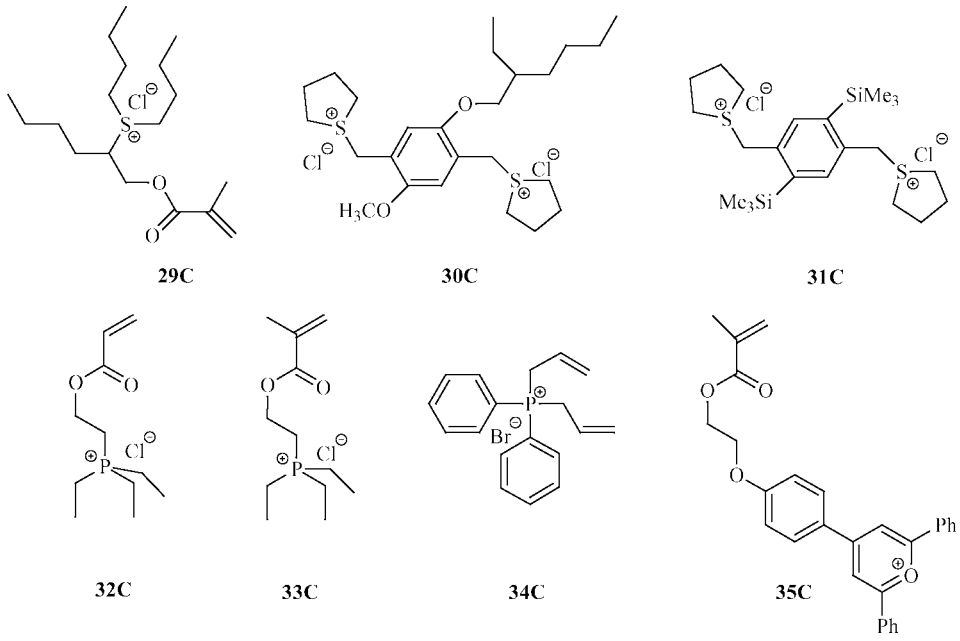

Fig. 43. Specialty cationic monomers.

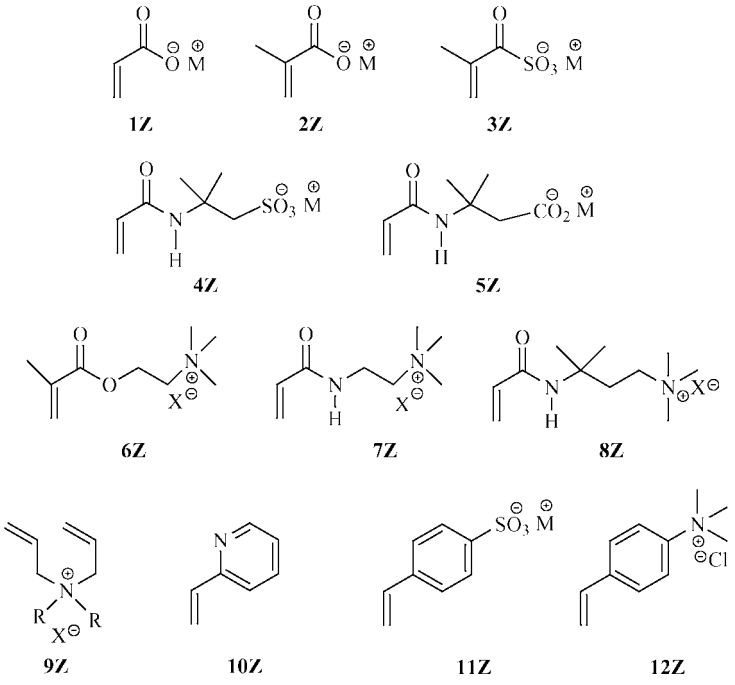

Fig. 44. Monomer pairs utilized in preparing polyzwitterions.

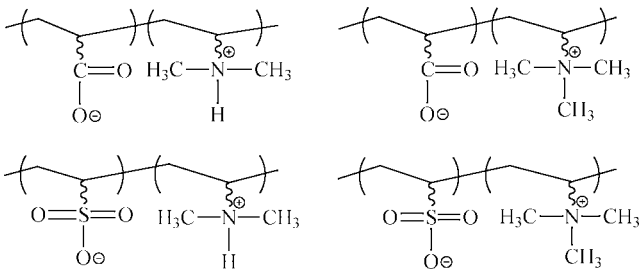

Fig. 45. Polyampholyte structures.

Polyampholytes. Polyampholytes are those materials in which the anionic and cationic charges reside on *different* mer units. Due to this, polyampholytes may be either charge balanced or unbalanced depending on the molar ratio of the anionic/cationic monomers. Polyampholytes may also be subdivided into four inherently different types. There are those in which the anionic and cationic residues may be neutralized, those where the cationic residue may be neutralized but the anionic residue is insensitive to changes in pH, those in which the anionic charges may be neutralized but the cationic residues are insensitive to pH changes, and finally those in which both the anionic and cationic residues are insensitive to changes in the pH (see Fig. 45).

Synthesis. Polyampholytes are most readily prepared by the direct statistical copolymerization of anionic and cationic monomers typically in aqueous media, via conventional free radical polymerization. Examples of such materials were first reported in the 1950s (240–244). Using this approach a wide range of copolymers and terpolymers, often with a neutral hydrophilic monomer such as acrylamide, have been reported. For example, early reports of statistical polyampholytes include the methacrylic acid-*stat*-2-(dimethylamino)ethyl methacrylate copolymers (245), from **1Z** and **2Z** with **6Z** and the *N*,*N*-diethylallylamine-*stat*-acrylic acid copolymers from **1Z** and **6Z** (246). More recently, synthesis and properties of novel polyampholytic terpolymers have been described (247–250). For example, the aqueous solution properties of novel ampholytic terpolymers of acrylamide, sodium 3-acrylamido-3-methylbutanoate **5Z** and 3-(acrylamidopropyl)trimethylammonium chloride **8Z** have been studied in detail (187).

It was not until the 1970s that the first block polyampholytes were reported (251,252). Anionic polymerization was used to prepare precursor AB diblock copolymers of 2-vinylpyridine **10Z** with trimethylsilyl methacrylate (TMSMA). The TMSMA residues were subsequently hydrolyzed to poly(methacrylic acid) residues to yield the corresponding AB diblock polyampholytes. Anionic polymerization has also been employed to prepare other block polyampholytes (253–258). GTP has also been successfully employed for the preparation of block polyampholytes. As with anionic polymerization, protected acid monomers must be employed since methacrylic acid (MAA) cannot be polymerized directly by this technique. A variety of protected monomers have been reported to be suitable as a means of introducing MAA residues, with 2-tetrahydropyranyl methacrylate being the most effective (Fig. 46).

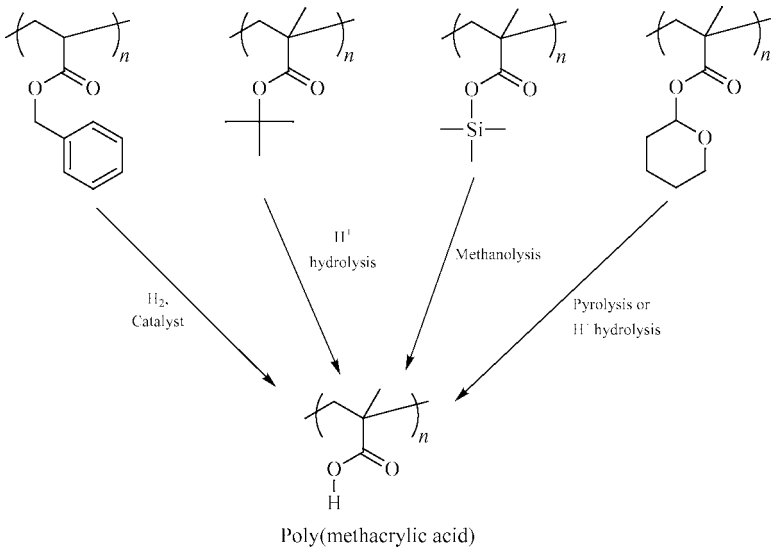

Fig. 46. Deprotection chemistry utilized to produce polymethacrylic acid or its salts.

For example, AB diblock and ABC triblock polyampholytes comprised of basic DMAEMA **6Z** and acidic MAA residues, and hydrophobic methyl methacrylate residues in the case of the triblocks, have been reported (128,259–262).

While these living polymerization techniques do offer the ability to prepare block polyampholytes they are both synthetically demanding and somewhat limiting with respect to monomer choice for example. There are a handful of reports detailing the synthesis of block polyampholytes using controlled/living polymerization techniques discussed earlier (Fig. 47). For example, Gabaston and co-workers have described the TEMPO-mediated SFRP of block copolymers of sodium 4-styrenesulfonate **11Z** with 4-(dimethylamino)methyl styrene **12Z** (133),

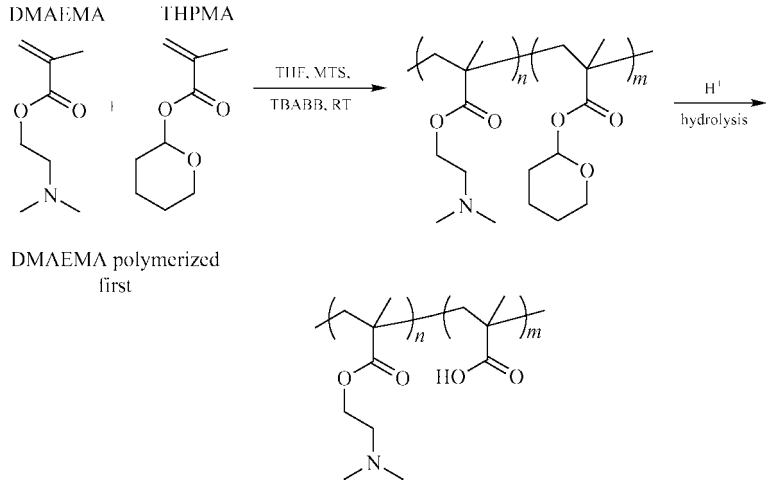

Fig. 47. GTP synthesis of AB diblock polyampholytes.

and several authors have reported the synthesis of block polyampholytes using ATRP although they still employed protecting group chemistry for the methacrylic acid residues (263–265).

Solution Properties. The aqueous solution behavior of polyampholytes is dictated by coulombic interactions between the basic and acidic residues. Polyampholytes have the ability to exhibit both polyelectrolyte and antipolylelectrolyte behavior in aqueous media. Which type of behavior is exhibited depends on factors such as solution pH, copolymer composition, the relative strengths of the acidic and basic residues, and the presence/absence of low molecular weight electrolyte (239). A feature of polyampholytes—in particular those comprised of weak acidic and basic residues—is the so-called *isoelectric point*, or IEP. This is simply defined as the solution pH at which the polyampholyte is electrically neutral. Statistical polyampholytes often remain soluble at and around the IEP whereas block polyampholytes tend to be soluble above and below but insoluble at this critical pH. The IEP may be determined either by titration or by measuring the reduced viscosity as a function of pH—the IEP also represents the point at which the polyampholyte chain is in its most compact conformation and thus corresponds to the minimum in reduced viscosity (239,266). With a knowledge of the respective pK_a's and copolymer composition it is also possible to predict the IEP (267).

Polybetaines. *Polybetaines* are materials in which the anionic and cationic functional species are part of the *same* mer unit (Fig. 48). Because of this the number of anionic, or potentially anionic, residues is always exactly equal to the number of cationic residues. The cationic residue in polymeric betaines is typically a quaternary ammonium species. The anionic functionality can vary and leads to the classification of polymeric betaines as sulfobetaines (sulfonate functional group), carbo or carboxybetaines (carboxylate functional groups), phosphobetaines (phosphate functional group), and etheneolatebetaines (dicyanoetheneolate functional group) (239).

Synthesis. Betaine monomers may be prepared in a number of different ways. For sulfobetaines, the most common, and easiest, method is to react a monomer containing a tertiary amine residue with either 1,3-propanesultone or 1,4-butanesultone (268). This is an extremely facile reaction and proceeds readily at RT in common solvents such as THF or CH_3CN to yield the corresponding sulfobetaine monomer. Alternatively, the tertiary amine functionality may be reacted

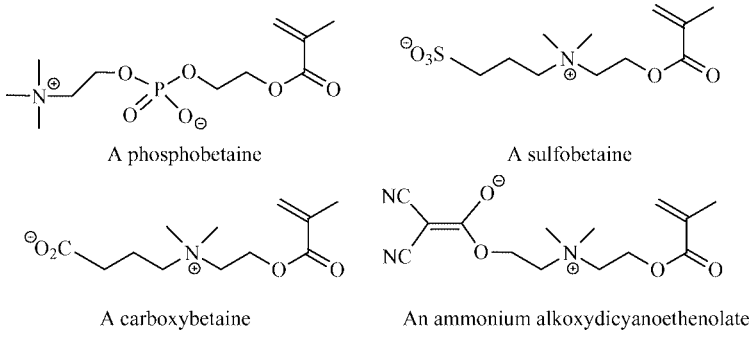

Fig. 48. General structures of selected methacrylic-based betaines.

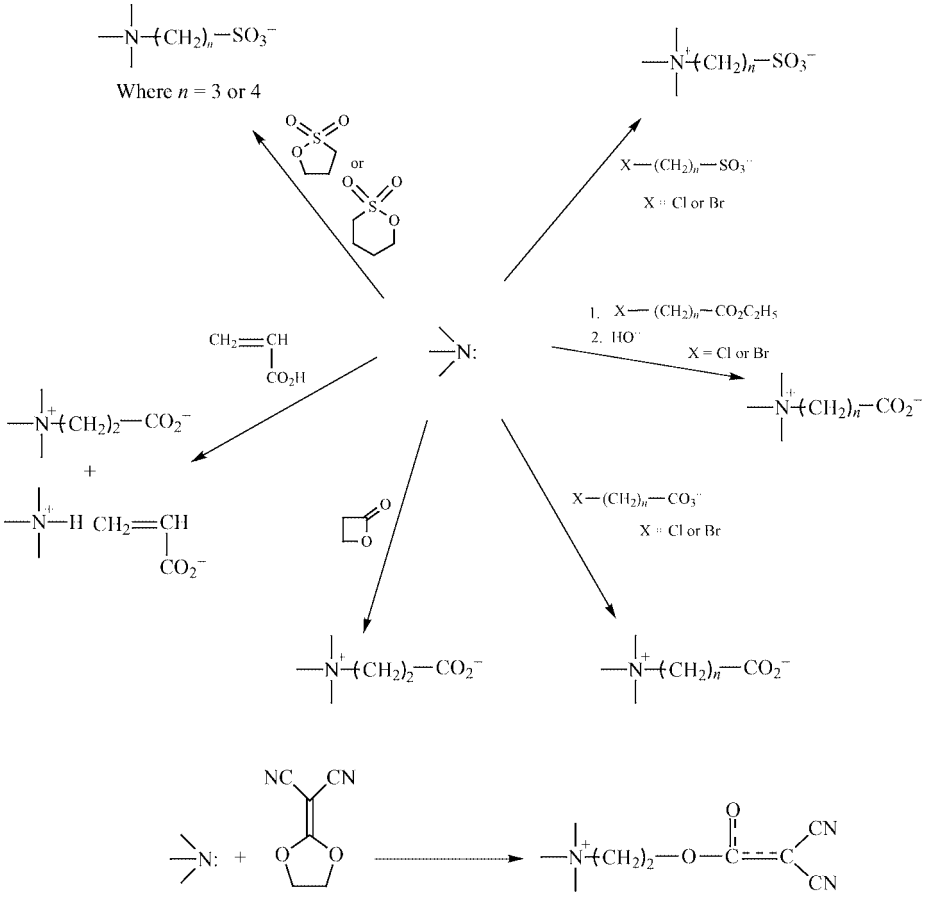

Fig. 49. General synthetic routes for sulfo/carboxybetaines.

with a haloalkylsulfonate species (269). Carboxybetaine monomers may be prepared via a number of different routes (Fig. 49). They may be obtained from the reaction of a suitable lactone (270) with a tertiary amine species, although this is somewhat limited to highly strained lactones to avoid competing nucleophilic attack at the carbonyl group. Alternatively they can be obtained from the Michael addition of a tertiary amine to acrylic acid (271), although again this route is prone to side reactions and simple salt formation. Perhaps the most versatile route for the preparation of carboxybetaines involves the reaction of a tertiary amine with a haloalkylcarboxylate to yield the carboxy betaine directly, or by reaction with the corresponding haloalkylester to yield the quaternized species followed by ester hydrolysis to yield the carboxybetaine (272,273).

Phosphobetaine monomers may also be prepared via a number of routes (239,274). Probably the most common phosphobetaine monomer is 2-(methacryloyloxy)ethyl phosphorylcholine (MPC), although other derivatives are also known (275–278). MPC is prepared from the reaction of 2-hydroxyethyl methacrylate with 2-chloro-2-oxo-1,3,2-dioxaphospholane, followed by ring

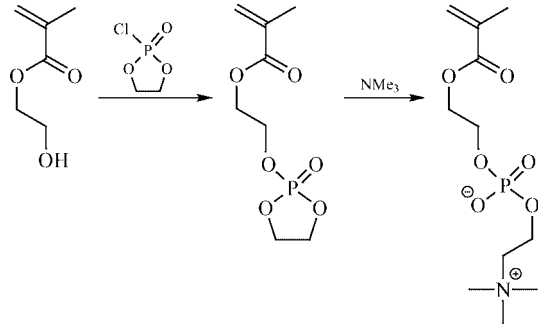

Fig. 50. Synthesis of MPC.

opening of the intermediate phospholane with trimethylamine (Fig. 50). This is a general synthetic procedure which can be applied to any alcohol functional monomer. There are very few examples of the dicyanoetheneolate betaines. These particular species are prepared from the reaction of a tertiary amine monomer with 2,2-dicyanoketene-1,2-ethylene acetal (279–281).

Polymeric betaines are most readily prepared by the direct polymerization of the betaine monomers, typically in aqueous salt solution. Since their initial report in 1957, by Ladenheim and Morawetz (282), there have been a large number of polymeric betaines reported based on many different families of monomers (239). Polymeric betaines may also be prepared under condensation polymerization conditions thus yielding polymers in which the betaine functionality is attached directly to the (co)polymer backbone (283–285).

Controlled structure polymeric betaines were reported for the first time only recently (286). The first examples were those prepared from the post-polymerization modification of poly(2-(dimethylamino)ethyl methacrylate) (PDMAEMA), and its block copolymers, which had been prepared under GTP conditions (286,287). Initial reports detailed the modification of hydrophilic-hydrophobic block copolymers, but this was subsequently extended to the selective modification of diamino hydrophilic-hydrophilic block copolymers (276).

The *direct* polymerization of betaine monomers in a controlled fashion has been reported by ATRP (288–291), and, most recently, via RAFT (38,43,292,293). Methacrylic derivatives of carboxy-, sulfo-, and phosphobetaines have been prepared via ATRP, while RAFT is more versatile with respect to monomer choice, and examples of styrenic, methacrylic and acrylamido sulfobetaines have been disclosed.

Solution Properties. Zwitterionic polymers show interesting aqueous solution behavior. As a general rule, they are *insoluble* in pure water due to the formation on intra- and interchain ion contacts resulting in an ionically cross-linked network-type structure. Polyampholytes and polybetaines which are not soluble become soluble upon the addition of low molecular weight electrolytes, such as NaCl (Fig. 51). This dissolution process can best be understood in terms of the low molecular weight electrolyte penetrating the ionically cross-linked network whereupon the ions screen the net attractive interactions between the polymer chains and hence promote solubility. The addition of the salt also results in antipolylelectrolyte behavior, ie chain expansion upon the addition of the salt.

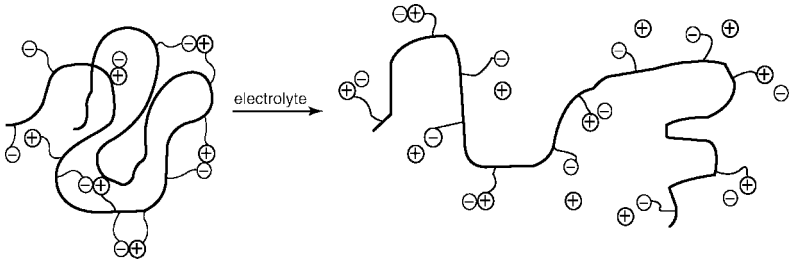

Fig. 51. Schematic illustration of polyampholyte response to added electrolyte.

Applications of Polyzwitterions. Polyzwitterions have wide-ranging applications. For example, statistical polyampholytes comprised of 2-vinylpyridine **10Z** and acrylic acid **1Z** have been evaluated as desalination membranes, while others have been used in sewage treatment, flocculation, coagulation, drilling fluids, enhanced oil recovery, and drag reduction.

Polymeric betaines have applications in areas similar to those of the polyampholytes described above. Additionally, phosphobetaines in particular have found application in the biomedical field. (Co)polymers comprised of MPC and various alkyl methacrylates (294,295) for example have been shown to exhibit both good bio and hemocompatability and have found application as coatings for medical devices such as catheters or arterial stents as well as materials for contact lens application. The success of MPC-based materials, and other phosphobetaines, is attributed to their biomimetic characteristics, ie their structural and chemical similarity to naturally occurring phospholipids. Recently, sulfobetaine-based materials were also shown to exhibit similar properties indicating that these bio/hemocompatability characteristics may not be unique to polymer phosphobetaines but perhaps to polybetaines in general (296).

Stimuli-Responsive Amphiphilic Polymers

Amphiphilic copolymers with appropriate balance of hydrophilic and hydrophobic sequences along or pendent to the micromolecular backbone can self-organize in water (297). In principle, intramolecular (closed) or intermolecular (open) associations can result. Intramolecular self assembly can, for example, lead to unimeric or multimeric micelles (Fig. 52**a,b**) with solution behavior resembling that of small molecule surfactants above their critical micelle concentration. Intermolecular assembly (Fig. 52**c**) often results in network or associative thickening behavior. Judicious choice of polymerization methods and conditions, monomer selection, post reactions, etc allows molecular construction of a wide variety of systems capable of self-assembly. Strategic placement of functional groups along the macromolecular backbone can also lead to reversible association in response to external stimuli including pH (298,299), ionic strength (300), light (301–303), temperature (304), and shear stress (297,305).

The earliest synthetic polymeric micelles, often referred to as *polysoaps*, were prepared as biological protein mimics (306–308). Copolymers synthesized

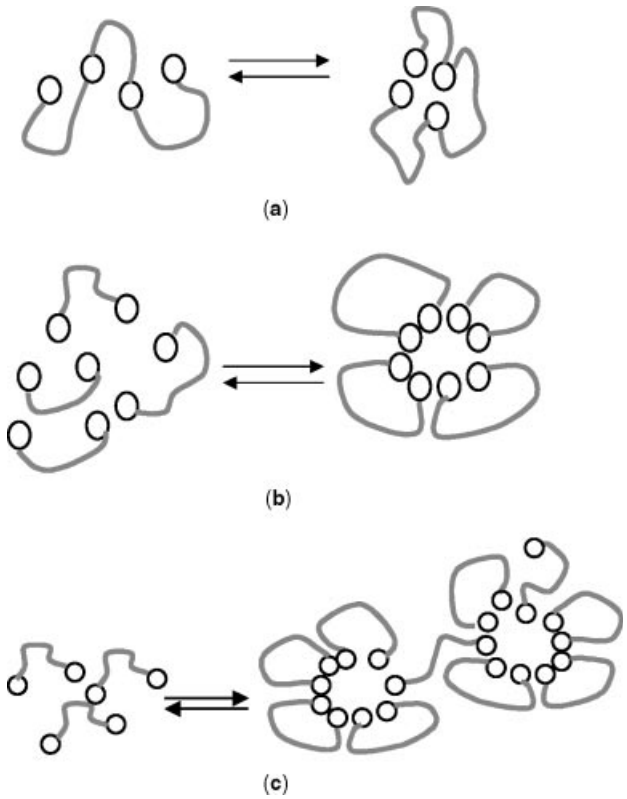

Fig. 52. Behavior of amphiphilic copolymers in response to stimuli.

by partial *n*-dodecylation of poly(2-vinyl pyridine) or by hydrolysis of poly(maleic anhydride-*alt*-alkylvinyl ethers) possessed surfactant-like properties in water (309–312). The initial associative thickeners, on the other hand, were prepared by (*1*) substitution of water-soluble cellulose derivatives with long chain alkyl groups (153,313–317) (*2*) partial esterification of poly(styrene-*alt*-maleic anhydride) with nonionic surfactants (318–321), (*3*) step growth polymerization of hydrophobically modified diisocyanates with poly(oxyethylene glycols) (322), or (*4*) by statistical chain growth free radical polymerization of a variety of hydrophobic and hydrophilic monomers under heterogeneous reaction conditions including emulsion polymerization (323,324) and micellar polymerization (325–330).

Despite a number of successes in preparing polymers with aqueous solution behavior depicted in Figs. 21**a** and 21**c**, little understanding of the nature of associative polymer domains existed prior to 1990. As well, studies of block copolymer associations had been limited to phase behavior in selective organic solvents. Since then, rapid developments in characterization of reversible microdomains via static and dynamic fluorescence spectroscopy (331–351), NMR spectroscopy (345,352–359) light scattering (171,175,360–364), and rheological techniques (365–370) have led to a better understanding of the structural parameters governing assembly/disassembly in water. Likewise, the development of

facile controlled/living free radical polymerization techniques for preparing block copolymers with well-defined structures has led to better models for study.

It can be established that the extent of closed or open associations depends on the architectures of the macromolecular chains. Molecular parameters affecting such associative behavior include hydrophilic and hydrophobic block lengths, placement and molecular weight of the segments, polymer concentration, flexibility and spacer lengths side-chain functionality. Responsiveness to pH, electrolyte, and to temperature changes depends markedly on the nature of the functional groups (cations, anions, zwitterions), their proximity to hydrophilic or hydrophobic units, and the ionic strength of the surrounding aqueous media. Some theoretical models have been put forth that describe unimolecular micelle formation progressing to bridged micelles and eventually networks (371–373).

Statistical Amphiphilic Polymers

Statistical amphiphilic polymers with ionic charges along the macromolecular backbone represent most of the stimuli-responsive systems reported in the literature. In principle, hydrophilic monomers from Figures 27, 33, 38, 43, or 44 can be copolymerized with hydrophobic comonomers or macromonomers under conditions allowing sufficient incorporation of the latter. The most successful methods have been "micellar" polymerization (324,325,347,348) in which high concentrations of surfactants are added to solubilize the hydrophobic monomer in the aqueous phase or emulsion polymerization utilizing macromonomers having amphiphilic character (323,324). Table 1 gives examples of associative polymers and the type of responsiveness reported in the literature. A comprehensive review (305) presents details of the synthetic routes to and behavioral characteristics of associative polyelectrolytes as determined by a wide variety of analytical techniques.

Well-Defined Amphiphilic Copolymers. Well-defined, controlled structure amphiphilic copolymers may be prepared using a range of polymerization techniques that includes anionic, cationic, and controlled free radical approaches. The materials may be "simple" AB diblock copolymers or more structurally complex species such as ABA or ABC triblock copolymers for example.

Hydrophilic-Hydrophobic Block Copolymers. These materials represent the "simplest" type of amphiphilic block copolymer. Materials are comprised of one block which is inherently hydrophobic, such as polystyrene or poly(methyl methacrylate), and a second block which is hydrophilic such as poly(methacrylic acid). For example, anionic polymerization may be employed for the synthesis of AB diblock copolymers comprised of styrene with 2- (438) or 4-vinylyridine (439). In the case of the styrene-2-vinylpyridine copolymers, self-assembly, under appropriate aqueous conditions, leads to the formation of block copolymer micelles with styrene forming the hydrophobic core and the 2-vinylpyridine forming the stabilizing corona. These block copolymer micelles are highly stable in 0.1 *M* HCl. Similarly, styrene–acrylic acid block copolymers may likewise be prepared via anionic polymerization using *tert*-butyl acrylate as a protected precursor for the acrylic acid residues. Such block copolymers exhibit similar self-assembly behavior in aqueous media (440,441). Other examples of such hydrophilic-hydrophobic

Table 1. Copolymer Compositions[a] Responsiveness, and References for Stimuli-Responsive Polyelectrolytes

Polymer Composition	Response	Ref.
K-S	pH, salt	(312,374–380)
K-T	pH, salt, shear	(336,374,381–383)
E-H-Fl	pH, salt, shear	(374,384)
I-P	salt, shear	(374,385–388)
G-B-R	salt, shear	(374,389,390)
E-Q-B	pH, salt, shear	(374,391,392)
E-B-Fl	pH, salt, shear	(374,393)
B-R-D	pH, salt, shear	(365,366,374)
E-Q	shear	(327,328,374,393–404)
E-R	shear	(327,328,374,393–404)
E-S	shear	(327,328,374,393–404)
E-U	shear	(374,405,406)
E-B-U	pH, salt, shear	(374)
B-Q	pH, salt, shear	(305,407)
B-Fl	pH	(305,408,410)
A-S	pH, salt, shear	(305,411)
B-Fl	pH, salt, shear	(305,412)
B-Q	pH, salt, shear	(305,345,413)
A-R	pH, salt, shear	(305,363,364)
B-E-Q	pH, salt, shear	(305,404,414,415)
B-Fl	pH, salt, shear	(305,349,409)
C-F-Q	pH, salt, shear	(305,416)
Y	pH, salt, shear	(305,417)
Z	pH, salt, shear	(305,418)
Z-T	pH, salt, shear	(305,382)
Z-T-Fl	pH, salt, shear	(305,336,381)
I-P-Fl	pH, salt, shear	(305,385,419–422)
I-R	pH, salt, shear	(305,423–426)
I-R-P	pH, salt, shear	(305,427)
E-A-R	pH, salt, shear	(305,428)
E-I-R	pH, salt, shear	(305,429,430)
O-V	pH, salt, shear	(305,431–436)
U-M	pH, salt, shear	(276,305)
U-N	pH, salt, shear	(305,437)

[a]Letters refer to repeating units in Figure 53.

block copolymers capable of supramolecular self-assembly include the poly(2-(dimethylamino)ethyl methacrylate-*block*-methyl methacrylate) (442). and the poly(3-(*N*-2-methacroyloyethyl)-*N*,*N*-dimethylammonio)propanesulfonate-*block*-methyl methacrylate) copolymers (287,443). In both instances the block copolymers were prepared via group transfer polymerization. Cationic polymerization also offers a route to amphiphilic vinyl ether-based AB diblock copolymers. For example, the synthesis and micellization properties of isobutyl vinyl ether-*block*-methyl tri(ethyleneglycol) vinyl ether copolymers have been reported (444). Also the self-association of AB diblocks comprised of methyl tri(ethyleneglycol) vinyl ether (hydrophilic block) and benzyl vinyl ether (hydrophobic block) have

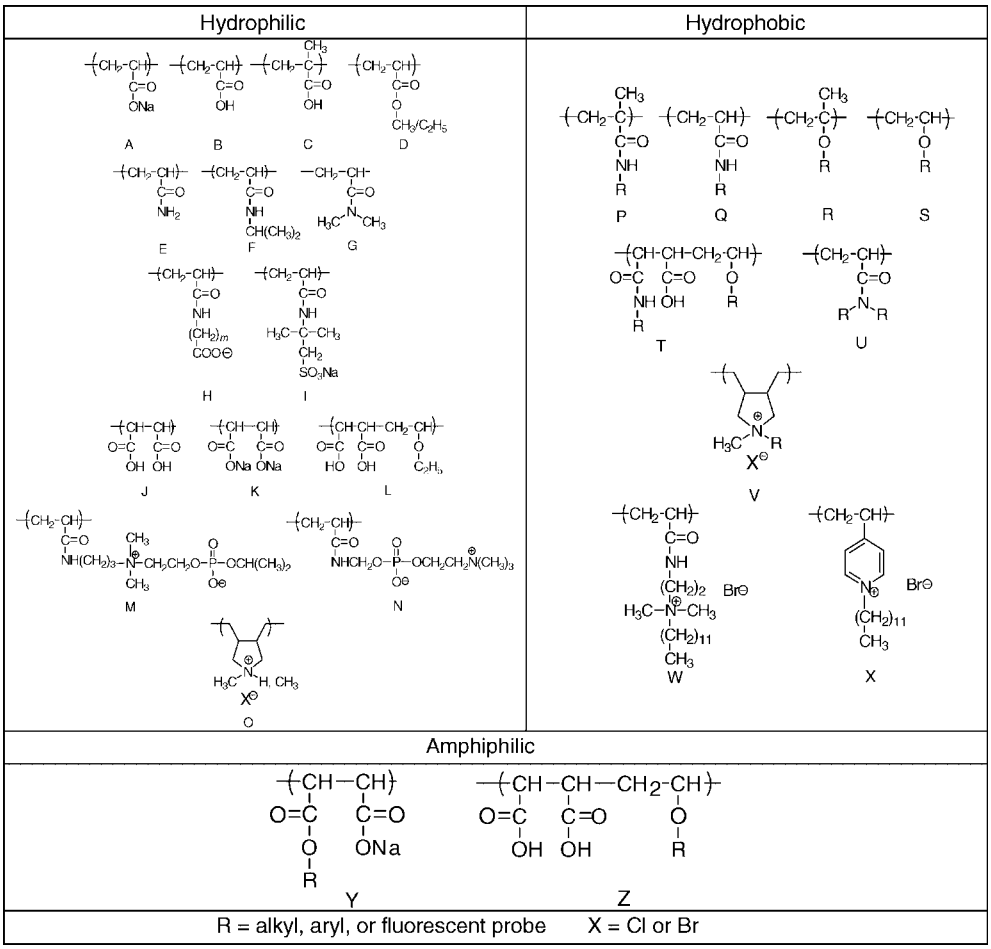

Fig. 53. Polymer segments utilized in statistical polymers with stimuli-responsive associative behavior in water. For polymers incorporating a fluorescent probe the letters Fl are used in Table 1.

been investigated (445). In water, micelles with hydrodynamic diameters in the range 10–26 nm were observed depending on the molar composition of the block copolymer.

Hydrophilic/Tunably Hydrophilic/Hydrophobic Block Copolymers. The next level of complexity for amphiphilic block copolymers are those comprised of one block which is permanently hydrophilic with the second block being tunably hydrophilic/hydrophobic, ie under a set of conditions A, the second block is readily water soluble and thus the block copolymer exists as unimers, but upon the application of a certain stimulus (change in pH or temperature for example) to condition B the second block becomes hydrophobic. Provided appropriate block copolymer compositions are employed this will lead to self-assembly. Additionally, such behavior is typically completely reversible. While there are now numerous examples of such “smart” self-assembly these types of systems have not been

as thoroughly investigated as the inherently hydrophilic/hydrophobic species, with perhaps one notable exception being the PEO/PPO and PEO/PPO/PEO, PPO/PEO/PPO block copolymers.

Group transfer polymerization has proven to be an extremely useful technique for the synthesis of such AB diblock copolymers. For example, the synthesis of AB diblock copolymers in which the A block was 2-(dimethylamino)ethyl methacrylate (**1C** in Fig. 38) and the B block was either **2C** or **3C** in Figure 33 have been reported. **1C** is temperature responsive whereas **2C** and **3C** are both pH responsive. At low pH when both the tertiary amine blocks (**1C** + **2C** or **1C** + **3C**) are protonated the block copolymers are molecularly dissolved. Raising the solution pH above the p*K*a of tertiary amine residues for **2C** and **3C** renders these blocks hydrophobic and as such the block copolymers self-assemble to form micelles with the hydrophobic **2C** (or **3C**) residues in the core, stabilized by coronal chains of 1. Supramolecular self-assembly is completely reversible—lowering of the pH back below the respective p*K*a's results in molecular redissolution (183).

More recently controlled free radical polymerization methodologies have been employed for the preparation of novel "smart" AB diblock copolymers. Nitroxide-mediated polymerization was utilized for the synthesis of sodium 4-styrenesulfonate-block-sodium 4-vinylbenzoate block copolymer (133). These strong acid/weak acid species exhibit reversible pH-induced self-assembly, with the sodium 4-styrenesulfonate residues remaining ionized and thus permanently hydrophilic over the useful pH range whereas the sodium 4-vinylbenzoate block can be reversible protonated (the carboxylate residue has a pK_a ~4.0). The same block polymers can also be prepared via RAFT, albeit with somewhat more control. Other workers reported the preparation of such AB diblock copolymers as well as some analogous amine-based styrenic diblock copolymers, (48) shown in Figure 54.

Similarly, such AB diblocks may be prepared based on the acrylamido family of monomers. For example, the synthesis of novel AB diblock copolymers comprised of the two anionic monomers sodium 2-acrylamido-2-methylpropanesulfonate (AMPS) and sodium 3-acrylamido-3-methylbutanoate (AMBA) have been reported (42,44). By analogy with the styrenic block copolymers, these AMPS-AMBA species also exhibit reversible pH-induced self-assembly by virtue of the fact that the AMBA residues may be reversible protonated, switching the residues from a hydrophilic (high pH) to a hydrophobic (low pH) state. Similar AB diblocks of AMPS with sodium 6-acrylamidohexanoate which also exhibit pH-induced micellization have been reported by Yusa and co-workers (45) RAFT has

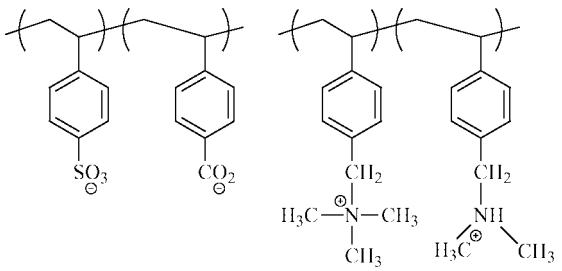

Fig. 54. Responsive AB block copolymers from ionic styrenic monomers.

additionally proven very useful for the preparation of AB diblock copolymers comprised of blocks from different monomer families. For example, AB diblocks of *N*,*N*-dimethylacrylamide (DMA) with *N*,*N*-dimethylbenzyl vinyl amine (DMBVA) were recently disclosed. These particular blocks are also capable of undergoing reversible pH-induced micellization (222). The DMA residues are nonionic, permanently hydrophilic whereas the styrenic-based DMBVA block is water soluble in its protonated form, but hydrophobic in its nonionized state. As such, simply raising the pH of an acidic solution of the block copolymer results in self-assembly and the formation of aggregates with the hydrophobic DMBVA blocks residing in the core which is stabilized by the DMA block. RAFT has also been utilized for the preparation of AB diblocks in which one of the blocks is a salt-responsive specie (293). For example, AB diblocks of *N*,*N*-dimethylacrylamide with 3-[2-(*N*-methylacrylamido)-ethyldimethylammonio]propanesulfonate (MAEDAPS).

Doubly "Smart" Block Copolymers. Doubly "smart" or responsive copolymers are those in which *both* the blocks of the copolymer are tunably hydrophilic/hydrophobic. As such this potentially facilitates the preparation of both normal and inverse micelles in the *same* solvent (NB: normal and inverse micelles are well known but switching between the two often requires a change of solvent). Some authors have termed such materials *"schizophrenic" block copolymers*. At present these represent the least studied of the amphiphilic block copolymers. Examples of such materials include the poly(2-(*N*-morpholino)ethyl methacrylate-*block*-2-(diethylamino)ethyl methacrylate) (177,446) and the poly(propylene oxide-*block*-2-(diethylamino)ethyl methacrylate) copolymers (447). A number of these types of block copolymers have been studied (263,264,448,449). As a representative example, a precursor poly(2-(dimethylamino)ethyl methacrylate-*block*-2-(*N*-morpholino)ethyl methacrylate) (DMAEMA-MEMA) copolymer was reacted with 1,3-propanesultone to yield the corresponding sulfopropylbetaine-MEMA block copolymer (Fig. 55) (448). At temperatures between 30 and 40°C a block copolymer comprised of an equimolar ratio of the two comonomers exists as molecularly dissolved unimeric chains. Upon raising the temperature above the cloud point of the MEMA block, the copolymer self-assembles forming polymeric micelles with the now-hydrophobic MEMA residues residing in the core with the sulfobetaine blocks in the corona.

Sulfobetaine-core micelles were obtained by lowering the solution temperature below 20°C at which point increased attractive electrostatic interactions result in phase separation of the sulfobetaine block and thus micelle formation. A similar doubly temperature responsive block copolymer, prepared via RAFT, was reported which was based on acrylamido monomers (292).

Shell and Core Cross-Linked Nanoassemblies. Shell or core cross-linked nanoassemblies represent a group of materials which can, in principle, be derived from any of the amphiphilic species described in the earlier sections. Clearly the self-assembled structures described above are dynamic species. However, one can envisage the need for "locked" structures for certain applications. One method to achieve this is via cross-linking of either the coronal or core chains. To facilitate either approach there must be a suitable reactive species in the core or corona susceptible to chemical modification after self-assembly.

Shell cross-linked micelles, also referred to as *knedel* or *SCK micelles*, were first reported in 1997 (450,451). For example, an amphiphilic AB diblock

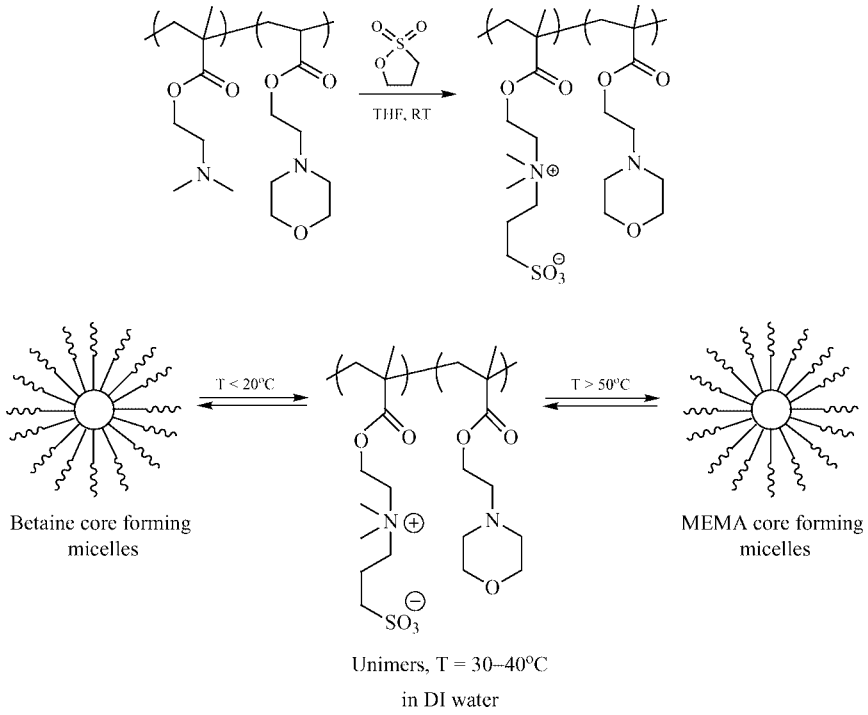

Fig. 55. An example of a "schizophrenic," methacrylic-based AB diblock copolymer and conditions leading to self-assembly.

copolymer comprised of hydrophobic polystyrene with hydrophilic partially quaternized poly(4-vinylpridine) was prepared by the sequential living anionic polymerization of styrene and 4-vinyl pyridine followed by quaternization of some of the 4-vinylpyridine residues with 4-vinylbenzyl chloride. Micelles are prepared by dissolving the quaternized block copolymer in a mixture of water and THF. Finally, shell cross-linking is accomplished by polymerizing the styrenic residues in the shell (present as a result of the quaternization reaction) in the presence of a free radical initiator (452). Examples in which the micelle coronal shell consists of hydrophilic acrylic acid residues, with a variety of hydrophobic cores, may be conveniently shell cross-linked using 2,2′-(ethylenedioxy)bis(ethylamine). Thus, cross-linking is achieved via an amidation reaction using a bifunctional primary amine (453–457). Other examples of these novel nanomaterials include those with polysilane cores and partially cross-linked poly(methacrylic acid) coronas (458,459), and micelles in which the reactive, cross-linkable functionality is either methacrylic acid or DMAEMA residues, with the actual cross-linking being achieved with bis-(2-iodoethoxy)ethane (460–462). The effectiveness of bis-(2-iodoethoxy)ethane as a cross-linking agent is illustrated in Figure 56.

Here so-called Type I and Type II zwitterionic SCK micelles can be prepared from the hydrophilic-hydrophobic precursors poly(2-(dimethylamino)ethyl methacrylate-*block*-2-tetrahydropyranyl methacrylate) (DMAEMA-THPMA) copolymers prepared via group transfer polymerization (128,129,461). Micellization of the DMAEMA-THPMA block copolymers in a water/THF mixture

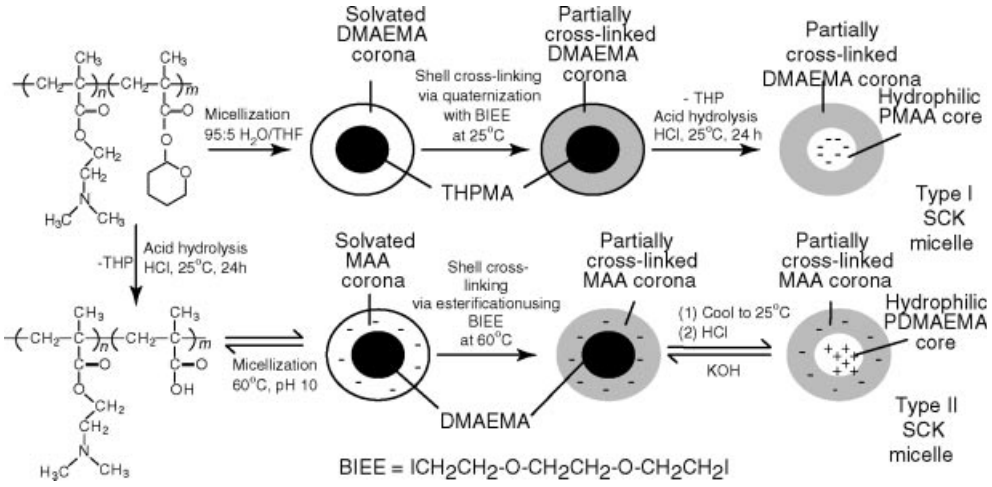

Fig. 56. An example of bis-(2-iodoethoxy)ethane as a cross-linking agent.

(95:5) results in the formation of core-shell structures in which the hydrophobic THPMA species forms the core and the hydrophilic DMAEMA species the corona. The reactive tertiary amine residues in the coronal may be cross-linked using bis-(2-iodoethoxy)ethane in a *quaternization* reaction (Menshutkin Reaction). Subsequent hydrolysis of the micelles cores leads to the formation of the Type I SCK species. Alternatively, the DMAEMA-THPMA precursor block copolymers may be initially deprotected to form the block polyampholytes. Heating an aqueous solution of this block polyampholyte above the cloud point of the DMAEMA residues results in the formation of inverse micelles in which the now-hydrophobic DMAEMA residues form the micelle core and ionized poly(methacrylic acid) chains form the corona. These carboxylate coronal chains may also be cross-linked using bis-(2-iodoethoxy)ethane, in this instance via an esterification reaction.

A potential drawback of shell cross-linking is the need to perform such chemistries under relatively dilute conditions to avoid the occurrence of inter-particle cross-linking. However it was recently demonstrated that SCK micelles could be successfully prepared at high solids with ABC triblock copolymers in which the *C block* forms the *micelle core*, the *A block the outer coronal chains* and the *cross-linkable B block the inner coronal chains*. Here, the outer A block is effectively acting as a steric barrier to inter-particle cross-linking (463,464).

Most recently the core cross-linking approach was adopted for the preparation of novel nanoassemblies derived from pH-responsive AB diblock copolymers prepared via RAFT (222). Here the A block was the permanently hydrophilic DMA species with the tunably hydrophilic/hydrophobic DMBVA forming the B block. In aqueous media, at high pH, these block copolymers form core-shell structures with the DMA residues forming the corona and the DMVBA chains in the core. Addition of a hydrophobic, difunctional, alkyl halide namely 1,4-bisbromomethylbenzene results in this species being sequestered into the hydrophobic core of the micelles where it reactions with the tertiary amine residues via the Menshutkin reaction to yield the core-cross-linked species. Successful core cross-linking was

verified via NMR spectroscopy, dynamic light scattering and transmission electron microscopy.

Concluding Remarks

Water-soluble polymers are an extremely important class of materials that permeate every facet of our lives. This class of materials encompasses a wide range of interesting species ranging from naturally occurring proteins, peptides, RNA, DNA, and sugars (carbohydrates) to complex synthetic nanoassemblies such as the well-defined core-cross-linked AB diblock polymeric micelles.

Clearly there have been significant advances in the field of water-soluble polymers since the previous edition of this encyclopedia. Arguably the most important development in recent years has been the discovery and application of more facile controlled/living polymerization techniques for the synthesis of highly functional, well-defined, model, materials. Of these, the controlled/living free radical polymerization techniques, and especially reversible addition–fragmentation chain transfer (RAFT) are proving to be especially versatile.

It is likely that such developments will continue to revolutionize water-soluble polymer synthesis in the years to come with chemists taking up the challenge to prepare ever more complex structures capable of supramolecular self-assembly for a wide variety of specialized applications.

BIBLIOGRAPHY

"Water-Soluble Polymers" in *EPSE* 2nd ed., Vol. 17, pp. 730–784, by C. L. McCormick, University of Southern Mississippi; J. Bock and D. N. Schulz, Exxon Research.

1. http://www.mathemagic.com/MOBM/fractals.html.
2. P. J. Flory, *Principles of Polymer Chemistry*, Cornell University Press, Ithaca, N.Y., 1953.
3. J.-L. Barrat and J.-F. Joanny, *Adv. Chem. Phys.* **94**, 1–66 (1996).
4. A. V. Dobrynin, R. Colby, and M. Rubinstein, *Macromolecules* **28**, 1859–1871 (1995).
5. F. Franks, ed., *Water: A Comprehensive Treatise*, Vol. 4, Plenum Press, New York, 1975.
6. P. Molyneaux, *Water-Soluble Synthetic Polymers*, Vols. 1 and 2, CRC Press, Inc., Boca Raton, Fla., 1984.
7. C. Tanford, *The Hydrophobic Effect: Formation of Micelles and Biological Membranes*, John Wiley & Sons, Inc., New York, 1973.
8. W. Saenger, *Annu. Rev. Biophys. Chem.* **16**, 93 (1987).
9. J. T. Edsal and H. A. McKenzie, *Adv. Biophys.* **16**, 53 (1978).
10. J. L. Finney, *J. Mol. Biol.* **119**, 415 (1978).
11. R. M. Fuoss, *J. Polym. Sci.* **3**, 603 (1948).
12. O. W. Webster, W. R. Hertler, D. Y. Cogah, W. B. Farnham, and T. V. TajanBabu, *J. Am. Chem. Soc.* **105**, 5706 (1983).
13. U.S. Pat. 4,417,034 (1984), O. W. Webster (to E. I. du Pont de Nemours & Co., Inc.).
14. Y. Nagasaki, Y. Sato, and M. Kato, *Macromol. Rapid Commun.* **18**, 827 (1997).
15. M. Vamvakaki, N. C. Billingham, and S. P. Armes, *Macromolecules* **32**, 2088 (1999).
16. G. Moad, D. H. Soloman, S. R. Johns, and R. I. Willing, *Macromolecules* **15**, 1188 (1982).

17. M. K. Georges, P. M. Veregin, P. M. Kazmeier, and G. K. Hamer, *Macromolecules* **26**, 2987 (1993).
18. M. Kato, M. Kamigaito, M. Sawamoto, and T. Higashimura, *Macromolecules* **28**, 1721 (1995).
19. M. Kato, M. Kamigaito, M. Sawamoto, and T. Higashimura, *Polym. Prep. Jpn.* **43**, 1792 (1994).
20. T. Ando, M. Kato, M. Kamigaito, and M. Sawamoto, *Macromolecules* **29**, 1070 (1996).
21. J.-S. Wang and K. Matyjaszewski, *Macromolecules* **28**, 7572 (1995).
22. J.-S. Wang and K. Matyjaszewski, *J. Am. Chem. Soc.* **117**, 5614 (1995).
23. T. E. Patten, J. Xia, T. Abernathy, and K. Matyjaszewski, *Science* **272**, 7970 (1996).
24. J. Chiefari, Y. K. Chong, F. Ercole, J. Krstina, J. Jeffrey, T. P. T. Le, R. T. A. Mayadunne, G. F. Meijs, C. L. Moad, G. Moad, E. Rizzardo, and S. H. Thang, *Macromolecules* **31**, 5559 (1998).
25. M. Desarac, D. Charmot, X. Franck, and S. A. Zard, *Macromol. Rapid Commun.* **21**, 1035 (2000).
26. R. T. A. Mayadunne, E. Rizzardo, J. Chiefari, Y. K. Chong, G. Moad, and S. H. Thang, *Macromolecules* **32**, 6977 (1999).
27. D. Charmot, P. Corpart, H. Adam, S. Z. Zard, T. Biadatti, and G. Bouhadir, *Macromol. Symp.* **150**, 23 (2000).
28. S. Yamago, K. Iida, and J.-I. Yoshida, *J. Am. Chem. Soc.* **124**, 2874 (2002).
29. S. Yamago, K. Iida, and J.-I. Yoshida, *J. Am. Chem. Soc.* **124**, 13666 (2002).
30. A. Goto, Y. Kwak, T. Fukuda, S. Yamago, K. Iida, M. Nakajima, and J. I. Yoshida, *J. Am. Chem. Soc.* **125**, 8720 (2003).
31. S. Yamago, K. Iida, M. Nakajima, and J.-I. Joshida, *Macromolecules* **36**, 3793 (2003).
32. D. M. Haddleton, E. Depaquis, E. J. Kelly, D. Kukulj, S. R. Morsley, S. A. F. Bon, M. D. Eason, and A. G. Steward, *J. Polym. Sci., Polym. Chem.* **39**, 2378–2384 (2001).
33. A. A. Gridnev and S. D. Ittle, *Chem. Rev.* **101**, 3611 (2001).
34. T. M. Trinka and R. H. Grubbs, *Acc. Chem. Res.* **34**, 18 (2001).
35. D. M. Lynn, B. Mohr, and R. H. Grubbs, *J. Am. Chem. Soc.* **120**, 1627 (1998).
36. D.-J. Liaw, C.-C. Huang, and P.-L. Wu, *Polymer* **42**, 9371 (2001).
37. E. Khosravi and Szymanska-T. Buzar, eds., *Ring Opening Metathesis Polymerization and Related Chemistry*, Kluwer Academic Publishers, Boston, Mass., 2002.
38. A. B. Lowe and C. L. McCormick, *Aust. J. Chem.* **55**, 367 (2002).
39. C. L. McCormick and A. B. Lowe, *Acc. Chem. Res.* **37**, 312 (2004).
40. K. Matyjaszewski, ed., *Controlled/Living Radical Polymerization*, Vol. 768, American Chemical Society, Washington, D.C., 2000.
41. K. Matyjaszewski, ed., *Advances in Controlled/Living Radical Polymerization*, Vol. 854., American Chemical Society, Washington, D.C., 2003.
42. B. S. Sumerlin, M. S. Donovan, Y. Mitsukami, A. B. Lowe, and C. L. McCormick, *Macromolecules* **34**, 6561 (2001).
43. M. S. Donovan, B. S. Sumerlin, A. B. Lowe, and C. L. McCormick, *Macromolecules* **35**, 8663 (2002).
44. B. S. Sumerlin, A. B. Lowe, D. B. Thomas, and C. L. McCormick, *Macromolecules* **36**, 5982 (2003).
45. S.-I. Yusa, Y. Shimada, Y. Mitsukami, T. Yamamoto, and Y. Morishima, *Macromolecules* **36**, 4208 (2003).
46. A. B. Lowe, B. S. Sumerlin, and C. L. McCormick, *Polymer* **44**, 6761 (2003).
47. D. B. Thomas, A. J. Convertine, R. D. Hester, A. B. Lowe, and C. L. McCormick, *Macromolecules* **37**, 1735 (2004).
48. Y. Mitsukami, M. S. Donovan, A. B. Lowe, and C. L. McCormick, *Macromolecules* **34**, 2248 (2001).

49. D. B. Thomas, A. J. Convertine, L. J. Myrick, C. W. Scales, A. B. Lowe, N. Ayres, and C. L. McCormick, *Macromolecules* (in press).
50. D. B. Thomas, B. S. Sumerlin, A. B. Lowe, and C. L. McCormick, *Macromolecules* **36**, 1436 (2003).
51. J. D. Watson and F. H. C. Crick, *Nature* **171**, 737 (1953).
52. E. Chargaff, *Experientia* **6**, 201 (1950).
53. M. H. F. Wilkins, A. R. Stokes, and H. R. Wilson, *Nature* **171**, 738 (1953).
54. D. L. Nelson and M. M. Cox, *Principles of Biochemistry*, 3rd ed., Worth Publishers, Inc., New York, 2000, p. 913.
55. D. Cooper, ed., *Nature Encyclopedia of the Human Genome*, Nature Publishing Group, London, 2003.
56. K. Itakura, J. J. Rossi, and R. B. Wallace, *Annu. Rev. Biochem.* **53**, 323 (1984).
57. D. Freifelder, *The DNA Molecule--Structure and Properties*, W. H. Freeman & Co., San Francisco, 1978.
58. V. Schranke and R. Allshire, *Science* **301**, 1069 (2003).
59. A. Kornberg, *DNA Replication*, W. H. Freeman & Co., San Francisco, 1980.
60. M. J. Chamberlin, *RNA Polymerasses: An Overview*, Cold Spring Harbor Laboratory, Cold Spring Harbor, N.Y., 1976.
61. N. Arnheim and H. Erlich, *Annu. Rev. Biochem.* **61**, 131 (1992).
62. M. E. Scott, *Am. Biotech. Lab.* **3**, 131 (1985).
63. D. M. Nelson, A. L. Lehninger, and M. M. Cox, *Principles of Biochemistry*, 3rd ed., Worth Publishers, Inc., New York, 2000.
64. A. L. Lehninger, *Principles of Biochemistry*, Worth Publishers, Inc., New York, 1982.
65. A. Fersht, *Protein Science: A Guide to Enzyme Catalysis and Protein Folding*, W. H. Freeman & Co., New York, 1999.
66. R. B. Merrifield, *J. Am. Chem. Soc.* **85**, 2149 (1963).
67. R. B. Merrifield, *Adv. Enzymol.* **32**, 221 (1969).
68. E. Gross and Meienhofer, eds., *The Peptides, Analysis, Synthesis, and Biology*, Academic Press, Inc., Orlando, Fla., 1979, pp. 43–48.
69. F. S. Collins, E. D. Green, A. E. Guthmacher, and M. S. Guyer, *Nature* **422**, 835 (2003).
70. R. S. Morrison, Y. Kinoshita, M. D. Honson, and T. P. Conrad, *Protein Chem.* **65**, 1 (2003).
71. A. G. Walton and J. Blackwell, *Biopolymers*, Academic Press, Inc., Orlando, Fla., 1973, pp. 12–13.
72. D. A. Brant and G. S. Buliga, in R. R. Colwell, ed., *Biotechnology of Marine Polysaccharides*, Hemisphere Publishers, Washington, D.C., 1985, pp. 30–73.
73. R. L. Whistler and E. F. Paschall, *Starch: Chemistry and Technology*, Academic Press, Inc., Orlando, Fla., 1965.
74. R. L. Whistler, *Industrial Gums*, 2nd ed. Academic Press, Inc., Orlando, Fla., 1973.
75. P. A. Sanford and A. Laskin, eds., *Extracellular Microbial Polysaccharides*, American Chemical Society, Washington, D.C., 1977.
76. R. L. Davidson, *Handbook of Water-Soluble Gums and Resins*, McGraw-Hill, Inc., New York, 1980.
77. P. M. Collins, ed., *Carbohydrates*, Chapman and Hall, London, 1987 p. 313.
78. R. F. Gould, ed., *Cabohydrate Sulfates*, American Chemical Society, Washington, D.C., 1978.
79. B. V. McCleary, A. H. Clark, I. C. Dea, and D. A. Rees, *Carbohydr. Res.* **139**, 237 (1985).
80. C. L. McCormick, in D. A. Brant and G. S. Buliga, eds., *Biotechnology of Marine Polysaccharides*, Hemisphere Publichers, Washington, D.C., 1985, pp. 232–245.
81. T. Bishop and H. J. Jennings, *The Polysaccharides*, Vol. I, Academic Press, Inc., Orlando, Fla., 1982, p. 291.
82. R. Moorhous, M. D. Walkinshaw, S. Arnott, ACS Symposium Series 45, American Chemical Society, Washington, D.C., 1977, pp. 90–98.

83. P. A. Sanford, *Pure Appl. Chem.* **56**, 879 (1984).
84. W. Pigman and D. Horton, eds., *The Carbohydrates*, Vols. IIA and IIB, Academic Press, Inc., Orlando, Fla., 1970.
85. E. Casu, in R. S. Tipson and D. Horton, eds., *Advances in Carbohydrate Chemistry and Biochemistry*, Academic Press, Inc., Orlando, Fla., 1985, p. 51.
86. T. P. Nevell and S. H. Zeronian, *Cellulose Chemistry and Its Applications*, John Wiley & Sons, Inc., New York, 1985.
87. R. Y. Lochhead, in R. Y. Lochhead, ed., *Encyclopedia of Polymers and Thickeners for Cosmetics*, Vol. 108, Allured Publishing Corp., 1993, pp. 95–135.
88. C. L. McCormick and P. A. Callais, *Polymer* **28**, 2317 (1987).
89. U.S. Pat. 4,278,790 (1981), C. L. McCormick.
90. U.S Pat. 4,024,335 (1977), M. D. Nicholson.
91. U.S. Pat. 3,447,939 (1969), D. L. Johnson.
92. R. A. A. Muzzarelli, *Carbohydr. Polym.* **3**, 53 (1983).
93. J. P. Zikakis, ed., *Chitin, Chitosan and Related Enzymes*, Academic Press, Inc., Orlando, Fla., 1984.
94. C. L. McCormick and D. K. Lichatowich, *J. Polym. Sci.* **17**, 479 (1979).
95. C. L. McCormick, D. K. Lichatowich, J. A. Pelezo, K. W. Anderson, and C. E. Carraher, eds., ACS Symposium Series 121, American Chemical Society, Washington, D.C., 1980, p. 371.
96. H. G. Elias, *Macromolecules* **2**, 1113 (1977).
97. Ref. 6, p. 31.
98. W. M. Kulicke, R. Kniewske, and J. Klein, *Prog. Polym. Sci.* **8**, 373 (1982).
99. R. A. M. Thomson, in C. A. Finch, ed., *Chemistry and Technology of Water Soluble Polymers*, Plenum Press, New York, 1983, pp. 31–70.
100. N. M. Bikales, in N. M. Bikales, ed., *Water Soluble Polymers*, Plenum Press, New York, 1973, pp. 213–225.
101. D. L. Visioli, M. S. El-Assar, and J. W. Vanderoff, *Polym. Prep. (Am. Chem. Soc., Div. Polym. Chem.)* **51**, 258 (1984).
102. J. M. Vanderhoff, D. L. Visioli, and M. S. El-Assar, *Polym. Prep. (Am. Chem. Soc. Div. Polym. Chem.)* **54**, 375 (1986).
103. U.S. Pat. 3,624,019, A. J. Frisque (to Nalco Chemical).
104. F. Candau, U. S. Leong, and R. M. Fitch, *J. Polym. Sci., Polym. Chem.* **23**, 167 (1984).
105. Y. K. Chong, T. P. T. Le, G. Moad, E. Rizzardo, and S. H. Thang, *Macromolecules* **32**, 2071 (1999).
106. C. Ladaviere, N. Dorr, and J. P. Claverie, *Macromolecules* **34**, 5370 (2001).
107. J. Loiseau, N. Doerr, J. M. Suau, J. B. Egraz, M. F. Llauro, C. Ladaviere, and J. Claverie, *Macromolecules* **36**, 3066 (2003).
108. D. Taton, Z.-Z. Wilczewska, and M. Destarac, *Macromol. Rapid Commun.* **22**, 1497 (2001).
109. N. Gaillard, A. Guyot, and J. Claverie, *J. Polym. Sci., Polym. Chem.* **41**, 684 (2003).
110. C. Burguiere, S. Pascual, C. Bui, J.-P. Vairon, B. Charleux, K. A. Davis, K. Matyjaszewski, and I. Betremieux, *Macromolecules* **34**, 4439 (2001).
111. L. Couvreur, C. Lefay, J. Belleney, B. Charleux, O. Guerret, and S. Magnet, *Macromolecules ASAP*, **36**, 8260 (2003).
112. R. H. Harding and J. K. Rose, in R. L. Davidson and M. Sittig, eds., *Water-Soluble Resins*, 2nd ed., Van Nostrand Reinhold, New York, 1982.
113. D. B. Braun, in R. L. Davidson, ed., *Handbook of Water-Soluble Gums and Resins*, McGraw Hill Book Co., Inc., New York, 1980.
114. W. H. Montgomery, in R. L. Davidson and M. Sittig, eds., *Water-Soluble Resins*, 2nd ed., Van Nostrand Reinhold, New York, 1962.
115. M. H. Stenzel, L. Cummins, G. E. Roberts, T. P. Davis, P. Vana, and C. Barner-Kowollik, *Macromol. Chem. Phys.* **204**, 1160 (2003).

116. C. Forder, C. S. Patrickios, N. C. Billlingham, and S. P. Armes, *Chem. Commun*. 883 (1996).
117. C. Forder, C. S. Patrickios, S. P. Armes, and N. C. Billingham, *Macromolecules* **29**, 8160 (1996).
118. C. S. Patrickios, C. Forder, S. P. Armes, and N. C. Billingham, *J. Polym. Sci., Polym. Chem.* **36**, 2547 (1998).
119. O. Fuchs, in J. Brandrup and E. H. Immergut, eds., *Polymer Handbook*, 3rd ed., Wiley-Interscience, New York, 1989, pp. vii–383.
120. S. R. Sandler and W. Karo, *Polymer Synthesis*, Vol. 2, Academic Press, Inc., New York, 1977.
121. L. Blecher, D. H. Lorenz, H. L. Lowd, A. S. Wood, and D. P. Wyman, in R. L. Davidson, ed., *Handbook of Water-Soluble Gums and Resins*, McGraw-Hill Book Co., Inc., New York, 1980.
122. J. L. Azorlosa and A. J. Martinelli, in W. H. Montgomery, R. L. Davidson, and M. Sittig, eds., *Water-Soluble Resins*, 2nd ed., Van Nostrand Reinhold, New York, 1962.
123. C. Tanford, *Physical Chemistry of Macromolecules*, John Wiley & Sons, Inc., New York, 1961.
124. G. S. Manning, *Annu. Rev. Phys. Chem.* **23**, 117 (1972).
125. J. Mykytiuk, S. P. Armes, and N. C. Billingham, *Polym. Bull.* **29**, 139 (1992).
126. S. P. Mannard, N. C. Billingham, S. P. Armes, and J. Mykytiuk, *Eur. Polym. J.* **29**, 407 (1993).
127. C. S. Patrickios, W. R. Hertler, N. L. Abbott, and T. A. Hatton, *Macromolecules* **27**, 930 (1994).
128. A. B. Lowe, N. C. Billingham, and S. P. Armes, *Chem. Commun*. 1035 (1997).
129. A. B. Lowe, N. C. Billingham, and S. P. Armes, *Macromolecules* **31**, 5991 (1998).
130. E. J. Ashford, V. Naldi, R. O'Dell, N. C. Billingham, and S. P. Armes, *Chem. Commun*. 1285 (1999).
131. D. M. Haddleton, E. Depaquis, E. J. Kelly, D. Kukulj, S. R. Morsley, S. F. A. Bon, M. D. Eason, and A. G. Steward, *J. Polym. Sci., Polym. Chem.* **39**, 2378 (2001).
132. B. Kesoshivianan, M. Georges, and D. Boils-Boissier, *Macromolecules* **28**, 6387 (1995).
133. L. J. Gabaston, S. A. Furlong, R. A. Jackson, and S. P. Armes, *Polymer* **40**, 4505 (1999).
134. U.S. Pat. 3,506,707 (1970), L. E. Miller and D. L. Murfin (to Lubrizol Corp.).
135. U.S. Pat. 3,332,904 (1967), E. M. LaCombe and W. P. Miller (to Union Carbide Corp.).
136. U.S. Pat. 3,692,673 (1972), D. I. Hoke (to Lubrizol Corp.).
137. U.S. Pat. 3,709,780 (1973), R. C. Slagel and G. D. Sinkovitz (to Calgon Corp.).
138. U.S. Pat. 3,709,816 (1973), J. E. Boothe III, and T. E. C. (to Calgon Corp.).
139. U.S. Pat. 3,709,816 (1973), J. L. Walker and J. E. Boother (to Calgon Corp.).
140. U.S. Pat. 3,679,000 (1972), P. R. Kaufman (to Lubrizol Corp.).
141. C. L. McCormick and G. S. Chen, *J. Polym. Sci. Chem.* **20**, 817 (1982).
142. C. L. McCormick and G. S. Chen, *J. Appl. Polym. Sci.* **29**, 713 (1984).
143. C. L. McCormick and C. B. Johnson, *Macromolecules* **21**, 694 (1988).
144. C. B. Johnson, Ph.D. dissertation, University of Southern Mississippi, Hattiesburg, Miss., 1987.
145. C. L. McCormick and K. P. Blackmon, *J. Polym. Sci. Chem. A* **24**, 2635 (1986).
146. C. L. McCormick, K. P. Blackmon, and D. L. Elliott, *J. Polym. Sci. Chem. A* **24**, 2619 (1986).
147. C. L. McCormick and K. P. Blackmon, *Macromolecules* **19**, 1512 (1986).
148. C. L. McCormick, K. P. Blackmon, and D. L. Elliott, *Macromolecules* **19**, 1516 (1986).
149. L. Shiyang and S. P. Armes, *Angew. Chem. Int. Ed.* **41**, 1413 (2002).
150. M. F. Hoover, *J. Macromol. Sci. Chem. A* **4**, 1327 (1970).

151. M. F. Hoover and G. B. Butler, *J. Polym. Sci., Polym. Chem.* **45**, 1 (1974).
152. E. W. Flick, *Water-Soluble Resins—An Industrial Guide*, Noyes, Park Ridge, N.J., 1986.
153. U.S. Pat. 4,663,159 (1987), G. L. Brode, R. L. Kreefer, D. Goddard, F. M. Merritt, and D. B. Braun, (to Union Carbide).
154. S. Wen, X. Yin, and W. T. K. Sevenson, *J. Appl. Polym. Sci.* **43**, 205 (1991).
155. S. Creutz, P. Tessie, and R. Jerome, *Macromolecules* **30**, 6 (1997).
156. F. L. Baines, N. C. Billingham, and S. P. Armes, *Macromolecules* **29**, 3416 (1996).
157. M. V. de Paz Banez, K. L. Robinson, and S. P. Armes, *Macromolecules* **41**, 451 (2000).
158. M. V. de Paz Banez, K. L. Robinson, M. Vamvakaki, S. F. Lascelles, and S. P. Armes, *Polymer* **41**, 8501 (2000).
159. K. Deboudt, M. Delporte, and C. Loucheux, *Macromol. Chem. Phys.* **196**, 279 (1995).
160. K. Deboudt, M. Delporte, and C. Loucheux, *Macromol. Chem. Phys.* **196**, 29 (1995).
161. M. Prady, J. Lokaj, M. Novotna, and S. Sevcik, *Makromol. Chem.* **190**, 2229 (1989).
162. T. Ohmae, S. Hosoda, H. Tanaka, H. Kihara, B. Jiang, Q. Ying, R. Qian, and T. Nakajima, *Pure Appl. Chem.* **65**, 1825 (1993).
163. F. Zeng, Y. Chen, S. Zhu, and R. Pelton, *J. Polym. Sci., Polym. Chem.* **38**, 382 (2000).
164. X. Zhang, J. Xia, and K. Matyjaszewski, *Macromolecules* **31**, 516 (1998).
165. X. Zhang and K. Matyjaszewski, *Macromolecules* **32**, 1763 (1999).
166. X. Zhang, J. Xia, and K. Matyjaszewski, *Macromolecules* **31**, 5167 (1998).
167. A. P. Narrainen, S. Pascual, and D. M. Haddleton, *J. Polym. Sci., Polym. Chem.* **40**, 439 (2002).
168. S. Liu, J. V. Weaver, M. Y. Tang, N. C. Billingham, and S. P. Armes, *Macromolecules* **35**, 6121 (2002).
169. L.-H. Gan, P. Ravi, B. W. Mao, and K.-C. Tam, *J. Polym. Sci., Polym. Chem.* **41**, 2688 (2003).
170. X. Bories-Azeau and S. P. Armes, *Macromolecules* **35**, 1024 (2002).
171. Y. Li, S. P. Armes, X. Jin, and S. Zhu, *Macromolecules ASAP* **36**, 8268 (2003).
172. J. Chiefari, Y. K. Chong, F. Ercole, J. Krstina, J. Feffery, T. P. T. Le, R. T. A. Mayadunne, G. F. Maijs, C. L. Moad, G. Moad, E. Rizzardo, and S. H. Thang, *Macromolecules* **31**, 5559 (1998).
173. A. B. Lowe and C. L. McCormick, Unpublished Results, 2003.
174. T. Alfrey, R. M. Fuoss, H. Morawetz, and H. Pinner, *J. Am. Chem. Soc.* **74**, 438 (1952).
175. V. Bηtηn, N. C. Billingham, and S. P. Armes, *Chem. Commun.* **7**, 671 (1997).
176. V. Bηtηn, C. E. Bennett, M. Vamvakaki, A. B. Lowe, N. C. Billingham, and S. P. Armes, *J. Mater. Chem.* **7**, 1693 (1997).
177. V. Bηtηn, N. C. Billingham, and S. P. Armes, *J. Am. Chem. Soc.* **120**, 11818 (1998).
178. M. R. Simmons and C. S. Patrickios, *Macromolecules* **31**, 9075 (1998).
179. M. R. Simmons and C. S. Patrickios, *J. Polym. Sci., Polym. Chem.* **37**, 1501 (1999).
180. M. V. de Paz Banez, K. L. Robinson, V. Bηtηn, and S. P. Armes, *Polymer* **42**, 29 (2001).
181. L.-H Gan, P. Ravi, B. W. Mao, and K.-C. Tam, *J. Polym. Sci., Polym. Chem.* **41**, 2688 (2003).
182. S. Creutz, P. Teyssie, and R. J. Jerome, *J. Polym. Sci., Polym. Chem.* **35**, 2035 (1997).
183. V. Bηtηn, S. P. Armes, and N. C. Billingham, *Polymer* **42**, 5993 (2001).
184. C. L. McCormick, K. P. Blackmon, and D. L. Elliott, *Polymer* **27**, 1976 (1986).
185. C. L. McCormick and L. C. Salazar, *J. Polym. Sci., Polym. Chem.* **31**, 1099 (1993).
186. D. B. Thomas, Ph.D. dissertation, University of Southern Mississippi, Hattiesburg, Miss., 2003.
187. M. J. Fevola, Ph. D. dissertation, University of Southern Mississippi, Hattiesburg, Miss., 2003.
188. G. B. Butler, *Cyclopolymerization and Cyclocopolymerization*, Marcel Dekker, Inc., New York, 1992.

189. R. S. Armentrout and C. L. McCormick, *Macromolecules* **33**, 419 (2000).
190. R. S. Armentrout and C. L. McCormick, *Macromolecules* **33**, 2944 (2000).
191. D. B. Thomas, *Macromolecules* **36**, 9710 (2003).
192. W. P. Shyluk, *J. Polym. Sci., Part A-2* **2**, 2191 (1964).
193. W. P. Shyluk, *J. Appl. Polym. Sci.* **8**, 1063 (1964).
194. W. P. Shyluk, *J. Polym. Sci., Part A-2* **6**, 2009 (1968).
195. W. P. Shyluk and R. W. Smith, *J. Polym. Sci., Part A-2* **7**, 27 (1969).
196. W. P. Shyluk, *J. Polym. Sci., Part A* **2**, 2191 (1964).
197. C. L. Lee, J. Smid, and M. Szwarc, *Trans. Faraday Soc.* **59**, 1192 (1963).
198. C. Tsitsiliani, G. A. Voyiatzis, and J. K. Kallitsis, *Macromol. Rapid Commun.* **21**, 1130 (2000).
199. N. Ekizoglou and N. Hajichristidis, *J. Polym. Sci., Polym. Chem.* **40**, 2166 (2002).
200. S. K. Varsheny, X. F. Zhong, and A. Eisenbert, *Macromolecules* **26**, 701 (1993).
201. F. Liu, Q. Wu, A. Eisenbert, 226th ACS National Meeting, American Chemical Society, New York, 2003.
202. T. Diaz, A. Fischer, A. Jonquieres, A. Brembilla, and P. Lochon, *Macromolecules* **36**, 2235 (2003).
203. Z. Chen, J. Cai, X. Jiang, and C. Yang, *Eur. Polym. J.* **37**, 33 (2001).
204. A. Fischer, A. Brembilla, and P. Lochon, *Eur. Polym. J.* **37**, 33 (2001).
205. M. Baumann and G. Schmidt-Naake, *Macromol. Chem. Phys.* **201**, 2751 (1999).
206. A. Fischer, A. Brembilla, and P. Lochon, *Macromolecules* **32**, 6069 (1999).
207. X. Z. Ding, A. Fischer, A. Brembilla, P. Lochon, *J. Polym. Sci., Polym. Chem.* **38**, 3067 (2000).
208. I. Chalari, S. Pispas, and N. Hadjichristidis, *J. Appl. Polym. Sci., Polym. Chem.* **39**, 2889 (2001).
209. J. Lokaj and P. Holler, *J. Appl. Polym. Sci.* **80**, 2024 (2001).
210. X. Ding, A. Fischer, and A. Brembilla, *J. Polym. Sci., Polym. Chem.* **38**, 3067 (2000).
211. J.-J. Yuan, R. Ma, Q. Gao, Y.-F. Want, S.-Y. Cheng, L.-X. Feng, A.-Q. Fan, and L. Jiang, *J. Appl. Polym. Sci.* **89**, 1017 (2003).
212. A. J. Convertine, B. S. Sumerlin, D. B. Thomas, and C. L. McCormick, *Macromolecules* **36**, 4679 (2003).
213. A. Ramakrishnan and R. Dhamodharan, *J. Macromol. Sci., Pure Appl. Chem. A* **37**, 621 (2000).
214. K. A. Davis and K. Matyjaszewski, *Macromolecules* **34**, 2101 (2001).
215. R. Yang, Y. Wang, X. Wang, W. He, and C. Pan, *Eur. Polym. J.* **39**, 2029 (2003).
216. G. B. Butler and N. Z. Zhang, in S. W. Shalaby, C. L. McCormick, and G. B. Butler, eds., *Water-Soluble Polymers Synthesis: Solution Properties, and Applications*, American Chemical Society, Washington, D.C., 1991, p. 37.
217. P. Molyeaux, *Water-Soluble Synthetic Polymers*, Vol. 2, CRC Press, Inc., Boca Raton, 1984, p. 50.
218. L. Y. Ji, E. T. Kang, K. G. Neoh, and K. L. Tan, *React. Func. Polym.* **46**, 145 (2000).
219. T. Ucchida, Furuzeno K. Ishihara, N. Nakabayashi, and M. Akashi, *J. Polym. Sci., Polym. Chem.* **38**, 3052 (2000).
220. K. Se, M. Kijima, R. Ohtomo, and T. Fujimoto, *J. Polym. Sci., Polym. Chem.* **35**, 1219 (1997).
221. K. Se, M. Kijima, and T. Fujimoto, *Polymer* **38**, 5755 (1997).
222. B. S. Sumerlin, A. B. Lowe, D. B. Thomas, A. J. Convertine, M. S. Donovan, and C. L. McCormick, *J. Polym. Sci., Polym. Chem. ASAP* **42**, 1724 (2004).
223. H. Wenker, *J. Am. Chem. Soc.* **57**, 2328 (1935).
224. D. Fischer, A. V. Harpe, K. Kunath, H. Peterson, Y. Li, and T. Kissel, *Bioconjugate Chem.* **13**, 1124 (2002).
225. G. Odian, *Principles of Polymerization*, 3rd ed. Wiley-Interscience, New York, 1991.

226. G. B. Butler and N. Z. Zhang, in S. W. Shalaby, C. L. McCormick, and G. B. Butler, eds., *Water-Soluble Polymers: Synthesis, Solution Properties and Applications*, ACS Symposium Series 467, American Chemical Society, Washignton, D.C., 1991, pp. 25–27.
227. K. Yamamoto, Y. Imamura, E. Nagatomo, T. Serizawa, Y. Muraoka, and M. Akashi, *J. App. Polym. Sci.* **89**, 1277 (2003).
228. Z. Hu, S. Zhang, and J. Yang, *J. App. Polym. Sci.* **89**, 3889 (2003).
229. L. Shi, T. M. Chapman, and E. J. Beckman, *Macromolecules* **36**, 2563 (2003).
230. D.-H. Hwang, J.-H. Chang, H.-K. Shim, and T. Zyung, *Syn. Met.* **119**, 393 (2001).
231. G. B. Butler, D. L. Skinner, W. C. Bond, and C. L. Rogers, *Polym. Prep.* **10**, 923 (1969).
232. G. B. Butler and N. Z. Zhang, *Water-Soluble Polymers: Synthesis, Solution Properties and Applications*, American Chemical Society, Washington, D.C., pp. 25–56.
233. C. C. Petropoulos, *J. Polym. Sci. A* **10**, 957 (1972).
234. T. Nonaka, L. Hua, T. Ogata, and S. Kurihara, *J. Appl. Polym. Sci.* **87**, 386 (2003).
235. T. Nonaka, H. Li, K. Makinose, T. Ogata, and S. Kurihara, *J. Appl. Polym. Sci.* **90**, 1139 (2003).
236. A. Kanazawa, T. Ikeda, and T. Endo, *J. Polym. Sci., Polym.Chem.* **31**, 335 (1993).
237. A. Kanazawa, T. Iked, and T. Endo, *J. Polym. Sci., Polym. Chem.* **31**, 3003 (1993).
238. D.-H. Hwang, I.-N. Kang, J.-I. Lee, L.-M. Do, H. Y. Chu, T. Zyung, Shim, and H.-K., *Polym. Bull.* **41**, 275 (1998).
239. A. B. Lowe and C. L. McCormick, *Chem. Rev.* **102**, 4177 (2002).
240. T. Alfrey, H. Morawetz, E. B. Fitzgerald, and R. M. Fuoss, *J. Am. Chem. Soc.* **72**, 1864 (1950).
241. T. Alfrey and H. Morawetz, *J. Am. Chem. Soc.* **74**, 436 (1952).
242. T. Alfrey, R. Fuoss, H. Morawetz, and S. H. Pinner, *J. Am. Chem. Soc.* **74**, 438 (1952).
243. T. Alfrey and S. H. Pinner, *J. Am. Chem. Soc.* **23**, 533 (1957).
244. A. Katchalsky and I. R. Miller, *J. Polym. Sci.* **14**, 57 (1954).
245. G. Ehrlich and P. Doty, *J. Am. Chem. Soc.* **76**, 3764 (1954).
246. F. Ascoli and B. Botre, *J. Polym. Sci.* **62**, S56 (1962).
247. C. L. McCormick and C. B. Johnson, *Macromolecules* **21**, 686 (1988).
248. C. L. McCormick and C. B. Johnson, *Macromolecules* **21**, 694 (1988).
249. C. L. McCormick and C. B. Johnson, *Polymer* **31**, 1100 (1990).
250. C. L. McCormick and C. B. Johnson, *J. Macromol. Sci. Chem. A* **27**, 539 (1990).
251. M. Kamachi, M. Kurihara, and J. K. Stille, *Macromolecules* **5**, 161 (1972).
252. M. Kurihara, M. Kamachi, and J. K. Stille, *J. Polym. Sci., Chem. Ed.* **11**, 587 (1973).
253. R. Varoqui, Q. Tran, and E. Pefferkorn, *Macromolecules* **12**, 831 (1979).
254. Y. Morishima, T. Hashimoto, Y. Itoh, M. Kamachi, and S. Nozakura, *J. Polym. Sci., Polym. Chem.* **20**, 299 (1982).
255. E. A. Bekturov, V. A. Frolova, S. E. Kudaibergenov, R. C. Schulz, and J. Zoller, *J. Makromol. Chem.* **191**, 457 (1999).
256. E. A. Bekturov, S. E. Kudaibergenov, R. E. Khamzamulina, V. A. Frolova, , E. E. Nurgalieva, R. C. Schulz, and J. Zoller, *J. Makromol. Chem. Rapid Commun.* **13**, 225 (1992).
257. S. Creutz, P. Teyssie, and R. Jerome, *Macromolecules* **30**, 6 (1997).
258. S. Creutz, J. V. Stam, F. C. D. Schryver, and R. Jerome, *Macromolecules* **31**, 681 (1998).
259. C. S. Patrickios, W. R. Hertler, N. L. Abbott, and T. A. Hatton, *Macromolecules* **27**, 930 (1994).
260. W. I. Chem, P. Alexandridis, C. K. Su, C. S. Patrickios, W. R. Hertler, and T. A. Hatton, *Macromolecules* **28**, 8604 (1995).
261. A. B. Lowe, N. C. Billingham, and S. P. Armes, *Macromolecules* **31**, 5991 (1998).
262. C. S. Patrickios, A. B. Lowe, N. C. Billingham, and S. P. Armes, *J. Polym. Sci., Polym. Chem.* **36**, 617 (1998).
263. S. Liu and S. P. Armes, *Angew. Chem. Int. Ed.* **41**, 1413 (2002).

264. S. Liu and S. P. Armes, *Langmuir* **19**, 4432 (2003).
265. S. Dai, P. Ravi, K. C. Tam, B. W. Mao, and L. H. Gan, *Langmuir* **12**, 5175 (2003).
266. F. Ascoli and C. Botre, *J. Polym. Sci.* **62**, S56 (1962).
267. C. S. Patrickios, *J. Colloid Interface Sci.* **175**, 256 (1995).
268. D. W. Roberts and D. L. Williams, *Tetrahedron* **43**, 1027 (1987).
269. U.S. Pat. 3,671,502 (1972), C. M. Samour and M. L. Flaxa (to The Kendall Co.).
270. M. Hahn, E. Gornitz, and H. Dautzenberg, *Macromolecules* **31**, 5616 (1998).
271. V. Barboiu, E. Streba, C. Luca, and C. I. Simionescu, *J. Polym. Sci., Polym. Chem.* **33**, 389 (1995).
272. N. Bonte and A. Laschewsky, *Polymer* **37**, 2011 (1996).
273. E. E. Kathmann, L. A. White, and C. L. McCormick, *Polymer* **38**, 879 (1997).
274. T. Nakaya and Y.-J. Li, *J. Prog. Polym. Sci.* **24**, 143 (1999).
275. K. Ishihara, T. Ueda, and N. Nakabayashi, *Polym. J.* **22**, 355 (1990).
276. Y. F. Wang, T. M. Chen, Y. J. Li, M. Kitamura, T. Nakaya, and I. Sakurai, *Macromolecules* **29**, 5810 (1996).
277. D. Hamaide, L. Germanaud, and P. L. Perchec, *Makromol. Chem.* **187**, 1097 (1986).
278. T. Nakaya, H. Toyoda, and M. Imoto, *Polym. J.* **18**, 881 (1986).
279. M.-L. Pujol-Fortin, and J.-C. Galin, *Polymer* **35**, 1462 (1994).
280. J.-C. Galin and M. Galin, *J. Polym. Sci., Polym. Phys.* **33**, 2033 (1995).
281. A. Biegle, A. Mathis, and J.-C. Galin, *Macromol. Chem. Phys.* **201**, 113 (2000).
282. H. Ladenheim and H. Morawetz, *J. Polym. Sci.* **26**, 251 (1957).
283. T. Umeda, T. Nakaya, and M. Imoto, *Makromol. Chem. Rapid Commun.* **6**, 285 (1985).
284. K. Sugiyama and T. Nakaya, *Makromol. Chem. Rapid Commun.* **7**, 679 (1986).
285. M. Yamada, Y.-J. Li, and T. Nakaya, *Macromol. Sci., Pure Appl. Chem. A* **32**, 1723 (1995).
286. A. B. Lowe, N. C. Billingham, and S. P. Armes, *Chem. Commun.* 1555 (1996).
287. Z. Tuzar, H. Posposil, J. Plestil, A. B. Lowe, F. L. Baines, N. C. Billingham, and S. P. Armes, *Macromolecules* **30**, 2509 (1997).
288. E. J. Lobb, I. Ma, N. C. Billingham, S. P. Armes, and A. L. Lewis, *J. Am. Chem. Soc.* **123**, 7913 (2001).
289. Y. Ma, S. P. Armes, and N. C. Billingham, *Polym. Mater. Sci. Eng.* **84**, 143 (2001).
290. I. Y. Ma, E. J. Lobb, N. C. Billingham, S. P. Armes, A. L. Lewis, A. Lloyd, and W. J. Salvage, *Macromolecules* **35**, 9306 (2002).
291. Y. Ma, Y. Tang, N. C. Billingham, S. P. A. L. Lewis, A. L. Lloyd, and J. P. Salvage, *Macromolecules* **36**, 3475 (2003).
292. M. Arotcarena, B. Heise, S. Ishaya, and A. Laschewsky, *J. Am. Chem. Soc.* **124**, 3787 (2002).
293. M. S. Donovan, A. B. Lowe, T. A. Sanford, and C. L. McCormick, *J. Polym. Sci., Polym. Chem.* **41**, 1262 (2003).
294. T. Ueda, H. Oshida, K. Kurita, K. Ishihara, and N. Nakabayashi, *Polym. J.* **24**, 1259 (1992).
295. K. Ishihara, *Trends Polym. Sci.* **5**, 401 (1997).
296. A. B. Lowe, M. Vamvakaki, M. A. Wassall, L. Wong, N. C. Billingham, S. P. Armes, and A. W. Lloyd, *J. Biomed. Mater. Res.* **52**, 88 (2000).
297. C. L. McCormick, ed. *Stimuli-Responsive Water Soluble and Amphiphilic Polymers*, ACS Symposium Series 780, American Chemical Society, Washington, D.C., 2000.
298. S. Y. Park and Y. H. Bae, *Macromol. Rapid Commun.* **20**, 269 (1999).
299. X. Qui, C. M. S. Kwan, and C. Wu, *Macromolecules* **30**, 6090 (1997).
300. M. Schops, H. Leist, A. DuChesne, and U. Wiesner, *Macromolecules* **32**, 2806 (1999).
301. I. Porcar, P. Sergot, and C. Tribet, *Stimuli-Responsive Water Soluble and Amphiphilic Polymers*, American Chemical Society, Washington, D.C., 2000, p. 82.
302. M. Irie and R. Iga, *Macromolecules* **19**, 2480 (1986).

303. H. Yamamoto, *Macromolecules* **19**, 2472 (1986).
304. Z. Tong, F. Zeng, X. Zheng, and T. Sato, *Macromolecules* **32**, 4488 (1999).
305. A. Hashidzume, Y. Morishima, and K. Szczubialka, in S. K. Tripathy, J. Kumar, and H. S. Nalwa, eds., *Handbook of Polyelectrolytes and Their Applications*, Vol. 2, American Chemical Society, Washington, D.C., 2002.
306. U. P. Strauss and E. G. Jackson, *J. Polym. Sci.* **6**, 649 (1951).
307. S. J. Assony and J. Layton, *J. Polym. Sci.* **9**, 509 (1952).
308. W. Kauzmann, ed., *Advances in Protein Chemistry*, Academic Press, Inc., Orlando, Fla., 1959.
309. P. Dubin and U. P. Strauss, *J. Phys. Chem.* **77**, 1558 (1973).
310. P. Dubin and U. P. Strauss, *J. Phys. Chem.* **71**, 2757 (1963).
311. P. Dubin and U. P. Strauss, *J. Phys. Chem.* **74**, 2842 (1967).
312. U. P. Strauss and G. Vesnaver, *J. Phys. Chem.* **79**, 1558 (1975).
313. U.S. Pat. 4,663,159, G. L. Brode and R. L. Kreeger (to Union Carbide Co.).
314. U.S. Pat. 4,352,916 (1982), L. M. Landoll.
315. U.S. Pat. 4,228,277 (1980), L. M. Landoll.
316. L. M. Landoll, *J. Polym. Sci., Polym. Chem.* **20**, 443 (1982).
317. U.S. Pat. 4,426,485 (1984), K. L. Hoy and R. C. Hoy (to Hercules, Inc.).
318. U.S. Pat. 3,779,970 (1973), S. Evani and R. H. Lalk (to Hercules, Inc.).
319. S. Evani and G. D. Rose, *Polym. Mater. Sci. Eng.* **57**, 477 (1987).
320. U.S. Pat. 3,963,684 (1976), S. Evani and E. P. Corson (to Union Carbide Co.).
321. U.S. Pat. 4,105,649 (1978), S. Evani and F. P. Corson (to Dow Chemical Co.).
322. J. E. Glass, *Polym. Mater. Sci. Eng.* **57**, 618 (1987).
323. U.S. Pat. 4,514,552 (1985), G. D. Shay, E. Eldridge, and J. E. Kail (to Dow Chemical Co.).
324. U.S. Pat. 4,600,761 (1986), C. G. Ruffner and J. M. Wilkerson (to Dow Chemical Co.).
325. J. Bock, D. B. D. N. Schulz, S. R. Turner, P. L. Valint, and S. J. Pace, *Polym. Mater. Sci. Eng.* **55**, 355 (1986).
326. U.S. Pat. 4,520,182 (1985), S. R. Turner, D. B. Siano, and J. Bock (to Exxon Research & Engineering Co.).
327. U.S. Pat. 4,528,348 (1985), S. R. Turner, D. B. Siano, and J. Bock (to Exxon Research & Engineering Co.).
328. C. L. McCormick and C. B. Johnson, *Polym. Mater. Sci. Eng.* **55**, 366 (1986).
329. C. L. McCormick and C. B. Johnson, T. Nonaka, *Polymer* **29**, 731 (1987).
330. C. B. Johnson, Ph.D. dissertation, University of Southern Mississippi, Hattiesburg, Miss., 1986.
331. S. A. Ezell and C. L. McCormick, *Macromolecules* **25**, 1881 (1992).
332. S. A. Ezell, C. E. Hoyle, and C. L. McCormick, *Macromolecules* **25**, 1887 (1992).
333. F. M. Winnik, M. A. Winnik, H. Ringsdorf, J. Venzmer, and S. E. Webber, *J. Phys. Chem.* **95**, 2583 (1991).
334. S. E. Webber, *Chem. Rev.* **90**, 1469 (1990).
335. H. Ringsdorf, J. Simon, and F. M. Winnik, *Macromolecules* **25**, 5353 (1992).
336. Y. Hu, M. C. Kramer, C. Boudreaux, and C. L. McCormick, *Macromolecules* **28**, 7100 (1995).
337. M. C. Kramer, J. A. Steger, Y. Hu, and C. L. McCormick, *Macromolecules* **29**, 1992 (1996).
338. Y. Morishima, *Prog. Polym. Sci.* **15**, 949 (1990).
339. Y. Morishima, T. Hashimoto, Y. Itoh, M. Kamaichi, and S. Nozakura, *J. Polym. Sci., Polym. Chem.* **20**, 299 (1982).
340. T. J. Martin and S. E. Webber, *Macromolecules* **28**, 8845 (1995).
341. S. Cruetz, J. V. Stam, S. Antoun, and R. Jerome, *Macromolecules* **30**, 4078 (1997).
342. C. K. Smith and G. Liu, *Macromolecules* **29**, 2060 (1996).

343. A. R. Eckert, T. J. Martin, and S. E. Webber, *J. Phys. Chem. A* **101**, 1646 (1997).
344. K. T. Wang, I. Illiopoulos, and R. Audibert, *Polym. Bull.* **20**, 577 (1988).
345. Y. Sato, A. Hashidzume, and Y. Morishima, *Macromolecules* **34**, 6121 (2001).
346. G. L. Smith and C. L. McCormick, *Macromolecules* **34**, 918 (2001).
347. G. L. Smith and C. L. McCormick, *Macromolecules* **34**, 5579 (2001).
348. G. L. Smith and C. L. McCormick, *Langmuir* **17**, 1719 (2001).
349. C. L. McCormick, C. E. Hoyle, and M. D. Clark, *Macromolecules* **23**, 3124 (1990).
350. C. L. McCormick and K. Kim, *J. Macromol. Sci., Chem. A* **25**, 285 (1988).
351. C. L. McCormick and K. Kim, *J. Macromol. Sci., Chem. A* **25**, 307 (1988).
352. F. Petit-Agnely, I. Iliopoulous, and R. Zana, *Langmuir* **16**, 9921 (2000).
353. F. Petit-Agnely and I. Iliopoulous, *J. Phys. Chem. B* **103**, 4053 (1999).
354. Z. Gao, A. Desjardins, and A. Eisenburg, *Macromolecules* **27**, 794 (1994).
355. J. K. Newman and C. L. McCormick, *Macromolecules* **27**, 5123 (1994).
356. H. Yamamoto and Y. Morishima, *Macromolecules* **32**, 7469 (1999).
357. M. Seki, Y. Morishima, and M. Kamachi, *Macromolecules* **25**, 6540 (1992).
358. Z. Gao, A. Desjardins, and A. Eisenberg, *Macromolecules* **25**, 1300 (1992).
359. K. Nagashima, V. Strashke, P. M. McDonald, R. D. Jenkins, and D. R. Bassett, *Macromolecules* **33**, 9329 (2000).
360. J. Selb and Y. Gallot, *Makromol. Chem.* **182**, 1491 (1981).
361. J. Selb and Y. Gallot, *Makromol. Chem.* **182**, 1513 (1981).
362. J. Selb and Y. Gallot, *Makromol. Chem.* **182**, 1775 (1981).
363. T. Noda, A. Hashidzume, and Y. Morishima, *Polymer* **42**, 9243 (2001).
364. T. Noda, A. Hashidzume, and Y. Morishima, *Langmuir* **17**, 5984 (2001).
365. V. Tirtaatmadja, K. C. Tam, and R. D. Jenkins, *Macromolecules* **30**, 1426 (1997).
366. V. Tirtaatmadja, K. C. Tam, and R. D. Jenkins, *Macromolecules* **30**, 3271 (1997).
367. S. Dai, K. C. Tam, R. D. Jenkins, and D. R. Bassett, *Macromolecules* **33**, 7021 (2000).
368. M. F. Islam and R. D. Jenkins, *Macromolecules* **33**, 2480 (2000).
369. S. Dai, K. C. Tam, and R. D. Jenkins, *Macromolecules* **33**, 404 (2000).
370. W. K. Ng, K. C. Tam, and R. D. Jenkins, *Polymer* **42**, 249 (2001).
371. P. G. deGennes, *Isr. J. Chem.* **35**, 33 (1995).
372. A. Halperin, *Macromolecules* **24**, 1418 (1991).
373. A. N. Semenov, J. Joanny, and A. Kholokov, *Macromolecules* **28**, 1066 (1995).
374. G. L. Smith, Ph.D. Dissertation, University of Southern Mississippi, Hattiesburg, Miss., 2001.
375. M. G. Baldwin, *J. Polym. Sci. A* **3**, 703 (1965).
376. W. Binana-Limele and R. Zana, *Macromolecules* **23**, 2731 (1990).
377. W. Binana-Limele and R. Zana, *Macromolecules* **20**, 1331 (1987).
378. U. P. Strauss and M. S. Schlesinger, *J. Phys. Chem.* **82**, 1627 (1978).
379. U. P. Strauss and M. S. Schlesinger, *J. Phys. Chem.* **82**, 571 (1978).
380. U. P. Strauss and G. Vesnaver, *J. Phys. Chem.* **79**, 2428 (1975).
381. C. L. McCormick and Y. Chang, *Macromolecules* **27**, 2151 (1994).
382. C. L. McCormick, C. E. Hoyle, and M. D. Clark, *Polymer* **33**, 243 (1992).
383. Y. Hu, M. C. Kramer, C. J. Boudreaux, and C. L. McCormick, *Macromolecules* **30**, 3526 (1997).
384. M. C. Kramer, C. G. Welch, J. R. Steger, and C. L. McCormick, *Macromolecules* **28**, 5248 (1995).
385. Y. Morishima, S. Nomura, T. Ikeda, M. Seki, and M. Kamachi, *Macromolecules* **28**, 2874 (1995).
386. Y. Morishima and M. Kamachi, *Proc. Am. Chem. Soc., Div. Polym. Mater. Sci. Eng.* **71**, 271 (1994).
387. Y. Morishima, in S. E. Webber, D. Tuzar, and P. Munk, eds., *Solvents and Self-Organization of Polymers*, Kluwer Academic Publishers, Dordrecht, the Netherlands, 1996, p. 331.

388. H. Yamamoto, M. Mizusaki, K. Yoda, and Y. Morishima, *Macromolecules* **31**, 3588 (1998).
389. F. Petit-Agnely and I. Iliopoulos, *J. Phys. Chem. B.* **103**, 4803 (1999).
390. L. Guillaumont, G. Bokias, and I. Iliopoulos, *Macromol. Chem. Phys.* **201**, 51 (2000).
391. C. L. McCormick, J. C. Middleton, and C. E. Grady, *Polymer* **33**, 4184 (1992).
392. K. D. Branham, Ph.D. dissertaion, University of Southern Mississippi, Hattiesburg, Miss., 1995.
393. K. D. Branham, C. L. McCormick, and G. S. Shafer, *Proc. Am. Chem. Soc. Div. Polym. Mater., Sci. Eng.* **71**, 423 (1994).
394. W. Peer, in J. E., Glass, ed., *Polymers in Acqueous Media: Performance Through Association*, Advances in Chemistry Series 223, American Chemical Society, Washington, D.C., 1989, p. 381.
395. S. A. Ezzell and C. L. McCormick, in W. Shalaby, C. L. McCormick, and G. B. Butler, eds., *Water Soluble Polymers, Synthesis, Solution Properties, and Applications*, ACS Symposium Series 467S, American Chemical Society, Washington, D.C., 1991, p. 130.
396. S. A. Ezzell and C. L. McCormick, *Macromolecules* **25**, 1881 (1992).
397. S. A. Ezzell, C. E. Hoyle, and C. L. McCormick, *Macromolecules* **25**, 1887 (1992).
398. U.S. Pat. 4,432,881 (1984), S. Evani (to Dow Chemical Co.).
399. C. L. McCormick, T. Nonaka, and C. B. Johnson, *Polymer* **29**, 731 (1988).
400. S. Biggs, A. Hill, J. Selb, and F. Candau, *J. Phys. Chem.* **96**, 1505 (1992).
401. C. Graillat, M. Lepais, and C. Pichot, *J. Dispersion Sci. Technol.* **11**, 455 (1990).
402. C. Holtzscherer and F. Candau, *J. Colloid Interface Sci.* **125**, 97 (1988).
403. F. Candau, Y. S. Leong, G. Pouyet, and S. Candau, *J. Colloid Interface Sci.* **101**, 167 (1984).
404. K. D. Branham, S. Snowden, and C. L. McCormick, *Macromolecules* **29**, 254 (1996).
405. E. Volpert, J. Selb, and F. Candau, *Macromolecules* **29**, 1452 (1996).
406. E. J. Regalado, J. Selb, and F. Candau, *Macromolecules* **32**, 8580 (1999).
407. C. Poncet, F. Tiberg, and R. Audebert, *Langmuir* **14**, 1697 (1998).
408. D. F. Anghel, V. Alderson, F. M. Winnik, M. Mizusaki, and Y. Morishima, *Polymer* **39**, 3035 (1998).
409. C. L. McCormick, C. E. Hoyle, and M. D. Clark, *Macromolecules* **24**, 2397 (1991).
410. C. J. Boudreaux, W. C. Bunyard, and C. L. McCormick, *J. Controlled Release* **40**, 223 (1996).
411. P.-L. Kuo, M.-N. Hung, and Y.-H. Lin, *J. Appl. Polym. Sci.* **47**, 1295 (1993).
412. C. J. Boudreaux, W. C. Bunyard, and C. L. McCormick, *J. Controlled Release* **44**, 171 (1997).
413. J. Chen, M. Jiang, Y. Zhang, and H. Zhou, *Macromolecules* **44**, 171 (1999).
414. R. Varadaraj, J. Bock, N. Brons, and S. Pace, *J. Phys. Chem.* **97**, 12991 (1993).
415. K. D. Branham, *Diss. Absstr. Int. B* **56**, 5518 (1996).
416. T. L. Lowe, J. Virtanen, and H. Tenhu, *Langmuir* **15**, 4259 (2000).
417. D. Tsiourvas, C. M. Paleos, and A. Malliaris, *J. Polym. Sci., Polym. Chem.* **31**, 387 (1993).
418. G. Akazome, S. Sakai, and K. Murai, *Kobunshi Kagaku* **17**, 618 (1960).
419. Y. Morishima, M. Kobayashi, and S. Nozakura, *Macromolecules* **20**, 1707 (1987).
420. Y. Morishima, T. Kobayashi, and S. Nozakura, *Polym. J.* **21**, 267 (1989).
421. Y. Morishima, Y. Tominaga, S. Nomura, and M. Kamachi, *Macromolecules* **25**, 861 (1992).
422. Y. Morishima, Y. Tominaga, S. Nomura, M. Kamachi, and T. Okada, *J. Phys. Chem.* **96**, 1990 (1992).
423. T. Noda and Y. Morishima, *Macromolecules* **32**, 4631 (1999).
424. A. Hashidzume, T. Noda, and Y. Morishima, in C. L. McCormick, ed., *Stimuli-Responsive Water Soluble and Amphiphilic Polymers*, ACS Series 780, American Chemical Society, Washington, D.C., 2001, p. 14.

425. T. Noda and Y. Morishima, *Macromolecules* **33**, 3694 (2000).
426. T. Noda, A. Hashidzume, and Y. Morishima, *Macromolecules* **34**, 1308 (2001).
427. S. Yusa, M. Kamachi, and Y. Morishima, *Langmuir* **15**, 6059 (1998).
428. J. C. Middleton, D. Cummins, and C. L. McCormick, *Polym. Prep. (Am. Chem. Soc., Div. Polym. Chem.)* **30**, 348 (1989).
429. J. C. Middleton, D. F. Cummins, and C. L. McCormick, in W. Shalaby, C. L. McCormick, and G. B., Butler, eds., *Water Soluble Polymers: Synthesis, Solution Properties, and Applications*, ACS Symposium Series 467S, American Chemical Society, Washginton, D.C., 1991, p. 338.
430. C. L. McCormick, J. C. Middleton, and D. F. Cummins, *Macromolecules* **25**, 1201 (1992).
431. Y. J. Yang and J. B. F. N. Egberts, *Recl. Trav. Chim. Pays-Bas* **110**, 384 (1991).
432. Y. J. Yang and J. B. F. N. Engberts, *J. Org. Chem.* **56**, 4300 (1991).
433. Y. J. Yang and J. B. F. N. Engberts, *Eur. Polym. J.* **28**, 881 (1992).
434. J. B. F. N. Engberts, *Pure Appl. Chem.* **64**, 1653 (1992).
435. G.-J. Wang and J. B. F. N. Engberts, *J. Org. Chem.* **59**, 4076 (1994).
436. G.-J. Wang and J. B. F. N. Engberts, *Langmuir* **10**, 2583 (1994).
437. Y.-F. Wang, T.-M. Chen, K. Okada, I. Sakurai, and T. Nakaya, *J. Polym. Sci., Part A: Polym. Chem.* **37**, 1293 (1999).
438. M. R. Talingting, P. Munk, S. E. Webber, and Z. Tuzar, *Macromolecules* **32**, 1593 (1999).
439. Z. Gao, S. K. Varshney, S. Wong, and A. Eisenberg, *Macromolecules* **27**, 7923 (1994).
440. L. Zhang and A. Eisenberg, *J. Am. Chem. Soc.* **118**, 3168 (1996).
441. L. Zhang and A. Eisenberg, *Macromolecules* **32**, 2239 (1999).
442. F. L. Baines, S. P. Armes, N. C. Billingham, and Z. Tuzar, *Macromolecules* **29**, 815 (1996).
443. A. B. Lowe, N. C. Billingham, and S. P. Armes, *Macromolecules* **32**, 2141 (1999).
444. C. S. Patrickios, C. Forder, S. P. Armes, and N. C. Billingham, *J. Polym. Sci., Polym. Chem.* **34**, 1539 (1996).
445. C. Forder, C. S. Patrickios, S. P. Armes, and N. C. Billingham, *Macromolecules* **30**, 5758 (1997).
446. V. Bητηn, S. P. Armes, N. C. Billingham, Z. Tuzar, A. Rankin, J. Eastoe, and R. K. Heenan, *Macromolecules* **34**, 1503 (2001).
447. S. Liu, N. C. Billingham, and S. P. Armes, *Angew. Chem. Int. Ed.* **40**, 2328 (2001).
448. J. V. M. Weaver, S. P. Armes, and V. Bητηn, *Chem. Commun.* 2122 (2002).
449. V. Bητηn, M. Vamvakaki, N. C. Billingham, and S. P. Armes, *Polymer* **41**, 3173 (2000).
450. K. B. Thurmond, T. Kowalewski, and K. L. Wooley, *J. Am. Chem. Soc.* **119**, 6656 (1997).
451. H. Huang, T. Kowalewski, E. E. Remsen, R. Gertzmann, and K. L. Wooley, *J. Am. Chem. Soc.* **119**, 11653 (1997).
452. K. B. Thurmond, T. Kowalewski, and K. L. Wooley, *J. Am. Chem. Soc.* **118**, 7239 (1996).
453. Q. Zhang, E. E. Remsen, and K. L. Wooley, *J. Am. Chem. Soc.* **122**, 3642 (2000).
454. K. S. Murthy, W. Ma, C. G. Clark, E. E. Remsen, and K. L. Wooley, *Chem. Commun.* 773 (2001).
455. Q. Ma, E. E. Remsen, T. Kowalewski, J. Schafer, and K. L. Wooley, *Nano Lett.* **1**, 651 (2001).
456. J. Liu, Q. Zhang, E. E. Remsen, and K. L. Wooley, *Biomacromolecules* **2**, 362 (2001).
457. M. L. Becker, E. E. Remsen, and K. L. Wooley, *J. Polym. Sci., Polym. Chem.* **39**, 4152 (2001).
458. T. Sanji, Y. Nakatsuka, F. Kitayama, and H. Sakurai, *Chem. Commun.* 2201 (2000).
459. T. Sanji, Y. Nakatsuka, S. Ohnishi, and H. Sakurai, *Macromolecules* **33**, 8524 (2000).
460. V. Bητηn, N. C. Billingham, and S. P. Armes, *J. Am. Chem. Soc.* **120**, 12135 (1998).
461. V. Bητηn, A. B. Lowe, N. C. Billingham, and S. P. Armes, *J. Am. Chem. Soc.* **121**, 4288 (1999).

462. V. Bητηn, and S. P. Armes, in C. L. McCormick, ed., *Stimuli Responsive Water Soluble and Amphiphilic Polymers*, American Chemical Society, Washington, D.C., 2000.
463. V. Bητηn, W.-S. Wang, M. V. de Paz Banez, K. L. Robinson, N. C. Billingham, and S. P. Armes, *Macromolecules* **33**, 1 (2000).
464. S. Liu and S. P. Armes, *J. Am. Chem. Soc.* **123**, 9910 (2001).

CHARLES L. MCCORMICK
NEIL AYRES
Department of Polymer Science,
University of Southern Mississippi
ANDREW B. LOWE
Department of Chemistry and Biochemistry,
University of Southern Mississippi

WEAR. See SURFACE MECHANICAL DAMAGE AND WEAR.

WEATHERING. See Volume 4.

WOOD COMPOSITES

Introduction

Wood composites can be defined as materials made by gluing together small pieces of wood, residue materials from wood processing operations, or other elements into larger materials to produce products with specific definable mechanical and physical properties. Wood composite products continue to be among the most widely utilized building materials throughout the world. They are commonly manufactured as lumber, flooring, roofing, paneling, palettes, decking, fencing, cabinets, furniture, millwork, structural beams, etc.

The increased number and importance of wood composite products are directly related to the decreased supply of high quality large timber, and as the quality and variety of wood composite products increases, and new applications for them are found, the trend toward increased use and importance of wood composites should continue. Wood composites offer numerous advantages over lumber. They can be produced from waste wood, agricultural residues, little used and low commercial value wood species, as well as smaller and fast growing trees, which can relieve stress on old growth forests that are increasingly unavailable for use. Also, the increased homogeneity of the raw material obtained by combining small wood elements allows a wide variety of composite products to be produced that have consistent, high quality properties. The properties can often surpass those of lumber (eg, have stronger and more uniform properties throughout the product, and be completely free of growth characteristics, weak spots, or defects such as knots), and often, the product can be produced with customized engineered properties, dimensions, and complex shapes (eg, complex roof shapes, cathedral ceilings, cantilevered supports).

The exact properties and the appropriate end use for a composite depend on the wood species and wood adhesive, and are very dependent on the size, shape,

Encyclopedia of Polymer Science and Technology. Copyright John Wiley & Sons, Inc. All rights reserved.

and arrangement of the wood in the composite. In fact, the names of the composite products are mostly based on the wood geometry (wood shape and size) and their arrangement in the product, without involving the name of the wood species or adhesive. These elements (species and adhesive) can be changed with far less effect on properties than changing wood geometry or arrangement.

The procedure for making a wood composite begins with the raw wood being processed by removal of leaves and bark, then being cut into pieces of the desired size and shape, followed by drying to the desired moisture content, and then going through a sorting process to ensure the wood pieces meet the selection criteria. This process is followed regardless of wood species or wood geometry. Some composite processes allow more than 90% of the tree stem to be utilized with either small or large diameter trees, while lumber can only be produced from large diameter trees and even then typically less than 50% of the tree can be converted to the intended product.

A large number of product types having quite different properties can be prepared using the same wood element. Processing conditions to convert the wood element into a composite product will depend on the type of adhesive selected and/or if the product being produced is pressed, impregnated, extruded, etc. Therefore, wood composites can be classified into two major types: (*1*) wood bonded with thermoset adhesives and (*2*) wood combined with other materials such as cement and thermoplastics.

This article outlines some of the features and components of wood composites, describes some major wood composite products and properties, and describes some future directions in the wood composites industry. For additional information the reader is referred to some recent reviews (1–7).

Wood Bonded with Thermoset Adhesives

Wood composite products are conventionally manufactured from wood materials having various geometries (eg, fibers, particles, strands, flakes, veneers, and lumber) combined with a thermoset resin and bonded in a press (4). The press applies heat (if needed) and pressure to activate (cross-link) the adhesive resin and bond the wood material into a solid panel, lumber, or beam having good mechanical (strength and stiffness) and physical (form, dimensional stability, etc) properties.

Types of Wood Elements. A wide range of wood elements are employed to produce an increasing number of wood composite products. These elements can be broadly divided into two categories: “long grain” and “short grain” elements based on their size and shape (Table 1). The largest of the commonly used long grain wood elements, excluding lumber itself, is veneer. Shorter grain elements include strands, flakes, wafers, particles, and fibers. It should also be noted that increasing numbers of wood composite products are employing recycled wood such as sawdust and wood flour, which can be considered to be a separate wood type. Agrofibers are increasingly being employed as a raw material to produce commercial products similar to wood composites but with varying degrees of success. Some of the reasons for the rising interest in agrofibers include their low density and low abrasion, the potential to improve some properties such as stiffness, and potential cost savings when used as a filler for thermoplastics, and because many

Table 1. Types of Wood Elements Used In Wood Composites[a]

	Length		Width		Thickness	
Elements	cm	in.	cm	in.	cm	in.
Lumber	120–600	48–240	10–30	4–12	12.5–50	0.5–2
Veneer	120–240	48–96	10–120	4–48	0.5–12.5	0.02–0.5
Strands	1.27–7.5	0.5–3	0.63–2.5	0.25–1	0.25–0.625	0.010–0.025
Flakes	1.25–7.5	0.5–3	0.125–7.5	0.5–3	dito	0.010–0.025
Wafers	3.3	1.3	2.5–7.5	1–3	0.625–1.25	0.025–0.05
Particles	0.125–1.25	0.05–0.5	0.0125–0.125	0.005–0.05	0.125–1.25	0.005–0.050
Fibers	0.1–0.63	0.04–0.25	0.0025–0.0075	0.001–0.003	0.025–0.075	0.001–0.003

[a]Adapted from Ref. 7.

of these materials are the by-products of annual crops (8). In the United States and Canada wheat straw is currently the most important agrofiber furnish but many other agrofibers are of interest. Agrofiber preferences vary with availability and geographical region of the world (9). Soybean and cotton stalks, kenaf, flax, coffee and rice husk, hemp, fescue straw, ramie, and sugarcane bagasse are just some of the agrofiber raw materials being used or studied. Composites made from various agrofibers include low density insulating board, medium density fiberboard, hardboard, and particleboard (9,10). The mechanical properties for some agrofiber composites are reported in the literature, but additional research is needed, particularly on the long-term durability and weathering properties of these composites (10).

Thermoset Wood Adhesives

A wide range of adhesive types and chemistries are used to bond wood elements to one another (Table 2), but relatively few adhesive types are utilized to form the composites themselves. The vast majority of pressed-wood products use synthetic thermosetting adhesives. In North America the most important wood adhesives are the amino resins (qv), eg, urea–formaldehyde (UF) and melamine–formaldehyde (MF), which account for 60% by volume of adhesives used in wood composite products, followed by the phenolic resins (qv) eg, phenol–formaldehyde (PF) and resorcinol–formaldehyde (RF), which account for 32% of wood composite adhesives (12,13). The remaining 9% consists of cross-linked vinyl (X-PVAc) compounds, thermoplastic poly(vinyl acetates) (PVA), soy-modified casein, and polymeric diphenylmethylene diisocyanate (pMDI). Some products may use various combinations of these adhesives to balance cost with performance.

The thermosetting amino and phenolic adhesives are by far the predominant adhesives used in making wood composites. These adhesives are described below, but more detailed information is available elsewhere (4,7,16–21) (see ADHESIVE COMPOUNDS).

Urea–Formaldehyde (UF) Adhesives. UF resins are produced in a two-stage condensation polymerization process through the reaction of urea with excess formaldehyde. In the first stage of the polymerization process, urea and

Table 2. Characteristics of Major Wood Composites Bonded with Thermoset Adhesives

Types of composites	Raw materials[a]	Adhesives used	Structural (S) vs nonstructural (NS)	Applications	Typical thickness, mm (in.)	Typical density, kg/m^3 (lb/ft^3)
Particleboard	Particles	UF, MF, MDI	Mostly NS	Furniture, cabinetry, floor underlay, stair treads,	6–57 ($\frac{1}{4}$–2$\frac{1}{4}$)	640–800 (40–50)
Medium density fiberboard (MDF)	Fibers	UF, pMDI	NS	Furniture, kitchen and bath cabinet, fixtures, molding, millwork, laminate flooring	5–38, max. 76 (3/16–1$\frac{1}{2}$, max. 3)	640–800 (40–50)
Construction and industrial plywood	Softwood veneer, some hardwood	PF	S	Roof, floor, wall sheathing, single-layer floor, siding, floor underlayment, preserved wood foundations, laminated veneer lumber	6–31.5 ($\frac{1}{4}$–1$\frac{1}{4}$)	450–500 (28–31)
Decorative plywood	Hardwood veneer, some softwoods	UF, MF, RF, PVAc	Mostly NS	Decorative wall paneling, furniture, cabinetry, decorative flooring	6–19 ($\frac{1}{4}$–$\frac{3}{4}$)	400–880 (25–55)
Oriented strandboard (OSB)	Strand, flake, wafer	PF, pMDI	S	Roof, floor, wall sheathing, floor underlayment, siding, I-beams web stock, hybrid products	6–32 ($\frac{1}{4}$–11/8)	580–700 (36–44)
Laminated veneer lumber (LVL)	Softwood veneer	PF, pMDI	S	Floor and roof joists, roof ridge beams, roof truss chords, window and doorheaders, wood I-joist flanges, concrete form, scaffold planking, window and door joinery	19–75 ($\frac{3}{4}$–3 in.), 27–50 in. wide, up to 24.4 m (80 ft) long	
Wood I-joist	Lumber, LVL, OSB, plywood	Cold setting glue (eg, RF, PRF), pMDI	S	Floor and roof construction	Flange sizes (1.5–3 in. in depth, 2.5–3.5 in. in width), Joist depths range from 9$\frac{1}{2}$ to 50 in. and lengths up to 50 ft	
Glulam beams	Lumber, some LVL	RF, PRF, MF		Headers, girders, purlins, beams, arches, bridges, marinas, power transmission structures	Up to 50 m long	
Parallel strand lumber (PSL)	Strands from softwood veneer	PF	S	Headers, beams, columns and posts; industrial uses such as bridge structures and power poles; and with CCA pressure treatment, post, beams and columns for decks, balconies, car-ports	280 by 430 cross section (11 by 17), length up to 66 ft	
Laminated strand lumber (LSL)	Strand	pMDI	S	Industrial and light structural applications	140 mm (5.5 in.) thick, 2.4 m wide, 10–15 m long	

[a] Refer to Table 1. The data in this table are adapted from various references 3–6,11–16.

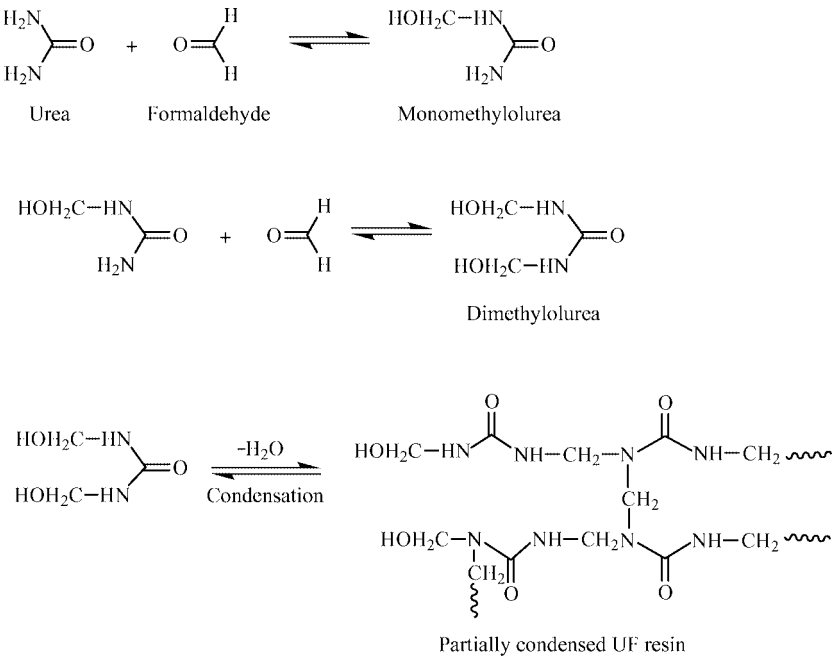

Fig. 1. Polymerization reaction of UF resin.

formaldehyde are heated under slightly alkaline conditions (pH 7–8) to produce methylolurea resins (Fig. 1). Depending on the synthesis conditions (eg, the *relative* urea-to-formaldehyde molar ratios, the reaction temperature, and pH), up to four molecules of formaldehyde can bond to urea owing to the four replaceable hydrogen atoms of urea. The methylolureas produced at this stage are low molecular weight prepolymer solutions that have no adhesive properties. During the second stage, these prepolymer solutions are slightly acidified, which causes the methylolureas produced in the first stage to condense with one another. As this occurs the prepolymer molecular weight increases, and as the polymerization of the UF resin advances further the growing chains begin to cross-link through the formation of methylene–ether links. At the desired point in this polymerization process the aqueous suspension of UF adhesive is neutralized, which stops the reaction before the resin precipitates, and cooled. Water is removed under reduced pressure (vacuum) to produce a final resin content of about 65% nonvolatile resin solids. The final stage of the condensation polymerization, which produces a solid cross-linked thermoset, is completed during production of the wood composite. It is accomplished by the addition of a small amount of acid catalyst to the UF suspension immediately prior to its application to the wood element and occurs during the pressing cycle to produce the wood composite.

UF resin is applied to wood furnish as an aqueous suspension. With the addition of a catalyst such as an acid, the curing can occur at room temperature in a few days, but most industrial processes employ high temperatures and ammonium salts to shorten the bonding cycle (7). In the presence of heat and catalyst, UF condenses into a cross-linked three-dimensional network of macromolecules

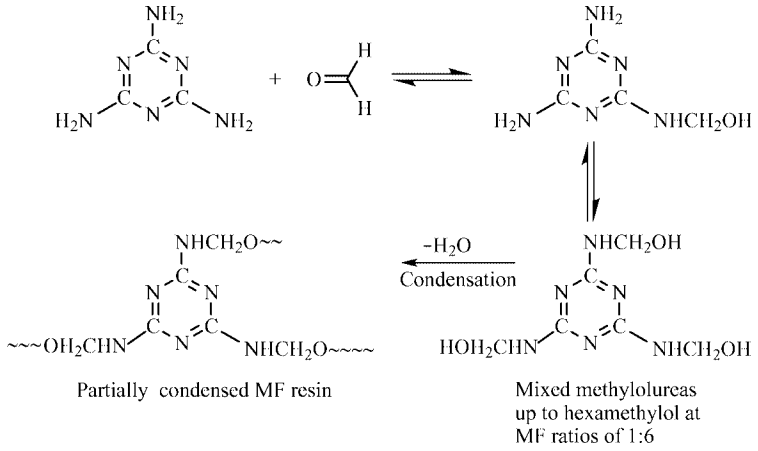

Fig. 2. Formation of MF resin.

that provide bonding. UF resin cures rapidly, provides strong adhesion in a permanently dry environment, and is the least expensive of the major wood adhesives. For these reasons, UF resin is by far the dominant commercial adhesive and is widely used throughout the world for bonding wood and wood-based composites. Despite these attributes, UF resins have three major drawbacks: (*1*) their brittleness once cured, (*2*) their limited resistance to moisture in the cross-linked state (limiting their use to interior products), and (*3*) the potential for formaldehyde emission from UF-bonded wood composites.

Although the urea (U) to formaldehyde (F) molar ratios can be in the range of 1:1.2 to 1:2, governmental regulations on the permissible level of free formaldehyde have forced resin producers and wood-composite manufacturers to lower the molar ratio, and so today resins with a U:F ratio as low as 1:1.1 are not uncommon. The potential for formaldehyde release from UF resin-bonded wood composites is caused by two factors: (*1*) release of a portion of the excess formaldehyde that did not react and (*2*) hydrolysis of susceptible bonds in the UF resin producing the urea and formaldehyde reactants (hydrolytic degradation), which can occur in the presence of moisture and heat during the pressing operation or subsequent installation (18,19). The low moisture resistance of UF resins limits their application to interior products, but if greater moisture resistance is required various urea derivatives or melamine are included in the UF formulation.

Melamine–Formaldehyde (MF) Adhesives. MF resins are produced by a condensation process by reacting melamine with excess formaldehyde (Fig. 2). The reaction proceeds in a manner similar to that between formaldehyde and urea but progresses to a greater extent (see MELAMINE–FORMALDEHYDE RESINS).

Cured MF resins are considerably more water-resistant than UF resins. This is attributed to the lower solubility of melamine in cold water compared to urea (18,19), and the overall greater hydrophobicity of the MF. These resins also have superior heat resistance and shorter curing times than UF resins because of the higher functionality of melamine compared to urea (up to six molecules of formaldehyde can react with melamine). Therefore, MF-bonded composites can be employed in both interior and in some exterior applications.

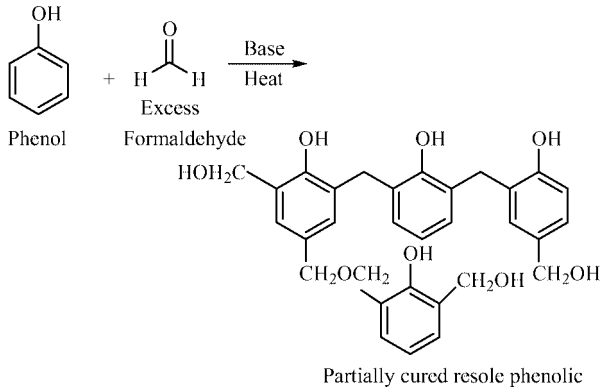

Fig. 3. Formation of resole PF resins.

However, MF resins are costly (about 3.5 times the price of UF based on 100% resin solids), and can only be cured properly at high temperature, which adds to the cost. This is a serious commercial drawback.

As previously mentioned, MF and UF resins are often combined. In the case of UF resins it is done to improve their moisture resistance, to accelerate their cure rate, and to reduce formaldehyde emission from UF-bonded wood composites, while in the case of MF resins it is done to reduce the cost. However, because of the differences in reactivity between urea and melamine mixing these components can complicate the curing. The conditions needed to cure the MF can overcure the UF, and conditions designed to properly cure the UF can leave the MF component undercured. However, when a suitable cure cycle is found for the blended resin, a good combination of properties can be achieved.

Phenol–Formaldehyde (PF) Adhesives. PF resins are produced by the reaction of a phenol and formaldehyde. Depending upon the phenol-to-formaldehyde (P:F) molar ratios and the type of catalyst, two types of PF resins can be produced: resole and novolac PF resins (Figs. 3 and 4).

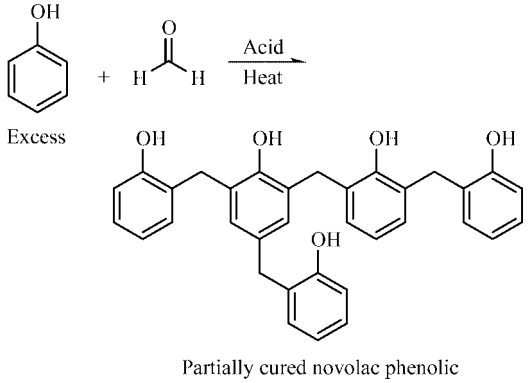

Fig. 4. Formation of novolac PF resins.

Resole PF resins are produced by the reaction of phenol with excess formaldehyde (P:F molar ratio 1:1.8 to 1:2.2) in the presence of an alkali catalyst (Fig. 3). Because resole resins contain reactive methylol groups, they are self-curing resins that can condense with active sites on the phenol rings to form a cross-linked network in the presence of heat even without additional hardener. Resole resins have a very branched structure (Fig. 3) and are by far the more important of the two types of PF resins for wood composites.

Conversely, novolac PF resins are produced by the reaction of excess phenol with formaldehyde (P:F molar ratio 1:0.8 to 1:1) in the presence of an acid catalyst. Unlike resole resins, novolac PF resins have a more linear structure (Fig. 4) and do not self-cure because they lack the residual reactive methylol groups of resoles. Therefore, an external curing agent such as hexamethylenetetraamine must be added to novolac resins to yield a cross-linked structure. Novalac PF resins cured under acidic conditions are not recommended for wood composites for long-term structural applications.

In the presence of heat and on the addition of sodium hydroxide (NaOH) or other catalyst, resole PF resins condense into a three-dimensional cross-linked network having reactive sites suitable for wood bonding. While too much heat accelerates the degradation of UF resins, use of heat is desirable in PF-bonded composites to achieve a high degree of cross-linking. It should also be mentioned that the curing rate of PF resins is strongly influenced by the amount of NaOH added to the resins, with the higher NaOH content affording a faster cure up to a point. However, use of an excessive amount of NaOH in PF resins has adverse effects, including increasing the affinity of the composite for absorbing moisture from the air, which in turn results in PF-bonded composites having a higher thickness swell. As is the case with UF bonding, the adhesion to the wood surfaces in PF-bonded wood composites is achieved through secondary and/or physical bonding. PF resins have greater moisture resistance and greater strength retention when exposed to a high moisture environment than UF resins, and so are employed extensively in the manufacture of wood composites slated for exterior applications. Long-term aging studies in which plywood specimens prepared using various adhesives bonds were exposed to natural weathering confirmed the superior moisture resistance of PF. The PF-bonded specimens retained up to 90% of their original strength even after 8 years, while the UF-bonded specimens lost 100% of their original strength after only 4 years in service (7).

Resorcinol–Formaldehyde (RF) Adhesives. RF resins are a type of phenolic adhesive that are distinguished by a very high reactivity relative to PF resins. This greater reactivity is due to the two phenolic hydroxyl groups on resole. The groups *activate* one another by making each other more electron-rich. Therefore, the first hydroxyl group is much more reactive than the phenol hydroxyl group, and following its reaction the remaining hydroxyl group is still highly reactive. Consequently, although RF adhesives are generally prepared using excess resorcinol to produce a novolac-type resin, in contrast to PF novalacs, these resins set rapidly *with the addition of hardener* even at low temperatures (eg, anywhere from 5 to 70°C). This is termed *cold curing*. The high reactivity between resorcinol and formaldehyde with additional hardener, eg paraformaldehyde, allows the cure to proceed rapidly to completion. The reaction can be further accelerated by applying heat. Attempts to produce a resole RF resin typically result in an unusable

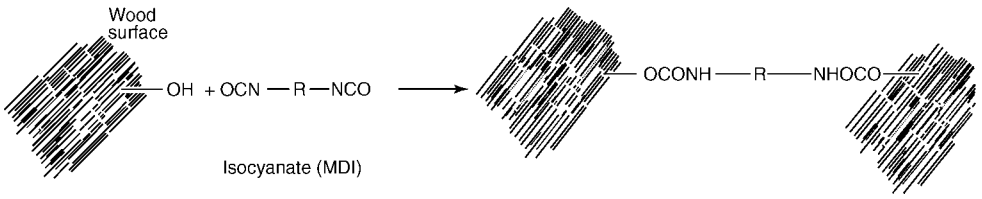

Fig. 5. Reaction of wood with MDI resin.

gel (18–20). Despite the ability to cure at room or elevated temperatures and give composite products having good moisture resistance, RF adhesives are not used extensively because they are among the most expensive of the thermoset adhesives, being second only to the isocyanates in cost. Nevertheless, RF adhesives are used as binders for selected wood products.

Isocyanates. Polymeric diphenylmethane diisocyanate (pMDI) is the most commonly used isocyanate wood adhesive mainly because of its lower volatility and toxicity when compared to other isocyanates such as toluene diisocyanate and dicylcohexylmethane diisocyanate. Some of the advantages enjoyed by pMDI include the fact that it is a liquid polymer, and so it does not require a solvent carrier for application, it is free of formaldehyde, and also it does not require acidic (the case with UF) or alkaline catalysts (the case with PF). It is an effective wood adhesive because the high reactivity of the isocyanate (—N=C=O) groups allows the resin to cure rapidly, and it has the potential to covalently bond directly to the wood by reacting with the hydroxyl groups on the wood surface (Fig. 5) (7,18–20).

The ability of pMDI to cure rapidly is due to the high reactivity of isocyanate (—N=C=O) groups that react rapidly with active hydrogen atoms. Wood possesses active hydrogens from hydroxyl groups on wood surfaces and from moisture in the wood. When the isocyanates react several reactions occur simultaneously but at different rates. The —N=C=O groups first add water to form unstable carbamic acid groups that then dissociate into an amine and carbon dioxide. The resulting amine is more reactive than water and reacts rapidly with another isocyanate to form a polyurea (22). The —N=C=O groups can also add cellulosic hydroxyl groups on the wood surface to form covalent bonds via urethane linkages (Fig. 5). pMDI can cure at ambient temperature in the presence of moisture and so it can also be used in cold pressing of wood-based composites, but hot pressing is usually preferred to shorten the press cycle.

pMDI forms covalent bonds and polar interactions with wood and tolerates both high moisture content in the wood and lower press temperatures during composite manufacture. When wood composites are prepared with equal amounts of adhesive and the bond strength and the dimensional stability of wood composites are compared it is found that pMDI's bond strength and dimensional stability of composites prepared with it are generally superior to those of amino and phenolic resins in both dry and moist environments. Despite these advantages, pMDI adhesives also have some disadvantages. There are some perceived health hazards associated with the manufacturing process, and it can bond to the metal surfaces of a hot press, which is undesirable, although this can be prevented by applying

release agents to the surfaces of the press. However, the primary drawback is cost. pMDI is the most expensive of the wood adhesives.

Other Wood Adhesives. There is considerable interest in developing adhesives from renewable resources that can be used as a primary adhesive or as an adhesive component (an "extender") to replace a portion of petroleum-based adhesives. These natural and renewable resources include lignin, tannins, and natural oils such as soy bean and proteins.

Lignin. Lignin is a waste product produced in large quantities by the pulp and paper industry that is often burned as fuel. Lignin-modified PF resins have been formulated to bond fiberboards, strandboards, and structural plywood (14,15,23–29). Lignin (qv) is employed in this manner primarily to reduce the consumption of oil-based products and to a lesser extent for cost savings since lignin can be less expensive than phenols. The lignin is usually methylolated *in situ* during the PF resin formulation, replacing anywhere from 15 to 35% of the phenol (12,13). Some lignins (eg, lignosulfonates) have also been added directly into the adhesive formulation as a PF resin extender (24–26). Although lignin-based adhesives are used in bonding wood composites, these adhesives require longer press times, produce darker coloration of the panel, and potentially have lower strength relative to PF without lignin (19,25). However, composites having good dimensional stability and good performance under conditions of high moisture have been reported for boards produced with lignin-extended resins, so interest in developing these adhesives continues (4).

Tannin. Tannin is an inexpensive naturally occurring polyphenol found mostly in the bark of trees but also as a component of the wood of some species. Tannin, like lignin, has also been used as a substitute for phenol in the manufacture of PF resins (4,30,31). Although using tannin-based adhesives in the manufacture of wood composites is thought to have potential, some reports indicate that these resins have lower cohesive strength and lower moisture resistance compared to common exterior wood adhesives (30). The poor performance of tannin-based adhesives is attributed to their limited ability to cross-link into a three-dimensional network, their high initial viscosity, and a short pot life owing to the high reactivity of tannin with formaldehyde. However, extensive research has been conducted in recent years to improve the performance of tannin-based adhesives. For example, the addition of small amounts of amino or phenolic resins (4) or metallic ion catalysts (18) has been shown to effectively increase the degree of cross-linking, thereby improving the strength and moisture resistance of tannin adhesives. Reducing the pH or adding hardeners such as hexamethylenetetramine during resin formulation has been shown to decrease the initial viscosity of some tannin-based adhesives (19) thus extending their pot life. These breakthroughs have allowed tannin-based glues to be used in the manufacture of wood composites in South Africa, New Zealand, India, South America, and to some extent in North America.

Other adhesives such as hot melt adhesives (HMA), poly(vinyl acetate) (PVA, catalyzed or uncatalyzed), pressure-sensitive adhesives (PSA), or elastomeric adhesives (based on natural or synthetic rubbers) are also used in wood bonding (7). However, their use is mostly limited to nonstructural applications (eg, secondary manufacturing processes such as kitchen furniture, interior joinery, decorative paper, and packaging) where strength and water resistance are of limited concern.

Advances in Wood Composite Adhesives

Improvements in wood composite properties can be achieved in three areas: (*1*) improvements in wood properties, (*2*) improvement in adhesive properties, and (*3*) improvement in the overall wood composite design. Most advances in wood composites witnessed over the last 10–15 years have been brought about by improved manufacturing equipment and improved composite design (eg, oriented strandboard, I-joist, parallel strand lumber, and laminated strand lumber), while significant advances in future wood composites seem likely to involve changes in wood properties (eg, genetic modification to produce species with some desired property such as improved resistance to decay). However, given the importance of developing alternatives to petroleum-based materials, development of new adhesives may yield the next generation of significant advances in wood composite products.

Some of the more recent research efforts that may lead to new adhesive types are categorized as follows: (*1*) adhesives from natural products, (*2*) adhesives generated *in situ* in the wood, (*3*) adhesive modifications to facilitate processing, and (*4*) adhesive modification for improved properties. Examples of these approaches are given below.

Prior to the 1930s all adhesives were based on natural products (eg, proteins such as animal blood, casein, soy protein). Use of adhesives from natural products steadily decreased thereafter with the development of synthetic polymers that had superior properties. Recently, renewed interest has been shown in using natural products to replace, entirely or in part, petroleum-based adhesive components with natural products, without sacrificing the performance levels achieved with modern petroleum-based adhesives. The purposes are often to reduce cost and dependence on petrochemicals, to reduce formaldehyde emissions, and improve selected properties (eg, biodegradability).

For example, there is renewed interest in using soy-based adhesives for fiber-based composites. New research is underway to develop soy-based adhesives that have improved properties and durability, and that have low volatile emissions (32).

Lignin-modified PF has been utilized for more than 20 years in a variety of different wood products (fiberboards, strandboards, structural plywood, etc.) where the lignin extender has lowered the cost. More recently lignosulfonates have been utilized as extenders to replace up to 35% of phenol in PF formulations (15). It has also been evaluated as an extender for other resins such as epoxy and polyurethane. Considerable research has recently been directed toward incorporating lignin into copolymers or grafting reactive monomers onto lignin allowing it to be copolymerized (33). One recent example of this approach describes using enzymes to copolymerize lignin with alkenes to produce well-defined lignin acrylate copolymers within fibers and pressing those fibers into medium density fiberboard (MDF) (34).

Work in South Africa and in South America has resulted in development of adhesives based largely or entirely on tannins. Tannins, which like lignins are renewable natural products, have the advantage of affording adhesives with low or no formaldehyde emissions, but tannin-based adhesives tend to be brittle. A useful tannin-based particleboard adhesive was reported using tannin extract

from radiata pine bark that was formulated with 5% isocyanate and 5% urea (13). Another report described a tannin-based adhesive in which a significant number of the phenolic groups of the tannin had been esterified to produce a less brittle adhesive (35). The partially esterified tannin was blended with paraformaldehyde and the resulting resin afforded a less brittle adhesive that had better properties than those of the unmodified tannin adhesive.

Because lignin and tannin are phenolic species they have both been evaluated as extenders for PF and UF adhesives. It was subsequently shown that they could be used as primary adhesives. Because these natural phenolics can function as primary adhesives, and because these and other phenolics are components of wood and bark, researchers are investigating reactions of wood's natural phenolic components *in situ* to form a composite without added adhesives. Bark contains not only high amounts of tannins, but also carbohydrates and various other reactive phenolic components. Composites have been prepared by subjecting bark particles to high temperature and pressure to react the phenolic components within the bark so that these components cross-link *in situ* to serve as the sole binder for composites (13). A 1999 publication reported a similar approach for binding wood (36). In that work, birch wood was heated for 1–15 min at 170–230°C under 2 MPa pressure from hot steam. These conditions were used to hydrolyze the polysaccharides within the wood. Under the acidic conditions (formic and acetic acid from hemicellulose and sugars) the resulting sugars reacted with phenolic fragments originating from hydrolyzed lignin. These reactions yield a polymeric binder *in situ*, and have several advantages over adding adhesives to wood. These advantages include eliminating the need for equipment to apply adhesive to wood, no formaldehyde emissions from added synthetic adhesive, and this approach accommodates a high moisture content in wood, which is a major processing advantage. Nevertheless, the long processing time required at high temperature is expensive and additional research is required to evaluate the composite properties, so it is not yet known if this approach will be cost-effective.

Research efforts have been directed towards developing new adhesives that address some disadvantages associated with the processing of pressed wood composites. Pressed wood composites using thermosetting adhesives typically employ a high temperature press cycle. This process requires that the wood furnish be dried to a moisture content typically below 5%. Pressing wood with higher moisture content at higher temperatures can produce a poor product because of "blows," delaminated wood produced when water vapor generated within the mat during the hot-press cycle is rapidly released. Development of effective adhesives that tolerate high moisture content wood has been a goal for many years because drying the wood furnish to a low moisture level is time-consuming and costly, and the potential exists for overdrying some of the wood furnish. Moisture-tolerant isocyanate and PF adhesives are currently available that can tolerate high moisture content furnish (above 15%). Isocyanate adhesives have been used for many years with composites that use higher moisture-content conditions such as "wet wood." Under these conditions isocyanate adhesives have less tendency to delaminate than other adhesives (37). This is probably because of several characteristics of isocyanate-bonded wood composites, including that they can be pressed at a lower temperature than is usual for UF and PF adhesives, isocyanates can chemically bond to the wood rather than rely only on mechanical adhesion, and the cured

adhesive retains greater flexibility than UF and PF adhesives. PF adhesives that can be used with wet wood are also available, but their exact composition and method of function is not clear, although these adhesives may make use of higher formaldehyde content, a coupling agent to promote wood bonding, and/or be a PF/isocyanate blend.

Approaches have been developed that allow some other adhesives to be used with wet wood. The simplest of these approaches uses foamed adhesives. Foaming allows the adhesive to be applied at a higher solid content, often having only 15–20% water, and so higher moisture content in wood can be tolerated, and the composite cures faster since less moisture needs to be removed during cure. A recent investigation reported use of a soy protein-modified PF as a foamed adhesive for plywood production (38). The soy replaced animal blood in the formulation, which not only improves durability but can alleviate health concerns.

Another major difficulty with hot-pressed wood composites is adequate thermal transfer across the thickness of the composite. Heat is transferred through the press platens, sometimes with the aid of steam. However, wood is a low thermal transfer medium and so there is risk of overcuring resin nearer the surfaces of the composite, while undercuring resin in the interior. This is particularly true with thicker composites. Also the pressing step is probably the most expensive of the processing steps so any adhesive modification that reduces the press time and facilitates a more uniform cure is a significant advantage for cost and properties. Matuana (39) reported using thermally conductive filler material such as synthetic graphite (carbon filler) in the mat or adhesive to facilitate thermal transfer. Use of the carbon filler not only reduced the required cure time but also significantly increased the internal bond strength of the wood composites.

Wood composites are now being considered for use under increasingly demanding conditions and so adhesive modifications to improve specific composite properties, such as improved strength, durability, and dimensional stability, are needed. These types of modifications which usually increase adhesive cost were previously considered not cost-effective, but now might find markets. Early efforts to improve properties included adding thermoplastic polymers to the reactive adhesive prepolymer and applying the thermoplastic-modified prepolymer to the wood furnish and pressing. Examples of this approach include adding poly(furfural alcohol), a water-soluble polymer, to a UF prepolymer (40) and using chlorinated natural rubber to modify PF (41). The poly(furfural alcohol) did not improve properties, while the chlorinated natural rubber did improve properties but required processing conditions that were not industrially viable. These efforts highlight issues that must be addressed for an industrially useful modification. Any modifications must allow the processing conditions to be similar to those used now. Therefore, solvent should not be required, and prepolymer viscosity, stability, and cure conditions should be similar to those used now, and the resulting properties must be improved sufficiently so that an increased resin cost is worthwhile. A series of publications by Ebewele and coworkers (42–45) described modifying UF resins with di- and trifunctional amines and ureas without excessive increases in viscosity or processing difficulty. Particleboard made with the modified UF resins had an internal bond (IB) strength that was significantly greater than the IB strength of the control particleboards before and after exposure to moisture. Recently a method was reported that yielded

thermoplastic-modified UF adhesives that could be processed in the same way as unmodified control UF and gave wood flour composites with improved mechanical properties and moisture resistance. A premade thermoplastic polymer suspension (46–48), or aqueous slurry of acrylic and vinylic monomers, and a radical polymerization initiator (49) were combined with the UF prepolymer. The modified UF was used to prepare hot-pressed wood flour composites with significant improvements in notched Izod impact strengths. Further development simplified the method and modified UF resins were employed for hot pressing of particleboards (50) that, depending on the choice of thermoplastic monomers employed, also gave a higher IB strength and the neat resin showed lower moisture uptake than unmodified UF neat resin. Zanetti and co-workers (51) recently reported substantial increases in the IB strength of melamine–urea–formaldehyde (MUF) resins by the addition of small amounts (10%) of acetals to MUF resins. The authors reported that the acetals worked by improving the solubility of melamine and higher molecular weight reactive oligomers in the MUF resin and also appeared to disrupt the clustering of colloidal particles of MUF. This modification afforded 25–50% increases in IB strength and yet required no additional modification of the MUF formulation or the processing conditions.

Wood Composites Bonded with Thermoset Adhesives

The principal wood composite products currently in use in the United States and Canada, based on volume, are plywood (17.5 million cubic meters), oriented strandboard (16.8 million cubic meters), particleboard (10.3 million cubic meters), medium density fiberboard (3.4 million cubic meters), hardboard (2.0 million cubic meters), hardwood plywood (1.0 million cubic meters), and laminated veneer lumber (1.2 million cubic meters) (13). These products are described below. While all of these composites occupy an important place in the market now, some of these products are gaining in importance while others appear to be losing market share to other composite products.

Wood composites for structural and nonstructural applications that are bonded with thermosetting glues can be produced in many different geometries, including panels (3 ft or more in width by 3/8 to 1 in. thick), lumber (2 in. or more in width by 2–4 in. thick), or beams ($3\frac{1}{8}$ in. wide by 9 in. or more in depth) (Table 2). The exact procedure for making wood composites depends on the type of wood furnish (wood geometry), the desired arrangement of the particles in the final product, and the adhesive to be used, as well as the cure cycle if the adhesive needs to be reacted during the process step. These processing variables determine the characteristics of the final products, including mechanical properties, water resistance, dimensional stability, surface quality, and workability. Regardless of the increasing number of wood composite products being introduced into the market, the different sizes and shapes of these products, and the different volumes of these products that are produced, the fabrication process is a highly automated one, and once the adhesive mixture is applied to the wood furnish the general manufacturing method for preparing these composites is similar (Fig. 6).

The composite fabrication process begins once the trees have been processed into a dried furnish and the furnish is transported to a device such as rotating drum (as is the case for flakes, particles, and fibers). Here, the adhesive and other

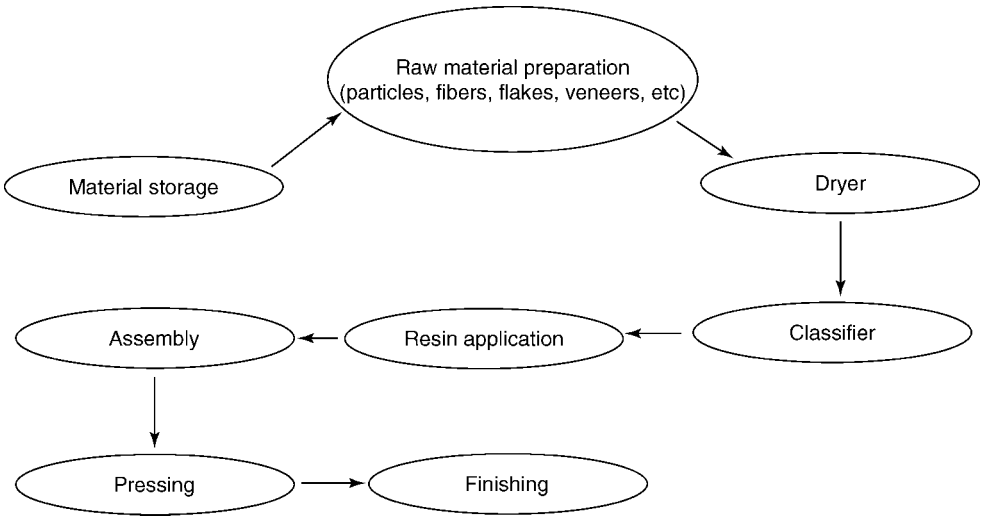

Fig. 6. A typical wood composites manufacturing process.

additives are applied to the furnish by air spray, airless spray, or a high shear atomizer. The rotating drum possesses nozzles that are fed by hose lines connected to resin storage drums. Adhesive resin mixtures are applied to veneer-based wood products (plywood, laminated veneer lumber) by a roll coater, curtain coater, spray coater, or liquid or foam extrusion. The amount of adhesive applied to the furnish varies with the product and adhesive type. Common additives are also applied during this step and include wax (to improve dimensional stability by reducing moisture absorption), wood preservatives (for protection against insect and fungal attack), and fire retardants.

After resin application, the coated wood furnish moves to a forming apparatus. The forming apparatus arranges the furnish appropriately into a mat having the specified dimensions and orientation of wood raw material to give the desired product type with the desired dimensions and density after pressing. This mat is then prepressed to remove much of the air, ie, consolidate a loosely formed mat into a rigid mat which has a certain degree of cohesion to reduce its thickness. The formed mat then goes to a hot press where it is subjected to a selected press cycle. Here it is heated and pressed at the desired temperature and pressure for specified periods of time to bond the wood into a composite part of the desired thickness. The pressed wood composite finally goes on to the finishing steps where the panel is sized, sanded, trimmed to the desired thickness and dimensions, edge sealed, and packaged for shipment. In some cases the hot composite product is stacked to help retain heat and continue the cure out of the hot press, as is the case with phenolic resins.

The biggest differences in processing for each type of wood composite reside in the geometry and arrangement of wood furnish, the adhesive type and amount applied, and the cure cycle. The following sections describe the main characteristics of the major wood composite products made with thermoset adhesives.

Plywood. Plywood panels have been produced and marketed in the United States for more than five decades. They are considered a material of choice in the building industry because of outstanding structural performance as defined by

a high strength-to-weight ratio, excellent dimensional stability, and durability compared to other building material (6). Plywood typically consists of an uneven number of thin layers of wood veneers, called plies, that are glued together into a panel. The individual plies are typically arranged in the panel so that their grains are perpendicular to one another (right angles of 90°). The plies are arranged at 90° to one another to improve the dimensional stability and make the properties of the plywood more uniform along both the vertical and horizontal axes. The anisotropic nature of wood results in a tendency to swell less parallel to the grain than perpendicular to the grain and simultaneously gives wood greater strength parallel to the grain than perpendicular to the grain. Therefore, arranging individual plies at 90° to one another affords greater dimensional stability, decreases the tendency to split, and generally evens out the strength properties in all directions. If the grain angles were not varied then the plywood would have less dimensional stability and be much stronger along the grain axis but weaker perpendicular to the axis. The appearance of the final product can be improved if desired by applying a decorative surface veneer to give the final plywood a desired appearance. The final overall properties of the plywood depend on many factors, including the wood species, the quality of wood veneers, the order of placement of the veneer plies in the panel, the type and amount of adhesive applied, and the curing or pressing conditions.

Both hardwood and softwood species are utilized in the manufacture of plywood. Softwoods (Douglas-fir, western hemlock, larch, white fir, ponderosa pine, redwood, and southern pine are examples) are generally preferred in construction applications where strength and stiffness are required. Hardwood plywood is generally preferred for decorative applications where appearance is most important and strength is a limited criterion, although hardwood plywood can also be designed for structural applications. In decorative applications, hardwood plywood often competes with thin MDF which can be given a high quality overlay giving it an appearance similar to that of hardwood plywood.

Oriented Strandboard (OSB). Oriented strandboard (OSB) panels have been developed as an alternative to plywood in building construction. The emergence of OSB was driven in part by a decreased supply of large diameter logs suitable for veneer production, and by innovation and productivity changes in the North American wood products industry over the past few decades as well as the structural performance of OSB products, which are suitable for use in most plywood applications but at a much lower cost. In addition, OSB manufacture allows small, low grade timber resources to be processed into a marketable product. This effectively saves raw materials that are in short supply and promotes efficient utilization of wood (3,5,6).

OSB panels are made up of rectangular strands (wafers or flakes) of wood approximately 0.030 in. thick, bonded together with exterior-grade adhesive under extreme heat and pressure to develop adequate strength properties in the panel. During this process, long grain strands are compressed and mechanically oriented more or less parallel to each other and arranged into three to five distinct layers. These layers are oriented at ca 90° to one another, ie, strands are aligned lengthwise in layers perpendicular to each other similar to veneer plywood. The strands near the surface are typically $\geq$ 3 in. long but shorter strands are

sometimes used in core layers. The core layers are also sometimes randomly arranged rather than oriented. The strands for the faces are typically oriented parallel with the long direction of the panel, whereas the core layers are oriented perpendicular to the length of the panel. Hardwood species, alone or in combinations with softwood species, can be used in the manufacture of OSB panels, but preferably lower density wood species (eg, aspen poplar in the northern part of North America and southern yellow pine in the south) are employed because strands of these woods can be compressed into medium density boards with sufficient contact between strands during pressing for good bonding (4).

The alignment of strands and the use of long strands give OSB panels improved mechanical (strength and stiffness) and physical (dimensional stability) properties in the direction of alignment, which make them acceptable in a wide range of industrial, residential, and commercial applications (Table 2). Even though OSB panels are being used as a substitute for plywood, their potential for use in some structural applications has been limited because of poor dimensional stability and durability compared to that of plywood. OSB panels will swell in thickness, and like all wood products decay when they come into extended contact with water. Since most of the thickness swelling is not reversed when the panels are re-dried, the products are regarded as unacceptable for some applications where high moisture contact is expected (52–54).

Particleboard. Particleboard is prepared using small dried-particles combined with a thermally curable adhesive or other suitable binder and bonded together under high heat and pressure into panels of the desired thickness. The raw materials used to produce particleboard consist of wood wastes from sawmills, primarily from milled or ground wood chips, sawdust, and planer shaving. In some cases recycled cellulosic materials and plant residues such as wheat straw and bagasse are utilized as furnish to make particleboard. Most particleboard is formed into flat panels. However, molded and extruded particleboard products such as furniture parts, molded door skins, and molded pallets are also produced.

Particleboard usually consists of a three-layered panel with two surface layers (outer layers) and one core layer (inner layer). The face furnish is usually thinner than that in the core. This permits the strength and stiffness of the panel to be tailored and the faces to be produced with smooth surfaces. The American National Standard for Particleboard, ANSI A208.1, classifies particleboard by density, properties, and class, and is the voluntary particleboard standard for the North American industry (Table 3).

Medium Density Fiberboard (MDF). MDF is manufactured from refined wood chips or other fine cellulosic materials combined with a synthetic resin. The adhesive coated furnish is joined together under heat and pressure to form a versatile material having varying characteristics depending on the composition and processing conditions (Tables 2 and 3).

The surface of MDF can be controlled so that it is smooth, flat, and uniform in appearance and free of wood growth features such as knots and grain patterns. MDF panels are highly valued by woodworkers because they machine well and are suitable for finishing operations such as direct printing (eg, wood grains), thin laminating (eg, paper, decorative foil laminates), and painting (eg, custom colors). These attributes allow MDF panels to serve as excellent substitutes for solid wood

Table 3. Selected Properties of Wood-Based Composite Panels

Physical properties	Plywood[a]	OSB[b]	Particleboard[c]	MDF[a]
Density, lb/ft^3[d]	28–31	36–44	40–48	<40 to >50
Thickness, in.	1/4–1$\frac{1}{4}$	1/4–3/4	1/2–1$\frac{1}{4}$	3/4 or higher
Internal bond (IB), psi[e]	Species specific	50	15–145	44–131
Modulus of rupture (MOR), psi[e]	3000–7000	3394–4206 (‖) 1392–1799 (⊥)	435–3408	2030–5003
Modulus of elasticity (MOE), 10^3 psi[e]	1000–1900	653–798 (‖) 189–218 (⊥)	79.8–449.6	203–500
Screw holding capacity—face, lb	Species specific	100–300	90–450	172–342
Screw holding capacity—edge, lbs	Species specific	100–300	180–348	147–294
Hardness, lb	Species specific	—	500–1,500	—
Linear expansion (max. avg. percent)	0.15	0.20–0.40	0.35	—

[a]Properties for various plywood grades or MDF (55).
[b]Properties obtained from the Canadian Standards Association, standard CAN3–0437.0-M85, Waferboard and Strandboard/Test Methods for Waferboard and Strandboard (June 1985). ‖ means parallel to the indicated direction of face alignment; ⊥ means perpendicular to the indicated direction of face alignment. The Wood Handbook (55) shows OSB having MOR values of 3000–4000 psi and MOE values of (700–1200) $\times$ 10^3 psi.
[c]Properties obtained from ANSI standard (ANSI A208.1–1999) for various grades of particleboard.
[d]To convert lb/ft^3 to kg/m^3, multiply by 16.
[e]To convert psi to MPa, divide by 145.

in many interior applications such as kitchen cabinets, furniture, door parts, and moldings (Table 2).

Composite Lumbers and Beams. Composite lumbers and beams comprise a large and diverse family of products known as engineered wood products (EWPs). EWPs include laminated veneer lumber (LVL), laminated strand lumber (LSL), parallel strand lumber (PSL), glulam, and I-joists, among others.

LVL [also known as structural composite lumber (SCL)] technology was developed in Finland. Trus Joist became the first U.S. producer of LVL in 1970 (3,6). LVL is a structural building material manufactured by layering dried and graded wood veneers with waterproof adhesive into billets of various thicknesses and widths. Generally, high quality laminates are used at the faces and low quality laminates in the center of the lumber. This specific arrangement gives LVL greater strength (by a factor of 2 or more) than conventional solid lumber having equivalent dimensions. In LVL billets, all veneers are laminated with the grain angle parallel to the longitudinal axis of the wood (one-grain direction) rather than arranging the veneer grains perpendicular to one another as in plywood. PF and pMDI are the resins that are typically employed to produce LVL and so the billets are hot-pressed or radio-frequency-pressed to consolidate the laminates. Common wood species used for LVL include Douglas fir, larch, southern yellow pine, and poplar, but other wood species can be used as the raw material. As an engineered wood product, LVL is an ideal structural building material for applications in housing, commercial, and industrial construction. Typical applications include floor and roof joists, roof beams, roof truss chords, flanges for prefabricated wood I-joists, concrete form, and scaffolding plank, among others (Table 2).

Wood I-joists are hybrid beam elements that are made by gluing together lumber and panel composites to produce a dimensionally stable lightweight member having specified engineering properties. The product utilizes the geometry of the I-shaped cross section composed of two flanges (top and bottom) of various widths linked by a web (or two webs) of various depths (Table 2). The flanges are typically LVL, or finger-jointed sawn lumber of various machine stress-rated grades, while the webs are either structural grade OSB or structural plywood. The flanges are designed to resist bending strength and provide stiffness, while the web is designed to resist shear forces in the beam. Thus, the I-shaped geometry of these products gives a high strength-to-weight ratio. I-joists are marketed as building products that do not warp, twist, or shrink, and their dimensions are more uniform than those of conventional sawn lumber joists. The wood I-joists performs much better than solid lumber because greater joist spacing can be used and their frames are lighter and more dimensionally stable than lumber, making their installation less costly for the builders. Wood I-joists are used in residential and light commercial construction in applications such as floor and roof joists, rafters, and purloins, among others (Table 2). Wood I-joists are certified by the APA-Engineered Wood Association as the APA-Engineered Wood System (APA-EWS), and are manufactured in compliance with Performance Rated I-Joists (PRI-400), Performance Standard for APA-EWS I-Joists.

Glued laminated timber, or glulam, is a structural beam element manufactured by gluing laminates of solid wood lumber, finger-jointed lumber, or LVL. The individual lumber elements are oriented parallel to the longitudinal axis of the beam and laminated flat-wise to bond along the entire length and width of the lumber elements. Based on the stiffness rating of the individual laminations high quality laminates are generally applied at the beam faces, while low quality laminates are placed in the middle of the beam. This combination is preferred since the load is carried by the beam in the top and bottom faces, while the middle only has to resist shear. A cold curing resin adhesive such as resorcinol or phenol–resorcinol is usually used to produce the beam by applying the adhesive and clamping or cold-pressing the laminates. Since little or no heat is required for the cure, curved glulam members and other customized shapes can easily be produced. Glulams are manufactured in accordance with the American National Standards Institute (ANSI) ANSI standard A190.1 for structural glued laminated timber. The strength values (bending and shear) for glulam are higher than for lumber. Glulam members are typically used as headers, beams, arches, etc (Table 2). The production of glulam is not expected to grow significantly in North America because of the scarcity and high cost of laminating grade lumber, combined with stiff competition from LVL and other engineered wood products such as LSL and PSL, which are expected to grow because they have excellent structural properties and they employ more readily available raw materials (5,6).

PSL is an engineered wood product developed by MacMillan Bloedel, Ltd., of Canada and was first commercialized in 1988 (3,6). PSL is made in a similar manner to glulam beams with the difference being that strands of broken-up veneer (about $\frac{1}{2}$ in. wide and up to about 37 in. long) are employed instead of solid lumber laminates. The strands are oriented and laid-up into a mat in a lengthwise direction, ie, aligned parallel to one another. The strands are glued with a water-resistant adhesive (PF) and are consolidated in a continuous microwave press. PSL is stronger, stiffer, and more stable than sawn lumber having the same

cross section and is free of splits, knots, and warp. PSL is employed in various applications such as head beams, trusses, and other structural frames (Table 2).

LSL is another type of engineered wood product in which all the strands are aligned in one direction, ie, LSL is an oriented strand lumber. The strands in LSL are shorter than in PSL and produced from strand wood rather than veneer. The strands are typically longer than strands utilized in oriented strandboard. Pressing includes steam injection rather than radio-frequency heating, and isocyanate resin is typically used rather than PF adhesive. LSL is used in industrial and light structural applications (Table 2).

Wood Thermoplastic Composites

Wood-based composites continue to be among the most widely used building materials throughout the world. While thermoset wood composites date back to the early 1900s (a wood flour/PF composite called Bakelite®), wood combined with thermoplastic composites have become of major commercial importance only since the 1980s in the United States, although they have been in use longer in Europe (2). Wood-plastic composites (WPCs) represent a rapidly growing industry in the United States in both the plastic processors and forest products industries (56–58).

To plastic processors wood and other lignocellulosic fibers (eg, agrofibers) represent a vast supply of readily available raw materials for all types of WPCs. Statistics show that 2.5 million tons of fillers were used in North America in 2001 with the most important fillers being inorganic materials (2.3 million tons) such as calcium carbonate (1 million tons), glass fiber (0.77 million tons), and other mineral fillers such as clay, talc, mica (0.55 million tons). Only 182,000 t was natural fibers (57). The inorganic materials enhance some composite properties (eg, strength and modulus) and are extensively employed as fillers, but have several drawbacks. They are produced from nonrenewable sources and they have high density, so products prepared with inorganic fillers tend to be heavy. Furthermore, these inorganic fillers cause equipment wear during processing (59). Therefore, on a volumetric basis, their use may not be very cost-effective. During the past two decades, wood fibers and other lignocellulosic materials have begun to penetrate the filled thermoplastic markets because they possess many advantages relative to the common inorganic fillers. These advantages include high specific stiffness and strength, easy availability, lower density, lower cost on a unit-volume basis, low hardness which minimizes wear of the processing equipment, renewability, recyclability, safety, and biodegradability (60,61). The replacement of inorganic fillers with lignocellulosic fibers also provides an opportunity to increase processing productivity rates (56).

The forest products companies, on the other hand, see plastics as a way to expand sustainable forest resource utilization through the use of wood waste, fibers from underutilized species, and reclamation and recycling of wood, other agricultural species and waste, and paper materials from municipal solid waste streams (62), as well as a way to make new construction materials with attributes that wood does not have (56).

WPCs are typically manufactured by first mixing dried cellulosic materials (in powder or fibrous form) with various plastics and other processing ingredients (eg, lubricants, fusion promoters, coupling agents, flame and smoke retardants, ultraviolet stabilizers). Cellulosic materials that are used in the production of WPCs include wood flour or particle, flax, jute, or other agricultural waste. The most commonly employed plastics are polyethylene (PE), polypropylene (PP), polystyrene (PS), and poly(vinyl chloride) (PVC). These thermoplastics are selected mainly because they can be processed at lower temperatures (150–220°C) to prevent the degradation of cellulosic materials (2). Generally, wood flour and other coarse particles (10–100 mesh size) are easier to handle during processing than long fibers which tend to agglomerate and cause dispersion problems during mixing. However, because of their higher aspect ratio, long fibers provide greater reinforcing effects in WPCs than particles. The fiber can be difficult to disperse but the dispersion problems can be offset by using compatibilizers during processing (60,63,64). Once mixed, the blended material is processed into the desired shape by conventional plastic processing equipment such as an extruder, injection molder, and a hot press (compression molding). Most of the WPCs used in construction applications are extruded to a profile of uniform cross section (solid or hollow) and any practical length, whereas products having more complex shapes such as those used in the automotive industry or other consumer products are injection- or compression-molded.

WPCs comprise an emerging class of materials that combine the favorable performance and cost attributes of both wood and plastics (Table 4). Because WPCs are true hybrid materials, they have strength and stiffness properties that are somewhere between both materials. They have outstanding bolt, drill, screw, and nail retention and they machine similarly to wood. Generally, WPCs are stiffer than neat plastics and have attributes that solid wood does not have. If properly manufactured, WPCs are more resistant to moisture (water absorption and thickness swell) than wood and resist attack by insects and fungi better than other wood

Table 4. Some Physicomechanical Properties of WPCs and Comparative Performance of WPCs with (Oak) and Softwood (Pine) Solid Wood

Tests	Test methods	HDPE/WF[a]	PVC/WF[a]	Northern oak[b]	Ponderosa pine[b]
Specific gravity	ASTM D143	0.96–1.1	1.36	0.56–0.63[b]	0.38–0.40[b]
MOR, psi[c]	ASTM D790	790–1423	2100–4500	14300[b]	9400[b]
MOE, 10^3 psi[c]	ASTM D790	160–510	700–980	1820[b]	1290[b]
Water absorption, %	ASTM D1037	0.7–4.3	1.2	—	17.2
Thickness swell, %	ASTM D1037	0.2	—	—	2.6
Nail withdrawal, lb	ASTM 1761	90–170	—	—	50
Screw withdrawal, lb	ASTM 1761	430–600	—	—	165
Hardness, lb	ASTM 143	1290	—	1290[b]	460[b]
Linear coefficient of expansion (per °F)	ASTM 696	16×10^{-6}	17×10^{-6}	—	25×10^{-6}

[a]HDPE/WF and PVC/WF contained 50–70% wood fiber.
[b]MOE and MOR values measured at 12% moisture content (7).
[c]To convert psi to MPa, divide by 145.

products. This outstanding performance is due to the fact that the plastic matrix encapsulates the individual wood fibers, thus interfering with moisture uptake by the wood element. Moisture can only be absorbed into the exposed sections of the wood. WPCs can be sanded, stained, painted, and finished just like natural solid wood. However, sealants and paints are not required for protection because WPCs resist moisture better than wood, and WPC products can be prepared with colorants and other additives during the processing phase, which eliminates the need for additional finishing.

Because of their performance, easy installation, and cost-effectiveness, WPC products are being selected by homebuilders over other materials such as solid wood, concrete, clay, and aluminum, especially as building materials for applications like decking, siding, and window and door frames. WPCs are also used as molded panel components for automotive interiors. The market for these composites continues to expand in the United States and other parts of the world. In 1999, 460 million pounds of WPCs were produced in North America (56). In 2000, production of these composites increased to 760 million pounds and experts believe that the production of WPCs will continue to grow particularly because of their acceptance as a substitute for chromated copper arsenate pressure-treated lumber (57,58).

Although a variety of WPC products have been commercialized, some drawbacks in their properties may limit the market potential of these products. For example, WPCs are more brittle and have lower impact resistance than neat plastic products (61,65). In addition, their high density (62–85 lb/ft^3), which is almost twice that of solid lumber (22–40 lb/ft^3 for various pine species), may hinder their acceptance in the conventional structural lumber market (66). In general, unfilled plastics are more ductile than WPCs because the incorporated brittle wood fibers alter the ductile mode of failure of the matrix making the composites more brittle (61,65,67). The higher density of WPCs compared to the unfilled plastic and solid wood is mainly due to the compression of wood cell walls during processing. The final specific gravity of WPCs manufactured by injection molding, extrusion, and compression molding, even when made with a 0.9 specific gravity thermoplastic resin, is over 1 because the wood cell walls are crushed or compressed nearly to the specific gravity of solid wood without air spaces (approximately 1.5), and voids between and within the wood fiber structure are completely filled with resin (68,69).

Several attempts have been made to overcome the drawbacks of dense WPCs (65,70–72). Significant improvements in the impact strength of WPCs are achieved by incorporating impact modifiers into the formulation (65). However, impact modification of WPCs does not enhance their ductility or reduce the density of the products (65). The creation of a microcellular void structure (wood-like structure) in WPCs through foaming has recently been found appropriate to reduce the weight of the composites (70–73). The lightweight WPCs, as a result of the presence of microcells, exhibit enhanced ductility and impact resistance. However, the reduced density can be achieved at the expense of other mechanical properties such as strength and stiffness (72,74) (Table 5).

There currently are no manufacturing standards for WPCs and the standard test methods for evaluating the mechanical and physical properties of WPC products are under development by the American Society for Testing and Materials (ASTM), committee D7 on Wood. The lack of manufacturing standards combined

Table 5. Mechanical Properties of Microcellular Pure Plastic and WPC Foams

	Mechanical properties[b]							
	Strength at break, MPa[c]		Tensile modulus (stiffness), GPa[d]		Elongation at break, %		Notched Izod impact strength, J/m[e]	
Samples[a]	Unfoamed	Foamed	Unfoamed	Foamed	Unfoamed	Foamed	Unfoamed	Foamed
Pure plastic (PVC)	17	14	0.06	0.07	84	126	72	206
WPC	14	13	0.37	0.20	28	63	31	87

[a]The density of pure PVC was 1.35 g/cm^3 whereas the densities of the composites with 30% wood fibers were in the range of 1.35–1.45 g/cm^3. The densities of foamed PVC and WPC samples were 0.60 g/cm^3.
[b]Properties are expressed as specific properties, ie, property divided by the specific density of the sample (72).
[c]To convert MPa to psi, multiply by 145.
[d]To convert GPa to psi, multiply by 145,000.
[e]To convert J/m to ft·lbf/in., divide by 53.38.

with the increased use of WPCs by the construction industry have also resulted in concern about the durability of these products exposed to outdoor environments. In applications such as decks and docks, landscaping timber, fencing, signposts, playground equipment, window frames, etc, the products can be in ground contact and/or are in an above-ground environment where there often are risks of material deterioration. When WPCs are in ground contact, biological agents such as fungi and subterranean termites may be the main cause of degradation (75,76). On the other hand, exposure to sunlight and moisture can cause degradation in an above-ground environment (77,78). Freeze-thaw durability may also be of significant importance in colder regions where freeze-thaw action is prevalent. These climatic environments may cause millions of dollars of material damage and high material cost may be involved to replace damaged products. Therefore, the durability of these composites is of special concern for their use in outdoor applications and is currently being extensively studied.

BIBLIOGRAPHY

"Composition Board" in *EPST* 1st ed., Vol. 4, pp. 75–118, by M. N. Carroll, Washington State University; "Composition Board" in *EPSE* 2nd ed., Vol. 4, pp. 47–66, by T. M. Maloney, Washington State University; "Wood, Polymer-Impregnated" in *EPSE* 2nd ed., Vol. 17, pp. 887–900, by J. A. Meyer. SUNY College of Environmental Science and Forestry.

1. J. L. Bowyer, R. Shmulsky, and J. G. Haygreen, *Forest Products and Wood Science: An Introduction*, 4th ed., Iowa Press, Ames, Iowa, 2003, p. 554.
2. C. Clemons, *Forest Products J.* **52**(6), 10–19 (2002).
3. T. M. Maloney, *Forest Products J.* **46**(2), 19–22 (1996).
4. T. M. Maloney, *Modern Particleboard and Dry-Process Fiberboard Manufacturing* (updated edition), Miller Freeman Publications, Inc., San Francisco, 1993, p. 681.
5. L. M. Guss, *Forest Products J.* **45**(7/8), 17–24 (1995).
6. D. A. Pease in J. A. Sowle, ed., *Panels: Products, Applications and Production Trends, A Special Report from Wood Technology*, Miller Freeman Publications, Inc., San Francisco, 1994, p. 272.

7. A. A. Marra, *Technology of Wood Bonding: Principles in Practice*, Van Nostrand Reinhold, New York, 1992.
8. R. M. Rowell, A. R. Sanadi, D. F. Caulfield, R. E. Jacobson, in A. L. Leao, F. X. Carvalho, E. Frollini, eds., *Proceedings of the First International Lignocellulosics-Plastics Composites, Mar. 13–15, 1996*, Sao Paulo, Brazil, 1997, pp. 23–51.
9. J. A. Youngquist, A. M. Krzysik, B. W. English, H. N. Spelter, and P. Chow, *The Use of Recycled Wood and Paper in Building Applications* (Proceedings of a 1996 symposium sponsored by the U. S. Department of Agriculture Forest Service, Forest Products Laboratory and the Forest Products Society, in cooperation with the National Association of Home Builders Research Center, the American Forest & Paper Association, the center for Resourceful Building Technology, and Environmental Building News), Proc. 7286, Forest Products Society, Madison, Wis., 1996, pp. 123–134.
10. J. A. Youngquist, A. M. Krzysik, P. Chow, and R. Meimban, in R. M. Rowell, R. A. Young, J. K. Rowell, eds., in *Paper and Composites from Agro-Based Resources*, CRC Lewis Publishers, Boca Raton, Fla., 1997, Chapt. 9, pp. 301–336.
11. Anonymous, Wood-based Panel Products: Technology roadmap (Canadian Cataloguing in Publication Data), 1998, http://strategis.ic.gc.ca/trm.
12. T. Sellers Jr., *Wood Technol.* **127**(3), 40–43 (2000).
13. T. Sellers Jr., *Forest Products J.* **51**(6), 12–22 (2001).
14. T. Sellers Jr., *Panel World* **35**(3), 22–26 (1994).
15. T. Sellers Jr., *Panel World* **31**(5), 26–29, 44 (1990).
16. T. Sellers Jr., *Plywood and Adhesive Technology*, Marcel Dekker, Inc., New York, 1985, p. 661.
17. A. Gardziella, L. A. Pilato, and A. Knop, *Phenolic Resins*, 2nd ed., Springer, New York, 2000, p. 560.
18. A. Pizzi, *Advanced Wood Adhesives Technology*, Marcel Dekker, Inc., New York, 1994, p. 89.
19. A. Pizzi and A. Pizzi, eds., in *Wood Adhesives: Chemistry and Technology*, Vols. 1 and 2, Marcel Dekker, Inc., New York, 1983, 1989.
20. A. Pizzi and K. L. Mittal, eds., *Handbook of Adhesive Technology*, Marcel Dekker, Inc., New York, 1994, p. 680.
21. A. V. Pocius, *Adhesion and Adhesives Technology: An Introduction*, Hanser–Gardner Publications, Inc., Cincinnati, Ohio, 1997.
22. Z. W. Wicks, F. N. Jones, and S. P. Pappas, *Organic Coatings, Vol. 1: Film Formation, Components, and Appearance*, Wiley-Interscience, New York, 1992, p. 190.
23. M. Turunen, L. Alvila, T. T. Pakkanen, and J. Rainio, *J. Appl. Polym. Sci.* **88**, 582–588 (2003).
24. J.-S. Kazayawoko, B. Riedl, and J. Poliquin, *Holzforschung* **46**, 349–354 (1992).
25. J. S. M. Kazayawoko, B. Riedl, J. Poliquin, A. O. Barry, and L. M. Matuana, *Holzforschung* **46**, 257–261 (1992).
26. L. M. Matuana, B. Riedl, and A. O. Barry, *Eur. Polym. J.* **29**, 483–490 (1993).
27. W. Peng and B. Riedl, *Polymer* **35**, 1280–1286 (1994).
28. A. O. Barry, W. Peng, and B. Riedl, *Holzforschung* **47**, 247–252 (1993).
29. D. J. Gardner and G. D. McGinnis, *J. Wood Chem. Technol.* **8**, 261–288 (1988).
30. M. Fechtal and B. Riedl, *Holzforschung* **47**, 349–357 (1993).
31. M. Fechtal, B. Riedl, and L. Calvé, *Holzforschung* **47**, 419–424 (1993).
32. United Soybean Board 2002. Market Opportunity Summary, Soy-Based Wood Adhesives, Feb. 2002, and Soy-Based Wood Adhesives and the Environment, Feb. 2002, www.unitedsoybean.org.
33. J. J. Meister, Presented at the *2nd Annual Partnerships for Environmental Improvement and Economic Development Conference on Wood and Cellulose, Building Blocks for Chemicals, Fuels and Advanced Materials*, Syracuse, New York, Apr. 9–11, 2000.

34. A. Huttermann, C. Mai, and A. Kharazipour, *Appl. Microbiol. Biotechnol.* **55**, 387–394 (2001).
35. A. P. Barbosa, E. B. Mano, and C. T. Andrade, *Forest Products J.* **50**, 89–92 (2000).
36. O. V. Startsev, B. N. Salin, Yu. G. Skuridin, R. M. Utemesov, and A. D. Nasonov, *Wood Sci. Technol.* **33**, 73–83 (1999).
37. R. D. Palardy, B. A. Haataja, S. M. Shaler, A. D. Williams, and T. L. Laufenberg, *Forest Products J.* **39**, 27–32 (1989).
38. Anonymous, Soy-Based Foaming Adhesive May Change Plywood Industry, http://www.unitedsoybean.org/feedstocks.pdf/fs9803.pdf, accessed May 26, 2003.
39. L. M. Matuana, *Forest Products J.* **53**(3), 40–42 (2003).
40. M. H. Schneider, Y. H. Chui, and S. B. Ganev, *Forest Products J.* **46**(9), 79–83 (1996).
41. J. Neetha and J. Rani, *J. Appl. Polym. Sci.* **68**, 1185–1189 (1998).
42. R. O. Ebewele, G. E. Myers, B. H. River, and J. A. Koutsky, *J. Appl. Polym. Sci.* **42**, 2997–3012 (1991).
43. R. O. Ebewele, G. E. Myers, B. H. River, and J. A. Koutsky, *J. Appl. Polym. Sci.* **43**, 1483–1490 (1991).
44. R. O. Ebewele, B. H. River, and G. E. Myers, *J. Appl. Polym. Sci.* **52**, 689–700 (1994).
45. R. O. Ebewele, B. H. River, and G. E. Myers, *J. Appl. Polym. Sci.* **49**, 229–245 (1993).
46. P. Rachtanapun, M.S. thesis, Michigan Technological University, 1999, p. 171
47. P. Rachtanapun and P. Heiden, *J. Appl. Polym. Sci.* **87**, 890–897 (2003).
48. P. Rachtanapun and P. Heiden, *J. Appl. Polym. Sci.* **87**, 898–907 (2003).
49. S. Das, M.S. thesis, Michigan Technological University, 2000, p. 169.
50. K. Carlborn, M.S. thesis, Michigan Technological University, 2002, p. 131.
51. M. Zanetti, A. Pizzi, M. Beaujean, H. Pasch, K. Rode, and P. Dalet, *J. Appl. Polym. Sci.* **86**, 1855–1862 (2002).
52. Can. Pat. 1,215,510 (1986), W. E. Hsu.
53. R. L. Geimer, and J. H. Kwon, *Wood Fiber Sci.* **31**(1), 15–27 (1999).
54. R. L. Geimer, J. H. Kwon and J. Bolton, *Wood Fiber Sci.* **30**, 326–338 (1998).
55. Wood Handbook: Wood as an Engineering Material, Forest Products Laboratory General Technical Report FPL-GTR-113, U.S. Department of Agriculture, Forest Service, Forest Products Laboratory, Madison, Wis., 1999.
56. J. Patterson, *J. Vinyl Additive Technol.* **7**(3), 138–141 (2001).
57. M. Defosse, *Mod. Plast.* 25–30 (Jan. 2003).
58. R. Donnell, *Timber Processing* 28–30 (Nov. 2000).
59. L. C. Czarnecki and J. L. White, *J. Appl. Polym. Sci.* **25**, 1217 (1980).
60. R. T. Woodhams, G. Thomas, and D. K. Rodgers, *Polym. Eng. Sci.* **24**, 1166–1177 (1984).
61. L. M. Matuana, C. B. Park, and J. J. Balatinecz, *J. Vinyl Additive Technol.* **3**, 265–273 (1997).
62. J. J. Balatinecz and R. T. Woodhams, *J. of Forestry* **91**(11), 22–26 (1993).
63. L. M. Matuana, R. T. Woodhams, J. J. Balatinecz, and C. B. Park, *Polym. Comp.* **19**, 446–455 (1998).
64. M. Kazayawoko, J. J. Balatinecz, and L. M. Matuana, *J. Mater. Sci.* **34**, 6189–6199 (1999).
65. F. Mengeloglu, L. M. Matuana, and J. A. King, *J. Vinyl Additive Technol.* **6**(3), 153–157 (2000).
66. F. Mengeloglu and L. M. Matuana, *J. Vinyl Additive Technol.* **7**(2), 142–148 (2001).
67. C. M. Clemons, A. J. Giacomin, and J. A. Koutsky, *Polym. Eng. Sci.* **37**, 1012–1018 (1997).
68. B. D. Park and J. J. Balatinecz, *J. Thermoplast. Comp. Mater.* **9**, 342–364 (1996).
69. R. L. Geimer, C. M. Clemons, and J. E. Wood Jr., *Wood Fiber Sci.* **25**(2), 163–169 (1993).
70. L. Matuana-Malanda, C. B. Park, and J. J. Balatinecz, *J. Cell. Plast.* **32**, 449–467 (1996).
71. L. M. Matuana, C. B. Park, and J. J. Balatinecz, *Polym. Eng. Sci.* **37**, 1137–1147 (1997).

72. L. M. Matuana, C. B. Park, and J. J. Balatinecz, *Polym. Eng. Sci.* **38**, 1862–1872 (1998).
73. L. M. Matuana and F. Mengeloglu, *J. Vinyl Additive Technol.* **7**(2), 67–75 (2001).
74. F. Mengeloglu and L. M. Matuana, *J. Vinyl Additive Technol.* **9**(1), 26–31 (2003).
75. P. I. Morris and P. Cooper, *Forest Products J.* **48**(1), 86–88 (1998).
76. W. Chetanachan, D. Sookkho, W. Sutthitavil, N. Chantasatrasamy, and R. Sinsermsuksakul, PVC/Wood: A New Look in Construction, in *Proceedings of Vinylitec 2000: Rigid PVC in the New Millennium: Innovations, Applications, Properties*, Sponsored by Vynil Division-SPE and Philadelphia Section, Philadelphia, Pa., Oct. 11–12, 2000, pp. 15–18.
77. L. M. Matuana and D. P. Kamdem, *Polym. Eng. Sci.* **42**, 1657–1666 (2002).
78. L. M. Matuana, D. P. Kamdem, and J. Zhang, *J. Appl. Polym. Sci.* **80**, 1943–1950 (2001).

LAURENT M. MATUANA
Michigan State University
PATRICIA A. HEIDEN
Michigan Technological University

WOOL

Raw Wool Specification

Wool is the fibrous covering from sheep (1) and is by far the most important animal fiber used in textiles. It appears to have been the earliest fiber to be spun and woven into cloth. In 2000–2001, world greasy wool production was 2.3×10^9 kg from 1×10^9 sheep, which is equivalent to 1.4×10^9 kg of clean wool (2) (Tables 1 and 2). This is down from a peak of 2.0×10^9 kg in 1989–1990.

Wool belongs to a family of proteins, the keratins, that also includes hair and other types of animal protective tissues such as horn, nails, feathers, beaks, and outer skin layers. The relative importance of wool as a textile fiber has declined over the past decades with the increasing use of synthetic fibers for textile products. Wool, however, is still an important fiber in the middle and upper price ranges of the textile market. It is also an extremely important export commodity for several nations, notably Australia, New Zealand, South Africa, and Argentina, and commands a price premium over most other fibers because of its outstanding natural properties. These include soft handle (the feel of the fabric), water absorption (and hence comfort), and superior drape (the way the fabric hangs). Table 2 shows wool production and sheep numbers in the world's principal wool-producing countries.

The principal characteristics of clean wool types are average diameter, measured in micrometers (referred to as microns), and average length, measured in millimeters. Essentially all fine diameter wool is produced by merino sheep or merino crossbreeds. Over 75% of the sheep in Australia (the world's largest wool producer) are merino sheep, which are also bred in large numbers in South Africa, Argentina, and the former USSR. The softness, fineness, and lightness of fabrics is determined primarily by fiber diameter, and so the price is very sensitive to the mean diameter (3) (Fig. 1).

Encyclopedia of Polymer Science and Technology. Copyright John Wiley & Sons, Inc. All rights reserved.

Table 1. World Production (10^6 kg) of Wool (2000/2001)[a]

Source	Fiber diameter, μm	Greasy	Clean
Merino	<24.5	932	572
Crossbred	24.6–32.5	540	308
Other (carpet)	>32.5	852	494
Total		*2324*	*1374*

[a]From Ref. 2.

Medium diameter wool includes sheep breeds of English origin, eg, southdown, hampshire, dorset, and cheviot, as well as crossbreds, eg, columbia, targhee, corriedale, and polwarth, from interbreeding with merinos. Coarse diameter wool comes from sheep chiefly bred for meat, eg, lincoln, cotswold, and leicester.

Raw wool from sheep contains other constituents considered contaminants by wool processors. These can vary in content according to breed, nutrition, environment, and position of the wool on the sheep. The main contaminants are a solvent-soluble fraction (wool grease), protein material, a water-soluble fraction (largely perspiration salts, collectively termed *suint*), dirt, and vegetable matter (VM) (eg, burrs and seeds from pastures).

In buying raw wool, wool processors are concerned about its quality, the quantity of pure fiber present, and its freedom from contamination (4). For the fine and medium wools used for apparel, the major characteristics are average fiber diameter, yield (ie, the percentage content of pure fiber), content and type of VM, average fiber length, strength of fiber staples, and the position of any weak spot along the fibers. For very fine wools, the frequency and clarity of waves (crimp) in the staples has a significant effect on price. The range of fiber diameters, color of the clean wool, and the number (if any) of naturally colored fibers present can also be important. For carpet-type wools (long wools), the important properties

Table 2. Wool Production and Numbers of Sheep in Principal Wool-Producing Countries (2000/2001)[a]

	Wool production (greasy)		
Country/region	10^6 kg	%	No. of sheep, (10^6)
Australia	652	28.1	113
China	291	12.5	135
New Zealand	258	11.1	45.3
South Africa	50	2.2	17.5
Argentina	62	2.7	13.4
Uruguay	57	2.5	13.0
United Kingdom	62	2.7	27.6
Turkey	70	3.0	30.2
Iran	74	3.2	53.9
Former USSR	128	5.5	49.2
Others	620	26.5	508
Total	*2324*	*100*	*1006*

[a]From Ref. 2.

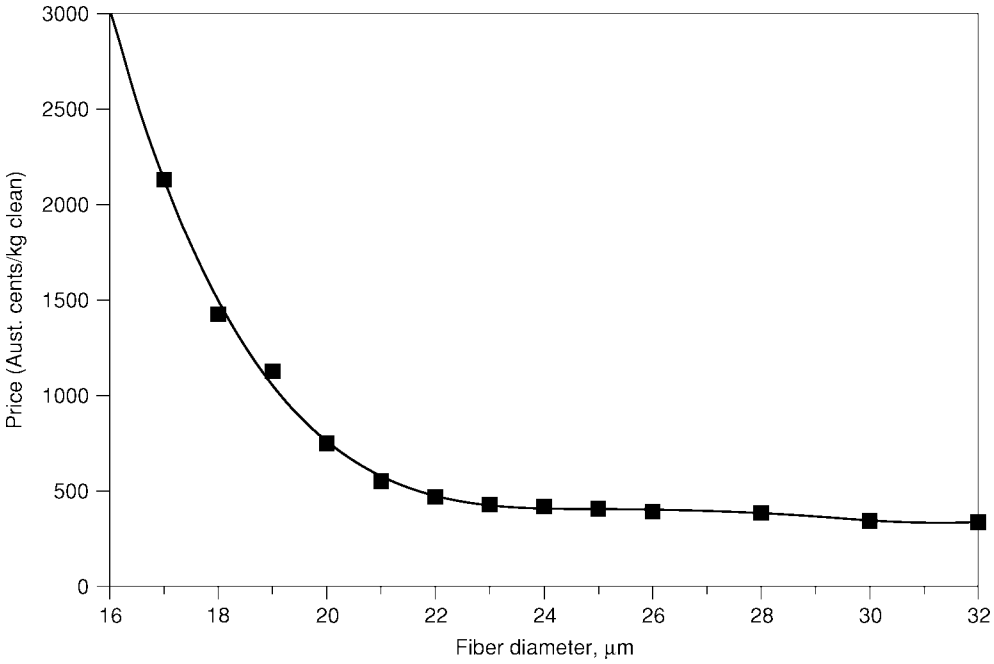

Fig. 1. Dependence of Australian wool prices on fiber diameter (1999/2000) (3).

(5) are yield, fiber diameter, fiber length, color, bulk (the volume occupied by the fibers in a yarn), and VM content. Also important for coarse wools is the degree of medullation. This is associated with cells containing air, arranged along the fiber axis. The presence of medulla cells increase light scattering by the fibers, restricting the use of these wools for some purposes.

Until the early 1970s, the characteristics of different wools were largely evaluated visually by wool classers and valuers. With the development of sampling techniques and equipment capable of rapid and economical measurement of yield, diameter, and VM (6,7), objective measurement and the sale of wool by sample became dominant in major wool-exporting countries. In sale by sample, cores are drawn from each lot and tested for yield, diameter, and VM content in accordance with international standards (8,9). Measurements of staple length, strength, and position of weakness are also now in routine commercial use. In addition, a full-length display sample, representative of each lot and obtained by standard procedure (10), is available for buyers to appraise other characteristics. Sale by sample decreased costs by reducing the handling of bulk wool in wool-brokers' stores and selling operations. It also enabled the processing performance of wool to be predicted in topmaking (11) and spinning (12).

Fiber Characteristics

New instrumentation for measuring fiber diameter (13,14) has meant that data on the range of diameters present (CV_D) and fiber curvature (related to crimp frequency) are now available. The impact of these is fairly well established (15).

These instruments have also been introduced on-farm so that the fleece quality of each animal can be assessed from a mid-side (16) or whole-fleece (17) sample. In some cases it is possible to gain increased returns from separating out the finest fleeces but bigger gains are possible from accelerating the rate of genetic progress. A remaining objective of research is to facilitate the introduction of a system of sale of raw wool by description in which a sale sample will not be required for inspection.

Fiber Growth. Wool fibers are produced from multicellular tube-like structures known as follicles. These follicles are located in the skin layers (dermis and epidermis) of sheep, and two types of follicles, primary and secondary, are usually identified. Primary and secondary follicles are described from the order of their initiation and development in foetal skin. The primary follicles develop first, in the unborn lamb. Secondary follicles develop later and in finer wooled sheep derived secondary follicles subsequently form by branching from the original secondaries, with which they share a common orifice (18). Each primary follicle has a sebaceous gland and a sweat gland together with an arrector muscle, whereas secondary follicles usually have only an associated sebaceous gland (19).

Fiber Morphology. Wool fibers consist of cells, where flattened overlapping cuticle cells form a protective sheath around cortical cells. A scanning electron micrograph of a clean merino wool fiber is shown in Figure 2. In some coarser fibers, a central vacuolated medullary cell type may be present.

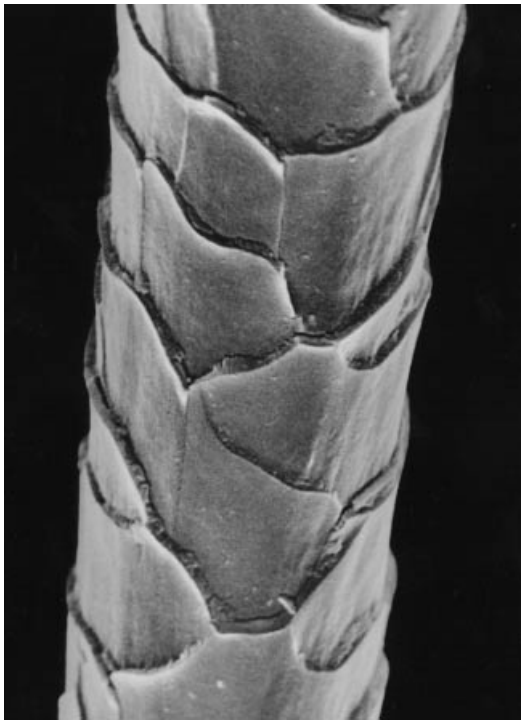

Fig. 2. Scanning electron micrograph of merino fiber, showing overlapping cuticle cells.

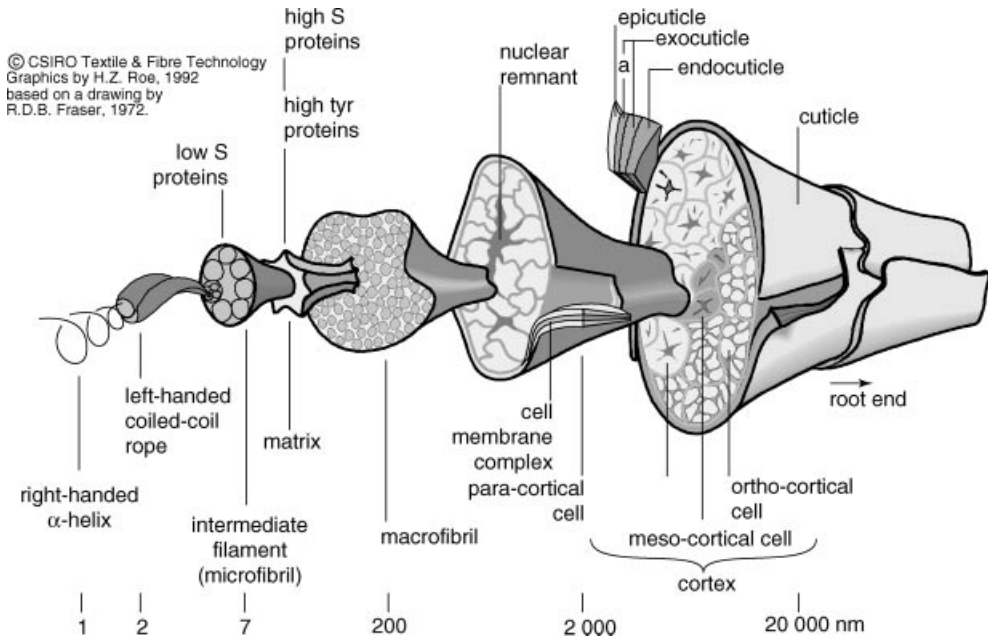

Fig. 3. Schematic of the structure of a fine merino wool fiber.

In fine wool, such as that obtained from merino sheep, the cuticle is normally one cell thick (approximately $20 \times 30 \times 0.5$ μm) and usually constitutes about 10% by weight of the total fiber. Sections of cuticle cells show an internal series of laminations (Fig. 3), comprising outer sulfur-rich bands known as the exocuticle and inner regions of lower sulfur content called the endocuticle (20). On the exposed surface of cuticle cells, a membrane-like proteinaceous band (epicuticle) and a unique lipid component form a hydrophobic-resistant barrier (21). These lipid and protein components are the functional moieties of the fiber surface and are important in fiber protection and textile processing (22).

The cortex comprises the main bulk and determines many mechanical properties of wool fibers (Fig. 3). Cortical cells are polyhedral, spindle-shaped, and approximately 100 μm long. They consist of a class of biological filaments known as intermediate filaments (23) embedded in a sulfur-rich matrix. The intermediate filaments (originally termed microfibrils), together with the matrix, are organized into large macrofibrillar units and these are often observed in sections of cortical cells. In fine merino wool, two main types of cortical cell, known as ortho- and para-, are arranged bilaterally. Orthocortical cells show different intermediate filament/matrix packing arrangements from those of paracortical cells (24). The arrangement of ortho- and paracortical cells differs among wool types. For example, in lincoln wool an annular (orthocortical core surrounded by paracortex) cellular arrangement is present. Merino fibers possess a characteristic crimp and in these fibers the orthocortex is located on the outer side of the crimp curvature.

A continuous intercellular material is present between cuticle and cortical cells which, despite being a relatively minor fraction of the total fiber weight, is of

increasing interest because of its presumed role in the penetration of water and chemical reagents into wool fibers. This region, called the cell membrane complex, is approximately 25 nm wide (25). It comprises a continuous phase of intercellular material, together with the apposing cellular membranes of the cuticle and cortical cells.

Over the past decade, major advances have been made in our knowledge of the cellular and molecular processes in wool follicles that lead to the formation of the wool fiber cuticle, fiber surface, and fiber cortex. In the wool follicle, presumptive cuticle cells undergo flattening during their passage up the follicle and are interlocked with the cuticle cells of the inner root sheath (IRS). When examined by transmission electron microscopy (TEM), the developing fiber cuticle cells demonstrate densely stained intracellular laminae forming in the outer regions of the cells. As the laminae develop, they separate to form an outermost layer, the a-layer, and an underlying layer. Together, these layers comprise the exocuticle.

The remaining cellular volume contains an innermost lightly stained endocuticle (20). In the final stages of cuticle differentiation, proteolipid complexes are formed on the presumptive fiber surface. Unusual mixtures of fatty acids are present in these complexes, which lead to the formation of a hydrophobic surface on the emergent wool fiber (26).

During their upward growth in the follicle, fiber cuticle cells remain adhered to the IRS cuticle by intercellular laminae that develop between two cell types (20). This produces a membrane complex that is different in appearance to that formed between differentiated cortical cells. The main differences exist in the presumptive surface of fiber cuticle cells, where the original plasma membrane appears to be disrupted. This process has been observed by using energy-filtered TEM (21), where it appears that the intercellular laminae are precursors to the formation of a new fiber cuticle surface membrane. It seems reasonable to conclude that a specialized hydrophobic membrane must be synthesized, because a plasma membrane is designed to exist only in a physiological environment and could not perform the protective and other specialist functions of the fiber surface membrane. The mechanism involving separation of inner root sheath cuticle and fiber cuticle cells is essentially unknown, but the cleavage plane appears to occur along a densely stained ultrafine band located in the center of the intercellular laminae (21).

Cortical cells form from a central or annular stream of germinal epithelia. During their early differentiation they undergo elongation and alignment processes. The initial sites for the formation of keratin structural components (arising concurrently with cell elongation) are at the outer boundaries (plasma membranes) of cortical cells, often in association with desmosomes (27,28). At high magnification, these initial keratin structures appear to consist of intermediate filaments (IFs) of 7–8 nm in diameter. These show appreciable staining when viewed after application of the heavy-metal preparations commonly used for contrast enhancement in TEM studies (28). After the formation and packing of IFs into lattice structures, a densely stained proteinaceous material appears to occupy the interfilamentous spaces. This proteinaceous material forms a matrix that is generally considered to be composed of high sulfur and high tyrosine proteins. The formation of these various structural components from their constituent proteins follows this two-stage sequential differentiation (29). As differentiation

proceeds, the IF matrix aggregates to form structures, often known as macrofibrils, which increase in size and eventually occupy the bulk of presumptive cortical cells (30).

Chemical Structure

Wool belongs to the family of proteins called α-keratins, which also include materials such as hooves, horns, claws, and beaks (31). A characteristic feature of these "hard" keratins is a higher concentration of sulfur than "soft" keratins, such as those in skin. Although clean wool consists mainly of proteins, wool also contains approximately 1% by mass of nonproteinaceous material. This consists mainly of lipids plus very small amounts of polysaccharide material, trace elements, and, in colored fibers, pigments called melanin. The lipids are both structural and free.

Protein Composition. Proteins, or polypeptides, are formed by multiple condensation of α-amino acids via their amino and carboxyl groups to form secondary amide (ie peptide) bonds (—CONH—). The general structure of all proteins or polypeptides may be represented as (—NHCHRCO—), where R represents the side chain of the amino acid. The peptide grouping is also known as an amino acid residue, because it is the part of the amino acid that remains after the condensation reaction. Complete acid hydrolysis of wool yields 18 amino acids, the relative amounts of which vary considerably between fibers from different sheep breeds, from different individuals of the same species, and sometimes along the length of single fibers from the same animal (31). These differences are the result of several factors, including genetic origin and nutrition. Studies on the chemical structure of wool have been largely confined to fine merino fibers, although aspects treated herein are relevant to all wool types. Typical figures for two different samples of wool are given in Table 3.

The side groups of the amino acids derived from wool vary markedly in size and chemical nature and play an important role in the physical and chemical properties of the fiber. Those containing nonpolar, hydrocarbon groups are hydrophobic and of low chemical reactivity. The polar, aliphatic hydroxyl groups of serine and threonine are chemically more reactive than the hydrocarbon residues. The side chains that have the most overall influence on the properties of wool are, however, the acidic groups of aspartic and glutamic acids and the basic groups of hystidine, arginine, and lysine. These acidic and basic groups give wool an amphoteric character and play an important role in wool dyeing. They are also responsible for wool's ability to combine with large amounts of acids or bases. The individual polypeptide chains of wool are held together and stabilized by both covalent and noncovalent bonds and interactions.

The most important of these is the disulfide bond (Fig. 4). This occurs by reaction of pairs of cysteine residues to form cystine (disulfide) linkages (—S—S—) between different polypeptide molecules, or between segments of the same molecules, as shown. The disulfide interchain cross-links have been compared with the rungs of a ladder. They are important because they prevent movement of chains and chain segments and, thus, are responsible for the higher stability and lower solubility of wool fibers compared with most proteins. The disulfide cross-links are readily rearranged through a thiol/disulfide interchange reaction

Table 3. Amino Acid Composition of Merino Wool

Amino acid[a]	Amino acid content, residues/100 residues: Sample 1[b]	Sample 2[c]	Nature of R group
Glycine	8.6	8.2	Aliphatic hydrocarbon
Alanine	5.3	5.4	Aliphatic hydrocarbon
Valine	5.5	5.7	Aliphatic hydrocarbon
Leucine	7.7	7.7	Aliphatic hydrocarbon
Isoleucine	3.1	3.1	Aliphatic hydrocarbon
Phenylalanine	2.9	2.8	Aromatic hydrocarbon
Tyrosine	4.0	3.7	Aromatic hydrocarbon
Serine	10.3	10.5	Hydroxyl
Threonine	6.5	6.3	Hydroxyl
Aspartic acid[d]	6.4	6.6	Acidic
Glutamic acid[e]	11.9	11.9	Acidic
Histidine	0.9	0.8	Basic
Arginine	6.8	6.9	Basic
Lysine	3.1	2.8	Basic
Methionine	0.5	0.4	Sulfur containing
Cystine[f]	10.5	10.0	Sulfur containing
Tryptophan	[g]	[g]	Heterocyclic
Proline	5.9	7.2	Heterolytic

[a] $(+H_3N{-}C(R){-}COO^-)$
[b] Ref. 32.
[c] Ref. 33.
[d] Includes asparagine.
[e] Includes glutamine.
[f] The amount of cystine is shown as the concentration of its reduction product, cysteine (also termed "half-cystine"). This includes any of the oxidation by-product, cysteic acid, that is present).
[g] Tryptophan is destroyed under the conditions used for these analysis; values of about 0.5 residues % have been obtained by alternative techniques (Refs. 34–36).

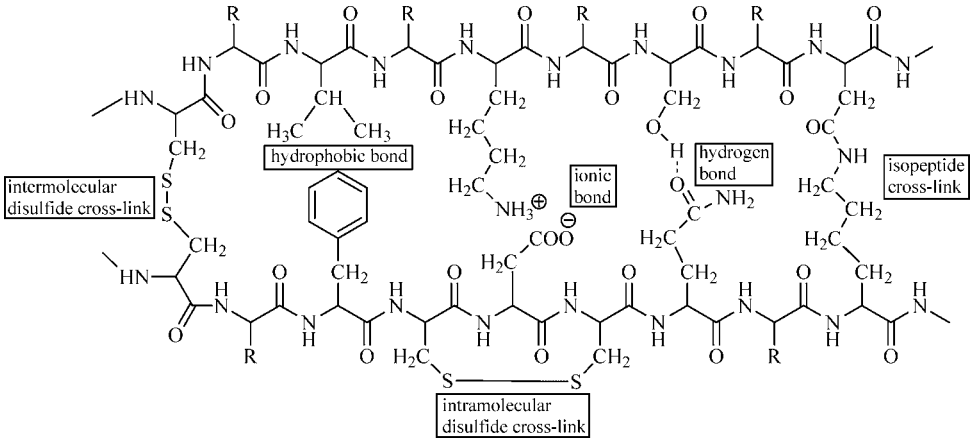

Fig. 4. Types of covalent and noncovalent bonds in wool.

under the influence of heat and water, or more rapidly on treatment with alkaline-reducing agents (eq. 1 where W = Wool).

$$WS_1—S_2W + —S_3^- \rightleftharpoons —S_1^- + WS_2—S_3W \quad (1)$$

Thiol/disulfide interchange facilitates conformational rearrangement of the wool proteins, leading to relaxation of molecular stress in the fiber. This property is employed in the permanent setting of wool fabrics. Another type of covalent cross-link present in wool is the isopeptide bond, formed between the side chains of lysine and either aspartic or glutamic acid (Fig. 4). Noncovalent bonds or interactions also make an important contribution to the properties of wool. These secondary bonds can occur within a single protein chain, or between different chains. They include hydrogen bonds between —CO and —NH groups in the polypeptide chains and the amino and carboxyl groups in the side chains, and also between suitable donor and acceptor groups in the amino acid side chains. Strong electrostatic interactions (ionic bonds, or "salt linkages") also occur between ionized carboxyl and amino groups in some of the side chains. Ionic bonds contribute to the dry mechanical properties of wool fibers. Hydrophobic interactions can occur between nonpolar groups in some of the side chains and these contribute to the mechanical properties of keratin fibers, particularly when wet. They are also important in wool setting.

Structure of Wool Proteins. The structure of wool proteins has been the subject of much research. Methods to solubilize, separate, and determine the amino acid sequence of these proteins have been reviewed (31,37). It is estimated that wool contains about 170 different types of polypeptides varying in relative molecular mass from below 10,000 to greater than 50,000 (37,38). Morphologically, wool fibers are biological composites, with each component having a different physical and chemical composition (Fig. 3). The groups of proteins that constitute wool are not uniformly distributed throughout the fiber, but are aggregated within the various regions.

Except for a small amount of the amino acid methionine, the sulfur in wool occurs in the form of the amino acid cystine. Only approximately 82% of clean wool consists of keratinous proteins, which are characterized by a high concentration of cystine. Approximately 17% of the fiber is protein material of relatively low cystine content (<3%); this has been termed nonkeratinous. As a result of the lower cystine content, the nonkeratinous proteins have a lower concentration of disulfide cross-links compared with the keratinous proteins in the fiber. The nonkeratinous material is, therefore, more labile and less resistant to chemical attack than the keratinous proteins. The nonkeratinous proteins are located primarily in the cell membrane complex between the cortical cells and in the endocuticle (Fig. 3). Approximately 13% of the total nonkeratinous material is also located within the cortical cells, where its distribution differs between the cells of the ortho- and paracortex.

The keratinous proteins of wool belong to three groups:

(1) low sulfur proteins, rich in amino acids that contribute to α-helix formation (glutamic acid, aspartic acid, leucine, lysine, arginine)

(2) high sulfur proteins, rich in cystine, proline, serine, and threonine
(3) high glycine, high tyrosine proteins which are also rich in serine.

The proteins derived from the rod-like intermediate filaments (microfibrils) of the cortical cells contain the helical segments of low sulfur proteins. These are surrounded by a relatively amorphous, nonfilamentous matrix, which consists principally of high sulfur and high glycine/high tyrosine proteins. It has been shown that the amino acid sequences of the helical portions are highly homologous with those of intermediate filament proteins derived from skin and other tissues. For this reason the microfibrils of wool are now generally referred to as intermediate filaments (37). Although the filament proteins of the ortho- and paracortex are similar, the orthocortex contains a higher proportion of intermediate filaments than the paracortex. The orthocortex is, therefore, richer in the low sulfur proteins that favor α-helix formation. The intermediate filaments contain a rod-like central helical domain in which the sequences show a heptad repeat, interrupted at three positions by short nonhelical segments. The ends of the polypeptides consist of nonhelical domains terminated in carboxyl and *N*-acetyl groups, respectively (37,39). The proportion of matrix (and hence of the high sulfur proteins) is greater in the paracortex than in the cells of the orthocortex (40). Furthermore, the proteins of highest sulfur content (ultrahigh sulfur proteins) are concentrated in the paracortex (41).

Wool Lipids. The lipids of wool are located mainly in the cell membrane complex. They constitute less than 1% of the fiber mass but play an important role in many properties, such as the intercellular diffusion of dyes and reagents (25,31). The free lipids are extractable with organic solvents and consist of fatty acids, fatty alcohols, sterols, sterol esters, and trace amounts of glycerides, sphinolipids, and glycolipids (26). Although phospholipid is present in the wool follicle membranes, only trace amounts of phospholipid are found in the keratinized fiber (42,43). Cholesterol and its biosynthetic precursor, desmosterol, are the main sterol components of the free lipids. In addition to the free lipids, wool contains some lipids that are believed to be covalently bound to proteins. These components are not readily removed by organic solvents, but those at the fiber surface can be released by alkaline hydrolysis under conditions where damage or modification of the fiber interior cannot occur (44). Covalently bound surface lipids represent approximately 0.025% of the fiber mass and are a distinct component of the fiber that has been termed the F-layer (44,45). This component is very important because it is responsible for the hydrophobicity of the fiber surface. The major component of the F-layer is an unusual branched-chain fatty acid (18-methyleicosanoic acid), which accounts for approximately 60% of the surface lipid material. Removal of the bound surface lipids generates a clean protein surface, which is more wettable, and has higher friction and better adhesion properties than the surface of clean untreated wool (44).

Physical Properties

Fiber Size and Shape. Wool is usually harvested from sheep by annual shearing. The fiber length is, therefore, determined largely by the rate of growth,

which in turn depends on both genetic and environmental factors. Typical merino fibers are 50–125 mm long. They have irregular crimp (curvature), with the finer fiber generally showing lower growth rates and higher crimp. The fiber surface is rough as a consequence of the outer layer of overlapping cuticle cells. By far the most important dimension is the fiber diameter. Wool fibers exhibit a range of diameters, which like fiber length is dependent on both genetics and environment. Coarse wool fibers (25–70 μm diameter) are used in carpets, while fine merino fibers (10–25 μm) are used in apparel because of their soft handle. Fibers from an individual sheep also exhibit a range of diameters. The mean diameter is the prime dictator of price; however, the distribution of diameters is also important. When worn next to the skin, the number of coarse fibers affects comfort as these fibers, rather than buckling, indent the skin and activate nerve receptors (46,47). This gives rise to a sensation of prickle and itch that has been incorrectly assumed, by some consumers, to be an allergic reaction. True allergies are rare, if they exist at all, and the irritation is mechanical and not immunological. Instruments that measure the full diameter distribution as well as fiber curvature have been developed recently (13,14). Individual fibers exhibit curvature in three dimensions; however, by measuring the circular curvature of short segments, a two-dimensional value can be obtained that correlates with the crimp frequency measured in staples. Crimp contributes to the excellent insulating properties of wool fabrics by improving their bulkiness and, hence, the amount of entrapped air.

Water Sorption. Wool is hygroscopic and able to absorb and desorb large amounts of water as the relative humidity surrounding the fiber changes. The water is believed to be associated with specific chemical groups in the amorphous regions, with polar side groups and peptide groups of the protein chains considered to be the most important (48). Debate continues, however, on the exact location of this water, its state, and the mechanism by which it enters the fiber (49–51). As a consequence of the lipid outer layer, the surface of wool is hydrophobic. It is dry to touch and not readily wet-out by liquid water. In line with other polymers having functional surfaces, the surface of wool is believed to rearrange in different environments (52). In textiles, the amount of water absorbed is generally expressed as a percentage of the dry weight. This is referred to as "regain" and is different to "water content", which is the mass of water in the fiber expressed as a percentage of the total mass of fiber plus water. A pronounced hysteresis is observed in the water sorption isotherm of wool. This is 2% higher on desorption than on absorption, at most relative humidities (53). The saturated regain of wool is about 33%, which is higher than that of most other fibers (54).

Heat is liberated when wool absorbs water; this increases comfort by helping to buffer the wearer against sudden environmental changes. The absorption of water by wool also results in other improvements to comfort during wear. At a given relative humidity, wool has similar water sorption to skin. Wool garments, therefore, act as an excellent buffer during physical activity by transporting perspiration away from the skin, thereby keeping its moisture content close to the comfort level. A new wool-containing product designed for active sportswear (SportWool^{TM}) utilizes the moisture-buffering properties of wool (CSIRO Textile and Fibre Technology Web site: http://www.tft.csiro.au; Sportwool Web site: http://www.sportwool.com). As can be seen from Table 4, most physical properties of the fiber are affected by (water) regain.

Table 4. Effect of Moisture Sorption on the Physical Properties of Wool Fibers at 25°C[a]

	Regain, %							
Property	0	5	10	15	20	25	30	33
Relative humidity, % (absorption)	0	15	42	68	85	94	99	100
Relative humidity, % (desorption)	0	8	32	58	79	92	98	100
Specific gravity, kg/m^3	1.304	1.314	1.315	1.313	1.304	1.292	1.277	1.268
Volume swelling, %	0	4.24	9.07	14.25	20.0	26.2	32.8	36.8
Length swelling, %	0	0.55	0.93	1.08	1.15	1.17	1.18	1.19
Radial swelling, %	0	1.82	4.00	6.32	8.88	11.69	14.57	16.26
Heat of wetting[b], kJ/kg wool	101	64.4	38.1	20.5	10.0	4.2	1.13	0
Young's modulus, relative[c]	2.69	2.54	2.36	2.02	1.59	1.27	1.05	1.00
Torsional rigidity modulus, GPa[d]	1.76	1.60	1.26	0.90	0.50	0.28	0.16	0.11
Electrical resistivity, $M\Omega \cdot m$	—	3×10^4	400	8	0.40	0.06	—	—

[a] Unless otherwise stated, data from Ref. 55.
[b] Heat evolves when wool, dry mass of 1 kg, at a particular regain is immersed in water.
[c] Ref. 56.
[d] To convert GPa to psi, multiply by 145,000.

Table 4 Effect of Water Sorption on the Physical Properties of Wool Fibers at 25°C

Wool is sold by weight; thus, allowance for uptake of water must be made. A premium is paid for fine wools and because the diameter changes with regain, diameter measurements must be made under standard conditions of temperature and humidity.

Thermal Properties. The regular packing of α-helical polypeptide chains within the intermediate filaments forms a crystalline phase that occupies about 70% of the dry volume of the fiber (57). This phase melts irreversibly at a temperature that is both time- and regain-dependent (58). During the dyeing and finishing of wool, no melting of the fiber occurs. Care should be taken, however, when processing blends of wool and synthetic fibers that require higher temperatures. The amorphous matrix phase contains a high concentration of the amino acid cystine and is, therefore, highly cross-linked. As with other amorphous materials, a glass transition T_g has been detected in the wool fiber (59,60) which is sensitive to physical aging (61). Water acts as a plasticizer, lowering the glass-transition temperature of the dry fiber from 170°C to below zero when saturated (Fig. 5).

The glass-transition temperature is an important parameter, as the properties and performance of wool are influenced by the environmental conditions (temperature and humidity) relative to the glass transition. The insertion of temporarily set creases or pleats in wool fabric (equivalent to thermally set creases in synthetic polymer fabrics) is achieved by subjecting wool to bending strain above T_g and fixed by transition to conditions below T_g. This can be done by heating and cooling, wetting and drying, or a combination of both, eg, steam pressing. Wrinkle recovery is poorer when wrinkles are inserted above T_g and recovery is below T_g. This is likely to occur under hot and humid conditions where local wetting (perspiration) and wrinkle insertion occurs simultaneously. When the fabric moves away

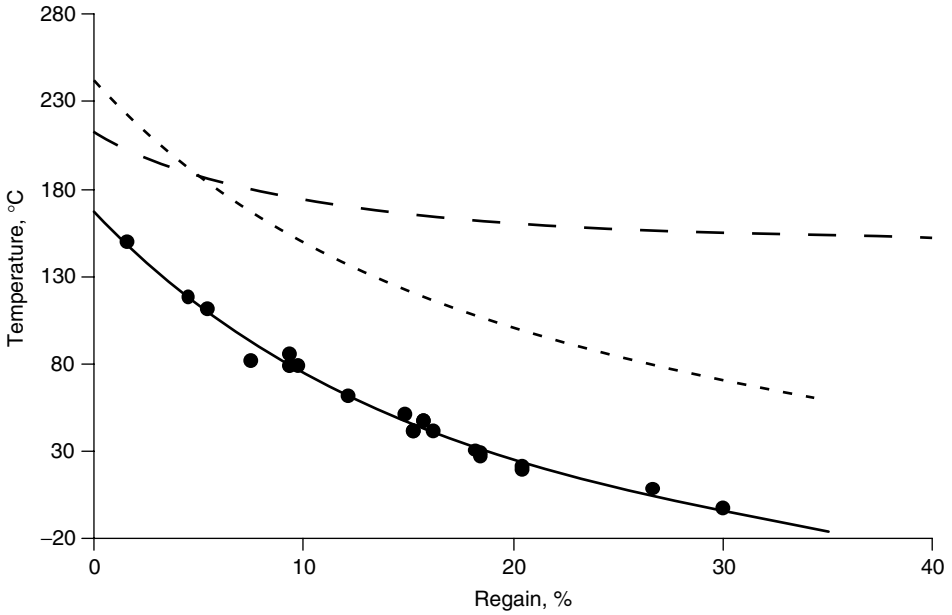

Fig. 5. Glass-transition (—) (60), indicative permanent setting temperature (----), and melting temperature (– – – –) (58) of wool as a function of regain.

from the skin, the wrinkle has insufficient time for complete recovery before the fabric dries. This causes the T_g of the fabric to rise to a temperature above that of the environment. The viscoelastic properties (59), physical aging (59), felting (62), and the water absorption isotherm of wool (50) are also influenced by the glass transition.

Tensile Properties. The tensile properties of wool are quite variable but, typically, at 65% RH and 20°C individual fibers have a tenacity of 110–140 N/ktex (140–180 MPa), a breaking elongation of 30–40%, and an initial modulus of 2100–3000 N/ktex (2.7–3.9 GPa) (54). Although wool has a complicated hierarchical structure (see Fig. 3), the tensile properties of the fiber are largely understood in terms of a two-phase composite model (63–65). In these models, water-impenetrable crystalline regions (generally associated with the intermediate filaments) oriented parallel to the fiber axis are embedded in a water-sensitive matrix to form a semicrystalline biopolymer. The parallel arrangement of these filaments produces a fiber that is highly anisotropic. While the longitudinal modulus of the fiber decreases by a factor of 3 from dry to wet (56), the torsional modulus (a measure of the matrix stiffness) decreases by a factor greater than 10 (Table 4 and Reference 66). The longitudinal stress–strain curves for a wool fiber at different relative humidities are shown in Fig. 6 (54).

Three distinct regions can be discerned, especially for fibers at higher relative humidity. Once the fiber crimp is removed, a near-linear region up to about 2% strain is obtained (pre-yield region). For the wet fiber, this is generally associated with stretching of the α-helices within the intermediate filaments. At lower (water) regain, the matrix phase plays an increasingly dominant role. Between 2 and 25%

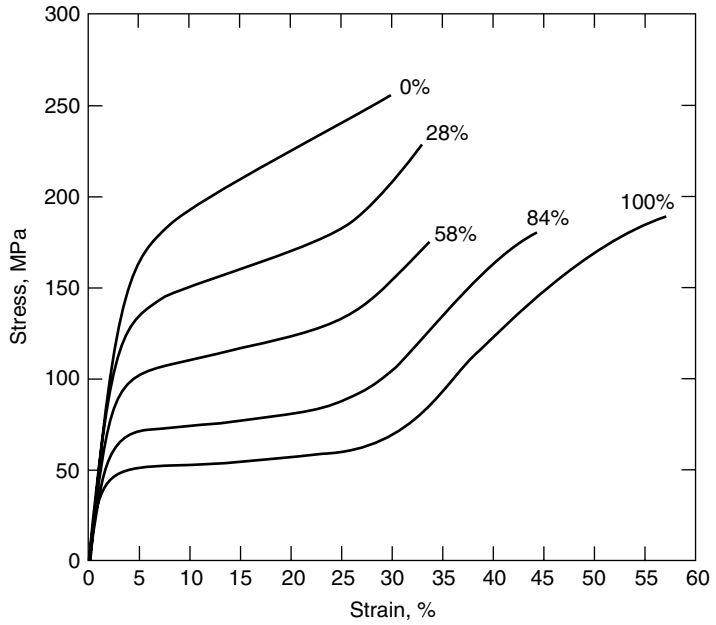

Fig. 6. Stress–strain curves of typical wool fibers at different relative humidities.

strain (yield-region) progressive unfolding of zones of α-helices to form a β-pleat configuration occurs. Very little increase in stress is observed during this stage and complete recovery is still possible, provided the fiber is allowed to relax in water. Beyond 25% strain (post-yield region), the fiber stiffens and breaks. At a molecular level, the reasons for this are still a matter of debate but include resistance to the unfolding of a stabilized region of the intermediate filaments (63,65) and the rubber-like response of the matrix (64). A recent review looks critically at the different models (67).

For a fiber immersed in water, the ratio of the slopes of the stress–strain curve in these three regions is about 100:1:10. While the apparent modulus of the fiber in the pre-yield region is both time- and water-dependent, the equilibrium modulus (1.4 GPa) is independent of water content and corresponds to the modulus of the crystalline phase (68). The time-, temperature-, and water-dependence can be attributed to the viscoelastic properties of the matrix phase.

Wool Processing

The conversion of raw wool into a textile fabric or garment involves a long series of separate processes. There are two main processing systems, worsted and woolen. A significant volume of wool is also processed on the semiworsted system, for carpet use. Some wool is processed on the short-staple (cotton) system. Details of the principal stages in the woolen and worsted systems and discussion of more recent developments can be found elsewhere (69,70).

The majority of the world's apparel wool clip is combing wool and this is processed on the worsted system. This process was so named because the combed wool spinning industry in England developed in the English town of Worsted in the fourteenth century (70). Fine, smooth yarns were produced by "spinsters" who placed the combed parallel array of fibers on top of a distaff (combed wool even today is known as top), drew the strand down to the required linear density, and inserted the twist using a spindle. Prior to the development of worsted spinning, and coexisting ever since with it, the traditional system produced yarns in which the fibers were much more disorientated. Although the texture was not as smooth, there was a high degree of bulk, and the finished woven fabrics produced coatings, blankets, and distinctive products such as tweeds and flannels. Woolen spinning is the mechanized form of the traditional system.

Besides scoured (cleaned) wool, the next saleable commodity in worsted processing is top, or combed wool. Generally the combing plant combines the processes of scouring and combing. Most often, a separate commercial enterprise which buys top from the topmaker carries out spinning. Although there are woolen sales-to-yarn spinners, particularly in the knitwear area, the production of woven woolen products in the one enterprise from raw wool is more common. The woolen process is characterized by a much higher degree of vertical integration than the worsted system.

Scouring. The first stage in wool processing is to remove the fleece impurities by scouring. The impurities consist principally of wool wax, dirt, proteinaceous contaminants, and suint. The latter is a water-soluble component, consisting mainly of potassium and other inorganic salts arising from perspiration. Scouring is carried out by washing the raw wool in an aqueous medium, a solvent medium, or a combination of the two. Aqueous scouring is used to process 99% of the world's wool. This involves washing the raw wool in aqueous solutions (neutral or slightly alkaline) of nonionic detergent or, less frequently, soap and alkali. This is followed by rinsing in water.

The process is carried out in a series of between four and seven tanks (called bowls), in which the wool is transported through the wash liquor by mechanical rakes, or by passing it around perforated drums (71,72). At the end of each bowl, the wool passes through a roller squeeze. Agitation of wool in anhydrous solvents does not cause felting, and several systems (71,73,74) have been operated to take advantage of this property, but none are still in commercial operation.

There are two broad categories of contaminants on raw wool: those that are easily removed and those that are hard to remove. The different rates of removal of these contaminants in the scouring process has led to the development by CSIRO of a new scouring technology, known as Siroscour™. This uses the principles of multistage scouring, rather than severe mechanical action, to optimize the removal of contaminants during aqueous scouring. The three separate stages which comprise the Siroscour process are a modified desuinting bowl, designed to remove as much dirt as possible; a hot scouring stage that removes the easy-to-remove contaminants; and a third stage, designed to remove the hard-to-remove contaminants. To achieve optimum performance, separate dirt and grease contaminant recovery loops are incorporated into the Siroscour process, as well as specific bowl designs for optimum scouring efficiency of Australian wools. Comparative trials have shown Siroscour to consistently produce wool of superior whiteness and

lower residual content of mineral contaminents (ash content) than other scouring systems (75).

In most situations, wastewater discharged from a scouring machine contains large quantities of wool wax and both water-soluble and water-insoluble material (organic and inorganic). The pollution load of a single modern scouring machine is equivalent to a population of 50,000 people. Disposal or treatment of the wastes to comply with environmental requirements is expensive. In the past, the least expensive approach involved biological treatment by irrigation of large land areas, or maturation in very large, shallow lagoons. The high levels of potassium present in scour effluent require 1000 ha of land for sustainable irrigation. These factors have forced scourers to install large evaporation ponds that cover many hectares. Technology has been developed that enables scourers to recover a large amount of the potassium from the scour liquor. This can be used as a potassium supplement in fertilizer.

Physicochemical methods of wastewater treatment have been investigated. These include flocculation with inorganic or polymeric flocculants, or with sulfuric acid, and also physical techniques, eg, membrane processes and solvent extraction. Few of these processes have proceeded beyond pilot-scale evaluation, however. One of the most recent processes that has proved to be commercially viable is the Sirolan CF™ technology developed by CSIRO (76). This is a chemical flocculation process that removes more than 75% biological oxygen demand, 80% chemical oxygen demand, and 99% of the suspended solids and wool wax. This is a simpler process with lower operating costs than other methods involving chemical flocculation. Sludge disposal technologies have been developed that can be used in conjunction with the Sirolan CF process. These include composting, incineration, and pelletizing (77). The centrate from the Sirolan CF process contains mainly suint salts. Plant growth trials, carried out by Agriculture Victoria and CSIRO, demonstrated that suint salts, which contain about 27% potassium, are equal or better than inorganic sources of potassium (78).

Carbonizing. Carbonizing is a process used to remove excessive amounts of cellulosic impurities, eg burrs and VM, from wool. It is carried out on loose wool, rags (79), and fabric (80). With loose wool and fabric, the wool is treated with aqueous sulfuric acid and then baked. The cellulosic matter is rapidly destroyed by the hot concentrated acid, by conversion into friable hydrocellulose, whereas wool is scarcely affected by the treatment. For dyed rags, hydrogen chloride gas is preferred as the mineral acid, because it has less effect on the colors. After acid treatment, the carbonized VM is crushed to facilitate its removal. The wool is then normally neutralized in alkali, although some mills omit this stage to facilitate subsequent dyeing under acid conditions.

Most industrial carbonizing is done on loose wool, the technology having changed little over the past 40 years. Australian carbonizers use surface-active agents to reduce fiber damage in the carbonizing process (81,82). The improved results depend on the use of high acid concentrations and rapid throughput (81).

Processing on the Worsted and Woolen Systems. The wool is dried after scouring and blended before carding. Carding individualizes the entangled fibers and reassembles them into a "sliver" weighing about 25 g/m. At the same time, up to 90% of the VM is removed. Lubrication (83) is used to minimize fiber breakage. After carding, there are three stages of gilling, to align fibers and remove

hooked fiber ends before combing. Here, the advancing beard of fibers is inserted into a circular comb, and the leading fibers are then gripped and pulled through a top comb before being reassembled, like overlapping tiles, in the output sliver. The process removes short and entangled fibers and almost all remaining VM. The waste (noil) can be carbonized and fed into the woolen system. The sliver is then given two more gillings and consolidated into top. Some combing plants also produce shrink-resist treated wool top. The current process incorporates chlorination followed by application of a polymer.

The worsted spinner converts top of about 25 g/m linear density into roving of between 200 and 2000 g/km, depending on the linear density of the yarn to be spun. The sequence of processes incorporates four or five drawing stages. The first three or four usually employ gills, whereas the last is commonly carried out on a roving frame in which the attenuated strands are rubbed or twisted to impart cohesion. For finer wool, dyed tops or after blending with synthetic fibers, it is normal to recomb the wool before the above drawing stages.

Long-staple ring spinning is similar to short-staple (cotton) ring spinning, except that the components are increased in approximate proportion to the length of the fibers. On the spinning frame, the rovings are drafted by a factor of about 20, twist is inserted, and at the same time the yarn is wound onto bobbins. The yarn on the bobbins is usually steam-set in an autoclave to reduce its twist liveliness, then wound onto packages or cones. Detection and removal of thick, thin, and colored faults can occur during winding. Following twisting into a twofold yarn and further setting, the yarns are ready for knitting or weaving. Open-end (rotor) spinning is rarely used for wool, and spinning and twisting are very costly operations, because of their low productivity: typically 40 spindles produce 1 kg/h of yarn.

In woolen processing, there are no highly efficient mechanical methods to remove VM. Generally, very clean scoured wool, combed wools, or carbonized wool must be used as inputs. Alternatively, fabrics must be carbonized. A much longer card than in worsted processing and shorter fibers are used. The web of fibers at the card delivery is split longitudinally into about 120 ends, rubbed to impart cohesion, and wound into cylindrical packages called slubbing. Twisting of these slubbings occurs on the woolen spinning frame with a draft of 1.3–1.5, to produce woolen singles yarn. This yarn can be woven without any further processing, other than a winding and clearing operation similar to that used in the worsted sequence. Woolen spinning is, thus, a very short sequence of operations compared to worsted processing. Woolen yarns, however, become economically uncompetitive with worsted yarns at relatively coarse yarn counts, because production is tied to the number of ends times their weight.

Woolen yarns cannot be spun as fine as worsted yarns, even when using the same fiber diameter. The fabric weights are greater and they have a harsher feel. For these reasons, woolen products have not been able to follow the modern trend to smoother lightweight clothing as easily as their worsted counterparts.

Setting

Setting operations form an important part of the processing of wool yarn, fabric, and garments. Yarn is set in steam to stabilize twist and prevent snarling

during winding and warping, while fabrics may be set after weaving to prevent the formation of distortions during wet processes, such as scouring and dyeing. Normally, fabrics are flat-set near the end of the finishing routine to impart dimensional stability and to confer the required handle. Finally, garments are set by steam pressing to form their desired shape, for example, to insert pleats and creases.

Two forms of set may be conferred to the wool fiber and these two forms can be distinguished on the basis of stability. Temporary set (or cohesive set as it is generally referred to in the wool industry) is imparted when wool fibers are dried, or steamed for a short time and then cooled while under strain. This set is readily lost when the fibers are gently steamed or allowed to relax in water at room temperature (84). Permanent set, as the name implies, is set that has a considerable degree of permanency. Set that remains after relaxation in water at 70°C for approximately 15 min is generally considered permanent, ie, the set is permanent to conditions in excess of those that a wool garment would normally encounter during use, eg machine washing.

At the molecular level, setting is a process of stress relaxation which results from the rearrangement of the protein macromolecules that form the fiber. Under ambient conditions of water content and temperature, the matrix regions of wool are glass-like (ie below the glass-transition temperature, see Fig. 5). When fibers are deformed under these conditions, stress relaxation is slow.

If wool is heated or becomes wet, the matrix regions become rubber-like and stress relaxation occurs much more rapidly. Cohesive or temporary setting occurs whenever the fibers are deformed under conditions where stress relaxation is high (rubbery state), and then cooled or dried to a glassy state before they are released. In the glassy state the relaxation rate is slow, so that the fiber will essentially maintain its new shape indefinitely, or until it is again wetted-out or heated to make it rubber-like.

The protein molecules, particularly those of the cuticle and matrix regions of the fiber, are stabilized by a number of covalent bonds and noncovalent interactions. The most important of these are disulfide bonds, which cross-link the peptide chains (Fig. 4). A unique feature of the wool fiber is the ability, under suitable conditions, for these disulfide bonds to rearrange and form a new cross-linked polymer network. This occurs via a mechanism involving thiol/disulfide interchange (eq. 1). Permanent setting will occur if this rearranged network, cross-linked by reformed disulfide bonds, is at equilibrium with the new shape of the fiber. The rate of disulfide rearrangement is "catalyzed" by the concentration of thiol anions in the fiber (85), as well as by the macromolecular mobility of the protein chains. Hence, the rate of disulfide rearrangement can be increased by increasing the pH, breaking disulfide bonds with a reducing agent to form additional thiol anions, or by increasing the regain or temperature to facilitate molecular mobility. In addition to the rearrangement of disulfide cross-links via thiol/disulfide interchange, other mechanisms are also involved. These include rearrangement of hydrogen bonds and the formation of new types of covalent cross-links that are formed from residues produced by breaking disulfide bonds. The new bonds include lanthionine and lysinoalanine cross-links (86). These cross-links are more stable than the disulfide bonds from which they were produced and make a significant contribution to the stability of permanently set wool fibers. In some circumstances,

hydrophobic bonds between suitably located nonpolar side chains can also contribute to the stabilization of permanent set (87). Figure 5 depicts a curve above which the temperature and regain are sufficient for imparting permanent set to wool within a few minutes. This curve is indicative only, as its actual position can vary between different wool types, previous treatments, and process conditions, because it is influenced by the thiol content and pH of the wool fiber, and also the definition of "permanent set."

During wool processing, the regain and temperature are carefully selected and controlled in order to impart either permanent or temporary set. As indicated in Figure 5, permanent setting can be achieved under wet or dry conditions (less than saturation, ie <33% regain). The most common form of wet permanent setting is continuous crabbing. This is an operation in which a wet fabric, sandwiched between a hot (up to 160°C) roller and an impermeable belt, is heated to temperatures above 100°C for up to 1 min, before being rapidly quenched in cold water. The amount of permanent set imparted in a continuous crab is less than that conferred by a traditional batch crabbing operation. The continuous method has greater productivity, however. The effectiveness depends on the pH of the wool and the treatment time and temperature. The rate of permanent setting can be increased by increasing the number of thiol groups within the fiber by impregnating the fabric with a reducing agent. Some dyeing operations can impart large amounts of permanent set to wool. This can be minimized by including in the dyebath a chemical that reacts with the thiol anions. Minimizing permanent set during dyeing is beneficial in maintaining fiber strength (88) and for maintaining yarn bulk (89).

Dry setting operations usually involve the use of steam. As is the case for wet setting, the amount of permanent set imparted in steam-setting depends on the wool pH, water content, and the time and temperature of setting. Fabrics are steam-set by decatizing. In this process, the wool fabric, interleaved with a cotton wrapper cloth, is wound onto a perforated drum, through which steam is forced. In continuous machines, the conditions are mild and little permanent set is imparted. In a batch process, in which the fabric roll is placed in a pressure vessel (autoclave), setting temperatures up to 130°C for 3–5 min are used. These conditions impart a higher degree of permanent set than continuous methods. The amount of temporary or cohesive set imparted in both batch and continuous machines depends on the temperature of the fibers when the fabric is released from the wrapper cloth. The cooler the fabric, the higher the level of cohesive set. Yarns on packages are normally cohesively set in an autoclave at temperatures up to 90°C, in order to reduce twist liveliness. A vacuum pump is used to remove air from the packages, which ensures even penetration of steam and, thus, a uniform level of set.

Normal pressing operations carried out during garment making impart only temporary set to the fibers. A number of commercial processes are used, however, to set permanent creases into wool garments (90–92). These include autoclave setting and wet or dry pressing in the presence of chemical assistants. Permanent pleats are fixed into skirts by autoclave setting at around 110°C. In the SIROSET™ process of CSIRO, for inserting permanent creases into trousers, a chemical assistant (monoethanolamine sulfite) is sprayed onto the trousers before steam-pressing.

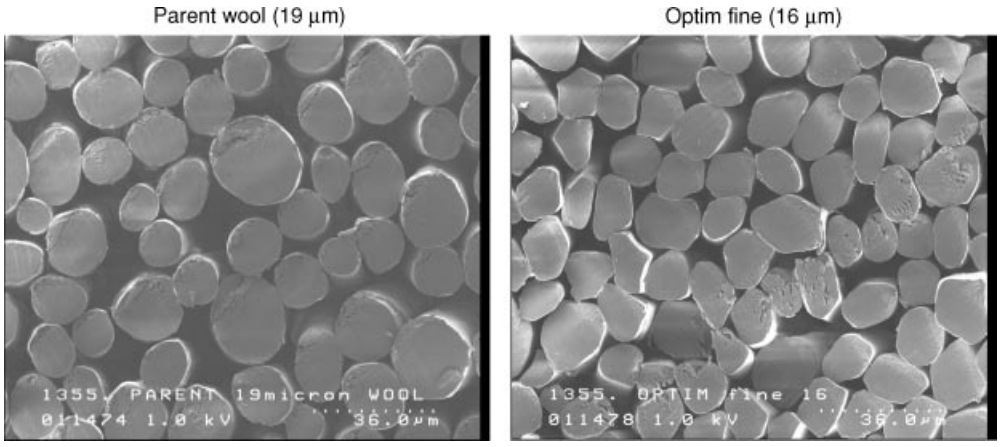

Fig. 7. Scanning electron micrograph of cross sections of normal wool and Optim fine fibers.

A New Textile Fiber from Wool. The most recent application of wool setting is in the manufacture of OPTIM^{TM} (CSIRO Textile and Fibre Technology Web site: http://www.tft.csiro.au), a new textile fiber produced from wool (93). The production process involves stretching and setting wool to create two new fiber types; Optim fine and Optim max (94). A key aspect of the continuous process is the use of false twist to maintain cohesion within a large fiber assembly during the whole operation.

In the Optim fine manufacturing process a chemical setting agent, such as sodium bisulphite, is applied to wool. A twisted assembly of the treated fibers is stretched by around 40–50% and then permanently set in the extended state. This procedure gives longer fibers of decreased diameter. Stretching and setting the fibers converts ordered intermediate filaments in the wool from an α-crystallite helical form to a β-pleated sheet structure that more closely resembles silk (95). Typically, the diameter is reduced by about 3–4 μm for a 19-μm parent wool fiber. The use of false twist to control fiber movement applies a large transverse force to the twisted assembly that changes the cross-sectional shape of the fibers so that common measures of diameter that assume a mostly circular cross section are no longer valid (Fig. 7).

Optim fine fibers are stronger and softer than the parent wool and exhibit an attractive lustre. They are used to produce fabrics with many of the aesthetic properties of silk. The modified wool is ideal for spinning into fine yarns, especially with other high value natural fibers, eg, silk, cashmere, and alpaca, where softness, lightness, and sheen are desirable attributes.

Optim max utilizes a key benefit of the manufacturing process that allows the extent of set in the fiber to be manipulated in a controlled manner. Optim max fiber is wool that has been temporarily set while stretched, so that the fiber retracts when released in hot moist conditions by about 25% in length. This fiber offers scope for innovation in yarn and fabric design. For example, when Optim max is blended with normal wool, spun into yarn, and relaxed in hank form in hot water, the Optim max fibers retract and force the normal wool fibers to buckle.

The yarn has an increased volume and this property produces increased "cover" in knitted fabric and decreased weight. When knitted to the same cover factor, a weight saving of 20–30% is possible compared with fabrics made from normal wool yarns.

Shrinkage of Wool Textiles

Two mechanisms of fabric shrinkage are observed for wool: relaxation shrinkage and felting shrinkage (22,96). Relaxation shrinkage occurs when a fabric or yarn made from any textile fiber is first immersed in water. It results from the release of temporarily set strains imparted during previous processing operations such as spinning, knitting, and fabric finishing. Relaxation shrinkage also occurs when a knitted garment or fabric is immersed in water after it has been dried while in a stretched state (for example by line drying). Felting results from the presence of cuticle cells (scales) on the wool fiber surface that point away from the fiber root and overlap like tiles on a roof (Fig. 2). The protruding scale edges result in differential friction between the with-scale and against-scale direction, which under some conditions results in irreversible migration of individual fibers toward their root ends. Felting is exploited in the "milling" of wool. This is a process of controlled, mild felting used to close up the structure of fabrics and garments. Milling is also used to produce wool felts, which are composed of a very dense matting of fibers. Felts are used for products as diverse as hats, polishing pads, table covers, and piano hammers.

Felting in garments and fabrics that leads to excessive shrinkage is, however, undesirable. It occurs when the wet material is subjected to severe mechanical action, for example, in laundering or tumble drying (22). Shrink-resist treatments are directed at preventing felting shrinkage, whereas minimization of relaxation shrinkage requires careful control during fabric finishing. Felting of loose fibers results in entanglement, whereas in fabrics fiber migration inside and between yarns reduces the fabric area, ie, shrinkage occurs. The mechanisms of felting shrinkage and its prevention have been discussed comprehensively (22). Many factors influence felting shrinkage; these include (*1*) yarn and fabric structure (woolen or worsted, knitted or woven, yarn twist level); (*2*) the method of wash-testing (pH, temperature of wash liquor, presence of detergents, electrolytes, or lubricants, and the severity of the mechanical action of the washing machine); (*3*) the properties of the fiber (elasticity, diameter, length). Recently, felting shrinkage has been related to the glass-transition temperature of wool (97). Important points to note are that products made from fine diameter wools felt more readily than those from coarse fibers, and that if a small amount of untreated wool is added to shrink-resist treated wool, the blend will felt as readily as the untreated material.

Shrink-Resistent Terminology and Testing. The term shrink-resistant is preferred to "shrinkproofed," although in recent years emphasis has switched to performance-related terms, such as hand-washable and machine-washable. A recent trend is to use the term easy-care, which for knitwear means resistance to felting shrinkage under severe conditions, including tumble drying. It also includes assessment of the fabric appearance after testing. For woven garments, this includes retention of pleats or creases as well as smooth drying performance.

All these terms are meaningless unless related to some standard testing sequence and criteria for passing the test.

Relaxation shrinkage tests usually involve mild agitation in water. Felting shrinkage is then determined after more severe agitation. Hence, in practice it may be difficult to say when relaxation ceases and felting starts. The most commonly used methods to test for felting shrinkage is to use multiple wash-test cycles in domestic-type washing machines (front loading in Europe, or top loading in the United States). The Woolmark Company (formally the International Wool Secretariat) has developed test methods for machine washability, together with performance criteria for different garment types and end uses. Woolmark test methods are widely used around the world, although in the United States AATCC methods predominate.

Development of Shrink-Resist Science and Technology. Felting of wool and its use in fabric finishing has been known for a very long time. Monge observed the differential friction effect in wool fibers in 1790 and Mercer chlorinated wool to improve dye affinity in printing in 1839, but chlorination was soon found to impart shrink-resistance (22). Chlorination was widely used during World War II to produce shrink-resistant wool socks and blankets for the military. From then on, two distinct trends in shrink-resist research and technology emerged. Firstly, better control of the reaction of chlorine or other oxidants with wool, and secondly, the use of synthetic polymers to bond adjacent wool fibers together. The reader is directed to Reference 98, which gives a good summary up to the early 1950s, and to Reference 22, which continues to the late 1970s and discusses the mechanism of felting. Recent research has been directed toward environmental aspects of the shrink-resist treatment of wool, particularly the reduction or elimination of organochlorine compounds in effluents from treatment plants. In future years, replacements for chlorination processes are likely to emerge.

Figures published by The Woolmark Company in 2002 show that approximately 40×10^6 kg of wool is shrink-resist-treated each year. This figure may include some low level chlorination treatments of fine wools, designed to prevent felting during wet processing or to improve garment appearance or dyeability. The products of these low level treatments are generally not claimed to be machine-washable. The fact that only 5–10% of all wool is shrink-resist-treated indicates that many end uses do not require an antifelting treatment. More than 90–95% of the treated wool is used in knitwear. The amount treated, however, varies markedly from country to country and also with the type of product, with those worn next to the skin, eg, underwear, being most likely to be treated. Wool can be shrink-resist-treated at various stages, from loose wool to garments. Approximately 5% is treated at the loose wool stage, mainly for use in bedding products such as futons; 80% at the top stage; very little as yarn; 10% as knitted garments; and about 5% as woven fabrics. The chlorine-Hercosett process for treating loose wool or top is by far the most important method used. In 2002 this method accounted for at least 80% of shrink-resist-treated wool.

Industrial Shrink-Resist Treatments. Mechanistically, shrink-resist treatments can be divided into degradative and additive types. Degradative treatments use an oxidizing agent to eliminate or reduce the differential friction effect of the fiber surface by modifying or removing the scales. In some cases, a polymer is also applied to the surface to mask the modified scales. The additive approach

prevents fiber migration by bonding fibers together with elastomeric polymers. Some polymer deposition processes involve a degradative chemical pretreatment, to improve the adhesion of the polymer to the fiber surface. Additive treatments must be applied after spinning (usually at the fabric stage), whereas degradative treatments can be used at any stage from loose wool through to garments.

Chlorine-Based Shrink-Resist Treatments. The principal oxidizing agent used in degradative shrink-resist treatments is chlorine. Free chlorine reacts very rapidly with wool; hence, it is difficult to treat a mass of wool fibers evenly. Two different types of chlorination methods are used commercially: continuous treatment and batch treatment. In the continuous method, top or loose wool is reacted with an aqueous solution of chlorine gas for a short time (<30 s). The batch treatment method involves a longer treatment time (5–30 min) with a less reactive chlorinating agent, such as DCCA (*N*,*N*′-dichloroisocyanuric acid). Batch treatments are mainly used on garments and fabrics but can also be applied to loose wool or tops. Generally, in both continuous and batch treatments a reactive polymer, usually cationic, is applied after the chlorination step.

The features and chemistry of chlorination shrink-resist treatments are best illustrated by consideration of the chlorine-Hercosett process for wool top (99). This process uses a dedicated plant, of which there are about 40 around the world. A web of parallel slivers is treated with water and chemicals in a series of bowls (tanks), separated by squeeze rollers. The wool is then dried. Usually, 30–40 slivers (20–30 g/m) are treated simultaneously at a speed of 5–10 m/min. Overall production rates range from 200 to 500 kg/h.

The first stage involves chlorination, either with chlorine gas dissolved in water or with sodium hypochlorite acidified with sulfuric acid. Chlorination is the most critical step of the process and modern plants incorporate features designed to achieve uniform treatment of the web. These include cooling the chlorine solution to 10–12°C, to slow down the rate of reaction with wool, and special application devices, eg, those produced by the Kroy or Fleissner companies, to rapidly contact the web with a large volume of dilute chlorine solution. The second stage of the process is a neutralization, or anti-chlor, treatment with sodium sulfite. In the third stage, the wool is treated with a cationic polyamide/epichlorohydrin polymer, usually Hercosett 57 (Hercules, Inc.). The final stage consists of treatment with a cationic softener and a lubricant to facilitate further processing, followed by drying to cross-link the polymer on the fiber surface. The reaction of chlorine with wool is complex, but the principal effect of the combination of the chlorination and neutralization stages is to remove surface lipid from the fiber. This increases the surface energy and shifts the isoelectric point of the fiber to a lower pH, by converting cystine disulfide residues to cysteic acid (sulfonic acid) groups. Some of the surface protein is also solubilized and removed, which softens the fiber cuticle. These changes allow the cationic Hercosett polymer to spread on the fiber surface. Virtually all the shrink-resistance is imparted by the chlorination step. The function of the Hercosett is to compensate for any weight loss arising from chlorination, prevent further loss of soluble protein during subsequent dyeing, and improve the shrink-resistance of any insufficiently chlorinated fibers.

Chlorine-Free Shrink-Resist Treatments. Commercially, the only other oxidizing agent used to any extent is permonosulfuric acid (PMS; $HOOSO_3H$). This is used in the form of its potassium triple salt, containing potassium sulfate and

bisulfate. It is employed in batch processes at elevated temperatures, because it reacts more slowly with wool than chlorine (100). The process sequence is similar to that used for chlorine-based treatments. It involves degradative oxidation with PMS, followed by neutralization with sodium sulfite and then application of a resin. Unlike chlorine, however, PMS does not remove the bound lipid or oxidize cystine to cysteic acid. The main product of the reaction is cystine sulfonic acid or Bunte salt groups.

Other chlorine-free shrink-resist technologies under development include plasma and ozone treatments for sliver and enzyme treatments for garments and fabrics.

Additive Shrink-Resist Treatments. The principal additive shrink-resist treatment for wool fabrics uses the polymer Synthappret BAP (Bayer AG). This is a poly(propylene oxide) polyurethane, containing reactive carbamoyl sulfonate (bisulfite adducts of isocyanate) groups, ie $-NHCOSO_3^- \ Na^+$. An aqueous solution of this polymer is padded onto woven fabrics. The polymer cross-links on drying to form flexible linkages between fibers and yarns (101). Other polymers may be applied at the same time to modify the handle.

Easy-Care Wovens

Dry-clean-only garments are increasingly becoming a turnoff to the modern consumer. Consumers now demand "total easy-care" garments that can withstand repeated machine washing and tumble drying, while maintaining their "just pressed" appearance with no more than minimal ironing. In addition to dimensional stability, wool-containing fabrics and garments must be specifically engineered so that, after laundering, seams remain flat and without pucker, the fabric remains wrinkle-free without the development of fuzz or pills, and the creases or pleats stay sharp.

To produce total easy-care garments from a blend, of wool and polyester, heat-setting the polyester component using a hot head press will generally impart sufficient set to the creases and pleats to make them stable to repeated laundering. A minimum of 20–30% polyester is needed for adequate stability. An alternative procedure that sets the entire garment is to impart temporary set to the wool component of the blend by steam-pressing the garment, followed by baking the entire garment in an oven to permanently set the polyester. The wool dries out in the oven and maintains the garment shape during setting of the polyester (102). A fabric-based treatment to prevent felting may be unnecessary, provided the polyester content is above 50% and a suitable fabric construction is used.

It is more difficult to produce pure wool total easy-care garments. The challenge is to obtain adequate permanent set rather than obtaining shrink resistance, because some wool setting processes are not stable to machine washing. The problem of set stability is further exacerbated when the garments are tumble-dried, because the tumbling action tends to flatten the creases and they become temporarily set in a distorted configuration, even if a high level of permanent set has been imparted to the garment. The application of a delay-cure polymer to the fabric, followed by curing in an oven after the garment has been made and pressed, appears to be the latest approach to producing total easy-care wool garments.

Dyeing

Commercially, wool is dyed from aqueous solutions, usually under acidic conditions. In the past, methods have been proposed for dyeing wool from organic solvents, in particular concentrated formic acid. More recently, the use of supercritical carbon dioxide has also been investigated. These solvent systems are, however, very unlikely to replace water as the preferred dyeing medium for wool, because of the relative cost of the solvent compared with water and also the specialized, expensive equipment required.

The majority of dyes used on wool are sodium salts of aromatic anions. Water solubility is usually provided by sulfonic acid groups, but in a few cases carboxyl or hydrophilic, nonionic substituents are used. In a typical wool dyeing operation, the ratio of the mass of dyestuff solution to the mass of wool ranges from approximately 10:1 to as high as 60:1, depending on the type of wool substrate and the equipment used. Wool is dyed as loose fiber, sliver, yarn, fabric, or in garment form by batch methods (103,104). In the case of fiber, sliver or yarn, the process involves pumping dye solution through the stationary substrate, whereas in fabric dyeing the material may be transported through the dye liquor or, alternatively, both liquor and fabric may be moved through the machine. Simultaneous circulation of liquor and wool substrate is also used in garment dyeing techniques. In a typical operation, the liquor is heated from around 40°C to a temperature of 98–100°C, where it is held for a period that can range from around 30 min to over 2 h. The actual time depends on the type of dye and depth of shade. Procedures have also been developed for continuously dyeing wool in loose, or sliver form and wool fabric can be dyed by a pad-batch method (105). These techniques have found only limited use, however, because they are uneconomic unless a large quantity of substrate is dyed to a single color, which is uncommon in the wool industry.

Dyeing Theory. Wool is composed mainly of a large number of different proteins, the fundamental structural units of which are α-amino acids (31). It is amphoteric in character because of the presence of basic amino groups in the side chains of lysine, hystidine, and arginine, and acidic carboxyl groups in the side chains of aspartic and glutamic acids. In an aqueous, acidic dyebath protonation of the amino and carboxyl groups results in a net positive charge on the fiber. Early workers explained the mechanism of wool dyeing in terms of electrostatic interactions between the positively charged amino groups and anionic dye molecules. The two most popular theories were the Gilbert–Rideal theory and the Donnan theory (106–108). Later studies, however, showed that the affinity and wetfastness properties of dyes on wool are largely determined by other types of interactions, namely, van der Waals' forces and interactions between hydrophobic regions in the fiber and hydrophobic parts of the dye molecules (109,110). Dyes differ markedly in their hydrophilic–hydrophobic character (105,110,111). Ionic forces are of greatest importance for dyes of relatively low molecular weight. With increasing molecular weight, van der Waals' and hydrophobic interactions become increasingly important, which is reflected in a higher affinity for the fiber and better wetfastness properties. Ionic interactions are important, however, for all wool dyes in determining the rate at which the dye is taken up by the fiber from the dye liquor. The dyeing rate can be controlled by varying the amount of acid added

to the dyebath, because this determines the size of the net positive charge on the wool, produced by protonation of amino groups.

In early studies on the uptake of dyes by wool, the fiber was treated as a cylinder of uniform composition. The main focus was on the thermodynamics of the dyeing process, in particular the situation applying when equilibrium had been attained. These studies provided little information, however, on the mechanism of the dyeing process itself. Recent work has clarified the relationship between fiber structure and the mechanism of wool dyeing (112,113).

Dyeing Mechanism. Wool fibers have a very complex morphological structure (Fig. 3). They can be considered as biological composite materials, in which the various regions are both chemically and physically different (31). Fine wool fibers contain two types of cell: those of the internal cortex and those of the external cuticle. Cortical cells, which constitute around 90% of the fiber, are spindle-shaped and are arranged in an overlapping pattern, parallel to the fiber axis. They are separated and held together by a continuous network, the cell membrane complex. This region of the fiber contains protein and also lipid material. The proteinaceous material in the cell membrane complex is relatively lightly cross-linked compared with the proteins in other regions of wool. The external cuticle cells are rectangular in shape and overlap, rather like tiles on a roof (Fig. 2). Dyes enter wool fibers at the junctions where the cuticle cells overlap and in the early stages of the dyeing process they diffuse into the interior along the lightly cross-linked network of the cell membrane complex (31,112,113). Later in the cycle, the dyes transfer, progressively, from the cell membrane complex into the cortical cells. The affinity of the dyes for wool is largely the result of their interaction with hydrophobic proteins located within the matrix of cortical cells.

Wool Dyes. The dyes used on wool can be divided into the following groups: acid dyes, chrome dyes, premetallized dyes, and reactive dyes (103,105,107,110, 111,114–116). Strictly speaking, all types of wool dyestuffs can be described as acid dyes, but in practice this term is confined to leveling acid dyes, half-milling dyes, milling dyes, and supermilling dyes (111,114). This subclassification of acid dyes arises out of the methods used for their application and their fastness properties on wool.

Levelling acid dyes (sometimes called level-dyeing or equalizing dyes) are the simplest type of dyes used on wool. They are of relatively low molecular weights (300–600) and have a comparatively low affinity for the fiber, because they interact largely by ionic attraction. They are applied at around pH 3, obtained with sulfuric acid. Under these conditions, the initial uptake of dye is usually uneven because the exhaustion rate is very rapid. As their name implies, levelling acid dyes have good migration properties and levelling occurs during the stage of the dyeing cycle when the dye liquor is held at the boil, thus producing a very even result. Levelling of the dyes is assisted by the presence of sodium sulfate in the dye bath, because the anionic sulfate ions compete with dye anions for the positively charged amino groups in the fiber. In general, these dyes are not particularly resistant to wet treatments, but are used when level dyeing is critically important.

Milling acid dyes are so named because they are more resistant than levelling acid dyes to extraction from wool during the milling process. They are of higher molecular weight (600–900) and are more hydrophobic than levelling acid dyes, which gives them a higher affinity for wool. The higher molecular weight and

lower dependence on ionic attraction means that they diffuse out of the fiber more slowly than levelling dyes, which is responsible for their higher fastness to wet treatments such as milling and laundering. Their migration properties, and hence their ability to level during application, is not as good as that of acid dyes. To obtain level results it is important to ensure that the rate of exhaustion is uniform and not too rapid. This is achieved by setting the dyebath at a higher pH (ca pH 4.5–6.0) with a weak acid, such as acetic acid, and also by the addition of a surfactant-type levelling agent, which promotes even uptake on wool. Half-milling dyes fall between levelling acid and milling dyes in molecular weight (500–600), migration properties, and wetfastness. They are applied at a pH in the range pH 4.0–4.5.

Supermilling acid dyes are similar in molecular weight to milling dyes, but contain long alkyl groups that make them more hydrophobic in character. This gives them a high affinity for wool that is virtually independent of ionic interactions with the fiber; consequently, they have very good wetfastness properties. They show good exhaustion under almost neutral (pH 5.5–7.0) dyeing conditions, but their high affinity means that they have poor migration and relatively poor levelling properties. Auxiliary products are often used to assist level application of these dyes.

Chrome dyes are acid dyes (mol. wt. 300–600) that contain groups capable of forming complexes by reaction with a metal salt, usually sodium or potassium dichromate (111,114). The chrome/dye complex has lower solubility, and hence better wetfastness, than the parent dyestuff. Reaction between the dye molecule and chromium salt can be carried out before, during or after application of the dye to the wool. Modern practice is to carry out the chroming step after dyeing. Chrome dyes are relatively cheap, and have good migration and level dyeing behavior and excellent wetfastness properties. Their popularity, except for black and navy blue shades, has declined in recent years. This is because of the need for prolonged dyeing cycles, fiber damage associated with oxidation of the fiber in the chroming step, and environmental concerns about the use of chromium salts in the textile industry.

In many applications, chrome dyes have been replaced by metal-complex dyes, which have a very high affinity for wool (111,115). In these dyes, the metal complex is preformed during manufacture of the dye, by reaction of one metal atom with either one (1:1 metal-complex dyes) or two (1:2 metal-complex dyes) dyestuff molecules that contain groups capable of coordinating with chromium or, occasionally, cobalt atoms. In general, metal-complex dyes produce duller shades than acid or milling dyes. The 1:1 metal-complex dyes are applied to wool from strongly acidic dyebaths at around pH 2. They are almost all monosulfonates (mol. wt. 400–500) and have good levelling behavior and wetfastness properties. Some degradation of the fiber can be caused by the low dyeing pH. The earliest type of 1:2 metal-complex dyes were unsulfonated; solubility was provided by nonionic polar groups, such as sulfonamide or methylsulfone. More recently, monosulfonated, disulfonated, and some carboxyl-containing types have become available. These dyes range in molecular weight from 700 to around 1000. They are applied at pH values ranging from pH 4.5 to 7.0, depending on the degree of sulfonation and molecular size of the dye.

Reactive dyes have molecular weights in the range 500–900 and usually contain two or three sulfonic acid groups (105,116). These dyes also contain groups

that react covalently with wool, which gives them outstanding wetfastness properties. They are characterized by bright colors and moderate migration and levelling properties, provided careful attention is given to ensuring that the exhaustion rate is not too rapid. This is achieved by careful control of the dyebath pH and by using special amphoteric levelling agents. Their ability to react with the fiber means that uneven uptake of these dyes is very difficult to rectify. Reactive dyes are relatively expensive and, currently, their most important application is on wools that have been treated to withstand shrinkage in machine washing. They are, however, becoming increasingly important as alternatives to chrome dyes for dyeing all types of wool. At present, reactive dyes offer the only viable alternative to chrome dyes for products where very high wetfastness properties are required.

Fiber Damage in Dyeing. When wool is dyed for prolonged times at the boil, the fiber can be damaged as a result of hydrolysis of the component proteins. Methods of dyeing wool substrates at temperatures below the boil (85–90°C) have been developed. One such method, the CSIRO Sirolan-LTD™ process employs a special chemical (Valsol LTA-N, APS Chemicals) that increases the rate of exhaustion and diffusion of dye into the fiber, thus enabling satisfactory dyeings to be obtained at temperatures below the boil (117). Wool dyed by this method suffers less degradation than wool dyed for a similar time at the boil. This leads to benefits in the processing performance of the dyed fiber and in improved quality of end products (118). Permanent setting of wool fibers during dyeing has been identified as a major factor that also contributes to deterioration of the quality of dyed wool (117). This effect is separate from hydrolytic degradation. Setting occurs via a mechanism involving thiol/disulfide interchange (eq. 1). Methods of inhibiting the permanent setting of wool fibers during dyeing have been developed (89). These involve addition to the dyebath of auxiliaries (antisetting agents such as Basolan AS, BASF) that block thiol groups and, thus, prevent thiol/disulfide interchange. Improvements in the properties of a range of products made from wool are obtained by reducing the amount of permanent set that occurs during dyeing.

Printing

Printing provides the means of transferring bright multicolor designs onto textiles. The amount of wool fabric printed is very small compared to cotton and synthetics. This is partly because the pigment printing systems widely used for cotton and synthetics have a severe adverse effect on the natural handle of wool. Furthermore, although the printing of wool using dyes maintains the natural qualities of the fiber, it requires a more complex processing sequence involving several stages, some of which are technically challenging.

The usual route for printing wool with dyestuffs is fabric preparation/print/dry/steam at 100°C (to fix dye to fabric)/wash off (to remove thickener and unfixed dye)/dry. Globally, an estimated 20 million meters per annum of high quality printed wool fabric is produced, with the center of excellence being in Northern Italy.

Fabric preparation is considered to be the most important stage for obtaining good color yields, levelness, and brightness on wool fabric (119,120). Currently, this

is done almost exclusively by an oxidative chlorination process. The most popular commercial methods use either a batch treatment with DCCA or a continuous fabric treatment with gaseous chlorine (the Kroy process). Chlorination has a profound effect on wool, especially near the fiber surface. The number of anionic groups is increased, with cystine residues oxidized to cysteic acid and accessible peptide bonds cleaved to form carboxyl groups. These reactions increase the wettability of the surface of wool, which facilitates spreading of the dye formulations. Chlorination also reduces the degree of cross-linking of wool, which increases the rate of dye diffusion into the fiber. Chlorination can have several adverse effects, however. At higher levels (4% on mass fabric of DCCA), there are problems in obtaining level treatments. Yellowing, especially after steaming, can also occur. These problems can be minimized by treating fabrics continuously in open width in a machine such as the Kroy chlorinator. With all chlorination processes, soluble protein and free oxidation products must be removed from the wool before drying. This is done by neutralization with a reducing agent, such as sodium bisulphite or sodium dithionite.

The effluent from the chlorination of wool contains adsorbable organohalogen compounds (AOX), which are now regarded as undesirable products to release into the environment, particularly in Europe. Several AOX-free methods for preparing wool for printing are currently being investigated. Plasma (121) and corona discharge (122) treatments have been investigated as potential prepare-for-print methods for wool, as they oxidize the surface of wool fibers and have the advantage of being dry processes. Although the wettability of fabrics prepared using these methods is high, the color yields of prints are significantly less than prints on chlorinated fabric and the fabric handle is inferior. An alternative approach is the CSIRO "Siroflash" process. This method involves continuous ultraviolet (UV) irradiation of dry wool fabric with the type of commercial UV source used for curing polymer films. This is followed by a conventional oxidative bleaching treatment with hydrogen peroxide (123). This process is surface-specific, giving a white fabric with good handle properties and similar color yields to DCCA treatment.

Most wool is printed directly onto the prepared fabric. Automatic flat-screen printing remains the most popular method over the rotary screen process used for most cotton printing, because of the shorter run lengths normally processed for wool fabrics. The dyestuffs most commonly used for wool printing are acid milling, metal complex, and reactive dyes. A simple dye paste is prepared using a suitable thickener, urea (to swell wool fibers during steaming), and the dyestuffs. Various additives may be included in the paste recipe, such as antifoam, glycerol to prevent screen blocking, an acid donor (to maintain a low pH), wetting agent, and a dye solvent such as thiodiglycol (120).

During the steaming stage, large aggregates of dye molecules break down into smaller entities which can then penetrate the swollen wool fibers, allowing fixation to take place. Typical steaming times are 10–15 min for reactive dyes and 30 min for acid milling and metal complex dyes. Saturated steam is essential for optimum penetration and fixation of dyes, especially for dyes of high molecular weight such as those based on copper phthalocyanine derivatives. Both continuous and batch steamers are used commercially. Chlorinated fabrics are highly prone to yellowing during steaming, which can be detrimental to printed pale shades.

The aim of washing off is to remove the thickener and any residual chemicals and unfixed dye from the fabric, without causing staining of any pale or unprinted areas. Fabrics printed with metal complex or acid milling dyes are usually washed off in water at 30–40°C, whereas reactive dyes require higher temperatures (60–80°C), with addition of ammonium hydroxide (120).

Discharge printing of wool remains popular, despite its technical difficulties (119,120). In this style of printing, a predyed fabric is printed with a reducing agent that destroys the background shade. Included in the print paste is a dye which is resistant to the discharge agent. The result is bleaching of the color in the printed areas and replacement with the illuminating color. It is often impossible to reproduce the designs and effects of discharge printing with direct printing. The reducing agents used in discharge printing are zinc, calcium or sodium formaldehyde sulfoxylate, or thiourea dioxide. The technique is limited by the choice of dyes that are resistant to the reducing agent.

Other techniques, such as resist printing, cold batch printing, and transfer printing have been applied to wool with some success, but these now occupy only a small share of the current wool printing market (119,120).

Digital inkjet printing is a recent development for printing textiles (124). It has the advantage that any design can be transferred rapidly from a personal computer onto a fabric, without the requirements to perform a color separation and make a separate screen to print each color. It is also more cost-effective for producing the short runs of printed fabric designs that are typical for wool compared with other methods. The wool fabric is prepared for printing using a conventional method, padded with a mixture of a thickening agent and urea and dried before digital printing. The padding process assists penetration of the dye into the wool fabric and avoids flushing of the prints during steaming.

Yellowing

In common with many other polymeric materials, yellowing of wool is an undesirable property that can be caused by several different mechanisms (see DEGRADATION). For wool, the most important of these are exposure to sunlight and heat.

The rate and extent of photoyellowing of wool exposed to direct sunlight is a serious shortcoming when compared with fibers such as cotton and synthetics. Photoyellowing is caused by the UV components of natural sunlight (285–380 nm), whereas exposure of wool to sunlight filtered through window glass, which absorbs most of the UV, causes photobleaching (125). Photoyellowing of wool by sunlight only occurs in the presence of oxygen and it has been proposed that it is a photo-oxidative process involving the formation of singlet oxygen (126,127). More recent work, however, has shown that in common with cotton, polyester, and nylon, wool in the wet state is capable of producing hydroxyl radicals ($OH^{\bullet}$) on irradiation with UV light at 366 nm and blue light at 430 nm (128). This reaction appears to be catalyzed by trace metals such as iron and copper. It has been proposed that the photoyellowing mechanism for wool may involve a free-radical chain reaction involving formation of hydroperoxide intermediates (as is the case for most other polymers), rather than a singlet oxygen mechanism

(128). There is now general agreement in the literature that yellow chromophores formed in irradiated wool are derived (at least in part) from tryptophan residues (129,130).

The use of some water-soluble benzotriazoles (a well-known class of UV absorber) can be effective against both photoyellowing and phototendering (see UV STABILIZERS). The effectiveness of these reagents relies on intramolecular hydrogen bonding and proton transfer, and intermolecular bonding of the compounds to wool fibers was found to be highly detrimental to their performance. Optimization of the photochemical properties of soluble benzotriazoles has resulted in a suitable formulation (Cibafast W) for use on both bleached and unbleached wool (131). Unfortunately, UV absorbers cannot be used on wool together with a fluorescent whitening agent (FWA) because they absorb the UV wavelengths necessary to excite fluorescence. FWA treatment is essential to achieve a high level of whiteness on wool, because even wool that has been bleached retains some of its natural cream color. An important problem for wool is the very rapid photoyellowing that occurs following treatment with FWAs (132). The poor lightfastness of bright white and pastel colors severely limits the range of possible shades for wool products. This is reflected in wool's limited market share in fashion and summer knitwear, sportswear, hosiery, and baby wear. Wet photoyellowing of whitened (FWA-treated) wool is extremely rapid and can cause unacceptable yellowing after a single laundering and drying cycle in direct sunlight. When wet FWA-treated wool is exposed to sunlight, hydrogen peroxide is formed (133). The rate of photoyellowing of FWA-treated wool is significantly increased by doping with hydrogen peroxide. This indicates that blocking the formation of peroxide (via the superoxide radical anion) could improve the photostability of whitened wools.

Treatment of wool with a FWA, followed by post-treatment with thiourea/formaldehyde by a pad/cure method, confers a high level of protection against photoyellowing and also improves the initial fabric whiteness (134). Unfortunately, this process is not commercially viable, partly because of environmental concerns about thiourea and formaldehyde and also because much of the benefit is lost after laundering. An alternative approach is to physically separate the FWA from the wool fiber by incorporating the whitener into a suitable polymer that can be applied as a surface treatment to wool fabrics (135). The photostability of the treated fabrics is somewhat better than for conventional FWA treatments (being similar to bleached wool) but the initial whiteness is significantly lower than that of FWA-treated wool.

Two comprehensive reviews on the photodegradation of wool keratin have been published recently by Smith (129) and by Davidson (136). There is also an excellent review dealing specifically with the problem of sunlight yellowing of wool treated with FWAs (126).

Thermal yellowing of wool can be a problem during wool processing, in particular during extended dyeing at the boil, in setting with superheated steam (decatizing), and in drying for extended times, particularly under alkaline conditions (137). The thermal yellowing of wet wool is far more rapid than for dry wool, which is similar to the behavior observed for photoyellowing. Thermal yellowing of wool during dyeing is influenced by pH, temperature, and time, chlorinated wools being especially sensitive. Yellowing during dyeing can be counteracted by adding a bleaching agent, based on sodium bisulfite or hydroxylamine sulphate, to the

dyebath (138). Addition of hydrogen peroxide to the dyebath after exhaustion of the dyestuffs can also be effective.

Bleaching and Fluorescent Whitening

The natural pale cream color of wool is due to absorption of light above 320 nm. This is the result of natural pigments and also photodecomposition products in the fiber. Reduction of the natural cream-yellow color of wool is sometimes necessary for improving the brightness of dyed shades, particularly pastel colors, and also for improving the whiteness of undyed wool fabrics. Commercially, wool bleaching is carried out using either an oxidative or a reductive system, or a combined oxidation/reduction process. Oxidative bleaching in the dyebath is also possible (138). In general, oxidative bleaching with hydrogen peroxide gives superior whiteness over reductive methods.

A batch treatment with hydrogen peroxide is used for most bleaching applications. An activator (eg an alkali) is normally added to increase the rate of bleaching. Typically, wool is bleached at pH 8–9 for 1 h at 60°C with a stabilized solution of hydrogen peroxide (0.75% w/w). It is generally accepted that, under alkaline conditions, the active bleaching species is the perhydroxy anion (OOH^-), the formation of which is encouraged by higher pH (139). Peroxide bleaching of wool under mild acidic conditions (pH 5–6) can also be carried out using a peracid activator such as Prestogen W (BASF) or citric acid (140). As wool sustains some damage in the presence of alkali, this method is useful for bleaching delicate fabrics. An undesirable side effect is the rapid decomposition of hydrogen peroxide to water and oxygen, a reaction catalyzed by transition-metal ions. A stabilizer, which sequesters these ions, is used to prevent this side reaction occurring. The most common stabilizers for alkaline wool bleaching are phosphates, particularly tetrasodium pyrophosphate. However, recent concerns over phosphates in effluents from textile treatment have led to the development of alternative stabilizers based on silicates (141). An alkaline peroxide bleaching process using the silicate-based product Stabicol BAC (Allied Colloids) has been developed (138).

Heavily pigmented fibers, such as Karakul wools, require a more severe approach known as mordant bleaching. In this method, the wool is treated with a metal salt and then with hydrogen peroxide. In the first step, the melanin pigment in the wool preferentially absorbs the metal cations; and in the second step, the cations catalytically decompose the peroxide to produce highly aggressive hydroxyl free radicals, which selectively attack and bleach the melanin (142).

The two most popular chemicals used for reductive bleaching of wool are stabilized sodium dithionite and thiourea dioxide. Most reductive bleaching of wool is carried out using stabilized dithionite (2–5g/L) at pH 5.5–6 and 45–65°C for 1 h. Thiourea dioxide is more expensive than sodium dithionite, but is an effective bleach when applied (1–3 g/L) at 80°C and pH 7 for 1 h. Whiter fabrics are produced when oxidative bleaching is followed by a reductive process—this is often referred to as "full bleaching."

To obtain a high level of whiteness, comparable to white cotton and synthetics, wool must be treated with a FWA after bleaching. The normal procedure is to carry out a full bleaching process and include the FWA in the reductive

bleaching bath. FWA-treated wool absorbs UV light and emits blue fluorescence, which makes it appear much whiter than bleached wool. Commercial FWAs for wool are usually based on a sulfonated stilbene, distyrylbiphenyl, or pyrazoline derivative.

Wool fabrics that have been bleached or treated with FWAs yellow rapidly when exposed to sunlight, especially when wet. This is a major problem when bright whites and pastel shades are required. Despite a significant amount of research into the chemistry of photoyellowing processes progress in this area has been limited (126).

Insect-Resist Treatment

Wool is a protein fiber but, because it is insoluble and highly cross–linked, it is not widely available as a food resource. Only a few keratin-digesting animals have developed specialized digestive systems that allow them to derive nutrition from the potential protein resource. These animals, principally the larvae of clothes moths and carpet beetles, perform a useful function in nature by scavenging the keratinous parts of dead animals (fur, skin, beak, claw, feathers) that are unavailable to other animals.

The principal insects that attack wool are the common clothes moth (*Tineola bisselliella*), the case-bearing clothes moths (*Tinea metonella, T. dubiella, T. translucens*, and *T. pellionella*), the brown house moth (*Hofmannophila pseudospretella*), the variegated carpet beetle (*Anthrenus verbasci*), the black carpet beetle (Attagenus piceus), and a few others. The taxonomy of the Tineid species has been comprehensively reviewed (143). These insects have different temperature sensitivities and tend to be found in different climates. Studies in Australia have shown that the native Tineids are rarely involved in domestic infestations. The introduced species, such as *T. translucens*, are the major textile pests and these are often associated with the nests of introduced urban bird species such as sparrows and swallows (144), while *T. bisselliella* is widely distributed and is common in domestic infestations.

All keratinous materials stored for long periods, including stored greasy wool in bales, animal skins, furs, and horns, are liable to attack. Strategies for protecting goods vary with the product type. Buildings used to store wool may be fumigated or sprayed periodically. Small articles of clothing may be isolated from the environment in sealed bags, often with the use of heat (sunlight), cold (refrigerated storage), or volatile repellent agents (mothballs), with varying degrees of success.

The most practical means of protecting wool textile products is treatment with an insecticide during manufacture (145). Wool products most commonly treated are carpets, furnishings, and insulation. Except for insulation, the most convenient point for treating wool goods is during dyeing, which is attractive because it avoids the needs for an additional wet processing step. Under ideal application conditions the pesticide will be adsorbed inside the highly swollen fiber. This ensures that the pesticide will have maximum resistance to desorption from the dry fiber, and also have optimum fastness to washing, dry-cleaning, and skin contact. An additional benefit of locating the pesticide inside the fiber is that there

is little contact action against nontarget pests, as the active agent is released only in the insect gut when the fiber is completely degraded.

Unfortunately, it is impossible under practical dyebath conditions to ensure 100% transfer of pesticide from dyebath to fiber. It is also extremely difficult and expensive to remove residual insect-resist agent from dyehouse effluents (146). Even if the pesticide is removed by absorption or flocculation, the fate of the adsorbed material also needs to be considered (147). As a result, there is inevitably some environmental contamination. With the current generation of insect-resist agents, discharge of residual pesticide from dyebaths is a cause of significant environmental concern in large processing centers. Insect-resist agents must have a broad spectrum of activity because of the variety of moth and beetle species that must be controlled. They must also be reasonably stable to the dyeing conditions used in their application and be durable on wool for long periods. It is also essential that the agent is relatively hydrophobic so that it exhausts effectively from the dyebath onto wool. Unfortunately, this combination of properties is likely to lead to adverse effects on aquatic insects and invertebrates. To minimize environmental damage an allowable environmental concentration for permethrin of 10 ng/L has been set in the United Kingdom (148,149). To meet this requirement, the U.K. carpet dyeing industry has introduced a range of "best practice" operational procedures. These include dyeing at low pH and high temperature, avoiding dyes and dyeing assistants that may decrease the efficiency of application of the insecticide, containing spillages, and avoiding the discharge of effluents from tape scouring machines. Additionally, a number of manufacturers are using alternative application procedures, where little or no aqueous effluent is produced (147,150–152).

Prior to the introduction of synthetic pyrethroids, insect-resist agents were based mainly on speciality materials, such as polychloro chloromethyl sulfonamido diphenyl ether (PSCDs) (Eulan U33, Eulan WA New). The production of these compounds has been discontinued, however, because of a combination of environmental toxicity (149) and cost. One speciality insect-resist agent based on sulcofuron (Mitin FF), released in 1939 (153), retains a small market share for specific applications where cost is less important and where high resistance to wet conditions is required. It has also been used on wool insulation where it also has low volatility and provides resistance to rotting (154).

The principal active agent used for insect-resist treatments since the late 1970s has been permethrin. Although other broad-spectrum agricultural insecticides (including other synthetic pyrethroids) have been examined, permethrin remains dominant as it is a nonirritant with a good human health profile, especially when strongly adsorbed into the wool fiber. Pyrethroids with a safer environmental profile, such as cycloprothrin, have also been examined (155). These, however, require higher application levels, which increases the cost of the treatment. Newer commercial insect-resist agents under development are based on lufenuron (an insect growth regulator) (147,156) and on bifenthrin (a synthetic pyrethroid). The latter agent includes a synergist to counter the resistance to synthetic pyrethroids that is being observed in Australia (147). Resistance is an inevitable result of using a single protective agent for more than two decades. Resistance to pyrethroids is common among other agricultural pests, and pyrethroid-resistant strains of the Australian carpet beetle and the case-bearing clothes moth have been found

in domestic infestations in northern Australia (157). In the future, it is unlikely that speciality insect-resist agents for the protection of wool will be developed, as the market is too small to support the testing required to demonstrate the safety of modern, biologically active agents. The focus remains, therefore, on the use of commercial insecticides for protecting wool against insect damage.

A diverse range of nonpesticidal approaches has also been studied (144). Attempts to find triggers for such behaviors as egg-laying and recognition of food were inconclusive. Although it has been long known that otherwise unrelated clothes moths and carpet beetles have developed unique reducing systems in the gut that allow them to digest wool, specific inhibitors of these systems have not yet been identified.

Flame-Resist Treatment

Wool is regarded as a naturally flame-resistant fiber, which is partly due to its high nitrogen content, high sulfur content, and high (water) regain under ambient conditions. It has a high ignition temperature (570–600°C), high limiting oxygen index (25–26%), and a low heat of combustion (4.9 kcal/g) (158). In most cases, when wool fabrics are ignited they will rapidly self-extinguish, because of the formation of a high volume, insulating ash, or char. Unlike thermoplastic materials, wool does not melt or drip when ignited. In many end uses, no additional fire-retardant treatment is needed.

If higher standards of flammability are needed, such as in aviation, furnishing fabrics, or protective clothing, durable protective treatments are available. These treatments evolved from the observation that wool treated with a chrome mordant, such as that used in chrome dyeing, has a markedly improved flame resistance (159). The chrome mordant, however, discolors undyed wool. It was shown, subsequently, that titanium or zirconium compounds give similar improvements in fire retardancy (160), with reduced discoloration of the wool. The Zirpro Process, developed by IWS (now, The Woolmark Company) has been used extensively for wool in aircraft interiors to meet FAA requirements. It is also used for protective clothing and for stage curtains and carpets in public buildings and similar areas, where high flame resistance is required by legislation (161,162). Other wool finishes (dyeing, insect-resist, shrink-resist) have been developed that are compatible with the Zirpro Process.

BIBLIOGRAPHY

"Keratin" in *EPST* 1st ed., Vol. 8, pp. 1–44, by E. G. Bendit and M. Feughelman, CSIRO Wool Research Laboratories; "Wool" in *EPST* 1st ed., Vol. 15, pp. 41–79, by K. R. Makinson, CSIRO Wool Research Laboratories; "Keratin" in *EPSE* 2nd ed., Vol. 8, pp. 566–600, by Max Feughelman, University of New South Wales.

1. *Textile Terms and Definitions*, 10th ed., Textile Institute, Manchester, England, 1996.
2. *Wool Statistics*, International Wool Textile Organisation (IWTO), London, 2000–2001.
3. *Australian Wool Statistics Yearbook*, 1999–2000, Australian Wool Exchange, 2000, p. 57.

4. *Seminar Proceedings CSIRO Woolspec 94*, CSIRO, Sydney, Australia, 1994.
5. G. A. Carnaby and A. J. McKinnon, *Aus. Text.* **2**, 11 (1982).
6. *Objective Measurement of Wool in Australia*, Australian Wool Corp., Melbourne, Australia, 1973.
7. B. H. Mackay, In *Proc. 6th Int. Wool Text. Res. Conf.*, South African Wool and Textile Research Institute (SAWTRI), Pretoria, South Africa, 1980, Vol. I, p. 59.
8. Core Test Regulations Test Methods IWTO 19–76.28–75, 3–73, 20–69, International Wool Textile Organisation (IWTO), London, 1968.
9. B. P. Baxter, In *Proc. Inaugural Wool Ind. Sci. Technol. Conf.*, Hamilton, Australia, 2002.
10. *Australian Standard 1363–1976*, Standards Association of Australia, Melbourne, Australia, 1976.
11. *Report on Trials Evaluating Additional Measurement, 1981–1988*, Australian Wool Corp., Melbourne, Australia, 1988.
12. P. R. Lamb and S. Yang, In *Proc. 9th Int. Wool Text. Res. Conf.*, Città degli Studi Biella and International Wool Secretariat (IWS), Biella, Italy, 1995, Vol. V, p. 159.
13. A. R. Edmunds, *Wool Tech. Sheep Breeding* **45**(3, 27 (1997).
14. B. P. Baxter, *Wool Tech. Sheep Breeding* **45**, 267 (1997).
15. P. R. Lamb, In *Proc. Inaugaural Wool Ind. Sci. Technol. Conf.*, Hamilton, Australia, 2002.
16. A. D. Peterson and S. G. Gherardi, *Wool Tech. Sheep Breed.* **49**(2), 110 (2001).
17. K. A. Hansford, *Wool Tech. Sheep Breed.* **47**(1, 19 (1999).
18. M. H. Hardy and A. G. Lyne, *Aust. J. Biol. Sci.* **9**, 423 (1965).
19. R. E. Chapman and K. A. Ward, in J. L. Black and P. J. Reis, eds., *Physiological and Environmental Limitations to Wool Growth*, University of New England Publishing Unit, Armidale, Australia, 1979, p. 193.
20. R. D. B. Fraser, T. P. MacRae, and G. E. Rogers, *Keratins, Their Composition, Structure and Biosynthesis*, Charles C. Thomas, Springfield, Ill., 1972.
21. L. N. Jones, T. J. Horr, and I. J. Kaplin, *Micron* **25**, 589 (1994).
22. K. R. Makinson, *Shrinkproofing of Wool*, Marcel Dekker, Inc., New York, 1979.
23. R. C. Marshall, D. F. G. Orwin, and J. M. Gillespie, *Electron Microsc. Rev.* **4**, 47 (1991).
24. I. J. Kaplin and K. J. Whiteley, In *Proc. 7th Int. Wool Text. Res. Conf.*, Society of Fiber Science and Technology, Tokyo, Japan, 1985, Vol. 1, p. 95.
25. J. D. Leeder, *Wool Sci. Rev.* **63**, 35 (1986).
26. D. E. Rivett, *Wool Sci. Rev.* **67**, 1 (1991).
27. M. S. C. Birbeck and E. H. J. Mercer, *Biophys. Biochem. Cytol.* **3**, 203 (1957).
28. R. E. Chapman and R. T. J. Gemmell, *Ultrastruct. Res.* **36**, 342 (1971).
29. K. M. Rudall, In *Proc. 1st Int. Wool Text. Res. Conf.*, Commonwealth Scientific and Industrial Research Organisation (CSIRO), Melbourne, Australia, 1955 Vol. F, p. 176.
30. D. F. G. Orwin, in D. A. D. Parry and L. K. Creamer, eds., *Fibrous Proteins: Scientific, Industrial and Mechanical Aspects*, Academic Press, New York, 1979, pp. 271–297.
31. J. A. Rippon, in D. M. Lewis, ed., *Wool Dyeing*, Society of Dyers and Colourists, Bradford, U.K., 1992, Chapt. 1.
32. J. H. Bradbury, G. V. Chapman and N. L. R. King, in W. G. Crewther, ed., *Symposium on Fibrous Proteins*, Butterworths, Australia, 1967, p. 368.
33. J. D. Leeder and R. C. Marshall, *Text. Res. J.* **52**, 245 (1982).
34. B. Milligan, L. A. Holt, and J. B. Caldwell, *Appl. Polym. Symp.* **18**, 113 (1971).
35. M. Cole, J. C. Fletcher, K. L. Gardner, and M. C. Corfield, *Appl. Polym. Symp.* **18**, 147 (1971).
36. L. A. Holt, B. Milligan, and L. J. Wolfram, *Text. Res. J.* **44**, 846 (1974).
37. J. M. Gillespie, in R. D. Goldman and P. M. Steinert, eds., *Cellular and Molecular Biology of Intermediate Filaments*, Plenum Press, New York, 1990, Chapt. 4.

38. H. Zahn and P. Kusch, *Melliand Textilber. (Eng. Ed.)* **10**, 75 (1981).
39. J. F. Conway, R. D. B. Fraser, T. P. Macrae and D. A. D. Parry, in G. E. Rogers, P. J. Reis, K. A. Ward, and R. C. Marshall, eds., *The Biology of Wool and Hair*, Chapman and Hall, London, 1988, p. 127.
40. I. J. Kaplin and K. J. Whiteley, *Aust. J. Biol. Sci.* **31**, 231 (1978).
41. L. M. Dowling, K. F. Ley, and A. M. Pearce, In *Proc. 8th Int. Wool Text. Res. Conf.*, Wool Research Organisation of New Zealand (WRONZ), Christchurch, New Zealand, 1990, Vol. I, p. 205.
42. J. Herrling and H. Zahn, In *Proc. 7th Int. Wool Text. Res. Conf.*, Society of Fiber Science and Technology, Tokyo, Japan, 1985, Vol. 1 p. 181.
43. A. Schwan, J. Herrling and H. Zahn, *Colloid Polym. Sci.* **264**, 171 (1986).
44. J. D. Leeder and J. A. Rippon, *J. Soc. Dyers Colour.* **101**, 11 (1985).
45. D. E. Evans, J. D. Leeder, J. A. Rippon, and D. E. Rivett, In *Proc. 7th Int. Wool Text. Res. Conf.*, Society of Fiber Science and Technology, Tokyo, Japan, 1985, Vol. 1, p. 135.
46. G. R. S. Naylor, D. G. Phillips, C. J. Veitch, M. Dolling, and D. J. Marland, *Text. Res. J.* **67**, 288 (1997).
47. G. R. S. Naylor and D. G. Phillips, In *Proc. 9th. Int. Wool Text. Res. Conf.*, Città degli Studi Biella and International Wool Secretariat (IWS), Biella, Italy, 1995, Vol. II, p. 203.
48. I. C. Watt, *J. Macromol. Sci.-Rev. Macromol. Chem., C* **18**(2), 169 (1980).
49. H. Sakabe, H. Ito, T. Miyamoto, and H. Inagaki, *Text. Res. J.* **57**, 66 (1987).
50. A. P. Pierlot, *Text. Res. J.* **69**, 97 (1999).
51. C. Popescu and F.-J. Wortmann, *Wool Tech. Sheep Breed.* **50**(1), 52 (2002).
52. D. J. Evans, R. J. Denning, and J. S. Church, *Encyclopedia of Surface and Colloid Science*, Marcel Dekker, Inc., 2002, p. 2628.
53. I. C. Watt and R. L. D'Arcy, *J. Text. Inst.* **70**, 298 (1978).
54. W. E. Morton and J. W. S. Hearle, *Physical Properties of Textile Fibres*, 3rd ed., The Textile Institute, Manchester, U.K., 1993.
55. *Wool Research*, Wool Industries Research Association, Leeds, U.K., 1955, Vol. 2.
56. M. G. Huson, *Text. Res. J.* **68**, 595 (1998).
57. M. Feughelman, *Text. Res. J.* **59**, 739 (1989).
58. A. R. Haly and J. W. Snaith, *Text. Res. J.* **37**, 898 (1967).
59. F.-J. Wortmann, B. J. Rigby, and D. G. Phillips, *Text. Res. J* **54**, 6 (1984).
60. J. M. Kure, A. P. Pierlot, I. M. Russell, and R. A. Shanks, *Text. Res. J.* **67**, 18 (1997).
61. M. G. Huson, *Polym. Int.* **26**(3), 157 (1991).
62. A. P. Pierlot, *Text. Res. J.* **67**, 616 (1997).
63. M. Feughelman, in J. I. Kroschwitz, ed., *Encyclopedia of Polymer Science and Engineering*, Vol. 8, 1987, p. 566.
64. J. W. S. Hearle and M. Susutoglu, In *Proc. 7th Int. Wool Text. Res. Conf.*, Society of Fiber Science and Technology, Tokyo, Japan, 1985, Vol. 1, 214.
65. F.-J. Wortmann and H. Zahn, *Text. Res. J.* **64**, 737 (1994).
66. T. W. Mitchell and M. Feughelman, *Text. Res. J.* **30**, 662 (1960).
67. J. W. S. Hearle, *Int. J. Biol. Macromol.* **27**, 123 (2000).
68. M. Feughelman and M. S. Robinson, *Text. Res. J.* **41**, 469 (1971).
69. A. Brearley and J. A. Iredale, *The Worsted Industry: An Account of the Worsted Industry and Its Processes from Fibre to Fabric*, Wira, Leeds, U.K. (1980).
70. R. G. Stewart and R. G. Jamieson, *Wool Sci. Rev.* **64**, 16 (Dec. 1987); J. R. Christoe, *Wool Sci. Rev.* **64**, 25 (Dec. 1987); B. V. Harrowfield, *Wool Sci. Rev.* **64**, 44 (Dec. 1987).
71. G. F. Wood, *Text. Prog.* **12**(1), 1 (1982).
72. *Text. Recorder* **81**, 69 (Jan. 1964).
73. CSIRO Division of Textile Industry Report No. G. 10, CSIRO Division of Textile Industry, Geelong, Australia, 1960.

74. J. Brach, *Wool Sci. Rev.* **36**, 38 (May 1969).
75. B. Robinson, C. P. S. Lee, and T. Shaw, Technical Information Letter, TIL/ET-14, International Wool Secretariat, Jan. 1993; J. R. Christoe and B. O. Bateup, CSIRO Division of Wool Technology Report, G70, CSIRO Division of Wool Technology, Geelong, Australia, 1992.
76. J. R. Christoe and B. O. Bateup, In *Proceedings of Third Asian Textile Conference*, Hong Kong Polytechnic University, Hong Kong, 1995.
77. B. O. Bateup, J. R. Christoe, F. W. Jones, A. J. Poole, C. Skourtis, and D. J. Westmoreland, *Enviro. 2000*, Sydney, Australia, 2000; B. O. Bateup, J. R. Christoe, F. W. Jones, A. J. Poole, C. Skourtis, and D. J. Westmoreland, *In 80th Textile Institute Conference*, Melbourne, Australia, 2001.
78. A. Elice-Invaso, J. Maheswaran, K. I. Peveril, J. R. Christoe, and C. Skourtis, *Wool Scour Effluent as a Potassic Fertiliser. ASSI & NZSS National Soils Conference, Aural Papers*, Melbourne, Australia, July 1996, p. 75.
79. N. C. Gee, *Shoddy and Mungo Manufacture*, Emmott & Co., Bradford, U.K., 1950.
80. H. K. Rouette and G. K. Kittan, *Text. Praxis Int.* **36**, 784 (1981).
81. W. G. Crewther, In *Proc. 1st Int. Wool Text. Res. Conf.*, Commonwealth Scientific and Industrial Research Organisation (CSIRO), Melbourne, Australia, 1955, Vol. E, p. 408.
82. W. G. Crewther and T. A. Pressley, *Text. Res. J.* **28**, 67 (1958).
83. Lubrication for Improved Worsted Top, CSIRO, Division of Textile Industry Report No. G.65, CSIRO Geelong, Australia, Oct. 1989.
84. D. G. Phillips, *Text. Res. J.* **55**, 171 (1985).
85. J. A. Maclaren and B. Milligan, *Wool Science: The Chemical Reactivity of the Wool Fibre*, Science Press, Marrickville, NSW, Australia, 1981.
86. K. Ziegler, In *Proc. 3rd Int. Wool Text. Res Conf.*, Institut Textile de France, Paris, 1965, Vol. II, p. 403.
87. R. S. Asquith and A. K. Puri, *J. Soc. Dyers Colour.* **84**, 461 (1968).
88. M. G. Huson, *Text. Res. J.* **62**, 9 (1992).
89. P. G. Cookson, P. R. Brady, K. W. Fincher, P. A. Duffield, S. S. Smith, K. Reincke, and J. Schreiber, *J. Soc. Dyers Colour.* **111**, 228 (1995).
90. M. A. White, CSIRO Division of Textile Industry Report No. G 44, CSIRO, Geelong, Australia, 1982.
91. A. J. Farnworth, *Am. Dyest. Rep.* **49**, 996 (1960).
92. J. R. Cook and J. Delmenico, In *Proc. 3rd Int. Wool Text. Res. Conf.*, Institut Textile de France, Paris, 1965, Vol. III, p. 619.
93. Aust. Pat. 645026 (May 20, 1994), D. G. Phillips and J. J. Warner (to CSIRO).
94. A. Y. Bhoyro, J. S. Church, D. G. King, G. J. O'Loughlin, D. G. Phillips, and J. A. Rippon, In *Proc. Text. Inst. 81st World Conf.*, Melbourne, Australia, 2001.
95. E. G. Bendit, *Text. Res. J.* **30**, 547 (1960).
96. P. Alexander, R. F. Hudson, and C. Earland, *Wool Its Chemistry and Physics*, 2nd ed., Chapman and Hall, London, 1963, Chapt. 2.
97. A. P. Pierlot, *Text. Res. J.* **67**, 616 (1997).
98. R. W. Moncrieff, *Wool Shrinkage and Its Prevention*, National Trade Press, London, 1953.
99. J. Lewis, *Wool Sci. Rev.* **55**, 23 (1978).
100. R. J. Denning, G. N. Freeland, G. B. Guise, and A. H. Hudson, *Textile Res. J.* **64**, 413 (1994).
101. J. A. Rippon and M. A. Rushforth, *Textilver.* **11**, 224 (1976).
102. A. G. De Boos, K. W. Fincher, and A. M. Wemyss, *Text. Chem. Colorist* **29**(10), 28 (1997).

103. C. L. Bird, *The Theory and Practice of Wool Dyeing*, Society of Dyers and Colourists, Bradford, U. K., 1972.
104. F. W. Marriott, in D. M. Lewis, ed., *Wool Dyeing*, Society of Dyers and Colourists, Bradford, U.K., 1992, Chapt. 5.
105. D. M. Lewis, *Rev. Prog. Colorat.* **8**, 10 (1977).
106. P. Alexander, R. F. Hudson, and C. Earland, *Wool Its Chemistry and Physics*, 2nd ed., Chapman and Hall, London, 1963, Chapts. 6 and 7.
107. L. Peters, in C. L. Bird and W. S. Boston, eds., *The Theory of Coloration of Textiles*, Dyers' Company Publications Trust, Bradford, U.K., 1975, p. 163.
108. R. H. Peters, *Textiles Chemistry*, Vol. III, Elsevier Publishing, Amsterdam, 1975, p. 203.
109. J. Meybeck and P. Galafassi, *Appl. Polym. Symp.* **1**, 463 (1971).
110. M. T. Pailthorpe, in D. M. Lewis, ed., *Wool Dyeing*, Society of Dyers and Colourists, Bradford, U.K., 1992, Chapt. 2.
111. J. A. Bone, J. Shore, and J. Park, *J. Soc. Dyers Colour.* **104**, 12 (1988).
112. J. D. Leeder, J. A. Rippon, F. E. Rothery, and I. W. Stapleton, In *Proc. 7th Int. Wool Text. Res. Conf.*, Society of Fiber Science and Technology, Tokyo, Japan, 1985, Vol. V, p. 14.
113. J. D. Leeder, L. A. Holt, J. A. Rippon, and I. W. Stapleton, In *Proc. 8th Int. Wool Text. Res. Conf.*, Wool Research Organisation of New Zealand (WRONZ), Christchurch, New Zealand, 1990, Vol. IV, p. 227.
114. P. A. Duffield, in D. M. Lewis, ed., *Wool Dyeing*, Society of Dyers and Colourists, Bradford, U.K., 1992, Chapt. 6.
115. S. M. Burkinshaw, in D. M. Lewis, ed., *Wool Dyeing*, Society of Dyers and Colourists, Bradford, U.K., 1992, Chapt. 7.
116. D. M. Lewis, in D. M. Lewis, ed., *Wool Dyeing*, Society of Dyers and Colourists, Bradford, U.K., 1992, Chapt. 8.
117. P. R. Brady and J. A. Rippon, *J. Soc. Dyers Colour.* **108**, 114 (1992).
118. J. A. Rippon, F. J. Harrigan, and A. R. Tilson, In *Proc. 9th Int. Wool Text. Res. Conf.*, Città degli Studi Biella and International Wool Secretariat (IWS), Biella, Italy, 1995, Vol. III p. 122.
119. V. A. Bell, *J. Soc. Dyers Colour.* **104**, 159 (1989).
120. V. A. Bell, in in D. M. Lewis, ed., *Wool Dyeing*, Society of Dyers and Colourists, Bradford, U.K., 1992, Chapt. 10.
121. D. Radetic, D. Josic, P. Jovancic, and R. Trajkovic, *Text. Chem. Colorist* **32**(4), 55 (2000).
122. J. Ryu, T. Wakida, and T. Takagishi, *Text. Res. J.* **61**, 595 (1991).
123. K. R. Millington, *J. Soc. Dyers Colour.* **114**, 286 (1998).
124. T. L. Dawson, *J. Soc. Dyers Colour.* **116**, 52 (2000).
125. M. G. King, *J. Text. Inst.* **62**, 251 (1971).
126. B. Milligan, In *Proc. 6th Int. Wool Text. Res. Conf.*, South African Wool and Textile Research Institute (SAWTRI), Pretoria, South Africa, 1980, Vol. V, p. 167.
127. C. H. Nicholls and M. T. Pailthorpe *J. Text. Inst.* **67**, 397 (1976).
128. K. R. Millington and L. J. Kirschenbaum, *Coloration Technol.* **118**, 6 (2002).
129. G. J. Smith, *J. Photochem. Photobiol., B: Biol.* **27**, 187 (1995).
130. S. Collins, R. S. Davidson, P. H. Greaves, M. Healy, and D. M. Lewis, *J. Soc. Dyers Colour.* **104**, 348 (1988).
131. I. H. Leaver and J. F. K. Wilshire, *Chem. Aust.* 174 (1990).
132. D. R. Graham and K. W. Statham, *J. Soc. Dyers Colour.* **72**, 434 (1956).
133. K. R. Millington, In *Proc. 9th Int. Wool Text. Res. Conf.*, Città degli Studi Biella and International Wool Secretariat (IWS), Biella, Italy, 1995, Vol. III, p. 174.
134. B. Milligan and D. J. Tucker, *Text. Res. J.* **34**, 681 (1964).
135. R. Levene, *Text. Res. J.* **57**, 298 (1987).

136. R. S. Davidson, *J. Photochem. Photobiol., B: Biol.* **33**, 3 (1996).
137. J. A. Maclaren and B. Milligan, *Wool Science: The Chemical Reactivity of the Wool Fibre*, Science Press, Marrickville, NSW, Australia, 1981, p. 85.
138. P. A. Duffield, IWS Review of Wool Bleaching Processes, International Wool Secretariat, Ilkley, U.K., 1996.
139. K. M. Thompson, W. P. Griffith, and M. Spiro, *J. Chem. Soc., Chem. Commun.* 1600 (1992).
140. A. W. Karunditu, C. M. Carr, K. Dodd, P. Mallinson, I. A. Fleet, and L. W. Tetler, *Text. Res. J.* **64**, 570 (1994).
141. J. Cegarra, J. Gacen, D. Cayuela, and M. C. Riva, *J. Soc. Dyers Colour.* **110**, 308 (1994).
142. A. Bereck, *Rev. Prog. Colorat.* **24**, 17 (1994).
143. G. Robinson and E. Nielsen, *Tineid Genera of Australia: Lepidoptera*, CSIRO Publications, Canberra, Australia, 1993.
144. D. E. Rivett, S. Ciccotosto, R. I. Logan, E. S. Nielsen, C. P. Robinson, L. G. Sparrow, and R. M. Traynier, In *Proc. 8th Int. Wool Text. Res. Conf.*, Wool Research Organisation of New Zealand (WRONZ), Christchurch, New Zealand, 1990, Vol. IV, p. 548.
145. R. J. Mayfield, *Text. Progress* **11**(4, 1 (1982); D. M. Lewis and T. Shaw, *Rev. Prog. Colorat.* **17**, 86 (1987).
146. P. I. Norman and R. Seddon, *J. Soc. Dyers Colour.* **107**, 215 (1991).
147. J. Barton, *Intern. Dyer*, 14 (Sept. 2000).
148. T. Zabel, J. Seager, and S. D. Oakley, Proposed Environmental Quality Standards For List 2 Substances in Water-Mothproofing Agents, Report TR261, Water Research Center, U.K., 1988.
149. T. Shaw, In *Proc. 8th Int. Wool Text. Res. Conf.*, Wool Research Organisation of New Zealand (WRONZ), Christchurch, New Zealand, 1990, Vol. IV, p. 533.
150. *Anon, Wool Rec.* **154**, 25 (Mar. 1995).
151. D. Allenach, In *Proc. 8th Int. Wool Text. Res. Conf.*, Wool Research Organisation of New Zealand (WRONZ), Christchurch, New Zealand, 1990, Vol. IV p. 568.
152. D. Allenach, *Wool Rec.* **151**, 35 (Mar. 1992).
153. R. W. Moncrieff, *Mothproofing*, Billing and Sons, Ltd., London, U.K., 1950, p. 70.
154. I. M. Russell, Combined Insect Resist and Rot-Resist Treatments for Wool Insulation, CSIRO Division of Wool Technology Report G69, CSIRO, Geelong, Australia, May 1992.
155. I. M. Russell, In *Proc. 8th Int. Wool Text. Res. Conf.*, Wool Research Organisation of New Zealand (WRONZ), Christchurch, New Zealand, 1990, Vol. IV, p. 606.
156. *Anon, WRONZ News* **44**, 2 (2001).
157. Specification of Insect Resistance. E 10, The Woolmark Co., Australia, 2001.
158. T. Shaw and M. A. White, in M. Lewin and S. B. Sello, eds., *Handbook of Fiber Science and Technology, Vol. II: Chemical Processing of Fibers and Fabrics*, Part B, Marcel Dekker, Inc., New York, 1984, Chapt. 5.
159. M. J. Koroskys, *Am. Dyes. Rept.* **60**(5), 48 (1971).
160. L. Benisek, *Text. Manuf.* **99**, 36 (Jan.–Feb. 1972); *Melliand Textilber.* **53**, 931 (1972).
161. L. Benisek, *J. Text. Inst.* **65**, 102 and 140 (1974).
162. P. Gordon and L. Stephen, *J. Soc. Dyers Colour.* **90**, 239 (1974).

GENERAL READING

Textile Terms and Definitions, 10th ed., Textile Institute, Manchester, England, 1996.
W. E. Morton and J. W. S. Hearle, *Physical Properties of Textile Fibres*, 3rd ed., The Textile Institute, Manchester, U.K., 1993.
P. Alexander, R. F. Hudson, and C. Earland, *Wool Its Chemistry and Physics*, 2nd ed., Chapman and Hall, London, 1963.

J. A. Maclaren and B. Milligan, *Wool Science: The Chemical Reactivity of the Wool Fibre*, Science Press, Marrickville, NSW, Australia, 1981.
R. S. Asquith, ed., *Chemistry of Natural Protein Fibers*, Plenum Press, New York, 1977.
A. Brearley and J. A. Iredale, *The Worsted Industry: An Account of the Worsted Industry and Its Processes from Fibre to Fabric*, Wira, Leeds, U.K., 1980.
D. M. Lewis, ed., *Wool Dyeing*, Society of Dyers and Colourists, Bradford, U.K., 1992.
K. R. Makinson, *Shrinkproofing of Wool*, Marcel Dekker, Inc., New York, 1979.
P. R. Brady, ed., *Finishing and Wool Fabric Properties: A Guide to the Theory and Practice of Finishing Woven Wool Fabrics*, CSIRO Division of Wool Technology, Victoria, Australia, 1997.
Proc. 1st Int. Wool Text. Res. Conf., Melbourne, Australia, 1955.
Proc. 2nd Int. Wool Text. Res. Conf., Harrogate, U. K., 1960.
Proc. 3rd Int. Wool Text. Res. Conf., Paris, 1965.
Proc. 4th Int. Wool Text. Res. Conf., San Francisco, 1970; Published in *Appl. Polym. Symp., No. 18*, Interscience Publishers, a Division of John Wiley & Sons, Inc., New York, 1971.
Proc. 5th Int. Wool Text. Res. Conf., Aachen, Germany, 1975.
Proc. 6th Int. Wool Text. Res. Conf., Pretoria, South Africa, 1980.
Proc. 7th Int. Wool Text. Res. Conf., Tokyo, 1985.
Proc. 8th Int. Wool Text. Res. Conf., Christchurch, NZ, 1990.
Proc. 9th Int. Wool Text. Res. Conf., Biella, Italy, 1995.

JOHN R. CHRISTOE
RON J. DENNING
DAVID J. EVANS
MICKEY G. HUSON
LESLIE N. JONES
PETER R. LAMB
KEITH R. MILLINGTON
DAVID G. PHILLIPS
ANTHONY P. PIERLOT
JOHN A. RIPPON
IAN M. RUSSELL
CSIRO Textile and Fibre Technology

XYLYLENE POLYMERS

Introduction

In a process capable of producing pinhole-free coatings of outstanding conformality and thickness uniformity through the unique chemistry of *p*-xylylene (PX) [502-86-3] (**1**), a substrate is simply exposed to a controlled atmosphere of pure gaseous monomer. The coating process is best described as a *vapor deposition polymerization* (VDP). The monomer molecule is thermally stable, but kinetically very reactive toward polymerization with other molecules of its kind. Although it is stable as a rarified gas, upon condensation it polymerizes spontaneously to produce a coating of high molecular weight, linear poly(*p*-xylylene) (PPX) [25722-33-2] (**2**). This article emphasizes recent VDP developments. There have been several reviews of the subject (1,2), which offer a more thorough treatment of early developments in the field.

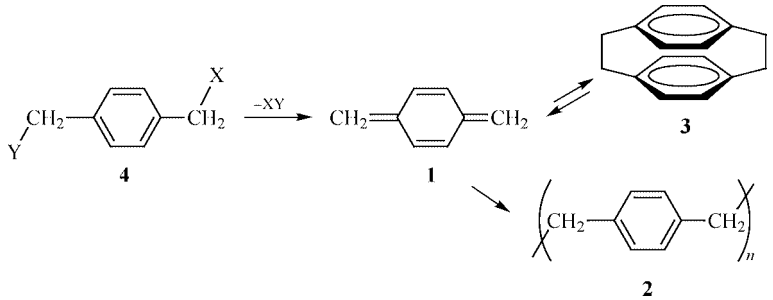

In the commercial Gorham process (3), the extremely reactive PX is conveniently generated by the thermal cleavage of its stable dimer, *cyclo*-di-*p*-xylylene

Encyclopedia of Polymer Science and Technology. Copyright John Wiley & Sons, Inc. All rights reserved.

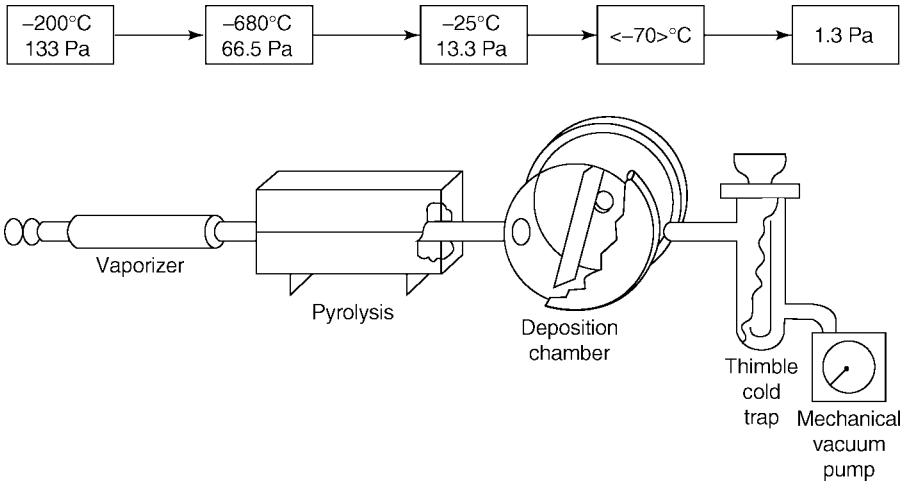

Fig. 1. Parylene deposition apparatus. To convert Pa to torr, multiply by 0.0075.

(DPX), a [2.2]paracyclophane [1633-22-3] (**3**). In many instances, substituents attached to the paracyclophane framework are carried through the process unchanged, ultimately becoming substituents of the polymer in the coating.

The process takes place in two stages that must be physically separate but temporally adjacent. Figure 1 presents a schematic of a typical parylene deposition process, also indicating the approximate operating conditions.

The PPXs formed as coatings in the Gorham process are referred to generically as the parylenes. The terms Parylene N [25722-33-2], Parylene C [9052-19-1], and Parylene D [52261-45-7] refer specifically to polymers produced as coatings by the Gorham process using the dimers DPXN, DPXC [28804-46-8], and DPXD [30501-29-2], respectively, originally marketed by Union Carbide Corp.

The parylene process has certain similarities with vacuum metallizing. The principal distinction is that truly conformal parylene coatings are deposited even on complex, three-dimensional substrates, including on sharp points and in hidden or recessed areas. Vacuum metallizing, on the other hand, is a line-of-sight coating technology. Whatever areas of the substrate cannot be "seen" by the evaporation source are "shadowed" and remain uncoated.

The *p*-xylylene species plays a central role in the coating process itself as well as in the making of the dimers which are used as feedstocks for the coating process. Polymers and dimers have both been made from precursor *p*-xylene compounds (**4**) featuring a variety of X and Y leaving groups. The conditions of the reaction determine the relative amounts of the resulting dimeric or polymeric products. Dilution is of course the key element in any procedure which offers a high yield of dimer.

The modest commercial success the *p*-xylylene dimer based Gorham process has achieved to date is readily attributed to the fact that thermal cleavage of cyclic dimer produces the *p*-xylylene monomer in essentially quantitative yield, while at the same time producing no gaseous by-products. In a gas-to-solid coating process, any gaseous entities generated from the leaving groups X and Y, necessarily formed in volumes comparable to the volume of the monomeric *p*-xylylene

generated, would at the very least need to be exhausted through the pumping system, thereby slowing the process down. Moreover, certain of the most effective leaving groups XY, such as halogens or halogenide acids, would create a corrosion hazard both for any sensitive substrates to be coated and for the deposition equipment itself.

Gorham Process Monomers

The eight-carbon monomer PX is generated in the first stage of the parylene process by heating gaseous dimer as it passes through a high temperature zone. Its intermediacy in the process was deduced by the earliest investigators. Apprehending the unusual properties of PX is an important aid to understanding the unique features of the coating process.

Chemical Evidence for PX Monomer. Establishing early on that PX is indeed the pyrolysis product, rather than the molecule formed by breaking only one of the original dibenzyl bonds, the dimer diradical (**5**), would prove to be an important development.

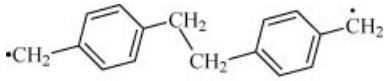

5

When the pyrolysis gases are quenched with a molar excess of iodine vapor, a yield of greater than 50% *p*-xylylene diiodide is recovered. The observation of this effect offered the first direct chemical support for the idea that DPX pyrolysis results in PX (**1**) (4).

Moreover, where *ar*-acetyldi-*p*-xylylene [10029-00-2] (**6**) is pyrolyzed, by adjusting temperatures in the deposition region, it is possible to isolate two different polymeric products, ie, poly(acetyl-*p*-xylylene) [67076-72-6] (**8**) and poly(*p*-xylylene) (PPX) (**2**). This of course requires the cleavage of the original dimer into two fragments.

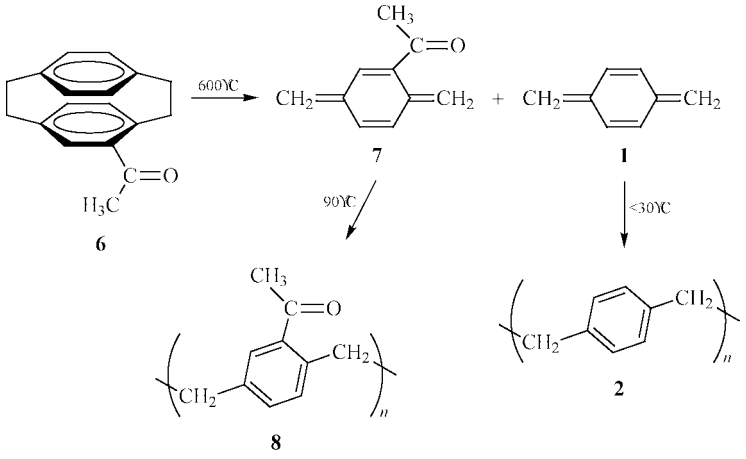

6 **7** **1** **8** **2**

Experiments with monoethyl and monocarbomethoxy di-*p*-xylylene (5) gave similar results. These experiments do not, however, shed any light on whether the rupture of the methylene–methylene bonds in the dimer upon pyrolysis is simultaneous or sequential.

Only one exception to the clean production of two monomer molecules from the pyrolysis of dimer has been noted. When α-hydroxydi-*p*-xylylene (**9**) is subjected to the Gorham process, no polymer is formed, and the 16-carbon aldehyde (**10**) is the principal product in its stead, isolated in greater than 90% yield. This transformation indicates that, at least in this case, the cleavage of dimer proceeds in stepwise fashion rather than by a concerted process in which both methylene–methylene bonds are broken at the same time. This is consistent with the predictions of Woodward and Hoffmann from orbital symmetry considerations for such [6 + 6] cycloreversion reactions in the ground state (**6**).

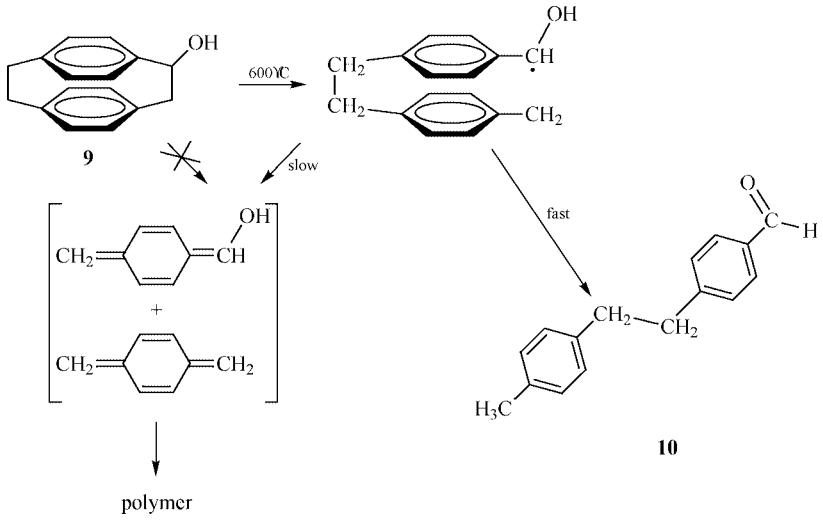

Monomer Properties. Despite difficulties involved in studying it owing to its great reactivity, a great deal is known about the structure of the parylene process monomer PX: the eight-carbon framework is planar (7); The molecule is diamagnetic, ie, all electron spins are paired in the ground state (spectroscopically, a singlet). Although many have ascribed its reactivity to its so-called biradical nature, the true biradical (triplet) form (**11**) of the molecule, an electronically excited state, is substantially more energetic, estimated at ca 50 kJ/mol (12 kcal/mol), and therefore cannot contribute to the monomer at equilibrium to any appreciable extent, even at pyrolysis temperatures. The PX molecule is instead a conjugated tetraolefin whose particular arrangement gives it extreme reactivity at its end carbons.

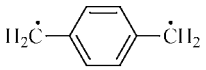

11

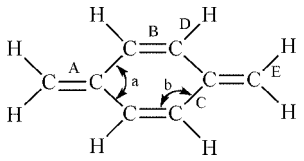

Fig. 2. Structure of PX monomer molecule from electron diffraction (9). Bond lengths: C═C A = B + 0.1381 ± 0.008; C—C, C = 0.1451 ± 0.0007 nm; C—H, D = E = 0.1116 ± 0.0035 nm. Bond angles: a = 122.2 ± 3.7°, b = 118.9 ± 1.9°.

This extreme reactivity of PX has precluded many experimental approaches that otherwise would have been useful in studying it. Most of the present structural knowledge has been gleaned from spectroscopic studies and molecular orbital calculations. A noteworthy exception is an electron diffraction study (8) in which an electron beam was directed at a stream of gaseous PX, generated much as it is in the parylene process, issuing from a nozzle in a specially constructed apparatus. The results of the study are shown in Figure 2. Although the study was unable to resolve the lengths of the two different C═C and C—H bonds, it clearly distinguished between the C—C and C═C bond lengths. Thus *p*-xylylene is experimentally demonstrated to have an olefinic geometry rather than that of an aromatic biradical.

By trapping PX at liquid nitrogen temperature and transferring it to THF at −80°C, the ^{1}H NMR spectrum could be observed (10). It consists of two sharp peaks of equal area at chemical shifts of 5.10 and 6.49 ppm downfield from tetramethylsilane (TMS). The fact that any sharp peaks are observed at all attests to the absence of any significant concentration of unpaired electron spins, such as those that would be contributed by the biradical (**11**). Furthermore, the chemical shift of the ring protons, 6.49 ppm, is well upfield from the typical aromatic range and more characteristic of an olefinic proton. Thus the olefin structure (**1**) for PX is also supported by NMR.

A particularly useful property of the PX monomer is its enthalpy of formation. Conventional means of obtaining this value, such as through its heat of combustion, are, of course, excluded by its reactivity. An experimental attempt was made to obtain this measure of chemical reactivity with the help of ion cyclotron resonance; a value of 209 ± 17 kJ/mol (50 ± 4 kcal/mol) was obtained (11). Unfortunately, the technique suffers from lack of resolution in addition to experimental imprecision. It is perhaps better to rely on molecular orbital calculations for the formation enthalpy. Using a semiempirical molecular orbital technique, which is tuned to give good values for heat of formation on experimentally accessible compounds, the heat of formation of *p*-xylylene has been computed to be 234.8 kJ/mol (56.1 kcal/mol) (12).

Successful *p*-Xylylene VDP Monomers. Within the limits mentioned above, it is frequently possible, and often desirable, to modify the *p*-xylylene monomer by attaching to it certain substituents. Limitations on such modifications lie in three areas: reactivity, performance in the coater, and cost.

Reactivity. Although the reactivity which enables the gas–solid polymerization to proceed is a characteristic of the eight-carbon *p*-xylylene tetraolefin system, it is possible to subdue that reactivity. For example, by attaching

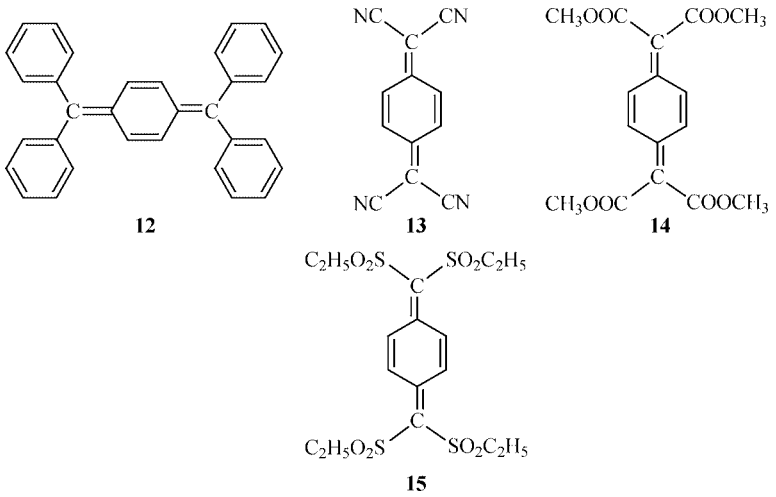

Fig. 3. Isolatable *p*-xylylene derivatives: **12**, Thiele's hydrocarbon—1904 [26392-12-1]; **13**, tetracyanoquinodimethane [1518-16-7] (TCNQ); **14**, tetrakis(methoxycarbonyl)-quinodimethan [65649-20-9]; **15**, tetrakis(ethylsulfonyl)quinodimethan [84928-90-5].

electron-withdrawing substituents to the alpha positions and thereby further delocalizing the π-electrons of the highly reactive *p*-xylylene nucleus, it is in several instances possible to prepare *p*-xylylenes that are so stable that they can be isolated and handled as normal organic compounds (Fig. 3). These sorts of substitutions must of course be avoided if the goal is to make polymer.

It is also possible to interfere with the polymerization by attaching at the alpha positions either too many groups, or groups which are too bulky. Four chlorine atoms (13) or four methyl groups (14) seem to be sufficient to hinder the production of polymer. These crowded *p*-xylylene monomers can be polymerized, but not through a VDP process.

Thus, except for electron-withdrawing or bulky substituents, at least from the standpoint of reactivity toward polymerization, modification by most other substituents is possible.

Performance in Coater. The modified monomer should perform well in commercial deposition equipment. Performance considerations include the growth rate of the coating, the uniformity of thickness of the coating over the chamber volume, and the efficiency with which the dimer is converted to useful coatings on the substrates.

An important further constraint is the fact that economic considerations in the construction of deposition equipment normally lead to a preference for an ambient-temperature deposition chamber. Control of deposition temperature is possible, but it adds to both equipment expense and operational complexity.

The vapor pressure of a parylene monomer is a prime factor in determining how rapidly a coating grows when exposed to an atmosphere of monomer at a given pressure. Vapor pressure is reduced as molecular weight increases, thereby increasing the monomer's tendency to condense and, along with it, increasing the VDP growth rate. The presence of polar functionality in the molecule further

depresses vapor pressure. But too low a vapor pressure makes it difficult to transport gaseous monomer from point to point in the deposition chamber. Hence, some optimum value of monomer volatility is expected.

The widely used Parylene C owes its popularity principally to the room-temperature volatility of its monomer. The Parylene C monomer, chloro-*p*-xylylene, has become the de facto performance standard. By comparison, the Parylene N monomer, *p*-xylylene itself, is too volatile and would perform better in a sub-ambient-temperature deposition system. The Parylene D monomer, dichloro-*p*-xylylene [85586-88-5] is too heavy, and causes distribution problems in larger deposition systems.

Cost. It is necessary to produce the feedstock from which the monomer is generated, viz, the dimer, at a cost which can be supported by the commercial application, and yet allow it to be economically competitive with all other alternative ways to achieve the same end result. This factor often, but not always, seriously limits the amount of effort that can be put into dimer synthesis and purification.

Other, Related Processes

VDP processes using means other than the pyrolytic cleavage of DPX (Gorham process) to generate the reactive monomer are also known, although none are practiced commercially at the time of this writing (ca 1997).

Photopolymerization and Plasma Polymerization. The use of ultraviolet light alone (15,16) as well as the use of electrically excited plasmas or glow discharges to generate monomers capable of undergoing VDP have been explored. The products of these two processes, called plasma polymers, continue to receive considerable scientific attention. Interest in these approaches is enhanced by the fact that the feedstock material from which the monomer capable of VDP is generated is often inexpensive and readily available. In spite of these widespread scientific efforts, however, commercial use of the technologies is quite limited.

When *p*-xylene is used as the monomer feed in a plasma polymer process, PX may play an important role in the formation of the plasma polymer. The plasma polymer from *p*-xylene closely resembles the Gorham process polymer in the infrared, although its spectrum contains evidence for minor amounts of nonlinear, branched, and cross-linked chains as well. Furthermore, its solubility and low softening temperature suggest a material of very low molecular weight (17).

VDP Polyimides. Polyimide films have also been prepared by a kind of VDP (18). The poly(amic acid) layer is first formed by the coevaporation and condensation of two monomers, followed by copolymerization on the substrate. The imidization is carried out in a separate baking step (see POLYIMIDES).

***o*-Xylylene/BCB.** Thermosetting resins based on benzocyclobutene (BCB)

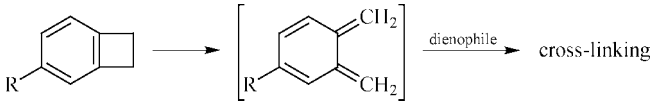

chemistry have been reported (19,20). In these condensed phase cures, the *o*-xylylene isomer is the key reactive intermediate. From the behavior of this energetically similar ortho isomer, the value of the para configuration's rendering any ring closure reaction—analogous to cyclobutene formation from the ortho isomer—geometrically forbidden can be appreciated.

Dimer

In contrast to the extreme reactivity of the monomeric PX (**1**) generated from it, the dimer DPX (**3**) feedstock for the parylene process is an exceptionally stable compound. Because of their chemical inertness, dimers in general do not exhibit shelf-life limitations. Although a variety of substituted dimers are known in the literature, at present only three are commercially available: DPXN, DPXC, and DPXD, which give rise to Parylene N, Parylene C, and Parylene D, respectively.

The unsubstituted C-16 hydrocarbon, [2.2]paracyclophane (**3**), is DPXN. Both DPXC and DPXD are prepared from DPXN by aromatic chlorination and differ only in the extent of chlorination; DPXC has an average of one chlorine atom per aromatic ring and DPXD has an average of two.

Manufacture. For the commercial production of DPXN (di-*p*-xylylene) (3), two principal synthetic routes have been used: the direct pyrolysis of *p*-xylene (**4**, X = Y = H) and the 1,6-Hofmann elimination of ammonium (HNR_3^+) from a quaternary ammonium hydroxide (**4**, X = H, Y = NR_3^+). Most of the routes to DPX share a common strategy: PX is generated at a controlled rate in a dilute medium, so that its conversion to dimer is favored over the conversion to polymer. The polymer by-product is of no value because it can neither be recycled nor processed into a commercially useful form. Its formation is minimized by careful attention to process engineering. The chemistry of the direct pyrolysis route is shown in equation 1:

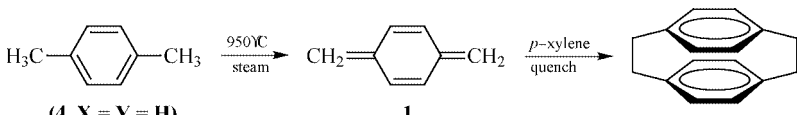

(1)

First, *p*-xylene is dehydrogenated pyrolytically in the presence of steam at about 950°C to give *p*-xylylene (PX), which in turn forms di-*p*-xylylene (DPX) when quenched in liquid xylene. The xylene is recycled to the pyrolysis vessel. Yields and conversion efficiency are satisfactory. However, several engineering challenges need to be overcome, including the choice of a suitable diluent; establishing optimal residence time, vapor velocity, and operating pressure during pyrolysis; and the design and construction of novel equipment to withstand the highly corrosive reaction environment.

The Hofmann elimination route, of which many versions exist, can be carried out at much lower temperatures in conventional equipment. The PX is generated by a 1,6-Hofmann elimination of amine from a quaternary ammonium hydroxide in the presence of a base. This route gives yields of 17–19%. Undesired polymeric

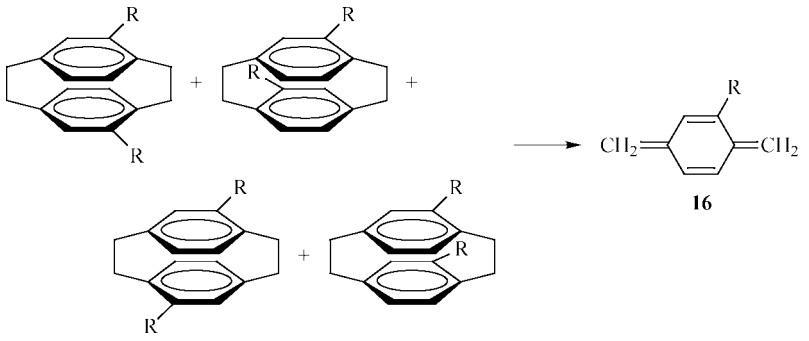

Fig. 4. Isomeric dichloro[2.2]paracyclophanes produce the same xylylene.

products can be as high as 80% of the product. In the presence of a polymerization inhibitor, such as phenothiazine, DPXN yields can be increased to 50%.

In the 1,6-elimination of *p*-trimethylsilylmethylbenzyltrimethylammonium iodide with tetrabutylammonium fluoride, yields as high as 56% have been reported (21). The starting materials are not readily accessible, however, and are costly.

The yield can be raised to 28% if the Hofmann elimination is conducted in the presence of a water-soluble copper or iron compound (22). Further improvements up to 50% were reported when the elimination was carried out in the presence of ketone compounds (23). Further beneficial effects have been found with certain cosolvents, with reported yields of greater than 70% (9).

DPXC and DPXD. The economic pressure to control dimer costs has had an important effect on what is in use today (ca 1997). Attaching substituents to the ring positions of a [2.2]paracyclophane does not proceed with isomeric exclusivity. Indeed, isomeric purity in the dimer is not an essential requirement for obtaining isomeric purity, eg, monosubstituted monomer, in the pyrolysis. Any mixture of the four possible heteronuclearly disubstituted dichloro[2.2]paracyclophanes, will, after all, if pyrolyzed produce the same monomer molecule, chloro-*p*-xylylene [10366-09-3] (**16**) (Fig. 4).

Although DPXC and DPXD prepared by the chlorination of DPXN are relatively complex mixtures, after pyrolytic cleavage the resulting mixture of monomers is considerably simpler. Thus DPXC, when pyrolyzed, gives predominantly monochloro PX, which is accompanied by small but significant amounts of PX and dichloro PX. The resulting polymer, Parylene C, consequently has an average of about one chlorine atom per repeat unit. However, it contains significant amounts of unchlorinated, as well as dichlorinated, repeat units.

DPXC and DPXD are prepared from DPXN by chlorinating to different extents. The conditions are controlled to favor aromatic ring chlorination to the exclusion of the free-radical chlorination of the ethylene bridges. However, the chlorination products are complex mixtures of the homologues DPXN, monochloro DPX, dichloro DPX, trichloro DPX, and tetrachloro DPX, and even higher homologues, as well as the several possible isomers of each.

New synthetic routes for the preparation of homologously pure dichloro DPX and tetrachloro DPX have been reported through the 1,6-Hofmann elimination of

Table 1. Properties of Parylene Dimers

Dimer	Melting point, °C	Density, g/cm^3
DPXN	284[a]	1.22
DPXC	140–160[b]	1.30
DPXD	170–195[b]	1.45

[a] Decomposes.
[b] Mixture of homologues and their isomers.

chlorinated *p*-methylbenzyltrimethylammonium hydroxide. In the case of dichloro DPX, yields of 30% were reported (24). In the presence of ketone compounds, yields were increased to 50% (23).

Purification. Unsubstituted di-*p*-xylylene (DPXN) is readily purified by recrystallization from xylene. It is a colorless, highly crystalline solid. The principal impurity is polymer, which fortunately is insoluble in the recrystallization solvent and easily removed by hot filtration.

In purifying DPXC and DPXD, care must be taken not to disturb the homologue composition, so that product uniformity is maintained. For example, a recrystallization of DPXC from ethanol would give a higher melting, more crystalline dimer material, at the expense of a decrease in yield owing to the removal of otherwise useful isomers, but the polymer made from it would not be identical to the historical Parylene C, as defined by its preparation from the chlorination mixture. The real purification issues are the removal of insoluble residues and any components that contain aliphatic side-chain chlorine. Although ring-substituted chlorine is stable, side-chain chlorine can give rise to hydrogen chloride gas under the conditions of the parylene process, or subsequent to it, which in certain applications could initiate substrate corrosion. Fortunately, the aliphatic chlorine problem can be minimized by proper attention to process detail.

Properties. The DPXs are all crystalline solids; melting points and densities are given in Table 1. Their solubility in aromatic hydrocarbons is limited. At 140°C, the solubility of DPXN in xylene is only about 10%. DPXC is more readily soluble in chlorinated solvents, eg, in methylene chloride at 25°C its solubility is 10%. In contrast, the corresponding figure for DPXN is 1.5%.

The structure of DPXN was determined in 1953 from X-ray diffraction studies (25). There is considerable strain energy in the buckled aromatic rings and distorted bond angles. The strain has been experimentally quantified at 130 kJ/mol (31 kcal/mol) by careful determination of the formation enthalpy through heat of combustion measurements (26). The release of this strain energy is doubtless the principal reason for success in the particularly convenient preparation of monomer in the parylene process.

Polymer

The linear polymer of PX, poly(*p*-xylylene) (PPX) (**2**), is formed as a VDP coating in the parylene process. The energetics of the polymerization set it apart from

all other known polymerizations and enable it to proceed as a vapor deposition polymerization.

Thermodynamic Considerations. On the basis of the value for the enthalpy of formation of *p*-xylylene, ΔH_f^0 (PX), the enthalpy of polymerization, $\Delta H^0_{polym} = \Delta H_f^0$(PPX) ΔH_f^0(PX), can be estimated. No experimental combustion data are available for high molecular weight poly(*p*-xylylene) as it is formed in the parylene process, ΔH^0_f (PPX).

For crystalline [2.2]paracyclophane [(1,2), DPXN], a ΔH^0_f of +154.4 kJ/mol (+36.9 kcal/mol) is reported (26). The hypothetical transformation of crystalline DPXN into polymer is accompanied by the release of 129.7 kJ/mol (31.0 kcal/mol) of paracyclophane strain energy per mole of paracyclophane, and 12.6 kJ/mol (3.0 kcal/mol) per polymer repeat unit as a result of the bibenzyl hyperconjugative stabilization, which is permitted in the polymer but excluded by geometry in the dimer. Thus the standard enthalpy of formation for the hypothetical 100% crystalline poly(*p*-xylylene) is estimated to be −0.3 kJ/mol (−0.05 kcal/mol), assuming that the energies associated with crystallinity are the same in both cases. Although it might be acceptable to assume that such energies per repeat unit are similar in the crystalline polymer and crystalline dimer, Parylene N, as produced by the parylene process, is typically only about 57% crystalline. Using a value of 14.1 kJ/mol (3.37 kcal/mol) for the heat of fusion for poly(*p*-xylylene) (27), the standard formation enthalpy for Parylene N, as it is typically deposited in the parylene process, ΔH^0_f (Parylene N), is +5.7 kJ/mol (+1.4 kcal/mol).

In estimating the enthalpy of polymerization, the physical state of both starting monomer and polymer must be specified. Changes in state are accompanied by ethalpy changes. Therefore, they also affect the level of the polymerization enthalpy. The ΔH^0_f for *p*-xylylene previously mentioned is applicable to the monomer as an ideal gas. To make comparisons with other polymerization processes, most of which start with condensed monomer, a heat of vaporization for *p*-xylylene is needed. It is assumed herein that it is the same as that for *p*-xylene, 42.4 kJ/mol (10.1 kcal/mol). Thus the ΔH^0_f of the liquid monomer *p*-xylylene is 192.3 kJ/mol (46.0 kcal/mol).

The enthalpy of polymerization of unannealed (57% crystalline) Parylene N, as it is deposited, starting with liquid monomer, $\Delta H^0_{polym(lu)}$, is −186.6 kJ/mol (−44.6 kcal/mol). This is an exceptionally high value compared with those of other addition polymers, which generally fall in the −60 to −100 kJ/mol (−14.3 to −23.8 kcal/mol) range. It quantifies the vigor of the polymerization. Because the source of polymerization enthalpy is within the *p*-xylylene system, substituents affect it only to a minor extent. All parylenes are expected to have a similar molar enthalpy of polymerization. An experimental value for the heat of polymerization of Parylene C has appeared. Using the gas evolution from the liquid nitrogen cold trap to measure thermal input from the polymer, and taking advantage of a peculiarity of Parylene C at −196°C to polymerize abruptly, perhaps owing to the arrival of a free radical, a ΔH^0_{polym} of −152 ± 8 kJ/mol (−36.4 ± 2.0 kcal/mol) at −196°C was reported (28). The correction from −196°C to room temperature is estimated at −17 kJ/mol, bringing this experimental value for Parylene C closer to the calculated value for Parylene N. It is assumed that S_{polym} is 0 at 0 K (third law), 125 J/(mol · K) [30 cal/(mol · K)] at 298 K, and proportional to *T* in between—a

crude assumption, but appropriate to the current level of knowledge. Thus experiment and calculation are in harmony in quantifying the exceptional exothermicity of parylene polymerization (see THERMODYNAMIC PROPERTIES OF POLYMERS).

The thermodynamic ceiling temperature (29) T_c for a polymerization is computed by dividing the ΔH^0_{polym} by the standard entropy of polymerization, ΔS^0_{polym}. The T_c is the temperature at which monomer and polymer are in equilibrium in their standard states at 25°C (298.15 K) and 101.3 kPa (1 atm). (In the case of *p*-xylylene, such a state is, of course, purely hypothetical.) The T_c quantifies the binding forces between monomer units in a polymer and measures the tendency of the polymer to revert back to monomer. In other systems, the T_c indicates a temperature above which the polymer is unstable with respect to its monomer, but in the case of parylene it serves rather as a means of comparing the relative stability of the polymer with respect to its reversion to monomer. For computing the T_c, however, the standard entropies of polymerization are required.

The standard polymerization entropies can be estimated from the following. The standard entropy S^0 for PX as an ideal gas is computed by a group-contribution method (30) to be 310.6 J/(mol · K) [74.24 cal/(mol · K)]. The entropy of vaporization for PX is assumed to be the same as that of *p*-xylene, 104.7 J/(mol · K) [25.03 cal/(mol · K)] (31). Therefore, the S^0 for liquid PX is 205.9 J/(mol · K) [49.21 cal/(mol·K)]. Noting that the experimental specific heat C_p of PPX follows that of polystyrene over the range of 160 to 340 K (32), it can be assumed that the proportionality continues down to 0 K and that the factor 135/116 at 298 K can be applied to the known S^0 for polystyrene [$S = 128.5$ J/(mol · K) or 30.70 cal/(mol · K) (33). It follows that the S^0 for as-deposited 57% crystalline Parylene N is 149.5 J/(mol · K) [35.73 cal/(mol · K)]. Therefore, $\Delta S^0_{polym(g)} = -161.1$ J/(mol · K) [−38.50 cal/(mol · K)] and $\Delta S^0_{polym(l)} = -56.4$ J/(mol · K) [−13.4 8cal/(mol · K)].

The results of the above polymerization thermodynamics calculations for parylene are compared to similar data for typical addition polymers in Table 2. The T_c quantifies the stability of the polymer only with respect to reversion to monomer. When PPX is thermally degraded (ca 500°C), a mixture of degradation

Table 2. Entropies, Enthalpies, and Ceiling Temperatures for the Polymerization of Various Monomers at 25°C (298.15 K) and 101.3 kPa (1 atm)[a]

	Liquid			Gas		
Monomer	$-\Delta H^0$, kJ/mol[b]	$-\Delta S^0$, J/(mol · K)[b]	T_c, °C	$-\Delta H^0$, kJ/mol[b]	$-\Delta S^0$ J/(mol · K)[b]	T_c, °C
Ethylene	108.4	173.6	351			
Propylene	81.6	116.3	429			
Isoprene	74.9	101.3	467	101.3	187.0	268
Styrene	69.9	104.6	395	113.4	212.1	262
Methyl methacrylate	55.2	117.2	198			
α-Methylstyrene	35.1	103.8	65			
p-Xylylene	186.6	56.4	3035	229.1	161.1	1149

[a] Ref. 26.
[b] To convert J to cal, divide by 4.184.

products including hydrogen gas, *p*-xylene, toluene, and *p*-methylstyrene is observed (34), suggesting that the path taken in thermal degradation requires the cleavage of bonds other than those formed in the polymerization, very likely starting with the methylene C—H bond. Complete replacement of the methylene hydrogens in PPX with fluorine gives a polymer with substantially better stability at elevated temperatures (35).

The enthalpy liberated on the VDP of parylene is real and in an adiabatic situation causes a rise in temperature of the coated substrate. For Parylene C, 229.1 kJ/mol (54.7 cal/mol) corresponds to 1654 J/g (395 cal/g) whereas its specific heat at 25°C is only 1.00J/(g · K) [0.239 cal/(g · K)] (36). In most practical situations, however, the mass of parylene deposited is dwarfed by the substrate mass, and the heat of polymerization is dissipated within the coated substrate over the time required to deposit the coating with minimal actual temperature rise.

Polymerization Mechanism. The physical processes of condensation and diffusion must be considered along with the *p*-xylylene polymerization chemistry for a proper understanding of what happens microscopically during vapor deposition polymerization (37). These processes point to an important distinction between VDP and vacuum metallization, ie, that in the latter, adsorption is followed by a surface reorganization of the existing deposited material, and diffusion of incoming species through the bulk is nonexistent. In most parylene depositions, a coating forms from gaseous monomer under steady-state conditions.

Gaseous monomer is transported to the location within the coating where it is to be consumed to produce polymer by an initial condensation, followed by diffusion. The net flux of monomer molecules through the growth interface, ie, the outer boundary of the coating, between the gaseous and condensed phases, needed to sustain growth at a given rate can be readily calculated [for Parylene C, 10 μm/h requires $1.55 \times 10^{15}/(\mathrm{cm}^2 \cdot \mathrm{s})$]. Comparing a net flux so obtained with the flux of molecules that according to the kinetic theory of gases are striking the growth surface ($Z = PN_0/\sqrt{2\pi MRT}$) for the conditions typical of parylene deposition, a large difference (two or three orders of magnitude) is observed. For Parylene C monomer at a pressure of 1.3 Pa (10 μm Hg) and 25°C, $Z = 6.7 \times 10^{17}/(\mathrm{cm}^2 \cdot \mathrm{s})$. For each molecule that eventually enters the coating, some hundred or thousand molecules strike the growth interface. Those that condense and do not react must, of course, evaporate. The term "sticking coefficient" has sometimes been borrowed from vacuum metallization to describe this ratio of incident molecules to consumed molecules. However, the VDP situation is not adequately described by hard spheres bouncing off a growth interface. Every incident molecule spends at least some time in the polymeric coating phase beyond the growth interface before it is lost again to the gas phase.

Because most of the condensing molecules evaporate, condensation equilibrium at the growth surface can be assumed, to a good approximation. The concentration of monomer dissolved in the coating near the growth interface is, therefore, governed by Henry's law, and monomer concentration in polymer solution increases proportionately to the partial pressure of monomer in the gas phase. Furthermore, as the temperature is lowered, or as higher molecular weight monomers of lower volatility are selected, monomer concentration at the growth interface increases. In most practical situations, these Henry's law effects

Table 3. Threshold Condensation Temperatures T_{tc} for Substituted *p*-Xylylene Monomers

Monomer	T_{tc}, °C
p-Xylylene	30
2-Methyl-*p*-xylylene	60
2-Ethyl-*p*-xylylene	90
2-Chloro-*p*-xylylene	90
2-Acetyl-*p*-xylylene	130
2-Cyano-*p*-xylylene	130
2-Bromo-*p*-xylylene	130
Dichloro-*p*-xylylene	130

dominate in determining growth rates for VDP coatings by regulating monomer concentration within the coating. For each monomer, there exists a threshold condensation temperature, T_{tc}, above which the rate of growth of coating is, for all practical purposes, zero (Table 3), but this phenomenon is governed by the competition between initiation and propagation chemistries, discussed herein.

Once it is in "solution" in the coating, the monomer moves about in random directions by diffusion until it evaporates or is consumed by chemical reaction. The polymer molecules that have already grown to higher molecular weight cannot relocate appreciably owing to entanglement with their neighbors. The rate of diffusion of monomer through the polymer bulk is adequate for the participation of diffusive transport in the mechanism of VDP (ca 10^{-10} cm^2/s at room temperature). This can be confirmed in swelling-rate experiments with solvents having similar physical properties, such as *p*-xylene.

The monomer is consumed by two chemical reactions: initiation, in which new polymer molecules are generated, and propagation, in which existing polymer molecules are extended to higher molecular weight. In steady-state VDP, both reactions proceed continuously inside polymeric coating, in the reaction zone just behind the growth interface.

The first step of the initiation reaction is the coupling of two monomer molecules to form the dimer diradical (**5**). The formation of this diradical is energetically uphill, ie, the energy of two benzyl radicals is greater than that of two starting *p*-xylylene systems. The rate of destruction greatly exceeds the rate of formation. Only a trace concentration of the dimer diradical species exists at equilibrium. Further reaction of the dimer diradical with monomer gives more stable diradicals. In these subsequent transformations, a *p*-xylylene is converted into a benzene with a net stabilizing effect. At some stage of oligomerization, the resulting *n*-mer diradical becomes more stable than the *n* *p*-xylylene molecules from which it was constructed. At this point, the new polymer molecule is formed. Thus the overall order of the initiation reaction, the reaction in which new polymer molecules are generated, is some $n > 2$. Initiation chemistry requires no species other than monomer, another unusual aspect of the polymerization chemistry of *p*-xylylene.

The order *n* of the initiation reaction has an important influence on the manner in which the VDP occurs. Because monomer molecules, even in solution

at low concentration, are closer together in the condensed phase than they are in the gaseous phase, the rate of initiation is greater in the condensed phase than in the gaseous phase. The higher the order n, the more the condensed phase is favored. The order n, according to the mathematical model (37) of *p*-xylylene VDP, at the same time governs the effect of monomer pressure on growth rate at a given deposition temperature. The model predicts that growth rate should vary with the pressure raised to the power $(n + 3)/4$. Thus, if $n = 3$, the growth rate should be proportional to $p^{1.5}$. In an early attempt to determine the pressure dependence of parylene growth rate γ, an expression of $\gamma = kp^2$ was reported (38). A pressure exponent of 2 would be interpreted as an initiation order of $n = 5$. Although such a high order would favorably deemphasize "snow," consideration of the energetics of oligomeric *p*-xylylene diradicals would seem to place the order nearer to 3. Perhaps the early investigators did not anticipate a nonintegral order for pressure dependence. A more recent report (39) places n at 3 for Parylenes N and C, and 4 for Parylene D. Thus, with $n \geq 3$, the parylenes are more likely to form a continuous coating than a dust or a snow, the physical form of the product of a gas-phase polymerization. To the extent that snow is included in the formation of a coating (ie, dual-phase polymerization), haze develops.

In the propagation reaction, the monomer molecule reacts with an existing free-radical polymer chain end to make the chain one repeat unit longer. The polymer chains have two active ends, and they grow from both ends at the same time. Under normal coating conditions, the consumption of monomer by propagation must be much higher than its consumption by initiation to obtain high molecular weight polymer. In fact, the number-average molecular weight is determined by the proportion of monomer consumed by the two reactions, and is diminished by increases in deposition temperature or monomer partial pressure.

The concentration of monomer within the coating decreases approximately exponentially with distance from the growth interface. With this decrease in monomer concentration, the rates of initiation and propagation reactions also decrease. Moving back into the polymer from the growth interface, through the reaction zone where polymer is being manufactured, a region in which the polymer formation is essentially complete is gradually entered. Because initiation is of higher order in monomer concentration, it tends to occur closer to the growth interface than does propagation. Under conditions prevailing during a typical deposition, the characteristic depth of the reaction zone is a few hundred nanometers, and the maximum concentration of monomer, ie, the concentration at the growth interface, is of the order of a few tenths percent by weight. Thus the parylene polymerization takes place just behind the growth interface in a medium that is best described as a slightly swollen, solid polymer.

During the vapor deposition process, the polymer chain ends remain truly alive, ceasing to grow only when they are so far from the growth interface that fresh monomer can no longer reach them. No specific termination chemistry is needed, although subsequent to the deposition, reaction with atmospheric oxygen, as well as other chemical conversions that alter the nature of the free-radical chain ends, is clearly supported experimentally.

Polymer Properties. The single most important feature of the parylenes, that feature which dominates the decision for their use in any specific situation, is the VDP process by which they are applied. VDP provides the room-temperature

coating process and produces the films of uniform thickness, having excellent thickness control, conformality, and purity. The engineering properties of commercial parylenes once they have been formed are given in Table 4. As crystalline polymers, the parylenes retain useful physical integrity up to temperatures approaching their crystalline melting points. However, their glass-transition temperatures, T_g, the temperature spans over which the continuous amorphous phase, usually the minority phase, changes from a rigid, vitreous condition to a more flexible, rubbery condition, are probably in the vicinity of ambient temperature. In the case of PPX (Parylene N), careful measurements have established the T_g

Table 4. Typical Engineering Properties of Commercial Parylenes

Property	Parylene N	Parylene C	Parylene D	ASTM method
General				
Density, g/cm^3	1.110	1.289	1.418	D1505
Refractive index, $n^{23}{}_D$	1.661	1.639	1.669	
Mechanical				
Tensile modulus, GPa[a]	2.4	3.2	2.8	D882
Tensile strength, MPa[b]	45	70	75	D882
Yield strength, MPa[b]	42	55	60	D882
Elongation to break, %	30	200	10	D882
Yield elongation, %	2.5	2.9	3	D882
Rockwell hardness	R85	R80		D785
Coefficient of friction				D1894
Static	0.25	0.29	0.35	
Dynamic	0.25	0.29	0.31	
Thermal				
Melting point, °C	420	290	380	
Linear coefficient of expansion to 25°C × 10^5, K^{-1}	6.9	3.5		
Heat capacity at 25°C, J/(g · K)[c]	1.3[d]	1.0[e]		
Thermal conductivity at 25°C, W/(m · K)	0.12	0.082		
Electrical				
Dielectric constant				D150
60 Hz	2.65	3.15	2.84	
1 kHz	2.65	3.10	2.82	
1 MHz	2.65	2.95	2.80	
Dissipation factor				D150
60 Hz	0.0002	0.020	0.004	
1 kHz	0.0002	0.019	0.003	
1 MHz	0.0006	0.013	0.002	
Dielectric strength at 25 μm, MV/m				D149
Short time	275	220	215	
Step-by-step	235	185		
Volume resistivity at 23°C, 50% RH, Ω	1.4×10^{17}	8.8×10^{16}	2×10^{16}	D257

Table 4. (Continued)

Property	Parylene N	Parylene C	Parylene D	ASTM method
Surface resistivity at 23°C, 50% RH, Ω	1×10^{13}	1×10^{14}	5×10^{16}	D257
Barrier				
Water absorption, %	< 0.1	< 0.1	<0.1	D570
Water vapor transmission at 37°C, ng/(Pa · s · m)[f]	0.0012	0.0004	0.0002	E96
Gas permeability at 25°C, amol/(Pa · s · m)[g]				D1434
N_2	15.4	2.0	9.0	
O_2	78.4	14.4	64.0	
CO_2	429	15.4	26.0	
H_2S	1590	26.0	2.9	
SO_2	3790	22.0	9.53	
Cl_2	148	0.7	1.1	

[a]To convert GPa to psi, multiply by 145,000.
[b]To convert MPa to psi, multiply by 145.
[c]To convert J to cal, divide by 4.184.
[d]Refs. 25 and 30.
[e]Ref. 34.
[f]To convernt ng/(Pa · s · m) to g·mil/(100 in^2 · day) at 90% RH, 37°C, multiply by 1240.
[g]To convert amol/(Pa · s · m) to cm^3 (STP) mil/(100 in^2 · day · atm), multiply by 0.498.

to be centered at 13°C, the range over which T affects heat capacity measurements extending from 240 to 330 K (−33 to + 57°C) (27). Because they have similar backbone structures, other parylenes are expected to have similar T_gs, although no measurements taken with equal care exist. Earlier reports have quoted a somewhat higher (60–90°C) range for the entire family (5). In either case, the parylenes as prepared by their VDP process are further distinguished from conventional polymers in having been generated in a medium that is at least to some extent vitreous.

During formation, the motions of the parylene polymer chains in the vitreous medium are restricted. The properties of freshly deposited parylenes, therefore, generally differ from those that have been aged or annealed. Restricted polymer chain motion during VDP severely limits their ability to organize into crystallites, and consequently freshly deposited parylenes are metastable. With the passage of time, and sooner if heated, they will reorganize into a thermodynamically more satisfactory configuration, increasing crystallinity. Certain physical properties of freshly deposited parylenes therefore can be expected to change upon aging or annealing. Of the commercial materials, Parylene C, perhaps as a result of the asymmetry of its repeat unit, is particularly subject to modifications subsequent to its initial formation.

Mechanical Properties. Many of the mechanical properties of the parylenes are similar to those of other conventional plastics. The values in Table 4 are typical of those quoted for the parylenes, but in any particular case can vary with aging or annealing. In an outstanding instance of this effect, the 200% elongation quoted for Parylene C is the value commonly observed on the freshly

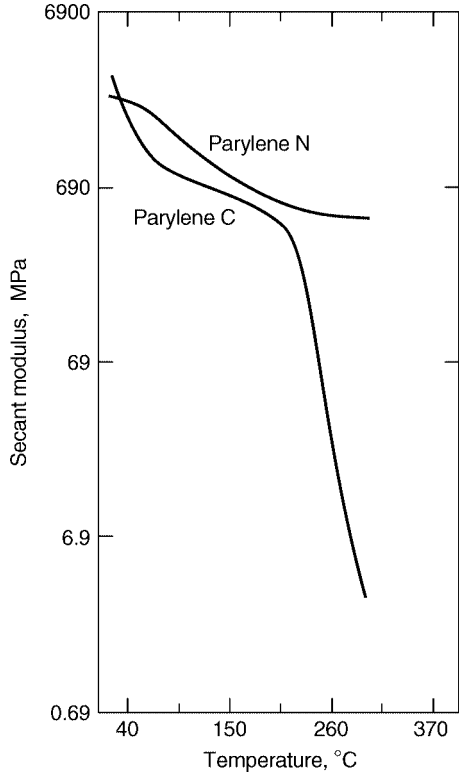

Fig. 5. Stiffness–temperature behavior of Parylenes N and C. To convert MPa to psi, multiply by 145.

deposited material. It drops dramatically as crystallinity builds. In general, an increase in crystallinity with aging or annealing results in a lowering of elongation to break and an increase in modulus and strength. The variation in mechanical rigidity of the parylenes as temperature increases is shown in Figure 5, which plots the logarithm of the secant modulus, a measure of stiffness, vs temperature. Generally, a small decrease in rigidity occurs near ambient temperature as the glass transition is traversed. Significant rigidity is then retained up to the point where the crystallites begin to melt.

It has been reported that Parylene N is deposited in a state of compressive stress (40). The inherent stress is 18 MPa (2300 psi) and is invariant with thickness. This congenital compressive stress can be removed and rendered tensile by a thermal cycle.

Electrical Properties. The bulk electrical properties of the parylenes make them excellent candidates for use in electronic construction. The dielectric constants and dielectric losses are low and unaffected by absorption of atmospheric water. The dielectric strength is quoted for specimens of 25 μm thickness because substantially thicker specimens cannot be prepared by VDP. If the value appears to be high in comparison with other materials, however, it should be noted that the usual thickness for such a measurement is 3.18 mm. Dielectric strength declines

Table 5. Dielectric Constants and Refractive Indexes of Parylenes

Parameter	Parylene N	Parylene C	Parylene D
Dielectric constant			
60 Hz	2.65	3.15	2.84
1 kHz	2.65	3.10	2.84
1 MHz	2.65	2.95	2.80
Refractive index			
n_D line	1.661	1.639	1.669
Squared	2.76	2.69	2.79

with the square root of increasing thickness. Viewed in this light, the dielectric strength of the parylenes is good, but not outstandingly high. The bulk resistivities are advantageously high because of the purity of the parylenes, their low moisture absorption, and in particular their freedom from the trace ionic impurities present in conventional polymers as residues. Such impurities might be the residues of the catalysts necessary for their formation. The surface resistivities are advantageously high in part because of their low affinity for atmospheric water. The experimental dependence of the electrical properties on temperature is shown in Figure 6.

The question of the value of the dielectric constant of the parylenes in the gigahertz range of frequencies is often of interest to designers of high frequency circuitry. Making such measurements on low loss, low dielectric constant, thin films is experimentally difficult, and no reliable data exist as of this writing (ca 1997). Fortunately, however, an indicator is available. For nonabsorbing, nonmagnetic materials such as the parylenes, the well-known Maxwell relation applies: at any particular frequency, the square of the index of refraction equals the relative permittivity, or dielectric constant (41). The refractive indices for the parylenes at the sodium D line (589 nm), a visible wavelength that corresponds to a frequency of 510 THz (5.1×10^{14} Hz), are shown in Table 5, along with their squares and the lower frequency measurement of dielectric constant. Because by virtue of the Maxwell relation the dielectric constants of the parylenes at the much higher frequency of visible light are close to those observed by conventional means, it seems likely that when reliable gigahertz dielectric constant measurements on the parylenes become available, similar values will be obtained.

Thermal Properties and Endurance. The heat capacity or specific heat, C_p is a quantity of theoretical thermodynamic significance as well as of practical importance. It has been determined for Parylene N over the temperature range of 220 to 620 K (-53 to $+ 347^\circ$C) (27,32).

Figure 7 gives the results of an experiment in which free-standing films were exposed to constant elevated temperatures in air-circulating ovens for periods of weeks to months; the failure criterion was a 50% loss in tensile strength. Because the test is destructive, each data point (failure time at a given temperature) required many specimens. In the degradation of many polymers, including the parylenes, tensile strength is maintained until chain scission has reduced molecular weight to the point at which entanglement is no longer a factor in

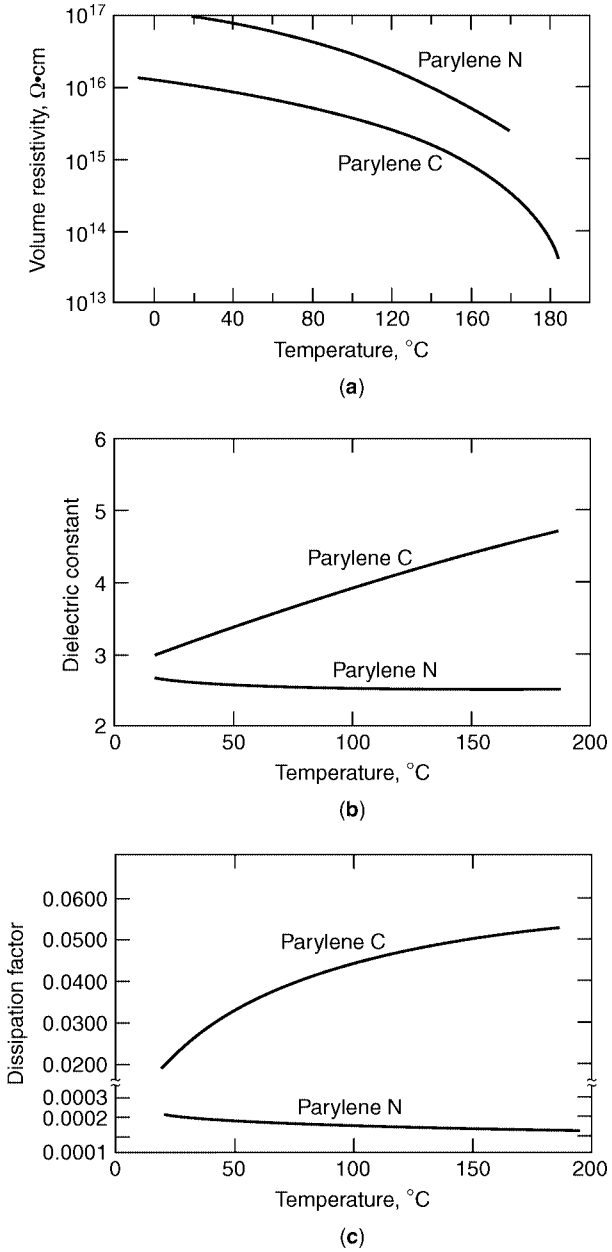

Fig. 6. Variation of electrical properties of Parylenes N and C with temperature.

determining physical properties. Beyond that point it drops abruptly. Thus despite the relatively large variance in tensile strength measurements, the 50% loss criterion allows a reasonably precise location of end of useful life on a log time scale (Fig. 8). The data of Figure 7 suggest that Parylenes N, C, and D perform in air without significant loss of physical properties for 10 years at 60, 80, and 100°C,

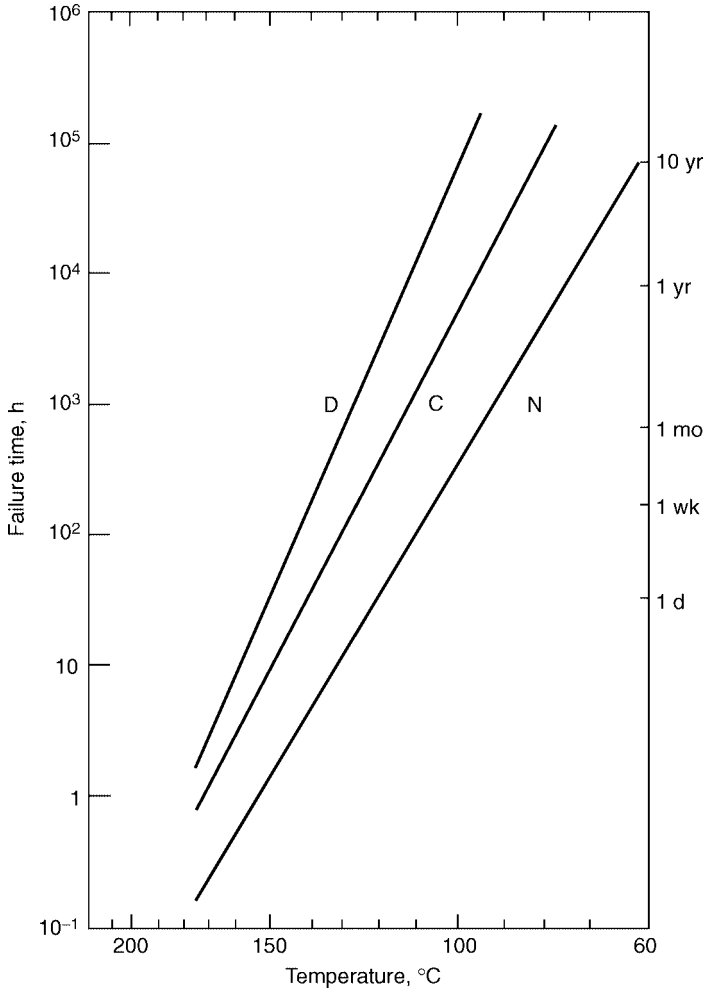

Fig. 7. Useful lifetime of Parylenes N, C, and D as a function of temperature in air. Failure = 50% loss in tensile strength.

respectively. Clearly, these data can justifiably be made to serve only as a guide for considering the parylenes for a specific application. Questions of thermal endurance tend to have no clear-cut answers. In situations where performance may be marginal, there is no substitute for retesting under conditions more directly relatable to the application.

Degradation. The most important mode of degradation for parylenes is oxidative chain scission. Significantly, hydrolytic degradation is chemically impossible. Oxidative degradation limits the use of parylenes at elevated temperatures in many common applications. Figure 9 shows the effect of exposure to elevated temperature in air or in vacuum on elongation to break, an indicator of toughness or lack of brittleness. The data are given for Parylene C, which suffers substantial change in mechanical properties as the freshly deposited material is annealed.

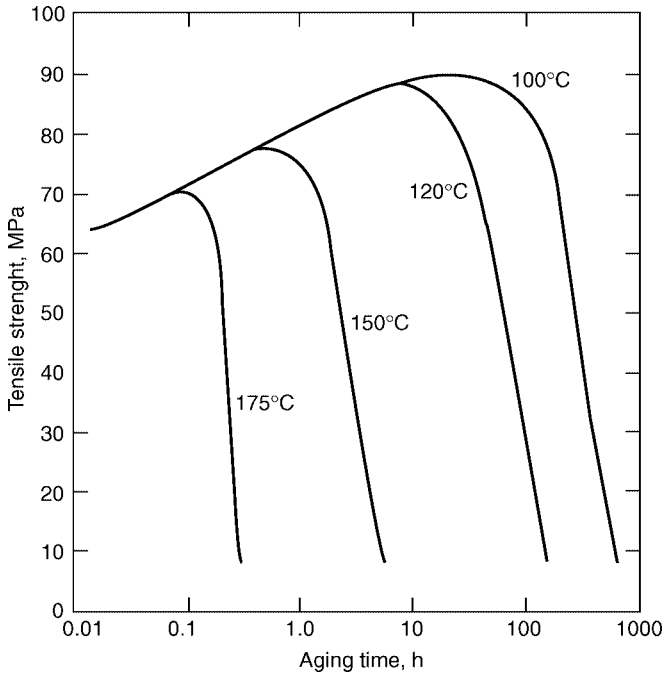

Fig. 8. Tensile strength of Parylene C on aging at elevated temperature. To convert Pa to psi, multiply by 0.145×10^3.

Aging in air at 150°C for ca 100 h causes the elongation to break to drop from its initially very high value to 0, at which point the specimen is mechanically useless. Aging in vacuum at yet higher temperatures (265°C) for a similar length of time gives a stronger, more rigid, stabilized material with 15% elongation at break, the result of annealing.

For applications where oxygen can be excluded, eg, in outer space, Figure 10 shows that 10-year-use projections exceed 200°C for Parylenes N, C, and D. Conventional antioxidants, incorporated during or after VDP, can extend the life of the parylenes at elevated temperatures (42,43).

Another factor in oxidative degradation is ultraviolet radiation, of which sunlight is a rich source. The oxidation of parylene appears to be enhanced by ultraviolet radiation. Ozone may play a mechanistic role in the ambient-temperature exposure of parylenes to ultraviolet radiation in the presence of oxygen. For the best physical endurance, exposure of the parylenes to ultraviolet light must be minimized.

Barrier Properties. The bulk barrier properties of parylenes are among the best of organic polymeric coatings. The data in Table 4 are the results of tests conducted some time ago, and certain entries seem unaccountably high, particularly the values for the permeability of Parylene N by SO_2 and H_2S. Because film damage might have been the cause of these high test values, experimental confirmation is advisable. More recent values for water transport rates in Parylene C films are available over the temperature range of 20–55°C in a comparative

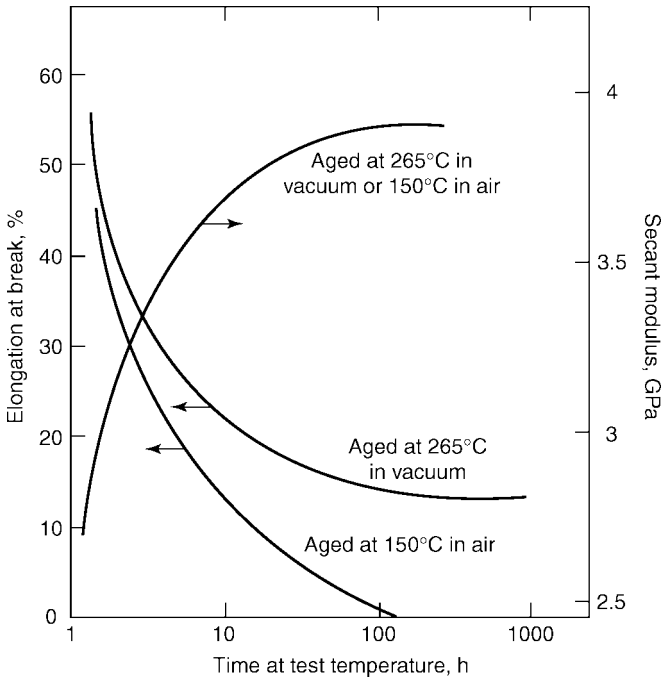

Fig. 9. Effect of temperature on the flexibility of Parylene C in air and vacuum. To convert GPa to psi, multiply by 145,000.

study which includes Mylar A and Kapton H (44). Similar information is provided for Parylene D in a study over the temperature range of 30–80°C (45).

Spectral and Optical Properties. The parylenes do not absorb visible light, and absorb only at the shorter wavelength, high energy end of the ultraviolet range (Fig. 11). Such absorption is expected for the electronic system of the parylenes' benzene ring. Films and coatings are colorless in the visible, becoming opaque to sufficiently short wavelength uv light.

The infrared transmission spectra of Parylenes N, C, and D are compared in Figure 12. Infrared spectra can be used to distinguish among sample films of the three commercial materials should a practical question of identity arise. The spectra in Figure 12 are taken on films of ca 18 μm thickness, which gives a good picture of a typical organic film in the standard infrared presentation format. It is, however, thicker than normally encountered in a typical parylene application. The amount of incident light absorbed at any given wavelength is predictably less than that indicated by the ordinate of Figure 12.

Interference effects, which arise because of the extraordinary uniformity of thickness of the film over the spectrometer sample beam, superimposed on the absorption of incident light by parylene films, can be observed. Experimentally, a sinusoidal undulation of the baseline of the spectrum is seen, particularly in the spectral regions where there is little absorption by the sample. These so-called "interference fringe" excursions can amount to some 15–20% transmission and are uniformly spaced in frequency. Larger excursions indicate greater uniformity

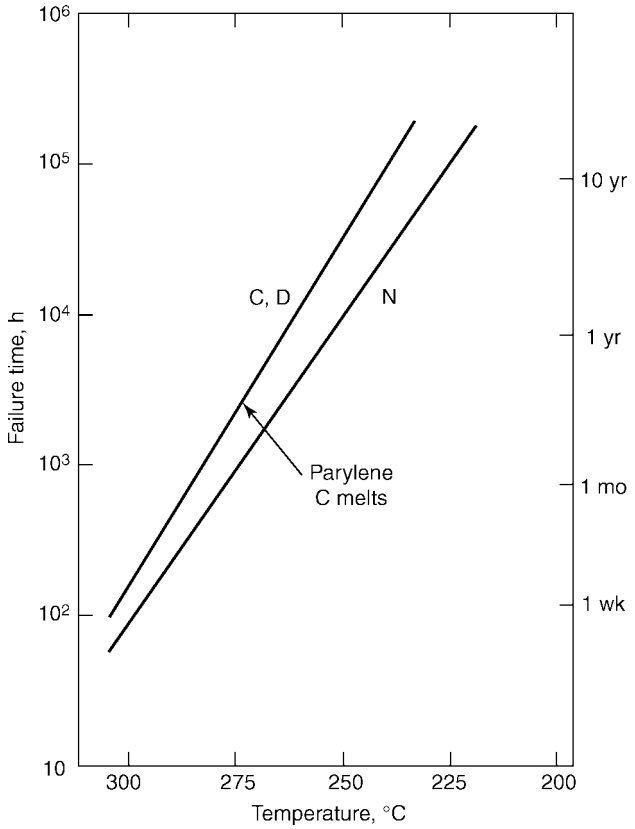

Fig. 10. Long-term effect of aging in vacuum on flexibility of Parylenes C, D, and N at elevated temperature. Failure = 50% loss in tensile strength.

in thickness. Such fringes are seen toward the left side of the experimental spectra of Figure 12. Although interference phenomena are also encountered experimentally in the visible and ultraviolet regions, their effects have been removed in the consolidation and replotting of the data of Figure 11. In transmission spectra, at the top of the interference fringes (the wavelengths of the sinusoidal maxima), constructive interference occurs in which all incident light that is not absorbed appears for detection. At the fringe troughs (the wavelengths of the sinusoidal minima), a condition of destructive interference exists, at which a portion of the incident beam is reflected back toward the source, thereby escaping detection even though it is not absorbed by the sample. By observing the wavelengths at which constructive interference occurs, the approximate thickness of the sample can be determined by using the expression

$$d = \frac{m\lambda_1\lambda_2}{2\,R(\lambda_1 - \lambda_2)}$$

where λ_1 and λ_2 are any two wavelengths at which interference transmission maxima (ie, constructive fringes) exist, separated by m-1 intervening

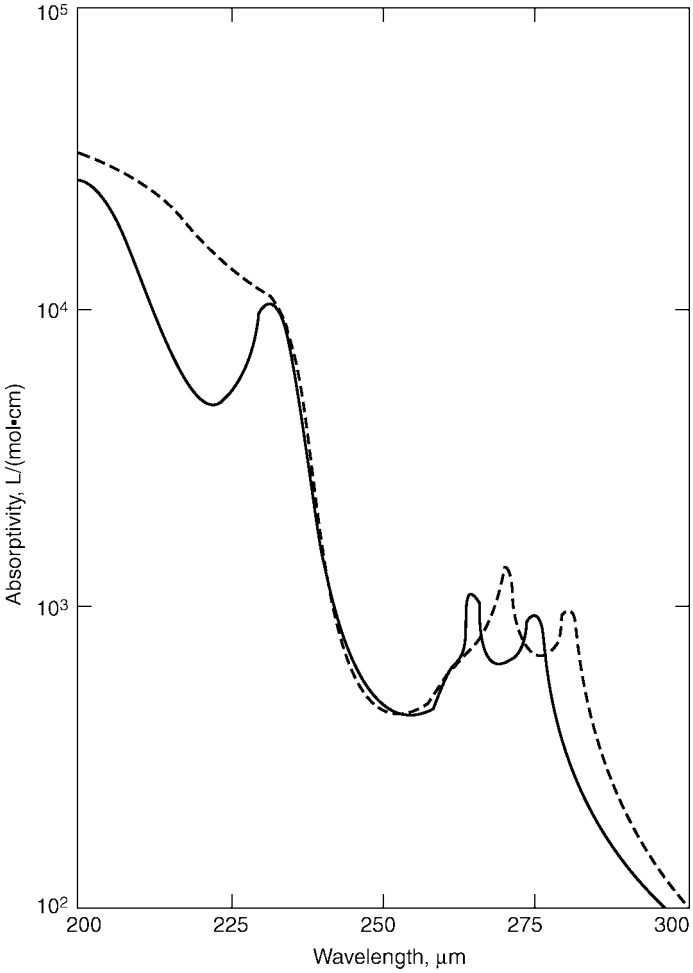

Fig. 11. Ultraviolet absorption spectra of Parylenes N (——) and C (– – –).

constructive fringes; R is the refractive index of the sample film. The thickness d takes the units of wavelength used for λ. At any condition of constructive interference (fringe), twice the thickness times the refractive index equals an integral number of wavelengths of the incident light. That integer is known as the order of the fringe. Much more precise and accurate thicknesses may be computed from the experimental optical spectra if the order of the fringe is known and if any variation of refractive index with wavelength is taken into consideration.

Unstretched PPX films exhibit an inherent negative birefringence, the optical axis of which is perpendicular to the plane of the film. The refractive index along the optical axis is lower than the refractive index observed in the plane of the film, the difference being $n_e - n_0 = -0.075 \pm 0.001$ (46). Where they are observed from the direction normal to the film plane, the films appear to be isotropic. Birefringence is observable only when the films are tilted, or observed in cross section. When stretched, PPX films exhibit a much greater birefringence. The

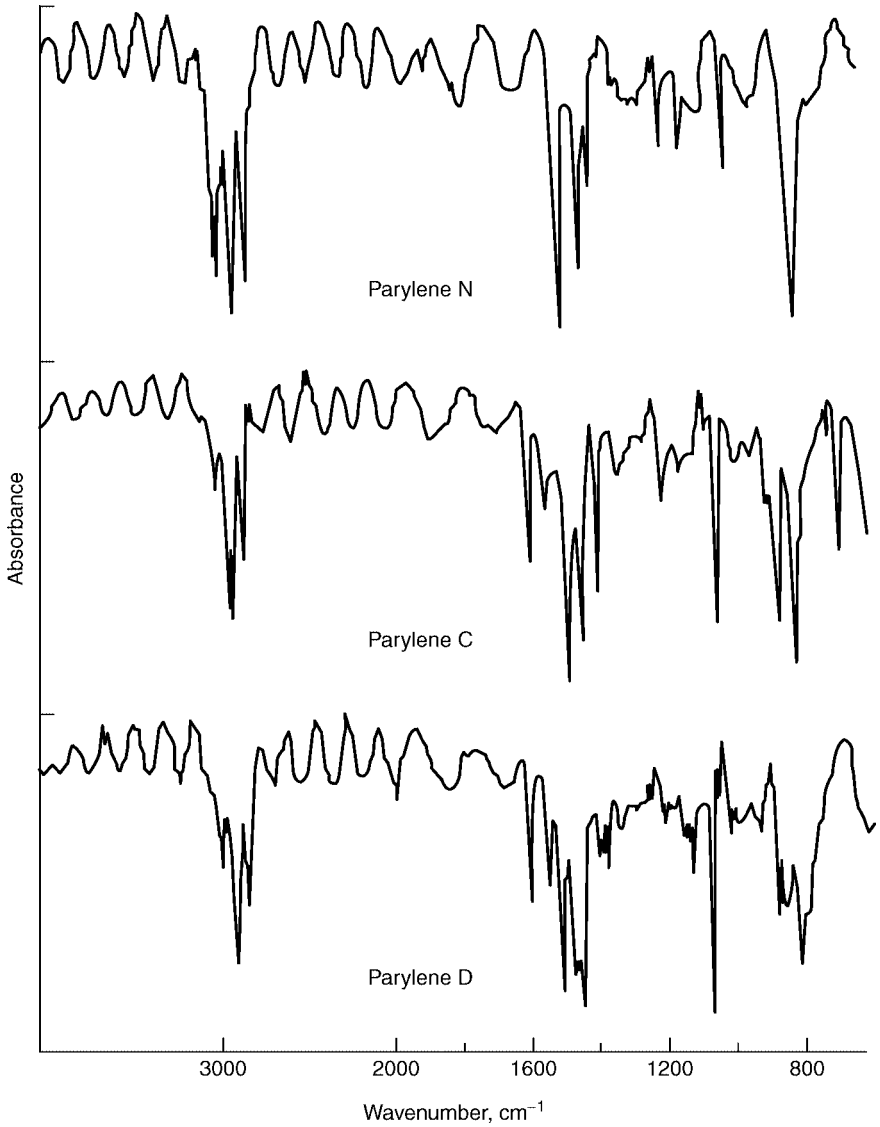

Fig. 12. Infrared absorption spectra of Parylenes N, C, and D films of 18-μm thickness.

stretch birefringence has an optical axis in the direction of stretch and is positive: $n_z - n_0 = +0.2$.

Surface Energy. The surface energies of Parylenes N, C, and D were measured by observing the contact angles for several standard probe liquids. All three have surface energies of approximately 45 mJ/m^2 (= dyn/cm), ie, all test liquids having less than 45 mJ/m^2 surface tension completely wet the as-deposited parylene surfaces (47).

Plasma treatments using reactive gases (N_2, O_2) as well as inert gases (Ar, He) seemed universally to lower the contact angle for water, an observation that

would imply that all such treatments raise the surface energy. Reflectance spectroscopy confirmed the presence of carbonyl in all plasma-treated specimens. Surprisingly, the inert-gas-plasma treatments affected the surface energies of the parylenes more than the reactive gas plasmas did, as indicated by a water contact angle. However, the surface energies of the plasma-treated specimens universally dropped toward the original value on standing in air, but stabilized in about 1 day, without recovering the original value. Plasma treatment of parylene surfaces markedly improves the adhesion of polyurethanes, a result that could be in part, at least, the result of the surface energy change.

Crystallinity. The crystallinity of the parylenes determines two of their most important practical characteristics: mechanical strength at elevated temperatures (see Fig. 5) and solvent resistance.

In a manner typical of crystalline polymers, the crystallinity of parylenes is confined to small-submicrometer domains that are randomly dispersed throughout an amorphous continuum. Adjacent polymer chains, in order to acquire greater overall system stability, exhibit a preference to be close to one another, but the extent to which they actually can be is limited by the tangles already present. Because a given polymer chain is long enough to participate successively in several crystallites, these crystallites function as cross-links to strengthen the bulk polymer. This structural role of the crystallites is retained as temperature rises, giving the bulk polymer physical strength even above its glass-transition temperature, where the amorphous phase is changed to a low modulus, rubbery consistency. Because the crystalline domains are much more resistant to permeation than the amorphous phase, they retain their reinforcing structural role even in the presence of permeants in the amorphous phase, thus giving the parylenes their resistance to solvent attack. The crystalline content increases in freshly deposited polymer as it ages, particularly when it is heated.

Parylene N (PPX) possesses a singularly complex crystalline morphology in which two distinct crystalline modifications are recognized. When deposited in the usual VDP fashion, the crystallites tend to be mostly of the α modification. On annealing at a temperature of about 220°C, the α form is converted to the β modification. This transition was originally thought to be irreversible, but studies have demonstrated that it can be made reversible (48). The crystalline phase undergoes further modifications at higher temperatures before reaching its melting point of 420°C; these modifications have not been fully explored. The detailed crystal structures of the α ($a = 592$ pm, $b = 1060$ pm, $c = 655$ pm, $\beta = 134.7°$ for two monomer repeat units per cell) (49) and β ($a = b = 2052$ pm, $c = 655$ pm, $\gamma = 120°$, for 16 monomer repeat units per cell) (50) modifications have been determined.

In Parylene C, the single crystalline form observed is very similar to the α form of Parylene N. Its detailed crystal structure has been determined [$a = 596$ pm, $b = 1269$ pm, c (chain axis) $= 666$ pm, $\beta = 135.2°$] (51). X-ray studies on the crystal structure of Parylene D have not been reported.

The diffraction pattern produced where X-rays or electrons are directed perpendicularly at the film is the familiar pattern of concentric rings (a powder pattern) produced where the crystallites within the sample are randomly oriented. When the incident beam is directed at an angle to the plane, however, the uniform rings break up into bands or spots, indicative of a preferred orientation of unit

Table 6. Swelling on Immersion in Various Solvents for the Commercial Parylenes at Room Temperature

	Volume change, %		
Solvent	Parylene N	Parylene C	Parylene D
Dichlorobenzene	0.2	3.0	1.8
Mixed xylenes	1.4	2.3	1.1
Monochlorobenzene	1.1	1.5	1.5
2,4-Pentanedione	0.6	1.2	1.4
Trichloroethylene	0.5	0.8	0.8
Acetone	0.3	0.9	0.4
Pyridine	0.2	0.5	0.5
Isopropyl alcohol	0.3	0.1	0.1
Freon	0.2	0.2	0.2
Water, deionized	0.0	0.0	0.0

cells. Tilted electron diffraction results (52) demonstrate that in Parylene N there is a preference for the ⟨100⟩ face of the unit cell to lie in the film plane. Because the polymer chain is oriented along the *c* axis of the unit cell with the benzene rings lying approximately in the plane of the ⟨100⟩ face, it follows that, at least among molecules within crystallites, there is a preference for the polymer chains and benzene rings to be oriented in the film plane. Within the film plane, however, the direction of the chains is random. That benzene rings are preferentially oriented in the plane of the film is supported by negative birefringence and by the Raman spectrum of the polymer (53).

Solvent Resistance. At temperatures below the melting of the crystallites, the parylenes resist all attempts to dissolve them. Although the solvents permeate the continuous amorphous phase, they are virtually excluded from the crystalline domains. Consequently, when a parylene film is exposed to a solvent a slight swelling is observed as the solvent invades the amorphous phase. In the thin films commonly encountered, equilibrium is reached fairly quickly, within minutes to hours. The change in thickness is conveniently and precisely measured by an interference technique. As indicated in Table 6, the best solvents, specifically those chemically most like the polymer (eg, aromatics such as xylene), cause a swelling of no more than 3%.

Applications

Although there is ample evidence in the literature that several industrial groups had a research interest in the PPXs during the 1950s, industrial exploitation was for the most part prevented by the obstacle the parylenes present to conventional fabrication technologies. Because they are generally insoluble in most solvents, even at elevated temperatures, they cannot be used as solvent-based coatings; neither can they be cast as films nor spun as fibers from solution. Because of their high crystalline melting points, melt-working (molding, extrusion, calendering, etc) is also difficult. Yet it is often just these features of solvent resistance and

high temperature mechanical strength that constitute the advantages of PPX materials.

It had been recognized from the outset that polymer forms spontaneously on surfaces exposed to the gaseous monomer PX, but the recognition of VDP as an industrially viable process was not immediate. The public announcement, in 1965, of the convenient generation of pure monomer by the Gorham process from the dimer marked the beginning of a period of a gradually increased understanding and acceptance of the unique features of the parylenes.

As a coating technique, VDP offers certain advantages over other coating techniques such as brushing, dipping, or spraying. These advantages stem principally from the fact that the solid coating is formed from the gaseous monomer directly, without an intermediate liquid stage. As a result, the forces of surface tension, which would cause a pulling away from sharp edges and a filling in of troughs in conventional methods, are not operative and therefore do not affect the cross-sectional profile of VDP coatings. Coatings of PPX grow from the substrate surface outward, producing a conformal layer of uniform thickness. Extensive tests (54) demonstrate that the coating so formed is pinhole-free at thicknesses well below those achievable with conventional coating techniques (see COATINGS).

The PPX coatings are formed spontaneously on substrates at or near room temperature; a cure cycle at elevated temperature is not necessary to complete the polymerization chemistry. The substrate need not be subjected to any temperatures above ambient, and no further time is required beyond that needed for the growth of the film. Because the polymerization is spontaneous, no catalyst is necessary. Catalysts that promote other polymerizations are often ionic or ionogenic and, to the extent that they remain in the coating after cure, their residues are capable of participating in charge mobilization, with resulting detrimental effects in electrical properties. Because the coating is formed at room temperature, stresses that might be induced by differential thermal expansion between the temperature of cure and room temperature are avoided. Because PPX coatings are generally much thinner than conventional coatings, any stress that they impart on the substrate is proportionately less.

Circuit Boards. The most important application of parylenes is as a conformal coating for printed wiring assemblies. The parylene VDP process has the ability to produce a continuous, thin, truly conformal coating on geometrically complex, delicate articles. These coatings provide excellent chemical resistance, especially to solvent attack, and resistance to fungal attack. In addition, they exhibit stable dielectric properties over the wide range of temperatures in which military boards are expected to perform, as well as low dielectric constants, which together with thinness minimize the undesirable loading of high frequency tuned circuits. The reliability with which the process operates substantially reduces labor-intensive touch-up and inspection operations otherwise required for conventional coatings.

Parylene C was included among the earliest MIL-I-46058 (55) qualified coatings (as type XY) and has since enjoyed a reputation for superior performance in protecting and preserving the operation of electronic circuits against the detrimental effects of their operating environments. Environmental water is, of course, chief among these adverse factors. Although the rate of water transport through a parylene coating is finite and well documented, the hydrophobic nature of the

parylenes makes them excellent barriers to penetration by ionic species. Once the circuit board is clean to the extent that surface ionic contamination is minimized and weak surface layers are eliminated, the parylene coating adheres well to the organic substrate material between the conductors. Ionic conduction along the coating–substrate interface, which would otherwise impair electrical performance in the short run and promote galvanic corrosion and dendritic growths in the long term, is minimized.

The SEM photographs of Figure 13 show a conventional FR-4 printed wiring board, coated with an 8-μm film of Parylene C, on which the copper conductor trace has been peeled back. The peeling reveals the rough texture of the epoxy gel coat produced during the original lamination against etched copper in order to achieve maximum laminate peel strength. The region covered with Parylene C in Figure 13 was of the same texture before coating, a fact that, along with parylene's conformality, accounts for much of the texture in the upper surface. Of particular interest is the mode of Parylene C failure as the conductor is peeled. There is evidence of substantial yield prior to failure in the filamentous nature of the failed regions and the web of stretched Parylene C at the apex of the peel. Furthermore, all tensile failure is cohesive, ie, the adhesion of Parylene C to the underlying epoxy gel coat is greater than the cohesive strength within the coating material. The higher magnification (Fig. 13) shows the line of demarcation between the regions covered with copper and with Parylene C prior to the peel, revealing that the breadth of the failed Parylene C exceeded by far its original thickness.

The circuit board with all its components attached presents a variety of surface types for the conformal coating, ranging from plastics through ceramics and glass to metals, in particular aluminum and tin–lead solder. No single mechanism for adhesion can serve all sites effectively. Of particular importance for the epoxy board are the surfaces between conductor traces. Because epoxy is an organic material that is permeable to PX monomer, the growth mechanism of the parylene coating provides adhesion by the interpenetrating network it produces. Care must be taken in cleaning the board surface before coating of leakage-producing ionic contamination as well as organic soils, which interfere with a secure xylylene interpenetration lock. In the cases of ceramic and metal surfaces, monomer penetration is impossible, and other adhesion mechanisms must be engaged. Adhesion to metals is often not essential to the performance of the board, but it is usually desirable. Adhesion to ceramics or glasses is vital in situations where electrical leakage across their surfaces is to be minimized, and is particularly necessary in hybrids. Because the outside surface of common metals is an adherent coating of native oxide, adhesion to metals, ceramics, and glasses can often be achieved using the same approach, ie, treatment with a compatibilizing layer of an organosilane (56). γ-Methacryloxypropyltrimethoxysilane (A-174) is the organosilane most commonly used for the purpose. In action, the trialkoxysilane end of the molecule hydrolyzes and bonds covalently with the oxide on the substrate surface. The methacrylic end of the molecule provides a hydrophobic surface to accommodate parylene deposition, as well as the opportunity to form covalent bonds with the *p*-xylylene polymer through its double bond. It is, of course, essential to provide no more than a monolayer of the organosilane. Water plays an important role in the bonding chemistry between the organosilane and the oxide, and the treatment is often applied from aqueous solution. An alternative treatment is by exposure

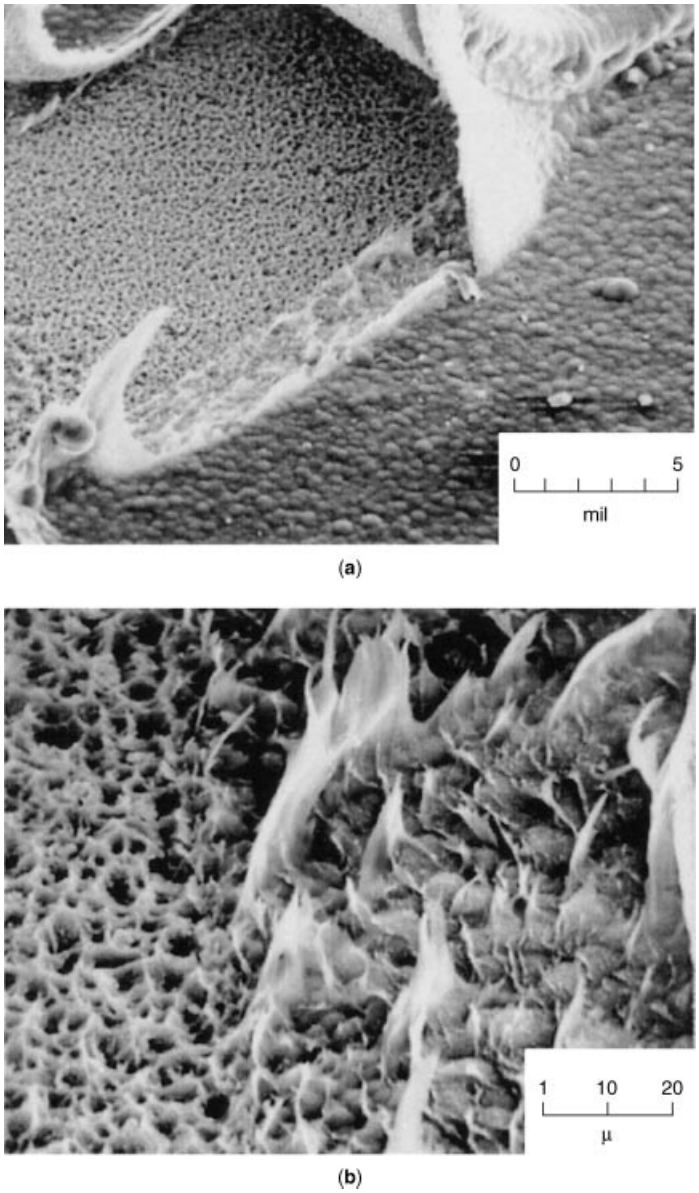

Fig. 13. Scanning electron microscope (SEM) photographs of Parylene C-coated printed circuit conductor peeled to demonstrate the adhesion of the coating to the substrate. To convert mil to meters, multiply by 2.54×10^{-5}.

of the substrate circuit boards to pure gaseous organosilane (57), a process which often takes several days to develop optimum adhesion.

Fluorescence is frequently required in a circuit-board coating to assist inspection of the board after it is coated. Fluorescent parylene coatings can be prepared by admixing a fluorescent agent into the dimer charge. The agent must have

just the right volatility to pass through the process and deposit with the polymer, yet it must be sufficiently stable that it survives the conditions it encounters during the process. Agents that have been used in this manner are anthracene and certain fluorescent whiteners of the Calcofluor family, the 7-dialkylamino-4-methylcoumarins.

Hybrid Circuits. The use of parylenes as a hybrid circuit coating is based on much the same rationale as its use in circuit boards. A significant distinction lies in obtaining adhesion to the ceramic substrate material, the success of which determines the eventual performance of the coated part. Adhesion to the ceramic must be achieved using adhesion promoters, such as the organosilanes.

In the coating of hybrid circuits, parylene provides certain other advantages. In certain technologies, chips are mounted with substrate clearances of as little as 10 μm. The parylene VDP process penetrates this narrow space, coating the underside of the chip as well as the substrate opposite it. Conventional coatings cannot flow into such a narrow space and must rely on simply sealing it off, leaving an air pocket under the chip. Where the fabrication technology uses wire bonds to connect the chips with substrate conductor patterns electrically, the fine (25-μm dia) wires are coated by the parylene VDP process to the same thickness as all other surfaces. A marked increase in wire-bond strength in pull tests on coated hybrids is observed. The increase in strength can be attributed to the strengthening effect of the coating on the wire (which typically exceeds in cross section the amount of metal in the wire) or to a reinforcement of the welded junction to the chip pad or substrate conductor.

A hybrid solid-state relay needed for a NASA space experiment underwent redesign to provide 2500-V dc isolation, input-to-output, while undergoing temperature cycling from -120 to $+ 180^{\circ}$C, as detailed in an instructive published case history (58). The electrical isolation requirement was met only by using a conformal coating, although several conventional coatings were evaluated along with parylene. These stresses in the thicker conventional coatings associated with temperature excursions resulted, in all cases other than parylene, in the rupture of the circuitry and the functional failure of the relay.

During the manufacture of hybrid circuits, it is possible to generate small metallic fragments such as wire chips and solder balls. If they are not removed before hermetic packaging, they can disrupt performance of the unit at some future time. In certain aerospace or military applications where no physical replacement of the unit is possible, such a failure could mean the loss of a mission. A program intended to improve the reliability of hermetic packages in critical systems concluded by finding a solution to this problem by applying a parylene coating to the inside of the hybrids. The coating confers electrical insulation to all surfaces and tends to anchor any loose particles; it also confers nonconductance should they break loose from their moorings. From the standpoint of coating technology, the most interesting part of this solution to the particle-immobilization problem is the throwing power, demonstrated by the fact that the entire internal surface of the hybrid is coated through a 0.5–1.0-mm hole in the lid of the hermetic package (59).

Semiconductors. The distinctive conformality of parylene is often regarded as a handicap for meeting the requirements of an interlayer dielectric (ILD) in large-scale integration (LSI) multilevel interconnection systems. After many

layers of successive patterning, a planarizing procedure is very much needed, not a procedure that would replicate the existing lumpiness. A polyimide, the first organic compound to be used in a commercial semiconductor structure, was selected for this application (60), because of the planarization inherent in its spinning application procedure. However, because parylene offers distinct advantages in purity and thickness control and low moisture absorption (particularly in comparison to the polyimides), it receives continued attention in the search for new fabrication techniques (61–63). Recognition of the need to lower the dielectric constant of ILD insulating materials as a means of improving device performance has generated a renewed interest in organics in general, and the parylenes in particular. To meet this opportunity, the intent to produce the dimer of the per-α-fluorinated version known as Parylene AF4, poly(α,α,α',α'-tetrafluoro-*p*-xylylene) [74952-03-7], has been announced (64). In addition to offering a dielectric constant in the vicinity of 2.35, its thermal stability is such that it can withstand back-end-of-line processing steps at temperatures up to 450°C without perceptible weight loss.

In an interesting extension of the conventional solid-state device concept, where a thin film covers the channel of a field-effect transistor (FET), the electron current in the channel may be made to respond to changes in the chemical environment on the opposite side of the film. Thus a silicon nitride film on a channel gives an ion-selective FET (ISFET) that responds to the pH of a solution with which it is in contact. The hydrophobic nature of parylene, on the other hand, enables the channel it covers to be independent of solution composition, and such a channel can be used as a reference electrode. An important advantage of parylene in this context is the thinness with which it can be deposited as a continuous film. The gate coatings are 0.1 μm thick, a thinness required if the sensor is to have a speedy response. An experimental probe-type all-solid-state pH sensor has been demonstrated (65). It was also demonstrated that chemically modifying the parylene surface with crown ether compounds can give an ISFET (known as a CHEMFET) that responds to potassium ion concentration.

Sensors for physical effects are also fabricated using standard semiconductor technology. A notable example is a silicon membrane pressure transducer, which, among its many other uses, is currently employed as a manifold pressure transducer in automobiles (66). The thin membrane of single-crystal silicon was prepared by etching most of the wafer thickness away, into which a resistive Wheatstone Bridge network that enables an electrical readout of the membrane's physical strain while flexing had previously been diffused. Although it is desirable to insulate the membrane electrically from the medium it measures, it is also desirable to do so without affecting the elasticity of the membrane, so that it retains its calibration of electrical output vs input pressure. A thin coating of Parylene C easily accomplishes both. In an inversion of roles, these same pressure transducers were used to sense the stresses imparted to coated substrates by a variety of MIL-I-46058C qualified coating materials (67). Whereas all other coatings, as a result of their cure shrinkages acting through their greater thicknesses modified by their assorted elastic moduli, affected sensor calibration in all cases, the presence of 13 μm of Parylene C was barely detectable.

Capacitors. The outstandingly low dielectric loss of parylenes make them superior candidates for dielectrics in high quality capacitors. Furthermore, their

dielectric constant and loss remain constant over a wide temperature range. In addition, they can be easily formed as thin, pinhole-free films. Kemet Flatkaps are fabricated by coating thin aluminum foil with Parylene N on both sides and winding the coated foils in pairs (68).

Parylenes are also used to coat the rotor and stator plates of miniature variable-air-gap tuning capacitors (69). Coating the plate raises the voltage that must be applied between two parallel plates for a discharge to occur in the air gap. Thus, a closer plate spacing is permitted, and a smaller unit having the same electrical function can be built. This is also beneficial in improving design capacitance per unit volume. Compared to the alternative of interleaving dielectric films between the plates, the coated-plate technique offers the advantages of simplicity in assembly as well as reliability of the unit. Uniformity and thickness control are of paramount importance in this case.

The Bathythermograph. The thermistor sensing probe of a disposable bathythermograph is coated with parylene. This instrument is used to chart the ocean water temperature as a function of depth. Parylene provides the needed insulation resistance and is thin and uniform enough to permit a rapid and accurate response to the temperature of the surrounding salt water (70).

Miniature Electrical Components. In the manufacture of miniature transformers and motor armatures, it is often necessary that the winding be electrically isolated from the bobbin. The insulating varnish of fine copper wire often does not survive the rigors of the winding operation, and, particularly in the case of the smaller devices, the bobbin requires insulation. However, a thicker insulation than is absolutely necessary takes up space that otherwise could be used for more turns of wire. Thus, thickness control in the coating of the bobbin means better performance of the finished device. Parylene is used in the manufacture of high quality miniature stepping motors, such as those used in wristwatches, and as a coating for the ferrite cores of pulse transformers, magnetic tape-recording heads, and miniature inductors, where the abrasiveness of the ferrite is particularly damaging. In the coating of complex, tiny objects such as these, the VDP process has an extra labor-saving advantage. It is possible to coat thousands of such articles simultaneously by tumbling them during the VDP operation (71).

Medical Uses. Under the auspices of the National Institutes of Health Artificial Heart program (72), Parylene C received considerable attention as a component of a novel scheme for achieving blood compatibility in a flexible pump chamber wall by anchoring the endothelial tissue of the host to it. A microfiber nonwoven fabric anchored to the flexible wall by an overcoating of Parylene C provides scaffolding for cellular ingrowth (73). Although the scheme is not used today, the program contributed a significant amount of favorable biocompatibility data on Parylene C, particularly in the area of cytotoxicity (74). Parylene's minimal perturbance of cells growing in its vicinity can be ascribed to its high purity and its ability to slow down impurity species that might otherwise diffuse out of a substrate material. The corrosive biological environment does not affect parylene, which cannot be hydrolytically degraded.

Parylene's use in the medical field is linked to electronics. Certain pacemaker manufacturers use it as a protective conformal coating on pacemaker circuitry (75). The coated circuitry is sealed in a metal can, so that the parylene coating serves only as a backup should the primary barrier leak. There is also interest in

its use as an electrode insulation in the fabrication of miniature electrodes for long-term implantation to record or to stimulate neurons in the central or peripheral nervous system, as the "front end" of experimental neural prostheses (76). One report describes the 3-year survival of functioning parylene-coated electrodes in the brain of a monkey (77).

Artifact Conservation. As books age, the paper of their pages becomes brittle. A relatively thin coating of parylene can make these embrittled pages stronger (78). Parylene coats the fibers conformally and welds them together at crossing points, providing added structural strength. Although parylene does little to retard the chemical processes that make the paper brittle, it restores some physical strength. Furthermore, the parylene coating can be applied to the existing book without disturbing the binding, thus saving the labor of disassembly. The concept has been extended to other fragile artifacts, such as fabrics.

Laser Fusion Targets. In the search for new energy sources, some research is directed toward the thermonuclear fusion of deuterium–tritium (DT) mixtures. In laser-driven inertial confinement fusion, a single laser pulse crushes a target containing the DT fuel to one thousandth of its normal volume and achieves a temperature of 10^8 K. The energy per pulse in current lasers is small, which limits the experimental targets to a diameter of about 100 μm. The outer layer of the spherical target absorbs the omnidirectionally incident laser energy and ablates as it is thermally destroyed, imparting a reactive compressive force on the inner portions of the target, thus compressing it. The dimensions of the outer layer are central to achieving hydrodynamic stability during the implosion process. Concentricity, sphericity, and thickness (ca 10 μm) must be better than 5%, and surface roughness must be no greater than 0.1 μm. Parylene is a leading contender for the outer layer, and considerable ingenuity has been applied in several methods for experimental target fabrication (79,80).

Contamination Control. In a number of developing technologies, contamination by small particles is a serious problem. To the extent that the generation of freely mobile particles is reduced by securing them to their initial locations, parylene coating of critical system components can be useful. In the manufacture of Winchester disk drive units, large magnesium castings are coated with parylene. This increases system reliability (81), presumably because the large surface within the sealed unit, if not coated, is capable of producing particles of the same destructive potential that the system seal is supposed to prevent from entering.

Barrier Coating. The bulk permeabilities of parylenes, although finite, are generally lower than those of most other types of plastic materials. The further advantage of coating continuity inherent in the VDP process allows the parylenes to realize the benefits of their low permeabilities to the fullest, without leakage of the permeant through coating defects such as cracks or pinholes. Thus the parylenes are uniquely suited as protective encapsulants or barrier coatings (see BARRIER POLYMERS).

Where pieces of lithium metal are coated with Parylene C, and their subsequent reaction to water vapor follows, the steady-state generation of hydrogen can be controlled exactly by the rate of water transport through the coating (82). Pellets of nitronium perchlorate, a potent oxidizer useful as a solid-rocket propellant component, can be rendered less moisture-sensitive and compatible with organic binders by applying a coating of Parylene C (83). The absorption of water by

particulate ammonium nitrate could be reduced tenfold by as little as a 0.7% coating of Parylene C (84). Particles of ammonium nitrate remain free-flowing after long exposures to ambient conditions of temperature and moisture when coated with as little as 0.2% Parylene C. The thermal sensitivity of Parylene C–coated ammonium nitrate (time to explosion) is unaffected by the coating. On the other hand, the 1.5–8% coating of particulate military-grade RDX explosive, cyclotrimethylene trinitramine, produced significant changes in physical and explosive properties. The changes were attributed to the chemical properties of the protective Parylene C coating and to the virtual absence of encapsulated agglomerates of RDX crystals (85).

In a recent report (86), a 150–200 mg/cm^2 Parylene C coating provided protection against moisture uptake by three-phase—polyimide, microballoons, and air—syntactic foams. In a previously reported coating of a similar foam, the stated purpose was strengthening (87).

Corrosion Control. The oxygen and water permeability and thinness of the parylene coatings notwithstanding, the rate of corrosion of a coated surface is often significantly reduced. In one case, the corrosion of a plated wire memory was reduced to the point where no bits were lost during 30 cycles of a MIL STD 202D-106C test by overcoating the permalloy plating, which had been previously coated with a Ni–P anticorrosive layer, with Parylene N (88).

Dry Lubricant. The static and dynamic coefficients of friction for the parylenes are low and virtually the same. This feature is an advantage in the use of a parylene coating as a dry lubricant on the bearing surfaces of miniature stepping motors. Coating a threaded ferrite core significantly reduces the abrasion to coil forms (89).

Pellicles and Membranes. By separating the coating from the substrate after deposition, the unique coating features of parylenes, especially continuity and thickness control and uniformity, can be imparted to a free-standing film. In practice, a sheet of smooth glass is coated with a layer of a hygroscopic substance before being coated with parylene. The film is then lifted from the glass by water immersion to activate the release agent. In this manner, uniform, continuous, free-standing parylene films with thicknesses of less than 0.1 μm can be prepared. Applications of such films include optical beam splitters (90), a window for a micrometeoroid detector (91), a detector cathode for an X-ray streak camera (92), windows for X-ray proportional counters (93), a charge stripper for converting a portion of the H-output beam of a 50 MV LINAC to neutral H^0 for diagnostic purposes (94), and a massless support for projectile abrasion testing (95); proposals have included the membrane structure for a solar sail (96).

Health and Safety

In a world increasingly conscious of the dangers of contact with chemicals, a process that is conducted within the walls of a vacuum chamber, such as the VDP process for parylene coatings, offers great advantages. Provided the vacuum pump exhaust is appropriately vented and suitable caution is observed in cleaning out the cold trap (trace products of the pyrolysis, which may possibly be dangerous,

would collect here), the VDP parylene process has an inherently low potential for operator contact with hazardous chemicals.

To an experienced operator trained in the handling of industrial chemicals, the dimers present little cause for concern in handling or storage. The finished polymer coating presents even less of a health problem; contact with the reactive monomer is unlikely. In the ancillary operations, such as cleaning or adhesion promotion, the operator must observe suitable precautions. Before using the process chemicals, operators must read and understand the current Material Safety Data Sheets, which are available from the manufacturers.

BIBLIOGRAPHY

"Xylylene Polymers" in *EPST* 1st ed., Vol. 15, pp. 98–124, by William F. Gorham and W. D. Niegisch, Union Carbide Corporation; "Xylylene Polymers" in *EPSE* 2nd ed., Vol 17, pp. 990–1025, by W. F. Beach, C. Lee, D. R. Bassett, and T. M. Austin, Union Carbide Corporation, and R. Olson, Nova Tran Corporation.

1. L. A. Errede and M. Szwarc, *Q. Rev. Chem. Soc.* **12**, 301 (1958); M. Szwarc, *Polym. Eng. Sci.* **16**(7), 473 (1976).
2. W. F. Gorham and W. D. Niegisch, in N. M. Bikales, ed., *Encyclopedia of Polymer Science and Technology*, Vol. 15, Wiley-Interscience, New York 1989, 98–124.
3. U. S. Pat. 3,342, 754 (Sept. 19, 1967), W. F. Gorham (to Union Carbide Corp.).
4. W. F. Gorham, *J. Polym. Sci. A-1* **4**, 3030 (1966).
5. W. F. Gorham, *J. Polym. Sci. A-1* **4**, 3027 (1966).
6. R. B. Woodward and R. Hoffmann, *The Conservation of Orbital Symmetry*, John Wiley & Sons, Inc., Hoboken, N.J., Chapt. 6, pp. 70, 85, and reference 96 therein.
7. L. K. Montgomery and co-workers, *J. Am. Chem. Soc.* **108**, 6004 (1986).
8. P. G. Mahaffy, J. D. Wieser, and L. K. Montgomery, *J. Am. Chem. Soc.* **99**, 4514 (1977).
9. U. S. Pat. 4,532,369 (July 30, 1985), H. Hartner (to Merck); U. S. Pat. 4,769,505 (Sept. 6, 1988), C. Lee and D. R. Bassett (to Union Carbide Corp.).
10. D. J. Williams, J. M. Pearson, and M. Levy, *J. Am. Chem. Soc.* **92**, 1436 (1970).
11. S. K. Pollak, B. C. Raine, and W. J. Hehre, *J. Am. Chem. Soc.* **103**, 6308 (1981).
12. M. J. S. Dewar, *J. Am. Chem. Soc.* **104**, 1449 (1982).
13. H. G. Gilch, *J. Polym. Sci. A-1* **4**, 438–439 (1966).
14. V. V. Korshak and S. L. Sosin, *Vysokomol. Soyed.* **7**, 232–238 (1965).
15. U. S. Pat. 3,787,382 (Jan. 22, 1974), A. N. Wright, W. R. Burgess, and E. V. Wilkus (to General Electric Co.).
16. M. Inoue, H. Fujioka, T. Sorita, and T. Tanaka, *ACS Polym. Prepr.* **28**, 332 (1987).
17. Y. Takai, Y. Hayase, T. Mizutani, and M. Ieda, *J. Phys. D.* **17**, 399 (1984).
18. J. R. Salem, F. O. Sequeda, J. Duran, W. Y. Lee, and R. M. Yang, *J. Vac. Sci. Technol.* **A4**, 369 (1986); Y. Takahashi, M. Iijima, K. Inagawa, and A. Itoh, *J. Vac. Sci. Technol.* **A5**, 2253 (1987).
19. F. E. Arnold and L. S. Tan, *31st Int. SAMPE Symp.* **31**, 1185 (1986).
20. U. S. Pat. 4,711,964 (Dec. 8, 1987), L. S. Tan and F. E. Arnold (to University of Dayton).
21. Y. Ito, S. Miyata, M. Nakatsuka, and T. Saegusa, *J. Org. Chem.* **46**, 1043 (1981).
22. Eur. Pat. 220,743 (May 6, 1987), R. Ungarelli, M. A. Baretta, and L. Sogli (to Montedison SpA).
23. Eur. Pat. 226,255 (June 24, 1987), R. Ungarelli, M. A. Baretta, and A. Malacrida (to Montedison SpA).
24. Eur. Pat. 220,744 (May 6, 1987), G. F. Pregaglia, M. A. Baretta, and A. Malacrida (to Montedison SpA).

25. C. J. Brown, *J. Chem. Soc*. 3265 (1953).
26. R. H. Boyd, *Tetrahedron* **22**, 119 (1966); D. L. Rodgers, E. F. Westrum, Jr., and J. T. S. Andrews, *J. Chem. Thermodyn.* **5**, 733–739 (1973).
27. D. E. Kirkpatrick, Ph.D. dissertation, Rensselaer Polytechnic Institute, Troy, N.Y., 1984.
28. M. Gazicki, G. Surendran, W. James, and H. Yasuda, *J. Polym. Sci., Polym. Chem. Ed.* **23**, 2255 (1985).
29. H. Sawada, *Thermodynamics of Polymerization*, Marcel Dekker, Inc., New York, 1976.
30. M. Souders and co-workers, *Ind. Eng. Chem.* **41**, 1048 (1949).
31. D. R. Stull, E. F. Westrum Jr., and G. C. Sinke, *The Chemical Thermodynamics of Organic Compounds*, Krieger, Malabar, Fla., 1987, p. 699.
32. D. E. Kirkpatrick, L. Judovits, and B. Wunderlich, *J. Polym. Sci., Polym. Phys. Ed.* **24**, 45 (1986).
33. R. W. Warfield and M. C. Petree, *J. Polym. Sci.* **55**, 497 (1961).
34. S. Y. Lazareva, *Vysokomol. Soedin.* **A21**, 1509 (1979).
35. B. L. Joesten, *J. Appl. Polym. Sci.* **18**, 439 (1974).
36. W. A. Alpaugh and D. R. Morrow, *Thermochim. Acta* **9**, 171 (1974).
37. W. F. Beach, *Macromolecules* **11**(1), 72 (1978).
38. F. E. Cariou, D. J. Vally, and W. E. Loeb, *IEEE Trans. Parts Mater. Packag.* **PMP-1**(1), 54 (1965).
39. J. F. Gaynor, S. B. Desu, and J. J. Senkevich, *Macromolecules* **28**, 7343–7348 (1996).
40. B. J. Bachman, in *Proceedings of the 1st International SAMPE Electronics Conference*, Santa Clara, Calif., June 23–25, 1987, 431–440.
41. A. von Hippel, in E. U. Condon and H. Odishaw, eds., *Handbook of Physics*, 2nd ed., McGraw-Hill Book Co., Inc., New York, 1968, Part 4, p. 104.
42. U. S. Pats. 4,163,828 (Aug. 7, 1979); 4,173,664 (Nov. 6, 1979), both to G. S. Cieloszyk (to Union Carbide Corp.); and U. S. Pat. 4,176,209 (Nov. 27, 1979), T. E. Baker, G. L. Fix, and J. S. Judge (to Raytheon).
43. T. E. Nowlin, D. F. Smith, and G. S. Cieloszyk, *J. Polym. Sci., Polym. Chem. Ed.* **18**(7), 2103 (1980). T. E. Baker, G. L. Fix, and J. S. Judge, *J. Electrochem. Soc.* **127**, 1851 (1980).
44. W. H. Hubbel Jr., H. Brandt, and Z. A. Munir, *J. Polym. Sci., Polym. Phys. Ed.* **13**, 493 (1975).
45. E. Sacher, *J. Appl. Polym. Sci.* **28**, 1535 (1983).
46. R. S. Corley, H. C. Haas, M. W. Kane, and D. I. Livingston, *J. Polym. Sci.* **13**, 137 (1954).
47. T. E. Nowlin and D. F. Smith, *J. Appl. Polym. Sci.* **25**, 1619 (1980).
48. D. E. Kirkpatrick and B. Wunderlich, *J. Polym. Sci., Polym. Phys. Ed.* **24**, 931 (1986).
49. R. Iwamoto and B. Wunderlich, *J. Polym. Sci., Polym. Phys. Ed.* **11**, 2403 (1973).
50. S. Isoda, M. Tsuji, M. Ohara, A. Kawaguchi, and K. Katayama, *Polymer* **24**, 1155 (1983).
51. S. Isoda, T. Ichida, A. Kawaguchi, and K. Katayama, *Bull. Inst. Chem. Res. Kyoto Univ.* **61**, 222 (1983).
52. W. D. Niegisch, *J. Appl. Phys.* **38**, 4110 (1967).
53. M. S. Mathur and G. C. Tabisz, *J. Cryst. Mol. Struct.* **4**, 23 (1973).
54. M. A. Spivack and G. Ferrante, *J. Electrochem. Soc.* **119**, 1592 (1969).
55. *MIL-I-46058C(6): Insulating Compound, Electrical (for Coating Printed Circuit-Assemblies)*, U.S. Dept. of Defense, Washington, D.C., Nov. 8, 1982.
56. U. S. Pat. 3,600,216 (Aug. 17, 1971), D. D. Stewart (to Union Carbide Corp.).
57. Ger. Pat. 2,737,792 (Mar. 2, 1978), D. M. Mahoney and W. F. Beach (to Union Carbide Corp.).

58. B. L. Slater, T. J. Riley, and W. Janssen, *Proceedings of the IEEE Power Electronics Specialists Conference*, Pasadena, Calif., June 11–13, 1973, 163–169.
59. V. S. Kale and T. J. Riley, *IEEE Trans. Parts Hybrids Packag.* **PHP-1**(3), 273 (1977).
60. D. L. Bergeron, J. P. Kent, and K. E. Morrett, *22nd Proceedings of the International Reliability Physics Symposium*, Las Vegas, Nev., 1984, 229–233.
61. J. M. Baker, J. H. Magerlein, and M. J. Palmer, *IBM Tech. Disel. Bull.* **27**, 4382 (Dec. 1984).
62. Jpn. Pat. 62 106456 (Nov. 1, 1986), M. Kanazawa and S. Kawanako (to Fujitsu, Ltd.).
63. W. F. Beach and T. M. Austin, *Hybrid Circ. Technol.*, 33–36 (Jan. 1990).
64. J. Wary, R. A. Olson, and W. F. Beach, in *2nd International Dielectrics for VLSI/ULSI Multilevel Insulation Conference (DUMIC)*, Santa Clara, Calif., Feb. 20–21, 1996, 207–213.
65. T. Matsuo, H. Nakajima, T. Osa, and J. Anzai, *Sens. Actuat.* **9**(2), 115 (1986).
66. R. Olson, *Electron. Packag. Prod.*, 213 (May 1980).
67. R. Olson, *Circuits Mfg*. 57 (Jan. 1986).
68. U. S. Pat. 3,327,184 (June 20,1967), D. J. Valley (to Union Carbide Corp.); U. S. Pat. 3,319,141 (May 9, 1967), F. E. Cariou, W. E. Loeb, and D. J. Valley (to Union Carbide Corp.).
69. U. S. Pat. 3,949,280 (Apr. 6, 1976), S. Odagiri, M. Nuka, N. Shinba, M. Baba, and Y. Iizuka (to Mitsumi Electric Co., Ltd.); Ger. Pat. 2,546,332 (Apr. 29, 1976), J. Lefeber and J. deJonge (to N. V. Philips Gloeilampenfabriken).
70. U. S. Pat. 3,389,604 (June 25, 1968), G. B. Williams (to Buzzards Corp.).
71. Ger. Pat. 2,329,186 (Jan. 3, 1974), F. R. Tittmann (to Union Carbide Corp.); U. S. Pat. 3,300,332 (Jan. 27, 1967), W. F. Gorham and H. L. Willard (to Union Carbide Corp.).
72. *Contract No. N01-HV-8-1388*, National Heart, Lung and Blood Institute, Division of Heart and Vascular Diseases, Bethesda, Md.
73. F. R. Tittmann and W. F. Beach, in M. Szycher and W. J. Robinson, eds., *Synthetic Biomedical Polymers: Concepts and Applications*, Technomic Publishing Co., Inc., Westport, Conn., 1980, 117–132.
74. R. H. Kahn and W. E. Burkel, *In Vitro* **8**, 451 (1973).
75. R. Olson, *Electron. Packag. Prod.*, 213 (May 1980).
76. E. M. Stemmed, *J. Electrophysiol. Tech. Eng.* **10**(1), 19 (1983); G. E. Loeb, M. Salcman, and E. M. Schmidt, *IEEE Trans. Bionwd. Eng.* **BME-24**(2), 121 (1977).
77. E. M. Schmidt, J. S. McIntosh, and M. J. Bak, *Med. Biolog. Eng. Comput.*, 96 (Jan. 1988).
78. B. J. Humphrey, *J. Am. Inst. Conserv.* **25**, 15 (1986); C. J. Shahani and W. K. Wilson, *Am. Sci.* **75**, 240 (1987).
79. D. F. Peiffer, T. J. Corley, G. M. Halpern, and B. A. Brinker, *Polymer* **22**, 450 (1981); R. Q. Gram, H. Kim, J. F. Mason, and M. Wittman, *J. Vac. Sci. Technol.* **A4**(3), 1145 (1986); K. W. Beig, *J. Vac. Sci. Technol.* **18**, 1231 (1981).
80. U. S. Pat. 4,381,963 (May 3, 1983), I. S. Goldstein, F. D. Kalk, and H. W. Deckman (to The University of Rochester).
81. R. Olson and R. Veague, *Microcontamination*, 57 (Jan. 1985).
82. M. A. Spivack, *Corrosion (Houston)* **26**, 371 (1970).
83. U. S. Pat. 3,523,839 (Aug. 11, 1970), L. Shechter and W. E. Loeb (to Union Carbide Corp.); U. S. Pat. 3,556,881 (Jan. 19, 1971), W. F. Gorham and W. E. Loeb (to Union Carbide Corp.).
84. T. C. Castorina and A. F. Smetana, *J. Appl. Polym. Sci.* **18**, 1373 (1974).
85. A. F. Smetana and T. C. Castorina, in *Proceedings of the Propellants, Explosives and Pyrotechnics Conference*, Dec. 3–4, 1974, Picatinny Arsenal, Dover, N.J.
86. A. Calahorra, O. Gara, and S. Kenig, *J. Cell. Plast.* **23**, 383 (1987).

87. R. J. McWhirter, *Report from Bendix Corp., BDX-613-2358*, Bendix Corp., Kansas City, Mo., Sept. 1980.
88. K. Makino, S. Kawakami, and S. Orihara, *Fujitsu Sci. Tech. J.* **9**(4), 153 (1973).
89. R. Olson, *Electron. Packag. Prod.*, 213 (May 1980).
90. M. A. Spivack, J. N. Pike, and W. M. Jayne, in *Proceedings of the Electro-Optical Systems Design Conference*, New York, Sept. 18–20, 1973, 362–371.
91. N. Pailer and E. Grun, *Planet. Space Sci.* **28**, 321 (1980).
92. P. L. Tassano, *J. Vac. Sci. Technol.* **A3**, 2036 (1980).
93. P. H. Sheather, *J. Physics E.* **6**, 319 (1973).
94. S. L. Kramer and D. R. Moffett, *IEEE Trans. Nucl. Sci.* **NS-28**, 2174 (1981).
95. U. S. Pat. 3,940,530 (Feb. 24, 1976), W. E. Loeb and M. A. Spivack (to Union Carbide Corp.); U. S. Pat. 3,864,202 (Feb. 4, 1975), W. E. Loeb and M. A. Spivack (to Union Carbide Corp.).
96. U. S. Pat. 4,321,299 (Mar. 23, 1982), R. A. Frosch and R. A. Frazer (to NASA).

W. F. BEACH
Alpha Metals

YIELD AND CRAZING IN POLYMERS

Introduction

Polymers serve increasingly in structural applications as lightweight replacements for more traditional materials such as metals and wood. In light of this it is important to understand and be able to characterize the engineering or mechanical properties over the likely service conditions (see MECHANICAL PERFORMANCE). Typically when a material fails in service it is thought of in terms of a catastrophic brittle failure and these modes have been partially discussed elsewhere (see FRACTURE; FATIGUE). However, polymers (both thermoplastics and thermosets) can also fail by yielding, and while generally this is not necessarily a catastrophic event (ie the material remains intact) it does mean the material retains a degree of permanent deformation and is usually considered a failure criterion in terms of structural integrity. Furthermore, the yield response of polymers affects the plastic zone at the crack tip and this is important in fracture events.

Another deformation mechanism common to many polymers is that of crazing. Crazes are generally a precursor to brittle failure, though on the local scale they are the result of highly localized yielding phenomena. As such they provide a significant source of energy absorption and, further, since the crazes remain load bearing, the time for their initiation and growth can be a significant portion of the overall lifetime of the material.

The present article focuses on yield and crazing in polymers and does not deal directly with the viscoelastic response, though it is recognized that yield and viscoelasticity share many of the same features—strain rate and temperature dependence (1) and even concepts such as time–temperature superposition (2) (see VISCOELASTICITY; AGING, PHYSICAL). We first present a summary of conventional yield criteria, these being methods to quantify the yield stress as a function of

Encyclopedia of Polymer Science and Technology. Copyright John Wiley & Sons, Inc. All rights reserved.

the applied stress field, ie uniaxial vs biaxial. Following this the phenomenology of yield is addressed by considering a number of models of the yield process in polymers, including the observation of strain softening and strain hardening. A brief overview of craze structure and morphology is given and several criteria for the initiation, growth, and failure of crazes are described.

Yield

A general definition of yield is the point at which a material ceases to deform elastically in a recoverable manner and undergoes permanent (irreversible) plastic deformation. Historically, the study of yield and the theories describing it were developed for metals (3) and, there, this definition works well, with elastic deformation arising from lattice distortions and plastic deformation from the motion of dislocations. In polymers the molecular processes involved in deformation cannot be so easily split into such distinct mechanisms. Further, it has long been recognized that polymers exhibit a viscoelastic response to deformation (4–7) and consequently the general mechanical properties are both rate and temperature dependent. Such a viscoelastic response is evidenced not only on deformation but also on recovery. The time-dependent nature of the recovery means that for polymers the determination of permanent (plastic) deformation can depend on how long one is prepared to conduct the relevant measurements. That said, general aspects of the large deformation behavior of amorphous glassy and semi-crystalline polymers can be usefully discussed in terms of conventional yield criteria.

We begin by examining general stress (load per unit area)–strain (fractional change in length) responses for polymers under uniaxial tensile loading and develop what is essentially an elastic–plastic analysis of the material behavior. Loading under compressive and shear forces is then considered. This is followed by general yield criteria: these can be considered macroscopic criteria relating the applied stress to some critical value for yielding (generally a critical shear stress) and their modification to introduce pressure dependence. While such criteria are useful engineering concepts, it is perhaps more satisfying to be able to describe yielding from a microscopic perspective, and this is addressed in the section on yield theories. Subsequent to the discussion of yield phenomena we present a section on another important aspect of polymer mechanical behavior, that of crazing. Crazing is a localized yielding process that may be dilatational in nature. It results in essentially load-bearing cracks that are generally a precursor to macroscopically brittle failure when the craze density is low.

Before describing the yield response of polymers in the next section, we remark here that polymer mechanical behavior depends strongly not only on the time (rate) and temperature, but also on the morphology of the material (8,9). Hence the yield phenomenology described below will approximately describe the behavior, but the details of the behavior will depend strongly on the morphology and where one is relative to the glass-transition temperature, T_g. For example, above the T_g, an amorphous polymer such as polystyrene does not yield but undergoes viscous flow. On the other hand, a material such as polyethylene, which is semi-crystalline, will undergo a yield process above the glass transition. Below T_g, both glassy amorphous and glassy semi-crystalline polymers can undergo

yielding, though the processes may differ between the two types of materials. Much of the development of the present article deals with yield of glassy amorphous polymers, though some discussion of yielding in semi-crystalline materials is also presented.

General Stress–Strain Curves under Uniaxial Tensile Loading. In uniaxial extension or compression, the true axial stress, σ_T, is given by the current load (P) divided by the current cross sectional area (A):

$$\sigma_T = P/A \tag{1}$$

If it is assumed that the deformation takes place at constant volume (a reasonable assumption under most conditions of plastic deformation where the volume changes are small compared to the total strain), then the instantaneous area (A) and length (l) are related to the original cross sectional area and length (A_0, l_0 respectively) by

$$Al = A_0 l_0 \tag{2}$$

We now define the engineering (or nominal) stress, σ_E, as

$$\sigma_E = P/A_0 \tag{3}$$

and the engineering strain, ε, as

$$\varepsilon = (l - l_0)/l_0 \tag{4}$$

so that

$$l/l_0 = (l + \varepsilon) \tag{5}$$

From equations 1-5 we find that

$$\sigma_E = \sigma_T/(l + \varepsilon) \qquad \sigma_T = \sigma_E(l + \varepsilon) \tag{6}$$

The deformation response of a material to a given loading regime is described by generalized equations known as constitutive relations. For uniaxial loading in the limit of small strains, the simplest of these is known as Hooke's Law and linearly relates the stress to the strain:

$$E = \frac{\sigma}{\varepsilon} \tag{7}$$

where E is Young's modulus.

The extreme temperature and rate sensitivity of polymers means that they can display a wide range of mechanical behaviors depending on the precise conditions under which they are tested. Figure 1 shows a set of typical engineering stress–strain curves that an amorphous polymer might be expected to exhibit as a function of rate or temperature in a uniaxial tensile test (10,11). At low temperatures or high rates polymers tend to fail in a brittle manner (Curve A)—the strain

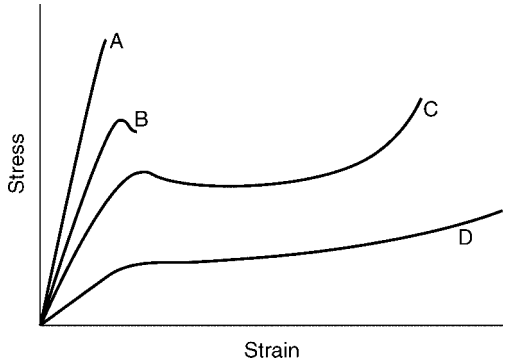

Fig. 1. Typical engineering stress–strain curves for an amorphous polymer as a function of temperature or strain rate.

to failure is low (of the order of a few percent) and the modulus high (of the order of a few GPa). As the temperature increases (or the strain rate decreases) the curves progress such that the material passes through a softening regime (Curve D), characterized by low moduli, an indistinct (or nonexistent) yield point, and large strains to failure (>100 percent). Ultimately, at a sufficiently high temperature (or low enough strain rate), the material may show a pure rubbery response with a modulus some orders of magnitude lower than those indicated in Figure 1 (curve omitted for clarity).

Of particular interest in this discourse is the behavior shown in Curves B and C. At small strains (typically <1%), the stress rises approximately linearly with increasing strain, ie the material displays Hookean-like behavior (note that this is not strictly true for polymers because of viscoelastic effects; however if the applied strain rate is faster than the relaxation time for the material then little relaxation will occur and it is a reasonable approximation). At larger strains (above the proportional limit) the engineering stress will continue to rise with strain, though less rapidly. Eventually, at a certain strain, the stress reaches a maximum and then falls with increasing strain. It is this peak stress which is generally taken to be the yield stress, σ_y, and the strain at which it occurs as the yield strain, ε_y. The nature of the load drop and the postyield behavior are discussed subsequently. Here it is sufficient to note that the peak in engineering stress is normally accompanied by macroscopic changes to the sample geometry. The plastic deformation is concentrated locally to a small portion of the specimen. This section is seen to reduce in width and to form what is called a "neck." Because of the change in cross-sectional area, the local stresses in the neck region can be significantly higher than the engineering stress and indeed may be rising while the load or engineering stress is falling (12,13). Accordingly it is instructive to look at the true stress–strain behavior. This is important because while strain localization is often associated with yield behavior, such localization is not necessary for yielding to occur.

Considère Construction (14). Referring back to equation 6 for the true and engineering stresses,

$$\sigma_E = \sigma_T/(1+\varepsilon); \qquad \sigma_T = \sigma_E(1+\varepsilon)$$

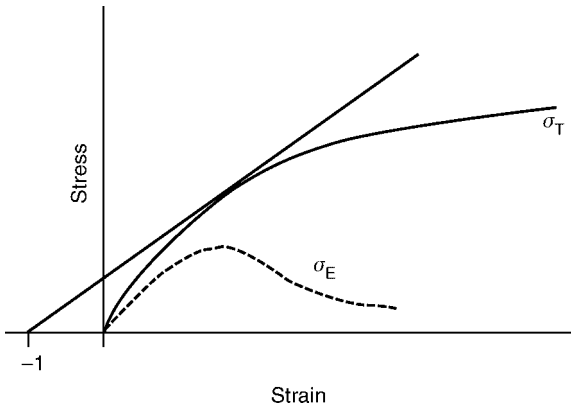

Fig. 2. Engineering (σ_E) and true stress (σ_T) as a function of strain in uniaxial tension. The Considère criterion for necking, that is the ability to draw a tangent to the true stress curve from $\varepsilon = -1$, is also shown.

we see that for all finite strains under uniaxial tensile loading, the true stress is greater than the engineering stress (for uniaxial compressive loading, the true stress is always lower than the engineering stress).

Figure 2 compares the engineering stress, σ_E, and true stress, σ_T, as a function of engineering strain for uniaxial tensile loading. As noted above, the neck is seen to form at the point where the load (or engineering stress) ceases to rise, ie where

$$\frac{d\sigma_E}{d\varepsilon} = 0 = \frac{1}{(1+\varepsilon)}\frac{d\sigma_T}{d\varepsilon} - \frac{\sigma_T}{(1+\varepsilon)^2} \tag{8a}$$

or

$$\frac{d\sigma_T}{d\varepsilon} = \frac{\sigma_T}{(1+\varepsilon)} \tag{8b}$$

In practice then, the point at which a polymer will form a neck is given by drawing a tangent to the true stress–strain curve from the point $\varepsilon = -1$, as illustrated in Figure 2. [We note here that in this condition, yielding is a localization phenomenon. It is also possible that yielding can be a material property unrelated to localization and this is touched upon in a subsequent section.]

Necking and Cold Drawing. Before further discussion of the Considère construction it would be useful to discuss the phenomenology of the yield and necking processes. As discussed above, yield in a material under uniaxial tensile loading is characterized by highly localized plastic deformation within the specimen and a corresponding decrease in the engineering stress. The exact position at which yield occurs on a nominally isotropic and uniform sample is impossible to predict. However, a small change in the local properties at some segment in the sample can lower the local yield stress such that yield will initiate there first. Alternatively, a flaw or inclusion can cause a stress concentration such that the

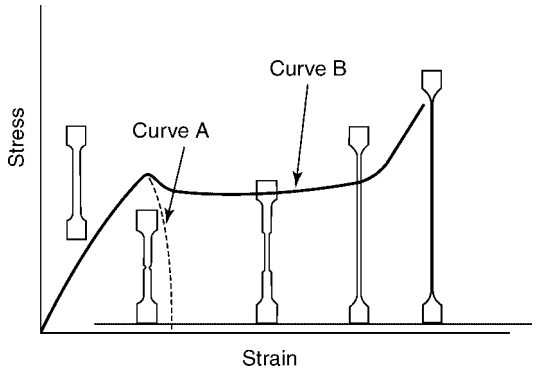

Fig. 3. Engineering stress–strain curves for a material showing, with increasing strain, strain localization(necking), cold drawing, and strain hardening. Also shown are schematics of the sample geometry at each stage.

local stress is higher than the yield stress. After this point one of two things may happen (refer to Fig. 3).

(1) The material in the neck may continue to draw down. As it does so, the true stress continues to rise in the segment, which leads rapidly to failure. This is the case shown in Curve A in Figure 3.

(2) The yielded material can undergo strain hardening. As the material yields and draws down, the polymer chains align along the stress direction, increasing the local stiffness (hence strain hardening is also known as orientation hardening). If the rate of strain hardening is greater than linear, this is sufficient to offset the increase in local stress due to area reduction, and the neck can stabilize. This is the case shown in Curve B in Figure 3. Also shown in Figure 3 are sketches of the deformation that would be seen in a typical tensile specimen as a function of cross-head displacement. Once the yielded material has hardened sufficiently to offset the increase in local stress, the stress (load) stabilizes to a constant value (the draw stress, σ_D) and the neck is seen to propagate along the remaining gage length of the sample until the whole sample has yielded. This process is known as cold drawing.

The oriented material in the strain-hardened section draws down to a characteristic extent under any given conditions and is known as the natural draw ratio, λ_D, and is given by the ratio of the length of the drawn section to its length before deformation. Further deformation can cause additional extension and hence further orientation and strain hardening, and the stress is seen to once again rise until eventually it exceeds the ultimate strength of the material and failure occurs.

In terms of the Considère construction, the criterion for a material to neck and cold draw is indicated by the ability to draw a second tangent to the true stress–strain curve from the point $\varepsilon = -1$ (Fig. 4). Another important aspect of yielding is that, while there is a clear drop in the engineering stress at (or near)

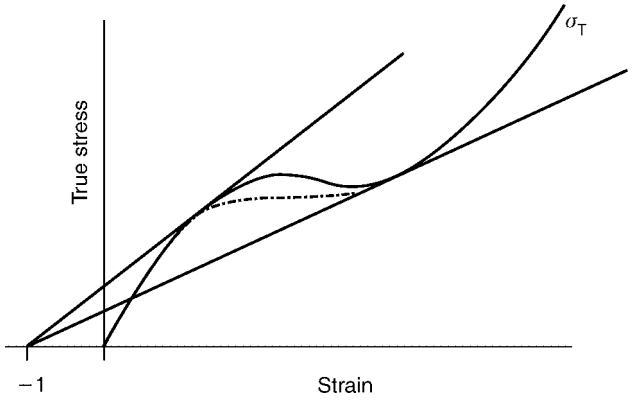

Fig. 4. True stress (σ_T) as a function of strain in uniaxial tension. The Considère criterion for cold drawing, that is the ability to draw a second tangent to the true stress curve from $\varepsilon = -1$, is also shown.

the yield point, there may also, though not necessarily, be a drop in the true stress after yield (Fig. 4). This drop in true stress is commonly referred to as strain softening. At the point of the second tangent, molecular orientation is sufficient to stiffen the material and strain hardening occurs.

Compressive Loading. The discussion above has been developed specifically for uniaxial tensile loading conditions, and this is still the most widely used method for testing of polymers. However, the formation of a localized neck means that it is difficult to measure the true strain at any given point and hence determine the true stress–true strain behavior. Moreover, because tests are generally carried out at a constant cross-head displacement rate, the spatially varying strain means the strain rate is poorly defined. G'Sell and co-workers (15,16) have gone some way to resolving this difficulty by using an optical system to monitor the local strain and a feedback mechanism to adjust the imposed deformation rate to perform constant true strain rate experiments. Alternatively, others (17,18) have used a video system to monitor the neck profile and so back-calculate the true stress–true strain rate profile in the neck region.

Some of the shortcomings of tensile testing are mitigated by the use of compressive loading, typically performed on cylindrical specimens. Since the localization seen when the sample necks is suppressed in this geometry it is experimentally easier to ensure a more uniform strain field; however, some care needs to be exercised to prevent buckling or barreling of the specimens. Barreling is caused by lateral constraint on the cylinder ends due to friction with the loading plates. A suitable (inert) lubricant or a thin PTFE film applied to the cylinder ends is often sufficient to prevent barreling. Buckling will occur if the aspect ratio of the cylinder (height-to-diameter) is too large—aspect ratios of 0.5 to 1 are typically used.

From tests conducted on polymer glasses under both tension and compression (19–23) the true stress versus true strain rate response can be determined and typical plots are shown in Figure 5 (19). As can be seen, qualitatively the true stress–true strain behaviors are similar for both deformation modes. Importantly

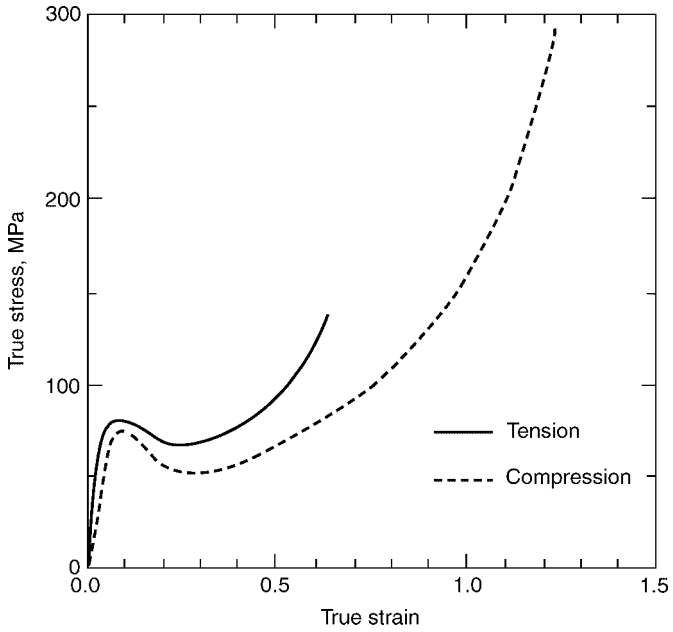

Fig. 5. True stress–strain curves for a polycarbonate under tension and compression. After Boyce and Arruda (19) with permission.

they both show a drop in true stress at the yield point. The observation of a drop in true stress without the localization (necking) seen in tensile tests confirms that the material is undergoing intrinsic strain softening. Importantly this shows that localization is not a necessary requirement for yield and further that the load drop seen in tensile tests is not necessarily simply the result of geometric changes.

While the true stress–true strain response is qualitatively similar in both compression and tension, the resulting deformation states are very different. Tensile loading leads to uniaxial molecular orientation along the loading axis. Compression on the other hand results in a biaxial orientation state in a plane perpendicular to the loading direction and so it is expected that quantitatively different stress–strain curves are seen. In addition, as discussed below, the hydrostatic pressure difference between tension and compression leads to differences in yield strength because yield in polymers is pressure dependent.

The preceding is a general overview of the main features of yield in polymers. From a practical point of view, structures are rarely subjected to simple uniaxial or shear loads and it is instructive to be able to determine when a material might yield under more complicated stress states. The following yield criteria attempt to do this from a phenomenological point of view, that is they do not address the fundamental mechanisms of yield but rather provide yield criteria for multiaxial loading conditions.

Yield Criteria. A practical yield criterion needs to describe the conditions under which yield will occur for a general stress state (eg tension, compression, shear, or some combination). Before we consider the various yield criteria which have been proposed, it is useful to very briefly recap the definition of the principal

stress components as these are generally the terms which are used to define the yield criteria (see VISCOELASTICITY for a more thorough introduction to the generalized stress and strain definitions).

If we take a small representative cube within a body, then the general stress state is given by the stress tensor of the forces acting on the faces of the cube:

$$\sigma_{ij} = \begin{bmatrix} \sigma_{11} & \sigma_{12} & \sigma_{13} \\ \sigma_{21} & \sigma_{22} & \sigma_{23} \\ \sigma_{31} & \sigma_{32} & \sigma_{33} \end{bmatrix} \tag{9}$$

and the generalized strain tensor as

$$\varepsilon_{ij} = \begin{bmatrix} \varepsilon_{11} & \varepsilon_{12} & \varepsilon_{13} \\ \varepsilon_{21} & \varepsilon_{22} & \varepsilon_{23} \\ \varepsilon_{31} & \varepsilon_{32} & \varepsilon_{33} \end{bmatrix} \tag{10}$$

where i refers to the axis normal to the plane on which the stress is acting and j the direction in which the stress acts.

For an isotropic, elastic material two elastic constants are sufficient to describe the material response, the elastic modulus E (eq. 7) and the Poisson's Ratio (ν), defined as the ratio of the axial to the (negative) transverse strain ($-\varepsilon_{11}/\varepsilon_{22}$).

Other mechanical functions such as the bulk modulus, K, and the shear modulus, G are interrelated by the following expressions:

$$\begin{aligned} G &= \frac{E}{2(1+\nu)} \\ K &= \frac{E}{(1-2\nu)} \\ E &= \frac{9KG}{3K+G} \end{aligned} \tag{11}$$

From equation 9, it is seen that the general stress state is described by nine independent components. However, if we assume that the sample is not undergoing rigid body rotation, then the shear components must give a net torque of zero, that is,

$$\sigma_{12} = \sigma_{21} : \sigma_{13} = \sigma_{31} : \sigma_{23} = \sigma_{32}: \tag{12}$$

Thus the stress state is defined by six independent components. Further, if the body is in equilibrium, then it is possible to define a set of orthogonal axes such that the shear components are zero. Such axes are termed the "principal axes"

and the resulting stress components the "principal stresses":

$$\sigma_i = \begin{bmatrix} \sigma_1 & 0 & 0 \\ 0 & \sigma_2 & 0 \\ 0 & 0 & \sigma_3 \end{bmatrix} \tag{13}$$

The sum of the three principle stresses is known as the first stress invariant (or trace), I_1,

$$\sigma_1 + \sigma_2 + \sigma_3 = \text{constant}$$

and the related quantity, the mean stress, σ_M

$$\sigma_M = \frac{\sigma_1 + \sigma_2 + \sigma_3}{3}$$

Tresca Yield Criterion. The earliest proposal for a yield criterion in metals is due to Tresca (24), and it stated that yield occurs when the maximum shear stress reaches a critical value. With $\sigma_1 > \sigma_2 > \sigma_3$ the criterion can be written as

$$1/2(\sigma_1 - \sigma_3) = \tau_s \tag{14}$$

For the simplest loading situation of a tensile test at a stress level of σ_1, with $\sigma_2 = \sigma_3 = 0$ we have

$$\tau_s = \sigma_1/2 \tag{15}$$

so that yield occurs when the applied tensile stress reaches twice the shear yield stress.

Von Mises Yield Criterion. The Von Mises yield criterion (also known as the maximum distortional energy criterion or the octahedral stress theory) (25) states that yield will occur when the elastic shear-strain energy density reaches a critical value. There are a number of ways of expressing this in terms of the principal stresses, a common one being

$$(\sigma_1 - \sigma_2)^2 + (\sigma_2 - \sigma_3)^2 + (\sigma_3 - \sigma_1)^2 = \text{constant} \tag{16}$$

If we again look at the case of simple tension, then we have $\sigma_2 = \sigma_3 = 0$. Defining the tensile yield stress as σ_Y, we see that the constant in equation 16 is $2{\sigma_Y}^2$.

If we look now at the case of pure shear, where we have $\sigma_1 = -\sigma_2 = \tau$ and $\sigma_3 = 0$, we find that

$$4\sigma_1^2 + \sigma_1^2 + \sigma_1^2 = 6\sigma_1^2 = 6\tau^2 = \text{constant} = 2\sigma_Y^2$$

ie

$$\tau = \frac{\sigma_Y}{\sqrt{3}} \tag{17}$$

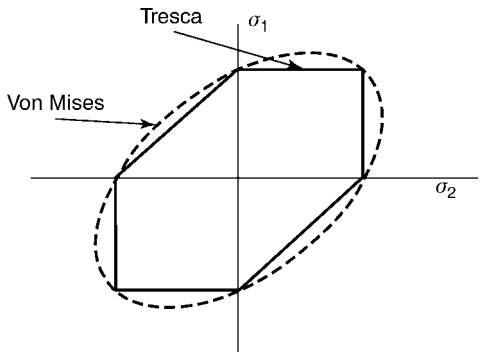

Fig. 6. The Tresca and von Mises yield criteria for plane strain conditions ($\sigma_3 = 0$).

Compare this to the prediction of $\sigma_Y/2$ from the Tresca criterion. The yield criteria for both the Tresca and Von Mises theories are shown graphically in Figure 6. For simplicity, the plots are shown for conditions of plane stress (ie $\sigma_3 = 0$). We can see that the Von Mises criterion describes an ellipse in stress space, with the Tresca criterion consisting of a series of straight lines bounded by the Von Mises limits.

Coulomb Yield Criterion. In 1773, Coulomb (26) identified two components important in the strength of building stone—cohesion and friction. He observed that the shear stress, τ, necessary to cause shear failure across a plane is resisted by the cohesion of the material S_0 and by the product, $\mu\sigma_N$, across that plane, where the constant μ is called the coefficient of internal friction and σ_N is the force normal to the shear plane:

$$\tau = S_0 + \mu\sigma_N \tag{18}$$

This criteria is often expressed in the form

$$\tau = \tau_c + \sigma_N \tan \phi \tag{19}$$

where τ_c is now the critical shear stress for yield and

$$\phi = 2\theta - \frac{\pi}{2} \tag{20}$$

and θ is the angle between the normal to the shear plane and the direction of the applied stress. Data from tensile, compressive, and torsional tests on a range of polymers under imposed hydrostatic pressure (20,27) have been successfully described by the Coulomb criterion, though it should be noted that the modified Von Mises criteria (see below) was equally successful.

Pressure-Modified Criteria. One major shortcoming of the criteria described above is that they predict that the yield stresses in tension and compression are the same. However, in practice it is generally found for polymers that the yield stress in compression is higher than that in tension. This effect is usually considered to be a consequence of the fact that the yield stress depends on the hydrostatic pressure that develops under load. The hydrostatic pressure component

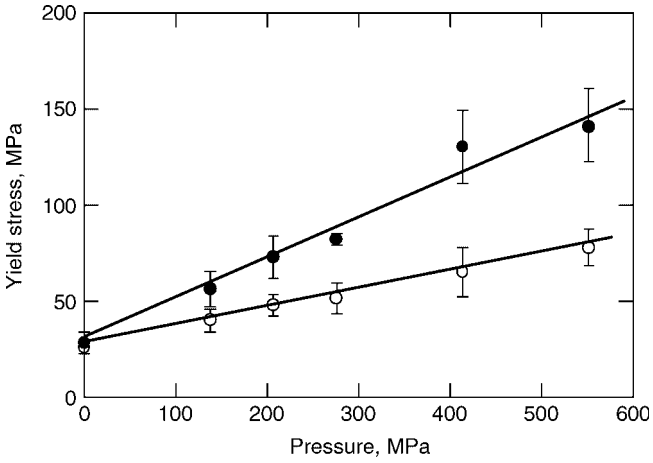

Fig. 7. Yield stress as a function of imposed hydrostatic pressure for polyethylene and polypropylene. Data from Ref. 28. ○, polyethylene, ●, Polypropylene.

of the load in tension is negative, while in compression it is positive. In fact, experiments in which measurements were made under imposed hydrostatic pressures exhibit a strong pressure dependence of the yield stress in polymers (27–29 see also the extensive review in Reference 30). In general it was seen that the yield stress increased linearly with imposed hydrostatic compression (Fig. 7).

Modified Tresca Criterion. A simple way to modify the Tresca criterion to allow for a pressure dependence is to make the critical shear yield stress a linear function of hydrostatic pressure:

$$\tau_T = \tau_T^0 + \mu_T P \tag{21}$$

where τ_T^0 is the critical shear stress with no hydrostatic pressure, P is the hydrostatic pressure, given by $P = -(\sigma_1 + \sigma_2 + \sigma_3)/3$ and μ is a constant. Substituting into equations 14 and 15, we find that the yield stresses in tension σ_{Yt} and compression σ_{Yc} are given by

$$\sigma_{Yt} = 2\tau_T^0/(1 + 2\mu/3) \tag{22}$$

$$\sigma_{Yc} = 2\tau_T^0/(1 - 2\mu/3) \tag{23}$$

Modified Von Mises Criterion. In the same manner as the modification to the Tresca yield criterion one can modify the Von Mises criterion by introducing a linear dependence of the critical shear stress on the hydrostatic pressure:

$$\tau_M = \tau_M^0 + \mu_M P \tag{24}$$

where τ_M^0 is the critical shear stress with no hydrostatic component, P is the hydrostatic pressure, and μ_M is a material constant.

It can be seen from the above criteria that for polymers under uniaxial loading, yield is essentially characterized as a shear-controlled process. There is good experimental evidence for this being the case, and is shown most clearly by the observation of the formation of shear bands on uniaxially loaded specimens. These are regions of locally strained material running at an angle to the applied load, typically at approximately 45°. For isochoric deformation in an isotropic material the angle is precisely 45°, which corresponds to the angle of maximum shear stress. Any preorientation in the material (which introduces an anisotropy to the material) or dilatation during deformation can cause the angle to change. Dilatation generally causes the angle to decrease in the loading direction, while the change due to preorientation depends on the direction of the applied load to the orientation direction.

The criteria discussed above are certainly useful from an engineering point of view and offer a method to estimate the likelihood of failure for a given loading situation. However, from a fundamental viewpoint, they are lacking as they provide no insight into the microscopic or molecular mechanisms that give rise to yield. The following section examines a number of theories that seek to explain yield to varying degrees of complexity.

Theories of Yield

Adiabatic Heating. As far back as 1949 (31–33) it was postulated that local adiabatic heating in polymers causes a temperature rise in the neck region, thereby lowering the local yield stress. While this may be a factor at high rates of deformation where the heat generated cannot be dissipated, experiments using, for example, thermal imaging techniques have shown that the temperature rise is not sufficient to account for yielding. In addition, experiments conducted at rates low enough such that the system is essentially under quasi-isothermal conditions still show yield behavior (34) and therefore simple heating is not an adequate explanation for polymer yield.

Strain-Induced Dilatation. An alternative view of yield in polymers comes from the fact that a tensile strain induces a hydrostatic tension in the material and a corresponding increase in the sample volume. This in turn translates to an increase in the free volume, which increases the polymer mobility and effectively lowers the glass-transition temperature (T_g) of the polymer (alternatively it can be looked upon as increasing the free volume to the value it would have at the normal measured T_g). The increased mobility results in a lowering of the yield stress. Knauss and Emri (35) used an integral representation of nonlinear viscoelasticity with a state-dependent variable related to free volume to model the yield behavior, with the free volume a function of temperature, time, and stress history. This model uses the concept of reduced time (see VISCOELASTICITY), where application of a tensile stress causes a volume dilatation and consequently causes the material time scale to change by a shift factor related to the magnitude of the applied stress. Yield occurs because the free-volume shift factor causes the molecular mobility to increase in such a way that yield can occur.

However yield and plastic deformation are also observed in uniaxial compression and shear (19–23). In the former case the hydrostatic component of stress is

compressive and this leads to a reduction in free volume. Further, as was shown above when discussing the yield criteria, yielding in either tension or compression seems, for polymers, to be associated with the deviatoric (shear) component of the stress tensor, and this intrinsically involves no volume change. Thus, it seems unlikely that strain-induced changes in volume are the underlying cause of yield.

Models of Yield Based on Activated Processes

Models put forward in the in the late 1960s and early 1970s (eg Robertson (36), Haward and Thackray (37), Argon(38)) suggested that for yield and large-strain plastic deformation to occur two distinct sources of resistance must be overcome. First, yield is thought to occur when the polymer is stressed sufficiently to be able to overcome intermolecular resistance to segmental motion. Once the material has started to flow, molecular alignment occurs and changes the configurational entropy of the system. This change in entropy of the system causes the second resistance and is seen physically as a strain-hardening effect.

Yield is generally taken to be an activated process, and the first three of the following theories address this aspect. Models are then presented which address not only the yield of the material but the subsequent strain-softening and strain-hardening events that are observed. The first of these is the Haward and Thackray (37) one-dimensional model, which, while not physically realistic, laid the groundwork for many of the theories that followed it. This is followed in some detail by the BPA model of Boyce, Parks, and Argon (39), which addresses the rate, temperature, and pressure dependence of the intermolecular resistance and also the temperature dependence of entropic hardening. The model proposed by Tervoort and co-workers (40) is then discussed as this addresses some of the shortcomings of the BPA model, specifically the omission of a spectrum of relaxation times to describe the material behavior. The section is finished by examining the model of Caruthers and co-workers (41,42), which approaches yield from the framework of Rational Thermodynamics and seeks to explain a range of behaviors using a set of unified constitutive equations.

Internal Viscosity Model (Eyring Model). If we think of amorphous polymers as essentially viscous fluids then it is reasonable to think of yield and plastic deformation as viscous flow. Eyring (43) in 1936 developed a theory for flow in viscous fluids based on transition-state theory and it is instructive to look at this in more detail as it shows the temperature and rate dependency of the flow process. The Eyring model treats segmental motion as an activated process in which for a given segment to "jump" to an alternative position it needs to cross an energy barrier of height E^*. In the unstrained state the likelihood of either a forward jump or backward jump is equal, ie the stable states on either side of the barrier are at the same energy level (Fig. 8). The rate at which the segments cross the barrier is given by the Arrhenius equation:

$$\nu_0 = A \exp\left[-\frac{E^*}{kT} \right] \tag{25}$$

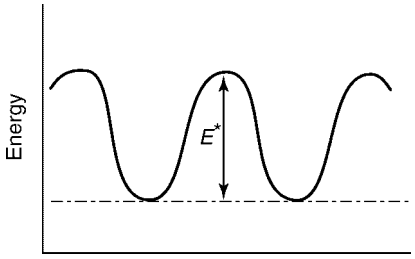

Fig. 8. Schematic of the energy landscape for an unstrained polymer for Eyring's model of viscous flow.

where A is a constant, E^* is the energy barrier height, k is Boltzmann's constant, and T the absolute temperature. According to the theory, application of a stress causes an asymmetric change in the stable energies on either side of the barrier of $+\tau V$ and $-\tau V$ for the forward and backward motions, respectively (Fig. 9). V is the Eyring activation volume and τ the applied shear stress. It is difficult to relate the activation volume V to a physical volume in the polymer, though the term τV in the model notionally represents the work required to move a polymer segment during flow. Under applied stress then, the frequency with which the segments jump in the forward direction is given by

$$\nu_f = A \exp\left(-\frac{E^* - \tau V}{kT}\right) \tag{26}$$

and the frequency they jump in the reverse direction is given by

$$\nu_b = A \exp\left(-\frac{E^* + \tau V}{kT}\right) \tag{27}$$

So, the net rate at which the segments jump is simply the difference in the forward and backward rates:

$$\nu_f - \nu_b = A \exp\left(-\frac{E^*}{kT}\right)\left[\exp\left(\frac{\tau V}{kT}\right) - \exp\left(-\frac{\tau V}{kT}\right)\right] \tag{28}$$

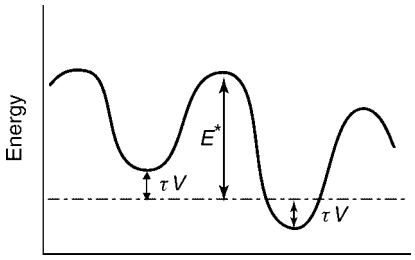

Fig. 9. Schematic of the energy landscape for a strained polymer for Eyring's model of viscous flow.

In a solid, the backward jump rate is negligible in comparison to the forward jump rate (the term τV being sufficiently large such that the term $e^{-\tau V/kT}$ becomes small), and taking the net jump rate $(\nu_f - \nu_b)$ to be proportional to the strain rate, $\dot{\varepsilon}$, then

$$\dot{\varepsilon} = A^* \exp\left(-\frac{E^*}{kT}\right)\exp\left(\frac{\tau V}{kT}\right) \tag{29}$$

As shown earlier, a simple criterion for yield is that the maximum shear stress reaches a critical value given by $\tau = \sigma_y/2$, where σ_y is the tensile yield stress (ie the Tresca yield criterion). Substituting and rearranging equation 29 gives

$$\sigma_Y = \left[k \ln\left(\frac{\dot{\varepsilon}}{A^*}\right) + \frac{E^*}{T}\right]\frac{2T}{V} \tag{30}$$

Equation 30 shows that the yield stress is both rate and temperature dependent, hence it captures some important features of yield in polymers. For example, Figure 10 (44) shows a plot of σ_Y/T (or σ_e/T in the notation of Reference (44)) as a function of log strain rate and, as predicted by equation 30, a linear relationship is seen at each temperature. It is worth noting that the Eyring equation (typically in the form of two activated processes acting in parallel) has been successfully applied not only to the yield behavior of polymers but also to the creep rupture behavior of isotropic and oriented polymers (45–48).

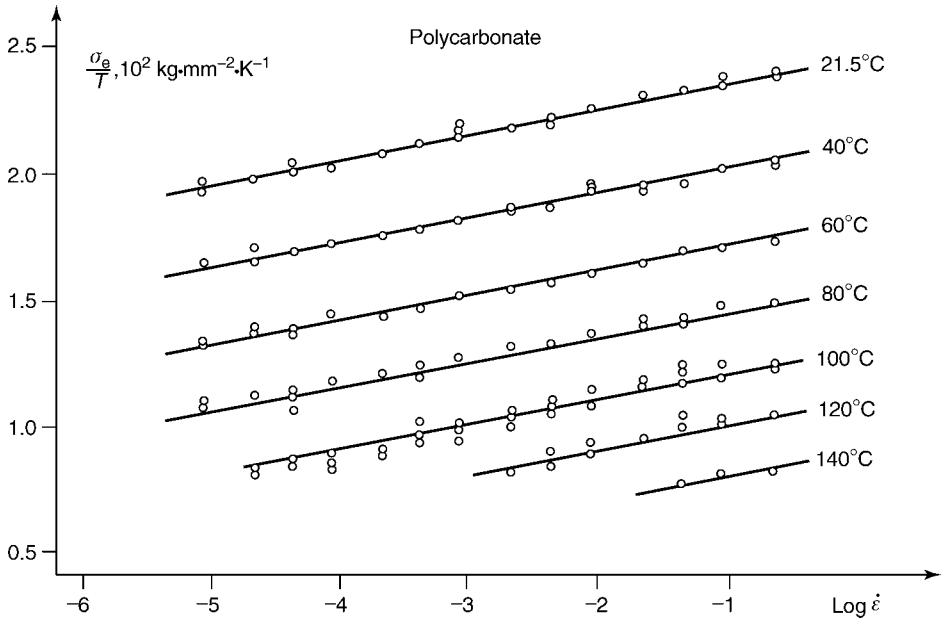

Fig. 10. Yield stress normalized to temperature as a function of logarithmic strain rate for polycarbonate. After Bauwens-Crowet and co-workers (44) with permission.

Robertson Model. The model developed by Robertson in 1966 (36) is also based on an activated process. He stated that the rigidity of a glass is a result of the intermolecular forces between adjacent chains, though for polymer glasses they suppose that the intramolecular forces are also important. Thus, to cause a glassy polymer to move into the liquid state it is necessary to reduce the effect of either the intramolecular or intermolecular forces. Robertson posited that a shear stress alone could achieve this and so induce Newtonian flow in the material. A shear stress field set up in the material can increase the number of flexed bonds (conformations) to a level above the preferred level of the equilibrium glass and may increase to the level that would be typically seen in a polymer liquid.

The model introduces the strain energy as a bias on the energy difference between bonds in the preferred (trans) and flexed (cis) conformations, with the simplifying assumption that the bonds can only exist in one of these two stable states. A polymer below the glass-transition temperature has a fixed, or "frozen-in," distribution of bond conformations in either the high energy (cis) or low energy (trans) states, with the difference in energy between the two states denoted as ΔE. Application of a stress causes conformations to shift from the trans to the cis state, effectively increasing the mobility to liquid-like levels. At sufficiently high stress levels the mobility is sufficiently increased such that yield can occur. More specifically the shear component of the stress (τ) causes a change in the energy difference between the two states by an amount $\tau v \cos \phi$, where v is the "flex volume" and is approximately the average volume of chain segments containing two bonds, and ϕ is the angle between the applied stress and vector displacement of the flexed bond (Fig. 11). The resulting energy difference between the two states (ΔE^*) is now given by

$$\Delta E^* = \Delta E - \tau \mathrm{v} \cos \phi \tag{31}$$

An assumption is then made that the material can be described by a term θ_g, which is the temperature at which the polymer structure in the glass would be an equilibrium structure and can be conveniently set to T_g. By performing a statistical average, the maximum number of flexed bonds for a given applied stress can be calculated and the current structure related to an "equivalent temperature," θ_1.

Using the WLF (49) equation to model the effect of temperature on the material viscosity Robertson went on derive an equation for the maximum shear strain

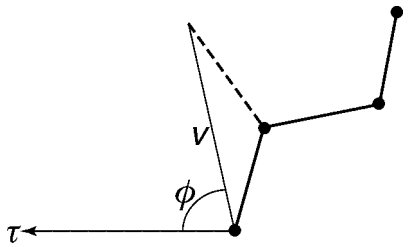

Fig. 11. Schematic of the Robertson (36) model for a shear-induced conformation change.

rate, $\dot{\gamma}_{MAX}$, induced by the shear stress, τ, as

$$\dot{\gamma}_{MAX} = \frac{\tau}{\eta_g} \exp\left\{-2.303\left[\left(\frac{c_1^g c_2^g}{\theta_1 - T_g + c_2^g}\right)\left(\frac{\theta_1}{T}\right) - c_1^g\right]\right\} \tag{32}$$

where c_1^g and c_2^g are the "universal" constants from the WLF equation, η_g is the "universal viscosity" at T_g, and θ_1 is as discussed above.

The model can be used to predict the shear rate as a function of shear stress for a range of temperatures. In the original paper a lack of shear stress data meant that the predictions were compared to tensile stress–strain data by decomposing the tensile data into shear and biaxial components. The point on the tensile stress–strain data that Robertson took to be the most appropriate stress to compare with the computed strain rate was the yield point. The model gives values for the yield stress and the temperature dependence of the yield stress that agree well with experiment for a number of polymers.

The model is attractive since the six parameters required above can be obtained independently and thus no fitting to the data is required. Of these six parameters, only two relate directly to the individual polymer, namely the glass-transition temperature, T_g, and the parameter v, the average volume of chain segments containing two bonds (though in practice Robertson took this to be the volume of a monomer unit in the glassy state at room temperature).

The Robertson model was extended by Duckett and co-workers in 1970 (29) to account for the pressure dependence of the yield stress. By their argument, if the two states are trans and cis and the effect of stress is to increase the number of cis conformations, then this implies a lower resulting density since the packing is less efficient. This in turn implies the change in conformations has an impact on the hydrostatic component of the applied stress. They further suggest that the hydrostatic component of the stress, p, will do work during the activation process leading to an overall energy difference between the two states of

$$\Delta E - \tau v + p\Omega \tag{33}$$

where p is positive in compressive loading and negative in tensile loading. The term Ω has units of volume. Using this modification they successfully correlated the torsional yield stress dependence of PMMA under hydrostatic pressure with the variation in the yield stress under compressive and tensile stresses as a function of temperature and strain rate.

Argon Model. Argon in 1973 (38) developed a molecular model for the initial yield based on the Gibbs free energy of the system. Again it considers that yield does not occur until the resistance to segmental rotation can be overcome by the application of stress. Strain in the sample is proposed to occur by the rotation of small molecular segments from an initially random orientation to a preferential orientation along the load axis. Such a process is modeled by introducing a "kink pair" into the molecule. The resistance to this kink formation is primarily from the surrounding molecular chains, and is modeled as an equivalent elastic medium. Argon derived an expression for the change in free energy, dG^*, required to produce

segmental rotation:

$$dG^* = \frac{3\pi G\omega^2\alpha^3}{16(1-\nu)}\left[1-\left(\frac{\tau}{\frac{0.077G}{1-\upsilon}}\right)^{5/6}\right] \tag{34}$$

where G is the temperature-dependent shear modulus, ν is Poisson's ratio, ω is the net angle of rotation between the two configurations, α is the mean molecular radius, and τ is the applied shear stress. This leads to an energy maximum as a function of the distance between molecular kinks and defines an energy barrier for kink formation. The rate of transfer between the ground and activated states is then modeled in a manner similar to that of a thermally activated Arrhenius process.

This leads to a plastic strain rate given by

$$\dot{\gamma}_P = \dot{\gamma}_0 \exp\left(\frac{-\mathrm{d}G^*}{kT}\right) \tag{35}$$

where $\dot{\gamma}_0$ is a pre-exponential factor having the units of s^{-1}, k is Boltzmann's constant, and T the absolute temperature.

Equation 35 can be rewritten as

$$\dot{\gamma}_p = \dot{\gamma}_0 \exp\left\{-\frac{As_0}{T}\left(1-\left(\frac{\tau}{s_0}\right)^{5/6}\right)\right\} \tag{36}$$

where

$$A = 39\pi\omega^2\alpha^3/16\kappa$$

and

$$s_0 = 0.077G/(1-\nu)$$

s_0 is termed the athermal shear yield strength and is the value of the shear yield strength as the temperature approaches absolute zero (and assuming finite strain rates). The above equation can be rearranged to give

$$\tau = s_0\left[1-\frac{T}{As_0}\ln\left(\frac{\dot{\gamma}_0}{\dot{\gamma}_P}\right)\right]^{6/5} \tag{37}$$

Equation 37 thus captures both rate and temperature dependencies of the shear yield stress.

Haward and Thackray Model. In 1968 Haward and Thackray (37) developed a one-dimensional model for yield using a spring in series with a parallel arrangement of a spring and dashpot (Fig. 12). The dashpot, rather than being Newtonian as with the standard Maxwell/Kelvin models, was instead an Eyring

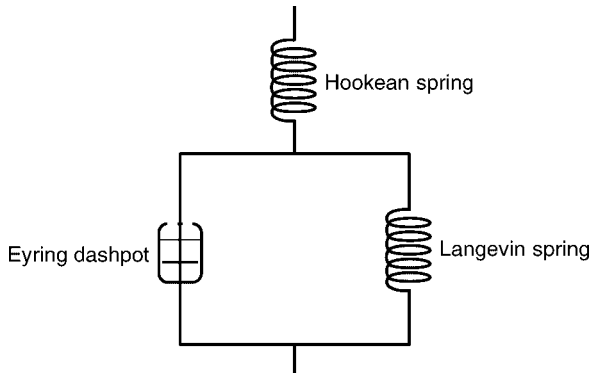

Fig. 12. Schematic of the one-dimensional model of Haward and Thackray.

dashpot. The standard Hookean-type spring was replaced with a Langevin (finite extensible) spring to account for the strain hardening (entropic resistance) observed at larger strains. The initial elastic response remains modeled with a Hookean spring in series. While the model correctly gives the dependence of the yield stress on strain rate it gives only a somewhat simple approximation to the realistic stress–strain response. Also, in common with all the previous models (Eyring, Robertson, and Argon), it does not address the issue of strain softening. However, the general principle of the model has been widely accepted and has been further refined and extended to address some of the shortcomings as discussed in the following sections.

Boyce, Parks, and Argon model (BPA Model). In a fashion that is conceptually the same as the Haward and Thackray (37) model, the BPA (39) model assumes that after an initial elastic response, the plastic resistance can be separated into a resistance to flow due to an activated process and an entropic resistance due to molecular alignment. The model builds on the Argon model to describe the initial yield in terms of the resistance to segmental motion and extends it to include pressure and strain-softening effects. It then goes on to model the second component of resistance to (large-strain) deformation, that of entropic resistance, in terms the "three chain" non-Gaussian (inverse Langevin) statistical model of Wang and Guth (50).

In the BPA model, it is the athermal shear strength given in the Argon model, s_0, which is modified to explain the observed strain-softening behavior. The reasoning behind this is that as the material undergoes the initial stages of plastic flow some restructuring of the molecular chains is assumed to occur and these changes are in turn assumed to cause a reduction in the athermal shear resistance. The evidence for this is discussed in detail in the paper by Boyce and co-workers (39). Briefly, tests carried out on polycarbonate after different thermal treatments and tested under identical conditions give different peak yield stress levels. However, the post-yield strain softening generally brings the stress levels down to the same value and this is interpreted as the material achieving a "preferred structure" during plastic flow. The decrease in the athermal shear resistance with strain is modeled phenomenologically by the following

expression:

$$\dot{s} = h\left(1 - \frac{s}{s_{ss}}\right)\dot{\gamma}_P \tag{38}$$

where s is the current value for the athermal shear resistance and is a function of the instantaneous structure, s_{ss} is the value s reaches at steady state, ie in the preferred structure, and $\dot{\gamma}_P$ is the plastic strain rate. Note that s_{ss} can itself be temperature and rate dependent. h is the slope of the yield drop with respect to strain, with the yield drop defined as the difference in the maximum stress before softening and the lowest stress level after plastic flow. The yield drop depends on temperature and strain rate and varies with strain as a function of structure and strain rate.

As noted above in discussing yield criteria, the shear yield strength generally increases linearly with applied hydrostatic pressure. Similar to the modified Tresca or von Mises yield criteria, where the shear yield stress is modified by a term linearly dependent on pressure, the BPA model introduces a term to modify the current athermal shear yield strength, s:

$$\tilde{s} = s + \alpha P \tag{39}$$

where α is the pressure coefficient, P the hydrostatic pressure, and s the athermal shear resistance modified for strain softening.

Thus the term s_0 in the original Argon model for yield (eq. 36) is replaced by $\tilde{s}$ to give

$$\dot{\gamma}_P = \dot{\gamma}_0 \exp\left\{-\frac{A\tilde{s}}{T}\left[1 - \left(\frac{\tau}{\tilde{s}}\right)^{5/6}\right]\right\} \tag{40}$$

where the pressure and strain-softening effects are contained in the $\tilde{s}$ term.

The second part of the BPA model concerns the entropic resistance resulting from molecular orientation and which leads ultimately to strain-hardening behavior. This is strictly a post-yield phenomenon and indeed the physics of the development of chain orientation and subsequent material behavior alone is the subject of books (eg Ward I.M. (51)). The BPA model uses the development of three-dimensional entropic resistance as first modeled by Parks and co-workers (52). Consider an amorphous polymer that is plastically deformed below its glass-transition temperature (T_g). If this material is then heated to above T_g it will recover to its original undeformed state. In order to prevent the material returning to the undeformed state at temperatures above T_g, it would be necessary to impose a stress on the sample. This restraining force then acts to counteract the shrinkage force or 'back stress' B_i. For the plastically deformed material below T_g, this back stress can be considered to be frozen-in to the deformed polymer at temperatures below T_g and is the source of resistance to further deformation. The recovery of the material deformation above T_g clearly has parallels with rubber elasticity and the orientation hardening is modeled using the statistical mechanics theories of rubber elasticity (Treloar 1975 (53)). For low

stretch ratios, the standard Gaussian statistical model of Treloar (53) is sufficient. However, the BPA model as originally developed used the non-Gausssian statistical mechanics network (Three-chain model) of Wang and Guth (50). This gave an expression for the back stress, B_i, as a function of the number of statistical segments between entanglements, the plateau rubber modulus (through which the temperature effects are taken into account) and the change in entropy as a function of the principal plastic stretches. The reader is referred to the original paper (39) for the specific details and development of this aspect of the model. The model has since been incorporated into commercial finite element codes (ABAQUS).

The model has been subsequently refined (Arruda and co-workers (54)) to more accurately describe the three-dimensional spatial orientation of the stretched molecular network using the eight-chain model (though comparison of the predictions from the eight-chain model with experimental results from natural rubber and polydimethylsiloxane has called into question the physics of that model (55)). The BPA model has been further developed (56) to account for aging effects (see, eg Reference 57). A model using the same underlying concepts, but again developed to improve the description of the strain hardening (entropic resistance), has been given by Wu and van der Giessen (58) using a "full chain" model.

Tervoort and co-workers Model. While the above models make reasonable predictions of the stress–strain behavior in monotonic loading conditions, a main drawback to them is that they use only a single stress-dependent characteristic (relaxation) time. As a consequence, the predicted behavior tends to show a sharp transition between elastic (solid-like) and plastic (fluid-like) behavior. However, it is found in practice that all polymers exhibit behavior consistent with a spectrum of relaxation times and this is clearly going to affect the stress–strain response at constant strain rate. In an effort to address this inconsistency Tervoort and co-workers (40) have developed a "modified compressible Leonov model."

The model is based on an earlier one by the same authors, the "compressible Leonov model" (59). In this, the behavior is modeled with a single Maxwell element where the dashpot and spring now have a relaxation time that is a function of the applied shear stress. This is similar in principle to the change seen in the relaxation time with a change in temperature (time–temperature superposition, (see VISCOELASTICITY), leading to the concept of time-stress superposition and a "stress clock" within the material. The model is developed with thermodynamically consistent constitutive equations by assuming that the free energy of the system (a measure of the stored energy) is given by two state variables, the relative volume deformation and the isochoric strain tensor. The volume deformation is coupled to the hydrostatic component of stress while the isochoric strain is determined by the deviatoric stress. It is assumed that the volume deformation remains elastic, whereas the accumulated isochoric elastic strain is reduced over time because of a plastic strain rate. This plastic strain rate is described by a three-dimensional Eyring equation. The single-element model is essentially an elastic–plastic model and still exhibits a sharp transition between the two behaviors. To make the model more realistic, it was extended (40) to include a discrete relaxation

spectrum by using an array of 18 Leonov modes, each with a unique relaxation time.

Tervoort and co-workers tested the multimode model using polycarbonate since it could be described with a single relaxation mechanism having a distribution of relaxation times at the temperature of interest. The model parameters for the Eyring term were determined from plateau creep rates and the linear Leonov parameters from a linear shear relaxation curve (obtained from inversion of the creep compliance curves). The resulting model predictions agreed excellently with stress–strain curves over a range of strain rates up to approximately 8% strain. However, the model lacks any term to account for the entropic resistance (strain hardening) and so is valid only up to the yield point.

In subsequent work, Govaert and co-workers (60,61) specifically address the postyield large-strain phenomenon of strain hardening, again for a polycarbonate. In an effort to minimize the effects of a localized, inhomogeneous strain deformation (neck), they adopted a technique of mechanical preconditioning. This technique aims to reduce the strain-softening characteristics of the material by conditioning the material through plastic deformation (61,62). The resulting true stress–true strain curves show a markedly reduced yield drop, while maintaining the same large-strain response. Interestingly, the authors found that the large-strain data could be modeled as simple neo-Hookean behavior and this was true up to the failure point (at a draw ratio of approximately 3). As the authors observed, this is in contrast with the results of eg Arruda and co-workers (63) for a different grade of polycarbonate where there was a deviation from neo-Hookean behavior indicating finite extensibility effects (ie a rapid upturn in the true stress–true strain response).

Caruthers and co-workers Model. The group of J.M. Caruthers at the Chemical Engineering Department of Purdue University has, over the last decade or so, been developing a set of unified constitutive equations that aim to realistically model a wide range of rheological and mechanical properties (41,42). A detailed description of the model is beyond the scope of this article and we mention here only the main ideas behind the development of the model (see also VISCOELASTICITY). The model addresses the time, temperature, and history (thermal and mechanical) dependence of the material behavior using a set of thermoviscoelastic constitutive equations based on Rational Thermodynamics (64,65). The model introduces a material (or reduced) time, where the material timescale is determined by the instantaneous thermodynamic state of the material, using the Adam–Gibbs (66) model, which relates the relaxation time to configurational entropy. This is a potentially important development in the context of this article, as it allows the prediction of nonlinear mechanical behavior including yield. The model is still in development, but has successfully predicted a range of behaviors including specifically isobaric volume relaxation, yielding under uniaxial extension, shear thinning, and stress overshoot in transient shear (42).

A particularly appealing aspect of the model is that all the model parameters can be determined from independent experiments and further that they are relatively few in number. Thus a material can be characterized in a relatively short period of time, though the mathematical framework of the model is somewhat intensive.

Dislocation Plasticity

The observation of microscopic shear bands in polymeric materials, coupled with the highly successful application of dislocation theory to plasticity in ductile metals, has led to the concept of dislocation plasticity in polymeric materials. The first application of dislocation mechanisms was, not surprisingly, to semi-crystalline polymers (67). Predeki and Statton (68,69) looked at the effect of chain ends on crystalline regions and introduced the idea of screw and edge dislocations occurring in nylon-6,6 (68). They further examined the effect of shear stress on such dislocations in polyethylene (69). Direct evidence for the presence of dislocations in polymer crystals was obtained by Petermann and Gleiter (70) from the electron microscopy of single crystals of polyethylene. Gilman (71,72) further suggested that dislocation mechanisms can be applied to amorphous solids such as glasses and polymers. Bowden and Raha (73) developed a model of yield in which micro–shear bands are created by the formation and growth of dislocation loops, the energetics of which are influenced by the shear stress and the thermal energy. Unlike metals, where the dislocations or defects are inherent, the dislocations in polymers are formed under the action of an applied stress. Once formed, they may grow with the aid of thermal activation, ultimately leading to yield. The authors emphasize that the dislocation process they envision as occurring in an amorphous solid is not the same as in the classic concept of crystal plasticity, though it is a close analogy.

The energy U of a dislocation loop of radius R is

$$U = (2\pi R)\frac{Gb^2}{4\pi}\ln\left(\frac{2R}{r_0}\right) - (\pi R^2)\tau b \tag{41}$$

where r_0 is the radius of the dislocation core, τ the applied shear stress, G the shear modulus and b the Burgers vector (essentially equal to the magnitude of the shear displacement). The first term in equation 41 is the elastic strain energy associated with a loop of length $2\pi R$ and the second term the work done by the applied stress to expand the loop to radius R (of the order of 1 nm). As the loop expands the energy at first increases then reaches a maximum at some critical radius (R_c), then will monotonically decrease. As expected, the height of this energy barrier decreases with increasing shear stress. The Bowden and Raha model is thus a thermally activated model whereby both the rate and temperature dependence are captured in the term U/kT. Interestingly, the model also implicitly accounts for strain softening—as the dislocation loop overcomes the peak in the energy barrier, further growth leads to a lower energetic state with the implication of reduced resistance to further extension. As the model is presented, the reduction in resistance (and hence the degree of strain softening) is monotonic, that is there is no limit to the extent to which the material will strain soften. This is clearly a major limitation of the model, though the authors have suggested a number of mechanisms that may limit the degree of strain softening.

The above model based on dislocation-type defects in polymer glasses is attractive in that it allows one to put some order and physical interpretation to

the (obviously complicated) processes occurring during deformation. Care must be exercised though in taking the analogy with dislocations in metals too far—the ordered structure of metals is not seen in polymers, hence the meaning of a defect such as a dislocation is unclear.

Ultimate Shear Strength

The maximum theoretical strength of a crystal had been estimated by Frenkel as far back as 1926 (74), and the same general ideas have been applied to amorphous polymers (73,75,76). Briefly, if an equilibrium crystal lattice is sheared to a strain of 1, each atom will have moved to a new equilibrium position. At a strain of 0.5, the atoms will be between one equilibrium position and the next and the shear stress required to hold it in position will be zero (albeit in an unstable state). Consequently, the maximum shear stress is assumed to occur at a shear strain of approximately 0.25. Since the initial slope of the stress–strain curve is the shear modulus G, this gives an estimate of the maximum shear stress to be approximately $G/6$. While the structure of an amorphous polymer is far from that of an ideal crystal it is reasonable to suppose that the molecular segments are at some equilibrium position and at a high enough shear stress most, if not all, will fall into a new equilibrium position (though the energy landscape, and hence equilibrium potentials, will not be as uniform as those in a crystal). The model as proposed did not allow for thermal fluctuations (ie it was effectively for a material at 0 K) and it is expected that taking account of such fluctuations would reduce the theoretical strength.

Other estimates of the ultimate shear strength of amorphous polymers have been made by a number of authors and generally all fall within a factor of 2 of each other (38,77,78). Stachurski (79) has expressed doubt as to the validity of the concept of an intrinsic shear strength based on the value of the shear modulus, G, for an amorphous solid. He questions which modulus is the correct value to use—the initial small strain value or the value at higher strain (the yield point or the ultimate extension). Further, the temperature and strain-rate dependence of both the yield strength and modulus (however defined) suggests that perhaps the ratio of yield strength to modulus is not a true intrinsic material property. We remark however that the temperature and strain-rate dependence of both the yield stress and the shear modulus are often similar.

A related issue is that the modulus is a viscoelastic property, as evidenced by the temperature/strain-rate dependence, and that for most polymers (at least those without a large beta transition near the alpha transition) time–temperature superposition of, for example, the shear relaxation modulus is valid (80). Further, G'Sell and McKenna (81) have shown that the yield stress vs strain rate also seems to obey time–temperature superposition. Hence there is a correlation between the viscoelastic properties and the yield response of polymers, though one that is not generally stated explicitly. We note that some of the models mentioned previously, such as those of Caruthers' group (41,42), Tervoort and co-workers (40), and Knauss and Emri (35), are (nonlinear) viscoelastic models that have yield arising due to the nonlinear response induced by the material clock (see VISCOELASTICITY).

Calorimetry and Dilatometry

When a polymer is deformed, work is necessarily done in the material. On subsequent unloading, the stress–strain curve does not generally follow the loading curve and the difference in the areas under the two curves gives the net work done on the material (W). This work can be subdivided into work done in changing the internal energy of the material ($\mathrm{d}U$) and heat liberated (Q):

$$W = \mathrm{d}U + Q \tag{42}$$

By measuring both the heat flow generated during deformation (Q) and the engineering stress–strain data (and from this the quantity W) it is possible to estimate the change in the internal energy of the sample. A pioneer in this field of study is Oleinik (also spelled Oleynik) (82). In a series of experiments, samples of polystyrene placed in a calorimeter were compressed to varying levels of strain (up to approximately 40%) and unloaded, and the W and Q were calculated. The total work (W) rises somewhat linearly with applied stress while the amount of heat liberated (Q) rises at an initially slower rate then increases to become parallel to the W curve at a strain of approximately 25%. This means that the stored internal energy ($\mathrm{d}U$) rises at lower strains then plateaus out at strains above 25%, with an inflection point at or near the yield strain of 12%.

The same effect can be observed by performing DSC tests on previously strained samples. Hasan and Boyce (83) subjected annealed polystyrene to compressive strains up to 170% followed by DSC scans up to and through the glass-transition temperature (T_g). Comparing the results to freshly annealed samples, it was seen that for samples that had been strained, a pre-T_g exotherm appeared that increased with increasing compressive strain. This pre-T_g exotherm increases in magnitude up to a strain of 25% and remains constant thereafter up to the maximum strain of 170%, in excellent agreement with the data of Oleinik. They also note that the exotherm is spread over a wide temperature range (starting at approximately T_g -35°C), which they attribute to the distributed nature of the structural state. In addition, there appears to be a similar inflection point at a strain near the yield strain (within the range 10–15%).

The exact nature of the storage mechanism that is reflected in the increase in internal energy remains unclear. Indeed it is not clear that the energy term $\mathrm{d}U$ can be considered simply as a storage term, especially at the higher strains where energy could be expended on chain scission or processes akin to phase changes occurring at and above yield.

Polymers are inherently viscoelastic, compressible materials and under conditions of dilatational deformation (eg uniaxial tension or compression) a full description of their behavior needs to take into account the volume changes due to, at least, the hydrostatic component of the stress (84). One of the earliest works on volume effects on yielding in glassy polymers was by Whitney and Andrews (85), who examined a range of polymers under uniaxial compression. In the study, the authors observed a volume contraction upon loading up to the yield point, after which the volume remained approximately constant. More recently (86), subyield tension and compression tests were performed on two commercial grades of polycarbonate (PC). These tests were performed under stress relaxation conditions and

showed that under tension the volume increased somewhat monotonically with strain while under compression the reverse was true, ie the volume decreased monotonically. While the volume at a small strain was found to recover toward the initial state, at strains approaching yield and in tension the material actually densified to a state of higher density than the undeformed polymer. It was postulated that the mobility that allowed the material to densify was related to its propensity to yield rather than fail in a brittle manner. A number of studies have been performed on the volume evolution during mechanical deformation [eg (87–89)]. Also studies on the changes in "free volume" with deformation using positron annihilation spectroscopy (PALS) (90–92), have been carried out. The reader is referred to the texts for further details.

Computer Modeling

With the advent in recent years of increasingly powerful and cheap computing power, molecular modeling of the deformation response of polymers has come to be of increasing importance (76). Molecular mechanics uses the Newtonian equations of motion to calculate the step-wise displacement of individual atoms within a molecule in small time intervals (typically of the order of femtoseconds). On each step, the atom's position is modified with reference to its previous state (position, velocity, etc) and taking into consideration, for example, its bond length and bond angle (bonded interactions) and Van der Waals forces (nonbonded interactions) with its nearest neighbor. The system as a whole is then optimized using potential energy functions to determine the equilibrium conformation. Molecular mechanics calculations are performed on systems that are generally considered to have little, if any, thermal energy (ie at low temperature). As such, the optimization procedure may only find the conformation representing the *local* minimum in the energy landscape and this will not necessarily (indeed rarely) be the lowest possible energy. Molecular dynamics, on the other hand, considers not only the force interactions but also the thermal motions of the molecule. By doing so, the molecule is allowed to overcome energy barriers and so explore its surroundings more effectively, assisting in finding the *global* energy minimum. Importantly, in molecular dynamics the thermal motion is always active and the molecules tend to oscillate about the energy minimum, giving additional information about the time-dependent motion of the molecules.

As noted, the field of molecular simulation is relatively new, and a detailed review of it is beyond the scope of this text and we introduce here a few of the more relevant references. One of the first applications of molecular mechanics to polymers was by Theodorou and Suter (93,94), who modeled atactic polypropylene as an amorphous cell subjected to a range of stress conditions (hydrostatic pressure, pure strain, and uniaxial strain). Such modeling generally gives reasonable estimates of the elastic constants of a material [within 15% (79)], providing the density of the glass is correctly modeled.

Argon and co-workers (95,96) have developed an atomistic mechanics model of polypropylene and related it to experiments performed at a temperature of 10°C below the glass-transition temperature. Stress–strain curves calculated after small strain increments showed a series of generally monotonically increasing

stress versus applied strain sections (elastic response), interspersed with sudden step-wise drops in the load (plastic events). Significantly, the authors note that the plastic events are not associated with any deformation process invoked by many of the molecular theories discussed above (ie a sudden conformation or configuration change, a dislocation motion or kink propagation). However, because this was an athermal model, the meaning of these events for a real viscoelastic or viscoplastic polymer is unclear.

Computer modeling can clearly help in the understanding of the deformation and yield behavior of polymeric systems by giving an insight into the individual molecular, indeed atomic, movements that occur. However, the simulations are typically run over a few tens of picoseconds at most and in a volume of a few cubic nanometers—such scales of time and dimensions cannot fully capture the processes involved in yield at the present state of development.

Semicrystalline Materials

The propensity of a polymer to crystallize is chiefly determined by its molecular architecture, specifically the regularity of the polymer chain. Polymers consisting of the same repeat unit, the simplest example being linear polyethylene, can fit together neatly to form the ordered crystalline phase and typically have 70–80% crystallinity. For polymers where a hydrogen from the ethylene monomer is replaced by a bulky side group [for example the methyl group ($-CH_3-$) in polypropylene or the phenyl group ($-C_6H_5$) in polystyrene], the polymer chain can exist in one of three forms of handedness, or tacticity. If all the side groups lie on the same side of the main chain the material is called isotactic; if they lie in a regularly alternating fashion left and right of the main chain the material is termed syndiotactic; and finally, if they occur randomly positioned along the main chain they are termed atactic. The least regular, atactic form generally does not crystallize to any degree, while both the isotactic and syndiotactic forms can crystallize, though the degree to which either form does so depends on the structure, polarity of the side group, etc.

Early X-ray studies on the structure of Semicrystalline Polymers (qv) showed that the longest dimension of the crystallites was typically of the order of a few tens of nanometers. This is a small fraction of the length of a typical polymer chain, which may be of the order of several thousands of nanometers, and it was originally thought that the polymer chain moved successively between different regions of amorphous and ordered crystalline phases in what is termed the "fringed micelle model." However, later work on single crystals grown from dilute solutions revealed that the polymer backbone was perpendicular to the longest dimensions of the crystal. Such a structure could only be produced if the polymer chains were folding back upon themselves.

The current prevailing view is that the crystalline regions in semi-crystalline polymers are made up of plate-like structures formed from mostly chain-folded molecules. These plate-like structures are termed lamella and are typically some 10–20 nm thick. As the molecules forming the lamella chain fold, they may either reenter adjacent to the current position, reenter at some position farther along the lamella, or stay in the amorphous region. Ultimately, farther along the molecular

chain, such molecules may enter another lamella thus forming "tie molecules," akin to entanglements in amorphous polymers. These lamellae may in turn form supramolecular structures called spherulites—aggregations of lamellae forming and growing from a central nucleation point.

Below the crystalline melting point, semi-crystalline polymers are then essentially two-phase systems consisting of a stiff, rigid crystal phase embedded in a more flexible amorphous phase. The amorphous phase may be either above its glass-transition temperature (semi-crystalline/rubber) or below it (semi-crystalline/glass). The yield behavior of semi-crystalline polymers depends critically on a number of factors, eg the degree of crystallinity, the lamellar thickness and interlamellar spacing, spherulite size, the number of tie molecules and, of course, temperature. That said, however, they still show the same general behavior as depicted in Figure 1: brittle at low temperatures, yield and possible strain hardening at intermediate temperatures, and rubbery or viscous flow behavior at higher temperatures.

At temperatures below the T_g of the amorphous phase, the crystallites and associated tie molecules can severely reduce the mobility of the polymer chains and thus tend to embrittle the material. This generally leads to a brittle-like failure (Fig. 13, curve A) though at slow enough rates yielding and drawing may be observed (Fig. 13, curve B).

At temperatures above the T_g of the amorphous phase, the crystallite regions still act to prevent the free movement of the amorphous region and the material does not behave in a rubber-like fashion as would be expected for a pure amorphous polymer. Under these conditions, where the amorphous fraction would not be expected to show a yield point, yield is associated purely with the crystallites. On initial deformation, the crystallites act as hard inclusions, and the strain in the material is carried predominantly within the amorphous fraction. Given that the yield strain in these materials is typically of the order of 0.25 it is unlikely that the (rubbery) network has been sufficiently stretched and strain hardened to

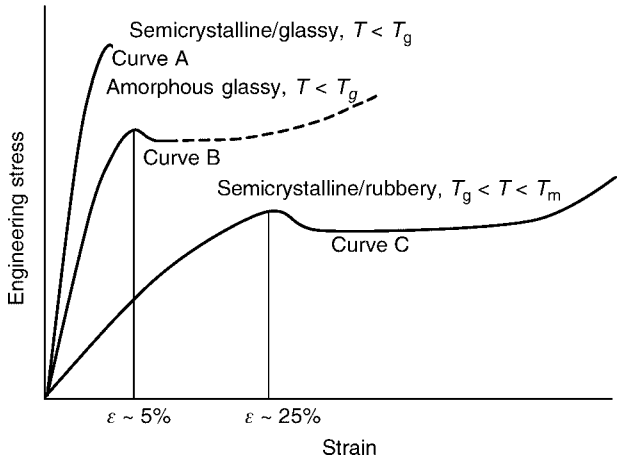

Fig. 13. Representative engineering stress–strain curves for a semicrystalline polymer as a function of temperature.

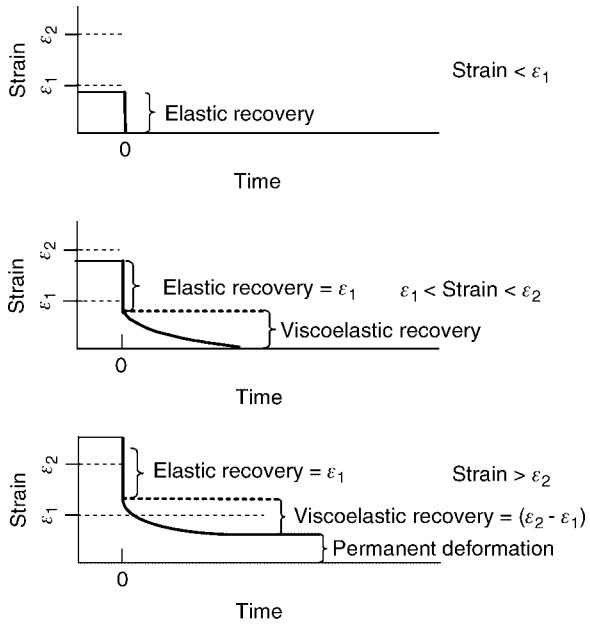

Fig. 14. Schematic of the strain recovery with respect to the double yield point observed in some semicrystalline materials (stress removed at time 0).

load the crystallites to yield. However, it is expected that the network has been sufficiently stretched, such that the tie molecules associated with the lamellae have become taut and so are able to transfer the load to the crystallites. The precise mechanisms associated with the subsequent yield of the crystallites are still not well understood. However, the observation of two yield points (double yield) in polyethylene (97–99) has provided some insight into the molecular processes at work. Up to the first yield point, the material is elastic and deformations are fully recoverable (Fig. 14). The first yield point occurs at low strains (∼5%) and marks the onset of recoverable deformation. This process has been associated with an interlamellar shear process or martensitic transformation within the lamellae and leads to a reorientation of the lamellae, with little or no destruction of the lamellae themselves. The second yield point occurs at a higher strain (20–50%) and marks the onset of permanent plastic deformation and is generally associated with the formation of a neck. At this point coarse slip occurs within the lamellae leading to fragmentation and destruction of the lamellae themselves. The post-yield behavior is largely associated with the amorphous regions and, like a pure amorphous polymer, is controlled by the entangled network. As such, phenomena such as strain hardening and cold drawing are commonly observed as discussed previously (Fig. 13, curve C).

Phenomenologically, the rate and temperature dependence of the yield stress of semi-crystalline polymers can be described by the Eyring activated state model, as discussed earlier, with either one (100,101) or two (46,102) activated processes. However, developing a theory for the yield of semi-crystalline polymers is clearly complicated by the presence of two distinct phases. It is unclear at present whether

the models discussed above are even applicable to the amorphous phase present in semi-crystalline polymers because of the topological constraints that the crystalline regions impose. Nevertheless, in light of the fact that above the T_g of the amorphous region, it is the crystallites that dominate the yield behavior the ideas of classical crystal plasticity are obviously attractive. Young (103) developed a theory along such lines in which the energy required to initiate a screw dislocation in the crystal lamellae determines the yield stress. The model correctly predicts the observed linear relation between yield stress and lamellar thickness, though the quantitative agreement with experiment is controversial (104–107). A model has been recently developed (108) wherein the driving force for the screw dislocations are thermally activated "chain twist" defects that transfer along the chain backbone.

In the early 1990s Bartczak, Argon, and Cohen conducted a series of tests on what they termed "single-crystal textured high density polyethylene" (109,110). These were samples that had been compressed under plain strain conditions, producing an axisymmetric texture that approximated to a macroscopic single crystal. X-ray scattering studies were conducted on the material at various stages of deformation (up to a strain of 1.86, after recovery) to monitor the structural evolution. The resulting material showed distinct crystallographic features indicating unique crystallographic planes, with the *c*-axis of the crystallites aligned along the flow direction (indicating that the lamellae are, broadly speaking, oriented perpendicular to the flow direction). Samples were then cut from the textured samples at particular orientations in order to investigate specific deformation mechanisms. Significant differences in the stress–strain response of samples tested at differing angles to the chain axis were observed under both tension and compression. The papers offer considerable insight into the contribution from different crystallographic deformation mechanisms. Interestingly, when such mechanisms could be isolated, it was found that the Coulomb criterion was an adequate description of the yield surface. The specifics of the various deformation mechanisms and their relation to the specific crystallographic planes is beyond the scope of this article, and the reader is referred to the original papers (109,110) for details.

Crazing

The previous section was concerned with what may be termed "macroscopic yield," which is the shear yield over an entire sample ligament area (albeit localized in the case of neck formation). Another mode of deformation that is commonly observed in thermoplastics is that of crazing. Unlike the shear yielding discussed above, crazing is a microscopically localized phenomenon. The crazes that result from the localized process can be looked upon as load-bearing cracks, where the load-bearing capacity is provided by highly drawn fibrils of material spanning the two interfaces. This is a unique aspect of crazing in polymers as the fibrils can support the crack and help prevent or delay failure.

Crazing generally occurs where the stress on the sample has become highly concentrated owing to, for example, surface defects such as flaws, scratches, or inclusions within the material such as dust or other contaminants. Crazes can also occur in homogenous polymers, ie those without any contaminants or additives

and which are flaw-free. An elegant series of experiments by Argon and co-workers (111) using samples carefully prepared from single pellets has shown that crazing can still occur without any tell tale origins relating to contaminants, a behavior denoted as "intrinsic crazing." While no obvious cause for the craze nucleation may be evident, it must nevertheless originate at a particular point because of an intrinsic local heterogeneity in the molecular structure, such as a local density variation. The stress required to craze such samples is higher than that observed in bulk (and implicitly contaminated) samples and indicates that while flaws or inclusions are not a necessary condition for crazing, they do lead to premature crazing.

The appearance of crazes in a material is generally a precursor to brittle failure. While such a mode is normally to be avoided, the presence of crazes can provide some beneficial effects. Because the crazes contain highly drawn fibrils of material, considerable plastic deformation and hence energy goes in to their formation and this can be a major source of fracture toughness. Indeed, the deliberate inclusion of small, typically rubber, particles into inherently brittle polymers is commonly undertaken to produce tough materials (112–115), because the presence of the particles dramatically increases the craze density.

The following is a brief overview of the subject matter which introduces the reader to the main features of craze morphology and current theories on their initiation, growth, and failure. The reader is pointed in particular to excellent reviews on many aspects of crazing by Kramer (116), Kramer and Berger (117), Kambour (118), and Donald (119,120), and much of the subsequent discussion follows the development in those reviews.

Crazing in polymers follows three distinct stages: craze initiation where the craze is nucleated, craze growth where the craze continues to grow in a direction perpendicular to the applied stress, and finally craze failure, the precursor to ultimate failure. Before discussing these three aspects of crazing, a general overview of craze morphology is given to familiarize the reader with the structure of the craze and the salient features involved in craze growth. The specific details and evolution of the structures are discussed in the relevant subsequent sections.

Craze Morphology. Figure 15 shows a schematic of craze nucleation and growth. The presence of an intrinsic or extrinsic heterogeneity causes the bulk stress to be locally modified. This results in an increase in the local triaxial stress field and forms a localized plastic zone (Fig. 15**a**). Small voids form in this plastic zone and, as the voids grow, they eventually coalesce with the original material between the voids forming the fibrils (Fig. 15**b**). The final craze structure (Fig. 15**c**) consists of the two surfaces bridged by a network of fibrils of drawn (highly anisotropic) polymer with a voided region at the craze tip from which craze growth may continue. Such fibrils typically have a diameter of a few tens of nanometers and a length (craze thickness) of the order of a micron. As the craze continues to grow, the fibrils extend by either a creep mechanism or by drawing in additional material from the bulk–fibril interface (Fig. 16) under the influence of the local stress at the craze boundary (σ_{CR}), which is typically slightly lower ($\sim$5%) than the applied bulk stress (σ_B) (Fig. 17, after Reference 121—the data shown is for an isolated craze in an "infinite" sheet, points on the x-axis denoting the distance from the centerline of the craze and is of course symmetrical about that line). Eventually a failure criterion is reached and the fibrils fail. The loss of the load-bearing

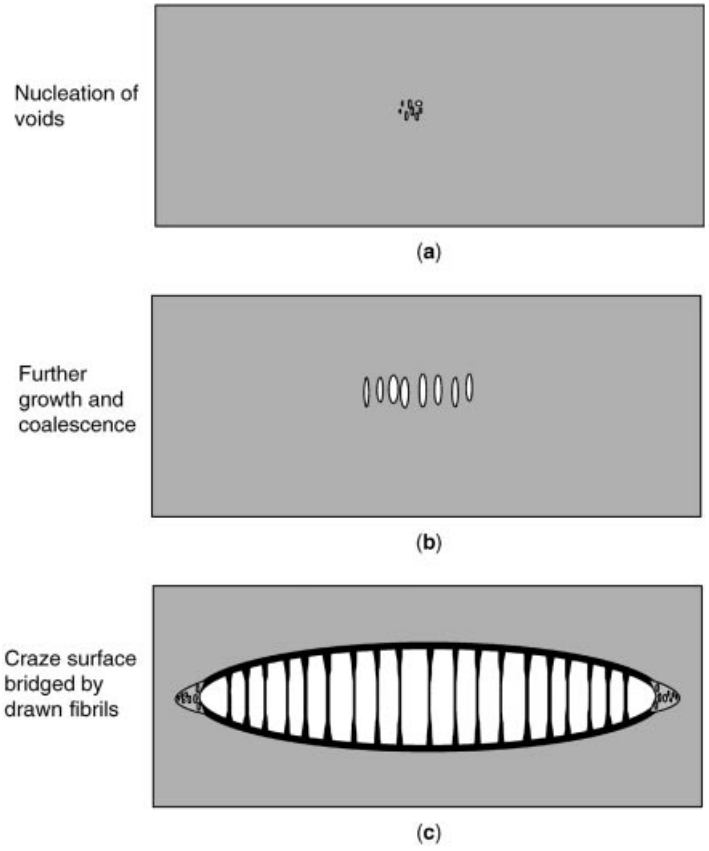

Fig. 15. Schematic of (**a**) void formation, (**b**) craze initiation, and (**c**) craze growth.

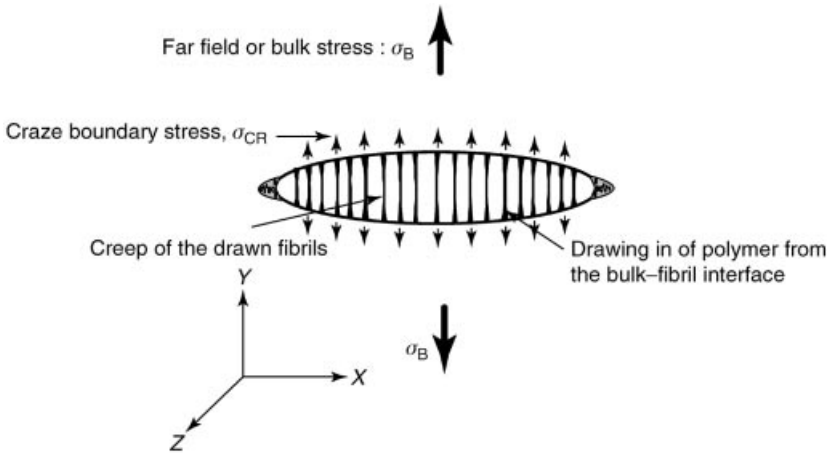

Fig. 16. Craze morphology and possible growth mechanisms.

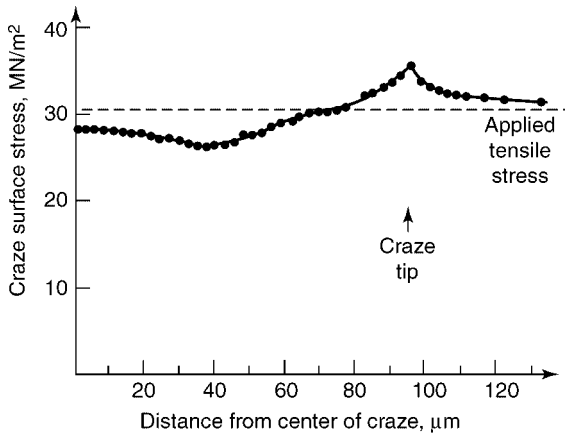

Fig. 17. Craze surface stress as a function of position from the craze centre for polystyrene. After Lauterwasser and Kramer (121), with permission of Taylor and Francis Ltd., http://www.tandf.cp.uk/journals.

capacity of the failed fibrils means the neighboring fibrils are subjected to an additional load and this can, under certain circumstances, lead to a runaway failure of the fibrils, true crack formation, and ultimately brittle failure.

Crazes also normally occur at surface crack tips. The presence of a crack causes a geometrically imposed increase in the local stress (stress concentration), which results in a dilatational stress field. This in turn leads to the formation of a local plastic zone and, in a manner similar to the above, to cavitation and the formation of a craze. The general features of a surface craze are the same as those of an internal craze (Fig. 15), though with the obvious lack of symmetry owing to the presence of the crack. Such crazes tend to stabilize a crack by blunting the crack tip, reducing the stress concentration while retaining a load-bearing capacity.

We now look in more detail at the individual stages of craze formation and subsequent growth.

Craze Initiation

Unlike the shear yield process, crazing is an inherently non-isovolume event. Cavitation of the material requires a dilatational component of the stress tensor, such as occurs in triaxial stress systems that may be found in samples subjected to plane strain conditions. In addition, it is found in practice that there is a time dependency on the appearance of crazing. That is, there is generally a time delay between application of the load and the first visible appearance of a craze. A number of models have been proposed which require either a critical cavitation stress, a critical strain, or the presence of inherent microvoids, which can grow under the applied local stress or strain.

Sternstein and Ongchin (1969). Considering that cavitation was required for craze nucleation, Sternstein and Ongchin (122) postulated that it is

the dilatational component of the stress tensor along with a stress bias σ_b (flow stress) that controls craze initiation:

$$\sigma_b = A + \frac{B}{I_1} \tag{43a}$$

where for plane stress, $\sigma_b = \sigma_1 - \sigma_2$, and

$$I_1 = \sigma_1 + \sigma_1 + \sigma_1 = 3p > 0 \tag{43b}$$

where I_1 is the first stress invariant ie the dilatational component of the stress tensor. A and B are temperature-dependent constants. We note that under this criterion, crazing will not occur under pure hydrostatic tension ($\sigma_1 = \sigma_2 = \sigma_3$), pure shear stress [$(\sigma_1 + \sigma_2 + \sigma_3)/3 = 0$, $I_1 = 0$], or compressive stress states ($I_1 < 0$). The model was extended beyond the specific case of plane (or biaxial) stress conditions to a general three-dimensional case by Sternstein and Meyers (123). Because they are essentially empirical, the Sternstein et al models have several shortcomings: (*1*) the stress bias, $\sigma_1 - \sigma_2$, is related to the shear stress and it is difficult to reconcile a shear stress component controlling initiation of a craze in a direction perpendicular to the principal stress component σ_1, (*2*) the parameters A and B have no direct or obvious physical interpretation, (*3*) no time dependency for the initiation of crazes.

Gent (1970). Gent (124) proposed a model in which the hydrostatic tensile stress at an inclusion or local heterogeneity increases the free volume and therefore effectively reduces the T_g of the material. At a sufficiently high stress concentration, the reduction in T_g is sufficient to reduce the local T_g to the test temperature. The reduced yield stress of the material in this rubber-like phase and the hydrostatic tensile stress then leads to cavitation and craze initiation. Implicit in this free-volume approach is that an imposed hydrostatic pressure will tend to prevent the formation of crazes in accordance with experimental observation. The criterion is summarized in the equation for the critical applied stress for initiation, σ_c:

$$\sigma_c = \frac{\beta(T_g - T) + P}{k} \tag{44}$$

where T_g is the glass temperature of the material, T is the test temperature, P is the bulk hydrostatic pressure, k is the stress concentration, and β is a constant related to the pressure dependence of T_g, and has a value of approximately 5 MPa/K. However, the inferred stress concentrations, k, required to induce crazing at room temperature were unrealistically large (of the order of 20) and the authors acknowledge it is a factor not easily accessible to experimental techniques. In addition, Lauterwasser and Kramer (121) calculated the reduction in T_g at the crack tip due to the imposed hydrostatic stress. Using the data in Figure 15 they calculated the hydrostatic pressure term to be one third of the bulk stress (σ_{bulk} = approximately 30 MPa) plus the additional surface stress at the craze tip of approximately 5 MPa, giving a total of 15 MPa. Using a value of 1°C/5 MPa for the

pressure dependence of T_g, they estimated the reduction in T_g at the crack tip to be a modest 3°C, certainly not enough to reduce the local T_g to the test temperature.

Oxborough and Bowden (1973). Addressing the lack of generality in terms of the usable stress states in the original Sternstein and Ongchin paper (122), which was limited to plane stress conditions, and concerns as to the physical interpretation of the critical stress (stress bias $\sigma_b = \sigma_1 - \sigma_2$) Oxborough and Bowden(125) proposed a criterion for craze initiation based on a critical strain. The form of the criterion is identical to that in the Sternstein and Ongchin paper, with the critical stress σ_b replaced by a critical strain ε_c:

$$\varepsilon_c = X' + \frac{Y'}{I_1} \tag{45}$$

where I_1 is again the first stress invariant and X' and Y' are time- and temperature-dependent variables. Noting that under a general stress state the maximum strain is in the direction of the principal stress and is given by

$$\varepsilon_1 = \frac{1}{E}(\sigma_1 - \nu\sigma_2 - \nu\sigma_3) \tag{46}$$

ν is the Poisson's ratio and assuming that crazing occurs at the critical strain given by equation 45, they derived a criterion for crazing that is written in terms of the principal stresses:

$$\sigma_1 - \nu\sigma_2 - \nu\sigma_3 = \frac{X}{\sigma_1 + \sigma_2 + \sigma_3} + Y \tag{47}$$

where $X = EX'$ and $Y = EY'$.

Using this criterion, Bowden and Oxborough could successfully fit the crazing data of Sternstein and Ongchin as well as their own data on four grades of polystyrene. Further, their data showed that the critical strain for crazing decreased with an increasing component of tensile hydrostatic stress and also decreased with increasing load time. Both the X and Y fitting parameters were shown to decrease with increasing temperature. The Y parameter also decreased with increasing load time, though the X parameter appeared to be relatively insensitive to loading time. Ultimately however, the X and Y parameters remain curve-fitting variables and offer little insight into the mechanisms or underlying structural parameters controlling craze initiation/growth.

Argon and Hannoosh (1977). The apparent time dependence for craze initiation after initial loading suggests the possibility that a thermally activated process may control initiation. Argon and co-workers (111,126,127) suggested a mechanism which considered that craze initiation occurs when a critical porosity is reached. The initial microscopic pores are formed when thermally activated micro-shear bands are blocked, the resulting local strain energy being sufficient to provide the surface energy for the formation of a microcrack. Allowing for additional free energy to form a stable pore, Argon and co-workers (111,126) derived

the following expression for the free energy required for pore formation:

$$\Delta G^*_{\text{pore}} = (0.15)^2 \pi (G/\tau)(\mu\phi^3) + \alpha L^3 \sigma_Y \tag{48}$$

where G is the shear modulus at the test temperature, τ the shear stress, φ a dimension related to the size of the sheared region (typically of the order of a molecular diameter), σ_Y the yield strength, L a length scale related to the spacing of molecular inhomogeneities, and α a factor of the order of 0.1. By considering the local stress field at an inclusion or groove and by taking the deviatoric stress, s, to be largest for a groove perpendicular to the maximum principal tensile stress, an expression was derived for the increase in the local porosity β as a function of time t, given by

$$\beta = \dot{\beta}_0 t \exp(-\Delta G^*_{\text{pore}}(s)/kT) \tag{49}$$

where $\dot{\beta}_0$ is a pre-factor characteristic of the vibrational frequency of the sheared region. Following these arguments, two criteria for the negative pressure p and the critical initial porosity β_i required for the expansion of the pores was determined (126):

$$p = \left(\frac{2\sigma_Y}{3}\right)\ln\left(\frac{1}{\beta}\right)Q \tag{50a}$$

$$\beta_i < \frac{1}{(1+2G/\sigma_Y)} \tag{50b}$$

where σ_Y is the yield stress, and Q a normalization factor. By further considering the negative pressure required to expand the porous region, an expression was derived for the initiation time, t_{in}, of craze nucleus formation (111):

$$t_{in} = \frac{1}{\dot{\beta}_0} \exp\left(\frac{\Delta G^*_{\text{pore}}}{kT} - \frac{\xi}{Q}\right) \tag{51}$$

where ξ is $(\sigma_1 + \sigma_2)/2\ \sigma_Y$, with σ_1 and σ_2 the principal stresses and σ_Y and Q are as before. The authors also recognized that while the craze may have initiated, it requires additional time for the craze to grow before it becomes visible (this is an inherent problem when discussing initiation times for crazes as it almost inevitably includes a period of craze growth for the crazes to be detectable). An estimate for the growth time, Δt_{growth} was derived based on a power law relationship between effective strain rate, $\dot{\varepsilon}_e$, and effective stress, σ_e:

$$\left(\frac{\dot{\varepsilon}_e}{\dot{\varepsilon}_{eo}}\right) = \left(\frac{\sigma_e}{\sigma_{e0}}\right)^m \tag{52}$$

where $\dot{\varepsilon}_e 0$, σ_{e0}, and m are temperature-dependent material constants.

Thus, the total time for craze nucleation is the sum of the time to initiation and the growth time to the point where the crazes are visible:

$$t_{\text{craze nucleation}} = t_{\text{in}} + \Delta t_{\text{growth}}$$

For small negative pressures, the growth time can be a significant proportion of the total time for nucleation. The model also predicts that under pure shear stress (an isovolume deformation), though considerable pore formation is present, no craze nucleation will occur because of the lack of a dilatational component of the stress. The authors went on to derive expressions to model the time dependence of the density of pore formation and subsequent craze saturation density (where the crazes have relieved the stress sufficiently that further craze nucleation is stopped) and expressions for biaxial craze nucleation. A set of such data from reference (111) is shown in Figure 18, where the surface density of crazes is plotted as a function of initiation time for polystyrene samples subjected to a combination of deviatoric stresses and negative pressures. The general features under each set of conditions are the same, with an increase in the craze density with time followed by saturation. It is also seen that the saturation density increases with increasing deviatoric stress and also with increasing negative pressure. The solid lines are the results from the model developed in reference (111). While the model captures the broad features of the material response, it should be noted that a number of parameters in the model cannot be easily determined from independent experiments. Consequently, a number of the parameters have been determined by optimizing the fit to experimental data such as that shown in Figure 18. These parameters, however, compare favorably with the expected ranges for such values. The reader is referred to the original paper for further discussions (111).

Kambour [1978]. Kambour, one of the pioneers in the area of crazing from as early as the mid-60's, has made significant contributions to the field and his thorough review article has already been mentioned (118). In 1978 Kambour and Gruner (128) reported a set of data for eight resins which showed a correlation between the critical strain for crazing in air, ε_c, and a combination of three factors, σ_y, the yield stress in tension, ΔT, the difference in the glass-transition temperature and the test temperature (T_g-T_{test}), and the solubility parameter (δ_p), [reported here in terms of the cohesive energy density, CED ($= \delta_p{}^2$)]:

$$e_c \propto \left[\frac{\text{CED} \cdot \Delta T}{\sigma_Y}\right] \tag{53}$$

In a follow-up paper in 1983 (129) it was shown that the correlation held for a further 29 polymers and copolymers, though in this case an additional correlation was used:

$$e_c \propto \left[\frac{\text{CED} \cdot \Delta T}{E}\right] \tag{54}$$

where E is the elastic modulus, and an implicit correlation between E and σ_Y is assumed. Figure 19 shows the data from the 1983 paper (129) and, while the correlations are shown to be satisfactory, the author acknowledges that the underlying

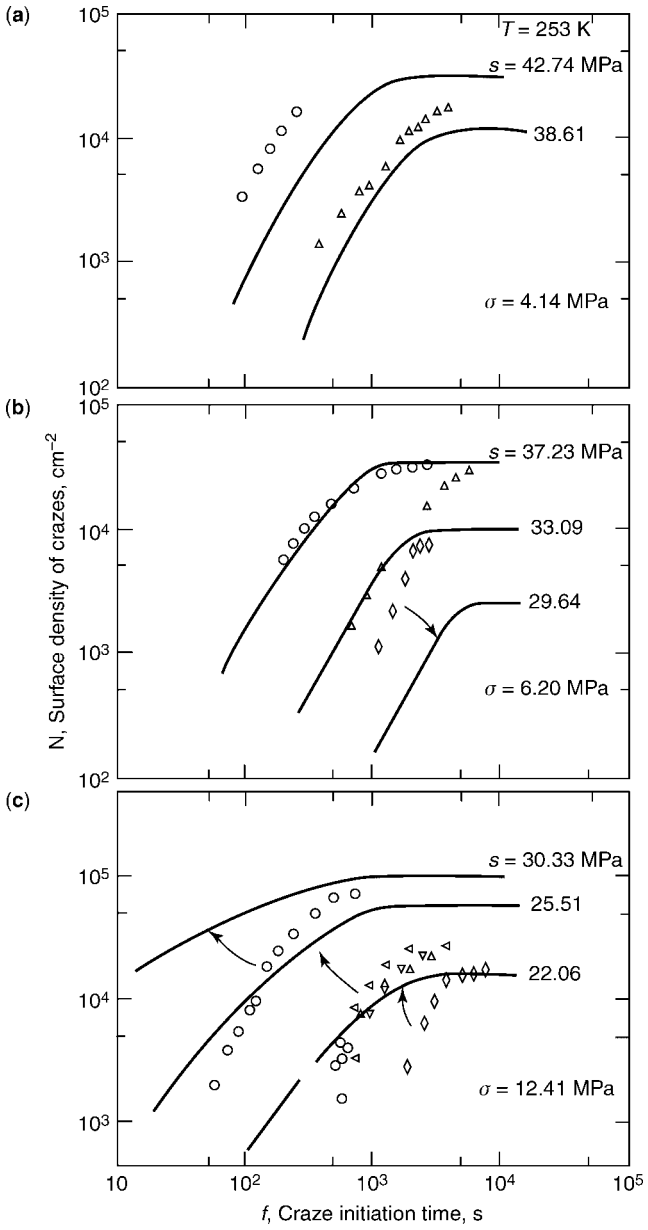

Fig. 18. Craze density as a function of initiation time for polystyrene subjected to a combination of deviatoric stresses (s) and negative pressures (σ). After Argon and Hannoosh (111), with permission of Taylor and Francis Ltd., http://www.tandf.cp.uk/journals.

source of the correlation is open to interpretation. [Note: In the 1983 paper (129), it appears that the abscissa labels have been inadvertently swapped between Figures 1 and 2, though the captions are correct. The abscissa has been corrected here.] Experimental craze growth studies as a function of temperature and aging

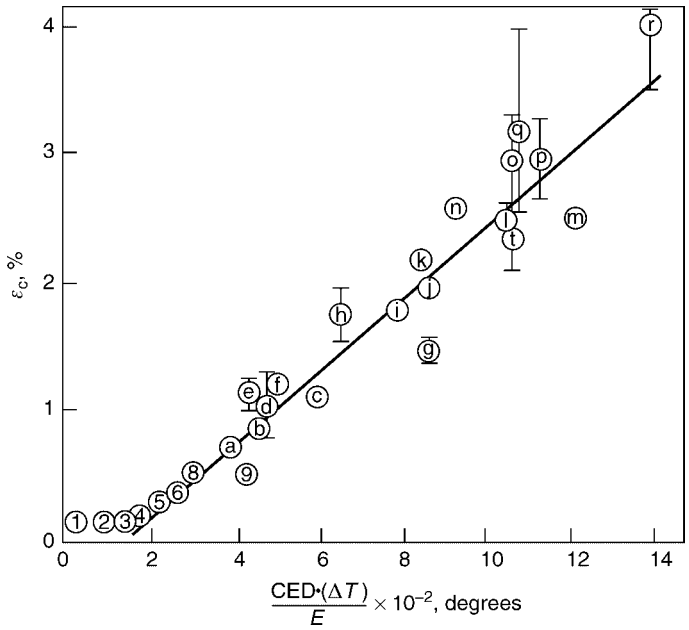

Fig. 19. Correlation between the critical strain for crazing, ε_c, and the product of the cohesive energy density (CED), the difference between the test temperature and the glass-transition temperature ΔT, and the elastic modulus E. Reprinted from Ref. 129, with permission from Elsevier.

time are compared with the general predictions of this and two of the models discussed above (Sternstein et al and Argon et al) in Reference (130).

Craze Growth

After initiation the craze starts to grow. There are two aspects to consider when considering craze growth:

(1) Growth of the craze in the plane perpendicular to the load direction and in the direction of the craze tip (direction X in Fig. 16).
(2) Craze thickening, ie opening of the craze–bulk interfaces and extension of the fibrils in the Y direction (Fig. 16).

Craze Tip Advance. The earliest explanation for the advance of the craze tip was the continued nucleation of isolated voids ahead of the craze tip and their subsequent expansion (127).

However, experimentally it has been observed that craze growth occurs faster than craze initiation and so it is difficult to explain growth with such a model as it is essentially the same mechanism as initiation. Also, some of the features of the craze predicted from such a mechanism, such as a closed cell structure formed

from the formation of isolated voids, are inconsistent with experiments that clearly show that the craze has an open structure.

The currently accepted model for craze tip advance is that proposed by Argon and Salama (131) and based on the Taylor meniscus instability mechanism (132,133). This is the same phenomenon that is observed when two wetted plates are pulled apart and is shown schematically in Figure 20. In this scenario, the craze–bulk interface is treated as the solid boundary, and the plastically deformed, strain-softened matter at the craze tip is the liquid. As the boundary layers separate an instability is set up owing to a negative pressure gradient in the "fluid." Small fingers propagate into the craze tip at a characteristic spacing of λ_c. The fingers expand as shown in Figure 20, eventually joining up to leave isolated columns of polymer. It is possible to calculate the minimum spacing, λ_M, necessary for the

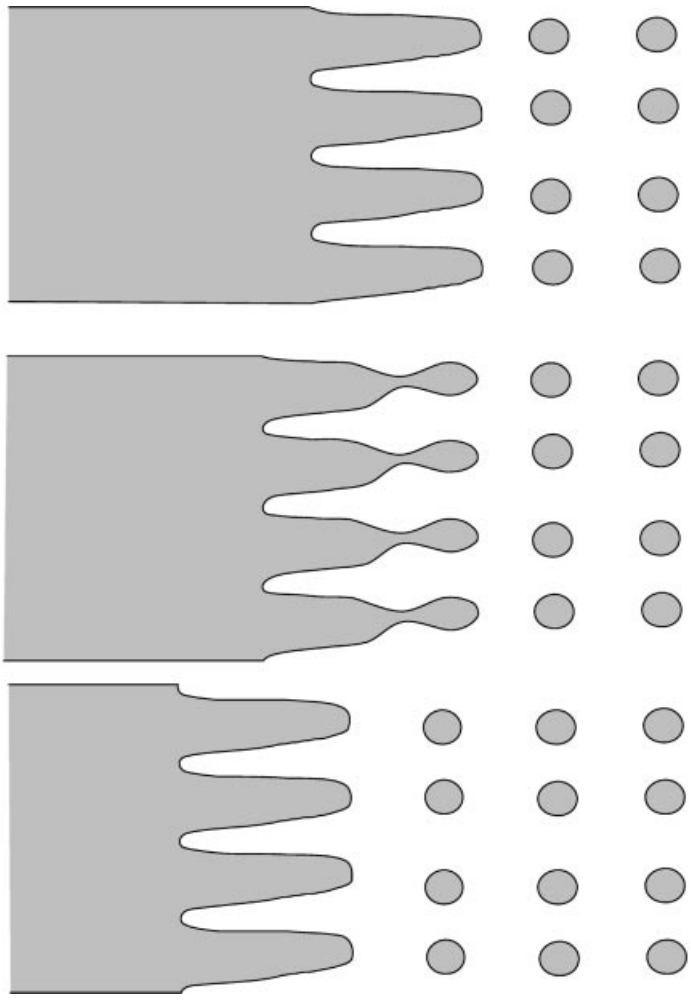

Fig. 20. Schematic for the Taylor meniscus instability mechanism for craze front advance. After Argon and Salama (131).

instability to grow (116):

$$\lambda_M = 2\pi\sqrt{\frac{\Gamma}{d\sigma_0/dx}} \tag{55}$$

where $d\sigma_0/dx$ is the hydrostatic stress gradient ahead of the craze and Γ is the surface energy. The fastest growing wavelength, λ_c, is given by (131,134)

$$\lambda_c = \sqrt{3}\lambda_M \tag{56}$$

Though a somewhat idealized picture of craze growth, the basic premise of the Taylor meniscus instability model has been verified by Donald and Kramer (135), who measured a critical wavelength in polystyrene crazes that was in close agreement with the interfibrillar distance. Further, following the procedure of Fields and Ashby (134) a steady-state craze tip velocity may be estimated by assuming a non-Newtonian fluid of the form

$$\left(\frac{\dot{\varepsilon}}{\dot{\varepsilon}_F}\right) = \left(\frac{\sigma}{\sigma_F}\right)^n \tag{57}$$

where $\dot{\varepsilon}_F$, σ_F, and n are material constants, leading to the expression for the tip velocity V_0:

$$V_0 = \frac{\sqrt{3}}{2}\frac{\dot{\varepsilon}_F h}{(n+2)}\left[\frac{\sqrt{3}h(\beta^* S_t)^2}{8\sigma_F\Gamma}\right]^n\left(1-\frac{2\Gamma}{\beta^* S_t h}\right)^{2n} \tag{58}$$

where h is the thickness of the craze at the crack front and $\beta^* S_t$ is the hydrostatic pressure between the void fingers.

The (relatively) simple form of equation 58 leading to a constant craze growth rate belies the complicated nature of craze growth in practice. While a linear growth in the craze length has been observed (136), equally a linear growth of the craze has been observed with logarithmic time (137–139). Undoubtedly the complicated, and possibly changing, nature of the stress field at the craze tip and even subtle differences in the morphology of the polymer can dramatically affect craze growth.

Craze Thickening. As indicated in Figure 16, two mechanisms exist for craze thickening:

(1) Drawing in of isotropic material from the bulk–craze interface
(2) Creep of the fibrillar material

Both processes can of course occur simultaneously, though it is generally accepted that it is the drawing in of fresh material that dominates the thickening of the craze in amorphous polymers. Evidence for this comes from a number of experiments aimed at examining either the volume fraction of craze material or the draw ratio of the fibrils as a function of position in the craze. If fibril creep

occurred to any significant extent, then the fibrils farther from the craze tip, which are naturally older and hence have been subjected to the interface stress for longer, would have a higher draw ratio. Evidence from crazes in PS (121) and poly-*tert*-butylstyrene (140) show an essentially constant draw ratio along the craze length, rising slightly at the craze tip owing to the locally high craze stresses present when they form (117)—this actually leads to a narrow band along the center line of the craze where the draw ratio is higher and volume fraction lower (127). Hence, the main mechanism of craze thickening is from material drawing in at the craze–fibril interface in a manner analogous with that of cold drawing under tensile loading. The material that is drawn in comes from what is termed the "active zone," a thin layer of material at the bulk–craze interface consisting of strain-softened material and which is typically of the order of a fibril diameter in size.

As noted, once the material has been drawn into the craze it appears to stabilize, and little, if any, further extension takes place. As with cold drawing, the fibrillar material is seen to take on a natural draw ratio, λ_N, the value of which is characteristic of the individual polymer. Kramer (116,141) found that the natural draw ratio correlated well with the maximum theoretical extension expected for an entangled network, λ_{max}:

$$\lambda_{max} = \frac{L_c}{k(M_e)^{1/2}} \text{ and } L_c = \frac{L_M M_e}{M_{m0}} \tag{59}$$

where M_e is the molecular weight between entanglements, L_M the monomer unit length, M_{m0} the monomer molecular weight, and k a constant. The molecular weight between entanglements, M_e, is a characteristic of any given polymer and can be determined experimentally from

$$M_e = \rho RT/G_N \tag{60}$$

where G_N is the measured rubbery plateau shear modulus, ρ the density, T the temperature, and R the gas constant. It is interesting to note that in polymers with a molecular weight less than approximately half the entanglement molecular weight, stable crazes are not seen to form and it seems then that entanglements are a necessary feature for stabilizing the craze–fibril structure.

During the surface drawing process in the active zone, it is inevitable that material that is destined to go into two neighboring fibrils can share a common molecule. Thus, as the fibrils form, the molecule must either disentangle such that the molecule flows into only one fibril or the chain must break. As we noted above, entanglements appear to be necessary for the formation of stable fibrils and, if the molecule is unable to disentangle, then it is inevitable that chain scission must occur during craze growth. On this basis Kramer (116,117) suggests that the energy required to create new surface (Γ) is given by the standard surface energy plus a component due to the energy required for chain scission:

$$\Gamma = \gamma + \frac{Uvd}{4} \tag{61}$$

where γ is the Van der Waals surface energy, U the polymer backbone bond energy, v the network strand density, and d is the root mean square end-to-end distance between entanglements. Kramer also estimated the force required to break a molecule, f_b, given approximately by

$$f_b = \frac{U}{2a} \tag{62}$$

where a is the bond length. If, during the fibril formation, the force should rise above this level breakage will obviously occur. If the force remains below this level then fibril formation can proceed via disentanglement.

Disentanglement of the polymer chains is generally accepted to occur by the mechanism of reptation as proposed by Doi and Edwards (142) and by deGennes (143). In this model, the movement of the chain is taken to be confined to a tube, the confinement coming from neighboring chains. The molecule moves through this tube in a snake-like motion by a series of cooperative steps. McLeish (144) has introduced the concept of "forced reptation" with regards to craze formation. Here, one end of the molecule is locked into a formed fibril and as material continues to be drawn in to the fibril, the molecule is pulled through its confining tube at a velocity v_f. From such considerations they determined that the maximum force acting on the molecule, f_d, is given by

$$f_d = v_f \xi \frac{M}{M_0} \tag{63}$$

where ξ is a monomeric friction coefficient, M the molecular weight, and M_0 the monomer molecular weight. Thus, if $f_d < f_b$ disentanglement will occur in preference to chain scission. It is worth noting also that if we assume that the velocity of the chain through the confining tube, v_f, is proportional to the applied strain rate and further that the monomeric friction coefficient is a thermally activated process (proportional to $e^{(1/T)}$) then equation 63 indicates that disentanglement is favored by low molecular weights, low strain rates, and high temperatures. However, while this approach correctly accounts for the dependence of craze growth on these parameters, in practice the majority of polymers are of a sufficiently high molecular weight (and hence chain length) that a single molecule will cross between the prefibril regions several times. Again, following the argument of McLeish this results in the polymer chain being pinned at several points along its length in what has been described as a 'block and tackle' arrangement (Fig. 21). This has the effect of increasing the velocity the chain must move at through the confining tube for a given macroscopic strain rate. On the basis of these concepts, Kramer (117) derived an expression for the maximum force on the chain (at its center) of

$$f_{max} = \xi v_f \frac{M^2}{16 M_0 M_e} \tag{64}$$

where M_e is the average molecular weight between the entanglements. It is seen then that the maximum force on the chain is proportional to the square of the

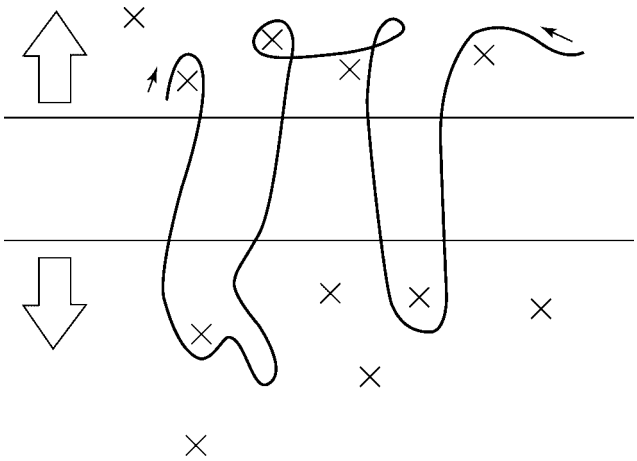

Fig. 21. Block-and-tackle arrangement for disentanglement at the craze boundary as proposed by McLeish and co-workers. Reprinted from Ref. 142 and 144, with permission from Elsevier.

molecular weight. During the formation of the fibril the chain is assumed to break randomly along its length, thereby reducing M, until the maximum force in the chain falls below the level required for scission. The concept of entangled molecules and the competition between chain scission and disentanglement is important not only for the growth kinetics but also, as we will see in the following section, for the ultimate failure of the fibrils/craze.

Craze Failure

Craze breakdown is obviously of fundamental importance since it is the mechanism by which the crack grows and so leads ultimately to failure. However, the mechanism of craze failure is still unclear. The two main mechanisms that have been proposed are

(1) Failure in the fibril, or
(2) Failure at the active zone

It is likely that both occur depending on the conditions and morphology of the material. The first step in considering the likelihood of fibril failure is to look at the stress levels within the fibril. Because of the reduced cross-sectional area in the craze region, the true stress on the fibrils (σ_{CT}) can be considerably higher than the stress at the craze boundary (σ_{CR}) by a factor given by the draw ratio of the fibril (λ):

$$\sigma_{CT} = \lambda \sigma_{CR} \tag{65}$$

λ is typically of the order of 2 to 4 for amorphous polymers and as noted above can be somewhat higher at the midrib of the fibril. Though at these stresses the creep contribution to the fibril length is minor, any small inhomogeneities in the local structure can lead to localized creep. Further, as discussed above, the material which forms the fibril has passed through the active zone at the craze–bulk boundary and has undergone chain scission. This results in the fibrillar material having a lower molecular weight and a reduced entanglement density. These conditions can then lead to chain disentanglement by essentially plastic flow. Such a mechanism can be facilitated by the small diameter of the fibrils leading to a reduction in the constraints that a polymer chain might otherwise see in the bulk. However, if fibril failure were the dominant mechanism in the breakdown of the craze, then it would be reasonable to expect failure to occur at the fibril midpoint where the fibril is oldest and has been subjected to the highest stresses for the longest length of time. While this has indeed been observed (145,146), it is more generally seen that the point of failure is at the craze–bulk interface, ie at the active zone. This in turn would imply that, for the majority of polymers, the reduction in entanglement density on traversing the active zone during fibril formation is not sufficient to destabilize the fibril.

We saw above that the material that flows into the active zone, and which may go on to form fibrils, has to undergo a degree of disentanglement or chain scission. This results in the material within the active zone having a lower entanglement density than the bulk material. Further the material in the active zone is in a strain-softened state, characterized by more liquid-like dynamics. If the entanglement density is low enough and the polymer strands dwell within the active zone for a sufficiently long period of time then the strands may fully disentangle. The material then loses its load-bearing capacity, and that particular fibril element will fail. In practice, because polymers generally have a broad distribution of molecular weights, there is a chance that the material destined to form a fibril will consist of relatively short chains with a low entanglement density. Thus, the likelihood of a given fibril failing is ultimately governed by a statistical distribution (note that, although not included in this analysis, the presence of inhomogeneities, inclusions, flaws etc can also lead to a breakdown in the active zone owing to a decreased load-bearing capacity). Kramer and Berger (117) developed such a statistical model and the reader is referred to the original paper for the full mathematical development. In brief, they based their calculations on the number of effectively entangled strands, n_e, that survive during the formation of the active zone, ie those which do not undergo chain scission. From this they formulated an expression for the probability that a given fibril would fail, P_F, given by the product of the probability that a strand survives fibril formation, $P_{survive}$, and the probability that it then disentangles, P_{dis}, summed over the total number of chains which go into fibril formation. The probability of a chain i surviving, $P_{survive}(i)$, is given by a normal distribution:

$$P_{survive}(i) = \frac{1}{\sqrt{2\pi n_e(1-q)}} \exp\left(\frac{(i-n_e)^2}{2(1-q)n_e}\right) \tag{66}$$

and where q is the fraction of originally entangled strands which do not undergo chain scission. The probability of disentanglement P_{dis} is given by

$$P_{\mathrm{dis}}(\mathrm{i}) \approx \exp\left(\frac{-t_{\mathrm{dis}}(\mathrm{i})}{\tau_{\mathrm{res}}}\right) \tag{67}$$

τ_{res} is a measure of the time the strand spends within the active zone and t_{dis} is the time for disentanglement, and is a function of strand molecular weight, the molecular weight between entanglements, the force on the strand, and the monomeric friction coefficient. Though the τ_{res} term is a fitting parameter, the model captures many of the features observed with craze stability such as the molecular weight dependence (117).

Other Considerations for Crazing

The preceding sections only touch upon the main characteristics of crazing and many of the additional factors that go into determining the initiation, growth, and failure of the craze have been omitted. Without elaboration, we mention several such factors and refer the reader to the relevant references.

The structure of the craze as discussed above has been idealized as a uniform array of isolated fibrils bridging the boundaries of the craze. In reality it is found that the main fibrils are connected to their neighbors by small "cross-tie" fibrils (117,147). The formation of these cross-tie fibrils has been modeled by Tijssens and van der Giessen (148), interestingly using many of the concepts presented in the section on yield. The presence of such cross-tie fibrils gives the craze some tangential load-bearing capacity, and a modeling of such a structure shows that their presence can lead to an increase in the stress on the main fibril, at times sufficient to cause failure of the polymer backbone (149,150).

A common, and potentially serious, drawback of polymers is their susceptibility to environmental factors, causing a greater likelihood to form crazes. Indeed, it has been estimated that environmental-stress cracking is responsible for as much as 30% of failures in engineering polymers in service (151). Environmental stress cracking (ESC), as the phenomenon is known, occurs predominately (though not exclusively) in amorphous polymers in contact with organic solvents. The other prerequisite for ESC is the presence of a stress since ESC is a result of the *physical* interaction of the polymer and solvent and is not due to a *chemical* interaction (ie no chemical degradation occurs).

One view of how the ESC agents act on the polymer is that they can diffuse into the polymer and cause it to swell. This in turn will increase the polymer chain mobility and so cause an effective decrease in the local T_{g}, leading to an increase in the propensity to craze ie crazing occurs at lower stresses or strain. An alternative view is that the liquid can wet the surface, reducing the energy required to create new surfaces and so aiding the formation of voids. This latter effect may be important in the early stages of craze initiation. The reviews by Kambour (118), Volynskii (152), Wright (153) and the work of, for example, Arnold (154–156) cover this area in detail and are briefly discussed in the chapter Fracture (qv) in this encyclopedia.

Just as crazing tends to be a precursor to failure under static loading, it is also seen to develop under cyclic loading conditions. The area of cyclic or fatigue failure of polymers has been extensively investigated, with much of the early work carried out by Hertzberg and co-workers (157–160) and Döll and co-workers (161–163). The reader is referred to the chapter Fatigue (qv) in this encyclopedia for a detailed review.

BIBLIOGRAPHY

"Crazing" in *EPST* 1st ed., Vol. 4, pp. 294–307, by R. W. Raetz, Catalin Corp.; in *EPSE* 2nd ed., Vol. 4, pp. 299–323, by R. P. Kambour, General Electric Co.; "Mechanical Properties" in *EPST* 1st ed., Vol. 8, pp. 445–516, by V. A. Kargin and G. L. Slonimsky; Akademii Nauk SSSR; in *EPSE* 2nd ed., Vol. 9 pp. 379–466, by D. W. Hadley, University of Reading, U.K., and I. M. Ward, University of Leeds, U.K.

1. G. Langford, W. Whitney, and R. D. Andrews, *Materials Research Laboratory Research Report No. R63-49*, MIT School of Engineering, Cambridge, 1963.
2. J. D. Ferry, *Viscoelastic Properties of Polymers*, 3rd ed., John Wiley & Sons, Inc., New York, 1980.
3. R. A. Hill, "A Theory of the Yielding and Plastic Flow of Anisotropic Materials", *Proc. R. Soc. London, Ser. A* **193**, 281–297 (1948).
4. W. Weber, "Über die Elastizität der Seidenfäden", *Pogg. Ann. Phys.* **4**, 247–257 (1835).
5. L. Boltzmann, "Zur Theorie der Elastischen Nachwirkung", *Sitzungsber Akad. Wiss. Wien. Mathem-Naturwiss Kl.* **70**, 275–300 (1874).
6. B. Bernstein, E. A. Kearsley, and L. J. Zapas, "A Study of Stress Relaxation with Finite Strains", *Trans. Soc. Rheol.* **7**, 391–410 (1963).
7. R. A. Schapery, "On the Characterization of Nonlinear Viscoelastic Materials", *Polym. Eng. Sci.* **9**, 295–310 (1969).
8. N. W. Brooks, M. Ghazli, R. A. Duckett, R. A. Unwin, and I. M. Ward, "Effects of Morphology on the Yield Stress of Polyethylene", *Polymer* **40**, 821–825 (1999).
9. R. O. Sirotkin and N. W. Brooks, "The Effects of Morphology on the Yield Behaviour of Polyethylene Copolymers", *Polymer* **42**, 3791–3797 (2001).
10. I. M. Ward, *Mechanical Properties of Solid Polymers* 2rd ed., John Wiley & Sons, Inc., Chichester, U.K., 1983.
11. I. M. Ward and D. W. Hadley, *An Introduction to the Mechanical Properties of Solid Polymers*, John Wiley & Sons, Inc., New York, 1993.
12. A. Nadai, *Theory of Flow and Fracture of Solids*, McGraw-Hill, New York, 1950.
13. E. Orowan, "Fracture and Strength of Solids", *Rep. Prog. Phys.* **12**, 185–232 (1949).
14. A. Considère, "Memoire sur l'Emploi du Fer et de l'Acier dans les Constructions", *Ann. Ponts et Chaussées* **9**, 574–775 (1885).
15. C. G'Sell and J. J. Jonas, "Yield and Transient Effects During the Plastic Deformation of Solid Polymers", *J. Mater. Sci.* **16**, 1956–1974 (1981).
16. C. G'Sell, J. M. Hiver, A. Dahouin, and A. Souahi, "Video-Controlled Tensile Testing of Polymers and Metals beyond the Necking Point", *J. Mater. Sci.* **27**, 5031–5039 (1992).
17. A. R. Haynes and P. D. Coates, "Semi-automated image analysis of the true tensile drawing behavior of polymers to large strains", *J. Mater. Sci.* **31**, 1843–1855 (1996).
18. S. Nazarenko, S. Bensason, A. Hiltner, and E. Baer, "The Effect of Temperature and Pressure on Necking of Polycarbonate", *Polymer* **35**, 3883–3892 (1994).
19. M. C. Boyce and E. M. Arruda, "An Experimental and Analytical Investigation of the Large Strain Compressive and Tensile Response of Glassy Polymers", *Polym. Eng. Sci.* **30**, 1288–1298 (1990).

20. W. Whitney and R. D. Andrews, "Yielding of Glassy Polymers: Volume Effects", *J. Polym. Sci., Part C* **16**, 2981–2990 (1967).
21. N. Brown and I. M. Ward, "Load Drop at the Upper Yield Point of a Polymer", *J. Polym. Sci., Part A* **2**, 607–620 (1968).
22. M. C. Boyce, E. M. Arruda, and R. Jayachandran, "The Large Strain Compression, Tension and Simple Shear of Polycarbonate", *Polym. Eng. Sci.* **34**, 716–725 (1994).
23. M. Kitagawa, D. X. Zhou, and J. H. Qiu, "Stress–Strain Curves for Solid Polymers", *Polym. Eng. Sci.* **35**, 1725–1732 (1995).
24. H. Tresca, "Sur l'écoulement des corps solids soumis ´ des fortes pression" *C. R. Acad. Sci. (Paris)* **59**, 754–758 (1864).
25. R. von Mises, "Die Mechanik der festen Körper im plastischen deformablen Zustand", *Göttinger Nachricten, Math-Phys. Klasse* 582–592 (1913).
26. C. A. Coulomb, "Sur une application des regles de Maximis et Minimis à quelques Problèmes de Statique, relatifs à l'Architecture", *Mem. Math et Phys.* **7**, 343–382 (1773).
27. S. Rabinowitz, I. M. Ward, and J. S. C. Parry, "The Effect of Hydrostatic Pressure on the Shear Yield Behavior of Polymers", *J. Mater. Sci.* **5**, 29–39 (1970).
28. D. R. Mears, K. D. Pae, and J. A. Sauer, "Effects of Hydrostatic Pressure on the Mechanical Behavior of Polyethylene and Polypropylene", *J. Appl. Phys.* **40**, 4229–4237 (1969).
29. R. A. Duckett, S. Rabinowitz, and I. M. Ward, "The Strain-rate, Temperature and Pressure Dependence of Yield of Isotropic Poly(Methyl Methacrylate) and Poly(Ethylene Terephthalate)", *J. Mater. Sci.* **5**, 909–915 (1970).
30. K. D. Pae and Bhateja, "The Effects of Hydrostatic Pressure on the Mechanical Behavior of Polymers", *J. Macromol. Sci., Chem.* **13**(1), 1–75 (1975).
31. F. H. Muller, "Zum Problem der Kaltverstreckung hochpolymerer Substanzen", *Kolloid Zeitschrift* **114**, 59–61 (1949).
32. F. H. Muller, "Zur Kaltverstreckung hochmolekularer Stoffe", *Kolloid Zeitschrift* **115**, 118–123 (1949).
33. F. H. Muller, "Weitere Versuche und Betrachtungen zur Kaltverstreckung", *Kolloid Zeitschrift* **126**, 65–72 (1956).
34. P. I. Vincent, "Necking and cold-drawing of rigid plastics", *Polymer* **1**, 7–19 (1960).
35. W. G. Knauss and I. Emri, "Volume Change and the Nonlinearly Thermoviscoelastic Constitution of Polymers", *Polym. Eng. Sci.* **27**(1), 86–100 (1987).
36. R. E. Robertson, "Theory of the Plasticity of Glassy Polymers", *J. Chem. Phys.* **44**, 3950–3956 (1966).
37. R. N. Haward and G. Thackray, "The Use of a Mathematical Model to Describe Isothermal Stress–Strain Curves in Glassy Polymers", *Proc. R. Soc., London, Ser. A* **302**, 453–472 (1968).
38. A. S. Argon, "A Theory for the Low-Temperature Plastic Deformation of Glassy Polymers", *Philos. Mag.* **28**, 839–865 (1973).
39. M. C. Boyce, D. M. Parks, and A. S. Argon, "Large Inelastic Deformation of Glassy Polymers. Part I: Rate Dependent Constitutive Model", *Mech. Mater.* **7**, 15–33 (1988).
40. T. A. Tervoort, E. T. J. Klompen, and L. E. Govaert, "A Multi-Mode Approach to Finite, Three-Dimensional, Nonlinear Viscoelastic Behavior of Polymer Glasses", *J. Rheol.* **40**, 779–797 (1996).
41. R. M. Shay and J. M. Caruthers, "A New Nonlinear Viscoelastic Constitutive Equation for Predicting Yield in Amorphous Solid Polymers", *J. Rheol.* **30**, 871–827 (1986).
42. S. R. Lustig, R. M. Shay, and J. M. Caruthers, "Thermodynamic Constitutive Equations for Materials with Memory on a Material Time Scale", *J. Rheol.* **40**, 69–106 (1996).

43. H. Eyring, "Viscosity, Plasticity and Diffusion as Examples of Absolute Reaction Rates", *J. Chem. Phys.* **4**, 283–291 (1936).
44. C. Bauwens-Crowet, J. C. Bauwens, and G. Homes, "Tensile Yield-Stress Behavior of Glassy Polymers", *J. Polym. Sci., Part A* **2**, 735–742 (1969).
45. J. S. Foot, R. W. Truss, I. M. Ward, and R. A. Duckett, "The Yield Behavior of Amorphous Polyethylene-teraphthalate—An Activated Rate Theory Approach", *J. Mater. Sci.* **22**, 1437–1442 (1987).
46. Y. Liu and R. W. Truss, "A Study of Tensile Yielding of Isotactic Polypropylene", *J. Polym. Sci, Part B: Polym. Phys.* **32**, 2037–2047 (1994).
47. M. Bonner, R. A. Duckett, and I. M. Ward, "The Creep Behaviour of Isotropic Polyethylene", *J. Mater. Sci.* **34**, 1885–1897 (1999).
48. I. M. Ward, "Creep and Yield Behavior of Polyethylene", *Macromol. Symp.* **98**, 1029–1041 (1995).
49. M. L. Williams, R. F. Landel, and J. D. Ferry, "The Temperature Dependence of Relaxation Mechanisms in Amorphous Polymers and Other Glass-Forming Liquids", *J. Am. Chem. Soc.* **77**, 3701–3706 (1955).
50. M. C. Wang and E. J. Guth, "Statistical Theory of Networks of Non-Gaussian Flexible Chains", *J. Chem. Phys.* **20**, 1144–1157 (1952).
51. I. M. Ward, *Structure and Properties of Oriented Polymers*, 2nd ed. Chapman and Hall, London, 1997.
52. D. M. Parks, A. S. Argon, and B. Bagepalli, "Large Elastic–Plastic Deformation of Glassy Polymers", *Program in Polymer Science and Technology*, Technical Report, MIT, 1984.
53. L. R. G. Treloar, *The Physics of Rubber Elasticity*, 3rd ed., Clarendon Press, Oxford, 1975.
54. E. M. Arruda and M. C. Boyce, "A 3-Dimensional Constitutive Model for the Large Stretch Behavior of Rubber Elastic Materials", *J. Mech. Phys. Solids* **41**, 389–412 (1993).
55. W. H. Han, F. Horkay, and G. B. McKenna, "Mechanical and Swelling Behaviors of Rubber: A Comparison of Some Molecular Models with Experiment", *Math. Mech. Solids* **4**(2), 139–167 (1999).
56. O. A. Hasan, M. C. Boyce, X. S. Li, and S. Berko, "An Investigation of the Yield and Post-Yield Behavior and Corresponding Structure of Poly(Methylmethacrylate)", *J. Polym. Sci., Part B: Polym. Phys.* **31**(2), 185–197 (1993).
57. C. G'Sell and G. B. McKenna, "Influence of Physical Ageing on the Yield Response of Model DGEBA/Poly(Propylene Oxide) Epoxy Glasses", *Polymer* **33**, 2103–2113 (1992).
58. P. D. Wu and E. van der Giessen, "On Improved Network Models for Rubber Elasticity and Their Applications to Orientation Hardening in Glassy Polymers", *J. Mech. Phys. Solids* **41**, 427–456 (1993).
59. A. Leonov, "Nonequilibrium Thermodynamics and Rheology of Viscoelastic Polymer Media", *Rheol. Acta* **15**, 85–98 (1976).
60. T. A. Tervoort and L. E. Govaert, "Strain Hardening Behavior of Polycarbonate in the Glassy State", *J. Rheol.* **44**, 1263–1277 (2000).
61. L. E. Govaert, P. H. M. Timmermans, and W. A. M. Brekelmans, "The Influence of Intrinsic Strain Softening Localization in Polycarbonate: Modeling and Experimental Validation", *J. Eng. Mater. Tech., Trans ASME* **122**(2), 177–185 (2000).
62. M. Aboulfaraj, C. G'Sell, D. Mangelinck, and G. B. McKenna, "Physical Aging of Epoxy Networks after Quenching and/or Plastic Cycling", *J. Non-Cryst. Solids* **172–174**, 615–621 (1994).
63. E. M. Arruda and M. C. Boyce, "Evolution of Plastic Anisotropy in Amorphous Polymers during Finite Straining", *Int. J. Plast.* **9**, 697–720 (1993).

64. B. D. Coleman, "Thermodynamics of Materials with Memory", *Arch. Ration. Mech. Anal.* **17**, 230–254 (1964).
65. W. Noll, "Mathematical Theory of the Mechanical Behavior of Continuous Media", *Arch. Ration. Mech. Anal.* **2**, 197–226 (1958).
66. G. Adam and J. H. Gibbs, "On the Temperature Dependence of Cooperative Relaxation Properties in Glass Forming Liquids" *J. Chem. Phys.* **43**, 139–146 (1965).
67. D. A. Zaukelies, "Observation of Slip in Nylon 66 and 610 and Its Interpretation in Terms of a New Model", *J. Appl. Phys.* **33**, 2797–2803 (1962).
68. P. Predecki and W. O. Statton, "Dislocations Caused by Chain Ends in Crystalline Polymers", *J. Appl. Phys.* **37**, 4053–4059 (1966).
69. P. Predecki and W. O. Statton, "A Dislocation Mechanism for Deformation of Polyethylene", *J. Appl. Phys.* **38**, 4140–4144 (1967).
70. J. Petermann and H. Gleiter, "Direct Observation of Dislocations in Polyethylene Crystals", *Philos. Mag.* **25**, 813–816 (1972).
71. J. J. Gilman, in A. R. Rosenfield, G. T. Hahn, A. L. Bement and R. I. Jaffee, eds., *Dislocation Dynamics*, John Wiley & Sons, Inc., New York, 1968.
72. J. J. Gilman, in A. S. Argon, ed., *Physics of Strength and Plasticity*, MIT, 1969.
73. P. B. Bowden and S. Raha, "A Molecular Model for Yield and Flow in Amorphous Glassy Polymers Making Use of a Dislocation Analogue", *Philos. Mag.* **29**, 149–166 (1974).
74. J. Frenkel, "Zur Theorie der Elastizitätsgrenze und der Festigkeit Kristallinischer Körper ", *Z. Physik* **37**, 572–609 (1926).
75. P. B. Bowden in R. N. Haward, ed. *The Physics of Glassy Polymers*, 1st ed., John Wiley & Sons, Inc., New York, 1973.
76. B. Crist, in R. N. Haward and R. J. Young, eds., *The Physics of Glassy Polymers*, 2nd ed., Chapman and Hall, London 1997.
77. A. Kelly and N. H. MacMillen, *Strong Solids*, 3rd ed., Oxford University Press, New York, 1986.
78. N. Brown, "A Theory of Yielding of Amorphous Polymers at Low Temperature–A Molecular Viewpoint" *J. Mater. Sci.* **18**, 2241–2254 (1983).
79. Z. H. Stachurski, "Deformation Mechanisms and Yield Strength of Amorphous Polymers", *Prog. Polym. Sci.* **22**, 407–474 (1997).
80. P. A. O'Connell and G. B. McKenna, "Large Deformation Response of Polycarbonate: Time–Temperature, Time–Aging Time and Time–Strain Superposition", *Polym. Eng. Sci.* **37**, 1485–1495 (1997).
81. C G'Sell and G. B. McKenna, "Influence of Physical Ageing on the Yield Response of Model DGEBA/Poly(Propylene Oxide) Epoxy Glasses", *Polymer* **33**, 2103–2113 (1992).
82. E. Oleynik, "Plastic Deformation and Mobility in Glassy Polymers", *Prog. Colloid Polym. Sci.* **80**, 140–150 (1989).
83. O. A. Hasan and M. C. Boyce, "Energy Storage During Inelastic Deformation of Glassy Polymers", *Polymer* **34**, 5085–5092 (1993).
84. Y. C. Yung, *Foundations of Solid Mechanics*, Prentice-Hall, Inc.,, Englewood Cliffs, N.J., 1965.
85. W. C. Whitney and R. D. Andrews, "Yielding of Glassy Polymers: Volume Effects", *J. Polym. Sci., Part B* **16**, 2981–2990 (1967).
86. D. M. Colucci, P. A. O'Connell, and G. B. McKenna, "Stress Relaxation Experiments in Polycarbonate: A Comparison of Volume Changes for Two Commercial Grades", *Polym. Eng. Sci.* **37**, 1469–1474 (1997).
87. W. G. Knauss and I. Emri, "Volume Change and Nonlinearly Thermo-Viscoelastic Constitution of Polymers", *Polym. Eng. Sci.* **27**(1), 86–100 (1987).

88. C. G'Sell, J. M. Hiver, and A. Dahoun, "Experimental Characterization of Deformation Damage in Solid Polymers under Tension, and Its Interrelation with Necking", *Int. J. Solids. Struct.* **39**, 3857–3872 (2002).
89. R. S. Duran and McKenna, "A Torsional Dilatometer for Volume Change Measurements on Deformed Glasses: Instrument Description and Measurements on Equilibrated Glasses", *J. Rheol.* **34**, 813–839 (1990).
90. L. Xie, D. W. Gidley, H. A. Hristov, and A. F. Yee, "Evolution of Nanometer Voids in Polycarbonate under Mechanical Stress and Thermal Expansion using Positron Spectroscopy", *J. Polym. Sci., Part B* **33**(1), 77–84 (1995).
91. O. A. Hasan, M. C. Boyce, X. S. Li, and S. Derko, "An Investigation of the Yield and Post-Yield Behavior and Corresponding Structure of Poly(Methyl Methacrylate)", *J. Polym. Sci., Part B* **31**, 185–197 (1993).
92. M. Y. Ruan, H. Moaddel, A. M. Jamieson, R. Simha, and J. D. McGervey, "Positron Annihilation Lifetime Studies of Free Volume Changes in Polycarbonate under Static Tensile Deformation", *Macromolecules* **25**, 2407–2411 (1992).
93. D. N. Theodorou and U. W. Suter, "Detailed Molecular Structure of a Vinyl Polymer Glass", *Macromolecules* **18**, 1467–1478 (1986).
94. D. N. Theodorou and U. W. Suter, "Atomistic Modeling of Mechanical Properties of Polymeric Glasses", *Macromolecules* **19**(1), 139–154 (1986).
95. P. H. Mott, A. S. Argon, and U. W. Suter, "Atomistic Modeling Cavitation of Glassy Polymers", *Philos. Mag.* **67**, 931–978 (1993).
96. P. H. Mott, A. S. Argon, and U. W. Suter, "Atomistic Modeling of Plastic Deformation of Glassy Polymers", *Philos. Mag.* **68**, 537–564 (1993).
97. N. W. Brooks, R. A. Duckett, and I. M. Ward, "Investigation into Double Yield Points in Polyethylene", *Polymer* **33**, 1872–1880 (1992).
98. N. W. Brooks, A. P. Unwin, R. A. Duckett, and I. M. Ward, "Double Yield Points in Polyethylene—Structural Changes under Tensile Deformation", *J. Macromol. Sci., Phys.* **B34**(1–2), 29–54 (1995).
99. R. Seguela and O. Darras, "Phenomenological Aspects of the Double Yield of Polyethylene and Related Copolymers under Tensile Loading", *J. Mat. Sci.* **29**, 5342–5352 (1994).
100. P. A. Botto, R. A. Duckett, and I. M. Ward, "The Yield and Thermoelastic Properties of Oriented Poly(Methyl-Methacrylate)", *Polymer* **28**, 257–262 (1987).
101. J. P. Chen, A. F. Yee, and E. J. Moskala, "The Molecular Basis for the Relationship between the Secondary Relaxation and Mechanical Properties of a Series of Polyester Copolymer Glasses", *Macromolecules* **32**, 5944–5955 (1999).
102. R. W. Truss, P. L. Clarke, and R. A. Duckett, "The Dependence of Yield Behavior on Temperature, Pressure and Strain Rate for Linear Polyethylenes of Different Molecular Weight and Morphology", *J. Polym. Sci., Polym. Phys.* **22**, 191–209 (1984).
103. R. J. Young, "A Dislocation Model for Yield in Polyethylene", *Philos. Mag.* **30**, 85–94 (1974).
104. M. A. Kennedy, A. J. Peacock, M. D. Failla, J. C. Lucas, and L. Mandelkern, "Tensile Properties of Crystalline Polymers—Random Copolymers of Ethylene", *Macromolecules* **28**, 1407–1421 (1995).
105. B. Crist, C. J. Fisher, and P. R. Howard, "Mechanical Properties of Model Polyethylenes—Tensile Elastic Modulus and Yield Stress", *Macromolecules* **22**, 1709–1718 (1989).
106. O. Darras, and R. Seguela, "Tensile Yield of Polyethylene in Relation to Crystal Thickness", *J. Polym. Sci., Part B: Polym. Phys.* **31**, 759–766 (1993).
107. N. W. J. Brooks and M. Mukhtar, "Temperature and Stem Length Dependence of the Yield Stress of Polyethylene", *Polymer* **41**, 1475–1480 (2000).

108. R. Seguela, "Dislocation Approach to the Plastic Deformation of Semicrystalline Polymers: Kinetic Aspects for Polyethylene and Polypropylene", *J. Polym. Sci., Part B: Polym. Phys.* **40**, 593–601 (2002).
109. Z. Bartczak, R. E. Cohen, and A. S. Argon, "Evolution of the Crystalline Texture of High-Density Polyethylene during Uniaxial Compression", *Macromolecules* **25**, 4692–4704 (1992).
110. Z. Bartczak, A. S. Argon, and R. E. Cohen, "Deformation Mechanisms and Plastic Resistance in Single Crystal Textured High Density Polyethylene", *Macromolecules* **25**, 5036–5053 (1992).
111. A. S. Argon and J. G. Hannoosh, "Initiation of Crazes in Polystyrene", *Philos. Mag.* **36**, 1195–1216 (1977).
112. A. Lazzeri and C. B. Bucknall, "Dilatational Bands in Rubber Toughened Polymers", *J. Mater. Sci.* **28**, 6799–6808 (1989).
113. C. B. Bucknall and A. Lazzeri, "Rubber Toughening of Plastics. Part XIII: Dilatational Yielding in PA6.6/EPR Blends", *J. Mater. Sci.* **35**, 427–435 (2000).
114. M. Todo, K. Takahasi, P. Y. B. Jar, and P. Beguelin, "Toughening Mechanisms of Rubber Toughened PMMA", *JSME Int. J., Ser. A: Solid. Mech. Mater. Eng.* **42**, 585–591 (1999).
115. Y. Huang and A. J. Kinloch, "Modeling of the Toughening Mechanisms in Rubber Modified Epoxy Polymers. Part I: Finite Element Analysis Studies", *J. Mater. Sci.* **27**, 2753–2762 (1992).
116. E. J. Kramer, "Microscopic and Molecular Fundamentals of Crazing" in *Adv. Polym. Sci.* **52/53**, 1–56 (1983).
117. E. J. Kramer and L. L. Berger, "Fundamental Processes of Craze Growth and Fracture" in *Adv. Polym. Sci.* **91/92**, 1–68 (1990).
118. R. P. Kambour, "A Review of Crazing and Fracture in Thermoplastics", *J. Polym. Sci., Macromol. Rev.* **7**, 1–154 (1973).
119. A. M. Donald, in W. Brostow, ed., *Performance of Plastics*, Hanser Publishers, Munich, pp. 283–296, 2000.
120. A. M. Donald, in R. N. Haward and R. J. Young, eds., *The Physics of Glassy Polymer*, Chapman and Hall, London, 1997.
121. B. D. Lauterwasser and E. J. Kramer, "Microscopic Mechanisms and Mechanics of Craze Growth and Fracture", *Philos. Mag. A* **39**, 469–495 (1979).
122. S. S. Sternstein and L. Ongchin, "Yield Criteria for Plastic Deformation of Glassy High Polymers in General Stress Fields", *Polym. Prepr.* **10**, 1117–1124 (1969).
123. S. S. Sternstein and F. A. Myers, "Yielding of Glassy Polymers in the Second Quadrant of Principal Stress Space", *J. Macromol. Sci., Phys.* **B8**, 539–571 (1973).
124. A. N. Gent, "Hypothetical Mechanism of Crazing in Glassy Plastics", *J. Mater. Sci.* **5**, 925–932 (1970).
125. R. J. Oxborough and P. B. Bowden, "A General Critical–Strain Criterion for Crazing in Amorphous Glassy Polymers", *Philos. Mag.* **28**, 547–559 (1973).
126. A. S. Argon, "Role of Heterogeneities in the Crazing of Glassy Polymers", *Pure Appl. Chem.* **43**, 247–272 (1975).
127. A. S. Argon, "Physical Basis of Distortional and Dilatational Plastic Flow in Glassy Polymers", *J. Macromol. Sci., Phys.* **B8**, 573–596 (1973).
128. R. P. Kambour and C. L. Gruner, "Effects of Polar Group Incorporation on Crazing of Glassy Polymers: Styrene–Acrylonitrile Copolymer and a dicyano Bisphenol Polycarbonate", *J. Polym. Sci., Polym. Phys.* **16**, 703–716 (1978).
129. R. P. Kambour, "Correlations of the Dry Crazing Resistance of Glassy Polymers with Other Physical Properties", *Polym. Commun.* **24**, 292–296 (1983).
130. G. M. Gusler and G. B. McKenna, "The Craze Initiation Response of a Polystyrene and a Styrene–Acrylonitrile Copolymer during Physical Aging", *Polym. Eng. Sci.* **37**, 1442–1448 (1997).

131. A. S. Argon and M. M. Salama, "The Mechanics of Fracture in Glassy Materials Capable of Some Inelastic Deformation", *Mater. Sci. Eng.* **23**, 219–230 (1977).
132. G. I. Taylor, "The Instability of Liquid Surfaces When Accelerated in the Direction Perpendicular to Their Planes", *Proc. R. Soc. London, Ser. A* **201**, 192–196 (1950).
133. P. G. Saffman and G. I. Taylor, "The Penetration of Liquid into Porous Medium or Hele–Shaw Cell Containing a More Viscous Liquid", *Proc. R. Soc. London, Ser. A* **245**, 312–329 (1958).
134. R. J. Fields and M. F. Ashby, "Finger-Like Crack Growth in Solids and Liquids", *Philos. Mag.* **33**, 33–48 (1976).
135. A. M. Donald and E. J. Kramer, "The Mechanisms for Craze Tip Advance in Glassy Polymers", *Philos. Mag. A* **43**, 857–870 (1981).
136. A. S. Argon and M. M. Salama, "Growth of Crazes in Glassy Polymers", *Philos. Mag. B* **36**, 1217–1234 (1977).
137. N. Verheulpen-Heymans, and J. C. Bauwens, "Effect of Stress and Temperature on Dry Craze Growth Kinetics during Low-Stress Creep of Polycarbonate", *J. Mater. Sci.* **11**, 1–6 (1976).
138. J. L. S. Wales, "Surface Crazing in PVC and Other Polymers", *Polymer* **21**, 684–690 (1980).
139. M. Delin and G. B. McKenna, "The Craze Growth Response in Stress Relaxation Conditions for a Styrene–Acrylonitrile Copolymer during Physical Aging", *Mech. Time Dep. Mater.* **4**, 231–255 (2000).
140. A. M. Donald, E. J. Kramer, and R. A. Bubeck, "The Entanglement Network and Craze Micromechanics in Glassy Polymers", *J. Polym. Sci., Polym. Phys.* **20**, 1129–1141 (1982).
141. A. M. Donald and E. J. Kramer, "Effect of Molecular Entanglements on Craze Microstructure in Glassy Polymers", *J. Polym. Sci., Polym. Phys.* **20**, 899–909 (1982).
142. M. Doi and S. F. Edwards, "Dynamics of Concentrated Polymer Systems. Part I: Brownian Motion in the Equilibrium State", *J. Chem. Soc., Faraday Trans. 2* **74**, 1789–1801 (1978).
143. P. G. deGennes, "Reptation of a Polymer Chain in the Presence of Fixed Obstacles", *J. Chem. Phys.* **55**, 572–579 (1971).
144. T. C. B. McLeish, C. J. G. Plummer, and A. M. Donald, "Crazing by Disentanglement–Non-Diffusive Reptation", *Polymer* **30**, 1651–1655 (1989).
145. R. Schirrer, J. Le Masson, and B. Tomatis, "The Disentanglement Time of the Craze Fibrils under Cyclic Load", *Polym. Eng. Sci.* **24**, 820–824 (1984).
146. W. Doll, "Optical Interference Measurements and Fracture Mechanics Analysis of Crack Tip Craze Zones", *Adv. Polym. Sci.* **52/53**, 105–168 (1983).
147. P. Behan, M. Bevis and D. Hull, "Fracture Processes in Polystyrene", *Proc. R. Soc.London, Ser. A* **343**, 525–535 (1975).
148. M. G. A. Tijssens and E. van der Giessen, "A Possible Mechanism for Cross-Tie Fibril Generation in Crazing of Amorphous Polymers", *Polymer* **43**, 831–838 (2002).
149. H. R. Brown, "A Molecular Interpretation of the Toughness of Glassy Polymers", *Macromolecules* **24**, 2752–2756 (1991).
150. Y. Sha, C. Y. Hui, A. Ruina, and E. J. Kramer, "Detailed Simulation of Craze Fibril Failure at a Crack Tip in a Glassy Polymer", *Acta. Mater.* **45**, 3555–3563 (1997).
151. D. C. Wright, *Environmental Stress Cracking of Plastics*, ChemTec, Ontario, 1996.
152. A. L. Volynskii and N. F. Bakeev, *Solvent Crazing of Polymers*, Elsevier, New York, 1995.
153. W. A. Woishnis and D. C. Wright, "Select Plastics to Avoid Product Failure", *Adv. Mater. and Proc.* **12**, 39–40 (1994).
154. J. C. Arnold, "Environmental Stress Crack Initiation in Glassy Polymers", *Trends Polym. Sci.* **4**, 403–408 (1996).

155. J. C. Arnold, "Craze Initiation during the Environmental Stress Cracking of Polymers", *J. Mater. Sci.* **30**, 655–660 (1995).
156. J. C. Arnold, "Environmental Stress Cracking Behavior of Urethane Methacrylate Based Resins. Part I: Environmental Crazing and Cracking under Bending Conditions", *J. Mater. Sci.* **29**, 3095–3101 (1994).
157. R. W. Hertzberg and J. A. Manson, *Fatigue in Engineering Plastics*, Academic Press, New York, 1980.
158. C. Rimnac, R. W. Hertzberg and J. A. Manson, "On the Nature of Craze Development and Breakdown During Fatigue", *J. Mater. Sci. Lett.* **2**, 325–328 (1983).
159. C. Rimnac, R. W. Hertzberg, and J. A. Manson, "Craze Development and Breakdown in PVC during Cyclic Loading", *J. Mater. Sci.* **19**, 1116–1124 (1984).
160. R. W. Lang, J. A. Manson, and R. W. Hertzberg, "Craze Development in Poly(Methyl-Methacrylate) during Stable Fatigue Crack Propagation", *Polym. Eng. Sci.* **24**, 833–842 (1984).
161. W. Döll and L. Könczöl, "Micromechanics of Fracture under Static and Fatigue Loading: Optical Interferometry of Crack Tip Craze Zones" *Adv. Polym. Sci.* **91/92**, 137–214 (1990).
162. R. Schirrer, M. G. Schinker, L. Konczol, and W. Döll, "Interference Optical Studies on Crack Propagation during Cyclic Loading in PMMA", *Colloid Polym. Sci.* **259**, 812–817 (1981).
163. W. Döll, L. Kinczol, and M. G. Schinker, "Size and Mechanical Properties of Craze Zones at Propagating Crack Tips in Poly(Methyl Methacrylate) during Fatigue Loading", *Polymer* **24**, 1213–1219 (1983).

PAUL A. O'CONNELL
GREGORY B. MCKENNA
Texas Tech University

ZIEGLER–NATTA CATALYSTS. See Volume 8.

Encyclopedia of Polymer Sceince and Technology
Copyright © 2005 John Wiley & Sons, Inc. All rights reserved.

FLAMMABILITY

Introduction

Plastics (polymers) are a large and growing fraction of the fire load in homes, commercial environments, and transportation (1–5). Moreover, the plastics that are most widely used are those that are least expensive and these tend to be the most flammable. *Flammability*, which generally refers to the propensity of a substance to ignite easily and burn rapidly with a flame, is one indicator of fire hazard. Figure 1 shows the relationship between two measures of flammability—heat release capacity (see under Heat Release Rate) and flame resistance (see under Testing for Regulatory Compliance) versus the truckload price of commercial polymers. Flammability and cost span over 2 orders of magnitude but the commodity polymers costing less than about $1/pound comprise over 95% of the polymers in use and these will continue to burn after brief exposure to a small flame. Engineering and specialty plastics costing over $2/pound are typically polymers with aromatic backbones and fluoropolymers, and these will self-extinguish or resist ignition because of high thermal stability or low fuel value. Figure 1 shows that the flame resistance of polymers does not always correlate with cost but does correlate reasonably well with heat release capacity.

Regulations (1–5) governing the flammability of plastics (eg, see section Testing for Regulatory Compliance) used in consumer electronics, electrical equipment, building and construction, home furnishings, automobiles, and public transportation have created an annual worldwide market of tens of billions of pounds for flame-retardant plastics (1). The designation flame retardant, flame resistant, or ignition resistant as it applies to these plastics typically refers to the tendency of a thin (2–3 mm) strip of the material to withstand a brief exposure to a Bunsen burner flame or a hot wire without continuing to burn. Flame or ignition resistance is a low level of fire safety that is intrinsic to heat-resistant polymers but can be achieved with commodity polymers by adding flame-retardant chemicals (1–4). The economic incentive to add flame retardants to commodity polymers in order to pass flammability requirements (ie, the slope in Fig. 1) has focused polymer flammability research over the past few decades on the mechanisms and efficacy of flame-retardant additives (6–10), rather than on polymer flammability as an intrinsic material property. This trend in research combined with the fact that flaming combustion of solids is a highly coupled, multiphase process, and that fire test results depend on the apparatus, test conditions, and sample geometry, has limited the understanding of polymer flammability to a descriptive/qualitative nature.

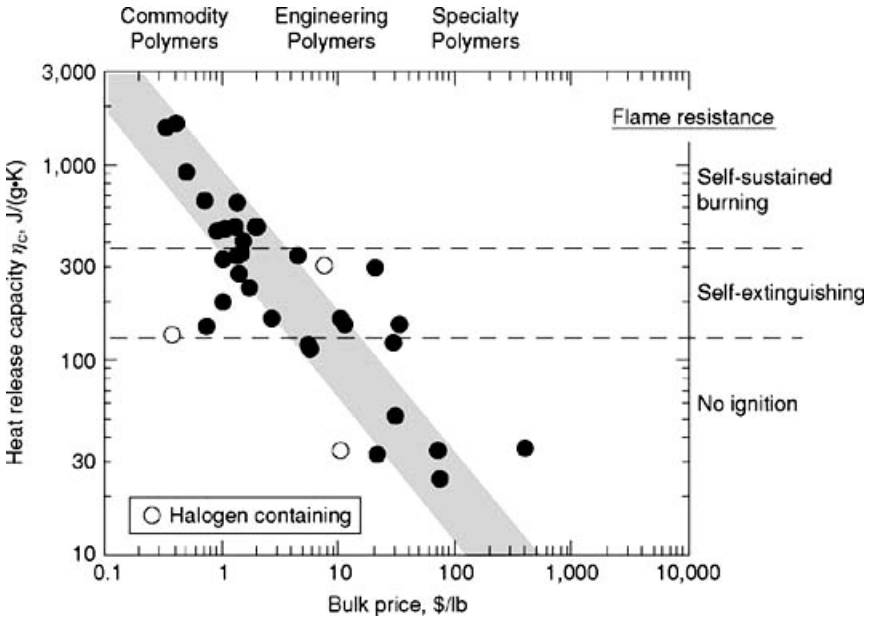

Fig. 1. Heat release capacity, cost, and flame resistance of commercial polymers.

In this article simplifying assumptions are made about the burning processes under well-defined (standardized) conditions in order to provide mathematical relationships between polymer chemical structure and flammability properties. Experimental data are used in lieu of, and in support of, analytic results drawn from the broad subject material that is referenced in the bibliography. The goal of this article is to provide a consistent, mechanistic interpretation of the burning process as it relates to synthetic polymers and to describe currently accepted test methods to quantify burning behavior.

The Burning Process

Gases and volatile liquids are small molecules that are held together by weak (<1 kJ/kg) secondary chemical bonds. These volatile compounds spontaneously form combustible mixtures with air that ignite easily and burn with a high velocity. Polymers are very large (macro) molecules with the same intermolecular and intramolecular forces as low molecular weight compounds, but their boiling temperature is essentially infinite because of their high molecular weight. Consequently, both intermolecular and intramolecular (backbone) chemical bonds of polymers must be broken to generate volatile fuel species, and this process requires a large (≈2 MJ/kg) and continuous supply of thermal energy for ignition and sustained burning.

Flaming combustion can be roughly divided into physical and chemical processes taking place in each of three separate phases: gas, mesophase, and condensed (liquid/solid) phase (6,7,10–16). The *mesophase* is the interface between

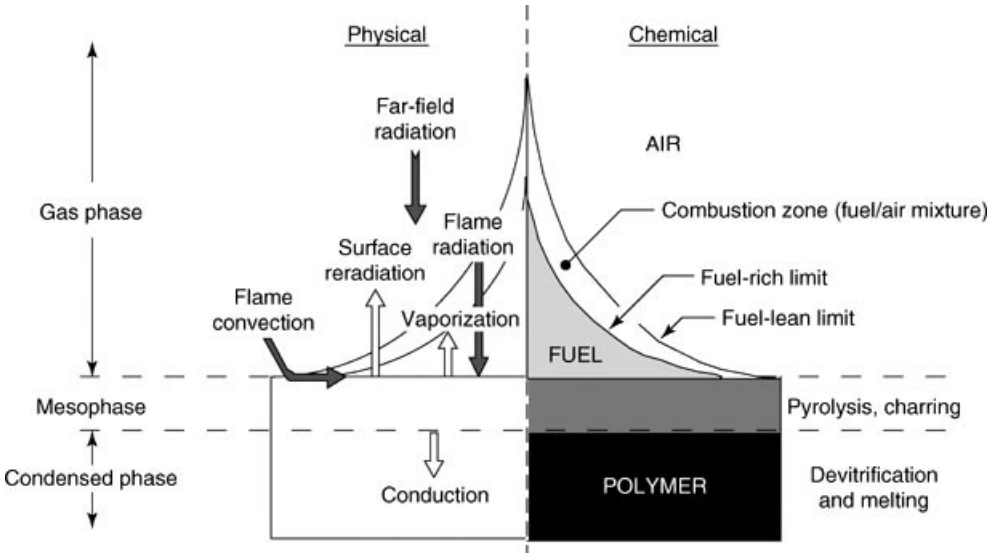

Fig. 2. Physical and chemical processes in the flaming combustion of polymers.

the gas and condensed phase during burning. Figure 2 is a schematic diagram of a horizontal polymer slab that is burning with a diffusion flame. Physical processes are shown on the left-hand side of Figure 2, and these include energy transport by radiation and convection between the gas phase (flame) and the mesophase; energy loss from the mesophase by mass transfer (vaporization of the pyrolysis gases); and conduction into the solid. At typical burning rates the polymer surface (mesophase) recedes at a velocity of about 10^{-6} m/s. Conservation of momentum at the gas–mesophase boundary shows that fuel gases evolve at a relatively low velocity ($\approx 10^{-3}$ m/s) compared to the burning velocity of these gases when mixed with air (≈ 1 m/s). Consequently, fuel generation is the rate-limiting step in polymer flaming combustion and it is governed primarily by the rate at which heat and mass are transported to and from the polymer, respectively.

The important chemical processes are shown on the right-hand side of Figure 2, and these are thermal degradation of the polymer in a thin surface layer (the mesophase) as a consequence of the physical (energy transport) processes; mixing of the volatile pyrolysis products with air by diffusion; and combustion of the fuel/air mixture in a combustion zone that produces radiant energy over a spectrum of wavelengths including visible. The combustion zone is bounded by a fuel-rich region on the inside and fuel-lean region on the outside. Increasing the concentration of oxygen in the environment is known to increase the flame heat flux, because of either a higher flame temperature, an increase in the volume of the combustion zone, or an increase in the soot concentration (luminosity) of the flame. The chemical and physical processes of flaming combustion particular to each of the gas, meso, and solid phase are treated separately below.

The Gas Phase.

Kinetics. Condensed phases (solids and liquids) of combustible compounds will only burn if they can be made to generate volatile fuel/air mixture, and so the

phenomena that lead to ignition and the release of heat are those of the gas phase (11–19). Although there are hundreds or thousands of chemical reactions going on in the flame that convert oxygen and fuel to stable combustion products, kinetic modeling and experimental data have shown that the burning velocity is most sensitive to the following reactions involving active radicals of fuel (R), hydroxyl (OH), hydrogen (H), and oxygen (O), and halogen or phosphorus (X):

$$\begin{aligned}
&\text{Initiation:} && \mathrm{RH} \xrightarrow{k_1} \mathrm{R^{\cdot}} + \mathrm{^{\cdot}H} \\
&\text{Branching:} && \mathrm{^{\cdot}H} + \mathrm{O_2} \xrightarrow{k_2} \mathrm{^{\cdot}OH} + \mathrm{^{\cdot}O} \\
&\text{Propagation (and primary heat producing reaction):} && \mathrm{^{\cdot}OH} + \mathrm{CO} \xrightarrow{k_3} \mathrm{CO_2} + \mathrm{^{\cdot}H} \\
&\text{Propagation:} && \mathrm{^{\cdot}OH} + \mathrm{H_2} \xrightarrow{k_4} \mathrm{H_2O} + \mathrm{^{\cdot}H} \\
&\text{Termination:} && \mathrm{^{\cdot}H} + \mathrm{O_2} \xrightarrow{k_5} \mathrm{^{\cdot}HO_2} \\
&\text{Inhibition:} && \mathrm{^{\cdot}H} + \mathrm{HX} \xrightarrow{k_6} \mathrm{H_2} + \mathrm{^{\cdot}X} \\
&\text{Inhibition:} && \mathrm{^{\cdot}OH} + \mathrm{HX} \xrightarrow{k_7} \mathrm{H_2O} + \mathrm{^{\cdot}X}
\end{aligned} \tag{1}$$

The set of seven radical reactions in equation 1 accounts for the key processes of initiation, branching, propagation, and termination typical of hydrocarbon fuels as well as the inhibition reactions that are important for polymers containing halogen or phosphorus in a low oxidation state. Because the concentrations of radicals are empirically related as $[\mathrm{H}] \approx [\mathrm{OH}] \approx 2[\mathrm{O}]$, the set of equations can be solved for the total concentration of active radicals, $[\mathrm{n}] = [\mathrm{H}] + [\mathrm{O}] + [\mathrm{OH}]$. Defining a rate of chain initiation, $\theta = k_1[\mathrm{RH}]$, a branching coefficient $f = (2/5)k_2[\mathrm{O_2}]$, and a linear termination coefficient $g = (2/5)\{k_5[\mathrm{O_2}] + (k_6+k_7)[\mathrm{HX}]\}$, the rate of change of radical concentration at time t is

$$\frac{\mathrm{d}[n]}{\mathrm{d}t} = \theta + f[\mathrm{n}] - g[\mathrm{n}] \tag{2}$$

The general solution of equation 2 for the total radical concentration at any time is

$$[\mathrm{n}] = \frac{\theta}{g-f}\{1 - e^{-(g-f)t}\} \tag{3}$$

Figure 3 is a schematic plot of equation 3 for three special cases:

(1) $f > g$: In this case the branching reactions dominate and the radical concentration increases exponentially as $[\mathrm{n}] = \{\theta \exp((f-g)t) - 1\}/(f-g)$, until the reactants are depleted.

(2) $g = f$: In this case the radical concentration increases steadily with time as $[\mathrm{n}] = \theta t$. It is the boundary between steady state and exponential growth.

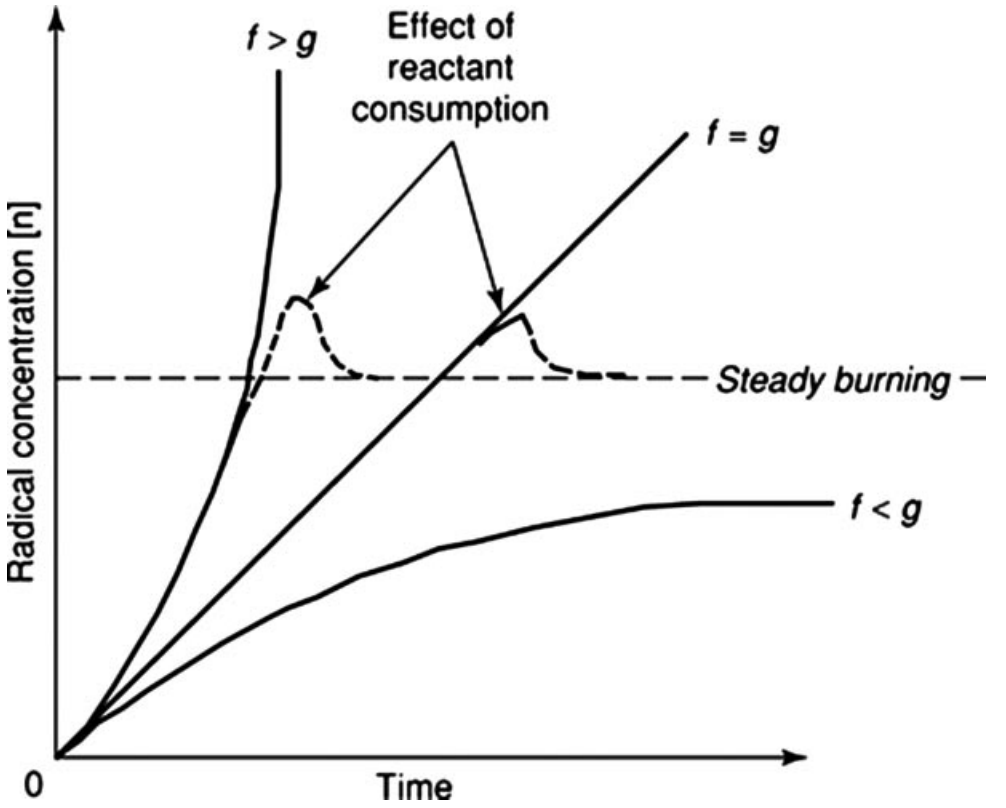

Fig. 3. Gas phase kinetics: accelerating ($f > g$), steady growth ($f = g$), and steady state ($f > g$) radical concentration histories at ignition.

(3) $g > f$: In this case the rate of chain termination is greater than branching and a steady-state concentration is reached at $[n] = \theta/(g - f)$. This steady state may be above or below the concentration for flame propagation.

The molar inhibition efficiency of the halogen atoms X = bromine (Br), chlorine (Cl), and fluorine (F) is found to be in the ratio Br/Cl/F = 10/2/1; ie, bromine is 10 times more efficient than fluorine and 5 times more efficient than chlorine on a mole basis. On a mass basis the inhibitor efficiency is Br/Cl/F = 2/1/1, which explains the widespread use of bromine-containing monomers and additives as flame retardants (4–10).

Thermochemistry. If the kinetics are such that the combustion reactions proceed to completion at a rate that sustains flaming combustion, the chemical reaction of a generic fuel with atmospheric oxygen yields carbon dioxide (CO_2), water (H_2O), nitrogen (N_2), and mineral acid (HX) in quantitative yield:

$$C_cH_hO_mN_nX_x + \left(c + \frac{h - x - 2m}{4}\right)O_2 \rightarrow c\ CO_2 + \frac{h - x}{2}H_2O + \frac{n}{2}\ N_2 + x\ HX \qquad (4)$$

Equation 4 assumes complete, 100% efficient, conversion of reactants (fuel gases, O_2) to products (CO_2, H_2O). Flaming combustion efficiency rarely exceeds 99% and typically ranges from 50 to 95%. Smoke is a combination of complete (CO_2, H_2O, acid gases) and incomplete (soot, carbon monoxide, partially oxidized fuel gases) combustion products that occurs when combustion inhibitors are present, oxygen concentration is low, or there is insufficient reaction time or temperature in the combustion zone. The composition of smoke is highly dependent on the chemical composition of the polymer and the ventilation conditions under which the polymer is burning. Acid gases are irritating to eyes and nasal passages which makes escape more difficult. Carbon monoxide is the primary toxic compound in smoke. Soot absorbs light which limits visibility and increases the luminosity or radiant power of the fire. Smoke is considered to be the main fire hazard but it depends on ventilation and the burning rate of the polymer, and so it is the latter quantity, ie, the burning or heat release rate, that is considered to be the primary indicator of fire hazard (4,11,12,20,21).

The chemical pathway to soot formation is recombination of aromatic radical fragments in the fuel-rich region inside the flame (see Fig. 2). Minute polycyclic aromatic hydrocarbon particles are formed that are 10–100 nm in diameter, and these elementary soot particles may oxidize in the combustion zone of the flame. However, the elementary soot particles will agglomerate and grow in size until they are large enough to interact with visible light (0.3–0.7 μm), ultimately reaching sizes of the order of a micron that absorb infrared radiation. Smoke is a combination of these soot particles in an aerosol with unburned liquid hydrocarbons, carbon dioxide/monoxide, water, and halogen acid gases, if present in the burning polymer (11–13).

Energetics. Regardless of the gas phase combustion kinetics and thermochemistry, burning will only be possible if the energy balance is favorable. The first law of thermodynamics for a constant pressure gas phase process in which all of the work is pressure–volume (P–V) work states that the internal energy change dU is related to the change in heat content dQ:

$$dU + P\,dV = dQ \tag{5}$$

If the volatile fuel and air are well-mixed and react to generate a power density $\dot{Q}'''$ (heat of combustion per unit volume per unit time, W/m^3), a portion of which accumulates in the reaction volume as a rise in the temperature of the fuel/air mixture and a portion of which is lost to the surroundings at ambient temperature T_a by convection and radiation, the first law energy balance for the fuel/air mixture during deflagration (burning) is

$$\rho c \frac{dT}{dt} + P\frac{dV}{V} = \dot{Q}''' - \frac{\bar{h}S}{V}(T - T_a) - \frac{\varepsilon\sigma S}{V}\left(T^4 - T_a^4\right) \tag{6}$$

where ρ, c, V, and T are the instantaneous density, heat capacity, volume, and temperature of the fuel/combustion products/air mixture, $\bar{h}$ is the average heat transfer coefficient at the boundary between the combustible mixture and the environment having surface area S at temperature T and pressure P. In equation 6, ε is the gas emissivity and σ is the Stefan–Boltzmann constant. Defining quantities

$\theta = T - T_a$ and $\tau = \rho c V/\overline{h}S$ and assuming a constant fraction ϕ of the power density is lost by radiation to the surroundings,

$$\frac{S}{V}\varepsilon\sigma\left(T^4 - T_a^4\right) \approx \phi\dot{Q}''' \tag{7}$$

Substituting equation 7 into equation 6, rearranging and separating variables

$$\frac{d\theta}{dt} - \frac{\theta}{\tau} = \frac{1}{\rho c}\{\dot{Q}'''(1-\phi) - P\,d\ln V\} \tag{8}$$

where $\dot{Q}'''$, ρ, and c are initial values for the mixture. If deflagration (burning) raises the temperature from T_a to T_f with a corresponding increase in volume from V_a to V_f at constant pressure over a short time interval (0, t_f) with $t_f \ll \tau$, and heat is transferred by radiation only, equation 8 becomes

$$T_f - T_a \approx \frac{1}{\rho c}\left\{Q'''(1-\phi) - P\ln\left(\frac{V_f}{V_a}\right)\right\} \tag{9}$$

where $Q''' = t_f\dot{Q}'''$ (J/m^3) is the energy density at ignition. If the moles of reactants (fuel and air) and combustion products (CO_2 and H_2O, principally) are equal and behave as ideal gases and T_f is the (quasi) adiabatic flame temperature, then

$$Q''' = \frac{\rho c(T_f - T_a) + P\ln(T_f/T_a)}{1-\phi} \tag{10}$$

The *lower flammability limit* (LFL), is the minimum volume (or mole) fraction of fuel in a fuel/air mixture that sustains ignition (11,12,18). The LFL has been measured for hundreds of gaseous and liquid hydrocarbon fuels including fuels that contain oxygen, nitrogen, sulfur, boron, phosphorus, and halogen (11). The average value of Q''' for 236 combustible compounds is

$$Q''' = \rho_f h_c^0 \mathrm{LFL} = 1864 \pm 278 \text{ kJ/m}^3 \tag{11}$$

where ρ_f and $h_c{}^0$ are the vapor density and heat of complete combustion of the fuel, respectively. If burning occurs at the lower flammability limit of the fuel, then equations 10 and 11 are equal and

$$\frac{\rho c(T_f - T_a) + P\ln(T_f/T_a)}{1-\phi} = 1.9 \text{ MJ/m}^3 \tag{12}$$

Equation 12 can be solved for the quasi-adiabatic flame temperature at standard temperature and pressure (STP). For $\phi < 0.2$, the flame temperatures calculated using equation 12 are in the range $T_f = 1720$–1420 K, compared to experimental values $T_f = 1600 \pm 100$ K (11,12). Equation 12 shows that the lower flammability limit corresponds to a temperature $T_f \approx 1600$ K at which the rate of heat losses from the flame equal the rate of heat production in the flame owing to the combustion reactions.

The Mesophase. The mesophase is the interface between the gas and condensed phases during burning. All of the thermal degradation chemistry that results in volatile fuel generation occurs in the mesophase (also known as the pyrolysis zone). A qualitative diagram of the mesophase properties is shown in Figure 4. The temperature distribution at the burning surface is primarily a consequence of the prevailing energy balance but the viscosity, density, and physical dimension of the mesophase shown qualitatively in Figure 4 is determined by the temperature field and thermal degradation chemistry. For polymers that thermally

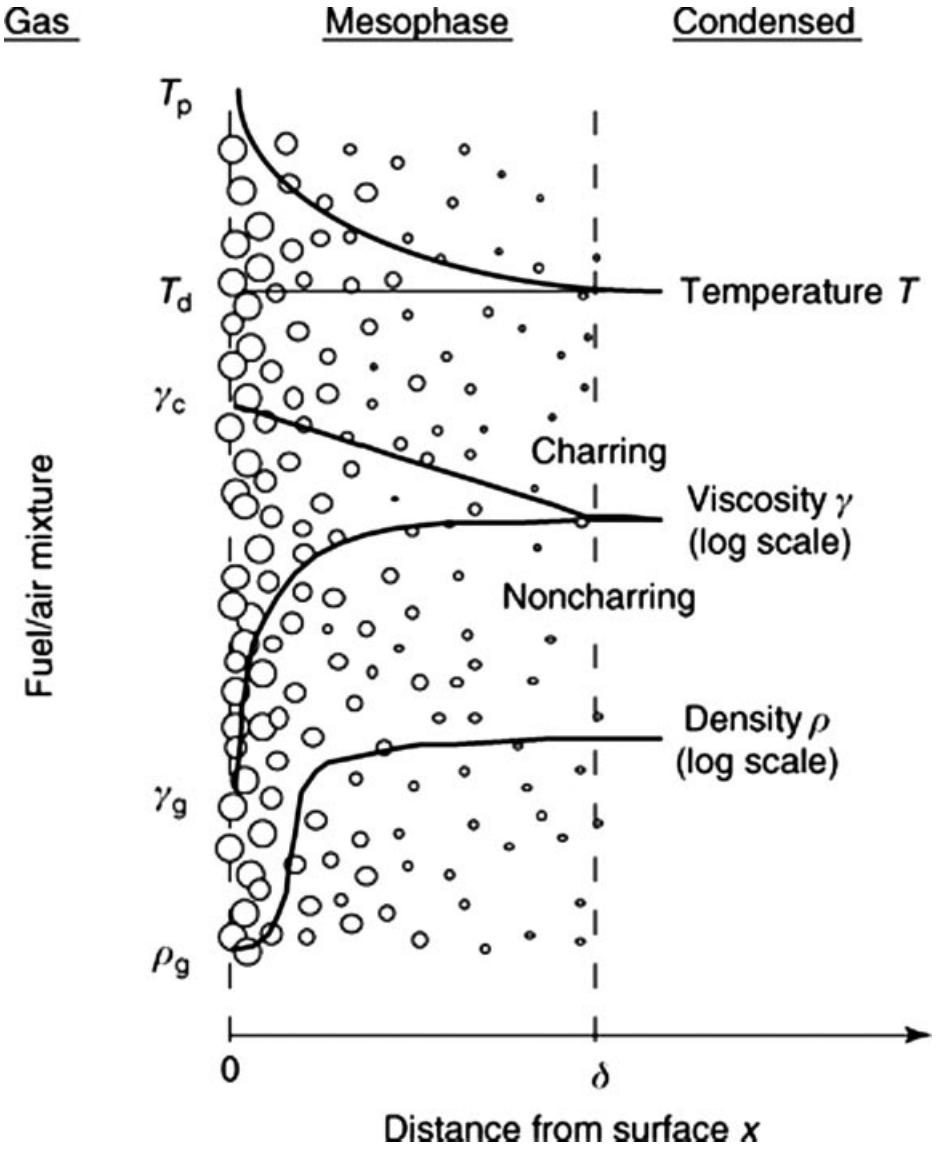

Fig. 4. Mesophase profiles of temperature, viscosity, and density during flaming combustion.

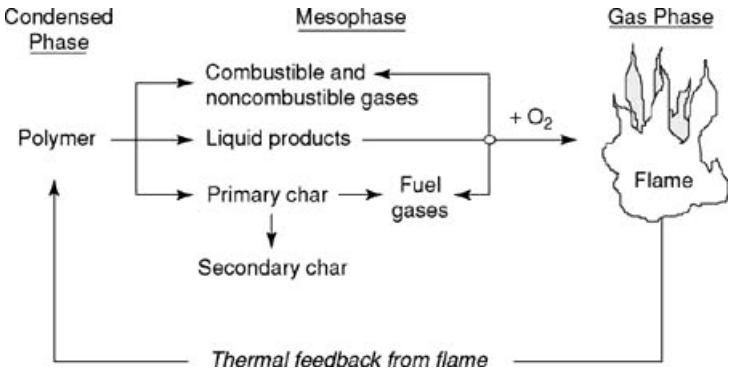

Fig. 5. Phenomenology of polymer burning.

degrade with the formation of a solid char the viscosity of the mesophase is higher than that of the molten polymer and probably comparable to that of the solid polymer. The mesophase is composed of thermal degradation products in a variety of phases including gas, liquid, and solid as indicated schematically in Figure 4 by the bubble density and in Figure 5 by a generic product distribution.

Figure 5 shows the phenomenology of polymer burning and illustrates the coupled nature of the flaming combustion of condensed phases. The sequence of events for self-sustained burning involves the application of heat sufficient to thermally degrade (pyrolyze) the solid polymer to low molecular weight volatile fuel species and possibly a nonvolatile/solid char depending on the polymer chemical structure. Mixing of the volatile thermal degradation products with atmospheric oxygen and ignition of this fuel/air mixture results in flaming combustion. Flaming combustion produces thermal energy in proportion to the heat of combustion of the volatile thermal degradation products and at a rate that is controlled by the fuel generation rate. The majority of the combustion energy from the flame is lost to the environment but a fraction is returned to the polymer surface by convection and radiation (see Fig. 2). If the feedback of thermal energy from the flame at the polymer surface is sufficient to generate fuel vapors, flaming combustion will continue after the ignition source is removed and burning will be self-sustained.

Kinetics. In Figure 5 the first stage of thermal degradation produces primary volatiles (gas and liquid products/tar) and possibly a primary char residue (see under Char Yield). If a primary char forms, further decomposition generates a secondary gas (principally hydrogen) and a thermally stable carbonaceous char. Figure 6 shows thermogravimetric data at a heating rate of 10 K/min for anaerobic pyrolysis of polybenzimidazole (2,2′-*m*-phenylene-5,5′-bibenzimidazole, PBI). Polybenzimidazole is a heat-resistant, char-forming polymer that thermally degrades by primary and secondary decomposition events as evidenced by distinct mass loss rate peaks for these processes. Models have been proposed that account for some or all of the pyrolysis products (gas, tar, primary char secondary char, secondary gas) as various combinations of sequential or simultaneous thermal degradation reactions. However, a detailed mechanism for the thermal degradation of most polymers, especially char-forming polymers, is unlikely and unnecessary for a phenomenological treatment of fuel generation chemistry.

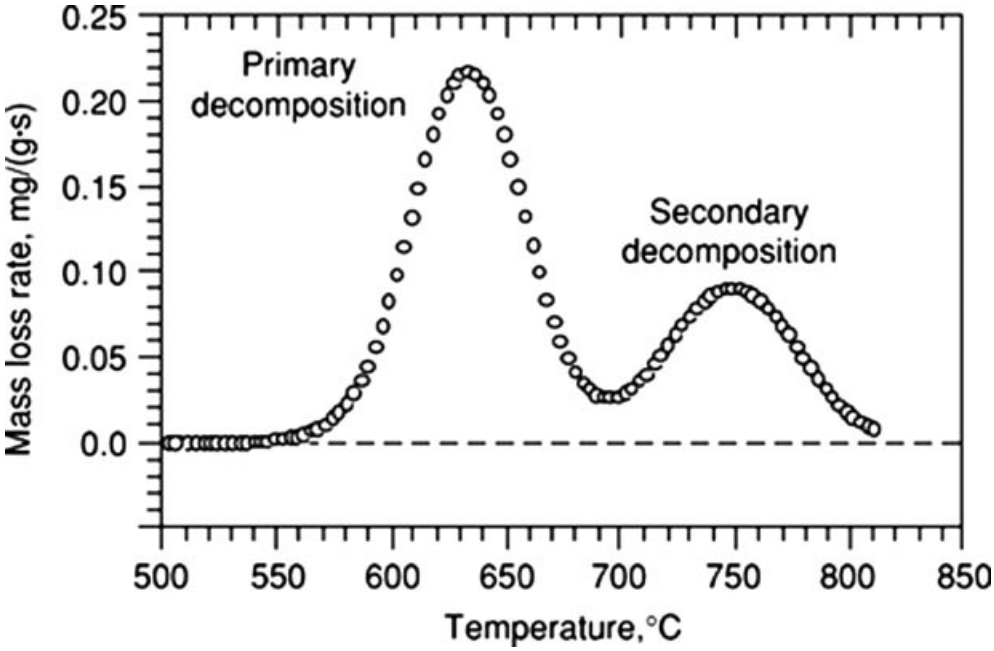

Fig. 6. Fractional mass loss rate versus temperature for polybenzimidazole in TGA ($\beta =$ 10 K/min).

Mechanistic reaction kinetics of polymer thermal degradation processes show that the overall mass loss (fuel generation) rate should be first order with respect to the instantaneous mass if the reactive intermediates (free radicals) maintain a steady-state concentration, regardless of whether thermal degradation occurs by random or end-chain scission. A first-order thermal degradation scheme that accounts for the main pyrolysis products is (4,7,10)

$$\text{Polymer (P)} \xrightarrow{k_d} \text{Intermediate (I*)} \tag{13}$$

$$\text{I*} \xrightarrow{k_g} \text{Gas (G)} \tag{14}$$

$$\text{I*} \xrightarrow{k_c} \text{Char (C)} \tag{15}$$

Equations 13–15 are a subset of the reactions shown in Figure 5 but they are sufficient to represent the mesophase fuel generation kinetics. In particular, polymer P thermally degrades to a reactive intermediate I^* with rate constant k_d. The intermediate produces gas G and/or char C, with rate constants k_g and k_c, respectively. Figure 7 shows data for a variety of pure, unfilled polymers plotted

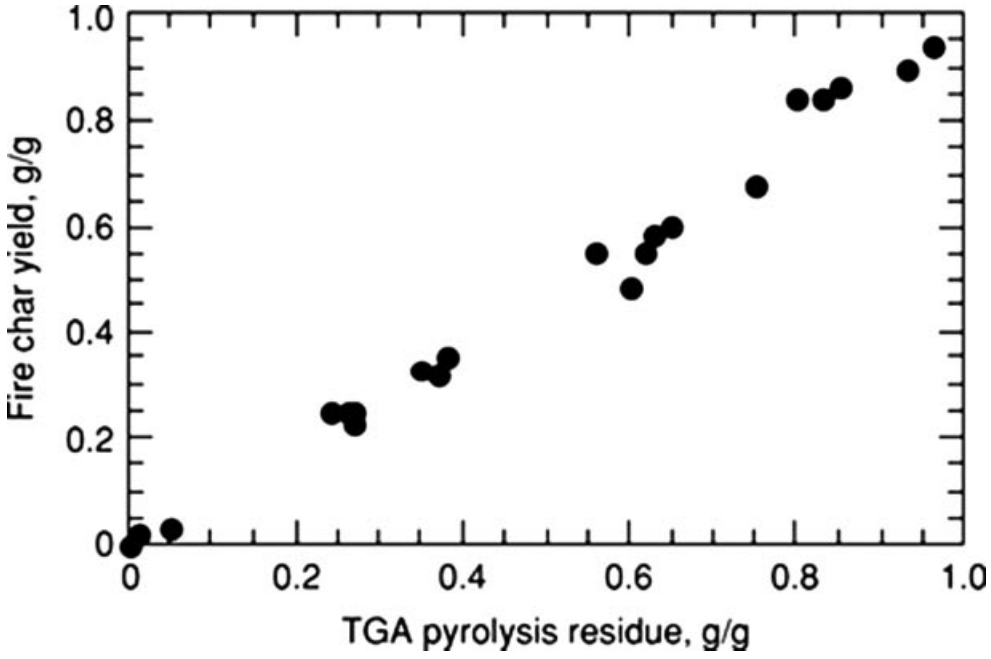

Fig. 7. Char mass fraction in fire versus anaerobic pyrolysis.

as the mass fraction of char measured immediately after flaming combustion has ceased in a fire calorimeter (see under Testing to Obtain Engineering Data) versus the char residue at 900 ± 100°C for the same material after anaerobic pyrolysis in a thermogravimetric analyzer at a heating rate of about 10 K/min. It is seen that the char yield of a material in a fire is essentially equal to its residual mass fraction after anaerobic pyrolysis at temperatures representative of the char temperature in a fire. Although oxidative degradation products have been identified at the surface of olefinic polymers after flaming combustion, the data in Figure 7 suggest that oxidation reactions in the solid *during* flaming combustion are not important to the overall fuel fraction. If the reactive intermediate I* in equations 13–15 is a stationary state then $dI^*/dt = 0$, and if thermal decomposition is an anaerobic process, the fuel generation rate is

$$-\frac{dm'}{dt} = k_p m' = A\, e^{-E_a/RT} m' \tag{16}$$

where m' is the mass of volatile fuel, k_p is the mass loss rate constant in terms of a global frequency factor A (1/s) and activation energy E_a (J/mol). Equation 16 is easily solved for the fuel generation rate at constant temperature (isothermal conditions). However, the polymer temperature changes rapidly from ambient to the pyrolysis temperature near the burning surface, and so a nonisothermal solution of equation 16 is required to capture the dynamics of the fuel generation process as it occurs in the mesophase. For an arbitrary temperature history $T(t)$

in the mesophase, the mass of fuel generated at any time t is

$$\ln\left\{\frac{m'(\tau)}{m'(0)}\right\} = -\int_0^t A\,\exp\left\{-\frac{E_a}{RT(t')}\right\}dt' \tag{17}$$

Equation 17 can be solved numerically for any specified temperature history. However, the mesophase temperature history is a function of both time and position (see Fig. 4), and so the transient temperature distribution $T(x, t)$ must be specified in order to obtain an analytic solution for equation 17. If the temperature distribution is static during steady burning of a thick sample as the surface $x = 0$ recedes at constant velocity $v = (dx/dt)_T$ and the mesophase is a thin surface layer, then the rate of temperature rise of the mesophase is constant, $(dT/dt)_{x=0} = -v(dT/dx)_t = \beta$. The assumption of a constant heating rate for the mesophase transforms the independent variable in equation 17 from time to temperature and allows for a solution in terms of the mass fraction of polymer remaining at temperature T

$$\frac{m(T)}{m_0} = \mu(T) + \{1 - \mu(T)\}\,e^{-y} \tag{18}$$

where

$$y = \frac{k_p R T^2}{\beta(E_a + 2RT)}$$

The equilibrium char fraction at temperature T is

$$\mu(T) = \frac{k_c}{k_c + k_g} = \left\{1 + \frac{A_g}{A_c}\,\exp\left(-\frac{E_g - E_c}{RT}\right)\right\}^{-1} \tag{19}$$

in terms of the frequency factors A_g, A_c and the activation energies E_g, E_c, for gas and char formation, respectively. A temperature-dependent equilibrium char fraction, which is the ratio of rate constants for gas and char formation, is consistent with the use of group contributions for the char-forming tendency of polymers (22) (see under Char Yield). The fractional mass loss rate at temperature T is obtained by differentiating equation 18 with respect to time. For $\mu\,(T) = \mu =$ constant, the result is

$$-\frac{1}{m_0}\frac{dm}{dt} = (1 - \mu)k_p\,e^{-y} \tag{20}$$

Setting the time derivative of equation 20 equal to zero shows that the maximum fuel generation rate occurs when

$$k_p(T_p) = A\,\exp\left(-\frac{E_a}{RT_p}\right) = \frac{\beta E_a}{RT_p^2} \tag{21}$$

Substituting k_p from equation 21 into equation 20 for $E_a \gg RT_p$ gives the maximum fuel generation rate

$$-\frac{1}{m_0}\frac{dm}{dt}\bigg|_{max} = (1-\mu)\frac{\beta E_a}{eRT_p^2} \tag{22}$$

The temperature T_p in equations 21 and 22 is the temperature at the maximum fuel generation rate during the course of the linear temperature history. Defining a characteristic heating rate $\beta^* = A\ \Delta T_p$, where $\Delta T_p = RT_p{}^2/E_a$ is the half-width of the pyrolysis temperature interval, equation 22 takes the form of a (statistical) thermodynamic phase transition temperature

$$T_p = \frac{E_a}{R\ln(\beta^*/\beta)} \tag{23}$$

Thermogravimetric analysis (TGA) is a common laboratory method for studying the thermal degradation kinetics of polymers at constant heating rate (6–10). The maximum fuel generation rate and T_p are readily obtained from these experiments as shown in Figure 8 for poly(methyl methacrylate) (PMMA) and polyamideimide (PAI). Figure 8 shows the onset thermal degradation temperature T_d, the temperature at peak mass loss rate T_p, and the char fraction μ for PAI. The range of temperatures over which pyrolysis takes place is of the order $eRT_p{}^2/(1-\mu)E_a$, which is seen to be very different for these two polymers of widely differing thermal stability and charring tendency. Table 1 contains T_d, T_p, and T_{ign} for a number of polymers.

Thermochemistry. The basic thermal degradation mechanism leading to volatile fuel generation in polymers involves primary and secondary decomposition events as illustrated in Figure 5. The primary decomposition step can be main-, end-, or side-chain scission of the polymer. Subsequent thermal degradation reactions depend largely on the chemical structure of the polymer but typically proceed by hydrogen transfer to α- or β-carbons, nitrogen or oxygen, intramolecular exchange (cyclization), side-chain reactions, small-molecule (SO_2, CO_2, S_2) elimination, molecular rearrangement, and/or unzipping to monomer (15). Unzipping or depolymerization of vinyl polymers is characterized by a *kinetic chain length or zip length* that is the average number of monomer units produced by a decomposing radical before the radical is deactivated by termination or transfer. Mathematically, the zip length is the ratio of the rate constants for initiation to termination.

Aromatic backbone polymers such as polycarbonate, polyimides, polyaramides, polyarylsulfones, and polyphenyleneethers tend to decompose in varying degrees to a carbonaceous char residue through a complex set of intramolecular rearrangements and side-chain reactions involving cross-linking and bond scission. The char yield is the mass fraction of carbonaceous char that remains after flaming combustion of the polymer. Charring competes with termination reactions that generate volatile species and thus reduces the amount of available fuel in a fire. In addition, char acts as a heat and mass transfer barrier that lowers the flaming heat release rate. Figure 7 demonstrated that the char yield in a fire is roughly equal to the anaerobic pyrolysis residue at high (flame) temperatures. Polymers

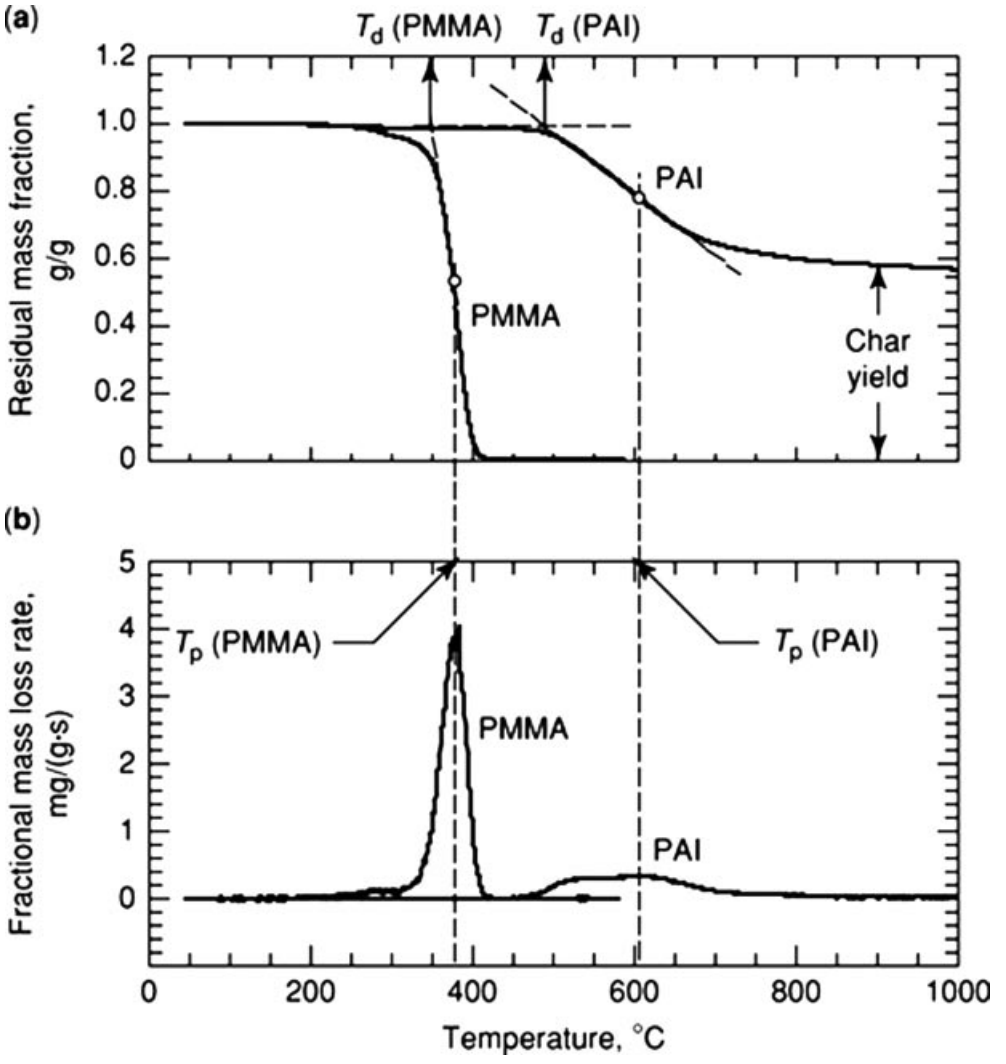

Fig. 8. Thermogravimetric analysis (TGA) data for poly(methyl methacrylate) (PMMA) and polyamideimide (PAI): (**a**) residual mass fraction versus temperature; (**b**) mass loss rate versus temperature.

that contain heterocyclic or aromatic structures in the backbone tend to form char during thermal decomposition in rough proportion to the carbon/hydrogen (C/H) ratio of the polymer. Figure 9 shows the mass fraction of char plotted versus the mole fraction of hydrogen in the polymer molecule. High C/H ratios favor termination by cross-linking between carbon radicals, and char is formed. Low C/H ratios favor termination of carbon radicals by hydrogen transfer, resulting in low molecular weight fuel species rather than char. The relative rates of intermolecular cross-linking and aromatization and intramolecular hydrogen transfer and cyclization reactions, ie, the ratio $k_c/(k_c + k_g)$ in equation 19, will determine the char yield at any particular hydrogen mole fraction.

Table 1. Onset Decomposition (T_d), Peak Mass Loss Rate (T_p), and Ignition (T_{ign}) Temperatures of Polymers (Average Values ± 10°C)

Polymer	ISO/ASTM abbreviation	T_d, °C	T_p, °C	T_{ign}, °C
Thermoplastics				
Acrylonitrile–butadiene–styrene	ABS	390	461	394
ABS FR	ABS-FR	—	—	420
Polybutadiene	BDR	388	401	378
Polyisobutylene (butyl rubber)	BR	340	395	330
Cellulose acetate	CA	250	310	348
Cyanate ester (typical)	CE	448	468	468
Polyethylene (chlorinated)	CPE	448	476	—
Polyvinylchloride (chlorinated)	CPVC	—	—	643
Polychloroprene rubber	CR	345	375	406
Polychlorotrifluoroethylene	CTFE	364	405	580
Poly(ethylene-chlorotrifluorethylene)	ECTFE	445	465	613
Phenoxy-A	EP	—	350	444
Epoxy (EP)	EP	427	462	427
Poly(ethylene-tetrafluoroethylene)	ETFE	490	520	540
Polyethylenevinylacetate	EVA	448	473	
Fluorinated ethylene propylene	FEP	—	—	630
Poly(styrene-butadiene)	HIPS	327	430	413
Poly(styrene-butadiene) FR	HIPS-FR	—	—	380
Poly(*p*-phenyleneterephthalamide)	KEVLAR	474	527	—
Polyarylate (liquid crystalline)	LCP	514	529	—
Melamine formaldehyde	MF	350	375	350
Polyisoprene (natural rubber)	NR	301	352	297
Polytrifluoroethylene	P3FE	400	405	—
Polyamide 12	PA12	448	473	—
Polyamide 6	PA6	424	454	432
Polyamide 610	PA610	440	460	—
Polyamide 612	PA612	444	468	—
Polyamide 66	PA66	411	448	456
Polyamide 6 (glass reinforced)	PA6-G	434	472	390
Polyamideimide	PAI	485	605	526
Polyacrylamide	PAM	369	390	—
Polyacrylonitrile	PAN	293	296	460
Polyarylate (amorphous)	PAR	469	487	—
Polybutene	PB	—	390	—
Polybenzimidazole	PBI	584	618	—
Polybutylmethacrylate	PBMA	261	292	—
Polybenzobisoxazole	PBO	742	789	—
Polybutyleneterephthlate	PBT	382	407	382
Polybutyleneterephthalate	PBT-G	386	415	360
Polycarbonate	PC	476	550	500
Polycarbonate/ABS (70/30)	PC/ABS	421	475	440
Polycarbonate (glass reinforced)	PC-G	478	502	420
Polycaprolactone	PCL	392	411	—
Polyethylene (high density)	PE HD	411	469	380
Polyethylene (low density)	PE LD	399	453	377
Polyethylacrylate	PEA	373	404	—

Table 1. (continued)

Polymer	ISO/ASTM abbreviation	T_d, °C	T_p, °C	T_{ign}, °C
Polyethylene-acrylic acid salt	PEAA	452	474	—
Polyetheretherketone	PEEK	570	600	570
Polyetherimide	PEI	527	555	528
Polyetherketone (eg, KADEL)	PEK	528	590	—
Polyetherketoneketone	PEKK	569	596	—
Polyethylmethacrylate	PEMA	246	362	—
Polyethylenenaphthalate	PEN	455	495	479
Polyethyleneoxide	PEO	373	386	—
Polyethersulfone	PESU	533	572	502
Polyethyleneterephthlate	PET	392	426	407
Phenol formaldehyde	PF	256	329	429
Polytetrafluoroethylene-perfluoroether	PFA	—	578	—
Phenol formaldehyde	PF-G	—	—	580
Polymethylmethacrylate	PMMA	354	383	317
Poly(4-methyl-1-pentene)	PMP	—	377	—
Poly(α-methyl)styrene	PMS	298	333	—
Poly(α-methylstyrene)	PMS	250	314	—
Polyoxymethylene	POM	323	361	344
Polypropylene	PP	354	424	367
Polypropylene (isotactic)	PP (iso)	434	458	—
Polyphthalamide (AMODEL)	PPA	447	488	—
Polyphenyleneether	PPE	—	418	426
Poly(2,6-dimethylphenyleneoxide)	PPO	441	450	418
Polypropyleneoxide	PPOX	292	343	—
Polyphenylenesulfide	PPS	504	545	575
Polyphenylsulfone	PPSU	557	590	575
Polystyrene	PS	319	421	356
Polysulfone	PSU	481	545	510
Polytetrafluoroethylene	PTFE	545	590	630
Polytetramethyleneoxide	PTMO	—	352	—
PU (isocyanurate/rigid)	PU	271	422	378
Polyetherurethane rubber	PUR	324	417	356
Polyvinylacetate	PVAC	319	340	—
Polyvinylbutyral	PVB	333	373	—
Polyvinylchloride (50% DOP)	PVC (flex)	249	307	318
Polyvinylchloride (rigid)	PVC (rigid)	273	285	395
Polyvinylchloride/polyvinylacetate blend	PVC/PVAC	255	275	—
Polyvinylidenechloride	PVDC	225	280	—
Polyvinylidenefluoride	PVDF	440	490	643
Polyvinylfluoride	PVF	361	435	476
Polyvinylcarbazole	PVK	356	426	—
Polyvinylalcohol	PVOH	298	322	—
Polyvinylpyridine	PVP	385	408	—
Polypara(benzoyl)phenylene	PX	476	602	—
Poly(styrene-acrylonitrile)	SAN	389	412	368
Phenylsilsesquioxane (silicone) resin	SI	475	541	—
Silicone rubber	SIR	456	644	407
Poly(stryene-maleic anhydride)	SMA	337	388	—

Table 1. (continued)

Polymer	ISO/ASTM abbreviation	T_d, °C	T_p, °C	T_{ign}, °C
Polyimide thermoplastic	TPI	523	585	600
Polyurethane thermoplastic	TPU	314	337	271
Unsaturated polyester	UPT	330	375	380
Unsaturated polyester	UPT-G	—	—	395

Energetics. In principle, the heat (enthalpy) of gasification is the difference between the enthalpy of the solid in the initial state at ambient temperature and pressure, T_0, P_0, and the enthalpy of the volatile thermal decomposition products at T_p, P_0. If the stored heat is Δh_s, the enthalpy of fusion (melting) for semicrystalline polymers is Δh_f, the bond dissociation enthalpy is Δh_d, and the enthalpy of vaporization of the decomposition products is Δh_v, then the enthalpy of gasification per unit mass of fuel is (10)

$$L_g = \Delta h_s + \Delta h_f + \Delta h_d + \Delta h_v = \int_{T_0}^{T_p} c(T)\,dT + \Delta h_f + \Delta h_d + \Delta h_v \tag{24}$$

The symbol L_g derives from latent heat, ie, the recoverable heat in a reversible process. Thermolytic cleavage of primary chemical bonds in the polymer backbone to produce volatile fuel and char is obviously not a reversible process, but the symbol L_g will be used throughout to conform with the literature in the fire sciences. Table 2 illustrates the magnitude of these enthalpic terms for amorphous PMMA, polystyrene (PS), and semicrystalline polyethylene (PE). The stored heat Δh_s was obtained by numerical integration of heat capacity versus temperature from ambient to the dissociation temperature as per equation 24. The dissociation

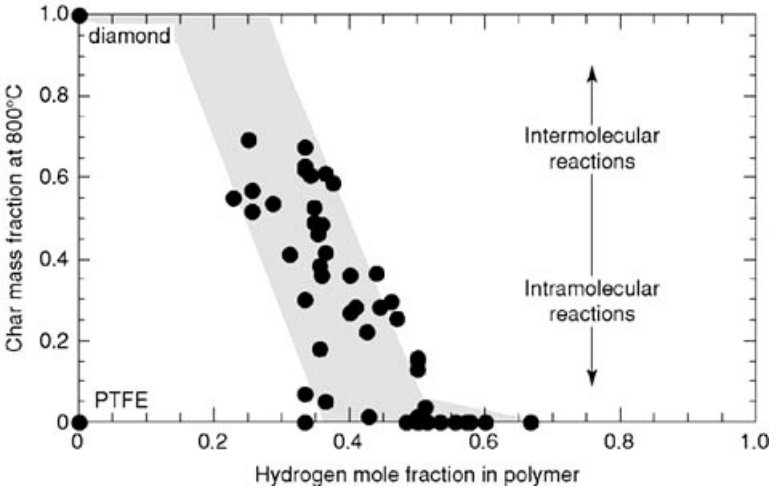

Fig. 9. Char mass fraction versus hydrogen mole fraction in polymer.

Table 2. Components of the Enthalpy of Gasification for poly(methyl methacrylate) (PMMA), polystyrene (PS), and polyethylene (PE)

	PMMA	PS	PE
Monomer molecular weight, g/mol	100	104	28
Fuel molecular weight, g/mol	100	104	112
Δh_s, J/g	740	813	803
Δh_f, J/g	Amorphous	Amorphous	243
Δh_d, J/g	550	644	910
Δh_v, J/g	375	387	345
$L_g = \sum \Delta h_i$, J/g	1665	1850	2301
L_g(measured), J/g	1700	1800	2200

(bond breaking) enthalpy Δh_d is assumed to be equal to the heat of polymerization but opposite in sign for these polymers which thermally degrade by random or end-chain scission. The degradation product for PE is assumed to be a tetramer (ie, octane with $M_g = 112$ g/mol) for the purpose of calculating the heats of dissociation and vaporization on a mass basis for this polymer, and the degree of crystallinity of PE is taken to be 90%. All other enthalpies in Table 2 were obtained from handbooks using monomer molecular weights to convert the energies to a mass basis. The values for h_g in the second to last row were obtained by summing the individual enthalpies according to equation 24 for each polymer.

In practice, the enthalpy of gasification is rarely calculated because detailed and reliable thermodynamic data for the polymer and its decomposition products are generally unavailable. Direct laboratory measurement of L_g using differential thermal analysis and differential scanning calorimetry has been reported, but L_g is usually measured in a constant heat flux gasification device or fire calorimeter (see under Steady Burning). In these experiments a plot of mass loss rate per unit surface area (mass flux) versus external heat flux has slope $1/L_g$ where

$$L_g = \frac{h_g}{1 - \mu} \tag{25}$$

h_g is the heat of gasification per unit mass of solid and μ is the nonfuel fraction (char or inert filler). The last row in Table 2 lists the average of h_g values for these noncharring polymers. Agreement is seen to be quite good between experimental values and thermochemical calculations of h_g. Table 3 contains L_g, μ, and h_g for 53 polymers. Analysis of the data in Table 3 shows that L_g and μ vary widely with polymer chemical structure but that h_g is relatively independent of composition with an average value $h_g = 2.0 \pm 0.5$ kJ/g.

The Condensed Phase.

Thermal Properties. The rate at which heat is transported and stored in the condensed phase is of fundamental importance because these processes determine the time to ignition and burning rate of polymers. Table 4 lists generic thermophysical properties at ambient temperature (295 ± 3 K) gathered from the

Table 3. Latent Heat of Gasification, Char Yield, and Enthalpy of Gasification of Polymers

Polymer	L_g, kJ/g	μ, g/g	h_g, kJ/g
ABS	2.3	0.00	2.3
ABS-FR	2.5	0.00	2.5
CEA	4.0	0.36	2.6
CEE	4.1	0.42	2.4
CEF	3.0	0.55	1.3
CEM	3.0	0.26	2.2
CEN	3.0	0.52	1.4
CET	3.5	0.35	2.3
CPE (25% Cl)	2.1	0.00	2.1
CPE (36% Cl)	2.8	0.20	2.2
CPVC	2.0	0.00	2.0
CR	2.0	0.13	1.7
ECTFE	1.5	0.00	1.5
EP	1.6	0.04	1.5
EPDM	1.9	0.00	1.9
EP (30% fiber glass)	2.3	0.30	1.6
ETFE	1.1	0.00	1.1
FEP	1.5	0.00	1.5
HIPS	2.0	0.00	2.0
HIPS-FR	2.1	0.10	1.9
PA6	1.5	0.02	1.5
PA66	2.1	0.04	2.0
PAI	4.8	0.61	1.9
PBI	5.5	0.75	1.4
PBT	1.4	0.07	1.3
PBT-FR	2.3	0.15	2.0
PC	2.4	0.25	1.8
PC-FR	3.5	0.52	1.7
PE HD	2.2	0.00	2.2
PE LD	1.9	0.00	1.9
PEEK	3.4	0.54	1.6
PEI	3.5	0.53	1.7
PEN	2.5	0.18	2.0
PESU	3.8	0.40	2.3
PET	1.4	0.05	1.3
PF	5.4	0.60	2.2
PMMA	1.7	0.00	1.7
POM	2.4	0.00	2.4
PP	1.9	0.00	1.9
PPS	3.8	0.50	1.9
PPSU	4.3	0.58	1.8
PS	1.8	0.00	1.8
PSU	2.0	0.28	1.4
PTFE	2.5	0.00	2.5
PU	2.3	0.13	2.0
PVC (flexible)	1.3	0.08	1.2
PVC (rigid)	2.3	0.09	2.1
PVDF	4.0	0.23	3.1

Table 3. (continued)

Polymer	L_g, kJ/g	μ, g/g	h_g, kJ/g
PVF	1.9	0.00	1.9
PX	6.4	0.66	2.2
SIR	2.3	0.00	2.3
TPU	2.4	0.13	2.1

literature for a number of common thermoplastics, thermoset resins, elastomers, and fiber-glass reinforced plastics (4). Entries are individual values, averages of values from different sources, or averages of a range of values from a single source and therefore represent in most cases a generic property value with an uncertainty of about 10–20%.

Neglecting changes in the slope or magnitude of thermal properties that occur at phase changes such as the glass transition, melting, and decomposition temperatures of polymers, the temperature dependence of κ, ρ, and c for an amorphous polymer can be roughly approximated

$$\kappa(T) = \kappa_0 \left(\frac{T}{T_0} \right)^{1/2} \tag{26}$$

$$\rho(T) = \rho_0 \left(\frac{T_0}{T} \right)^{1/2} \tag{27}$$

$$c(T) = c_0 \left(\frac{T}{T_0} \right) \tag{28}$$

These properties are plotted in reduced form in Figure 10 as $P(T)/P(T_0)$ versus T/T_0, where $P(T)$, $P(T_0)$ are the values of κ, ρ, or c at temperature T and standard temperature (298 K), respectively.

The product $\kappa\rho c$ is a quantity called the thermal inertia that emerges from the transient heat transfer analysis of ignition time (see eq. 40). The temperature dependence of κ, ρ, and c in equations 26–28 suggests that the product of these terms (ie, the thermal inertia) should have the approximate temperature dependence:

$$\kappa(T)\rho(T)c(T) \approx \kappa_0\rho_0 c_0 T/T_0 = (\kappa\rho c)_0 T/T_0 \tag{29}$$

where κ_0, ρ_0, c_0, are the room temperature (T_0) values listed in Table 4.

Another thermal parameter that emerges from unsteady heat transfer analyses is the thermal diffusivity $\alpha = \kappa/\rho c$, which, according to equations 26–28, should be relatively independent of temperature

$$\alpha(T) = \frac{\kappa(T)}{\rho(T)c(T)} = \alpha_0 \tag{30}$$

Room temperature values of polymer thermal diffusivity are listed in Table 4.

Table 4. Polymer Thermal Conductivity, Density, Heat Capacity, and Thermal Diffusivity at Room Temperature

Polymer	κ, W/(m · K)	ρ, kg/m^3	c_p, kJ/(kg · K)	α, (10^7 m^2/s)
ABS	0.26	1050	1.50	1.65
BDR	0.22	970	1.96	1.16
BR	0.13	920	1.96	0.72
CA	0.25	1250	1.67	1.20
CAB	0.25	1200	1.46	1.43
CAP	0.25	1205	1.46	1.42
CE	0.19	1230	1.11	1.39
CN	0.23	1375	1.46	1.15
CP	0.20	1300	1.46	1.05
CPVC	0.48	1540	0.78	4.00
CR	0.19	1418	1.12	1.20
CTFE	0.23	1670	0.92	1.50
DAP	0.21	1350	1.32	1.18
DAP-G	0.42	1800	1.69	1.38
EAA	0.26	945	1.62	1.70
ECTFE	0.16	1690	1.17	0.81
EP	0.19	1200	1.7	1.12
EPDM	0.20	930	2.0	1.08
EP-G	0.42	1800	1.60	1.46
EPN	0.19	1210	1.26	1.25
ETFE	0.24	1700	1.0	0.66
EVA	0.34	930	1.37	2.67
FEP	0.25	2150	1.17	0.99
HIPS	0.22	1045	1.4	1.54
LCP	0.20	1350	1.20	1.24
MF	0.25	1250	1.67	1.20
MF-G	0.44	1750	1.67	1.51
NBR	0.25	1345	1.33	1.40
NR	0.14	920	1.55	0.98
P3FE	0.31	1830	1.08	1.41
PA11	0.28	1120	1.74	1.44
PA11-G	0.37	1350	1.76	1.56
PA12	0.25	1010	1.69	1.46
PA6	0.24	1130	1.55	1.37
PA610	0.23	1100	1.51	1.38
PA612	0.22	1080	1.59	1.28
PA66	0.23	1140	1.57	1.29
PA6-G	0.22	1380	1.34	1.19
PAEK	0.30	1300	1.02	2.27
PAI	0.24	1420	1.00	1.69
PAN	0.26	1150	1.30	1.74
PAR	0.18	1210	1.20	1.24
PB	0.22	920	2.09	1.14
PBI	0.41	1300	0.93	3.40
PBT	0.22	1350	1.61	1.01
PC	0.20	1200	1.22	1.36
PC-G	0.21	1430	1.10	1.34
PE (HD)	0.43	959	2.00	2.24

Table 4. (contined)

Polymer	κ, W/(m · K)	ρ, kg/m^3	c_p, kJ/(kg · K)	α, (10^7 m^2/s)
PE (LD)	0.38	925	1.55	2.65
PE (MD)	0.40	929	1.70	2.53
PEEK	0.20	1310	1.70	0.90
PEI	0.23	1270	1.22	1.48
PEKK	0.22	1280	1.00	1.72
PEMA	0.18	1130	1.47	1.08
PEO	0.21	1130	2.01	0.90
PESU	0.18	1400	1.12	1.15
PET	0.20	1345	1.15	1.29
PET-G	0.29	1700	1.20	1.42
PF	0.25	1300	1.42	1.35
PFA	0.25	2150	1.0	1.16
PF-G	0.40	1850	1.26	1.72
PI	0.11	1395	1.10	0.72
PI-TS	0.21	1400	1.13	1.33
PMMA	0.20	1175	1.40	1.19
PMP	0.17	834	1.73	1.18
PMS	0.20	1020	1.28	1.53
POM	0.23	1420	1.37	1.18
PP	0.15	880	1.88	0.89
PPA	0.15	1170	1.40	0.92
PPE	0.23	1100	1.19	1.76
PPO	0.16	1100	1.25	1.16
PPO-G	0.17	1320	1.31	0.98
PPS	0.29	1300	1.02	2.19
PPSU	0.18	1320	1.01	1.35
PS	0.14	1045	1.25	1.04
PS-G	0.13	1290	1.05	0.96
PSU	0.26	1240	1.11	1.89
PTFE	0.25	2150	1.05	1.11
PU	0.21	1265	1.67	0.99
PUR	0.19	1100	1.76	0.98
PVAC	0.16	1190	1.33	1.03
PVC (flex)	0.17	1255	1.38	0.98
PVC (rigid)	0.19	1415	0.98	1.34
PVDC	0.13	1700	1.07	0.91
PVDF	0.13	1760	1.12	0.68
PVF	0.13	1475	1.30	0.72
PVK	0.16	1265	1.23	1.02
PVOH	0.20	1350	1.55	0.96
PX	0.32	1220	1.3	2.02
SAN	0.15	1070	1.38	1.02
SBR	0.17	1100	1.88	0.82
SI-G	0.30	1900	1.17	1.35
SIR	0.23	970	1.59	1.49
UF	0.25	1250	1.55	1.29
UPT	0.17	1230	1.30	1.06
UPT-G	0.42	1650	1.05	1.85
VE	0.25	1105	1.30	1.74

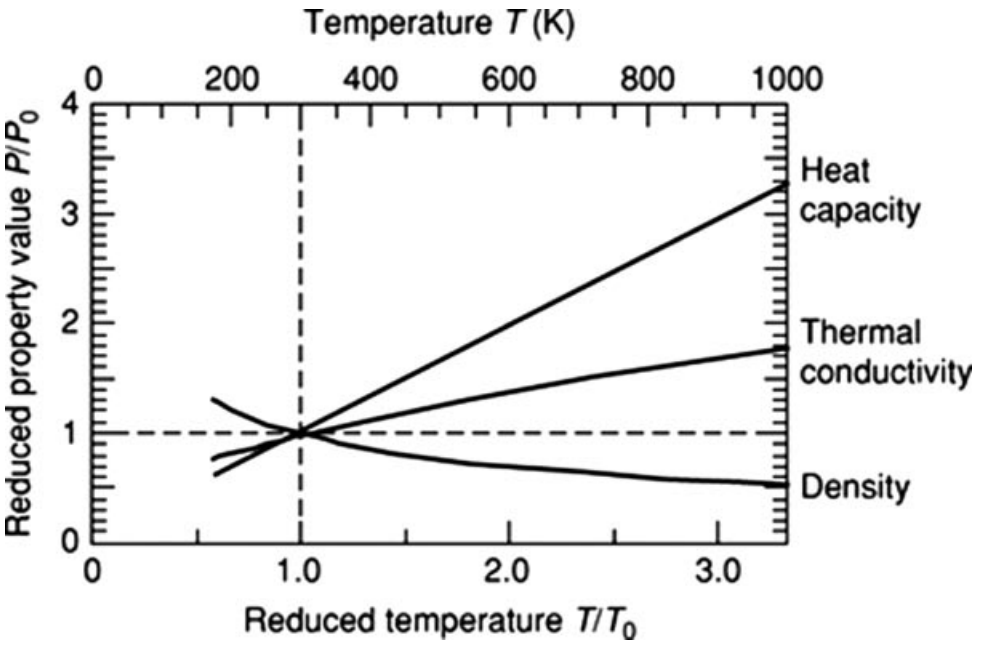

Fig. 10. Temperature dependence of polymer heat capacity, thermal conductivity, and density.

Another thermal property that affects the response of a polymer to the exposure from an external heat source is the surface absorptivity. It is generally assumed that polymers behave as gray surfaces, ie that the total hemispherical surface absorptivity is equal to the total hemispherical emissivity, ε. Hallman (23) measured ε for many polymers and different radiant heat sources. Some of Hallman's measurements are given in Table 5. These values are applicable prior

Table 5. Surface Absorptivity of Polymers

	Radiant Energy Source			
Polymer	1000 K blackbody	1500 K blackbody	Flames	Solar
BR	0.92	0.93	0.92	0.95
CR	0.72	0.63	0.71	0.62
HIPS	0.86	0.75	0.88	0.29
NR	0.88	0.82	0.89	0.69
PA66	0.93	0.90	0.93	0.63
PC	0.87	0.83	0.88	0.69
PE LD	0.92	0.88	0.93	0.57
PMMA (black)	0.94	0.94	0.94	0.96
PMMA (clear)	0.85	0.69	0.89	0.097
PP	0.87	0.83	0.86	0.62
PPO	0.86	0.78	0.88	0.48
PS (clear)	0.75	0.60	0.78	0.095
PVC (flex)	0.90	0.90	0.91	0.89
SIR	0.79	0.66	0.79	0.62

to ignition and it is reasonable to assume that $\varepsilon = 1$ for the flaming surface of a polymer.

Fire Behavior of Solid Polymers

The continuum level treatment of the fire behavior of polymers disregards the discrete (molecular) structure of matter so that the temperature distribution, and more importantly its derivatives, are continuous throughout the material. In addition, the polymer is assumed to be thermally thick and have identical properties at all points (homogeneous) and in all directions (isotropic). In this way analytic results for ignition and burning can be derived from unsteady and steady heat transfer analyses, respectively, using simplified mass and energy balances. The continuum level treatment provides scaling relationships between the properties of polymers and their fire response, but ignores many important characteristics of burning behavior such as the effect of char formation on heat and mass transfer, swelling (intumescence), and dripping that can only be captured empirically or through detailed numerical modeling and analyses.

Ignition. Ignition is the initiation of combustion of a fuel/air mixture that is uniformly heated (autoignition) or comes in contact with a flame, spark, or glowing wire (piloted ignition). The ignition of volatile liquid and gaseous fuels is fairly well understood because only the global or local thermodynamic state of the system need be considered (17–19). As shown in section The Gas Phase, the reaction of gaseous fuels with air will be self-sustaining if the combustion energy density of the mixture is above a minimum (critical) value of about 2 MJ/m^3. The burning of condensed phases is more complicated because there is dynamic coupling of heat and mass transfer between the gas phase and condensed (meso, solid) phase (11–13). Consequently, a variety of criteria have been proposed for piloted ignition of solids and these can be roughly divided into thermal (condensed phase) and chemical (gas phase) (11,24). The primary example of a thermal criterion is an ignition temperature for the solid, while chemical criteria extend to a critical mass flux or a critical heat release rate. Any of these criteria can be expressed in terms of an external heat flux at which the temperature or the flux of mass/energy reaches some critical value. The criteria for piloted ignition of polymer solids are examined separately below.

Chemical Criteria. Chemical criteria for ignition of condensed phases include a boundary layer reaction rate and a critical mass flux of fuel gases, both of which are equivalent to establishing a lower flammability limit at the ignition source for a fixed test geometry and ventilation rate. Table 6 lists mass fluxes at incipient piloted ignition and incipient burning/extinction for over 20 polymers measured in a fire calorimeter (see under Testing to Obtain Engineering Data) or similar device. Also listed is the effective heat of combustion (HOC) of the fuel gases and the product of the mass flux and HOC at ignition or extinction, ie, the heat release rate (HRR). The mass flux at ignition in Table 6 varies between polymers because of differences in the lower flammability limit of their pyrolysis products/fuel gases. If piloted ignition occurs when the concentration of pyrolysis gases in air reaches the LFL of the particular fuel species and $\dot{m}''_{\mathrm{f}}$ and $\dot{m}''_{\mathrm{a}}$ are the mass fluxes of fuel and air in a well-mixed volume at the igniter, then for

Table 6. Mass Loss Rate (MLR), Effective Heat of Combustion (HOC), and Heat Release Rate (HRR) at Ignition (Flashpoint) and Incipient Burning/Extinction (Firepoint)

		Flashpoint		Firepoint	
Polymer	HOC, kJ/g	MLR, g/(m^2 · s)	HRR, kW/m^2	MLR, g/(m^2 · s)	HRR, kW/m^2
POM	14.4	0.88	13	1.7–4.5	40
PMMA	24.8	0.97–1.01	25	1.9–3.2	61
PE	40.3	0.88	35	1.3–2.5	73
PP	41.9	0.60	25	1.1–2.7	72
PS	27.9	0.57	16	0.8–4.0	50
PS FR	9.6	2.0	19	6–8	67
PUR	23.7	0.83	20	2.0	47
PA6	29.8	0.88	26	3.0	89
PBT	21.7	0.77	17	3.4	74
PC	21.2	0.78	17	3.4	72
PPS	23.5	0.81	19	3.6	85
PPZ	15.4	1.23	19	3.0	46
PEN	22.9	0.71	16	2.7	62
PEEK	21.3	0.72	15	3.3	70
PESU	22.4	0.9	20	3.7	83
EP	21.3	1.0	21	3.4	72
CE	22.8	1.3	30	4.4	100
PBI	16.2	1.5	24	—	—
PI	12.0	1.30	16	4.0	48
PEI	16.7	0.82	14	—	—
PAI	19.3	1.63	31	2.5	48
Average		1.0	21	3.2	66
Standard deviation		0.4	6	1.2	17

LFL $\ll 1$,

$$\frac{\dot{m}_{\mathrm{f}}''}{\dot{m}_{\mathrm{a}}''} = \frac{m_{\mathrm{f}}}{m_{\mathrm{a}}} = \frac{\rho_{\mathrm{f}}}{\rho_{\mathrm{a}}}\left(\frac{\mathrm{LFL}}{1-\mathrm{LFL}}\right) \approx \frac{\rho_{\mathrm{f}}}{\rho_{\mathrm{a}}}\mathrm{LFL} \tag{31}$$

The average convective heat transfer coefficient at the polymer surface at incipient ignition is

$$\bar{h} = c_{\mathrm{a}}\dot{m}_{\mathrm{a}}'' \tag{32}$$

The mass flux at ignition from equations 11, 31, and 32 is

$$\dot{m}_{\mathrm{f}}|_{\mathrm{LFL}} = \frac{\rho_{\mathrm{f}}}{\rho_{\mathrm{a}}}\frac{\bar{h}}{c_{\mathrm{a}}}\mathrm{LFL} = \frac{\bar{h}Q'''}{\rho_{\mathrm{a}}c_{\mathrm{a}}}\frac{1}{h_{\mathrm{c}}^0} = \frac{\mathrm{HRR}^*}{h_{\mathrm{c}}^0} \tag{33}$$

Equation 33 shows that there is a parameter with the units and significance of a virtual heat release rate $\mathrm{HRR}^* = \bar{h}Q'''/\rho_{\mathrm{a}}c_{\mathrm{a}}$ that is independent of the type of polymer but depends on the nature of the convective environment, ie, the test

conditions. Piloted ignition of a solid polymer will occur under a particular set of test conditions when

$$\dot{m}''_{\text{ign}} = \dot{m}''|_{\text{LFL}} \geq \frac{\text{HRR}^*}{h_c^0} \tag{34}$$

or when

$$h_c^0 \dot{m}''_{\text{ign}} \geq \text{HRR}^* \tag{35}$$

In fire calorimeters (see under Testing to Obtain Engineering Data) HRR* is of the order

$$\text{HRR}^* \frac{\bar{h}\bar{Q}'''}{\rho_a c_a} = \frac{(10\ \text{W/(m}^2 \cdot \text{K)})(1.9\ \text{MJ/kg})}{(1\ \text{kg/m}^3)(1\ \text{kJ/(kg} \cdot \text{K)})} \approx 20\ \text{kW/m}^2$$

Equations 34 and 35 are physically based criteria for ignition of polymers in typical (see under Testing to Obtain Engineering Data) convective environments where a spark is located 25 mm from the heated polymer surface. Equation 35 is a steady-state, two-dimensional analog of the combustion energy density criterion for gaseous ignition (eq. 11) and, like that criterion, is independent of the chemical composition of the fuel gases. Using HRR* = 20 kW/m^2 and the indicated HOCs in Table 6, equation 34 predicts $\dot{m}''_{\text{ign}} = 1.00 \pm 0.37$ g/(m^2·s) at the flashpoint, which is indistinguishable from the average experimental result. Equation 35 predicts that piloted ignition is imminent when $h_c{}^0\ \dot{m}''_{\text{ign}} = \text{HRR} \geq \text{HRR}^* = 20$ kW/m^2, which is also indistinguishable from the experimental result HRR = 21 ± 6 kW/m^2 at incipient ignition (the flashpoint). Table 6 also lists the mass flux and heat release rate for the majority of polymers at the firepoint when the flame is first established. It seems that the mass flux and HRR increase by a factor of 2–3 between the flashpoint and the firepoint as additional heat flux is imparted to the surface from the flame at incipient burning.

Thermal Criterion. A chemical criterion (eq. 34 or 35) is probably sufficient for ignition to occur but a surface temperature in the vicinity of the thermal decomposition temperature is necessary to begin the fuel generation process. The thermal theory of ignition assumes that the surface temperature at ignition is a characteristic property of the polymer. If fuel gasification obeys a simple energy balance such as equation 24 and the temperature dependence of the heat capacity is equation 28, ie, $c(T) = c_0 T/T_0$, then the enthalpy of gasification at ignition is

$$\frac{c_0}{T_0}\int_{T_0}^{T_{\text{ign}}} T\,\text{d}T + \Delta h_f + \Delta h_d + \Delta h_v = L_g \tag{36}$$

The heat capacity–temperature integral in equation 36 can be solved explicitly with the result

$$\frac{c_0 T_{\text{ign}}^2}{2T_0} + \left(\Delta h_f + \Delta h_d + \Delta h_v - \frac{c_0 T_0}{2}\right) = L_g \tag{37}$$

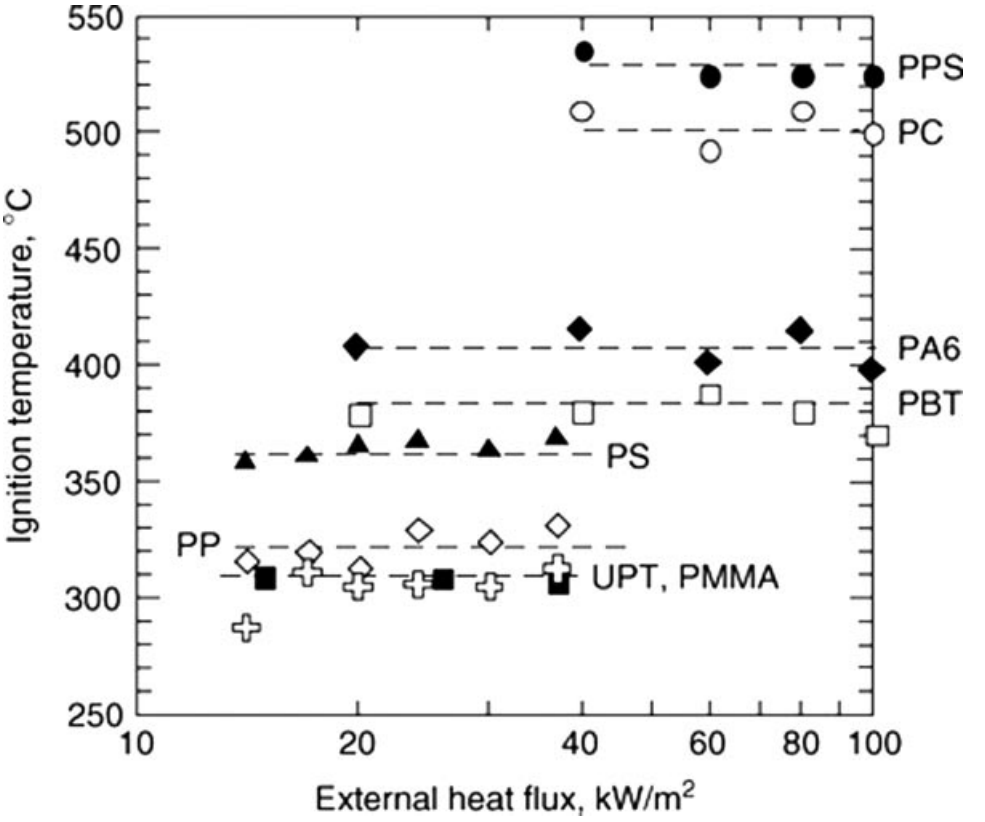

Fig. 11. Ignition temperature versus external heat flux for PPS (●), PC (○), PA6 (◆), PBT (□), PS (▲), PP (◇), UPT (■), and PMMA (✙).

The data in Table 2 suggest that $(\Delta h_f + \Delta h_d + \Delta h_v - c_0 T_0/2) \approx L_g/2$, which allows equation 37 to be solved for T_{ign}:

$$T_{ign} \approx \left(\frac{T_0 L_g}{c_0}\right)^{1/2} \tag{38}$$

Figure 11 is a plot of measured surface temperature at piloted ignition in a fire calorimeter (see under Testing to Obtain Engineering Data) or similar device over a range of external heat fluxes for polyphenylenesulfide (PPS), polycarbonate (PC), polycaprolactam (PA6), polystyrene (PS), polybutylene terephthalate (PBT), polypropylene (PP), unsaturated polyester thermoset (UPT), and PMMA. The ignition temperature of each polymer is relatively independent of heat flux as per equation 38, which also accounts for the large differences between polymers (see Table 1). Using typical properties for commodity and engineering polymers,

$$T_{ign} = \left(\frac{T_0 L_g}{c_0}\right)^{1/2} = \left\{\frac{(298\ \text{K})(2\ \text{MJ/kg})}{1.5\ \text{kJ/(kg}\cdot\text{K)}}\right\}^{1/2} = 630\ \text{K} = 357^\circ\text{C}$$

which approximates the ignition temperature of these materials in lower part of Figure 11. For a constant ignition temperature, unsteady heat transfer (4,11,12) gives the time to ignition, t_{ign}, for a thermally thick sample at a constant external heat flux $\dot{q}''_{ext}$

$$\frac{1}{\sqrt{t_{ign}}} = \frac{\dot{q}''_{ext} - \dot{q}''_{loss}}{TRP} \tag{39}$$

where

$$TRP = \frac{\sqrt{\pi \kappa \rho c}}{2}(T_{ign} - T_0) \tag{40}$$

is a quantity known as the thermal response parameter (TRP). Equation 39 states that a plot of the reciprocal square root of the time-to-ignition versus the external heat flux has a slope equal to average value of the thermal response parameter. The product $\kappa \rho c$ in equation 40 is an effective property called the thermal inertia that can be approximated using equation 29 and tabulated values for κ, ρ, and c (see Table 4) or from the thermal response parameter if T_{ign} is measured separately or calculated (see eq. 38 and section on Ignition Temperature). The intercept $\dot{q}''_{loss}$/TRP of equation 39 can also provide an estimate of T_{ign} if an additional expression is introduced to account for the surface heat losses at incipient ignition

$$\dot{q}''_{loss} = \bar{h}(T_{ign} - T_0) + \varepsilon\sigma\left(T_{ign}^4 - T_0^4\right) \tag{41}$$

For a thermally thin sample of thickness b and at low external heat fluxes near the critical value, the ignition time and external heat flux are related

$$\frac{1}{t_{ign}} = \frac{\dot{q}''_{ext} - \dot{q}''_{loss}}{\rho b c (T_{ign} - T_0)} \tag{42}$$

Equations 39 and 42 state that $t_{ign} \to \infty$ as $\dot{q}''_{ext} \to \dot{q}''_{loss}$ at the flashpoint. In other words, the minimum (critical) value of the external heat flux that can cause ignition is

$$CHF = \dot{q}''_{loss}(\text{ignition}) = \bar{h}(T_{ign} - T_0) + \varepsilon\sigma\left(T_{ign}^4 - T_0^4\right) \tag{43}$$

At the firepoint, flaming combustion is first established. If a flame covers a polymer surface having $\varepsilon \approx 1$ and heat losses are by reradiation only from a surface for which the burning and ignition temperatures are the same, then the first term on the right-hand side of equation 43 is zero and the critical heat flux (CHF) for burning is

$$CHF_b = \dot{q}''_{loss}(\text{burning}) \approx \dot{q}''_{rerad} = \sigma T_{ign}^4 \tag{44}$$

Equations 43 and 44 explain why thermally stable/heat-resistant polymers with high thermal decomposition/ignition/burning temperatures require a higher heat

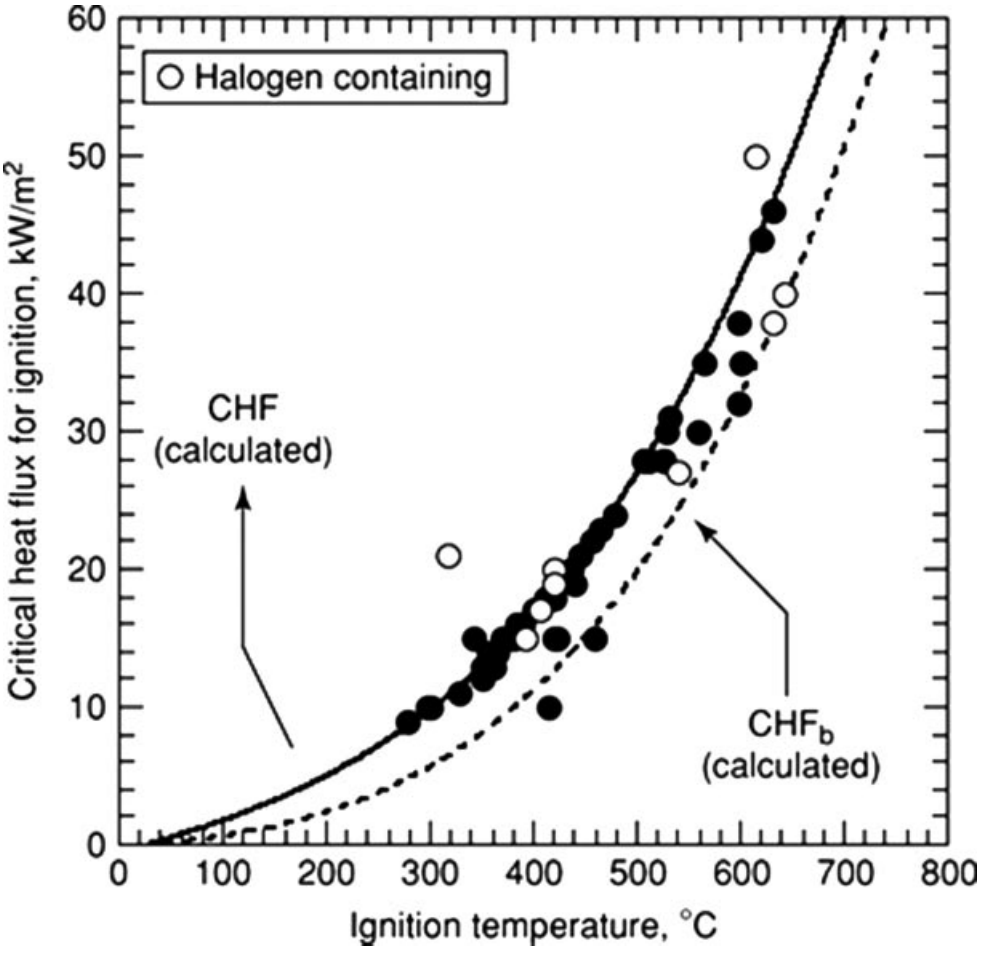

Fig. 12. Critical heat flux versus ignition temperature. Symbols are measurements at sustained ignition. Lines are calculated from abscissa for incipient ignition (solid) and incipient burning (dashed).

flux to ignite and burn. Figure 12 is a plot of the critical heat flux versus the ignition temperature of common polymers measured separately. The solid line is calculated from the abscissa using equation 43 and the dotted line using equation 44.

Steady Burning. Once ignition is sustained and the burning rate reaches a constant value, the HRR (W/m^2) of the polymer in steady flaming combustion is (4,11,12,20,21)

$$\mathrm{HRR} = \chi h_c^0 \dot{m}'' = \chi \frac{h_c^0}{L_g} \dot{q}''_{net} \tag{45}$$

where χ is the combustion efficiency in the flame and

$$\dot{q}''_{net} = \dot{q}''_{ext} + \dot{q}''_{flame} - \dot{q}''_{loss} \tag{46}$$

is the net heat flux for steady flaming combustion with $\dot{q}''_{\text{flame}}$ the total convective and radiative heat flux from the flame to the polymer surface (see Fig. 2). The dimensionless ratio of the heat of combustion to the heat of gasification in equation 45 is the heat release parameter (HRP)

$$\chi \frac{h_c^0}{L_g} = \chi(1-\mu)\frac{h_c^0}{h_g} = \text{HRP} \tag{47}$$

Fire calorimetry (4,11,20,25) (see under Testing to Obtain Engineering Data) is used to obtain HRP as the slope of heat release rate versus external heat flux or as the ratio $\chi {h_c}^0/L_g = \text{HOC}/L_g$, from individual measurements. Table 7 contains HOC and χ ($\equiv$HOC/${h_c}^0$) for common polymers while HRP are listed in Table 8. The heat of combustion of the fuel gases, ${h_c}^0$, was measured separately in a pyrolysis-combustion flow calorimeter (26) (see section on The Pyrolysis-Combustion Flow Calorimetry).

Figure 13 shows representative HRR histories for thermally thick and thin samples of polymers that gasify completely or form a char during burning. It is apparent that none of these heat release rate histories show a constant (steady-state) value of heat release rate over the burning interval as presumed in equation 45.

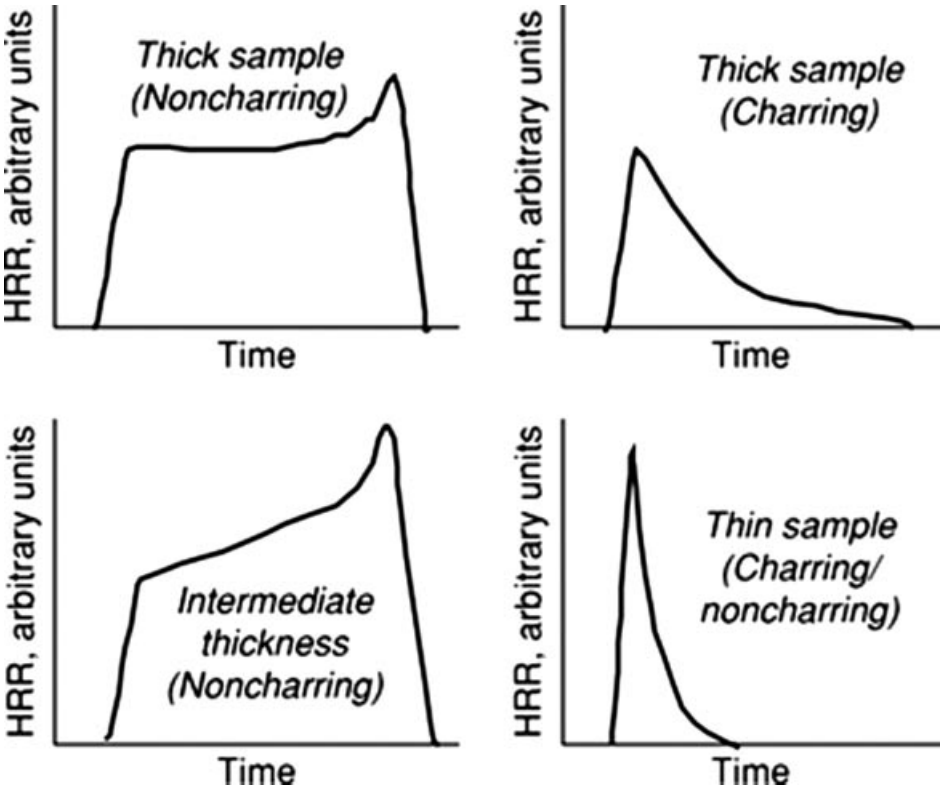

Fig. 13. Representative heat release rate histories in flaming combustion for thick and thin samples of charring and noncharring polymers.

Table 7. Effective Heat of Combustion (HOC), Heat of Complete Combustion of Fuel Gases (h_c^0), and Flaming Combustion Efficiency (χ)

Polymer	HOC, kJ/g	h_c^0, kJ/g	χ
CEN	20.6	20.7	1.00
CEE	25.1	25.3	0.99
PMMA	24.8	25.0	0.99
PP	41.9	43.0	0.97
PE LD	40.3	41.4	0.97
PUR	24.0	24.7	0.97
PE HD	40.3	41.6	0.97
CET	25.9	26.9	0.96
PAI	15.3	15.9	0.96
CR	17.6	18.5	0.95
CEM	28.9	30.6	0.94
PEI	21.8	23.2	0.94
CEA	25.9	27.6	0.94
UPT	23.4	25.0	0.94
POM	14.4	15.4	0.94
TPU	23.5	25.4	0.93
PPA	24.2	26.2	0.92
CEF	16.9	18.3	0.92
PA66	25.2	27.4	0.92
PEEK	21.3	23.2	0.92
PBT	21.7	23.8	0.91
PSU	20.4	22.4	0.91
PC	21.2	23.3	0.91
PEN	22.9	25.2	0.91
PPZ	15.0	16.6	0.90
PESU	22.4	24.9	0.90
PA6	25.8	28.7	0.90
PPSU	23.5	27.0	0.87
PPS	25.4	29.3	0.87
PBI	22.0	26.5	0.83
SBR	31.5	38.0	0.83
EVA	30.8	37.9	0.81
NR	30.2	37.9	0.80
SIR	21.7	27.2	0.80
PPO/PS	21.3	26.9	0.79
ABS	29.0	36.6	0.79
EPDM	29.2	37.9	0.77
CTFE	6.5	8.5	0.76
HIPS	28.1	37.2	0.76
EP	20.4	27.1	0.75
PET	18.0	24.1	0.75
LCP	14.8	20.6	0.72
CPE (25% Cl)	22.6	31.6	0.72
VE	22.0	31.1	0.71
ETFE	7.3	10.8	0.68
PS	27.9	42.0	0.66
PU	16.3	25.4	0.64
PX	20.0	31.3	0.64

Table 7. (continued)

Polymer	HOC, kJ/g	$h_c{}^0$, kJ/g	χ
PVC (flexible)	11.3	19.3	0.59
PTFE	4.6	8.4	0.55
PVC (rigid)	9.3	18.6	0.50
PS-FR	13.8	33.0	0.42
CPE (36% Cl)	10.6	26.3	0.40
TPI	12.0	31.6	0.38
ABS-FR	10.2	26.9	0.38
PVDF	3.8	10.4	0.36
CPE (48% Cl)	7.2	20.2	0.36
ECTFE	4.6	13.6	0.34
CPVC	3.9	12.8	0.30
PVF	4.1	18.5	0.22
FEP	1.3	7.7	0.17

Consequently, an average heat release rate for the entire test or over some time interval is typically used in place of a steady HRR. In fact, the interpretation of time varying heat release rate histories is a subject of active research in fire science. The curves on the left-hand side of Figure 13 are characteristic of noncharring ($\mu = 0$) plastics of different thickness. The heat release histories for the charring plastics on the right-hand side of Figure 13 show the typical peak in heat release rate soon after ignition followed by a depression in the heat release rate as the char layer forms and increases in thickness. The growing char layer insulates the underlying plastic from the surface heat flux so that the net heat flux at the in-depth pyrolysis front decreases with time. Char can also act as a mass diffusion barrier to the volatile fuel. Charring polymers can be linear, branched, or cross-linked thermoplastics, elastomers, or thermosets having amorphous or semicrystalline morphologies.

In all cases in Figure 13 the time integral (area under), the heat release rate history per unit mass of polymer consumed by burning, is the effective heat of flaming combustion, HOC (J/kg). The effective heat of combustion is determined primarily by the fuel chemistry, ventilation rate, and combustion efficiency in the flame. Combustion efficiency is low when halogens are present in the polymer molecule or added as flame- retardant chemicals, when soot or smoke is produced in large yield, or when there is insufficient oxygen for complete conversion of the organic fuel to carbon dioxide and water. Flaming combustion efficiency appears to be relatively independent of the charring tendency of a polymer (compare Tables 2 and 5).

Figure 14 shows fire calorimetry data for the average heat release rate of plastics versus their char yield after burning or pyrolysis. The nonlinear dependence of heat release rate on char yield in Figure 14 indicates that charring suppresses the HRR more than can be accounted for by the fuel fraction alone (eg, eq. 47). In fact, charring correlates with thermal stability (L_g) and acts as a barrier to the transfer of mass and heat during burning as illustrated schematically in Figure 13, all of which tend to reduce HRR.

Table 8. Limiting Heat Release Rate (HRR_0), Heat Release Parameter (HRP), Limiting Oxygen Index (LOI), UL 94 Rating, and Heat Release Capacity (η_c)

Polymer	HRR_0, kW/m^2	HRP, kJ/kJ	LOI, $[O_2]$, % v/v	UL 94 rating	η_c, J/(g · K)
HIPS	510 ± 77	14 ± 2	18	HB	893
PP	369 ± 79	22 ± 2	17	HB	1200
PET	424 ± 168	13 ± 4	20	HB	402
PS	410 ± 66	17 ± 2	18	HB	1040
ABS	359 ± 66	13 ± 2	18	HB	669
PBT	341 ± 106	15 ± 3	23	HB	474
PE (chlorinated)	—	—	21	HB	693
UPT	261 ± 105	11 ± 2	20	HB	—
PC/ABS	259 ± 43	11 ± 1	—	HB	—
PA66	240 ± 59	18 ± 2	24	HB	600
PMMA	217 ± 47	13 ± 1	17	HB	574
PS-FR	205 ± 27	7 ± 1	—	V2	—
PPO/PS	192 ± 22	15 ± 1	—	HB	—
PA6	187 ± 55	18 ± 2	24	HB	487
PC/ABS-FR	178 ± 36	7 ± 1	—	V1	—
VET	169 ± 44	13 ± 1	—	HB	805
PESU	168 ± 23	4 ± 0	36	V1	345
HIPS-FR	164 ± 30	5 ± 1	—	V2	—
POM	162 ± 30	6 ± 1	15	HB	398
EP	160 ± 46	10 ± 1	19	HB	657
PE	145 ± 93	21 ± 3	17	HB	1560
PBT-FR	141 ± 130	6 ± 3	—	V2	—
CEA	112 ± 22	7 ± 2	24	V1	273
ABS-FR	117 ± 33	6 ± 1	—	V2	301
HIPS-FR	114 ± 36	4 ± 1	—	V0	—
PVC (flex)	91 ± 19	4 ± 0	—	V2	—
SIR (filled)	90 ± 13	5 ± 0	32	V0	88
PC	89 ± 32	9 ± 1	25	V2	390
PEN	57 ± 13	5 ± 0	32	V2	309
ETFE	44 ± 31	6 ± 0	30	V0	198
PVC (rigid)	9 ± 25	3 ± 1	45	V0	138
CR	—	9	40	V0	188
KEVLAR	—		32	V0	302
UPT-FR	−31 ± 10	2 ± 0	—	V0	—
CPVC	−34 ± 9	3 ± 0	52	V0	—
PE (cross-linked)-FR	−38 ± 28	5 ± 5	—	V0	—
PAI	−64 ± 16	2 ± 0	45	V0	33
PPSU	−83 ± 25	4 ± 0	38	V0	115
PTFE	−84 ± 9	2 ± 0	95	V0	35
PEEK	−94 ± 20	3 ± 0	35	V0	155
NOMEX	—	—	28	V0	152
PEI	−113 ± 19	3 ± 0	47	V0	121
ECTFE	−127 ± 6	4 ± 0	60	V0	—
PPS	−147 ± 30	6 ± 1	44	V0	164
PBI	−150 ± 36	3 ± 0	36	V0	41
PC-FR	−191 ± 51	4 ± 1	56	V0	30
FEP	—	2	95	V0	57

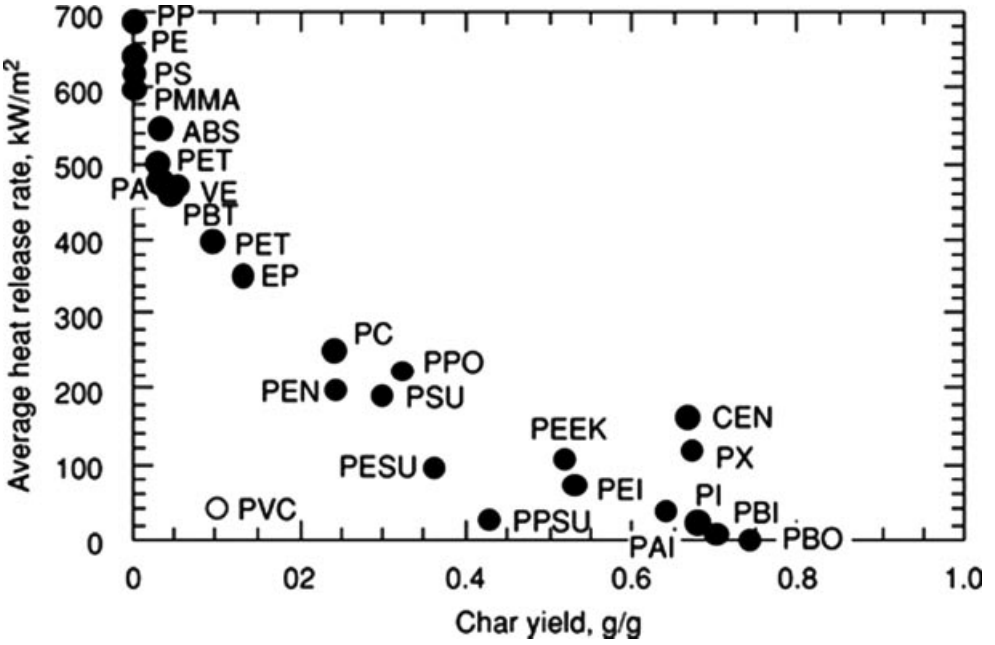

Fig. 14. Average heat release rate in flaming combustion versus char yield of polymers.

Unsteady Burning. Unsteady burning or transient ignition is the fire behavior that is most relevant to flammability tests (5,25,27). In flammability tests of flame resistance a thin strip of polymer is typically subjected to a Bunsen burner flame for several seconds to force ignition, after which the sample is removed from the flame and the duration, extent, and characteristics of burning are recorded. Polymers that continue to burn after removal from the ignition source are considered relatively flammable while polymers that self-extinguish are relatively flame resistant. Flame resistance is related to fire behavior by combining equations 45–47 and separating the heat release rate into unforced (HRR_0) and forced (HRP $\dot{q}''_{ext}$) components

$$HRR = HRR_0 + HRP\ \dot{q}''_{ext} \tag{48}$$

where the heat release rate in unforced flaming combustion, ie, in the absence of an external heat flux, is

$$HRR_0 = HRP(\dot{q}''_{flame} - \dot{q}''_{loss}) \tag{49}$$

Equation 49 states that the surface flame must provide all of the energy to sustain burning in unforced combustion. However, $\dot{q}''_{flame}$ contains convective and radiative components and will depend on the size and orientation of the sample with respect to its flaming surface while $\dot{q}''_{loss}$ depends on sample thickness and heat transfer boundary conditions for unsteady burning. Consequently, HRR_0 is generally apparatus- or test-specific. The fire parameters HRP and HRR_0 for a fire

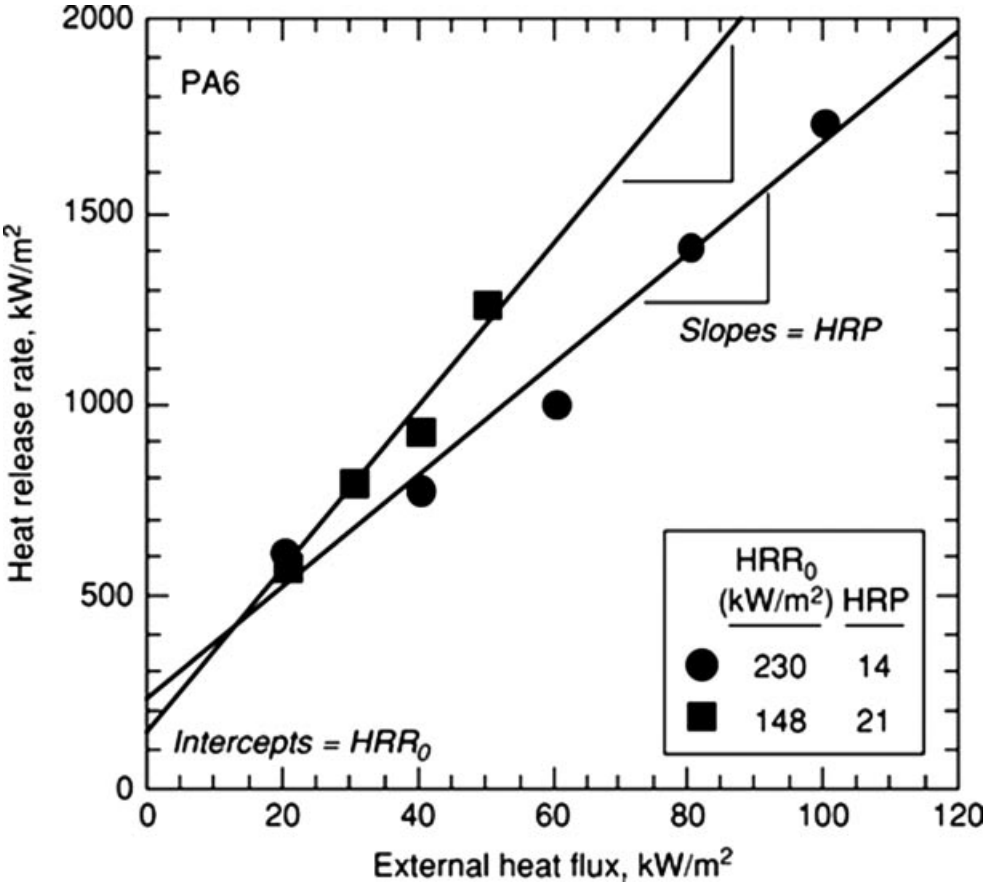

Fig. 15. Heat release rate versus external heat flux data for polycaprolactam (PA6) from different sources. Slopes are HRP. Intercepts are HRR_0.

calorimeter (see under Testing to Obtain Engineering Data) can be determined from the slope and intercept, respectively, of a plot of HRR versus external heat flux in a fire calorimeter as shown in Figure 15 for PA6 data from two different sources (4).

If extinction occurs when the gas phase combustion energy density falls below a minimum (critical) value, analogous to the phenomenon that governs ignition, then equations 38 and 48 provide a criterion for flame extinction in a flammability test. After the sample ignites and the flame is removed $\dot{q}''_{ext} = 0$, and the sample will self-extinguish if

$$HRR_0 < HOC\ \dot{m}''_b = HRR^*_b \tag{50}$$

where $\dot{m}''_b$ and $HRR_b{}^*$ are the critical mass flux and heat release rate for sustained burning, respectively, in the flammability test (see eqs. 36–38). From equations

49 and 50, the flame heat flux at the firepoint is

$$\dot{q}''_{\text{flame}}\,(\text{extinction}) \leq \frac{\text{HRR}^*_b}{\text{HRP}} + \dot{q}''_{\text{loss}} \tag{51}$$

Since $\text{HRR}_b{}^*$ is test-dependent, the same value that governs horizontal burning/extinction in fire calorimeters ($\text{HRR}_b* \approx 70$ kW/m^2; see Table 6) will not necessarily apply to extinction in an upward flame spread test of a thin strip of polymer. Table 8 lists HRR_0 for common polymers along with their flammability rating in the upward vertical (V) or horizontal (H) burning Underwriters Laboratory (UL) test for flammability of plastic materials (a Bunsen burner ignition test). Table 8 shows that when $\text{HRR}_0 < 50$ kW/m^2 as measured in a fire calorimeter, self-extinguishing behavior is observed exclusively in the vertical burning test. Equation 49 shows that HRR_0 decreases as the difference between the heat influx from the flame and the heat efflux by reradiation. Negative HRR_0 values toward the bottom of Table 8 are observed for halogen-containing/flame retarded (FR) plastics that may burn with a low flame heat flux. Negative HRR_0 values are also observed for heat-resistant/thermally stable polymers that have high losses and a thermally insulating char. In either case, $\dot{q}''_{\text{flame}}$ can be less than $\dot{q}''_{\text{loss}}$ and negative HRR_0 values are expected and observed.

Another widely used flammability test is the limiting oxygen index (LOI) (25) test (see section on The Limiting Oxygen Index Test). The LOI is a downward-burning test of a thin ($3 \times 6 \times 150$ mm) polymer strip in a flowing gas stream whose oxygen concentration is adjusted until the sample flame is on the verge of extinguishing. The dependent variable in the LOI test is the flame heat flux, which increases in rough proportion to the oxygen concentration in the combustion atmosphere (independent variable). The concentration of oxygen in the combustion atmosphere at incipient burning/extinction is the LOI, and this corresponds to a flame heat flux in equation 51:

$$\text{LOI} \propto \dot{q}''_{\text{flame}}(\text{extinction}) = \frac{\text{HRR}^*_b}{\text{HRP}} + \dot{q}''_{\text{loss}} \tag{52}$$

A value $\text{HRR}_b{}^* \approx 100$ kW/m^2 has been observed for the LOI test. This value is somewhat higher than the critical heat release rate for incipient burning/extinction of horizontal slabs ($\text{HRR}_b* \approx 70$ kW/m^2; see Table 6) and upward burning of vertical strips ($\text{HRR}_b* \approx 50$ kW/m^2) because heat transfer from the flame is less efficient in downward burning, and so a higher HRR is necessary for sustained ignition in the LOI test.

The equations for ignition, steady burning, and unsteady burning show that flammability tests measure the fire behavior of the polymer in unforced burning, whether as an afterflame time in a Bunsen burner test (see under Testing for Rugulatory Compliance) or as an oxygen concentration at incipient extinction (see under Testing for Quality Assurance and Research). Substituting equations 44 and 38 into equation 51 or 52 gives the efficiency of heat transfer from the

flame to the polymer surface in terms of the fire parameter HRP:

$$\frac{\dot{q}''_{\text{flame}}(\text{extinction})}{\text{HRR}_b^*} = \frac{\text{HRP}}{1+(\lambda/\text{HRP})} \tag{53}$$

where $\lambda = (\sigma/\text{HRR}_b{}^*)(\chi h_c{}^0\ T_0/c_0)^2$ is a dimensionless quantity that is test-dependent by virtue of χ and $\text{HRR}_b{}^*$. Table 8 shows that self-extinguishing behavior in the UL 94 V test and an LOI above 30 is observed exclusively for HRP $\leq$ 5 in these tests where $\text{HRR}_b{}^* = 75 \pm 25$ kW/m^2. Substituting HRP $= 4.5 \pm 0.5$ into equation 53 for typical $\lambda = 20 \pm 5$ (see Tables 3, 4, and 7) gives $\dot{q}''_{\text{flame}}/\text{HRR}_b{}^* \approx 0.8$ at incipient extinction in tests of flame resistance. Thus, at incipient extinction/burning when the combustion zone of the flame is in close proximity to the sample surface, a large fraction ($\approx$80%) of the heat released by combustion is used to sustain the burning process.

Chemical Structure and Fire Properties

A powerful tool to study the effect of chemical structure on the properties of polymers is the additivity principle. The additivity principle, pioneered by Van Krevelen (22), assumes that polymer properties when expressed per mole of substance can be calculated by summation of atomic, chemical group, or bond contributions:

$$\mathbf{P} = \sum_j n_i P_i$$

where $\mathbf{P}$ is a molar property, n_i is the number of moles of component i in the polymer repeat unit contributing to the property, and P_i is the numerical value of the contribution. In the study of fire behavior, the use of specific (mass-based) properties p is more convenient, and these are related to the molar properties and molecular weight M of the repeat unit

$$p = \frac{\mathbf{P}}{M}\frac{\sum_j n_i P_i}{\sum_j n_i M_i}$$

where M_i is the molar mass of component i. Additive molar contributions to polymer fire properties κ, ρ, c, $h^0{}_{c,p}$, T_p, and μ are well documented and their calculation from molar group contributions is straightforward. However, it is often the case that the molar group contributions are not available in the literature for new polymers with novel backbone and pendant structures. Recognizing this limitation of Van Krevelen's group contribution method, Bicerano generalized the additive scheme using graph theory to develop atomic connectivity indices which replace the larger chemical groups in the traditional additive approach as the principal descriptors of the topology of the polymer repeat unit (28). Bicerano's approach is still empirical in that the connectivity indices must be determined from experimental data or by correlation with known group contributions. However, once the connectivity indices are determined for a particular property, that

property may be predicted for any chemical structure for which the atomic (as opposed to group) composition is known. The connectivity index method of predicting polymer properties from atomic composition can be accomplished with a hand calculator but is more typically implemented using a stand-alone computer code or accessed as a module in molecular modeling software. Reactive molecular dynamics (RMD) simulations of thermal degradation is a semiempirical method that has recently been applied to the calculation of fuel species and fuel generation rates of polymers (10). RMD simulations are the most fundamental and powerful approach to understanding and predicting polymer flammability because, unlike the additive approaches, RMD has the potential to predict the products and rates of thermal decomposition, ie, the fuel generation chemistry.

Heat Transport. There are no good fundamental theories to predict the thermal conductivity κ (W/(m · K)), heat capacity c (kJ/(kg · K)), or density ρ (kg/m^3) of condensed phases (eg, solid or molten polymers) from chemical structure but empirical structure–property correlation allows calculation of these properties from additive atomic or chemical group contributions if the chemical structure of the polymer is known. Table 4 lists thermal properties of polymers, some of which were calculated from the chemical structure using additive contributions (22,28) when experimental values were not available.

Heat of Combustion. Thermodynamics allow calculation of the heat of combustion, $h_c{}^0$, as the difference between the free energy of the products and reactants in equation 4. Additive molar contributions to the free energy of gaseous, liquid, and solid fuels have been tabulated and used successfully to estimate heats of combustion. A simpler method for calculating or measuring combustion heat is based on the observation that the net heat of complete combustion of organic fuels per mole of oxygen consumed is independent of the chemical composition of the fuel (20),

$$C = h_c^0 \left(\frac{nM}{n_{O_2} M_{O_2}} \right) = \frac{h_c^0}{r_0} = 13.1 \pm 0.7 \text{ kJ/g } O_2 \tag{54}$$

where $h_c{}^0$ is the net heat of complete combustion of the fuel with all products in their gaseous state, n and M are the number of moles and molecular weight of the molecule or polymer repeat unit, respectively, n_{O_2} is the number of moles of O_2 consumed in the balanced thermochemical equation, and r_0 is the stoichiometric oxygen-to-fuel mass ratio. To illustrate the thermochemical calculation of the net heat of combustion, consider PMMA, which thermally degrades by end-chain scission/unzipping/depolymerization to monomer in quantitative yield. PMMA has the following chemical structure:

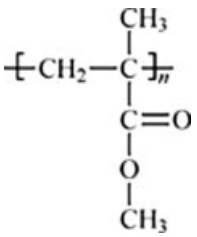

The methyl methacrylate (MMA) repeat unit in brackets is the volatile fuel species when PMMA burns and it has the atomic composition $C_5H_8O_2$; so the balanced chemical equation for complete combustion of PMMA is

$$C_5H_8O_2 + 6\ O_2 \rightarrow 5\ CO_2 + 4\ H_2O$$

Thus, 6 moles of O_2 are required to completely convert 1 mole of PMMA repeat unit to carbon dioxide and water. Inverting equation 54, the heat of combustion of the MMA fuel is

$$h_c^0 = C\left(\frac{n_{O_2}M_{O_2}}{nM}\right) = \frac{(13.1\ \text{kJ/g}\ O_2)(6\ \text{moles}\ O_2)(32\ \text{g}\ O_2/\text{mol})}{(1\ \text{mole MMA})(100\ \text{g MMA/mol})} = 25.15\ \text{kJ/g} \tag{55}$$

Net heats of complete combustion of polymers are available in the literature. If the mass fraction of char that remains after burning is μ, the fuel fraction is $(1 - \mu)$, and the heat of complete combustion of the fuel gases, ${h_c}^0$, is related to the heat of combustion of the char, ${h_{c,\mu}}^0$, and polymer, ${h_{c,p}}^0$,

$$h_c^0 = \frac{h_{c,p}^0 - \mu h_{c,\mu}^0}{1 - \mu} \tag{56}$$

Experimental values for ${h_c}^0$ determined by pyrolysis-combustion flow calorimetry (see below) are listed in Table 7. The elemental analysis of chars gives typical chemical formula C_5H_2 from which the heat of combustion of the char calculated from oxygen consumption is ${h_{c,\mu}}^0 \approx 37$ kJ/g, which can be used to estimate the heat of combustion of the fuel gases of charring polymers using equation 56 if μ is known.

Enthalpy of Gasification. In principle, the enthalpy of gasification, L_g, could be estimated from chemical structure using additive molar contributions or estimated from equation 25 if μ is known and h_g is taken to be 2 MJ/kg. Also relevant to the energetics of fuel generation is the observation that the activation energy for pyrolysis, E_a (J/mol), measured from laboratory TGAs approximates the molar enthalpy of gasification if M_g is the molecular weight of the fuel gases (10):

$$L_g = \frac{E_a}{M_g} \tag{57}$$

If M is the molar mass of the polymer repeat unit it follows from equation 57 that the ratio

$$\frac{M_g}{M} = \frac{E_a}{ML_g} \tag{58}$$

should be characteristic of the mode of thermal degradation. For example, polymers such as PMMA, polyoxymethylene (POM) and, to a first approximation, PS that thermally degrade by end-chain scission (depolymerize/unzip) produce monomer at near-quantitative yield. Consequently, these polymers should have

Table 9. Heats of Gasification, Pyrolysis Activation Energy, Char Yield, as well as Calculated and Measured Molecular Weights of Decomposition Products for Some Polymers

Polymer	M, g/mol	L_g, kJ/g	μ, g/g	h_g, kJ/g	E_a, kJ/mol	M_g/M	Pyrolysis products
				Chain cracking			
PP	42	1.9	0	1.9	243	3.0	C_2–C_{90} saturated and unsaturated hydrocarbons
PE	28	2.2	0	2.2	264	4.3	
				Unzipping			
PS	104	1.8	0	1.8	230	1.2	40–60% monomer
PMMA	100	1.7	0	1.7	160	0.94	100% monomer
POM	30	2.4	0	2.4	84	1.2	100% monomer
				Intramolecular scission			
PA66	226	2.1	0	2.1	160	0.3	H_2O, CO_2, C_5 HCs
PVC	62	2.7	0.1	2.4	110	0.7	HCl, benzene, toluene
Cellulose	162	3.2	0.2	2.6	200	0.5	H_2O, CO_2, CO
PT	131	5.0	0.6	2.0	178	0.3	Complex mixture of low molecular weight products
PC	254	2.4	0.3	1.7	200	<1	
PEI	592	3.5	0.5	1.8	≈275	<1	
PPS	108	3.8	0.5	1.9	≈275	<1	
PEEK	288	3.4	0.5	1.7	≈275	<1	
PAI	356	4.8	0.6	1.9	≈275	<1	
PX	180	6.4	0.7	1.9	≈275	<1	

$M_g \approx M$, or $M_g/M \approx 1$. Polymers such as PE and PP that decompose by main chain scission (cracking) to multimonomer fragments will have $M_g/M > 1$. Conversely, polymers with complex molecular structures and high molar mass repeat units ($M \geq 200$ g/mol) such as polyamides (PA), cellulose, poly(ethylene terephthalate) (PET), or polycarbonate (PC) that degrade by random scission, cyclization, small-molecule splitting, or by chain stripping of pendant groups such as poly(vinyl chloride) (PVC) yield primarily low molar mass species (water, carbon dioxide, alkanes, mineral acids) relative to the repeat unit so that for these materials $M_g/M < 1$. Table 9 shows fuel/monomer molar mass ratios M_g/M calculated as E_a/ML_g according to equation 58 for some of the polymers in Table 3. Global pyrolysis activation energies for the thermally stable engineering plastics listed in the last four rows of Table 9 are estimated to be in the range $E_a = 275 \pm 25$ kJ/mol. Qualitative agreement is observed between the modes of pyrolysis (end-chain scission, random scission, chain stripping) and the calculated fragment molecular weight using equation 58, suggesting that the global pyrolysis activation energy determined from TGA experiments approximates the molar enthalpy of pyrolysis of the degradation products.

Ignition Temperature. Common sense and much experimental data suggest that the ignition temperature and thermal decomposition temperature of polymers should be related since mass loss/fuel generation begins in earnest at these temperatures. However, the heating rate in a fire is of the order of 10–20

Table 10. Thermokinetic Properties of PMMA, PE, and Phenolic Triazine

Polymer	$\ln(\beta^*)$, K/s	c_0, kJ/(kg · K)	E_a, kJ/mol	M_g, kg/mol
PMMA	30	1.4	160	0.10
PE	43	1.5	264	0.11
Phenolic triazine	36	1.5	178	0.12

times higher than the heating rates normally used to measure thermal decomposition temperatures in laboratory thermogravimetry experiments. Figure 11 and equation 38 show that the ignition temperature of polymers is not particularly sensitive to heat flux (heating rate) while equation 23 states that the thermal decomposition temperature of polymers in TGA experiments increases by about 45°C for each 10-fold increase in heating rate. Consequently, there should be a heating rate β_{ign} in a TGA experiment for which the ignition and decomposition temperatures of polymers are equal, ie, $T_{ign} = T_p(\beta_{ign})$. Substituting equation 57 into equation 38

$$T_{ign} = \left(\frac{T_0 L_g}{c_0}\right)^{1/2} = \left(\frac{T_0 E_a}{M_g c_0}\right)^{1/2} \tag{59}$$

Setting this result equal to T_p in equation 23

$$\left(\frac{T_0 E_a}{c_0 M_g}\right)^{1/2} = \frac{E_a}{R \ln(\beta^*/\beta_{ign})} \tag{60}$$

Equation 60 can be evaluated at $T_0 = 293$ K using the properties in Table 10, with the result that the heating rate for which $T_{ign} = T_p(\beta_{ign})$ is of the order

$$\beta_{ign} = \beta^* \exp\left(-\frac{E_a\, c_0 M_g}{R^2 T_0}\right)^{1/2} \approx 1 - 3 \text{ K/min} \tag{61}$$

which is at the lower range of heating rates typically used in nonisothermal TGA experiments, $\beta = 10$–20 K/min. From equations 59–61, the ignition and decomposition temperatures are related as

$$\frac{1}{T_{ign}} = \frac{1}{T_p} + \frac{R \ln(\beta/\beta_{ign})}{E_a}$$

Consequently, T_p measured in a TGA in an inert environment at heating rates $\beta/\beta_{ign} \approx 10$ can be 25–50 K higher than T_{ign} (see Table 1) for typical $E_a \approx 200$ kJ/mol. Figure 16 is a plot of the data in Table 1 for the measured ignition temperature of polymers versus their mean thermal decomposition temperature $(T_d + T_p)/2$. The use of a mean thermal decomposition temperature rather than T_p as an estimate of T_{ign} compensates for most of the heating rate effects described by equations 59–61. Also contained in Figure 16 are data for the incipient burning (firepoint) and incipient ignition (flashpoint) temperatures of hydrocarbon oils plotted on the ordinate and abscissa, respectively.

Because of its importance to flammability, Van Krevelen identified a number of experimental indices that can be used to characterize the short-term thermal

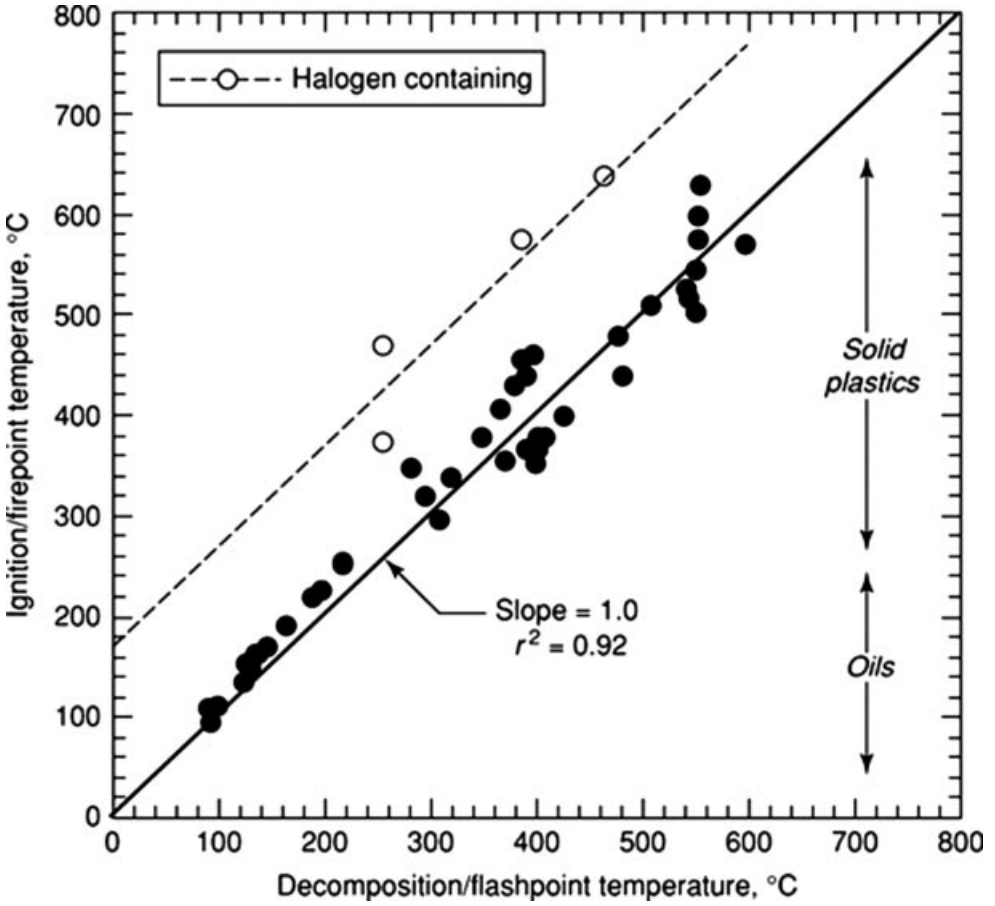

Fig. 16. Ignition/firepoint temperature versus decomposition/flashpoint temperature for solid/liquid fuels.

stability of a polymer (22). The indices, which are determined from temperature scanning thermogravimetry experiments at constant heating rates of 3–10 K/min, are T_d, the temperature (in Kelvin) at which the polymer weight loss is just measurable; $T_{d,1/2}$, the temperature at which the weight loss reaches 50% of its final value; $T_{d,max}$, the temperature at the maximum rate of weight loss; and E_a, the activation energy for pyrolysis. Noting that all of these temperatures depend on heating rate and that $T_{d,max}$ is identical to T_p in the present work, Van Krevelen proposed the following interrelationships based on tabulated data for 37 polymers (all temperatures are in Kelvin):

$$T_d = 0.9T_{d,1/2} \tag{62}$$

$$T_{d,max} = T_p \approx T_{d,1/2} \tag{63}$$

$$T_p \approx 423 + E_a \text{ (kJ/mol)} \tag{64}$$

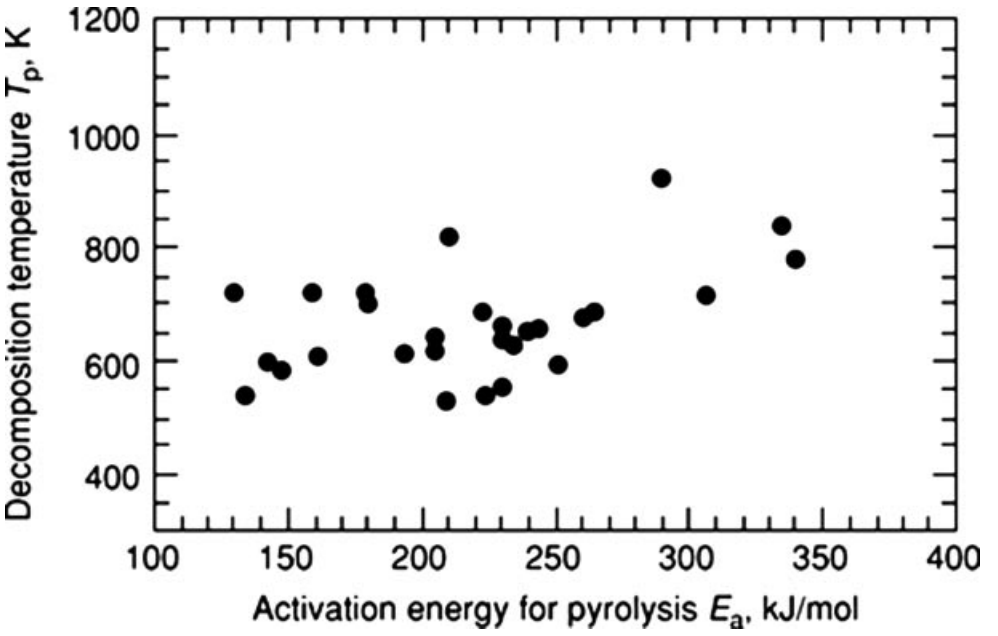

Fig. 17. Pyrolysis temperature versus activation energy of polymers.

Equation 64 can be cast in the form of equation 23 by defining a reference temperature $T_0 = E_a/R \ln(\beta*/\beta_0) = 423$ K. Equations 62–64 imply that T_p or $T_{d,1/2}$ can be used as the primary indicator of thermal stability with the other indices being roughly estimated from it. A plot of T_p versus E_a from thermogravimetric analyses of various polymers at heating rates of the order of 10 K/min is shown in Figure 17. The trend is in qualitative agreement with equation 64 but the correlation coefficient is too low (<0.5) for predictive purposes. For this reason, Van Krevelen extended the use of additive molar group contributions to the calculation of the thermal decomposition temperature. In Van Krevelen's method of calculating the thermal decomposition temperature, the molar thermal decomposition function $Y_{d,1/2}$ is related to the product of the polymer repeat unit molecular weight M and the decomposition temperature, viz.

$$MT_{d,1/2} = Y_{d,1/2} \tag{65}$$

The decomposition temperature is calculated by summing the individual molar decomposition functions $Y^i{}_{d,1/2}$ for each chemical group of molar mass M_i comprising the repeat unit:

$$T_{d,1/2} = \frac{Y_{d,1/2}}{M} = \frac{\sum_j n_i Y^i_{d,1/2}}{\sum_j n_i M_i} \tag{66}$$

The molar group contribution $Y^i{}_{d,1/2}$ for each of the chemical groups comprising the polymer was determined for decomposition temperatures measured at

Table 11. Group Contributions to the Decomposition Temperature of Polybenzimidazole

Structural group, i	n_i	M_i, g/mol	$Y^i_{d,1/2}$, g · K/mol
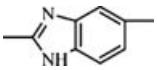	2	116.12	105
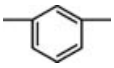	1	76.09	65

a linear heating rate ≈ 3 K/min. For example, the decomposition temperature of PBI having the chemical repeat unit structure

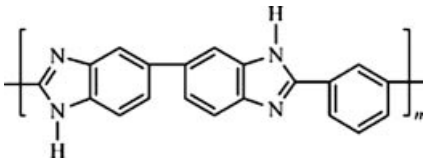

is calculated from the $Y^i_{d,1/2}$ given in Table 11 and equation 66 as

$$T_p = \frac{(2)(105)+(1)(65)}{(2)(116.12)+(1)(76.09)} \times 1000 = 892\ \text{K} = 619^\circ\text{C}$$

which is in general agreement with the literature value $T_p \approx 903$ K and the data in Table 1 and Figure 6.

Char Yield. Pyrolysis/char residue has the character of a thermodynamic quantity since it depends only on temperature and the composition of the material through the enthalpy barriers to gas and char formation, E_g, E_c, in equation 19. The char-forming tendency of different groups is additive and roughly proportional to the aromatic (ie, nonhydrogen) character of the group (see Fig. 9). The char yield is calculated by summing the char-forming tendency per mole of carbon of the chemical groups, $C_{FT,i}$, and dividing by the molecular weight of the repeat unit (22)

$$Y_c = \frac{C_{FT}}{M} \times M_{carbon} = \frac{\sum_j n_i C_{FT,i}}{\sum_j n_i M_i} \times 12 \qquad (67)$$

The $C_{FT,i}$ are the moles of carbon remaining as char per mole of chemical group i in the polymer measured at 850°C. Negative corrections are made for aliphatic groups containing hydrogen atoms in proximity to char-forming groups because of the possibility for disproportionation and subsequent volatilization of hydrogen-terminated chain fragments that are no longer capable of recombining/cross-linking to make char. Table 12 lists the char-forming tendency of the structural units comprising bisphenol-A polycarbonate (PC) whose chemical structure is

Table 12. Group Contributions to the Char Yield of Bisphenol-A Polycarbonate

Structural group, i	n_i	M_i, g/mol	$C_{\mathrm{FT},i}$, mol · C/mol
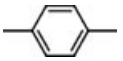	2	76.10	4
	1	42.08	−3
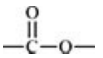	1	44.01	0
—O—	1	16.00	0

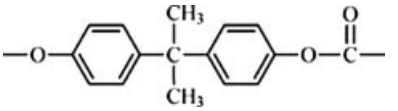

From the data in Table 12 and equation 67 the char yield of PC is calculated to be

$$Y_c = \frac{(2)(4)+(1)(1-3)+(1)(0)+(1)(0)}{(2)(76)+(1)(42)+(1)(16)+(1)(44)} \times 12 = 0.24 = 24\%$$

which compares with the measured value $Y_c = 0.25$ in Table 3. The method is empirical and relatively simple to use and good agreement is obtained with other measured pyrolysis residues in Table 3. The char yield of polymers under anaerobic conditions is thus well described using the additive molar contributions of the individual structural groups comprising the polymer.

Heat Release Rate. Individually, the material and combustion properties κ, ρ, c, ${h_{c,p}}^0$, T_p, and μ have found limited success as descriptors of fire behavior because the coupling of gas and condensed phase burning processes is complex (eg, Fig. 2). Direct measurement of fire behavior or flammability requires about 1 kg of material from which to prepare samples and is therefore prohibitively expensive for research where only gram quantities are typically available. Separate determination of thermochemical and combustion properties using laboratory thermal analyses and combustion calorimetry requires only gram quantities of material but the process is time-consuming. Consequently, recent work has focused on identifying a flammability parameter that captures the chemical dynamics of flaming combustion in a single laboratory test using research (gram) quantities of material (10,26,29).

The heat release rate in flaming combustion, HRR, is the amount of heat Q released by gas phase combustion of unit mass of fuel m, released by pyrolysis per unit time t, and per unit area of burning surface, S. A simple dimensional analysis

gives

$$\mathrm{HRR} = \frac{1}{S}\frac{\mathrm{d}Q}{\mathrm{d}t} = \rho\delta\left(\frac{1}{m}\frac{\mathrm{d}Q}{\mathrm{d}t}\right) = \rho\delta\dot{Q}_\mathrm{c} \tag{68}$$

where ρ and δ are the average density and thickness of the mesophase, respectively. If a specific heat release rate is defined that is equation 22 multiplied by the heat of combustion of the pyrolysis/fuel gases, ${h_\mathrm{c}}^0$,

$$\dot{Q}_\mathrm{c} = \beta\left\{\frac{h_c^0(1-\mu)E_\mathrm{a}}{eRT_\mathrm{p}^2}\right\} = \beta\eta_\mathrm{c} \tag{69}$$

where

$$\eta_\mathrm{c} = \frac{h_\mathrm{c}^0(1-\mu)E_\mathrm{a}}{eRT_\mathrm{p}^2} \approx \frac{h_{\mathrm{c,p}}^0}{\Delta T_\mathrm{p}} \tag{70}$$

is a collection of thermal and combustion properties with the units [J/(kg · K)] and significance of a heat *release* capacity. The heat release capacity is the maximum amount of heat released by combustion per degree of temperature rise per unit mass of polymer in the mesophase. If the heating rate in the mesophase is β, then η_c is related to HRR

$$\mathrm{HRR} = \eta_\mathrm{c}(\chi\rho\delta\beta) = \eta_\mathrm{c} f(\dot{q}''_\mathrm{net}) \tag{71}$$

where $f(\dot{q}''_\mathrm{net}) = \chi\rho\delta\beta$ is an increasing function of the external heat flux with units of (kg · K)/(m^2 · s). Figure 18 is a plot of the average heat release rate at an external heat flux of about 50 ± 10 kW/m^2 versus η_c for the same or similar polymers. The proportionality between HRR and η_c in Figure 18 is reasonably good considering that the coefficient of proportionality $f(\dot{q}''_\mathrm{net}) = f(\dot{q}''_\mathrm{ext} + \dot{q}''_\mathrm{flame} - \dot{q}''_\mathrm{loss})$ varies with thermal stability, char-forming tendency, mesophase density, and flaming combustion efficiency in a complex way.

Equation 70 is an explicit result for a parameter, η_c, that contains most of the properties known to correlate with flammability. In particular, η_c is proportional to the fuel fraction and heat of combustion of the fuel, and inversely proportional to thermal stability (heat resistance). Because η_c is a combination of a material properties each of which is calculable from additive molar group contributions, η_c itself should be calculable from the same or similar molar groups if it is a material property.

From the additivity principle for polymer properties, a molar heat release capacity Ψ is defined (29) with units of J/(mol · K) whose functional form is equation 70 but with the thermal stability and combustion properties written as additive molar quantities **H, V, E**, and **Y/M** in place of ${h_\mathrm{c}}^0$, $(1-\mu)$, E_a, and T_p, respectively. If each chemical group i in the polymer adds to the component molar properties according to its mole fraction n_i in the repeat unit, then in terms of molar quantities

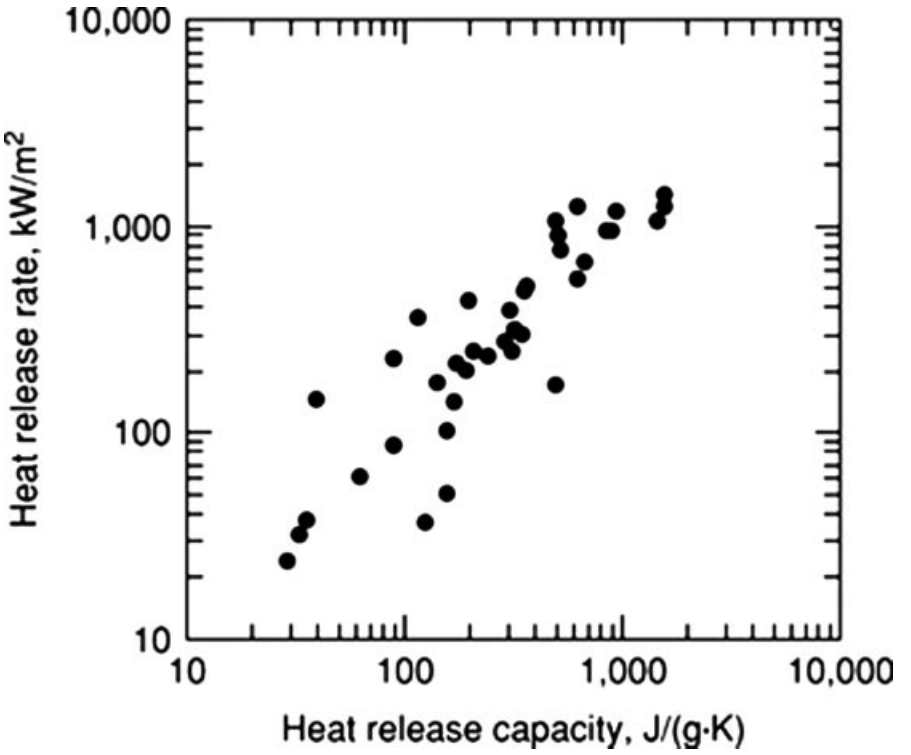

Fig. 18. Average heat release rate versus heat release capacity of polymers.

equation 70 becomes

$$\Psi = \frac{\text{HVE}}{eR(\mathbf{Y}/\mathbf{M})^2} = \frac{\left(\sum_i n_i H_i\right)\left(\sum_i n_i V_i\right)\left(\sum_i n_i E_i\right)}{eR\left(\sum_i n_i Y_i / M_i\right)} \tag{72}$$

with H_i, V_i, E_i, Y_i, and M_i being the molar heat of combustion, mole fraction of fuel, molar activation energy, molar thermal decomposition function, and molar mass of component i, respectively. Expanding the summations in equation 72 and retaining only the noninteracting terms for which $i = j = k \ldots$ (ie, neglecting terms containing products and quotients with mixed indices), the heat release capacity on a mass basis is

$$\eta_c = \frac{\Psi}{M} = \frac{\sum_j n_i \Psi_i}{\sum_j n_i M_i} = \frac{\sum_j N_i \Psi_i}{\sum_j N_i M_i} \tag{73}$$

Experimental heat release capacities η_c have been measured for over 200 polymers and the results are used to generate over 30 additive molar group contributions by treating the Ψ_i as adjustable parameters in equation 73 for polymers with known chemical structures (29). Table 8 contains η_c for a few dozen polymers. Figure 19 compares calculated and measured heat release capacities for 50 polymers using

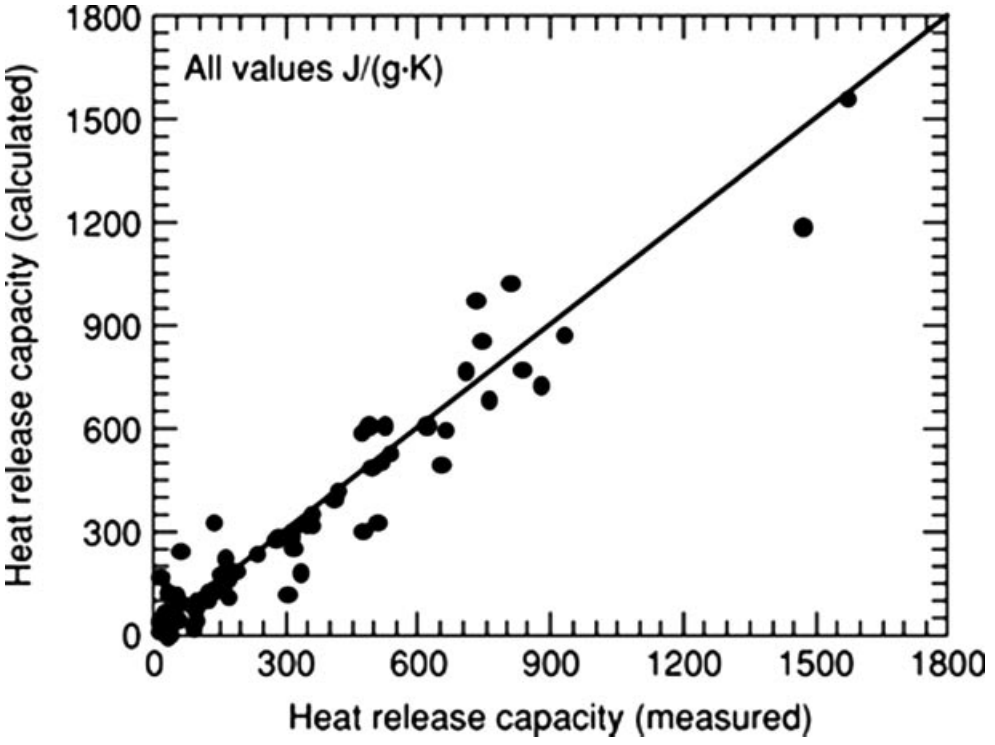

Fig. 19. Polymer heat release capacities: calculated versus measured values.

the 30 empirical Ψ_i determined by Walters and Lyon (2003). Overall agreement between measured and calculated values is about 15%, which is encouraging at this early stage of research. Additive contributions to the heat release capacity are being updated as more polymers are tested and the measurement technique improves. As an example of the additive procedure for calculating the heat release capacity, the chemical repeat unit for PET is

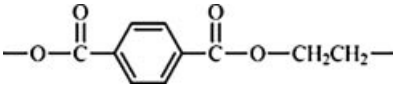

for which the most recent chemical group contributions are listed in Table 13. Combining the N_i, M_i, and Ψ_i for PET as per equation 73,

$$\eta_c = \frac{\sum N_i \Psi_i}{\sum N_i M_i} = \frac{(1)(28.8)+(2)(0)+(2)(16.7)}{(1)(76.10)+(2)(44.01)+(2)(14.03)} = \frac{62.2\ \text{kJ/(mol}\cdot\text{K)}}{192.18\ \text{g/mol}}$$

$$= 324\ \text{kJ/(kg}\cdot\text{K)}$$

The predicted heat release capacity for PET compares favorably with typical experimental values for this polymer, $\eta_c = 326 \pm 52$ kJ/(kg · K) (see Table 8),

Table 13. Group Contributions to the Heat Release Capacity of Poly(ethylene terephthalate)

Structural group, i	n_i	M_i, g/mol	Ψ_i, kJ/(mol · K)
	1	76.10	28.8
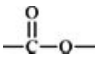	2	44.01	0.0
	2	14.03	16.7

considering that the group contributions are average values derived from several different polymers.

Flame Resistance. *Flame resistance* is the ability to withstand flame impingement or give protection from it. Equation 53 shows that a critical heat release rate criterion for incipient burning/extinction gives a simple scaling relationship between flame resistance and fire behavior in terms of the heat release parameter. At the molecular level, HRR is governed by the heat release capacity (see under Heat Release Rate) which is proportional to HRR in steady burning (eq. 71) for a particular set of test conditions and material properties. Heat release capacity can be related to flame resistance in the same way that HRR was related to flame resistance (see Unsteady Burning). If the heat release rate is equation 71 and the criterion for flame extinction in flammability tests is equation 50, then flame extinction is related to heat release capacity

$$\mathrm{HRR} = \eta_c f(\dot{q}''_{\mathrm{flame}} - \dot{q}''_{\mathrm{loss}}) \leq \mathrm{HRR}^*_b \tag{74}$$

Equation 74 states that (analogous to HRR) there is a critical value of η_c below which flame extinction will occur in a flammability test:

$$\eta_c \leq \frac{\mathrm{HRR}^*_b}{f(\dot{q}''_{\mathrm{flame}} - \dot{q}''_{\mathrm{loss}})} \tag{75}$$

Figure 1 showed generic η_c and flame resistance results for commercial polymers. Figure 20 shows grouped ratings for 50 polymers in the Underwriters Laboratory vertical (V) and horizontal (H) test for flammability of plastics (27) (see section on Testing for Regulatory Compliance and Table 14). Three ranges of flammability are observed with respect to η_c in Figures 1 and 20: No ignition in a vertical test (UL 94 V0 rating or better) for $\eta_c < 200$ kJ/(kg · K); self-extinguishing (UL 94 V) behavior after 10–30 s of burning in a vertical test for $\eta_c = 200$–400 kJ/(kg · K); a self-propagating flame in a horizontal burning (HB) test for $\eta_c > 400$ kJ/(kg · K).

With regard to flammability as measured in the LOI test (25) (see section on The Limiting Oxygen Index Test), if Equation 52 applies and $\dot{q}''_{\mathrm{flame}}(\mathrm{extinction}) = \varphi \mathrm{LOI}$, then equation 74 gives the criterion for flame extinction

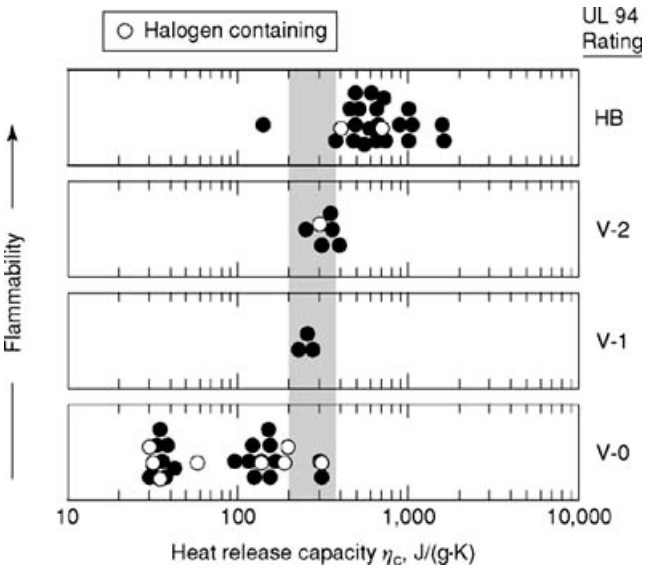

Fig. 20. Flammability rating in UL 94 test versus heat release capacity of 50 polymers.

in the LOI test:

$$\eta_c \leq \frac{\mathrm{HRR}_b^*}{f(\varphi \mathrm{LOI} - \dot{q}''_{\mathrm{loss}})} \tag{76}$$

Equation 76 suggests that LOI and η_c are inversely related. Figure 21 is a plot of generic values of LOI versus η_c (see Table 8). A power law $\mathrm{LOI} = 125/\eta_c^{1/4}$ can be fit to the data with reasonable accuracy (correlation coefficient = 0.84), confirming the inverse relationship between LOI and η_c suggested by equation 76.

Smoke. The *smoke extinction area* (SEA; m^2/kg) is a global measure of the condensed phase (liquid and solid) products of flaming combustion having units of square meters of particulate scattering surface per kilogram of material burned. The SEA is measured in a fire calorimeter under well-ventilated conditions from optical extinction of the combustion gas stream (25). Table 15 lists the specific SEA for a variety of polymers averaged from the literature. Figure 22 is a plot of SEA in Table 15 versus the flaming combustion efficiency of the same polymer

Table 14. UL 94 20-mm Vertical Burning Test Classification Criteria

	Classification		
Observation	V-0	V-1	V-2
t_1 or t_2 for any specimen	10 s	30 s	30 s
$t_1 + t_2$ for 5 specimens	50 s	250 s	250 s
$t_2 + t_3$ for any specimen	30 s	60 s	60 s
Afterflame or afterglow up to clamp, any specimen	No	No	No
Ignition of cotton	No	No	Yes

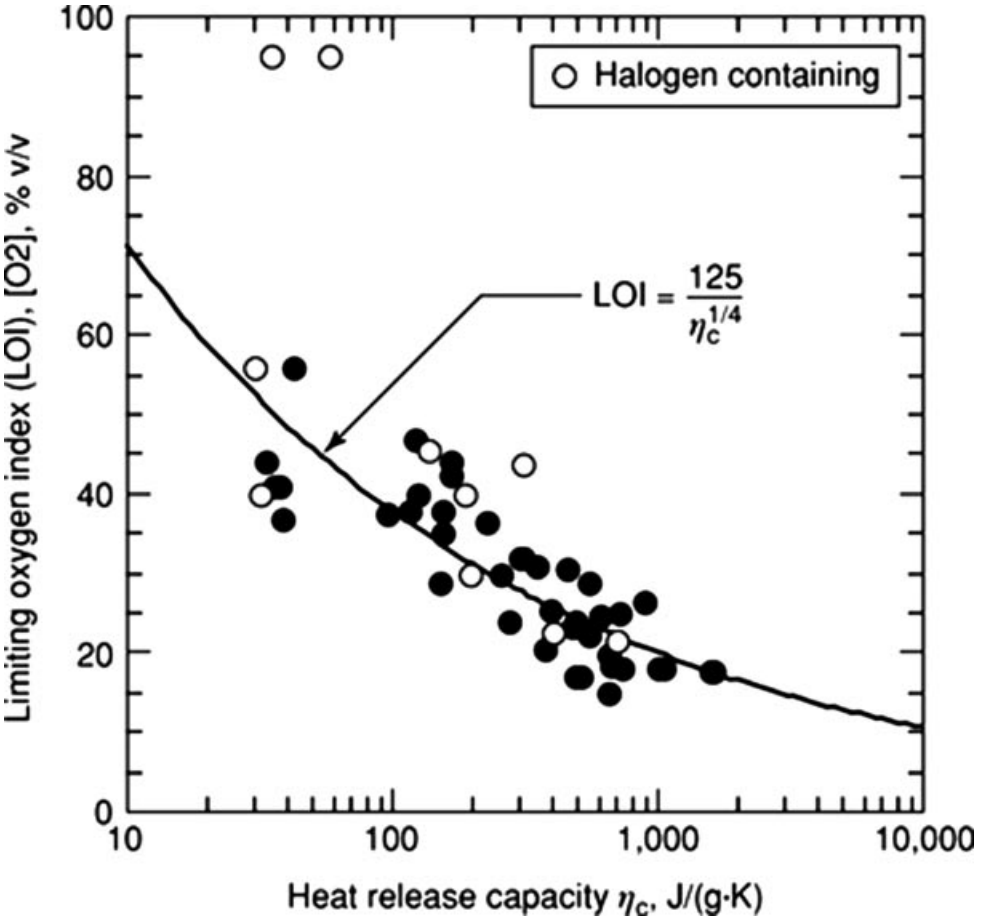

Fig. 21. Limiting oxygen index versus heat release capacity for 50 polymers.

listed in Table 7. It is seen that SEA varies by a factor of 100 between different polymers and is particularly sensitive to combustion efficiency in the range $\chi = 0.8–1.0$. Below $\chi = 0.8$, SEA is essentially independent of combustion efficiency.

The effect of chemical structure on smoke production can generally be described as follows. Aliphatic oxygenated fuels (POM, PMMA, PA) and those with high thermal stability (PBI, PAI, PEI, PES, PEEK, PAS) or extremely low burning rate (PTFE, CPVC, wood) tend to produce less smoke per unit mass of material burned than aliphatic (PE, PP), aromatic oxygen- and nitrogen-containing (PET, PBT, EP, PC, PU, BMI, VE, PPO) or aromatic sulfur-containing (PSU, PPS) polymers.

Polymers with low thermal stability and pendant (ABS, PS) or backbone (EP, UPT, VE, PPO) aromatic groups produce a large amount of smoke because their thermal degradation products (fuel gases) contain the aromatic nucleus for soot formation (see under The Gas Phase).

Low thermal stability aromatic polymers with high SEA (ABS, EP, PS) produce 50% more smoke per unit mass when brominated flame retardants are added

Table 15. Smoke Extinction Area of Polymers

Polymer	SEA, m^2/kg
PTFE	33
CPVC	33
POM	50
Douglas fir (wood)	75
PI	75
PMMA	100
PBI	100
PAI	120
PA6	134
Hemlock (wood)	150
PEI	150
PES	150
PA66	230
PEEK	292
PAS	300
PE	325
PF	325
PET	400
PP	455
PSU	475
PU	550
PBT	623
PPS	646
PVC flex/FR	770
PEKK	800
UPT	800
PC	891
PMMA/PVC alloy	900
EP	907
ABS	925
BMI	950
PVC rigid	1015
VE	1050
PVC flex	1078
PS	1150
PPO	1300
ABS (Br FR)	1500
Silicone elastomers	1500
EP (Br FR)	1600
PS (Br FR)	1650

to inhibit combustion. These materials, listed at the bottom of Table 15, produce 5–20 times more smoke per unit mass than the commodity and engineering polymers in the top half of the table. Silicones are anomalous with respect to SEA because the scattering particles are silica (SiO_2), which is a complete (rather than incomplete) combustion product of the backbone silicon.

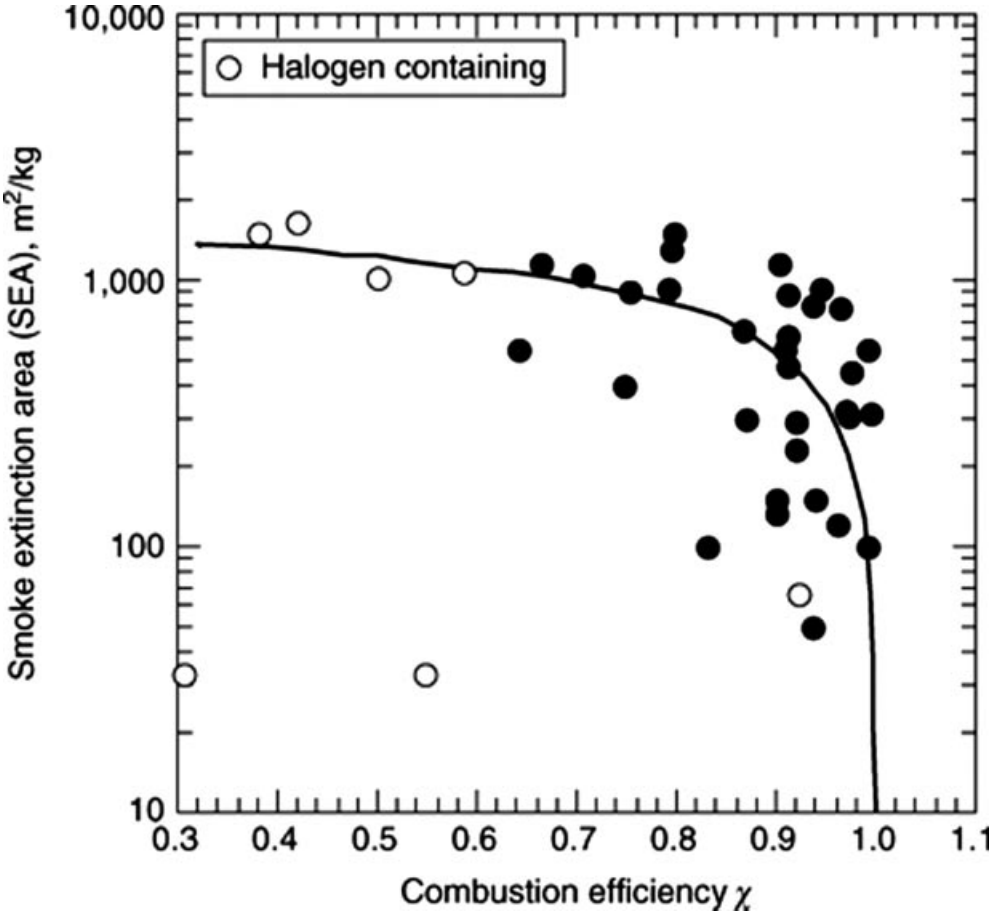

Fig. 22. Smoke extinction area (SEA) versus flaming combustion efficiency (χ) for 40 polymers.

The highest SEAs are associated with halogen-containing polymers (rigid and flexible PVC, PMMA/PVC alloy) apparently because of combustion inhibition by chlorine (see equations 1–3 and Fig. 22).

The smoke point is another measure of the tendency of a fuel to produce smoke and this quantity, like SEA, is related to the chemical composition and structure of the fuel. The *smoke point* is defined as the minimum fuel mass flow rate at which smoke first escapes from the tip of a laminar diffusion flame (see Fig. 2), ie, the residence time of the smoke in the combustion zone becomes too short to effect complete oxidation. The results of the smoke point test are qualitatively similar to the SEA data in Table 15 with respect to chemical structure and smoke-forming tendency. In particular, it is found that the smoke-forming tendency, as determined by smoke point measurements, is lowest for oxygenated fuels (alcohols, aldehydes, esters, ethers) and increases through the series alkanes, branched alkanes, alkenes, and aromatics.

Fire and Flammability Tests

Terminology: Fire versus Flammability. There is no universal agreement on the definition of flammability tests and how they are different from fire tests. A common application of fire and flammability tests is to obtain data for regulatory compliance, as will be discussed in the next section. Fire safety codes and regulations are generally based on two strategies. The first strategy involves preventing, or at least minimizing the likelihood of ignition. Since in practice it is not possible to completely eliminate ignition, the second strategy involves managing the impact of a subsequent fire.

Flammability tests are typically associated with the first strategy. A small specimen (linear dimensions of the order of centimeters or inches) of a polymer is exposed to a small heat source (Bunsen burner-type flame, hot wire, etc.) for a short duration (seconds). Pass/fail criteria are based on ignition of the specimen during exposure, formation of flaming droplets, and/or sustained flaming or smoldering after removal of the heat source.

For the purpose of this article, fire tests are associated with the second strategy and defined as experimental methods to characterize the behavior of polymers under more severe thermal exposure conditions that are representative of the growth phase of a compartment fire. These conditions are simulated with a gas-fired or electrical heater or a large gas burner turbulent diffusion flame (flame length of the order of a meter or several feet). The incident heat flux to the specimen is primarily radiative when heaters are used, and mainly convective for flame exposure. Total incident heat flux varies from approximately 1 kW/m^2 to more than 100 kW/m^2. Note that the maximum radiant heat flux from the sun on earth is approximately 1 kW/m^2. Polymers that are not treated with fire retardant chemicals typically ignite when exposed to heat fluxes of 10–20 kW/m^2 in the presence of a small pilot flame or hot spark.

The aforementioned definitions imply that flammability tests are concerned with a lower level of performance. Passing a flammability tests does not mean that a material will be less hazardous when involved in a fire. This is consistent with one definition of the term *flammable*, which in ASTM E176, *Terminology of Fire Standards*, is described as, subject to easy ignition and rapid flaming combustion (25).

The characteristics that are measured in a fire test are indicative of the performance of the material under the conditions of the test and are therefore referred to as fire-test-response characteristics. They may or may not be indicative of the hazard of a material under actual fire conditions. The most common fire-test-response characteristics that are measured in fire tests are the ease of ignition, flame spread, heat release, smoke generation and toxic potency of smoke (20,25).

Fire and Flammability Test Applications. There are three distinct applications of fire and flammability tests as discussed below.

Regulatory Compliance. Codes and regulations have been developed in many countries to ensure a level of public fire safety that is acceptable to society. The main objectives of these codes and regulations in terms of fire and flammability of materials are to limit the likelihood of ignition and to reduce the rate of fire growth to the critical stage of flashover in the compartment of fire origin. In addition, codes and regulations also limit the quantities of particulate matter

(affects visibility) and of toxic/corrosive products of combustion that can cause human casualties and excessive damage to equipment.

Codes and regulations are intended to provide a minimum level of safety based on loss objectives that are acceptable to society. Other stakeholders often specify additional requirements. For example, an insurance company might have more stringent requirements to reduce the risk of incurring excessive losses in the event of a fire. Building owners and operators might require a level of safety that exceeds the building code. Manufacturers of transportation vehicles might issue specifications for their product suppliers that go beyond the regulations.

Codes, regulations, and specifications specify acceptance criteria for the products that are used in specific areas of the environment that is regulated. These criteria are based on performance in one or more fire or flammability tests. This approach has been applied extensively to two environments where the potential exists for large life loss: buildings and transportation vehicles. Some important fire and flammability tests that are used in different parts of the world to ensure a specific level of safety in these two environments are summarized in subsequent sections of this article.

Quality Assurance and Research. Fire and flammability tests are also used in support of production control. The objective of a production control program is to ensure that a product that is sold in the marketplace is identical to the specimen that was originally tested for regulatory compliance. Often it is not practical or economically feasible to use the qualification test(s) in a follow-up production control program and a simple test is often adequate to verify consistency of the product. Relatively simple flammability tests are therefore most often used for the purpose of quality assurance. The same tests are then also used in research and development of new products.

Data for Fire Safety Engineering Design and Analysis. Fire safety codes and regulations are largely prescriptive. This means that they contain acceptance criteria for materials, products, and assemblies based on performance in one or several tests. The overall level of safety that is accomplished is not explicitly stated. Sometimes it is not possible to demonstrate that a material, product, or assembly meets the specified acceptance criteria. For example, it might not be possible to obtain a valid test result for a product that melts and shrinks away from the heat source in a fire test. Fire safety codes and regulations generally contain a clause that gives the enforcing official the authority to accept a variance from the specified acceptance criteria. To persuade the enforcing official it is necessary to demonstrate that the material, product, or assembly does not compromise the level of safety that is implicit in the code or regulation. This usually requires an engineering analysis and tests to obtain material properties that are needed in support of the analysis.

In recent years performance-based codes and regulations have become increasingly popular. Such codes and regulations explicitly state the minimum level of performance of the system (building, railcar, etc.) in case of fire. That a particular design meets the specified level of performance is again based on an engineering analysis. Similar analyses are performed in support of the investigation and reconstruction of actual fire incidents.

Fire and Flammability Test Standards. Regardless of the application, it is important that fire and flammability test methods be free of systematic error

(bias). It is also essential that consistent results can be obtained from experiments repeated at different times within one laboratory (repeatability) and that there is reasonable agreement between the results for the same material, product, or assembly tested in different laboratories (reproducibility). These are the reasons why fire safety codes, regulations, and specifications refer to standardized fire and flammability test methods and why test data needed in support of fire engineering are obtained with standardized experimental protocols.

Consensus-Based Test Standards. Most fire and flammability test standards are developed by consensusbased committees. The rules and procedures by which these committees operate ensure that the development cannot be dominated by a single interest group and that there is reasonable agreement between the different interest groups represented on the committee.

The primary consensus-based organizations in the United States developing and maintaining fire and flammability test standards are ASTM International (previously the American Society for Testing and Materials) and the National Fire Protection Association (NFPA). Committee E05 on Fire Tests is the primary committee in ASTM that develops fire and flammability test standards (25). Several material- or product-oriented Committees have subcommittees that develop fire and flammability test standards as well. For example, Committee D20 on Plastics has a subcommittee on thermal properties (D20.30) that develops and maintains some fire and flammability test standards for plastics. The Fire Test Committee is responsible for all fire and flammability test standards that are used by any of the fire safety codes and standards published by NFPA. A number of test laboratories in the United States, such as Underwriters Laboratories and FM Global, have established a consensus process that meets the requirements of the American National Standards Institute (ANSI) so that they now can publish American National Standards.

International fire and flammability test standards are developed by the International Organization for Standardization (ISO) and the International Electrotechnical Committee (IEC). The latter is concerned with electrical products only. Technical committees TC 92 and TC 89 are the primary committees that develop and maintain fire and flammability test standards in ISO and IEC respectively. As in ASTM, there are a number of product- or industry-specific committees in ISO that also develop fire and flammability test standards. For example, SC1 on Test Methods of ISO TC 136 on Furniture has published two ignition tests for upholstered seating. An important difference between ISO and IEC vs ASTM and NFPA is that the international committees establish consensus on a geographical basis. Each country that actively participates in the work can be a voting member on an ISO or IEC committee. Committees are composed in a similar manner in CEN and CENELEC, which are the European counterparts of ISO and IEC respectively. However, member countries can have multiple votes in CEN and CENELEC committees. The number of votes is a function of the population of the country.

Other Types of Test Standards. There are also many fire and flammability tests methods that are not developed by a consensus-based process. In the United States these types of test standards are typically promulgated by regional or federal government agencies. The latter are published as part of the regulations that refer to these test methods in the Code of Federal Regulations (CFR), although

many federal regulations rely on consensus-based test standards. Some federal fire and flammability test standards are also described in military specifications (MIL specs) issued by the different agencies of the Department of Defense. The U.S. government has recognized the advantages of using test standards that have been subjected to a review and are accepted by all interest groups and is now actively supporting the adoption of consensus-based tests standards. Examples of regional fire and flammability test standards that are not consensus-based are the California Technical Bulletins to assess the fire and flammability characteristics of upholstered furniture and mattresses. Finally, specifications for suppliers issued by manufacturers of passenger airplanes, railcars, etc., might also rely on fire and flammability test procedures that have not been developed by a consensus-based process. For example Airbus, Boeing, and Bombardier all have their own fire and flammability test standards.

Testing for Regulatory Compliance. There are literally hundreds of fire and flammability tests for polymers (5,25). It is not possible to provide an overview of these tests in this article. A few important tests have been selected to illustrate the key concepts. These tests include the ones that are referred to in the first four sections of this article: the UL 94 20-mm vertical burning test (27), the limiting oxygen index test (25), the cone calorimetry (25), and the pyrolysis combustion flow (29) calorimetry. For guidance on available fire and flammability test methods to evaluate polymers, the reader is referred to ASTM D3814, *Standard Guide for Locating Combustion Test Methods for Polymeric Materials* (25). A comprehensive review of fire and flammability tests used in support of codes and regulations in different parts of the world can be found in Troitzsch (5).

Typical Example of a Flammability Test. The UL 94 standard provides procedures for bench-scale tests to determine the acceptability of plastic materials for use in appliances or other devices with respect to flammability under controlled laboratory conditions. The standard includes several test methods that are employed depending upon the intended end use of the material and its orientation in the device. The standard outlines two horizontal burning tests, three vertical burning tests, and a radiant panel flame spread test. The most commonly used method is summarized below as a typical example of a flammability test.

The first vertical burning test described in the UL 94 standard is the "20-mm Vertical Burning Test; V-0, V-1, or V-2." A photograph of the test cabinet is shown in Figure 23. The V-0, V-1, or V-2 classification is based on the duration of afterflaming or afterglowing following the removal of the burner flame, as well as the ignition of cotton by dripping particles from the test specimen.

In this test, specimens measuring 125 mm in length and 13 mm in width are suspended vertically and clamped at the top end. A thin layer of cotton is positioned 300 mm below the test specimen to catch any molten material that may drop from the specimen. A 20-mm-long flame from a methane burner is applied to the center point on the bottom end of the specimen. The burner is positioned such that the burner barrel is located 10 mm below the bottom end of the material specimen. The flame is maintained for 10 s, and then removed to a distance of at least 150 mm. Upon flame removal, the specimen is observed for afterflaming and its duration time recorded (t_1). As soon as the afterflame ceases, the burner flame is reapplied for an additional 10 s, and then removed again. Durations of afterflaming (t_2) and/or afterglowing (t_3) are noted. On the basis of the results,

Fig. 23. UL 94 cabinet. Photo Courtesy of Fire Testing Technology © 2004.

the material is classified as either V-0, V-1, or V-2 based on the criteria outlined in Table 14.

Typical Examples of Fire Tests. The following two examples are commonly used tests that illustrate two distinct approaches to simulate the thermal exposure conditions in a pre-flashover compartment fire. The steiner tunnel test uses a gas burner to heat the specimen primarily by convection. The radiant flooring panel test relies on a gas-fired panel that exposes a flooring specimen to a radiant heat flux profile.

The Steiner Tunnel Test. The primary intent of the steiner tunnel test is to quantify the wind-aided flame spread propensity of the material tested. It is

Fig. 24. The steiner tunnel test. Photo Courtesy of Southwest Research Institute © 2004.

the most common reaction-to-fire test method prescribed by U.S. model building codes. The steiner tunnel test is described in ASTM E84, *Standard Test Method for Surface Burning Characteristics of Building Materials*, and NFPA 255, *Standard Method of Test of Surface Burning Characteristics of Building Material.* The apparatus, as shown in Figure 24, consists of a long tunnel-like enclosure measuring 8.7 × 0.45 × 0.31 m. The test specimen is 7.6 m long and 0.51 m wide, and is mounted in the ceiling position. It is exposed at one end, designated as the burner end, to a 79 kW gas burner. There is a forced draft through the tunnel from the burner end, with an average initial air velocity of 1.2 m/s. A smoke photometer is mounted on the exhaust duct. The photometer consists of a white light source on one side of the duct and a photocell on the opposite side of the duct.

The measurements consist of flame spread over the surface and light absorption in the exhaust duct of the tunnel. Test duration is 10 min. A flame-spread index (FSI) is calculated on the basis of the area under the curve of flame tip location versus time. The FSI is 0 for an inert board, and is normalized to approximately 100 for red oak flooring. The smoke developed index (SDI) is equal to 100 times the ratio of the area under the curve of light absorption versus time for the 10-min test duration to the area under the curve for red oak flooring. Thus, the SDI of red oak flooring is 100, by definition.

The classification of linings in the model building codes in the United States is based on the FSI. There are three classifications: Class A, or I, for products with FSI $\leq$ 25, Class B, or II, for products with 25 $<$ FSI $\leq$ 75, and Class C, or III, for products with 75 $<$ FSI $\leq$ 200. Class A, or I, products are generally permitted in

stairways. Class B, or II, products can be used in corridors, and Class C, or III, products are allowed in other rooms and areas. The model building codes do not permit interior finishes that produce excessive amounts of light-obscuring smoke. Products that have to be tested according to the tunnel test must have an SDI of 450 or less.

The Radiant Flooring Panel Test. The National Bureau of Standards (NBS; currently the National Institute of Standards and Technology, or NIST) conducted a series of full-scale fire tests in the 1970s to investigate the fire hazard of floor coverings. The main concern was flame spread from a fire room to a connected corridor. This work resulted in the development of the radiant flooring panel test. This test is described in ASTM E648, *Standard Test Method for Critical Radiant Flux of Floor Covering Systems Using a Radiant Heat Energy Source*, and NFPA 253*, Standard Method of Test for Critical Radiant Flux of Floor Covering Systems Using a Radiant Heat Energy Source*. The international version of this test method, ISO 9239-1*, Reaction to Fire Tests for Floor Coverings—Determination of the Burning Behavior Using a Radiant Heat Source*, includes a photometer in the exhaust stack to measure smoke optical density (see Fig. 25).

The Radiant Flooring Panel Test apparatus consists of an air–gas-fueled radiant heat panel inclined at 30° to and directed at a horizontally mounted floor covering system specimen. The radiant panel generates a heat flux distribution along the 1-m length of the test specimen from a nominal maximum of 10 kW/m^2 (1 W/cm^2) to a minimum of 1 kW/m^2 (0.1 W/cm^2). The test is initiated by open-flame ignition from a pilot burner. The heat flux at the location of maximum flame propagation is reported as the critical radiant flux.

Rate of Heat Release Test for Aircraft Cabin Materials. The Federal Aviation Administration requires (14 CFR 25.853) that large areas including interior ceiling and wall panels, partitions, galley structures, cabinets, and stowage compartments of commercial transport aircraft pass a rate of heat release test in addition to flammability and smoke tests. The rate of heat release apparatus (see Fig. 26) is a modified version of the ASTM E906, *Standard Test Method For Heat And Visible Smoke Release Rates of Materials and Products (configuration A)*. Samples are 150 × 150 mm and are cut from cabin components or tested in representative thickness. Samples are exposed to a radiant heat flux of 35 kW/m^2 in a vertical orientation and ignited by an impinging pilot flame. The rate of heat released by flaming combustion is deduced from the calibrated temperature rise of the air stream passing over the sample surface at a prescribed flow rate. The maximum rate of heat release cannot be greater than 65 kW/m^2 over the entire duration of the 5-min test and the heat released during the first 2-min of the test cannot be greater than 65 (kW · min)/m^2.

Testing for Quality Assurance and Research.

The Limiting Oxygen Index Test. The LOI test is a typical example of a method that is used to control the production of materials, products, and assemblies and in research to develop new products. This test is standardized in North America as ASTM D2863, *Standard Test Method for Measuring the Minimum Oxygen Concentration to Support the Candle-Like Combustion of Plastics (Oxygen Index)*, and internationally as ISO 4589-2 *Plastics—Determination of Burning Behavior by Oxygen Index—Part 2: Ambient-Temperature Test*. The test does not correlate well with other fire and flammability tests nor does it provide a reliable

Fig. 25. The radiant flooring panel test. Photo Courtesy of Fire Testing Technology © 2004.

indication of material performance in real fires. However, the results appear to be very sensitive to the composition of the material and the test is therefore ideally suited to serve as a quality assurance tool of fire-retardant-treated materials.

The LOI test apparatus consists of a glass tube of 75–100 mm in diameter and 450–500 mm in height. Figure 27 shows a photograph of the apparatus. A specimen with a height between 70 and 200 mm and a width of 10–20 mm is

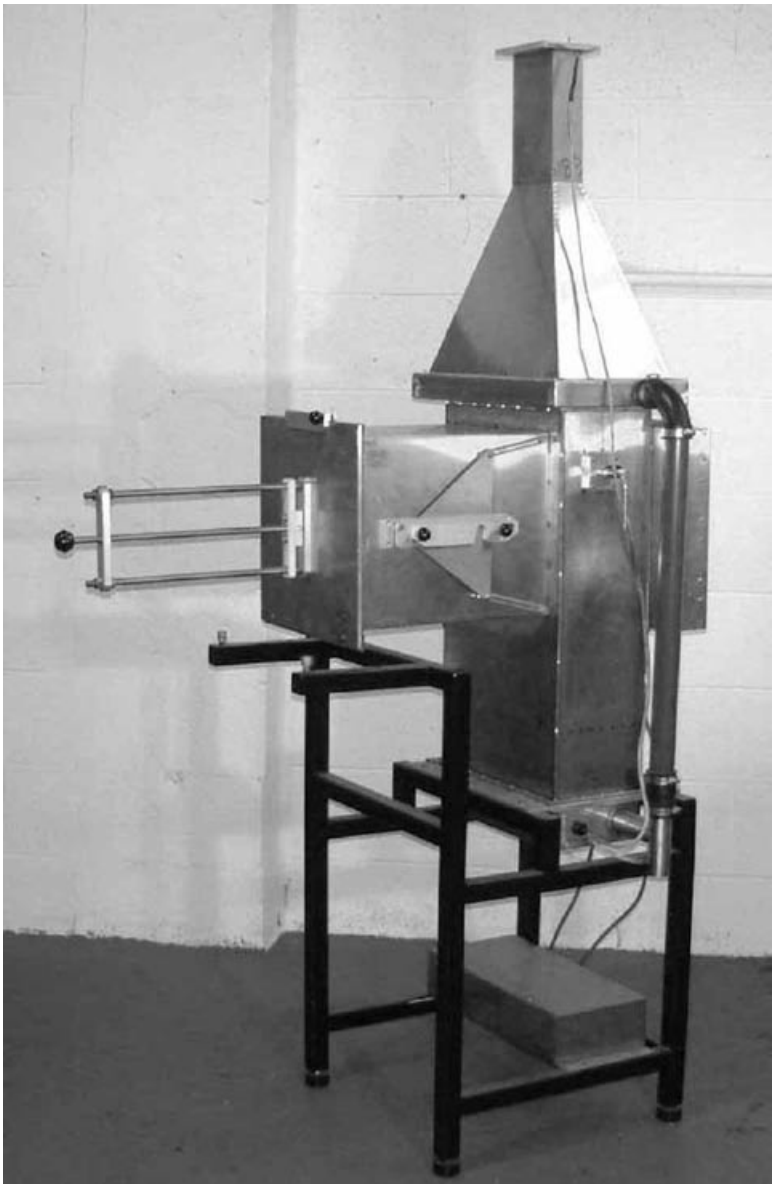

Fig. 26. Rate of heat release apparatus. Photo Courtesy of The Govmark Organization, Inc.

supported inside the glass tube. A gas mixture of oxygen and nitrogen is supplied at the bottom of the tube and a small candle-like flame is applied to the top of the specimen in an attempt to ignite it. The objective is to find the minimum oxygen concentration in nitrogen that will result in sustained combustion for at least 3 min or excessive flame propagation down the specimen. The dimensions of the specimen and the limit of excessive flame propagation depend on the type of material that is being tested.

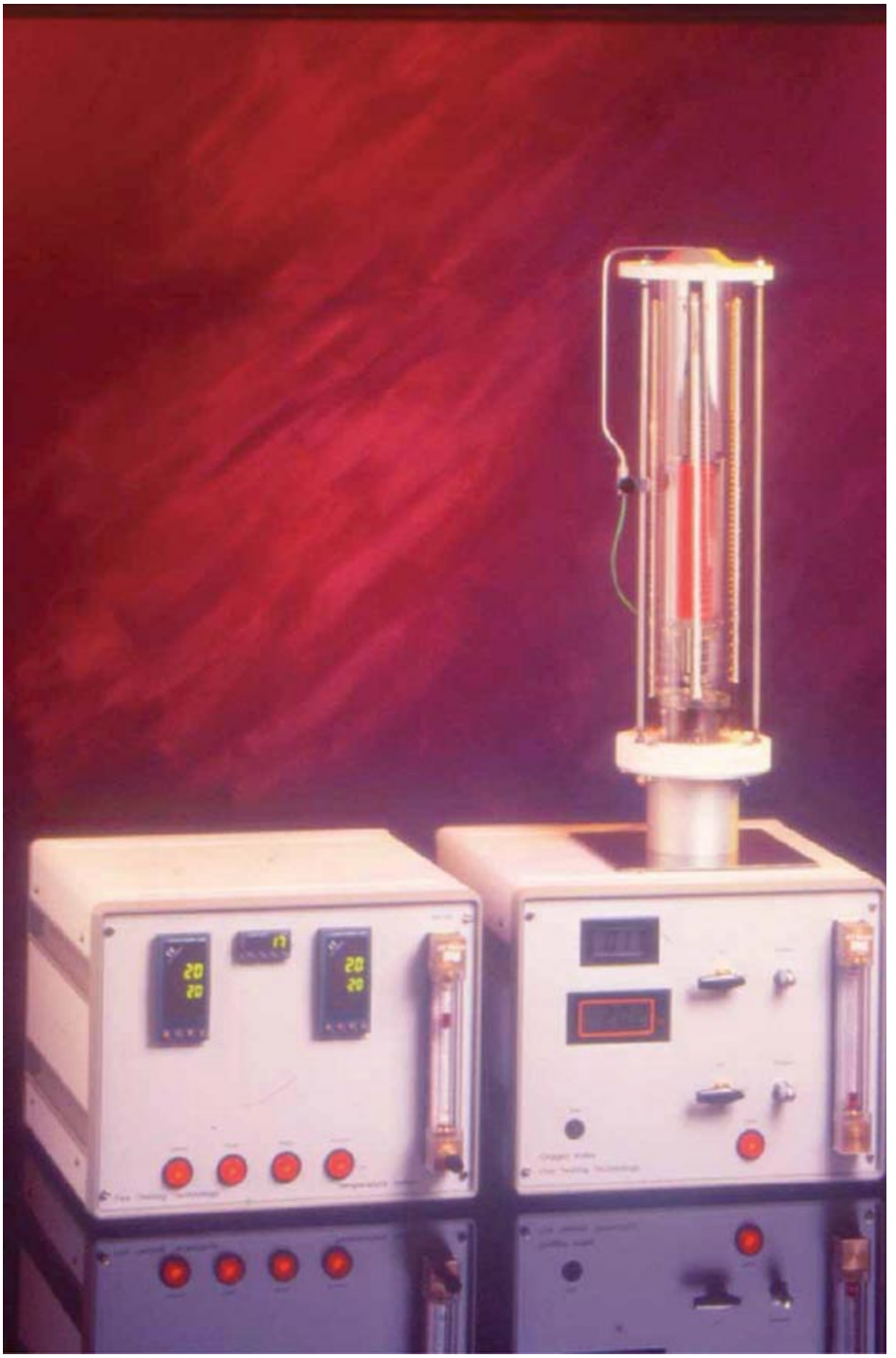

Fig. 27. The limiting oxygen index test. Photo Courtesy of Fire Testing Technology © 2004.

The Pyrolysis-Combustion Flow Calorimetry. Pyrolysis-combustion flow calorimetry (PCFC) is a method for measuring quantitative flammability parameters of combustible materials and is used in research to develop new polymers with improved fire performance (see Lyon and Walters). In PCFC the condensed-phase and gas-phase processes of flaming combustion are separately reproduced through controlled pyrolysis of milligram samples in an inert gas stream and high temperature thermal oxidation (combustion) of the pyrolyzate in excess oxygen. The rate of heat released by combustion per unit mass of sample during the test (specific heat release rate; see under Heat Release Rate) is measured by oxygen consumption calorimetry (see Enthalpy of Gasification). Time integration of the specific heat release rate gives the net heat of combustion of the fuel gases, $h_c{}^0$. The maximum value of the specific heat release rate, normalized for the sample heating rate, is a material flammability parameter with the units and significance of a heat (release) capacity that is a good predictor of flame test results and fire performance. The temperature at maximum specific heat release rate is a good approximation of the ignition temperature (see sections on Ignition; Ignition Temperature as well as Table 1).

Testing to Obtain Engineering Data. Heat release rate is the primary characteristic to quantify the fire hazard of a material. Most fire tests to obtain engineering data therefore measure heat release rate. The rate of heat release is generally determined using oxygen consumption calorimetry. In 1917, Thornton showed that for a large number of organic liquids and gases, a nearly constant net amount of heat is released per unit mass of oxygen consumed for complete combustion. Sixty years later, researchers at NBS also found this to be true for organic solids and obtained an average value for this constant of 13.1 MJ/kg of O_2. This value may be used for practical applications and is accurate with very few exceptions to within ±5%. Thornton's rule implies that it is sufficient to measure the oxygen consumed in a combustion system in order to determine the net heat released. This method, generally referred to as "oxygen consumption calorimetry," is now the most widely used and accurate method for measuring heat release rate in experimental fires. A summary of the most commonly used oxygen consumption calorimeters follows.

Bench-Scale Calorimeters.

The Cone Calorimeter. The cone calorimeter is standardized in North America as ASTM E1354, *Test Method for Heat and Visible Smoke Release Rates for Materials and Products Using an Oxygen Consumption Calorimeter*, and internationally as ISO 5660-1*, Fire Tests—Reaction to Fire—Part 1: Rate of Heat Release from Building Products (Cone Calorimeter Method)*. A photograph of a commercial version of the cone calorimeter is shown in Figure 28.

A square sample of 100 × 100 mm is exposed to the radiant flux of an electric heater. The heater has the shape of a truncated cone (hence the name of the instrument) and is capable of providing heat fluxes to the specimen up to 100 kW/m^2. An electric spark plug is used for piloted ignition. Heater temperature is measured as an average of the readings of three thermocouples in contact with the coil. It is set and maintained at a certain level by a three-term controller. Calibration of heat flux as a function of heater temperature is performed with a total heat flux meter of the Schmidt-Boelter type. Prior to testing, the heater temperature is set at the appropriate value resulting in the desired heat flux.

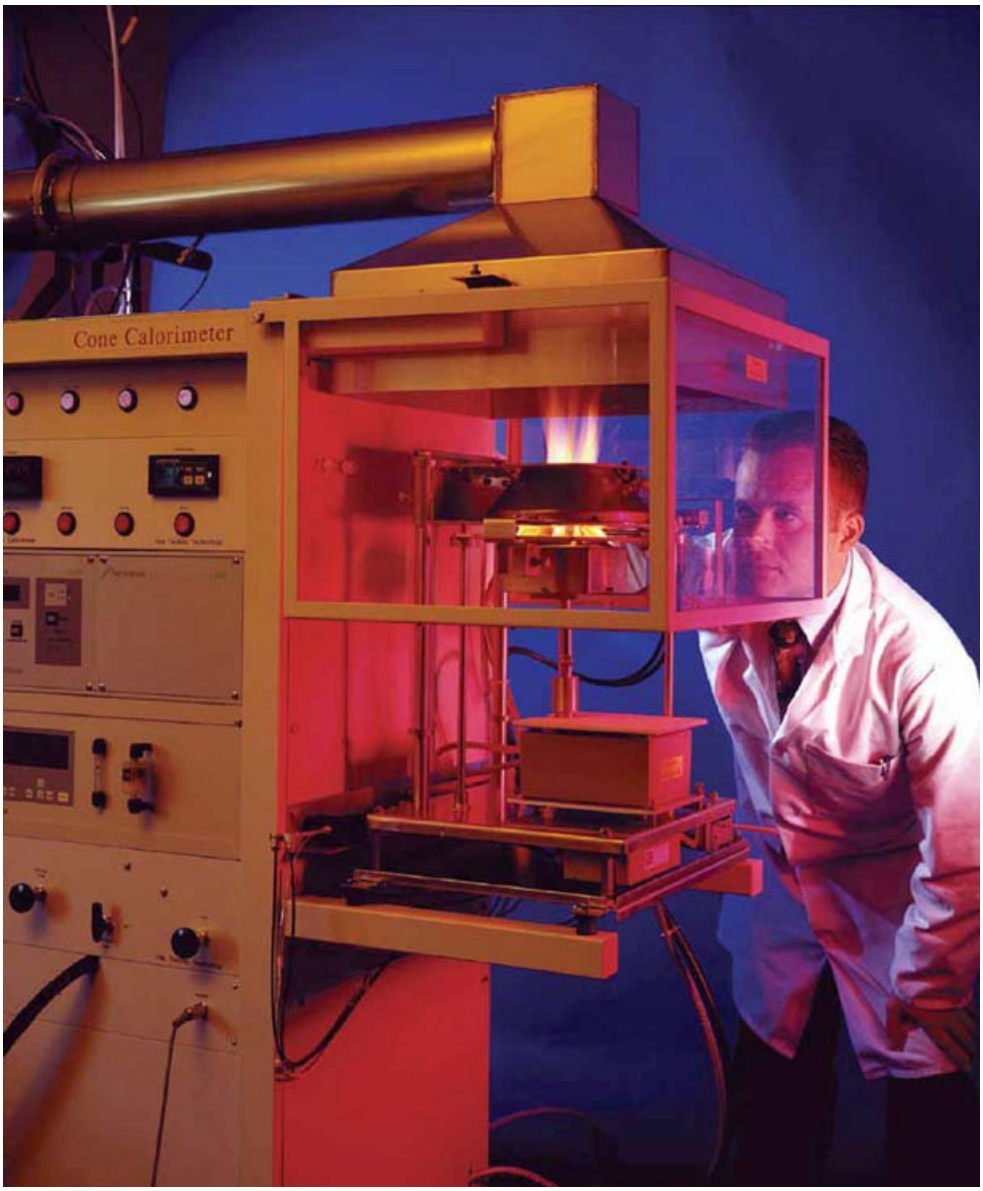

Fig. 28. Commercial version of the cone calorimeter. Photo Courtesy of Fire Testing Technology © 2004.

At the start of a test, the specimen in the appropriate holder is placed on the load cell, which is located below the heater. The load cell has a tare adjustment so that high accuracy mass loss measurements can be made, even if the mass of the holder and a possible substrate are much higher than that of the specimen. As soon as the pyrolysis products released by the specimen ignite, the electric spark plug is removed. All combustion products and entrained air are collected in the hood. An orifice plate at the entrance of the exhaust duct results in an almost uniform

gas mixture. At a sufficient distance downstream from the mixing orifice, a gas sample is taken and analyzed for O_2. A laser photometer is located close to the gas sampling point to measure light extinction by the smoke. The exhaust gases are removed by a high temperature blower. The flow rate can be adjusted between 0 and 50 L/s. For standard testing, the cone calorimeter is used in constant volume mode and the fan speed is set at 24 L/s. Downstream of the fan is a second orifice plate. Measurements of the differential pressure across and gas temperature at the orifice plate are used for calculating the mass flow of the exhaust gases.

The cone calorimeter can also be used to obtain other data in support of fire safety engineering analysis. For example, the instrument can be used to determine ignition characteristics of a material by measuring the time to ignition at different heat flux levels. A laser smoke photometer is mounted on the duct to determine the smoke production rate. A continuous gas sample can be taken from the exhaust duct and analyzed to determine the concentration of different toxic and corrosive products of combustion in the effluents. Fourier transform infrared spectroscopy is now a common method to measure the concentration of toxic and irritant gases in the exhaust duct of the cone calorimeter.

The Fire Propagation Apparatus. The fire propagation apparatus was developed by FM Global Research (previously Factory Mutual Research Corp.). The test is described in ASTM E2058, *Standard Test Methods for Measurement of Synthetic Polymer Material Flammability Using a Fire Propagation Apparatus (FPA)*. A photograph of a commercial version of the fire propagation apparatus is shown in Figure 29.

Fig. 29. Commercial version of the fire propagation apparatus. Photo Courtesy of Fire Testing Technology © 2004.

The fire propagation apparatus is similar to the cone calorimeter and can be used to obtain the same types of measurements. However, there are some significant differences that are briefly summarized below:

(1) The products of pyrolysis are ignited with a small hydrogen flame that is located 10 mm above the center of the specimen.
(2) The specimen is surrounded by a quartz tube. This makes it possible to conduct tests in a vitiated or oxygen-enriched atmosphere. The tube allows for a forced flow over the specimen surface and reduces the effect of external heat flux and specimen surface temperature on convective heat losses prior to ignition.
(3) Specimens are heated by high temperature (approximately 2300 K) tungsten filament lamps that are located outside the quartz tube. Since the spectral response of many materials is different for a radiant heat source at this temperature compared to heat fluxes in fires from sources at much lower temperatures, specimens have to be blackened. In addition, because of the type of heaters that is used and the quartz tube arrangement, the maximum incident heat flux that can be obtained is 70 kW/m^2.

Large-Scale Calorimeters.

The Room/Corner Test. The room/corner test is used to evaluate the fire growth characteristics of wall and ceiling linings. The walls and/or ceiling of a 2.4 $\times$ 3.6 $\times$ 2.4 m room are lined with the test material. A gas burner is placed in one of the rear corners of the room opposite the 0.8 $\times$ 2.0 m open doorway in the front wall. Products of combustion are collected in a hood located in front above the door opening and extracted by a high temperature blower through the exhaust duct. The instrumentation in the exhaust duct is similar to that in the cone calorimeter, except that flow rate is typically determined on the basis of bidirectional probe measurements of centerline velocity and the smoke photometer often uses a white light source instead of a He–Ne laser. Several room/corner test standards have been developed and are used for regulatory purposes. For example, NFPA 265, *Standard Methods of Fire Tests for Evaluating Room Fire Growth Contribution of Textile Wall Coverings*, is required in the United States to qualify textile wall coverings for use in unsprinklered spaces of certain types of buildings. ISO 9705, *Fire Tests—Full-Scale Room Test for Surface Products*, is more severe than NFPA 265 and is used to qualify materials as fire restricting for high speed craft (small passenger ferries operating with short distance from shore). Figure 30 shows an ISO 9705 test in progress.

The Furniture Calorimeter. Often it is very difficult to determine the burning behavior of complex objects on the basis of the fire performance of its individual components. For example, it is very hard to determine the burning behavior of upholstered furniture on the basis of the fire characteristics of the foam, fabric, and framing materials and to account for the geometry and configuration of the furniture and how it is ignited. It is much more practical to measure the heat release rate and related properties for the complete object. This can be done in a furniture calorimeter. The object is placed on a load platform to measure the mass loss rate during the test. It is ignited with a standardized ignition source and the products

Fig. 30. ISO 9705 room/corner test in progress. Photo Courtesy of Southwest Research Institute © 2004.

of combustion are collected in a hood and extracted through an exhaust duct. Measurements of oxygen concentration, flow rate and light transmission in the exhaust duct are used to determine the heat release rate and smoke production rate from the object as a function of time. Furniture calorimeter test standards have been developed in ASTM for chairs, mattresses and stacked chairs. The corresponding designations are ASTM E1537, ASTM E1590, and ASTM E1822 respectively.

The Intermediate-Scale Calorimeter (ICAL). One of the limitations of the Cone Calorimeter is that only relatively small samples can be evaluated. As a

result, products that have joints or layered materials with a thickness exceeding 50 mm can generally not be tested in the Cone Calorimeter in a representative manner. For those types of products or assemblies, a larger calorimeter is required. Such an intermediate scale calorimeter forms the subject of ASTM standard E1623, *Standard Test Method for Determination of Fire and Thermal Parameters of Materials, Products, and Systems Using an Intermediate Scale Calorimeter (ICAL)*.

The ICAL apparatus consists of an array of gas heaters, forming a vertical radiant panel with a height of approximately 1.33 m and width of approximately 1.54 m. The test specimen measures 1×1 m, and is positioned parallel to the radiant panel. The heat flux to the specimen is preset to a maximum of 60 kW/m^2 by adjusting the distance to the panel. Gas flow to the panel is controlled to maintain the temperature to the panel, and consequently the heat flux to the specimen. The products of pyrolysis from the specimen are ignited with hot wires located close to, but not in contact with, the specimen at its top and bottom. The specimen is placed in a holder that is put on a load cell to measure mass loss during testing. Panel and specimen are positioned beneath the hood of the standard ISO 9705 room/corner test. All products of combustion are collected in the hood and continuously extracted through the exhaust duct. Instrumentation is provided in the duct for measuring heat release rate on the basis of oxygen consumption. A smoke photometer is also included for measuring smoke obscuration in the duct.

The Fire Products Collector. The first industrial-size calorimeter for fires into the MW range was built at Factory Mutual (currently FM Global) around 1980. This calorimeter, also referred to as the FM fire products collector, was designed to measure heat and other fire products from test fires up to a size associated with sprinkler activation in commodity warehouse storage and other representative occupancies. Approximately 10 years later, a similar industrial-size calorimeter for heat release rate measurements up to 10 MW was constructed at the National Testing Laboratory (SP) in Sweden. Since then several other laboratories, such as the National Research Council of Canada, the Fire Research Station in the United Kingdom, Underwriters Laboratories and Southwest Research Institute in the United States developed the capability of measuring heat release rate from large fires into the MW range.

Disclaimer

Certain commercial equipment, instruments, materials, and companies are identified in this article in order to adequately specify the experimental procedure. This in no way implies endorsement or recommendation by the Federal Aviation Administration.

BIBLIOGRAPHY

1. C. J. Hilado, *Flammability Handbook for Plastics*, 5th ed., Technomic Publishing Co., Lancaster, Pa., 1998.

2. A. H. Landrock, *Handbook of Plastics Flammability and Combustion Toxicology*, Noyes Publications, Park Ridge, N.J., 1983.
3. F. L. Fire, *Combustion of Plastics*, Van Nostrand Reinhold, New York, 1991.
4. C. A. Harper, ed., *Handbook of Building Materials for Fire Protection*, McGraw Hill, New York, 2004.
5. J. Troitzsch, *Plastics Flammability Handbook*, Hanser Publishers, Munich, 2004.
6. M. Le Bras, G. Camino, S. Bourbigot, and R. Delobel, *Fire Retardancy of Polymers: The Use of Intumescence*, The Royal Society of Chemistry, Cambridge, UK, 1998.
7. A. R. Horrocks and D. Price, eds., *Fire Retardant Materials*, Woodhead Publishing, Ltd., Cambridge, England, 2001.
8. G. L. Nelson, ed., *Fire and Polymers: Hazards Identification and Prevention* (ACS Symposium Series 425), American Chemical Society, Washington, D.C., 1990.
9. G. L. Nelson, ed., *Fire and Polymers II: Materials and Tests for Hazard Prevention* (ACS Symposium Series 599), American Chemical Society, Washington, D.C., 1995.
10. A. F. Grand and C. A. Wilkie, eds., *Fire Retardancy of Polymeric Materials*, Marcel Dekker, New York, 2000.
11. SFPE, *Handbook of Fire Protection Engineering*, 3rd ed., Society of Fire Protection Engineers, Boston, MA, 2002.
12. D. D. Drysdale, *An Introduction to Fire Dynamics*, 2nd ed., John Wiley & Sons, Inc., New York, 1998.
13. G. Cox, ed., *Combustion Fundamentals of Fire*, Academic Press, Publishers, London, UK, 1995.
14. R. Friedman, *Principles of Fire Protection Chemistry and Physics*, National Fire Protection Association, Quincy, MA, 1998.
15. C. F. Cullis and M. M. Hirschler, *The Combustion of Organic Polymers*, Clarendon Press, Oxford, England, 1981.
16. G. Pal and H. Macskasy, *Plastics:Their Behavior in Fires*, Elsevier, New York, 1991.
17. R. A. Strehlow, *Combustion Fundamentals*, McGraw Hill, New York, 1984.
18. R. Turns, *An Introduction to Combustion—Concepts and Applications*, McGraw Hill, New York, 1996.
19. I. Glassman, *Combustion*, 3rd ed., Academic Press, New York, 1996.
20. V. Babrauskas and S. J. Grayson, eds., *Heat Release in Fires*, Elsevier Applied Science, London, UK, 1992.
21. J. G. Quintiere, *Principles of Fire Behavior*, Del Mar Publishers, Albany, N.Y., 1998.
22. D. W. Van Krevelen, *Properties of Polymers*, 3rd ed., Elsevier Scientific, New York, 1990.
23. J. R. Hallman, Ph.D Thesis, The University of Okhlahama, 1971.
24. V. Babrauskas, *Ignition Handbook*, Fire Science Publishers, Issaquah, WA, 2003.
25. *ASTM Fire Test Standards*, 5th ed., American Society for Testing and Materials, West Conshohocken, Pa., 1999.
26. R. E. Lyon and R. N. Walters, *J. Anal. Appl. Pyrolysis* **71**, 27–46 (2004).
27. *Flammability of Plastic Materials*, UL 94 Section 2 (Horizontal: HB) and Section 3 (Vertical: V-0/1/2), Underwriters Laboratories Inc., Northbrook, Ill., 1991.
28. J. Bicerano, *Prediction of Polymer Properties*, 2nd ed., Marcel Dekker, New York, 1996.
29. R. N. Walters and R. E. Lyon, *J. Appl. Polym. Sci.* **87**, 548–563 (2003).

RICHARD E. LYON
W. J. Hughes Technical Center, Federal Aviation Administration
MARC L. JANSSENS
Southwest Research Institute

Glossary

A_i
: frequency factor for kinetic process, where i = initiation, branching, gasification, charring, etc

α
: thermal diffusivity, $= \kappa/\rho c$ (m^2/s)

$\beta*$
: kinetic heating rate (K/s)

β
: experimental heating rate (K/s)

c_i
: heat capacity of substance, where i = gas, air, polymer, etc ($J/(kg \cdot K)$)

C
: heat of combustion of oxygen, =13.1 kJ/g O_2

$C_{FT,i}$
: molar char-forming tendency of chemical group i in polymer (dimensionless)

χ
: combustion efficiency of fuel gases in flame (dimensionless)

δ
: mesophase dimension (m)

E_i
: activation energy for kinetic process, where i = initiation, branching, gasification, charring, pyrolysis, etc (J/mol)

ε
: emissivity (dimensionless)

ϕ
: radiative fraction of power density at ignition (dimensionless)

γ
: viscosity (Pa)

$\overline{h}$
: average surface convective heat transfer coefficient ($W/(m^2 \cdot K)$)

$h_c{}^0$
: heat of combustion of fuel gases (J/kg)

h_g
: enthalpy of gasification per unit mass of polymer (J/kg)

HOC
: heat released by flaming combustion of fuel gases (J/kg)

HRP
: heat release parameter, $= \chi h_c{}^0/L_g$ (dimensionless)

HRR
: heat release rate per unit area of burning surface in flaming combustion (W/m^2)

HRR^*
: apparatus-dependent ignition parameter (W/m^2)

$HRR_b{}^*$
: critical heat release rate for incipient burning/extinction (W/m^2)

HRR_0
: heat release rate in unforced burning (W/m^2)
η_c
: heat release capacity ($J/(kg \cdot K)$)
k_i
: rate constant for kinetic process, where i = initiation, branching, gasification, charring, etc (s^{-1})
κ
: thermal conductivity ($W/(m \cdot K)$)
L_g
: latent heat of gasification per unit mass of volatile fuel (J/kg)
LOI
: limiting oxygen index/concentration of oxygen at extinction (dimensionless)
$\dot{m}''_a$
: mass flux of air ($kg/(m^2 \cdot s)$)
$\dot{m}''_f$
: mass flux of fuel gases ($kg/(m^2 \cdot s)$)
M_i
: molar mass of substance, where i = fuel gases, oxygen, monomer, chemical group, etc (kg/mol)
μ
: mass fraction of char or inert residue after burning or pyrolysis (dimensionless)
n_i
: number of moles of substance i
$\dot{q}''_{ext}$
: external heat flux from fire or radiant heater (W/m^2)
$\dot{q}''_{flame}$
: heat flux to surface from flame by convection and radiation (W/m^2)
$\dot{q}''_{loss}$
: rate of heat loss from surface per unit area (W/m^2)
$\dot{q}''_{net}$
: net heat flux to surface (W/m^2)
$\dot{q}''_{rerad}$
: heat flux reradiated to environment from surface (W/m^2)
Q'''
: heat of combustion per unit volume (energy density) for ignition in air, =1.9 MJ/m^3
$\dot{Q}'''$
: heat of combustion per unit volume per unit time (power density) at ignition
R
: gas constant, =8.314 $J/(mol \cdot K)$
ρ
: mass density (kg/m^3)
σ
: stefan–boltzmann constant, $= 5.7 \times 10^{-8}$ $W/(m^2 \cdot K^4)$
SEA
: smoke extinction area (m^2/kg)

t_{ign}
: time to ignition (s)
T_{a}
: ambient temperature (K)
T_{f}
: flame temperature (K)
T_{ign}
: ignition temperature (K)
T_{p}
: pyrolysis temperature (K)
T_0
: standard temperature = 298 K ≈ room temperature
$Y_{\text{d},1/2}$
: molar thermal decomposition function ((kg · K)/mol)
Ψ_i
: molar group contribution to the heat release capacity (J/(mol · K))

Encyclopedia of Polymer Sceince and Technology
Copyright © 2005 John Wiley & Sons, Inc. All rights reserved.

IONIC LIQUIDS, POLYMERIZATION IN

Introduction

The first room temperature ionic liquid (RTIL), $[EtNH_3][NO_3]$ (mp 12°C), was reported in 1914 (1), and since then a great deal of research effort has been exerted to exploit possible applications of these compounds. Initially, RTILs were used mainly as electrolytes in batteries or for metal electrodeposition; however, nowadays they are finding an ever increasing range of applications.

Ionic liquids may be viewed as molten salts and are liquids containing only cations and anions at ambient or near ambient (<100°C) temperature. They exhibit a relatively wide electrochemical window, good electronic and ionic conductivities, a broad range of room temperature liquid compositions, and may have negligible vapor pressure, and excellent chemical, thermal, air and moisture stability (2–6). They are composed of weakly coordinating anions, for example, BF_4^- and PF_6^- and, hence, are highly polar yet noncoordinating solvents. Most imidazolium and pyridinium ionic liquids have polarities similar to those of small molecule alcohols (7,8). Their hydrophilicity/lipophilicity is tunable by varying the combination of cations and anions. Thus, RTILs have been referred to as "designer solvents" (9), and millions of different RTILs could potentially be synthesized and optimized for specific applications. Depending on their structures, RTILs are able to dissolve a variety of organic, inorganic, and organometallic compounds. Their ease of handling, low vapor pressures, and potential for recycling make them promising potentially environmentally benign reaction media to replace volatile molecular solvents in both the chemical industry and in academic research.

Furthermore, RTILs have limited miscibility with some common organic solvents but high compatibility with transition metals. As a consequence, a biphasic or phase-separable (organic/RTIL biphasic systems) catalysis concept can be developed in which a homogeneous catalyst is immobilized in one liquid phase (RTIL) and the reactants and/or products reside largely in another liquid phase (organic) (10), thus enabling easy product and catalyst separation with the retention of the transition metal catalyst in an ionic liquid phase. Various common organic reactions employing metal catalysts have been conducted by employing ionic liquids as alternative reaction media, including Diels-Alder reactions (11), Friedel-Crafts reactions (12), hydrogenations (13), hydroformylations (14), alkylations (15), dimerizations (16), Heck reactions (17), Suzuki couplings (18), Sonogashira couplings (19), ring-closing olefin metathesis reactions (20), alcohol oxidations (21), and nucleophilic substitutions (22).

	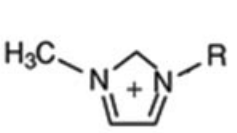	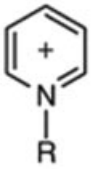	$^{+}NR_3R'$
Cl^-	Easy to synthesize, hydrophilic	Easy to synthesize, hydrophilic	Inexpensive, hydrophilic
NO_3^-	Anion can produce reactive RTIL	Hydrophilic	Inexpensive, hydrophilic
PF_6^-	High thermal stability	Less thermally stable	Dopant RTIL to decrease cost
$N(CF_3SO_2)_2^-$	Low viscosity, hydrophobic, expensive	Hydrophobic	Low viscosity

Fig. 1. Matrix of RTIL cations and anions.

Some typical RTILs and how structure affects properties are shown in Figure 1. Representative common cations and anions used to prepare RTILs are shown in Figure 2. RTILs are commercially available from ACROS Organic (Fisher Scientific, UK), Chemada Fine Chemicals (Israel), Covalent Associates (Boston, Mass.), C-TRI (Korea), CYTEC (Canada), Sigma-Aldrich (US), BASF (US), Merck KGaA (Germany), QUILL (UK), Sachem (Austin, Tex.), Scionix (UK), and Solvent-Innovation (Germany).

Ionic Liquids for Polymerization

One of the earliest examples of polymerization in RTILs was reported in 1990 in a Lewis acidic ionic liquid: $AlCl_3$-1-ethyl-3-methylimidazolium chloride [EMIM]Cl

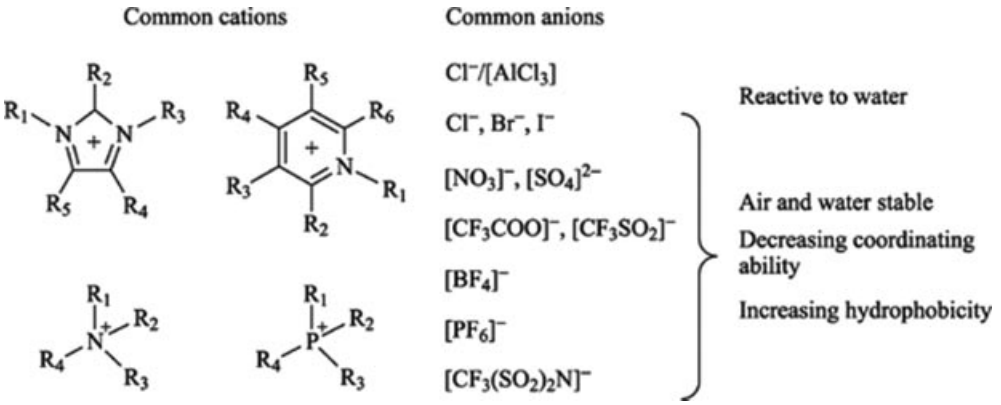

Fig. 2. Representative common cations and anions used to prepare room temperature ionic liquids.

(23). It was found that the combination of $TiCl_4$ and $AlEthylCl_2$ in $AlCl_3$/[EMIM]Cl can be catalytically active for ethylene polymerization, although the yield of polyethylene (PE) was low. This work opened a new route for making polymers using RTILs as alternative reaction media. Later, replacing $TiCl_4$ with Cp_2TiCl_2 was shown to give higher yields of PE using the same RTIL (24). More examples of related work on using ionic liquids for polymerization or oligomerization of olefins can be found in the literature and in patents (25,26). It was believed that the active sites are cationic alkyl–metal complex generated by the interaction of added transition metal catalyst with alkylaluminum moieties present in the ionic liquids via halogen abstraction and alkylation. The electrochemical polymerization of benzene in various ionic liquids has been described as a method for synthesis of poly(*p*-phenylene) (27). In these studies, ionic liquids were used mainly as convenient electrolytes. Carlin and Osteryoung produced a new electroactive material by electrochemical oxidation of triphenylsilyl chloride (Ph_3SiCl) in the acidic ionic liquid ($AlCl_3$-[EMIM]Cl) (28). The film formed exhibited reversible redox behavior and was electronically conducting in the oxidized state by incorporation of the cation of the ionic liquid into the film. However, most of the RTILs mentioned above are the 1st generation ionic liquids, which are haloaluminate-based ionic liquids and thus easily undergo hydrolysis to form undesirable HCl by-products.

Free Radical Polymerization

Free radical polymerization is extensively used for the synthesis of a variety of polymeric materials due to its versatility, synthetic ease, and compatibility with a wide variety of functional groups, which is also coupled with its tolerance to water and protic media. However, conventional free radical polymerization has a significant drawback, which is related to the reactivity of the propagating free radical chain ends and their propensity to undergo a variety of termination and chain transfer reactions. The materials obtained are therefore polydisperse with limited control over molecular weight and architecture. Ionic polymerizations (anionic or cationic) were for many years the only "living" polymerization techniques available that achieved efficient control over the structure and architecture of vinyl polymers. Although these techniques can generate polymers with low polydispersity, controlled molecular weight, and control over chain ends and macromolecular architectures, they are not suitable for the polymerization and copolymerization of many vinylic monomers. This limitation is due to the incompatibility of the growing polymer chain ends (carbanion or carbocation) with numerous functional groups and certain monomer families. In addition, stringent reaction conditions, including the use of ultrapure reagents and the need for total or near-total exclusion of water and oxygen, limit the widespread commercial use of these techniques. These challenges spurred polymer chemists to develop new concepts which allow a living or controlled polymerization using special free radical polymerization techniques. As a consequence, nitroxide-mediated polymerization (NMP), atom transfer radical polymerization (ATRP), and radical addition-fragmentation and transfer (RAFT) were developed. The general strategy behind these processes is the reversible termination of the growing polymeric chain with a mediating radical to reduce the overall concentration of the propagating radical chain ends.

In the absence of other reactions leading to initiation of new polymer chains (ie, no reaction of the mediating radical with the vinylic monomer), the concentration of reactive chain ends is extremely low, minimizing irreversible termination reactions, such as combination or disproportionation. All chains would thus be initiated only from the desired initiating species, and growth should occur in a living fashion, allowing a high degree of control over the entire polymerization process with well-defined polymers being obtained (29).

Although polymerization in moisture-sensitive ionic liquids has certain advantages when compared to traditional solvents, little polymerization work was done in RTILs until the introduction of the 2nd generation of air, moisture, and thermally stable, neutral ionic liquids, composed of dialkylimidazolium cations and PF_6 or BF_4 anions. In spite of the fact that these ionic liquids are anticipated to be potentially useful solvents for ionic polymerization due to their highly polar nature, the first report of polymerization in the new nonhygroscopic ionic liquids was based on a free radical polymerization process—atom transfer radical polymerization (ATRP). Carmichael and co-workers (30) observed first-order kinetic behavior over a wide range of reaction temperatures using ethyl-2-bromoisobutyrate initiator and CuBr/*N*-propyl-2-pyridylmethanimine as the catalyst pair in a 50/50 (V/V) MMA/[BMIM]PF_6 system. The reactions are faster as compared to those in common solvents, while the polydispersities (M_w/M_n, where M_w is weight-average molecular weight and M_n is number-average molecular weight) are narrow: 1.30–1.43. By extraction with toluene, the polymer can be separated from the solution while copper catalyst remains in the ionic liquid phase, which facilitates catalyst re-use by adding fresh monomer. The use of the RTIL medium also eliminated the need for postpurification to eliminate toxic copper salts, which entails passing the polymer solution through purification columns. Carmichael and co-workers attributed this polymerization behavior to the increased polarity of ionic liquids, because a similar increase in the rate has been observed with other polar/co-ordinating solvents. In a recent communication (31), Hong and co-workers reported large increases in both the rate of polymerization and the molecular weights that were obtained in the polymerizations of methyl methacrylate (MMA) in [BMIM]PF_6 as compared to identical polymerizations carried out in conventional organic solvents. These dramatic increases were believed to be at least in part because of the high viscosity of the polymerization media. Thus, a "diffusion-controlled termination" mechanism was proposed to explain the diminished chain terminations in such a viscous system, which would account for a simultaneous increase in both rate of polymerization and degree of polymerization. Very recently, Benton and Brazel (32) reported similar behavior, high molecular weights and rapid polymerization rates, for MMA in [BMIM]PF_6. Harrison and co-workers (33) used a pulse laser polymerization (PLP) technique to polymerize MMA in [BMIM]PF_6, which is the IUPAC-recommended standard procedure for measuring the rate constant of propagation (k_p). They found that both the propagation and termination rates were significantly affected by [BMIM]PF_6. They attributed the increase of the propagation rate to the increased polarity of the ionic liquid solution, which lowers the activation energy of propagation through charge-transfer interactions. The termination rate is decreased simply because of the increased viscosity of the polymerization medium. Both an increase of k_p and decrease of k_t contribute a roughly ten-fold increase of overall rate of polymerization. Quite

recently, Cheng and co-workers (34) reported free radical polymerization of acrylonitrile in [BMIM]BF_4 using AIBN as initiator. These workers also note that ionic liquids are excellent media for achieving high molecular weight polymers. They attribute this result to low chain transfer constants for RTILs and the ability of these solvents to stabilize the growing radical chain ends.

Clearly most of the early studies on polymerization in RTILs used [BMIM]PF_6 as the medium. This was largely due to the commercial availability and easy synthesis of this material. However, [BMIM]PF_6 can readily hydrolyze to release toxic HF as a by-product, and there is an ever increasing focus on the use of more benign RTILs in polymer systems. Zhang and co-workers (35) measured the polarity and viscosity of over a dozen RTILs based upon a wide range of cations and anions, and attempted to correlate these physical data with the *low conversion* conventional free radical polymerization behavior of styrene and MMA in these RTILs. This study revealed no obvious trends between polarity or viscosity of RTILs and polymerization rate or molecular weight of the formed polymer. At around the same time, Strehmel and co-workers (36) reported that the higher the viscosity of the RTIL, the higher the yields and molecular weights of the polymers. However, unlike in the work by Zhang and co-workers, these workers carried their polymerizations to high (near quantitative) conversions, where the Trommsdorff effect strongly impacts polymerization behavior. Clearly, the higher viscosities will affect polymerization behavior in this regime and make it difficult to ascertain polymerization behavior in the non-Trommsdorf regime. The RTILs employed in this latter study were composed of cations and anions of similar structures except the alkyl length and positions on the cation, while either cations or anions are structurally different in the former case. In our opinion, it is still too early to make a conclusion regarding the effects of polarity and viscosity of the RTIL on polymerization behavior. It would be very interesting to repeat the experiments of Strehmel and co-workers (36) but keep conversions low. The polarity of molecular solvents is a complex of many interactions including: H-bonding, π-interaction, or van der Waals forces. In RTILs, the situation is even more complicated since both cations and anions may have their own distinct interactions. Zhang and co-workers used solvatochromic dye (Nile red) to measure the polarities of RTILs and the results had similar trend as those in Reference (37). Since Nile red is a positively solvatochromic, it preferentially interacts with anions of RTILs. The apparent polarities deduced may be not reflect the real values, thus further experiments need to be carried out to address this problem. In addition, the polymers synthesized in RTILs all have similar glass transition temperatures and microstructures as compared to those obtained in benzene or in bulk, based upon thermal analysis and ^{13}C NMR experiments (38).

Biedroń and co-workers (39) reported heterogeneous ATRP in [BMIM]PF_6. Alkyl acrylates (methyl, butyl, hexyl, and dodecyl) are either soluble, partly soluble, or completely insoluble in this RTIL depending on the length of the alkyl substituent. For the heterogeneous systems, the alkyl acrylate formed an upper monomer phase while the CuBr/pentamethyldiethylenetriamine (PMDETA) catalyst remained in the lower RTIL phase. Methyl acrylate (MA) and poly(methyl acrylate) (PMA) are miscible with [BMIM]PF_6 and form a homogeneous polymerization system, therefore, all reactions proceed in one phase. For the three other acrylates, the growing macromolecular chains react with the monomer at the

interface but reside predominantly in the monomer phase. In all cases, the reactions were living radical polymerizations. The advantages of heterogeneous ATRP are easy separation of polyacrylate from the RTIL phase after reaction, with less copper catalyst contamination and reduction of side reactions due to the absence of catalyst in the upper monomer phase, as compared to bulk ATRP. It was found that using a chiral RTIL (1-(*R*-(+)-2′-methylbutyl)-3-methylimidazolium hexafluorophosphate) could impact the stereoregularity of polymer produced by ATRP (40).

Sarbu and co-workers (41) used different catalyst systems (iron or copper halides) to successfully carry out ATRP in a range of 1-butyl-3-methylimidazolium ionic liquids. In iron-mediated ATRP, no additional ligand was required to achieve a controlled polymerization of MMA although both initiation rates and rates of reaction were low. Systems without organic ligands were effective only in a phosphonate ionic liquid for copper-mediated ATRP of MMA, while a ligand was required in ionic liquids with halide or carbonate anions. ATRP in ionic liquids proceeds with low initiation efficiency. This has been attributed to the high concentration of the catalyst in the RTIL phase, into which the small initiators can easily diffuse and thus generate high concentration of free radicals. The free radical can undergo irreversible termination and cause the low initiation efficiency. However, initiator efficiency can be improved by employing macroinitiators, which have little tendency to diffuse into the RTIL phase. In addition, the catalyst can be regenerated after removal of polymer and unreacted monomer.

Reversible atom transfer radical polymerization of MMA in [BMIM]PF_6, [BMIM]BF_4, and [DMIM]BF_4 (1-dodecyl-3-methylimidazolium tetrafluoroborate) has been described (42). In [BMIM]PF_6, the reverse ATRP of MMA was achieved with 2,2′-azobisisobutyronitrile (AIBN)/$CuCl_2$/2,2′-bipyridine initiation system, in which the system is homogeneous throughout the reaction. Due to a cage effect with ionic liquids molecules, the termination of the primary radicals through decomposition of AIBN might occur before they can initiate polymerization, which accounts for the low initiation efficiency of AIBN. The Cu catalyst is also soluble in the ionic liquid. As a consequence of both factors, less catalyst is needed to effectively mediate the polymerization process in ionic liquids than in other reverse ATRPs. The ionic liquids and catalyst can be recovered and reused.

Zhang and co-workers (43) used both a bimolecular initiation system (benzoyl peroxide (BPO) + 2,2,6,6-tetramethylpiperidine 1-oxyl (TEMPO)) and a universal initiator system (2,2,5-trimethyl-3-(1-phenylethoxy)-4-phenyl-3-azahexane (TMPPAH)) for the attempted nitroxide-mediated polymerization of MMA and St. Polymers were produced but polymerizations were not living/controlled for either monomer. Possible reasons are the low diffusion rates of mediating radicals and slow degradation of free TEMPO at elevated temperatures in the presence of [BMIM]PF_6. Ryan and co-workers (44) demonstrated a controlled/living nitroxide-mediated polymerization of MA in 50% V/V of [HMIM]PF_6 initiated by the initiator pair AIBN + 4-oxo-2,2,6,6-tetramethyl-1-piperidinyl-*N*-oxyl (4-oxo-TEMPO) at 140°C–155°C. The reaction rates under these conditions were greater than for similar reactions conducted in anisole. In both of these studies, self-polymerization (thermal polymerization) was observed because of the high temperatures used. Other kinds of living free radical polymerization, such as RAFT and charge transfer polymerization, have also been reported in RTILs (45).

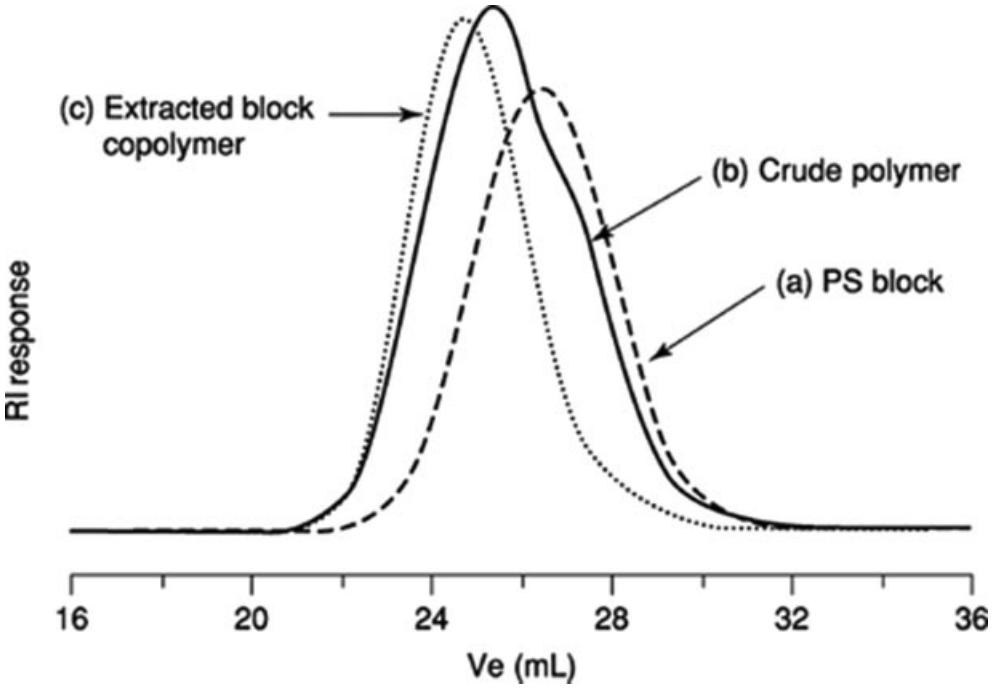

Fig. 3. SEC traces of (a) PS block from BPO in [BMIM]PF6, (b) PS-*b*-PMMA before extraction, and (c) PS-*b*-PMMA after extracting with cyclohexane and acetonitrile.

Combined with CuBr/PMDETA catalyst, dendritic polyarylether 2-bromoisobutyrates (G*n*-Br, n=1–3) can be used as effective macroinitiators for ATRP of *N*-hexylmaleimide and styrene in [BMIM]PF_6 at lower temperature than in anisole. The afforded polymers had well-defined molecular weights and low polydispersities ($1.18 < PDI < 1.36$) (46). The two monomers showed a stronger tendency to form alternating structures in RTILs as compared to polymerizations conducted in anisole.

Limited solubility of some monomers and polymers in ionic liquids presents opportunities to make diblock copolymers by sequential addition polymerization. Zhang and co-workers (47) demonstrated the formation of PSt-b-PMMA by sequential addition in [BMIM]PF_6 through conventional free radical polymerization using benzoyl peroxide (BPO) as initiator. St was polymerized first and the polymer gradually precipitated out when the conversion reached around 50% due to the insolubility of PSt in [BMIM]PF_6. The chain coils wrapped the macroradicals inside resulting in prolonged lifetimes because of diminished termination. Unreacted St monomer was pumped out on a high vacuum line. After adding the second monomer (MMA), diblock copolymers were formed at room temperature although the re-initiation was not 100% (see Figure 3). Reversal of the polymerization sequence only afforded homopolymer, PMMA. Kubisa and co-workers used a similar strategy to produce PBA-b-PMA and PMA-b-PBA block copolymers (PBA is poly(butyl acrylate) by different sequences of addition of monomers using the ATRP method in the same ionic liquid (48). They found that when conversion of

MA, used as first monomer, exceeded 70%, a significant percentage of dead PMA chains contaminated the final diblock copolymer. Conversely, when MA was added to the solution of PBA in [BMIM]PF_6, "clean" diblock was formed, essentially free of homopolymer, and BA can be polymerized to complete conversion. Ma and co-workers (42,49) also described successful synthesis of block copolymers, where St was polymerized by chlorine-end-capped PMMA as macroinitiator through reverse ATRP in [BMIM]PF_6, [BMIM]BF_4, and [C_{12}MIM]BF_4.

The effect of solvents on reactivity ratios and sequence length distributions for free radical polymerization has been extensively studied. The calculated reactivity ratios of St and MMA ($r_{St} = 0.381 \pm 0.02$ and $r_{MMA} = 0.464 \pm 0.02$) in [BMIM]PF_6 by nonlinear method (CONTOUR computer program (50)) are significantly different from those ($r_{St} = 0.54 \pm 0.04$ and $r_{MMA} = 0.50 \pm 0.04$) in benzene at 60°C (51). The "boot-strap" model (52), polarity of the solvents, interaction between solvent and monomers (eg solvent–monomer complex), viscosity and system heterogeneity all possibly contribute to the different reactivity ratios in RTILs and in benzene.

[BMIM]PF_6 was found to be an efficient plasticizer for PMMA, prepared by *in situ* radical polymerization in this ionic liquid (53). The polymers have physical characteristics comparable with those containing traditional plasticizers (phthalates, adipates, and trimellitates) and retain greater thermal stability. RTILs are normally used as inert solvents for polymerization. However, Mays and co-workers discovered that polymerization of MMA can be carried out at ambient temperature in the ionic liquid trihexyl-tetradecyl-phosphonium bis(2,4,4-trimethylpentyl)phosphinate ([H_3TDP] [$(PM_3)_2$P]) via a redox-initiated polymerization mechanism (54). The cation of [H_3TDP][$(PM_3)_2$P] apparently reacts with BPO in a redox reaction, with the cation as reductant and BPO as oxidant. The generated radical efficiently initiated polymerization at room temperature to produce PMMA with high yield and high molecular weight.

Ionic Polymerization

Living anionic polymerization usually gives narrower molecular weight distribution polymers as compared to those obtained by living free radical polymerizations. These polymerizations can proceed to complete conversion with far fewer side reactions such as termination and chain transfer. The ability to introduce terminal functional groups by using selective termination agents is an additional advantage of anionic polymerization. On the other hand, the stringent purification requirements for living anionic polymerization put some limits on the commercial synthesis of polymers using this method. Even though RTILs are in some ways ideal potential solvents for ionic polymerizations, because the RTIL can possibly help to stabilize the growing carbanions or carbocations due to their ionic nature, there are no reports in the literature on anionic polymerization in ionic liquids. This is primarily because it is very difficult to adequately purify ionic liquids to the standards required for anionic polymerizations. Our preliminary data (not yet published) indicate that termination occurs due to impurities in the RTIL. Vijayaraghavan and co-workers (55) reported the first case of cationic polymerization of styrene in *N*-butyl-*N*-methylpyrrolidinium bis(trifluoromethanesulfonyl)amide

([P_{14}][Tf_2N]). The cationic initiator used was a Brønsted acid: bis(oxalato)boric acid (HBOB). The polymerization proceeded in a living manner but the reaction temperature was high (60°C). PSt produced had low molecular weights (1300–1700) and moderate polydispersities (1.3–1.5). The author suggested that RTILs might promote the dissociation of the acid that can efficiently initiate polymerization. Biedron and Kubisa (56) conducted cationic polymerization of styrene in [BMIM]PF_6 with a 1-phenetyl chloride/$TiCl_4$ initiating system. Polymers were obtained but chain transfer was significant, resulting in a lack of control over molecular weight and molecular weight distribution.

Ring-Opening Polymerization

Ring-opening metathesis polymerization of norbornene using cationic allenylidene precatalys, [(*p*-cymene)RuCl(Pcy_3)(=C=C=CPh_2)][OTf], in a biphasic medium, (1-butyl-2,3-dimethylimidazolium hexafluorophosphate ([BDMIM]PF_6)/toluene), was carried out (57). The catalyst was in the ionic liquid phase, and the upper toluene phase dissolved the polymer that was formed. Both the ionic liquid and catalyst could be reused up to six times without significant loss of catalytic activity and with quantitative yields of polymer. After reloading of catalyst, the catalyst system can still be re-used up to five times. The enhanced recycling capabilities as compared to other alkylidene catalysts were attributed to the ionic character of the cationic allenylidene complex, while the other systems gradually lost their catalytic abilities within three successive runs.

Biedroń and co-workers (58) presented the results of the cationic ring opening polymerization of 3-ethyl-3-hydroxymethyloxetane in the most common hydrophilic ionic liquid, [BMIM]BF_4, using the BF_3-Et_2O initiation system. The advantage of carrying out this reaction in ionic liquids over solution or bulk polymerizations is the high reaction temperature that can be used (up to 180°C because intermolecular hydrogen bonding that leads to the formation of aggregates is reduced at the elevated temperature). The intramolecular H-bonding, facilitating intramolecular chain transfer, is not significantly affected. The multihydroxyl, branched structure was preserved, and the molecular weights of the polymers were in the same range as those made in organic solvents or in bulk. On the contrary, the application of ionic liquids can also help to reduce the reaction temperature. At higher temperatures, side reactions may be significant. Polycarbonate made by ring opening polymerization of ethylene carbonate experiences decarboxylation when the reaction is carried out at 180–200°C (59). In acidic ionic liquids such as [BMIM]Cl-$AlCl_3$ or [BMIM]Cl-$SnCl_2$, the reaction can take place at temperatures of 100–120°C depending on the ionic liquid used. The drawback of these new reaction systems is that decarboxylation was still not negligible, and low levels of ethylene carbonate polymers were formed.

Enzyme-Catalyzed Polymerization

Candida Antarctica lipase (lipase CA) catalyzed formation of biodegradable polyesters in [BMIM]PF_6 and [BMIM]BF_4 has been reported (60). Ring-opening

polymerization of ε-caprolactone and polycondensation of dicarboxylic acid diesters with 1,4-butanediol were examined. Higher molecular weight products and improved conversions suggest the potential for green polymer chemistry by the combination of nontoxic enzyme catalyst, mild reaction conditions with potentially environmentally benign solvents.

Condensation Polymerization

Polyimides and polyamides are important materials due to their attractive thermal, mechanical, and electrical properties. Usually, the synthesis of high molecular weight polyimides in organic solvents requires high temperatures and the presence of an acidic catalyst. Vygodskii and co-workers (61) studied the condensation polymerization behavior in RTILs composed of different anions and cations. High molecular weight polyimides and polyamides were obtained using RTILs as novel reaction media, without addition of catalyst.

Transition-Metal Catalyzed Polymerization

Poly(phenyl-acetylene) (PPA) is a conjugated polymer with interesting photoconductivity, photoluminescence, nonlinear optical, and membrane properties. It can be obtained by different polymerization methods including radical, cationic, metathesis catalyst or Ziegler–Natta polymerizations. High molecular weight PPA can also be obtained by Rh(I) catalyzed phenylacetylene polymerization in ionic liquids such as *n*-butylpyridinim tetrafluoroborate ([bupy]BF_4) or [BMIM]PF_4 (62). The catalyst used was either (diene)Rh(acac) or [(diene)$RhCl_2$]$_2$, and the cocatalyst used was triethylamine. The polymer was separated from the ionic liquid using either extraction with toluene or filtration by adding methanol into ionic liquids to form a suspension of PPA in the solvent mixture methanol/RTIL. Extraction usually facilitates catalyst recycling, but cannot permit the maximum product recovery. While more polymers can be recovered through the filtration method, the Rh(I) complex solution after filtration shows no catalytic activity. The molecular weights ranged from 55,000 to 200,000.

Rogers and co-workers (63) used 1-hexylpyridinium bis(trifluoromethanesulfonyl) imide ([C_6Pyr][NTf_2])/methanol as a solvent pair for palladium-catalyzed alternating copolymerization of styrene and carbon monoxide, in which the palladium catalyst was L$Pd(OAc)_2$ (L=2,2′-bipyridine and 1,10-phenanthroline). [C_6Pyr][NTf_2] and catalyst can be recycled, and the yields and molecular weights were higher as compared to those obtained when the polymerization was carried out in methanol alone. Furthermore, the catalyst stability and propagation rate were improved due to the inhibited chain transfer and catalyst decomposition in [C_6Pyr][NTf_2].

Electrochemical Polymerization

Electrochemical polymerization is a major method to synthesize conducting polymer for potential application in energy storage devices, electrochromic devices,

and light-emitting diodes. This process shows some advantages over chemical synthesis including faster reactions, simple procedures, generation of the polymer in the doped state, and easy control of the film thickness. Naudin and coworkers (64) have used ionic liquids for the electrochemical polymerization of poly(3-(4-fluorophenyl)thiophene) (PFPT). The electrochemical behavior was similar to that in common nonaqueous electrolyte. However, X-ray photoluminescence spectroscopy revealed the presence of some ionic liquid residue in the formed film. Other kinds of conjugated polymers such as polypyrrole, polyaniline, and unsubstituted polythiophene were also synthesized in ionic liquid (65).

Other Applications of Ionic Liquids in Polymers Systems

Polyaniline nanoparticles with diameters from about 30–80 nm can be fabricated by interfacial polymerization at the interface between aqueous media and RTILs (66). Electronic devices such as electrochemical mechanic actuators have improved cycle life and larger generated strain using [BMIM]PF_6, [BMIM]BF_4, or [BMIM][NTf_2] as electrolytes as compared to traditional organic or aqueous solvents, because ionic liquids have high ion conductivity, large electrochemical windows, and fast ion mobility (67). Single-ion conductive membrane material, made out of polymerizable ionic liquids by incorporating some ethylene oxide spacer cross-linkers, has high ionic conductivity (1.37×10^{-4} S cm^{-1}), and the film formed is transparent and free standing (68). In order to overcome migration of ions of RTILs along with potential gradient with target ions in membrane application, poly(VdF-co-HFP) containing zwitterionic ionic liquids was reported as a new polymer gel electrolyte which only transports target ions (69). RTILs have been used as porogens in cross-linked polymer systems formed by free radical polymerization of cross-linking monomers (70). RTILs are also effective solvents for regenerating cellulose via the aid of microwave irradiation (71). Forming hydrogen-bonding between hydroxyl functions on the polymer chains and anions of RTILs such as Cl^-, Br^-, and SCN^-, which are hydrogen bond acceptors, can break the intermolecular hydrogen bonding between linear glucose polymer chains. A recent review on application of ionic liquids in polymerization is available in the literature (72).

Conclusions

Room temperature ionic liquids have proved over recent years to be useful and unique reaction media for a variety of chemical reactions. Some potential benefits of working with RTILs as solvents for polymerization are wide and varied (Table 1):

Faster reaction rates and better selectivities are often observed in RTILs as compared to those in common organic solvents. In addition to these advantages, the nonvolatility, nonflammability, and recycling potential also help RTILs become a preferred alternative reaction medium to meet environmental and other requirements. Although polymerization in 1st generation RTILs was not very attractive when compared to similar reactions carried out in organic solvents, the 2nd generation RTILs are showing much greater promise. This is evidenced by

Table 1. Potential Benefits of Polymerization in RTILs

• Ability to rapidly generate high molecular weight polymers with low residual monomer
• Simplified methods to synthesize complex molecular architectures such as block- and graft copolymers, and copolymers with new monomer sequences, as compared with more complicated techniques such as anionic, cationic and living radical polymerization
• Ability to design reactions to be carried out at much higher temperatures, as RTIL volatility is much lower and thermal stability is much higher than traditional solvent
• Improvement in polymer physical properties, such as tensile strength, elastic modulus and impact strength, based on the reaction mechanism in RTILs
• Ability to work with biological components in a nondenaturing environment during reactions that incorporate enzymes, proteins, and other biologically active agents into polymer networks.

the increasing number of papers published in this area every year, and interesting and important discoveries. When conventional free radical polymerizations are carried out in RTILs, there is an increase in the propagation rate due to the high polarity of the RTIL and a decrease in the termination rate because of the high viscosity of the RTILs, and thus the overall reaction rate is greatly increased. For living/controlled polymerization such as ATRP, the reactions in RTILs are still controllable with faster reaction rates and easy separation of catalysts and/or ligands from the resulting polymers. Several other polymerization processes have been conducted in RTILs, with the notable exception of anionic polymerization, which needs careful work in order to find the right RTILs, purification techniques, and polymerization conditions.

BIBLIOGRAPHY

1. P. Walden, *Bull. Acad. Imper. Sci. (St. Petersburg)* 1800 (1914).
2. C. L. Hussey, *Pure Appl. Chem.* **60**, 1763–1772 (1988).
3. K. R. Seddon, in G. Mamantov and R. Marassi, eds., *Molten Salt Chemistry*, Reidel Publishing Co., Dordrecht, The Netherlands, 1987, p. 365.
4. J. S. Wilkes, J. A. Levisky, R. A. Wilson, and C. L. Hussey, *Inorg. Chem.* **21**, 1263–1264 (1982).
5. C. L. Hussey, in G. Mamantov and C. Mamantov, eds., *Advances in Molten Salts Chemistry*, Vol. 5, Elsevier Science Publishing Co., New York, 1983, pp. 185–230.
6. (a) M. K. Dieter, C. J. Dymek Jr., N. E. Heimer, J. W. Rovang, and J. S. Wilkes, *J. Am. Chem. Soc.* **110**, 2722 (1988); (b) J. S. Wilkes and M. J. Zaworotko, *J. Chem. Soc., Chem. Commun*. 965–967 (1992); (c) H. L. Ngo, K. LeCompte, L. Hargens, and A. B. McEwen, *Thermochim. Acta* **357–358**, 97–102 (2000).
7. S. N. V. K. Aki, J. F. Brennecke, and A. Samanta, *Chem. Commun*. 413 (2001).
8. H. Zhang, K. Hong, and J. W. Mays, in *Abstract of Papers, ACS 227th National Meeting*, Anaheim, CA, USA, 2004.
9. M. Freemantle, *Chem. Eng. News* 32 (Mar. 30, 1998); 37 (May 15, 2000); 21 (Jan. 1, 2001); 26 (May 3, 2004).
10. B. Cornils and W. A. Herrmann, in B. Cornils and W. A. Herrmann, eds., *Applied Homogeneous Catalysis with Organometallic Compounds*, Weinheim, New York, 1996, Chap. 4.1, p. 1167.

11. T. Fischer, A. Sethi, T. Welton, and J. Woolf, *Tetrahedron Lett.* **40**, 793 (1999).
12. A. Stark, B. L. MacLean, and R. D. Singer, *J. Chem. Soc., Dalton Trans.* 63 (1999).
13. Y. Chauvin, L. Mussmann, and H. Olivier, *Angew. Chem. Int. Ed.* **34**, 2698 (1995).
14. C. P. Mehnert, R. A. Cook, N. C. Dispenziere, and M. Afeworki, *J. Am. Chem. Soc.* **124**, 12932 (2002).
15. M. Badri, J. J. Brunet, and R. Perron, *Tetrahedron Lett.* **33**, 4435 (1992).
16. (a) J. E. L. Dullius, P. A. Z. Suarez, S. Einloft, R. F. de Souza, J. Dupont, J. Fischer, and A. De Cian, *Organometallics* **17**, 815 (1988); (b) S. M. P. Silva, A. Z. Suarez, R. F. de Souza, and J. Dupont, *Polym. Bull.* **40**, 401 (1998).
17. D. E. Kaufmann, M. Nouroozian, and H. Henze, *Syn. Lett.* 1091 (1996).
18. (a) C. J. Mathews, P. J. Smith, and T. Welton, *Chem. Commun.* 1249 (2000); (b) R. Rajagopal, D. V. Jarikote, and K. V. Srinivasan, *Chem. Commun.* 616 (2002); (c) J. McNulty, A. Capretta, J. Wilson, J. Dyck, G. Adjabeng, and A. Robertson, *Chem. Commun.* 1986 (2002).
19. (a) S. B. Park, H. Alper, *Chem. Commun.* 1306 (2004); (b) T. Fukuyama, M. Shinmen, S. Nishitani, M. Sato, and I. Ryu, *Org. Lett.* **4**, 1691 (2002).
20. (a) Q. Yao and Y. Zhang, *Angew. Chem. Int. Ed.* **42**, 3395 (2003); (b) N. Audic, H. Clavier, M. Mauduit, J. C. Guillemin, *J. Am. Chem. Soc.* **125**, 9248 (2003).
21. I. A. Ansari and R. Gree, *Org. Lett.* **4**, 1507 (2002).
22. D. Kim and D. Chi, *Angew. Chem. Int. Ed.* **43**, 483 (2004).
23. R. T. Carlin, R. A. Osteryoung, J. S. Wilkes, and J. Rovang, *Inorg. Chem.* **29**, 3003 (1990).
24. R. T. Carlin and J. S. Wilkes, *J. Mol. Catal.* **63**, 125 (1990).
25. (a) M. F. Pinheiro, R. S. Mauler, and R. F. de Souza, *Macromol. Rapid Commun.* **22**, 425 (2001); (b) P. Wasserscheid, C. M. Gordon, C. Hilgers, M. J. Muldoon, and I. R. Dunkin, *Chem. Commun.* 1186 (2001); (c) O. Stenzel, R. Brüll, U. M. Wahner, R. D. Sanderson, and H. G. Raubenheimer, *J. Mol. Catal. A: Chem.* **192**, 217 (2003).
26. (a) EP 558187 (1993), P. W. Ambler, P. K. G. Hodgson, and N. J. Stewart; (b) WO 9521871 (1995), A. A. K. Abdul-Sada, P. W. Ambler, P. K. G. Hodgson, K. R. Seddon, and N. J. Stewart; (c) EP 791643 (1997), P. M. Atkins, M. R. Smith, and B. Ellis; (d) WO 0032658 (2000), V. Murphy.
27. (a) V. M. Kobryanskii and S. A. Arnautov, *J. Chem. Soc., Chem. Commun.* **9**, 727 (1992); (b) V. M. Kobryanskii and S. A. Arnautov, *Makromol. Chem.* **193**, 455 (1992); (c) D. C. Trivedi, *J. Chem. Soc., Chem. Commun.* **544** (1989); (d) S. A. Arnautov, *Synth. Met.* **84**, 295 (1997); (e) L. M. Goldenberg, R. A. Osteryoung, *Synth. Met.* **64**, 63 (1994).
28. R. T. Carlin and R. A. Osteryoung, *J Electrochem. Soc.* **141**, 1709 (1994).
29. (a) C. J. Hawker, A. W. Bosman, and E. Harth, *Chem. Rev.* **101**, 3661 (2001); (b) M. Kamigaito, T. Ando, and M. Sawamoto, *Chem. Rev.* **101**, 3689 (2001); (c) K. Matyjaszewski and J. Xia, *Chem. Rev.* **101**, 2921 (2001).
30. A. J. Carmicheal, D. M. Haddleton, S. A. F. Bon, and K. R. Seddon, *Chem. Commun.* **1237** (2000).
31. (a) K. Hong, H. Zhang, J. W. Mays, A. N. Visser, C. S. Brazel, J. D. Holbrey, W. M. Reichert, and R. D. Rogers, *Chem. Commun.* 1368 (2002);
32. (b) M. G. Benton and C. S. Brazel, *Polym. Int.* **53**, 1113 (2004).
33. (a) S. Harrison, S. R. MacKenzie, and D. M. Haddleton, *Chem. Commun.* 2850 (2002); (b) S. Harrison, S. R. MacKenzie, and D. M. Haddleton, *Macromolecule* **36**, 5072 (2003).
34. A. L. Cheng, Y. Zhang, T. Zhao, and H. Wang, *Macromol. Symp.* **216**, 9 (2004).
35. H. Zhang, K. Hong, and J. W. Mays, in R. Rogers and C. S. Brazel, eds., *Ionic Liquids in Polymer System, ACS Symposium Series*, Anaheim CA, Spring, 2004, in press.
36. V. Strehmel, H. Kraudelt, H. Wetzel, E. Görnitz, and A. Laschewsky, in R. Rogers and C. S. Brazel, eds., *Ionic Liquids in Polymer System, ACS Symposium Series*, Anaheim CA, Spring, 2004, in press.

37. (a) J. F. Deye, T. A. Berger, and A. G. Anderson, *Anal. Chem.* **62**, 615 (1990); (b) A. J. Carmicheal and K. R. Seddon, *J. Phys. Org. Chem.* **13**, 591 (2000); (c) S. V. Dzyuba and R. A. Bartsch, *Tetrahedron Lett.* **43**, 4657 (2002).
38. H. Zhang, L. Bu, M. Li, K. Hong, A. E. Visser, R. D. Rogers, and J. W. Mays, in R. D. Rogers and K. R. Seddon, eds., *Ionic Liquids: Industrial Application for Green Chemistry, ACS Symposium*, 2001.
39. T. Biedroń and P. Kubisa, *Macromol. Rapid Commun.* **22**, 1237 (2001).
40. T. Biedroń and P. Kubisa, *Polym. Int.* **52**, 1584 (2003).
41. T. Sarbu and K. Matyjaszewski, *Macromol. Chem. Phys.* **202**, 3379 (2001).
42. (a) H. Ma, X. Wan, X. Chen, and Q. Zhou, *J. Polym. Sci.. Part A: Polym. Chem.* **41**, 143 (2003); (b) H. Ma, X. Wan, X. Chen, and Q. Zhou, *Polymer* **44**, 5311 (2003).
43. H. Zhang, K. Hong, and J. W. Mays, *Polym. Bull.* **52**, 9 (2004).
44. J. Ryan, F. Aldabbagh, P. B. Zetterlund, and B. Yamada, *Macromol. Rapid Commun.* **25**, 930 (2004).
45. (a) S. Perrier, T. P. Davis, A. J. Carmichael, and D. M. Haddleton, *Chem Commun.* 2226 (2002); (b) S. Perrier, T. P. Davis, A. J. Carmichael, and D. M. Haddleton, *Euro. Polym. J.* **39**, 417 (2003); (c) R. Vijayaraghavan and D. R. MacFarlane, *Aust. J. Chem.* **57**, 129 (2004).
46. Y. Zhao, J. Zhang, J. Jiang, C. Chen, and F. Xi, *J. Polym. Sci., Part A: Polym. Chem.* **40**, 3360 (2002).
47. H. Zhang, K. Hong, and J. W. Mays, *Macromolecules* **35**, 5738 (2002).
48. T. Biedroń and P. Kubisa, *J Polym. Sci., Part A: Polym. Chem.* **40**, 2799 (2002).
49. (a) H. Ma, X. Wan, X. Chen, and Q. Zhou, *J Polym. Sci., Part A: Polym. Chem.* **41**, 143 (2003); (b) H. Ma, X. Wan, X. Chen, and Q. Zhou, *Polymer* **44**, 5311 (2003).
50. A. M. van Herk, *J. Chem. Educ.* **72**, 138 (1995).
51. H. Zhang, K. Hong, M. Jablonsky, and J. W. Mays, *Chem Commun.* 1356 (2003).
52. H. Harwood, *J. Macromol. Sci. Macromol Symp.* **10/11**, 331 (1987).
53. M. P. Scott, C. S. Brazel, M. G. Benton, J. W. Mays, J. D. Holbrey, and R. D. Rogers, *Chem. Commun.* 1370 (2002).
54. H. Zhang and J. W. Mays, manuscript in preparation (2005).
55. R. Vijayaraghavan, and D. R. MacFarlane, *Chem. Commun.* 700 (2004).
56. T. Biedroń and P. Kubisa, *J. Polym. Sci., Part A: Polym. Chem.* **42**, 3230 (2004).
57. S. Csihony, C. Fischmeister, C. Bruneau, I. T. Horváth, and P. H. Dixneuf, *New J. Chem.* **26**, 1667 (2002).
58. T. Biedroń, M. Bednarek, and P. Kubisa, *Macromol. Rapid Commun.* **25**, 878 (2004).
59. J. Kadokawa, Y. Iwasaki, and H. Tagaya, *Macromol. Rapid Commun.* **23**, 757 (2002).
60. H. Uyama, T. Takamoto, and S. Kobayashi, *Polym. J.* **34**, 94 (2002).
61. Y. S. Vygodskii, E. I. Lozinskaya, and A. S. Shaplov, *Macromol. Rapid Commun.* **23**, 676 (2002).
62. P. Mastrorilli, C. F. Nobile, V. Gallo, G. P. Suranna, and G. Farinola, *J. Mol. Catal. A: Chem.* **184**, 73 (2002).
63. M. A. Klingshirn, G. A. Broker, J. D. Holbrey, K. H. Shaughnessy, and R. D. Rogers, *Chem Commun.* 1394 (2002).
64. E. Naudin, H. A. Ho, S. Branchaud, L. Breau, D. Bélanger, *J. Phys. Chem. B* **106**, 10585 (2002).
65. (a) K. Sekiguchi, M. Atobe, and T. Fuchigami, *J. Electroanal. Chem.* **557**, 1 (2003); (b) J. M. Pringle, J. Efthimiadis, P. C. Howlett, J. Efthimiadis, D. R. MacFarlane, A. B. Chaplin, S. B. Hall, D. L. Officer, G. G. Wallace, and M. Forsyth, *Polymer* **45**, 1447 (2004); (c) J. H. Shi, C. H. Yang, G. Y. Gao, and Y. F. Li, *Chin. J. Chem. Phys.* **17**, 503 (2004).
66. H. Gao, T. Jiang, B. Han, Y. Wang, J. Du, Z. Liu, and J. Zhang, *Polymer* **45**, 3017 (2004).

67. (a) J. Ding, D. Zhou, G. Spinks, G. Wallace, S. Forsyth, M. Forsyth, and D. MacFarlane, *Chem. Mater.* **15**, 2392 (2003); (b) W. Lu, A. G. Fadeev, B. Qi, E. Smela, B. R. Mattes, J. Ding, G. Spinks, J. Mazurkiewics, D. Zhou, G. G. Wallace, D. R. MacFarlane, S. A. Forsyth, and M. Forsyth, *Science* **297**, 983 (2002).
68. S. Washiro, M. Yoshizawa, H. Nakajima, and H. Ohno, *Polymer* **45**, 1577 (2004).
69. H. Ohno, M. Yoshizawa, and W. Ogihara, *Electrochim. Acta.* **48**, 2079 (2003).
70. P. Snedden, A. I. Cooper, K. Scott, and N. Winterton, *Macromolecule* **36**, 4549 (2003).
71. R. P. Swatloski, S. K. Spear, J. D. Holbrey, and R. D. Rogers, *J. Am. Chem. Soc.* **124**, 4974 (2002).
72. P. Kubisa, *Prog. Polym. Sci.* **29**, 3 (2004).

HONGWEI ZHANG
University of Tennessee
JIMMY W. MAYS
Oak Ridge National Laboratory

Encyclopedia of Polymer Sceince and Technology
Copyright © 2005 John Wiley & Sons, Inc. All rights reserved.

MICROENCAPSULATION

Introduction

Microencapsulation is the coating of small solid particles, liquid droplets, or gas bubbles with a thin film of coating or shell material. In this article, the term *microcapsule* is used to describe particles with diameters between 1 and 1000 μm. Particles smaller than 1 μm are called *nanoparticles*; particles greater than 1000 μm can be called *microgranules* or *macrocapsules*.

Many terms have been used to describe the contents of a microcapsule: active agent, actives, core material, fill, internal phase (IP), nucleus, and payload. Many terms have also been used to describe the material from which the capsule is formed: carrier, coating, membrane, shell, or wall. In this article the material being encapsulated is called the *core material*; the material from which the capsule is formed is called the *shell material*.

Although virtually any coating material, conceptually, is a candidate microcapsule shell material, most commercial microcapsules produced to date utilize a relatively small number of different shell materials. Table 1 lists representative examples of these materials along with typical applications. Microcapsule shell material selection for a specific application is determined by a number of factors including cost, availability, processing ease, and inherent barrier properties. Shell materials for pharmaceutical, food, and personal care products are limited to materials that are approved by regulatory agencies responsible for such products. Defining an optimal shell material for a given application can be complex, since many interacting parameters determine success of a given capsule shell material. Fortunately, many suppliers of candidate shell materials provide valuable information concerning the use of their products in various encapsulation processes.

Microcapsules can have a wide range of geometries and structures. Figure 1 illustrates three possible capsule structures. Parameters used to characterize microcapsules include particle size, size distribution, geometry, actives content, storage stability, and core material release rate. Characterization studies provide valuable insight into the nature of various types of capsules and how they function in specific applications.

Throughout the world, research and development activity dedicated to advancing microcapsulation technology is producing a steadily increasing number of commercially successful products that utilize microcapsules. Many established encapsulation processes like spray drying and fluidized bed coating are being refined and improved while new processes continue to be developed. Various reviews of this subject exist (1–6). Pan coating, a well-established means of producing coated

Table 1. Shell Materials Used to Produce Commercially Significant Microcapsules

Shell material	Regulatory status	Chemical class	Encapsulation process	Applications
Gum arabic	Edible	Polysaccharide	Spray drying	Food flavors
Gelatin	Edible	Protein	Spray drying	Vitamins
Gelatin–gumarabic[a]	Nonedible[b]	Protein–polysaccharide complex	Complex coacervation	Carbonless paper
Ethylcellulose	Edible	Cellulose either	Wurster process or polymer–polymer incompatibility	Oral pharmaceuticals
Polyurea or polyamide	Nonedible	Cross-linked polymer	Interfacial polymerization *in situ* polymerization	Agrochemicals and carbonless paper
Aminoplasts	Nonedible	Cross-linked polymer		Carbonless paper, fragrances, and adhesives
Maltodextrins	Edible	Low molecular weight carbohydrate	Spray drying and desolvation	Food flavors
Hydrogenated vegetable oils	Edible	Glycerides	Fluidized bed	Assorted food ingredients

[a] Treated with glutaraldehyde.
[b] For intended application, ie, carbonless paper.

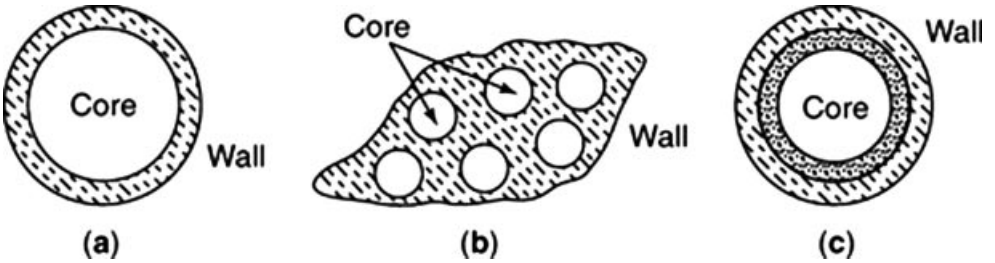

Fig. 1. Schematic diagrams of several possible capsule structures: (**a**) continuous core/shell microcapsule in which a single continuous shell surrounds a continuous region of core material; (**b**) multinuclear microcapsule in which a number of small domains of core material are distributed uniformly throughout a matrix of shell material; and (**c**) continuous core capsule with two different shells.

particles for the pharmaceutical industry, is not discussed because it produces particles larger than 1000 μm.

Encapsulation Processes

Because there are so many encapsulation processes, various schemes have been created in order to classify them. Some schemes classify encapsulation processes as chemical or physical even though so-called chemical processes may be based exclusively on physical phenomena, while physical processes may involve chemical reactions. This author prefers to simply classify encapsulation processes as type A or type B. Type A processes are defined as those in which capsule formation occurs entirely in a liquid-filled stirred tank or tubular reactor. Type B processes are processes in which capsule formation occurs because a coating is sprayed or deposited in some manner onto the surface of a liquid or solid core material dispersed in a gas phase or vacuum. This latter category includes processes in which liquid droplets containing core material are sprayed into a gas phase and subsequently solidified to produce microcapsules. Emulsion and dispersion stabilization play a key role in the success of both type A and B processes.

Differences in some type A and type B processes can be subtle, but significant. For example, solvent evaporation is a key step in spray dry encapsulation protocols (type B), and protocols involving solvent evaporation from an emulsion (type A). The difference in these protocols is that evaporation in the former case occurs directly from a liquid to a gas phase, whereas in the latter case evaporation involves transfer of a volatile liquid from a dispersed phase to a continuous liquid phase from which it is subsequently evaporated. Another example is encapsulation by gelation. In type A gelation processes, the droplets that are gelled and become microcapsules are formed by dispersion in a liquid phase and are gelled in this phase. In type B gelation processes, droplets formed by atomization or extrusion into a gas phase are subsequently gelled either in the gas phase or a liquid gelling bath.

Representative examples of both types of processes follow. Type B processes tend to be promoted by organizations that sell and service equipment for producing

microcapsules. Most type A processes are developed and used in-house by organizations that produce microcapsules.

Type A processes	Type B processes
Complex coacervation	Spray drying
Polymer–polymer incompatibility	Fluidized bed
Interfacial polymerization at liquid–liquid and solid–liquid interfaces	Interfacial polymerization at solid–gas or liquid–gas interfaces
In situ polymerization	Centrifugal extrusion
Solvent evaporation or in-liquid drying	Extrusion or spraying into a desolvation bath
Submerged nozzle extrusion	Rotational suspension separation (spinning disk)

Type A Processes

Complex Coacervation. This process occurs in aqueous media and is used primarily to encapsulate water-immiscible liquids or water-insoluble solids (4,5). In the complex coacervation of gelatin with gum arabic (Fig. 2), a water-insoluble core material is dispersed to a desired drop size in a warm gelatin solution. After gum arabic and water are added to this emulsion, pH of the aqueous phase is typically adjusted to 4.0–4.5. This causes a liquid complex coacervate of gelatin, gum arabic, and water to form. When the coacervate adsorbs on the surface of the core material, a liquid complex coacervate film surrounds the dispersed

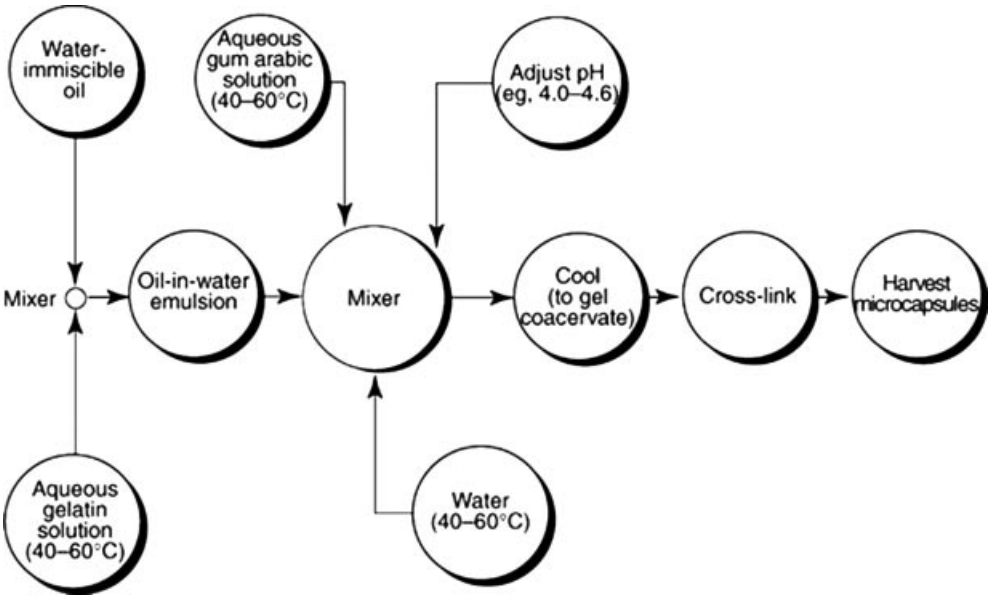

Fig. 2. Flow diagram of a typical encapsulation process based on the complex coacervation of gelatin with gum arabic.

core material, thereby forming embryo microcapsules. The system is subsequently cooled, often below 10°C, thereby gelling the liquid coacervate shell. After gelation, the coacervate gel typically is chemically cross-linked. For many years, glutaraldehyde was the preferred cross-linking agent, but an enzyme, transglutaminase, has now emerged as a candidate cross-linking agent, particularly when the capsules are for food or cosmetic applications.

Many pairs of oppositely charged Polyelectrolytes (qv) are able to form a liquid complex coacervate suitable for microcapsule formation. Normally, gelatin is the positively charged polyion, because it is readily available and forms suitable complex coacervates with a wide range of polyanions. Polyanions typically used include gum arabic, polyphosphate, poly(acrylic acid), and alginate.

Chemically cross-linked complex coacervate capsule shells generally are highly water-swollen, but can be dried in a spray dryer or fluidized bed dryer. If such capsule shells are treated with urea and formaldehyde under acidic conditions, these materials polymerize within the water-swollen complex coacervate capsule shell, thereby greatly, increasing the degree of chemical cross-linking, reducing water content of the shell, and enhancing ease of drying to a free-flow powder.

A wide variety of capsules loaded with water-immiscible or water-insoluble materials have been prepared by complex coacervation. Capsule size typically ranges from 20 to 1000 μm, but capsules outside this range can be prepared. Although core contents are often 80–95 wt%, capsules with lower loadings can be made. Complex coacervation processes are adversely affected by active agents that have finite water solubility, are surface-active, or are unstable at pH values of 4.0–5.0. The shell of dry complex coacervate capsules is sensitive to variations in atmospheric moisture content and becomes plasticized at elevated humidities.

Simple Coacervation. Aqueous solutions of water-soluble polymers are phase-separated in aqueous media when sufficient salt is added to such solutions. This phenomenon is called *simple coacervation*. As long as phase separation produces a liquid polymer-rich phase, simple coacervation can be used to produce microcapsules (5). Microcapsules with a gelatin or poly(vinyl alcohol) shell have been formed in this manner. The use of poly(vinyl alcohol) as a capsule shell material is of great interest in various applications because it is a widely available synthetic polymer with excellent oxygen and oil barrier properties (see BARRIER POLYMERS; VINYL ALCOHOL POLYMERS).

Polymer–polymer Incompatibility. Two chemically different polymers dissolved in a common solvent are usually incompatible. That is, they spontaneously separate into two liquid phases, with each phase containing predominately one polymer. When a core material insoluble in the solvent is dispersed in such systems, it is spontaneously coated by a thin film of the liquid phase that contains the polymer designed to be the capsule shell material; this polymer must be preferentially adsorbed by the core material which is not difficult to arrange. Microcapsules are harvested by desolvating this coating either by chemical cross-linking or addition of a nonsolvent (Fig. 3) (4,5). In the latter case, the embryonic capsule as slurry is often added to a very large excess of nonsolvent in order to minimize capsule agglomeration during isolation.

Polymer–polymer incompatibility encapsulation processes can be carried out in aqueous or nonaqueous media but, thus far, have primarily been carried out in

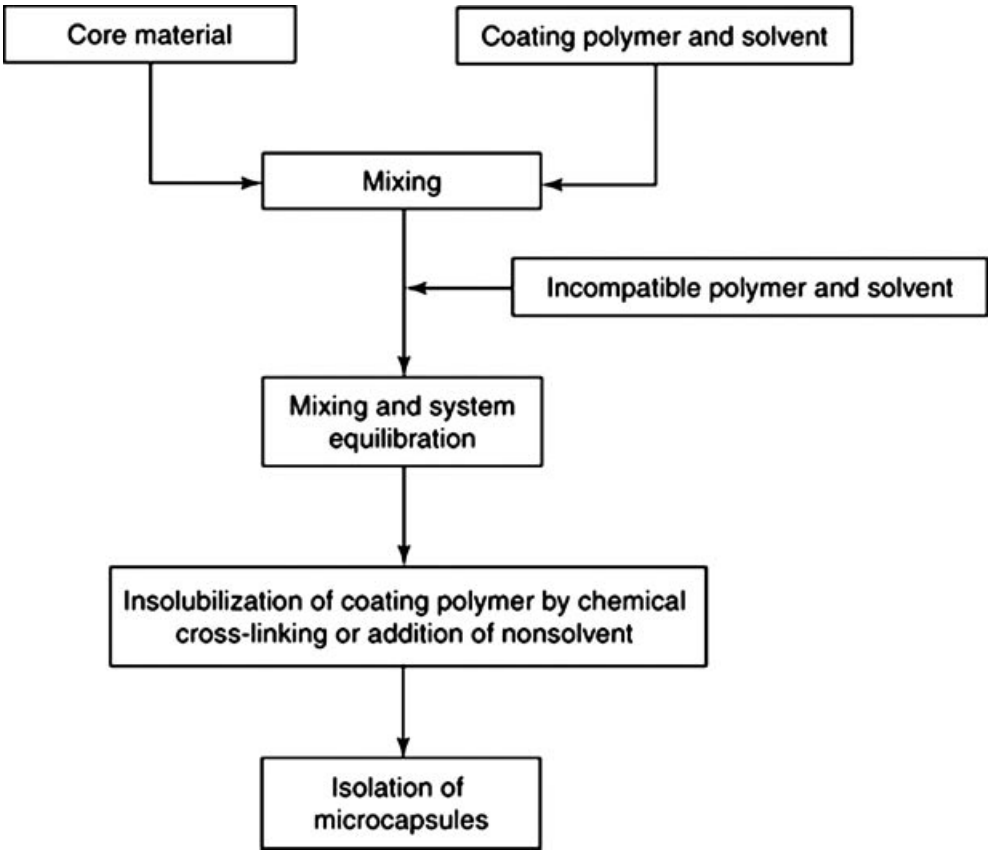

Fig. 3. Flow diagram of a typical encapsulation process based on polymer–polymer incompatibility.

organic media. Core materials encapsulated tend to be polar solids with a finite degree of water solubility. Historically, ethylcellulose has been the shell material used. Biodegradable shell materials such as poly(D,L-lactide) and lactide–glycolide copolymers have received much attention. In these latter cases, the object has been to produce biodegradable capsules that carry proteins or polypeptides. Such capsules tend to be below 100 μm in diameter and are for oral or parenteral administration (7).

Interfacial Polymerization. Many types of polymerization reactions can be made to occur at interfaces, or produce polymers that concentrate at interface, thereby producing microcapsules. Accordingly, this approach to encapsulation has steadily developed into a versatile family of encapsulation processes. Figure 4 schematically illustrates five types of encapsulation processes that utilize these types of reactions.

Figure 4**a** represents interfacial polymerization encapsulation processes in which shell formation occurs at the core material–continuous phase interface due to reactants in each phase diffusing and rapidly reacting there to produce a capsule shell (1,8). The continuous phase normally contains a dispersing agent in order

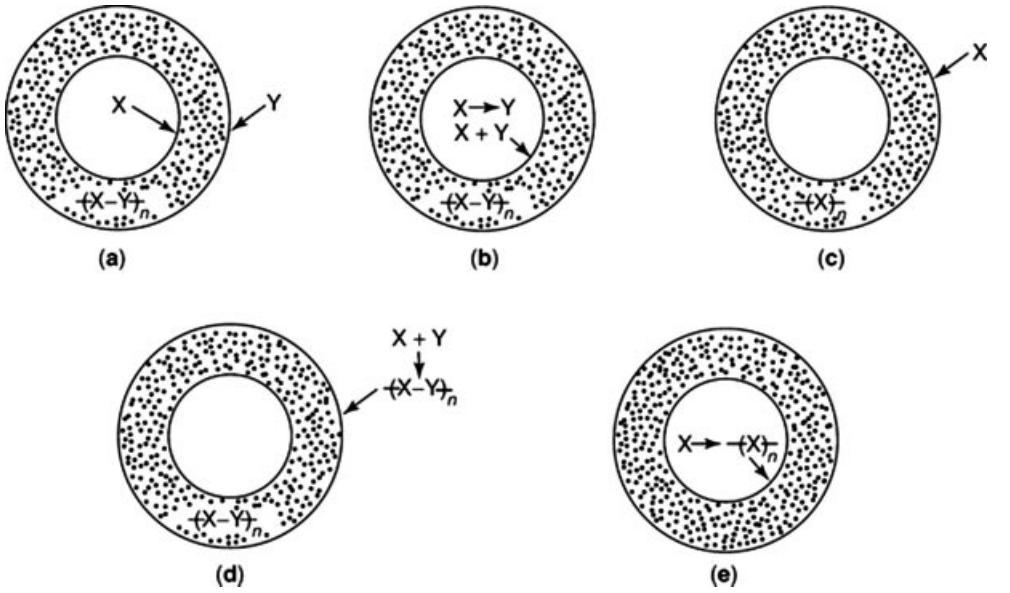

Fig. 4. Schematic diagrams that illustrate the different types of interfacial polymerization reactions used to form microcapsules. Reactants: X, Y; polymerization product: $(X{-}Y)_n$ or $-(X-)_n$. See text for descriptions of cases (**a**)–(**e**).

to facilitate formation of the dispersion. The dispersed core phase encapsulated can be water, or a water-immiscible solvent. The reactant(s) and coreactant(s) in such processes generally are various multifunctional acid chlorides, isocyanates, amines, and alcohols. For water-immiscible core materials, a multifunctional acid chloride, isocyanate, or a combination of these reactants is dissolved in the core, and a multifunctional amine(s) or alcohol(s) is dissolved in the aqueous phase used to disperse the core material. For water or water-miscible core materials, the multifunctional amine(s) or alcohol(s) is dissolved in the core, and a multifunctional acid chloride(s) or isocyanate(s) is dissolved in the continuous phase. Both cases have been used to produce capsules.

Figure 5 illustrates the type of encapsulation process, shown in Figure 4**a**, when the core material is a water-immiscible liquid. Reactant X, a multifunctional acid chloride, isocyanate, or a combination of these reactants, is dissolved in the core material. The resulting mixture is emulsified in an aqueous phase that contains an emulsifier such as partially hydrolyzed poly(vinyl alcohol) or a lignosulfonate. Reactant Y, a multifunctional amine or a combination of amines such as ethylenediamine, hexamethylenediamine, or triethylenetetramine, is added to the aqueous phase, thereby initiating interfacial polymerization and formation of a capsule shell. If reactant X is an acid chloride, a base is added to the aqueous phase in order to act as an acid scavenger.

A key feature of encapsulation processes (Figs. 4**a** and 5) is that the reagents for the interfacial polymerization reaction responsible for shell formation are present in two mutually immiscible liquids. They must diffuse to the interface in order to react. Once reaction is initiated, the capsule shell that forms becomes

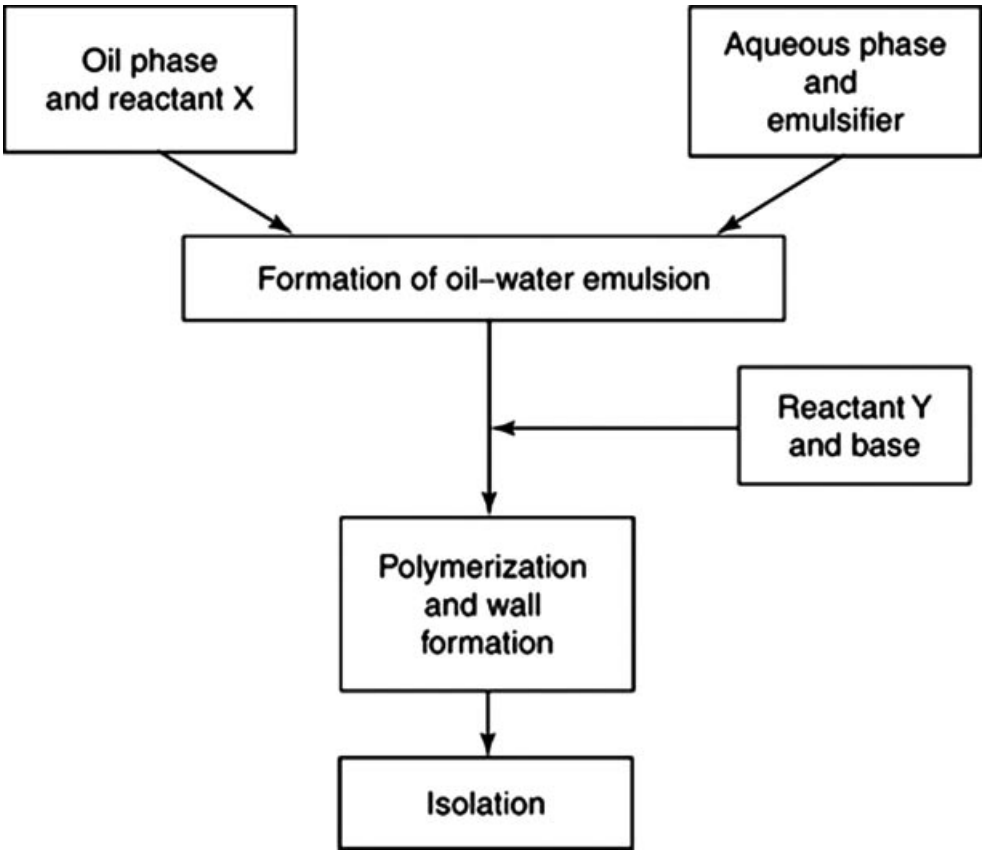

Fig. 5. Flow diagram of a typical interfacial polymerization encapsulation process in which reactants X and Y are dissolved in separate mutually immiscible phases (see Fig. 4**a**).

a barrier to diffusion and ultimately begins to limit the rate of the interfacial polymerization reaction. This, in turn, influences morphology and uniformity of thickness of the capsule shell. Kinetic analyses of the process have been published (8). A drawback to the technology for some applications is that aggressive or highly reactive molecules must be dissolved in the core material in order to produce microcapsules. Such molecules can react with sensitive core materials.

Figure 4**b** represents the case where a reactant dissolved in the dispersed phase reacts with the continuous phase to produce a co-reactant. The co-reactant and any unreacted original reactant left in the dispersed phase then proceed to react with each other at the dispersed phase side of the interface and produce a capsule shell. Capsule shell formation occurs entirely because of reaction of reactants present in the droplets of the dispersed phase. No reactant is added to the aqueous phase. As in the case of the process described by Figure 4**a**, a reactive species must be dissolved in the core material in order to produce a capsule shell.

A specific example of the process represented by Figure 4**b** occurs when a multifunctional isocyanate is dissolved in a liquid, water-immiscible core mate-

rial and the mixture produced is dispersed in an aqueous phase that contains a dispersing agent. The aqueous phase reacts with some of the isocyanate groups to produce primary amine functionalities. These amino groups react with unreacted isocyanate groups to produce a polyurea capsule shell (9).

Figure 4**c** illustrates interfacial polymerization encapsulation processes in which the reactant(s) that polymerizes to form the capsule shell is transported exclusively from the continuous phase of the system to the dispersed phase–continuous phase interface where polymerization occurs and a capsule shell is produced. This type of encapsulation process has been carried out at liquid–liquid and solid–liquid interfaces. An example of the liquid–liquid case is the spontaneous polymerization reaction of cyanoacrylate monomers at the water–solvent interface formed by dispersing water in a continuous solvent phase (10). The poly(alkyl cyanoacrylate) produced by this spontaneous reaction encapsulates the dispersed water droplets. An example of the solid–liquid process is where a core material is dispersed in aqueous media that contains a water-immiscible surfactant along with a controlled amount of surfactant. A water-immiscible monomer that polymerizes by free-radical polymerization is added to the system and free-radical polymerization localized at the core material–aqueous phase interface is initiated, thereby generating a capsule shell (11).

Figure 4**c** also describes the spontaneous polymerization of *para*-xylylene diradicals on the surface of solid particles dispersed in a gas phase that contains this reactive monomer (12) (see XYLYLENE POLYMERS). The poly(*p*-xylylene) polymer produced forms a continuous capsule shell that is highly impermeable to the transport of many penetrants, including water. This is an expensive encapsulation process, but it has produced capsules with impressive barrier properties. It is a type B encapsulation process, but is included here for the sake of completeness.

Figure 4**d** represents *in situ* encapsulation processes (13,14), an example of which is presented in more detail in Figure 6 (14). The first step is to disperse a water-immiscible liquid or solid core material in an aqueous phase that contains urea, melamine, water-soluble urea–formaldehyde condensate, or water-soluble urea–melamine condensate. In many cases, the aqueous phase also contains a system modifier that enhances deposition of the aminoplast capsule shell (14). This is an anionic polymer or copolymer (Fig. 6). Shell formation occurs once formaldehyde is added and the aqueous phase acidified, eg, pH 2–4.5. The system is heated for several hours at 40–60°C.

A unique feature of *in situ* encapsulation technology is that polymerization occurs in the aqueous phase, thereby producing a condensation product that deposits on the surface of the dispersed core material where polymerization continues. This ultimately produces a water-insoluble, highly cross-linked polymer capsule shell. The polymerization chemistry occurs entirely on the aqueous phase side of the interface, and so reactive agents do not have to be dissolved in the core material. The process has been commercialized and produces a range of commercial capsules.

Figure 4**e** represents interfacial polymerization processes in which a solution of water-immiscible vinyl monomer(s), vinyl monomer initiator, and core material is dispersed in an aqueous phase that contains a dispersing agent. Polymerization is then initiated, eg, by heating. The polymer produced within the droplets of the core material is designed to precipitate or deposit at the core material–aqueous

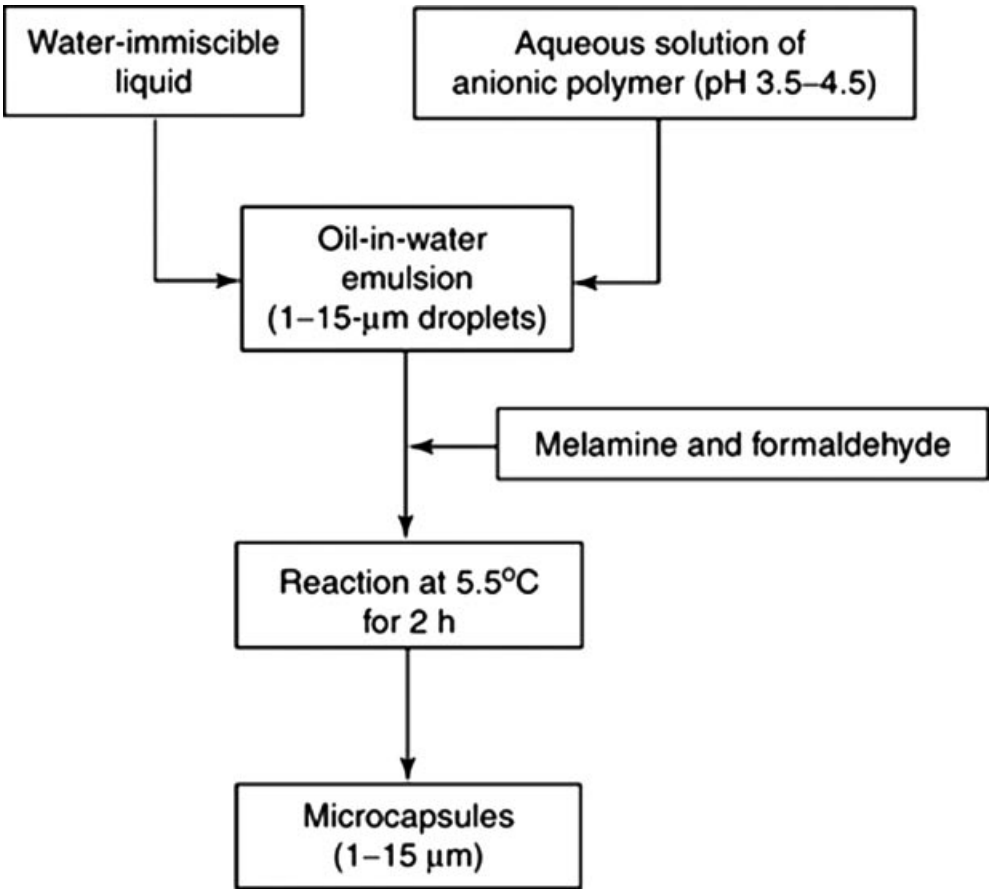

Fig. 6. Flow diagram of a microencapsulation process that utilizes acid-catalyzed *in situ* polymerization of melamine or urea with formaldehyde to form a capsule shell (see Fig. 4**d**).

phase interface, thereby producing a microcapsule shell. Although this technology was disclosed many years ago, it has not been much in use, presumably because the capsules produced do not have acceptable barrier properties.

Solvent Evaporation. This encapsulation technology involves removing a volatile solvent from an oil-in-water, oil-in-oil, or water-in-oil-in-water emulsion (4,15). In most cases, the shell material is dissolved in a volatile solvent, such as methylene chloride or ethyl acetate. The active agent to be encapsulated is dissolved, dispersed, or emulsified into this solution. Water-soluble core materials like hormonal polypeptides are dissolved in water that contains a thickening agent before dispersion in the volatile solvent phase that contains the shell material. This dispersed aqueous phase is gelled thermally to entrap the polypeptide in the dispersed aqueous phase before solvent evaporation occurs (16).

Once the active agent is dispersed in the volatile solvent phase, the dispersion produced is typically emulsified into an aqueous phase that contains a dispersing agent. The solvent used to dissolve the shell material is subsequently

removed from this emulsion at atmospheric or reduced pressure. Significantly, solvent evaporation processes can be based on nonaqueous media. In such cases, a volatile organic solvent is removed by evaporation from an organic solvent that has low volatility.

The microcapsules produced by solvent evaporation processes can range in size from below 1 μm to over several hundred micrometers. The technique is used often to form drug-loaded microparticles from biodegradable polymer shell materials (15,16). Significantly, solvent removal from the dispersed phase of a solvent evaporation process occurs by partitioning or extraction of a volatile solvent into the continuous phase of the emulsion, rather than by direct evaporation into a gas phase. The solvent is removed from the continuous phase by evaporation. Because of this, a range of mass-transfer events can occur during the solvent evaporation process. These may have a negative effect on microcapsule formation, such as causing loss of core material to the continuous phase. Because of this, solvent evaporation encapsulation processes have also been described as solvent removal, in-liquid drying, or emulsion solvent evaporation encapsulation processes.

Centrifugal Force and Submerged Nozzle Processes. A variety of type A encapsulation processes have used centrifugal force or submerged nozzles to produce microcapsules. For example, a device in which a perforated cup was immersed in an oil bath and spun at a fixed rate has been described (17). An emulsion of core and shell material fed into the spinning cup is thrown in droplet form into the oil outside the spinning cup by centrifugal force. Such droplets are gelled by cooling to thereby yield gel beads loaded with an oil that are subsequently dried.

Capsules have also been produced by extruding in droplet form a liquid core and liquid shell formulation through a submerged two- or three-fluid nozzle into a moving stream of carrier fluid. The liquid shell formulation is gelled, usually by cooling, to yield gel beads that can be dried (18). By using a three-fluid nozzle, capsules with unique multiple shell structures can be produced. To date, type A centrifugal force and submerged nozzle encapsulation processes have been used primarily for the encapsulation of various vitamin or flavor oils, and probiotics. The capsules tend to be relatively large and typically are formed from natural shell materials capable of being gelled thermally.

Type B Processes

Spray Drying. Spray-dry encapsulation processes (Fig. 7) consist of spraying an intimate mixture of core and shell material into a heated chamber where rapid desolvation occurs to thereby produce microcapsules (19,20). The first step in such processes is to form a solution of the carrier or shell material in the solvent from which spray drying is to be done. Water is the most common solvent for spray drying. Any film-forming shell material can, in principle, be used, but water-soluble polymers, such as gum arabic, modified starch, and hydrolyzed gelatin, are used most often. Solutions of these shell materials at 50 wt% solids have sufficiently low viscosities so that they can still be atomized without difficulty. It is not unusual to blend gum arabic and modified starch with maltodextrins, sucrose, or sorbitol.

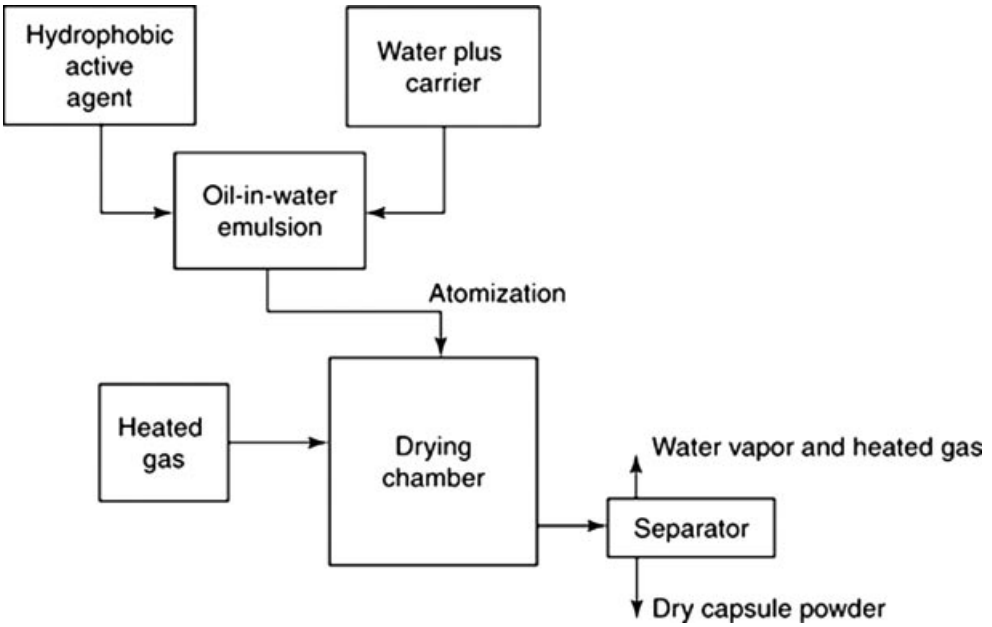

Fig. 7. Flow diagram of a typical spray-dry encapsulation process.

The second step is to disperse the core material being encapsulated in the solution of shell material. Usually, the core material is a hydrophobic or water-immiscible oil, although solid powders have been encapsulated. A suitable emulsifier is used to aid formation of the dispersion or emulsion. In the case of oil core materials, the oil phase is typically reduced to a drop size of 1–3 μm. This is done in order to minimize free oil on the surface of the dried capsules. Once a suitable dispersion or emulsion has been prepared, it is sprayed into a heated chamber. The small droplets produced have a high surface area and are rapidly converted to a fine powder by desolvation in the chamber. Residence time in the spray-drying chamber is 30 s or less. Inlet and outlet air temperatures are important process parameters, as is relative humidity of the inlet air stream.

Capsules produced by spray drying often have a diameter of 10–40 μm. They may be individual particles or aggregates. In either case, capsule geometry varies from irregular to spherical. Core material loadings of commercial spray-dried capsules are typically 20–30 wt%, although loadings as high as 60 wt% have been reported. The core material is dispersed as small droplets or particles throughout spray-dried capsules. Hydrocolloid carriers such as gum arabic and modified starch produce spray-dried capsules that are dispersible in cold water, but warm or hot water is needed to dissolve them completely. Maltodextrins and hydrolyzed gelatins give capsules soluble in cold and hot water.

Spray-dry encapsulation is a low cost process capable of producing a range of microcapsules in good yield. It is often used to produce commercial capsules loaded with fragrance or flavor oils. A number of research workers have prepared drug-loaded biodegradable capsules from nonaqueous media by spray drying (20). This technology has steadily improved over the years, but the capsules produced may

contain a small amount of free or unencapsulated active agent. If this active agent is an oil that contains components capable of oxidizing on storage, an objectionable odor or taste may be produced. Another problem is loss of volatiles during the atomization and drying steps if the active agent contains low boiling, polar active agents such as ethyl acetate and acetaldehyde. Such agents can be difficult to encapsulate by this technology. Their retention is favored by maximizing initial concentration of carrier material.

Spray chilling, cooling, and congealing are essentially variations of conventional spray drying. These processes use a chilled gas to solidify molten capsule shell material formulations rather than volatilize a solvent, as is done in the case of spray drying (21,22). Various fats, waxes, fatty alcohols, or fatty acids are used as shell materials. In such encapsulation procedures, the active agent is dispersed in a molten shell material with the aid of an emulsifier, if necessary (see EMULSIFIERS). This dispersion is atomized through heated nozzles into a cooling chamber analogous to that shown in Figure 7. The shell material is solidified by cooling and solid particles are isolated. If the chamber is at room temperature, the coating material has a melting point between 45 and 122°C. If the chamber is cooled, material melting at 32–43°C can be used. Particles produced by this method have water-insoluble shells. The influence of processing temperature on shell material polymorphism, a phenomenon characteristic of many fats, has been discussed (23).

Fluidized-Bed Coating. Fluidized-bed encapsulation technology involves spraying shell material in solution or hot melt form onto solid particles suspended in a stream of heated gas, usually air (2,6,24). Although several types of fluidized-bed units exist, the so-called top and bottom spray units have been used most often to produce microcapsules. In top-spray units, hot melt shell materials such as fats and waxes are sprayed onto the top of a fluidized bed of solid particles (25). The coated particles are subsequently cooled producing capsules with a solid shell. This technology is used to prepare a variety of encapsulated water-soluble food and pharmaceutical ingredients. Top-spray units are generally not recommended for applying solutions of shell material because the spray droplets move countercurrent to the gas stream that suspends the fluidized bed. This favors solvent evaporation and deposition of a poor coating of shell material.

In bottom-spray or Wurster units (Fig. 8), the coating material is sprayed as a solution into the bottom of a column of fluidized particles. The freshly coated particles are carried away from the nozzle by the airstream and up into the coating chamber where the coating solidifies due to evaporation of solvent. At the top of the column or spout, the particles settle. They ultimately fall back to the bottom of the chamber, where they are guided once again by the airstream past the spray nozzle and up into the coating chamber. The cycle is repeated until a desired capsule shell thickness is reached. Coating uniformity and final coated particle size are strongly influenced by the nozzle(s) used to apply the coating formulation. This technology is routinely used to encapsulate solids, especially pharmaceuticals (qv). It can coat a wide variety of particles, including irregularly shaped particles. The technology generally produces capsules larger than 100–150 μm, but can produce coated particles smaller than 100 μm. An important feature of the Wurster process is that it can be used to apply a wide range of coating materials and multiple layers of different coating materials. Candidate coating materials include various

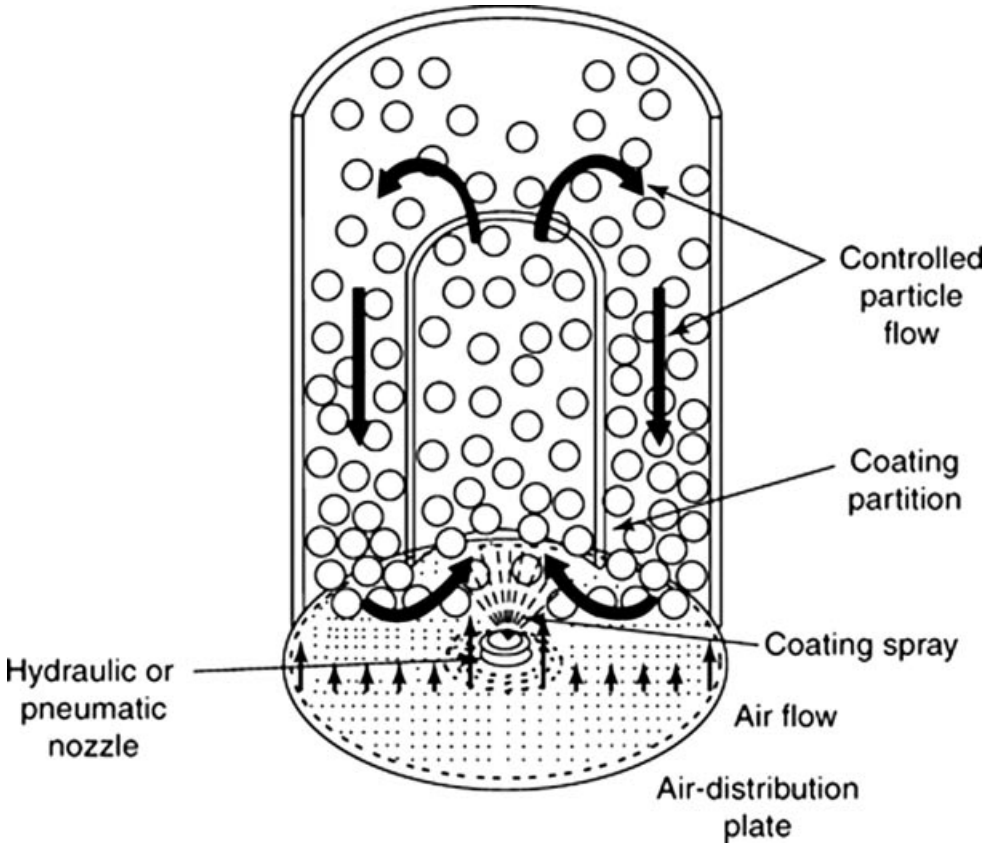

Fig. 8. Schematic diagram of a Wurster coating chamber. Courtesy of the Coating Place.

water-soluble polymers or hydrocolloids, solvent-soluble polymers, sugars, and pseudolatices. The latter are aqueous dispersions of small polymer particles which fuse together during desolvation to form a continuous capsule shell.

Centrifugal Force Processes. Several type B encapsulation processes utilize centrifugal force to form microcapsules. In one process, two mutually immiscible liquids, the core and shell material, are pumped through a two-fluid nozzle that is spun rapidly (26). The two-fluid column produced breaks up spontaneously into a series of droplets. Each droplet contains a core region surrounded by a continuous film of fluidized shell material. The shell is solidified either by cooling or by immersion in a gelling bath to produce microcapsules that can be harvested. In the former case, the shell material is typically a molten wax or fat that has relatively low melt viscosity and solidifies by cooling as it falls away from the nozzle. It may contain a small amount of polymer added in order to toughen the final capsule shell. The core material is, typically, water or an aqueous solution. In the latter case, the fluidized shell material, typically, is an aqueous sodium alginate solution. This solution is gelled ionically by immersion in an aqueous $CaCl_2$ solution to form a gel bead which can subsequently be dried and isolated. The core material is a water-immiscible liquid. This type of encapsulation technology tends

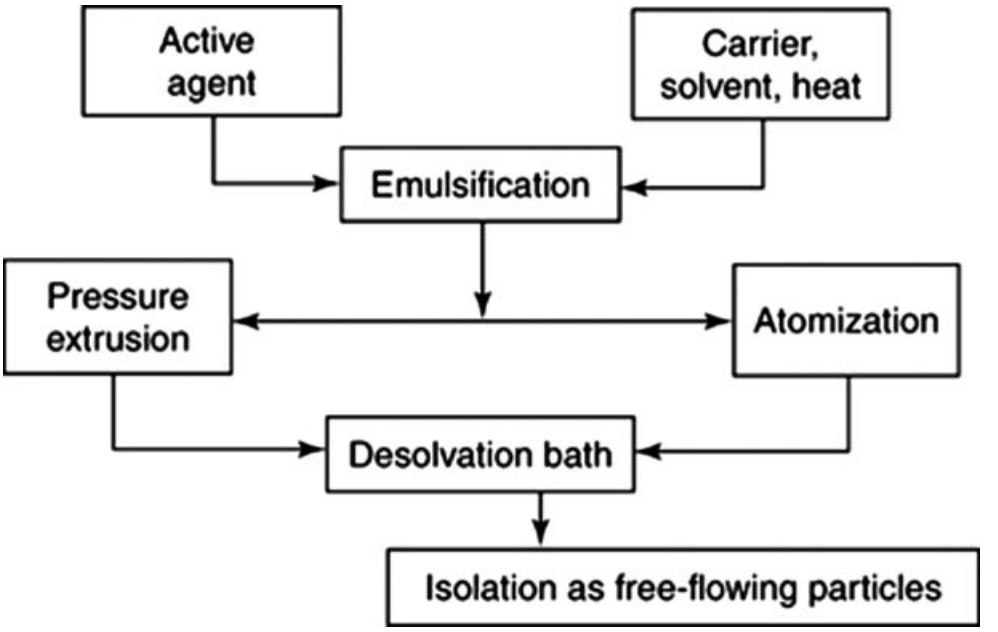

Fig. 9. Desolvation process.

to favor production of larger microcapsules. The lower particle size limit is approximately 250 μm; the upper particle size limit is several millimeters.

A second type B encapsulation process that uses centrifugal force is called *rotational suspension separation* (6). It utilizes a rapidly spinning disk to produce particles of core material surrounded by shell material. The fluidized shell material formulation, often a wax, fat, or a solution of a polymer in these materials, is mixed with particles of core material. The resulting dispersion is fed onto a rotating disk placed at the top of a chamber. Individual particles of liquid-coated droplets are flung off the edge of this disk into the chamber producing solid particles of core material enclosed in a thin film of liquid shell material. The shell formulation solidifies as the embryonic capsules fall to the bottom of the chamber producing solid microcapsules. Droplets of pure coating material are also flung off the edge of the disk, and fall in a circumferential area or zone below the disk at a closer distance to the disk than the capsules.

A number of hot-melt shell formulations have been applied in this manner to produce a range of capsules. It is claimed that the process is capable of rapidly producing capsules smaller than 100 μm in large amounts at low cost. Candidate core materials must act like solids on the rotating disk and should have a spherical geometry. Candidate coating formulations must solidify rapidly on cooling and not have high viscosities. For these reasons, preferred shell formulations, typically, are waxes and fats or polymer solutions in these materials.

Desolvation or Extractive Drying. This encapsulation technology (Fig. 9) has been used to produce commercial water-soluble capsules loaded with a range of flavor compounds (27,28). Water-soluble shell materials used are maltodextrins, sugars, and gums (qv). The shell material is dissolved in as little wa-

ter as possible and the core material is dispersed in this solution. Heat, up to 124°C, is used to reduce the viscosity of the shell formulation so that dispersion can be achieved readily. The dispersion of core material and shell formulation is either extruded or atomized into a desolvation solvent. Preferred desolvation solvents are water-miscible alcohols such as 2-propanol or polyglycols. This step solidifies the particles. Because the core materials used in this process are miscible with the desolvation solvents used, capsules with no free core material are produced. Such capsules have excellent storage stability properties. The problem with this approach to encapsulation has been that it uses solvents other than water which must be recycled. It also produces capsules with relatively low core loadings. Core loadings as high as 15% can be achieved, but forming stable emulsions in the concentrated hot aqueous core solutions used poses serious problems.

A steady stream of encapsulation technologies continues to appear in the patent literature. Some are simply modifications or improvements of established technologies, whereas others are new technologies such as very low temperature casting (29), deposition of coating material from a supercritical fluid (30), and polymer phase separation induced by evaporation of a volatile solvent from a two-component solvent mixture (31).

Applications

Microcapsules are incorporated in a number of products produced by the pharmaceutical, graphic arts, food, agrochemical, cosmetic, and adhesive industries. In order to illustrate the wide range of microcapsule applications, it is appropriate to describe briefly a number of commercial microcapsule-based products and the role that microcapsules play in these products.

Graphic Arts. Carbonless copy paper was the first large-scale commercial application of microcapsules. This product has consumed thousands of tons of capsules annually for many years, although the rate of usage has begun to decline significantly. Figure 10, a schematic diagram of a three-part business form, illustrates the concept of carbonless copy paper. The bottom surface of the top sheet of this form (sheet A) and the second sheet (sheet B) is coated with a layer of small microcapsules. The coating includes inert spacer particles, often starch particles, that are larger than the microcapsules. They protect the microcapsules from premature rupture. The capsules, filled with a colorless solution of 2–6% leuco dye dissolved in a high boiling organic solvent, rupture under pressures encountered in normal handwriting or impact printing. The dye solution released is transferred from the bottom surface of sheets A and B to the top surface of sheets B and C, respectively, where it reacts to form an image. The reactive coating on the top surface of sheets B and C contains acidic sites that activate leuco dyes. Reactive materials often used are attapulgite clay (see Clays) or phenolic resins. Sheet A in Figure 10 is called a coated back (CB) sheet; sheet B, a coated front back (CFB) sheet; and sheet C, a coated front (CF) sheet. The capsules and reactive coating can be coated on the same paper surface. In this case, the product is called self-contained carbonless copy paper.

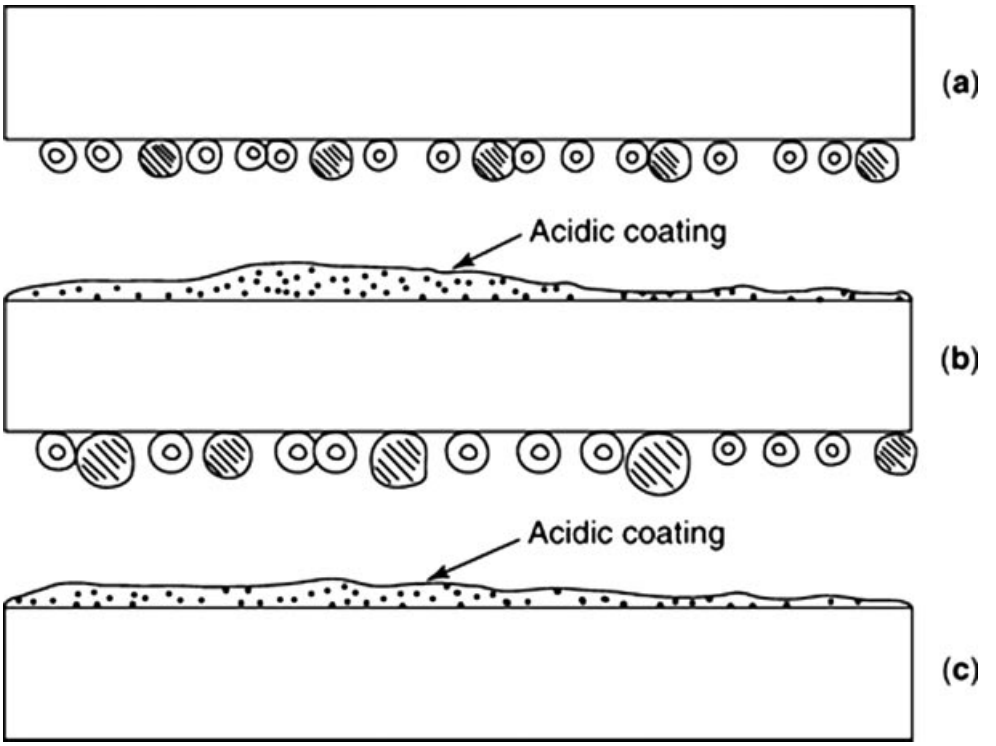

Fig. 10. Cross section of a three-part business form prepared from carbonless copy paper, where ◎ are microcapsules and ● are starch: (**a**), CB sheet; (**b**), CFB sheet; and (**c**), CF sheet.

Blythe and co-workers (32) discuss the industrial and commercial aspects of microcapsules for carbonless paper. Such capsules must be small enough to give a sharp image on the reactive coating of the transfer sheet and large enough to be broken by pressures encountered in normal writing and impact printing. The upper size limit is approximately 20 μm, since capsules larger than this produce a fuzzy image. The lower size limit is approximately 1–2 μm. Capsules smaller than this tend to fall into the crevices of the paper where they are protected from breakage. Capsules that meet these size requirements and are able to retain leuco dye solutions can be produced by complex coacervation, interfacial polymerization, or *in situ* polymerization. Solvents for dyes used in carbonless copy paper are high boiling ($>200^{\circ}$C) organic liquids that experience minimal solvent loss during product storage. Candidate solvents include benzylated ethylbenzene, benzyl butyl phthlate, isopropylbiphenyl, and diisopropylnaphthalene. Solvent choice is determined by cost, availability, toxicity, and the ability to dissolve the dye system, produce the desired color intensity on the transfer sheet, and form acceptable microcapsules.

Microcapsules have many imaging applications other than carbonless paper. They are used in toners for electrophotography, thermomsensitive printing

papers, various thermosensitice recording products, photosensitive recording materials, and thermofixing photosensitive paper (33). Encapsulated liquid crystal formulations coated on polyester film produce a variety of temperature-sensitive display products, while polyester film coated with capsules loaded with leuco dyes is used as a means of measuring line and force pressures.

So-called microencapsulated electronic inks have received much publicity in recent years. They consist of microencapsulated electrophoretic media that change color (eg, black to white) when an electric field is applied to thin microcapsule layers placed between thin electrodes. This color change occurs because the microcapsules contain a mixture of two color components dispersed in a dielectric fluid. The two color components can conceptually be two different colored particles (eg, white titanium dioxide and carbon black) or particles of one color (eg, titanium dioxide) dispersed in a dyed dielectric fluid. In either case, application of an external electrical field causes the color components to migrate or separate inside the microcapsules, thereby forming different colored images. Such inks make it possible to create flexible electronic paper displays that require low power and can receive and display information electronically (34–36).

Pharmaceuticals. The concept of microencapsulation has intrigued the pharmaceutical industry for many years, because it offers the possibility of providing a number of important new oral and parenteral dosage forms. Microcapsules in oral dosage forms can conceptually taste-mask bitter pharmaceuticals, provide extended release *in vivo*, provide enteric release, improve the stability of incompatible drug mixtures, provide resistance to oxidation, reduce volatility, and distribute a drug in many small carrier particles so that effects of the drug on the sensitive walls of the stomach are minimized. Microencapsulated parenteral formulations can provide prolonged delivery of drugs with short half-lives *in vivo* and perhaps even achieve targeted drug delivery. For these reasons, microencapsulation has received much attention by pharmaceutical scientists (37) and yielded a number of commercial pharmaceutical formulations. Initially, many of the microcapsules in these formulations had an ethylcellulose shell and were produced by a polymer–polymer phase-separation process carried out in hot cyclohexane (5). More recent formulations tend to have an acrylic copolymer coating and are prepared by using a fluidized bed coating process. Core materials encapsulated tend to be solids with finite water solubility. Encapsulated potassium chloride, KCl, has been used extensively because the KCl dispersed in many small capsules minimizes high localized KCl concentrations that can irritate the lining of the stomach and induce bleeding. Encapsulated aspirin for arthritic patients is an example of using microencapsulation to extend time of release of a drug in the gastrointestinal tract. In this case, the encapsulated aspirin formulation provides overnight relief. Finally, encapsulated oral acetaminophen formulations for children are used to provide taste-masking. One application that has received much attention in recent years is the development of microcapsules with a biodegradable poly(lactide–glycoilide) copolymer shell for delivery of vaccines (38,39) (see CONTROLLED RELEASE TECHNOLOGY).

Several commercial parenteral formulations utilize microcapsules. The core materials are polypeptides with hormonal activity. The shell materials are poly(lactide–glycolide) copolymers. The capsules are produced by solvent evaporation, polymer–polymer phase separation, or spray-dry encapsulation processes.

Core material release can occur over a 30–90 day period *in vivo*, although not at a constant rate.

Injectable encapsulated leuprolide acetate formulations (Lupron Depot) have developed into a major tool for treating cancer of the prostrate. Lupron Depot dosages that last 30 and 90 days *in vivo* are available. Biodegradable poly(lactide–glycolide) polymers are the shell materials used to form these microcapsules. The capsules are produced by removing volatile solvent from a water-in-oil-in-water emulsion. Okada reviewed their preparation and release behavior (16). An encapsulated formulation of bromocryptin [25614-03-3] is used to inhibit milk production in women after pregnancy. Injectable biodegradable microcapsules loaded with fertility control agents have been under development for a number of years and have been carried to various stages of clinical development (40) (see BIODEGRADABLE POLYMERS, MEDICAL APPLICATIONS).

The development of injectable microcapsules for delivery of chemotherapy agents remains an active area of research. The ultimate goal is to achieve targeted delivery of chemotherapy agents to specific sites in the body, ideally by injection of drug-loaded microcapsules that would seek out and destroy diseased cells. Intra-arterial infusion chemotherapy is a direct approach to targeted delivery. The clinical applications of microspheres and microcapsules in embolization and chemotherapy have been assessed (41).

Biomedical and Biotechnology. The use of microcapsules for a variety of biomedical and biological applications has been promoted for many years (42,43). Several biomedical microcapsule applications are in clinical use or have approached clinical use. One application is the use of liquid-filled microcapsules or microbubbles as ultrasound contrast agents. Such microcapsules can be formed in several different ways (44). Perfluorocarbon-gas-filled microbubbles with a human albumin shell (45) are FDA (U.S. Food and Drug Administration) approved.

Another biomedical application is the encapsulation of live mammalian cells for transplantation into humans. The purpose of encapsulation is to protect the transplanted cells or organisms from rejection by the host. The capsule shell must prevent entrance of harmful agents into the capsule, allow free transport of nutrients necessary for cell functioning into the capsule, and allow desirable cellular products to freely escape from the capsule. This type of encapsulation has been carried out with different types of live cells, but studies with encapsulated pancreatic islets or islets of Langerhans are most common. The alginate–poly(L-lysine) encapsulation process originally developed in 1981 (46) catalyzed much of the cell encapsulation work carried out since. In 1993, Vos and co-workers (47) reviewed the obstacles that must be overcome for successful application of microcapsules in islet transplantation. Work on this approach to islet transplantation has continued. Vos and co-workers (48) recently reported a study of the long-term biocompatibility, chemistry, and function of encapsulated pancreatic islets. These authors report that capsules prepared with purified alginate are biocompatible and stable *in vivo* up to two years after implantation. Yin and co-workers (49) describe microcapsules loaded with hepatocytes for use in a bioartificial liver assist device.

The microencapsulation or immobilization of a variety of live cells and organisms has been examined. The capsules prepared often are larger than 1000 μm and may not have a well-defined capsule shell, but they are designed to provide

many of the capabilities traditionally associated with microcapsules. Rokstad and co-workers (50) evaluated several different types of alginate microcapsules that contained endostatin secreting cells. Park and Chang (51) reviewed the microencapsulation of microbial cells. Goosen discussed animal cell encapsulation (52). A wide range of applications has been explored, including the use of alginate microcapsules gel beads to shorten the handling time for preparing champagne.

Other biomedical and biological applications of microcapsules exist. For example, the encapsulation of enzymes continues to attract interest even though loss of enzyme activity due to harshness of the encapsulation protocols used has been a persistent problem (53). Microencapsulated activated carbons can be used as sorbents to remove metabolic wastes and/or toxins from blood (54). The use of microcapsules in antibody hormone immunoassays has been reviewed (55). The encapsulation of hemoglobin as a red blood substitute has received much attention because of AIDS and blood transfusions (56).

Food Ingredients. A number of food ingredients or additives have been encapsulated and are available commercially. Solid ingredients encapsulated are typically water-soluble and are often encapsulated with a hydrophobic hot-melt coating material applied by a fluidized-bed coating process. Preferred hydrophobic coating materials are partially hydrogenated vegetable oils of varying melting points, monoglycerides, and diglycerides. If a hydrophilic coating is used, it tends to be gum arabic, modified starch, or mixtures of these materials with a maltodextrin. Such capsules typically are produced by spray drying. All coating materials used are well-accepted food-grade products.

Several reviews (57–59) and books (60,61) examine in some detail many aspects of the formation, properties, and uses of microencapsulated food ingredients. Encapsulation is designed to provide taste-masking, possibly a degree of prolonged release, stabilization of the core material against oxidation, and minimization of reaction with other ingredients in the final product. Dziezak discussed the function of a number of commercially available encapsulated solid food ingredients (62). Acidulants like citric and lactic acid encapsulated in partially hydrogenated vegetable oil are used in meat processing, where they provide direct acidification and shorten processing time. Sodium acid pyrophosphate encapsulated in hydrogenated vegetable oil is used in frozen cake batters in order to aid mixing and reduce gas release during batter make-up. In both types of applications, release of core material occurs during a heating cycle that melts the shell formulation and releases the core material. Figure 11 illustrates the nature of commercial NaCl-loaded microcapsules with a lipid coating produced by fluidized-bed coating.

Acidulants like citric, lactic, and fumaric acids encapsulated in a water-soluble maltodextrin shell formulation are used in dry mix beverages and desserts, as well as prepared premixes for the baking and dairy industries. The maltodextrin coating is designed to minimize hygroscopicity, reduce dusting, and minimize reactions with incompatible ingredients. It dissolves in the presence of liquid water to rapidly release the contents of the capsules during a mixing cycle. Figure 12 is a photomicrogrpah of commercial spray dried microcapsules that contain an oxygen-sensitive supplemen oil.

Various iron compounds have been encapsulated in order to provide food products with enhanced iron contents. Boccio and co-workers (63) studied the

Fig. 11. Scanning electron micrograph of commercial NaCl microcapsules with a lipid coating produced by fluidized-bed coating. Magnification: x.

bioavailability in mice and storage stability in milk of ferrous sulfate encapsulated with a lecithin shell. They report high bioavailability of the encapslated ferrous sulfate and found that the capsule-containing milk was stable to heat processing (100°C, 30 min) as well as 6-month storage at room temperature.

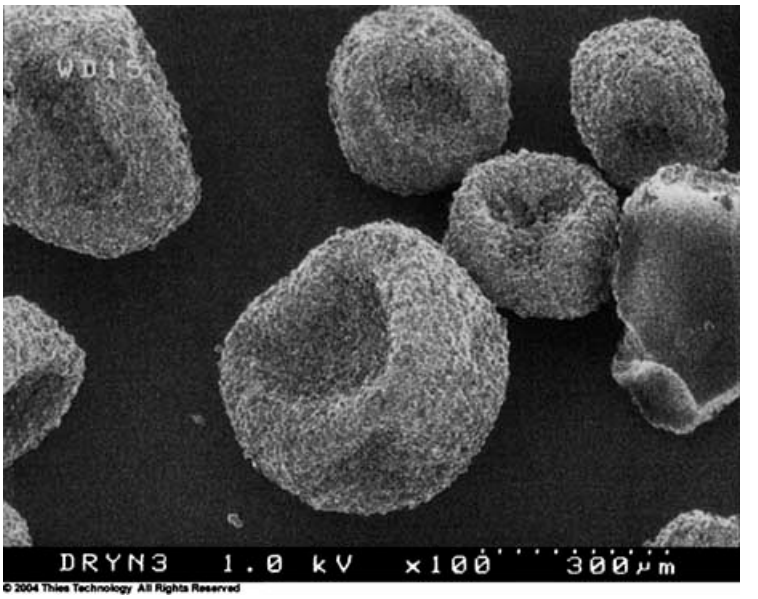

Fig. 12. Scanning electron photomicrograph of commercial PFUA-loaded microcapsules.

Calcium proprionate [4075-81-4] and sodium bicarbonate [144-55-8] encapsulated in hydrogenated vegetable oil are used in chemically leavened products. Release typically occurs during the baking cycle due to melting of the hydrogenated shell material. Sodium bicarbonate encapsulated with maltodextrin is used in dry mix baking and other chemically leavened products. In this case, release occurs during the mixing step. Sodium chloride [7647-14-5] encapsulated in a hydrogenated vegetable shell is used in various meat products, yeast-containing mixes, and assorted doughs. The capsules are designed to minimize inhibition of yeast activity, rancidity, and excessive salt binding during product storage.

Liquid food ingredients encapsulated traditionally have been oil-soluble flavors, spices, and vitamins. However, in recent years, the encapsulation of 3-*n* polyunsaturated fatty acids (PUFAs) for improved cardiovascular health has received much interest recently. Fish oils contain desired PUFAs and are microencapsulated in order to increase resistance of the PUFAs to oxidation. Encapsulation also provides taste-masking. A human feeding study established that the *n*-3 PUFAs in a microencapsulated fish oil have the same desired effect on platlet *n*-3 fatty acid profile as unencapsulated fish oil (64). Figure 12 is a photomicrograph of commercial capsules loaded with PUFAs.

Hydrophobic flavors, food oils, and fats are often encapsulated with a water-soluble shell material applied by spray drying from water (65), but gelatin-based shells formed by complex coacervation can also be used (66). Water-soluble shell materials applied by spray drying include milk protein (casein), modified starches, gum arabic, maltodextrins, or blends of these polysaccharide polymers with maltodextrins. Vitamins are encapsulated with zero bloom strength gelatin by spray drying.

A range of spray-dried flavor-filled capsules with water-soluble shell formulations are used in various dry beverage mixes and other dry food products. Flavors containing ethyl acetate and other low boiling point components pose problems for successful spray-dry encapsulation. Such components are either lost during the initial emulsification process or during the actual dewatering step as a result of azeotrope formation. Another problem with spray-dry encapsulation is the formation of free surface oil. The rapid desolvation that occurs in the drying chamber can produce blow holes in the capsules, essentially leaving a small amount of flavor oil or free or surface oil, which oxidizes on storage and detrimentally affects product quality. This effect generally limits the flavor content of capsules produced by spray drying to 20–30 wt%. Another approach to the encapsulation of food flavors is desolvation by pressure extrusion. The rod-like particles produced in this manner typically have a relatively low loading (8–10 wt%), although higher loadings (15%) have been reported. The advantage of this technology is that it yields essentially defect-free particles with superb shelf-life storage stability. Macrocapsules loaded with a flavor oil are produced by dropwise extrusion through a submerged multifluid nozzle. Figure 13**a** shows the outer surface of commercial capsules produced in this manner. Figure 13**b** is a photomicrograph of a cut capsule that shows the thickness of the capsule shell and lack of macrosopic defects in the shell. Another approach to the encapsulation of food flavors, spray chilling, should be particularly well suited to the encapsulation of aqueous flavor compositions. Release occurs during a product heating cycle, eg, bake or microwave.

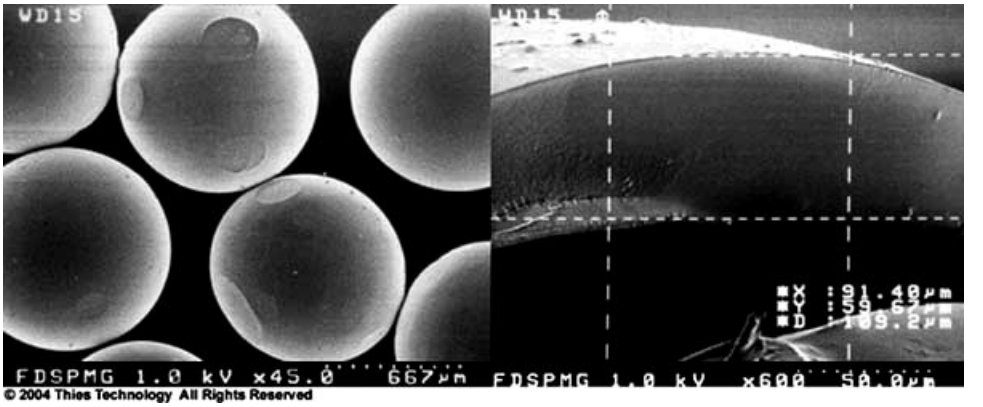

Fig. 13. Scanning electron photomicrographs of commercial flavor-loaded macrocapsules produced by dropwise extrusion through a multifluid submerged nozzle. (**a**), Outer surface of the capsules. Magnification: x. (**b**), Cut macrocapsule that shows uniformity and thickness of the capsule shell. Magnification: x.

The food industry has increasingly realized that microencapsulation offers much potential for the development of new products. For example, Talwlkar and Kailasapathy (67) discuss the effect of microencapsulation on oxygen toxicity in probiotic bacteria, another appplication area of current interest. Hagenbart gives a valuable discussion of the problems that must be overcome when an effort is made to develop microcapsule formulations for use in food products (68).

Agrochemicals. The microencapsulation of pesticides, herbicides, and other pest control agents has been an active area of development. Several books or book chapters (69–72) summarize much of these efforts. Wilkins (69, pp. 314–315) and Tsuji (71) list commercial microencapsulated formulations of pest control agents available in 1990 and 1999, respectively. Most of the microcapsules in these formulations are prepared by interfacial polymerization.

Pest control agents are microencapsulated in order to prolong activity while reducing mammalian toxicity, volatilization losses, phytotoxicity, environmental degradation, and movement in the soil. Ideally, encapsulation would also reduce the amount of agrochemical needed. Penncap-M was the first of several encapsulated pesticide formulations commercialized by Atochem North America (Pennwalt) (8). It is sold as an emulsifiable concentrate of encapsulated methyl parathion. The 30–50-μm capsules are prepared by interfacial polymerization. Encapsulation reduces mammalian toxicity of methyl parathion and prolongs its activity. Significantly, the use of highly toxic pesticides, including microencapsulated forms like Penncap-M, is declining. Microencapsulated chlorpyriphos is no longer sold in the United States.

A significant trend in current agrochemical development work is the on-going transition from highly toxic pesticides to pest control agents with markedly less mammalian toxicity. Examples of the latter include insect pheromones to disrupt mating, insect growth regulators, and pyrethins. Microencapsulation enhances the effectiveness of these compounds. For example, methoprene [40596-69-8],

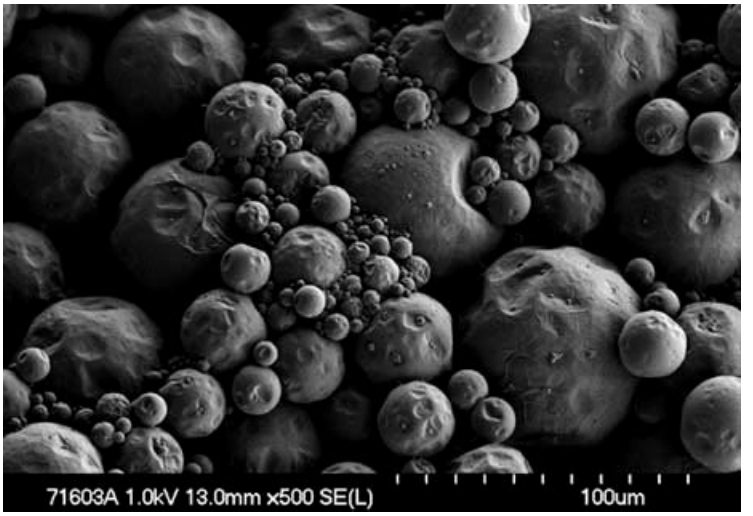

Fig. 14. Scanning electron photomicrograph of pheromone-loaded microcapsules produced by interfacial polymerization. Magnification: x.

a mosquito growth regulator, has been sold as an encapsulated formulation that provides release over a 5–7 day period in the field. A microencapsulated pyrethin formulation is used to control crawling insects such as cockroaches. The capsules are sold as an aqueous-based suspension that provides protection for at least 30 days. Field tests indicate that effectiveness of the encapsulated pyrethin compares favorably with several nonencapsulated pesticides although the capsule formulation leaves a visible residue. Encapsulated fenitrothion [122-14-5] is also available commercially. The capsules are 20 μm in diameter and have a polyurethane shell formed by interfacial polymerization (73). Commrcial microencapsulated pheromone formulations are available and provide pheromone release in the field for 14–28 days. Figure 14 is a photomicrograph of the outer surface of pheromone-loaded microcapsules produced by interfacial polymerization.

The encapsulation of biopesticides has been studied for many years, but the author is not aware of any commercialized encapsulated biopesticide formulations. Hunter-Fujita and co-workers (74) summarize the techniques and shell materials used to produce past encapsulated biopesticide formulations. More recently, Behle and co-workers (75) describe the storage stability and field activity of a spray-dried nucleopolyhedrovirus formulation. Cost and long-term stability of encapsulated biopesticides remain issues to be resolved.

Several encapsulated herbicide formulations exist. Encapsulated alachlor herbicide has been sold as a liquid or dry granule formulation. The capsules, produced by interfacial polymerization, are spherical with a diameter of 2–15 μm. Two thiocarbamate herbicides, EPTC and vernolate [1929-77-7], were encapsulated by interfacial polymerization because they are volatile compounds. When applied in unencapsulated form, they must be incorporated in the soil within 2 h in order to provide effective weed control. When applied as a microencapsulated formulation, the rate of volatilization is lower and soil incorporation can be

delayed by 24 h (76). Microencapsulation of clomazone reduces the risk of bleaching of nontargeted foilage (77).

Various workers have explored the use of microencapsulation as a means of preparing formulations for feeding fish at various stages of development (78). Encapsulated fish food is currently commercially available (79).

Consumer and Industrial Products. Many encapsulated consumer and industrial products exist. Advertising inserts that utilize encapsulated perfumes and flavors contain a coating of scent-filled capsules which break and release scent when the insert is torn open. This product is widely used as a marketing tool, primarily for new perfumes. Various paper products are coated with scent-filled capsules that break when the coated area is rubbed.

Microcapsules are present in a number of personal care and cosmetic products (80). For example, deodorants may contain capsules that release their core contents due to moisture developed because of sweating. Microcapsules are incorporated in various cosmetic creams, powders, and personal cleansing products. Kiyama (81) summarizes the preparation and use of poy(vinyl alcohol) microcapsules in cosmetic products. Miyazawa and co-workers (82) describe the formation of agar capsules designed for cosmetic use. They note that residual glutaraldehyde in capsules with gelatin shells formed by complex coacervation may be an issue for microcapsules intended for cosmetic applications.

Microcapsules are used in several film coatings other than carbonless paper. Encapsulated liquid crystal formulations coated on polyester film produce a variety of temperature-sensitive display products, including thermometers. Polyester film coated with capsules loaded with leuco dyes analogous to those used in carbonless copy paper is used as a means of measuring line and force pressures.

Microcapsules loaded with phase change materials (PCMs) have been incorporated into various textiles (83). They provide enhanced heat capacity not easily achieved in other ways. Nelson (84) discusses a variety of textile applications of microcapsules including encapsulated PCMs. Encapsulated PCMs offer much promise as a means of improving the thermal capacity of various heat-transfer fluids (85).

Several groups have described the fabrication of microcapsules loaded with a catalyst. Catalysts encapsulated include palladium(II) acetate (86) and osmium tetraoxide (87). Microencapsulated catalysts are described as effective, easily isolated from a reaction system by filtration, and reusable. Shchukin and co-workers (88) recognized that chemical processes can be performed within microcapsules to produce unique products that are retained within the microcapsules. They produced crystalline WO_3 nanoparticles inside microcapsules with a polyelectrolyte shell.

Pernot and co-workers (89) discussed a number of one- and two-component adhesive systems that utilize microencapsules. A majority of fasteners used in automobiles are coated with microcapsules loaded with an adhesive. When the fastener is installed, a fraction of the capsules in the coating rupture, releasing the adhesive payload. The adhesive essentially glues the fasteners in place, preventing them from becoming loose and causing rattles. The capsules are designed so that only a fraction of them break each time a fastener is taken off and put back. The on/off cycle can be repeated three or four times.

Encapsulated ammonium polyphosphate [10124-31-9] incorporated in plastics acts as a fire-retardant. In Japan, microcapsules loaded with naramycin are incorporated into poly(vinyl chloride) (PVC). The capsule-loaded PVC is used to coat a range of electrical cables. Rodents bite and gnaw on cables coated with PVC free of capsules, ultimately causing power interruptions; but when rodents bite into cables coated with capsule-loaded PVC coatings, they break the capsules in the coating, thereby releasing the naramycin [66-81-9], a taste-repellent to the rodents. The encapsulation of fillers and pigments for engineering plastics as well as inks and toners is an active area of development (90).

The oil industry uses microencapsulated oil-field chemicals. For example, microencapsulated breaker is delivered into a subterranean formation, where it breaks the fracturing liquid used to stimulate the recovery of fluids such as crude oil or natural gas. Examples of breakers encapsulated include oxidizers, enzymes, and various mineral or organic acids.

Microcapsules designed to serve as inertial confinement fusion targets represent an intriguing potential capsule application that is currently under active development. Schultz and co-workers (91) reviewed the status of this effort in the United States in 1999. Capsules for this application must meet strict spherical geometry and shell thickness uniformity requirements. Tsai and co-workers (92) note that desired properties of candidate shell materials include high gas permeability, high Young's modulus and tensile strength, and good optical transparency. They described the formation of candidate capsules with a polyimide shell by vapor deposition polymerization.

New Developments. Creation of novel microencapsulation technology and applications of microcapsules are goals that many research and development groups are pursuing globally. Technical deficiencies of current capsules, unanticipated problems in marketing, and poor product design are problems that handicapped past efforts. The growing number of products that utilize microcapsules indicates that these issues are increasingly resolved successfully.

BIBLIOGRAPHY

"Microencapsulation, Survey" in *EPST* 1st ed., Vol. 8, pp. 179–736, by James A. Herbig, The National Cash Register Co., and "Microencapsulation with Polyethylene," pp. 736–752, by D. F. Herman, National Lead Co.; "Microencapsulation" in *EPSE* 2nd ed., Vol. 9, pp. 724–745, by Curt Thies, Washington University.

1. A. Kondo, *Microcapsule Processing and Technology*, Marcel Dekker, Inc., New York, 1979.
2. R. Arshady, ed., *Microspheres, Microcapsules and Liposomes*, Citus Books, London, 1999, p. 576
3. P. B. Deasy, *Microencapsulation and Related Drug Processes*, Marcel Dekker, Inc., New York, 1984.
4. E. Mathiowitz, M. R. Kreitz, and L. Brannon-Peppas, in E. Mathiowitz, ed., *Encylopedia of Controlled Drug Delivery*, Vol. 2, John Wiley & Sons, Inc., New York, 1999, p. 493.
5. J. A. Bakan, in J. Swarbrick and J. C. Boylan, eds., *Encyclopedia of Pharmaceutical Technology*, Vol. 9, Marcel Dekker, Inc., New York, 1994, p. 423.
6. R. E. Sparks, I. C. Jacobs, and N. S. Mason, in K. E. Avis, A. J. Shukla, and R.-K. Chang, eds., *Pharmaceutical Unit Operations: Coating*, Vol. 3, Interpharm Press, Buffalo Grove, Ill., 1999, p. 177.

7. J. M. Ruiz, B. Tissier, and J. P. Benoit, *Int. J. Pharm.* **49**, 69 (1989).
8. R. C. Koestler, in A. F. Kydonieus, ed., *Controlled Release Technologies: Methods, Theory, and Applications*, Vol. II, CRC Press, Boca Raton, Fla., 1980, p. 117.
9. G. J. Marrs and H. B. Scher, in R. M. Wilkins, ed., *Controlled Delivery of Crop-Protection Agents*, Taylor & Francis, London, 1990, p. 65.
10. D. A. Wood, T. L. Whatley, and A. T. Florence, *Int. J. Pharm.* **8**, 35 (1981).
11. M. Bakhshaee, R. A. Pethrick, H. Rashid, and D. C. Sherrington, *Polym. Comm.* **26**, 185 (1985).
12. W. D. Jayne, in J. E. Vandegaer, ed., *Microencapsulation: Processes and Applications*, Plenum Press, New York, 1973, p. 103.
13. U.S. Pat. 3,516,941 (June 23, 1970), G. W. Matson (to 3M Corp.).
14. U.S. Pat. 4,087,376 (May 2, 1978), P. L. Foris, R. W. Brown, and P. S. Phillips (to the National Cash Register Co.).
15. C. Thies, in M. Donbrow, ed., *Microcapsules and Nanoparticles in Medicine and Pharmacy*, CRC Press, Boca Raton, Fla., 1992, p. 47.
16. H. Okada, *Adv. Drug Delivery Rev.* **28**, 43 (1997).
17. U.S. Pat. 2,299,929 (Oct. 27, 1942), J. A. Reynolds (to Atlantic Vitamin Corp.).
18. U.S. Pat. 3,389,194 (June 1968), G. R. Somerville (to Southwest Research Institute).
19. M. I. Re, *Drying Technol.* **16**, 1195 (1998).
20. S. Wendel and M. Celik, *Pharm. Technol.* **21**, 124, 1997.
21. A. H. Taylor, *Food Flav. Ingred. Proc. Pckg.* **5**, 48 (Sept. 1983).
22. A. Atilla Hincal and H. Suheyla Kas, in I. Ghebre-Sellassie, ed., *Multiparticulate Oral Drug Delivery*, Marcel Dekker, Inc., New York, 1994, p. 17.
23. R. Lamb, *Food Flav. Ingred. Proc. Pckg.* **9**, 39 (1987).
24. K. Lehmann, in M. Donbrow, ed., *Microcapsules and Nanoparticles in Medicine and Pharmacy*, CRC Press, Boca Raton, Fla., 1992, Chapt. 4.
25. D. M. Jones and P. J. Percel, in I. Ghebre-Sellassie, ed., *Multiparticulate Oral Drug Delivery*, Marcel Dekker, Inc., New York, 1994, p. 113.
26. J. T. Goodwin and G. R. Sommerville, *CHEMTECH* **4**, 623 (1974).
27. U.S. Pat. 3,704,137 (Nov. 28, 1972), E. E. Beck.
28. S. J. Risch, in S. J. Risch and G. R. Reineccius, eds., *Flavor Encapsulation* (ACS Symposium Series 370), American Chemical Society, Washington, D.C., 1988, p. 55.
29. U.S. Pat. 5,019,400 (May 28, 1991), W. R. Gombotz, M. S. Healy, and L. R. Brown (to Enzytech).
30. I. Ribeiro Dos Santos, J. Richard, B. Pech, C. Thies, and J. P. Benoit, *Int. J. Pharm.* **242**, 69 (2002).
31. K. Teshima, *Adv. Eng. Mater.* **5**, 512 (2003).
32. D. Blythe, D. Churchill, K. Glanz, and J. Stutz, in R. Arshady, ed., *Microspheres, Microcapsules and Liposomes*, Citus Books, London, 1999, p. 391.
33. T. Usami, S. Sano, and S. Yoshida, in R. Arshady, ed., *Microspheres, Microcapsules and Liposomes*, Citus Books, London, 1999, p. 391.
34. B. Commiskey, J. D. Albert, H. Yoshizawa, and J. Jacobson, *Nature* **394**, 253 (1998).
35. S. Inoue, H. Kawai, S. Kanbe, T. Saeki, and T. Shimoda, *IEEE Trans. Electron Devices* **49**, 1532, 2002.
36. P. T. Kazlas and M. D. McCreary, *MRS Bull.* **27**, 894 (2002).
37. C. Thies, *CRC Crit. Rev. Biomed. Eng.* **8**, 335 (1983).
38. M. Murillo, C. Gamazo, M. M. Goni, J. M. Irache, and M. J. Blanco-Prieto, *Int. J. Pharm.* **242**, 341 (2002).
39. C. A. Gilligan and A. Li Wan Po, *Int. J. Pharm.* **75**, 1, 1991.
40. H. Ziyan and X. Rubqiu, *Int. J. Gynaecol. Obstet.* **22**, 319 (1984).
41. P. M. J. Flandroy, C. Grandfils, and R. J. Jerome, in A. Rolland, ed., *Pharmaceutical Particulate Carriers*, 1993, p. 321.

42. T. M. S. Chang, *Artificial Kidney, Artificial Liver, and Artificial Cells*, Plenum Publishing Corp., New York, 1978.
43. T. M. S. Chang, *Biomater., Artif. Cells Immobilization Biotechnol.* **21**, 291 (1993).
44. P. Narayan, D. Marchant, and M. A. Wheatley, *J. Biomed. Mater. Res.* **56**, 333 (2001).
45. J. H. Wible, Jr., K. P. Galen, J. K. Wojdyla, M. S. Hughes, A. L. Klibanov, and G. H. Brandedburger, *Ultrasound Med. Biol.* **28**, 1535 (2002).
46. F. Lim and R. D. Moss, *J. Pharm. Sci.* **70**, 351 (1981).
47. P. De Vos, G. H. J. Wolters, W. M. Fritschy, and R. Van Schilfgaarde, *Int. J. Artif. Organs* **16**, 205 (1993).
48. P. de Vos, C. G. van Hoogmoed, J. van Zanten, S. Netter, J. H. Strubbe, and H. J. Busscher, *Biomaterials* **24**, 305 (2003).
49. C. Yin, S. M. Chia, C. H. Quek, H. Yu, R.-X. Z, K. W. Leong, and H.-Q. Mao, *Biomaterials* **24**, 1771 (2003).
50. A. M. Rokstad, B. Strand, K. Rian, B. Steinkjer, B. Kulseng, G. Skjak-Braek, and T. Espevik, *Cell Transplantation* **12**, 351 (2003).
51. J. K. Park and H. N. Chang, *Biotechnol. Adv.* **18**, 303 (2000).
52. M. F. A. Goosen, ed., *Fundamentals of Animal Cell Encapsulation and Immobilization*, CRC Press, Boca Raton, Fla., 1993.
53. C. Thies, in K. L. Kadam, ed., *Granulation Technology for Bioproducts*, CRC Press, Boca Raton, Fla., 1991, p. 179.
54. C.-J. Lee and S.-T. Hsu, *J. Biomed. Mater. Res.* **24**, 243 (1990).
55. A. M. Wallace, *Drug Targeting Delivery* **1**, 177 (1992).
56. T. M. S. Chang, ed., *Blood Substitutes and Oxygen Carriers*, Marcel Dekker, Inc., New York, 1992.
57. F. Shahidi and X.-Q. Han, *Crit. Rev. Food Sci. Nutr.* **33**, 501 (1993).
58. B. F. Gibbs, S. Kermasha, I. Alli, and C. N. Mulligan, *Int. J. Food Sci. Nutr.* **50**, 213 (1999).
59. P. M. M. Schrooyen, R. ven der Meer, and C. G. De Kruif, *Proc. Nutr. Soc.* **60**, 475 (2001).
60. P. Vilstrup, ed., *Microencapsulation of Food Ingredients*, Leatherhead Publishing, Surrey, U.K., 2001.
61. S. J. Risch and G. A. Reineccius, eds., *Encapsulation and Controlled Release of Food Ingredients* (ACS Symposium Series 590), American Chemical Society, Washington, D.C., 1995.
62. J. D. Dziezak, *Food Technol*. 136 (Apr. 1988).
63. J. R. Boccio, M. B. Zubillaga, R. A. Caro, C. A. Gotelli, M. J. Gotelli, and R. Weill, *J. Nutr. Sci. Vitaminol.* **42**, 233 (1996).
64. J. M. W. Wallace, A. J. McCabe, P. J. Robson, M. K. Keogh, C. A. Murray, P. M. Kelly, G. Marquez-Ruiz, H. McGlynn, W. S. Gilmore, and J. J. Strain, *Ann. Nutr. Metab.* **44**, 157 (2000).
65. X.-D. Liu, T. Atarashi, T. Furuta, H. Yoshii, S. Aishima, M. Ohkawara, and P. Linko, *Drying Technol.* **19**, 1361 (2001).
66. J. C. Soper, in S. J. Risch and G. A. Reineccius, eds., *Encapsulaton and Controlled release of Food Ingredients* (ACS Symposium Series 590), American Chemical Society, Washington, D.C., 1995, p. 104.
67. A. Talwlkar and K. Kailasapathy, *Aust. J. Dairy Technol.* **58**, 1 (2003).
68. S. Hagenbart, *Food Prod. Des*. 28 (Apr. 1993).
69. R. M. Wilkins, ed., *Controlled Delivery of Crop-Protection Agents*, Taylor & Francis, London, 1990.
70. H. B. Scher, ed., *Controlled-Release Delivery Systems for Pesticides*, Marcel Dekker, Inc., New York, 1999.
71. K. Tsuji, in R. Arshady, ed., *Microspheres, Microcapsules and Liposomes*, Citus Books, London, 1999, p. 349.

72. R. C. Koestler, G. Janes, and J. A. Miller, in A. F. Kydonieus, ed., *Treatise of Controlled Drug Delivery*, Marcel Dekker, Inc., New York, 1992, p. 491.
73. K. Tsuji, in R. Arshady, ed., *Microspheres, Microcapsules and Liposomes*, Citus Books, London, 1999, p. 373.
74. F. R. Hunter-Fujita, P. F. Entwistle, H. F. Evans, and N. E. Crook, *Insect Viruses and Pest Management*, John Wiley & Sons, Inc., Chichester, U.K., 1998, Chapt. 7.
75. R. W. Behle, P. Tamez-Guerra, and M. R. McGuire, *J. Econ. Entomol.* **96**, 1066 (2003).
76. B. E. Greenwold, F. Pereiro, T. J. Purnell, and H. B. Scher, *Proceedings of the 1980 British Crop Protection Conference on Weeds*, British Crop Protection Society, London, p. 185.
77. P. K. Bollich, D. L. Jordan, D. M. Walker, and A. B. Burns, *Weed Technol.* **14**, 89 (2000).
78. D. A. Jones, D. L. Holland, and S. Jabborie, *Appl. Biochem. Biotech.* **10**, 275 (1984).
79. I. Ben Khemis, C. Audet, R. Fournier, and J. de la Noue, *Aquaculture Res.* **34**, 445 (2003).
80. Y. Vinetsky and S. Magdassi, in S. Magdassi and E. Touitou, eds., *Novel Cosmetic Delivery Systems*, Marcel Dekker, Inc., New York, 1999, p. 295.
81. K. Kiyama, in S. Magdassi and E. Touitou, eds., *Novel Cosmetic Delivery Systems*, Marcel Dekker, Inc., New York, 1999, p. 315.
82. K. Miyazawa, I. Yajima, I. Kaneda, and T. Yanaki, *J. Cosmet. Sci.* **51**, 239 (2000).
83. J. Kim and G. Cho, *Textile Res. J.* **72**, 1093 (2002).
84. G. Nelson, *Int. J. Pharm.* **242**, 55 (2002).
85. Y. Yamagishi, H. Takeuchi, A. T. Pyatenko, and N. Kayukawa, *AIChE J.* **45**, 696, 1999.
86. S. V. Ley, C. Ramarao, R. S. Gordon, A. B. Holmes, A. J. Morrison, I. F. McConvey, I. M. Shirley, S. C. Smith, and M. D. Smith, *Chem. Commun.* **2002**, 1134.
87. S. Nagayama, M. Endo, and S. Kobayashi, *J. Org. Chem.* **63**, 6094 (1998).
88. D. G. Shchukin, W. Dong, and G. B. Sukhorukov, *Macromol. Rapid Commun.* **24**, 462 (2003).
89. J.-M. Pernot, B. Pouyet, H. Brun, and S. Briancon, in R. Arshady, ed., *Microspheres, Microcapsules and Liposomes*, Citus Books, London, 1999, p. 441.
90. A. M. van Herk and A. L. German, in R. Arshady, ed., *Microspheres, Microcapsules and Liposomes*, Citus Books, London, 1999, p. 457.
91. K. R. Schultz, J. L. Kaae, W. J. Miller, D. A. Steinman, and R. B. Stephens, *Fusion Eng. and Des.* **44**, 441 (1999).
92. F. Y. Tsai, D. R. Harding, S. H. Chen, and T. N. Blanton, *Polymer* 44, 995 (2003).

CURT THIES
Thies Technology, Inc.

Encyclopedia of Polymer Sceince and Technology
Copyright © 2005 John Wiley & Sons, Inc. All rights reserved.

NONDESTRUCTIVE TESTING

Introduction

Polymers are macromolecules that contain repetitive, regular or irregular arrangements of organic molecular groups, ie, carbon atoms covalently bonded with other carbon and/or heteroatoms. Technical polymers usually contain additives, fillers, and pigments. Polymer–matrix composites (PMC) contain at least a second, insoluble phase, frequently in the form of fibers or particles. The structure and morphology of polymers and PMC can be quite complex; see, eg, AMORPHOUS POLYMERS; SEMICRYSTALLINE POLYMERS; MORPHOLOGY, ADDITIVES, VISCOELASTICITY, PHASE TRANSFORMATION, and Reference 1. Properties of polymers and PMC that may be relevant for nondestructive testing (NDT) are as follows: (*1*) (pronounced) temperature dependence, viscoelastic behavior, and, in some cases, specific transition temperatures; (*2*) limited thermal stability, upper limit set by incipient decomposition or melting; (*3*) relatively low density; (*4*) transparency, semitransparency, or opaqueness with respect to the visible part of the electromagnetic spectrum; (*5*) electrical insulation and relatively low electrical conductivity for specially formulated compositions; and (*6*) possible changes in volume, properties, and, in some cases, even chemical reactions induced by absorption or diffusion of media.

The literature on NDT of polymers and PMC comprises the classes shown in Table 1. References illustrate the available range of literature or a specific topic. Omission or inclusion of a reference does not imply a rating by the authors. The amount of information available in electronic format only is steadily increasing, eg, References 2–8, and many journals feature electronic on-line editions. Electronic database searches are sensitive to spelling, eg, "non-destructive" yields 27, and "nondestructive" 384, active standards of the American Society for Testing and Materials International. Most NDT methods apply to various material classes. Those documents that explicitly mention polymers or PMC deal with effects specific to certain materials, eg, the Felicity effect in PMC (9), or with polymer products used in large quantities (10–14). Standards tend to lag behind technical developments, as discussed for acoustic emission (15), but similar arguments hold for other NDT methods.

Nondestructive testing (NDT) is the development and application of technical methods for the detection, location, measurement, and evaluation of discontinuities, defects and other imperfections, the assessment of integrity, the assessment of properties and composition, or the measurement of geometrical characters without impairing the intended use or application of the test object (31).

Table 1. Classes of Literature on NDT of Polymers and PMC

Source type	Sample references	Remarks
Handbooks	(16–26)	Some volumes available in 3rd edition, others in preparation; 3rd edition also available in electronic format on compact disc with supplemental information
Monographs	(27,28)	
Normative codes and standards	(9–14)	Few codes and standards are explicitly on NDT applied to polymers and PMC, but most NDT codes and standards are applicable to polymers and PMC, except when explicitly stating another class of materials; up-to-date information can be obtained on the Web sites of standards-issuing organizations, eg (2–5)
Guidelines (without normative character)	(29,30)	A few guidelines are explicitly on NDT applied to polymers and PMC, but most NDT guidelines apply to polymers and PMC, except when stating explicitly another class of materials
Journals	Electronic journals Class A (6,7) Class B (8)	Literature on NDT of polymers and PMC comprises two classes (see Bibliography for examples): A. journals dealing with NDT B. journals dealing with polymers and PMC
Conference proceedings	Class A Class B	Conferences again comprise two classes: A. general or topical (on specific NDT methods and/or applications) NDT conferences B. conferences on polymers and PMC Information on many conferences is available on the Internet, eg, through links on the Web sites of national NDT societies[a]
Technical documents	Equipment descriptions, technical manuals, application notes	Provided, eg, by equipment manufacturers or test agencies
Educational documents	Lecture notes, training manuals	Provided, eg, by lecturers, national NDT societies, NDT training and certification agencies

[a]Web sites of most national NDT societies can be found at www.icndt.org/directory.htm (however, some listings may not be up-to-date).

Composites are a combination of at least two materials, insoluble in one another, combined to yield a material with certain properties not possessed by the constituents (32). In PMC, polymers form a continuous constituent, called *matrix*, in which the other phase(s) are embedded (see COMPOSITE MATERIALS).

The distinction between "natural" and "synthetic" polymers or PMC (eg, natural versus synthetic rubber, plastics versus biopolymers, wood versus fiber-reinforced composites) is of limited relevance for the application of NDT methods.

Classes of Nondestructive Test Methods. NDT methods are classified according to the physical principle or effect that constitutes their base (26), corresponding to the probe-type or energy source (Table 2, the list of methods is incomplete). Each NDT method can be characterized by its type of (*1*) probe or energy source, (*2*) interaction with the test object, (*3*) signal detection, (*4*) signal recording, and (*5*) signal interpretation (26). Other categories for grouping NDT methods are, eg, (*1*) "imaging" versus "nonimaging" methods, (*2*) "volume" versus "local" method, (*3*) noncontact versus contacting methods, (*4*) *in situ* versus *ex situ* or "field" versus "laboratory" testing, (*5*) real-time versus post-test indication and (*6*) "small" or "specific" specimen size versus full-scale testing.

Mechanical Test Methods

Determination of mechanical properties is one, although indirect, way of finding indications of defects (see MECHANICAL PERFORMANCE OF PLASTICS). The elastic modulus of polymers and PMC depends, among others, on porosity or microcrack content. Quantitative evaluation requires comparison with specimens with known content from destructive analysis or others (33). Qualitative, relative comparison is feasible, but still requires careful conditioning, since mechanical properties depend on humidity content and temperature. The tensile elastic modulus of samples from one batch typically yields standard deviations of 3–5% for carbon fiber-reinforced polymers (CFRP) and of 5–7% for glass fiber-reinforced polymers (GFRP). Values around 2% have been obtained for high quality CFRP laminates.

Dynamic Mechanical Analysis (qv) (DMA) or dynamic thermal mechanical analysis (DTMA) indicate damage in polymers or PMC (34), and aging effects in polymers by a shift in the transition temperature (35). Limitations are the volume of the test chamber or the required specimen shape.

Compliance, ie, the displacement-to-load ratio, is used in fracture mechanics tests to determine crack length or to monitor crack growth (36).

Vibration or modal analysis yield indications of defects in structural elements or parts when excited by suitable loads (37) (also see SONIC AND ULTRASONIC TEST METHODS). The literature mainly describes applications to PMC laminates, aiming at detecting critical delaminations (38). A relative comparison for a specific element with time, loading, or exposure may be sufficient to find indications of a defect or of a change in the behavior of the structure. Comparison with finite element calculations is one approach for quantitative evaluation (39). Recent research on monitoring of PMC elements or structures also investigates the use of piezoelectric sensors for detection of delaminations by external excitation (40).

Table 2. Classes of NDT Methods

Class	Methods (examples)	Remarks
Mechanical	E-modulus measurement Vibration analysis Modal analysis Scanning probe microscopy	Mostly indirect indications of defects
Optical	Visual inspection Optical microscopy Brillouin scattering Photoelasticity Projection moiré Shearography Optical holography	Using visible part of electromagnetic spectrum (wavelength roughly between 400 and 700 nm)
Penetrating radiation	X-ray radiography X-ray tomography γ-ray radiography Neutron radiography Neutron scattering Electron microscopy	Electromagnetic (wavelengths below about 1 nm) and particle radiation
Electromagnetic	Dielectric spectroscopy Resistance measurement Eddy-current testing	X-ray and γ-ray classified among penetrating radiation
Sonic/ultrasonic	Tap testing Acoustic emission Acousto-ultrasonics Ultrasonics Acoustic microscopy	
Thermal/infrared	Thermography	Infrared spectrometry is classified among chemical/analytical
Chemical/analytical	Infrared spectrometry Raman spectrometry Ultraviolet spectrometry X-ray spectrometry Magnetic resonance imaging	

Scanning probe microscopy of polymers (listing of web sites on Atomic Force and Scanning Probe Microscopy, with images, is available at http://www.ou.edu/research/electron/www-vl/afm.shtml) and PMC (41,42), beside images indicating possible defects, yields mechanical properties, eg, force-stiffness relations (43), and quantitative surface roughness or corrugation relating to tribology (44), on a microscopic scale (see also MECHANICAL PERFORMANCE OF PLASTICS).

Optical Test Methods

Optical test methods use the visible part of the electromagnetic spectrum; ie, they comprise a subset of the electromagnetic test methods.

Visual inspection by eye is certainly the oldest method and is widely used, but subject to physiological limitations. Optical and electronic equipment, eg, endoscopes originally developed for medical applications, and electronic image recording and processing have become standard tools for visual inspection.

Composition and/or morphology of many polymers and PMC limit NDT visual inspection to surface and near-surface features. Transparent polymers and semitransparent PMC allow for the detection of inhomogeneities, such as voids, pores, or cracks, as well as qualitative or semiquantitative estimates of fiber volume fraction and/or fiber alignment. Light sources enhance sensitivity in visual through-thickness and surface inspection.

Standards for visual inspection of polymer products are in preparation (12). Evaluation requires experience and is operator-dependent. Indications can be documented with photography. Digital photography or digitization of photographs allow for image processing and automated image analysis.

Conventional dye penetrant testing for surface crack detection in PMC is described in older literature (45), but is now rarely used, except for highlighting cracks in PMC after destructive sectioning (46).

Optical microscopy has also profited from recent advances. Scanning near field optical microscopy (SNOM) (47) (SNOM images of polymers and other materials are available at, eg, http://wwwex.physik.uni-ulm.de/SNOMWeb/), eg, reaches spatial resolution at the molecular level when using fluorescent molecules, competing with the scanning probe methods (48). The limitations are typical specimen size and scanning area.

Using coherent or structured light to illuminate the test object can reveal information that is not accessible to visual inspection (25,49,50). Commonly, a film or camera is used to record this information.

Interferometric methods use laser illumination to measure surface deformations under thermal, mechanical, vibration, or pressure loading (51). By virtue of the high sensitivity of a few tens of nanometer, inhomogeneities in the interference fringe pattern due to cracks, delaminations, or material inhomogeneities can be revealed using small loads. Because the laser light is only used to record the information, care must be taken to set up the appropriate loading scheme that enhances the type of defect to be found. Well-known methods in composite testing, especially for aerospace and spacecraft applications, are electronic or digital speckle pattern (correlation) interferometry (ESPI or DSPI) (52–55) and shearography, also termed shearing speckle pattern interferometry (SSPI) (56). The methods are used to find indications of delaminations, voids, and cracks. Quantitative evaluation of deformation and strain is also important (57) and can be used to measure stress concentrations, vibration modes (58,59), or material parameters. By nature, the techniques discussed are surface techniques and therefore most appropriate for surface or close-to-surface defects. However, when combined with transient loads, some information on the depth of a flaw can be gained (60).

(Digital) holographic interferometry (61) basically yields the same information as DSPI, but is limited because it requires a development step (photographic processing or numerical reconstruction) before indicating the load effect on the object.

Limitations of the interferometric techniques are due to the required mechanical stability of the measurement head relative to the object of better than 1 μm. Safety regulations for using high power lasers also have to be observed.

Structured light methods comprise shadow moiré, projection moiré, and fringe projection (25,62). They use a structured intensity pattern, most commonly a set of parallel fringes, to illuminate the object. A camera records the fringes on the object surface from a triangulation angle. In moiré methods (63) fine pitch gratings can be used, because the imaged fringes are demodulated by a reference grating in front of the camera before recording. Moiré methods are usually used to measure deformations or to compare the shape of objects, eg, in production control, with a resolution of roughly 1/10,000 of the field of view (64–66). The physics of fringe projection is basically the same (67), but the fringes are directly recorded by the camera. Hence, the pitch of the grating is limited by the camera resolution.

By using a sequence of ever coarser gratings and a calibrated setup, the absolute shape of an object is acquired with a resolution of roughly 1/1,000 of the field of view (68).

Penetrating Radiation Test Methods

Penetrating radiation comprises electromagnetic radiation in the wavelength range below about 1 nm (roughly equivalent to 1 keV energy) or particle radiation. The former is generated in the electronic shell of atoms (X-rays) or by processes in the atomic nuclei (γ-rays). Particle radiation can be generated with particle accelerators, sometimes requiring special targets. Neutrons, eg, come from a spallation source (69) or a nuclear reactor. X-rays are produced by electron beam impact on targets in evacuated tubes or in accelerators by *Bremsstrahlung*, the "braking" radiation emitted by accelerated, charged particles. Ultraviolet and low energy X-ray radiation of high intensity from synchrotrons is used for analysis (70) and processing (71) of polymers and PMC. A list of currently operational synchrotron sources is available, eg, at http://www.src.wisc.edu/community/sr_sources.html (see SYNCHROTRON RADIATION).

Polymers and PMC are of relatively low density and hence do not absorb X-rays or γ-rays efficiently. "Low" energy radiation (typically 10–40 keV) yields enhanced contrast for X-ray radioscopy or radiography of polymers and PMC due to the nonlinear shape of the absorption versus energy curve (72). Higher energy γ- and X-ray sources are hence less suitable.

Contrast can be enhanced by X-ray contrast agents or X-ray dye penetrants (73). These consist of high density materials, eg, liquid halogen compounds (ZnI, methylenediiodide, or diiodobutane) and are different from the dye penetrants used in visual penetrant testing. Test objects are immersed or the contrast agent is injected into, eg, cracks or delaminations extending to the surface of the test object. Any pore, void, crack, or delamination not extending to the surface hence escapes detection. Sufficient wetting between contrast agent and material is important for complete penetration. Even then, a minimum amount of contrast agent is necessary to obtain detectable contrast. Many commercial contrast agents (*1*) are toxic or carcinogenic requiring appropriate safety measures, (*2*) are volatile to some degree, limiting immersion time and imaging duration, (*3*) are of limited

shelf live, and (*4*) raise concerns about inducing deleterious effects (73). There is at least one documented case of suspected dye penetrant induced microcracking in PMC (74).

Penetration and absorption of the electromagnetic or particle radiation results in energy deposition (heating) and implantation of beam particles. Energy deposition and particle irradiation may affect the microstructure and induce breaking or formation of new molecular bonds. Examples are gamma radiation effects (75) and cross-linking in polyethylene by electron irradiation (71). The intensity needed for cross-linking usually exceeds that obtained from NDT beam sources.

Conventional X-ray tubes with an energy range from 10 to 450 keV have a typical source diameter (focal spot) of a few millimeters. Microfocal X-ray sources (76) with a source diameter of about 5 to 10 μm allow for magnification in X-ray radiography by projection imaging (test object close to source, imaging system at a distance). The small source size limits the blur due to geometrical projection with conventional X-ray sources. Energy—microfocal X-ray sources operate up to about 200 keV—and intensity limit the maximum distance between source and imaging system. Magnification can be up to 100 times, but frequently the size of details to be imaged or the maximum size of the imaging system set lower limits.

At energies below 40 keV, X-ray absorption in air is a major limitation, and replacing air by low density helium has been recommended (77). This requires a special enclosure for X-ray source and imaging system, often limiting the size of the test object. *X-ray beam hardening* (78), ie, the preferential absorption of low energy X-rays in the test object, also occurs in polymers and PMC, but to a lesser extent than in denser materials.

Low X-ray intensity yields longer exposure times; for a 1-mm thick CFRP plate a G2 class X-ray film (79) (ie, a D4 class film at that time), 17–18 keV X-ray energy, 1000 mm imaging system–focus distance, and a focus–object distance of 150 mm, resulted in an exposure of about 600 s (80).

X-ray image intensifiers converting the incident X-rays into an image on a scintillating screen allow time-resolved X-ray imaging when recorded with a video camera. Crack initiation in PMC, eg, was investigated with a microfocal X-ray source and X-ray image intensifier with 25-Hz video imaging at magnifications between 5 and 10 times (81). Digitized frames of the video recording can be electronically processed and analyzed. Conventional or X-ray film still images can also be digitized for electronic processing (82).

X-ray radiography is moving from X-ray film to computed radiography (CR). Reusable imaging plates with 25 or 50 μm resolution are commercially available. Manufacturers data sheets indicate that up to 1000 record–erase cycles can be performed (83). Special electronic filters may improve detection of indications. Electronic image recording and storage allow for easy processing and electronic data transmission. However, long-term storage and readability of the records may pose problems in the future. Development of standards in CR is under way (84,85).

X-ray Compton back-scattering can yield indications of delaminations in PMC without the use of contrast agents, ie, including those that do not extend to the surface. The basis is a special source–detector arrangement (86).

X-ray laminography was developed for investigating specific layers of fiber-reinforced laminate sheets by multiple exposure on the same film. Recently, it has been developed into a computer tomography (CT) method (87), but is rarely used.

X-ray CT with commercial CT equipment or synchrotron radiation (70) is increasingly used in research and development, and industrial use is incipient. X-ray micro-CT yields spatial resolution of around 10–20 μm for microfocal (76) and down to 1–2 μm for synchrotron X-ray sources (88). These resolutions require "small" test objects, around a few cubic decimeters in the microfocal and a few cubic centimeters in the synchrotron X-ray source.

X-ray refraction, based on small angle X-ray scattering (SAXS), may prove useful in the detection of microdamage in PMC, such as crack growth (89) and fiber debonding (90). SAXS images of polymer nanocomposites are shown in Reference 91. Near-edge X-ray absorption fine structure (NEXAFS) and related X-ray techniques provide information on composition and morphology of polymers on a microscopic scale (see X-RAY MICROSCOPY).

Neutrons find various applications in the characterization of polymers and PMC (92). Neutron scattering experiments investigate structure and behavior of polymers at the atomic level (93). Neutron absorption as a function of the atomic number of the elements differs from that of X-rays, and the power of neutron radiography (94) for polymers and PMC, even combined with metals, is illustrated at, eg, http://neutra.web.psi.ch/gallery/index.html. Currently operational neutron radiography sources are listed at www.anlw.anl.gov/nr/oldindex.htm.

Positron annihilation spectroscopy (PAS) is used in research on free volume (95) or on aging effects in polymers (96), and muon spin resonance with muon beams (97) yields information on dynamic processes in polymers (98), but specimen size may be limited.

Electron microscopy is one example of electron beam analysis of polymers and PMC. Beam charging effects occur in most polymers and PMC (99), unless when coated with a thin conductive layer (carbon, gold, or platinum). Environmental scanning electron microscopes (ESEM) do not require such coatings (100). Size and shape of the test object and possible electron beam heating effects then decide whether the method is NDT.

Electromagnetic Test Methods

Many polymers and most PMC show no or only comparatively low electrical conductivity, which limits application of electromagnetic test methods. One of the main exceptions is CFRP. The continuous network of carbon fibers in CFRP allows for electrical resistance measurements, eg, based on the four-probe method. Electrical potential (101) or resistance methods are used in fracture mechanics to detect delaminations (102) and to monitor damage in CFRP (103). Whether the application of electrodes is nondestructive depends on the intended use.

Electrical conductivity measurements have also been developed as tomography (104). Eddy-current testing (ET) of CFRP laminates is feasible (105). ET is noncontact and NDT, as long as thermal effects from resistive heating and energy dissipation are sufficiently small. Superconducting quantum interference devices (SQUID) have been used for ET to detect damage in CFRP (106). However, SQUID

may soon be replaced by sensors based on giant magnetoresistance (GMR) or giant magnetoimpedance (GMI) effects (107).

Dielectric measurements are performed on polymers and PMC for research and industrial applications, specifically to find materials with low dielectric losses (108) (see DIELECTRIC RELAXATION).

Fractoluminescence (109), ie, the emission of visible light, and electromagnetic emission from fracture of polymers or PMC (110) have not yet been investigated as NDT tools. Microwave testing is applicable to nonconducting materials (111) and used, eg, for exciting ultrasonic waves in PMC (112) or the characterization of anisotropic materials, such as short fiber–reinforced injection molded parts (113). The energy deposition due to microwave radiation, on the other hand, is applied in processing of polymers and PMC (114).

Sonic and Ultrasonic Test Methods

Sonic and ultrasonic test methods use elastic waves propagating in solid or fluid media and are classified into "active" and "passive" methods. The former requires emission of waves into the test object; the latter, waves emitted by the material itself.

Tap testing a PMC structure by hand or by a suitable instrument, an experienced operator can tell whether the structure is sufficiently defect-free (115).

Acoustic emission (AE) analysis is an example of a passive method (21). Beside piezoceramic lead zirconate titanate (PZT) sensors, thin piezoelectric poly(vinylidene fluoride) (PVDF) films (116) and noncontact interferometry (117) also sense the rapid, transient elastic waves generated inside most materials. Composites (118) made from PZT fibers have recently been characterized as AE sensors (119). AE of polymers and PMC is affected by (*1*) relatively large signal attenuation limiting the maximum distance between sensor and signal source, and mainly in PMC; (*2*) anisotropy, limiting location accuracy; and (*3*) several source mechanisms that can act simultaneously. In PMC, the so-called Felicity effect ie, the appearance of AE activity at the same sensitivity but lower load levels than previously attained (31), forms the base of commercial AE applications in integrity assessment of PMC structures (9).

Quantitative AE analysis for characterizing damage accumulation in PMC is described in Reference 120, approaches for signal analysis and identification of mechanisms in Reference 121, and a practical AE application to automotive composites in Reference 122.

Ultrasonic waves (typically in the MHz range) can be excited by piezoelectric transducers coupled to the test object. Electromagnetic acoustic transducers (EMAT) (123) cannot be used for ultrasonics of polymers and PMC; alternatives are discussed in Reference 124. The waves propagate and are scattered and attenuated in the material. The signal can be detected in either reflection or transmission mode (by the transducer emitting the ultrasonic pulse for reflection or by additional transducers at other locations in transmission). Acousto-ultrasonics (AU) (11) records low frequency guided waves (typically 30–500 kHz) emitted at another location to detect changes in the test objects, eg, in carbon–carbon

composites (125). Recently developed stacked transducers look promising for low frequency applications (126).

Ultrasonic A-, B-, and C-scans (23) can be obtained from polymers and PMC. Isotropic or anisotropic elastic constants, attenuation, and phase transitions are detected in detailed A-scan data analysis (127,128). Ultrasonics is also used for process monitoring in manufacturing of polymeric or PMC parts (129).

Ultrasonic C-scan is standard for quality inspection of PMC plates (28), but the large signal attenuation with penetration depth limits this to "thin" plates. Lower frequency waves, eg, 0.5 MHz, yield larger penetration for equivalent attenuation, but the longer wavelengths limit the spatial resolution (eg, 6 mm for 0.5 MHz at 3000 m/s).

Another limitation is posed by the shadowing effect in PMC. The delamination closest to the transducer will reflect the ultrasonic pulse to such an extent that delaminations below will be masked, unless their lateral size is larger. Even C-scans taken on both sides do not necessarily guarantee detection of delaminations in all layers. In the reflection mode, repeat echoes from multiple reflections have to be distinguished from "real" indications, especially in relatively thin PMC shells.

The shape of certain structures, eg, shells or thin rods with small radii of curvature, limits the application of ultrasonics, but there is equipment that allows three-dimensional movement of the transducer (130).

The standard coupling via immersion in water or use of water jets may be prohibited, since many polymers and PMC change mechanical properties or chemical composition due to penetration of water (swelling, softening, leaching of components, hydrolysis). If immersion in water is used, formation of gas-bubbles from dissolved air has to be prevented. Gel-like coupling agents may leave stains on the surface, but now wheel array sensors for dry coupling (131,132) are available, eg, for the inspection of aerospace structures (133). Air-coupled ultrasonics also offer an alternative (131,134,135). Ultrasonic pulses in polymers and PMC can also be generated by laser (136,137), but this may lead to heating effects. Ultrasonic imaging is widely used for electronic components, where indications of defects (delaminations, cracks, pores) in the epoxy packaging have to be detected (138).

Ultrasonic computer tomography (CT) of polymers is feasible (139).

Recently, phased-array technology (140) has become a novel ultrasonic scanning technique. Multielement transducers in conjunction with high speed electronics allow for electronic focusing and steering of the ultrasonic beam. Since no mechanical movement is involved, the "scanning speed" can be enhanced, enabling imaging for on-line control of manufacturing (141,142).

Ultrasonic transducers can excite various wave modes, eg, guided Lamb waves that may be suitable for specific applications (143). Ultrasonic excitation is also used to detect the so-called acoustic nonlinearity associated with defects, eg, in PMC (144,145). The combination of recording guided ultrasonic waves with numerical back-calculation of wave propagation for detecting indications of defects in PMC pipes also looks promising (146). Surface-bonded fiber optics can detect ultrasonic waves via interferometric techniques (147). Beyond frequencies of 1 GHz, ultrasonics is called *acoustic microscopy*; for details, the reader is referred to Reference 148. This technique can be applied to polymers or PMC (149), specifically to polymeric microelectronics packaging (150).

Thermal and Infrared Test Methods

Thermal and infrared methods can also be classified as passive or active (see THERMAL ANALYSIS). *Passive thermography*, ie, recording the temperature distribution, is rarely used for detecting indications, but probably found useful in polymer and PMC process monitoring (151). The emissivity of the specimen and other factors have to be considered for accurate measurements (152).

Active thermography requires the application of a stimulus (thermal heat), either as single pulse (153) or continuously varying with time (154). The pulse, typically from flash lights, its duration, and intensity, as well as direction (surface or back side of test object) will affect the detectability of the indications (155). Surface finish or paint coats may affect the absorption of the pulse. In CFRP, excitation by short ultrasonic pulses (156) and noncontact eddy currents is also feasible.

In lock-in thermography (154), the selected frequency of the heat "wave" to which the detector is tuned (locked) is important. *Heat waves* are diffusion waves that yield a quadratic dependence on time for the observation of indications at a certain depth of the test object. For thin-walled PMC shells (a few millimeters) this does not constitute a severe limitation (157). Limited operating temperature, pronounced temperature-dependent properties, and thermal degradation may pose limits on the application of active thermography to polymers and PMC. A recent example of a possible application of active thermography in PMC is the determination of the fiber orientation of CFRP (158) that, in the future, may replace the conventional destructive methods.

Chemical and Analytical Test Methods

Chemical analysis of polymers typically deals with monomers or functional groups rather than constituent atoms. Thermal infrared and laser optical Raman spectrometry are the typical tools (36) (see TEST METHODS; VIBRATIONAL SPECTROSCOPY), but frequently, specific specimen size or form is required. For physical properties, mechanical and sonic/ultrasonic NDT methods are available (see above). Molecular mass distribution and related properties of polymers, or fiber or particle volume fraction and distribution for PMC, are usually determined destructively (see TEST METHODS).

Detection, Sizing, and Evaluation of Indications with Nondestructive Test Methods

Basic Approaches. The morphology of polymers and PMC comprises several levels, each with specific defects (see MORPHOLOGY). In NDT, a defect is an aggregate of or a single imperfection or discontinuity that exceeds specified acceptance criteria. These criteria may depend on and vary with location, size, or orientation of the indication. The indications can further be (*1*) relevant, (*2*) nonrelevant, or (*3*) false (31). Hence, not all detected indications are "defects."

Locating the indication is frequently performed with "imaging" methods that also image reference points on the test object. Some nonimaging methods also yield information on location, eg, from source location algorithms in acoustic emission analysis (21).

Locating is a prerequisite for *sizing*, ie, the determination of geometrical dimensions required by specified size criteria. This relates to the spatial resolution of the NDT method. For nonimaging methods, sizing may be replaced, eg, in acoustic emission by defect severity evaluation (159). Principles, limitations, and accuracy of defect location and sizing in polymers and PMC with specific NDT methods are described in (16–26).

Defect types frequently relate to the mechanism causing the indication. Many NDT methods have an intrinsic sensitivity for specific types of indications. Examples are (*1*) ultrasonic C-scans sensitive to boundaries between materials of different acoustic impedance (eg, voids, delaminations), (*2*) X-ray radiography sensitive to variations in density (eg, inclusion of foreign objects, voids), and (*3*) acoustic emission sensitive to microscopic stress release (eg, crack growth).

Determination of Structural Integrity with Nondestructive Test Methods. Some commercial NDT applications, mainly on PMC, do not aim at detection and evaluation of individual indications, but rather at the so-called structural integrity. Most technical structures contain flaws that may evolve into defects that accumulate and grow with time. Structural integrity analysis evaluates test objects with respect to critical defect accumulation, beyond which further use may lead to catastrophic failure. A prime method for determination of the integrity of PMC structures is acoustic emission analysis (9,21). Driven in part by economic considerations, predicting the remaining service-life is increasing in importance. NDT monitoring is hence expected to contribute to, or to be incorporated into, service-life engineering approaches to design.

Smart Monitoring of Polymer–Matrix Composites Elements. The increasing use of PMC in structural elements or as reinforcement or for repair may, at least in critical applications, require periodic inspection or even continuous monitoring. Intermittent or continuous, smart monitoring of PMC aims at automatic detection of specified defects. One research direction develops intelligent materials or structures that sense indications, assess their significance, eg, with computer-based evaluation or expert systems (160), and, if considered significant, take appropriate corrective measures. A full review of smart monitoring of PMC structures is beyond the scope of this article, but a few examples will illustrate this active research area.

Fiber optics based monitoring of PMC includes, eg, strain (161), temperature, acoustic emission signals, and other measurements (162). Electromagnetic resistance measurements yield information on strain changes and defect accumulation (101–104). Even carbon nanotubes are now investigated as strain sensors in PMC (163). Piezoelectric thin wafers or plates (164) or active fiber composites made from piezoelectric fibers (165) also yield, eg, strain and acoustic emission signals. The performance of fiber optics and piezoelectric sensors for detection of microdamage in CFRP is compared in Reference 166.

Another area receiving increasing attention recently is the application of electroactive polymers in actuators and sensors (167). Quite likely, this could lead

to new approaches for NDT of polymers and PMC in the context of smart monitoring of structural elements.

Special Applications of Nondestructive Test Methods

Determination of Geometry or Size and Reverse Engineering. So far, determination of geometrical characteristics has only been discussed with respect to defect location and sizing. However, NDT also comprises determining geometrical characteristics of test objects per se (31). Determination of size and shape, with calipers by hand, with gauges, or with computer-controlled tactile coordinate-measuring machines, is a routine quality assurance procedure, but noncontact methods are also used (168). Size and shape of the test object may pose some limitations. Another example is wall thickness measurements with dedicated ultrasonic thickness gauges (169). As discussed above, the maximum thickness is limited by the frequency-dependent, attenuating properties of polymers and PMC. Requirements on spatial resolution, eg, for test objects where the wall thickness varies over distances that are short compared with the size of the probe, pose another limitation. CT offers another approach for determining geometrical characteristics, X-ray CT being most widely used. CT based on other probe types (see Table 2), eg, ultrasonics (139), magnetic resonance imaging (MRI), also called Nuclear Magnetic Resonance (NMR) imaging (170) (see NUCLEAR MAGNETIC RESONANCE), optical coherence tomography (mainly applicable to GFRP but with limited penetration in CFRP and not suitable for aramide fiber–reinforced PMC) (171), thermal impedance tomography (172), and positron emission tomography (173) are feasible as well.

The driving force behind the development of industrial CT has been and still is the medical field; new methods and improvements are likely to originate there (174). Spatial resolution in X-ray CT depends on the type of X-ray source and on the size and shape of the test object (76,88). X-ray and MRI CT, however, yield more than geometrical characteristics; the data can be converted into distributions of, eg, density, elemental composition (175), or even velocity (176). Three-dimensional CT representations of the geometry, converted into computer-aided design (CAD)-compatible files (177), are used for quality control by comparing with CAD design data for deviations from specification and tolerances, or for computer-aided manufacturing, such as rapid prototyping or reverse engineering (178,179).

Nondestructive Testing of Adhesive Joints. Many commercially available adhesives are based on polymers. NDT of adhesive joints (180) poses challenges because of (*1*) the small size of possibly deleterious defects (eg, porosity), (*2*) the thinness of the adhesive layers, and (3) sometimes, the size, shape, and material of the adherends. Acousto-ultrasonics (181) and various types of ultrasonics (182,183) are applicable to adhesive joints. Ultrasonics can be combined with noncontact optical methods (184) and pulsed thermography (185). However, the assessment of the "quality" or of the quantitative strength of the adhesive bond based on the NDT data often proves difficult.

Process Monitoring and Process Control with Nondestructive Test Methods. NDT plays an important role in quality assurance for products from

all classes of materials and is increasingly used in process monitoring and control. NDT monitoring of polymers and PMC comprises, eg, cure monitoring of molding with thermography (151), infrared methods (186), fiber optics (187), dielectric spectroscopy (188), or ultrasonics (129). Phased-array ultrasonics may be used for on-line manufacturing control (142). NDT process control requires sufficiently fast data analysis and feedback into the process management or steering facility. Some approaches for smart monitoring of PMC, eg, AE, show potential for NDT process control.

Cost may limit process control to either crucial or most effective parameters, eg, pressure and temperature in extrusion (189). Process simulation for optimization of parameters (190) prior to process implementation is also a cost-effective tool (see PROCESSING, MODELING).

Summary and Outlook

Beside technical aspects mentioned above, there are additional considerations for selecting NDT methods for a specific purpose. Cost, frequently, is decisive and major cost factors are (*1*) test duration, including time used for setup and post-test analysis and assessment; (*2*) type of equipment, its sophistication, calibration, and maintenance (compatibility with previous records from periodic inspection may require costly maintenance of aging equipment); (*3*) equipment operator, specifically operator training and certification (191); (*4*) accreditation of test agency; (*5*) qualification or validation of the NDT method (192); and (*6*) accuracy and precision estimates required by test standards or quality management systems.

NDT may hence be effective and economic in scientific research, product or process development, manufacturing process control, quality assurance, and in-service monitoring of crucial or high performance rather than mass produced, low cost polymer and PMC products.

Size and shape of the test object relative to the required spatial and, sometimes, temporal resolution may significantly influence the choice of the NDT method. "Small" objects are readily tested with commercial equipment, while "large" objects may require portable equipment or robots, special test rigs, or several operators. "Single shot" imaging, if satisfying the specification, is to be preferred over scanning, where test duration mainly depends on scan time, ie, scan step to scan area ratio. The shape of test objects may preclude the use of imaging methods, eg, because of hidden areas or uneven spatial resolution. Large size combined with high spatial and/or temporal resolution increases the amount of data and duration of analysis.

Five trends seem to govern the development of NDT, namely, (*1*) increasing sensitivity, (*2*) increasing spatial resolution, (*3*) decreasing test and analysis duration, (*4*) increasing automation of testing, analysis, and evaluation, and (*5*) increasing use of so-called real-time NDT methods (80). The increase in computing power at constant or even lower cost, frequently projected to follow an exponential growth, called *Moore's law* (http://www.intel.com/research/silicon/mooreslaw.htm), is still defying predictions that computer technology will reach physical limits. Hence, the last three trends may continue, while the first two may reach physical or economic limits sooner.

Applying a combination of NDT methods is advisable in many cases. A useful guiding principle is to choose NDT methods that yield complementary information, eg, based on different probe types (Table 2). One example is acoustic emission monitoring with high sensitivity for potentially critical areas, followed by high spatial resolution inspection of such areas by, eg, ultrasonic or X-ray methods to quantitatively locate and size the indication.

The general problem of selecting the "optimum" NDT method for polymers and PMC requires consideration and balancing of several aspects. These are (*1*) requirements on type and size of indications that have to be detected with specified confidence compared to size and shape of the test object; (*2*) technical feasibility of the test method, including behavior of the material under the applied stimulus; (*3*) availability of the test method; (*4*) (eventually) formal requirements, eg, operator certification, test facility accreditation, test method validation; (*5*) (eventually) compatibility with previous measurements; and (*6*) overall cost. It would be of interest to have more quantitatively evaluated, comparative tests applying different NDT methods to specimens with simulated, known defects (80) or to real test objects. A comparative study of the cost of different NDT methods for polymer and PMC would also be welcome.

BIBLIOGRAPHY

1. M. Stamm and B. Carlowitz, *Ullmann's Encyclopedia of Industrial Chemistry*, Wiley-VCH Verlag GmbH, Weinheim, Germany, 2002.
2. International Organization for Standardization Web site: http://www.iso.ch.
3. Comité Européen de Normalisation Web site: http://www.cenorm.be.
4. International Electrotechnical Commission Web site: http://www.iec.ch.
5. American Society for Testing and Materials International Web site: http://www.astm.org.
6. *J. ASTM Int.* Electronic journal starting Jan. 2004, see Ref. 5.
7. *NDT.net*. Electronic journal available at http://www.ndt.net.
8. *e-polymers*. Electronic journal available at http://www.e-polymers.org.
9. ASTM E1067, Standard Practice for Acoustic Emission Examination of Fiberglass Reinforced Plastic Resin (FRP) Tanks/Vessels, *Annual Book of ASTM Standards*, Vol. 03.03, American Society for Testing and Materials International, West Conshohocken, Pa., 2004.
10. ASTM E1118, Standard Practice for Acoustic Emission Examination of Reinforced Thermosetting Resin Pipe (RTRP), *Annual Book of ASTM Standards*, Vol. 03.03, American Society for Testing and Materials International, West Conshohocken, Pa., 2004.
11. ASTM E1736, Standard Practice for Acousto-Ultrasonic Assessment of Filament-Wound Pressure Vessels, *Annual Book of ASTM Standards*, Vol. 03.03, American Society for Testing and Materials International, West Conshohocken, Pa., 2004.
12. EN 13100-1, *Nondestructive testing of welded joints of thermoplastics semi-finished products*, Part 1: Visual examination.
13. prEN 13100-2, *Nondestructive testing of welded joints of thermoplastics semi-finished products*, Part 2: X-ray radiographic testing.
14. prEN 13100-3, *Nondestructive testing of welded joints of thermoplastics semi-finished products*, Part 3: Ultrasonic testing.
15. A. J. Brunner and J. Bohse, *NDT.net* **7**(9), 10 (2002).

16. C. N. Jackson, C. N. Sherlock, and P. O. Moore, eds., *Nondestructive Testing Handbook, Vol. 1: Leak Testing*, 3rd ed., American Society for Nondestructive Testing, Columbus, Ohio, 1998.
17. N. Tracy and P. O. Moore, eds., *Nondestructive Testing Handbook, Vol. 2: Liquid Penetrant Testing*, 3rd ed., American Society for Nondestructive Testing, Columbus, Ohio, 1999.
18. X. P. V. Maldague and P. O. Moore, eds., *Nondestructive Testing Handbook, Vol. 3: Infrared and Thermal Testing*, 3rd ed., American Society for Nondestructive Testing, Columbus, Ohio, 2001.
19. R. H. Bossi, F. A. Iddings, G. C. Wheeler, and P. O. Moore, eds., *Nondestructive Testing Handbook, Vol. 4: Radiographic Testing*, 3rd ed., American Society for Nondestructive Testing, Columbus, Ohio, 2002.
20. S. S. Udpa and P. O. McIntire, eds., *Nondestructive Testing Handbook, Vol. 4: Electromagnetic Testing*, 3rd ed., American Society for Nondestructive Testing, Columbus, Ohio, 2004.
21. R. K. Miller and P. McIntire, eds., *Nondestructive Testing Handbook, Vol. 5: Acoustic Emission Testing*, 2nd ed., American Society for Nondestructive Testing, Columbus, Ohio, 1987.
22. Th. J. Schmidt, K. Skeie, and P. McIntire, eds., *Nondestructive Testing Handbook, Vol. 6: Magnetic Particle Testing*, 2nd ed., American Society for Nondestructive Testing, Columbus, Ohio, 1989.
23. A. S. Birks, R. E. Green Jr., and P. McIntire, eds., *Nondestructive Testing Handbook, Vol. 7: Ultrasonic Testing*, 2nd ed., American Society for Nondestructive Testing, Columbus, Ohio, 1991.
24. M. W. Allgaier, S. Ness, P. McIntire, and P. O. Moore, eds., *Nondestructive Testing Handbook, Vol. 8: Visual and Optical Testing*, 2nd ed., American Society for Nondestructive Testing, Columbus, Ohio, 1993.
25. R. K. Stanley, P. O. Moore, and P. McIntire, eds., *Nondestructive Testing Handbook, Vol. 9: Special Nondestructive Testing Methods*, 2nd ed., American Society for Nondestructive Testing, Columbus, Ohio, 1995.
26. S. Ness, C. N. Sherlock, P. O. Moore, and P. McIntire, eds., *Nondestructive Testing Handbook, Vol. 10: Nondestructive Testing Overview*, 2nd ed., American Society for Nondestructive Testing, Columbus, Ohio, 1996.
27. J. Summerscales, ed., *Non-Destructive Testing of Fibre-Reinforced Plastics Composites*, Vol. 1, Elsevier Science, Ltd., Oxford, 1987.
28. J. Summerscales, ed., *Non-Destructive Testing of Fibre-Reinforced Plastics Composites*, Vol. 2, Elsevier Science, Ltd., Oxford, 1990.
29. Committee on Acoustic Emission from Reinforced Plastics, CARP of the Society of Plastics Industries, *J. Acoustic Emission* **11**(3), C1–C24 (1993).
30. ASTM E1495, Standard Guide for Acousto-Ultrasonic Assessment of Composites, Laminates, and Bonded Joints, *Annual Book of ASTM Standards*, Vol. 03.03, American Society for Testing and Materials International, West Conshohocken, Pa., 2004.
31. ASTM E1316, Standard Terminology for Nondestructive Examinations, *Annual Book of ASTM Standards*, Vol. 03.03, American Society for Testing and Materials International, West Conshohocken, Pa., 2004.
32. ASTM D3878, Standard Terminology for Composite Materials, *Annual Book of ASTM Standards*, Vol. 15.03, American Society for Testing and Materials International, West Conshohocken, Pa., 2004.
33. ASTM WK581, Standard Guide for Assessing the Porosity of Polymeric Scaffolds for Use in Tissue-Engineered Medical Products, New Work Item, ASTM Subcommittee F04.42, see information in Ref. 5.

34. D. S. Jones, *Int. J. Pharm.* **179**, 167–178 (1999).
35. C. Saron and M. I. Felisberti, *Mater. Sci. Eng. A* **370**, 293–301 (2004).
36. P. Davies, A. J. Brunner, and B. R. K. Blackman, *Appl. Compos. Mater.* **5**(6), 354–364 (1998).
37. S. S. Kessler, S. M. Spearing, M. J. Atalla, C. E. S. Cesnik, and C. Soutis, *Compos., Part B: Eng.* **33**, 87–95 (2002).
38. S. Vanlanduit and P. Guillaume, *Mech. Systems Signal Process.* **18**, 79–88 (2004).
39. J. Cugnoni, Th. Gmür, and A. Schorderet, *Compos., Part A: Appl. Sci. Manuf.* **35**(7/8), 977–987 (2004).
40. P. Tan and L. Tong, *J. Compos. Mater.* **38**(4), 321–325 (2004).
41. D. W. Bonnell, *Scanning Probe Microscopy and Spectroscopy, Theory, Techniques, and Applications*, 2nd ed., Wiley-VCH, New York, 2001.
42. B. D. Ratner and V. V. Tsukruk, eds., *Scanning Probe Microscopy of Polymers* (ACS Symposium Series 694), American Chemical Society Division of Polymer Chemistry, Calif. ACS Meeting, Orlando, 1996.
43. R. J. Colton, D. R. Baselt, Y. F. Dufrêne, J.-B.D. Green, and G. U. Lee, *Curr. Opin. Chem. Biol.* **1**, 370–377 (1997).
44. G. V. Dedkov, *Phys. Status Solidi A* **179**, 3–75 (2000).
45. R. Vipond and C. J. Daniels, *Composites* **16**(1), 14–18 (1985).
46. S. A. Hitchen and S. L. Ogin, *Compos. Sci. Technol.* **47**(3), 239–244 (1993).
47. K. D. Jandt, *Mater. Sci. Eng. R* **21**, 221–295 (1998).
48. J. Michaelis, C. Hettich, J. Mlynek, and V. Sandoghdar, *Nature* **405**, 325–328 (2000).
49. P. K. Rastogi and D. Inaudi, eds., *Trends in Optical Non-destructive Testing and Inspection*, Elsevier, Amsterdam, 2000.
50. P. K. Rastogi, ed., *Optical Measurement Techniques and Applications*, Artech House, London, 1997.
51. R. Jones and C. Wykes, *Holographic and Speckle Interferometry*, 2nd ed., Cambridge University Press, Cambridge, 1989.
52. M. V. Rao, R. Samuel, and A. Ananthan, *Opt. Lasers Eng.* **40**, 563–571 (2003).
53. G. Georgeson, *Proc. Int. Soc. Opt. Eng. SPIE* **4704**, 104–115 (2002).
54. M. O. W. Richardson, Z.-Y. Zhang, M. Wisheart, J. R. Tyrer, and J. Petzing, *Compos., Part A: Appl. Sci. Manuf.* **29**(7), 721–729 (1998).
55. W. C. Wang, C. H. Day, C. H. Hwang, and T. B. Chiou, *Res. Nondestr. Eval.* **10**(1), 1–15 (1998).
56. H. O. Nyongesa, A. W. Otieno, and P. L. Rosin, *Compos. Struct.* **54**(2/3), 313–318 (2001).
57. V. Shchepinov and V. Pisarev, eds., *Strain and Stress Analysis by Holographic and Speckle Interferometry*, John Wiley & Sons, Inc., New York, 1996.
58. M. Whelan, *Key Eng. Mater.* **167/168**, 122–31 (1999).
59. M. Roesel, K. Herstrass, and P. Bajons, *Ultrasonics* **41**, 663–669 (2003).
60. A. Davila, P. D. Ruiz, G. H. Kaufmann, and J. M. Huntley, *Opt. Lasers Eng.* **40**, 447–458 (2003).
61. T. Kreis, *Holographic Interferometry*, Akademie Verlag, Berlin, 1996.
62. M. Heredia-Ortiz and E.-A. Patterson, *Strain* **39**(3), 95–100 (2003).
63. O. Kafri and I. Glatt, *The Physics of Moiré Metrology*, John Wiley & Sons, Inc., New York, 1990.
64. H. R. Meyer-Piening, M. Farshad, B. Geier, and R. Zimmermann, *Compos. Struct.* **53**(4), 427–35 (2001).
65. A. H. Fagg, B. Hales, and H. P. Stahl, *Proc. Int. Soc. Opt. Eng. SPIE* **1779**, 68–72 (1992).
66. T. M. Wang, I. M. Daniel, and J. T. Gotro, *J. Compos. Mater.* **26**(6), 883–899 (1992).
67. P. Tatasciore and E. K. Hack, *Opt. Eng.* **34**(7), 1887–1898 (1995).
68. W. Osten, *Opt. Eng.* **39**(1), 232–243 (2000).

69. G. S. Bauer, *Nucl. Instrum. Methods Phys. Res. Sect. B* **139**, 65–71 (1998).
70. R. J. Cernik and P. Barnes, *Radiat. Phys. Chem.* **45**(3), 445–457 (1995).
71. R. L. Clough, *Nucl. Instrum. Methods Phys. Res. Sect. B* **185**, 8–33 (2001).
72. R. C. Barry and R. A. Betz, *Mater. Eval.* **49**, 474–477 (1991).
73. G. Sala, *Compos., Part B: Eng.* **31**, 357–373 (2000).
74. A. Paige Clifton Furrow, D. A. Dillard, T. L. St. Clair, J. Hinkley, *J. Compos. Mater.* **32**, 31–48 (1998).
75. J. C. M. Suarez and R. S. de Biasi, *Polym. Degrad. Stab.* **82**(2), 221–227 (2003).
76. R. V. Ely, ed., *Microfocal Radiography*, Academic Press, London, U.K., 1980.
77. I. Rudich, L. Lesensky, and F. Kapelewski, *Mater. Eval.* **44**, 1158–1184 (1986).
78. R. Ferreira de Paiva, J. Lynch, E. Rosenberg, and M. Bisiaux, *NDT&E Int.* **31**(1), 17–22 (1998).
79. EN 584-1, Non-destructive testing—Industrial radiographic film—Part 1: Classification of film systems for industrial radiography, Comité Européen de Normalisation, 1994.
80. A. J. Brunner and J. Neuenschwander, in C. A. Mota Soares, C. M. Mota Soares, and M. J. M. Freitas, eds., *Mechanics of Composite Materials and Structures* (NATO Science Series E: Applied Science 361), Kluwer Academic Publishers, Boston, Mass., 1999, pp. 261–278.
81. A. J. Brunner, *Comput. Methods Appl. Mech. Eng.* **185**(2/4), 161–172 (2000).
82. M. K. Choong, M. Bister, P. Sathyamoorthy, Zaharah, H. Y. Boey, and Y. C. Wong, *Int. Congr. Ser.* **1256**, 285–291 (2003).
83. U. Ewert, Y. Onel, U. Zscherpel, J. Stade, and P. Willems, in *Proceedings of the 7th European Conference on Nondestructive Testing*, Vol. 3, 2004, pp. 2725–2732.
84. ASTM WK670, Test Method for Classification of Computed Radiology Systems, New Work Item, ASTM Subcommittee E07.01, see information in Ref. 5.
85. ASTM WK4511, Standard Practice for the Qualification of Computed Radiography Systems, New Work Item, ASTM Subcommittee E07.01, see information in Ref. 5.
86. J. Kosanetzky, G. Harding, H. H. Fischer, and A. Meyer, *Proceedings of the 4th European Conference on Nondestructive Testing*, Pergamon Press, New York, 1988, pp. 2118–2132.
87. S. Gondrom, J. Zhou, M. Maisl, H. Reiter, M. Kröning, and W. Arnold, *Nucl. Eng. Des.* **190**, 141–147 (1999).
88. B. Müller, F. Beckmann, M. Huser, F. Maspero, G. Székely, K. Ruffieux, Ph. Thurner, and E. Wintermantel, *Biomol. Eng.* **19**, 73–78 (2002).
89. K.-W. Harbich, M. P. Hentschel, and J. Schors, *NDT&E Int.* **34**, 297–302 (2001).
90. M. P. Hentschel, K.-W. Harbich, and A. Lange, *NDT&E Int.* **27**(5), 275–280 (1994).
91. S. S. Ray and M. Okamoto, *Prog. Polym. Sci.* **28**, 1539–1641 (2003).
92. M. W. Johnson, *Appl. Radiat. Isot.* **46**(6/7), 673–680 (1995).
93. R.-J. Roe, *Methods of X-Ray and Neutron Scattering in Polymer Science* (Topics in Polymer Science Series), Oxford University Press, New York, 2000.
94. S. Fujine, K. Yoneda, K. Yoshii, M. Kamata, M. Tamaki, K. Ohkubo, Y. Ikeda, and H. Kobayashi, *Nucl. Instrum. Methods Phys. Res., Sect. A* **424**, 190–199 (1999).
95. D. Fink, M. Müller, S. Ghosh, K. K. Dwivedi, J. Vacik, V. Hnatowicz, J. Cervena, Y. Kobayashi, and K. Hirata, *Nucl. Instrum. Methods Phys. Res., Sect. B* **156**, 170–176 (1999).
96. D. M. Bigg, *Polym. Eng. Sci.* **36**(6), 737–743 (1996).
97. H. Daniel, *Nucl. Instrum. Methods Phys. Res., Sect. B* **68**, 459–467 (1992).
98. F. L. Pratt, S. J. Blundell, Th. Jestädt, B. W. Lovett, A. Husmann, I. M. Marshall, W. Hayes, A. Monkman, I. Watanabe, K. Nagamine, R. E. Martin, and A. B. Holmes, *Physica B* **289/290**, 625–630 (2000).

99. G. Czeremuszkin, M. Latrèche, and M. R. Wertheimer, *Nucl. Instrum. Methods Phys. Res., Sect. B* **185**, 88–99 (2001).
100. C. M. Ramsdale, I. C. Bache, J. D. MacKenzie, D. S. Thomas, A. C. Arias, A. M. Donald, R. H. Friend, and N. C. Greenham, *Physica E* **14**, 268–271 (2002).
101. A. Todoroki, H. Kobayashi, and K. Matuura, *JSME Int. J. Ser. A* **38**(4), 524–530 (1995).
102. A. Todoroki and Y. Tanaka, *Compos. Sci. Technol.* **62**(5), 629–639 (2002).
103. D. D. L. Chung and S. K. Wang, *Polym. Polym. Compos.* **11**(7), 515–525 (2003).
104. R. Schueler, S. P. Joshi, and K. Schulte, *Compos. Sci. Technol.* **61**(6), 921–930 (2001).
105. G. Mook, R. Lange, and O. Koeser, *Compos. Sci. Technol.* **61**(6), 865–873 (2001).
106. Y. Hatsukade, N. Kasai, M. Kurosawa, R. Kawai, H. Takashima, F. Kojima, and A. Ishiyama, *Physica C* **372–376**, 267–270 (2002).
107. A. E. Mahdi, L. Panina, and D. Mapps, *Sens. Actuators, A* **105**, 271–285 (2003).
108. M. Bini, R. Olmi, A. Ignesti, J. Abusleme, M. Bassi, and A. Sanguineti, *Mater. Res. Innovations* **8**(1), 23–26 (2004).
109. L. M. Sweeting, *ChemMatters* **8**(3), 10–12 (1990).
110. C. Sklarczyk, S. Winkler, and B. Thielicke, *Materialwissenschaft und Werkstofftechnik* **27**, 559–566 (1996) (in German).
111. W. Saleh, N. Qaddoumi, and M. Abu-Khousa, *Compos. Struct.* **62**(3/4), 403–407 (2003).
112. E. Guilliorit, B. Hosten, C. Bacon, and D. E. Chimenti, *Ultrasonics* **41**, 97–103 (2003).
113. L. Diener, *Rev. Prog. Quant. Nondestr. Eval.* **14**, 615 (1995).
114. S. Zhou and M. C. Hawley, *Compos. Struct.* **61**, 303–309 (2003).
115. D. K. Hsu, D. J. Barnard, and J. J. Peters, *Proc. Int. Soc. Opt. Eng. SPIE* **4336**, 100–107 (2001).
116. R. Stiffler and E. G. Henneke, *Mater. Eval.* **41**, 956–960 (1983).
117. M. Enoki, M. Watanabe, P. Chivavibul, and T. Kishi, *Sci. Technol. Adv. Mater.* **1**, 157–165 (2000).
118. A. Bent and N. W. Hagood, *J. Intell. Mater. Syst. Struct.* **8**(11), 903–919 (1997).
119. M. Barbezat, A. J. Brunner, P. Flüeler, C. Huber, and X. Kornmann, *Sens. Actuators, A* **114**(1), 13–20 (2004).
120. R. A. Nordstrom, A. J. Brunner, and P. Flüeler, *J. Acoustic Emission* **13**(3/4), 67–77 (1995).
121. J. Bohse, *Compos. Sci. Technol.* **60**(8), 1213–1226 (2000).
122. N. Sato and T. Kurauchi, *Res. Nondestr. Eval.* **9**, 119–136 (1997).
123. S. Dixon and S. B. Palmer, *Ultrasonics* **42**(10), 1123–1136 (2004).
124. W. M. D. Wright, D. A. Hutchins, A. Gachagan, and G. Hayward, *Ultrasonics* **34**, 825–833 (1996).
125. P. K. Raju and U. K. Vaidya, *Polym. Compos.* **17**(2), 275–287 (1996).
126. A. Cochran, P. Reynolds, and G. Hayward, *Ultrasonics* **36**, 969–977 (1998).
127. S. Baudouin and B. Hosten, *Ultrasonics* **34**(2–5), 379–382 (1996).
128. K. Matsushige, N. Hiramatsu, and H. Okabe, *Adv. Polym. Sci.* **125**, 147–186 (1996).
129. M. Rath, J. Döring, W. Stark, and G. Hinrichsen, *NDT&E Int.* **33**(2), 123–130 (2000).
130. D. J. Cotter, J. E. Michaels, T. E. Michaels, I. V. Ivakhnenko, and D. Kass, in *Proceedings of the 15th World Conference on Non-Destructive Testing*, Paper No. 216, 2000; available in Ref. 7.
131. D. J. Cotter, T. E. Michaels, J. E. Michaels, D. Kass, M. E. Stanton, I. V. Kosenko, and F. H. C. Hotchkiss, in *Proceedings of the 15th World Conference on Non-Destructive Testing*, Paper No. 215, 2000; available in Ref. 7.
132. S. J. Bourne, M. Newborough, and D. J. Highgate, *INSIGHT* **43**(1), 26–28 (2001).
133. C. J. Brotherhood, B. W. Drinkwater, and R. J. Freemantle, *INSIGHT* **45**(11), 729–734 (2003).

134. J. Buckley, in *Proceedings of the 15th World Conference on Non-Destructive Testing*, Paper No. 507, 2000; available in Ref. 7.
135. A. Neild, D. A. Hutchins, and D. R. Billson, *Ultrasonics* **42**(1–9), 859–864 (2004).
136. F. H. Chang, T. E. Drake, M. A. Osterkamp, R. S. Prowant, J. P. Monchalin, R. Heon, P. Bouchard, C. Padioleau, D. A. Froom, W. Frazier, and J. P. Barton, *Rev. Prog. Quant. Nondestr. Eval.* **12A**, 611–616 (1993).
137. J. P. Monchalin, *Rev. Prog. Quantitative Nondestr. Eval.* **23A**, 3–31 (2004).
138. G. Pfannschmidt, in A. Briggs and W. Arnold, eds., *Advances in Acoustic Microscopy*, Vol. 2, 1996, pp. 1–38.
139. T. H. Gan, D. A. Hutchins, D. R. Billson, and F. C. Wong, *Res. Nondestr. Eval.* **13**, 131–152 (2001).
140. X. E. Gros, N. B. Cameron, and M. King, *INSIGHT* **44**(11), 673–6768 (2002).
141. M. Lethiecq, C. Pejot, M. Berson, P. Guillemet, and A. Roncin, *NDT&E Int.* **27**(6), 311–315 (1994).
142. J. Neuenschwander, B. Blau, I. L. Horvath, T. Lüthi, and H. Marti, *IEEE Trans. Appl. Supercond.* **12**, 1199–1202 (2002).
143. M. Castaings and B. Hosten, *NDT&E Int.* **34**(4), 249–258 (2001).
144. D. Donskoy, A. Sutin, and A. Ekimov, *NDT&E Int.* **34**, 231–238 (2001).
145. N. Krohn, R. Stoessel, and G. Busse, *Ultrasonics* **40**, 633–637 (2002).
146. T. Leutenegger and J. Dual, *Ultrasonics* **41**(10), 811–822 (2004).
147. T. S. Jang, S. S. Lee, and Y. G. Kim, *Ultrasonics* **42**(1–9), 837–841 (2004).
148. A. Briggs, *Acoustic Microscopy*, Clarendon Press, Oxford, 1992.
149. F. Lisy, A. Hiltner, E. Baer, J. L. Katz, and A. Meunier, *J. Appl. Polym. Sci.* **52**(2), 329–352 (1994).
150. J. Yang, *Microeletron. Reliability* **36**(9), 1291–1295 (1996).
151. A. R. Greenberg, S. S. Shojaie, W. B. Krantz, and S. B. Tantekin-Ersolmaz, *J. Membr. Sci.* **107**, 249–261 (1995).
152. M. Honner, P. Litoš, and M. Švantner, *Infrared Phys. Technol.* **45**, 131–142 (2004).
153. S. M. Shepard, J. R. Lhota, T. Ahmed, and Y. L. Hou, *SAMPE J.* **39**(5), 53–59 (2003).
154. D. Wu and G. Busse, *Revue Générale de Thermique* **37**, 693–703 (1998).
155. G. Giorleo and C. Meola, *NDT&E Int.* **35**, 287–292 (2002).
156. A. Mian, X. Han, S. Islam, and G. Newaz, *Compos. Sci. Technol.* **64**, 657–666 (2004).
157. H. Berglind and A. Dillenz, *NDT&E Int.* **36**, 395–399 (2003).
158. W. Karpen, D. Wu, and G. Busse, *Res. Nondestr. Eval.* **11**, 179–197 (1999).
159. B. R. A. Wood and R. W. Harris, *Int. J. Pressure Vessels Piping* **77**, 125–132 (2000).
160. S. N. Dwivedi and A. Sharan, *J. Mater. Process. Technol.* **141**, 155–162 (2003).
161. P. M. Nellen, R. Brönnimann, A. Frank, P. Mauron, and U. Sennhauser, *Proc. Int. Soc. Opt. Eng. SPIE* **3860**, 44–54 (1999).
162. P. Clark, J. Boriniski, M. Gunther, S. Poland, D. Wigent, and S. Watkins, *Smart Mater. Bull.* **2001**(6), 8–11 (2001).
163. A. H. Barber, Q. Zhao, H. D. Wagner, and C. A. Baillie, *Compos. Sci. Technol.* **64**, 1915–1919 (2004).
164. G. Mook, J. Pohl, and F. Michel, *Smart Mater. Struct.* **12**, 997–1004 (2003).
165. X. Kornmann, C. Huber, M. Barbezat, and A. J. Brunner, in *Proceedings of the 11th European Conference on Composite Materials*, 2004, p. 9, Paper B047.
166. J.-M. Park, S.-I. Lee, O.-Y. Kwon, H.-S. Choi, and J.-H. Lee, *Compos. Part A: Appl. Sci. Manuf.* **34**, 203–216 (2003).
167. Y. Bar-Cohen, ed., *Proc. Int. Soc. Opt. Eng. SPIE* 5385, 2004.
168. W. Li and P. Gu, *Computer-Aided Des.* **36**, 1395–1417 (2004).
169. prEN 1427 Non-Destructive Testing—Ultrasonic Thickness Measurement, Comité Européen de Normalisation, Brussels, Belgium, Oct. 2003.

170. D. E. Demco and B. Blümich, *Curr. Opin. Solid State Mater. Sci.* **5**, 195–202 (2001).
171. J. P. Dunkers, F. R. Phelan, D. P. Sanders, M. J. Everett, W. H. Green, D. L. Hunston, and R. S. Parnas, *Opt. Lasers Eng.* **35**, 135–147 (2001).
172. R. Smallwood, P. Metzerall, D. Hose, M. Delves, H. Pollock, A. Hammiche, C. Hodges, V. Mathot, and P. Willcocks, *Thermochim. acta* **385**, 19–32 (2002).
173. C. Degueldre, H. Pleinert, P. Maguire, E. Lehmann, J. Missimer, J. Hammer, K. Leenders, H. Böck, and D. Townsend, *Earth Planet. Sci. Lett.* **140**, 213–225 (1996).
174. G. Sakas, *Comput. Graphics* **26**, 577–587 (2002).
175. D. H. Phillips and J. J. Lannutti, *NDT&E Int.* **30**(6), 339–350 (1997).
176. R. Kimmich, A. Klemm, and M. Weber, *Magnetic Resonance Imaging* **19**, 353–361 (2001).
177. A. F. Obrist, A. Flisch, and J. Hofmann, *NDT&E Int.* **37**(5), 373–380 (2004).
178. X. Yan and P. Gu, *Computer-Aided Des.* **28**(4), 307–318 (1996).
179. B. Schillinger, W. Blümlhuber, A. Fent, and M. Wegner, *Nucl. Instrum. Methods Phys. Res., Sect. A* **424**, 58–65 (1999).
180. R. D. Adams and B. W. Drinkwater, *NDT&E Int.* **30**(2), 93–98 (1997).
181. O.-Y. Kwon, T.-H. Kim, and K.-J. Lee, *Proceedings 15th World Conference on Non-Destructive Testing*, Paper No. 473, 2000; available in Ref. 7.
182. C. J. Brotherhood, B. W. Drinkwater, and S. Dixon, *Ultrasonics* **41**(7), 521–529 (2003).
183. A. M. Robinson, B. W. Drinkwater, and J. Allin, *NDT&E Int.* **36**, 27–36 (2003).
184. F. Lanza di Scalea, M. Bonomo, D. Tuzzeo, *Res. Nondestr. Eval.* **13**, 153–171 (2001).
185. J. A. Schroeder, T. Ahmed, B. Chaudhry, and S. Shepard, *Compos. Part A: Appl. Sci. Manuf.* **33**, 1511–1517 (2002).
186. J. Mijović and S. Andjelić, *Polymer* **37**(8), 1295–1303 (1996).
187. C. Li, M. Cao, R. Wang, Z. Wang, Y. Qiao, L. Wan, Q. Tian, H. Liu, D. Zhang, T. Liang, and C. Tang, *Compos. Sci. Technol.* **63**, 1749–1758 (2003).
188. J.-M. Gonnet, J. Guillet, C. Raveyre, G. Assezat, R. Fulchiron, and G. Seytre, *Polym. Eng. Sci.* **42**(6), 1171–1180 (2002).
189. S. A. Nield, H. M. Budman, and C. Tzoganakis, *Control Eng. Practice* **8**, 911–920 (2000).
190. A. Gokce, K.-T. Hsiao, and S. G. Advani, *Compos. Part A: Appl. Sci. Manuf.* **33**, 1263–1272 (2002).
191. EN 473, Nondestructive Testing: Qualification and Certification of NDT Personnel—General Principles, Comité Européen de Normalisation, Brussels, Belgium, Oct. 2000.
192. prCEN/TR 14748, Non-Destructive Testing—Methodology for Qualification of Non-destructive Tests, Comité Européen de Normalisation, Brussels, Belgium, Aug. 2003.

ANDREAS J. BRUNNER
ERWIN HACK
JÜRG NEUENSCHWANDER
Center for Nondestructive Testing, EMPA,
Swiss Federal Laboratories for Materials Testing and Research

Encyclopedia of Polymer Sceince and Technology
Copyright © 2005 John Wiley & Sons, Inc. All rights reserved.

N-VINYLAMIDE POLYMERS

Introduction

N-Vinylamide-based polymers, especially the *N*-vinyllactams, such as poly(*N*-vinyl-2-pyrrolidinone) [9003-39-8] or simply polyvinylpyrrolidinone (PVP), continue to be of major importance to formulators of personal-care, pharmaceutical, agricultural, and industrial products because of desirable performance attributes and very low toxicity profiles. Because of hydrogen bonding of water to the amide group, many of the *N*-vinylamide homopolymers are water soluble or dispersible. Like proteins, they contain repeating (but pendant) amide (lactam) linkages and share several protein-like characteristics (1). Many studies have actually employed PVP as a substitute for proteins, eg, in simplifying the chemistry of the effects of radiation on polymers (2). Proteins are extremely complicated molecules with not only sequence distribution but tertiary bonding and structural complexity and it is an oversimplification to compare them to PVP, but the effects of radiation on PVP can be more readily studied. PVP can even be considered as a uniform synthetic protein-like analogue. By itself it does not enter into intermolecular hydrogen bonding, thus affording low viscosity concentrates, and also, unlike the proteins, PVP is soluble in polar solvents like alcohol. But even given these differences, the chemistry of PVP, the most commercially successful polymer of the class, is in many respects similar to that of proteins because of amide linkages sharing with them complexation to large anions such as polyphenols, anionic dyes, and surfactants. In addition to the ability to complex, PVP and its analogues along with a large assortment of copolymers are excellent film formers. They exhibit the ability to interact with a variety of surfaces by hydrogen or electrostatic bonding, resulting in protective coatings and adhesive applications of commercial significance such as hair-spray fixatives, tablet binders, disintegrants, iodophors, antidye redeposition agents in detergents, protective colloids, dispersants, and solubilizers, among many others.

Monomers

N-Vinylamides and *N*-vinylimides can be prepared by reaction of amides and imides with acetylene (3), by dehydration of hydroxyethyl derivatives (4), by pyrolysis of ethylidenebisamides (5), or by vinyl exchange (6), among other methods; the monomers are stable when properly stored.

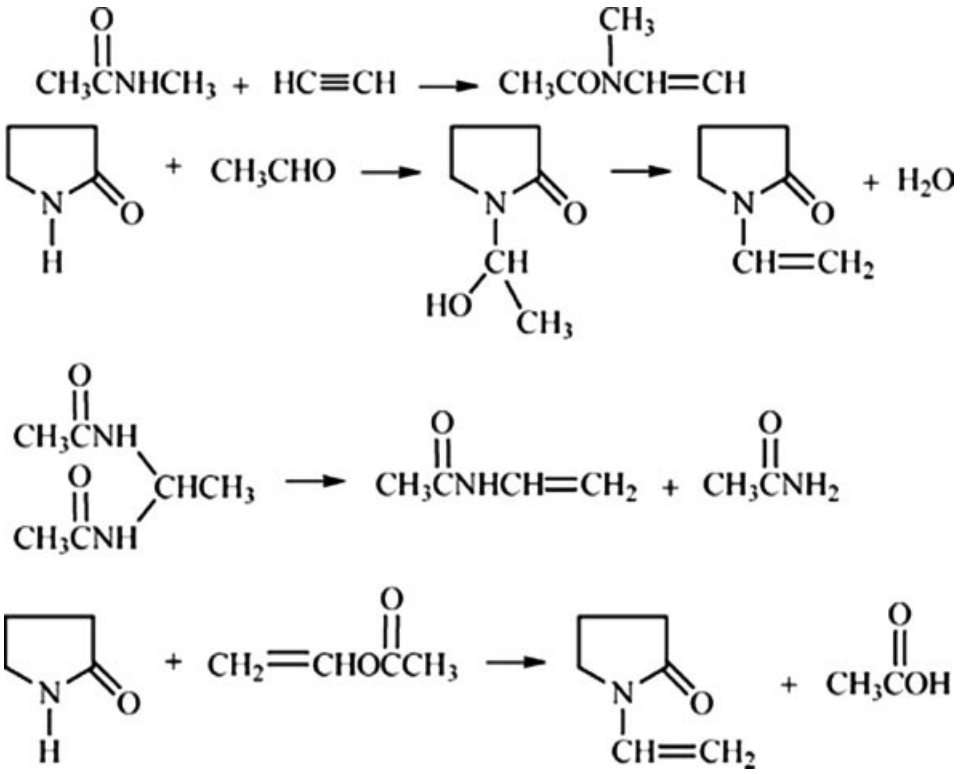

Poly *N*-vinyl-2-pyrrolidinone (VP) [88-12-0] is of significant commercial importance and hence is the principal focus of this article. Vinylcaprolactam is available (BASF) and is growing in importance, and vinyl formamide is available as a developmental monomer (Air Products). Some physical properties are given in Table 1.

***N*-Vinyl-2-Pyrrolidinone.** Commonly called vinylpyrrolidinone or VP, *N*-vinyl-2-pyrrolidinone was developed in Germany at the beginning of World War II. It is a clear, colorless liquid that is miscible in all proportions with water and most organic solvents. It can polymerize slowly by itself but can be easily inhibited by small amounts of ammonia, sodium hydroxide (caustic pellets), or

Table 1. Physical Properties of Selected Vinylamides and Vinylimides

Compound	CAS Registry Number	Bp, °C$_{kPa}$[a]	Mp, °C
N-Vinylacetamide	[5202-78-8]	107–109	
N,*N*-Methylvinylacetamide	[3195-78-6]	$70_{3.3}$	
N-Vinylacetanilide	[4091-14-9]	$102–105_{0.13}$	52
N-Vinyl-2-piperidinone	[4370-23-4]	$125–126_{3.3}$	45
N-Vinylcaprolactam	[2235-00-9]	$129–130_{2.7}$	34.5
N-Vinylphthalimide	[3485-84-5]	$128–130_{3.3}$	86.5
N-Vinyl-2-oxazolidinone	[4271-26-5]	$77–78_{0.067}$	
N-Vinyl-5-methyl-2-oxazolidinone	[3395-98-0]	$105–108_{0.33}$	

[a] To convert kPa to mmHg, multiply by 7.5. Pressure = 101.3 kPa (760 mmHg) if not shown.

Table 2. Properties of *N*-Vinyl-2-Pyrrolidinone (Commercial Production)

Property	Value
Molecular wt.	111
Assay, %	98.5[a]
Moisture content, %	0.2[b]
Color (APHA)	100[b]
Vapor pressure, Pa[c] at	
17°C	6.7
24°C	13.3
45°C	67
54°C	133
64°C	266
77°C	667
Boiling point at 400 mmHg	193
Freezing point	13.5
Flash point (open cup)	98.4
Fire point	100.5
Viscosity at 25°C, mPa·s (=cP)	2.07
Specific gravity (25/4°C)	1.04
Refractive index, $n^{25}{}_{D}$	1.511
Solubility	Completely miscible in water and most organic solvents, including methanol, ethyl acetate, methylene chloride, ethyl ether, and hydro-carbons in general
Ultraviolet spectrum	No significant absorption at wavelengths longer than 220 nm

[a]Value is minimum.
[b]Value is maximum.
[c]To convert Pa to mmHg, multiply by 0.0075.

antioxidants such as *N,N′*-di-*sec*-butyl-*p*-phenylenediamine. It is stable in neutral or basic aqueous solution but readily hydrolyzed in the presence of acid to form 2-pyrrolidinone and acetaldehyde. Properties are given in Table 2.

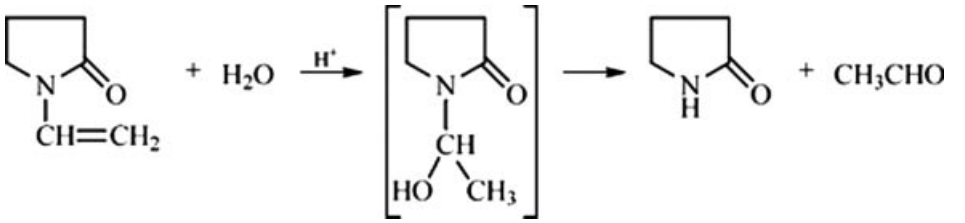

Commercially available VP is usually over 99% pure but does contain several methyl-substituted homologues and 2-pyrrolidinone. Even at this high level of purity, further purification is required if reliable kinetic data concerning rates of polymerization are desired. This can be accomplished only by recrystallization, because distillation will not separate methyl-substituted isomers (7).

Manufacture. The principal manufacturers of *N*-vinyl-2-pyrrolidinone are ISP and BASF. Both consume most of their production captively as a monomer for the manufacture of PVP and copolymers. The vinylation of 2-pyrrolidinone is carried out under alkaline catalysis analogous to the vinylation of alcohols. 2-Pyrrolidinone is treated with ca 5% potassium hydroxide, then water and some pyrrolidinone are distilled at reduced pressure. A ca 1:1 mixture (by vol) of acetylene and nitrogen is heated at 150–160°C and ca 2 MPa (22 atm). Fresh 2-pyrrolidinone and catalyst are added continuously while product is withdrawn. Conversion is limited to ca 60% to avoid excessive formation of by-products. The *N*-vinyl-2-pyrrolidinone is distilled at 70–85°C at 670 Pa (5 mmHg) and the yield is 70–80% (8).

Shipment and Storage; Specifications. *N*-Vinyl-2-pyrrolidinone is available in tank cars and tank trailers and in drums of various sizes. Shipping containers are normally steel or stainless steel. Tank cars are provided with heating coils to facilitate unloading in cold weather. Rubber, epoxy, and epoxy–phenolic coatings are attacked and must be avoided. Carbon steel has been successfully used for storage tanks, but stainless steel preserves product quality better. Aluminum and certain phenolic coatings are also satisfactory.

Toxicity Data on N-Vinyl-2-Pyrrolidinone. Results of a chronic inhalation study in rats warrant a review of industrial hygiene practices to assure that VP vapor concentrations are maintained at a safe level. One of the manufacturers, ISP, recommends that an appropriate workplace exposure limit be set at 0.1 ppm (vapor) (9). Additionally, normal hygienic practices and precautions are recommended, such as prompt removal from skin and avoidance of ingestion. In case of accidental eye contact, immediately flush with water for at least 15 min and seek medical attention. Refer to the manufacturers' Material Safety Data Sheets for more detailed information. Table 3 provides some toxicity data.

Table 3. Summary of Toxicity Data for *N*-Vinyl-2-Pyrrolidinone

Test	Result
Acute oral LD_{50}	1.5 mL/kg (rats)
Acute dermal LD_{50}	0.56 g/kg (rabbits)
Acute inhalation LC_{50}	700 ± 100 ppm(rats)
Eye irritation	Severe (rabbits)
Primary irritation index (PII)	0.38 (rabbits)
Skin Repeated Insult Patch Test	Not a primary irritant or sensitizer (humans)
Subacute inhalation	No gross or clinical abnormal effects; subacute/chronic inflammation of respiratory tract at 16.5 and 66 ppm (rats)
Subchronic inhalation	Evidence of liver damage at 15, 45, and 120 ppm; no evidence of toxicity at 1 ppm (rats)
Chronic inhalation	Benign and malignant tumors of the nasal mucosa at the 10 and 20 ppm levels; liver tumors noted at 20 ppm
Mutagenicity	Negative in a battery of five assays

Homopolymerization of *N*-Vinyl-2-Pyrrolidinone

VP was originally polymerized in bulk by heating in the presence of small amounts of hydrogen peroxide. This neat polymerization was a difficult process to work-up, requiring crushing of the solidified polymer mass and extraction with ether to remove unreacted monomer and by-products. However, it was important to the original application as a blood substitute because it afforded low molecular weight (10,11). Low molecular weight is necessary for excretion from the kidneys (12). Bulk polymerization favors the tendency of VP to undergo chain transfer to monomer. Neat VP polymerized with di-*tert*-butyl peroxalate in the presence of a nitroxide scavenger that exclusively traps carbon centered radicals generates considerable nonvinyl radicals by chain transfer (13,14). VP (and presumably PVP) can, under the right circumstances, undergo chain transfer, and this route is more prevalent as the concentration of monomer is increased.

Because VP and PVP are soluble in water, early workers realized that polymerization could be more easily controlled in such a high heat capacity solvent. In the presence of acid, VP readily hydrolyzes, and when initiated with hydrogen peroxide, the pH drops quickly into the acidic range. The problem this presents was solved by buffering with bases. Of all of the bases tried by the early German chemists, ammonia not only prevented hydrolysis by neutralizing acidic by-products, it accelerated the polymerization. The early workers found that with an optimized concentration of monomer and ammonia level, the molecular weight was reproducibly controlled by the hydrogen peroxide level. Even relatively high molecular weight could be achieved by small amounts of hydrogen peroxide, but such levels might easily be compromised by unproductive side reactions. High molecular weight homopolymers are more reliably produced by initiation with organic peroxides and azo initiators.

Ammonia H_2O_2 Initiation. The lower molecular weight grades (K-15 and K-30) of PVP are prepared industrially with an ammonia/H_2O_2 initiation system. Such products are the standards for the pharmaceutical industry and conform to the various national pharmacopeias. Several papers have appeared concerning the mechanism of this polymerization (15).

The proposed rate expression for the ammonia/H_2O_2 process is as follows:

$$R_p = k[H_2O_2]^{1/2}[NH_3]^{1/4}[VP]^{3/2} \tag{1}$$

Comparing this to the theoretical expression based on the steady state approximation suggests that the mechanism is not straightforward:

$$R_p = k_p[M]\,\frac{(fkd[I])^{1/2}}{kt} \tag{2}$$

Higher than first order for monomer, such as the 3/2 power suggests that VP is involved in initiation (16). If the efficiency of initiation is a function of the monomer concentration, then $f = f^1[M]$, and substituting in equation 2 gives

$$R_p = k_p[M]^{3/2}\,\frac{(f^1kd[I])^{1/2}}{k_t} \tag{3}$$

The $[I]^{1/2}$ is reflected in $[H_2O_2]^{1/2}$ but $[NH_3]^{1/4}$ can be explained by the finding (17) that the rate of polymerization is proportional to $[NH_4^+]^{1/2}$. If the equilibrium expression for $NH_3/[NH_4^+]$ is solved for $[NH_4^+]$ and this expression substituted, the quarter power for ammonia is apparent.

Several papers (6,18) have appeared that attempt to reconcile the ability of H_2O_2 to act as a rather strong transfer agent (hydrogen donor), generating the weakly initiating species $HOO^\bullet$, with its ability to act as a source of $HO^\bullet$ hydroxy radicals that are known to be active vinyl initiators. Such studies demonstrate that $HO^\bullet$ generated by photolysis behaves classically as an initiator for PVP (the rate is, as expected, first order in VP and half order in H_2O_2). Polymerization with 2,2′-azobisisobutyronitrile (AIBN) in the presence of H_2O_2 demonstrates that H_2O_2 in this case acts as a proton donor, reducing molecular weight, suggesting it also functions similarly during NH_3/H_2O_2 initiation. Even with other water-soluble initiators, VP behaves classically, with the rate expression being first order in monomer and half order in initiator (19,20). This would indicate that VP is a vinyl monomer with normal behavior and hence the H_2O_2/NH_3 initiation system is unusual. The evidence clearly demonstrates that it is a redox initiator system requiring trace amounts of cuprous or ferrous salt (21). Other bases such as NaOH or KOH can be employed to replace NH_3 if precautions are taken to sequester these metal ions, preventing them from being deactivated in the redox complex (22).

In one of the few published studies of H_2O_2 initiation, it is shown that in the case of methacrylamide, the monomer participates in its own initiation by reacting with H_2O_2, forming an intermediate hydroperoxide (23). Subsequently, this hydroperoxide generates hydroxyl radicals capable of initiation. Like that of methacrylamide, VP polymerization is very sensitive to molecular oxygen reacting faster with it than propagation to polymer (18), and a similar reaction might be at work with VP that would be expected to generate an intermediate hydroperoxide capable of entering into a redox initiation system. The proposed mechanism would also explain the formation of 2-pyrrolidinone as a consequence of redox polymerization, dispelling the previous belief that 2-pyrrolidinone was a result of primary radical termination caused by reaction of hydroxyl radicals with the growing chain, followed by hydrolysis of the hemiacetal (24,25) subsequently formed. Hydroxyl radicals afford PVP with one hydroxyl per chain, correlating well with a mechanism that relies on hydroxyl radical initiation and strong H_2O_2 chain transfer (26). In this case, one end of the polymer is not an aldehyde but rather a hydroxyl group, and no evidence for other than proton termination could be found, producing a methylene terminus at the other end of the polymer chain. Figure 1 illustrates the proposed mechanism and explains the formation of acidic by-products responsible for the acidic pH drift during polymerization.

Organic Peroxides and Azo Initiation

The H_2O_2/ammonia initiation system is not employed commercially in the manufacture of higher molecular weight homologues; they are prepared with organic initiators. Such polymerizations follow simple chain theory and are usually performed in water commercially. The rate of polymerization is at a maximum in aqueous media at pH 8–10 and at 75 wt% monomer (27,28). Polymerization rates

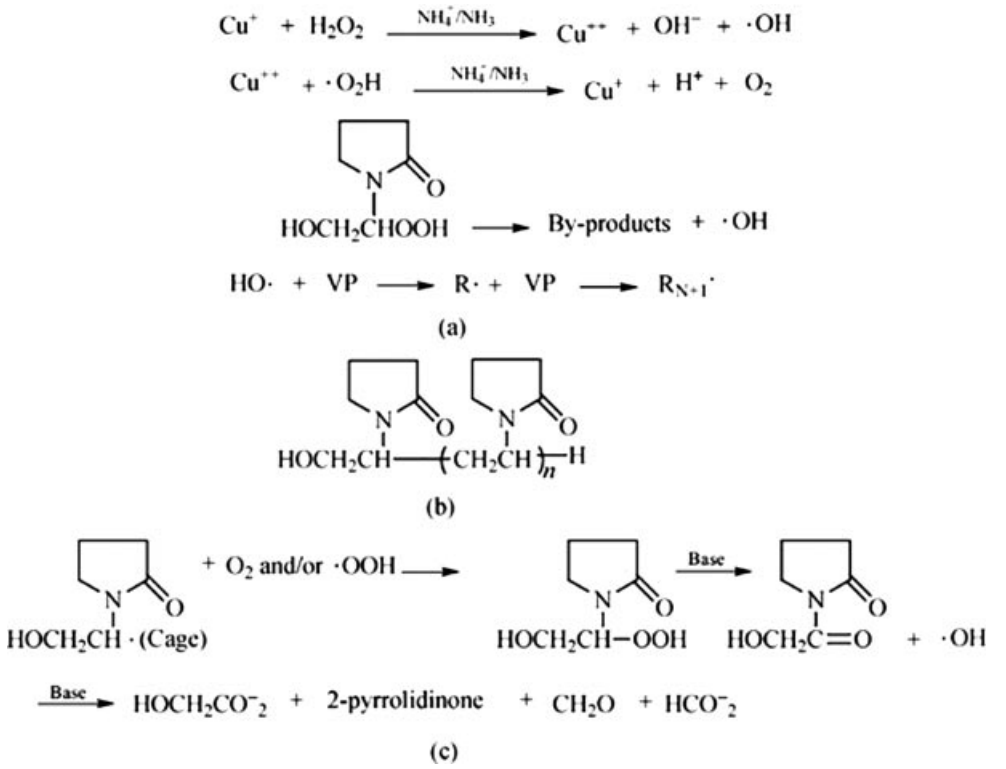

Fig. 1. Mechanism of NH_3/H_2O_2 polymerization of VP: (**a**) initiation; (**b**) end groups; (**c**) 2-pyrrolidinone generation.

follow the polarity and hydrogen bonding capability of the solvent (29). One possible explanation for this fact is that water is most capable of reducing the apparent negative charge on the beta carbon VP's vinyl group by hydrogen bonding to the pyrrolidinone carbonyl and polar interactions. Such a reduction permits the electron-rich radical terminus to more easily approach another VP and hence allows the acceleration (29). Alternatively, PVP may be somewhat more hydrophobic than VP forming associates ("micelles") capable of enhancing the rate of polymerization by concentrating monomer close to the reacting polymer terminus. This is the reason why even in relatively dilute aqueous solutions the rate can be substantial. The hydrophobic effect accounts for a higher VP concentration at the reactive polymer terminus (30).

Cationic Polymerization. VP polymerizes to low molecular weight (oligomers) with typical cationic initiators, such as boron trifloride etherate (31). This reaction requires high concentrations, if not neat, of monomer and scrupulously anhydrous conditions for high yields; VP will readily hydrolyze to 2-pyrrolidinone and acetaldehyde even in the presence of trace moisture when catalyzed by strongly acidic reagents. Pyrrolidinone derivatives apparently complex and deactivate cationic polymerization catalysts and generally present an unfavorable environment for polymerization (32). Thus, initiating species are relatively

short-lived and readily deactivated, or undergo chain transfer; hence, more than catalytic amounts of initiator are required for high yields.

Interest has been rekindled in cationic polymerization by the discovery that carboxylic acid groups trapped in insoluble matrices like activated carbon or poly(glutamic acid) can generate higher mol wt. polymers (33–35). Additionally, oxoaminium salts (36) derived from 2,2,6,6-tetramethylpiperidine-1-oxyl (TEMPO) or anodic polymerization (37) on platinum electrode surfaces will also afford higher molecular weight polymers. Such cationically generated polymers would be expected to afford microstructure and greater tacticity because of the higher activation energy for inversion associated with a growing cationic terminus vs a growing free-radical terminus. Unfortunately, none of the above references present detailed polymer structural characterizations.

Microstructure. Interest in PVP microstructure and the potential for tacticity has been reviewed (38,39). PVP generated by free radicals has been shown to be atactic except when polymerization is conducted in water. In this case, some syndiotacticity is observed (39). In the presence of syndiotactic templates of poly(methacrylic acid) (or poly(MAA)), VP will apparently polymerize with syndiotactic microstructure, although proof is lacking (40–44). The reverse, polymerization of MAA in the presence of PVP, affords, as expected, atactic poly(MAA) (45,46).

Advances in VP cationic polymerization hold out the possibility of tacticity, and the study of this route to crystalline homologues continues to be of interest.

Proliferous Polymerization. Early attempts to polymerize VP anionically resulted in proliferous or "popcorn" polymerization (47). This was found to be a special form of free-radical addition polymerization, and not an example of anionic polymerization, as originally thought. VP contains a relatively acidic proton alpha to the pyrrolidinone carbonyl. In the presence of strong base such as sodium hydroxide, VP forms crosslinkers *in situ*, probably by the following mechanism:

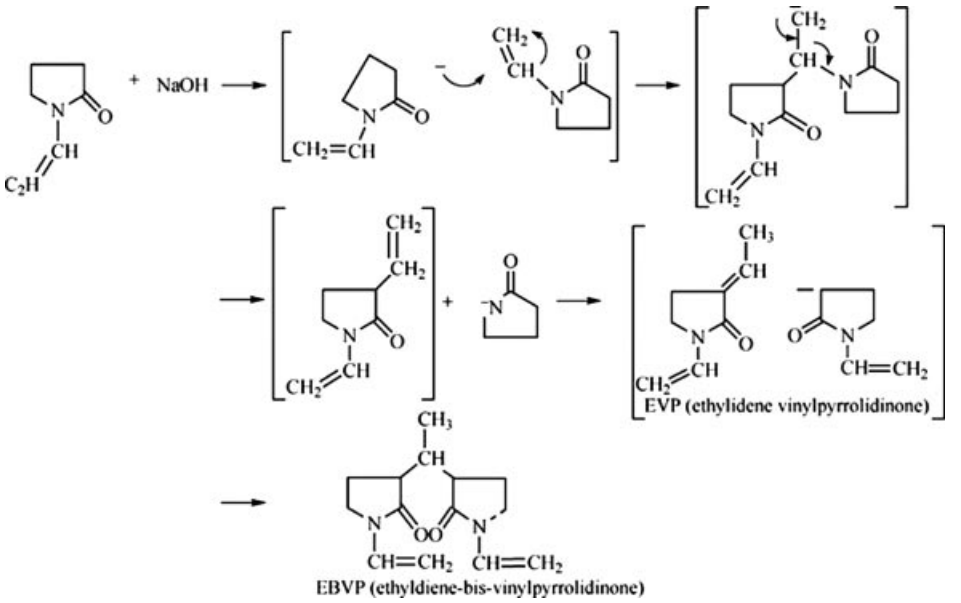

Both ethylidene vinyl pyrrolidinone (EVP) and ethylidene-bis-vinylpyrrolidinone (EBVP) are generated in about a 10:1 ratio, respectively (24). At the temperature required to generate these cross-linkers and when their concentration reaches some minimum level, usually a few percent, proliferous polymerization begins (48). The same situation can be reached by the addition of a suitable cross-linker (49). Although no initiator is required, the polymerization can be prevented in the presence of typical free-radical inhibitors or initiated by very small amounts of AIBN. Reviews indicate that the rate of polymerization accelerates because the initially formed cross-linked seeds swell to generate active sites by bond homolysis and that growing chains resist termination because of the rigid cross-linked structure. Very high conversions can be achieved and the resulting product, a granular "popcorn" mass, can be freed of residual monomer/soluble polymer by careful washing. Drying results in a free-flowing white powder (50).

Crospovidones are produced commercially by these two processes, ie, *in situ* generation of cross-linker or addition of divinylimidazoline, and they are indistinguishable by ir. Both types exhibit a T_g of 190–195°C, which is not that much above the 175°C of high molecular weight, soluble PVP (24). Proliferous polymers prepared with easily hydrolyzed cross-linker containing an imine linkage do not further swell even when the cross-links are hydrolyzed (49). In order to reach the low swell volume typical of these resins with a typical VP/cross-linker polymerized with free-radical initiator, sizeable amounts of cross-linker are actually required, resulting in much higher (240°C) T_gs. The crospovidones are therefore unusually high molecular weight, highly chain-entangled polymers having covalent cross-links that most likely retard the termination reaction during polymerization and are not entirely responsible for the resulting mechanical properties, such as swell ratio. Even hydrolyzing such cross-links is not sufficient to cause dissolution.

The crospovidones are easily compressed when anhydrous but readily regain their form upon exposure to moisture. This is an ideal situation for use in pharmaceutical tablet disintegration and they have found commercial application in this technology. PVP strongly interacts with polyphenols, the crospovidones can readily remove them from beer, preventing subsequent interaction with beer proteins and the resulting formation of haze. The resin can be recovered and regenerated with dilute caustic.

PVP Hydrogels

Cross-linked versions of Water-Soluble Polymers (qv) swollen in aqueous media are broadly referred to as Hydrogels (qv) and have a growing commercial utility in such applications as oxygen-permeable soft contact lenses (Table 4) and controlled-release pharmaceutical drug delivery devices (51). Cross-linked PVP and selected copolymers fit this definition and are of interest because of the following structure/performance characteristics:

Structure	Performance	Benefit
Nonionic	Compatibility with other ingredients	Stable formulation
Pyrrolidinone	Low toxicity	Nonirritating/nonthrombogenic
	Complexation actives/O_2	Controlled release transport
	High T_g	Mechanical stability
	Hydrolytic stability	Storage stable
Ethylene backbone	Nonbiodegradable, hydrolytic stability	Resists biocontamination storage-stable
Cross-links	Swell volume/viscosity	Mechanical stability/diffusion control

Cross-linked PVP can be prepared by several routes other than proliferous polymerization PPVP (crospovidones). Although a hydrogel, the swell volume of this type of polymer cannot be controlled over a large increment because the granular particles cannot be formed into larger uniform assemblies. These limitations can be overcome by the polymerization of VP in the presence of a few percent of suitable cross-linker utilizing standard free-radical initiation by, for example, AIBN (52–54) or actinic radiation (gamma rays) (55,56). This results in a lightly cross-linked PVP. If the polymerization is carried out incorrectly, significant amounts of uncross-linked soluble polymer may be present that must be removed before a meaningful physical analysis such as swell ratio can be accomplished. The solution to this problem is to balance the reactivity ratios of the cross-linker and other comonomers with those of VP to obtain uniform copolymerization and cross-linking (57,58). Not only does this reduce the level of soluble uncross-linked polymer but affords crystal-clear hydrogels so important for use in contact lenses. Allyl-substituted sugars used to generate cross-linked polyacrylic acid gels,

Table 4. Generic Names of Polymeric Compositions Used in Soft Contact Lenses

USAN Generic Name	Polymer composition[a]	Water, %	Trademarks	Manufacturer
Droxifilcon-A	Copolymer of HEMA and MA modified with poly(2-vinyl-pyrrolidone)	47	Accugel	Strieter Labs
Lidofilcon-B	Copolymer of MMA and 2-vinylpyrro-lidone (VP)	79	Sauflon PW	American Medical Optics
Surfilcon-A	Copolymer of MMA, VP, and other methacrylates	74	Permaflex	Cooper Vision, Inc.
Tetrafilcon-A	Terpolymer of HEMA, MMA, and VP cross-linked with divinylbenzene	42.5	Aosoft Aquaflex	American Optical Corp., Cooper Vision, Inc.
Vifilcon-A	Copolymer of HEMA and MA with PVP cross-linked with EGDM	55	Softcon	American Optical Corp.

[a] HEMA, hydroxyethylmethacrylate; EGDM, ethyleneglycoldimethacrylate.

carbomers, employed as thickeners in pharmaceutical formulations, have been shown to work well with VP (59).

Cross-linked PVP can also be obtained by cross-linking the preformed polymer chemically (with persulfates, hydrazine, or peroxides) or with actinic radiation (60). This approach requires a source of free radicals capable of hydrogen abstraction from one or another of the labile hydrogens attached alpha to the pyrrolidone carbonyl or lactam nitrogen. The subsequently formed PVP radical can combine with another such radical to form a cross-link or undergo side reactions such as scission or cyclization (61,62), thus:

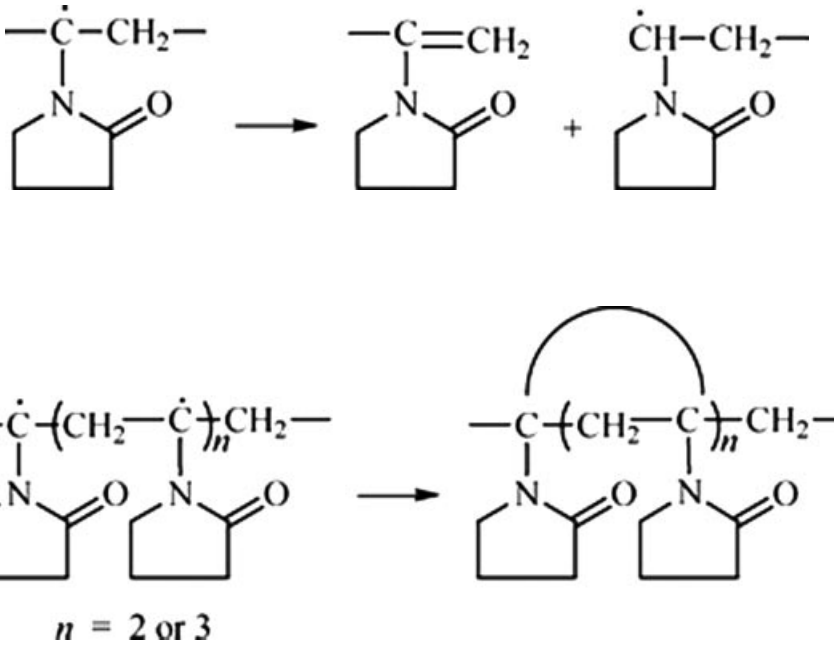

If the starting PVP homopolymer is too low in molecular weight or too dilute, cyclization or cleavage is preferred (62,63). However, because of the high T_g of PVP, the backbone is sufficiently rigid to avoid reorientation during bond homolysis so that the same bond has a good chance of reforming; hence, PVP yields cross-linked structures in preference to cleavage (64) and PVP hydrogels formed by e-beam have become commercially important for use as conductive electrodes for medical applications (65).

Poly(*N*-Vinyl-2-Pyrrolidinone)

Poly(*N*-vinyl-2-pyrrolidinone) (PVP) is undoubtedly the best characterized and most widely studied *N*-vinyl polymer. It derives its commercial success from its biological compatibility, low toxicity, film-forming and adhesive characteristics, unusual complexing ability, relatively inert behavior toward salts and acids, and thermal and hydrolytic stability.

First developed in Germany by I. G. Farben (W. Reppe) during the 1930s, PVP was subsequently widely used in Germany as a blood–plasma substitute and extender during World War II (66). In the United States, it has been manufactured since 1956 by ISP, and more recently by BASF.

Molecular Weight and *K* Value. Poly(*N*-vinyl-2-pyrrolidinone) is described in the *United States Pharmacopeia* (67) as consisting of linear *N*-vinyl-2-pyrrolidinone groups of varying degrees of polymerization. The molecular weights of PVP samples are determined by size-exclusion chromatography (sec), osmometry, ultracentrifugation, light scattering, and solution viscosity techniques. The most frequently employed method of determining and reporting the molecular weight of PVP samples utilizes the sec/low angle light-scattering (lalls) technique (68,69).

A frequently used and commonly recognized method of distinguishing between different molecular weight grades of PVP is the K value. Its nomenclature is accepted by the USP, FDA, and other authoritative bodies worldwide. The *Pharmacopeia* (USP) specifies that for very low molecular weight, a 5% solution whereas for very high molecular weight, a 0.1% solution be measured. All other molecular weights employ a 1% solution. The relative viscosity is obtained with an Ostwald–Fenske or Cannon–Fenske capillary viscometer, and the K value is derived from Fikentscher's equation (70).

$$\log \frac{\eta_{\text{rel}}}{c} = \frac{75K_{\text{o}}^2}{1 + 1.5K_{\text{o}}c} + K_{\text{o}}$$

where $K = 1000K_{\text{o}}\eta_{\text{rel}}$ = relative viscosity, and c = concentration of the solution in g/100 mL. Solving directly for K, the Fikentscher equation is converted to

$$K = [300c \log Z + (c + 1.5c \log Z)^2 + 1.5c \log Z - c]/(0.15c + 0.0003c^2)$$

where $Z = \eta_{\text{rel}}$. Table 5 illustrates a correlation chart where the K value is simply read off from a knowledge of η_{rel}.

The intrinsic viscosity $[\eta]$ may be approximated from the Fikentscher equation by

$$[\eta] = 2.303\ (0.001K + 0.000075K^2)$$

where $[\eta]$ = intrinsic viscosity and $K = K$ value of sample.

Table 5. K_{o} Value vs Relative Viscosity at 1% Concentration (wt/vol)[a]

K value	Relative viscosity	K value	Relative viscosity
20	1.120	60	2.031
25	1.175	65	2.258
30	1.243	70	2.527
35	1.325	75	2.846
40	1.423	80	3.225
45	1.539	85	3.678
50	1.677	90	4.219
55	1.839	95	4.870

[a] Ref. 68.

Table 6. *K* Value vs Weight-Average Molecular Weight for PVP[a]

K value	$\overline{M}_w$, amu	*K* value	$\overline{M}_w$, amu
10	2,600	70	626,900
15	8,100	75	761,500
20	18,300	80	913,500
25	34,400	85	1,084,000
30	57,500	90	1,273,000
35	88,800	95	1,483,000
40	129,300	100	1,714,000
45	180,300	105	1,967,000
50	242,700	110	2,242,000
55	317,600	115	2,542,000
60	405,900	120	2,866,000
65	508,600		

[a]Ref. 68.

Utilizing the Mark–Houwink equation (71)

$$[\eta] = K\bar{M}_v^a$$

it is possible to relate the viscosity-average molecular weight ($\bar{M}_v$) to the *K* value.

For commercial grades of unfractionated PVP prepared by similar means (presumed to exhibit similar molecular weight distribution (MWD) and degree of branching), the following regression formula can be employed (68):

$$\log \text{mol wt.} = 2.82 \log K + 0.594$$

Table 6 indicates mol wt. vs *K* value obtained by this technique. Table 7 lists M_n obtained by osmometry methods. The specifications for Technical and Pharmaceutical grades are given in Tables 8 and 9.

Glass-Transition Temperature. The T_g of PVP is sensitive to residual moisture (72) and unreacted monomer. It is even sensitive to how the polymer was prepared, suggesting that MWD, branching, and cross-linking may play a part (73). Polymers presumably with the same molecular weight prepared by bulk polymerization exhibit lower T_gs compared to samples prepared by aqueous solution polymerization, lending credence to an example, in this case, of branching caused by chain transfer to monomer.

Table 7. Osmometry Molecular Weights for PVP[a]

Sample	Technique	$\overline{M}_n$
K-90	Membrane osmometry	37,4000
K-60	Membrane osmometry	67,500
K-30	Vapor pressure osmometry	8,430
K-15	Vapor pressure osmometry	5,170

[a]Ref. 69.

Table 8. Specifications of Technical PVP Grades

Designation	Form	K range	Water, %max	Ash, %max	$M_v(\times 10^{-3})^a$
K-15	Powder	13–19	5	0.02	10
K-15	Aqueous solution	13–19	72		10
K-30	Powder	26–34	5	0.02	40
K-60	Aqueous solution	50–62	55	0.02	220
K-90	Aqueous solution	80–100	80	0.02	630
K-90	Powder	88–100	5	0.02	630
K-120	Powder	115–125	5	0.02	1450

[a] Performed at 25°C, in H_2O, using Mark–Houwink constants of $K = 1.4 \times 10^{-4}$ and $a = 0.7$.

Table 9. Specifications of Pharmaceutical PVP Grades (Povidone)

Assay	Value[a]
K value	
10–15	85–115% of stated supplier's value
16–90	90–107% of stated supplier's value
Moisture, %	5
pH[b]	3.0–7.0
Residue on ignition, %	0.02
Aldehydes, %[c]	0.02
N-Vinyl-2-pyrrolidinone, %	0.20
Lead, ppm	10
Arsenic, ppm	1
Nitrogen, %	11.5–12.8

[a] All single values are maximum.
[b] Of a 5% solution in distilled water.
[c] Calculated as acetaldehyde.

Molecular weight also plays a significant role in T_g, which increases to a limiting value of 180°C for high purity samples above K-90 in molecular weight. The following equation applies:

$$T_g(^\circ\mathrm{C}) = 175 - \frac{9685}{K^2}$$

and Table 10 illustrates this relationship with commercially available samples.

Table 10. Glass-Transition Temperatures of PVP

Sample[a]	Measured K value	T_g, °C
Plasdone K-15	14.0	126
PVP K-15	14.9	130
Plasdone K-25	22.5	160
PVP K-30	27.5	163
Plasdone K-29/32	28.7	164
PVP K-60	55.5	170
PVP K-90	89.6	174

[a] Courtesy of ISP Corp.

Solubility. One of PVP's more outstanding attributes is its solubility in both water and a variety of organic solvents. PVP is soluble in alcohols, acids, ethyl lactate, chlorinated hydrocarbons, amines, glycols, lactams, and nitroparaffins. Solubility means a minimum of 10 wt% PVP dissolves at room temperature (moisture content of PVP can influence solubility). PVP is insoluble in hydrocarbons, ethers, ethyl acetate, *sec*-butyl-4-acetate, 2-butanone, acetone, cyclohexanone, and chlorobenzene. Both solvent polarity and Hbonding strongly influence solubility (74).

Swelling Behavior. One way to visualize the interaction of solvents with PVP is to examine the effect the former have on lightly cross-linked PVP, as a model for the linear polymer (75).

Such gels can be prepared from a minimum of diallyl cross-linker and VP to afford products that are mechanically stable and easy to handle as hydrogels. Such samples must be extracted because soluble polymer competes for solvent, affording lower swell volumes than those expected. The extracted and dried samples are swollen to equilibrium in a variety of solvents (Table 11). Three groups of solvents can be distinguished: the first includes those in which the cross-linked polymer swells 15–25 times. VP, H_2O, CH_3OH, C_2H_5OH, benzylamine, and chloroform are examples. Swelling drops off with longer chain-length alcohols. Aromatic derivatives like benzyl alcohol and aniline afford similar swelling ratios to each other and to aliphatic analogues. This indicates that simple aromatic groups do not interact. When comparing volume instead of weight, water actually causes a 0.36% shrinkage of the gel. Water can therefore cross-link by hydrogen bonding to a limited but measurable extent. The second group consists of acetone, MEK, and dioxane solvents that not only increase the swell ratio (to a much lesser extent) but also increase the swell volume by 60–100%. The third group consists of hydrocarbons, benzene, carbon tetrachloride, isopropyl ether, and triethyl amine. In this case, they have little or no effect on swelling. The hallmark of this group is lack of hydrogen-bonding capability.

In water, the swell ratio actually decreases with temperature at a constant rate of $-0.12\%/^{\circ}C$. PVP gels therefore swell exothermically in water, and, as expected, heat reverses the process. Cooling back to a lower temperature results in the expected higher swell ratio being reestablished. Alcohols and other

Table 11. Swelling of Cross-linked Polyvinylpyrrolidone in Various Liquids at 20°C[a]

Liquid	Degree of swelling	Liquid	Degree of swelling
1-Propanol	25.6	Chloroform	16.7
Ethanol	24.8	Ethylenediamine	15.6
Isoamyl alcohol	24.8	Acetone	2.1
Methanol	24.0	Methyl ethyl ketone	2.0
Water	19.7	Cyclohexanone	1.9
Benzyl alcohol	19.5	Dioxane	1.6
n-Octanol	19.1	Trimethylamine	1.07
Benzylamine	17.1	Carbon tetrachloride	1.03
Prim-phenyl ethyl alcohol	16.9	Benzene	1.02
		Isopropyl ether	1.0

[a]Ref. 75.

hydrogen bonding solvents cause the same effect but to a lesser extent. Nonhydrogen-bonding solvents actually cause an increase in swelling with temperature (Table 12).

Rheology. PVP solubility in water is limited only by the viscosity of the resulting solution. The heat of solution is −16.61kJ/mol (−3.97 kcal/mol) (76); aqueous solutions are slightly acidic (pH 4–5). Figure 2 illustrates the kinematic

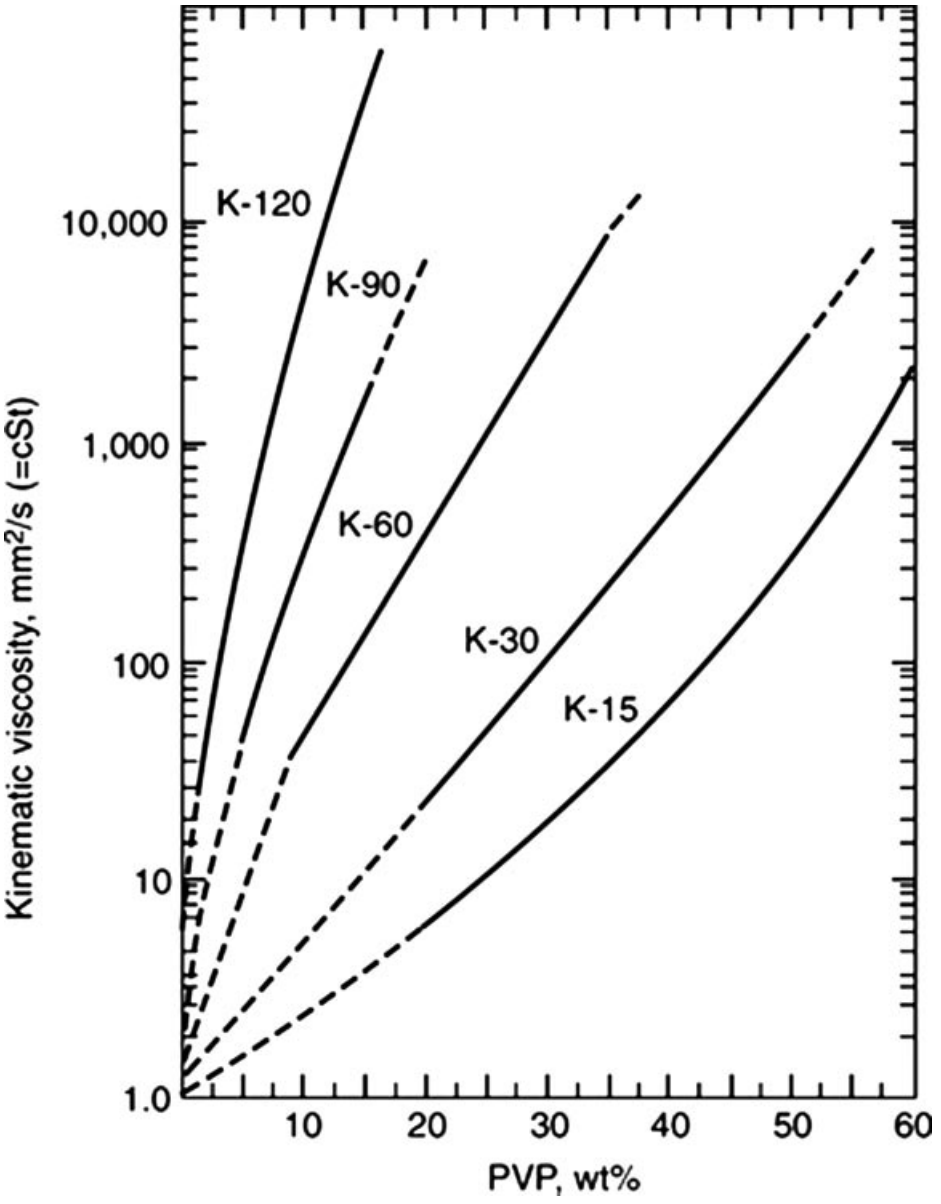

Fig. 2. Kinematic viscosity of PVP in aqueous solutions.

Table 12. Temperature-Dependence of Degree of Swelling in Four Liquids[a]

Liquid	Temperature, °C	Degree of swelling
Dioxane	20	1.57
	50	2.34
Methyl ethyl ketone	20	1.69
	50	2.86
Ethanol	20	18.3
	50	17.3
Chloroform	20	24.6
	50	24.0

[a]Ref. 75.

viscosity of PVP in aqueous solution. The kinematic viscosity of PVP K-30 in various organic solvents is given in Table 13.

Aqueous Solutions of PVP. Although it is soluble in a variety of polar solvents, PVP has generated significant interest because of its aqueous solubility. Water can readily hydrogen bond to the polar, negatively charged pyrrolidinone carbonyl oxygen because pyrrolidinone, a five-membered planar lactam, affords maximum π, π-orbital overlap. The canonical resonance forms highlight the

Table 13. Kinematic Viscosity of PVP K-30 in Organic Solvents

	Kinematic viscosity,[a] mm^2/s (=cSt)	
Solvent	2% PVP	10% PVP
Acetic acid (glacial)	2	12
1,4-Butanediol	101	425
Butyrolactone	2	8
Cyclohexanol	80	376
Diacetone alcohol	5	22
Diethylene glycol	39	165
Ethanol (absolute)	2	6
Ethyl lactate	4	18
Ethylene glycol	24	95
Ethylene glycol monoethyl ether	3	12
Glycerol	1480	2046
2-Propanol	4	12
Methyl cyclohexanone	3	10
N-Methyl-2-pyrrolidone	2	8
Methylene dichloride	1	3
Monoethanolamine	27	83
Nitroethane	1	3
Nonylphenol	3300	
Propylene glycol	66	261
Triethanolamine	156	666

[a]Kinematic viscosity = absolute viscosity/density.

potential for a partial negative charge to form on oxygen:

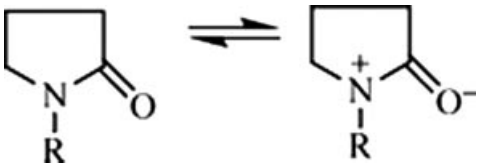

The partial charge on nitrogen is sterically shielded by the polymer backbone and the surrounding pyrrolidinone methylenes. Because of high dipole moment and polarity, PVP has a noticeable effect on water structure and various methods have been proposed to measure bound water (77). One study even illustrates the different categories of water generated by freezing aqueous PVP solutions (78). The results are summarized in Figure 3, and, as can be seen, PVP is hydrated with

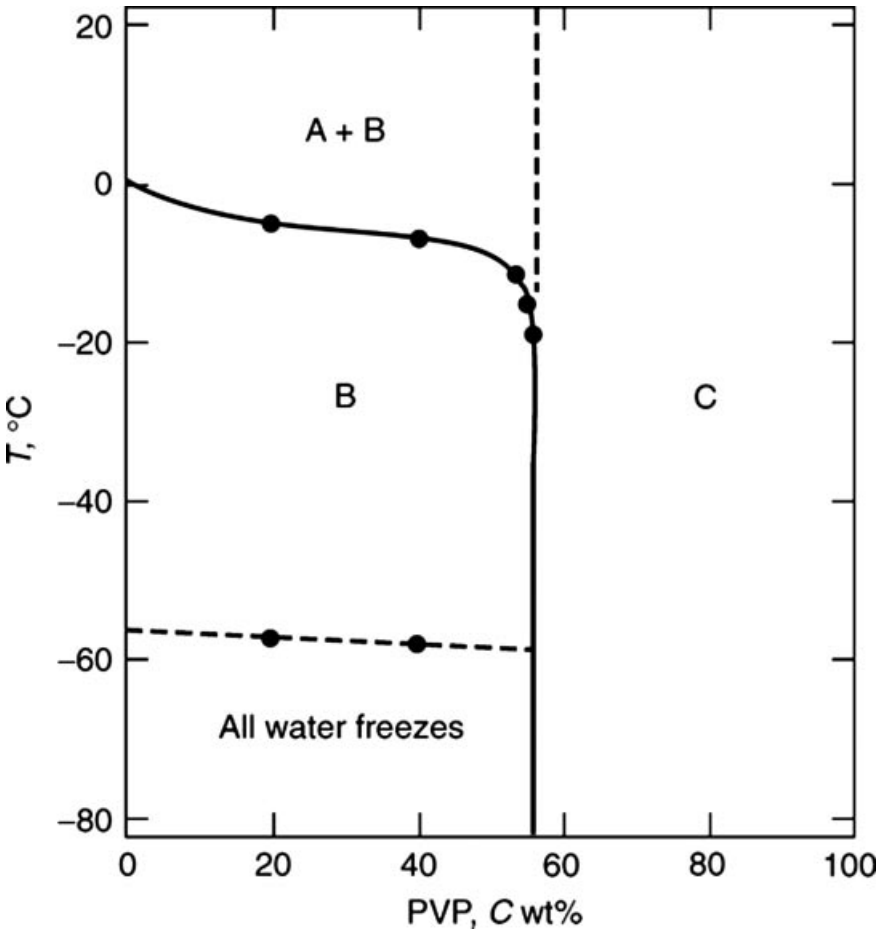

Fig. 3. Phase diagram for the three kinds of water in PVP aqueous solutions (78). A, freezable water; B, bound, nonfreezable water (six per repeat unit); C, nonfreezable water.

bound water that will not freeze (concentrated solutions >57% will not freeze). PVP is therefore used as a protectorate in cryobiology (79).

The actual amount and structure of this "bound" water have been the subject of debate (80), but the key factor is that in water, PVP and related polymers are water structure organizers, which is a lower entropy situation (81). Therefore, it is not unexpected that water would play a significant role in the homopolymerization of VP, because the polymer and its reactive terminus are more rigidly constrained in this solvent and termination k_t is reduced (82).

Complexation

The combination of electrostatic interaction (induced dipole–dipole interaction) with an increase in entropy resulting from the discharge of bound water is fundamental to PVP's ability to complex with a variety of large anions.

Other factors that can stabilize such a forming complex are hydrophobic bonding by a variety of mechanisms (van der Waals, Debye, ion dipole, charge transfer, etc). Such forces complement the stronger hydrogen bonding and electrostatic interactions.

Approximately a minimum $\bar{M}_n$ of 1–5000 is required before complexation is no longer dependent on molecular weight for small anions such as KI_3 and 1-anilinonaphthaline-8-sulfonate (ANS) (83,84). The latter anion is a fluorescent probe that, when bound in hydrophobic environments, will display increased fluorescence and, as expected, shows this effect in the presence of aqueous PVP. PVP, when complexed with HI_3, shrinks in size as it loses hydrodynamic volume, possibly because of interchain complexation. ANS, on the other hand, causes the polymer to swell by charge repulsion because it behaves like a typical polyelectrolyte (85).

Adsorption Isotherms. Equilibrium dialysis studies indicate around 10 repeat VP units (base moles) are required to form favorable complexes (86,87). This figure can rise to several hundred for methyl orange and other anions depending on structure (88,89).

Although hydrophobic bonding is well established as a significant force stabilizing such complexes, some work suggests that such generalizations do not apply to every case (89). However, a study of the complexes of PVP with tetraanionic porphyrins has shown that the reaction of porphyrin with cupric ion is slowed dramatically in the presence of PVP. This is interpreted as demonstrating the existence of hydrophobic pockets preventing a reaction that is clearly favored if both species are in aqueous environments (90). Hydrophobic bonding has been illustrated by comparing competitive binding of butyl orange (BO) with 1-amino-4-methylamino anthraquinone-2-sulfonate (AQ) (91). The thermodynamic data for BO show that the binding process is athermal and stabilized entirely by the entropy term. On the other hand, AQ exhibits a large enthalpy and small entropy value and its binding is by the stronger and energetic interaction caused by hydrogen bonding (NH groups of AQ) and hydrophobic interaction of the polynuclear aromatic AQ; both structural features are missing from BO (91).

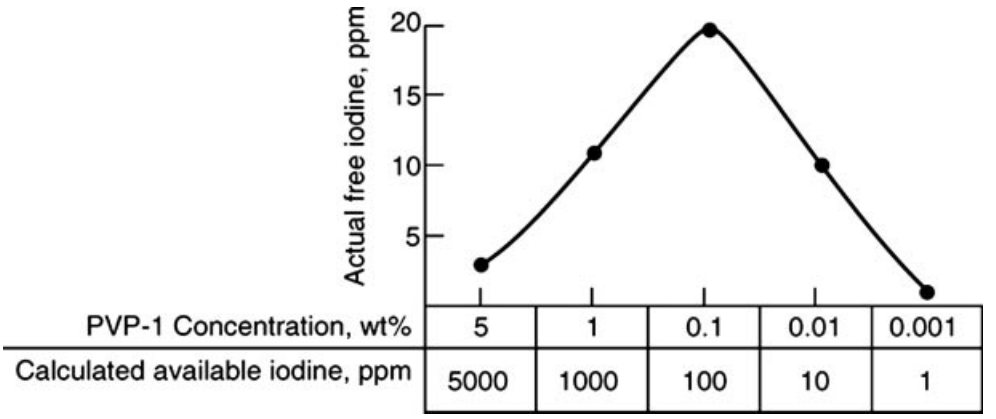

Fig. 4. Free iodine in povidone–iodine aqueous solutions (96).

Iodine Complexes. The small molecule/PVP complex between iodine and PVP is probably the best-known example (92) and can be represented as follows:

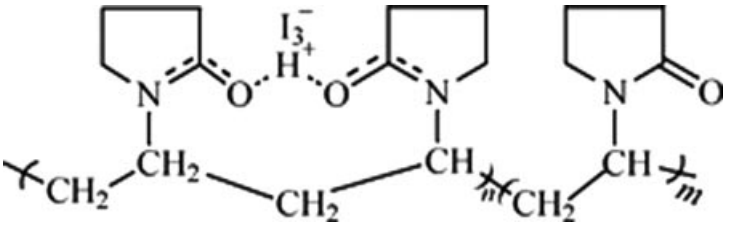

It is widely employed as a disinfectant in medicine (povidone–iodine) because of its mildness, low toxicity, and water solubility. In actuality, the complex is based on HI_3 since HI is formed *in situ* from iodine during the manufacturing process (93). According to the *U.S. Pharmacopeia*, povidone–iodine is a free flowing, brown powder that contains from 9 to 12% available iodine. It is soluble in water and lower alcohols. When dissolved in water, the uncomplexed free-iodine level is very low (Fig. 4) (94); however, the complexed iodine acts as a reservoir and by equilibrium replenishes the free iodine to the equilibrium level. This prevents free iodine from being deactivated because the free form is continually available at effective biocidal levels from this large reservoir (95). The structure of the complex has been studied and in essence is similar to the representation above (95,96). PVP will interact with other small anions and resembles serum albumin and other proteins in this regard (97). It can be "salted in" with anions such as NaSCN or "out" with Na_2SO_4 much like water-soluble proteins (98).

Phenolics. PVP readily complexes phenolics of all types to some degree, the actual extent depending on structural features such as number and orientation of hydroxyls and electron density of the associated aromatic system. A model has been proposed (99). Complexation with phenolics can result in reduced PVP viscosity and even polymer-complex precipitation (100).

One practical result of this strong interaction is the employment of PVP to remove unwanted phenolics such as bitter tanins from beer and wine. This process is more easily carried out with insoluble crospovidone, which can be regenerated for reuse with dilute base (101). Soluble PVP has been employed to prevent photoyellowing of paper by complexing free-phenolic hydroxyl groups in lignin (102).

Dyes. PVP is currently (ca 1997) employed in a variety of antidye redeposition detergents as a result of its strong interaction with fugitive anionic dyes (103,104). This interaction depends on the structure of the dye. Cationic dyes complex only if they also contain hydrogen-bonding functionality. Anionic dyes complex more easily, depending on the number of anionic groups, size of the aromatic nucleolus, and number and orientation of phenolic hydroxyl groups, etc.

Anionic Surfactants. PVP also interacts with anionic detergents, another class of large anions (105). This interaction has generated considerable interest because addition of PVP results in the formation of micelles at lower concentration than the critical micelle concentration (CMC) of the free surfactant the mechanism is described as a "necklace" of hemimicelles along the polymer chain, the hemimicelles being surrounded to some extent with PVP (106). The effective lowering of the CMC increases the surfactant's apparent activity at interfaces. PVP will increase foaming of anionic surfactants for this reason.

Because of this interaction, PVP has found application in surfactant formulations, where it functions as a steric stabilizer for example to generate uniform particle-size polystyrene emulsions (107–109). In a variety of formulations, a surfactant's ability to emulsify is augmented by PVP's ability to stabilize colloids sterically and to control rheology.

Polymer/Polymer Complexes. PVP complexes with other polymers capable of interacting by hydrogen bonding, ion dipole, or dispersion forces. For example mixing of PVP with poly(acrylic acid) (PAA) in aqueous solution results in immediate precipitation of an insoluble complex (110). Addition of base results in disruption of hydrogen bonding and dissolution (111–113). Complexes with a variety of polyacids (114) and polyphenols (115) have been reported. The interest in compatibility on a molecular level, an interesting phenomenon rarely found to exist between dissimilar polymers, is favored by the ability of PVP to form polymer/polymer complexes.

Practical applications have been reported for PVP/cellulosics (105,116,117) and PVP/polysulfones (118,119) in membrane separation technology, eg, in the manufacture of dialysis membranes. Electrically conductive polymers of polyaniline are rendered more soluble and hence easier to process by complexation with PVP (120). Addition of small amounts of PVP to nylon 66 and 610 causes significant morphological changes, resulting in fewer but more regular spherulites (121).

Copolymerization

The Q and e values of VP are 0.088 and −1.62, respectively (122). This indicates resonance interaction of the double bond of the vinyl group with the electrons of the lactam nitrogen, whence the electronegative nature. With high $e+$ monomers such as maleic anhydride, VP forms alternating copolymers, much as expected

Table 14. VP Copolymerization Parameters[a]

Comonomer (M_2)	r_1	r_2	Reference
N-Vinyl caprolactam	2.80	1.70	125
Maleic anhydride	−0.027	0.074	126
Methyl methacrylate	0.01	4.04	127
Styrene	0.057	17.2	128
Vinyl acetate	3.40	0.195	128
Acrylic acid	0.100	0.880	129
Dimethylaminoethyl	0.07	4.7	130
Methacrylate	0.69	11.16	131

[a]Ref. 124.

(123). With other monomers between these Q and e extremes a wide variety of possibilities exist. Table 14 lists reactivity ratios for important comonomers.

Copolymerizations can be conveniently carried out in aqueous solution or in a variety of solvents, depending on monomer/polymer solubilities. Various strategies have been employed to compensate for the divergence in reactivity ratios in order to form uniform (statistical) copolymers such as semibatch or mixed monomer feeds, the goal being to add the more reactive monomer at the rate at which it is being consumed (132). Clearly, if the difference in reactivity is too great, then the amount of more reactive monomer that can be uniformly incorporated is significantly reduced. Of the monomers listed, styrene fits this category (133).

Poly(Vinylpyrrolidinone-co-Vinyl Acetate). The first commercially successful class of VP copolymers, poly(vinylpyrrolidinone-*co*-vinyl acetate) is currently manufactured in sizeable quantities by both ISP and BASF. A wide variety of compositions and molecular weights are available as powders or as solutions in ethanol, isopropanol, or water (if soluble). Properties of some examples of this class of copolymers are listed in Table 15.

Table 15. Properties of PVP/VA Copolymers[a]

	PVP–VA copolymer						
	E-735	E-635	E-535	E-335	I-735	I-535	I-335
Physical form at 25°C	Clear liquid				Light yellow liquid		
Solvent	SDA-40 anhydrous ethanol				2-propanol		
Solids after infrared drying, %		50 ± 2	50 ± 2	50 ± 2	50 ± 2	50 ± 2	50 ± 2
Vinylpyrrolidinone–vinyl Acetate ratio	70:30	60:40	50:50	30:70	70:30	50:50	30:70
K value of 1% ethanol solution	30–50	30–50	30–50	25–35	30–40	25–35	20–30
Moisture as is, Karl Fischer, %max	0.5	0.5	0.5	0.5	0.5	0.5	0.5
Nitrogen, dry basis, Kjeldahl, %	8–9	7–8	5.8–6.8	3.1–4.1	8–9	5.9–6.9	3.9–4.9
Specific gravity at 25°C	0.955 ± 0.01						

[a]Ref. 134.

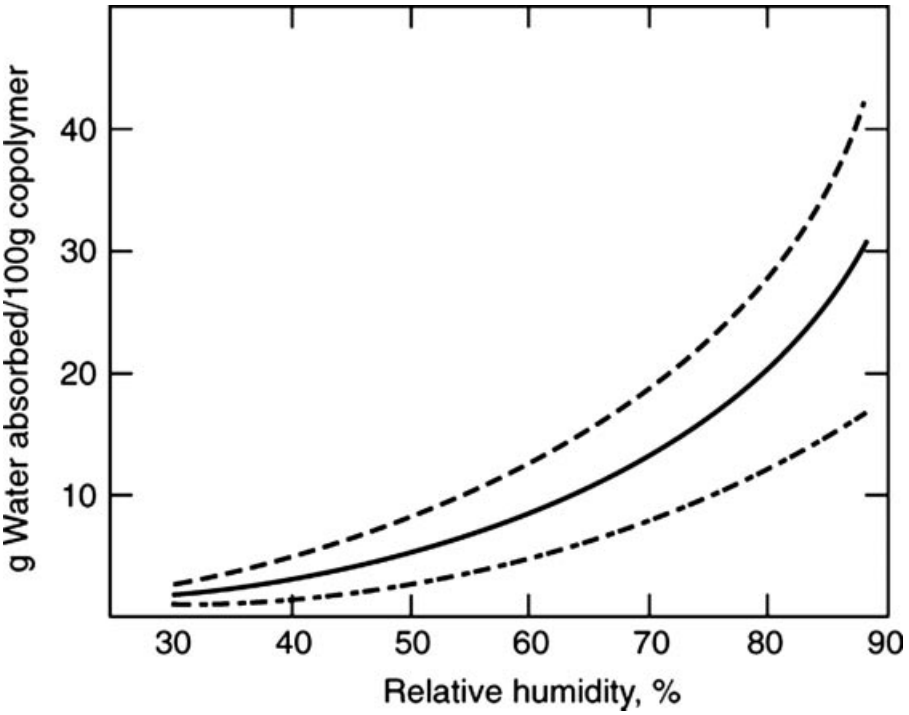

Fig. 5. Hydrophilicity of three wt% monomer ratios of PVP/VA: (– – –), 70/30; (—), 50/50; (—·—·), 30/70.

Although reactivity ratios indicate that VP is the more reactive monomer, reaction conditions such as solvent polarity, initiator type, percent conversion, and molecular weight of the growing radical can alter these ratios (135). Therefore, depending on polymerization conditions, copolymers produced by one manufacturer may not be identical to those of another, especially if the end use application of the resin is sensitive to monomer sequence distribution and MWD.

An important reason for the ongoing interest in these copolymers is that vinyl acetate reduces hydrophilicity so that applications that require less moisture-sensitive films such as those employed to set hair are less prone to plasticize and become tacky under high humidity conditions (136) (Fig. 5).

As shown in Figure 6, desirable fixative properties superior to PVP homopolymer can be specified by judicious selection of the amount of vinyl acetate. Hair sprays are limited in the molecular weight of the resin because if they are too high the resulting viscosity of the formulation will result in a poor (coarse) spray pattern. Increasing the VP/VA ratio causes properties to increase in the direction shown by the arrows.

Other applications for VP/VA copolymers are uses as water-soluble or remoistenable hot-melt adhesives (137), pharmaceutical tablet coatings, binders, and controlled-release substrates.

Tertiary Amine-Containing Copolymers. Copolymers based on dimethylaminoethyl methacrylate (DMAEMA) in either free-amine form or

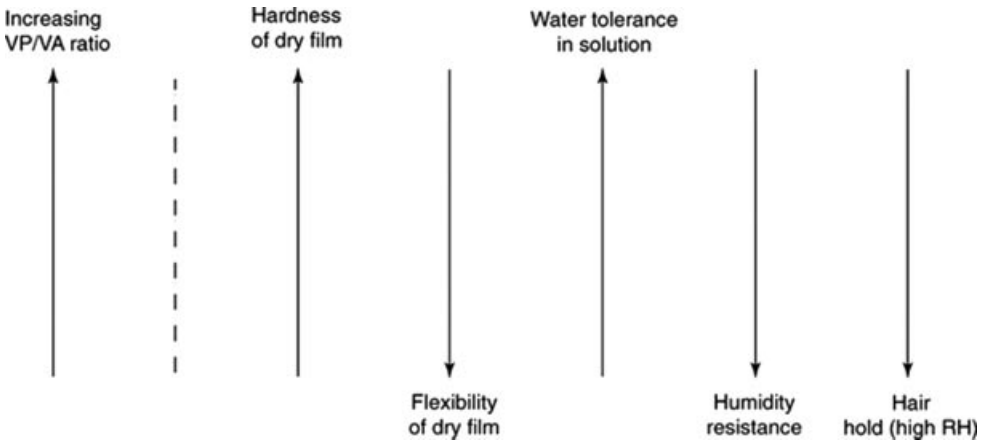

Fig. 6. Effect of VP/VA monomer ratio on properties of VP/VA copolymers.

quaternized with diethyl sulfate or methyl chloride have achieved commercial significance as fixatives in hair-styling formulations, especially in the well-publicized "mousses" or as hair-conditioning shampoo additives. This success has occurred because the cationic charge affords substantive resins that strongly adhere to the hair (138).

The most successful of these products contain high ratios of VP to DMAEMA and are partially quaternized with diethyl sulfate (Polyquaternium 11) (139–141). They afford very hard, clear, lustrous, nonflaking films on the hair that are easily removed by shampooing. More recently, copolymers with methylvinylimidazolium chloride (Polyquaternium 16) (142) or methacrylamidopropyltrimethyl ammonium chloride (MAPTAC) (Polyquaternium 28) have been introduced. Replacement of the ester group in DMAEMA with an amide analog as in Polyquaternium 28 results in a resin resistant to alkaline hydrolysis and hence greater utility in alkaline permanent wave and bleach formulations (see QUATERNARY AMMONIUM COMPOUNDS).

Unquaternized DMAEMA copolymers afford resins that are mildly cationic and less hydroscopic. They provide more moisture-resistant fixatives (143). Further refinements have been accomplished by adding a third comonomer such as *N*-vinylcaprolactam (VCl). In this case, replacement of VP with VCl results in a terpolymer (VP/VCl/DMAEMA) with even greater high humidity moisture resistance and curl retention.

Copolymers Containing Carboxylic Groups. A new line of VP/acrylic acid copolymers in powdered form prepared by precipitation polymerization (144) from heptane have been introduced commercially (145). A wide variety of compositions and molecular weights are available, from 75/25 to 25/75 wt% VP/AA and from 20×10^3 to 250×10^3 molecular weights.

The copolymers are insoluble in water unless they are neutralized to some extent with base. They are soluble, however, in various ratios of alcohol and water, suggesting applications where delivery from hydroalcoholic solutions (146) but subsequent insolubility in water is desired, such as in low volatile organic

Table 16. Properties and Applications of Commercial PVPs

Polymer	Mfr/Trade name	Grades	Properties/applications
		Homopolymers	
PVP	ISP/PVP, Plasdone BASF/Luviskol, Kollidon	K-15 to K-120 K-12 to K-90	Film former, adhesive, binder, com-plexant, stabilizer, crystallization inhibitor, dye scavenger, detoxi-cant, viscosity modifier
		Cross-linked	
Proliferous polymerization	ISP/Polyclar, Polyplasdone BASF/Divergan	Various (by particle size) various (by particle size)	Pharmaceutical tablet disintegrant, adsorbent for polyphenols (tanins), beverage clarification
		Copolymers	
PVP/VA	BASF/ISP/PVP–VA copolymers	Various monomer ratios in ethanol, IPA or water in ethanol, IPA or water	Film forming adhesives for hairsprays, mousses, gels, shampoos, styling lotions, bio-adhesives, water-remoist-enable or removable adhesives
PVP/DMAEMA	ISP/copolymer	845/937/958	Mildly cationic, hair styling aids and conditioners, with strong hold; sub-stantive, lustrous film-formers
PVP/DMAEMA DES quaternary	ISP/Gafquat BASF/Luviquat	755N/734PQ11	Strongly cationic, substantive, mousse and gel hair fixative ingredients
PVP/imidazolinum quaternary	BASF/Luviquat FC		
PVP/styrene[a]	ISP/Polectron 430	30% VP	Opacifier for personal care products; very stable styrene emulsion
PVP/alpha-olefins[a]	ISP/Ganex	Various (olefin chain length and monomer ratios)	Surface active film formers; waterproofing of sunscreens
		Terpolymers	
VP/VCl/DMAEMA	ISP/Gaffix VC-713	VC-713	Cationic water-soluble hair styling aid hair fixatives
VP/tBMA/MA	BASF/Luviflex	Various	

[a] Graft copolymers.

compound (VOC) hair-fixative formulations or tablet coatings. Unneutralized, their T_gs are higher than expected, indicating interchain hydrogen bonding (147).

Miscellaneous Copolymers. VP has been employed as a termonomer with various acrylic monomer–monomer combinations, especially to afford resins useful as hair fixatives. Because of major differences in reactivity, VP can be copolymerized with alpha-olefins, but the products are actually PVP grafted with olefin or olefin oligomers (148,149). Likewise styrene can be polymerized in the presence of PVP and the resulting dispersion is unusually stable, suggesting that this added resistance to separation is caused by some grafting of styrene onto PVP (150). The literature contains innumerable references to other copolymers but at present (ca 1997), those reviewed in this article are the only ones known to have commercial significance.

Applications

An overview of the various product categories is given in Table 16.

The Chemical Abstracts Services Registry Number and IUPAC nomenclature for PVP are [9003-39-8] and 1-ethenyl-2-pyrrolidinone homopolymer, respectively; however, it is known by a variety of approved names by foreign and domestic regulatory authorities. For example:

Name	Chemical name
Povidone	Poly(*N*-vinyl-2-pyrrolidinone)
Polyvidone	
Polyvidon	Poly(*N*-vinylbutyrolactam)
Polyvidonum	Poly(1-vinyl-2-pyrrolidinone)
	1-Vinyl-2-pyrrolidinone polymer
	Poly{1-(2-oxo-1-pyrrolinyl)ethylene}

Trade names for nonpharmaceutical grades are PVP, Peregal ST, Albigen A, and Luviskol; for pharmaceutical grades, Plasdone and Kollidon. The insoluble or crospovidones likewise exist as two grades: nonpharmaceutical are Polyclar and Divergan; pharmaceutical, Polyplasdone XL and Kollidon Cl.

BIBLIOGRAPHY

"*N*-Vinyl Amide Polymers" in *EPST* 1st ed., Vol. 11, pp. 239–251, by Donald H. Lorenz, GAF Corporation; "*N*-Vinyl Amide Polymers" in *EPSE* 2nd ed., Vol. 17, pp. 198–257, by E.S. Barabas, GAF Chemicals Corporation.

CITED PUBLICATIONS

1. P. Molyneux, in G. Starnsby, ed., *The Chemistry and Rheology of Water-Soluble Gums and Colloids*, S.C.I. Monograph No. 24, Society of Chemical Industries, London, 1966, p. 91.

2. A. Charlesby, *Radiat. Phys. Chem. V* **18**(1–2), 59 (1981).
3. W. Reppe and co-workers, *Justus Leibig's Ann. Chem.* **601**, 134 (1956).
4. J. Falbe and H. J. Schulze-Steinem, *Brennst. Chem.* **48**, 136 (1967).
5. D. J. Dawson, R. D. Gless, and R. E. Wingard Jr., *JACS* **98**, 5996 (1976).
6. T. M. Karaputudze and co-workers, *Vysokomol. Soedin., Ser. B.* **24**, 305 (1982).
7. C. Bramford, E. Schofield, and D. Michael, *Polymer* **26**, 946 (1985).
8. S. A. Miller, *Acetylene, Its Properties, Manufacture, and Uses*, Vol. **2**, Academic Press, New York, 1965, pp. 338–339.
9. *Vinylpyrrolidone (VP) Toxicity*, Update No. 2303-222R′ 2M-292, ISP Corp., Wayne, N.J., 1992.
10. G. M. Kline, *Mod. Plastics* **22**, 157 (1945).
11. J. W. Copenhaver and M. H. Bigelow, *Acetylene and Carbon Monoxide Chemistry*, Reinhold Publishing Corp., New York, 1949.
12. B. V. Robinson and co-workers, *PVP, A Critical Review of the Kinetics and Toxicology of Polyvinylpyrrolidone (Povidone)*, Lewis, Chelsea, Mich., 1990.
13. J. W. Breitenbach, *J. Polym. Sci.* **23**, 949 (1957).
14. S. Bottle and co-workers, *Eur. Polym. J.* **23**, 671 (1989).
15. Y. E. Kirsh, *Polym. Sci.* **35**(2), 98 (1993).
16. G. Odian, *Principles of Polymerization*, 3rd ed., Wiley-Interscience, 1991, p. 217.
17. R. T. Woodhams, Ph.D. Dissertation, Polytechnic Institute of Brooklyn, Brooklyn, N.Y., 1954.
18. V. Shtamm and co-workers, *Zh. Fiz. Khim.* **55**, 2289 (1981).
19. M. V. Encinas, E. A. Lissit, and J. Quiroz, *Eur. Polym. J.* **28**, 471 (1992).
20. K. C. Gupta, *J. Appl. Polym. Sci.* **53**, 71 (1994).
21. W. Kern and H. Cherdron, *Houben Weyl, Methoden der Organische Chemie*, 4th ed., Vol. **14**, Verlag, Stuttgart, Germany, 1961, p. 1106.
22. Ger. Pat. DE 3,532,747 (1987), A. Nuber and co-workers (to BASF).
23. S. C. Ng, *Eur. Polym. J.* **18**, 917 (1982).
24. F. Haaf, A. Sanner, and F. Straub, *Polym. J.* **17**(1), 143 (1985).
25. V. V. Kopeikin, Y. G. Santuryan, and M. Y. Danilova, *Khim. Farm. Zh.* **22**, 1253 (1988).
26. I. G. Gulis and co-workers, *Khim. Farm. Zh.* **25**(9), 82 (1991).
27. E. Senogles and R. Thomas, *J. Polym. Sci. Polym. Symp.* **49**, 203 (1975).
28. E. Senogles and R. Thomas, *J. Polym. Sci. Polym. Lett. Ed.* **16**, 555 (1978).
29. T. M. Karaputadze, V. I. Shumskii, and Y. E. Kirsh, *Vysokomol. Soedin. Ser. A* **20**, 1854 (1978).
30. V. R. Gromov and co-workers, *Eur. Polym. J.* **27**, 505 (1991).
31. M. Biswas and P. K. Mishra, *Polymer* **16**, 621 (1970).
32. G. D. Jones, in P. H. Plesch, ed., *The Chemistry of Cationic Polymerization*, Macmillan, New York, 1963, p. 554, Chapt. 14.
33. N. Tsubokawa, N. Takeda, and A. Kanamaru, *J. Polym. Sci. Polym. Lett. Ed.* **18**, 625 (1980).
34. N. Tsubokawa, H. Maruyama, and Y. Sone, *J. Macromol. Sci. Chem. A* **25**(2), 171 (1988).
35. N. Tsubokawa and co-workers, *J. Polym. Sci. Polym. Chem. Ed.* **31**, 3193 (1993).
36. E. Yoshida and co-workers, *J. Polym. Sci. Polym. Chem. Ed.* **31**, 1505 (1993).
37. E. Leonard-Stibbe and co-workers, *J. Polym. Sci. Polym. Chem. Ed.* **32**, 1551 (1994).
38. H. N. Cheng, T. E. Smith, and D. M. Vitus, *J. Polym. Sci. Polym. Lett. Ed.* **19**, 29 (1981).
39. J. R. Ebdon, T. N. Hackerby, and E. Senogles, *Polymer* **24**, 339 (1983).
40. T. Bartels, Y. Y. Tan, and G. Challa, *J. Polym. Sci.* **15**, 341 (1977).
41. D. W. Koetsier, G. Challa, and Y. Y. Tan, *Polymer* 1709 (1980).
42. D. W. Koetsier, Y. Y. Tan, and G. Challa, *J. Polym. Sci.* **18**, 1933 (1980).

43. G. O. R. Alberda van Ekenstein, D. W. Koetsie, and Y. Y. Tan, *Eur. Polym. J.* **17**, 845 (1981).
44. V. S. Rajan and J. Ferguson, *Eur. Polym. J.* **18**, 633 (1982).
45. I. V. Kotlyarskii and co-workers, *Vysokomol. Soedin. Ser. A* **31**, 1893 (1989).
46. J. Matuszewska-Czerwik and S. Polowinski, *Eur. Polym. J.* **26**, 549 (1990).
47. U.S. Pat. 2,938,017 (1960), F. Grosser (to AF).
48. U.S. Pat. 5,286,826 (Feb. 15, 1994), J. S. Shih and S. Y. Tseng (to ISP).
49. J. W. Breitenbach and H. Axmann, in N. Platzer, ed., *Polymerization Kinetics and Technology*, Chapt. 7 (Advances in Chemistry Series 128, ACS, 1973).
50. E. Barabas and C. Adeyeye, *Anal. Profiles Drug Subst. Excipients* **24**, 87–163 (1996).
51. B. I. Da Silveira, *Eur. Polym. J.* **29**, 1095 (1993).
52. J. W. Breitenbach, *J. Polym. Sci.* **23**, 949 (1957).
53. J. W. Breitenbach and E. Wolf, *Makromol. Chem.* **18/19**, 217 (1956).
54. J. W. Breitenbach and A. Schmidt, *Monatsh. Chem.* **85**(1), 52 (1954).
55. T. P. Davis and M. B. Huglin, *Makromol. Chem.* **191**, 331 (1990).
56. O. Guven and M. Sen, *Polymer* **32**(13), 2491 (1991).
57. M. B. Huglin and M. Zakaria, *Polymer* **25**, 797 (1984).
58. T. Davis, M. Huglin, and D. Yip, *Polymer* **29**, 701 (1988).
59. J. Shih, J. C. Chuang, and R. B. Login, *Polym. Mater. Sci. Eng.* **72**, 374 (1995).
60. C. C. Anderson, F. Rodriguez, and D. A. Thurston, *J. Appl. Polym. Sci.* **23**, 2453 (1979).
61. H. Tenhu and F. Sundholm, *Makromol. Chem.* **185**, 2011 (1984).
62. P. Alexander and A. Charlesby, *J. Polym. Sci.* **23**, 355 (1957).
63. A. Chapiro and C. Legris, *Eur. Polym. J.* **25**, 305 (1989).
64. J. E. Davis and E. Senogles, *Aust. J. Chem.* **34**, 1413 (1981).
65. U.S. Pat. 4,699,146 (Oct. 13, 1987), D. L. Sieverding (to Valley Lab).
66. J. W. Copenhaver and M. H. Bigelow, *Acetylene and Carbon Monoxide Chemistry*, Reinhold Publishing Corp., New York, 1969, pp. 67–74.
67. *USP 23*, The United States Pharmacopeial Convention, Inc., Rockville, Md., 1995.
68. C. Wu, in C. Wu, ed., *Handbook of Size Exclusion Chromatography*, Marcel Dekker, Inc., New York, 1995, Chapt. 12.
69. L. Senak, C. Wu, and E. Malawer, *J. Liq. Chrom.* **10**, 1127 (1987).
70. H. Fikentscher and K. Herrle, *Mod. Plast.* **23**, 157, 212, 214, 216, 218 (1945).
71. J. Brandrup and E. H. Immergut, eds., *Polymer Handbook*, 3rd ed., John Wiley & Sons, Inc., New York, p. VII 18.
72. Y. Y. Tan and G. Challa, *Polymer* **17**, 739 (1976).
73. D. T. Turner and A. Schartz, *Polymer* **26**, 757 (1985).
74. P. Molyneux, in F. Franks, ed., *Water: A Comprehensive Treatise*, Vol. **4**, New York, 1975, pp. 569–801, Chapt. 7.
75. J. W. Breitenbach and E. Wolf, *Makromol. Chem.* **18/19**, 217 (1956).
76. R. Meza and L. Gargallo, *Eur. Polym. J.* **13**, 235 (1977).
77. Y. E. Kirsh, *Prog. Polym. Sci.* **18**, 519–542 (1993).
78. N. Shinyashiki and co-workers, *J. Phys. Chem.* **98**, 13612 (1994).
79. S. K. Jain and G. P. Johari, *J. Phys. Chem.* **92**, 5851 (1988).
80. M. J. Blandamer and J. R. Membrey, *J. Chem. Soc. Perkin II* 1400 (1974).
81. V. V. Kobyakov and co-workers, *Vysokomol. Soedin. Ser. A* **23**(1), 150 (1981).
82. D. A. Topchiev, personal communication, 1995.
83. Y. E. Kirsh and co-workers, *Eur. Polym. J.* **15**, 223 (1979).
84. Y. E. Kirsh and co-workers, *Eur. Polym. J.* **18**, 639 (1983).
85. E. Killmann and R. Bittler, *J. Polym. Sci. Part C* **39**, 247 (1972).
86. B. P. Molyneux and H. P. Frank, *J. Am. Chem. Soc.* **83**, 3169 (1961).
87. H. P. Frank, S. Barkin, and F. R. Eirich, *J. Am. Chem. Soc.* **61**, 1375 (1957).
88. W. Scholtan, *Makromol. Chem.* **11**, 131 (1953).

89. R. L. Reeves, S. A. Harkaway, and A. R. Sochor, *J. Polym. Sci.* **19**, 2427 (1981).
90. F. M. El Torki and co-workers, *J. Phys. Chem.* **91**, 3686 (1987).
91. T. Takagishi and co-workers, *J. Polym. Sci.* **22**, 185 (1984).
92. W. Gottardi, in S. Block, ed., *Disinfection, Sterilization and Preservation*, Lea & Febiger, 1991, Chapt. 8.
93. H. Schenck, P. Simak, and E. Haedicke, *J. Pharm. Sci.* **68**, 1505 (1979).
94. J. L. Zamora, *Am. J. Surg.* **151**, 400 (1986).
95. D. Horn and W. Ditter, in G. Hierholzer and G. Gortz, eds., *PVP-Iodine in Surgical Medicine*, Springer, New York, 1984.
96. H. N. Cheng, T. E. Smith, and D. M. Vitus, *J. Polym. Sci. Polym. Phys. Ed.* **23**, 461 (1985).
97. L. Turker and co-workers, *Colloid Polym. Sci.* **268**, 337 (1990).
98. A. Guner and M. Ataman, *Colloid Polym. Sci.* **272**, 175 (1994).
99. P. Molyneuz and S. Vekavakaynondha, *J. Chem. Soc., Faraday Trans. 1* **82**, 291 (1986).
100. P. Molyneuz and S. Vekavakaynondha, *J. Chem. Soc., Faraday Trans. 1* **82**, 635 (1986).
101. D. Oechsle and B. Fussnegger, *Brauwelt* **41**, 1780 (1990).
102. M. Ratto and co-workers, *Tappi* **76**(6), 67 (1993).
103. J. C. Hornby, *Tappi* **88** (Jan., 1995).
104. H. U. Jager and W. Denzinger, *Tenside* **6**, 428 (1991).
105. M. Paillet and co-workers, *Colloid Polym. Sci.* **271**, 311 (1993).
106. Y. J. Nikas and Blankschtein, *Langmuir* **10**, 3512 (1994).
107. Y. Almog, S. Reich, and M. Levy, *Brit. Polym. J.* **14**, 131 (1982).
108. A. J. Paine, *J. Polym. Sci. Polym. Chem. Ed.* **28**, 2485 (1990).
109. C. M. Tseng and co-workers, *J. Polym. Sci. Polym. Chem. Ed.* **28**, 2569 (1990).
110. H. L. Chen and H. Morawetz, *Eur. Polym. J.* **19**, 923 (1983).
111. I. Iliopoulos and R. Audebert, *J. Polym. Sci. Polym. Lett. Ed.* **26**, 2093 (1988).
112. I. Iliopoulos, J. L. Halary, and R. Audebert, *J. Polym. Sci. Polym. Chem. Ed.* **26**, 275 (1988).
113. I. Iliopoulos and R. Audebert, *Eur. Polym. J.* **24**(2), 171 (1988).
114. K. R. Shah, *Polymer* **28**, 1212 (1987).
115. M. J. Fernandez-Berridi and co-workers, *Polymer* **31**(1), 38 (1993).
116. M. T. Qurashi, H. S. Blair, and S. J. Allen, *J. Appl. Polym. Sci.* **46**, 255, 263 (1992).
117. J. F. Masson and R. St. John Manley, *Macromolecules* **24**, 6670 (1991).
118. C. M. Tam, M. Dal-Cin, and M. D. Guiver, *J. Membr. Sci.* **78**, 123 (1993).
119. C. M. Tam and co-workers, *Desalination* **89**, 275 (1993).
120. W. B. Stockton and M. F. Rubner, *Polym. Prepr.* **19**, 319 (1978).
121. H. D. Keith, F. J. Padden Jr., and T. P. Russell, *Macromolecules* **22**, 666 (1989).
122. R. Z. Greenley, in J. Brandrup and E. H. Immergut, eds., *Polymer Handbook*, 4th ed., John Wiley & Sons, Inc., New York, p. 318, Chapt. II.
123. G. Georgiev, C. Konstantinov, and V. Kabaivanov, *Macromolecules* **25**, 6302 (1992).
124. Ref. 125, p. II, 247.
125. E. E. Skorikova and co-workers, *Vysokomol. Soedin., Ser. B* **27**, 869 (1985).
126. W. M. Culbertson, in J. I. Kroschwitz, ed., *Encyclopedia of Polymer Science and Engineering*, 2nd ed., Vol. **9**, John Wiley & Sons, Inc., NY, 1987, p. 240.
127. M. Orbay, R. Laible, and L. Dulog, *Makromol. Chem.* **47**, 183 (1982).
128. J. F. Bork and L. E. Coleman, *J. Polym. Sci.* **43**, 413 (1960).
129. Van Paesschen and G. Smets, *Bull. Soc. Chem. Belg.* **64**, 173 (1955).
130. A. Chapiro and L. D. Trung, *Eur. Polym. J.* **10**, 1103 (1974).
131. K. Deboudt, M. Delporte, and C. Loucheux, *Macromol. Chem. Phys.* **196**, 279 (1995).
132. K. Y. Choi, *J. Appl. Polym. Sci.* **37**, 1429 (1989).
133. M. B. Huglin and K. S. Khairou, *Eur. Polym. J.* **24**, 239 (1988).

134. PVP/VA brochure No. 2302-194, ISP, 1990.
135. Yu. D. Semchikov and co-workers, *Eur. Polym. J.* **26**, 889 (1990).
136. R. Y. Lochhead, *Cosmet. Toiletries* **103**, 23 (1988).
137. G. Russell, *Eur. Adhes. Sealants* (June, 1989).
138. J. Jachowicz, M. Berthiaume, and M. Garcia, *Colloid Polym. Sci.* **263**, 847 (1985).
139. U.S. Pat. 3,910,862 (1975), E. S. Barabas and M. M. Fern (to GAF).
140. U.S. Pat. 3,914,403 (1975), K. Valan (to GAF).
141. Bulletin No. QO394, *International Specialty Products*, 1994.
142. Ger. Pat. 4,138,763 (1991), H. Meyer and A. Sanner (BASF).
143. U.S. Pat. 4,223,009 (1980), P. M. Chakrabarti (to GAF).
144. U.S. Pat. 5,015,708 (1991), J. S. Shih, T. E. Smith, and R. B. Login (to GAF).
145. J. S. Shih, J. C. Chuang, and R. B. Login, Vol. 67, American Chemical Society, Division of Polymeric Materials (Fall, 1992), p. 226.
146. U.S. Pat. 5,219,906 (1993), J. S. Shih and T. E. Smith (to ISP).
147. J. C. Hornby, J. D. Pelesko, and D. Jon, *Soap/Cosmet. Specialt*. (June, 1993).
148. S. L. Kopolow, R. B. Login, and M. Tazi, in C. G. Gebelein, T. C. Cheng, and U. C. Yang, eds., *Cosmetic and Pharmaceutical Application of Polymers*, Plenum Publishing Co., New York, 1991.
149. *Ganex Bulletin* (2302-191 5M-989), ISP Corp., 1989.
150. *Polectron Emulsion Copolymers Bulletin* (2302-104), GAF Corp., 1984.

ROBERT B. LOGIN
Sybron Chemicals Inc.

Encyclopedia of Polymer Sceince and Technology
Copyright © 2005 John Wiley & Sons, Inc. All rights reserved.

PHOTOREFRACTION

Introduction

This article introduces the field of photorefraction and the photorefractive effect in polymer composites. The photorefractive effect is expected to play a significant role in the development of all-optical information processing techniques. Photorefractive materials, including polymers, have been proposed for use in high density optical data storage; associative image processing techniques, including dynamic holography, novelty filtering and image amplification; spatial light modulation, such as beam fanning, optical limiters, phase conjugators, self-induced optical resonators, programmable interconnections in integrated optics; and simulations of neural networks and associative memories with parallel signal processing (1–8).

The photorefractive effect requires a specific mechanism for the spatial modulation of the index of refraction of a material arising from an intensity modulation of the incident light (as in a diffraction pattern or hologram). The specific mechanism is the generation, transport, and trapping of charge through photoconduction in the illuminated regions to set up space-charge fields between the light and dark regions. These space-charge fields cause the modulation of the index of refraction acting through electro-optic and molecular orientation effects (9–11).

Scope of Article. The Photorefractive Process section describes the photorefractive process in detail, including theoretical models for photorefraction that are used to determine optimized material properties for applications using polymers. That section also describes how photorefraction can be distinguished from other photo-induced refractive index changes. Composition of Polymeric Photorefractive Materials section describes many of the ways polymeric composite materials have been formulated for their photorefractive properties, primarily by incorporating different functionalities via doping with electro-optic chromophores, photo-charge generation and transport agents, and plasticizers. Test Methods section briefly describes important experimental techniques for studying photorefraction, including four-wave mixing, two-beam coupling, and ellipsometry. Test Methods section also highlights several techniques for studying photoconductivity specifically for the photorefractive response. Finally, Applications section discusses recent progress in developing polymeric photorefractive devices.

Because of the extensive overlap with electro-optics and nonlinear optics, the reader is referred to separate articles on these topics in this encyclopedia. See ELECTROOPTICAL APPLICATIONS for a discussion of the changes in the optical response of polymers due to an applied AC or DC electric field from the so-called Pockels or Kerr effects. Also see, for an overview, NONLINEAR OPTICAL PROPERTIES.

Similarly, because photoconductivity is essential to photorefraction, readers may refer to CONDUCTIVE POLYMER COMPOSITES.

In addition to those cited above, many other helpful review articles have appeared in the archived research literature, for example, References 12–18.

History and Advantages of Polymeric Photorefractive Materials. The research literature on photorefraction dates back to its discovery as optical damage in the inorganic ferroelectric crystal, lithium niobate in 1966 (19). The first reports on photorefraction in an organic crystal appeared in 1990 (20) and in a polymeric material in 1991 (21). Application of crystalline photorefractive materials has been limited due to (1) the difficulty of crystal growth and processing and (2) fundamental limits on the maximum possible variation in the index of refraction of inorganic crystals in which large optical nonlinearities, measured by the electro-optic coefficient, r_e, are generally accompanied by large dielectric constants, ε_r, leading to screening of the space-charge distribution through polarization effects (1). For the linear electro-optic contribution, the relevant figure of merit is defined by $Q = n^3 r_e/\varepsilon_r$, where n is the index of refraction. Q values for organic photorefractive materials can exceed those of inorganic materials by more than an order of magnitude. The electro-optic mechanism in polymers is intrinsically different from that in inorganic crystals. In ferroelectric crystals, acoustic and optical phonons contribute significantly to the electro-optic effect, where the polarizability is largely ionic. The linear electro-optic response in organic polymers is primarily due to the electronic excitations of individual molecules and/or molecular units, thus yielding low dielectric constants and minimizing dispersion over DC to optical frequencies (22).

Because of these advantages as well as orientational enhancement effects and the superior compositional flexibility of polymers, the number of studies of polymers for photorefraction grew rapidly during the 1990s and into the current decade. It is now common to see a chapter on polymeric photorefraction in treatises that once emphasized only inorganic crystalline materials (for example, see References 23–27) and to see specific sections on photorefraction in overviews of nonlinear optical properties of polymers (for example, See references 28–31).

The Photorefractive Process

The essential property of photorefraction is the writing of a refractive index grating due to a nonuniform incident optical field, typically through interference and/or diffraction of the incident light beam(s). The photorefractive effect can be understood as four distinct sequential steps, shown schematically in Figure 1. (*1*) The incident light generates mobile charges, usually positively charged "holes" in polymeric materials, through the photoionization of light sensitive constituents called sensitizers or photocharge generation agents (32). (*2*) The photo-induced charge carriers (holes) drift away due to an applied electric field, E_B, separating the positive from the negative charges by the charge-transfer photoconducting properties of the material, while the negative charges generally remaining localized (33). Other transport mechanisms including diffusion and photovoltaic processes are possible and, though significant in inorganic materials, they have not been found significant in photorefractive polymers. These first two steps show the

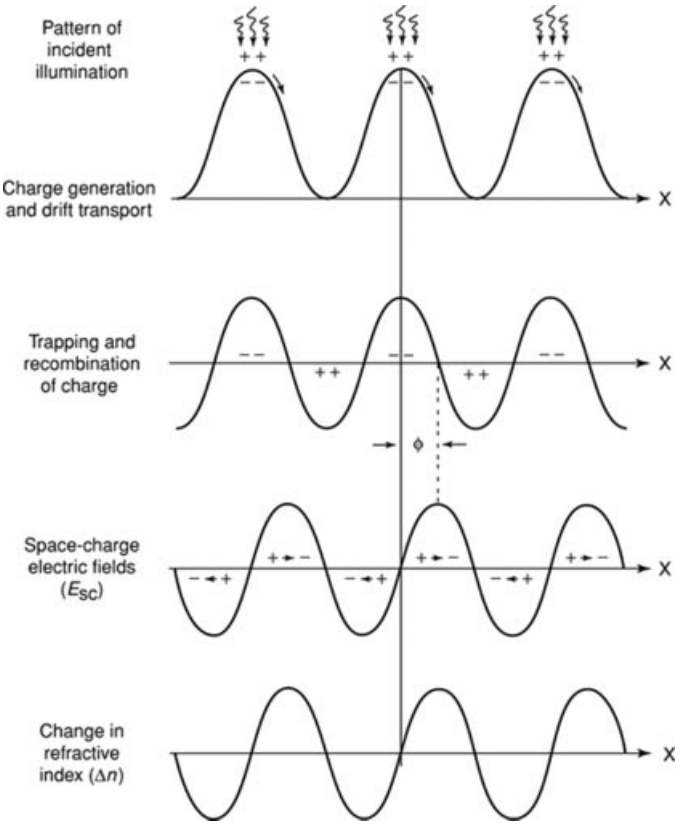

Fig. 1. Schematic of the photorefractive process. Note the phase shift, ϕ, between the incident intensity grating and the resulting photorefractive grating in the material. Depending upon the trapping depth and depth of modulation of the intensity of light incident on the material, the phase shift can vary between 0 and $\pi/2$. The absence of this phase shift indicates that mechanisms of photoinduced refractive index change other than photorefraction are involved. Many photorefractive applications require phase shifts approaching $\pi/2$.

importance of the photoconductivity of the material which must provide for the transport of the charge over distances many times greater than the wavelength of the illumination. (*3*) Because the photorefractive material does not generate mobile charge in dark regions (where destructive interference occurs), the third step in the process is the trapping of the mobile charges at suitable charge trapping sites. These trapped charges establish charge density gradients in the material that produce a patterned internal ("space-charge") electric field, shifted from the incident light pattern by the migration of the mobile charges into dark regions. (*4*) Lastly, the space-charge field arising between the dark and light regions modulates the index of refraction of the material via the electro-optic effect and reorientation of the molecular dipoles in the space-charge field (11,34–36). The resulting index-of-refraction pattern then stores the information in the original illumination pattern. This index-of-refraction grating will diffract an incoming reference beam to reproduce the pattern that created it as in a hologram.

Not surprisingly, different material functions are required for each of the steps in the formation of a photorefractive grating, leading to development of multifunctional composite materials and the search for optimal combinations of material properties as discussed in Composition of Polymeric Photorefractive Materials section.

One of the most important results of these processes is that a phase shift ϕ appears between the index of refraction grating and the incident light intensity pattern, ideally by as much as 90° when the centers of mobile and fixed charge density correspond to the regions of minimum and maximum light intensity, respectively (as shown in Fig. 1). As discussed further in Test Methods section and Applications section, this phase shift makes possible an energy exchange between two incident crossed beams (two-beam coupling) necessary for many optical data processing applications requiring optical gain, amplifying one beam at the expense of another.

Refractive Index Modulation by E_{sc}. Photorefractive behavior in polymers can be very roughly modeled by assuming a one-dimensional index of refraction change caused by the vector sum of the applied "bias" field E_B and a space-charge field resulting from separated, trapped charges within the material E_{sc}, $E_T(x) = E_{sc} + E_B$ (4,37),

$$\Delta n(x) \approx -\frac{n^3 r_e}{2} E_T(x) + \frac{3 r_K}{2n} E_T^2(x) \tag{1}$$

where n is the index of refraction, r_e is the effective Pockels (linear) electro-optic coefficient, and r_K is the effective Kerr (quadratic) coefficient due to chromophore reorientation. As further discussed below, E_{sc} is inversely proportional to the relative permittivity ε_r (as seen in eq. 3).

For a common alternate representation of the quadratic field dependence, see equation 2.

Refractive index modulations on the order of $\Delta n \sim 10^{-2}$ have been suggested with known materials at field strengths of only 28 V/μm (38).

Orientational Enhancement Effect. In addition to a strictly electronic and linear (Pockels) electro-optic response given by the first term on the right side of equation 1, the quasi-one-dimensional nonlinear optical chromophores incorporated into the polymer for their electro-optic response often exhibit large differences in the polarizability parallel versus perpendicular to the chromophore long axis (36,39–42). This so-called "polarization anisotropy" ($\Delta\alpha \approx \alpha_\parallel - \alpha_\perp$, where $\alpha_\parallel$ and $\alpha_\perp$ are the linear polarizabilities along and perpendicular, respectively, to the long molecular axis) typically arises from strong light absorption and a large ground state dipole moment μ_g (14) as found in highly colored nonlinear optical chromophores. In fact, reorientation of these chromophores in the space-charge field usually plays the dominant role in determining the depth of the index-of-refraction grating in polymeric composite materials (4). The orientational effect can be interpreted either in terms of the optical Kerr effect (4) as in the second term on the right in equation 1 or as a polarization anisotropy appearing with a quadratic dependence on the space-charge field (14,43). In the latter case, the quadratic dependence is often represented using the following expression based

upon an oriented gas model (14).

$$\Delta n_{\text{orient}}(x) \approx \frac{N(\alpha_{\parallel} - \alpha_{\perp})}{45n} \left(\frac{\mu_{\text{g}} E_{\text{T}}}{k_{\text{B}} T} \right)^2 \tag{2}$$

where N is the density of reorienting nonlinear optical molecules, k_{B} is the Boltzman constant and T is the temperature.

To understand the significance of the orientational enhancement effect and how it increases the depth of the refractive index change beyond that of the linear electro-optic effect found in crystalline materials, it is helpful to recall that the bulk linear electro-optic effect can only occur when the material lacks inversion symmetry (see ELECTROOPTICAL APPLICATIONS). To induce the asymmetric order in amorphous polymers, the polymer is typically subject to electric-field poling to align the dipoles. In this poling process (see NONLINEAR OPTICAL PROPERTIES), the polymer is heated above its glass-transition temperature (T_{g}) (see GLASS TRANSITION) and then cooled during the application of the poling field to freeze in polar order.

In room-temperature experiments with low T_{g} polymers ($<100^{\circ}$C), it is found that the polymers will not maintain the polar order needed for the linear electro-optic effect when the poling field is turned off. These materials must therefore be poled *in situ* for the requisite asymmetry to appear. At the same time, an external electric field (also called the bias or drift field) must be applied across the photorefractive polymer *in situ* to enable the mobile charges to move efficiently into the dark regions. Thus, the requisite external poling field is already present for polymeric photorefractive materials. This applied bias field serves two purposes: (*1*) The dominant mechanism for charge transport is drift of the holes in the direction of the applied field (as further discussed below). (*2*) The external field strengthens the alignment of the polymer polar order required for the linear electro-optic effect and for the electric-field-induced birefringence.

The applied bias field is not the only field experienced by the molecules, however. The creation of space-charge fields E_{sc} will also modulate the orientation of the nonlinear chromophores. This so-called orientational enhancement effect was discovered by Moerner and co-workers when they found that the measured diffraction efficiency of a low T_{g} photorefractive polymer required E_{sc} to be an order of magnitude larger than should have been permitted by the projection of E_{B}, using only the linear electro-optic effect (11). In effect, the sinusoidal space-charge grating produced a sinusoidal variation in the electro-optic r_{e} coefficients *and* a sinusoidal birefringence of the polymer. Additional enhancements were obtained upon adding a plasticizer to the composite in order to further reduce T_{g} (44).

A schematic of the typical oblique transmission experimental geometry used to measure the diffraction efficiency of a photorefractive polymer this way is shown in Figure 2. The sample must be tilted with respect to the bisector of the two beams because the applied field must have a component parallel to the grating wavevector in order to move charges along the grating. This experimental geometry complicates analysis of the relationship between the vector fields and the tensor elements of the resulting refractive index change. A more complete

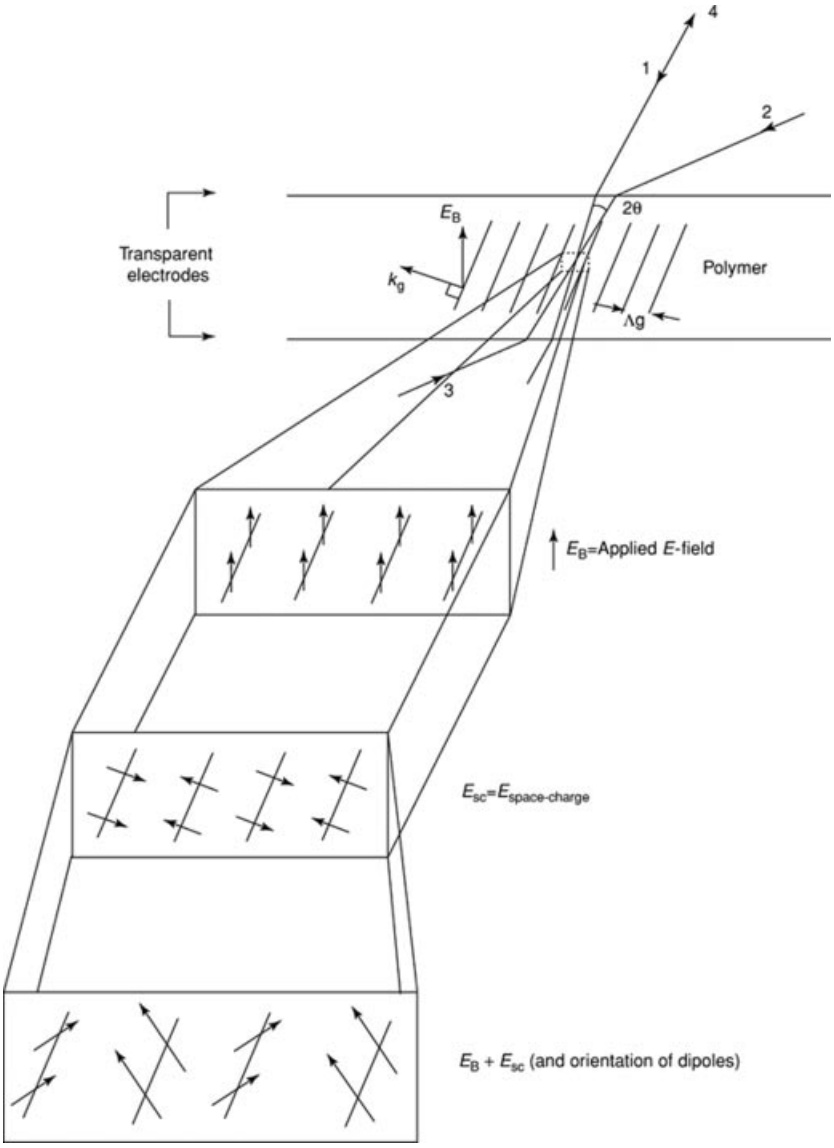

Fig. 2. Oblique geometry typically used for characterizing bulk photorefractive polymers. The magnified portion illustrates the orientational enhancement effect described in the text due to the modulated poling of the electro-optic chromophore in the combined $E_B + E_{sc}$ fields. The beam and grating geometry applies for both four-wave mixing (beams 1–4) and two-beam coupling (beams 1 and 2).

treatment, including the tensorial nature of the index of refraction modulation, as well as figures of merit, may be found in Reference 45.

Understanding the effects of orientational enhancements has been made more complex, however, by the need to account for supramolecular interactions such as dipolar aggregation, the tendency of dipoles to adopt align antiparallel

with their neighbors (38). Several studies have explored the effects of glass transition temperature on polymeric photorefractive properties (46–48).

Origin of the Space-Charge Field E_{sc}. For a photorefractive index grating, the space-charge field E_{sc} can be described approximately by (49)

$$E_{sc} \approx \left(\frac{\Phi}{h\nu}\right)(eL_{eff})\left(\frac{mI_0\alpha}{\varepsilon_0\varepsilon_r}\right) \tag{3}$$

where Φ is the photocarrier generation efficiency, $h\nu$ the photon energy, e the electronic charge, L_{eff} the effective transport length traveled by the mobile charge, α the absorption coefficient, and ε_0 the vacuum permittivity. The modulation index m is a function of the grating geometry and is given by $m = 2\sqrt{I_1 I_2}/I_0$, where the interference arises from two crossed beams of combined irradiance $I_0 = I_1 + I_2$. For this elementary hologram, the resulting irradiance distribution is

$$I(x) = I_0[1 + m\cos(k_g x)] \tag{4}$$

where k_g is the wavevector defined by the spacing Λ_g between adjacent irradiance maxima in the incident grating (the grating "wavelength"). Thus, $k_g = 2\pi/\Lambda_g = 4\pi n \sin\theta/\lambda_g$, where λ_g and θ are the incident optical wavelength (assuming the interfering beams are the same wavelength) and the crossing half-angle between those beams inside the sample. For visible wavelengths, Λ_g ranges from 0.3 to 20 μm, due to the limited range of accessible angles between the two beams (see Fig. 2).

Photoconduction. The generation, transport, and trapping of charge necessary to create E_{sc} and the resulting index-of-refraction modulation are each steps in the process of photoconduction in the photorefractive material (50). The literature on photoconductivity in polymers is voluminous and the variety of effects to be accounted for mirrors the variety of applications to which polymers may be adapted (see, for example, References 51–53). The original rate equations developed by Kukhtarev for inorganic materials (54) are inadequate for polymers due to the electric-field dependence of the charge photogeneration efficiency (55) and the complexities of charge trapping in the transport of charge (56). Unlike the photoconductive effects in inorganic materials, photoconduction in polymers is generally modeled using temperature-activated hopping mechanisms, not the standard band transport model used for inorganic ferroelectric crystals (57–59). In high-mobility polymers, however, the transport involves both traps associated with polymer transport and the conduction band associated with the ordered phase of the material. These combined effects require a hybrid model for the transport, and its dependence on field (60–62). The hopping model assumes conductivity is controlled not by the size and accessibility of the conduction band, but by the presence and location of suitable trapping and recombination centers between which charges move via electric-field dependent or thermally activated jumps. In polymeric photoconduction, the charge hopping is between traps which are sensitized by the presence of a drift (DC) electric field across the sample as in the Poole–Frankel model (21,33,63–66). Traps are parametrized by their "depth," ie, by the likelihood that charge may be released from the trap thermally as well as optically (a "shallow" trap) or may only be released, if at all, by absorption of a

photon (a "deep" trap, either active or inactive depending upon its photoionizability) (67). Traps may be shallow or deep based on their thermal ionizability and photoionizability and are distinguished from recombination centers by the relative likelihood of the charge either being released from a *trap* to participate further in conduction or being neutralized through *recombination* with a carrier of the opposite sign. Thus, photoconductivity is also an increasing function of incident photon energy.

The time evolution of the charge generation and trapping process has been the subject of particular study because of significant interest in the development of photorefractive materials with a faster response. Notable recent developments include the numerical simulation of the kinetics of E_{sc} as a function of the light intensity, grating vector, electric field and density of deep inactive traps (68), the introduction of both shallow and deep traps with different, nonzero, excitation rates into the theory (69), and the experimental study of rise, decay, and steady-state photocurrents with pulsed light (70). The rate limiting step in the photorefractive process varies between materials, primarily being due to either the photocarrier generation efficiency or the charge mobility (1,69). Preillumination of the sample has been shown to affect the timing of the response significantly (69–72).

Photocarrier Generation Efficiency. The photocarrier generation efficiency Φ_g depends upon the applied electric field, and is usually approximated as having a power-law dependence of $\Phi_g \sim E^p$, where p varies between 1.5 and 3.5, depending upon the material (1,50,73). The reason for this dependence is that even if the initial quantum yield from the incident photons is large, the photogeneration efficiency is limited by geminate recombination or back electron transfer due to the small thermalization radius of many polymers, ie, freed carriers cannot separate sufficiently so that the energy of their Coulombic attraction is less than $k_B T$ (55). A strong applied field will help to separate the charge carriers and so improve the effective carrier generation efficiency (34). Typically, the field dependence of the charge generation and the effects of geminate recombination are understood using the Onsager model (74,75). That model is inadequate, however, in accounting for the slow recombination rate of electron–hole pairs in polymeric materials and has been augmented by the Marcus theory of electron transfer in more recent treatments to model slow recombination rates found in photoconductive polymers (76).

Charge Transport, Mobility and Free Charge Lifetime. An important parameter for understanding charge transport in photorefractive polymers is the quantity L_{eff}, which describes the transport length of the generated photocarriers. L_{eff} depends on the presence of applied fields, the grating geometry, and the intrinsic mechanisms of carrier transport (77). It is important to maximize L_{eff}, which is defined so as to be always less than the inverse grating wavevector (on the order of 0.1–2.0 μm) (35). In its simplest form for one carrier and only drift transport, we can represent L_{eff} in terms of the grating wavevector k_g and the average drift length L_E

$$L_{eff} = \frac{L_E}{\left[1 + (k_g L_E)^2\right]^{\frac{1}{2}}} \tag{5}$$

where $L_E = \mu\tau|\boldsymbol{E}_B + \boldsymbol{E}_{sc}|$ is the transport length due to the combined fields. Here, μ is the effective carrier mobility (also a strongly increasing function of E_B) and τ is the effective free lifetime of the carrier over distances large compared to the distances between traps.

From equation 5, it can be seen that maximization of L_{eff} for a given grating spacing requires maximization of the μ–τ product or application of a large external field. Because of the dispersive nature of the transport, μ and τ are not easily defined quantities in polymers (78). The mobilities are field dependent, often in a highly nonlinear way, and the presence of significant trapping in a polymer complicates their determination (33,79). Furthermore, τ in many polymers may be effectively limited by the presence of "deep traps" from which further photoionization is inhibited.

A major trade-off in the development of poled polymers for photorefraction arises from the need both to maximize the mobility for photoconductive transport and yet to minimize the dark conductivity to allow poling and subsequent storage of the photorefractive grating (80). Unfortunately, because poling introduces charge carriers into the sample, if the mobility of carriers in the photoconducting polymer is appreciable, the sample will short-circuit in the presence of a large applied poling or drift field before the molecules have adequately aligned (4).

On the other hand, another advantage of polymers over inorganic photorefractives is that the space-charge fields attainable are not generally limited by the trap density, so that large diffraction efficiencies have been realized by the application of large external fields. Thin-film polymers are amenable to the application of large external field, which has led to large efficiencies by compensating for small values of the $\mu\tau$ product. Destruction of samples due to dielectric breakdown remains a problem and materials with large Δn in a relatively small applied field are of significant interest (38).

One potential benefit of using high mobility polymers is in reducing the response time of the materials in the cases when neither charge generation (69) nor rotational mobility (81) of the chromophores are the rate limiting factors in the PR process. Unlike diffraction efficiency, which can be increased by application of a stronger external field, the application of a strong external field cannot fully compensate for slow speed due to low mobility. While the mobility in some polymeric photorefractives has been found generally to be an increasing function of applied field, negative-field dependence has been predicted and observed in other cases (75,79).

Perhaps a better model for describing the disorder in charge generation and transport in molecularly doped polymers is the so-called "disorder formalism" proposed by Bässler for xerographic photoreceptors (82). In this model, transport occurs through hopping between localized states with a Gaussian distribution of energies and separation distances. A random distribution of permanent dipoles due to the nonlinear optical chromophores produces a local variation of the electrostatic potential and an increasing energy width, and position disorder appears with increasing dipolar molecule concentration. Increasing concentrations of molecules with large dipole moments led to increased disorder and reduced carrier mobility and photorefractive speed (79).

Distinguishing Photorefraction from Other Photoinduced Refractive Index Changes. A variety of photoinduced effects, such as photochromism,

thermochromism, thermorefraction, conventional electronic $\chi^{(3)}$ effects and photochemical changes, may lead to changes in the refractive indices of a polymer in ways other than photorefraction, or even so-called, pseudo-photorefraction (83–86). Each of these lacks the physical separation of internal space-charge that leads to a phase shift between the incident light intensity and the refractive index modulation. Though not always experimentally simple, there are many ways to distinguish true photorefraction from competing mechanisms, such as cis–trans isomerization, which lead to refractive index changes (75,87).

Two Beam Coupling via a Phase Shift of the Index Grating. The most unmistakable sign of photorefraction (and one of its most promising features) is asymmetric two-beam coupling (88). A critical element in this coupling is the nonzero phase shift between the phase grating and the incident interference pattern (indicated by ϕ in Fig. 1). For absorption gratings from photochemical or photochromic effects, the index and intensity gratings are in phase. Two-beam coupling techniques for measuring the grating phase are discussed in (88) and in Test Methods section. Two-beam coupling in the absence of a moving grating (89) or an AC applied field is the strongest evidence of photorefraction. Its absence, however, does not alone signify the absence of photorefraction (21,90).

Hologram Erasability. The photorefractive effect is reversible. The traps that lead to the space-charge fields in photorefractive materials must themselves be photoionizable. If so, the photorefractive diffraction grating is erased simply by bathing the material in a uniform field of the proper photon energies. For photochemical effects, reversibility generally requires heating or other chemical treatment. Photochromic gratings tend to be only partially erasable under uniform illumination.

Enhancement by External Fields. The photoconductive response generally increases at least as the square root of the applied drift field. Application of an external field enhances photocarrier generation both by reducing the barrier to charge release and, as previously discussed, by assisting the separation of photogenerated charges to lessen the effects of geminate recombination.

Correlation with Photoconductivity. To confirm that the refractive index grating is due to the photoconduction of mobile charges into dark regions, comparisons between the absorption spectrum and the wavelength dependence of the photoconductivity and photorefractivity of a material help identify the underlying photoconduction mechanism and resultant charge density gradients (33). These comparisons are complicated by the fact that the mobility and photocharge generation efficiency of photorefractive materials can be orders of magnitude lower than those properties appearing in materials developed solely for photoconduction. Some of the difficulties in quantifying relevant photoconductivity parameters in polymeric photorefractives are discussed in Reference 91 and in Test Methods section.

Polarization Anisotropy of the Grating Readout. The photorefractive response is dependent upon the polarization of the incident beam. If pure *s*- or *p*-polarized light is used in writing the grating, the depth of the index grating and thus the diffraction efficiency will be different depending upon whether the polarization of the beam has components parallel to the poling field (75). As discussed

in Test Methods section, the writing beams in a four-wave mixing configuration usually are *s*-polarized beams to limit the coupling between the illuminating interference pattern and the diffraction of one beam into the other, which is maximized when the reading beam is *p*-polarized to sample the refractive index change parallel to the applied poling field. In addition, the polarization of the writing beams will change the energy-transfer direction in two-beam coupling measurements due to the orientational enhancement effect (11).

Composition of Polymeric Photorefractive Materials

In this section, in addition to reviewing common ingredients for photorefractive polymeric materials, some of the problems that are being overcome in the formulation of useful multifunctionality in multicomponent polymers are explored. Current polymeric materials are limited in some cases by their slow response times and short wavelengths of operation (44,92) and in other cases by the need for large external electric fields and tendencies towards dielectric breakdown and other material instabilities. Typically, photorefractive polymers require the application of fields around 40–100 V/μm, severely limiting sample thicknesses to under 100 μm. Higher speed operation is required for data processing using these materials. Also, further work is needed to develop polymeric photorefractives with a longer wavelength response for compatibility with current optical communications standards (for example, typical near infrared telecommunications operate at 1550 μm).

Formulation of the ideal photorefractive polymer requires finding or mixing materials that combine necessary photogeneration, charge transport and trapping response with electro-optic and orientational anisotropy properties. With respect to the electro-optic response in organic materials, the largest nonlinearities have been in polymers that combine an extended system of highly mobile π-electrons with electron donor and acceptor groups at para positions. To make these materials photorefractive, it is necessary to include one or more additional functionalities, usually by doping after polymerization. Charge generation, transport and trapping properties can be tailored by attaching molecules to the polymer structure with the appropriate ionization energy or electron affinity (63). For instance, charge transfer complexing is accomplished by adding donor sensitizers to acceptor polymers, or vice versa, so that the charge released by the donor is taken by the acceptor to create an absorption band corresponding to the difference between the donor and acceptor energies. Also, because many otherwise appropriate polymers tend to absorb primarily in the ultraviolet spectrum, dye sensitization of these polymers leads to greater absorption of visible light or longer through the release of photocarriers in the dye (4,33).

When combining functions by adding plasticizers, sensitizers, charge transport agents, and other functional groups, one may be limited to having less than the optimum amount of the nonlinear response to accommodate these functionalities. Also, doping of materials often leads to an increase in phase segregation, which causes undesirable light scattering and can severely limit the useful lifetime of the polymer and/or its processability (21). In the trade-off between using

fully-functionalized polymers with better stability and the improved responsiveness of guest–host systems, guest–host systems currently lead in terms of the depth of the index grating, the achievable two-beam coupling gain, and, surprisingly, even in the speed of grating dynamics (4).

Electro-Optic and Electric-Field-Induced Birefringent Materials. As can be seen from the analysis of The Photorefractive Process section, one material parameter to be optimized is the electro-optic and orientational response. This can be accomplished either by finding compatible materials with large linear electro-optic coefficients or by optimizing the orientational effects using materials with large birefringence (polarization anisotropy). One major difference in these approaches is the response speed of the photorefractive effect in that the orientational approach is expected to be slower, but submillisecond responses of low T_g materials have been demonstrated (93–96).

Optimizing the nonlinear response of the polymer usually requires saturating the polymer with the appropriate chromophore, typically 25–35 wt% (38). The most common electro-optic molecules used with these polymers are azo-dyes, such as ethyl-hexyloxy-dimenthyl-nitrophenylazo benzene (EHDNPB) (61,97–102), and dimethyl-*p*-nitrophenylazo anisole (DMNPAA) (103–105), and dicyanostyrene (DCST) derivatives, such as diethylaminodicyanostyrene and (DDCST) (106), though the range of molecules used includes simple donor–acceptor units and complex oligomers (107). The chromophore unit is the most common distinguishing factor among demonstrably photorefractive materials. The photorefractive response tends to decrease with an increase in the size of the chromophore (5,108).

Plasticizers. To optimize the reorientational effects, either polymers with low glass transition temperature (T_g) values (after incorporating other material properties, as discussed below) are used or a plasticizer is added to depress the T_g value and enable molecular rotations (109), which may or may not be desirable depending upon the need to better fix the grating in the polymer with a high T_g or to deepen the index-of-refraction modulation through orientation of the chromophores in the space-charge field (11,48).

The most common plasticizer used is ethylcarbazole (ECZ), typically added at 15–30 wt% (110–114). One trade-off in the use of inert plasticizers is the accompanying decreased concentration of other active ingredients. Thus, the use of functionalized plasticizers or materials that fulfill dual roles is preferred (115). However, others used include benzyl butyl phthalate (BBP) (40,110,112,116), polybutylacrylate (PBA) (117), and diphenyl phthalate (DPP) (118), and several systems have been developed in which the amount of plasticizer needed is either decreased significantly (119) or eliminated entirely (59,60,106,120,121), using triphenylamine units.

Photogeneration Sensitizers. As discussed in Origin of the Space-Charge Field E_{sc} section, charge generation is often the rate limiting step in achieving the fastest photorefractive response. Though only a small amount is required, typically from 0.1 to 1 wt%, the sensitizer's role is critical. When adding a photogeneration sensitizer, it is important that it absorbs at a longer wavelength than the nonlinear optical chromophore so that attenuation of the beam by the sensitizer is minimized. Obviously, this requires careful balancing of functions that compete for absorbance within the polymer. Sensitizers for photogeneration

are available throughout the visible and near infrared spectra that may permit tuning of the photorefractive effect for an otherwise identical polymer (4,58,65).

Charge-generation agents are typically variations on C60 (see, for example, References 116,122–125) or trinitrofluorenone (TNF) derivatives (see, for example, References 126–130), although squaraines, phthalocyanines (131), difluorobenzontrile (FTCN) (113), and others have also been used. TNF is a charge-transporting molecule/sensitizer, long wavelength photosensitizer. Addition of this charge-generating agent increases the absorption of the material at wavelengths larger than 550 nm as well as increasing the shallow trap concentration. The absorption coefficient increases approximately linearly as a function of concentration of charge-generation agent.

Also, in order to increase the sensitivity of polymer photorefractives, researchers have also investigated the effects of incorporation of nanoparticles (99,132,133). For example, CdSe quantum dots (99,102,133) have come into favor as sensitizers because of their nanoscale and ability to be made to suit specific applications with wavelength sensitivity.

Charge-Transport Agents. The charge-transport agents in a photorefractive polymer must provide a closely-spaced network or oxidizable molecules for charge hopping. For the backbone of the photorefractive composite material, poly(*N*-vinylcarbazole) (PVK) is the most common polymer used because of its excellent charge-transport properties and because the photocharge generation efficiency can be improved by adding acceptor molecules that form a charge transfer complex with the carbazole moiety (16,134). Other common transport agents include hydrozanes, such as diethylaminobenzaldehyde-diphenylhydrazone (DEH), polyphenylvinylene (PPV), and arylamines, such as tritolylamine (TTA) (1,71). Typically, the photoconductive polymer requires 40–60 wt% to provide sufficient density of transport sites (1).

The most common reasons for not using polyvinylcarbazole (PVK) are phase separation and higher glass transition temperature (T_g), and therefore the need for high amounts of plasticizer, as discussed above. As previously mentioned, the use of a fully-functionalized polymer helps to minimize phase separation while significantly reducing orientational enhancement effects and requiring higher temperature electric field poling. In a fully-functionalized polymer, a polymer main chain or side chains are linked to the chromophore, charge generator, and sensitizer, thereby providing all the necessary photorefractive components in one polymer (17,135–144). Another recent technique to overcome the limitations of PVK systems is to dope polyimides with dyes that form nanocrystalline J-aggregates. Such systems exhibit high third-order macroscopic polarizability (145,146). Sol-gel glasses with low T_g have also been used (147,148). For any of these materials, the highest occupied energy level of the transporting agent must be higher than that of the photogenerating agent (1).

Combinations with Liquid Crystals. Because polymeric photorefraction is greatly enhanced by the fast reorientation of the nonlinear optical component, many researchers have investigated the use of liquid crystals as ingredients in polymer-composite photorefractives (149–152). Readers looking for a more detailed understanding of liquid crystalline polymers should also see Liquid Crystalline Polymers, Side-Chain. A major advantage with these materials is that

the liquid crystal alignment can be accomplished with very low fields, on the order of $\sim$1 V/μm (153). One of the most common liquid crystals used as the nonlinear optical material is pentylcyanobiphenyl (5CB) (154). It has been used either doped with a photoionizable dye sensitizer, but without a photoconducting polymer or mixed into either polymer-disperse liquid crystal form (155) or a homogeneous photorefractive polymer/nematogen composite (120) to take advantage of photoconducting properties of the polymer.

The resolution of gratings in bulk nematic liquid crystals is too low for most applications leading researchers to develop polymer-dispersed liquid crystal (PDLC) photorefractives. In these materials, liquid crystal domains are dispersed throughout a solid polymer matrix (156). One of the largest two-beam coupling gains recorded, 3700 cm^{-1}, was obtained from a mixture of a commercial liquid crystal mixture in a PVK/TNF complex (157). For many liquid crystal polymer composites, the use of PVK is not as common; other polymers such as poly(methyl methacrylate) (PMMA) (89,158–161), poly(vinyl alcohol) (PVA) (162–164), photocross-linkable polymers (PCP) (165), and phenylenevinylene (PPV) (166) are more commonly used than PVK, often requiring additional photoconducting agents (122,149,163). The polymer PMMA is also used in a number of related holographic data storage applications (103,158,167) because of its ease of fabrication and thus low cost, as well as its low index of refraction and high melting point.

Test Methods

The two most common techniques for characterizing the photorefractive efficiency of a material are degenerate four-wave mixing (DFWM) and two-beam coupling (2BC), both of which use similar configurations, as shown in Figure 3. Ellipsometric techniques are used to measure the electric-field-induced birefringence. Standard time-of-flight and xerographic discharge methods are used to measure photoconductivity, as well as specialized techniques that take advantage of the holographic gratings in photorefractive materials.

Four Wave Mixing. In a DFWM experiment, a refractive index grating is recorded by two interfering writing beams (beams 1 and 2 in Fig. 3), which is then read by a weaker third beam (beam 3, which diffracts as beam 4). A maximum index change is obtained when the writing beams are *s*-polarized and the reading beam is *p*-polarized (158). This technique is particularly useful in evaluating the rise time or decay time of hologram formation (168). Different times may be seen, however, depending upon whether or how long the bias electric field is applied before the beams are incident on the sample or whether one of the two writing beams is applied well before the other. Theoretical evaluation of the rise time or the decay time is also complicated by the use of different analytical functions to fit the time dependence of the diffraction efficiency (1,4).

One figure of merit in DFWM is given by the energy required to achieve a specified diffraction efficiency in a given thickness of material. The diffraction efficiency is the ratio of the diffracted beam intensity $I_{\text{diffracted}}$ to the incident reading beam intensity I_{reading}. This criterion may be difficult to compare for different device structures such as waveguide versus bulk materials. The theoretical

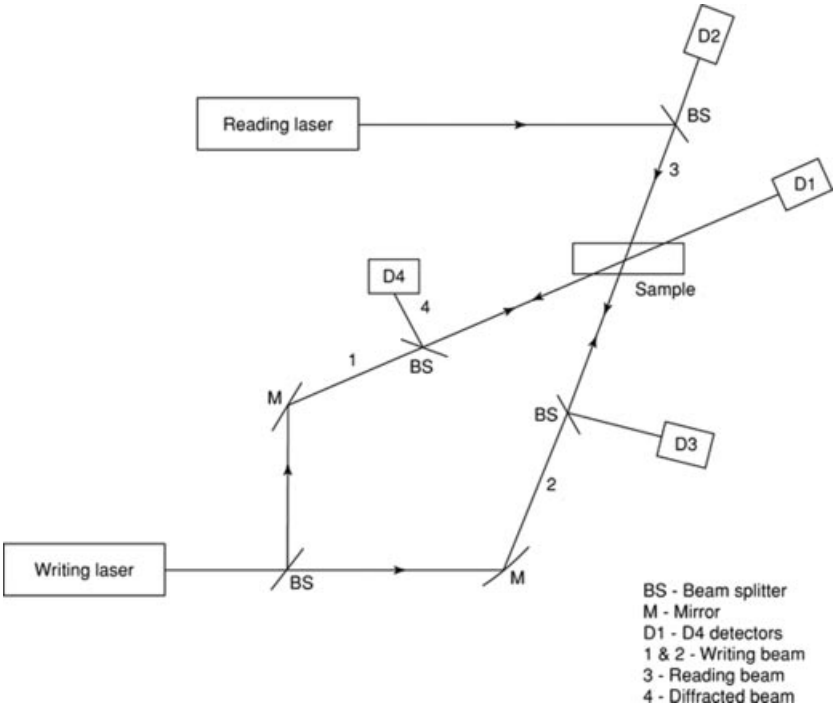

Fig. 3. Experimental schematic for four-wave mixing. The diffraction grating is written by beams 1 and 2 and read by beam 3, which need not be of the same wavelength as the writing beams. In the absence of a reading beam, the same geometry may be used to measure two-beam coupling between the writing beams.

diffraction efficiency can be expressed as (35)

$$\eta = \frac{I_{\text{diffracted}}}{I_{\text{reading}}} = \mathrm{e}^{-\alpha d/\cos\theta} \sin^2\left(\frac{\pi G d \Delta n}{\lambda}\right) \tag{6}$$

where α is the absorption coefficient, d is the interaction length of the beams and G is function of the geometry and polarization of the incident and reading beams on the material (for example, $G = 1/\sqrt{\cos\theta_1 \cos\theta_2}$ in a simplified quasi-one-dimensional model, where θ_1 and θ_2 are the internal angles of the intersecting beams (37,75). For thin films or materials where the absorption is small, it is usually sufficiently accurate to drop the exponential decay factor and even to approximate the sine function by its argument (35). Using the measured diffraction efficiency to determine Δn and combining with equation 1, one can determine the magnitude of the space-charge field E_{sc} in the material. Diffraction efficiencies of nearly 100% have been reported at applied electric fields as low as 58 V/μm in polymeric photorefractives (44,161,169) or even lower fields for polymer-dispersed liquid crystals (170).

In some cases it is important to also compare diffraction efficiency to the diffraction sensitivity of the sample. Sensitivity is a measure of the depth of the refractive index change as a function of the incident power. A material may be

sensitive for very low intensities yet not diffract sufficient power for device needs. The sensitivity may be important in that the change in the index of refraction may saturate at a specific laser power density (49).

Two-Beam Coupling. In a 2BC experiment, the additional reading beam is not used. Instead, the transmitted intensities of the two writing beams are monitored as a function of the applied external electric field. The writing beams will be deflected or diffracted with respect to the original beams, interfering constructively with one, destructively with the other. Sometimes a piezo transducer is used to measure the phase shift by causing a time-varying energy transfer between beams. These energy shift oscillations depend on the spatial phase shift ϕ of the incident diffraction pattern and the refractive-index grating (171–173).

One important figure of merit in the case of 2BC is the optical gain coefficient Γ, which can be determined by comparing the energies of the two beams when the other is momentarily blocked. If γ_i represents the ratio of the incident powers in front of the sample and γ_f the ratio behind the sample, then the gain is given by

$$\Gamma = \frac{1}{L}[\ln(\gamma_i\gamma_f) - \ln(\gamma_i + 1 - \gamma_f)] \approx \frac{4\pi n_1}{\lambda\cos\theta}\sin\phi \tag{7}$$

where L is the interaction length within the sample, θ is the half-angle between the beams, ϕ is the phase shift, and n_1 is the nonlinear refractive index (4,174). Gains in polymer photorefractives as large as $\sim$400 cm^{-1} have been reported, a factor of 10 larger than seen in inorganic crystals (175,176). The actual transferred power, given by $\exp(\Gamma d)$, is limited in polymers due to the small sample thickness d required to attain large applied fields. The 2BC experiment is also used to characterize the response time of the photorefractive polymer, with the fastest responses being around 5 ms at relatively high powers of 1 W/cm^2 (177).

Two beam coupling measurements can be complicated by the presence of beam fanning, by which additional coupling to randomly scattered light in the sample leads to loss of energy to the scattered light (178). Though not a measurement technique, it is a potentially important application of photorefractive polymers and is discussed further in Applications section.

Ellipsometry. Because of the importance of the orientational enhancement effect, the electric-field-induced birefringence is independently measured using a transmission ellipsometry technique. In this experiment, the photorefractive polymer is placed between two crossed polarizers with the normal to the sample tilted 45° from the x-axis of the propagating laser beam, as shown in Figure 4. Any change in the refractive index of the sample will result in a change of the polarization state of the laser beam, allowing light to emerge through the polarizers. The index change is then measured by observing the transmittance of the plane-polarized light after passing through both polarizers and the sample (179). Use of ellipsometry is further discussed in Reference 180. Transient ellipsometry techniques are discussed in Reference 46.

Photoconductivity. As outlined in Introduction section, the first three steps of the photorefractive process are related to photoconduction, which controls the rate of grating formation and the amplitude of the charge grating, as well as the rate of erasure under uniform illumination. Therefore, to understand and optimize the physical processes involved in photorefractive polymers, it is

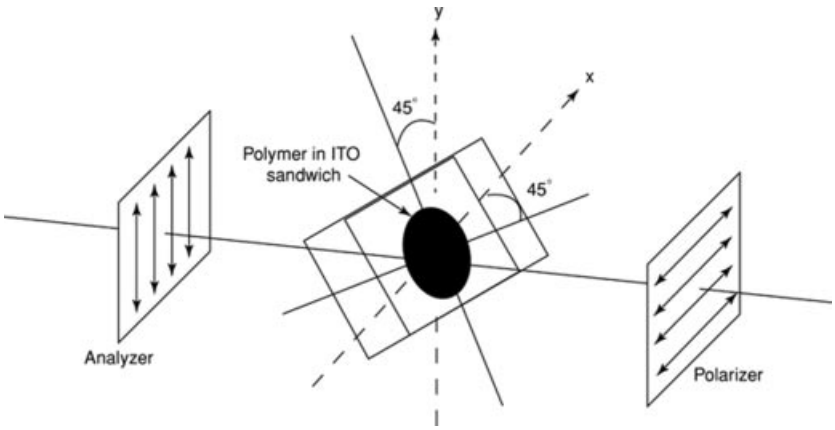

Fig. 4. Schematic for ellipsometry measurements.

important to measure their photoconductivity. The most common methods for characterizing the photoconductivity and the hole mobility and effective trapping of photorefractive polymers are conventional DC techniques, xerographic discharge, and time-of-flight mobility measurements (65,181,182).

In the conventional DC technique, a direct comparison is made between the current through the sample under the drift field both in the dark and under uniform illumination. The photoconductivity σ_{ph} is related to the charge mobility μ when the absorption is low by $\sigma_{\mathrm{ph}} = pe\mu = [\Phi\ \alpha\ I\ \tau_{\mathrm{eff}} / h\nu]\ e\mu$, where p is the density of mobile holes produced at intensity I, e the elementary charge, $h\nu$ the photon energy, Φ the quantum efficiency of charge generation, and α the absorption coefficient. Recall that the mobility, together with the effective carrier lifetime, determine the speed of response of the material (the effective carrier lifetime τ is then controlled by recombination and trapping processes).

The photoconduction sensitivity is usually determined by using a xerographic discharge technique that is applicable to thin films under low intensity illumination, because the measurement of small magnitudes might be confused by sample heating effects. In this experiment one charges the sample using a corona poling apparatus similar to that used for poling, then views the thin film sample as a discharging capacitor and measures the rate of decay of the surface potential with an electrometer and transparent probe under a high light source, using filters or the monochrometer to control the range of wavelengths illuminating the sample. This method can be used with even very low conductivity samples by monitoring the decay rate over long times (91).

One difficulty with bulk photoconductivity measurements is the analysis of the effects of different electrode materials. Comparisons are needed to determine the effects of Ohmic (free supply of charges) versus blocking electrodes (1). To determine the carrier mobilities and the effects of trapping, a relatively unusual approach used for photorefractive polymers is to supplement conventional time-of-flight mobility measurements, during which the flow of photoinduced charge across the bulk sample is monitored on an oscilloscope, with holographic time-of-flight (HTOF) measurements (183). In these measurements, an interference

pattern from two short laser pulses in a four-wave mixing geometry creates a sinusoidal distribution of charge carriers that can drift in the presence of an external field (66). As the charge separation advances, the space-charge field is probed with a cw laser through the electro-optic effect. The diffraction efficiency is a function then of the coincidence and anti-coincidence of the mobile carriers with the stationary charge. From the plot of the diffraction efficiency versus time one can determine the drift mobility and the degree of charge transport disorder due to the highly dispersive transport that appears in amorphous polymeric materials. Dispersive transport leads to a length-dependent mobility in these materials (66). A significant advantage of HTOF over conventional time-of-flight measurements is the ability to vary the drift length by varying the angle between the writing beams and between the beams and the applied field and to monitor the motion of charge internally, rather than across the bulk sample (184).

Applications

Data Storage. When a reference beam intersects with the scattered light from an object in a photorefractive material, a hologram is recorded, stored in the form of a refractive index pattern in the material. The image can then be reconstructed by diffracting a third beam on this hologram (in the same manner as DFWM as shown in Figure 3, except that the reading beam need not be of the same wavelength). The use of a photorefractive material in the recording of a hologram eliminates the need for chemical processing in the development of the hologram. Digital data storage is one of the earliest applications of photorefractive polymers (4,185,186).

The high optical damage threshold, low dielectric constants, high photosensitivity, and low cost of photorefractive polymers make them more efficient than inorganic materials (129). Optical data storage in PMMA-based photorefractive polymers has been demonstrated as a cheap and compact way improve data storage on compact discs and digital versatile discs (103). Polysiloxane-based photorefractive polymers have demonstrated the highest optical clarity and lowest optical scattering to date (105).

A significant drawback to the use of photorefractive polymers for data storage is the lack of easy fixing mechanisms and the resulting volatility of the recording. Dark lifetimes and the grating growth rate tend to be inversely proportional to each other (4). Using high T_g materials, the grating can be written above the glass transition temperature and frozen-in by cooling the sample during writing, but this scheme has not yet proved practical (187). Other photoinduced refractive index change mechanisms may be preferable for long-term holographic storage where optical gain is not required.

Another drawback of many photorefractive polymer composites is the need to use a thin film geometry that is not as amenable to high storage density as a bulk crystalline material. Multiple holograms have many applications including parallel holographic memory, template matching, and optical neural networks, interconnects, and correlators (188). Additionally, various types of multiplexing including angular and rotation (189,190) multiplexing allow for the storage of many holograms on the same material A nonmechanical angular multiplexed

holographic memory system has been demonstrated in liquid crystalline materials using a moving LCD window that is controlled electronically (191). Using these techniques, each hologram is recorded in the photorefractive polymer using a uniquely oriented setup; the individual holograms can be similarly read using a unique read setup. In this manner, several thousand data pages may be stored in the same element. Polymers are advantageous because large samples can be fabricated, allowing a larger recording volume to hold more holograms.

Materials combining photopolymers with liquid crystals are ideal for wavelength tunable storage devices. Such polymer-dispersed liquid crystal composites (PDLCCs) provide a medium for switchable holograms; when the refractive index of the polymer is matched to one of two principal refractive indices of the liquid crystal (LC) an applied electric field alters the orientation of the LC molecules, turning the recorded grating on or off (3,104). As previously mentioned, liquid crystals have the advantage of only requiring a few volts to induce an index grating because of their high nonlinearities (192).

To overcome volatility problems, two-photon absorption (TPA) is the most promising long-term data storage technique to date. TPA can be observed in all materials and lacks the noncentrosymmetric symmetry requirements of even-order nonlinear optical effects. Nevertheless, in centrosymmetric polymers two-photon absorption is allowed between states that have the same parity according to parity selection rules (112). Such a system has been demonstrated with nondestructive readout (113). Additionally, use of two-photon absorption on photorefractive polymer dispersed liquid crystals has been used to record a high 3D data density of 204.8 Gbits/cm^3 (158).

The formation of thick phase holograms has been demonstrated by fabricating photorefractive polymers by injection molding (193).

Adding fluorescent molecules to photopolymers also provides a method for optical data storage. In such a system, the fluorescent molecules bond to the polymer matrix and become more concentrated in the polymerized regions causing the required refractive index pattern (194).

Optical Correlation, Imaging through Scattering Media, and Novelty Filtering. Using a photorefractive polymer, optical correlation can be made all-optical, eliminating the need for a computer or any other such devices. Such a device was demonstrated in a 100-μm-thick photorefractive polymer using a low power laser. The document is optically encoded and authenticity is validated by correlating the encoded information with a master copy. Such a setup is used in such applications as the identification of individual pupils and fingerprints, searching of large databases and navigation. Spatial correlation is accomplished by creating a hologram by recording the interference pattern of the optical wavefront of the object with a reference beam in the material. Optical correlation is performed by overlapping the Fourier transform of the master copy with the hologram in the polymer. If the two optical codes match, a correlation peak can be observed and the document under test may be considered valid (4,195,196).

One common application of optical correlation in photorefractive polymers is in edge enhancement, a form of high pass image filtering which uses a Fourier transform holographic operation with a photorefractive composite. Two beams, the more intense one containing the image, interfere in a photorefractive material. The resulting interference pattern is stronger at the edges due to a closer matching of

intensities at the edges. Thus, the refractive index change is greatest at the edges and more of the readout beam is deflected or diffracted. A third beam recovers the reconstructed image with enhanced edges. The reconstructed image is an exact copy of the object only if the signal beam intensity is less than that of the reference beam. Violating this condition produces an image only at the edges of the object where the largest index modulation occurs (149,192).

Time-gated holographic imaging through scattered media has been demonstrated at wavelengths appropriate for medical imaging. In these demonstrations, the hologram is formed by the temporal overlap of direct light from the object that has been temporally stretched (without scattering) and a reference pulse (197).

In vibration analysis, or novelty filtering, the hologram acts as an adaptive beam splitter with exact wavefront matching: a plane-wave reference beam is diffracted into the signal beam that is reflected from the surface of the object. The applied field is reversed so that the exponential gain coefficient becomes negative, thus transferring energy from the signal beam to the reference beam, reducing the signal intensity. Only objects moving faster than approximately the inverse of the response time of the photorefractive material are observed. The fast moving parts are constantly changing in time and do not interact long enough with the reference beam to lead to the recording of a hologram. An image amplification configuration may be used build a device to observe an object under low light levels (116,198). This technique can also be used to visualize the mode patterns of a vibrating object; the mode patterns can reveal defects and areas under particular stress. Such devices have typically been made with PVK (199). Applications include remote sensing and inspection, especially in hazardous environments.

Beam Fanning. Beam fanning is the spontaneous amplification of scattered light in a photorefractive material arising from an energy exchange between the incident beam and light randomly scattered from impurities or defects (178). It results from a redistribution of charges in the nonlinear material and can complicate two-beam coupling measurements or provide promise for novel applications, such as self-pumped phase conjugation (200) and some forms of optical limiting (201,202). The effect of beam fanning is the depletion of the pump beam and the appearance of a fanned beam that is swept to one side of the material.

Waveguides. Utility in waveguides generally imposes additional restrictions on the polymer composition. The geometry required to couple an external static drift field to the optical field in the waveguide dictates the use of channel waveguides to reach maximum efficiency so that the poling direction has a component along the space-charge field. The bias field is then applied across the width of the channel. Narrow channels are preferred although coupling into the channels becomes more difficult in this case. Problems with the use of waveguides in the study of photorefractive effects also include the presence of thermo-optic changes in the guide and/or coupling mechanism, whereby small temperature changes may significantly change the coupling angles. Thus, temperature control may be imperative in practical applications. All polymer dopants, of course, should be soluble in an appropriate spin-coating solvent for making thin films ($\approx 1\ \mu$m) and of sufficiently high molecular weight so as not to evaporate with the solvent. Waveguides may be utilized in optical data storage applications (203–206).

To summarize, the benefits from the development of photorefractive polymers are many but there are still significant problems to overcome before these benefits

can be realized (1). Foremost among the problems may be balancing the competing needs for both steady-state performance and fast response speed, as well as the often competing factors of stability, high mobility and fast orientational response to attain fast, highly sensitive, and efficient response. It will be necessary to better understand the trade-off between dark and photoconductivity and the effects of preillumination history (207). Better understanding is also needed of the nature and depth of charge trapping sites in polymers to optimize the dark lifetimes of the gratings.

BIBLIOGRAPHY

1. O. Ostroverkhova and W. E. Moerner, *Chem. Rev.* **104**, 3267–3314 (2004).
2. L. Solymar, D. J. Webb, and A. Grunnet-Jepson, *The Physics and Applications of Photorefractive Materials*, Clarendon Press, Oxford, 1996.
3. C. Gu, Y. Xu, Y. Liu, J. J. Pan, F. Zhou, and H. He, *Opt. Mater.* **23**, 219–227 (2003).
4. S. J. Zilker, *Chem. Phys. Chem.* **1**, 72–87 (2000).
5. W. E. Moerner and S. M. Silence, *Chem. Rev.* **94**, 127–155 (1994).
6. K. Meerholz, B. Kippelen, and N. Peygambarian, in D. L. Wise, G. E. Wnek, D. J. Trantolo, T. M. Cooper, and J. D. Gresser, eds., *Photonic Polymer System: Fundamentals, Methods, and Applications*, Marcel Dekker, Inc., New York, 1998, pp. 571–631.
7. D. M. Pepper, J. Feinberg, and N. V. Kukhtarev, *Sci. Am*. 63–74 (1990).
8. K.-S. Lee, ed., *Polymers for Photonics Applications II: Nonlinear Optical, Photorefractive and Two-Photon Absorption Polymers*, Springer-Verlag, Berlin, 2003.
9. P. Günter and J.-P. Huignard, in P. Günter and J.-P. Huignard, eds., *Photorefractive Materials and Their Applications I*, Springer-Verlag, Berlin, 1988.
10. P. Yeh, *Introduction to Photorefractive Nonlinear Optics*, John Wiley & Sons, Inc., New York, 1993.
11. W. E. Moerner, S. M. Silence, F. Hache, and G. C. Bjorkland, *J. Opt. Soc. Am. B* **11**, 320–330 (1994).
12. S. R. Marder, B Kippelen, A. K.-Y. Jen, and N. Peyghambarian, *Nature* **388**, 845–851 (1997).
13. Ch. Bosshard, K. Sutter, Ph. Pretre, J. Hulliger, M. Florsheimer, P. Kaatz, and P. Gunter, *Organic Nonlinear Optical Materials*, Gordon & Breach, Basil, Switzerland, 1995, pp. 193–241.
14. W. E. Moerner, A. Grunnet-Jepson, and C. L. Thompson, *Annu. Rev. Mater. Sci.* **27**, 585–623 (1997).
15. B. Kippelen, K. Meerholz, and N. Peygambarian, in H. S. Nalwa and S. Miyata, eds., *Nonlinear Optics of Organic Molecules and Polymers*, CRC Press, Inc., Boca Raton, Fla., 1997, pp. 465–513.
16. T. Wada and H. Sasabe, *J. Mater. Chem.* **8**, 809–828 (1998).
17. J. V. Grazulevicius, P. Strohriegl, J. Pielichowski, and K. Pielichowski, *Prog. Polym. Sci.* **28**, 1297–1353 (2003).
18. Q. Wang, L. Wang, and L. Yu, *Macromol. Rapid Commun.* **21**, 723–745 (2000).
19. A. Ashkin, G. D. Boyd, J. M. Dziedzic, R. G. Smith, A. A. Ballman, J. J. Levinstein, and K. Nassau, *Appl. Phys. Lett.* **9**, 72–74 (1966).
20. K. Sutter and P. Günter, *J. Opt. Soc. Am. B* **7**, 2274–2278 (1990).
21. S. Ducharme, J. C. Scott, R. J. Twieg, and W. E. Moerner, *Phys. Rev. Lett.* **66**, 1846–1849 (1991).
22. Y. Shuto, M. Amano, and T. Kaino, *Jpn. J. Appl. Phys.* **30**, 320–326 (1991).

23. H. S. Nalwa, ed., *Handbook of Advanced Electronic and Photonic Materials and Devices, Vol. 9: Nonlinear Optical Materials*, Academic Press, Inc., San Diego, Calif., 2001.
24. G. S. He, and S. H. Lui, *Physics of Nonlinear Optics*, World Scientific, Singapore, 1999, Chapt. 6.
25. G. Motemezzani, C. Medrano, and M. Zgonik, in P. Gunter, ed., *Nonlinear Optical Effects and Materials*, Springer-Verlag, Berlin, 2000, pp. 301–374.
26. L. Wang, M.-K. Ng, and Q. Wang, in V. Ramamurthy, K. S. Schanze, eds., *Optical Sensors and Switches*, Marcel Dekker, Inc., New York, 2001, pp. 257–319.
27. B. Kippelen, in H. J. Coufal, D. Psalis, and G. Sincerbox, eds., *Holographic Data Storage*, Springer-Verlag, Berlin, 2000, pp. 159–170.
28. N. Peyghambarian, B. Kippelen, K. B. Ferio, J. Herlocker, J. L. Maldanado, E. Hendrickx, S. Mery, A. Golemme, and S. R. Marder, in S. Miyata and H. Sasabe, eds., *Light Wave Manipulation Using Organic Nonlinear Optical Materials*, Gordon & Breach, Amsterdam, the Netherlands, 2000, pp. 223–232.
29. M. Blanchard-Desce, M. Barzoukas, F. Chaput, B. Darracq, M. Mladenova, L. Ventelon, K. Lahlil, J. Reyes, J.-P. Boilot, and Y. Levy, in F. Kajzar and M. V. Agronovich, eds., *Multiphoton and Light Driven Multielectron Processes in Organics: New Phenomena, Materials and Applications*, Kluwer Academic Publishers, Amsterdam, the Netherlands, 2000, pp. 183–198.
30. B. Kippelen, H. S. Kackritz, and R. O. Claus, eds., *Organic Nonlinear Optical Materials and Devices*, Materials Research Society, Warrendale, Pa., 1999.
31. M. Pope and C. E. Swenberg, *Electronic Processes in Organic Crystals and Polymers*, Oxford University Press, New York, 1999, Chapts. XVIII and XX.
32. Cf. K. Okamoto, T. Momura, S.-H. Park, K. Ogino, and H. Sato, *Chem. Mater.* **11**, 3279–3284 (1999).
33. P. J. Reucroft, in A. V. Patsis and D. Z. Seanor, eds., *Photoconductivity in Polymers: An Interdisciplinary Approach*, Technomic Publishing, Co., Inc., Westport, Conn., 1976.
34. J. Feinberg, D. Heiman, Jr, A. R. Tanguay, and R. W. Hellwarth, *J. Appl. Phys.* **51**, 1297–1305 (1980); *Erratum*, **52**, 537 (1980).
35. A. M. Glass and J. Strait, in P. Günter and J.-P. Huignard, eds., *Photorefractive Materials and Their Applications I*, Springer-Verlag, Berlin, 1988, pp. 237–262.
36. W. E. Moerner, S. M. Silence, F. Hache, and G. C. Bjorkland, *J. Opt. Soc. Am. B* **11**, 320–330 (1994).
37. A. M. Glass, I. P. Kaminow, A. A. Ballman, and D. H. Olson, *Appl. Opt.* **19**, 276–281 (1980).
38. F. Wurthner, R. Wortmann, and K. Meerholz, *Chem. Phys. Chem.* **3**, 17–31 (2002).
39. G. Cipparrone, A. Mazzulla, and P. Pagliusi, *Opt. Commun.* **185**, 171–175 (2000).
40. O. Ostroverkhova, A. Stickrath, and K. D. Singer, *J. Appl. Phys.* **91**, 9481–9486 (2002).
41. Th. G. Pedersen, K. Jespersen, and P. M. Johansen, *Opt. Mater.* **18**, 95–98 (2001).
42. I. C. Khoo, *IEEE J. Quantum. Electron.* **32**, 525–534 (1996).
43. M. G. Kuzyk, J. E. Sohn, and C. W. Dirk, *J. Opt. Soc. Am. B* **7**, 842–858 (1990).
44. K. Meerholz, B. L. Volodin, Sandalphon, B. Kippelen, and N. Peyghambarian, *Nature* **371**, 497–500 (1994).
45. R. Wortmann, C. Poga, T. J. Twieg, C. Geletneky, C. Moylan, P. M. Lindquist, R. G. DeVoe, P. M. Cotts, H. Horn, J. E. Rice, and D. M. Burland, *J. Chem. Phys.* **105**, 10637–10647 (1996).
46. R. Bittner, C. Bräuchle, and K. Meerholz, *Appl. Opt.* **37**, 2843–2851 (1998).
47. H. Chun, I. K. Moon, D.-H. Shin, S. Song, and N. Kim, *J. Mater. Chem.* **12**, 858–862 (2002).
48. D. V. Steenwinckel, E. Hendrickx, C. Samyn, C. Engels, and A. Persoons, *J. Mater. Chem.* **10**, 2692–2697 (2000).

49. K. D. Singer and J. H. Andrews, in J. Zyss, ed., *Molecular Nonlinear Optics: Materials Physics, and Devices*, Academic Press, Inc., San Diego, Calif., 1994, Chapt. 6.
50. T. K. Däubler, R. Bittner, K. Meerholz, V. Cimrová, and D. Neher, *Phys Rev. B* **61**, 13515–13527 (2000).
51. M. Biswas, A. Mukherjee, and V. Mylnikov, *Photoconducting Polymers/Metal-Containing Polymers*, Springer-Verlag, Berlin, 1994.
52. N. A. Davidenko and A. A. Ishchenko, *Theor. Exp. Chem.* **38**, 88–108 (2002).
53. R. H. Bube, *Photoelectronic Properties of Semiconductors*, Cambridge University Press, Oxford, 1992.
54. N. V. Kukhtarev, V. B. Markov, S. G. Odulov, M. S. Soskin, and V. L. Vinetskii, *Ferroelectrics* **22**, 949–964 (1979).
55. A. Twarowski, *J. Appl. Phys.* **65**, 2833–2837 (1991).
56. J. S. Schildkraut and A. V. Buettner, *J. Appl. Phys.* **72**, 1888–1893 (1992).
57. H. Scher and E. W. Montroll, *Phys. Rev. B* **12**, 2455–2477 (1975).
58. J. Mort and G. Pfister, in J. Mort and G. Pfister, eds., *Electronic Properties of Polymers*, John Wiley & Sons, Inc., New York, 1982.
59. M. Thelakkat, *Macromol. Mater. Eng.* **287**, 442–461 (2002).
60. J. Ostrauskaite, H. R. Karickal, A. Leopold, D. Haarer, and N. Thelakkat, *J. Mater. Chem.* **12**, 58–64 (2001).
61. M. Thelakkat, J. Ostrauskaite, A. Leopold, R. Bausinger, and D. Haarer, *Chem. Phys.* **285**, 133–147 (2002).
62. P. Strohriegl and J. V. Grazulevicius, *Adv. Mater.* **14**, 1439–1452 (2002).
63. B. E. Jones, S. Ducharme, M. Liphardt, A. Goonesekera, J. M. Takacs, L. Zhang, and R. Athalye, *J. Opt. Soc. Am. B* **11**, 1064–1072 (1994).
64. J. S. Schildkraut, *Appl. Phys. Lett.* **58**, 340–342 (1991).
65. W. D. Gill, in J. Mort and D. Pai, eds., *Photoconductivity and Related Phenomena*, Elsevier, Amsterdam, the Netherlands, 1976.
66. G. G. Malliaras, V. V. Krasnikov, H. J. Bolink, and G. Hadziioannou, *Appl. Phys. Lett.* **66**, 1038–1040 (1995).
67. J. S. Schildkraut and Y. Cui, *J. Appl. Phys.* **72**, 5055–5060 (1992).
68. B. H. Yuan, X. D. Sun, Y. Y. Jiang, C. F. Hou, and Z. X. Zhou, *J. Mod. Opt.* **48**, 1161–1170 (2001).
69. O. Ostroverkhova and K. D. Singer, *J. Appl. Phys.* **92**, 1727–1743 (2002).
70. L. Kulikovsky, D. Neher, E. Mecher, K. Meerholz, H.-H. Horhold, and O. Ostroverkhova, *Phys. Rev. B* **69**, 125216-1-11 (2004).
71. E. Mecher, F. Gallego-Gomez, H. Tillmann, H. H. Horhold, J. C. Hummelen, and K. Meerholz, *Nature* **418**, 959–964 (2002).
72. J. Wolff, S. Schloter, U. Hofmann, D. Haarer, and S. J. Zilker, *J. Opt. Soc. Am. B* **16**, 1080–1086 (1999).
73. K. Khand, D. J. Binks, and D. P. West, *J. Appl. Phys.* **89**, 2516–2519 (2001).
74. S. C. Freilich, *Macromolecules* **20**, 973–978 (1987).
75. W. E. Moerner, C. Walsh, J. C. Scott, S. Ducharme, D. M. Burland, G. C. Bjorklund, and R. J. Twieg, *SPIE Proc.* **1560**, 148–161 (1991).
76. Y. Wang and A. Suna, *J. Phys. Chem. B* **101**, 5627–5638 (1997).
77. A. Leopold, M. Grasruck, U. Hofmann, M. A. Kol'chenko, and S. J. Zilker, *Appl. Phys. Lett.* **76**, 1644–1646 (2000).
78. T. Jakob, S. Schloter, U. Hofmann, M. Grasruck, A. Schreiber, and D. Haarer, *J. Chem. Phys.* **111**, 10633–10639 (1999).
79. A. Goonesekera, S. Ducharme, and J. M. Takacs, *Proc. SPIE* **3144**, 195–206 (1997).
80. O. Ostroverkhova, M. He, R. J. Twieg, and W. E. Moerner, *Chem. Phys. Chem.* **4**, 732–744 (2003).
81. J.-C. Ribierre, L. Mager, A. Fort, and S. Méry, *Macromolecules* **36**, 2516–2525 (2003).

82. H. Bassler, *Phys. Status Solidi B* **175**, 15 (1993).
83. A. Ohshima, A. Momotake, and T. Arai, *J. Photochem. Photobiol., A: Chem.* **162**, 473–479 (2004).
84. S. Anguille, P. Brun, and R. Guglielmetti, *Appl. Organomet. Chem.* **18**, 68–70 (2004).
85. M. Levitus and P. F. Aramendia, *J. Phys. Chem. B* **103**, 1864–1870 (1999).
86. E. H. Chung, J. Shim, and W. K. Chae, *J. Photochem. Photobiol., A: Chem.* **129**, 43–48 (1999).
87. G. H. Brown, ed., *Photochromism*, Vols. I–III, Wiley InterScience, New York, 1971).
88. C. A. Walsh and W. E. Moerner, *J. Opt. Soc. Am. B* **9** 1642–1647 (1992).
89. J. Mun, J. W. Lee, J. K. Park, K. S. Lee, and C. S. Yoon, *Opt. Mater.* **21**, 379–383 (2003).
90. J.-W. Lee, J. Mun, C. S. Yoon, K.-S. Lee, and J.-K. Park, *Adv. Mater.* **14**, 144–147 (2002).
91. J. C. Scott, L. T. Pautmeier, and W. E. Moerner, *J. Opt. Soc. Am. B* **9**, 2059–2064 (1992).
92. M. Liphardt, A Goonesekera, B. E. Jones, S. Ducharme, J. M. Takacs, and L. Zhang, *Science* **263**, 367–369 (1994).
93. J. A. Herlocker, K. B. Ferrio, E. Hendrickx, B. D. Guenther, S. Mery, B. Kippelen, and N. Peyghambarian, *Appl. Phys. Lett.* **74**, 2253–2255 (1999).
94. D. V. Steenwinckel, E. Hendrickx, A. Persoons, K. Van den Broeck, and C. Samyn, *J. Chem. Phys.* **112**, 11030–11037 (2000).
95. J. C. Ribierre, G. Cheval, F. Huber, L. Mager, A. Fort, R. Muller, S. Méry, and J. F. Nicoud, *J. Appl. Phys.* **91**, 1710–1712 (2002).
96. D. Wright, M. A. Diaz-Garcia, J. D. Casperson, M. DeClue, and W. E. Moerner, *Appl. Phys. Lett.* **73**, 1490–1492 (1998).
97. D. J. Binks and D. P. West, *J. Chem. Phys.* **115**, 6760–6765 (2001).
98. D. J. Binks and D. P. West, *Appl. Phys. B: Lasers Opt.* **74**, 279–282 (2002).
99. D. J. Binks, D. P. West, S. Norager, and P. O'Brien, *J. Chem. Phys.* **117**, 7335–7341 (2002).
100. M. Thelakkat, *Macromol. Mater. Eng.* **287**, 442–461 (2002).
101. D. P. West, M. D. Rahn, C. Im, and H. Bässler, *Chem. Phys. Lett.* **326**, 407–412 (2000).
102. J. G. Winiarz and P. N. Prasad, *Opt. Lett.* **27**, 1330–1332 (2002).
103. D. Day, M. Gu, and A. Smallridge, *Adv. Mater.* **13**, 1005–1007 (2001).
104. D. Day and M. Gu, *Appl. Phys. Lett.* **80**, 2404–2406 (2002).
105. C. Poga, P. M. Lundquist, V. Lee, R. M. Shelby, R. J. Twieg, and D. M. Burland, *Appl. Phys. Lett.* **69**, 1047–1049 (1996).
106. O.-P. Kwon, S.-H. Lee, G. Montemezzani, and P. Günter, *Adv. Funct. Mater.* **13**, 434–438 (2003).
107. W. E. Douglas, A. Kuzhelev, S. Alexandar, I. Yurasova, O. L. Antipov, L. G. Klapshina, V. V. Semenov, G. A. Domrachev, T. I. Lopatina, and D. M. H. Guy, *Phys. Chem. Chem. Phys.* **4**, 109–114 (2002).
108. H. Cun, I. K. Moon, D.-H. Shin, S. Song, and N. Kim, *J. Mater. Chem.* **12**, 858–862 (2002).
109. L. Li, R. J. Jeng, J. Y. Lee, J. Kumar, and S. K. Tripathy, *SPIE Proc.* **1560**, 243–250 (1991).
110. A. V. Afanas'ev, O. L. Antipov, R. E. Benfield, B. A. Bushuk, S. B. Bushuk, G. A. Domrachev, W. E. Douglas, Zh. Fominikh, R. G. Jones, L. G. Klapshina, A. S. Kuzhelev, T. I. Lopatina, A. Mustafa, A. N. Rubinov, V. V. Semenov, I. V. Yurasova, and A. P. Zinoviev, *Silicon Chem.* **1**, 145–154 (2002).
111. P. A. Blanche, B. Kippelen, A. Schlzgen, C. Fuentes-Hernandez, G. Ramos-Ortiz, J. F. Wang, E. Hendrickx, N. Peyghambarian, and S. R. Marder, *Opt. Lett.* **27**, 19–21 (2002).
112. W. E. Douglas, A. S. Kuzhelev, I. V. Yurasova, O. L. Antipov, L. G. Klapshina, V. V. Semenov, G. A. Domrachev, T. I. Lopatina, and D. M. H. Guy, *Phys. Chem. Chem. Phys.* **4**, 109–114 (2002).

113. B. Kippelen, P. A. Blanche, A. Schülzgen, C. Fuentes-Hernandez, G. Ramos-Ortiz, and co-workers, *Adv. Funct. Mater.* **12**, 615–620 (2002).
114. I. V. Yurasova and O. L. Antipov, *Opt. Commun.* **224**, 329–336 (2003).
115. Z. Zhang and K. D. Singer, *Appl. Phys. Lett.* **72**, 2948–2950 (1998).
116. A. Goonesekera, D. Wright, and W. E. Moerner, *Appl. Phys. Lett.* **76**, 3358–3360 (2000).
117. Z. Rui-Zhi, Z. You-Yuan, M. Ke, W. Chang-Chun, and L. Fu-Ming, *Chin. Phys. Lett.* **19**, 795–797 (2002).
118. D. J. Suh, O. O. Park, T. Ahn, and H.-K. Shim, *Opt. Mater.* **21**, 365–371 (2003).
119. C. Castè, V. Castelvetro, F. Ciardelli, A. Colligiani, A. Mazzotta, D. Michelotti, G. Ruggeri, and C. A. Veracini, *Synth. Met.* **138**, 341–345 (2003).
120. J. Zhang and K. D. Singer, *Appl. Phys. Lett.* **72**, 2948–2950 (1998).
121. S.-H. Park, K. Ogino, and H. Sato, *Polym. Adv. Technol.* **11**, 349–358 (2000).
122. Y. Bai, X. Chen, X. Wan, Q.-F. Zhou, H. Liu, B. Zhang, and Q. Gong, *Appl. Phys. B: Lasers Opt.* **73**, 35–37 (2001).
123. Y. Bai, X. Chen, X. Wan, Q. Zhou, H. Liu, B. Zhang, and Q. Gong, *Appl. Phys. Lett.* **80**, 10–12 (2002).
124. D. J. Binks and D. P. West, *J. Opt. Soc. Am. B* **19**, 2349–2356 (2002).
125. O. Ostroverkhova, D. Wright, U. Gubler, W. E. Moerner, M. He, A. Sastre-Santos, and R. J. Twieg, *Adv. Funct. Mater.* **12**, 621–629 (2002).
126. Y. Chen, Q. Gong, F. Wang, B. Zhang, and Z. Chen, *Mater. Lett.* **57**, 4372–4377 (2003).
127. L. Zhang, G. Zhang, G. O. Carlisle, and G. A. Crowder, *J. Mater. Sci.* **11**, 229–234 (2000).
128. S. Wu, F. Zeng, F. Li, and J. Li, *React. Funct. Polym.* **46**, 225–231 (2001).
129. P. Wang, Z. Feng, Y. Chang, C. Ye, F. Wang, and Q. Gong, *J. Appl. Polym. Sci.* **75**, 447–451 (2000).
130. A. Leopold, M. A. Kol'chenko, U. Hofmann, and S. J. Zilker, *J. Lumin.* **86**, 371–374 (2000).
131. Z. Peng, A. R. Gharavi, and L. Yu, *J. Am. Chem. Soc.* **119**, 4622–4632 (1997).
132. R. Termine, I. Aiello, D. Dattilo, M. Ghedini, and A. Golemme, *Adv. Mater.* **15**, 723–726 (2003).
133. K. R. Choudhury, J. G. Winiarz, M. Samoc, and P. N. Prasad, *Appl. Phys. Lett.* **82**, 406–408 (2003).
134. V. S. Mylnikov, *Photoconducting Polymers/Metal-Containing Polymers, Advances in Polymer Science*, Vol. 115, Springer-Verlag, Berlin, Heidelberg, 1994.
135. Z. Bo, L. Hui, G. Qi-Huang, J. Sohn, J. Hwang, S. Y. Park, J. K. Lee, J.-H. Lee, J.-S. Chang, and G. J. Lee, *Chin. Phys. Lett.* **19**, 66–68 (2002).
136. K. D. Belfield, O. Najjar, and S. R. Sriram, *Polymer* **41**, 5011–5020 (2000).
137. F. Brustolin, V. Castelvetro, F. Ciardelli, G. Ruggeri, and A. Colligiani, *J. Polym. Sci., Part A: Polym. Chem.* **39**, 253–262 (2001).
138. Y. Chen, Z. Chen, Q. Gong, and M. Schroers, *Mater. Lett.* **57**, 2271–2276 (2003).
139. Y.-W. Chen, Y.-K. He, H.-Y. Chen, F. Wang, Z.-J. Chen, and Q.-H. Gong, *J. Appl. Polym. Sci.* **77**, 189–194 (2000).
140. J. V. Grazulevicius, P. Strohriegl, J. Pielichowski, and K. Pielichowski, *Prog. Polym. Sci.* **28**, 1297–1353 (2003).
141. H. Tang, J. Li, and J. Qin, *React. Funct. Polym.* **48**, 193–199 (2001).
142. Q. Wang, L. Wang, J. Yu, and L. Yu, *Adv. Mater.* **12**, 974–978 (2000).
143. Z. Li, J. Luo, J. Li, C. Zhan, and J. Qin, *Polym. Bull.* **45**, 105–111 (2000).
144. C. Jung, T. Aoyama, T. Wada, H. Sasabe, M. Jikei, and M. Kakimoto, *High Perform. Polym.* **12**, 205–212 (2000).
145. A. V. Vannikov, A. D. Grishina, B. I. Shapiro, L. Y. Pereshivko, T. V. Krivenko, V. V. Savel'ev, V. V. Savel'ev[1], V. I. Berendyaev[3], and R. W. Rychwalski, *High Energy Chem.* **36**, 38–43 (2002).

146. A. V. Vannikov, A. D. Grishina, B. I. Shapiro, L. Y. Pereshivko, T. V. Krivenko, V. V. Savelyev, V. I. Berendyaev, and R. W. Rychwalski, *Chem. Phys.* **287**, 261–271 (2003).
147. W. J. Kuo, G. H. Hsiue, and R. J. Jeng, *Macromol. Chem. Phys.* **202**, 1782–1790 (2001).
148. D. H. Choi, W. Jun, K. Y. Oh, and J. H. Kim, *Polym. Bull.* **49**, 173–180 (2002).
149. G. P. Wiederrecht, *Annu. Rev. Mater. Res.* **31**, 139–169 (2001).
150. L. Hui, Z. Bo, G. Qi-Huang, B. Yao-Wen, C. Xiao-Fang, W. Xin-Hua, and Z. Qi-Feng, *Chin. Phys. Lett.* **18**, 909–911 (2001).
151. H. Ono, T. Kawamura, N. Mocam Frias, K. Kitamura, N. Kawatsuki, H. Norisada, and T. Yamamoto, *J. Appl. Phys.* **88**, 3853–3858 (2000).
152. H. Ono, T. Kawamura, N. M. Frias, L. Kitamura, N. Kawatsuki, and H. Norisada, *Adv. Mater.* **12**, 143–146 (2000).
153. P. G. de Gennes, *The Physics of Liquid Crystals*, Clarendon Press, Oxford, 1974.
154. I. C. Khoo, H. Li, and Y. Liang, *Opt. Lett.* **19**, 1723–1725 (1994).
155. A. Golemme, B. L. Volodin, B. Kippelen, and N. Peyghambarian, *Opt. Lett.* **22**, 1226–1228 (1997).
156. N. Peyghambarian, in I. Khan and J. Harrison eds., *ACS Symposium Series*, Vol. 726, American Chemical Society, Washington, D.C., 1999, Chapt. 14, pp. 204–225.
157. S. Bartkiewicz, K. Matczyszyn, A. Miniewicz, and F. Kajzar, *Opt. Commun.* **187**, 257–261 (2001).
158. D. McPhail and M. Gu, *Appl. Phys. Lett.* **81**, 1160–1162 (2002).
159. H. Ono, A. Emoto, F. Takahashi, N. Kawatsuki, and T. Hasegawa, *J. Appl. Phys.* **94**, 1298–1303 (2003).
160. H. Ono, H. Shimokawa, A. Emoto, and N. Kawatsuki, *J. Appl. Phys.* **94**, 23–30 (2003).
161. C. Engels, D. V. Steenwinckel, E. Hendrickx, M. Schaerlaekens, A. Persoons, and C. Samyn, *J. Mater. Chem.* **12**, 951–957 (2002).
162. J. E. Hall and D. A. Higgins, *Rev. Sci. Instrum.* **73**, 2103–2107 (2002).
163. J. Mun, C. S. Yoon, H.-W. Kim, S.-A. Choi, and J.-D. Kim, *Appl. Phys. Lett.* **79**, 1933–1935 (2001).
164. P. Pagliusi and G. Cipparrone, *J. Appl. Phys.* **92**, 4863–4869 (2002).
165. N. Kawatsuki, T. Kawakami, and T. Yamamoto, *Adv. Mater.* **13**, 1337–1339 (2001).
166. M. J. Fuller, C. J. Walsh, Y. Zhao, and M. R. Wasielewski, *Chem. Mater.* **14**, 952–953 (2002).
167. U. Gubler, D. Wright, W. E. Moerner, and M. B. Klein, *Opt. Lett.* **27**, 354–356 (2002).
168. J. A. Herlocker, C. Fuentes-Hernandez, K. B. Ferrio, E. Hendrickx, Y. Zhang, J. F. Wang, P. A. Blanche, S. R. Marder, N. Peyghambarian, and B. Kippelen, *Appl. Phys. Lett.* **77**, 2292–2294 (2000).
169. S. Schloter, U. Hofmann, P. Strohriegl, H. W. Schmidt, and D. Haarer, *J. Opt. Soc. Am B* **15**, 2473–2475 (1998).
170. A. Golemme, B. Kippelen, and N. Peyghambarian, *Appl. Phys. Lett.* **73**, 2408–2410 (1998).
171. J. E. Hall and D. A. Higgins, *Rev. Sci. Instrum.* **73**, 2103–2107 (2002).
172. Z. Bo, L. Hui, G. Qi-Huang, J. Sohn, J. Hwang, S. Y. Park, J. K. Lee, J.-H. Lee, J.-S. Chang, and G. J. Lee, *Chin. Phys. Lett.* **19**, 66–68 (2002).
173. A. Grunnet-Jepsen, C. L. Thompson, and W. E. Moerner, *J. Opt. Soc. Am. B* **15**, 905–913 (1998).
174. K. Kuroda, ed., *Progress in Photorefractive Nonlinear Optics*, Taylor & Francis, London, 2002, pp. 4–6.
175. D. Wright, U. Gubler, Y. Roh, W. E. Moerner, M. He, and R. J. Twieg, *Appl. Phys. Lett.* **79**, 4274–4276 (2001).
176. D. J. Suh, O. O. Park, T. Ahn, and H. K. Shim, *Jpn. J. Appl. Phys., Part 2* **41**, L428–L430 (2002).

177. D. Wright, M. A. Diaz-Garcia, J. D. Casperson, M. DeClue, and W. E. Moerner, *Appl. Phys. Lett.* **73**, 1490–1492 (1998).
178. A. Grunnet-Jepsen, C. L. Thompson, R. J. Twieg, and W. E. Moerner, *J. Opt. Soc. Am. B* **15**, 901–904 (1998).
179. J. D. Shakos, M. D. Rahn, D. P. West, and K. Khand, *J. Opt. Soc. Am. B* **17**, 373–380 (2000).
180. Sandalphon, B. Kippelen, K. Meerholz, N. Peyghambarian, *Appl. Opt.* **35**, 2346–2354 (1996).
181. V. S. Mylnikov, *Photoconducting Polymers/Metal-Containing Polymers, Advances in Polymer Science* vol. 115, Springer-Verlag, Berlin, 1994.
182. A. Rose, *Concepts in Photoconductivity and Allied Problems*, Interscience Publishers, New York (1963).
183. G. G. Malliaras, V. V. Krasnikov, H. J. Bolink, and G. Hadziioannou, *Phys. Rev. B* **52**, R14324–R14327 (1995).
184. S. J. Zilker, M. Grasruck, J. Wolff, S. Schloter, A. Leopold, M. A. Kol'chenko, U. Homann, A. Schreiber, P. Strohriegl, C. Hohle, and D. Haarer, *Chem. Phys. Lett.* **306**, 285–290 (1999).
185. H. Chun, W. J. Joo, N. J. Kim, I. K. Moon, and N. Kim, *J. Appl. Polym. Sci.* **89**, 368–372 (2003).
186. P. M. Lindquist, C. Poga, R. G. DeVoe, Y. Jia, W. E. Moerner, M.-P. Bernal, H. Coufal, R. K. Grygier, J. A. Hoffnagle, C. M. Jefferson, R. M. Macfarlane, R. M. Shelby, and G. T. Sincerbox, *Opt. Lett.* **21**, 890–892 (1996).
187. N. Cheng, B. Swedek, and P. N. Prasad, *Appl. Phys. Lett.* **71**, 1828–1830 (1999).
188. H.-W. Kim, K.-S. Choi, J. Mun, S. Jung, C.-S. Yoon, and J.-D. Kim, *Opt. Mater.* **21**, 657–662 (2003).
189. G. J. Steckman, R. Bittner, K. Meerholz, and D. Psaltis, *Opt. Commun.* **185**, 13–17 (2000).
190. K. Curtis, A. Pu, and D. Psaltis, *Opt. Lett.* **19**, 993–994 (1994).
191. S. G. Kim, H. S. Lee, K. T. Kim, E. S. Kim, and B. Lee, *Opt. Quantum. Electron* **32**, 419–430 (2000).
192. H. Ono, T. Kawamura, N. Kawatsuki, and H. Norisada, *Appl. Phys. Lett.* **79**, 895–897 (2001).
193. J. A. Herlocker, C. Fuentes-Hernandez, J. F. Wang, N. Peyghambarian, B. Kippelen, Q. Zhang, and S. R. Marder, *Appl. Phys. Lett.* **80**, 1156–1158 (2002).
194. M. M. Wang and S. C. Esener, *Appl. Opt.* **39**, 1826–1834 (2000).
195. B. L. Volodin, B. Kippelen, K. Meerholz, B. Javidi, and N. Peyghambarian, *Nature* **383**, 58–59 (1996).
196. D. Vacar, A. J. Heeger, B. Volodin, B. Kippelen, and N. Peyghambarian, *Rev. Sci. Instrum.* **68**, 1119–1121 (1997).
197. D. D. Steele, B. L. Volodin, O. Savina, B. Kippelen, N. Peyghambarian, H. Rockel, and S. R. Marder, *Opt. Lett.* **23**, 153–155 (1998).
198. M. B. Klein, G. D. Bacher, A. Grunnet-Jepsen, D. Wright, and W. E. Moerner, *Opt. Commun.* **162**, 79–84 (1999).
199. E. Hendrickx, D. Van Steenwinckel, C. Engels, E. Gubbelmans, K. Van den Broeck, D. Beljonne, J.-L. Bredas, C. Samyn, and A. Persoons, *Mater. Sci. Eng., C* **18**, 25–35 (2001).
200. W.-J. Joo, N.-J. Kim, H. Chun, I. K. Moon, and N. Kim, *Polymer* **42**, 9863–9866 (2001).
201. M. R. Leahy, and D. J. McGee, *Opt. Commun.* **187**, 277–282 (2001).
202. A. N. Simonov, A. V. Larichev, V. P. Shibaev, and A. I. Stakhanov, *Opt. Commun.* **197**, 175–185 (2001).
203. S. Mookherjea and A. Yariv, *Phys. Rev. E* **64**, 066602(6) (2001).

204. T. Sassa, T. Wada, H. Sasabe, M. Yokoyama, and S. Umegaki, *Opt. Lett.* **26**, 995–997 (2001).
205. Y. Hayasaki, N. Ishikura, H. Yamamoto, and N. Nishida, *Rev. Sci. Instrum.* **74**, 3693–3696 (2003).
206. Z. Chen, M. Asaro, O. Ostroverkhova, W. E. Moerner, M. He, and R. J. Twieg, *Opt. Lett.* **28**, 2509–2511 (2003).
207. J. Obrzut, M. J. Obrzut, and F. E. Karasz, *Synth. Met.* **29**, E103–E108 (1989).

FURTHER READING

In addition to previously cited materials, the reader interested in ongoing developments may also want to consider regular topical symposia on organic photorefractives sponsored by, among others, the Materials Research Society, The Optical Society of America, and the Society of Photo-Optical Instrumentation Engineers (SPIE). Recent related proceedings of SPIE include

K. Meerholz, *Organic Photorefractive and Photosensitive Materials for Holographic Applications*, 4802 SPIE, Bellingham, Wash., 2002.
S. Ducharme and J. W. Stasiak, *Organic Photorefractive Materials and Xerographic Photoreceptors*, 2850 SPIE, Bellingham, Wash., 1996.
S. Ducharme and J. W. Stasiak, *Xerographic Photoreceptors and Organic Photorefractive Materials II*, 3144 SPIE, Bellingham, Wash., 1997.
S. Ducharme and J. W. Stasiak, *Xerographic Photoreceptors and Organic Photorefractive Materials IV*, 3471 SPIE, Bellingham, Wash., 1998.
C. M. Lawson and K. Meerholz, *Nonlinear Optical Transmission Processes and Organic Photorefractive Materials*, 4462 SPIE, Bellingham, Wash., 2002.
G. V. Klimusheva and A. G. Iljin, eds., *Eighth International Conference on Nonlinear Optics of Liquid and Photorefractive Crystals*, 4418 SPIE, Bellingham, Wash., 2001.
G. V. Klimusheva and A. G. Iljin, *Nonlinear Optics of Liquid and Photorefractive Crystals*, 2795 SPIE, Bellingham, Wash., 1996.
G. V. Klimusheva, *Nonlinear Optics of Liquid and Photorefractive Crystals II*, 3488 SPIE, Bellingham, Wash., 1998.

JAMES H. ANDREWS
KAREN ZREBIEC
Youngstown State University

Encyclopedia of Polymer Sceince and Technology
Copyright © 2005 John Wiley & Sons, Inc. All rights reserved.

POLYMER BLENDS

Polymer Blends

Mixing of two or more different polymers together makes it possible to achieve various property combinations of the final material—usually in a more cost-effective way than in the case of synthesis of new polymers. Therefore, great attention has been paid to the investigation of these systems, as well as to the development of specific materials. Recently, the problem of polymer blends has also become important for recycling industrial and/or municipal plastics scrap. A considerable amount of information has been collected during more than three decades, summarized in dozens of monographs (see General References).

Basic problems associated with the equilibrium and interfacial behavior of polymers, compatibilization of immiscible components, phase structure development, and the methods of its investigation are described herein. Special attention is paid to mechanical properties of heterogeneous blends and their prediction. Commercially important types of polymer blends as well as the recycling of commingled plastic waste are briefly discussed.

Equilibrium Phase Behavior

Mixing of two amorphous polymers can produce either a homogeneous mixture at the molecular level or a heterogeneous phase-separated blend. Demixing of polymer chains produces two totally separated phases, and hence leads to macrophase separation in polymer blends. Some specific types of organized structures may be formed in block copolymers due to microphase separation of block chains within one block copolymer molecule.

Two terms for blends are commonly used in literature—miscible blend and compatible blend. The terminology recommended by Utracki (1) will be used in this article. By the *miscible polymer blend*, we mean a blend of two or more amorphous polymers homogeneous down to the molecular level and fulfilling the thermodynamic conditions for a miscible multicomponent system. An *immiscible polymer blend* is the blend that does not comply with the thermodynamic conditions of phase stability. The term *compatible polymer blend* indicates a commercially attractive polymer mixture that is visibly homogeneous, frequently with improved physical properties compared with the constituent polymers.

2 POLYMER BLENDS

Equilibrium phase behavior of polymer blends complies with the general thermodynamic rules (2–6)

$$\Delta G_{\text{mix}} = \Delta H_{\text{mix}} - T\Delta S_{\text{mix}} < 0 \tag{1}$$

and

$$\mu_i^{'} = \mu_i^{''}\ i = 1,2,\ldots,n \tag{2}$$

where ΔG_{mix}, ΔH_{mix}, and ΔS_{mix} are the Gibbs energy, enthalpy, and entropy of mixing of a system consisting of i components, respectively, $\mu_i{}'$ and $\mu_i{}''$ are the chemical potentials of the component i in the phase μ' and μ''. The condition given in equation 1 is necessary but it is not sufficient. Equation 2 must be also fulfilled.

Generally for a compressible polymer blend the following requirement must be satisfied (5–7):

$$\left(\frac{\partial^2 \Delta G_{\text{mix}}}{\partial v_i^2}\right)_{T,P} = \left(\frac{\partial^2 \Delta G_{\text{mix}}}{\partial v_i^2}\right)_V + \left(\frac{\partial V}{\partial P}\right)_{T,v_i}\left(\frac{\partial^2 \Delta G_{\text{mix}}}{\partial v_i \partial V}\right) > 0 \tag{3}$$

where v_i is the volume fraction of component i, V molar volume of blend, P and T are pressure and temperature of the system. If we consider an incompressible system with $\Delta V_{\text{mix}} = 0$, the application of equation 3 to the simple Flory–Huggins relationship for ΔG_{mix} (4) leads to the condition of these stability

$$\frac{1}{N_1 v_1} + \frac{1}{N_2 v_2} - 2\chi_{12} \geq 0 \tag{4}$$

where N_1, N_2 are the numbers of segments of polymer 1 or 2, and χ_{12} is the interaction parameter between polymers 1 and 2. The entropy contribution (the first and second terms on the left-hand side of equation 4 supporting miscibility of polymers is practically zero ($N_1, N_2 \gg 1$). In this case, the miscibility is controlled by the enthalpy of mixing (interaction parameter χ_{12}). For nonpolar polymers without strong interactions, the temperature dependence of χ_{12} (Fig. 1, curve 1) is given as

$$\chi_{12} = A + \frac{B}{T} \tag{5}$$

where A and B are positive constants characterizing enthalpy and entropy parts of interaction parameter χ_{12}, respectively. Its positive value indicates a very poor miscibility of high molecular weight nonpolar polymers.

Relationships describing the compressibility of polymer blends are based on the equations-of-state theories (5,6,8–16). These relationships include contributions to the entropy and enthalpy of mixing resulting from volume changes during mixing. The temperature dependence of free-volume interaction is schematically presented as curve 2 in Fig. 1. This value plays a decisive role in determining phase behavior of a polymer blend at high temperature range.

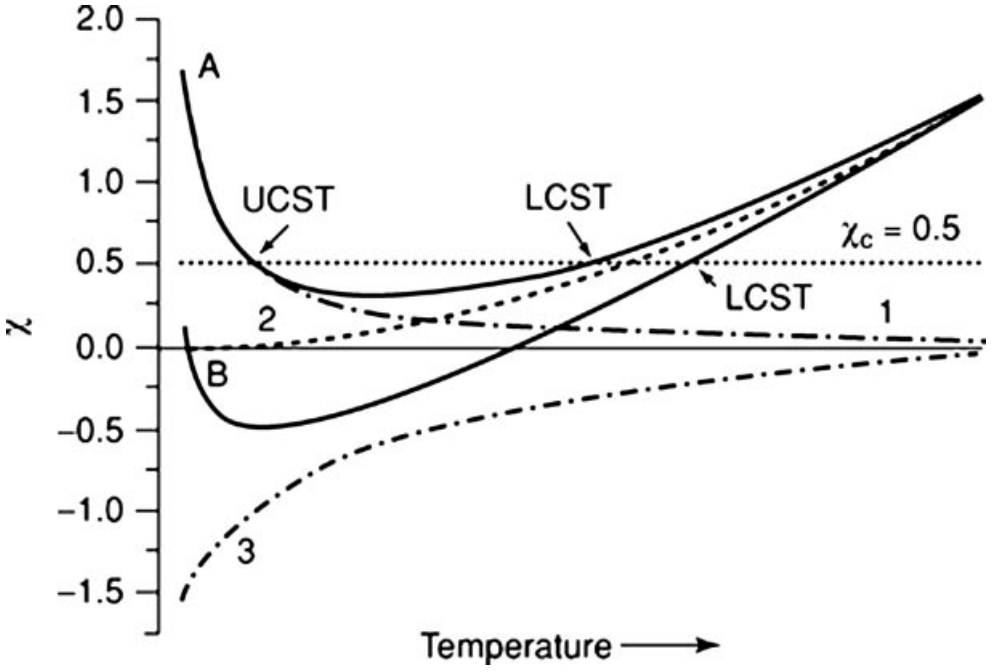

Fig. 1. Schematic temperature dependence of interaction parameters resulting from different types of interactions in a polymer blend. (1-dispersive interactions, 2-free-volume interactions, 3-specific interactions, A-sum of 1+2, B-sum of 1+2+3).

From the equation 4 it follows that the negative value of parameter χ_{12} is necessary to obtain a stable homogeneous polymer blend. The negative value of χ_{12} is characteristic of systems with specific interactions such as dipole–dipole or hydrogen bond interactions (1,5,6,17). A schematic representation of the temperature dependence of a specific interaction parameter, according (13), is given in Figure 1, curve 3.

The critical value of interaction parameter χ_c for "symmetric" polymer blends of polymers 1 and 2 ($N_1 = N_2 = N$, N-number of segments in polymer chain) is $\chi_c = 2/N$. When χ_{12} value crosses the critical value, a polymer blend separates into two macrophases. The character of the temperature dependence of χ_{12} determines the shape of the phase diagram (Fig. 1). Figure 2 shows schematic binodal and spinodal curves corresponding to the different types of interaction parameters presented in Figure 1. Binodal curves (Fig. 2, curves 1–4), defining the two-phase region, are calculated from equation 2 (2,4–6,18). A spinodal curve is obtained by solving of equation 4. The spinodal curve defines the region of absolute instability of the polymer blend. The point common to the binodal and spinodal curves is the critical point. The position of the critical point of a blend of monodisperse polymers coincides with the maximum (UCST-upper critical solution temperature) or minimum (LCST-lower critical solution temperature) of a binodal curve (18) (Fig. 2). If only dispersive interactions among polymer molecules are effective in a blend (Fig. 1, curve 1), partial miscibility can be expected at low temperatures. Above the UCST, the polymer blend is homogeneous (Fig. 2 curve 1) (4–6). Values

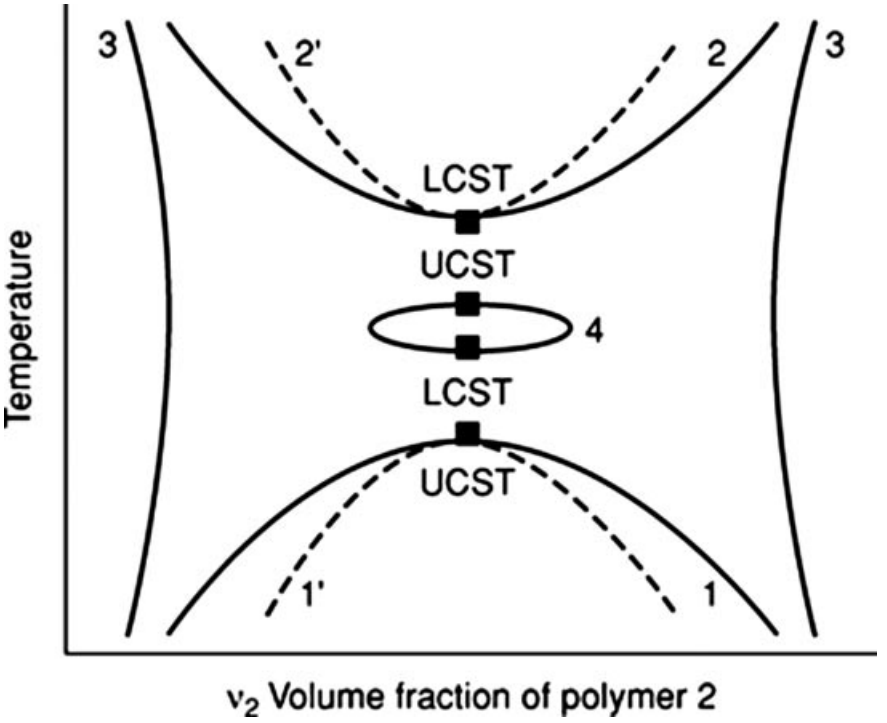

Fig. 2. Possible types of phase diagrams corresponding to interactions in Figure 1 (—— ——binodal curves, ———- spinodal curves, UCST—upper critical solution temperature, LCST—lower critical solution temperature).

of interaction parameters of nonpolar polymers can be found in literature (1,5,6) or estimated from the solubility parameters, δ_1 and δ_2, of the neat components

$$\chi \approx (\delta_1 - \delta_2)^2 \tag{6}$$

The χ parameter of disperse interactions is always positive, and miscibility is driven only by combinatorial entropy of mixing. In general, nonpolar polymers are rarely miscible with each other. Considerable data relevant to interaction energies obtained by different techniques can be found in the literature (5,6,19,20).

The area below the spinodal curve is the region of absolute instability of a polymer blend. The phase separation in this region is controlled by a spinodal mechanism. The region between spinodal and binodal curves is called the metastable region. Phase separation in this region is controlled by a nucleation mechanism.

Phase structure at an initial stage of phase decomposition depends on the type of decomposition mechanisms. The characteristic trait of the spinodal decomposition in an absolutely unstable region is phase separation in the whole volume of a blend. Initially, the resulting structure is very fine, but gradually gets coarse (5,21), and the final stage of separation is full macrophase separation. If the phase separation takes place in the metastable region, the decomposition of a blend

depends on the formation of a nucleus of a new phase. The resulting structure at the initial stage is grainy. The critical sizes of existing nuclei increase by Ostwald ripening mechanism (16)—small grains dissolve and large grains grow due to the dependence of the concentration gradient of dissolved molecules of the nucleating component, which are in turn dependent on grain radius. At the final stage, when the separation is finished, the full phase-separated structure is again obtained (5).

In unstable region, appearing fluctuations increase. The fluctuations can be considered as a set of sinusoidal waves with a constant length (6,16). The amplitude of the fluctuations appearing in the initial stage of the phase separation increases with time, as described by Kwei and Wang in Reference 6. The phase structure of the system is co-continuous for a broad range of blend compositions. At the end of the process, separated phases are identical to the blend components. Theories describing various stages of spinodal decomposition (using various approximations) have been developed (16). Scattering methods have been used for many experimental studies of phase structure decomposition in polymer blends. The initial, intermediate, and late stages of phase structure separation, differing in the time dependence of the domain size of individual phases were identified. The individual stages of the phase structure development are described by different time dependences of the phase domain size. The development of spatial concentration fluctuation is generally described by Ginsburg–Landau equation, considering chemical potential as a function of the order parameter, contribution of the random forces, and the hydrodynamic interaction between polymer molecules (16). Similar equations also describe polymer dissolution if, due to a change in thermodynamics parameters, an immiscible blend passes to a miscible one. The phase separation is affected by the presence of a copolymer and by a shear flow (16). A more detailed description of the kinetics of phase decomposition in polymer blends can be found in Reference 16.

If we have a system with free-volume or specific interactions, an increase in temperature causes phase separation at LCST. In real systems, where several types of interactions are effective, phase behavior with two regions of partial miscibility of components with UCST and LCST (Fig. 2, binodals 1 and 2) or hourglass-shaped binodal and spinodal curves (Fig. 2, binodal 3) can be expected (5,6,9,13–16). In some cases, a closed loop of immiscibility with LCST and UCST (Fig. 2, binodal 4) or a closed loop and region of partial immiscibility at high temperatures with LCST (Fig. 2, binodals 2 and 4) are observed. This pattern of phase behavior is caused by a diminishing intensity of specific interactions with increasing temperature.

Whether polymers are miscible or not depends on a delicate balance of interactions among all components in a system (6). Any favorable gain in the energy of mixing is accompanied by an unfavorable noncombinatorial entropy effect (22,23).

The effective value of the interaction parameter χ_{eff} of a multicomponent polymer blend is controlled by its composition. Blends containing statistical copolymers of A and B monomers can be used as examples. Using the mean field-theory leads to the following relation for χ_{eff}

$$\chi_{\text{eff}} = \sum_i \sum_{j>i} \chi_{ij} \left(v_i^{\text{A}} - v_j^{\text{B}}\right)\left(v_i^{\text{B}} - v_j^{\text{A}}\right) \tag{7}$$

where χ_{ij} is the interaction parameter between segments i and j. For the identical type of segments, its value is zero. It follows from equation 7 that at a proper composition of copolymers, the value of χ_{ij} can be negative, and the resulting blend is homogeneous.

The former discussion deals with liquid–liquid phase behavior; however, one or both components of the blend can sometimes crystallize. For a polymer pair that is miscible in the melt, cooling well below the melting point of pure crystallizable component leads to a pure crystalline phase of that component. Far below the melting point, the free energy of crystallization is considerably larger than that of mixing. Because polymers never become 100% crystalline, the pure crystals coexist with a mixed amorphous phase consisting of the material that did not crystallize (6,7).

The morphology of heterogeneous polymer blends is controlled by interfacial tension. The interfacial tension, σ, is intrinsically positive and can be defined as the change in the Gibbs free energy when the interfacial area A is reversibly increased at constant temperature and pressure at closed system (24).

$$\sigma = \left(\frac{\partial G}{\partial A}\right)_{T,P} \tag{8}$$

In a multicomponent system, the tendency to minimize the system Gibbs free energy leads to migration of the minor component on the interface. The resulting increase in concentration of this component at the interface (compared to its concentration in the bulk) (24) decreases the interfacial tension, as follows from equation 9

$$\frac{\partial \sigma}{\partial \ln c_2} = -RT\left(\frac{\Delta N_2}{VN_1}\right) \tag{9}$$

where c_2 is the molar concentration of the component 2, ΔN_2 is the excess number of molecules of the component 2 on the interface, N_1 is the number of molecules of the component 1, and V is volume of the system. Therefore low energy additives can greatly reduce the interfacial tension between polymers, and hence are expected to increase the degree of dispersion in blends. Block and graft copolymers are the most effective interfacial agents. They show considerable surface activity of the low energy components, and their emulsifying property depends on their structure.

Compatibilization

As it follows from thermodynamics, the blends of immiscible polymers obtained by simple mixing show a strong separation tendency, leading to a coarse structure and low interfacial adhesion. The final material then shows poor mechanical properties. On the other hand, the immiscibility or limited miscibility of polymers enables formation of a wide range structures, some of which, if stabilized, can impart excellent end-use properties to the final material. To obtain such a stabilized structure, it is necessary to ensure a proper phase dispersion by decreasing interfacial tension to suppress phase separation and improve adhesion. This can

be achieved by modification of the interface by the formation of bonds (physical or chemical) between the polymers. This procedure is known as compatibilization, and the active component creating the bonding as the compatibilizer (1,6,7). Two general methods are used for compatibilization of immiscible polymers: (i) incorporation of suitable block or graft copolymers, or (ii) reactive compatibilization.

Incorporation of Copolymers (Nonreactive Compatibilization). Block or graft copolymers with segments that are miscible with their respective polymer components show a tendency to be localized at the interface between immiscible blend phases. The copolymers anchor their segments in the relevant polymer, reducing interfacial tension and stabilizing dispersion against coalescence (24–52). Random copolymers, sometimes also used as compatibilizers, reduce interfacial tension, but their ability to stabilize the phase structure is limited (53). Finer morphology and higher adhesion of the blend lead to improved mechanical properties. The morphology of the resulting two-phase (multiphase) material, and consequently its properties, depend on a number of factors, such as copolymer architecture (type, number, and molecular parameters of segments), blend composition, blending conditions, and the like (25,38,39). Creton and co-workers (54) have reviewed the molecular criteria for copolymers linking two immiscible homopolymers that must be fulfilled to achieve a good stress-transfer ability of the interface. In Figure 3, the conformation of different block, graft, or random copolymers at the interface is schematically drawn.

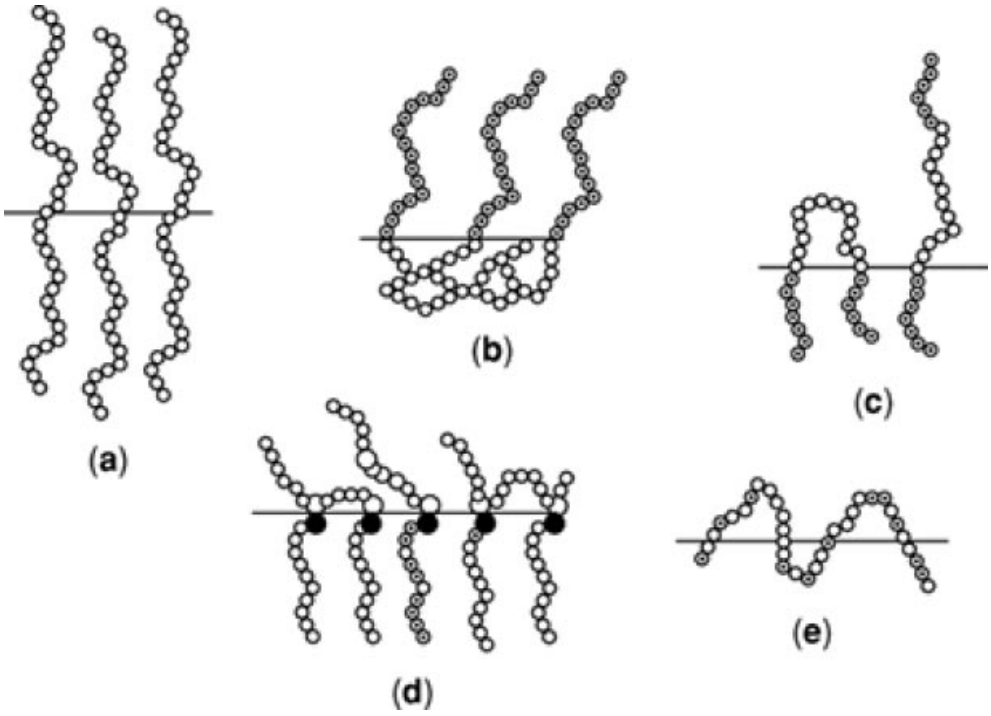

Fig. 3. Possible localization of A-B copolymer at the A/B interface. Schematic of connecting chains at an interface, a-diblock copolymers, b-end-grafted chains, c-triblock copolymers,d-multiply grafted chain, and e-random copolymer.

Besides copolymers synthesized specially for compatibilization of immiscible polymers, commercial products (typically used as impact modifiers) are utilized as compatibilizers in research as well as in practice. Typical examples are styrene-butadiene block copolymers and their styrene-hydrogenated butadiene analogues used for compatibilization of styrene polymers (PS, HIPS, SAN, ABS), with polyolefins (49), or ethylene–propylene copolymers for compatibilization of various polyolefins (50).

Mechanical properties that are sensitive to stress transfer (impact strength, tensile strength, elongation) are usually considered as criteria of compatibilization efficiency because they indirectly characterize interface adhesion (1,7,45). Morphological characteristics, such as particle size of the dispersed phase, structure homogeneity, character of interfacial layer, existence of micelles, or mesophases, also give evidence on the compatibilization efficiency (25,29,40–44).

This process, however, inherently bears two practical limitations. Blending of an immiscible polymer pair requires a specific block or graft copolymer. Consequently, a specific synthetic procedure is necessary to obtain the desired copolymer. This can be costly, and sometimes there is no feasible technology at manufacturer's disposal. Moreover, the amount of the copolymer to be added is often significantly higher than that for saturation of the interface. A part of the copolymer may be trapped in the bulk phase during blending and never reach the interface. This fact can negatively affect the blend morphology and may lead to a higher compatibilizer consumption.

During more than three decades, much information on nonreactive compatibilization has been obtained and successfully applied in the development of new multiphase materials. Moreover, the prove efficiency of block or graft copolymers in the controlling of the phase structure development has led to new, more effective approaches to producing these copolymers directly during the blending. This process is known as reactive compatibilization.

Reactive Compatibilization. Reactive compatibilization is the process that allows generating graft or block copolymers acting as compatibilizers *in situ* during melt blending (46,55). These copolymers are formed by reactions at the interfaces between suitably functionalized polymers, and they link the immiscible phases by covalent or ionic bonds. In this process, the copolymers are formed directly at the interfaces, where they act like preformed copolymers, ie, they reduce the size of the dispersed phase and improve adhesion. For this reason, the problem with transport of the compatibilizer to interface is not relevant and structure control is easier than in the case of adding preformed copolymers. In order to achieve efficient compatibilization of polymer blends, the reactions between the functional groups should be selective and fast, and the mixing conditions should minimize the limitation of mass transfer in the course of the reaction.

There are several types of reactive compatibilization. If the mixed polymers contain reactive groups, the reaction is straightforward. The polymers without reactive groups have to be functionalized or a miscible polymer containing proper reactive groups is added to the respective component. Therefore, reactive groups such as anhydride, hydroxy, amine, or carboxy are incorporated, into one or both of the polymers to be compatibilized. Maleic anhydride-grafted polymers, such as PP, PE, EPR, EPDM, SEBS, or ABS (46,55), which can react with polymers

containing amino group can serve as examples:

Reactive compatibilization of polymers through copolymer formation is also possible with the help of low molecular weight compounds (56), eg by combination of a peroxide with an oligomer coagent for preparation of PE/PP blends (57) or bis-maleic imide for PE/PBT (58). Special cases of reactive compatibilization can be considered radical-initiated reactions of monomers forming homopolymers and grafts on the chains of dissolved polymers. This process is used for manufacture of such important polymers as HIPS or ABS (59).

Preparation and Phase Structure Development

Methods of Blend Preparation. Most polymer pairs are immiscible, and therefore, their blends are not formed spontaneously. Moreover, the phase structure of polymer blends is not equilibrium and depends on the process of their preparation. Five different methods are used for the preparation of polymer blends (60,61): melt mixing, solution blending, latex mixing, partial block or graft copolymerization, and preparation of interpenetrating polymer networks. It should be mentioned that due to high viscosity of polymer melts, one of these methods is required for size reduction of the components (to the order of μm), even for miscible blends.

Melt mixing is the most widespread method of polymer blend preparation in practice. The blend components are mixed in the molten state in extruders or batch mixers. Advantages of the method are well-defined components and universality of mixing devices—the same extruders or batch mixers can be used for a wide range of polymer blends. Disadvantages of the method are high energy consumption and possible unfavorable chemical changes of blend components. Evolution of the phase structure in polymer blends during melt mixing and rules for prediction of the structure of the formed phases are discussed in the next section.

During several past years, novel solid state processing methods, such as shear pulverization or cryogenic mechanical alloying, have been developed to provide efficient mixing of polymer blends (62). The polymers are disintegrated in pulverizers at cryogenic temperatures, and nanoscale blend morphologies are achieved. Since the blends are prepared as solid powders, they must be consequently processed in the melt for concrete manufacture. Mechanochemistry of this process makes it possible to obtain block or graft copolymers acting as compatibilizers. In spite of these advantageous results, this procedure has not been used so far in industrial practice because of large energy consumption.

Solution blending is frequently used for preparation of polymer blends on a laboratory scale. The blend components are dissolved in a common solvent and intensively stirred. The blend is separated by precipitation or evaporation of the

solvent. The phase structure formed in the process is a function of blend composition, interaction parameters of the blend components, type of the solvent, and history of its separation. Advantages of the process are rapid mixing of the system without large energy consumption and the potential to avoid unfavorable chemical reactions. On the other hand, the method is limited by the necessity to find a common solvent for the blend components, and in particular, to remove huge amounts of organic (frequently toxic) solvent. Therefore, in industry, the method is used only for preparation of thin membranes, surface layers, and paints.

A blend with heterogeneities on the order of 10 μm can be prepared by mixing of latexes without using organic solvents or large energy consumption. Significant energy is needed only for removing water and eventually achievement of finer dispersion by melt mixing. The whole energetic balance of the process is usually better than that for melt mixing. The necessity to have all components in latex form limits the use of the process. Because this is not the case for most synthetic polymers, the application of the process in industrial practice is limited.

In partial block or graft copolymerization, homopolymers are the primary product. But, an amount of a copolymer sufficient for achieving good adhesion between immiscible phases is formed (59). In most cases, materials with better properties are prepared by this procedure than those formed by pure melt mixing of the corresponding homopolymers. The disadvantage of this process is the complicated and expensive startup of the production in comparison with other methods, eg, melt mixing.

Another procedure for synthesis of polymer blends is by formation of interpenetrating polymer networks. A network of one polymer is swollen with the other monomer or prepolymer; after that, the monomer or prepolymer is crosslinked (63). In contrast to the preceding methods used for thermoplastics and uncrosslinked elastomers, blends of reactoplastics are prepared by this method.

Phase Structure Development in Molten State.

Starting Period of Melt Mixing. Most polymer blends are prepared by melt mixing and processed in the molten state. Therefore, the phase structure of a blend is formed during melt flow and is petrified by solidification. Formation of the phase structure at the initial stage of the mixing was intensively studied by Macosko's group (64–68). It was found that sheets of minor phase are formed after the start of mixing. Quite rapidly, holes are formed in these sheets that coalesce. Further, the sheets transform to fibers or co-continuous structures, which can pass (depending on blend composition and properties of the components) to a dispersed structure (see Figs. 4**a**–4**e**). If the softening or melting transition temperature of the minor phase is lower than that of the major phase, switching of phase continuity occurs at this stage of mixing (67). It was found that the reduction of characteristic size of phase domains from millimeters (characteristic size of polymer pellets) to micrometers is rapid. This reduction has been achieved during the first 2 min in batch mixers and in the first mixing zones in extruders.

Type of Phase Structure. For application of polymer blends, type and fineness of their phase structure are important. In blends of immiscible polymers 1 and 2 with low content of 2, particles of component 2 are dispersed in the matrix of component 1. With rising fraction of 2, partially continuous structure of 2 appears. With further increase in the amount of 2, fully co-continuous structure is formed (see Fig. 5). After that, phase inversion occurs, where 2 forms the matrix and 1

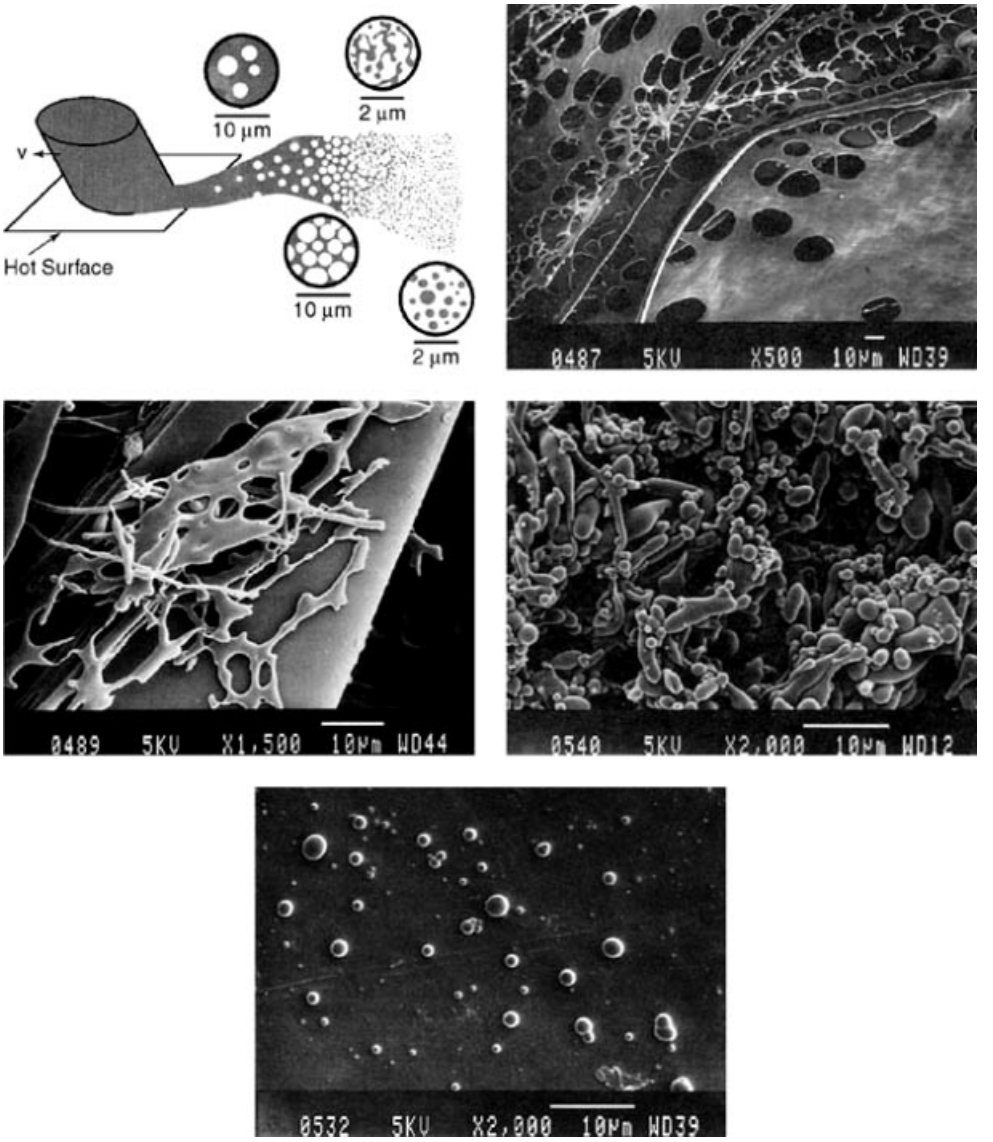

Fig. 4. (**a**) Scheme of initial morphology development. (**b**) Holes and lace structure observed in ribbons at 1.0 min mixing. (**c**) Broken lace structure and small spherical particles at 1.0 min mixing. (**d**) Morphology of the dispersed phase particles at 1.5 min mixing. (**e**) Morphology of the dispersed phase particles at 7 min. mixing. Reproduced with permission from Reference 64.

the dispersed phase (69,70). Dependencies of continuity indexes or percentages of continuity (the continuous fraction of a component, determined as a fraction of the component that can be dissolved with a selective solvent) on volume fraction of component 2 are schematically shown on Figure 15. In contrast to low molecular weight emulsions, where phase inversion occurs in one point or in a very narrow

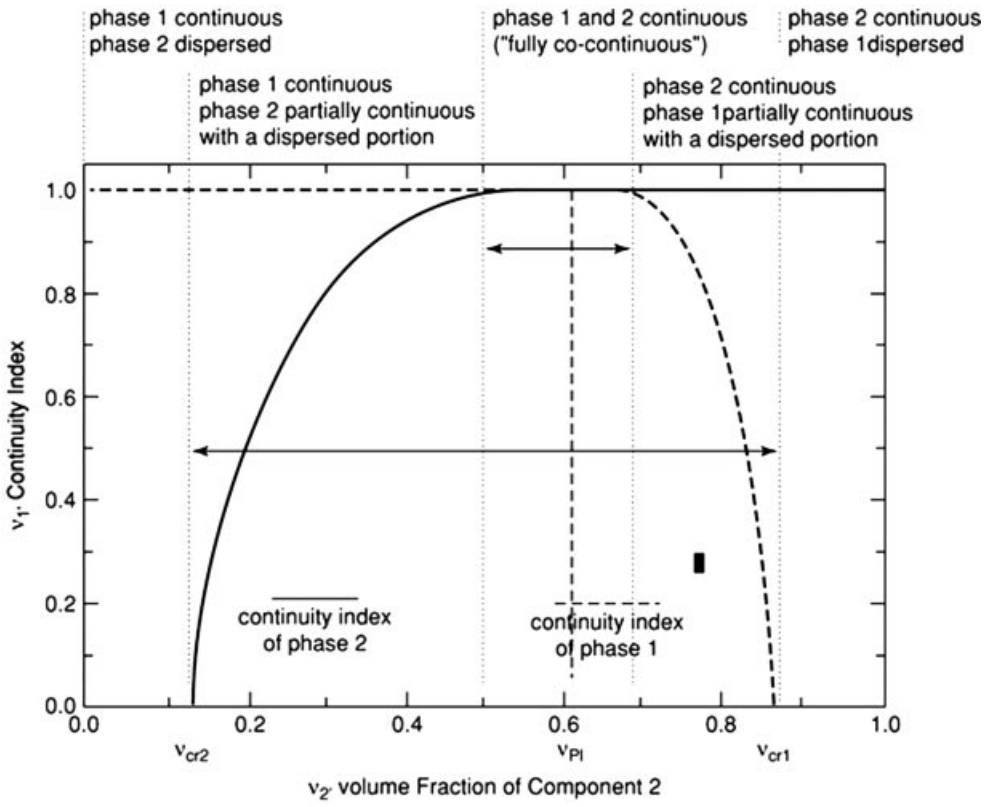

Fig. 5. Composition range of co-continuous structure. Full line continuity index of phase 2, broken line continuity index of phase 1. v_{cr1}, v_{cr2}, v_{f1} a v_{f2} are volume fractions of phase 1 or 2 at which partial or full co-continuity of the related phase start. v_{PI} designate phase inversion composition. Reproduced with permission from Reference 69.

interval of composition, co-continuous range for polymer blends is frequently quite wide. Phase inversion points calculated as the center of the interval with full co-continuity of both the components and of the interval between critical volume fractions, v_{cr1} and v_{cr2} for starting continuity of components 1 and 2, need not be the same. The interval of volume fractions of the components in which the blend structure is co-continuous depends on rheological properties of the components, interfacial tension, and mixing conditions. There have been several attempts to formulate a rule for prediction of the phase inversion point from the knowledge of viscosity of the components (69,71–74). They qualitatively describe the experimentally verified tendency of a less viscous component to be continuous down to low volume fractions. However, all fail in quantitative evaluation of a substantial portion of experimental data (69). The proposed rules for prediction of the phase inversion from the knowledge of elastic properties of the components (75–77) contain unknown parameters or have limited validity.

Utracki and Lyngaae-Jørgensen (78) proposed a theory based on the assumption that the critical volume fractions relate to the percolation thresholds of droplets, and phase inversion appears at the composition at which the blend

with dispersed component 1 and matrix 2 has the same viscosity as the blend with dispersed component 2 and matrix 1. The theory qualitatively describes dependencies of the continuity indexes on the blend composition found experimentally. However, for some blends, v_{cr} does not relate to the percolation threshold for spheres, and the predicted point of phase inversion does not agree with the experimental one for a number of systems.

A model for formation of fully co-continuous morphology based on material properties and processing conditions was proposed (79). It is based on the assumption that full co-continuity is achieved when randomly oriented cylindrical particles, formed by deformation of droplets of a minor component, are closely packed. For the volume fraction of a minor component, v_{dl}, at which co-continuous structure is formed, the following equation was derived

$$\frac{1}{v_{dl}} = 1.38 + 0.0213\left(\eta_m \dot{\gamma} \frac{R_0}{\sigma}\right)^{4.2} \tag{10}$$

where η_m is viscosity of the matrix, $\dot{\gamma}$ is the shear rate, σ is the interfacial tension, and R_0 is the radius of equivalent sphere related to a droplet of the minor phase. The model qualitatively describes the fact found experimentally that the width of the co-continuity interval increases with decreasing interfacial tension. Unfortunately, the model cannot be used in a predictive manner because R_0 has to be determined afterwards.

Recent studies (80,81) showed that at long mixing in batch mixers, transition from co-continuous to dispersed morphology appears. The mixing time, at which the transition was determined, is about one order of magnitude longer than the time necessary for reduction of the characteristic size of phase domains from millimeters to micrometers. At present, it is not clear whether co-continuous structure is only transient, or in some cases, steady (relating to certain steady mixing conditions) morphology. Elucidation of this problem is complicated by the fact that transitions between co-continuous and dispersed structures frequently occur after a long time of mixing, where it is very difficult to avoid strong degradation of the blend components.

In addition to co-continuous morphology, droplet-within-droplet (composite droplets, subinclusion, salami-like) morphologies are sometimes formed in blends with a higher content of minor component (see Fig. 6) (70,82). In some systems, ribbon like or stratified morphology was detected instead of classic co-continuous one (75). Rules for formation of individual types of morphology have not been formulated so far.

Prediction of the type of morphology in polymer blends containing three and more components is a more difficult task than for binary blends. Generally, properties of the components, interfacial tensions between them, and mixing conditions should be considered. A quite successful predictive scheme was proposed for blends with matrix component 2 and two minor dispersed components 1 and 3. It was proposed (70,83) that component 3 encapsulates the component 1 if the spreading coefficient λ_{31} is positive. λ_{31} is defined as

$$\lambda_{31} = \sigma_{12} - \sigma_{32} - \sigma_{13} \tag{11}$$

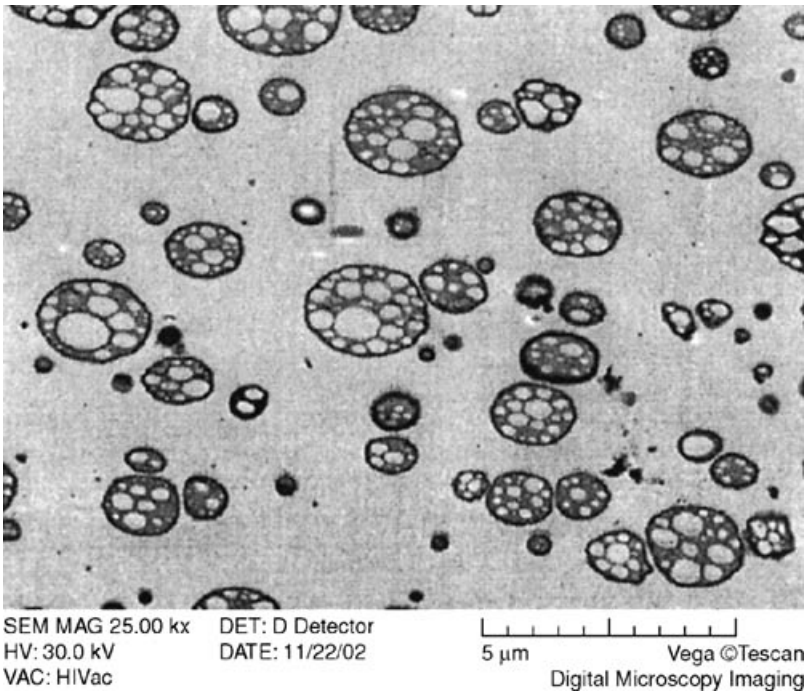

Fig. 6. Micrograph of droplet-within-droplet (composite droplets, subinclusion, salami-like) morphology.

where σ_{12}, σ_{32}, and σ_{13} are the interfacial tensions for each component pair. If spreading coefficient λ_{13} is positive, the component 1 encapsulates component 3. For both λ_{31} and λ_{13} negative, separated droplets of 1 and 3 are formed. The concept of spreading coefficients was extended taking into account the overall interface Gibbs free energy by including interfacial area of each component (84). Predictions of these schemes agree with a substantial number of experimental results (70,83–86), but the effect of rheological properties of the components on the type of phase structure was reported in some papers (87–89). The results of Reference 89 were plausibly explained if effective interfacial tensions, relating to flow, considering elasticity of the components were used in the predictive schemes. No rule for prediction of the continuity degree of the components is available for ternary blends.

Binary Polymer Blends.

Size of Dispersed Droplets in Flow. The effects of the properties of blend components and mixing conditions on fineness of the phase structure are well understood qualitatively for binary polymer blends with dispersed structure. It is broadly accepted that the size of dispersed droplets in flowing blends is controlled by the competition between the droplet breakup and coalescence (70,90–94). On the other hand, the droplet breakup and coalescence in blends with viscoelastic components are complex events described only approximately. Moreover, the flow field in mixing devices is also complex, which further complicates correct description of the phase structure development (70,92–94).

Deformation of a droplet in a flow field is controlled by the competition of the deforming stress, τ, setting on the droplet by external flow field and the shape conserving interfacial stress, σ/R, where R is the droplet radius (70,90–96). For characterization of the deformation, the dimensionless capillary number, Ca, defined as $Ca = \tau R/\sigma$, is used. Above a critical value, Ca_c, the external stress overrules the interfacial stress, the droplet is stretched and finally breaks into fragments. For Newtonian droplets in a Newtonian matrix, Ca_c is a function of the ratio, $p = \eta_d/\eta_m$, of the viscosities of the dispersed phase and matrix. For blends with viscoelastic components, Ca_c is also a function of their elasticity parameters. A minimum Ca_c was found for η_d/η_m between 0.1 and 1 for shear and extensional flows. At shear flow, Ca_c gradually increases with decreasing p for $p < 0.1$. For $p > 1$, Ca_c steeply increases with increasing p and goes to infinity for $p \approx 3$–4. At extensional flow, the minimum is flat and an increase in Ca_c for high and low p is weak. For flow in mixing devices, the dependence of Ca_c on p lies between those for shear and extensional flow (94). Two main breakup mechanisms were recognized: stepwise, ie, a repeated droplet breakup into two fragments, and transient, where the droplet is stretched into a long fiber that bursts into a chain of small droplets (70,90,92–94,97). It seems that the stepwise mechanism operates for Ca only slightly higher than Ca_c and the transient one for $Ca \gg Ca_c$. Other breakup mechanisms such as tip streaming (or erosion) of small droplets from the surface of deformed droplets and breakup into two main and several satellite droplets were detected (70,94–96). So far, the role of individual breakup mechanisms in complex flow fields generated in mixing devices has not been fully understood, and it is the object of intensive investigation.

Flow-induced coalescence is caused by droplet collisions due to the difference in their velocities (91–94,98–100) (see Fig. 7). The coalescence is usually described in "ballistic approximation," ie, the number of fusions of droplets in a time period is expressed as a product of the number of collisions of noninteracting

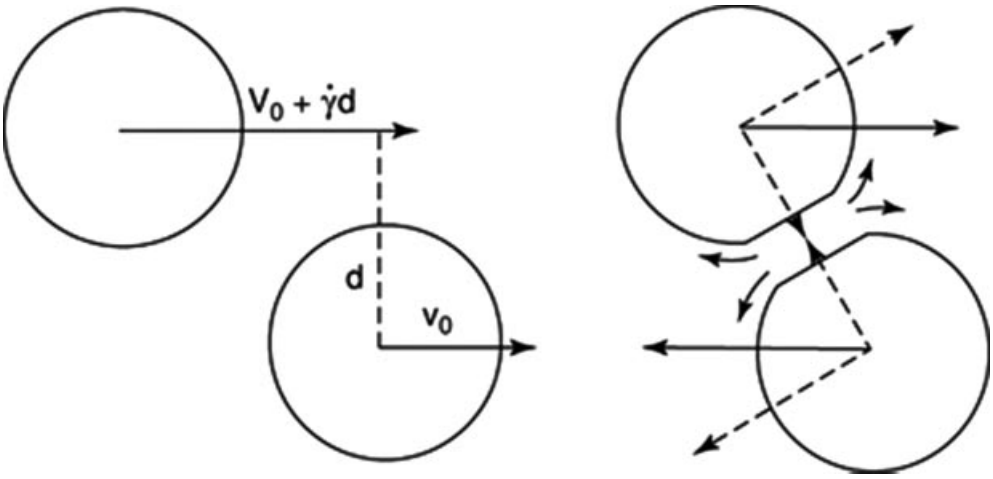

Fig. 7. Shear flow induced coalescence of droplets with the same coordinate in neutral direction. Forces causing droplet approach and rotation in coordinate system moving with the center of inertia are indicating.

droplets and probability, P_c, that the collision will be followed by droplet fusion (91,92,94,100,101). A more or less intensive flattening of the droplets appears during their collision in dependence on properties of the blend components and flow field (100,102). Most calculations of P_c were focused on the case where droplets keep spherical shape during coalescence (102,103) or where the radius of flattened area is substantially larger than interdroplet distance (91,92,100). Unfortunately, the dependences of P_c on system parameters are quite different in these cases. In the former case, P_c is a decreasing function of p and the ratio of radii of large and small droplets and is independent of the average droplet size and deformation rate. On the other hand, in the latter case, P_c is independent of the ratio of droplet radii and depends on average R and the deformation rate. Therefore, inadequate application of any of these extreme cases can lead to a serious misinterpretation of experimental results. Recent calculations (104,105) have shown that for deformable droplets, P_c is given by the value for the spherical particles in the region of small R and steeply decreases at a certain R where a substantial flattening appears (for the shape of P_c, see Fig. 8). It should be mentioned that the so far developed theories describe dilute systems (simultaneous collisions of three and more droplets are not considered) of Newtonian droplets in a Newtonian matrix.

Generally, the distribution of droplet sizes in flow can be obtained as a solution of the generalized Smoluchowski (balance population) equation describing the competition between the droplet breakup and coalescence. Various approximate approaches to the solution of the equation with various expressions for breakup and coalescence frequencies have been used in the literature (101,105–115). For rather long mixing in batch mixers, achievement of a steady state in the droplet size distribution is assumed. For mixing in extruders, development of the droplet

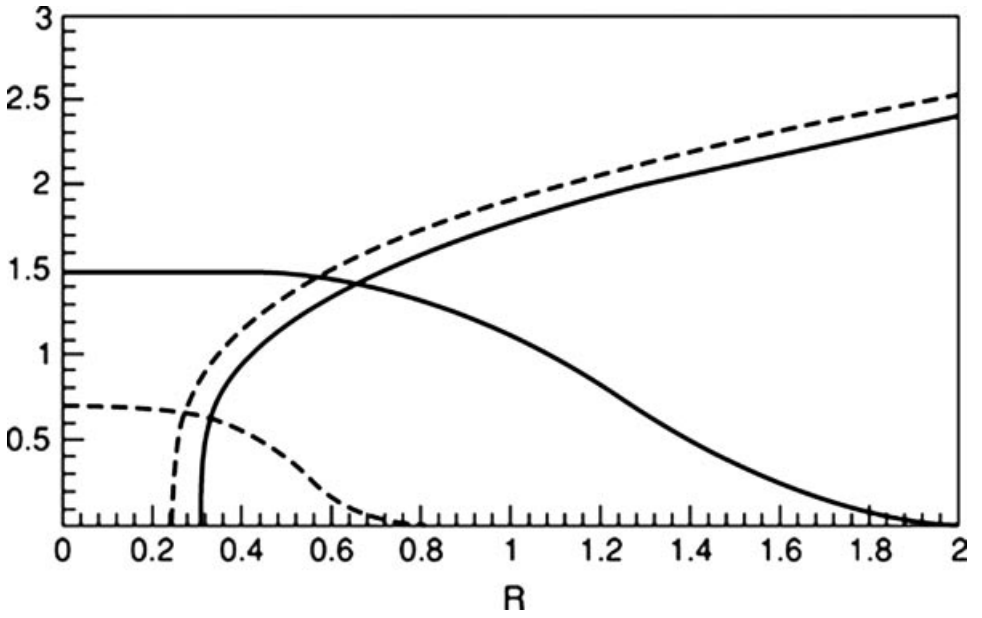

Fig. 8. Scheme of graphic solution of equation 12. Full and broken lines relate to blends with and without a compatibilizer. Y-axis shows $F(R)$ and $(4/\pi)\dot{\gamma}vP_c(R)$ in arbitrary units.

size distribution during throughput in individual zones of the extruders should be studied. A simplified model, where a system of droplets is still monodisperse and breakup leads to a decrease and coalescence to an increase in droplet size, can be helpful in understanding the dependence of average droplet size on parameters of a system (116). The steady droplet radius for this model in shear flow can be calculated from the equation (116)

$$\left(\frac{\mathrm{d}n}{\mathrm{d}t}\right)_{\mathrm{B}} = \left(\frac{\mathrm{d}n}{\mathrm{d}t}\right)_{\mathrm{C}} \Rightarrow F(R) = \left(\frac{4}{\pi}\right)\dot{\gamma} v P_{\mathrm{c}}(R) \tag{12}$$

where $(\mathrm{d}n/\mathrm{d}t)_{\mathrm{B}}$ and $(\mathrm{d}n/\mathrm{d}t)_{\mathrm{C}}$ are changes in the droplet number in a time unit due to their breakup and coalescence, respectively, and the breakup frequency $F(R) = 0$ for $R < R_{\mathrm{c}} = \sigma Ca_{\mathrm{c}}/(\eta_{\mathrm{m}}\dot{\gamma})$. The dependence of F on R for $R > R_{\mathrm{c}}$ has not been well established, and very different expressions have been used in literature (116). It seems, based on recent results, that F increases with R slower than linearly (96, 117). This assumption is in agreement with experiments showing a steeper than linear increase in R with increasing v in a certain blend under constant mixing conditions (70,90,93,94,116). In spite of the approximations used in calculation of P_{c}, the shape of the dependence P_{c} on R is always similar to that in Figure 8. It follows from graphic solution of equation 12, shown in Figure 8, that for R_{c} smaller than R, at which P_{c} falls to very low value, steady state can be achieved during reasonable time. In the opposite case, regions of R exist where only coalescence or practically only breakup occurs.

Under constant mixing conditions, an increase in average droplet radius with increasing volume fraction of the dispersed phase has been observed (70,93,94,99,106,118). The increase is a consequence of the fact that the breakup frequency is in first approximation independent of v, but the frequency of coalescence is an increasing function of v. An increase in interfacial tension leads to an increase in R (118) due to a decrease in Ca. The effect of viscosity ratio, p, can be directly studied by changing η_{d} while keeping η_{m} constant. For a system containing a low v, the effect of p on droplet breakup is decisive and the dependence of R on p for stepwise breakup is controlled by the dependence of Ca_{c} versus p. For a transient breakup mechanism, the situation is different and an increase in p can lead to smaller R also for $p > 1$ (91,92,112). Generally, P_{c} decreases with increasing p. Therefore, a lower R at $v \to 0$ and a steeper increase in R with v should appear for lower p if the stepwise breakup mechanism is decisive. This type of dependency was observed for polypropylene/ethylene-propylene elastomer blends mixed in the chamber of a Plasticorder (94,119). For the transient breakup mechanism, R should be smaller for larger p for all volume fractions of the dispersed phase. If η_{m} is changed at a constant η_{d}, p and Ca are changed simultaneously. In most cases, an increase in η_{m} at constant η_{d} and mixing conditions leads to a decrease in the droplet size in the whole concentration range (94,119). The effect of elasticity of the components has not been fully understood so far. Available experimental results show that the deformation and breakup of droplets more elastic than the matrix are more difficult than in the related Newtonian system (70,120,121). Generally, the dependence of the droplet size on shear stress (mixing intensity) is affected by the concentration of the dispersed phase because R_{c} (R for $v \to 0$) depends on stress (deformation rate) in a different way than P_{c}.

While R in dilute blends typically decreases with increasing stress applied during mixing (94,122–124), in concentrated systems, R is a complex function of system parameters and it can be a decreasing, increasing, or nonmonotonic function of the applied stress (70,94,125,126). Only a weak dependence of R on processing parameters was frequently observed (70,127–129), apparently due to a non-Newtonian character of the matrix, increase in temperature in a mixer at growing mixing rate, and increasing P_c with decreasing R. Usually, quite fine morphology is achieved after a short time of mixing in batch mixers or in first zones of extruders (64–68,70,128–130). On the other hand, large particles of dispersed phase with high viscosity surrounded by material with fine phase structure were found in blends with low interfacial tension (94,131–133). Uniform fine morphology was achieved in these systems only after long and intensive mixing.

Phase Structure Evolution During Annealing. Substantial changes in the phase structure of molten blends of immiscible polymers appear at rest, and are driven by the tendency to achieve a minimum interfacial area. Deformed (elongated) droplets either retract to spheres or break up into smaller fragments. Relaxation occurs by one of several mechanisms, depending on initial deformation (the ratio of long and short semiaxes a/b) and the viscosity ratio (96,134,135). A droplet with the a/b less than approximately 9 retracts to a single sphere. Very elongated droplets (about $a/b > 60$) break up by the capillary wave (Rayleigh) instability, ie, by the transient breakup mechanism mentioned above, into a chain of small droplets. In this case, the amplitude of the perturbation wave grows exponentially with time and the growth rate increases with interfacial tension and decreases with viscosity of both the components and fibril radius (70,91–94,96). For droplets with intermediate deformation, the breakup is dominated by end pinching (96,134,135). Co-continuous structures stay either co-continuous and show increase in the phase size with time or break up into droplet/matrix morphologies (136,137). The breakup of fibers between crossing points of the structure is controlled by the capillary wave mechanism and it can occur if the length of fibers between the crossing points is substantially larger than the fiber thickness. Therefore, the coarsening of co-continuous structures is typical of blends with compositions near 1/1 and their breakup appears for blends with asymmetric compositions. The coarsening rate increases with interfacial tension and decreases with the viscosity of blend components (137). A substantial increase in the size of dispersed particles after annealing in the molten state was found for many polymer blends with particulate morphology (138). Two main mechanisms were suggested: coalescence driven by molecular forces and Brownian motion (139), and Ostwald ripening (140,141). Analysis of these mechanisms showed that the rate of coarsening should increase for coalescence and decrease for Ostwald ripening with increasing interfacial tension (138). A clear increase in the coarsening rate with interfacial tension was found experimentally (138). Moreover, coalescing droplets were detected in some experiments (142,143). Therefore, it seems that the coalescence induced by molecular forces and Brownian motion is the main mechanism of droplet coarsening, at least for blends with moderate or high interfacial tension.

Blends Containing a Compatibilizer.

The Effect of Compatibilizer on a Blend Microrheology. The presence of a compatibilizer at the interface substantially affects the development of the phase structure of molten blends in the flow and quiescent state. The position

and width of the concentration region related to co-continuous morphology are affected by two competing mechanisms. A decrease in interfacial tension caused by a compatibilizer favors the formation and stability of co-continuous structures. On the other hand, the compatibilizer suppresses the coalescence, which is assumed to be a reason for the co-continuity formation (69). Experimentally, narrowing of the concentration region with co-continuous structure was observed for some systems (69,144,145), but no change was found in other systems (69,146,147). Fixation of co-continuous structure in a blend containing 20% of minor component by the addition of a compatibilizer was also observed (148).

The effect of a compatibilizer on fineness of the phase structure can be understood through its effects on droplet breakup and coalescence. The decrease in interfacial tension mentioned above leads to a decrease in the critical droplet radius, R_c, at a constant Ca_c. Generally, Ca_c of a compatibilized blend differs from that of the related binary blend without compatibilizer (149,150). The bulk flow convects the compatibilizer towards the ends of the droplets causing a gradient in interfacial tension along the droplet surface. The lower interfacial tension on the tips promotes tip streaming, tending to reduce Ca_c. On the other hand, Marangoni stresses oppose deformation. An increase in the droplet surface due to deformation leads to compatibilizer dilution and, therefore, to an increase in interfacial tension. The last two effects tend to increase Ca_c (149,150). At breakup by the transient mechanism, a compatibilizer causes an increase in the breakup time due to a decrease in interfacial tension and existence of interfacial tension gradients (149–151). A decrease in interfacial tension due to the presence of a compatibilizer decreases the droplet radius, R, at which the probability of coalescence, P_c, falls to a negligible value. Two other mechanisms contributing to coalescence suppression were proposed (149,152). The first involves immobilization of the interface (suppression of liquid circulation in droplet) due to the Marangoni stress. The Marangoni stress is induced by convection of a compatibilizer out of the gap between approaching droplets, which leads to a gradient of interfacial tension (149,150). The immobilization of the interface decreases P_c for small R. The other mechanism, repulsion of the droplets arises mainly from the compression of the compatibilizer block extending into the matrix phase (149,152). This mechanism is applied only if the dilution of a compatibilizer in the gap between droplets is not large. The effect of a compatibilizer on the breakup frequency and P_c (decrease in interfacial tension and the Marangoni effect are considered) is schematically illustrated in Figure 8. Figure 8 shows that the situation when steady state is not achieved is more probable for blends with a compatibilizer. In the calculation of steady R, changes in interfacial tension induced by changing interfacial area in droplet breakup and coalescence should be considered (153). The above effect can be quantified if the distribution of a copolymer between the interface and bulk phases, relationship between copolymer concentration at the interface and interfacial tension, and the rate of copolymer migration along the interface and between the interface and bulk phases are known.

Effect of the Compatibilizer Architecture. Compatibilization efficiency of various copolymers follows from their thermodynamic and microrheological effects. It has been generally accepted that the total molecular weight of the copolymer, molecular weight of its blocks and their number are the main structural compatibilizer characteristics affecting the phase structure of the final blend.

Contradictory results have been published on the effect of block copolymers with different numbers of blocks. In some papers, diblock copolymers have been found more efficient compatibilizers than triblock copolymers (51,154,155), whereas in several other studies, the opposite results have been obtained (156–158). Still others state that there is no difference between diblocks and triblocks (159). Some more recent articles show the compatibilizing efficiency of multiblock (tetrablock, pentablock, heptablock) copolymers (160–162), which seems to be supported also by some theoretical studies (163,164).

It has been believed that proper molecular weight of the copolymer blocks should be close to that of the relevant homopolymer. However, some results show that copolymers with differing lengths can be efficient compatibilizers. A complex situation also occurs when the copolymer blocks are not chemically identical with homopolymer chains, but only similar, and thus they exhibit limited miscibility. The complexity of these issues have been shown in a number of studies.

Thus Xu and Lin (154) successfully compatibilized a high molecular weight blend of *i*PS and *i*PP with a *i*PS-*i*PP diblock copolymer, where the molecular weight of both blocks amounted to 150,000. Feng (165) has shown that for PS/polyolefin blends, even PE-*g*-PS graft copolymers can be suitable compatibilizers.

Cavanaugh and co-workers (166) have studied the compatibilization efficiency of various styrene-butadiene copolymers in polystyrene (PS, M_w = 202,000)/polybutadiene (PB, M_w = 320,000) blends. The most effective compatibilizer proved to be a long, asymmetric diblock (M_w = 182,000; PS content 30%), which could entangle in both homopolymer phases. Short diblock copolymers and most of the random copolymers were inadequate as interfacial agents. Moderate improvement in impact strength was observed for a S-B multiblock.

The effects of the block length and block number in linear S-B block copolymers on compatibilization efficiency in low molecular weight PS/PB blends were studied also by Horák and co-workers (167). For this detailed stucture study, PS (M_w = 40,000), PB (M_w = 60,000), and di-, tri-, and pentablock S-B copolymers, having M_w of the PS block either 10,000 or 40,000, were prepared. Besides standard slow cooling, also quenched samples, having the structure close to that of the molten state, were prepared. It shows that in quenched samples, all block copolymers, with an exception of large 40S–60B–40S, are molecularly dispersed (probably at the PS/PB interface). Escape of the S-B copolymers from the interface is observed for the copolymers having short PS blocks, while the copolymers with long PS blocks remain a part of the PS/PB interfacial layer, and this phenomenon manifests itself by the formation of a finer morphology and better stress-transfer properties than in blends containing S-B copolymers with short PS blocks.

Segregation of a poly(2-vinylpyrrolidone-*block*-styrene-d_8-*block*-2-vinylpyrrolidone) (PVP-dPS-PVP) triblock and dPS-PVP diblock copolymers between the PS and PVP homopolymers was studied by Dai and co-workers (169). Both the block copolymers show an increase in the interfacial excess beyond the saturation plateau, due to condensation of copolymer micelles adjacent to the PS/PVP interface in the PS phase (Fig. 9). A significantly lower critical micelle condensation (CMC) was determined for the triblock copolymer when compared with the diblock. While the condensation of the diblock copolymer micelles at the PS/PVP surface occurs above the CMC, no such preferential segregation is observed for the triblock copolymer.

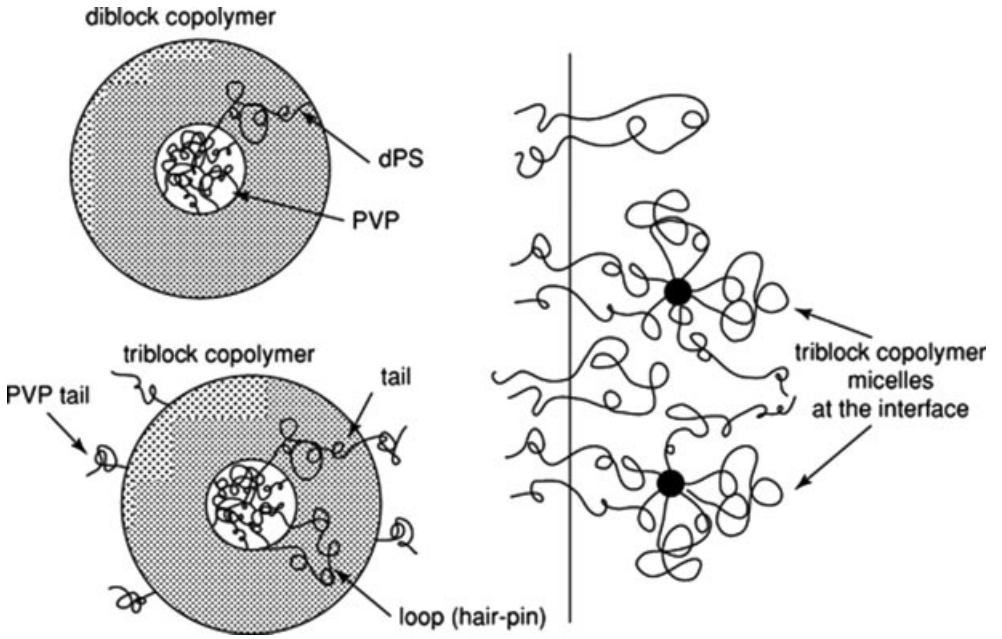

Fig. 9. Condensation of PVP-dPS-PVP triblock copolymer micelles adjacent to the PS/PVP interface in the PS phase. Schematics of (left) the isolated micelle structure for diblock and triblock copolymers and (right) triblock copolymer micelles adsorbed onto an interfacial brush of triblock copolymers.

The compatibilization process becomes more complicated when one of the copolymer blocks is not completely miscible with the corresponding blend component, ie, interaction parameter $\chi > 0$. This problem has been studied in polystyrene (PS)/polyolefin (PO) blends compatibilized with various block copolymers, consisting of styrene and aliphatic hydrocarbon sequences different from the used polyolefin (161,162,168,170–173). It was found that in these blends, the most important factor controlling localization of the block copolymers at the PS/PO interface is the length of the styrene block in the block copolymers. Copolymers having the styrene blocks long enough to form entanglements with the styrene homopolymer in the blend, are entrapped in the final compatibilized blends in this phase. Hence, their transport to the PS/PO interface is difficult and their compatibilization efficiency is low. Critical molecular weight for the formation of the entanglements of PS chains, $M*$, cca 18,000 was determined (174,175). Surprisingly, in these blends, block copolymers with "long" styrene blocks are less efficient compatibilizers than those with "short" blocks.

Also the interfacial layer between the homopolymers differs in A/B + A-*block*-B' blends from that in A/B + A-*block*-B blends. In blends compatibilized with block copolymers having the corresponding blocks miscible with the blend components, they are supposed to be molecularly dispersed to a high degree at the A/B interface (Figs. 9, 3). In A/B/A-*block*-B′ blends, block copolymers with "short" A blocks are localized at the A/B interface as well, but they do not lose their ordered supermolecular structure (Fig. 10). Block copolymers having "long" A blocks are

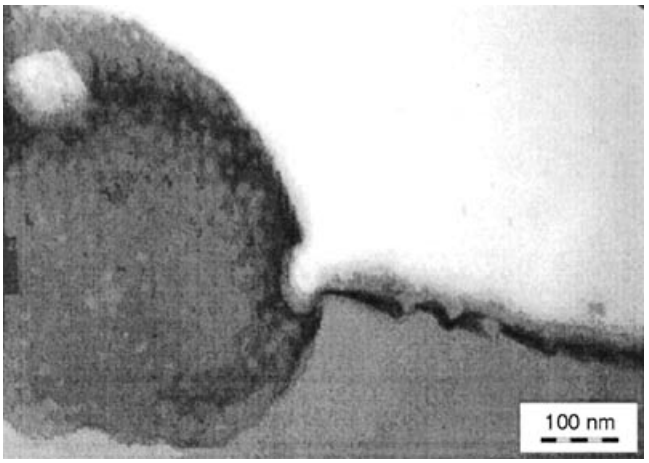

Fig. 10. TEM micrographs of the interface in PS/PP (4/1) blend with addition of 10S-60B-10S block copolymer.

entrapped in the A homopolymer in the form of micelles or small particles, swollen by homopolymer chains (Fig. 11**a**). Additional annealing of these blends leads to pronounced migration of the entrapped copolymers to the A/B interface (Fig. 11**b**) and improvement of mechanical properties. On the other hand, coalescence and worsening of the A/B interface coverage were observed in annealed blends on addition of copolymers having "short" styrene blocks (168). In general, morphology of the A/B/A-*block*-B′ blends depends on the conditions of blend mixing and processing, and cannot be predicted using only the rules of equilibrium thermodynamics. This dependence on the processing conditions is more pronounced in blends with an excess of the A phase, ie, of the homopolymer that is fully miscible with one block of the block copolymer used (168).

Different behavior of block copolymers having blocks miscible with the corresponding homopolymers and those where one block differs chemically from the

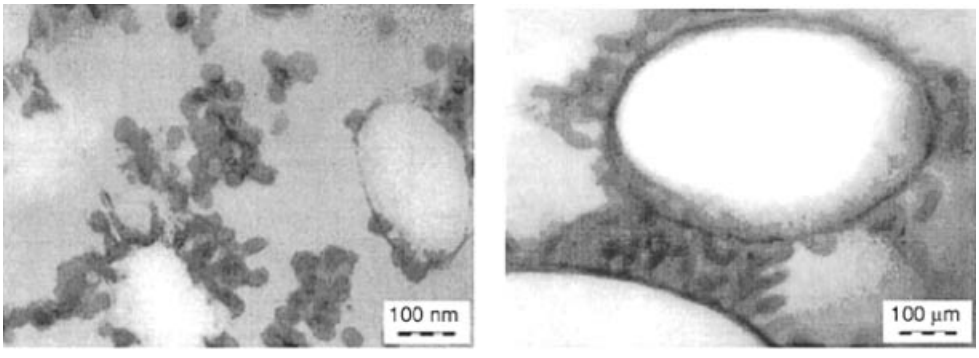

Fig. 11. TEM micrographs of the interface in PS/PP (4/1) blend with addition of 40S-60B-40S block copolymer: (**a**) as prepared sample; (**b**) annealed sample.

homopolymer was observed also by other authors. Barlow and Paul (176) and Appleby and coworkers (157) reported remarkable improvement of ductility and impact or tensile strength in PS/PP blends compatibilized by the commercial material Kraton G1652. This poly(styrene-*block*-ethene-*co*-butene-*block*-styrene) (S-EB-S) triblock copolymer has an M_n value of one PS block approximately equal to 8,000, that is, considerably below the critical value $M*$ necessary for the entanglement formation. Tjong and Xu (177) found that the presence of this BC in PS/high density polyethylene blends leads to increased adhesion between the two phases as well as decreased particle dispersion. Cigana and co-workers (178) observed improvement of mechanical properties in PS/ethene-*co*-propene rubber blends (PS/EPR) with Kraton G1652, unlike with the S-EB-S triblock copolymer, where the molecular weight of the S block was about 24,000 (Kraton G1651).

In the PS/EPR blends, Radonjič and co-workers (179) found the S-B-S triblock copolymer with M_n of the PS blocks of 7,000, to be localized at the PS/EPR interface. The compatibilization efficiency of this block copolymer was further confirmed by finer dispersion in the resulting PS/EPR/S-B-S blends, as well as by improved PS/EPR adhesion. This short triblock copolymer appears to be a good compatibilizer also in *i*PP/*a*PS blends. According to Šmit and Radonjič (180), S-B-S forms an interfacial layer between dispersed honeycomb-like PS/S-B-S particles and PP matrix and influences also crystallization in *i*PP.

Hence, the compatibilization efficiency of block and graft copolymers is influenced by many factors, such as their chemical composition with respect to the character of the corresponding blend components, the number of the blocks, their molecular weights, and consequently, the total molecular weight. Also, in blends where one block of a compatibilizer is not miscible, but only compatible with, the corresponding blend component, achievement of thermodynamic equilibrium can be difficult, as it depends on the processing conditions. However, it seems that triblock copolymers can be considered the most efficient compatibilizers for most of the blends studied.

We can conclude that despite extensive studies performed during more than three decades, no reliable rules for the prediction of the effect of molecular characteristics of block copolymers on the structure and properties of polymer blends have been formulated to date.

Effect of Compatibilizer Concentration. The compatibilizing efficiency of the copolymers is, besides the architecture, a function of their concentration. The effect of a compatibilizer concentration has been quantitatively characterized by the emulsification curve—the dependence of the average particle diameter of the minor dispersed phase on copolymer concentration (70). The particle diameter decreases with increase of copolymer concentration until a constant value is obtained. For most systems, this value is achieved if the copolymer amount is 15–25% of the dispersed phase. There are systems where saturation was detected only at substantially higher concentration of a copolymer (181).

Structure Determination of Polymer Blends. Properties of polymer blends are closely associated with their structure on several scale levels, such as crystallinity and supermolecular structure of the blend components, and, of course, morphology of the final blend. Thus, a series of methods that enable one to characterize these different structure parameters should be employed, including WAXS, SAXS, SANS, SEM, TEM, LS, and DSC.

Wide angle X-ray scattering (WAXS) affords information on the level of interatomic distances, ie, this method can be used for determination of crystalline modification in partially crystalline polymers, degree of crystallinity. Also, dimensions of the crystallites can be estimated from the width of the crystalline reflections (182). Small-angle X-ray scattering (SAXS) experiments lead to determination of supermolecular structure, such as ordered two-phase separation in block copolymers (183,184), long period in semicrystalline polymers (185), or micellar structure (186,187). Classic experimental techniques used in SAXS have been reviewed by Stein (188). Small-angle neutron scattering (SANS), a related and often complementary method to SAXS, is also a very useful tool for determination of supermolecular structure in polymer blends (189). Moreover, by using SANS, interactions in polymer blends can be studied if one of the blend components is deuterated in order to obtain scattering contrast (190). Recently an ultrasmall-angle neutron scattering spectrometer (USANS) was developed (191), lifting the upper resolution limit of SAXS and SANS instruments by an order of magnitude, and thus permitting an overlap with light scattering techniques.

The most suitable and comparatively rapid method used for determination of the morphology of polymer blends appears to be electron microscopy. Techniques employed in scanning electron microscopy (SEM) have been reviewed by Shaw (192). In addition to the use of SEM for determination of particle size and shape in a blend, and adhesion between the blend components (193, Fig. 12), evolution of the structure based on the processing conditions and blend homogeneity can be quickly studied (194, Figs. 13, 14). Transmission electron microscopy (TEM) is a much more time-consuming method. Polymer samples need to be stained with OsO_4 or RuO_4 in order to obtain sufficient contrast, and in addition, very thin sections are necessary (195,196). The simplest result obtained by means of TEM is, similarly to SEM, description of the blend morphology. However, there is a wider scale of possibilities, such as localization of a block copolymer used as a compatibilizer in blends of immiscible polymers (197). Chi-An Dai and co-workers (198) published a study of the morphology development of poly(2-vinyl pyrrolidone)-*block*-(deuterated polystyrene)-*block*-poly(2-vinyl pyrrolidone

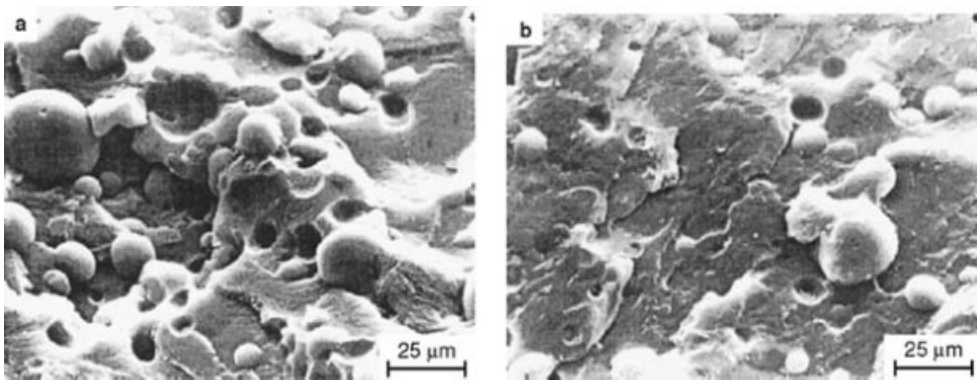

Fig. 12. Scanning electron micrographs of cryofractured surfaces of HDPE/HIPS (80/20) blend with H77 copolymer concentration of: (**a**) 0 wt%, (**b**) 5 wt%.

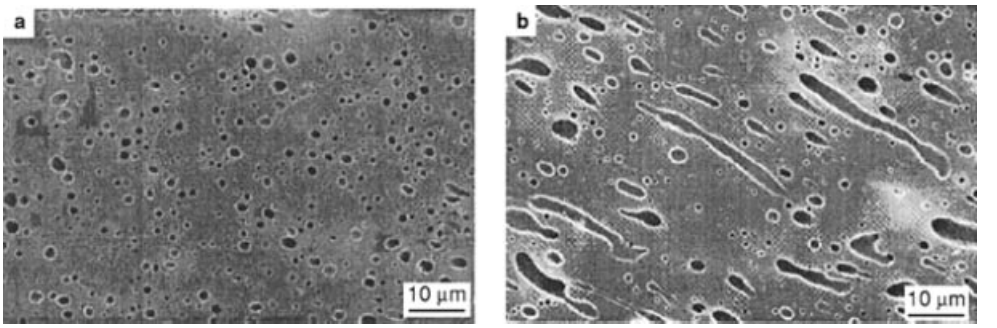

Fig. 13. Phase structure of PP/PS/SBS (71/24/5) blends mixed in microextruder at 250°C for 2 min: (**a**) small particles; (**b**) large particles.

(PVP-*block*-dPS-*block*-PVP) triblock copolymer at the PS/PVP interface, observed by TEM (Fig. 15).

Light scattering can be used for determination of the blend morphology, not only in the solid, but also in the molten state (199,200). This method was successfully used in detection of phase transitions in polymer blends, and in determination of changes in droplet size in immiscible polymer blends due to breakup and/or coalescence. In comparison with microscopic methods, scattering methods can easily examine larger blend volume, and therefore, give more reliable average values of morphological parameters. On the other hand, microscopic methods provide more straightforward and complex information (201).

Differential scanning calorimetry (DSC) is used especially for discrimination between miscible and immiscible polymer blends (202). One T_g depending on blend composition indicates a miscible system, two T_g coinciding with related T_g of the components indicate an immiscible blend, and two T_g shifted to the direction of their average is typical of partially miscible systems.

As polymer blends are very complex systems, a combination of different methods for complete description of their structure is of great importance. Several examples of typical combinations are described below.

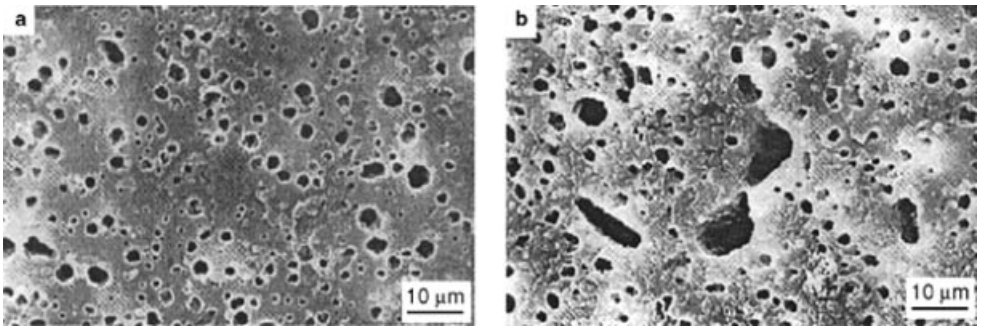

Fig. 14. Phase structure of PP/PS/SBS (71/24/5) blends mixed in microextruder at 250°C for 20 min: (**a**) smaller particles; (**b**) larger particles.

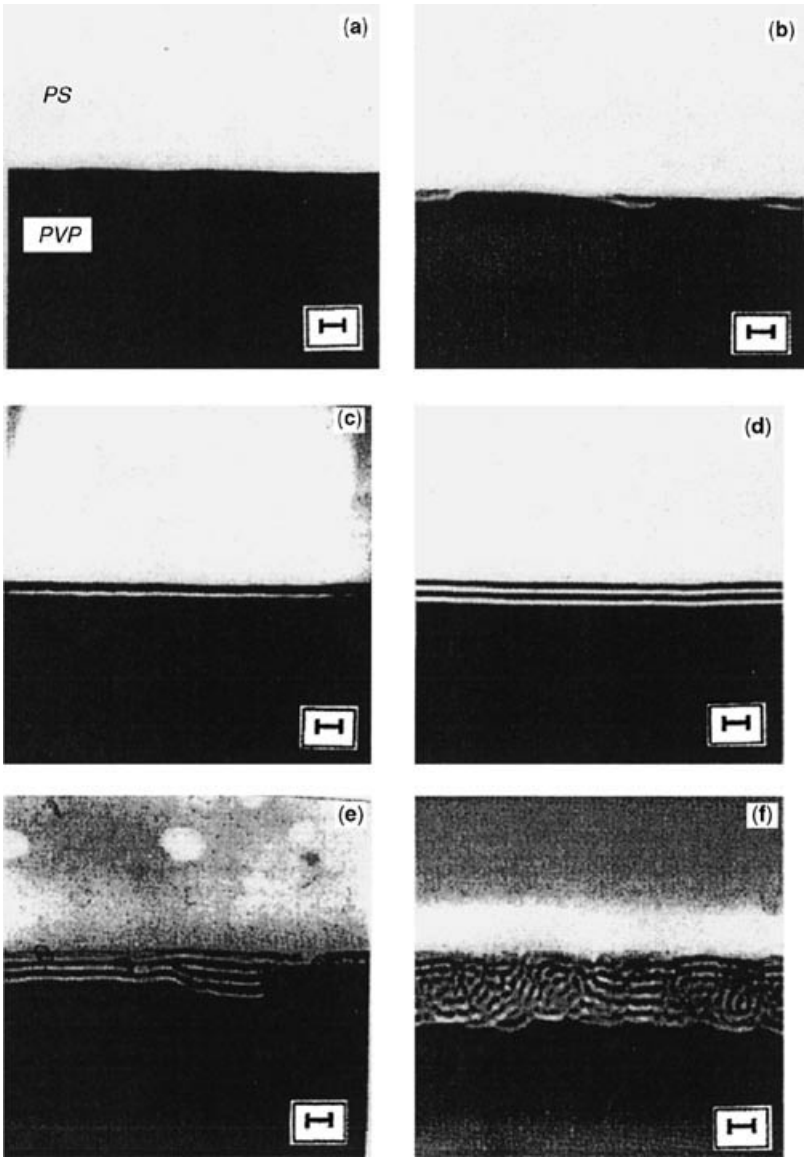

Fig. 15. TEM micrographs of the morphology of the PVP-dPS-PVP triblock copolymer microstructure near the interface for (**a**) area chain density, $\Sigma = 0.09$, (**b**) $\Sigma = 0.17$, (**c**) $\Sigma = 0.22$, (**d**) $\Sigma = 0.4$, (**e**) $\Sigma = 0.6$, (**f**) $\Sigma = 1.0$ chains/nm^2. Note that disordered lamellae are found for $\Sigma > 0.6$ chains/nm^2. The bar scale denotes 100 nm.

Combination of WAXS and SAXS is a very efficient way of detailed description of crystallization in blends of semicrystalline polymers. Baldrian and co-workers (203,204) has studied isothermal melt crystallization of blends of low molecular weight poly(ethylene oxide) (PEO) and poly(methyl methacrylate) (PMMA) using time resolved SAXS/WAXS measurements on the ELETTRA synchrotron (205). He has reported the formation of unstable PEO lamellae of nonintegrally folded

chains at the very beginning of crystallization and subsequent transformation of these lamellae into stable PEO crystals with one-folded or extended chains. Amorphous PMMA plays a decisive role in structure development. A similar study was performed by Campoy and co-workers (205) with polyamide (PA6) and the liquid-crystalline copolyester Vectra using calorimetric data and X-ray diffraction.

Structure development in blends of polyaniline doped with camphor sulfonic acid (PANI-HCSA) and PA was studied by Hopkins and co-workers (206) using SAXS and SANS. At 3 vol% PANI loading concentration, salt domains with characteristic length of 22 nm are expected to be present in the blend with PA12. This differs from the blend of PA6 where a fractal geometry was found. For higher salt concentrations, no simple structural model was found.

Wignal and co-workers (207) investigated phase separation of linear (high density) and short-chain branched (linear low density) polyethylenes (HDPE/LLDPE) by of combination of SAXS, SANS, DSC, and TEM. According to SANS, this blend is homogeneous in the melt when the ethyl branch content in LLDPE is low, but due to the structural and melting point differences between HDPE and LLDPE, the components may phase-separate in the solid state.

Block copolymers, usually used as compatibilizers in additive compatibilization, are very often organized in an ordered supermolecular structure, which manifests itself by an interference maximum in the region of SAXS (183,184). The compatibilization efficiency of a block copolymer is associated with its interaction with the blend components, and consequently, with the changes of its supermolecular structure. Hence it is convenient to begin the study of its structure in compatibilized blends using SAXS. Additionally, SAXS gives information on a comparatively large sample volume, even if the information concerns the reciprocal space. Microscopic methods show the real structure, but of a very small part of the sample, which can be inhomogeneous. Thus, combination of scattering and microscopic methods appears to be a very useful for investigation of the compatibilization process. Moreover, TEM and SEM experiments are relatively time consuming, while measurement of one SAXS curve takes several minutes. Thus, it is possible to check samples obtained under preparation conditions, when the steady state is achieved by comparison of SAX curves. Then, several selected samples can be studied by electron microscopic methods (168). Kinning shows in his study (208) a very instructive comparison of different orderings of a styrene-butadiene block copolymer in a styrene homopolymer, obtained by TEM together with corresponding SAXS curves (Figs. 16, 17)

Physical Properties of Polymer Blends

Preparation of heterogeneous polymer blends ranks among the effective ways of upgrading polymers and preparing new cost-effective materials. Tensile modulus, E_b, or shear modulus, G_b, tensile yield strength, σ_{yb}, tensile strength (stress at break), σ_{ub}, fracture resistance, permeability, P_b, to gases and vapors, etc. are viewed as very important physical properties that simultaneously predetermine possible applications of the blends of industrially useful polymers. Phase structure (morphology), which depends on blend composition, relative viscosities of components, interfacial energy, mixing machine and adopted conditions of the mixing

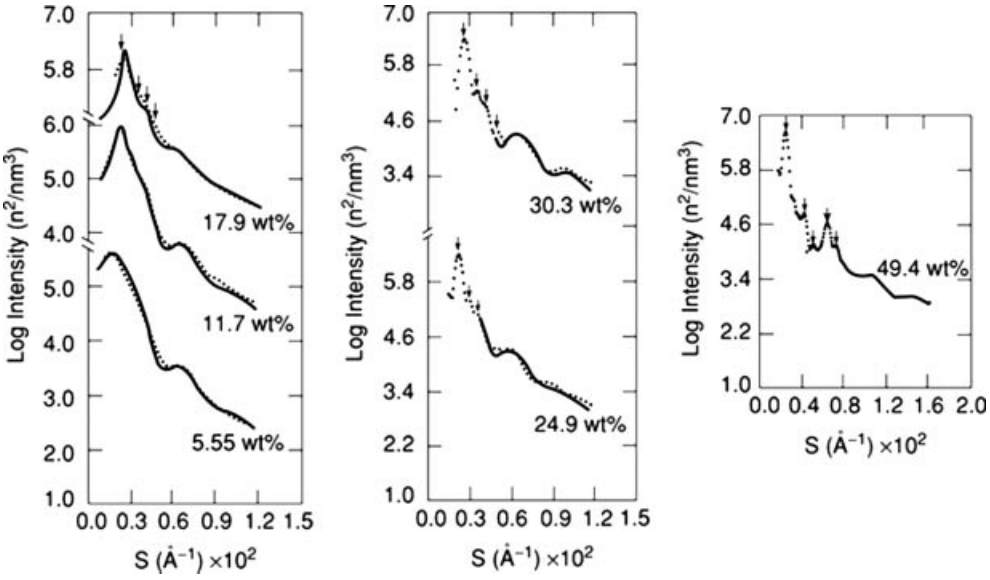

Fig. 16. SAXS curves of blends consisting of copolymer SB 20/20 in 3900 PS homopolymer at various copolymer concentrations.

process, annealing, reprocessing, etc., is essential for the properties of heterogeneous melt-mixed blends consisting of immiscible or partly miscible polymers (209,210). As the phase structure of a blend formed in a mixing machine does not correspond to a state with the lowest Gibbs free energy, the phase structure

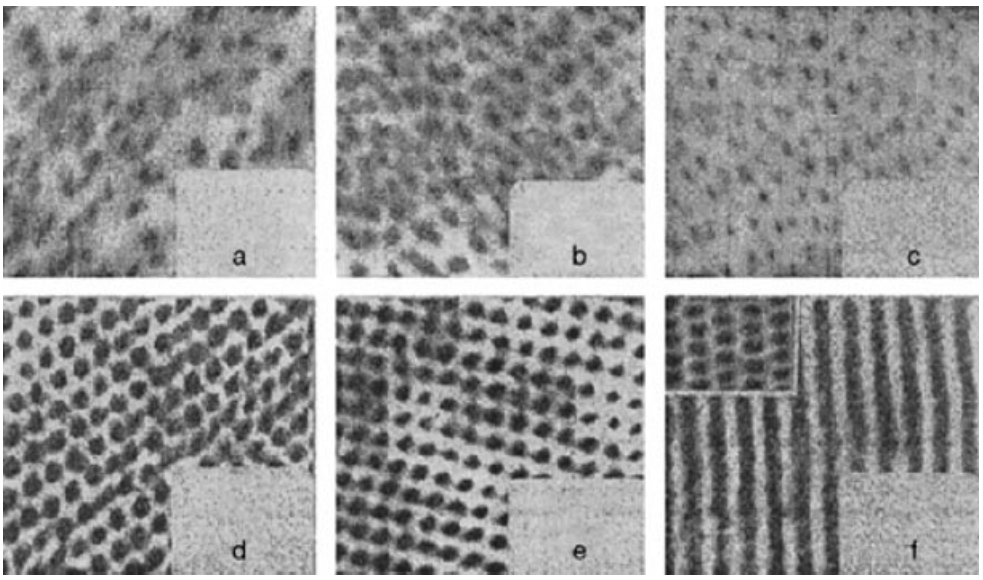

Fig. 17. Transmission electron micrographs of blends containing copolymer SB 20/20 in 3900 PS homopolymer. Copolymer concentrations are (**a**) 5.55 wt%, (**b**) 11.7 wt.%, (**c**) 17.9 wt%, (**d**) 24.9 wt%, (**e**) 30.3 wt%, and (**f**) 49.4 wt%. The bar scale denotes 100 nm.

coarsening begins to take place immediately after completion of the mixing process and is stopped only by freezing-in the melt. The coarsening process is reinitiated whenever blends are heated to processing temperatures in the course of following operations, such as injection or compression molding, reprocessing, and quiescent annealing. In practice, the coarsening is undesirable phenomenon because it usually accounts for deterioration of physical (mechanical) properties of annealed or reprocessed blends.

Heterogeneous blends of immiscible or partially miscible polymers are isotropic heterogeneous materials with three-dimensional spatial continuity of one or more components (69,211). In binary blends, the co-continuity (duality) of constituents occurs in the central composition interval delimited by the critical fractions, v_{1cr} and v_{2cr}, of the components (69,78,212,213). From the viewpoint of mechanical properties, blends can be divided into two basic categories: (1) at $v_1 < v_{1cr}$ or $v_2 < v_{2cr}$, the minority component is dispersed as spherical particles in the continuous majority component (matrix); (2) at $v_1 > v_{1cr}$ and $v_2 > v_{2cr}$, both components become partially continuous. As soon as the volume fraction of a component exceeds v_{cr}, continuous entities are formed in the mixed blend, but a spectrum of particles still coexists. With increasing volume fraction, the degree of continuity (continuity index) of the component increases, so that in a narrower interval delimited by the volume fractions $v_{1dl} > v_{1cr}$ and $v_{2dl} > v_{2cr}$, both components are fully co-continuous (213–215). The coarsening process manifests itself by narrowing the interval of the phase duality and/or by an increase in the particle size of the minority component. Physical properties of solid heterogeneous blends primarily depend on respective properties of the components, frozen-in phase structure, and interfacial adhesion. Typical dependencies of physical properties on the blend composition are schematically visualized in Figure 18.

Predictive Formats for Selected Physical Properties of Polymer Blends. Tailoring of heterogeneous polymer blends with balanced physical properties for specific applications is a frequent task of materials engineering. A great number of heterogeneous polymer blends have been studied and reported in available literature. A review of empirical knowledge gathered so far is beyond the scope of this basic treatment. Instead, the existing means applicable in projecting polymer blends will be outlined. To reduce experimental time and costs of a blend development, it is highly desirable to have reliable formats for the prediction of considered physical properties, eg, E_b, σ_{yb}, σ_{ub}, P_b. Although modeling and simulations cannot fully replace experimental investigation, their role in the designing and structural analysis of blends is ever increasing.

Physical properties of blends consisting of a continuous matrix and one or more dispersed (discrete) components can be predicted by using adapted models proposed for particulate composite systems (216–220). Most of these models do not consider effects of the particle size, but only of volume fractions of components in the system. Thus, the increase in particle size due to particle coalescence is not presumed to perceptibly affect mechanical properties, except for fracture resistance, which is controlled by particle size and properties of dispersed rubbers. As polymer blends with three-dimensional continuity of two or more components are isotropic materials, simple parallel or series models or models for orthotropic or quasi-isotropic materials are not applicable. Physical properties of blends with partially co-continuous constituents can be calculated by means of a predictive

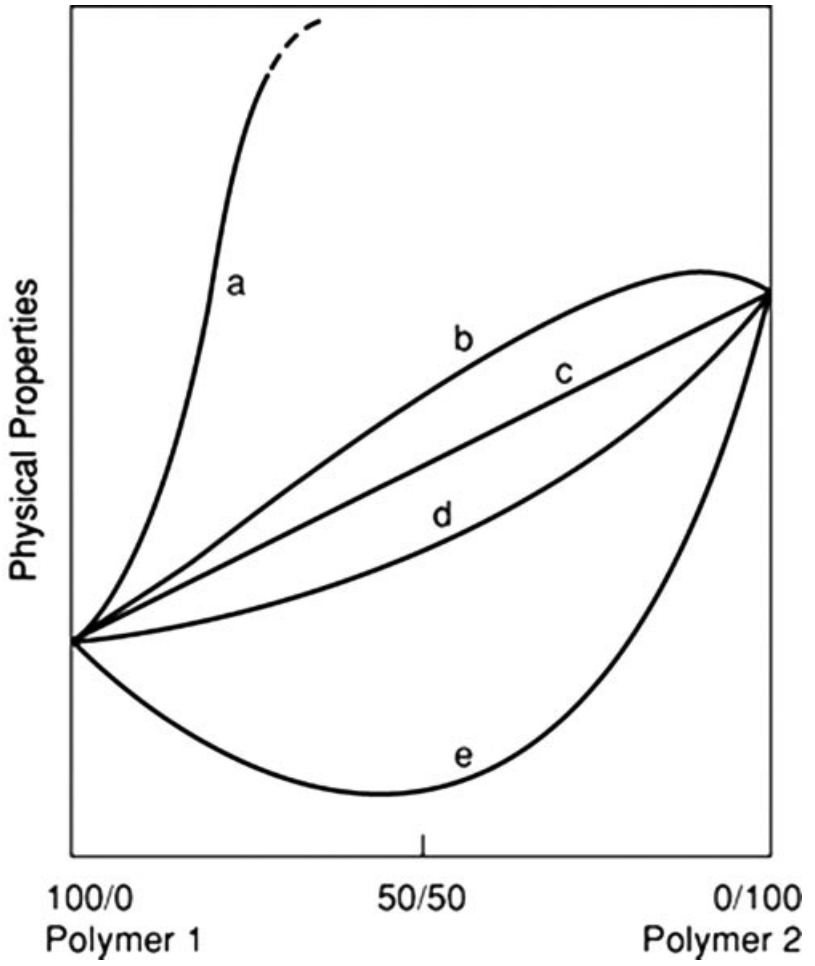

Fig. 18. Effect of the composition of heterogeneous binary blends on their physical properties (schematically). (**a**) Fracture resistance, toughness and impact resistance of commercial rubber-toughened polymers; (**b**) modulus and tensile (yield) strength of blends consisting of partially miscible polymers; (**c**) density (straight line corresponds to the rule of mixtures); (**d**) modulus, compliance, tensile yield strength, stress at break, permeability to gases, thermal conductivity of compatible blends with good interfacial adhesion; (**e**) tensile yield strength and stress at break of blends with poor interfacial adhesion; fracture and/or impact resistance of nontoughened blends.

format (221–223) based on a two-parameter equivalent box model (EBM) (Fig. 19) and modified equations rendered by the percolation theory for two-component systems (78,212,224–227). This combination is necessitated by the fact that the EBMs are not self-consistent models. The EBM assumes that either component consists of a fraction continuous in the direction of the acting force (v_{1p} or v_{2p}) and a fraction discontinuous in that direction (v_{1s} or v_{2s}). In this concept, the lines of force do not cross any interface in the fractions v_{1p} and v_{2p}, while the phase continuity is completely disrupted in the fractions v_{1s} and v_{2s}, where all

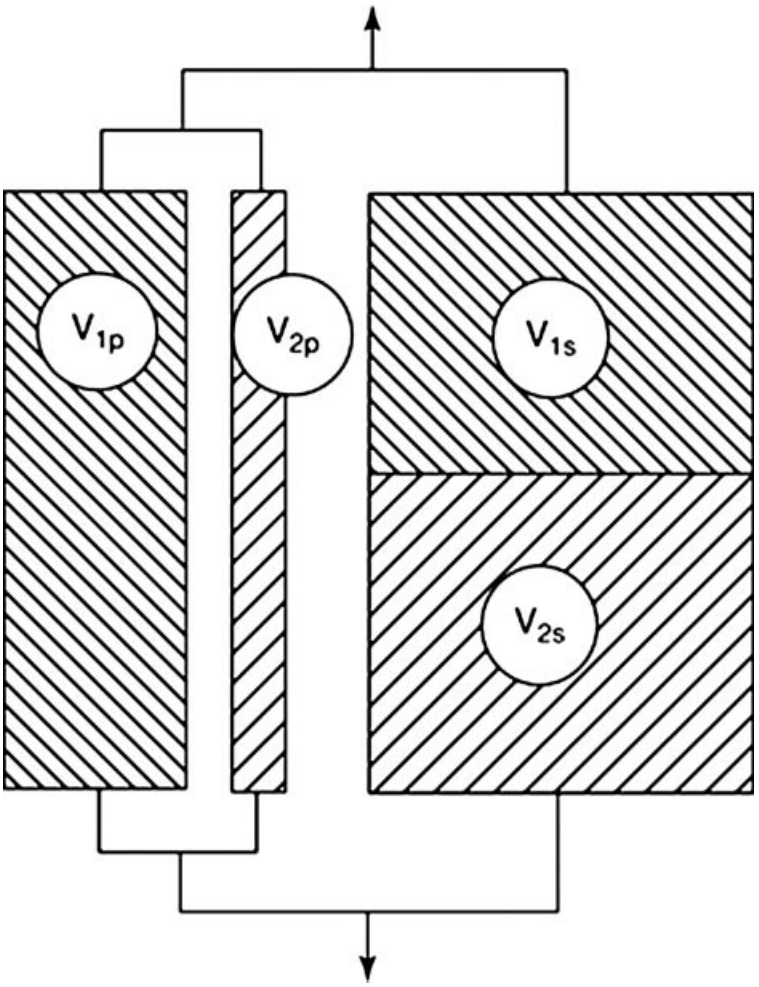

Fig. 19. Equivalent box model for a heterogeneous binary blend (schematically).

stress is transmitted through the present interfaces. (Obviously, the continuity of blend components evaluated by means of extraction methods (69,210,228) has a different meaning). The predictive format takes into account (i) the respective properties of components, (ii) the co-continuity interval of components, (iii) interfacial adhesion and (iv) partial miscibility (if any) of components. Application of the EBM to the prediction of physical properties of blends requires (1) calculation the volume fractions v_{ij} and (2) derivation of equations for the properties under consideration in terms of the EBM. Simultaneously predicted physical properties of blends are interrelated because they are calculated by using an identical set of input parameters characterizing a certain phase structure. The model is likely to fail if the blending process produces a significant change in the structure (eg, in crystallinity), and consequently, in the considered properties of one or both constituents.

Calculation of the Volume Fractions in the EBM. The EBM is a two-parameter model because out of four volume fractions v_{ij}, only two are independent; the volume fractions visualized in Figure 19 are interrelated as follows:

$$\nu_1 = \nu_{1p} + \nu_{1s}; \nu_2 = \nu_{2p} + \nu_{2s}; \nu_1 + \nu_2 = \nu_p + \nu_s = 1 \tag{13}$$

The percolation theory (224–227) provides a universal formula for some physical properties of binary systems (modulus, permeability) where the contribution of the second component is negligible. The formula has been experimentally shown (212,229) to plausibly fit the modulus of model blends with $E_1 \gg E_2$ in the range $v_{1cr} \leq v_1 \leq 1$. Modifying this approach for binary blends, the following equations were derived (221–223):

$$\nu_{1p} = [(\nu_1 - \nu_{1cr})/(1 - \nu_{1cr})]^q, \tag{14a}$$

$$\nu_{2p} = [(\nu_2 - \nu_{2cr})/(1 - \nu_{2cr})]^q \tag{14b}$$

where q is the critical exponent. The remaining v_{1s} and v_{2s} are evaluated by using equation 13. The theoretical critical volume fraction (percolation threshold) $v_{cr} = 0.156$ was calculated (78,219,226,227) for random spatial array of discrete spherical domains. Most reported values of q are located in the interval 1.6–2.0, which complies well with the theoretical prediction (224,227) or $q = 1.8$. In a first approximation, "universal" values $v_{1cr} = v_{2cr} = 0.156$ and $q = 1.8$ can be employed in the EBM, which may provide a good prediction for blends whose components show similar viscosity and elasticity under mixing conditions. Experimental values of v_{1cr} and/or v_{2cr} have usually been found in the interval 0.15–0.25; however, extreme values around 0.03 or 0.46 have also been observed (230). Any considerable change in viscosity of one component influences both v_{1cr} and v_{2cr} (230,231), wherein the component with lower viscosity exhibits a stronger tendency to continuity, which manifests itself in a lower v_{cr} and an asymmetric interval of the phase duality. Owing to enormous complexity, only recently has a quantitative prediction of v_{cr} been attempted (213), which operates with rheological characteristics of components and of the blending equipment. Despite a number of simplifying assumptions, it provides useful guidelines for minimizing v_{cr} of one component in binary blends. In the marginal zone, $0 < v_1 < v_{1cr}$ (or $0 < v_2 < v_{2cr}$), where only component 2 (or 1) is continuous, simplified relations can be used for the minority component in the EBM, ie, $v_{1p} = 0$, $v_{1s} = v_1$ (or $v_{2p} = 0$, $v_{2s} = v_2$), to obtain an approximate prediction of physical properties.

Moduli of Binary Heterogeneous Blends. A linear stress–strain relationship, indispensable for modulus measurements, is granted only at very low strains, typically below 1%, where virtually all blends show interfacial adhesion sufficient for transmission of acting stress. At strains exceeding the linearity limit, blend modulus (or compliance) decreases (or rises) with the strain. The tensile modulus of a two-component blend (Fig. 19) is given as (222)

$$E_b = E_1\nu_{1p} + E_2\nu_{2p} + \nu_s^2/[(\nu_{1s}/E_1) + (\nu_{2s}/E_2)] \tag{15}$$

where $v_s = v_{1s} + v_{2s}$. Along with the tensile modulus from stress–strain measurements (Fig. 18, curve d), the storage modulus E_b' and the loss modulus E_b'' are frequently used. Dynamic mechanical thermal analysis (DMTA) at a constant frequency is the case of steady state harmonic conditions to which the elastic-viscoelastic correspondence principle is applicable (232). Thus, isochronous DMTA is a method allowing the use of the models for elastic materials also for viscoelastic materials by replacing elastic constants by complex (viscoelastic) counterparts (233,234). Introducing $E_1* = E_1' + iE_1''$, $E_2* = E_2' + iE_2''$ and $E_b* = E_b' + iE_b''$ into equation 15 and separating real and imaginary terms, one obtains

$$E_b' = E_1' v_{1p} + E_2' v_{2p} + v_s^2 N'/M \tag{16a}$$

$$E_b'' = E_1'' \nu_{1p} + E_2'' \nu_{2p} + \nu_s^2 N''/M \tag{16b}$$

where

$$N' = \nu_{1s} E_1' \left(E_2'^2 + E_2''^2\right) + \nu_{2s} E_2' \left(E_1'^2 + E_1''^2\right) \tag{17a}$$

$$N'' = \nu_{1s} E_1'' \left(E_2'^2 + E_2''^2\right) + \nu_{2s} E_2'' \left(E_1'^2 + E_1''^2\right) \tag{17b}$$

$$M = \left(\nu_{1s} E_2' + \nu_{2s} E_1'\right)^2 + \left(\nu_{1s} E_2'' + \nu_{2s} E_1''\right)^2 \tag{17c}$$

A possible occurrence of an additional mechanical transition (loss peak) in the dynamic mechanical spectrum of polymer blends was ascribed to the geometrical arrangement of phases, rather than to a molecular relaxation process within the interfacial area (235).

In boundary regions, ie, $v_1 < v_{1cr}$ or $v_2 < v_{2cr}$, the blend modulus can be calculated from the Kerner – Nielsen equation (216,217,219), which for dispersed component 2 with $E_2 > E_1$ reads

$$E_{b1} = E_1(1 + A_1 B_1 v_2)/(1 - B_1 \psi_2 v_2). \tag{18a}$$

The quantities A_1, B_1, ψ_2 are defined as follows:

(1) $A_1 = (7 - 5\mu_1)/(8 - 10\mu_1)$, where μ_1 is the Poisson ratio of the (glassy) matrix;
(2) $B_1 = (E_2/E_1 - 1)/(E_2/E_1 + A_1)$; $\psi_2 = 1 + [(1 - \nu_{2max})/(\nu_{2max})^2]\nu_2$, where v_{2max} is the maximum packing fraction of the dispersed particles (the value $v_{2max} = 0.63$ for random close packing of monodisperse spheres is usually used (217).

If component 1 with lower modulus E_1 is dispersed in a stiffer matrix 2, eg, in rubber-toughened plastics, then inverted relations can be employed (216,217):

$$E_{b2} = E_2(1 - B_2 \Psi_1 \nu_1)(1 + A_2 B_2 \nu_1) \tag{18b}$$

where $A_2 = (8 - 10\mu_2)/(7 - 5\mu_2)$; $B_2 = (E_2/E_1 - 1)/(E_2/E_1 + A_2)$; the formulas for ψ_1 and ψ_2 are analogous. Alternatively, similar equations derived by other

authors (218,219,236) for particulate systems can be used; the differences in moduli predicted by existing theories are not significant.

Compliance of Heterogeneous Binary Blends. As end products made of thermoplastics and their blends are frequently exposed to a long-lasting dead load, their resistance to creep becomes a significant characteristic of their dimensional stability. By introducing a co-continuous creep-resistant component, the creep of blends can be substantially reduced. To anticipate the time-dependent compliance $D_b(t)$ of a blend, the corresponding functions $D_1(t)$ and $D_2(t)$ of the components are to be experimentally evaluated. In analogy to the blend modulus (Fig. 18, curve d), the compliance of heterogeneous binary blends with co-continuous components reads (237–239):

$$D_b(t) = \left\{v_{1p}/D_1(t) + v_{2p}/D_2(t) + (v_{1s} + v_{2s})^2/[D_1(t)v_{1s} + D_2(t)v_{2s}]\right\}^{-1} \tag{19}$$

To describe the compliance of blends with one continuous component and one discontinuous component, equation 19 can provide a first approximation by using $v_{1p} = 0$, $v_{1s} = v_1$ or $v_{2p} = 0$, $v_{2s} = v_2$. More accurate equations can be obtained by modifying existing equations (213). If the minority polymer 2 of the volume fraction v_2 having a lower compliance $D_2(t) < D_1(t)$ is dispersed in polymer 1, the compliance $D_{b1}(t)$ of the blend is (237)

$$D_{b1}(t) = D_1(t)[1 - B_1(t)\psi_2 v_2]/[1 + A_1 B_1(t) v_2] \tag{20a}$$

where $B_1(t) = [D_1(t)/D_2(t) - 1]/[D_1(t)/D_2(t) + A_1]$; A_1 and ψ_2 are defined for equation 18a. If the component 1 is dispersed in the component 2, then the inverted relation applies:

$$D_{b2}(t) = D_2(t)[1 + A_2 B_2(t) v_1]/[1 - B_2(t)\psi_1 v_1] \tag{20b}$$

where $B_2(t) = [D_1(t)/D_2(t) - 1]/[D_1(t)/D_2(t) + A_2]$; A_2 and ψ_1 are defined for equation 18b.

As the stress–strain linearity limit of most thermoplastics and their blends is very low, nonlinear viscoelastic behavior of heterogeneous blends needs to be considered in most cases. The nonlinearity is at least partly ascribed to the fact that the strain-induced expansion of materials with Poisson's ratio smaller than 0.5 markedly enhances the fractional free volume (240). Consequently, the retardation times are perpetually shortened in the course of a tensile creep in proportion to the achieved strain. Thus, knowledge of creep behavior over appropriate intervals of time and stress is of great practical importance. The handling and storage of the compliance curves $D(t,\sigma)$ in a graphical form is impractical, so numerous empirical functions have been proposed (241), eg,

$$D(t,\sigma) = W(\sigma)(t/\tau_{rm})^n \tag{21}$$

where $W(\sigma)$ is a function of the stress, τ_{rm} is the mean retardation time, and $0 \leq n \leq 1$ is the creep curve shape parameter reflecting the distribution of retardation times. Parameters characterizing the nonlinear compliance of the parent polymers

can be extracted from generalized creep dependencies obtained by means of time-strain superposition. The predictive format based on equations 14a, 14b, 19 and 21 allows the prediction of corresponding parameters for blends and the construction of the creep curves of blends for selected stresses in the region of recoverable stress-strain behavior (238,239).

Yield and/or Tensile Strength of Heterogeneous Binary Blends. If blend components show yielding (usually at a strain of 3–6%), the yield strength in tension σ_{yb} of the resulting blend obeys the following equation, derived in terms of the EBM in Fig. (19) (221,242):

$$\sigma_{yb} = \sigma_{y1}\nu_{1p} + \sigma_{y2}\nu_{2p} + A\sigma_{y1}\nu_s, \tag{22}$$

where $\sigma_{y1} < \sigma_{y2}$ characterize the parent polymers and $0 \leq A \leq 1$ the extent of interfacial debonding. Two limiting values of σ_{yb}, identified with the lower or upper bound, can be distinguished by means of equation 22: (i) Interfacial adhesion is so weak that complete debonding occurs before yielding between the fractions of constituents coupled in series ($A = 0$ at the yield stress). As a function of blend composition, the lower bound of σ_{yb} passes through a minimum (Fig. 18, curve e). (ii) Interfacial adhesion is strong enough to transmit the acting stress between constituents so that no debonding ($A = 1$) appears in the course of yielding; then the contribution of the series branch in the EBM is added to that of the parallel branch (the effect of different strain rates in the parallel and series branches on σ_{y1} and σ_{y2} is neglected). However, if two components differing in the yield strength are coupled in series, then this branch yields at σ_{y1} or σ_{y2}, whichever is lower. The upper bound of σ_{yb} is a monotonic function of the blend composition (Fig. 18, curve d). Whenever a partial or complete debonding occurs before yielding, then σ_{yb} passes through a minimum as a function of blend composition (211). A good correlation was found between the partial miscibility of blend components and their interfacial adhesion (243).

The yield strength σ_{yb1} of particulate systems, where dispersed particles do not yield and have a good adhesion to the matrix, is approximately equal to that of the matrix σ_{y1} (244). In the case of "zero" adhesion, the yield strength σ_{yb2} drops with the volume fraction of particles (219,245):

$$\sigma_{yb2} = \sigma_{y2}\left[1 - (\nu_1/\nu_{1max})^{2/3}\right] \tag{23}$$

The latter formula also holds for glassy matrices with rubber-like inclusions, because yield strength of the dispersed component is negligible (219).

With regard to the experience that equation 23 is suitable for the evaluation of the yield as well as tensile strength of particulate systems, equation 22 can also be tentatively applied (221–223) for the tensile strength σ_{ub} of blends by replacing the yield strengths σ_{y1} and σ_{y2} by the tensile strengths σ_{u1} and σ_{u2}, respectively. If fracture mechanisms in the blend components are very different, the format may not fit the σ_{ub} versus v_2 dependence.

Application of the Predictive Formats. In addition to the prediction of selected physical properties of envisaged blends, subsequent comparison of model calculations with experimental data allows the experimentalists (i) to analyze the phase structure of prepared blends, (ii) to evaluate interfacial adhesion or the

extent of interfacial debonding, and (iii) to assess to which extent the potential of a material has been exploited, etc. A great advantage of the EBM approach is that several physical properties can be simultaneously evaluated, eg, modulus, yield, or tensile strength, and permeability to gases (222,223,246). If no information is available about the phase structure of blends, the properties can be predicted by using the "universal" values $v_{1cr} = v_{2cr} = 0.16$ and $q = 1.8$. However, this should be regarded as a first approximation that may not well approximate experimental data due to the fact that v_{1cr} and v_{2cr} of a studied system may be different, being affected by the relative viscosities of components, conditions of blend mixing, phase structure coarsening, etc. Conversely, as soon as some experimental data for a specific system are available, it is possible to determine actual v_{1cr} and v_{2cr} by a fitting procedure; thus the formats can be alternatively viewed as an efficient tool for analysis of the phase structure of blends. In a similar way, the phase structure of ternary blends (242,247) and/or the extent of interfacial debonding (248) can be evaluated. The outlined format for the modulus was successfully used in the structure analysis of interpenetrating epoxy and silica networks (249). Blends consisting of partially miscible polymers often show positive deviations (Fig. 18, curve b) of the moduli and yield strength, (250,251) which are ascribed to two effects: (i) respective properties of one or both conjugate phases are higher than those of parent polymers; (ii) molecular mobility in conjugate phases is reduced due to associative interactions (heterocontacts) between the chains of components. The properties of these blends can be modeled by combining the predictive formats with an empirical equation expressing the composition of conjugate phases as a function of blend composition (251). The predictive format was also used for manifestation of the effects of the phase structure coarsening (narrowing of the co-continuity interval) on the modulus, yield or tensile strength, and gas permeability of heterogeneous polymer blends characterized by good or poor interfacial adhesion (252). If postmixing treatments (quiescent annealing before freezing-in the melt, molding, reprocessing) account for a more profound drop in blend properties, then it is likely that—in addition to phase structure coarsening of the blend—the respective properties of constituents have deteriorated due to changes in their structure or due to chemical degradation.

Toughness of Polymer Blends. Toughness (fracture resistance) ranks among the most closely watched properties of polymer materials because it is an important prerequisite in most applications. It is commonly defined as the ability to resist fracture by absorbing mechanical energy (253–256). In general, toughness is an extremely complex phenomenon, depending on polymer composition (molar mass, chain flexibility, chain-entanglement density), surface energy, density, crystallinity, modulus, and yield strength as well as on testing conditions (specimen geometry and dimensions, mode of loading, strain rate, temperature, presence of notches, etc.). Only parameters based on fracture mechanics can separate the effects of testing conditions from the effects of intrinsic material properties. Relevant material characteristics can be derived from either the energy balance approach or the stress intensity approach. Linear elastic fracture mechanics (LEFM), which is appropriate for (semi)brittle materials, operates with the strain energy release rate and the stress intensity factor. Nonlinear fracture mechanics (257,258) developed for ductile materials—including toughened polymers and blends—has introduced the J-integral fracture toughness, which can be

considered as a nonlinear elastic energy release rate. A widely used method is that of the essential work of fracture (EWF), which is a material property related to the J-integral (255). Despite an enormous amount of empirical knowledge gathered so far, there are no quantitative means for anticipating the toughness of new materials.

Amorphous glassy polymers show two types of localized deformation mechanisms, ie, crazing and shear yielding (256,259–261). A craze can be described as a microcrack bridged by polymer fibrils (5 – 20 nm in diameter) partially bearing the load. Crazes initiated by pre-existing defects or flaws typically develop in a plane perpendicular to a maximum principal stress in polymers, whose crazing stress is lower than yield stress (under the conditions of testing) (262–264). Crazing involves formation of microvoids that account for an increase in volume. Crazes grow through drawing of fibrils formed from the bulk polymer, and at the final stage give rise to cracks at a stress below that necessary to cause bulk shear yielding. The energy absorption per unit volume is relatively high within the craze deformation zone, but the amount of material involved in that absorption is very limited, so ensuing brittle fracture requires a very low mechanical energy. Brittle polymers have a low crack initiation energy (unnotched toughness) as well as a low crack propagation energy (notched toughness) (265). Brittle fracture is typical of PS, SAN, PMMA and highly crosslinked glassy polymers (256,259,260).

Shear yielding involves localized or homogeneous plastic deformation occurring without any volume change. A number of glassy polymers possess some degree of ductility (at room temperature) at moderate rates of straining, eg, polycarbonate (PC), polysulfone, and polyethersulfone (260). Ductile fracture requires sufficient molecular (segmental) mobility for shear yielding (plastic flow) to occur. Yielding localized in planar zones with high shear strains gives rise to "shear bands" at an angle of about 45° to the acting force, ie, in the direction of maximum shear stress. The strain hardening due to chain orientation eventually imposes a limit of the achievable plastic deformation. Ductile behavior is favored by uniaxial stress conditions, low strain rates, elevated temperature and smaller specimen cross-section (256,260). Ductile polymers have high crack initiation energy and low crack propagation energy (265,266). The transition between crazing and shear yielding is mainly predetermined by the entanglement and/or crosslinking density, because an increasing network density hampers the void formation in the process of crazing. Thus, the craze initiation stress is lower than the shear band initiation stress, and crazing prevails in polymers with a network density lower than a critical value. Shear yielding is typical of highly entangled thermoplastics with flexible chains.

In semicrystalline polymers, the main energy-absorbing mechanism is shear yielding (261,267,268). Local crazing may take place as a part of the fracture process ahead of a running crack without being an important energy-absorbing mechanism. Semicrystalline polymers usually have high toughness at temperatures above their T_g. Their toughness decreases with increasing crystallinity and perfection of the crystallites because shear yielding is impeded. Rising spherulite size has negative effects on toughness because larger defects and voids are created, and cracks propagate more easily along the interfaces between coarser spherulites. Higher molar mass accounts for the enhanced number of tie molecules between crystallites and spherulites, which improve the fracture resistance (260).

Molecular mobility, crazing, and shear yielding are thermally activated rate processes that follow the Eyring equation (256,264). For this reason, all plastics are brittle under extreme testing conditions (low temperatures and high strain rates permit only crazing because the yield stress is higher than the craze initiation stress). The brittle/ductile transition temperature $T_{b/d}$ of a polymer means that at $T < T_{b/d}$ the fracture is brittle, while at $T > T_{b/d}$ the fracture is ductile. The transition is a consequence of the fact that the yield strength decreases faster with rising temperature than the brittle strength so that yielding starts to be a dominating deformation mechanism at $T > T_{b/d}$. This temperature, which is of major engineering importance, always lies below T_g. However, it increases with the strain rate, crosslinking density, presence of notches, etc. (264).

Advanced characterization of the fracture processes in polymers and their blends is provided by the methods of fracture mechanics. Comprehensive reviews of this topic can be found in References 253, 255–259. Despite the achieved progress in this field, the plastics industry traditionally employs standard empirical tests for evaluating toughness (259,269). The Charpy or Izod impact test and falling-weight impact tests are widely used, although they provide only a semiquantitative basis for selection of materials. The impact resistance is a measure of the ability of a material to withstand the application of a sudden load without failure (259); however, it is not a material property because it depends on testing method and conditions, specimen geometry, and other factors. The obtained values are suitable for simple ranking of available materials or for evaluation of achieved improvements in material formulations. It should be noted that it is extremely difficult to correlate the impact strength found for a type of specimen with the impact performance of the manufactured article (260). In practice, it is advisable to select a method and testing conditions resembling the service conditions. Instrumented impact devices, which register the load-displacement curves in the course of impact, provide a deeper insight into the fracture mechanisms.

Toughening of rigid polymers consists of the involvement of their large fractions in energy absorption processes. To achieve this goal, a suitable amount of rubbery particles (of proper size, modulus, crosslinking density, and interfacial adhesion) is to be evenly dispersed in the brittle matrix to function as stress concentrators and to initiate multiple energy-absorbing plastic microdeformations. A good dispersal of rubbery component and formation of an optimum size of particles are often aided by suitable compatibilization. During initial deformation, cavitation (formation of voids of the order of 10 nm) occurs within or around the rubber particles, which triggers either multiple crazing, in polymers prone to crazing, or shear deformations (bands) in shear-yielding matrices (256). Cavitation is an essential step in the toughening process because it relieves the triaxial tension built up in the proximity of the crack tip. After cavitation, only biaxial tension remains, which is more favorable to shear yielding. A spectacular upswing in the toughness occurs at a certain rubber volume fraction, which indicates a percolation character of the underlying process. In this way, the toughness can routinely exceed by 1–2 orders of magnitude the value characterizing a neat rigid matrix (Fig. 18, curve a). However, in practice there is always a need to balance fracture resistance against other properties, eg, stiffness, resistance to creep, and dimensional stability.

As the optimum fraction of the rubber component is rather low (0.05–0.30), the term “rubber-toughened polymers” (instead of “blends”) is commonly used.

Almost any engineering plastic can be made tougher in its rubber-modified version, but at the expense of modulus and yield strength. Although the mechanism of plastic deformation in such materials depends on the properties of matrix (molecular weight, crystallinity, entanglement density, cohesive energy), dispersed rubber (modulus, cohesive energy, particle size, crosslinking), and adopted test conditions (test specimen dimensions, test speed, test temperature, notch dimensions), the fracture resistance of toughened polymers is primarily derived from the deformation and failure behavior of the rigid matrix, where most of the mechanical energy is absorbed via multiple crazing and/or shear yielding during straining and fracture. Semicrystalline polymers usually fracture in a ductile manner due to high resistance to crack initiation; however, in the presence of a sharp defect (notch) they show brittle fracture, because their resistance to crack propagation is low (255). For this reason, impact resistance of the notched test specimens is an important criterion of the achieved toughening. The quantitative theory of toughening based on the energy balance model (270) correctly predicts trends in the deformation and fracture behavior of toughened plastics with various structures. However, due to extreme complexity of the toughening phenomenon, there has been no format for the prediction of fracture resistance of rubber-modified plastics to date.

Rubber particle cavitation and subsequent multiple matrix crazing is the dominant mechanism of toughening in rubber-modified brittle matrices such as HIPS, SAN, PMMA, and ABS polymer (260,271,272). In less brittle matrices, such as SAN and PMMA, mixed crazing and shear yielding can occur (265). In the beginning, application of external stress causes the biggest rubber particles to cavitate and initiate the first series of crazes, which grow by increasing their area and thickness. The rising deformation initiates secondary cavitation of smaller rubber particles and further crazing. Thus, crazes lying close to a craze plane begin to connect together; a rapid craze thickening follows, involving the drawing of fresh polymer from the walls of rising crazes. The latter stage can be identified with an effective energy-consuming process. Fibrillation occurs in an increasing fraction of rubber particles, which stretch in parallel with the crazes up to a saturation point. The rupture of a blend deformed by multiple crazing is assumed to be associated with failure in the fibrillated rubber particles when the local tensile strain exceeds their limiting value. The light scattering from microvoids formed in the matrix crazes and/or in the rubber particle cavities accounts for the stress whitening (273).

In HIPS, where the "salami" rubber particles consist of hard polystyrene subinclusions embedded in the matrix of crosslinked rubber, a specific type of cavitation was revealed (256). Cavitation in the rubber "membranes" results in a craze-like structure where rubber fibrils form bridges between the PS subinclusions and between the subinclusions and the PS matrix. Yielding in the matrix allows the rubber fibrils to stretch and the rubber particles to expand until strain hardening stops the process. PVC and poly (oxymethylene) (POM) also show very high values of the notched Izod toughness when the incorporated rubber forms an intermeshed (network) structure (265) instead of discrete particles. A higher effectivity of intermeshed rubber phase morphology was ascribed to a lower percolation threshold in comparison with that for an assembly of spherical particles. The toughening mechanism of ABS consists in the formation of numerous shear

bands in addition to massive crazing (259). A similar effect can be produced in SAN by bimodal-sized rubber particles (265).

Shear yielding is the process by which most intrinsically ductile polymers achieve high strains. The incorporation of a rubbery component still enhances the toughness so that supertough materials can be produced (260,265,274), but the main purpose of the modification is to improve the resistance to crack propagation (notch sensitivity) (259). The high stress concentrations generated in the matrix by rubber particles bring about a spectacular rise in the rate of plastic deformation, because the adjacent matrix is free to yield and stretch in the way that was not possible in the neat matrix. The main factors controlling the shear yield stress of toughened plastics are the yield behavior of the rigid matrix and the volume fraction, shear modulus, and particle size of the dispersed rubber. Essential gains in toughness are achieved only when the cohesive failure within the rubber particles induces accelerated shear yielding in the matrix, which is then followed by strain hardening of the yield zone due to stretching of both rubber and rigid matrix. In this plastic deformation process, chain segments slip past each other, so that the material in the yield zone changes its shape, while only minor changes in density are due to disturbed molecular packing. Yielding localized in planar zones with high shear strains gives rise to pronounced shear bands; strain hardening due to the chain orientation eventually imposes a limit of the achievable plastic deformation. Toughening is particularly effective in the case of an array of closely spaced rubber particles, which assures that the ligaments between particles become fully yielded (256). The maximum degree of macroscopic toughness can be achieved if the local ligament thickness (surface-to-surface interparticle distance) decreases below its critical value (261,266), which is related to the experimental finding that brittle polymers become ductile below a critical specimen thickness (less than 1 μm). The critical ligament thickness is characteristic of the matrix for a given loading mode, temperature, and rate of deformation (266).

Toughness of semicrystalline polymers is enhanced by means of techniques similar to those developed for glassy polymers (260,267,275). Rubbery particles usually initiate both massive crazing and shear banding, which depend on blend composition, morphology, rubber particle size, and interfacial adhesion. An additional positive effect of the rubber component may consist in that its nucleating effect leads to finer spherulitic structure, thus improving the inherent toughness of the crystalline phase. Specific nucleating agents can markedly increase the toughness of the PP matrix by modifying crystalline structure and increasing the concentration of tie molecules (276,277).

Because of profound differences in the deformation and fracture behavior of polymer matrices, the optimum size of toughening rubber particles depends on the inherent fracture mechanism of a matrix. On the other hand, these optimum dimensions are affected by some properties of the rubber used, eg, modulus, viscosity, and crosslinking density. Rubber particles of improper size are ineffective in the toughening process. The existence of a minimum particle size for efficient toughening corresponds to the minimum particle size required for cavitation (256). Extensive experimental work has established that the particle size of a toughener should lie within an optimum range. The optimum diameter of rubber particles for efficient toughening of brittle glassy polymers tending to craze decreases with their entanglement density; the values reported (265) for PS, SAN, and PMMA

are 2.5, 0.75, and 0.25 μm, respectively. On the other hand, matrices absorbing fracture energy via shear yielding (polycarbonate, polyamides, PET, PBT, PVC) are commonly toughened with particles of 0.5 μm or less, eg, 0.2–0.3 μm for polyamides, added in the amounts necessary for the critical interparticle distance. The critical ligament thickness in a matrix depends on temperature, strain rate, loading mode, and other factors (265). Thermoset resins are routinely toughened by liquid carboxy-terminated butadiene rubbers (CTBN) dissolved in the resin mixture, and after curing, form separate domains 0.2 – 0.5 μm in diameter (253).

A fine dispersion of rubber in a polymer matrix is facilitated by a low interfacial tension between blended components in the molten state. Under these conditions, the rubber particles may not be well bonded to the matrix for efficient stress transfer (54). At any rate, the final particle size strongly depends on the rubber relative viscosity and blending conditions. The goal of concurrently optimizing dispersion and adhesion of a rubbery modifier is rather difficult to achieve. An elegant solution is offered by core-shell impact modifiers with a well-defined size and a narrow particle-size distribution (278). A major advantage of core-shell particles is that their size is set during their synthesis (emulsion polymerization) and remains the same after the dispersal in a host matrix. A soft core, made up of a rubbery polymer, is surrounded by a shell of grafted rigid polymer. The core of the particles provides the soft component that induces toughening mechanisms. The shell of a much higher T_g than the core has two primary functions: (i) to facilitate isolation of the particles from emulsion and to keep the cores from adhering to one another; (ii) to act as the interlayer binding the matrix to the core. Core-shell particles of acrylate rubber-PMMA, polybutadiene-PMMA, or polybutadiene-SAN are used for PA, PET, and PBT; ABS core-shell materials are effective in toughening PBT and PC. The amount of incorporated modifier particles varies from 5 to 30% by weight of the matrix.

A key factor in the performance of core-shell particles as impact modifiers is their adhesion to the host matrix, determined by the composition of both shell and matrix (278). If the latter polymers are compatible (miscible or partly miscible), the toughener will be effective. However, in most cases, the matrix and shell consist of dissimilar polymers. Also in this situation, solubilization of the matrix polymer into the grafted shell needs to be ensured to develop proper interfacial adhesion. High degrees of solubilization are favored by negative values of the interaction energy density, high molecular weight of the shell relative to the matrix, and a low shell thickness. If the matrix and shell are highly incompatible, introduction of a suitable compatibilizer can enhance the efficiency of core-shell impact modifiers. Alternatively, the matrix/shell adhesion can be enhanced by employing possible reactions between functional groups introduced in the shell and reactive sites of the matrix. Recent advances in polymerization techniques permit synthesis of various types of modified polyolefins (279), eg, polypropylene toughened with evenly distributed particles of ethylene-propylene rubber bound to the matrix.

The transition of dispersed particles from the rubbery to glassy state defines the lowest temperature at which the incorporated rubber is able to reduce the matrix yield stress and account for significant toughening (280,281). The effect of added rubber usually fades away at temperatures 10–20 K above its T_g, which is manifested as a sharp drop in the fracture energy (256). An equation was derived for the brittle-ductile transition temperature as a function of the particle

volume fraction, size, distribution, and matrix ligament thickness (282). However, this critical temperature is also affected by testing conditions. In proportion to their fraction, rubbery impact modifiers reduce the modulus and yield strength of toughened polymers as quantified by equations 18b and 22, respectively.

Impact resistance of ductile polymers was also improved by blending with 5–15% of a brittle component, eg, polycarbonate with SAN (283) or polyamide 6 with poly(styrene-*co*-maleic anhydride) (SMA) (284). Although the enhancement of impact resistance is lower than in the ductile matrix/rubber systems, the advantage of rigid particles is a simultaneous increase in toughness and stiffness. To achieve these effects, brittle inclusions should be small and interfacial adhesion should be high. Then, the brittle inclusions having a sufficiently higher modulus and a lower Poisson's ratio than the matrix become ductile under the action of the compressive component of stress (285,286) and absorb mechanical energy. To prevent formation of a co-continuous brittle component at higher volume fractions, it is convenient to add two brittle and incompatible minority components. To achieve their separate dispersion, the surface energy of one minority component should be higher than that of the matrix, while the reverse relation holds for the other minority component (242). Ternary blends of polyamide 6 containing rigid particles of SMA (about 5%) and particles of maleated ethylene-propylene rubber (about 5%) are an example of blends with balanced mechanical properties (286,287). In these blends, the losses in stiffness and tensile strength caused by rubbery component are (more than) compensated by the action of the brittle component, while both minority components contribute to the toughness enhancement.

Recently, specific conditions have been elucidated under which isometric filler particles (calcium carbonate) can account for a considerable toughening of PE (288) and PP (289). The notched Izod impact energy of PE/$CaCO_3$ materials rose by one order of magnitude when the mean interparticle ligament thickness of the PE matrix dropped to values below 0.6 μm. Under these conditions, the stiff filler brought about a substantial increase in both the modulus and toughness. The achieved improvements of the toughness of PP/$CaCO_3$ were smaller, while polyamide 6/$CaCO_3$ (290) showed brittle behavior, probably due to a high plastic resistance of the matrix. In all cases, dispersal of fine filler particles and elimination of their agglomerates were critical for enhancing the toughness.

Rheological Properties of Molten Blends. The dependence of shear viscosity, first normal stress difference or storage modulus on blend composition varies very substantially from system to system. According to the type of relation between the logarithm of viscosity and concentration, blends were classified into four categories (291–293). Additive blends fulfill the log-additivity rule:

$$\log\eta = \sum_i v_i \log \eta_i \tag{24}$$

where v_i and η_i denote, respectively, volume fraction and viscosity of the component i. Other categories are blends showing a positive deviation from log-additivity, blends with a negative deviation, and blends where both the positive and negative deviation have been observed. Because polymer blends are non-Newtonian liquids with η dependent on $\dot{\gamma}$, dependences of η on the blend composition determined at a constant shear rate and at a constant shear stress can be different. Dependences

at a constant stress are more plausible, because the stress is continuous at the interface in contrast with the deformation rate. Different types of the dependence of η on v at different shear stresses were found for some systems (291). Therefore, the above classification does not characterize polymer pairs only, but it is also a function of flow conditions. Dependences of the first normal stress difference and storage modulus on blend composition are similar to those for viscosity (291).

Generally, there is interrelation between rheological properties and morphology of flowing blends. Therefore, the morphology must be assumed in calculation of rheological properties or both characteristics must be calculated simultaneously. Great attention has been paid to the development of the theory of viscosity for blends containing a small amount of a dispersed component (96,291,292). A number of expressions for viscosity were derived using various approximations for these blends. For blends containing a very small volume fraction, v, of Newtonian droplets in the Newtonian matrix, the following equation was derived for $C_a \ll 1$.

$$\eta = \eta_m\left(1 + \frac{5p+2}{2p+2}v\right) \tag{25}$$

Equations considering somewhat higher contents of dispersed droplets, higher C_a and viscoelasticity of the components were derived. Also, these expressions predict for blends containing dispersed droplets that viscosity of a blend is higher than that of its matrix also for $p \ll 1$. This is a general feature of all theories describing rheological properties of dispersed droplets in matrix and assuming stick condition at the interface.

The Palierne model (294,295) describes a linear viscoelastic response of a dispersion of droplets that are spherical in stress-free state. The model may account for viscoelastic properties of both matrix and droplets, effects of finite concentration, distribution of size and composition of the droplets, and interfacial tension effects (also for compatibilized blends). The agreement of its predictions with experimental results is good (295). Description of rheological properties of blends with co-continuous structure is more complicated. In this case, it is useful to characterize the interface. The interfacial area per unit volume Q and specific anisotropy tensor q, characterizing anisotropy of the microstructure are used as proper characteristics for blends with a general shape of the interface (96). Development of theories for prediction of time evolution of Q and q and average stress tensor, which would serve for prediction of rheological properties, is in progress (96).

A reasonable explanation of negative deviation of η from log-additivity rule (eq. 24) was proposed by Utracki (293). It is assumed that the interlayer slip at the interface should be considered in immiscible polymer blends. A semiempirical theory considering the emulsion behavior and interlayer slip factor can predict all the above-mentioned categories of blend behavior with respect to log-additivity rule depending upon the system parameters. More recently, the origin of the slip at the interface was discussed in more detail (296). Suppression of the slip at the interface by the presence of a compatibilizer can explain the typically observed higher viscosity of compatibilized blends than that of the related blends without compatibilizer (297). Most polymer blends have the dependence of shear viscosity on the shear rate similar to that of homopolymers only with a somewhat shorter

Newtonian plateaus due to the effect of the interface (291,295). In contrast, dynamically vulcanized blends show yield stress, ie, a strong increase in η with decreasing shear rate in the region of low $\dot{\gamma}$ (298–300). It seems that the yield stress is induced by long-living entanglements between crosslinked domains of characteristic size of about 1 μm.

Permeability of Blends to Gases and Vapors. The permeation of gases, vapors, and liquids through films (layers, walls) of blends is of primary importance in many applications (packaging, pipes, tanks, etc.). The permeability of polymers is mainly determined by their polarity and crystallinity. Polyolefins are good barriers to moisture, but are highly permeable to hydrocarbons. On the other hand, aliphatic polyamides have outstanding resistance to hydrocarbons, but poor resistance to moisture. Thus, there are many reasons for blending various polymers to tailor materials with balanced and acceptable physical properties (301).

For a miscible polymer pair, the blend permeability P_b was empirically found to approximately obey the semilogarithmic additivity rule (302):

$$1nP_b = \nu_1 1nP_1 + \nu_2 1nP_2 \tag{26}$$

where P_1 and P_2 are the permeabilities of components. In the free volume approach (303,304), it is assumed that the free volume of the mixture consists of the additive contributions from each component, which leads to the following equation:

$$\ln(P_b/Q) = [\nu_1/\ln(P_1/Q) + \nu_2/\ln(P_2/Q)]^{-1} \tag{27}$$

where Q is a characteristic constant for the gas. The transport through blends consisting of miscible polymers is comprehensively reviewed in References 301–303.

Heterogeneous blends of immiscible or partially miscible polymers are much more important engineering materials than homogeneous blends. The permeability of blends consisting of a continuous matrix and dispersed particles of another polymer can be approximated by models developed for particulate systems (301,302). However, these models (assuming dispersed components in the form of spheres, cylinders, cubes, lamellar structures of random orientation, etc.) were found inadequate for the prediction of the blend permeability throughout the composition range (225,305–307), a part of which necessarily corresponds to blends with co-continuous components. Thus, the EBM (Fig. 19) combined with the percolation approach was found (301) to be the most convenient predictive model for the permeability of heterogeneous blends. The permeability of binary blends consisting of partially continuous components can be predicted (223,230,308) using the format formally analogous to that for tensile modulus given in the previous section on mechanical properties (Fig. 18, curve d):

$$P_b = (P_1 v_{1p} + P_2 v_{2p}) + v_s^2/[(v_{1s}/P_1) + (v_{2s}/P_2)] \tag{28}$$

The data are usually presented as the relative permeability $P_{br} = P_b/P_1$ (relative to the component 1 with a lower permeability) versus blend composition. The "basic" curve calculated for $v_{1cr} = v_{2cr} = 0.16$ and $q = 1.8$ by means of equations

14 and 28 may deviate from experimental data if component 2 with a higher permeability, which controls P_{br}, is characterized by v_{2cr} different from 0.16. *Vice versa*, it is possible to evaluate realistic values of v_{1cr} and v_{2cr} in individual series of blends by fitting experimental data. For blends consisting of components that differ by 2–4 orders of magnitude in their permeability, the semilogarithmic plot is more instructive (308); moreover, it indicates v_{2cr} as a break (discontinuity), so that v_{2cr} can be adjusted with an accuracy of about 0.01. In this way, the format becomes an efficient tool for the analysis of the phase structure of polymer blends. In marginal regions $0 < v_1 < v_{1cr}$ (or $0 < v_2 < v_{2cr}$), simplified relations can be used for the EBM, ie, $v_{1p} = 0$, $v_{1s} = v_1$ (or $v_{2p} = 0$, $v_{2s} = v_2$), to obtain an approximate prediction of permeability. The permeability of layered materials can be modeled as the series coupling of components.

The outlined format was found to match up well the permeability of a number of permeant-blend systems, eg, water–HDPE/LDPE, toluene–HDPE/polyamide 6, methanol–polyethylene/silicone rubber, oxygen–PVC/chlorinated PE (230); oxygen–PMMA/siloxane copolymer, oxygen–PE/poly (vinylidene chloride), oxygen–poly(ethylene-*co*-vinyl alcohol)/poly(ethylene-*co*-vinyl acetate) (308). The agreement with experimental data was very good throughout the composition range. Moreover, the format is suitable for simultaneous prediction or fitting of several physical properties, such as modulus and permeability (246) or modulus, tensile strength, and permeability (223).

Commercially Important Polymer Blends

There are three practical reasons for blending of polymers: (i) developing materials with desired properties, (ii) extending performance of expensive polymers by diluting it with a low cost polymer and (iii) utilizing plastic scrap by mechanical recycling. It is estimated that about one third of all commercially produced polymer materials are blends of two or more polymers. These multicomponent and largely multiphase materials show various combinations of properties unattainable in any one polymer alone. Major concern is focused on increasing impact strength, processability, tensile strength, stiffness, and heat resistance (309). It should be emphasized that an improvement in one property leads usually to deterioration of another property, and therefore the main efforts have been devoted to attaining well balanced properties of the final material required for the pertinent applications. Commercially produced polymer blends are the subject of several excellent monographs (1,55,56,310–312). Thus, only several examples of technically important polymer blends prepared by different compatibilization procedures are briefly presented in this chapter together with basic information on the recycling of mixed plastic waste.

High Impact Polystyrene (HIPS). Polystyrene shows excellent processability, good appearance, tensile strength, and thermal and electrical characteristics; however, its brittleness considerably limits its use in high performance products. Therefore, modification of its toughness made possible rapid growth of high impact polystyrene grades (60,272,313). Polystyrene whose impact strength is modified by the incorporation of rubber can be manufactured either by

mechanical blending of components under controlled conditions or by grafting of the polymerizing styrene onto the rubber.

Mechanical blending of PS with PB is not very effective, and in its classic form is a matter of the past. Blending technology is still used for modification of polystyrenes with special rubber components such as thermoplastic elastomers, eg, SBS or SEBS. HIPS is also sometimes blended with styrene homopolymer to yield material with reduced cost but intermediate properties still acceptable for some applications.

At the present time, HIPS is produced by polymerization of styrene containing 5–10% of dissolved polybutadiene. The process yields both the styrene homopolymer and the polybutadiene-*graft*-polystyrene, where PS side chains are grafted onto the main polybutadiene chain. The process can be carried out technologically as mass (bulk) polymerization or as a mass suspension process, either batchwise or continuously. It is initiated thermally or by suitable initiator (such as dibenzoyl peroxide). As conversion reaches 2–3%, phase separation occurs as a result of immiscibility of PS and PB. The system forms so called polymeric oil-in-oil emulsion, in which the dispersed phase is a solution of PS in styrene, and the continuous phase is a solution of PB in styrene. Grafted copolymer is formed at the interface and acts as an emulsion stabilizer. As the volume ratio of PS and PB in styrene approaches one, and the mixture is subjected to sufficiently strong shearing agitation—phase inversion takes place. Sufficient agitation of the reaction mixture in the phase inversion region is essential for morphology control of the final polymer blend. Particles of newly formed dispersed phase still contain permanently included residues of the original dispersed styrene phase as isolated particles. The presence of polystyrene subinclusions in polybutadiene particles is characteristic of HIPS, increasing its impact strength due to an increase in the "effective volume" of the PB phase. Near the completion of polymerization, crosslinking of the rubber component takes place. Rubber crosslinking must be sufficient to prevent disintegration during processing.

The HIPS performance is controlled by the amount and type of rubber, particle size distribution, rubber-phase volume, degree of grafting and crosslinking, as well as by molecular characteristics of the PS matrix. Most HIPS grades contain 5–7% of rubber, which covers the total volume fraction from 20 to 30%. For optimum toughening, the rubber particles of several micrometers are required. For good surface appearance a bimodal particle size distribution of rubber phase (eg, 2 and 0.2 μm) is desirable. The presence of rubber phase in the PS matrix substantially improves not only impact strength but affects also other properties compared with styrene homopolymer. Thus elasticity modulus, tensile strength, and hardness somewhat decrease while elongation and melt viscosity increase. All things considered, HIPS shows balanced complex end-use properties, which is advantageous in a broad application sphere.

HIPS is currently processed by procedures such as injection molding, extrusion, blow-molding, and thermoforming. HIPS properties can be further modified by incorporation of special additives such as flame retardants, stabilizers, antistatic agents, etc. The main production fraction of HIPS is consumed in the manufacture of packaging materials, technical products, toys, and various consumer goods.

Acrylonitrile-Butadiene-Styrene Polymer. The name acrylonitrile–butadiene–styrene (ABS) polymer is reserved for a family of thermoplastics with the SAN matrix containing dispersed elastomer particles.The oldest approach to the ABS preparation, similarly as in the case of HIPS, is mechanical blending of individual components. At present the graft polymerization of a mixture of styrene with acrylonitrile in the presence of a suitable rubber component is the current process of ABS polymer manufacture. Most producers employ some form of emulsion technology, but the mass or mass-emulsion polymerization is also technologically feasible (60,272).

Common types of ABS have an average composition of 21–27% acrylonitrile, 12–25% butadiene, and 54–63% styrene. The styrene component contributes good processability and stiffness to the final ABS, butadiene increases the impact strength, and acrylonitrile improves chemical and heat deformation resistance. The two-phase system where rubber particles are dispersed in the matrix of SAN shows a morphology similar to HIPS, but the particle size is smaller with fewer SAN subinclusions than those in HIPS. ABS polymer shows excellent toughness combined with good thermal and chemical resistance, high elastic modulus, and good appearance.

ABS can be processed by all common molding technologies. The main consumption of this polymer is for household appliances, automotive parts, business machine and telephone components, electrical devices, pipes and fittings, and leisure-time equipment.

Poly(2,6-dimethyl-1,4 phenylene oxide)/High Impact Polystyrene (PPO/HIPS). Poly (phenylene oxide) is a polymer with high heat deformation resistance, excellent electrical properties, and high resistance to acids and bases. Because of high melt viscosity, PPO is blended with styrene polymers to achieve rheological properties necessary for processing by current technologies. Improvement in PPO toughness is obtained simultaneously with viscosity decrease if HIPS is used as a modifier. Rubber particles distributed uniformly throughout the new matrix are responsible for an increase in toughness, and polystyrene improves its processability. Unlimited PPO/PS miscibility enables preparation of blends of broad composition scale with well-balanced end-use properties. For high performance applications in electrotechnical and automotive industries, high impact blends of PPO with ABS, PA, or PC are manufactured.

Polypropylene/Rubber. Polypropylene (PP) is a versatile polymer with good resistance to heat, chemicals and solvents, and good electrical properties. Other properties can be improved by compounding with various nonpolymeric additives as well as with polymers. Blending with elastomers and copolymerizing with other monomers are used for toughening of this polymer (314,315). Synthetic elastomers as EPM, SEBS, PIB, and natural rubber are incorporated into PP matrix by mechanical blending. Especially PP/EPM blends are of considerable practical importance. These blends with a low EPM content are used as high impact polypropylene, the blends with high content of this elastomer can be used as thermoplastic elastomers. Phase structure control of modified PP depends strongly on molecular characteristics of the matrix (crystallinity, crosslinked part etc.) and therefore it is relatively difficult to achieve the desired and sufficiently stabile blend morphology. The presence of rubber particles in PP matrix increases the

impact strength, but leads to lower tensile strength, stiffness, and heat deformation resistance. The set of end-use properties is convenient mainly for application in automotive industry.

Poly(vinylchloride)/Rubber. PVC is an important commodity polymer with good chemical resistance and low flammability. Without modification, however, it is not practically processable, and its mechanical properties and heat resistance are very poor. Therefore, various additives as lubricants, stabilizers, and impact modifiers are incorporated to PVC grains to obtain versatile polymer.

To achieve good toughness, required for many applications, impact modifiers are added to PVC. Chlorinated polyethylenes, ethylene-vinyl acetate copolymers, styrene-methyl methacrylate grafted elastomers, vinyl rubbers, and polyacrylates are the most frequently used (316). These polymers are blended together with other additives. Blending conditions are extraordinarly important for morphology control and consequently for final properties of the blends.

Most of high impact PVC blend production is consumed in civil engineering applications. Because of low price and ability to be properly modified, this oldest commercially produced polymer remains one of the most important synthetic materials.

Polyamide/Rubber Blends. The family of polyamides (PA) encompasses polymers with a variety of chemical compositions. A characteristic feature of these polymers is poor toughness at low temperature and/or in the presence of notches. Multi-year efforts to improve their toughness has resulted in numerous modification procedures (317). Most are based on melt blending of acid or anhydride-containing elastomers with PA. At present, producers of toughened PA typically use rubbers containing small amount of maleic anhydride (up to 2%). During blending, reactive compatibilization takes place. The maleic-anhydride groups react with amino groups of PA giving rise to graft copolymers at the interface. Saturated rubbers, eg, EPDM, SEBS, or BR are used. The obtained morphology shows the dispersed rubber particles of size between 0.001–0.1 μm. Compatibilization based on the reaction of anhydride and amino groups is also utilized for preparation of engineering materials as PA/PP, PA/ABS, or PA/PPO blends.

Polycarbonate Blends. Polycarbonates (PC) are classified as construction plastics because of their high heat deformation temperature, electric properties, and mechanical characteristics including impact strength. Similarly, as in the case of polyamides, they do not achieve the required toughness if notched or if exposed to low temperature. Therefore, polycarbonates are blended with ABS polymer to combine their properties with the toughness of ABS. No compatibilizer is needed in the blending of both the components as SAN and PC are partly miscible (313).

PC/ABS blends are materials with an excellent combination of end-use properties, improved processability and, moreover, an acceptable cost. A broad scale of PC/ABS types is used in the automotive industry and other engineering applications.

Recyclates of Polymers. Blending of polymers is an important aspect of the recycling technologies that aim to overcome the problem of separation (sorting) mixed polymeric waste into pure feedstock streams by direct processing of mixed materials with or without compatibilizers (318,319). Mechanical recycling of commingled plastic waste may be viewed as a compromise between conflicting

requirements. That is, sorting of the waste is expensive, but can give recyclates of higher quality; on the other hand, reprocessing of commingled plastics is relatively inexpensive, but the resulting product shows lower mechanical and aesthetic properties. In any case, under certain circumstances, the mechanical blending of mixed plastics waste can be advantageous from both the economical and ecological viewpoints.

For reprocessing of mixed plastics, either current processing machines or special machinery for manufacturing large profiles are used. The recyclates, called plastic lumber, suffer from inferior mechanical performance due to immiscibility, and thus poor adhesion of components. Moreover, the presence of heterogeneities and particulate contamination restricts application of the products. Therefore, commingled plastics are often processed into large profiles which can rather fulfill requirements for strength characteristics. For manufacture of such profiles, specific procedures have been developed. Thus, the intrusion process combines extrusion of mixed plastics with melt filling to a large mold without using screenpack or an extrusion nozzle (Klobbie process) (319). Continuous extrusion produces linear profiles with large cross-sections of molten polymer materials that are then extruded into cooled dies.

For more demanding applications, the commingled plastic wastes as well as partially sorted plastics mixture can be processed using compatibilizers. Recyclates with good mechanical properties as well as appearance have been reported. Thus, a mixture of polyolefins blended with organic peroxides or with a combination of peroxides and liquid PB gives materials of the same or higher impact resistance than the virgin HDPE (57). A mixture of polyolefins and styrene plastics blended with a multicomponent compatibilizer (combination of SB and EPDM copolymers) shows excellent impact strength and acceptable mechanical properties. Still better results have been obtained with a compatibilization system containing, besides copolymers, stabilizers based on aromatic amines. This combination shows even a synergistic effect (320). It seems that in case, the mixed polymers are not seriously damaged during their life cycle the compatibilization and restabilization can be an advantageous way of material recycling.

BIBLIOGRAPHY

"Polyblends" in *EPST* 1st ed., Suppl. Vol. 2, pp. 458–484, by R. D. Deanin, University of Lowell; "Polymer Blends" in *EPSE* 2nd ed., Vol. 12, pp. 399–461, by D. P. Paul, J. W. Barlow, and H. Keskkula, University of Texas.

1. L. A. Utracki, *Polymer Alloys and Blends, Thermodynamic and Rheology*, Hanser Publishers, Munich, 1989.
2. J. W. Gibbs, *Trans. Conn. Acad. Sci.* **3**, 228 (1976).
3. G. L. Lewis and M. Randall, *Thermodynamics*, McGraw-Hill, New York, 1961.
4. P. J. Flory, *Principles of Polymer Chemistry*, Cornell University Press, Ithaca, N.Y., 1953.
5. O. Olabisi, L. Robeson, and M. T. Shaw, *Polymer—Polymer Miscibility*, Academic Press, Inc., New York, 1979.
6. D. R. Paul and S. Newman, eds., *Polymer Blends*, Vols. I, II, Academic Press, Inc., New York, 1978.

7. D. R. Paul, J. W. Barlow, and H. Keskula, in J. I. Kroschwitz, ed.-in-ch, *Encyclopedia of Polymer Science and Engineering* 2nd ed., Wiley-Interscience, New York, 1985.
8. P. J. Flory, *J. Am. Chem. Soc.* **86**, 1833 (1965).
9. L. P. McMaster, *Macromolecules* **6**, 760 (1973).
10. P. J. Flory, R. A. Orwoll, and A. Vrij, *J. Am. Chem. Soc.* **86**, 3515 (1964).
11. B. E. Eichinger and P. J. Flory, *Trans. Faraday Soc.* **64**, 2035 (1968).
12. D. Patterson, *Macromolecules* **2**, 672 (1969).
13. D. Patterson and A. Robard, *Macromolecules* **11**, 690 (1978).
14. I. C. Sanchez and R. H. Lacombe, *J. Phys. Chem.* **80**, 2352 (1976).
15. I. C. Sanchez, *Polym. Eng. Sci.* **24**, 79 (1984).
16. Yu. S. Lipatov and A. E. Nesterov, *Thermodynamics of Polymer Blends*, Technomic Publishing Co., Lancaster, Pa., 1997, Chap. 5, pp. 275–361.
17. Coleman, J. F. Graf, and P. C. Painter, *Specific Interactions and the Miscibility of Polymer Blends*, Technomic Publishing Co., Lancaster, Pa., 1991.
18. R. Koningsveld, W. H. Stockmayer, and E. Nies, *Polymer Phase Diagrams*, Oxford University Press, Oxford, U.K. 2001.
19. H. J. Jeon, J. H. Lee, and N. P. Balsara, *Macromolecules* **31**, 3328 (1998).
20. S. Zhu and D. R. Paul, *Polymer* **44**, 5671 (2003).
21. J. W. Cahn, *Trans. Metall. Soc., AIME* **242**, 166 (1968).
22. E. Roerdink and G. Challa, *Polymer* **21**, 1161 (1980).
23. J. W. Schurer, A. deBoer, and G. Challa, *Polymer* **16**, 201 (1975).
24. I. C. Sanchez, *Physics of Polymer Surfaces and Interfaces*, Butterworth-Heiemann, Boston, Mass., 1992.
25. S. Wu, *Polymer Interface and Adhesion*, Dekker, Inc., New York, 1982.
26. L. Leibler, *Makromol. Chem., Macromol. Symp.* **16**, 1 (1988).
27. D. Broseta, G. H. Fredrickson, E. Helfand, and L. Leibler, *Macromolecules* **23**, 132 (1990).
28. L. Leibler, H. Orland, and J. C. Wheeler, *J. Chem. Phys.* **79**, 3550 (1983).
29. D. Mathur, R. Hariharan, and E. B. Neuman, *Polymer* **40**, 6077 (1999).
30. S. B. Chun and C. D. Han, *Macromolecules* **32**, 4030 (1999).
31. R. B. Thompson and M. W. Matsen, *J. Chem. Phys.* **112**, 6863 (2000).
32. J. R. Kim, A. M. Jamieson, S. D. Hudson, I. Manas-Zloczower, and H. Ishida, *Macromolecules* **31**, 5383 (1998).
33. A. Adedeji, S. D. Hudson, and A. I. Jamieson, *Polymer* **38**, 737 (1997).
34. D. Gersappe, P. K. Horn, D. Irvine, and A. C. Balazs, *Macromolecules* **27**, 720 (1994).
35. E. A. Eastwood and M. D. Dadmun, *Macromolecules* **35**, 5069 (2002).
36. M. D. Dadmun, *Macromolecules* **33**, 9122 (2000).
37. B. D. Edgecombe, J. A. Stein, J. M. J. Frechet, Z. Xu, and E. J. Kramer, *Macromolecules* **31**, 1292 (1998).
38. J. Li and D. Favis, *Polymer* **43**, 4935 (2002).
39. N. Marin and D. Favis, *Polymer* **43**, 4723 (2002).
40. L. Leibler, *Makromol. Chem., Rapid Commun.* **2**, 393 (1981).
41. H. S. Jeon, J. H. Lee, and N. P. Balsara, *Macromolecules* **31**, 3328 (1998).
42. H. S. Jeon, J. H. Lee, N. P. Balsara, and N. C. Newstein, *Macromolecules* **31**, 3340 (1998).
43. J. H. Lee, N. P. Balsara, A. K. Chakraborty, R. Krishnamorti, and B. Hammouda, *Macromolecules* **35**, 7748 (2002).
44. L. Corte, K. Yamauchi, F. Court, M. Cloitre, T. Hashimoto, and L. Leibler, *Macromolecules* **36**, 7695 (2003).
45. S. Datta and D. J. Lohse, *Polymeric Compatibilizers*, Carl Hanser Verlag, Munich 1996, pp. 41–59.

46. W. E. Baker, C. Scott, and G. H. Hu, eds., *Reactive Polymer Blending*, Carl Hanser Verlag, Munich, 2001.
47. M. J. Folkes and P. S. Hope, eds., *Polymer Blends and Alloys*, Chapman & Hall, London, 1993.
48. D. R. Paul and C. B. Bucknall, eds., *Polymer Blends*, John Wiley & Sons, New York, 2000, pp. 539–579.
49. R. Fayt, R. Jerome, and Ph. Teyssie, *J. Polym. Sci., Polym. Phys.* **20**, 2209 (1982).
50. R. Fayt, R. Jerome, and Ph. Teyssie, *Polym. Eng. Sci.* **27**, 328 (1987).
51. R. Fayt, R. Jerome, and Ph. Teyssie, *J. Polym. Sci., Polym. Phys.* **27**, 775 (1989).
52. R. Fayt, R. Jerome, and Ph. Teyssie, *Polym. Eng. Sci.* **30**, 937 (1990).
53. G. P. Hellmann and M. Dietz, *Macromol. Symp*. **170**, 1 (2001).
54. C. Creton, E. J. Kramer, H. R. Brown, and C. Y. Hui, *Adv. Polym. Sci.* **156**, 53 (2002).
55. S. Al Malaika, ed., *Reactive Modifiers for Polymers*, Chapman & Hall, London, 1997, pp. 84–159.
56. W. E. Baker, C. Scott, and G. H. Hu, eds., *Reactive Polymer Blending*, Carl Hanser Verlag, Munich, 2001, pp. 255–280.
57. Z. Kruliš, Z. Horák, F. Lednický, J. Pospíšil, and M. Sufčák, *Angew. Makromol. Chem.* **258**, 63 (1998).
58. H. X. Zhang and D. J. Hourston, *J. Appl. Polym. Sci*. **71**, 2049 (1999).
59. J. Schies and D. B. Priddy eds., *Modern Styrenic Polymers: Polystyrene and Styrenic Copolymers*, John Wiley & Sons, Chichester, U.K., 2003.
60. B. D. Gesner, *Encyclopedia of Polymer Science and Technology*, Vol. 10, Interscience, New York, 1969, pp. 694–709.
61. R. D. Deanin, in H. F. Mark, N. G. Gaylord, and N. M. Bikales, eds., *Encyclopedia of Polymer Science and Technology*, Suppl. Vol. 2, Wiley-Interscience, New York, 1977, p. 458.
62. A. P. Smith, H. Ade, S. D. Smith, C. C. Koch, and R. J. Spartac, *Macromolecules* **34**, 1536 (2001); N. Furgiuele, A. H. Lebowitz, K. Khait, and J. M. Torkelson, *Polym. Eng. Sci.* **40**, 1447 (2000).
63. L. H. Sperling, *Interpenetrating Polymer Networks and Related Materials*, Plenum Press, New York, 1981.
64. C. E. Scott and C. W. Macosko, *Polym. Bull.* **26**, 341 (1991).
65. C. E. Scott and C. W. Macosko, *Polymer* **36**, 461 (1995).
66. U. Sundararaj, C. W. Macosko, A. Nakayama, and T. Inoue, *Polym. Eng. Sci.* **35**, 100 (1995).
67. U. Sundararaj, C. W. Macosko, and Chi-Kai Shih, *Polym. Eng. Sci.* **36**, 1769 (1996).
68. C. W. Macosko, *Macromol. Symp.* **149**, 171 (2000).
69. P. Pötschke and D. R. Paul, *J. Macromol. Sci.* **C43**, 87 (2003).
70. B. D. Favis, in D. R. Paul and C. B. Bucknall, eds., *Polymer Blends Vol. 1: Formulations*, John Wiley & Sons, Inc., New York, 2000, Chap. 16.
71. D. R. Paul and J. W. Barlow, *J. Macromol. Sci., Rev. Macromol. Chem.* **C18**, 108 (1980).
72. S. Miles and A. Zurek, *Polym. Eng. Sci.* **28**, 796 (1988).
73. V. I. Metelkin and V. P. Blekht, *Colloid J. USSR* **46**, 425 (1984).
74. V. Everaert, L. Aerts, and G. Groeninckx, *Polymer* **40**, 6627 (1999).
75. H. Van Oene, in D. R. Paul and S. Newman, eds., *Polymer Blends*, Vol. 2, Academic Press, Inc., New York, 1978, p. 295.
76. D. Bourry and B. D. Favis, *J. Polym. Sci., Part B: Polym. Phys.* **36**, 1889 (1998).
77. S. Steinmann, W. Gronski, and C. Friedrich, *Rheol. Acta* **41**, 77 (2002).
78. J. Lyngaae-Jørgensen and L. A. Utracki, *Makromol. Chem., Macromol. Symp.* **48/49**, 189 (1991).
79. R. Willemse, A. Posthuma de Boer, J. van Dam, and A. D. Gotsis, *Polymer* **39**, 5879 (1998).

80. J. K. Lee and C. D. Han, *Polymer* **40**, 6277 (1999).
81. C. Z. Chuai, K. Almdal, and J. Lyngaae-Jørgensen, *Polymer* **44**, 481 (2003).
82. B. D. Favis, C. Lavalle, and A. Derdouri, *J. Mater. Sci.* **27**, 4211 (1992).
83. S. Y. Hobbs, M. E. J. Dekkers, and W. H. Watkins, *J. Mater. Sci.* **23**, 1598 (1988).
84. H. F. Guo, S. Packirisamy, N. V. Gvozdic, and D. J. Meier, *Polymer* **38**, 785 (1997).
85. I. Luzinov, C. Pagnoulle, and R. Jérôme, *Polymer* **41**, 7099 (2000).
86. N. Henmati, H. Nazokdast, and H. S. Panahi, *J. Appl. Polym. Sci.* **82**, 1129 (2001).
87. N. Nemirovski, A. Siegmann, and M. Narkis, *J. Macromol. Sci., Phys.* **B34**, 459 (1995).
88. A. K. Gupta and K. R. Shrinivasan, *J. Appl. Polym. Sci.* **47**, 167 (1993).
89. J. Reignier, B. D. Favis, and M.-C. Heuzey, *Polymer* **44**, 49 (2003).
90. J. Lyngaae-Jørgensen, in M. J. Folkes and P. S. Hope, eds., *Polymer Blends and Alloys*, Blackie Academic & Professional, London, 1993, Chap. 4.
91. J. M. H. Janssen, in H. E. H. Meijer, ed., *Materials Science and Technology, Vol. 8: Processing of Polymers*, Wiley-VCH, Weinheim, 1997, Chap. 3.
92. H. E. H. Meijer and J. M. H. Janssen, in I. Manas-Zloczower and Z. Tadmor, eds., *Mixing and Compounding of Polymers*, Hanser Publishers, Munich, 1994, Chap. 4.
93. L. A. Utracki and Z. H. Shi, *Polym. Eng. Sci.* **32**, 1824 (1992).
94. I. Fortelný, J. Kovář, and M. Stephan, *J. Elastomers Plast.* **28**, 106 (1996).
95. H. A. Stone, *Annu. Rev. Fluid Mech.* **26**, 65 (1994).
96. C. L. Tucker and P. Moldenaers, *Annu. Rev. Fluid Mech.* **34**, 177 (2002).
97. J. M. H. Janssen and H. E. H. Meijer, *J. Rheol.* **37**, 597 (1993).
98. J. T. Overbeek, in H. K. Kruyt, ed., *Kinetic of Flocculation, Colloid Science* Vol. 1, Elsevier, Amsterdam, The Netherlands, 1952, p. 278.
99. J. J. Elmendorp, in C. Rauwendaal, ed., *Mixing in Polymer Processing*, Marcel Dekker, Inc., New York, 1991, p. 17.
100. I. Fortelný, *Macromol. Symp.* **158**, 137 (2000).
101. S. T. Milner, H. Xi, *J. Rheol.* **40**, 663 (1996).
102. A. K. Chesters, *Trans. I. Chem. E.* **69A**, 259 (1991).
103. H. Wang, A. Z. Zinchenko, and R. H. Davis, *J. Fluid Mech.* **265**, 161 (1994).
104. M. A. Rother and R. H. Davis, *Phys. Fluids* **13**, 1178 (2001).
105. I. Fortelný and A. Živný, *Rheol. Acta* **42**, 454 (2003).
106. N. Tokita, *Rubber Chem. Technol.* **50**, 292 (1977).
107. J. J. Elmendorp and A. K. Van der Vegt, *Polym. Eng. Sci.* **26**, 1332 (1986).
108. I. Fortelný and J. Kovář, *Eur. Polym. J.* **25**, 317 (1988).
109. J. Lyngaae-Jørgensen and A. Valenza, *Makromol. Chem., Macromol. Symp.* **38**, 43 (1990).
110. I. Fortelný and A. Živný, *Polym. Eng. Sci.* **35**, 1872 (1995).
111. M. Huneault, Z. H. Shi, and L. A. Utracki, *Polym. Eng. Sci.* **35**, 115 (1995).
112. J. M. H. Janssen and H. E. H. Meijer, *Polym. Eng. Sci.* **35**, 1766 (1995).
113. L. Delamare, B. Vergnes, *Polym. Eng. Sci.* **36**, 1685 (1996).
114. S. A. Patlazhan and J. T. Lindt, *J. Rheol.* **40**, 1095 (1996).
115. H. Potente and M. Bastian, *Polym. Eng. Sci.* **40**, 727 (2000).
116. I. Fortelný, *Rheol. Acta* **40**, 485 (2001).
117. P. Van Puyvelde, H. Yang, J. Mewis, and P. Moldenaers, *J. Rheol.* **44**, 1401 (2000).
118. B. D. Favis and J. M. Willis, *J. Polym. Sci., Part B: Polym. Phys.* **28**, 2259 (1990).
119. I. Fortelný, D. Kamenická, and J. Kovář, *Angew. Makromol. Chem.* **164**, 125 (1988).
120. P. G. Ghondgaonkar and U. Sundararaj, *Polym. Eng. Sci.* **36**, 1656 (1996).
121. W. Lerdwijitjarud, A. Sirivat, and R. G. Larson, *Polym. Eng. Sci.* **42**, 798 (2002).
122. Z. H. Shi and L. A. Utracki, *Polym. Eng. Sci.* **32**, 1834 (1992).
123. I. Fortelný, D. Michálková, and J. Mikešová, *J. Appl. Polym. Sci.* **59**, 155 (1996).
124. N. Grizzuti and O. Bifulco, *Rheol. Acta* **36**, 406 (1997).
125. A. P. Plochocki, S. S. Dagli and R. D. Andrews, *Polym. Eng. Sci.* **30**, 741 (1990).

126. I. Fortelný, Z. Černá, J. Binko, and J. Kovář, *J. Appl. Polym. Sci.* **48**, 1731 (1993).
127. B. D. Favis and J. P. Chalifoux, *Polym. Eng. Sci.* **27**, 1591 (1987).
128. B. D. Favis, *J. Appl. Polym. Sci.* **39**, 285 (1990).
129. O. Franzheim, T. Rische, M. Stephan, and W. J. MacKnight, *Polym. Eng. Sci.* **40**, 1143 (2000).
130. H. Potente, S. Krawinkel, M. Bastian, M. Stephan, and P. Pötschke, *J. Appl. Polym. Sci*. **82**, 1986 (2001).
131. I. Fortelný, D. Michálková, J. Koplíková, E. Navrátilová, and J. Kovář, *Angew. Makromol. Chem.* **179**, 185 (1990).
132. I. Fortelný, R. Rosenberg, and J. Kovář, *Polym. Networks Blends* **3**, 35 (1993).
133. M. A. Huneault, F. Mighri, G. H. Ko, and F. Watanabe, *Polym. Eng. Sci*. **41**, 672 (2001).
134. H. A. Stone, B. J. Bentley, and L. G. Leal, *J. Fluid Mech.* **173**, 131 (1989).
135. H. A. Stone and L. G. Leal, *J. Fluid Mech.* **198**, 399 (1989).
136. R. C. Willemse, R. J. J. Ramaker, J. Van Dam, and A. Posthuma de Boer, *Polym. Eng. Sci.* **39**, 1717 (1999).
137. H. Veenstra, J. Van Dam, and A. Posthuma de Boer, *Polymer* **41**, 3037 (2000).
138. I. Fortelný, A. Živný, and J. Jza, *J. Polym. Sci., Part B: Polym. Phys.* **37**, 181 (1999).
139. I. Fortelný and A. Živný, *Polymer* **39**, 2669 (1998).
140. F. M. Mirabella, *J. Polym. Sci., Polym. Phys. Ed.* **32**, 1205 (1995).
141. B. Crist and A. R. Nesarikar, *Macromolecules* **28**, 890 (1995).
142. W. R. White and P. Wiltzius, *Phys. Rev. Lett.* **75**, 3012 (1995).
143. K. Wallheinke, P. Pötschke, C. W. Macosko, and H. Stutz, *Polym. Eng. Sci.* **39**, 1022 (1999).
144. J. Lyngaae-Jørgensen, K. Lunde Rasmussen, E. A. Chtcherbakova, and L. A. Utracki, *Polym. Eng. Sci.* **39**, 1060 (1996).
145. D. Boury and B. D. Favis, *J. Polym. Sci., Part B: Polym. Phys.* **36**, 1889 (1998).
146. P. T. Hijetaoja, R. M. Holsti-Miettinen, J.V. Sepälä, and O. T. Ikkala, *J. Appl. Polym. Sci.* **54**, 1613 (1994).
147. I. Fortelný, D. Michálková, J. Hromádková, and F. Lednický, *J. Appl. Polym. Sci.* **81**, 570 (2001).
148. R. Fayt and P. Teyssié, *Polym. Eng. Sci.* **30**, 937 (1990).
149. P. Van Puyvelde, S. Velankar, and P. Moldenaers, *Curr. Opin. Colloid Interface Sci.* **6**, 457 (2001).
150. I. Fortelný, *J. Macromol. Sci.-Phys.* **B39**, 67 (2000).
151. J. F. Palierne and F. Lequeux, *J. Non-Newtonian Fluid Mech.* **40**, 289 (1991).
152. Su Ping Lyu, T. D. Jones, F. S. Bates, and C. W. Macosko, *Macromolecules* **35**, 7845 (2002).
153. I. Fortelný and A. Živný, *Polymer* **41**, 6865 (2000).
154. G. Xu and S. Lim, *Polymer* **37**, 421 (1996).
155. M. Taha and J. Frerejean, *J. Appl. Polym. Sci.* **61**, 969 (1996).
156. M. Wagner and B. A. Wolf, *Polymer* **34**, 1460 (1993).
157. T. Appleby, F. Czer, G. Moad, E. Rizzardo, and C. Stavropulos, *Polym. Bull.* **32**, 479 (1994).
158. Z. Horák, V. Fořt, D. Hlavatá, F. Lednický, and F. Večerka, *Polymer* **37**, 66 (1996).
159. T. Li, V. A. Topolkaraev, A. Hiltner, E. Baer, X. Y. Ji, and R. P. Quirk, *J. Polym. Sci., Part B: Polym. Phys.* **33**, 667 (1995).
160. E. Kroeze, G. ten Brinke, and G. Hadziioannou, *Polym. Bull. (Berlin)* **38**, 210, (1997).
161. D. Hlavatá, Z. Horák, F. Lednický, and Z. Tuzar, *Polym. Networks Blends* **7**, 195 (1997).
162. D. Hlavatá, Z. Horák, J. Hromádková, F. Lednický, and A. Pleska *J. Polym. Sci., Part B: Polym. Phys.* **37**, 1647 (1999).
163. J. Noolandi, *J. Macromol. Chem. Theory Simul.* **1**, 295 (1992).

164. G. Gersappe, P. K. Harm, D. Irvine, and A. C. Balazs, *Macromolecules* **27**, 720 (1994).
165. H. Feng, J. Tian, and C. Ye, *J. Appl. Polym. Sci.* **61**, 2265 (1996).
166. T. J. Cavanaugh, K. Buttle, J. N. Turner, and E. B. Nauman, *Polymer* **39**, 4191 (1998).
167. Z. Horák, D. Hlavatá, J. Hromádková, J. Kotek, V. Hašová, J. Mikešová, and A. Pleska, *J. Polym. Sci., Part B: Polym. Phys.* **40**, 2612 (2002).
168. D. Hlavatá, J. Hromádková, I. Fortelný, V. Hašová, and J. Pulda, *J. Appl. Polym. Sci.* **92**, 2431(2004).
169. K. H. Dai, J. Washiyama, and E. J. Kramer, *Macromolecules* **27**, 4544 (1994).
170. D. Hlavatá, Z. Horák, F. Lednický, J. Hromádková, A. Pleska, and V. Zanevskii, *J. Polym. Sci., Part B: Polym. Phys.* **39**, 931 (2001).
171. I. Fortelný, D. Hlavatá, J. Mikešová, D. Michálková, L. Potroková, and I. Šloufová, *J. Polym. Sci., Part B: Polym. Phys.* **41**, 609 (2003).
172. I. Fortelný, J. Mikešová, J. Hromádková, V. Hašová, and Z. Horák, *J. Appl. Polym. Sci.* **90**, 2303 (2003).
173. Z. Horák, D. Hlavatá, I. Fortelný, and F. Lednický, *Polym. Eng. Sci.* **42**, 2042 (2002).
174. S. Wu, *Polym. Eng. Sci.* **30**, 753 (1990).
175. T. A. Kavassalis and J. Noolandi, *Macromolecules* **22**, 2709 (1989).
176. J. W. Barlow and D. R. Paul, *Polym. Eng. Sci.* **24**, 525 (1984).
177. S. C. Tjong and S. A. Xu, *J. Appl. Polym. Sci.*, **68**, 1099 (1998).
178. P. Cigana, B. D. Favis, C. Albert, and T. Vu-Khanh, *Macromolecules* **30**, 4163 (1997).
179. G. Radonjič, V. Musil, and I. Šmit, *J. Appl. Polym. Sci.* **69**, 2625 (1998).
180. I. Šmit and G. Radonjič, *Polym. Eng. Sci.* **40**, 2144 (2000).
181. C. Harrats, R. Fayt, and R. Jerome, *Polymer* **43**, 863 (2002).
182. L. E. Alexander, *X-Ray Diffraction Methods in Polymer Science*. Wiley-Interscience, New York, 1969.
183. C. Sadron and B. Galott, *Makromol. Chem.* **164**, 301 (1973).
184. F. S. Bates, R. E. Cohen, and C. V. Berney, *Macromolecules* **15**, 589 (1982).
185. F. J. Balta-Calleja and C. G. Vonk, *X-ray Scattering of Synthetic Polymers*. Elsevier, Amsterdam, The Netherlands, 1989.
186. L. Leibler, *Makromol. Chem., Macromol. Symp.* **16**, 1 (1988).
187. D. Mathur, R. Hariharan, and E. B. Nauman, *Polymer* **40**, 6077 (1999).
188. R. S. Stein, in D. R. Paul, and S. Newman, eds., *Polymer Blends*, Vols. I and II, Academic Press, Inc., New York, 1978, Chapt. 9.
189. R. J. Composto, J. W. Mayer, E. J. Kramer, and D. M. White, *Phys. Rev. Lett.* **57**, 1312 (1986).
190. G. D. Wignall and J. I. Kroschwitz, eds., *Encyclopedia of Polymer Science and Engineering*, Vol. 10, Wiley-Interscience, New York, 1987, p. 112.
191. M. M. Agamalian, R. G. Alamo, J. D. Londono, L. Mandelkern, and G. D. Wignall, *J. Appl. Cryst.* **33**(1), 843 (2000).
192. M. T. Shaw, in D. J. Walsh, J. S. Higgins, and A. Maconnachie, eds., NATO Series E No. 89, Martinns Nijhoff Publishers, Dordrecht, The Netherlands, 1985.
193. B. Brahimi, A. Ait-Kadi, A. Ajji, and R. Fayt, *J. Polym. Sci., Part B: Polym. Phys.* **29**, 945 (1991).
194. I. Fortelný and D. Michálková, *Plast., Rubber Compos. Process. Appl.* **27**(2), 53 (1998).
195. K. Kato, *J. Electron Microsc. Jpn.* **14**, 219 (1965).
196. J. S. Trent, J. I. Scheinbeim, and P. R. Couchman, *Macromolecules* **16**, 589 (1983).
197. G. Radonjič, *J. Appl. Polym. Sci.* **72**, 291 (1999).
198. Chi-An Dai, K. D. Jandt, D. R. Iyengar, N. L. Slack, K. H. Dai, W. B. Davidson, E. J. Kramer, and Chung-Yuen Hui, *Macromolecules* **30**, 549 (1997).
199. K. Sondergaard and J. Lyngaae-Jorgensen, *Rheo-Physics of Multiphase Polymer Systems*, Tecnomic, Lancaster, Pa., 1995.

200. G. Schlatter, C. Serra, M. Bouquey, R. Muller, and J. Terrisse, *Polym. Eng. Sci.* **42**(10), 1965 (2002).
201. Y. A. Akpalu and Y. Y. Lin, *J. Polym. Sci., Part B: Polym. Phys.* **40**, 2714 (2002).
202. W. J. Macknight, F. E. Karasz, and J. R. Fried, in *Polymer Blends*, D. R. Paul and S. Newman, eds., Academic Press, Inc., New York, 1978, Chap. 5.
203. J. Baldrian, M. Steinhart, P. Vlček, M. Horký, P. Laggner, H. Amenitsch, and S. Bernstorff, *J. Macromol. Sci., Part B-Physics* **41**, 1023 (2002).
204. H. Amenitsch, S. Bernstorff, M. Kriechbaum, D. Lombardo, H. Mio, M. Rappolt, and P. J. Lagner, *Appl. Crystallogr.* **30**, 872 (1997).
205. I. Campoy, M. A. Gomez, and C. Marco, *Polymer* **40**, 4259 (1999).
206. A. R. Hopkins, P. G. Rasmussen, R. A. Basheer, B. K. Annis, and G. D. Wignall, *Synth. Met.* **95**, 179 (1998).
207. G. D. Wignall, R. G. Alamo, J. D. Londono, L. Mandelkern, M. H. Kim, J. S. Lin, and G. M. Brown, *Macromolecules* **33**, 551 (2000).
208. D. J. Kinning, E. L. Thomas, and L. J. Fetters, *J. Chem. Phys.* **90**, 15 (1989).
209. J. Furukawa, *Physical Chemistry of Polymer Rheology*, Springer-Verlag, Berlin, 2003, p. 217.
210. J. Lyngaae-Jorgensen, K. Lunde Rasmuseen, E. A. Chtcherbakova, and L. A. Utracki, *Polym. Eng. Sci.* **39**, 1060 (1999).
211. J. Kolařík, *Polym. Compos.* **18**, 433 (1997).
212. J. Lyngaae-Jorgensen, A. Kuta, K. Sondergaard, and K. V. Poulsen, *Polym. Networks Blends* **3**, 1 (1993).
213. J. Lyngaae-Jorgensen and L. A. Utracki, *Polymer* **44**, 1661 (2003).
214. R. C. Willemse, A. Posthuma de Boer, J. van Dam, and A. D. Gotsis, *Polymer* **40**, 827 (1999).
215. H. Veenstra, J. van Dam, and A. Posthuma de Boer, *Polymer* **40**, 1119 (1999).
216. L. E. Nielsen, *Predicting the Properties of Mixtures: Mixture Rules in Science and Engineering*, Marcel Dekker, Inc., New York, 1978, p. 51.
217. L. E. Nielsen and R. F. Landel, *Mechanical Properties of Polymers and Composites*, Marcel Dekker, Inc., New York, 1994, p. 384.
218. S. McGee and R. L. McCullough, *Polym. Compos.* **2**, 149 (1981).
219. J. Kolařík, G. L. Agrawal, Z. Kruliš, and J. Kovář, *Polym. Compos.* **7**, 463 (1986).
220. J. Kolařík, J. Velek, G. L. Agrawal, and I. Fortelný, *Polym. Compos.* **7**, 472 (1986).
221. J. Kolařík, *Polym. Networks Blends* **5**, 87 (1995).
222. J. Kolařík, *Polym. Eng. Sci.* **36**, 2518 (1996).
223. J. Kolařík, *Eur. Polym. J.* **34**, 585 (1998).
224. P.G. De Gennes, *J. Phys., Lett. (Paris)* **37**, L1 (1976).
225. J. Sax and J. M. Ottino, *Polym. Eng. Sci.* **23**, 165 (1983).
226. W. Y. Hsu and S. Wu, *Polym. Eng. Sci.* **33**, 293 (1993).
227. H. Matsuyama, M. Teramoto, and M. Tsuchyia, *J. Membr. Sci.* **118**, 177 (1996).
228. N. Marin, B. D. Favis, *Polymer* **43**, 4723 (2002).
229. J. Kolařík, *Polym. Eng. Sci.* **36**, 2518 (1996).
230. J. Kolařík and G. Geuskens, *Polym. Networks Blends* **7**, 13 (1997).
231. D. E. Kirkpatrick, J. K. McLemore, and M. A. Wright, *J. Appl. Polym. Sci.* **46**, 377 (1992).
232. R. M. Christensen, *Mechanics of Composite Materials*, John Wiley & Sons, Inc., New York, 1979.
233. J. Kolařík, J. Janáček, and L. Nicolais, *J. Appl. Polym. Sci.* **20**, 841 (1976).
234. J. Kolařík, A. Pegoretti, L. Fambri, and A. Penati, *J. Polym. Res.* **7**, 7 (2000).
235. D. Colombini and F. H. J. Maurer, *Macromolecules* **35**, 5891 (2002).
236. J. A. Faucher, *J. Polym. Sci., Part B: Polym. Phys.* **12**, 2153 (1974).

237. J. Kolařík, L. Fambri, A. Pegoretti, A. Penati, and P. Goberti, *Polym. Eng. Sci* **42**, 161 (2002).
238. J. Kolařík, A. Pegoretti, L. Fambri, and A. Penati, *J. Appl. Polym. Sci.* **88**, 641 (2003).
239. J. Kolařík, A. Pegoretti, L. Fambri, and A. Penati, *Macromol. Mater. Eng.* **288**, 629 (2003).
240. J. Kolařík, *J. Polym. Sci., Part B: Polym. Phys.* **41**, 736 (2003).
241. R. W. Garbella, J. Wachter, and J. H. Wendorff, *Prog. Colloid Polym. Sci.* **71**, 164 (1987).
242. J. Kolařík, F. Lednický, G. C. Locati, and L. Fambri, *Polym. Eng. Sci* **37**, 128 (1997).
243. L. Buki, E. Gonczy, E. Fekete, G. P. Hellmann, and B. Pukanszky, *Macromol. Symp.* **170**, 9 (2001).
244. J. Jančář, A. DiAnselmo, and A. T. DiBenedetto, *Polym. Eng. Sci* **32**, 1394 (1992).
245. L. Nicolais and M. Narkis, *Polym. Eng. Sci.* **10**, 97 (1971).
246. Z. Horák, J. Kolařík, M. Šípek, V. Hynek, and F. Večerka, *J. Appl. Polym. Sci.* **69**, 2615 (1998).
247. J. Kolařík, L. Fambri, A. Pegoretti, and A. Penati, *Polym. Adv. Technol.* **11**, 75 (2000).
248. J. Kolařík, *Polymer* **37**, 887 (1996).
249. L. Matějka, O. Dukh, and J. Kolařík, *Polymer* **41**, 1449 (2000).
250. J. Kolařík, G. C. Locati, L. Fambri, and A. Penati, *Polym. Networks Blends* **7**, 103 (1997).
251. J. Kolařík, *J. Macromol. Sci. Phys. B* **39**, 53 (2000).
252. J. Kolařík and L. Fambri, *Macromol. Mater. Eng.* **283**, 41 (2000).
253. C. B. Bucknall, *Toughened Plastics*, Applied Science Publisher, London, 1977, p. 243.
254. L. H. Sperling, *Polymeric Multicomponent Materials*, John Wiley & Sons, Inc., New York, 1997, p. 223.
255. Y.-W. Mai, S.-C. Wong, and X.-H. Chen, in D. R. Paul and C. B. Buckmall, eds., *Polymer Blends*, John Wiley & Sons, Inc., New York, 1999, p. 17.
256. C. B. Bucknall, in D. R. Paul, and C. B. Bucknall, eds., *Polymer Blends*, John Wiley & Sons, Inc., New York, 1999, p. 83.
257. W. Grellmann and S. Seidler, *J. Polym. Eng.* **11**, 71 (1992).
258. S. Seidler and W. Grellman, *Polym. Test.* **14**, 453 (1995).
259. A. F. Yee, *Encyclopedia of Polymer Science and Engineering* Vol. 8, Wiley-Interscience, New York, 1986, p. 36.
260. W. G. Perkins, *Polym. Eng. Sci.* **39**, 2445 (1999).
261. M. C. M. van der Sanden, in R. W. Cahn, P. Haasen, and E. J. Kramer, eds., *Materials Science and Technology*, Wiley-VCH, Weinheim, 1997, p. 579.
262. E. J. Kramer, *Adv. Polym. Sci.* **52/53**, 1 (1983).
263. E. J. Kramer, *Plast. Rubber Compos. Process. Appl.* **26**, 241 (1997).
264. G. M. Swallowe, in G. M. Swallowe, ed., *Mechanical Properties and Testing of Polymers*, Kluwer Academic Publishers, Dordrecht, 1999, p. 40.
265. S. Wu, *Polym. Eng. Sci.* **30**, 753 (1990).
266. S. Wu, *J. Appl. Polym. Sci.* **35**, 549 (1988).
267. R. J. Gaymans, in D. R. Paul, and C. B. Buckmall, eds., *Polymer Blends*, John Wiley & Sons, Inc., New York, 1999, p. 177.
268. K. Friedrich, *Adv. Polym. Sci.* **52/53**, 225 (1983).
269. C. B. Bucknall, in D. R. Paul, and C. B. Bucknall, eds., *Polymer Blends*, John Wiley & Sons, Inc., New York, 1999, p. 59.
270. A. Lazzeri and C. B. Bucknall, *J. Mater. Sci.* **28**, 6799 (1993).
271. A. S. Argon, R. E. Cohen, O. S. Gebizlioglu, and C. E. Schwier, *Adv. Polym. Sci.* **52/53**, 275 (1983).

272. P. Švec, L. Rosík, Z. Horák, and F. Večerka, *Styrene-Based Plastics and Their Modifications*, E. Horwood, London, 1990, p. 109.
273. W. Döll, *Adv. Polym. Sci.* **52/53**, 105 (1983).
274. A. Arostegui and J. Nazabal, *Polymer* **44**, 239 (2003).
275. J. Z. Liang and R. K. Y. Li, *J. Appl. Polym. Sci.* **77**, 409 (2000).
276. M. Raab, J. Kotek, J. Baldrian, and W. Grellmann, *J. Appl. Polym. Sci.* **69**, 2255 (1998).
277. J. Kotek, M. Raab, J. Baldrian, and W. Grellmann, *J. Appl. Polym. Sci.* **85**, 1174 (2002).
278. C. A. Cruz-Ramos, in D. R. Paul and C. B. Buckmall, eds., *Polymer Blends*, John Wiley & Sons, Inc., New York, 1999, p. 137.
279. P. Galli, *J. Macromol. Sci., Pure Appl. Chem. A* **36**, 1561 (1999).
280. W. Jiang, S. C. Tjong, and R. K. Y. Li, *Polymer* **41**, 3479 (2000).
281. W. Jiang, L. An, and B. Jiang, *Polymer* **42**, 4777 (2001).
282. Z. H. Liu, X. D. Zhang, X. G. Zhu, Z. N. Qi, and F. S. Wang, *Polymer* **38**, 5267 (1997).
283. T. Kurauchi and T. Ohta, *J. Mater. Sci.* **19**, 1699 (1984).
284. M. Lu, H. Keskkula, and D. R. Paul, *Polymer* **34**, 1874 (1993).
285. K. Matsushige, S. V. Radcliffe, and E. Baer, *J. Appl. Polym. Sci.* **20**, 1853 (1976).
286. I. Kelnar, M. Stephan, L. Jakisch, and I. Fortelný, *J. Appl. Polym. Sci.* **74**, 1404 (1999).
287. I. Kelnar, J. Kotek, B. S. Munteanu, and I. Fortelný, *J. Appl. Polym. Sci.* **89**, 3647 (2003).
288. Z. Bartczak, A. S. Argon, R. E. Cohen, and M. Weinberg, *Polymer* **40**, 2347 (1999).
289. W. C. J. Zuiderduin, C. Westzaan, J. Hueting, and R. J. Gaymans, *Polymer* **44**, 261 (2003).
290. M. W. L. Wilbrink, A. S. Argon, R. E. Cohen, and M. Weinberg, *Polymer* **42**, 10155 (2001).
291. C. D. Han, *Multiphase Flow in Polymer Processing*, Academic Press, Inc., New York, 1981.
292. L. A. Utracki, *Polymer Alloys and Blends*, Carl Hanser-Verlag, Munich, 1990.
293. L. A. Utracki, *J. Rheol.* **35**, 1615 (1991).
294. J. F. Palierne, *Rheol. Acta* **29**, 204 (1990).
295. R. Muller, in G. O. Shonaike and G. P. Simon, eds., *Polymer Blends and Alloys*, Marcel Dekker, Inc., New York, 1999, Chap. 16.
296. M. Bousmina, J. F. Palierne, and L. A. Utracki, *Polym. Eng. Sci.* **39**, 1049 (1999).
297. M. Iza, M. Bousmina, and R. Jérôme, *Rheol. Acta* **40**, 10 (2001).
298. P. K. Han and J. L. White, *Rubber Chem. Technol.* **68**, 728 (1995).
299. Z. Kruliš and I. Fortelný, *Eur. Polym. J.* **33**, 513 (1997).
300. M. A. López-Manchado and M. Arroyo, *Rubber Chem. Technol.* **74**, 211 (2001).
301. P. M. Subramanian and I. G. Plotzker, in D. R. Paul and C. B. Buckmall, eds., *Polymer Blends*, John Wiley & Sons, Inc., New York, 1999, p. 359.
302. H. B. Hopfenberg and D. R. Paul, in D. R. Paul, and S. Newman, eds., *Polymer Blends*, Academic Press Inc., New York, 1978, p. 445.
303. J. S. Chiou and D. R. Paul, *J. Appl. Polym. Sci.* **33**, 2935 (1987).
304. C. K. Kim, M. A. Vega, and D. R. Paul, *J. Polym. Sci., Part B: Polym. Phys.* **30**, 1131 (1992).
305. T. F. Blahovici and G. R. Brown, *Polym. Eng. Sci.* **27**, 1611 (1988).
306. Y. Nir, M. Narkis, and A. Siegmann, *Polym. Networks Blends* **7**, 139 (1998).
307. J. B. Faisant, A. Ait-Kadi, M. Bousmina, and L. Deschenes, *Polymer* **39**, 533 (1998).
308. J. Kolařík, L. Fambri, A. Pegoretti, and A. Penati, *Polym. Eng. Sci.* **40**, 127 (2000).
309. L. A. Utracki, *Polymer Alloys and Blends, Thermodynamic and Rheology*, Carl Hanser-Verlag, Munich, 1989, p. 10.
310. L. A. Utracki, *Encyclopaedic Dictionary of Commercial Polymer Blends*, Chem Tec Publishing, Toronto, Canada, 1994.

311. L. A. Utracki, *Commercial Polymer Blends*, Chapman & Hall, London, 1998.
312. S. Datta, D. J. Lohse, *Polymeric Compatibilizers*, Carl Hanser-Verlag, Munich 1996.
313. W. E. Baker, C. Scott, and G. H. Hu, eds., *Reactive Polymer Blending*, Carl Hanser-Verlag, Munich 2001.
314. A. H. Hogt, J. Meijer, and J. Jelenič, in S. Al-Malaika, ed., *Reactive Modifiers for Polymers* Chapman & Hall, London, 1997, p. 84.
315. Utracki, *Encyclopaedic Dictionary of Commercial Polymer Blends*, ChemTec Publishing, Toronto, pp. 183–189, 1994.
316. S. Datta and D. J. Lhose, *Polymeric Compatibilizers*, Carl Hanser-Verlag, Munich, 1996, pp. 315–321.
317. M. van Duin and R. J. M. Borggreve, in S. Al-Malaika, ed., *Reactive Modifiers for Polymers*, Chapman & Hall, London, p. 133, 1997.
318. J. Scheirs, *Polymer Recycling*, John Wiley & Sons, Inc., New York, 1998.
319. R. J. Ehrig, ed., *Plastic Recycling*, Carl Hanser-Verlag, Munich, 1989.
320. I. Fortelný, D. Michálková, and Z. Kruliš, *Polym. Degrad. Stab.* **85**, 975 (2004).

GENERAL REFERENCES

P. J. Flory, *Principles of Polymer Chemistry*, Cornell University Press, Ithaca, N.Y., 1953.
G. L. Lewis and M. Randall, *Thermodynamics*, McGraw-Hill, New York, 1961.
B. D. Gesner, *Encyclopedia of Polymer Science and Technology*, Vol. **10**, Wiley-Interscience, New York, 1969.
J. A. Manson and L. H. Sperling, *Polymer Blends and Composites*, Plenum Press, New York, 1976.
C. B. Bucknall, *Toughened Plastics*, Applied Science Publishers, London, 1977.
R. D. Deanin, in H. F. Mark, N. G. Gaylord, and N. M. Bikales, eds., *Encyclopedia of Polymer Science and Technology*, Supple. Vol. 2, Wiley-Interscience, New York, 1977.
D. R. Paul and S. Newman, eds., *Polymer Blends*, Vols. I, II, Academic Press, Inc., New York, 1978.
O. Olabisi, L. Robeson, and M. T. Shaw, *Polymer—Polymer Miscibility*, Academic Press, Inc., New York, 1979.
L. Sperling, *Interpenetrating Polymer Networks and Related Materials*, Plenum Press, New York, 1981.
D. R. Paul, J. W. Barlow, and H. Keskula, in J. I. Kroschwitz, Ed.-in-ch., *Encyclopedia of Polymer Science and Engineering*, 2nd edition, John Wiley & Sons, New York, 1985.
L. A. Utracki, *Polymer Alloys and Blends*, Hanser Publishers, Munich, 1990.
I. C. Sanchez, *Physics of Polymer Surfaces and Interfaces*, Butterworth-Heiemann, Boston, Mass., 1992.
M. J. Folkes and P. S. Hope, *Polymer Blends and Alloys*, Chapman & Hall, Cambridge, U.K., 1993.
L. A. Utracki, *Encyclopaedic Dictionary of Commercial Polymer Blends*, ChemTec Publishing, Toronto, 1994.
S. Datta and D. J. Lhose, *Polymeric Compatibilizers*, Carl Hanser-Verlag, Munich, 1996.
L. H. Sperling, *Polymeric Multicomponent Materials*, John Wiley & Sons, Inc., New York, 1997.
S. Malaika, *Reactive Modifiers for Polymers*, Chapman & Hall, London, 1997.
L. A. Utracki, *Commercial Polymer Blends*, Chapman & Hall, London, 1998.
G. O. Shonaike and G. P. Simon, *Polymer Blends and Alloys*, Marcel Dekker, Inc., New York, 1999.
D. R. Paul and C. B. Bucknall, eds., *Polymer Blends*, Vols. 1 and 2, John Wiley & Sons, Inc., New York, 2000.

W. E. Baker, C. E. Scott, and G-H. Hu, *Reactive Polymer Blending*, Carl Hanser-Verlag, Munich, 2001.
W. Grellmann, S. Seidler, eds., *Deformation and Fracture Behaviour of Polymers*. Springer-Verlag, Berlin, 2001.
C. Vasile and A. K. Kulshreshtha, eds., *Handbook of Polymer Blends*, Vol. 3A, Rapra, Shawbury, 2003.
C. Vasile and A. K. Kulshreshtha, eds., *Handbook of Polymer Blends*, Vol. 3B, Rapra, Shawbury, 2003.
C. Vasile and A. K. Kulshreshtha, eds., *Handbook of Polymer Blends*, Vol. 4A, Rapra, Shawbury, 2003.
C. Vasile and A. K. Kulshreshtha, eds., *Handbook of Polymer Blends*, Vol. 4B, Rapra, Shawbury, 2003.

ZDENĚK HORÁK
IVAN FORTELNÝ
JAN KOLAŘÍK
DRAHOMÍRA HLAVATÁ
ANTONÍN SIKORA
Institute of Macromolecular Chemistry,
Academy of Sciences of the Czech Republic

Encyclopedia of Polymer Sceince and Technology
Copyright © 2005 John Wiley & Sons, Inc. All rights reserved.

POLYMER VESICLES

Introduction

Vesicles (latin: *vesicula* = small bubble) are self-supported closed bilayer assemblies of several thousand amphiphiles that enclose an aqueous interior volume. The bilayer is a two-dimensional fluid composed of amphiphiles with their hydrophilic head groups exposed to the aqueous solutions and their hydrophobic tails aggregated to exclude water (Fig. 1). The bilayer structure is highly ordered yet dynamic because of the rapid lateral motion of the amphiphiles within the plane of each half of the bilayer.

Cells exploit bilayer structures to create anatomical boundaries, eg in the case of cell membranes which are composed of lipids, proteins, and carbohydrates. During the early 1960s researchers demonstrated that certain classes of lipids, especially phospholipids, could be used to form protein- and carbohydrate-free *model membranes*. Methods were developed for the preparation of supported bilayer lipid *membranes* (1), and it was discovered that dried thin films of phospholipids spontaneously hydrate to yield lipid *vesicles* (2). Vesicles have since then been used as model systems for fluid interfaces and biomembranes (3). Practical applications involving vesicles are in the area of cosmetics and pharmaceutics.

The term *liposome* is frequently interchanged with the term *vesicle* and is usually reserved for vesicles of glycerophospholipids or other natural lipids. *Lipids* (greek: *lipos* = fat) are amphiphiles consisting of two hydrophobic hydrocarbon chains and a polar hydrophilic head group. The most important classes of lipids are phospho- and glycolipids, which contain a phosphate group or a sugar group as head groups. Head groups may in general be ionic, zwitterionic, or dipolar. The typical chemical structures of phospho- and glycolipids are shown in Figure 2.

Since Bangham's 1960s description of lipid vesicles as *liposomes* (4), many other *somes* have been created such as *virosomes* by integrating a cell-binding HIV protein into liposomes (5), *niosomes* made from nonionic amphiphiles similar in size to lipids (6), *polymersomes* formed by amphiphilic block copolymers (7), *peptosomes* made of block copolymers containing polypeptide chains (8,9), and *novasomes*, multilamellar niosomes developed for topical and cosmetic application (10).

In recent years the number of studies on polymer vesicles or polymersomes has strongly increased after first reports by the groups of Eisenberg (11,12), and Bates and Discher (7,13). Since then, amphiphilic block copolymers, rod-coil polymers (14–16), dendrimers (17), and amphiphilic fullerene derivatives (18) have been reported to form vesicular structures. Vesicles can now be made from various polymers, from modified biological to wholly synthetic, from diblock, triblock,

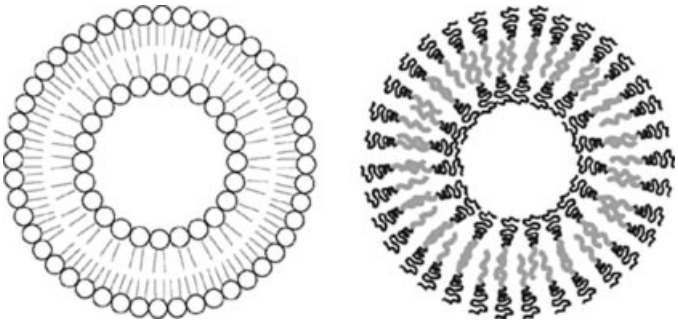

Fig. 1. Lipid and block copolymer vesicles with their typical bilayer structure.

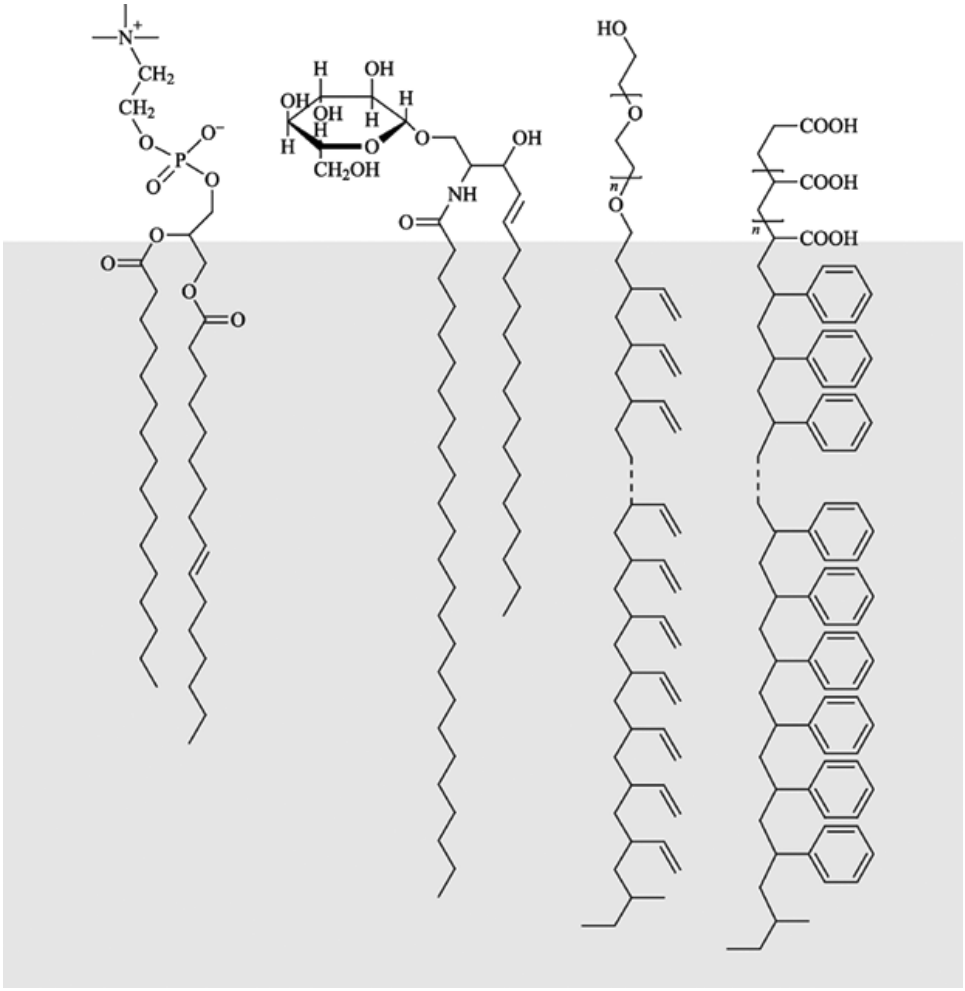

Fig. 2. Chemical structures of a typical phospholipid (phosphatidylcholine), a glycolipid (galactocerebroside), and two vesicle-forming block copolymers, poly(butadiene-*b*-ethylene oxide) and poly(styrene-*b*-acrylic acid.) The grey region indicates the hydrophobic interior of the bilayer.

multiblock, and even statistical copolymers in media ranging from complex to neat organics and water (19–21). A summary of vesicle-forming block copolymers is given in Table 1.

Bilayer and Vesicle Formation

The formation of vesicles can be viewed as a two-step self-assembly process where first the amphiphile forms a bilayer which in a second step closes to form a vesicle (Fig. 3). In the following we will first discuss conditions that lead to the formation of bilayers and then consider their closure to form vesicles.

Energy and Kinetic Aspects.

Thermodynamics of Bilayer Formation. The free energy of a bilayer is mainly determined by the interfacial energy F_{int} of the hydrophobic/hydrophilic interface and the repulsive energy F_{rep} of adjacent amphiphiles (96):

$$F = 2F_{\text{int}} + 2F_{\text{rep}} = 2\gamma a + \frac{2k}{a} = 4\gamma a_0 + \frac{2\gamma}{a}(a - a_0)^2 \tag{1}$$

where γ is the interfacial tension, k is a constant describing the repulsion between the hydrophilic part of the amphiphiles, and a is the interfacial area per amphiphile. The factors 2 arise from the contribution of the two monolayers of the bilayer. A further contribution arises from the elastic stretching energy for the molecules to fit into the planar assembly. The minimum free energy can be obtained by setting $\partial F/\partial a = 0$, which yields an equilibrium interfacial area per chain

$$a_0 = \sqrt{\frac{k}{\gamma}} \tag{2}$$

which allows to recast the expression for the free energy in equation 1 in terms of γ and a_0. The last term in equation 2 then corresponds to a harmonic potential with an area elasticity modulus γ/a, which will be considered in more detail below. Typical values for the interfacial area per chain are $a_0 \approx 0.5$ nm^2 for phospholipids and $a_0 \approx$ 1–50 nm^2 for block copolymers (37,46).

Closure to Vesicles. A flat bilayer disk has a rim energy $F_{\text{disk}} = 2\pi\gamma R_{\text{disk}}$ (Fig. 3), which can be prevented by bending and closing the bilayer to form a

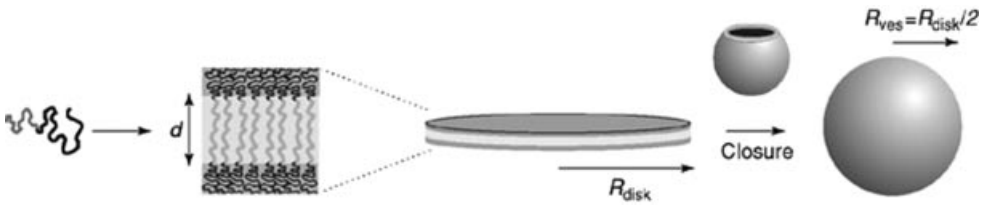

Fig. 3. Scheme of the formation of bilayers and their closure to form a vesicle. From Ref. 20, with permission from John Wiley & Sons, Inc.

Table 1. Overview of Vesicle-Forming Di- and Triblock Copolymers with Corresponding Solvents and Co-solvents

Polymer	Solvent	Co-solvent	Reference
Diblock copolymers			
Poly(dimethylsiloxane-*b*-ethylene oxide), PDMS-PEO	Water		22,23
Poly(methylphenylsiloxane-*b*-ethylene oxide), PMPS-PEO	Water		24
Poly(styrene-*b*-ethylene oxide), PS-PEO	Water	THF, DMF	25–28
Poly(styrene-*b*-acrylic acid), PS-PAA	Water, alcohols	DMF, THF, dioxane	11,12,29–45
Poly(ethylenepropylene-*b*-ethylene oxide), PEP-PEO	Water		46,47
Poly(butadiene-*b*-ethylene oxide), PB-PEO	Water	THF	48
	Water		23,49–54
Poly(2-vinylpyridine-*b*-ethylene oxide), P2VP-PEO	Water		55
Poly(butadiene-*b*-acrylic acid), PB-PAA	Water	THF	48
Poly(ethylethylene-*b*-styrenesulfonic acid), PEE-PSSH	Water		56
Poly(butadiene-*b*-2-vinylpyridine), PB-P2VP	Water		57–59
Poly(styrene-*b*-4-vinylpyridine), PS-P4VP	Water	DMF	60
	$CHCl_3$	HCOOH	61
Poly(styrene-*b*-poly2-β-D-glucopyranosyloxy)ethyl acrylate)	Water	THF, DMF	62
Poly(styrene-*b*-AlaAla)	Water		63,64
Poly(styrene-*b*-*N*,*N*-dimethylaminoisoprene), PS-PDMAI	Water	THF, DMF, dioxane	65
Poly(butadiene-*b*-glutamic acid)	Water		8,66,67
Poly(styrene-*b*-phenylquinoline)	TFA/CH_2Cl_2		15,16
Poly(isoprene-*b*-2-cinnamoylethyl methacrylate)	THF/hexane		68–70
Poly(4-aminomethylstyrene-*b*-styrene)	Water	THF, DMF, dioxane	71
Poly(propylene sulfide-*b*-ethlyene oxide), PPS-PEO	Water		72–74
Poly(styrene-*b*-propyleneimine dendron)	Water		17

C_{60}-(C_5H_{11})$_5$K	Water		18
Poly(dimethylsiloxane-*b*-2-methyloxazoline), PDMS-PMOX	Water		75
Cyclic poly(styrene-*b*-isoprene), PS-PI	Heptane, decane		76
Poly(lactic acid-*b*-N-isopropylacrylamide), PLA-PNIPAM	Water		77
Poly(lactic acid-*b*-ethylene oxide), PLA-PEO	Water		78
Poly(caprolactone-*b*-ethylene oxide), PCL-PEO	Water		78
Poly(3-(trimethylsilyl)propyl methacrylate-*b*-ethylene oxide), PTMSPMA-PEO	Water	methanol	79,80
Poly(dimethylsiloxane-*b*-ferrocenylsilane), PDMS-PFS	Water		81
Poly(N-2-(2-(2-methoxyethoxy)ethoxy)acetyl-lysine-*b*-leucine), PAcOLys-PLeu	Water		82,83
Poly(ethylene oxide-*b*-butylene oxide), PEO-PBO	Water		84
Triblock copolymers			
Poly(styrene-*b*-methylmethacrylate-*b*-acrylic acid), PS-PMMA-PAA	Water	DMF, dioxane, THF	85
Poly(acrylic acid-*b*-styrene-*b*-4-vinylpyridine), PAA-PS-P4VP	Water	DMF/THF	86
Poly(2-methyloxazoline-*b*-dimethylsiloxane-*b*-2-methyloxazoline), PMOX-PDMS-PMOX	Water		87–89
Poly(ethylene oxide-*b*-propylene oxide-*b*-ethylene oxide), PEO-PPO-PEO	Water		90–92
Poly(ethylene oxide-*b*-propylene sulphide-*b*-ethylene oxide), PEO-PPS-PEO	Water		72
Poly(dimethylaminoisoprene-*b*-styrene-*b*-dimethylaminoisoprene), PDMAI-PS-PDMAI	Water		65
Poly(ethylene oxide-*b*-dimethylsiloxane-*b*-2-methyloxazoline), PEO-PDMS-PMeOX	Water		75,93,94
Poly(lactic acid-*b*-PEO-PPO-PEO-*b*-lactic acid), PLA-PEO-PPO-PEO-PLA	Water		95

vesicle. The corresponding bending energy is given by $F_{\mathrm{bend}} = 8\pi\kappa$ (eq. 9), where κ is the bending elastic constant. For a fixed bilayer area $A = \pi R^2{}_{\mathrm{disk}} = 4\pi R^2{}_{\mathrm{ves}}$, a flat bilayer will bend to form vesicles if $F_{\mathrm{bend}} < F_{\mathrm{disk}}$, or if the vesicle radius R_{ves} is larger than

$$R_{\mathrm{ves}} > R_{\mathrm{min}} \approx \frac{2\kappa}{\gamma} \tag{3}$$

The minimal vesicle radius R_{min} is increasing with increasing bending modulus and decreasing interfacial tension. Rigid amphiphiles with in-plane order have large bending moduli and therefore form large vesicles. In the case of fluorosurfactants the crystallinity of the bilayers leads to high values of the bending moduli such that rigid bilayer sheets are formed which are unable to bend into vesicles (97). At a given bending modulus an increase of the interfacial tension can induce a transition from planar bilayers to closed vesicles as has been shown for PS-PAA (39). If the interfacial tension is the dominant contribution to the free energy, the bending modulus is $\kappa \sim \gamma\, d^2$ (eq. 17), and the minimal radius is just dependent on the bilayer thickness $R_{\mathrm{min}} \sim d^2$.

Since the bending energy $F_{\mathrm{bend}} = 8\pi\kappa$ is independent of R, there is no distinguished equilibrium radius for $R_{\mathrm{ves}} > R_{\mathrm{min}}$. After preparation one mostly obtains polydisperse vesicle samples. The increase in translational entropy will slightly favor the formation of small vesicles. As will be outlined below, a control of the vesicle radius is possible by inducing an asymmetry between the outer and the inner monolayer.

Energy Scales. The interfacial energy is in nearly all cases the dominant contribution to the free energy. It is related to the interaction energy ε between the hydrophilic and hydrophobic domains, where typical values are $\varepsilon \approx 5$–10 kJ/mol ($\varepsilon \approx 2 - 4$ k_{B}T) per repeat unit, ie CH_2— or monomer. ε is related to the Flory-Huggins interaction parameter $\chi = z\varepsilon/k_{\mathrm{B}}\,T$, where z is the coordination number. For a typical value of $z = 6$ the interaction parameter is $\chi \approx 12$–24. The interfacial tension is given by $\gamma = \varepsilon/a$, which for $a \approx 0.5$ nm^2 has values in the range $\gamma \approx$ 17–34 mN/m ($\gamma \approx 4$–$8 k_{\mathrm{B}}$T/nm^2).

The key parameter for block copolymer thermodynamics is the segregation parameter $\chi\, N$, where $N = N_{\mathrm{A}} + N_{\mathrm{B}}$ is the degree of polymerization of the block copolymer given by the degrees of polymerization of block A and block B, N_{A} and N_{B}, respectively. Throughout the article, "A" will denote the hydrophobic block and "B" the hydrophilic block, respectively. The molar fraction of the hydrophilic block is given by $f = N_{\mathrm{B}}/N$. For typical values of $N \approx 10$–1000, the segregation parameter is $\chi N \gg 100$, which corresponds to the limit of strong segregation. The segregation parameter χN together with the relative block length f dictates the phase behavior of block copolymers, eg the formation of micelles (98), lyotropic phases (99,100) and bulk phases (101,102).

A characteristic parameter for amphiphiles is the critical micelle concentration (CMC), which is related to the interaction energy as $c_{\mathrm{CMC}} \sim \mathrm{e}^{-N\varepsilon/KT}$. The CMC corresponds to the number of free chains in equilibrium with micelles. For single chain surfactants, typical values are in the range of $c_{\mathrm{CMC}} \approx 10^{-2}$–$10^{-4}\,M$, whereas for double chain lipids typical values are in the range of $c_{\mathrm{CMC}} \approx 10^{-9}\,M$. For block copolymers the CMC is expected to be much smaller. Luo and co-workers

(123) estimated the fraction of free chains to be between 10^{-14} and 10^{-32} M depending on segregation strength. For most vesicle forming systems, the fraction of single free chains is negligibly small.

Exchange Kinetics and Freezing. There are two processes that lead to exchange of amphiphiles between micelles or vesicles (103):

(1) Exit/insertion of single free amphiphiles: This is the classical mechanism for low molecular weight surfactants; the exchange rate is practically independent of concentration
(2) Merger/splitting of two micelles or vesicles upon contact with exchange of amphiphiles: The exchange rate increases with concentration because the number of collisions is increasing

The exchange of amphiphiles for both processes is a thermally activated process. As such, the average exchange time (residence time in a micelle or vesicle) is of the order $\tau \sim e^{N\varepsilon/kT}$. With increasing interaction energy ε or interfacial tension γ, and as the alkyl or polymer chain becomes longer, the exit rate of a chain becomes appreciably lower. Exchange times for single chain surfactants are $\tau \approx 10^{-5}$–10^{-3} s, whereas typical values for lipids are $\tau \approx 10^5$ s, ie of the order of several hours to days. For polymeric amphiphiles the exchange times are still orders of magnitude larger.

The small fraction of single free chains together with slow exchange kinetics essentially freezes the exchange process. A sufficiently fast exchange of amphiphiles is, however, necessary to sustain thermodynamic equilibrium. Therefore vesicles, once formed, are in a metastable, trapped, or quenched thermodynamic state. The number of amphiphiles and therefore their bilayer area is essentially constant on timescales of most experiments. An extreme case is glassy polymers with very slow lateral mobility which can even impede shape changes of polymer vesicles ("frozen" vesicles).

The presence of co-solvents can fluidize and activate polymer exchange rates. The influence of solvent composition on vesicle exchange kinetics has been investigated for PS-PAA in DMF/water mixtures (30). When the water content was <6.5 wt%, the formation of the aggregates was reversible. When the water content was >7.5 wt%, the morphology of the aggregates depended on the method of sample preparation and the morphological reversibility decreased significantly. Shape transitions such as spheres → cylinders → bilayers were not achievable within a period of several days. The kinetics could be accelerated by increasing the efficiency of adhesive collisions through addition of ions or increase of the polymer concentration.

Packing and Geometry.

Packing parameter and Curvature. An important factor determining the shape of self-assembled amphiphilic structures is the size of the hydrophobic part of the amphiphile relative to the hydrophilic part. The shape can be parameterized in terms of the packing parameter Δ, which is given by

$$\Delta = \frac{v}{al_c} = 1 - Hl_c + \frac{Kl_c^2}{3} \tag{4}$$

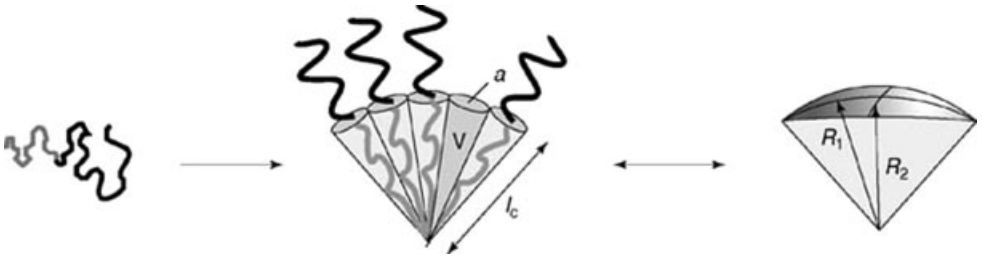

Fig. 4. Packing of amphiphiles at curved interfaces. The volume v, the surface area a, and the chain length l_c determine the interfacial curvature, which is characterized by the two principal radii R_1 and R_2.

where v is the volume of the hydrophobic chain, l_c is the contour length of the hydrophobic chain, and a is the interfacial area, as shown in Figure 4. The packing parameter is related to the curvature of the hydrophobic/hydrophilic interface as described by its mean curvature H and its Gaussian curvature K (104,105), which are given by the two principal radii of curvature, R_1 and R_2

$$H = \frac{1}{2}\left(\frac{1}{R_1} + \frac{1}{R_2}\right)$$
$$K = \frac{1}{R_1 R_2} \tag{5}$$

The simplest shapes are spheres, cylinders, and bilayers which have values of the packing parameter and curvature as shown in Table 2.

Conditions for Bilayer Formation. In order to obtain bilayers or vesicles for an amphiphile of length l_c, one needs to adjust the interfacial area until the surfactant parameter Δ approaches unity. With the optimum head group area a_0 from equation 2 and the definition of the packing parameter (eq. 4), one obtains a simple expression that can serve to rationalize the influence of different parameters on the packing parameter

$$\Delta \sim \frac{\gamma^{1/2} v}{k^{1/2} l_c} \tag{6}$$

Thus, for fixed length l_c, the packing parameter can be increased by

(1) increasing the interfacial tension γ, eg by working in aqueous solutions or adding water to organic solvents;

Table 2. Values for the Packing Parameter, the Principal Radii of Curvature, Mean and Gaussian Curvature for Different Amphiphile Aggregate Shapes

Shape	Δ	R_1	R_2	H	K
Sphere	1/3	R	R	$1/R$	$1/R^2$
Cylinder	1/2	R	∞	$1/(2R)$	0
Bilayer	1	∞	∞	0	0

Table 3. Variation of Different Parameters to Drive Self-Assembly towards Vesicle Formation

Parameter	Realization	Polymer	Reference
k↓	Decreasing N_B	PS-PAA	11,37,39,44, 50,111,112
		PS-PEO	113
		PB-PEO	46,114
		PEE-PEO	46
		PEO-PEE-PEO	46
$\gamma \uparrow$	Addition of water	PS-PAA; dioxane/water	32,39,112
$k \downarrow$	Addition of ions; screens Coulomb interaction	PS-PAA	12,115
		PEE-PSSH	56
k	pH	P4VP-PS; DMF/water; P4VP-PS-PAA; DMF/THF/water	60,86
$k \downarrow$	Addition of ionic surfactant (SDS)	PS-PAA; dioxane/water	116
$v \uparrow$	Core-swelling, screening of PAA	PS-PAA; Dioxane, THF, DMF	38,117

(2) decreasing the chain repulsion, k, eg by decreasing the hydrophilic block length (decreasing hydrophilic fraction f), screening of electrostatic repulsion via the addition of ions, or screening adjacent chain repulsion by increasing the polymer concentration;

(3) increasing the volume, v, eg by swelling with organic solvents.

By variation of these factors it is possible to drive amphiphile association in the direction spheres → cylinders → bilayers/vesicles. Detailed theoretical investigations have recently been performed by molecular dynamics simulations (106). Further factors involve temperature and added homopolymer, which affects the stretching energy of the core chains. The variation of these factors and their effects on aggregate morphology have been reviewed (29,32–36,107–110) and are summarized in Table 3.

Shape Transitions. The influence of the hydrophilic block length on the micellar shape has been systematically investigated for PS-PAA in DMF/water mixtures (10). As the length of the PAA block decreased, the morphology of the aggregates changed progressively from spheres for PS_{200}-PAA_{21} → cylinders for PS_{200}-PAA_{15} → bilayers (vesicles and lamellae) for PS_{200}-PAA_8. It was noted that for block copolymers of similar hydrophobic block length, the values of the interfacial area per chain a_0 decrease as the morphology changes from sphere → cylinder → vesicle, which is in accord with the reduced chain repulsion (eq. 2) leading to larger packing parameters for shorter hydrophilic chains (37).

As another example, Figure 5 shows the morphologies for a series of PB-PEO block copolymers in aqueous solutions, where a decrease of the hydrophilic block ratio f leads to shape changes from sphere → cylinder → vesicle (102). Similarly,

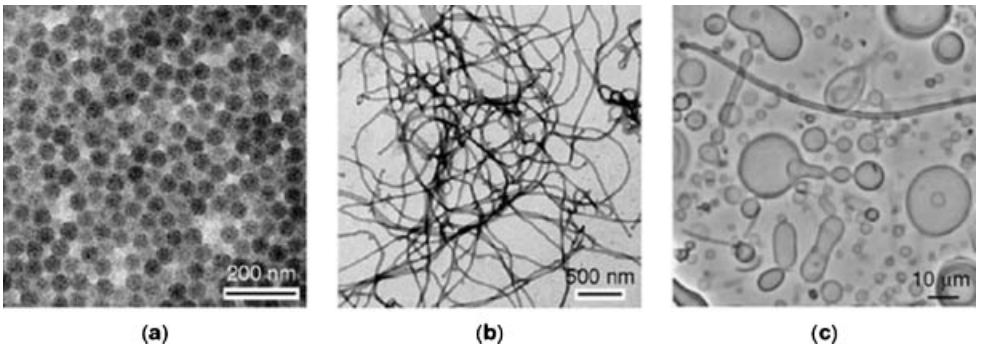

Fig. 5. TEM (**a**, **b**) and optical micrographs (**c**) of different shapes for a series of PB-PEO block copolymers, ranging from spherical micelles (PB_{202}-PEO_{360}, $f = 0.64$), cylindrical micelles (PB_{125}-PEO_{155}, $f = 0.55$) to vesicles (PB_{25}-PEO_{40}, $f = 0.38$). It illustrates the influence of the hydrophilic block fraction f on the self-assembly structure. From Ref. 20, with permission from John Wiley & Sons, Inc.

an increase of the size of the hydrophobic part at a given hydrophilic block length decreases f, leading to the same series of shape transition as shown for dendron-block copolymers with increasing dendron generation (17). This sequence of shape transitions induced by changes in block length is well known for low molecular weight nonionic surfactants (C_xE_y- series) (118).

Phase Diagrams. A phase diagram with the boundaries for the micellar shape transitions as a function of block copolymer composition has been determined for PEO block copolymers (Fig. 6**a**). The vertical lines are the boundaries separating different micellar shapes. As a rule of thumb, the hydrophilic fraction

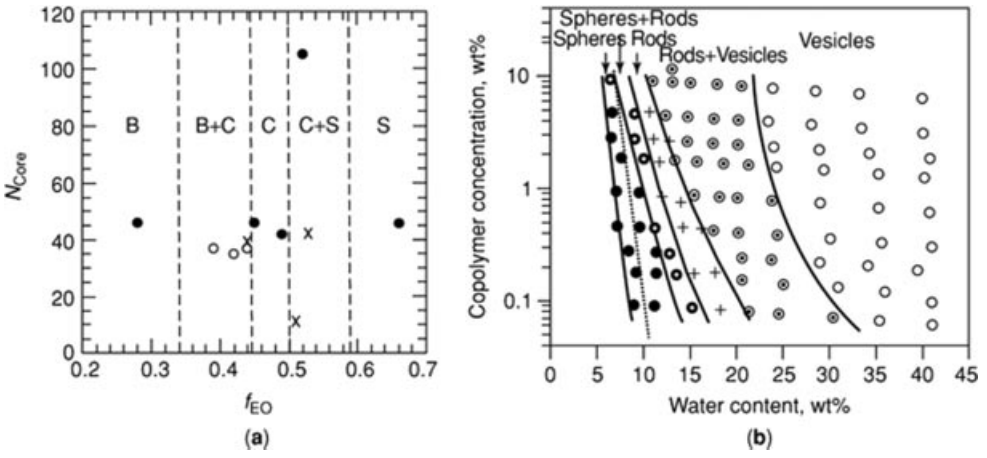

Fig. 6. Phase diagrams with shape transition boundaries for block copolymers as a function of (**a**) hydrophilic fraction f (from Ref. 46, with permission from ACS Publication Division) and (**b**) water content in dioxane/water solutions (from Ref. 39, with permission from ACS Publication Division). B: bilayers/vesicles; C: cylindrical micelles; S: spherical micelles.

of the block copolymer should be in a range $f \approx 30$–40%, a range which is similar to that for phospholipids, to obtain vesicles (46).

The influence of the interfacial tension γ on the micellar shape has been investigated for PS-PAA block copolymers in dioxane/water mixtures. With increasing water content the expected sequence of morphologies, sphere → cylinder → bilayer, is observed (115). Bilayers include vesicles, lamellae, and more complicated structures. The addition of water to dioxane solutions induces aggregation of the polystyrene segments and increases the interfacial tension γ. Figure 6**b** shows the corresponding phase diagram (39).

Not only the water content but also the polymer concentration affects the morphologies and the sizes of the aggregates. It was found that the boundaries of the morphological transitions shift to lower water contents with increasing total block length and with decreasing PAA block length. Further it was found that long core-forming blocks and high water contents favor the formation of vesicles and that short core-forming blocks and low water contents favor the formation of open bilayers. The addition of homopolystyrene changed the morphologies from bilayers or cylinders to spheres (37).

Intermediate Shapes. Details of the cylinder → vesicle shape transition have been investigated for PS-PAA block copolymers in dioxane/water mixtures (119). Accordingly, the morphological transition proceeds through a flattening of the rods via a lamellar intermediate state and their closing to form vesicles. The reverse shape transition proceeds via a collapse of the vesicle followed by a rearrangement to form dumbbell aggregates and finally smooth cylinders (40). For amphiphilic block copolymers with compositions f that are intermediate between cylinders and vesicles, Y-junctions and three-dimensional networks leading to a considerable morphological complexity were reported (120). Other complex structures involve the formation of filaments in polyelectrolyte bilayers as a consequence of the balance of long-range repulsive Coulomb interactions and short-range attractive hydrophobic interactions (59,121,122).

Segregation and Localization.

Strong Segregation Limit. So far flexible chain amphiphiles have been considered where a balance of chain repulsion, chain stretching, and interfacial tension together with the hydrophilic/hydrophobic ratio of the amphiphile dictates the aggregate shape. Vesicle formation is generally observed if the hydrophilic fraction of the amphiphiles is in a range $f \approx 30$–40%. This range can be much larger if the bilayer structure is further stabilized. This is typically the case for systems with

(1) large interfacial energy F_{int}: high energy interfaces in order of increasing interfacial tension are water/oil < water/silicone < water/fluorinated hydrocarbon;

(2) small stretching energy F_{el}, which is the case for polymers with small conformational entropy which are typically stiff polymer chains with low internal degrees of freedom or chains with highly localized segments;

(3) small repulsive energy F_{rep}, where the repulsion between adjacent polymer chains at the interface is screened, eg by addition of ions or increasing polymer concentrations to high volume fractions.

Under these conditions the interfacial energy is the most dominant thermodynamic contribution and hydrophobic and hydrophilic domains are highly segregated (strong segregation limit). The system globally minimizes the interfacial area per unit volume, which is given by

$$A_V = d\frac{\phi}{l} \tag{7}$$

where ϕ is the volume fraction of the hydrophobic domains and d is the dimensionality. Since for planar structures the dimensionality has the lowest value of $d = 1$, such interfaces are preferred compared to cylindrical ($d = 2$) or spherical ($d = 3$) domains. In this regime bilayer structures are preferred irrespective of the shape of the amphiphiles.

Secondary Valence Interactions. Under these conditions, the range of stability of planar bilayer structures and vesicles can be quite extended. Low entropy chains include fullerenes, rod-like polymers, and polymers carrying mesogens as well as polymer chains with highly localized chain segments such as branch points in dendrimers (covalent binding) or segments involved in strong functional or complementary interactions including H-bonds, Coulombic, dipolar or π–π interactions, ligand binding, α-helix/β-sheet formation, or other secondary valence interactions. These structures are schematically shown in Figure 7.

A well-known case where Coulombic interactions stabilize bilayer structures are mixtures of cationic and anionic surfactants, so-called catanionics (123). A related single component surfactant system which forms equilibrium vesicles over the whole range of volume fractions is single chain sulfonium surfactants (124). Here, the polarizability of the sulfur head group and H-bridges stabilize the bilayer morphology. Vesicle formation was described by Chu and co-workers (18) for pentaphenylfullerene anions, which form small vesicles of 17 nm diameter. Kukula and co-workers described vesicle formation of polybutadiene-*b*-poly(L)glutamates (7), where the hydrophilic glutamic acid blocks form α-helices. Schlaad and co-workers used polyelectrolyte ionic complex formation of double hydrophilic

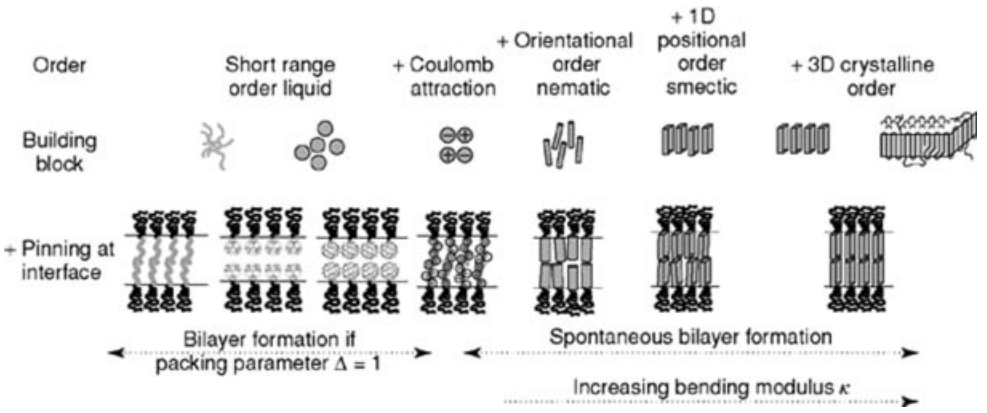

Fig. 7. Different amphiphile structures arranged, from left to right, with increasing in-plane order, which is an additional driving force for bilayer and vesicle formation. From Ref. 20, with permission from John Wiley & Sons, Inc.

block copolymers to form asymmetric equilibrium vesicles (125). Complexes of block ionomers and surfactants have also been reported to form vesicles (126,127). Even statistical copolymers can form well-defined vesicles by complementary functionalization with diaminopyridine and thymine groups, which are DNA-binding motives (128).

Liquid Crystalline Packing. A further factor that stabilizes bilayer structures is a hydrophobic part of the amphiphile, which is shape persistent and has a tendency to form ordered structures. One distinguishes *liquid-like* structures with short-range order (eg dendrimers, flexible polymer chains) from *nematics* with additional orientational order (eg rod-like polymers), *smectics* with additional one-dimensional positional order, and *crystalline materials* with three-dimensional positional order. Increasing in-plane order leads to an increase of the bending modulus of the bilayer resulting in large vesicles. For example, Jenekhe and coworkers (15,16) described giant vesicles that spontaneously formed from rod-coil block copolymers even in organic solvents.

The factors leading to bilayer or vesicle formation are schematically summarized in Figure 7, where amphiphiles are arranged according to their in-plane state of order. The pinning of hydrophobic mesogens to an interface is sufficient for the formation of stable bilayer structures. In summary, amphiphiles can be made to assemble into bilayers by adjusting the packing parameter toward unity, for high energy interfaces, or by using amphiphiles with low conformational entropy or using mesogenic amphiphiles.

Vesicle Preparation and Size Control. As outlined, the size and shape of vesicles depend to a large extent on preparation conditions. Several procedures are available for the formation of lipid vesicles (129,130), which are in most cases also suitable for the preparation of polymer vesicles.

Direct hydration. The simplest procedure is to hydrate a thin film or a solid piece of lipid or block copolymer with an aqueous solution, which leads to the spontaneous formation of vesicles. For film rehydration the amphiphile is dissolved in an organic solvent, which then is evaporated under vacuum or using a nitrogen stream to yield a thin film on a glass or Teflon substrate (131). Upon addition of water, the film swells under formation of a lamellar bilayer phase with vesicles budding or separating at lamellar defects from the film surface (Fig. 8). This method often yields multilamellar vesicles with a broad size distribution. For bulk rehydration stirring, vortexing or sonication is required for a complete hydration of the sample.

Electroformation. For electroformation (132), a thin film is deposited on adjacent electrodes (Pt, Au, ITO-coated glass) and the budding process is induced by an alternating current at typically 10 Hz (10 V) (7). The electric field decreases the membrane tension and thereby facilitates vesicle formation. This method yields the largest vesicles (giant vesicles) with diameters up to 100 μm.

Hydrating under shear, eg by vigorous stirring, reduces the vesicle size to the submicron range. Details of the shear-induced formation of vesicles from swollen lamellar phases have been investigated (92).

Organic Co-solvents. In this method the amphiphile is dissolved in an organic solvent and then mixed with an aqueous solution where it forms vesicles. It is a convenient way for the large-scale preparation of vesicles. Vesicle size and size distribution depends on the details of the mixing process, ie dropwise addition/

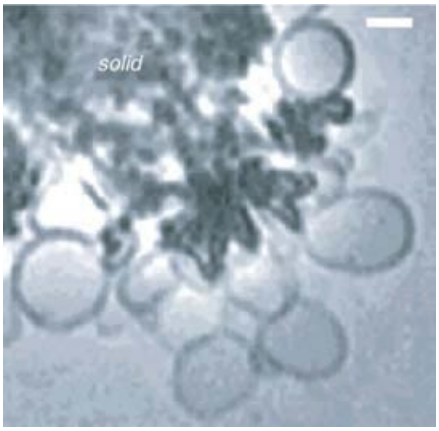

Fig. 8. Block copolymer vesicles budding-off from a swollen lamellar phase. After separation, there is no further exchange of block copolymers between vesicles. from Ref. 50, with permission from ACS Publications Division.

injection of the organic solution into water or addition/injection of water into the organic solution both with or without agitation by stirring or sonication. The organic solvent can subsequently be removed by reduced pressure, dialysis, gel filtration, or ultrafiltration.

Size Control. Once the vesicles are formed, they will keep their size and size distribution. In order to reduce their size one has to disrupt the vesicle membrane, which is done by strong shear forces, eg by ultrasonic irradiation, ball milling, and high-pressure extrusion through membranes or slits ("French press"). Extrusion through polycarbonate membranes, which are available with pore diameters between 50 and 800 nm, allows a reduction and control in vesicle size and polydispersity to obtain small unilamellar vesicles with size distributions within 10–20%. Fast and direct preparation of small monodisperse vesicles in the size range of 50–200 nm is possible using inkjet printers (133). By appropriate choice of sample preparation method, it is thus possible to tailor the size of the vesicle between 50 nm and 10 μm with narrow size distribution.

Glassy Polymers. Vesicle preparation for high molecular weight or glassy block copolymers requires the use of co-solvents. First, the block copolymer is dissolved in a water-miscible common solvent for both blocks (eg dioxane, THF, DMF). Then water is added, which induces the aggregation into micelles. Further addition of water increases the interfacial tension and drives shape transitions to cylindrical micelles, bilayers, and vesicles. Under optimal conditions, it is possible to obtain small, uniform unilamellar vesicles as is shown in Figure 9. In another method, the polymers are dissolved at high temperatures close to their glass-transition temperature. In case of low-boiling solvents, confinement under pressure is required. The formation of vesicles is subsequently induced by cooling (31).

Vesicle Shapes

Lipid and polymer vesicles can possess numerous shapes that can be systematically categorized and their energy described by concepts derived from differential geometry.

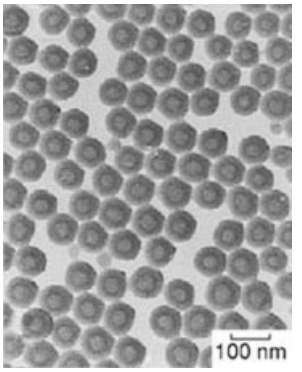

Fig. 9. Small, narrow disperse block copolymer vesicles prepared using organic cosolvents. From Ref. 115, with permission from ACS Publications Division.

Curvature Energy.

Membrane Energy. Any three-dimensional geometrical object can be characterized by its volume V, surface area A, and its mean and Gaussian curvature H and K, respectively. For bilayer membranes, a further contribution arises from the difference ΔA of the area of the outer and inner monolayer. This leads to five contributions to the free energy (134), which are obtained by integrating over the volume and the surface area of the vesicle as

$$\begin{aligned} F &= F_{\mathrm{V}} + F_{\mathrm{A}} + F_{\mathrm{H}} + F_{\mathrm{K}} + F_{\Delta \mathrm{A}} \\ &= \int \Pi \mathrm{d}V + \frac{k_{\mathrm{A}}}{2} \oint \bar{\rho}^2 \mathrm{d}A + \frac{\kappa}{2} \oint (2H)^2 \mathrm{d}A + \kappa_{\mathrm{G}} \oint K \mathrm{d}A + \frac{k_{\mathrm{A}}}{2} \oint (\rho - \mathrm{d}H)^2 \mathrm{d}A \end{aligned} \tag{8}$$

where Π is the osmotic pressure, V is the volume of the vesicle, k_{A} is the area elastic modulus, $\overline{\rho}$ is the deviation from the equilibrium area per chain a_0 (eq. 2), κ is the elastic bending modulus, H is the mean curvature (eq. 4), κ_{G} is the Gaussian bending modulus, K is the Gaussian curvature (eq. 4), ρ is the area difference between outer and inner bilayer, and d is the bilayer thickness. Integration of the osmotic pressure $\Pi = RT(n_{\mathrm{in}}/V - c)$ over the volume of the vesicle, and of the mean curvature H and area differences $\overline{\rho}$ and ρ over the area of the vesicle yields (134)

$$F = \frac{RTc}{2V_0}(V - V_0)^2 + \frac{k_{\mathrm{A}}}{2A}(A - A_0)^2 + 8\pi\kappa + \kappa_{\mathrm{G}} \oint K \mathrm{d}A + \frac{k_{\mathrm{A}}}{8A}(\Delta A - \Delta A_0) \tag{9}$$

where c is the concentration of solute outside the vesicle, n_{in} is the moles of solute inside the vesicle, $V_0 = n_{\mathrm{in}}/c$ is the volume for which the osmotic pressure vanishes, A_0 is the area of the relaxed bilayer, and ΔA and ΔA_0 are the actual area difference and the relaxed area difference between the outer and the inner monolayer.

Osmotic Pressure. The osmotic contribution to the free energy, F_{V}, arises from the presence of molecules in the solution to which the membrane is impermeable on the timescale of the experiment. This leads to an osmotic pressure $\Pi = RT\Delta c$, where Δc is the concentration difference between the solutions outside and inside the vesicle. The concentration difference that can be sustained by a curved membrane can be estimated by comparing the osmotic energy to the bending energy $F_{\mathrm{H}} = 8\pi\kappa$. For typical values of the bending modulus $\kappa \approx 1.5 \times 10^{-19}$

J (7,53) one finds at room temperature $\Delta c \approx 1$ mmol/L. Thus, only minute concentration differences between interior and exterior solution can be balanced by the curvature energy. Large osmotic pressure differences will instead lead to the inward/outward permeation of water and concomitantly an increase/decrease of the vesicle volume until the concentration difference is $\Delta c = 0$ and thus $V = V_0$. In practice, this allows one to control the vesicle volume by the molar concentration ("osmolarity") difference of the inner and outer solutions.

Membrane Area. Similar to the osmotic energy, the energy F_A involving the total area of the vesicle vastly exceeds the energy of the bending elasticity. Thus the vesicle will adapt an area $A = A_0 = \overline{N}a_0$ that is given by the number $\overline{N}$ of amphiphiles in the bilayer. The average area of the vesicles is in most cases fixed after sample preparation and may slightly depend on temperature or pH.

Genus. As a consequence of the Gauss–Bonnet theorem

$$\oint K \mathrm{d}A = 2\pi(2 - 2g) \tag{10}$$

the energy due to the Gaussian curvature F_K is related to a topological invariant of the vesicle, its genus g. The genus of a surface is given by its number of "holes" or "handles" (see Fig. 10). Therefore, local variations in the Gaussian curvature K have no effect on the global Gaussian curvature as long as the topology is fixed. For any fixed topology or genus, the energy F_K is thus constant and can be neglected by setting $\kappa_G = 0$.

Membrane Elasticity. For a vesicle with fixed volume $V = V_0$, area $A = A_0$, and genus the curvature energy of the bilayer membrane reduces to the sum of the remaining two terms of equation 9

$$F = F_H + F_{\Delta A} = \frac{\kappa}{2}\oint (2H - C_0)^2 \, \mathrm{d}A + \frac{k_A}{2A}(\Delta A - \Delta A_0)^2 \tag{11}$$

which correspond to the two modes of membrane deformation shown in Figure 11. C_0 is the spontaneous curvature, which has been introduced to account for a locally preferred curvature of the membrane due to the molecular structure of the amphiphile.

Area Difference. ΔA is the area difference between the inner and outer monolayer, which is related to the radius of the vesicle and the bilayer thickness d (see Fig. 12) via

$$\Delta A = A_{\mathrm{out}} - A_{\mathrm{in}} = 8\pi \, \mathrm{d}R \tag{12}$$

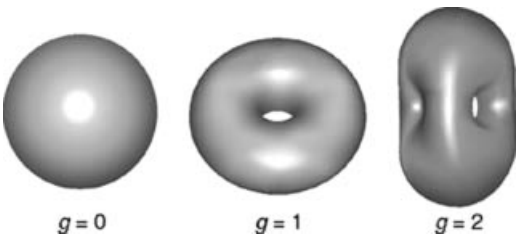

Fig. 10. Closed surfaces with genus (number of holes) of zero, one, and two.

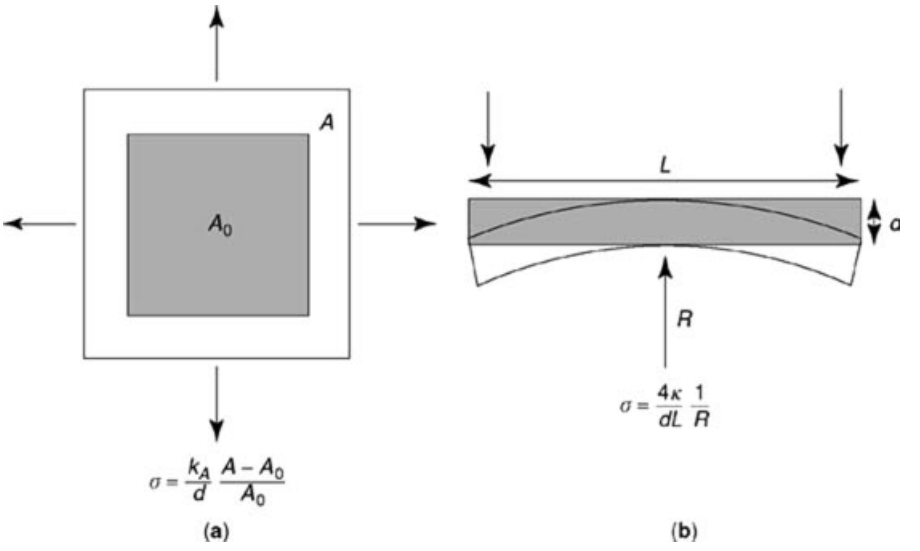

Fig. 11. Stretching (**a**) and bending (**b**) of a membrane with the corresponding elastic stretching modulus k_A and elastic bending modulus κ. In case of stretching, the stress σ is the force per unit area $A = L^2$, whereas in the case of bending, the stress is the force per unit cross-sectional area dL. According to simple elasticity theory for thin plates, the two moduli are related by $4\kappa = k_A d^2/12$ (135).

The actual area difference will, in general, differ from the optimal area difference ΔA_0

$$\Delta A_0 = (N_{out} - N_{in})a_0 = \Delta N a_0 \tag{13}$$

which is determined by the number of amphiphiles in each monolayer and the equilibrium area per amphiphile a_0. If the interfacial area per amphiphile is the

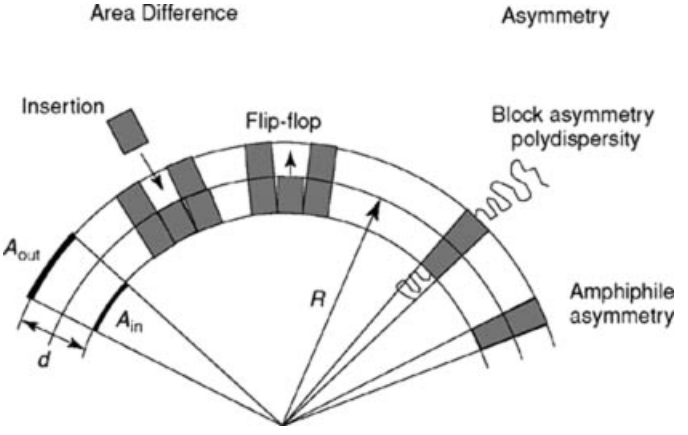

Fig. 12. Sources of area difference curvature ΔA (insertion, flip-flop) and spontaneous curvature C (block and amphiphile asymmetry, polydispersity) for bilayer structures. The vesicle will adapt a curvature that is a compromise between the two, depending on the related energy.

same in the outer and inner monolayer, ie $a_{out} = a_{in} = a$, then the relative area difference $\Delta A/A$ is related to the relative difference in the number of amphiphiles $\Delta N/N$ by

$$\frac{\Delta A}{A} = \frac{\Delta N}{N} = \frac{d}{2R} \tag{14}$$

with the mean bilayer area $A = Na$. Thus, for small lipid vesicles with a bilayer thickness $d = 3$ nm and a radius eg, $R = 20$ nm, there is a large ($\Delta N/N = 30\%$) difference in the number of lipids in the inner compared to the outer bilayer. This leads to a large free energy contribution related to ΔA, and so small vesicles are often relatively unstable. The area difference ΔA can change by the exchange of lipids between the inner and outer monolayer ("flip-flop"), or the addition (insertion, adsorption, anchoring) of amphiphiles to one monolayer (136) (Fig. 12).

Spontaneous Curvature. A different chemical environment on both sides of the membrane (eg different surface charge density, different electrolyte concentrations), an asymmetric molecular shape of the amphiphile, or a different chemical composition of the two monolayers tends to locally curve the membrane (Fig. 12). This membrane-asymmetry-related curvature is described by the spontaneous curvature

$$C_0 = \frac{1}{R} \tag{15}$$

of the bilayer. Different chemical environments on both sides of the membrane will in general also lead to differences in the interfacial area per amphiphile $a_{out} \neq a_{in}$ and thus in the area difference ΔA.

Bilayer asymmetry can already be caused by chain length segregation of polydisperse polymeric amphiphiles between the two monolayers. To reduce steric repulsion, short hydrophilic chains will tend to segregate to the inner monolayer, whereas long chains will preferentially segregate to the outer monolayer as schematically shown in Figure 12. The segregation of block copolymers of different length across the bilayer has been demonstrated by Luo and Eisenberg (41) using pyrene-labeled PS-PAA. Upon addition of a fluorescence quencher (Tl^+), vesicles prepared with the labeled short hydrophilic blocks experience minimum quenching, since these chains preferably segregate to the inside of the vesicles and are thus largely inaccessible to the quencher. Pyrene residues in the vesicles prepared from the longest labeled hydrophilic chains are 12 times more accessible to the quencher than the pyrene in the vesicles prepared from the shortest labeled hydrophilic chains (Fig. 13). This asymmetry leads to a certain spontaneous curvature C_0. If there is sufficient flip-flop of amphiphiles to adjust the corresponding area difference ΔA, there will be a thermodynamically preferred average radius $R \approx {C_0}^{-1}$ of the vesicles. As expected, the spontaneous curvature increased, and thus the size of the vesicles decreased with increasing PAA polydispersity, ie increasing bilayer asymmetry (137). This allows to asymmetrically localize two different types of polymer chains if the corona blocks are of sufficiently different length (138). In a further study (42,139), fluorescence quenching

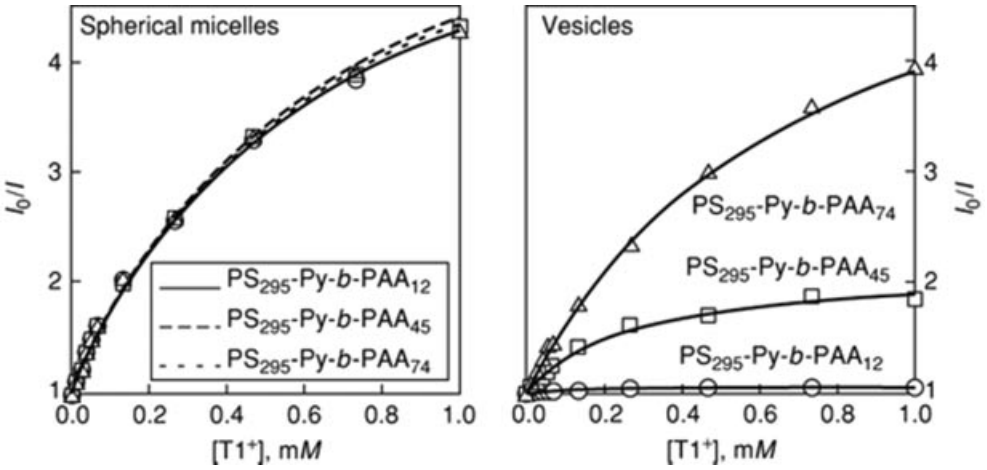

Fig. 13. Experiments showing preferential quenching of long, fluorescently labeled chains due to their accumulation in the outer monolayer of vesicles. In case of spherical micelles, preferential quenching is neither expected nor observed. From Ref. 41, with permission from the ACS Publications Division.

experiments have shown that this segregation is size dependent. The larger the vesicles, the lower the degree of segregation becomes.

The average radius of PS-PAA vesicles could also be changed in solvent mixtures of dioxane/THF/water or DMF/THF/water by changing the water content (11,42,43,111,139). An increase in vesicle size from $R \sim 45$ nm to $R \sim 100$ nm could be induced by increasing the water content from 25 to 70%, while a decrease in vesicle size could be induced by decreasing the water content by addition of THF/dioxane. The observed change has been attributed to minimization of the interfacial energy, but may also be related to changes in membrane diameter d. The addition of water extracts DMF/THF from the bilayer thereby decreases d, which according to equation 12 leads to an increase of the radius for a given area difference ΔA. The addition of DMF/THF will then lead to the reverse effect. The effect of block lengths, solvent composition, and additives on the vesicle size has been summarized in Reference (45).

Equilibrium Curvature. The two sources of curvature (ΔA, C_0) correspond to two different radii R. In general, a vesicle will thus be in a stressed state, its radius and shape minimizing the bending energy for a given difference ΔN of the number of amphiphiles in the inner and outer monolayer. The compromise between changes in area difference ΔA and local curvature C_0 in equilibrium depends on the relative magnitude of the two bending energies F_{H} and $F_{\Delta A}$. Only if the area difference is $\Delta A = \Delta A_0$, so that the corresponding radius $R = (\Delta A/8\pi d) = (1/C_0)$, then $H = C_0/2$ and the corresponding free energy of the membrane (eq. 11) is equal to zero. Under these conditions the vesicle is said to be in its "relaxed" thermodynamic state.

An illustrative example for the introduction of spontaneous curvature is bolaamphiphiles. *Bolaamphiphiles* are membrane-spanning bipolar amphiphiles. They are the most important lipid fraction from archebacteria that exhibit unusual

stability at extreme conditions of pH and heat. Single chain bolaamphiphiles form extended single-molecule-thick membranes. They are unable to form small vesicles because their vanishing spontaneous curvature requires a large difference ΔN of lipids in the outer and inner monolayer, which leads to a large free energy contribution related to ΔA. If the spontaneous curvature is increased by addition of cholesterol, small vesicles can be formed by sonication (140). The cholesterol is preferentially incorporated into the outer monolayer of the vesicle bilayer. Bolaamphiphiles with one large and one small head group form asymmetric vesicles with the larger group on the outside surface (141).

Chemically Asymmetric Bilayers. Vesicles from the asymmetric triblock copolymer PAA-PS-P4VP have been prepared in DMF/THF/water mixtures (86). Since the ionization of the two hydrophilic P4VP and PAA chains occurs in different pH ranges (for PAA at high pH, P4VP at low pH), a pH-induced flip-flop of the hydrophilic chains could be observed. Vesicles prepared at low pH contained P4VP chains on the outside and PAA chains on the inside membrane to minimize Coulombic repulsion, whereas vesicles prepared from the same triblock at high pH contained PAA outside and P4VP inside. This could be shown by measurements of the ς potential, which changed characteristically when changing the pH of the outside solution. A similar concept has been used for a one-step preparation of block copolymer vesicles with preferentially segregated acidic and basic corona chains (138). Asymmetric PEO-PDMS-PMOX vesicles have been prepared with a preferred orientation of the shorter hydrophilic blocks to the inside of the vesicles (142). The asymmetry was demonstrated by fluorescence quenching experiments similar as in Reference (41).

Vesicle Shapes and Shape Transitions.

Phase Diagram. As the surface area A is usually fixed for a vesicle after its preparation, it is useful to consider an area-equivalent radius $\overline{R} = (A/4\pi)^{1/2}$, which is defined via the radius of a spherical vesicle with the same surface area A. Using the radius $\overline{R}$ the reduced spontaneous curvature c_0, the reduced volume v, the reduced optimal area difference Δa_0, and the effective reduced area difference $\Delta \hat{a}_0$ are introduced which are given in Table 4. Reduced quantities are convenient measures of vesicles shapes irrespective of vesicle size.

The effective spontaneous curvature $\Delta \hat{a}_0$ is reflecting the different sources of membrane curvature. The constant $\alpha = \overline{\kappa}/\kappa$ gives the relative importance of the two bending moduli with the non-local bending rigidity given by $\overline{\kappa} = 2k_{\mathrm{A}}\, d^2/\pi$.

Table 4. Parameters Describing the Shape of Vesicles

		Spherical vesicle	
Reduced volume	$v = 3V/4\pi\ \overline{R}^3$	$v = 1$	$v < 1$: deflated vesicle
Reduced spontaneous curvature	$c_0 = \overline{R}C_0$	$c_0 = 1$	
Reduced relaxed area difference	$\Delta a_0 = \Delta A_0/8\pi\ d\overline{R}$	$\Delta a_0 = 1$	
Effective reduced relaxed area difference	$\Delta \hat{a}_0 = \Delta a_0 + (c_0/2\pi\ \alpha)$	$\Delta \hat{a}_0 = 1 + (1/2\pi\ \alpha)$	$\Delta \hat{a}_0 > 1$: prolate vesicles $\Delta \hat{a}_0 < 1$: oblate vesicles

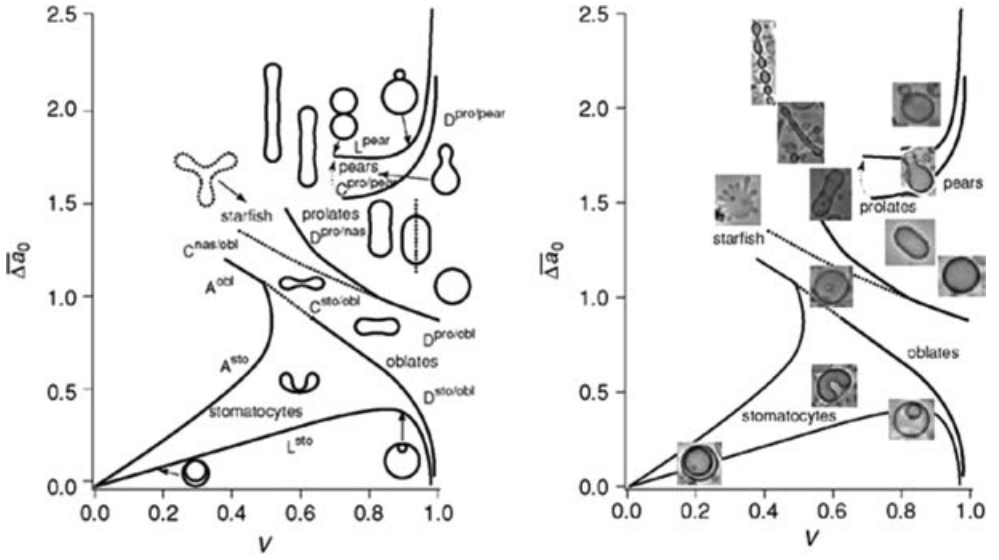

Fig. 14. (**a**) Theoretical phase diagram of vesicle shapes. From Ref. 3, with permission from Elsevier BV. (**b**) Experimentally observed vesicle shapes of PB-PEO block copolymer vesicles. From Ref. 144. Lipid and block copolymer vesicles show the same structural polymorphism.

For most bilayer systems the constant has values of $\alpha \approx 1$. A large area difference $\Delta\hat{a}_0 > 1$ tends to curve the membrane outward, whereas a smaller or negative value leads to inward curvature or invaginated vesicle shapes.

For a fixed value of α, the two parameters v and $\Delta\hat{a}_0$ determine the shape of vesicles which can be placed in a two-dimensional phase diagram as shown in Figure 14**a** (143). There are numerous shapes including spherical, tubular, oblate, and starfish vesicles. Vesicles with outwardly curved shapes and prolate vesicles are in the upper part of the diagram for $\Delta\hat{a}_0 > 1$, and inwardly curved shapes and oblate vesicles are in the lower part for $\Delta\hat{a}_0 > 1$. In this phase diagram, all the shapes are drawn to scale, have the same area, and differ only in their values of v and $\Delta\hat{a}_0$. Lipid and block copolymers exhibit a similar multitude of shapes as shown for PB-PEO block copolymer vesicles in Figure 14**b** (144).

Polymorphism. As during vesicle preparation the number of amphiphiles in the outer and inner monolayer and thus ΔN is fixed for each vesicle, each vesicle carries its own value of $\Delta\hat{a}_0$ and thus its own shape. This often leads to a zoo of different vesicle shapes within the same vesicle preparation. From the definition of Δa_0 and equation 12, it follows that

$$\Delta a_0 = \frac{\bar{R}}{2\mathrm{d}} \frac{\Delta N}{N} \tag{16}$$

which means that for a given relative difference $\Delta N/N$ between the number of amphiphiles in each monolayer, changes in Δa_0 and thus of vesicle shapes are particularly pronounced for large vesicles ($>1\ \mu$m) because of the large prefactor

$(\overline{R}/2d) \approx 10^3$. The polymorphism of vesicle shapes is quite commonly observed for large, micron-sized vesicles.

Shape Transitions. Shape transitions can be induced by changes in the reduced volume v and the effective spontaneous curvature $\Delta\hat{a}_0$ and can be mapped as a trajectory in the phase diagram in Figure 14. Changes in v can be induced by osmotic swelling or deswelling of vesicles, eg by changing the concentration ("osmolarity") of solutes outside the vesicles. Changes in $\Delta\hat{a}_0$ can occur via changes in area difference ΔA and spontaneous curvature C_0. Changes in temperatures can affect the membrane area and therefore the reduced volume v, but also $\Delta\hat{a}_0$ which leads to oblique trajectories in the phase diagram. For large reduced volumes, ie quasi-spherical vesicles, there is hardly any membrane area available for shape changes. For $v \leq 0.97$ required changes in $\Delta\hat{a}_0$ for shape transitions are of the order of unity or less, so that shape transitions become achievable. If, on the other hand, by permeation of solvent into the vesicle interior the reduced volume is adjusted to approach unity, all vesicles will become spherical.

Common shape transitions include

(1) the "pearling" transition, a sequential beading of tubular vesicles;
(2) the "budding" transition, where a small vesicle is expelled from the "parent" vesicle; and
(3) the vesicle-tubule transition.

Pearling Transition. The pearling transition has been investigated for giant tubular PB-PEO block copolymer vesicles. Thermal quenches lead to pearling of the tubes starting symmetrically from the two ends (see Fig. 15) (52). The pearling transition is slow because of the high membrane surface viscosity. The necks close one by one with velocities of the order of a few tens of nanometers per minute, and so complete pearling takes about 2 h.

The pearling transition of giant tubular lipid vesicles has also been induced by insertion of *O*-palmitoyl dextrans into the outside monolayer of the membrane. The insertion leads to an increase in the membrane curvature, which induces the

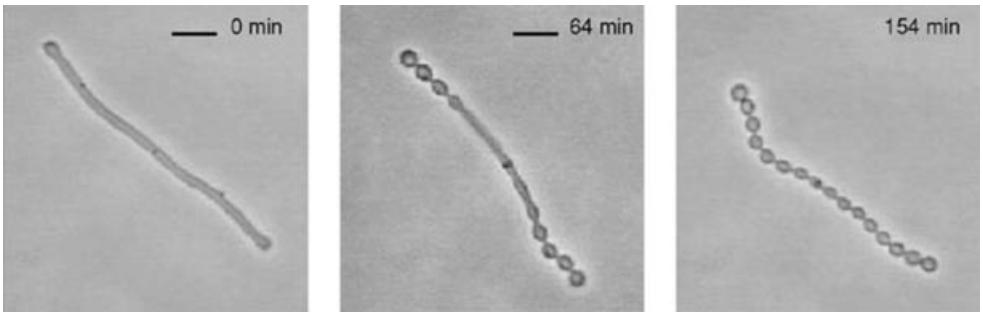

Fig. 15. Different stages of the pearling transition for a tubular PB-PEO block copolymer vesicle after a thermal quench from 38 to 25°C. Compared to lipid vesicles, the transition is extremely slow. The necks close one by one with effective velocities of a few tens of narometers per minute. From Ref. 52, with permission from ACS Publications Division.

pearling transition (145,146). The concentration critical for the shape transition depends on both the palmitoyl substitution frequency along the dextran and the size of the dextran.

Budding Transition. In cells, the budding of vesicles from internal organellae or the plasma membrane is an ubiquitous process and a key process for cellular traffic. In case of giant lipid vesicles, asymmetric insertion of fluorescently labeled PEO with cholesteryl anchor groups into the outer monolayer lead to an increase of the spontaneous curvature and induced budding of starfish vesicles (136). The addition of the cholesteryl anchor increases both components of the effective spontaneous curvature $\Delta\hat{a}_0$, the area difference, and the local spontaneous curvature as locally the membrane curves away from the polymer (147).

The budding transition is directly related to the fission and fusion process of vesicles. In case of block copolymer vesicles, details of this process have been investigated for PS-PAA using transmission electron microscopy of quenched intermediate states (13,42,139). Accordingly, the fusion proceeds via contact, adhesion, coalescence, and formation of a central, connecting wall. Destabilization of the wall leads to its asymmetric detachment and retraction with final formation of a uniform outer wall. The fission process starts with the elongation of the vesicle, formation of an internal waist, narrowing of the external waist, and final complete separation (Fig. 16). Vesicle fusion and fission kinetics have been followed by turbidity changes after jumps in water content and are found to have relaxation times as fast as seconds.

Vesicle-Tubule Transition. Transitions between spherical and tubular vesicles have been reported for a glycopolymer-containing amphiphilic block copolymer by varying the ratio of the co-solvents THF and DMF in aqueous solutions, and by changing the temperature at which the aggregates were prepared (62). Shape transitions involving tubular and starfish vesicles as well as connected tubules have been observed for PS-PEO as a function of water content, polymer concentration, and added ions (25).

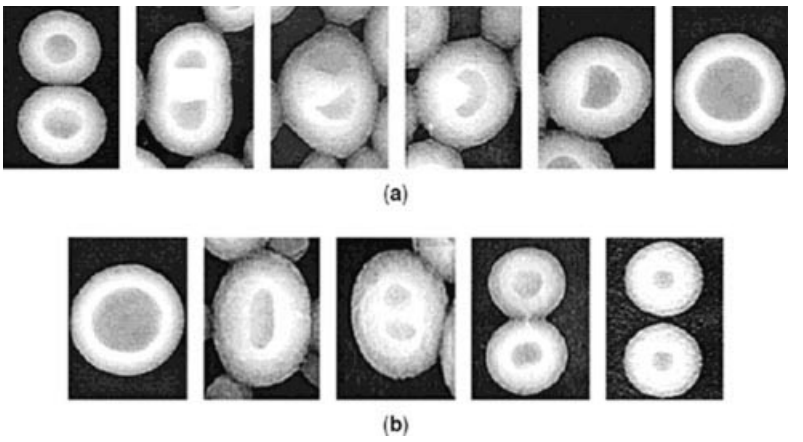

Fig. 16. Reconstruction of different stages of the fusion (a) and fission process (b) of block copolymer vesicles. From Ref. 42, with permission from the ACS Publications Division.

Shape transitions from vesicles to inverted hexagonally packed (hollow) rods were studied for PS-PEO in THF/water mixtures by increasing the water content. The transition proceeds via the formation of hollow regions in the walls of the vesicles, thickening of the walls, and alignment of the rods in a hexagonal pattern leading to the formation of quasihexagonal structures and eventually to the full development of inverted hexagonally packed rods. This mechanism is different from the usually observed fusion of vesicles (25,26). Fascinating intermediate structures such as undulating tubules (44) and ordered toroids (27,148) have been reported for transitions between cylinders and vesicles.

High Genus Vesicles. Block copolymer vesicles can also exhibit shapes, which are unknown for lipid vesicles such as stable high genus vesicles (51). Block copolymer vesicles can easily have a genus $g > 100$, as shown in Figure 17. The local membrane shape indicates that the bilayer has nonzero spontaneous curvature. Experimentally found shapes include vesicles with small and large passages, budded vertices, connected tubes, and spindles, which are stable for different values of the reduced volume and spontaneous curvature $\Delta\hat{a}_0$. The range of stability of these shapes can be depicted in a phase diagram similar to Figure 14.

The development and stability of holes or pores in bilayer membranes have been studied by poration experiments. These experiments show that pore stability depends strongly on the thickness d of the bilayer (149). For small d, poration leads to large unstable pores and the resulting membrane fragments reassemble into vesicles within minutes. For large d, submicron pores form and are extremely long-lived.

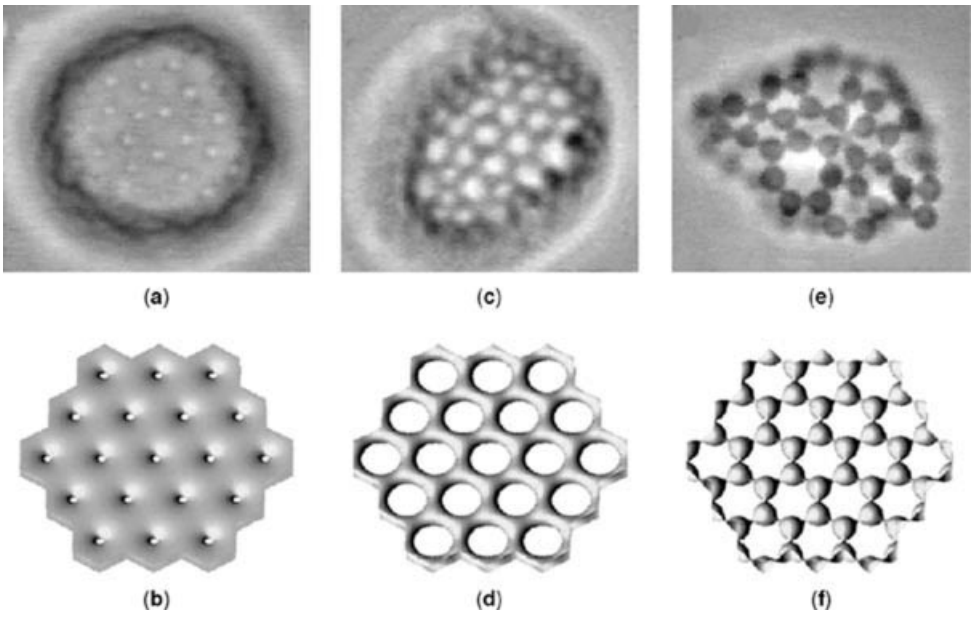

Fig. 17. Comparison of experimental and theoretical shapes for giant high genus PB-PEO vesicles with small passages (**a**, **b**), large passages (**c**, **d**), and budded vertices (**e**, **f**). The scale bar is 10 μm. From Ref. 51, with permission from the APS Associate Publisher.

Bilayer Properties

Physical properties of the vesicle membranes such as elasticity, toughness, stability, and permeability determine to a large extent the performance of vesicles in applications. These properties are largely determined by the interfacial tension and membrane thickness, the latter being adjustable via the chain length of the membrane forming block copolymer. This allows one to tailor membrane characteristics within a range outlined in the following sections.

Mechanical Properties. The mechanical properties of bilayers such as their bending elasticity (Fig. 11) can be understood by a rather simple model. If the bilayer is assumed to be a thin, solid-like film, there is a simple relation between the area elasticity modulus k_A and the bending modulus κ (19,135,150) (Fig. 11), ie

$$\kappa = \frac{1}{48} k_A d^2 \tag{17}$$

where d is the bilayer thickness. If the interfacial tension is the dominant contribution to the elastic properties of the membrane, then a comparison of the coefficients of the area elastic energy terms in equations 2 and 9 implies (96)

$$k_A = 4\gamma \tag{18}$$

Thus, both the bending modulus and area elasticity are directly related and are determined by the interfacial tension.

Thickness. The thickness of polymersome bilayers is several times greater than that of typical phospholipid bilayers in natural membranes. Lipid bilayers have a hydrophobic core thickness that is in a very narrow range of $d \approx 3$–4 nm to be compatible with integral membrane proteins. For self-assembled bilayers of PEE-PEO vesicles, the hydrophobic core thickness increases with increasing molecular weight from $d \approx 8$–21 nm (see Fig. 18) to more than 100 nm (53,151–153). The observed $d \sim M^{0.5}$ scaling is typical for random coil polymers and agrees with molecular dynamics simulations of block copolymer bilayers (106).

Elasticity. The elastic behavior of membranes has been studied using micropipette techniques on giant vesicles (>5 μm). These techniques allow one to simultaneously measure membrane stretching and bending moduli. The experiments show an interface-dominated elasticity. Membrane stretching moduli are found to be independent of chain length (Fig. 19**a**). A value of $k_A \approx 120$ mN/m is reported for PEE-PEO vesicles, which is in good agreement with $\gamma = k_A/4 \approx 30$ mN/m consistent with an oil/water interface (eq. 18). Bending and stretching elastic constants are in a range of values typical for lipid membranes (53). The well-investigated unsaturated lipid DPPC (dipalmitoyl phosphatidylcholine) mixed with cholesterol (1:1) has a value of $k_A = 102$ mN/m corresponding to $\gamma \approx 25$ mN/m (155). For polymersomes, the bending elastic constant κ is reported to be ~35 kT (7), which is in good agreement with equation 17. Data confirm the expected square dependence of the bending modulus on membrane thickness (Fig. 19**b**) (154).

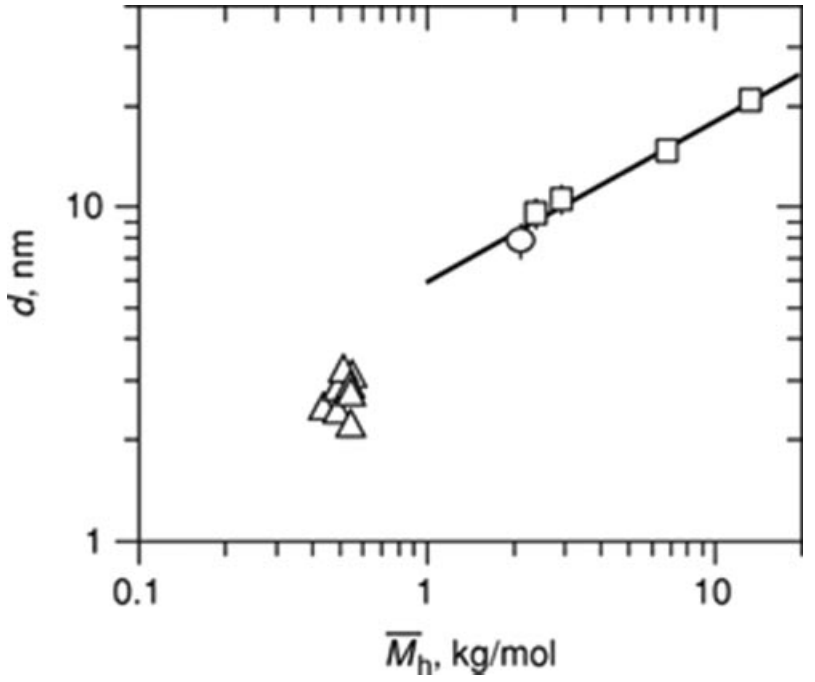

Fig. 18. Increase of the membrane thickness d with the hydrophobic molecular weight for PEE-PEO vesicles. Data (triangles) are also shown for membranes of various phospholipids. Block copolymer vesicle bilayers can be more than an order of magnitude thicker compared to phospholipid vesicles. From Ref. 151, with permission from the ACS Publications Division.

Toughness. Membrane stability as defined by the maximal area strain $\alpha_c = (A_c - A_0)/A_0$ increases with increasing molecular weight, approaching a universal limit set by the interfacial tension. The sustainable critical strain is $\alpha_c \approx 0.19$, which considerably exceeds the range of $\alpha_c = 0.03$–0.06 typical of natural lipid membranes (Fig. 20); lipid membranes cannot be strained without rupture, osmotically or otherwise, by more than about 5% in surface area. Polymersomes are almost an order of magnitude tougher and sustain far greater area strain before rupture compared to lipids. From the data, a critical yield stress of $\sigma_c = \frac{k_A \alpha_c}{d} \approx 1$ MPa can be estimated. One expects that both critical yield tensions and strains increase linearly with the bilayer thickness. Nonlinear responses and memory effects emerge with increasing molecular weight, indicating the onset of chain entanglements at higher molecular weight (151).

Dynamics. For polymersomes, measurements of the lateral diffusivity (47) and the membrane viscosity (152) indicate that membrane fluidity decreases strongly with increasing molecular weight. The decreases are most drastic when the chains are long enough to entangle.

Fluorescence recovery after photobleaching has been used to determine lateral diffusion in block copolymer bilayers (Fig. 21). The experiments yield a time constant τ from which the lateral diffusion coefficient $D = l^2/2\tau$ is calculated. In the fluid L_α phase, lipid molecules have lateral diffusion coefficients of

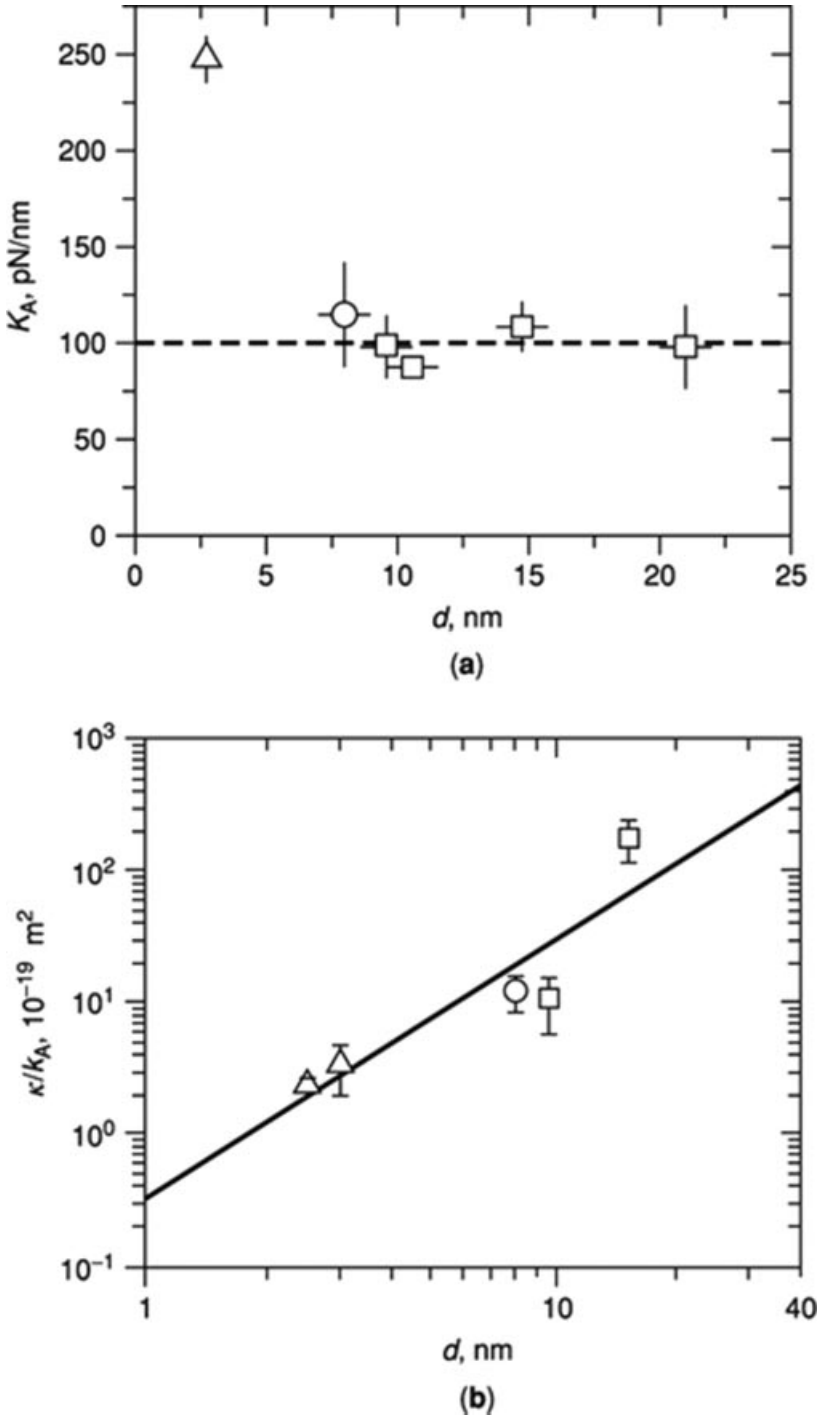

Fig. 19. (**a**) Area elasticity modulus k_A and (**b**) bending modulus κ as a function of the bilayer thickness d. The experiments are in agreement with equations 17 and 18. From Refs. 151 and 154, with permission from the ACS Publications Division.

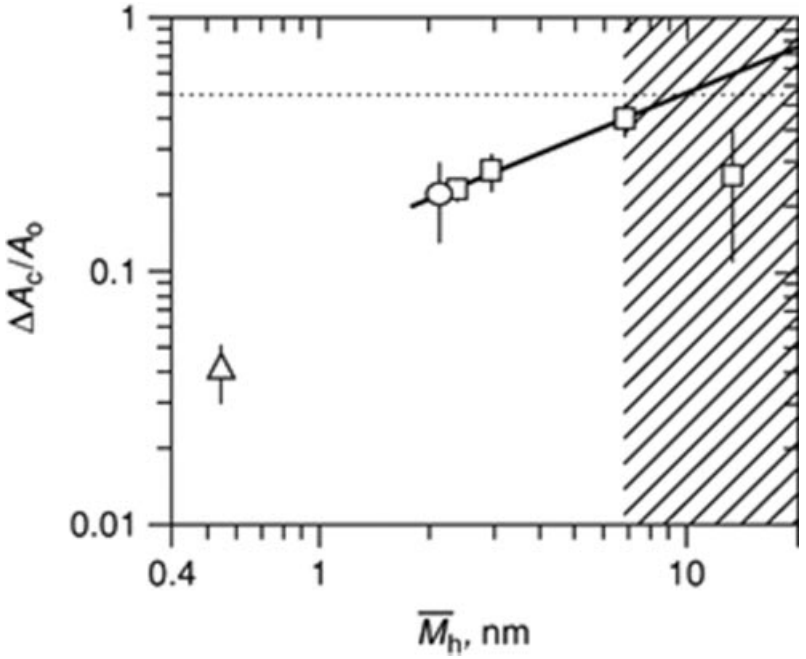

Fig. 20. Maximum area strain for lipid and block copolymer bilayers as function of molecular weight. This experiment demonstrates the increased toughness of block copolymer vesicles compared to lipid vesicles. From Ref. 151, with permission from the ACS Publications Division.

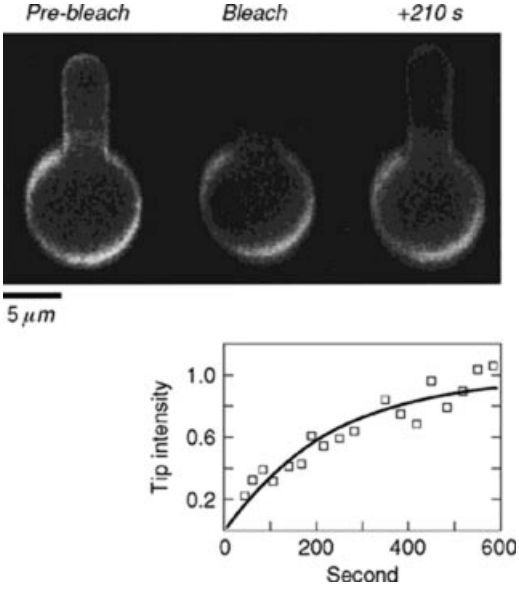

Fig. 21. Fluorescence recovery after photobleaching for a polymersome tip pulled into a glass micropipette. The recovery of the tip intensity can be monitored by fluorescence imaging showing the lateral diffusivity in the bilayer. From Ref. 47, with permission from the ACS Publications Division).

$D \approx 10^{-7}$–10^{-8} cm^2/s. Depending on molecular weight, block copolymers have much lower values of $D \approx 10^{-9}$–10^{-11} cm^2/s for molecular weights between 4000 and 10,000 g/mol (47).

The surface shear viscosity of block copolymer vesicles is about 500 times higher than those found in common phospholipid bilayers (53). The experiments involve pulling out a tether from an immobilized polymersome and following its relaxation back to the vesicle body. This provides an estimate of the viscous coupling between the two monolayers composing the polymer membrane. For giant vesicles of approx. 100 μm diameter, typical relaxation times for thin tethers of 50 μm length and 0.1 μm diameter are of the order of 30–90 s. The detected intermonolayer friction is about an order of magnitude higher than for phospholipid membranes.

Stability. Because of their increased toughness and bending elastisticity, block copolymer vesicles are more stable compared to lipid vesicles. Block copolymer vesicles have been reported to be stable over several years with no changes in size or size distribution (156).

Electromechanical Stability. The electromechanical stability of diblock copolymer membranes is several times larger compared to lipid membranes (152). At zero mechanical tension, the breakdown potential V_c for polymersomes with a membrane thickness of $d = 15$ μm is $V_c = 9$ V, compared to 1 V for liposomes with $d = 3$ nm. The breakdown potential increases with membrane thickness up to a limit set by the interfacial tension (53,152). The electromechanical stresses at breakdown universally exhibit a V_c^2 dependence. The membrane capacitance shows the expected strong d dependence.

Thermal Stability. The thermal expansion coefficient for lipid membranes far from phase transitions is generally in the range $\alpha_T = 0.001$–0.01 K^{-1} (157), which is similar for polymersomes with values of $\alpha_T \approx 0.002$ K^{-1} (49), albeit with no thermal transitions. The thermal stability of vesicles is of importance, if autoclaving is needed for sterilizing vesicles that are too large for filtration through 0.22 μm filters. When polymersomes are autoclaved in dilute suspension for 15 min at a maximum cycle temperature of 121°C (2 atm), about 10% of the vesicles have retained their contents (sucrose solution). Interestingly, the distribution of vesicle sizes shifts to smaller and tighter distribution. It is speculated that because of area expansion, small vesicles have budded off (49).

Stability to Lysis. The addition of surfactants eventually leads to lysis of vesicles. In general, the stability of polymer vesicles against lysis is expected to be higher compared to lipid vesicles, because of the reduced entropy of mixing of polymer and surfactant chains which leads to a reduced partition of surfactants in the polymer membrane. When using Triton-X as a nonionic surfactant, it was found that the concentration of surfactant required for dissolution after a fixed amount of time increases nearly linearly with membrane thickness (158). Because of low partition of hydrocarbon surfactants, vesicles formed by siloxane and fluorinated polymers are expected to have relatively high stability.

The incorporation of PEO-PPO-PEO (Pluronic L31) surfactants into preformed giant PEE-PEO vesicles has been investigated and was found to be weak and reversible (159). The incorporation reduced the area expansion modulus k_A by almost a factor of 2, while dramatically increasing the vesicles susceptibility to lysis. Additionally, water permeability was increased by a factor

of 2. Surfactant incorporation rates were proportional to the free surfactant concentration.

Permeability.

Permeation Coefficient. Vesicles will slowly release encapsulated molecules by permeation through the vesicle bilayer. The release rate is determined by the permeation coefficient P (in m^2/s), which is related to the solubility or the partition coefficient S of the compound between the aqueous phase and the bilayer, and to the rate of diffusion or diffusivity D of the compound in the bilayer, ie

$$P = S\mathrm{D} \tag{19}$$

In a fluid membrane, diffusion coefficients of small molecules have the same magnitude as in bulk solvents. Therefore, the factor determining the permeability is the partition coefficient. Small ions whose low solubility in hydrophobic environment leads to very small values of the partition coefficient exhibit very low permeabilities.

The permeability of small polar solutes across a bilayer or membrane can be greatly enhanced by introducing specific carriers. A small solute X can be transported by a carrier C such that the complex CX has a much higher partition coefficient compared to the bare solute X. Common ion carriers, or ionophores, are valinomycin for K^+ and crown ethers for alkali ions. Solutes can also cross the membrane through channel proteins, eg gramicidin.

If the permeation occurs via Fickian diffusion driven by the concentration gradient across the bilayer, the permeation time τ is related to the permeation coefficient as

$$\tau = \frac{R}{3}\frac{\mathrm{d}}{P} = \frac{V}{A}\frac{\mathrm{d}}{P} \tag{20}$$

where R is the radius, V the volume, A the surface area of the vesicles, and d is the bilayer thickness. Smaller vesicles exhibit a faster release because of the larger surface/volume ratio compared to larger vesicles. Often, the permeation of molecules is compared in terms of their permeability $p = Pd$ (in m/s), since most lipid bilayers have a similar bilayer thickness of $d \approx 3$ nm. For practical applications, equation 20 allows one to tailor release rates τ^{-1} via bilayer thickness and vesicle radius, which themselves can be controlled via polymer block length and vesicle preparation method. Because of the larger thickness of polymer bilayers compared to lipid bilayers, the permeability of molecules can be adjusted to be much slower.

Permeation Experiments. Encapsulated fluorescent and radiochemical labels are commonly used to evaluate permeabilities. Three different types of experiments allow to determine the permeation coefficient.

(1) In one experiment the release of labeled molecules into the exterior solution is monitored in a closed cell. If the initial concentration of the label inside the vesicle is c_0, and in the exterior solution is equal to zero, and if the volume encapsulated by the vesicles is much smaller than the volume of

the sample cell, $V_{ves} \ll V_{cell}$, then the concentration of the labeled molecule in the exterior solution is increasing with time t as

$$c(t) = c_\infty(1 - e^{-t/\tau}) \tag{21}$$

where $c_\infty = V_{ves}c_0/V_{cell}$ is the saturation concentration in the exterior solution for $t \to \infty$. For short times ($t \ll \tau$), $c(t) = c_\infty t/\tau$, which allows to obtain the permeation time and thus the permeation coefficient from the initial linear increase of the concentration with time. The concentration c_∞ can be obtained after lysing the vesicles via addition of a surfactant, where all labeled molecules are released into the exterior solution.
Conveniently, one monitors the increase of the fluorescence intensity of an encapsulated self-quenched dye, eg 50 m*M* 6-carboxyfluorescein (6-CF) (160) or calcein (161), as it permeates the vesicles. [^{3}H]Glucose is more generally applicable because it does not interact with charged lipid membrane surfaces and can be used at low ionic strength. Alternatively, a dilute solution of 6-CF (10 μm) is encapsulated and Co^{2+} (500 μm) is added to the external solution which quenches the fluorescence. Permeation of either Co^{2+} ions or the dye across the membranes causes a reduction in fluorescence intensity.

(2) In the second type of experiment the vesicle with encapsulated solute is placed in an ultrafiltration cell which is continuously flushed with solvent at a rate v_1 (in mL/min) (162,163)

$$c_1(t) = \frac{V_{ves}}{v_1\tau} c_0\, e^{-t/\tau} \tag{22}$$

The permeation coefficient can be obtained from the exponential decay, provided that the elution rate is faster than the permeation rate of the vesicles, $v_1 \gg V_{ves}/\tau$. This method does not rely on fluorescence labels and can be used for any solute. In addition, this method more closely resembles the *in vivo* situation where vesicles release solutes that are instantaneously carried away by the blood stream.

(3) In a third type of experiment the vesicles are investigated under equilibrium with free exchange between encapsulated and nonencapsulated solute. The exchange rate and fraction of encapsulated solute can be determined with pulsed field gradient nuclear magnetic resonance (PFG-NMR). Using this technique, the permeability of polyethylene oxide PEO through P2VP-PEO vesicle bilayers has been determined as a function of molecular weight of PEO (55). The analysis yielded a nearly linear dependence of the logarithmic transmembrane exchange rate on the hydrodynamic radius of the polyethylene glycol (PEG) molecules. The method does not require to separate encapsulated from nonencapsulated molecules. It allows to estimate the encapsulated molar fraction of PEO chains, which was in the range of 2%.

Barrier Properties. The water permeability p of lipid bilayers is reported to be in a range of $p = (5–100) \times 10^{-6}$ m/s. In comparison, polar solutes such as

glucose, glycerol, and urea have much smaller values of $p = (5–300) \times 10^{-10}$ m/s. Small ions such as Na^+, K^+, and Cl^- have the lowest permeabilities, in the range of $p = (1–100) \times 10^{-14}$ m/s (164). Even though the bilayers are only 3 nm thick, they provide an effective barrier to ions and other polar compounds.

The permeability of polymersome membranes for a given solute has been reported to be at least 10 times smaller compared to common phospholipid membranes (8). Retention of encapsulants (eg dextrans, sucrose, physiological saline) over periods of months has been observed for small ∼100 nm polymersomes prepared by liposome-type extrusion techniques (49) as well as with ∼10 μm giant vesicles. Permeability and membrane hydration have been shown to be inversely related to the bending modulus (165). It is suggested that membrane permeability and membrane hydration are related to the ability of the membrane to locally bend so as to create holes for solute permeation.

Cross-Linking, Anchoring, and Templating of Membranes

A major problem of lipid vesicles in pharmaceutical applications has always been their minor stability. Stabilization of vesicles can be achieved by introduction of covalent cross-links or the attachment of stabilizing polymers (87,166–168). The most common methods involve the

(1) formation of vesicles with polymerizable amphiphiles and subsequent polymerization (166,167,169);
(2) solubilization or association of polymerizable monomers to the amphiphile or vesicle bilayer with subsequent polymerization;
(3) association or anchoring of polymers for vesicle bilayer stabilization.

The polymerization of lipid assemblies was first demonstrated in monolayers, vesicles, and extended bilayers and subsequently in cast multilayers, black lipid membranes, and tubules. During the 1970s several groups demonstrated that fatty acids with an incorporated reactive group, eg photopolymerizable diacetylenes, could be polymerized in a monolayer (170,171). The introduction of synthetic double-tail amphiphiles, coupled with the successful demonstration of polymerization of fatty acid monolayers, led directly to the next step in the early 1980s. Vesicles of a polymerizable double-chain ammonium salt have been described with a methacrylate at the end of one hydrocarbon chain (**1**) (Fig. 22) (172). In short order three additional groups (173–175) reported the synthesis and polymerization of lipid diacetylenes (**2, 3**) in bilayer membranes. Within a year, the synthesis and polymerization of dienoyl lipids (**4**) (176,177), methyacroyl lipids and other diacetylenes (178), and styryl lipids (179) were reported.

Polymerizable Amphiphiles. Polymerization of amphiphiles with only one reactive group per lipid such as **1–3** yield vesicles that contain several polymer chains, termed polymerized vesicles. The presence of a second polymerizable group per molecule (**4**) allows cross-linking of the polymer chains and thus cross-linking of the bilayer structure. Such reactive groups include diacetylene, acryloyl, methacryloyl, itaconyl, dienoyl, muconyl, styryl, vinyl, thiol, and isocyanates. The

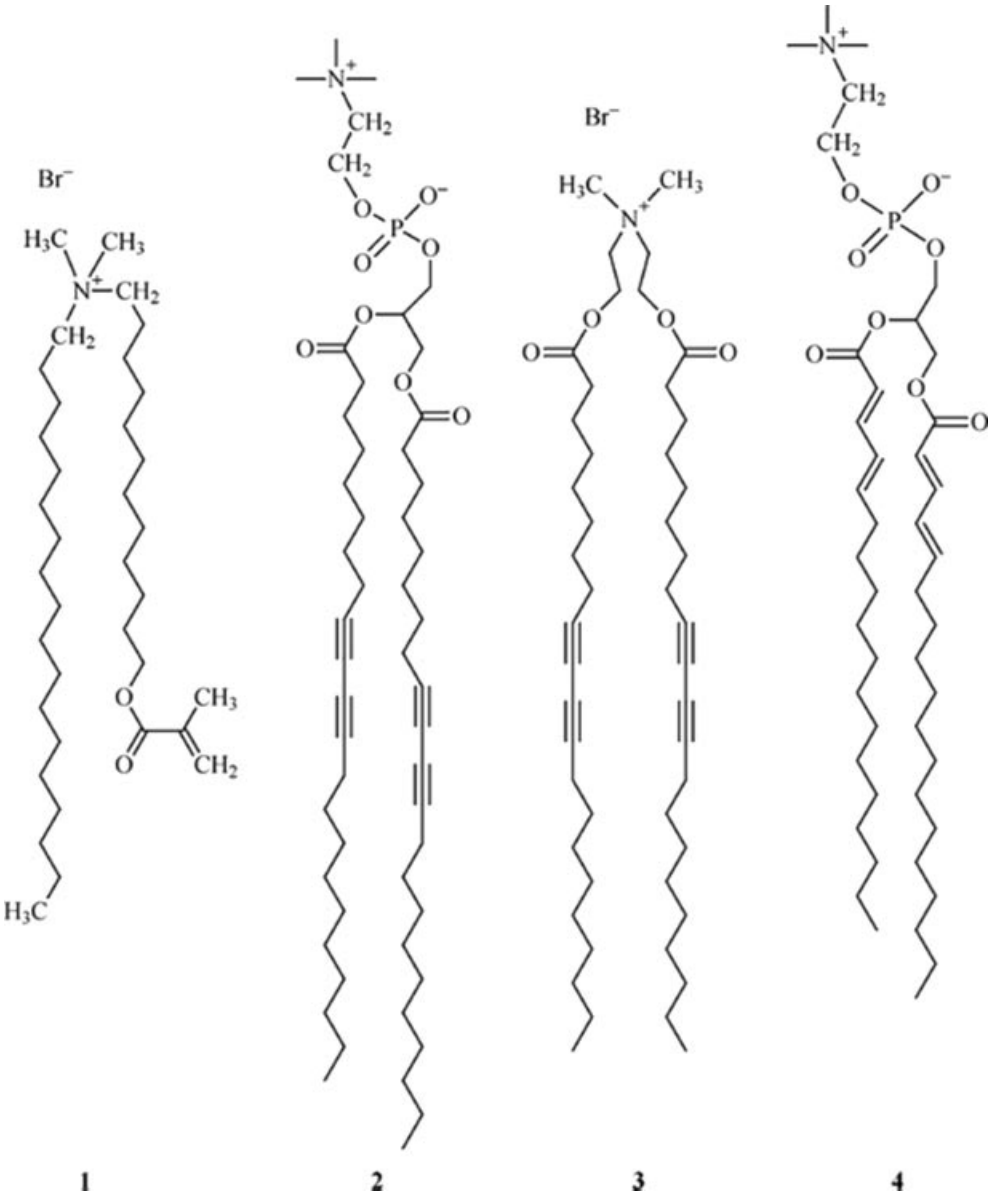

Fig. 22. Chemical structure of polymerizable and cross-linkable lipids.

use of carotene side chains for the preparation of cross-linked vesicles has also been demonstrated (180). Polymerization can be induced by photo, thermal, or redox initiation. In most cases, the vesicle size and shape are not significantly changed by the polymerization reaction.

Cross-Linking. Cross-linking increases membrane stability to detergents and organic solvents. The polymerization of monosubstituted lipids **1–3** in vesicles leads to moderate changes in stability, whereas more significant changes are

found only after polymerization of bis-substituted lipids. For example, polymerized vesicles from mono-methacryloyl lipids may still be disrupted by detergents and organic solvents, albeit at somewhat higher concentrations than required for unpolymerized vesicles. In contrast, polymerized vesicles from the bisdienoyl PC (**4**) are quite stable to detergents and organic solvents (181). The polymerization of **4** yields vesicles that are stable enough to maintain their spherical shape in the vacuum chamber of a scanning electron microscope (182). Polybisdienoyl PC vesicles are not solubilized by 2 m*M* sodium dodecyl sulfate (183).

Measurements of the release rate of encapsulated [^{3}H]glucose through vesicles before and after polymerization show that the permeabilities of vesicles of mono-methacryloyl lipids are reduced upon complete polymerization to 30–50% of the unpolymerized control vesicles (181). A much larger reduction (2 orders of magnitude) in membrane permeability is observed on photopolymerization of the bis-methacryloyl lipid **4**, which allows cross-linking of the vesicle bilayer. Thus the formation of linear chain polymers in vesicles does not significantly alter the physical properties, whereas polymerization of disubstituted lipids can lead to cross-linked polymer networks with a corresponding large change in vesicle properties.

Polymerizable Counterions. Ion exchange of the counterions of ionic lipids vs polymerizable counterions such as choline methacrylate presents an additional route for vesicle stabilization much like the formation of the actin network of natural membranes. Photopolymerization yields vesicles with surface-associated polyelectrolytes. These vesicles were reported to have a similarly reduced permeability as polymerized mono-methacryloyl lipid vesicles (184).

Polymerizable Block Copolymers. Unsaturated hydrocarbon polymers with a large number of polymerizable double bonds can be used to prepare fully cross-linked vesicle membranes. This has been demonstrated for polybutadiene block copolymers (23,168) and methacroyl-functionalized block copolymers (87) using free-radical polymerization, and for polycinnamoylethylmethacrylate block copolymers using a [2+2] photoaddition (68). Poly(ethylene oxide-*b*-3-(trimethoxysilyl)propyl methacrylate) vesicles could be efficiently cross-linked with triethylamine (79,80). PLA-PNIPAM block copolymer vesicles were cross-linked by chain extension of the PNIPAM block using hexamethylene diacrylate (77).

In case of the polybutadiene vesicles, the membrane transformation from liquid to solid state is directly observable upon osmotic deflation of the originally spherical vesicle as creases, folds, wrinkles, and dents proliferate like the deflation of a micron-sized rubber ball (Fig. 23). The cross-linked vesicles do not dissolve in chloroform, a common solvent for both blocks. Encapsulated sucrose was not lost in chloroform, indicating membrane stability on a molecular scale. The results imply defect-free membranes many microns-squared in area. Surface elastic moduli as well as sustainable wall stresses are orders of magnitude greater than any natural lipid membrane. Cross-linked vesicles could be dried, stored at room temperature for days, and then rehydrated to their original average diameter and volume (87). Mixing of saturated (PEE) and unsaturated (PB) block copolymers allows to tune the bilayer elastic constants as well as the rupture strength over a broad range (168). Preblending with a non-cross-linkable diblock copolymer of PEO-polylactic acid undermines vesicle stability in chloroform/water solutions (185). The results prove miscibility and stable integration of a binary block

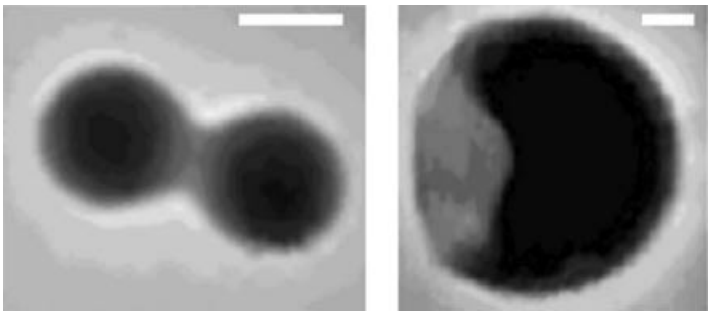

Fig. 23. Deflation of a non-cross-linked (left) and a cross-linked polymersome (right). The latter deflates with dents and wrinkles, characteristic of a solid-like membrane. From Ref. 168, with permission from the ACS Publications Division.

copolymer mixture in a membrane, and allow to realize a first-order scheme for controlled release of encapsulants.

Solubilization of Monomers. Hydrophobic monomers such as methacrylates (186) and styrene (187) can be solubilized into the bilayers of lipid vesicles. These monomers can subsequently be polymerized within the membranes by an UV-induced free-radical polymerization, which leads to the formation of a quasi-two-dimensional polymer entanglement network. The polymerized vesicles are stable to addition of surfactant (bare liposomes are not), can be isolated by lyophilization, and subsequently redispersed in aqueous media by sonification. Depending on the dimensions of the templating vesicles, polymer hollow spheres can be produced with diameters ranging from several tens of nanometers up to hundreds of micrometers (188–191). After extraction of the surfactant matrix, the polymer particles contract considerably without loss of their spherical shape. By the same method, water-soluble polyelectrolyte nanocapsules have been prepared (192–194). These particles show a reversible pH- and ionic strength-dependent swelling transition, causing a considerable increase (decrease) of their radius together with a change of the permeability of the polyelectrolyte walls, which can be used to trigger the release of encapsulated materials.

Adsorption of Polyelectrolytes. Some water-soluble polymers adsorb to neutral or charged membrane surfaces by hydrophilic or ionic interactions which can stabilize or destabilize vesicles. Polyelectrolytes such as polyionene-6,6 (195,196) and poly(L-lysine) (197,198) have been adsorbed to negatively charged lipid vesicles and effects on bilayer thickness and polymer conformation have been investigated. Studies of the adsorption of polyanions to positively charged lipid vesicles are of importance for gene transfection of plasmid-DNA in gene therapy. The adsorption of poly(α-ethylacrylic acid) (PEAA) has been used to make lipid vesicles pH-sensitive. Acidification induces conformational changes of PEAA, leading to disruption of the vesicles (199,200).

Anchoring of Polymers. Synthetic polymers with hydrophobic side groups interact with membranes by insertion of these so-called anchors into the bilayer. Polysaccharides such as pullulan and amylopectin, which were derivatized with palmitoyl groups, are sufficiently hydrophobic to insert into lipid bilayers (201). If a sufficient amount of polysaccharide is added after vesicle formation, the

vesicles are coated only on the exterior surface. The bound polysaccharide reduces the vesicle permeability to water-soluble markers and decreases the sensitivity of the vesicle lipids to enzymatic hydrolysis by phospholipases (201). The surface characteristics of such polysaccharide vesicles are sufficiently different from those of uncoated vesicles in that they display an unusual distribution of vesicles in the body. The lung uptake of vesicle-encapsulated label is five times greater for *O*-palmitoyl amylopectin-coated vesicles than for uncoated vesicles. Monoclonal antibody fragments attached to polysaccharide-coated vesicles bind to specific cells with a higher frequency than those attached to antibody-free coated vesicles (202).

Pluronic-type PEO-PPO-PEO triblock copolymers were anchored into bilayers of soybean lecithin to prepare sterically stabilized vesicles (203–205). Vesicles with anchored polymer are reported to have an increased stability with respect to cation (Na^+, Mn^{2+})-induced flocculation. Also the addition of other hydrophobically modified polymers to lipid vesicles lead to a stabilization of the vesicles (206).

Templating. Solutions of multilamellar block copolymer vesicles could be used as templates for the preparation of vesicular structured monolithic silica using a sol/gel process (57). This method can be used to freeze vesicular structure for analysis, and also for the preparation of mesoporous silica with slit pores. Thin films of templated multi-bilayer vesicular structures of PS-PEO could also be prepared using sol/gel chemistry (28). The films were prepared from dilute PS-PEO/THF/water/silica precursor mixtures via solvent evaporation. For the silica/diblock copolymer films with regular mesophases, copolymer removal produced also mesoporous structures.

Biomedical Applications

Vesicles are intensely investigated with respect to their use as transportation systems for pharmaceutical and cosmetic applications (207,208). The potential of lipid vesicles is rooted in the notion that natural lipids will be at least partially biocompatible (209). Via conjugation with biological ligands different biomedical functions can be implemented into the vesicle (Fig. 24), including

(1) actuator functions for temperature-, pH-, salt-, and light-triggered release;
(2) the incorporation of adhesion sites, eg RGD sequence, sialyl-Lewis^x, HIV-TAT sequence;
(3) the conjugation of recognition sites, eg antibodies like anti-PECAM to target lung endothelia or anti-CD3 to peripheral blood cells (210);
(4) a "stealth" layer to prevent unspecific recognition; and
(5) integral proteins that provide channel and transport functions.

Conjugation can be achieved by covalently attaching a ligand to the end group of the peripheral polymer block, eg via activated ester synthesis, or by reconstitution of a protein or ligand into the vesicle bilayer. By using a mixture of functionalized and unfunctionalized block copolymers, vesicles with optimal ligand spacing can be prepared for efficient binding to cell surfaces.

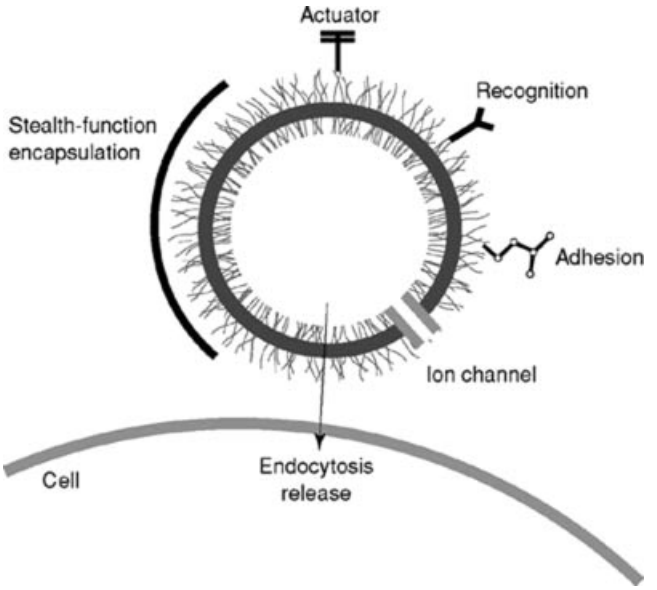

Fig. 24. Biomedical functions that can be implemented into vesicles. From Ref. 20, with permission from John Wiley & Sons, Inc.

Problems can consist in the chemical and colloidal stability, eg upon oral administration, and in the low permeation through cellular membranes. For this reason vesicles are mostly administered parenterally, ie intravenously, subcutaneously, or intramuscularly. Their tissue specificity is first confined to the cells of the reticuloendothelial system which recognizes them as foreign microparticles and transports them to liver and spleen. Their biodistribution can be regulated by surface modification, eg by placing PEO (*stealth* systems) or monoclonal antibodies (*site-specific targeting*) to the vesicle surface. By this means their residence time and bioavailablity can be increased (211).

Biocompatibility. The biocompatibility of materials is influenced predominantly by the material surface. Materials with hydrophilic surfaces are often well-suited, because hydrophilic, noninteracting surfaces are difficult to recognize by living systems and have low cytotoxicity.

Stealth Layers. It is known that PEO (or PEG, which is chemically the same) enhances the biocompatibility of polymeric materials. PEO is water soluble, chemically stable under physiological conditions, and shows low unspecific binding of proteins. Liposomes containing lipid-conjugated PEO as a hydrophilic layer do not interact with and are difficult to be recognized by living systems and have been called "stealth" liposomes. Blood plasma proteins, which generally adsorb to artificial surfaces and mediate clearance by immune system cells, are sterically delayed in deposition into or onto "stealth" membranes. After intravenous injection stealth liposomes are cleared more slowly from the blood circulation than are conventional liposomes. PEO chains can prolong circulation half-lives from a few hours to tens of hours. The extended circulation time allows stealth vesicles loaded with anticancer drugs (eg doxorubicin) to be distributed to distant and well-hidden

tumors (212). Eventually, liposomes are engulfed by phagocytic cells of the liver and spleen.

For optimal stealth properties, liposomes would have to be densely covered by a PEO layer. However, PEO liposomes are limited in their ability to integrate high molar ratios of PEO lipid because of shape transitions to micellar structure as a result of the increasing interfacial curvature and lower packing parameter. Polymersomes have the advantage that vesicles are entirely composed of PEO-based block copolymer amphiphiles and are not limited by PEO-driven micellization.

Blood Plasma Stability. Polymer vesicles are found to be stable for at least 5 days in plasma when suspended at room temperature and kept well-mixed (49). Under quiescent conditions vesicles are stable for almost 60 h. At longer times, aggregation of settled-out vesicles is observed. Within the aggregates, no vesicle fusion is observed because of the steric stabilization of the PEO chains.

Phagocyte Stability. Of particular importance is the assessment of the interaction of vesicles with the cellular components of blood, particularly granulocytes, which are the predominant circulating phagocytes. Neither adhesion nor stimulation of phagocytes are apparent when giant polymersomes are held in direct contact. When placed in contact with a white cell (Fig. 25**b**), vesicles do not exhibit any adhesion or other cellular response for up to 30 min, despite the presence of 20% plasma. In comparison, 1–2 min of contact between a yeast particle and a white cell (neutrophil leukocyte) leads to strong adhesion (49).

Proliferating cells are unaffected when cultured for an extended time with an excess of polymersomes. Similar *in vitro* tests with macrophages, endothelial cells, and myoblasts further indicate the inertness of the polymersome surface. The dense PEO layer prevents the deposition of phagocytic ligands such as plasma C3b on the vesicle surface, thereby repelling phagocyte adhesion. The lack of polymersome recognition by phagocytes is important for prolonged circulation upon intravital injection.

In Vivo Performance. Polymersomes are found to have *in vivo* circulation times of $\tau_{1/2} \approx 18$ h, which is about twofold longer than PEGylated or stealth

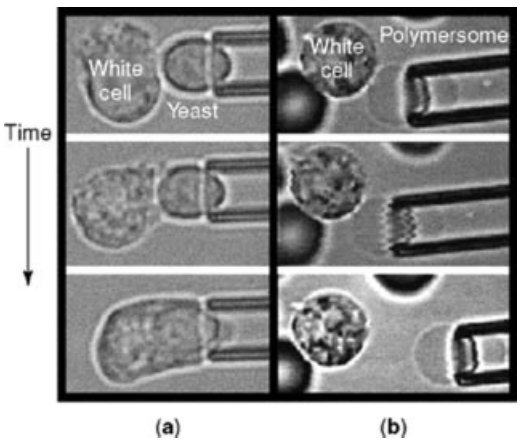

Fig. 25. Exposure of a yeast cell (**a**) and a polymersome (**b**) to a white cell. The yeast cell is rapidly engulfed, whereas there is no response upon contact with the polymersome. From Ref. 49, with permission from John Wiley & Sons, Inc.

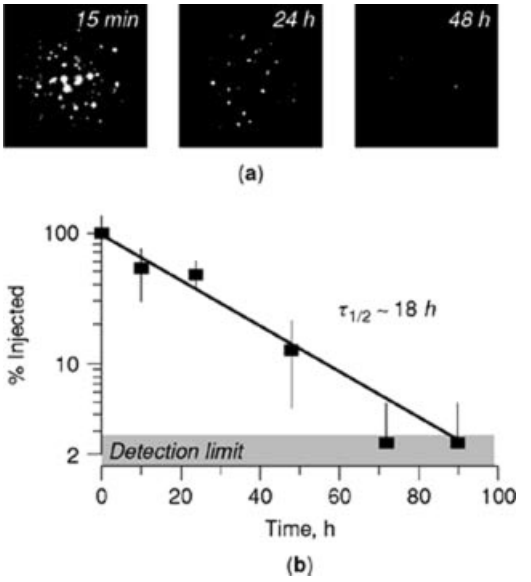

Fig. 26. Fluorescence images (**a**) and number of polymersomes (**b**) after different circulation times in rats. The experiment shows the delayed clearance of polymersomes from the blood stream. From Ref. 213, with permission from Elsevier B.V.

liposomes. Fluorescently labeled vesicles were injected into rat tail veins with subsequent bleeds taken to monitor vesicle clearance from the circulation (213) by taking a fluorescence image of centrifuged platelet-poor plasma (Fig. 26). From image analysis, the decay of the number of vesicles with time is obtained, which is fitted to an exponential to derive the circulation half time $\tau_{1/2}$.

As with lipid vesicles, the circulation time is limited by uptake into the liver and spleen. *In vitro* incubations of polymersomes in plasma indicate plasma protein adsorption during circulation, which leads to engulfment of the vesicles by phagocytes.

Toxicity. Toxicity is found to be a minor problem and many vesicle systems have passed standard toxicity tests. The hydrophilic PEO block effectively screens the influence of the hydrophobic cores on timescales of the measured circulation half-life $\tau_{1/2}$. With respect to long-time applications, PEE is structurally similar to low-density polyethylene, which is commonly used in implants and is generally considered bioinert (214). PB is also understood to be bioinert as it is commonly chosen for the hydrophobic block in triblock copolymers (215,216). In a more prolonged model test of biocompatibility, nondifferentiated C_2C_{12} cells were incubated with polymersomes. The cells remained well spread with no evidence of cytotoxicity. As shown by the Trypan blue exclusion assay, polymersomes had no significant effect on cell survival.

Encapsulation and Release.

Encapsulation Methods. Vesicles can solubilize and encapsulate hydrophilic as well as hydrophobic compounds. Hydrophobic compounds (eg carotene, vitamin E, Taxol, CdTe-quantum dots (20)) are solubilized into the hydrophobic interior of the bilayer. Solubilization can be achieved by stirring the

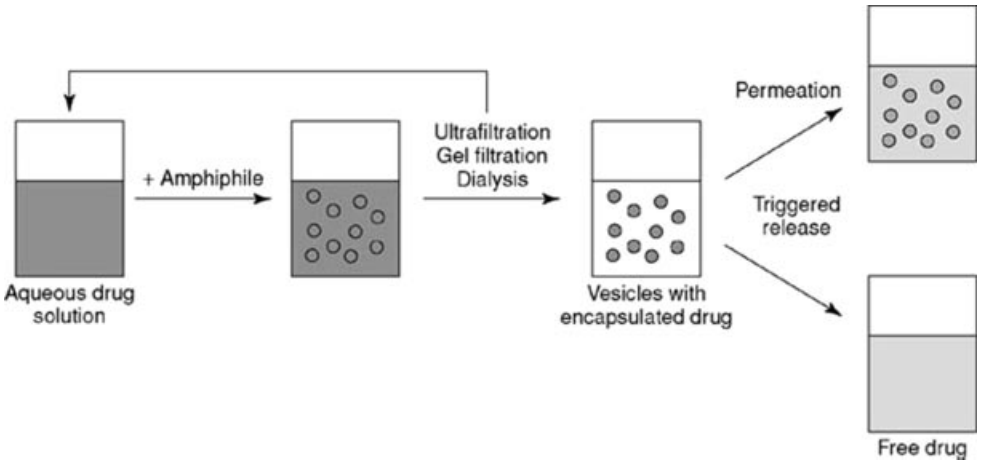

Fig. 27. Methods for encapsulation and release of hydrophilic drugs using vesicles. From Ref. 20, with permission from John Wiley & Sons, Inc.

hydrophobe in the aqueous vesicle solution or by dissolving the vesicle-forming amphiphile and the hydrophobe in an organic co-solvent with subsequent transfer into water. Because of the small mixing entropy, polymer vesicles have a higher selectivity for the solubilization of hydrophic compounds compared to lipid vesicles.

Hydrophilic drugs can be encapsulated by dissolving the vesicle-forming amphiphile in the aqueous drug solution (Fig. 27). Removal and recycling of nonencapsulated molecules is possible by ultrafiltration, gel filtration, dialysis, or centrifugation. Polymer vesicles can retain encapsulated molecules over periods of days to weeks. Encapsulated substances include fluorescein (7,102), rhodamin (68), eosin, myoglobin, hemoglobin (7), BSA (7), dextrans (7), PEG (55), sucrose (7), physiological saline, doxorubicin (78,217), β-lactamase (218), and cylindrical micelles (219). As has been shown, encapsulation of enzymes into liposomes or polymer nanocapsules protects them against proteases and denaturation (218). Particularly interesting is the integration of channel proteins into bilayers, which is discussed below.

Sustained Release. Depending on permeation coefficient, vesicle radius, and bilayer thickness, encapsulated low molecular weight solutes will be released on timescales of minutes to days. This can be used for the controlled release of drugs, where the dose can be predicted from the encapsulated volume and the initial drug concentration in the vesicle using equation 21. Large ionic solutes, in particular proteins, will have low release rates and are practically permanently encapsulated until the vesicle is ruptured.

Triggered Release. By triggering solution conditions vesicles can be spontaneously dissolved with a concomitant release of the encapsulated substance. This can be achieved with vesicles containing polymer blocks with solubilities responding to changes in pH, temperature, and ionic strength. Other stimuli include UV, light, enzymes, and reducing agents which degrade the polymer block.

pH-Triggered Release. The pH-induced release is of relevance for the delivery of drugs and genes into the cytosol via endolysosomal acidification and

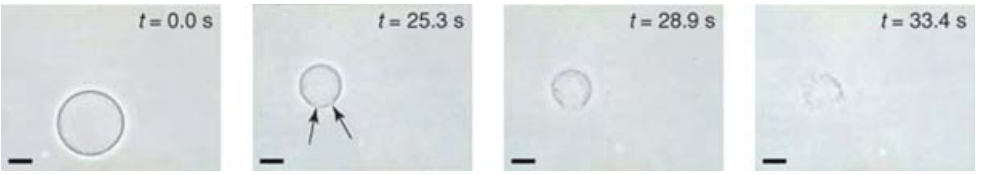

Fig. 28. Shrinking and lysis of P2VP-PEO vesicles by addition of dilute acetic acid. The arrows indicate the formation of holes in the membrane. From Ref. 224.

escape for applications in chemo- and gene therapy. The acid-catalyzed and thus pH-dependent hydrolysis of plasmenylcholine vesicles has been used to release encapsulated calcein (220). With the pH decreasing from 6.3 to 2.3, the time to release 50% of the calcein decreased by 3 orders of magnitude from 50 h down to 3 min. The acid-catalyzed hydrolysis of the vinylether linkage of PEG-DOPC lipids has been used to trigger the release of calcein from lipid vesicles at pH <4.5 (221–223). A pH response can also be realized by using polybase blocks which can be rendered water soluble by protonation at low pH (224). A pH-induced lysis is shown in Figure 28 for P2VP-PEO vesicles upon addition of acetic acid. A protonation of L-lysine residues in the hydrophobic domain of polypeptide diblock copolymer bilayers was used to destabilize vesicles to release encapsulated Fura-2 dye (82,83).

Reducing Agents. The release of eosin induced by addition of a reducing agent has been demonstrated for polymerized lipid vesicles. Immiscible lipid mixtures can laterally phase separate within the membrane to form domains. This can be achieved by using a mixture of hydrocarbon and fluorocarbon lipids, eg, a polymerizable dienoyl lipid and a labile fluorocarbon disulfide lipid in the ratio 9:1 (146), or a polymerizable fluorinated lipid together with a labile bolaamphiphile in the same ratio 9:1 (146). Photopolymerization of the lipid domains stabilizes the vesicles, which can efficiently entrap the fluorescent dye eosin. Exposure of the vesicles to dithiothreitol reduces the disulfide over several minutes and divides the lipid in half at the head group. The reduction product, a single-chain cysteine, prefers a micellar rather than a lamellar structure; therefore, the polymerized vesicles become leaky by the formation of holes, accompanied by release of the eosin (50% loss over 10 min) from the vesicle.

Oxidizing Agents. In case of PEO-PPS block copolymers, the thioether groups of the hydrophobic PPS blocks can be converted into the more hydrophilic sulfoxides and sulfones by exposure to an oxidative environment. This changes the hydrophilic–hydrophobic balance and can be used to destabilize PEO-PPS vesicles. In a study by Napoli and co-workers, hydrogen peroxide was used as the oxidizing agent, which was produced by glucose oxidase (GOx) upon reaction with glucose (73,74). When using PEO-PPS-PEO vesicles with encapsulated GOx, addition of glucose triggers the oxidation with a concomitant destabilization and dissolution of the vesicles.

Enzymatic. Another method of lipid cleavage involves the enzymatic hydrolysis of phospholipids. The enzyme phospholipase A_2 catalyzes the hydrolytic cleavage of phospholipids into fatty acids and lysolecithins, which disrupts the vesicle bilayer (225,226). However, it does not attack the polymerizable bisdienoyl

4. Therefore the selective hydrolysis of DPPC in mixed lipid membranes is possible (146) as shown by the release of 6-CF that had been encapsulated in vesicles of DPPC and **4** (1:1).

Hydrolysis. PLA-PEO and PCL-PEO block copolymers have been investigated for the release of doxorubicin (78). The release is induced by the hydrolysis of the PLA- and PCL-polyester blocks. PCL has a smaller degradation rate compared to PLA. The block copolymers were blended with PB-PEO prior to formation of the vesicles to increase the release times τ by a factor of 10, ie from 21 to 208 h.

Polymerization-Induced. Two-component vesicles of a polymerizable PC and a PE form stable vesicles. Photopolymerization induces a lateral phase separation of polymerized PC domains and unpolymerized PE domains. As pure PE does not form bilayers, this leads to a destabilization of the vesicles as shown by the release of calcein or other water-soluble self-quenched fluorescent markers (227).

Photo- and UV-Induced. The bacteriochlorophyll-sensitized photooxidation of plasmenylcholine vesicles was used to trigger the dissolution and release of Ca^{2+} ions (228). The photorelease of Ca^{2+} ions subsequently activated calcium-dependent phospholipase A2, leading to the enzymatic cleavage of DPPC phospholipid vesicles containing calcein. In effect, this lead to a light-induced release of encapsulated calcein via a two-step cascade process. Block copolymer vesicles (PMPS-PEO) containing encapsulated fluorescent dye can be broken up using UV irradiation, which photolytically cleaves the PMPS segments (229).

Conjugation with Membrane Proteins.

Reconstitution. The reconstitution of membranes from purified protein and lipid components is a well-known method for the study of membrane protein functionality. Membrane proteins that have been reconstituted into liposomes of polymerizable lipids include ATP synthetase (230), bacteriorhodopsin (231,232), rhodopsin (233,234), and porins.

ATP Synthetase. Membrane-bound proteins that utilize the proton gradient across the membrane to form ATP from ADP and phosphate are known as ATP synthetases. The synthetase complex, composed of a hydrophobic part (F0) and a water-soluble domain (F1, catalytic center) from Rhodospirillum rubrum, was incorporated into liposomes of a polymerizable sulfolipid (235). Lipid-free synthetase has a very low enzymatic activity. If the sulfolipid liposome is partially photopolymerized and the protein complex is incorporated into the liposome, the observed enzymatic activity is comparable to that of the natural lipid membranes.

Rhodopsin. Rhodopsin is the principal membrane protein of the light-harvesting and energy-transducing rod outer segment (ROS) cell. Light absorption by the chromophore of the transmembrane rhodopsin initiates spectral and structural changes in the protein that enable it to interact with several peripheral membrane enzymes, a G protein (transducin), and a phosphodiesterase. Recombination of these ROS enzymes with rhodopsin-lipid bilayers yields a system that displays the native activation sequence. Light stimulation (a millisecond flash) of the rhodopsin results in the activation of both peripheral proteins and a rapid hydrolysis of the cyclic GMP to decrease the pH of the aqueous buffer. These rhodopsin membranes are functional, with a high yield (10^5) of protons produced per photon.

Porins. In natural cell walls the rate and selectivity of substrate permeation is controlled by porins. Porins are transmembrane proteins that form trimeric water-filled channels that allow passive diffusion of small solutes, such as ions,

nutrients, or antibiotics, across the membrane. The most prominent of these porins is OmpF (outer membrane protein F). Molecules with a molecular weight above 400 g/mol are sterically excluded from the OmpF channels. In addition, it has stereospecific binding sites for maltooligosaccharides inside the aqueous channels, which enhance the diffusion of sugars across membranes. It is also the pathway of β-lactam antibiotics intrusion into the bacteria. OmpF has further the interesting property of being closed if a transmembrane voltage above a certain threshold is applied. Porins are quite stable and are not denatured at temperatures up to 70°C or in 2% SDS. They can be produced on large scales in Escherichia coli using recombinant technology.

OmpF was successfully reconstituted into lipid vesicles (186,218), which could be demonstrated using an encapsulated enzyme, β-lactamase, which is able to hydrolyze the antibiotic ampicillin. The hydrolysis product, ampicillinoic acid, can reduce iodine to iodide, which can be monitored by iodometry, ie via the decolorization of a starch/iodine complex in the exterior solution. The enzyme and the membrane channel have been shown to preserve their activity in the presence of hydrophobic methacrylate monomers before and after their cross-linking polymerization. Polymerization of hydrophobic *N*-butylmethacrylate and ethylene glycol dimethacrylate (186) lead to partial expulsion of some reconstituted channels during the cross-linking reaction, thereby decreasing the enzymatic activity.

OmpF has also been reconstituted into the membrane of PMOX-PDMS-PMOX triblock copolymer vesicles carrying polymerizable end groups (236). The triblock copolymer membrane had a thickness of 10 nm, which is two to three times thicker than a conventional lipid bilayer (237). Nevertheless, the channel-forming OmpF could be reconstituted and remained functional, showing similar activities as in lipid membranes, despite the extreme thickness of the membranes. The functionality even remained after polymerization of the reactive end groups, which was demonstrated by monitoring the ampicillin hydrolysis of encapsulated β-lactamase (156,218,237–240).

The maltooligosaccharide-specific channel LamB, or maltoporin, of E. coli forms trimeric channels in the outer cell wall of Gram-negative bacteria that allow a specific transport of maltose and maltodextrins. Simultaneously, it serves as a receptor for phage-λ. Because during infection the phages transfer their genome into the host cells, it has been proposed that the channels of LamB could be a major intrusion path for the viral DNA.

For this purpose LamB was reconstituted into membranes of PMOX-PDMS-PMOX vesicles and the binding to phage λ was studied (156). It was demonstrated that the functionality of the LamB protein is fully preserved, in particular its binding to phage λ (Fig. 29). The transfer of DNA into the vesicles was quantified by labeling the viral DNA with the fluorescent dye YO-PRO-1. After injection of the phage, the intensity is increasing because of partial capsoid lysis. The further increase of the intensity after lysis of the vesicles demonstrates the injection of DNA (156).

Generally, integral membrane proteins are vectorial molecules with distinct cytoplasmic and extracellular parts. They insert into cell membranes with a specific orientation. A reconstitution of aquaporin 0 with preferred orientation has been achieved by using vesicles consisting of an asymmetric PEO-PDMS-PMOX bilayer (94). The amino terminus of the porin orients to the cytoplasmatic side

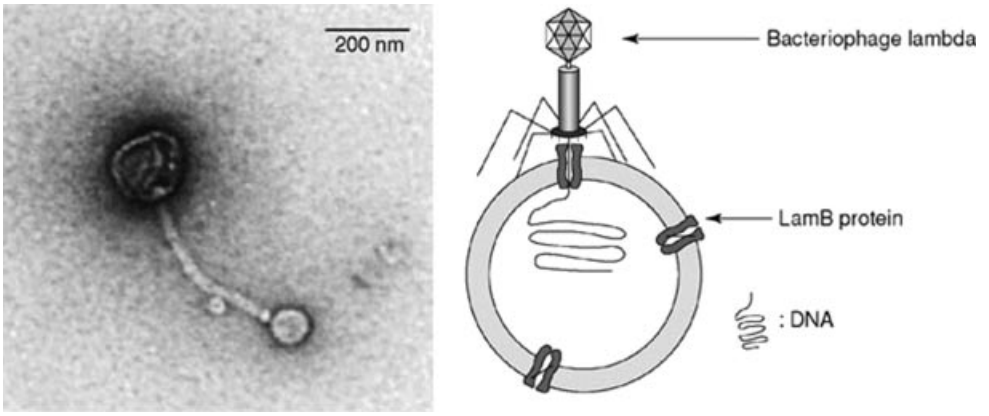

Fig. 29. Injection of virus-DNA through reconstituted LamB protein. The λ-capsid is icosahedral with an outer diameter at 63 nm and the inner diameter at 55 nm. From Ref. 156, with permission from the The National Academy of Sciences, USA.

of cell membranes and was labeled with a His tag to monitor its orientation by immunolabeling with nanogold-labeled antibodies.

Ionophores. Ionophores have been inserted into the bilayers of PMOX-PDMS-PMOX vesicles with encapsulated K_3PO_4 solution (241). The ionophore-assisted metal-ion transport across the block copolymer membranes was studied for Ca^{2+}, which without ionophores does not permeate the triblock copolymer membrane from the external solution. The incorporation of ionophores such as Lasalocid A, ETH5234, or alamethicin into the vesicle membrane led to permeation of Ca^{2+} as shown by the precipitation of calcium phosphate inside the vesicles (241).

Leukocyte Adhesion. A future challenge is the integration of adhesive sites into vesicle membranes to mimic leukocyte adhesion, allowing vesicles to target and exploit the same pathways that cells use to traffic throughout the body. To traffic from blood into tissues, cells adhere to blood vessel walls via specific receptor-ligand binding. The adhesion is initiated through proteins (selectins) that bind to carbohydrates, in particular to sialylated-fucosylated carbohydrate ligands such as sialyl-Lewis^x. Thus, sialyl-Lewis^x or closely related carbohydrates can be viewed as the minimum functional binding element. For this purpose, vesicle surface groups may be derivatized with specific ligands such as streptavidin, allowing the attachment of a wide array of adhesive functions such as biotinylated forms of sialyl-Lewis^x. First steps in this direction have been the investigation of the adhesion between biotinylated polymersomes and avidin-coated microspheres (242).

Outlook

In recent years there has been significant progress in the preparation of stable polymer vesicles over a size range of tens of nanometers to tens of micrometers by either polymerization of lipid vesicles or self-assembly of amphiphilic block

copolymers. The molecular parameters governing the formation of vesicles have been elucidated, enabling the preparation of a variety of chemically different vesicles in different solvents with specific physical, chemical, and biological functions. In particular the use of block copolymers has provided stability, a means to tailor membrane properties like thickness, bending elasticity, and permeability, and to attach biofunctional groups via appropriate choice of block length and block chemistry. Different functions can be implemented into a vesicle either by implementing them into a single block copolymer chain, or by assembling differently functionalized block copolymers into a vesicle.

An important use of vesicles will be the encapsulation and controlled release of hydrophilic compounds for pharmaceutical and cosmetic applications. Different release modes such as first-order release via membrane permeation, zero-order release using channel proteins, and instantaneous release triggered by environmental stimuli have already been realized. The encapsulation of enzymes for protection against proteases and detergents, of hemoglobin for use in erythrocyte mimics, of magnetic particles for application in diagnostics and therapy, of plasmid DNA for gene transfection in gene therapy, of vitamins in body care products, and of fertilizers in agro-chemistry are being discussed. In some cases stealth and conventional liposomes loaded with anticancer agents have recently overcome cost, scale-up, sterility, toxicity, and stability hurdles, and have demonstrated clinical efficacy (209).

The use of vesicles and membranes in nature is a constant source of challenge and inspiration. In cells, vesicles and membranes are used to separate metabolistic pathways, as intracellular transport systems, and for electrophysiological signaling, eg in neurons. The realization of such functions by using self-assembling, functionalized polymers may provide further understanding and use of nature's efficient self-organization principles (243,244). This also includes the assembly of photosynthetic centers into membranes for efficient light harvesting and separation of photogenerated charge carriers. Further, polymer bilayers are discussed as stable alternatives for lipid bilayer systems for use in biosensors. Reconstituted ion channels or encapsulated enzymes provide substrate selectivity necessary for selective detection of small amounts of solutes.

After some years of consolidation in vesicle and liposome research, the field is currently rapidly expanding, particularly in the field of block copolymer vesicles. It brings together scientists from many disciplines such as physics, chemistry, biology, pharmacy, medicine, materials science and engineering. New approaches and solutions to current challenges in biomedical, pharmacological, and cosmetic research are investigated with new and promising materials and methodology.

BIBLIOGRAPHY

1. P. Mueller, D. O. Rudin, H. T. Tien, and W. C. Wescott, *Nature* **194**, 979 (1962).
2. A. D. Bangham and R. W. Horne, *J. Mol. Biol.* **8**, 660 (1964).
3. H. G. Döbereiner, *Curr. Opin. Coll. Interface Sci.* **5**, 256–253 (2000).
4. A. D. Bangham, *Chem. Phys. Lipids* **64**, 275 (1993).
5. B. Cornet, E. Decroly, D. Thines-Sempoux, J. M. Ruysschaert, and M. Vandenbranden, *AIDS Res. Hum. Retroivruses* **8**, 1823 (1992).

6. I. F. Uchegbu, ed., Drug Targeting and Delivery, Vol. 11: *Synthetic Surfactant Vesciles: Niosomes and Other Non-Phospholipid Vesicular Systems*, Harwood Academic, Amsterdam, 2000.
7. B. M. Discher, Y.-Y. Won, D. S. Ege, J. C. M. Lee, F. S. Bates, D. E. Discher, and D. A. Hammer, *Science* **284**, 1143 (1999).
8. H. Kukula, H. Schlaad, M. Antonietti, S. Förster, *J. Am. Chem. Soc.* **124**, 1658 (2002).
9. H. Schlaad and M. Antonietti, *Eur. Phys. J. E* **10**, 17 (2003).
10. R. Mathur and P. Capasso, *ACS Symp. Ser.* **610**, 219 (1995).
11. L. F. Zhang and A. Eisenberg, *Science* **268**, 1728 (1995).
12. L. F. Zhang, K. Yu, and A. Eisenberg, *Science* **272**, 1777 (1996).
13. D. E. Discher and A. Eisenberg, *Science* **29**, 967 (2002).
14. S. I. Stupp, V. Lebonheur, K. Walker, L. S. Li, K. E. Huggins, M. Keser, and A. Amstutz, *Science* **276**, 384 (1997).
15. S. A. Jenekhe and X. L. Chen, *Science* **283**, 372 (1999).
16. S. A. Jenekhe and X. L. Chen, *Science* **279**, 1903 (1998).
17. J. C. M. Van Hest, D. A. P. Delnoye, M. W. P. L. Baars, M. H. P. Van Genderen and E. W. Meijer, *Science* **268**, 1592 (1995).
18. S. Q. Zhou, C. Burger, B. Chu, M. Sawamura, N. Nagahama, M. Toganoh, U. E. Hackler, H. Isobe and E. Nakamura, *Science* **291**, 1944 (2001).
19. B. M. Discher, D. A. Hammer, F. S. Bates, and D. E. Discher, *Curr. Opin. Coll. Interface Sci.* **5**, 125–131 (2000).
20. M. Antonietti and S. Förster, *Adv. Mater.* **15**, 1323 (2003).
21. D. A. Hammer and D. E. Discher, *Annu. Rev. Mater. Sci* **31**, 387 (2001).
22. G. Kickelbick, J. Bauer, N. Husing, M. Andersson, and A. Palmqvist, *Langmuir* **19**, 3198–3201 (2003).
23. M. Maskos and J. R. Harris, *Macromol. Chem. Rapid Commun.* **22**, 271 (2001).
24. S. J. Holder, R. C. Hiorns, N. A. J. M. Sommerdijk, S. J. Williams, R. G. Jones, and R. J. M. Nolte, *Chem. Commun.* **14**, 1445 (1998).
25. K. Yu and A. Eisenberg, *Macromolecules* **31**, 3509–3518 (1998).
26. K. Yu, C. Bartels, and A. Eisenberg, *Langmuir* **15**, 7157–7167 (2000).
27. K. Yu, C. Bartels, and A. Eisenberg, *Macromolecules* **31**, 9399–9402 (1998).
28. K. Yu, A. J. Hurd, A. Eisenberg, and C. J. Brinker, *Langmuir* **17**, 7961–7965 (2001).
29. H. W. Shen and A. Eisenberg, *Angew. Chem., Int. Ed.* **39**, 3310 (2000).
30. L. F. Zhang and A. Eisenberg, *Macromolecules* **32**, 2239–2249 (1999).
31. L. Desbaumes and A. Eisenberg, *Langmuir* **15**, 36–38 (1999).
32. L. F. Zhang and A. Eisenberg, *Polym. Adv. Tech.* **9**, 677–699 (1998).
33. N. S. Cameron, M. K. Corbierre, and A. Eisenberg, *Can. J. Chem.* **77**, 1311–1326 (1999).
34. L. F. Zhang and A. Eisenberg, *Macromol. Symp.* **113**, 221–232 (1997).
35. S. Burke and A. Eisenberg, *High Performance Polym.* **12**, 535–542 (2000).
36. A. Choucair and A. Eisenberg, *Eur. Phys. J. A* **10**, 37–44 (2003).
37. L. F. Zhang and A. Eisenberg, *J. Am. Chem. Soc.* **118**, 3168–3181 (1996).
38. Y. S. Yu, L. F. Zhang, and A. Eisenberg, *Macromolecules* **31**, 1144–1154 (1998).
39. H. W. Shen and A. Eisenberg, *J. Phys. Chem. B* **103**, 9473–9487 (1999).
40. S. E. Burke and A. Eisenberg, *Polymer* **42**, 9111–9120 (2001).
41. L. Luo and A. Eisenberg, *J. Am. Chem. Soc.* **123**, 1012 (2001).
42. L. B. Luo and A. Eisenberg, *Langmuir* **17**, 6804–6811 (2001).
43. A. A. Choucair, A. H. Kycia, and A. Eisenberg, *Langmuir* **19**, 1001–1009 (2003).
44. K. Yu, L. F. Zhang, and A. Eisenberg, *Langmuir* **12**, 5980–5984 (1996).
45. A. Choucair, C. Lavigueur, and A. Eisenberg, *Langmuir* **20**, 3894 (2004).
46. Y. Y. Won, A. K. Brannan, H. T. Davis, and F. S. Bates, *J. Phys. Chem. B* **106**, 3354–3364 (2002).

47. J. C. M. Lee, M. Santore, F. S. Bates, and D. E. Discher, *Macromolecules* **35**, 323–326 (2002).
48. Y. S. Yu, L. F. Zhang, and A. Eisenberg, *Langmuir* **13**, 2578–2581 (1997).
49. J. C. M. Lee, H. Bermudez, B. M. Discher, M. A. Sheehan, Y.-Y. Won, F. S. Bates, and D. E. Discher, *Biotech. Bioeng.* **73**, 135 (2001).
50. B. M. Discher, H. Bermudez, D. A. Hammer, D. E. Discher, Y. Y. Won, and F. S. Bates, *J. Phys. Chem. B* **106**, 2848 (2002).
51. C. K. Haluska, W. T. Gozdz, H.-G. Döbereiner, S. Förster, and G. Gompper, *Phys. Rev. Lett.* **89**, 238302 (2002).
52. A. A. Reinecke and H. G. Döbereiner, *Langmuir* **19**, 605–608 (2003).
53. R. Dimova, H.-G. Döbereiner, S. Förster, B. Pouligny, and U. Seifert, *Eur. Phys. J. E* **7**, 241 (2002).
54. J. J. Lin, J. A. Silas, H. Bermudez, V. T. Milam, F. S. Bates, and D. A. Hammer, *Langmuir* **20**, 5493 (2004).
55. A. Rumplecker, S. Förster, M. Zähres, and C. Mayer, *J. Chem. Phys.* **120**, 8740 (2004).
56. M. Regenbrecht, S. Akari, S. Förster, and H. Möhwald, *J. Phys. Chem. B* **103**, 6669–6675 (1999).
57. E. Krämer, S. Förster, C. Göltner, and M. Antonietti, *Langmuir* **14**, 2027 (1998).
58. M. Regenbrecht, S. Akari, S. Förster, H. Möhwald, *Surf. Interface Anal.* **27**, 418 (1999).
59. S. Förster, V. Abetz, and A. H. E. Müller, *Adv. Polym. Sci.* **166**, 173 (2004).
60. H. W. Shen, L. F. Zhang, and A. Eisenberg, *J. Am. Chem. Soc.* **121**, 2728–2740 (1999).
61. H. Peng, D. Chen, and M. Jiang, *Langmuir* **19**, 10989 (2003).
62. Z. C. Li, Y. Shen, Y. Z. Liang, and F. M. Li, *Chin. J. Polym. Sci.* **19**, 297–301 (2001).
63. J. J. L. M. Cornelissen, M. Fischer, N. A. J. M. Sommerdijk, and R. J. M. Nolte, *Science* **280**, 1427 (1998).
64. D. Vriezema, A. Kros, R. De Gelder, J. L. M. Jeroen, A. E. Rowan, and R. J. M. Nolte, *Macromolecules* **37**, 4736 (2004).
65. I. C. Riegel, D. Samios, C. L. Petzhold, and A. Eisenberg, *Polymer* **44**, 2117–2128 (2003).
66. F. Checot, S. Lecommandoux, Y. Gnanou, and H.-A. Klok, *Angew. Chem., Int. Ed.* **41**, 1340 (2001).
67. F. Checot, S. Lecommandoux, H.-A. Klock, and Y. Gnanou, *Eur. Phys. J. E* **10**, 25 (2003).
68. J. Ding and G. Liu, *J. Phys. Chem. B* **102**, 6107 (1998).
69. J. Ding and G. Liu, *Macromolecules* **30**, 655 (1997).
70. J. Ding and G. Liu, *Chem. Mater.* **10**, 537 (1998).
71. S. M. Gravano, M. Borden, T. von Werne, E. M. Doerffler, G. Salazar, A. Chen, E. Kisk, J. A. Zasadzinski, T. E. Patten, and M. L. Longo, *Langmuir* **18**, 1938 (2002).
72. A. Napoli, N. Tirelli, G. Kilcher, and J. A. Hubbell, *Macromolecules* **34**, 8913 (2001).
73. A. Napoli, M. Valentini, N. Tirelli, M. Mueller, and J. A. Hubbell, *Nat. Mater.* **3**, 183 (2004).
74. A. Napoli, M. J. Boerakker, N. Tirelli, R. J. M. Nolte, N. A. J. M. Sommerdijk, and J. A. Hubbell, *Langmuir* **20**, 3487 (2004).
75. R. Stoenescu and W. Meier, *Chem. Commun.* **24**, 3016–3017 (2002).
76. J.-L. Putaux, E. Minatti, C. Lefebvre, R. Borsali, M. Schappacher, and A. Deffieux, *Faraday Disc.* **128**, 163 (2004).
77. M. Hales, C. Barner-Kowollik, T. P. Davis, and M. H. Stenzel, *Langmuir* 20 (2004).
78. F. Ahmed and D. E. Discher, *J. Controlled Release* **96**, 37 (2004).
79. J. Du, Y. Chen, Y. Zhang, C. C. Han, K. Fischer, and M. Schmidt, *J. Am. Chem. Soc.* **125**, 14710 (2003).
80. J. Du and Y. Chen, *Macromolecules* **37**, 5710 (2004).

81. K. N. Power-Billard, R. J. Spontak, and I. Manners, *Angew. Chem., Int. Ed.* **43**, 1260 (2004).
82. E. G. Bellomo, M. D. Wyrsta, L. Pakstis, D. J. Pochan, and T. J. Deming, *Nat. Mater.* **3**, 244 (2004).
83. T. J. Deming, E. G. Bellomo, M. Wyrsta, L. Pakstis, and D. Pochan, *Polym. Mater. Sci. Eng.* **90**, 302 (2004).
84. J. K. Harris, G. D. Rose, and M. L. Bruening, *Langmuir* **18**, 5337 (2002).
85. G. E. Yu and A. Eisenberg, *Macromolecules* **31**, 5546–5549 (1998).
86. F. T. Liu and A. Eisenberg, *J. Am. Chem. Soc.* **49**, 15059–15064 (2003).
87. C. Nardin, T. Hirt, J. Leukel, and W. Meier, *Langmuir* **16**, 1035–1041 (2000).
88. C. Nardin, T. Hirt, J. Leukel, and W. Meier, *Langmuir* **16**, 1035 (2000).
89. W. Meier, C. Nardin, and M. Winterhalter, *Angew. Chem., Int. Ed.* **39**, 4599 (2000).
90. K. Schillen, K. Bryskhe, and Y. S. Mel'nikova, *Macromolecules* **32**, 6885 (1999).
91. K. Bryskhe, J. Jansson, D. Topgaard, K. Schillen, and U. Olssson, *J. Phys. Chem. B* **108**, 9710 (2004).
92. J. Zipfel, J. Berghausen, G. Schmidt, P. Lindner, P. Alexandridis, and W. Richtering, *Macromolecules* **35**, 4064–4074 (2002).
93. R. Stoenescu and W. Meier, *Mol. Cryst. Liq. Cryst.* **417**, 185 (2004).
94. R. Stoenescu, A. Graff, and W. Meier, *Macromol. Biosci.* **4**, 930 (2004).
95. X. Y. Xiong, K. C. Tam, and L. H. Gan, *Macromolecules* **36**, 9979 (2003).
96. J. N. Israelachvili, *Intermolecular and Surface Forces*, Academic Press, London, 1985.
97. Monduzzi M: Self-assembly in fluorocarbon surfactant systems, *Curr. Opin. Coll. Interfac. Sci.* **3** 467–477 (1998).
98. S. Förster, M. Zisenis, E. Wenz, and M. Antonietti, *J. Chem. Phys.* **104**, 9956 (1996).
99. D. A. Hajduk, M. B. Kossuth, M. A. Hillmyer, and F. S. Bates, *J. Phys. Chem. B.* **102**, 4269 (1998).
100. S. Förster, B. Berton, H. P. Hentze, E. Krämer, M. Antonietti, and P. Lindner, *Macromolecules* **34**, 4610 (2001).
101. F. S. Bates and G. H. Fredrickson, *Phys. Today* **52**, 32 (1999).
102. S. Förster and T. Plantenberg, *Angew. Chem. Int. Ed.* **41**, 688 (2002).
103. T. Haliloglu, I. Bahar, B. Erman, and W. L. Mattice, *Macromolecules* **29**, 4764 (1996).
104. J. N. Israelachvili, D. J. Mitchell, and B. W. Ninham, *J. Chem. Soc., Faraday Trans. 2* **72**, 1525 (1976).
105. S. T. Hyde, *J. Phys. C* **7**, 209 (1990).
106. G. Srinivas, D. E. Discher, and M. L. Klein, *Nat. Mater.* **3**, 638 (2004).
107. S. Burke, H. W. Shen, and A. Eisenberg, *Macromol. Symp.* **175**, 273–283 (2001).
108. P. L. Soo and A. Eisenberg, *J. Polym. Sci. B* **42**, 923 (2004).
109. J. A. Opsteen, J. J. L. M. Cornelissen, and J. C. M. van Hest, *Pure Appl. Chem.* **76**, 1309 (2004).
110. K. Kita-Tokarczyk, J. Grumeland, T. Haefele, and W. Meier, *Polymer*, in press.
111. H. Shen, L. Zhang, and A. Eisenberg, *J. Phys. Chem. B.* **101**, 4697 (1997).
112. H. W. Shen and A. Eisenberg, *Macromolecules* **33**, 2561–2572 (2000).
113. K. Yu and A. Eisenberg, *Macromolecules* **29**, 6359–6361 (1996).
114. K. Yu and A. Eisenberg, *Macromolecules* **31**, 3509 (1998).
115. L. F. Zhang and A. Eisenberg, *Macromolecules* **29**, 8805–8815 (1996).
116. S. E. Burke and A. Eisenberg, *Langmuir* **17**, 8341–8347 (2001).
117. Y. S. Yu and A. Eisenberg, *J. Am. Chem. Soc.* **119**, 8383–8384 (1997).
118. D. J. Mitchell, G. J. T. Tiddy, L. Waring, B. Bostock, and M. P. McDonald, *J. Chem. Soc. Faraday Trans.* **79**, 975 (1983).
119. L. Chen, H. W. Shen, and A. Eisenberg, *J. Phys. Chem. B* **103**, 9488–9497 (1999).
120. S. Jain and F. S. Bates, *Science* **300**, 460–464 (2003).

121. S. Förster, N. Hermsdorf, C. Böttcher, and P. Lindner, *Macromolecules* **35**, 4096 (2002).
122. N. Hermsdorf, Ph.D. dissertation, University of Potsdam, 1999.
123. E. W. Kaler, A. K. Murphy, B. E. Rodriguez, J. A. N. Zasadzinski, *Science* **245**, 1371 (1989).
124. B. zu Putlitz, K. Landfester, S. Förster, and M. Antonietti, *Langmuir* **16**, 3003 (2000).
125. S. Schrage, R. Sigel, and H. Schlaad, *Macromolecules* **36**, 1417–1420 (2003).
126. A. V. Kabanov, T. K. Bronich, V. A. Kabanov, K. Yu, and A. Eisenberg, *J. Am. Chem. Soc.* **120**, 9941–9942 (1998).
127. T. K. Bronich, O. Y. Ming, V. A. Kabanov, A. Eisenberg, F. C. Szoka, and A. V. Kabanov, *J. Am. Chem. Soc.* **124**, 11872–11873 (2002).
128. F. Ilhan, T. H. Galow, M. Gray, G. Clavier, and V. M. Rotello, *J. Am. Chem. Soc.* **122**, 5895 (2000).
129. F. Szoka and D. Papahadjopoulos, *Annu. Rev. Biophys. Bioeng.* **9**, 467 (1980).
130. R. R. C. New, ed., *Liposomes—A Practical Approach*, Oxford University Press, Oxford, 1990.
131. E. Evans and D. Needham, *J. Phys. Chem.* **91**, 4219 (1987).
132. M. I. Angelova, S. Soleau, P. Meleard, J. F. Faucon, and P. Bothorel, *Progr. Coll. Polym. Sci.* **89**, 127 (1992).
133. S. Hauschild, U. Lipprandt, A. Rank, R. Schubert, and S. Förster, submitted.
134. U. Seifert, *Adv. Phys.* **46**, 13 (1997).
135. L. Landau and E. Lifshitz, *Elastizitätstheorie*, Akademie-Verlag, Berlin, 1989.
136. H.-G. Döbereiner, A. Lehmann, W. Goedel, O. Selchow, and R. Lipowsky, *Mater. Res. Soc. Symp. Proc.* **489**, 101 (1998).
137. O. Terreau, L. B. Luo, and A. Eisenberg, *Langmuir* **19**, 5601–5607 (2003).
138. L. B. Luo and A. Eisenberg, *Angew. Chem., Int. Ed.* **41**, 1001 (2002).
139. L. B. Luo and A. Eisenberg, *Langmuir* **18**, 1952 (2002).
140. H. Bader and H. Ringsdorf, J. *Polym. Sci., Polym. Chem. Ed.* **20**, 1623 (1982).
141. J.-H. Fuhrhop, K. Ellermann, H. H. David, and J. Mathieu, *Angew. Chem., Int. Ed.* **21**, 440 (1982).
142. R. Stoenescu and W. Meier, *Chem. Commun*. 3016 (2002).
143. B. L.-S. Mui, H.-G. Döbereiner, T. D. Madden, P. R. Cullis, *Biophys. J.* **69**, 930 (1995).
144. U. Borchert, Ph.D. dissertation, University of Hamburg, 2005.
145. K. Fricke and E. Sackmann, *Biochim. Biophys. Acta* **554**, 145 (1984).
146. H. Ringsdorf, B. Schlarb, and J. Venzmer, *Angew. Chem., Int. Ed.* **27**, 113 (1988).
147. H. G. Döbereiner, E. Evans, M. Kraus, U. Seifert, and M. Wortis, *Phys. Rev. E* **55**, 4458 (1997).
148. L. Zhang, C. Bartels, Y. Yu, H. Shen, and A. Eisenberg, *Phys. Rev. Lett.* **79**, 5034 (1997).
149. H. Bermudez, H. Aranda-Espinoza, D. A. Hammer, and D. E. Discher, *Europhys. Lett.* **64**, 550–556 (2003).
150. R. Goetz, G. Gompper, and R. Lipowsky, *Phys. Rev. Lett.* **82**, 221 (1999).
151. H. Bermudez, A. K. Brannan, D. A. Hammer, F. S. Bates, and D. E. Discher, *Macromolecules* **35**, 8203–8208 (2002).
152. H. Aranda-Espinoza, H. Bermudez, F. S. Bates, and D. E. Discher, *Phys. Rev. Lett.* **87**, 208301 (2001).
153. D. Marsh, *CRC Handbook of Lipid Bilayers*, CRC Press, Boca Raton, Fla., 1990.
154. H. Bermudez, D. A. Hammer, and D. E. Discher, *Langmuir* **20**, 540 (2004).
155. R. Lipowsky and E. Sackmann, eds., *From Cells to Vesicles*, Elsevier, Amsterdam, 1995, pp. 1–5A.
156. A. Graff, M. Sauer, P. Van Gelder, and W. Meier, *Proc. Natl. Acad. Sci. U.S.A.* **99**, 5064 (2002).
157. E. Evans and D. Needham, *J. Phys. Chem.* **91**, 4219 (1987).
158. V. Pata, F. Ahmed, D. E. Discher, and N. Dan, *Langmuir* **20**, 3888 (2004).

159. M. M. Santore, D. E. Discher, Y. Y. Won, F. S. Bates, D. A. Hammer, *Langmuir* **18**, 7299–7308 (2002).
160. J. N. Weinstein, S. Yoshikami, P. Henkart, R. Blumenthal, and W. A. Hagins, *Science* **195**, 489 (1977).
161. T. M. Allen and L. G. Cleland, *Biochim. Biophys. Acta* **591**, 418 (1980).
162. C. Washington, *Int. J. Pharm.* **58**, 1 (1990).
163. U. Borchert and S. Förster, submitted.
164. L. Stryer, *Biochemistry*, 3rd ed., W. H. Freeman and Co., San Francisco, Calif., 1988.
165. J. C. M. Lee, R. J. Law, and D. E. Discher, *Langmuir* **17**, 3592–3597 (2001).
166. H. Ringsdorf, B. Schlarb, and J. Venzmer, *Angew. Chem., Int. Ed.* **27**, 113 (1988).
167. S. C. Liu and D. F. O'Brien, *J. Am. Chem. Soc.* **124**, 6037 (2002).
168. B. M. Discher, H. Bermudez, D. A. Hammer, D. E. Discher, Y. Y. Won, and F. S. Bates, *J. Phys. Chem. B* **106**, 2848–2854 (2002).
169. D. F. O'Brien, R. T. Klingbiel, D. P. Specht, and P. N. Tyminski, *Ann. N.Y. Acad. Sci.* **446**, 282 (1985).
170. D. R. Day and H. Ringsdorf, *J. Polym. Sci., Polym. Lett. Ed.* **16**, 205 (1978).
171. D. R. Day and H. Ringsdorf, *Makromol. Chem.* **180**, 1059 (1979).
172. S. L. Regen, B. Czech, and A. Singh, *J. Am. Chem. Soc.* **102**, 6638 (1980).
173. D. S. Johnston, S. Sanghera, M. Pons, and D. Chapman, *Biochim. Biophys. Acta* **602**, 57 (1980).
174. H. Hub, B. Hupfer, H. Koch, and H. Ringsdorf, *Angew. Chem., Int., Ed.* **19**, 938 (1980).
175. D. F. O'Brien, T. H. Whitesides, and R. T. Klingbiel, *J. Polym. Sci., Polym. Lett. Ed.* **19**, 95 (1981).
176. L. Gros, H. Ringsdorf, and H. Schupp, *Angew. Chem., Int. Ed. Engl.* **20**, 305 (1981).
177. A. K. Akimoto, K. Dorn, L. Gros, H. Ringsdorf, and H. Schupp, *Angew. Chem., Int. Ed. Engl.* **20**, 90 (1981).
178. E. Lopez, D. F. O'Brien, and T. H. Whitesides, *J. Am. Chem. Soc.* **104**, 305 (1982).
179. P. Tundo, D. J. Kippenberger, P. L. Klahn, N. E. Prieto, T. C. Jao, and J. H. Fendler, *J. Am. Chem. Soc.* **104**, 456 (1982).
180. T. Komatsu, E. Tsuchida, C. Böttcher, D. Donner, C. Messerschmidt, U. Siggel, W. Stocker, J. P. Rabe and J.-H. Fuhrhop, *J. Am. Chem. Soc.* **119**, 11660 (1997).
181. K. Dorn, R. T. Klingbiel, D. P. Specht, P. N. Tyminski, H. Ringsdorf, and D. F. O'Brien, *J. Am. Chem. Soc.* **106**, 1627 (1984).
182. R. Büschl and D. F. O'Brien, Unpublished data, 1984.
183. B. Hupfer, H. Ringsdorf, and H. Schupp, *Chem. Phys. Lipids* **33**, 355 (1983).
184. H. Ringsdorf, B. Schlarb, P. N. Tyminski, and D. F. O'Brien, *Macromolecules* **21**, 671 (1988).
185. F. Ahmed, A. Hategan, D. E. Discher, and B. M. Discher, *Langmuir* **19**, 6505–6511 (2003).
186. A. Graff, M. Winterhalter, and W. Meier, *Langmuir* **17**, 919–923 (2001).
187. W. Meier, A. Graff, A. Diederich, and M. Winterhalter, *Phys. Chem. Chem. Phys.* **2**, 4559–4562 (2000).
188. J. Hotz and W. Meier, *Langmuir* **14**, 1031–1036 (1998).
189. J. Hotz and W. Meier, *Adv. Mater.* **10**, 1387 (1998).
190. W. Meier, *Chimia* **53**, 214–215 (1999).
191. W. Meier, *Chem. Soc. Rev.* **29**, 295–303 (2000).
192. M. Sauer and W. Meier, *Chem. Commun.* **1**, 55–56 (2001).
193. M. Sauer, D. Streich, and W. Meier, *Adv. Mater.* **13**, 1649–1651 (2001).
194. M. Sauer and W. Meier, *Aust. J. Chem.* **54**, 149–151 (2001).
195. D. A. Tirrell, A. B. Turek, D. A. Wilkinson, and T. J. McIntosh, *Macromolecules* **18**, 1513 (1985).
196. D. Y. Takigawa and D. A. Tirrell, *Makromol. Chem. Rapid Commun.* **6**, 653 (1985).

197. D. Carrier and M. Pezolet, *Biochemistry* **25**, 4167 (1986).
198. A. Walter, C. J. Steer, and R. Blumenthal, *Biochim. Biophys. Acta* **861**, 319 (1986).
199. D. A. Tirrell, D. Y. Takigawa, and K. Seki, *Ann. N.Y. Acad. Sci.* **446**, 237 (1985).
200. K. Seki and D. A. Tirrell, *Macromolecules* **17**, 1692 (1984).
201. M. Takada, T. Yuzuriha, K. Katayama, K. Lwamoto, and J. Sunamoto, *Biochim. Biophys. Acta* **802**, 237 (1984).
202. J. Sunamoto, T. Sato, M. Hirota, K. Fukushima, K. Hiratani, and K. Hara, *Biochim. Biophys. Acta* **898**, 323 (1987).
203. K. Kostarelos, M. Kipps, T. F. Tadros, and P. F. Luckham, *Coll. Surf. A* **136**, 1–9 (1998).
204. K. Kostarelos, P. F. Luckham, and T. F. Tadros, *J. Chem. Soc. Faraday Trans.* **94**, 2159–2168 (1998).
205. K. Kostarelos, T. F. Tadros, and P. F. Luckham, *Langmuir* **15**, 369–376 (1999).
206. M. L. Hwang, R. K. Prud'homme, J. Kohn, and J. L. Thomas, *Langmuir* **17**, 7713 (2001).
207. C. Allen, A. Eisenberg, and D. Maysinger, *S.T.P. Pharma Sci.* **9**, 139–151 (1999).
208. D. E. Discher, P. Photos, F. Ahmed, R. Parthasrathy, and F. S. Bates, in V. Muzykantov and V. Torchilin, eds., *Biomedical Aspects of Drug Targeting*, Kluwer, 2002, pp. 459–471.
209. D. D. Lasic and D. Papahadjopoulos, eds., *Medical Applications of Liposomes*, Elsevier Science, Amsterdam, 1988.
210. T. Merdan, J. Kopecek, T. Kissel, *Adv. Drug Delivery Rev.* **54**, 715 (2002).
211. A. L. Klibanov, K. Maruyama, V. P. Torchilin, and L. Hung, *FEBS Lett.* **268**, 235 (1990).
212. D. D. Lasic and D. Papahadjopoulos, eds. *Medical applications of liposomes*, Elsevier Science, Amsterdam, 1998.
213. P. J. Photos, L. Bacakova, B. Discher, F. S. Bates, and D. E. Discher, *J. Controlled Release* **90**, 323–334 (2003).
214. S. I. Ertel, B. D. Ratner, A. Kaul, M. B. Schway, and T. A. Horbett, *J. Biomed. Mater. Res.* **28**, 667, (1994).
215. A. Kidane, T. McPherson, H. S. Shim, and K. Park, *Coll. Surf. B* **18**, 347 (2000).
216. A. Kidane and K. Park, *J. Biomed. Mater. Res* **48**, 640 (1999).
217. R. H. Müller and G. E. Hildebrand, eds., *Pharmazeutische Technologie: Moderne Arzneimittelformen*, Wissenschaftliche Verlagsgesellschaft, Stuttgart, 1998.
218. C. Nardin, J. Widmer, M. Winterhalter, and W. Meier, *Eur. Phys. J. A* **4**, 403–410 (2001).
219. P. Dalhaimer, H. Bermudez, and D. E. Discher, *J. Polym. Sci. B* **42**, 168–176 (2004).
220. O. V. Gerasimov, A. Schwan, and D. H. Thompson, *Biochim. Biophys. Acta* **1324**, 200 (1997).
221. J. Shin, P. Shum, and D. H. Thompson, *J. Controlled Release* **91**, 187 (2003).
222. J. A. Boomer, H. D. Inerowicz, Z.-Y. Zhang, N. Bergstrand, K. Edwards, J.-M. Kim, and D. H. Thompson, *Langmuir* **19**, 6408 (2003).
223. N. Bergstrand, M C. Arfvidsson, J.-M. Kim, D. H. Thompson, and K. Edwards, *Biophys. Chem.* **104**, 361 (2003).
224. S. Förster, U. Borchert, U. Lipprandt, P. Lindner, A. Kimpfler, and R. Schubert, submitted.
225. K. Jorgensen, J. Davidsen, and O. G. Mouritsen, *FEBS Lett.* **531**, 23 (2002).
226. J. Davidsen, K. Jorgensen, T. L. Andresen, and O. G. Mouritsen, *Biochim. Biophys. Acta* **1609**, 95 (2003).
227. U. Liman, D. A. Frankel, and D. F. O'Brien, *Biohys. J.* **53**, 325a (1988).
228. N. J. Wymer, O. V. Gerasimov, and D. H. Thompson, *Bioconj. Chem.* **9**, 305 (1998).
229. A. Kros, J. A. Jansen, S. J. Holder, R. J. M. Nolte, and N. A. J. M. Sommerdijk, *J. Adhes. Sci. Technol.* **16**, 143–155 (2002).

230. N. Wagner, K. Dose, H. Koch, and H. Ringsdorf, *FEBS Lett.* **132**, 313 (1981).
231. R. Pabst, H. Ringsdorf, H. Koch, and K. Dose, *FEBS Lett.* **154**, 5 (1983).
232. P. Yager, *Biosensors* **2**, 363 (1986).
233. P. N. Tyminski, L. H. Latimer, and D. F. O'Brien, *J. Am. Chem. Soc.* **107**, 7769 (1985).
234. P. N. Tyminski, L. H. Latimer, and D. F. O'Brien, *Biochemistry* **27**, 2696 (1988).
235. N. Wagner, K. Dose, H. Koch, and H. Ringsdorf, *FEBS Lett.* **132**, 313 (1981).
236. W. Meier, *Chimia* **56**, 490–493 (2002).
237. W. Meier, C. Nardin, and M. Winterhalter, *Angew. Chem., Int. Ed.* **39**, 4599 (2000).
238. M. Winterhalter, C. Hilty, S. M. Bezrukov, C. Narind, W. Meier, and D. Fournier, *Talanta* **55**, 965–971 (2001).
239. W. Meier, C. Nardin, M. Winterhalter, *Angew. Chem., Int. Ed.* **39**, 4599. (2000).
240. C. Nardin, S. Thoeni, J. Widmer, M. Winterhalter, and W. Meier, *Chem., Commun.* **15**, 1433–1434 (2000).
241. M. Sauer, T. Haefele, A. Graff, C. Nardin, and W. Meier, *Chem. Commun.* **23**, 2452–2453 (2001).
242. J. J. Lin, J. A. Silas, H. Bermudez, V. T. Milam, F. S. Bates, and D. A. Hammer, *Langmuir* **20**, 5493 (2004).
243. P. Dalhaimer, F. S. Bates, H. Aranda-Espinoza, and D. E. Discher, *C. R. Physique* **4**, 251–258 (2003).
244. D. A. Hammer and D. E. Discher, *Annu. Rev. Mater. Res.* **31**, 387–404 (2001).

STEPHAN FÖRSTER
KWE BORCHERT
University of Hamburg

Encyclopedia of Polymer Sceince and Technology
Copyright © 2005 John Wiley & Sons, Inc. All rights reserved.

POLYPEPTIDE SYNTHESIS, RING-OPENING POLYMERIZATION OF α-AMINO ACID *N*-CARBOXYANHYDRIDES

Introduction

α-Amino acid *N*-carboxyanhydrides (NCAs) were first described in 1906 by Hermann Leuchs (1). Leuchs discovered that heating *N*-ethoxycarbonyl and *N*-methoxycarbonyl α-amino acid chlorides under reduced pressure resulted in the formation of the corresponding NCAs. Upon exposure to water, he observed that these NCAs reacted and were transformed into an insoluble mass. The concept of polymers not being established at that time, Leuchs described this product as cyclic oligopeptides. It was not until the 1920s, when the existence of macromolecules became widely accepted, that systematic studies on the synthesis and polymerization of NCAs were started (2–3). Since then, the NCA polymerization has matured and has become the most commonly applied technique for the large-scale (ie, multigram) synthesis of high molecular weight polypeptides and polypeptide-based block copolymers. A survey of the number of publications describing polypeptide synthesis via NCA ring-opening polymerization reveals that after a strong increase in the 1960s and 1970s, the interest in this technique decreased until the mid 1990s (Fig. 1). The renewed interest in the NCA ring-opening polymerization since then may be attributed to two factors, which are closely related to each other: (*1*) the development of novel methods for the polymerization of NCAs and (*2*) the notion that polypeptides and polypeptide-based hybrid block copolymers may be potentially interesting materials for a variety of applications in biomedicine and biomineralization, and analysis.

Much of the interest in the development of novel materials based on polypeptides is driven by their ability to fold in a variety of stable secondary, tertiary, and quaternary structures (see PROTEIN FOLDING). Polypeptides can self-assemble into complex, hierarchically organized nanoscale morphologies, which cannot be produced from conventional nonbiological polymers. These characteristics may allow the preparation of ordered films or organic/inorganic composites that could be of interest for a multitude of advanced applications. Since the folding properties of natural peptide polymers (proteins) are, amongst others, due to their uniform chain lengths and well-defined monomer sequences, synthetic methods that allow the polymerization of NCAs with precise control of molecular weight, molecular weight distribution, and composition are important to explore the full potential of novel synthetic polypeptide materials. This article provides an overview of the

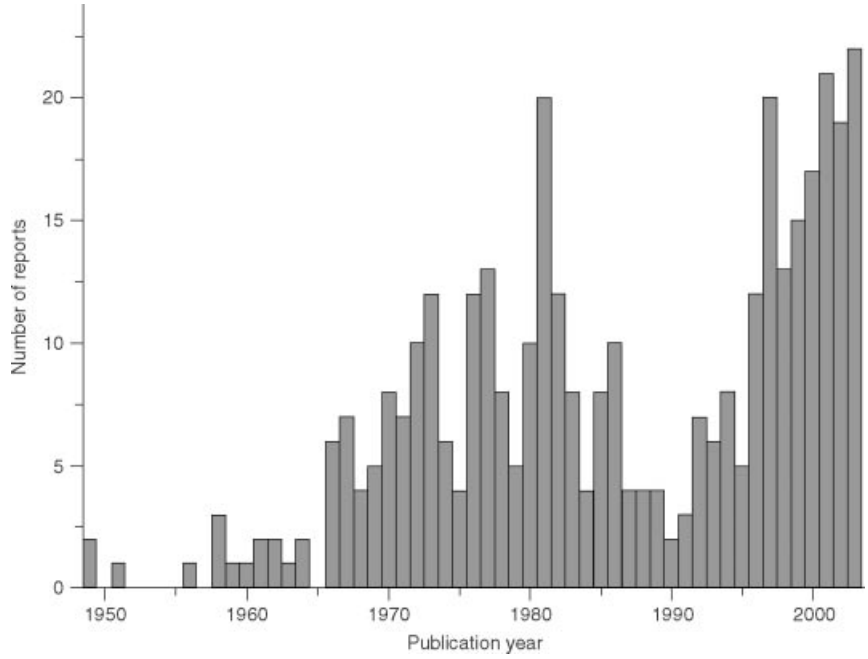

Fig. 1. Survey of the number of reports describing polypeptide synthesis via NCA ring-opening polymerization. *Source*: SciFinder Scholar, Dec. 2003.

different methodologies that have been developed for the polymerization of NCAs and discusses the scope and limitations of each of these techniques for the preparation of polypeptides with controlled molecular weights and narrow molecular weight distributions.

NCA Synthesis

One obvious method for the preparation of NCAs is of course by cyclization of *N*-alkoxycarbonyl amino acid chlorides, as originally discovered by Leuchs (eq. 1) (1). Over the years, various improvements of this so-called Leuchs method have been made. While the original procedure used thionylchloride for the chlorination of *N*-alkoxycarbonyl α-amino acids, it was found that phosphorus bromide is more convenient, allowing cyclization to take place at lower temperatures (4). The rate of cyclization depends on the nature of the alkoxycarbonyl group and decreases in the following order: ethyl < methyl < allyl < benzyl. Equation 1 shows a mechanism that is in line with these observations.

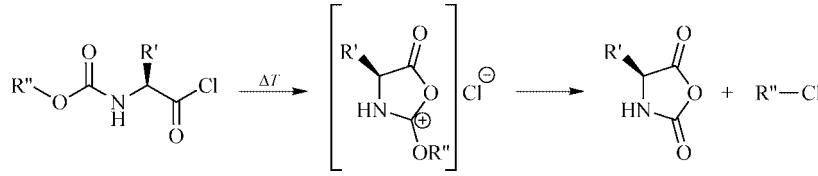

(1)

One of the most widely applied methods for the preparation of NCAs involves the direct phosgenation of free α-amino acids (5). This synthesis, which is referred to as the Fuchs–Farthing method, is usually carried out in inert, low boiling solvents such as tetrahydrofuran, dioxane, or ethyl acetate. Mixtures of these solvents with methylene chloride have also been reported and have the advantage of a lower solubility for the hydrochloric acid that is released during the reaction. A low concentration of hydrochloric acid is important in order to prevent cleavage of the NCA ring. The liberated hydrochloric acid may also lead to problems in the synthesis of NCAs derived from trifunctional amino acids that carry acid-sensitive protective groups. To avoid premature cleavage of such protective groups, hydrochloric acid scavengers such as AgCN (6) or triethylamine (7) are added. Another method that prevents the formation of hydrochloric acid and allows the synthesis of NCAs carrying acid-sensitive protective groups starts with the preparation of the corresponding silylated amino acid derivatives. Upon treatment with phosgene, thionylchloride, or phosphorous trihalides, silylated amino acids react to produce the NCA and trimethylsilylchloride (8). The original Fuchs–Farthing procedure used phosgene, but modifications of this method have been developed in which phosgene is replaced by diphosgene (trichloromethyl chloroformate) (9) or triphosgene (bis(trichloromethyl)carbonate) (10). Instead of the gaseous phosgene, which can be difficult to handle, diphosgene and triphosgene are liquid and solid, respectively, which makes them much easier to handle and allows the use of stoichiometric quantities.

Monomer purity is of critical importance for the success of the NCA polymerization; the presence of traces of hydrochloric acid or other contaminants can lead to premature termination of chain growth and result in broadening of the molecular weight distribution. Advanced procedures have been developed, which allow the preparation of NCAs in high purities (11). These procedures involve washing an organic solution containing the NCA with chilled, aqueous bicarbonate. Polymerization of NCAs purified following this method by primary amine functionalized polystyrene macroinitiators was found to result in synthetic-peptide hybrid block copolymers with polydispersities that were smaller than those obtained using NCAs prepared and isolated according to the traditional procedures (12).

Traditional NCA Polymerization Methods

Traditionally, the most important classes of initiators for the NCA ring-opening polymerization included a broad range of nucleophiles and bases, such as primary amines, tertiary amines, and alkoxide and hydroxide ions (4,13). Other initiating systems, such as temperature, metal salts, and organometallic compounds, have also been used, but these have not found widespread application (4). Polymerization of NCAs using nucleophilic or basic initiators is thought to proceed along two main pathways, the amine mechanism (eq. 2) and the activated-monomer mechanism (Fig. 2) (4,13). The amine mechanism is a nucleophilic ring-opening chain growth process. The activated-monomer mechanism, on the other hand, starts with deprotonation of an NCA, which subsequently acts as the nucleophile that initiates chain growth. If decarboxylation is slow, chain growth may proceed

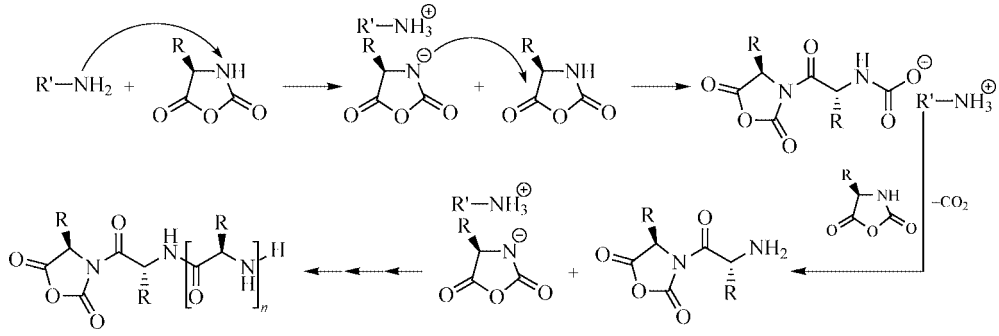

Fig. 2. NCA polymerization via the activated monomer mechanism.

along a third pathway, the carbamate mechanism (eq. 3). The preferred pathway of polymerization for a given initiator is determined by its nucleophilicity/basicity ratio. Generally, NCA polymerizations initiated by primary amines, which have a high nucleophilicity/basicity ratio, predominantly follow the primary amine mechanism. NCA polymerizations initiated by tertiary amines or alkoxide/hydroxide ions, which are more basic than nucleophilic, mainly proceed along the activated monomer mechanism. This classification, however, is by no means unambiguous, and it is important to note that a given polymerization can switch back and forth many times between the different mechanisms during the course of the reaction. In other words, a propagation step for one mechanism is a side reaction for the other, and vice versa.

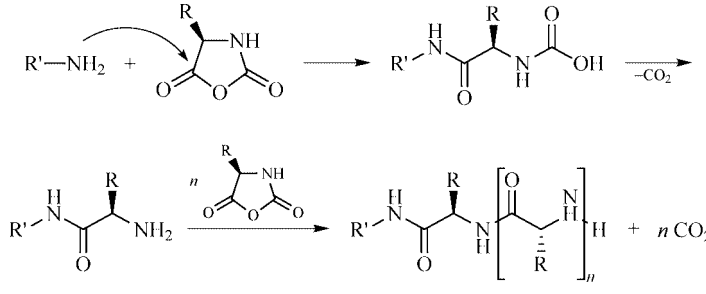

(2)

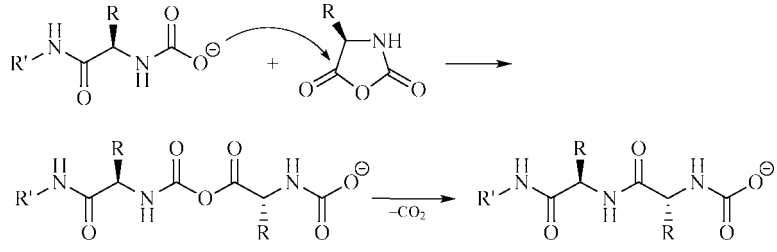

(3)

The existence of multiple, competitive mechanisms, which may act simultaneously during the course of a polymerization reaction, restricts control over the molecular weight and the molecular weight distribution of the resulting

polypeptide and also hampers the formation of well-defined block copolymers. Using very nucleophilic or basic initiators, the NCA polymerization can be biased toward the amine and activated-monomer mechanism, respectively. These initiators allow a certain level of control over the polymerization and can produce polypeptides with molecular weights which roughly correlate with the monomer-to-initiator ratio.

Especially primary amines and primary amine functionalized macroinitiators have been extensively used for the preparation of a broad range of polypeptides and polypeptide-containing hybrid polymers. In addition to simple polypeptide homopolymers, random copolymers have been prepared by co- or terpolymerization of different NCAs. Polypeptide copolymers have attracted attention, eg, as polymeric drug carriers (14). Furthermore, random copolypeptides have been used to study the conformational properties of amino acids (15). Polypeptides and polypeptide-containing block copolymers have been obtained by sequential copolymerization of different NCAs and by using primary amine end-functionalized nonpeptidic macroinitiators for the NCA ring-opening polymerization, respectively. Amongst other, triblock copolypeptides have been used to investigate the helix-forming propensities of amino acids (16). The solid-state structures of synthetic-peptide hybrid block copolymers have been studied in considerable detail (17). Most of these block copolymers form lamellar superstructures, with the polypeptide chains folded and arranged in an hexagonal array. Furthermore, peptide-synthetic hybrid block copolymers can possess good antithrombogenic properties, which make them of interest for medical applications.

In addition to simple, linear polypeptides, the NCA polymerization has also been used to prepare branched macromolecular architectures. Star polypeptides, probably the simplest example of branched polypeptides, can be obtained via NCA polymerization using multiple, primary amine functionalized initiators. Examples of multifunctional initiators include hexakisamines derived from 1,3,5-tris(bromomethyl)benzene (18), tetra-amino functionalized perylene chromophores (19) and cyclotriphosphazenes (20). Interestingly, Teflon-supported films of hexaarmed, ethylene glycol substituted polyglutamic acid star polymers based on a cyclotriphosphazene core were found to be excellent enantioselective membranes for amino acids (21). A further class of initiators that has been frequently used to prepare star-shaped polypeptides are poly(amido amine) (PAMAM) dendrimers (22-23). PAMAM dendrimers have been used as initiators for the ring-opening polymerization of sugar-substituted NCAs (eg, *O*-(tetra-*O*-acetyl-β-D-glucopyranosyl)-L-serine *N*-carboxyanhydride and *O*-(2-acetamido-3,4,6-tri-*O*-acetyl-2-deoxy-β-D-glucopyranosyl)-L-serine *N*-carboxyanhydride) (23) as well as γ-benzyl-L-glutamate *N*-carboxyanhydride (23). It was found that the helicity of the PAMAM-based star polypeptides was significantly enhanced compared to their linear analogues. This effect was attributed to the aggregation of peptide segments on the dendrimer surface.

More complex branched polypeptides can be obtained following iterative reaction schemes involving several NCA ring-opening polymerization steps. Graft copolypeptides, which have also been termed multichain polypeptides, have been prepared using a linear poly(L-lysine) as initiator for the NCA ring-opening polymerization (24). These graft polypeptides were designed with the aim of developing polymer–drug and polymer–epitope conjugates (25–26). This synthetic

approach can be further extended by utilizing these graft copolymers as initiators for a next NCA ring-opening polymerization step. Repetition of this graft-on-graft strategy leads to highly branched, so-called dendritic-graft, polypeptides (27). In addition to the graft-on-graft strategy, branched polypeptides can also be prepared by end-functionalization of a peptide chain with an appropriate N^{α},N^{ε}-diprotected lysine derivative (28). Deprotection of the lysine amino groups doubles the number of end groups that can be used to initiate a subsequent NCA ring-opening polymerization step. Repetition of this NCA ring-opening polymerization–end-functionalization–deprotection sequence has been successfully used to prepare highly branched poly(L-lysine)s with molecular weights up to 33 kDa in small number of reaction steps.

Primary amine initiated NCA polymerizations have not only been carried out in homogeneous solution but also under heterogeneous conditions. The use of primary amine functionalized surfaces allows the preparation of thin, directionally aligned polypeptide films (29). If the density of the peptide chains at the surface is sufficiently high, the chains are mainly oriented normal to the surface. Such polypeptide films have been grown from a variety of surfaces, including silicon, aluminum, gold, indium-tin-oxide, quartz, and polytetrafluoroethylene (Teflon). Surface-initiated NCA polymerizations can be carried out either by exposing the amino-functionalized substrate to a solution containing the appropriate NCA monomer or by vapor phase deposition of the NCA monomer (30). Sequential addition of two different NCA monomers allows the preparation of surface-grafted polypeptide block copolymers (31). Surface-grafted polypeptide films obtained via NCA polymerization have been found to possess piezoelectric properties, (32) indicative for the parallel alignment of the peptide helices. Furthermore, the water permeability of porous Teflon membranes, which were modified with a surface-grafted layer of poly(L-glutamic acid) could be modulated by pH-induced variations in the secondary structure of the peptide chains (33).

Transition-Metal-Mediated NCA Polymerization

Transition-metal complexes have already been explored as initiators for the NCA ring-opening polymerization since the 1960s (34–35). Unfortunately, most of these complexes were characterized by relatively low initiator efficiencies and did not permit the synthesis of polypeptides with precise control of molecular weight and narrow molecular weight distributions in high yields. This situation changed dramatically, however, with the discovery of zero-valent nickel and cobalt complexes, which were found to be able to promote very efficient "living" polymerization of NCAs (36–37). The putative mechanism for the polymerization of NCAs using these initators, bipyNi(COD) and $(PMe_3)_4Co$, is outlined in Figure 3 (35). These transition-metal initiators were found to offer unprecedented control over molecular weight and allowed the high yield synthesis of polypeptides with molecular weights between 500 and 500,000 Da and polydispersities <1.20. Sequential addition of two different NCA monomers allowed the formation of well-defined block copolypeptides.

Peptide block copolymers prepared via transition-metal-mediated NCA polymerization have been investigated, eg, to direct the biomimetic synthesis of

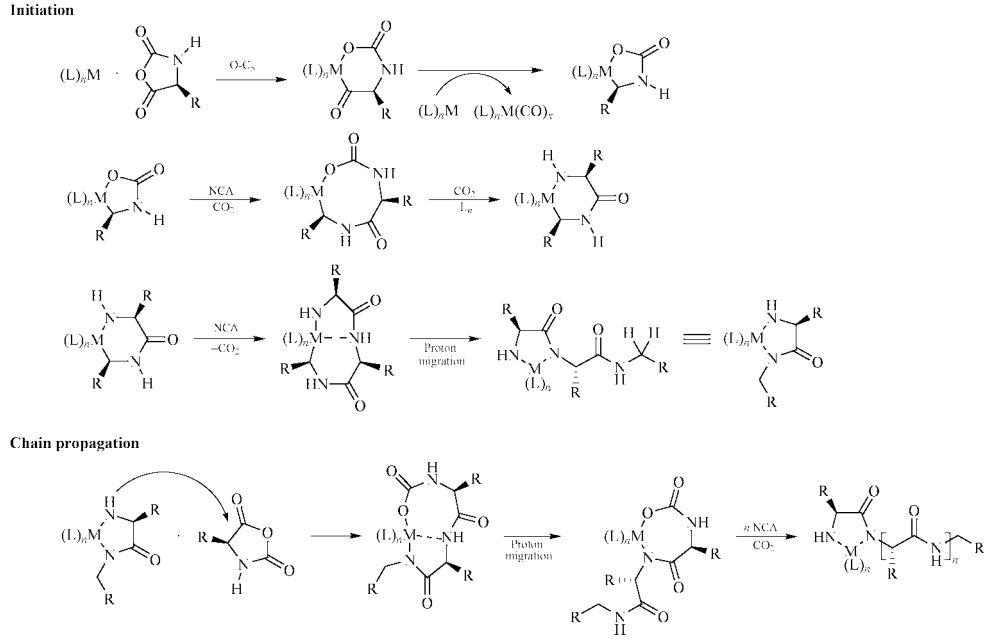

Fig. 3. Proposed mechanism for NCA polymerization using the initiators bipyNi(COD) and $(PMe_3)_4$ Co.

ordered silica structures (38) or to prepare self-assembled polypeptide hydrogels (39). Furthermore, such block copolypeptides have found application to generate hollow, organic/inorganic hybrid microspheres, which are composed of a thin inner layer of gold nanoparticles surrounded by a thick layer of silica nanoparticles (40). Alternatively, hollow spheres could be prepared that consisted of a thick inner layer of core–shell CdSe/CdS nanoparticles that are surrounded by a thicker silica nanoparticle layer (41). The latter spheres allow for microcavity lasing without the use of additional mirrors, substrate spheres, or gratings.

Initially, a major drawback of the transition-metal-mediated NCA polymerization, as it is outlined in Fig. 3, was the lack of control over the chain end functionality of the polypeptide chains. This is in great contrast to, eg, primary amine initiated NCA polymerizations, which are widely explored for the preparation of synthetic-peptide block copolymers and other peptide-hybrid architectures. This limitation could be overcome by the direct synthesis of the amido amidate metallacycle propagating species (eq. 4) (42).

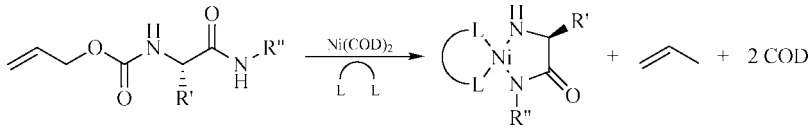

(4)

These complexes allowed controlled polymerization of NCAs, which also provided additional support for their validity as polymerization intermediates. The initiating ligand was found to be quantitatively incorporated as a C-terminal

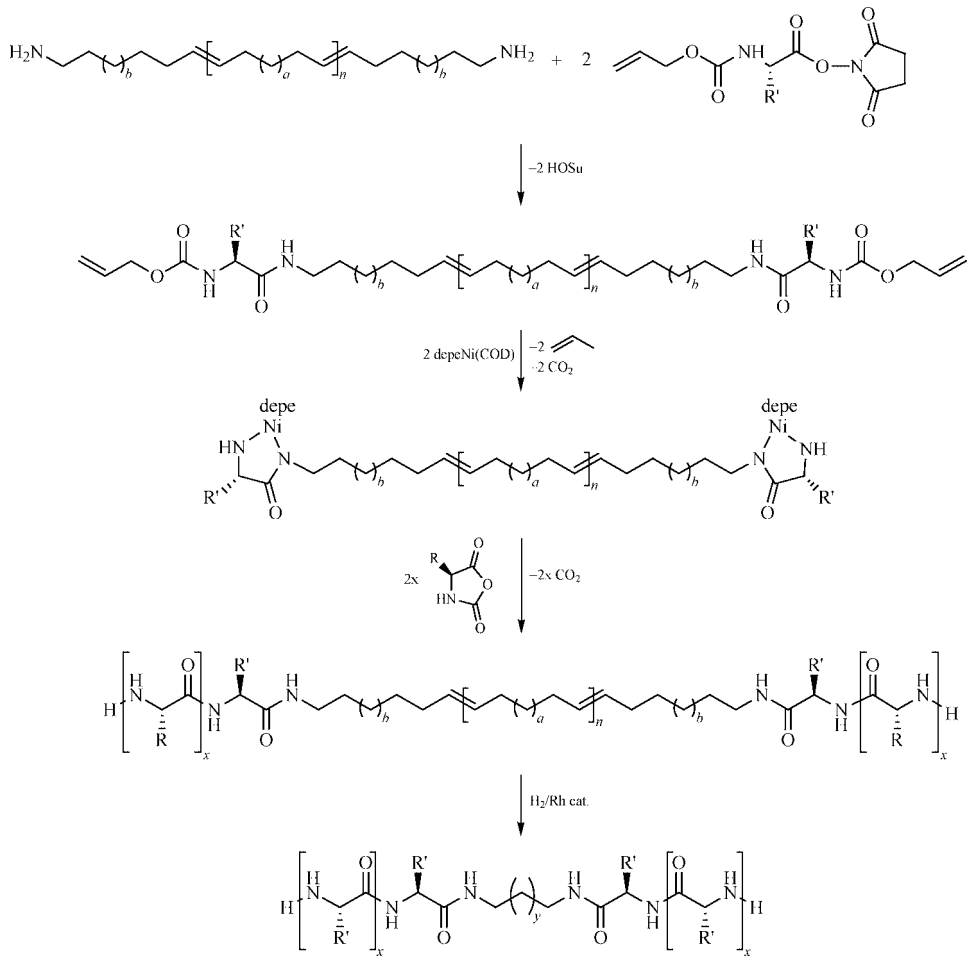

Fig. 4. Synthesis of poly(γ-benzyl-L-glutamate)-polyethylene-poly(γ-benzyl-L-glutamate) triblock copolymers from metallacyle-substituted macroinitiators.

group, which would allow the introduction of a broad variety of functional end groups. Interestingly, the direct synthesis of functional amido amidate metallacycles is not restricted to low molecular weight substituents, but can also be extended to polymeric macroinitiators (43). This is outlined in Fig. 4, which shows the transformation of α,ω-amino polyoctenamers obtained via ADMET into metallacycle-substituted macroinitiators. These macroinitiators were used to polymerize γ-benzyl-L-glutamate *N*-carboxyanhydride (Bn-Glu NCA). Selective hydrogenation of the polyoctenamer double bonds subsequently afforded poly(γ-benzyl-L-glutamate)–polyethylene–poly(γ-benzyl-L-glutamate) triblock copolymers. Transition-metal-mediated NCA polymerization is not restricted to homogeneous solutions, but can also be adapted to allow controlled polymerization of NCAs from surfaces (44).

Replacement of the achiral bipyridyl ligand in bipyNi(COD) by an optically active 2-pyridinyloxazoline ligand results in a metal complex (**1**) that can act

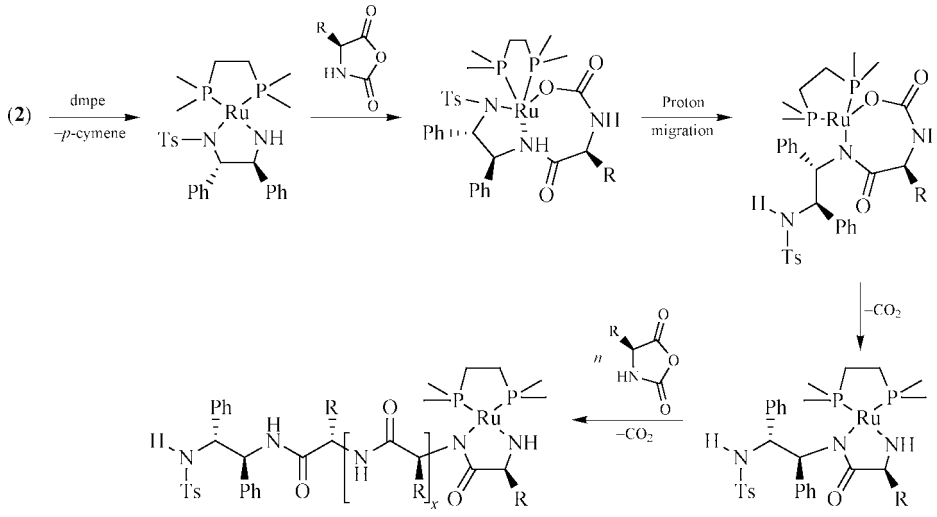

Fig. 5. Proposed mechanism for the polymerization of Bn-Glu NCA by **2**.

as an initiator for the stereoselective polymerization of Bn-Glu NCA (45). Complex **1** has polymerization properties identical to bipyNi(COD), ie, it can produce narrow polydispersity polypeptides with molecular weights corresponding to the monomer–initiator ratio in high yields. For the chiral 2-pyridinyloxazoline complexes, however, the polymerization rate constant for the D enantiomer (k_D) was found to be five times larger than that of the L enantiomer. These enantioselectivities are higher than those reported for many other chiral initiators and catalysts that have been explored for the stereoselective polymerization of NCAs (46). Even better results were obtained with chiral ruthenium initiators derived from the Noyori complex (**2**) (47).

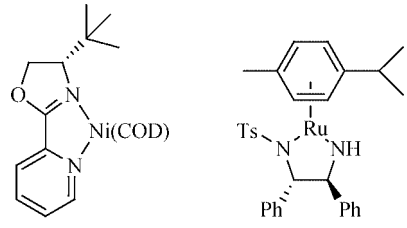

1 **2**

The presence of 1 equiv 1,2-bis(dimethylphosphino)ethane (dmpe) resulted in an initiator that can promote living NCA polymerization of Bn-Glu NCA with a rate constant (k) that was found to be eight times larger for the L enantiomer in comparison with the D antipode. A putative model for the polymerization of Bn-Glu NCA by ruthenium complex (**2**) is shown in Fig. 5. It has been proposed that the observed enantioselectivity is due to the rigid, chiral coordination geometry at the metal center, which is located at the propagating chain end.

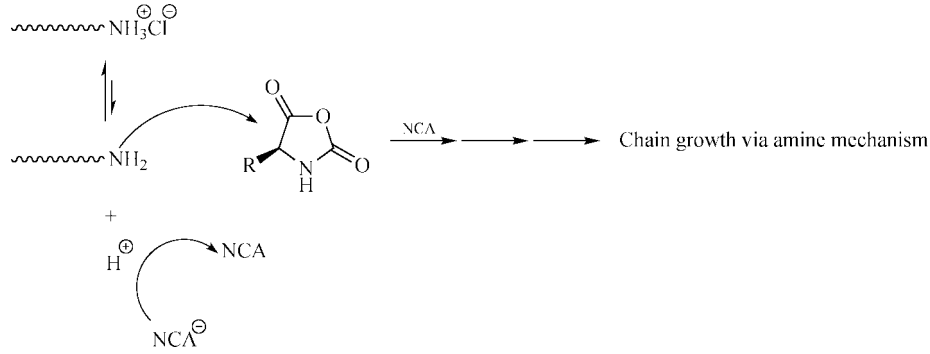

Fig. 6. Proposed mechanism for NCA polymerization in the presence of primary amine hydrochlorides.

Polymerization of NCAs Using Primary Amine Hydrochlorides

The inherent problem of the use of any of the traditional initiators for the NCA ring-opening polymerization is that the amino group at the growing peptide's *N*-terminus can act as both a nucleophile and a base. As a result, chain growth may proceed via both the amine and the activated-monomer mechanism. In the previous paragraph, the use of transition-metal complexes to control the reactivity of the growing polymer chain end has been described. An interesting alternative approach, which allows chain growth to take place preferentially via the amine mechanism and suppresses the activated-monomer pathway is to use primary amine hydrochlorides as initiators for the NCA ring-opening polymerization (48). The use of primary amine hydrochlorides is based on early work by Knobler and co-workers (49) who investigated stoichiometric reactions between primary amine hydrochlorides and NCAs. Their investigations revealed that this reaction proceeds smoothly and without the formation of polypeptides. When anionically prepared polystyrene macroinitiators with a primary amine end group were used for the ring-opening polymerization of ε-benzyloxycarbonyl-L-lysine NCA, hybrid block copolymers with very narrow polydispersities (<1.03) were obtained (48). These narrow polydispersities, which are close to a Poisson distribution, suggest that primary amines promote polymerization of NCAs in a well-controlled fashion. The mechanism proposed for the polymerization of NCAs in the presence of primary amine hydrochlorides is outlined in Figure (6). As illustrated in the figure, the primary amine hydrochloride is regarded as a dormant species, which is in equilibrium with the corresponding free amine and $H^+(Cl^-)$. While the primary amine end group is responsible for chain growth via the amine mechanism, the liberated $H^+(Cl^-)$ serves to protonate any NCA anion that may be present, thereby preventing polymerization via the activated monomer mechanism.

Polymerization of NCAs under High Vacuum Conditions

The two approaches that have been discussed so far, viz transition-metal-mediated and primary amine hydrochloride initiated NCA ring-opening polymerization,

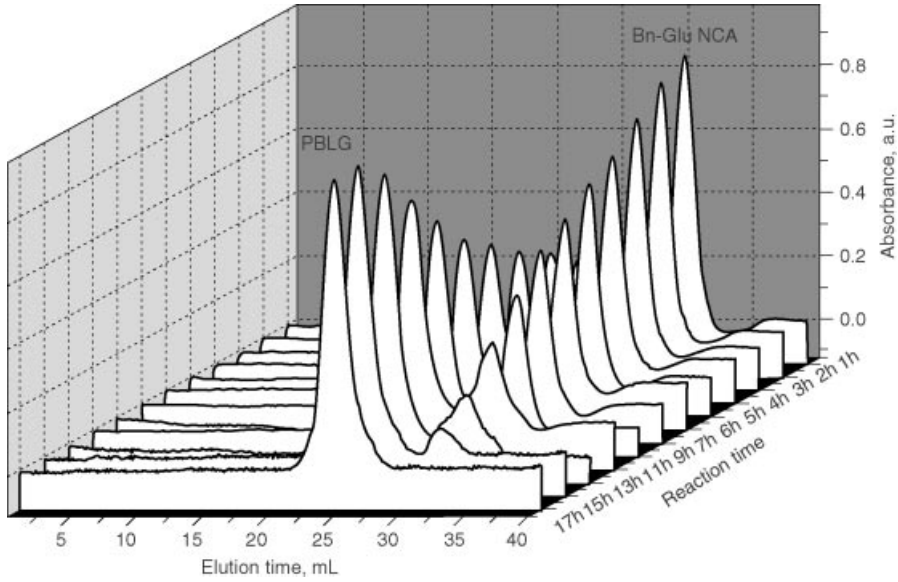

Fig. 7. GPC traces illustrating the evolution of polypeptide molecular weight and monomer consumption during the polymerization of γ-benzyl-L-glutamate *N*-carboxyanhydride (Bn-Glu NCA). Targeted number-average degree of polymerization was ~440. After 17 h, monomer consumption is >99%.

suggest that the limited control over molecular weight and molecular weight distribution of polypeptides produced from NCAs using traditional initiators such as primary amines is due to the polymerization mechanism. However, polypeptide homopolymers and block copolypeptides with molecular weights corresponding to the monomer–initiator ratio and with narrow molecular weight distributions can also be prepared using high vacuum techniques, which have traditionally been used for the anionic polymerization of vinyl monomers (50). High vacuum techniques allow careful purification of all reagents and can provide a reaction environment that is virtually free of any impurities that can interfere with polymerization. Under these conditions, using monomers purified via high vacuum techniques and thoroughly dried solvents, primary amine initiated NCA polymerizations can produce polypeptide homo and block copolymers with precise control of molecular weight and composition and narrow polydispersities (51). These primary amine initiated NCA ring-opening polymerizations fulfill all the requirements to be considered truly living polymerizations. For example, poly(benzyl-L-glutamate) homopolymers with a number-average degree of polymerization of ~440 ($M_n \approx 100{,}000$ Da) could be produced with a polydispersity of 1.18. Monomer consumption could be monitored using gel-permeation chromatography and was found to be quantitative after 17 h (Fig. 7).

Summary and Conclusions

Since its initial discovery by Leuchs in the early twentieth century, the NCA ring-opening polymerization has grown to become the most convenient strategy

for the large-scale preparation of polypeptides and synthetic-polypeptide hybrid materials. Traditionally, initiators for the NCA ring-opening polymerization were nucleophiles and bases, such as primary amines and KOtBu, which, however, only provided limited control over the molecular weight and molecular weight distribution of the resulting polypeptides. This is due to the existence of multiple, competing reaction pathways, which may act simultaneously during polymerization. To overcome these problems and enhance control over molecular weight, molecular weight distribution, and polymer composition, which is required for the preparation of advanced, complex macromolecular architectures, several alternative strategies have been developed. One approach involves the use of transition-metal complexes to control the reactivity of the growing polymer chain end. An alternative strategy, which has been successfully used to bias the NCA ring-opening polymerization to proceed exclusively via one pathway relies on the use of primary amine hydrochlorides as initiators. While these two examples suggest that the limited control over molecular weight, molecular weight distribution, and composition of polypeptides produced via NCA ring-opening polymerization using traditional nucleophilic or basic initiators can be solely attributed to the polymerization mechanism, the picture may be more complex. When high vacuum techniques are used to purify the NCA monomer and to conduct the polymerization, primary amines can also generate polypeptide homopolymers and block copolypeptides with narrow polydispersities and predictable molecular weights. These primary amine initiated NCA ring-opening polymerizations were shown to fulfill all the requirements to be characterized as truly living polymerizations. This last example underlines the importance of monomer purity and the absence of other contaminants that can interfere with the polymerization. Almost 100 years after its discovery, the mechanistic details of the NCA polymerization have not yet been fully unravelled. Nevertheless, great advances have been made in the development of novel synthetic methodologies, which allow controlled polymerization of NCAs, ie, the production of peptide polymers with controlled architecture, predictable molecular weight, and narrow molecular weight distributions. These advanced synthetic methodologies will prove useful to further exploit the potential of these materials, in particular for applications in biomedicine and biomineralization.

BIBLIOGRAPHY

"Polypeptides" in *EPSE* 2nd ed., Vol. 12, pp. 786–811, by E. Peggion, University of Padua, Italy, and M. Goodman, University of California at San Diego.

1. H. Leuchs, *Ber. Dtsch. Chem. Ges.* **39**, 857 (1906); H. Leuchs and W. Manasse, *Ber. Dtsch. Chem. Ges.* **40**, 3235 (1907); H. Leuchs and W. Geiger, *Ber. Dtsch. Chem. Ges.* **41**, 1721 (1908).
2. F. Wessely, *Z. Physiol. Chem.* **146**, 72 (1925); F. Sigmund and F. Wessely, *Z. Physiol. Chem.* **157**, 91 (1926); F. Wessely and F. Sigmund, *Z. Physiol. Chem.* **159**, 102 (1926); F. Wessely and M. John, *Z. Physiol. Chem.* **170**, 38 (1927); F. Wessely and J. Mayer, *Monatsh. Chem.* **50**, 439 (1928).
3. E. Katchalski, *Adv. Protein Chem.* **6**, 123 (1951).
4. H. R. Kricheldorf, *α-aminoacid-N-carboxyanhydrides and Related Heterocycles—Synthesis, Properties, Peptide Synthesis, Polymerization*, Springer-Verlag, Berlin, 1987.

5. F. Fuchs, *Chem. Ber.* **55**, 2943 (1922); C. J. Brown, D. Coleman, and A. C. Farthing, *Nature* **163**, 834 (1949); A. C. Farthing, R. J. W. Reynolds, *Nature* **165**, 647 (1950); A. C. Farthing, *J. Chem. Soc*. 3213 (1950).
6. R. Hirschmann, H. Schwam, R. G. Strachan, E. F. Schoenewaldt, H. Barkemeyer, S. M. Miller, J. B. Conn, V. Garsky, D. F. Veber, and R. G. Denkewalter, *J. Am. Chem. Soc.* **93**, 2746 (1971).
7. R. Wilder and S. Mobashery, *J. Org. Chem.* **57**, 2755 (1992).
8. H. R. Kricheldorf, *Chem. Ber.* **103**, 3353 (1970); *Chem. Ber.* **104**, 87 (1971).
9. M. Oya, R. Katakai, H. Nakai, and Y. Iwakura, *Chem. Lett*. 1143 (1973); R. Katakai and Y. Iizuka, *J. Org. Chem.* **50**, 715 (1985).
10. W. H. Daly and D. S. Poché, *Tetrahedron Lett.* **29**, 5859 (1988).
11. D. S. Poché, M. J. Moore, and J. L. Bowles, *Synth. Commun.* **29**, 843 (1999).
12. I. Dimitrov, H. Kukula, H. Cölfen, and H. Schlaad, *Macromol. Symp*. (in press).
13. T. J. Deming, *Adv. Mater.* **9**, 299 (1997); T. J. Deming, *J. Polym. Sci., Part A: Polym. Chem.* **38**, 3011 (2000).
14. J. M. Anderson, D. F. Gibbons, R. L. Martin, A. Hiltner, and R. Woods, *J. Biomed. Mater. Res. Symp.* **5**, 197 (1974); R. Duncan, *CRC Crit. Rev. Biocompat.* **2**, 127 (1986); H. C. Chiu, P. Kopeckova, S. D. Deshmane, and J. Kopecek, *J. Biomed. Mater. Res.* **34**, 381 (1997).
15. R. K. Scheule, F. Cardinaux, G. T. Taylor, and H. A. Scheraga, *Macromolecules* **9**, 23 (1976).
16. F. Cardinaux, J. C. Howard, G. T. Taylor, and H. A. Scheraga, *Biopolymers* **16**, 2005 (1997); D. M. Rothwarf, V. G. Davenport, P.-T. Shi, J.-L. Peng, and H. A. Scheraga, *Biopolymers* **39**, 531 (1996).
17. B. Gallot, *Prog. Polym. Sci.* **21**, 1035 (1996); H.-A. Klok and S. Lecommandoux, *Adv. Mater.* **13**, 1217 (2001); H. Schlaad and M. Antonietti, *Eur. Phys. J. E* **10**, 7 (2003), and references cited therein.
18. W. H. Daly, D. Poche, P. S. Russo, and I. Negulescu, *Polym. Prepr.* **33**(1), 188 (1992); W. H. Daly, D. S. Poche, P. S. Russo, and I. I. Negulescu, *J. Macromol. Sci., A* **31**(Suppl. 6/7), 795 (1994).
19. H.-A. Klok, J. Rodriguez-Hernandez, S. Becker, and K. Müllen, *J. Polym. Sci., Part A: Polym. Chem.* **39**, 1572 (2001).
20. K. Inoue, H. Sakai, S. Ochi, T. Itaya, and T. Tanigaki, *J. Am. Chem. Soc.* **116**, 10783 (1994); K. Inoue, S. Horibe, M. Fukae, T. Muraki, E. Ihara, and H. Kayama, *Macromol. Biosci.* **3**, 26 (2003).
21. K. Inoue, A. Miyahara, and T. Itaya, *J. Am. Chem. Soc.* **119**, 6191 (1997).
22. K. Aoi, K. Tsutsumiuchi, A. Yamamoto, and M. Okada, *Tetrahedron* **53**, 15415 (1997).
23. N. Higashi, T. Koga, N. Niwa, and M. Niwa, *Chem. Commun*. 361 (2000); N. Higashi, T. Koga, and M. Niwa, *Adv. Mater.* **12**, 1373 (2000).
24. M. Sela, S. Fuchs, and R. Arnon, *Biochem. J.* **85**, 223 (1962); M. Sakamoto and Y. Kuroyanagi, *J. Polym. Sci., Part A: Polym. Chem.* **16**, 1107 (1978); G. Mezo, J. Remenyi, J. Kajtar, K. Barna, D. Gaal, and F. Hudecz, *J. Control. Release* **63**, 81 (2000).
25. F. Hudecz, *Anti-Cancer Drug* **6**, 171 (1995).
26. F. Hudecz, in A. Aggeli, N. Boden, and S. Zhang, eds., *Self-Assembling Peptide Systems in Biology, Medicine and Engineering*, Kluwer Academic Publishers, Boston, Mass., 2001, Chapt. 11.
27. H.-A. Klok and J. Rodríguez-Hernández, *Macromolecules* **35**, 8718 (2002).
28. J. Rodríguez-Hernández, M. Gatti, and H.-A. Klok, *Biomacromolecules* **4**, 249 (2003).
29. J. K. Whitesell and H. K. Chang, *Science* **261**, 73 (1993); R. H. Wieringa and A. J. Schouten, *Macromolecules* **29**, 3032 (1996).
30. Y.-C. Chang and C. W. Frank, *Langmuir* **14**, 326 (1998); Y. Wang and Y.-C. Chang, *Langmuir* **18**, 9859 (2002).

31. R. H. Wieringa, E. A. Siesling, P. J. Werkman, E. J. Vorenkamp, and A. J. Schouten, *Langmuir* **17**, 6491 (2001).
32. T. Jaworek, D. Neher, G. Wegner, R. H. Wieringa, and A. J. Schouten, *Science* **279**, 57 (1998).
33. Y. Ito, Y. Ochiai, Y. S. Park, and Y. Imanishi, *J. Am. Chem. Soc.* **119**, 1619 (1997).
34. T. J. Deming, *Adv. Mater.* **9**, 299 (1997), and references therein.
35. T. J. Deming, *J. Polym. Sci., Part A: Polym. Chem.* **38**, 3011 (2000), and references therein.
36. T. J. Deming, *Nature* **390**, 386 (1997).
37. T. J. Deming, *Macromolecules* **32**, 4500 (1999).
38. J. N. Cha, G. D. Stucky, D. E. Morse, and T. J. Deming, *Nature* **403**, 289 (2000).
39. A. P. Novak, V. Breedveld, L. Pakstis, B. Ozbas, D. J. Pine, D. Pochan, and T. J. Deming, *Nature* **417**, 424 (2002).
40. M. S. Wong, J. N. Cha, K.-S. Choi, T. J. Deming, and G. D. Stucky, *Nano Lett.* **2**, 583 (2002).
41. J. N. Cha, M. H. Bartl, M. S. Wong, A. Popitsch, T. J. Deming, and G. D. Stucky, *Nano Lett.* **3**, 907 (2003).
42. S. A. Curtin and T. J. Deming, *J. Am. Chem. Soc.* **121**, 7427 (1999).
43. K. R. Brzezinska and T. J. Deming, *Macromolecules* **34**, 4348 (2001).
44. P. Witte and H. Menzel, *Polym. Prepr.* **44**, 423 (2003).
45. J. Cheng and T. J. Deming, *Macromolecules* **32**, 4745 (1999).
46. T. Tsuruta, S. Inoue, and K. Matsuura, *Makromol. Chem.* **63**, 219 (1963); K. Matsuura, S. Inoue, and T. Tsuruta, *Makromol. Chem.* **80**, 149 (1964); T. Makino, S. Inoue, and T. Tsuruta, *Makromol. Chem.* **150**, 137 (1971); H. G. Bührer and H. G. Elias, *Makromol. Chem.* **169**, 145 (1973); S. Yamashita, N. Yamawaki, and H. Tani, *Macromolecules* **7**, 724 (1974); N. Oguni, H. Kuboyama, and A. Nakamura, *J. Polym. Sci., Part A: Polym. Chem.* **21**, 1559 (1983).
47. S. W. Seidel and T. J. Deming, *Macromolecules* **36**, 969 (2003).
48. I. Dimitrov and H. Schlaad, *Chem. Commun*. 2944 (2003).
49. Y. Knobler, S. Bittner, and M. Frankel, *J. Chem. Soc*. 3941 (1964); Y. Knobler, S. Bittner, D. Virov, and M. Frankel, *J. Chem. Soc*. 1821 (1969).
50. N. Hadjichristidis, H. Iatrou, S. Pispas, and M. Pitsikalis, *J. Polym. Sci., Part A: Polym. Chem.* **38**, 3211 (2000).
51. T. Aliferis, H. Iatrou, and N. Hadjichristidis, *Biomacromolecules* (in press).

HARM-ANTON KLOK
Ecole Polytechnique Fédérale de Lausanne

Encyclopedia of Polymer Sceince and Technology
Copyright © 2005 John Wiley & Sons, Inc. All rights reserved.

RADIATION CHEMISTRY OF POLYMERS

Introduction

The fundamental property of polymeric materials which sets them apart from other materials is their very large molecular weight. The arrangement of a large number of structurally similar chemical units into linear or branched chains provides polymers with their unique viscoelastic properties. This large molecular weight necessarily leads to both transient and permanent molecular entanglements, which determine the response of the polymer to applied loads. It is essentially this property which is altered, or deliberately manipulated, when a polymer is subjected to ionizing radiation.

High energy radiation leads to a succession of chemical reactions which ultimately lead to either an increase or a decrease in the molecular weight of a polymer. As will be discussed below, either result may be desirable. The initial processes which occur when a high energy photon interacts with an organic polymer are reasonably well established and do not depend essentially on the chemical structure of the material. However, these primary processes lead to a cascade of further reactions, the nature of which depends sensitively on the nature of the polymeric material; for example, the ability to dissipate excess energy, the relative bond energies within various structures, and the presence of oxygen, radical scavengers, and other moderating factors.

This article approaches the field of radiation chemistry of polymers from a mechanistic viewpoint, and does not describe in detail the growing list of applications of high energy radiation in polymer science. The basic principles of radiation chemistry are described, and subsequently the interaction of radiation with specific classes of polymers. The mechanisms of reaction are described by reference to specific materials. Furthermore, the means by which these mechanisms have been determined, ie, the methods of analysis, are described in detail. Finally, an attempt is made to draw overall conclusions about the radiation sensitivity of the constituent units of synthetic polymers.

Interaction of High Energy Radiation with Organic Matter. The passage of a high energy photon or particle through matter leads to a complex cascade of processes which results in the dissipation of the initial energy, ultimately as thermal energy and chemical reactions (1–5). If the source of radiation consists of high energy photons, the energy is deposited in a highly nonuniform manner via a number of processes. In organic polymers the most important mechanism of energy loss is *Compton scattering*, in which a photon interacts with an electron resulting in ejection of the electron and deflection of the photon with reduced

energy. The probability of the photon undergoing Compton scattering and the resultant energy of the ejected electron and scattered photon depend on the incident energy of the photon and the electron density of the material through which it is traversing.

Of less importance for high energy photons is the *photoelectron effect*, in which the entire energy of the photon is transferred to a single electron, which is ejected with energy equal to the incident photon energy minus the binding energy of the electron. Also of less importance for most commercial sources of ionization radiation is the mechanism of *pair production*. This also involves complete absorption of the incident photon energy, and results in the formation of an electron–positron pair. The combination of the two particles results in emission of two 0.51-MeV γ-rays, which may undergo further interaction with the material as described above. Pair production is only of importance when the incident photons have energies greater than 1.02 MeV.

If on the other hand the source of ionization is high energy electrons, the initial steps toward loss of the energy to the material involves *inelastic collisions* resulting in ionization and excitation of the material and loss of energy of the incident particle. On ejection of the secondary electrons, the resultant processes occurring are identical to those occurring on irradiation with high energy photons. These can be summarized as follows.

Initial interaction with photons:

$$\mathrm{R}\sim\sim\sim\sim\sim\sim\rightarrow\mathrm{R}^{+}+\mathrm{e}^{-} \tag{1}$$

Interaction of primary electrons with other structures:

$$\mathrm{R}+\mathrm{e}^{-}\rightarrow\mathrm{R}^{+}+2\,\mathrm{e}^{-} \tag{2}$$

As the energy of the electrons is reduced, there is increased probability of recombination of the cations and secondary electrons to form excited states:

$$\mathrm{R}^{+}+\mathrm{e}^{-}\rightarrow\mathrm{R}^{*} \tag{3}$$

The excited-state molecules may return to the ground state through radiationless decay, or undergo homolytic dissociation reactions to form free radicals, which are believed to be the main protagonists in subsequent radiochemical reactions. Heterolytic bond cleavage may in addition result in the formation of charged species.

Linear Energy Transfer and Recombination Reactions. The vast majority of studies on the radiation stability of polymeric systems have been concerned with either incident γ photons or electrons. This clearly reflects the greater availability of γ sources or electron accelerators. However, there has been a smaller but increasing interest in the effects of heavier charged particles on polymers, either because of interest in ion implantation or concern for the effects of heavy ions on materials in, for example, the space environment, or indeed processing of polymers using ion beams. Of most interest is the effect of the increased linear energy transfer (LET) of heavier charged particles on the mechanism of the

radiation chemistry. The results presented so far are conflicting. For example, While Parkinson and co-workers (6) and Boyett and Becker (7) did report differences between neutron and γ irradiation, others have indicated identical changes in properties (8). The effect of proton irradiation was found to be identical to electron irradiation for aliphatic polymers; however, some differences were observed for aromatic materials (9,10). However, Hill and Hopewell (11) found no difference between the mechanical properties of polyimides irradiated with γ rays or photons. A survey of several studies of the effects of ion beam irradiation on various polymers (12–17) again does not present a clear picture. This is clearly an area for further investigation.

Energy Transfer and Dissipation. From early times it was recognized that the presence of small concentrations of certain structures in a material can lead to a pronounced decrease in the radiation sensitivity of the material as a whole. The earliest observations of this type were of the evolution of gases from mixtures of small aromatic and aliphatic molecules. For example, Manion and Burton (18) reported in 1952 that the yields of reactions in irradiated mixtures of cyclohexane and benzene were reduced significantly compared to the yield expected from the linear addition of the yields of the pure individual molecules. This led to the concept of *protection effect*, in which the introduction of aromatic groups results in significant protection of the surrounding aliphatic structures. The mechanism of "protection" afforded by the aromatic molecules has been a subject of considerable discussion.

Since these early studies of mixtures of aromatic and aliphatic liquids (18,19), the phenomenon of radiation protection has been observed in copolymers of styrene with other monomers (20–25), in a range of alkylbenzenes (26), and in miscible polymer blends (27). The description of the mechanism of radiation protection has often in the past relied upon the assumption that the amount of energy deposited in each molecule or molecular segment within a polymer is proportional to its electron fraction. As a consequence the decrease in radiation sensitivity of one component must be due to either transfer of energy or charge prior to dissociation, or scavenging of intermediates in systems where significant mobility is present. It has been reported, however, that the assumption that the cross section is proportional to electron density is not at all times obeyed (28). Therefore the assignment of protection effects wholly to transfer processes must be made with caution, although the relative stabililizing effect of aromatic structures is not in question.

Yields and Units. The unit of radiation dose used in this text is the Gray (Gy); 1 Gy corresponds to an energy absorption of 1 J/kg of material. Typical applied doses in the field of radiation modification of polymers are in the range of tens of kGy; however, in some cases irradiation up to 10 MGy has been required to induce sufficiently large yields of new molecular structures. The yield of radiochemical events is expressed as the *G value* [written, for example, G(X) for the G value of cross-linking]. The G-value is defined as the number of products formed for every 100 eV, or 16 aJ, of energy absorbed by the material. Thus, 1 kGy of radiation will produce $G \times 1.036 \times 10^{-7}$ moles of product per gram of irradiated polymer (4). The SI unit for radiation yield is μmol/J, which is equivalent to 10 Gy (29).

Summary of Radiation-Induced Reactions in Polymers

The preceding section has described briefly the primary reactions occurring on interaction of high energy radiation with organic molecules in general. Following the succession of reactions detailed above, a number of subsequent combination and bond-breaking reactions lead to permanent changes in the properties of the material. Much experimental evidence exists to support the contention that most of these reactions are initiated by free radicals. The observation, by electron spin resonance (ESR) spectroscopy, of relatively large concentrations of radicals in polymers irradiated at low temperatures is one example of this.

In the vast majority of experimental studies of the radiation chemistry of polymers, we observe usually the final products of the passage of the high energy photons. Attempts to trap radical and charged species at low temperatures usually succeed in revealing part of the radiochemical history of the material. An indication of this can be obtained by consideration of the relative yields of products on radiolysis of simple alkane molecules. The respective bond energies of C—H and C—C bonds in linear alkanes are 4.3 and 3.4 eV (415 and 328 kJ/mol) (1). On consideration of these numbers alone, one would expect that the predominant products of radiolysis of linear alkanes would be due to rupture of C—C bonds. However, the main product of the radiolysis of linear alkanes, and indeed of polyethylene, is hydrogen gas. Furthermore, there is some debate as to whether permanent cleavage of the main-chain C—C bond actually occurs at all on irradiation of polyethylene. The origin of these results is of course the "cage" effect. The larger radical fragments formed on cleavage of C—C bonds are unlikely to escape from the reaction cage, and recombination reactions tend to occur. The smaller, perhaps thermally excited, hydrogen radicals formed by cleavage of C—H bonds have a much greater probability of escaping and undergoing recombination and other reactions. This simple and important observation also helps us understand the differences in the radiation chemistry of hydrocarbon polymers and perfluorocarbon polymers, as discussed below. In addition the unusual temperature dependence of the radiochemical yields of a number of materials can be explained by the cage effect. For example, the radiochemical G-values for formation of *stable* free radicals in γ-irradiated fluorinated ethylene–propylene copolymers (FEP) are 0.22 at 77 K, and 2.0 at 298 K (30), since at low temperatures cage recombination of the primary radicals is very effective, while at higher temperatures sufficient thermal energy is available to remove the radical fragments from the reactive cage.

Additional evidence of the very large number of nonpermanent bond cleavages initiated by ionizing radiation is the observation of large changes in the stereochemistry of initially highly stereoregular polymers, such as isotactic poly(methyl methacrylate) (iPMMA) and related polymers (31–34), as well as isotactic polypropylene (iPP) (35–38). The loss of stereoregularity arises from a racemization reaction occurring as a result of temporary scission of either the main chain or the side chain. The latter mechanism is favored for syndiotactic PMMA. The yield of temporary chain scissions is approximately 10 times greater than the yield of permanent chain scissions determined by measurement of gel fraction or molecular weight of the soluble polymers.

Cross-Linking and Chain Scission. The most important reactions occurring during radiolysis of polymers are those that lead to permanent changes in their molecular weight. The reactions leading to either increases or decreases in molecular weight are referred to as cross-linking and chain scission, respectively. End-linking, ie, reaction between a polymer main-chain species and a polymer chain end, is regarded as a cross-linking reaction of lower functionality. In general cross-linking and scission processes can occur simultaneously in any irradiated material; however, it is often observed that one tends to dominate over the other, and thus polymers can be broadly placed into the categories *cross-linking* or *degrading*. Over the past 50 years a solid understanding of the relationship between polymer structure and the relative yields of cross-linking and chain scission has been acquired. Thus, for linear polyolefins, the proportion of chain scission reactions increases as the number of tertiary and especially quaternary carbons along the backbone is increased. Polyethylene undergoes primarily cross-linking reactions, polypropylene undergoes approximately equal amounts of scission and cross-linking, which ultimately leads to an increase in molecular weight, and finally polyisobutylene undergoes chain-scission reactions exclusively. However, it must be clearly stated here that respective and absolute yields of the two types of reactions depend also on a number of extrinsic factors, such as the presence of a crystalline phase, the temperature, the presence of chain-end unsaturation, and perhaps most profoundly the presence of oxygen gas. In Table 1 below, we attempt to classify the various polymer types as either cross-linking or degrading on exposure to ionizing radiation in the absence of oxygen. Specific examples are discussed later in this article.

Evolution of Gases. When polymers are exposed to high energy radiation, the reactions induced will lead to the formation of low molecular weight gaseous molecules. A study of the structure and yields of the gaseous products

Table 1. Cross-Linking vs Chain Scission for the Polymer Classes on Exposure to Ionizing Radiation in Vacuum

Cross-linking dominates	Chain scission dominates
Polyethylene	Polyisobutylene
Polypropylene	
Polydienes	
Polystyrene	Poly(α-methyl styrene)
Polyacrylates	Polymethacrylates
Polyacrylamide	Polymethacrylamide
Fully fluorinated elastomers	Fully fluorinated thermoplastics
Poly(vinyl chloride)	Poly(vinylidene chloride)
	Polychlorotrifluoroethylene
Polyamides	Cellulosics
Polyesters	
Polysiloxanes	
Poly(vinyl alcohol)	
Poly(*N*-vinylpyrollidinone)	
Main-chain aromatic polymers	

can provide great insight into the mechanisms of the reactions occurring on radiolysis. In general, gaseous products can arise either from primary cleavage of the main-chain bonds or from cleavage at the side chains.

Polymers that fall into the class of degrading polymers can, on irradiation at elevated temperatures (more specifically at temperatures approaching their ceiling temperature), yield high concentrations of monomers among the gaseous products. The *ceiling temperature* is the temperature at which the reversible addition of monomers to a radical chain end is balanced by the tendency of the monomers to depolymerize. Thus, it was noted as early as 1953 (39) that poly(methyl methacrylate) foams on irradiation due to the formation of gaseous products, including methyl methacrylate monomer. Subsequently, it was reported that the yield of methyl methacrylate monomer increased substantially to a limiting yield around 180°C (40,41). Related to this is the pronounced tendency of these materials to undergo depolymerization after exposure to high energy radiation.

The most important commercial exploitation of this phenomenon has been the development of positive radiation resists for use in the semiconductor industry. A number of methacrylates and butene sulfones have been developed for these applications (42–44). Another important class of materials which undergo large-scale degradation of the main chain are the aliphatic polysulfones. For example, in 1981 Bowmer and O'Donnell (45) examined the yields of a number of aliphatic polysulfones as a function of temperature and discussed these results in terms of the change in the equilibrium between polymerization and depolymerization as the ceiling temperature is approached. This aspect of radiation chemistry has had far-reaching consequences for our modern society.

The second major mechanism leading to the formation of volatile products on irradiation of polymers is cleavage of the side-chain groups. In the case of linear polymers, such as polyethylene, scission of the C—H bond leads to the formation of thermally activated hydrogen atoms. As discussed above, these small entities are able to escape the reactive cage and undergo subsequent reaction. These include addition reactions to double bonds, and also abstraction of hydrogen atoms and recombination with hydrogen atoms to form molecular hydrogen gas. Thus, the main gaseous product formed on radiolysis of hydrocarbons is hydrogen gas. The yield of hydrogen gas in polymers of the cross-linking type is often in excess of that expected from consideration of the yield of alkyl radicals leading to the formation of cross-links. As early as 1954, Dole and co-workers (46) determined that up to 80% of the hydrogen gas measured after irradiation of polyethylene arose from the formation of vinylene unsaturation, with cross-linking reactions accounting for the remainder. The presence of hydrogen gas has an important influence on the kinetics of radical reactions, and in principle on the overall product distribution in irradiated polymers. It has been suggested (47,48) that hydrogen gas is capable of enhancing the rate of diffusion of free radical species via reaction with alkyl radicals as depicted below:

$$R'\bullet + H{-}H + H{-}R \rightarrow R' \cdots H \cdots H \cdots H \cdots R \rightarrow R'H + H{-}H + \bullet R \qquad (4)$$

The importance of the presence of hydrogen gas was first demonstrated by Dole and Cracco in 1961 (49–51) by measuring the rate of hydrogen exchange from irradiated high density polyethylene to gaseous D_2, and explored more completely

by Dole and co-workers over the next decade (47). Clough (48) much later provided a detailed analysis of the mechanism of migration of radicals through the solid state in aliphatic hydrocarbon polymers, including an analysis of the number of these "hydrogen-hopping" reactions expected on the production of main-chain radicals. The calculations accounted for localized hydrogen–deuterium exchange reactions in linear alkanes irradiated in the presence of D_2 gas. It should also be noted that in aromatic polymers, hydrogen atom addition to aromatic rings results in the formation of cyclohexadienyl radicals and, potentially, initiation of cross-linking reactions (22,24,52–54).

The great importance of the hydrogen-hopping reaction can be appreciated by considering the differences in the radiation chemistry of polyhydrocarbons and polyfluorocarbons. In the latter materials, reaction 4 is of course not operative, and the corresponding reaction involving fluorine radicals is believed to be unimportant after consideration of the respective C—F and F—F bond energies (approximately 510 and 155 kJ/mol, respectively). Thus, the reactivity of fluorocarbon radicals in irradiated fluoropolymers is much more dependent on the inherent mobility of the polymer chains than in hydrogenated polymers. Thus, cross-linking reactions, which require two alkyl radicals to meet each other, are unlikely to occur in fluoropolymers irradiated at normal temperatures. Thus, polytetrafluoroethylene (PTFE) undergoes chain scission at all temperatures below the melting temperature (55,56). On the other hand the fluoroelastomer Kalrez (DuPont), a copolymer of tetrafluoroethylene and perfluorinated methyl vinyl ether, can be readily cross-linked by exposure to γ radiation, because of the mobility of the polymer chains and related higher probability of radical recombination reactions (57). A corollary to this is the marked long-term stability of free radicals in irradiated fluoropolymers. Indeed, Judeikis and co-workers (58) and others have proposed the use of PTFE as a radiation dosimeter. Of more practical concern is the propensity of these stable radicals to react slowly with dissolved oxygen, a phenomenon leading to the well-known poor radiation stability of fluoropolymers.

Finally, examination of the volatile products of irradiation of branched polymers reveals the importance of loss of the side chains. For example, irradiation of branched copolymers of ethylene and α-olefins results in volatile products characteristic of both the frequency and structure of the side chain (59,60). In this work the authors also highlight the influence of radiation temperature and morphology of the irradiated semicrystalline polymer.

Formation of Unsaturated Groups. As indicated above, an important result of the radiolysis of polymer is the formation of unsaturated groups. In 1954, Dole and co-workers (46) reported the formation of main-chain unsaturation in irradiated polyethylene and demonstrated that the yield of these groups was proportional to the yield of hydrogen gas. In these materials the mechanism of formation of unsaturation was thus established at an early time. In this and a subsequent article (46,61), Dole and co-workers also indicated that other types of unsaturated groups, for example vinyl and vinylidene groups, are rather consumed in the radiation-induced reactions. Later, this same group deduced from measurements of gel fractions that the terminal unsaturation was reacting via an end-linking reaction, a result confirmed much later by Randall and co-workers (62–64) and Horii and co-workers (65,66).

Perhaps the most well-known system in which large amounts of unsaturated groups are formed is poly(vinyl chloride). It is well established that irradiation leads to the formation of alkyl radicals, which are the locus for subsequent dehydrochlorination reactions. This results in characteristic changes in the infrared and visible absorption spectra (67–69), as well as the formation of stable polyenyl radicals (67,68).

Color Centers. An obvious corollary of the formation of polyenyl radicals and conjugated double bonds in irradiated poly(vinyl chloride) is a marked changed in the visible appearance of the polymer (67–70). Color changes on irradiation of polymers may have important implications for a number of commercial applications, for example when the appearance of the material is of importance, as in medical applications, or when the optical properties of the material must be maintained in a high dose environment, for example in polymeric fiber optics in particle physics detectors. On the other hand, color development for radiation dosimeters has been exploited by a number of workers, most notably the group of McLaughlin (71–74).

Until recently the phenomenon of color changes in irradiated polymers has not received detailed attention. Clough and co-workers (75–77), however, have recently reviewed studies of color changes in a number of important synthetic polymers. They report that there are two classes of color centers in polymers, annealable and permanent. The former class of color center appears to be associated with free radicals trapped within the polymer matrix, whereas permanent color centers are stable chromophores formed as a result of radiochemical reactions. The free radicals can be destroyed by the application of heat, or often through reaction with atmospheric oxygen. Clough and coworkers (77) also reported that whereas the incorporation of aromatic groups provides a degree of protection against radiochemical damage to polymers, it does not necessarily protect against color formation, because presumably the products of reaction in aromatic polymers tend to have high extinction coefficients.

Changes in Molecular Weight of Polymers on Exposure to Radiation

The effects of cross-linking and main-chain scission on the molecular weight and the molecular weight distribution of polymers have been examined in great detail by a number of authors (78–89). The exact method of treatment of the problems depends on the molecular weight distribution of the polymer prior to irradiation, and on whether it can be described by a most-probable distribution or recourse must be made to a higher-order distribution. For simplicity, in this article we shall consider the effects of cross-linking and scission on polymer having an initial most-probable distribution; however, reference will be made to more complete analyses where appropriate.

Effects of Chain Scission. In the early 1950s, Charlesby and co-workers were considering theoretical approaches to the description of the changes in molecular weight of polymers during irradiation. In 1954 they reported that the molecular weight of PMMA, measured by solution viscometry, was inversely proportional to the radiation dose (80,90). Since that time a number of

refinements to these initial observation and theoretical expression have been made (81,91–94).

In summary, the number- and weight-average molecular weights change as described below:

$$\frac{1}{M_n(D)} = \frac{1}{M_n(0)} + 2k_1 G(S)D \tag{5}$$

$$\frac{1}{M_w(D)} = \frac{1}{M_w(0)} + k_1 G(S)D \tag{6}$$

In these expressions the constant k_1 is equal to 5.18×10^{-8} if the dose D is expressed in units of kGy. Most importantly, equations 5 and 6 are applicable to any initial molecular weight distribution, because in the case of degrading polymers, the molecular weight distribution will approach the most-probable distribution.

Effects of Simultaneous Cross-Linking. Charlesby (78) was also the first to describe the relationship between the molecular weight of a polymer and the radiation-induced chain cross-linking. He reported in 1954 that the dose required to produce incipient gel formation, known as the gel dose D_g, was inversely proportional to the initial molecular weight of the irradiated siloxane.

$$\frac{1}{M_n(D)} = \frac{1}{M_n(0)} + 2k_1[G(S) - G(X)]D \tag{7}$$

$$\frac{1}{M_w(D)} = \frac{1}{M_w(0)} + k_1[G(S) - 4G(X)]D \tag{8}$$

In this case, equation 7 applies to all initial molecular weight distributions, whereas equation 8 applies only to polymers having an initial most-probable distribution undergoing H-linking reactions. Expressions for changes in molecular weight in polymers having other initial molecular weight distributions, and also for the case of cross-linking via a Y-linking mechanism, have been developed, and these have been summarized by various authors (86–88,93).

The above expressions have been derived for the first two moments of the molecular weight distribution, M_n and M_w. However, the third moment, the z-average molecular weight, M_z, is experimentally accessible through measurement of sedimentation velocity of polymer chains. O'Donnell and co-workers (85,86) have reported the respective relationships between M_z and the radiochemical yields for scission and cross-linking. The results of analysis of the changes in M_z and M_w of irradiated poly(acrylic acid) and poly(methacrylic acid) (85) and polystyrene have also been reported (86).

Soluble Fractions. The above descriptions of the change in molecular weight on irradiation presuppose the ability to accurately measure the molecular weight distribution of the polymer after irradiation. A number of authors have pointed out that for polymers for which cross-linking dominates chain scission, measurement of molecular weight is limited to doses well below 50% of the gel

dose. More conveniently measured parameters are therefore the gel dose, that is, the dose to achieve incipient gel formation, and the residual soluble fraction beyond the gel dose.

The most widely used expression for analysis of the soluble fraction is also due to Charlesby and Pinner (95).

$$S + S^{0.5} = \frac{G(\mathrm{S})}{2G(\mathrm{X})} + k_2/[G(\mathrm{X})M_\mathrm{n}(0)D] \tag{9}$$

The constant k_2 is equal to 4.82×10^6 if the dose is expressed in kGy. Equation 9 assumes a post-probable initial molecular weight distribution, random scission and cross-linking reactions, and cross-linking by an H-linking mechanism. If cross-linking occurs by a Y-linking mechanism, the relationship between soluble fraction and dose is given by (96)

$$S + S^{0.5} = \frac{2G(\mathrm{S})}{G(\mathrm{X})} + k_3/[G(\mathrm{X})M_\mathrm{n}(0)D] \tag{10}$$

The constant k_3 is equal to 1.93×10^4 if the dose is expressed in kGy. Clearly, the choice of application of either equation 9 or equation 10 must be directed by additional evidence of the mechanism of cross-linking. Finally, a number of workers have derived expressions for the relationship between the soluble fraction and radiation dose for more general initial molecular weight distributions (81,88, 91–93,97).

The Radiation Chemistry of Specific Polymers

The radiation chemistry of polymers has attracted enormous interest since the initial studies by Charlesby, Dole, and Chapiro in the early 1950s. This interest has been a result of the recognition of the tremendous commercial importance of the radiation chemistry of polymers, and of the importance of an understanding of radiation chemistry to other fields. A number of excellent reviews have appeared over the past 45 years, including the seminal texts by Charlesby (1) and Chapiro (2), and the comprehensive review texts edited by Dole (98,99). Since then, a number of broad reviews of the effects of radiation have been published. For example, the *Polymer Handbook* has previously tabulated lists of the radiochemical yields reported elsewhere (100). The American Chemical Society has published a number of collections of papers presented at radiation chemistry meetings (101,102), and the two journals *Radiation Physics and Chemistry* and *Polymer Degradation and Stability* are of much interest. The 11 international meetings on radiation processing, which have been published in *Radiation Physics and Chemistry* (103–113), and the text by Singh and Silverman (114), provide an excellent overview of the field.

A number of more specific reviews have also been published. For example, Reichmanis has written about the use of radiation chemistry for electronics applications (43,115). Clough (116,117) has written a number of excellent reviews with

an emphasis on commercial applications of radiation chemistry, and the effects of oxygen on radiochemical events. The radiation chemistry of fluoropolymers has been reviewed recently by Lyons (118) and Forsythe and Hill (119). Burillo and co-workers (120) have addressed the use of radiation in the polymer recycling industry. Rosiak (121,122) has reviewed the emerging field of the radiation processing of biomedical polymers. More recently, Pruitt (123) has reviewed the major changes induced in medical polymers on irradiation, and given specific case studies of a number of materials. Hill and Whittaker (124) have detailed the importance of NMR spectroscopy in this field.

Polyethylene. It has been known for many years that polyethylene undergoes cross-linking on exposure to high energy radiation. In 1952 Charlesby (125) reported that exposure of polyethylene to pile radiation resulted in chemical changes consistent with cross-linking reactions. This initial observation prompted extensive work by him and others, most notably Dole, which has laid the foundations for the modern field of radiation chemistry of materials. The main findings of these and subsequent workers are summarized below (see Ethylene Polymers).

Free-Radical Intermediates. From an early time the participation of free radicals in the radiation chemistry of polymers has been well understood. Charlesby (125) in 1952 invoked a free-radical mechanism of cross-linking of polyethylene, although for other materials the participation of ionic species has also been suggested (126–137). The primary radicals observed at 77 K, at which temperature a significant proportion of the radicals are assumed to be trapped and prevented from further reaction, are the secondary alkyl radicals **I** (49,138–148).

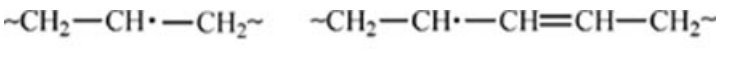

I **II**

Dole and co-workers have reported yields of alkyl free radicals in polyethylene irradiated at 77 K ranging from 2.7 to 3.7 (141,145,149). Furthermore, Cracco, Arvia, and Dole (49) reported that on warming, alkyl radicals decay by a first-order process, and they attributed this to reactions between alkyl radicals within isolated spurs. The persistent free radicals on warming to room temperature are the allyl radicals **II**. The impact of long-term stability of radical species on the stability of polyethylene has been underlined by studies of Jahan and co-workers (150–157) of ultrahigh molecular weight polymer used in medical implants.

Cross-Linking. In addition to conversion of alkyl radicals to more thermally stable allyl radicals, a significant proportion can undergo radical–radical recombination reactions (eq. 11).

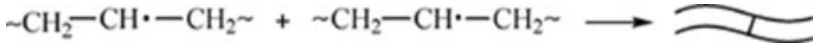

(11)

The product shown on the right of equation 11 is called an H-type cross-link. A number of alternative mechanisms of cross-linking have been proposed,

the most important being the formation of Y-type cross-links through either radical recombination reactions (eq. 12) or end-linking to terminal vinyl groups (eq. 13).

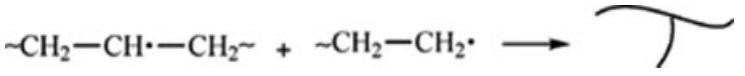

(12)

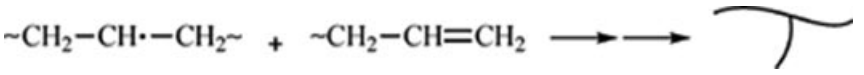

(13)

In the case of polyethylene the initial cleavage of carbon–carbon main-chain bonds is believed to be relatively unimportant compared with end-linking reactions. Evidence for this includes the absence of a contribution from chain-end free radicals in the ESR spectra of polyethylene irradiated at low temperatures, and careful analysis of the residual soluble fractions formed on irradiation at higher temperatures. Dole and Katsuura (158) suggested that if main-chain scission does occur, the cage effect is responsible for an overwhelming proportion undergoing recombination reactions. Not long after this, Kang, Saito, and Dole (159) measured the yields of cross-linking and main-chain scission in high density polyethylene at a range of temperatures by analyzing the residual soluble fractions with a Charlesby–Pinner equation modified for a Wesslau molecular weight distribution. They found that at each temperature over 308–393 K, the ratio of scission to cross-linking reactions was significant (ca 0.2) and decreased slightly at higher doses, an effect they ascribed to the reactions of vinylene double bonds to form cross-links. Similar results were reported by Dole and co-workers (149,160). In contrast to these articles, Lyons and Fox (161) reported negligible dose-dependence of $G(X)$ and 0.03 as the ratio of the yield of scission to that of cross-linking reactions.

The yields of cross-linking reactions in polyethylene have been reported extensively (97,149,159,160,162) and generally fall in the range $G(X) = 0.8–2.5$ for samples irradiated at ambient temperatures. The principle reason for this wide range of values of cross-link yields is the variation in crystallinity in the materials studied. It is reasonably well accepted that cross-linking reactions do not occur within the crystalline lamellae of polyethylene; Patel and Keller (163) confirmed this by analyzing the residual molecular weights of the chains within the crystalline regions of irradiated high density polyethylene after the amorphous regions had been removed by exposure to ozone. There was no evidence for cross-linking reactions between the chains previously within the crystalline regions. To further underline this relationship, O'Donnell and Whittaker (164) have reported that the value of $G(X)$ decreases progressively with increasing crystalline content for a range of materials having a similar initial molecular weight distribution.

In this same article, O'Donnell and Whittaker (164) compared the yields of cross-linking and scission, and other radiochemical products, in fully amorphous ethylene–propylene rubber (EPR) with the yields measured by them and reported by other workers for semicrystalline polyethylene and polypropylene. The yields of cross-linking and scission were significantly lower than those expected from extrapolation of the G-values for the homopolymers to zero crystalline content. In

other words, the yields for the fully amorphous materials were much lower than expected from considering yields within the amorphous regions of the semicrystalline polymers. It was concluded that the radiation-induced reactions must be favored at the crystalline–amorphous interface and that this might be a result of the stabilization of free-radical intermediates at the interface.

The relative importance of reactions 11–13 in the radiation cross-linking of polyethylene has been resolved to a large extent through a number of elegant studies of the structures of polymer irradiated to doses below the gelation dose, using high resolution solution-state ^{13}C NMR spectroscopy. The initial use of ^{13}C NMR to study radiochemical reactions was by Bennett and co-workers (165), who reported structural changes in irradiated liquid model compounds of polyethylene, *n*-hexadecane, and *n*-eicosane. These authors reported the formation of H-link structures apparently via recombination of two secondary main-chain alkyl radicals. Not long after this, Bovey and co-workers (166) reported the identification of both H- and Y-type links in *n*-$C_{44}H_{90}$ irradiated in the melt using solution-state ^{13}C NMR. Irradiation in the crystalline state produced only linear dimers, apparently through the end-linking of molecules at the crystal surfaces.

Several years after this, Randall and co-workers (62–64) studied irradiated high density polyethylenes using ^{13}C NMR, and identified a number of new structures, including internal double bonds and Y-type cross-links. The materials under consideration initially contained a high concentration of vinyl end groups, which react readily with secondary alkyl radicals (reaction 12 above) to form Y-links. The authors were unable to identify H-links in their irradiated HDPE samples, and suggested that for these materials irradiated to low doses, the H-linking mechanism is relatively unimportant.

More recently, Horii and co-workers (65,66) examined changes in the solution-state ^{13}C NMR spectra of relatively low molecular weight PE samples irradiated under a range of experimental conditions. The lower viscosity of the solutions as a result of the low molecular weight was manifested in narrow line widths in the NMR spectra, and thus the authors were able to observe resonances in the spectra due to H-type cross-links in all samples. The yields of H-links and Y-links were measured as a function of temperature (66), and it was found that H-links were the dominant product when PE was irradiated in the molten state, whereas Y-links were more commonly formed on irradiation at ambient temperatures. It was suggested that at higher temperatures the probability of reaction of the primary radicals (in reaction 12 above) with hydrogen radicals is higher in the molten state, and thus recombination of the longer-lived secondary radicals (reaction 11) dominates. These conclusions are supported by the study of O'Donnell and Whittaker (167) in which the formation of H-type cross-links in fully saturated ethylene–propylene rubber (EPR) irradiated well above T_g was confirmed. In addition, O'Donnell and Whittaker (168) have reported the observation of resonances due to H-type cross-links in LLDPE irradiated to very high doses.

Volatile Products. As discussed above, Dole and co-workers were the first to observe that hydrogen gas was a major product formed on the irradiation of polyethylene (46). Gaseous hydrogen was formed by recombination of hydrogen atoms formed by cleavage of C—H bonds, as illustrated in reaction 4 above, or by abstraction of hydrogen atom from the polymer main-chain by this ejected,

perhaps thermally activated, hydrogen atom itself. The role of the hydrogen gas so formed in radical migration was fully described by Dole and Cracco in 1961 and 1962 (50,51), and later through observation of the catalytic effect of hydrogen gas on the kinetics of decay of alkyl free radicals by Waterman and Dole (169) and Johnson and co-workers (145).

The yield of hydrogen gas in irradiated polyethylene has been reported by a number of workers to fall in the range of $G(H_2) = 3–4$, and shown by Kang and co-workers (159) to increase with increasing irradiation temperature. There is also evidence that the yield does depend to some extent on radiation dose (159) and polymer crystallinity (164).

In addition to hydrogen gas, small quantities of hydrocarbon gas reflective of the concentration and identity of side chains are produced on irradiation of polyethylene containing short chain branches. Bowmer and co-workers in 1983 (59) reported that the primary scission process leading to the formation of these small alkanes must occur at the tertiary carbon on the main chain. They also reported that the relative yields of volatile saturated products were essentially constant with increasing temperature, but that the total overall yield of gases did increase. On the other hand the formation of unsaturated products, principally ethylene and butylene, attributed to thermal depolymerization, increased markedly at elevated temperatures.

Unsaturation. The formation and reaction of unsaturated groups in polyethylene has been extensively studied by Dole and co-workers over a number of years, with a particular emphasis on the relationship between the rate of formation and decay of unsaturation with other radiochemical reactions. The main unsaturated product formed on irradiation of polyethylene is internal vinylene unsaturation. Dole and co-workers (46) suggested that up to 80% of the hydrogen gas evolved on irradiation resulted from processes leading to formation of vinylene groups. Dole and co-workers (61) further reported that the rate of formation of vinylene unsaturation was scarcely affected by irradiation at 77 K, at which temperature migration reactions are presumably retarded. This led them to suggest that molecular detachment of hydrogen molecules may be involved. Later, this group (159) reported that the *G*-value for the formation of vinylene groups was close to 2.4 at all temperatures in the solid state.

In addition to the formation of vinylene unsaturation, evidence for the formation of conjugated double bonds can be found in the appearance of new absorption bands in the UV spectrum of irradiated polyethylene (170–172). The rate of formation of dienes is significantly higher than that expected from consideration of the statistics of formation of vinylene unsaturation; Fallgatter and Dole (170) speculate on possible cooperative mechanisms of formation. The formation of more highly conjugated species is suggested to result from secondary reaction (171,172).

The kinetics of decay of double bonds initially present in the material have also been studied in detail. Dole and co-workers (61) reported that the decay of terminal vinyl or vinylene groups follows first-order kinetics until the formation of vinylene groups, mentioned immediately above, becomes significant. The exact mechanism of reaction of the vinyl end groups remains unclear; however, the participation of these groups in end-linking reactions (reaction 12) has been confirmed by Randall and co-workers (62–64) and Horii and co-workers (65,66).

Polypropylene. Polypropylene undergoes net cross-linking when exposed to ionizing radiation in the absence of oxygen. However, the radiation chemistry of polypropylene differs markedly from that of polyethylene as a consequence of the presence of tertiary carbons along the polymer backbone. Therefore, polypropylene undergoes significant levels of main-chain scission on irradiation (see PROPYLENE POLYMERS (PP)).

Initial studies of this polymer were mainly concerned with understanding the changes in molecular weight and the rate of gel formation on irradiation. Much of this work was concerned with the development of fundamental relationships between the radiochemical yields and molecular weights. The reported yields of chain scission and cross-linking fall in the ranges $G(S) = 0.198–0.62$ and $G(X) = 0.0645–0.272$, respectively (81,82,95,173–176). The apparent large variation in values of $G(S)$ and $G(X)$ are in part due to the difficulty in analysis of molecular weight or solubility changes in materials having broad molecular weight distributions, and also possibly due to a dose dependence of the G-value for chain scission (81,175,176).

Despite the increased probability of main-chain scission in polypropylene compared with polyethylene, there is no evidence of the formation of stable scission radicals on irradiation at low temperatures. Rather extensive ESR evidence has been accumulated that the stable free-radical intermediates are those listed below:

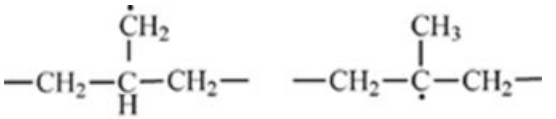

III **IV**

On irradiation at low temperatures, alkyl radicals (**III** and **IV**) are formed with a radiochemical yield $G(R)$ of 2.4–2.6, depending on the crystallinity of the material (99,164).

A particularly informative set of experiments which reveal the extent of initial bond cleavage has been conducted by Busfield and co-workers (35–38). They have studied the radiation-induced changes in the stereochemistry of isotactic polypropylene (iPP). The changes in the stereochemistry are a result of initial chain scission, isomerization, and rehealing of the broken bond, as shown below in Figure 1.

Studies of irradiated iPP (35–38,177) have provided evidence that the racemization reactions do not occur as isolated events, but rather that they may occur in clusters. The methyl region of the solution-state ^{13}C NMR spectrum of iPP can be resolved to the pentad level. The changes in the pentad distribution on irradiation are not consistent with random reactions occurring along the polymer backbone (35–38). A number of mechanisms have been suggested to account for the observed changes in tacticity, involving for example an increased probability of reaction after initial reaction, but all schemes have in common the observation that the proportion of syndiotactic sequences formed on irradiation is high and that the rate of equilibration of these sequences is low. It was also found that

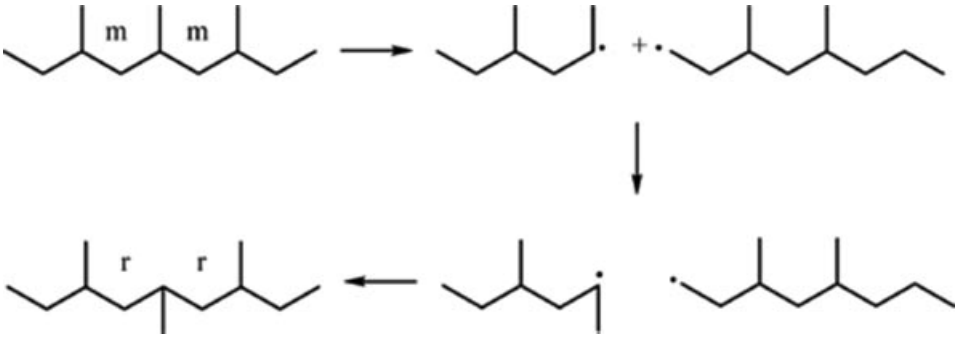

Fig. 1. The racemization of an initially isotactic polymer through chain scission, isomerization, and bond reforming.

electron-beam irradiation at high dose rates was much more effective in promoting changes in tacticity than γ irradiation to comparable doses (37).

Polyisobutylene. In 1954 Charlesby (80) noted that the molecular weight of polyisobutylene (PIB) decreased rapidly on exposure to high energy radiation. It has since been well understood that the presence of quaternary carbons in the main chain of polymers predisposes such a material to degradation (see BUTYL RUBBER). In the case of PIB, the primary reactions during radiolysis have been suggested by Alexander and co-workers (178) and Chapiro (179) to be those described in Figure 2. On the other hand Miller and co-workers (180) suggested that the initial chemical changes involve loss of a methyl hydrogen to form radical **VII**, followed by spontaneous β-cleavage (Fig. 3). In addition, Il'icheva and Slovokhotova (181) have suggested that the energetically favoured radical **VIII** can also undergo β-cleavage, as in Figure 4.

The ESR spectra of PIB irradiated at low temperature consists of a broad doublet with a hyperfine coupling constant of 2 mT, attributed to either radical **VIII** (182) or a combination of contributions from radicals **VII** and **VIII** (183, 184). The primary radicals **V** and **VI** (Fig. 2) have not been observed by ESR spectroscopy. Despite extensive studies of the radiochemical changes in PIB by ESR, volatile product analysis, and UV and IR spectroscopy, the mechanism of degradation had been uncertain until the advent of high resolution ^{13}C NMR methods. In a comprehensive study, Bremner and co-workers (185) and Hill and

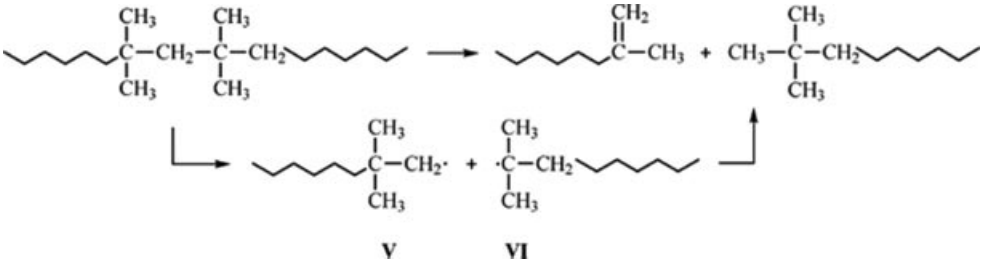

Fig. 2. Proposed mechanism of degradation of PIB via initial main-chain cleavage.

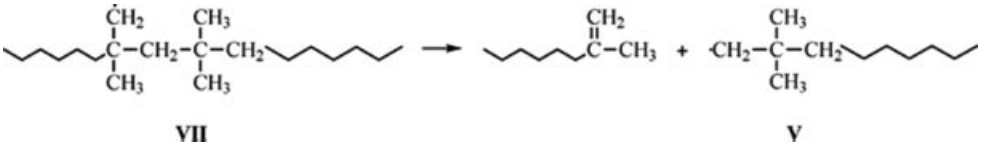

VII V

Fig. 3. Proposed mechanism of degradation of PIB via β scission of the side-chain methylene radical.

co-workers (186) identified the major products of degradation by NMR and other methods. They concluded that the schemes shown in Figures 2–4 are all possible degradation pathways, and that the major products are structures formed through the reaction scheme shown in Figure 2.

Polyethers. The radiation chemistry of the polyethers has received relatively little attention. It is known, however, that all of this class of materials undergoes net cross-linking reactions. A comprehensive study of the radiation chemistry of polyoxymethylene (POM) has been reported by Fischer and Langbein (187). These authors reported that irradiation at the high dose rates of 150 kGy/min with 1-MeV electrons at 287 K resulted in a reduction in the total mass of the sample of approximately 1% per 100 kGy absorbed dose. There was a corresponding increase in the yield of new acetate chain ends determined by IR spectroscopy. The evolved gases consisted of many products, however the main products were hydrogen ($G = 1.7$), methane ($G = 0.14$), and CO ($G = 0.013$). The gases also included formaldehyde and higher molecular weight molecules. These results were combined with ^{1}H NMR analysis of the polymer after irradiation. Peaks due to new acetate and methoxy chain ends, and H-type cross-links, were observed. The yields of products obtained from the NMR spectra appear to be high, perhaps reflecting the difficulty in obtaining quantitative NMR spectra of irradiated materials. Despite this, they were able to confirm that this polymer does crosslink on irradiation.

The effects of irradiation on the properties of poly(ethylene oxide) (PEO) have been examined by a number of workers (see ETHYLENE OXIDE POLYMERS). A number of these studies have been concerned with irradiation cross-linking of PEO in solution (188–201). When irradiated in the solid state, PEO undergoes net cross-linking with the reported gel doses of 3.5 and 1.1 kGy, respectively, for highly crystalline, lower molecular weight and more highly disordered, high molecular weight materials (202). King reported earlier changes in solution viscosity of PEO irradiated in air and in vacuum (203). Other studies have been concerned with changes in the crystalline structure on irradiation; the crystalline order is reduced at moderate radiation doses consistent with cross-linking reactions (202,204,205).

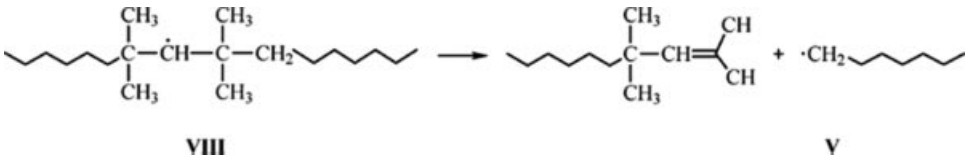

VIII V

Fig. 4. Proposed mechanism of degradation of PIB via β scission of the main-chain methine radical.

Finally, the effects of radiation cross-linking on the chain dynamics have been examined by Schilling and co-workers (206) using solid-state ^{13}C NMR techniques.

Poly(propylene oxide) (PPO) has also been observed to form a gel on irradiation (207). Roberts and co-workers (207) reported G(S) values of 0.22 and 0.55 and G(X) values of 0.15 and 0.31 for atactic and isotactic PPO, respectively. In this article the products of degradation are compared with previous reports of products of irradiation of PP and POM. It was found that the radiation chemistry is broadly consistent with that expected from previous studies.

Poly(vinyl alcohol). The radiation chemistry of poly(vinyl alcohol) (PVA) is similar in many respects to the degradation of PVC, described below (see VINYL ALCOHOL POLYMERS). PVA undergoes a progressive darkening on irradiation at elevated temperatures or gets heated subsequent to irradiation due to the formation of sequences of conjugated double bonds (208). The mechanism of degradation proposed by Zhao and co-workers (208), and shown in Figure 5 below, involves the participation of radical cations. Previous studies have indicated that hydrogen gas is a primary product of the degradation of PVA (209,210), leading to the formation of the α-carbon radicals, as shown in Figure 5. More recently, using ESR spectroscopy, Zainuddin and co-workers (211) have examined in detail the radical species formed on irradiation of PVA. They identified contributions for three radical species at low temperatures: the α-carbon radical (triplet ESR spectrum), a radical anion (doublet spectrum), and an unidentified neutral species (doublet radical). The latter two species contribute 62% of the total radical concentration at 77 K. These results are broadly consistent with the mechanism proposed in Figure 5; however, neither article comments on the expected changes in molecular weight on irradiation. Lu and co-workers (212) have shown that the molecular weight of PVA decreases on irradiation, with the polymer remaining soluble up

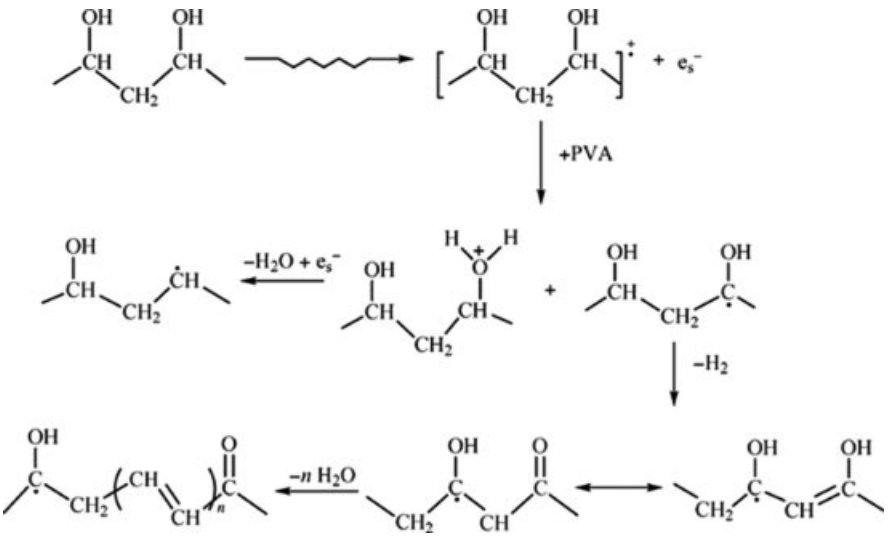

Fig. 5. Proposed mechanism of formation of conjugated structures during the radiolysis of poly(vinyl alcohol).

to doses greater than 1000 kGy. It is apparent that chain scission reactions must dominate over cross-linking reactions.

Poly(vinyl chloride). The mechanism of radiation chemistry of poly(vinyl chloride) (PVC) in many ways resembles the well-known thermal degradation of this polymer (see VINYL CHLORIDE POLYMERS). The principal results of exposure of PVC to ionizing radiation are evolution of hydrochloric acid and development of intense absorption bands in the UV and visible regions of the electromagnetic spectrum (67–69,213). The result of dehydrochlorination is the formation of polyene radicals. For example, absorption peaks at 252, 291, and 330 nm were assigned to allyl, dienyl, and trienyl radicals, respectively. The dehydrochlorination reactions dominate the radiation chemistry; the yield of cross-linking reactions is very low, as reported by Chapiro (69). Salovey and Gebauer (214) later reported from the changes in the polydispersity of irradiated PVC that chain scission and cross-linking are occuring simultaneously on irradiation in air.

Aliphatic Polyesters. Over the past 10 years the linear aliphatic polyesters, the polyalkanoates, and the copolymers of lactic and glycolic acids have attracted enormous interest as a result of their widespread use as biomedical materials. The radiation stability of these materials is of importance because of the potential to effect sterilization through exposure to ionizing radiation (215–225).

Polyhydroxybutyrate. Copolymers of hydroxybutyrate and hydroxyvalerate possess many mechanical properties in common with synthetic polyolefins, and so have attracted much attention as replacements for these materials in environments where biodegradability is an important parameter (see POLY(3-HYDROXYALKANOATES)). Carswell-Pomerantz and co-workers (217,218) have reported a detailed study of the radicals formed on irradiation of such materials. They found that the yield of radicals at 77 K was $G(\mathrm{R}) = 1.7 \pm 0.2$, independent of copolymer composition, but that on irradiation at 300 K, the yield of radicals was reduced for the copolymers because of their lower glass-transition temperatures compared with the homopolymer. At low temperatures a significant contribution to the ESR spectra from radical anions was noted. These radicals were observed to decay on warming to produce scission radicals. At still higher temperatures, radicals produced by abstraction of a methylene proton adjacent to the carbonyl group were detected.

The predominant reaction on radiolysis of polyalkanoates is chain scission. Carswell-Pomerantz and co-workers (218) have shown that the main volatile products of radiolysis are CO, CO_2, and H_2. Scission at the ester unit results in a reduction in the molecular weight of these materials, and the G-value for scission $G(\mathrm{S})$ for PHB was calculated to be 1.3. Using solution NMR, a very similar yield of reactions was determined from measurement of the yield of new chain ends. Cross-linking is not important in the radiation chemistry of PHB; however, analysis of the changes in molecular weights of irradiated PHBV copolymers provided evidence of some cross-linking, with the ratio of scission to cross-linking being 9 and 6.8 for materials having valerate mole fractions of 0.184 and 0.263, respectively.

Poly(lactic acid-co-glycolic acid). The degradation of the homopolymers and copolymers of lactic and glycolic acids (PLGA) has been reported by a number of authors (220–223). Babanalbandi and co-workers (220) have measured the G-radical values at 77 K for poly(L-lactic acid) (L-PLA) and poly(D,L-lactic acid)

(D,L-PLA) and reported these to be 2.0 and 2.4, respectively. They also reported $G(S) = 2.3$ and $G(X) = 0.0$ for D,L-PLA and $G(S) = 2.4$ and $G(X) = 0.28$ for L-PLA. These results are in contrast to the values of Collett and co-workers, who suggested that rather than chain scission dominating the radiation chemistry, these polymers form a gel on irradiation.

The results of Babanalbandi and co-workers (221), in which new aliphatic chains ends formed by cleavage of the main chain at the ester unit are observed, are in support of a mechanism in which chain scission dominates cross-linking. These authors reported *G*-values for the formation of chain end structures comparable with earlier study. Furthermore, the main volatile products of radiolysis of PLA and poly(glycolic acid) (GPA) are CO_2 and CO, consistent with chain scission being the most important reaction. In addition, small amounts of hydrogen and ethane gas were observed on the radiolysis of PLA. Finally, Montanari and co-workers (226) have examined the effects of radiation sterilization on the stability of PLGA microparticles used for drug delivery.

Aliphatic Polysulfones. The class of copolymers of olefins and sulfur dioxide are well known for undergoing extensive degradation on exposure to high energy radiation. In 1965 Ayscough and co-workers (227) reported an ESR study of the degradation products of sulfones and poly(olefin sulfone)s. They were able to confirm that the relatively weak C—S bonds are more susceptible to rupture compared with the C—H bonds. Later, Brown and O'Donnell (228,229) confirmed that this initial chain breakage leads to loss of SO_2 and permanent chain scission and reduction of molecular weight. The yield of scission reactions was found to increase progressively up to the ceiling temperature for the propagation–depropagation equilibrium, at which temperature rapid depropagation occurred. The yield of olefin gas evolved on radiolysis was observed to be lower than the yield of sulfur dioxide, because of the cationic homopolymerization of the olefins initiated by a polymeric carbonium ion (45,230). Isomerization of the olefin via a carbonium ion intermediate was also confirmed. The mechanisms of these reactions are summarized in Figure 6.

Polymethacrylates and Polyacrylates. The high energy radiation chemistries of polyacrylates and polymethacrylates were some of the first studied in detail for any polymer (see ACRYLIC ESTER POLYMERS; METHACRYLIC ESTER POLYMERS). For example, in the 1950s, Charlesby and co-workers reported extensively on the breakdown of poly(methyl methacrylate) (PMMA) on exposure to high energy radiation, and also on studies of coloration and gas formation associated with the loss of the side chains (20,39,80). The molecular weight of PMMA was shown to decrease on irradiation (80,231), with the decrease inversely proportional to the irradiation dose. The latter observation was later rationalized through the famous Charlesby–Pinner relationship (95), which allowed *G*-values of chain scission and cross-linking to be evaluated. Shultz and co-workers (232) reported that for 1-MeV electron irradiation of PMMA under vacuum, $G(S) = 0$ and $G(X) = 1.65$, and Wall and Brown (231) examined the yields for the principal gases formed on γ radiolysis under vacuum: H_2, CH_4, CO, and CO_2, for which the *G*-values were 0.21, 0.54, 0.45, and 0.32, respectively [$G(\text{gas}) = 1.6$].

ESR studies by Ovenall and co-workers (233–236) during the same period identified the natures of the spectra of the radicals formed in PMMA on radiolysis over a temperature range from ambient to 77 K. They identified the multiline

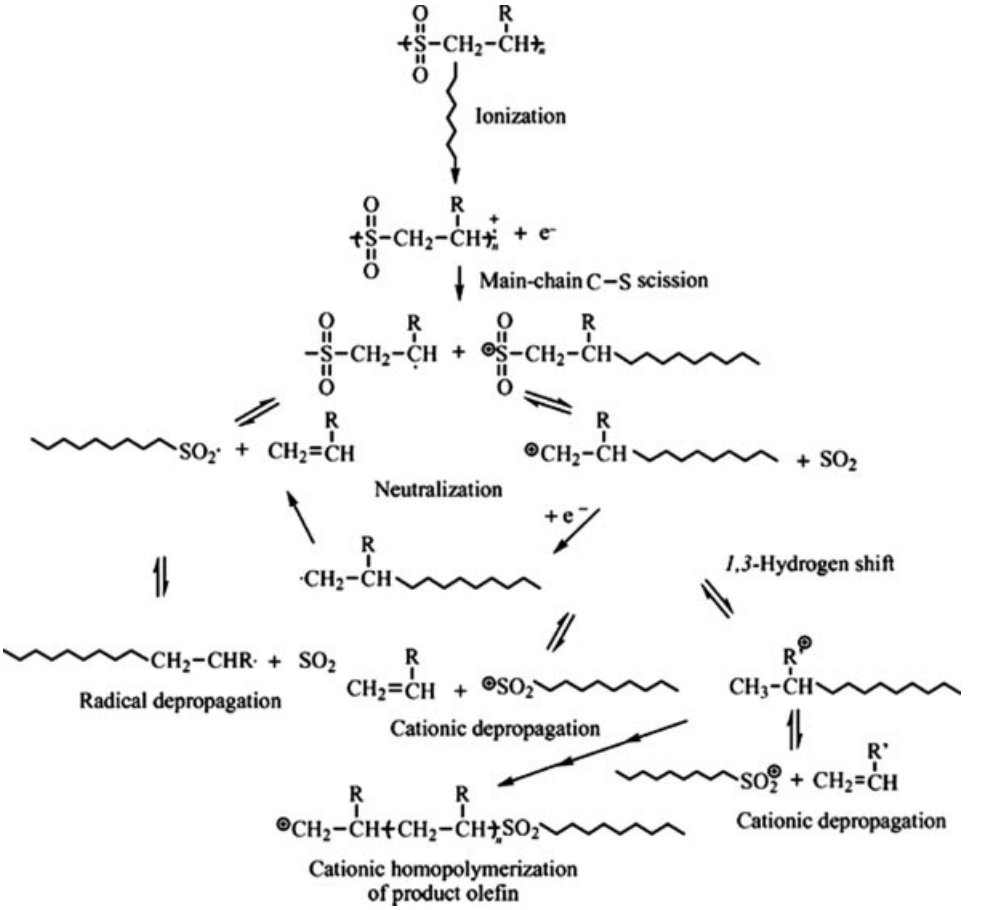

Fig. 6. Proposed mechanism of degradation of poly(olefin sulfone)s.

spectra observed at room temperature as being principally associated with chain-end radicals, which were characterized by a nine-line spectrum at room temperature, with $G(\mathrm{R}) = 2.5$. Later, O'Donnell and co-workers (237) were able to account for the nine lines in terms of two overlapping spectra, one consisting of five and the other of four lines, arising from two conformations of the chain-end radicals. Bowden and O'Donnell (238) later showed that the relative contributions of the two conformations varied with the observation temperature.

A consideration of the molecular weight changes and the natures and yields of the gaseous and radical products formed on radiolysis at room temperature allowed a mechanism for the radiolysis of PMMA to be formulated. The principal process associated with the degradation was scission of the ester side chain, forming the principal gaseous products and a main-chain radical which can further undergo β-scission to form the propagating radical and a chain-end double bond. It was also thought that some direct main-chain scission may occur at the α-carbon. The coloration of PMMA on radiolysis was believed to arise from the formation of oxygen and temperature-sensitive radical and charged species.

David and co-workers (32) confirmed the occurrence of direct main-chain scission and reported that racemization also occurred during radiolysis of syndiotactic PMMA. In the presence of a radical scavenger, no racemization was found to take place, suggesting that radical processes are involved in the racemization process (33). These results therefore indicate that irradiation must induce some temporary main-chain scission, which is followed by recombination of the scission radicals within the cage leading to a concomitant change in the stereochemistry of the polymer. The extent of the racemization observed for a γ-ray dose of 8 MGy was reported to be approximately 24%.

Because PMMA has a low ceiling temperature, the formation of propagating radicals on radiolysis at 453 K, with $G(S) = 10$, Charlesby and Moore (40) found spontaneous depolymerization of the polymer to monomer at this temperature. In a later article, David and co-workers (239) showed that depolymerization also occurred when PMMA was irradiated at ambient temperature and then heated to 433 K, and that the yield of monomer was independent of the absorbed dose and the initial molecular weight of the PMMA.

By contrast with PMMA, poly(methyl acrylate), PMA, and several other aliphatic polyacrylates were found by Shultz and Bovey (240) to undergo cross-linking and gel formation on irradiation with 1-MeV electron beams. They reported $G(S) = 0.15$ and $G(X) = 0.52$ for PMA. Graham (241,242) reported that the phenyl, benzyl, and 2-phenyl ethyl acrylate polymers also undergo cross-linking on γ radiolysis under vacuum. There was evidence of side-chain scission also, and according to Fox and co-workers (243,244) the major volatile products were similar to those observed for PMMA.

In these early years, the high energy radiation induced reactions of PMA and PMMA were not the only polyacrylates and polymethacrylates investigated, but they were found to be representative of the radiation chemistries of the two polymer families with different ester side-chains.

With improvements in the sensitivities of NMR and ESR spectrometers during the 1970s and the growing importance of microlithography in the production of solid-state devices, extra interest was directed to studies of the radiation-induced reactions of both polymethacrylates and polyacrylates. Because the methacrylate polymers almost entirely undergo scission on exposure to radiation under vacuum and the acrylates undergo cross-linking, they can be utilized as the basis for positive and negative resists, respectively. Thompson and co-workers (42) and Bowden (245) reported studies of the applications of PMMA in resist development, and examined the effect of incorporation of heavy atoms to enhance the sensitivity of PMMA to X-rays. Bowden (245) found that the sensitivity of a resist depends not only on the nature of the polymer but also on its molecular weight and molecular weight distribution, and that it increases with deceasing polydispersity. The development dose was found to decrease with increasing $G(S)$ for positive resists such as the polymethacrylates.

In a series of articles, Busfield, O'Donnell and co-workers reexamined the radical yields, gaseous products, molecular weight, and material property changes on γ radiolysis of PMMA and PMA (22,23,27,246–248).

O'Donnell and co-workers (22,248) have reevaluated radical formation on irradiation of PMMA at 77 K and room temperature. At 77 K the spectrum was analyzed in terms of the presence of $CHO\bullet$, $CH_3\bullet$, $\bullet COOCH_3$, and $-COOCH_2\bullet$,

as well as the propagation radical. At room temperature, only the propagating radical spectrum was observed. The *G*-value for overall radical formation at 77 K was 0.58, which is lower than that found at room temperature, 2.2, indicating the importance of radical recombination within the cage at 77 K. On annealing of the radicals produced at 77 K to room temperature and above, the radical decay is not linear, but reflects the onset of thermal transitions in PMMA (249).

A wide range of gaseous products have been identified by Busfield and co-workers (246) on γ radiolysis of PMMA at room temperature, which arise principally from a breakdown of the ester side-chains. The principal products and their yields G are respectively H_2, 0.34; CH_4, 0.66; CO, 1.08; CO_2 0.68; CH_3OH, 0.36; HCO_2CH_3, 0.69; dimethoxymethane, 0.11; and CH_3Ac, 0.02. Kudoh and co-workers (250) have measured the yields of H_2, CH_4, CO, and CO_2 on radiolysis at 77 K and report that whereas the hydrogen yields are the same at 77 K and room temperature, those for the other gases are lower at 77 K. This is in accord with the temperature dependence of the observed radical yields (248) and with the mechanical properties (251).

Busfield and co-workers (246) have examined the molecular weight dependence for γ radiolysis of PMMA in vacuum at room temperature, and Kudoh and co-workers (250) have also reported the dependence at 77 K. The values of G(S) at room temperature were 1.3 (246) and 1.7 (250) and at 77 K, 0.24 (250). These reflect the reported radical yields at the two temperatures. The variation of the molecular weight distribution with dose for e-beam irradiation of PMMA has been studied by Viswanathan (83). He has modeled the dependence of the distributions for use in predicting the sensitivities of positive resists in terms of product solubilities for development following exposure.

Busfield and O'Donnell (23) have examined the correlations between the changes in the molecular weight and the tensile properties of PMMA following radiolysis at room temperature. Both the flexural and compressive strengths decrease with increasing dose, reflecting the falling molecular weight of the polymer. Kudoh and co-workers have drawn similar conclusions for radiolysis at 77 K and ambient temperature (251).

The racemization of PMMA on radiolysis has been studied by Luo and co-workers (34), Dong and co-workers (31), and Thominette and Verdu (252) by use of NMR. Luo and co-workers (34) reported that for radiolysis of isotactic PMMA in solution, the yield of scission was greater than that for racemization, but the order was reversed for radiolysis in the solid state, indicating an important role for molecular motion of the scissioned chains. Dong and co-workers (31) investigated the γ radiolysis of both highly isotactic and highly syndiotactic PMMA. They found that their results were consistent with a temporary chain scission G-value of 18.6 at 353 K, and the polymers tended to approach a common average tacticity with increasing absorbed dose, which was the same as that found for PMMA prepared by free-radical polymerization.

By comparison with PMMA, the radiolysis of PMA has received much less recent attention. Busfield and co-workers (247) have measured the G-values for gaseous product formation at room temperature and 423 K, and they have also measured the dose to gel. The major volatile products were the same as those observed for the radiolysis of PMMA, but the total gas yield was much smaller: $G(\text{gas}) = 1.6$ compared with 3.9 for PMMA. However, the gas yield increased with

temperature, reaching 3.9 at 423 K. At 195 K the dose to gel was approximately 0.25 MGy, and decreased with increasing temperature.

The sensitivities of a wide range of other acrylate and methacrylate polymers to γ radiation have also been investigated, including poly(acrylic acid) (85,253), poly(methacrylic acid) (85,254–263), poly(hydroxyethyl methacrylate) (264,265), polymethacrylates with longer ester side-chains (266,267), and poly(ethylene glycol dimethacrylate) (268). In general, the behaviors of these polymers mirror the behaviors of the related methyl ester polymers, but some observations are worthy of special mention.

Hill and co-workers (85) have reported a study of the scission and cross-linking yields on γ radiolysis of poly(acrylic acid) and poly(methacrylic acid) using sedimentation equilibrium to obtain the weight- and Z-average molecular weights as a function of absorbed dose. The values $G(\mathrm{S}) = 0$, $G(\mathrm{X}) = 0.44$ and $G(\mathrm{S}) = 6.0$, $G(\mathrm{X}) = 0$, respectively, were obtained for the two polymers, highlighting the significant role of the substituent methyl group in determining the outcome of the radiolysis. Kudoh and co-workers (259) have investigated LET effects for electron radiolysis of PMMA. A comparison of the scission probabilities for γ radiation (0.5 Gy/s) and high energy electron beams (up to 4×10^{10} Gy/s) showed no evidence for dose rate effects; thus they found no evidence for spur overlapping at the high electron beam dose rates. Dong and co-workers (267) studied the role of the length of the aliphatic side chains in a series of highly syndiotactic polymethacrylates and found that poly(heptyl methacrylate) indeed undergoes gelation on γ radiolysis, via the heptyl side chain.

Heavy ion irradiation of PMMA has also received some attention, particularly by researchers at the Japan Atomic Energy Research Institute. Kudoh and co-workers (269–273) have compared the effects of γ radiation and electron beams with those for 30 and 45 MeV protons and heavier ion beams on the tensile and molecular weight properties of PMMA. They have found no difference between the sensitivities of the tensile properties of PMMA to γ-rays and electron and proton beams as a function of dose. However, the molecular weight dependence for PMMA showed a clear LET dependence for heavy ions above a critical LET, indicating overlapping between spurs. For low LET radiation the scission probability remains constant, but the scission probability decreases with increasing LET for high LET radiation. The critical LET level for PMMA is a few hundred $\mathrm{MeV} \cdot \mathrm{cm}^2/\mathrm{g}$.

Esters of Other Acids. Poly(*tert*-butyl crotonate) (PtBC) is an analogue of poly(*tert*-butyl methacrylate) (PtBMA) but it does not have the disubstituted main-chain carbon atom. Thus, on these grounds, PtBC might potentially undergo cross-linking, but this process may potentially be hampered by the severe steric hindrance involved in the formation of a cross-link at the main-chain ester–carbon atom. O'Donnell and co-workers (274,275) have reported studies of the yields for radical formation, cross-linking and scission, and the gaseous products on radiolysis of PtBC. Three major radicals were observed on radiolysis at 77 K: tertiary butyl radicals, oxygen centred radicals formed by loss of the tertiary butyl groups, and a third unidentified radical. The value of $G(\mathrm{R})$ was 1.28. The major gaseous radiolysis products were the same as those observed by Ungar and co-workers (276) for PtBMA, and the yield of CO_2 ($G = 1.0$) was greater than that for CO ($G = 0.26$), in contrast to the observations for PMMA and PMA. This is consistent

with the preferential loss of the labile *t*-butyl ester group. The values of $G(S) = 0.59$ and $G(X) = 0.66$ for PtBC can be compared with those for PtBMA, $G(S) = 0.21$ and $G(X) = 0.17$, reported by Shultz and Bovey (240). These values indicate that PtBC indeed undergoes cross-linking, while PtBMA undergoes net scission. However, the nature of the cross-links formed in PtBC have not been identified.

Polysiloxanes. Poly(dimethyl siloxane) (PDMS) undergoes cross-linking on exposure to ionizing radiation. As early as 1954, Charlesby (78,277,278) had reported that PDMS can be cross-linked to form a transparent rubbery material, and that the dose to achieve a cross-linked network was inversely proportional to the initial polymer molecular weight (see SILICONES). Early work also reported that the main volatile products of irradiation are hydrogen, methane, and ethane gases (277,279,280). Other chemical changes observed with IR spectroscopy were Si—H structures and new, unidentified —Si-O— structures (280,281). ESR studies have revealed that on irradiation at 77 K $CH_3\cdot$, $—CH_2\cdot$, —Si·, and —O· radicals are produced, and that, as expected, the radicals react on warming above the glass-transition temperature (127,282,283). *G*-values between 2.3 and 2.7 for cross-linking have been reported (279,284,285).

Whereas some evidence for chain-scission structures has been obtained from these previous studies, not until recently have conclusive measurements of the yields of scission reactions been reported (286–288). Hill and co-workers (286,287) have identified new structures formed in PDMS using solid-state ^{29}Si and ^{13}C NMR. They were able to measure the rate of formation of a number of chain-end, side-chain, and cross-link structures. The mechanism of cross-linking is dominated by Y-linking, although two minor H-linking products were also observed. On irradiation at 303 K, the radiochemical yields were $G(S) = 1.3$, $G(H) = 0.34$, and $G(Y) = 1.7$.

Fluorinated Polymers.

Fully Fluorinated Polymers. The radiation chemistry of fully fluorinated polymers shows remarkable temperature dependence, with all of the fluorinated thermoplastics undergoing degradation, ie, chain scission, at ambient temperatures, but with an increasing yield of cross-linking reactions at elevated temperatures. Over the past 10 years, this has led to renewed interest in the radiation chemistry and applications of these materials (see PERFLUORINATED POLYMERS, POLYTETRAFLUOROETHYLENE).

As discussed in a number of reviews (1,2,289), the parent of the fluoropolymer family, polytetrafluoroethylene (PTFE), undergoes degradation on irradiation. Over a number of years, this process has been exploited commercially to reduce the molecular weight of PTFE resins. Despite this recognition, the details of the mechanism of reaction have remained unclear, in part due to the paucity of experimental techniques available to study these materials. The inherent insolubility of PTFE has until recently restricted studies of radiation chemistry of PTFE to measurements of mechanical and thermal properties, and melt viscosity. For example, Bro and co-workers (290) reported in 1963 that the melt viscosity of PTFE decreased on irradiation followed by heating. This effect was more pronounced in the presence of air. In another example, Hedvig (291) in 1969 showed that the mechanical strength and in particular the elongation at break of irradiated PTFE dropped dramatically on irradiation, but that these properties disappeared on irradiation in air.

As mentioned above, the mechanism of degradation of PTFE is unclear, particularly the location of radiation-induced chemical reactions. However, ESR spectroscopy (290–293) has confirmed that the stable free-radical species at low temperatures are the chain-end radicals **IX** (shown below) and that at higher temperatures the secondary radicals **X** dominate the spectrum. Hedvig (291) has suggested that chain-end radicals terminate by abstraction to form the more stable secondary radical. These radicals persist for very long times, and this leads some authors (58) to suggest the suitability of PTFE as a radiation dosimeter.

IX **X**

The effect of irradiation at elevated temperatures was initially investigated by Lovejoy and co-workers (294), who found that irradiation of PTFE above the glass-transition temperature resulted in a decrease in the molecular weight of the material, as evidenced by a decrease in melt viscosity. In a later series of articles Tutiya (295–299) studied the effect of various irradiation conditions on the broad-line ^{19}F NMR spectra of PTFE. He reported in 1972 (295) that on irradiation above the melting temperature there was a significant decrease in the crystalline content, ascribed in part to the increased melt viscosity of the irradiated polymer. It was not until about 20 years later that these observations were pursued. In 1994 and the early 1990s, Sun and co-workers (55,300) and Oshima and co-workers (56) reported the radiation-cross-linking of PTFE above its melting temperature. Since then, Oshima and co-workers (56,301–310) have examined in detail the mechanism of formation and properties of radiation-cross-linked PTFE. It was found that cross-linked PTFE had significantly enhanced radiation stability compared with the uncross-linked resin despite the radical yield at low temperatures being significantly higher (304,308,309).

PTFE undergoes cross-linking via a Y-type mechanism (reaction 12 above). This has been confirmed by solid-state ^{19}F NMR measurements both by Katoh and co-workers (307,310) and Fuchs and co-workers (311,312). Initially, the Y-linking mechanism was favored over the H-linking mechanism after considering steric effects. However, it has been conclusively shown that branch points are formed and that the yield of branch points is superior to the yield of new chain ends (312), whereas Oshima (310) has suggested that double bond structures may also participate in the branching reactions.

In an early article Lovejoy and co-workers (294,313) reported that the copolymer of tetrafluoroethylene and hexafluoropropylene (FEP) would undergo degradation on irradiation at room temperature, but that it cross-links at higher temperatures. In 1985 Seguchi and co-workers (8) confirmed that FEP indeed undergoes cross-linking reactions through measurements of the soluble fractions after irradiation. The primary free radicals have been identified by Hill and co-workers (30) to be radicals **IX** and **X** above. In addition the yield of free radicals is significantly enhanced at room temperature compared with irradiation at 77 K. This is a consequence of the lower probability of cage recombination of the primary species at higher temperatures. In a later series of articles

(314–316) these authors have measured the yields of new structures by solid-state ^{19}F NMR spectroscopy and found that, as with PTFE, irradiation below the melting temperature resulted in predominately new chain ends due to chain scission. On the other hand, upon irradiation at 523 K, just above the melting temperature, new branch or cross-link structures were formed in significant quantities.

Similar conclusions have been reached for the third commercially important fully fluorinated polymer, namely the copolymer of tetrafluoroethylene and perfluoropropyl vinyl ether (317–320). This is not unexpected, because this material typically contains approximately 2 mol% of the vinyl ether. Irradiation at elevated temperatures by electron beam or with γ-rays resulted in increased yields of cross-links. Finally, Forsythe and co-workers (321) have also reported the radiation chemistry of members of the Teflon AF DuPont family of thermoplastics, and found that degradation proceeded through loss of hexafluoroacetone of the dioxole ring, leading to chain-scission reactions.

Fluoroelastomers. The above discussion has highlighted the importance of molecular motion on the ultimate radio-chemical products formed in fluorinated polymers. This is a consequence of the limited number of mechanisms of termination of radicals in fluorinated polymers when compared with protonated polymers. Specifically, in fluoropolymers there is no mechanism of radical migration equivalent to the hydrogen-hopping mechanism at work in irradiated hydrogen-containing polymers. The three-body intermediate suggested to participate in the hydrogen-hopping mechanism (eq. 4) is unlikely to form on radiolysis of fluorocarbons, on purely energetic grounds. Thus, the radicals produced in fluoropolymers are particularly long-lived, and when they do react it is usually through combination reactions. This means that the radicals must have sufficient mobility to be able encounter one another; hence the probability of chain cross-linking increases with increasing temperature, and in the semicrystalline materials discussed above, sufficient mobility is only achieved above the crystalline melting temperature.

The situation is somewhat similar for fluorinated elastomers (see FLUOROCARBON ELASTOMERS). The radiation chemistry of the copolymer of tetrafluoroethylene (TFE) and perfluoro-methyl vinyl ether (PFMVE), known commercially as Kalrez, has been studied in detail by Hill and co-workers (57,322–327) This material is a random copolymer of these two monomers with a TFE to PFMVE molar ratio of 2:1. It is a fully amorphous polymer with a glass-transition temperature close to 273 K. On irradiation at room temperature it undergoes cross-linking, as confirmed by measurement of structural changes by NMR spectroscopy (57), and changes in mechanical and solubility properties (327). When this material is irradiated below its glass transition temperature, chain scission tends to dominate over cross-linking reactions (326).

Partially Fluorinated Polymers. The radiation chemistry of fluoropolymers is very sensitive to the presence of hydrogen in the chemical structure. The introduction of hydrogen to the backbone generally results in a marked increase in the probability of cross-linking reactions occurring. Presumably, this is a result of the increased mobility of radicals as discussed immediately above. In addition, as pointed out by Wall and co-workers (328), the introduction of hydrogen leads to the formation of HF on irradiation, with concomitant formation of main-chain

Table 2. Radiochemical Yields of Cross-Linking and Scission for Several Partially Fluorinated Polymers

Polymer[a]	G(X)	G(S)	p_0/q_0	Ref.
PVDF	1.0	0.3	0.15	319
PVDF	0.95–1.05	0.2–0.4	0.18–0.21	317
PVF	3–8	1.8–4.0	0.28–0.35	317
PTrFE	1.1	0.4	0.18	319
PTrFE	1.1–1.2	0.3–0.5	0.16–0.21	317
ECTFE			0.3	322

[a]PVDF, poly(vinylidene fluoride); PVF, poly(vinyl fluoride); PtrFE, poly(trifluoroethylene); ECTFE, poly(ethylene-*co*-trifluoroethylene).

double bonds. These double bonds act as efficient sites for subsequent cross-linking reactions.

Of this class of polymers, the radiation chemistry of poly(vinylidene fluoride) (PVDF) has been examined in most detail. In 1962, Timmerman and Greyson (329) compared the mechanical properties of PVDF with PTFE and found that overall PVDF was more resilient to exposure to radiation. Not long after this, Yoshida and co-workers (330) reported the yields of cross-linking and scission reactions in irradiated PVDF, and that cross-linking dominated. The radiochemical yields of scission and cross-linking of PVDF and a number of other materials are listed in Table 2. The identity of the radical species formed on irradiation has been confirmed by Seguchi and co-workers (331). They found that the chain-end radical **XI** dominated the ESR spectrum at low temperatures, but that the main-chain radical **XII** became more important on warming. On long standing the polyenyl radical **XIII** came to dominate the ESR spectrum, highlighting the importance of loss of HF, and the increased radical mobility compared with fully fluorinated polymers.

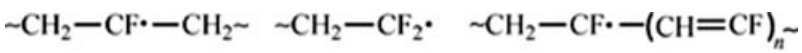

XI **XII** **XIII**

As mentioned above, all of this class of polymers undergoes cross-linking on irradiation in vacuum. The yields of cross-linking and scission for these polymers are listed in Table 2. Of note also are the reports of cross-linking predominating in the copolymers of ethylene with TFE (332) and of ethylene with chlorotrifluoroethylene (333).

Polychlorotrifluoroethylene. In contrast to the above materials, the homopolymer of polychlorotrifluoroethylene (PCTFE) undergoes radiation degradation on exposure to ionizing radiation. Florin and Wall reported in 1961 that PCTFE undergoes chain scission, and calculated a G-value of 0.67 for scission from the dose to achieve zero strength. A relatively low yield of volatile products was reported: G(volatiles) = 0.11. Very recently, Hill and co-workers reexamined the radiation chemistry of this polymer (334,335). They measured the yields of free radicals to be 1.55 at 77 K decreasing to 0.32 at room temperature (335). The

ESR spectra were difficult to identify because of the large anisotropic hyperfine coupling to the fluorine nuclei. These authors also examined the radio-chemical products using solid-state ^{19}F NMR and FTIR spectroscopies (334). On irradiation below the melting temperature, there was no evidence of branch/cross-link formation. However, the yields of chain ends, double bonds, and branch points on irradiation at 493 K were 3.6, 0.2, and 0.5, respectively. The structure of the branches could not be confirmed; however, the respective yields of chain ends and branches indicate that scission dominates for this polymer.

Polydienes. The polydienes undergo cross-linking on radiolysis in vacuum. The principle reactions occurring are cross-linking, consumption of double bonds, isomerization of double bonds, and evolution of hydrogen gas. There is considerable variation in the reported *G*-values for these reactions, arising primarily from differences in the experimental techniques used in their determination. For example, physical measurements, usually of soluble fraction or swelling ratio, used to determine yields of cross-linking and scission reactions are particularly susceptible to errors in the case of polydienes. These techniques assume a random distribution of cross-linking and scission reactions; as will be seen below, this assumption may break down in the case of radiolysis of polydienes.

Polybutadiene. The primary products of irradiation of polybutadiene (PBD) are allyl free radicals. The yield of radicals has been reported to range from 0.19 to 0.44 (336,337). On heating the radicals decay in a monotonic fashion to low concentrations just above the glass-transition temperature of the polymer (337) (see BUTADIENE POLYMERS).

As mentioned above, the net result of irradiation of PBD is cross-linking. *G*-values for cross-linking, determined as described immediately above, range from 3.2 to 6.7 (338–343). In one case a *G*(S) value of 0.52 has been reported, although it is more generally accepted that the *G*-value for scission in irradiated PBD is much smaller than this (343).

As will be discussed below, these *G*-values contrast with the very high yield of reactions which consume double bonds in these polymers. The reason for this is the highly nonuniform cross-linking reactions in polydienes. The advent of solid-state ^{13}C NMR allowed direct observation and quantitation of the cross-link structures in irradiated polymers. In the case of poly(1,4-butadiene), O'Donnell and Whittaker (344,345) have reported very high *G*-values for consumption of double bonds, and formation of cross-link structures. The authors have suggested a chain reaction through successive double bonds to form a highly nonuniform network structure. As a result, the effective cross-link density is much lower than the measured chemical cross-link density. Similar results were reported for materials having different initial microstructure.

A number of workers have reported a very high rate of disappearance of double bonds on irradiation of PBD. Using IR spectroscopy, Parkinson and Sears (346) determined *G*(cis) to be 15, G(-trans) 11–22, and G(cis–trans) 7. The last reaction is the isomerization of a cis double bond to a trans double bond via an allylic radical intermediate. The rate of consumption of 1,2-vinyl groups was found to depend on the initial vinyl content; values from 0.2 to 40 were reported. Similarly, Golub (347,348) reported a *G*-value of 7.9 for consumption of double bonds, and 7.2 for isomerization. He suggested the formation of cyclic structures. O'Donnell and Whittaker (344) have reported the yields of these reactions for a number

of polybutadienes. The calculated G-value for loss of double bonds was initially 41.8 over a dose range of 0–1 MGy and decreased to 6.3 at higher doses (4–10 MGy). For poly(1,2-butadiene) the G-value for loss of double bonds was 237 (0–0.5 MGy), because of, it was suggested, an intramolecular chain reaction of the vinyl groups.

Polyisoprene. As with polybutadiene, polyisoprene (PIP) and natural rubber are cross-linking polymers. The radical intermediates have been identified as allyl radicals (336,337,342). Radical yields at 77 K ranging from 0.28 to 0.73 have been reported. It is also clear that the mechanism of reaction of these radicals is similar to that discussed above for polybutadiene. A G-value of 6.7 for the decrease in unsaturation has been reported by Golub and Danon (347). Much later, using solid-state NMR, Whittaker (349) obtained a G(d.b.) value of 45.8 (0–1 MGy). Significantly lower yields of cross-links have been reported; Boehm (350) has compiled a list of G(X) values ranging from 0.4 to 3.5 as determined by measurement of physical properties.

Polychloroprene. In contrast to PBD and PIP, the radiation cross-linking of polychloroprene does not appear to proceed by a chain-reaction mechanism (see CHLOROPRENE POLYMERS). The yields of cross-links [G(X)] were measured by a number of methods and determined to be 3.9 (NMR), 4.8 (swelling ratio), and 3.2 (sol. fraction) (351). This close correlation, and the observation of a narrow resonance in the ^{13}C NMR spectrum assigned to cross-link structures, indicated that cross-linking in this material occurs randomly throughout the material. Peaks are observed in the NMR spectra because of new chain structures formed on irradiation.

Aromatic Polymers.

Polystyrene. Polystyrene undergoes net cross-linking on irradiation (see STYRENE POLYMERS). In 1953 Charlesby (352) reported that the polymer undergoes gelation on irradiation, and that the yield of permanent chain scission reactions is small or negligible. Furthermore, he reported that despite cross-link reactions dominating the radiation chemistry, the overall yield of cross-linking is very small compared with nonaromatic polymers, because of the presence of the benzene ring. A major study of the changes in molecular weight (viscosity) and formation of volatile products was subsequently undertaken by Wall and Brown in 1957 (231). The major volatile product, hydrogen gas, is produced in low yields [$G(H_2) = 0.022–0.026$] compared with nonaromatic polymers.

Since these early reports, a number of further studies have appeared (6,231,339) and these have been summarized in 1973 by Parkinson and Keyser (353). Since that date, efforts have been made to understand the relatively wide discrepancies in reported yields of radiochemical reactions, and also the effect of temperature on the radiolysis products. For example, values of the yield of radicals, G(R), measured at 77 K after irradiation at that temperature range from 0.04 to 0.50 (22,100,354–357). O'Donnell and co-workers (358) have proposed that the variation in reported yields of radical formation, and of chain scission and cross-linking, may be in part due to the presence of trace amounts of residual oxygen.

Using ESR spectroscopy, the mechanism of radiation-induced cross-linking of polystyrene has been revealed to a large extent by careful studies of radical intermediates. The major free-radical products formed on irradiation are the

α-carbon radical **XIV** and the cyclohexadienyl radical **XV** shown below. The contribution of radical anions to the ESR spectra was confirmed by Garrett (357) and Hill and co-workers (24). On heating these samples toward the glass-transition temperature (ca. 373 K), free-radical reactions occur until at room temperature the ESR spectrum resembles that observed for a sample irradiated at the elevated temperature. The radical concentration has decayed to negligible values at the glass-transition temperature. The mechanism of cross-linking has not been confirmed, but is suggested to involve recombination reactions between radicals **X** and **XI**. Measurements of gel doses for materials having different initial molecular weight distributions have suggested that H-linking rather than end-linking is the major mechanism of cross-linking (359).

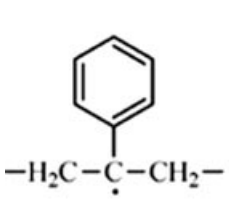

XIV

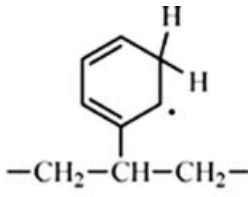

XV

The effect of irradiation temperature has been examined in some detail. A number of workers have reported that the yield of cross-links decreases progressively above room temperature with a corresponding increase in the yield of chain-scission reactions (302,360–362). Burlant and co-workers (363) initially suggested that as the temperature increases, an increasing proportion of main-chain radicals **XIV** undergo a β-cleavage reaction to form terminal unsaturation and chain-end radical. On the other hand, from analysis of changes in molecular weights, Bowmer and co-workers (360) reported that the ratio of yields of scission to cross-linking reactions, $G(S)/G(X)$, increases from 0.02 at 303 K to 2.8 at 423 K. These authors suggest that competition between combination and disproportionation reactions between temporary scission radicals is responsible for this trend, with disproportionation, and hence permanent chain scission, becoming more likely at higher temperatures. A comparison was made with the mechanism of termination in the free-radical polymerization of styrene. Seguchi and co-workers (302,362) have also examined in detail the effects of temperature and tacticity on the relative yields of cross-linking and scission reactions in irradiated polystyrene, and have arrived at similar conclusions.

Poly(α-methyl styrene). Poly(α-methyl styrene) (PαMSTY) is one of the class of degrading polymers, having along its backbone a quaternary carbon, at which a stable scission radical can be formed. In addition to this, PαMSTY has a low polymerization ceiling temperature of 334 K (364). At and above this temperature, the polymer will undergo depolymerization to its monomers. Garrett and co-workers (365) measured the yield of chain scission $G(S)$ and the rate of depolymerization at temperatures of 298, 353, and 536 K. At the two lower temperatures the weight loss due to depropagation was negligible and the authors were able to calculate yields of chain scission from changes in the number-average molecular

weights (see eq. 5 above). The values of $G(S)$ were 0.29 ± 0.01 and 0.48 ± 0.06 at 298 K and 353 K, respectively. However, at the highest temperature, extensive and rapid first-order weight loss occurred. The G-value for depolymerization $[G(-M)]$ was found to be 320 ± 45. The results of a Monte Carlo simulation of this process resulted in an estimate of the yield of chain scission $[G(S)]$ of 1.8 and the average unzipping length of 400 (365).

This same group has also reported an ESR study of the radicals formed on irradiation at 77 K and room temperature (54). The authors identified a number of radical species including a propagation radical formed by direct chain scission, and radicals associated with the side chain and the aromatic ring.

Main-Chain Aromatic Polymers. The above discussion highlights the relative stability of polymers containing aromatic rings, due to the ability of these structures to dissipate excess energy through resonance effects (1). For example the yields of cross-links and free radicals in irradiated polystyrene are approximately 50 times lower in polyethylene. It has also been noted from comparisons of the radiation sensitivity of polymers having similar structures that those in which the structures are incorporated into the main chain are less sensitive to degradation than those with similar side-chain structures. This is partly due to the more effective cage effect in main-chain polymers, which tend to have higher glass-transition temperatures than those of side-chain polymers, but also due to more effective resonance coupling to the aromatic rings. It follows therefore that main-chain aromatic polymers represent some of the most radiation-resistant organic materials discovered so far.

Aromatic Polysulfones. The presence of the relatively labile sulfone linkage in Polysulfones (qv) results in these materials having a tendency to undergo degradation reactions. Under many conditions, however, aromatic sulfones are relatively stable and undergo net cross-linking. Brown and O'Donnell (366) initially reported the radiation chemistry of copolymers of bisphenol A and 4,4′-dichlorodiphenyl (Table 3). They found that on irradiation in vacuum at ambient temperatures, this material undergoes cross-linking with relative yields of cross-linking and scission reactions being respectively 0.051 and 0.012. These studies lead to a large body of work considering the effect of chemical structure on the radiation sensitivity of aromatic polymers. In general for all aromatic polysulfones, on irradiation at ambient temperature, cross-linking predominates. In addition, as aliphatic groups are introduced into the main chain, the radiation sensitivity is increased.

Lewis and co-workers (367) have reported a detailed study of the effect of polymer structure on the yields of chemical reactions for a series of polysulfone terpolymers containing varying amounts of bisphenol A and biphenyl units. They found a close to linear relationship between the yields of radicals and volatile sulfur dioxide with the ratio of the bisphenol A and biphenyl units. They report that the biphenyl unit imparts significantly higher radiation stability. As with other polymers, the details of the radiation chemistry are affected by the irradiation temperature, with Hill and co-workers (368) providing evidence of enhanced chain scission on irradiation of polysulfone copolymers (Table 3) at temperatures approaching the glass-transition temperature.

The ESR spectra of irradiated aromatic polysulfones, and aromatic polymers in general, are often poorly resolved, because of the effect of delocalization of

Table 3. Radiochemical Yields[a] of Formation of Free Radicals in Aromatic Main-Chain Polymers

Unit 1	Unit 2	Name	Radical Yield 10^{20} spins/kg	Ref.
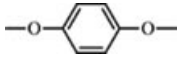	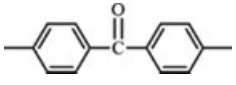	PEEK	1.0	379
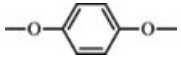	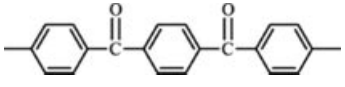	PEEKK	1.1	379
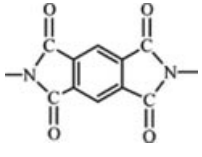	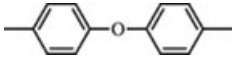	Kapton	1.7	371
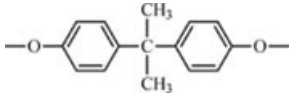	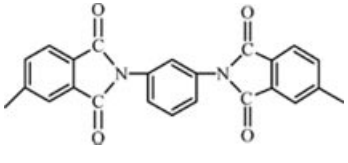	Ultem	2.2	371

Table 3. (Continued)

Unit 1	Unit 2	Name	Radical Yield 10^{20} spins/kg	Ref.
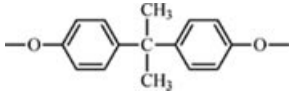	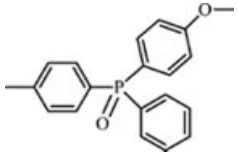	Bis-A PEPO	2.5	371
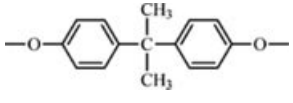	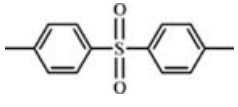	Bis-A PSO	2.8	371
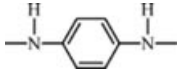	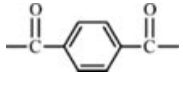	Kevlar	5.6	371
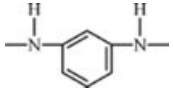	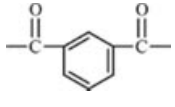	Nomex	5.6	371
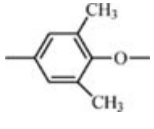		PPO	5.7	371

[a]The yield of free radicals is expressed in the units of spins/kg after irradiation to a dose of 10 kGy, rather than a G value, since the increase in radical concentration with dose is highly nonlinear with dose in the initial stages. To obtain a single-point G value at 10 kGy, divide the radical yield by 6.24×10^{20}.

the electron spin across aromatic structures, and the contribution from radical anions to the spectra at low temperatures. For example, Lewis and co-workers (367) reported that up to 75% of the total area of the ESR spectra of bisphenol A polysulfone irradiated to 10 kGy arose from radical anions, which were susceptible to photobleaching with UV radiation. These relatively uninformative spectra offer little information to assign reaction mechanisms. On the other hand, Hill and co-workers (96) have deduced, from measurements of changes in molecular weights and the formation of new structures detected on irradiation using solution-state ^{13}C NMR, that the main cross-linking mechanism involves Y-linking.

Polyimides. The two most important commercial Polyimides (qv) are Kapton and Ultem (structures shown in Table 3). Whereas Kapton is insoluble in most convenient solvents, Ultem is soluble and hence amenable to detailed study by standard methods. In 1985 Basheer and Dole (369) reported the yields of cross-linking and scission in irradiated Ultem to be respectively 0.014 and 0.005 on irradiation at room temperature. The gel dose of commercial Ultem film is of the order of 10 MGy. Devasahayam and co-workers (370) have reported a more detailed analysis of the changes in molecular weights on irradiation, and calculated *G*-values for scission and cross-linking for either H- or Y-linking mechanisms.

Basheer and Dole (369) reported that the ESR spectrum of irradiated Ultem was composed of contributions from radicals from scission at the isopropylidene unit and aromatic ether group. Recently, Devasahayam and co-workers (370) reported a detailed study of the free-radical yields and radical reactions in irradiated Ultem. At 77 K, the spectra contain significant contributions from radical anions, which were susceptible to thermal or photolytic annealing. Potential scission sites were identified from the radical products. Similarly, the formation of methylene radicals through loss of hydrogen atoms from the isopropylidene unit was suggested as a precursor to cross-linking reactions. Associated NMR analysis (371) of the radiolysis products identified a large number of products, the majority of which were identified with chain-scission products.

Kapton polyimide is an intractable material under usual conditions, and hence studies of its radiation chemistry are confined to measurements of volatile and free-radical products. The ESR spectrum of irradiated Kapton is a featureless singlet, and the yield of free radicals (1.7×10^{20} spins/kg after 10 kGy irradiation) was the one of the lowest of a large number of aromatic polymers compared in this study (372). Earlier, Hegazy and colleagues (373,374) confirmed the very high radiation stability of Kapton by measurement of the yields of volatile products of this polymer and other aromatic materials, including several aromatic polyimides. For Kapton, the evolved gases, in decreasing yields, were CO_2, CO, nitrogen, and hydrogen. Again Kapton was the most stable material studied.

A number of other polyimides have been studied by Hill and co-workers Devasahayam and co-workers (375) reported changes in the optical properties, and formation of free radicals in a series of fluorinated polyimides, and found that all materials were less stable than Kapton film. The fluorinated groups are incorporated in the polyimides to reduce coloration, and to provide oxygen atom resistance for space applications. Alexander and co-workers (376) have measured the radical yields for two fluorinated polyimide containing phosphine oxide groups attached to the aromatic main chain. The phosphine oxide unit also provides protection for the polymer against degradation from atomic oxygen. The relatively

high yields of radicals at 77 K, $G(R) = 0.50$ and 0.42 indicate, however, that this protection has been gained at the expense of radiation stability. Prior to this, Hopewell and co-workers (129) measured the radical yields and the solution viscosity of a number of phosphine oxide containing polyimides, and found that for these materials chain scission and cross-linking occur simultaneously on irradiation, but that scission is predominant on irradiation at room temperature.

Polyarylene Ether Ketones. The polyarylene ether ketone, known commercially as PEEK, is a semicrystalline thermoplastic of high melting temperature, and is insoluble in common organic solvent. The fully aromatic structure of PEEK imparts very high radiation resistance to this material. In a series of articles, Sasuga and co-workers (377,378) and Hegazy and co-workers (373,374,379) have measured a number of properties of PEEK and compared its radiation stability to a number of materials. The main volatile products, in decreasing yields at 15 MGy, are methane, hydrogen, CO, and CO_2. The source of the methane is not discussed. However, the overall yield of gases is very low compared to other aromatic polymers. The effect of crystallinity on the radiation chemistry is also demonstrated through the significantly higher yields of gases obtained from irradiation of a fully amorphous polymer.

In a related study, Hegazy and co-workers (379) examined the changes in the thermal properties of irradiated PEEK. An increase in glass-transition temperature and a small decrease in the heat of crystallization are both evidence of cross-linking formation. Similarly, the decrease and broadening of the recrystallization transition is due to cross-links.

Heiland and co-workers (380) have examined the radiation sensitivity of a series of polyarylene ether ketones using ESR spectroscopy and gas chromatography. The yields of radicals formed in all materials at 77 K were very low (approximately $1–2 \times 10^{20}$ spins/kg after 10 kGy irradiation). Introduction of methyl groups on the main-chain aromatic rings decreased the radiation stability, and further substitution of isopropylidene units into the main chain reduced the radiation stability even further.

Polycarbonates. The most commercially important Polycarbonates (qv) is bisphenol A polycarbonate (Bis-A PC). The effects of radiation on this material have been studied for a number of years, with a particular interest in the identity of the species responsible for a pronounced color change in Bis-A PC after irradiation. The radiation-induced green coloration has been assigned variously to trapped electrons (381) or a combination of trapped electron and radical ions (382,383). Golden and co-workers (384–386) have also in some detail examined the evolution of gases on irradiation (386), and found that the major volatile products are carbon dioxide and oxygen, with small amounts of hydrogen, methane, and benzene.

Bis-A PC undergoes net chain scission during irradiation in vacuum, presumably because of the high sensitivity of the carbonate group to chain scission. Evidence for this is the decrease in limiting viscosity after irradiation (384,386,387). More recently, further insight into the radiation degradation of Bis-A PC has been gained in a study by Babanalbandi and co-workers (388). In this the authors were able to confirm that the G-value for radical formation at 77 K is 0.5 ± 0.02, and that approximately 50% of the observed radicals are able to be photobleached with visible light, and hence are radical anions. NMR analysis of the soluble polymer after irradiation revealed new peaks, assigned to phenol-type chain end structures,

with a G-value for formation of 0.7. This observation confirmed that the main site of radiation degradation of Bis-A PC is the carbonate unit.

Aromatic Polyesters. The degradation of aromatic polyester has been investigated by a number of authors (7,53,389–398). The most commercially important material of this class is poly(ethylene terephthalate), a semicrystalline material of high melting temperature ($T_m \sim 538$ K) and moderate glass-transition temperature ($T_g \sim 343$ K) (see POLYESTERS, THERMOPLASTIC). On irradiation at low temperatures the observed ESR signal is primarily attributed to the secondary alkyl radicals formed by loss of a hydrogen atom from ethylene segments (53,391,394). The yield of radicals at room temperature was 0.025 (394). Since then, Choi and co-workers (132,398–401) have reported the radical yields of a number of allied main-chain aromatic polyesters. They found that for series of polymers containing fluorinated isopropylidene units the radiation stability was enhanced with higher content of the fluorinated residues (400). The yields of free radicals at 77 K were found to fall in the range 0.38–0.46. Later, this same group reported the radical yields for a number of linear halogenated aromatic polyesters [$G(R) = 0.41$–0.81] (401), terephthalate-based polyesters [$G(R) = 0.19$–0.41] (398), and naphthalene-containing polyesters [$G(R) = 0.08$–0.12] (132,399). In the last study the yield of radicals was found to increase, as expected, with the length of the aliphatic chain in the polyester, with, for example, $G(R)$ at 77 K increasing from 0.19 to 0.27 to 0.41 for terephthalate polyesters with the increasing length of the alkyl chain (n) of 2, 4, and 10, respectively (394).

Limited data is available on the respective rates of cross-linking and scission of the aromatic polyesters under radiolysis. Turner (394) has collected the data available from measurements of residual soluble fractions of irradiated poly(ethylene terephthalate), and reported values of $G(S)$ and $G(X)$ ranging from 0.07 to 0.17 and 0.07 to 0.14, respectively. The large range reflects the experimental difficulties and the range of irradiation conditions employed.

Babanalbandi and co-workers (388) have used ESR and NMR to determine the yields of radical intermediates and final products in irradiated U-polymer, a polyester of bisphenol A and terephthalic acid. The radical yield $G(R) = 0.5$ at 77 K was consistent with previous studies of similar polyesters. The NMR spectra of polymer irradiated to very high doses at room temperature revealed that phenol-type chain ends were the main stable products. The results are consistent with the observation of CO and CO_2 being the main gaseous products of the degradation of polyesters. For this material no evidence of cross-linking reactions was found.

Copolymers. The properties of polymers can be enhanced extensively through Copolymerization (qv) or blending of homopolymers. The effects of radiation on copolymers and blends might be expected to show behaviors that are related to the behaviors of the homopolymer constituents, modified by the polymer mole fraction composition and the electron densities of the components. For simple polymers, eg, those composed of carbon, hydrogen, and oxygen, random copolymers show a linear relationship between the properties of the homopolymers and the weight fraction of the components, eg, for copolymers of aliphatic esters (402). Although this behavior has been found to apply for many copolymer and blend systems, major differences from linear relationships are also common.

Aromatic components in mixtures of low molecular weight materials have long been known (18) to exhibit a protective effect on other components. This

protective effect is also found in random copolymers, such as the copolymers of styrene and methyl methacrylate, which have been studied by Busfield and co-workers (246), where the presence of styrene lowers the yields for radical intermediates, volatile products, and chain scission below those expected from the linear additivity rule. Similar observations have been made for radical formation in copolymers of glutamic acid and tyrosine (403), and several other systems.

On the other hand, positive deviations from the additivity rule for copolymers have also been reported. For example, Fox and co-workers (404) have reported that the radical yields at 77 K for γ radiolysis of the copolymers of methacrylic acid and acrylonitrile exhibit a positive deviation from the rule. They have attributed this to the breakup of the hydrogen bonding between methacrylic acid units by the acrylonitrile units in the copolymer.

Polymer Blends (qv) can be classified as being either compatible or incompatible. Most blends fall into the latter category. If this is the case, the additivity rule might be expected to apply, even for blends of homopolymers such as PS and PMMA, because the two components are phase separated. Garrett (357) has shown that this is indeed the case when homopolymers of comparable molecular weight are blended. However, if PS of low molecular weight is blended with PMMA of high molecular weight, a level of compatibility is achieved, and the PS then provides protection of the PMMA against degradation (357).

Many other instances of deviations from the additive rule and of protective effects in copolymers and blends have been reported in some of the studies discussed elsewhere in this article. The use of aromatic groups to provide protection against degradation has been utilized in some commercial materials. One example of this has been the incorporation of aromatic groups into polyester medical sutures (405) in order to protect the sutures against damage during radiation sterilization.

The Influence of Oxygen

Oxygen is a diradical, and so it can readily react at diffusion-controlled rates with free radicals formed in a polymer during radiolysis. This process has been well researched because it also occurs as a result of the thermal degradation of polymers, and consequently occurs during polymer processing. The mechanisms of these oxidation processes have been well documented in the literature and involve propagation, termination, and branching steps as part of a chain reaction. These mechanisms are summarized in Figure 7 (P = polymer).

Methods for stabilizing polymers by the addition of antioxidants and hydroperoxide decomposers are also well known, and are generally used with polymers which undergo radiolysis. For example, so called antirads are added to polypropylene to allow medical goods manufactured from it to be radiation-sterilized without discoloration or degradation.

The mechanism and kinetics of the reactions of oxygen with polymer radicals produced during radiolysis have been studied and extensively reviewed by Gillen, Clough, and co-workers (117,406–409), who have contributed greatly to this field. The roles of added polymer antioxidants and stabilizers have also been reviewed

Initiation

$$P \longrightarrow P\cdot$$

Propagation

$$P\cdot + O_2 \longrightarrow POO\cdot$$
$$PO_2\cdot + PH \longrightarrow POOH + P\cdot$$

Bimolecular termination

$$P\cdot + P\cdot \longrightarrow \text{Products}$$
$$PO_2\cdot + P\cdot \longrightarrow \text{Products}$$
$$PO_2\cdot + PO_2\cdot \longrightarrow \text{Products} + O_2$$

Unimolecular termination

$$PO_2\cdot \longrightarrow \text{Products}$$
$$P\cdot \longrightarrow \text{Products}$$

Branching

$$POOH \longrightarrow PO\cdot + \cdot OH$$
$$\cdot OH + PH \longrightarrow H_2O + P\cdot$$
$$PO\cdot + PH \longrightarrow POH + P\cdot$$
$$PO\cdot \longrightarrow P{=}O + P\cdot$$

Fig. 7. A summary of the reaction pathways in the oxidative degradation of polymers.

in a treatise edited by Clough, Billingham, and Gillen (410). Therefore, a detailed review will not be presented herein, and only some recent developments will be discussed.

In many polymers, radicals can have very long lifetimes, particularly if they are located in crystalline regions where they are protected from any added stabilizer. Jahan and co-workers (153), for example, have reported that long-lived radicals formed during sterilization of PE artificial joint components are at least partially responsible for their long-term deterioration. In addition, Young and

Slemp (411) have found that polymers exposed to space irradiation can exhibit a slow deterioration of properties on their return to earth atmosphere. These processes are just two examples of slow polymer aging due to polymer oxidation in air.

Clough and co-workers (409,412,413) have recently studied the structural changes induced in polymers and model compounds by oxidation through the use of ^{17}O-labeled oxygen and by the analysis of the polymer using ^{17}O NMR. This approach has provided a new insight of the oxidation and subsequent aging of irradiated polymers.

The Influence of Irradiation Temperature

The chemical changes that occur when polymers are irradiated include the formation of free-radical intermediates, the scission of main-chain bonds, the loss or modification of side-chains, the cross-linking of chains, the formation of new polymer structures, and the production low molecular weight products. One of the most important factors determining the extent to which these processes can occur is the prevailing temperature. For example, the crystalline melting and the α-transition temperatures, along with the temperatures of other secondary transitions in a polymer, play an important role in controlling chain motions, and hence the rates of reactions. In addition, the ceiling temperature determines the overall thermodynamic stability of a polymer chain when propagating radicals are present.

The temperature dependences of the rates of radiolysis reactions are determined by their activation energies, and can be predicted through the Arrhenius equation. In polymers, the activation energies for radiolysis reactions are positive, so that the rates of these reactions show a positive dependence on temperature. However, the activation energies for radiolysis reactions can show a considerable variation depending on both chemical and physical factors. For example, the activation energies for reactions can be quite different in the crystalline and amorphous regions of a polymer. Thus, the overall rates for formation of radiolysis products depend on the morphology of the polymer, which can vary from sample to sample. In addition, the rates of radiolysis reactions are likely to exhibit discontinuities at any first- and second-order polymer transition temperatures, which are characteristic of a polymer.

Thermodynamic considerations must also be considered. Negative enthalpies and negative entropies of reaction characterize free-radical polymerization reactions. Thus, whereas the free energy change for polymerization of a vinyl monomer may be negative at a low temperature, it will become zero at a higher temperature, the ceiling temperature. Above this temperature, spontaneous depolymerization of the polymer is thus thermodynamically possible.

Some representative examples of the effects of temperature drawn from reported work are presented below.

Secondary Transitions. The secondary transitions in polymers characterize the onset chiefly of side-chain motions and the motions of chain ends. The secondary transitions for PMMA and PS are given in Table 4. In these polymers, the β transitions occur below room temperature, and are associated with the

Table 4. Transition Temperatures for PMMA and PS

Transition	PMMA, K	PS, K
T_α	378 K	370 K
T_β	270 K	300 K
T_γ	103 K	138 K
T_δ	4 K	48 K

large-scale motions of the side chains. The γ and δ transitions occur at much lower temperatures.

At 77 K the polymer chain motions in PMMA and PS are very restricted, but as the temperature is increased to room temperature, the side chains become mobile. Thus, the polymer radicals formed in PMMA and PS on radiolysis at 77 K are relatively stable, but they decompose on annealing to higher temperatures.

Garrett (357) has reported a careful study of the reactions of the radicals formed on irradiation of PMMA and PS at 77 K when they are annealed to higher temperatures. For PS a small decrease in the radical concentration was observed at approximately 140 K and a further decrease occurs at about 270 K. The temperatures at which these changes occur coincide closely with the δ- and β-transition temperatures, respectively, for PS.

The radical concentration for PMMA decreased by approximately 45% at about 190 K and is associated chiefly with the loss of the anion formed on radiolysis (357). The temperature of 190 K corresponds to the temperature at which a change in the spin-lattice relaxation time has been reported to occur in s-PMMA (414), which is believed to be associated with the superposition of the motions of the α-methyl group and rapid fluctuations of the adjacent main chain.

Wundrich and co-workers (415) has examined the variation in G(S) for PMMA following radiolysis from 77 K to room temperature. From 77 K to approximately 140 K, G(S) was found to be constant, but above 140 K the values increased with temperature. He observed a second discontinuity at approximately 268 K. His reported values of G(S) in these regions are as follows: 0.3, 77–140 K; 0.3–0.9, 140–268 K; and 0.9–1.15, 268–293 K. Although there is no reported chain transition at 140 K, 268 K corresponds to the β transition in PMMA.

It has been proposed that the loss of the ester side group is the precursor for main-chain scission in PMMA, and so the lower G-values for scission below the β-transition temperature should be associated with lower G-values of volatile side-chain products. Kudoh and co-workers (250) found that the yield for hydrogen for PMMA was not sensitive to the radiolysis temperature. However, the yields of the products of ester side-chain scission and decomposition, principally CO and CO_2, were depressed by a factor of about 5 to 10 times when compared with those found for room temperature radiolysis. Kudoh and co-workers (260) also found a large difference in the tensile properties consistent with less chain scission at 77 K.

α Transition. The α transition in polymers, T_g, is associated with the onset of significant main-chain motion spread over several adjacent carbon atoms. Above T_g the free volume of the polymer increases, and so the rates of radical and other reactions may increase significantly. The effect of the glass-transition temperature

on radical reactions was clearly demonstrated by the work of Hill and co-workers (186) on polyisobutene (PIB). Annealing of PIB beyond its glass-transition temperature, 203 K, results in a rapid decrease in the radical concentration. At room temperature the radical concentration is very small and cannot be measured effectively by ESR spectroscopy. Many other polymers have been reported to behave similarly. However, Garrett and co-workers (416) found no evidence for a discontinuity in G(S) of PMMA at its α transition, 378 K. They reported that the value of G(S) increases continuously with temperature between 268 and 400 K and rises smoothly from 1.3 at 303 K to 3.9 at 413 K.

A similar observation has been reported by Bowmer and co-workers (360) for PS, which undergoes cross-linking on radiolysis at room temperature, $G(\mathrm{S}) = 0.0086$ and $G(\mathrm{X}) = 0.043$. However, as the temperature increases, G(S) increases and G(X) decreases. As a result, although no significant discontinuity was observed in the scission and cross-linking yields, in the neighborhood of the α transition, the behavior of PS changes, and it becomes a polymer which undergoes net scission on radiolysis [at 423 K $G(\mathrm{S}) = 0.074$, $G(\mathrm{X}) = 0.027$].

So, although the α transition does not appear to have a significant influence on the scission and cross-linking in PMMA or PS, it does play an important role in PIB and several other polymers. For example, the temperature dependence of G(S) has been found to increase significantly above this transition temperature for PIB (186), and for Kalrez, Forsythe and co-workers (57,383) have demonstrated that cross-linking only occurs on radiolysis above T_g.

Although no discontinuity has been found for G(S) at the α-transition in PMMA, Dong and co-workers (31) have shown conclusively that tacticity changes do occur in i-PMMA and s-PMMA with high yield above T_g. Similar changes in the tacticity of isotactic polypropylene have also been observed by Busfield and co-workers (35) for radiolysis at room temperature, which is above its α-transition temperature. The G-value for the loss of isotactic triads was estimated to be 64 at 298 K.

Crystalline Melting. Many of the radiolysis reactions of polymers are believed to occur principally in the amorphous regions or interphase regions at the crystalline boundaries. A strong influence of morphology has been reported by Busfield and Hanna (38) for the radiolysis of i-PP. They found that above the crystalline melting temperature the values of G(S) and G(X) at low dose are 11.6 and 3.5, respectively, whereas below the crystalline melting temperature the values are approximately equal and fall in the range 0.1–0.9. They also report that in the molten state the G-values for inversion of isotactic sequences in i-PP are also much higher: $G(\text{inversion}) = 106$.

Another recently reported difference in radiation chemistry above the crystalline melting temperature has been for polytetrafluoroethylene (PTFE). In the solid state PTFE is known to undergo scission readily. However, Oshima and co-workers (56) have found that just above the melting temperature of 600 K, PTFE undergoes cross-linking on e-beam irradiation, with a concomitant enhancement in the mechanical and chemical properties of the polymer.

Ceiling Temperature. For some polymers, for example PTFE, the ceiling temperature, T_c, is very high (693 K), whereas for others it may be below room temperature. Polymers with quaternary carbon atoms in the main chain, such as PMMA, PIB, and poly(α-methyl styrene), PαMS, are particularly susceptible

Table 5. The Temperature Dependence for $G(-M)$ for Poly(α-methyl styrene)

T, K	$G(-M)$
303	0.3
373	95
383	153
393	182
453	529

to radiation-induced depolymerization at elevated temperatures, because they have relatively low ceiling temperatures. For example, the ceiling temperature for PαMS is only slightly above room temperature, 339 K (for the pure liquid monomer standard state). Hill and co-workers (417) have reported the G-values for loss of monomer, $G(-M)$, on radiolysis of PαMS over a range of temperatures (see Table 5). Clearly, $G(-M)$ increases significantly for radiolysis above T_c where spontaneous depolymerization can occur.

Property discontinuities which can be associated with temperature transitions in many polymers have been observed, and the cases discussed above serve only as a few examples. Attention has been drawn to many other cases elsewhere in the article.

Summary and Major Conclusions

The radiation chemistry of polymers is an extremely rich field of study, both from an intellectual and a practical viewpoint. The very large body of research devoted to this field is testament to this fact. The overall outcome of this work is a clear understanding of the effect of radiation on this class of materials, and the factors which influence the rates of reaction and the product distribution. These include factors intrinsic to the polymers, and extrinsic factors more readily under the control of the experimental scientist or engineer. These are summarized below.

Intrinsic Factors.

Aliphatic Polymers. The main reactions occurring on radiolysis of aliphatic polymers are cross-linking, chain scission, evolution of gaseous molecules, formation of unsaturation, and reaction of unsaturated groups. Changes in physical properties of polymers on irradiation depend on the balance and overall yields of cross-linking and chain-scission reactions. For polyolefins, the presence of secondary, tertiary, and quaternary carbons in the main-chain leads to a progressively higher probability of chain scission. The presence of main-chain units such as sulfone, ester, and amide groups results in a higher probability of main-chain scission. Cross-linking can proceed through H- or Y-type linking. The rate of gel formation depends on the mechanism of cross-linking. The introduction of double bonds, either as terminal double bonds, or main-chain double bonds in polydienes, results in an increased probability of cross-linking reactions. Fully fluorinated thermoplastics tend to undergo chain scission reactions on irradiation at ambient temperature.

Aromatic Polymers. The introduction of aromatic groups results in significantly higher stability to radiation due to the resonant structure of the aromatic rings. Main-chain aromatic groups provide the highest stability to degradation.

Morphology. In semicrystalline polymers, chemical reaction is largely confined to the disordered, amorphous regions. Chemical reactions appear to be enhanced by the presence of an interface between crystalline and amorphous phases.

Extrinsic Factors. The temperature of irradiation can dramatically affect the radiation stability of a polymer. Irradiation of degrading polymers above their ceiling temperatures leads to extensive depolymerization. Unsaturated polyolefins tend to undergo increasing amounts of H-linking as opposed to Y-linking as the temperature is raised. Irradiation of fluoroplastics immediately above their melting temperature, or of fluoroelastomers above T_g, increases the probability of cross-linking reactions. Irradiation in the presence of oxygen increases the probability of long-term degradation reactions.

BIBLIOGRAPHY

"Cross-linking with Radiation" in *EPST* 1st ed., Vol. 4, pp. 398–414, by Allan R. Schultz, General Electric Co.; in *EPSE* 2nd ed., Vol. 4, pp. 418–449, by Vincent D. McGinniss, Battelle Columbus Laboratories; "Radiation-Induced Reactions" in *EPST* 1st ed., Vol. 11, pp. 702–755, by A. Chapiro, Laboratoire de Chimie des Radiations du CNRS, Bellevue, France; "Radiation-Resistant Polymers" in *EPST* 1st ed., Vol. 11, pp. 783–809, by W. W. Parkinson, Oak Ridge National Laboratory; in *EPSE* 2nd ed., Vol 13, pp. 667–708, by Roger Clough, Sandia National Laboratories.

1. A. Charlesby, *Atomic Radiation and Polymers*, Vol. 1, Permagon Press, Oxford, 1960.
2. A. Chapiro, ed. *Radiation Chemistry of Polymeric Systems*, Vol. XV, Interscience, New York, 1962.
3. F. Williams, *Radiat. Chem. Macromol.* **1**, 7–23 (1972).
4. J. H. O'Donnell and D. F. Sangster, *Principles of Radiation Chemistry*, Edward Arnold, London, 1970, p. 176.
5. J. W. T. Spinks and R. J. Woods, *An Introduction to Radiation Chemistry*, 3rd ed., John Wiley & Sons, Inc., New York, 1990.
6. W. W. Parkinson, C. D. Bopp, D. Binder, and J. E. White, *J. Phys. Chem.* **69**, 828–833 (1965).
7. R. H. Boyett and K. Becker, *J. Appl. Polym. Sci.* **14**, 1654–1656 (1970).
8. T. Seguchi, N. Hayakawa, K. Yoshida, N. Tamura, Y. Katsumura, and Y. Tabata, *Radiat. Phys. Chem.* **26**, 221–225 (1985).
9. T. Sasuga, S. Kawanishi, T. Seguchi, and I. Kohno, *Polymer* **30**, 2054–2059 (1989).
10. T. Sasuga, H. Kudoh, and T. Seguchi, *Polymer* **40**, 5095–5102 (1999).
11. D. J. T. Hill and J. L. Hopewell, *Radiat. Phys. Chem.* **48**, 533–537 (1996).
12. T. Sasuga, S. Kawanishi, M. Nishii, T. Seguchi, and I. Kohno, *Radiat. Phys. Chem.* **37**, 135–140 (1991).
13. S. Seki, K. Kanzaki, Y. Kunimi, S. Tagawa, Y. Yoshida, H. Kudoh, M. Sugimoto, T. Sasuga, T. Seguchi, and H. Shibata, *Radiat. Phys. Chem.* **50**, 423–427 (1997).
14. T. Seguchi, H. Kudoh, M. Sugimoto, and Y. Hama, *Nucl. Instrum. Methods Phys. Res., Sect. B* **151**, 154–160 (1999).
15. S. Seki, K. Maeda, Y. Kunimi, S. Tagawa, Y. Yoshida, H. Kudoh, M. Sugimoto, Y. Morita, T. Seguchi, T. Iwai, H. Shibata, K. Asai, and K. Ishigure, *J. Phys. Chem. B* **103**, 3043–3048 (1999).

16. Y. Hama, T. Oka, K. Inoue, M. Kitoh, M. Washio, H. Kudoh, M. Sugimoto, and T. Seguchi, *Res. Chem. Intermed.* **27**, 469–473 (2001).
17. A. Oshima and M. Washio, *Nucl. Instrum. Methods Phys. Res., Sect. B* **208**, 380–384 (2003).
18. J. P. Manion and M. Burton, *J. Phys. Chem.* **56**, 560–569 (1952).
19. M. Burton and S. Lipsky, *J. Phys. Chem.* **61**, 1461–1467 (1957).
20. P. Alexander and A. Charlesby, *Nature (London)* **173**, 578–579 (1954).
21. P. Alexander and A. Charlesby, *Proc. R. Soc. London, Ser. A* **230**, 136–145 (1955).
22. J. H. O'Donnell and P. J. Pomery, *J. Polym. Sci., Polym. Symp.* **55**, 269–278 (1976).
23. W. K. Busfield and J. H. O'Donnell, *J. Polym. Sci., Polym. Symp.* **49**, 227–237 (1975).
24. D. J. T. Hill, A. P. Lang, J. H. O'Donnell, and P. J. Pomery, *Polym. Degrad. Stab.* **38**, 205–218 (1992).
25. L. Dong, D. J. T. Hill, J. H. O'Donnell, and P. J. Pomery, *Polym. Degrad. Stab.* **48**, 71–77 (1995).
26. A. Zeman and H. Heusinger, *J. Phys. Chem.* **77**, 3374–3376 (1966).
27. R. W. Garrett, J. H. O'Donnell, P. J. Pomery, and E. C. Shum, *J. Appl. Polym. Sci.* **24**, 2415–2418 (1979).
28. J. Kroh and S. Karolczak, *Radiat. Res. Rev.* **1**, 411–470 (1969).
29. J. H. O'Donnell, *ACS Symp. Ser.* **475**, 402–413 (1991).
30. D. J. T. Hill, S. Mohajerani, P. J. Pomery, and A. K. Whittaker, *Radiat. Phys. Chem.* **59**, 295–302 (2000).
31. L. Dong, D. J. T. Hill, J. H. O'Donnell, T. G. Carswell-Pomerantz, P. J. Pomery, A. K. Whittaker, and K. Hatada, *Macromolecules* **28**, 3681–3691 (1995).
32. C. David, A. Verhasselt, and G. Geuskens, *Polymer* **9**, 287–288 (1968).
33. G. Geuskens, D. Fuld, and C. David, *Makromol. Chem.* **160**, 347–348 (1972).
34. Y. Luo, H. Yang, S. Li, B. Yu, M. Ding, and B. Jiang, *Radiat. Phys. Chem.* **42**, 233–236 (1993).
35. W. K. Busfield, J. V. Hanna, J. H. O'Donnell, and A. K. Whittaker, *Br. Polym. J.* **19**, 223–226 (1987).
36. P. F. Barron, W. K. Busfield, and J. V. Hanna, *J. Polym. Sci., Part C: Polym. Lett.* **26**, 225–228 (1988).
37. P. F. Barron, W. K. Busfield, and J. V. Hanna, *Polym. Commun.* **29**, 70–72 (1988).
38. W. K. Busfield and J. V. Hanna, *Polym. J. (Tokyo)* **23**, 1253–1263 (1991).
39. A. Charlesby and M. Ross, *Nature (London)* **171**, 1153 (1953).
40. A. Charlesby and N. Moore, *Int. J. Appl. Radiat. Isot.* **15**, 703–708 (1964).
41. A. Charlesby and D. K. Thomas, *Proc. R. Soc. London, Ser. A* **269**, 104–124 (1962).
42. L. F. Thompson, E. D. Feit, M. J. Bowden, P. V. Lenzo, and E. G. Spencer, *J. Electrochem. Soc.* **121**, 1500–1503 (1974).
43. E. Reichmanis, O. Nalamasu, F. M. Houlihan, and A. E. Novembre, *Polym. Int.* **48**, 1053–1059 (1999).
44. M. J. Bowden, *Crit. Rev. Solid State Mater. Sci.* **8**, 223–264 (1979).
45. T. N. Bowmer and J. H. O'Donnell, *J. Polym. Sci., Polym. Chem. Ed.* **19**, 45–50 (1981).
46. M. Dole, C. D. Keeling, and D. G. Rose, *J. Am. Chem. Soc.* **76**, 4304–4311 (1954).
47. M. Dole, *Radiat. Chem. Macromol.* **1**, 335–347 (1972).
48. R. L. Clough, *J. Chem. Phys.* **87**, 1588–1595 (1987).
49. F. Cracco, A. J. Arvia, and M. Dole, *J. Chem. Phys.* **37**, 2449–2457 (1962).
50. M. Dole and F. Cracco, *J. Am. Chem. Soc.* **83**, 2584–2585 (1961).
51. M. Dole and F. Cracco, *J. Phys. Chem.* **66**, 193–201 (1962).
52. D. J. T. Hill, D. S. Hunter, D. A. Lewis, J. H. O'Donnell, and P. J. Pomery, *Radiat. Phys. Chem.* **36**, 559–563 (1990).
53. K. Araki, D. Campbell, and D. T. Turner, *J. Polym. Sci.* **3**, 993–996 (1965).

54. R. W. Garrett, D. J. T. Hill, T. T. Le, J. H. O'Donnell, and P. J. Pomery, *Radiat. Phys. Chem.* **39**, 215–221 (1992).
55. J. Sun, Y. Zhang, and X. Zhong, *Polymer* **35**, 2881–2883 (1994).
56. A. Oshima, Y. Tabata, H. Kudoh, and T. Seguchi, *Radiat. Phys. Chem.* **45**, 269–273 (1995).
57. J. S. Forsythe, D. J. T. Hill, A. L. Logothetis, T. Seguchi, and A. K. Whittaker, *Macromolecules* **30**, 8101–8108 (1997).
58. H. S. Judeikis, H. Hedgpeth, and S. Siegel, *Radiat. Res.* **35**, 247–262 (1968).
59. T. N. Bowmer, S. Y. Ho, and J. H. O'Donnell, *Polym. Degrad. Stab.* **5**, 449–456 (1983).
60. T. N. Bowmer, S. Y. Ho, and J. H. O'Donnell, G. S. Park, and M. Saleem, *Eur. Polym. J.* **18**, 61–66 (1982).
61. M. Dole, D. C. Milner, and T. F. Williams, *J. Am. Chem. Soc.* **80**, 1580–1588 (1958).
62. J. C. Randall, F. J. Zoepfl, and J. Silverman, *Radiat. Phys. Chem.* **22**, 183–192 (1983).
63. J. C. Randall, F. J. Zoepfl, and J. Silverman, *ACS Symp. Ser.* **247**, 245–267 (1984).
64. J. C. Randall, F. J. Zoepfl, and J. Silverman, *Makromol. Chem., Rapid Commun.* **4**, 149–157 (1983).
65. F. Horii, Q. Zhu, R. Kitamaru, and H. Yamaoka, *Macromolecules* **23**, 977–981 (1990).
66. Q. Zhu, F. Horii, R. Kitamaru, and H. Yamaoka, *J. Polym. Sci., Part A: Polym. Chem.* **28**, 2741–2751 (1990).
67. R. Salovey, R. V. Albarino, and J. P. Luongo, *Macromolecules* **3**, 314–318 (1970).
68. R. Salovey, J. P. Luongo, and W. A. Yager, *Macromolecules* **2**, 198–200 (1969).
69. A. Chapiro, *J. Chim. Phys.* **53**, 895–902 (1956).
70. R. V. Albarino and E. P. Otocka, *J. Appl. Polym. Sci.* **16**, 61–68 (1972).
71. M. F. Desrosiers, J. M. Puhl, and W. L. McLaughlin, *Appl. Radiat. Isot.* **44**, 325–326 (1993).
72. W. L. McLaughlin, *Radiat. Phys. Chem.* **41**, 45–56 (1993).
73. W. L. McLaughlin and M. F. Desrosiers, *Radiat. Phys. Chem.* **46**, 1163–1174 (1995).
74. W. L. McLaughlin, J. Silverman, M. Al-Sheikhly, W. J. Chappas, L. Zhan-Jun, A. Miller, and W. Batsberg-Pedersen, *Radiat. Phys. Chem.* **56**, 503–508 (1999).
75. K. T. Gillen, J. S. Wallace, and R. L. Clough, *Radiat. Phys. Chem.* **41**, 101–113 (1993).
76. R. L. Clough, G. M. Malone, K. T. Gillen, J. S. Wallace, and M. B. Sinclair, *Polym. Degrad. Stab.* **49**, 305–313 (1995).
77. R. L. Clough, K. T. Gillen, G. M. Malone, and J. S. Wallace, *Radiat. Phys. Chem.* **48**, 583–594 (1996).
78. A. Charlesby, *Nature (London)* **173**, 679–680 (1954).
79. A. Charlesby, *J. Polym. Sci.* **14**, 547–553 (1954).
80. A. Charlesby, *Proc. R. Soc. London, Ser. A* **224**, 120–128 (1954).
81. M. Inokuchi and M. Dole, *J. Chem. Phys.* **38**, 3006–3009 (1963).
82. N. S. Marans and L. J. Zapas, *J. Appl. Polym. Sci.* **11**, 705–718 (1967).
83. N. S. Viswanathan, *J. Polym. Sci., Polym. Chem. Ed.* **14**, 1553–1555 (1976).
84. J. H. O'Donnell, C. A. Smith, and D. J. Winzor, *J. Polym. Sci., Polym. Phys. Ed.* **16**, 1515–1518 (1978).
85. D. J. T. Hill, J. H. O'Donnell, C. L. Winzor, and D. J. Winzor, *Polymer* **31**, 538–542 (1990).
86. J. H. O'Donnell, C. L. Winzor, and D. J. Winzor, *Macromolecules* **23**, 167–172 (1990).
87. W. T. Bremner, K. A. Milne, and J. O'Donnell, *Polym. Bull. (Berlin)* **35**, 525–532 (1995).
88. C. L. Moad and D. J. Winzor, *Prog. Polym. Sci.* **23**, 759–813 (1998).
89. J. H. O'Donnell, N. P. Rahman, C. A. Smith, and D. J. Winzor, *Macromolecules* **12**, 113–119 (1979).
90. P. Alexander, A. Charlesby, and M. Ross, *Proc. R. Soc. London, Ser. A* **223**, 392–404 (1954).
91. O. Saito, H. Y. Kang, and M. Dole, *J. Chem. Phys.* **46**, 3607–3616 (1967).

92. H. Y. Kang, O. Saito, and M. Dole, *J. Polym. Sci., Polym. Symp.* **25**, 123–130 (1968).
93. O. Saito, *Radiat. Chem. Macromol.* **1**, 223–261 (1972).
94. M. Tsuda and S. Oikawa, *J. Polym. Sci., Polym. Chem. Ed.* **17**, 3759–3773 (1979).
95. A. Charlesby and S. H. Pinner, *Proc. R. Soc. London, Ser. A* **249**, 367–386 (1959).
96. D. J. T. Hill, D. A. Lewis, J. H. O'Donnell, and A. K. Whittaker, *Polym. Adv. Technol.* **9**, 45–51 (1998).
97. V. N. Handlos and K. A. Singer, *J. Appl. Polym. Sci.* **20**, 3375–3386 (1976).
98. M. Dole, ed. *Radiat. Chem. Macromol.* **1**, (1972).
99. M. Dole, ed. *Radiat. Chem. Macromol.* **2**, (1973).
100. J. Brandrup and E. H. Immergut, eds., *Polymer Handbook*, 3rd. ed., Vol. 3, John Wiley & Sons, Inc., New York, 1989, Chapt. 2.
101. R. L. Clough and S. W. Shalaby, *Irradiation of Polymers: Fundamentals and Technological Applications*, Vol. 620, American Chemical Society, Washington, D.C., 1996.
102. R. L. Clough and S. W. Shalaby, *Radiation Effects on Polymers*, Vol. 475, American Chemical Society, Washington, D.C., 1991.
103. *Radiat. Phys. Chem.* **7**, 1 (1977).
104. *Radiat. Phys. Chem.* **57**, 203 (2002).
105. *Radiat. Phys. Chem.* **18**, 1 (1981).
106. *Radiat. Phys. Chem.* **22**, 1 (1983).
107. *Radiat. Phys. Chem.* **25**, 1 (1985).
108. *Radiat. Phys. Chem.* **31**, 1 (1988).
109. *Radiat. Phys. Chem.* **35**, 1 (1990).
110. *Radiat. Phys. Chem.* **42**, 1 (1993).
111. *Radiat. Phys. Chem.* **46**, 399 (1995).
112. *Radiat. Phys. Chem.* **52**, 1 (1998).
113. *Radiat. Phys. Chem.* **14**, 1 (1979).
114. A. Singh and J. Silverman, *Radiation Processing of Polymers*, Hanser, Munich, 1992.
115. E. Reichmanis, *ACS Symp. Ser.* **381**, 132–154 (1989).
116. R. L. Clough, *Nucl. Instrum. Methods Phys. Res., Sect. B* **185**, 8–33 (2001).
117. R. L. Clough and K. T. Gillen, and M. Dole, *Irradiat. Eff. Polym*. 79–156 (1991).
118. B. J. Lyons, *Mod. Fluoropolym*. 335–347 (1997).
119. J. S. Forsythe and D. J. T. Hill, *Prog. Polym. Sci.* **25**, 101–136 (2000).
120. G. Burillo, R. L. Clough, T. Czvikovszky, O. Guven, A. Le Moel, W. Liu, A. Singh, J. Yang, and T. Zaharescu, *Radiat. Phys. Chem.* **64**, 41–51 (2002).
121. J. M. Rosiak and P. Ulanski, *Radiat. Phys. Chem.* **55**, 139–151 (1999).
122. J. M. Rosiak and F. Yoshii, *Nucl. Instrum. Methods Phys. Res., Sect. B* **151**, 56–64 (1999).
123. L. A. Pruitt, *Adv. Polym. Sci.* **162**, 63–93 (2003).
124. D. J. T. Hill and A. K. Whittaker, *Annu. Rep. NMR Spectrosc.* **46**, 1–35 (2002).
125. A. Charlesby, *Proc. R. Soc. London* **215A**, 187–214 (1952).
126. A. Charlesby, *Polym. J. (Tokyo)* **19**, 649–657 (1987).
127. H. Menhofer and H. Heusinger, *Radiat. Phys. Chem.* **29**, 243–251 (1987).
128. D. J. T. Hill, J. H. O'Donnell, P. J. Pomery, and C. L. Winzor, *Radiat. Phys. Chem.* **39**, 237–241 (1992).
129. J. L. Hopewell, D. J. T. Hill, J. H. O'Donnell, P. J. Pomery, J. E. McGrath, D. B. Priddy Jr., and C. D. Smith, *Polym. Degrad. Stab.* **45**, 293–299 (1994).
130. A. Faucitano, A. Buttafava, V. Patruno, P. A. Guadra, and G. Marchionni, *Radiat. Phys. Chem.* **45**, 23–30 (1995).
131. D. J. T. Hill, J. L. Hopewell, J. H. O'Donnell, and P. J. Pomery, *JAERI-Conf.* **95–003**, 115–119 (1995).
132. D. J. T. Hill, B.-K. Choi, H.-K. Ahn, and E. J. Choi, *Polym. Int.* **48**, 956–962 (1999).
133. S. Y. Ho and J. H. O'Donnell, *Eur. Polym. J.* **20**, 421–424 (1984).

134. R. Basheer and M. Dole, *J. Polym. Sci., Polym. Phys. Ed.* **22**, 1313–1329 (1984).
135. T. N. Bowmer, J. H. O'Donnell, and P. R. Wells, *Makromol. Chem., Rapid Commun.* **1**, 1–6 (1980).
136. M. G. Ormerod and A. Charlesby, *Polymer* **5**, 67–88 (1964).
137. A. Charlesby and J. Morris, *J. Polym. Sci.* **4**, 1127–1133 (1964); discussion 1132–1123.
138. C. F. Albert, W. K. Busfield, and P. J. Pomery, *Polym. Int.* **27**, 285–291 (1992).
139. V. I. Feldman, *Appl. Radiat. Isot.* **47**, 1497–1501 (1996).
140. R. Basheer and M. Dole, *J. Polym. Sci., Polym. Phys. Ed.* **21**, 957–967 (1983).
141. N. Gvozdic and M. Dole, *Radiat. Phys. Chem.* **15**, 435–440 (1980).
142. S. Shimada, M. Maeda, Y. Hori, and H. Kashiwabara, *Polymer* **18**, 19–24 (1977).
143. Y. Hori, S. Shimada, and H. Kashiwabara, *Polymer* **18**, 151–154 (1977).
144. Y. Hori, S. Shimada, and H. Kashiwabara, *Polymer* **18**, 567–572 (1977).
145. D. R. Johnson, W. Y. Wen, and M. Dole, *J. Phys. Chem.* **77**, 2174–2179 (1973).
146. D. C. Waterman and M. Dole, *J. Phys. Chem.* **74**, 1906–1912 (1970).
147. M. Iwasaki, T. Ichikawa, and T. Ohmori, *J. Chem. Phys.* **50**, 1984–1990 (1969).
148. M. Dole, G. G. A. Boehm, and D. C. Waterman, *Eur. Polym. J.* 93–104 (1969).
149. M. Dole and V. M. Patel, *Radiat. Phys. Chem.* **9**, 433–444 (1977).
150. H. H. Trieu, D. E. Thomas, M. Shah Jahan, W. O. Haggard, R. L. Conta, and J. E. Parr, *ASTM Spec. Tech. Publ. STP* **1307**, 109–119 (1998).
151. M. S. Jahan, D. E. Thomas, and M. D. Ridley, *Mater. Sci. Forum* **426–432**, 3139–3144 (2003).
152. N. Naheed, M. S. Jahan, and M. Ridley, *Nucl. Instrum. Methods Phys. Res., Sect. B* **208**, 204–209 (2003).
153. M. S. Jahan, M. C. King, W. O. Haggard, K. L. Sevo, and J. E. Parr, *Radiat. Phys. Chem.* **62**, 141–144 (2001).
154. M. C. Buncick, D. E. Thomas, K. S. McKinny, and M. S. Jahan, *Appl. Surf. Sci.* **156**, 97–109 (2000).
155. M. S. Jahan, K. S. McKinny, *Nucl. Instrum. Methods Phys. Res., Sect. B* **151**, 207–212 (1999).
156. M. S. Jahan, D. E. Thomas, K. Banerjee, H. H. Trieu, W. O. Haggard, and J. E. Parr, *Radiat. Phys. Chem.* **51**, 593–594 (1998).
157. M. S. Jahan, J. C. Stovall, J. A. Davidson, and G. Hines, *Appl. Radiat. Isot.* **46**, 637–638 (1995).
158. M. Dole and K. Katsuura, *J. Polym. Sci., Part B: Polym. Lett.* **3**, 467–472 (1965).
159. H. Y. Kang, O. Saito, and M. Dole, *J. Am. Chem. Soc.* **89**, 1980–1986 (1967).
160. R. Basheer and M. Dole, *J. Polym. Sci., Polym. Phys. Ed.* **21**, 949–956 (1983).
161. B. J. Lyons and A. S. Fox, *J. Polym. Sci., Polym. Symp.* **21**, 159–170 (1968).
162. H. Mitsui and Y. Shimizu, *J. Polym. Sci., Polym. Chem. Ed.* **17**, 2805–2813 (1979).
163. G. N. Patel and A. Keller, *J. Polym. Sci., Polym. Phys. Ed.* **13**, 323–331 (1975).
164. J. H. O'Donnell and A. K. Whittaker, *J. Macromol. Sci., Chem.* **29**, 1–9 (1991).
165. R. L. Bennett, A. Keller, J. Stejny, and M. Murray, *J. Polym. Sci., Polym. Chem. Ed.* **14**, 3027–3033 (1976).
166. F. A. Bovey, F. C. Schilling, and H. N. Cheng, *ACS Symp. Ser.* **169**, 133–141 (1978).
167. J. H. O'Donnell and A. K. Whittaker, *Polymer* **33**, 62–67 (1992).
168. J. H. O'Donnell and A. K. Whittaker, *Radiat. Phys. Chem.* **39**, 209–214 (1992).
169. D. C. Waterman and M. Dole, *J. Phys. Chem.* **74**, 1913–1922 (1970).
170. M. B. Fallgatter and M. Dole, *J. Phys. Chem.* **68**, 1988–1997 (1964).
171. D. M. Bodily and M. Dole, *J. Chem. Phys.* **45**, 1428–1432 (1966).
172. D. M. Bodily and M. Dole, *J. Chem. Phys.* **45**, 1433–1439 (1966).
173. D. O. Geymer, *Makromol. Chem.* **99**, 152–159 (1966).
174. W. Schnabel and M. Dole, *J. Phys. Chem.* **67**, 295–299 (1963).
175. R. W. Keyser, B. Clegg, and M. Dole, *J. Phys. Chem.* **67**, 300–303 (1963).

176. M. Inokuti and M. Dole, *J. Polym. Sci.* **1**, 3289–3302 (1963).
177. T. Asanuma, T. Shiomura, Y. Hirase, T. Matsuyama, H. Yamaoka, A. Tsuchida, M. Ohoka, and M. Yamamoto, *Polym. Bullet. (Berlin)* **29**, 79–83 (1992).
178. P. Alexander, R. M. Black, and A. Charlesby, *Proc. R. Soc. London, Ser. A* **232**, 31–48 (1955).
179. A. Chapiro, *J. Chim. Phys. Phys.-Chim. Biol.* **53**, 306–307 (1956).
180. A. A. Miller, E. J. Lawton, and J. S. Balwit, *J. Polym. Sci.* **14**, 503–504 (1954).
181. Z. F. Il'icheva and N. A. Slovokhotova, *Khim. Vysokikh Energii* **3**, 272–273 (1969).
182. B. Ranby and P. Carstensen, *Adv. Chem. Ser.* **66**, 256–270 (1967).
183. Y. Hori and H. Kashiwabara, *J. Polym. Sci., Polym. Phys. Ed.* **19**, 1141–1149 (1981).
184. J. Bartos, *Collect. Czech. Chem. Commun.* **50**, 1699–1713 (1985).
185. T. Bremner, D. J. T. Hill, J. H. O'Donnell, M. C. S. Perera, and P. J. Pomery, *J. Polym. Sci., Part A: Polym. Chem.* **34**, 971–984 (1996).
186. D. J. T. Hill, J. H. O'Donnell, M. C. S. Perera, and P. J. Pomery, *ACS Symp. Ser.* **620**, 139–150 (1996).
187. H. Fischer and W. Langbein, *Kolloid Z. Z. Polym.* **216/217**, 329–336 (1967).
188. H. Savas and O. Guven, *Radiat. Phys. Chem.* **64**, 35–40 (2002).
189. R. A. Van Brederode, F. Rodriguez, and G. G. Cocks, *J. Appl. Polym. Sci.* **12**, 2097–2104 (1968).
190. U. Borgwardt, W. Schnabel, and A. Henglein, *Makromol. Chem.* **127**, 176–184 (1969).
191. W. Schnabel and U. Borgwardt, *Makromol. Chem.* **123**, 73–79 (1969).
192. P. A. King and J. A. Ward, *J. Polym. Sci., Polym. Chem. Ed.* **8**, 253–262 (1970).
193. J. W. Stafford, *Makromol. Chem.* **134**, 99–111 (1970).
194. J. W. Stafford, *Makromol. Chem.* **134**, 87–97 (1970).
195. J. W. Stafford, *Makromol. Chem.* **134**, 71–86 (1970).
196. J. W. Stafford, *Makromol. Chem.* **134**, 57–69 (1970).
197. J. W. Stafford, *Makromol. Chem.* **134**, 113–119 (1970).
198. R. A. Van Brederode and F. Rodriguez, *J. Appl. Polym. Sci.* **14**, 979–987 (1970).
199. J. A. Ward, *J. Polym. Sci., Polym. Chem. Ed.* **9**, 3555–3561 (1971).
200. A. Charlesby and M. Byrne, *Radiat. Phys. Chem.* **12**, 129–131 (1978).
201. P. Kofinas, V. Athanassiou, and E. W. Merrill, *Biomaterials* **17**, 1547–1550 (1996).
202. L. Zhang, W. Zhang, Z. Zhang, L. Yu, H. Zhang, Y. Qi, and D. Chen, *Radiat. Phys. Chem.* **40**, 501–505 (1992).
203. P. A. King, *Adv. Chem. Ser.* **66**, 113–126 (1967).
204. E. Nedkov and S. Tsvetkova, *Radiat. Phys. Chem.* **44**, 251–256 (1994).
205. E. Nedkov and S. Tsvetkova, *Radiat. Phys. Chem.* **43**, 397–401 (1994).
206. F. C. Schilling, A. E. Tonelli, and A. L. Cholli, *J. Polym. Sci., Part B: Polym. Phys.* **30**, 91–96 (1992).
207. G. P. Roberts, M. Budzol, and M. Dole, *J. Polym. Sci., Polym. Phys. Ed.* **9**, 1729–1745 (1971).
208. W. Zhao, Y. Yamamoto, and S. Tagawa, *J. Polym. Sci., Part A: Polym. Chem.* **36**, 3089–3095 (1998).
209. J. Pacansky and S. Schneider, *J. Phys. Chem.* **94**, 3166–3179 (1990).
210. G. Burillo, G. Canizal, and T. Ogawa, *Radiat. Phys. Chem.* **33**, 351–354 (1989).
211. Zainuddin, D. J. T. Hill, and T. T. Le, *Radiat. Phys. Chem.* **62**, 283–291 (2001).
212. G. Lu, H. Chen, and D. Liu, *Radiat. Phys. Chem.* **42**, 229–232 (1993).
213. P. L. Walker Jr. and D. E. Kline, *Carbon* **6**, 739–741 (1968).
214. R. Salovey and R. C. Gebauer, *J. Polym. Sci., Polym. Chem. Ed.* **10**, 1533–1537 (1972).
215. A. Babanalbandil and D. J. Hill, *Polym. Int.* **48**, 963–970 (1999).
216. T. Carswell-Pomerantz, D. J. T. Hill, J. H. O'Donnell, and P. J. Pomery, *Polym. Prepr. (Am. Chem. Soc., Div. Polym. Chem.)* **35**, 913, 918 (1994).

217. T. Carswell-Pomerantz, D. J. T. Hill, J. H. O'Donnell, and P. J. Pomery, *Radiat. Phys. Chem.* **45**, 737–744 (1995)
218. T. Carswell-Pomerantz, L. Dong, D. J. T. Hill, J. H. O'Donnell, and P. J. Pomery, *ACS Symp. Ser.* **620**, 11–27 (1996)
219. S. Luo and A. N. Netravali, *J. Appl. Polym. Sci.* **73**, 1059–1067 (1999).
220. A. Babanalbandi, D. J. T. Hill, J. H. O'Donnell, P. J. Pomery, and A. Whittaker, *Polym. Degrad. Stab.* **50**, 297–304 (1995).
221. A. Babanalbandi, D. J. T. Hill, and A. K. Whittaker, *Polym. Degrad. Stab.* **58**, 203–214 (1997).
222. A. Babanalbandi, D. J. T. Hill, D. S. Hunter, and L. Kettle, *Polym. Int.* **48**, 980–984 (1999).
223. J. H. Collett, L. Y. Lim, and P. L. Gould, *Polym. Prepr. (Am. Chem. Soc., Div. Polym. Chem.)* **30**, 468–469 (1989).
224. O. Wollersheim, H. Zumaque, J. Hormes, D. Kadereit, J. Langen, L. Haeussling, P. Hoessel, and G. Hoffmann, *Nucl. Instrum. Methods Phys. Res., Sect. B* **97**, 273–278 (1995).
225. O. Wollersheim and J. Hormes, *Chem. Phys.* **204**, 129–134 (1996).
226. L. Montanari, M. Costantini, E. C. Signoretti, L. Valvo, M. Santucci, M. Bartolomei, P. Fattibene, S. Onori, A. Faucitano, B. Conti, and I. Genta, *J. Controlled Release* **56**, 219–229 (1998).
227. P. B. Ayscough, K. J. Ivin, and J. H. O'Donnell, *Trans. Faraday Soc.* **61**, 1110–1117 (1965).
228. J. R. Brown and J. H. O'Donnell, *Macromolecules* **3**, 265–267 (1970).
229. J. R. Brown and J. H. O'Donnell, *Macromolecules* **5**, 109–114 (1972).
230. T. N. Bowmer, J. H. O'Donnell, and P. R. Wells, *Polym. Bull. (Berlin)* **2**, 103–110 (1980).
231. L. A. Wall and D. W. Brown, *J. Phys. Chem.* **61**, 129–136 (1957).
232. A. R. Shultz, P. I. Roth, and J. M. Berge, *J. Polym. Sci., Part A: Gen. Pap.* **1**, 1651–1669 (1963).
233. D. W. Ovenall, *Nature (London)* **184**, 181–182 (1959).
234. D. W. Ovenall, *J. Polym. Sci.* **41**, 199–211 (1959).
235. D. W. Ovenall, *J. Polym. Sci.* **39**, 21–27 (1959).
236. R. J. Abraham, H. W. Melville, D. W. Ovenall, and D. H. Whiffen, *Trans. Faraday Soc.* **54**, 1133–1139 (1958).
237. J. H. O'Donnell, B. McGarvey, and H. Morawetz, *J. Am. Chem. Soc.* **86**, 2322–2325 (1964).
238. M. J. Bowden and J. H. O'Donnell, *J. Phys. Chem.* **72**, 1577–1582 (1968).
239. C. David, D. Fuld, G. Geuskens, and A. Charlesby, *Eur. Polym. J.* **5**, 641–648 (1969).
240. A. R. Shultz and F. A. Bovey, *J. Polym. Sci.* **22**, 485–493 (1956).
241. R. K. Graham, *J. Polym. Sci.* **37**, 441–444 (1959).
242. R. K. Graham, *J. Polym. Sci.* **38**, 209–212 (1959).
243. R. B. Fox, L. G. Isaacs, S. Stokes, and R. E. Kagarise, *J. Polym. Sci*. 2085–2092 (1964).
244. R. B. Fox, L. G. Isaacs, R. E. Kagarise, and S. Stokes, *Am. Chem. Soc., Div. Org. Coatings, Plastic Chem., Prepr.* **22**, 205–210 (1962).
245. M. J. Bowden, *J. Polym. Sci., Polym. Symp.* **49**, 221–226 (1975).
246. W. K. Busfield, J. H. O'Donnell, and C. A. Smith, *Polymer* **23**, 431–434 (1982).
247. W. K. Busfield, J. H. O'Donnell, and C. A. Smith, *J. Macromol. Sci., Chem.* **A17**, 1263–1272 (1982).
248. T. G. Carswell, R. W. Garrett, D. J. T. Hill, J. H. O'Donnell, P. J. Pomery, and C. L. Winzor, *Polym. Spectrosc*. 253–274 (1996).
249. D. J. T. Hill, *Radiat. Chem. (Japan)* **59**, 20–27 (1995).
250. H. Kudoh, N. Kasai, T. Sasuga, and T. Seguchi, *Radiat. Phys. Chem.* **48**, 95–100 (1996).

251. H. Kudoh, N. Kasai, T. Sasuga, and T. Seguchi, *Radiat. Phys. Chem.* **43**, 329–334 (1994).
252. F. Thominette and J. Verdu, *J. Polym. Sci., Part A: Polym. Chem.* **34**, 3221–3223 (1996).
253. H. J. Glasel, E. Hartmann, R. Mehnert, D. Hirsch, R. Bottcher, and J. Hormes, *Nucl. Instrum. Methods Phys. Res., Sect. B* **151**, 200–206 (1999).
254. N. W. Isaacs, C. H. L. Kennard, and J. H. O'Donnell, *Nature (London)* **216**, 1104 (1967).
255. R. P. Kusy, M. J. Katz, and D. T. Turner, *Thermochim. Acta* **26**, 415–425 (1978).
256. R. Jenkins and R. S. Porter, *J. Polym. Sci., Polym. Lett. Ed.* **18**, 743–750 (1980).
257. D. J. T. Hill and J. H. O'Donnell, *J. Chem. Educ.* **58**, 174–176 (1981).
258. Y. Katsumura, Y. Tabata, T. Seguchi, N. Hayakawa, K. Yoshida, and N. Tamura, *Radiat. Phys. Chem.* **26**, 211–220 (1985).
259. H. Kudoh, M. Celina, M. Malone, R. J. Kaye, K. T. Gillen, and R. L. Clough, *Radiat. Phys. Chem.* **48**, 555–562 (1996).
260. H. Kudoh, N. Kasai, T. Sasuga, and T. Seguchi, *ACS Symp. Ser.* **620**, 313–322 (1996).
261. O. Schmalz, M. Hess, and R. Kosfeld, *Angew. Makromol. Chem.* **239**, 79–91 (1996).
262. N. M. Bol'bit, V. B. Taraban, E. R. Klinshpont, I. P. Shelukhov, and V. K. Milinchuk, *High Energ. Chem.* **34**, 229–235 (2000).
263. A. A. Koptelov and S. V. Karyazov, *Dokl. Chem.* **384**, 135–139 (2002).
264. F. M. Veronese, G. Ceriotti, G. Keller, S. Lora, and M. Carenza, *Radiat. Phys. Chem.* **35**, 88–92 (1990).
265. D. J. T. Hill, J. H. O'Donnell, P. J. Pomery, and G. Saadat, *Radiat. Phys. Chem.* **48**, 605–612 (1996).
266. L. Dong, D. J. T. Hill, J. H. O'Donnel, P. J. Pomery, and I. M. Brereton, *Macromol. Chem. Phys.* **196**, 3379–3390 (1995).
267. L. Dong, D. J. T. Hill, J. H. O'Donnell, P. J. Pomery, and K. Hatada, *J. Appl. Polym. Sci.* **59**, 589–597 (1996).
268. L. Brown, T. G. Carswell-Pomerantz, J. T. Hill, and P. J. Pomery, *Radiat. Phys. Chem.* **48**, 627–630 (1996).
269. H. Kudoh, T. Sasuga, and T. Seguchi, *Radiat. Phys. Chem.* **48**, 545–548 (1996).
270. H. Kudoh, T. Sasuga, T. Seguchi, and Y. Katsumura, *Polymer* **37**, 4663–4665 (1996).
271. H. Kudoh, T. Sasuga, T. Seguchi, and Y. Katsumura, *Polymer* **37**, 2903–2908 (1996).
272. H. Kudoh, T. Sasuga, and T. Seguchi, *ACS Symp. Ser.* **620**, 2–10 (1996).
273. H. Kudoh, T. Sasuga, and T. Seguchi, *Radiat. Phys. Chem.* **50**, 299–302 (1997).
274. J. H. O'Donnell, N. P. Rahman, and D. J. Winzor, *J. Polym. Sci., Polym. Chem. Ed.* **15**, 131–139 (1977)
275. J. H. O'Donnell, P. J. Pomery, N. P. Rahman, C. A. Smith, and D. J. Winzor, *J. Appl. Polym. Sci., Appl. Polym. Symp.* **35**, 527–536 (1979).
276. I. S. Ungar, J. F. Kircher, W. B. Gager, F. A. Sliemers, and R. I. Leininger, *J. Polym. Sci., Part A: Polym. Chem.* **1**, 277–288 (1963).
277. A. Charlesby, *Proc. R. Soc. London, Ser. A* **230**, 120–135 (1955).
278. A. Charlesby, *J. Polym. Sci.* **17**, 379–390 (1955).
279. L. E. St. Pierre, H. A. Dewhurst, and A. M. Bueche, *J. Polym. Sci.* **36**, 105–111 (1959).
280. A. A. Miller, *J. Am. Chem. Soc.* **82**, 3519–3523 (1960).
281. A. M. Bueche, *J. Polym. Sci.* **19**, 297–306 (1956).
282. S. Okamura, H. Inagaki, and K. Ohdan, *Doitai Hoshasen* **1**, 214–216 (1958).
283. M. G. Ormerod and A. Charlesby, *Polymer* **4**, 459–470 (1963).
284. C. G. Delides, *Radiat. Phys. Chem.* **16**, 345–352 (1980).
285. A. Charlesby and P. G. Garratt, *Proc. R. Soc. London, Ser. A* **273**, 117–132 (1963).
286. D. J. T. Hill, C. M. L. Preston, A. K. Whittaker, and S. M. Hunt, *Macromol. Symp.* **156**, 95–102 (2000).
287. D. J. T. Hill, C. M. L. Preston, and A. K. Whittaker, *Polymer* **43**, 1051–1059 (2001).

288. D. J. T. Hill, C. M. L. Preston, D. J. Salisbury, and A. K. Whittaker, *Radiat. Phys. Chem.* **62**, 11–17 (2001).
289. M. Dole, *Radiat. Chem. Macromol.* **2**, 167–177 (1973).
290. M. I. Bro, E. R. Lovejoy, and G. R. McKay, *J. Appl. Polym. Sci.* **7**, 2121–2133 (1963).
291. P. Hedvig, *J. Polym. Sci., Polym. Chem. Ed.* **7**, 1145–1152 (1969).
292. H. N. Rexroad and W. Gordy, *J. Chem. Phys.* **30**, 399–403 (1959).
293. D. W. Ovenall, *J. Chem. Phys.* **38**, 2448–2454 (1963).
294. E. R. Lovejoy, M. I. Bro, and G. H. Bowers, *J. Appl. Polym. Sci.* **9**, 401–410 (1965).
295. M. Tutiya, *Jpn. J. Appl. Phys.* **11**, 1542–1546 (1972).
296. M. Tutiya, *Jpn. J. Appl. Phys.* **11**, 1219 (1972).
297. M. Tutiya, *Jpn. J. Appl. Phys.* **9**, 1204–1209 (1970).
298. M. Tutiya, *J. Phys. Soc. Japan* **25**, 1518 (1968).
299. M. Tutiya, *Polym. J. (Tokyo)* **6**, 39–44 (1974).
300. J. Sun, Y. Zhang, X. Zhong, and W. Zhang, *Radiat. Phys. Chem.* **42**, 139–142 (1993).
301. Y. Ito, H. F. M. Mohamed, T. Seguchi, and A. Oshima, *Radiat. Phys. Chem.* **48**, 775–779 (1996).
302. Y. Tabata, A. Oshima, K. Takashika, and T. Seguchi, *Radiat. Phys. Chem.* **48**, 563–568 (1996).
303. A. Oshima, S. Ikeda, H. Kudoh, T. Seguchi, and Y. Tabata, *Radiat. Phys. Chem.* **50**, 611–615 (1997).
304. A. Oshima, T. Seguchi, and Y. Tabata, *Radiat. Phys. Chem.* **50**, 601–606 (1997).
305. A. Oshima, S. Ikeda, T. Seguchi, and Y. Tabata, *Radiat. Phys. Chem.* **49**, 581–588 (1997).
306. A. Oshima, S. Ikeda, T. Seguchi, and Y. Tabata, *Radiat. Phys. Chem.* **49**, 279–284 (1997).
307. E. Katoh, H. Sugisawa, A. Oshima, Y. Tabata, T. Seguchi, and T. Yamazaki, *Radiat. Phys. Chem.* **54**, 165–171 (1999).
308. A. Oshima, T. Seguchi, and Y. Tabata, *Polym. Int.* **48**, 996–1003 (1999).
309. A. Oshima, T. Seguchi, and Y. Tabata, *Radiat. Phys. Chem.* **55**, 61–71 (1999).
310. A. Oshima, S. Ikeda, E. Katoh, and Y. Tabata, *Radiat. Phys. Chem.* **62**, 39–45 (2001).
311. B. Fuchs, U. Lappan, K. Lunkwitz, and U. Scheler, *Macromolecules* **35**, 9079–9082 (2002).
312. B. Fuchs and U. Scheler, *Macromolecules* **33**, 120–124 (2000).
313. G. H. Bowers and E. R. Lovejoy, *Ind. Eng. Chem. Prod. Res. Dev.* **1**, 89–92 (1962).
314. D. J. T. Hill, S. Mohajerani, A. K. Whittaker, and U. Scheler, *Polym. Int.* **52**, 1725–1733 (2003).
315. K. K. Gleason, D. J. T. Hill, K. K. S. Lau, S. Mohajerani, and A. K. Whittaker, *Nucl. Instrum. Methods Phys. Res., Sect. B* **185**, 83–87 (2001).
316. J. S. Forsythe, D. J. T. Hill, S. Mohajerani, and A. K. Whittaker, *Radiat. Phys. Chem.* **60**, 439–444 (2001).
317. U. Lappan, U. Geissler, U. Scheler, and K. Lunkwitz, *Radiat. Phys. Chem.* **67**, 447–451 (2003).
318. T. R. Dargaville, D. J. T. Hill, and A. K. Whittaker, *Radiat. Phys. Chem.* **62**, 25–31 (2001).
319. T. R. Dargaville, G. A. George, D. J. T. Hill, U. Scheler, and A. K. Whittaker, *Macromolecules* **35**, 5544–5549 (2002).
320. T. R. Dargaville, G. A. George, D. J. T. Hill, U. Scheler, and A. K. Whittaker, *Macromolecules* **36**, 7138–7142 (2003).
321. J. S. Forsythe, D. J. T. Hill, A. L. Logothetis, and A. K. Whittaker, *Polym. Degrad. Stab.* **63**, 95–101 (1998).
322. J. S. Forsythe, D. J. T. Hill, A. L. Logothetis, P. J. Pomery, and A. K. Whittaker, *J. Appl. Polym. Sci.* **75**, 1447–1452 (2000).

323. J. S. Forsythe, D. J. T. Hill, A. L. Logothetis, P. J. Pomery, and A. K. Whittaker, *J. Appl. Polym. Sci.* **73**, 169–175 (1999).
324. J. S. Forsythe, D. J. T. Hill, A. K. Whittaker, and A. L. Logothetis, *Polym. Int.* **48**, 1004–1009 (1999).
325. J. S. Forsythe, D. J. T. Hill, N. Calos, A. L. Logothetis, and A. K. Whittaker, *J. Appl. Polym. Sci.* **73**, 807–812 (1999).
326. J. S. Forsythe, D. J. T. Hill, A. L. Logothetis, T. Seguchi, and A. K. Whittaker, *Radiat. Phys. Chem.* **53**, 611–621 (1998).
327. J. S. Forsythe, D. J. T. Hill, A. L. Logothetis, T. Seguchi, and A. K. Whittaker, *Radiat. Phys. Chem.* **53**, 657–667 (1998).
328. L. A. Wall, S. Straus, and R. E. Florin, *J. Polym. Sci., Polym. Phys. Ed. A* **14**, 349–365 (1966).
329. R. Timmerman and W. Greyson, *J. Appl. Polym. Sci.* **6**, 456–460 (1962).
330. T. Yoshida, R. E. Florin, and L. A. Wall, *J. Polym. Sci., Part A: Gen. Pap.* **3**, 1685–1712 (1965).
331. T. Seguchi, K. Makuuchi, T. Suwa, N. Tamura, T. Abe, and M. Takehisa, *Nippon Kagaku Kaishi* 1309–1314 (1974).
332. A. Oshima, S. Ikeda, T. Seguchi, and Y. Tabata, *Radiat. Phys. Chem.* **50**, 519–522 (1997).
333. Y. X. Luo, F. C. Pang, and J. X. Sun, *Radiat. Phys. Chem.* **18**, 445–457 (1981).
334. D. J. T. Hill, K. J. Thurecht, and A. K. Whittaker, *Radiat. Phys. Chem.* **67**, 729–736 (2003).
335. D. J. T. Hill, K. J. Thurecht, and A. K. Whittaker, *Radiat. Phys. Chem.* **68**, 857–864 (2003).
336. V. T. Kozlov and Z. N. Tarasova, *Vysokomol. Soedin.* **8**, 943–948 (1966).
337. V. T. Kozlov, *Vysokomol. Soedin., Ser. A* **9**, 515–521 (1967).
338. A. S. Kuzminskii, T. S. Nikitina, E. V. Zhuravskaya, L. A. Oksentevich, L. L. Sunitsa, and N. I. Vitushkin, *Proc. 2nd Int. Conf. U.N. Peaceful Uses At. Energy, 1958* **29**, 258–265 (1959).
339. E. Witt, *J. Polym. Sci.* **41**, 507–518 (1959).
340. B. Jankowski and J. Kroh, *J. Appl. Polym. Sci.* **9**, 1363–1366 (1965).
341. V. T. Kozlov, A. G. Evseev, and P. I. Zubov, *Vysokomol. Soedin., Ser. A* **11**, 2230–2237 (1969).
342. V. T. Kozlov, M. V. Gur'ev, A. G. Evseev, N. G. Kashevskaya, and P. I. Zubov, *Vysokomol. Soedin., Ser. A* **12**, 592–601 (1970).
343. D. S. Pearson, B. J. Skutnik, and G. G. A. Boehm, *J. Polym. Sci., Polym. Phys. Ed.* **12**, 925–939 (1974).
344. J. H. O'Donnell and A. K. Whittaker, *J. Polym. Sci., Part A: Polym. Chem.* **30**, 185–195 (1992).
345. P. F. Barron, J. H. O'Donnell, and A. K. Whittaker, *Polym. Bull. (Berlin)* **14**, 339–346 (1985).
346. W. W. Parkinson and W. C. Sears, *Adv. Chem. Ser.* **66**, 57–70 (1967).
347. M. A. Golub and J. Danon, *Can. J. Chem.* **43**, 2772–2785 (1965).
348. M. A. Golub, *J. Phys. Chem.* **69**, 2639–2645 (1965).
349. A. K. Whittaker, Department of Chemistry, University of Queensland, Brisbane, 1986.
350. G. G. A. Boehm, *Radiat. Chem. Macromol.* **2**, 195–260 (1973).
351. D. J. T. Hill, J. H. O'Donnell, M. C. Senake Perera, and P. J. Pomery, *ACS Symp. Ser.* **527**, 74–94 (1993)
352. A. Charlesby, *J. Polym. Sci.* **11**, 521–529 (1953).
353. W. W. Parkinson and R. M. Keyser, *Radiat. Chem. Macromol.* **2**, 57–96 (1973).
354. R. Basheer and M. Dole, *Int. J. Chem. Kinet.* **13**, 1143–1150 (1981).
355. R. Basheer and M. Dole, *Radiat. Phys. Chem.* **18**, 1053–1060 (1981).

356. H. Moenig, *Makromol. Chem.* **181**, 2293–2303 (1980).
357. R. W. Garrett, Department of Chemistry, University of Queensland, Brisbane, 1984.
358. J. H. O'Donnell, N. P. Rahman, C. A. Smith, and D. J. Winzor, *J. Polym. Sci., Polym. Chem. Ed.* **17**, 4081–4088 (1979).
359. J. G. Spiro and C. A. Winkler, *J. Appl. Polym. Sci.* **8**, 1709–1717 (1964).
360. T. N. Bowmer, J. H. O'Donnell, and D. J. Winzor, *J. Polym. Sci., Polym. Chem. Ed.* **19**, 1167–1174 (1981).
361. Y. Tabata and A. Oshima, *Macromol. Symp.* **143**, 337–358 (1999).
362. K. Takashika, A. Oshima, M. Kuramoto, T. Seguchi, and Y. Tabata, *Radiat. Phys. Chem.* **55**, 399–408 (1999).
363. W. Burlant, J. Neerman, and V. Serment, *J. Polym. Sci.* **58**, 491 (1962).
364. J. G. Kilroe and K. E. Wearle, *J. Chem. Soc., Abstr*. 3849–3854 (1960).
365. R. W. Garrett, T. Le, D. J. T. Hill, J. H. O'Donnell, and P. J. Pomery, *Polym. Microelectron. Proc. Int. Symp*. 47–62 (1990).
366. J. R. Brown, J. H. O'Donnell, *J. Polym. Sci., Part B: Polym. Phys.* **8**, 121–126 (1970)
367. D. A. Lewis, J. H. O'Donnell, J. L. Hedrick, T. C. Ward, and J. E. McGrath, *ACS Symp. Ser.* **381**, 252–261 (1989).
368. D. J. T. Hill, D. A. Lewis, and J. H. O'Donnell, *J. Macromol. Sci., Chem.* **29**, 11–18 (1991).
369. R. Basheer and M. Dole, *Radiat. Phys. Chem.* **25**, 389–398 (1985).
370. S. Devasahayam, D. J. T. Hill, P. J. Pomery, and A. K. Whittaker, *Radiat. Phys. Chem.* **64**, 299–308 (2002).
371. I. Brereton, S. Devasahayam, D. J. T. Hill, and A. K. Whittaker, *Radiat. Phys. Chem.* **69**, 65–77 (2004).
372. K. Heiland, D. J. T. Hill, J. L. Hopewell, D. A. Lewis, J. H. O'Donnell, P. J. Pomery, and A. K. Whittaker, *Adv. Chem. Ser.* **249**, 637–649 (1996).
373. E. S. A. Hegazy, T. Sasuga, M. Nishii, and T. Seguchi, *Polymer* **33**, 2897–2903 (1992).
374. E. S. A. Hegazy, T. Sasuga, M. Nishii, and T. Seguchi, *Polymer* **33**, 2904–2910 (1992).
375. S. Devasahayam, D. J. T. Hill, and J. W. Connell, *Radiat. Phys. Chem.* **62**, 189–194 (2001).
376. M. A. Alexander, D. J. T. Hill, J. W. Connell, and K. A. Watson, *High Perf. Polym.* **13**, 67–78 (2001).
377. T. Sasuga and M. Hagiwara, *Polymer* **28**, 1915–1921 (1987).
378. T. Sasuga, T. Seguchi, H. Sakai, T. Nakakura, and M. Masutani, *J. Mater. Sci.* **24**, 1570–1574 (1989).
379. E. S. A. Hegazy, T. Sasuga, and T. Seguchi, *Polymer* **33**, 2911–2914 (1992).
380. K. Heiland, D. J. T. Hill, J. H. O'Donnell, and P. J. Pomery, *Polym. Adv. Technol.* **5**, 116–121 (1994).
381. A. Davis and J. H. Golden, *J. Macromol. Sci., Rev. Macromol. Chem.* **3**, 49–68 (1969).
382. Y. Hama and K. Shinohara, *J. Polym. Sci., Polymer Chem. Ed.* **8**, 651–663 (1970).
383. A. Torikai, T. Murata, and K. Fueki, *Polym. Degrad. Stab.* **7**, 55–64 (1984).
384. J. H. Golden, B. L. Hammant, and E. A. Hazell, *J. Polym. Sci.* **2**, 4787–4794 (1964).
385. J. H. Golden, *Makromol. Chem.* **66**, 73–81 (1963).
386. J. H. Golden and E. A. Hazell, *J. Polym. Sci., Part A: Gen. Pap.* **1**, 1671–1686 (1963).
387. R. C. Giberson, *Mod. Plast.* **39**, 143, 146, 228 (1962).
388. A. Babanalbandi, D. J. T. Hill, and A. K. Whittaker, *Polym. Adv. Technol.* **9**, 62–74 (1998).
389. S. P. Burow, D. T. Turner, G. F. Pezdirtz, and G. D. Sands, *Am. Chem. Soc., Div. Polymer Chem., Prepr.* **5**, 396–402 (1964).
390. S. D. Burow, D. T. Turner, G. F. Pezdirtz, and G. D. Sands, *J. Polym. Sci., Polymer Chem. Ed.* **4**, 613–622 (1966).

391. D. Campbell, K. Araki, and D. T. Turner, *J. Polym. Sci., Polym. Chem. Ed.* **4**, 2597–2606 (1966).
392. D. T. Turner, G. F. Pezdirtz, and G. D. Sands, *J. Polym. Sci., Polym. Chem. Ed.* **4**, 252–254 (1966).
393. D. T. Turner and R. P. Kusy, *Macromolecules* **4**, 337–341 (1971).
394. D. T. Turner, *Radiat. Chem. Macromol.* **2**, 137–166 (1973).
395. V. Stannett, T. Memetea, M. Dole, and J. Salik, *J. Polym. Sci., Polym. Lett. Ed.* **16**, 63–65 (1978).
396. Y. Komaki and T. Seguchi, *Polymer* **23**, 1143–1146 (1982).
397. V. L. Bell and G. F. Pezdirtz, *J. Polym. Sci., Polym. Chem. Ed.* **21**, 3083–3092 (1983).
398. E. J. Choi, D. J. T. Hill, K. Y. Kim, J. H. O'Donnell, P. J. Pomery, and A. K. Whittaker, *Polym. Int.* **48**, 971–979 (1999)
399. D. J. T. Hill, B. K. Choi, H. K. Ahn, and E. J. Choi, *Radiat. Phys. Chem.* **62**, 195–201 (2001).
400. E. J. Choi, D. J. T. Hill, K. Y. Kim, J. H. O'Donnell, and P. J. Pomery, *Polymer* **38**, 3669–3676 (1997).
401. E. J. Choi, D. J. T. Hill, K. Y. Kim, J. H. O'Donnell, and P. J. Pomery, *Polym. Adv. Technol.* **9**, 52–61 (1998)
402. A. Babanalbandi, D. J. T. Hill, J. H. O'Donnell, and P. J. Pomery, *Polym. Degrad. Stab.* **52**, 59–66 (1996).
403. D. J. T. Hill, S. Y. Ho, J. H. O'Donnell, and P. J. Pomery, *Radiat. Phys. Chem.* **36**, 467–474 (1990)
404. P. A. Fox, D. J. T. Hill, A. P. Lang, and P. J. Pomery, *Polym. Int.* **52**, 1719–1724 (2003).
405. D. D. Jamiolkowski, R. S. Bezwada, and S. W. Shalaby, *ACS Symp. Ser.* **527**, 320–325 (1993).
406. K. T. Gillen and R. L. Clough, *Irradiat. Eff. Polym*. 157–223 (1991).
407. M. Celina, K. T. Gillen, J. Wise, and R. L. Clough, *Radiat. Phys. Chem.* **48**, 613–626 (1996).
408. M. Celina, K. T. Gillen, G. M. Malone, R. L. Clough, and W. H. Nelson, *Radiat. Phys. Chem.* **62**, 153–161 (2001).
409. R. A. Assink, M. Celina, T. D. Dunbar, T. M. Alam, R. L. Clough, and K. T. Gillen, *Macromolecules* **33**, 4023–4029 (2000).
410. R. L. Clough, N. C. Billingham, and K. T. Gillen, *Adv. Chem. Ser.* **249** (1996).
411. P. R. Young and W. S. Slemp, *ACS Symp. Ser.* **527**, 278–304 (1993).
412. T. M. Alam, *Radiat. Phys. Chem.* **62**, 145–152 (2001).
413. T. M. Alam, M. Celina, R. A. Assink, R. L. Clough, and K. T. Gillen, *Radiat. Phys. Chem.* **60**, 121–127 (2001).
414. B. Gabrys, F. Horii, and R. Kitamaru, *Macromolecules* **20**, 175–177 (1987).
415. K. Wundrich, in *International Symposium on Radiation Degradation of Polymers and Radiation Resistant Materials*, JAERI, Takasaki, Japan, 1989, p. 159.
416. R. W. Garrett, D. J. T. Hill, T. T. Le, K. A. Milne, J. H. O'Donnell, S. M. C. Perera, and P. J. Pomery, *ACS Symp. Ser.* **475**, 146–155 (1991).
417. D. J. T. Hill, T. T. Le, J. H. O'Donnell, M. C. Senake Perera, and P. J. Pomery, *ACS Symp. Ser.* **527**, 50–61 (1993).

DAVID J. T. HILL
ANDREW K. WHITTAKER
The University of Queensland

Encyclopedia of Polymer Sceince and Technology
Copyright © 2005 John Wiley & Sons, Inc. All rights reserved.

STARCH

Introduction

In nature, starch represents a link with the energy of the sun, which is partially captured during photosynthesis. Starch serves as a food reserve for plants and provides a mechanism by which nonphotosynthesizing organisms, such as man, can utilize the energy supplied by the sun.

Today, starch is inexpensive and is available annually from corn and other crops, and is produced in excess of current market needs in the United States and Europe (1). Starch is totally biodegradable in a wide variety of environments and could permit the development of totally degradable products for specific market demands. Degradation or incineration of starch products would recycle atmospheric CO_2 trapped by starch-producing plants and would not increase potential global warming (2) (see also ENVIRONMENTALLY DEGRADABLE PLASTICS).

For these reasons there has been renewed interest in starch-based plastics in recent years. Earlier studies of starch esters and ethers (3–10) indicated that they had inadequate properties in comparison with cellulose derivatives for most applications. More recently, starch graft copolymers (2), starch plastic composites (11,12), and starch itself (13–17) have been proposed as plastic materials.

Starch consists of two major components: amylose, a mostly linear α-D(1-4)-glucan and amylopectin, an α-D-(1-4)-glucan which has α-D(16) linkages at the branch point. The linear amylose molecules of starch have a molecular weight of 0.2–2 million, whereas the branched amylopectin molecules have molecular weights as high as 100–400 million (18,19) (see POLYSACCHARIDES AND CARBOHYDRATE POLYMERS).

In nature, starch is found as crystalline beads of about 15–100 μm in diameter, in three crystalline modifications designated A (cereal), B (tuber), and C (smooth pea and various beans), all characterized by double helices: almost perfect left-handed, six-fold structures, as elucidated by X-ray diffraction experiments (18,20,21). Starch beads may also show V crystallinity, characterized by a single helix when starch is in presence of fatty acids (22).

Crystalline starch beads in plastics can be used as Fillers (qv) or can be transformed into thermoplastic starch, which can be processed alone or in combination with specific synthetic polymers. To make starch thermoplastic, its crystalline structure has to be destroyed by pressure, heat, mechanical work, and Plasticizers (qv) such as water, glycerol, or other polyols.

This article reviews the main results obtained in the fields of starch-filled plastics and thermoplastic starch, with particular attention to the concepts of gelatinization, destructurization, extrusion cooking, and the complexation of

amylose by means of polymeric complexing agents with the formation of specific supramolecular structures. The behaviors of products now in the market are considered in terms of processability, physical-chemical and physical-mechanical properties, and biodegradation rates.

Starch-Filled Plastics

Starch can be used as a natural filler in traditional plastics (11,23–33) and particularly in polyolefins. When blended with starch beads, polyethylene films (34) biodeteriorate on exposure to a soil environment. The microbial consumption of the starch component, in fact, leads to increased porosity, void formation, and the loss of integrity of the plastic matrix. Generally (32,35–38), starch is added at fairly low concentrations (6–15%); the overall disintegration of these materials is achieved by the use of transition-metal compounds, soluble in the thermoplastic matrix, as pro-oxidant additives which catalyze the photo- and thermooxidative process (39–44).

Starch-filled polyethylenes containing pro-oxidants are commonly used in agricultural mulch film, in bags, and in six-pack yoke packaging. Commercial products based on this technology have been sold first by Ecostar and Archer Daniels Midland Cos. (45,46). In the St. Lawrence Starch (47,48) technology, bought by Ecostar, regular corn starch was treated with a Silane Coupling Agents (qv) to make it compatible with hydrophobic polymers, and dried to less than 1% of water content. It was then mixed with the other additives such as an unsaturated fat or fatty acid autoxidant to form a master batch, which is added to a commodity polymer. The polymer can then be processed by convenient methods, including film blowing, Injection Molding (qv) and Blow Molding (qv).

The temperature had to be kept below 230°C to prevent decomposition of the starch, and exposure of the master batch to air had to be minimized to avoid water absorption. Direct addition of starch and autoxidant without the master batch step can also be used; as this requires some specific equipment, it is only practical for large volumes (42). It was claimed that under appropriate conditions, the disintegration time of a buried carrier bag, containing an Ecostar additive to reach 6% starch, will be reduced from hundreds of years to 3–6 years (38). However there is no evidence of a compliance of such materials with the norms of biodegradability and compostability already in place at the international level. Moreover, the destabilization of polyethylene induced by the pro-oxidants may significantly affect its in-use performance as a function of time.

Within the field of starch-filled materials other systems were studied, some of which were completely biodegradable, such as starch/poly(ε-caprolactone) (49), and others partially biodegradable, such as starch/PVC/poly (ε-caprolactone) and its derivatives (50) or starch/modified polyesters (51). ln all these cases starch granules are used to increase the surface area available for attack by microorganisms.

Thermoplastic Starch

Starch can be gelatinized by extrusion cooking technology (52–66). As described by Conway in 1971, extrusion cooking and forming is characterized by sufficient work

and heat being applied to a cereal-based product to cook or gelatinize completely all the ingredients. In general the main components of high pressure cooking extruders are feeders, compression screws, barrels, dies, and heating systems (52). The effects of processing conditions on the gelatinization of starch and on the texture of the extruded product have been studied by several researchers (53–70). Gelatinized materials with different starch viscosity, water solubility, and water absorption have been prepared by altering the moisture content of the raw product and the temperature or the pressure in the extruder. It has been demonstrated that an extrusion-cooked starch can be solubilized without any formation of maltodextrins, and that the extent of solubilization depends on extrusion temperature, moisture content of the starch before extrusion, and the amylose/amylopectin ratio. Mercier (69) analyzed the properties of different types of starch and considered the influence of the following parameters: moisture content between 10.5 and 28%, barrel temperature between 70 and 250°C, residence time between 20 s and 2 min, in a twin-screw extruder. Corn starch, after extrusion cooking, gave a solubility lower than 35%, whereas potato starch solubility was up to 80% (Fig. 1).

Starch gelatinization is a difficult term to clearly define and it was used in the past to describe loss of crystallinity of starch granules, notwithstanding the process conditions applied (18), namely, extrusion cooking, spray drying, or heating of diluted starch slurries. The work carried out by Donovan in 1979 (71) and by Colonna and Mercier in 1985 (72) gave, however, a clear explanation of two different conditions for the loss of crystallinity of starch. Colonna reported that all starches exhibit a pure gelatinization phenomenon, which is the disorganization of the semicrystalline structure of the starch granules during heating in the presence of a water fraction >0.9. For normal genotypes, gelatinization occurs in two stages. The first step, at around 60–70°C, corresponds mainly to swelling of the granules, with limited leaching. Loss of birefringence, demonstrating that macromolecules are no longer oriented, occurs prior to any appreciable increase in viscosity. By contrast, differential scanning calorimetry (DSC) permits the determination of the gelatinization temperature more easily and precisely than microscopy and, additionally, the energy input needed to disorganize the crystalline structure of the granules. The second step, above 90°C, implies the complete disappearance of granular integrity by excessive swelling and solubilization. Nevertheless this last transition is not detectable by DSC. Only at this stage the swollen granules can be destroyed by shear.

As observed by Donovan (71) and Colonna (72), at low water volume fractions ($V_1 < 0.45$) loss of crystallinity occurred by two (pea and high amylose maize) or three (standard maize) crystalline melting steps, according to the Flory equation (Fig. 2):

$$1/T_m - 1/T_{m_o} = (R/\Delta H_u)(V_u/V_1)(V_1 - X_1 V_1)$$

where R is the gas constant, ΔH_u the fusion enthalpy per repeating unit (anhydroglucose), V_u/V_1 the ratio of the molar volume of the repeating unit to the molar volume of the diluent (water), T_m (K) the melting point of the crystalline polymer plus diluent, T_{m_o} (K) the true melting point of undiluted polymer crystallites, V_1 the volume fraction of the diluent, and X_1 the Flory–Huggins interaction parameter. At high water volume fractions, melting of crystallites and swelling are cooperative processes. According to Colonna, during extrusion cooking and

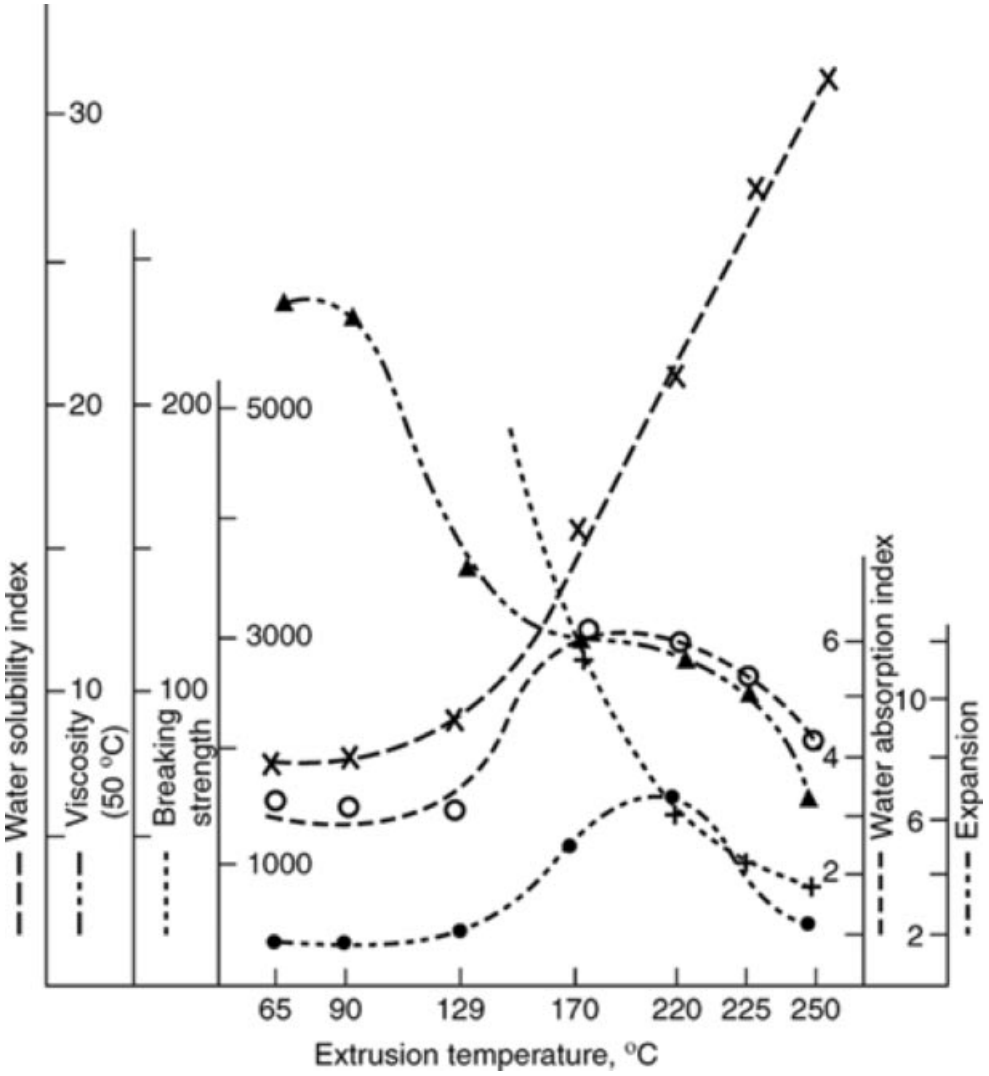

Fig. 1. Effects of extrusion temperature on expansion (●), breaking strength (+), viscosity at 50°C (▲), water absorption index (○), and water-solubility index (x) of extruded products from corn grits. Initial moisture content before extrusion was 18.2% by weight (69).

mainly under the conditions described by Mercier (water volume fraction <0.28) (68) starch undergoes a real melting.

In the patent literature the term *destructurized starch* (73–91) refers to a form of thermoplastic starch described as molecularly dispersed in water (92). Destructurization of starch is defined as melting and disordering of the molecular structure of the starch granules and as a molecular dispersion (75,92). The molecular structure of the starch granules is molten and consequently the granular structure disappears. This is achieved by heating the starch above the glass-transition and the melting temperature of its components until they undergo endothermic

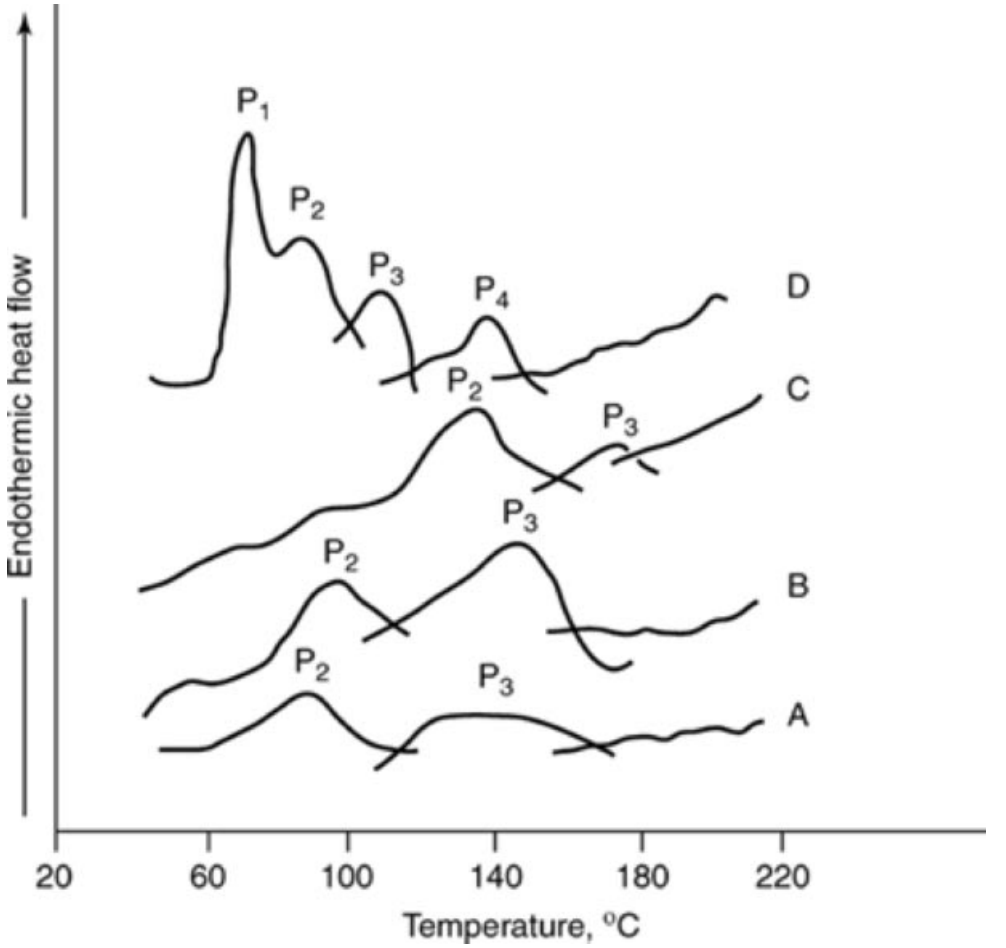

Fig. 2. Typical DSC curves for pea and maize starch. Water volume fractions (V_1): wrinkled pea (A), $V_1 = 0.35$; smooth pea (B) $V_1 = 0.29$; high amylose maize (C), $V_1 = 0.20$; and normal maize (D), $V_1 = 0.55$. Reprinted from Ref. 72, copyright 1985, with kind permission from Elsevier Science.

transitions. In the melt stage both the crystalline and the granular structure of the starch are destroyed and the starch–water system forms a single phase in which no structure is discernible microscopically. The disappearance of the molecular structure of the starch granule may be determined using conventional light microscopy techniques (93).

If starch is heated above the glass-transition and melting temperatures in presence of plasticizers, the endothermic transition can be replaced by an exothermic transition. Destructurized starch, in simple terms, is a form of thermoplastic starch suitable for applications in the sector of plastics, with minimized defects tied to the granular structure of native starch (17,94,98).

Thermoplastic starch alone can be processed as a traditional plastic (69, 92,99); its sensitivity to humidity, however, makes it unsuitable for most of the

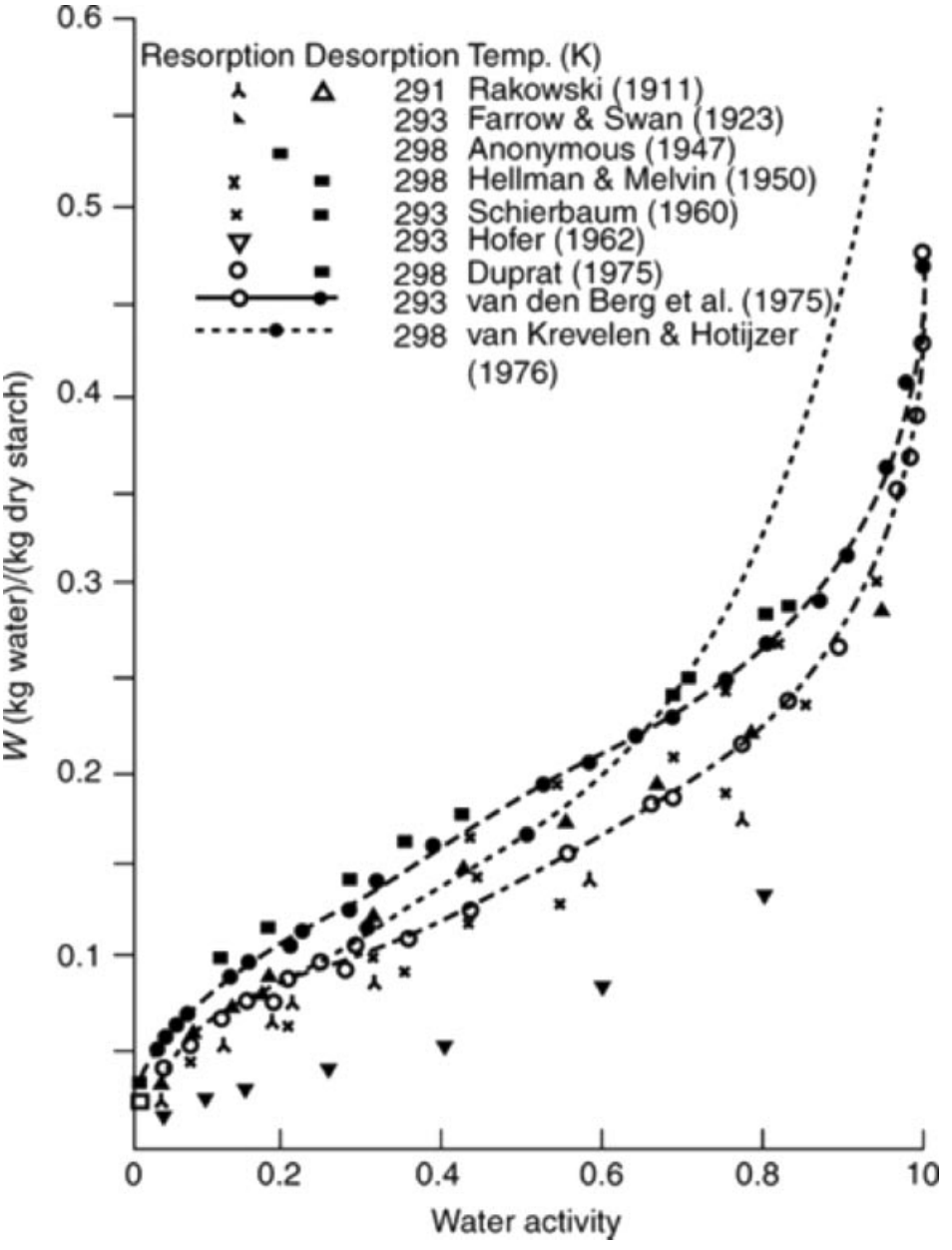

Fig. 3. Some sorption isotherms of water vapor on native potato starch as reported in the literature (100).

applications (Fig. 3). Starch can be also made thermoplastic at water contents lower than 10%, in the presence of high boiling point plasticizers (14,17), to avoid expansion phenomena at the die.

Another term which can be found in the literature is *thermoplastically processable starch* (TPS), defined as a thermoplastic starch substantially water-free.

Table 1. Influence of Starch/EAA Ratio and of Partial Replacement of EAA with PE or PVOH on the Tensile Strength and Elongation of Starch/EAA Films[a]

Starch, phr	EAA, phr	PE, phr	PVOH, phr	Elongation, %	UTS,[b] MPa
10	90	—	—	260	23.9
30	70	—	—	150	22.2
40	60	—	—	92	26.7
40	40	20	—	66	23.9
40	25	25	—	85	21.7
40	20	40	—	34	20.1
40	55	—	5	97	32.0
40	40	—	20	59	39.7

[a]From Refs. 112 and 118.
[b]Ultimate tensile strength.

Thermoplastically processable starch is a modified native starch which is obtained without water, since instead of water, use is made of a plasticizer or additive. The starch is thermoplastically processed together with the additive, and the thermal transition taking place here is exothermic (101–106).

Starch can be destructured in combination with different synthetic polymers to satisfy a broad spectrum of needs for the market. In this case it is possible to reach starch contents higher than 50%. Otey has studied EAA (ethylene–acrylic acid copolymer)/thermoplastic starch composites since 1977 (107–117) and has demonstrated that the addition of ammonium hydroxide to EAA makes it compatible with starch. Urea, in these formulations, enhances the film tear propagation resistance and reduces aging phenomena due to segmental motions in amorphous starch (118,119). The films obtained with a content of plasticized starch of about 50% showed good tensile properties (Table 1) (112). The sensitivity to environmental changes and in particular the susceptibility to tear propagation precluded their use in most packaging applications (118); moreover, EAA is not biodegradable at all.

In 1989 studies on EAA–thermoplastic starch films, containing 40% by weight of EAA, processed at water contents lower than 2%, led to improved processability and film properties with elongation at break up to 200% (93). By microscopic analysis it was possible to observe at least three different phases: one consisting of destructured starch, one consisting of the synthetic polymer alone, and a third one described as "interpenetrated," characterized by a strong interaction between the two components. As a confirmation, phase changes observed by DSC, nuclear magnetic resonance (NMR) (113,117,120–124), for starch–EAA–PE films showed at least four phases. DSC endotherms and extraction of free starch with hot water demonstrated the existence of a starch phase. DSC showed melting of an EAA phase and a low density polyethylene (LDPE) phase but did not indicate the presence of EAA in amorphous regions of the PE. NMR, X-ray diffraction, and extraction indicated the presence of an insoluble starch–EAA complex (124). It was demonstrated that a portion of the starch forms complexes (122,123) with EAA when EAA is salified by ammonium hydroxide or other salts during extrusion cooking, providing partial miscibility between the two polymers.

Rheological studies were performed on a product consisting of 60% starch and natural additives and 40% of an EAA copolymer, containing 20 mol % of

acrylic acid (125). A strong non-Newtonian behavior was shown by the viscosity curves at high shear rates; at intermediate shear rates the material seemed to approach a Newtonian plateau, whereas at low shear rates a viscosity upturn was observed, suggesting the presence of yield stress. Breaking-stretching data for the same material are also reported in the literature, together with those of LDPE (125).

Starch/vinyl alcohol copolymer systems (126–131) can generate a wide variety of morphologies and properties, depending on the processing conditions, the starch type, and the copolymer composition. Different microstructures have been observed, from droplet-like to layered, as a function of different hydrophilicity of the synthetic copolymer. Furthermore, for this type of composite, materials containing starch with an amylose–amylopectin ratio >20/80 wt/wt do not dissolve even with stirring in boiling water. Under these conditions a microdispersion, consisting of microsphere aggregates is produced; individual particle diameters are under 1 μm (Fig. 4). A droplet-like structure is also confirmed by transmission electron microscopic (TEM) analysis of film slices (127). The droplet size is comparable with that of the microdispersion obtained by boiling.

For these products, high melt elasticity is monitored by exit pressure data, whereas its recoverable fraction is almost negligible (low die swell) (129,130). The morphology of materials in film form, containing starch with an amylose–amylopectin ratio lower than 20/80 wt/wt, gradually loses the droplet-like form, generating layered structures (Fig. 5). In this case no microspheres are produced by boiling and the starch component becomes partially soluble. Fourier transform infrared (FTIR) second derivative spectra of materials with droplet-like structure, in the range of starch ring vibrations between 960 and 920 cm^{-1}, gives an absorption peak at about 947 cm^{-1} (Fig. 6). This peak, observed also when starch is

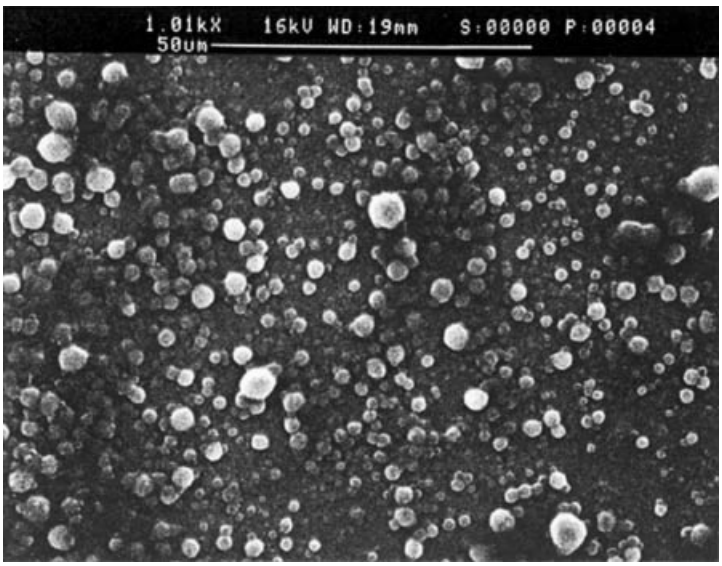

Fig. 4. Droplet-like structure of thermoplastic corn starch/EVOH blend in film from, after disagregation in boiling water (129).

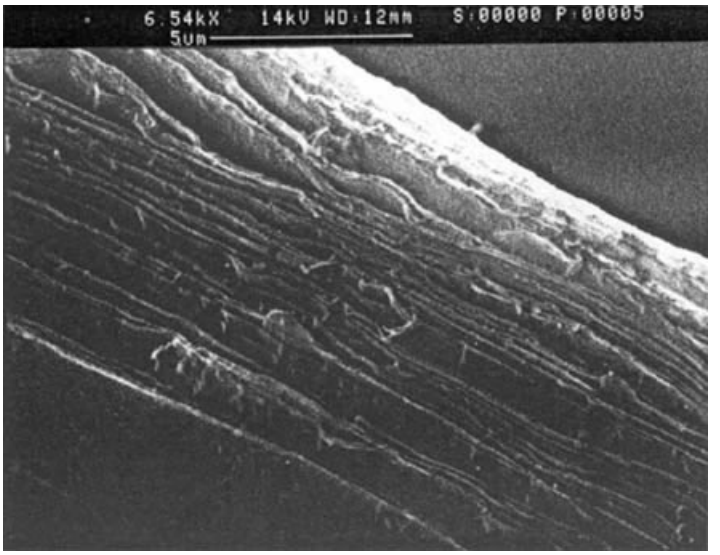

Fig. 5. Layered structure of thermoplastic waxy maize/EVOH film after 3 days of soil burial test (129).

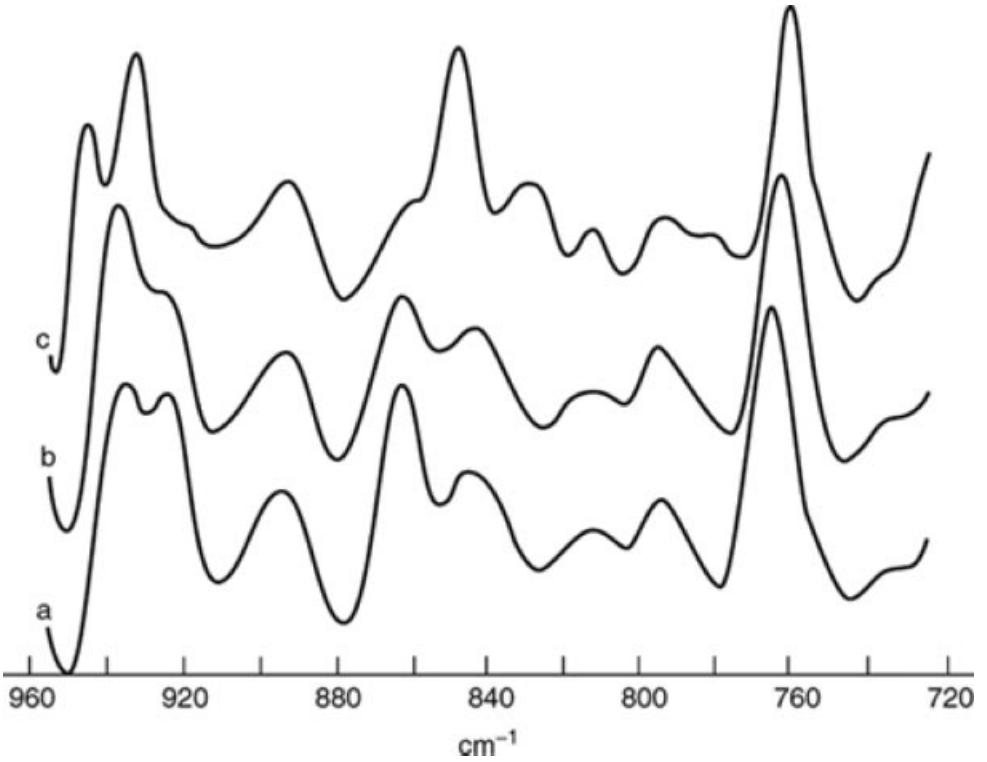

Fig. 6. FTIR second derivative spectrum of corn starch: a, cystalline; b, gelatinized; c, blended with EVOH (129).

Table 2. Insoluble Residue of Starch/EVOH 1:1 Films after Disagregation in Boiling Water as a Function of Starch Composition[a]

Amylose content, %	Insoluble residue,[b] %
5	58.3
10	67.5
15	75.3
20	92.1
25	97.5
28	96.8
70	97.1

[a]From Ref. 129.
[b]Dry starch plus EVOH = 100%.

complexed with butanol, is attributed (21) to ring vibrations, which result when amylose assumes a conformation known as the V form (a left-handed single helix). Therefore, the absorption at 947 cm^{-1} does not correspond to crystalline or gelatinized amylose, but to a complexed one (V-type complex), as in the presence of low molecular weight molecules such as butanol and fatty acid (21,129). Starch-based materials with an amylose content close to zero, even in the presence of vinyl alcohol copolymers, do not show any peak at 947 cm^{-1}, demonstrating that vinyl alcohol copolymers, as well as butanol, leave the amylopectin conformation unchanged.

On the other hand, the V complex formed by starch, having an amylose–amylopectin ratio higher than 20 wt%, with ethylene–vinyl alcohol (EVOH) copolymers makes even amylopectin insoluble in boiling water (Table 2). The experimental evidence was accounted for by a model considering large invididual amylopectin molecules interconnected at several points per molecule as a result of hydrogen bonds and entanglements by chains of amylose–vinyl alcohol copolymer V complexes (129). The biodegradation rate of starch in these materials is inversely proportional to the content of amylose–vinyl alcohol complex. Furthermore FTIR second derivative spectra show the 947 cm^{-1} peak increasing with biodegradation, which means a delayed microbial attack of complexed amylose relative to amylopectin (129). In addition, water permeability of starch/EVOH films is a function of the V-type complex and can range from about 2.46–1 $g \cdot cm/m^2 \cdot day$ 820–334 $g \cdot 30\ \mu m/m^2 \cdot 24h$ (130) (see BARRIER POLYMERS for units).

A general study of shear flow characteristics was performed on a material containing about 60% of starch and natural additives and 40% of ethylene–vinyl alcohol copolymer 40/60 mol/mol (131). A strong pseudoplastic behavior at high shear stresses as well as yield stress at lower ones was detected (Fig. 7). The nonlinear Bingham fluid model (132) well described its viscous behavior over a wide range of shear rates. High levels of melt elasticity were detected from steady shearing tests, whereas its recoverable fraction was almost negligible, at least for a reasonable time scale. The peculiar viscous and elastic behavior has been explained on the basis of the droplet-like morphology generated by the ability of starch to form V complexes in the presence of EVOH. Notwithstanding the peculiar rheological behavior shown by starch/EVOH systems, traditional processing techniques such as film blowing can be easily applied.

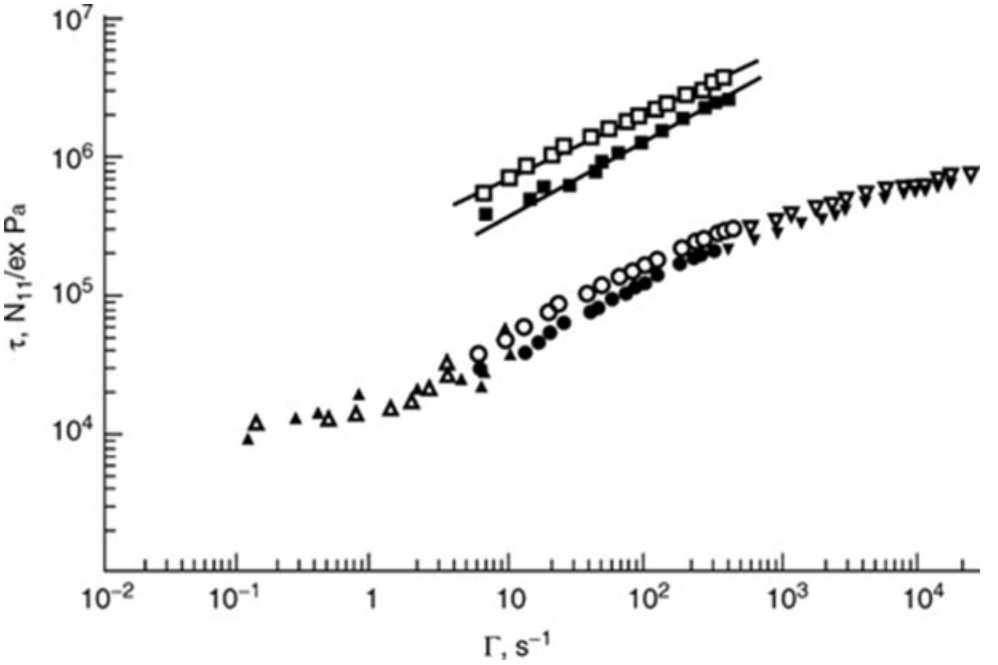

Fig. 7. Shear stress (○,●) and normal stress difference (N_{11}/ex) (□,■) versus wall shear rate of a thermoplastic starch/EVOH blend at 140 (open circles/squares) and 150°C (filled circles/squares) (131).

The products based on starch/EVOH show mechanical properties good enough to meet the needs of specific industrial applications (133). Their moldability is comparable with that of traditional plastics such as polystyrene (PS) and acrylonitrile–butadiene–styrene copolymer (ABS). Nevertheless, they continue to be highly sensitive to low humidities, especially when in film form, with evident embrittlement.

In terms of biodegradation, 10 months of aerobic biological treatment, performed by a high sensitivity respirometric test, provoked the degradation of more than 90% wt/wt of a product constituted by 60% of maize starch and natural additives and by 40% of EVOH copolymer at 40% mol/mol of ethylene. Furthermore, it has also been demonstrated that the synthetic component was degraded to about 80% wt/wt, notwithstanding interrupting the test when CO_2 evolution was still relevant (127,128). A material with the same composition, containing an EVOH copolymer, characterized by a lower ethylene content (29% instead of 40% mol/mol) and, therefore, by a reduced ability to generate interpenetrated structures, showed, in the Sturm test, an initial biodegradation rate significantly higher (127). The semicontinuous activated sludge (SCAS) test and biodegradation in lake water of a product constituted of 70% maize starch and natural additives and 30% EVOH support the hypothesis of substantially different biodegradation mechanisms for the two components (128):

(1) the natural component, even if significantly shielded by the interpenetrated structure, appeared to be initially hydrolyzed by extracellular enzymes;

(2) the synthetic component appeared to be biodegraded through surface adsorption of microorganisms, assisted by the increase of available surface area during the hydrolysis of the natural component.

Other evidences for disappearance of ethylene–vinyl alcohol copolymers have been produced to a limited extent by Roemesser (134) and Kaplan and co-workers (135). The presence of starch improves the biodegradation rate of these synthetic polymers; a fundamental role is also played by size and distribution of ethylene blocks. The degradation rate is too slow to consider these materials as compostable (128).

Specific types of plasticizers were selected in order to avoid migration phenomena and physical aging (133). The possibility of speeding up the biodegradation process was considered by modifying the ethylene–vinyl alcohol copolymer by introducing carbonyl groups, making it more sensitive to photodegradation (136). The transparency of the material was also improved by adding additives such as boric acid, borax, and other saline compounds (137). Surface treatment by wax lamination or coextrusion was also considered (138). With this kind of material it is possible to obtain finished parts by film blowing, injection molding, blow molding, thermoforming, etc. It is also possible to make foamed parts (139), particularly by an expansion process based on injection molding technology. The technology consists of a breathable mold connected with a vacuum pump, applied to an ordinary injection molding madrine (140). Cushioning characteristics of these materials are close to expanded polystyrene (EPS-55) (Fig. 8); moreover, the foam density is of 0.040 g/mL.

Starch can also be destructured in the presence of more hydrophobic polymers such as aliphatic polyesters (141). It is known that aliphatic polyesters with low melting points are difficult to process by conventional techniques for thermoplastic materials, such as film blowing and blow molding. With reference particularly to poly(ε-caprolactone) and its copolymers, films produced thereby are tacky as extruded, and rigid, and have low melt strength over 130°C; moreover, because of the slow crystallization rate of such polymers, the crystallization process proceeds for a long time after production of the finished articles with an undesirable change of properties with time.

Novamont's Mater-Bi starch-based technology implies processing conditions able to almost completely destroy the crystallinity of amylose and amylopectin, in the presence of macromolecules which are able to form a complex with amylose such as specific polyesters. They can be of natural or synthetic origin and are biodegradable. The complex formed by amylose with the complexing agent is generally crystalline, and it is characterized by a single helix of amylose formed around the complexing agent. Unlike amylose, amylopectin does not interact with the complexing agent and remains in its amorphous state. The specification of the starch, ie, the ratio between amylose and amylopectin, the nature of the additives, the processing conditions, and the nature of the complexing agents, allows engineering of various supramolecular structures with very different properties.

The scheme of a "droplet-like" and a "layered" structure which can be produced as a result of Mater-Bi technology is reported in Figures 9 and 10. The droplet-like structure (Fig. 9) is constituted by a core of an almost amorphous

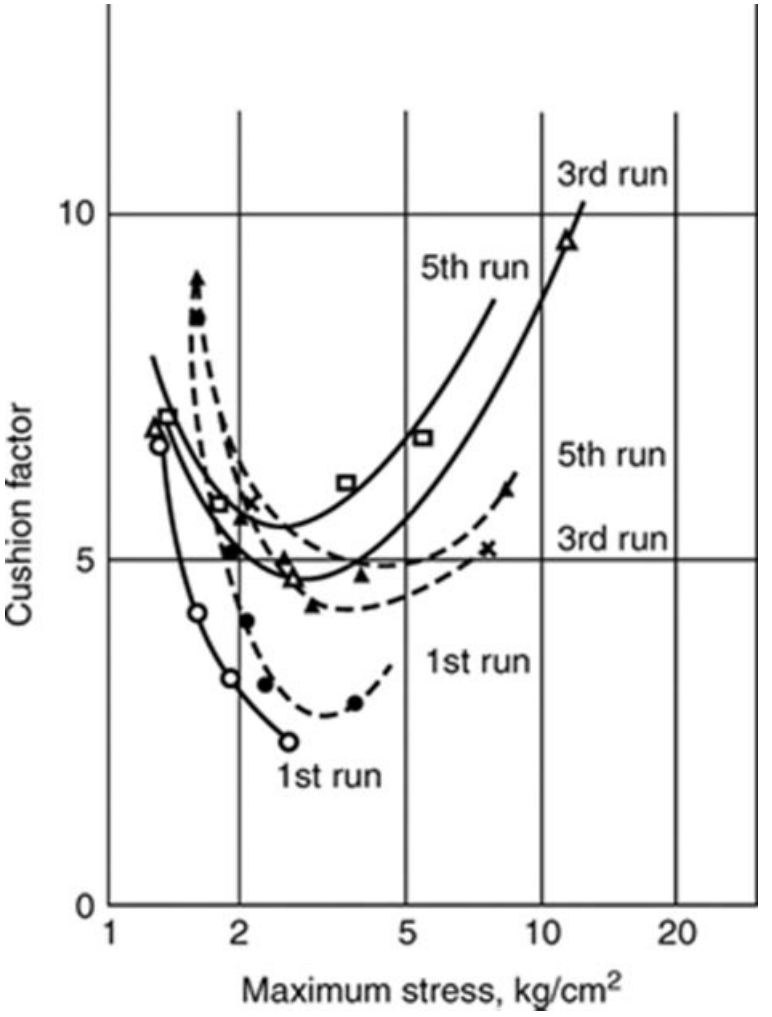

Fig. 8. Dynamic cushioning properties of Mater-Bi molded foams. □, Mater-Bi molded foam; ———, EPS-55. Reprinted from Ref. 140, copyright 1994, with kind permission from Elsevier Science.

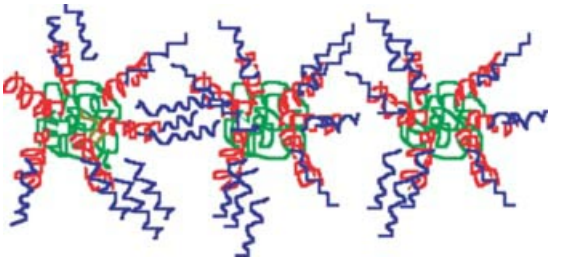

Fig. 9. Mater-Bi technology: droplet-like structure. Green, amylopectin; red, amylose; blue, complexing agent.

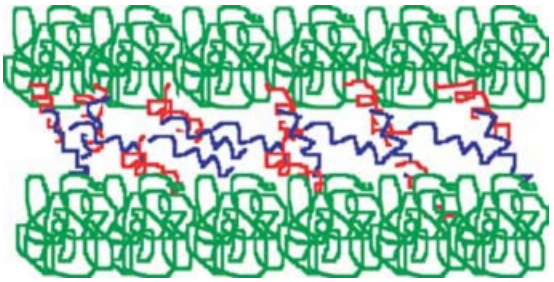

Fig. 10. Mater-Bi technology: layered structure. Green, amylopectin; red, amylose; blue, complexing agent.

amylopectin molecule screened by complexed amylose molecules which render amylopectin insoluble (142–144).

The layered structure is constituted by submicronic layers of amylopectin molecules intercalated by layers of complexing agent; such layers are compatibilized by complexed amylose (Fig. 10). The two structures and the many others derived from them explain the wide range of mechanical, physical-chemical, and rheological properties and the different biodegradation rates of Mater-Bi products.

Blending of starch with aliphatic polyesters improves their processability and biodegradability. Particularly suitable polyesters are poly(ε caprolactone) and its copolymers, or polymers of higher melting point formed by the reaction of 1,4-butandiol with succinic acid or with sebacic acid, azelaic acid, or poly(lactic acid), poly(hydroxyalkanoates), and aliphatic–aromatic polyesters.

The compatibilization between starch and aliphatic polyesters can be promoted either by the processing conditions and or by the presence of compatibilizers between starch and aliphatic polyesters such as amylose/EVOH V-type complexes (129) and starch-grafted polyesters. Chain extenders like diisocyanates, epoxides, etc. are preferred. These types of materials are characterized by excellent compostability and mechanical properties and reduced sensitivity to water.

Thermoplastic starch can also be blended with polyolefins (145). In this case, about 50% of thermoplastically processable starch is mixed with 40% of polyethylene and 10% of ethyl acrylate–maleic anhydride copolymer. During this mixing process an esterification reaction takes place between the maleic anhydride groups in the copolymer and the free hydroxyl groups in starch. Other studies have been performed on polyamide/high amylose (75,146,147) and acrylic copolymers/high amylose starch systems (75,147,148). The problem of partial biodegradability and a too high sensitivity to humidity persists.

Starch/cellulose derivative systems are also reported in other publications (137,141,149,150), particularly, cellulose acetate and butyrate/starch blends in presence of glycerol and epoxidized soybean oil (149).

The combination of starch with a water-soluble polymer such as poly(vinyl alcohol) (PVOH) and/or polyalkylene glycols has been widely considered since 1970 (151). More recently, the thermoplastic starch/PVOH system has been mainly studied for producing starch-based loose fillers as a substitute for expanded polystyrene (152–158). As an example, Altieri and Lacourse developed a technology based on hydroxy propylated high amylose starch containing small amounts of

PVOH for improving foam resiliency and density (152–156). In this case loose fill was produced directly by a twin-screw extruder. More advanced processes and alloys have been developed which have resulted in foams with lower foam densities (8–6 kg/m^3) and better performance (159–161).

Starch-Based Materials on the Market

The market of destructurized and complexed starch-based bioplastics accounts for about 25,000 ton/year, 75% of which is for packaging applications, including soluble foams for industrial packaging and films for bags and sacks. The market share of these products accounts for about 75–80% of the global market of bioplastics (162).

Leading producers with well-established products in the market are Novamont, National Starch, main Novamont partner and licensee in the sector of loose-fills and of foamed sheets, and, finally, Biotec with a capacity of about 2000 ton/year.

Following the recent start-up of its third line dedicated to the production of Mater-Bi film grades in Terni, Novamont's internal production capacity is of 20,000 ton/year. The total capacity, including the network of licensees in the sector of loose fills, is about 35,000 ton/year. The technology for the production of starch-based loose fills is licensed together with National Starch and Chemical Co.

The wide patent portfolio of Novamont covers the technologies of complexed starch developed by Novamont and of destructurized starch developed by Warner Lambert and acquired by Novamont in 1997 after the exit of Warner Lambert from the market in 1993. Moreover, on August 2001 Novamont acquired the film technology of Biotec which included an exclusive license of the Biotec's patents on TPS in the sector of film (162).

In recent years companies such as Earthshell, Apack, and Avebe dedicated significant efforts to the development of food containers through the "baking technology." Market tests are in place in the United States and Europe to check their performances (163). Moreover, very recently in the Netherlands, Rodemburg built up a plant for the transformation of potato wastes generated by the industry of fried potatoes in a granulate to be used for the injection molding of slow release devices. The claimed capacity is 40,000 ton/year.

The price of starch-based bioplastics ranges from 1.25 to 4 Euro/kg, with possibilities to compete even with traditional materials in some limited areas (163).

The properties achieved by starch-based bioplastics in certain applications and the commitment of the companies today dealing with this family of bioplastics give more confidence in the future possibilities of this market sector. Bioplastics from renewable origin, either biodegradable or nonbiodegradable, still constitute a niche market which requires high efforts in the areas of material and application development; the technical and economical breakthroughs achieved in the last three years, however, open new possibilities for such products in the mass markets. Novamont today boasts a diversified portfolio of industrial tailor-made materials for a wide range of applications, which explains its position as market leader (162).

After more than 12 years of research and development, Mater-Bi products are able to fulfil specific in-use performances in different application sectors, and offer original solutions both from the technical and the environmental point of view.

Under the Mater-Bi trademark today, Novamont produces a wide range of materials, divided into five families, according to the processing technologies: film, extrusion/thermoforming, injection molding, foaming, and tires technology. Mater-Bi products are mainly used in specific applications where biodegradability is required; examples include composting bags and sacks, fast food tableware (cups, cutlery, plates, straws, etc), packaging (soluble and insoluble foams for industrial packaging), film wrapping, laminated paper, food containers, agricultural film products (mulch film, nursery pots, plant labels, slow release devices, etc.), and hygiene (diaper backsheet, cotton swabs).

New sectors are also growing outside biodegradability, driven by the unique technical performance of some Mater-Bi products versus traditional materials, as in the case of breathable films with silky hand for diapers, chewable items for pets, or biofillers for tires. The new tire Biotred GT3, launched by Goodyear in 2001 and recently adopted by BMW and Ford, is an example of the high tech performances reached by Mater-Bi products (164).

Mater-Bi starch-based materials are characterized by the following properties:

(1) complete biodegradability and compostability according to existing standards (Fig. 11) (165–167)
(2) significant reduction of environmental impact, particularly with respect to CO_2 emissions and energy consumption, in comparison with traditional materials in specific uses (168,169)
(3) in-use performances similar to traditional plastics
(4) processability similar or improved in comparison with traditional plastic materials (162).

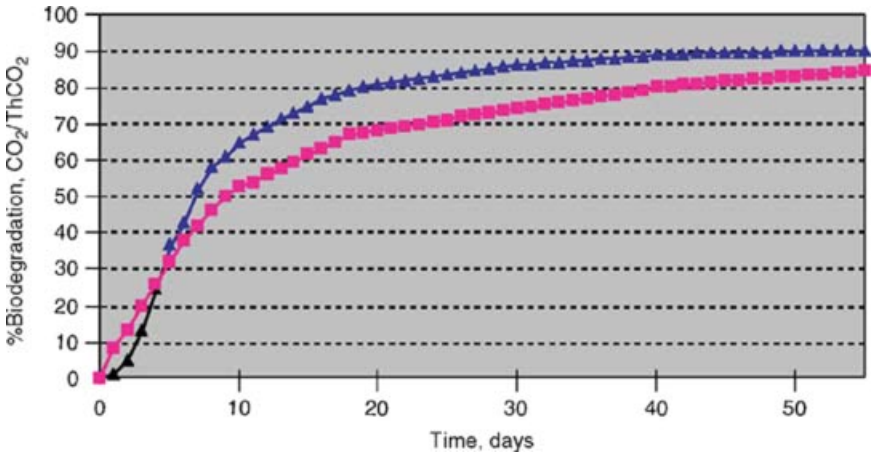

Fig. 11. Aerobic biodegradation of Mater-Agro under controlled composting conditions (EN13432), in comparison with pure cellulose (test performed by OWS, Belgium). ▲, positive control; ■, Mater-Bi.

Table 3. Some Physical Properties of Mater-Bi Grades for Film, in Comparison with Traditional Plastics

Test	Procedure	Unit	Mater-Bi	LDPE
MFI	ASTM D1338	g/10 min	2–8[a]	0.1–22[b]
Strength at break	ASTM D882	MPa[c]	24–30	8–10
Elongation at break	ASTM D882	%	200–1000	150–600
Young's modulus	ASTM D882	MPa[c]	100–400	100–200
Tear strength	ASTM D1938			
Primer		N/mm[d]	30–90	60
Propagation		N/mm[d]	30–90	60

[a] 150°C, 5kg.
[b] 190°C, 2.16 kg.
[c] To convert MPa to psi, multiply by 145.
[d] To convert N/mm to ppi, divide by 0.175.

Other properties of Mater-Bi films of the last generation can be summarized as follows:

(1) soft, silky handle
(2) wide range of permeability to water vapor from 0.75 to 3 $g \cdot cm/m^2 \cdot day$ (250 to 1000 $g \cdot 30\mu m/m^2 \cdot 24h$)
(3) wide range of mechanical properties from soft and tough materials to rigid ones, with no significant aging after one year of storage, (163) (Table 3 and 4)
(4) antistatic behavior
(5) colorability with food contact approved pigments
(6) compostability in a wide range of composting conditions: from home composting and static windrows to rotary fermenting reactors

They are biodegradable and compostable according to the present European standards and are certified by AIB Vincotte in Belgium, by DINCERTCO in Germany, and by IIP in Italy, according to CEN EN13432, DIN 54900, and

Table 4. Some Physical Properties of Mater-Bi Grades for Injection Molding, in Comparison with Traditional Plastics

Test	Procedure	Unit	Mater-Bi[a]	PP[b]	PS[c]
MFI	ASTM D1238	g/10 min	20–10	0.3–40	1.2–25
Strength at break	ASTM D638	MPa[d]	20–30	23	30–60
Elongation at break	ASTM D638	%	20–500	400–900	1–4.5
Young's modulus	ASTM D638	MPa	200–2000	1400–1800	3000–3500
IZOD (notched impact)	ASTM D256	kJ/m^2[e]	1–80	3–10	2–3

[a] 170°C, 5 kg.
[b] 23°C, 2.16 kg.
[c] 200°C, 5 kg.
[d] To convert MPa to psi, multiply by 145.
[e] To convert kJ/m^2 to $ftlbf/in^2$, divide by 2.1.

UNI 10785 standards, respectively (see DEGRADABLE POLYMERS AND PLASTICS IN LANDFILL SITES).

After the acquisition of Enpac in 1998 and the subsequent agreement with Novamont, National Starch is licensing two technologies for the production of loose fills: one from hydroxypropilated high amylose starch and a second from almost unmodified starch. The loose fills' densities range from 6 to 10 kg/m^3. The main licensees are Unisource, American Excelsior, Storopack, and Flow Pack in the United States.

Biotec, the German company which acquired in 1994 the patents of Fluntera, was acquired by EKI (Essem Kashoggi Industries) in 1998. Biotec, after the sale of the film business to Novamont in 2000 is concentrated on foodserviceware products and on pharmaceutical products.

Conclusions

Starch-based bioplastics constitute a new generation of materials able to significantly reduce the environmental impact in terms of energy consumption and green-house effect in specific applications, to perform as traditional plastics when in use, and to completely biodegrade within a composting cycle through the action of living organisms when engineered to be biodegradable. They offer a possible alternative to traditional materials when recycling is inpractical or not economical, or when environmental impact has to be minimized.

After more than 12 years of research and development, starch-based materials have begun to fulfil specific in-use performances in different application sectors. They are able to offer original solutions both from the technical and the environmental point of view.

Today some of the bioplastics available in the market are used in specific applications where biodegradability is required, such as the sectors of composting (bags and sacks), fast food tableware (cups, cutlery, plates, straws etc), packaging (soluble foams for industrial packaging, film wrapping, laminated paper, food containers), agriculture (mulch film, nursery pots, plant labels), hygiene (diaper back sheet, cotton swabs) and slow release devices in agricultural and pharmaceutical sectors. Moreover, new sectors are growing outside biodegradability, driven by improved technical performances versus traditional materials, as in the case of biofillers for tires and chewable items for pets.

The price of bioplastics from renewable origin is decreasing and ranges from 1.25 to 4 Euro/kg, with possibilities to compete even with traditional materials in some limited areas.

The world market for biodegradable plastics is still small, but it has grown significantly in the last few years, reaching about 33000 ton/year in the year 2000; products totally or partially from renewable resources represent nearly 85–90% of this market (170).

BIBLIOGRAPHY

1. *Corn Annual Report*, Corn Refiners Assoc., Inc., Washington, D.C., 1991, p. 20.
2. E. B. Bagley, G. F. Fanta, R. C. Burr, W. M. Doane, and C. R. Russell, *Polym. Eng. Sci.* **17**, 311–316 (1977).

3. Seiberlich, *J. Mod. Plast.* **18**(7), 64–65 (1941).
4. U.S. Pat. 40,26,849 (May 31, 1977), E. B. Bagley, G. F. Fanta, W. M. Doane, L. A. Gugliemelli, C. R. Russell (to The United States of America as represented by the Secretary of Washington, DC).
5. U.S. Pat. 43,82,813 (May 10, 1983), B. S. Shasha (to The United States of America as represented by the Secretary of Washington, DC).
6. U.S. Pat. 44,39,488 (Mar. 27, 1984), D. Trinmell and B. S. Shasha (to The United States of America as represented by the Secretary of Washington, DC).
7. U.S. Pat. 43,44,857 (Aug. 17, 1982), B. S. Shasha, W. M. Doane, and C. R. Russel (to The United States of America as represented by the Secretary of Washington, DC).
8. U.S. Pat. 43,48,492 (Sept. 7, 1982), B. S. Shasha and T. P. Abbott (to The United States of America as represented by the Secretary of Washinvgton, DC).
9. U.S. Pat. 44,83,950 (Nov. 20, 1984), G. F. Fanta, W. M. Doane, and E. I. Stout (to The United States of America as represented by the Secretary of Washington, DC).
10. U.S. Pat. 43,30,443 (May 18, 1982), J. C. Rankin (to The United States of America as represented by the Secretary of Washinvgton, DC).
11. U.S. Pat. 40,16,117 (Apr. 5, 1977), G. J. L. Griffin (to Coloroll Ltd., London).
12. F. H. Otey, R. P. Westhoff, and C. R. Russell, *Symposium Papers, Technical Symposium*, Nonwoven Product Technology, Miami Beach, Fla., 1975, pp. 40–47.
13. F. T. Stepto and I. Tomka, *Chimia* **41**(3), 76–81 (1987).
14. PTC Int. Pat. Appl. WO 90/05161 (May 17, 1990), I. Tomka (to Dr. Troesch, AG).
15. Eur. Pat. Appl. 03 76 201 (July 4, 1990), N. L. Lacourse and P. A. Altieri (to Nat Starch Chem Corp US).
16. PCT Int. Pat. Appl. WO 90/14938 (Dec. 13, 1990), A. T. Knight (to Goodman Fielder Wattie Austral, AU).
17. Eur. Pat. Appl. EP 0400531 (Dec. 5, 1990), C. Bastioli, R. Lombi, G. F. Del Tredici, and I. Guanella (to Butterfly Srl, Italy).
18. F. H. Otey and W. M. Doane, in R. L. Whistler, J. N. BeMiller, and E. F. Paschall, eds., *Starch Chemistry and Technology*, Academic Press, London, 1984, pp. 154–155, pp. 667–669.
19. F. H. Otey and W. M. Doane, in R. L. Whistler, J. N. BeMiller, and E. F. Paschall, eds., *Starch Chemistry and Technology*, Academic Press, London, 1984, pp. 397–403.
20. J. J. Cael, J. L. Koening, and Blackwell, *J. Biopolymers* **14**, 1885–1903 (1975).
21. B. Casu and M. Reggiani, *Die Starke* **7**, 218–228 (1966).
22. Henry F. Zobel, in R. L. Whistler, J. N. BeMiller, and E. F. Paschall, eds., *Starch Chemistry and Technology*, Academic Press, London, 1984, pp. 287.
23. PCT Int. Pat. Appl. W091/04286 (1991), G. J. L. Griffin.
24. IT 10,24,922 (July 20, 1978), G. J. L. Griffin (to Coloroll Ltd. GB).
25. U.S. Pat. 4,02,13,88 (May 3, 1977), G. J. L. Griffin (to Coloroll Ltd.).
26. U.K. Pat. 14,85,833 (Sept. 14, 1977), G. J. L. Griffin (to Coloroll Ltd.).
27. U.S. Pat. 41,25,495 (Nov. 14, 1978), G. J. L. Griffin (to Coloroll Ltd.).
28. U.S. Pat. 43,24,709 (Apr. 13, 1982), G. J. L. Griffin (to Coloroll Ltd.).
29. Eur. Pat. 363 383 B (Apr. 18, 1990), G. J. L. Griffn (to Epron Ind Ltd., GB).
30. Int. Pat. Appl. WO 92/01741 (Feb. 6, 1992), G. J. L. Griffin (to Epron Ind Ltd., GB).
31. G. J. L. Griffin, *Prog. Biotechnol.* **1**, 201–210 (1985).
32. R. Warren, *Bridges* 23–25 (1989).
33. G. J. L. Griffin, *Pure Appl. Chem.* **52**, 399–407 (1980).
34. J. L. Griffin, *ACS Adv. Chem. Ser., No. 18424* (1975).
35. J. D. Evans and S. K. Sikdar, *CHEMTECH* **20**, 38–42 (1990).
36. R. Johnson, in *Proceedings of Symposium on Degradable Plastics*, Society of the Plastics Industry, Washington, D.C., June 10, 1987, pp. 6–13.
37. W. Hiltz, *Nat. Living* 13 (1989).

38. W. J. Maddever, in *Proceedings of Symposium on Degradable Plastics*, Society of the Plastics Industry, Washington, D.C., June 10, 1987 pp. 41–44.
39. U.K. Pat. 1,356,107 (June 12, 1974), G. Scott.
40. U.S. Pat. 4,519,161 (May 28, 1985), D. Gilead and G. Scott.
41. U.S. Pat. 5,216,043 (June 1, 1993), A. J. Sipinen, J. T. Jaeger, D. R. Rutherford, and E. C. Edblom (to Minnesota Mining and Manufacturing Co.).
42. P. J. Hocking, *J. Macromol. Sci.—Rev. Macromol. Chem. Phys.* **C32**(1), 35–54 (1992).
43. A. L. Andrady, J. E. Pegram, and S. J. Nakatsuka, *Environ. Polym. Degrad.* **1**(1), 31–43 (1993).
44. A. L. Andrady, J. E. Pegram, and Y. J. Tropsha, *Environ. Polym. Degrad.* **1**(3), 171–179 (1993).
45. R. Wilder, *Mod. Plast. Int*. (Sept. 1989).
46. R. Narayan and W. Lafayette, *Kunstoffe German Plast.* **79**, 92–95 (1989).
47. R. H. Thomas, *Polym. News* **14**(9), 271–273 (1989).
48. *High-Tech Mater. Alert* **7**(3), 4–6 (1990).
49. Jpn. Pat. Appl. 146953 (1992), (to Chuo Chemical Co.).
50. U.S. Pat. 48,73,270 (Oct. 10, 1989), J. M. Aime, G. Mention, and A. Thouzeau (to Charbonnages De France, Paris, FR).
51. U.S. Pat. 5,219,646 (June 15, 1993), F. G. Gallagher, H. Shin, and R. F. Tietz (to E. I. Du Pont de Nemours and Co. Inc., Wilmington, DE).
52. H. F. Conway, *Food Prod. Dev*. pp. 141–131 (1971).
53. B. Y. Chiang and A. J. Johnson, *Cereal Chem.* **54**(3), 429–435 (1977).
54. H. F. Conway, E. B. Lancester, and G. N. Bookwalter, *Food Eng*. 1021 (1968).
55. C. Mercier, *Feedstufs* **4**, 33–39 (1971).
56. B. T. Lawton, G. A. Henderson, and E. J. Derlatka, *Can. J. Chem. Eng.* **50**, 168–172 (1972).
57. R. A. Anderson, H. F. Conway, and V. F. Pfeifer, *Griffin Cereal Sci. Today* **14**(1), 4–7 (1969).
58. R. L. Derby, B. S. Miller, and H. B. Trimbo, *Cereal Chem.* **52**(5), 702–713 (1975).
59. D. V. Harmann and J. M. Harper, *Trans. ASAE* 1175–1178 (1973).
60. J. F. De La Gueriviere, *Bull. Anc. Eleves Ec. Fr. Meum.* **276**, 305–314 (1976).
61. D. J. Stevens and G. A. H. Elton, *Die Starke* **23**(1), 8–11 (1971).
62. R. A. Anderson, H. F. Conway, and A. Peplinski, *J. Die Starke* **22**(4), 130–135 (1970).
63. H. H. Mottern, J. J. Spadaro, and A. S. Gallo, *Food Technol.* **23**, 169–171 (1969).
64. R. M. Shetty, D. R. Lineback, and P. A. Seib, *Cereal Chem.* **51**, 364–375 (1974).
65. B. S. Miller, R. I. Derby, and H. B. Trimbo, *Cereal Chem.* **50**, 271–280 (1973).
66. B. Y. Chiang and A. J. Johnson, *Cereal Chem.* **54**(3), 436–443 (1977).
67. R. A. Anderson, H. F. Conway, V. F. Pfeifer, and E. L. Griffin, *Cereal Sci. Today* **14**, 372–381 (1969).
68. C. Sterling, *J. Texture Stud.* **9**, 225–255 (1978).
69. C. Mercier and P. Feillet, *Cereal Chem.* **52**(3), 283–297 (1975).
70. R. A. Anderson, H. F. Conway, V. F. Pfeifer, and Griffin, *Cereal Sci. Today* **14**(1), 4–7 (1969).
71. J. W. Donovan, *Biopolymers* **18**, 263 (1979).
72. P. Colonna and C. Mercier, *Phytochemistry* **24**(8), 1667–1674 (1985).
73. U.S. Pat. 4,900,361 (Feb. 13, 1990), J. P. Sacchetto, R. F. T. Stepto, H. Zeller (to Warner-Lambert Co., Morris Plains, NJ).
74. Eur. Pat. 0 326 517 B (Aug. 2, 1989), R. F. T. Stepto and B. Dobler (to Warner Lambert Co., US).
75. Eur. Pat. 0 327 505 B (Aug. 9, 1989), G. Lay, J. Rehm, R. F. T. Stepto, and M. Thoma (to Warner Lambert Co., US).

76. Eur. Pat. Appl. 0 391 853 (Oct. 10, 1990), J. P. Sacchetto, M. Egil, R. F. T. Stepto, and J. Zeller (to Warner Lambert Co., US).
77. Eur. Pat. 0 404723 B (Dec. 27, 1990), J. P. Sacchetto, D. J. Lentz, and Silbiger (to Warner Lambert Co., US).
78. Eur. Pat. Appl. 0404 728 (Dec. 27, 1990), J. Silbiger, J. P. Sacchetto, and D. J. Lentz (to Warner Lambert Co., US).
79. Eur. Pat. Appl. 0 407 350 (Jan. 9, 1991), J. P. Sacchetto and J. Rehm (to Warner Lambert Co., US).
80. Eur. Pat. Appl. 0408501 (Jan. 16, 1991), J. Silbiger, J. P. Sacchetto, and D. Lentz (to Warner Lambert Co., US).
81. Eur. Pat. Appl. 0 408502 (Jan. 16, 1991), J. P. Sacchetto, J. Silbiger, and D. J. Lentz (to Warner Lambert Co., US).
82. Eur. Pat. 0 408 503 B (Jan. 16, 1991), J. Silbiger, D. Lentz, and J. P. Sacchetto (to Warner Lambert Co., US).
83. Eur. Pat. 0 409 781 B (Jan. 23, 1991), J. P. Sacchetto, J. Silbiger, and D. J. Lentz (to Warner Lambert Co., US).
84. Eur. Pat. 0 409 782 B (Jan. 23, 1991), D. Lentz, J. P. Sacchetto, and J. Silbiger (to Warner Lambert Co., US).
85. Eur. Pat. 0 409 783 B (Jan. 23, 1991), J. P. Sacchetto, J. Silbiger, and D. J. Lentz (to Warner Lambert Co., US).
86. Eur. Pat. 0 409 788 B (Jan. 23, 1991), D. Lentz, J. P. Sacchetto, and J. Silbiger (to Warner Lambert Co., US).
87. Eur. Pat. 0 409 783 B (Jan. 23, 1991), J. Silbiger, D. J. Lentz, and J. P. Sacchetto (to Warner Lambert Co., US).
88. Eur. Pat. Appl. 0 500 885 (Sept. 2, 1992), E. T. Cole and M. Egli (to Warner Lambert Co., US).
89. Eur. Pat. Appl. 0 679 172 (Sept. 2, 1995), M. J. Izbicki, G. Loomis, and A. Flammino (to Novon International Inc., US).
90. Eur. Pat. Appl. 1 109 858 (June 27, 2001), F. Degli Innocenti, R. Lombi, C. Bastioli, M. Nicolini, and M. Tosin (to Novamont Spa, Italy).
91. Eur. Pat. Appl. 965 615 (Dec. 22, 1989), V. Bellotti, R. Lombi, C. Bastioli, I. Guanella, and G. Del Tredici (to Novamont Spa, Italy).
92. Eur. Pat. 0 I 18 240 (Sept. 12, 1984), F. Wittwer and I. Tomka (to Warner Lambert Co., US).
93. H. B. Wigman, W. W. Leathen, and M. J. Brackenbeyer, *Food Technol.* **10**, 179–184 (1956).
94. U.S. Pat. 52,62,458 (Nov. 16, 1993), C. Bastioli, V. Bellotti, L. Del Giudice, G. Del Tredici, R. Lombi, A. Rallis (to Novamont SpA, Milan, Italy).
95. Eur. Pat. Appl. EP 0400532 (Dec. 5, 1990), C. Bastioli, V. Bellotti, L. Del Giudice, and R. Lombi (to Butterfly Srl, Italy).
96. Int. Pat. Appl. EP 0437561 (July 24, 1991), C. Bastioli, V. Bellotti, L. Del Giudice, and R. Lombi (to Butterfly Srl Italy).
97. Eur. Pat. Appl. EP 0437589 (July 24, 1991), C. Bastioli, V. Bellotti, and G. F. Del Tredici (to Butterfly Srl, Italy).
98. Int. Pat. Appl. EP 0494287 (July 15, 1992), C. Bastioli, V. Bellotti, A. Montino, G. del Tredici, and R. Lombi (to Butterfly Srl Italy). U.S. Pat. 4,673,438 (Apr. 6, 1987), F. Wittwer and I. Tomka.
99. U.S. Pat. 27,88,546 (Apr. 6, 1957), C. R. Russell and L. Hellies (to USDA).
100. C. Van den Berg, *Vapour Sorption Equilibria and Other Water-Starch Interactions: A Physico-Chemical Approach*, Agricultural University, Wageningen, The Netherlands 1981, p. 49.
101. Eur. Pat. 0 397819 B (Nov. 22, 1990), I. Tomka.

102. Eur. Pat. 0 539 544 B (May 5, 1993), I. Tomka.
103. Eur. Pat. 0 537 657 B (Apr. 21, 1993) I. Tomka, J. Meissner, and R. Menard.
104. Eur. Pat. 0 542 155 B (May 19, 1993), I. Tomka.
105. U.S. 6,242 102 (June 5, 2001), I. Tomka (to Biotec Biologische Natuverpackungen GmbH & Co., KG).
106. Eur. Pat. 0 596 437 B (May 11, 1994), I. Tomka (to Fluntera Ag, CH).
107. U.S. Pat. 41,33,784 (Jan. 9, 1979), F. H. Otey (to The United States of America as represented by the Secretary of Washington, DC).
108. Eur. Pat. 1,32,299 (Jan. 30, 1985), R. P. Westhoff and F. H. Otey (to US Commerce, US).
109. U.S. Pat. 44,54,268 (June 12, 1984), F. H. Otey and R. P. Westhoff (to The United States of America as represented by the Secretary of Washington, DC).
110. U.S. Pat. 43,37,181 (June 29, 1982), F. H. Otey and R. P. Westhoff (to The United States of America as represented by the Secretary of Washington, DC).
111. F. H. Otey, R. P. Westhoff, and W. M. Doane, *Ind. Eng. Chem. Res.* **26**, 1659–1663 (1987).
112. F. H. Otey, R. P. Westhoff, and W. M. Doane, *Ind. Eng. Chem. Prod. Res. Dev.* **19**, 592–595 (1980).
113. R. P. Westhopp, F. H. Otey, Ch. L. Mehltretter, and C. R. Russell, *Ind. Eng. Chem. Prod. Res. Dev.* **13**(2), 123–125 (1974).
114. F. H. Otey, *Polym. Plast. Technol. Eng.* **7**(2) 221–234 (1976).
115. F. H. Otey, R. P. Westhofh, and C. R. Russell, *Ind. Eng. Chem. Prod. Res. Dev.* **15**(2), 1392 (1976).
116. F. H. Otey, A. M. Mark, Mehltretter, and C. R. Russell, *Ind Eng. Chem. Prod. Res. Dev.* **13**(1), 90–92 (1974).
117. U.S. Pat. 48,39,450 (June 13, 1989), G. F. Fanta and F. H. Otey (to The United States of America as represented by the Secretary of Washington, DC).
118. C. L. Swanson, R. L. Shogren, G. F. Fanta, and S. H. Imam, *J. Environ. Polym. Soc.* **1**(2), 155–166 (1993).
119. R. L. Shogren, *Carbohydr. Polym.* **19**, 83–90 (1992).
120. G. F. Fanta, C. L. Swanson, and W. M. Doane, *Polym. Prepr. (Am. Chem. Soc., Div. Polym. Chem.)* **29**(2), 453–454 (1988).
121. G. F. Fanta, C. L. Swanson, and W. M. Doane, *J. Appl. Polym. Sci.* **40**, 811–821 (1990).
122. G. F. Fanta, C. L. Swanson, and W. M. Doane, *Carbohydr. Polym.* **17**, 51–58 (1992).
123. G. F. Fanta, C. L. Swanson, and R. L. Shogren, *J. Appl. Polym. Sci.* **44**, 2037–2042 (1992).
124. R. L. Shogren, A. R. Thompson, F. C. Felker, R. E. Harry-Ökuru, S. H. Gordon, R. V. Greene, and J. M. Gould, *J. Appl. Polym. Sci.* **44**, 1971–1978 (1992).
125. C. Bastioli, A. Rallis, F. Cangiatosi, M. Vert, J. Feijen, A. Albertsson, G. Scott, E. Chiellini, *Proceeding of the Polymer Processing Society—European Regional Meeting*, Palermo, Sept. 15–18, 1991.
126. C. Bastioli and V. Bellotti, *Agrobiotecnologie e nuove produzioni chimiche da risorse rinnovabili*, Accademia Nazionale dei Lincei, Rome, Nov. 26–27, 1990.
127. C. Bastioli, V. Bellotti, L. Del Giudice, and G. Gilli, *J. Environ. Polym. Degrad.* **1**(3), 181–191 (1993).
128. C. Bastioli, V. Bellotti, L. Del Giudice, and G. Gilli, in M. Vert, J. Feijen, A. Albertson, G. Scott, and E. Chiellini, eds., *Biodegradable Polymers and Plastics*, The Royal Society of Chemistry, Cambridge, UK, 1992, pp. 101–110.
129. C. Bastioli, V. Bellotti, M. Camia, L. Del Giudice, and A. Rallis, in Y. Doi and K. Fukuda, eds., *Biodegradable Plastics and Polymers*, Elsevier Science, Inc., Elmeford, N.Y., 1994, pp. 200–213.

130. Ital. Appl. EP 0560244 (Sept. 15, 1993), C. Bastioli, V. Bellotti, G. F. Del Tredici, A. Montino, R. Ponti (to Novamont Spa, Italy).
131. C. Bastioli, V. Bellotti, and A. Rallis, *Rheol. Acta* **33**, 307–316 (1994).
132. W. H. Herschel and R. Bulkley, *Proc. ASTM* **26**, 621 (1926).
133. Int. Pat. Appl. 92/14782 (Sept. 3,1992), C. Bastioli, V. Bellotti, and A. Montino (to Novamont Spa, Italy).
134. J. Roemesser, *Presentation at Plastics Waste Management Workshop*, American Chemical Society, Polymer Chemistry Division, New Orleans, LA, Dec. 1991.
135. D. L. Kaplan, J. M. Mayer, and D. Ball, in *Proceedings Biodegradable Packaging Symposium*, Natick, Mass., June 1992.
136. Int. Pat. Appl. WO 91/02024 (Feb. 21, 1991), C. Bastioli, V. Bellotti, L. Del Giudice, and R. Lombi (to Butterfly Srl, Italy).
137. Int. Pat. Appl. WO 92/01743 (Feb. 6, 1992), C. Bastioli, V. Bellotti, A. Montino, and co-workers (to Butterfly Srl Italy).
138. Int. Pat. Appl. WO 92/02363 (Feb. 20, 1992), C. Bastioli, V. Bellotti, G. C. Romano, and M. Tosin (to Butterfly Srl, Italy).
139. Int. Pat. Appl. WO 91/02023 (Feb. 21, 1991), C. Bastioli, V. Bellotti, and L. Del Giudice (to Butterfly Srl Italy).
140. Y. Yoshida and T. Uemura, in Y. Doi and K. Fukuda, eds., *Biodegradable Plastics and Polymers*, Elsevier, pp. 443–450 (1994).
141. Int. Pat. Appl. WO 92/19680 (Sept. 12, 1992), C. Bastioli, V. Bellotti, G. F. Del Tredici, R. Lombi, A. Montino, R. Ponti (to Novamont Spa, Italy).
142. C. Bastioli, *Polym. Degrad. Stab.* **59**, 263–272 (1998).
143. C. Bastioli, *Starch Based Materials: Properties and Applications—Renewable Bioproducts, Industrial Outlets and Research for the 21st Century Wageningen*, The Netherlands, 1997.
144. C. Bastioli, *Global Status for Biodegradable Polymers Production*, 7th Annual Meeting of Bio/Environmentally Degradable Polymer Society, Cambridge, Mass., 1998.
145. Int. Pat. Appl. WO 92/20740 (Nov. 26, 1992), I. Tomka.
146. Eur. Pat. Appl. 0541050 A2 (May 12, 1993), F. S. Buehler, V. Baron, E. Schmid, and P. Meir (to Inventa Ag, CH).
147. Eur. Pat. Appl. 0522358 (Jan. 13, 1993), E. Schmid and F. S. Buehler (to Inventa Ag, CH).
148. Int. Pat. 437 589 (July 24, 1961), C. Bastioli, V. Bellotti, and G. F. Del Tredici (to Butterfly Srl, Italy).
149. Eur. Pat. Appl. 0542155 (May 19, 1993), I. Tomka.
150. Eur. Pat. 0 551 125 B (July 14, 1993), J. Schroeter (to Buck Chem Tech Werke, Germany).
151. C. S. Maxwell, *Tappi J.* **53**(8), 1464–1466 (1970).
152. U.S. Pat. 48,63,655 (Sept. 5, 1989), N. L. Lacourse and R. A. Alteri (to National Starch and Chemical Corporation, Bridgewater, NJ).
153. Eur. Pat. Appl. 0375831 (July 4, 1990), N. L. Lacourse and P. A. Altieri (to Nat Starch Chem Corp, US).
154. Eur. Pat. 0 376 201 B (July 4, 1990), N. L. Lacourse and P. A. Altieri (to Nat Starch Chem Corp, US).
155. U.S. Pat. 50,35,930 (July 30, 1991), N. L. Lacourse and P. A. Altieri (to National Starch and Chemical Investment Holding Corporation, Wilmington, DE).
156. U.S. Pat. 50,43,196 (Aug. 27, 1991), N. L. Lacourse and P. A. Altieri (to National Starch and Chemical Investment Holding Corporation, Wilmington, DE).
157. U.S. Pat. 51,85,382 (Feb. 9, 1993), P. E. Neumann (to Kansas State University Research Foundation, Manhattan, KS).

158. Int. Pat. Appl. WO 92/08759 (July 29, 1992), J. R. Anfinsen and R. R. Garrison (to DuPoint, US).
159. Eur. Pat. Appl. 0 667 369 (Aug. 16, 1995), C. Bastioli, V. Bellotti, G. Del Tredici, and A. Rallis (to Novamont Spa, Italy).
160. Eur. Pat. 0 696 611 (Feb. 14, 1996), C. Bastioli V. Bellotti, G. Del Tredici, A. Montino, and R. Ponti (to Novamont Spa Italy).
161. Eur. Pat. Appl. 0 696 612 (Feb. 14, 1996), C. Bastioli V. Bellotti, G. Del Tredici, and A. Rallis (to Novamont Spa, Italy).
162. C. Bastioli and S. Facco, in *Biodegradabile Plastics 2001 Conference*, Frankfurt, Germany, Nov. 26–27, 2001.
163. C. Bastioli, in *Global Status of the Production of Biobased Materials*, Actin Conference, Birmingham, U.K., 2001.
164. *Automotive News Eur*. 15 (Oct. 22, 2001).
165. Prufung der Kompostierbarkeit von Kunstoffen, DIN V 54900-2, 1998.
166. Requirements for Packaging Recoverable through Composting and Biodegradation—Test Scheme and Evaluation Criteria for the Final Acceptance of Packaging, EN 13432.
167. Compostabilita' dei Materiali Plastici—Requisiti e Metodi di Prova, UNI10785, Jan. 1999.
168. Life Cycle Assessment of Mater-Bi Bags for the Collection of Compostable Waste, Composto, Switzerland, 1998.
169. Life Cycle Assessment of Mater-Bi and EPS Loose-Fills, Composto, Switzerland, 2000.
170. Actual Situation and Prospects of EU Industry using Renewable Raw Materials, E.1, 2002. Edited by DG Enterprise.

CATIA BASTIOLI
Novamont SpA

Encyclopedia of Polymer Sceince and Technology
Copyright © 2005 John Wiley & Sons, Inc. All rights reserved.

THERMAL ANALYSIS OF POLYMERS

Introduction

Thermal analysis is defined by the International Confederation of Thermal Analysis and Calorimetry (ICTAC) (1,2) as "a group of techniques in which a property of a sample is monitored against time or temperature while the temperature of the sample, in a specified atmosphere, is programmed." In practice, the temperature of the oven that contains the sample actually is programmed, while the temperature of the sample in some cases may differ from the programmed temperature. Exothermic or endothermic reactions or phase transitions in the sample subjected to the programmed temperature variation may cause variations in the temperature between the sample and oven up to several degrees.

The more common thermal analysis (TA) methods are listed in Table 1 (3). Acronyms used for the techniques are included in the right-hand column. The present discussion will be limited to the major techniques that are used to characterize polymer samples. These are differential thermal analysis (DTA), differential scanning calorimetry (DSC), thermogravimetry (TGA), thermomechanical analysis (TMA), dynamic mechanical analysis (DMA), and dielectric analysis (DEA). The most popular technique for polymer applications is DSC followed by TGA (along with its derivative, DTGA). The use of the other methods is not as widespread as DSC and TGA but is gaining in popularity. The realization of the potential for TMA as a valuable tool for polymer characterization is comparatively recent. DMA and DEA were originally developed by rheologists over 50 years ago and have been adopted by thermal analysts more recently.

In addition to the individual techniques cited above, there are situations where individual samples are subjected to a common atmosphere and thermal environment. This is referred to as a *concurrent analysis*. An example of this is the combined DTA and TGA measurement, where two separate measurement devices share the same oven. In some cases two or more measurements are performed on the same sample. There is also the possibility of interfacing several techniques, such as TGA combined with some form of evolved gas analysis such as gas chromatography, Mass Spectrometry (qv), or infrared spectroscopy (or some combination of these) (see CHROMATOGRAPHY, AFFINITY; VIBRATIONAL SPECTROSCOPY). This situation is referred to as '*coupling*' or a *coupled technique*. Since the possibilities for interfacing several analytical techniques are quite large, concurrent or coupled techniques will not be considered further in this presentation.

Prior to the advent of DSC (ca 1964–65), DTA was first used in the field of geology to study clay mineralogy and pyrometry. The evolution of DSC has its

Table 1. Principal Thermoanalytical Methods[a]

Property	Technique	Acronym
Mass	Thermogravimetry	TGA, TG
Apparent mass[b]	Thermomagnetometry	TM
Volatiles	Evolved gas detection	EGD
	Evolved gas analysis	EGA
	Thermal desorption	
Radioactive decay	Emanation thermal analysis	ETA
Temperature	Differential thermal analysis	DTA
Heat[c] or heat flux[d]	Differential scanning calorimetry	DSC
Dimensions	Thermodilatometry	TD
Mechanical properties	Thermomechanical analysis	TMA
	Dynamic mechanical analysis	DMA, DMTA
Acoustical properties	Thermosonimetry (emission)	TS
	Thermoacoustimetry (velocity)	
Electrical properties	Thermoelectometry (resistance)	DETA, DEA
	(voltage)	
	(current)	
	(dielectric)	
Optical properties	Thermooptometry (spectroscopy)[e]	TPA
	Thermoluminescence (emission)	
	Thermomicroscopy (structure)	
	Thermoparticulate analysis	

[a]From Ref. 3.
[b]Change induced by an imposed magnetic field gradient.
[c]Power-compensated DSC.
[d]Heat flux DSC.
[e]Absorption, fluorescence, Raman, etc. Nonoptical forms of spectroscopy, eg, NMR, ESR, Mössbauer, etc, are also applicable.

origins in DTA, driven by applications in polymers and the timely development of techniques, instruments, and advanced software. In recent years, DSC has largely supplanted DTA for use in polymers, except for applications at high temperatures. Most commercial DSC instruments have a temperature range from -150°C up to 750°C, which is quite adequate for most polymer applications.

Differential Thermal Analysis

Description of the Method. As shown in Table 1 and Figure 1, DTA measures the differential temperature between a sample and a reference pan, which are closely matched thermally and arranged symmetrically within the oven. As the sample goes through the programmed dynamic temperature change, there is no temperature difference until the sample undergoes an exothermic or endothermic chemical reaction or change of physical state. In the case of an exotherm, the sample's temperature will increase, while in the case of an endotherm, it will decrease. In either case, the thermal event will be recorded as the sample temperature departs from the baseline and then returns to the base line when the

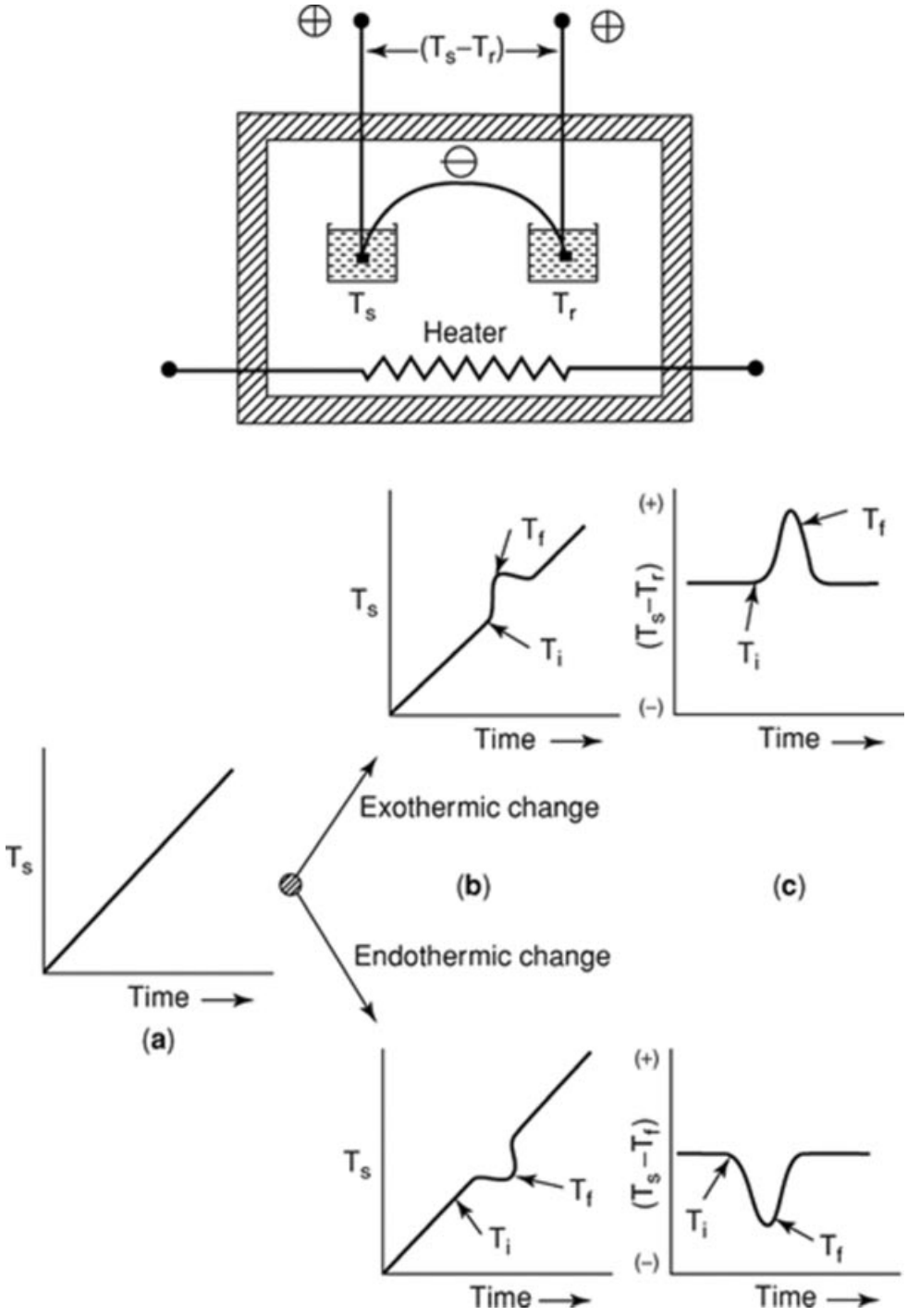

Fig. 1. General principle of operation for DTA and schematic of a DTA apparatus (4). The subscripts represent: s-sample, r-reference, i-initial, f-final.

Table 2. Some Applications of DTA and DSC to Polymers

Melting ranges	Release of strains
Rates of crystallization and reaction	Purity determination
Degree of crystallinity	Quality control
Glass-transition phenomena	Phase diagrams
Heat capacity	Energy storage
Enthalpy of transitions	Hazards evaluation
Identification—Fingerprints	Mesophase *transitions*
Thermal and oxidative stability	Nucleation of crystals
Analysis of copolymers and blends	Catalysis
Nucleation phenomena	Thermal conductivity

reaction or transformation is complete. Also, a change in the heat capacity of the sample will show as a change in slope (eg, Glass Transition (qv)) in the ΔT versus time or temperature plot. Modern DTA instruments generally use matched thermocouples as sensors, one each in contact with the sample or its container and the reference material or its container. The output of the differential signal is amplified and sent to a data acquisition system. Further details about DTA instrumentation and the appropriate experimental parameters can be found in several references by Wendlandt (4), Gallagher (Ref 5, Chapt. 1), and Wunderlich (Ref. 5, Chapt. 2). Some consideration of sample preparation, the effect of experimental parameters (eg, rate of heating and cooling), and methods for enthalpy and temperature calibration will be considered in the subsequent discussion of DSC.

Applications of DTA for Polymers. Table 2 (Ref. 5, Chapt. 1) describes some of the many applications of DTA and DSC. Both DTA and DSC can be used to determine the temperature of the transitions, cited in Table 2. However, the DSC peak area, in addition, gives quantitative calorimetric information (heat of reaction, transition, or heat capacity). DTA can only do so when calibration with a standard material allows the quantitative conversion of ΔT to heat flow and, ultimately, heat of transition (ΔH) or heat capacity (C_p). Also, the response of DTA with increasing temperature may be affected by poor heat transfer in the system, detector sensitivity, etc (4). For these reasons, when there is a choice between DSC and DTA, DSC is the preferred method. The illustrations shown below for applications of DSC in characterization of polymers also generally apply for DTA, with the limitations mentioned above. Therefore, DTA applications will not be considered here. Illustrations of polymer applications for DTA can be found in the Thermal Analysis section by Bacon Ke (6) in the previous edition of this encyclopedia.

Differential Scanning Calorimetry

Instrumentation. The development and introduction of DSC in 1964 (7) was a major innovation in thermal analysis. Several competitive commercial instruments were developed shortly afterward. Basically, there are two types of DSC instruments. The Perkin-Elmer version is called the "power compensation" DSC.

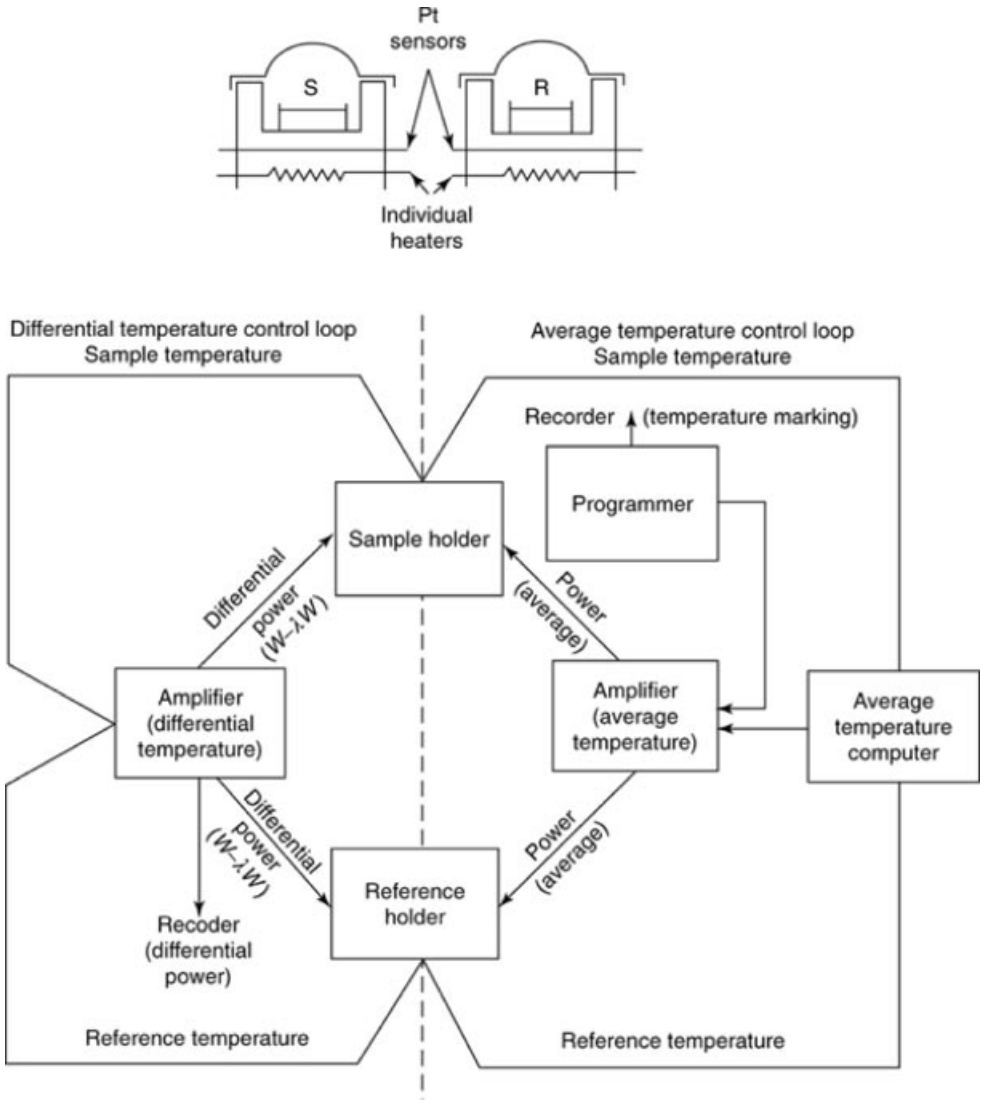

Fig. 2. A schematic representation of a power compensation DSC instrument and its operation (7).

Zahra and Zahra (8) reviewed a recent version of this type of DSC instrumentation. Figure 2 provides a schematic representation of the power compensation DSC.

The concept of operation of this instrument is based on keeping the temperature of R and S the same. This is achieved by placing the temperature sensors (platinum resistance thermometers) in a bridge circuit. Any change in temperature in either the sample or in the reference (by virtue of any exo- or endothermic event) is immediately compensated for by an equivalent amount of current flow required to drive a heater to keep them at the same temperature. Thus, the

integral of the power input during the transition (or the heat capacity change) is equal to the energy difference (ΔH) supplied to the sample or the reference during the particular event. The event would be endothermic or exothermic depending on whether the current travels to the sample or the reference pan, respectively. This results in an exothermic peak pointing downward and an endothermic peak pointing upward. This is in conformity with the thermodynamic convention, but differs with the sign convention for the DTA and the DSC "heat flux" for instruments made by other manufacturers, as discussed below. For DTA, ICTAC (2) recommends plotting "an upward deflection as a positive temperature differential and a downward deflection as a negative temperature differential with respect to the reference." In other words, exo is upward and endo is downward.

The second type of DSC unit operates in a "heat flux" mode. This type of instrument is offered by TA Instruments, Mettler-Toledo, Setaram, Netszch, and other manufacturers. Its operation is similar to that of DTA (ie, it generates a ΔT signal). However, the associated hardware and software, carefully integrated into the system, quantitatively converts ΔT to ΔH and compensates for other deficiencies, such as the temperature dependence of thermal transport and sensor sensitivity. Figure 3 shows two types of heat-flux calorimeters along with a schematic diagram taken from Boerio-Goates and Callanan (9). Figure 3**a** represents the Boersma-type instrument used by TA Instruments. In this unit, single thermocouples are in good thermal contact with the sample and the reference holders. In the Tian–Calvet-type calorimeter, shown in Figure 3**b**, a thermopile is used. The latter tends to give greater temperature sensitivity and better temperature averaging over the entire sample and reference containers. The schematic representation in Figure 3**c** notes the temperatures and thermal resistances that are necessary for mathematical analysis of the heat-flux DSC. The analysis is described by Wunderlich (5). Each type of DSC gives satisfactory enthalpy data (10) with an accuracy of around 1–2%. Some heat-flux DSC instruments can operate at temperatures up to 1500°C, while the power-compensation instrument operation is limited to 725°C.

Calibration and Standards. Thermal analysis methods are not absolute and calibration is needed to record the correct abscissa value of temperature T (in Kelvin) and time t (in seconds or minutes). On the ordinate, calibration is necessary for the amplitude of deflection, ΔT, expressed as the difference in temperature (in Kelvin) for DTA or as heat flux, dQ/dT (in joules per second or watts) for DSC. Each instrument manufacturer provides methods and standard materials for these calibrations. In addition, ICTAC, in collaboration with the National Institute of Standards and Technology (NIST), has developed a series of materials as calibration standards for DSC/DTA. These reference materials can be used to calibrate both the temperature scale (K, abscissa) and heat flow (J/g, ordinate) on the basis of the integrated area under the curve. Figure 4 shows the heat flow–temperature relationship for various solid–solid and solid–liquid melting standards. Table 3 lists the solid_1-to-solid_2 transitions, melting points, and Curie temperatures of various pure metals, and also their transition enthalpies (J/g) (11).

Figure 5 illustrates temperature calibration curves for both DTA/DSC and TGA using high purity nickel as a magnetic material (Curie point = 358.4°C). Unlike T_m, the Curie point temperature is practically unaffected by the changing of the heating rate between 1 to 20°C/min.

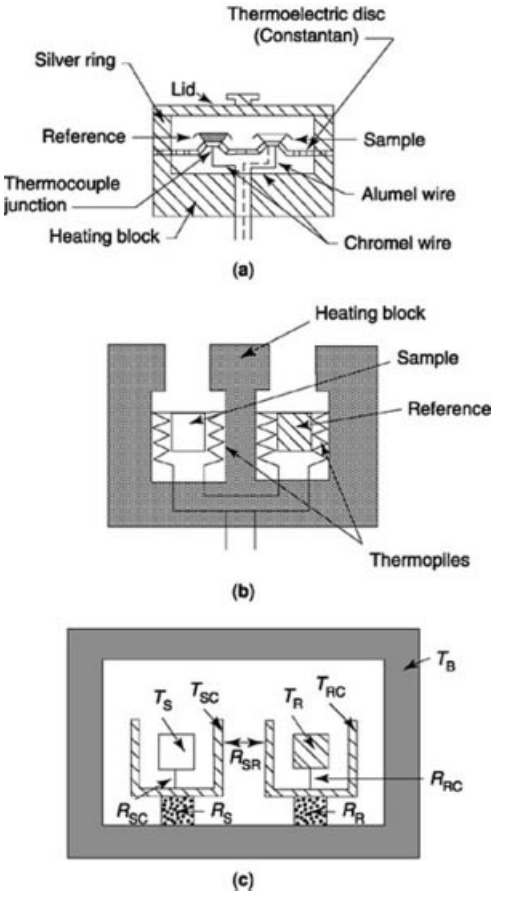

Fig. 3. Representation of a two heat-flux calorimeter showing (**a**) Boersma thermocouple placement and (**b**) the Tian–Calvet design. The schematic diagram (**c**) is appropriate for analysis of the response of both types of calorimeters. Symbols in (**c**) are: subscript T refers to temperature, R refers to reference; the temperatures of the block, sample, container, reference, and reference containers given by T_B, T_{SC}, T_R, T_{RC}, respectively; capital R refers to heat transfer resistance in the instrument (9).

Hakvoort (16) and also Della Gatta and Barczynska (17) advocate certain solid-state first-order transitions for use as subambient temperature standards. For relatively low temperature ranges, such as the glass transitions (T_g) for elastomers, Tan and Sabbah (18) have proposed the melting transitions of various organic compounds. Certified reference materials for heat capacity calibration, which are recommended by International Union of Pure and Applied Chemistry (IUPAC), are also available (Ref. 5, pp. 46 and 353–356). Two ASTM standards document procedures for temperature (ASTM E967) and heat-flow (ASTM E968) calibration in DSC.

Operating Parameters for DSC/DTA.

Sample Size. In order to avoid temperature gradients inside a sample, a small sample size is preferred. A small sample size also gives better resolution.

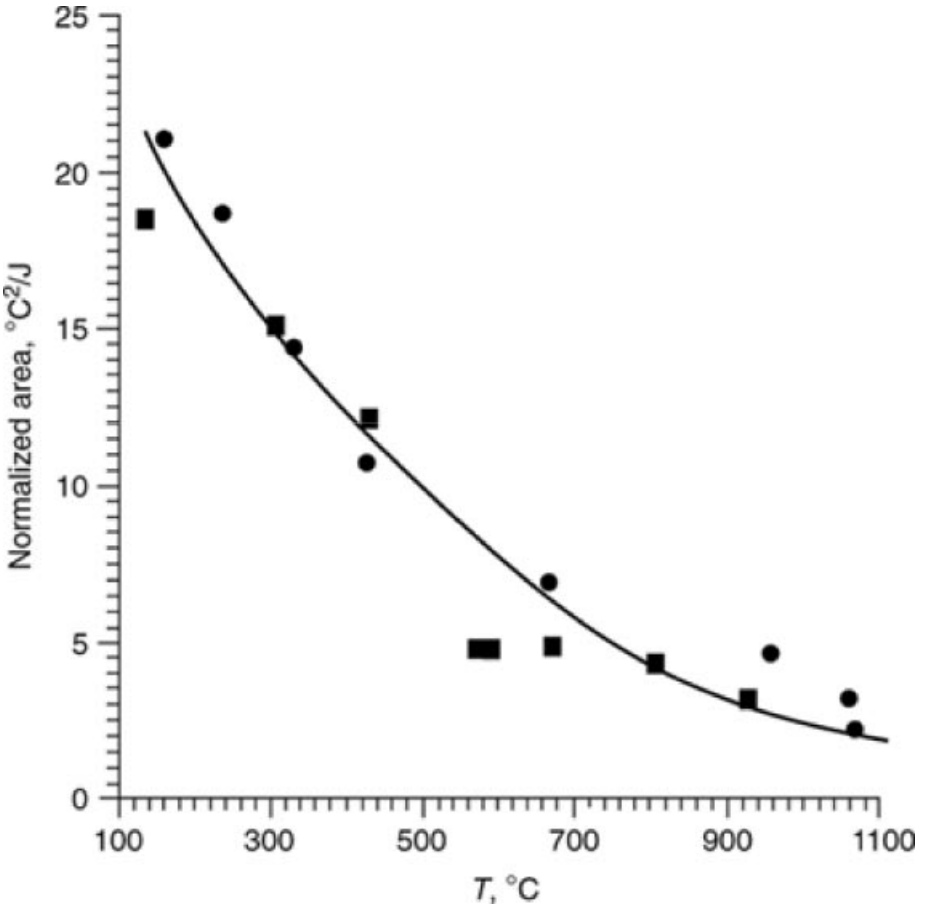

Fig. 4. Typical enthalpy calibration curve for DSC. ● Salt ($Solid_1$–$solid_2$ standard); ■ Metal (melting standard) (14).

Table 3. Some Reference Materials for DTA and DSC

Melting points[a]			$Solid_1$–$solid_2$[b]		
Material	Temperature, °C	Enthalpy, J/g	Material	Temperature, °C	Enthalpy, J/g
Hg	−38.8344	11.5	Cyclohexane	−83.1	Unavailable
In	156.5985	28.42	KNO_3	127.7	50.48
Sn	231.928	59.2	$KClO_4$	299.5	99.32
Pb[c]	327.502	23.16	Ag_2SO_4	412	59.85
Zn	419.527	112.0	SiO_2	573	12.1
Al	660.323	400.1	K_2SO_4	583	48.49
Ag	961.78	104.7	K_2CrO_4	665	51.71
Au	1064.18	63.7	$BaCO_3$	810	89.00
Cu	1084.62	205.4	$SrCO_3$	925	133.23

[a] International Temperature Scale 1990 for temperatures, and Ref. 12 for the enthalpies.
[b] NBS–ICTA Certificates GM-758, GM-759, GM-760 for the recommended temperatures, and Ref. 13 for the enthalpies.
[c] Downgraded to a secondary temperature point.

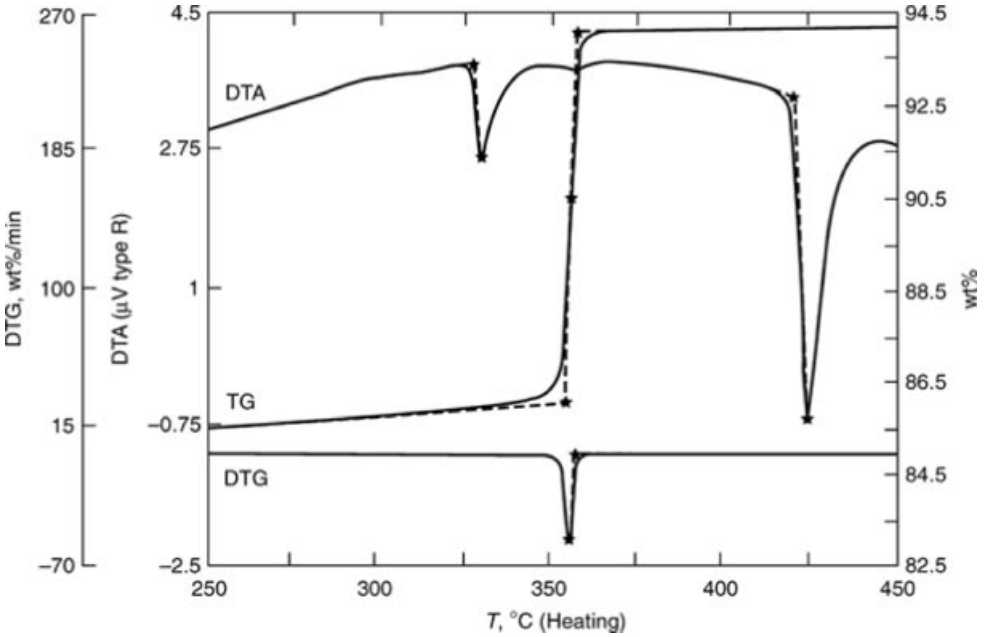

Fig. 5. Thermomagnetometry (TM)/DTA curves for accurate determination of T_c for magnetic materials (15).

On the other hand, sensitivity of the instrument increases with increasing sample size. The choice of sample size for DSC/DTA depends on the composition of the sample. For pure polymers, 3–10 mg is sufficient. For heterogeneous materials, such as blends and filled polymers or those containing several other compounding ingredients (such as elastomer vulcanizates), larger samples in the range of 10–20 mg may be necessary. However, for characterization of all materials in an air or oxygen environment, thin samples weighing only 0.2–0.5 mg are recommended in order to minimize diffusional effects with respect to oxygen or air, inhibit secondary reactions, and improve reproducibility. In the case of heterogeneous materials it is advisable to run multiple samples in order to verify that the data are representative of the composition.

Sample History. A factor that is characteristic of polymers is the dependence of morphology on thermal history. Significant variations in the degree of crystallinity as well as temperatures for glass transition (T_g), crystallization (T_c), and crystalline melting (T_m) can be obtained by varying the crystallization and annealing temperatures, or by changing cooling and heating rates. Additional types of sample history may be due to the viscoelastic character of the polymer. Elastomer samples that have been pressed, molded, or extruded may exhibit appreciable elastic "memory," which eventually may result in severe distortion of the sample during the TGA, DSC, and DMA experiments. This would result in anomalous data. Another type of time-dependent sample history variation can be encountered with thermoplastic block copolymers. Here changes in dimensional stability and/or polymer transition temperature may occur because of changes in the morphology of the material during the thermal measurement. This might

result from changes in the phase distribution resulting from aggregation of the hard or soft block segments. A further complication is physical aging or enthalpy relaxation that occurs in the amorphous phase due to the tendency of a polymer in a nonequilibrium state to spontaneously shift toward the equilibrium state. This is a complex subject that is not considered here but is covered in some detail by Chartoff in Reference 5.

In order to obtain a representative DSC curve for the polymer sample that is consistent and reproducible, it is necessary to destroy the prehistory. This is achieved by preheating the sample above the crystalline melting temperature in an inert atmosphere, holding it there for a few minutes (generally, 5 min) and then cooling slowly to the start temperature. If the crystallization rate is slow, it may be necessary to hold the polymer (ie, anneal) at a temperature below the melting point for some time in order for crystallization to go to completion.

In certain cases, whenever a special kind of prehistory is imparted to a polymer (eg, either through processing or aging, such as in fiber and film processing from the melt), it is important to study the prehistory. Here it may be desirable *not* to destroy the prehistory because the DSC response of the material may be correlated with a process parameter, thus extending the usefulness of the DSC curve. In this case, one should always record the first heat DSC/DTA curve followed by a second run using the reheat procedure noted above.

Base Line. Selecting a proper base line for integrating the area under the curve is essential for enthalpy determinations. In the absence of detailed information about overall error in different alternative modes, a simple straight-line approach is adequate. However, for partial area measurements in kinetics, a more accurate base line may be needed. The following texts may be consulted for further information on this topic: Wendlandt (4), Brown (19), and Wunderlich (11). Many modern instruments have the ability to manipulate the base line. In the case of irreversible transformations without any weight loss, a simple rerun of a sample (after the transformation), under the same conditions should give a suitable base line. All current computerized instruments can subtract one base line from another that is generated under identical experimental conditions.

Thermal Transport. Heat transfer to the sample can be affected by the following factors: (*1*) physical arrangement of the sample and reference relative to the furnace; (*2*) the choice of sensor, its size and position; and (*3*) the type of construction materials. These factors determine the thermal coupling. They also influence the shape and size of the peak for a thermal event. The better the thermal coupling between the sample and the reference, the smaller the original ΔT signal and the faster the return to the base line, thus improving resolution. A higher thermal conductivity environmental gas, such as helium, will result in better thermal coupling. Placing a metal lid on the sample pan also markedly improves the thermal properties of the system by helping to press the sample into good contact with the pan and reducing heat flow to the environment.

Effect of Heating Rate. The thermal lag between the sample and the sensor increases as the heating rate increases and, generally, the resolution of a transition (or other thermal event) decreases. However, the amplitude of the ΔT signal increases with heating rate because the transition takes place in a shorter period of time and the rate of change is greater. With modern instruments, amplification of the ΔT signal at a lower heating rate is not a problem, but it increases

Table 4. Compromises in Operation and Construction for DTA and DSC

Parameter	Maximum resolution	Maximum sensitivity
Sample size	Small	Large
Heating rate	Slow	Fast
Sample–reference	Linked	Isolated
Particle size	Small	Large
Atmosphere[a]	High conductivity	Low conductivity

[a] In the absence of any reaction.

the signal-to-noise ratio. Therefore, compromises must be made. Typical heating rates for DSC experiments are in the 10–20°C/min range. For unknown polymer samples, a range of heating rates with different amounts of sample should be explored. This should provide information on the optimum conditions for detection and resolution of minor thermal events and would be a background study for establishing a routine procedure for subsequent analyses. The effects of different parameters on resolution and sensitivity are summarized in Table 4 (Ref. 5, p. 87).

DSC Applications in Polymers

The numerous applications of DSC in characterizing polymeric materials are quite varied. Therefore, it is only possible to cast a glimpse on the subject. Figure 6 shows a schematic DSC curve (20) for a pure polymer as it is progressively heated from a low temperature to a high temperature in an oxidative (A) or inert (B) atmosphere. The actual temperature, for a given polymer to undergo all of the thermal events shown in Figure 6, depends on the structure of the polymer. For an elastomer, a low temperature transition (glass-transition temperature T_g) may be as low as −140°C, whereas for a thermoplastic polymer, T_g values of room temperature or higher may be more common. As noted before, the DSC experiment should be started at a temperature at least 20–50°C lower than the region of interest and continued to at least 20°C higher than the highest transition temperature. The elevated temperature at which most carbon-chain polymers degrade is usually less than 500°C.

Starting from the lowest temperature, the first discontinuity observed is the glass transition, which appears as a shift of the base line corresponding to the heat capacity difference of the sample before and after the transition. There are various methods to mark the exact location in the curve where the glass-transition temperature T_g is recorded. This will be discussed below. The magnitude of base line shift (ΔC_p) during the glass transition is related to the concentration of amorphous chains in the sample and is affected by other factors such as molecular mobility and free volume.

As the temperature increases, there may be a cold crystallization peak (T_c, exotherm), followed by a crystalline melting peak (T_m, endotherm). The intensity of the cold crystallization peak depends on the prehistory of the sample. It will not be present at all if the sample were cooled under controlled conditions from the melt state or if it were annealed at a fixed temperature below T_m so as to complete

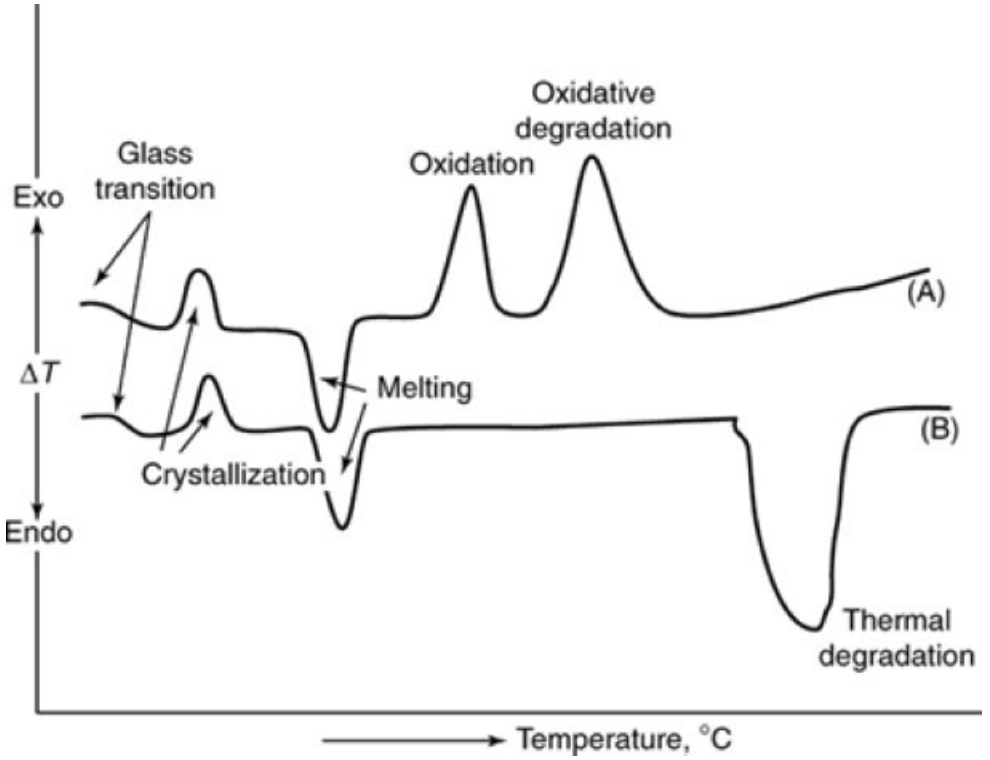

Fig. 6. Schematic DSC curves showing different transitions and reactions of a polymer, ranging from low temperatures to progressively higher temperatures. A, in oxygen; B, in nitrogen (20).

the crystallization process. If the sample is heated above T_m and then cooled slowly to a low temperature, and scanned again, the enthalpy or the area under the melting curve will relate directly to the amount of crystalline material in the polymer or the degree of crystallinity. Up to this point, the transitions mentioned are due to physical changes and they are reversible. Physical transitions are not accompanied by any weight change and are not affected by the environment (nitrogen or oxygen). Thus, they cannot be monitored using TGA, since there is no weight loss involved.

At a still higher temperature (150–220°C), if the polymer is an elastomer, formulated with all the vulcanizing ingredients or uncured thermosetting type monomer, an exotherm should occur indicating the curing reaction (not shown in Figure 6). DSC enthalpy determination (from the area under the exotherm) is one of the methods for determining the degree of cure of an elastomer formulation or a thermoset and can be used as a quality control tool.

At still higher temperatures (250–500°), the polymer undergoes degradation, resulting in main-chain scission, cross-linking, cyclization, and loss of volatile fragments. In an inert atmosphere, the degradation pattern may be endothermic, exothermic, or both, whereas in oxygen or air, it is always exothermic. As expected, degradation occurs at a much lower temperature in oxygen than in nitrogen. The

DSC degradation patterns in nitrogen and oxygen have been used to identify many polymers (21). Many authors, including Goh (22) and Savasçi and Baysal (23) have attempted to use oxidation exotherms to characterize the oxidative stability of elastomers, and, subsequently, to evaluate the effectiveness of added antioxidants. DSC curves in the degradation regime may tend to be erratic because of the loss of mass that may occur during the degradation event.

Glass-Transition Temperature.

Specifying T_g by DSC. All Amorphous Polymers (qv) become stiff and ultimately brittle like a glass, if sufficiently cooled. The temperature region where the physical transition from a rubbery to a glassy state takes place is called the "Glass Transition (qv)." It is characterized by a step change in C_p. As shown in Figure 7, the glass transition covers a wide range of temperature (10–15°C for pure, uncross-linked polymers and wider for blends, filled, and cross-linked polymers). A defined point in this temperature range is called the glass-transition temperature or T_g.

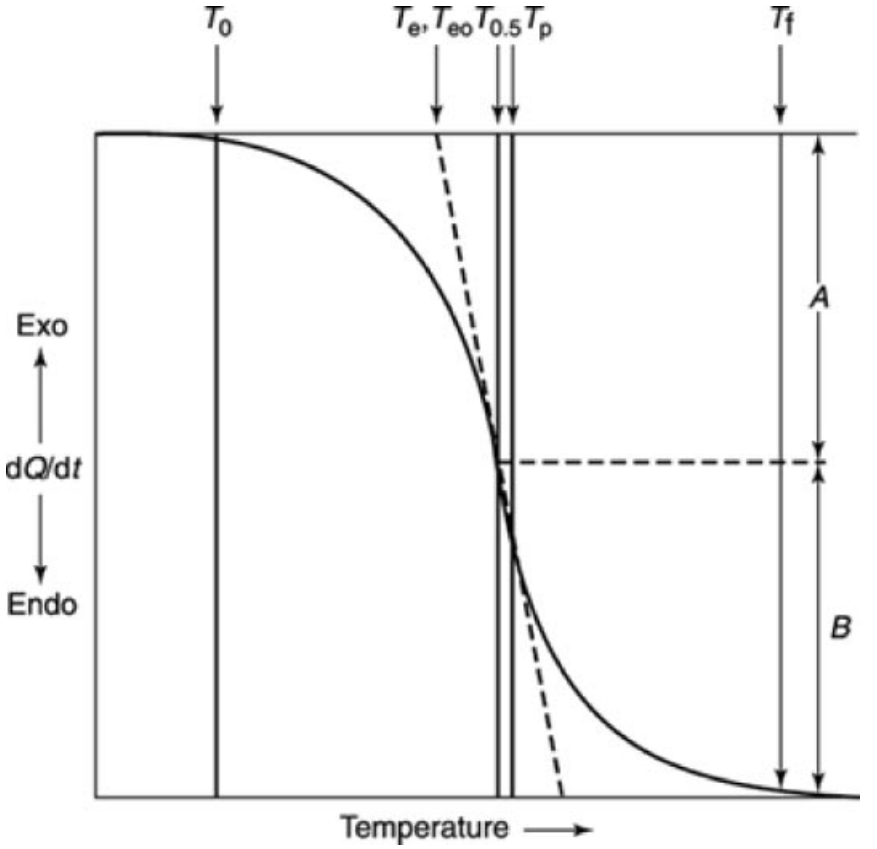

Fig. 7. Representative curve of heat flow versus temperature in the region of the T_g of a polymer: T_o, temperature of departure from the base line; T_e or T_{eo}, temperature of intercept of extrapolated base line and tangent to steepest slope; $T_{0.5}$, temperature of 50% transition (A = B); T_p, temperature of maximum slope (peak of derivative plot); T_f, temperature at completion of the transition (24).

Figure 7 shows five characteristic temperatures associated with a glass transition on the DSC curve. All five have been cited in various places in the literature as T_g, often without mention of the specific location actually picked (24). The assignment of T_g by thermal analysis methods was the topic of a recent ASTM symposium (25). T_o, the "onset" temperature, defines the point at which the first deviation from the base line on the low temperature side is observed. T_o is very subjective and often difficult to determine because of the base line slope; and it is not reproducible. T_e or T_{eo} (extrapolated onset, also called the fictive temperature) is the temperature at the intersection of the extrapolated base line and tangent taken at the point of maximum slope. It is generally reproducible and is the most quoted value in many early publications on thermal methods. $T_{0.5}$, the endotherm half-height (also called half-vitrification) is the temperature preferred in recent years for specifying T_g. The autoanalysis feature available with all modern thermal analysis equipment makes this determination easy and reproducible. It has better reproducibility than the extrapolation method and locates a temperature where the thermal transition has approximately reached the inflection point. ASTM E1356 and ASTM D3418 recommend either T_e or $T_{0.5}$ for specifying T_g.

Wunderlich (Ref. 5, p. 278) advises that T_g should be measured as the sample is progressively cooled, rather than heated. The advantage here is that the sample is in thermal equilibrium at the start of the measurement and enthalpy relaxation, often encountered in T_g measurements, is avoided. However, instrumental drawbacks, such as precise control of the cooling rates in some DSC models, preclude general use of cooling curves for determining T_g. If T_g is obtained by progressive heating of a cooled sample, it is advisable to cool the sample somewhat faster than the subsequent heating rate to avoid enthalpy relaxation. This is also discussed by Wunderlich (5). The heating or cooling rate and the location on the DSC curve where T_g is taken always should be specified along with the reported T_g value.

Another method for locating T_g is by taking the derivative of the DSC glass-transition curve. (The acronym DerDSC for "derivative DSC" is used here.) The derivative curves exhibit a peak corresponding to the maximum slope of the endothermic step in C_p accompanying T_g. In Figure 7, T_p is very close to $T_{0.5}$, the midpoint value. This is illustrated in Figure 8 for natural rubber (26). Note the small endotherm at the high temperature end, presumably due to enthalpy relaxation. The derivative curves may also be helpful in locating multiple transitions close in temperature and not resolved by the T_g curve (Ref. 25, p. 229). The disadvantage of this method is the high signal-to-noise ratio for the DerDSC curves.

For amorphous thermoplastic polymers, T_g at the extrapolated onset is technically more significant, since it defines the initial temperature for the loss of structural properties (eg, modulus) as the polymer softens through the glass-transition region. Thus, it defines both a low temperature limit for the processing of amorphous thermoplastic polymers and an upper use temperature. For elastomers, the temperature for useful elastomeric properties lies above the glass-transition region, (to the right of the T_g curve) shown in Figure 7. Therefore, T_f, the temperature at the completion of the glass transition, should be technically more significant (26). If the elastomer is cooled beyond this point it enters the glass-transition region and starts losing its elastic properties, becoming progressively stiffer as the temperature decreases. As noted above, ASTM E1356 describes the test method for determining the glass-transition temperature by DSC or DTA.

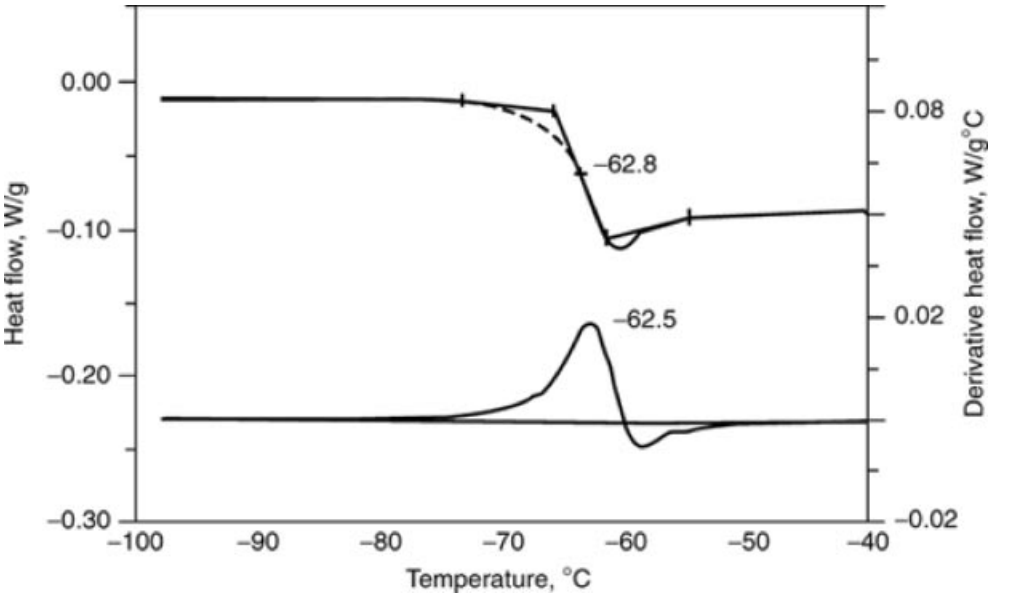

Fig. 8. DSC glass transition of natural rubber showing $T_{0.5}$ and T_p; heating rate 10°C/min (26).

Degree of Cure Using T_g. For many thermosets, T_g can be correlated with the conversion or degree of cure (Ref. 5, Chapt. 6). Therefore, simultaneously with the heat of reaction, measured by enthalpy, T_g can be used as a measure of the degree of cure. In the final stages of cure, where T_g is actually the more sensitive measure, it may be preferred to the residual heat of reaction, ΔH_1, as a measure of the degree of cure. This may happen when the glass transition immediately precedes the small residual exotherm. This is illustrated in Figure 9 (27) for epoxy–anhydride samples, previously cured to *apparent* completion at different temperatures. Note that the exotherms are facing downward, as would be expected for a power compensation DSC instrument; ΔH_c is the exothermic heat of reaction for 100% conversion, expressed as heat per mole of reacting groups (kcal/mole or kJ/mole) or per mass of material (cal/g or J/g) at the time t. The fractional degree of conversion is given by

$$\alpha_1 = \Delta H_1 / \Delta H_c \tag{1}$$

where α_1 is the fractional conversion or extent of reaction and ΔH_1 the heat generated up to time t_1.

The measurement of the degree of conversion by enthalpy measurement applies to elastomer cure also, since the vulcanization reaction is highly exothermic. Unlike for thermosets, T_g is not a measure of degree of cure for elastomers. Sircar discusses this and numerous other aspects of the characterization of elastomeric materials using thermal analysis in chapter 5 of Reference 5.

Melting in Semicrystalline Polymers.

Traditional DSC Methods. Many commercially available thermoplastics [eg, polyethylene (PE), polypropylene (PP), poly(ethylene terephthalate) (PET),

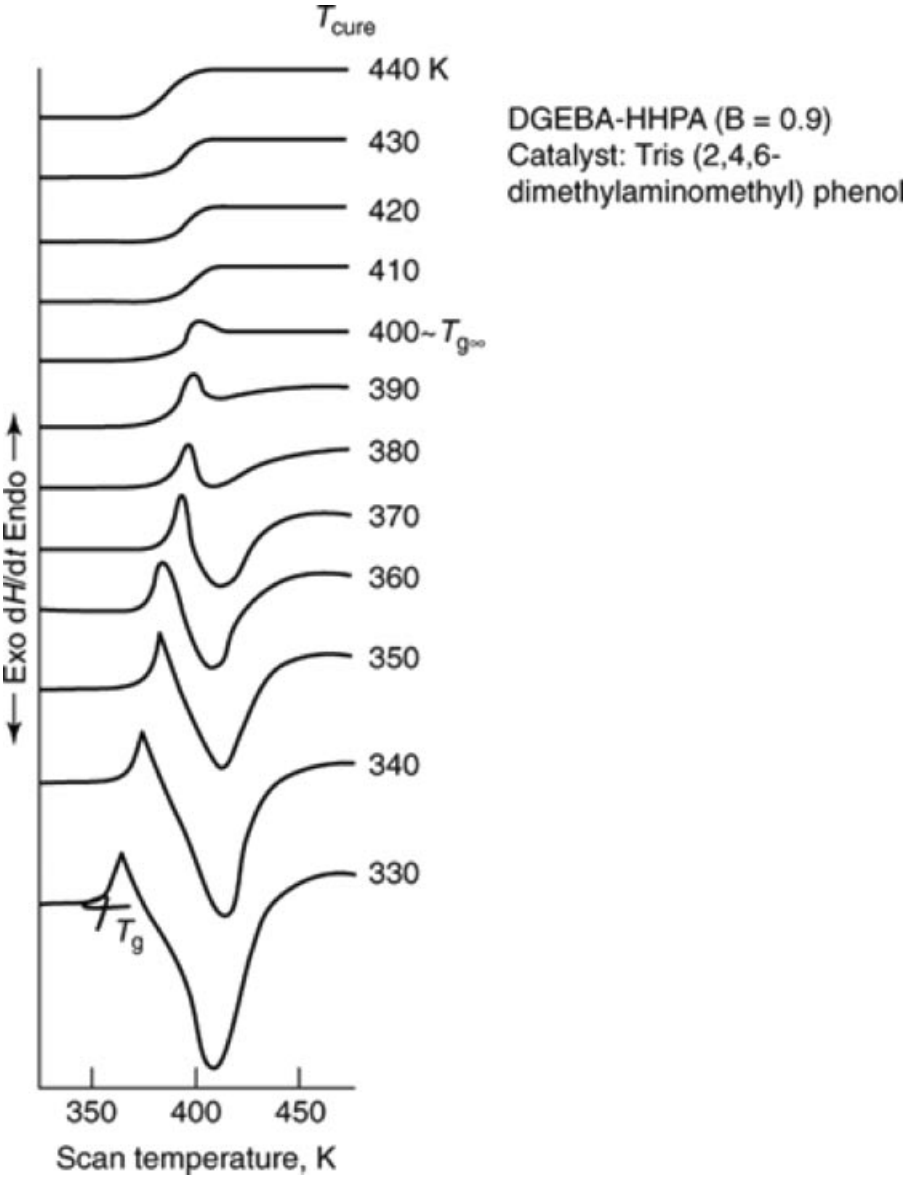

Fig. 9. DSC scans at 8°C/min on epoxy–anhydride samples previously reacted to apparent completion at indicated temperatures. Note increasing T_g followed by residual exotherm for samples cured below $T_{g\infty}$. Diminishing T_g at highest cure temperature suggests possible degradation (27).

various nylons, and numerous others] and some elastomers [eg, polychloroprene, known commercially as neoprene (CR), *cis*-1,4 -poly(butadiene) (BR), ethylene–propylene–diene polymer (EPDM)] are morphologically semicrystalline. These are virtually two-phase systems where a crystalline phase and an amorphous phase coexist. However, the crystalline phase and the amorphous phase are not

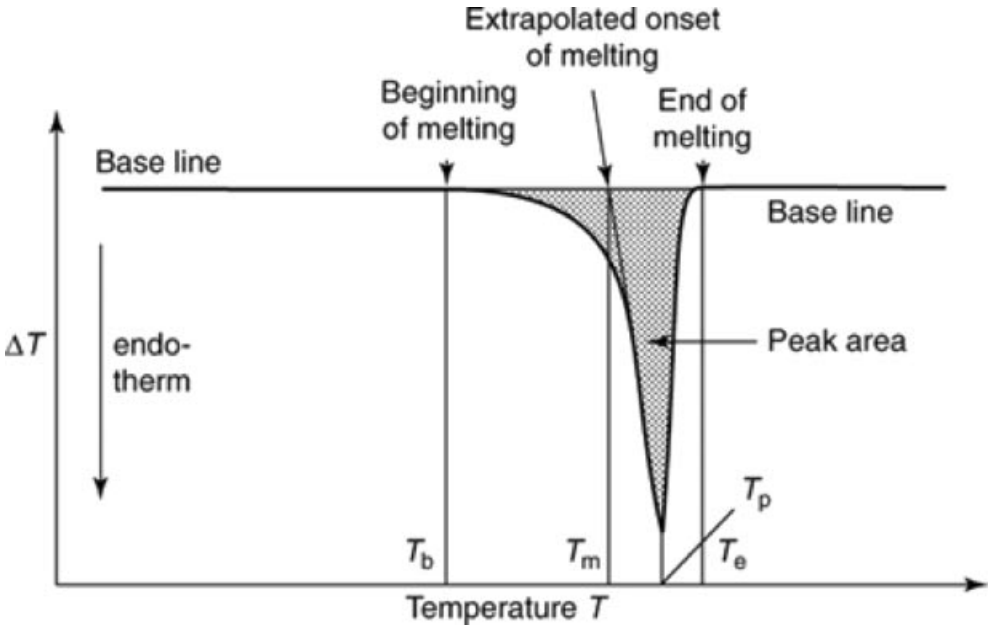

Fig. 10. Four characteristic temperatures for melting transitions. In addition, the peak area (heat of transition) and the time scale of the experiment should be recorded (11).

completely homogeneous. The crystals generally are of different sizes and forms and the amorphous phase near the crystallite interfaces is constrained and less mobile than the amorphous chains far from the crystallite boundaries. DSC is a useful tool for characterizing these semicrystalline materials.

Other important characteristics of Semicrystalline Polymers (qv) are that melting takes place over a range of temperatures (in some cases, over a range of 100°C or more) and supercooling always occurs, so that there is a hysteresis between the melting and crystallization cooling curves. Semicrystalline polymers melt at characteristic temperatures when heated in DSC. Wunderlich (Ref. 5, p. 277) describes reasons for designating the melting temperature T_m at different locations of the melting curve (Fig. 10). If there is a large temperature gradient within the sample, it has been observed empirically that the peak temperature often represents the actual melting temperature. Also, a sample with a broad melting range and a small melting rate (as are the semicrystalline polymers with crystals of different perfection, shape, and size) should be better characterized by its melting peak temperature, since T_p represents the temperature where the largest fraction of the sample melts. This is the most frequently quoted T_m for semicrystalline polymers. Lastly, the temperature for recovery of the base line, T_e, is a function of the design of the instrument. For a polymer with a very broad melting range, the instrument lag becomes negligible and T_e would indicate the melting temperature of the most perfect, highest melting crystals of the sample.

Another important characteristic of melting for semicrystalline polymers using DSC is the enthalpy or the value of the heat of fusion, ΔH_f. It should be noted that the value of ΔH_f, determined by DSC, denotes only the amount of crystallinity

present in the sample and not the inherent value of the enthalpy of fusion of a fully crystalline polymer, ΔH_u. Methods for determining ΔH_u are described by Starkweather and co-workers (28). If the enthalpy of fusion of the fully crystalline polymer is known, the degree of crystallinity of an unknown polymer sample can be determined as follows:

$$\text{Degree of crystallinity } (\%) = (\Delta H_f / \Delta H_u) \times 100 \tag{2}$$

As in the case of the glass transition, another important item to be reported is the heating or cooling rate. Equilibrium melting should be independent of heating rate, but rarely do polymer crystals represent equilibrium crystals, nor do they melt in DTA or DSC under equilibrium conditions. Under such nonequilibrium conditions, the time scale of a first-order transition (such as melting) is an important experimental parameter. It should be noted again that the magnitude of the step change in the base line during the glass transition relates to the amorphous content of the polymer. Similarly, the magnitude (area) of the melting transition enthalpy relates to the degree of crystallinity of the polymer. The degree of crystallinity of a semicrystalline polymer is an important parameter that correlates with most major engineering mechanical properties including elastic modulus, strength, and elongation to break. DSC is the most efficient method for accurately measuring the degree of crystallinity.

Modulated Differential Scanning Calorimetry. A relatively recent development in DSC instrumentation allows heating or cooling a sample under a constant underlying rate while simultaneously superimposing a sinusoidally varying time–temperature wave. This is shown in Figure 11 for the modulated differential scanning calorimetry [MDSC, TA Instruments; Sauerbrunn and co-workers (29)]. As described below, the accepted name for this method has since been changed to modulated temperature DSC, or MTDSC, after this term was introduced in 1996. A similar technology [dynamic DSC or step scan DSC (SCDSC) developed by Perkin-Elmer] is based on a series of isothermal holds, each followed by a linear heating segment (ramp) instead of the sinusoidal cycle of MTDSC. Schawe (30) compares the two methods (MTDSC versus DDSC) using the glass transition as an example. The results are virtually identical.

A major advantage of the MTDSC technique and analysis is that the total heat flow rate can be separated into two other signals by deconvolution of the raw data (Fig. 11**b**). One of these is a reversible signal, in phase with the modulated heating rate, and the other a nonreversible signal out of phase with the modulated heating but dependent on the rate of heat flow. Examples of polymer thermal events that are nonreversible are molecular relaxation, cold crystallization, evaporation, thermoset cure, elastomer vulcanization, and decomposition. The utility of having two response components is demonstrated in Figure 11**c** for PET, where the glass transition and the melting endotherm are reversible but the endothermic enthalpy relaxation at T_g and the exothermic cold crystallization are not. Another advantage of MTDSC is that once the instrument is calibrated for the amplitude and period, heat capacity data can be obtained directly in the same run by measuring the modulated heat flow signal, and dividing by the amplitude of the heating rate.

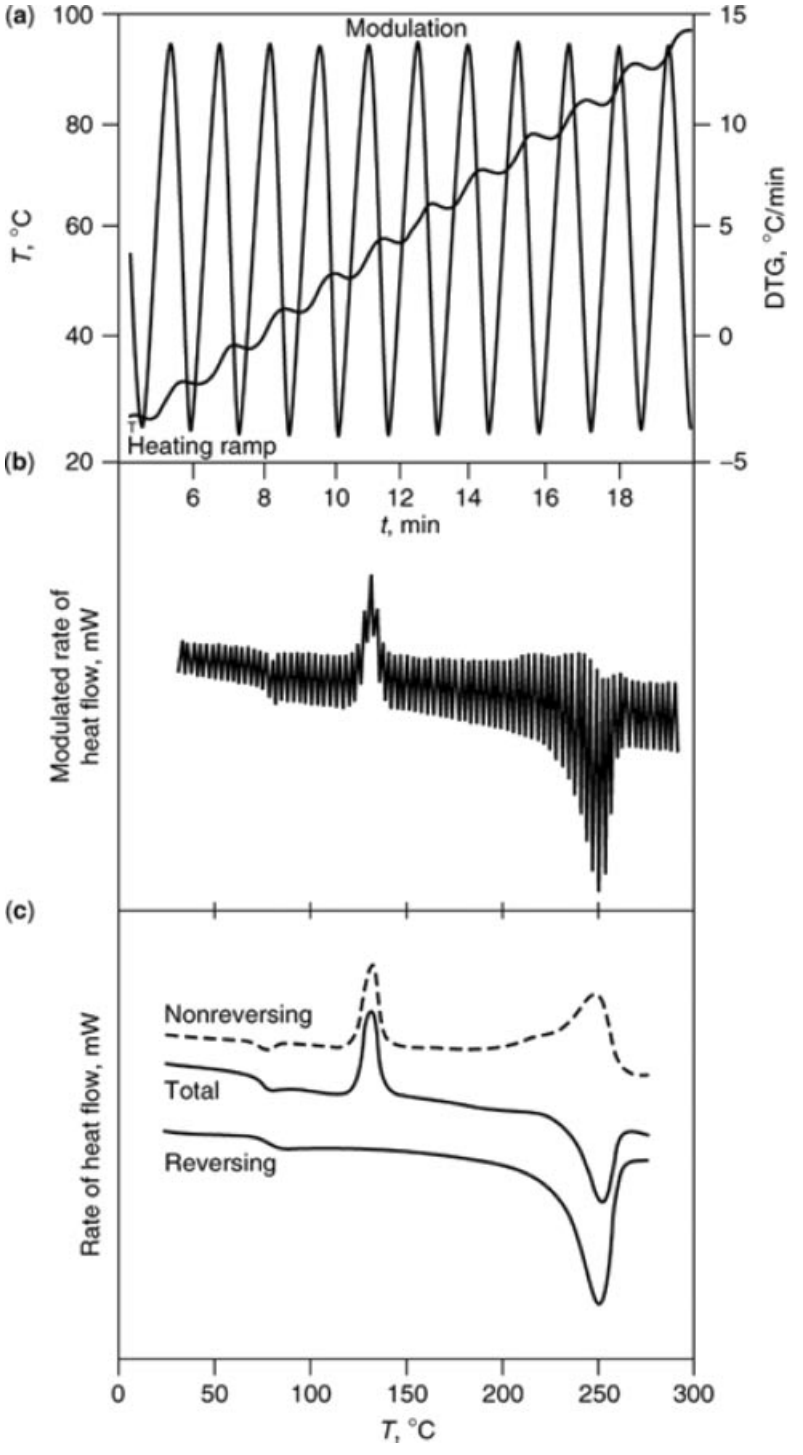

Fig. 11. Examples of MDSC data: (**a**) typical temperature–time profile; (**b**) raw data for an MDSC scan of quenched PET; (**c**) Deconvolution and analysis of the curve (29).

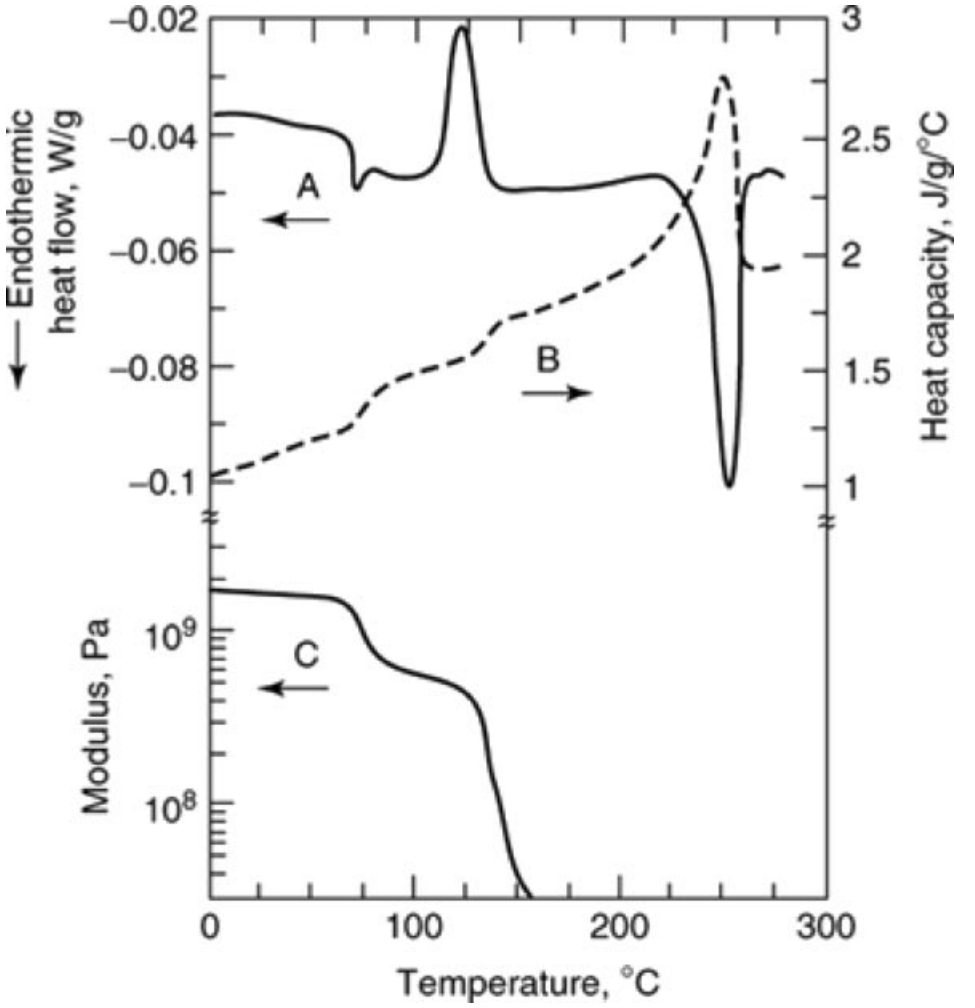

Fig. 12. Modulated DSC curve for Makroblend UT-400, an impact-modified polycarbonate/poly(ethylene terephthalate) blend. Curve A shows the conventional DSC curve; curve B shows the heat capacity extracted from the reversing component of the signal; curve C shows the modulus of the same material measured by DMA (Hale and Bair, in Ref. 5).

An interesting analysis of a blend of PET/polycarbonate (PC), using MTDSC, was reported by Hale and Bair (Ref. 5, p. 804) (Fig. 12). The conventional DSC curve (A) has all the indications of PET, but PC cannot be detected without the deconvoluted reversing curve (B) that indicates PC is present by virtue of its T_g that occurs in the same temperature range as the cold crystallization of PET. Further confirmation of the presence of PC is obtained from the dynamic mechanical storage modulus (curve C). The dynamic modulus technique will be discussed later in this article.

In the MTDSC technique, C_p (heat capacity) data from the convoluted MDSC is replaced with the term C_p^*, called a complex heat capacity. C_p^* can then be

further deconvoluted into an out-of-phase C_p'', and an in-phase (C_p'), component relative to the imposed temperature modulation. The vector sum of these components is equal to complex heat capacity, the data traditionally generated by MDSC. For most polymers, C_p'' is very small. In those cases, C_p and C_p^* will be virtually identical. However, a phase correction in MDSC should be relevant for time-dependent heat capacity phenomena. Aubochon and Gill (31) present a good comparison of MDSC and MTDSC with illustrations. The attention of interested readers is also directed to the papers on MDSC and MTDSC presented at the 11th ICTAC conference (1996), and later published in three volumes of the *Journal of Thermal Analysis* (1997). NATAS, the North American Thermal Analysis Society, has sponsored symposia on MDSC at each of its meetings for the past several years.

DSC Modifications and Simultaneous Techniques. DSC and other thermal analysis instrumentation have undergone many modifications and developments in recent years. Among these innovations is the coupling of various methods. In this context the terms *parallel*, *concurrent*, and *simultaneous* should be defined. Parallel techniques use separate samples, each in its own unique thermal environment. Concurrent or combined techniques also use separate samples, but the experiment is carried out in a common atmosphere and thermal environment. Simultaneous techniques use the same sample in the same atmospheric and thermal environment. Such methods are increasing in popularity. While a detailed treatment of this topic is outside the scope of this discussion, a brief list will be presented in order to provide input for those new to the subject area. Interested readers should consult the chapter by Gallagher (5) and the additional references mentioned therein.

Some of the simultaneous instruments available commercially are as follows: TGA/DTA/DSC, TGA/DTA/FTIR, DTA(DSC)/EGA(EGD), and DSC/FTIR. Also, high pressure DSC and photo-DSC instruments are available commercially. In addition, individual researchers have used simultaneous DSC/XRD (X-ray diffraction), DSC/EGA/XRD, and DSC/TRXRD (time-resolved X-ray diffraction). Experiments with parallel, combined, and simultaneous techniques help to affirm the conclusions drawn from a single technique and very often offer definitive clues to the actual mechanisms taking place during thermal analysis.

Thermal conductivities can be measured using DSC. Chiu and Fair (32) irreversibly modified a DSC cell to determine thermal conductivity. Sircar and Wells (33) developed a modification of this approach, which allowed the use of the same cell for conventional DSC work as well as for the measurement of thermal conductivity. Marcus and Blaine (34) discuss the possibilities for using MTDSC for measuring thermal conductivity.

Thermogravimetry

The terms, *thermogravimetry* (TG) and *thermogravimetric analysis* (TGA) are synonymous. Both ICTAC and International Union of Pure and Applied Chemistry (IUPAC) accept either of them. This is because of the early use and popularity of the term TGA, as well as an interest in avoiding verbal confusion with the glass transition T_g. There may also be potential problems with computer searching.

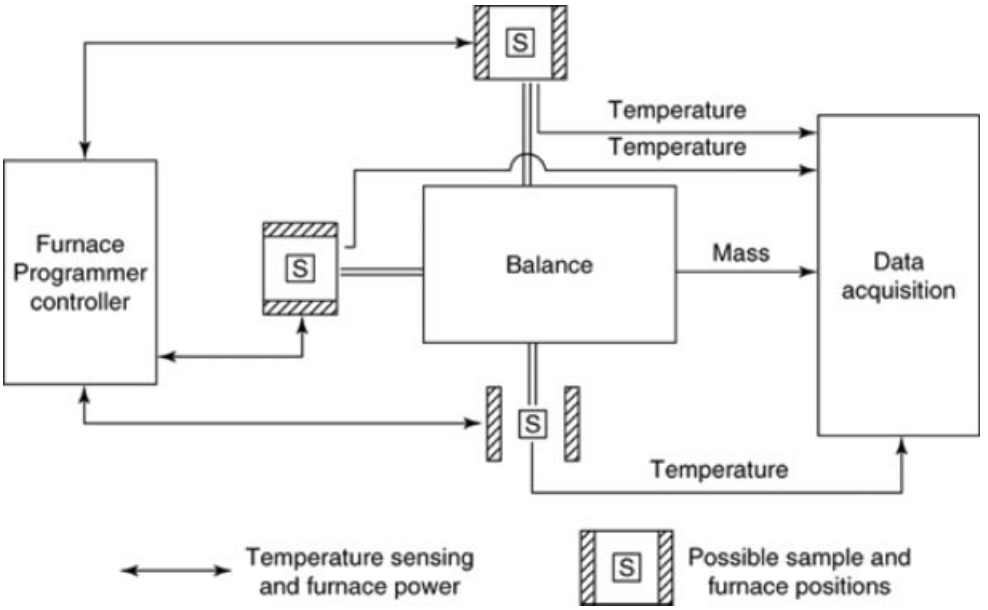

Fig. 13. Typical arrangement for the components of a TGA instrument (3).

Thermogravimetry involves the continuous recording of mass versus temperature or time as a sample is heated in a furnace with a controlled environment. The sample may be heated at a constant rate or held at an isothermal temperature. Madorsky (35) and Jellinek (36) authored major books dealing with thermogravimetry of polymers. The era of modern automated thermogravimetry started with the introduction of the electrobalance by Cahn and Schultz (37). Other competitors, such as DuPont, Mettler, and Perkin-Elmer, introduced their products in rapid succession.

Description of a TGA Instrument. The components of the instrument are the microbalance, the furnace, the programmer controller, and a computer or data acquisition system. Typical arrangements of the components for TGA are shown in Figure 13. The sample can be linked to the balance in three different ways: (*1*) above the balance, (*2*) below the balance, and (*3*) beside the balance as a horizontal extension to the beam.

Arrangement 1 is the most common. However, arrangement 3 is actually preferred because it minimizes the heat effects of the furnace that may be encountered in arrangement 2 and is less influenced by the flow patterns of the gases within the balance and furnace chamber. It also lengthens the balance lever arm, increasing sensitivity, and minimizes the problem of condensation of volatiles on the sample support. In order to minimize thermal expansion of the balance lever arm, quartz is frequently the beam material of choice.

The Balance. Figure 14 shows a schematic of the Cahn electrobalance (38) most frequently used in thermogravimetry work (arrangement 1). A photodetection system monitors the beam position. If the beam moves from the horizontal, enough current flows to the torque motor to move the beam back to its original

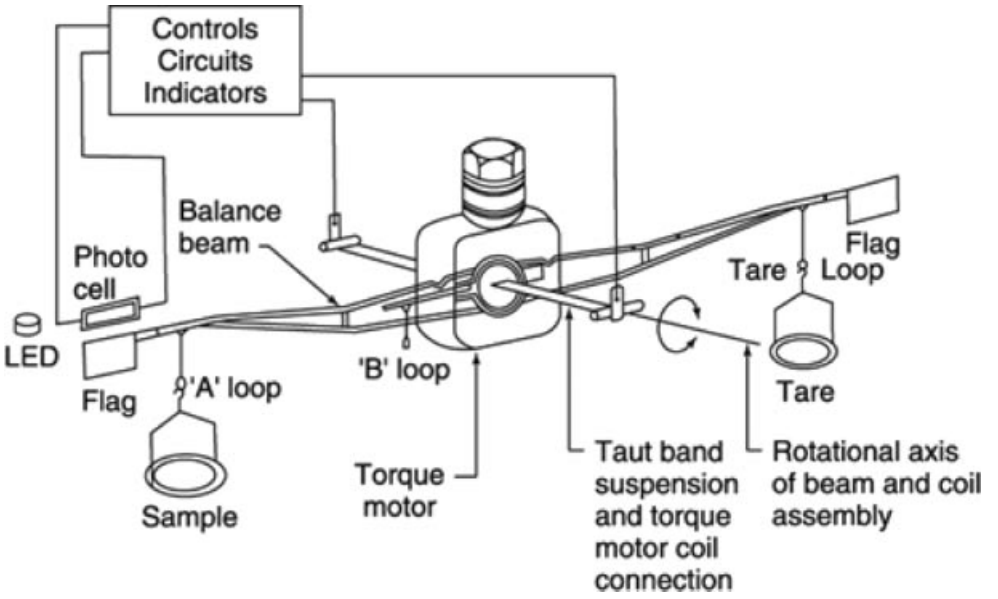

Fig. 14. The Cahn electrobalance (19).

position. The restoring force generated by the current is proportional to the change in mass. A sensitivity of 1 μg is easily achieved. The sensitivity and total capacity of the balance have an inverse relationship. A commercial instrument with high sensitivity (ELCHEMA of Potsdam, New York) has a sensitivity of 0.1 μg and an operating range of up to 100 μg.

The Furnace and Controller. The heating elements of the furnace are most often resistance heaters. Nichrome and Kanthal elements are used for the temperature range up to 1000–1200°C. This range is sufficient for most polymer applications. Aluminum sample pans are often used for low temperatures up to 600°C. For higher temperatures, platinum pans are frequently used as sample containers. For higher temperatures in the range up to 1500–1700°C, molybdenum disilicide (Super Kanthal) or silicon carbide (Globar) is used for heating elements, and platinum or platinum alloys for sample pans. Ceramic refractories such as mullite or alumina are needed to contain the controlled atmosphere. Only a few manufacturers, such as Linseis, Netzsch, and Setaram, market instruments for use above 1700°C. They are expensive and perform poorly below 300°C. Such high temperatures usually are unnecessary for polymers.

Most instrument manufacturers offer several furnace options in interchangeable modules to cover a broad range of temperatures. Thermal shock, oxidation, and vaporization shorten the life span of the resistance elements and refractories so that they may need occasional replacement. The higher the temperature of operation, the more severe this problem is. To enhance TGA instrument lifetime, Gallagher (5) recommends current limiting devices, thermocouple protection circuits and conservative ratings. Also, short times at elevated temperatures and less cycling to high temperatures will help. The use of dedicated computers and microprocessor chips has markedly improved the effective sensitivity and temperature

control of modern instruments. Speyer (39) describes many of the fundamental considerations for the proper design of TGA equipment.

For checking uniform heating rates, the temperature (T) versus time plot (t) is suggested. Wendlandt (40) found that replacing T in the above plot with the derivative dT/dt shows temperature fluctuations better than those of the temperature versus time plot. For further details, refer to the chapter by Gallagher (5).

Major Factors Affecting Thermogravimetry. Mass and temperature are the two most important parameters that must be determined accurately for proper characterization of a material by TGA. Table 5 (Ref. 5, p. 24) shows all of the factors that need to be taken into account for accurate determination of either mass (left-hand side) or temperature (right-hand side). However, it is easier to deal with corrections for mass than it is for temperature. The following discussion summarizes these factors.

Mass. The factors that may affect mass determination are buoyancy, atmospheric turbulence, condensation and reaction, electrostatic and magnetic forces, and electronic drift. Buoyancy corrections arise because the sample is in a lighter gas environment as the temperature of the environment increases. This shows up as a greater weight for the sample. The correction for this is minimal and, except for most accurate or demanding work, it can be neglected. If needed, there are suggestions for both instrumental and software adjustments that will take care of the correction. Atmospheric turbulence depends on the specific gas, its flow rate and pressure, as well as geometrical considerations. Wendlandt (4) discusses these factors in detail and suggests necessary compromises.

Evolved volatile products may condense on the cooler parts of the sample suspension system, thus altering the measured mass loss. The direction of flow of the evolved gases must be manipulated to protect the vulnerable parts of the balance mechanism, temperature sensor, and furnace windings from chemical attack. Also, in case the TGA system becomes contaminated from the products of the high temperature decomposition, subsequent experiments (particularly at high temperature) may be affected. An easy solution for this is to heat the system to around 600°C in an oxidizing atmosphere. This will eliminate most organic condensation products. If there is a chemical reaction with a component in the environment, there may be specific effects on the reversibility and the chemical equilibrium involved. Examples of this are the decomposition of carbonates, sulfates, hydroxides, and hydrates in the presence of CO_2, SO_3 and water, respectively. The partial pressure of the gases present will determine the extent of the respective reactions. Consequently, the degree of decomposition will be determined by the ability to sweep away the decomposition products.

Table 5. Major Factors Affecting Thermogravimetry

Mass	Temperature
Buoyancy	Heating rate
Atmospheric turbulence	Thermal conductivity
Condensation and reaction	Enthalpy of the process
Electrostatic and magnetic forces	Sample, furnace, and sensor arrangement
Electronic drift	Electronic drift

Catalytic reaction of the sample pan with the environment can also affect the environment. Moreover, potential reactions of a sample with the sample holder must be considered. For example, a silica crucible will lower the decomposition temperature of $CaCO_3$ by about 600°C in the presence of the self-generated atmosphere of CO_2. There is potential for reactions of materials such as alkalis and alkaline earth carbonates to react with ceramic or metal parts of the sample holder.

The form or packing of the sample is another factor that will determine excess of the degree of contact with gaseous environment and the rate of escape of the volatile products. Thus, decomposition may be diffusion controlled and dependent on the sample geometry instead of chemically controlled and dependent only on the sample composition. Packing will also affect the thermal gradients in the sample. Thus, results for a single "lump" of a sample, rather than a powder, may differ.

Low humidity of the surroundings and purge gases can generate electrostatic forces that can cause the sample holder to be attracted to or even stick to the nearest wall, thus disturbing the mass signal. This effect tends to be seasonal (dry winter) and there are simple remedies, such as wiping glass surfaces with conducting liquids or surfactants and providing a ground connection through thin metallic film on the glass surface. If moisture can be tolerated, the gas stream can be humidified to eliminate electrostatic charges or, if it is not too hot, the outer wall surface can be wrapped with a moist covering. The electronic drift problem usually is relatively minor and only becomes a problem for experiments lasting for several hours.

Temperature. As mentioned above, accurate temperature control is more of a problem in TGA than is weighing mass accurately. Referring again to the five factors affecting accurate temperature measurement as listed on the right-hand side of Table 5, geometrical placement of the sensor, the sample, and the furnace are particularly important. The sample should be as near to the thermocouple as possible in order to sense accurately the temperature of the sample, but should not affect the measurement of weight. It should not undermine effective control of the programmed rate of heating and cooling by virtue of the heating or cooling generated by any exothermic and endothermic reactions that take place. Also, the products of decomposition may have a corrosive effect on the thermocouple and balance parts. Thus, these volatile products should not come in contact with system components. Some of these requirements are contradictory, and compromises must be made.

The most common configurations for the placement of the sample and the thermocouple are shown in Figure 15 (Ref. 5, p. 30). This emphasizes the contradictions in the above requirements and the uncertainty in measuring the actual temperature of a sample. Very often, thermal runaway reactions caused by highly exothermic processes (e. g., oxidative decomposition of polymers) show as foldback curves (where the temperature increases and then decreases as heat is released) in the mass or weight % versus temperature plot. There is no completely satisfactory remedy for this. Using a high thermal conductivity atmosphere (helium) reduces the response time for temperature control and permits better heat dissipation or absorption by the sample but cannot completely alleviate the problem. Also, at a high flow rate, the high thermal conductivity gas will increase the heat loss from the furnace causing an increase in the power level necessary to obtain the same temperature.

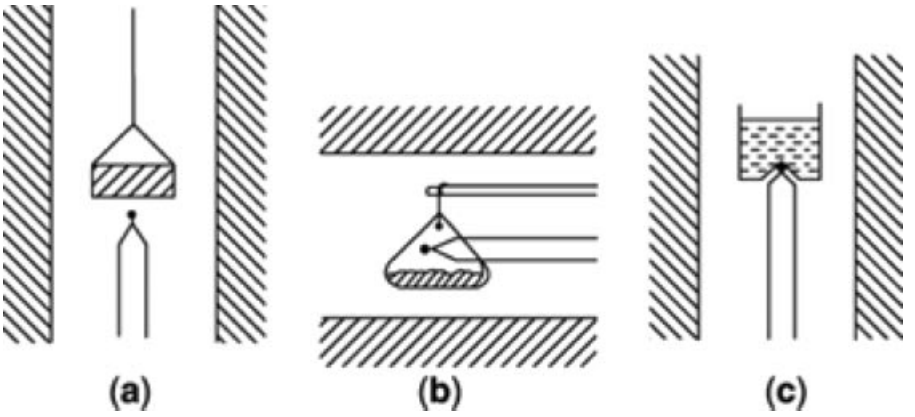

Fig. 15. Possible placements of the thermocouple relative to the sample in TGA (Gallagher, in Ref. 5).

Sartorius-Werke GmbH developed a clever solution (41). Here the balance and the sample chamber are completely separate, linked magnetically with a simple suspension (Fig. 16), thus alleviating the problem of corrosive gases coming in contact with the balance mechanism. A modern version of this "Thermosuspension balance" is available from Netzsch.

A number of manufacturers supply TGA instruments capable of operation in high vacuum or high pressure. A TGA with a magnetic suspension system is available from Rubotherm (Bochum, Germany). The magnetic suspension separates the high pressure sample environment from the delicate balance. The system can operate up to 1000°C or 450 atm. The readers should note that the pressure and temperature limits cited throughout this article represent the manufacturers' specifications, rather than any practical limits determined and recommended by the editor or the authors. Operation at reduced pressure is particularly valuable for determining the adsorption or absorption characteristics of materials. High pressure instruments may be used for studies of combustion, pyrolysis, catalysis, or nonstoichiometry.

Mass and Temperature Calibrations and Standards.

Calibration of Mass. Calibration of mass is conducted by weighing a standard mass (over 1 μg) at a controlled temperature. Room temperature is preferable, since buoyancy and aerodynamics add to the uncertainty when the experiment is conducted over a wide range of temperatures. Any changes due to these factors go into a blank or background correction.

For experiments over an extended period of time, such minor factors as fluctuations in room heating and air conditioning, exposure to sunlight, drafts, and other sources of temperature, and variable heat transfer from the furnace should be taken into consideration. These factors, along with vibration stability, should be considered when choosing a location for a TGA instrument. Generally, all TGA equipment gives precise data with only infrequent checks of the calibration with a standard mass. The starting mass for a TGA experiment is generally larger than that for DTA/DSC and is in the range of 6–10 mg for pure polymers and around 15 mg for filled or blended polymers.

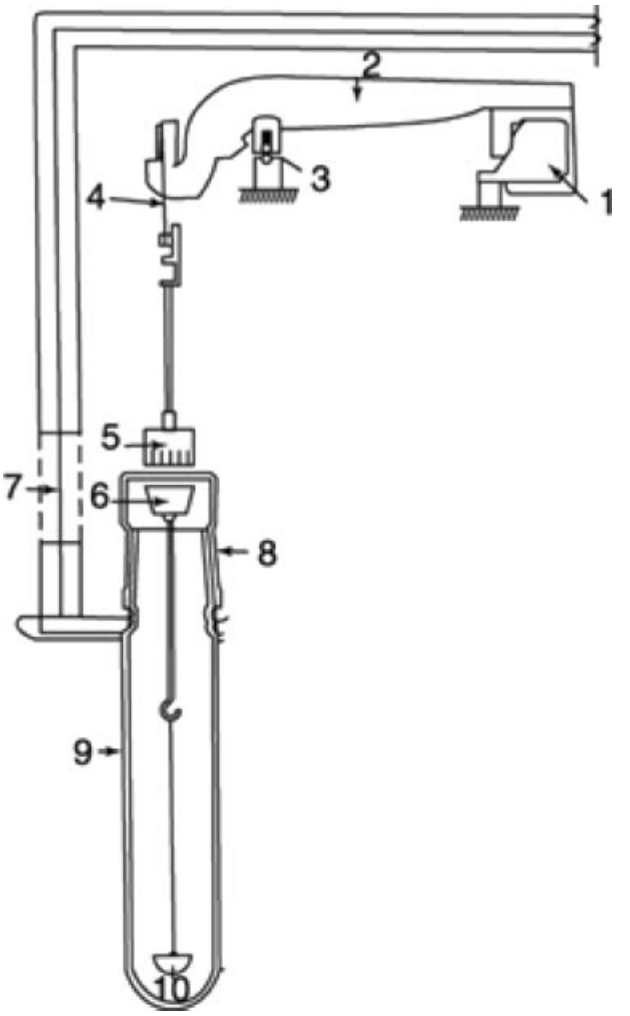

Fig. 16. Sartorius Model 4201 magnetic suspension balance. 1, Magnet and coil; 2, beam; 3, beam fulcrum; 4, suspension ribbon; 5, beam magnet; 6, suspension magnet; 7, observation window; 8, upper glass body; 9, lower glass body; 10, sample pan (41).

For a simple calibration of weight loss, the weight loss of a standard material can be checked under reproducible conditions of sample mass, packing, heating rate, sample holder configuration and atmosphere type, flow, and pressure. The TGA of calcium oxalate monohydrate ($CaC_2O_4 \cdot H_2O$) is often used as a standard for the calibration of mass loss in thermogravimetry. This is due to three well-resolved steps in its thermal decomposition.

The three steps in Figure 17 are (*1*) the loss of H_2O to form anhydrous oxalate, (*2*) the loss of CO to form the carbonate, and (*3*) the loss of CO_2 to form CaO. The observed weight losses, determined from the integral curve (TGA), may be compared with the theoretical values obtained from the known stoichiometry of the process. Potential differences in the sample temperatures indicated by the

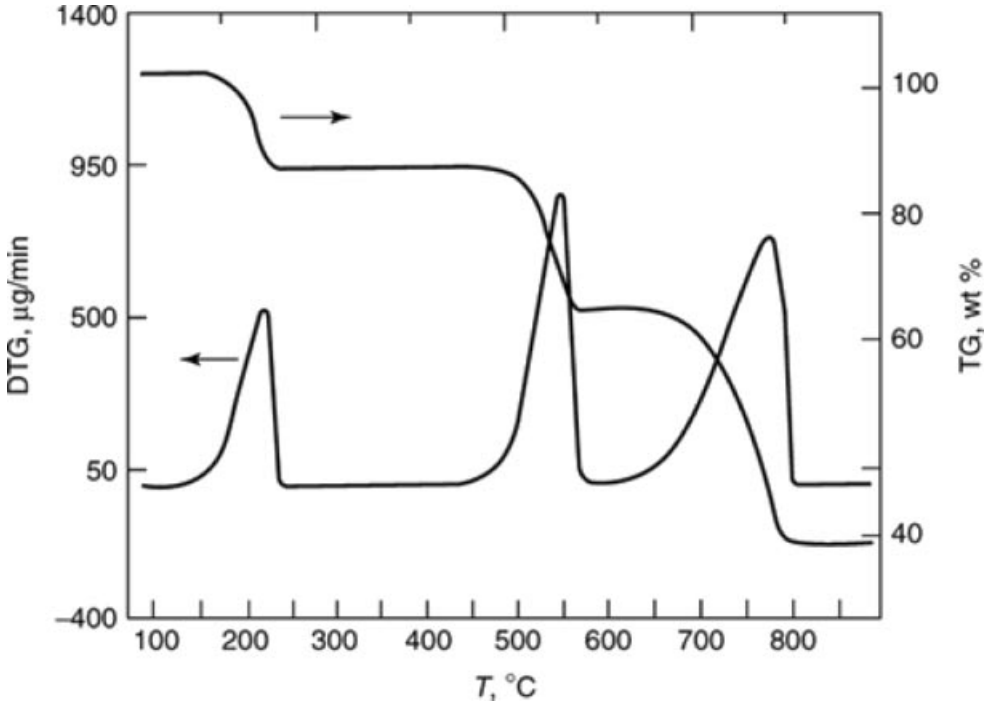

Fig. 17. TGA and DTGA curves for the thermal decomposition of calcium oxalate (CaC_2O_4, H_2O) in argon at 20°C/min (3).

TGA curve can arise when the starting masses differ significantly among the experiments. Plots of weight versus time should reveal the linearity of the heating rate in the range of the experiments. The derivative TGA curve (DTGA), shown in Figure 17, enhances resolution and gives a "fingerprint" of the decomposition process. DTGA curves always should accompany a TGA analysis. Such curves also are important for kinetic studies, since they are related to the actual rate of the reaction. Weight loss is, however, more readily evaluated from the integral curve. There is no international standard method for TGA, because all of the instrumental and experimental variables noted above cannot be fixed for different instruments and different laboratories. However, for a given instrument, standards for mass loss under carefully controlled conditions can be adopted for routine checks of reproducibility.

Temperature Calibration. As mentioned, temperature control and calibration of TGA equipment is more difficult. Not only are the sample and the thermocouple a finite distance apart, so as not to interfere with the weight measurement, but also the heat transfer between sample and oven in TGA is usually across an air or an inert gas gap. In addition, sample masses are often larger than those in DTA/DSC. There may be a large temperature gradient inside the sample. There are also other factors noted in the right-hand side of Table 5 that would affect temperature control.

Wunderlich (5) recommends that the actual sample temperature should be measured by using an external thermocouple in contact with the sample in the

crucible and then running a heating scan. The thermocouple adds additional weight to the balance pan. Therefore, the mass information is lost. Two methods commonly used to measure sample temperature in relation to the sensor temperature are (*1*) magnetic standards and (*2*) "fusible links." They have been found to work equally well in a comparison study (42).

In the "fusible link" method a small weight hangs at the end of a metal link. The link takes the normal position of the sample. When the link melts, there is a sharp break in the TGA curve. The temperature at the break point is the T_m of the metal, which should be known beforehand. The second method uses the Curie temperature (T_c) of a ferromagnetic material. A pellet of the reference material is placed in the field of a magnet, placed outside the balance. Because of the effect of the magnet, the actual weight measured by the thermobalance is either less or more than the true weight. As the Curie temperature of the standard material is reached, the magnetic effect vanishes and an equivalent increase or decrease of weight is recorded. A nice feature of using magnetic materials is that there is no interaction between different samples and multimetal sandwiches of magnetic standards can be used in a single experiment to obtain several calibration points. Representative curves for a series of magnetic standards are shown in Figure 18 (43). The heating and flow rates used for calibration should be the same as those chosen for subsequent experiments.

A series of magnetic reference metals are available from NIST. Gallagher (5) lists the selected metals and alloys for potential use as magnetic standards. The ICTAC Committee for Standardization has conducted an extensive round-robin study to establish the calibration procedures and recommended temperatures for various standards (44). An inert gas (N_2, Ar) whose thermal conductivity approximates that of the gas to be used in subsequent experiments should be used instead of oxygen, since these metals are liable to be oxidized. An ASTM method describes the practice for evaluating the temperature scale for thermogravimetry (ASTM E914). A recent proposal (Ref. 5, p. 48) is to use the ignition temperature of selected organometallic compounds for temperature calibration. There is an abrupt weight loss at the ignition temperature of these compounds. The temperature of ignition can be previously calibrated using DSC or DTA, which again has been calibrated using metallic standards to conform to the International Temperature Scale. ICTAC recommendations should be followed in reporting TGA data.

The present trend in thermal analysis is toward smaller samples and furnaces, as well as faster heating and cooling rates in order to obtain minimum turnaround times. As these trends continue, temperature calibration will remain a major consideration and probably increase in importance. For recommendations on the presentation of data, the reader should consult ICTA recommendations (2).

Application of TGA/DTGA in Polymers

The principal applications of TGA/DTGA in polymers are (*1*) determination of the thermal stability of polymers, (*2*) compositional analysis, and (*3*) identification of polymers from their decomposition pattern. Also, TGA curves are used to determine the kinetics of thermal decomposition of polymers and the kinetics of cure

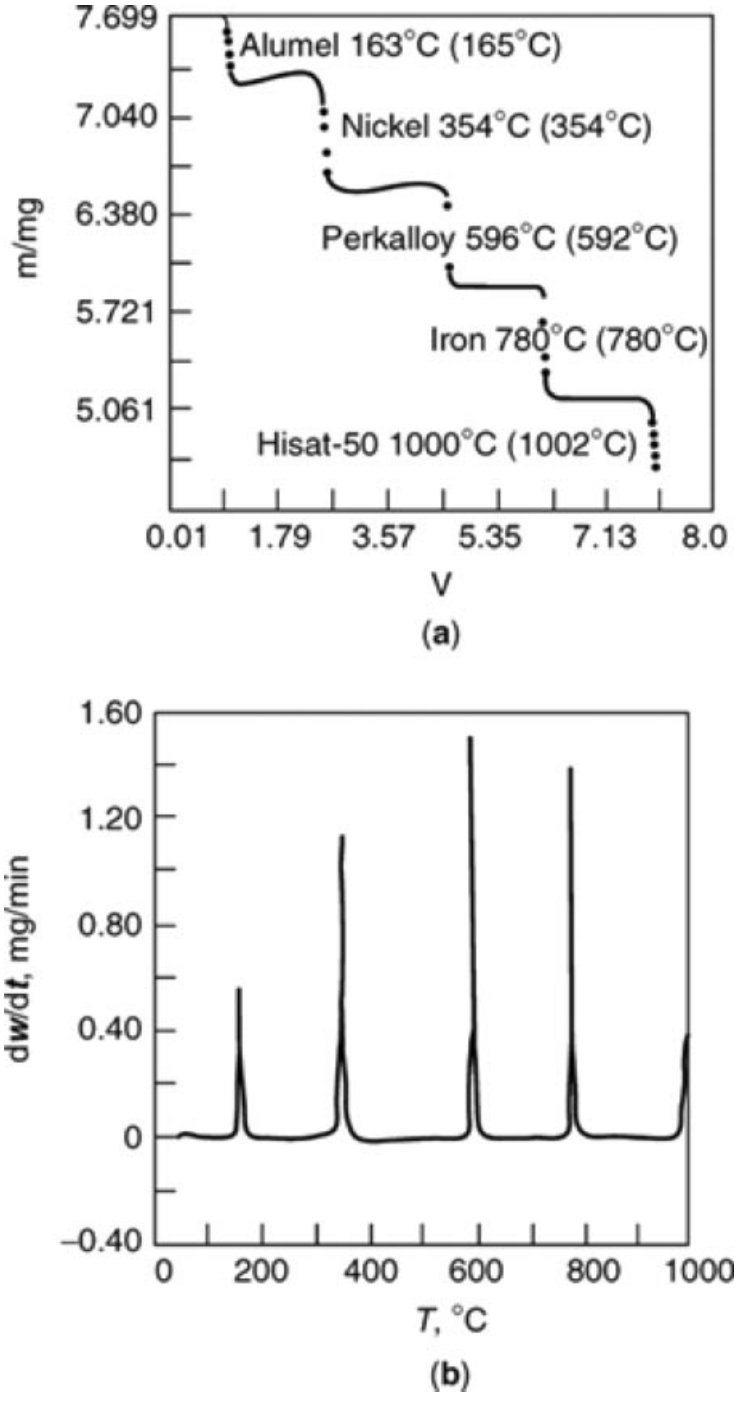

Fig. 18. Representative curves for a series of magnetic standards: (**a**) Thermomagnetometry (TM) curves using Perkin-Elmer TGS-1 and their materials and recommended temperatures. The values in parentheses were the observed values prior to calibration. (**b**) DTM (derivative) curves after conversion of the sensor voltage to actual temperature (43).

where weight loss accompanies the cure reaction (eg, as in condensation polymerizations, such as cure of phenolic resins). The latter will not be discussed here.

Thermal Stability of Polymers. Thermogravimetry has become a general method for comparing the thermal stability of polymers. In comparing thermal stability, it should be remembered that TGA measurements only record the loss of volatile fragments of polymers, caused by decomposition. TGA/DTGA cannot detect any chemical changes or degradation of properties caused by cross-linking. Examples of Degradation (qv) involving cross-linking without weight loss are the degradation of styrene-*co*-butadiene rubber (SBR) and butadiene rubber (BR) or their blends, although at high temperature they decompose into fragments with loss of weight that can be detected by TGA/DTGA. Small sample sizes and low heating rates prevent any dramatic influence of reaction heat that accumulates faster at high heating rates. However, there are some exceptions when small sample size and low heating rate do not yield satisfactory results.

A strict comparison of thermal stability can only be made when the samples are evaluated under identical conditions. Figure 19 shows an example of the stability determination of poly(vinyl chloride) (PVC) and polystyrene (PS) and a

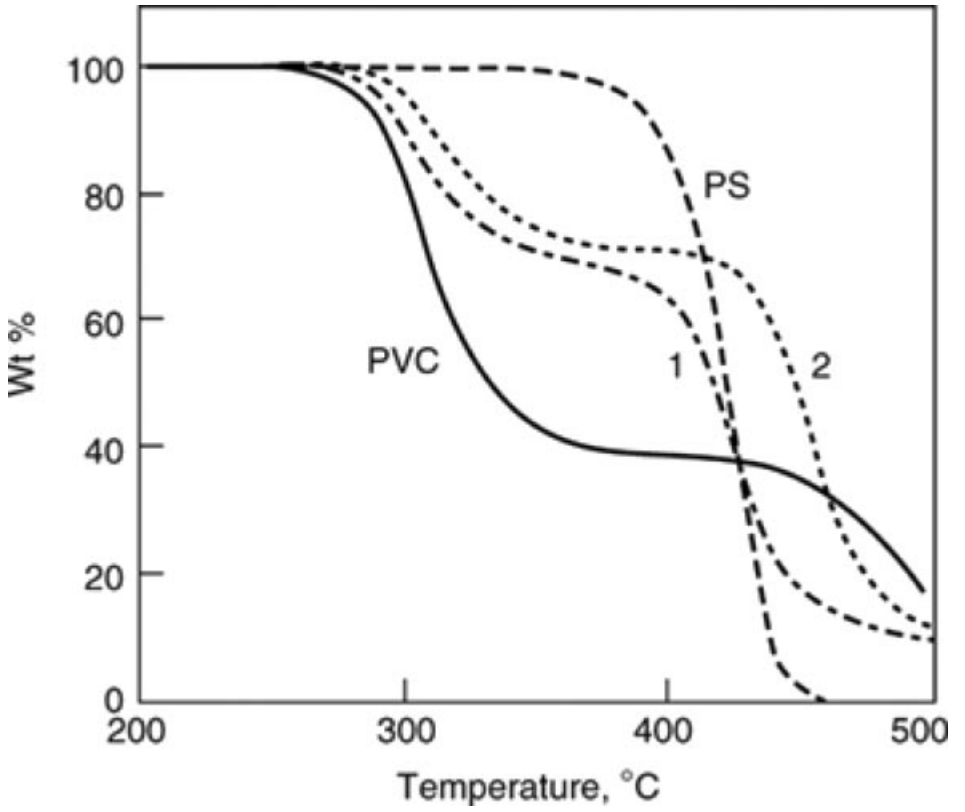

Fig. 19. TGA curves for PVC and PS films for 1:1 (by weight) blend of PVC and PS: 1, predicted behavior for the blend based upon the PVC and PS curves; 2, behavior observed experimentally for the blend (45).

50:50 blend of the two polymers by weight (45). The two inside curves are for (*1*) the predicted behavior for the blend, based on the neat PVC and PS curves, and (*2*) the actual experimental curve for the blend. Under thermal decomposition conditions, there is some possibility that any of the components or their degradation products can interact with one another causing either (*1*) greater stability for the blend, (*2*) less stability for the blend, or (*3*) no change in stability. The case of PVC and PS seems to be one where the blend is more stable than the individual pure polymers (Fig. 19). The shift of curve 2 to higher temperatures as compared to curve 1 indicates that some interaction between the components is taking place leading to mutual stabilization. This may be due to reducing the kinetic chain length (and rate) for dehydrohalogenation of HCl in the PVC component. It will also be dependent on the degree of mixing of PVC and PS in the blend. Examples of polymer blends that are less stable than the pure polymers, to name a few, are PVC/PMMA poly(methyl methacrylate) and (PVC)/PVA poly(vinyl acetate). PS and PMMA blends show no evidence of interaction; thus the thermal stability of their blends neither increases nor decreases.

Compositional Analysis of TGA/DTGA.

Copolymers. If different segments of the copolymer chain have different thermal stabilities, it is possible to quantitatively analyze certain polymers by TGA. The classical example is the polyethylene-*co*-(vinyl acetate) polymer or EVA. When EVA is thermally degraded in an inert atmosphere, the first product emitted at about 350°C is acetic acid. The rest of the hydrocarbon chain decomposes at a higher temperature (430°C). This is shown in Figure 20 (Ref. 5, p. 870). The weight loss at 350°C corresponds to the amount of vinyl acetate present in the copolymer.

The amount of vinyl acetate can be calculated from the weight loss as follows:

$$\%\text{vinyl acetate} = \%\text{weight loss} \times (1.43) \tag{3}$$

Rubber Vulcanizates. One of the common uses of TGA/DTGA analysis in the rubber industry is to determine the composition of a rubber formulation, either cured or uncured. The general TGA/DTGA procedure for elastomer vulcanizate analysis is illustrated in Figure 21 (46). The standard test method for compositional analysis by TGA (47) provides a method for determining four arbitrarily defined components: (*1*) highly volatile matter, (*2*) matter of medium volatility, (*3*) combustible material, and (*4*) ash, left after oxidative decomposition of inorganic components. The materials fitting this description in the case of elastomer vulcanizates are depicted in Figure 21 and described in Table 6. The definition of each component is based on its relative volatility. The success of the method depends on each component having a different thermal stability range in an inert atmosphere and in an oxidizing atmosphere. The standard method for compositional analysis by thermogravimetry is described in ASTM E1131.

The analysis is performed by first taring the microbalance and then introducing the sample. The initial weight is set after establishing an inert atmosphere. Next the desired heating program is started and the specimen weight continuously monitored in the recorder. The ordinate setting can be either weight in milligrams or percentage of the original sample weight. As noted in Table 6, the first weight loss (~150–350°C) is due to highly volatile matter. For a vulcanized rubber, this

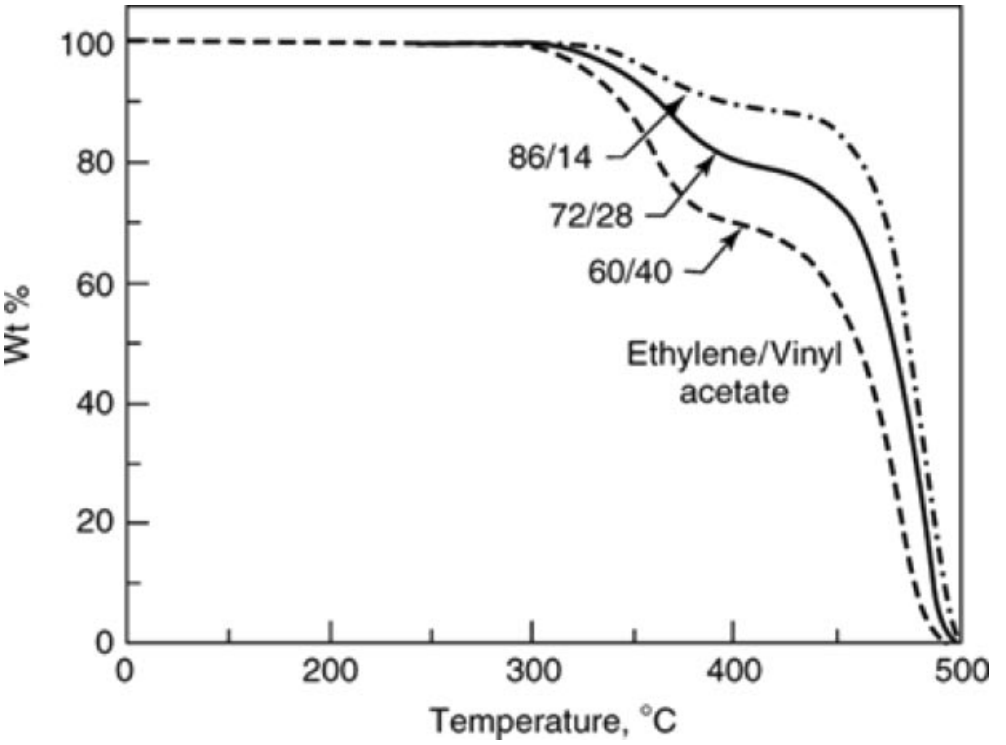

Fig. 20. Weight loss curves of several ethylene/vinyl acetate copolymers. The ethylene/vinyl acetate composition is shown next to each curve. The heating rate was 10°C/min (Hale and Bair, in Ref. 5).

generally consists of the amount of oil added as a processing agent and a small amount (∼1–2%) of decomposed fragments of the vulcanizing agent (sulfur peroxide), vulcanization accelerators and antioxidants, emulsifiers, etc. Moisture, if present, evolves at a lower temperature. The second fraction (∼350–550 or 600°C) represents the amount of polymer decomposed. After the plateau of the second or "medium volatile matter" weight loss has been established (∼600°C), the atmosphere is changed from inert to oxidative.

In the case of an elastomer vulcanizate that contains Carbon Black (qv), the sample is first cooled to ∼300 to 400°C before changing to air or oxygen. This is to ensure that the initial oxidation atmosphere is at a lower temperature than the carbon black oxidation temperature. The modified procedure often permits the identification of carbon blacks from the weight-loss profile (48). The combustible material refers to oxidizable material (eg, carbon black, graphite), which is not volatile in an inert atmosphere at temperatures up to 750°C. In the absence of nonblack fillers, the ash is mostly composed of zinc oxide, which is a component in most vulcanization recopies. The analysis is complete when a weight-loss plateau, corresponding to the residual sample mass, is established. Several reviewers have stressed the use of smaller sample sizes (for better resolution, lower heating rate) and an inert atmosphere of high thermal conductivity (eg, helium). In using small

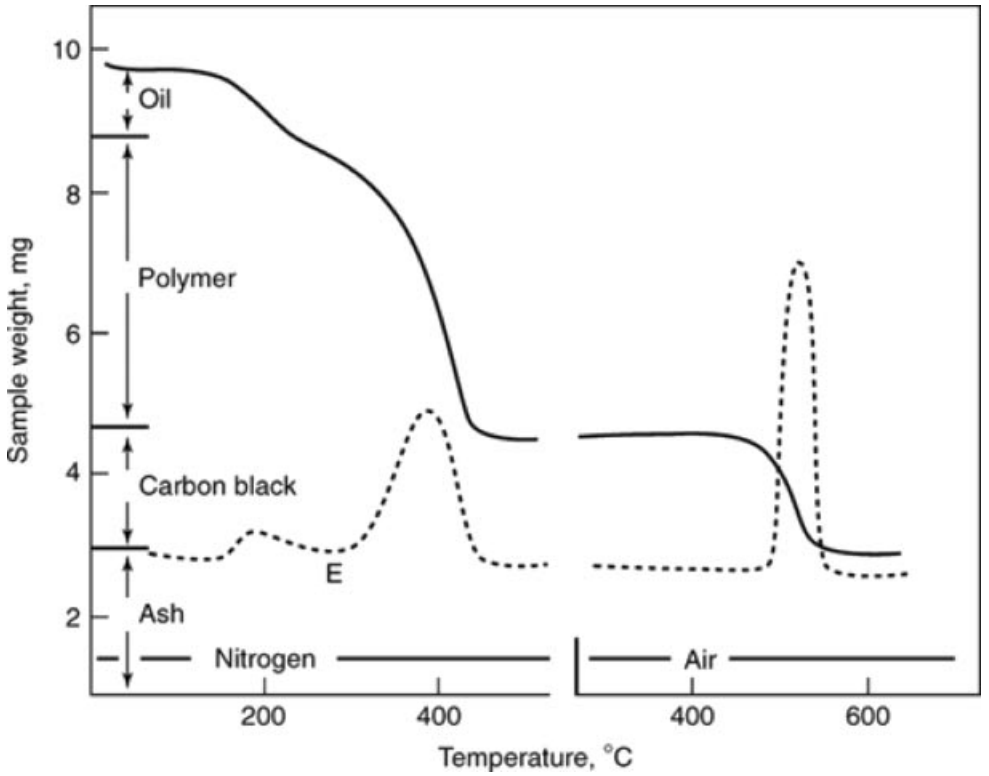

Fig. 21. Schematic TGA and DTGA curve for compositional analysis of a rubber vulcanizate (46).

Table 6. Definitions of Different Fractions in Thermogravimetric Analysis of Elastomers[a]

Highly volatile matter	Refers to moisture, polymer, diluent, oil, plasticizer, emulsifiers (eg, in styrene–butadiene rubbers), curatives (sulfur, accelerator), antioxidants, antiozonants, and other low boiling components (approx. 300°C or lower)
Medium volatile matter	Refers to medium volatility material such as processing oil, processing aid, elastomer, resin (used as curing agent), etc. In general, these materials degrade at 300 to 750°C.
Combustible material	Refers to oxidizable material, not volatile (in the unoxidized form) at 750°C or some stipulated temperature dependent on the material (eg, carbon black, graphite, etc).
Ash	Refers to nonvolatile residues in an oxidizing atmosphere which may include metallic oxides, filler or inert reinforcing material (eg silica). In the absence of nonblack fillers, the ash is composed of zinc oxide which is a component in most vulcanizates. A small amount of ash (<1%) may be due to elastomer residue.

[a]From Ref. 47.

samples it may be useful to characterize multiples to ensure that the results are representative of bulk material. The residue may be analyzed to determine the nature and amount of inorganic components by using X-ray fluorescence.

Factors that influence the accuracy of the component analysis procedure are the following. The above discussion assumes that there is no high boiling oil present as a processing aid that can interfere with detecting clearly the initial breakdown point of the polymer and no mineral filler (which may have water of crystallization or other constituents that escape around the temperature of the "highly volatile matter"). Also, it is important to note that the determination of carbon black by the suggested method is accurate only for hydrocarbon elastomers, which degrade cleanly in an inert atmosphere at temperatures below 500°C Elastomers with a heteroatom in the molecule leave a char residue, which volatilizes along with carbon black during the oxidation stage. Resin curing agents also will interfere with polymer determination. Graphite, if present, can be determined by oxidation at a higher temperature (~800°C). These and numerous other considerations, as well as possible remedies, have been discussed in considerable detail by Sircar (49).

Despite the above-cited difficulties, TGA-DTGA analysis remains a useful tool for the compositional analysis of rubber vulcanizates. It is a straightforward, reasonably accurate process and is much faster than classical extraction methods. Also, it is an excellent quality control tool for determining possible weighing errors and reproducibility for elastomer batches in a production setting. Thus, TGA-DTGA is the method of choice for compositional determinations for cured and uncured elastomer compounds, as well as for many other polymer compositions.

Identification of Elastomers. Sircar and co-workers (Ref. 5, p. 1278) developed a unique and very useful DSC and TGA/DTGA protocol for identifying elastomers. It involves using the measurement of T_g and the degradation patterns for many elastomers and their blends in both nitrogen and oxygen. On the basis of this, they classified elastomers into three principal groups according to their degradation characteristics in nitrogen: (*1*) those exhibiting an endotherm (eg, polyethylene, EPDM, butyl rubber); (*2*) those exhibiting an exotherm (eg, SBR, BR, NBR); and (*3*) those exhibiting multiple peaks, both exotherm and endotherm (eg, NR, IR). For details on using the protocol, the reader is referred to the above reference.

Controlled Rate Thermogravimetry. Gallagher (5) describes controlled rate thermal analysis. In the case of mass loss, the rate of change of temperature is controlled by a preset rate of weight loss or change in partial pressure. Gallagher describes three different modes of controlled rate TGA and also dynamic TGA with isothermal rest periods. In the first mode, the operator chooses a fixed rate of weight loss (eg, X%/min) and the temperature programmer maintains that rate of change, sometimes by both heating and cooling at different times. The second mode is similar to the first mode, except that the sample is always dynamically heated. TA Instruments, Inc. (50) markets a commercial software package called "Hi-Res TGA." It operates so that the heating rate approaches a preset maximum during periods of no mass loss. As the mass change is sensed, however, the heating rate automatically slows depending upon two parameters set by the operator (resolution and sensitivity). The aim is to improve resolution while minimizing the total time for the experiment. The third controlled rate option is called stepwise

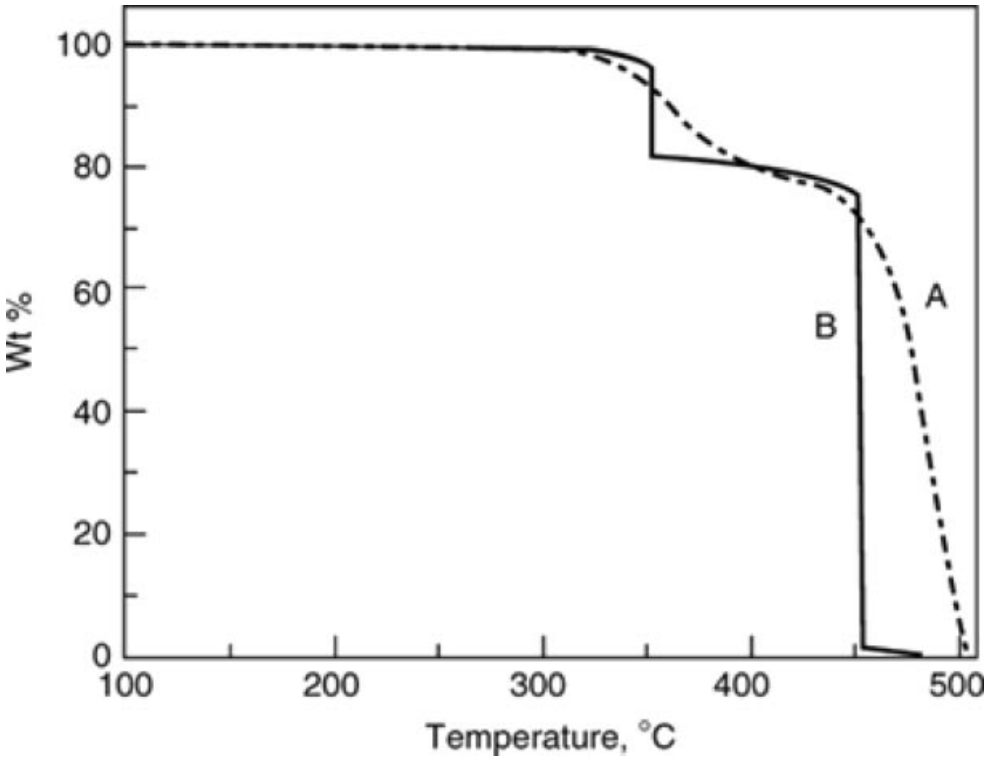

Fig. 22. Weight loss curves for a 72:28 ethylene/vinyl acetate copolymer. Curve **A** was obtained at 10°C/min rate of heating. Curve **B** was obtained using Autostepwise software, which automatically slows down the heating rate when a sharp change in weight loss is detected, and increases the rate when little change in weight loss is observed (from Hale and Bair, in Ref. 5).

(or autostepwise) isothermal measurement and involves one or more isothermal steps as the weight loss reaches a threshold level. The necessary software and instrumentation are available through Seiko Instruments (currently marketed by Mettler-Toledo) (51).

An example of autostepwise TGA shows an improvement in resolution for weight-loss curves of EVA samples. Without the autostepwise rate control it is evident (Fig. 20) that the end point for the acetic acid evolution is not distinct. The acetic acid weight loss curves are not completely level before the residual polymer fraction starts decomposing. As shown in Figure 22, the resolution can be much improved by using the High-Res or autostepwise TGA technique enabling more quantitative information. The figure shows an initial weight loss of 18.4%, corresponding to a vinyl acetate content of 26.3% versus the known value (supplied by the manufacturer) of 28%.

Simultaneous or Combined Techniques. Many of the simultaneous or combined techniques that include TGA as a component have been described while discussing DSC/DTA techniques. Others with TGA as a component are TGA-EGA or EGD, TGA-MS, TGA-FTIR, TGA-GC-MS, TGA-MS-MS, and TGA-APCI-MS. APCI stands for atmospheric pressure chemical ionization. More details are

available in the reference by Gallagher (5). The other acronyms, not mentioned in Table 1, are as follows: mass spectrometry (MS), Fourier transform infrared spectrometry (FTIR).

Thermomechanical Analysis

Thermomechanical analysis (TMA) measures the deformation of a material contacted by a mechanical probe, as a function of a controlled temperature program, or time at constant temperature. TMA experiments are generally conducted under static loading with a variety of probe configurations in expansion, compression, penetration, tension, or flexure. In addition, various attachments are available to allow the instrument to operate in special modes, such as stress relaxation, creep, tensile loading of films and fibers, flexural loading, parallel-plate rheometry, and volume dilatometry. The type of probe used determines the mode of operation of the instrument, the manner in which stress is applied to the sample, and the amount of that stress.

TMA Instrumentation. For accurate measurements of the change in dimension of small samples, the device generally used by most manufacturers of TMA is called a linear voltage differential transformer (LVDT). This device, as configured in a Perkin-Elmer TMA module, is shown in Figure 23. For distinguishing between expansion and contraction, the sign of the output voltage changes with the direction of motion. The device can readily detect changes of the order of 0.1 μm. Testing for linearity of the range of output voltage of an LVDT (mV/μm) is frequently performed by measuring gauge blocks of a sheet metal. For accurate work, it is necessary to provide compensation for the dependence of the output on temperature. The instrument shown in Figure 23 is typical of a single rod module, based on LVDT. Contemporary TMA instruments use closed loop electromagnetic circuits to accomplish constant loading and positioning of the probe as compared to older instruments where mechanical placement of the weights was used. The instrument in Figure 23 is reported to be capable of detecting changes as small as 3 nm and can operate in the temperature range -170 to 1000°C. The resolution is around 0.1 μm, when the instrument is operated carefully over a range of temperatures. Temperature-sensitive components such as the LVDT generally are isolated from the high temperature environment of the sample.

Optical instruments that use laser interferometry have much greater sensitivity with an accuracy of 0.02 μm or 1/32nd of the laser wavelength used. The surfaces for the sample and the reference specimens need to be polished for this kind of accuracy. Also, the high temperature limit is governed by the loss of reflection from the mirrored surfaces and is around 700°C, as compared to a maximum of 2000°C for the LVDT-based instruments.

For determining the coefficient of linear expansion, it is a common practice to generate $\Delta L/L_0$ curves with and without the sample. The two curves are subsequently subtracted to compensate for the expansion of the sample holder. For convenience, it is best to use a standard reference material, eg, an isotropic metal such as aluminum or platinum (52), as the sample holder. In Figure 24, we see that, compared to other isotropic materials, quartz (fused silica) has a very low thermal expansion coefficient (0.6×10^{-6}/°C). It is also easily formed. If the upper

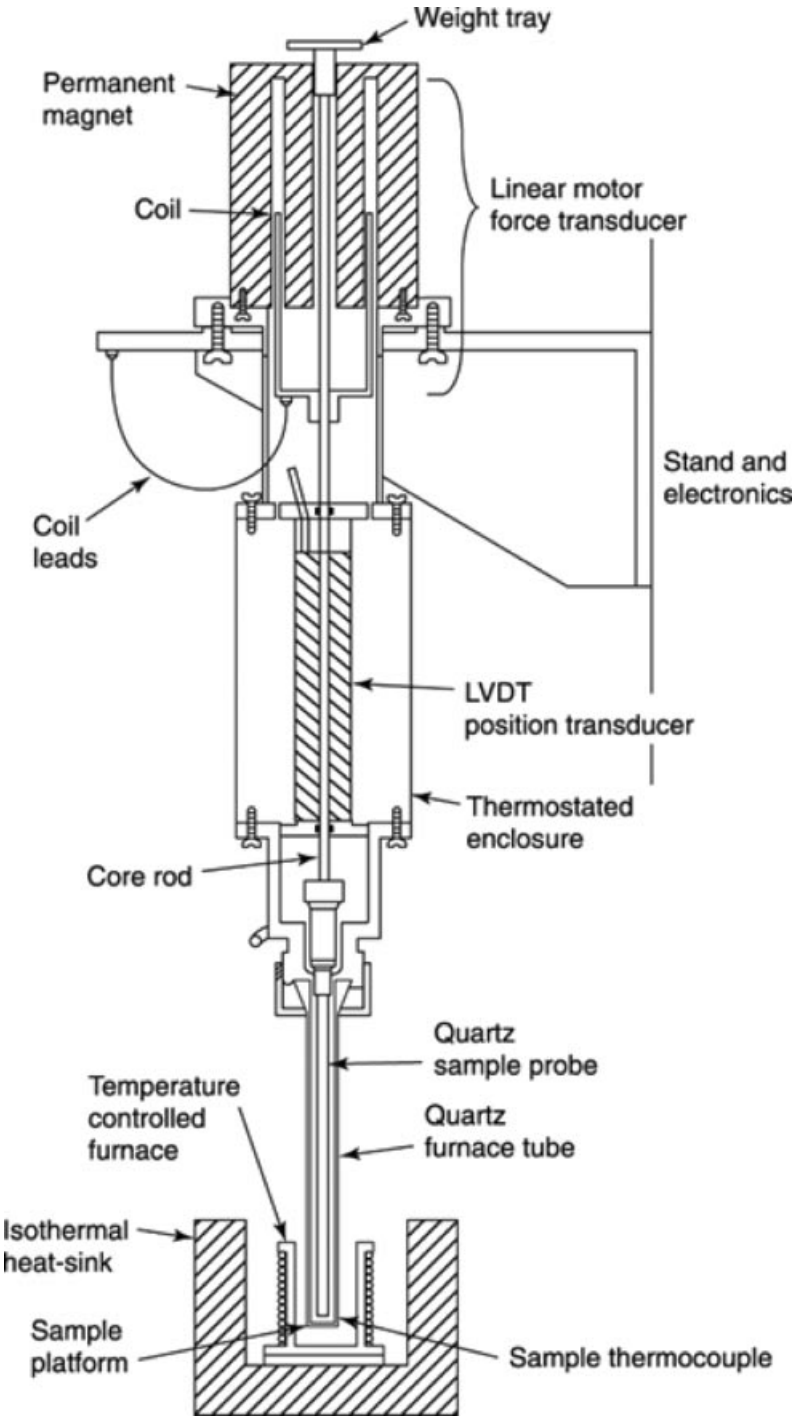

Fig. 23. Schematic representation of a typical thermomechanical analyzer (TMA), Perkin-Elmer Model TMA 7, based on an LVDT (3).

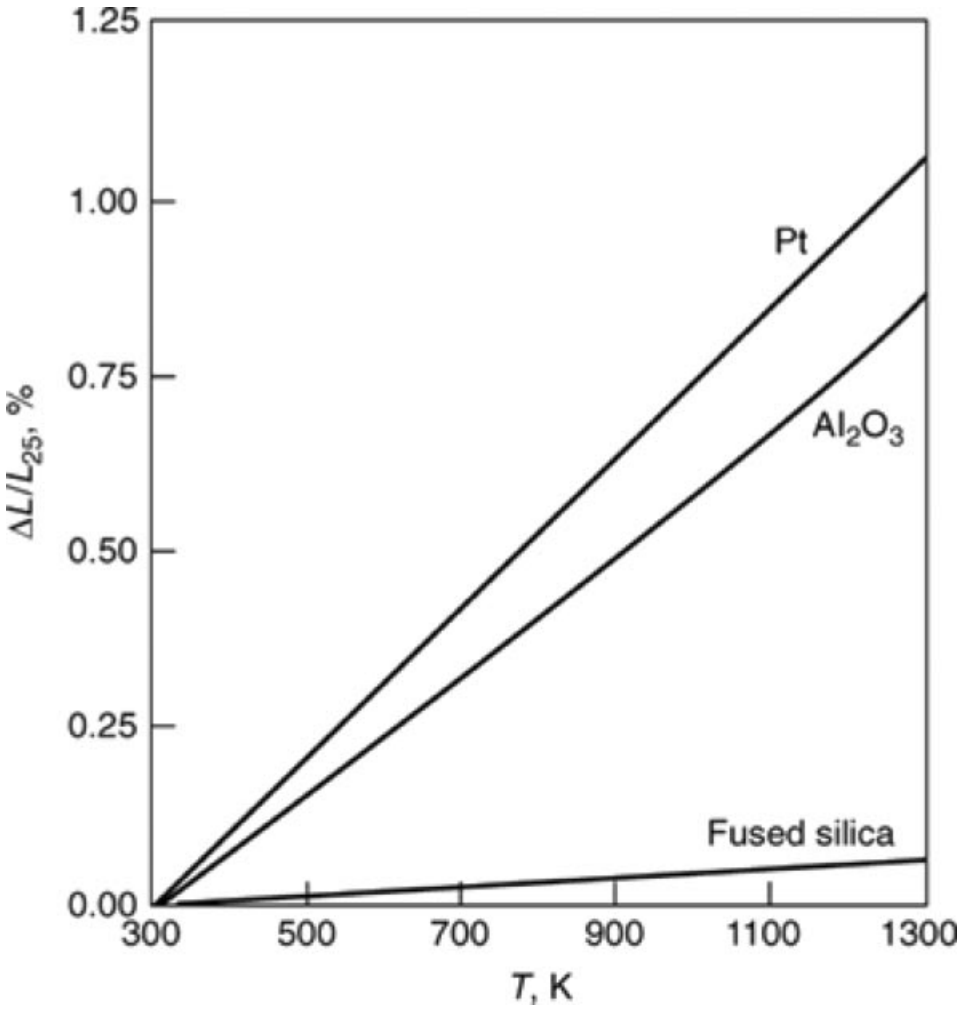

Fig. 24. TMA thermal expansion curves for platinum, alumina, and fused quartz (52).

temperature limit ($<1100^{\circ}$C) is acceptable, then use of a quartz sample holder may permit ignoring the small correction for the linear thermal expansion of the sample holder, with very little effect on accuracy. If the upper temperature limit is over 1100°C, a high temperature material such as alumina or platinum is the material of choice and the correction is substantial. Another way to reduce the correction is to use the instrument in a differential fashion. Both the optical and the LVDT instruments can be used in this fashion with the reference (a standard material) pushrod connected to the coil and the sample rod to the core. To obtain the correction accurately, the sample and the reference should have the same length. It is also necessary to maintain thermal equilibrium by keeping the heating and cooling rate low. This also avoids a thermal gradient inside the larger-sized samples typically used for TMA. It is necessary to allow sufficient time to equilibrate if programming several isothermal steps is the temperature profile followed.

A temperature calibration procedure for TMA has been proposed (53–55) and subsequently included as an ASTM method (Test Method for Temperature Calibration of Thermomechanical Analyzers, E1363-90). It uses a penetration probe and the melting temperature of one or more standard materials. Pure metals with sharp melting points are the standards often used. An open DSC pan may be used to contain the calibrant material. Another potential material would be the selected shape memory alloy, reported to be reproducible to $\pm 1^{\circ}$C (56). Several reviews on temperature calibration for TMA have been published based on ASTM efforts in this area (54,55). Sircar (26) suggests that, when used for elastomer evaluation, temperature calibration for TMA should be conducted with low melting liquids as in DSC. For calibration of the expansion, one manufacturer's manual (TA Instruments) recommends aluminum for calibrating the linear expansion parameter. Other calibration standards suggested for the linear coefficient of thermal expansion (CTE) are lead (57) and copper (58).

Sample Preparation and Procedure. Sample preparation for CTE measurement is somewhat more rigorous for TMA than for either DSC or TGA. Samples with flat parallel faces ($\sim$7 mm^2 $\times$ 1 to 2.5 mm in thickness) may be used. The larger the sample thickness, the greater will be the possibility of thermal gradients developing within the sample. ASTM D696 describes a recommended procedure for determining the coefficient of linear expansion of plastics. A general test method for solids (Test Method for Linear Expansion of Solid Materials by Thermomechanical Analysis, E831-86) is also available. Not all polymers and, particularly some elastomers, are amenable to TMA study. For example, a flat surface, to allow intimate contact of the sample and the probe, cannot be cut from a gum elastomer of high molecular weight. Maurer (59) has recommended hot pressing, which works for lower molecular weight gum rubbers. Silica powder also has been used to level the surface of gum elastomers (60). For penetration measurements the surface does not need to be smooth.

For Thermosets (qv), a flat surface can be achieved by molding, machining, or melt-pressing the sample. If the sample is punched, the burred edges must be removed or the sample placed burred edge up. Prime (Ref. 5, p. 1447) advises that the sample be conditioned in the TMA apparatus by heating to just above T_g and cooling with the loaded probe in place. This helps in relieving the internal stress, removes thermal history (eg, the effects of physical aging), and allows the sample to conform to the probe. For samples that are not fully cured, care must be taken not to advance the degree of cure while following this procedure.

For T_g studies in elastomers, the ASTM E831-86 procedure must to be modified (26). After the probe is zeroed at room temperature, the sample is placed on the TMA platform and cooled to -120°C under liquid nitrogen purge at 50 mL/min. After equilibration at -120°C for 10 min, a 0.5–1-g weight (10 mN) or equivalent force is placed on the top of the pan. This places the probe in contact with the hardened elastomer sample. The thickness of the sample is measured and the probe zeroed. The sample is ramped at a low rate of heating (2–5°C/min) under 50 mL/min of nitrogen purge from -120°C to 100°C. For presentation of data, the ICTAC recommendations (2) are followed.

The above procedure differs from ASTM E831 in two important ways. First, the weight should be added only after the elastomer sample is rigid (below T_g) to avoid compression; and second, a small weight of only around 0.5 g or less is

necessary to ensure intimate contact. Larger weights (1–3 g, as recommended for plastics by ASTM E831) may again compress the elastomer as it reaches temperatures above T_g. A static weight of 10 g or more or the equivalent force is generally used with a penetration probe.

Probe Configuration for TMA. Typical probe configurations for TMA have been described by Maurer (59) and Earnest (25). Figures 25**a** to 25**e** are from Earnest (25), whereas 25**f** and 25**g** are from Wendlandt (4). The coefficient of linear expansion uses a probe of greater surface area and is operated under negligible load (Fig. 25**a**). A high loading converts it to a compression probe for elastomeric materials and the results differ with load. Figures 25**b**, 25**c**, and 25**f** show various penetration probes. The hemispherical probe can also be used as an expansion probe. Ennis and Williams (61) used the hemispherical probe to determine linear

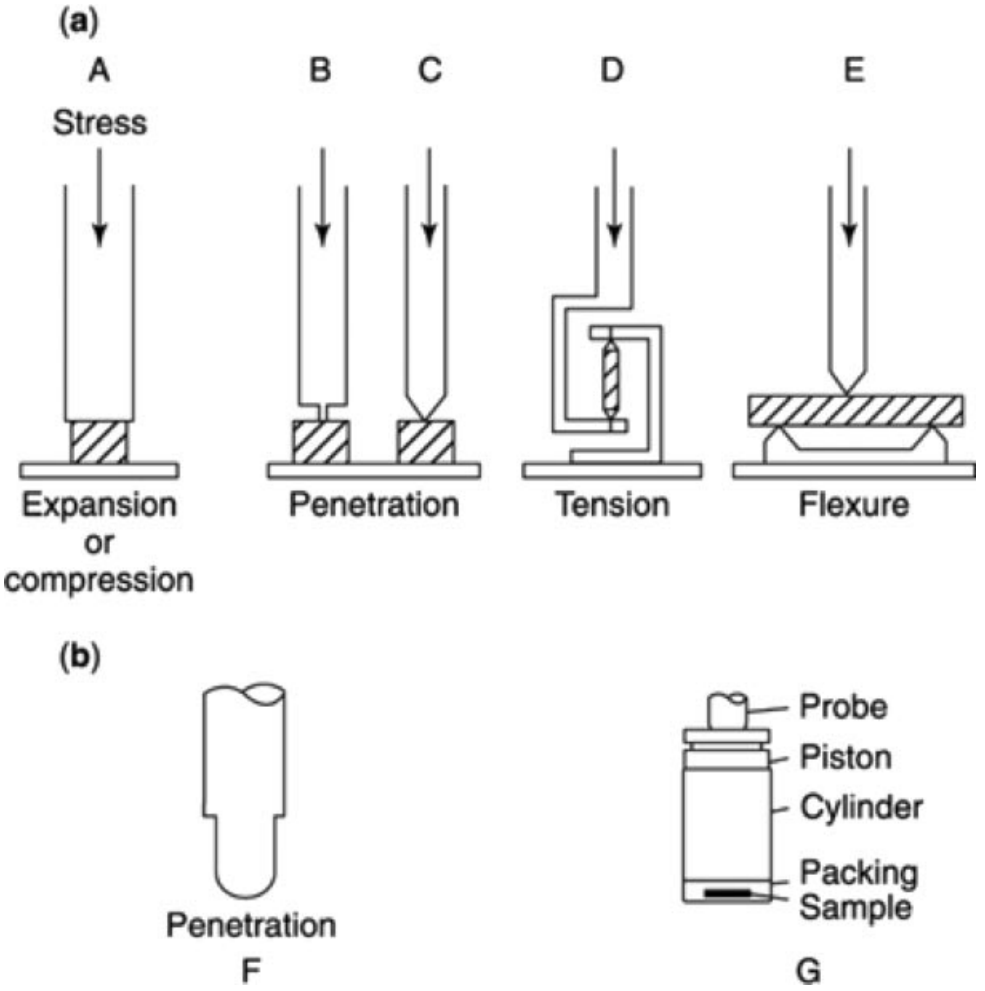

Fig. 25. Examples of probe geometry or operation modes for TMA: (**a**) from Neag (62); two Perkin-Elmer TMA sample probes for penetration and dilatometry (**b**) from Wendlant (4).

expansion of thermosets and claim better accommodation of probe misalignment with this type of probe. Figures 25**d** and 25**e** are for tensile and flexure modes, respectively. For anisotropic materials, the determination of linear expansion does not give the volume expansion by a simple calculation. However, TMA also can be used to determine volume expansion by using a fluid to surround the sample in a cylinder and piston arrangement, as shown in Figure 25**g**. This is similar to a dilatometer. Another method uses a vitreous silica dilatometer (ASTM E228). Special instrumentation has been designed to determine the coefficient of thermal expansion of fibers using TMA (Ref. 5, p. 1974). For "fingerprinting" of fibers, TMA offers more detail than either DSC or DTA. Therefore, TMA is the preferred technique if the study is limited to only a single method.

Derivative TMA. An example illustrating the use of different probe configurations for determining linear expansion in both the glassy and the rubbery states, as well as T_g of chloroprene rubber (neoprene, CR) (62), is presented in Figure 26. Note the use of the derivative signal (DTMA) for both the loaded expansion (penetration) and tension measurements. The derivative plot aids in locating the transitions or relaxations, which are not prominent, and also defines a reproducible transition point in cases where a diffuse transition is encountered. DTMA of tension measurements is a sensitive technique for evaluating polymer blends. Several transitions are reproducibly detected by this method when other modes may fail. The T_{go} values are the glass-transition temperatures reported in the literature. They correspond to the inflection point of the DSC curves (T_{eo}) in Figure 7. T_{gd} is slightly different and corresponds to the peak of the derivative DSC curve (see T_p in Figs. 7 and 8). Sircar (26) determined T_g values for eight elastomers using TMA (expansion and penetration probes), DSC, and DMA. He found that T_g(expansion) and T_g(penetration) have somewhat different values and the latter is closer to that determined by DSC. The differences in the T_g values are due to the differences in the temperature dependence of the different thermal properties being measured by different techniques: specific heat capacity in the case of DSC, linear expansion with the TMA expansion probe, and modulus in the case of the TMA penetration probe.

Illustrative Examples for TMA.

Expansion Mode. Figure 27 (64) illustrates the calculation of the CTE from the slope of the TMA curve of an epoxy printed circuit board and the use of the derivative (DTMA) to directly record the coefficient of linear expansion (α). Thermosetting polymers, especially when highly filled, can absorb moisture from the atmosphere. Moisture acts as a plasticizer and has the effect increasing α and lowering T_g. The process is reversible. While moisture in polar polymers is often tightly bound, desorption may occur on heating during the measurement. This will be discussed at greater length below. In this case the measurement will reflect the sum of thermal expansion and hygroscopic contraction. Purely thermal expansion then can be measured in a second run after the sample has been thoroughly dried.

Penetration Mode. TMA in the penetration mode can be used to evaluate the degree of cure of thermoset materials (64). A large load (typically, 10–100 g or 0.1–1.0 N) is employed for these experiments. The probe measures the softening associated with the large decrease in modulus as the temperature approaches T_g. The softening point correlates well with T_g (65,66). The penetration probe referred to in Figure 28 is a small-radius (0.48 mm) hemispherical probe. The

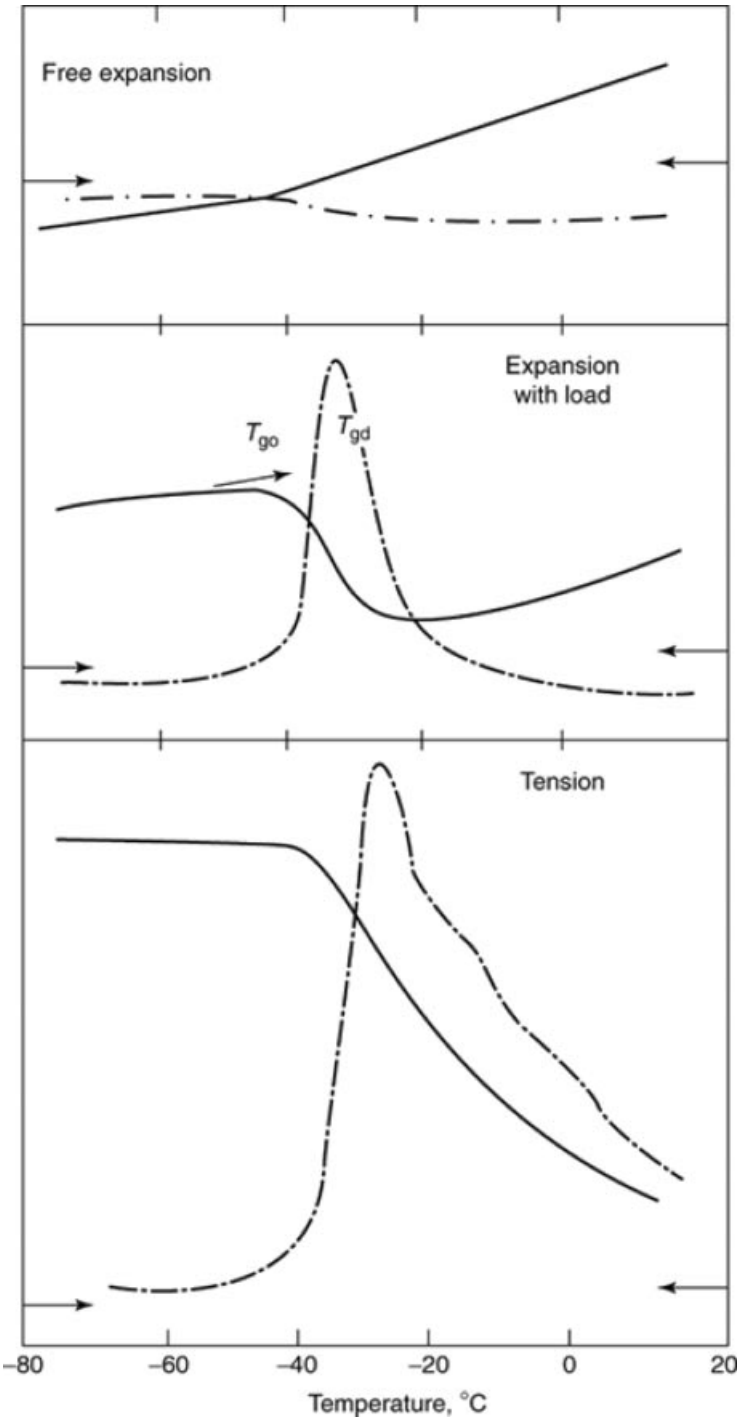

Fig. 26. TMA free expansion, indentation, and tension curves for polychloroprene (neoprene) vulcanizates; 5°C/min, 50-*g* load in indentation and tension.—, Δl versus temperature; -˙-˙-, $d(\Delta l/dT)$ versus temperature (63).

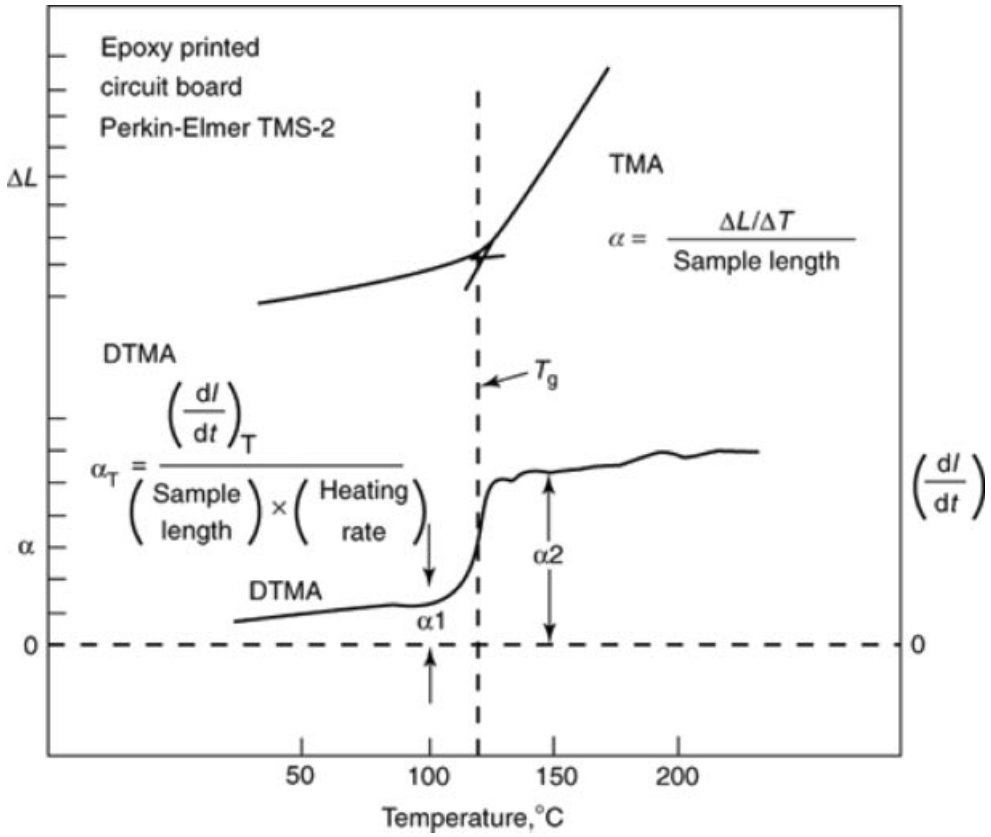

Fig. 27. Linear expansion before and after the glass-transition range using TMA-DTMA. Linear expansion coefficient α from TMA trace requires measurement of the slope; DTMA allows direct recording of α (64).

smaller amount of penetration for sample A indicates that this is more highly cross-linked of the two samples.

Flexure Mode. Figure 29 illustrates TMA data for a two-layer insulation wire coating. Using the knife-edged three-point bend flexure probe (67) accentuates the softening that occurs at the glass-transition temperature. It is remarkable that the softening of both the outer layer of polyester and the inner layer of poly(amide–imide) were easily detected.

Degree of Cure. As shown in Figure 27, the T_g is taken as the extrapolated intersection for the glassy and rubbery state curves. Typically, thermal expansion in the rubbery state is about three times that in the glassy state. The T_g determined by TMA (using either an expansion or penetration probe), is often related to the degree of cure for thermosetting polymers, as was mentioned in the discussion of DSC and illustrated in Figure 9. As the degree of cure increases, T_g increases and the coefficient of linear expansion (α) decreases. Thus, a relationship between T_g and conversion, independent of the temperature of cure, exists for most thermosetting systems. This will be discussed further later in this presentation. Also, a direct proportionality exists between the deflection temperature under load (ASTM D648) and the TMA T_g determined in either the expansion or

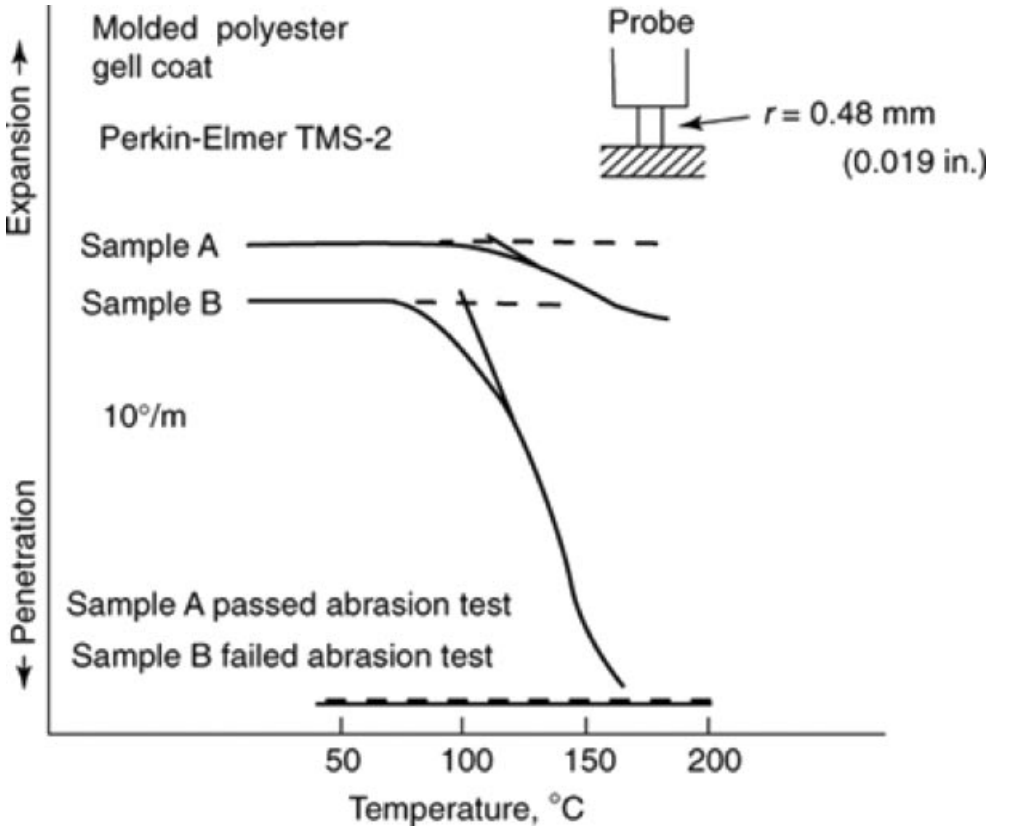

Fig. 28. TMA penetration tests to detect relative states of cure of a thermoset polyester. The more highly cross-linked material softens at a higher temperature, undergoes less penetration, and is more abrasion-resistant. – – – No load; ——— 50-g load (64).

the penetration mode. Sykes and co-workers (68) describe a fixture to measure a TMA heat distortion temperature (HDT) as defined in ASTM D648. For printed circuit board materials, Lamoureux (66) observed a correlation between T_g by TMA expansion and softening temperature determined by TMA penetration (as described above by Sykes and co-workers). For an elastomer compound, Brazier and Nickel (63) found a correlation between T_g, determined by TMA (expansion and penetration mode) and Gehman rigidity temperature.

Unlike thermosetting materials, the T_g of elastomers does not increase significantly with the degree of cure. However, the penetration temperature under a fixed load will increase with cure and can be used as a measure of the degree of cure of an elastomer compound. This is illustrated in Figure 30 (69) and is based on the fact that the elastomer modulus increases with cure.

Dynamic Mechanical and Dielectric Analysis

Dynamic mechanical (DMA) and dielectric analysis (DEA) methods are used both to study molecular relaxation processes in polymers and to determine inherent

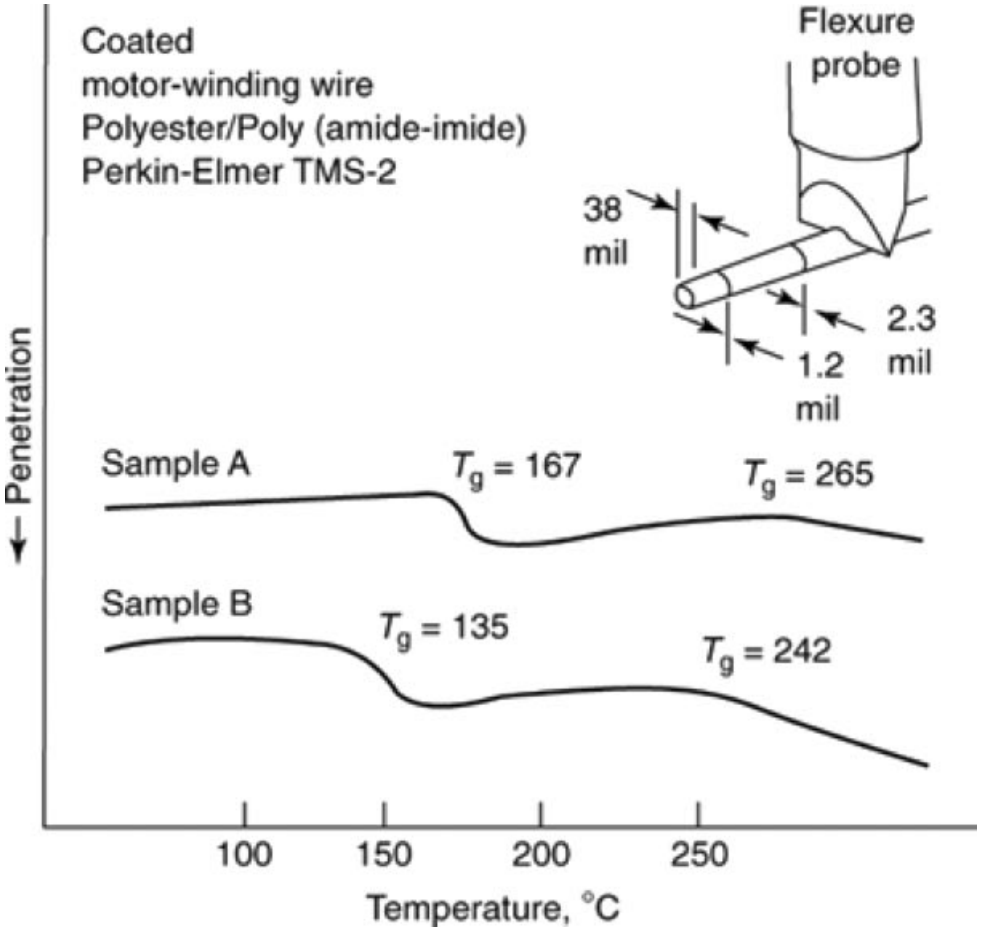

Fig. 29. Use of the TMA knife-edged flexure probe to determine the softening point of both the outer and inner coatings of a motor-winding wire (67).

mechanical and dielectric properties. DMA measurements involve mechanical excitation by imposing a small cyclic deformation to a sample and measuring the stress response. DEA involves imposing a cyclic (or alternating) electric field to a sample and observing the electric polarization or current induced in the sample (see DYNAMIC MECHANICAL ANALYSIS; DIELECTRIC RELAXATION).

DMA methods are widely used by thermal analysts to determine the viscoelastic properties of polymers for a number of purposes (see VISCOELASTICITY). The primary application of these techniques to the study of polymeric solids and melts is well documented. Excellent general discussions covering the subject are provided in References 70–72. Linear Amorphous Polymers (qv) exist in a number of characteristic physical states depending on the time scale and temperature of measurement. These are illustrated in Figure 31 in terms of an arbitrary modulus function and are classified as glassy, leathery, rubbery, rubbery flow, and viscous (73). All linear amorphous polymers exhibit these five physical states when they

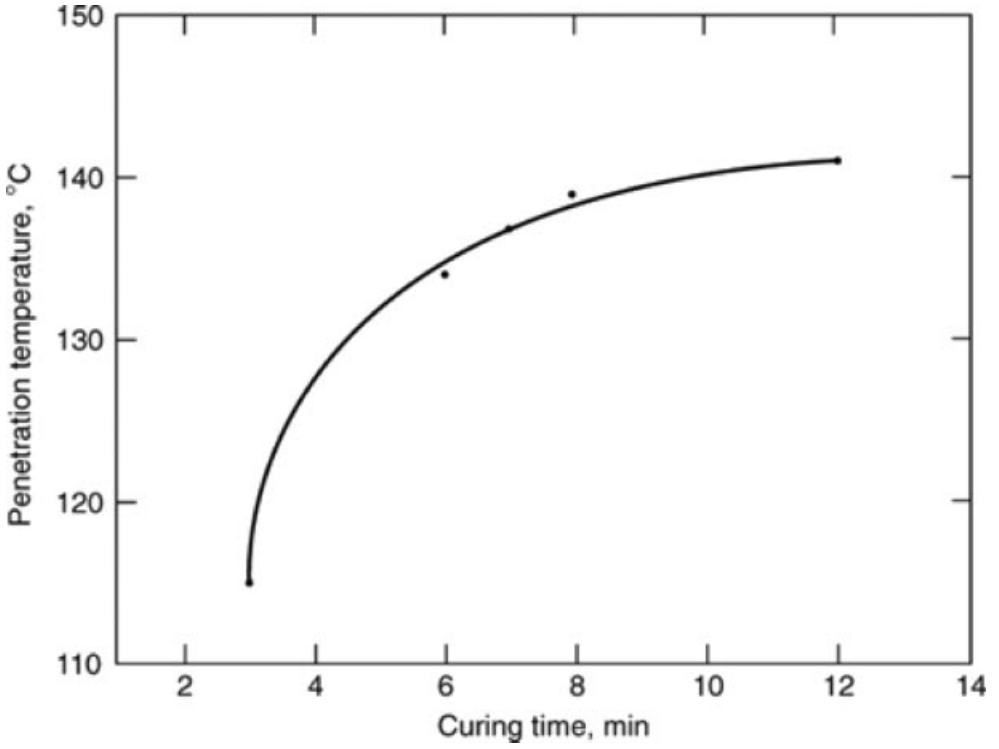

Fig. 30. Evaluation of the degree of cure of an elastomer by TMA penetration probe; sample is a carbon black filled rubber stopper (69).

are observed over a wide range of time or temperature. Polymers that are either cross-linked or crystalline do not exhibit the rubbery flow and viscous responses as illustrated.

Region 2 in Figure 31 corresponds to the Glass Transition (qv), which serves as an important benchmark or corresponding state for viscoelastic response. The particular physical state that the polymer exhibits during a DMA measurement reflects the extent to which the rate of molecular motion or relaxation compares to the test rate at a given temperature. In general, the modulus decreases either with decreasing test rate or increasing temperature. In fact, there is a strong relationship between time and temperature.

In most commercial dynamic mechanical instruments a steady-state alternating strain is applied such that

$$\varepsilon\,(u) = \varepsilon_0\, \mathrm{e}^{i\omega u} \tag{4}$$

is the generalized sinusoidal strain function in complex notation, where ε_0 is the strain amplitude, ω is the radian angular frequency of the sine wave (rad/s), and u is the historical time, $u \leq t$ ($u = 0$ at $t = 0$). An analysis of the cyclic stress and strain provides that the steady-state ratio of stress to strain is (70,73) a complex quantity having both in-phase and out-of-phase components.

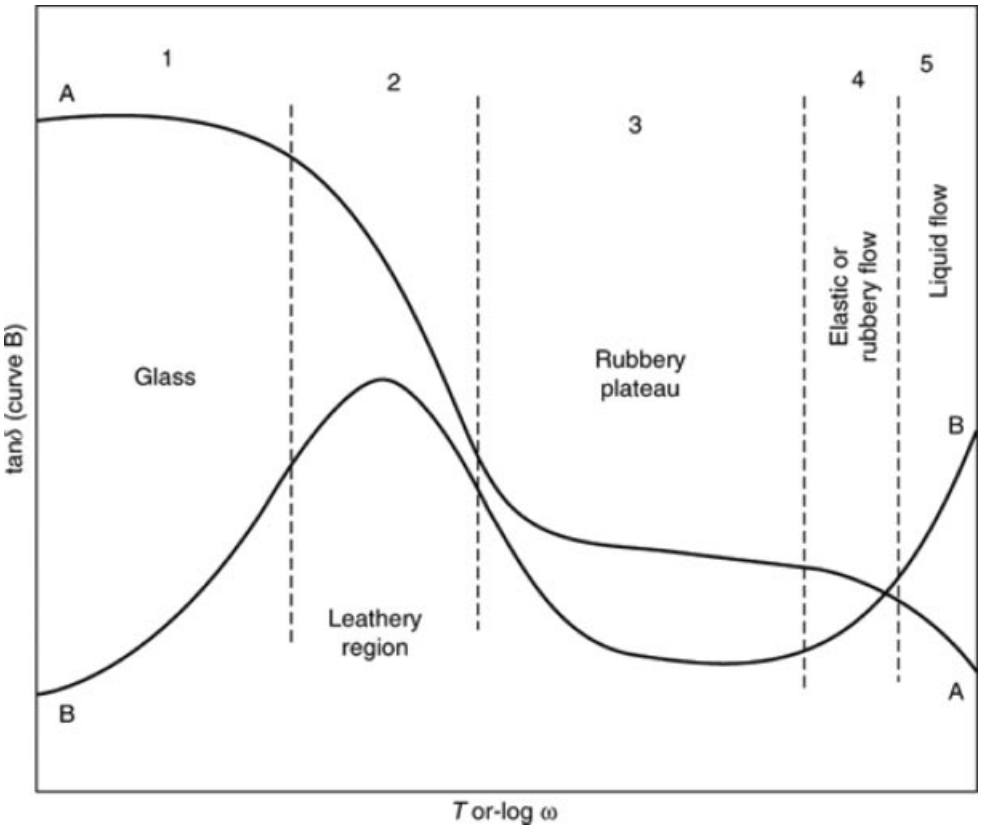

Fig. 31. Diagram of master curves for modulus and loss tangent for a typical amorphous polymer showing five characteristic physical states (73).

$$\frac{\sigma\ (t)}{\varepsilon\ (t)} = E^* = E^{'} + iE^{''} \tag{5}$$

Here $\sigma(t)$ is the stress at time t and ε is the strain; E^* is the complex dynamic mechanical modulus, E' is the ratio of in-phase stress to the applied strain, and E'' is the ratio of out-of-phase stress to strain. The out-of-phase stress leads the strain by 90°. Further, it can be shown that E' is related to the mechanical energy stored per cycle and E'' is related to the energy converted to heat through viscous dissipation. As a result, E' is referred to as the storage modulus and E'' is called the loss modulus. The material loss factor or loss tangent is

$$\tan\delta = E^{''}/E^{'} \tag{6}$$

representing the ratio of energy dissipated to energy stored per cycle of deformation. In a physical sense the storage modulus is related to the stiffness of the material and the loss modulus is reflected in the damping capacity of the material.

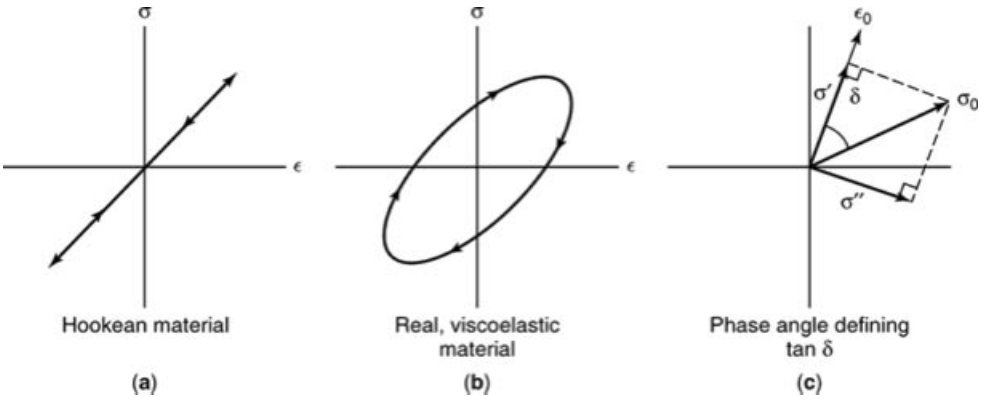

Fig. 32. Simple relationship between stress (σ) and strain (ε) in dynamic mechanical tests illustrating the role of the phase angle, showing (**a**) Hookian elastic response, (**b**) viscoelastic response, and (**c**) vectorial representations of complex oscillatory stress/strain response (74).

On the basis of the complex representation for the dynamic mechanical modulus, the relationships between stress and strain can be considered on a complex plane in terms of vectors (74), as shown in Figure 32**c**. The applied strain of magnitude ε_0 is out of phase with the resulting stress of magnitude σ_0 by an amount represented by angle δ. The stress components of σ^* are resolved as σ', in-phase, and σ'', 90° out-of-phase with $\varepsilon^* = \varepsilon_0$.

Further, Figure 32**b** illustrates that the phase shift between the cyclic stress and strain for a viscoelastic material results in a hysteresis loop, the size of which reflects the rate of viscous dissipation or heat generation during the cyclic deformation. For an ideal Hookean material, there is a zero-area loop (Fig. 32**a**). But as tan δ increases, so does the size of the hysteresis loop. This notion is particularly important in applications such as the damping of vibration and sound.

DMA experiments are performed under conditions of very small strain so that the material response is in the "linear viscoelastic" range. This means that the magnitude of stress and strain are linearly related and the deformation behavior is completely described by the complex modulus function, which is a function of time only. The theory applies both for the case of a tensile deformation or simple extension and for shear. In the latter case the comparable modulus is $G^*(t)$, with components $G'(\omega)$ and $G''(\omega)$. As a first-order approximation, $E = 3G$. The theory is developed assuming deformation under isothermal conditions, and temperature does not appear (nor is implicit) as a variable.

Dielectric analysis (DEA) measures changes in the properties of a polymer as it is subjected to a periodic (or alternating) electric field. In DEA a sample is placed between two electrodes. The traditional electrode geometry used for thermoplastics is a parallel-plate capacitor. The parallel-plate electrode measures the bulk dielectric response of the material subjected to a sinusoidal voltage applied to the electrodes. The electrodes typically are formed by vapor deposition or sputtering of a metal onto the polymer surfaces. A more contemporary dielectric electrode geometry is the interdigitated comb type of electrode which is particularly well

suited for *in situ* process monitoring. This will be discussed in more detail in a later section.

In DEA the applied voltage establishes an electric field in the sample. In response to this field, the sample becomes electrically polarized and conducts a net charge from one electrode to the other. This gives rise to a current whose amplitude is dependent on the frequency of the measurement as well as the temperature and structural properties of the polymer (or dielectric) being tested. The measured current is at the same frequency as that of the field (voltage) but shifted in phase and amplitude. The phase angle δ and the relative difference in amplitude between current and voltage provide data on dielectric properties.

In the following discussion it should be noted that we use the same symbol, ε, to represent both mechanical strain and the electrical dielectric constant. This is based on common terminology from the literature and should not cause the reader any difficulty, since both are used in differing contexts. ε^* represents the complex dielectric constant, ε' the in-phase component or permittivity, and ε'' the out-of-phase component or dielectric loss factor. It is also important to note that the dielectric "constant" is not a constant but is strongly dependent on both frequency and temperature.

A dielectric experiment is analogous to a DMA experiment where the charge is mathematically comparable to the strain and the voltage is comparable to the stress. The mathematical analysis is similar and, assuming a single relaxation time model for simplicity, it can be shown that the complex dielectric constant ε^* has the form $\varepsilon^* = \varepsilon' - i\varepsilon''$ with

$$\varepsilon' = \left[\varepsilon_u + \frac{(\varepsilon_r - \varepsilon_u)}{1 + (\omega\tau)^2}\right] \times E'_p \tag{7}$$

$$\varepsilon'' = \left[\frac{\sigma}{\omega\varepsilon_0} + \frac{(\varepsilon_r - \varepsilon_u)\omega\tau}{1 + (\omega\tau)^2}\right] \times E''_p \tag{8}$$

Here σ is the bulk ionic or dc conductivity; ω is the angular frequency ($2\pi f$); τ is the dipole relaxation time; ε_r is the relaxed dielectric constant or low frequency/high temperature dielectric constant (relative permittivity due to induced plus static dipoles); ε_u is the unrelaxed dielectric constant or high frequency/low temperature dielectric constant (relative permittivity due to induced dipoles only); ε_0 is the permitivity of free space; E'_p is the electrode polarization term for permittivity; and E''_p is the electrode polarization term for loss factor. The value of E'_p and E''_p is usually unity, except when ionic conduction is very high (75).

Many polymeric materials consist of dipoles (chemical bonds which have an unbalanced distribution of charge in a molecule) and traces of ionic impurities. If a polymer containing polar groups is heated so that an immobile dipole becomes mobile, an increase in permittivity is observed as the dipole starts to oscillate in the alternating electric field. This effect is referred to as a dipole transition and has a characteristic relaxation time (τ) associated with it (76). When exposed to an electric field, the dipoles tend to orient parallel to the field direction and the ions move toward the electrodes, where they form layers. The dipole relaxation time

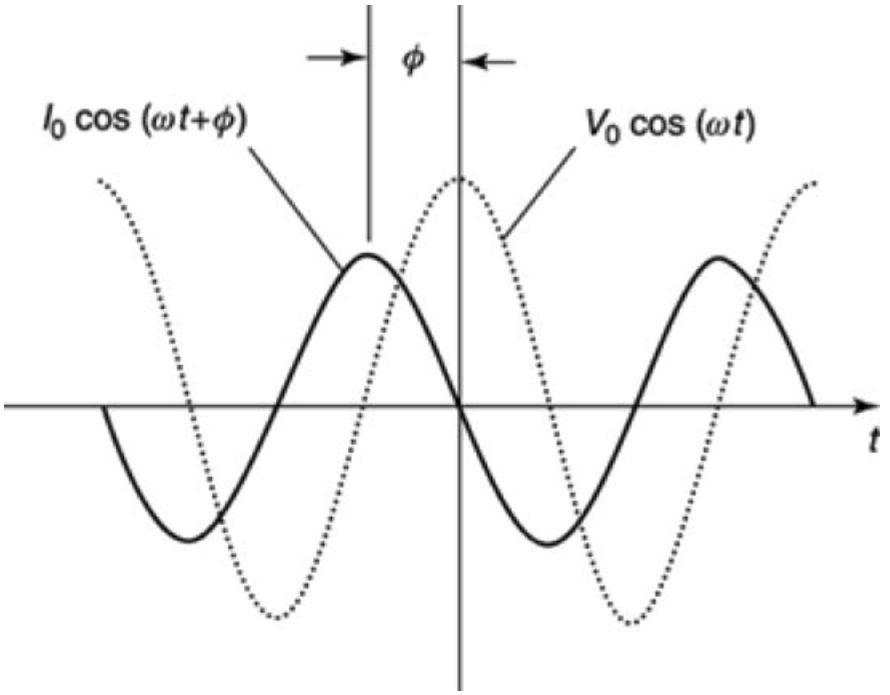

Fig. 33. Diagram of the phase shift between the current I and voltage V in a dielectric experiment that results from the lag in dipole response to the applied electric field.

is the time required for the dipoles to fully align, and the cycle time (reciprocal of frequency) is the time required for the electric field to change polarity.

The permittivity is a measure of the alignment of the dipoles in the applied electric field, while the loss factor represents the energy required to align the dipoles and to move the free ionic impurities. Both of these dielectric parameters depend on the temperature and the structure or composition of the material. The loss tangent

$$\tan \delta = \varepsilon'' / \varepsilon' \tag{9}$$

relates to the phase shift between the current, $I(t)$, and voltage $V(t)$, which results from the lag in dipole response with respect to the applied field, as indicated in Figure 33. Tan δ is often referred to as the dissipation factor. The functional forms of ε', ε'', and tan δ are shown in Figure 34, which represents the mathematical relationships for the dielectric functions calculated for a simple single relaxation model (71).

Most organic materials have permittivities ranging from 2 to 10. Polymers at temperatures well below the T_g generally have loss factors less than 0.1. When heated to T_g and above, they can have loss factors as high as 10^9 (71). Because of its large variation with the physical state of a material, the loss factor is a most useful function for the cure monitoring of thermosets.

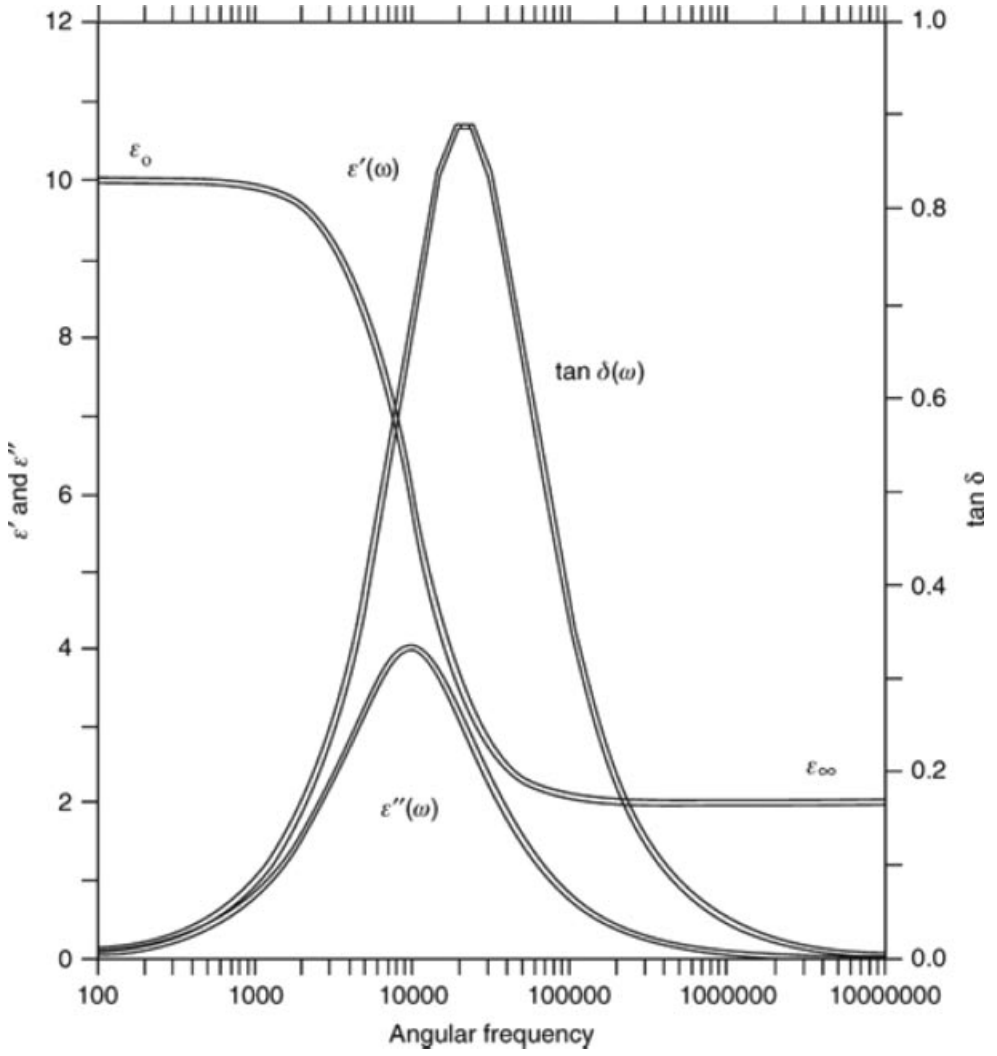

Fig. 34. Single relaxation time model curves for dielectric parameters ε', ε'', and tan δ. The curves were calculated using $\varepsilon_0 = 10$, $\varepsilon_\infty = 2$ and a relaxation time of 10^{-4} sec. (discussed in McCrum and co-workers, Ref. 69).

Dielectric analysis is used most frequently with thermoplastics to provide information on and an understanding of the molecular basis for relaxations. This is a more traditional context for DEA and ample information with numerous interesting examples is available in the literature, particularly in the text by McCrum (71) and the review by Chartoff (77). The reader is referred to these references for further insights. More recently, DEA has had extensive applications in the characterization and *in situ* process monitoring of the cure of thermosets, particularly in the manufacturing of composites. Since this topic is not as well known, we summarize in a subsequent section some of the more salient aspects of the use of DEA for the cure characterization of thermosets.

Applications of DMA in Characterization of Thermoplastics

Determining T_g by Dynamic Mechanical Analysis. Dynamic mechanical methods are popular among thermal analysts for measuring thermomechanical properties. Identifying the glass transition and how various system modifications affect T_g is a major application for DMA. Generally, the glass transition is easily identified from dynamic mechanical data because of the sharp decrease in storage modulus E' (or shear storage modulus G'), and the corresponding loss dispersion in E'' (shear loss G'') or tan δ that occur at T_g, as shown in Figure 35. These data are for a typical amorphous polymer (78). It is evident that there is latitude in how the exact value of T_g is chosen from a set of dynamic data, and this often leads to confusion in the literature. The criterion for selection of T_g from DMA data is usually either the peak in loss modulus E'' or peak in tan δ. While the peak tan δ is often used in the literature, the T_g value obtained is several degrees higher than peak E''. The tan δ peak corresponds more closely to the transition midpoint of the decreasing log E' curve, while the loss modulus peak more closely denotes the initial drop from the glassy state into the transition. In this respect the E'' peak T_g value is generally close to the intersection of the two tangents to the log storage modulus curve originating from both the glassy region and the transition region, the so-called "onset" temperature.

In general, the maximum loss modulus is the most appropriate value. This is the method prescribed by ASTM D4065. It is a reasonable criterion from a practical point of view because the upper use temperature of many amorphous polymers is the "softening" point. It is clear that by the transition midpoint (peak tan δ) the softening point has been exceeded.

For most linear amorphous polymers the transition region is rather narrow, covering around 15°C. In these cases the distinction between peak E'' and tan δ is not substantial. There are cases such as in crystalline polymers or cross-linked thermosets where the T_g region is broad and neither peak E'' or tan δ may be appropriate. Also in the case of both highly crystalline polymers and cross-linked polymers, T_g is a less prominent event and may be difficult to observe because the loss dispersion is not distinct. This is illustrated in Figure 36 (79). These data will be discussed further in a subsequent section. However, in general, the glass transition in crystalline and cross-linked polymers may be observed more clearly in DMA than by DSC, because the base line deflection ($\Delta E'$) at T_g is much larger than the ΔC_p measured in DSC. The change in modulus at T_g is often of the order of 10 to 10^3, while the ΔC_p change will be of the order of 10–30%.

Viscoelastic Relaxation Processes. There are several relaxation processes that are observed in polymers at temperatures below T_g. These relaxations, in addition to the major glass–rubber relaxation, are of continuing scientific interest and engineering importance. They are intimately associated with the stiffness of engineering thermoplastics, impact toughness, diffusion rates of low molecular weight vapors and liquids, and the effectiveness of plasticization, among others. A more detailed review of these is presented by Chartoff (77).

For isochronal (constant frequency) experiments on Semicrystalline Polymers (qv) in the temperature range between the crystalline melting point and liquid nitrogen temperature (−196°C or 77 K), at least three relaxation processes are often found. The high temperature α process is often related to the crystalline

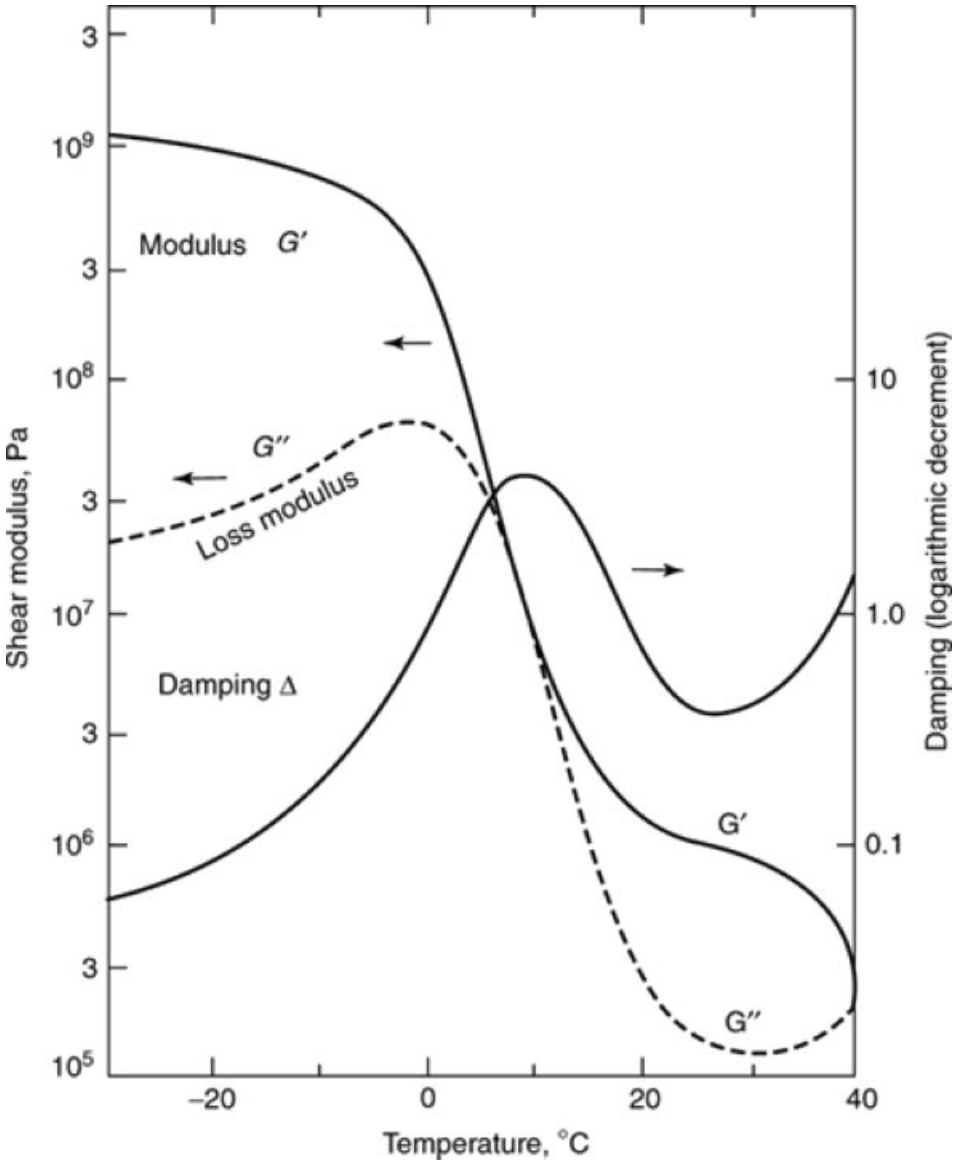

Fig. 35. Typical dynamic mechanical behavior for viscoelastic functions and G' and G'' and log damping decrement $= \pi \tan \delta$ (isochronal plot, constant frequency = 1 Hz) for a styrene–butadiene copolymer (78). To convert Pa to dynes/cm^2, multiply by 10.

fraction. The β process in these polymers is related to the amorphous phase and usually represents the glass transition. The low temperature γ process is generally considered to originate in the amorphous phase but may also have an important component associated with the crystalline phase. In amorphous polymers the highest temperature relaxation is the glass transition, also referred to as α, while β and γ relaxations also are commonly observed. Of course, in this case these are all associated with the amorphous phase.

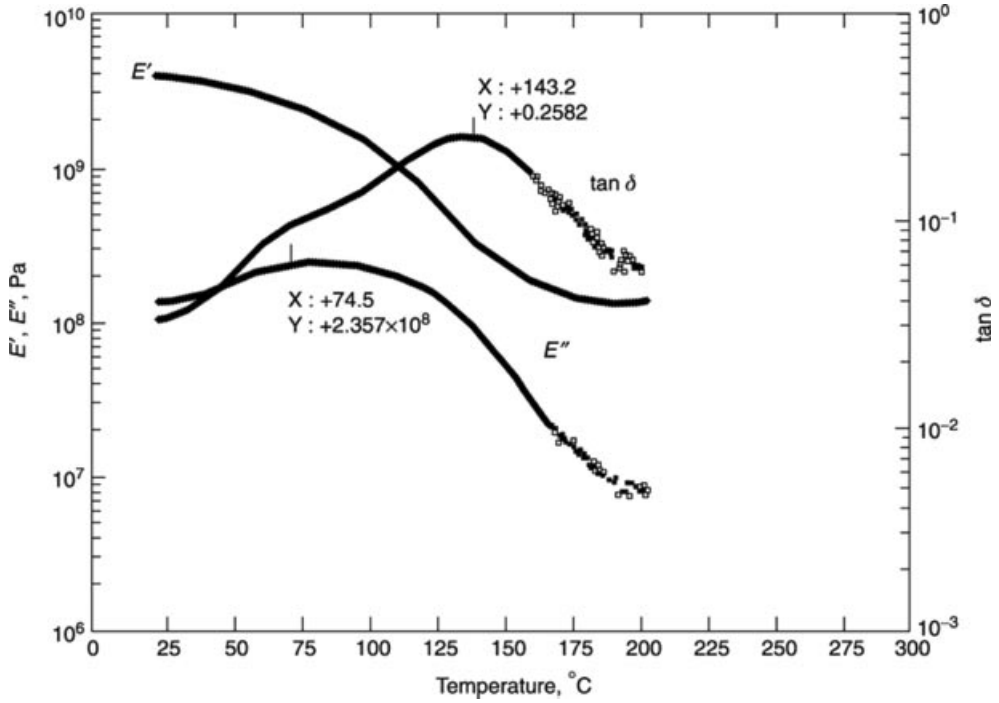

Fig. 36. DMA data at 1 Hz for a UV-cured acrylate polymer which is representative of a highly cross-linked system (79). The highly cross-linked acrylate represented has a very broad transition region that illustrates the problem involved in assigning T_g in such cases; the broad transition is due to multiple phases formed during cure. Δ, E'; $\diamond$, E''; ◘ tan δ.

The three points of greatest interest in relation to characterizing relaxation processes are (*1*) determining in what phase they originate, (*2*) describing the molecular processes underlying them, and (*3*) relating relaxation behavior to engineering properties and practical applications. DMA and DEA have proved most useful in helping to address these issues. DEA has been used extensively for studying the origin and mechanisms of relaxation processes. However, it is restricted to systems with active dipoles. As a result some relaxation processes that are active mechanically are not active dielectrically (the converse is also true), for example, the β relaxations in polyethylene and polytetrafluoroethylene.

Relaxations That Occur in Amorphous and Crystalline Polymers. In isochronal experiments on amorphous polymers, for the temperature interval between the melt and liquid nitrogen temperature, commonly each of the relaxation processes has distinct characteristics related to the specific motions associated with the relaxation processes. The highest temperature or α process is the glass transition involving the cooperative motion of several molecular segments or subunits (between 5 and 10). The glassy-state β and γ relaxations take place in polymers either with or without flexible side groups and are believed to be due to local rotational motions of the main chain and/or motions of side groups with differing degrees of cooperativity, and a distribution of relaxation times. The sub-T_g relaxations are characterized by an Arrhenius-type temperature dependence

of relaxation times. The more complex the cooperative motions associated with a relaxation process, the greater the activation energies. Thus each relaxation process has a different activation energy. This will be discussed further below.

In crystalline polymers there are at least two, and often three, processes observed below the melting point. In polymers that show all three, the high temperature α process commonly is connected with the crystal fraction in the semicrystalline material. The β process in such polymers is connected with the amorphous fraction and is the glass–rubber relaxation. In polymers where the α process is not of the above type, it is the glass transition. The low temperature process, γ(or β where α is missing), is generally agreed to originate in the amorphous phase but may also be affected by the crystalline phase.

There are some generalizations that can be made about the relaxation behavior of the above types (80). Inherently low crystallinity polymers show no crystalline high temperature process but do possess a well-developed amorphous fraction glass–rubber relaxation (α). Inherently easily crystallizable, high crystallinity polymers show both α and β relaxations where the α relaxation is associated with the crystalline phase. However, the β process tends to be less prominent than the amorphous phase α relaxation in the less easily crystallizable polymers. All crystalline polymers show the low temperature γ (referred to as β when α is missing) process.

The study of relaxation processes in Semicrystalline Polymers (qv) is a subject of continuing technological interest because of its practical importance. This is based on the observation that the stiffness of typical crystalline engineering thermoplastics at room temperature may be only one-third to one-fifth that of the same material at a low temperature. The drop in stiffness or modulus takes place in regions of temperature associated with a relaxation process.

Similarly, in Amorphous Polymers (qv) the drop in modulus accompanying sub–glass relaxations can have an important effect on engineering properties, particularly brittleness and impact resistance. This is discussed below in a section on impact behavior.

Effects of Plasticizers and Moisture. In amorphous polymers the glass transition and the relaxation behavior associated with it are very sensitive to the addition of small amounts of diluents. The relaxation is shifted to lower temperature isochronally or higher frequency isothermally. The usual explanation is that since the diluent molecules are small and mobile, they act to effectively increase the available free volume for segmental motion and hence speed it up. Similar plasticizing effects on the glass–rubber relaxation in crystalline polymers are observed. One example is the case of polyvinyl alcohol (PVOH), which is water-soluble. As shown in Figure 37 (81), PVOH can absorb large amounts of water, which shifts the glass transition to lower temperatures. As the relaxation shifts to lower temperatures, it also narrows. The shift to lower temperatures (as noted above) reflects the improved segmental mobility due to additional free volume imparted by the addition of moisture dispersed into the molecular network. The narrowing is likely due to a more uniform distribution of free volume, so that the formerly less-mobile amorphous phase fraction residing near the crystalline interface has become more mobile due to moisture plasticization.

These effects of moisture are also observed in aliphatic polyamides such as nylon-6,6 (82), nylon-6,10 (83,84), and nylon-12 (85), among others. There are

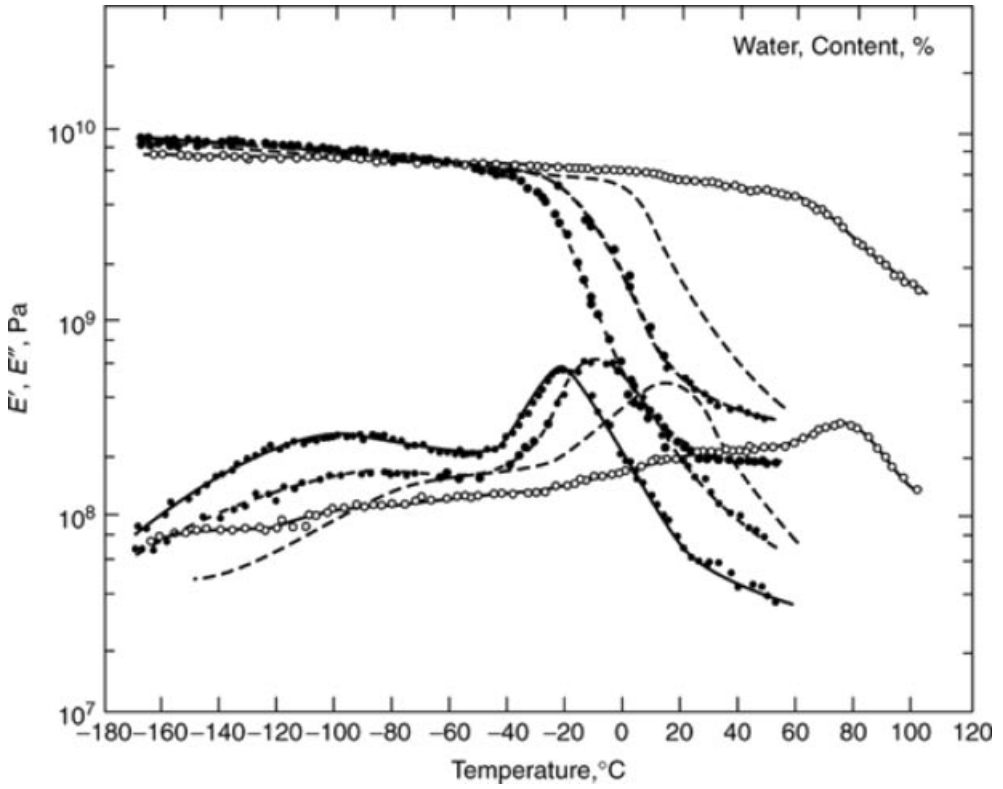

Fig. 37. Effect of moisture content on DMA glass transition of poly(vinyl alcohol) (81); E' and E'' vs temperature at 138 Hz with water contents indicated (T_g ~70°C for dry sample). ○, 0; – – – –, 8; ●, 20; ●, 30.

three major relaxations in nylon-6,6 (71,82,86,87). The α relaxation is the glass transition reflecting motion in fairly long chain segments in amorphous regions. The β relaxation has been attributed to the motion of labile amide groups and may be absent in dry, annealed specimens. The γ relaxation has been assigned to motion of short polymethylene segments with some involvement of adjacent amide groups. The addition of small amounts of water or alcohols (which readily dissolve in the amorphous fraction by virtue of hydrogen bonding) moves the α loss peak to lower temperatures (or higher frequencies isothermally) and narrows it, a result similar to that described above for PVOH. Moisture also reduces the temperatures of the β and γ relaxations to a lesser degree than the α relaxation.

The sorption of water by nylon has a major effect on major mechanical properties of engineering importance. For example, in molded nylon-6,6 at room temperature, the modulus decreases by about a factor of 5, the yield stress decreases by more than half, and there are major increases in the elongation and energy to break as the water content is increased from dryness to saturation (82,88). The reported properties of nylon are frequently those of nylon containing some amount of absorbed water. Thus, it is important to specify the water content or the relative humidity with which the polymer is in equilibrium.

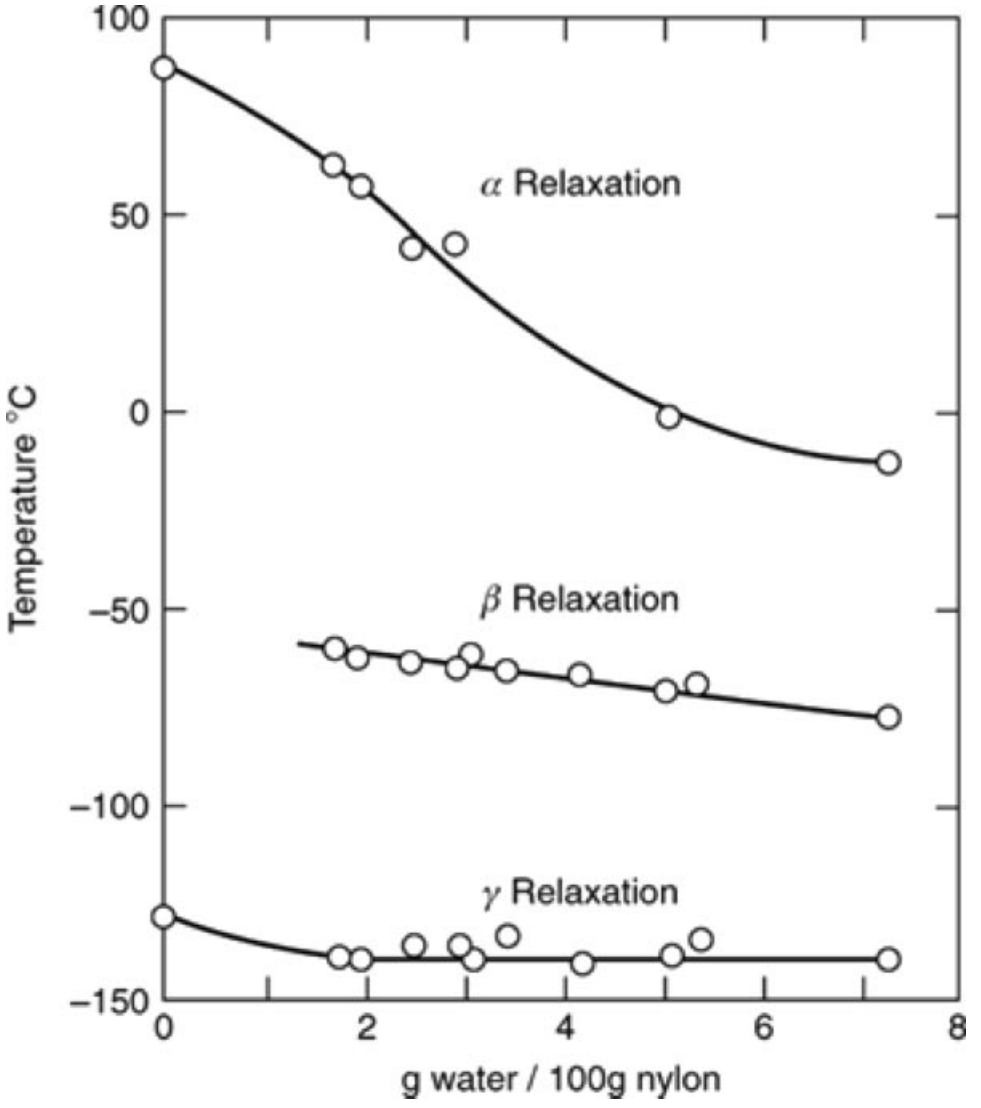

Fig. 38. Temperature position of loss modulus peaks in nylon-6,6 vs moisture content (1 Hz) (82).

The dependence of the relaxation temperatures on the level of absorbed water is known from dynamic mechanical studies (82,87,89) as well as dielectric studies (90). The temperature variations with sorbed moisture of the loss modulus peaks for the three relaxations are shown in Figure 38 (82). The test frequency for the three relaxations varies slightly but is around 1 Hz. The data indicate that the temperature of the α relaxation at a given frequency decreases by about 100°C between dryness and saturation. The β relaxation is also shifted to lower temperatures and higher frequencies by absorbed water, while the temperature of the γ relaxation is only slightly affected, shifting somewhat to lower temperatures and higher frequencies.

In addition, it is found that moisture increases the intensity of the β relaxation and reduces its activation energy, as well as decreases the peak height of the γ relaxation with little change in activation energy. The decrease in γ intensity has been referred to as an "antiplasticization" effect, since it is associated with an increase in modulus and decrease in impact strength. This is discussed further below in reference to impact behavior. The increase in β intensity has been associated with the motion of water molecules H-bonded with carbonyl and amide groups about the H-bond axis (84,90).

Moisture is an effective plasticizer for highly polar, phenylene polymers with α relaxations in excess of the 100°C boiling point of water. This is particularly noted in polyamides where strong hydrogen bonding prevents the loss of moisture even at high temperatures up to T_g. The polyamide derived from hexamethylenediamine and a 70/30 mixture of isophthalic and terephthalic acids (nylon 6I/T, 70/30) is quite hydrophillic. A considerable reduction in the dielectric α loss peak temperature (at frequency of 1 kHz) with increasing moisture content has been documented for this polymer (91). The α peak temperature is a linear function of relative humidity decreasing from 154°C at 0% RH to 60°C at 100% RH. The DSC T_g at 10°C/min decreased from 128°C for a dry sample to 48°C for one conditioned at 97% RH.

The hydrophilic character of nylon 6I/T (70/30) combined with a relatively low permeability to oxygen makes it an attractive candidate as a food-packaging material. The low permeability to O_2 is related to the antiplasticization of nylon 6I/T (70/30) by moisture. Moisture in this material decreases the γ relaxation strength as in other nylons, reducing the activation entropy for the γ process to zero. It is thought that water forms bridges between amide groups that are stable at low temperatures. These bridges serve as effective constraints, reducing the mobility of the adjacent aliphatic segments. Avakian and co-workers (91) contend that the permeability of O_2 is associated with the mobility of the aliphatic segments and will therefore decrease with suppression of the γ relaxation.

DMA data for samples of an aromatic poly(amide–imide) polymer containing various amounts of moisture are shown in Figures 39 and 40 (92). These data indicate a decrease in T_g of over 100°C at 4.25% moisture sorption. The dry T_g value is around 285°C. Each α loss dispersion has the same shape, indicating that moisture was not lost during the measurement (if moisture were lost, the loss dispersion would broaden because of a gradual shift in the relaxation to higher temperatures during the measurement). Since the α relaxation in this polymer occurs at temperatures well in excess of 100°C, the data show that water is indeed tightly bound in such systems. A broad β relaxation at around 100°C is seen to sharpen, increase in intensity, and shift upward to around 140°C in the wet specimens.

The effect of moisture on the β relaxations in amorphous phenylene polymers is well documented (93–95) for many of the systems cited previously. For example, Allen and co-workers (93) determined that both the dielectric and mechanical β relaxations in polysulfone, polycarbonate, polyphenylene oxide, and polyether sulfone were dependent on the water content of the samples. In addition, the amount of water absorbed depended on the polarity of the molecule. The effect of moisture on the dielectric β process in these polymers appears to be greater than for the mechanical loss process, as illustrated in Figures 41 and 42 (93).

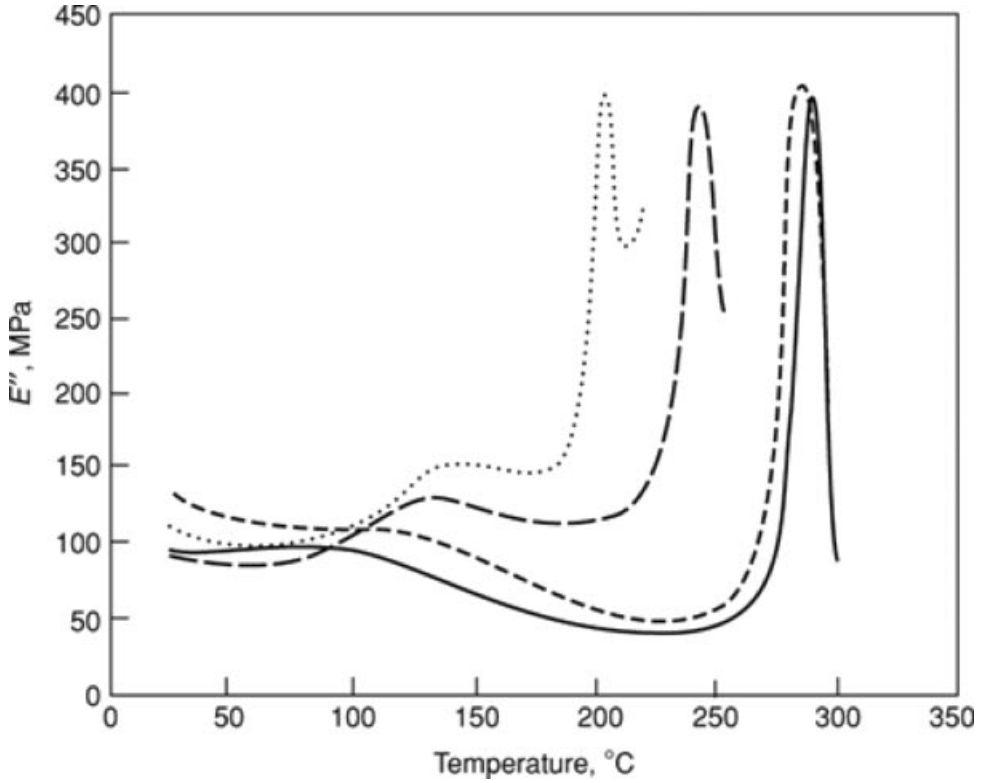

Fig. 39. Effect of moisture content on DMA glass transition of an aromatic poly(amide–imide). Note that a large moisture effect is noted even though T_g is well above the bp of water. ———, 0.90% water; – –, 0.85% water; —, 2.80% water; ●●●, 4.25% water (92).

These results indicate that the absorbed water hydrogen bonds to polar groups along the polymer chain and, as such, takes part in the molecular processes which give rise to the β relaxation. This is consistent with the other examples cited previously.

The polymers studied by Allen and co-workers (93) are modestly polar with maximum moisture uptakes of less than 1%. In more polar phenylene polymers such as polyimides (94) and poly(amide–imide)s (92), the mechanical β relaxation shows a more significant effect because of the larger amounts (1.5 to >4%) of moisture absorbed.

As in other crystalline polymers the glass–rubber (β) relaxation in linear or high density polyethylene (HDPE) is sensitive to plasticizing diluents. CCl_4 is effective in this regard (96–98). Loss data for HDPE containing absorbed CCl_4 such as those of Figure 43 (96) show a prominent E'' β peak in the -60 to -80°C range compared to a very weak (or nonexistent) relaxation peak in the -30 to -50°C range for the unplasticized material. It is evident that the diluent is effective in removing constraints on the amorphous segments, thus increasing their mobility (reduction in T_β), and in making more conformations available to reorientation (increase in β intensity).

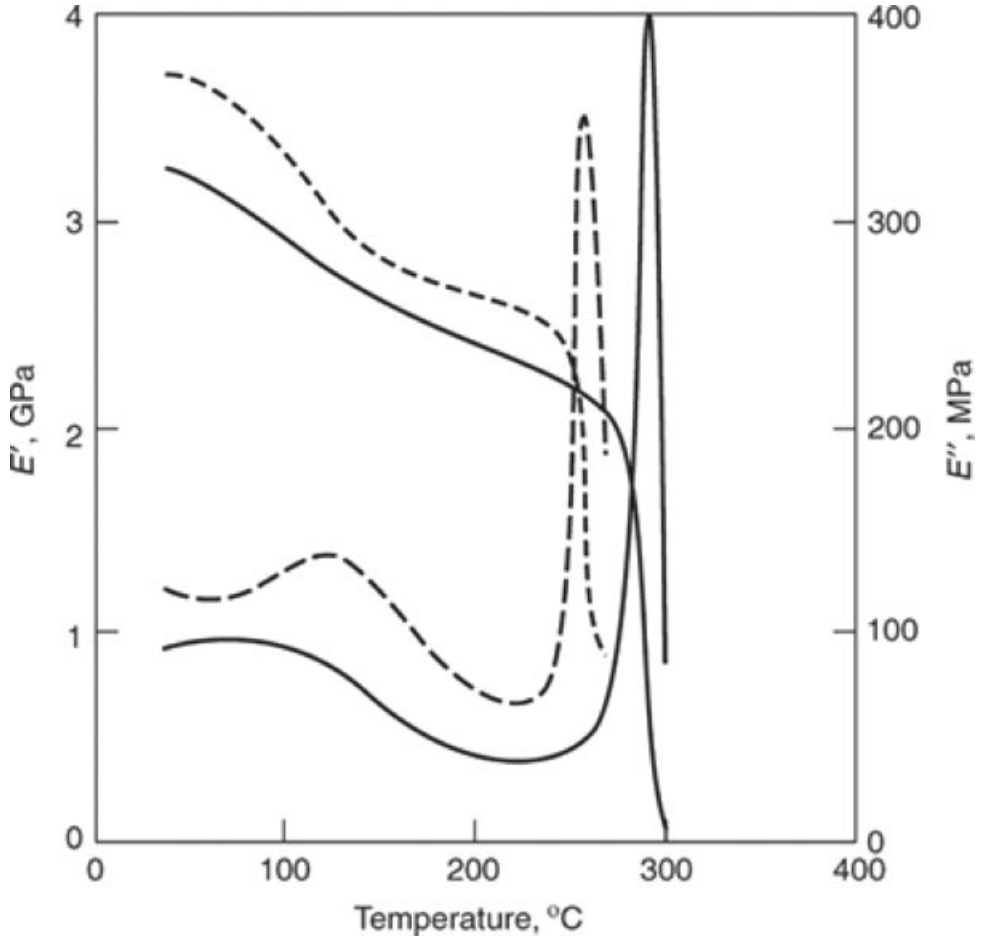

Fig. 40. Storage and loss moduli for a sample of dry poly(amide–imide) compared with one stored under ambient conditions of temperature and humidity. –, Ambient; —, dried (92).

Impact Behavior. The Fracture (qv) behavior of polymers under large-scale deformations is of considerable interest for engineering applications of polymers. It is important for material selection to have some practical criteria for decision making. Such criteria are discussed by Menges and Boden (99), who indicate how linear viscoelastic DMA data can be of benefit as a decision-making aid.

The cause of brittle fracture in polymers is the inability of the material to quickly dissipate by molecular relaxation processes the internal stresses generated as a result of the imposed deformation. Brittle fracture occurs when the time to failure is the same order of magnitude (or faster) than the speed of the relaxation process that dominates the mechanical behavior in the temperature range of interest. The relevant relaxation processes are the first $T < T_g$ secondary relaxation (β or γ). A qualitative criterion for determining whether the relaxation

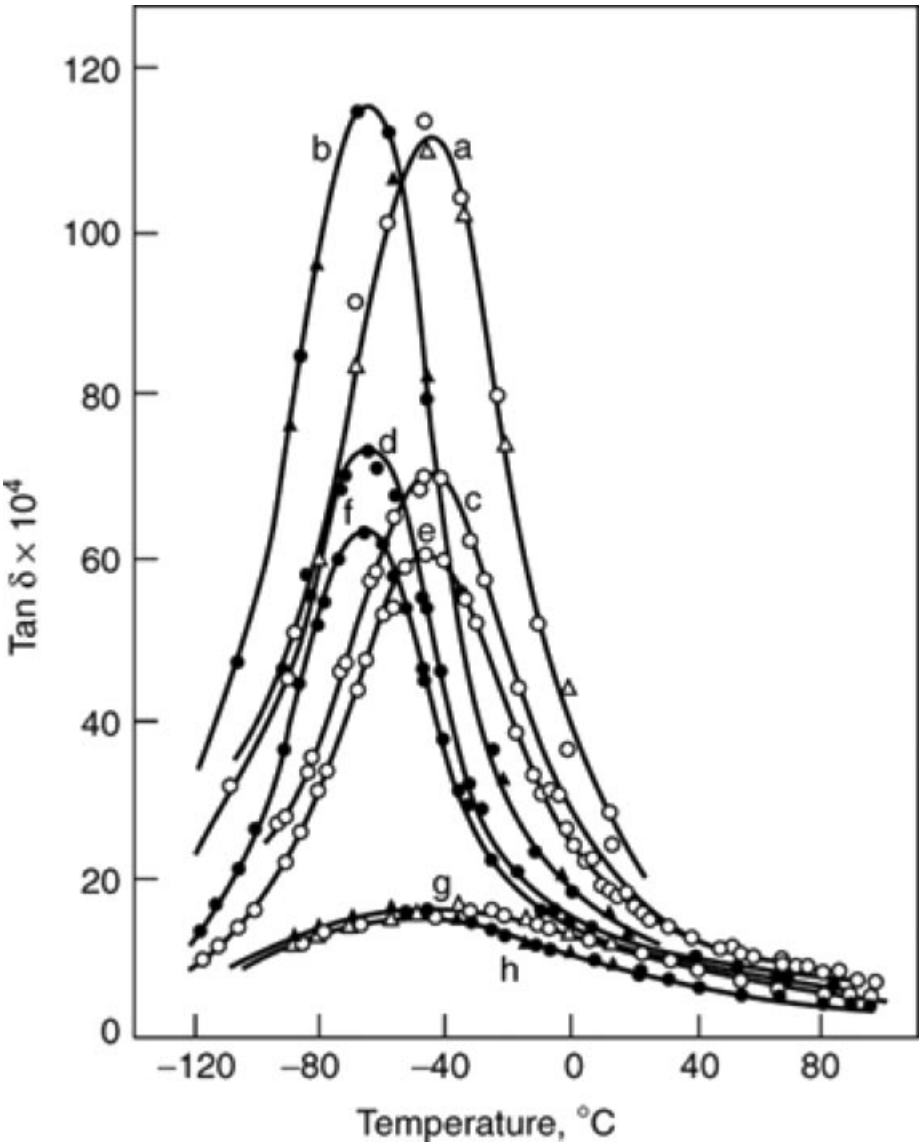

Fig. 41. Effect of H_2O and D_2O on the low temperature dielectric β relaxation in polysulfone at 1 and 10 KHz (93); circles, H_2O; triangles, D_2O; closed symbols, 1 KHz; open symbols, 10 KHz. The β peak intensity increases as absorbed moisture level increases.

will significantly influence the impact properties is whether the isochronal storage modulus (on a log modulus vs T plot) exhibits a distinct step at the damping maximum. The size of the step is related to the relaxation intensity. It has been known for some time that polymers with relatively intense low temperature relaxations may be expected to be "tough" at room temperature (100–102).

The occurrence of a secondary relaxation loss peak by itself is not a necessary and sufficient condition for improved impact strength (99,100). Additional

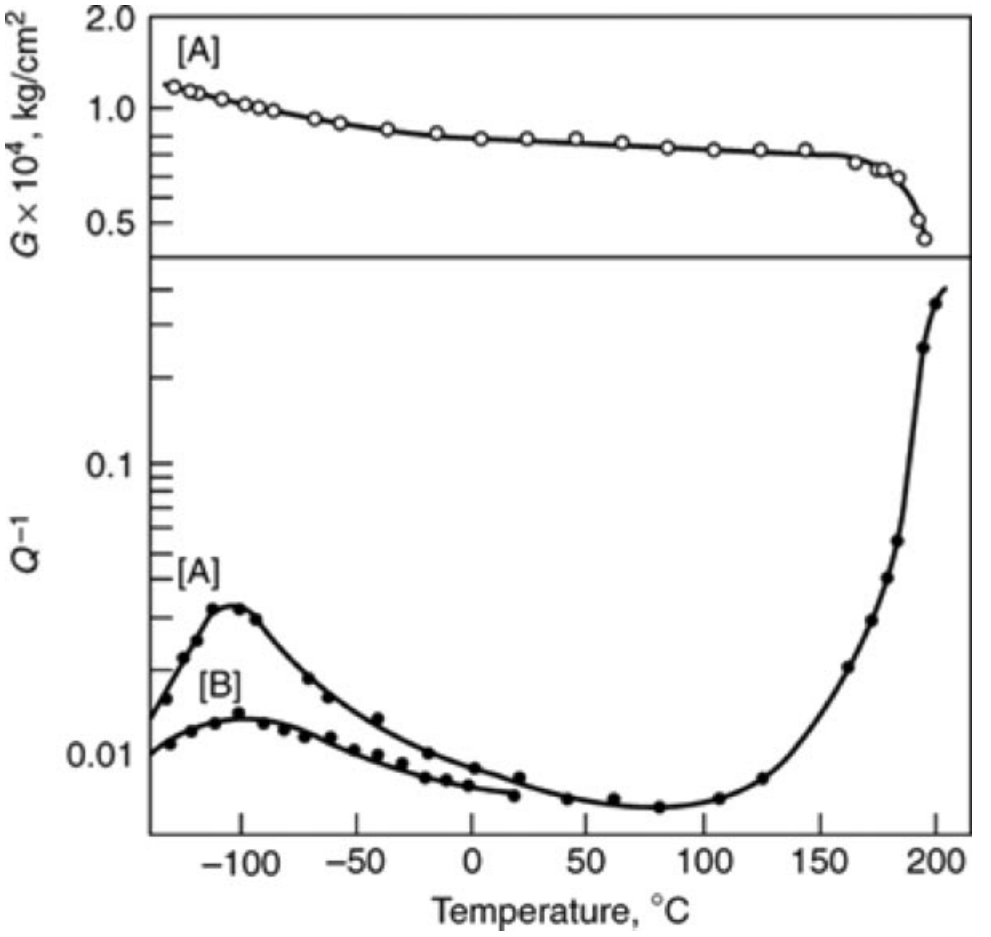

Fig. 42. Effect of H_2O on mechanical damping behavior of polysulfone at 1 Hz; (**A**) 0.31% H_2O, (**B**) 0.07% H_2O (93).

information such as actual impact test data, at temperatures above and below the relaxation, should be used to verify whether a given relaxation process has a significant influence on the impact behavior (see IMPACT RESISTANCE).

Evidence of the importance of secondary ($T < T_g$) relaxations in determining the impact strength of polymers is provided by numerous examples of changes in these relaxations by the addition of certain diluents that act as "antiplasticizers." The term *antiplasticizer* relates to the fact that, while these diluents lower T_g, they also cause increases in storage (and tensile) modulus and tensile strength but lower impact strength and elongation-at-break. Figures 44**a** and 44**b** (103) show storage modulus and tan δ curves for antiplasticized polysulfone and polycarbonate. As noted previously, both polymers in the pure state have well-defined β relaxations at about -100°C (173 K). It is readily apparent that at high diluent levels these relaxations are greatly reduced and virtually eliminated.

The presence of an antiplasticizer in these systems and the resulting near elimination of the β relaxation leads to a higher modulus value at temperatures

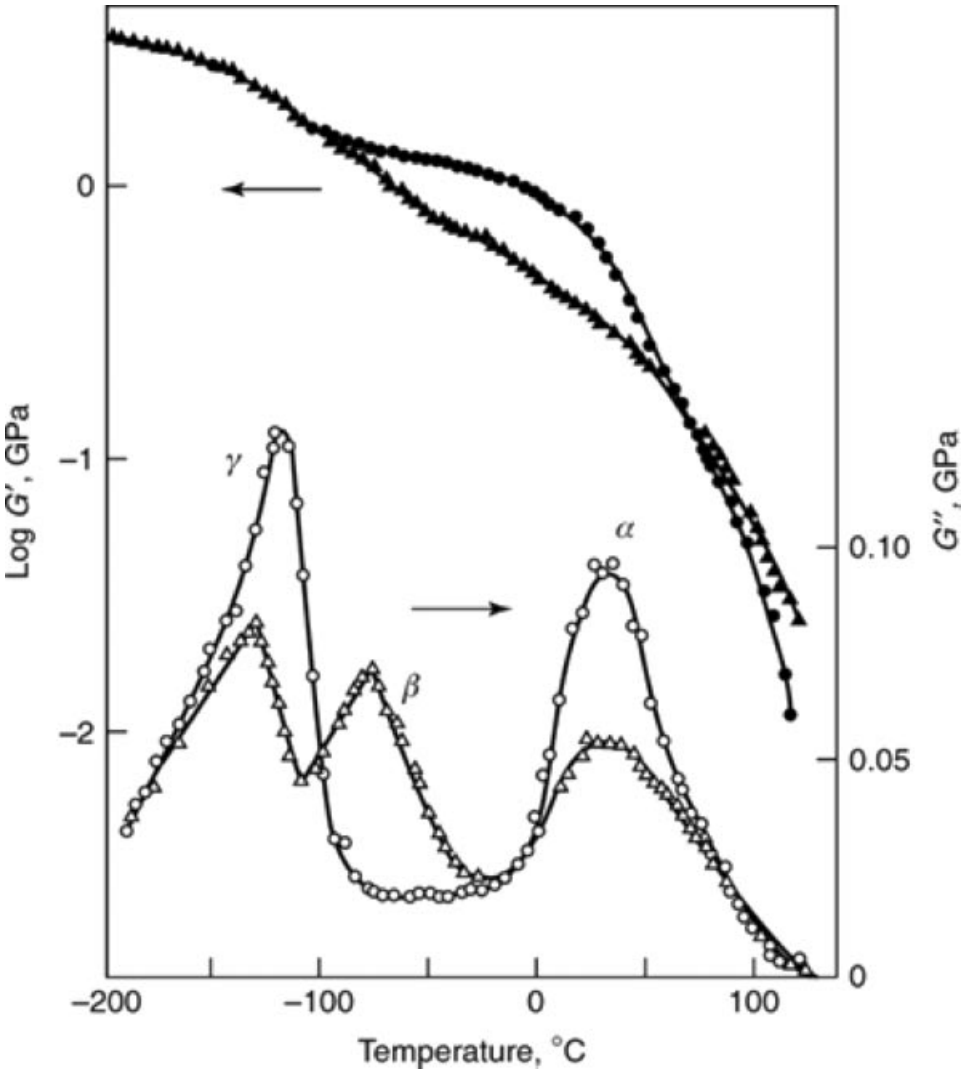

Fig. 43. DMA shear storage and loss moduli for linear polyethylene (LPE) unswollen (○,●) compared to LPE swollen with CCl_4 (11 wt%) (△,▲) (97).

above the relaxation range up through room temperature. This also results in higher tensile strength, lower elongation at break, and reduced impact strength, as noted in Table 7. Specific volume data suggest a qualitative explanation of antiplasticization in these systems, where the antiplasticizer molecules fill polymer free volume and restrict the local mode relaxations associated with the β relaxation.

Similar observations are found in the case of PVC (104,105), where the addition of normal plasticizers actually results in antiplasticization until the 15–20% plasticizer level is reached. At this point modulus and tensile strength begin to decrease because the T_g has been reduced to below room temperature. Pezzin

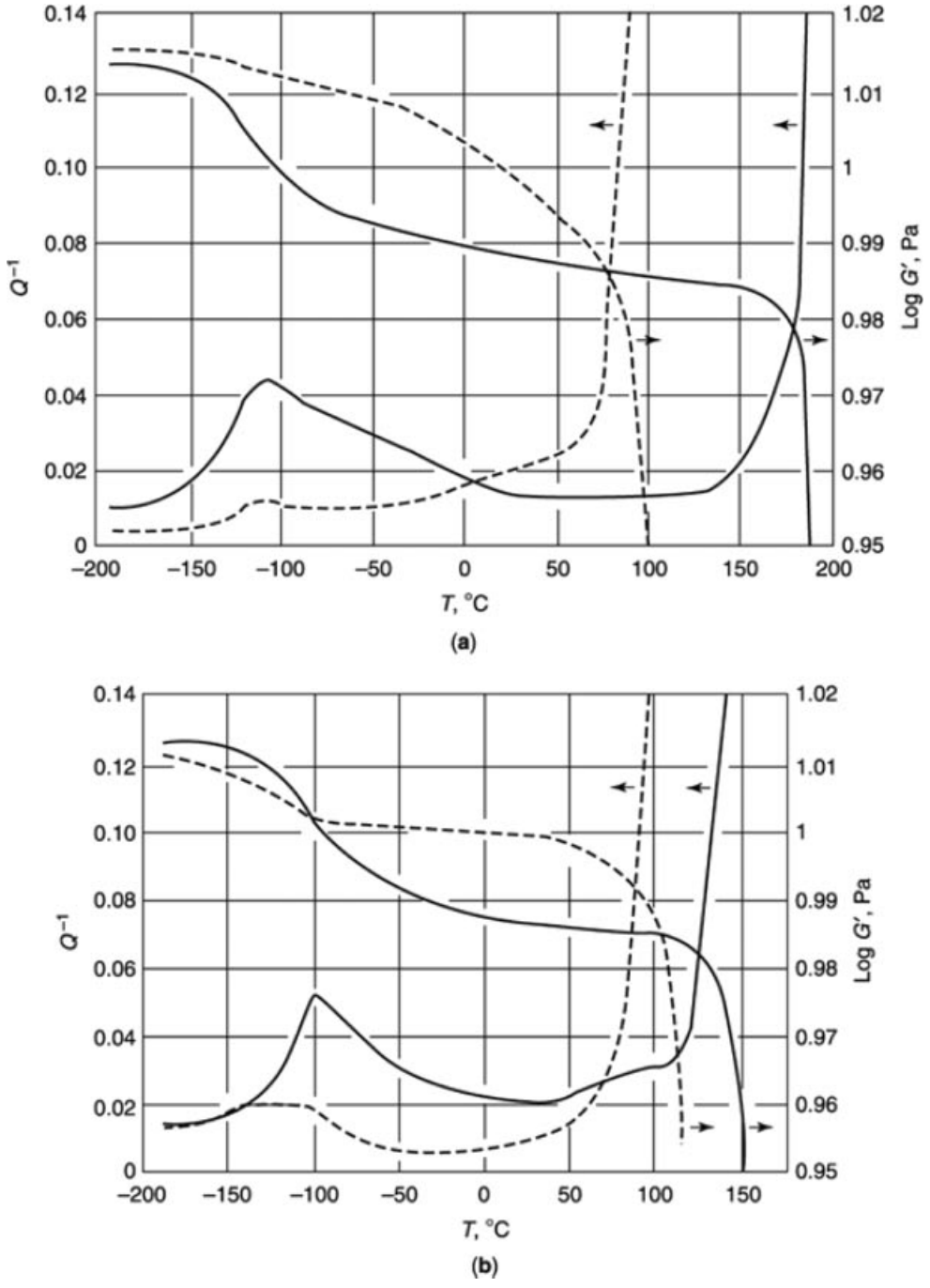

Fig. 44. DMA shear storage modulus and loss tangent curves at 1 Hz for (**a**) polysulfone (—) and 30% 4,4′-dichlorodiphenyl sulfone/70% polysulfone(—), and (**b**) polycarbonate (—) and 30% arochlor 5460 and 70% polycarbonate (—) (103). To convert Pa to dynes/cm^2, multiply by 10.

Table 7. Mechanical Property Data for Various Antiplasticized Aromatic Polymer Systems[a]

	Antiplasticizer, wt%	Tensile modulus, GPa[b]	Tensile strength, MPa[c]	Elongation at break, %	Izod impact, J/m[d]	T_g, °C
Polysulfone-*N*-phenyl-	0	2.55	75.1	50	80.1	189
2-naphthylamine	10	3.10	88.6	7.8	26.7	137
($T_g \cong -16$°C)[e]	20	3.18	85.2	7.5	21.4	110
Polysulfone-4,4′-	10	3.12	85.4	9.2	48.0	148
dichlorodiphenyl	20	3.23	80.7	6.7	26.7	125
sulfone ($T_g \cong 0$°C)[f]	30	3.30	77.5	6.0	16.0	102
Bisphenol A	0	2.28	62.6	50–100	641–854	147
polycarbonate-	10	2.88	78.6	30.0	69.4	131
Arochlor 5460	20	3.06	85.5	6.2	53.4	120
($T_g \cong 55$°C)	30	3.31	84.1	9.0	26.7	112

[a] From Ref. 103.
[b] To convert GPa to psi, multiply by 145,000.
[c] To convert MPa to psi; multiply by 145.
[d] To convert J/m to ft·lbf/in. (of notch), divide by 53.38.
[e] Determined by measurement on torsion pendulum.
[f] Determined by extrapolation.

and co-workers (105) show that this antiplasticization effect is closely related to a reduction in the intensity of the β relaxation centered around -40°C.

We noted previously that various workers (82,85,89,95) have reported similar effects for nylons including nylon-6,6, an amorphous nylon 6I/T (70/30) based on iso- and terephthalic acids, and nylon-12. It was noted that at temperatures below the α relaxation, water is an antiplasticizer for nylon, increasing the modulus and tensile strength and reducing the intensity of the γ relaxation. Absorbed water reduces the activation entropy for the γ relaxation from a substantial positive value in the dry state to zero at saturation (91,106). It was suggested that this is explained by water forming bridges between amide groups and that these bridges reduce the mobility of the aliphatic segments adjacent to the amide groups. It is known that local mode relaxations of the aliphatic groups in cooperation with the amide groups give rise to the γ relaxation in nylon.

One further note on antiplasticization is that the ability of polymers to be antiplasticized will be related to the strength of their secondary relaxations. Thus, polymers with small relaxations should be unaffected by antiplasticizers (103).

Finally, we consider the question: What determines whether a given polymer will have a secondary relaxation strong enough to impart toughness as described above? This is discussed by Tanaka and co-workers (107), who examined the temperature/frequency dependence of α and β dielectric relaxations in a series of polyarylates with respect to Matsuoka's cooperative domain model for relaxation (108–110).

The cooperative domain model specifies that when a stress is applied to a polymer, the free energy of the system momentarily increases. As a result, conformers will readjust themselves and shift back to the lower free-energy state. In

general, for a conformer to complete a rotational relaxation its nearest neighbors must also rotate in cooperation. However, below the glass transition, polymer segments are pinned in place, making it very difficult for motions to take place. While intermolecular cooperative motions are locked in place during the stress application period, some intramolecular rearrangements are possible between the points along the chain that are pinned by their neighbors. The β relaxation process (or γ in certain cases) involves such motions. Tanaka and co-workers (107) noted that the size of a conformer in the β process is usually equal to the α conformer, such as for polycarbonate and PET. But in the arylates, with 2,2′-dicarboxy biphenyl groups, the rotation of conformers within a repeat unit becomes nearly impossible when one of the conformers is pinned. Thus, their β conformers are often several times larger than their α conformers. Such polymers exhibit very low β relaxation intensities and small values for the activation energy. As a result they have low impact strengths and a tendency for brittle behavior.

DMA Characterization of Cross-Linked Polymers

The Glass Transition. Highly cross-linked polymers are an important class of materials used as adhesives, coatings, and matrices for composites, to name just a few applications. Many of this class are referred to as *thermosets* and almost all are completely amorphous (an exception is the case of liquid crystal thermosets). The glass transition is a most significant parameter for this group and the difficulty in specifying T_g arises from the effect of crosslinking on relaxation in the transition region (79). The general effect on the glass transition by increasing crosslink density is shown in Figure 45. The transition loss dispersion decreases in intensity, broadens, and shifts to higher temperatures. Also, the transition slope of the storage modulus decreases. The broadening of the relaxation spectrum is further enhanced by network heterogeneity and microphase separation introduced into systems formed from the mixtures of reactive monomers that have different functionalities. The data of Figure 36 for a UV-cured acrylate polymer are representative of such a system.

The highly cross-linked acrylic represented in Figure 36 has a very broad transition region that well illustrates the problem involved in assigning T_g in such cases. The question to consider is: What criterion do we use for specifying T_g? The loss dispersion in Figure 36 covers a span of approximately 100°C and is very flat, with no well-defined maximum value. The E'' maximum which was determined numerically is 70°C lower than the peak tan δ. Furthermore, the E'' peak appears to occur in the transition region above the temperature where E' begins to decrease gradually from the glassy-state value. Our recommendation in such cases, where the T_g range is unusually broad, is based on practical considerations. Since network polymers are frequently used in structural applications as adhesives and composite matrix materials, the point where E' begins to drop from its glassy value is the most appropriate T_g assignment based primarily on the criterion of retention of structural integrity. This is most easily specified by the onset point, defined by intersection of the tangents to the storage modulus glassy-state curve and transition-region curve.

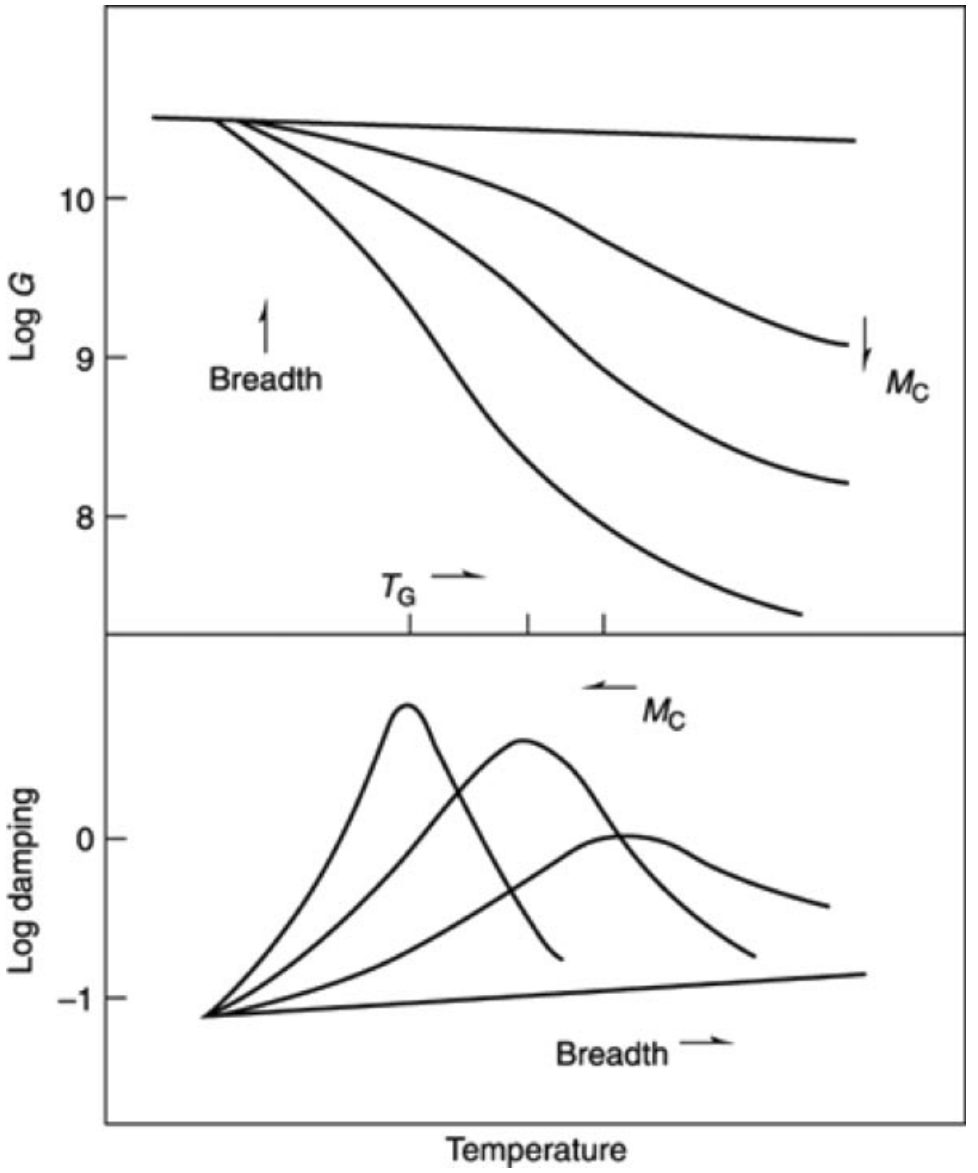

Fig. 45. Schematic diagram showing the effects of cross-linking on modulus and damping (loss tangent) vs temperature behavior at T_g.

Thermoset Cure Chracterization by DMA. On the basis of the information on crosslinking and T_g noted above, DMA can be used for the cure characterization of Thermosets (qv). There are two aspects of this. First, as the chemical conversion (extent of cure) and the degree of crosslinking advance, T_g increases. Thus the T_g measured by DMA correlates with the cure state of the material. In cases where T_g is not overly broad and a well-defined maximum in the loss modulus is evident, the T_g value obtained is related to crosslink density. Second,

the magnitude of the plateau modulus above T_g increases with crosslink density. This can be used to estimate the average crosslink density (or molecular weight between crosslinks) of the network. We present a brief review of these issues in the following paragraphs.

It has been shown that in many cases for thermoset systems, there is a quantitative relationship between the chemical conversion of the thermoset and its T_g value, independent of the time–temperature cure history (111). This is very convenient from an applications standpoint because measurement of T_g is equivalent to a direct measurement of conversion. It implies that either the molecular structure at a given degree of conversion is the same, regardless of the reaction path, or that differences in the structures produced for different reaction paths do not affect T_g. While a T_g–degree of cure relationship has been found valid for many epoxy–amine and other thermoset materials, it has been observed not to hold in some cases, which include some epoxy–DICY, cyanate–ester, and phenolic systems. It has also been found not to hold for a given resin system cured by two different methods such as thermal and microwave (112) or thermal and electron beam cures (113).

The reasons why a T_g–conversion relationship is not valid in some instances are not fully understood. One explanation is that the relationship is not likely to hold under conditions where the cured molecular network has a significant degree of heterogeneity due to composition or molecular weight heterogeneities in the initial monomer, or resulting from phase separation, or even the partial formation of a liquid crystal phase during polymerization. In the case of the epoxy–DICY and cyanate–ester systems, composition heterogeneity may arise, since the crosslinking agents are catalysts that are added initially as crystalline powders. In such cases there is always some degree of incomplete mixing of the catalyst so that the cross-linked network is heterogeneous, with multiple phases having different crosslink densities occurring on a microscale (114). These phase differences will correspond to local variations in catalyst concentration resulting in local "hot spots." In the phenolic systems the starting material is generally a mixture of oligomers, with a range of chemical functionalities. This also leads to a heterogeneous cross-linked phase distribution. For practical reasons, in dealing with thermoset cure, it is recommended that T_g–conversion data be generated as part of any cure characterization study. This will be useful even if there is not a direct correlation between T_g and conversion. The easiest way to develop a T_g–conversion relationship is via DSC. Where degree of conversion cannot be measured directly, T_g is a good means for evaluating cure advancement.

DMA also has been used to determine thermoset vitrification times by running the DMA in an isothermal or temperature-programmed mode that simulates actual processing conditions. The methodology for this is discussed in detail by Prime (115). In general, when thermoset reactions proceed at a given temperature, the uncured thermoset (which may be a solid) is initially converted to a liquid phase before reaction begins. Once the sample is in the liquid phase, crosslinking continues until the viscosity of the system becomes extremely high and the sample passes into the glassy state or vitrifies. At this point the reaction is inhibited due to restrictions on diffusion of reactive groups. So the reaction slows down drastically and, in most instances, essentially stops even though the chemical reaction is not complete. The increase in storage modulus (which parallels the rise in viscosity) of

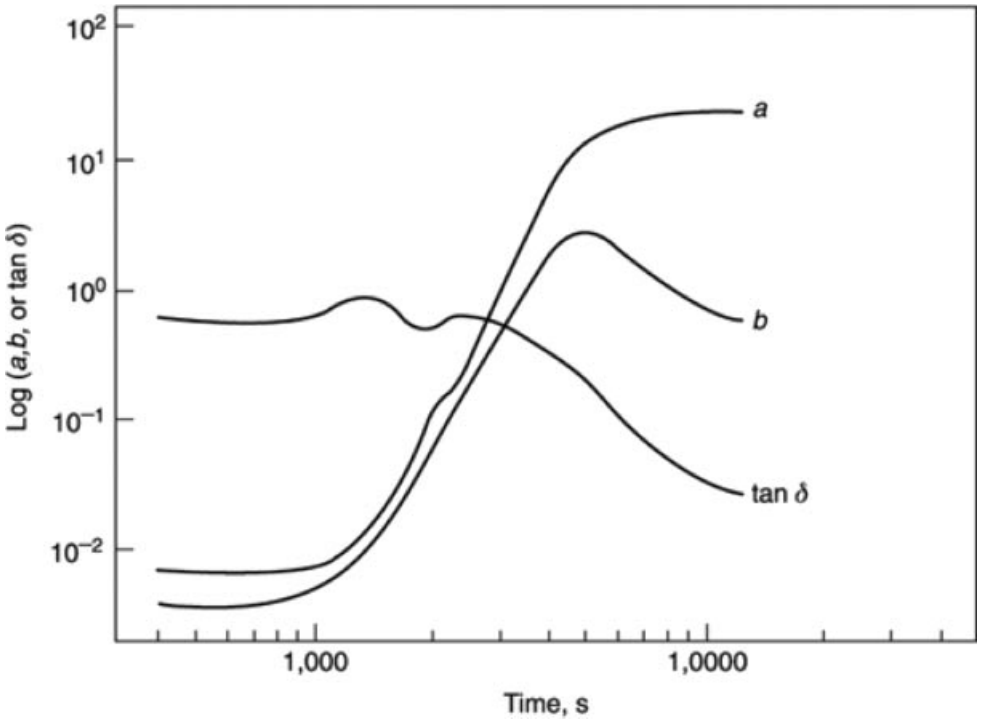

Fig. 46. DMA isothermal modulus and tan δ vs cure time plot for a supported epoxy resin sample (resin coated onto an inert fiber glass substrate); (**a**) storage modulus, (**b**) loss modulus (116).

the system from the onset of reaction can be mapped by DMA either for supported samples (resin coated onto an inert substrate) or unsupported samples. As shown in Figure 46, an isothermal modulus vs cure time plot (116), the storage modulus rises and then levels off at a high value characteristic of the glassy state.

When the modulus reaches its plateau, the polymer has vitrified or attained the glassy state due to the advance of the crosslinking reaction. If the cure reaction is carried out at a temperature T_i , the cure reaction continues until the sample vitrifies (becomes glassy) at T_i . The effective T_g of the partially cross-linked, vitrified polymer will be equal to or slightly greater than the cure temperature T_i because the reaction rate slows down gradually upon vitrification. If the temperature is then raised above T_g , the curing reaction will continue and T_g will gradually increase until the reaction is completed, or T_g again increases to the reaction temperature. If an isochronal DMA scan is run for a partially cured sample, the storage modulus will decrease with temperature at T_g in the usual manner until the reaction starts again. Then the modulus will increase with temperature.

Dielectric Measurement Methods Applied to Thermoset Cure

Dielectric analysis (DEA) has the capability for following the transformation of a thermoset from a low molecular weight liquid resin to a solid cross-linked network.

In this respect it provides some detail beyond that from a DMA run with supported samples, because it more accurately follows changes that occur in the low viscosity state, as well as during the large viscosity increase leading up to vitrification. Using disposable microdielectric sensors (117), dielectric data can be obtained in the laboratory as well as *in situ* during reactive manufacturing processes with minimal disturbance of the process. Thus, DEA is well suited for process monitoring and process control in real time. DEA can provide information on key characteristics of thermosetting materials, including molecular relaxations, thermal transitions, onset of flow and viscosity minima, rate of cure, and degree of cure. Some of the topics of interest concerning the dielectrometry of thermosets are as follows: (*1*) ionic conductivity often dominating the observed dielectric properties; (*2*) the correlation between viscosity and conductivity early in cure; (*3*) the contribution of dipoles and sample heterogeneities to the measured dielectric properties; and (*4*) the importance of electrode polarization at low frequencies (118).

We noted previously that in DEA, a sample is placed between two electrodes and a sinusoidal voltage is applied to one of the electrodes. The traditional electrode is a parallel-plate capacitor, as illustrated in Figure 47. The applied voltage establishes an electric field in the sample. In response to this field, the sample becomes electrically polarized and also can conduct a net charge from one electrode to the other. Both the electric polarization and ionic conduction give rise to a current whose amplitude is dependent on the frequency of the measurement and

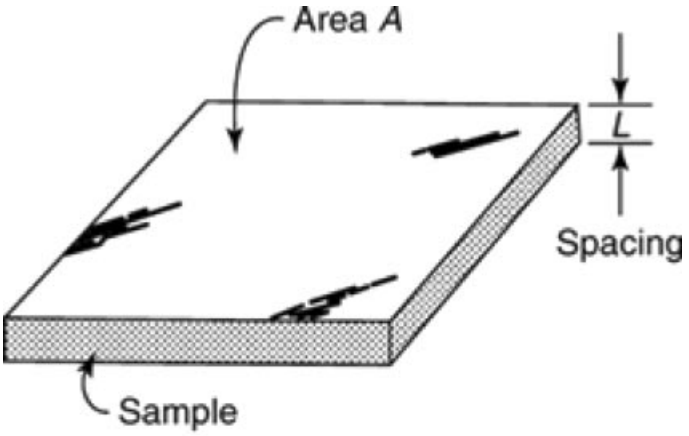

$$C_x = \frac{\epsilon'_x \epsilon_0 A}{L}$$

$$R_x = \frac{L}{\omega A \epsilon''_x \epsilon_0}$$

Fig. 47. Parallel-plate electrode geometry for dielectric measurements; capacitance is related to permitivity and resistance is related to loss factor.

the temperature and structural properties of the medium being tested. The DEA electrode assembly both transmits the applied voltage to the sample and senses the response signals.

Most thermosetting materials possess both permanent and induced dipoles. Static or permanent dipoles consist of inherently polar moieties (not induced by the electric field) within the material, such as amine or hydroxyl groups. The static dipoles, if sufficiently mobile, may rotate in an alternating electric field, thus also storing energy and contributing to the capacitive nature of a material. Even nonpolar polymers can be dielectrically active. In the presence of an electric field, electron clouds may be slightly shifted, inducing a small polarization that is aligned with the electric field. This acts to store energy and contributes to the capacitive nature of a material. These induced dipoles are responsible for nonpolar or symmetrically polar materials having permittivities greater than 2.

Static dipoles also contribute to the loss factor, as can be seen from equation 8. This contribution arises from viscous drag as the dipole rotates through the surrounding medium. As a result of this drag, there can be a significant phase lag between the maximum applied field and maximum dipole deflection. The energy lost because of this phase lag reaches a peak as ω approaches τ^{-1}. At higher frequencies the dipole hardly moves, because it is not able to keep pace with the changing field, and so little energy is lost, while at lower frequencies the dipole can keep up with the field more easily and, as a result, less energy is expended.

Ionic conduction is the result of current flow due to the motion of mobile ions within the material under test. It has been demonstrated that concentrations well below 1 ppm are sufficient to cause significant ionic conduction levels (118). From equations 7 and 8, it is evident that ionic conduction contributes only to the loss factor and does not affect the permittivity. Epoxy resins typically contain sodium and chloride ions, which are residuals from their manufacture. These impurities are quite sufficient to cause ionic charge transport. Thus, it is common to observe large loss factors in such thermosetting materials when the temperature is above T_g, because of the ionic conduction contribution to the loss factor.

An artifact that affects the dielectric properties when ionic conductivity is high is known as electrode polarization. This results from the thermosetting resin acting in combination with the electrodes used to introduce the electric field. Electrode polarization occurs when ionic conduction is extremely high, causing ions to collect at the material–electrode interface during a half-cycle of the oscillating electric field. As ions build up at the interface, they accumulate in a thin boundary layer and build up a considerable charge density, and therefore a large capacitance is formed. This has the effect of artificially decreasing the measured values of loss factor and increasing the measured values of permittivity. The measured permittivities attained through electrode polarization are usually large enough (greater than 100) to render electrode polarization easy to identify. A detailed discussion of the electrode polarization effect is given in Reference 75.

There are two electrode sensor geometries that are common in dielectric analysis. As noted previously, the traditional electrode is a parallel-plate capacitor (Fig. 47). However, this geometry is not well suited for thermoset cure monitoring. In order to obtain high signal levels with the classical parallel-plate technique, thin specimens with large areas are required, and the dielectric properties are an average of the bulk. In addition, low frequency measurements, which can reveal

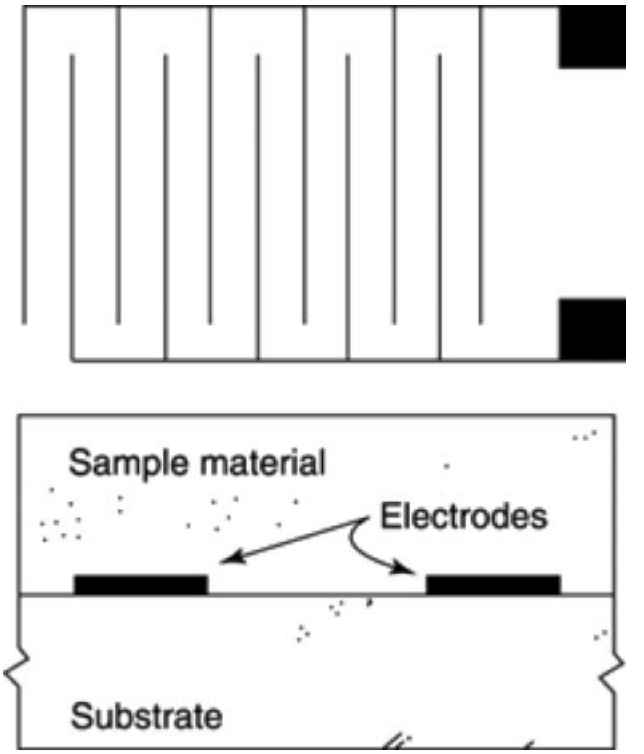

Fig. 48. Interdigitated or comb electrode geometry for contemporary microdielectric sensors (117,118).

much about glass transitions and the mechanical properties of the material, are often difficult to obtain using the parallel-plate technique, since the signal current is proportional to the test frequency. The principal disadvantage, however, is the need to accurately control or measure the plate spacing. Thermosets during cure frequently undergo dimensional changes due to temperature, reaction-induced shrinkage, or pressure. In order to obtain quantitative values for the dielectric properties, the plate spacing must be known throughout the experiment.

The interdigitated or comb electrode (117) is a contemporary, alternative geometry, as illustrated in Figure 48. For this type of sensor, metal electrodes are fabricated on an insulating substrate by photopatterning. The substrate is typically a ceramic or a silicon integrated circuit. Sampling is simplified. Either a small amount of sample is placed over the electrode sensor, or the sensor may be embedded in the test medium. The comb electrode has been miniaturized as a microdielectric sensor, which combines the electrode with a pair of field-effect transistors in a silicon, integrated microcircuit. For thermosets these microsensors circumvent the problems associated with parallel-plate capacitors while achieving comparable sensitivities. The microsensor is small, around 0.5 in. in size. This design permits a one-sided, very localized measurement of dielectric properties, is particularly well suited for thin films, and can be inserted directly into a part being cured. The modern measurement circuitry also circumvents the traditional

lower frequency limits, thus permitting dielectric analysis at frequencies as low as 0.001 Hz. Very fast response times of considerably less than 1 s are possible so that the microsensors can monitor very fast reactions.

Dielectric Analysis of Thermoset Glass Transitions. As a polymer is heated through its glass transition, static dipoles gain mobility and start to oscillate in the electric field. This causes an increase in permittivity, with a corresponding loss factor peak. At the low temperature side of the glass transition, dipoles are able to respond only to low frequency excitation, because their mobility is low. Dipole mobility increases as the polymer is heated through T_g and above. Charged ions also gain mobility as a material is heated through T_g and will start to contribute to conductive losses above T_g. The contribution of ion conductive loss to the measured loss factor may be large and can often overshadow the smaller dipole loss contributions. The loss dispersion observed in dielectric measurements is analogous to that observed for mechanical measurements. Low frequency dipole loss peaks (less than 1 Hz) correspond well to other thermal analysis measurements of T_g.

Figure 49 shows temperature-dependent data for the permittivity and loss factor of a diglycidal ether of bisphenol A (DGEBA) epoxy resin in the vicinity of its glass transition ($T_g = -17^\circ$C), measured at frequencies between 0.1 and 10,000 Hz (118). At temperatures well below T_g, the permittivity at all frequencies has a value of 4.2 (the unrelaxed permittivity, ε_u) and the loss factor is less than 0.1. As the temperature approaches T_g, the dipoles gain sufficient mobility to contribute to the permittivity, with evidence of this mobility increase occurring first at the lowest frequency. With a further increase in temperature, the permittivity for each given frequency levels off at the relaxed permittivity ε_r, and then decreases because of increasing temperature (118). This is then followed by an abrupt increase in ε' as a result of ionic conductivity and electrode polarization. At each frequency, a dipole peak is observed in the loss factor at T_g. ε'' then rises continuously with temperature because of an increase in ionic conductivity. The frequency at which the dipole loss peak occurs is proportional to the ionic mobility. Both the frequency of the loss factor maximum and the ionic conductivity increase by many orders of magnitude over a narrow temperature range, a characteristic of relaxation processes very close to the glass-transition temperature. Note in Figure 49, that the 0.1-Hz loss peak temperature is similar to the T_g as measured by DSC (-17°C). A similar correlation was observed between the onset of the modulus decrease by DMA at 0.1 Hz and the T_g as measured by DSC (119).

Cure Characterization. With considerations concerning the DEA observations related to T_g in mind, it is apparent that dielectric properties can be particularly useful in following chemical and physical changes in real time during thermoset cure. At the beginning of cure, the dipole relaxation time is much shorter than the cycle time, and the dipoles and ions move easily and align themselves with the field as the polarity changes, as illustrated in Figure 50**a**. Hence, both the permittivity and the loss factor have high values initially. As cure proceeds, crosslinking produces larger and more complex molecules and the viscosity of the medium increases. This restricts the motion of the dipoles and ions and causes an increase in the relaxation time. If the frequency of the electric field is fixed, then the relaxation time will approach the cycle time, and there will be less alignment of dipoles and less ion transport, as shown in Figure 50**b**. Eventually,

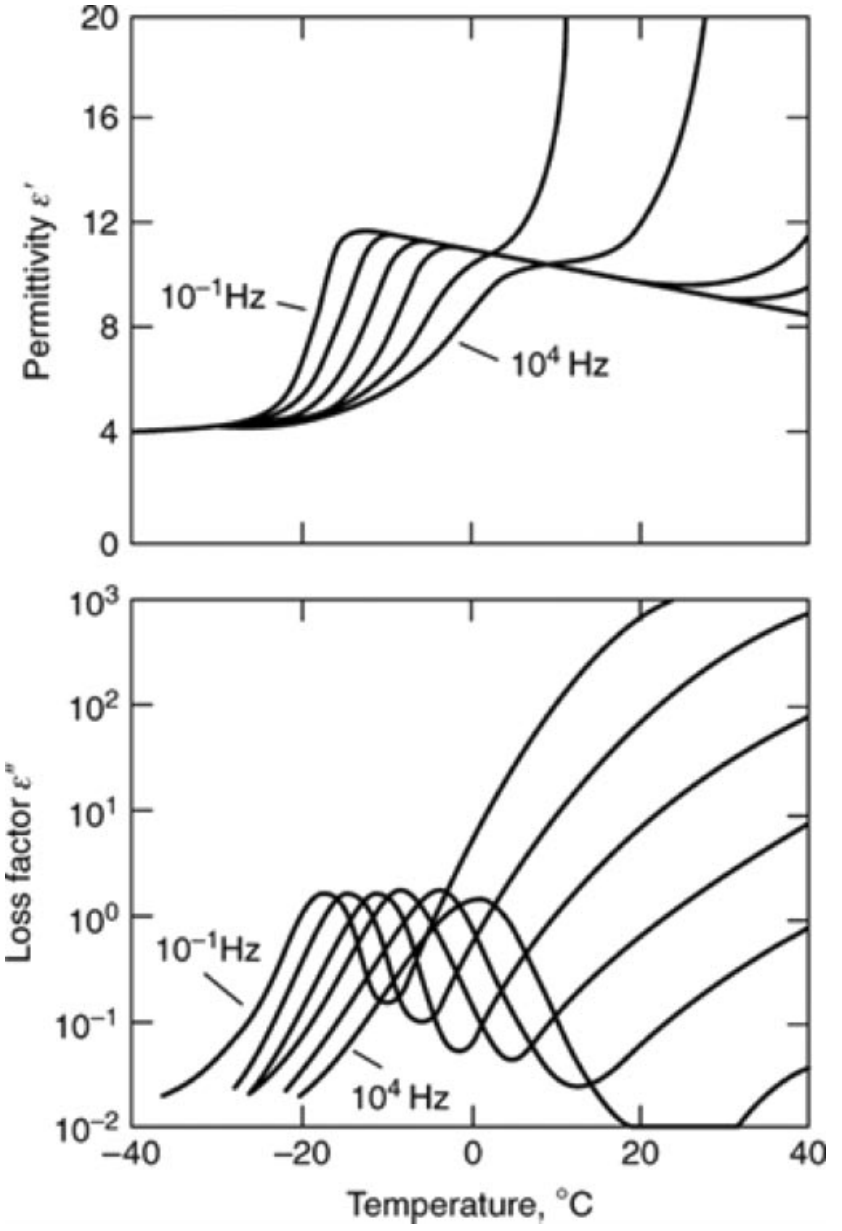

Fig. 49. Temperature-dependent data for the permittivity and loss factor of an uncured DGEBA epoxy resin (Epon 825) in the vicinity of its glass transition ($T_g = -17^\circ$C), measured at frequencies between 0.1 and 10,000 Hz (118).

as the relaxation time becomes large relative to the cycle time, the dipoles will be randomly oriented, as illustrated in Figure 50**c**. Concomitantly, as the curing polymer becomes more viscous and/or glassy, it offers increasing resistance to the motion of free ions, and ion mobility decreases. This results in both a low permittivity and a low loss factor.

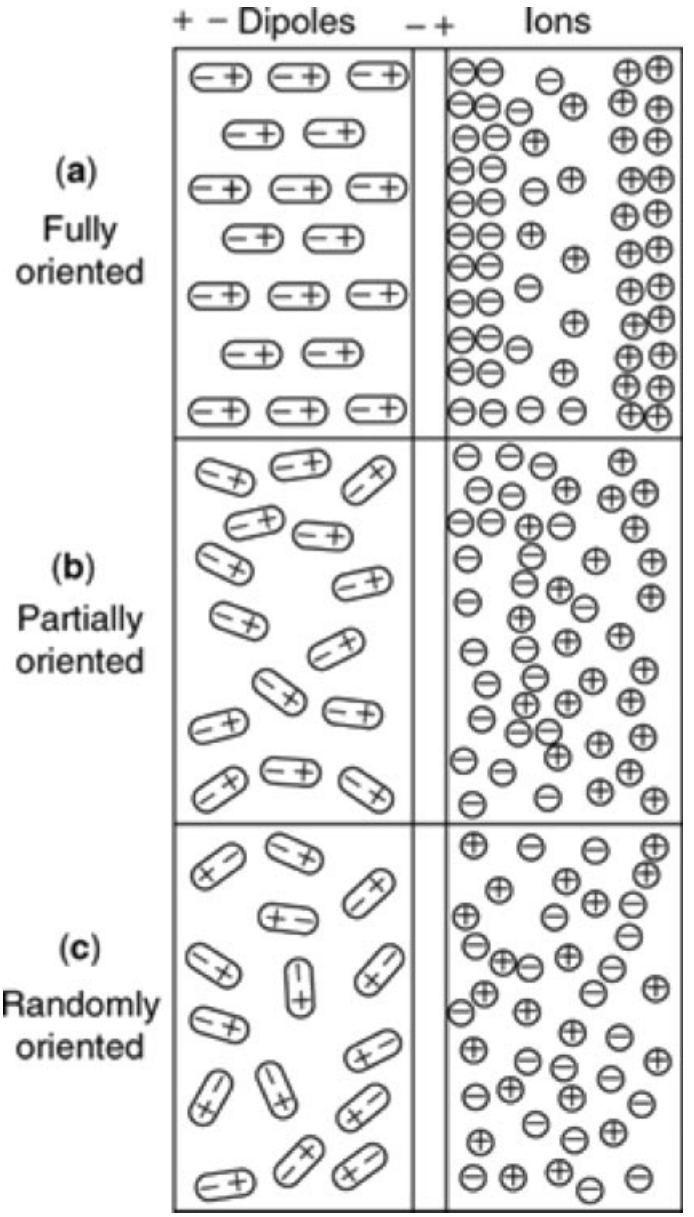

Fig. 50. Schematic representation of ion and dipole behavior at various stages of thermoset cure: (**a**) beginning of cure in liquid state, (**b**) during cure as viscosity begins to increase, and (**c**) after sharp rise in viscosity severely restricts dipole mobility (75).

During cure, ε'' generally will change by several orders of magnitude. As a result, ε'' is a particularly useful function for evaluating the progression of cure. The loss factor can be expressed as

$$\varepsilon'' = \varepsilon''_{\mathrm{d}} + \frac{\sigma}{\omega \varepsilon_0} \tag{10}$$

where ε''_d is the energy loss arising from dipole orientation, and σ, ω, and ε_0 are as previously defined in equations 7 and 8. At low frequencies, the conductivity term will usually be considerably larger than the dipole term, and the value for conductivity, σ, then can be extracted from the loss factor by equating σ to $\varepsilon''\omega\varepsilon_0$. The ionic conductivity is very useful for distinguishing frequency-dependent dipolar phenomena, such as the glass transition, from frequency-independent phenomena, such as the onset of flow and the viscosity minimum.

Examples and Applications of DEA in Curing of Thermosets

Valuable information about the molecular and rheological behavior of thermosets during processing can be obtained from DEA, particularly for on-line cure monitoring and process control. This is illustrated in the following example representing the cure of a DGEBA/diaminodiphenylsulfone, epoxy–amine system (DGEBA/DDS).

The permittivity change measured over a range of frequencies during the isothermal cure of a DGEBA/DDS resin is shown in Figure 51 (120). The cure temperature is 137°C. To a first approximation, these data are the mirror image of those in Figure 49, consistent with the idea that the change in dielectric properties due to crosslinking during isothermal cure is similar to the effect of a decrease in temperature at fixed T_g. Examination of Figure 51 shows an important difference between the temperature and cure time dependencies, namely, that the relaxed permittivity continues to decrease with cure time under isothermal conditions. This is a direct result of the changing chemistry. The permittivity decreases during cure because of the decreasing ability of the molecules (dipoles) to completely align during the cycle time. Early in the cure at long cycle times (ie, at low frequencies), the measured permittivity is high because of electrode polarization (121). The relaxed permittivity ε_r (ie, the maximum dipole alignment that can be achieved, assuming no electrode polarization) is indicated by the shoulder early in the polymerization at high frequencies. The relaxed permittivity for this system is ~14. As cure proceeds, the dipoles find it more difficult to align themselves with the periodic field and an unrelaxed permittivity, ε_u, of ~4 is achieved. The loss factor during cure is also illustrated in Figure 51. ε'' is a function of the energy required for both dipole orientation and ionic conduction. Early in the cure, ε'' is inversely proportional to the frequency ω (see eq. 10), indicating that ion mobility dominates the loss factor. In Figure 51, the conductivity σ can be seen to decrease (eq. 11) with cure because of the increasing viscosity of the resin. This decrease is followed by a peak in ε''. Here the highest frequency peak occurs at the shortest time. This loss peak is due to the restriction of dipole rotation in the cross-linked resin, and its maximum has been correlated with vitrification (120,122). Similar dielectric relaxation results during isothermal cure have been reported for a DGEBA/DDM (diaminodiphenyl methane) resin (121). Corresponding measurements may be made by dynamic mechanical analysis (see Figs. 52 and 53).

From equation 11, the ionic conductivity (σ) can be calculated from the frequency-independent portion of the loss factor data, that is, where a log–log plot of loss factor versus frequency has a slope of −1, using the relation

$$\varepsilon'' = \frac{\sigma}{\omega\varepsilon_0} \tag{11}$$

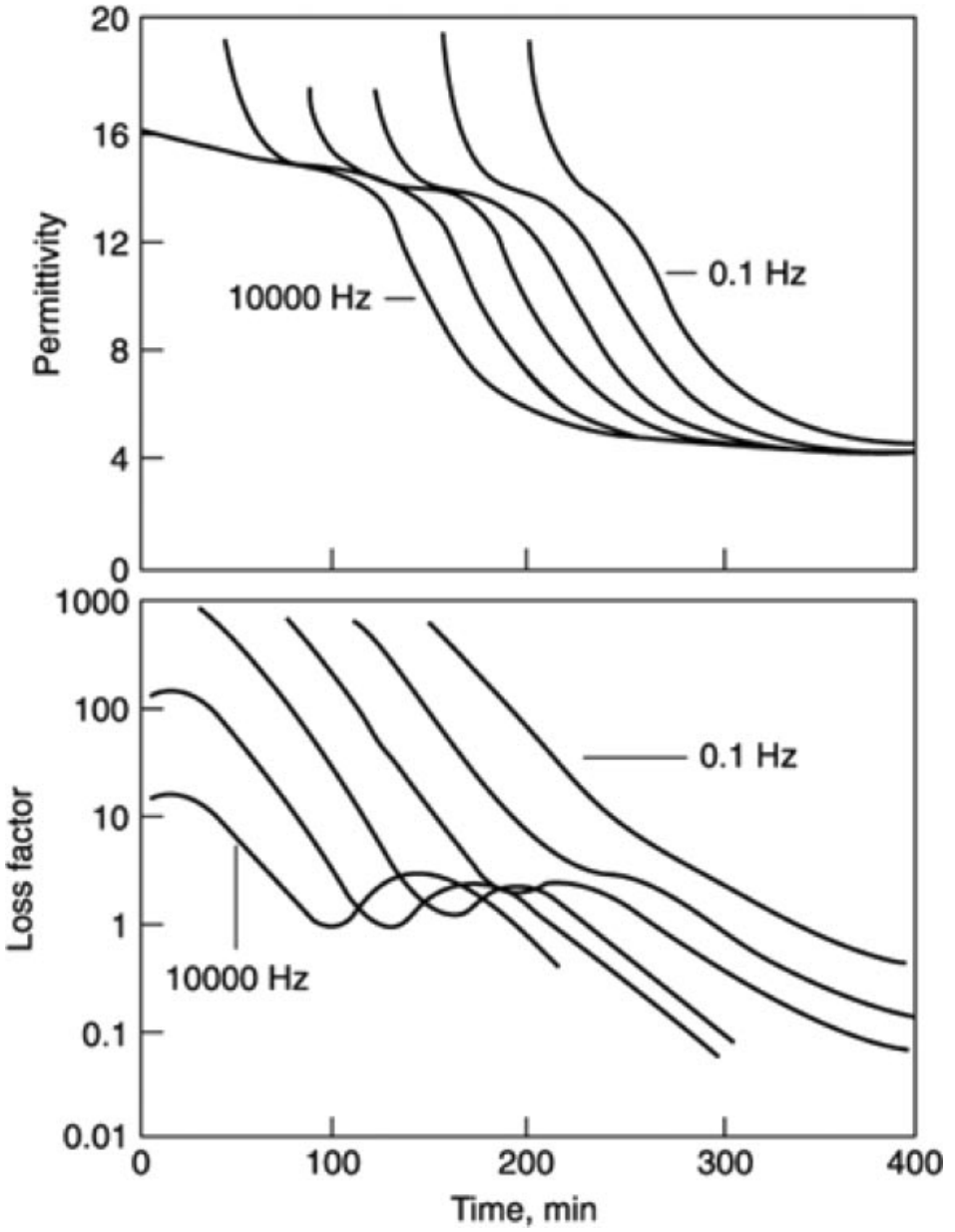

Fig. 51. Permittivity change measured over a range of frequencies during the isothermal cure at 137°C of an epoxy–amine system (DGEBA/DDS) (120).

Conductivity versus reaction time data for the isothermal cure of the DGEBA/DDS epoxy at six different cure temperatures are shown in Figure 54 (123). If the ion concentration does not change during cure, then σ is directly proportional to ion mobility. Early in the reaction, the ionic impurities move freely in the system and the ionic conductivity is high. The ionic conductivity decreases as

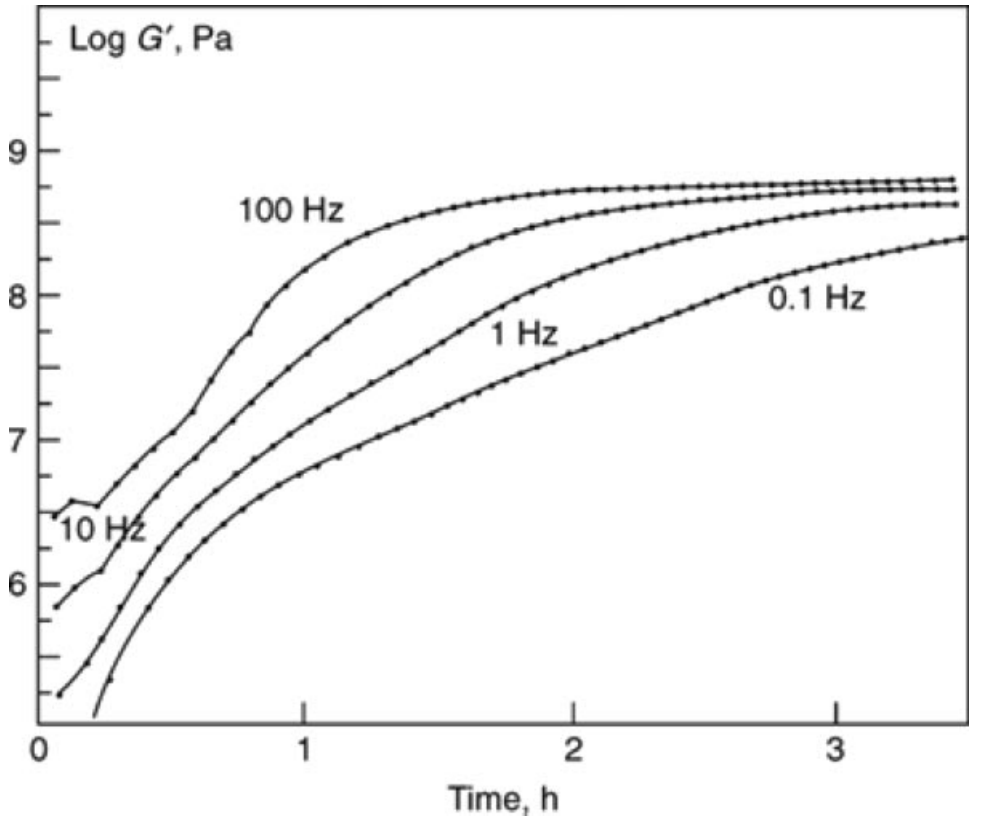

Fig. 52. Dynamic mechanical storage modulus data measured over a range of frequencies during the isothermal cure (137°C) of the same epoxy–amine system (DGEBA/DDS) as in Figure 51 (120).

the cure proceeds and viscosity increases, offering more resistance to the transport of ions. Hence, conductivity is related to the viscosity of the polymer system (124) and the density or "tightness" of the crosslink network. Eventually, there is an inflection in the conductivity versus cure time curve that marks the slowing of the reaction. When there is no further change in conductivity with cure time (ie, $d\sigma/dt \rightarrow 0$), the reaction is considered to be complete (125).

As noted above the ionic conductivity is related to the viscosity of the system prior to up to vitrification, where the reaction becomes diffusion-controlled (126). This is demonstrated by observing conductivity and viscosity changes during dynamic curing at a constant heating rate. Figure 55 illustrates the dynamic cure of a brominated epoxy–phenolic system at a heating rate of 7°C/min (125). Superimposed on the dielectric loss factor plot are dynamic viscosity data taken in a rheometrics rheometer specially adapted to simultaneously measure both dielectric and flow properties of a curing resin. At short times (corresponding to low temperatures), where the reaction is insignificant, the loss factor increases with temperature because of decreasing viscosity. After ∼18 min of ramped heating, the reaction rate becomes significant, resulting in a viscosity increase, while

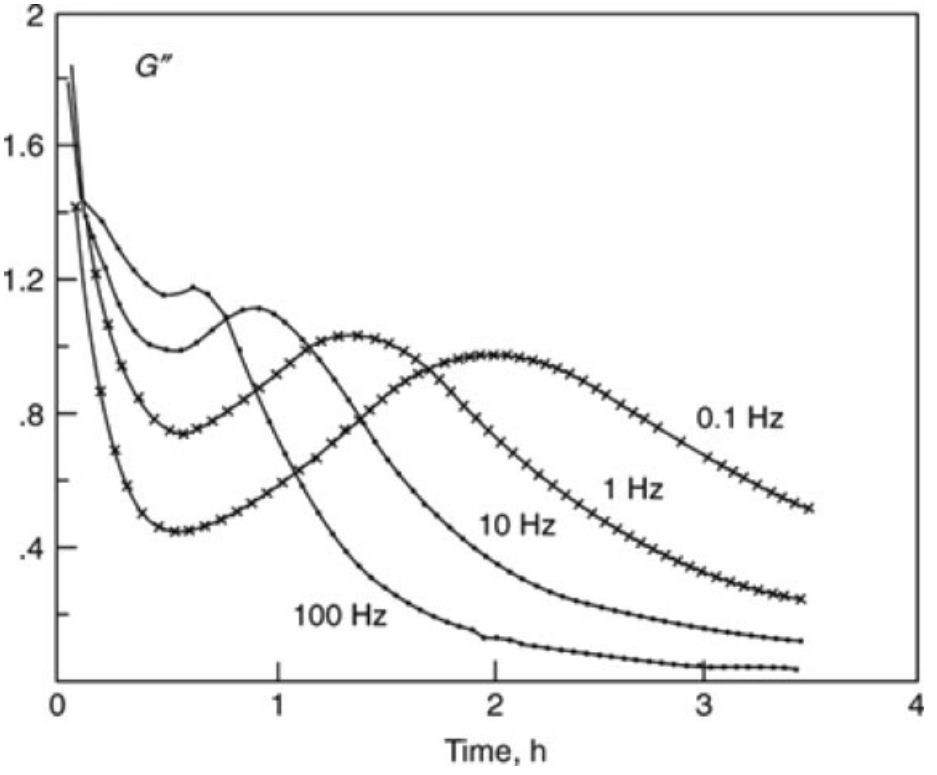

Fig. 53. Dynamic mechanical loss modulus data measured over a range of frequencies during the isothermal cure (137°C) of the same epoxy–amine system (DGEBA/DDS) as in Figure 51 (120).

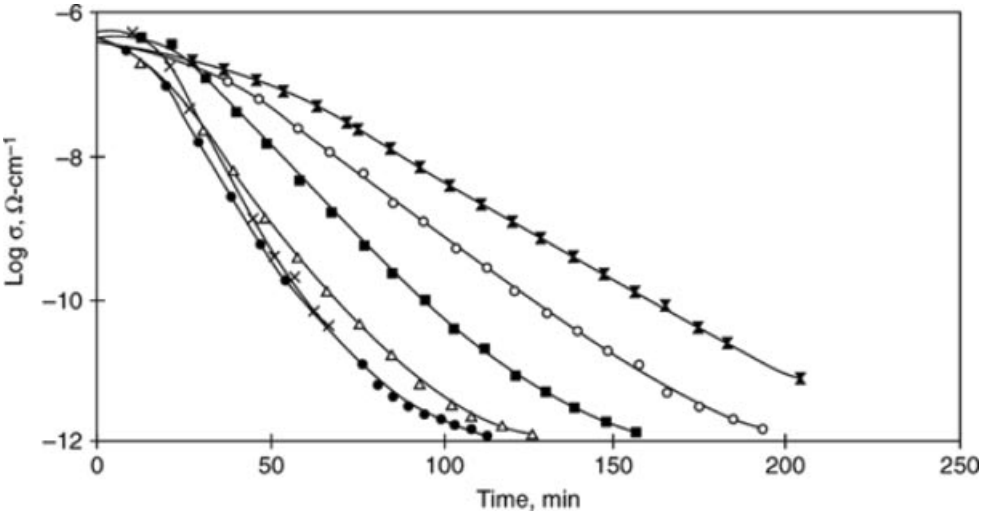

Fig. 54. Isothermal ionic conductivity data for the DGEBA/DDS resin of Figure 51 at various cure temperatures (76,120). ⧗, 135°C; ○, 145°C; ■, 162°C; △, 167°C; ●, 173°C; ×, 188°C.

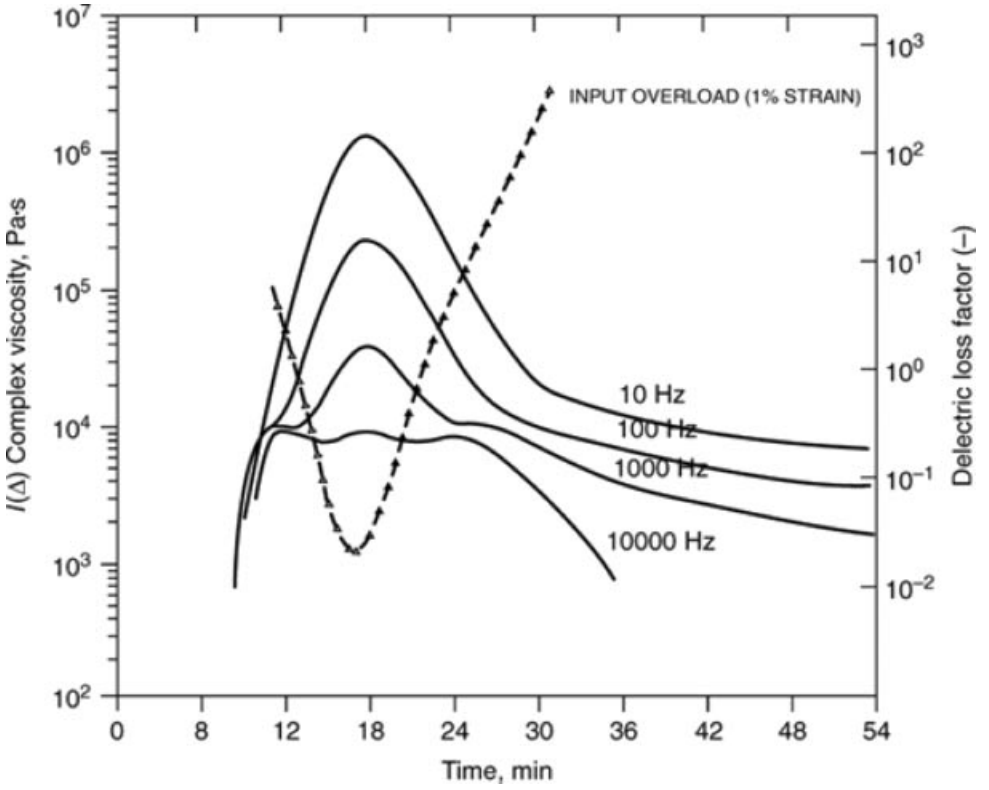

Fig. 55. Dynamic cure of a brominated epoxy–phenolic system at a heating rate of 7°C/min (125); superimposed on the dielectric loss factor plot are dynamic viscosity data taken with a rheometrics rheometer. 1 Pa · s = 10 P.

conductivity decreases. The loss factor maximum peak is frequency-independent and occurs in the same time range as the minimum viscosity. In addition, frequency-dependent dipole peaks preceding the loss factor maximum correspond to the softening of the resin system upon heating as the neat resin passes through the glass transition. The dipole peaks observed following the loss factor maximum occur near the time at which the torque input overloads on the rheometer, indicating that they correspond to vitrification (127,128). Similar studies were reported for a bismaleimide–triazine resin system (129).

Figure 56 shows the results of dielectric analysis for the DGEBA/DDS system at a heating rate of 3°C/min, presented as log ε'' versus temperature. The glass transition is detected by the frequency-dependent dipole peaks (Fig. 56**b**) between 0 and 50°C (T_g by DSC would be more typical of values at 0.1–1 Hz, perhaps 20–30°C lower than these data) (76). The frequency-independent viscosity minimum is also evident near 150°C.

For more detail on DEA characterization of thermoset cure as well as other aspects of thermosets, the reader is referred to the excellent presentation by Prime (115) and the entry on thermosets by Prime and Gotro in this encyclopedia.

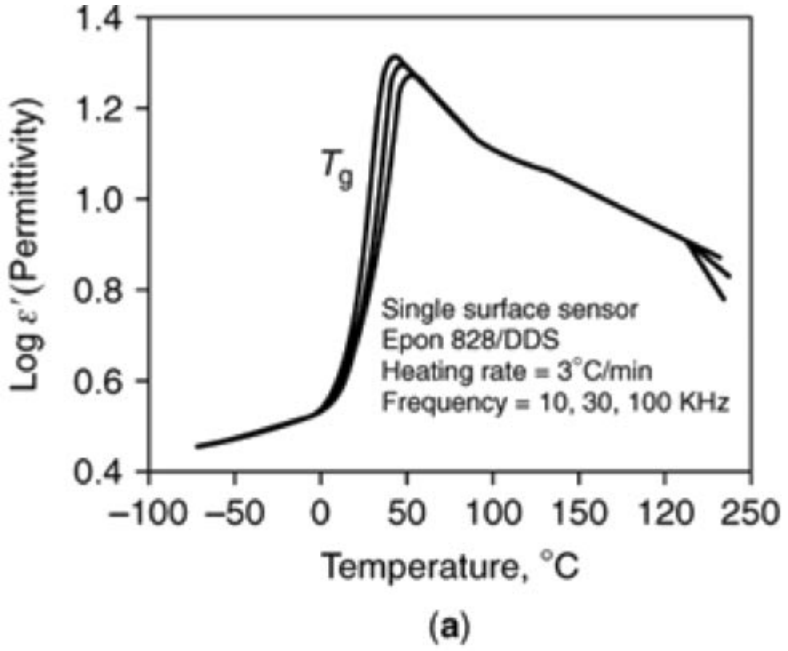

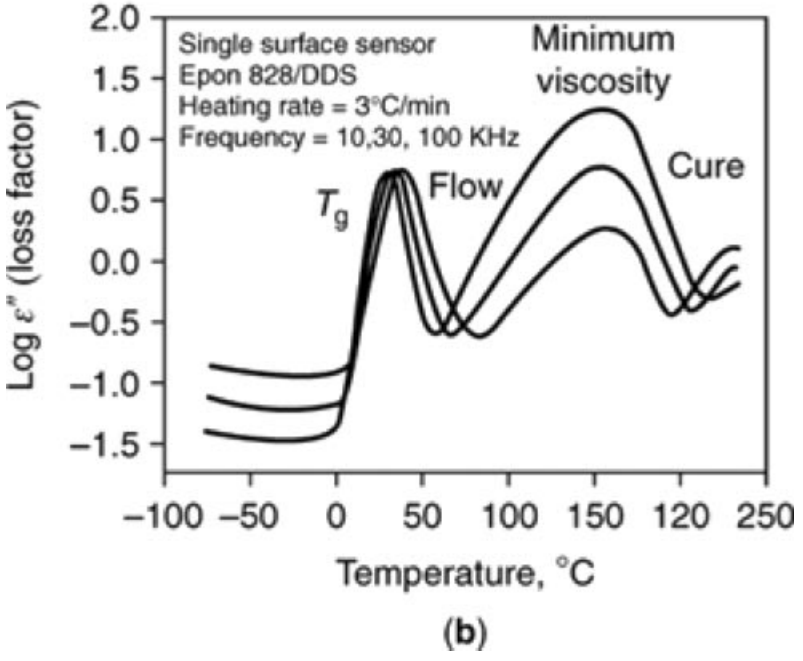

Fig. 56. Dielectric analysis data for the DGEBA/DDS system at a heating rate of 3°C/min, presented as log (ε'') vs temperature. The glass transition is indicated by the frequency-dependent dipole peaks between 0 and 50°C (76).

BIBLIOGRAPHY

"Thermal Analysis" in *EPSE* 2nd ed., Suppl. Vol, pp. 690–723, by Joseph H. Flynn, Sci. Thermal Research & Data Analysis.

1. R. C. Mackenzie, in I. M. Kolthoff, P. J. Elving, and E. B. Sandell, eds., *Treatise on Analytical Chemistry*, Vol. 12, Pt. 1, John Wiley & Sons, Inc., New York, 1983, p. 1.
2. J. O. Hill, *For Better Thermal Analysis and Calorimetry*, ICTA, 3rd ed., CPC Reprographics, Portsmouth, U.K., 1991.
3. P. K. Gallagher, *Adv. Anal. Geochem.* **1**, 211 (1993).
4. W. W. Wendlandt, *Thermal Analysis*, 3rd ed., John Wiley & Sons, Inc., New York, 1986.
5. E. A. Turi, ed., *Thermal Characterization of Polymeric Materials*, 2nd ed., Academic Press, New York, 1997.
6. B. Ke, in *Encyclopedia of Polymer Science and Technology*, Vol. 5, John Wiley & Sons, Inc., New York, 1970.
7. E. S. Watson, M. J. O'Neill, J. Justin, and N. Brenner, *Anal. Chem.* **36**, 1233 (1964).
8. C. Y. Zahra and A. M. Zahra, *Thermochim. Acta* **276**, 161 (1996).
9. J. Boerio-Goates and J. E. Callanan, in B. W. Rossitor and R. C. Baetzold, eds., *Physical Methods in Chemistry*, Vol. 6, Wiley-Interscience, New York, 1992, p. 621.
10. G. W. H. Ohne, J. Schawe, and C. Schick, *Thermochim. Acta* **221**, 129 (1993).
11. B. Wunderlich, *Thermal Analysis*, Academic Press, San Diego, Calif., 1990.
12. R. Hultgren and co-workers, *Selected Values of the Thermodynamic Properties of the Elements*, American Society of Metals, Metals Park, Ohio, 1973.
13. I. Barin, *Thermochemical Data of Pure Substances*, Wiley-VCH, Weinheim, Germany, 1989.
14. Z. Zhong and P. K. Gallagher, *Thermochim. Acta* **186**, 199 (1991).
15. P. K. Gallagher, Z. Zhong, E. L. Charsely, and S. A. Mikhail, *J. Therm. Anal.* **40**, 1323 (1990).
16. G. Hakvoort, *Calorim. Anal. Therm.* **24**, 177 (1993).
17. G. Della Gatta and J. Barczynska, *Calorim. Anal. Therm.* **24**, 543 (1993).
18. Z. Tan and R. Sabbah, *J. Therm. Anal.* **41**, 1577 (1994).
19. M. E. Brown, *Introduction to Thermal Analysis*, Chapman and Hall, London, 1988.
20. A. K. Sircar, *J. Sci. Ind. Res. (India)* **41**, 536 (1982).
21. A. K. Sircar and T. G. Lamond, *Rubber Chem. Technol.* **45**, 329 (1972).
22. S. H. Goh, *Polym. Degrad. Stab.* **8**, 123 (1984).
23. O. T. Savasçi and S. M. Baysal, *J. Appl. Polym. Sci.* **31**, 2157 (1986).
24. M. J. R. Loadman, *J. Therm. Anal.* **30**, 929 (1985).
25. A. K. Sircar and R. P. Chartoff, in R. J. Seyler, ed., *Assignment of Glass Transition*, ASTM STP 1249, American Society for Testing and Materials, Philadelphia, Pa., 1994, pp. 226–238.
26. A. K. Sircar, *Rubber Chem. Technol.* **72**, 513 (1999).
27. R. A. Fava, *Polymer* **9**, 137 (1968).
28. H. W. Starkweather, Jr., P. Zoller, and G. A. Zones, *J. Polym. Sci., Polym. Phys. Ed.* **21**, 295 (1983).
29. S. Sauerbrunn, B. Crowe, and M. Reading, *Am. Lab.* **24**(12), 44 (1992).
30. J. E. K. Schawe, C. Schick, and G. W. H. Höhne, *Thermochim. Acta* **244**, 49 (1994).
31. S. R. Aubochon and P. S. Gill, *J. Therm. Anal.* **49**, 1039 (1997).
32. J. Chiu and P. G. Fair, *Thermochim. Acta* **34**, 267 (1979).
33. A. K. Sircar and J. L. Wells, *Rubber Chem. Technol.* **54**, 191 (1982).
34. S. M. Marcus and R. L. Blaine, *Thermochim. Acta* **243**, 231 (1994).
35. S. L. Madorsky, *Thermal Decomposition of Organic Polymers*, Wiley-Interscience, New York, 1964.

36. H. H. G. Jellinek, *Aspects of Degradation and Stabilization of Polymers*, Elsevier, Amsterdam, 1978.
37. L. Cahn and H. Schultz, *Anal. Chem.* **35**, 1729 (1963).
38. M. E. Brown, T. T. Bhengu, and D. R. Sanyal, *Thermochim. Acta* **242**, 141 (1994).
39. R. F. Speyer, *Thermal Analysis of Materials*, Marcel Dekker, Inc., New York, 1993.
40. W. W. Wendlandt, *Thermochim. Acta* **12**, 109 (1975).
41. B. Schubert and E. Knothe, *Prog. Vac. Microbalance Tech.* **1**, 207 (1972).
42. P. K. Gallagher and E. M. Gyorgy, *Thermochim. Acta* **109**, 193 (1986).
43. P. K. Gallagher and F. Schrey, *Thermochim. Acta* **1**, 465 (1970).
44. P. D. Garn, O. Menis, and H. G. Wiedeman, in H. G. Wiedeman, ed., *Thermal Analysis*, Vol. 1, Birkhaeuser, Basel, p. 201.
45. B. Dodson and I. C. McNeill, *J. Polym. Sci., Polym. Chem. Ed.* **14**, 353 (1976).
46. A. K. Sircar, *Thermochim. Acta* **27**, 337 (1978).
47. D. E. Larkin, in C. M. Earnest, ed., *Compositional Analysis in Thermogravimetry*, ASTM STP 997, American Society for Testing and Materials, Philadelphia, Pa., 1988, p. 28.
48. J. J. Maurer, in E. I. Turi, ed., *Thermal Characterization of Polymeric Materials*, Academic Press, New York, 1981, p. 571.
49. A. K. Sircar, *Rubber Chem. Technol.* **65**, 503 (1992).
50. P. S. Gill, S. R. Sauerbrunn, and B. S. Crowe, *J. Therm. Anal.* **38**, 255 (1992).
51. W. J. Sichina, *Am. Lab.* **25**, 45 (1993).
52. G. Goldsmith, T. E. Waterman, and H. J. Hirschhorn, *Handbook of Thermophysical Properties of Solid Materials*, rev. ed., Macmillan, New York, 1961.
53. C. M. Earnest and R. J. Seyler, in A. Riga, ed., *Material Characterization by Thermomechanical Analysis*, ASTM STP 1136, American Society for Testing and Materials, Philadelphia, Pa., 1991, p. 22.
54. C. M. Earnest and R. J. Seyler, *J. Test Eval.* **20**, 430 (1992).
55. R. J. Seyler and C. M. Earnest, *J. Test Eval.* **20**, 434 (1992).
56. W. F. Hemminger and W. Gorsky, *Thermochim. Acta* **69**, 137 (1983).
57. D. D. Gray, *American Institute of Physics Handbook*, McGraw-Hill, New York, 1963.
58. T. A. Hahn, *J. Appl. Phys.* **41**, 5096 (1970).
59. J. J. Maurer, in S. W. Shalaby, ed., *Thermal Methods of Polymer Analysis*, Franklin Institute Press, Philadelphia, Pa., 1978, p. 129.
60. J. J. Maurer, *Anal. Calorim.* **1**, 107 (1968).
61. B. C. Ennis and J. G. Williams, *Thermochim. Acta* **21**, 355 (1977).
62. C. M. Neag, in A. T. Riga and C. M. Neag, ed., *Material Characterization by Thermomechanical Analysis*, ASTM STP 1136 American Society for Testing and Materials, Philadelphia, Pa., 1991. pp. 3–21.
63. D. W. Brazier and G. H. Nickel, *Thermochim. Acta* **26**, 399 (1978).
64. B. Cassel, Perkin-Elmer TAAS 19; Perkin-Elmer TAAS 20; product bulletins from Thermal Analysis Application Series, PerkinElmer Life and Analytical Sciences, Inc., Boston, Mass.
65. F. M. Angeloni, *Polym. Prepr. (Am. Chem. Soc., Div. Polym. Chem.)* **8**, 950 (1967).
66. R. T. Lamoureux, *Proc. Tech. Program—Natl. Electron Packag. Prod. Conf.*, 1978, p. 161.
67. B. Cassel, DSC Product Document MA-29, product bulletins from PerkinElmer Life and Analytical Sciences, Boston, Mass.
68. G. F. Sykes, H. D. Burkes, and J. B. Nelson, Proc. Natl. SAMPE Symp. Exhib., 22nd, 1977, p. 350.
69. S. W. Schmit, Proc. Int. Rubber Conf., Munich, 1974, Paper No. 305.
70. J. D. Ferry, *Viscoelastic Properties of Polymers*, 3rd ed., John Wiley & Sons, Inc., New York, 1980, p. 641.

71. General references on dielectric characterization include: N. G. McCrum, B. E. Read, and G. Wiliams, *Anelastic and Dielectric Effects in Polymeric Solids*, John Wiley & Sons, Inc., New York, 1967; C. W. Reed, in F. E. Kraus, ed., *Dielectric Properties of Polymers*, Plenum Press, New York, 1972; P. Hedvig, *Dielectric Spectroscopy of Polymers*, McGraw-Hill, New York, 1977; D. R. Day, in Ho-Ming Tong and Luu T. Nguyen, eds., *New Characterization Techniques for Thin Polymer Films*, John Wiley & Sons, Inc., New York, 1990.
72. L. E. Nielsen and R. F. Landel, *Mechanical Properties of Polymers and Composites*, 2nd ed., Marcel Dekker, Inc., New York, 1994, p. 557.
73. E. A. Collins, J. Bares, and F. W. Billmeyer, Jr., *Experiments in Polymer Science*, Wiley-Interscience, New York, 1973; A. V. Tobolsky, *Properties and Structure of Polymers*, John Wiley & Sons, Inc., New York, 1960, p. 331.
74. L. H. Sperling, *Introduction to Physical Polymer Science*, 3rd ed., Wiley-Interscience, New York, 2001, p. 352.
75. D. R. Day, T. J. Lewis, H. L. Lee, and S. D Senturia, *J. Adhes.* **18**, 73 (1985).
76. S. A. Bidstrup and D. R. Day, in R. J. Seyler, ed., *Assignment of the Glass Transition*, American Society for Testing and Materials, Philadelphia, Pa., 1994, pp. 108–119.
77. R. P. Chartoff, in E. Turi, ed., *Thermal Characterization of Polymeric Materials*, 2nd ed., Academic Press, New York, Chapt. 3, 1997, pp. 483–743.
78. L. E. Nielsen, *Mechanical Properties of Polymers*, Van Nostrand-Reinhold, Princeton, N.J., 1962, p. 23.
79. R. P. Chartoff, P. Weissman, and A. Sircar, in R. J. Seyler, ed., *ASTM STP 1249, Assignment of the Glass Transition*, American Society for Testing and Materials, Philadelphia, Pa., 1994, p. 308.
80. R. H. Boyd, *Polymer* **26**, 323 (1985).
81. M. Takayanagi, *Proceedings of the Fourth International Congress on Rheology*, Part 1, Wiley-Interscience, New York, 1965, p. 161.
82. H. W. Starkweather, *ACS Symp. Ser.* **127**, 433 (1980).
83. R. H. Boyd, *J. Chem. Phys.* **30**, 1276 (1959).
84. A. E. Woodward, J. M. Crissman, and J. A. Sauer, *J. Polym. Sci.* **44**, 23 (1960).
85. J. Varlet, J. Y. Cavaillé, J. Perez, and G. P. Joharie, *J. Polym. Sci.: Part B: Polym. Phys.* **28**, 2691 (1990).
86. K. Schmieder and K. Wolf, *Kolloid-Z.* **134**, 148 (1953).
87. H. W. Starkweather, *J. Polym. Sci., Polym. Phys. Ed.* **11**, 587 (1973).
88. H. W. Starkweather, in M. I. Kohan, ed., *Nylon Plastics*, John Wiley & Sons, Inc., New York, 1973.
89. D. C. Prevorsek, R. M. Butler, and H. K. Reimschussel, *J. Polym. Sci.* **9**, 867 (1971).
90. H. W. Starkweather and J. R. Barkley, *J. Polym. Sci., Polym. Phys. Ed.* **19**, 1211 (1981).
91. P. Avakian, R. R. Matheson, Jr., and H. W. Starkweather, Jr., *Macromolecules* **24**, 4698 (1991).
92. J. Hiltz and I. A. Keough, *Thermochim. Acta* **212**, 151–162, (1992).
93. G. Allen, J. McAinsh, and G. M. Jeffs, *Polymer* **12**, 85 (1971).
94. T. Lim, V. Frosini, V. Zaleckas, D. Morrow, and J. A. Sauer, *Polym. Eng. Sci.* **13**, 51 (1973).
95. C. I. Chung and J. A. Sauer, *J. Polym. Sci.: Part A: Polym. Chem.* **9**, 1097 (1971).
96. K. H. Illers, *Kolloid Z. Z. Polym.* **250**, 426 (1972).
97. H. Arai, and I. Kuriyama, *Colloid Polym. Sci.* **254**, 967 (1976).
98. H. Sha, I. R. Harrison, and X. Zhang, in *Proceedings of the 19th North American Thermal Analysis Society Conference*, 1990, p. 179.
99. G. Menges and H.-E. Boden, in W. Brostow and R. D. Corneliussen, eds., *Failure of Plastics*, Hanser, Munich, 1986, Chapt. 9, pp. 169–195.
100. R. F. Boyer, *Polym. Eng. Sci.* **8**, 161 (1968).

101. W. Retting, *Rheol. Acta* **8**, 259 (1969).
102. B. Hartmann and G. F. Lee, *J. Appl. Polym. Sci.* **23**, 3639 (1979).
103. L. M. Robeson and J. A. Faucher, *J. Polym. Sci., Polym. Lett. Ed.* **7**, 35 (1969).
104. L. Bohn, *Kunstoffe* **53**, 826 (1963).
105. G. Pezzin, G. Ajroldi, and C. Garbuglio, *J. Appl. Polym. Sci.* **11**, 2553 (1967).
106. H. W. Starkweather, Jr., *Macromolecules* **21**, 1798 (1988).
107. T. Tanaka, G. E. Johnson, and S. Matsuoka, in *Proceedings of the 20th NATAS Conference*, 1991, pp. 144–149.
108. S. Matsuoka and X. Quan, *Macromolecules* **24**, 2770 (1991).
109. S. Matsuoka, in *Proceedings of 20th NATAS Conference*, 1991, pp. 8–15.
110. S. Matsuoka, *Relaxation Phenomena in Polymers*, Hanser Publishers, Munich, New York, 1992.
111. A. Hale, C. W. Macosko, and H. E. Bair, *Macromolecules* **24**, 2610–2621 (1991); R. A Venditti and J. K. Gillham, *J. Appl. Polym. Sci.* **64**, 3 (1997).
112. J. Wei, M. C. Hawley, and M. T. DeMeuse, *Polym. Eng. Sci.* **35**, 461–470 (1995).
113. D. Klosterman, R. Chartoff, T. Tong, and M. Galaska, *Thermochim. Acta* **396**, 199–210 (2003).
114. See for example, E. G. Bobalek, E. R. Moore, S. S. Levey, and C. C. Lee, *J Appl. Polym. Sci.* **8**, 635–657 (1964); J. A. Manson, L. H. Sperling, S. L. Kim, Influence of Crosslinking on the Mechanical Properties of High Tg Polymers, AFML-TR-77-109 (US Air Force Technical Report, Wright Patterson Air Force Base), July, 1977.
115. R. B. Prime, in E. Turi, ed., *Thermal Characterization of Polymeric Materials*, 2nd ed., Academic Press, New York, 1997, Chapt. 6, pp. 1379–1766.
116. C. Y.-C. Lee and I. J. Goldfarb, *Polym. Eng. Sci.* **21**, 390 (1981); **21**, 787 (1981).
117. N. F. Sheppard, S. L. Garverick, D. R. Day, and S. D. Senturia, in *Proceedings of the 26th SAMPE Symposium*, 1983, p. 65.
118. S. D. Senturia and N. F. Sheppard, Jr., *Adv. Polym. Sci.* **80**(1), 1–47 (1986).
119. N. F. Sheppard and S. D. Senturia, *J. Polym. Sci., Part B: Polym. Phys.* **27**, 753–762 (1989).
120. N. F. Sheppard, Jr., Dielectric Analysis of the Cure of Thermosetting Epoxy/Amine Systems, Ph.D. dissertation, Department of Electrical Engineering, Massachusetts Institute of Technology, Cambridge, Mass., 1986.
121. N. F. Sheppard, M. C. W. Coln, and S. D. Senturia, in *Proceedings of 29th National SAMPE Symposium and Exhibition*, 1984, pp. 1243–1250.
122. B. Cassel and B. Twombly, in A. T. Riga and M. Neag, ed., *Material Characterization by Thermomechanical Analysis*, ASTM STP 1136, American Society for Testing and Materials, Pa., 1991, pp. 108–119.
123. T. Koike, *J. Appl. Polym. Sci.* **44**, 679–690 (1992).
124. S. A. Bidstrup, N. F. Sheppard, and S. D. Senturia, *Polym. Eng. Sci.* **29**, 325–328 (1989).
125. J. T. Gotro and M. Yandrasits, *Polym. Eng. Sci.* **29**, 278 (1989).
126. J. O. Simpson and S. A. Bidstrup, *J. Polym. Sci., Polym. Phys. Ed.* **31**, 609–618 (1993).
127. B. Fuller, J. T. Gotro, and G. C. Martin, *ACS Adv. Chem. Ser.* **227**, 215–234 (1990).
128. J. T. Gotro, B. K. Appelt, and K. I. Papathomas, *Polym. Compos.* **8**, 39–45 (1987); *IBM J. Res. Dev.* **32**, 616–625 (1988).
129. "Dielectric Analysis" brochure, Courtesy of TA Instruments, Inc., New Castle, Del.; available at www.tainst.com.

RICHARD P. CHARTOFF
University of Arizona
ANIL K. SIRCAR
University of Dayton (retired)